Polyhedron Vol. 10, No. 1, pp. 1–9, 1991
Printed in Great Britain

0277–5387/91 $3.00+.00
© 1991 Pergamon Press plc

TEMPLATE SYNTHESIS OF SUBSTITUTED CYCLOPENTANONES BY ZIRCONOCENE/OLEFIN/CO SYSTEMS*

MUNETAKA AKITA, HAJIME YASUDA,†‡ HITOSHI YAMAMOTO and AKIRA NAKAMURA†

Department of Macromolecular Science, Faculty of Science, Osaka University, Toyonaka, Osaka 560, Japan

(*Received* 6 *July* 1990; *accepted* 17 *July* 1990)

Abstract—A series of 3,4-dialkylcyclopentanones was synthesized by template reactions on the "Cp_2Zr" moiety generated from Cp_2Zr(2,4-hexadiene) or Cp_2Zr(olefin) complexes by ligand exchange reactions. The addition of a 1-olefin or 1,7-octadiene to the Cp_2Zr species followed by CO insertion and acid hydrolysis gave a *cis*- or *trans*-disubstituted cyclopentanone in high yield.

Conjugated diene complexes of zirconium of the type Cp_2Zr(diene) are unique in their mode of coordination for the diene. For example, when prepared from Cp_2ZrCl_2 and butenediylmagnesium at low temperature, the simplest member exists in a mixture of complexes with s-*cis* and s-*trans* butadiene ligands.[1,2] Our subsequent study has indicated a remarkable difference in the nature of the bonding of these metal–diene complexes. The s-*cis* isomer has a metallacyclopentene structure in which the reactive metal–carbon σ-bonds readily react with organic homo- and hetero-unsaturated species [eq. (1)].[3,4] In the s-*trans* isomers, η^4-diene coordination is found and thus the diene is prone to dissociate partially to a η^2-diene species (monoene coordination) or completely to a solvent-coordinated metallocene species in solution [eq. (2)].

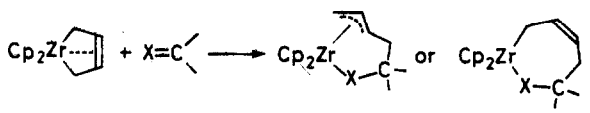

(1)

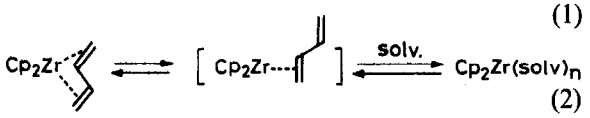

(2)

We have found that alkyl or aryl substitution at the terminal positions of the diene enhances the stability of the s-*trans* coordination.[1a,5] Thus, (*E*,*E*)-2,4-hexadiene in the zirconium complex, $Cp_2Zr(C_6H_8)$, exists exclusively in the s-*trans* form. In the reaction with 1-olefin, the s-*cis* complexes give metallacycles by olefin insertion into the Zr—C bond of the diene. In contrast, the s-*trans* complexes, especially complex **1**, release the diene and give metallacyclopentanes by oxidative coupling of two olefin molecules [eq. (3)]. Thus, the s-*trans*-2,4-hexadiene complex can serve as an equivalent of coordinatively unsaturated "Cp_2Zr".

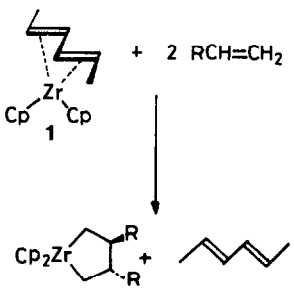

(3)

This latter reaction seems remarkable since η^4-coordination of a diene is generally known to be more stable than the η^2-coordination of olefins.

Factors influencing regio- and stereochemistry of the metallacyclization step are important for the selective synthesis of disubstituted cyclopentanones utilizing metallacyclopentanes.[6] Regioselectivity in the formation of metallacyclopentanes has been

* Paper presented at the Symposium on Applied Organometallic Chemistry, Pokolbin, N.S.W., Australia, 10–12 July 1989.

† Authors to whom correspondence should be addressed.

‡ Present address: Department of Applied Chemistry, Hiroshima University, Kagamiyama 1-4-1, Higashi-Hiroshima 724, Japan.

theoretically investigated by Lauher and Hoffmann and McKinney, and the importance of overlap between the antibonding olefin orbitals has been pointed out.[7] The validity of this prediction may be tested in the present example.

Carbonylation of alkyl–zirconium species has been extensively investigated and mechanisms involving η^2-acyl or oxycarbene ligands have been proposed.[8] The bicyclic structure of zirconahydrindane may offer a unique opportunity for investigation of this type of carbonylation. The stereochemical fate of the bicyclic ring fusion upon carbonylation and the influence of the bicycle on the carbonylation mechanism are also of interest.

In this report, we describe a template synthesis of metallacyclopentanes from a labile s-*trans* hexadiene or an olefin complex, and the formation of substituted cyclopentanones by subsequent reaction with CO followed by acid hydrolysis.

RESULTS AND DISCUSSION

Reaction of Cp_2Zr(*hexadiene*) *with* 1-*olefin*

The addition of one equiv. of 1-olefin to Cp_2Zr(2,4-hexadiene) (**1**) was found to provide a zirconacyclopentane (**2**) together with the 1 : 1 insertion product (**3**) and a trace amount (< 5%) of its isomer (**4**) [eq. (4)].

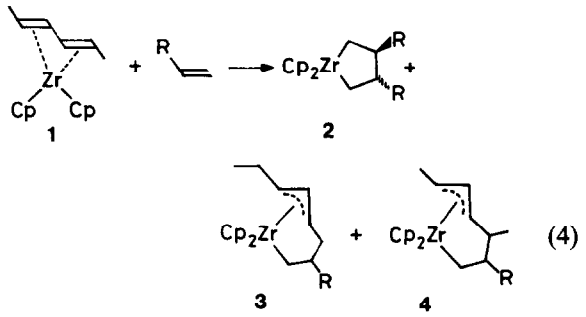

(4)

In the initial stage of this reaction (for example, at room temperature for 2–4 h), the formation of zirconacyclopentane species (**2**) was predominant as a result of ligand exchange and subsequent metallacyclization. Progress of the reaction was monitored by GLC after acidic hydrolysis of the resulting products; the results of reactions (30°C for 3 h) are summarized in Table 1.

Terminal olefins readily give rise to the formation of **2** in more than 80% yield. The product from 1-pentene prefers the *trans*-configuration in sharp contrast to the *cis*-form for the 1,7-octadiene derivatives (*vide infra*). Butadiene was also converted into a metallacycle by C—C coupling at the terminal position of two butadiene molecules, liberating the ligated 2,4-hexadiene in quantitative yield, to give a zirconacyclo-3,7-nonadiene derivative (**11**) in 93% yield. Reaction with styrene, however, gave different products (the structure of the major product is unknown because of the polymeric nature). Although the 2,4-hexadiene ligand was expelled completely, the formation of a styrene dimer was not detected from the hydrolyzate. Only a small amount of ethylbenzene, presumably derived from Cp_2Zr(styrene), was detected upon hydrolysis. Inner olefins such as 2-pentene and 3-hexene were found to be completely inert to **1** under conditions employed here. By contrast, 2-butyne rapidly reacts with **1** to afford 2,3,4,5-tetramethylzirconacyclopentadiene (**12**) in high yield.

Table 1. Mode of reaction between Cp_2Zr(2,4-hexadiene) and olefins[a]

Olefins	Distribution of products (%) 2(*trans*/*cis*)	3	Others	Total yield (%)
1-Pentene	86(95/5)	14	0	96
1-Heptene	78(95/5)	22	0	94
1,7-Octadiene	89(12/88)	11	0	92
Styrene	0	0	80	20
Butadiene			95	95
2-Heptene	0	0	0	0

[a] Result of the reaction after stirring at 30°C for 2 h.

The zirconacyclopentanes (**2**) thus formed from 1-pentene and 1-heptene in the initial stage of the reaction were gradually transformed to diene adducts (**3**) on standing the mixture at room temperature for 4 days or heating them at 60°C for 6 h. However, when the liberated 2,4-hexadiene was removed in the initial stage of the reaction by flash distillation, compound **2** could be isolated as a dark brown oily product. Thus, the 2,4-hexadiene ligand once liberated from the metal again participates in coupling with the 1-olefin to give **3** [eq. (5)]. This type of reaction has not been observed previously when 1-olefins rather than 2,4-hexadiene were added to **2**.

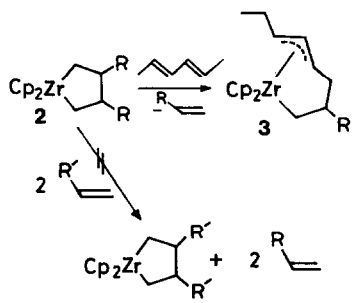

Consequently, reductive cyclization occurs competitively on the metal sphere of **1** to predominantly

produce the *trans*-3,4-dialkylzirconacyclopentane under thermodynamic equilibrium. Two C_2 fragments may be arranged so as to facilitate the C—C bond formation between carbon atoms bearing the biggest olefinic π^* lobes, as shown below. Steric repulsion between Cp and alkyl groups of coordinating olefins should hamper the formation of 2,4- and 2,5-dialkylzirconacyclopentanes.

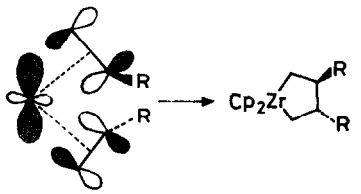

(6)

Reaction of $Cp_2Zr(C_6H_8)$ *with* 1,7-*octadiene*

Metallabicyclization occurs more readily by using a chelating linear diolefin, 1,7-octadiene. A high yield of the *cis*-isomer of zirconahydrindane (**5a**) starting from **1** indicates that the favourable orientation of the two olefinic units towards Cp_2Zr species is the *cis*-arrangement. However, prolonged heating of the *cis*-zirconahydrindane (**5a**) at 60°C for 6 h was found to result in quantitative conversion to the *trans*-isomer, **5b** [eq. (7)]. The configurational change may occur through an η^2,η^2-bis(olefin)metal intermediate **6a** → **6b** shown in Scheme 1.

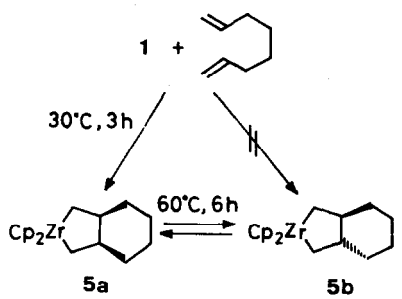

(7)

Both of the present bicyclic complexes, **5a** and **5b**, are thermally more stable than 3,4-dialkylated zirconacyclopentanes which decompose at 60–70°C. Thus, the *cis*-isomer **5a** is concluded to be a kinetic product and the *trans*-isomer **5b** a thermodynamic product.

On the other hand, Gell and Schwartz reported that the addition of 1,7-octadiene to a zirconocene–phosphine complex produced a 1 : 1 mixture of **5a** and **5b** [eq. (8)].[9]

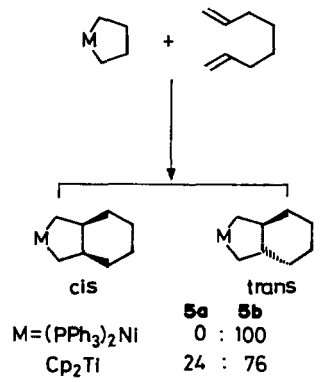

	5a	5b
$M=(PPh_3)_2Ni$	0	100
Cp_2Ti	24	76

(8)

Similar behaviour was also observed for other metallahydrindanes as reported by Grubbs and Miyashita, who prepared the corresponding titanium compounds by a ligand exchange reaction using parent monocyclic complexes.[10] Ready conversion of a nickelacycle from the *cis*-form to the *trans*-isomer, which is prepared from $(Ph_3P)_2NiCl_2$ and *cis*-1,2-di(lithiomethyl)cyclohexane, clearly confirms that the *trans*-isomer is the thermodynamic product. The formation of a mixture of *cis*- and *trans*-isomers (*ca* 1 : 1) was also found in the synthesis of a bicyclic tantalacycle, as reported by McLain and Schrock.[11]

Preference for the *cis*- or *trans*-configuration should largely depend on the strength of ligand coordination to the metal. The complexes with strongly coordinated ligands, such as phosphines, ethylene and even terminal olefins, bring about the

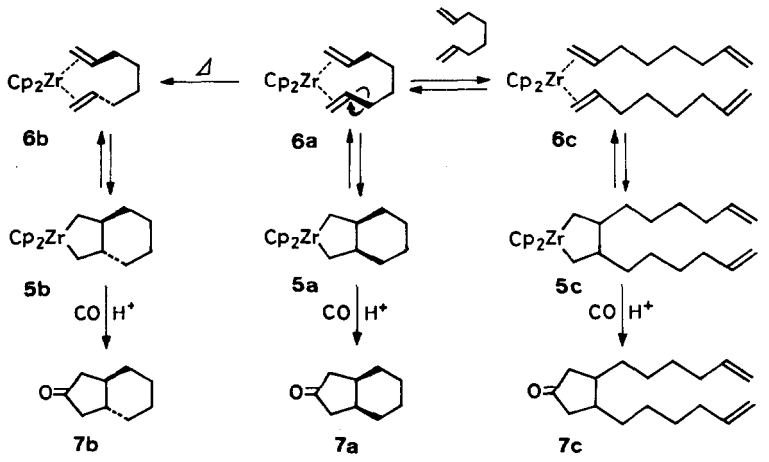

Scheme 1.

Table 2. Formation of 3,4-dialkylcyclopentanones by carbonylation of zirconacyclopentanes obtained from **1** and olefins[a]

Olefins	Yield (*trans*/*cis*) (%)
1-Pentene	78(95/5)
1-Heptene	76(96/4)
1,7-Octadiene	75(10/90)
Styrene	15(52/48)
Butadiene	0
2-Heptene	0

[a] Reaction conditions for carbonylation with CO, 30°C for 6 h in benzene.

interconversion between *cis*- and *trans*-isomers and finally produce the stable *trans*-isomer. By contrast, highly hindered 2,4-hexadiene was readily liberated irreversibly from Cp_2Zr(2,4-hexadiene) and the analytically pure *cis*-zirconahydrindane could be obtained by utilizing this unique ligand exchange reaction. Thus, we can control the stereochemistry in the formation of substituted metallacyclopentanes by choosing appropriate ligands in Cp_2ML_2 or $(R_3P)ML_2$.

Carbonylation of 3,4-disubstituted zirconacyclopentanes

(a) *Reaction route using* Cp_2Zr(*diene*). Bicyclic zirconium complexes, **5a** and **5b**, synthesized from **1**, demonstrated an interesting series of carbonylation reactions, as shown in Scheme 1. The addition of CO to isolated **5a** and **5b**, in benzene under atmospheric pressure, afforded *cis*-hydrindanone (**7a**) and *trans*-hydrindanone (**7b**) in high yield (> 85%), respectively. The reaction occurs with retention of configuration as confirmed by the ^{13}C NMR studies. However, the corresponding reaction of **5a** in the presence of 3 equiv. of 1,7-octadiene led to the formation of a 1 : 2 adduct, 3,4-di(5-hexenyl)cyclopentanone (**7c**), in 85% yield. A reaction pathway through $Cp_2Zr(\eta^2$-1,7-octadiene$)_2$ (**6c**) seems most likely for this coupling. Although complexes **5a** and **5b** could be trapped by hydrolysis as a form of *cis*- and *trans*-1,2-dimethylcyclohexane, respectively, the expected 7,8-dimethyl-1,13-tetradacadiene was not detected from the reaction mixture obtained from **1** and excess 1,7-octadiene (4 equiv.) in the presence or absence of CO. This result indicates that the initially formed complexes, **5a** and **5b**, become labile under a CO atmosphere due to the ligation of CO and generate an intermediate **8**, a zirconocene (olefin)(carbonyl) complex [eq. (9)].

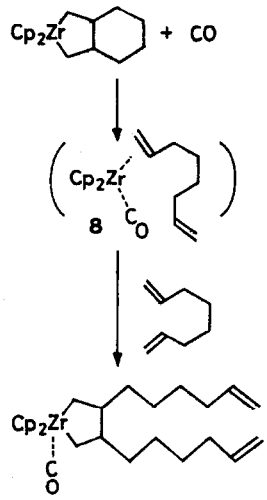

(9)

The subsequent reductive coupling of 1,7-octadiene followed by CO insertion occurs very rapidly.

On the other hand, the isolated complex **3** also could be converted into *trans*-hydrindanone in 67% yield by the addition of CO at room temperature for 3 h. However, complexes **9**, **10** and **12**, prepared from Cp_2Zr(butadiene) with 1-butene, 2-butyne or butadiene, were completely inert to CO under the usual conditions. Compound **11** is also inert to CO even at high temperature. On the basis of these results, we attribute the ease of liberation of coordinated 2,4-hexadiene to its great steric hindrance. Thus an equilibrium shown in eq. (10) is proposed, where the zirconocene species contains a σ,π-diene unit.

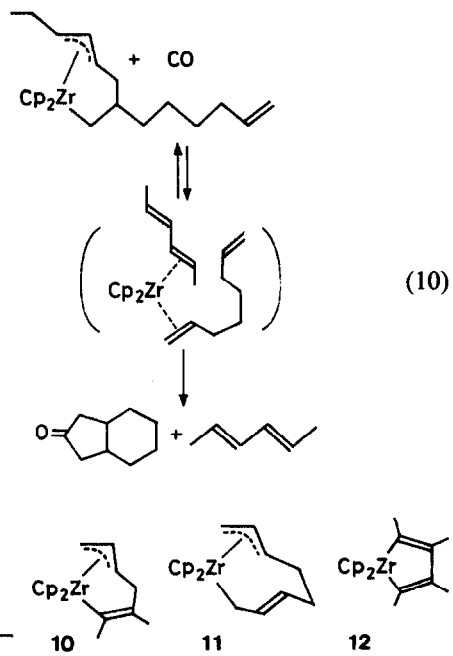

(10)

The inertness of **9–12** along with **3** (direct insertion of CO into **3** was not observed) suggests that the 18-electronic zirconium does not accept the initial coordination of CO.

The reaction of **1** with a 1-olefin (1 : 3) followed by carbonylation and protonolysis gave a simple product in high yield as shown in Table 2. The exception is the low yield (15%) observed for the zirconacyclopentane system derived from styrene. Although the formation of 3,4-diphenylzirconacyclopentane was not detected upon hydrolysis of the reaction mixture before carbonylation (only ethylbenzene was formed), the *in situ* reaction afforded 3,4-diphenylcyclopentanone. This reaction should proceed in essentially the same way as described for the formation of 3,4-di(5-hexenyl) cyclopentanone.

(b) *Reaction route using* Cp_2Zr(*olefin*) *complexes.* Recently the isolation of zirconocene–olefin complexes has been attained by Alt *et al.* and Takahashi *et al.* either by reaction of a zirconocene–phosphine complex with olefin[12] or by the 1 : 2 reaction of zirconocene dichloride with RCH_2Li or RCH_2MgX.[13] Since the Zr–olefin bond is presumed to be rather weak, these olefin complexes are expected to act as an equivalent of Cp_2Zr(2,4-hexadiene) or the coordinatively unsaturated "Cp_2Zr". Actually, a convenient one-pot synthesis of dialkylcyclopentanones has been realized by using these olefin complexes generated *in situ* [eq. (11)].[14]

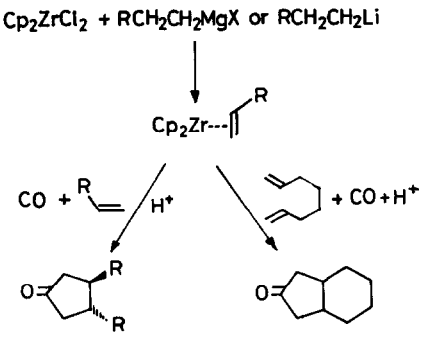

(11)

The addition of excess 1-olefin to Cp_2Zr(ethylene) or Cp_2Zr(butene), followed by the reaction with CO, gave the desired cyclopentanone derivatives in high yield (Table 3). The use of EtLi or n-BuLi is favourable for obtaining high yields of the product. The use of Grignard reagents was found to be less favourable, presumably due to the stabilization of the resulting zirconacyclopentanes by coordination with ether, a donor solvent. Actually, the addition of ether, THF, triethylamine or pyridine to n-BuLi (4 : 1 ratio) resulted in a significant decrease in the product yield (< 5%). When 1,7-nonadiene or 1,9-decadiene was used in similar reaction conditions,

Table 3. Carbonylation of zirconacyclopentanes generated by reactions of Cp_2ZrCl_2 with RLi or RMgX in the presence of 1-olefins

Reducing agents[a]	Reaction temperature (°C)[e]	1-Olefins	Yield of cyclopentanones (*trans*/*cis*) (%)
EtLi	30°C, 6 h	1-Pentene	33.6 (98/2)
n-BuLi	30°C, 6 h	1-Pentene	67.4 (98/2)
t-BuLi	30°C, 6 h	1-Pentene	9.9 (97/3)
EtMgBr	30°C, 6 h	1-Pentene	0.8
i-PrMgBr	30°C, 6 h	1-Pentene	0.6
EtLi	30°C, 6 h	1,7-Octadiene	58.2 (2/98)[b]
n-BuLi	30°C, 6 h	1,7-Octadiene	84.5 (1/99)
EtLi	60°C, 6 h	1,7-Octadiene	54.4 (82/18)
n-BuLi	60°C, 6 h	1,7-Octadiene	69.4 (83/12)
EtMgBr	30°C, 6 h	1,7-Octadiene	16.4 (3.97)
i-PrMgBr	30°C, 6 h	1,7-Octadiene	0.6
n-BuLi	30°C, 6 h	1,8-Nonadiene	61.3 (66/34)[c]
n-BuLi	30°C, 6 h	1,9-Decadiene	91.7 (98/2)[d]

[a] Alkyllithium was used as a hexane solution and RMgX as an ether solution.

[b] Total yield of hydrindanone.

[c] Ratio of 3,4-di(6-heptenyl)cyclopentanone and bicyclo[5.3.0]decan-9-one.

[d] Ratio of 3,4-di(7-octenyl)cyclopentanone and 3-ethyl-4-(7-octenyl) cyclopentanone.

[e] Reaction conditions for carbonylation with CO.

the formation of 3,4-dialkenylcyclopentanones (for example, **7d**) was predominant due to preference of the intermolecular cyclization [eq. (12)]. Although the reaction with 1,8-nonadiene provided a bicyclic cyclopentanone derivative (**7e**) as a minor product, the corresponding reaction was not observed with 1,9-decadiene.

Analogous metallabicyclization reactions starting from enynes[15] and diynes[16] have also been reported recently, and the carbonylation leading to cyclopentenone derivatives was successful only in the former case.

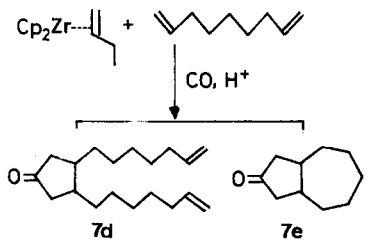

(12)

Reaction mechanism for formation of cyclopentanone

Two reaction sequences (shown in Scheme 2) are to be considered for the carbonylation of alkylzirconium complexes. Path A illustrates a reductive elimination from the alkylacyl intermediate (**13**) which is generated by CO insertion into zirconacyclopentanes (**5**). On the other hand, path B pursues migratory insertion of a transient oxycarbene intermediate (**14**) into the Zr—C bond affording zirconaoxiran (**15**), which subsequently rearranges to a hydridoenolato complex (**16**).

The reaction pathway has been analysed based on ^{13}C NMR studies. Four absorptions assignable to **5a** promptly disappeared upon the addition of CO and a set of seven signals emerged. This spectral change clearly confirms an unsymmetrical structure, i.e. hydrido-enolate, for the intermediate.

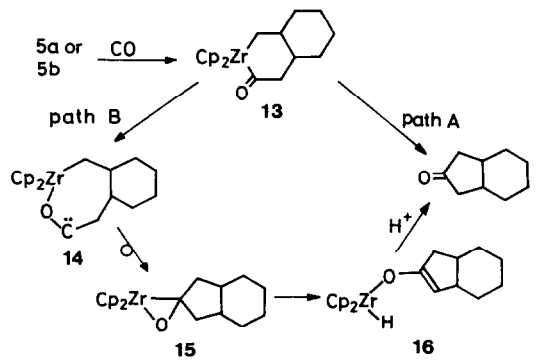

Scheme 2.

Actually, signals assignable to quarternary carbon and olefinic carbon are observed at 165.5 and 111.3 ppm, respectively. If **13** is the intermediate, the signal should be observed at around 300 ppm as found for $Cp_2Zr(Ar)(COAr)$.[17] Thus the carbonylation in the present work most likely proceeds through the migratory insertion mechanism.

The preference of the *cis*- or *trans*-configuration of the cyclopentanones may be largely effected by the mode of coordination of the acyl ligand. It is well established, based on MO calculations, that geometry **18** shown in eq. (13) is far more stable than its geometrical isomer **19**. However, the presence of a metallacyclic skeleton in **21** [eq. (14)] should prevent the rearrangement to the other isomer corresponding to **18** and hence the formation of η^2-hydrindanone **21** becomes favourable.

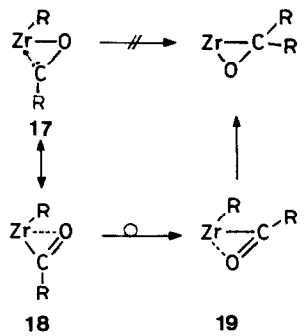

(13)

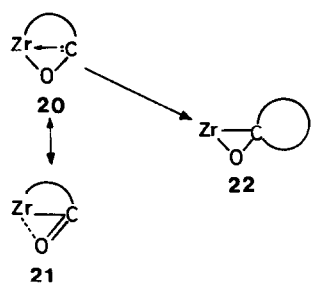

(14)

On the other hand, the species like **18** will not cause a migratory insertion via **17** because high energy is required for the geometrical inversion.

Concluding remarks

A series of 3,4-disubstituted cyclopentanones has been successfully synthesized by the carbonylation of dialkyl-substituted zirconacyclopentanes generated by the reaction of zirconocene-2,4-hexadiene or zirconocene–olefin complexes with two equiv. of 1-olefin or one equiv. of α,ω-unconjugated dienes. This type of reaction should have a broad application in the synthesis of cyclopentanones with a variety of substituents.

EXPERIMENTAL

Materials

Cp_2Zr(2,4-hexadiene) was prepared from $Cp_2Zr(H)Cl$ and hexadienylpotassium.[5] The 1:1 adducts of Cp_2Zr(butadiene) with 1-butene and 2-butyne were prepared as reported previously.[18]

Olefins were obtained commercially and CO was used without further purification.

Formation and carbonylation of zirconacyclopentanes from **1**

To a stirred benzene solution (10 cm^3) of Cp_2Zr(2,4-hexadiene) (**3**) (3 mmol), the 1-olefin (10 mmol) was added dropwise under argon. The mixture was stirred at room temperature for 2 h and the extent of the reaction was monitored by GLC after hydrolysis of the product. The solvent was then removed under reduced pressure. The amount of liberated (*E,E*)-2,4-hexadiene was determined by GLC analysis of the distillate. Benzene (10 cm^3) was added to the residue and the solution was cooled to −78°C. After the reaction mixture was purged with CO, reaction with CO was carried out at room temperature for 6 h. The solution was evaporated to dryness and the product was extracted with ether (20 cm^3). On addition of acetic acid (1 cm^3) the dark brown solution turned to pale yellow. Following work-up, analytically pure 3,4-dialkylcyclopentanones were obtained. Separation of the *cis*- and *trans*-isomers was carried out by preparative GLC.

Formation and carbonylation of zirconacyclopentanes from olefin complexes

A typical example of the one-pot synthesis of 3,4-dialkylcyclopentanones is shown below. Cp_2ZrCl_2 (0.5 mmol) and 1-olefin (5 mmol) were dissolved in oxygen-free, dried benzene (6 cm^3). To the stirred solution was added n-BuLi (0.63 cm^3, 1.6 M) at 0°C. The colour of the solution turned yellow–orange and finally brown by continuing the stirring for 4 h at 30°C. The reaction mixture was then cooled to −78°C and purged with CO gas using a rubber balloon. The resulting solution was stirred for 6 h at 30°C and treated with acetic acid (0.2 cm^3). On the addition of acetic acid, the colour changed to pale yellow. After the usual work-up, the sample was distilled to obtain analytically pure 3,4-dialkylcyclopentanone.

The reduction of Cp_2ZrCl_2 with RMgX in the presence of 1-olefin or 1,7-octadiene was carried out in essentially the same way as described above.

Structure determination of the products

The stereochemistry of the products was determined by ^{13}C NMR spectra with reference to the literature: *cis*- and *trans*-1,2-dimethylcyclohexane,[19] (*RS*)-6,7-dimethyldodecane,[20] *cis*-hydrindanone,[21] *trans*-3,4-diphenylcyclopentanone, cyclopentanol[22] and dimethylcyclopentanones.[23]

cis-*Zirconahydrindane* (**5a**). ^{13}C NMR: δ 24.6, 35.0, 42.1, 43.1, 111.6, 111.7.

trans-*Zirconahydrindane* (**5b**). ^{13}C NMR: δ 27.3, 41.3, 45.9, 49.3, 111.3.

cis-1,2-*Dimethylcyclohexane* (*hydrolysis product of* **5a**). ^1H NMR ($CDCl_3$): δ 0.82 (CH_3), 1.39 (CH_2), 1.63 (CH_2). ^{13}C NMR ($CDCl_3$): δ 23.7 [C(4), C(5)], 31.4 [C(3), C(6)], 34.3 [C(1), C(2)], 16.1 (CH_3).

trans-1,2-*Dimethylcyclohexane* (*hydrolysis product of* **5b**). ^1H NMR ($CDCl_3$): δ 0.85 (CH_3), 0.98 (CH), 1.30 (CH_2). ^{13}C NMR ($CDCl_3$): δ 27.0 [C(4), C(5)], 36.0 [C(3), C(6)], 39.5 [C(1), C(2)], 20.4 (CH_3).

6,7-*Dimethyldecane* (*hydrolysis product of* **2**, R = C_5H_{11}). ^1H NMR ($CDCl_3$): δ 0.86, 0.90 (CH_3), 1.29–1.35 (CH_2). ^{13}C NMR ($CDCl_3$): δ 14.2, 14.6 (CH_3), 22.9, 27.5, 32.4, 35.1 (CH_2).

(E)-7-*methyl*-1,9-*tridecadiene* (*hydrolysis product of* **3**, *where* R = 5-*hexenyl*). ^1H NMR: δ 0.84 (3H, d, J = 6.0 Hz, $CHCH_3$), 0.87 (3H, t, J = 6.0 Hz, CH_2CH_3), 1.05–1.65 [9H, m, $=CHCH_2CH_2CH_3$ and $CH(CH_3)(CH_2)_3CH_2CH=CH_2$], 1.70–2.30 (6H, m, $CH_2CH=CHCH_2$ and $CH_2CH=CH_2$), 4.80–5.10 (2H, $CH=CH_2$), 5.24–5.42 (2H, m, $CH=CH$), 5.55–6.00 (1H, m, $CH=CH_2$). IR (neat): 3070, 2960, 2920, 2850, 1642, 1465, 1378, 991, 969, 912 cm^{-1}. MS: m/z 194 (M^+). Found: C, 86.5; H, 13.4. Calc. for $C_{14}H_{26}$: C, 86.5; H, 13.5%.

trans-3,4-*Dipropylcyclopentanone*. ^1H NMR: δ 0.92 (6H, t, J = 6.0 Hz, CH_3), 1.04–1.54 (8H, m, $CHCH_2CH_2CH_3$), 1.54–2.00 [4H, m, O=C($CHHCH$)$_2$], 2.44 (2H, dd, J = 11.0 and 22.0 Hz, O=CCHH). ^{13}C NMR: δ 14.3 [C(3′)], 21.5 [C(2′)], 36.4 [C(1′)], 42.6 [C(3) and C(4)], 45.1 [C(2) and C(5)], 218.7 (CO). IR (neat): 2955, 2930, 2870, 1745, 1468, 1407, 1380, 1241, 1197, 1160 cm^{-1}. MS: m/z 168 (M^+). Found: C, 78.5; H, 11.5. Calc. for $C_{11}H_{20}O$: C, 78.5; H, 12.0%. *trans* Geometry was determined with reference to the ^{13}C NMR data.

cis-*Hydrindanone* (**7a**) (*bicyclo*[4.3.0]*nonan-9-one*). ^1H NMR ($CDCl_3$): δ 1.05–1.80 (CH_2), 2.00–2.51 (CH, CH_2CO). ^{13}C NMR ($CDCl_3$): δ 22.5 [C(3), C(4)], 27.5 [C(2), C(5)], 35.6 [C(7), C(9)], 43.3 [C(1), C(6)], 220.5 [C(8)]. IR (neat): 2920, 2845, 1743,

1450, 1405, 1160 cm^{-1}. EIMS: *m/z* 138 (M^+). Found: C, 78.6; H, 10.7. Calc. for $C_9H_{14}O$: C, 78.2; H, 10.2%.

trans-*Hydrindanone* (**7a**) (*bicyclo*[4.3.0]*nonan-9-one*). ^1H NMR ($CDCl_3$): δ 1.00–2.10 (CH_2), 2.10–2.50 (CH_2, CH). ^{13}C NMR ($CDCl_3$): δ 26.4 [C(3), C(4)], 31.5 [C(2), C(5)], 44.0 [C(7), C(9)], 45.7 [C(1), C(6)], 218.3 [C(8)]. IR (neat): 2925, 2850, 1746, 1450, 1410, 1193, 1156, 1103, 1085 cm^{-1}. EIMS: *m/z* 138 (M^+). Found: C, 78.2; H, 10.5. Calc. for $C_9H_{14}O$: C, 78.2; H, 10.2%.

trans-3,4-*Di*(5-*hexenyl*)*cyclopentanone* (**7c**). ^1H NMR: δ 1.00–1.90 [12H, m, $CH(CH_2)_3CH_2CH{=}CH_2$], 1.90–2.20 [8H, m, $O{=}C(CHHCH(CH_2)_3CH_2CH{=}CH_2)_2$], 2.45 (2H, dd, $J = 12.0$ and 22.5 Hz, $O{=}CCHH$), 4.80–5.10 (4H, m, $CH{=}CH_2$), 5.54–6.00 (2H, m, $CH{=}CH_2$). ^{13}C NMR: δ 27.5, 29.0, 33.7, 33.9 [C(1′)–C(4′)], 42.7 [C(3) and C(4)], 45.1 [C(2) and C(5)], 114.5 [C(6′)], 138.8 [C(5′)], 192.5 [C(1)]. IR (neat): 3070, 2920, 2845, 1740, 1640, 1463, 1404, 992, 910 cm^{-1}. MS: 248 (M^+). Found: C, 82.4; H, 11.0. Calc. for $C_{17}H_{20}O$: C, 82.2; H, 11.4%.

trans-3,4-*Di*(6-*heptenyl*)*cyclopentanone* (**7d**). ^1H NMR ($CDCl_3$): δ 1.1–1.4 (16H, m, CH_2), 1.6–2.1 (8H, m, $CH_2C{=}C$ and $OCCHH$), 2.45 (2H, m, $OCCHH$), 4.85–5.1 (4H, m, $C{=}CH_2$) 5.78 (2H, m, $CH{=}C$). ^{13}C NMR ($CDCl_3$): δ 28.0, 28.9, 29.3, 33.8, 34.1 [C(1′)–C(5′)], 42.8 [C(2), C(5)], 45.2 [C(3), C(4)], 114.4 [C(7′)], 139.1 [C(6′)]. EIMS: *m/z* 276 (M^+).

Bicyclo[5.3.0]*decan-9-one* (**7e**). ^1H NMR ($CDCl_3$): δ 1.2–2.1 (CH_2), 2.3–2.6 ($OCCH_2$, CH). ^{13}C NMR ($CDCl_3$): δ 26.8 [C(4)], 27.2 [C(3), C(5)], 34.6 [C(3), C(6)], 43.6 [C(8), C(10)], 48.1 [C(1), C(7)], 219.0 [C(9)]. EIMS: *m/z* 152 (M^+).

trans-3,4-*Di*(7-*octenyl*)*cyclopentanone*. ^1H NMR ($CDCl_3$): δ 1.1–1.4 (10H, m, CH_2), 1.6–2.1 (8H, m, $OCCHH$, CH and $CH_2C{=}C$), 2.45 (2H, m, $OCCHH$), 4.85–5.1 (4H, m, $C{=}CH_2$), 5.80 (2H, m, $CH{=}C$). ^{13}C NMR ($CDCl_3$): δ 28.0, 29.0, 29.4, 29.6, 32.6, 34.2 [C(1′)–C(6′)], 42.8 [C(2), C(5)], 45.2 [C(3), C(4)], 114.3 [C(8′)], 139.2 [C(7′)], 218.9 [C(1)]. EIMS: *m/z* 304 (M^+).

Hydridoenolato complex (**16**). ^{13}C NMR: δ 23.2, 23.7, 29.0, 30.6, 36.8, 40.2, 40.9, 112.9, 165.6.

REFERENCES

1. H. Yasuda, Y. Kajihara, K. Mashima, K. Lee and A. Nakamura, *Chem. Lett.* 1981, 519; H. Yasuda, Y. Kajihara, K. Mashima, K. Nagasuna and A. Nakamura, *Organometallics* 1982, **1**, 388; H, Yasuda, K. Tatsumi and A. Nakamura, *Accts Chem. Res.* 1985, **15**, 120; H. Yasuda and A. Nakamura, *Angew. Chem. Int. Edn Engl.* 1987, **26**, 723.
2. G. Erker, J. Wicher, K. Engel, F. Resenfeldt, W. Dietrich and C. Krüger, *J. Am. Chem. Soc.* 1980, **102**, 6346; G. Erker, C. Krüger and G. Muller, *Adv. Organomet. Chem.* 1985, **24**, 1.
3. H. Yasuda, Y. Kajihara, K. Mashima, K. Nagasuna and A. Nakamura, *Chem. Lett.* 1981, 671; Y. Kai, N. Kanehisa, K. Miki, N. Kasai, M. Akita, H. Yasuda and A. Nakamura, *Bull. Chem. Soc. Jpn* 1983, **56**, 3735; M. Akita, Y. Matuoka, K. Asami, H. Yasuda and A. Nakamura, *J. Organomet. Chem.* 1987, **327**, 193; H. Yasuda, T. Okamoto, K. Mashima and A. Nakamura, *J. Organomet. Chem.* 1989, **363**, 61.
4. G. Erker, K. Engel, K. L. Atwood and W. E. Hunter, *Angew. Chem. Int. Edn Engl.* 1983, **22**, 494; G. Erker and U. Dorf, *Angew. Chem. Int. Edn Engl.* 1983, **22**, 777.
5. Y. Kai, N. Kanehisa, K. Miki, N. Kasai, K. Mashima, K. Nagasuna, H. Yasuda and A. Nakamura, *J. Chem. Soc., Chem. Commun.* 1982, 191; K. Tatsumi, H. Yasuda and A. Nakamura, *Isr. J. Chem.* 1983, **23**, 145; H. Yasuda, K. Nagasuna, M. Akita, K. Lee and A. Nakamura, *Organometallics* 1984, **3**, 1470.
6. J. P. Collman and L. S. Hegedus, *Principles and Applications of Organotransition Metal Chemistry*. University Science Books, Mill Valley, California (1980).
7. J. W. Lauher and R. Hoffmann, *J. Am. Chem. Soc.* 1976, **98**, 1729; R. J. McKinney, *J. Chem. Soc., Chem. Commun.* 1980, 490.
8. J. M. Manriquez, D. R. McAlister, R. D. Sanner and J. E. Bercaw, *J. Am. Chem. Soc.* 1978, **100**, 2716; G. Erker, *Accts Chem. Res.* 1984, **17**, 103.
9. K. I. Gell and J. Schwartz, *J. Chem. Soc., Chem. Commun.* 1979, 244.
10. R. H. Grubbs and A. Miyashita, *J. Chem. Soc., Chem. Commun.* 1977, 964; R. H. Grubbs and A. Miyashita, *Organomet. Chem.* 1978, **161**, 371.
11. S. McLain and R. R. Schrock, *J. Am. Chem. Soc.* 1978, **100**, 1315.
12. H. G. Alt, C. E. Denner, U. Thewalt and M. D. Raush, *J. Organomet. Chem.* 1988, **356**, C83.
13. T. Takahashi, T. Seki, M. Saburi, Y. Uchida and E. Negishi, *Chem. Lett.* 1989, 761.
14. For prenary report see, M. Akita, PhD thesis. Osaka University (1984).
15. E. Negishi, S. J. Holms, J. M. Tour and J. A. Miller, *J. Am. Chem. Soc.* 1985, **107**, 2568; E. Negishi, D. R. Swanson, F. E. Cederbaum and T. Takahashi, *Tetrahedron Lett.* 1987, **28**, 917.
16. T. V. Rajanbabu, W. A. Nugent, D. F. Taber and P. J. Fagan, *J. Am. Chem. Soc.* 1988, **110**, 7128.
17. G. Erker and F. Resenfeldt, *Angew. Chem. Int. Edn Engl.* 1978, **17**, 605.
18. H. Yasuda, Y. Kajhihara, K. Nagasuna, K. Mashima and A. Nakamura, *Chem. Lett.* 1981, **719**; Y. Kai, N. Kanehisa, N. Kasai, K. Mashima, K. Nagasuna, H. Yasuda and A. Nakamura, *Chem. Lett.* 1982, 1979.

19. D. K. Dalling and D. M. Grant, *J. Am. Chem. Soc.* 1967, **89**, 6612.
20. A. Zambelli and G. Gatti, *Macromolecules* 1978, **11**, 485.
21. A. Warshawsky and B. Fuchs, *J. Am. Chem. Soc.* 1979, **101**, 3567.
22. D. A. Clark and P. L. Fuchs, *Tetrahedron* 1969, **25**, 2633.
23. J. B. Stothers and C. T. Tan, *Can. J. Chem.* 1974, **52**, 308.

Polyhedron Vol. 10, No. 1, pp. 11–17, 1991
Printed in Great Britain

0277–5387/91 $3.00+.00
© 1991 Pergamon Press plc

COMPLEX FORMATION EQUILIBRIA BETWEEN ASTATINE(I) AND SULPHUR-CONTAINING CHELATING LIGANDS

R. LUDWIG, S. FISCHER and R. DREYER*

Technische Universität Dresden, Sektion Chemie, WB SRC 3, Mommsenstr. 13, Dresden 0-8027, F.R.G.

and

R. JACOBI and J. BEGER

Bergakademie Freiberg, Sektion Chemie, WB OC, Leipziger Str., Freiberg 0-9200, F.R.G.

(*Received* 27 *February* 1990; *accepted* 1 *August* 1990)

Abstract—Complex compounds between [^{211}At] astatine(I) and chelating ligands were characterized by electromigration in free electrolytes. O, S and N served as donor atoms in the ligands. Complexes of the type (AtXL) ($X^- = Cl^-$ and Br^-) are formed in ligand exchange reactions, and their stability constants were assessed for X^- being Br^-. In the case of astatine(I) the stability depends on the kind and number of donor atoms, as well as on substituents at the nitrogen and on the basicity of the ligand. The behaviour of astatine(I) is typical for a strongly polarizable acceptor. The experiments were carried out at 298 K in anhydrous ethanolic solutions at constant ionic strength adjusted to 0.05 ± 0.01 M with $Na(H)ClO_4$.

The characterization of complex compounds between [^{211}At] astatine(I) and thiourea (tu), selenourea (su), as well as their derivatives,[1,2] provided some information about the influence of the donor atoms O, S and Se and the substituents at N on the stability of complexes of the types $[AtL_2]^+$ and [AtXL] ($X^- = Cl^-$, Br^-, I^-; L = tu, su). The aim of this work was to extend these investigations on representatives of classes of chelating ligands and aliphatic sulphides (Table 1). Studies on extraction equilibria with copper(II) and silver(I) already exist for some of these compounds.[3,4] The ligands contain aliphatic substituents which provide them with higher basicity in comparison with aromatic substituents.[5]

The method of horizontal zone electromigration in free electrolyte solution[6,7] was chosen for the characterization of complex formation equilibria. Thus, redox reactions, which could occur during extraction of astatine(I) or multivalent metals,[8,9] can be avoided provided redox-stable ligands are used. Ethanol (EtOH) was used as solvent because other astatine(I) complex compounds have already been characterized in this medium[10,11] and the solubility of the ligands was sufficient. In order to prevent the hydrolysis of astatine(I) in neutral solutions, $HClO_4$ was added (see Experimental). Some of the ligands contain nitrogen, which is completely protonated in acidic solutions, as is shown from basicity constants of similar compounds[12–16] and from titration measurements.

Numerous coordinative properties of sulphur-containing chelating ligands are known.[17–19] The complex formation behaviour of the astatine(I) cation can be compared with polarizable cations, for example silver(I).[20] The following order (Scheme 1) of decreasing affinity of ligands can be derived from stability data for the complexes of some compounds with silver(I) {log K_1 for $[AgL]^+$, $T = 293$–303 K, the ligand number according to ref. 13 in parentheses}.

The donor effect decreases in the order S > N > O. However, the analogous macroheterocycles hint at the order N > S > O in silver(I)

* Author to whom correspondence should be addressed.

Table 1. Ligands for the complex formation with astatine(I)

Structural formula	Empirical formula	Ligand type/number	Molecular weight (g mol^{-1})	Reference
$Bu_2N\,S\,O\,O\,S\,NBu_2$	$C_{26}H_{56}O_2N_2S$	A1	492.9	3, 27
$Bu_2N\,S\,O\,S\,NBu_2$	$C_{24}H_{52}ON_2S_2$	A2	448.8	3, 27
$Bu_2N\,S\text{-}(CH_2)_5\text{-}S\,NBu_2$	$C_{25}H_{54}N_2S$	A3	446.5	27
$Bu_2N\,S\,S\,NBu_2$	$C_{22}H_{48}N_2S_2$	A4	404.8	3, 27
$HexN\,S\,NHex$ (H, H)	$C_{16}H_{36}N_2S$	B1	288.5	27, 28
$Hex_2N\,S\,NHex_2$	$C_{28}H_{60}N_2S$	B2	456.9	28
$Hex_2N\,S\,NHex_2$	$C_{30}H_{64}N_2S$	B3	484.9	27, 28
$PrS\,N\,SPr$ (Dodec)	$C_{22}H_{47}NS_2$	C1	389.7	27
$HexS\,N\,SHex$ (Hex)	$C_{22}H_{47}NS_2$	C2	389.7	3
$BuS\,N\,SBu$ (Bu)	$C_{16}H_{35}NS_2$	C3	305.6	3, 27
$HO\,S\,S\,S\,OH$	$C_8H_{18}OS_3$	D1	242.4	26
$Hex\,S\,S\,S\,SHex$ [a]	$C_{18}H_{38}S_4$	D2	382.8	—
$BuS\text{-}SBu$	$C_8H_{18}S_2$	D3	178.4	30
$Bu\,S\,S\text{-}(CH_2)_4\text{-}S\,SBu$ [b]	$C_{16}H_{34}S_4$	D4	354.7	—
$Bu\,S\,S\text{-}(CH_2)_6\text{-}S\,SBu$ [c]	$C_{18}H_{38}S_4$	D5	382.8	—
$HexS\,O\,O\,SHex$	$C_{18}H_{36}O_2S_2$	D6	350.6	28
$HexS\,O\,SHex$	$C_{16}H_{34}OS_2$	D7	306.6	28
$Hex\,S\,Hex$	$C_{12}H_{26}S$	D8	202.4	29

[a] Fp 66–68°C (acetone).
[b] Fp 34°C (methanol).
[c] Fp 39°C (methanol–chloroform).

Symbols: Pr = propyl, Bu = butyl, Hex = hexyl, Dodec = dodecyl, ⌒ = $-\overset{H}{\underset{H}{C}}-\overset{H}{\underset{H}{C}}-\overset{H}{\underset{H}{C}}-$.

$H_2N\,S\,S\,NH_2$ > $H_2N\,N\,N\,NH_2$ (H, H) > $H_2N\,S\,NH_2$ > $H_2N\,N\,NH_2$ (H) > $H_2N\,O\,NH_2$ > $H_2N\,S\,OH$ > $H_2N\,NH_2$

	(487)	(407)	(268)	(231)	(266)	(271)	(120)
$\log K_1$:	8.34	7,7	7,0	6,1	5,59	4,97	4,7
$\log K$:	5,79	5,8	-	3,2	-	-	2,35

symbols: ⌒ : $-\overset{H}{\underset{H}{C}}-\overset{H}{\underset{H}{C}}-$

K_1, K : see text

Scheme 1.

complexes.[21] On comparing the stability of silver(I) complexes with the ligands, in which one of the nitrogen atoms is protonated, differences between the donor strength of S and N are hard to find. However, the donor strength decreases considerably, which can be concluded from the log K values in Scheme 1 {log K for $Ag^+ + HL^+ = [AgHL]^{2+}$}. The order N > S > O can be determined for complexes between chelating ligands and copper(II) as a somewhat less polarizable cation.[22–24] Furthermore, the stability of these complexes decreases with shorter chain length of the alkyl groups at N.

EXPERIMENTAL

Production of ^{211}At

The ^{211}At isotope was obtained via irradiation of bismuth with 28 MeV alpha particles on the U-120 cyclotron at the Central Institute for Nuclear Research in Rossendorf. After which, a two-step gasthermochromatographical separation of astatine was carried out.[25] This aqueous solution of carrier-free astatine is represented by "$At^0 \times H_2O$".

Chemicals and apparatus

"$At^0 \times H_2O$" was diluted with a ten-fold volume of a 0.5 M solution of $NaClO_4$ or $LiClO_4$ in EtOH and was mixed with a surplus of ligand-containing electrolyte solution. As was shown in preparatory experiments, the oxidation state +1 was stabilized by the presence of ligands in solution without adding an oxidizing agent as described in ref. 1.

For the measurement of cationic complexes the ethanolic solutions contained 0.001–0.005 M of the ligand, 0.05 M $NaClO_4$ and $HClO_4$. For the characterization of ligand exchange equilibria the solutions consisted of ligands with a constant concentration per measurement series in the range 0.0001–0.004 M, 0.05 M LiCl or 0.05 M (NaBr + $NaClO_4$), as well as $HClO_4$. The ionic strength, μ, was adjusted to 0.05 ± 0.01 M using $Na(H)ClO_4$. $HClO_4$ was added to the solutions in order to prevent hydrolysis of astatine(I) by the following method: each solution containing the organic ligand and the salts mentioned above was titrated potentiometrically with concentrated $HClO_4$ from a microburette. A glass electrode (stored in EtOH, type GA 60 N from Forschungsinstitut Meinsberg) and a calomel electrode connected via a current key with the solutions serving as electrodes were used. The titrations were stopped at a measured pH* of 3 ± 0.3, when the nitrogen-containing ligands are completely protonated. Because EtOH is a protic solvent, the measured pH* and the calculated pH for aqueous solutions of the same composition are qualitatively comparable.

The chemicals used were of p.a. grade. Ethanol was dried over CaO and molecular sieves and distilled under flowing nitrogen. The solutions contained less than 0.3% water and were freshly prepared. The apparatus described in ref. 7 was used for the experiments, allowing measurement of the mediate ion mobility, u_m, which represents the sum of all individual ion mobilities multiplied by their partial molar fraction in the investigated solution. The temperature, T, was found to be 298 ± 0.5 K.

Synthesis of ligands

For the synthesis of compound D1 (Table 1) bis-(2-mercaptoethyl)sulphide was converted using ethylene oxide.[26] The other ligands in groups A, C and D were accessible by reaction of the corresponding thiols and α,ω-dichloro or dibromo compounds according to the usual method of nucleophilic substitution.[3,27,28] The melting points of the new D2, D4 and D5 tetrathioalkanes are given in Table 1. The B type compounds resulted from the reaction of sodium sulphide with the corresponding 1-halogenide compounds. Sulphide D8 and disulphide D3 were produced by following the methods given in refs 29 and 30.

RESULTS AND DISCUSSION

Cationic complexes

In solutions containing $NaClO_4$, $HClO_4$, 0.005 M ligand and astatine(I), cationic complexes were formed with the ligands shown in Table 2. As shown in Table 2, only type A and B ligands form cationic

Table 2. Cationic complexes of ligands with astatine(I) and their ion mobility, u_m, in EtOH (μ = 0.05 M, T = 298 K, pH* = 3)

Ligand	Concentration of ligand (M)	$u_m \pm$ error ($cm^2 V^{-1} s^{-1}$)
A1	0.005	(2.2 ± 0.4) E-05
A2	0.005	(3.4 ± 0.4) E-05
A3	0.0025	(2.9 ± 0.5) E-05
A4	0.0015	(1.7 ± 0.5) E-05
A4	0.004	(2.4 ± 0.5) E-05
B1	0.004	(4.1 ± 0.2) E-05
B2	0.004	(4.1 ± 0.3) E-05
B3	0.0025	(1.7 ± 0.5) E-05

species. At a pH* value less than four the ion mobility, u_m, was independent of the $HClO_4$ concentration but dependent on the ligand concentration. An equilibrium corresponding to eq. (1), with $X^- = ClO_4^-$ and L being the organic ligand, probably dominates in solution:

$$[AtX] + L = [AtXL]. \quad (1)$$

Complexes of this stoichiometry but with Ag^+ and Cu^{2+} as cations and partly other anions are known.[9,17,36] A positive charge on L, resulting from protonation and partial association with ClO_4^-, would be responsible for the formation of cations with type A and B ligands. Type C ligands, which are almost completely associated in these solutions, thus existing neutrally, in addition to type D ligands form neutral complexes.

Ligand exchange reactions with chloride

The u_m values were measured in ethanolic solutions containing astatine(I), 0.05 M LiCl, $HClO_4$ (pH* = 3) and 0.0025 M ligand. The data are summarized in Fig. 1. The astatine(I) ion mobility in solution under analogous conditions but without an organic ligand is $u_m = -2.06$ E-04 $cm^2\ V^{-1}\ s^{-1}$ (standard). From Fig. 1, initial conclusions on the graduation of complex stabilities can be drawn. For these purposes the following equilibria for the characterization of the ligand exchange reactions are assumed ($X^- = Cl^-$):

$$[AtX] + X^- = [AtX_2]^- \quad K_2 \quad (2)$$

$$[AtX] + L = [AtXL] \quad K. \quad (3)$$

The smaller the measured u_m value, the larger the concentration of [AtXL] in solution. Due to the high chloride concentration in solution and possible association reactions, comparison of the ligands would be useful only within the groups.

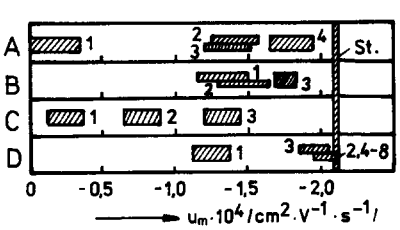

Fig. 1. Ion mobility, u_m, of astatine(I) in chloride-containing ethanolic solutions of the ligands A1–D8 at 298 K. [0.0025 M ligand, 0.05 M LiCl, $HClO_4$ (pH* = 3), EtOH, st = standard 0.05 M LiCl without second ligand].

Ligand exchange reactions with bromide

In ethanolic solutions containing astatine(I), NaBr, $NaClO_4$, $HClO_4$ and a chelating ligand, u_m was measured at different bromide concentrations and constant organic ligand concentration per measurement series ($T = 298$ K, pH* = 3, $\mu = 0.05$). Eleven chelating ligands were chosen for this purpose. Figure 2 shows the average data for u_m measured per concentration of bromide, as well as the electromigrational curve for equilibrium (2) with $X^- = Br^-$ (standard).

The electromigrational equation (4)[32] for the ligand exchange equilibria was derived from eqs (2) and (3) by modelling the measuring points:

$$u_m = \frac{u(AtBr_2^-)}{1. + \frac{1.}{K_2 \cdot [Br]} + \frac{K \cdot [L]}{K_2 \cdot [Br]}} \quad (4)$$

For two parameters, previously calculated data can be used:[10] $\log K_2 = 3.42$ and $u(AtBr_2^-) = -2.54$ E-04 $cm^2\ V^{-1}\ s^{-1}$. Thus, modelling concentrates on the calculation of K. Only anions have been measured in the investigated concentration range in the ligand exchange reactions, therefore the [AtXL] charge can be set to zero and the protonation and association of ligands do not have to be considered. This fact allows the use of the same equilibrium model for all the ligands.

The equilibrium concentration of bromide was calculated according to the method used by Schwabe,[33] taking into consideration the association with Na^+ in EtOH. For that purpose the thermodynamical association constants for NaBr ($\log K_A = 1.73$) and $NaClO_4$ ($\log K_A = 1.91$) had to be assessed from conductivity data.[34] The medium activity coefficient was evaluated according to the Debye–Hückel theory.

The parameter K in the electromigrational equation (4) was optimized with the MINUIT program[35] in such a way that the chi-square sum became minimal. Table 3 provides the $\log K$ data, and the electromigrational curves (2–14) calculated on the basis of these data are plotted in Fig. 2.

Comparison with the $\log K_2$ value of 3.42 for $[AtBr_2]^-$ shows that all type A and C, as well as ligands B1 and D1, are more likely to coordinate with AtBr than Br^-. The order of stability constants corresponds to that which can be derived from Fig. 1.

In comparing the measurements with protonated amines and diamines free of heteroatoms, *no* complexes of these compounds with astatine(I) could be proved. This is an indication that under the measurement conditions (pH* being 3) no bonding of astatine(I) to nitrogen is established.

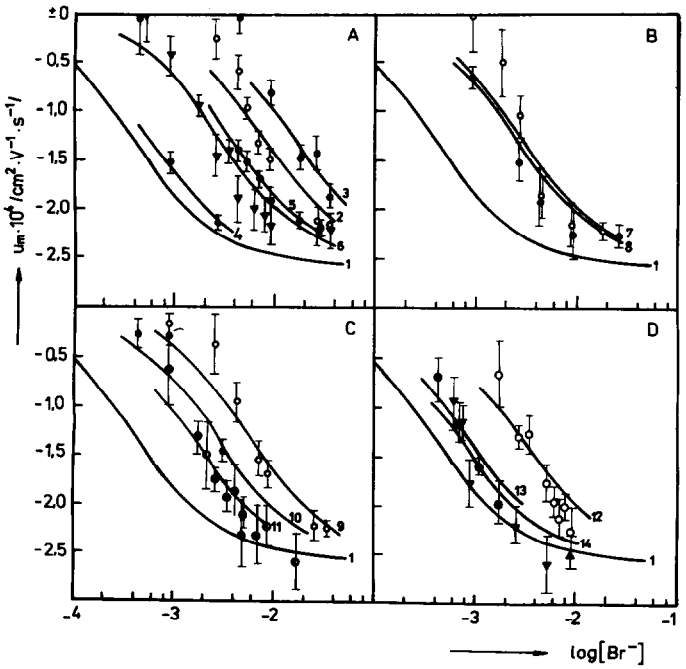

Fig. 2. Ion mobility, u_m, of astatine(I) in bromide-containing ethanolic solutions of 11 ligands at 298 K [0.05 M ($NaBr+NaClO_4$), $HClO_4$ (pH* = 3)]: 1, without organic ligand; 2, A1 0.002 M; 3, A1 0.004 M; 4, A2 0.00011 M; 5, A3 0.002 M; 6, A4 0.002 M; 7, B1 0.002 M; 8, B2 0.002 M; 9, C1 0.002 M; 10, C1 0.0008 M; 11, C2 0.00052 M; 12, D1 0.002 M; 13, D2 0.002 M; 14, D7 0.004 M.

The A1 ligand shows the strongest donor effect for astatine(I). The similarly constructed ligand D6 which is free of nitrogen is clearly less apt to complex formation. By comparing the log K values it can be stated, in general, that nitrogen-containing ligands form more stable [AtXL] complexes than nitrogen-free ligands. The undissociated [AtX] complex is probably coordinated by the chelating ligand. An interaction between the protonated nitrogen and the X^- halogenide in [AtXL] could cause the increase in stability.

Table 3. Stability constants, log K, for AtBrL {[AtBr]+L = [AtBrL]; $\mu = 0.05$ M, $T = 298$ K, pH* = 3, EtOH}

Ligand	Log K Error	n
A1	3.99±0.02	17
A3	3.64±0.02	7
A2	3.60±0.04	16
A4	3.59±0.03	23
B1	3.63±0.04	7
B2	3.42±0.04	8
C1	3.83±0.02	26
C2	3.71±0.03	15
D1	3.49±0.02	21
D2	2.75±0.04	7
D7	2.24±0.04	15

The D1 ligand with a relatively high stability constant is an exception among the type D ligands. A similar effect of increased stability was reported for alkali ion complexes in which chelating ligands with OH-groups at the chain ends are involved.[17] In the case of astatine(I), an interaction between two OH-groups at the chain ends or their lower steric hindrance in comparison with alkyl groups (D2) may be decisive.[36]

The C1, C2 and C3 ligands differ in donor effect which correlates with the length of the alkyl group at nitrogen. The A1, A2 and A4 ligands differ in the number of oxygen atoms among the sulphur atoms which influences the complex stability. A similar effect was noticed in the complex formation of silver(I) with open-chain ligands[4] and with macrocycles.[37] Thereby, the $—S(CH_2)_2O(CH_2)_2S$ group showed a stronger donor affinity than $—S(CH_2)_2S—$; this was explained due to less steric hindrance occurring in chelate formation between the metal and sulphur. The number of oxygen atoms in sulphur-containing chelating ligands influences the complex stability and extraction behaviour in the case of copper(II) also.[3]

The slight difference between A3 and A4 can be based on steric effects of the CH_2 groups. The ligands B1 (secondary amine) and B2 (tertiary amine) differ in the basicity of the nitrogen atom and in the required space of the end groups. The complex stability decreases with growing substitution at nitrogen and decreasing basicity. There is only a slight difference in affinity between B2 and B3. This effect is also found in the case of copper(II) complexes with similar ligands.[12]

The exchange of oxygen (D7) for nitrogen, as well as the exchange of nitrogen (B2) for S(C2), leads to an increase in the complex stability of the [AtXL] type of complexes. It would be of interest to study the stability of astatine complexes with cyclic analogues of the investigated ligands or with cyclic sulphides[38–40] such as (14)-ane-S_4, (18)-ane-S_6 and (28)-ane-S_8. Considering the size of the astatine(I) cation (r = 122 pm[41]), sulphur-containing analogues of 16-crown-5[42] could be suitable for that purpose.

Acknowledgements—We wish to thank Professor Dr sc. G.-J. Beyer and his team at the ZfK Rossendorf cyclotron for their cooperation. Furthermore, thanks are due to Dr Beckert (Friedrich-Schiller University, Jena) for the synthesis of D3 and D8 compounds, as well as to Mrs C. Reizenstein for drawing the figures.

REFERENCES

1. R. Dreyer, I. Dreyer, S. Fischer, H. Hartmann and F. Rösch, *J. Radioanal. Nucl. Chem. Lett.* 1985, **96**, 333.
2. H. Hussein, Diss. Rer. Nat. TU Dresden (1989).
3. J. Beger, R. Jacobi, H. Merkwitz, K. Gloe and P. Mühl, *Z. Chemie* 1984, **24**, 230.
4. F. Dietze, K. Gloe, R. Jacobi, P. Mühl, J. Beger, M. Petrich, L. Beyer and E. Hoyer, *Solv. Extract. Ion Exch.* 1989, **7**, 223.
5. A. F. Brugger, Diss. Rer. Nat. Eidgen. TH Zürich, No. 7855 (1985).
6. M. Milanov, W. Doberenz, R. Dreyer, M. Noack and V. A. Chalkin, *Radiokhimiya* 1982, **24**, 520.
7. I. Hoffmann, R. Münze, I. Dreyer and R. Dreyer, *J. Radioanal. Chem.* 1982, **74**, 53.
8. W. Doberenz, S. Fischer and R. Dreyer, *Isotopenpraxis* 1987, **23**, 339.
9. V. G. Torgov, *Isotopenpraxis* 1984, **20**, 352.
10. R. Ludwig, R. Dreyer and S. Fischer, *Radiochim. Acta* 1989, **47**, 129.
11. R. Ludwig, S. Fischer and R. Dreyer, *Isotopenpraxis* 1990, **26**, 27.
12. L. G. Sillen and A. E. Martell, *Stability Constants of Metal Ion Complexes*, and refs therein. The Chemical Society, London (1964).
13. D. D. Perrin, *Stability Constants of Metal Ion Complexes, Part B* and refs therein. Pergamon Press, Oxford, (1979).
14. F. Arnaud-Neu and M. J. Schwing-Weill, *Inorg. Nucl. Chem. Lett.* 1977, **13**, 17.
15. F. Arnaud-Neu and M. J. Schwing-Weill, *Inorg. Nucl. Chem. Lett.* 1975, **11**, 655.
16. D. D. Perrin, *Dissociation Constants of Organic Bases in Aqueous Solution.* Butterworth, London (1965).
17. F. Vögtle and E. Weber, *Angew. Chem.* 1979, **91**, 813 and refs therein.
18. F. Vögtle and E. Weber (Eds), *Host Guest Complex Chemistry of Macrocycles.* Izdat. Mir, Moscow (1988) (in Russian).
19. E. Weber and F. Vögtle, in *Host Guest Complex Chemistry I* (Edited by F. L. Boschke), p. 11. Springer-Verlag, Berlin (1982).
20. G. W. M. Visser, Dissertation. University of Amsterdam (1982).
21. H. K. Frensdorff, *J. Am. Chem. Soc.* 1971, **93**, 600.
22. S. Ahrland, J. Chatt and N. R. Davies, *Q. Rev.* (*Chem. Soc.*) 1958, **12**, 265.
23. J. R. Lotz, B. P. Block and W. C. Fernelius, *J. Phys. Chem.* 1959, **63**, 541.
24. F. J. C. Rossotti, in *Modern Coordination Chemistry* (Edited by J. Lewis and R. G. Wilkins), p. 48. Interscience, New York (1960).
25. W. Doberenz, D. D. Nhan, R. Dreyer, M. Milanov, Yu. V. Norseev and V. A. Chalkin, *Radiochem. Radioanal. Lett.* 1982, **52**, 119.
26. P. Bergthaler and P. Wenzel, DE-OS 2934948; *Chem. Abstr.* 1981, **95**, 24266d.
27. H. J. Pietzsch, M. Spiess, S. Hofmann, J. Beger and R. Jacobi, G.D.R. patent registration WP CO7F/3242717.
28. K. Gloe, P. Mühl, J. Beger, R. Jacobi and A. Urban, *Z. Chemie* 1985, **25**, 99.
29. A. Schöberl and A. Wagner, in *Methoden der Organischen Chemie*, Vol. IX (Edited by E. Müller), p. 97. Georg Thieme, Stuttgart (1955).
30. W. A. Schulze and J. P. Lyon, A. P. 2517934(1946) Phillips Petroleum Co., ref. *ibid.*, p. 55.
31. F. Vögtle, H. Sieger and W. M. Müller, in *Host Guest Complex Chemistry I* (Edited by F. L. Boschke), p. 143. Springer-Verlag, Berlin (1982).
32. A. V. Stepanov and E. K. Korchemnaya, *The Electromigrational method in the Inorganic Analysis.* Izdat. Khimija, Moscow (1979) (in Russian).
33. K. Schwabe, *Physikalische Chemie*, Vol. II, p. 127. Akademie Verlag, Berlin (1986).
34. Landolt Börnstein, *Zahlenwerte und Funktionen*, 6th edn, Vol. II, Pt 7, p. 389. Springer-Verlag, Berlin (1960).
35. P. James and M. Roos, MINUIT Program. CERN Computer 6000 Services Program Library, Long Write-Up D 506, D 516 (1971).
36. E. Weber, R. Jacobi and R. Ludwig, private communication.
37. R. Louis, F. Arnaud-Neu, R. Weiss and M. J.

Schwing-Weill, *Inorg. Nucl. Chem. Lett.* 1977, **13**, 31.
38. M. Schröder, *Pure Appl. Chem.* 1988, **60**, 517.
39. A. J. Blake, R. O. Gould, A. J. Holder, T. I. Hyde and M. Schröder, *Polyhedron* 1989, **8**, 513.
40. D. Sevdic and H. Meider, *J. Inorg. Nucl. Chem.* 1977, **39**, 1403.
41. V. A. Chalkin and E. Herrmann, *Isotopenpraxis* 1975, **11**, 333.
42. C. J. Pedersen, *J. Am. Chem. Soc.* 1970, **92**, 391.

Polyhedron Vol. 10, No. 1, pp. 19–25, 1991
Printed in Great Britain

0277–5387/91 $3.00+.00
© 1991 Pergamon Press plc

BINDING OF THE LATE TRANSITION METAL IONS TO THE MIXED N_2S DONOR MACROCYCLIC LIGAND 1-THIA-4,7-DIAZACYCLONONANE (= L^1). X-RAY CRYSTAL STRUCTURES OF $[Pt^{IV}(L^1)Br_3]Br_{0.5}Cl_{0.5}\cdot 2H_2O$, $[Au^{III}(L^1)Cl_2][AuCl_4]$ AND $[Ag_4(L^1)_4](CF_3SO_3)_4$

ULRICH HEINZEL and RAINER MATTES*

Anorganisch-Chemisches Institut der Westfälischen Wilhelms-Universität, Wilhelm-Klemm-Straße 8, 4400 Münster, F.R.G.

(*Received* 9 *May* 1990; *accepted* 6 *August* 1990)

Abstract—Complexes of the nine-membered macrocyclic ligand 1-thia-4,7-diazacyclononane (L^1) with platinum(IV), gold(III) and silver(I) have been prepared and the X-ray crystal structures of $[Pt^{IV}(L^1)Br_3]Br_{0.5}Cl_{0.5}\cdot 2H_2O$ (**1a**), $[Au^{III}(L^1)Cl_2][AuCl_4]$ (**2a**) and $[Ag_4(L^1)_4](CF_3SO_3)_4$ (**3a**) determined. In the octahedral cation of **1a** the ligand is bound facially. Complex **2a** contains a planar $AuCl_2N_2$ unit and the thioether group is weakly donating [Au—S = 2.973(3) Å] to an axial site. In **3a**, four AgL^1 units are bridged by thioether groups to a centrosymmetrical $[Ag_4(L^1)_4]^{4+}$ tetramer. The exodentate Ag—S [2.403(2) and 2.415(2) Å] bonds are rather short.

The nine-membered macrocyclic ligands 1,4,7-triazacyclononane (L^2) and 1,4,7-trithiacyclononane (L^3) have been shown to bind to a range of transition metal ions whose coordinative properties are not fully compatible with facial binding of these ligands, e.g. Pd^{II},[1,2] Pt^{II},[1] Ag^I,[3] and Au^I and Au^{III}.[4] This has led to a number of complexes with unusual stereochemical and redox properties. We have been investigating this aspect recently using the mixed N_2S donor set macrocyclic ligand 1-thia-4,7-diazacyclononane (L^1).[5] We have shown that in $[Pd(L^1)_2]^{2+}$ the central ion is octahedrally coordinated and in addition to the square-planar PdN_4 group the S-donor atoms are weakly donating towards the axial positions. In $[Pt(L^1)_2]^{2+}$, however, the S-donor atoms are bent away from the central ion, which then is in a square-planar N_4 environment only. The electrochemical properties of both complexes are also different.[5,6] The platinum(II) complex is easily oxidized to a platinum(IV) species, even by atmospheric oxygen. The structure of this species, $[Pt^{IV}(L^1)Br_3]Br_{0.5}Cl_{0.5}\cdot 2H_2O$ (**1a**), is described in this paper.

Gold(III) is isoelectronic with palladium(II) and platinum(II). We have, therefore, prepared gold (III) complexes of L^1 in order to compare their structures with the aforementioned palladium(II) and platinum(II) complexes, especially with respect to the binding of the thioether group. Complexes of silver(I) exhibit a preference for linear two-coordination, and occasionally, tetrahedral four-coordination. Polydentate macrocyclic ligands enforce higher coordination numbers and irregular geometries.[7,8] L^3 forms monomeric trigonal-antiprismatic silver(I) complexes, $[Ag(L^3)]^+$, tetrahedral, $[Ag(L^3)Cl]$, and trimeric, $[Ag_3(L^3)_3]^{3+}$, complexes.[3] Silver(I) complexes of L^2 are unknown so far. Therefore, it seemed interesting to investigate the binding properties of 1-thia-4,7-diazacyclononane with silver(I) as well. A monomeric complex of the related hexadentate bis-coronand L^4 has been characterized very recently.[9]

EXPERIMENTAL

Preparation of 1-*thia*-4,7-*diazacyclononane* (L^1)

$L^1\cdot 2HBr$ was prepared as described previously.[10] To obtain the free ligand, NaOH (1 g) was added to an aqueous solution (10 cm^3) of

* Author to whom correspondence should be addressed.

$L^1 \cdot 2HBr$ (0.34 g, 1.1 mmol), which was extracted several times with $CHCl_3$. The solutions were combined and dried over Na_2SO_4. The solvent was distilled off, and the resultant yellow oil dissolved in a suitable solvent.

Preparation of $[Pt(L^1)Br_3]Br_{0.5}Cl_{0.5} \cdot 2H_2O$ (**1a**) *and* $[Pt(L^1)Br_3]Br_{0.5}Cl_{0.5} \cdot H_2O$ (**1b**)

To an aqueous solution of K_2PtCl_6 (0.2 g, 0.4 mmol) a solution of $L^1 \cdot 2HBr$ was added. After several days yellow prismatic crystals of **1a** and orange crystals of **1b** (as thick needles) precipitated in approximately equal amounts. Yield 0.16 g (60%). They were separated mechanically (**1a**: Found: C, 11.2; H, 2.8; N, 4.5. Calc. for $[Pt(L^1)Br_3]Br_{0.5}Cl_{0.5} \cdot 2H_2O$: C, 10.7; H, 2.7; N, 4.1%. **1b**: Found: C, 11.1; H, 2.3; N, 4.6. Calc. for $[Pt(L^1)Br_3]Br_{0.5}Cl_{0.5} \cdot H_2O$: C, 11.0; H, 2.5; N, 4.3%.) Probably the bulk material of **1a** had a higher bromine content than the crystals used for X-ray diffraction (see below).

Preparation of $[Au(L^1)Cl_2][AuCl_4]$ (**2a**)

A small amount of well-formed dark red crystals was obtained in a U-shaped tube by slow interdiffusion of solutions of $HAuCl_4$ (0.68 g, 2 mmol) and of L^1 (0.3 g, 2 mmol) in methanol (5 cm^3) through a porous glass membrane. (Found: C, 9.3; H, 1.8; N, 3.6. Calc. for $[Au(L^1)Cl_2][AuCl_4]$: C, 9.6; H, 1.9; N, 3.7%.)

Preparation of $[Au(L^1)Cl_2]Cl$ (**2b**)

L^1 (0.15 g, 1 mmol) dissolved in methanol (10 cm^3) was added to a solution of $HAuCl_4$ (0.34 g, 1 mmol) also in methanol (20 cm^3). After a few minutes, orange–red needles appeared from the solution. Yield 0.11 g (50%). (Found: C, 16.2; H, 3.1; N, 6.4. Calc. for $[Au(L^1)Cl_2]Cl$: C, 16.0; H, 3.1; N, 6.2%.)

Preparation of $[Ag_4(L^1)_4](CF_3SO_3)_4$ (**3a**)

$Ag(CF_3SO_3)$ (0.3 g, 1.2 mmol) was added to a solution of L^1 (1.1 mmol) in CH_3CN (10 cm^3) under nitrogen. After some minutes the complex precipitated as a white powder. Yield 0.13 g (30%). Crystals of X-ray quality were obtained by recrystallization from CH_3CN. (Found: C, 20.8; H, 3.5; N, 7.0. Calc. for $[Ag_4(L^1)_4](CF_3SO_3)_4$; C, 20.8; H, 3.5; N, 6.9%.)

Preparation of $[Ag_4(L^1)_4](PF_6)_4$ (**3b**)

A solution of $AgNO_3$ (0.17 g, 1 mmol) and $NaPF_6$ (0.5 g) in CH_3CN (10 cm^3) was added to a solution of L^1 (1.1 mmol) in CH_3CN (10 cm^3). The complex precipitated immediately. Yield 0.31 g (70%). Large octahedral crystals of X-ray quality were obtained by recrystallization from CH_3CN. The crystals were slightly sensitive to light. (Found: C, 18.1; H, 3.5; N, 7.0. Calc. for $[Ag_4(L^1)_4](PF_6)_4$: C, 17.8; H, 3.3; N, 7.0%.)

Preparation of $[Ag(L^1)][ClO_4)$ (**3c**)

L^1 (0.15 g, 1 mmol) dissolved in CH_3OH (40 cm^3) was dropped slowly into a solution of $AgClO_4$ (0.21 g, 1 mmol) in CH_3OH (10 cm^3). During the addition a white compound precipitated. Yield 0.23 g (65%). Recrystallization from water yielded colourless thin needles. (Found: C, 20.7; H, 3.9; N, 7.7. Calc. for $[Ag(L^1)][ClO_4)$: C, 20.4; H, 4.0; N, 7.9%.)

X-ray crystallography

Details of the crystal structure determinations are summarized in Table 1. Suitable crystals were sealed in Lindemann capillaries, and the unit cells and space groups obtained using Weissenberg photography. Diffraction studies were performed on CAD4 or Syntex $P2_1$ automated diffractometers. Graphite monochromatized Mo-K_α radiation ($\lambda = 0.71073$ Å) was used. Unit cells and orientation matrices were determined by least-squares treatment of 20–25 machine-centred reflections having $2\theta > 20°$. Two or three check reflections were measured periodically to monitor crystal decay. Data were corrected for Lorentz and polarization effects. Empirical absorption corrections were applied to all data. The structures were solved by Patterson or direct methods and refined by full-matrix least-squares methods by using the SHELXTL-PLUS[11] program. Anisotropic thermal parameters were refined for all non-hydrogen atoms. Hydrogen atoms were included in calculated positions with isotropic thermal parameters fixed ($U_H = 0.008$ Å) or tied to the bonded carbon atom ($U_H = 1.2U_C$). The weighting scheme $w^{-1} = \sigma(F)^2 + gF_o^2$ (for g see Table 1) was used. Individual features of the structures are outlined below.

$[Pt(L^1)Br_3]Br_{0.5}Cl_{0.5} \cdot 2H_2O$ (**1a**). Due to the preparative routine the single crystal studied contained both Br^- and Cl^- as non-complexing anions. The halide ions occupy statistically the same crystallographic site. Refinement of the site occupation

Table 1. Crystal data and data collection parameters

Compound	$[Pt(L^1)Br_3]Br_{0.5}Cl_{0.5}\cdot 2H_2O$	$[Au(L^1)Cl_2][AuCl_4]$	$[Ag_4(L^1)_4](CF_3SO_3)_4$
Formula	$C_6H_{18}Br_{3.5}Cl_{0.5}N_2O_2PtS$	$C_6H_{14}Au_2Cl_6N_2S$	$C_{28}H_{56}Ag_4F_{12}N_8O_{12}S_8$
f_w	674.3	752.9	1612.8
Crystal system	Monoclinic	Monoclinic	Monoclinic
Space group	$P2_1$	$P2_1/n$	$P2_1/c$
a (Å)	7.265(9)	7.697(4)	13.153(5)
b (Å)	12.44(2)	13.637(2)	13.036(4)
c (Å)	8.34(1)	15.576(3)	15.330(5)
β (°)	99.36(7)	94.31(3)	93.56(3)
V (Å^3)	744.6	1630.3	2628.5
Z	2	4	2
D_c (g cm^{-3})	3.01	3.07	2.04
D_o (g cm^{-3})	2.85	3.05	2.06
$F(000)$	579.83	1179.21	1599.82
μ(Mo-K_α) (cm^{-1})	178.91	127.9	18.46
Crystal size (mm)	$0.16\times0.21\times0.08$	$0.31\times0.12\times0.18$	$0.17\times0.25\times0.1$
Scan type	ω–2θ	ω–2θ	ω–2θ
Scan speed (° min^{-1})	5–29	5–29	5–29
Data collected	$+h, +k, +l$	$+h, +k, +l$	$\pm h, +k, +l$
$2\theta_{max}$ (°)	54	54	54
Reflections measured	1854	3974	6388
Unique reflections	1785	3382	5826
Reflections with $I \geqslant 3.92\sigma(I)$	1673	2957	3568
Number of variables	145	157	326
Structure solved with	Direct methods	Direct methods	Patterson methods
Weight	0.0004	0.0003	0.0003
R	0.032	0.039	0.076
R_w	0.034	0.046	0.074
S	1.59	0.096	2.66
Max. Δ/σ (final cycle)	0.171	0.027	0.001
Residual density (eÅ^{-3})	−2.63 to 2.24	−1.52 to 3.18	−0.2728 to 2.195

factors resulted in the composition $Br_{0.51(2)}$ and $Cl_{0.49(2)}$.

$[Ag_4(L^1)_4](CF_3SO_3)_4$ (**3a**). During data acquisition the intensities of the check reflections dropped to approximately 56%. A correction for decay was therefore applied to the data.

$[Pt(L^1)Br_3]Br_{0.5}Cl_{0.5}\cdot H_2O$ (**1b**). Crystal data: orthorhombic, space group *Pnma*, $a = 14.515(5)$, $b = 36.593(7)$, $c = 12.822(3)$ Å, $V = 6810.4$ Å^3, $Z = 20$. This structure was also solved (5869 reflections, $R = 0.0601$). The unit cell contains three independent $[Pt(L^1)Br_3]^+$ ions with the same bonding parameters as the cation of **1a**. The structure is not therefore further discussed.

$[Ag_4(L^1)_4](PF_6)_4$ (**3b**). Crystal data: tetragonal, $a = 12.918(7)$, $c = 14.864(9)$ Å, $V = 2476.7$ Å^3, $Z = 2$. Using a twinned crystal the structure of **3b** was refined to $R = 0.22$. Like **3a** the structure contains tetrameric, S-bridged $[AgL^1]_4^{4+}$ ions. No further efforts were made, therefore, to determine the twinning law and the true space group of **3b**.

RESULTS AND DISCUSSION

(a) *Platinum*(IV) *compounds*

Compounds **1a** and **1b** were prepared from K_2PtCl_6. In reactions of K_2PtCl_4 with L^1, which were performed in air, considerable amounts of **1a** or **1b** were also detected.[6] Obviously, platinum(II) is easily oxidized to platinum(IV) in the presence of L^1. The loss of the d_{z^2} electrons is considerably favoured, because the thioether donor atoms of L^1 closely approach the axial sites of the square planar platinum(II) coordination sphere. After oxidation a strong Pt^{IV}—S bond is formed. Both **1a** and **1b** contain $[PtL^1Br_3]^+$ cations and statistically distributed over the same crystallographic site, Cl^- or Br^- anions. In the cation, platinum(IV) is octahedrally coordinated (see Fig. 1) with L^1 in a facial position. The bond angles between all donor atoms are close to 90 or 180°. The Pt—Br, Pt—N and Pt—S bond distances are in the expected range,

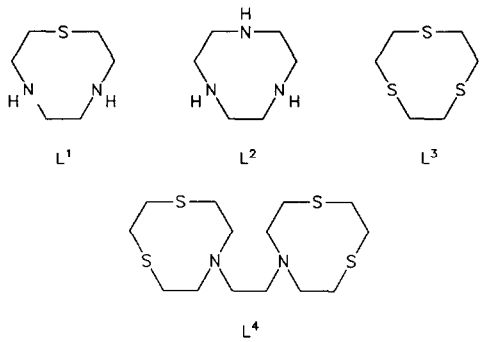

Scheme 1.

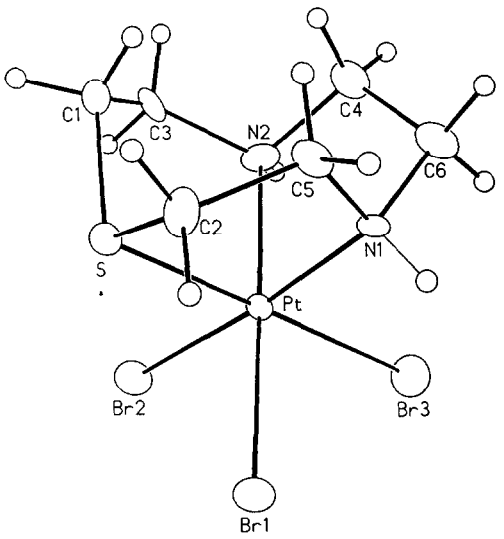

Fig. 1. Structure of the $[Pt(L^1)Br_3]^+$ ion in **1a**.

close to the sums of the respective covalent radii (see Table 2). The Pt—S bond shows a distinct *trans* effect; the Pt—Br bond opposite to the Pt—S bond is significantly ($\geqslant 10\sigma$) larger than the Pt—Br bonds in the adjacent positions.

Strong hydrogen bonds connect the non-complexed Cl^- and Br^- anions with N(1) and the water molecule O(2). Further hydrogen bonds exist between N(2) and O(2), and O(1) and O(2).

(b) *Gold compounds*

The gold(III) complexes **2a** and **2b** were easily prepared from stoichiometric solutions of L^1 and $HAuCl_4$. Only the structure of **2a** has been determined so far. According to the IR spectra **2b** contains, very probably, the same type of cation as well. In **2a** the metal centre of the $[Au(L^1)Cl_2]^+$ ion is bound in a planar fashion by two Cl atoms (mean Au—Cl = 2.27 Å) and by the two N-donors of L^1 (see Fig. 2). The mean Au—N distance (2.07 Å) is slightly shorter than in $[Au(dmp)Cl_3]$[12] or $[Au(en)(SO_3)_2]^-$,[13] where the distances 2.09 and 2.12 Å, respectively, have been found. The S-donor participates in a long-range apical coordination with the metal centre [Au—S = 2.973(3) Å]. Gold is lying 0.07 Å out of the Cl_2N_2 plane towards the S-donor. The Au—S vector is inclined 82.8° to this plane. Thus, the binding of the ligand is very similar to $[Au(L^3)_2]^{3+}$, where four Au—S bonds define a square (mean Au—S = 2.35 Å), while the remaining two donors are weakly interacting apically (Au—S = 2.929 Å). Apical interactions of the third donor atom of the nine-membered macrocyclic ligands, L^1, L^2 and L^3, have been observed so far in $[Pd(L^1)_2]^{2+}$,[5] $[Pd(L^3)_2]^{2+}$ and $[Pt(L^3)_2]^{2+}$,[1] but not in $[Pt(L^1)_2]^{2+}$,[5] $[Pt(L^2)_2]^{2+}$ [1] and $[Pd(L^2)_2]^{2+}$.[14] Obviously the affinity to the S-donor of L^1 increases from platinum(II) to gold(III). The structure of **2a** is completed by two $[AuCl_4]^{2-}$ anions, positioned in inversion centres of the unit cell; the mean Au—Cl distance is 2.27 Å, as in the cationic part of the structure.

Table 2. Relevant bond lengths and bond angles in $[Pt(L^1)Br_3]$ $Br_{0.5}Cl_{0.5} \cdot 2H_2O$

Pt—Br(1)	2.454(1)	Pt—N(2)	2.038(2)
Pt—Br(2)	2.457(1)	O(1)···Br(4)	3.049(4)
Pt—Br(3)	2.477(1)	O(2)···Br(4)	3.162(4)
Pt—S	2.283(3)	O(2)···O(1)	2.723(3)
Pt—N(1)	2.057(8)	O(2)···N(2)	2.741(3)
Br(1)—Pt—Br(2)	91.4(1)	Br(3)—Pt—S	179.0(1)
Br(1)—Pt—Br(3)	90.6(0)	Br(1)—Pt—N(1)	92.4(3)
Br(2)—Pt—Br(3)	91.0(0)	Br(2)—Pt—N(1)	175.0(4)
Br(1)—Pt—S	88.4(1)	Br(3)—Pt—N(1)	92.2(3)
Br(2)—Pt—S	89.0(1)		

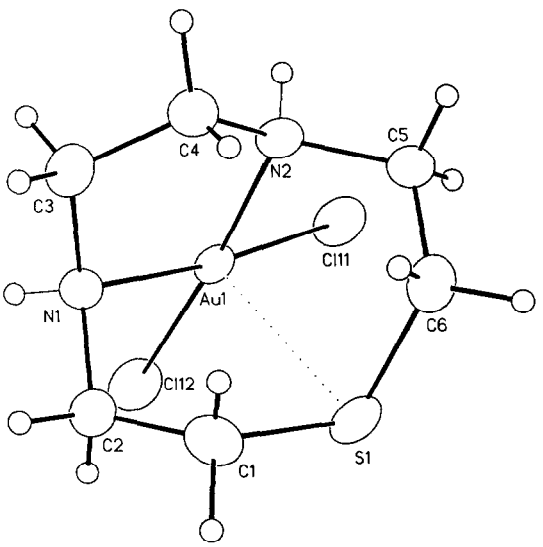

Fig. 2. Structure of the $[Au(L^1)Cl_2]^+$ ion in **2a**.

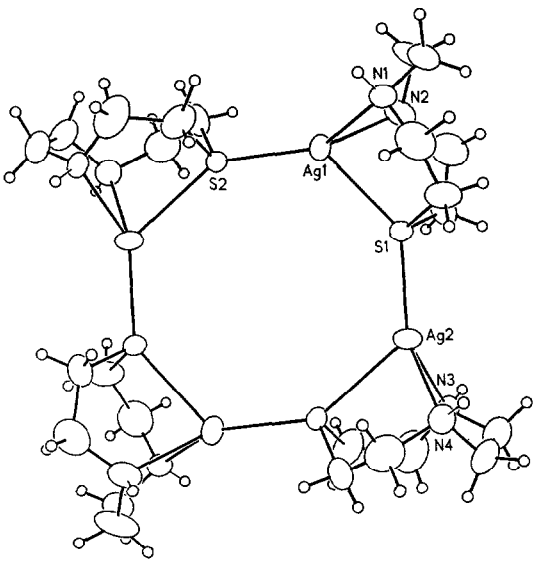

Fig. 3. Structure of the tetrameric $[Ag_4(L^1)_4]^{4+}$ ion in **3a**.

The $[AuCl_4]^-$ ions form hydrogen bridge bonds via Cl(32) and Cl(22) to N(1) [3.22(1) Å] and N(2) [3.295(1) Å], respectively. Further intermolecular contacts exist between Cl(21) and Au(1) (3.524 Å), in the direction of the empty apical site and, similarly, between Au(3) and Cl(11) (3.982 Å).

(c) *Silver compounds*

Using the non-complexing counterions $CF_3SO_3^-$ and PF_6^- and the metal : ligand ratio of 1 : 1, silver(I) forms cyclic tetranuclear complexes, $[Ag_4(L^1)_4]^{4+}$, with L^1, as shown by structure determination of **3a** and **3b**. The fully refined structure of **3a** contains the cyclic tetranuclear $[Ag_4L_4]^{4+}$ ion (see Fig. 3). Silver(I) is coordinated four-fold by two nitrogen and two sulphur atoms. Each sulphur atom in turn coordinates to two separate silver(I) ions to yield the cyclic tetramer, surrounding an inversion centre of the space group. The AgN_2S_2-tetrahedra are severely distorted; three X—Ag—X angles (X = nitrogen or sulphur within one macrocycle) are less than 80°, three X—Ag—S angles, with sulphur in the neighbouring ligand, are 127–140°. The coordination polyhedra of Ag(1) and Ag(2) differ slightly (see Table 4). The exodentate Ag—S distances [2.403(2) and 2.415(2) Å] are to our knowledge the shortest Ag—S bonds in thioether macrocyclic complexes observed so far. In the related thioether bridged trimer, $[Ag_3(L^3)_3]^{3+}$, the shortest exodentate Ag—S distance is 2.480(2) Å.[3] Ag—S distances in octahedrally coordinated sil-

Table 3. Relevant bond lengths and bond angles in $[Au(L^1)Cl_2][AuCl_4]$

Au(1)—Cl(11)	2.286(3)	Au(2)—Cl(2a)	2.270(3)
Au(1)—Cl(12)	2.269(4)	Au(2)—Cl(2b)	2.275(3)
Au(1)—N(1)	2.065(8)	Au(3)—Cl(31)	2.279(3)
Au(1)—N(2)	2.068(8)	Au(3)—Cl(32)	2.264(3)
Au(2)—Cl(21)	2.270(3)	Au(3)—Cl(3a)	2.279(3)
Au(2)—Cl(22)	2.275(3)	Au(3)—Cl(3b)	2.264(3)
Cl(11)—Au(1)—Cl(12)	92.7(1)	Cl(31)—Au(3)—Cl(32)	89.7(1)
Cl(11)—Au(1)—N(1)	174.0(2)	Au(1)—N(1)—C(2)	112.1(6)
Cl(12)—Au(1)—N(1)	91.2(2)	Au(1)—N(1)—C(3)	105.3(6)
Cl(11)—Au(1)—N(2)	91.8(2)	C(2)—N(1)—C(3)	120.3(8)
Cl(12)—Au(1)—N(2)	174.6(2)	Au(1)—N(2)—C(5)	111.5(6)
N(1)—Au(1)—N(2)	84.1(3)	Au(1)—N(2)—C(4)	110.8(6)
Cl(21)—Au(2)—Cl(22)	90.0(1)	C(5)—N(2)—C(4)	112.1(8)

Table 4. Relevant bond lengths and bond angles in $[Ag_4(L^1)_4](CF_3SO_3)_4$

Ag(2)—S(1)	2.403(2)	S(4)—O(4)	1.389(9)
Ag(2)—S(2)	2.705(2)	S(4)—O(6)	1.387(9)
Ag(2)—N(4)	2.306(8)	S(4)—O(5)	1.407(8)
Ag(2)—N(3)	2.339(9)	S(4)—C(14)	1.79(2)
Ag(1)—S(1)	2.635(2)	F(1)—C(13)	1.31(1)
Ag(1)—S(2a)	2.415(2)	F(3)—C(13)	1.30(1)
Ag(1)—N(1)	2.332(8)	F(4)—C(14)	1.29(2)
Ag(1)—N(2)	2.369(9)	F(5)—C(14)	1.29(2)
S(2)—C(11)	1.80(1)	F(6)—C(14)	1.29(2)
S(3)—O(1)	1.396(8)	C(14)—F(4)	1.29(2)
S(3)—O(2)	1.432(9)	C(14)—C(5)	1.29(2)
S(3)—O(3)	1.415(8)	C(14)—F(6)	1.29(2)
S(3)—C(13)	1.80(1)		

S(1)—Ag(2)—S(2)	127.9(1)	Ag(2)—S(1)—C(4)	106.6(4)
S(1)—Ag(2)—N(4)	140.1(2)	Ag(2)—S(1)—C(2)	108.9(3)
S(2)—Ag(2)—N(4)	78.5(2)	C(4)—S(1)—C(2)	104.0(5)
S(1)—Ag(2)—N(3)	134.0(2)	Ag(2)—S(1)—Ag(2b)	139.8(1)
S(2)—Ag(2)—N(3)	77.8(2)	C(4)—S(1)—Ag(2b)	95.3(4)
N(4)—Ag(2)—N(3)	74.5(3)	C(2)—S(1)—Ag(2b)	97.5(4)
S(1)—Ag(1)—S(2a)	126.9(1)	Ag(2)—S(2)—C(8)	94.3(4)
S(1)—Ag(1)—N(1)	79.4(2)	Ag(2)—S(2)—C(11)	96.5(4)
S(2a)—Ag(1)—N(1)	135.2(2)	C(8)—S(2)—C(11)	104.1(6)
S(1)—Ag(1)—N(2)	78.7(2)	Ag(2)—S(2)—Ag(1a)	145.3(1)
S(2a)—Ag(1)—N(2)	138.5(2)	C(8)—S(2)—Ag(1a)	103.3(4)
N(1)—Ag(1)—N(2)	75.0(3)	C(11)—S(2)—Ag(1a)	107.6(4)

ver(I) complexes with mixed N,S-donor and pure S-donor macrocycles are usually in the range 2.6–2.8 Å.[3,7–9] The endodentate Ag—S distances of **3a** [2.635(2) and 2.705(2) Å] also belong to this range.

The Ag—N distances in **3a** fall into the small range, 2.308(8)–2.369(9) Å, with the mean, 2.337 Å. There are no reports of other complexes of mixed N,S-donor macrocycles, where the central ion is coordinated tetrahedrally. In complexes with higher coordination numbers the Ag—N distances are larger and range from 2.368(7) for Ag—N (pyridine) to 2.589(10) for Ag—N (amide).[7–9]

In three dimensions, the tetrameric cations are positioned at the origin of the pseudo-tetragonal unit cell. In the cell centre and along the *c*-axis pairs of triflate ions are located. All N—H bonds of L^1 are engaged in weak hydrogen bridge bonds to oxygen atoms of the CF_3SO_3 anion. Besides **3a** and **3b**, $[AgL^1]ClO_4$ (**3c**) very probably forms a tetrameric complex cation as well.

(d) *Conformation of* L^1

According to an analysis of the torsional angles, L^1 shows in **1a** and **3a** the common [333] conformation, which is also typical for L^2 and L^3. The chelate rings have either $\lambda\lambda\lambda$ or $\delta\delta\delta$ conformation. In the gold complex **2a** the ligand adopts the [234] conformation which is usually observed in complexes of L^1, when the difference between the lengths of the M—N and M—S bonds exceeds approximately 0.3 Å, as with $[Cu(L^1)_2]$.[16] In this case the chelate rings show the $\lambda\lambda\delta$ or $\delta\delta\lambda$ conformation. According to Parker *et al.* the [333] and [234] conformations differ only slightly in energy.[4]

REFERENCES

1. K. Wieghardt, M. Köppen, W. Swiridoff and J. Weiss, *J. Chem. Soc., Dalton Trans.* 1983, 1896; K. Wieghardt, H. J. Küppers, E. Raabe and C. Krieger, *Angew. Chem.* 1986, **98**, 1136; *Angew. Chem. Int. Ed. Engl.* 1986, **25**, 1101; A. J. Blake, R. O. Gould, A. J. Lavery and M. Schröder, *Angew. Chem.* 1986, **98**, 282; *Angew. Chem. Int. Ed. Engl.* 1986, **25**, 274; A. J. Blake, R. O. Gould, A. J. Lavery and M. Schröder, *J. Chem. Soc., Chem. Commun.* 1987, 118; A. J. Blake, A. J. Holder, T. I. Hyde, Y. V. Roberts, A. J. Lavery and M. Schröder, *J. Organomet. Chem.* 1987, **323**, 267.
2. A. J. Blake and M. Schröder, *J. Chem. Soc., Chem. Commun.* 1988, 1452.
3. H. J. Küppers, K. Wieghardt, Yi-Hung Tsay, C. Krüger, B. Nuber and J. Weiss, *Angew. Chem.* 1987, **99**, 583; *Angew. Chem. Int. Ed. Engl.* 1987, **26**, 575;

J. Clarkson, R. Yagbasan, P. J. Blower, S. C. Rawle and S. R. Cooper, *J. Chem. Soc., Chem. Commun.* 1987, 950; P. J. Blower, J. A. Clarkson, S. C. Rawle, J. R. Hartman, R. E. Wolf, R. Yagbasan, S. G. Bott and S. R. Cooper, *Inorg. Chem.* 1989, **28**, 4040.

4. D. Parker, P. S. Roy, G. Ferguson and M. M. Hunt, *Inorg. Chim. Acta* 1989, **155**, 227; A. J. Blake, R. O. Gould, J. A. Greig, A. J. Holder, T. I. Hyde and M. Schröder, *J. Chem. Soc., Chem. Commun.* 1989, 876.
5. P. Hoffmann and R. Mattes, *Z. Naturfor.* 1987, **43b**, 261.
6. U. Heinzel and R. Mattes, unpublished results.
7. G. Ferguson, A. S. Craig, D. Parker and R. E. Matthes, *Acta Cryst.* 1989, **C45**, 741; A. S. Craig, R. Kataky, D. Parker, H. Adams, N. Bailey and H. Schneider, *J. Chem. Soc., Chem. Commun.* 1989, 1870.
8. U. Kallert and R. Mattes, *Inorg. Chim. Acta*, in press.
9. D. Parker, A. S. Craig, G. Ferguson and A. Lough, *Polyhedron* 1989, **8**, 2951.
10. P. Hoffmann, A. Steinhoff and R. Mattes, *Z. Naturfor.* 1987, **42b**, 867.
11. SHELXTL-PLUS, Siemens Analytical X-ray Instruments, Inc., Madison, Release 3.4 (1989).
12. A. Dunand and R. Gerdil, *Acta Cryst.* 1975, **B31**, 370.
13. W. T. Robinson and E. Sinn, *J. Chem. Soc., Dalton Trans.* 1975, 726.
14. G. Hunter, A. McAuley and T. W. Whitcombe, *Inorg. Chem.* 1988, **27**, 2634.
15. A. J. Blake, R. O. Gould, A. J. Holder, T. I. Hyde and M. Schröder, *Polyhedron* 1989, **8**, 513.
16. J. C. Boeyens, S. M. Dobson and R. D. Hancock, *Inorg. Chem.* 1985, **24**, 3073.

Polyhedron Vol. 10, No. 1, pp. 27–31, 1991
Printed in Great Britain

0277–5387/91 $3.00+.00
© 1991 Pergamon Press plc

SYNTHESIS AND THERMAL STABILITY OF MIXED-LIGAND LANTHANIDE ORGANOMETALLICS INVOLVING BOTH CYCLOPENTADIENYL AND *o*-NITROPHENOLATO OR α-NITROSO-β-NAPHTHOLATO LIGANDS

ZHONGZHI WU* and ZHONGWEN YE

Institute of Organic Chemistry, Anhui Normal University, Wuhu, Anhui 241000, P.R.C.

(*Received* 18 *January* 1990; *accepted* 13 *August* 1990)

Abstract—By reaction of Cp_3Nd or Cp_3Yb ($Cp = C_5H_5$) with *o*-nitrophenol (HNP) or α-nitroso-β-naphthol (HNN), eight new mixed-ligand lanthanide organometallics of the general formula $Cp_nLn(NP)_{3-n}$ and $Cp_nLn(NN)_{3-n}$ ($n = 1, 2$; NP = *o*-nitrophenolato ligand; NN = α-nitroso-β-naphtholato ligand; Ln = Nd, Yb) have been synthesized. All the complexes were characterized by elemental analyses, and IR and MS spectra, showing that they are chelates with NP and NN as bidentate chelate ligands. Their thermal stability has been studied and discussed.

Many inorganic and organometallic complexes are extremely susceptible to heat, and some of them may disproportionate at low temperatures.[1–3] Recently, we reported studies on the thermal stability of lanthanide complexes $Cp_2Sm(L)$ ($L = OCOCH_3$, Cl, Br, I)[4] and $Cp_nLn(L)_{3-n}$ ($n = 1, 2$; L = β-diketonato, 8-quinolinolato, *o*-aminophenolato, *o*-aldehydophenolato, furfuralcoholato ligand; Ln = Nd, Yb)[2,5–7] and found that they are thermally unstable and tend to disproportionate at moderately high temperatures. In continuation of our previous studies, we have now carried out the synthesis and the study of the thermal stability of eight new mixed-ligand (Nd, Yb) organometallic complexes containing both cyclopentadienyl (Cp) and *o*-nitrophenolato (NP) or α-nitroso-β-naphtholato (NN) ligands, and the results are reported in this paper.

RESULTS AND DISCUSSION

By adopting the very versatile method of liberating cyclopentadiene from a Cp_3Ln moiety by the action of protonic acids stronger than C_5H_6, we have synthesized the mixed-ligand lanthanide organometallic complexes by reaction of Cp_3Nd or Cp_3Yb with *o*-nitrophenol (HNP) or α-nitroso-β-naphthol (HNN) in tetrahydrofuran (THF) at room temperature. They are:

1 : 1 mole ratio of reactants	1 : 2 mole ratio of reactants
$Cp_2Nd(NP)$ (**1**)	$CpNd(NP)_2$ (**5**)
$Cp_2Nd(NN)$ (**2**)	$CpNd(NN)_2$ (**6**)
$Cp_2Yb(NP)$ (**3**)	$CpYb(NP)_2$ (**7**)
$Cp_2Yb(NN)$ (**4**)	$CpYb(NN)_2$ (**8**)

All these complexes were characterized by elemental analyses (Table 1), and IR (Table 2) and MS (Table 3) spectra.

The elemental analyses for all the complexes are in compliance with the general formula $Cp_nLn(L)_{3-n}$. They are soluble in THF and insoluble in pentane, n-hexane and other alkane solvents, but sparingly soluble in benzene and toluene. None of the complexes have melting points; decomposition is observed in a sealed capillary in the range 90–200°C.

The IR spectra of all the complexes show absorptions at approx. 250, 780, 1010, 1440 and 3080 cm^{-1}, characteristic of the η^5-Cp group.[8] All the complexes exhibit two bands in the IR spectra in the regions 1115 and 470 cm^{-1}. We attribute the first band to a Ln—O—C vibration mode and the second band to the ν(Ln—O) stretching.[9,10] Complexes **1**, **3**, **5** and **7** exhibit two absorptions at *ca* 1325 and 1510 cm^{-1}, attributable to the symmetric

* Author to whom correspondence should be addressed.

Table 1. Analytical and physical data for complexes **1–8**

Complex	Formula	Colour	Yield (%)	Decomposition temperature (°C)	Found(Calc.) (%) Ln	C	H	N
1	$(C_{16}H_{14}NO_3)Nd$	Yellow–orange	72	120	34.6 (34.9)	46.2 (46.5)	3.0 (3.4)	3.3 (3.3)
2	$(C_{20}H_{16}NO_2)Nd$	Brown	80	140	32.6 (32.3)	53.1 (53.7)	3.2 (3.6)	3.4 (3.2)
3	$(C_{16}H_{14}NO_3)Yb$	Red–orange	72	170	38.9 (39.2)	42.9 (43.5)	2.9 (3.2)	3.4 (3.2)
4	$(C_{20}H_{16}NO_2)Yb$	Brown	33	200	37.0 (36.4)	50.6 (50.5)	3.1 (3.4)	3.1 (2.9)
5	$(C_{17}H_{13}N_2O_6)Nd$	Orange	91	90	29.6 (29.1)	42.0 (42.1)	2.8 (2.7)	5.9 (5.8)
6	$(C_{25}H_{17}N_2O_4)Nd$	Brown	82	120	26.5 (26.1)	53.7 (54.2)	3.3 (3.1)	5.2 (5.1)
7	$(C_{17}H_{13}N_2O_6)Yb$	Orange	74	150	33.6 (33.6)	39.1 (39.7)	2.7 (2.6)	5.6 (5.4)
8	$(C_{25}H_{17}N_2O_4)Yb$	Brown–black	86	180	29.7 (29.7)	51.4 (51.6)	2.9 (2.9)	4.7 (4.8)

and antisymmetric stretching vibrations of the NO_2 group, respectively. In the spectrum of the sodium salt of the ligand HNP, $\nu(NO_2)$ appears at 1334 and 1546 cm^{-1}. Therefore, the shift of the stretching vibrations of the NO_2 group to lower frequencies in these complexes may indicate the coordination of the NO_2 group.[10] The IR spectra of complexes **2**, **4**, **6** and **8** reveal that the ν(NO) in the sodium salt of the ligand HNN located at 1530 cm^{-1} is shifted to lower frequency on complexation to approx. 1476 cm^{-1}, suggesting coordination of the NO group.[11] In addition, the strong band of the phenolic-OH stretching vibration for the free ligand HNP or HNN at *ca* 3000 cm^{-1} does not appear in the IR spectra of any of the complexes. This also proves the presence of the Ln—O—C bond in each complex.

In the mass spectra of these complexes, the molecular ion peaks and main resulting fragments all appear. All the molecular ion intensities are low.

Table 2. IR spectral data for complexes **1–8** (4000–200 cm^{-1})

Complex	Main absorption peaks (cm^{-1})
$Cp_2Nd(NP)$ **(1)**	3082w, 3057w, 1600m, 1511m, 1500s, 1443m, 1324m, 1253m, 1115m, 1013m, 777m, 748m, 480m, 255w
$Cp_2Nd(NN)$ **(2)**	3058w, 3025w, 1617s, 1596s, 1554s, 1463m, 1450s, 1259m, 1113m, 1013s, 810m, 767s, 722s, 475w, 252w
$Cp_2Yb(NP)$ **(3)**	3085w, 3035w, 1602s, 1510s, 1501s, 1442s, 1328s, 1256s, 1140m, 1014m, 781s, 751s, 463m, 250w
$Cp_2Yb(NN)$ **(4)**	3060m, 3020w, 1592m, 1465m, 1440m, 1260, 1259m, 1115m, 1010m, 769m, 721m, 469w, 245w
$CpNd(NP)_2$ **(5)**	3080w, 3052w, 1602m, 1512m, 1501s, 1445s, 1325m, 1254m, 1114m, 1020m, 784m, 750m, 470m, 252w
$CpNd(NN)_2$ **(6)**	3065m, 3030w, 1614s, 1595s, 1555s, 1465s, 1445s, 1260m, 1115m, 1015m, 785m, 766m, 721m, 471w, 248w
$CpYb(NP)_2$ **(7)**	3078w, 3032w, 1600w, 1512m, 1501s, 1438m, 1328m, 1253m, 1138m, 1018m, 779m, 749s, 470m, 248w
$CpYb(NN)_2$ **(8)**	3075w, 3025w, 1613s, 1597s, 1554s, 1435m, 1464m, 1262m, 1114m, 1009m, 770s, 722m, 466m, 250w

Table 3. MS data for complexes **1–8** at different evaporation temperatures

Complexes $Cp_nLn(L)_{3-n}$ ($Cp = C_5H_5$) and molecular species	Temperature of evaporation (°C)	Main ion peaks (m/z)[a]
1 $n = 2$, $L = C_6H_4(o\text{-}NO_2)O$, $M = Cp_2NdL$, $M' = Cp_3Nd$	80–120	410(M), 380(M−NO), 345(M−Cp), 272(M−L), 207(M−Cp−L), 142(Nd)
	140–180	337(M′), 272(M′−Cp), 207(M′−2Cp), 142(Nd)
2 $n = 2$, $L = \underline{CH:CHCH:CHC}_6H_2(o\text{-}NO)O$, $M = Cp_2NdL$, $M' = Cp_3Nd$	100–140	444(M), 414(M−NO), 379(M−Cp), 314(M−2Cp), 272(M−L), 207(M−Cp−L), 142(Nd)
	160–200	337(M′), 272(M′−Cp), 207(M′−2Cp), 142(Nd)
3 $n = 2$, $L = C_6H_4(o\text{-}NO_2)O$, $M = Cp_2YbL$	180–300	442(M), 396(M−NO_2), 377(M−Cp), 312(M−2Cp), 174(Yb)
4 $n = 2$, $L = \underline{CH:CHCH:CHC}_6H_2(o\text{-}NO)O$, $M = Cp_2YbL$	160–250	476(M), 446(M−NO), 411(M−Cp), 346(M−2Cp), 174(Yb)
5 $n = 1$, $L = C_6H_4(o\text{-}NO_2)O$, $M = CpNdL_2$, $M' = Cp_2NdL$, $M'' = Cp_3Nd$	50–70	483(M), 437(M−NO_2), 418(M−Cp), 345(M−L), 207(M−2L), 142(Nd)
	90–130	483(M), 437(M−NO_2), 418(M−Cp), 410(M′), 345(M′−Cp), 280(M′−2Cp), 142(Nd)
	140–180	337(M″), 272(M″−Cp), 207(M″−2Cp), 142(Nd)
6 $n = 1$, $L = \underline{CH:CHCH:CHC}_6H_2(o\text{-}NO)O$, $M = CpNdL_2$, $M' = Cp_2NdL$, $M'' = Cp_3Nd$	60–100	551(M), 521(M−NO), 491(M−2NO), 486(M−Cp), 314(M−Cp−L), 142(Nd)
	120–140	444(M′), 414(M′−NO), 379(M′−Cp), 314(M′−2Cp), 207(M′−Cp−L), 142(Nd)
	160–200	337(M″), 272(M″−Cp), 207(M″−2Cp), 142(Nd)
7 $n = 1$, $L = C_6H_4(o\text{-}NO_2)O$, $M = CpYbL_2$, $M' = Cp_2YnL$	120–160	515(M), 469(M−NO_2), 450(M−Cp), 312(M−Cp−L), 174(Yb)
	180–300	515(M), 469(M−NO_2), 442(M′), 377(M′−Cp), 312(M′−2Cp), 174(Yb)
8 $n = 1$, $L = \underline{CH:CHCH:CHC}_6H_2(o\text{-}NO)O$, $M = CpYbL_2$, $M' = Cp_2YbL$	100–140	583(M), 553(M−NO), 518(M−Cp), 346(M−Cp−L), 142(Yb)
	160–300	583(M), 553(M−NO), 518(M−Cp), 476(M′), 411(M′−Cp), 346(M′−2Cp), 174(Yb)

[a] MS data are given for the isotopes ^{142}Nd, ^{174}Yb, ^{14}N and ^{16}O, the peak patterns correspond to theoretical values based on the natural abundance of the isotopes.

They are characterized by ready loss of the Cp group with the $(M-Cp)^+$ ion as the base peak in the mass spectra. The ion peaks of $(M-L)^+$ (L = NP, NN) formed by direct loss of the NP or NN ligand of the molecular ion are very low. This is consistent with the results that Cp groups form η^5-bonds with metals, whereas NP and NN ligands chelate with the metal atom to form a chelating ring. Thus, the Ln—Cp bond is weaker than the Ln—L bond, and the former breaks easily under electron impact. However, it was observed that in the mass spectra, the loss of NO_2 or NO fragments occurs during cleavage. This feature can be attributed to the existence of the electron-withdrawing group NO_2 or NO weakening the C—NO_2 or C—NO bond strength, thus leading to easy fragmentation of the molecular ion.

From the above elemental and spectral analyses, it may be assumed that all the complexes are chelates with NP or NN as bidentate chelate ligands. This is in agreement with the fact that the greatest tendency to form chelate complexes is found with polyfunctional ligands whose donor atoms are separated by two or three carbon atoms, the chelating ring produced by chelate formation will be five- or six-membered. Therefore, the following structure for the eight new mixed-ligand complexes may be proposed (**1**, **2**).

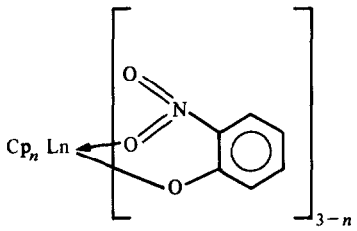

(1)

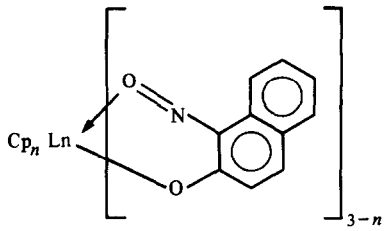

(2)

In order to study the thermal stability of these complexes, their mass spectra were recorded at different evaporation temperatures. It is interesting to note that when the evaporation temperature of a sample of CpLnL-type complexes reaches a certain value, not only are the molecular ions $CpLnL_2^+$ observed in the spectra, but the peaks corresponding to Cp_2LnL^+ and their fragments are observed also. Furthermore, by increasing the evaporation temperature, the molecular ion peaks of $CpLnL_2^+$ gradually disappear and the peaks of Cp_2LnL^+ and its fragments are enhanced. In addition, we interestingly found that when the evaporation temperature reaches a moderately high value, the ion peaks of Cp_2NdL^+ completely disappear and the strong peaks corresponding to Cp_3Nd^+ and its fragments are observed instead. However, no Cp_3Yb^+ ion peak is observed in the mass spectra of complexes of $CpYbL_2$ or Cp_2YbL. Thus, based on the above results, we predict that the complexes may undergo the following disproportionation reactions during the course of raising the temperature:

$$2CpLnL_2 \rightarrow Cp_2LnL + LnL_3 \quad (1)$$

$$3Cp_2LnL \rightarrow 2Cp_3Ln + LnL_3. \quad (2)$$

This feature is consistent with the results reported in our previous studies.[6,7] The ion peaks of disproportionation products LnL_3 do not appear in the mass spectra.

In view of the mass spectra, we also found that complexes of ytterbium, either of the Cp_2LnL- or $CpLnL_2$-type, are thermally more stable than the analogues of neodymium. Above 160°C, the disproportionations of four neodymium complexes are apparently complete. But even at 300°C, the Cp_2YbL-type complexes still remain unchanged. We assume that the greater thermal stability of the ytterbium complexes compared with their neodymium analogues is due to the lanthanide contraction. As the radius of Yb^{3+} is smaller than Nd^{3+}, the attraction of the Yb—ligand bond formed by Yb^{3+} and an anionic ligand will be stronger than the Nd—ligand bond. Another reason for the superior thermal stability of ytterbium complexes may be due to the greater steric saturation present around the smaller metal centre.[12,13]

Probably due to the large radii and coordinative unsaturation of light lanthanides, their organometallic complexes involving both Cp and Cl groups, such as unsolvated Cp_2LnCl and $CpLnCl_2$ (Ln = La, Ce, Pr and Nd), have not yet been synthesized at room temperature.[3,14] The reported facile preparation of the unsolvated and room-temperature stable complexes $Cp_nNd(L)_{3-n}$ (n = 1, 2; L = NP, NN) is obviously due to stabilization of the species by the chelation effect. This also revealed that the steric bulky ligands are favourable for the stabilization of the Ln—C bond.

EXPERIMENTAL

Materials

All operations were carried out in an atmosphere of dry oxygen-free argon using standard Schlenk techniques or in a glove box. All solvents were dried over sodium, refluxed over sodium benzophenone or finely divided $LiAlH_4$, and distilled immediately before use. HNP and HNN were of chemically pure grade, and were dried *in vacuo* before use. Cp_3Nd and Cp_3Yb were prepared and purified by the literature method.[15]

Physical measurements and elemental analyses

IR spectra were recorded on a Perkin–Elmer 983G IR spectrophotometer as Nujol and Fluorolube mulls between CsI plates (200–4000 cm^{-1}). All the mass spectrometric measurements were performed on a MAT 312 mass spectrometer operating in the EI mode at a resolving power of 1000 (electron energy, 70 eV; emission current, 1 mA; ion acceleration, 3 kV). The samples were introduced by direct inlet techniques with a source temperature of 130°C and a sample evaporation temperature in the range 20–300°C.

Metal analyses for lanthanides were accomplished using the literature method.[16] Elemental analyses for carbon, hydrogen and nitrogen

were carried out on a Yanaco MT2 CHN analyser. Decomposition points were determined in a sealed capillary filled with argon and are uncorrected.

Preparation of complexes $Cp_2Ln(NP)$ *and* $CpLn(NP)_2$

A THF solution (20 cm^3) of HNP (1.5 mmol or 3.0 mmol) was added dropwise to a THF solution 30 cm^3) of Cp_3Nd or Cp_3Yb (1.5 mmol) at room temperature. After stirring for 24 h at room temperature, the resulting solution was concentrated via vacuum to *ca* 15 cm^3. On the addition of 40 cm^3 of n-hexane, a solid precipitated out, which was recrystallized twice from THF–n-hexane, washed with n-hexane and dried *in vacuo* to afford the product. Yields and elemental analyses are given in Table 1.

Preparation of complexes $Cp_2Ln(NN)$ *and* $CpLn(NN)_2$

A THF solution (20 cm^3) of HNN (1.5 or 3.0 mmol) was added dropwise to a THF solution (30 cm^3) of Cp_3Nd or Cp_3Yb (1.5 mmol) at room temperature. The reaction solution was allowed to stir for 24 h at room temperature. A solid gradually precipitated, which was separated out by centrifugation, washed twice with n-hexane and dried *in vacuo* to afford the product. Yields and elemental analyses are listed in Table 1.

Acknowledgements—This research was financially supported by the National Science Foundation. The authors are grateful to the mass spectra group of Fujian Institute of Research on the Structure of Matter for the measurements of mass spectra. Thanks are also due to Dr Baohui Du and Jiping Hu for assistance.

REFERENCES

1. M. R. Litzow and T. R. Spalding, *Mass Spectrometry of Inorganic and Organometallic Compounds*. Elsevier, Amsterdam (1973).
2. Lanping Yang, Liang Dai, Huaizhu Ma and Zhongwen Ye, *Organometallics* 1989, **8**, 1129.
3. R. E. Maginn, S. Manastyskj and M. Dubeck, *J. Am. Chem. Soc.* 1963, **85**, 672.
4. Zhongwen Ye, Huaizhu Ma and Yongfei Yu, *J. Less-Common Metals* 1986, **125**, 405.
5. Huaizhu Ma and Zhongwen Ye, *J. Organomet. Chem.* 1987, **326**, 369.
6. Zhongwen Ye and Zhongzhi Wu, *Synth. React. Inorg. Met.-Org. Chem.* 1989, **19**, 157.
7. Zhongzhi Wu, Zhongwen Ye and Zhennan Zhou, *Polyhedron* 1989, **8**, 2109.
8. C. Qian, C. Ye, H. Lu, Y. Li, J. Zhou, Y. Ge and M. Tsutsui, *J. Organomet. Chem.* 1983, **247**, 161.
9. R. Lozano, J. Roman and F. D. Jesus, *Polyhedron* 1989, **8**, 947.
10. K. Nakamoto, *Infrared and Raman Spectra of Inorganic and Coordination Compounds*, 3rd edn. Wiley-Interscience, New York (1978) (and refs cited therein).
11. Yulan Qi, Gaocong Peng, Xiaojing Li, Yuansheng Wu and Rudong Yang, *Univer. J. Chem.* (Chinese) 1988, **9**, 844.
12. W. J. Evans, *Polyhedron* 1987, **6**, 803.
13. R. D. Fischer and Li Xing-Fu, *J. Less-Common Metals* 1985, **112**, 303.
14. T. J. Marks, *Prog. Inorg. Chem.* 1978, **24**, 51.
15. G. Wilkinson and J. M. Birmingham, *J. Am. Chem. Soc.* 1956, **78**, 42.
16. Changqin Ye and Yuqin Li, *J. Org. Chem.* (Chinese) 1981, 210.

Polyhedron Vol. 10, No. 1, pp. 33–35, 1991
Printed in Great Britain

0277–5387/91 $3.00+.00
© 1991 Pergamon Press plc

ACCEPTOR BEHAVIOUR OF A $Mo^{VI}O_2$(ONO) COMPLEX WITH IMIDAZOLE LIGANDS

R. N. MOHANTY, V. CHAKRAVORTTY and K. C. DASH*

Department of Chemistry, Utkal University, Vani Vihar, Bhubaneswar-751004, India

(*Received* 3 *May* 1990; *accepted* 13 *August* 1990)

Abstract—A molybdenum(VI) complex of the type MoO_2(ONO) (ONO is a dibasic tridentate Schiff base ligand H_2SAE), reacts with imidazole or its derivatives (L) to yield [MoO_2(ONO)(L)] complexes that are yellow, diamagnetic, non-electrolytic octahedral complexes. The IR spectra have three characteristic bands in the region 890–940 cm^{-1}, attributable to the *cis*-MoO_2 stretching vibrations in addition to the vibrations of the Schiff base ligand and the imidazole ligand. The ^{1}H NMR spectra reveal the coordination of the ligands to the MoO_2^{2+} core. Cyclic voltammetric measurements provide the cathodic reduction potentials (E_{pc}) for the irreversible reduction of the molybdenum(VI) complexes and in all cases this value spans the range from −1.1 to −1.2 V vs Ag/AgCl.

Molybdenum is an important trace metal in enzymes.[1–3] It has a range of stable and accessible oxidation states in which coordination numbers can vary from four to eight.[4] The one- and two-electron transfer capability associated with molybdenum and its ability to couple ion (e.g. O^{2-}) transfer with electron transfer may be crucial to the chemical role played by molybdenum in enzymes. Many simple molybdenum(VI) complexes contain the *cis*-MoO_2^{2+} ion, which has been shown to be present in certain enzymes[5,6] on the basis of EXAFS studies.

This paper reports some dioxomolybdenum(VI) complexes, where the *cis*-MoO_2^{2+} group is attached to a planar tridentate ligand spanning three coordination positions and leaving the fourth position to be bonded by a substrate like imidazole or its derivatives; significantly important molecules from a biological point of view. Similar complexes involving other tridentate ligands have been reported by us[7] and others.[8,9]

EXPERIMENTAL

Materials

Salicylaldehyde (BDH) and 2-amino-1-ethanol (Sisco-Chem, India) were used as available commercially. Although the tridentate dibasic Schiff base ligand, N-(hydroxyethyl) salicylideneimine (H_2SAE), has been reported[10] to have been obtained as an amber oil, no attempt was made to isolate it. This ligand could be conveniently generated in solution phase by mixing the components in EtOH (*in situ*) and was then available for reaction with the metal component.

$MoO_2(acac)_2$ is a very convenient source of the MoO_2^{2+} ion and could be prepared either from Na_2MoO_4[11] or from $(NH_4)_6Mo_7O_{24}\cdot 4H_2O$[8] and acetylacetone by adjusting the pH.

Synthesis of complexes

MoO_2(SAE)(Im) (Im = *imidazole*). Salicylaldehyde (0.12 cm^3, 1 mmol) and 2-amino-1-ethanol (0.06 cm^3, 1 mmol) were dissolved in 5 cm^3 of EtOH and refluxed for about 30 min to give a yellow solution containing the H_2SAE ligand *in situ*. To this ligand solution was added imidazole (0.136 g, 2 mmol) in EtOH (2 cm^3) and the mixture was magnetically stirred for 10–15 min before $MoO_2(acac)_2$ (0.33 g, 1 mmol) dissolved in EtOH (10 cm^3) was added slowly. The entire mixture was held under reflux for 60 min with continued stirring, after which the volume of the solvent was reduced to almost half. On cooling the mixture and storing in a refrigerator overnight the yellow solid separated out and was collected on a glass frit, washed

* Author to whom correspondence should be addressed.

several times with EtOH followed by ether and dried *in vacuo* over P_4O_{10}. Yield 0.2 g, 55%.

All other complexes involving the substituted imidazoles were prepared in a similar manner.

Physical measurements and analyses

The FT–IR spectra in KBr phase, FT–NMR spectra in $(CD_3)_2CO$ medium, electrical conductivities in $MeNO_2$ and the determinations of Mo, C, H and N were carried out as reported earlier.[12] Cyclic voltammetric measurements were made using PAR equipment comprising a three-electrode system of glassy carbon, platinum wire and Ag/AgCl (satd LiCl) electrodes as the working, auxillary and reference electrodes, respectively, using $(Bu_4N)(PF_6)$ (0.1 M) as the supporting electrolyte. All potential measurements were standardized by comparing with a ferrocenium/ferrocene couple.[13]

RESULTS AND DISCUSSION

The biological activity of molybdenum mostly involves the molybdenum(VI) state,[3] the chemistry of which is largely centred around the oxomolybdenum compounds, MoO_2^{2+}, with the two oxygens mutually *cis*. Five-coordinated molybdenum(VI) complexes with the *cis*-MoO_2^{2+} core are rare and the dioxomolybdenum(VI) complexes are mostly octahedrally coordinated.[4,14] The reaction of a dibasic, tridentate ligand with MoO_2^{2+} renders the sixth coordination site vacant in the electrically neutral molybdenum(VI) complex[9,15–17] and this may be envisaged as providing a suitable bonding site for substrates during a catalytic cycle. The tridentate ligand which was made to react with MoO_2^{2+} in the presence of imidazole base was obtained[10] by condensation of 2-amino-1-ethanol with salicylaldehyde and is abbreviated as H_2SAE. The source of the MoO_2^{2+} core was $MoO_2(acac)_2$ which could be easily prepared[8] in pure form and partial or total exchange of acac groups by other ligands takes place readily.[12,18] The displacement of both the acac groups from $MoO_2(acac)_2$ to form compounds of the type $MoO_2(SAE)(Im)$ has been confirmed by the isolation of $Cu(acac)_2$ quantitatively from the filtrate after the reaction of $MoO_2(acac)_2$ with H_2SAE and imidazole ligands. Further confirmation of the formation of these compounds, reported in Table 1, has been obtained from IR and ^1H NMR spectra. All compounds are yellow, diamagnetic and non-electrolytic. The ligand H_2SAE has an intense band at 1638 cm^{-1} assigned to coupled ν(C=N) vibrations,[10] which is shifted to lower frequencies and appears as a split band in the region close to 1600 cm^{-1}, suggesting coordination as an anionic ligand through the O and N atoms.[19,20] The aromatic ν(C—O) and the aliphatic ν(C—O) vibrations occur at 1550 and 1040 cm^{-1}, respectively. The broad hydrogen-bonded

Table 1. Analytical, conductivity, cyclic voltammetry and prominent IR data for molybdenum(VI) complexes

Complex $MoO_2(SAE)L$[a]	Colour	Melting point (°C)	Found (Calc.) (%) Mo	C	H	N	Λ_M[b] ($\Omega^{-1}cm^2$ mol^{-1})	E_{pc}, (V)[c]	IR (cm^{-1}) ν(C=N)	ν(Mo=O)
L = Im	Yellow	210	26.5 (26.7)	40.3 (40.1)	3.8 (3.6)	11.8 (11.7)	5.1	−1.10	1619, 1599	937, 922, 912
1-EtIm	Yellow	120	24.5 (24.7)	43.1 (43.4)	4.3 (4.4)	10.9 (10.8)	8.5	−1.16	1617, 1599	936, 919, 904
1-BuIm	Pale yellow	152	23.2 (23.1)	46.4 (46.2)	5.2 (5.1)	10.3 (10.1)	3.5	—	1614, 1600	928, 912, 898
1-ViIm	Yellowish-white	170	24.7 (24.9)	43.8 (43.6)	3.7 (3.9)	10.7 (10.9)	3.3	−1.20	1616, 1601	930, 922, 904
1-AlIm	Pale yellow	150	24.2 (24.0)	45.3 (45.1)	4.1 (4.3)	10.3 (10.5)	5.0	−1.18	1600, 1594	938, 928, 917
2-MeIm	Yellow	180	25.6 (25.7)	41.9 (41.8)	4.2 (4.0)	11.1 (11.2)	4.3	—	1602, 1598	933, 903, 890
BzIm	Pale cream	210	23.1 (23.4)	46.7 (46.9)	3.8 (3.7)	10.3 (10.2)	6.2	—	1615, 1603	928, 910, 902

[a] Abbreviations: H_2SAE = N-(hydroxyethyl)salicylideneimine, Im = imidazole; Et = ethyl; Bu = butyl; Vi = vinyl; Al = allyl; Me = methyl; BzIm = benzimidazole.

[b] All measurements in $MeNO_2$.

[c] Volts vs Ag/AgCl.

—OH stretch near 2700 cm^{-1} of the free ligand is absent in the complexes, suggesting coordination of the ligand as a deprotonated, dianionic ligand. The IR bands due to the imidazole derivatives occur in almost identical positions and can be easily assigned.[21] The formation of Mo—O bonds with the Schiff base results in the appearance of few medium to strong bands in the 550–650 cm^{-1} region,[22] and formation of Mo—N bonds with the Schiff base and imidazole results in the appearance of additional bands in the 520–600 cm^{-1} region.[23] All the complexes exhibit three IR bands in the region 890–938 cm^{-1} due to the *cis*-MoO_2^{2+} group.[8] The *trans*-MoO_2^{2+} configuration would have resulted in a single ν(Mo=O) band.

The ^{1}H NMR spectra of complexes in $(CD_3)_2CO$ reveal the coordination of the ligands to the MoO_2^{2+} core. The aldiminic proton (—N=CH—) appears as one proton singlet at 8.19 ppm in the ligand,[10] shifting somewhat down field to 8.67 ppm for the complexes. The aromatic protons are observed as a multiplet centred around 7.5 ppm. The methylene signals of the ligand backbone are seen as two sets of triplets at 3.89 and 4.51 ppm in the complexes. The imidazole protons in the complexes appear[24] at 7.84, 7.08 and 7.07 ppm for H-2, H-4 and H-5, respectively, and the proton signals for the substituents in the imidazole ring are appropriately assigned. The proton signals at 2.4 ppm for the 2-Me; at 1.3 and 4.0 ppm for the CH_3 and CH_2 of 1-Et; at 5.14, 5.46 and 6.95 ppm for 1-Vi and at 4.05, 4.95 and 5.30 ppm for 1-allyl substituents in the imidazole ring are observed.

The cyclic voltammetric measurements provide the values for cathodic reduction potentials. The complexes do not show any observable oxidation wave after the reverse anodic scan in the cyclic voltammogram indicating irreversible redox behaviour.[25,26] The reductions observed are irreversible and the cathodic reduction potentials (E_{pc}) in CH_3CN medium are all obtained in the narrow range of -1.1 to -1.2 V vs Ag/AgCl.

Acknowledgements—The authors are grateful to Professor A. Schmidpeter, Munich University, Munich, F.R.G. for FT–NMR (^{1}H) spectra; Professor K. Wieghardt, Ruhr University, Bochum, F.R.G. for cyclic voltammetric measurements; and Dr C. R. Panda, Chemical Centre, Lund University, Sweden for FT–IR measurements. One of the authors (R.N.M.) is thankful to the UGC for financial assistance and to the Government of Orissa for leave of absence.

REFERENCES

1. A. G. Sykes, *Comprehensive Coordination Chemistry* (Edited by G. Wilkinson, R. D. Gillard and J. A. McCleverty), Vol. 3, p. 1229. Pergamon Press, Oxford (1987).
2. R. C. Bray, *Enzymes* (Edited by P. Boyer), 3rd edn, Vol. 12, p. 299. Academic Press, New York (1975).
3. M. P. Coughlan (Ed.), *Molybdenum and Molybdenum Containing Enzymes*. Pergamon Press, Oxford (1980).
4. E. I. Stiefel, *Prog. Inorg. Chem.* 1977, **22**, 1.
5. T. D. Tullius, D. M. Kurtz Jr, S. D. Conradson and K. O. Hodgson, *J. Am. Chem. Soc.* 1979, **101**, 2776.
6. S. P. Cramer, H. B. Gray and K. V. Rajagopalan, *J. Am. Chem. Soc.* 1979, **101**, 2772.
7. P. K. Nath and K. C. Dash, *Transition Met. Chem.* 1985, **10**, 262.
8. O. A. Rajan and A. Chakravorty, *Inorg. Chem.* 1981, **20**, 660.
9. J. Topich, *Inorg. Chem.* 1981, **20**, 3704.
10. E. C. Alyea and A. Malek, *Can. J. Chem.* 1975, **53**, 939.
11. H. Gehrke Jr and J. Veal, *Inorg. Chim. Acta* 1969, **3**, 623.
12. R. N. Mohanty and K. C. Dash, *Polyhedron* 1990, **9**, 1011.
13. R. R. Gagne, C. A. Koval and G. C. Lisensky, *Inorg. Chem.* 1980, **19**, 2854.
14. A. J. Wilson, B. R. Penfold and C. J. Wilkins, *Acta Cryst.* 1983, **39C**, 329.
15. J. Topich and J. T. Lyon III, *Polyhedron* 1984, **3**, 55.
16. J. M. Berg and R. H. Holm, *Inorg. Chem.* 1983, **22**, 1768.
17. C. P. Marabella, J. H. Enemark, K. F. Miller, A. E. Bruce, N. Pariyadath, J. L. Corbin and E. I. Stiefel, *Inorg. Chem.* 1983, **22**, 3456.
18. S. Lee, C. Floriani, A. Chiesi-Villa and C. Guastini, *J. Chem. Soc., Dalton Trans.* 1989, 145.
19. J. R. Dilworth, C. A. McAuliffe and B. J. Sayle, *J. Chem. Soc., Dalton Trans.* 1977, 849.
20. K. Yamanouchi and S. Yamada, *Inorg. Chim. Acta* 1975, **12**, 9.
21. K. C. Dash and P. Pujari, *J. Inorg. Nucl. Chem.* 1975, **37**, 2061.
22. C. Knobler, B. R. Penfold, W. T. Robinson, C. J. Wilkins and S. H. Yong, *J. Chem. Soc., Dalton Trans.* 1980, 248.
23. L. J. Willis, T. M. Loehr, K. F. Miller, A. E. Bruce and E. I. Stiefel, *Inorg. Chem.* 1986, **25**, 4289.
24. G. Roy Choudhury and K. C. Dash, *J. Molec. Struct.* 1980, **68**, 319.
25. R. D. Taylor, J. P. Street, M. Minelli and J. T. Spence, *Inorg. Chem.* 1978, **17**, 3207.
26. C. A. Cliff, G. D. Fallon, B. M. Gatehouse, K. S. Murray and P. J. Newman, *Inorg. Chem.* 1980, **19**, 773.

Polyhedron Vol. 10, No. 1, pp. 37–40, 1991
Printed in Great Britain

0277–5387/91 $3.00+.00
© 1991 Pergamon Press plc

PREPARATION AND X-RAY CRYSTAL STRUCTURE OF DEPROTONATED S-METHYL-β-N-(PYRIDINE N-OXIDE-2-YLMETHYLIDENE)DITHIOCARBAZATE PYRIDINE NICKEL(II) PERCHLORATE: $[Ni(C_8H_8N_3OS_2)(C_5H_5N)]ClO_4$

ZHONGYUAN ZHOU and KEIBE YU

Chengdu Center of Analysis and Determination, Academia Sinica, Chengdu, P.R.C.

and

SHAOHUA GOU,* XIAOZENG YOU and ZHENG XU

Coordination Chemistry Institute, Nanjing University, Nanjing, P.R.C.

(*Received* 5 *June* 1990; *accepted* 13 *August* 1990)

Abstract—A nickel(II) complex with S-methyl-β-N-(pyridine N-oxide-2-ylmethylidene) dithiocarbazate (LH) and pyridine (Py) as ligands with the formula $[NiLPy]ClO_4$ has been synthesized. The crystal structure has been determined by X-ray diffraction analysis. Sulphur, nitrogen and oxygen atoms of the tridentate ligand, as well as a nitrogen atom of one additive pyridine, adopt a planar conformation to produce the square planar geometry at each nickel atom. Magnetic susceptibility and IR spectra are interpreted in accordance with the proposed stereochemistry.

Transition metal complexes with Schiff base ligands containing sulphur and nitrogen atoms have been widely studied for their unique anti-tumour and anti-bacterial activities in recent years.[1–4] Although many papers focused on the characteristic and spectroscopic properties of these complexes, X-ray structure determinations are few. Recently, we reported two new tridentate Schiff base ligands derived from S-alkyldithiocarbazate with 2-pyridinecarboxaldehyde N-oxide and their four-coordinate copper(II) complexes.[5] To further explore the relationship between structure and activity of such complexes, the crystal structure of [NiL Py]ClO_4 has been studied and is reported in this paper.

EXPERIMENTAL

Preparation of the complex

A solution of $Ni(ClO_4)_2 \cdot 6H_2O$ (1 mmol) and LH[5] (1 mmol) in ethanol (60 cm^3) was refluxed for 5 min, then pyridine (2 mmol) dissolved in ethanol (10 cm^3) was added. After refluxing for 10 min, the mixture was filtered while hot. The filtrate was left at room temperature, brown–red crystals were obtained with a yield of 80%. Found: C, 33.7; H, 2.8; N, 11.7. Calc. for $NiC_{13}H_{13}ClN_4O_2S_2$: C, 33.6; H, 2.8; N, 12.1%.

Crystallographic analysis

Crystal data are given in Table 1. A suitable crystal (0.25 × 0.32 × 0.60 mm) obtained from slow diffusion of ether (20 cm^3) into an acetonitrile solution (5 cm^3) of the complex was mounted on a glass fibre in random orientation. Unit cell and intensity data were obtained using a R3M/E four-circle diffractometer and graphite-monochromatized Mo-K_α radiation in a ω–2θ scan mode with a range of $2° < 2\theta < 45°$. The structure was solved by the direct method, Lorentz and polarization corrections but no absorption corrections were made. Hydrogen atoms were located on the difference Fourier map. The coordinate parameters of all the atoms, anisotropic thermal parameters for non-hydrogen atoms and isotropic thermal parameters

*Author to whom correspondence should be addressed.

Table 1. Crystallographic data

Formula	$NiC_{13}H_{13}ClN_4O_5S_2$
Molecular weight	463.53
Space group	Monoclinic, $P2_1/n$
a (Å)	7.923(2)
b (Å)	17.325(4)
c (Å)	13.317(3)
β (°)	98.16(2)
V (Å^3)	1809.6
Z	4
D_c (g cm^{-3})	1.70
μ (cm^{-1})	14.76
F(000)	916
Temperature (K)	293
Radiation	λ(Mo-K_α) = 0.71073 Å
Maximum Bragg angle	θ_{max} = 22.5
Number of independent reflections	2761
Number of observed reflections	1954 for $I > 3\sigma(I)$
Number of refined parameters	287
R and R_w	0.031 and 0.045
Weighting scheme	Unit weight

for hydrogen atoms, were refined by the full-matrix least-squares method.

Atomic scattering factors and anomalous dispersion corrections for all non-hydrogen atoms were taken from *International Tables for X-Ray Crystallography*.[6] Final atomic coordinates and thermal parameters and lists of F_o/F_c values have been deposited as supplementary material with the Editor, from whom copies are available on request.

Measurements

Magnetic susceptibility was measured in the solid state at room temperature (283 K) using a Gouy balance with $[Ni(en)_3]S_2O_3$ as calibrant. IR absorption spectra from 4000 to 400 cm^{-1} were obtained on a 170SX FT–IR instrument with samples prepared as solid KBr pellets.

RESULTS AND DISCUSSION

Crystal structure

The X-ray crystal structure of $[NiLPy]ClO_4$ is shown in Fig. 1 with the atomic numbering scheme. Figure 2 is a view of the packing and selected bond lengths and angles are listed in Table 2.

The geometry of the tetra-coordinated nickel atom is square planar. S(1), N(3) and O(1) atoms of the tridentate ligand, and the N(1) atom of the additive pyridine form a least-squares plane, deviations (Å) of atoms from their least-squares plane are S(1), −0.0399; N(3), 0.0429; O(1), −0.0461; and N(1), 0.0430 Å. The nickel atom is located in the centre of that plane, with a deviation < 0.01 Å. Ni—N, Ni—O, Ni—S distances are standard for low-spin nickel(II) compounds. Bond angles of S(1)—Ni—N(3), N(3)—Ni—O(1), O(1)—Ni—N(1) and N(1)—Ni—S(1) are 87.6, 94.6, 85.9 and 92.0°, respectively. X-ray data show that the ligand is uninegative in the complex, but the hybridization of C(12) is still sp^2. Bond lengths of O(1)—N(2), C(10)—C(11), C(11)—N(3), N(3)—N(4), N(4)—C(12) and C(12)—S(1), which are between values of corresponding normal single bonds and double bonds, indicate a large degree of electronic delocalization of these atoms.

The least-squares plane composed of O(1), N(2), C(6), C(7), C(8), C(9), C(10) and C(11), with maximum deviation not greater than 0.026 Å, is nearly parallel to that of O(1), S(1), N(3) and N(1); the dihedral angle between them is only 8.2°. The additive pyridine is co-planar, deviations of ring

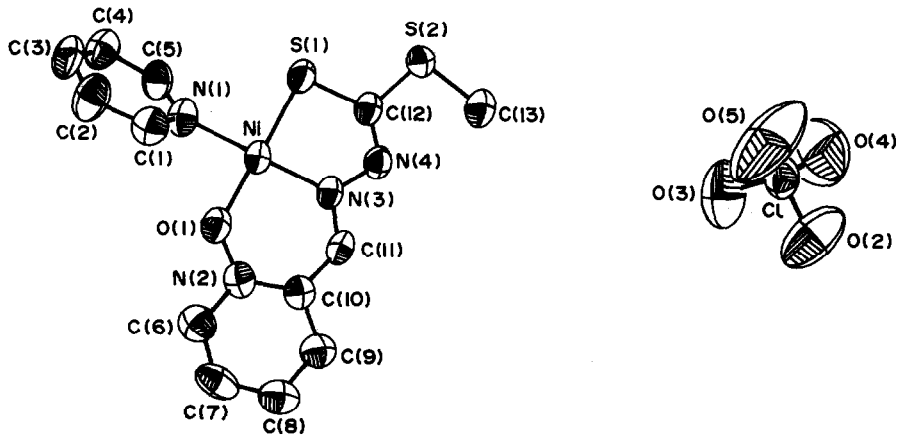

Fig. 1. Molecular structure of $[NiLPy]ClO_4$.

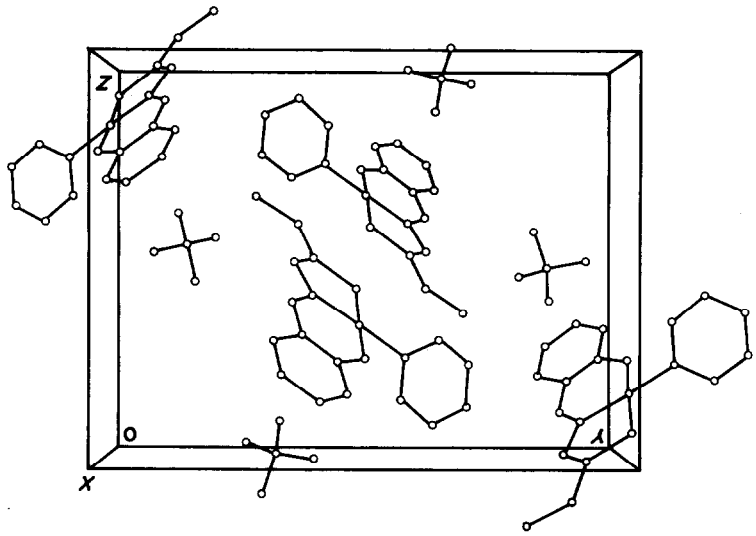

Fig. 2. The view of molecular packing.

atoms are C(1), 0.035; C(2), −0.054; C(3), 0.003; C(4), 0.0069; C(5), −0.0092; and N(1), 0.040 Å. The pyridine ring plane and the coordination plane around the nickel(II) atom have a dihedral angle of 50.8°.

The molecule is in a low symmetry. In the crystal (Fig. 2), two molecules of the complex, separated by a longer distance which results from the existence of the larger additive pyridine moiety, are situated in the opposite direction to decrease steric hindrance.

Magnetic properties and IR spectra

The magnetic susceptibility of solid samples at 283 K indicates that the complex is diamagnetic, confirming the square planar structure of the nickel(II) atom, and compatible with the proposed stereochemistry.

The IR spectra contain a very strong band at 1439 cm^{-1} assigned to ν(C=N) of the ligand. The stretching vibration of the N—O bond is observed at 1205 cm^{-1}, which is consistent with values

Table 2. Selected bond lengths (Å) and angles (°)

Ni—S(1)	2.140(2)	Ni—N(1)	1.912(4)
Ni—N(3)	1.845(4)	Ni—O(1)	1.843(4)
S(1)—C(12)	1.727(5)	S(2)—C(12)	1.735(6)
N(2)—O(1)	1.320(6)	N(2)—C(10)	1.366(6)
N(3)—N(4)	1.398(6)	N(3)—C(11)	1.297(7)
N(4)—C(12)	1.300(7)	N(1)—C(1)	1.350(7)
N(2)—C(6)	1.360(8)	C(1)—C(2)	1.367(9)
S(1)—Ni—N(1)	92.0(1)	S(1)—Ni—N(3)	87.6(1)
N(1)—Ni—N(3)	176.8(2)	S(1)—Ni—O(1)	177.1(1)
N(1)—Ni—O(1)	85.9(2)	N(3)—Ni—O(1)	94.6(2)
Ni—S(1)—C(12)	95.4(2)	C(12)—S(2)—C(13)	102.6(3)
Ni—N(1)—C(1)	118.3(4)	Ni—N(1)—C(5)	123.9(3)
C(1)—N(1)—C(5)	117.8(4)	O(1)—N(2)—C(6)	115.9(4)
O(1)—N(2)—C(10)	123.0(4)	C(6)—N(2)—C(10)	121.0(5)
Ni—N(3)—N(4)	122.0(3)	Ni—N(3)—C(11)	124.5(4)
N(4)—N(3)—C(11)	113.5(4)	N(3)—N(4)—C(12)	111.5(4)
Ni—O(1)—N(2)	128.1(3)	N(2)—C(10)—C(9)	118.5(5)
C(9)—C(10)—C(11)	119.7(5)	N(2)—C(10)—C(11)	121.8(5)
S(1)—C(12)—S(2)	115.2(3)	S(1)—C(12)—N(4)	123.4(4)
S(2)—C(12)—N(4)	121.3(4)		

reported in the literature.[7–13] Both ν(C=N) and ν(N—O) frequencies decrease by *ca* 41 and 16 cm^{-1} upon complex formation, respectively. The ν(C—S) frequency is at 1045 cm^{-1} with a weak band, whereas ν(C=S) and ν(N—H) frequencies are not observed. This confirms that the ligand coordinates the nickel(II) ion in the form of thiolate and is uninegative in the complex.[14–16] A strong broad band at 1088 cm^{-1} corresponds to the vibrations of Cl—O bonds.

REFERENCES

1. D. L. Klayman, J. P. Scovill, J. F. Bartosevich and J. Bruce, *J. Med. Chem.* 1983, **26**, 35, and refs therein.
2. J. P. Scovill, D. L. Klayman and C. F. Franchino, *J. Med. Chem.* 1982, **25**, 1261.
3. J. P. Scovill, D. L. Klayman, C. Lambros, G. E. Childs and J. D. Nortsh, *J. Med. Chem.* 1984, **27**, 87.
4. D. X. West and L. K. Pannell, *Transition Met. Chem.* 1989, **14**, 457.
5. S. H. Gou, X. Z. You, Z. Xu, K. B. Yu and Z. Y. Zhou, *Polyhedron* 1990, **9**, 2981.
6. *International Tables for X-ray Crystallography*, Vol. 4. Kynoch Press, Birmingham (1974).
7. A. E. Landers and D. J. Phillips, *Inorg. Chim. Acta* 1977, **25**, L39.
8. A. E. Landers and D. J. Phillips, *Inorg. Chim. Acta* 1981, **51**, 109.
9. A. E. Landers and D. J. Phillips, *Inorg. Chim. Acta* 1982, **59**, 41.
10. A. E. Landers and D. J. Phillips, *Inorg. Chim. Acta* 1982, **59**, 125.
11. A. E. Landers and D. J. Phillips, *Inorg. Chim. Acta* 1983, **74**, 43.
12. A. E. Landers and D. J. Phillips, *Inorg. Chim. Acta* 1984, **86**, 77.
13. N. M. Carayannis, L. L. Pylewski and C. M. Mikulski, *Coord. Chem. Rev.* 1973, **11**, 93.
14. M. Das and S. E. Livingstone, *Inorg. Chim. Acta* 1976, **19**, 5.
15. M. A. Ali and M. T. H. Tarafdar, *J. Inorg. Nucl. Chem.* 1977, **39**, 1785.
16. M. A. Ali and S. E. Livingstone, *Coord. Chem. Rev.* 1974, **13**, 101.

Polyhedron Vol. 10, No. 1, pp. 41–45, 1991
Printed in Great Britain

0277–5387/91 $3.00+.00
© 1991 Pergamon Press plc

TETRAHEDRAL HgS_4 AND LINEAR HgS_2 COORDINATION IN THE CRYSTAL STRUCTURE OF $Na_2Hg_3S_4(H_2O)_2$

R. M. HERATH BANDA, DON CRAIG, IAN G. DANCE* and MARCIA SCUDDER

School of Chemistry, University of New South Wales, PO Box 1, Kensington, N.S.W. 2033, Australia

(*Received* 21 *June* 1990; *accepted* 13 *August* 1990)

Abstract—The colourless crystalline compound $Na_2Hg_3S_4(H_2O)_2$ obtained from the heterogeneous reaction of HgS and Na_2S in DMF containing residual water, contains mercury sulphide chains $\{[Hg_2S_3]^{2-}\}_\infty$ in which tetrahedral HgS_4 units [D_2 site symmetry, Hg—S = 2.558(2) Å] are linked along the chain by pairs of digonal mercury atoms [C_2 site symmetry, Hg—S = 2.362(2) Å, S—Hg—S = 166.2(1)°]. These chains are separated by $\{[Na_2(OH_2)_2]^{2+}\}_\infty$ chains, and connected to them by O–H—S hydrogen bonds [3.261(7) Å] and Na—S contacts [2.946(5), 2.974(5) Å]. The structure embodies and mimics the coordination in both of the HgS minerals, cinnabar and metacinnabar.

We have been using the reactions of metal sulphides, MS (M = Cd, Hg), with Na_2S and S_8 in aprotic solvents such as DMF to prepare solutions of cadmium and mercury polysulphide complexes, which are characterized by metal NMR in solution and by diffraction methods after crystallization.[1,2] As part of this programme we carried out the control reaction of HgS plus Na_2S to determine whether $[Hg(S)_n]^{2-2n}$ complexes might form in DMF, as they do in water.[3,4] We observed heterogeneous reaction of black HgS and Na_2S to form almost colourless crystalline products, and here report on these reactions and on the non-molecular crystal structure of one product, $Na_2Hg_3S_4(H_2O)_2$.

RESULTS

Preparations

Although black HgS dissolves with reaction in concentrated aqueous Na_2S solution, it is not appreciably co-soluble with dehydrated Na_2S in DMF. There is, however, a heterogeneous reaction, as evinced by the colour change from black to white solids. The reaction that yielded $Na_2Hg_3S_4(H_2O)_2$ used $Na_2S \cdot 9H_2O$ that had been incompletely dehydrated, with a molar ratio of $3Na_2S$ per HgS, in deoxygenated DMF. The mixture was ultrasonicated at room temperature, converting the solid mixture from grey through yellow to white. When the mixture was heated briefly to 110°C there was no evidence that the white solids were soluble or would crystallize.† The sealed reaction mixture was ignored, and after several months it was discovered that large prismatic crystals with a very pale yellow colour had grown into the solution. On removal from the mother liquor these crystals appeared to attract atmospheric moisture within minutes and to undergo a slight morphological change leading to crystals which were less hygroscopic. Longer exposure to the atmosphere caused these crystals to revert to black HgS, but a covering of vaseline prevented this decomposition during the period of X-ray diffraction analysis.

Repetition of this preparation is difficult, and despite numerous attempts it has not yet been achieved. Heating similar mixtures at *ca* 100°C accelerates the heterogeneous conversions and colourless crystalline products appear within hours. All of these are very hygroscopic, but the X-ray diffraction patterns of the crystalline phases generated during the hydration provide no evidence for the formation of $Na_2Hg_3S_4(H_2O)_2$. Variations of the Na_2S–HgS ratio and of the water content in the reaction mixture also did not yield $Na_2Hg_3S_4(H_2O)_2$. It appears that there are at least two crystalline hydrates in this Na–Hg–S system: all are hygroscopic, and with

* Author to whom correspondence should be addressed.

† Temperature dependent blue/green colours characteristic of the $(S_6)^{2-} \rightleftharpoons 2(S_3)^-$ equilibrium in DMF were apparent.

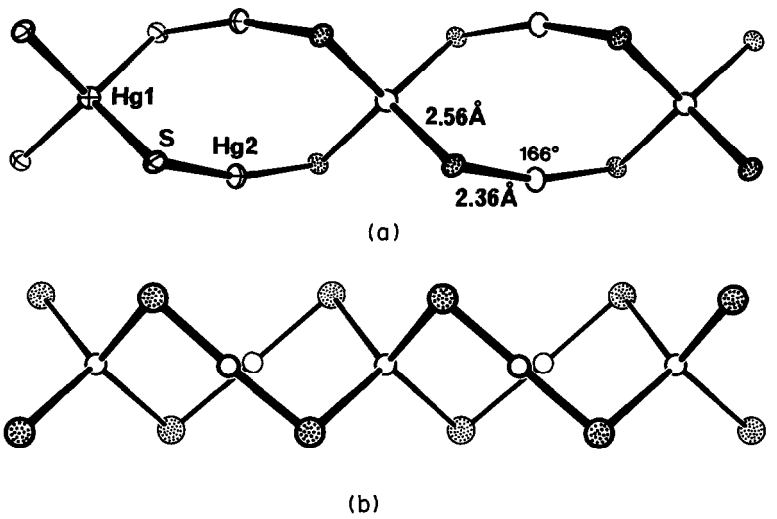

Fig. 1. Part of the $\{[Hg_2S_3]^{2-}\}_\infty$ chain in $Na_2Hg_3S_4(H_2O)_2$. (a) The three atoms, Hg(1) (tetrahedral), Hg(2) (digonal) and S, of the asymmetric unit are labelled and drawn with 50% probability ellipsoids. There is a crystallographic two-fold axis along the length of the chain, and transverse crystallographic two-fold axes through the Hg(1) and Hg(2) atoms. (b) The same chain viewed from the side, almost parallel to the transverse two-fold axes.

sufficient water undergo dissociative reversion to black HgS.

Crystal structure

The crystal structure is non-molecular. It is composed of two types of chain, one containing the Hg and S atoms and formulated $\{[Hg_2S_3]^{2-}\}_\infty$, the other the Na ions and water molecules, $\{[Na_2(OH_2)_2]^{2+}\}_\infty$. There is strong bonding within the chains and weaker bonding between chains of different types.

Appreciation of the structure is facilitated by examining first the $\{[Hg_2S_3]^{2-}\}_\infty$ chain, which is shown in Fig. 1. There are tetrahedral HgS_4 units [Hg(1)] with D_2 (222) site symmetry, linked along the chain by pairs of digonal Hg atoms [Hg(2)] with C_2 site symmetry. At the tetrahedral Hg the Hg—S distance is 2.558(2) Å, and the S—Hg—S angles are 108.2(1), 108.8(1) and 111.4(1)°. At the digonal Hg the Hg—S distance is 2.362(2) Å, and the S—Hg—S angle is 166.2(1)°. It is evident from Fig. 1 that within the chain two digonal S—Hg—S segments are directly opposed, with two Hg(2) atoms lying on the same two-fold axis: this Hg(2)—Hg(2) distance is 3.452(1) Å. The non-linearity of the digonal S—Hg—S segments is in the sense that increases the separation of the opposing Hg(2) atoms: if the S—Hg(2)—S angles were 180° the Hg(2)—Hg(2) separation would be reduced to 2.885 Å, which is at least 0.2 Å less than the sum of the normally accepted van der Waals' radius of Hg atoms (1.55 Å[5]). Thus, the observed outward bending of the opposed digonal segments along the chain is interpreted to be a consequence of repulsive Hg—Hg interactions. The Hg(1)—S—Hg(2) angle is 98.0(1)°: in many other systems with $M(\mu\text{-}S)_2M$ moieties[6] smaller values of M—S—M angles are well known, and therefore angular strain at S is not considered to be the reason for the outward bending of the digonal Hg atoms.

Each digonal Hg atom has two long contacts at 3.119(3) Å with S atoms in the adjacent $\{[Hg_2S_3]^{2-}\}_\infty$ chain: the two S atoms involved both belong to one HgS_4 tetrahedron.

The Na^+ ions and water molecules form zigzag —Na—OH_2—Na—OH_2— chains also parallel to the crystallographic *a* axis, with the Na and O atoms lying on crystallographic mirror planes. As shown in Fig. 2, each $\{[Na_2(OH_2)_2]^{2+}\}_\infty$ chain lies between four $\{[Hg_2S_3]^{2-}\}_\infty$ chains, and is connected to them by O–H—S hydrogen bonds and Na—S contacts. Along the —Na—OH_2—Na—OH_2— chain the Na—O distances alternate as 2.339(11) and 2.372(11) Å, the O—Na—O angle is 174.7(5)°, and the Na—O—Na angle is 88.7(3)°. Each Na^+ ion makes contact with four S atoms, two at 2.946(5) Å and two at 2.974(5) Å, and in the $Na(S)_4(OH_2)_2$ octahedral coordination the angles are all within 5° of 90°. Note that each S atom contacts two contiguous Na^+ ions along the $\{[Na_2(OH_2)_2]^{2+}\}_\infty$ chain. While the Na^+ ions link to the closest S

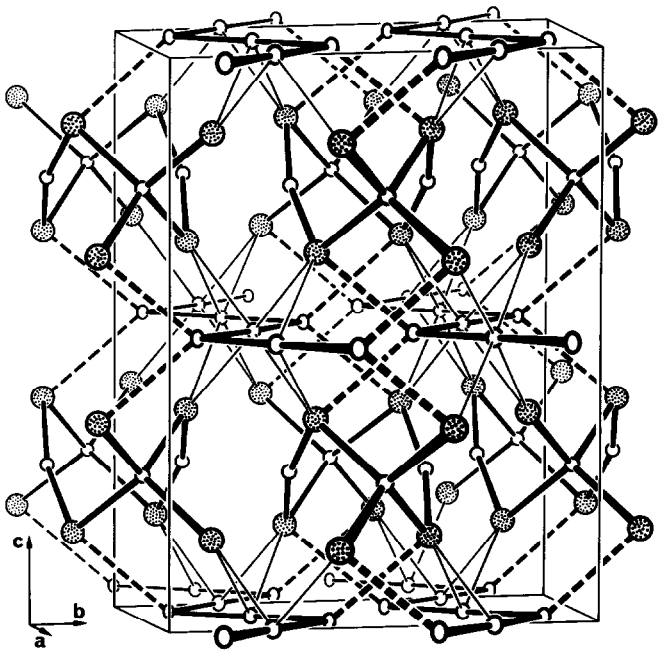

Fig. 2. The crystal lattice of $Na_2Hg_3S_4(H_2O)_2$. The dotted circles are S atoms, the small circles at $z = 0.25, 0.75$ are Hg atoms, the zigzag chains on the mirror planes at $z = 0, 0.5$ contain the Na ions (almost linear, with thin line connections to S) and O atoms of the water molecules (for which the hydrogen bonds to S are marked with thick broken lines).

atoms of the four surrounding $\{[Hg_2S_3]^{2-}\}_\infty$ chains, the O–H—S hydrogen bonds are to the more distant S atoms of the same four chains (see Fig. 2). The S—O distance is 3.261(7) Å, and the S—O—S angle 80.0(2)°. Although the hydrogen atoms were not located, it is clear that they would be slightly displaced from the O—S lines to allow H—O—H angles close to 100°. It is significant that, along *a*, the S---S separations are commensurate with the water---water separations and therefore the two chemically different chains fit together remarkably well.

DISCUSSION

HgS is dimorphic. The black form usually obtained by precipitation from aqueous solution is the same as the cubic mineral metacinnabar, with the zinc blende structure type. Metacinnabar reverts to the red stable trigonal form, cinnabar, below 344°C, while there is a first-order transformation of cinnabar to metacinnabar above 344°C.[7,8] In metacinnabar there is tetrahedral HgS_4 coordination, with Hg—S = 2.534 Å.[9] In cinnabar, helical S—Hg—S—Hg chains are present: the primary digonal HgS_2 coordination has Hg—S = 2.368 Å, S—Hg—S of 172°, while Hg—S—Hg is 105°.[10,11] Thus it is evident that the $\{[Hg_2S_3]^{2-}\}_\infty$ chains in $Na_2Hg_3S_4(H_2O)_2$ embody the structural features of both HgS minerals. The correspondence extends to the metrical details, with digonal Hg—S distances and angles of 2.362 Å, 166° and 2.368 Å, 172° in $Na_2Hg_3S_4(H_2O)_2$ and cinnabar, respectively, and tetrahedral Hg—S distances of 2.558 and 2.534 Å in $Na_2Hg_3S_4(H_2O)_2$ and metacinnabar, respectively. The significant helicity of cinnabar is not maintained in crystalline $Na_2Hg_3S_4(H_2O)_2$. The absence of visible charge-transfer absorption in $Na_2Hg_3S_4(H_2O)_2$ differentiates it from both HgS minerals, and is evidence that more extensive non-molecular interactions, rather than the primary Hg coordination, are responsible for the charge-transfer absorption of the minerals.

The motif of opposed linear digonal coordination segments occurs in many silver thiolate compounds.[12] Other relevant related compounds are the molecular ions $[HgE_2]^{2-}$, E = S, Se, Te,[3,13] the anion $[S_2W(S—Au—S)_2WS_2]^{2-}$ which contains the tetrahedral and linear components connected with the same topology,[14] and many partially hydrated alkali salts of thiometallate anions, with O–H—S hydrogen bonds.[6]

Investigations of the formation reaction for $Na_2Hg_3S_4(H_2O)_2$ and of the alternative product phases are continuing.

EXPERIMENTAL

Synthesis

$Na_2S \cdot 9H_2O$ (0.72 g, 3.0 mmol) was partially dehydrated in a stream of N_2 at 80°C, and black HgS (0.23 g, 1.0 mmol) was added. Deoxygenated and dried DMF (5 cm^3) was introduced, the vessel sealed under dinitrogen, and the mixture subjected to low power ultrasonication at room temperature. After 24 h the solid was yellow and the solution pale green: after 40 h the solid was white, and after 52 h the volume of the white solid had grown to about 4 cm^3. When the mixture was heated briefly to 110°C the pale yellow mother liquor changed to green, and returned to pale yellow on cooling, but there was no evidence that the polycrystalline solid was soluble or would crystallize. On standing at room temperature for several months large buff-coloured prismatic crystals grew in the solution. The mother liquor was removed and the crystals dried in a stream of dinitrogen. The crystals were hygroscopic and on brief exposure to the atmosphere, while mounting for X-ray diffraction, appeared to undergo a morphological change without losing single crystallinity. The sample used for collection of the X-ray diffraction data was coated with a thin layer of vaseline.

X-ray diffraction

The diffraction data were collected using a CAD4 diffractometer, at 21°C. The essential crystallographic data are as follows: crystal system orthorhombic, space group *Ibam*, $a = 6.5823(6)$, $b = 10.922(1)$, $c = 14.379(2)$ Å, $V = 1033.7(2)$ $Å^3$, $Z = 4 \times Na_2Hg_3S_4(H_2O)_2$, $D_{calc} = 5.22$ gm cm^{-3}, Mo-K_α radiation ($\lambda = 0.7107$ Å), $\mu = 452$ cm^{-1}, crystal dimensions $0.25 \times 0.08 \times 0.08$ mm^3, absorption corrections calculated and applied, max/min values of transmission coefficient = 0.028/0.092, 476 reflections measured in octant $+h$, $+k$, $+l$ to $2\theta = 50°$, 346 observed reflections [$I/\sigma(I) \geqslant 3$], 31 refined parameters, $R = 0.031$, $R_w = 0.048$.

Structure solution and refinement

There are two different Hg atoms in the structure, both located on two-fold axes: one labelled Hg(1) is on the four-fold special positions *b* of the space group *Ibam*, the other Hg(2) on the eight-fold special positions *g*. The one type of S atom is on the

Table 1. Bond distances (Å) and angles (°) in $Na_2Hg_3S_4(H_2O)_2$ (ESD in parentheses)

Hg(1)—S	2.558(2)	S—Na^f	2.946(5)
Hg(1)—S^a	2.558(2)	Na—S^c	2.946(5)
Hg(1)—S^b	2.558(2)	Na—S^h	2.946(5)
Hg(1)—S^c	2.558(2)	S—Na^g	2.974(5)
Hg(2)—S^c	2.362(2)	Na—S^j	2.974(5)
Hg(2)—S^d	2.362(2)	Na—S^k	2.974(5)
S—Hg(2)^e	2.362(2)	Na—O^l	2.339(11)
		Na—O^m	2.372(11)
S—Hg(1)—S^a	108.2(1)	S^h—Na—S^j	89.8(1)
S—Hg(1)—S^b	108.8(1)	S^h—Na—S^k	177.4(2)
S—Hg(1)—S^c	111.4(1)	S^h—Na—O^l	86.2(2)
S^a—Hg(1)—S^b	111.4(1)	S^h—Na—O^m	97.5(2)
S^a—Hg(1)—S^c	108.8(1)	S^c—Na—S^j	177.4(2)
S^b—Hg(1)—S^c	108.2(1)	S^c—Na—S^k	89.8(1)
S^d—Hg(2)—S^c	166.2(1)	S^c—Na—O^l	86.2(2)
Hg(1)—S—Hg(2)^e	98.0(1)	S^c—Na—O^m	97.5(2)
Hg(1)—S—Na^f	168.9(1)	S^j—Na—S^k	89.6(2)
Hg(1)—S—Na^g	110.6(2)	S^j—Na—O^l	91.3(2)
Hg(2)^e—S—Na^f	88.2(1)	S^j—Na—O^m	84.9(2)
Hg(2)^e—S—Na^g	143.9(2)	S^k—Na—O^l	91.3(2)
Na^f—S—Na^g	67.6(2)	S^k—Na—O^m	84.9(2)
S^h—Na—S^c	90.7(2)	O^l—Na—O^m	174.7(5)

Symmetry operators: ^{a} $1-x, -y, z$; ^{b} $x, -y, \frac{1}{2}-z$; ^{c} $1-x, y, \frac{1}{2}-z$; ^{d} $x-1, y, z$; ^{e} $1+x, y, z$; ^{f} $1-x, y, z-\frac{1}{2}$; ^{g} $\frac{1}{2}-x, \frac{1}{2}-y, z-\frac{1}{2}$; ^{h} $1-x, y, \frac{1}{2}+z$; ^{j} $\frac{1}{2}-x, \frac{1}{2}-y, \frac{1}{2}+z$; ^{k} $\frac{1}{2}-x, \frac{1}{2}-y, \frac{1}{2}-z$; ^{l} $x-\frac{1}{2}, \frac{1}{2}+y, \frac{1}{2}+z$; ^{m} $x-1, -y, \frac{1}{2}+z$.

general 16-fold position *k*, the Na^+ ion and the water oxygen atom (labelled O) are located on the mirror planes at $z = 0$, 1/2 (the eight-fold special position *j*). The hydrogen atoms were not directly located, and were not included in the refined model. Scattering factors for neutral atoms were taken from *International Tables for X-ray Crystallography*.[15] The least-squares refinement involved anisotropic thermal parameters for all atoms and an isotropic extinction coefficient. On completion of refinement, $R = \Sigma^m|\Delta F|/\Sigma^m|F_o| = 0.031$ and $R_w = [\Sigma^m w|\Delta F|^2/\Sigma^m w|F_o|^2]^{1/2} = 0.048$.

Important distances and angles are given in Table 1.

Acknowledgements—We thank the Australian Research Council and the Australian International Development and Assistance Bureau (R.M.H.B.) for financial support.

REFERENCES

1. I. G. Dance, R. M. Herath Banda, D. C. Craig, M. L. Scudder and T. D. Bailey, *Inorg. Chem.* 1989, **28**, 1862.
2. T. D. Bailey, R. M. Herath Banda, D. C. Craig, I. G. Dance, I. N. L. Ma and M. L. Scudder, *Inorg. Chem.* 1990, in press.
3. R. P. J. Cooney and J. R. Hall, *Aust. J. Chem.* 1966, **19**, 2179 and refs cited therein.
4. G. Svehla, *Vogel's Qualitative Inorganic Analysis*, 6th edn, p. 72. Longmans Scientific and Technical Publishers (1987).
5. A. Bondi, *J. Phys. Chem.* 1964, **68**, 441.
6. B. Krebs, *Angew. Chem., Int. Ed. Engl.* 1983, **22**, 113.
7. F. Jellinek, in *Inorganic Sulfur Chemistry* (Edited by G. Nickless). Elsevier, Amsterdam (1968).
8. D. J. Vaughan and J. R. Craig, *Mineral Chemistry of Metal Sulfides*, p. 64. Cambridge University Press, Cambridge (1978).
9. K. L. Aurivillius, *Acta Chem. Scand.* 1964, **18**, 1552; 1965, **19**, 522.
10. K. L. Aurivillius, *Acta Chem. Scand.* 1950, **4**, 1413.
11. P. Auvray and F. Genet, *Bull. Soc. Fr. Mineral* 1973, **96**, 218.
12. I. G. Dance, L. J. Fitzpatrick, D. C. Craig and M. L. Scudder, *Inorg. Chem.* 1989, **28**, 1853.
13. R. C. Burns, L. A. Devereux, P. Granger and G. J. Schrobilgen, *Inorg. Chem.* 1985, **24**, 2615.
14. A. Muller, H. Dornfeld, G. Henkel, B. Krebs and M. P. A. Viegers, *Angew. Chem., Int. Ed. Engl.* 1978, **17**, 52.
15. J. A. Ibers and W. C. Hamilton (Eds), *International Tables for X-Ray Crystallography*, Vol. 4, Tables 2.2A, and 2.3.1. Kynoch Press, Birmingham, England (1974).

Polyhedron Vol. 10, No. 1, pp. 47–53, 1991
Printed in Great Britain

0277–5387/91 $3.00+.00
© 1991 Pergamon Press plc

COMPLEXATION AND THERMODYNAMICS OF THE URANYL ION WITH PHOSPHATE

J. N. MATHUR

Radiochemistry Division, Bhabha Atomic Research Centre,
Trombay, Bombay 400 085, India

(*Received* 4 *July* 1990; *accepted* 15 *August* 1990)

Abstract—Complexation of UO_2^{2+} with the $H_2PO_4^-$ anion at various ionic strengths (0.1–1.0 M $NaClO_4$) has been studied using the solvent extraction technique. The equilibrium constants (β_1 and β_2) for the formation of the species $UO_2H_2PO_4^+$ and $UO_2(H_2PO_4)_2$ were fit to the following extended Debye–Hückel expressions:

$$\log \beta_1(I) = 3.47 - \frac{2.044\, I^{1/2}}{1+1.6\, I^{1/2}} + 0.273\, I$$

and

$$\log \beta_2(I) = 5.77 - \frac{3.066\, I^{1/2}}{1+1.6\, I^{1/2}} + 0.364\, I.$$

The thermodynamic parameters for these systems have been computed using the temperature coefficient method. The reactions are favoured by entropy and opposed by enthalpy. The complexes are predominantly the "inner sphere" type.

Complexing of UO_2^{2+} with various phosphate moieties has been a subject of interest for over four decades. Apart from the interest in the basic nature of the complexes formed, the acquired data are of great relevance in the recovery of uranium from phosphate solutions. In earlier studies, the concentrations of the UO_2^{2+} ion used were in the macro range and the methods employed were solubility,[1–4] spectrophotometry and solvent extraction[5] and anion exchange.[6] In a few recent publications,[7,8] di-2-ethylhexyl phosphoric acid has been used as an extractant for the study of uranyl–phosphoric acid complexes at very high phosphoric acid concentrations. Formation of various species like $UO_2(H_2PO_4)H_6P_2O_8^+$, $UO_2(H_5P_2O_8)\cdot H_3PO_4$, etc., has been reported. Recent interest in the environmental aspects of natural and waste waters and migration of radionuclides has re-emphasized the importance of phosphate complexation of actinide and lanthanide ions.[9,10]

The present work deals with the complexing of UO_2^{2+} with the $H_2PO_4^-$ anion at pH 2.50 and different ionic strengths. With the use of a ^{233}U tracer (concentration $\sim 10^{-6}$ M) the problems due to precipitation have been avoided. Also, as the studies were carried out at low phosphoric acid concentrations (< 0.02 M), the formation of species such as $UO_2H_3PO_4^{2+}$, $UO_2(H_2PO_4)_2\cdot H_3PO_4$, etc., as reported in earlier publications,[3–8] is also ruled out. This is the first systematic study at such low UO_2^{2+} ion concentrations where a direct complexation between UO_2^{2+} and $H_2PO_4^-$ ions is being reported. The thermodynamic parameters for the formation of the species $UO_2H_2PO_4^+$ and $UO_2(H_2PO_4)_2$ are also reported for the first time.

EXPERIMENTAL

The ^{233}U tracer was purified by the usual methods and its radiochemical purity was checked by alpha spectrometry. The stock solution was kept at pH 2.0 ($HClO_4$). A benzene solution of dinonylnaphthalene sulphonic acid (HD) from Vanderbilt Inc., U.S.A. was converted to its sodium salt (NaD) by shaking the solution thrice with 4 M NaCl solution. *o*-Phosphoric acid (A.R.) was obtained from Glaxo Laboratories, India. All other chemicals used were of A.R. grade.

For the present studies a solution of ^{233}U in 0.0016 F NaD/benzene was prepared by extracting an appropriate quantity of this tracer from the aqueous phase at pH 2.50 and was used for all the extraction experiments.

Variation of phosphoric acid concentrations at various ionic strengths

2 cm^3 of the aqueous phase containing $[H_3PO_4]_t$, in the range 0.0–0.02 M at pH 2.50 and ionic strengths 0.1, 0.3, 0.5, 0.7 and 1.0 M, were equilibrated with an equal volume of the NaD/benzene phase containing the ^{233}U tracer for 1 h by slow rotation in a thermostated bath at 25±0.1°C. In an earlier experiment this time was found to be sufficient to attain the equilibrium. The solutions were allowed to settle for 30 min, centrifuged and aliquots of the two phases taken for radioassay. The activities were measured with a liquid scintillation counter using a toluene–HDEHP scintillator cocktail. In a few test cases 5 cm^3 of the aqueous and organic phases were employed, and after equilibration the pH of the aqueous phases was checked, which was found to remain constant at 2.50±0.01.

Variation of phosphoric acid concentrations at 1.0 *M* $NaClO_4$ *and various temperatures*

2 cm^3 of the aqueous solutions containing $[H_3PO_4]_t$ (as mentioned above), at 1.0 M $NaClO_4$, were shaken with the same volume of organic solutions (NaD/benzene containing ^{233}U tracer) for 1 h at 10, 25, 40 and 50±0.1°C. After settling and centrifuging the activities in the two phases were measured as detailed above.

pH-*titration of phosphoric acid at various ionic strengths*

To determine the p*K*a values of phosphoric acid at different ionic strengths (0.1, 0.3, 0.5, 0.7 and 1.0 M $NaClO_4$), 45 cm^3 of an appropriate concentration of phosphoric acid at a fixed ionic strength was titrated with NaOH solution (keeping the ionic strength constant). The water used for this work was distilled and deionized and was boiled to remove dissolved CO_2. During the course of the titrations, care was taken to avoid any adsorption of CO_2 by the solutions.

Calculation of stability constants

The uptake of UO_2^{2+} into the NaD/benzene phase from the aqueous phase can be written as:

$$UO_{2(a)}^{2+} + (NAD)_{m(o)} \rightleftharpoons UO_2(Na_{m-2}D_m)_{(o)} + 2Na_{(a)}^{+}, \quad (1)$$

where (a) and (o) represent the aqueous and organic phases. The validity of this mechanism has been confirmed from the plot of log D (D = distribution ratio), at different $[Na^+]$ concentrations, vs log a_{Na^+} (activity of sodium ion), where the straight line had a slope of 1.7 (Fig. 1). The distribution ratio under such conditions is given by

$$D_o = \frac{[UO_2(Na_{m-2}D_m)]_{(o)}}{[UO_2^{2+}]_{(a)}}. \quad (2)$$

In the presence of a complex anion, $H_2PO_4^-$, the extraction of UO_2^{2+} is affected by the complexes formed in the aqueous phase. The complex formation equilibria can be written as:

$$UO_2^{2+} + H_2PO_4^- \overset{\beta_1}{\rightleftharpoons} UO_2H_2PO_4^+ \quad (3)$$

and

$$UO_2^{2+} + 2H_2PO_4^- \overset{\beta_2}{\rightleftharpoons} UO_2(H_2PO_4)_2. \quad (4)$$

Now D will become

$$D = \frac{[UO_2(Na_{m-2}D_m)]_{(o)}}{[UO_2^{2+}]_{(a)} + [UO_2H_2PO_4^+]_{(a)} + [UO_2(H_2PO_4)_2]_{(a)}} \quad (5)$$

$$= \frac{[UO_2(Na_{m-2}D_m)]_{(o)}}{[UO_2^{2+}]_{(a)}\{1 + \beta_1[H_2PO_4^-] + \beta_2[H_2PO_4^-]^2\}}. \quad (6)$$

By combining eqs (2) and (6) and simplifying, we can write

$$\frac{1}{D} = \frac{1}{D_0} + \frac{\beta_1}{D_0}[H_2PO_4^-] + \frac{\beta_2}{D_0}[H_2PO_4^-]^2. \quad (7)$$

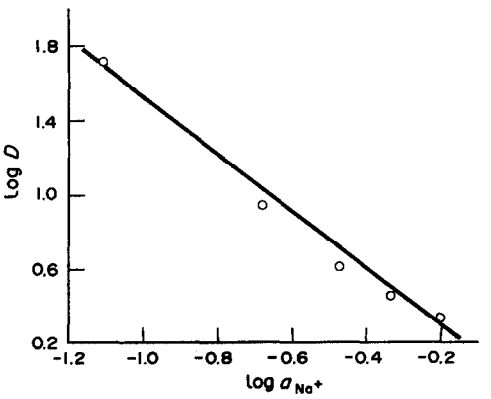

Fig. 1. Plot of log D vs log a_{Na^+} at fixed NaD concentration in the absence of phosphate ions.

At very low $H_2PO_4^-$ concentrations, where only the first complex is formed, β_1 values were evaluated using a linear least-square program (LLSP) fitting $1/D$ and $[H_2PO_4^-]$ data. The β_2 values were computed fitting $(D_0/D-1)/[H_2PO_4^-]$ and $[H_2PO_4^-]$ data at higher $[H_2PO_4^-]$ concentrations using the same program.

Calculation of thermodynamic parameters

Values of ΔG for the UO_2^{2+}–$H_2PO_4^-$ complexes were calculated from the stability constants at 25°C. Values of ΔH with their standard deviations were computed by LLSP fitting the log (stability constant) and $1/T$ (in Kelvin) data using the Van't Hoff equation. Values of ΔS were evaluated form the ΔG and ΔH values using the Gibbs–Helmholtz equation.

RESULTS AND DISCUSSION

Stability constants

For the calculation of the stability constants of UO_2^{2+}–$H_2PO_4^-$ complexes at pH 2.50, the $H_2PO_4^-$ concentrations at this pH had to be evaluated. For this purpose, the pKa_1 values at different ionic strengths were determined using the pH titration technique. The pKa_1 values thus obtained, along with the activity coefficients of $NaClO_4$ at different ionic strengths (from ref. 11), are given in Table 1. In all the calculations in this work $[H^+]$, the hydrogen ion concentration and not the hydrogen ion activity (as given by pH-meter), has been used. The molar concentrations of H_3PO_4, $H_2PO_4^-$, HPO_4^{2-} and PO_4^{3-}, at pH 2.50, 1.0 M $NaClO_4$ and $[H_3PO_4]_t = 0.02$ M were calculated by using protonation constant values from ref. 12 (log $K_1 = 1.70 \pm 0.02$, log $K_2 = 6.30 \pm 0.02$ and log $K_3 = 10.99 \pm 0.03$) and are given in Table 2. It is evident from this table that the concentrations of

Table 1. pKa_1 of phosphoric acid and activity coefficients of $NaClO_4$ at different ionic strengths

Ionic strength	pKa_1	Activity coefficient[a]
0.1	2.09 ± 0.02	0.775
0.3	2.01 ± 0.02	0.701
0.5	1.95 ± 0.03	0.668
0.7	1.86 ± 0.02	0.648
1.0	1.70 ± 0.02	0.629

[a] From ref. 11.

Table 2. Molarities of H_3PO_4, $H_2PO_4^-$, HPO_4^{2-} and PO_4^{3-} at pH 2.50, $I = 1.0$ and total phosphate = 0.02 M

Species	Molarities
H_3PO_4	4.01×10^{-3}
$H_2PO_4^-$	1.599×10^{-2}
HPO_4^{2-}	1.583×10^{-6}
PO_4^{3-}	3.226×10^{-15}

HPO_4^{2-} and PO_4^{3-} are negligibly small even at the highest $[H_3PO_4]_t$ concentration and hence the probabilities for the participation of any anions other than $H_2PO_4^-$ under these experimental conditions have been ruled out.

Figure 2 gives the plots of $1/D$ vs $[H_2PO_4^-]$ at pH 2.50 and various ionic strengths (I). It is clear from these curves that under the present experimental conditions more than one complex species is formed. However, due to the good fit of the $(D_0/D-1)/[H_2PO_4^-]$ vs $[H_2PO_4^-]$ data into a straight line it was concluded that complex species higher than $UO_2(H_2PO_4)_2$ are not formed. Table 3 gives the values of β_1 and β_2 [eqs (3) and (4)] at different values of I. Due to the uncertainty about the quality of experimental conditions such as ionic strength, high concentrations of H^+ ion, very high concentrations of phosphoric acid, uncertainty in pKa_1 values or the mixed nature of equilibrium

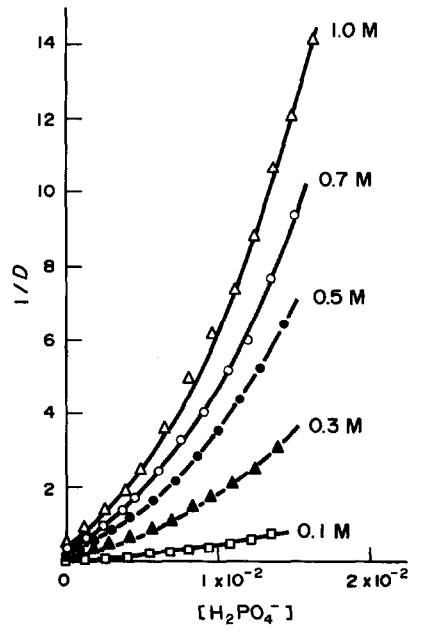

Fig. 2. Dependence of $1/D$ on $[H_2PO_4^-]$ at pH 2.50 and different ionic strengths.

Table 3. Stability constants of UO_2^{2+} complexes with the $H_2PO_4^-$ anion at different ionic strengths

Ionic strength	$\log \beta_1$	$\log \beta_2$
0.0[a]	3.47±0.02	5.77±0.02
0.1	3.04±0.03	5.15±0.02
0.3	2.97±0.01	4.97±0.03
0.5	2.95±0.02	4.96±0.02
0.7	2.94±0.02	4.94±0.03
1.0	2.94±0.02	4.93±0.02

[a] Calculated using the extended Debye–Hückel expression.

constants, it is not correct to compare the equilibrium constant values reported in refs 3, 5 and 6 with the values obtained in the present work. However, the only equilibrium constant values for the UO_2^{2+}–phosphate systems quoted in the recent critical stability constant book[12] are those given in ref. 4. These $\log \beta_1^*$ and β_2^* values correspond to the reactions

$$UO_2^{2+} + H_3PO_4 \rightleftharpoons UO_2(H_2PO_4)^+ + H^+ \quad (8)$$

and

$$UO_2^{2+} + 2H_3PO_4 \rightleftharpoons UO_2(H_2PO_4)_2 + 2H^+ \quad (9)$$

and are given at $I = 0.0$. This study has been carried out by equilibrating the solid uranyl phosphate compound with aqueous solutions, and estimating the uranyl, phosphate and hydrogen ion concentrations in the equilibrated solutions. After applying a correction for the dissociation of H_3PO_4 at $I = 0.0$ ($pKa_1 = 2.148$[13]), the values of $\log \beta_1$ and $\log \beta_2$ equivalent to our systems were calculated. These values are 3.65 and 5.60, which agree well with the values computed from the extended Debye–Hückel expression at $I = 0.0$ (Table 3). In recent work[14] on the complexing of NpO_2^{2+} with $H_2PO_4^-$ at pH 2.50, 1.0 M $NaClO_4$ and 25°C, $\log \beta_1$ for the formation of the $NpO_2H_2PO_4^+$ species was reported to be 2.52±0.07. This value is smaller than the one obtained for the similar uranyl complex (2.94) in the present work. A similar order, i.e. the NpO_2^{2+} complex stability constant being smaller than that of UO_2^{2+}, has also been reported for the first fluoride complexes.[15] Such an order could arise due to the order of effective cationic charge on the metal atoms in the dioxoactinyl ions, UO_2^{2+} (+3.2±0.1) and NpO_2^{2+} (+3.0±0.1).[15]

The stability constant values at different ionic strengths were fitted to the extended Debye–Hückel expression:

$$\log \beta(I) = \log \beta(0) + \frac{A\Delta Z^2 I^{1/2}}{1 + BI^{1/2}} + CI + DI^2, \quad (10)$$

where $\log \beta(I)$ is the equilibrium constant at a particular ionic strength I, $\log \beta(0)$ that at $I = 0.0$, $\Delta Z^2 = \Sigma Z^2(\text{products}) - \Sigma Z^2(\text{reactants})$ and $A = 0.511$. A fixed value of $B = 1.6$ was taken for our calculations, since this value has been proposed for general use in hydrolytic systems[16] and substantiated to be so from the uranyl diglycolate complex studies.[17] The value of D was set at 0.0 as has normally been done at such ionic strengths. With these values the non-linear expression (10) was fitted for two unknowns, the $\log \beta(0)$ and C. The following expressions gave the best fit with a minimum of error:

$$\log \beta_1(I) = 3.47 - \frac{2.044 I^{1/2}}{1 + 1.6 I^{1/2}} + 0.273 I \quad (11)$$

and

$$\log \beta_2(I) = 5.77 - \frac{3.066 I^{1/2}}{1 + 1.6 I^{1/2}} + 0.364 I. \quad (12)$$

The error in $\log \beta(0)$ values was computed as ±0.02. The $\log \beta(0)$ values so obtained agree well with the modified values at $I = 0.0$ reported in ref. 4.

Figure 3 gives a plot of $\log \beta_1$ and $\log \beta_2$ values of uranyl complexes with SCN^-, HSO_4^-, $H_2PO_4^-$ and F^- anions vs the pKa of these anions at 25°C and 1.0 M $NaClO_4$. The data for SCN^-, HSO_4^- and F^- complexes have been taken from ref. 13. Good fitting of these data into straight lines (separate for β_1 and β_2) suggests that the stability constant values of UO_2^{2+} complexes increase with

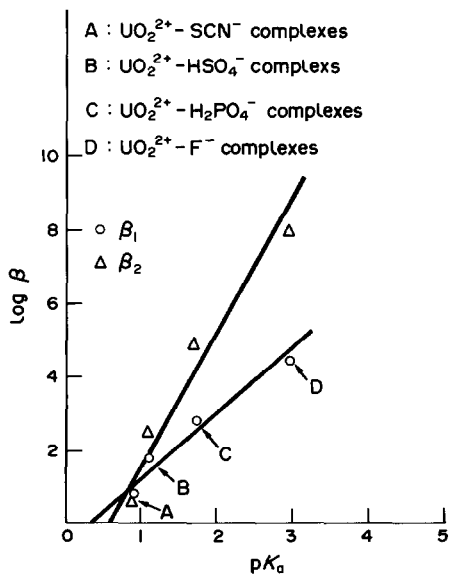

Fig. 3. Plots of pKa of HSCN, HSO_4^-, H_3PO_4 and HF vs the stability constants of these anions with UO_2^{2+} at 25°C and 1.0 M $NaClO_4$.

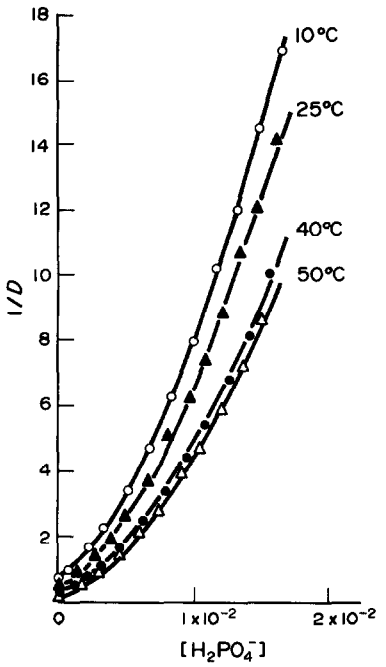

Fig. 4. Dependence of $1/D$ on $[H_2PO_4^-]$ at pH 2.50, 1.0 M $NaClO_4$ and various temperatures.

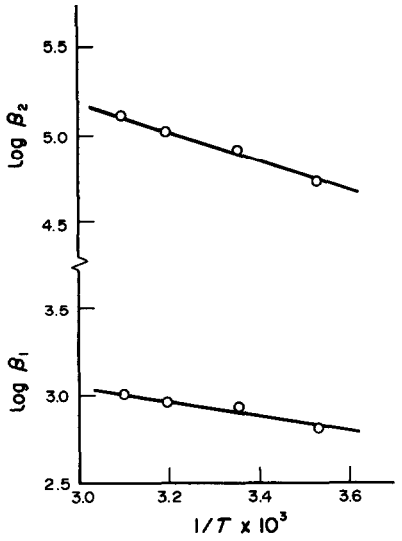

Fig. 5. Dependence of stability constants of UO_2^{2+} with $H_2PO_4^-$ complexes on temperature at 1.0 M $NaClO_4$.

increasing pKa of the inorganic ligands. Such a correlation could be of help in assessing the stability constants of uranyl complexes with other inorganic ligands.

Thermodynamic data

Figure 4 gives the plots of $1/D$ vs $[H_2PO_4^-]$ at 10, 25, 40 and 50 ± 0.1°C and a fixed ionic strength of 1.0 M $NaClO_4$. For the calculation of $[H_2PO_4^-]$ concentrations at 10, 40 and 50°C, the pKa_1 values at such temperatures and 1.0 M $NaClO_4$ are not known. However, from the knowledge of pKa_1 values at these temperatures and 0.0 ionic strength we have assessed these values as 1.64, 1.77 and 1.83 at 10, 40 and 50°C and 1.0 M $NaClO_4$ and used them for our calculations. Values of log β_1 and log β_2 (Table 4) at these temperatures were evaluated as discussed earlier. The plot of log β vs $1/T$ (in Kelvin) (Fig. 5) gave straight lines. The ΔH and ΔS values were calculated as discussed earlier and are given in Table 5. Also included in this table are the thermodynamic parameters for the uranyl complexes of SCN^-, F^- and HSO_4^- at 1.0 M $NaClO_4$ and 25°C from ref. 13. The positive enthalpy and positive entropy changes associated with the formation of both the species $UO_2H_2PO_4^+$ and $UO_2(H_2PO_4)_2$ are similar to those observed for the F^- and HSO_4^- complexes. In the case of SCN^- complexes, small exothermic ΔH and very small entropy changes have been reported. The large positive entropy changes associated with the formation of uranyl–$H_2PO_4^-$ complexes suggest the inner-sphere nature of these complexes. The positive enthalpy values observed are due to a cumulative effect of the following factors: (1) heat energy needed to break uranyl–water bonds, (2) heat energy needed to break $H_2PO_4^-$–water bonds and (3) the heat energy liberated during the formation of UO_2^{2+}–$H_2PO_4^-$ bonds. The positive ΔH values encountered in the present systems suggest that in these aqueous phase reactions the heat energy needed by factors (1) and (2) together is much more than that evolved by factor (3).

For the formation of UO_2A^+ and $UO_2(A)_2$, where $A^- = F^-$, $H_2PO_4^-$ or HSO_4^-, the ΔS values are nearly the same, while the endothermic ΔH follows the order $F^- < H_2PO_4^- < HSO_4^-$. Of the three factors mentioned above, for a cumulative effect on the ΔH values, factor (1) will be the same for all the three systems. Hence the difference in ΔH

Table 4. Stability constants of UO_2^{2+} complexes with the $H_2PO_4^-$ anion at various temperatures and 1.0 M $NaClO_4$

Temperature (°C)	log β_1	log β_2
10	2.79 ± 0.01	4.71 ± 0.01
25	2.94 ± 0.02	4.93 ± 0.02
40	2.96 ± 0.01	5.00 ± 0.02
50	2.98 ± 0.03	5.11 ± 0.01

Table 5. Thermodynamic parameters of UO_2^{2+} complexes with inorganic ligands at 25°C and 1.0 M $NaClO_4$

Parameter	Reaction: $UO_2^{2+}+A^- \rightleftharpoons UO_2A^+$, where A^- = SCN^- [a]	F^- [a]	$H_2PO_4^-$ [b]	HSO_4^- [a]
ΔG_1 (Kcal mol^{-1})	−1.02	−6.17	−3.99±0.03	−2.46
ΔH_1 (Kcal mol^{-1})	−0.8	0.4	1.9±0.4	4.4
ΔS_1 (cal deg^{-1} mol^{-1})	1	22	20±1	24
	Reaction: $UO_2^{2+}+2A^- \rightleftharpoons UO_2A_2$			
ΔG_2 (Kcal mol^{-1})	−0.98	−10.83	−6.70±0.03	−3.40
ΔH_2 (Kcal mol^{-1})	−2.1	0.5	3.9±0.4	8.4
ΔS_2 (cal deg^{-1} mol^{-1})	−4	38	36±1	41

[a] From ref. 13.
[b] Present work.

values could arise due to factor (2) and/or factor (3). It may be noted that since the F^- ion is smaller than the $H_2PO_4^-$ or HSO_4^- ions, the affinity for water will be higher for the F^- ion rather than for the other two. If the contribution due to factor (2) was predominant, one would expect a higher positive ΔH for the fluoride complexes rather than the sulphate or phosphate complexes. Hence it could be concluded that for these complexes contributions due to factor (3) are more predominant for the changes in ΔH values. The order of ΔH observed for these systems is an indication of the bonding strength of UO_2^{2+} with these anions, which follows the order $F^- > H_2PO_4^- > HSO_4^-$.

Speciation

For the UO_2^{2+}–$H_2PO_4^-$ system, the total uranyl concentration can be written as:

$$[UO_2^{2+}]_t = [UO_2^{2+}]+[UO_2H_2PO_4^+] +[UO_2(H_2PO_4)_2]. \quad (13)$$

This could be simplified to

$$[UO_2^{2+}]_t = [UO_2^{2+}]+[UO_2^{2+}]\beta_1[H_2PO_4^-] +[UO_2^{2+}]\beta_2[H_2PO_4^-]^2. \quad (14)$$

Normalizing to $[UO_2^{2+}]_t = 1$ and rearranging, eq. (14) becomes

$$[UO_2^{2+}] = \frac{1}{1+\beta_1[H_2PO_4^-]+\beta_2[H_2PO_4^-]^2}, \quad (15)$$

by knowing values of β_1 and β_2 one could easily

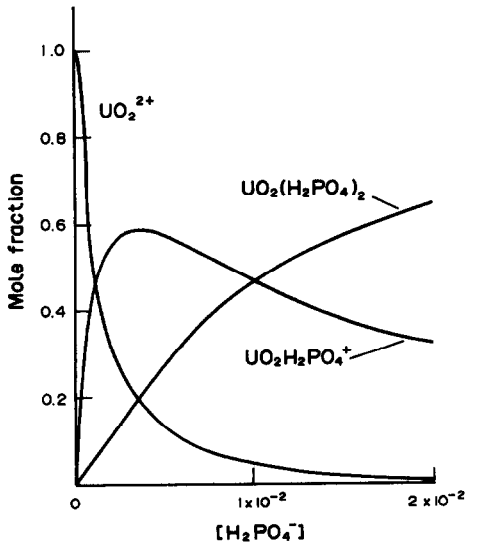

Fig. 6. Mole fraction of UO_2^{2+} species as a function of $H_2PO_4^-$ concentration at $I = 1.0$ M, pH = 2.50 and 25°C.

evaluate the value of $[UO_2^{2+}]$ at different $[H_2PO_4^-]$ concentrations. The fraction of each complexed species can be given by:

$$[UO_2H_2PO_4^+] = [UO_2^+][H_2PO_4^-]\cdot\beta_1 \quad (16)$$

and

$$[UO_2(H_2PO_4)_2] = [UO_2^{2+}][H_2P_4^-]^2\cdot\beta_2. \quad (17)$$

Figure 6 gives a plot of mole fractions of $[UO_2^{2+}]$, $[UO_2H_2PO_4^+]$ and $[UO_2(H_2PO_4)_2]$ vs $[H_2PO_4^-]$ concentration at pH 2.50.[18] It can be seen from the figure that at very low $[H_2PO_4^-]$ concentration only the first complex is predominant. With increasing $H_2PO_4^-$ concentration the formation of the $UO_2(H_2PO_4)_2$ complex increases and at a $\sim 1\times10^{-2}$ M concentration of $H_2PO_4^-$ anion both the complex species are present in almost equal quantities. At still higher $H_2PO_4^-$ concentrations the $UO_2(H_2PO_4)_2$ species predominates.

Acknowledgements—The author thanks Dr P. R. Natarajan, Head, Radiochemistry Division, B.A.R.C. for his encouragement and keen interest, and Dr Tarun Datta of this Division for his help in writing the computer programs used in this work.

REFERENCES

1. G. R. Leader, Report CN-2195. University of Chicago Metallurgical Laboratory (26 December 1944).
2. J. M. Schreyer and C. F. Baes Jr, *J. Phys. Chem.* 1955, **59**, 1179.
3. C. F. Baes Jr, *J. Phys. Chem.* 1956, **60**, 878.
4. M. Markovic and N. Pavkovic, *Inorg. Chem.* 1983, **22**, 978.
5. B. J. Thamer, *J. Am. Chem. Soc.* 1957, **79**, 4298.
6. Y. Marcus, *Proc. U.N. Int. Conf. Peaceful Uses At. Energy* 1958, **3**, 465.
7. A. Elyahyaoui, S. Bouhlassa, M. Hussonnois, L. Brillard and R. Guillaumont, *J. Less-Common Metals* 1987, **135**, 147.
8. A. Elyahyauoui, S. Bouhlassa, M. Hussonnois, L. Brillard and R. Guillaumont, *J. Less-Common Metals* 1988, **143**, 195.
9. V. K. Rao, G. R. Mahajan and P. R. Natarajan, *Radiochim. Acta* 1986, **40**, 145.
10. L. S. Bingler and R. H. Bryne, *Polyhedron* 1989, **8**, 1315.
11. *Handbook of Chemistry and Physics* CRC (1969).
12. *Critical Stability Constants* (Compiled by R. M. Smith and A. E. Martell), Vol. 6, 2nd Suppl. Plenum Press, New York (1989).
13. *Critical Stability Constants* (Compiled by R. M. Smith and A. E. Martell). Plenum Press, New York (1976).
14. J. N. Mathur and G. R. Choppin, unpublished work.
15. G. R. Choppin and L. F. Rao, *Radiochim. Acta* 1984, **37**, 143.
16. S. L. Phillips, Lawrence Berkley Laboratory LBL-14313 (1982).
17. M. S. Caceci and G. R. Choppin, *Radiochim. Acta* 1983, **33**, 207.
18. K. L. Nash and J. M. Cleveland, *Radiochim. Acta* 1983, **33**, 105.

Polyhedron Vol. 10, No. 1, pp. 55–60, 1991
Printed in Great Britain

0277–5387/91 $3.00+.00
© 1991 Pergamon Press plc

THE CHEMISTRY OF SIMPLE CERAMIC GLAZES—III. A MASNMR STUDY OF SIMULATED FELDSPARS AND THEIR REACTIONS WITH CaO, SrO, BaO OR Li_2O ON HEATING TO 1300°C

ARVIND-PAL S. MANDAIR and WILLIAM R. McWHINNIE*

Department of Chemical Engineering and Applied Chemistry, Aston University, Aston Triangle, Birmingham B4 7ET, U.K.

(*Received* 9 *July* 1990; *accepted* 13 *August* 1990)

Abstract—The influence of additions of CaO, SrO, BaO or Li_2O to a synthetic albite feldspar glass was investigated by ^{29}Si, ^{27}Al and ^{23}Na MASNMR spectroscopy. All oxides induce more ordering of the "SiO_4", "AlO_4" tetrahedra in the glass when present in greater (CaO > 60 mol % relative to SiO_2) or lesser (Li_2O > 30 mol %) proportions. Larger additions of CaO (80, 100 mol %) induced crystallization of calcium silicate phases but similar additions of SrO or BaO stabilized the glass phase. ^{27}Al MASNMR data suggested that large additions of CaO caused the separation of an aluminate phase; the data also revealed the presence of octahedral Al^{3+} sites for all additions of MO (M = Ca, Sr, Ba), however, no octahedral aluminium was seen in the presence of LiO_2. The apparent ^{23}Na chemical shift generally moved to lower field as the proportion of "AlO_4" in the glass increased.

In previous papers the use of the non-invasive, resonance spectroscopies to probe the thermolysis of the clay minerals illite and montmorillonite[1] (^{57}Fe Mössbauer), and laponite together with hectorite[2] (MASNMR), has been demonstrated. Subsequently, ^{57}Fe Mössbauer spectroscopy was used to probe the fate of iron compounds in a feldspathic ceramic glaze,[3] and MASNMR (^{29}Si, ^{27}Ai, ^{23}Na) followed the modifications produced to the pattern of thermolysis of laponite by additions of oxides such as Na_2O, CaO or Al_2O_3.[4]

X-ray powder diffraction (XRD) supplied extra, though sometimes incomplete and ambiguous, information in the above studies.[1–4] In this paper ^{29}Si, ^{23}Na and ^{27}Al MASNMR spectroscopies are used alone to explore the influence of added oxides (CaO, SrO, BaO or Li_2O) to a simulated sodium feldspar, albite ($NaAlSi_3O_8$). Albite and anorthite ($CaAl_2Si_2O_8$) are regarded as end members of a complete series of solid solutions which constitute the plagioclase feldspars.[5] The natural minerals usually contain paramagnetic impurities, often iron, which may lead to some loss of resolution in the ^{29}Si MASNMR spectrum, although reports have been published on studies of these natural minerals;[6–9] however, it was decided to simulate albite as $(Na_2O)(Al_2O_3)(SiO_2)_6$ using pure sources of oxides. Since the identification of reaction products obtained at 1300°C was the objective of the work, the use of a simulated feldspar, which provided the constituent oxides in the correct stoichiometric ratio, was deemed satisfactory.

EXPERIMENTAL

The basic simulated albite was constituted from silica, alumina and sodium carbonate of the highest available purity to give the oxide ratios $(Na_2O)(Al_2O_3)(SiO_2)_6$. To this basic mixture was added the carbonates of either calcium, strontium, barium or lithium to give the following composition ranges (based on oxides):

$(CaO)_x(Na_2O)(Al_2O_3)(SiO_2)_6$

x = 1.2, 2.4, 3.6, 4.8, 6.0

* Author to whom correspondence should be addressed.

$(SrO)_x(Na_2O)(Al_2O_3)(SiO_2)_6$

$x = 0.6, 1.2, 2.4, 4.0, 6.0$

$(BaO)_x(Na_2O)(Al_2O_3)(SiO_2)_6$

$x = 0.6, 1.2, 2.4, 3.0, 6.0$

$(Li_2O)_x(Na_2O)(Al_2O_3)(SiO_2)_6$

$x = 0.3, 0.6, 1.2, 1.8, 2.4, 3.0.$

Each individual batch was placed in a new, porcelain crucible and fired to 1300°C (monitored with a Pt/Rh thermocouple) for 4 h in a carbolite furnace. After cooling, the crucible was broken and care taken to use only a sample obtained from the centre of the melt to ensure no contamination with the material of the crucible. The sample was ground to a fine powder using an agate mortar and pestle.

Physical measurements

MASNMR spectra were obtained with a Bruker AC(E) 300 MHz spectrometer. The "magic angle" was set with KBr, and Delrin rotors were spun at approximately 5000 Hz. Frequencies were 59.580 MHz (^{29}Si), 78.206 MHz (^{27}Al) and 79.392 MHz (^{23}Na).

RESULTS

The now well accepted "Q" notation is used to classify the ^{29}Si MASNMR data in Tables 1 and 2. Thus Q^2 signifies a SiO_4 tetrahedron sharing two vertices with similar tetrahedra, whereas Q^4 (3Al), for example, indicates that the SiO_4 tetrahedron shares *all* vertices, in this case with one other SiO_4 and three AlO_4 tetrahedra.

Table 1 details the changes that occur when the simulated albite is fired in the presence of varying amounts of alkaline earth oxides. The spectrum of the simulated albite consists of a broad ($\Gamma_{1/2} = 1300$ Hz) resonance with a maximum placed in the Q^4 (2Al) range; the breadth of the signal probably reflects both a range of Q^4 (nAl) sites as well as variable OSiO angles within the glassy matrix. Small additions of CaO did not influence the breadth of the peak but shifted the maximum to high field, suggesting that Q^4 (2Al) was the dominant environment. Larger additions of CaO, e.g. 40 mol % (w.r.t. SiO_2), induced the appearance of sharp resonances (−83.6 ppm vs TMS) attributable to crystalline phases. Although the broad resonance remained discernable at 60% CaO addition, by 100% essentially only resonances from crystalline

Table 1. Variation of the ^{29}Si chemical shift of simulated albite glass as a function of added alkaline earth oxides

Per cent MO	Q^0	Q^1	Q^2	Q^3	Q^4(4Al)	Q^4(3Al)	Q^4(2Al)	Q^4(0Al)
Silica								−109
Quartz								−108
0% MO							−93.3	
20% MO								
CaO							−99.5	
SrO					−85.9			
BaO					−81.1			
40% MO								
CaO					−83.6	−89.9		
SrO					−85.0			
BaO					−81.5			
60% MO								
CaO	−69.7				−83.6			
80%								
CaO	−71.5				−83.8			
100% MO								
CaO	−71.5	−73.8			−83.9(w)			
SrO	−69.7				−80.6(s)			
BaO	−70.5				−81.5(s)			
10% MO								
SrO					−86.1			
BaO						−88.0		

Table 2. Solid state NMR data (^{29}Si, ^{27}Al, ^{23}Na) for simulated albite treated with lithium oxide fired to 1300°C

Added Li_2O (mol %)	^{29}Si MAS data (δ)[a]					^{27}Al	^{23}Na data	
	Q^0	Q^4(4Al)	Q^4(3Al)	Q^4(2Al)	Q^4(1Al)	δ[b]	δ[c]	$\Gamma_{1/2}$[d]
5					−97.1	53.3	−21.0	2500
10				−95.5		52.4	−20.9	2500
20			−89.3			56.8	−16.7	3400
30		−87.9				58.8	−15.3	2750
40		−85.9				57.4	−13.3	2700
50	−69.7	−83.1				58.4	−11.4	3250

[a] vs TMS.
[b] vs $[Al(H_2O)_6]^{3+}$.
[c] vs NaBr(aq).
[d] $\Gamma_{1/2}$ = width at half height (Hz).

phases are noted. The influence of added SrO and BaO was similar, but different in some respects to that of CaO. Thus smaller additions of these oxides are noted to be effective in changing the spectrum, and the line widths are less than for the calcium oxide case ($\Gamma_{1/2}$ = 920 Hz). The differences in the spectra for 100 mol % additions of CaO, SrO or BaO are illustrated in Fig. 1.

Table 3 combines ^{27}Al and ^{23}Na MASNMR data for the CaO, SrO and BaO modified feldspathic glazes. Both sets of spectra showed many spinning side bands, but these were readily distinguished from the true resonances by changing the rotor spinning rate. For simulated albite, both the ^{27}Al and ^{23}Na spectra consist of a broad resonance, characteristic of tetrahedral aluminium in the ^{27}Al case. Additions of the oxides certainly induced change. An octahedral signal appeared and large additions of CaO shifted the tetrahedral resonance to lower field, an effect much less marked on addition of SrO or BaO. Addition of the oxides produced an apparent deshielding of the sodium ion; in the case of BaO, the effect of small additions was quite dramatic, but the resonance underwent a high field shift on larger additions. In some cases, e.g. 60 mol % CaO, 30 mol % BaO, exceptionally broad resonances were noted.

Table 2 reports the ^{29}Si, ^{27}Al and ^{23}Na MASNMR data for simulated albite modified by additions of Li_2O, and fired to 1300°C. Even small additions (5 mol %) are effective in shifting the "albite" resonance and narrowing the resonant line width, although in an absolute sense $\Gamma_{1/2}$ remains large at 900–1100 Hz. It was only at 50 mol % addition that a weak resonance of −69.7 ppm vs TMS was perceived, which could possibly be assigned to a crystalline phase. Only a tetrahedral

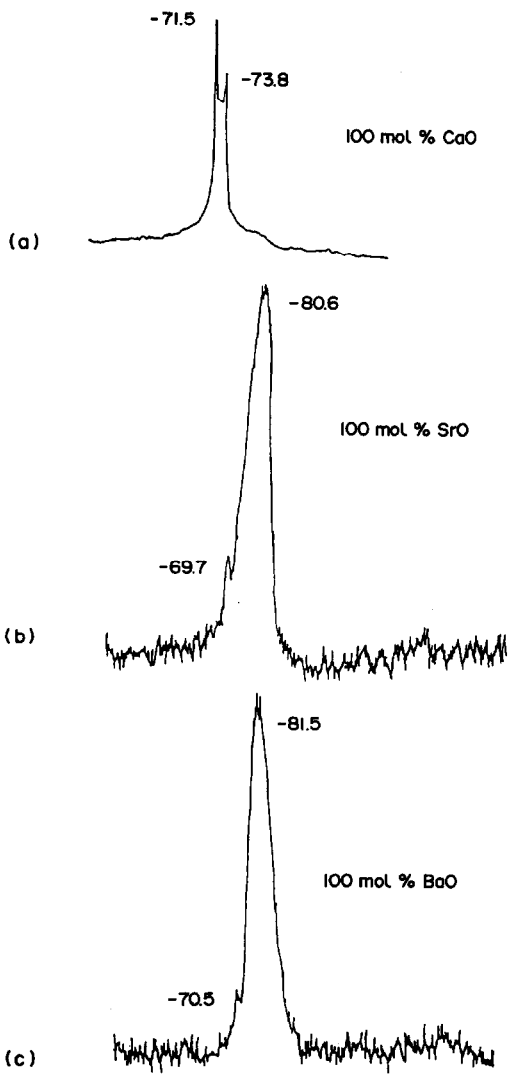

Fig. 1. ^{29}Si MASNMR spectra of simulated albite to which has been added 100 mol % (w.r.t. SiO_2) CaO (a), SrO (b) or BaO (c).

Table 3. ^{27}Al and ^{23}Na resonances of a simulated albite glass to which was added alkaline earth oxides in the indicated proportions

Per cent MO	^{27}Al Resonance		^{23}Na Resonance	
	δ^a (TET)	δ^a (OCT)	δ^b	$\Gamma_{1/2}{}^c$
0%				
	52.9		−21.5	2000
10%				
SrO	52.3	−4.2	−21.1	1800
BaO	59.3	1.8	−15.9	2500
20%				
CaO	52.7	6.2	−21.1	2250
SrO	61.4	4.5	−20.9	2400
BaO	62.9	7.0	−8.5	3800
30%				
SrO	61.9	6.2	−20.7	2800
BaO	61.8	5.4	−0.4	11,100
40%				
CaO	54.2		−20.9	2250
SrO	59.9	3.2	−13.8	2500
BaO	70.2	8.7	−12.9	4750
50%				
SrO	62.3	4.5	−14.3	2750
BaO	69.6	8.7	−12.9	4250
60%				
CaO	54.9	8.1	−18.0	17,350
80%				
CaO	81.3	4.2	−12.4	3000
100%				
CaO	80.4	7.5	−10.5	2250
SrO	65.3	8.3	−10.5	230
BaO	67.7	8.3	−13.1	4050

[a] vs $[Al(H_2O)_6]^{3+}$.
[b] vs $NaBr_{(aq)}$.
[c] $\Gamma_{1/2}$ = width at half height (Hz).

site was observed in the ^{27}Al spectra, whilst the sodium resonance maximum shifted to lower field as the amount of Li_2O increased.

DISCUSSION

An earlier study of iron in air-fired feldspathic glaze modified by addition of CaO, SrO or BaO revealed, via the ^{57}Fe Mössbauer parameters, that the influence of the heavier alkaline earth oxides as glaze modifiers was in a subtle way distinct from that of CaO. This investigation was initiated, in part, to pursue this matter further. Also, an opportunity was provided to evaluate the sole use of multinuclear MASNMR to monitor the chemical changes occurring in relatively intractable systems such as ceramic glazes.

The structure of crystalline feldspars is based on a vertex-linked framework of SiO_4 and AlO_4 tetrahedra; the ratio of aluminium to silicon may range from 1:3 to 1:1. Taylor and Brown[10] concluded that albite and anorthite glasses had essentially different structures. Thus, X-ray radial distribution analysis data were consistent with a glass structure based on rings comprising six vertex-linked MO_4 (M = Si, Al) tetrahedra (trydymite type) for an albite glass, whereas anorthite glasses gave data consistent with the presence of rings based on a feldspar crystalline structure, i.e. formulated from four vertex-sharing MO_4 tetrahedra. Kirkpatrick *et al.*[9] reported a ^{29}Si resonance at −98 ppm for an albite glass constituted from the component oxides, which may be compared with the value of −93.3 ppm in Table 1. The fact that in both studies a broad, featureless peak was observed probably implies that no great significance should be attached to the different δ_{max} values since a range of $Q^4(n\text{Al})$ environments will be present, which will also depend on the rate of cooling. What can be said, is that both investigations were in agreement that the dominant silicon site was $Q^4(2\text{Al})$. The ^{27}Al spectrum (Table 3) gives a single broad resonance at 52.9 ppm relative to $[Al(H_2O)_6]^{3+}$, characteristic of a tetrahedral environment and consistent with a model in which all the aluminium is present in an AlO_4 environment. Kirkpatrick *et al.* saw a quadrupole split ^{23}Na resonance (second-order quadrupole effects are not averaged to zero by spinning at the magic angle) with maxima at −13.1 and −21.9 ppm for crystalline albite, but for albite glass a broad symmetric band centred at −18.3 ppm (vs aqueous NaCl) was observed. The ^{23}Na resonance observed in this work was broad, but relatively symmetrical, with the maximum [w.r.t. NaBr(aq)] at −21.5 ppm.

The effect of added CaO at a 20 mol % level was unspectacular. Although the maximum of the ^{29}Si resonance underwent a high field shift, the dominant environment did remain $Q^4(2\text{Al})$. However, the ^{27}Al MASNMR spectrum showed the presence of octahedral as well as tetrahedral aluminium. It was only at 40 mol % additions of CaO that significant changes in the ^{29}Si spectra occurred. The broad peak shifted to −89.9 ppm, just within the $Q^4(3\text{Al})$ range, indicating further ordering of the aluminosilicate network. In addition, a sharp resonance indicative of a new crystalline phase was seen. Crystalline synthetic anorthite was reported to give ^{29}Si resonances at −82.9, −84.8 and −89.6 ppm. It is possible that anorthite has been formed,

the higher field resonances being hidden under the major broad peak. A 60 mol % addition of CaO gives a spectrum in which the maximum of a very broad resonance arising from a glassy phase is virtually coincident with that of the same sharp resonance (−89.9 ppm) seen at 40% addition. The resonance arising from the glass has been assigned as $Q^4(4Al)$ implying a glass structure of almost perfect ordering of SiO_4 and AlO_4 tetrahedra; this glass co-exists with the same crystalline phase described above. Further additions of CaO produce dramatic spectral changes. At 80 mol %, the sharp resonance at −83.8 ppm is now very weak and a new strong, sharp band at −71.5 ppm dominates. At 100 mol % CaO the spectrum is dominated by two sharp resonances at −71.5 and −73.8 ppm. These resonances are assigned to β- and γ-Ca_2SiO_4.[11] Thus large additions of CaO encourage the formation of crystalline phases and depolymerization.

The ^{27}Al and ^{23}Na MASNMR spectral data are given in Table 3. Although arguments based on changes of shielding of these quadrupolar nuclei must be advanced with caution (MAS does not average second-order quadrupole effects to zero), there were some significant changes in the observed peak maxima for the tetrahedral ^{27}Al resonance and the ^{23}Na resonance. This is best illustrated graphically in Fig. 2 where it can be noted that the

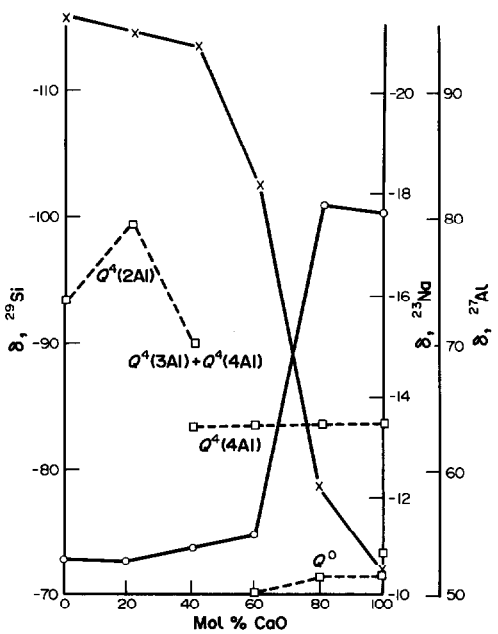

Fig. 2. Plots of chemical shift (δ) for ^{23}Na, ^{27}Al and ^{29}Si for a synthetic albite glass to which has been added the indicated mol % of CaO (—×—, ^{23}Na; —○—, ^{27}Al; --□-- ^{29}Si).

maximum change in the apparent chemical shift of both nuclei occurs between 60 and 80 mol % addition of CaO. In particular, the tetrahedral aluminium resonance undergoes a significant downfield shift to 80.4 ppm on 100% CaO addition, a region which has been correlated with aluminate (as opposed to aluminosilicate) phases.[12] A reasonable interpretation is that addition of CaO in large (>80 mol %) proportions encourages the crystallization of calcium silicate phases with the concurrent formation of, essentially, sodium aluminate phases. The ^{27}Al MASNMR data also reveal that even low additions of CaO cause one aluminium to occupy an "AlO_6" environment.

The effect of SrO and BaO was different in two respects. Firstly, their influence was felt at lower concentration (e.g. 10 mol %—see Table 1); secondly, at 100% mol % additions a *broad* resonance centred at −80.6 ppm (SrO) or −81.5 ppm (BaO) was dominant with lower field resonances characteristic of crystalline phases as weak spectral features. An earlier study using ^{57}Fe Mössbauer spectroscopy to track the fate of iron in feldspathic glazes noted differences produced by the use of different alkaline earth oxides; it was contemplated that either SrO and BaO modified the glass structure or encouraged the precipitation of "ferrate" phases. It would appear that the presence of Sr^{2+} or Ba^{2+} stabilizes the glass and discourages the precipitation of crystalline materials. Further evidence for this hypothesis comes from the ^{27}Al MASNMR data which do not give evidence of separate "aluminate" phases at high SrO, BaO additions. The ^{23}Na data are less informative; although the resonance maximum undergoes a low field shift with increasing mol % addition of MO (M = Sr, Ba), particularly for BaO, this occurs in an erratic fashion. As for CaO, some aluminium is located in an octahedral "AlO_6" site.

Lithium oxide is a strong flux. Since earlier investigations had considered the thermochemistry of laponite,[1] and how the thermal decomposition was modified by additions of oxides,[4] it was of interest to consider the influence of additions of Li_2O (up to 50 mol %) on the synthetic feldspar. The data in Table 2 reveal that lithium, in quite small additions, creates more ordering in the glass phase. The major resonance was, in all cases, broad but at 50% addition a weak resonance, possibly characteristic of a crystalline phase, was noted at −69.7 ppm. Also of interest is the fact that no aluminium was discernible in octahedral coordination. All firings were carried out under identical conditions; it is possible that the rate of reaction of alumina was slower in the presence of MO (M = Ca, Sr, Ba) than when the strong flux Li_2O was present. Alternatively, the octahedral site occupied by Al^{3+} in the

presence of M^{2+} may be preferentially occupied by Li^+. The ^{23}Na resonance shows a monotonic shift to lower field as the degree of ordering in the glass phase increases, i.e. a general conclusion from this work is that the incorporation of more aluminium in the glass leads to an apparent deshielding of the sodium ion.

Acknowledgements—A-P.S.M. thanks Aston University for a studentship. Dr M. C. Perry is thanked for his patient help in obtaining the spectra.

REFERENCES

1. P. J. Michael and W. R. McWhinnie, *Polyhedron* 1989, **8**, 2709.
2. A-P. S. Mandair, P. J. Michael and W. R. McWhinnie, *Polyhedron* 1990, **9**, 517.
3. N. J. Ali, P. A. Gillespie and W. R. McWhinnie, *Polyhedron* 1990, **9**, 999.
4. A-P. S. Mandair and W. R. McWhinnie, *Polyhedron* 1990, **9**, 1709.
5. J. V. Smith, *Feldspar Minerals. Part 1. Crystal Structure and Physical Properties*. Springer-Verlag, Berlin (1974).
6. E. Lippmaa, M. Mägi, A. Samoson, G. Engelhardt and A-R. Grimmer, *J. Am. Chem. Soc.* 1980, **102**, 4889.
7. B. L. Sherriff and J. S. Hartman, *Can. Miner.* 1985, **23**, 205.
8. J. V. Smith, C. S. Blackwell and G. L. Hovis, *Nature* 1984, **309**, 140.
9. R. J. Kirkpatrick, R. A. Kinsey, K. A. Smith, D. M. Henderson and E. Oldfield, *Am. Miner.* 1985, **70**, 106.
10. M. Taylor and G. E. Brown, *Geochim. Cosmochim. Acta* 1979, **3**, 61.
11. E. Oldfield and N. Janes, *J. Am. Chem. Soc.* 1985, **107**, 6769.
12. D. Müller, W. Gessner, A. Samoson, E. Lippmaa and G. Scheler, *J. Chem. Soc., Dalton Trans.* 1986, 1277.

Polyhedron Vol. 10, No. 1, pp. 61–65, 1991
Printed in Great Britain

0277–5387/91 $3.00+.00
© 1991 Pergamon Press plc

HYDROXYCARBOXYLATO OXO-OSMIUM(VI) COMPLEXES

CATHERINE F. EDWARDS and WILLIAM P. GRIFFITH*

Inorganic Chemistry Research Laboratories, Imperial College of Science, Technology and Medicine, London SW7 2AY, U.K.

(*Received* 9 *July* 1990; *accepted* 13 *August* 1990)

Abstract—The new complexes OsO_2py_2L (L = oxalate, lactate, atrolactate, citrate, quinate), OsO_2pic_2L (L = oxalate, oxoisobutyrate; pic = 3-methylpyridine), $(OsO_2py_2)_2$(tartrate), $K_2[OsO_2L_2]$ (L = glycolate, quinate) and $K_4[(OsO_2)_2(tartrate)_3]$ are reported. On the basis of IR, Raman and ^{13}C NMR studies we believe them to contain *trans* OsO_2 osmyl linkages. X-ray photoelectronic and mass spectral data are also reported for some of them.

In connection with work which we have recently started on complexes of osmium with glycols and carbohydrates we have been studying oxo-osmium(VI) complexes of α-hydroxycarboxylic acids since these are good models for glycols and the aldonic acid forms of sugars. Few osmium complexes of such ligands are known; salts of $[OsO_2L_2]^{2-}$ (L = salicylate,[1] oxalate and malonate[2]) and of OsO_2py_2L' (L' = glycolate, oxoisobutyrate, mandelate and salicylate)[3] have been reported and the X-ray crystal structure of OsO_2py_2L' (L' = glycolate,[4] salicylate[5]) shows the O═Os═O, "osmyl", linkage to be essentially *trans* in these species.

RESULTS AND DISCUSSION

(a) OsO_2py_2L *and* OsO_2pic_2L

By using hydrophobic co-ligands such as pyridine (py) or 3-picoline (pic) we were able to precipitate complexes of this type. Hinckley's procedure[3] for obtaining OsO_2py_2L (L = glycolate, oxoisobutyrate, mandelate, salicylate) was semi-heterogeneous and worked with few acids: a suspension of *trans*-$K_2[OsO_2(OCH_3)_4]$ was reacted with pyridine to give a suspension, to which was added the acid. In our method we react OsO_4 with the acid in ethanolic solution in the presence of excess pyridine; it is likely that $Os_2O_6py_4$ is formed *in situ* with the ethanol having reduced osmium(VII) to osmium(VI). A similar procedure is successful for 3-picoline, but we were unable to obtain tractable products using 2,2′-bipyridyl or 1,10-phenanthroline. Complexes were obtained with a wide variety of acids, though we were unable to isolate the products with malic, tartronic or gluconic acids.

The complexes were characterized by elemental analysis, IR and Raman spectroscopy (see Table 1), and in some cases by ^{13}C NMR, mass spectral and X-ray photoelectronic spectroscopic techniques. The vibrational spectra are discussed below (Section c).

The citrato and tartrato complexes are of particular interest because citrate and tartrate can function as terminal or bridge ligands. The analysis of the citrato complex is close to that for a monomer, OsO_2py_2(citrate), and the ^{13}C NMR spectrum [Section c(i)] is consistent with this. Unfortunately the tartrato complex is not sufficiently soluble for ^{13}C NMR studies, but its IR spectrum (see below) suggests that the tartrate has a bridging role; elemental analyses and the FAB^+ mass spectrum are in agreement with its formulation as $(OsO_2py_2)_2$(tartrate).

(b) $K_2[OsO_2L_2]$

Species of this type are not easy to isolate. Methods used in the literature include reaction of *trans*-$K_2[OsO_2(OH)_4]$,[2] OsO_4 with alkali[6,7] or $K_4[Os_2O_6(NO_2)_4]$[6,7] with the acid; the species so produced were $[OsO_2ox_2]^{2-}$,[2,6,7] $[OsO_2(salicylate)_2]^{2-}$[1] and $[OsO_2(malonate)_2]^{2-}$.[2] We

* Author to whom correspondence should be addressed.

Table 1. Analytical and spectral data for osmium hydroxycarboxylate complexes

Compound	Analyses (%)[a]				Vibrational data (cm^{-1})					ESCA binding energies ($4f_{7/2}$ in eV)
	C	H	N	K	ν(C=O)	ν(C—O_A)	ν(C—O_B)	$\nu^s(OsO_2)$[b]	$\nu^{as}(OsO_2)$	
OsO_2py_2ox	30.9 (30.8)	2.0 (2.2)	6.0 (6.0)	—	1732vs, 1702s	1327vs, 1220m		907s	864vs	54.7
OsO_2pic_2ox	33.8 (33.9)	2.7 (2.8)	5.7 (5.6)	—	1735vs, 1703s	1342vs		904s	856vs	
OsO_2py_2(glycolate)	32.1 (31.7)	2.8 (2.7)	6.0 (6.2)	—	1704vs, 1664s	1335s	1046m	887s	848vs	
OsO_2py_2(lactate)	33.6 (33.3)	3.0 (3.0)	5.8 (6.0)	—	1682vs	1359m	1103w	887s	843vs	
OsO_2py_2(atrolactate)	41.6 (41.2)	3.1 (3.3)	5.2 (5.1)	—	1694vs	1363m	1124	887s	840vs	
$(OsO_2py_2)_2$(tartrate)	32.0 (31.8)	2.7 (2.4)	6.0 (6.2)	—	1697vs	1320m	1114m 1070m	889s	847vs	
OsO_2py_2(citrate)	34.4 (33.7)	3.1 (2.8)	5.1 (4.9)	—	1595s	1366s	1187m 1078m	895s	853vs	54.6
OsO_2py_2(quinate)	35.4 (35.8)	3.3 (3.5)	5.5 (4.9)	—	1686s, 1639m	1300m	1116m	886s	838vs	54.6
OsO_2py_2(oxoisobutyrate)	35.0 (34.8)	3.2 (3.4)	5.8 (5.8)	—	1691vs	1304s	1129w	887s	837vs	
OsO_2pic_2(oxoisobutyrate)	38.2 (37.6)	3.9 (3.9)	5.5 (5.5)	—	1687vs	1300s	1113w	886s	843vs	
$K_2[OsO_2ox_2]$	10.0 (10.0)	Nil (Nil)	—	16.0 (16.4)	1718vs, 1702vs	1347, 1202		889s	863s	
$K_4[Os_2O_6ox_2]\cdot 2H_2O$	5.5 (5.7)	0.7 (0.5)	—	17.8 (18.5)	1705s, 1674vs	1386, 1260		895s	837s	
$K_2[OsO_2(glycolate)_2]$	10.8 (10.7)	0.8 (0.9)	—	16.6 (17.5)	1647vs	1343s	1051s		835s	54.9
$K_4[Os_2O_4(tartrate)_3]\cdot 4H_2O$	11.9 (12.9)	1.3 (1.6)	—	13.7 (14.0)	1710sh, 1645vs	1344s	1123m, 1050m		844vs	
$K_2[OsO_2(quinate)_2]\cdot 6H_2O$	20.1 (21.3)	3.7 (4.0)	—	8.7 (9.9)	1641vs	1337s	1117w		829vs	

[a] Calculated values in parentheses.
[b] Raman band.

find that a better method is to use a solution of *trans*-$K_2[OsO_2(OMe)_4]$ in methanol with the acid; in this way we have prepared the known salt $K_2[OsO_2ox_2]$ as well as the new salts listed in Table 1. These salts are not very stable and tend to decompose even in the solid state after a few days, while in solution they rapidly decompose to give OsO_2. Analyses of the compounds obtained with citric and tartaric acids do not fit the general formula $K_2[OsO_2L_2]$. These ligands (and also malic and tartronic acids which give complexes of variable composition) would have free hydroxyl and carboxylate groups in an $[OsO_2L_2]^{2-}$ structure and hence a propensity to oligomerization. Such a problem is lessened in the $[OsO_2py_2L]$ type of complexes since pyridine occupies two of the coordination sites on the metal and so decreases the possibilities of oligomerization.

(c) *Spectroscopic data and structures*

None of the new complexes gave crystals suitable for X-ray examination. However, on the basis of vibrational and, in some cases, ^{13}C NMR and X-ray photoelectronic spectroscopic evidence we believe them all to contain the linear *trans* $O{=}Os^{VI}{=}O$, "osmyl", unit, and in the case of the hydroxycarboxylic acids, that coordination occurs from the deprotonated hydroxy and carboxylate groups forming a five-membered ring. Thus the coordination around the osmium in both types of complex is likely to be as shown in Fig. 1.

(i) ^{13}C NMR. We were able to measure the ^{13}C NMR spectra of OsO_2py_2(glycolate) and OsO_2py_2(lactate) in C^2HCl_3 and of OsO_2py_2(citrate) in ^2H_2O; the other complexes (apart from OsO_2py_2ox for which ^{13}C data would not be useful) were either too unstable in solution or were insufficiently soluble.

The spectrum of OsO_2py_2(glycolate) shows two resonances assignable to the glycolato ligand, at δ 188.5 and at 76.1 [all δ in ppm vs $Si(CH_3)_4$]. The former we assign as arising from the carboxylate carbon atom and the latter to the hydroxy-bearing carbon atom. The large downfield shift of the latter resonance relative to its position in free glycolic acid (δ 62.0)[8] is consistent with the alcoholic OH group coordinating, with the loss of a proton. Comparable shifts and assignments have been made for solutions of $K_2[MoO(O_2)_2$(glycolate)$]\cdot 2H_2O$, in which X-ray data showed the hydroxy group to be deprotonated,[9] and in other molybdenum, tungsten[8] and uranyl[10] glycolato complexes. For OsO_2py_2(lactate), shifts at δ 189.5, 82.1 and 20.1 are assigned to the carboxylate, deprotonated hydroxy-bearing and methyl carbon centres, respectively (observed at δ 180.4, 67.4 and 19.6 in the free ligand);[11] highly comparable shifts have been reported for lactato complexes of molybdenum(VI),[8,11] tungsten(VI)[8] and of the uranyl entity.[10] The ^{13}C NMR spectrum of OsO_2py_2(citrate) shows four resonances at δ 192.7, 176.9, 88.8 and 46.4. If a five-membered ring is formed of $(citrate)^{2-}$ involving the deprotonated hydroxy group and the central carboxylate group both bound to the central metal atom, as we have demonstrated by X-ray work to be the case in $K_2[MoO(O_2)_2$(citrate)$]\cdot 1/2H_2O_2\cdot 3H_2O$,[12] the four resonances will be as follows. That at δ 46.4 arises from the methylene carbon atoms, the tertiary deprotonated hydroxy-bearing carbon is at δ 88.8, the non-coordinating carboxylate carbon atoms at δ 176.9, while the lowest field resonance at δ 192.7 would arise from the carbon atom of the unique central coordinating carboxyl group. Similar assignments have been made for gallium[13] and aluminium[14] citrato complexes.

(ii) *Raman and IR data.* All the complexes show very strong, sharp IR bands near 840 cm^{-1} and rather weaker, broader bands near 570 cm^{-1}. The former we assign to $\nu^{as}(OsO_2)$, the asymmetric stretch of the osmyl unit as in other complexes of this type,[2,15] while the 570 cm^{-1} band, or bands in that region, are likely to arise from Os—O stretches for the coordinated ligands {in $(Bu^n{}_4N)_2[OsO_2ox_2]$ these modes were identified near 570 cm^{-1}}.[3] For those complexes whose colours do not preclude the measurement of Raman spectra strong, sharp bands are observed near 890 cm^{-1}, assigned to the symmetric stretch $\nu^s(OsO_2)$ of the osmyl unit; as expected for these centrosymmetric or quasi-centrosymmetric moieties $\nu^s(OsO_2)$ is not observed in the IR and $\nu^{as}(OsO_2)$ is not observed in the Raman. In the cases of OsO_2py_2(citrato) and OsO_2py_2(glycolate), where solubilities are sufficient to allow recording of the Raman spectra of solutions, the 890 cm^{-1} bands are found to be polarized as expected for $\nu^s(OsO_2)$ vibrations.

The bands likely to be due to C—O stretches are complex and our assignments are necessarily tentative, following those of others on analogous

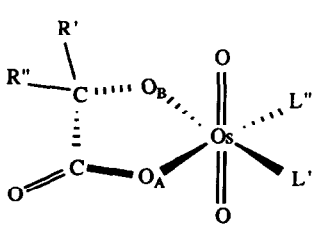

Fig. 1.

complexes. In the table we give assignments of ν(C=O), ν(C—O_A) and ν(C—O_B) where O is the *exo* carbonyl oxygen atom, O_A is the deprotonated carboxylate hydroxyl group and O_B is the deprotonated hydroxyl adjacent to the carboxyl group (see Fig. 1). Generally it is observed that there was a shift of both ν(C=O) and ν(C—O_A) towards lower frequency upon complexation, as expected.[16,17] For OsO_2py_2ox, OsO_2pic_2ox and the known *trans*-$K_2[OsO_2ox_2]$ we follow the assignments of Preetz and Schultz,[2] assigning IR bands near 1718 and 1702 cm^{-1} to ν^{as}(C=O) and ν^{s}(C=O), respectively, and at 1340 and 1205 cm^{-1} to ν^{as}(C—O) and ν^{s}(C—O), respectively. Likewise in the complexes OsO_2py_2(glycolate) and $K_2[OsO_2(glycolate)_2]$ bands near 1650 cm^{-1} are assigned to ν(C=O_A) and near 1388 cm^{-1} to ν(C—O_B), as in other glycolato complexes.[10,18] In the lactato complex, $[OsO_2py_2(lactate)]$, bands are similarly assigned by comparison with the literature for lactato complexes.[10]

The citrato and tartrato complexes are of interest here because these ligands can function as terminal or bridging ligands. The analysis of OsO_2py_2(citrate) fits well for this formula with terminal bidentate citrate, and the IR spectrum is similar to that observed for $K_2[MoO(O_2)_2(citrate)]\cdot 1/2H_2O_2\cdot 3H_2O$[12] and for $Na_2[\{VO(citrate)\}_2O]\cdot 12H_2O$.[19] As well as the band at 1595 cm^{-1} due to the complexed carboxylate group, another at 1727 cm^{-1} is seen which may be assigned to the asymmetric stretch of free carboxylic groups. A salt approximating in composition to $K_4[(OsO_2)_2(citrate)_3]$ was obtained from $K_2[OsO_2(OMe)_4]$ and citric acid; IR bands due to citrate were complicated and could arise from both terminal and bridging citrate groups. The IR spectrum of $(OsO_2py_2)_2$(tartrate), in which it is likely that the tartrate ligand bridges two osmium atoms as in the case of $K_4[Mo_2O_2(O_2)_4(tartrate)]\cdot 4H_2O$,[9] shows bands similar to those in the latter but different from those in a uranyl complex[8] in which tartrate behaves as a terminal ligand only. As would be expected for a bridging tartrate, the osmium complex shows no band assignable to a free carboxylate group.

The complex formulated by Wintrebert as $K_2[OsO_3ox]$[20] has been reformulated as $K_2[OsO_2(OH)_2ox]$ on the basis of IR data,[21] but we now reformulate it as a dimer, $K_4[Os_2O_6ox_2]\cdot 2H_2O$ (Fig. 2). This is consistent with the reformulation of "$K_2[OsO_3(NO_2)_2]$"[20] as $K_4[OsO_2O_6(NO_2)_4]$, proven by X-ray crystallography[22] to have an analogous structure. An IR band at 651 cm^{-1} and the weak Raman band at 519 cm^{-1} are likely to arise from the Os_2O_2 bridge.[23]

(iii) *X-ray photoelectron spectroscopy*. We also list in the table X-ray photoelectron spectroscopy (XPS) $4f_{7/2}$ binding energies for four of the complexes, since it is known[24,25] that such data are indicative of the oxidation state of the osmium. The values are relative to a C_{1s} binding energy of 285 eV; by comparison with $4f_{7/2}$ binding energies for standard compounds {$K_2[Os^{VI}O_2(OH)_4]$ 54.5 eV, $K_2[Os^{IV}Cl_6]$ 53.0 eV, $Os^{III}Cl_2(acac)(PPh_3)_2$ 51.9 eV} it is clear that they are likely to contain osmium in the hexavalent oxidation state. For these compounds minor peaks near 53 or 52 eV were also seen, suggesting that some decomposition had occurred under the conditions of the experiment.

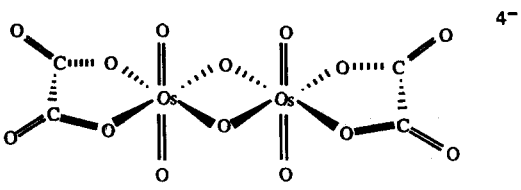

Fig. 2.

(d) *Mass spectroscopy*

We have determined the mass spectra of most of our neutral complexes using positive fast atom bombardment (FAB^+) conditions. For each of the complexes OsO_2py_2L (L = ox, lactate, atrolactate) which were run in a matrix of *meta*-nitrobenzylalcohol (MNBA) the molecular ions $[OsO_2py_2LH]^+$ are observed, as well as peaks corresponding to step-wise ligand loss giving $[OsO_2pyLH]^+$, $[OsO_2py_2]^+$, $[OsO_2py]^+$ and pyH^+; the ion $[OsO_2LH]^+$ is not seen. Similar results were obtained for the complexes OsO_2pic_2L' (L' = ox, oxoisobutyrate). For OsO_2py_2(citrate) however, which was run in glycerol $[OsO_2(citrateH)]^+$ is seen, but not $[OsO_2py_2]^+$ or $[OsO_2py]^+$. The parent ion for $(OsO_2py_2)_2$(tartrate) is seen at m/z = 909, which confirms its dimeric, tartrate-bridged structure. The spectra of all complexes studied contained peaks suggesting fragmentation of the coordinated hydroxycarboxylic acid and each osmium containing fragment gave a characteristic set of signals for which isotopic simulation gave a very similar pattern.

EXPERIMENTAL

OsO_2py_2L (L = *hydroxycarboxylate*)

OsO_4 (0.05 g, 0.19 mmol) was dissolved in ethanol (2 cm^3). The hydroxycarboxylic acid (0.19

mmol) was added, followed by pyridine (1 cm^3) (or 3-picoline in the case of two of the complexes). The reaction mixture was then placed in a freezer and left until the product precipitated. This was filtered off, washed with diethyl ether and vacuum dried. The complexes are various shades of brown in colour and slowly decompose in solution.

$K_2[OsO_2L_2]$ (L = *hydroxycarboxylate*)

$K_2[OsO_2(OMe)_4]$ (0.05 g, 0.12 mmol) prepared by the method of Criegee *et al.*,[26] was dissolved in methanol (5 cm^3). The hydroxycarboxylic acid (0.24 mmol) (or in the case of tartaric acid, 0.18 mmol), dissolved in minimum methanol, was added while stirring, whereby a colour change to green occurred. The volume of solution was reduced until the product began to precipitate. The product was centrifuged off, washed with methanol, then diethyl ether and stored under vacuum. All the complexes were dark green and decomposed readily, particularly in aqueous solution, depositing OsO_2.

$K_4[Os_2O_6ox_4]$ was prepared according to the literature for $K_2[OsO_3ox]$,[20] with the addition of a few drops of ethanol to accelerate the reaction.

IR spectra were measured on a Perkin–Elmer 1720 Infrared Fourier Transform spectrometer with samples as KBr discs. Raman spectra were measured on a Spex Ramalog 5 instrument with a Datamate data acquisition unit as spinning discs on a KBr matrix, using the red 6471 Å line of a Coherent Radiation Innova-90 krypton ion laser. XPS measurements were recorded of powdered samples mounted on a sample stub using chlorine-free, double-sided adhesive tape and analysed using Mg-K_α radiation at 15 kV and 10 mA using 6 mm slits on a Kratos XSAM 800 instrument. ^{13}C NMR spectra were measured in C^2HCl_3 or ^2H_2O on a Bruker WM 250 Fourier Transform spectrometer. Mass spectra were recorded by Mr G. Tucker and Mr J. Bilton on a VG-Micromass 7070E-HS spectrometer.

Microanalyses were provided by the Microanalytical Department of Imperial College.

Acknowledgements—We thank the SERC and Johnson Matthey PLC for a CASE award to one of us (C.F.E.), and Johnson Matthey for loan of osmium tetraoxide. We also thank Dr J. A. Busby for measurement and interpretation of the XPS data, Sue Johnson for running the NMR spectra and Dr P. D. Savage for helpful discussions.

REFERENCES

1. G. A. Barbieri, *Atti Accad. Linc.* 1916, **25**(II), 75.
2. W. Preetz and H. Schultz, *Z. Naturf.* 1983, **38B**, 183.
3. C. C. Hinckley and P. A. Kibala, *Polyhedron* 1986, **5**, 1119.
4. P. D. Robinson, C. C. Hinckley and P. A. Kibala, *Acta Cryst.* 1988, **48C**, 1365.
5. C. C. Hinckley, P. A. Kibala and P. D. Robinson, *Acta Cryst.* 1987, **47C**, 842.
6. M. Vèzes and L. Wintrebert, *Bull. Soc. Chim. Fr.* 1902, **27**, 569.
7. L. Wintrebert, *Annls Chim. Phys.* 1903, **28**(7), 15.
8. M. M. Caldeira, M. L. Ramos and V. M. S. Gil, *Can. J. Chem.* 1987, **65**, 827.
9. A. C. Dengel, W. P. Griffith, R. D. Powell and A. C. Skapski, *J. Chem. Soc., Dalton Trans.* 1987, 991; A. C. Dengel, W. P. Griffith, R. D. Powell and A. C. Skapski, *J. Chem. Soc., Chem. Commun.* 1986, 555.
10. M. Kakihana, T. Nagumo, M. Okamoto and H. Kakihana, *J. Phys. Chem.* 1987, **91**, 6128.
11. M. M. Caldeira and V. M. S. Gil, *Polyhedron* 1986. **5**, 381.
12. N. C. Campbell, J. Flanagan, W. P. Griffith, A. C. Skapski and R. W. Wiggins, *Inorg. Chim. Acta* 1985, **96**, L23; N. C. Campbell, thesis, University of London (1984).
13. C. H. F. Chang, P. P. Pitner, R. E. Lenkinski and J. D. Glickson, *J. Am. Chem. Soc.* 1977, **99**, 5858.
14. J. E. Grego and H. K. J. Powell, *Austr. J. Chem.* 1986, **39**, 1851.
15. W. P. Griffith, *J. Chem. Soc. A* 1969, 211.
16. K. Nakamoto, *J. Am. Chem. Soc.* 1957, **79**, 4904.
17. K. Nakamoto, *J. Am. Chem. Soc.* 1961, **83**, 4528.
18. K. Nakamoto, P. J. McCarthy and B. Miniatas, *Spectrochim. Acta* 1987, **21**, 379.
19. B. M. Nikolova and G. St. Nikolov, *J. Inorg. Nucl. Chem.* 1967, **29**, 1013.
20. L. Wintrebert, *Annls Chim. Phys.* 1903, **28**, 102.
21. W. P. Griffith, *J. Chem. Soc.* 1964, 245.
22. L. O. Atovyman and O. A. D'Yachenko, *J. Struct. Chem. (Engl. Translation)* 1974, **15**, 733.
23. A. M. R. Galas, M. B. Hursthouse, E. J. Behrman, W. R. Midden, G. Green and W. P. Griffith, *Transition Met. Chem.* 1981, **6**, 194.
24. W. P. Griffith, N. T. McManus and A. D. White, *J. Chem. Soc., Dalton Trans.* 1986, 1035.
25. D. J. Salmon and R. A. Walton, *Inorg. Chem.* 1978, **17**, 2179.
26. R. Criegee, B. Marchand and H. Wannowius, *Annalen* 1942, **550**, 99.

Polyhedron Vol. 10, No. 1, pp. 67–72, 1991
Printed in Great Britain

0277–5387/91 $3.00+.00
© 1991 Pergamon Press plc

THE CHEMICAL STRUCTURE AND THERMAL PROPERTIES OF ALKALI ULTRAPHOSPHATES

MAKOTO WATANABE* and KAZUHIRO NAKAMURA

Department of Industrial Chemistry, Chubu University, Kasugai, Aichi 487, Japan

(*Received* 16 *March* 1990; *accepted* 22 *August* 1990)

Abstract—Amorphous sodium and lithium ultraphosphates with M_2O/P_2O_5 (M = Na or Li) ratios of 1.0–0.3 have been prepared by mixing 85% phosphoric acid and sodium carbonate or lithium carbonate and then heating the mixture at 400–700°C, in air and in dry nitrogen. The ultraphosphates contained combined water and the amount of the water increased with a decrease in the M_2O/P_2O_5 ratio. When the ultraphosphates were heated in air, branching points in the ultraphosphates were hydrolysed to produce polyphosphates with shorter chain lengths.

Polyphosphates have been used in chemical fertilizers, detergents, food additives, chemical manufacture, ceramics, etc.,[1] and use of the compounds has recently expanded to other fields, for example, electrical manufacture and biomaterials.[2,3] The group of polyphosphates which are called ultraphosphates have a M_2O/P_2O_5 ratio smaller than unity and larger than zero, where M stands for a univalent cation or radical. Structurally, the ultraphosphates have branching points which are chemically active making them unstable materials. Studies on ultraphosphates lag behind in comparison with the studies on chain and ring polyphosphates. This paper describes the synthesis of alkali ultraphosphates by a heating process in air and in dry nitrogen, and the effect of the heating process on the chemical structure of the ultraphosphates. Thermal analysis of the ultraphosphates was also carried out to investigate the thermal properties of their branching points.

EXPERIMENTAL

Preparation

Sodium and lithium ultraphosphates with M_2O/P_2O_5 (M = Na or Li) ratios of 1.0–0.3 were prepared by mixing 85% phosphoric acid and sodium carbonate or lithium carbonate in a platinum crucible, carefully heating the mixture at 100–200°C for 1–2 h and then at 400–700°C (depending on the M_2O/P_2O_5 ratio) for 1 h, and finally, rapidly cooling the resulting melt in a desiccator containing silica-gel. The heating was carried out in air and in dry nitrogen.

Measurement of the mean degree of polymerization

The ultraphosphates made by the above process were dissolved in CO_2-free water. The mean degree of polymerization in an aqueous solution was measured by the end group titration method.[4,5]

Paper chromatography and colorimetry

One-dimensional paper chromatographic separation and colorimetric determination were employed for the measurement of the distribution of the phosphate species in a sample.[6]

Differential thermal analysis (DTA)

A sample was heated at a rate of 5°C min^{-1} in air and in dry nitrogen by means of a Rigaku DTA instrument.

X-ray diffractometry (XRD)

An X-ray diffraction diagram of a powder sample was taken with nickel-filtered Cu-K_α radiation by using a Rigaku X-ray diffractometer, RAD-1B.

* Author to whom correspondence should be addressed.

RESULTS

Sodium ultraphosphates

The phosphate composition of the prepared sodium ultraphosphates with Na_2O/P_2O_5 ratios of 1.0–0.3 are shown in Table 1. DTA curves of the ultraphosphates prepared in air are given in Fig. 1. The phosphate composition of the thermal products, as numbered in Fig. 1, are also listed in Table 1 together with the thermal equation given in the next section. It was not possible to obtain XRD data of thermal products 9 and 12 because the samples were too soft to be powdered. The sodium ultraphosphates prepared in dry nitrogen showed the same thermal properties as those ultraphosphates prepared in air.

Lithium ultraphosphates

Phosphate composition of the prepared lithium ultraphosphates with Li_2O/P_2O_5 ratios of 1.0–0.3 are indicated in Table 2. DTA curves of the ultraphosphates are given in Fig. 2. The phosphate composition of the thermal products numbered in Fig. 2 are also listed in Table 2. The thermal products 18, 19 and 20 were too soft to be powdered and XRD data could not be obtained.

DISCUSSION

Sodium ultraphosphates

The relation between M_2O/P_2O_5 ratio (R) and mean degree of polymerization (n) of chain poly-

Table 1. Phosphate composition of the sodium ultraphosphates and their thermal products

R	Ultra and thermal products	Temperature (°C)	XRD	Phosphates (P%)						Eq.[a]
				Ortho-	Di-	Tri-	Cyclo-tri-	Cyclo-tetra-	Higher	
1.0	—	—	AM[b]	—	—	—	4.0	—	96.0	—
	1	320[c]	$NaPO_3$I (JCPDS 11-648)	0.8	0.8	0.3	95.2	—	2.6	4
0.9	—	—	AM	1.1	2.1	1.9	4.0	—	90.9	—
	2	300[c]	$NaPO_3$I	0.4	0.9	0.2	92.8	—	5.7	4
	3	400[d]	$NaPO_3$I	0.8	0.6	0.5	70.5	—	27.6	5
0.8	—		AM	2.0	2.6	2.0	4.0	—	89.4	—
	4	280[c]	$Na_2H(PO_3)_3$ (JCPDS 9-101)	2.7	3.2	1.6	91.5	—	1.0	6
	5	370[d]	$(NaPO_3)_x$ (JCPDS 11-650)	3.7	5.0	4.6	4.6	—	82.1	8
0.7	—	—	AM	2.5	1.6	1.1	2.8	—	92.0	—
	6	300[c]	$Na_2H(PO_3)_3$	6.5	4.1	8.3	80.0	—	1.1	6
	7	350[d]	UK[e]	7.5	6.2	7.8	3.3	—	75.2	8
0.6	—	—	AM	2.3	2.1	3.3	2.4	—	89.9	—
	8	300[c]	UK	8.2	8.1	10.0	26.7	18.4	28.6	7
	9	370[d]	—	2.5	2.3	2.6	1.8	—	90.8	—
0.5	—	—	AM	1.5	2.2	2.2	4.2	—	89.9	—
	10	280[c]	$Na_2H_2(PO_3)_4$ (JCPDS 9-100)	2.6	2.2	2.2	4.0	47.0	42.0	9
0.4	—	—	AM	4.0	4.3	3.2	3.8	—	84.7	—
	11	250[c]	$Na_2H_2(PO_3)_4$	5.7	2.3	1.7	2.9	31.5	55.9	9
0.3	—		AM	5.2	4.0	4.3	2.7	—	83.8	—
	12	300[c]	—	9.5	3.8	4.7	1.6	3.2	77.2	—

[a] Thermal equations presented in this paper.
[b] Amorphous.
[c] Exotherm.
[d] Endotherm.
[e] Unknown crystalline.

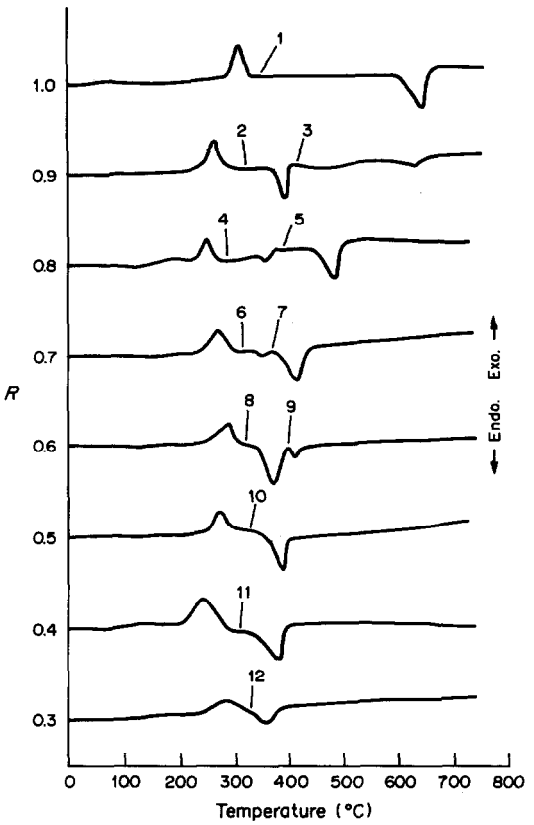

Fig. 1. DTA curves of the sodium ultraphosphates.

phosphates can be expressed by the following equation:

$$R = (n+2)/n \quad (1)$$

Ultraphosphates have branching points and these points must be considered as the factor which affects their chain length. Equation (1) can be modified as follows:

$$R+f = (n+2)/n, \quad (2)$$

where f stands for the number of branching points per atom of phosphorus. If there are no factors other than sodium and branching point which affect the lowering of the degree of polymerization, $R+f$ and n are unity and infinity, respectively. As Table 3 shows, n for the sodium ultraphosphates was a relatively small, finite number. Accordingly, it was concluded that there were some other factors which affect the degree of polymerization of the ultraphosphates. The most likely factor is the presence of combined water which exists as P—OH. If the number of hydrogens per atom of phosphorus is f', eq. (2) can be rewritten as the following:

$$R+f+f' = (n+2)/n. \quad (3)$$

One can calculate f' using the equation and the calculated values are listed in Table 3. The f' value

Table 2. Phosphate composition of the lithium ultraphosphates and their thermal products

R	Ultra and thermal products	Temperature (°C)	XRD	Phosphates (P%)					
				Ortho-	Di-	Tri-	Cyclo-tri-	Cyclo-tetra	Higher
1.0	—	—	AM[a]	—	—	1.7	1.8	9.7	86.8
	13	400[b]	$LiPO_3$ (JCPDS 13-438)	(27.8)[c]	—	—	—	—	(72.2)
0.9	—	—	AM	—	1.2	0.8	2.4	10.4	85.2
	14	380[b]	$LiPO_3$	(1.8)	—	—	(1.8)	(1.1)	(95.3)
0.8	—	—	AM	—	1.9	1.4	3.5	3.2	90.0
	15	300[b]	$LiPO_3$	(1.7)	(0.7)	(0.6)	(2.9)	(2.0)	(92.1)
0.7	—	—	AM	5.9	3.5	1.6	3.7	6.1	79.2
	16	230[b]	$LiPO_3$	(2.4)	(1.7)	(4.6)	(2.6)	—	(88.7)
0.6	—	—	AM	3.6	3.5	2.8	2.9	2.9	84.3
	17	300[b]	$LiPO_3$	(1.3)	(2.3)	(4.2)	(51.8)	(24.0)	(16.4)
0.5	—	—	AM	1.9	1.8	5.2	3.6	—	87.5
	18	300[b]	—	3.3	2.6	2.5	2.5	—	89.2
0.4	—	—	AM	2.7	2.9	3.0	2.3	—	89.1
	19	300[b]	—	4.1	8.9	9.4	0.8	—	76.8
0.3	—	—	AM	4.1	7.4	6.7	1.0	—	80.8
	20	300[b]	—	8.4	20.3	17.3	0.8	—	53.2

[a] Amorphous.
[b] Exotherm.
[c] Samples containing water-insoluble components are in parentheses.

Table 3. f, n and f' values of the sodium ultraphosphates

		In air		In dry nitrogen	
R	f	n	f'	n	f'
1.0	0.0	90.7	0.02	183.6	0.01
0.9	0.1	26.5	0.08	26.7	0.07
0.8	0.2	14.5	0.14	20.6	0.10
0.7	0.3	13.6	0.15	18.0	0.11
0.6	0.4	13.1	0.15	16.2	0.12
0.5	0.5	13.2	0.15	15.1	0.13
0.4	0.6	12.0	0.17	14.8	0.14
0.3	0.7	11.8	0.17	13.6	0.15

increased with a decrease in R and this means that the amount of combined water increases with a decrease in R. The measured mean degree of polymerization and the calculated f' values of the sodium ultraphosphates which were prepared in dry nitrogen are also listed in Table 3. Since the f' values of the ultraphosphates prepared in dry nitrogen are smaller than those of the ultraphosphates prepared in air, the dry atmosphere reduces the amount of combined water in the ultraphosphates, although it seemed impossible to remove all of it. It should be noted that f does not always indicate the number of branching points. Part of the f value can be responsible for the number of hydrogens which exist as combined water in the phosphates. Accordingly, f' expresses the minimum number of hydrogens per atom of phosphorus. From the above discussion, the following general chemical structure can be given for the ultraphosphates:

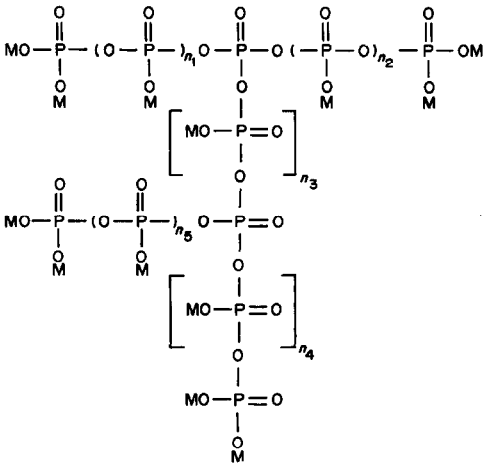

where M stands for sodium and/or hydrogen.

As the results of XRD and PC in Table 1 show, the amorphous polyphosphate with an Na_2O/P_2O_5 ratio of 1.0 was transformed to crystalline $NaPO_3I$, known as sodium cyclotriphosphate, through the exotherm at about 320°C.

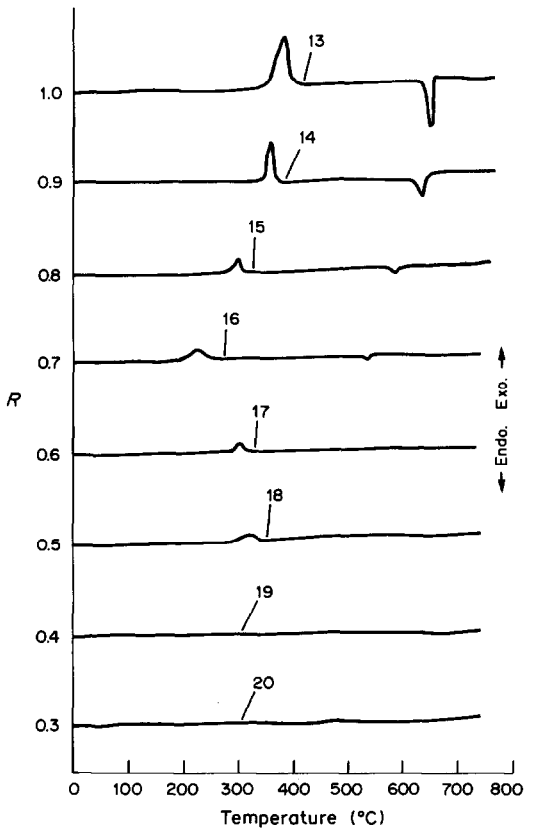

Fig. 2. DTA curves of the lithium ultraphosphates.

$$(NaPO_3)_n \longrightarrow n/3(NaPO_3)_3. \quad (4)$$

The endothermic peak at about 650°C was due to melting of the cyclotriphosphate. These results agree well with those which are given in the literature. Sodium ultraphosphate with an Na_2O/P_2O_5 ratio of 0.9 showed an exothermic peak at about 300°C. According to the XRD and PC data of thermal product 2 in Table 1, the exotherm seemed to be caused by reaction (4). Thermal product 3 showed the X-ray diffraction pattern of $NaPO_3I$, but, in comparison with the data of thermal product 2, the cyclotriphosphate content of thermal product 3 had decreased and the long chain polyphosphate content, increased. Therefore, the endothermic peak at about 400°C may be due to the transformation of part of the cyclotriphosphate to polyphosphates with longer chain lengths:

$$(NaPO_3)_3 \longrightarrow 3/n(NaPO_3)_n. \quad (5)$$

The phosphates melted through the small endotherm at about 630°C. Thermal product 4 showed the X-ray diffraction diagram of $Na_2H(PO_3)_3$ and

its cyclotriphosphate content was 91.5%. Accordingly, the ultraphosphate with an Na_2O/P_2O_5 ratio of 0.8 was changed to the cyclotriphosphate through the exotherm at about 280°C:

Sodium ultraphosphate ($R = 0.8$)

$$\xrightarrow{280°C} Na_2H(PO_3)_3. \quad (6)$$

The ultraphosphate contained 0.14 atoms of hydrogen per atom of phosphorus and therefore the hydrogen content of this ultraphosphate is less than that of $Na_2H(PO_3)_3$. It was concluded that the following hydrolysis of a branching point to an end group and/or a middle group took place during heating to 300°C:

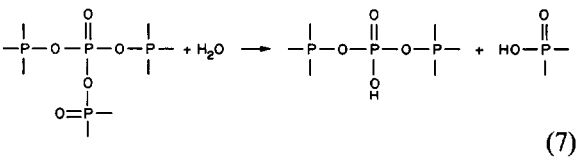

(7)

The water in the above equation can come from the moisture in air. After the next small endothermic reaction at about 370°C, the thermal product showed weak X-ray diffraction peaks of Maddrell's salt and most of the thermal product was long chain polyphosphates. Cyclophosphates seem to be transformed to polyphosphates with longer chain lengths by condensation and reorganization:

$$n Na_2H(PO_3)_3 \longrightarrow Na_{2n}H_n(PO_3)_{3n}. \quad (8)$$

The phosphates melted after the last large endothermic peak at about 500°C. Ultraphosphates with an Na_2O/P_2O_5 ratio of 0.7 showed similar thermal changes to ultraphosphates with a ratio of 0.8; because thermal products 6 and 7 had similar X-ray diffraction patterns and phosphate contents to thermal products 4 and 5. After the first exothermic peak of the ultraphosphate with an Na_2O/P_2O_5 ratio of 0.6 at about 300°C, thermal product 8 exhibited an unknown X-ray diffraction pattern. The phosphate content indicated that considerable amounts of long chain polyphosphates were transformed to cyclotri-, cyclotetra-, and other phosphates with shorter chain lengths. This result indicates that the hydrolysis of branching points proceeds according to reaction (7) during heating. The thermal product melted partly through the endotherm at about 370°C and the phosphates with short chain lengths were reorganized to phosphates with longer chain lengths. After the last small endothermic peak, the sample melted completely. The ultraphosphates with Na_2O/P_2O_5 ratios of 0.5 and 0.4 showed similar thermal changes to each other. After the exotherm at about 250–300°C, thermal products 10 and 11 gave an X-ray diffraction pattern of $Na_2H_2(PO_3)_4$. The phosphate content of these thermal products supported the above result because they contained fairly large amounts of cyclotetraphosphate. The thermal reaction can be given for the process:

Sodium ultraphosphates ($R = 0.5$ and 0.4)

$$\xrightarrow{250\text{–}300°C} Na_2H_2(PO_3)_4. \quad (9)$$

The reaction may progress by the hydrolysis shown in reaction (7) and the resulting reorganization of phosphates. Through the first exothermic peak at about 250–320°C, the ultraphosphates with Na_2O/P_2O_5 ratios of 1.0–0.7 were reorganized to cyclotriphosphate, and the ultraphosphates with Na_2O/P_2O_5 ratios of 0.5 and 0.4 were transformed to cyclotetraphosphate. The ultraphosphate with an Na_2O/P_2O_5 ratio of 0.6 formed both of the cyclophosphates. Accordingly, it can be said that the formation of six-membered and eight-membered ring phosphates from sodium ultraphosphates by a thermal process depends on the sodium content. Thermal products 10 and 11 melted completely through the last large endothermic peaks at about 380–400°C. The ultraphosphate with an Na_2O/P_2O_5 ratio of 0.3 was hygroscopic and thermal product 12 contained only a small amount of cyclotetraphosphate. The reorganization of the ultraphosphate to cyclotri- and cyclotetraphosphates may be difficult because the sodium content of the ultraphosphate is too low.

Lithium ultraphosphates

The mean degree of polymerization of the ultraphosphates with Li_2O/P_2O_5 ratios of 1.0–0.3, prepared in air and in dry nitrogen, was measured and the results are shown in Table 4 together with the f' values calculated using eq. (3). The f' value of the ultraphosphates prepared in air and in dry nitrogen increased with a decrease in R and therefore the combined water content in the ultraphosphates also increases. The f' value of the ultraphosphates prepared in air was larger than that of the ultraphosphates prepared in dry nitrogen. Accordingly, a dry atmosphere can help to reduce the combined water content of the ultraphosphates. Since these results for lithium ultraphosphates are the same as those for sodium ultraphosphates, the same chemical structure can be used to describe them.

Some of the thermal products in Table 2 contained a water-insoluble substance (crystalline

Table 4. f, n and f' values of the lithium ultraphosphates

		In air		In dry nitrogen	
R	f	n	f'	n	f'
1.0	0.0	29.0	0.07	68.1	0.03
0.9	0.1	28.5	0.07	31.7	0.06
0.8	0.2	20.7	0.10	23.7	0.08
0.7	0.3	18.9	0.12	19.6	0.10
0.6	0.4	13.3	0.15	17.0	0.12
0.5	0.5	11.5	0.17	15.2	0.13
0.4	0.6	10.4	0.19	14.3	0.14
0.3	0.7	8.1	0.25	14.0	0.14

$LiPO_3$). The phosphate contents in parentheses indicate soluble components of the thermal products. The lithium ultraphosphates with Li_2O/P_2O_5 ratios of 1.0–0.6 were reorganized to crystalline long chain polyphosphates, $LiPO_3$, through the first exothermic peaks at about 230–400°C. The formation of ring oligophosphates, which was observed in the thermal reactions of the sodium ultraphosphates, was not detected in the thermal processes of the lithium compounds. The small exotherm of the ultraphosphate with a Li_2O/P_2O_5 ratio of 0.6 at about 300°C seemed to be due to the formation of crystalline lithium metaphosphate, but thermal product 18 was so soft that it precluded the recording of XRD data. The ultraphosphates with Li_2O/P_2O_5 ratios of 0.4 and 0.3 did not show any detectable thermal change. Thermal products 19 and 20 which were taken out of a furnace at about 300°C showed that the ultraphosphates had degraded to phosphates with shorter chain lengths. This means that branching points in the ultraphosphates were hydrolysed according to reaction (7) during heating. After the endotherm at about 550–650°C, the ultraphosphates with Li_2O/P_2O_5 ratios of 1.0–0.7 melted completely. The ultraphosphates with R smaller than 0.7 did not show a clear thermal change on melting and were fused gradually by heating up to 500°C.

REFERENCES

1. J. R. Van Wazer, *Phosphorus and its Compounds*, Vol. 2, p. 987. Interscience, New York (1961).
2. S. Oae, *Kagaku To Kogyo* 1984, **37**, 207.
3. T. Kanazawa, *Ceramics Japan* 1985, **20**, 1066.
4. J. R. Van Wazer, E. J. Griffith and J. F. McCulough, *Analyt. Chem.* 1954, **26**, 1775.
5. E. J. Griffith, *Analyt. Chem.* 1956, **28**, 525.
6. M. Watanabe, T. Inagaki and S. Sato, *Bull. Chem. Soc. Japan* 1983, **56**, 458.

Polyhedron Vol. 10, No. 1, pp. 73–77, 1991
Printed in Great Britain

0277–5387/91 $3.00+.00
© 1991 Pergamon Press plc

THE CRYSTAL AND MOLECULAR STRUCTURE OF N,N′-BIPYRIDYL, N-METHOXY IMINODIACETATE OXOVANADIUM(IV)

MARIA A. A. F. DE C. T. CARRONDO,* M. TERESA LEAL S. DUARTE,†
J. ARMANDO L. SILVA and J. J. R. FRAÚSTO DA SILVA

Centro de Química Estrutural, Complexo I, I.S.T., 1096 Lisboa, Portugal

(*Received* 1 *June* 1990; *accepted* 22 *August* 1990)

Abstract—The structure of N,N′-bipyridyl, N-methoxy iminodiacetate oxovanadium(IV) has been determined by X-ray diffraction. The complex shows a distorted octahedral geometry with the vanadium atom coordinating to the oxo oxygen, two carboxyl oxygen atoms and an imino nitrogen of the N-methoxy iminodiacetate ligand, and two nitrogen atoms of the bipyridyl ligand. The V—O and V—N equatorial distances are 1.970(4), 1.982(4), 2.088(4) and 2.094(4) Å, respectively, while the axial V=O and V—N distances are 1.602(4) and 2.379(4) Å.

Some species of *Amanita* toadstools have relatively high contents of a rather simple iminodicarboxylic acid, namely, N-hydroxyimino-α,α′-dipropionic acid HIDPA.[1] For some years, the molecular structure of its oxovanadium complex was thought to be as **1** below, *i.e.* a penta-coordinated 1 : 2 complex of the vanadyl ion VO^{2+} with the above mentioned ligand. Recently, we demonstrated that with an analogue of HIDPA, namely N-hydroxyiminodiacetate acid (HIDA), an octa-coordinated vanadium(IV) bis-complex of the totally ionized ligand (including the N-hydroxyl group) is formed, as **2**, in which the oxo group of the vanadyl ion has been removed.[2]

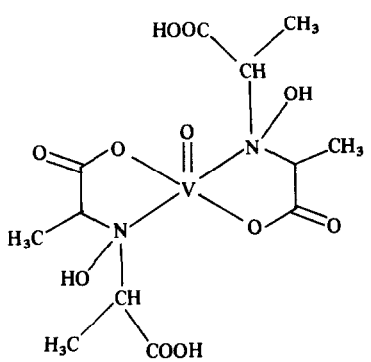

1

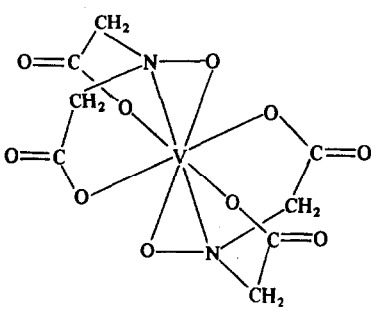

2

This was the first example of an octa-coordinated vanadium(IV) complex having only nitrogen and oxygen atoms as donors. Given the close similarity of chemical properties, EPR and IR spectra, and the analogous unusually high values of the stability constants of their vanadium complexes, it seems likely that the natural HIDPA vanadium complex, named "amavadin" by the researchers who first isolated it,[1] has a structure identical to that depicted as **2** above.

The ionization of the N-hydroxyl group of the ligand seems to be a prerequisite for coordination to the metal, to enable an octa-coordinated V^{4+} bis-complex to be formed. The very high stability of this species ($\log \beta_2$ *ca* 22–23) allows the removal of the oxo group of the vanadyl ion, which is commonly considered to be the most stable oxo-ion in aqueous solution.

To confirm this idea, we have prepared another

* Present address: Centro de Tecnologia Química e Biológica, R. da Quinta Grande 6, 2780 Oeiras, Portugal.
† Author to whom correspondence should be addressed.

analogue of HIDPA in which the N-hydroxyl group cannot ionize, namely, N-methoxyiminodiacetic acid (METIDA), and studied its complexion reactions with vanadium. Several differences emerged in the first studies in aqueous solution: first METIDA behaved as other common aminopolycarboxylic ligands and a predominant 1:1 complex was formed, which hydrolysed at neutral and basic pH; secondly, its EPR spectrum showed the presence of tetravalent vanadium, but the calculated g and A parameters are typical of vanadyl aminopolycarboxylate complexes, not of a vanadium(IV) complex.[3]

In these conditions, and since the $VO^{2+} \cdot L^{2-}$ species is neutral, its isolation as a crystalline form should not be too difficult, particularly if the two free coordination positions could be occupied by a rather bulky ligand. We were able to obtain good crystals of N,N′-bipyridyl,N-methoxy iminodiacetate oxovanadium(IV), and the X-ray diffraction study of the crystal and molecular structures is now described.

EXPERIMENTAL

Preparation

Bromoacetic acid (20.8 g, 0.15 mol) was added to 4.2 g of methoxylamine hydrochloride (0.05 mol) in 100 cm^3 H_2O; 140 cm^3 of 10% NaOH were added dropwise for a period of 36 h, keeping the pH always below 7. After that, the pH was lowered to about 4 with 2 N HCl, 12.8 g (0.05 mol) of barium acetate in 50 cm^3 H_2O were added. The solution was allowed to stand and 10.4 g of a white precipitate of barium N-methoxy iminodiacetate was formed which was filtered and dried *in vacuo* (yield 66%). Found: C, 19.1; H, 2.5; N, 4.3. Calc. for $C_5H_9NO_6Ba$: C, 19.0; H, 2.8; N, 4.4%.

$VOSO_4 \cdot 5H_2O$ (63.3 mg, 0.25 mmol) was added to 158 mg (0.5 mmol) of this salt in 10 cm^3 H_2O. The solution was left to stand overnight and the deposited material was filtered; 39 mg of N,N′-bipyridyl (0.25 mmol) in 5 cm^3 ethanol were added and the mixture was stirred and slowly evaporated *in vacuo*, whereupon brownish-violet crystals were obtained. No recrystallization was attempted. Found: C, 41.2; H, 4.8; N, 9.6. Calc. for $C_{15}H_{21}N_3O_9V$: C, 41.1; H, 4.8; N, 9.6%.

X-ray data

Intensity data were collected on an Enraf Nonius CAD 4 diffractometer using graphite monochromatized Mo-K_α radiation ($\lambda = 0.71069$ Å). The $\omega/2\theta$ scan mode was used for measuring the 4718 reflections with $1.5 \leqslant \theta \leqslant 25.0°$ in the reflection quadrant h −15–15, k 0–14, l 0–25. Three standard reflections were monitored but no decay was detected.

The crystal is monoclinic, space group $P2_1/c$, with $a = 10.954(2)$, $b = 9.944(2)$, $c = 17.822(6)$ Å and $\beta = 97.06(2)°$, $V = 1926.6(8)$ Å^3, $Z = 4$, $D_x = 1.45$ g cm^{-3}, μ(Mo-K_α) = 5.45 cm^{-1}, $F(000) = 1192$, $M = 421.9$ for $C_{15}H_{21}N_3O_9V$.

Data were corrected for Lorentz and polarization effects, an empirical absorption correction[4] was applied yielding the values of 0.9518 and 0.9996, respectively, for the minimum and maximum transmission factors.

SOLUTION AND REFINEMENT

3502 unique reflections with $|F_o| \geqslant 3\sigma|F_o|$ were used for solution and refinement with SHELX86[5] and SHELX76,[6] respectively.

The heavy atom position was located from a Patterson synthesis and all the remaining non-hydrogen atoms, including three oxygens of water molecules, were obtained from successive difference Fourier syntheses. The isotropic refinement gave $R = 0.108$ which lowered to 0.063 when anisotropic parameters were admitted.

Hydrogen atoms were introduced in positions obtained in the difference density map and were refined isotropically with no restrictions.

Final $R(F)$* = 0.043 and $R_w(F)$† = 0.048 were obtained for 337 refined parameters, using a weighting scheme $w = 1.0/[\sigma^2(F_o) + |g|F_o^2]$ with $g = 0.0007$. The highest peak on the final difference Fourier map was 0.3 e/Å^{-3}.

Atomic scattering factors were taken from International Tables.[7] All calculations were carried out on a VAX 11/780 computer at Instituto Superior Tecnico.

Fractional atomic coordinates and anisotropic temperature factors for non-hydrogen atoms, hydrogen fractional atomic coordinates and isotropic temperature factors can be obtained from the Cambridge Crystallographic Database. Tables of best least-squares planes in the ligands and lists of observed and calculated structure factors have been submitted as supplementary material.

RESULTS AND DISCUSSION

A molecular diagram presenting the numbering scheme is shown in Fig. 1, and bond lengths and bond angles are listed in Tables 1 and 2, respectively.

* $R(F) = \Sigma(|F_o| - |F_c|)/\Sigma|F_o|$.
† $R_w(F) = [\Sigma w(|F_o| - |F_c|)^2/\Sigma w|F_o|^2]^{1/2}$.

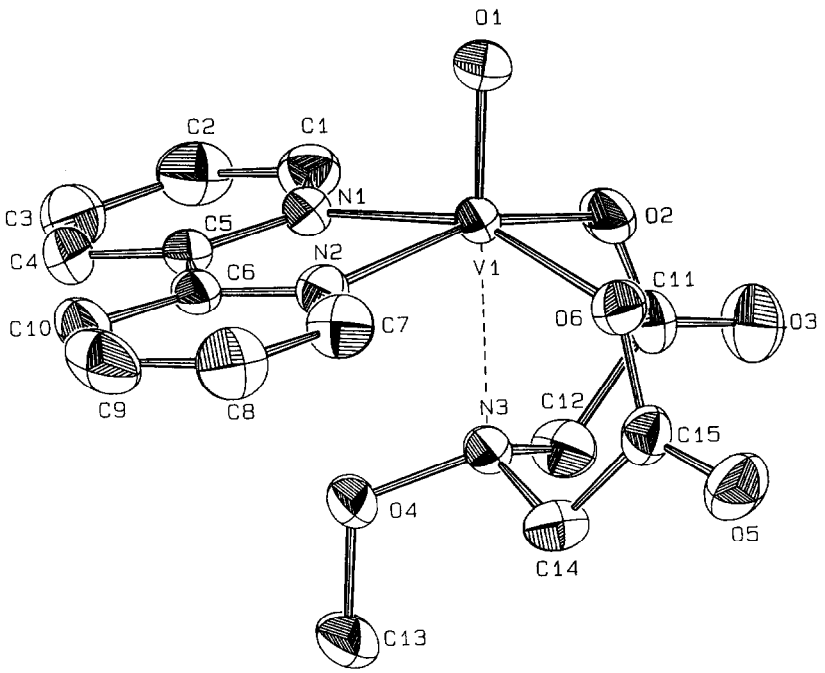

Fig. 1. Molecular diagram (ORTEP II)[8] of the complex.

The complex exhibits essentially an octahedral geometry, formed in the equatorial plane by the two nitrogen atoms of the bipyridyl ligand and the two oxygens from the N-methoxy iminodiacetate ligand; the six-fold coordination around the metal is completed by the oxo oxygen and by a weak interaction to the nitrogen atom of the imino group.

Atoms N(1) N(2) O(2) O(6) are almost coplanar with a slightly tetrahedral distortion. The vanadium atom is 0.373(1) Å away from that plane and towards the vanadyl oxygen. In other vanadyl hexa and penta-coordinated complexes with a quadrangular equatorial plane, the vanadium atom is normally out of that plane by a similar distance.[9,10]

The coordination about the vanadium atom can also be described by the angles formed between planes defined by atoms O(1) O(6) N(3) N(1) and O(1) O(2) N(3) N(2) and the equatorial plane. In our complex that angle is 94.62(5)°, and both planes are almost orthogonal to the equatorial plane. Table 3 lists the parameters of these least-squares planes, deviations of atoms and angles between the planes.

The vanadyl complex 2,2′-bipyridyl(iminodiacetate)oxovanadium(IV)[11] in which the aminopolycarboxylate ligand instead of a methoxyl group has one hydrogen atom attached to the nitrogen atom [N(3)] of the imino group, has the same type of coordination and geometry as that found in the title complex. Thus a close comparison will be made between the two complexes.

In the complex studied the V=O group is slightly tilted relative to the normal to the equatorial plane, making an angle of 1.64(9)° with this line. The corresponding angle of tilt in the other complex[11] is 1.8(2)°.

Holloway and Melnick made a survey[10] on vanadyl complexes, and found a correlation between the vanadyl V=O distance and the coordination geometry on the metal atom. Tetra and hexa-coordinated complexes have similar V=O distances,

Table 1. Bond lengths (Å) for the complex

N(1)—V(1)	2.088(4)	N(2)—V(1)	2.094(4)
O(1)—V(1)	1.602(4)	O(2)—V(1)	1.970(4)
N(3)—V(1)	2.379(4)	O(6)—V(1)	1.982(4)
C(1)—N(1)	1.346(4)	C(5)—N(1)	1.351(4)
C(6)—N(2)	1.351(4)	C(7)—N(2)	1.340(4)
C(2)—C(1)	1.376(5)	C(3)—C(2)	1.384(6)
C(4)—C(3)	1.374(6)	C(5)—C(4)	1.389(5)
C(6)—C(5)	1.477(5)	C(10)—C(6)	1.389(4)
C(8)—C(7)	1.389(5)	C(9)—C(8)	1.370(6)
C(10)—C(9)	1.372(6)	C(11)—O(2)	1.287(4)
O(3)—C(11)	1.221(4)	C(12)—C(11)	1.518(6)
N(3)—C(12)	1.467(4)	O(4)—N(3)	1.442(3)
C(14)—N(3)	1.462(4)	C(13)—O(4)	1.431(4)
C(15)—C(14)	1.513(6)	O(5)—C(15)	1.223(4)
O(6)—C(15)	1.286(4)		

Table 2. Bond angles (°) for the complex

N(2)—V(1)—N(1)	77.4(2)	O(1)—V(1)—N(1)	99.2(2)
O(1)—V(1)—N(2)	99.5(2)	O(2)—V(1)—N(1)	93.8(2)
O(2)—V(1)—N(2)	159.2(1)	O(2)—V(1)—O(1)	100.5(2)
N(3)—V(1)—N(1)	83.3(2)	N(3)—V(1)—N(2)	84.2(2)
N(3)—V(1)—O(1)	175.9(1)	N(3)—V(1)—O(2)	76.0(2)
O(6)—V(1)—N(1)	156.6(1)	O(6)—V(1)—N(2)	91.3(2)
O(6)—V(1)—O(1)	102.9(2)	O(6)—V(1)—O(2)	89.8(2)
O(6)—V(1)—N(3)	75.1(2)	C(1)—N(1)—V(1)	124.5(3)
C(5)—N(1)—V(1)	116.7(3)	C(5)—N(1)—C(1)	118.8(3)
C(6)—N(2)—V(1)	116.1(3)	C(7)—N(2)—V(1)	124.2(3)
C(7)—N(2)—C(6)	119.6(3)	C(2)—C(1)—N(1)	122.4(4)
C(3)—C(2)—C(1)	118.5(4)	C(4)—C(3)—C(2)	119.8(4)
C(5)—C(4)—C(3)	119.0(4)	C(4)—C(5)—N(1)	121.4(3)
C(6)—C(5)—N(1)	114.5(3)	C(6)—C(5)—C(4)	124.1(3)
C(5)—C(6)—N(2)	115.2(3)	C(10)—C(6)—N(2)	120.8(4)
C(10)—C(6)—C(5)	124.0(3)	C(8)—C(7)—N(2)	121.8(4)
C(9)—C(8)—C(7)	118.4(4)	C(10)—C(9)—C(8)	120.4(4)
C(9)—C(10)—C(6)	119.0(4)	C(11)—O(2)—V(1)	124.4(3)
O(3)—C(11)—O(2)	123.8(3)	C(12)—C(11)—O(2)	116.1(3)
C(12)—C(11)—O(3)	120.1(3)	N(3)—C(12)—C(11)	111.4(3)
C(12)—N(3)—V(1)	106.2(2)	O(4)—N(3)—V(1)	110.3(2)
O(4)—N(3)—C(12)	110.4(3)	C(14)—N(3)—V(1)	106.2(2)
C(14)—N(3)—C(12)	113.3(3)	C(14)—N(3)—O(4)	110.2(3)
C(13)—O(4)—N(3)	114.3(3)	C(15)—C(14)—N(3)	111.5(3)
O(5)—C(15)—C(14)	119.3(3)	O(6)—C(15)—C(14)	116.8(3)
O(6)—C(15)—O(5)	124.0(3)	C(15)—O(6)—V(1)	125.1(3)

with mean values of 1.612 and 1.615 Å, respectively, while penta-coordinated complexes normally have shorter distances, with a mean value of 1.518 Å. In ours and the iminodiacetate complexes, these distances are 1.602(4) and 1.596(2) Å, close to the hexa-coordinate mean value but on the short side of this range. This is not surprising since the six-fold coordination is indeed achieved via a weak interaction to the N(3) atom (see Fig. 1).

The V—O and V—N equatorial distances are within the normal range observed in vanadium(IV) complexes,[9,10,12,13] whilst the V—N axial distance 2.379(4) Å is longer than expected for a vanadium to nitrogen single bond. The corresponding V···N

Table 3. Best least-squares planes in the coordination sphere

Equations of the planes

Plane 1 [N(1)N(2)O(2)O(6)]: $-0.9398(3)x+0.3164(8)y-0.1293(7)z+5.006(7)=0$

Plane 2 [O(1)O(6)N(3)N(1)]: $-0.0720(7)x-0.4627(6)y-0.8836(3)z+8.158(5)=0$

Plane 3 [O(1)O(2)N(3)N(2)]: $0.2954(7)x+0.8723(4)y-0.3897(7)z-4.568(7)=0$

Deviations of atoms from planes (Å)

Plane 1		Plane 2		Plane 3	
N(1)	−0.018(2)	O(1)	0.101(2)	O(1)	0.069(2)
N(2)	0.020(2)	O(6)	−0.103(2)	O(2)	−0.072(2)
O(2)	0.015(2)	N(3)	0.102(2)	N(3)	0.068(2)
O(6)	−0.015(2)	N(1)	−0.109(2)	N(2)	−0.071(2)
V(1)	0.373(1)	V(1)	0.0442(8)	V(1)	0.0367(9)

Angles between planes (°)

Planes 1 and 2	87.96(6)
Planes 1 and 3	87.20(6)
Planes 2 and 3	94.62(5)

interaction in the iminodiacetate complex is 2.328(3) Å.

In the N-methoxy iminodiacetate ligand the two rings formed due to its tri-coordinative behaviour, V(1) O(6) C(15) C(14) N(3) and V(1) O(2) C(11) C(12) N(3), respectively, are almost planar with maximum deviations from the mean-squares planes of ±0.258(3) and ±0.197(3) Å, and are perpendicular to each other with an angle of 85.55(6)°. Bond distances and angles within the ligand are typical of the iminodiacetate molecule.[11,14,15]

The geometry found for bipyridyl is usual in this ligand. Steric repulsions between hydrogens at C(4) and C(10), which are 2.16(4) Å away in this complex, are believed[11,16,17] to be the cause of a common distortion observed, trying to alleviate this short intramolecular contact. This is achieved with a twist of 5.3(1)° in the two benzene rings and a dihedral angle of 9.0(1)° between the axes through C(2)—C(5) and C(6)—C(8). In the analogous complex these values compare with ours as: 6.6(3)° and 10.1(3)°, respectively. The angles at C(5) and C(6) are also different from normal benzenic angles. The smaller values inside the five membered ring, N(1)—C(5)—C(6) 114.5(3)° and N(2)—C(6)—C(5) 115.2(3)°, and larger values on the other side, C(4)—C(5)—C(6) 124.1(3)° and C(5)—C(6)—C(10) 124.0(3)°, are comparable to the mean values of 115° and 124°, respectively, in the iminodiacetate complex.[11] However, the aromatic character is still present in the rings, as can be observed by their planarity and C—C and C—N bond distances.

There are some hydrogen bonds between the solvent water molecules and the complex molecules. The stronger interactions are between the water hydrogen atoms and the exocyclic oxygens O(3) and O(5) [2.855(8) and 2.740(8) Å, respectively].

CONCLUSION

The results obtained show that ionization of a N-hydroxyl group is necessary to form a complex of vanadium(IV), whose high thermodynamical stability (octa-coordination of a 4-charged metal ion) is more than enough to compensate for the energy required to remove the oxo-group from the complex anion. The substitution of a N-hydroxyl by a N-methoxyl group forbids that possibility, and a normal aminopolycarboxylate complex with the vanadyl ion VO^{2+} is formed in which not even the oxygen atom of the methoxy group interacts with the metal ion.

REFERENCES

1. E. Bayer and H. Kneifel, *Z. Naturforsch.* 1972, **27B**, 20.
2. M. A. A. F. de C. T. Carrondo, M. T. N. L. S. Duarte, J. C. Pessoa, J. A. L. Silva, J. J. R. Fraústo da Silva, M. C. T. A. Vaz and L. F. Vilas-Boas, *J. Chem. Soc., Chem. Commun.* 1988, 1158.
3. G. Benski, J. Felcman, J. J. R. Fraústo da Silva, I. Moura, J. J. G. Moura, M. C. Vaz and L. F. Vilas-Boas, in *Frontiers in Bioinorganic Chemistry* (Edited by A. Xavier), p. 97. VCH, Weinheim (1986).
4. A. C. T. North, D. C. Philips and F. S. Mathews, *Acta Cryst.* 1968, **A24**, 351.
5. G. M. Sheldrick, in *Crystallographic Computing* (Edited by C. Kruger and R. Goddard), pp. 175–189. O.U.P., Oxford (1985).
6. G. M. Sheldrick, SHELX76, A program for crystallographic calculation. University of Cambridge (1976).
7. *International Tables for X-Ray Crystallography*, Vol. A. Reidel, Dordrecht (1983).
8. C. K. Johnson, ORTEPII Report ORNL-5138. Oak Ridge National Laboratory, Tennessee (1976).
9. L. Vilas-Boas and J. C. Pessoa, in *Comprehensive Coordination Chemistry* (Edited by G. Wilkinson, R. D. Gillard and J. A. McCleverty), Vol. 3. Pergamon Press, Oxford (1987).
10. C. Holloway and M. Melnick, *Rev. Inorg. Chem.* 1985, **7**, 75.
11. M. Ghosh and S. Ray, *Acta Cryst.* 1981, **C39**, 1367.
12. V. A. Nuber and J. Weiss, *Acta Cryst.* 1976, **B37**, 947.
13. K. Wieghardt, U. Quilitzsch, B. Nuber and J. Weiss, *Angew. Chem. Int. Ed. Engl.* 1978, **17**, 351.
14. Å. Oskarsson, *Acta Cryst.* 1976, **B32**, 2163.
15. A. Podder, J. K. Dattagupta and N. N. Saha, *Acta Cryst.* 1979, **B35**, 53.
16. W. D. Harrison and B. J. Hathaway, *Acta Cryst.* 1978, **B34**, 2843.
17. T. J. R. Weakley, *Acta Cryst.* 1978, **B34**, 281.

Polyhedron Vol. 10, No. 1, pp. 79–87, 1991
Printed in Great Britain

0277–5387/91 $3.00+.00
© 1991 Pergamon Press plc

FURTHER STUDIES ON THE REACTIVITY OF COMPLEXES OF THE TYPE *cis*-$Re_2(\mu\text{-}O_2CR)_2X_2(\mu\text{-dppm})_2$. THE STRUCTURAL CHARACTERIZATION OF *cis*-$Re_2(\mu\text{-}O_2CCH_3)_2(NCBH_3)_2(\mu\text{-dppm})_2$ AND $[Re_2Cl_3(\mu\text{-dppm})_2(1,2\text{-}C_6H_4(CN)_2)_2]PF_6$

DANIEL R. DERRINGER,* KENG-YU SHIH, PHILLIP E. FANWICK and RICHARD A. WALTON†

Department of Chemistry, Purdue University, West Lafayette, IN 47907, U.S.A.

(*Received* 31 *May* 1990; *accepted* 28 *August* 1990)

Abstract—The reactions of *cis*-$Re_2(O_2CC_2H_5)_2Cl_2(dppm)_2$ (dppm = $Ph_2PCH_2PPh_2$) with the nitriles RCN (R = CH_3 or C_2H_5) in the presence of $HBF_4 \cdot Et_2O$ or HPF_6 (aq.) afford salts of the *cis*-$[Re_2Cl_2(dppm)_2(NCR)_4]^{2+}$ cations. Studies on the reactivity of *cis*-$[Re_2Cl_2(dppm)_2(NCC_2H_5)_4](PF_6)_2$ with CO in acetone show that the mixed carbonyl–nitrile complexes $[Re_2Cl_3(dppm)_2(CO)_2(NCC_2H_5)]PF_6$ and $Re_2Cl_3(dppm)_2(CO)_2(NCC_2H_5)$ are the major products; these reactions involve the displacement of nitrile by CO and the uptake of Cl^- through the sacrifice of a portion of the starting dirhenium complex. Attempts to grow crystals of *cis*-$[Re_2Cl_2(dppm)_2(NCC_2H_5)_4](PF_6)_2$ led to its conversion to $[Re_2Cl_3(dppm)_2(NCC_2H_5)_2]PF_6$. The related complex $[Re_2Cl_3(dppm)_2(1,2\text{-}C_6H_4(CN)_2)_2]PF_6$ has been prepared by the reaction of $Re_2Cl_4(dppm)_2$ with $1,2\text{-}C_6H_4(CN)_2$ and KPF_6 in acetone, and its structure established by X-ray crystallography. The crystallographic data are as follows: orthorhombic space group $P2_12_12_1$, $a = 18.242(6)$, $b = 19.197(6)$, $c = 19.789(6)$ Å, $V = 6929(7)$ Å^3 and $Z = 4$. The structure was refined to $R = 0.081$ ($R_w = 0.098$) for 3511 data with $I > 3.0\sigma(I)$. The structure, which can be represented as $[Cl_2Re(\mu\text{-dppm})_2ReCl(1,2\text{-}C_6H_4(CN)_2)_2]PF_6$, contains monodentate $1,2\text{-}C_6H_4(CN)_2$ ligands and possesses a staggered rotational geometry. The Re—Re bond length is 2.265(1) Å. The reaction of *cis*-$Re_2(O_2CCH_3)_2Cl_2(dppm)_2$ with $NaBH_3CN$ in THF gives *cis*-$Re_2(O_2CCH_3)_2(NCBH_3)_2(dppm)_2$, in which the structure of the parent complex is retained but with N-bound cyanotrihydroborato ligands in place of the axially bound chlorides. The crystallographic data for *cis*-$Re_2(O_2CCH_3)_2(NCBH_3)_2(dppm)_2 \cdot CH_2Cl_2$ are as follows: orthorhombic space group *Pbca*, $a = 18.072(2)$, $b = 19.982(2)$, $c = 31.795(6)$ Å, $V = 11481(5)$ Å^3 and $Z = 8$. The structure was refined to $R = 0.035$ ($R_w = 0.045$) for 4613 data with $I > 3.0\sigma(I)$. The Re—Re bond distance in this complex is 2.2938(7) Å.

The development of the chemistry of the *cis* and *trans* isomeric forms of the triply-bonded dirhenium(II) complexes $Re_2(\mu\text{-}O_2CR)_2X_2(\mu\text{-LL})_2$ (R = CH_3, C_2H_5, C_6H_5 or $4\text{-}C_5H_5N$; X = Cl or Br; LL = $Ph_2PCH_2PPh_2$, $Ph_2PNHPPh_2$ or $Ph_2AsCH_2AsPh_2$) has been a focus of recent studies in our laboratory.[1–3] Among the characteristics of these systems is their ease of oxidation to the corresponding paramagnetic monocations with retention of stereochemistry.[1,2] In the present study we set out to examine the lability of the bridging carboxylate and axial halide ligands to substitution by other nucleophiles, especially nitrile-containing ligands. We now describe the results of these investigations as they relate to the complexes *cis*-$Re_2(O_2CR)_2Cl_2(dppm)_2$ (R = CH_3 or C_2H_5; dppm = $Ph_2PCH_2PPh_2$), and we include in this report the details of the full structural characterizations of the new complexes $[Re_2Cl_3(\mu\text{-dppm})_2(1,2\text{-}C_6H_4(CN)_2)_2]PF_6$ and *cis*-$Re_2(\mu\text{-}O_2CCH_3)_2(NCBH_3)_2(\mu\text{-dppm})_2$.

* Present address: Department of Chemistry, Hollins College, Roanoke, VA 24020, U.S.A.

† Author to whom correspondence should be addressed.

EXPERIMENTAL

Starting materials

The compounds $Re_2Cl_4(dppm)_2$,[1] *cis*-$Re_2(O_2CR)_2Cl_2(dppm)_2$ (R = CH_3 or C_2H_5)[1,3] and $[(Ph_3P)_2N]O_2CCH_3$[3,4] were prepared as described previously. The $HBF_4 \cdot Et_2O$ and HPF_6 (60% aq. solution) reagents were purchased from Aldrich Chemical Co., while carbon monoxide (99.9%) was obtained from Matheson Gas Products. These reagents were used without further purification. Solvents used in the preparation of the complexes were of commercial grade and were thoroughly deoxygenated prior to use.

Reaction procedures

Syntheses were performed in an atmosphere of dry nitrogen under the pressure provided by passing the outlet nitrogen through a mineral oil bubbler. All solvents were freshly distilled prior to use.

A. *Reactions of* cis-$Re_2(O_2CC_2H_5)_2Cl_2(dppm)_2$ *with* $HBF_4 \cdot Et_2O$ *or* HPF_6(aq.) *in the presence of nitriles*

(i) CH_3CN. A small volume of $HBF_4 \cdot Et_2O$ (*ca* 0.1 cm^3) was added to a mixture of *cis*-$Re_2(O_2CC_2H_5)_2Cl_2(dppm)_2$ (0.140 g, 0.103 mmol), acetone (5 cm^3) and acetonitrile (1 cm^3). The green solution thereby produced was stirred at room temperature for 15 min. The product was obtained as a pale green powder upon the slow addition of diethyl ether (*ca* 25 cm^3) to this solution. This solid was filtered off, washed with diethyl ether and dried *in vacuo*; yield 0.144 g (88%). Found: C, 42.5; H, 3.6; Cl, 4.8. Calc. for $C_{58}H_{62}B_2Cl_2F_8N_4O_3P_4Re_2$ {i.e. for $[Re_2Cl_2(dppm)_2(NCCH_3)_4](BF_4)_2 \cdot 3H_2O$}: C, 43.4; H, 3.9; Cl, 4.4%. This complex showed absorptions at 3538 (m–s,br) and 1630 (m–w,br) cm^{-1} in its IR spectrum (Nujol mull) assignable to ν(O—H) and δ(O—H) modes, respectively. The source of the water of crystallization is presumably the small quantity of water that is present in the $HBF_4 \cdot Et_2O$ reagent.

A related procedure was used to react a mixture of *cis*-$Re_2(O_2CC_2H_5)_2Cl_2(dppm)_2$ (0.20 g, 0.147 mmol), dichloromethane (6 cm^3) and acetonitrile (0.6 cm^3) with HPF_6(aq.) (0.05 cm^3). The colour of the reaction mixture changed from orange–brown to dark green within *ca* 2 min at room temperature. The solution was stirred for an additional 20 min and the product was obtained as a pale green powder upon the addition of a large excess of diethyl ether (*ca* 50 cm^3). The product was filtered off, washed with diethyl ether and dried *in vacuo*; yield 0.19 g (74%). Found: C, 40.2; H, 3.2. Calc. for $C_{59}H_{58}Cl_4F_{12}N_4P_6Re_2$ {i.e. for $[Re_2Cl_2(dppm)_2(NCCH_3)_4](PF_6)_2 \cdot CH_2Cl_2$}: C, 40.5; H, 3.3%. The presence of lattice CH_2Cl_2 was confirmed by ^1H NMR spectroscopy.

(ii) C_2H_5CN. Procedures similar to those described in section A(i) were used to obtain green products that we formulate as the propionitrile derivatives $[Re_2Cl_2(dppm)_2(NCC_2H_5)_4]X_2$ (X = BF_4^- or PF_6^-) on the basis of the similarities of their spectroscopic and electrochemical properties to those of the acetonitrile complexes. The propionitrile complex was also obtained from $[Re_2Cl_2(dppm)_2(NCCH_3)_4](BF_4)_2 \cdot 3H_2O$ by a nitrile exchange reaction. A quantity of the acetonitrile complex (0.23 g) was treated with an excess of propionitrile and the mixture stirred at room temperature for a few minutes. A small volume (2 cm^3) of acetone was added to the solution, followed by the slow addition of diethyl ether to initiate precipitation of the green propionitrile product, which was filtered off, washed with diethyl ether and dried *in vacuo*.

During attempts to grow single crystals of $[Re_2Cl_2(dppm)_2(NCC_2H_5)_4](PF_6)_2$ from dichloromethane–diethyl ether, this complex converted to the much more stable bis(propionitrile) derivative, $[Re_2Cl_3(dppm)_2(NCC_2H_5)_2]PF_6$. The crystals that were obtained proved to be of composition $[Re_2Cl_3(dppm)_2(NCC_2H_5)_2]PF_6 \cdot 2CH_2Cl_2$.[5]

B. *Synthesis of* $[Re_2Cl_3(dppm)_2(1,2\text{-}C_6H_4(CN)_2)]PF_6$

A mixture of $Re_2Cl_4(dppm)_2$ (0.10 g, 0.08 mmol), 1,2-dicyanobenzene (0.15 g, 1.17 mmol) and KPF_6 (0.10 g, 0.54 mmol) was treated with 6 cm^3 of acetone and stirred for 1 h at room temperature. An excess of diethyl ether was added to precipitate a red solid, which was filtered off, extracted into dichloromethane (15 cm^3) and reprecipitated upon the addition of excess diethyl ether; yield 0.11 g (83%). Found: C, 47.8; H, 3.5. Calc. for $C_{66}H_{52}Cl_3F_6N_4P_5Re_2$: C, 48.1; H, 3.9%. The identity of this product was confirmed by a single crystal X-ray structure analysis.

C. *Reactions of* $[Re_2Cl_2(dppm)_2(NCR)_4]X_2$ (X = BF_4^- *or* PF_6^-)

(i) $[(Ph_3P)_2N]O_2CCH_3$. Acetonitrile (10 cm^3) was added to a mixture of $[Re_2Cl_2(dppm)_2(NCCH_3)_4](BF_4)_2 \cdot 3H_2O$ (0.036 g, 0.002 mmol) and $[(Ph_3P)_2N]O_2CCH_3$ (0.055 g, 0.092 mmol). This reaction mixture was stirred at room temperature for 30

min. The orange product was filtered off, washed with ethanol and diethyl ether and dried; yield 0.015 g. It was identified as *cis*-$Re_2(O_2CCH_3)_2Cl_2(dppm)_2$ on the basis of its cyclic voltammetric properties as measured on 0.1 M TBAH–CH_2Cl_2 solutions. These data are in excellent agreement with the literature values of $E_{1/2}(ox) = +0.28$ V and $E_{1/2}(ox) = +1.34$ V vs Ag/AgCl.[1]

(ii) *Carbon monoxide.* A quantity of $[Re_2Cl_2(dppm)_2(NCC_2H_5)_4](PF_6)_2 \cdot CH_2Cl_2$ (0.10 g, 0.055 mmol) was dissolved in 10 cm^3 of deoxygenated acetone and a slow stream of carbon monoxide bubbled through the solution for 10 min. The green–brown solution was then stirred for 2 h, evaporated to dryness and the residue extracted with 10 cm^3 of dichloromethane. The resulting extract was added to 30 cm^3 of diethyl ether to precipitate a yellow–green product, which was washed with diethyl ether and dried *in vacuo*; yield 0.051 g (62%). Its identity as $[Re_2Cl_3(dppm)_2(CO)_2(NCC_2H_5)]PF_6$ was established by a comparison of its cyclic voltammetric properties and ^1H NMR and IR (Nujol mull) spectra with those reported in the literature for an authentic sample of this complex.[6]

In an alternative work-up of this reaction product, the initial green–brown reaction solution was subjected to chromatography on an Al_2O_3 column (80–200 mesh, 20 cm, CH_2Cl_2 as eluent) and a blue band collected. This was evaporated to low volume and treated with an excess of pentane to precipitate a blue solid; yield 0.02 g. Found: C, 48.3; H, 4.0. Calc. for $C_{55}H_{49}Cl_3NO_2P_4Re_2$ [i.e. for $Re_2Cl_3(dppm)_2(CO)_2(NCC_2H_5)$]: C, 48.6; H, 3.6%. The cyclic voltammetric properties and IR (Nujol mull) and X-band ESR spectral properties of this product were also in agreement with literature data.[6]

D. *Reactions of* cis-$Re_2(O_2CC_2H_5)_2Cl_2(dppm)_2$ *with carbon monoxide*

A quantity of the title complex (0.14 g, 0.10 mmol) was dissolved in 8 cm^3 of dichloromethane, a slow stream of carbon monoxide bubbled through the solution for 5 min, and a small volume (0.10 cm^3) of HPF_6(aq.) added. The resulting mixture was stirred at room temperature for a further 20 min under an atmosphere of carbon monoxide, and a large excess of diethyl ether added to precipitate a brown solid that was filtered off and recrystallized from dichloromethane–pentane; yield 0.09 g (61%). The identity of this product as $[Re_2Cl_3(dppm)_2(CO)_3]PF_6$ was established by the similarity of its cyclic voltammetric properties and IR (Nujol mull) spectrum to those of an authentic sample.[7] Further confirmation came from its ready reduction to the blue paramagnetic neutral species, $Re_2Cl_3(dppm)_2(CO)_3$.[7]

When $HBF_4 \cdot Et_2O$ was used in place of HPF_6(aq.) in the above procedure, the analogous BF_4^- salt was obtained, viz. $[Re_2Cl_3(dppm)_2(CO)_3]BF_4$. Found: C, 44.9; H, 3.3. Calc. for $C_{53}H_{44}BCl_3F_4O_3P_4Re_2$: C, 44.9; H, 3.1%. Its cyclic voltammogram (recorded on a 0.1 M TBAH–CH_2Cl_2 solution) showed reversible redox processes at $E_{1/2}(ox) = +0.33$ V and $E_{1/2}(red) = -0.70$ V vs Ag/AgCl. Its IR spectrum (Nujol mull) had characteristic ν(CO) modes at 2045 s and 2010 s cm^{-1} (terminal C—O stretches), and 1976 m cm^{-1} (bridging C—O stretch). These data are in excellent agreement with those reported for the PF_6^- salt.[7]

E. *Reaction of* cis-$Re_2(O_2CCH_3)_2Cl_2(dppm)_2$ *with* $NaBH_3CN$

A suspension of *cis*-$Re_2(O_2CCH_3)_2Cl_2(dppm)_2$ (0.20 g, 0.15 mmol) and $NaBH_3CN$ (0.05 g, 0.80 mmol) in 10 cm^3 of THF was stirred at room temperature for several hours until a rust coloured precipitate deposited. This product was filtered off and extracted into dichloromethane (*ca* 25 cm^3). The extract was evaporated to half volume and then treated with a large excess of pentane to precipitate *cis*-$Re_2(O_2CCH_3)_2(NCBH_3)_2(dppm)_2$; yield 0.11 g (54%). Found: C, 50.1; H, 4.5. Calc. for $C_{56}H_{56}B_2N_2O_4P_4Re_2$: C, 50.2; H, 4.2%.

Preparation of single crystals for structure determination

Red crystals of $[Re_2Cl_3(dppm)_2(1,2\text{-}C_6H_4(CN)_2)_2]PF_6$ (**1**) were grown by the diffusion of diethyl ether into a dichloromethane solution of the complex, while crystals of composition *cis*-$Re_2(O_2CCH_3)_2(NCBH_3)_2(dppm)_2 \cdot CH_2Cl_2$ (**2**) were obtained as red cubes from a dichloromethane–pentane mixture.

X-ray crystallography

The structures were determined by the use of standard procedures. A summary of the crystallographic data for both structures is given in Table 1. The cell constants are based on 25 reflections with $7 < \theta < 13°$ for **1** and $16 < \theta < 20°$ for **2**. Three standard reflections were measured after 5000 s of beam time during data collection. There were no systematic variations in intensity. Calculations were performed on a microVAX II com-

Table 1. Crystal data and data collection parameters for $[Re_2Cl_3(dppm)_2(1,2\text{-}C_6H_4(CN)_2)_2]PF_6$ (**1**) and *cis*-$Re_2(O_2CCH_3)_2(NCBH_3)_2(dppm)_2 \cdot CH_2Cl_2$ (**2**)[a]

	1	**2**
Formula	$Re_2Cl_3P_5F_6N_4C_{66}H_{52}$	$Re_2Cl_2P_4O_4N_2C_{57}B_2H_{58}$
Formula weight	1648.80	1423.93
Space group	$P2_12_12_1$ (No. 19)	*Pbca* (No. 61)
a (Å)	18.242(6)	18.072(2)
b (Å)	19.197(6)	19.982(2)
c (Å)	19.789(6)	31.795(6)
V (Å^3)	6929(7)	11481(5)
Z	4	8
d_{calc} (g cm^{-3})	1.580	1.647
Crystal dimensions (mm)	$0.56 \times 0.47 \times 0.41$	$0.25 \times 0.25 \times 0.15$
Temperature (°C)	20	20
Radiation (wavelength)	Mo-K_α (0.71073 Å)	Mo-K_α (0.71073 Å)
Monochromator	Graphite	Graphite
Linear absorption coefficient (cm^{-1})	38.24	45.20
Absorption correction applied	Empirical[b]	Empirical[b]
Transmission factors: min., max.	0.62, 1.00	0.72, 1.00
Diffractometer	Enraf–Nonius CAD4	Enraf–Nonius CAD4
Scan method	ω–2θ	ω–2θ
$h\,k\,l$ limits	0–19, 0–20, 0–21	0–19, 0–21, 0–34
2θ range (°)	4.00–45.00	4.00–45.00
Scan width (°)	$0.80 + 0.35 \tan(\theta)$	$0.42 + 0.35 \tan(\theta)$
Take-off angle (°)	3.15	2.95
Programs used	Enraf–Nonius SDP	Enraf–Nonius SDP
$F(000)$	3224.0	5600.0
p-Factor used in weighting	0.040	0.040
Data collected	5029	8183
Unique data	5029	8183
Data with $I > 3.0\sigma(I)$	3511	4613
Number of variables	425	658
Largest shift/ESD in final cycle	0.43	0.02
R[c]	0.081	0.035
R_w[d]	0.098	0.045
Goodness of fit[e]	2.270	1.040

[a] Numbers in parentheses following certain data are ESDs occurring in the least significant digit.
[b] N. Walker and D. Stuart, *Acta Cryst.* 1983, **A39**, 158.
[c] $R = \Sigma ||F_o| - |F_c|| / \Sigma |F_o|$.
[d] $R_w = [\Sigma w (|F_o| - |F_c|)^2 / \Sigma w |F_o|^2]^{1/2}$; $w = 1/\sigma^2(F_o)$.
[e] Goodness of fit $= [\Sigma w (|F_o| - |F_c|)^2 / (N_{obs} - N_{parameters})]^{1/2}$.

puter using the Enraf–Nonius structure determination package.

The crystals selected for the structure determinations belong to the orthorhombic space groups $P2_12_12_1$ (No. 19) with $Z = 4$ for **1** and *Pbca* (No. 61) with $Z = 8$ for **2**. Lorentz and polarization corrections were applied to the data. The structures were solved by the use of the Patterson heavy-atom method, which revealed the positions of the rhenium atoms in the asymmetric units. The remaining atoms were located in succeeding difference Fourier synthesis. The positions for the hydrogen atoms of the ligand molecules were calculated by assuming idealized geometry and a C—H bond distance of 0.95 Å. For the methyl groups of the acetate ligands and BH_3 groups of the $NCBH_3$ ligands, one hydrogen was located in a difference Fourier map, its position idealized, and the remaining positions calculated. We assumed that the value of B(H), i.e. the isotopic equivalent thermal parameter for the hydrogen atoms, was equal to $1.3[B_{eqv}(C)]$ at the time of the inclusion of this parameter in the refinement procedure. While these hydrogen atoms were used in the calculation of F_{calc} their positions

Table 2. Selected bond distances (Å) and angles (°) for $[Re_2Cl_3(dppm)_2(1,2\text{-}C_6H_4(CN)_2)_2]PF_6$ (**1**)[a]

Bond distances (Å)			
Re(1)—Re(2)	2.265(1)	Re(2)—P(22)	2.475(7)
Re(1)—Cl(11)	2.344(7)	Re(2)—N(210)	2.00(2)
Re(1)—Cl(12)	2.381(8)	Re(2)—N(220)	2.09(3)
Re(1)—P(11)	2.411(7)	N(210)—C(210)	1.10(3)
Re(1)—P(12)	2.371(9)	N(220)—C(220)	1.13(3)
Re(2)—Cl(21)	2.492(6)	N(2162)—C(2161)	1.14(4)
Re(2)—P(21)	2.466(8)	N(2262)—C(2261)	1.17(4)

Bond angles (°)			
Re(2)—Re(1)—Cl(11)	107.3(2)	Cl(21)—Re(2)—P(22)	86.1(2)
Re(2)—Re(1)—Cl(12)	106.2(2)	Cl(21)—Re(2)—N(210)	87.4(6)
Re(2)—Re(1)—P(11)	96.5(2)	Cl(21)—Re(2)—N(220)	85.4(7)
Re(2)—Re(1)—P(12)	96.3(2)	P(21)—Re(2)—P(22)	171.7(2)
Cl(11)—Re(1)—Cl(12)	146.5(3)	N(210)—Re(2)—N(220)	169.1(9)
P(11)—Re(1)—P(12)	167.2(2)	Re(2)—N(210)—C(210)	171(2)
Re(1)—Re(2)—Cl(21)	177.8(2)	Re(2)—N(220)—C(220)	172(3)
Re(1)—Re(2)—P(21)	93.0(3)	N(210)—C(210)—C(211)	162(3)
Re(1)—Re(2)—P(22)	95.3(2)	N(220)—C(220)—C(221)	175(3)
Re(1)—Re(2)—N(210)	91.3(5)	N(2162)—C(2161)—C(216)	172(3)
Re(1)—Re(2)—N(220)	96.2(7)	N(2262)—C(2261)—C(226)	177(4)
Cl(21)—Re(2)—P(21)	85.6(2)		

[a] Numbers in parentheses are ESDs in the least significant digits.

were not refined. An empirical absorption correction was used,[8] the linear absorption coefficients being 38.24 cm^{-1} for **1** and 45.20 cm^{-1} for **2**. No corrections for extinction were applied. The structures were refined in full-matrix least-squares, where the function minimized was $\Sigma w(|F_o|-|F_c|)^2$, with the weighting factor w defined as $w = 1/\sigma^2(F_o)$. For **1**, the Re, Cl, P and F atoms were refined anisotropically. All non-hydrogen atoms for complex **2** were refined anisotropically, including the C and Cl atoms of the crystallographically unique lattice CH_2Cl_2 molecule which is located about a general position (eight symmetry related sites per unit cell). Corrections for anomalous scattering were applied to all atoms that were refined anisotropically.[9]

The refinement of the PF_6^- anion in the structure of **1** was not entirely satisfactory; the thermal parameters for the F atoms were rather large, implying high thermal motion, and the P—F distances covered a fairly large range [1.37(3)–1.68(4) Å]. Nonetheless, our modelling of the PF_6^- makes sense based upon our knowledge of the stoichiometry and spectroscopic properties of the complex. The highest peaks in the final difference Fourier maps of **1** and **2** were 2.49 and 0.77 e Å^3, respectively. Since these were not at any bonding distance to the atoms of the dirhenium molecules they were not considered to be of any chemical significance.

Further details concerning the data sets and structure solutions and refinements may be obtained from Dr P. E. Fanwick. Tables 2 and 3 list important bond distances and angles for these structures.*

Physical measurements

Perkin–Elmer 1420 and 1800 spectrophotometers were used to record the IR spectra of compounds as mineral oil (Nujol) mulls supported on KBr plates in the region 4000–400 cm^{-1}. Electrochemical measurements were carried out on dichloromethane solutions that contained 0.1 M tetra-*n*-butylammonium hexafluorophosphate (TBAH) as the supporting electrolyte. $E_{1/2}$ values, determined as $(E_{p,a}+E_{p,c})/2$, were referenced to the silver/silver chloride (Ag/AgCl) electrode at room temperature and are uncorrected for junction potentials. Under our experimental conditions, $E_{1/2} = +0.47$ V vs Ag/AgCl for the ferro-

* Atomic positional and thermal parameters and full listings of bond lengths and angles have been deposited with the Editor and with the Director, Cambridge Crystallographic Data Centre.

Table 3. Selected bond distances (Å) and angles (°) for *cis*-$Re_2(O_2CCH_3)_2(NCBH_3)_2(dppm)_2 \cdot CH_2Cl_2$ (**2**)[a]

Bond distances (Å)			
Re(1)—Re(2)	2.2938(7)	Re(2)—O(21)	2.117(8)
Re(1)—P(11)	2.411(3)	Re(2)—O(22)	2.140(7)
Re(1)—P(12)	2.409(3)	Re(2)—N(4)	2.29(1)
Re(1)—O(11)	2.138(8)	N(1)—C(2)	1.16(2)
Re(1)—O(12)	2.096(8)	N(4)—C(5)	1.14(2)
Re(1)—N(1)	2.30(1)	C(2)—B(3)	1.54(2)
Re(2)—P(21)	2.400(3)	C(5)—B(6)	1.51(3)
Re(2)—P(22)	2.399(3)		

Bond angles (°)			
Re(2)—Re(1)—P(11)	94.89(8)	O(11)—Re(1)—O(12)	80.4(3)
Re(2)—Re(1)—P(12)	98.85(8)	O(11)—Re(1)—N(1)	78.7(4)
Re(2)—Re(1)—O(11)	88.0(2)	O(12)—Re(1)—N(1)	80.6(3)
Re(2)—Re(1)—O(12)	88.6(2)	Re(1)—Re(2)—P(21)	98.84(8)
Re(2)—Re(1)—N(1)	164.0(3)	Re(1)—Re(2)—P(22)	96.62(8)
P(11)—Re(1)—P(12)	94.7(1)	Re(1)—Re(2)—O(21)	88.7(2)
P(11)—Re(1)—O(11)	171.6(2)	Re(1)—Re(2)—O(22)	88.2(2)
P(11)—Re(1)—O(12)	91.7(2)	Re(1)—Re(2)—N(4)	167.7(3)
P(11)—Re(1)—N(1)	97.2(3)	Re(1)—N(1)—C(2)	164(1)
P(12)—Re(1)—O(11)	92.7(2)	Re(2)—N(4)—C(5)	179(1)
P(12)—Re(1)—O(12)	169.7(2)	N(1)—C(2)—B(3)	178(2)
P(12)—Re(1)—N(1)	90.6(3)	N(4)—C(5)—B(6)	175(2)

[a] Numbers in parentheses are ESDs in the least significant digits.

cenium/ferrocene couple. Voltammetric experiments were performed with a Bioanalytical Systems Inc. Model CV-1A instrument in conjunction with a Hewlett–Packard Model 7035 B *x–y* recorder. Conductivity measurements were performed on 1×10^{-3} M acetone solutions of the complexes on an Industrial Instruments Inc. Model RC-16B2 conductivity bridge. $^{31}P\{^1H\}$ NMR spectra were recorded on a Varian XL-200 spectrometer operated at 80.98 MHz with the use of an internal deuterium lock and 85% H_3PO_4 as an external standard. ^1H NMR spectra were obtained on Varian XL-200 and GE QE-300 spectrometers. Resonances were referenced internally to the residual protons in the incompletely deuteriated solvents. ^{11}B NMR spectra were recorded on a Varian FT-80 spectrometer with the use of $BF_3 \cdot OEt_2$ as an external standard.

Analytical procedures

Elemental microanalyses were performed by Dr H. D. Lee of the Purdue University Microanalytical Laboratory.

RESULTS AND DISCUSSION

A. *Synthesis of and characterization of* cis-$[Re_2Cl_2(dppm)_2(NCR)_4]^{2+}$

Our initial objective in preparing salts of these cations was accomplished in the case of R = CH_3 and C_2H_5 through the reactions of the complex *cis*-$Re_2(O_2CC_2H_5)_2Cl_2(dppm)_2$ with the appropriate nitrile, admixed with a suitable reaction solvent, in the presence of the strong acid $HBF_4 \cdot Et_2O$ or HPF_6(aq.). While the spectroscopic properties of the products showed the absence of propionate ligands and the presence of the appropriate nitrile, microanalytical data (supported by IR and NMR spectroscopy) indicated that lattice water, and/or solvent, was also present in the products. These are doubtless quite strongly hydrogen-bonded to the BF_4^- and PF_6^- anions. Since our attempts to free the complexes from these molecules were not successful, all subsequent studies were carried out on products that we formulate as *cis*-$[Re_2Cl_2(dppm)_2(NCR)_4](BF_4)_4 \cdot 3H_2O$ (the actual amount of water present seemed to vary somewhat from

run to run) and *cis*-$[Re_2Cl_2(dppm)_2(NCR)_4](PF_6)_2 \cdot CH_2Cl_2$.

In all instances, these salts had IR spectra (Nujol mulls) that showed the presence of coordinated nitrile ligands [ν(C≡N) at *ca* 2290 (w) cm^{-1}] and the anions $[BF_4]^-$ [ν(B—F) at *ca* 1060 (s) cm^{-1}] or $[PF_6]^-$ [ν(P—F) at *ca* 840 (s) cm^{-1}]. Further evidence as to the identity of these complexes came from conductivity measurements which showed that solutions of $[Re_2Cl_2(dppm)_2(NCR)_4](PF_6)_2 \cdot CH_2Cl_2$ in acetone ($c_m \simeq 1.0 \times 10^{-3}$ M) have conductivities characteristic of 1 : 2 electrolytes, viz 162 Ω^{-1} cm^2 mol^{-1} for R = CH_3 and 159 Ω^{-1} cm^2 mol^{-1} for R = C_2H_5. Furthermore, the reconversion of *cis*-$[Re_2Cl_2(dppm)_2(NCCH_3)_4](BF_4)_2 \cdot 3H_2O$ to *cis*-$Re_2(O_2CCH_3)_2Cl_2(dppm)_2$ upon its reaction with $[(Ph_3P)_2N]O_2CCH_3$ in acetonitrile implies that the structural integrity of the dirhenium core has been retained throughout these reactions.

The 200 MHz ^1H NMR spectrum of $[Re_2Cl_2(dppm)_2(NCC_2H_5)_4](BF_4)_2$, recorded in CD_3CN, showed that the propionitrile ligands had been displaced by CD_3CN. The resonances of propionitrile were at δ +2.35 (quartet, —C*H*$_2$—, 8H) and +1.19 (triplet, —C*H*$_3$, 12H) and integrated in accordance with there being four C_2H_5CN ligands in the complex. The spectrum of this complex in CD_2Cl_2 showed multiplets at δ *ca* +2.65 and *ca* +1.35 that are assigned to the coordinated propionitrile ligands. The complexity of these patterns implies that inequivalent nitrile ligands are present. This is supported by the $^{31}P\{^1H\}$ NMR spectrum of this complex (also recorded in CD_2Cl_2) which is an AA′BB′ pattern, the main components of which are centred at δ *ca* −2.6, −3.4, −16.9 and −17.4. These properties may be in accordance with the following structure:

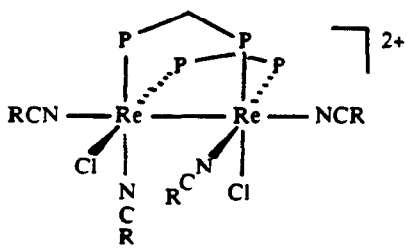

Unfortunately, attempts to determine the structure of the $[Re_2Cl_2(dppm)_2(NCR)_4]^{2+}$ cations by X-ray crystallography were thwarted by our failure to obtain suitable single crystals. In fact, solutions of these salts were unstable and converted to the much more stable $[Re_2Cl_3(dppm)_2(NCR)_2]^+$ cation[11] during the crystal growing procedures. This presumably occurs by a complicated reaction involving nitrile dissociation and chloride transfer between dirhenium species. In one such instance, the structure of $[Re_2Cl_3(dppm)_2(NCC_2H_5)_2]PF_6$ was determined[5] in the mistaken belief that the crystals were in fact those of $[Re_2Cl_2(dppm)_2(NCC_2H_5)_4](PF_6)_2$.

Attempts to derivatize $[Re_2Cl_2(dppm)_2(NCR)_4]X_2$ (X = BF_4^- or PF_6^-) by displacing some or all of the nitrile ligands led to products that are more conveniently prepared directly from $Re_2Cl_4(dppm)_2$. Thus, the reaction of $[Re_2Cl_2(dppm)_2(NCC_2H_5)_4](PF_6)_2$ with CO afforded $[Re_2Cl_3(dppm)_2(CO)_2(NCC_2H_5)]PF_6$ and $Re_2Cl_3(dppm)_2(CO)_2(NCC_2H_5)$, both of which have been prepared previously and are known to have edge-shared bioctahedral structures with an all-*cis* disposition of chloride ligands.[6] Once again, an additional chloride ligand, over and above the number that are present in the starting complex, becomes incorporated into the product. As an alternative strategy, the complex *cis*-$Re_2(O_2CC_2H_5)_2Cl_2(dppm)_2$ was reacted with CO in the presence of $HBF_4 \cdot Et_2O$ or HPF_6(aq.), with dichloromethane as the reaction solvent in place of CH_3CN or C_2H_5CN. The products were $[Re_2Cl_3(dppm)_2(CO)_3]X$ (X = BF_4^- or PF_6^-) in which the $[Re_2Cl_3(dppm)_2]$ unit is again present. The PF_6^- salt had been prepared previously and structurally characterized.[7]

B. *Synthesis and crystal structure of* $[Re_2Cl_3(dppm)_2(1,2\text{-}C_6H_4(CN)_2)_2]PF_6$ (1)

In the course of the present study, we investigated the reactivity of dirhenium complexes such as $Re_2Cl_4(dppm)_2$ and *cis*-$Re_2(O_2CC_2H_5)_2Cl_2(dppm)_2$ towards dinitrile ligands with the objective of ascertaining their ability to link dirhenium units so as to form small clusters or polymers. Our attempts to prepare salts of the $[Re_2Cl_2(dppm)_2(1,2\text{-}C_6H_4(CN)_2)_x]^{2+}$ cation (x = 2 or 4) from *cis*-$Re_2(O_2CC_2H_5)_2Cl_2(dppm)_2$ were not successful, and the best characterized product we isolated proved to be the title complex. It was obtained by the reaction of $Re_2Cl_4(dppm)_2$ with 1,2-dicyanobenzene and KPF_6 in acetone, a procedure that resembles the one used previously to prepare other complexes of the type $[Re_2Cl_3(dppm)_2(NCR)_2]PF_6$.[11] These compounds have an unsymmetrical structure that can be represented as $[Cl_2Re(\mu\text{-dppm})_2ReCl(NCR)_2]PF_6$.[5,11] The properties of the 1,2-dicyanobenzene complex are in accordance with those of other such derivatives. Most notably, its $^{31}P\{^1H\}$ NMR spectrum (recorded in CD_2Cl_2) consists of an AA′BB′ pattern (the most intense components are at δ −2.03 and −5.48), while a cyclic voltammetric measurement

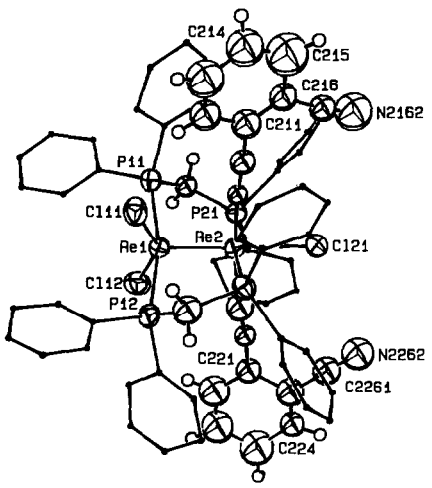

Fig. 1. ORTEP representation of the structure of the dirhenium cation in $[Re_2Cl_3(dppm)_2(1,2\text{-}C_6H_4(CN)_2)_2]PF_6$ (**1**) showing the atomic numbering scheme. The thermal ellipsoids are drawn at the 50% probability level except for the phenyl carbon atoms which are shown as circles of arbitrary radius.

on a solution of the complex in 0.1 M TBAH–CH_2Cl_2 revealed a rich redox chemistry with a reversible oxidation [$E_{1/2}(ox) = +0.75$ V vs Ag/AgCl], a reversible reduction [$E_{1/2}(red) = -1.20$ V], and an irreversible reduction at $E_{p,c} \simeq -1.8$ V. The IR spectrum (Nujol mull) of this complex has a $\nu(C{\equiv}N)$ mode at 2240 (m–w) cm^{-1}, with a shoulder at *ca* 2230 cm^{-1}, and a characteristic $\nu(P—F)$ mode for the PF_6^- anion at 842 (vs) cm^{-1}. A single crystal X-ray structure analysis, which confirmed the identity of this complex, showed that the two dinitrile ligands are bound in a monodentate fashion.

An ORTEP representation of the structure of the cation in the salt $[Re_2Cl_3(dppm)_2(1,2\text{-}C_6H_4(CN)_2)_2]PF_6$ is shown in Fig. 1. Important bond distances and angles are listed in Table 2. The dirhenium unit possesses no crystallographically-imposed symmetry. The Re—Re distance of 2.265(1) Å is essentially identical to the Re—Re distances in the analogous propionitrile[5] and benzonitrile[11] complexes, which are 2.266(1) and 2.270(1) Å, respectively. As expected, the axial Re—Cl bond [Re(2)—Cl(21)] is longer than the pair of equatorial Re—Cl bonds [2.492(6) Å vs 2.344(7) and 2.381(8) Å], a feature that is common to all three structures. All other bond lengths are normal and, with one exception, do not merit further discussion. The one exception concerns the C—N distances of the coordinated and free cyano groups of the $1,2\text{-}C_6H_4(CN)_2$ ligands. Within the significance level of 3σ, these distances are the same. The bond angles for the dirhenium cation are similar to those for the other two bis(nitrile) structures.[5,11] Thus, the Cl(11)—Re(1)—Cl(12) angle of 146.5(3)° can be compared with angles of 142.9(3) and 140.5(3)° in the propionitrile and benzonitrile complexes, respectively, while the N(210)—Re(2)—N(220) angle of 169.1(9)° compares with the values of 171.3(8) and 169.6(5)°. The conformation about the Re—Re bond is staggered as shown by values for the four torsional angles P(11)—Re(1)—Re(2)—P(21), P(12)—Re(1)—Re(2)—P(22), Cl(11)—Re(1)—Re(2)—N(210) and Cl(12)—Re(1)—Re(2)—N(220) of 33.3(4), 31.5(4), 24.5(8) and 31.2(10)°, respectively.

C. *The synthesis and characterization of* cis-$Re_2(O_2CCH_3)_2(NCBH_3)_2(dppm)_2$ (2)

A further reaction we studied was that involving an anionic nitrile ligand, namely $[BH_3CN]^-$. While we have been unable to identify the product from the reaction of $NaBH_3CN$ with $Re_2Cl_4(dppm)_2$, we found that *cis*-$Re_2(O_2CCH_3)_2Cl_2(dppm)_2$ reacts with $NaBH_3CN$ in THF at room temperature to form *cis*-$Re_2(O_2CCH_3)_2(NCBH_3)_2(dppm)_2$ (**2**). Interestingly, the electrochemical properties of this complex, as measured by the cyclic voltammetric technique on a 0.1 M TBAH–CH_2Cl_2 solution of the complex, are quite different from the related behaviour of the chloride precursor complex. While *cis*-$Re_2(O_2CCH_3)_2Cl_2(dppm)_2$ has two processes with $E_{1/2}$ values of +0.28 and +1.34 V vs Ag/AgCl, which correspond to one-electron oxidations of the bulk complex,[1,3] the cyanotrihydroborate complex shows an oxidation at $E_{1/2} = +0.60$ V and two irreversible reductions at $E_{p,c} = -1.29$ and $E_{p,c} = -1.48$ V vs Ag/AgCl.

The $^{31}P\{^1H\}$ NMR spectrum of **2** (recorded in CD_2Cl_2), like the analogous chloride,[3] appears as a singlet (δ −9.48). The ^1H NMR spectrum displays resonances for the phenyl protons in the range δ +7.6 to +6.9, and multiplets for the dppm bridgehead methylene protons (—CH_AH_M—) at δ_A +6.50 and δ_M +4.89. The latter patterns resemble closely those reported previously in the spectrum of *cis*-$Re_2(O_2CCH_3)_2Cl_2(dppm)_2$. The methyl protons of the acetate ligands appear as a singlet at δ +2.45. A very broad double-humped feature spanning the range δ +0.4 to −0.4 may be due to the protons of the $[BH_3CN]^-$ ligands. The ^{11}B NMR spectrum shows a broad resonance, exhibiting some poorly-defined structure, at δ *ca* −43; this becomes a sharp singlet at δ −41.7 in the proton-decoupled mode. In the IR spectrum (Nujol mull) there are characteristic bands associated with the cyanotrihydro-

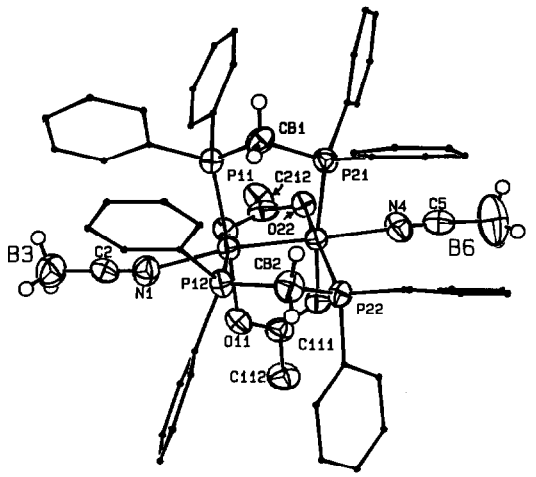

Fig. 2. ORTEP representation of the structure of the dirhenium unit in *cis*-$Re_2(O_2CCH_3)_2(NCBH_3)_2(dppm)_2 \cdot CH_2Cl_2$ (**2**) showing the atomic numbering scheme. The thermal ellipsoids are drawn at the 50% probability level except for the phenyl carbon atoms which are shown as circles of arbitrary radius.

borato ligands at 2328 (m–s,br) and 2154(s) cm^{-1} that are assigned to ν(B—H) and ν(C≡N) modes, respectively.[12–18] The C≡N stretch is unusual in being at a *lower* frequency than that of the free ligand; coordination of $[BH_3CN]^-$ to a metal ion invariably leads to an increase in this stretching frequency.[12–18] We attribute this decrease to the weakness of the Re—$NCBH_3$ interaction, a conclusion that is supported by the crystal structure data (*vide infra*).

A single crystal X-ray structure determination on this complex has confirmed its close structural relationship to *cis*-$Re_2(O_2CCH_3)_2Cl_2(dppm)_2$.[1,3] An ORTEP representation of the structure is shown in Fig. 2. The Re—Re distance in *cis*-$Re_2(O_2CCH_3)_2(NCBH_3)_2(dppm)_2$ is 2.2938(7) Å, a value that is very similar to that reported for the chloride complex [2.2763(7) Å];[3] the small difference presumably reflects the differing effects of the weakly bound axial ligands (BH_3CN^- versus Cl^-). The axial Re—N distances [2.30(1) and 2.29(1) Å] are much longer (by *ca* 0.3 Å) than the related equatorial Re—N distances in dirhenium(II) complexes that contain organic nitrile ligands,[5,11] and the Re—N distance to the $[BH_3CN]^-$ ligand in $Re(CO)_3(bpy)(NCBH_3)$.[18] The weakness of this interaction is also reflected by the IR spectral properties of this complex (*vide supra*). While the Re—N and N—C distances for the two terminal Re—$NCBH_3$ units are the same (Table 3), there is a modest difference between the associated Re—N—C angles [164(1) and 179(1)°]. These angles, as well as the related Re—Re—N angles [164.0(3) and 167.7(3)°], approach linearity. The structural parameters for the terminally bound $[BH_3CN]^-$ ligands are in satisfactory agreement with data reported in the literature for other M—$NCBH_3$ complexes.[14,17]

Acknowledgements—We thank the National Science Foundation (Grant No. CHE88-07444) for supporting this work, and for providing funds for the purchase of the microVAX II computer and diffractometer (Grant No. CHE86-15556). We also acknowledge the National Institutes of Health (Grant No. RR-01077) and the National Science Foundation (Grant No. 87-14258) for funds for the purchase of the NMR spectrometers.

REFERENCES

1. A. R. Cutler, D. R. Derringer, P. E. Fanwick and R. A. Walton, *J. Am. Chem. Soc.* 1988, **110**, 5024.
2. D. R. Derringer, P. E. Fanwick, J. Moran and R. A. Walton, *Inorg. Chem.* 1989, **28**, 1384.
3. D. R. Derringer, E. A. Buck, S. M. V. Esjornson, P. E. Fanwick and R. A. Walton, *Polyhedron* 1990, **9**, 743.
4. A. Martinsen and J. Songstad, *Acta Chem. Scand.* 1977, **A31**, 645.
5. P. E. Fanwick, J.-S. Qi, K.-Y. Shih and R. A. Walton, *Inorg. Chim. Acta* 1990, **172**, 65.
6. F. A. Cotton, K. R. Dunbar, L. R. Falvello and R. A. Walton, *Inorg. Chem.* 1985, **24**, 4180.
7. P. E. Fanwick, A. C. Price and R. A. Walton, *Inorg. Chem.* 1987, **26**, 3920.
8. N. Walker and D. Stuart, *Acta Cryst.* 1983, **A39**, 158.
9. D. T. Cromer, *International Tables for X-ray Crystallography*, Vol. IV, Table 2.3.1. Kynoch Press, Birmingham, U.K. (1974); For the scattering factors used in the structure solution see: D. T. Cromer and J. T. Waber, Table 2.2B of above.
10. W. J. Geary, *Coord. Chem. Rev.* 1971, **7**, 81.
11. T. J. Barder, F. A. Cotton, L. R. Falvello and R. A. Walton, *Inorg. Chem.* 1985, **24**, 1258.
12. S. J. Lippard and P. S. Welcker, *Inorg. Chem.* 1972, **11**, 6.
13. D. G. Holah, A. N. Hughes, B. C. Hui and K. Wright, *Inorg. Nucl. Chem. Lett.* 1973, **9**, 835.
14. B. G. Segal and S. J. Lippard, *Inorg. Chem.* 1974, **13**, 822.
15. B. G. Segal and S. J. Lippard, *Inorg. Chem.* 1977, **16**, 1623.
16. D. G. Holah, A. N. Hughes and N. I. Khan, *Can. J. Chem.* 1984, **62**, 1016.
17. R. J. Barton, D. G. Holah, H. Shengzhi, A. N. Hughes, S. I. Khan and B. E. Robertson, *Inorg. Chem.* 1984, **23**, 2391.
18. J. Guilhem, C. Pascard, J.-M. Lehn and R. Ziessel, *J. Chem. Soc., Dalton Trans.* 1989, 1449.

Polyhedron Vol. 10, No. 1, pp. 89–93, 1991
Printed in Great Britain

0277–5387/91 $3.00+.00
© 1991 Pergamon Press plc

ISOLATION OF A TETRAKIS(μ-THIOLATO)TRIPALLADIUM COMPLEX: CRYSTAL STRUCTURE OF *TRANS*-$Pd_3(\mu\text{-}SCy)_4Cl_2(PMe_3)_2$

ESTHER M. PADILLA and CRAIG M. JENSEN*

Department of Chemistry, University of Hawaii, Honolulu, HI 96822, U.S.A.

(*Received* 7 *June* 1990; *accepted* 28 *August* 1990)

Abstract—Reaction of excess cyclohexyl mercaptan with $[PdCl(PMe_3)\mu\text{-}Cl]_2$ (**1**) in refluxing chloroform produces the unusual tetrakis(μ-thiolato)tripalladium complex, $Pd_3(\mu\text{-}SCy)_4Cl_2(PMe_3)_2$ (**2**), rather than the more common (μ-thiolato)dipalladium complexes, $Pd_2(\mu\text{-}SCy)_2Cl_2(PMe_3)_2$ (**3**) or $Pd_2(\mu\text{-}SCy)(\mu\text{-}Cl)Cl_2(PMe_3)_2$ (**4**), which are obtained, respectively, from the reactions of **1** with excess and stoichiometric amounts of the thiol under ambient conditions. The molecular structure of **2**·$CHCl_3$ has been determined by single crystal X-ray crystallography. The coordination about each of the palladium centres is essentially square planar although the bond angles are severely distorted from an idealized geometry. The complex is non-planar with a Pd(1)—Pd(2)—Pd(3) angle of 132.2(1)°. In contrast to the *cis* configuration which is generally preferred by bis(μ-alkylthiolato)dipalladium complexes, the phosphine ligands are arranged in a *trans* configuration. The cyclohexyl groups of the μ-thiolate ligands which are situated *cis* about Pd(2) are in all cases in anti conformations. Crystallographic data for **2**: orthorhombic $P2_12_12_1$, $Z = 4$; $a = 11.027(4)$; $b = 11.230(6)$; $c = 12.676(6)$ Å; $V = 4621(3)$ Å^3.

There has been recent interest in diplatinum[1,2] and dipalladium[3] μ-thiolato complexes as homogeneous catalysts. A variety of dipalladium[4–7] and diplatinum[1,2,4,5,8] μ-alkylthiolato complexes have been prepared by the reaction of thiols with $[PdCl(PR_3)\mu\text{-}Cl]_2$ at ambient conditions. We have found that the reaction of excess cyclohexyl mercaptan (CySH) with $[PdCl(PMe_3)\mu\text{-}Cl]_2$ (**1**) in refluxing chloroform does not produce a bis(μ-thiolato)dipalladium complex, but rather the tetrakis(μ-thiolato)tripalladium complex, *trans*-$Pd_3(\mu\text{-}SCy)_4(PMe_3)_2Cl_2$(**2**). Although bis($\mu$-thiolate)dipalladium complexes have been known for nearly 40 years,[4] reports of the synthesis of tetrakis(μ-thiolato)tripalladium complexes are, to our knowledge, lacking. We wish to report the synthesis and the results of the X-ray structural determination of the tripalladium complex (**2**).

* Author to whom correspondence should be addressed.

EXPERIMENTAL

General details

The following were purchased from Aldrich Chemical Co. and used without further purification: cyclohexyl mercaptan, acetone (reagent-grade), chloroform (reagent-grade), chloroform-d_1 and dichloromethane-d_2. The complex $[PdCl(PMe_3)\mu\text{-}Cl]_2$ was prepared by the method of Chatt and Venanzi.[9]

The ^1H and $^{31}P\{^1H\}$ NMR spectra were recorded on a Nicolet NT300 spectrometer at 300 and 122 MHz, respectively. The ^1H NMR data are listed in ppm downfield from TMS at 0.00 ppm. ^{31}P NMR chemical shifts were measured relative to the deuterium resonance of the solvent by using the internal frequency lock of the spectrometer so that the resonance from a capillary of 85% H_3PO_4, centred in a 5 mm NMR tube containing the deuterated solvent, appeared at 0.0 ppm at 20°C. Microanalyses were

performed by Oneida Research Services Inc. (Whitesboro, New York).

Preparation of $Pd_3(\mu\text{-SCy})_4Cl_2(PMe_3)_2$ (**2**)

A solution of $[PdCl(PMe_3)\mu\text{-Cl}]_2$ (2.026 g, 4.00 mmol) and cyclohexyl mercaptan (1.65 cm^3, 13.49 mmol) in chloroform (150 cm^3) was refluxed for 30 min. The initial orange solution became green–yellow within 2 min. The resulting yellow crystalline product was isolated (2.124 g) by filtration from the reaction mixture. Reduction of the volume of the mother-liquor to 40 cm^3 resulted in the precipitation of an additional 0.3134 g of product (2.437 g combined yield, 91%). ^1H NMR (CD_2Cl_2): δ 3.18 m, 2.90 m, 2.36 m, 2.08 m, 1.69 m, 1.37 m, 1.18 m $S(C_6H_{11})$; 1.49 [d, J_{P-H} = 11 Hz, $P(CH_3)_3$]. $^{31}P\{^1H\}$ NMR ($CDCl_3$): δ −9.7 (s).

Preparation of $Pd_2(\mu\text{-SCy})_2Cl_2(PMe_3)_2$ (**3**)

The procedure involves variations of the synthesis of $Pd_2(\mu\text{-SEt})_2(PPr_3)_2Cl_2$ reported by Chatt and Hart.[4] A solution of $[PdCl(PMe_3)\mu\text{-Cl}]_2$ (0.508 g, 1.00 mmol) in acetone (50 cm^3) was treated at 25°C with cyclohexyl mercaptan (0.41 cm^3, 3.35 mmol). The initially orange solution became green–yellow within 2 min and was stirred at room temperature for 24 h. The resulting green–yellow crystalline product was isolated (0.440 g, 66%) by filtration from the reaction mixture. ^1H NMR (CD_2Cl_2): δ 3.18 m, 2.90 m, 2.38 m, 2.07 m, 1.67 m, 1.39 m, 1.18 m $S(C_6H_{11})$; 1.49 [d, J_{P-H} = 11 Hz, $P(CH_3)_3$]. $^{31}P\{^1H\}$ NMR ($CDCl_3$): δ −8.6 (s). Found: C, 32.2; H 5.6. Calc.: C, 32.4; H, 6.0%.

Preparation of $Pd_2(\mu\text{-SCy})(\mu\text{-Cl})Cl_2(PMe_3)_2$ (**4**)

The procedure involves variations of the synthesis of $Pd_2(\mu\text{-SEt})(\mu\text{-Cl})Cl_2(PPr_3)_2$ reported by Chatt and Hart.[4] A solution of $[PdCl(PMe_3)\mu\text{-Cl}]_2$ (0.414 g, 0.82 mmol) in acetone (50 cm^3) was treated at 25°C with cyclohexyl mercaptan (0.10 cm^3 0.82 mmol). The initial orange solution became yellow within 2 min and was stirred at room temperature for 24 h. The resulting green–yellow crystalline product (0.126 g) was isolated from the reaction mixture by filtration. Reduction of the volume of the mother-liquor to 5 cm^3 resulted in the precipitation of an additional 0.296 g of product (0.634 g combined yield, 87%). ^1H NMR (CD_2Cl_2): δ 3.50 m, 2.44 m, 1.78 m, 1.44 m, $S(C_6H_{11})$; 1.64 [d, J_{P-H} = 13 Hz, $P(CH_3)_3$]. $^{31}P\{^1H\}$ NMR ($CDCl_3$): δ 5.1 (s).

Crystallographic study

Crystals suitable for X-ray diffraction were obtained by slow evaporation of a chloroform solution of **2**. The crystal was mounted on a glass fibre with epoxy and centred on a Nicolet P3 automated diffractometer. The unit-cell parameters were obtained by least-square refinement of the setting angles of 20 reflections. Crystal and instrument stability were monitored with a set of three standard reflections measured every 97 reflections; no significant variations were found. Details of other crystal data and relevant information are summarized in Table 1.

The structure was solved by direct methods using SHELX PLUS computer programs (Nicolet Instrument Corp.) and refined by full-matrix least-squares procedures. All non-hydrogen atoms were refined with anisotropic coefficients. The hydrogen atoms were introduced in fixed calculated positions and the coordinates and isotropic thermal parameters for hydrogens were allowed to vary in the final cycles of full-matrix least-squares refinement. During the refinement, a group of peaks not associated with the palladium complex became apparent in the

Table 1. Summary of crystal and collection data for $Pd_3(\mu\text{-SCy})_4Cl_2(PMe_3)_2 \cdot CHCl_3$ (**2**·$CHCl_3$)

Formula	$Pd_3C_{31}H_{63}Cl_5P_2S_4$
fw	1122.4
Crystal dimensions (mm)	0.2 × 0.2 × 0.4
Crystal system	Orthorhombic
Space group	$P2_12_12_1$
a (Å)	11.027(4)
b (Å)	11.230(6)
c (Å)	12.676(6)
V (Å^3)	4621(3)
Z	4
$\rho_{calc.}$ (g cm^{-3})	1.614
λ (Å) (Mo-K_α radiation)	0.71073
Temperature (K)	295
Scan type	2θ–θ
Scan rate (° min^{-1})	1.5–15
2θ range (°)	4.0–55.0
μ (cm^{-1})	16.97
Transmission coefficient	0.373–0.540
Extinction correction (χ)	0.00025(5)
Reflections collected	6065
Unique data with $I > 3\sigma(I)$	5277
R^a (%)	3.60
$R_w{}^b$ (%)	6.14
Goodness of fit^c	0.77

$^a R = \Sigma||F_o| - |F_c||/\Sigma F_o$.
$^b R_w = [\Sigma w(|F_o| - |F_c|)^2/\Sigma w F_o{}^2]^{1/2}$.
^{c} GOF $= [\Sigma w(|F_o| - |F_c|)^2/(N_o - N_v)]^{1/2}$.

difference Fourier maps. The peaks were refined as a chloroform solvate.

Tables of the final fractional atomic coordinates and thermal parameters, as well as full lists of bond distances and angles for $2 \cdot CHCl_3$, have been deposited as supplementary material with the Editor.

RESULTS AND DISCUSSION

At ambient conditions the reaction of $[PdCl(PMe_3)\mu\text{-}Cl]_2$ (**1**) with cyclohexyl mercaptan with excess cyclohexyl mercaptan gives the expected bis(μ-thiolato) complex, $Pd_2(\mu\text{-}SCy)_2Cl_2(PMe_3)_2$ (**3**) while reaction with stoichiometric amounts of mercaptan gives $Pd_2(\mu\text{-}SCy)(\mu\text{-}Cl)Cl_2(PMe_3)_2$ (**4**). The trimetallic complex, *trans*-$Pd_3(\mu\text{-}SCy)_4Cl_2(PMe_3)_2$ (**2**) was obtained by refluxing chloroform solutions of **1** with excess cyclohexyl mercaptan for 30 min as shown in Scheme 1. The product was isolated upon filtration of the reaction mixture and an additional amount of **2** was obtained upon concentration of the mother-liquor (91% total yield). The approximately 2 : 1 ratio of the integrated intensities of the signals for thiolate cyclohexyl and phosphine methyl protons in the ^1H NMR spectrum of the sample in CD_2Cl_2 indicated that neither **3** nor **4** had been produced in this reaction. Complex **2** can also be distinguished from the dipalladium complexes **3** and **4** by ^{31}P NMR spectroscopy. The chemical shifts observed for the coordinated phosphorous of **2** and **3** in $CDCl_3$ solution of −9.7 and −8.6 ppm, respectively, are quite similar. However, the $^{31}P\{^1H\}$ NMR spectrum of a sample containing equal amounts of authentic samples of **2** and **3** in $CDCl_3$ solution contained baseline resolved signals for both complexes. The trimetallic nature of **2** became apparent only upon X-ray structural analysis.

Structure of $Pd_3(\mu\text{-}SCy)_4Cl_2(PMe_3)_2 \cdot CHCl_3$ ($2 \cdot CHCl_3$)

An ORTEP projection of the molecular structure of **2** is seen in Fig. 1. Selected bond distances and angles are presented in Table 2. The Pd(1)—Pd(2) and Pd(2)—Pd(3) distances of 3.234(2) and 3.230(2) Å, respectively, reflect the lack of bonding interactions between the palladium atoms. The coordination about each of the palladium centres is essentially square planar, although the bond angles are severely distorted from an idealized geometry to alleviate steric congestion of the cyclohexyl groups. The complex is non-planar with a Pd(1)—Pd(2)—Pd(3) angle of 132.2(1)° and dihedral angles between the coordination plane of Pd(2) and those of Pd(1) and Pd(3) of 130 and 131°, respectively. The $M_3(\mu\text{-}SR)_4$ core is very similar to that which

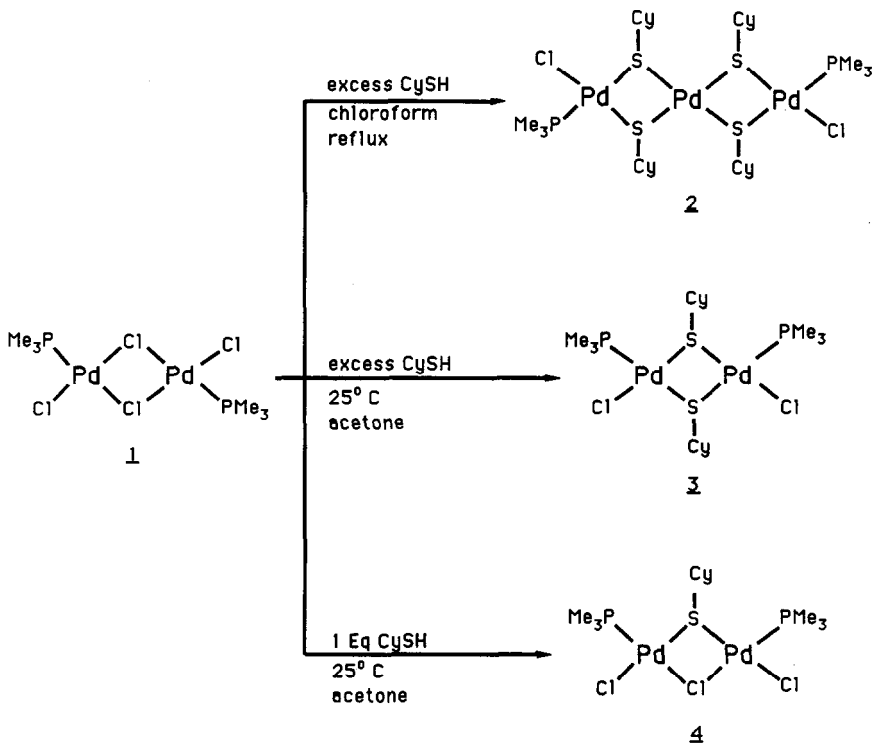

Scheme 1.

Table 2. Selected bond distances (Å) and angles (°) for $Pd_3(\mu\text{-}SCy)_4Cl_2(PMe_3)_2$ (**2**)

		Distances	
Pd(1)—S(1)	2.294(2)	Pd(2)—S(3)	2.318(2)
Pd(1)—S(2)	2.398(2)	Pd(2)—S(4)	2.339(2)
Pd(1)—P(1)	2.271(3)	Pd(3)—S(3)	2.400(2)
Pd(1)—Cl(1)	2.336(3)	Pd(3)—S(4)	2.295(2)
Pd(2)—S(1)	2.319(2)	Pd(3)—P(2)	2.264(3)
Pd(2)—S(2)	2.323(2)	Pd(3)—Cl(2)	2.337(3)
		Angles	
S(1)—Pd(1)—P(1)	93.8(1)	S(3)—Pd(2)—S(4)	81.4(1)
P(1)—Pd(1)—Cl(1)	86.9(1)	S(1)—Pd(2)—S(4)	178.2(1)
S(2)—Pd(1)—Cl(1)	99.1(1)	S(2)—Pd(2)—S(3)	178.2(1)
S(1)—Pd(1)—S(2)	80.2(1)	S(3)—Pd(3)—S(4)	80.6(1)
P(1)—Pd(1)—S(2)	174.0(1)	S(4)—Pd(3)—P(2)	93.1(1)
Cl(1)—Pd(1)—S(1)	179.3(1)	S(3)—Pd(3)—Cl(2)	99.7(1)
S(1)—Pd(2)—S(2)	81.3(1)	P(2)—Pd(3)—Cl(2)	86.6(1)
S(1)—Pd(2)—S(3)	97.6(1)	S(3)—Pd(3)—P(2)	173.7(1)
S(2)—Pd(2)—S(4)	99.7(1)	S(4)—Pd(3)—Cl(2)	178.3(1)

has been found[10] for $[Ni_3\{o\text{-}(SCH_2)_2C_6H_4\}_4]^{2-}$. Unlike bis($\mu$-alkylthiolato)dipalladium complexes in which *cis*-phosphine configurations are preferred,[4-6] the phosphine ligands in **2** are arranged in a *trans* configuration. The cyclohexyl groups of the μ-thiolate ligands which are situated *cis* about Pd(2) are in all cases in anti conformations.

In contrast to the large number of known dipalladium complexes, tripalladium complexes are quite rare. Several triangular clusters[11] as well as the linear cluster, $[Pd_3(MeNC)_6(PPh_3)_3]$[12] have been structurally characterized. Palladium acetate has been found[13] to be trimeric, consisting of a triangular arrangement of non-bonded palladium.

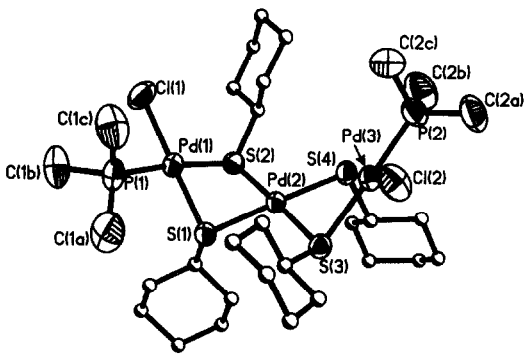

Fig. 1. ORTEP projection of $Pd_3(\mu\text{-}SCy)_4Cl_2(PMe_3)_2$ (**2**), thermal ellipsoids at 50% probability except for the cyclohexyl carbons which are shown as spheres of arbitrary radius. The hydrogen atoms have been omitted for clarity.

The structures of both $Pd_3[\eta^3\text{-}1,3\text{-di(pyvaloyl)allyl}]_2(\mu,\eta^2\text{-acetate})_4$[14] and $Pd_3[1\text{-}3\eta^3\text{-}6\text{-}(\alpha\text{-chloroethyl})\text{cyclooctenyl}]_2Cl_4$[15] have been found to be linear tripalladium complexes, which like **2** contain four bridging ligands and palladium atoms at non-bonding distances. However, $[Pd_3\{\eta^3\text{-}1,2,3\text{-tri}(p\text{-methoxyphenyl})\text{allyl}\}_2(acac)_2]$[16] and $Pd_3(\eta^3\text{-}2\text{-methylallyl})_2Cl_4$[17] are the only other examples of structurally characterized non-planar tripalladium complexes of which we are aware. In the case of the allyl complexes, it is believed[15] that the bent structures may result from crystal packing forces rather than steric interactions, as appears to be the case with **2**. Bent trimetallic structures have also been proposed for $Pd_3(\mu\text{-}PPh_2)_2(\mu\text{-}Cl)_2Cl_2(PPh_3)_2$[18] and $[NEt_4]_2[Pd_3(\mu\text{-}Cl)_4(C_6F_5)_4]$.[19]

In view of the wide variety of palladium[4-6] and platinum[1,4,5,8] $M_2(\mu\text{-}SR)_2(PR_3)_2Cl_2$ complexes which have been synthesized from the reaction of $M_2(\mu\text{-}Cl)_2(PR_3)_2Cl_2$ with thiols, it is surprising that there have been no prior reports of the isolation of $M_3(\mu\text{-}SR)_4(PR_3)_2Cl_2$ complexes. The rarity of these complexes has been somewhat clarified by our examination of the reaction of **1** with other thiols in refluxing chloroform. We have found the formation of trimetallic complexes to be surprisingly sensitive to the alkyl group of the thiol. For example, the exclusive product of the reaction of **1** with t-butyl mercaptan in refluxing chloroform is the structurally characterized[7] dimetallic complex, $Pd_2(\mu\text{-S-}t\text{-Bu})(\mu\text{-Cl})Cl_2(PMe_3)_2$.

Acknowledgements—We thank the University of Hawaii Research Council for the support of this research. The

assistance of Professor R. E. Cramer in the X-ray diffraction studies is gratefully acknowledged.

REFERENCES

1. H. C. Clark, V. K. Jain and G. S. Rao, *J. Organomet. Chem.* 1985, **279**, 181.
2. V. K. Jain and G. S. Rao, *Inorg. Chim. Acta* 1987, **127**, 161.
3. E. M. Padilla and C. M. Jensen, manuscript in preparation.
4. J. Chatt and F. A. Hart, *J. Chem. Soc.* 1953, 2363.
5. P. L. Goggin, R. J. Goodfellow and F. J. S. Reed, *J. Chem. Soc. A* 1971, 2031.
6. (a) V. K. Jain, *Inorg. Chim. Acta* 1987, **133**, 261; (b) V. K. Jain, R. P. Patel, K. V. Muralidharan and R. Bohra, *Polyhedron* 1989, **8**, 2151.
7. E. M. Padilla, P. N. Richmann, J. A. Golen and C. M. Jensen, *Polyhedron*, submitted.
8. (a) J. Chatt and F. A. Hart, *J. Chem. Soc.* 1960, 2807; (b) M. P. Brown, R. J. Puddephatt and C. E. E. Upton, *J. Chem. Soc., Dalton Trans.* 1976, 2490.
9. J. Chatt and L. M. Venanzi, *J. Chem. Soc.* 1957, 2351.
10. W. Tremel, B. Krebs and G. Henkel, *Angew. Chem. Int. Ed. Engl.* 1984, **23**, 634.
11. (a) E. M. McPartlin and N. C. Stephenson, *Acta Cryst.* 1969, **B25**, 1659; (b) S. Otsuka, Y. Tatsuno, M. Miki, M. Aoki, M. Matsumoto, H. Yasioka and K. Nakatsu, *J. Chem. Soc., Chem. Commun.* 1973, 445; (c) J. P. Fackler and W. J. Zegarski, *J. Am. Chem. Soc.* 1973, **95**, 8566; (d) G. W. Bushnell, K. R. Dixon, P. M. Moroney, A. D. Rattray and C. Wan, *J. Chem. Soc., Chem. Commun.* 1977, 709; (e) C. G. Francis, S. I. Khan and P. R. Morton, *Inorg. Chem.* 1984, **23**, 3680.
12. A. L. Balch, J. R. Boehm, H. Hope and M. M. Olmstead, *J. Am. Chem. Soc.* 1976, **98**, 1431.
13. A. C. Skapski and M. L. Smart, *J. Chem. Soc., Chem. Commun.* 1970, 658.
14. L. Y. Ukhin, N. A. Dolgopolova, L. G. Kuz'mina and Y. T. Struchkov, *J. Organomet. Chem.* 1981, **210**, 263.
15. M. Parra-Hake, M. F. Rettig and R. M. Wing, *Organometallics* 1983, **2**, 1013.
16. P. M. Bailey, A. Keasey and P. M. Maitlis, *J. Chem. Soc., Dalton Trans.* 1978, 1825.
17. P. M. Bailey, E. Kelly and P. M. Maitlis, *J. Organomet. Chem.* 1978, **144**, C52.
18. S. J. Cartwright, K. R. Dixon and A. D. Rattray, *Inorg. Chem.* 1980, **19**, 1120.
19. R. Uson, J. Fornies, M. Tomas, B. Menjon, J. Carnicer and A. J. Welch, *J. Chem. Soc., Dalton Trans.* 1990, 151.

Polyhedron Vol. 10, No. 1, pp. 95–99, 1991
Printed in Great Britain

0277–5387/91 $3.00+.00
© 1991 Pergamon Press plc

NEUTRAL COMPLEXES OF GALLIUM DI-IODIDE CONTAINING Ga—Ga BONDS

JOHN C. BEAMISH, ALAN BOARDMAN* and IAN J. WORRALL

Department of Chemistry, The University, Lancaster LA1 4YA, U.K.

(*Received* 23 *April* 1990; *accepted* 29 *August* 1990)

Abstract—The complexes $Ga_2I_4 \cdot 2L$ (L = pyridine, 2-methylpyridine, 3-methylpyridine, 4-methylpyridine, morpholine, N-methylmorpholine, 1,4-dioxan, tetrahydrofuran, tetrahydropyran, dimethylsulphide, diethylsulphide, tetrahydrothiophene, 1,4-thioxan, 1,4-dithiane and tetramethylbiphosphine) have been prepared. Vibrational spectra indicate that the complexes adopt disubstituted ethane-like structures containing Ga—Ga bonds. We were unable to synthesize complexes of stoichiometry $Ga_2I_4 \cdot 4L$ which had previously been reported.

Brewer *et al.*[1–3] were first to isolate coordination compounds of the ionic gallium dihalides, $Ga^+GaX_4^-$ (X = Cl, Br, I). Complexes of structure $GaL_2^+GaX_4^-$ for ligands with two donor atoms, and $GaL_4^+GaX_4^-$ for monodentate ligands were proposed, mainly from analytical and electrical conductivity data. By using many of the monodentate and potentially bidentate ligands originally chosen by Brewer *et al.*, we have prepared numerous complexes of one stoichiometry only, $Ga_2X_4 \cdot 2L$ (X = Cl, Br).[4] Ga—Ga bonded, ethane-like structures were proposed from spectroscopic studies, later confirmed by crystallographic investigations of $Ga_2X_4 \cdot 2diox$[5,6] and $Ga_2X_4 \cdot 2py$.[4,7] Given the difference between Brewer's conclusions and our recent studies, a re-investigation of the chemistry of Ga_2I_4 seemed necessary.

EXPERIMENTAL

Since Ga_2I_4 and its complexes are moisture-sensitive, all reactions were carried out in a nitrogen-filled glove box, or on a vacuum line. Ga_2I_4 was prepared by shaking, in warm water, a sealed pre-evacuated tube containing benzene, gallium and iodine, until all the metal had reacted.[8] All ligands were rigorously dried and purified before use. Raman spectra (40–3500 cm^{-1}) were obtained on a Carey model 81L spectrometer, using the 4880 and 5145 Å lines. IR spectra (200–3500 cm^{-1}) were recorded using a Nicolet MX-1 machine. Reliable IR data were obtained for few complexes, since many discoloured when ground with sodium-dried Nujol. Gallium was determined by atomic absorption analysis and iodine by the Volhard method.

Attempts to repeat Brewer's work by using his experimental methods have been largely unsuccessful.[9,10] Brewer's methods involve slow addition of a benzene solution of ligand to a benzene solution of Ga_2I_4 and, for volatile ligands, prolonged attack of vapour on Ga_2I_4–benzene solutions. Such reactions were performed at ambient temperature. In this work, closely related or identical ligands were deliberately chosen in an attempt to repeat the Brewer studies. The former method gave satisfactory complexes with diox, morph and DMS, other ligands producing Ga and GaI_3 adducts. These complexes were identified as Ga—Ga bonded $Ga_2I_4 \cdot 2L$ species, by chemical and spectral analysis. The latter method resulted in decomposition of Ga_2I_4 to Ga, such reactions not proceeding further. Our successful synthetic routes require direct reaction of the ligand with frozen Ga_2I_4, or ligand replacement reactions. We were unable to isolate Ga_2I_4 adducts with acetylacetone and anisole, two ligands successfully used by Brewer *et al.*[3]

* Author to whom correspondence should be addressed. Present address: Johnson Matthey Technology Centre, Blount's Court Road, Sonning Common, Reading RG4 9NH, U.K.

Synthesis of $Ga_2I_4 \cdot 2L$ (L = *1,4-dioxane, tetrahydrofuran, tetrahydropyran, morpholine,* N*-methylmorpholine, dimethylsulphide, diethylsulphide, tetrahydrothiophene,* 1,4*-thioxan and tetramethylbiphosphine*)

Ga_2I_4 was cooled to liquid nitrogen temperature and excess dry ligand condensed on *in vacuo*. The temperature was slowly allowed to rise to the ligand's melting point and the resultant slurry rapidly stirred. A colourless solution soon formed, and the excess ligand was then slowly removed to reveal colourless, crystalline solids, which dried to chalky white powders. An exception, the tetramethylbiphosphide adduct, formed as an oil, which partially solidified with age. It was not analysed because of its inflammability.

Synthesis of $Ga_2I_4 \cdot 2L$ (L = *pyridine,* 2*-methylpyridine,* 3*-methylpyridine and* 4*-methylpyridine*)

These adducts could not be isolated in a pure form by the above method. They could be easily prepared from O- and S-donor complexes by ligand replacement reactions. Excess ligand was condensed onto liquid nirogen-cooled $Ga_2I_4 \cdot 2$diox, *in vacuo*, and the temperature allowed to rise to the melting point of the ligand. The resulting slurry was stirred until a clear solution formed. Excess solvent was removed under a vacuum, and the white powder which precipitated, dried.

Unlike chloride and bromide analogues, $Ga_2I_4 \cdot 2$diox solutions were sensitive to prolonged standing under warm conditions, or rapid warming, producing Ga and $(GaI_3 \cdot \text{diox}) \cdot 2$diox. Our unpublished crystallographic studies on $(MI_3 \cdot \text{diox}) \cdot 2$diox (M = Ga, In) show the geometry around the five coordinate metal to be trigonal bipyramidal, with bridging dioxan chairs binding the MI_3 units together in an infinite polymer. Two rows of interstitial dioxan molecules, easily removed by vacuum pumping, lie disordered between the polymer chains. Because of its rapid and easy preparation, $Ga_2I_4 \cdot 2$DMS was found to be a more suitable precursor. Its solutions were stable to rapid warming and the volatile ligand could be quickly removed. By simply dissolving uncooled $Ga_2I_4 \cdot 2$DMS in warm pyridine, or methylpyridine, large diamond-shaped crystals of $Ga_2I_4 \cdot 2L$ (L = py, 3-Mepy, 4-Mepy) were deposited on cooling, whereas $Ga_2I_4 \cdot 2$(2-Mepy) gave fine oval-shaped needles.

Crystallographic studies on these complexes were unsuccessful, due to sample deterioration. Even when stored in the absence of light, all colourless crystals slowly turned dark orange.

Synthesis of $Ga_2I_4 \cdot 2$dithiane

A dilute solution of dry dithiane in CS_2 was added dropwise to a stirred suspension of Ga_2I_4 in CS_2. The first drops caused a blood-red coloration, which slowly turned orange and then yellow. Further addition caused this colour sequence to be repeated, until all the dithiane had been added. The insoluble yellow precipitate formed was recovered, washed with CS_2, and dried to a lemon powder *in vacuo*.

DISCUSSION

Structure of complexes; chemical evidence

Our analytical data (Table 1) shows the isolation of complexes of stoichiometry $Ga_2I_4 \cdot 2L$, regardless of the donor atom involved, or the number of donor atoms on the ligand. This conflicts with Brewer's results, where the availability of donor atoms on the ligand influences the stoichiometry of the resultant complex. Thus, monodentate O-, N- and S-donors produce 1 : 4 complexes, whereas bidentate ligands chelate to give 1 : 2 complexes.

Electrical conductivity measurements, obtained by Brewer *et al.*, from solutions of Ga_2X_4 complexes, provide the main evidence for their ionic formulations. Our conclusions are largely based on solid-state spectroscopic data, and we have not studied the structure of complexes in solution.

It should be noted that complexes of 1 : 2 and 1 : 4 stoichiometry are known for closely related In_2X_4 (X = Cl, Br, I),[11,12] but that mixed species $InGaX_4$ (X = Cl, Br)[13] give only 1 : 2 complexes.

Table 1. Analytical data

Compound	Found (Calc.) (%) Ga	I
$Ga_2I_4 \cdot 2$pyridine	17.3 (17.3)	63.0 (63.1)
$Ga_2I_4 \cdot 2$(2-methylpyridine)	16.5 (16.7)	60.5 (60.9)
$Ga_2I_4 \cdot 2$(3-methylpyridine)	16.5 (16.7)	60.4 (60.9)
$Ga_2I_4 \cdot 2$(4-methylpyridine)	16.5 (16.7)	60.5 (60.9)
$Ga_2I_4 \cdot 2$morpholine	17.0 (17.0)	61.5 (61.8)
$Ga_2I_4 \cdot 2$(NMe-morpholine)	16.7 (16.4)	60.7 (59.8)
$Ga_2I_4 \cdot 2$dimethylsulphide	17.8 (18.1)	65.8 (65.8)
$Ga_2I_4 \cdot 2$diethylsulphide	16.7 (16.8)	61.7 (61.4)
$Ga_2I_4 \cdot 2$tetrahydrothiophene	17.4 (16.9)	61.0 (61.7)
$Ga_2I_4 \cdot 2$dithiane	16.1 (15.7)	57.8 (57.2)
$Ga_2I_4 \cdot 2$thioxan	16.3 (16.3)	58.9 (59.4)
$Ga_2I_4 \cdot 2$dioxan	16.9 (16.9)	61.3 (61.7)
$Ga_2I_4 \cdot 2$tetrahydrofuran	17.6 (17.6)	64.0 (64.2)
$Ga_2I_4 \cdot 2$tetrahydropyran	17.2 (17.0)	62.5 (62.0)

Vibrational spectroscopy indicates that these materials are covalent, with metal–metal bonds. Such conclusions have been crystallographically confirmed for $In_2Br_3I \cdot 2tmed$ (tmed = N,N,N^1,N^1-tetramethylethanediamine), which comprises two X_2(tmed)In units joined by an In—In bond giving favoured five-coordinate indium.[14] A similar structure is proposed for $Ga_2I_4 \cdot 2L$ complexes, with GaI_2L units linked by a Ga—Ga bond giving favoured four-coordinate gallium. This structure can be substantiated by chemical evidence, which suggests that in ligand replacement reactions the Ga—Ga bond is retained. Firstly, the reaction of $Ga_2I_4 \cdot 2diox$ with $Me_4N^+I^-$ readily proceeds giving $(Me_4N)_2Ga_2I_6$, a well-characterized Ga—Ga bonded compound.[15] Secondly, reaction of $Ga_2I_4 \cdot 2diox$ with excess pyridine, or methylpyridine, gives complexes in which the 1 : 2 stoichiometry is retained, i.e. $Ga_2I_4 \cdot 2py$. If $Ga_2I_4 \cdot 2diox$ consisted of Brewer's ionic structure $Ga(diox)_2^+GaI_4^-$, then bidentate dioxan should have been displaced by four pyridines giving $Ga(py)_4^+GaI_4^-$. Since this definitely does not occur, it leads to a rejection of the Brewer structures in the solid state.

Structure of complexes; spectral evidence

Our structural diagnosis heavily depends on Raman spectroscopy, which has previously been successful in distinguishing between gallium iodides containing GaI_4^- anions, and those with Ga—Ga bonds.[16] We have previously discussed the similar spectral pattern exhibited by $Ga_2X_4 \cdot 2L$ (X = Cl, Br) complexes and $Ga_2X_6^{2-}$ anions in terms of their mutual Ga—Ga bonded, ethane-like structure.[4] We can now confirm that this spectral likeness is extendable, to a lesser degree, to analogous iodide species. Crystallographic studies, confirming the close structural relationship, exist for $Ga_2X_4 \cdot 2L$ (X = Cl, Br; L = diox, py),[4–7] $(Me_4N)_2Ga_2Cl_6$[17] and $(n\text{-}Pr_4N)_2Ga_2Br_6$,[18] whereas $(Ph_3PH)_2Ga_2I_6$ is known to be isomorphous with its chloride counterpart.[19] Detailed spectral assignments exist for $Ga_2X_6^{2-}$ (X = Cl, Br, I),[15,20] and their spectra are very different to those of GaX_4^-.[21–23] In particular, their Raman spectra each contain an intense band, which has been assigned to a totally symmetric mode, in which the Ga—Ga bond stretches in phase with Ga—X bonds. This dominant band has been used to identify Ga—Ga bonds in new gallium compounds.[4]

In all $Ga_2I_4 \cdot 2L$ spectra, normally two Raman-active ν(Ga—I) bands could be identified, appearing in the ranges 207–239 and 294–317 cm^{-1}. They were distinguished by comparison amongst $Ga_2X_4 \cdot 2L$ (X = Cl, Br, I) spectra, and by their similar position and intensity within the di-iodide series (Table 2).

Generally, for $Ga_2I_4 \cdot 2L$ spectra, Raman bands at low values, e.g. $Ga_2I_4 \cdot 2diox$ (93m, 141vs, 226w, 239w, *302w* cm^{-1}) and $Ga_2I_4 \cdot 2THP$ (47s, 56sh, 87s, 141vs, 226m, *302w* cm^{-1}) show some resemblance to those found in $Ga^+(GaI_4)^-$ (52m, 85m, 142vs, 214vw, 235vw cm^{-1}),[16] and $H^+GaI_4^-$ (52m, 73m, 145vs, 222w cm^{-1}).[22] This suggests a possible ionic structure for the complexes, as proposed by Brewer *et al.*, i.e. $GaL_4^+GaI_4^-$ and $GaB_2^+GaI_4^-$, where L and B are monodentate and bidentate ligands, respectively.[3] However, this ionic formulation fails to account for the full distribution of bands in $Ga_2I_4 \cdot 2L$ complexes. Notable discrepancies include bands around 150–190 cm^{-1} in most N- and S-donor adducts, but more importantly, the constant appearance of a ν(Ga—I) band near 300 cm^{-1} in all complexes. This band displays close positional similarity to the highest ν(Ga—I) assignment at 285 cm^{-1} in $Ga_2I_6^{2-}$ and in the Ga—Ga bonded iodides Ga_3I_5 and Ga_4I_6, which contain this anion.[16]

Rejection of the presence of GaI_4^- and the Brewer formulation, in favour of a Ga—Ga bonded structure, requires the intense band, around 140 cm^{-1} in the complexes, to be attributed to ν(Ga—Ga). This is entirely plausible. The shift of the strong ν(Ga—Ga) mode from 118 cm^{-1} in heavy $Ga_2I_6^{2-}$ to higher values in the lighter $Ga_2I_4 \cdot 2L$ complexes is not surprising in view of Tan and Taylor's work[23] on the mixed species $Ga_2X_nY_{6-n}^{2-}$ (X and Y are different halogens: n = 0–6). In these anions the position of the strong ν(Ga—Ga) band changes appreciably with halide ion replacement. To a large extent this is associated with mass change. For the anions $Ga_2I_4Br_2^{2-}$ and $Ga_2I_4Cl_2^{2-}$, the ν(Ga—Ga) mode has been assigned at 131 and 145 cm^{-1}, respectively.[23] This compares favourably with the proposed ν(Ga—Ga) assignment in $Ga_2I_4 \cdot 2L$.

Impressive comparisons are provided by $Ga_2I_4 \cdot 2L$ (L = 2-Mepy, 3-Mepy), which display intense bands at 135 and 132 cm^{-1}, respectively, and have a similar mass to $Ga_2I_4Br_2^{2-}$. A similar situation occurs for ν(Ga—I) modes. As the total mass of anion decreases, the ν(Ga—I) bands move to higher values to give a better correlation with $Ga_2I_4 \cdot 2L$ complexes. However, slight discrepancies may be anticipated, due to differences in mixing of modes in the complexes and associated anions.

The spectra of some coordinated ligands provide further evidence untenable with the Brewer ionic structure. Ligand spectra of $Ga_2I_4 \cdot 2diox$ indicate the absence of chelating boat-form dioxan,[2] as

Table 2. Vibrational spectra of $Ga_2I_4 \cdot 2L$ in the ranges 200–400 cm^{-1} (IR) and 100–400 cm^{-1} (R)[a]

L		ν(Ga—Ga)	ν(Ga—I)	ν(Ga—L)	δ(Ga—Ga—L)	Internal ligand mode
THF	R	143vs	229m 308w			
THP	R	141vs	226m 302w			
Diox	R	141vs	226w 239w 302w			
Dt	R	145vs	222m 296m	286m		340vw 374vw
Thiox	R	142vs	223m 297m	243w	185w	372vw 397vw
DMS	R	142vs	216w 225w 299w	260w	185w	285w
	IR		226s	260s		285m
THT	R	140s	222m 317w	246w		
	IR		227s	276m		
DES	R	135vs	222m 294w			
Py	R	143vs	216m 316m	226sh	187m	
	IR		227s	238s		
2-Mepy	R	135vs	209m 302m		156w	
3-Mepy	R	132vs	216m 300w	226sh	157m	
4-Mepy	R	136vs	207m 303m		168m	
Morph	R	141s	283w		172w	
N-Memorph	R	134s	214m 298w		172m	
Me_4P_2	R	135s	239m 294w	331w	176m	
$(Ga_2I_4Br_2)^{2-}$	R	131s				
$(Ga_2I_4Cl_2)^{2-}$	R	145s				
$(Ga_2I_6)^{2-}$	R	118vs	184m 285s			
	IR		155s 200vs			

[a] R, Raman; IR, infrared; THF, tetrahydrofuran; THP, tetrahydropyran; Diox, 1,4-dioxane; Dt, 1,4-dithiane; Thiox, 1,4-thioxane; DMS, dimethylsulphide; DES, diethylsulphide; THT, tetrahydrothiophene; Py, pyridine; *n*-Mepy, *n*-methylpyridine ($n = 2, 3, 4$); Morph, morpholine; N-Memorph, N-methylmorpholine; vs, very strong; s, strong; m, medium; w, weak; vw, very weak; sh, shoulder.

required for $Ga(diox)_2^+$, and the presence of monodentately attached dioxan chairs. Bands assignable to both free and coordinated ν(C—O) modes are observed for all Ga_2X_4 dioxanates. The loss of free dioxan's centrosymmetric structure when monodentately linked[24] leads to a number of its bands becoming both IR- and Raman-active in the complexes, e.g. 616, 870 and 1256 cm^{-1}.

Other potentially bidentate or chelating ligands are also attached in a monodentate fashion. $Ga_2I_4 \cdot$ 2thiox gives sharp IR- and Raman-active bands at 826 and 1100 cm^{-1}, due to ν(C—O) bands, which remain at their free ligand values, whereas ν(C—S) bands at 648 and 685 cm^{-1} are lowered by coordination from 665 and 692 cm^{-1} in liquid thioxan.[25] Ir- and Raman-active ν(N—H) bands at 3336 and 3298 cm^{-1} in morpholine[26] are replaced by a single band at 3268 cm^{-1} in $Ga_2I_4 \cdot$ 2morph, unlike bands in the ν(C—O) region near 1100 cm^{-1} which do not shift.

Comparison of Raman data for S-donor complexes of Ga_2I_4 allows a tentative ν(Ga—L) assignment to bands in the 240–290 cm^{-1} region, but for complexes with pyridine-type ligands a ν(Ga—L) Raman assignment is restricted to shouldering near 226 cm^{-1}. This weak band is mainly concealed by the strong ν(Ga—Ga) emission, but is more discernable in other halide analogues. A strong IR

band at 227 cm^{-1}, noted only in $Ga_2I_4 \cdot 2L$ complexes, is assigned to ν(Ga—I), leaving bands at 238(py), 260(DMS) and 276(THT) cm^{-1} as ν(Ga—L) candidates. Bands arising from Ga—O bonds are expected in the range 400–550 cm^{-1} but are weak, broad and often not observed.[27,28] Since many of the ligands used have bands in this region no reliable assignment could be made. Raman bands in the 157–187 cm^{-1} range are tentatively assigned to Ga—Ga—L bends because of the small degree of positional change noticed in pyridine and methylpyridine adducts and their general dependence on the type of ligand present. Bands of similar appearance, with slightly higher values, are observed in chloride and bromide counterparts.[10] Bands below 400 cm^{-1}, arising from internal ligand modes, are observed at their free ligand values although the Raman band of methylpyridines at 210 cm^{-1} is probably masked by the stronger ν(Ga—I) emission.

Crystallographic studies have so far determined two configurations of the ethane-like $Ga_2X_4 \cdot 2L$ structure. $Ga_2X_4 \cdot 2py$ (X = Cl, Br) adopt the *trans* (C_{2h}) conformation, and $Ga_2X_4 \cdot 2diox$ (X = Cl, Br) possess a less symmetric, staggered (C_i) structure. Vibrational spectroscopy should distinguish between *trans* and lower symmetry structures, since for the former, mutual exclusion should be operative.[29] Although, we could not practically confirm this for most complexes, the simple spectral behaviour of $Ga_2I_4 \cdot 2L$ (L = py, Mepy) is indicative of the *trans* conformation, whereas $Ga_2I_4 \cdot 2L$ (L = diox, DMS) seem likely to have structures of lower symmetry, a consequence of their more complicated spectra. This has recently been confirmed by Japanese workers,[30] who have studied the NQR spectra of $Ga_2X_4 \cdot 2diox$ (X = Cl, Br, I) and have concluded the iodide complex adopts the staggered (C_i) structure at room temperature. They have also observed a temperature-dependent conformational change for $Ga_2Cl_4 \cdot 2diox$.

REFERENCES

1. S. M. Ali, F. M. Brewer, J. Chadwick and G. Garton, *J. Inorg. Nucl. Chem.* 1959, **9**, 124.
2. F. M. Brewer, J. R. Chadwick and G. Garton, *J. Inorg. Nucl. Chem.* 1961, **23**, 45.
3. F. M. Brewer, G. S. Reddy and P. L. Goggin, *J. Indian Chem. Soc.* 1967, **44**, 179.
4. J. C. Beamish, A. Boardman, R. W. H. Small and I. J. Worrall, *Polyhedron* 1985, **4**, 983.
5. J. C. Beamish, R. W. H. Small and I. J. Worrall, *Inorg. Chem.* 1979, **18**, 220.
6. R. W. H. Small and I. J. Worrall, *Acta Cryst.* 1982, **B38**, 250.
7. R. W. H. Small and I. J. Worrall, *Acta Cryst.* 1982, **B38**, 86.
8. J. C. Beamish, M. Wilkinson and I. J. Worrall, *Inorg. Chem.* 1978, **17**, 2026.
9. J. C. Beamish, PhD thesis. University of Lancaster, England (1984).
10. A. Boardman, PhD thesis. University of Lancaster, England (1984).
11. I. Sinclair and I. J. Worrall, *Can. J. Chem.* 1982, **60**, 695.
12. M. J. Taylor, D. G. Tuck and L. Victoriano, *Can. J. Chem.* 1982, **60**, 690.
13. I. Sinclair and I. J. Worrall, *Inorg. Nucl. Chem. Lett.* 1981, **17**, 279.
14. M. A. Khan, C. Peppe and D. G. Tuck, *Can. J. Chem.* 1984, **62**, 601.
15. C. A. Evans, K. H. Tan, S. P. Tapper and M. J. Taylor, *J. Chem. Soc., Dalton Trans.* 1973, 988.
16. L. G. Waterworth and I. J. Worrall, *J. Inorg. Nucl. Chem.* 1973, **35**, 1535.
17. K. L. Brown and D. Hall, *J. Chem. Soc., Dalton Trans.* 1973, 1843.
18. H. J. Cumming, D. Hall and C. E. Wright, *Cryst. Struct. Commun.* 1974, **3**, 107.
19. M. Khan, C. Oldman, M. J. Taylor and D. G. Tuck, *Inorg. Nucl. Chem. Lett.* 1980, **16**, 469.
20. C. A. Evans and M. J. Taylor, *J. Chem. Soc., Chem. Commun.* 1969, 1201.
21. L. A. Woodward and A. A. Nord, *J. Chem. Soc.* 1956, 2655 and 3721.
22. L. A. Woodward and G. H. Singer, *J. Chem. Soc.* 1958, 716.
23. K. H. Tan and M. J. Taylor, *Inorg. Nucl. Chem. Lett.* 1974, **10**, 267.
24. G. W. A. Fowles and W. F. Tidmarsh, *Inorg. Chem.* 1969, **8**, 631.
25. O. H. Ellestad, P. Klaboe and K. Hagan, *Spectrochim. Acta* 1972, **28A**, 137.
26. D. Vedal, O. H. Ellestead, P. Klaboe and K. Hagen, *Spectrochim. Acta* 1976, **32A**, 877.
27. M. T. Bories, J. Roziere, A. Manteghetti and A. Potter, *Can. J. Chem.* 1974, **52**, 3274.
28. A. J. Carty, H. A. Patel and P. M. Boorman, *Can. J. Chem.* 1970, **48**, 492.
29. J. D. Odom, V. F. Kalasinsky and J. R. Durig, *Inorg. Chem.* 1975, **14**, 434.
30. T. Okuda, M. Sato, H. Hamamoto, H. Ishihara, K. Yamada and S. Ichiba, *Inorg. Chem.* 1988, **27**, 3656.

Polyhedron Vol. 10, No. 1, pp. 103–106, 1991
Printed in Great Britain

0277–5387/91 $3.00+.00
© 1991 Pergamon Press plc

SYNTHESIS, CHARACTERIZATION AND MAGNETIC PROPERTIES OF SEVERAL COPPER(II)–NICKEL(II) HETERODINUCLEAR OXAMIDO COMPLEXES

JUAN RIBAS,* AUXILIADORA GARCIA and MONTSERRAT MONFORT

Departament de Química Inorgànica, Universitat de Barcelona, Diagonal 647, 08028-Barcelona, Spain

(*Received* 5 *April* 1990; *accepted* 29 *August* 1990)

Abstract—Seven new heterodinuclear copper(II)–nickel(II) complexes, have been synthesized from the planar monomeric fragment Cu(oxpn) (oxpn = N,N′-bis(3-aminopropyl)oxamido and its 2,2′-dimethyl derivative) and characterized. Magnetic measurements between 4 K and room temperature have been carried out to study the magnetic coupling between the two paramagnetic ions. The J values thus calculated indicate a strong antiferromagnetic coupling in all cases ($J = -104$ to -115 cm^{-1}), in accordance with the nature of the oxamido group. The average isotropic g values occur over a range of 2.09–2.25. The EPR spectra at room temperature confirm these values. All the complexes are soluble in most common organic solvents, but attempts to obtain single crystals suitable for X-ray structure determination have so far been unsuccessful.

The field of heteropolymetallic systems with two different paramagnetic centres is very important from both biological and physical aspects. The copper–iron site in cytochrome oxidase is a good example of the first type;[1] the intramolecular ferrimagnetism which can be extended in a 3D array to achieve molecular ferromagnets, is an example of the second, corresponding to the design of new magnetic materials.[2] Very recently, Kahn[3] has reviewed this kind of complex and clearly indicates that accurate magnetic data on heteropolymetallic systems is much less extensive than with homopolymetallic complexes.

The copper(II)–nickel(II) complexes with the local spins $S_{Cu} = 1/2$ and $S_{Ni} = 1$, represent one of the most comprehensive examples of heterobimetallic systems.[3–8] Very recently,[9] starting from propylene-1,3-bis(oxamato)cuprate(II) we have synthesized the first fully characterized Ni—Cu—Ni trinuclear complex, in which both terminal nickel(II) ions were blocked with bis(3-aminopropyl)amine. During the synthesis, it was possible to synthesize and characterize the corresponding Cu—Ni dinuclear complex, in which $J = -94.6$ cm^{-1}, $g_{Cu} = 2.02$ and $g_{Ni} = 2.24$. To avoid the possibility of forming trinuclear species, we decided to start from Cu(oxpn) (**I**), where oxpn is N,N′-bis(3-aminopropyl)oxamido, and its 2-hydroxy (**II**) or 2,2′-dimethyl (**III**) derivatives.

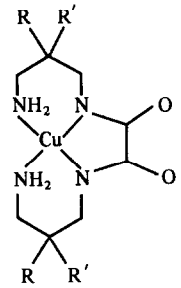

(**I**) R = R′ = H

(**II**) R = H; R′ = OH

(**III**) R = R′ = CH_3

With Cu(oxpn) Ojima and Nonoyama[10] synthesized the complex $[Cu(oxpn)Ni(bipy)_2](NO_3)_2 \cdot 2H_2O$, the magnetism and EPR spectra of which were studied by Journaux *et al.*[11] In this work, four new $[Cu(oxpn)Ni(ligand)](ClO_4)_2$ and three new $[Cu(Me_2oxpn)Ni(ligand)](ClO_4)_2$ complexes, in which the terminal nickel(II) ion is blocked with

* Author to whom correspondence should be addressed.

2,2-bipyridine (bipy), 1,10-phenanthroline (phen), 1,4,8,11-tetraazacyclotetradecane (cyclam) and 1,3-diaminopropane (tmd) have been synthesized. All attempts to start from [Cu(2-OHoxpn)] derivatives were unsuccessful, only the starting materials being obtained.

EXPERIMENTAL

Synthesis of starting mononuclear copper(II) complexes

Cu(oxpn) was obtained by the literature method.[12,13] Its dimethyl derivative [Cu(Me_2oxpn)] was obtained by the same procedure starting from 2,2′-dimethyl-1,3-diaminopropane (Fluka, without purification). The red products so formed were very soluble in water and insoluble in common organic solvents. They can be recrystallized from hot water.

Synthesis of heterodinuclear copper–nickel complexes

Hereafter we abbreviate the new complexes as [Cu(oxpn)Ni(ligand)] to indicate the hydrogen-derivatives and [Cu(Me_2oxpn)Ni(ligand)] to indicate the dimethyl-derivatives.

(a) [Cu(oxpn)Ni(cyclam)]$(ClO_4)_2$. An ice-cold solution of Cu(oxpn) (0.26 g, 1 mmol) in 20 cm^3 of water was added with constant stirring to an ice-cold solution of [Ni(cyclam)]$(ClO_4)_2$[14] (0.46 g, 1 mmol) in 30 cm^3 of water. A pink precipitate was immediately formed, which was separated by filtration and recrystallized in acetonitrile. Yield: 75%. The new compound was very soluble in acetone, acetonitrile and nitromethane; soluble in ethanol and methanol and insoluble in water. Found: C, 29.7; H, 5.3; N, 15.6; Cu, 8.8; Ni, 8.3. Calc. for $C_{18}H_{40}N_8O_2CuNi(ClO_4)_2$: C, 29.9; H, 5.5; N, 15.5; Cu, 8.8; Ni, 8.1%.

(b) [Cu(oxpn)Ni(tmd)$_2$]$(ClO_4)_2 \cdot H_2O$. An ice-cold solution of Cu(oxpn) (0.26 g, 1 mmol) in 20 cm^3 of methanol was added with constant stirring to an ice-cold solution of $Ni(ClO_4)_2$(aq) (0.36 g, 1 mmol) and 1,3-diaminopropane (0.15 g, 2 mmol) in 20 cm^3 of methanol. No precipitate was formed. Four times volume of ether was added, whereupon a red–violet precipitate was immediately formed. This was filtered and air-dried. Yield: 60%. The compound was soluble in all common solvents, including water. Found: C, 24.7; H, 5.5; N, 16.4; Cu, 9.3; Ni, 8.7. Calc. for $C_{14}H_{38}N_8O_3CuNi(ClO_4)_2$: C, 24.4; H, 5.5; N, 16.3; Cu, 9.2; Ni, 8.5%.

(c) [Cu(oxpn)Ni(bipy)$_2$]$(ClO_4)_2$. A hot solution of Cu(oxpn) (0.53 g, 2 mmol) in 25 cm^3 of methanol was added with constant stirring to a hot solution of $Ni(ClO_4)_2$(aq) (0.73 g, 1 mmol) and bipyridine (0.62 g, 4 mmol) in 25 cm^3 of methanol. After heating, a blue solution was formed, which was filtered to eliminate impurities. After several days, a microcrystalline powder was formed by slow evaporation, which was filtered and air-dried. Yield: 55%. The new complex was soluble in water, acetonitrile, nitromethane and acetone. Found: C, 41.0; H, 3.9; N, 13.5; Cu, 7.5; Ni, 7.1. Calc. for $C_{28}H_{32}N_8O_2CuNi(ClO_4)_2$: C, 40.3; H, 3.8; N, 13.4; Cu, 7.6; Ni, 7.0%.

(d) [Cu(oxpn)Ni(phen)$_2$]$(ClO_4)_2$. The product was obtained by using the same procedure as for the bipy derivative [see (c)]. Yield: 70%. It was insoluble in water and ethanol, but soluble in acetonitrile. Found: C, 43.1; H, 5.4; N, 12.5; Cu, 7.2; Ni, 6.6. Calc. for $C_{32}H_{48}N_8O_2CuNi(ClO_4)_2$: C, 42.7; H, 5.3; N, 12.5; Cu, 7.1; Ni, 6.5%.

(e) [Cu(Me_2oxpn)Ni(cyclam)]$(ClO_4)_2$. An ice-cold solution of Cu(Me_2oxpn) (0.32 g, 1 mmol) in 20 cm^3 of water was added, with constant stirring to an ice-cold solution of [Ni(cyclam)]$(ClO_4)_2$[14] (0.46 g, 1 mmol) in 25 cm^3 of water. A red solution was formed, without precipitation. After several days at room temperature, microcrystals of this compound were formed. Yield: 55%. The complex was filtered and air-dried. It was slightly soluble in ethanol and soluble in acetonitrile and nitromethane. Found: C, 34.1; H, 6.3; N, 14.6; Cu, 8.3; Ni, 7.5. Calc. for $C_{22}H_{48}N_8O_2CuNi(ClO_4)_2$: C, 33.9; H, 6.2; N, 14.4; Cu, 8.2; Ni, 7.5%.

(f) [Cu(Me_2oxpn)Ni(bipy)$_2$]$(ClO_4)_2$. The new complex was obtained by using the same procedure as for [Cu(oxpn)Ni(bipy)$_2$]$(ClO_4)_2$ [see (c)]. With Cu(Me_2oxpn) the precipitate obtained by mixing the starting complexes could be redissolved by boiling the solution. After concentration, the violet solution was allowed to stand at room temperature. Red microcrystals were formed after several days, which were filtered, washed and air-dried. Yield: 65%. The new complex is soluble in acetonitrile and nitromethane, slightly soluble in water and insoluble in ethanol. Found: C, 43.3; H, 4.5; N, 12.7; Cu, 7.3; Ni, 6.7. Calc. for $C_{32}H_{40}N_8O_2CuNi(ClO_4)_2$: C, 43.1; H, 4.5; N, 12.6; Cu, 7.1; Ni, 6.6%.

(g) [Cu(Me_2oxpn)Ni(phen)$_2$]$(ClO_4)_2$. The new product was synthesized as the bipy derivative [see (f)]. Yield: 75%. It was soluble in acetonitrile and nitromethane, but insoluble in ethanol. Found: C, 45.6; H, 5.9; N, 12.0; Cu, 6.8; Ni, 6.2. Calc. for $C_{36}H_{56}N_8O_2CuNi(ClO_4)_2$: C, 45.3; H, 5.9; N, 11.7; Cu, 6.6; Ni, 6.1%.

Physical measurements

IR spectra (4000–200 cm^{-1}) were recorded as KBr pellets with a Perkin–Elmer 1330 spec-

trophotometer. Magnetic measurements were carried out with a Faraday type magnetometer equipped with a helium continuous-flow cryostat working in the 4.2–300 K temperature range. For all the compounds the independence of the magnetic susceptibility versus the applied field was checked at each temperature. Mercury tetrakis(thiocyanato) cobaltate was used as a susceptibility standard. Diamagnetic corrections were estimated from Pascal Tables. EPR measurements were recorded with a Brucker ER-200 spectrometer working at X-band frequency.

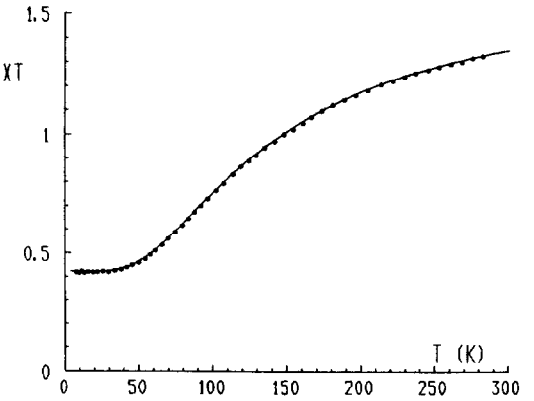

Fig. 1. XT vs T for $[Cu(oxpn)Ni(bipy)_2](ClO_4)_2$. (● experimental values; —— theoretical values). The XT curves for the other six complexes are very similar (see J and g values in Table 1).

RESULTS AND DISCUSSION

In the IR spectra all the characteristic bands attributed to the amine, oxamido and perchlorate anions are present. The most characteristic features are the very strong and wide band centred at 1600 cm^{-1} and the strong and sharp band centred at *ca* 800 cm^{-1}, due to the presence of the oxamido group. On the other hand, the two characteristic bands attributable to the perchlorate anion (non-coordinated) appear at 1100 cm^{-1} (very strong and wide) and at 620 cm^{-1} (strong and sharp). Many bands (from 3500 to 400 cm^{-1}) attributable to the bondings N—H, C—N (amine) are also present in all cases.

Magnetic measurements

Starting from the isotropic Hamiltonian $H = -J_{1,2}S_1S_2$, the interaction between copper(II) and nickel(II) leads to only two pair states (a doublet and a quartet) separated by $3J/2$.

The theoretical expression for the magnetic susceptibility, assuming that the isotropic interaction is much larger than the other terms of the spin Hamiltonian, is derived from the general Van Vleck equation as:[3,15]

$$XT = \frac{N\beta^2}{4k} \times \frac{g_{1/2}^2 + 10g_{3/2}^2 \exp(3J/2kT)}{1+2\exp(3J/2kT)}$$

where $g_{1/2} = (4g_{Ni} - g_{Cu})/3$ and $g_{3/2} = (2g_{Ni} + g_{Cu})/3$.

In this formula we have neglected the possible zero-field splitting within the excited quartet state. The magnetic properties of one of the seven new complexes, which are almost equal to those of the other six, are shown in Fig. 1. When the sample is cooled, XT decreases, then reaches a plateau with XT = 0.45 $cm^3\ mol^{-1}\ K$ corresponding to the temperature range where only the ground doublet state is thermally populated. Data for all complexes is given in Table 1. In all cases, R is less than 10^{-4}.

Such a value of J (approx. $-110\ cm^{-1}$) agrees perfectly with that reported by Journaux *et al.*[11] for $[Cu(oxpn)Ni(bipy)_2](NO_3)_2$ ($J = -110.6\ cm^{-1}$). On the other hand, this value indicates that the

Table 1. Magnetic and EPR data for the dinuclear complexes (g_{Cu} and g_{Ni} are obtained from the fitting of susceptibility data. With only one average g factor, the fitting is almost equal)

Compound	J (cm^{-1})	g_{Cu}	g_{Ni}	g(EPR)
$[Cu(oxpn)Ni(cyclam)](ClO_4)_2$	−104.2	2.12	2.23	2.24
$[Cu(oxpn)Ni(tmd)_2](ClO_4)_2$	−103.4	2.09	2.24	2.20
$[Cu(oxpn)Ni(bipy)_2](ClO_4)_2$	−104.5	2.10	2.24	2.21
$[Cu(oxpn)Ni(phen)_2](ClO_4)_2$	−103.8	2.11	2.22	2.20
$[Cu(Me_2oxpn)Ni(cyclam)](ClO_4)_2$	−107.3	2.15	2.25	2.22
$[Cu(Me_2oxpn)Ni(bipy)_2](ClO_4)_2$	−107.1	2.15	2.22	2.22
$[Cu(Me_2oxpn)Ni(phen)_2](ClO_4)_2$	−113.2	2.12	2.25	2.20

doublet–quartet gap ($3J/2$) is *ca* 165 $cm^{-1} \gg D$; therefore the employed equation for XT is correct. Lacking structural data we only can compare these results with those reported by Journaux *et al.*[11] for the trinuclear complex Cu—Ni—Cu with the same Cu(oxpn) as the bridging ligand ($J = -98.7\ cm^{-1}$). The slight difference may be attributed to the structural factors.

We can also compare these results with those reported by Journaux *et al.*[12] for [Cu(oxpn)Cu(bipy)]$(ClO_4)_2$ ($J = -439.7\ cm^{-1}$). The magnetic orbital in the central copper(II) ion ($d_{x^2-y^2}$) is the same in all cases. For the terminal ions, the magnetic orbitals are $d_{x^2-y^2}$ for copper(bipy) and both $d_{x^2-y^2}$ and d_{z^2} for nickel(II). Then, taking into account that the d_{z^2} orbital is not magnetically active with this kind of geometry, the overlap between the magnetic orbitals should be very similar. But, even with the correction due to the $1/n_1 \times n_2$,[16] n being the number of unpaired electrons (1×1 for CuCu and 1×2 for CuNi), the results are not comparable ($-110\ cm^{-1}$ for CuNi and $-220\ cm^{-1}$ for CuCu). Assuming a ferromagnetic contribution in CuNi which diminishes the antiferromagnetic factor is not realistic, as has been clearly indicated by Journaux.[17] Then, the only possible explanation is the less diffuse character and higher energy of the nickel(II) d orbitals: their interaction with the orbitals of the ligands is less pronounced and, consequently, the delocalization of these d orbitals into the oxamato bridge is greater in copper(II) than in nickel(II). The antiferromagnetic coupling would be more efficient in a CuCu pair than in a CuNi pair.

EPR spectra

The values of g for all complexes are collected in Table 1. There is a very wide band centred at approx. $g = 2.2$–2.3. At room temperature the complexes exhibit a smaller band centred at approx. $g = 4$, as has been also reported by Journaux *et al.*[11] for [Cu(oxpn)Ni(bipy)$_2$](NO$_3$)$_2$·2H$_2$O. The explanation would be the same as given by this author.[11] Since there is lack of structural data for this kind of complex, we hope, in the future, to obtain single crystals suitable for X-ray structural determination to examine whether the intermolecular interactions between the dimers could be the appropriate explanation.

Acknowledgement—We are very grateful for financial assistance from the CICYT (Grant no. MAT88-0545).

REFERENCES

1. B. G. Malstrom, in *Metal-ion Activation of Dioxygen* (Edited by T. G. Spiro), p. 181. Wiley, New York (1980).
2. (a) A. Gleizes and M. Verdaguer, *J. Am. Chem. Soc.* 1984, **106**, 3727; (b) Y. Pei, J. Sletten and O. Khan, *J. Am. Chem. Soc.* 1986, **108**, 3143; (c) Y. Pei, M. Verdaguer, O. Kahn, J. Sletten and J. P. Renard, *Inorg. Chem.* 1987, **26**, 138; (d) Y. Pei, M. Verdaguer, O. Kahn, J. Sletten and J. P. Renard, *J. Am. Chem. Soc.* 1986, **108**, 7427; (e) M. Drillon, E. Coronado, D. Beltran, J. Curely, R. Georges, R. Nugteren and L. de Jongh, *J. Magn. Mater.* 1986, **54**, 1507; (f) D. Beltran and M. Drillon, *J. Chem. Soc., Faraday Trans.* 1982, **78**, 1773.
3. O. Kahn, *Structure and Bonding* 1987, **68**, 89.
4. P. Tola, O. Kahn, C. Chauvel and H. Coudanne, *Nouv. J. Chim.* 1977, **1**, 647.
5. J. P. Costes, J. F. Serra, F. Dahan and J. P. Laurent, *Inorg. Chem.* 1986, **25**, 2790.
6. I. Morgenstern-Badarau, O. Khan, J. Jaud and J. Galy, *Inorg. Chem.* 1982, **21**, 3050.
7. E. Buluggiu, *J. Phys. Chem. Solids* 1980, **41**, 1175.
8. A. Bencini, A. Caneschi, A. Dei, D. Gatteschi, C. Zanchini and O. Kahn, *Inorg. Chem.* 1986, **25**, 1374.
9. J. Ribas, R. Costas, C. Diaz, O. Kahn, Y. Journaux and A. Gleizes, *Inorg. Chem.* 1990, **29**, 2042.
10. H. Ojima and K. Nonoyama, *Z. Anorg. Allg. Chem.* 1977, **429**, 282.
11. Y. Journaux, J. Sletten and O. Kahn, *Inorg. Chem.* 1986, **25**, 439.
12. Y. Journaux, J. Sletten and O. Kahn, *Inorg. Chem.* 1985, **24**, 4063.
13. H. Ojima and K. Nonoyama, *Z. Anorg. Allg. Chem.* 1972, **389**, 75.
14. B. Bosnich, M. L. Tobe and G. A. Webb, *Inorg. Chem.* 1965, **4**, 1109.
15. D. Gatteschi and S. Bencini, in *Magneto-structural Correlations in Exchange Coupled Systems* (Edited by R. Willet, D. Gatteschi and O. Kahn), NATO ASI Ser. C, Vol. 140. D. Reidel, Dordrecht (1984).
16. (a) O. Kahn and B. Briat, *J. Chem. Soc., Faraday Trans.* II 1976, **72**, 268; (b) O. Kahn and B. Briat, *J. Chem. Soc., Faraday Trans.* 1976, **72**, 1441.
17. Y. Journaux, Thèse. Université Paris-Sud, Orsay (1985).

Polyhedron Vol. 10, No. 1, pp. 107–112, 1991
Printed in Great Britain

0277–5387/91 $3.00+.00
© 1991 Pergamon Press plc

PHOTOCHEMISTRY OF THE μ-HYDROXO-μ-PEROXO-BIS[TRIETHYLENETETRAAMINE)COBALT(III)] COMPLEX IN BASIC AQUEOUS SOLUTIONS

NOBUYOSHI SHINOHARA,* SHIGEO MATSUFUJI and WATARU OKUBO

Department of Chemistry, Yokohama City University, Seto, Kanazawa-ku, Yokohama 236, Japan

(*Received* 8 *May* 1990; *accepted* 5 *September* 1990)

Abstract—Photochemical reaction of the title complex $[(trien)Co(\mu\text{-}OH,O_2)Co(trien)]^{3+}$ (**1**) was studied in basic, aqueous solution. The photo-induced cobalt(II)–trien complexes, $[Co(trien)(H_2O)_2]^{2+}$ and $[Co(OH)(trien)(H_2O)]^{+}$, react with dioxygen in oxygenated basic, aqueous solution to give the intermediates, $[(OH)(trien)Co\text{-}O_2\text{-}Co(trien)(H_2O)]^{3+}$ and $[(OH)(trien)Co\text{-}O_2\text{-}Co(trien)(OH)]^{2+}$, which are transformed reversibly into **1**. The transient absorption spectra of the monobridged μ-peroxo complexes, which have an absorption maximum near 313 nm, were measured using a flash photolysis method. The rate constants of the reaction of cobalt(II)–trien complexes with dioxygen were measured as a function of pH. A small amount of $[Co(trien)(H_2O)_2]^{3+}$ (**2**) was detected on prolonged irradiation in both the presence and absence of dioxygen. The photochemical reaction mechanisms are discussed, and the kinetic data of the reaction of cobalt(II)–trien complexes with dioxygen are compared with those obtained by a stopped-flow method.

Of the many transition metal complexes that have the ability to absorb dioxygen, the most outstanding complexes are those of cobalt(II).[1–3] The interaction of dioxygen with cobalt(II) complexes containing ligands such as aliphatic polyamines,[4–8] salicylidenamines,[9] amino acids[10] and macrocyclic tetraamines,[11–13] has been extensively studied because of their similarity to biological oxygen carriers. The general reaction mechanism of cobalt(II)–polyamine with dioxygen involves reactions (1) and (2):[1]

$$CoL^{2+} + O_2 \rightleftharpoons CoLO_2^{2+} \quad (1)$$

$$CoLO_2^{2+} + CoL^{2+} \rightleftharpoons LCo\text{-}O_2\text{-}CoL^{4+}. \quad (2)$$

There are several reports on the photochemical reactions of μ-superoxo dicobalt(III) complexes.[14–16] However, information about the photochemical reaction of μ-peroxo cobalt(III) complexes is relatively scanty.[13,17] Kikkawa *et al.*[17] have reported that the $[(en)_2Co(\mu\text{-}OH,O_2)Co(en)_2]^{3+}$ ion, undergoes deoxygenation in steady photolysis of basic, aqueous solution to give a photo-induced equilibrium (3):

$$[(en)_2Co(\mu\text{-}OH,O_2)Co(en)_2]^{3+} \overset{h\nu}{\rightleftharpoons} 2[Co(en)_2(H_2O)_2]^{2+} + O_2. \quad (3)$$

Miller and Wilkins[5] have investigated the reaction of the cobalt(II)–trien complex with dioxygen using a stopped-flow method, and found that the cobalt(II)–trien complex reacts with dioxygen to give the doubly bridged species **1**.

We have studied the photolysis of **1** in oxygenated aqueous solution and obtained the transient spectra of the O_2 adduct of the photo-induced cobalt(II)–trien complex and the kinetic data of the oxygenation reaction, using a flash photolysis method. The kinetic data obtained were compared with those obtained by a stopped-flow method.[5]

EXPERIMENTAL

Materials

Methods of synthesizing $[(trien)Co(\mu\text{-}OH,O_2)Co(trien)](ClO_4)_3 \cdot H_2O$ have been reported previ-

* Author to whom correspondence should be addressed.

ously.[18-20] The μ-hydroxo-μ-peroxo complex was prepared as follows.[19] $Co(ClO_4)_2 \cdot 6H_2O$ (30 g) was dissolved in a solution containing 20 cm^3 of water and 18 cm^3 of 60% $HClO_4$. Then, triethylenetetraamine (12 g) was added to the Co^{2+} solution with stirring. The solution was cooled in an ice bath and air-bubbled for 4 h. After filtering or decanting out tarry material containing small amounts of impurities, air-bubbling was continued for a further 2 h. The solution was left to stand overnight in a refrigerator and then the brown precipitate was filtered off and washed with cooled water and ethanol. Found: C, 18.2; H, 5.0; N, 14.3; Co, 15.0; ClO_4^-, 38.2. Calc. for $C_{12}H_{39}N_8O_{16}Cl_3Co_2$: C, 18.6; H, 5.1; N, 14.4; Co, 15.2; ClO_4^-, 38.5%. The spectrum in water gave λ_{max} 276 nm ($\varepsilon = 4.9 \times 10^3$ M^{-1} cm^{-1}) and λ_{max} 356 nm ($\varepsilon = 6.4 \times 10^3$ M^{-1} cm^{-1}), in good agreement with the λ_{max} 355 nm obtained by other methods.[18,20] The value of ε was larger than that found by another method.[20] When necessary, de-aeration of the solutions used for photolysis was carried out by bubbling with pure nitrogen.

Photochemical and analytical procedures

The flash photolysis apparatus was the same as that used previously.[21] Steady irradiations were carried out by using a high-pressure mercury lamp (100 W) or Xenon lamp (500 W), at room temperature. Monochromatic light was obtained by a combination of solution and glass filters. Ion-exchange chromatography on a cation resin (SP-Sephadex C-25 in sodium form) was used for the separation of products, which were determined by spectrophotometric analysis.

RESULTS AND DISCUSSION

Flash photolysis

Oscillograms obtained by the flash photolysis of **1** in basic, aqueous solution are shown in Fig. 1. The oscillogram A, obtained in an oxygen-saturated solution, showed an immediate decrease in absorbance at 310 nm after the flash, which was followed by an increase in absorbance. On the other hand,

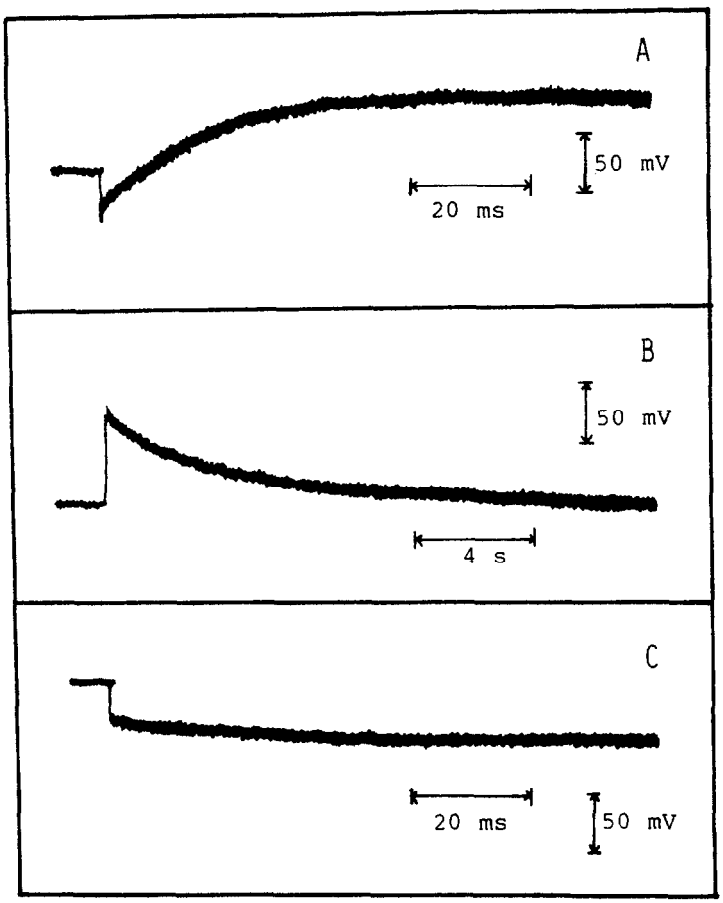

Fig. 1. Oscillograms showing changes in absorption after flashing aqueous solutions of 2.0×10^{-5} M [(trien)Co(μ-OH,O_2)Co(trien)]$^{3+}$ at pH = 10.1. The transmittance was monitored at 310 nm.

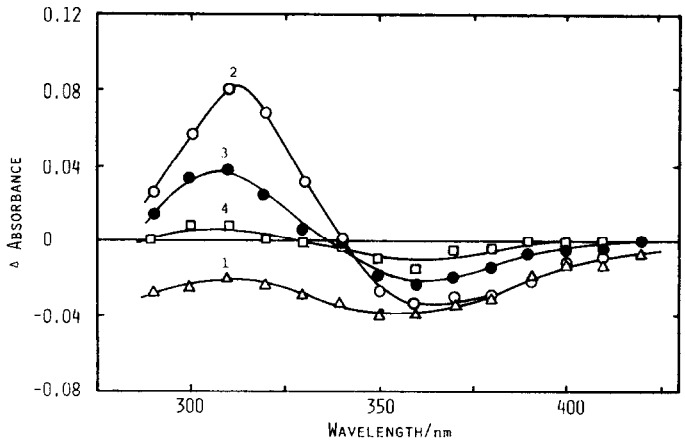

Fig. 2. Difference spectra of intermediates generated by the flash photolysis of dioxygen-saturated 2.0×10^{-5} M $[(trien)Co(\mu\text{-}OH,O_2)Co(trien)]^{3+}$ solutions at pH = 10. Spectra were obtained at the following reaction times; △ : immediately after the flash, ○ : 80 ms, ● : 1.8 s, □ : 9 s.

such an increase in absorbance was not observed in the flash photolysis of an oxygen-free solution (oscillogram C). The difference spectra obtained in the oxygen-saturated solutions are shown in Fig. 2. Spectrum 1 shows a decrease of the original two peaks at 276 and 356 nm, which is attributed to the decomposition of the bridge in the μ-peroxo dicobalt complex, similar to that suggested in the steady photolysis of $[(en)_2Co(\mu\text{-}OH,O_2)Co(en)_2]^{3+}$.[17] The absorbance in the wavelength region of < 380 nm increases progressively and reached a maximum value at about 80 ms after the flash. The spectrum of the intermediate has an absorption maximum at 313 nm (spectrum 2 in Fig. 2) and the spectrum did not change appreciably in the examined pH region.

The photochemical reaction mechanism in oxygenated, basic solution is explained in Scheme 1, where oxygenation reactions are similar to those proposed by Miller and Wilkins.[5] The first step of

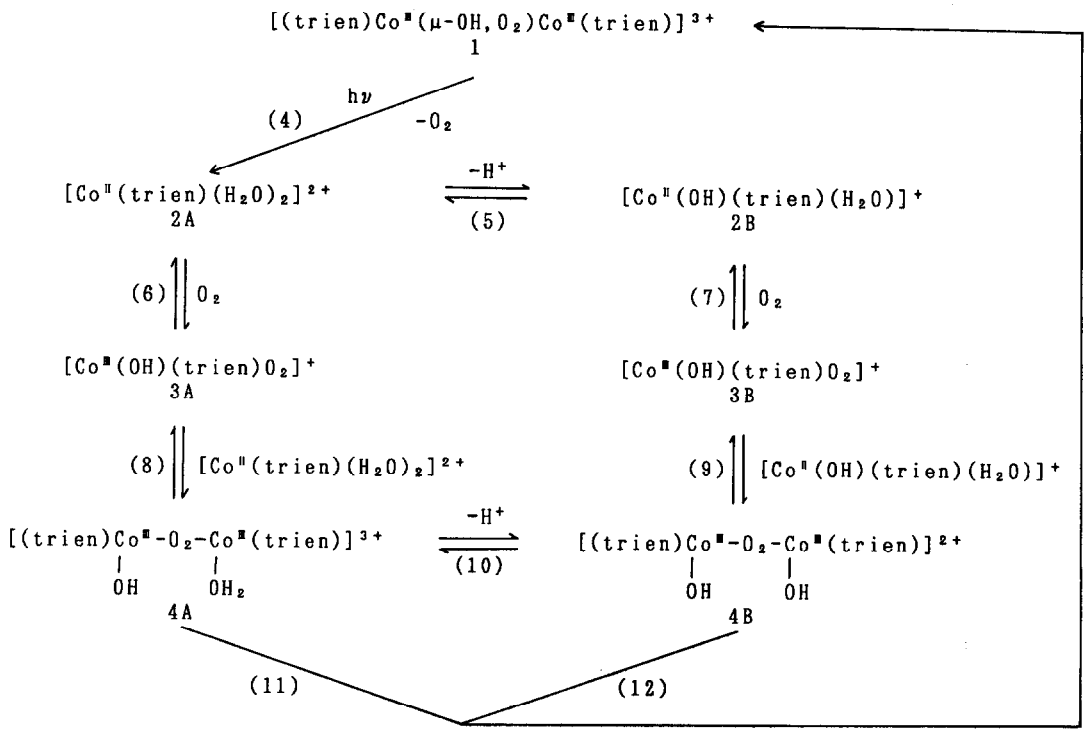

Scheme 1.

Table 1. Kinetic data for the formation of O_2 adducts[a]

First step:			
pH	$k_{obs}\times10^{-4}$ ($M^{-1}s^{-1}$)	pH	$k_{obs}\times10^{-4}$ ($M^{-1}s^{-1}$)
9.1	2.4±0.3	11.2	13.5±0.8
9.4	2.3±0.2	11.4	15.0±1.0
10.0	3.2±0.2	11.6	17.9±1.2
10.3	4.6±0.4	11.8	18.0±0.9
10.6	6.0±0.3	12.0	20.1±1.2
10.9	9.4±0.6	12.2	19.9±1.3
11.0	8.2±0.7	12.6	20.6±1.1
11.1	10.3±0.8		
Second step:			
pH	k'_{obs} (s^{-1})	pH	k'_{obs} (s^{-1})
9.2	1.86±0.19	11.3	0.42±0.08
9.8	1.84±0.20	11.4	0.40±0.08
9.9	1.68±0.21	11.6	0.34±0.09
10.0	1.75±0.19	12.0	0.21±0.04
10.6	1.40±0.26	12.3	0.13±0.04
10.7	1.00±0.17	12.6	0.05±0.03
11.2	0.56±0.09		

[a] I = 0.2 M $NaClO_4$. Concentration of $[(trien)Co(\mu\text{-}OH,O_2)Co(trien)]^{3+}$: 2.0×10^{-5} M. Monitored at 310 nm.

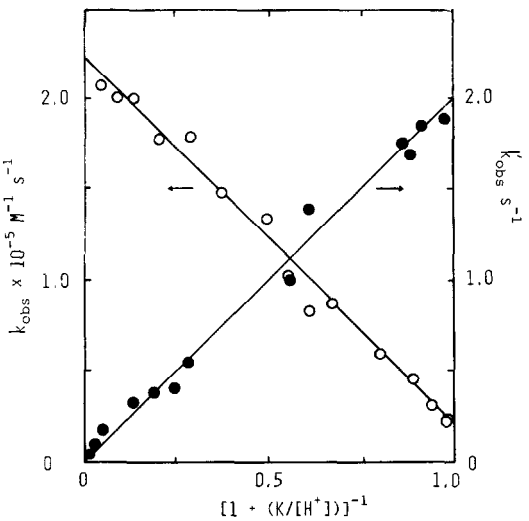

Fig. 3. Plots of k_{obs} vs $[1+(K_5/[H^+])]^{-1}$ for the first step (○) and k'_{obs} vs $[1+(K_{10}/[H^+])]^{-1}$ for the second step (●).

the oxygenation of the photo-induced cobalt(II)–trien complex **2A** or **2B** is the formation of activated dioxygen (**3A** or **3B**), followed by the rapid formation of the monobridged μ-peroxo dicobalt(III) complex **4A** or **4B**. The transient absorption spectrum 2 in Fig. 2 is attributed to the monobridged μ-peroxo dicobalt complex. The kinetics of the oxygenation of cobalt(II)–trien complexes was found to obey a pseudo-first-order rate law. The observed rate constants (k_{obs}) were independent of the initial O_2 concentration and increased with increasing pH (Table 1). Thus, k_{obs} for the first step can be given in eq. (13), where $k_a = k_7$, $k_b = k_6$ and $K_c = K_5$:

$$k_{obs} = \frac{k_a - k_b}{1+(K_c/[H^+])} + k_b. \qquad (13)$$

The plot of k_{obs} vs $[1+(K_5/[H^+])]^{-1}$ was linear (Fig. 3), the intercepts being k_6 (when the x coordinate = 0) and k_7 (when the x coordinate = 1) when the known value of $K_5 = 6.3\times10^{-12}$ M[5] was used. The rate constants, $k_7 = (2.1\pm0.1)\times10^4$ and $k_6 = (2.2\pm0.1)\times10^5\ M^{-1}s^{-1}$, estimated by a least-squares method are in good agreement with those obtained by a stopped-flow method ($k_7 = 2.5\times10^4$ and $k_6 = 2.8\times10^5\ M^{-1}s^{-1}$).[5]

An intermediate generated by the increase of absorbance at 310 nm decayed on a slow time scale (oscillogram B in Fig. 1). The absorption spectrum of the intermediate changes with an isosbestic point at 343 nm (Fig. 2). Spectrum 4, obtained at 9 s after the flash, appears to be still in the course of the change of the spectrum. We could not measure it on a longer time scale because of the limitations of the apparatus used. However, it can be expected that finally the absorbance would almost return to the original one. This observation indicates that reactions (11) and (12) really occur. The kinetics of the transformation into **1** (second step) obeyed a first-order rate law and the rate constant k'_{obs} decreased with increasing pH (Table 1) which can be given by eq. (13), where $k_a = k_{11}$, $k_b = k_{12}$ and $K_c = K_{10}$. Calculations were performed for a series of K_{10} values by using a computer, where K_{10} must be close to 10^{-11} M as can be seen from Table 1. The best plot (Fig. 3) gives $k_{11} = 2.0\pm0.1\ s^{-1}$, $k_{12} \approx 4\times10^{-2}\ s^{-1}$ and $K_{10} = (1.6\pm0.1)\times10^{-11}$ M, which are in good agreement with 2.0 s^{-1}, $\sim 1.2\times10^{-2}\ s^{-1}$ and 1.2×10^{-11} M obtained by a stopped-flow method, respectively.[5]

Steady photolysis

The spectral changes in the steady photolysis of **1** in oxygen-saturated and oxygen-free aqueous solutions are given in Fig. 4. Similar spectral changes were obtained upon irradiation with monochromatic lights, 313 and 365 nm, however, spectral changes hardly occurred upon irradiation at 436

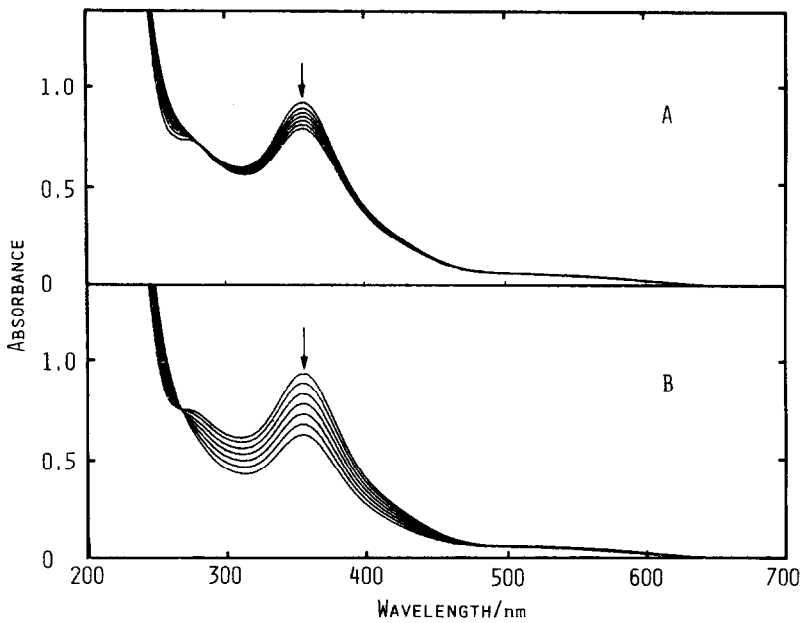

Fig. 4. Changes in the absorption spectra of 1.5×10^{-4} M $[(trien)Co(\mu\text{-}OH,O_2)Co(trien)]^{3+}$ solutions upon continuous irradiation at > 310 nm by a Xenon lamp: (A) irradiated at intervals of 5 min in the oxygen-saturated system; (B) irradiated at intervals of 2.5 min in the oxygen-free system.

nm. In the photolysis of **1** in oxygen-saturated solution, an initial small increase of absorbance in the wavelength region 240–310 nm was observed, which was followed by a slower change with an isosbestic point at 276 nm [Fig. 4(A)]. The initial and rapid equilibrium can probably be attributed to the formation of the *trans*-form of a monobridged μ-peroxo dicobalt(III) complex. The extinction coefficient of such a complex is unknown, however it can be expected to be larger than that of the μ-hydroxo-μ-peroxo dicobalt(III) complex, judging from the extinction coefficient of $[\{(H_2O)(cyclam)Co\}_2O_2]^{4+}$ ($\varepsilon > 10^4$ M^{-1} cm^{-1} at 280 nm, cyclam = 1,4,8,11-tetraazacyclotetradecane).[13,22] Whereas in the photolysis of **1** in oxygen-free solution, an initial and very small decrease was observed which can be attributed to equilibrium (14)

$$[(trien)Co(\mu\text{-}OH,O_2)Co(trien)]^{3+} \overset{h\nu}{\rightleftharpoons} 2[Co(trien)(H_2O)_2]^{2+} + O_2. \quad (14)$$

The oxygenation reaction of the photo-induced cobalt(II)–trien complexes will start to occur with the accumulation of dioxygen by reaction (4). The decomposition of the peroxo complex in the oxygen-free system takes place more rapidly than in the oxygen-saturated system, as shown in Fig. 4(B). In the oxygen-free system, the absorbance partially recovered by bubbling dioxygen through the solution after irradiation [Fig. 5(A)]. The difference spectra given in Fig. 5(B) were similar to the spectrum of **1**, which means that the photo-induced cobalt(II)–trien complexes are transformed reversibly into **1**. This fact suggests that, in the oxygen-free system, the photo-induced cobalt(II) complexes partially remain in the solution without dioxygen uptake. The final product obtained on prolonged irradiation was $[Co(trien)(H_2O)_2]^{3+}$ ($pK_1 = 5.4$ and $pK_2 = 7.3$[23]) in both systems in the presence and absence of dioxygen.

In conclusion, in the photolysis of **1** the photo-induced products were mainly cobalt(II)–trien complexes and dioxygen and the cobalt(II) complexes reacted with dioxygen, reversibly, to give μ-peroxo dinuclear complexes. The absorption spectra of the monobridged μ-peroxo complexes produced as intermediates have a maximum near 313 nm. The mononuclear cobalt(III) complex, $[Co(trien)(H_2O)_2]^{3+}$, was produced on prolonged irradiation. The kinetic data for the oxygenation of cobalt(II)–trien, obtained by the flash photolysis method, were in good agreement with those obtained by the stopped-flow method. By using the flash photolysis method with μ-peroxo cobalt complexes in oxygenated basic, aqueous solution, the oxygenation reactions of cobalt(II)–polyamine complexes can be studied easily without any interference from the oxidized reactive ligand produced by charge-transfer.

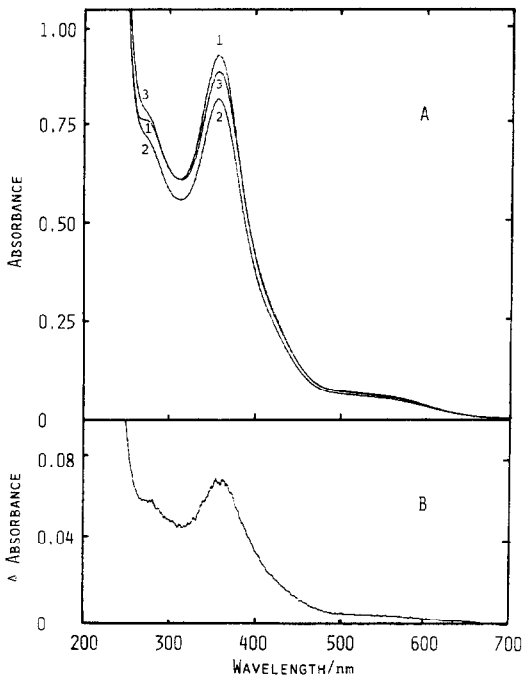

Fig. 5. Changes in absorption spectra by bubbling oxygen in the irradiated oxygen-free solution: (A) 1, before irradiation; 2, irradiated for 10 min at > 310 nm by a Xenon lamp; 3, bubbled oxygen for 1 min; (B) the difference between curve 3 and curve 2.

REFERENCES

1. R. G. Wilkins, *Adv. Chem. Ser.* 1971, **100**, 111.
2. E. C. Niderhoffer, J. H. Timmons and A. E. Martell, *Chem. Rev.* 1984, **84**, 137.
3. R. D. Jones, D. A. Summerville and F. Basolo, *Chem. Rev.* 1979, **79**, 139.
4. F. Miller, S. Simplicio and R. G. Wilkins, *J. Am. Chem. Soc.* 1969, **91**, 1962.
5. F. Miller and R. G. Wilkins, *J. Am. Chem. Soc.* 1970, **92**, 2687.
6. R. Nakon and A. E. Martell, *J. Am. Chem. Soc.* 1972, **94**, 3026.
7. S. A. Bedell, J. H. Timmons, A. E. Martell and I. Murase, *Inorg. Chem.* 1982, **21**, 874.
8. (a) Y. Sasaki, J. Fujita and K. Saito, *Bull. Chem. Soc. Japan* 1969, **42**, 146; (b) *Bull. Chem. Soc. Japan* 1971, **44**, 3373.
9. A. Puxddu and G. Costa, *J. Chem. Soc., Dalton Trans.* 1981, 1115.
10. W. R. Harris, G. McLendon and A. E. Martell, *J. Am. Chem. Soc.* 1976, **98**, 8378.
11. K. Kumar and J. F. Endicott, *Inorg. Chem.* 1984, **23**, 2447; C. L-. Wong and J. F. Endicott, *Inorg. Chem.* 1981, **20**, 2233; C. L-. Wong, J. A. Switzen, K. P. Balakrishnan and J. F. Endicott, *J. Am. Chem. Soc.* 1980, **102**, 5511.
12. M. Kodama and E. Kimura, *Inorg. Chem.* 1980, **19**, 1871; E. Kimura, M. Kodama, R. Machida and K. Ishizu, *Inorg. Chem.* 1982, **21**, 595; R. Machida, E. Kimura and M. Kodama, *Inorg. Chem.* 1983, **22**, 2055.
13. N. Shinohara, K. Ishii and M. Hirose, *J. Chem. Soc., Chem. Commun.* 1990, 700.
14. J. E. Barness, J. Barrett, R. W. Brett and J. Brown, *J. Inorg. Nucl. Chem.* 1968, **30**, 2207.
15. J. S. Valentine and D. Valentine Jr, *J. Am. Chem. Soc.* 1971, **93**, 1111; *Inorg. Chem.* 1971, **10**, 393; *Inorg. Chem.* 1973, **12**, 1697.
16. N. Shinohara, E. Kose and W. Ohkubo, *Bull. Chem. Soc. Japan* 1988, **61**, 3338.
17. M. Kikkawa, Y. Sasaki, S. Kawata, Y. Hatakeyama, F. Ueno and K. Saito, *Inorg. Chem.* 1985, **24**, 4096.
18. M. Zehnder and S. Fallab, *Helv. Chim. Acta* 1972, **55**, 1691.
19. N. Shinohara, M. Sugiyama and M. Hada, *J. Yokohama City Univ., Chem. Phys. Ser.* 1974, **2**, 1.
20. N. Al-Shatti, M. Ferrer and A. G. Sykes, *J. Chem. Soc., Dalton Trans.* 1980, 2533.
21. N. Shinohara, K. Mori and M. Inoue, *Chem. Lett.* 1986, 661; N. Shinohara and M. Inoue, *Bull. Chem. Soc. Japan* 1989, **62**, 730.
22. T. Geiger and F. C. Anson, *J. Am. Chem. Soc.* 1981, **103**, 7489.
23. C. J. Hawkins, A. M. Sargeson and G. H. Searle, *Aust. J. Chem.* 1964, **17**, 598.

Polyhedron Vol. 10, No. 1, pp. 113–120, 1991
Printed in Great Britain

0277–5387/91 $3.00+.00
© 1991 Pergamon Press plc

REACTION OF DIRUTHENIUM(II,III) ACETATE WITH TRIPHENYLPHOSPHINE

M. C. BARRAL, R. JIMÉNEZ-APARICIO,* E. C. ROYER and F. A. URBANOS

Departamento de Química Inorgánica, Facultad de Ciencias Químicas, Universidad Complutense, Ciudad Universitaria, 28040 Madrid, Spain

and

A. MONGE and C. RUIZ-VALERO

Instituto de Ciencias de los materiales, sede D, CSIC, Serrano 113, 28006 Madrid, Spain and Laboratorio de Rayos X, Facultad de Ciencias Químicas, Universidad Complutense, Ciudad Universitaria, 28040 Madrid, Spain

(*Received* 25 *June* 1990; *accepted* 5 *September* 1990)

Abstract—The reaction of $[Ru_2(\mu\text{-}O_2CCH_3)_4(thf)_2]BF_4$ with triphenylphosphine in thf or toluene is described. In this reaction, a yellow compound of formula $Ru(O_2CCH_3)_2(PPh_3)\cdot CH_3C_6H_5$ (**1**), and a violet, diamagnetic oxo-bridged compound, formulated as $Ru_2(\mu\text{-}O)(\mu\text{-}O_2CCH_3)_2(O_2CCH_3)_2(PPh_3)_2$ (**2**) are obtained. The compounds have been characterized by elemental analysis, magnetic susceptibility measurements and spectroscopic techniques. The structure of **2** has been determined by X-ray crystallography. Two pseudo-octahedral ruthenium(III) atoms are bridged by an oxo and two acetate ligands. The hexacoordination of each ruthenium atom is completed with a bidentate acetate and a triphenylphosphine ligand. Some spectroscopic evidence for the formation of a tetranuclear intermediate compound is also presented.

The reactions of $M_2(\mu\text{-}O_2CR)_4$ (M = Mo, W or Rh, R = alkyl or aryl) with phosphines, to give compounds of the type $M_2(\mu\text{-}O_2CR)_4(PR'_3)_2$ (R′ = alkyl or aryl) with the phosphine ligands on the axial or equatorial sites of the M—M core have been intensively studied.[1–8] However, in the case of ruthenium, similar compounds have not been isolated. For example Wilkinson and co-workers,[9] have reported the synthesis of the compound $Ru_2(\mu\text{-}O_2CCH_3)_4(PPh_3)_2$, but the crystal structure of this compound has been shown to be in fact, $Ru_3(\mu\text{-}O)(\mu\text{-}O_2CCH_3)_6(PPh_3)_3$.[10] A yellow complex of stoichiometry $Ru_2(\mu\text{-}O_2CCH_3)_4(PPh_3)_2$ has also been described,[11] but the compound was too insoluble for molecular weight studies and no structural information was obtained.

The reactivity of PPh_3 towards $Ru_2Cl(O_2CR)_4$ (R = Me, Ph, C_6H_4-*p*-OMe) has been recently investigated.[12,13] In the reaction of $Ru_2Cl(\mu\text{-}O_2CAr)_4$ (Ar = Ph, C_6H_4-*p*-OMe) and PPh_3, in a MeCN–H_2O mixture, an asymmetric, mixed-valance diruthenium(II,III) compound of formula $Ru_2(OH_2)Cl(MeCN)(O_2CAr)_4(PPh_3)_2$ was isolated.[13] However, several unsuccessful attempts to obtain similar adducts of diruthenium(II,III) compounds, with bridging ligands other than carboxylate, have been made.

The reaction of diruthenium(II,III) amidates with triarylphosphines led to the transfer of an aryl group from the triarylphosphine onto the metal centre, giving diruthenium(III,III) compounds.[14,15] Similarly, the reaction of $Ru_2Cl(\mu\text{-}O_2CCH_3)_4$ with the lithium salt of 2-aminopyridine followed by addition of PMe_2Ph gave a new diruthenium (III,III) compound of formula $Ru_2(C_5NH_4NH)_6(PMe_2Ph)_2$.[16]

The preparation of $[Ru_2(\mu\text{-}O_2CCH_3)_4(thf)_2]BF_4$ has been recently described.[17] The reaction of this complex with triphenylphosphine leads to the

* Author to whom correspondence should be addressed.

formation of a violet product formulated as $[Ru(\mu\text{-}O_2CCH_3)(O_2CCH_3)(PPh_3)]_x$ ($x \geqslant 3$) and an uncharacterized yellow product.[17] In this paper we report a more detailed study of this reaction, including the crystal structure of the violet product.

RESULTS AND DISCUSSION

The reaction of $[Ru_2(\mu\text{-}O_2CCH_3)_4(thf)_2]BF_4$ with triphenylphosphine carried out in thf leads to a violet solution. When this solution is pumped dry, extracted with toluene, treated with active carbon and allowed to stand at room temperature for several days, a yellow crystalline solid is formed. A violet compound is obtained from the residual solution when the solvent is removed. Similar results are achieved if the reaction is carried out in toluene.

The yellow crystals are stable in a toluene atmosphere, but in an air or nitrogen atmosphere lose solvent very quickly and the crystals are destroyed. The compound is soluble in polar organic solvents, but insoluble in diethyl ether, toluene and petroleum ether.

Magnetic susceptibility measurements indicate that the compound is diamagnetic, suggesting that the formal oxidation state for the ruthenium atom is two.

Analytical data for the yellow compound are in accordance with the stoichiometry, $Ru(O_2CCH_3)_2PPh_3 \cdot CH_3C_6H_5$ (**1**). The IR spectrum of this compound shows absorption bands due to the triphenylphosphine ligand and absorptions assigned to the symmetric and anti-symmetric vibrations of the carboxylate groups. No bands for the tetrafluoroborate anion are observed.

The ^1H NMR spectrum of this yellow complex shows a singlet at 1.26 ppm assigned to the methyl group of the acetate ligand and a singlet at 2.35 ppm assigned to the methyl group of the toluene. In the aromatic region a multiplet due to the triphenylphosphine and toluene protons is observed. The $^{13}C\{^1H\}$ NMR spectrum of this compound shows resonances due to the acetate ligands at 24.07 and 193.79 ppm, corresponding to the $—CH_3$ and $—CO_2$ groups, respectively. The signals corresponding to the aromatic carbons are observed in the region 125–135 ppm. The $^{31}P\{^1H\}$ NMR spectrum of this compound shows a singlet at 47.15 ppm, indicating the presence of only one type of phosphine. The NMR data are summarized in Table 1.

All these data are in accordance with a compound containing two bidentate acetate ligands, one phosphine ligand and a toluene molecule occupying the sixth coordination position, in accordance with the formula $Ru(O_2CCH_3)_2(PPh_3) \cdot CH_3C_6H_5$ (**1**). This compound is analogous to $Ru(O_2CCH_3)_2(PPh_3) \cdot CH_3OH$, the formation of which has been suggested by Wilkinson and co-workers[11] in the reduction of $Ru_3(\mu\text{-}O)(O_2CCH_3)_6(PPh_3)_3$.

The violet compound was initially formulated as $[Ru(\mu\text{-}O_2CCH_3)(O_2CCH_3)(PPh_3)]_x$ ($x \geqslant 3$),[17] but a more detailed study, including X-ray structural determination, has showed that it is, instead, $[Ru(\mu\text{-}O_2CCH_3)(O_2CCH_3)(PPh_3)]_2(\mu\text{-}O)$. The calculated analyses of carbon and hydrogen in these compounds are very similar, but the experimental results are in better agreement with the new formulation.

The magnetic moment for the ruthenium(III)

Table 1. NMR data for the compounds

	δ ^1H		δ $^{13}C\{^1H\}$			δ $^{31}P\{^1H\}$
Complex	CH_3COO	PPh_3	CH_3COO	CH_3COO	PPh_3	PPh_3
(**1**)	1.26(s)	6.8–7.4(m)	24.07(s)	193.79(s)	134.75(s) 132.65(d) J = 45.8 Hz 130.29(s) 127.99(s)	47.15(s)
(**2**)	174(s) 1.69(s)	7.2–7.1(m)	23.13(s) 22.29(s)	182.70(s) 181.96(s)	134.07(pt) J = 5.3 Hz 131.12(d) J = 49.9 Hz 129.65(s) 127.83(pt) J = 5.0 Hz	51.92(s)

s, singlet; d, doublet; pt, pseudo triplet; m, multiplet.

compounds must correspond to one unpaired electron per metal atom, but the magnetic susceptibility measurements at various temperatures show that the violet compound is diamagnetic. This behaviour has been observed in other oxo-bridged compounds of ruthenium(III) in which the spin-pairing occurs via the oxo groups.[10,11,18-24]

The IR spectrum of the oxo-dimer shows absorptions due to triphenylphosphine ligands and absorptions due to the presence of two types of acetate ligands.

The ^1H NMR spectrum of the oxo-dimer shows two singlets assigned to two, unequivalent acetate ligands and a multiplet due to the phenyl protons. The $^{13}C\{^1H\}$ NMR spectrum of this compound confirms the presence of two, unequivalent acetate groups. The aromatic region of this spectrum shows several resonances due to the carbons of the phenyl groups. The $^{31}P\{^1H\}$ NMR spectrum shows one singlet, which indicates the presence of only one type of phosphine (Table 1).

We have made numerous attempts to derive single crystals of the violet compound obtained from $[Ru_2(\mu\text{-}O_2CCH_3)_4(thf)_2]BF_4$. Finally, a toluene solution in air over several days gave single crystals of an unsolvated compound identified as $[Ru(\mu\text{-}O_2CCH_3)(O_2CCH_3)(PPh_3)]_2(\mu\text{-}O)$. This compound has been also obtained, as a methanol solvate, from $RuCl_3 \cdot 3H_2O$, NaO_2CCH_3 and PPh_3 in methanol, by a published procedure.[11] This method can be improved by bubbling a stream of oxygen for 30 min through the reaction mixture allowing the aforementioned compound to be obtained in shorter periods of time and in higher yield.

An ORTEP[25] drawing of the violet compound appears in Fig. 1. The distances, angles and some torsion angles are summarized in Table 2.

The molecule, $Ru_2(\mu\text{-}O)(\mu\text{-}O_2CCH_3)_2(O_2CCH_3)_2(PPh_3)_2$ (**2**), consists of two ruthenium(III) ions bridged by an oxo and two acetate ligands. Each ruthenium atom is also bonded to one bidentate acetate group and one PPh_3 ligand. Both ruthenium(III) atoms are in a distorted octahedral environment, with the oxo and phosphine ligands in *cis* positions. The $Ru—O_{oxo}$ distances are very short, indicating considerable double bond character. This situation is similar to that seen in other structurally characterized oxodiruthenium complexes. The Ru—O—Ru angle in this compound is 121.2°. The $Ru—O_{oxo}$ distances and the Ru—O—Ru angle are similar to those described for $[L_2Ru_2(\mu\text{-}O)(\mu\text{-}O_2CCH_3)_2](PF_6)_2 \cdot 0.5H_2O$ (L = 1,4,7-trimethyl-1,4,7-triazacyclononane),[20] {(tpm) $Ru(\mu\text{-}O)[\mu\text{-}O_2P(O)(OH)]_2Ru(tpm)\} \cdot 8H_2O$ [tpm = tris(1-pyrazolyl)methane][18] and $[Ru_2(\mu\text{-}O)(\mu\text{-}O_2CCH_3)_2(py)_6](ClO_4)_2 \cdot 4H_2O$,[21] and contrast with other oxoruthenium complexes in which the Ru—O—Ru angle is near 180°. The Ru—Ru distance is 3.216 Å, suggesting a weak intramolecular Ru—Ru interaction similar to that observed in other analogous oxo-dimer compounds.[18,20,21]

The bridging and bidentate acetate ligands are asymmetrically bonded to the ruthenium atoms. This asymmetrical disposition could be due to a pronounced *trans* effect of the oxo bridge and the triphenylphosphine ligands.

In order to isolate some intermediates in this reaction, it was stopped after 2 h of stirring. When

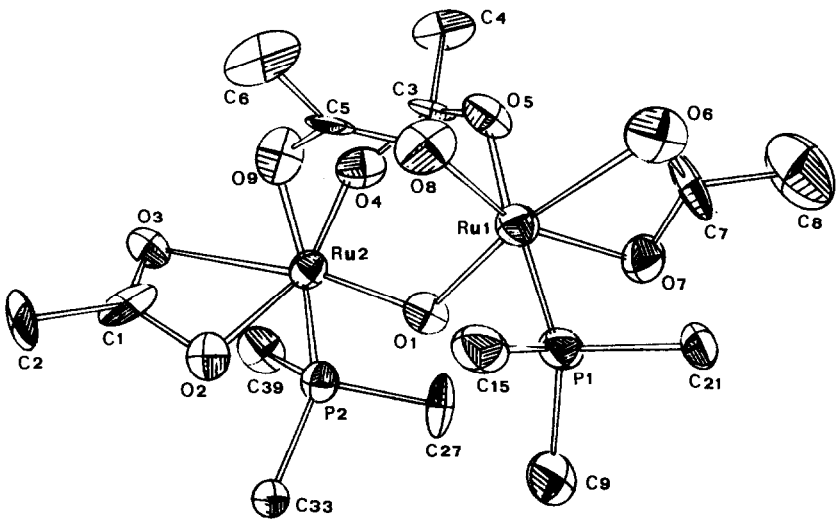

Fig. 1. ORTEP view of $Ru_2(\mu\text{-}O)(\mu\text{-}O_2CCH_3)_2(O_2CCH_3)_2(PPh_3)_2$ (**2**). The phenyl rings are omitted for clarity.

Table 2. Principal bond lengths (Å) and angles (°) with ESDs

Bond lengths

Ru(1)—Ru(2)	3.2158(28)	P(2)—C(27)	1.8560(267)
Ru(1)—P(1)	2.2722(75)	P(2)—C(33)	1.8164(281)
Ru(1)—O(1)	1.8473(159)	P(2)—C(39)	1.8539(275)
Ru(1)—O(5)	2.1171(189)	O(2)—C(1)	1.3205(310)
Ru(1)—O(6)	2.1666(216)	O(3)—C(1)	1.2679(333)
Ru(1)—O(7)	2.1208(194)	O(4)—C(3)	1.3179(301)
Ru(1)—O(8)	1.9841(216)	O(5)—C(3)	1.2486(306)
Ru(2)—P(2)	2.2798(77)	O(6)—C(7)	1.2012(412)
Ru(2)—O(1)	1.8478(151)	O(7)—C(7)	1.2633(401)
Ru(2)—O(2)	2.1156(168)	O(8)—C(5)	1.2563(356)
Ru(2)—O(3)	2.1868(158)	O(9)—C(5)	1.3222(364)
Ru(2)—O(4)	2.0186(189)	C(1)—C(2)	1.4923(406)
Ru(2)—O(9)	2.1229(211)	C(3)—C(4)	1.4921(385)
P(1)—C(9)	1.8182(334)	C(5)—C(6)	1.5205(466)
P(1)—C(15)	1.7880(328)	C(7)—C(8)	1.4944(517)
P(1)—C(21)	1.7959(253)		

Bond angles

Ru(1)—O(1)—Ru(2)	121.2(9)	P(2)—Ru(2)—O(1)	90.7(6)
P(1)—Ru(1)—O(1)	89.2(6)	P(2)—Ru(2)—O(2)	93.7(5)
P(1)—Ru(1)—O(5)	177.1(5)	P(2)—Ru(2)—O(3)	96.4(5)
P(1)—Ru(1)—O(6)	95.5(5)	P(2)—Ru(2)—O(4)	92.9(5)
P(1)—Ru(1)—O(7)	92.4(6)	P(2)—Ru(2)—O(9)	173.9(6)
P(1)—Ru(1)—O(8)	92.2(6)	O(1)—Ru(2)—O(2)	96.6(7)
O(1)—Ru(1)—O(5)	93.2(7)	O(1)—Ru(2)—O(3)	156.4(7)
O(1)—Ru(1)—O(6)	159.8(7)	O(1)—Ru(2)—O(4)	99.7(7)
O(1)—Ru(1)—O(7)	99.9(7)	O(1)—Ru(2)—O(9)	94.9(7)
O(1)—Ru(1)—O(8)	100.9(8)	O(2)—Ru(2)—O(3)	60.6(6)
O(5)—Ru(1)—O(6)	81.7(7)	O(2)—Ru(2)—O(4)	162.4(7)
O(5)—Ru(1)—O(7)	85.7(7)	O(2)—Ru(2)—O(9)	83.4(7)
O(5)—Ru(1)—O(8)	88.9(8)	O(3)—Ru(2)—O(4)	102.5(7)
O(6)—Ru(1)—O(7)	60.3(7)	O(3)—Ru(2)—O(9)	77.6(7)
O(6)—Ru(1)—O(8)	98.5(8)	O(4)—Ru(2)—O(9)	88.4(8)
O(7)—Ru(1)—O(8)	158.7(8)	O(2)—C(1)—O(3)	113.4(2)
O(6)—C(7)—O(7)	122.3(3)		

Torsion angles[34]

P(1)—Ru(1)—Ru(2)—P(2)	−78.2(3)	O(8)—Ru(1)—Ru(2)—O(9)	12.2(8)
O(5)—Ru(1)—Ru(2)—O(4)	11.7(8)		

this reaction mixture was pumped dry, extracted with toluene, treated with active carbon and pumped dry again, a diamagnetic violet solid was obtained.

The IR spectrum of this solid is very similar to **2**, showing absorption bands due to the triphenylphosphine ligand and two types of acetate ligands but giving no additional information.

The NMR spectrum show the resonances due to the oxo-dimer and **1** described above (Table 1), however, new signals are also observed. Thus, in the ^1H NMR spectrum, two new singlets at 1.83 and 1.95 ppm, assigned to two inequivalent acetate groups, are observed and in the region of the phenyl groups, new signals are also present. In the $^{13}C\{^1H\}$ NMR spectrum two new signals appear at 30.30 and 29.63 ppm due to two different acetate groups and in the region of the aromatic carbons new signals appear due to coordinated phosphine. Finally, in the $^{31}P\{^1H\}$ NMR spectrum a new signal at 35.45 ppm was observed. All these data indicate the presence of a new compound containing two classes of acetate group and an equivalent phosphine ligand.

In the FAB mass spectrum of the violet solid obtained after 2 h of reaction, the base peak is observed at $m/z = 980$, corresponding to a $[Ru_2(\mu\text{-}O)(\mu\text{-}O_2CCH_3)_2(O_2CCH_3)_2(PPh_3)_2]^+$ ion. In addition, the spectrum shows other peaks at higher

Table 3. Mass spectral data

m/z	Ion
1911	$[Ru_4(O_2CCH_3)_8(PPh_3)_4-CH_3]^+$
1713	$[Ru_4(O_2CCH_3)_7(PPh_3)_3(PPh)]^+$
1577	$[Ru_4(O_2CCH_3)_6(PPh_3)_3(P)]^+$
1465	$[Ru_4(O_2CCH_3)_7(PPh_3)(PPh_2)(POPh_2)]^+$
1430	$[Ru_3(O_2CCH_3)_5(O_2C)(PPh_3)_3]^+$
980	$[Ru_2(O)(O_2CCH_3)_4(PPh_3)_2]^+$

m/z than this base peak. The highest observed peak is at $m/z = 1911$, in accordance with a $\{[Ru(O_2CCH_3)_2(PPh_3)]_4-CH_3\}^+$ fragment. Signals corresponding to the fragmentation of this tetramer compound at $m/z = 1465$, 1577 and 1430 are observed. In Table 3 these peaks are summarized and their possible assignments shown. Figure 2 shows the experimental and calculated isotopic distribution for some of the peaks which appear in this mass spectrum. The peak at $m/z = 1911$ seems to suggest that in this reaction a tetramer compound of formula $[Ru(O_2CCH_3)_2(PPh_3)]_4$ is formed. Accordingly with the NMR data it is possible to propose the existence of a tetranuclear intermediate with bridging and monodentate acetates and a phosphine ligand bonded to ruthenium. Without a crystal structure determination, a precise structure assignment cannot be made but it seems reasonable to assume the structure for this intermediate shown in Scheme 1. This tetramer can be formed by the coupling of two dimer units. A similar reaction in which two dimer units of molybdenum are coupled to give a planar tetranuclear compound has been described by McCarley and co-workers.[26]

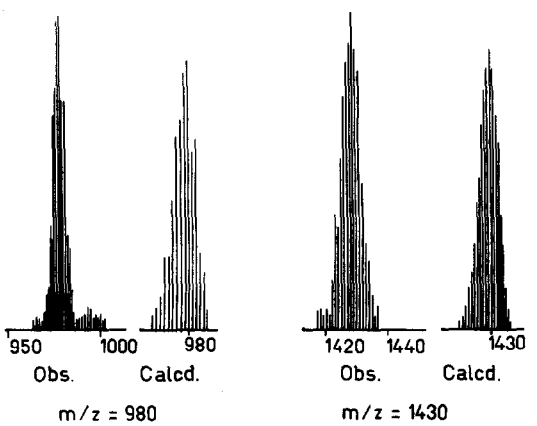

Fig. 2. Observed and calculated isotope ratios for some peaks of the mass spectrum.

We have made numerous attempts to isolate the pure tetramer compound, but in all cases we have obtained a mixture with the oxo-dimer, which indicates very similar solubility. Nonetheless all attempts to crystallize this compound have been unsuccessful, because in solution it is transformed.

In the reaction described, the formation of a compound of ruthenium(III) and of ruthenium(II), from a diruthenium(II,III) compound, indicates a formal disproportionation process. An analogous process of dismutation has been observed by Cotton *et al.*[27] in the reaction of $Ru_2Cl(\mu\text{-}O_2CCH_3)_4$ with L-mandelic acid (Hmand) to give $Ru_3(\mu\text{-}O)(mand)_6(H_2O)_3(mand)$ and $Ru_2(mand)_4(H_2O)_2$. Other disproportionations of chlorotetra-μ-acetatediruthenium(II,III) have been observed by Wilkinson and co-workers.[28,29]

The formation of an oxo-dimer instead of an oxo-trimer, as described by Cotton *et al.*,[27] could be due to the lower stability of the oxo-trimer in solution with the ligand triphenylphosphine compared with the oxo-dimer. The reaction of $[Ru_2(\mu\text{-}O_2CCH_3)_4(thf)_2]BF_4$ with PPh_3 must lead initially to the substitution of the thf ligands by PPh_3, giving $[Ru_2(\mu\text{-}O_2CCH_3)_4(PPh_3)_2]BF_4$. This compound must be unstable, giving a ruthenium(III) compound, **2**, and one of ruthenium(II), $Ru_2(\mu\text{-}O_2CCH_3)_4(PPh_3)_2$. The ruthenium(II) compound undergoes a coupling reaction giving a tetramer compound of the type $[Ru(\mu\text{-}O_2CCH_3)(O_2CCH_3)(PPh_3)]_4$. This compound is slowly converted in toluene solution to **1** (Scheme 1).

The behaviour of the tetra-μ-acetatediruthenium(II,III) unit towards the triphenylphosphine ligand contrasts with the existence of other adducts of the type $[Ru_2(\mu\text{-}O_2CH_3)_4L_2]^+$.[15,30,31] On the other hand, it has been demonstrated, by electrochemical studies,[32] that the tetra-μ-acetatediruthenium(III,III) unit cannot be obtained. Although some studies have questioned the π-acceptor character of the triphenylphosphine,[33] the existence of empty orbitals of low energy in this ligand can permit the existence of a π-backbonding interaction. Thus, the triphenylphosphine ligand could produce a decrease in the electron density of the $[Ru_2(\mu\text{-}O_2CCH_3)_4]^+$ unit, similar to that observed in the oxidation process of this core, leading to the rupture of the metal—metal bond.

Finally, although the oxo-dimer compound is also formed in the reaction of $Ru_2Cl(\mu\text{-}O_2CCH_3)_4$ with triphenylphosphine in alcohol,[11,13] MeCN[13] or MeCN–H_2O,[14] the mechanism of formation of this compound could be different from that observed in the reaction of $[Ru_2(\mu\text{-}O_2CCH_3)_4(thf)_2]BF_4$ and triphenylphosphine in thf or toluene described above.

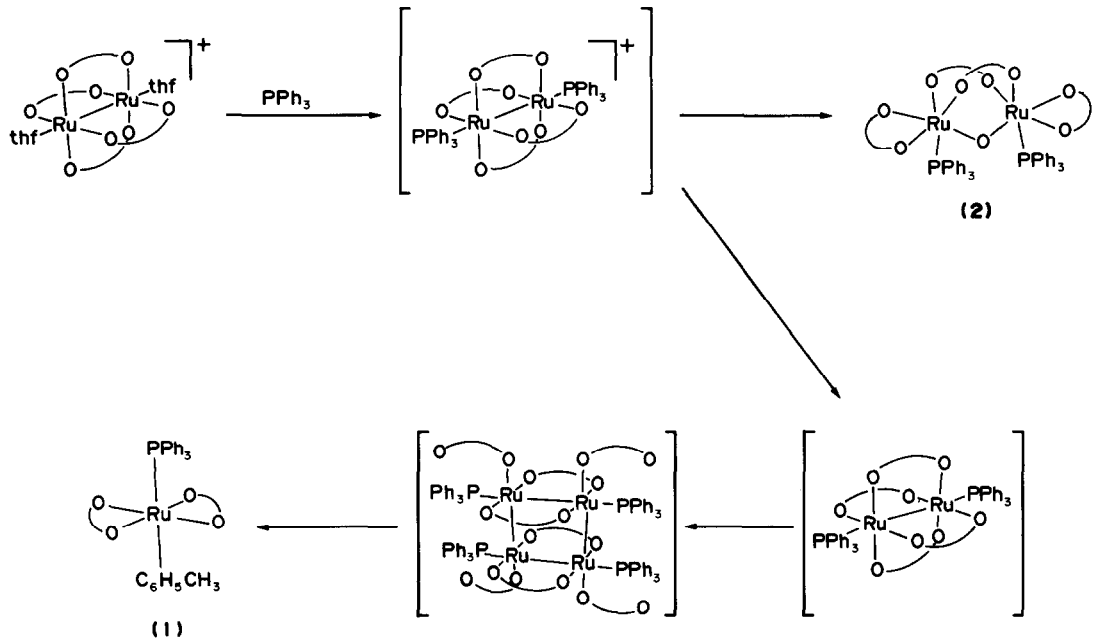

Scheme 1. Proposed mechanism for the formation of **1** and **2**.

EXPERIMENTAL

Ruthenium trichloride, triphenylphosphine and sodium acetate were purchased from commercial sources and used without purification. Tetrahydrofuran, toluene and diethyl ether were distilled from sodium/benzophenone. Dichloromethane was distilled from calcium hydride. Methanol was used without previous purification. The preparative method for $[Ru_2(\mu\text{-}O_2CCH_3)_4(thf)_2]BF_4$ is available in a previous report.[17] All manipulations were performed under a nitrogen atmosphere using Schlenk techniques.

All ^1H, ^{13}C and ^{31}P spectra were recorded with a Varian VXR-300 spectrometer using $CDCl_3$ as solvent. ^1H and ^{13}C NMR chemical shifts are reported in ppm relative to TMS and ^{31}P NMR chemical shifts are reported in ppm relative to external 85% H_3PO_4. IR spectra were recorded on a Perkin–Elmer 1330 as KBr disks. FAB mass spectra were obtained on a Kratos MS-80 mass spectrometer. Magnetic measurements were made with a magnetometer DSM-5 in the range 85–295 K. Elemental analyses were performed on a Perkin–Elmer 240B microanalyser.

Synthesis of $Ru(O_2CCH_3)_2(PPh_3)\cdot CH_3C_6H_5$ (1)

To a solution of $[Ru_2(\mu\text{-}O_2CCH_3)_4(thf)_2]BF_4$ (0.5 g, 0.75 mmol) in thf (30 cm^3) was added PPh_3 (0.78 g, 2.99 mmol). The solution was stirred at room temperature overnight and changed from red to violet. The solvent was removed to leave a dry residue, which was extracted with toluene (3×20 cm^3). The combined extracts were treated with active carbon and filtered. The solution was allowed to stand for 4 days to obtain a yellow crystalline solid, and the crystals were isolated by filtration, washed with toluene (2×5 cm^3) and dried in a stream of nitrogen. Yield: 28%. Found: C, 50.6; H, 4.9. Calc. for $Ru(O_2CCH_3)_2(PPh_3)\cdot CH_3C_6H_5$: C, 60.7; H, 5.1%.

Synthesis of $Ru_2(\mu\text{-}O)(\mu\text{-}O_2CCH_3)_2(O_2CCH_3)_2(PPh_3)_2$ (2)

Procedure 1. The residual solution from the preparation of **1** was pumped dry. The violet solid obtained was washed with cold diethyl ether (2×5 cm^3) and dried *in vacuo*. Yield: 32%. Found: C, 54.0; H, 4.7. Calc. for $Ru_2(\mu\text{-}O)(\mu\text{-}O_2CCH_3)_2(O_2CCH_3)_2(PPh_3)_2$: C, 54.0; H, 4.3%.

Procedure 2. The preparation of this complex as methanol solvate was achieved by an improved method from that previously described by Wilkinson and co-workers.[11] A mixture of $RuCl_3\cdot 3H_2O$ (0.15 g, 0.57 mmol), PPh_3 (0.30 g, 1.15 mmol) and $NaO_2CCH_3\cdot 3H_2O$ (0.31 g, 2.29 mmol), in methanol (40 cm^3), was heated at reflux for 15 min, during which time the solution changed to violet. After which, a slow stream of oxygen was bubbled for 30 min through the boiling solution. On cooling to room temperature, the violet solution

was filtered and the solvent was concentrated under reduced pressure to one-third of its initial volume. On standing at −15° for 12 h, violet crystals of the product were formed. Found: C, 53.3; H, 4.6. Calc. for $Ru_2(\mu\text{-}O)(\mu\text{-}O_2CCH_3)_2(O_2CCH_3)_2(PPh_3)_2 \cdot CH_3OH$: C, 53.5; H, 4.6%.

More violet product can be obtained from the mother liquor when this is pumped dry; the obtained solid is washed with diethyl ether and extracted with toluene. The resulting solution is evaporated to dryness to give the unsolvated violet compound. Total yield: 65%.

X-ray crystallographic procedures

A violet prismatic single crystal of $Ru_2(\mu\text{-}O)(\mu\text{-}O_2CCH_3)_2(O_2CCH_3)_2(PPh_3)_2$ was introduced into a Lindeman capillary and mounted on a Nonius CAD-4 diffractometer. The unit cell dimensions were determined by least-squares refinement of the observed setting angles of 25 accurately centred reflections. The crystal data are summarized in Table 4. Intensities within $1 < 2\theta < 30°$ were measured at 295 K, considering as observed those with $I > 2\sigma(I)$. The data were corrected for Lorentz and polarization effects. Scattering factors for neutral atoms and anomalous dispersion corrections for ruthenium and phosphorus were taken from *International Tables for X-ray Crystallography*.[35]

The structure was solved by conventional Patterson and Fourier techniques. An empirical absorption correction,[36] applied at the end of the isotropic refinement using unit weights, led to a conventional R value of 0.085. The hydrogen atoms were fixed at the calculated positions. Final refinement with fixed atomic coordinates and isotropic temperature factors for hydrogen atoms and unit weights led to $R = 0.067$. Most of the calculations were performed with X-ray 80.[37]

Complete tables of distances and angles as well as atomic positional and anisotropic thermal parameters and structure factors have been deposited as supplementary material.

Table 4. Crystallographic data for $Ru_2(\mu\text{-}O)(\mu\text{-}O_2CCH_3)_2(O_2CCH_3)_2(PPh_3)_2$ (**2**)

Formula	$Ru_2O_9C_{44}H_{42}P_2$
Fw	978.9
Space group	$P2_1/n$
a (Å)	23.209(4)
b (Å)	10.205(3)
c (Å)	19.927(3)
β (°)	98.56(1)
V (Å^3)	4667.1
Z	4
$d_{calc.}$ (g cm^{-3})	1.39
Crystal dimensions (mm^3)	0.2 × 0.3 × 0.2
μ(Mo-K_α) (cm^{-1})	7.49
Radiation, λ (Å)	Mo-K_α, 0.71069
Temperature (K)	295
Data collection range 2θ (°)	$1 < \theta < 30$
Number of reflections used	2378 [$I > 2\sigma(I)$]
R^a	0.067
R_w^b	0.092

[a] $R = \Sigma ||F_o| - |F_c|| \Sigma F_o$.
[b] $R_w = [\Sigma w(|F_o| - |F_c|)^2 / \Sigma w|F_o|^2]^{1/2}$; $w = 1/\sigma^2(|F_o|)$.

Acknowledgement—We are grateful to the Dirección General de Investigación Científica y Técnica (DGICYT) (Spain) for financial support (project PS87-0028).

REFERENCES

1. F. A. Cotton and R. A. Walton, *Struct. Bonding* 1985, **1**. 62.
2. F. A. Cotton and R. A. Walton, *Multiple Bonds Between Metal Atoms*. Wiley, New York (1982).
3. T. R. Felthouse, *Prog. Inorg. Chem.* 1982, **29**, 73.
4. J. L. Templeton, *Prog. Inorg. Chem.* 1979, **26**, 211.
5. E. B. Boyar and S. T. Robinson, *Coord. Chem. Rev.* 1983, **50**, 109.
6. R. J. H. Clark and A. J. Hempleman, *Inorg. Chem.* 1989, **28**, 746 and refs therein.
7. D. J. Santure, J. C. Huffman and A. P. Sattelberger, *Inorg. Chem.* 1984, **23**. 938.
8. D. J. Santure and A. P. Sattelberger, *Inorg. Chem.* 1985, **24**, 3477.
9. P. Legzdins, R. W. Mitchell, G. L. Rempel, J. D. Ruddick and G. Wilkinson, *J. Chem. Soc. A* 1970, 3322.
10. F. A. Cotton and J. G. Norman Jr, *Inorg. Chim. Acta* 1972, **6**, 411.
11. R. W. Mitchell, A. Spencer and G. Wilkinson, *J. Chem. Soc., Dalton Trans.* 1973, 846.
12. S. K. Mandal and A. R. Chakravarty, *Inorg. Chim. Acta* 1987, **132**, 157.
13. B. K. Das and A. R. Chakravarty, *Inorg. Chem.* 1990, **29**, 1783.
14. A. P. Chakravarty, F. A. Cotton and D. A. Tocher, *J. Am. Chem. Soc.* 1984, **106**, 6409.
15. A. R. Chakravarty and F. A. Cotton, *Inorg. Chem.* 1985, **24**, 3584.
16. A. R. Chakravarty, F. A. Cotton and D. A. Tocher, *Inorg. Chem.* 1984, **23**, 4030.
17. F. A. Urbanos, M. C. Barral and R. Jiménez-Aparicio, *Polyhedron* 1988, **7**, 2597.
18. A. Llobet, M. E. Curry, H. T. Evans and T. J. Meyer, *Inorg. Chem.* 1989, **28**, 3131.
19. P. Neubold, K. Wieghardt, B. Nuber and J. Weiss, *Angew. Chem. Int. Ed. Engl.* 1988, **27**, 933.
20. P. Neubold, K. Wieghardt, B. Nuber and J. Weiss, *Inorg. Chem.* 1989, **28**, 459.
21. Y. Sasaki, M. Suzuki, A. Tokiwa, M. Ebihara, T.

Yamaguchi, C. Kabuto and T. Ito, *J. Am. Chem. Soc.* 1988, **110**, 6251.
22. A. Spencer and G. Wilkinson, *J. Chem. Soc., Dalton Trans.* 1972, 1570.
23. A. Spencer and G. Wilkinson, *J. Chem. Soc., Dalton Trans.* 1974, 786.
24. S. Davis and R. S. Drago, *Inorg. Chem.* 1988, **27**, 4759.
25. C. K. Johnson, ORTEP, Report ORNL-3794. Oak Ridge National Laboratory, Tennessee (1965).
26. R. N. McGinnis, T. R. Ryan and R. E. McCarley, *J. Am. Chem. Soc.* 1978, **100**, 7900.
27. F. A. Cotton, V. M. Miskowski and B. Zhong, *J. Am. Chem. Soc.* 1989, **111**, 6177.
28. A. J. Lindsay, R. P. Tooze, M. Motevally, M. B. Hursthouse and G. Wilkinson, *J. Chem. Soc., Chem. Commun.* 1984, 1383.
29. R. P. Tooze, G. Wilkinson, M. Motavally and M. B. Hursthouse, *J. Chem. Soc., Dalton Trans.* 1986, 2711.
30. M. C. Barral, R. Jiménez-Aparicio, E. C. Royer, C. Ruíz-Valero, F. A. Urbanos, E. Gutierrez-Puebla and A. Monge, *Polyhedron* 1989, **8**, 2571.
31. A. Bino, F. A. Cotton and T. R. Felthouse, *Inorg. Chem.* 1979, **8**, 2599.
32. F. A. Cotton, M. Matusz and B. Zhong, *Inorg. Chem.* 1988, **27**, 4368.
33. Md. M. Rahman, H. Liu, K. Eriks, A. Prock and W. P. Giering, *Organometallics* 1989, **8**, 1.
34. M. Nardelli, A. Musatti, P. Domiano and G. D. Andreeti, *Ric. Sci. Parte 2: Sez. A* 1965, **8**, 807.
35. *International Tables for X-ray Crystallography*, Vol. IV, pp. 72–98. Kynoch Press, Birmingham (1974).
36. N. Walker and D. Stuart, *Acta Cryst.* 1983, **A39**, 158.
37. J. M. Stewart, F. A. Kundell and J. C. Baldwin, *The X-ray 80System*. Computer Science Center, University of Maryland, College Park, Maryland (1980).

Polyhedron Vol. 10, No. 1, pp. 121–122, 1991
Printed in Great Britain

0277–5387/91 $3.00+.00
© 1991 Pergamon Press plc

BIS(ACETATO-2,4-PENTANEDIONATO)DIZINC: REFORMULATION OF A ZINC CARBOXYLATE DIKETONATE COMPLEX

PETER G. PRITCHARD and PETER THORNTON*

Department of Chemistry, Queen Mary and Westfield College, University of London, Mile End Road, London E1 4NS, U.K.

(*Received* 10 *August* 1990; *accepted* 12 *September* 1990)

Abstract—NMR (^{1}H) spectra, supported by IR data, show that the compound previously formulated as $Zn_2(O_2CCH_3)(acac)_3$ (acac = 2,4-pentanedionate) is in fact $Zn(O_2CCH_3)$(acac), which probably has a dimeric structure with bridging acetate ligands.

Mixed carboxylate diketonate complexes of stoichiometry $[M(RCO_2)\{R'C(O)CHC(O)R''\}]$ have been recorded for a few transition elements. The most thorough investigations have been carried out on eight rhodium(II) complexes.[1] These studies involved acetate complexes of a number of diketonates, some fluorinated. The use of ^{1}H and ^{19}F NMR and IR spectra strongly indicated a structure (I) which can be considered as derived from

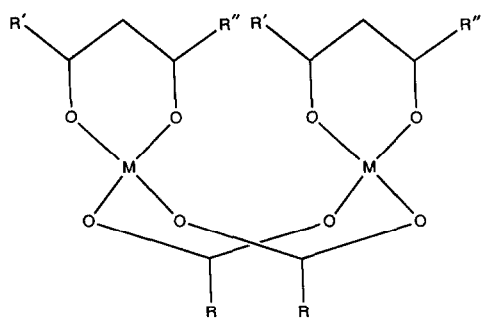

(I)

the familiar dimeric $[M_2(O_2CR)_4]$ structure for carboxylates,[2] well-known for rhodium(II),[3] by replacement of two of the four bridging carboxylate ligands by diketonates. These ligands are more likely to coordinate in a bidentate fashion to one Rh atom than to bridge two, giving complexes with the dimeric formulation $[Rh_2(O_2CR)_2\{R'C(O)CHC(O)R''\}_2]$. Most of the complexes contained two axial ligands (water, pyridine, etc.) along the line of the Rh—Rh bond, required by the complexes' diamagnetism.

Some cobalt(II) analogues have also been prepared using long chain carboxylates.[4] These were suggested to be trimers or tetramers but the evidence is ambiguous. The copper(II) complex $Cu(O_2CCl_3)$(acac) has also been reported.[5] For this complex the magnetic moment was given as $1.93\mu_B$ (temperature not stated) and it was suggested that the compound was monomeric. However, the IR data and green colour also fit structure **I** which avoids the constraint of a four-membered ring required by a chelating acetate, while the magnetic moment was not confirmed by measurements over a temperature range. Calcium acetate reacts with ammonium pentanedionate in water to give $[Ca(O_2CCH_3)(acac)(OH_2)_2]$, but the necessity to accommodate two water molecules on each calcium atom results in an eight-coordinate polymeric structure,[6] the only one to be confirmed crystallographically in this area.

With these results in mind we were surprised to read[7] that 2,4-pentanedione reacts with Zn $(O_2CCH_3)_2(OH_2)_2$ to give, apparently, $Zn_2(O_2CCH_3)(acac)_3$ which was formulated as the $[Zn(acac)_3]^-$ salt of the improbable cation $[Zn(O_2CCH_3)]^+$. We have reinvestigated this reaction.

We have found that the white solid reported[7] to form from this reaction is indeed produced. However, the ^{1}H NMR spectrum in $CDCl_3$ showed the methyl protons (δ2.0) to be nine times as abundant as the γ-H protons of the diketonate. This can only be

* Author to whom correspondence should be addressed.

reconciled with the formula $Zn(O_2CCH_3)(acac)$; the earlier formulation of $Zn_2(O_2CCH_3)(acac)_3$ requires a methyl to γ-proton ratio of 7:1. The acetate protons could not be distinguished from those of the diketonate. It is possible that the earlier workers were misled by erroneous elemental analyses, as we found the carbon content of our product to be appreciably higher than that required by the formula. Nevertheless, the NMR and IR spectra are very clean and there is no insoluble residue when the compound is dissolved in $CDCl_3$ or common organic solvents.

The formula $Zn(O_2CCH_3)(C_5H_7O_2)$ indicated by the NMR spectrum suggests that zinc resembles rhodium(II) in forming the dinuclear structure (**I**), which would avoid the improbabilities of three-coordination from monodentate acetate and a strained four-membered chelate ring given by bidentate acetate in monomeric formulations. The observation of CO_2 stretching frequencies at 1520 and 1400 cm^{-1} supports the dimeric formulation, but does not distinguish this from acetate chelation.[8] An interesting question, which the material's non-crystallinity prevented us answering, is whether zinc would adopt the square planar disposition of oxygens which is probably found in the rhodium compounds of structure **I**, or whether there is some distortion towards the tetrahedral geometry more usually found in zinc chemistry.

EXPERIMENTAL

Reagents were all commercially available. Spectroscopic techniques have already been described.[9]

$Zn(O_2CCH_3)(C_5H_7O_2)$

Zinc acetate dihydrate (1.00 g, 4.56 mmol) was dissolved in an excess of boiling 2,4-pentanedione (10 cm^3), and the resulting solution was concentrated by prolonged heating on a hotplate, after which it was filtered hot. On cooling, the product separated out as a white powder which was filtered off, washed with petroleum ether (60–80°C) and dried. Yield 0.77 g, 75.6%. Found: C, 40.0; H, 4.7%. $C_7H_{10}O_4Zn$ requires: C, 37.61; H, 4.52%.

Acknowledgement—We thank the SERC for a research studentship to P.G.P.

REFERENCES

1. S. Cenini, R. Ugo and F. Bonati, *Inorg. Chim. Acta* 1967, **1**, 443.
2. J. Catterick and P. Thornton, *Adv. Inorg. Chem. Radiochem.* 1977, **20**, 291.
3. T. R. Felthouse, *Progr. Inorg. Chem.* 1982, **29**, 73.
4. O. P. Singh, B. P. Baranwal and S. C. Tripathi, *Ind. J. Chem.* 1985, **24A**, 118.
5. M. M. Aly, *Inorg. Nucl. Chem. Lett.* 1973, **9**, 253.
6. J. J. Sahbari and M. M. Olmstead, *Acta Cryst.* 1985, **41C**, 360.
7. G. Rudolph and M. C. Henry, *Inorg. Chem.* 1964, **3**, 1317; 1965, **4**, 1076.
8. G. B. Deacon and R. J. Phillips, *Coord. Chem. Rev.* 1980, **33**, 227.
9. M. B. Hursthouse, O. D. Sloan, P. Thornton and N. P. C. Walker, *Polyhedron* 1986, **5**, 1475.

Polyhedron Vol. 10, No. 1, pp. 123–126, 1991
Printed in Great Britain

0277–5387/91 $3.00+.00
© 1991 Pergamon Press plc

COMMUNICATION

ANIONIC, FOUR-COORDINATE, 10-ELECTRON BISMUTH COMPLEXES

WILLIAM CLEGG, NEVILLE A. COMPTON, R. JOHN ERRINGTON, GEORGE A. FISHER, DAVID C. R. HOCKLESS and NICHOLAS C. NORMAN†

Department of Chemistry, The University, Newcastle upon Tyne NE1 7RU, U.K.

and

A. GUY ORPEN

Department of Inorganic Chemistry, The University, Bristol BS8 1TS, U.K.

(*Received* 7 *September* 1990; *accepted* 25 *September* 1990)

Abstract—The synthesis and structures of $[PPN][BiCl_2\{Fe(CO)_2(\eta\text{-}C_5H_5)\}_2]$ and $[PPN][BiCl_2\{Mo(CO)_3(\eta\text{-}C_5H_5)\}_2]$ (PPN = Ph_3PNPPh_3) are described; both bismuth complexes adopt structures intermediate between tetrahedral and equatorially vacant trigonal bipyramidal, possible electronic reasons for which are presented and discussed.

The syntheses of the bismuth complexes $[BiCl\{Fe(CO)_2(\eta\text{-}C_5H_4R)\}_2]$ [R = H (**1a**); R = Me (**1b**)][1] and $[BiCl\{Mo(CO)_3(\eta\text{-}C_5H_5)\}_2]$ (**2**)[2] have recently been described and, in the solid state, these compounds oligomerize by way of intermolecular bismuth–chlorine interactions such that the former exists as a cyclotrimer (**X**)[1] whilst the latter forms one-dimensional infinite chains (**Y**).[2] Solution

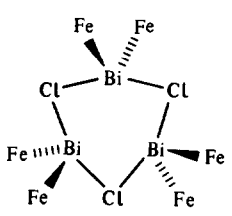

(**X**)

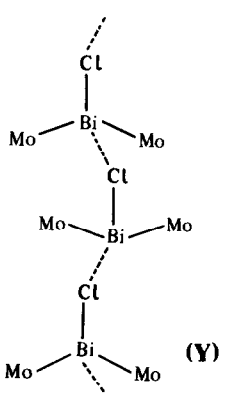

(**Y**)

EXAFS data obtained for **2** in THF solution, however, show that the species present is probably $[BiCl(THF)\{Mo(CO)_3(\eta\text{-}C_5H_5)\}_2]$ (**2a**).[3] These structural data, which will be discussed in more detail in a future publication,[3] indicate that the bismuth centres in **1** and **2** have appreciable Lewis acidic character, in common with many BiX_3 species, and therefore that discrete acid–base adducts of the general formula $(ML_n)_2BiCl(L)$ should be reasonable targets for chemical synthesis. Moreover, the nature of **2** in THF (i.e. **2a**) implies that such compounds might be monomeric, and thus furnish examples of four-coordinate, 10-electron bismuth species, rather than the dimeric or oligomeric structures more usually observed [e.g. $Bi_2Cl_8^{2-}$, $(BiBr_4)_n^{n-}$][4].

Accordingly, we examined the reaction between **1a**/**2** and [PPN]Cl (PPN = Ph_3PNPPh_3). Treatment of either **1a** or **2**, in THF solution, with one equivalent of solid [PPN]Cl led to no observable colour change (both **1** and **2** are dark green), but after stirring for 24 h, filtration through Celite and crystallization from THF–hexane mixtures, > 90% yields of the dark green crystalline complexes $[PPN][BiCl_2\{Fe(CO)_2(\eta\text{-}C_5H_5)\}_2]$ (**3**) and $[PPN][BiCl_2\{Mo(CO)_3(\eta\text{-}C_5H_5)\}_2]$ (**4**) were

† Author to whom correspondence should be addressed.

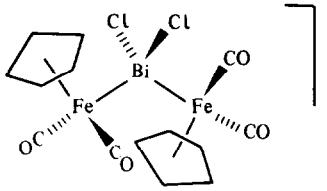

(3)

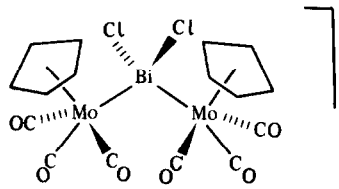

(4)

obtained. Spectroscopic and analytical data† were consistent with the anticipated formulae and their structures were confirmed by X-ray crystallography,‡ the results of which are shown in Figs 1 and 2. Both structures contain isolated $[PPN]^+$ cations and $[BiCl_2(ML_n)_2]^-$ anions with no short interionic contacts. In the anions, a central bismuth atom is bonded to two chlorine atoms and either two $Fe(CO)_2(\eta\text{-}C_5H_5)$ fragments (**3**) or two $Mo(CO)_3(\eta\text{-}C_5H_5)$ fragments (**4**). In complex **3** the

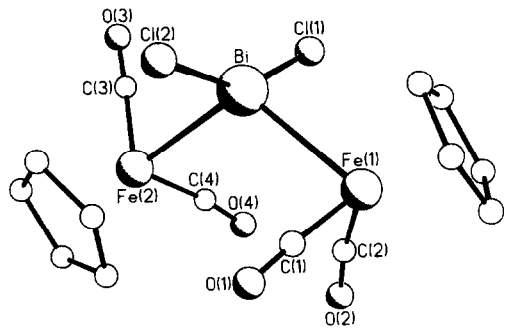

Fig. 1. A view of the molecular structure of $[BiCl_2\{Fe(CO)_2(\eta\text{-}C_5H_5)\}_2]^-$ (**3**), hydrogen atoms omitted for clarity; important bond lengths (Å) and angles (°):

Bi—Cl(1)	2.773(6)	Bi—Fe(1)	2.679(3)
Bi—Cl(2)	2.818(8)	Bi—Fe(2)	2.679(3)

Cl(1)—Bi—Cl(2)	155.6(2)
Cl(1)—Bi—Fe(1)	98.4(2)
Cl(2)—Bi—Fe(1)	95.6(2)
Cl(1)—Bi—Fe(2)	94.1(2)
Cl(2)—Bi—Fe(2)	99.4(2)
Fe(1)—Bi—Fe(2)	111.4(1)

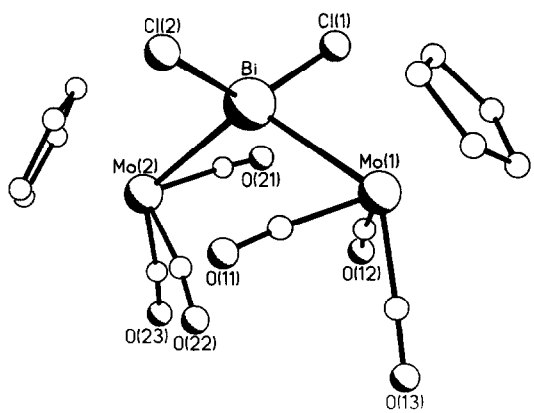

Fig. 2. A view of the molecular structure of $[BiCl_2\{Mo(CO)_3(\eta\text{-}C_5H_5)\}_2]^-$ (**4**), hydrogen atoms omitted for clarity; important bond lengths (Å) and angles (°):

Bi—Cl(1)	2.709(6)	Bi—Mo(1)	2.944(1)
Bi—Cl(2)	2.850(4)	Bi—Mo(2)	3.032(2)

Cl(1)—Bi—Cl(2)	138.5(1)
Cl(1)—Bi—Mo(1)	95.6(2)
Cl(2)—Bi—Mo(1)	96.3(1)
Cl(1)—Bi—Mo(2)	104.0(1)
Cl(2)—Bi—Mo(2)	105.8(1)
Mo(1)—Bi—Mo(2)	116.4(1)

† *Selected spectroscopic data.* $[PPN][BiCl_2\{Fe(CO)_2(\eta\text{-}C_5H_5)\}_2]$ (**3**): IR ν(C≡O) (THF): 1998m, 1974s, 1937m cm^{-1}. NMR ^1H (CD_2Cl_2): δ 4.96 (C_5H_5), 7.6–7.4 (m, phenyls, PPN); $^{13}C\{^1H\}$ (CD_2Cl_2): δ 85.4 (C_5H_5), 134.1, 132.5, 129.9 (m, *o*, *m*, *p* phenyls, PPN). $C_{50}H_{40}Cl_2BiFe_2NO_4P_2$ requires: N, 1.2; C, 51.2; H, 3.4. Found: N, 1.1; C, 50.6; H, 3.2%. $[PPN][BiCl_2\{Mo(CO)_3(\eta\text{-}C_5H_5)\}_2]$ (**4**): IR ν(C≡O) (THF): 2052w, 1996s, 1962m, 1899br, s, 1781m cm^{-1}. NMR ^1H (CD_2Cl_2): δ 5.49 (C_5H_5), 7.7–7.4 (m, phenyls, PPN). $C_{52}H_{40}Cl_2BiMo_2NO_6P_2$ requires: N, 1.1; C, 47.7; H, 3.1. Found: N, 1.1; C, 47.2; H, 2.9%. In the IR spectrum, the absorption at 1781 cm^{-1} is due to $[Mo(CO)_3(\eta\text{-}C_5H_5)]^-$, indicating that some dissociation takes place in this solvent. Full details on the solution-state behaviour of these complexes will be reported in a future full paper.

‡ Crystal data for **3**: $C_{50}H_{40}NO_4P_2Cl_2Fe_2Bi$, $M = 1172.4$, monoclinic, $P2_1/n$, $a = 9.009(2)$, $b = 35.049(9)$, $c = 14.796(5)$ Å, $\beta = 91.81(3)°$, $U = 4669.6$ Å^3, $Z = 4$, $D_c = 1.667$ g cm^{-3}, λ(Mo-K_α) = 0.71073 Å, $\mu = 4.588$ mm^{-1}, $F(000) = 2312$, $T = 295$ K. The structure was determined by Patterson and difference syntheses and refined[5] to a minimum of $\Sigma w\Delta^2$ [$\Delta = |F_o| - |F_c|$, $w^{-1} = \sigma^2(F) = \sigma_c^2(F) + 2 + 792G + 9G^2 - 18S + 150S^2 - 1583GS$, $G = F_o/F_{max}$, $S = \sin\theta/\sin\theta_{max}$][6] from 3564 reflections with $2\theta < 45°$ and $F > 4\sigma_c(F)$ (σ_c from counting statistics only), measured with a Stoë–Siemens diffractometer and on-line profile fitting.[7] Anisotropic thermal parameters were refined for all non-hydrogen atoms. Hydrogen atoms were constrained. Final $R = 0.074$, $R_w = (\Sigma w\Delta^2/\Sigma wF_o^2)^{1/2} = 0.063$ for 487 parameters. For **4**: $C_{52}H_{40}NO_6P_2Cl_2Mo_2Bi$, $M = 1308.6$, monoclinic, $P2_1/c$, $a = 14.197(2)$, $b = 9.556(2)$, $c = 37.190(7)$ Å, $\beta = 92.12(2)°$, $U = 5042.05$ Å^3, $Z = 4$, $D_c = 1.724$ g cm^{-3}, $\mu = 4.166$ mm^{-1}, $F(000) = 2552$, $T = 295$ K. The structure was determined as above [$w^{-1} = \sigma^2(F) = \sigma_c^2(F) + 51 + 353G + 1060G^2 - 133S + 151S^2 - 953GS$] from 4758 reflections with $2\theta < 50°$ and $F > 4\sigma_c(F)$. Final $R = 0.058$, $R_w = 0.064$ for 520 parameters. Atomic coordinates, bond lengths and angles, and thermal parameters have been deposited at the Cambridge Crystallographic Data Centre.

angles and distances around the bismuth atom are similar to those found in **1a** [for **3**, Bi—$Cl_{av.}$ 2.795 Å, Cl(1)—Bi—Cl(2) 155.6(2)°, Fe(1)—Bi—Fe(2) 111.4(1)°; for **1a**,[1b] Bi—$Cl_{av.}$ 2.907 Å, Cl—Bi—$Cl_{av.}$ 154.2°, Fe—Bi—$Fe_{av.}$ 109.8°]. In **2** the Bi—Cl bond lengths are markedly asymmetric (see ref. 2 for details), but the angles at bismuth are similar to those in **4** [for **4**, Cl(1)—Bi—Cl(2) 138.5(1)°, Mo(1)—Bi—Mo(2) 116.4(1)°; for **2**,[2] Cl—Bi—Cl 151.6(1) and 141.6(1)°, Mo—Bi—Mo 118.3(1) and 116.4(1)° for two crystallographically-independent molecules]. The coordination geometry around bismuth for these two structures can be described as between tetrahedral and equatorially vacant trigonal bipyramidal (evtb). As judged by the latter geometry, the chlorine atoms in **3** and **4** are pseudo-axial with the angle α [defined as in Fig. 3] equal to 155.6(2) and 138.5(1)°, respectively. Ideally this angle would be either 109.5 or 180° for the aforementioned limiting geometries.

The only other anionic, 10-electron, four-coordinate bismuth complex, related to **3** and **4** is $[Bi\{Co(CO)_4\}_4]^-$ (**5**), which has been structurally characterized by Leigh and Whitmire[8] and Martinengo *et al.*,[9] and found to be tetrahedral. Clearly a range of structures are possible for $[BiX_y(ML_n)_{4-y}]^-$ complexes, ranging from tetrahedral (**5**) to almost evtb for **3**, with **4** intermediate between the two. Although steric effects cannot be

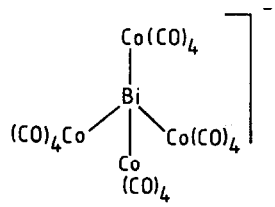

(5)

ruled out as a major contributory factor, an electronic origin involving negative hyperconjugation is a possibility.[10]

In general, the Lewis acidity of the three-coordinate $[BiCl(ML_n)_2]$ species, where ML_n is a 17-electron metal-based fragment such as $Fe(CO)_2(\eta\text{-}C_5H_5)$ (**1**) or $Mo(CO)_3(\eta\text{-}C_5H_5)$ (**2**), derives from the presence of a low-lying Bi—Cl σ^*-orbital. Moreover, the interaction of an incoming nucleophile, here Cl^-, with this orbital leads to a geometry in which the nucleophile is approximately *trans* to the pre-existing Bi—Cl bond which accounts for the observed positions of the chlorine atoms around the bismuth centres in **1**–**4**. However, the pseudo-axial Bi—Cl σ^*-orbital (**A**) of the resulting acid–base adduct will fall in energy as the Cl—Bi—Cl angle (α) decreases, as illustrated in Fig. 3,[11] due to a decrease in overlap and a corresponding reduction of antibonding character. In addition this orbital (**A**) can also play an important role in Bi—ML_n π-

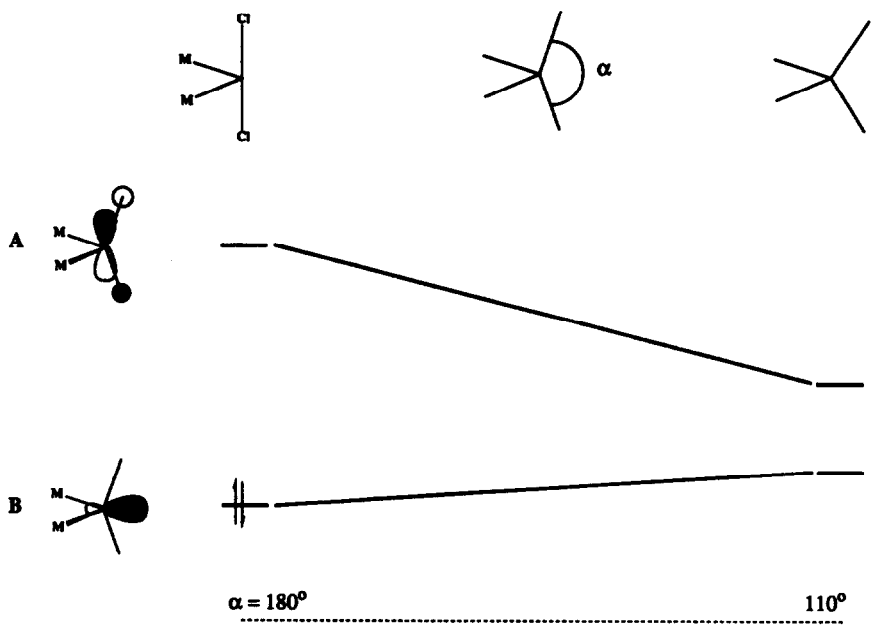

Fig. 3. Partial orbital correlation diagram[11] for the equatorially vacant trigonal bipyramidal to tetrahedral distortion of a $[BiCl_2(ML_n)_2]^-$ fragment (ML_n = 17-electron metal fragment).

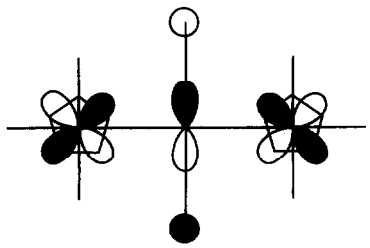

(C)

bonding as shown in **C** (see refs 10 and 12 for discussion of similar π-interactions). The effectiveness of the π-overlap will be enhanced by lowering the energy of orbital **A**, and (partial) occupancy of **A** will, therefore, promote a reduction of the angle α. Thus the presence of π-donating substituents (Z) in the pseudo-equatorial sites of a $BiCl_2Z_2$ species would be expected to lead to a distortion of the sort depicted in Fig. 3, and observed in **3** and **4**. Further evidence that metal-to-bismuth π-donation is present is provided by the observed orientations of the $Mo(CO)_3(\eta\text{-}C_5H_5)$ fragments in **4**. $(C_5H_5)ML_3$ fragments have two π-donor orbitals as described in detail in ref. 13. One of these, which lies in a plane orthogonal to the symmetry plane of the fragment, is the better disposed towards π-bonding and the orientation of both molybdenum-based fragments in **4** is such as to allow overlap of this orbital with the π-acceptor bismuth-based orbital **A**. This is shown diagrammatically in **C**.† Similar arguments can be advanced to account for the orientation of the $Fe(CO)_2(\eta\text{-}C_5H_5)$ fragments in both **1** and **3**.[3] It remains to be shown whether these distortions are indeed sterically or electronically driven, but π- to σ^*-donation, or negative hyperconjugation, is known to have pronounced effects on the angles within hypervalent main group compounds.[10] We note, also, that tetrahedral **5** is paramagnetic,[8] implying that the HOMO–LUMO gap is small or zero. As indicated in Fig. 3, this is to be expected if the "lone pair" orbital **B** is sufficiently destabilized, and the Bi—X σ^*-orbital(s) sufficiently stabilized by reduction of the X—Bi—X angles to tetrahedral values.

Further synthetic, structural and theoretical studies on these and related compounds are in progress.

Acknowledgement—We thank the SERC for financial support.

REFERENCES

1. (a) W. Clegg, N. A. Compton, R. J. Errington and N. C. Norman, *J. Chem. Soc., Dalton Trans.* 1988, 1671; (b) J. M. Wallis, G. Müller and H. Schmidbaur, *J. Organomet. Chem.* 1987, **325**, 159.
2. W. Clegg, N. A. Compton, R. J. Errington, N. C. Norman, A. J. Tucker and M. J. Winter, *J. Chem. Soc., Dalton Trans.* 1988, 2941.
3. N. A. Compton, R. J. Errington, N. C. Norman, P. S. Jarrett, N. A. L. Williams and A. G. Orpen, manuscript in preparation.
4. N. N. Greenwood and A. Earnshaw, *Chemistry of the Elements*. Pergamon Press, Oxford (1984).
5. G. M. Sheldrick, SHELXS-86, Program for Crystal Structure Determination, University of Göttingen (1986); SHELXTL, An Integrated System for Solving, Refining and Displaying Crystal Structures from Diffraction Data, Revision 5 (1985).
6. H. Wang and B. E. Robertson, *Structure and Statistics in Crystallography* (Edited by A. J. C. Wilson), p. 125. Adenine Press, New York (1985).
7. W. Clegg, *Acta Cryst. Sect. A* 1981, **A37**, 22.
8. J. S. Leigh and K. H. Whitmire, *Angew. Chem.* 1988, **100**, 399; *Angew. Chem. Int. Edn Engl.* 1988, **27**, 396.
9. S. Martinengo, A. Fumagalli, G. Ciani and M. Moret, *J. Organomet. Chem.* 1988, **347**, 413.
10. A. E. Reed and P. v. R. Schleyer, *J. Am. Chem. Soc.* 1990, **112**, 1434.
11. See for example, B. M. Gimarc, *Molecular Structure and Bonding*, p. 64. Academic Press, New York (1979); T. A. Albright, J. K. Burdett and M. H. Whangbo, *Orbital Interactions in Chemistry*, p. 268. John Wiley, New York (1985).
12. A. G. Orpen and N. G. Connelly, *Organometallics* 1990, **9**, 1206.
13. P. Kubacek, R. Hoffmann and Z. Havlas, *Organometallics* 1982, **1**, 180.

† For maximum overlap, the conformation about the Bi—Mo bonds should be such that the torsion angles defined as Cl(1), Cl(2) midpoint–Bi—Mo—C_5H_5 ring centroid equal 0°. The observed values in **4** are +29.4 and +12.4° for Mo(2) and Mo(1), respectively. Clearly, on the basis of electronic arguments alone, torsion angles at or close to 180° are also possible and the adoption of angles near 0° (as in **4**) or 180° is probably determined by steric factors.

Polyhedron Vol. 10, No. 1, pp. 127–132, 1991
Printed in Great Britain

0277–5387/91 $3.00+.00
© 1991 Pergamon Press plc

COMMUNICATION

MOLECULAR HELICITY IN INORGANIC COMPLEXES: THE CRYSTAL AND MOLECULAR STRUCTURE OF 2,6-DIACETYLPYRIDINE BIS(6-CHLORO-2-PYRIDYLHYDRAZONE) SILVER(I) HEXAFLUOROPHOSPHATE DIMER

EDWIN C. CONSTABLE,* JEREMY M. HOLMES and PAUL R. RAITHBY

University Chemical Laboratory, Lensfield Road, Cambridge CB2 1EW, U.K.

(*Received* 12 *September* 1990; *accepted* 25 *September* 1990)

Abstract—The crystal and molecular structure of the complex $[Ag_2L^1{}_2][PF_6]_2$ [L^1 = 2,6-diacetylpyridine bis(6-chloro-2-pyridylhydrazone)] have been determined. The cation is binuclear with each silver in a distorted four-coordinate environment, showing weak interactions with a fifth ligand and with a short Ag—Ag distance of 3.142 Å. The two equivalent ligands are wrapped around the binuclear core in a double-helical array. This is stabilized by π-stacking interactions between parallel pyridyl rings. The double-helical array is generated in a spontaneous self-assembly process which is dictated by the relative acceptor properties of the silver(I) ion and the donor properties of the ligand.

There has been considerable recent interest in the design of ligands which facilitate the spontaneous self-assembly of complexes[1–6] and host–guest compounds[7–9] with novel chemical, biological or topological properties. The assembly of double-helical polynuclear complexes has been studied by several groups.[10–24] We have investigated the ability of the oligopyridines to assemble flexible, but non-labile, double-helical ligand environments with a view to designing photo- and redox-active binuclear complexes.[18–24] The double-helical ligand array may be viewed as a spring which can expand or contract; in molecular terms this allows the accommodation of a wide range of metal–metal distances within the same ligand array, a feature that is not commonly observed in macrocyclic systems. In order to further probe the subtle features dictating the formation of the double-helical array, we have investigated the use of sterically demanding ligands related to the oligopyridines, and we report herein the crystal and molecular structure of the silver(I) complex of the potentially pentadentate ligand 2,6-diacetylpyridine bis(6-chloro-2-pyridylhydrazone) (L^1).

* Author to whom correspondence should be addressed.

EXPERIMENTAL

The ligand 2,6-diacetylpyridine bis(6-chloro-2-pyridylhydrazone) and its silver complex were prepared as previously reported.[25] ^{1}H NMR spectra were recorded on a Bruker WM250 spectrometer at ambient temperature.

Crystal structure determination

Pale yellow prisms of the complex were obtained by the recrystallization of $[Ag_2L^1{}_2][PF_6]_2$ from hot methanol. The crystals were stable in air, and several were mounted on glass fibres. The space group and unit cell dimensions were derived from preliminary Weissenberg photography. Pertinent crystallographic parameters are given in Table 1.

The position of the silver atom was determined from the Patterson function. Remaining non-hydrogen atoms were determined from Fourier difference maps. The structure was refined (Ag, Cl, P, F, N and C anisotropic, H isotropic in calculated positions; C—H, 1.08 Å) to $R = 0.0490$ ($R_w = 0.0554$). A final difference map showed no significant regions of electron density except for ripples of *ca* 0.75 e Å^{-3} close to the position of the

Table 1. Crystallographic data for $[Ag_2L^1{}_2][PF_6]_2$

Formula	$Ag_2C_{38}F_{12}H_{34}N_{14}P_2$
fw	1334.3
Space group	$C2/c$
a (Å)	23.854(3)
b (Å)	13.083(1)
c (Å)	15.505(2)
β (°)	98.36(1)
V (Å^3)	4787
Z	8
$F(000)$	2640
d_{calc} (g cm^{-3})	1.86
Crystal size (mm)	$0.65 \times 0.30 \times 0.21$
μ(Mo-K_α) (cm^{-1})	11.41
Data collection instrument	Stoë-Siemens four-circle
Radiation	Mo-K_α ($\lambda = 0.7107$ Å)
Data collection range	$20 \leqslant 2\theta \leqslant 30.0°$
Temperature (°C)	20
Number of unique data	3129
Total with $F \geqslant 4\sigma(F)$	2750
R^a	0.0490
R'^b	0.0554
Weighting scheme	$w = 0.541/[\sigma^2F + 0.001F^2]$
Largest peak (e/Å^3)	0.75

$^a R = \Sigma\,[|F_o| - |F_c|]/\Sigma\,|F_o|$.

PF_6^- anion. Scattering factors were taken from ref. 9. Calculations were performed using SHELX 76 on the IBM 370/165 computer at the University of Cambridge.[27] Selected dimensions within the coordination sphere are presented in Table 2. Tables of all final coordinates and thermal parameters, bond lengths, bond angles, hydrogen atom coordinates and tables of observed and calculated structure factors have been deposited with the Editor, from whom copies are available.

RESULTS AND DISCUSSION

We have previously reported the preparation and coordination chemistry of pentadentate N_5-donor macrocyclic ligands incorporating a 2,2′:6′,2″-terpyridyl functionality (L^2, R = H or Ph).[28–34] These macrocyclic ligands are relatively inflexible and possess a bonding cavity with a "hole-size" of 2.1 ± 0.5 Å. In contrast, the open-chain ligand 2,2′:6′,2″:6″,2‴:6‴,2⁗-quinquepyridine (L^3) possesses considerably more flexibility. In a planar configuration, L^3 presents the five nitrogen atoms to the metal with an effective "hole-size" of 2.45 ± 0.3 Å.

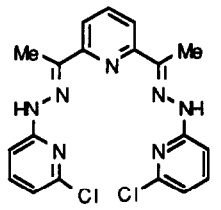

L^1

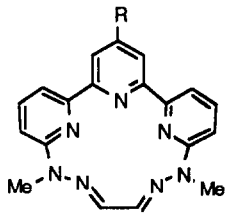

L^2

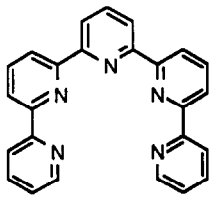

L^3

This corresponds to a pentagonal-planar geometry for metals with an ionic radius 1.0 ± 0.1 Å, and we have recently demonstrated such a geometry (with *no* axial interactions) in the complex $[AgL^3][PF_6]$.[22] The introduction of sterically demanding substituents into analogues of L^3 is

Table 2. Bond lengths (Å) and interbond angles (°) within the coordination sphere of the cation for $[Ag_2L^1{}_2][PF_6]_2$

Ag(1)—N(1)	2.428(4)	Ag(1)—N(2)	2.324(5)
Ag(1)—N(5)	2.371(5)	Ag(1)—N(7)	2.320(5)
Ag(1)···Ag(1a)	3.141(1)		
N(1)—Ag(1)—N(5)	133.8(1)	N(1)—Ag(1)—N(2)	70.0(1)
N(2)—Ag(1)—N(7)	153.4(1)	N(1)—Ag(1)—N(7)	108.5(1)
Ag(1)—N(1)—C(1)	126.1(3)	N(5)—Ag(1)—N(7)	70.2(1)
Ag(1)—N(2)—N(3)	121.2(3)	Ag(1)—N(1)—C(5)	113.2(3)
N(2)—Ag(1)—N(5)	131.0(1)	Ag(1)—N(2)—C(6)	120.1(4)

expected to increase the effective hole-size of the bonding cavity such that silver(I) is too small to be accommodated by the ligand in a planar pentadentate mode.

We have previously shown that the consequence of interaction of potentially planar pentadentate ligands with metal ions which are too small for the bonding cavity in the planar coordination mode is to introduce twisting within the ligand.[18-24] This results in the formation of double-helical binuclear coordination compounds from the interaction of first-row transition metal ions with $\mathbf{L}^3$. This process is illustrated schematically in Fig. 1, which also emphasizes that the double-helical geometry is partially dependent upon the coordination geometry of the metal ions involved. In the case of $\mathbf{L}^3$ complexes of stoichiometry $[M_2\mathbf{L}^3{}_2]^{n+}$ are formed. In these complexes the ligands have twisted around the interannular C—C bonds to adopt the helical configuration. One of the principal structural features of these complexes is the "stacking" of the planar aromatic rings, and this is responsible for the structural integrity of the double-helical array; so favourable is the $[M_2\mathbf{L}^3{}_2]^{n+}$ structural unit that it may be cycled between a range of oxidation levels ($\{Cu^I,Cu^I\}$, $\{Cu^{II},Cu^I\}$ and $\{Cu^{II},Cu^{II}\}$ for example). In fact, the double-helical array of ligands undergoes a "concertina" motion to accommodate the changes in the metal ion radius. We would anticipate that the interaction of $\mathbf{L}^1$ (which is a sterically hindered analogue of $\mathbf{L}^3$) with silver(I) might also lead to the formation of a double-helical ligand array, although the coordination properties of the silver(I) ion might preclude the formation of an octahedral centre.

The structurally developed ligand $\mathbf{L}^1$ is readily prepared by the condensation of 2,6-diacetylpyridine with 6-chloro-2-hydrazinopyridine.[25] The reaction of $\mathbf{L}^1$ with silver(I) hexafluorophosphate in methanol results in the formation of a pale yellow solution, from which pale yellow crystals of a complex of stoichiometry $[Ag\mathbf{L}^1][PF_6]$ separate on cooling.

The IR spectrum of the complex exhibits a strong absorption at 3103 cm^{-1}, which may be assigned to the hydrazino NH stretching mode. This is confirmatory evidence that the ligand has not deprotonated. A strong absorption at 1597 cm^{-1} is assigned to the C=N stretching mode.

The ^1H NMR spectrum (Fig. 2) of a solution of the complex in CD_3COCD_3 is also consistent with the presence of a complex of $\mathbf{L}^1$. The presence of a single methyl resonance centred at δ 2.88 indicates that the two methyl groups in the ligand are equivalent on the NMR time scale. The NH protons are observed as a slightly broadened resonance centred at δ 10.03. The resonances are all shifted with respect to the salt $[H\mathbf{L}^1][PF_6]$ (Table 3). The changes in chemical shift upon coordination ($\Delta\delta$) vary from +0.6 to −0.83, which is indicative of a major

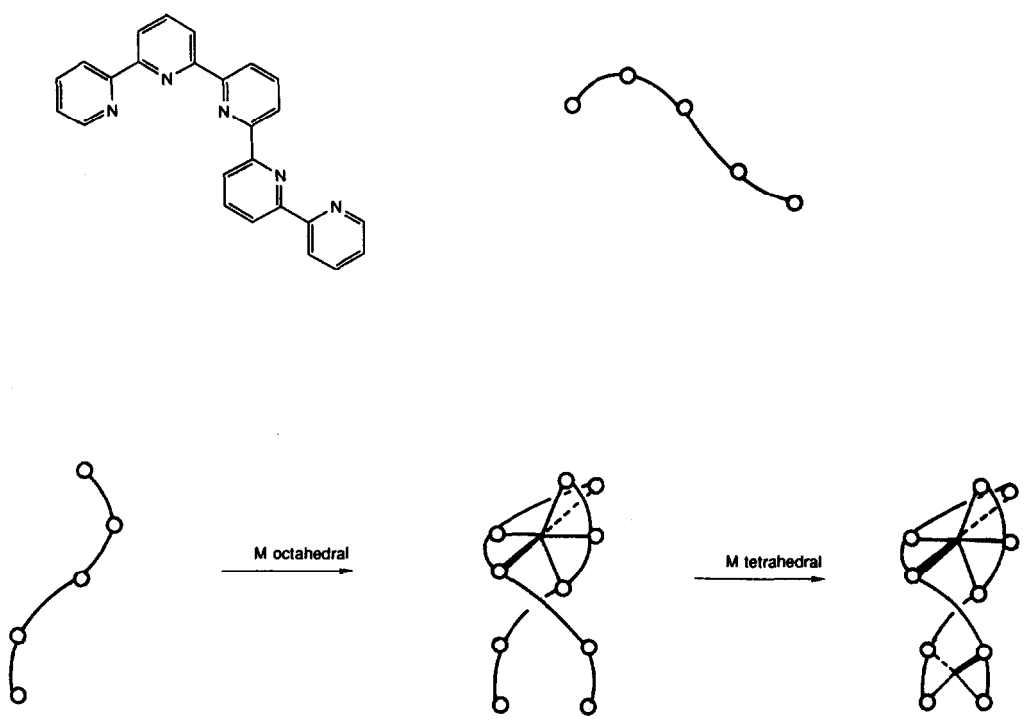

Fig. 1. Schematic representation of the formation of a binuclear double helical complex of $\mathbf{L}^3$.

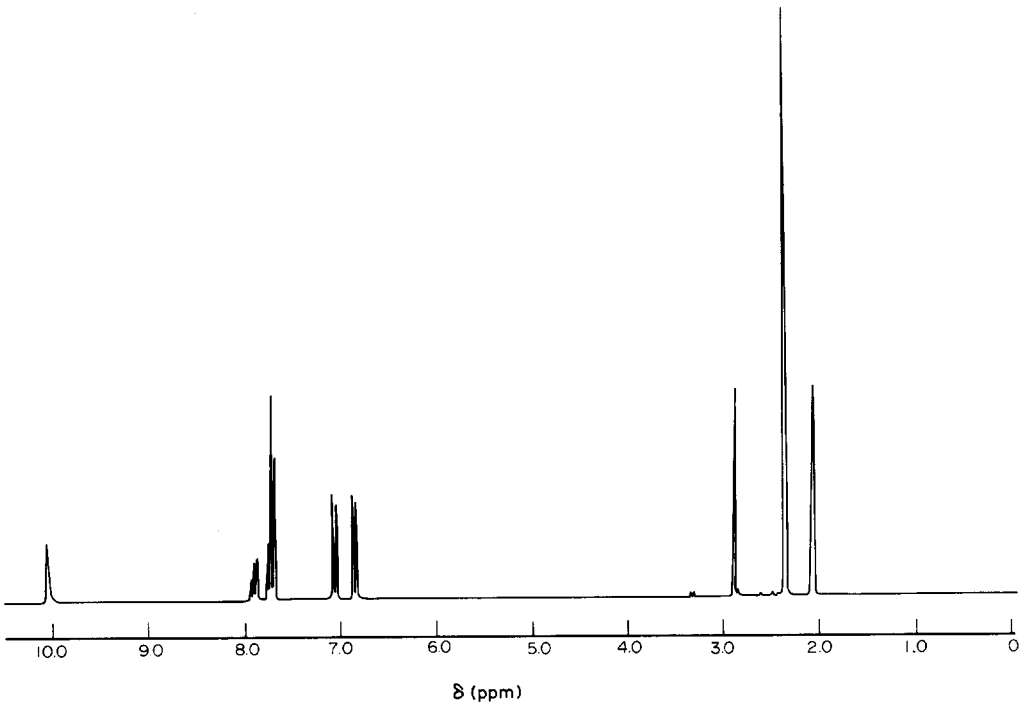

Fig. 2. 250 MHz ^{1}H NMR spectrum of a CD_3COCD_3 solution of $[Ag_2L^1{}_2][PF_6]_2$.

Table 3. ^{1}H NMR chemical shift data for a CD_3COCD_3 solution of $[Ag_2L^1{}_2][PF_6]_2$

Proton	δ	$\Delta\delta$
H(3′,5′)	6.83 (*d*, $J_{3',4'}$ 7.5 Hz)	−0.21
H(4′)	7.88 (*t*, $J_{3',4'}$ 7.5 Hz)	−0.83
H(3,3″)	7.04 (*d*, $J_{3,4}$ 8.3 Hz)	−0.42
H(4,4″)	7.71 (*m*)	+0.60
H(5,5″)	7.71 (*m*)	−0.67

change in ligand environment. We have previously demonstrated that $[HL^1][PF_6]$ adopts a configuration with the pyridyl nitrogen atoms facing *away* from the bonding cavity. If the chemical shift changes were associated simply with the rotation of these pyridyl groups about the C_{ring}—NH bond, dramatic changes are not expected at the central pyridyl ring.

In order to understand more fully the nature of the metal–ligand interactions in this complex we have determined its crystal and molecular structure. The molecular structure of the cation is presented in Fig. 3(a); selected bond parameters are listed in Table 2. The cation is dimeric and of stoichiometry $[Ag_2L^1{}_2]^{2+}$. The two silver atoms are in identical environments, in a very irregular coordination geometry. Each silver atom is bonded to *both* of the ligands, with each ligand acting as a bidentate donor to each metal. The geometry around each silver may be described as a flattened tetrahedron. Each silver is bonded to *one* terminal pyridyl ring [N(7)—Ag, 2.320(4) Å] and the associated imine nitrogen of one ligand [N(5)—Ag, 2.371(5) Å], and to the central pyridine [N(1)—Ag, 2.428(4) Å] and remaining imine nitrogen [N(2)—Ag, 2.324(5) Å]. The remaining pyridyl group of each ligand is not directly bonded to the metal, but interacts weakly with one silver atom [N(4)···Ag, 2.723(4)]. The distance between the two silver atoms is short [Ag···Ag, 3.14(1) Å], but significantly longer than that observed in silver metal (Ag···Ag, 2.899 Å). There is no direct silver–silver bond, but it seems likely that there is some degree of interaction between the two metals. However, the position of the two metals is to a great extent dictated by interligand interactions between the two ligands in the complex cation, and the question of the metal–metal interaction must remain unresolved. It is relevant that previous attempts to impose a pentadentate geometry upon silver(I) have led to complexes with short silver–silver vectors,[35–39] although this is *not* the case with L^3.[22]

The conformation of the ligands is of particular interest in this cation. The two ligands are wrapped around the binuclear silver core in a double-helical array, extremely reminiscent of that observed for the various binuclear complexes of L^3 with first-row transition metal ions. This is emphasized in Fig.

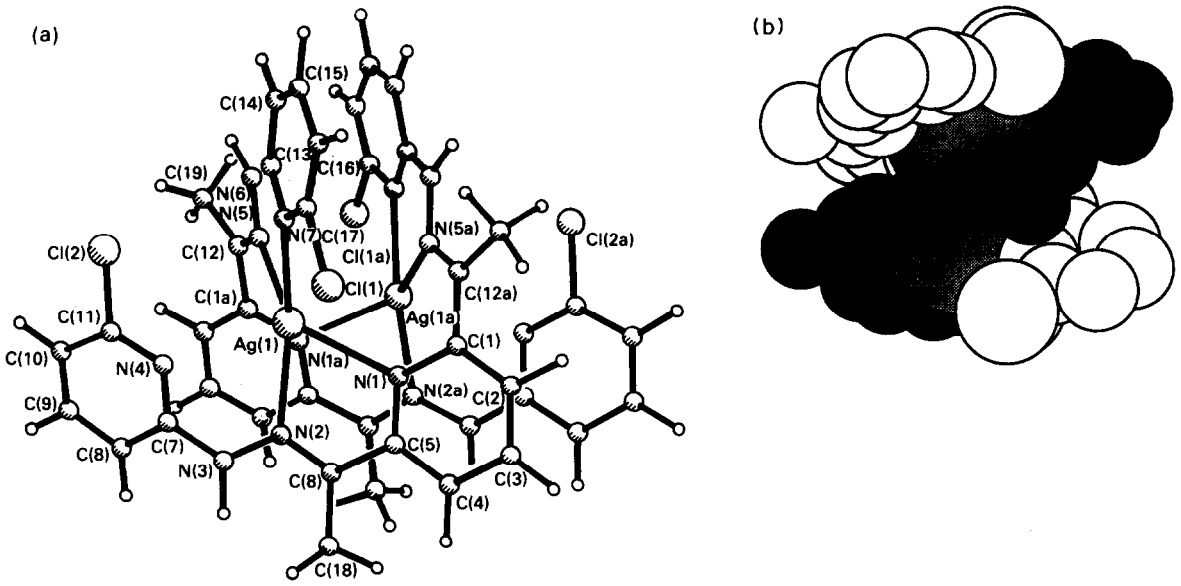

Fig. 3. (a) The molecular structure of the cation $[Ag_2L^1_2][PF_6]_2$, showing the atom numbering scheme. Hydrogen atoms have been omitted for clarity. (b) Representation of the cation $[Ag_2L^1_2]^{2+}$ showing the helical twisting of the two ligands. The two ligand molecules are represented by the different shading.

3(b), in which the two equivalent ligands are shaded to emphasize the helicity of the molecule. A further similarity with the double-helical structures of the binuclear complexes of L^3 is seen when we consider the stacking interactions of the planar aromatic rings. In the L^3 complexes, a very important component in the bonding is the stacking of parallel pyridine rings with mean interplanar separations of 3.4–4.0 Å. A very striking stacking interaction is observed between the weakly coordinated 6-chloropyridyl ring of one ligand and the central pyridine ring of the other ligand. The two rings are stacked directly one over the other, and are near parallel. The interplanar separation varies from 3.794 to 4.009 Å, indicative of a strong donor–acceptor interaction. The two coordinated 6-chloropyridyl rings are also nearly co-planar, but do not lie in a co-facial arrangement.

The helical arrangement of the ligand is achieved by a series of twists about the interannular bonds. The molecular structure of the free ligand[22] reveals it to be non-planar, with the terminal 6-chloropyridyl rings in a skewed *transoid* arrangement with the nitrogen atoms pointing away from the bonding cavity. The two terminal rings are non-equivalent, forming dihedral angles of 32.2 and 12.9°, respectively, with the central pyridine ring. In the silver complex, the helical configuration is achieved by a twist about the central 2,6-pyridyldiimine moiety, as shown in the projection in Fig. 3. The twist about the C_{ring}—C_{imine} bonds results in a dihedral angle of 45.1° between the planes of the two imine groups. This distortion from planarity is extremely unusual, and the loss of conjugation is presumably countered by the enhanced π-stacking which is possible. The twist results in dihedral angles of 37 and 11.7° between the two non-equivalent 6-chloropyridyl rings and the central pyridine ring.

We are currently further investigating the structural requirements for the spontaneous assembly of such double-helical binuclear complexes.

Acknowledgements—We should like to thank the SERC for the award of a studenthsip (J.M.H.) and the Université Louis Pasteur, Strasbourg for a visiting Professorship (E.C.C.).

REFERENCES

1. F. Stoddart, *Nature, Lond.* 1988, **334**, 10.
2. J. Libman, Y. Tor and A. Stanzer, *J. Am. Chem. Soc.* 1987, **109**, 5880.
3. G. Stuckmeier, U. Thewalt and J.-H. Furhop, *J. Am. Chem. Soc.* 1976, **98**, 278.
4. A. J. Blake, C. O. Dietrich-Bucherer, T. I. Hyde, J.-P. Sauvage and M. Schröder, *J. Chem. Soc., Chem. Commun.* 1989, 1663 and refs therein.
5. C. O. Dietrich-Bucherer and J.-P. Sauvage, *Angew. Chem. Int. Edn Engl.* 1989, **28**, 189 and refs therein.
6. C. O. Dietrich-Bucherer and J.-P. Sauvage, *Chem. Rev.* 1987, **87**, 795 and refs therein.

7. J.-Y. Ortholand, A. M. Z. Slawin, N. Spencer, J. F. Stoddart and D. J. Williams, *Angew. Chem. Int. Edn Engl.* 1989, **28**, 1394.
8. P. R. Ashton, T. T. Goodnow, A. E. Kaifer, M. V. Reddington, A. M. Z. Slawin, N. Spencer, J. F. Stoddart, C. Vicent and D. J. Williams, *Angew. Chem. Int. Edn Engl.* 1989, **28**, 1396.
9. R. Pease, *Nature, Lond.* 1989, **342**, 859.
10. J.-M. Lehn and A. Rigault, *Angew. Chem. Int. Edn Engl.* 1988, **27**, 1095.
11. J.-M. Lehn, *Angew. Chem. Int. Edn Engl.* 1988, **27**, 89.
12. J.-M. Lehn, A Rigault, J. Siegel, J. Harrowfield, B. Chevrier and D. Moras, *Proc. Natl. Acad. Sci., U.S.A.* 1987, **84**, 2565.
13. J.-M. Lehn, J.-P. Sauvage, J. Simon, R. Ziessel, C. Piccinni-Leopardi, G. Germain, J.-P. Declerq and M. Van Meerssche, *Nouv. J. Chim.* 1983, 7, 413.
14. J.-P. Gisselbrecht, M. Gross, J.-M. Lehn, J.-P. Sauvage, R. Ziessel, C. Picinni-Leopardi, J. M. Arrieta, G. Germain and M. Van Meerssche, *Nouv. J. Chim.* 1984, **8**, 661.
15. B. Lippert, *Nachr. Chem. Tech. Lab.* 1990, **38**, 186.
16. E. C. Constable, *Nature, Lond.* 1990, **346**, 314.
17. U. Koert, M. M. Harding and J-M. Lehn, *Nature, Lond.* 1990, **346**, 339.
18. E. C. Constable, S. M. Elder, J. A. Healy, M. D. Ward and D. A. Tocher, *J. Am. Chem. Soc.* 1990, **112**, 4590.
19. C. J. Cathey, E. C. Constable, M. J. Hannon, M. D. Ward and D. A. Tocher, *J. Chem. Soc., Chem. Commun.* 1990, 621.
20. E. C. Constable, M. D. Ward and D. A. Tocher, *J. Am. Chem. Soc.* 1990, **112**, 1256.
21. E. C. Constable, M. D. Ward, M. G. B. Drew and G. A. Forsyth, *Polyhedron* 1989, **8**, 2551.
22. E. C. Constable, M. G. B. Drew, G. Forsyth and M. D. Ward, *J. Chem. Soc., Chem. Commun.* 1988, 1450.
23. M. Barley, E. C. Constable, S. A. Corr, M. G. B. Drew, R. C. S. McQueen, J. C. Nutkins and M. D. Ward, *J. Chem. Soc., Dalton Trans.* 1988, 2655.
24. E. C. Constable, M. G. B. Drew and M. D. Ward, *J. Chem. Soc., Chem. Commun.* 1987, 600.
25. E. C. Constable and J. M. Holmes, *Inorg. Chim. Acta* 1987, **126**, 187.
26. *International Tables for X-ray Crystallography*, Vol. 4. Kynoch Press, Birmingham (1974).
27. G. M. Sheldrick, SHELX 76, Program for Crystal Structure Determination. University of Cambridge (1976).
28. E. C. Constable, J. Lewis, M. C. Liptrot, P. R. Raithby and M. Schröder, *Polyhedron* 1983, **2**, 301.
29. E. C. Constable and J. Lewis, *Polyhedron* 1982, **1**, 303.
30. E. C. Constable, J. Lewis, M. C. Liptrot, P. R. Raithby and M. Schroder, *J. Chem. Soc., Dalton Trans.* 1984, 2177.
31. E. C. Constable, F. K. Khan, J. Lewis, M. C. Liptrot and P. R. Raithby, *J. Chem. Soc., Dalton Trans.* 1985, 333.
32. E. C. Constable, J. M. Holmes and R. C. S. McQueen, *J. Chem. Soc., Dalton Trans.* 1987, 5.
33. E. C. Constable and J. M. Holmes, *Polyhedron* 1988, **7**, 2531.
34. E. C. Constable, M. J. Doyle, J. Healy and P. R. Raithby, *J. Chem. Soc., Chem. Commun.* 1988, 1262.
35. S. M. Nelson, S. G. McFall, M. G. B. Drew and A. H. B. Othman, *J. Chem. Soc., Chem. Commun.* 1977, 370.
36. M. G. B. Drew, C. P. Waters, S. G. McFall and S. M. Nelson, *J. Chem. Res. (M)* 1979, 360.
37. G. C. van Stein, G. van Koten, B. de Lok, L. C. Taylor, K. Vrieze and C. Brévard, *Inorg. Chim. Acta* 1984, **89**, 29.
38. G. C. van Stein, G. van Koten, F. Black, L. C. Taylor, K. Vrieze, A. L. Spek, A. J. M. Duisenberg, A. M. M. Schreurs, B. Kojic-Prodic and C. Brévard, *Inorg. Chim. Acta* 1985, **98**, 107.
39. G. C. van Stein, H. van der Poel, G. van Koten, A. L. Spek, A. J. M. Duisenberg and P. S. Pregosin, *J. Chem. Soc., Chem. Commun.* 1980, 1016.

Polyhedron Vol. 10, No. 1, pp. 133–134, 1991
Printed in Great Britain

0277–5387/91 $3.00+.00
© 1991 Pergamon Press plc

COMMUNICATION

REACTIVITY OF THE Mo—Sn BOND. REACTIONS OF $[MoSnPh_3(CO)_3(n\text{-}C_5H_5)]$ WITH HgX_2 (X = Cl, $OCOCF_3$)

M. CANO* and J. A. CAMPO

Departamento de Química Inorgánica, Facultad de Ciencias Químicas,
Universidad Complutense, 28040-Madrid, Spain

(*Received* 1 *June* 1990; *accepted* 2 *October* 1990)

Abstract—The cleavage of the Mo—Sn bond has been studied in the reactions of $[MoSnPh_3(CO)_3(n\text{-}C_5H_5)]$ with HgX_2 (X = Cl, $OCOCF_3$). Two new compounds were isolated, their formation depending on the reaction conditions.

The cleavage of the Mo—Sn bond in complexes of the type $[MoSnMe_3(CO)_3(n\text{-}C_5H_5)]$ by reaction with HgX_2 (X = Cl, Br, I) or RHgX (X = Cl; R = CH_3,C_6H_5) has produced the Mo—Hg—X and Mo—Hg—R species, respectively. Analogous behaviour has also been observed in the iodation reactions of the complexes $[MoSnR_3(CO)_3(n\text{-}C_5H_5)]$ (R = CH_3, C_6H_5).[1,2] The above results are summarized schematically in Table 1.

In some of the above reactions, cleavage of the Sn—C bond has been observed, giving compounds of the type $[MoSnR_2X(CO)_3(n\text{-}C_5H_5)]$.[1,2]

In a previous paper,[3] we found that the related $[MoSnPh_3(CO)_3(n\text{-}CH_3C_5H_4)]$ compound reacts with HgX_2 (X = Cl, Br, I, SCN) to give Mo—Hg—X complexes through the cleavage of the Mo—Sn bonds.

In order to obtain more information about the bonds which break (Sn—C or Mo—Sn) in the heterobimetallic compounds, we have tried to analyse the influence of different factors such as the nature of the mercury derivative, solvent and stoichiometric relations.

In this work, we describe the behaviour of the complex $[MoSnPh_3(CO)_3(n\text{-}C_5H_5)]$ with HgX_2 (X = Cl, $OCOCF_3$) in acetone and CCl_4 as solvents and at different molar ratios (1 : 1 or 1 : 5).

(1) *Reactions with* $HgCl_2$

This reaction afforded the complex $[MoHgCl(CO)_3(n\text{-}C_5H_5)]$ when a 1 : 1 molar ratio and acetone as solvent were used, but no reaction was observed in CCl_4.

(2) *Reactions with* $Hg(OCOCF_3)_2$

The reactivity of the complex with $Hg(OCOCF_3)_2$ also varied according to the reaction conditions employed and two new products, **1** and **2**, have been isolated (Scheme 1).

(a) *Reactions in acetone.* When a 1 : 1 molar ratio was used the $Hg[Mo(CO)_3(n\text{-}C_5H_5)]_2$ complex was evidently formed, as shown by the spectroscopic data.[4] However, if a 1 : 5 molar ratio was employed, a new asymmetrical complex $[Mo(HgOCOCF_3)(CO)_3(n\text{-}C_5H_5)]$ (**1**) was obtained {IR in KBr pellets: ν(CO) 2010, 1995, 1920, 1900; $\nu[CO_2(as)]$ 1678; $\nu[CO_2(sym)]$ 1422; γ(CH) 828 cm^{-1}. ^1H NMR in $CDCl_3$–TMS: 5.62 ppm}. We then proved that the asymmetrization reaction of $Hg[Mo(CO)_3(n\text{-}C_5H_5)]_2$ with $Hg(OCOCF_3)_2$, yielded the same product (**1**). This fact was consistent with our above results and suggested that in the 1 : 5 reactions the excess of $Hg(OCOCF_3)_2$ causes the asymmetrization of an intermediate, $Hg[Mo(CO)_3(n\text{-}C_5H_5)]_2$.

(b) *Reactions in* CCl_4. The reaction of $[MoSnPh_3(CO)_3(n\text{-}C_5H_5)]$ with $Hg(OCOCF_3)_2$ in CCl_4 (Scheme 1) led to a new yellow compound (**2**) in all cases. The ^1H NMR spectrum shows unexpected behaviour, no signals attributable to the phenyl and cyclopentadienyl groups appear. The IR spectrum, in KBR discs, presents carbonyl absorptions [ν(CO) 2040, 1992sh, 1945 cm^{-1}] shifted to higher frequencies than the starting

* Author to whom correspondence should be addressed.

Table 1. Reactions of the $[MoSnR_3(CO)_3(n\text{-}C_5H_5)]$ complexes

R	Solvent	Reagent	Cleavage observed	
			Mo—Sn	Sn—C
CH_3	All	I_2	Yes	
C_6H_5	CCl_4	I_2	Yes	Detected
CH_2—CH=CH_2	DMSO	I_2	Yes	Possible
CH_3	CH_3OH	HgX_2	Yes	
CH_2—CH=CH_2	DMSO	HgX_2	No	Detected
CH_3	Acetone	CH_3HgX	Yes	
CH_3	DMSO	C_6H_5HgX	Yes	

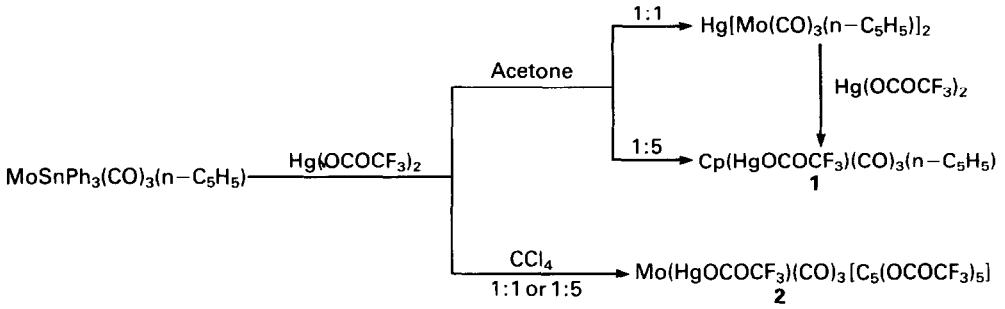

Scheme 1.

material and the asymmetrical compound (**1**). Strong and broad bands of the carboxyl group are present $\{\nu[CO_2(as)]\ 1685;\ \nu[CO_2(sym)]\ 1420\ cm^{-1}\}$.

The above results and the analytical data suggest that formulation of the type $[Mo(HgOCOCF_3)(CO)_3\{n\text{-}C_5(OCOCF_3)_5\}]$ is appropriate for **2**. There is no evidence for the formation of the symmetrical compound, $Hg[Mo(CO)_3(n\text{-}C_5H_5)]_2$ and so we suggest a different route for the formation of this product (**2**).

On the other hand, it is remarkable to note that in this reaction we have also isolated a white product, identified as $PhHgOCOCF_3$; this fact is consistent with the breaking of Sn—C bonds. It seems likely that Mo—Sn fission is dominant and that stable species containing the Mo—Hg—$OCOCF_3$ moiety are formed, but that other competing Sn—C fissions and subsequent reactions occur.

Further studies of multinuclear NMR and other possible reactions with related compounds containing substituted cyclopentadienyl ligands are proposed in order to continue this investigation.

Acknowledgement—Financial support for this work from the Comisión Asesora de Investigación Científica y Técnica (CAICYT) is gratefully acknowledged (Project No. 367/84).

REFERENCES

1. R. M. G. Roberts, *J. Organomet. Chem.* 1972, **40**, 359.
2. J. R. Chipperfield, J. Ford, A. C. Hayter and D. E. Webster, *J. Chem. Soc., Dalton, Trans.* 1976, 360.
3. M. Cano, R. Criado, E. Gutiérrez-Puebla, A. Monge and M. P. Pardo, *J. Organomet. Chem.* 1985, **292**, 375.
4. M. M. Kubicki, R. Kergoat, J. Y. Le Gall, J. E. Guerchais, J. Douglade and R. Mercier, *Aust. J. Chem.* 1982, **35**, 1543.

Polyhedron Vol. 10, No. 2, pp. 135–173, 1991
Printed in Great Britain

0277–5387/91 $3.00 + .00
Pergamon Press plc

POLYHEDRON REPORT NUMBER 36

HOMOLEPTIC AND RELATED ARYLS OF TRANSITION METALS

STEFAN U. KOSCHMIEDER and GEOFFREY WILKINSON*

Johnson Matthey Laboratory, Chemistry Department, Imperial College of Science and Technology, London SW7 2AY, U.K.

CONTENTS

1. INTRODUCTION 135

2. NEUTRAL COMPOUNDS 136
2.1. Group 3: Lanthanides 136
2.2. Group 4: Titanium, zirconium and hafnium 136
2.3. Group 5: Vanadium, niobium and tantalum 137
2.4. Group 6: Chromium, molybdenum and tungsten 139
2.5. Group 7: Manganese and rhenium 141
2.6. Group 8: Iron, ruthenium and osmium 142
2.7. Group 9: Cobalt, rhodium and iridium 143
2.8. Group 10: Nickel, palladium and platinum 144
2.9. Group 11: Copper, silver and gold 145

3. HOMOLEPTIC ANIONIC ARYL COMPLEXES 147
3.1. Group 3: Lanthanides and actinides 147
3.2. Groups 4 and 5: Titanium, vanadium, niobium and tantalum 148
3.3. Group 6: Chromium, molybdenum and tungsten 150
3.4. Group 7: Manganese and rhenium 152
3.5. Group 8: Iron 154
3.6. Group 9: Cobalt and rhodium 156
3.7. Group 10: Nickel, palladium and platinum 157
3.8. Group 11: Copper, silver and gold 159

4. FUNCTIONALIZED ARYLS 162
4.1. Lanthanides 162
4.2. Groups 4 and 5: Titanium and vanadium 163
4.3. Group 6: Chromium and molybdenum 164
4.4. Groups 7 and 8: Manganese, rhenium and iron 166
4.5. Groups 9 and 10: Cobalt, nickel, palladium and platinum 166
4.6. Group 11: Copper, silver and gold 167

1. INTRODUCTION

While sigma bonded homoleptic alkyl compounds of transition metals are now well characterized and have been the focus of much study, the analogous homoleptic aryl systems have received relatively little attention. Early reports have described often poorly characterized species. The synthesis and reaction chemistry of several examples of homoleptic transition metal aryl complexes has recently been reported and X-ray structural studies provided for their conclusive identification.

* Author to whom correspondence should be addressed.

There are numerous reviews on compounds with transition metal to carbon bonds, often including homoleptic alkyls and aryls,[R1] but it seemed pertinent in view of recent work to survey only the homoleptic and some related aryl compounds.

The report consists of three sections each covering a specific type of aryl complex (neutral, anionic, and *ortho*-functionalized). For the sake of completeness special cases will be included where the aryl complex is isolable only as an adduct of solvent molecules, although strictly speaking they are not homoleptic. Sections covering the metals copper, silver and gold will include only literature from 1980 to 1990 as excellent reviews have been published for material prior to 1980.[R2] Each section contains a table listing the aryl complexes known for the respective elements.

2. NEUTRAL COMPOUNDS

2.1. *Group* 3: *Lanthanides*

The neutral homoleptic *triphenyls* of scandium and yttrium were synthesized by interaction of the metal chlorides with phenyl lithium; they were characterized on the basis of IR spectra, analyses and reactions with small molecules;[1] no structural information is available.

Table 1. Neutral homoleptic aryls of lanthanide and Group 3 metals

Complex	Comments	References
MPh_3	MCl_3+PhLi (M = Sc, Yb); air-sensitive powder	1
$M(C_6F_5)_2(THF)_4$	$M^0+Hg(C_6F_5)_2$ (M = Eu, Yb)	2, 3
$Yb(C_6F_4H)_2(THF)_n$	*ortho*- and *meta*-isomers	2, 3
$Sm(C_6F_5)_2$	Decomposes in solution	2
$Sm(C_6F_5)_3$	Decomposes in solution	2

Several fluorophenyl complexes are reported. Divalent ytterbium complexes with C_6F_5 or C_6F_4H groups are obtained on reaction of ytterbium metal and $(C_6F_5)_2Hg$.[2] The pentafluoro complex was isolated as a THF adduct but the 2,3,5,6-tetrafluorophenyl was characterized in solution, the isolation being hampered by thermal instability. The bis(2,3,4,5-tetrafluorophenyl) was even less stable than the others and this was attributed to a decomposition pathway involving abstraction of the *ortho*-hydrogen atom.[3] Interaction of $Yb(C_6F_5)_2$ with $Ph_2PC_5H_5$ gives $(\eta^5\text{-}C_5H_4PPh_2)_2Yb$.[4a]

Di- and trivalent C_6F_5 compounds of samarium were considered as initial products in the reaction of samarium and $(C_6F_5)_2Hg$, but rapid decomposition gave solutions containing, on the basis of IR and electronic spectra, the species $(C_6F_5)SmF$ and $(C_6F_5)SmF_2$.

While attempts to obtain diphenyls by interaction of lanthanide metals and $HgPh_2$ were unsuccessful,[2] the compounds $M[(C_6H_5)Cr(CO)_3]_2$ (M = Sm, Eu and Yb) were obtained from the mercury reagent and the metal (see Section 4.1).[4b]

No neutral homoleptic aryls of actinide elements are reported.

2.2. *Group* 4: *Titanium, zirconium and hafnium*

A number of syntheses and characterizations of *tetraphenyltitanium* have appeared in the early literature. Latyaeva *et al.* have reported the synthesis by reaction of PhLi and $TiCl_4$ in benzene.[5] The $TiPh_4$ thus produced was said to decompose at $-10°C$ to form diphenyltitanium and biphenyl [eq. (1)]:

$$TiCl_4+4PhLi \xrightarrow{C_6H_6} TiPh_4 \longrightarrow TiPh_2+C_{12}H_{10}. \quad (1)$$

This mode of decay is thought to take place via a radical mechanism and is a common pathway to metal–aryl bond scission. Further reaction with ammonia yielded the adduct $(Ph)_2Ti(NH_3)$.[5] Reac-

Table 2. Neutral homoleptic aryls of Group 4

Complex	Comments: synthesis characterization	References
$Ti(Ph)_2(Et_2O)_n$	From $TiPh_4$ in Et_2O	5
$Ti(Ph)_4$	Decomposes > −20°C, TiX_4+MPh_5 (X = Cl, OPr^i, M = Li, BrMg)	7–17
$Ti(2,4,6\text{-}Me_3C_6H_2)_4$	$Ti(C_9H_{11})_4Li+O_2$; air-stable	19
$Ti(C_6F_4)_4(Et_2O)$	Stable to 100°C, $TiCl_4+LiC_6F_5$	18
$Zr(Ph)_2(Et_2O)$	From $ZrPh_4$, dimer in solution, black crystals	20
$ZrPh_4$	Decomposes to $ZrPh_2$	20

tion of $Cp_2Ti(Ph)_2$ with an excess of PhLi was also reported to give $TiPh_4$.[6] A curious series of reports by Jacot-Guillard and co-workers describes several routes to $TiPh_4$ by reaction of Grignard or diphenylmagnesium reagents with titanium(IV) alkoxides.[7–16] When prepared in the presence of 2,2′-bipyridine a product identified as $TiPh_4$ was said to be stable at elevated temperatures in the presence of a Lewis base (e.g. Et_2O). In a later paper $TiPh_4$ is reported as a complex with LiCl, $Li[Ti(Ph)_4Cl](THF)_4$.[17] It should be noted that these results should be treated with caution as in most cases the formulae are assigned on the basis of hydrolysis products, elemental analyses and by the products formed on reaction of filtered reaction mixtures with $HgCl_2$. Only very sparse spectroscopic information is provided. The *perfluoro* derivative, $(C_6F_5)_4Ti(Et_2O)_2$, was prepared via salt elimination from C_6F_5Li and $TiCl_4$ and is stable to 100°C.[18]

Tetramesityltitanium (mesityl = 2,4,6-$Me_3C_6H_2$) has been prepared via the route in eqs (2) and (3).

$$TiCl_3+4LiC_9H_{11} \xrightarrow{THF} LiTi(C_9H_{11})_4+3LiCl \quad (2)$$

$$LiTi(C_9H_{11})_4+O_2 \longrightarrow Ti(C_9H_{11})_4+\text{“lithium oxides”}. \quad (3)$$

The oxidation is best carried out in the solid state.[19] In contrast to the extreme air and water sensitivity of other titanium(IV) alkyls and aryls, $Ti(mes)_4$ is stable in dry air but is light sensitive.

Razuvaev *et al.* have prepared *tetraphenylzirconium* from $ZrCl_4$ and four equivalents of PhLi in Et_2O at −40°C.[20] The product thus obtained decomposed in a fashion similar to that of $TiPh_4$ to yield $(Ph)_2Zr(Et_2O)$ which could be recrystallized from benzene as shiny black crystals. Cryoscopic molecular weight measurements indicate a dimeric structure in solution. Reaction with ethanol gave the zirconium(IV) product $Zr(OEt)_4$, benzene and hydrogen gas [eq. (4)]:

$$(Ph)_2Zr(Et_2O)+4EtOH \xrightarrow{20°C} 2C_6H_6+Zr(OEt)_4+H_2. \quad (4)$$

2.3. *Group 5: Vanadium, niobium and tantalum*

Trimesitylvanadium was first reported by Seidel and Kreisel in 1974 with the formula $V(C_9H_{11})_3(THF)_n$.[21] The 2,6-xylyl was also prepared but the triphenyl complex could not be isolated.[22] The structure of the mesityl has confirmed the formula $V(C_9H_{11})_3(THF)$.[23] The metal atom is coordinated in a pseudo-tetrahedral fashion. The bending of the *ortho*-methyl carbon atoms out of the phenyl plane by 0.023–0.165 Å was ascribed to steric factors. The *tetramesityl*, $V(mes)_4$, was later prepared by addition of 1 equivalent of mesLi to $V(mes)_3THF$ in THF–Et_2O, and air oxidation of the intermediate formed $[V(mes)_4]Li$ [eqs (5) and (6)].[24]

$$V(mes)_3THF+mesLi \longrightarrow [V(mes)_4]Li \quad (5)$$

$$[V(mes)_4]^- + O_2 \longrightarrow V(mes)_4. \quad (6)$$

An X-ray study shows $V(mes)_4$ to have a slightly distorted tetrahedral structure.[25] Structures of $V(mes)_3THF$ and $V(mes)_4$ are shown in Figs 1 and 2, respectively. The tris-mesityl product reacts

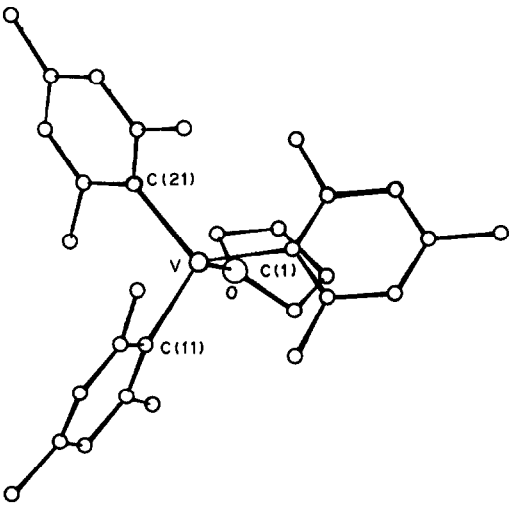

Fig. 1. Molecular structure of $V(mes)_3THF$ (reprinted by permission from ref. 23).

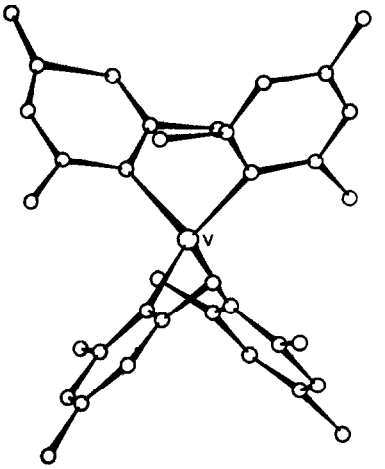

Fig. 2. Molecular structure of $V(mes)_4$ (reprinted by permission from ref. 25).

Table 3. Neutral homoleptic aryls of Group 5

Complex	Comments	References
VPh_2	From VPh_4	18
VPh_4	Decomposes to VPh_2	27, 28
$V(2,6\text{-}Me_2C_6H_3)_3(THF)$	$VCl_3(THF)_3+3(2,6\text{-}Me_2C_6H_3MgBr)$	22
$V(2,4,6\text{-}Me_3C_6H_2)_3(THF)$	X-ray, adds RLi to give $[V(mes)_3R]Li$ (R = aryl, alkyl)	21–23
$V(2,4,6\text{-}Me_3C_6H_2)_4$	X-ray; from oxidation of $[V(mes)_4]^-$	24, 25
$V(C_6F_5)_3(THF)$	$VCl_3+3C_6F_5BrMg$	29
$V(C_6F_5)_4(THF)_2$	Stable at room temperature	29, 30
$TaPh_5$	$Ta(OAr)_2Cl_3$ + excess PhLi; decomposes before isolation	31

with bulky silanols to give tris-siloxy complexes and mesitylene [eq. (7)]:[26]

$$V(mes)_3 + 3Bu^tMe_2SiOH \longrightarrow V(OSiMe_2Bu^t)_3 + 3C_9H_{12}. \quad (7)$$

Tetraphenylvanadium is obtained by reaction of VCl_4 and 4 equivalents of PhLi in diethyl ether at $-80°C$. The VPh_4 quickly decomposes at $-40°C$ to VPh_2 and biphenyl.[27] Compounds of formula $V(Ph)_2(OBu^t)_2$ could be isolated by reacting VPh_4, formed *in situ*, with Bu^tOH [eqs (8) and (9)]:[28]

$$VCl_4 + 4PhLi \longrightarrow VPh_4 \longrightarrow VPh_2 + C_{12}H_{10} \quad (8)$$

$$VPh_4 + Bu^tOH \longrightarrow V(Ph)_2(OBu^t)_2 + 2C_6H_6. \quad (9)$$

Pentafluorophenyl complexes of tri- and tetravalent vanadium have also been described. Reaction of VCl_3 and C_6F_5MgBr yields the vanadium(III) species $(C_6F_5)_3V(THF)$,[29] whereas VCl_4 and C_6F_5Li gives the tetravalent $V(C_6F_5)_4$[30] as a solvent complex with 2 moles of THF.

The neutral tantalum(V) complex, $TaPh_5$, has been postulated as a product in the reaction of $Ta(O\text{-}2,6\text{-}Me_2C_6H_2)_2Cl_3$ and excess PhLi; however no attempt at isolation was made.[31] Neutral homoleptic aryls of niobium have not been reported.

2.4. *Group 6: Chromium, molybdenum and tungsten*

The synthesis and characterization of *triphenylchromium-tris-tetrahydrofuran* in 1957 by Herwig and Zeiss represented a milestone in organometallic chemistry.[32] This complex received much attention in the time after its discovery and was found to be a key intermediate in the σ–π shift reactions investigated by Hein and co-workers in the 1920s and 1930s;[33] their "polyphenyl" chromium compounds were, of course, η^6-arene species. Many other triarylchromium complexes were synthesized soon thereafter, including the complete range of tolyls[34–37] and biphenyls.[36,37] The *trimesityl* was shown to form an adduct with only one molecule of THF,[38] while the others occurred as tris-tetrahydrofuranates. Only very recently has an X-ray structure become available for $(Ph)_3Cr(THF)_3$.[39] The chromium atom has the expected octahedral coordination geometry with the ligands lying in a *cis*(facial) configuration (Fig. 3). Each sigma-bound phenyl group lies *trans* to a coordinated THF molecule. The Cr—C bonds [$Cr—C_{av} = 2.060(10)$ Å] are much shorter than the Cr—O bonds [$Cr—O_{av} = 2.225(10)$ Å], an effect thought to be due to the stabilizing influence of $p\pi$–$d\pi$ backbonding from the metal atom to the phenyl carbon of the aryl ligand.[39]

The *tetramesityl* complexes of chromium and molybdenum have been prepared by oxidation of their parent M^{III} tetraaryl "ate" complexes.[40,41] Distorted tetrahedral structures are postulated on the basis of ESR and photoelectron spectral data.[42,43] The molybdenum complex undergoes oxidation with iodine or bromine to give molybdenum(V) salts of formula $[Mo(mes)_4][X_3]$ (X = I, Br), which also contain metal atoms in distorted tetrahedral geometries.[44] The only other Group 6 d^1

Table 4. Neutral homoleptic aryls of Group 6

Complex	Comments	References
$Cr(Ph)_3(THF)_3$	X-ray, $CrCl_3(THF)_3 + 3PhMgBr$	32, 39, 99
$Cr(MePh)_3(THF)_3$	*ortho*-, *meta*-, *para*-isomers	34–37
$Cr(\sigma\text{-}PhC_6H_5)_3(THF)_3$		37
$Cr(2,4,6\text{-}Me_3C_6H_2)_3(THF)$		38
$Cr(2,4,6\text{-}Me_3C_6H_2)_2$	$CrCl_2 + 2mesMgBr$; THF adduct	48, 49, 98
$Cr(C_{10}H_7)_2(THF)_3$	Decomposes to π complex	49
$M(2,4,6\text{-}Me_2C_6H_2)_4$	M = Cr, Mo; molybdenum species may be oxidized to $[Mo(mes)_4]^+$	40–44
$M(o\text{-}tol)_4$	M = Cr, Mo, W. X-ray for Mo; react with Lewis bases to form benzynes (Mo, W) or reduced species (Cr)	46
$W(C_6F_5)_5$	$WCl_6 + 6C_6F_5Li \longrightarrow [W(C_6F_5)_5]^- \xrightarrow{\Delta} W(C_6F_5)_5$	45

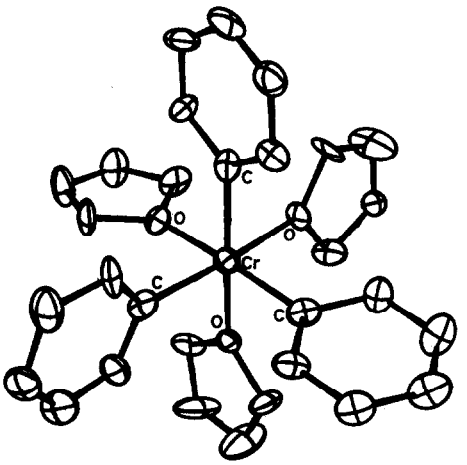

Fig. 3. Molecular structure of $(Ph)_3Cr(THF)_3$ showing the *trans* arrangement of the ligands (reprinted by permission from ref. 39).

homoleptic aryl characterized to date, the *perfluorophenyl*, $W(C_6F_5)_5$, was synthesized by thermal decomposition of $(C_6F_5)_5W(LiEt_2O)$.[45]

The *tetra*-o-*tolyl complexes* of chromium, molybdenum and tungsten are known.[46] The X-ray structure of the molybdenum derivative shows a slightly distorted tetrahedral geometry about the metal atom (Fig. 4).[47] The chromium tetratolyl is made in an oxidation reaction from $CrCl_3$ and *o*-tolLi, the molybdenum compound from $MoCl_4(THF)_2$, involving neither reduction or oxidation, and the tungsten derivative in a reduction from $W(OPh)_6$ and *o*-tolMgBr [eqs. (10)–(12)]:

$$(THF)_3CrCl_3 + 4\text{-}o\text{-tolLi} \longrightarrow Cr(o\text{-tol})_4 + 3LiCl + \text{other products} \quad (10)$$

$$MoCl_4(THF)_2 + 4\text{-}o\text{-tolLi} \longrightarrow Mo(o\text{-tol})_4 + 4LiCl \quad (11)$$

$$W(OPh)_6 + 6\text{-}o\text{-tolMgBr} \longrightarrow W(o\text{-tol})_4 + 6BrMg(OPh) + \text{bitolyl} \quad (12)$$

$$M(o\text{-tol})_4 + 2L \longrightarrow M(o\text{-tol})_2(\eta^2\text{-}2\text{-}MeC_6H_3)(L)_2 \quad (M = Mo, W;\ L = PMe_3, PMe_2Ph). \quad (13)$$

On addition of small tertiary phosphines, the molybdenum and tungsten complexes undergo facile *ortho*-hydrogen elimination to give M^{IV} aryne complexes[46] [eq. (13)], while the chromium derivative reductively eliminates bitolyl to give $[Cr(o\text{-tol})(\mu\text{-}o\text{-tol})(PMe_3)]_2$.[46] In comparison with homoleptic aryls of Groups 3–5, the Group 6 aryls are stable at room temperature as solids or in solution.

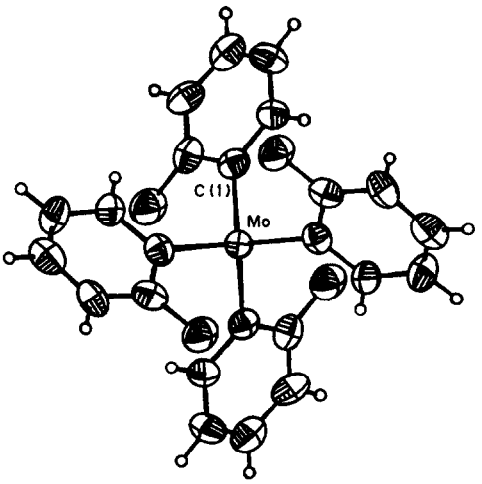

Fig. 4. Molecular structure of $Mo(o\text{-tol})_4$ (reprinted by permission from ref. 47).

While the tungsten and molybdenum aryls are extremely air- and moisture-sensitive, the chromium complex may be handled in air for short periods without decomposition.

Bis-mesityl and *bis-naphthyl* complexes of chromium(II) have been identified as products of the reaction of $CrCl_2$ and ArMgBr in THF.[48,49] It is likely these species exist only as THF adducts as dimesitylchromium has been structurally characterized only as complexes of Lewis bases.[50]

2.5. *Group 7: Manganese and rhenium*

Neutral homoleptic aryls of Group 7 are very scarce and none are known for technetium. *Bis(mesityl)manganese* has been structurally characterized and shown to exist as a trimer with the central metal atom bonded to four bridging aryls in a tetrahedral fashion (Fig. 5).[51] The terminal metal atoms have trigonal geometries with two bridging and one terminal aryl groups. Although magnetic behaviour indicates some metal–metal interaction, the metal–metal distances of 2.851(3) Å were considered too long for any significant metal–metal bonding in the solid state.[51]

*Tetra-o-tolyl*rhenium has been structurally characterized and is very similar to the tetratolyls of chromium, molybdenum and tungsten in possessing a slightly distorted tetrahedral coordination environment.[52] The synthesis involves the reaction of $ReCl_4(THF)_2$ and a deficiency of *o*-tolyl Grignard (1 : 2.4). The excess $ReCl_4$ is thought to act as an oxidant for the intermediate formed $[Re(o\text{-tol})_4]^-$ (see Section 2) to give moderate yields of the neutral compound.[47,52] As noted for the Group 6 tetra-*o*-tolyls the rhenium complex reacts with tertiary phosphines to yield benzyne species of formula $Re(2\text{-}MeC_6H_4)_2(\eta^2\text{-}2\text{-}MeC_6H_3)L_2$ ($L = PMe_3$, PMe_2Ph).[53] Air oxidation cleanly gives the rhenium(VI) *oxo-aryl* $ORe(o\text{-tol})_4$ [eq. (14)]:[52]

$$Re(o\text{-tol})_4 + 1/2O_2 \longrightarrow ORe(o\text{-tol})_4. \tag{14}$$

Table 5. Neutral homoleptic aryls of Group 7

Complex	Comments	References
$[Mn(2,4,6\text{-}Me_3C_6H_2)_2]_3$	X-ray; linear trimer	51
$Re(2\text{-}MeC_6H_4)_4$	X-ray; facile elimination of toluene and benzyne formation on addition of tertiary phosphines	52, 53

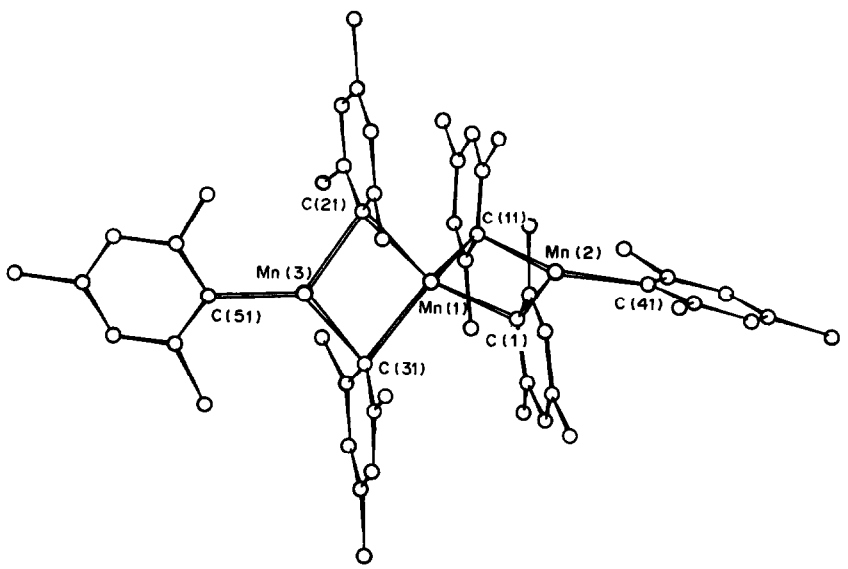

Fig. 5. Molecular structure of the trimer $[Mn(mes)_2]_3$ (reprinted by permission from ref. 51).

2.6. *Group 8 : Iron, ruthenium and osmium*

Divalent *bis(mesityl)iron* was first reported as a THF complex of formula $(mes)_2Fe(0.2THF)$;[24] however, in a later paper by the same group it is described as $Fe(mes)_2$.[54] The homoleptic aryl has a magnetic moment of 2.69 BM, indicating a low-spin electronic configuration, while the dipyridyl adduct $(mes)_2Fe(bipy)$ has a high-spin magnetic moment.[24]

Table 6. Neutral homoleptic aryls of Group 8

Complex	Comments	References
$Fe(2,4,6\text{-}Me_3C_6H_2)_2$	Forms high-spin adducts with chelating ligands	24, 54
$M(2\text{-}MeC_6H_4)_4$	M = Ru, Os; X-ray; reductive elimination of bitolyl on addition of Lewis bases (Os)	47, 52,[a] 58
$OsPh_4$	X-ray; isostructural with $Os(o\text{-tol})_4$ decomposes in solution to give biphenyl	47

[a] Synthesis also of RuR_4, R = $2,6\text{-}Me_2C_6H_3$, $2,4,6\text{-}Me_3C_6H_2$ and $4\text{-}Bu^tC_6H_4$.

Reactive iron powders prepared by the Riecke method* react with C_6F_5I in a disproportionation manner to form solvated complexes of $(C_6F_5)_2Fe$ and FeI_2 [eq. (15)].[55] Further reaction with carbon monoxide gives the known complex $Fe(C_6F_5)_2(CO)_2(THF)_2$.[55]

$$2Fe^0 + 2C_6F_5I \longrightarrow (C_6F_5)_2Fe(S)_x + FeI_2(S)_y \quad (S = \text{solvent}). \tag{15}$$

The X-ray structures, reactivity, spectroscopic and electrochemical behaviour of a series of *ruthenium and osmium tetraaryl* complexes have been described in several recent papers.[47,52,56,57] The tetra-*o*-tolyls of ruthenium and osmium are isostructural, having tetrahedral coordination environments about the metal atoms. Complexes of both metals are diamagnetic showing four equivalent *o*-tolyl groups in the ^1H NMR spectrum. Thermally very robust, the ruthenium aryl exhibits the parent ion in the mass spectrum as well as peaks due to sequential loss of *o*-tolyl groups. The ruthenium aryl was synthesized by reaction of $[Et_4N][RuCl_5(MeCN)]$ with 5 equivalents of *o*-tolMgBr or by reaction of $Ru_2(OAc)_4Cl$ and 8 equivalents of *o*-tolMgBr. The mesityl, 2,6-xylyl and $p\text{-}Bu^tC_6H_4$ complexes were also synthesized in this manner. The $Os(o\text{-tol})_4$ was obtained from OsO_4 and 8 equivalents of the aryl Grignard. The $OsPh_4$ is much less stable than $Os(o\text{-tol})_4$ and slowly decomposes in solution over a period of days to give biphenyl and an amorphous black solid. The solid-state structure of $OsPh_4$ is very similar to that of $Os(o\text{-tol})_4$ with an approximately tetrahedral coordination (Fig. 6).[56]

The reactivity of $Os(o\text{-tol})_4$ with Lewis bases was examined and proved to be quite different from that of the tetra-*o*-tolyls of molybdenum, tungsten and rhenium. Small tertiary phosphines, carbon monoxide and t-butyl isocyanide all induce reductive coupling to form species of formula $(2\text{-}MeC_6H_4)_2Os(\eta^6\text{-}C_{12}H_{10})_yL_x$ [L = CO, $x = 1$, $y = 1$; L = PMe_3, $x = 1$, $y = 1$; L = Bu^tNC, $x = 4$, $y = 0$ (Scheme 1)].[58]

The osmium complex also exhibits an interesting redox chemistry. Cyclic voltammetry studies[47] in CH_2Cl_2 and THF show reversible oxidation [+0.33 V (CH_2Cl_2), +0.41 (THF)] and reversible reduction [−1.96 V (CH_2Cl_2), −1.89 V (THF)] waves. Reaction of the neutral complex with one-electron oxidants $AgBF_4$ or AgO_3SCF_3 in CH_2Cl_2 [eq. (16)] allowed the isolation of the homoleptic osmium(V) cation, $[Os(o\text{-tol})_4]^+$, which could also be prepared via bulk electrolysis of $Os(o\text{-tol})_4$ at (+0.7 V) in CH_2Cl_2 with $[Bu^n{}_4N][PF_6]$ as supporting electrolyte.[47] An X-ray analysis again revealed an approximate tetrahedral arrangement for the OsC_4 core with only slight changes relative to the starting $Os(o\text{-tol})_4$.[57]

$$Os(o\text{-tol})_4 + AgO_3SCF_3 \longrightarrow [Os(o\text{-tol})_4]^+[O_3SCF_3]^-. \tag{16}$$

* This involves reducing suspensions of the appropriate metal halide with sodium to give fine suspensions of the metal and sodium salts.

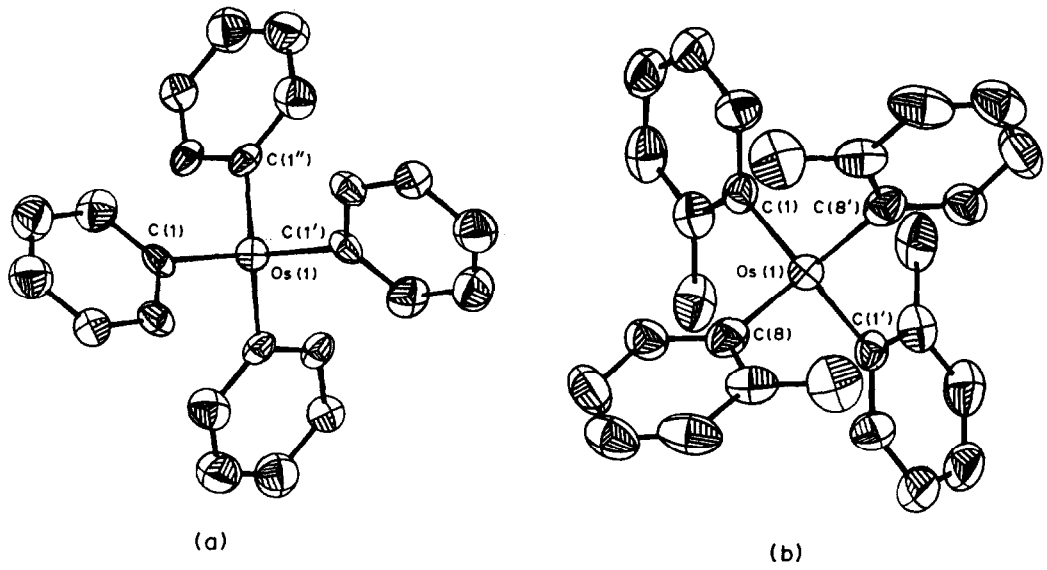

Fig. 6. Molecular structures of tetraaryl osmium complexes: (a) $OsPh_4$ and (b) $Os(o\text{-tol})_4$ (reprinted by permission from ref. 56).

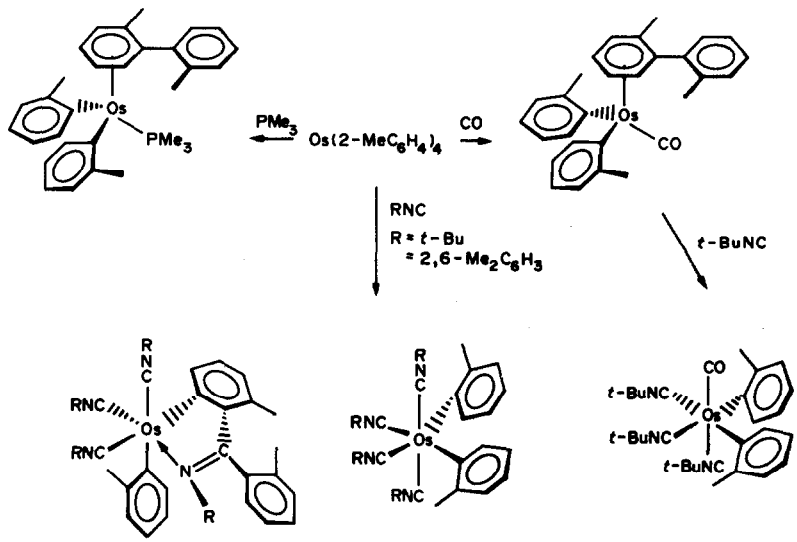

Scheme 1. Reactivity of $Os(o\text{-tol})_4$ with Lewis bases.

2.7. *Group 9: Cobalt, rhodium and iridium*

Dimesitylcobalt exists as a dimer in the solid state with the cobalt atoms lying in an almost planar coordination geometry (Fig. 7).[59] The average Co—Co distance (2.516 Å) of the two independent molecules found in the unit cell is indicative of metal–metal bonding even though the molecule exhibits a high degree of temperature-independent paramagnetism. An EHMO study supports the presence of metal–metal bonding. The *ortho*-methyls of the bridging mesityl ligands were found to have close contacts to the metal atoms, the shortest of which (2.79 Å) was within the range expected for agostic interactions.[60] Several elegant NMR experiments were undertaken to determine whether an agostic interaction was present, and on the basis of these experiments (C—H coupling, partial deuteriation isotopic effects) it was concluded that no agostic M---H—C bond was present. The

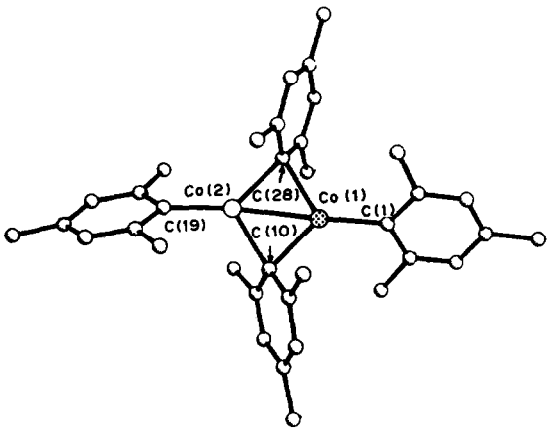

Fig. 7. Molecular structure of $[Co(mes)_2]_2$ (reprinted by permission from ref. 59).

Table 7. Neutral homoleptic aryls of Group 9

Complex	Comments	References
$Co(C_6F_5)_2(S_n)$	Isolated as solvent adduct (DME, THF, toluene)	55, 61
$Co(2,4,6\text{-}Me_3C_6H_2)_2$	X-ray; dimeric with M—M bonding. EHMO study	59
$Rh(2,4,6\text{-}Me_3C_6H_2)_3$	X-ray; pseudo-octahedral via close contacts between Rh and *ortho*-methyl groups	63

distortions noted in the solid state were ascribed to steric factors arising from contact between the *ortho*-methyl substituents of the two bridging mesityl ligands.

Other cobalt(II) homoleptic aryls include the bis(pentafluorophenyl)cobalt species generated either by reaction of cobalt(II) halides and C_6F_5MgBr in THF,[61] or by reaction of C_6F_5I and elemental cobalt generated by the Riecke method [eq. (17)].[55] In both cases the products are likely to be adducts of labile solvent molecules (DME, THF, toluene) (Table 7). An X-ray structure of $(C_6F_5)_2Co(\eta^6\text{-}C_7H_8)$ has appeared.[62]

$$2Co^0 + C_6F_5I \xrightarrow{\text{toluene}} (C_6F_5)_2Co(\eta^6\text{-}C_7H_8). \tag{17}$$

The *tris(mesityl)rhodium*(III), $Rh(mes)_3$, also has close contacts between the metal atom and the hydrogen atoms of one *ortho*-methyl group from each mesityl ligand. As is the case with $[Co(mes)_2]_2$, the absence of agostic interactions in solution was confirmed by NMR, and the aromatic rings shown to be rotating.[63]

No homoleptic aryls of iridium have been reported.

2.8. *Group* 10: *Nickel, palladium and platinum*

The aryl chemistry of nickel is much like that of its neighbour cobalt.[48] The bis(*pentafluorophenyl*) complex has been synthesized via several routes: interaction of $(C_6F_5)MgBr$ and $NiBr_2$ in THF,[64] the Riecke method using C_6F_5I and nickel^0,[55] or by direct reaction of nickel metal and C_6F_5I by metal vapour techniques [eqs (18) and (19)].[62,65,66]

$$2C_6F_5MgBr + NiBr_2 \longrightarrow (C_6F_5)_2Ni(THF)_x \tag{18}$$

$$2Ni^0 + 2C_6F_5I \longrightarrow Ni(C_6F_5)_2 + NiI_2. \tag{19}$$

Table 8. Neutral homoleptic aryls of Group 10

Complex	Comments	References
$Ni(2,4,6\text{-}Me_3C_6H_2)_2$	$NiBr_2$+mesMgBr	48
$Ni(C_6F_5)_2$	$NiBr_2+(C_6F_5)MgBr$, $Ni^0+C_6F_5I$	55, 62
	X-ray of mesitylene adduct	64–66, 68
$M(C_6F_5)_2(THT)_2$	M = Pd, Pt, $MCl_2(THT)_2+2LiC_6F_5$	67, 68

The palladium and platinum analogues were synthesized by Usón and co-workers as tetrahydrothiophene (THT) complexes from the metal halides and lithium or Grignard arylating agents.[67,68]

2.9. *Group* 11: *Copper, silver and gold*

The complete series of univalent *mesityl complexes* has been prepared and characterized by X-ray crystallography. Each complex exists as a cyclic oligomer with mesityl groups bridging the metal atoms.

Both the gold[69] and copper[70] compounds are pentamers in the solid state while the silver mesityl complex crystallizes as a cyclic tetramer.[71] Addition of THT to $[Cu(mes)]_5$ leads to ring contraction and formation of the tetrameric species $[Cu(mes)]_4(THT)_2$ [eq. (20)]:[70]

$$4[Cu(mes)]_5+\text{excess THT}\longrightarrow 5[Cu(mes)]_4(THT)_2 \tag{20}$$

The molecular structure of each aryl is shown in Fig. 8.

An equilibrium between cyclic oligomeric and dimeric structures was detected in solution by ^1H NMR and cryoscopic measurements.[72] Addition of the chelate phosphine, $Ph_2PCH_2PPh_2$, to solutions of the copper and silver mesityl complexes releases mesitylene and forms new complexes of formula $M_3(Ph_2PCHPPh_2)_3$ [eq. (21)]:

$$[M(mes)]_n+Ph_2PCH_2PPh_2\longrightarrow M_3(Ph_3PCHPPh_2)_3+\text{mesitylene}. \tag{21}$$

Addition of the chelate phosphine to the gold complex gave the Lewis base adduct $Au_2(mes)_2(\mu\text{-}Ph_2PCH_2PPh_2)$.[72]

When the sterically more demanding aryl 2,4,6-*triisopropylphenyl* is used in place of mesityl, a compound with a tetrameric structure involving a distorted square plane of copper atoms is obtained. A bonding description incorporating σ-M—C and π-M—C interactions was used to explain the cluster aggregate structure (Fig. 9).[73] If an even bulkier ligand, 2,4,6-*triphenylphenyl*, is employed, monomeric structures are favoured for both copper and silver.[74] No reaction is observed between

Table 9. Neutral homoleptic aryls of Group 11

Complex	Comments	References
$[M(2,4,6\text{-}Me_3C_6H_2)]_n$	M = Cu, n = 5; M = Ag, n = 4; M = Au, n = 5. X-ray; solution equilibria between oligomeric and dimeric forms	69–72
$Cu(2,4,6\text{-}Pr^i{}_3C_6H_2)$	X-ray; tetranuclear cluster	73
$M(2,4,6\text{-}Ph_3C_6H_2)$	M = Cu, Ag. X-ray; monomeric, inserts acetylenes and isocyanates	74
$[Ag(C_6F_5)]_n$	Polymeric	68, 75
$[AuAg(C_6Cl_5)_2]_n$	$[n\text{-}Bu_4N][Au(C_6Cl_5)_2]+AgClO_4\longrightarrow AuAg(C_6Cl_5)_2$	77
$Au(C_6F_5)_3(THT)$	$Au(C_6F_5)(THT)+Tl(C_6F_3)_2Cl\longrightarrow Au(C_6F_5)_3(THT)+TlCl$	76, 68

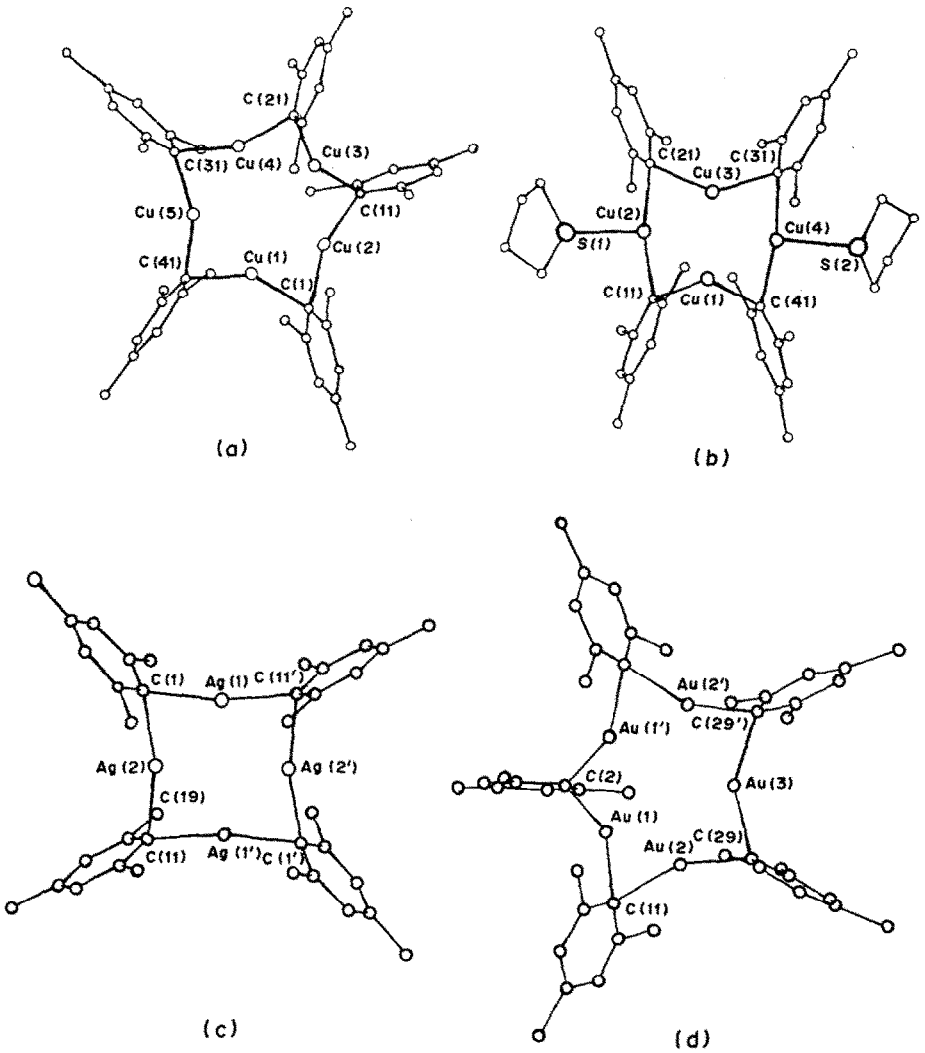

Fig. 8. Molecular structures of oligomeric group 11 mesityl complexes; (a) $[Cu(mes)]_5$, (b) $[Cu(mes)]_4(THT)_2$, (c) $[Ag(mes)]_4$, (d) $[Au(mes)]_5$ (reprinted by permission from ref. 72).

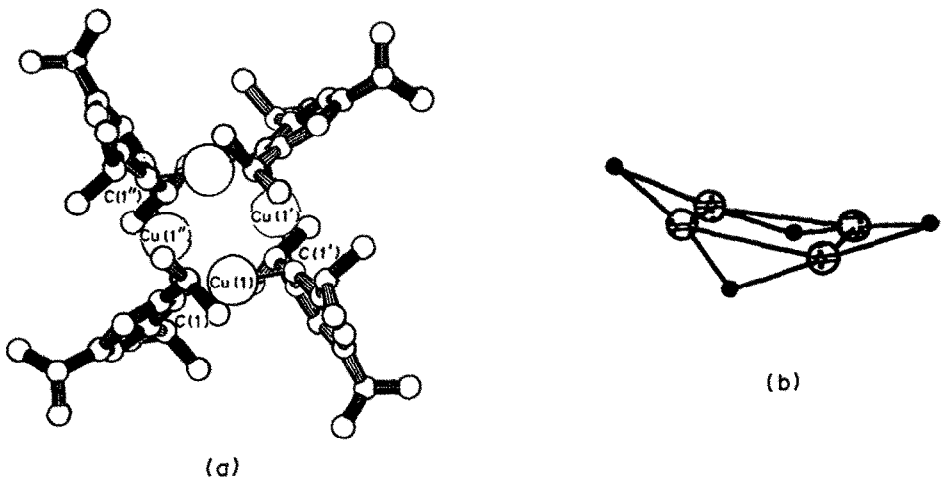

Fig. 9. Molecular structure of (a) $[Cu(Pr^i{}_3C_6H_2)]_4$ and (b) the $[Cu—C]_4$ core (reprinted by permission from ref. 73).

$M(Ph_3C_6H_2)$ (M = Cu, Ag) and large Lewis bases (pyridine, t-butyl isocyanide), but smaller bases (CO, NO) give 1 : 1 adducts.[74]

The *perhaloaryl chemistry* of *silver* and *gold* has been extensively explored by Usón and co-workers.[68] The silver aryl complexes, AgAr (Ar = C_6F_5, 2,4,6-$C_6F_3H_2$, C_6Cl_5) may be reacted with gold(I) chloride compounds to give perhaloaryl gold species [eq. (22)]:[75]

$$Ag(C_6F_5)+AuCl(THT)\longrightarrow Au(C_6F_5)(THT) \quad (22)$$

$$Au(C_6F_5)+Tl(C_6F_5)_2Cl_2\longrightarrow Au(C_6F_5)_3(THT). \quad (23)$$

Further reaction of the gold(I) species with $Tl(C_6F_5)_2Cl_2$ gives the oxidation product $Au(C_6F_5)_3(THT)$, eq. (23).[76] *Mixed silver–gold perhaloaryls* are prepared from the gold(I) salt $[Bu^n{}_4N][Au(C_6Cl_5)_2]$ and silver perchlorate, as shown in eq. (24):[77]

$$[Bu^n{}_4N][Au(C_6Cl_5)_2]+AgClO_4\longrightarrow [AuAg(C_6Cl_5)_2]_n. \quad (24)$$

3. HOMOLEPTIC ANIONIC ARYL COMPLEXES

In general, the primarily lithium compounds of anionic homoleptic or "ate" complexes are more numerous and better characterized than their neutral counterparts. This is especially true for chromium for which a large variety of complexes in several oxidation states has been isolated. This disproportionate amount of work for chromium stems from Hein's discovery that stable organochromium complexes may be isolated from the reaction of $CrCl_3$ and aryl Grignards in Et_2O.[33] Anionic aryl complexes, mainly of copper, have also been receiving attention as synthons in organic chemistry.[78,R2]

3.1. *Group* 3 : *Lanthanides and actinides*

"Ate" complexes of the lanthanide metals may be isolated by reaction of the trivalent metal chloride with four equivalents of PhLi [eq. (25)]:

$$LnCl_3+4PhLi\longrightarrow [Ln(Ph)_4]Li+3LiCl \quad (Ln = Pr, Lu). \quad (25)$$

In the solid state the lutetium and ytterbium derivatives, $LiM(Ar)_4$ (Ar = 2,6-$Me_2C_6H_3$), contain the metal in an approximately tetrahedral arrangement within the aryl ligand framework (Fig. 10).[79]

Table 10. Anionic homoleptic aryls of lanthanide and Group 3 metals

Complex	Comments	References
$M(Ph)_4Li$	M = La, Pr; $MCl_3+4PhLi$	1
$[M(2,6\text{-}Me_2C_6H_3)_4][Li(THF)_4]$	M = Lu, Yb; X-ray Lu. Discreet cation/anion pair	79
$U(C_6H_5)_6Li_2(Et_2O)_8$	Thermally unstable	80
$U(2\text{-}Me_2NCH_2C_6H_4)_6Li_2(Et_2O)_8$	Thermally unstable	80
$U(2\text{-}Me_2NCH_2C_6H_4)_6Li_2(TMEDA)_3$	Thermally unstable	80

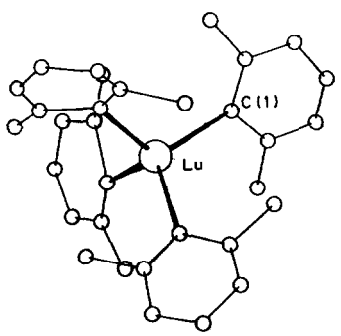

Fig. 10. Molecular structure of the anion $[Lu(xylyl)_4]^-$ (reprinted by permission from ref. 79).

The lithium counterion is surrounded by four molecules of Et_2O and does not interact strongly with the anionic portion of the molecule. Several polyphenyl and functionalized polyphenyl complexes of uranium(IV) have been isolated and found to be thermally unstable.[80]

3.2. *Groups* 4 *and* 5: *Titanium, vanadium, niobium and tantalum*

Anionic homoleptic aryl complexes of the earlier transition metals are fairly rare. The *titanium*(III) anion, $LiTi(mes)_4$, can be obtained in 20% yield from $TiCl_3$ and mesityl lithium in Et_2O–THF mixtures. A solution magnetic moment of 1.87 BM is indicative of one unpaired electron.[19]

No anionic aryl complexes have been reported for zirconium or hafnium. The *vanadium* arylate, $LiV(mes)_4$, was synthesized from the neutral $V(mes)_3$ and mesityl lithium. A distorted tetrahedral coordination environment for the vanadium atom was postulated on the basis of spectroscopic data.[81,82] Both vanadium and titanium tetramesityl anions can be converted to the neutral tetramesityl complexes by air oxidation.[24] Reaction of $V(mes)_3THF$ with other aryl lithium reagents leads to the formation of anionic mixed aryl complexes of formula $LiV(mes)_3(Ar)$ [Ar = C_6H_5, 2-MeC_6H_4 or 2,6-$(MeO)_2C_6H_3$]. The dimer $Li_2(THF)_8V_2(\mu\text{-}C_6H_4)(mes)_6$, containing a bridging C_6H_4 unit, was synthesized by reaction of $V(mes)_3$ and 1,2-$Li_2C_6H_4$ in a 2:1 stoichiometry and characterized by its magnetic, spectroscopic and thermal properties.[83]

The tris ortho-*diphenylether* complex $[Ti(C_6H_4OC_6H_4)_3](LiEt_2O)_2$ is one of a complete series of first-row anionic complexes reported by Drevs in 1975. It is diamagnetic and presumably represents a titanium(IV) species;[84] the analogous vanadium species, $[V(C_6H_4OC_6H_4)_3][Li(THF)_2]_3$, was shown to contain two unpaired electrons.

Two anionic vanadium complexes of 2,6-dimethoxyphenyl (DMOP) have been reported. The vanadium(II) species, $Li_2V(DMOP)_4$, is obtained by reaction of vanadocene with LiDMOP, and the vanadium(III) species, $LiV(DMOP)_4$, from $VBr_3(THF)_3$ and LiDMOP; both decompose to yield the well characterized $[V(DMOP)_2]_2$ [eq. (26) and (27)]:[85]

$$(C_5H_5)_2V + 4Li\text{-}2,6\text{-}(MeO)_2C_6H_3 \longrightarrow Li_2V[2,6\text{-}(MeO)_2C_6H_3]_4 \xrightarrow{\Delta} \{V[2,6\text{-}(MeO)_2C_6H_3]_2\}_2 \tag{26}$$

$$VBr_3(THF)_3 + 4Li\text{-}2,6\text{-}(MeO)_2C_6H_3 \longrightarrow LiV(2,6\text{-}(MeO)_2C_6H_3)_4. \tag{27}$$

A note has described the synthesis of $Li_4V(Ph)_6(Et_2O)_{3.5}$ from ethereal PhLi and $VCl_3(THF)_3$.[86] Characterization consisted of reaction with protic molecules and $HgCl_2$ to yield benzene and PhHgCl, respectively. If the synthesis is carried out with the Grignard in place of phenyl lithium, bis(benzene)vanadium can be isolated from the reaction mixture after hydrolysis (as is found for

Table 11. Anionic homoleptic aryls of Groups 4 and 5

Complex	Comments	References
$Ti(2,4,6\text{-}Me_3C_6H_2)_4Li$	$TiCl_3$+4 mesLi. Red, crystalline	19
$Ti[2,2'\text{-}C_6H_4OC_6H_4]_3Li_2(Et_2O)_2$	Yellow/diamagnetic	84
$V[2,6\text{-}(MeO)_2C_6H_3]_4Li_2$	$(C_5H_5)_2V$+4DMOPLi	85
$V[2,6\text{-}(MeO)_2C_6H_3]_4Li$	$VBr_3(THF)_3$+4DMOPLi	85
$V(C_6H_5)_6Li_4(Et_2O)_4$	X-ray; $VCl_3(THF)_3$+excess PhLi	86, 87
$V(2,4,6\text{-}Me_3C_6H_2)_3ArLi(THF)_4$	V(mesityl)$_3$+ArLi, Ar = ph, tol, DMOP	83
$V_2(\mu\text{-}C_6H_4)(2,4,6\text{-}Me_3C_6H_2)_6Li_2(THF)_8$	V(mesityl)$_3$+$Li_2C_6H_{11}$	83
$V(2,4,6\text{-}Me_3C_6H_2)_4Li$	V(mesityl)$_3$+mesLi	24, 81, 82
$Nb(\eta^2\text{-}C_6H_4)_2(C_6Ph)_3(LiPh)Li(THF)_2$	X-ray; bis-benzyne complex	90, 92, 89
$[Ta(\eta^2\text{-}C_6H_4)_2(Ph)_4(LiTHF)_2]^{2-}$	X-ray; bis-benzyne complex	
	$TaCl_5$+excess PhLi	92, 88
$Ta(4\text{-}MeC_6H_4)_6(LiEt_2O)$	Characterized by NMR spectroscopy	94

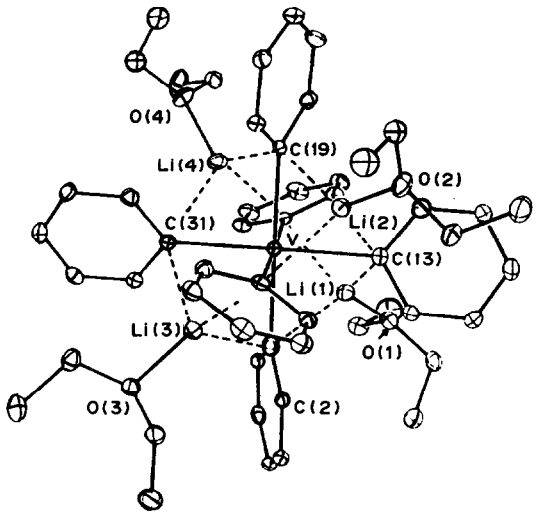

Fig. 11. Molecular structure of the hexaphenyl vanadate species $V(Ph)_6Li_4(Et_2O)_4$ (reprinted by permission from ref. 87).

chromium).[86] A recent crystallographic analysis of $Li_4V(Ph)_6(Et_2O)_{3.5}$ indicates an almost perfect octahedral geometry about vanadium, with an average V—C distance of 2.35 Å. The lithium atoms form an integral part of the molecule and each is bonded in a triply-bridging fashion to the faces of the VC_6 octahedron (C—Li_{av} = 2.225 Å) (Fig. 11).[87]

Anionic *polyphenyl complexes* of *niobium* and *tantalum* were first reported by Sarry and co-workers in the late 1960s and were originally formulated as $M(Ph)_2[Li(Ph)]_4(Et_2O)_{3.5}$ (M = Nb, Ta).[88–90] On the basis of ^7Li and ^1H NMR studies, benzyne structures were later favoured for these species.[91] The structures by X-ray diffraction show the species to be the bis-benzyne complexes $[Nb(\eta^2\text{-}C_6H_4)_2(Ph)_3(LiPh)(THF)][(LiTHF)](THF)_{0.5}(C_6H_{14})_{0.5}$ and $[Ta(\eta^2\text{-}C_6H_4)_2(Ph)_4(LiTHF)_4][Li_4Cl_2(THF)_6]$;[92] see Figs 12 and 13.

The niobium anion contains a five-coordinate metal in a roughly trigonal bipyramidal coordination geometry if the midpoint of the C—C bond of the benzyne ligands is taken to occupy one site of the coordination sphere. The equator of the bipyramid is made up of one phenyl group and two benzyne ligands. Niobium–C(phenyl) distances average 2.34 Å, while the Nb–benzyne distances are shorter in the range 2.17–2.22 Å. As was found in the structure of the polyphenyl vanadium ion described earlier, the lithium counterions are closely associated with the MC_7 core. There is one

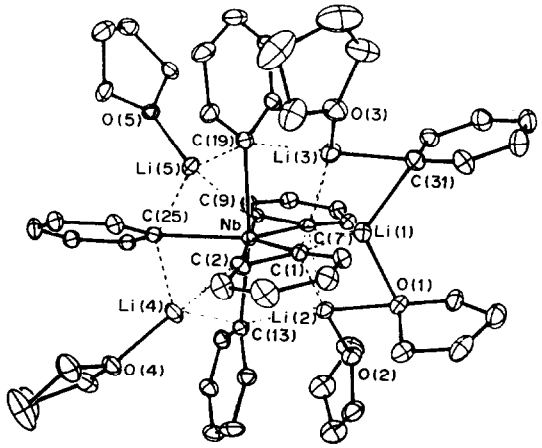

Fig. 12. Molecular structure of the benzyne niobate anion $[Nb(\eta^2\text{-}C_6H_4)_2(Ph)_3(LiPh)(THF)]^-$ (reprinted by permission from ref. 92).

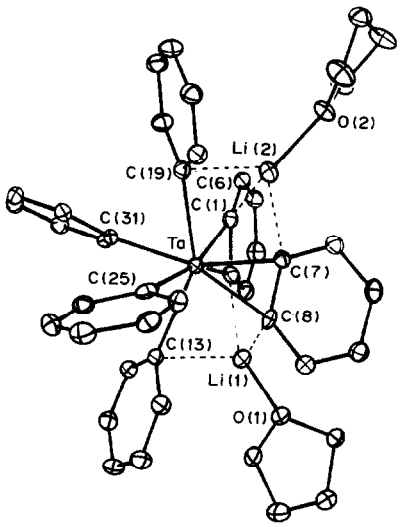

Fig. 13. Molecular structure of the polyphenyl benzyne tantalum complex $[Ta(\eta^2\text{-}C_6H_4)_2(Ph)_4(LiTHF)_2]^{2-}$ (reprinted by permission from ref. 92).

"extra" phenyl group with no bonds to niobium instead bridging two lithium atoms. The electron-rich nature of the niobium(II) complex is mirrored in the long benzyne C—C bonds relative to C—C bonds in other early transition metal benzyne complexes.[93]

The tantalum complex has a quite different structure with the metal residing in a distorted octahedron if the benzyne ligands are again assumed to occupy only one coordination site. The benzyne ligands lie *cis* to one another and are bridged by two lithium atoms which also have close contacts to two other η^1-phenyl ligands. The slight shortening of the benzyne C—C distances in the tantalum compound, relative to niobium, was ascribed to the greater electron deficiency in the former. The para-*tolyl tantalum* complex, "$LiTa(p\text{-tol})_6(Et_2O)$", has also been characterized spectroscopically as a benzyne species.[91,94]

3.3. *Group* 6: *Chromium, molybdenum and tungsten*

A brief mention of the chromium(III) p-*dimethylaminoaryl anion*, $Cr(p\text{-}Me_2NC_6H_4)_3Li$, has appeared in the literature but it is only poorly characterized.[95]

The dimeric chromium(II) phenyls $[Cr(Ph)_3Na]_2(Et_2O)_3$ and $[Cr(Ph)_3Li]_2(Et_2O)_3$ were synthesized by reaction of the compounds $M_2Cr(Ph)_5$ (M = Na, Li) with $CrCl_3$.[96] The reaction is thought to proceed via an intermediate chromium(III) complex $MCr(Ph)_4$, which disproportionates to $[MCr(Ph)_3]_2$ and biphenyl [eqs (28) and (29)]:

$$4M_2Cr(Ph)_5 + CrCl_3 \longrightarrow 5MCr(Ph)_4 + MCl \quad (M = Li, Na) \tag{28}$$

$$5MCr(Ph)_4 \longrightarrow 5MCr(Ph)_3 + 2.5(Ph)_2. \tag{29}$$

The lithium derivative could also be synthesized by reaction of $CrCl_3(THF)_3$ and PhLi in a 1:4 stoichiometry.[96] Lowered magnetic moments were thought to be due to metal–metal interaction within the molecule.[96] The monomeric high-spin chromium(II) complex $[Cr(Ph)_4Li_2](THF)_2$ was synthesized from $(PhCH_2)Cr(Ph)_2$ and two moles of PhLi in a reductive manner.[97]

More recently two *mesityl* chromium compounds have been reported, $[Cr(mes)_3][Li(dioxane)(Et_2O)]$ and $[Li(THF)_2]_2[Cr(mes)_4]$. The latter was assigned a tetrahedral structure from magnetic and spectroscopic data.[98] The synthesis involves the stepwise addition of mesLi to $Cr(mes)_2(THF)_3$ [eq. (30)]:

$$Cr(mes)_2(THF)_3 + mesLi \longrightarrow Cr(mes)_3Li + mesLi \longrightarrow [Li(THF)_2]_2[Cr(mes)_4]. \tag{30}$$

Table 12. Anionic homoleptic aryls of Group 6

Complex	Comments	References
$Cr(4\text{-}Me_2NCH_2C_6H_4)_3Li$	Poorly characterized, also 2-$MeOC_6H_4$, biphenyl	95
$[Cr(C_6H_5)_3M]_2(Et_2O)_3$	M = Na, Li; $Cr(Ph)_5M_2 + CrCl_3$	96
$Cr(C_6H_5)_4Li_2(THF)_4$	High-spin Cr^{II}. X-ray	97
$Cr(Ph)_4M$	M = Na, Li; four-coordinate metal centre	99
$Cr(2,4,6\text{-}Me_3C_6H_2)_3Li$	$Cr(mes)_2$ + mesLi	98
$[Cr(2,4,6\text{-}Me_3C_6H_2)_4Li_2(THF)_2](THF)$	$Cr(mes)_3Li$ + mesLi. X-ray	97
$Cr(Ph)_5Na_2(Et_2O)_3$	X-ray; distorted trigonal bipyramid with closely associated sodium ions	99–101
$Cr(Ph)_6Li_3(Et_2O)_{2.5}$	X-ray; distorted octahedron	87, 99, 102
$Cr(mes)_4Li(THF)_4$	$Cr(mes)_3THF$ + mesLi	40, 81, 82
$Cr(2,2'\text{-}C_6H_4OC_6H_4)_3Li_3$	High-spin, yellow	84
$Mo(\eta^2\text{-}C_6H_4)_2(Ph)_4(LiEt_2O)_4$	Bis-benzyne species characterized by NMR	104, 107, 106
$Mo(4\text{-}MeC_6H_4)_6(LiEt_2O)_4$	Paramagnetic in solution	107
$W(\eta^2\text{-}C_6H_4)_2(Ph)_4(LiEt_2O)_4$	Bis-benzyne species characterized by NMR	104, 106, 107
$W(C_6F_5)_5Li(Et_2O)_2$	WCl_6 + 6PhLi; decomposes to WPh_5	45

The analogous reaction of $Cr(mes)_3(THF)$ and mesLi gives the chromium(III) *tetramesityl anion* which again has a distorted tetrahedral structure.[82] Four-coordinate chromium(III) complexes of formula $MCr(Ph)_4(DME)_4$ (M = Na, Li) were formed in the presence of moisture during synthesis of chromium(II) aryl anions.[99] The ortho-*anisole* complex has also been described.[95]

An X-ray crystallographic analysis of the *pentaphenyl anion* $[Cr(Ph)_5][Na_2(Et_2O)_3(THF)]$[100] (Fig. 14) shows the distorted trigonal bipyramidal CrC_5 core.[101] The sodium ions maintain close contacts with the phenyl ligands, forming a secondary coordination sphere much like that found in the lithium polyphenyl chromates. The odd blue–green colour of the complex (other phenyl chromates are light yellow–orange) stimulated an investigation into its electronic spectrum which did not, however, prove informative because strong charge-transfer bands obscured all but one *d–d* transition.[161] Several other chromium(III) polyphenylates of formula $Cr(Ar)_6Li_3$ are known (Ar = *p*-$Me_2NC_6H_4$, biphenyl, diphenylether).[84,95] Both the tris *sodium* and tris *lithium hexaphenylchromium*(III) complexes have been reported[99,100,102] and the lithium salt structurally char-

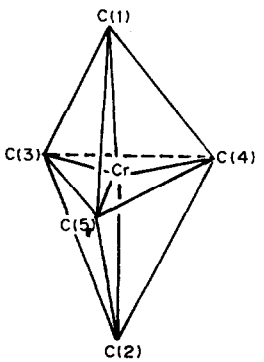

Fig. 14. The CrC_5 core of the polyphenyl chromate species $Cr(Ph)_5Na_2$; important bond angles are C(1)—Cr—C(4) = 86°, C(1)—Cr—C(5) = 84°, C(1)—Cr—C(3) = 102°, C(4)—Cr—C(5) = 145°, C(5)—Cr—C(3) = 97°, C(3)—Cr—C(4) = 104°, C(4)—Cr—C(2) = 94°, C(5)—Cr—C(2) = 85°, C(3)—Cr—C(2) = 97°.

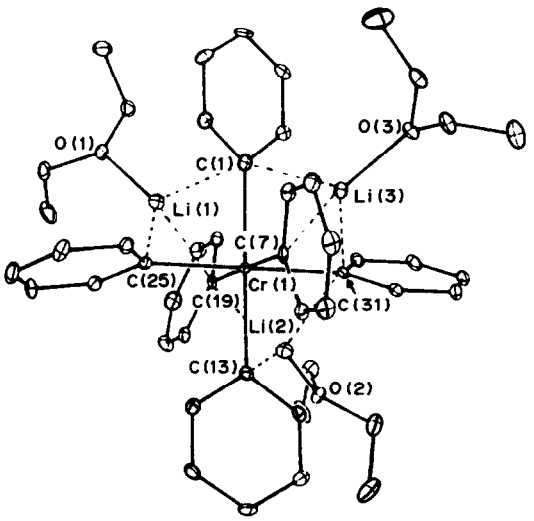

Fig. 15. Molecular structure of the Cr^{III} phenylate $Cr(Ph)_6Li_3(Et_2O)_3$ (reprinted by permission from ref. 87).

acterized.[87] This chromium complex is quite similar to the vanadium(III) complex mentioned earlier and has a central CrC_6 core in a distorted octahedron. The lithium ions cap faces of the octahedron in a triply-bridging fashion (Fig. 15).

The polyarylates of molybdenum and tungsten have also been investigated by Sarry and co-workers. As was found for the tantalum and niobium polyphenylates the original formulations, $M(Ar)_6Li_3$, were later revised to reflect the presence of aryne groups and the species reformulated as $M(\eta^2\text{-aryne})_2(Ar)_4(LiEt_2O)_4$ (M = Mo, Ar = Ph; M = W, Ar = *p*-tol, Ph) on the basis of NMR data.[106,107] No definitive conclusions were reached as to the exact nature of the coordination environments about the metal atoms. In the solid state the phenylate compounds were found to be diamagnetic with slight paramagnetism developing on dissolution. The hexatolylate of molybdenum was paramagnetic in solution (μ_{eff} = 3.9 BM) and NMR investigations were not possible.[107]

Lastly, a *perfluorophenylate* of tungsten(IV) has been synthesized in a reduction manner from PhLi and WCl_6.[45] The product was characterized by its reaction chemistry and magnetic behaviour.

3.4. *Group 7: Manganese and rhenium*

The *manganese*(II) *complexes*, $Mn(Ph)_3Li$, $Mn(p\text{-tolyl})_3Li$ and $Mn(p\text{-}MeOC_6H_4)_3Li$, reported in the early literature were prepared by the room temperature reaction of MnI_2 and the appropriate aryl lithium reagent.[108] Their characterization is questionable and formulation as monomers has been proven incorrect by Power and co-workers.[109]

Table 13. Anionic homoleptic aryls of Group 7

Complex	Comments	References
$[Mn(Ph)_3Li(S)_x]_2$	X-ray; S = Et_2O, x = 1; S = THF, x = 4	99
$[Mn(2,4,6\text{-}Me_3C_6H_2)_3][Li(THF)_4]$	X-ray; discrete cation/anion pair	105, 109
$Mn(2,2'\text{-}C_6H_4OC_6H_4)_2Li(THF)_2$	Yellow–brown; two unpaired electrons	84
$Mn(2,2'\text{-}C_6H_4OC_6H_4)_2Li_2(THF)_6$	Yellow–orange; high-spin d^5	84
$[Re(2\text{-}MeC_6H_4)_4]^-$	Initial reaction product of $ReCl_4(THF)_2$ + 4(2-MeC_6H_4)MgBr and Na/Hg reduction Re(*o*-tol)$_4$. Not isolated	47

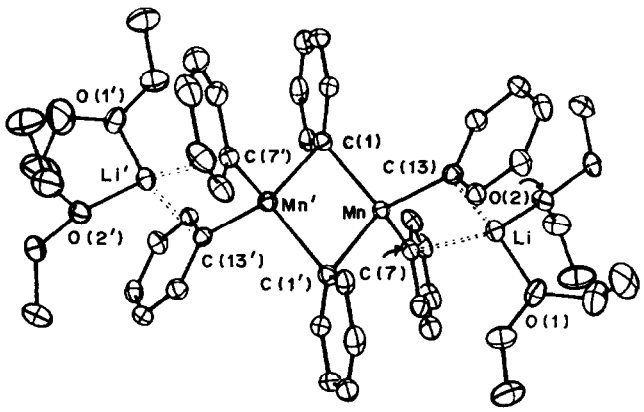

Fig. 16. Molecular structure of the dimeric manganate complex $[Mn(Ph)_3Li(Et_2O)_2]_2$ (reprinted by permission from ref. 109).

The dimer $[Mn(Ph)_3Li(Et_2O)_2]_2$ (Fig. 16) was shown to have one bridging and two terminal phenyl groups for each manganese atom. The terminal phenyl groups are closely associated with the lithium counterions and close contacts exist to the *ipso*-phenyl carbons (Li—C = 2.429 Å). If the synthesis is carried out in an Et_2O–THF mixture, crystals of $[Mn(Ph)_3]_2[Li(THF)_4]_2$ are obtained. Although there is no association between the cationic and anionic portions of the molecule, the structure (Fig. 17) is very similar to the diethyl ether analogue, although the free anion contains shorter Mn—C bonds for both bridging and terminal aryl groups [Mn—C_{av}^{free} = 2.146 (terminal), Mn—C_{av}^{free} = 2.255 Å (bridging): vs Mn—$C_{av}^{ass.}$ = 2.178 (terminal), Mn—$C_{av}^{ass.}$ = 2.285 Å (bridging)]. Distorted tetrahedral arrangements are common to metal atoms in both types of molecule.[109]

The tris-*mesityl anion*, whose preparation had been reported previously,[105] was synthesized in the same manner as the phenyl analogues and crystallized from THF–Et_2O–hexane mixtures as discrete cation–anion pairs. The molecular structure is composed of monomers containing planar MnC_3 cores (Fig. 18). This monomeric nuclearity is no doubt due to the greater steric demands of the mesityl ligands relative to the phenyl ligands. The solution magnetic moment of 5.9 BM corresponds to a high-spin complex containing five unpaired electrons. There were no distortions indicative of M---H—C interactions noted in the solid-state structures of any of these molecules.[109]

Manganese complexes of diphenyl ether have been isolated and characterized. The high-spin manganese(II) complex $Mn(C_6H_4OC_6H_4)_2Li_2(THF)_6$ is yellow–orange and the manganese(III) complex $Mn(C_6H_4OC_6H_4)_2Li(THF)_2$ is yellow–brown.[84]

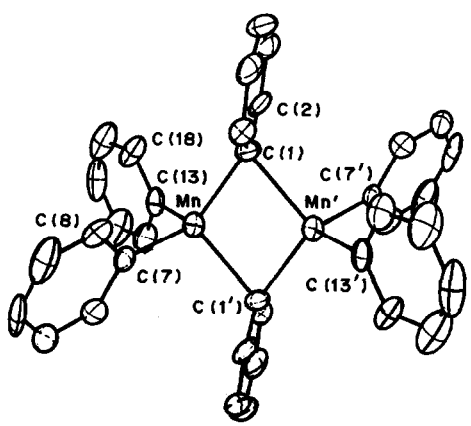

Fig. 17. Molecular structure of the anion in $[Mn(Ph)_3]_2[Li(THF)_4]_2$ (reprinted by permission from ref. 109).

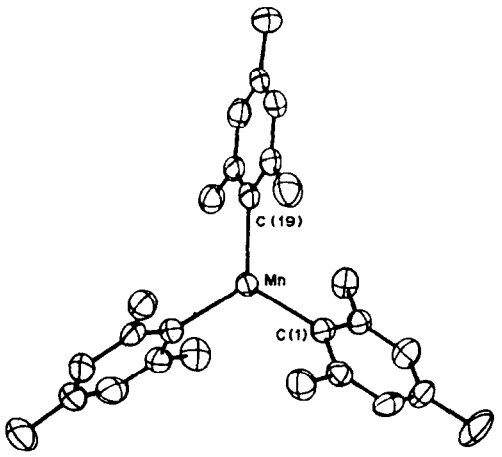

Fig. 18. Monomeric structure of the anionic portion of $[Mn(mes)_3][Li(THF)_4]$ (reprinted by permission from ref. 109).

No technetium compounds are known and the only *rhenium* compound is $[Re(o\text{-tol})_4]^-$. The presence of this anion in deep blue solutions arising from the attempted preparation of $Re(o\text{-tol})_4$ was deduced by oxidation of the solutions with CuCl to give $Re(o\text{-tol})_4$ and by reduction of $Re(o\text{-tol})_4$ with sodium amalgam to give similar deep blue solutions.[47]

3.5. *Group* 8 : *Iron*

Two aryl lithium complexes of iron(0) have been shown to have remarkable reactivity with dinitrogen. The *tetraphenyl complex*, $[Fe(Ph)_4][Li(Et_2O)_4]$, is synthesized by reaction of $FeCl_3$ and 10 equivalents of phenyl lithium in diethyl ether [eq. (31)]:[110]

$$FeCl_3 + \text{excess PhLi} \longrightarrow [Fe(Ph)_4][Li(Et_2O)_4]. \quad (31)$$

The FeC_4 core is close to being a rectangle (Fig. 19). There are close contacts between *ipso*-carbons of each pair of phenyl groups (C—C = 2.09 Å) suggesting some ligand–ligand interaction. The lithium atoms lie above and below the plane of the FeC_4 core and are coordinated to one solvent molecule and one pair of phenyl ligands.[110] The ability of the molecule to fix nitrogen was thought to be due to the ease with which a dinitrogen molecule could approach and coordinate to the metal centre and subsequently react with a nearby lithium atom to give a Fe—N=N—Li moiety. One mole of hydrazine per mole of iron is formed on acidolysis of the $Fe—N_2$ adduct with HCl.[110] A similar proposition has been put forward to explain the release of hydrazine from the acidolysis

Table 14. Anionic homoleptic aryls of Group 8

Complex	Comments	References
$[Fe(Ph)_4][Li(Et_2O)_4]$	X-ray; forms a dinitrogen complex which releases hydrazine on treatment with HCl	110
$Fe(C_{10}H_7)_3Li_3$	Obtained by reduction of $Fe(C_{10}H_7)_4Li_2$ with alkyl lithium reagents. Complex fixes N_2	111
$Fe(Ph)_5Li_5$	$FeCl_3$ + excess PhLi	112
$Fe(C_{10}H_7)_4(LiEt_2O)_2$	X-ray; distorted tetrahedral geometry	113, 114
$[Fe(mes)_3]_nM$	M = Li, $n = 1$; M = Mg, $n = 2$	54
$Fe[2,6\text{-}(MeO)_2C_6H_3]_4Li_2$	$FeBr_2$ + 4DMOPLi	115
$Fe[2,2'\text{-}C_6H_4OC_6H_4]_2Li_2(THF)_5$	$\mu_{eff} = 4.54$ BM, dark red	84
$Fe(C_6F_5)_2(THF)$	$Fe^0 + C_6F_5I$	55

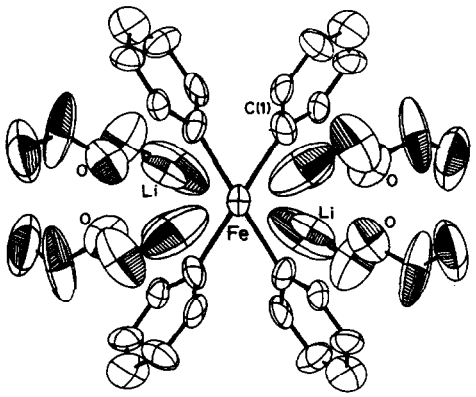

Fig. 19. Molecular structure of the ferrate complex $[Fe(Ph)_4][Li(Et_2O)]_4$ (reprinted by permission from ref. 110).

of the dinitrogen complex obtained from the iron(0) *naphthyl*, $Fe(naphthyl)_3Li_3$.[111] The black phenyl iron(0) complex, $Fe(Ph)_5Li_5$, has been reported as another product of $FeCl_3$/phenyl lithium mixtures.[112]

The tris-mesityl "ate" complexes, $Fe(mes)_3Li(dioxane)_4$ and $[Fe(mes)_3]_2Mg(THF)_{5.75}$, were synthesized in an attempt to find molecular precursors which would yield $Fe(mes)_3$ on oxidation.[54] Another iron(II) complex has been structurally characterized $Fe(naphthyl)_4(LiEt_2O)_2$.[113,114] In contrast to the rectangle found in the phenyl iron(0) complex, the naphthyl derivative has a distorted tetrahedral arrangement (Fig. 20). The lithium atoms maintain contact with the phenyl coordination sphere but no Fe—Li interaction is noted. Excess naphthyl lithium was not effective in reducing the iron to the metal(0) oxidation state. Non-bulky lithium reagents did, however, give the $[Li_3Fe(naphthyl)_3](Et_2O)_n$ complex [eq. (32)].[112,114]

$$Fe(naphthyl)_4(LiEt_2O)_2 + LiC_3H_5 \longrightarrow [Li_3Fe(naphthyl)_3](Et_2O)_n \qquad (32)$$

Drevs has reported d^6 iron(II) ferrate complexes of diphenyl ether, $Li_2Fe(C_6H_4OC_6H_4)_2(THF)_5$, and dimethoxybenzene (DMOP), $Li_2Fe(DMOP)_4(LiBr)(THF)_4$; no structural information other than magnetic moments is available.[84,115]

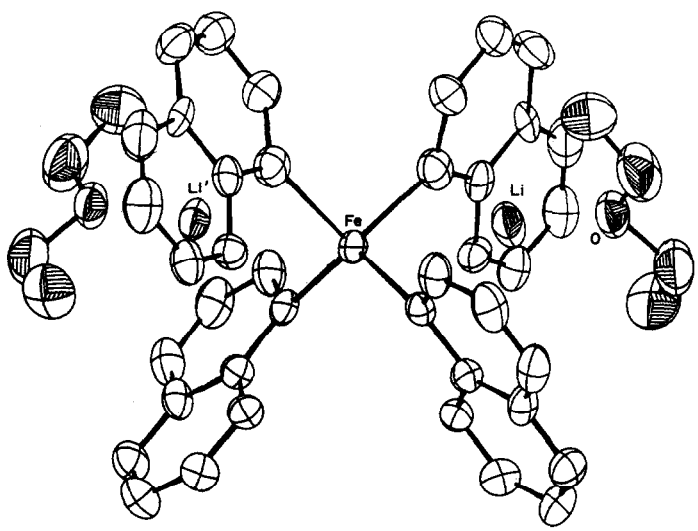

Fig. 20. Molecular structure of the iron(II) arylate complex $[Fe(naphth)_4][Li(Et_2O)]_2$ (reprinted by permission from ref. 114).

No compounds of ruthenium or osmium are known, although CV study showed reduction waves for $Os(o\text{-tol})_4$.[47]

3.6. *Group 9: Cobalt and rhodium*

The chemistry of the cobaltate $Co(Ph)_4Li_2(THF)_4$ has been examined and an interesting redox system discovered. If the compound is shaken at room temperature for 24 h biphenyl is lost and $Co_2(Ph)_4Li_4(THF)_4$ is formed [eq. (33)]:

$$2Co(Ph)_4Li_2(THF)_4 \longrightarrow Co_2(Ph)_4Li_4(THF)_4 + 2C_{12}H_{10}. \quad (33)$$

The identity of the cobalt(0) compound was determined by elemental analysis, cryoscopic molecular weight determination and reactivity with small molecules. It is believed the compound derives its stability from M–ligand π-backbonding and direct metal–lithium interaction.[116] A structure much like that of $Ni(Ph)_3Li_3(THF)_3$[117] was proposed.

Reaction of the cobalt(0) complex with four equivalents of PhLi gave the Co^{-1} species $Co(Ph)_3Li_4(THF)_5$ as a diamagnetic black–brown crystalline substance [eq. (34)]:[116]

$$Co_2(Ph)_4Li_4(THF)_4 + 4PhLi \longrightarrow 2Co(Ph)_3Li_4(THF)_5 + C_{12}H_{10}. \quad (34)$$

A monomeric structure containing two terminal phenyl ligands and an η^6-bonded phenyl lithium moiety was proposed on the basis of NMR evidence and comparison to $(C_6F_5)_2Co(\eta^6\text{-toluene})$, which has been structurally characterized.[116] As is the case for $Co_2(Ph)_4Li_4(THF)_4$, direct Co—Li interaction may be partly responsible for the stability of the molecule.

Complexes of diphenyl ether and DMOP similar to those of iron have also been characterized for cobalt. The cobalt(II) species $Co(DMOP)_4Li_2(THF)_3$ and $Co(C_6H_4OC_6H_4)_2Li_2(THF)_4$ are thermally sensitive, paramagnetic materials with magnetic moments of 3.18 and 2.79 BM, respectively.[84,115]

The cobalt(II) *mesityl* complex, $Li[Co(mes)_3(THF)]$, first reported in 1977,[105] has recently been the subject of more detailed investigation.[59] The complex shows temperature-dependent, paramagnetically-shifted ^1H NMR resonances, and the solution magnetic moment of 3.8 BM corresponds with that for a high-spin d^7 system in a trigonal environment.[59] Reaction with HBF_4 in THF gave the neutral $[Co(mes)_2]_2$ and mesitylene [eq. (35)]:[59]

$$2Li[Co(mes)_3(THF)] + HBF_4 \longrightarrow [Co(mes)_2]_2 + 2C_9H_{12}. \quad (35)$$

The *perhalophenyl* derivatives $[Bu^n{}_4N]_2[Co(C_6X_5)_4]$ (X = Cl, F) were synthesized by reaction of tetrahalocobaltate dianions with four equivalents of the appropriate lithium reagent [eq. (36)]:[118]

$$[Bu^n{}_4N]_2[CoCl_4] + 4C_6X_5Li \xrightarrow{-4LiCl} [Bu^n{}_4N]_2[Co(C_6X_5)_4]. \quad (36)$$

Table 15. Anionic homoleptic aryls of Group 9

Complex	Comments	References
$Co(Ph)_3Li_4(THF)_5$	$[Co(Ph)_4]^{2-} + 4PhLi$	116
$[Co(Ph)_2Li_2]_2$	Decomosition product of $[Co(Ph)_4]^{2-}$	116
$Co(Ph)_4Li_2(THF)_4$	Decomposes to Co^0 products in solution	116
$Co(2,4,6\text{-}Me_3C_6H_2)_3Li$	Gives neutral $Co(mes)_2$ on reaction with HBF_4	59, 105
$Co[2,6\text{-}(MeO)_2C_6H_3]_4Li_2$	Paramagnetic $\mu_{eff} = 3.18$ BM	115
$Co(2,2'\text{-}C_6H_4OC_6H_4)Li_2$	Paramagnetic $\mu_{eff} = 2.79$ BM	84
$Co(2,2'\text{-}C_6H_4OC_6H_4)Li_3(THF)_4$	Diamagnetic	84
$[Co(C_6X_5)_4][NBu^n{}_4]_2$	X = F, Cl; $[MCl_4][NBu^n{}_4]_2 + 4C_6X_5Li$	68, 118
$Rh(C_6F_5)_5Li_2$	X-ray of $PPh_3(CH_2Ph)^+$ salt, adds 2 moles of CO to give $[Rh(C_6F_5)_4(CO)_2]^{2-}$	119

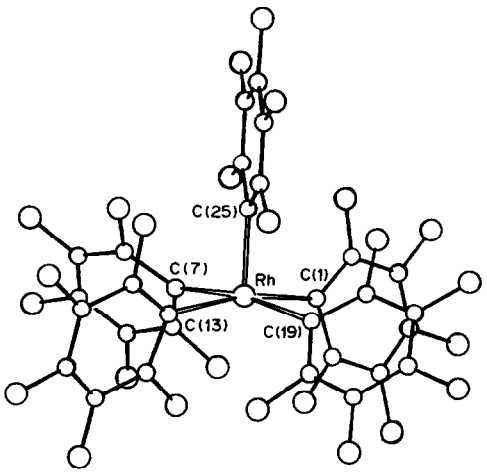

Fig. 21. Structure of anion $[Rh(C_6F_5)_5]^{2-}$ (reprinted by permission from ref. 119).

For *rhodium*[119] the pentacoordinate $[Rh(C_6F_5)_5]^{2-}$ dianion [eq. (37)] has been characterized crystallographically and contains a rhodium atom lying slightly above the base of a square pyramid (Fig. 21). The reaction with carbon monoxide is shown in eq. (38).

$$RhCl_3(THT)_3 + 5C_6F_5Li \longrightarrow Li_2[Rh(C_6F_5)_5] + 3LiCl \tag{37}$$

$$[Rh(C_6F_5)_5]^{2-} \xrightarrow{CO} [Rh(C_6F_5)_5(CO)]^{2-} \xrightarrow{CO} [Rh(C_6F_5)_4(CO)_2]^{-}. \tag{38}$$

3.7. *Group* 10: *Nickel, palladium and platinum*

Taube has reported both *tetraphenyl-* and *triphenylnickelate* complexes.[117,120] The tetraphenyl dianion was synthesized from the nickel(II) chelate complex Ni(dpi) [dpi = 1,3-bis(2-pyridylimino)isoindoline] and phenyl lithium [eq. (39)]:

$$Ni(dpi) + 4PhLi \longrightarrow Ni(Ph)_4Li_2. \tag{39}$$

Attempts to prepare the compound from $NiBr_2(THF)_2$ gave yields lower than 5%. It was thought the unique chelate ligand dpi had a stabilizing effect on intermediates formed during the course of the reaction.[120] The tris-phenyl complex $Ni(Ph)_3Li_2(THF)_3$, obtained either by reduction of $Ni(Ph)_4Li_2$ or from $Ni(COD)_2$ (COD = 1,5-cyclooctadiene), was thought to utilize Ni—Li π-

Table 16. Anionic homoleptic aryls of Group 10

Complex	Comments	References
$Ni(Ph)_3(LiTHF)_3$	Stabilized by Ni—Li π-back-bonding	117
$Ni(Ph)_4Li_2(THF)_4$	Ni(dpi) + 4PhLi	120
$Ni[2,6\text{-}(MeO)_2C_6H_4]_4Li_2(THF)_3$	Stable to 240°C; yellow	115
$Ni(2,2'\text{-}C_6H_4OC_6H_4)_2Li_2(THF)_4$	Yellow; crystalline complex	84
$[Ni(C_6X_5)_4][NBu^n_4]_2$	X = F, Cl; $[NiCl_4][NBu^n_4]_2 + 4LiC_6X_5$	118
$[M(C_6X_5)_4][NBu^n_4]_2$	M = Pd, Pt; X = F, Cl; X-ray for chloro derivative of Pt	67, 68, 121–124
$[Pt(C_6Cl_5)_4][NBu^n_4]$	X-ray; obtained by oxidation of Pt^{II} complex with $Tl(C_6F_5)_2Cl$, X_2 (X = Cl, Br, Ir)	68, 121, 122
$[Pt_2Ag(C_6F_5)_6Et_2O][NBu^n_4]$	X-ray; silver atom acts as counter ion with close contacts to Pt atoms	124

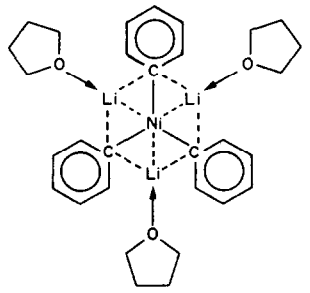

Fig. 22. Proposed structure for $Ni(Ph)_3Li_3(THF)_3$, Ni—Li backbonding is indicated by dashed lines.

backbonding and Li—C contacts to stabilize the molecule,[117] and a structure like that shown in Fig. 22 was proposed.

As with cobalt and iron, divalent complexes of both DMOP and diphenyl ether are known for nickel.[84,115] The DMOP compound is stable to 240°C and may be exposed to air for prolonged periods without decomposition. Its diamagnetic nature suggested a tetragonal coordination about the metal atom with the methoxy groups lying above and below the MC_4 plane.[115]

Usón and co-workers have synthesized a comprehensive series of tetra- and tri*perhalophenyl* derivatives of nickel,[118] palladium[67] and platinum[67,68] by reaction of ammonium salts of formula $[Bu^n_4N]_2[MCl_4]$ with lithium or Grignard C_6F_5 transfer reagents. The triaryl complexes are isolated as monosolvent adducts [eqs (40)–(42)]:[67,118]

$$[Bu^n_4N]_2[NiCl_4]+4C_6F_5Li \longrightarrow [Bu^n_4N]_2[Ni(C_6F_5)_4]+4LiCl \quad (40)$$

$$[Bu^n_4N]_2[M_2(\mu\text{-}Br)_2Br_4]+4C_6F_5Li \longrightarrow [Bu^n_4N]_2[M(C_6F_5)_4] \quad (M = Pd, Pt) \quad (41)$$

$$MCl_2(THT)_2+3C_6F_5Li \longrightarrow [M(C_6F_5)_3(THT)]Li+2LiCl \quad (M = Pd, Pt). \quad (42)$$

The platinum(II) complex $[Bu^n_4N]_2[Pt(C_6Cl_5)_4]$ may be oxidized to the platinum(III) complex $[Bu^n_4N][Pt(C_6Cl_5)_4]$ by reaction with Cl_2, Br_2, I_2 and $TlCl_3$, eq. (43):

$$[Bu^n_4N]_2[Pt(C_6Cl_5)_4]+1/2Cl_2 \longrightarrow [Bu^n_4N][Pt(C_6Cl_5)_4]+[Bu^n_4N][Cl]. \quad (43)$$

The solid-state structure of the platinum(III) compound was compared to that of its platinum(II) parent and no significant differences were discovered. Metal atoms in both compounds have a virtually identical square geometry and are shown together in Fig. 23.[121,122]

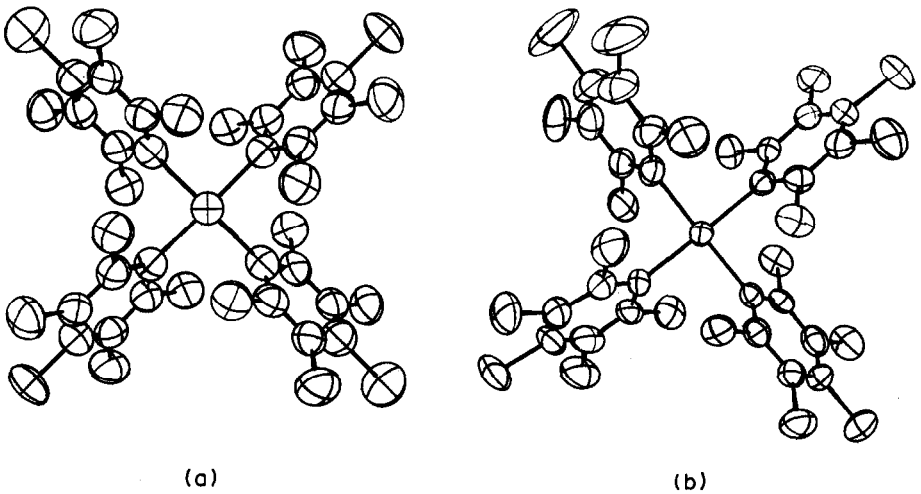

Fig. 23. Molecular structures of the platinate complexes (a) $[Pt(C_6F_5)_4]^{2-}$ and (b) $[Pt(C_6F_5)_4]^-$ (reprinted by permission from refs 121 and 122).

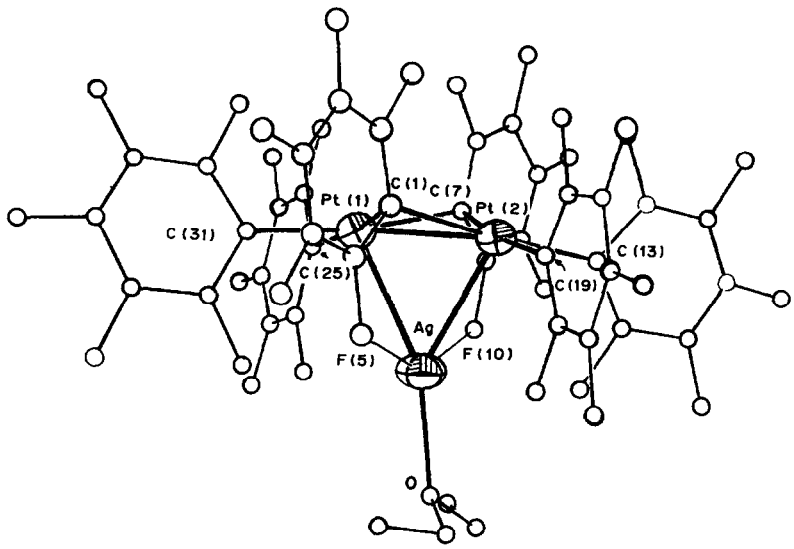

Fig. 24. Molecular structure of the mixed Pt—Ag cluster $[Pt_2Ag(C_6F_5)_6(Et_2O)]^-$ (reprinted by permission from ref. 124).

Species of formula $[M_2(\mu\text{-}X)_2(Ar)_4]^{2-}$ (M = Pd, Pt; Ar = C_6Cl_5; X = Cl, Br) are obtained when monomeric $[M(Ar)_4]^{2-}$ anions are reacted with HCl [eq. (44)]:[123]

$$[M(C_6Cl_5)_4]^{2-} + HCl \longrightarrow [M_2(\mu\text{-}Cl)_2(C_6Cl_5)_4]^{2-} + C_6Cl_5H. \quad (44)$$

The unique mixed-metal cluster $[Bu^n_4N][Pt_2Ag(C_6F_5)_6(Et_2O)](Et_2O)$ was synthesized by the route in eq. (45). An X-ray analysis revealed two closely associated $[Pt(C_6F_5)_3]^-$ units [Pt—Pt = 2.698(1) Å] bridged by two C_6F_5 ligands (Fig. 24). Weak Pt—Ag interactions are implied by short Pt—Ag distances (Pt—Ag_{av} = 2.821 Å) and the absence of bridging ligands across the Pt—Ag gaps.

$$2[Bu^n_4N]_2[PtCl(C_6F_5)_3] \xrightarrow{AgClO_4/CH_2Cl_2}$$

$$2AgCl + 3[Bu^n_4N][ClO_4] + [Bu^n_4N][Pt_2Ag(C_6F_5)_6(Et_2O)](Et_2O). \quad (45)$$

3.8. *Group* 11: *Copper, silver and gold*

Since 1980 (see Reviews for previous studies) the structural characterization of aryl cuprates has advanced dramatically. Monomeric structures are obtained for $[Cu(Ar)_2]^-$ (Ar = mes, Ph) when either a bulky aryl ligand is used[125] or the lithium counterion is complexed to a crown ether (12-C-4) to prevent it from associating closely with the anionic portion of the molecule.[126] The complexes are generated by the routes shown in eqs (46)–(47):

$$CuI \xrightarrow{PhLi} ICuPhLi \xrightarrow{PhLi} (Ph)_2CuLi(LiI) \xrightarrow{12\text{-}C\text{-}4} [(Ph)_2Cu][Li(12\text{-}C\text{-}4)] \quad (46)$$

$$2[Cu(mes)] + 2dppe \longrightarrow [Cu(mes)_2]^-[Cu(dppe)_2]^+$$

(dppe = 1,2-bis(diphenylphosphino)ethane). (47)

In the solid state both cuprate complexes have essentially linear C_{ipso}—Cu—C_{ipso} bonding.

If the diphenyl cuprate is crystallized from diethyl ether without added crown ether a dimeric species is obtained. In this case the lithium atoms play a significant role in the structural composition of the complex. An X-ray analysis shows a cyclic structure consisting of two C—Cu—C—Li units with the lithium atoms in bridging positions between two phenyl groups (Fig. 25).[127] The same C—Cu—C—Li arrangement is also found in $Cu_2Li_2(2\text{-}Me_2NCH_2C_6H_4)_4$ (see Section 4.6) where

Table 17. Anionic homoleptic aryls of Group 11

Complex	Comments	References
$[Cu(Ph)_2][Li(12\text{-crown-4})]$	X-ray; monomeric linear C—Cu—C	126
$[Cu(Ph)_2Li(Et_2O)_2]_2$	X-ray; dimeric Li—C—Cu—C cyclic structure	127
$[Cu(2,4,6\text{-}Me_3C_6H_2)_2]^-$	X-ray; $2Cu(mes)+2dppe \longrightarrow [Cu(dppe)_2]^+[Cu(mes)_2]^-$	125
$Cu_2(2\text{-}Me_2NCH_2C_6H_4)_4Li_2$	X-ray; cyclic structure with N—Li dative bonding	128
$[Cu_3(Ph)_6Li_2]_2$	X-ray; Cu_3Li_2 framework in solid state	130
$[Cu_2(Ph)_5Li_3]$	X-ray; complex of $[Cu(Ph)_2]^-$ and $[Cu(Ph)_3]^{2-}$	125
$[Cu_4(Ph)_6M]^{n-}$	M = Mg, $n = 0$; M = Li, $n = 1$. X-ray; Cu_4M framework in solid state	131
$[Cu_5(Ph)_6]^-$	X-ray; Cu_5 framework in solid state	132
$[Ag(C_6X_5)_2]^-$	X = F, Cl; $CF_3CO_2Ag+2LiC_6X_5$	139
$[Ag_3(Ph)_6Li_2]^-$	X-ray; trigonal bipyramidal structure with Ag_3Li core	140
$[Au(C_6F_5)_2]^-$	X-ray; linear C—Au—C linkage	136–138
$Au_2(2\text{-}Me_2NCH_2C_6H_4)_4Li_2$	X-ray; cyclic C—Au—C—Li structure with N-bonded lithium atoms	129
$[Au(C_6X_5)_4]^-$	X = H, F. X-ray; both complexes have square configurations	135, 134

the amino side groups are coordinated to the bridging lithium atoms (Fig. 26).[128] The same structural features are found in the gold complex $Au_2Li_2(2\text{-}Me_2NCH_2C_6H_4)_4$.[129]

Several copper phenylate clusters having solid-state structures based on distorted trigonal bipyramidal Cu_xLi_y ($x = 3$, $y = 2$; $x = 4$, $y = 1$; $x = 5$, $y = 0$) frameworks have been synthesized and characterized.[130–132] The exact composition of the molecule is dependent on slight variations in the

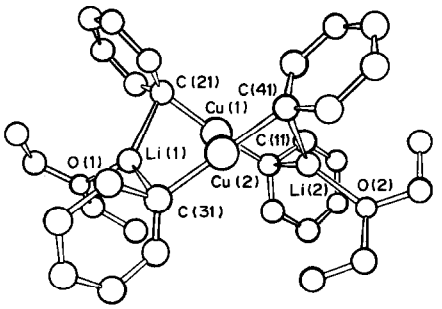

Fig. 25. Molecular structure of phenyl cuprate $[Cu(Ph)_2Li(Et_2O)]_2$ (reprinted by permission from ref. 127).

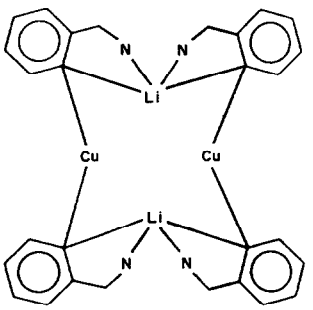

Fig. 26. Diagram of the cuprate $[Cu(2\text{-}Me_2NC_6H_4)_2Li]_2$ showing the secondary N—Li interaction (reprinted by permission from ref. 128).

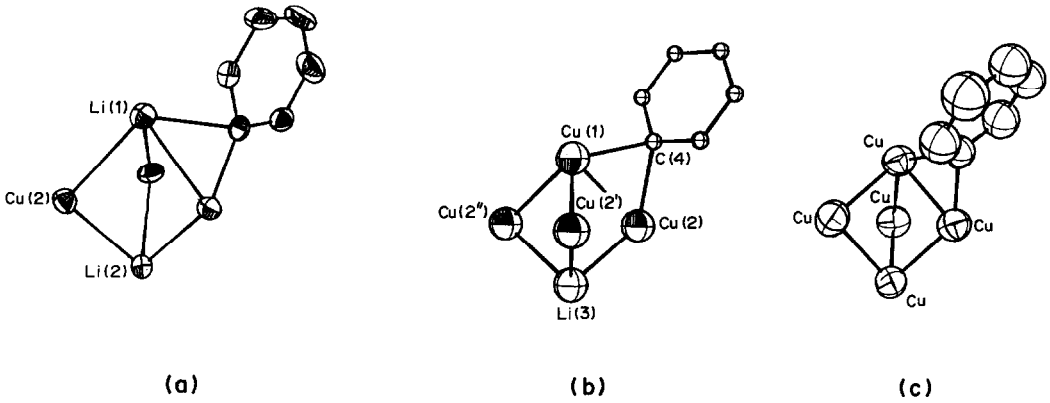

Fig. 27. Trigonal bipyramidal core structures found in the cuprate clusters (a) $[Cu_3Li_2(Ph)_6]^-$, (b) $[Cu_4Li(Ph)_6]^-$, (c) $[Cu_5(Ph)_6]^-$; only one bridging phenyl group is shown for clarity (represented by permission from refs 130, 131 and 132).

synthesis and conditions under which it was crystallized. In each case the copper atoms occupy equatorial positions with the axial positions taken by either lithium or copper atoms depending on the formula of the complex. The phenyl ligands take bridging positions across axial and equatorial sites. Any extra charge for the anion is compensated by a cation having no interaction with the Cu_xLi_y core. The structures of the Cu_xLi_y complexes are shown in Fig. 27. No significant change is noted when magnesium replaces lithium in $[Cu_4Li(Ph)_6][Li(Et_2O)_4](Et_2O)_2$ to give $Cu_4Mg(Ph)_6(Et_2O)$.[131]

A cluster compound $Cu_2Li_3(Ph)_5(SMe_2)_4$ different to those containing Cu_xLi_y trigonal bipyramidal cores and having a phenyl to copper ratio of greater than 2 : 1 may be isolated from PhLi–CuBr mixtures in Me_2S.[133] The molecular structure is shown in Fig. 28. The cluster may be viewed as two cuprate species, $[Cu(Ph)_2]^-$ and $[Cu(Ph)_3]^{2-}$, connected by bridging lithium atoms. The $[Cu(Ph)_3]^{2-}$ unit found in the molecule is the first of its kind to be structurally characterized. The bending of the copper atoms towards each other was thought to be indicative of either a weak Cu—Cu interaction or a directional influence of the phenyl groups caused by deviations in C_{ipso}—Cu planes due to the bridging lithium atoms.[133]

Both *tetraphenylaurate*(III)[134] and *tetra(perfluorophenyl)aurate*(III)[135] species have been structurally characterized and have essentially isostructural square coordination geometries with the aryl groups in a propeller configuration (Fig. 29). If the perhalo gold(I) compound $(C_6F_5)Au(THT)$ is treated with either *o*-phenylenebis(dimethylarsine) (pdma) or triphenylstibine the aurates,

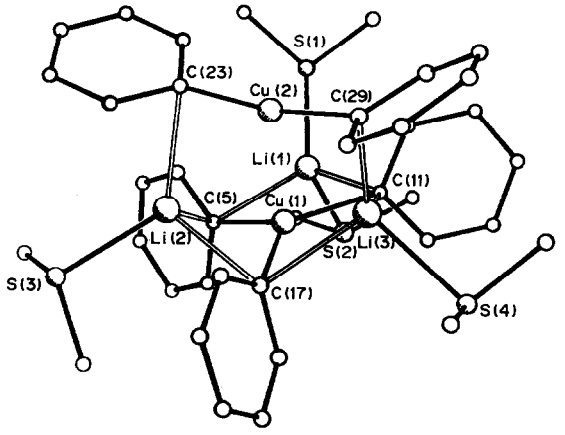

Fig. 28. Molecular structure of the $[Cu(Ph)_2]^-/[Cu(Ph)_3]^{2-}$ aggregate $Cu_2(Ph)_5Li_3(SMe_2)_4$ (reprinted by permission from ref. 133).

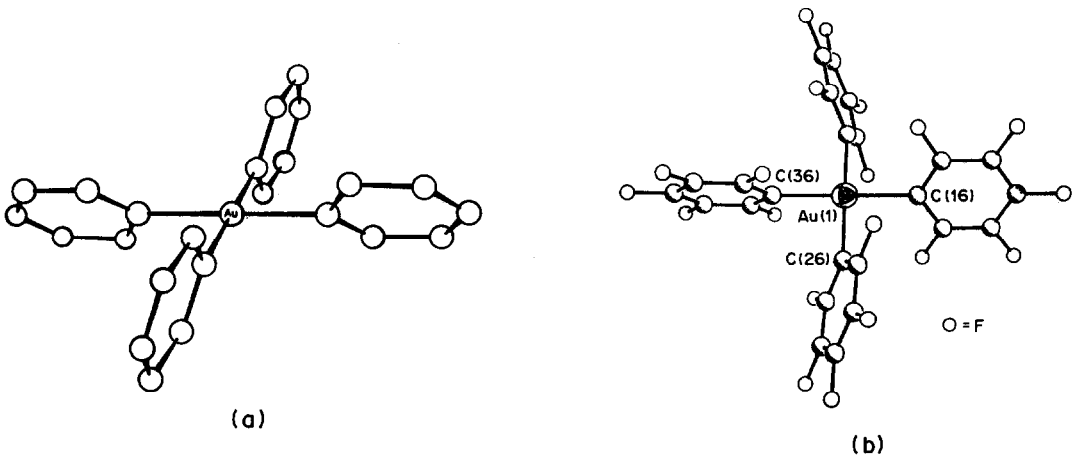

Fig. 29. Molecular structures of (a) $[AuPh_4]^-$ and (b) $[Au(C_6F_5)_4]^-$ showing nearly identical square geometries (reprinted by permission from refs 134 and 135).

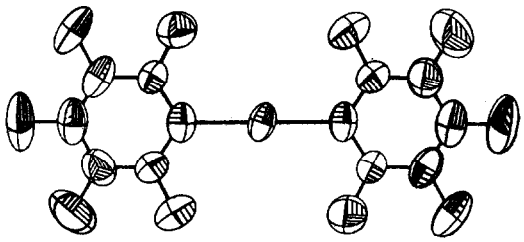

Fig. 30. Molecular structure of $[Au(C_6F_5)_2]^-$ showing the linear C—Au—C vector (reprinted by permission from ref. 138).

$[AuL_x][Au(C_6F_5)_2]$ (L = pdma, $x = 2$; L = $SbPh_3$, $x = 4$), are obtained.[136] Crystallographic analysis shows a monomeric anion with linear C_{ipso}—Au—C_{ipso} coordination (Fig. 30).[136–138]

The syntheses [eq. (48), X = F, Cl] of the aryl silver anions $[Bu^n_4N][AgAr_2]$ (Ar = C_6Cl_5, C_6F_5) have been reported but no structural details were given:[139]

$$CF_3CO_2Ag + 2LiC_6X_5 + [CF_3CO_2][Bu^n_4N] \longrightarrow [Bu^n_4N][Ag(C_6X_5)_2]. \quad (48)$$

The argentate $[Ag_3Li_2(Ph)_6]^-$ was characterized crystallographically and has the same basic structure as its copper counterpart $[Cu_3Li_2(Ph)_6]^-$.[140]

4. FUNCTIONALIZED ARYLS

4.1. *Lanthanides*

Functionalized aryl complexes of samarium, europium and ytterbium can be obtained by reaction of $Hg[PhCr(CO)_3]_2$ and lanthanide metal filings in THF [eq. (49)].[4b]

$$Ln^0 + Hg[(CO)_3CrPh]_2 \longrightarrow Hg^0 + Ln[PhCr(CO)_3]_2(THF)_n. \quad (49)$$

Low energy ν(C—O) stretches (1600–1800 cm^{-1}) in the IR spectrum of the products were ascribed to Ln—O≡C interactions. It is not clear whether these interactions are inter- or intramolecular.[4]

The scandium chelate complex $Sc(2\text{-}Me_2NCH_2C_6H_4)_3$ is thought to owe its stability to the dative bonding of the *ortho*-amino groups.[141] This ubiquitous dimethylaminoaryl ligand has also been used in the synthesis of a number of lanthanide hydrocarbyls (Lu, Er, Yb)[142] and the solid-state structure of the lutetium derivative has been determined (Fig. 31).[143] All three ligands are bonded

Table 18. Homoleptic functionalized aryls of the lanthanide, actinide and Group 3 metals

Complex	Comments	References
$M[(Ph)Cr(CO)_3]_2(THF)_n$	M = Sm, Eu, Yb; M---O≡C contacts in solid state	4b
$Lu(2\text{-}Me_2NCH_2C_6H_4)_3$	X-ray; six-coordinate metal centre with inequivalent aryl groups	143
$Sc(2\text{-}Me_2NCH_2C_6H_4)_3$	Stability attributed to chelating aryl ligand	141

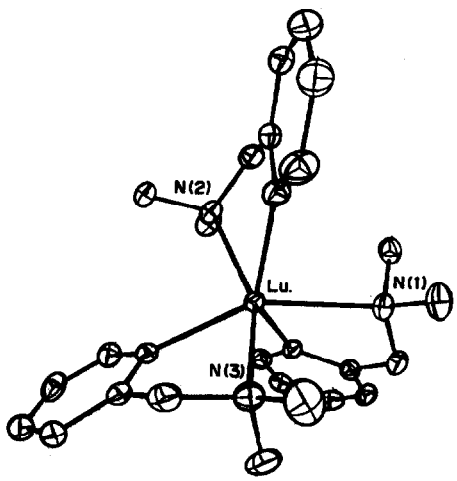

Fig. 31. Molecular structure of the *ortho*-amino-functionalized aryl complex $Lu(2\text{-}Me_2NC_6H_4)_3$ (reprinted by permission from ref. 143).

in a chelate fashion. The variation in Lu—N bond lengths (two short and one long; $Lu—N_{av}^{short} = 2.473$ Å, $Lu—N^{long} = 2.588$ Å) was attributed to either steric forces within the molecule or packing effects which influenced the "arm" of the chelate ligand.[143]

4.2. *Groups* 4 *and* 5: *Titanium and vanadium*

The tris ortho-*pyrazolylphenyl* complex of *titanium*(III) is thought to have an octahedral coordination geometry. Stable for short periods in air, protolytic cleavage of the Ti—C bond is rapid on reaction with protic molecules.[142] The analogous *vanadium* complex $V[2\text{-}(N_2C_3H_2)C_6H_4]_3$ has also been reported.[142] A very similar compound may be obtained using the aryl group *o*-$(Ph)_2PCH_2C_6H_4$[144] where stabilization is afforded by dative P—V bonding.

A class of molecules which have received a great deal of attention, due to their relevance towards metal–metal multiple bonding, are species containing the DMOP [DMOP = 2,6-$(MeO)_2C_6H_3$] aryl group. Reduction of vanadium(III) to vanadium(II) by reaction of VCl_3 and LiDMOP produces a

Table 19. Homoleptic functionalized aryls of Groups 4 and 5

Complex	Comments	References
$M[2\text{-}(N_2C_3H_3)C_6H_4]_3$	M = Ti, V; *ortho*-chelating pyrazolyl group	142
$V[2\text{-}(Ph_2PCH_2)C_6H_4]_3$	Diphenyl phosphine bonds to V centre	144
$\{V[2,6\text{-}(MeO)_2C_6H_3]_2\}_2$	X-ray; dimer with two pairs equivalent aryl ligands: V—V triple bond	85, 145, 146

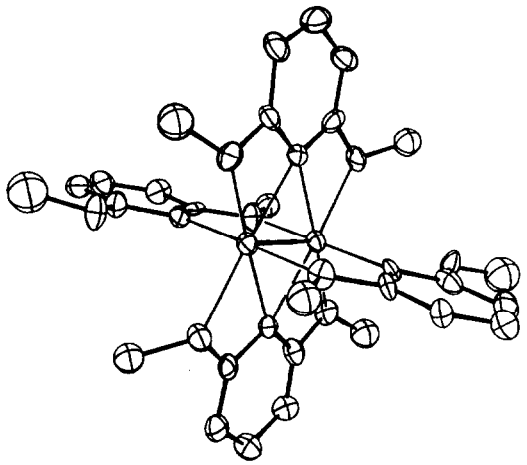

Fig. 32. The vanadium dimer $V_2(DMOP)_4$ showing two sets of inequivalent DMOP ligands (reprinted by permission from ref. 146).

compound which analyses for $V_2(DMOP)_4(THF)$ [eq. (50)]:

$$VCl_3 + 3Li[2,6\text{-}(MeO)_2C_6H_3] \longrightarrow \{V[2,6\text{-}(MeO)_2C_6H_3]_2\}_2(THF)_2. \quad (50)$$

The compound was originally thought to contain a vanadium–vanadium triple bond and four bridging DMOP ligands each using one available methoxy unit to bind the neighbouring atom.[145] A later crystal structure by Cotton and co-workers, one of a *series* (V, Mo, Cr) to appear involving metal complexes containing the DMOP ligand, showed two sets of unique DMOP ligands (Fig. 32). One set utilized only one methoxy oxygen atom while the other ligand set used both and contained the *ipso*-carbon in a bridging position between the vanadium atoms. A V≡V triple bond was presented as credible in comparison with other V—V bond distances.[146]

4.3. *Group* 6: *Chromium and molybdenum*

Ortho-*methoxyaryl* complexes of *chromium* are common and have been the subject of several structural investigations. The first report describing the structure of $Cr_2(DMOP)_4$ was remarkable in that the Cr—Cr distance of 1.847(1) Å was the shortest metal–metal distance known and was more than 0.6 Å shorter than the M—M separations found in the metallic element.[147] The DMOP ligands adopt a *trans*-parallel arrangement to the Cr—Cr bond forming two perpendicular planes (Fig. 33). In contrast to the vanadium derivative where one pair of DMOP ligands utilized only one

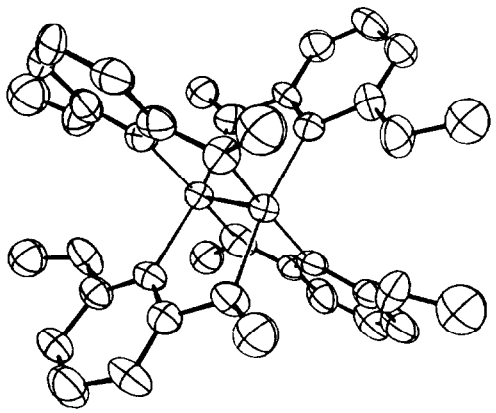

Fig. 33. The quadruply M—M bonded chromium dimer $Cr_2(DMOP)_4$ having equivalent DMOP ligands (reprinted by permission from ref. 147).

Table 20. Homoleptic functionalized aryls of Group 6

Complex	Comments	References
$Cr(2\text{-}MeOC_6H_4)_2$	Low solubility prevents crystallization	95, 150, 151
$Cr(2\text{-}MeOC_6H_4)_3$	Paramagnetic, decomposition studied	151, 153
$Cr(4\text{-}MeOC_6H_4)_2$	No intramolecular chelation	151
$Cr(2\text{-}Ph_2PCH_2C_6H_4)_3$	Secondary Cr—P bonding	144
$Cr[2\text{-}(N_2C_3H_3)C_6H_4]_3$	pz = pyrazolyl	142
$Cr(2\text{-}R_2NCH_2C_6H_4)_3$	R = Me, Et. X-ray for R = Me; distorted octahedral coordination environment	141, 159, 156
$[Cr(2\text{-}MeO\text{-}5\text{-}MeC_6H_3)_2]_2$	X-ray; M—M quadruple bond	152
$Cr(2\text{-}ox\text{-}C_6H_4)_3$	ox = oxazolinyl; X-ray	157
$\{Cr[2,6\text{-}(MeO)_2C_6H_4]_2\}_2$	X-ray	148, 147
$\{Cr[2,4,6\text{-}(MeO)_3C_6H_4]_2\}_2$	X-ray	148, 149
$\{Mo[2,6\text{-}(MeO)_2C_6H_3]_2\}_2$	X-ray	148
$[Mo(2\text{-}MeOC_6H_4)_2]_2$	Characterized by NMR	154

methoxy oxygen and the other DMOP ligands used both in metal–ligand bonding, the DMOP ligands in $Cr_2(DMOP)_4$ were equivalent and all four ligands used only one methoxy oxygen in secondary metal–ligand bonding. The same result was obtained for molybdenum, where a longer metal–metal bond was found [2.064(1) Å].[147] The X-ray structure of $Cr_2(DMOP)_4$ was solved to determine what effect the extra methoxy substituent would have on the metal–metal distance and no significant difference was noted.[148–149] The 5-methylanisole complex was also examined as the unsubstituted anisole derivative, which had previously been identified as a polymer,[95,150,151] proved too difficult to crystallize.[152] The gross structural features were found to be almost identical to the DMOP analogue, although some variation in metal–metal bond lengths was present: $Cr_2(5\text{-}Me\text{-}2\text{-}MeOC_6H_3)$ [Cr—Cr = 1.828(2) Å].

The 2,3- and 4-*methoxybenzene* complexes of chromium and molybdenum have also been synthesized. The 3-anisole and 4-anisole complexes do not seem to show the chelate effect displayed in the *ortho*-anisole dimers.[151,153] The *ortho*-anisole molybdenum compound, $Mo_2(2\text{-}MeOC_6H_4)_4$, has a structure very similar to the chromium analogue.[154] Chromium(III) tris(2-anisole) was the subject of thermal decomposition studies and at 100°C gave $Cr_2(2\text{-}MeOC_6H_4)_4$, 1,1,2,2-tetrakis(2-methoxyphenyl)ethane, anisole and 2,2′-(dimethoxy)biphenyl.[153]

Chromium(III) complexes with varying *ortho* "sidearm" substituents are quite abundant. The $Cr(2\text{-}Me_2NCH_2C_6H_4)_3$[141,155] compound has been structurally characterized (Fig. 34). The metal

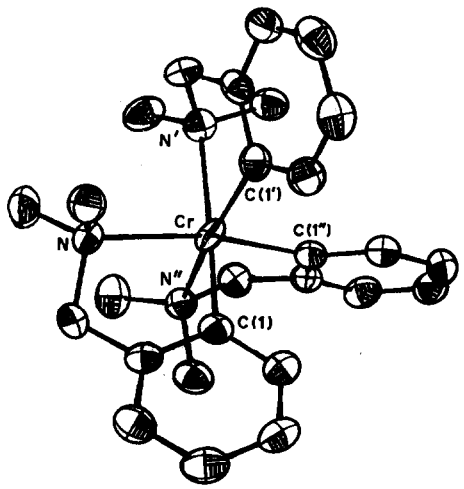

Fig. 34. Molecular structure of $Cr(2\text{-}Me_2NC_6H_4)_3$ (reprinted by permission from ref. 155).

atom resides in a distorted octahedron with a facial arrangement of ligands. Each M—C bond is *trans* to a dative M—N bond.[156] The same general features are found in the 1,3-dioxolano-substituted species, $Cr[2\text{-}(O_2C_3H_8)C_6H_4]_3$,[157] whose solid-state structure shows a chromium atom in a slightly more distorted octahedral CrC_3O_3 environment.[157] Other paramagnetic d^3 *ortho*-substituted chromium aryl complexes $Cr(2\text{-}XC_6H_4)_3$ [X = Et_2NCH_2, pyridyl, $(C_6H_5)_2PCH_2$, pyrazolyl, Me_2N] are likely to possess the same molecular geometries.[95,142,144,158,159]

4.4. *Groups* 7 *and* 8: *Manganese, rhenium and iron*

The same ligands used in the synthesis of group 6 chelate complexes have also seen application in the group 7 and 8 metal aryl complexes. The *manganese chelate* $Mn(2\text{-}Me_2NCH_2C_6H_4)_2$ is obtained from $(LiTHF)_2MnI_2(2\text{-}Me_2NCH_2C_6H_4)_2$ by removal of coordinated LiI in dioxane [eq. (51)]:

$$2Li(2\text{-}Me_2NCH_2C_6H_4) + MnI_2 \longrightarrow (LiTHF)_2MnI_2(2\text{-}Me_2NCH_2C_6H_4)_2$$

$$\xrightarrow{C_4H_8O_2} Mn(2\text{-}Me_2NCH_2C_6H_4)_2. \quad (51)$$

A dimeric structure similar to that of the benzyl chelate, $[Mn(2\text{-}Me_2NC_6H_4CH_2)_2]_2$, which was characterized crystallographically, is postulated.[155] The 2,6-dimethoxy complex of *rhenium*(III), $Re_2(2\text{-}MeOC_6H_4)_6$, has a core structure in solution (by NMR) similar to that of $Cr_2(2\text{-}MeOC_6H_4)_4$ with an additional $2\text{-}MeOC_6H_4$ ligand σ-bonded to each rhenium at the ends of the Re—Re vector.[154]

A ligand similar to 2-MeOPh was used to synthesize the *iron*(II) chelate $[Fe(2\text{-}MeOCH_2C_6H_4)_2]_n$ whose structure was thought to be polymeric.[160] Other iron chelates of ligands *o,o*-$C_6H_4CH_2N(Me)CH_2CH_2N(Me)CH_2C_6H_4$ and *o,o*-$C_6H_4CH_2OCH_2CH_2OCH_2C_6H_4$ have been reported.[160]

Table 21. Homoleptic functionalized aryl complexes of Groups 7 and 8

Complex	Comments	References
$[Re(2\text{-}MeOC_6H_4)_3]_2$	$[Re(DMOP)_2]_2$ core with two DMOP ligands bonded at ends of Re—Re bond	154
$Mn(2\text{-}Me_2NCH_2C_6H_4)_2$	Chelate structure	155
$Fe[2,2'\text{-}C_6H_4XCH_2CH_2XC_6H_4]$	X = N, O; bis-aryl bis-chelate ligand	160
$Fe(2\text{-}MeOCH_2C_6H_4)_2$		160

4.5. *Groups* 9 *and* 10: *Cobalt, nickel, palladium and platinum*

The *cobalt*(III) *chelate*, $Co(2\text{-}Me_2NCH_2C_6H_4)_3$, is obtained by *oxidation* of $CoCl_2$ with $Li(2\text{-}Me_2NCH_2C_6H_4)$ [eq. (52)].[161] The distorted octahedral facial geometry, found in chromium complexes is likely to be the favoured structure for this complex also.

$$CoCl_2 + 3Li(2\text{-}Me_2NCH_2C_6H_4) \longrightarrow Co(2\text{-}Me_2NCH_2C_6H_4)_3. \quad (52)$$

The same synthetic procedure was employed for the diamagnetic $Co[2\text{-}(pyrazolyl)C_6H_4]_3$.[142] The ortho-*pyrazolyl series* is completed with $Ni[2\text{-}(pyrazolyl)C_6H_4]_2$.[42] No mention of Ni—N bonding is made.

Many tetracoordinate bis-*chelate* complexes of the group 10 metals, having d^8 electronic configurations, are known. The $2\text{-}Me_2NCH_2C_6H_4$ ligand has been used to prepare compounds of nickel,[162] palladium[162–164] and platinum[162] via a salt elimination reaction using the lithium aryl and metal dichloride [eq. (53)]:

$$MCl_2 + 2Li(2\text{-}Me_2NCH_2C_6H_4) \longrightarrow 2LiCl + M(2\text{-}Me_2NCH_2C_6H_4)_2 \quad (M = Ni, Pd, Pt). \quad (53)$$

Different isomers are obtained depending on the metal and aminoalkyl substituent used. Table 21 contains a list of isomers identified by NMR {^{1}H and ^{31}P} and dipole moments.[162] The mixed-ligand compound Pd[2-$Me_2NCH_2C_6H_4$][2-(pyrazolyl)C_6H_4] was found to prefer a *trans* orientation.[164]

The reactivity of each complex with carbon monoxide was examined. The predominant products from the nickel and palladium aryls were $Ni(CO)_4$ and palladium metal, respectively. The *trans*-platinum isomer yielded an adduct Pt(2-$Me_2NCH_2C_6H_4)_2$(CO) while the *cis* isomer inserted one mole of CO to form Pt(2-$Me_2NCH_2C_6H_4$)(2-$Me_2NCH_2C_6H_4C$(O)) (Scheme 2).[162]

The analogous 2-$(C_6H_5)_2PCH_2C_6H_4$ complexes, where the amino group has been replaced by $(Ph)_2P$, have been reported and shown to exist as a mixture of isomers, Table 21.[165] The *cis* planar structure of Pt(2-CH_2=$CHCH_2C_6H_4)_2$ was also based on dipole and NMR data.[166]

Table 22. Homoleptic functionalized aryl complexes of Groups 9 and 10

Complex	Comments	References
M[2-$(N_2C_3H_3)C_6H_4$]$_3$	M = Ni, Co; diamagnetic, orange–yellow	142
Co(4-X,2-$Me_2NCH_2C_6H_3)_3$	X = Bu^t, H; octahedral; eliminates *ortho*-substituted biphenyl on decomposition	161
Pt(2-CH_2=$CHC_6H_4)_2$	*cis*-planar	166
M(2-$Me_2NCH_2C_6H_4)_2$	M = Ni (*trans*), M = Pd (*cis*), M = Pt (*cis*/*trans*)	162–164
M(2-$Et_2NCH_2C_6H_4)_2$	M = Pd (*cis*), M = Pt (*cis*/*trans*)	162
M(2-$Ph_2PCH_2C_6H_4)_2$	M = Ni, M = Pd (*cis*/*trans*), M = Pt (*cis*/*trans*)	165
Pd(2-$Ph_2PCH_2C_6H_4$)(4-Bu$^t_2$-$PCH_2C_6H_4$)	*cis*	165
Pd(2-$Me_2NCH_2C_6H_4$)(2-$(N_2C_3H_3)C_6H_4$)		164

4.6. *Group* 11 : *Copper, silver and gold*

Ortho-*chelated* copper, silver and gold complexes are common and have an established structural chemistry. In contrast to *ortho*-functionalized aryl complexes of the nickel triad which are monomeric and have both the σ-bound aryl carbon and *ortho*-functionality connected to the same metal atom, the Group 11 species adopt oligomeric structures in which the aryl and *ortho* moieties bond to separate metal atoms. The structures range from the simple dimer found in the oxazolinyl phenyl complex[167] and gold complexes of formula [Au(*o*-XC_6H_4)]$_2$ (X = PPh_2, PEt_2, $AsPh_2$,

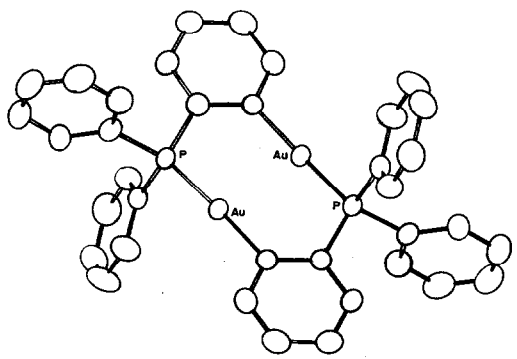

Fig. 35. Molecular structure of [Au(2-$(Ph)_2PC_6H_4$)]$_2$ (reprinted by permission from ref. 168).

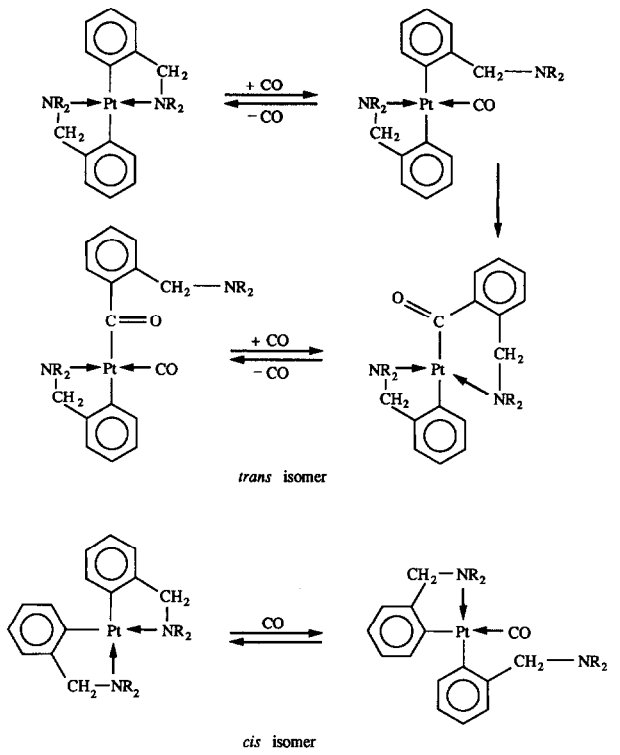

Scheme 2. Reactivity of *cis* and *trans* isomers of $Pt(2\text{-}Me_2NCH_2C_6H_4)_2$ with carbon monoxide.

Table 23. Homoleptic functionalized aryl complexes of Group 11 metals

Complex	Comments	References
$[Cu(8\text{-}Me_2NC_{10}H_6)]_4$	X-ray; cyclic tetramer with bridging chelate ligands	169
$[Cu_4Br_2(2,6\text{-}Me_2NCH_2C_6H_3)_2]_2$	X-ray; $Cu_2L_2(CuBr)_2$ aggregate containing four inequivalent copper atoms	171
$\{Cu[2\text{-}(C_5NOH_2)C_6H_3]\}_2$	Dimer containing oxazolinyl bridge; CuBr adduct also identified by X-ray	170,167
$[Au(2\text{-}EC_6H_4)]_2$	E = Ph_2P, Et_2P, Ph_2As, Me_2As; X-ray	168
$[Au(2\text{-}PhN_2C_6H_4)_2]^+$	X-ray; dimer with bridging phenyl azo unit	172

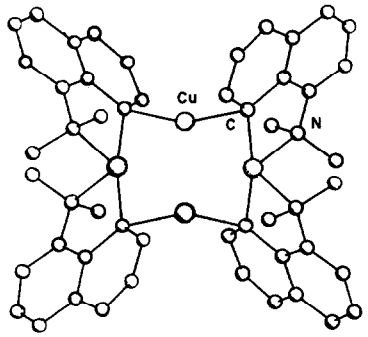

Fig. 36. Molecular structure of $[Cu(8\text{-}Me_2NC_{10}H_6)]_4$ (reprinted by permission from ref. 169).

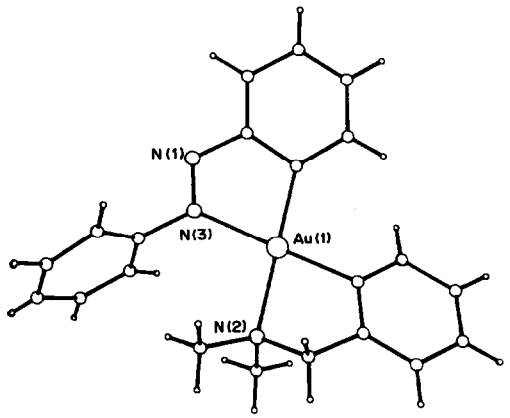

Fig. 37. Molecular structure of the mixed ligand cation $[Au(2\text{-}Me_2NCH_2C_6H_4)(2\text{-}C_6H_5N_2C_6H_4)]^+$ (reprinted by permission from ref. 173).

$AsMe_2$),[168] (Fig. 35) to higher oligomers found for the 8-(dimethylamino)naphthyl complex, $[Cu(8\text{-}Me_2NC_{10}H_6]_4$ (Fig. 36),[169] and the CuBr adduct of the oxazolinephenyl dimer [{Cu[2,4-dimethyl-2-oxazolinyl)phenyl]}$_2$CuBr]$_2$.[170]

The bis ortho-*substituted* species $[Cu_4Br_2(2,6\text{-}Me_2NCH_2C_6H_3)_2]_2$ has both *ortho*-amino groups bonded to copper atoms.[171]

A mixed-ligand cationic gold(III) species having a monomeric square coordination geometry with the nitrogen atoms in *cis* positions has been reported (Fig. 37).[172,173]

Acknowledgements—We are greatly indebted for permission to reprint figures as in the legends to the American Chemical Society, Elsevier Publishers, the Royal Society of Chemistry and V.C.H. Publishers.

REFERENCES

R1. (a) P. J. Davidson, M. F. Lappert and R. Pearce, *Accts Chem. Res.* 1974, **7**, 209; (b) P. J. Davidson, M. F. Lappert and R. Pearce, *Chem. Rev.* 1976, **76**, 219; (c) R. R. Schrock and G. W. Parshall, *Chem. Rev.* 1976, **76**, 243; (d) See appropriate chapters in, *Comprehensive Organometallic Chemistry* (Edited by G. Wilkinson, F. G. A. Stone and E. W. Abel). Pergamon Press, Oxford (1982).

R2. (a) G. H. Posner, *An Introduction to Organic Synthesis Using Organocopper Reagents*. Wiley-Interscience, New York (1980); (b) *Comprehensive Organometallic Chemistry* (Edited by G. Wilkinson, F. G. A. Stone and E. W. Abel). Pergamon Press, Oxford (1982); J. G. Noltes and G. van Koten, Ch. 14, Vol. 2; R. J. Puddephat, Ch. 15, Vol. 2; W. Carruthers, Ch. 49, Vol. 7.

1. F. A. Hart, A. G. Massey and M. S. Saran, *J. Organomet. Chem.* 1970, **21**, 147.
2. G. B. Deacon, A. J. Koplick, W. D. Raverty and D. G. Vince, *J. Organomet. Chem.* 1979, **182**, 121.
3. G. B. Deacon, W. D. Raverty and D. G. Vince, *J. Organomet. Chem.* 1977, **135**, 103.
4. (a) G. B. Deacon, A. Dietrich, C. M. Forsyth and H. Schumann, *Angew. Chem. Int. Edn Engl.* 1989, **28**, 1370; (b) G. Z. Suleimanov, V. N. Khandozhko, P. V. Petrovskii, R. Y. Mekhdiev, N. E. Kolobova and I. P. Beletskaya, *J. Chem. Soc., Chem. Commun.* 1985, 596.
5. V. N. Latyaeva, G. A. Razuvaev, A. V. Malisheva and G. A. Kiljakova, *J. Organomet. Chem.* 1964, **2**, 388.
6. V. N. Latyaeva, L. I. Vyshinskaya, V. B. Shur, L. A. Fyodorov and M. E. Volpin, *J. Organomet. Chem.* 1969, **16**, 103.
7. R. Tabacchi and A. Jacot-Guillarmod, *Chimia* 1970, **24**, 271.
8. G. J. Dubsky, K. S. Boustany and A. Jacot-Guillarmod, *Chimia* 1970, **24**, 17.
9. A. Jacot-Guillarmod, R. Tabacchi and J. Causse, *Chimia* 1969, **23**, 188.
10. R. Tabacchi and A. Jacot-Guillarmod, *Helv. Chim. Acta* 1970, **53**, 1977.
11. R. Tabacchi, K. S. Boustany and A. Jacot-Guillarmod, *Helv. Chim. Acta* 1970, **53**, 1971.
12. G. J. Dubsky and A. Jacot-Guillarmod, *Helv. Chim. Acta* 1970, **53**, 1965.
13. K. S. Boustany, K. Bernauer and A. Jacot-Guillarmod, *Helv. Chim. Acta* 1967, **50**, 1305.
14. K. S. Boustany, K. Bernauer and A. Jacot-Guillarmod, *Helv. Chim. Acta* 1967, **50**, 1120.
15. K. S. Boustany, K. Bernauer and A. Jacot-Guillarmod, *Helv. Chim. Acta* 1967, **50**, 1080.

16. R. Tabacchi, K. S. Boustany and A. Jacot-Guillarmod, *Helv. Chim. Acta* 1970, **53**, 1971.
17. V. J. Müller, H. Rau, P. Zolunneck and K. H. Thiele, *Z. Anorg. Allg. Chem.* 1973, **401**, 113.
18. G. A. Razuvaev, V. N. Latyaeva, G. A. Kilyakova and G. Y. Mal'kova, *Dokl. Akad. Nauk SSSR* 1970, **191**, 620.
19. W. Seidel and I. Bürger, *Z. Chem.* 1977, **17**, 185.
20. G. A. Razuvaev, V. N. Latyaeva, L. I. Vishinskaya and A. M. Rabinovitch, *J. Organomet. Chem.* 1973, **49**, 441.
21. W. Seidel and G. Kreisel, *Z. Chem.* 1974, **14**, 25.
22. W. Seidel and G. Kreisel, *Z. Anorg. Allg. Chem.* 1977, **435**, 146.
23. S. Gambarotta, C. Floriani, A. Chiesi-Villa and C. Gaustini, *J. Chem. Soc., Chem. Commun.* 1984, 886.
24. W. Seidel and G. Kreisel, *Z. Chem.* 1976, **16**, 115.
25. T. Glowiak, R. Grobelny and B. Jesowska-Trzebiatowska, *J. Organomet. Chem.* 1978, **155**, 39.
26. W. Seidel and U. Weinzierl, *Z. Chem.* 1989, **29**, 29.
27. G. A. Razuvaev, V. N. Latyaeva, B. G. Zateev and G. A. Kilyakova, *Dokl. Akad. Nauk SSSR* 1967, **172**, 1337.
28. G. A. Razuvaev, V. N. Latyaeva, V. V. Drobotenko, A. N. Linyova, L. I. Vishinskaya and V. K. Cherkasov, *J. Organomet. Chem.* 1977, **131**, 43.
29. G. A. Razuvaev, V. N. Latyaeva, L. I. Vishinskaya and V. V. Drobotenko, *J. Organomet. Chem.* 1981, **208**, 169.
30. G. A. Razuvaev, V. N. Latyaeva, A. N. Lineva and N. N. Spiridonova, *J. Organomet. Chem.* 1972, **46**, C13.
31. B. D. Steffey, P. E. Fanwick and I. P. Rothwell, *Polyhedron* 1990, **9**, 963.
32. W. Herwig and H. H. Zeiss, *J. Am. Chem. Soc.* 1957, **79**, 6561.
33. H. H. Zeiss, *A.C.S. Monograph* 1960, **147**, 380.
34. G. Stolze and J. Hähle, *J. Organomet. Chem.* 1966, **5**, 545.
35. R. P. A. Sneeden, H. H. Zeiss and A. Anderes, *J. Organomet. Chem.* 1965, **4**, 355.
36. G. M. Whitesides and W. J. Ehmann, *J. Am. Chem. Soc.* 1970, **92**, 5625.
37. S. W. Kirtley, *Comprehensive Organometallic Chemistry* (Edited by G. Wilkinson, F. G. A. Stone and E. W. Abel), Vol. 3, Ch. 26. Pergamon Press, Oxford (1982).
38. G. Stolze, *J. Organomet. Chem.* 1966, **6**, 383.
39. S. I. Khan and R. Bau, *Organometallics* 1983, **2**, 1896.
40. W. Seidel and I. Bürger, *Z. Anorg. Allg. Chem.* 1976, **426**, 155.
41. W. Seidel and I. Bürger, *J. Organomet. Chem.* 1979, **171**, C45.
42. R. Kirmse and W. Seidel, *Z. Anorg. Allg. Chem.* 1982, **490**, 19.
43. C. Cauletti and R. Zanoni, *Z. Anorg. Allg. Chem.* 1983, **496**, 143.
44. W. Seidel and I. Bürger, *J. Organomet. Chem.* 1979, **177**, C19.
45. E. Kinsella, V. B. Smith and A. G. Massey, *J. Organomet. Chem.* 1972, **34**, 181.
46. S. U. Koschmieder, B. S. McGilligan, J. Arnold, G. Wilkinson, B. Hussain-Bates and M. B. Hursthouse, *J. Chem. Soc., Dalton Trans.* 1990, 324.
47. J. Arnold, G. Wilkinson, B. Hussain and M. B. Hursthouse, *J. Chem. Soc., Dalton Trans.* 1989, 2149.
48. M. Tsutsui and H. Zeiss, *J. Am. Chem. Soc.* 1960, **82**, 6255.
49. G. Stolze and J. Hähle, *J. Organomet. Chem.* 1967, **7**, 301.
50. A. R. Hermes, R. J. Morris and G. S. Girolami, *Organometallics* 1988, **7**, 2372.
51. S. Gambarotta, C. Floriani, A. Chiesi-Villa and C. Gaustini, *J. Chem. Soc., Chem. Commun.* 1983, 1128.
52. P. D. Savage, G. Wilkinson, M. Motevalli and M. B. Hursthouse, *J. Chem. Soc., Dalton Trans.* 1988, 669.
53. J. Arnold, G. Wilkinson, B. Hussain and M. B. Hursthouse, *Organometallics* 1989, **8**, 415.
54. W. Seidel and K. J. Lattermann, *Z. Anorg. Allg. Chem.* 1982, **488**, 69.
55. A. V. Kavaliunas and R. D. Rieke, *J. Am. Chem. Soc.* 1980, **102**, 5944.
56. P. D. Savage, P. Stavropoulos, R. P. Tooze, G. Wilkinson, B. Hussain, M. Motevalli and M. B. Hursthouse, *J. Chem. Soc., Dalton Trans.* 1987, 557.
57. J. Arnold, G. Wilkinson, B. Hussain and M. B. Hursthouse, *J. Chem. Soc., Chem. Commun.* 1988, 1349.
58. J. Arnold, G. Wilkinson, B. Hussain and M. B. Hursthouse, *Organometallics* 1989, **8**, 1362.
59. K. H. Theopold, J. Silvestre, E. K. Byrne and D. S. Richeson, *Organometallics* 1989, **8**, 2001.
60. M. Brookhart, M. L. H. Green and L. L. Wong, *Prog. Inorg. Chem.* (Edited by S. J. Lippard), Vol. 36, Ch. 1. John Wiley, New York (1988).
61. C. F. Smith and C. Tamborski, *J. Organomet. Chem.* 1971, **32**, 257.
62. B. B. Anderson, C. L. Behrens, L. J. Radonovich and K. J. Klabunde, *J. Am. Chem. Soc.* 1976, **98**, 5390.
63. R. S. Hay-Motherwell, G. Wilkinson, B. Hussain-Bates and M. B. Hursthouse, *J. Chem. Soc., Chem. Commun.* 1990, 1242.
64. A. Arcas and P. Royo, *Inorg. Chim. Acta* 1978, **30**, 205.

65. B. B. Anderson, M. Bader, K. J. Klabunde and L. J. Radonovich, *J. Am. Chem. Soc.* 1978, **100**, 1313.
66. L. J. Radonovich, F. J. Koch and T. A. Albright, *Inorg. Chem.* 1980, **19**, 3373.
67. R. Usón, J. Fornies, F. Martinez and M. Tomás, *J. Chem. Soc., Dalton Trans.* 1980, 888.
68. R. Usón and J. Fornies, *Advances in Organometallic Chemistry* (Edited by F. G. A. Stone and R. West), Vol. 28, p. 219. Academic Press, London (1988).
69. S. Gambarotta, C. Floriani, A. Chiesi-Villa and C. Gaustini, *J. Chem. Soc., Chem. Commun.* 1983, 1304.
70. S. Gambarotta, C. Floriani, A. Chiesi-Villa and C. Gaustini, *J. Chem. Soc., Chem. Commun.* 1983, 1156.
71. S. Gambarotta, C. Floriani, A. Chiesi-Villa and C. Gaustini, *J. Chem. Soc., Chem. Commun.* 1983, 1087.
72. E. M. Meyer, S. Gambarotta, C. Floriani, A. Chiesi-Villa and C. Gaustini, *Organometallics* 1989, **8**, 1067.
73. D. Nobel, G. van Koten and A. L. Spek, *Angew. Chem. Int. Edn Engl.* 1989, **28**, 208.
74. R. Lingnau and J. Strähle, *Angew. Chem., Int. Edn Engl.* 1988, **27**, 436.
75. R. Usón, A. Laguna, E. J. Fernàndez, A. Mendia and P. G. Jones, *J. Organomet. Chem.* 1988, **350**, 129.
76. R. Usón, A. Laguna, M. Laguna, E. Fernàndez, P. G. Jones and G. M. Sheldrick, *J. Chem. Soc., Dalton Trans.* 1982, 1971.
77. R. Usón, A. Laguna, M. Laguna, B. R. Manzano and A. Tapia, *Inorg. Chim. Acta* 1985, **101**, 151.
78. J. F. Normant and G. Cahiez, *Modern Synthetic Methods* (Edited by B. Schefford), Vol. 3. Salle and Savenlander, Frankfurt (1983).
79. S. A. Cotton, F. A. Hart, M. B. Hursthouse and A. J. Welch, *J. Chem. Soc., Chem. Commun.* 1972, 1225.
80. E. R. Sigurdson and G. Wilkinson, *J. Chem. Soc., Dalton Trans.* 1977, 812.
81. W. Seidel and G. Kreisel, *Z. Anorg. Allg. Chem.* 1976, **426**, 150.
82. N. G. Connelley, *Comprehensive Organometallic Chemistry* (Edited by G. Wilkinson, F. G. A. Stone and E. W. Abel), Vol. 3, Ch. 24. Pergamon Press, Oxford (1982).
83. G. Kreisel, P. Scholz and W. Seidel, *Z. Anorg. Allg. Chem.* 1980, **460**, 51.
84. H. Drevs, *Z. Chem.* 1975, **15**, 451.
85. W. Seidel, P. Scholz and G. Kreisel, *Z. Anorg. Allg. Chem.* 1979, **458**, 263.
86. E. Kurras, *Angew. Chem.* 1960, **72**, 635.
87. M. M. Olmstead, P. P. Power and S. C. Shoner, *Organometallics* 1988, **7**, 1380.
88. B. Sarry and M. Schön, *J. Organomet. Chem.* 1968, **13**, 9.
89. B. Sarry, V. Dobrusskin and H. Singh, *J. Organomet. Chem.* 1968, **13**, 1.
90. G. Heppke, E. Lippert, A. Lange and B. Sarry, *J. Molec. Struct.* 1970, **5**, 146.
91. B. Sarry and R. Schaffernicht, *Z. Naturfor.* 1981, **36b**, 1238.
92. R. A. Bartlett, P. P. Power and S. C. Shoner, *J. Am. Chem. Soc.* 1988, **110**, 1966.
93. M. A. Bennett and H. P. Schweinlein, *Angew. Chem. Int. Edn. Engl.* 1989, **28**, 1296.
94. B. Sarry and P. Velling, *Z. Anorg. Allg. Chem.* 1976, **426**, 107.
95. F. Hein and D. Tille, *Z. Anorg. Allg. Chem.* 1964, **329**, 72.
96. F. Hein and K. Schmiedeknecht, *J. Organomet. Chem.* 1966, **6**, 45.
97. J. J. H. Edema, S. Gambarotta, F. van Bolhuis, W. J. J. Smeets, A. L. Spek and M. Y. Chiang, *J. Organomet. Chem.* 1990, **389**, 47.
98. K. Schmiedeknecht, *J. Organomet. Chem.* 1977, **133**, 187.
99. F. Hein and K. Schmiedeknecht, *J. Organomet. Chem.* 1967, **8**, 503.
100. F. Hein and K. Schmiedeknecht, *J. Organomet. Chem.* 1966, **5**, 454.
101. E. Müller, J. Krause and K. Schmiedeknecht, *J. Organomet. Chem.* 1972, **44**, 127.
102. F. Hein and R. Weiss, *Z. Anorg. Allg. Chem.* 1958, **295**, 10.
103. B. Sarry and H. Grossman, *Z. Anorg. Allg. Chem.* 1968, **359**, 234.
104. B. Heyn, *Z. Chem.* 1968, **8**, 426.
105. B. Sarry and M. Schön, *Z. Chem.* 1968, **8**, 151.
106. B. Sarry, H. Singh, B. Hahn and R. Schaffernicht, *Z. Anorg. Allg. Chem.* 1979, **456**, 181.
107. B. Sarry and P. Velling, *Z. Anorg. Allg. Chem.* 1983, **500**, 199.
108. R. Reimschneider, H. G. Kassahn and W. Schneider, *Z. Naturfor.* 1960, **15b**, 547.
109. R. A. Bartlett, M. M. Olmstead, P. P. Power and S. C. Shoner, *Organometallics* 1988, **7**, 1801.
110. T. A. Bazhenova, R. M. Lobkovskaya, R. P. Shibaeva, A. E. Shilov, A. K. Shilova, M. Gruselle, G. Leny and B. Tchoubar, *J. Organomet. Chem.* 1983, **244**, 265.
111. T. A. Bazhenkova, I. N. Ivleva, L. M. Kachapina, A. K. Shilova, A. E. Shilov and B. Tchoubar, *J. Organomet. Chem.* 1985, **296**, 95.
112. B. Sarry and S. Noll, *Z. Anorg. Allg. Chem.* 1972, **394**, 141.
113. T. A. Bagenova, A. K. Shilova, E. Deschamps, M. Gruselle, G. Leny and B. Tchoubar, *J. Organomet. Chem.* 1981, **222**, C1.
114. T. A. Bazhenova, R. M. Lobkovskaya, R. P. Shibaeva, A. K. Shilova, M. Gruselle, G. Leny and E. Deschamps, *J. Organomet. Chem.* 1983, **244**, 375.
115. H. Drevs, *Z. Chem.* 1978, **18**, 31.

116. R. Taube and N. Stransky, *Z. Anorg. Allg. Chem.* 1982, **490**, 91.
117. R. Taube, *Z. Chem.* 1979, **19**, 412.
118. R. Usón, J. Fornies, P. Espinet, R. Navarro, F. Martinez and M. Tomás, *J. Chem. Soc., Chem. Commun.* 1977, 789.
119. M. P. Garcia, L. A. Oro and F. J. Lahoz, *Angew. Chem. Int. Edn Engl.* 1988, **27**, 1700.
120. R. Taube and G. Honymus, *Angew. Chem. Int. Edn Engl.* 1975, **14**, 261.
121. R. Usón, J. Fornies, M. Tomás, B. Menjón, R. Bau, K. Sünkel and E. Kuwabara, *Organometallics* 1986, **5**, 1576.
122. R. Usón, J. Fornies, M. Tomás, B. Menjòn, K. Sünkel and R. Bau, *J. Chem. Soc., Chem. Commun.* 1984, 751.
123. R. Usón, J. Fornies, F. Martinez, M. Tomás and I. Reoyo, *Organometallics* 1983, **2**, 1386.
124. R. Usón, J. Fornies, M. Tomás, J. M. Casas, F. A. Cotton and L. R. Falvello, *J. Am. Chem. Soc.* 1985, **107**, 2556.
125. P. Leoni, M. Pasquali and C. A. Ghilardi, *J. Chem. Soc., Chem. Commun.* 1983, 240.
126. H. Hope, M. M. Olmstead, P. P. Power, J. Sandell and X. Xu, *J. Am. Chem. Soc.* 1985, **107**, 4337.
127. N. P. Lorenzen and E. Weiss, *Angew. Chem. Int. Edn. Engl.* 1990, **29**, 300.
128. G. van Koten, J. T. B. H. Jastrzebski, F. Muller and C. H. Stam, *J. Am. Chem. Soc.* 1985, **107**, 697.
129. G. van Koten, J. T. B. H. Jastrzebski, C. H. Stam and N. C. Niemann, *J. Am. Chem. Soc.* 1984, **106**, 1880.
130. H. Hope, D. Oram and P. P. Power, *J. Am. Chem. Soc.* 1984, **106**, 1149.
131. S. I. Khan, P. G. Edwards, H. S. H. Yuan and R. Bau, *J. Am. Chem. Soc.* 1985, **107**, 1682.
132. P. G. Edwards, R. W. Gellert, M. W. Marks and R. Bau, *J. Am. Chem. Soc.* 1982, **104**, 2072.
133. M. Olmstead and P. P. Power, *J. Am. Chem. Soc.* 1989, **111**, 4135.
134. H. H. Murray, J. P. Fackler Jr, L. C. Porter, D. A. Briggs, M. A. Guerra and R. J. Lagow, *Inorg. Chem.* 1987, **26**, 357.
135. A. J. Markwell, *J. Organomet. Chem.* 1985, **293**, 257.
136. R. Usón, A. Laguna, J. Vincente, J. Garcia, P. G. Jones and G. M. Sheldrick, *J. Chem. Soc., Dalton Trans.* 1981, 656.
137. P. G. Jones, *Z. Naturfor.* 1982, **37b**, 937.
138. K. Moss, R. V. Parish, A. Laguna, M. Laguna and R. Usón, *J. Chem. Soc., Dalton Trans.* 1983, 2071.
139. R. Usón, A. Laguna and J. A. Abad, *J. Organomet. Chem.* 1983, **246**, 341.
140. M. Y. Chiang, E. Böhlen and R. Bau, *J. Am. Chem. Soc.* 1985, **107**, 1679.
141. L. E. Manzer, *J. Am. Chem. Soc.* 1978, **100**, 8068.
142. H. Drevs, *Z. Chem.* 1976, **16**, 493.
143. A. L. Wayda, J. L. Atwood and W. E. Hunter, *Organometallics* 1984, **3**, 939.
144. K. Schmiedeknecht, M. Rudolph and H. P. Abicht, *Z. Anorg. Allg. Chem.* 1980, **462**, 106.
145. W. Seidel, G. Kreisel and H. Mennenga, *Z. Chem.* 1976, **16**, 492.
146. F. A. Cotton and M. Millar, *J. Am. Chem. Soc.* 1977, **99**, 7886.
147. F. A. Cotton, S. Koch and M. Millar, *J. Am. Chem. Soc.* 1977, **99**, 7372.
148. F. A. Cotton, S. A. Koch and M. Millar, *Inorg. Chem.* 1978, **17**, 2087.
149. F. A. Cotton and M. Millar, *Inorg. Chim. Acta* 1977, **25**, L105.
150. R. P. A. Sneeden and H. H. Zeiss, *J. Organomet. Chem.* 1973, **47**, 125.
151. R. P. A. Sneeden and H. H. Zeiss, *J. Organomet. Chem.* 1972, **40**, 163.
152. F. A. Cotton, S. A. Koch and M. Millar, *Inorg. Chem.* 1978, **17**, 2084.
153. J. J. Daly, F. Sanz, R. P. A. Sneeden and H. H. Zeiss, *J. Chem. Soc., Perkin II* 1972, 1614.
154. R. A. Jones and G. Wilkinson, *J. Chem. Soc., Dalton Trans.* 1979, 472.
155. L. E. Manzer and L. J. Guggenberger, *J. Organomet. Chem.* 1977, **139**, C34.
156. F. A. Cotton and G. N. Mott, *Organometallics* 1982, **1**, 38.
157. J. J. Daly, F. Sanz, R. P. A. Sneeden and H. H. Zeiss, *Helv. Chim. Acta* 1974, **57**, 1863.
158. K. Madeja, E. Hüsing and N. Ahrens, *Z. Chem.* 1967, **7**, 22.
159. G. Bähr and H. Zohm, *Angew. Chem. Int. Edn Engl.* 1963, **1**, 42.
160. F.-W. Küpper, *J. Organomet. Chem.* 1968, **13**, 219.
161. A. C. Cope and R. N. Gourley, *J. Organomet. Chem.* 1967, **8**, 527.
162. G. Longoni, P. Fantucci, P. Chini and F. Canziani, *J. Organomet. Chem.* 1972, **39**, 413.
163. A. Kasahara and T. Izumi, *Bull. Chem. Soc. Japan* 1969, **42**, 1765.
164. S. Trofimenko, *Inorg. Chem.* 1973, **12**, 1215.
165. H. P. Abicht and K. Issleib, *J. Organomet. Chem.* 1978, **149**, 209.
166. M. Aresta and R. S. Nyholm, *J. Chem. Soc., Chem. Commun.* 1971, 1459.
167. E. Wehman, G. van Koten and J. T. B. H. Jastrzebski, *J. Organomet. Chem.* 1986, **302**, C35.
168. M. A. Bennett, S. K. Bhargava, K. D. Griffiths, G. B. Robertson, W. A. Wickramasinghe and A. C. Wells, *Angew. Chem. Int. Edn Engl.* 1987, **26**, 258.

169. E. Wehman, G. van Koten, M. Knotter, H. Spelten, D. Heijdenrijk, A. N. S. Mak and C. H. Stam, *J. Organomet. Chem.* 1987, **325**, 293.
170. E. Wehman, G. van Koten, J. T. B. H. Jastrzebski, M. A. Rotteveel and C. H. Stam, *Organometallics* 1988, **7**, 1477.
171. E. Wehman, G. van Koten, C. J. M. Erkamp, D. M. Knotter, J. T. B. H. Jastrzebski and C. H. Stam, *Organometallics* 1989, **8**, 94.
172. J. Vicente, M.-T. Chicote, M.-D. Bermúdez, X. Soláns and M. Font-Altaba, *J. Chem. Soc., Dalton Trans.* 1984, 557.
173. J. Vicente, M.-T. Chicote, M.-D. Bermúdez, M. J. Sanchez-Santano, P. G. Jones, C. Fittschen and G. M. Sheldrick, *J. Organomet. Chem.* 1986, **310**, 1401.

ADDENDUM (1 DECEMBER 1990)

174. J. J. H. Edema, S. Gamberotti, F. van Bolhuis, W. J. J. Smeets, A. L. Spek and M. Y. Chiang, *J. Organomet. Chem.* 1990, **389**, 47. X-ray structures: $[Cr(mes)_2(THF)_2]THF$ and $[Cr(mes)_2bipy]THF$ (planar, cf. Section 3.4); $[Cr(mes)_4Li_2(THF)_2]THF$ and $[Cr(Ph)_4Li_2(THF)_4]$ (cf. Section 3.3).
175. M. M. Olmstead and P. P. Power, *J. Am. Chem. Soc.* 1990, **112**, 8908. X-ray structures: $Cu_4(Ph)_4(SMe_2)_2$ (cyclic tetramer); $Li_2Cu_2(Ph)_4(SMe_2)_3$, $[Cu(Ph)_2^-$ units bridged by Li]; $Li_3(CuPh)_2Cu(Ph)_3(SMe_2)_4$ and $Li_5[Cu(Ph)_2]_3Cu(Ph)_3(SMe_2)_4$ have rare $[Cu(Ph)_3]^{2-}$ units (cf. Section 3.8).
176. R. Uson, A. Laguna, M. Laguna, J. Jimenez and E. M. Durana, *Inorg. Chim. Acta* 1990, **168**, 89. $Au(C_6F_5)_3L$ and $[Au(C_6F_5)_3L]^+$, L = THF, Et_2O, EtOH, etc. (cf. Section 2.9).

Polyhedron Vol. 10, No. 2, pp. 175–178, 1991
Printed in Great Britain

0277–5387/91 $3.00+.00
© 1991 Pergamon Press plc

PREPARATION AND X-RAY CRYSTAL STRUCTURE DETERMINATION OF AN OCTAHEDRAL POLYMERIC LUTETIUM COMPOUND WITH CILIATINE; $\{Lu(PO_3HCH_2CH_2NH_3)_3(ClO_4)_3 \cdot 3D_2O\}_n$

T. GŁOWIAK, E. HUSKOWSKA and J. LEGENDZIEWICZ*

Institute of Chemistry, University of Wrocław, Joliot-Curie 14, 50-383 Wrocław, Poland

(*Received* 30 *March* 1990; *accepted* 20 *July* 1990)

Abstract—The new octahedral compound of lutetium with ciliatine of the formula $Lu(PO_3HCH_2CH_2NH_3)_3(ClO_4)_3 \cdot 3D_2O$ was prepared in the form of single crystals from D_2O solutions and subjected to X-ray structure determination. Each lutetium ion is coordinated by six oxygen atoms from the phosphonic groups. The coordination polyhedron is an almost ideal octahedron with a mean Lu—O distance of 2.201(6) Å. The lutetium ions are bridged by two oxygen atoms from each of three phosphonic groups. In this manner the linear polymer is formed along the x axis.

Recently, great efforts have been made to understand the role of aminoalkanephosphonic acids, the analogues of amino acids. The reason for this is that several synthetic and natural phosphonic acids have rather interesting biological properties. Aminophosphonates are found in tissues as the free compounds, but their most frequent form of occurrence include complex structures, such as lipids, peptides, proteins and polysaccharides.[1–3] Since the lanthanide ions are often used as metal probes in studies of important biological systems, it seemed reasonable to study the interaction of lanthanide ions with the simplest natural aminophosphonate, ciliatine.

Recently we reported potentiometric and ^{31}P NMR investigations on Nd^{3+} and Ho^{3+} complex formation with α-aminoethanophosphonic (α-PAla) and β-aminoethanophosphonic (β-PAla) acids in solution.[4] It was found from the potentiometric studies that the forms MAH, $M(AH)_2$ and MA_2H exist in solutions of β-PAla. However, the ^{31}P NMR data at lower pH revealed the interaction of Ln^{3+} ions with the zwitterionic form of ciliatine, which means an additional form could probably exist under these conditions. To confirm this phenomenon we have attempted to obtain this form in the solid state.

In this paper we describe the X-ray studies of the compound $Ln(PO_3HCH_2CH_2NH_3)_3(ClO_4)_3 \cdot 3D_2O$ and comparison of the results with related lanthanide single crystal structural data.

EXPERIMENTAL

Sample preparation

Crystals of the lutetium compound were grown from a concentrated D_2O solution of $Lu(ClO_4)_3$ at pH < 1. The concentration of phosphonic acid was maintained well below the lanthanide concentration.

It is worth mentioning that the growth of crystals is more difficult and slower than those of its amino acid analogue. The Lu^{3+} ion concentration in the crystal was determined by EDTA titration, using Xylenol Orange as the end point indicator. The density, measured by the flotation method using a mixture of bromoform and ethylene bromide, was $d = 2.17$ g cm^{-3}.

X-ray measurements

A crystal of dimensions 0.25 mm × 0.3 mm × 0.4 mm was used for the structure determination. A Syntex $P2_1$ diffractometer and MoK_α radiation with the graphite monochromator were used for the lattice parameter and intensity measurements. The intensities of the reflections were measured by the

* Author to whom correspondence should be addressed.

Table 1. Crystal data

Molecular weight	908.6
Space group	$P2_1/a$
Crystal system	Monoclinic
a (Å)	10.176(3)
b (Å)	18.840(7)
c (Å)	14.587(6)
β (°)	97.76(4)
V (Å^3)	2770.9
Z	4
D_c (g cm^{-3})	2.18
D_m (g cm^{-3})	2.17
$F(000)$	1784
μ (MoK_α) (cm^{-1})	43.1
Unique observed reflections	4762 [$I > 3.0\sigma(I)$]
$R = \Sigma\|\|F_o\|-\|F_c\|\|/\Sigma\|F_o\|$	0.040
$R = \{\Sigma w(\|F_o\|-\|F_c\|)^2/\Sigma w\|F_o\|^2\}^{1/2}$	0.051
$S = \{\Sigma w(F_o-F_c)^2/(n-p)\}^{1/2}$	3.223

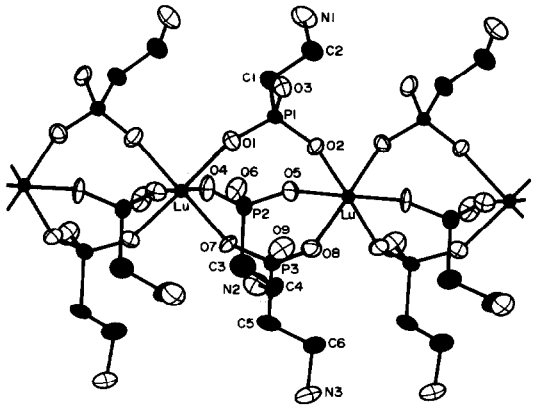

Fig. 1. An ORTEP drawing of the Lu($PO_3HCH_2CH_2NH_3$)$_3$(ClO_4)$_3$·3D_2O compound; the atoms of the crystallographic unit are labelled as in the text.

θ–2θ scan technique up to $2\theta_{max} = 55°$. The scan rate varied from 2.0 to 29.0° min^{-1}. The data were corrected for Lorentz, polarization and absorption effects. 4762 reflections, with $I > 3.0\,\sigma(I)$, were used for the structure determination. All calculations were performed using Syntex XTL programs[5] and scattering factors for neutral atoms were taken from the *International Tables for X-ray Crystallography*.[6] The structure was solved by the heavy-atom method. Full-matrix least-squares refinement was terminated at $R = 0.040$ and $R_w = 0.051$.

Crystal data are listed in Table 1. Final atomic and anisotropic thermal parameters, with estimated standard deviations, have been deposited.

CRYSTALLOGRAPHIC DESCRIPTION OF THE STRUCTURE AND DISCUSSION

Figure 1 shows the perspective view of a characteristic fraction of the title structure and the labelling of the atoms in the crystallographic unit. The geometric data for the coordination around the lutetium cation, and the covalent bond lengths and bond angles within the phosphonic acid residue, are listed in Tables 2 and 3. In the unit cell two polymeric chains are parallel to the x-axis at $y \sim 0.25$ and ~ 0.75.

The lutetium ions are six-coordinated by the oxygen atoms belonging only to the six phosphonic acids. The water molecules and perchlorate ions are not involved in coordination. The exclusion of the water molecule, while the coordination number remains so low, is very unusual for lanthanide compounds. The coordination number six is also rather rare, another example reported is cerium diethyl phosphate, Ce[$PO_2(OC_2H_5)_2$]$_3$.[7]

The coordination polyhedron is almost ideal octahedron; only some small deviations in the Ln—O distances are observed. The Ln—O distances range from 2.194(6) to 2.210(5) Å, with an average value of 2.201[6] Å. These distances are comparable with the Ln—O distances in the octahedral compound Pr($OPN_3C_6H_{18}$)$_3$$Cl_3$[8] (Pr—O = 2.35 Å) when the lanthanide contraction is considered (ER, Pr = 1.013 Å, Lu = 0.848 Å, Δr = 0.165 and ΔMe—O = 0.150), and differ significantly from the Ln—O distances found in lanthanide phosphates, where the coordination number is nine.[9] Two oxygen atoms from each of three phosphonic groups bridge the lutetium ions, so that a linear polymer along the x-axis is formed. The distance between the bridged lanthanide atoms is 5.093(1) Å. The phosphonic acid molecules exist in the structure as zwitterions. The bond distances and angles within them conform with expected values.

The P—O distance clearly indicates the coordination of two oxygen atoms of the phosphonic group to the lutetium ion. The torsion angles indicate an almost planar arrangement of the atoms. The distances of the donor groups (H_2O, NH_3^+, OH) between themselves and between the oxygen atoms of ClO_4^- groups, ranging from 2.6 to 3.0 Å, indicate the rich hydrogen bonding system formed in the structure. The crystal structure consists of parallel lutetium–phosphonic acid chains. The perchlorate anions and non-coordinating water molecules reside in the cavities between the chains and stabilize the crystal packing by forming hydrogen bonds.

The results of X-ray studies show that the coordination of the lanthanide cation in the title compound differs significantly from that in the amino acid compounds.[10–15] Although in both types of compound polymeric forms are created (by the bridges of the type M—O—P—O—M, M—O—C—

Table 2. Selected bond distances (Å) and angles (°) with ESDs in parentheses

Bond distances (Å)			
Lu—O(1)	2.200(5)	P(2)—O(4)	1.484(6)
Lu—O(2)^i	2.209(5)	P(2)—O(6)	1.578(6)
Lu—O(4)	2.195(6)	P(2)—O(5)	1.487(6)
Lu—O(5)^i	2.196(6)	P(2)—C(3)	1.813(9)
Lu—O(7)	2.194(6)	C(3)—C(4)	1.486(1)
Lu—O(8)^i	2.210(5)	C(4)—N(2)	1.505(1)
P(1)—O(1)	1.494(5)	P(3)—O(7)	1.494(6)
P(1)—O(2)	1.504(6)	P(3)—O(8)	1.501(5)
P(1)—O(3)	1.571(6)	P(3)—O(9)	1.587(6)
P(1)—C(1)	1.795(10)	P(3)—C(5)	1.782(9)
C(1)—C(2)	1.535(1)	C(5)—C(6)	1.514(1)
C(2)—N(1)	1.481(1)	C(6)—N(3)	1.480(1)
Bond angles (°)			
O(1)—Lu—O(2)^i	178.9(2)	O(4)—P(2)—O(5)	116.8(3)
O(1)—Lu—O(4)	89.6(2)	O(5)—P(2)—O(6)	109.6(4)
O(1)—Lu—O(5)^i	91.3(2)	O(6)—P(2)—O(4)	106.7(4)
O(1)—Lu—O(7)	89.3(2)	O(4)—P(2)—C(3)	108.4(4)
O(1)—Lu—O(8)^i	90.5(2)	O(5)—P(2)—C(3)	108.1(4)
O(2)^i—Lu—O(4)	90.3(2)	O(6)—P(2)—C(3)	109.9(4)
O(2)^i—Lu—O(5)	89.8(2)	O(7)—P(3)—O(8)	116.9(3)
O(2)^i—Lu—O(7)	89.6(2)	O(8)—P(3)—O(9)	108.4(3)
O(2)^i—Lu—O(8)	89.6(2)	O(7)—P(3)—O(9)	105.6(3)
N(2)—C(4)—C(3)	109.9(7)	O(7)—P(3)—C(5)	109.1(4)
N(3)—C(6)—C(5)	111.9(7)	O(8)—P(3)—C(5)	109.8(4)
O(4)—Lu—O(5)^i	90.7(2)	O(9)—P(3)—C(5)	106.7(4)
O(4)—Lu—O(7)	90.3(2)	Lu—O(1)—P(1)	143.4(3)
O(4)—Lu—O(8)^i	179.3(2)	Lu^{ii}—O(2)—P(1)	148.7(4)
O(5)^i—Lu—O(8)^i	88.6(2)	Lu—O(4)—P(2)	154.3(4)
O(7)—Lu—O(8)^i	90.4(2)	Lu^{ii}—O(5)—P(2)	150.3(4)
O(5)—Lu—O(7)	178.9(2)	Lu—O(7)—P(3)	151.7(4)
O(1)—P(1)—O(2)	115.3(3)	Lu^{ii}—O(8)—P(3)	144.6(3)
O(2)—P(1)—O(3)	108.5(3)	P(1)—C(1)—C(2)	115.4(7)
O(1)—P(1)—O(3)	110.2(3)	N(1)—C(2)—C(1)	111.5(8)
O(1)—P(1)—C(1)	109.5(4)	P(2)—C(3)—C(4)	112.8(6)
O(2)—P(1)—C(1)	109.7(4)	P(3)—C(5)—C(6)	113.6(6)
O(3)—P(1)—C(1)	103.0(4)		

Symmetry codes: (i) $-0.5+x, 0.5-y, z$; (ii) $0.5+x, 0.5-y, z$.

O—M and M—O—C—O—M), the coordination number of the lanthanide ions changes drastically.

The six-coordination found in the title compound is close to that observed for the calcium ion in phosphate,[16] therefore one might expect substitution of the Ca^{2+} ion by Ln^{3+} in biological systems in which phosphonic residues exist.

Table 3. Selected torsion angles (°) with ESDs in parentheses

Lu—O(1)—P(1)—C(1)	63.2(14)
Lu^i—O(2)—P(1)—C(1)	−51.8(24)
P(1)—C(1)—C(2)—N(1)	−79.5(24)
Lu—O(4)—P(2)—C(3)	−172.6(11)
Lu^i—O(5)—P(2)—C(3)	163.5(19)
P(2)—C(3)—C(4)—N(2)	172.4(9)
Lu—O(7)—P(3)—C(5)	75.4(12)
Lu^i—O(8)—P(3)—C(5)	−61.4(24)
P(3)—O(5)—O(6)—N(3)	−173.0(16)

The structure of $\{Lu(PO_3HCH_2CH_2NH_3)_3(ClO_4)_3 \cdot 3D_2O\}_n$ also differs from the structure of α-aminomethylphosphonic analogues of transition metals (Mn^{2+}, Cu^{2+}, Zn^{2+}, Co^{2+}).[17–19] Monomers or some polymers were observed but in none of the cases were the triple phosphate bridges formed.

The crystal structure of the title compound confirms the interaction between Lu^{3+} and the AH_2 form of the ligand found by ^{31}P NMR at low pH, which was undetectable using potentiometric methods.[4]

Acknowledgement—This work was supported by the Polish Academy of Sciences and MEN.II.W.

REFERENCES

1. M. Horiguchi and M. Kandatsu, *Nature* 1959, **184**, 901.
2. J. S. Kittredge, E. Roberts and D. G. Simonson, *Biochemistry* 1962, **1**, 624.
3. P. Kafarski and P. Mastalerz, *Beitr. Wirkst Forsch.* 1984, **21**, 1.
4. E. Huskowska, J. Legendziewicz, E. Brücher, I. Toth and L. Zékány, *Book of Abstracts XXIV ICCC Athens 1986*, p. 485.
5. *XTL/XTLE Structure Determination System.* Syntex Analytical Instruments, Cupertino, California (1976).
6. *International Tables for X-ray Crystallography*, Vol. IV. Kynoch Press, Birmingham (1974).
7. Yu-Zhen Han, Zuo-Hua Pan *et al. Book of Abstracts of XXV ICCC Nanjing China 1987*, p. 192.
8. L. J. Radonovich and M. D. Glick, *J. Inorg. Nucl. Chem.* 1973, **35**, 2745.
9. D. F. Mollica, W. O. Milligan, D. A. Grossie, G. W. Beall and L. A. Boatner, *Inorg. Chim. Acta* 1984, **95**, 231.
10. I. Csöregh, P. Kierkegaard, J. Legendziewicz and E. Huskowska, *Acta Chim. Scand.* 1987, **A41**, 453.
11. I. Csöregh, P. Kierkegaard, J. Legendziewicz and E. Huskowska, *Acta Chim. Scand.* 1989, **A43**, 636.
12. C. N. Dao, T. Głowiak, E. Huskowska and J. Legendziewicz, *J. Less-common Met.* 1988, **136**, 339.
13. J. Legendziewicz, T. Głowiak, E. Huskowska and C. N. Dao, *Polyhedron* 1988, **7**, 2495; 1989, **8**, 2139.
14. J. Legendziewicz, E. Huskowska, Gy. Argay and A. Waśkowska, *J. Less-common Met.* 1989, **146**, 33.
15. T. Głowiak, C. N. Dao, J. Legendziewicz and E. Huskowska, *Acta Cryst.*, in press.
16. N. M. Antraptseva, L. N. Shchegrov and I. V. Rudiy, *Book of Abstracts XXV ICCC Nanjing 1987*, p. 796.
17. T. Głowiak, W. Sawka-Dobrowolska, B. Jeżowska-Trzebiatowska and A. Antonów, *Inorg. Chim. Acta* 1980, **45**, L105.
18. T. Głowiak, W. Sawka-Dobrowolska, B. Jeżowska-Trzebiatowska and A. Antonów, *J. Cryst. Molec. Struct.* 1980, **10**, 1.
19. P. Fenot, J. Darriet and C. Garrigou-Lagrange, *J. Molec. Struct.* 1978, **43**, 49.

Polyhedron Vol. 10, No. 2, pp. 179–185, 1991
Printed in Great Britain

0277–5387/91 $3.00+.00
© 1991 Pergamon Press plc

MOLECULAR AND CRYSTAL STRUCTURE OF FLUXIONAL BIS[1-ISOPROPYL-3-METHYL-4-N-ALKYL(ARYL)ALDIMINOPYRAZOLE-5-THION]ATO NICKEL(II) COMPLEXES [pyr(N-CH_3)$_2S_2$]Ni, [pyr(N-Ph)$_2S_2$]Ni, [pyr(N-t-Bu)$_2S_2$]Ni

A. L. NIVOROZHKIN,* L. E. NIVOROZHKIN and V. I. MINKIN

Institute of Physical and Organic Chemistry, Rostov University, 344711 Rostov on Don, U.S.S.R.

and

T. G. TAKHIROV and O. A. DIACHENKO

Department of Institute of Chemical Physics of the Academy of Science of the U.S.S.R., 142432 Chernogolovska, U.S.S.R.

(*Received* 23 *April* 1990; *accepted* 6 *August* 1990)

Abstract—X-ray crystallographic studies of fluxional bis[1-isopropyl-3-methyl-4-N-alkyl(aryl)aldiminopyrazole-5-thion]ato nickel(II) complexes [pyr(N-CH_3)$_2S_2$]Ni, [pyr(N-Ph)$_2S_2$]Ni and [pyr(N-t-Bu)$_2S_2$]Ni show them to possess pseudo-tetrahedral configurations with the values of dihedral angles θ between chelate planes being 81.9 and 82.4; 68.7; 96.3° respectively. The values of θ as well as those of the NNiN′ valence angles have been found to correlate with the energy barriers against intramolecular enantiomerization of tetrahedral nickel configuration R $\rightleftharpoons$ S.

In nickel(II) metal chelates possessing the coordination site of type NiN_2X_2 (X = O, S, Se), the stereoconfiguration of the central atom is strongly affected by the type of ligating atom X, ligand structure and steric volume of the substituent attached to the coordinated nitrogen atom.[1,2] Of these compounds, 1,3-substituted bis[4-N-alkyl(aryl) aldiminopyrazole-5-thion(seleno)]ato nickel(II) complexes display a significant stabilization of the tetrahedral form both in solution and in the solid state, which has been established by ^{1}H NMR spectral study, measurements of magnetic moments and by X-ray structure investigation of two of these complexes.[3–6] In solution, the above complexes undergo a rapid interconversion of their enantiomeric forms R $\rightleftharpoons$ S, with the free activation energy of the inversion process falling within the range of 40–75 kJ mol^{-1}.[4] The magnitude of the energy barrier increases when going from N-n-alkyl and aryl to N-s-alkyl and t-Bu substituents presumably owing to the steric strain developed by bulky substituents in the transition or intermediate planar structure inherent in the mode of enantiomerization.

In the present work a crystallographic study of complexes **Ia–c** containing aryl and alkyl groups at

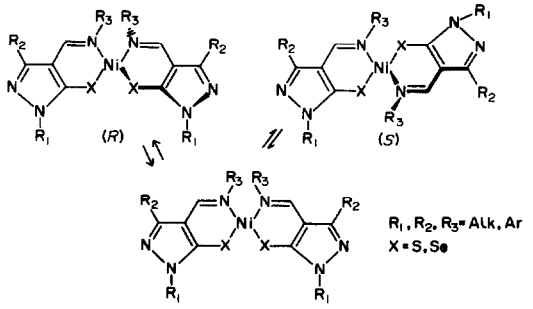

Scheme 1.

* Author to whom correspondence should be addressed.

coordinated nitrogen has been carried out with the aim of clarifying whether a correlation exists between the tetrahedral-to-planar distortion of the metal bond configuration and the energy barriers to the R⇌S interconversion. The previously reported[5] structural data on the complex [pyr(N-C_6H_{11}-cyclo)$_2S_2$]Ni (**Id**) are also discussed in this connection.

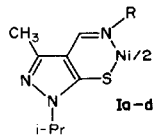

Ia–d

R=CH_3(a), Ph(b), t-Bu(c), C_6H_{11}-cyclo(d)

EXPERIMENTAL

The crystal samples have been obtained by slow crystallization from toluene–octane (1 : 1) mixture.

Crystal data, details of intensity measurement and refinement for **Ia–c** are given in Table 1. The unit-cell dimensions were refined on a DRON-1 diffractometer with a monocrystal attachment. The absorption corrections were introduced for **Ib,c** by Gaussian integration[7] using Udelnov's program.[8] The structures **Ia–c** were determined by direct methods and refined by the least-squares technique, with full-matrix anisotropic (Ni, S, N and C atoms) and isotropic (H atoms) approximation using the Cruickshank weighting scheme. The hydrogen atoms in **Ib,c** were located by difference Fourier synthesis. Selected bond distances are listed in Table 2. Calculations were carried out on a BESM-6 computer using the RENTGEN-75 program package.[9] The stereoprojections (Figs 1–3) were obtained by the use of the ELLIDS program.[10]

RESULTS AND DISCUSSION

The complexes **Ia–c** possess pseudo-tetrahedral structures. The values of dihedral angles θ between the planes of chelate rings, which indicate the degree of the tetrahedral-to-planar distortion ($\theta = 90°$ for ideal tetrahedron), are equal to 81.9, 82.4 (**Ia**), 68.7 (**Ib**) and 96.3 (**Ic**). The value of θ exceeding 90° as is the case with complex **Ic** corresponds to the S···S *trans*-planar distorted structure. For the complexes **Ia,b** ($\theta < 90°$) a distortion towards the *cis*-planar geometry occurs.

The diagonal twist mechanism of the R⇌S enantiomerization includes reciprocal rotation of

Table 1. Crystal data, details of intensity measurement and refinement

Compound	**Ia**	**Ib**	**Ic**
Formula	$C_{18}H_{28}N_6NiS_2$	$C_{28}H_{32}N_6NiS_2$	$C_{24}H_{40}N_6NiS_2$
Molecular weight	451.3	575.4	535.4
Melting temperature (°C)	213	215	260
Crystal system	Monoclinic	Monoclinic	Monoclinic
a (Å)	29.966(8)	21.387(6)	18.095(5)
b (Å)	12.640(4)	17.326(6)	17.086(5)
c (Å)	6.105(2)[a]	9.375(4)	9.394(2)
γ (°)	79.55(2)	121.93(4)	76.64(4)
Volume (Å^3)	2274(1)	2948(4)	2826(3)
Space group	$B2/b$	$B2/b$	$P2_1/b$
Z	4	4	4
D_c (g cm^{-1})	1.33	1.30	1.26
μ (cm^{-1})	10.8	23.3	23.9
Crystal dimensions (mm^3)	0.35 × 0.45 × 0.60	0.04 × 0.55 × 0.18	0.18 × 0.07 × 0.21
Data collection instrument	DAR-UM	DAR-UM	RED-4
Radiation	Mo-K_α	Cu-K_α	Cu-K_α
Min $\sin\theta/\lambda$	0.034	0.055	0.028
Max $\sin\theta/\lambda$	0.067	0.604	0.499
Scan method	ω–$\omega/2\omega$	ω–$\omega/2\omega$	ω–$\omega/2\omega$
Number of observed reflections	1468$I \geqslant 2\sigma(I)$	1584$I \geqslant 2\sigma(I)$	1613$I \geqslant 3\sigma(I)$
Reflections used in refinement	1260	1426	1459
Final R	0.072	0.055	0.051

[a] The structure was determined for pseudo-unit-cell [$c' = 2c = 12{,}210(4)$ Å].

chelate rings about the C(2) axis towards the achiral planar structure. Therefore, a correlation between the values of energy barriers of the tetrahedral inversion and the degree of the tetrahedral-to-planar distortion may, in principle, take place in accordance with the structure correlation concept.[11,12] The preference of *cis*-planar structures for the numerous bis-chelate complexes with the NiN_2S_2 coordination site has been revealed,[1,2] thus the gradual decrease of θ values may be associated with the decrease of the energy barriers to the enantiomerization of complexes **I**, $\Delta G^{\ddagger}$, as found from ^1H dynamic NMR spectral data.

Indeed, a comparison of θ and $G^{\ddagger}$ values (Table 3)

Table 2. Selected bond distances and valence angles of complexes (**Ia–d**)

Bond	D (Å)		Angle	ω (°)	
			(**Ia**) R = CH_3		
	Mol. A	Mol. B		Mol. A	Mol. B
Ni—S	2.237(2)	2.247(2)	S—Ni—S′	117.5(1)	116.5(1)
Ni—N(1)	1.975(7)	1.985(7)	S—Ni—N(1)	100.9(2)	101.8(2)
S—C(1)	1.715(8)	1.726(8)	S—Ni—N(1′)	118.2(2)	117.6(2)
N(1)—C(3)	1.28(1)	1.28(1)	N(1)—Ni—N(1′)	100.9(3)	101.2(3)
N(2)—N(3)	1.38(1)	1.38(1)	Ni—S—C(1)	105.1(3)	103.6(3)
N(2)—C(1)	1.36(1)	1.36(1)	Ni—N(1)—C(3)	129.7(6)	128.0(7)
N(3)—C(5)	1.31(1)	1.30(1)	S—C(1)—C(2)	129.5(6)	131.5(7)
C(1)—C(1)	1.41(1)	1.41(1)	C(1)—C(2)—C(3)	130.1(8)	128.6(7)
C(2)—C(3)	1.43(1)	1.43(1)	N(1)—C(3)—C(2)	124.7(9)	126.5(8)
C(2)—C(5)	1.43(1)	1.42(1)			
			(**Ib**) R = Ph		
Ni—S	2.229(1)		S—Ni—S′	98.9(1)	
Ni—N(1)	1.984(3)		S—Ni—N(1)	100.2(1)	
S—C(1)	1.708(4)		S—Ni—N(1′)	128.6(1)	
N(1)—C(3)	1.300(6)		N(1)—Ni—N(1′)	104.0(1)	
N(2)—N(3)	1.380(6)		Ni—S—C(1)	105.7(1)	
N(2)—C(1)	1.344(6)		Ni—N(1)—C(3)	128.5(3)	
N(3)—C(10)	1.311(5)		S—C(1)—C(2)	130.2(4)	
C(1)—C(2)	1.403(5)		C(1)—C(2)—C(3)	128.8(5)	
C(2)—C(3)	1.412(5)		N(1)—C(3)—C(2)	126.2(4)	
C(2)—C(10)	1.419(7)				
			(**Ic**) R = t-Bu		
Ni—S(1)	2.254(1)		S(1)—Ni—S(2)	105.22(7)	
Ni—S(2)	2.253(1)		S(1)—Ni—N(1)	102.0(1)	
Ni—N(1)	1.984(4)		S(1)—Ni—N(4)	106.7(1)	
Ni—N(4)	1.995(4)		S(2)—Ni—N(1)	105.2(1)	
S(1)—C(1)	1.697(4)		S(2)—Ni—N(4)	102.2(1)	
S(2)—C(13)	1.694(7)		N(1)—Ni—N(4)	133.0(2)	
N(1)—C(3)	1.288(5)		Ni—S(1)—C(1)	103.9(2)	
N(2)—N(3)	1.372(5)		Ni—S(2)—C(13)	104.4(2)	
N(2)—C(1)	1.362(6)		Ni—N(1)—C(3)	125.8(4)	
N(3)—C(8)	1.311(6)		Ni—N(4)—C(15)	124.6(4)	
N(4)—C(15)	1.289(6)		S(1)—C(1)—C(2)	131.8(4)	
N(5)—N(6)	1.383(5)		C(1)—C(2)—C(3)	128.1(4)	
N(5)—C(13)	1.340(6)		N(1)—C(3)—C(2)	128.4(5)	
N(6)—C(20)	1.308(7)		S(2)—C(13)—C(14)	130.5(4)	
C(1)—C(2)	1.396(6)		C(13)—C(14)—C(15)	128.5(4)	
C(2)—C(3)	1.427(6)		N(4)—C(15)—C(14)	129.3(5)	
C(2)—C(8)	1.416(6)				
C(13)—C(14)	1.416(7)				
C(14)—C(15)	1.413(8)				
C(14)—C(20)	1.409(6)				

continued

Table 2—*continued*

Bond	D (Å)	Angle	ω (°)
		(Id) R = C_6H_{11}-cyclo[a]	
Ni—S(1)	2.243(1)	S(1)—Ni—S(2)	114.74(4)
Ni—S(2)	2.258(1)	S(1)—Ni—N(1)	100.85(8)
Ni—N(1)	1.975(2)	S(1)—Ni—N(4)	125.71(8)
Ni—N(4)	1.992(2)	S(2)—Ni—N(1)	108.69(8)
S(1)—C(1)	1.720(3)	S(2)—Ni—N(4)	100.37(8)
S(2)—C(15)	1.724(3)	N(1)—Ni—N(4)	105.6(1)
N(1)—C(3)	1.276(4)	Ni—S(1)—C(1)	104.5(1)
N(2)—N(3)	1.366(3)	Ni—S(2)—C(15)	104.0(1)
N(2)—C(1)	1.357(4)	Ni—N(1)—C(3)	128.1(2)
N(3)—C(10)	1.318(4)	Ni—N(4)—C(17)	125.6(2)
N(4)—C(17)	1.290(4)	S(2)—C(1)—C(2)	131.6(2)
N(5)—N(6)	1.375(3)	C(1)—C(2)—C(3)	127.2(3)
N(5)—C(15)	1.344(4)	N(1)—C(3)—C(2)	127.7(3)
N(6)—C(24)	1.309(3)	S(2)—C(15)—C(16)	129.9(3)
C(1)—C(2)	1.389(4)	C(15)—C(16)—C(17)	128.7(3)
C(2)—C(3)	1.436(4)	N(4)—C(17)—C(16)	128.2(3)
C(2)—C(10)	1.497(4)		
C(15)—C(16)	1.392(4)		
C(16)—C(17)	1.417(4)		
C(16)—C(24)	1.410(4)		

[a] Data from ref. 5.

for the complexes of type **I** shows that the compounds with alkyl substituents **Ia**,**c**,**d** are consistent with anticipated correlation. For the complex **Ib**, containing the phenyl substituent, the value of θ falls appreciably, and is not accompanied by a corresponding change in $\Delta G^{\ddagger}$. Moreover, the correlation of activation energies with steric constants of N-alkyl substituents, E_s,[13] has been observed.

It may be assumed that, apart from θ, some other structural parameters reflect the steric strain in **Ia**–**d**. These include the valence angles at the nickel atom. Actually, the unusually high value of the

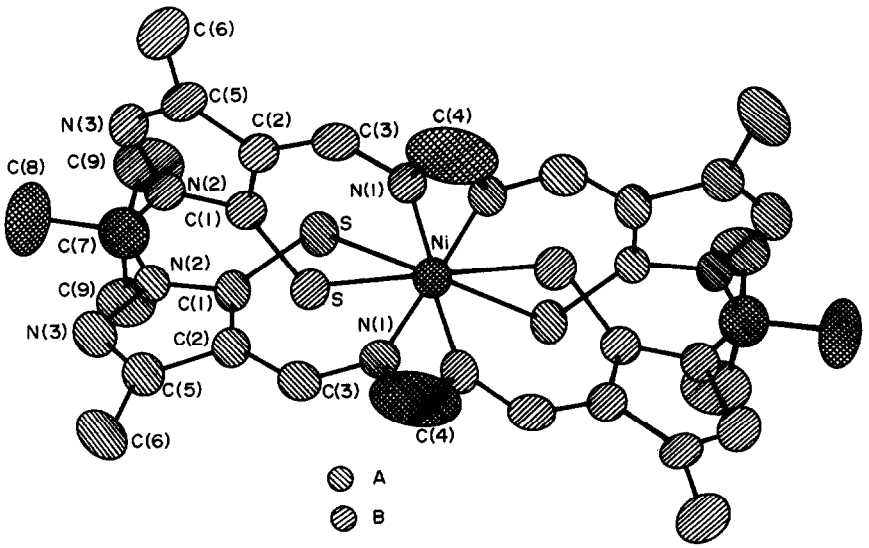

Fig. 1. Molecule of complex **Ia** (R = CH_3). A and B correspond to the molecules of **Ia** occupying the different positions within the same unit cell. The positions of Ni, C(4), C(7) and C(8) atoms have not been separated.

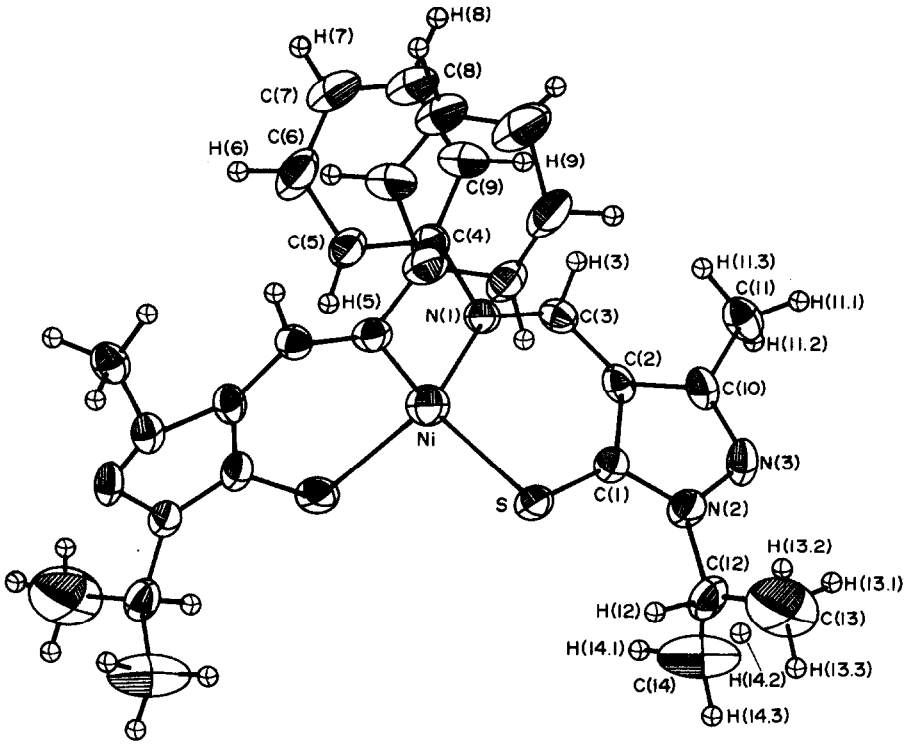

Fig. 2. Molecule of complex **Ib** (R = Ph).

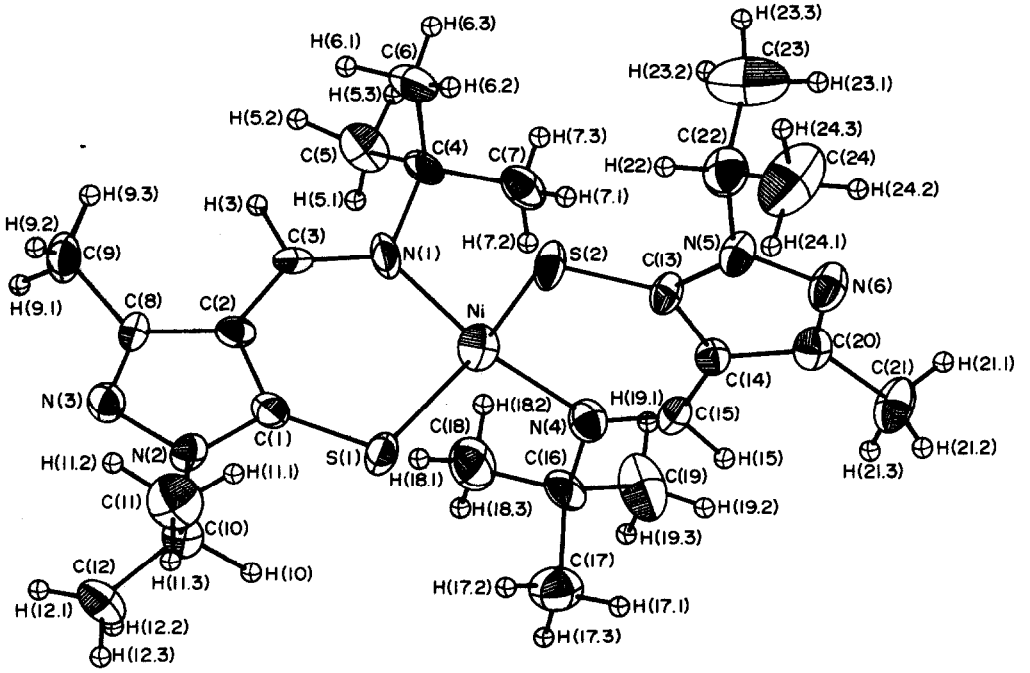

Fig. 3. Molecular of complex **Ic** (R = t-Bu).

Table 3.

	Ia (R = CH_3)	**Id** (R = C_6H_{11}-cyclo)[a]	**Ic** (R = t-Bu)	**Ib** (R = Ph)
θ (grad)	81.9; 82.4	85.3	96.3	68.7
NNiN′ (grad)	100.9; 101.2	115.0	133.0	104.3
$\Delta G^{\ddagger}$ (kJ mol^{-1})	42.7	49.5[b]	73.7	45.2
E_s	0.00	−0.79	−1.54	

[a] Structural data from ref. 5.

[b] The value obtained after re-examination of ^{1}H NMR spectral patterns observed earlier.[4]

NNiN′ angle in **Ic**, 133.0°, is considerably larger than the standard tetrahedral one of 109°. It is similar to that of the bis(N-t-butylsalicylideneiminato) nickel(II) complex, 128.6°.[14] Perhaps, such a bisphenoidal torsion arises by virtue of steric repulsion of t-Bu groups. A decrease in the steric volume of R for **Ia,b,d** as compared with **Ic** leads to the decrease in the NNiN′ angle in the order as follows **Ic** > **Id** > **Ib** > **Ia**. Noteworthy is that the enhancement of the bisphenoidal distortion rigorously follows the rise of enantiomerization barriers.

According to the recent consideration by Haaland[15] based on the VSEPR theory, the increase in valence angles formed by metal–ligand bonds can be provoked by their larger covalency, manifesting itself in the shortening of the bond lengths. The examination of Ni—S and Ni—N bond lengths in **Ia–d** shows that Ni—N bonds remain practically unchanged, *ca* 1.98 Å, whilst Ni—S demonstrates a tendency towards shortening, with the decrease of the value of the angle NNiN′. The changes in the Ni—S bond lengths span the range 2.253 (**Ic**) to 2.229 Å (**Ib**). The disagreement with what might be expected in view of the above concept can be explained in that the VSEPR approach is not fully extended to transition metal complexes.

For all complexes **Ia–c** studied, the chelate rings have nearly planar conformation. The deviations from the plane common to the pyrazole and chelate ring do not exceed 4°.

The structure **Ib** contains a highly shortened intramolecular S···S contact, 3.388(2) Å, similar to the known reference value of 3.43 Å,[16] as well as shortened contacts between phenyl substituents, C(9)···C(9′) 3.241(8) Å, C(4)···C(4′) 3.346(7) Å. Phenyl rings, which are rotated by 54° along the C—N axis relative to the chelate ring, form a contact with the CH=N moiety 0.2–0.3 Å less than the conventional value.

As seen from the bond lengths in complexes **Ia–d**, the electron structure of the coordinated ligand is consistent with the delocalized iminothiolato form. It can be illustrated by the values of the bond lengths in the SC(1)C(2)C(3)N(1) portion of the chelate ring, which are intermediate between the lengths in the model aminothione moiety S=C(1)—C(2)=C(3)—N(1) for 1-isopropyl-3-methyl-4-N-cyclohexylenamine-5-pyrazolethione, and iminothiol S—C(1)=C(2)—C(3)=N(1) for 1-phenyl-3-methyl-4-cyclohexylaldimine-5-mercaptomethylpyrazole: C(1)=S 1.696, C(1)—S 1.742 Å; C(1)—C(2) 1.462, C(1)=C(2) 1.396 Å; C(2)=C(3) 1.387, C(2)—C(3) 1.425 Å; C(3)=N(1) 1.251, C(3)—N(1) 1.306 Å.[17]

REFERENCES

1. R. H. Holm and M. J. O'Connor, *Prog. Inorg. Chem.* 1971, **14**, 241.
2. G. V. Panova, N. K. Vikulova and V. M. Potapov, *Usp. Khim.* 1980, **49**, 1234.
3. L. E. Nivorozhkin, L. E. Konstantinovsky, V. I. Minkin, O. A. Osipov, A. D. Garnovsky, V. P. Kurbatov and I. Ya. Kvitko, *Zh. Neorg. Khim.* 1975, **20**, 3012.
4. L. E. Nivorozhkin, A. L. Nivorozhkin, M. S. Korobov, L. E. Konstantinovsky and V. I. Minkin, *Polyhedron* 1985, **4**, 1701.
5. T. G. Takhirov, O. A. Diachenko, D. B. Tagiev, A. L. Nivorozhkin, L. E. Nivorozhkin and V. I. Minkin, *Koord. Khim.* 1988, **14**, 237.
6. A. I. Uraev, A. L. Nivorozhkin, A. S. Frenkel, A. S. Antsishkina, M. A. Porai-Koshits, L. E. Konstantinovsky, G. K.-I. Magomedov and A. D. Garnovsky, *J. Organomet. Chem.* 1989, **368**, 303.
7. W. R. Busing and H. A. Levy, *Acta Cryst.* 1961, **10**, 180.
8. A. I. Udelnov and Yu. T. Struchkov, *Kristallografia* 1976, **21**, 484.
9. V. I. Andrianov and Z. Sh. Safina, *RENTGEN-75*, Program package for the crystal structures interpretation. Chernogolovka (1975).
10. A. N. Chekhlov, *Kristallografia* 1981, **26**, 596.
11. J. D. Dunitz, *X-ray Analysis and the Structure of Organic Molecules*. Cornell University Press, Ithaca, N.Y. (1979).
12. H. B. Burgi and J. D. Dunitz, *Acc. Chem. Res.* 1983, **16**, 153.
13. O. Exner, in *Correlation Analysis in Chemistry.*

Recent Advances (Edited by N. B. Chapman and J. Shorter), p. 439. Plenum Press, New York (1978).
14. E. E. Castellano, O. J. R. Hodder, C. K. Prout and P. J. Sadler, *J. Chem. Soc. A.* 1971, 2620.
15. V. A. Haaland, *Angew. Chem.* 1989, 1017.
16. T. G. Koetzle, W. C. Hamilton and R. Parthasarathy, *Acta Cryst.* 1972, **B28**, 2083.
17. T. G. Takhirov, O. A. Diachenko, D. B. Tagiev, A. L. Nivorozhkin, L. E. Nivorozhkin and V. I. Minkin, *Koord. Khim.* In press.

Polyhedron Vol. 10, No. 2, pp. 187–196, 1991
Printed in Great Britain

0277–5387/91 $3.00+.00
© 1991 Pergamon Press plc

REACTIVITY OF PYRIDINECARBOXYLATE COMPLEXES OF RHODIUM(I) TOWARDS $Hg(OOCCF_3)_2$ AND $Hg(Ph)(OOCCF_3)$. CRYSTAL STRUCTURE OF $Rh(C_{10}H_6NO_2)(OOCCF_3)_2(H_2O)[P(4\text{-}CH_3\text{-}C_6H_4)_3]$—III*

M. CANO,† J. V. HERAS, M. A. LOBO, M. MARTINEZ and E. PINILLA

Departamento de Química Inorgánica I, Facultad de Ciencias Químicas, Universidad Complutense, 28040-Madrid, Spain

and

E. GUTIERREZ and M. A. MONGE

Laboratorio Difracción de Rayos X, Facultad de CC. Químicas, Universidad Complutense de Madrid and Instituto de Materiales, C.S.I.C., Serrano 113, Madrid, Spain

(*Received* 15 *June* 1990; *accepted* 10 *August* 1990)

Abstract—Reactions of $Rh(N\text{-}O)(CO)[P(4\text{-}X\text{-}C_6H_4)_3]$ [(N-O) = 2-C_5NH_4COO(pyC) and 2-C_9NH_6COO (quin), X = CH_3O, CH_3, F, Cl] with $Hg(R)(OOCCF_3)$ (R = Ph, $OOCCF_3$) lead to the hexacoordinate rhodium(III), $Rh(HgR)(OOCCF_3)(N\text{-}O)(CO)[P(4\text{-}X\text{-}C_6H_4)_3]$, complexes. The new compounds evolve in solution to the decarbonylated species $Rh(R)(OOCCF_3)(N\text{-}O)(H_2O)[P(4\text{-}X_6\text{-}C_6H_4)_3]$. The crystal of one of the above derivatives, $Rh(OOCCF_3)_2(quin)(H_2O)[P(4\text{-}CH_3\text{-}C_6H_4)_3]$, is reported, and a distorted octahedral coordination around the rhodium atom with the two monodentate $OOCCF_3$ ligands in *cis* positions is found.

Synthetic and structural aspects of the chemistry of complexes containing bonds between dissimilar metal atoms are of continuing interest.[1,2] In particular, the reactions of mercury(II) compounds with complexes of transition metals have been extensively studied[2] and different types of reactions have been found. Thus, when the transition metal complex is an electron-rich one, a donor–acceptor complex with mercury derivatives is usually formed.[3,4] However, when the transition metal complex is less nucelophilic and amenable to oxidation, oxidative addition products are obtained. For this reason, Vaska's complex is easily oxidized by mercury(II) halides or pseudohalides[5] but a similar reaction does not occur for analogous rhodium(I) complexes.

It is reasonable to consider that if more basic ligands, like pyridinecarboxylates, were used, facile oxidation would occur.

In previous papers[6,7] we reported the formation of oxidative addition products of the rhodium(I) complexes, $Rh(pyC)(CO)[P(4\text{-}X\text{-}C_6H_4)_3]$, by their reactions with I_2, CH_3I or HgX_2.

As an extenstion of these results, we have been studying the reactivity of new pyridinecarboxylate complexes of rhodium(I) with bulky, acidic, mercury(II) derivatives.[8]

In this paper, we describe the reaction of rhodium(I) pyridinecarboxylate complexes, $Rh(N\text{-}O)(CO)[P(4\text{-}X\text{-}C_6H_4)_3]$ [(N-O) = 2-C_5NH_4COO(pyC) and 2-C_9NH_6COO (quin), X = CH_3O, CH_3, F, Cl] with $Hg(OOCCF_3)_2$ and $Hg(Ph)(OOCCF_3)$. The new heterobimetallic Rh—Hg derivatives are stable in the solid state, but a slow evolution in solution with the formation of new decarbonylated products, $Rh(R)(OOCCF_3)(N\text{-}O)(H_2O)[P(4\text{-}X\text{-}C_6H_4)_3]$ (R = Ph, $OOCCF_3$), has been observed.

* For part II, see ref. 7.

† Author to whom correspondence should be addressed.

Table 1. Analytical and IR spectral data

Complex	Analyses: Found (Calc.)			IR (KBr, cm^{-1})		
	C(%)	H(%)	N(%)	ν(C═O)	ν_{as}(OCO)	ν(O—H)
$Rh(HgOOCCF_3)(OOCCF_3)(pyC)(CO)[P(4\text{-}CH_3O\text{-}C_6H_4)_3]$	36.8 (37.2)	2.4 (2.4)	1.4 (1.4)	2060 vs	1720–1640 vs, b	—
$Rh(HgOOCCF_3)(OOCCF_3)(pyC)(CO)[P(4\text{-}CH_3\text{-}C_6H_4)_3]$	38.1 (39.0)	2.6 (2.6)	1.5 (1.4)	2050 vs	1730–1640 vs, b	—
$Rh(HgOOCCF_3)(OOCCF_3)(pyC)(CO)[P(4\text{-}F\text{-}C_6H_4)_3]$	34.5 (35.0)	1.5 (1.6)	1.5 (1.4)	2050 vs	1730–1640 vs, b	—
$Rh(HgOOCCF_3)(OOCCF_3)(pyC)(CO)[P(4\text{-}Cl\text{-}C_6H_4)_3]$	32.6 (33.3)	1.6 (1.5)	1.4 (1.3)	2060 vs	1715–1635 vs, b	—
$Rh(HgOOCCF_3)(OOCCF_3)(quin)(CO)[P(4\text{-}CH_3O\text{-}C_6H_4)_3]$	40.4 (40.0)	2.6 (2.5)	1.3 (1.3)	2028 vs	1684 sh, 1660 vs, 1640 sh	—
$Rh(HgOOCCF_3)(OOCCF_3)(quin)(CO)[P(4\text{-}CH_3\text{-}C_6H_4)_3]$	42.8 (41.8)	2.5 (2.6)	1.4 (1.3	2034 vs	1683 sh, 1660 vs, 1638 sh	—
$Rh(HgOOCCF_3)(OOCCF_3)(quin)(CO)[P(4\text{-}F\text{-}C_6H_4)_3]$	38.3 (37.9)	2.1 (1.7)	1.4 (1.3)	2060 sh 2024 vs	1685 sh, 1658 vs, 1635 sh	—
$Rh(HgOOCCF_3)(OOCCF_3)(quin)(CO)[P(4\text{-}Cl\text{-}C_6H_4)_3]$	37.2 (36.2)	1.7 (1.6)	1.3 (1.3)	2040 vs	1685 sh, 1662 vs, 1634 sh	—
$Rh(OOCCF_3)_2(pyC)(H_2O)[P(4\text{-}CH_3O\text{-}C_6H_4)_3]$	45.0 (45.3)	3.4 (3.3)	1.8 (1.7)			
$Rh(OOCCF_3)_2(pyC)(H_2O)[P(4\text{-}CH_3\text{-}C_6H_4)_3]$	48.3 (48.2)	3.6 (3.5)	1.9 (1.8)	—	1750–1635 vs, b	3300 s, b
$Rh(OOCCF_3)_2(pyC)(H_2O)[P(4\text{-}F\text{-}C_6H_4)_3]$	42.3 (42.8)	2.4 (2.3)	1.8 (1.8)	—	1750–1635 vs, b	3300 s, b

$Rh(OOCCF_3)_2(pyC)(H_2O)[P(4\text{-}Cl\text{-}C_6H_4)_3]$	40.0 (40.3)	2.2 (2.1)	1.7 (1.7)	—	1740–1630 vs, b	3300 s, b
$Rh(OOCCF_3)_2(quin)(H_2O)[P(4\text{-}CH_3O\text{-}C_6H_4)_3]$	48.5 (48.3)	3.4 (3.3)	1.6 (1.6)			
$Rh(OOCCF_3)_2(quin)(H_2O)[P(4\text{-}CH_3\text{-}C_6H_4)_3]$	51.2 (51.1)	3.6 (3.5)	1.7 (1.7)	—	1740–1630 vs, b	3300 s, b
$Rh(OOCCF_3)_2(quin)(H_2O)[P(4\text{-}F\text{-}C_6H_4)_3]$	45.9 (46.0)	2.4 (2.4)	1.7 (1.7)	—	1740–1625 vs, b	3360 s
$Rh(OOCCF_3)_2(quin)(H_2O)[P(4\text{-}Cl\text{-}C_6H_4)_3]$	43.1 (43.4)	2.3 (2.3)	1.6 (1.6)	—	1740–1620 vs, b	3300 s, b
$Rh(HgPh)(OOCCF_3)(quin)(CO)[P(4\text{-}CH_3O\text{-}C_6H_4)_3]$	45.2 (45.9)	3.2 (3.1)	1.1 (1.3)	2031 vs	1657 vs, 1640 sh	—
$Rh(HgPh)(OOCCF_3)(quin)(CO)[P(4\text{-}CH_3\text{-}C_6H_4)_3]$	49.2 (48.1)	3.6 (3.2)	1.5 (1.4)	2037 vs	1655 vs, 1635 sh	—
$Rh(HgPh)(OOCCF_3)(quin)(CO)[P(4\text{-}F\text{-}C_6H_4)_3]$	45.0 (44.0)	2.2 (2.3)	1.5 (1.4)	2044 vs	1658 vs, 1632 sh	—
$Rh(HgPh)(OOCCF_3)(quin)(CO)[P(4\text{-}Cl\text{-}C_6H_4)_3]$	41.5 (42.0)	2.3 (2.2)	1.4 (1.3)	2044 vs	1655 vs, 1633 sh	—
$Rh(Ph)(OOCCF_3)(quin)(H_2O)[P(4\text{-}CH_3O\text{-}C_6H_4)_3]$	56.3 (56.1)	4.1 (4.2)	1.7 (1.7)	—	1710 sh, 1657 vs, 1640 vs	3275 s, b
$Rh(Ph)(OOCCF_3)(quin)(H_2O)[P(4\text{-}CH_3\text{-}C_6H_4)_3]$	60.0 (59.5)	4.4 (4.3)	1.9 (1.8)			
$Rh(Ph)(OOCCF_3)(quin)(H_2O)[P(4\text{-}F\text{-}C_6H_4)_3]$	54.4 (54.1)	3.2 (3.1)	1.8 (1.7)			
$Rh(Ph)(OOCCF_3)(quin)(H_2O)[P(4\text{-}Cl\text{-}C_6H_4)_3]$	51.1 (51.0)	3.0 (2.9)	1.6 (1.6)			

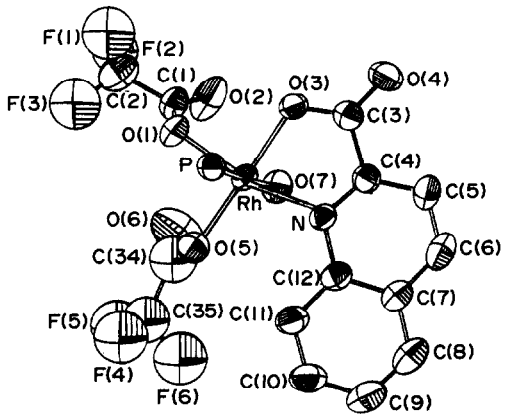

Fig. 1. Geometry of the molecule. (The phenyl groups of the triphenylphosphine have been omitted for clarity.)

The crystal structure of one these derivatives, $Rh(OOCCF_3)_2(quin)(H_2O)[P(4\text{-}CH_3\text{-}C_6H_4)_3]$, has been determined (Fig. 1).

RESULTS AND DISCUSSION

Reactions of $Rh(N\text{-}O)(CO)[P(4\text{-}X\text{-}C_6H_4)_3]$ [(N-O) = 2-pyridinecarboxylate anion (pyC) and 2-quinaldinate anion (quin), X = CH_3O, CH_3, F, Cl] with an excess of $Hg(OOCCF_3)_2$ yield oxidative addition products formulated as $Rh(HgOOCCF_3)(OOCCF_3)(N\text{-}O)[P(4\text{-}X\text{-}C_6H_4)_3]$ on the basis of their analytical and spectroscopic data.

The IR spectra of the new complexes in the solid state (Table 1) show two strong absorption bands in the carbonyl and carboxylic stretching regions.

The bands at *ca* 2060–2030 cm^{-1} attributed to $\nu(CO)$ of the carbonyl group appear at higher frequencies relative to those of the parent monocarbonyl compounds, showing a shift of 75–95 and 70–80 cm^{-1} for the pycolinate and quinaldinate complexes, respectively. This fact is consistent with an increase in the oxidation state of the rhodium atom by the addition of $Hg(OOCCF_3)_2$.

The strong absorption at *ca* 1730–1635 cm^{-1} due to $\nu_{as}(OCO)$ appears as a broad band. However, in the quinaldinate complexes this band is split into three components. The highest and the lowest could be tentatively assigned to the $\nu_{as}(OCO)$ of the CF_3COO moieties bonded to the mercury and rhodium atoms, respectively.[9] The middle band appears at the same position as for the parent $Rh(quin)(CO)[P(4\text{-}X\text{-}C_6H_4)_3]$ complexes, for which a bidentate N,O-coordination of the quinaldinate ligand is proposed.[6,10,11] However, in the absence of structural data it is not possible to unambiguously assign the different carboxylic groups present in these compounds.

Bands associated with the phosphine ligands are also observed in their characteristic regions.[12]

Thus, on the basis of the above data it appears that a pseudo-octahedral stereochemistry occurs, with $HgOOCCF_3$ and $OOCCF_3$ groups providing the fifth and sixth coordination sites.

The products are stable in the solid state, but in acetone or CH_2Cl_2 solutions evolution with Hg^0 deposition was observed and new decarbonylated products could be obtained. This evolution, which is faster for the pycolinate than the quinaldinate derivatives, sometimes prevents further studies. However, the quinaldinate derivative containing $P(4\text{-}CH_3O\text{-}C_6H_4)_3$ is more stable in $CDCl_3$ solution and we have been able to achieve good NMR spectra.

For this complex, $Rh(HgOOCCF_3)(OOCCF_3)(quin)(CO)[P(4\text{-}CH_3O\text{-}C_6H_4)_3]$, both ^1H NMR and ^{31}P NMR spectra (Table 2) show two groups of signals. In the former case, these appear as two singlets at δ 3.8 and 3.7 ppm, assigned to the protons of the CH_3O group of the phosphine ligand. In the second case, two doublets at δ 31.8 and 29.5 ppm [^1J(Rh—P) 124.0 and 120.9 Hz, respectively] were observed. A similar spectrum is obtained for the $Rh(HgOOCCF_3)(OOCCF_3)(pyC)(CO)[P(4\text{-}CH_3\text{-}C_6H_4)_3]$ complex. The presence in solution of a mixture of rhodium(III) isomers[7] could therefore be suggested.

The decarbonylated products obtained from the above compounds in acetone solution can be formulated as $Rh(OOCCF_3)_2(N\text{-}O)(H_2O)[P(4\text{-}X\text{-}C_6H_4)_3]$ on the basis of the analytical and spectroscopic data.

The IR spectra of these compounds in KBr pellets (Table 1) do not exhibit a CO stretching frequency. An absorption at *ca* 3300 cm^{-1} was assigned to $\nu(OH)$ of the coordinated water. A complicated group of bands appears in the region 1750–1620 cm^{-1}. Due to the presence of different carboxylate groups and coordinated water in the complex, the assignment of these bands is very difficult.

The complex $RH(OOCCF_3)_2(quin)(H_2O)[P(4\text{-}CH_3O\text{-}C_6H_4)_3]$ exhibits two singlets at δ 3.9 and 3.8 ppm in its ^1H NMR spectrum (Table 2), suggesting that two isomer species could be present in the decarbonylated derivatives. This fact is also confirmed by the ^{31}P NMR spectrum, and the presence of two doublets at δ 29.7 ppm, ^1J(Rh—P) 119.6 Hz and δ 27.9 ppm, ^1J(Rh—P) 116.6 Hz were observed, the first more intense than the second.

In order to characterize unambiguously these carboxylate rhodium(III) species, the crystal structure of one of these complexes, $Rh(OOCCF_3)_2(quin)(H_2O)[P(4\text{-}CH_3\text{-}C_6H_4)_3]$, has been determined. Bond lengths and angles are shown in Table

Table 2. ^{1}H NMR and ^{31}P NMR spectral data [δ (ppm), J(Hz)]

Complex	^{1}H NMR[a]		^{31}P NMR[b]	
	δ (aromatic H)	δ (CH_3O—)	δ	^1J(Rh—P)
$Rh(HgOOCCF_3)(OOCCF_3)(quin)(CO)[P(4\text{-}CH_3O\text{-}C_6H_4)_3]$	8.4–6.6 m	3.8 s	31.8 d	124.0
		3.7 s	29.5 d	120.9
$Rh(OOCCF_3)_2(quin)(H_2O)[P(4\text{-}CH_3O\text{-}C_6H_4)_3]$	8.4–6.7 m	3.9 s	29.7 d	119.6
		3.8 s	27.9 d[c]	116.6
$Rh(HgPh)(OOCCF_3)(quin)(CO)[P(4\text{-}CH_3O\text{-}C_6H_4)_3]$	8.5–6.2 m	3.8 s	31.8 d	124.0
		3.7 s[c]	31.9 d[c]	123.0
$Rh(Ph)(OOCCF_3)(quin)(H_2O)[P(4\text{-}CH_3O\text{-}C_6H_4)_3]$	8.5–6.7 m	3.8 s	29.6 d	120.9
		3.8 s[c]	26.1 d[c]	126.3
$Rh(HgOOCCF_3)(OOCCF_3)(pyC)(CO)[P(4\text{-}CH_3\text{-}C_6H_4)_3]$[d]			33.4 d	123.1
			30.5 d[c]	120.9

[a] $CDCl_3$ solvent, TMS as internal reference.
[b] $CDCl_3$ solvent, 85% H_3PO_4 as external reference.
[c] Weak signal.
[d] C_6D_6 solvent.

3. The geometry of the molecule is shown in Fig. 1.[13]

The coordination around the rhodium is a distorted octahedral with the equatorial positions occupied by the bidentate quinaldinate ligand and two O-monodentate $OOCCF_3$ ligands. One apical position is occupied by the $P(4\text{-}CH_3\text{-}C_6H_4)_3$ ligand and the other one is occupied by a molecule of water.

The oxygen atom [O(7)] of the water molecule is linked with one oxygen atom [O(4)] of the quinaldinate ligand of the nearest neighbouring molecule through an intermolecular hydrogen bond. It is also linked with two oxygen atoms [O(2), O(6)] of the two trifluoroacetate ligands through an assymetrically, bifurcated, intramolecular hydrogen bond. The geometrical features of the hydrogen bonds' network are shown in Fig. 2.

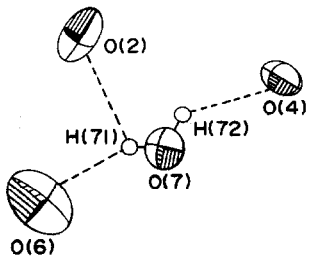

Fig. 2. The geometrical features of the hydrogen bonds. Bond distances (Å) and angles (°): O(7)—H(71), 0.707(123); O(7)—H(72), 0.747(120); O(2)—H(71), 2.413(118); O(6)—H(71), 2.081(135); O(4)—H(72), 2.134(216). H(71)—O(7)—H(72), 116.1(13.5).

So, it appears that in the evolution of the initial Rh—Hg compounds the ligands linked to mercury migrate to the rhodium atom in the decarbonylated complex.

As an extension of the above results we have studied the reactivity of the Rh(N-O)(CO)[P(4-X-$C_6H_4)_3$] complexes towards $Hg(Ph)(OOCCF_3)$. We have then obtained new σ-Rh—Ph organometallic compounds. The crystal structure of one of these complexes has been recently published.[8]

The reactions of Rh(quin)(CO)[P(4-X-$C_6H_4)_3$] with $Hg(Ph)(OOCCF_3)$ lead to the compounds formulated as $Rh(HgPh)(OOCCF_3)$(quin)(CO) [P(4-X-$C_6H_4)_3$] on the basis of analytical and spectroscopic data.

When the starting compounds were Rh(pyC)(CO) [P(4-X-$C_6H_4)_3$], we have not been able to obtain pure reaction products. In a 1 : 1 molar ratio, Rh : Hg, at low temperature and very short reactions times, mixtures of the parent compound and oxidative addition product were obtained. An increase in the molar ratio and/or the reaction time led to decomposition products. This difference in behaviour between 2-pycolinate and 2-quinaldinate starting compounds can be explained by the higher electron density of the rhodium atom in the 2-quinaldinate, than in the 2-pycolinate derivatives.

The IR spectra in the solid state (Table 1) of the new compounds $Rh(HgPh)(OOCCF_3)$(quin)(CO)[P(4-X-$C_6H_4)_3$] show the characteristic absorptions of the present ligands. The values of the ν(CO) relative to the parent compounds are consistent with the formation of oxidative addition

Table 3. Bond distances (Å) and angles (°) with ESDs in parentheses

Rh—P	2.277(2)	F(3)—C(2)	1.283(14)
Rh—N	2.060(7)	F(4)—C(35)	1.327(0)
Rh—O(1)	2.039(6)	F(5)—C(35)	1.270(0)
Rh—O(3)	1.996(6)	F(6)—C(35)	1.244(0)
Rh—O(5)	2.044(7)	C(1)—C(2)	1.537(17)
Rh—O(7)	2.171(7)	C(3)—C(4)	1.512(13)
O(1)—C(1)	1.257(12)	C(4)—C(5)	1.393(13)
O(2)—C(1)	1.199(13)	C(5)—C(6)	1.373(17)
O(3)—C(3)	1.284(11)	C(6)—C(7)	1.392(15)
O(4)—C(3)	1.217(11)	C(7)—C(8)	1.405(16)
O(5)—C(34)	1.244(13)	C(7)—C(12)	1.432(14)
O(6)—C(34)	1.224(16)	C(8)—C(9)	1.355(17)
N—C(4)	1.320(11)	C(9)—C(10)	1.384(18)
N—C(12)	1.385(11)	C(10)—C(11)	1.368(15)
F(1)—C(2)	1.260(11)	C(11)—C(12)	1.401(14)
F(2)—C(2)	1.285(13)	C(34)—C(35)	1.563(12)
P—Rh—N	94.2(2)	F(2)—C(2)—C(1)	114.4(9)
P—Rh—O(1)	88.5(2)	F(2)—C(2)—F(3)	107.1(9)
P—Rh—O(3)	88.5(2)	F(3)—C(2)—C(1)	112.1(1.0)
P—Rh—O(5)	92.4(2)	O(3)—C(3)—O(4)	124.1(9)
P—Rh—O(7)	177.3(2)	O(3)—C(3)—C(4)	115.0(8)
N—Rh—O(7)	173.3(3)	O(4)—C(3)—C(4)	121.0(8)
N—Rh—O(3)	81.1(3)	N—C(4)—C(3)	115.9(8)
N—Rh—O(5)	100.4(3)	N—C(4)—C(5)	125.4(8)
N—Rh—O(7)	83.2(3)	C(3)—C(4)—C(5)	118.8(8)
O(1)—Rh—O(3)	92.8(3)	C(4)—C(5)—C(6)	116.6(9)
O(1)—Rh—O(5)	85.6(3)	C(5)—C(6)—C(7)	121.6(1.0)
O(1)—Rh—O(7)	94.1(3)	C(6)—C(7)—C(8)	122.7(1.0)
O(3)—Rh—O(5)	178.1(3)	C(6)—C(7)—C(12)	117.7(9)
O(3)—Rh—O(7)	90.3(3)	C(8)—C(7)—C(12)	119.5(9)
O(5)—Rh—O(7)	88.9(3)	C(7)—C(8)—C(9)	120.7(1.1)
Rh—N—C(4)	111.3(6)	C(8)—C(9)—C(10)	120.4(1.1)
Rh—N—C(12)	130.0(6)	C(9)—C(10)—C(11)	122.7(1.2)
C(4)—N—C(12)	118.2(8)	C(10)—C(11)—C(12)	119.4(1.0)
Rh—O(1)—C(1)	124.8(6)	O(5)—C(34)—O(6)	128(1.2)
Rh—O(3)—C(3)	115.6(6)	O(5)—C(34)—C(35)	128.9(1.2)
Rh—O(5)—C(34)	125.1(7)	O(6)—C(34)—C(35)	117.6(1.0)
O(1)—C(1)—O(2)	131.0(1.0)	C(34)—C(35)—F(4)	112.1(4)
O(1)—C(1)—C(2)	112.0(9)	C(34)—C(35)—F(5)	113.3(4)
O(2)—C(1)—C(2)	117.0(1.0)	C(34)—C(35)—F(6)	115.5(5)
F(1)—C(2)—C(1)	112.8(9)	F(4)—C(35)—F(5)	115.1(0)
F(1)—C(2)—F(2)	107.2(9)	F(4)—C(35)—F(6)	96.8(0)
F(1)—C(2)—F(3)	102.4(9)	F(5)—C(35)—F(6)	102.6(0)

products. A strong absorption at 1658–1655 cm^{-1} with a shoulder at 1640–1633 cm^{-1} was assigned to the ν_{as}(OCO) of the carboxylate groups of the $OOCCCF_3$ and quinaldinate ligands. In contrast to the IR spectra of the above $Hg(OOCCF_3)_2$ derivatives, no bands attributed to the $OOCCF_3$ group bonded to the mercury atom appear in these spectra. This suggests that in the derivatives with $Hg(Ph)(OOCCF_3)$ the $OOCCF_3$ group is directly bonded to the rhodium atom.

The ^1H NMR spectrum of $Rh(HgPh)(OOCF_3)$(quin)(CO)[P(4-CH_3O-$C_6H_4)_3$] (Table 2) shows two singlets, one which is very intense at δ 3.75 ppm and the other weaker at δ 3.7 ppm. The ^{31}P NMR spectrum (Table 2) exhibits an intense signal centred at δ 31.8 ppm, split by coupling with the rhodium atom [^1J(Rh—P) 124.0 Hz], and a weak doublet centred at δ 31.9 ppm with ^1J(Rh—P) 123.0 Hz. The above data seem to confirm again the presence, in solution, of two isomeric forms of the new

rhodium(III) complexes, one of them more abundant than the other.

The addition of the (HgPh) and ($OOCCF_3$) groups to the rhodium atom of the square-planar parent compounds agrees with the related reactions with HgPhCl.[4,7]

The ^{13}C NMR spectrum of Rh(HgPh)($OOCCF_3$)(quin)(CO)[P(4-CH_3O-C_6H_4)$_3$] (Table 4) confirms this behaviour by the appearance of ^{199}Hg satellites on the signals of the carbon atoms of the phenyl ligand. The J(Hg—C) values are lower than in the free Hg(Ph)($OOCCF_3$), and they appear intermediate between those of $Hg(Ph)_2$ and HgPhCl.[14] The above results agree with the bonding of the phenyl group to the mercury atom in the oxidative addition products.

The aromatic carbons show two signals of different intensity in almost all of these cases. This fact agrees with the presence of the isomer mixture suggested above. It has not been possible to detect the carbonyl signal after 2 h, and it was not possible to use a longer time period because of the evolution of the compound in solution.

This evolution of the carbonylated rhodium(III) compounds leads to the formation of the crystalline complexes Rh(Ph)($OOCCF_3$)(quin)(H_2O)[P(4-X-C_6H_4)$_3$]. The crystal structure of one of these derivatives (X = F) has been described[8] and shows that new σ-organometallic compounds can be obtained in this way.

The ^1H NMR and ^{31}P NMR spectra of Rh(Ph)($OOCCF_3$)(quin)(H_2O)[P(4-CH_3O-C_6H_4)$_3$] (Table 2) show the same pattern that we have observed in all of the compounds studied above.

In the ^{13}C NMR spectrum of this complex (Table 4), the signals assigned to the carbon atoms of the phenyl group appear at lower δ values than in the mercuric starting compound. The spectrum shows the signals of the α- and β-carbons in the phenyl as doublets by coupling with the rhodium atom. As in the mercuric starting compound, two signals of different intensity for most of the carbon atoms of the phenyl and phosphine ligands are observed due to the presence of isomers in solution. The signals from the CF_3 group and quinaldinate ligand are weak and their assignment is not straightforward.

The ^{13}C NMR spectra of Hg(Ph)($OOCCF_3$) and Rh(quin)(CO)[P(4-CH_3O-C_6H_4)$_3$] have also been recorded for comparison (Table 4).

EXPERIMENTAL

IR spectra were recorded on a 1300 Perkin–Elmer spectrophotometer (over the 4000–200 cm^{-1} range) with KBr pellets. Analyses (C, H, N) were carried out by Elemental Microanalyses Laboratories Ltd., Devon, U.K. ^1H, ^{31}P and ^{13}C NMR spectra were recorded on a Varian XR-300 spectrometer at room temperatures, using TMS and 85% H_3PO_4 as standards. The reactions were carried out at room temperature, under oxygen-free nitrogen. Complexes Rh(N-O)(CO)[P(4-X-C_6H_4)$_3$] were prepared by our published methods.[6,10] Commercial $Hg(OOCCF_3)_2$ was used. Hg(Ph)($OOCCF_3$) was prepared by the method of Abbate and Ulrich.[16]

Solution and refinement of the crystal structure

A summary of the fundamental crystal data for the Rh($OOCCF_3$)$_2$(quin)(H_2O)[P(4-CH_3-C_6H_4)$_3$] is given in Table 5.

The heavy atom was located from the three dimensional Patterson map. The remaining non-hydrogen atoms were located in a Fourier synthesis.

An empirical absorption correction[17] was applied at the end of the isotropic refinement. Mixed full-matrix refinement with unit weights led to $R = 0.076$. The fluorine atoms of the trifluoroacetate ligands were refined isotropically because of some unsolved disorder from thermal motion. A difference synthesis calculated with reflections having $\sin\theta/\lambda < 0.5$ A^{-1} showed all hydrogen atoms as the highest peaks of the map. Final refinement with isotropic temperature factors and coordinate for the hydrogen atoms, except the hydrogen atom of the coordinated water molecule, produced $R = 0.073$.

Most of the calculations were carried out with the X-Ray 80 system.[18] Final atomic positional and thermal parameters, bond lengths and angles, and F_o/F_c values have been deposited as supplementary material with the Editor, from whom copies are available on request. Atomic coordinates have also been submitted to the Cambridge Crystallographic Data Centre.

Preparation of the complexes

Rh(HgO$OCCF_3$)($OOCCF_3$)(pyC)(CO)[P(4 - X - C_6H_4)$_3$] (X = CH_3O, CH_3, F, Cl). To a suspension of Rh(pyC)(CO)[P(4-X-C_6H_4)$_3$] (0.1 mmol) in acetone, a 1 : 3 molar excess of $Hg(OOCCF_3)_2$ was added in the dark. After 30 min of stirring Hg^0 appeared and the solution was filtered through Kiesselghur. The solvent was partially removed and the yellow product was precipitated by addition of diethyl ether and n-hexane, filtered off, washed with Et_2O/hexane and dried *in vacuo*. Yield: 60–75%.

Rh(HgO$OCCF_3$)($OOCCF_3$)(quin)(CO)[P(4 - X - C_6H_4)$_3$] (X = CH_3O, CH_3, F, Cl). The procedure was similar to the above synthesis except the reac-

Table 4. ^{13}C NMR spectral data

Assignment		Hg(Ph)(OOCCF$_3$)[a]		Rh(quin)(CO)[P(4-CH$_3$O-C$_6$H$_4$)$_3$][b]		Rh(HgPh)(OOCCF$_3$)(quin)(CO)[P(4-CH$_3$O-C$_6$H$_4$)$_3$][b]		Rh(Ph)(OOCCF$_3$)(quin)(H$_2$O)[P(4-CH$_3$O-C$_6$H$_4$)$_3$][b]	
		δ (ppm)	J(Hz)	δ (ppm)	J(Hz)	δ (ppm)	J(Hz)	δ (ppm)	J(Hz)
Ph	C—M(α)	142.8 s	^1J(Hg—C): —			144.7 s	^1J(Hg—C): —	140.6[c]	^1J(C—Rh): 59.7
	C (β)	137.6 s	^2J(Hg—C): 127.4			135.4 s 135.3 s	^2J(Hg—C): 100.3 ^2J(Hg—C): 100.4	133.1 d 133.1 d[c]	^2J(C—Rh): 6.0 ^2J(C—Rh): 5.5
	C (γ)	129.5 s	^3J(Hg—C): 227.1			128.9 s	^3J(Hg—C): 127.3	128.0 s	
	C (δ)	129.7 s	^4J(Hg—C): 39.7			128.7 s 128.7 s	^4J(Hg—C): 21.3 ^4J(Hg—C): 21.8	128.3 s 128.3 s[c]	
	CF$_3$	119.7 q[c]	^1J(C—F): 288.6						
	COO$^-$(CF$_3$)	161.0 q	^2J(C—F): 37.6			151.2 m[c]		146.6 q	^2J(C—F): 25.6
P(4-CH$_3$O-C$_6$H$_4$)$_3$	—OCH$_3$			55.1 s		55.5 s 55.4 s[c]		55.2 s 55.1 s	
	C—P			123.2 d	^1J(C—P): 57.5	120.1 d 120.2 d[c]	^1J(C—P): 63.8 ^1J(C—P): 64.1	118.4 d 118.5 d[c]	^1J(C—P): 59.9 ^1J(C—P): 61.4
	C(*o*) with respect to C—P			135.6 d	^2J(C—P): 12.9	135.d 136.1 d[c]	^2J(C—P): 11.1 ^2J(C—P): 11.1	135.9 d 135.8 d[c]	^2J(C—P): 10.9 ^2J(C—P): 11.2
	C(*m*) with respect to C—P			113.8 d	^3J(C—P): 11.8	114.7 d 114.2 d[c]	^3J(C—P): 12.1 ^3J(C—P): 13.1	114.0 d 113.9 d	^3J(C—P): 12.7 ^3J(C—P): 12.8
	C(*p*) (C—OMe)			161.2 d	^2J(C—P): 2.0	152.1 s 162.1 s[c]		161.6 s	
	CO			190.8 dd	^1J(C—Rh): 74.7 ^2J(C—P): 24.1				
	COO$^-$(quin)			172.6 d	^{2-3}J(C—Rh): 3.8	172.5 s		171.9 s	

[a] (CD)$_3$CO$_2$ solvent, TMS as internal reference.
[b] CDCl$_3$ solvent, TMS as internal reference.
[c] Weak signal.

Table 5. Crystal and refinement data for $[Rh(C_{10}H_6NO_2)(OCOCF_3)_2(P(4\text{-}CH_3C_6H_4)_3)(H_2O)]$

Formula	$RhC_{35}F_6H_{29}NO_7P$
Crystal system	Monoclinic
Space group	$P2_1/c$
a (Å)	10.629(3)
b (Å)	17.152(4)
c (Å)	19.549(4)
β (°)	98.93
V (Å^3)	3520(1)
Z	4
F(000)	1664
ρ (calc.) (g cm^{-3})	1.55
Temperature (°C)	22
μ (cm^{-1})	6.08
Crystal dimensions (mm)	$0.2 \times 0.2 \times 0.3$
Diffractometer	Enraf–Nonius CAD4
Radiation	Graphite-monochromated Mo-K_α (λ = 0.71069 Å)
Scan technique	ω–2θ
Data collected	(−14, 0, 0) to (14, 22, 25)
Reflections collected	9157
Unique data	8639
Unique data (I) $\geqslant 2\sigma(I)$	5267
R(int) (%)	1.3
Standard reflections	3/92 reflections
RF (%)	7.3
R_wF (%)	8.6
Average shift/error	0.02

tion time was 2 h and the molar ratio was 1:2 Rh:Hg. Yield: 65–80%.

$Rh(OOCCF_3)_2(pyC)(H_2O)[P(4\text{-}X\text{-}C_6H_4)_3]$ (X = CH_3O, CH_3, F, Cl). These complexes were obtained as above with more prolonged reaction times, *ca* 3 h. Yield: 50–55%.

$Rh(OOCCF_3)_2(quin)(H_2O)[P(4\text{-}X\text{-}C_6H_4)_3]$ (X = CH_3O, CH_3, F, Cl). Solutions of $Rh(HgOOCCF_3)(OOCCF_3)(quin)(CO)[P(4\text{-}X\text{-}C_6H_4)_3]$ in acetone/Et_2O/hexane yielded after 3 days under N_2, yellow crystals of $Rh(OOCCF_3)_2(quin)(H_2O)[P(4\text{-}X\text{-}C_6H_4)_3]$ and the deposition of mercury. The crystals were filtered, washed with hexane and dried *in vacuo*. Yield: 25–30%.

$Rh(HgPh)(OOCCF_3)(quin)(CO)[P(4\text{-}X\text{-}C_6H_4)_3]$ (X = CH_3O, CH_3, F, Cl). An excess of $Hg(Ph)(OOCCF_3)$ (X = CH_3O, 50%; X = CH_3, 10%; X = F, 75%; X = Cl, 100% of excess) was added to a suspension of $Rh(quin)(CO)[P(4\text{-}X\text{-}C_6H_4)_3]$ (0.1 mmol) in acetone. The light yellow solutions were stirred (X = CH_3O, 55 min; X = CH_3, 30 min; X = F, 70 min; X = Cl, 85 min) and filtered through Kiesselghur to eliminate the Hg^0 that had appeared. The solutions were concentrated under reduced pressure and the yellow solids were precipitated by addition of cold Et_2O/hexane, filtered off, washed with hexane and dried *in vacuo*. Yield: 75–85%.

$Rh(Ph)(OOCCF_3)(quin)(H_2O)[P(4\text{ - }X\text{ - }C_6H_4)_3]$ (X = CH_3O, CH_3, F, Cl). These compounds were obtained by evolution of the above compounds in acetone/Et_2O/hexane solution under N_2. After 2 days, the yellow crystals were filtered, washed with hexane and dried *in vacuo*. Yield: 30–35%.

Acknowledgement—We gratefully acknowledge the Comisión Asesora de Investigación Cientifica y Técnica (CAICYT) (Spain) for financial support (Project PR 84-0367).

REFERENCES

1. D. L. Kepert and K. Vrieze, *Comprehensive Inorganic Chemistry* (Edited by J. C. Baylar Jr, H. J. Emeleus, Sir R. Nyholm and A. F. Trotman-Dickenson), Vol. 4, Ch. 47. Pergamon Press, Oxford (1973).
2. G. Wilkinson, F. G. A. Stone and E. W. Abel (Eds), *Comprehensive Organometallic Chemistry*, Vol. 6, Chaps 40–43. Pergamon Press, Oxford (1982).
3. D. J. Cook, J. L. Dawes and R. D. W. Kemmitt, *J. Chem. Soc. A* 1967, 1547.

4. J. L. Dawes and R. D. W. Kemmitt, *J. Chem. Soc. A* 1968, 1072; 1968, 2093.
5. R. S. Nylhom and K. Vrieze, *J. Chem. Soc. A* 1965, 5337.
6. J. V. Heras, E. Pinilla and M. Martínez, *Polyhedron* 1983, **2**, 1009.
7. M. Cano, J. V. Heras, M. Martínez, E. Pinilla and C. Alvarez, *Polyhedron* 1989, **8**, 1085.
8. M. Cano, J. V. Heras, M. A. Lobo, E. Pinilla, E. Gutiérrez and M. A. Monge, *Polyhedron* 1989, **8**, 2727.
9. P. I. van Vliet, J. Kuyper and K. Vrieze, *J. Organomet. Chem.* 1976, **122**, 99.
10. J. V. Heras, M. Cano, M. A. Lobo and E. Pinilla, *Polyhedron* 1989, **8**, 167.
11. A. J. Crowe, R. Hill, P. J. Smith, J. S. Brooks and R. Formstone, *J. Organomet. Chem.* 1981, **204**, 47.
12. G. B. Deacon and J. H. S. Green, *Spectrochim. Acta* 1968, **24A**, 845.
13. C. K. Johnson, ORTEP, Report ORNL-3794. Oak Ridge National Laboratory, Tennessee (1985).
14. J. Browning, P. L. Goggin, R. J. Goodfellow, N. W. Hurst, L. G. Mallinson and M. Murray, *J. Chem. Soc., Dalton Trans.* 1978, 872.
15. *International Tables for X-Ray Crystallography*, Vol. 4, p. 72. Kynoch Press, Birmingham (1974).
16. F. W. Abbate and H. Ulrich, *J. Appl. Polym. Sci.* 1969, **13**, 1929.
17. N. Walker and D. Stuart, *Acta Cryst.* 1983, **A39**, 158.
18. J. M. Stewart, *The X-Ray 80 System*. Computer Science Center, University of Maryland, College Park, Maryland (1980).

Polyhedron Vol. 10, No. 2, pp. 197–202, 1991
Printed in Great Britain

0277–5387/91 $3.00+.00
© 1991 Pergamon Press plc

ELECTROCHEMICAL SYNTHESIS OF PYRIDINE-2-THIONATO COMPLEXES OF ZINC(II) AND CADMIUM(II): THE CRYSTAL STRUCTURE OF 1,10-PHENANTHROLINE-BIS(PYRIDINE-2-THIONATO)ZINC(II)

M. L. DURAN, J. ROMERO, J. A. GARCIA-VAZQUEZ, R. CASTRO, A. CASTIÑEIRAS and A. SOUSA*

Departamento de Química Inorgánica, Universidad de Santiago, Santiago de Compostela, Spain

(*Received* 16 *February* 1990; *accepted* 30 *August* 1990)

Abstract—Zinc and cadmium pyridine-2-thionato complexes, $M(pyt)_2$, were prepared by direct electrochemical oxidation of the metal into a solution of pyridine-2-thione (pytH) in acetonitrile. Adducts of type $[M(pyt)_2L]$ (L = 2,2′-bipyridine or 1,10-phenanthroline) were obtained by addition of the ligand to the electrolyte phase. X-ray structure determination of $[Zn(pyt)_2phen]$ shows the molecule to have a distorted octahedral *trans*-ZnS_2N_4 core, with average bond distances of 2.182 Å for Zn—N(phen), 2.061 Å for Zn—N(pyt) and 2.586 Å for Zn—S. The vibrational, ^1H and ^{13}C NMR spectra of the compounds are discussed.

The coordination chemistry of heterocyclic thione donors is an area of great interest, especially due to their wide ranging applications.[1] Particular attention has been focussed on metal-containing compounds of pyridine-2-thione (pytH) because of their useful biological activity (see for example,[1] the use of zinc and platinum pyridine-2-thione complexes as antibacterial and anti-tumour agents, respectively) and also due to their important biological role; pytH can be considered as a model of a thiolated nucleoside such as 6-thioguanosine.[2] Moreover, the importance of zinc–sulphur compounds in biochemical processes has been known for the last few years, since they are present, from cysteine, in a number of DNA and RNA binding proteins.[3] Consequently, there is much current interest in preparing complexes of ligands bearing sulphur atoms to act as models for zinc–cysteine centres in metalloproteins.[4–6] Among sulphur ligands, pyridine-2-thione is one of the most versatile and unique, since it can behave in two ways: (i) as a neutral ligand (pytH) through the sulphur atom (**1**),[7–9] (ii) as an anionic ligand (pyt), acting in this case as a monodentate (**2**)[9,10] bidentate (**3**)[9–11] or bridging (**4**,[8,12] **5**)[13] ligand.

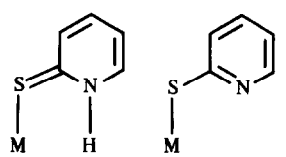

(1) (2)

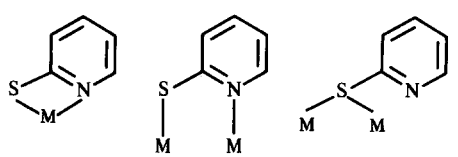

(3) (4) (5)

This paper reports the electrochemical synthesis and properties of some thionato complexes of zinc and cadmium. Although the compound $[Zn(pyt)_2]$ has been prepared before by another method, and has been attributed a dimeric structure on the basis of mass spectral data and osmometric molecular weight determination,[14] the other compounds reported in this article have not, as far as we know,

* Author to whom correspondence should be addressed.

been synthesized before. The X-ray structure of 1,10 - phenanthroline - bis(pyridine - 2 - thionate) zinc(II) is also described. This compound, to our knowledge, represents the first example of an octahedral complex of zinc(II) with thiolate ligands, which contrasts with the tetrahedral geometry commonly observed in other zinc thiolate complexes.[15-18]

EXPERIMENTAL

Acetonitrile, pyridine-2-thione (pytH), 1,10-phenanthroline (phen) and 2,2'-bipyridine (bipy) were all commercial products and were used without further purification. Zinc and cadmium (Ega Chemie) were used as plates (*ca* 2 × 2 cm).

Preparation of complexes

The electrochemical procedure followed was similar to that described in an earlier paper.[19] A solution of pytH in acetonitrile together with a few milligrams of tetramethylammonium perchlorate, added as a supporting electrolyte, were placed into the electrochemical cell containing a platinum wire cathode and an anode derived from zinc or cadmium foil, suspended from a platinum wire. During electrolysis hydrogen was evolved at the cathode and a precipitate of the complex, $M(pyt)_2$, appeared within a few hours. The introduction of phen or bipy into the cell led to the isolation of the corresponding adducts $[M(pyt)_2L]$ (L = phen or bipy).

The cells used can be summarized as:

$$Pt(-)/CH_3CN + pytH/M(+)$$

$$Pt(-)/CH_3CN + pytH + L/M(+)$$

L = phen or bipy.

At the end of electrolysis the products to be isolated were collected, washed with acetonitrile and dried *in vacuo*. The solution composition and electrochemical conditions are given in Table 1.

Physical measurements

The C, N and H contents of the complexes were determined on a Perkin–Elmer 240B microanalyser. The analytical data are given in Table 2. IR spectra were recorded as KBr mulls on a Perkin–Elmer 180 spectrophotometer. ^1H and ^{13}C NMR were recorded on a Bruker WM 250 MHz using $CDCl_3$ or DMSO-d_6 as solvent. The chemical shifts were determined against TMS as an internal standard.

Crystal structure determination

Crystal data for $[Zn(pyt)_2(phen)]$: $C_{22}H_{16}N_4S_2Zn$, $M = 465.90$, monoclinic, space group $P2_1/c$, $a = 15.116(2)$, $b = 9.918(2)$, $c = 14.181(3)$ Å, $\beta = 108.20(3)°$, $U = 2019.7$ Å^3, $Z = 4$, $D_c = 1.532$ g cm^{-3}, $F(000) = 952$, $\lambda(Mo\text{-}K_\alpha) = 0.71073$ Å, $\mu = 14.585$ cm^{-1}.

A prismatic crystal (dimensions 0.80 × 0.12 × 0.20 mm) was used for the data collection on a CAD4 automated four-circle diffractometer at room temperature, by the ω–θ scan technique with graphite-monochromated Mo-K_α radiation. 3912 intensities registered to θ_{max} 25, 3536 unique (R_{int} 0.030) of which 1176 with $I > 3\sigma(I)$ were used in refinement. They were corrected for Lorentz–polarization factors; an empirical absorption correction[20] was applied (minimum and maximum values 0.599–1.095). The structure was solved by direct methods. Positional and anisotropic thermal parameters for Zn, S and N atoms and isotropic thermal parameters for remaining non-hydrogen atoms were refined by full-matrix least-squares. Hydrogen atoms were not located. Weighting scheme $W^{-1} = \sigma^2(F)$. The agreement factor converged to $R = \Sigma(|F_o| - |F_c|)/\Sigma|F_o| = 0.065$,

Table 1. Experimental conditions for the electrochemical synthesis

Compound	Amount of pytH (g)[a]	Amount of ligand (g)	Initial voltage (V)[b]	Time (h)	Metal dissolved (mg)	E_f (mol F^{-1})
$Zn(pyt)_2$	0.300	—	25	2	50.7	0.52
$[Zn(pyt)_2bipy]$	0.165	0.300	20	2	45.0	0.46
$[Zn(pyt)_2phen]$	0.400	0.300	25	2	52.0	0.53
$Cd(pyt)_2$	0.150	—	20	1.5	65.0	0.52
$[Cd(pyt)_2phen]$	0.400	0.300	15	2	83.0	0.49

[a] Plus $[NEt_4]ClO_4$ (*ca* 10 mg).
[b] Voltage to produce a current of 20 mA.

Table 2. Analytical data for the complexes

Compound	Found (calc.) (%)		
	C	N	H
$Zn(pyt)_2$	42.4(42.1)	9.2(9.8)	3.0(2.8)
$[Zn(pyt)_2bipy]$	54.3(54.4)	12.7(12.7)	3.5(3.6)
$[Zn(pyt)_2phen]$	56.5(56.7)	12.2(12.0)	3.6(3.4)
$Cd(pyt)_2$	36.5(36.1)	8.1(8.4)	2.4(2.4)
$[Cd(pyt)_2phen]$	51.0(51.5)	10.8(10.9)	3.2(3.1)

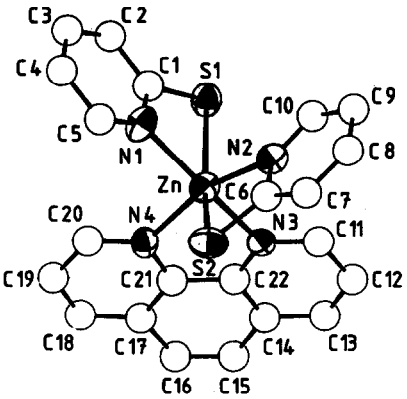

Fig. 1. The molecular structure of $[Zn(pyt)_2phen]$.

$R' = [\Sigma w(|F_o| - |F_c|)^2 / \Sigma w|F_o|^2]^{1/2} = 0.070$, 153 parameters; S 3.408; maximum Δ/σ 0.001; maximum $\Delta\rho$ 0.488 eA^{-3}. Neutral scattering factors were used.[21] Computations were performed on a DEC MicroVAXII computer using SHELXS[22] and SPD/VAX.[23] The atomic positions, full lists of bond lengths and angles and other crystallographic data have been deposited as Supplementary Material.

RESULTS AND DISCUSSION

The electrochemical oxidation of zinc or cadmium in non-aqueous solutions of pyridine-2-thione is an efficient and simple route to the appropriate $M(pyt)_2$ compounds, and a slight modification, such as the introduction of the neutral bidentate donors 2,2'-bipyridine or 1,10-phenanthroline into the electrochemical cell, serves to provide $[M(pyt)_2L]$ adducts.

The electrochemical efficiency, defined as the amount of metal dissolved per Faraday of charge, is close to 0.5 mol F^{-1} for the synthesis of both $M(pyt)_2$ and $[M(pyt)_2L]$ compounds, showing clearly that adduct formation takes place via a process occurring after the anodic formation of $M(pyt)_2$. This E_F value, together with the evolution of hydrogen gas at the cathode, is compatible with the following reaction scheme:

$$\text{Cathode} \quad 2pytH + 2e^- \longrightarrow H_2(g) + 2pyt^-$$

$$\text{Anode} \quad 2pyt^- + M \longrightarrow [M(pyt)_2] + 2e^-$$

$$2pyt^- + M + L \longrightarrow [M(pyt)_2L] + 2e^-$$

M = Zn or Cd; L = phen or bipy.

The compounds obtained were characterized by IR and ^1H and ^{13}C NMR spectroscopy, and in the case of 1,10-phenanthroline-bis(pyridine-2-thionato)zinc(II) by X-ray diffraction.

Structure of $[Zn(pyt)_2phen]$. The molecular structure of $[Zn(pyt)_2phen]$ (Fig. 1) is based on ZnN_4S_2 octahedral geometry, necessarily distorted as the result of the bidentate character of the ligands. The coordination at zinc involves one bidentate 1,10-phenanthroline molecule and two bidentate pyridine-2-thionato ligands. The arrangement of the pyridine-2-thionato ligands is such that the sulphur atoms are *trans* to each other. The basal plane is formed by the 1,10-phenanthroline nitrogen atoms and two nitrogen atoms from the pyridine-2-thiolato ligands and the inner coordination sphere is completed by two sulphur atoms at greater distances from the zinc atom. The four "in plane" atoms N(1), N(2), N(3) and N(4) are not coplanar; N(2) and N(4), which are *trans* to each other, lie −0.2541 and −0.3153 Å, respectively, below the least-squares plane through the four atoms, while N(1) and N(3) are +0.2553 and +0.3141 Å, respectively, above this plane; the zinc atom lies nearly in the plane, sitting 0.06 Å above it. This non-planarity gives rise to N(1)—Zn—N(3) and N(2)—Zn—N(4) angles of 156.2(2) and 162.9(2)°, respectively, instead of the anticipated 180°.

Further distortion is caused by the small bite of the 1,10-phenanthroline and the pyridine-2-thionato ligands, whose N(3)—Zn—N(4) and S—Zn—N chelate angles are *ca* 76 and 66°, respectively. The S(1)—Zn—S(2) angle is also distorted from 180 to 160.32(9)°. These values are hardly different from those reported for other bidentate 1,10-phenanthroline[24,25] or pyridine-2-thionato[9,26,27] metal complexes.

The phenanthroline ligand is essentially planar, with no atom deviating from the least-squares plane by more than 0.02 Å. The bond lengths and angles within the ligand are similar to those found in other phenanthroline complexes.[25,28] The pyridine portion of the pyridine-2-thionate ligands is also planar, while the associated sulphur atoms are above the plane [0.106 Å for S(1) and 0.129 Å for S(2)] of the pyridine ring to which they are bound. The average N—C (1.338 Å), S—C (1.716 Å) and

C—C (1.41 Å) bond distances in the pyridine-2-thionato ligand are close to those observed in other bidentate pyridine-2-thionato metal complexes, in which this ligand is bound in its thionate form.[9,26,27]

As can be seen in Table 3, the Zn—N(phen) bond distances (average value 2.182 Å) do not differ significantly from those found for the octahedral $[Zn(O_2C_6H_4)(phen)_2]$ (2.189 Å),[24] but they are slightly greater than those in the tetrahedral $[phenZnCl_2]$ [2.072(7), 2.050(7) Å],[29] corresponding to the change in coordination number from four to six. The Zn—N(pyt) bond lengths (average value 2.106 Å) are considerably larger than those reported for several tetrahedral pyridine complexes of zinc(II), which have Zn—N distances in the range 2.040–2.060 Å[30] and are even slightly greater than those found in the octahedral dinitritobis (pyridine)zinc(II), 2.063, 2.068 Å and dinitritobis(2-methylpyridine)zinc(II), 2.071 Å.[31] It is clear that Zn—N bond distances in $[Zn(pyt)_2phen]$ are somewhat longer than those generally observed in analogous complexes. This is probably due to the steric strain produced by the four-membered chelate rings. The Zn—S bond lengths, 2.627(2) and 2.546(3) Å, are significantly larger than those reported for several distorted tetrahedral thiolate complexes, which have Zn—S distances in the range 2.25–2.36 Å.[6,15,32] At present, no Zn—S(thiolate) bond distance estimation in octahedral complexes is available for comparison with the Zn—S bond length in $[Zn(pyt)_2phen]$.

Vibrational spectra. The IR spectra of the complexes show no bands which are assignable to ν(N—H) (3160 cm^{-1} in the free ligand) and the shifts exhibited by the ring stretching, C—H in-plane deformation and ring breathing bands are essentially identical in all complexes, suggesting that the cordination of the pyt ligand must be similar in these compounds. In addition, the mixed complexes show IR absorptions typical of coordinated 1,10-phenanthroline and 2,2′-bipyridine.[33]

NMR spectra. The ^1H NMR spectra show that

Table 3. Selected bond distances and angles

Bond lengths (Å)			
Zn—S(1)	2.627(2)	N(3)—C(11)	1.33(2)
Zn—S(2)	2.546(3)	N(3)—C(22)	1.350(9)
Zn—N(1)	2.085(6)	N(4)—C(20)	1.31(2)
Zn—N(2)	2.128(7)	N(4)—C(21)	1.359(9)
Zn—N(3)	2.162(6)	C(1)—C(2)	1.45(2)
Zn—N(4)	2.202(7)	C(2)—C(3)	1.41(1)
S(1)—C(1)	1.714(7)	C(3)—C(4)	1.39(1)
S(2)—C(6)	1.719(9)	C(4)—C(5)	1.42(1)
N(1)—C(1)	1.336(9)	C(6)—C(7)	1.43(1)
N(1)—C(5)	1.34(1)	C(7)—C(8)	1.37(1)
N(2)—C(6)	1.328(9)	C(8)—C(9)	1.43(1)
N(2)—C(10)	1.34(1)	C(9)—C(10)	1.41(1)
Bond angles (°)			
S(1)—Zn—S(2)	160.22(9)	C(11)—N(3)—C(22)	119.5(7)
S(1)—Zn—N(1)	65.1(2)	C(20)—N(4)—C(21)	119.3(8)
S(1)—Zn—N(2)	98.5(2)	S(1)—C(1)—N(1)	114.8(6)
S(1)—Zn—N(3)	95.3(2)	S(1)—C(1)—C(2)	125.4(6)
S(1)—Zn—N(4)	96.2(2)	N(1)—C(1)—C(2)	119.7(8)
S(2)—Zn—N(1)	103.8(2)	C(1)—C(2)—C(3)	117.1(8)
S(2)—Zn—N(2)	66.6(2)	C(2)—C(3)—C(4)	121(1)
S(2)—Zn—N(3)	98.6(2)	C(3)—C(4)—C(5)	119(1)
S(2)—Zn—N(4)	100.9(2)	N(1)—C(5)—C(4)	119.4(8)
N(1)—Zn—N(2)	101.5(3)	S(2)—C(6)—N(2)	115.9(7)
N(1)—Zn—N(3)	156.6(2)	S(2)—C(6)—C(7)	124.7(7)
N(1)—Zn—N(4)	92.7(3)	N(2)—C(6)—C(7)	119.4(9)
N(2)—Zn—N(3)	94.0(2)	C(6)—C(7)—C(8)	118.6(8)
N(2)—Zn—N(4)	162.9(2)	C(7)—C(8)—C(9)	121.7(9)
N(3)—Zn—N(4)	75.8(2)	C(8)—C(9)—C(10)	115.6(9)
C(1)—N(1)—C(5)	123.6(7)	N(2)—C(10)—C(9)	121.7(8)
C(6)—N(2)—C(10)	123.0(7)		

Table 4. NMR (^{1}H and ^{13}C) data for complexes

Compound	^{1}H		^{13}C	
	pyt$^-$	Ligand	pyt$^-$	Ligand
$Zn(pyt)_2$	7.63d H(6) 6.75t H(5) 7.42m H(4) 7.28d H(3)		175.7 C(2) 131.4 C(3) 139.0 C(4) 119.2 C(5) 148.1 C(6)	
$[Zn(pyt)_2bipy]$	7.83d H(6) 6.80t H(5) 7.38m H(4) 7.20d H(3)	8.73 H(3,3′) 8.48 H(4,4′) 8.06 H(5,5′) 7.66 H(6,6′)		
$[Zn(pyt)_2phen]$	7.66d H(6) 6.74t H(5) 7.33m H(4) 7.17d H(3)	9.13 H(2,9) 8.83 H(4,7) 8.22 H(5,6) 8.03 H(3,8)	173.8 C(2) 128.4 C(3) 136.5 C(4) 115.4 C(5) 146.0 C(6)	149.1 C(2) 140.0 C(10b,4) 127.2 C(4a) 125.8 C(5) 125.0 C(3)
$Cd(pyt)_2$	7.82d H(6) 6.81t H(5) 7.38m H(4) 7.24d H(3)		124.7 C(3) 136.5 C(4) 116.0 C(5) 146.8 C(6)	
$[Cd(pyt)_2phen]$	7.83d H(6) 6.77t H(5) 7.33m H(4) 7.22d H(3)	9.21 H(2,9) 8.79 H(4,7) 8.14 H(5,6) 8.07 H(3,8)	172.9 C(2) 128.8 C(3) 136.4 C(4) 115.9 C(5) 146.7 C(6)	149.8 C(2) 140.7 C(10b) 139.1 C(4) 127.1 C(4a) 125.2 C(5) 124.8 C(3)

the NH broad singlet of the free pyridine-2-thione at about 13.43 ppm is absent in the metal complexes, indicating that deprotonation of this group has occurred and, therefore, that this ligand is coordinated in the thionato form. Moreover, the complexes exhibit four distinct and widely separated signals of equal intensity, assignable to the four non-equivalent hydrogens of pyt$^-$ ligands. The lowest field signals attributable to H(6) appear as doublets, which is consistent with the chelating character of pyt$^-$ ligands.[9]

In the case of the mixed complexes, $[M(pyt)_2phen]$, the signals attributable to 2,9- and 3,8-protons undergo a small down-field shift with respect to the free ligand. This shift has been taken as proof of coordination of 1,10-phenanthroline,[34,35] in agreement with the X-ray diffraction structure for the corresponding zinc complex (*vide supra*). In the case of $[Zn(pyt)_2bipy]$, the coordination of 2,2′-bipyridine is inferred by the down-field shift of the signal attributed to the 3,3′- and the up-field shift of the signal of the 6,6′-protons.[36] This behaviour can be taken as proof that the coordination number of the zinc and cadmium atoms in these mixed complexes is six.

The ^{13}C NMR spectra of free ligand (pytH), phen and those complexes which are sufficiently soluble are shown in Table 4. Significant changes occur in the position of the signals of carbons of the pytH ligand[37] whereas smaller shifts are observed in the spectrum of 1,10-phen upon coordination. The most important feature of the spectrum is the C(2) signal, which is shifted towards high field with respect to the free ligand (pytH). This behaviour has been interpreted in terms of a reduction of the C=S bond order,[38] which is consistent with the ligand (pyt$^-$) having a higher contribution of the thionato form (*vide supra*) in the complex than in the free pyridine-2-thione.

REFERENCES

1. E. S. Raper, *Coord. Chem. Rev.* 1985, **61**, 115 and refs cited therein.
2. I. P. Evans and G. Wilkinson, *J. Chem. Soc., Dalton Trans.* 1974, 946.

3. D. T. Corwin Jr, E. S. Gruff and S. A. Koch, *Inorg. Chim. Acta* 1988, **5**, 151 and refs cited therein.
4. D. T. Corwin Jr, E. S. Gruff and S. A. Koch, *J. Chem. Soc., Chem. Commun.* 1987, 966.
5. D. T. Corwin Jr, R. Fikar and S. A. Koch, *Inorg. Chem.* 1987, **26**, 3079.
6. D. T. Corwin Jr and S. A. Koch, *Inorg. Chem.* 1988, **27**, 493 and refs cited therein.
7. B. P. Kennedy and A. B. P. Lever, *Can. J. Chem.* 1972, **50**, 3488; S. C. Kokkou, S. Fortier, P. J. Rentzeperis and P. Karagiannidis, *Acta Cryst.* 1983, **C39**, 178.
8. A. J. Deeming, M. N. Meah, H. M. Dawes and M. B. Hursthouse, *J. Organomet. Chem.* 1986, **25C**, 299.
9. A. J. Deeming, K. I. Hardcastle, M. N. Meah, P. A. Bates, H. M. Dawes and M. B. Hursthouse, *J. Chem. Soc., Dalton Trans.* 1988, 227.
10. P. Mura, B. G. Olby and S. D. Robinson, *J. Chem. Soc., Dalton Trans.* 1985, 2101; *Inorg. Chim. Acta* 1985, **98**, L21.
11. S. R. Fletcher and A. C. Skapski, *J. Chem. Soc., Dalton Trans.* 1972, 635; M. Masaki, S. Matsunami and H. Ueda, *Bull. Chem. Soc. Japan* 1978, **51**, 3298.
12. J. D. Gilbert and G. Wilkinson, *J. Chem. Soc. A.* 1969, 1749; N. Lenhart and H. Singer, *Z. Naturf.* 1975, **30B**, 284; I. Kinoshita, Y. Yasuba, K. Matsumoto and S. Ooi, *Inorg. Chim. Acta* 1983, **80**, L13.
13. D. Mentzafos, A. Terzis, P. Karagiannidis and P. Aslanidis, *Acta Cryst.* 1989, **C45**, 54.
14. M. Masaki and S. Matsunami, *Bull. Chem. Soc. Japan* 1976, **49**, 3274.
15. D. Swenson, N. C. Baenziger and D. Coucouvanis, *J. Am. Chem. Soc.* 1978, **100**, 1933.
16. I. G. Dance, *J. Am. Chem. Soc.* 1980, **102**, 3445.
17. I. G. Dance, *Polyhedron* 1986, **5**, 1037; P. J. Blower and J. R. Dilworth, *Coord. Chem. Rev.* 1987, **76**, 121.
18. T. L. Cremers, D. R. Bloomquist, R. D. Willet and G. A. Crosby, *Acta Cryst.* 1980, **B36**, 3097.
19. J. J. Habeeb, D. G. Tuck and F. H. Walters, *J. Coord. Chem.* 1978, **8**, 27.
20. N. Walker and D. Stuart, *Acta Cryst.* 1983, **A39**, 158.
21. *International Tables for X-Ray Crystallography*, Vol. IV, Table 2.2A. Kynoch Press, Birmingham (1974).
22. G. M. Sheldrick, SHELXS-86, Program for the solution of crystal structures from diffraction data. University of Göttingen, F.R.G.
23. B. A. Frenz, The Enraf–Nonius CAD4 SDP, a real-time system for concurrent X-ray data collection and crystal structure determination, in *Computing in Crystallography*, pp. 64–71 (1978). Delft University Press, Delft. Version 3.0. SDP/VAX (1986).
24. L. Bustos, J. H. Green, J. L. Hencher, M. A. Khan and D. G Tuck, *Can. J. Chem.* 1983, **61**, 2141.
25. H. E. Mabrouk, D. G. Tuck and M. A. Khan, *Inorg. Chim. Acta* 1987, **129**, 75.
26. S. G. Rosenfield, H. B. Berends, L. Gelmini, D. W. Stephan and P. K. Mascharak, *Inorg. Chem.* 1987, **26**, 2792 and refs cited therein.
27. S. G. Rosenfield, S. A. Swedberg, S. K. Arora and P. K. Mascharak, *Inorg. Chem.* 1986, **25**, 2109.
28. V. H. Hennig, J. Sieler, R. Benedix, J. Kaiser, L. Sjölin and O. Lindquist, *Z. Anorg. Allg. Chem.* 1980, **464**, 151; R. K. Chadha, R. Kumar, J. Romero and D. G. Tuck, *Can. J. Chem.* 1988, **66**, 2151.
29. M. A. Khan and D. G. Tuck, *Acta Cryst.* 1984, **C40**, 60.
30. H. Lynton and M. C. Sears, *Can. J. Chem.* 1971, **49**, 3418; W. L. Steffen and G. J. Palenik, *Acta Cryst.* 1976, **B32**, 298; W. L. Steffen and G. J. Palenik, *Inorg. Chem.* 1977, **16**, 1119.
31. M. A. Hitchman, R. Thomas, B. W. Skelton and A. H. White, *J. Chem. Soc., Dalton Trans.* 1983, 2273.
32. N. Ueyama, T. Sugawara, K. Sasaki, A. Nakamura, S. Yamashita, Y. Watatsuki, H. Yamazaki and N. Yasuoka, *Inorg. Chem.* 1988, **27**, 741.
33. A. A. Schilt and R. C. Taylor, *J. Inorg. Nucl. Chem.* 1959, **9**, 211; R. G. Inskeep, *J. Inorg. Nucl. Chem.* 1982, **24**, 763.
34. S. Yamazaki, *Polyhedron* 1985, **4**, 1915.
35. T. A. Annan, R. K. Chadha, D. G. Tuck and K. D. Watson, *Can. J. Chem.* 1987, **65**, 2670.
36. S. Castellano, H. Gunther and S. Ebersole, *J. Phys. Chem.* 1965, **69**, 4166; H. E. Mabrouk and D. G. Tuck, *J. Chem. Soc., Dalton Trans.* 1988, 2539.
37. A. Schanck, J. M. Dereppe and A. Van Meerssche, *Bull. Soc. Chim. Belg.* 1983, **92**, 199.
38. J.-M. Bret, P. Castan, G. Commenges and J.-P. Laurent, *Polyhedron* 1983, **2**, 901.

Polyhedron Vol. 10, No. 2, pp. 203–213, 1991
Printed in Great Britain

0277–5387/91 $3.00+.00
Pergamon Press plc

ELECTRONIC PROPERTIES OF MONOCAPPED PRISMANE AND BASKET IRON–SULPHUR CLUSTERS

B. S. SNYDER, M. S. REYNOLDS and R. H. HOLM*

Department of Chemistry, Harvard University, Cambridge, MA 02138, U.S.A.

and

G. C. PAPAEFTHYMIOU and R. B. FRANKEL†

Francis Bitter National Magnet Laboratory, Massachusetts Institute of Technology, Cambridge, MA 02139, U.S.A.

(*Received* 23 *June* 1990; *accepted* 11 *September* 1990)

Abstract—The ground state electronic properties of the mixed-valence clusters $Fe_7S_6(PEt_3)_4Cl_3$ (**1**), $Fe_6S_6(PEt_3)_4L_2$ [L = Cl^- (**2**), Br^- (**4**), I^- (**5**) and PhS^- (**6**)], $Fe_6Se_6(PEt_3)_4Cl_2$ (**3**) and $[Fe_6S_6(PEt)_6]^{1-}$ (**9**), have been investigated by magnetic susceptibility, magnetization and Mössbauer spectroscopic measurements. Cluster **1** has a (idealized C_{3v}) monocapped prismane structure and clusters **2–6** and **9** adopt the C_{2v} "basket" configuration based on the $[Fe_6(\mu_2\text{-}S)(\mu_3\text{-}S)_4(\mu_4\text{-}S)]^{2+,1+}$ core unit. From magnetic properties, the ground states $S = 1/2$ (**1**, **9**) and $S = 1$ (**2–5**) were established. Unlike the other clusters, **6** did not show a Curie region of susceptibility; its ground state was not directly determined but is probably $S = 1$. Mössbauer spectra were successfully analysed in terms of a 1 : 1 : 1 iron site population. Isomer shifts and quadrupole splittings were assigned to each site. Magnetically perturbed spectra obtained in applied fields of 60–80 kOe were analysed to give the magnetic hyperfine parameters and magnetic hyperfine fields in clusters **1–5** and **9**. The magnetic spectra demonstrate antiferromagnetic spin coupling which affords the indicated ground states.

Nearly all iron–sulphur clusters are characterized by core structures that are built up entirely by vertex-sharing and/or edge fusion of Fe_2S_2 rhombs.[1,2] The prototype single planar rhomb is found in the binuclear species $[Fe_2S_2L_4]^{2-}$. Clusters proceed in complexity from this type to those with nuclearities 3, 4, 6, 7, 8 and 18.[2,3] Excluding organometallics and with the exception of $[Fe_6S_8(PEt_3)_6]^{2+,1+}$ [4,5] in the preceding set, these clusters have as terminal ligands, halide, RS^- or RO^-. The electronic properties of many of these materials have been probed by application of Mössbauer spectroscopy and by magnetization and magnetic susceptibility measurements. For example, the ground spin states and associated matters of the electronic structures of cubane-type $[Fe_4S_4(SR)_4]^{3-,2-,1-}$ clusters have been eluciated in some detail by these methods.[6–8] All of these clusters have the common property of molecular antiferromagnetism.

As part of our work on higher-nuclearity Fe—S clusters, we have recently prepared and described the structures and certain reactivity aspects of a new series of hexa- and heptanuclear clusters.[3,9–12] These differ from the above in having a mixed ligand set that includes tertiary phosphines and core structures not yet found in the absence of phosphine. With reference to Fig. 1, the core geometry of $Fe_7S_6(PEt_3)_4Cl_3$[9] (**1**) approaches that of a monocapped hexagonal prism, while that of $Fe_6S_6(PR_3)_4L_2$, L = halide[10,11] (**2–5**, **7**) and thiolate[3] (**6**, **8**), and $[Fe_6S_6(PEt_3)_6]^{1+}$ [12] (**9**) resembles a basket, with the lower Fe—S—Fe fragment, which

* Author to whom correspondence should be addressed.
† Present address: Department of Physics, California Polytechnic State University, San Luis Obispo, CA 94307, U.S.A.

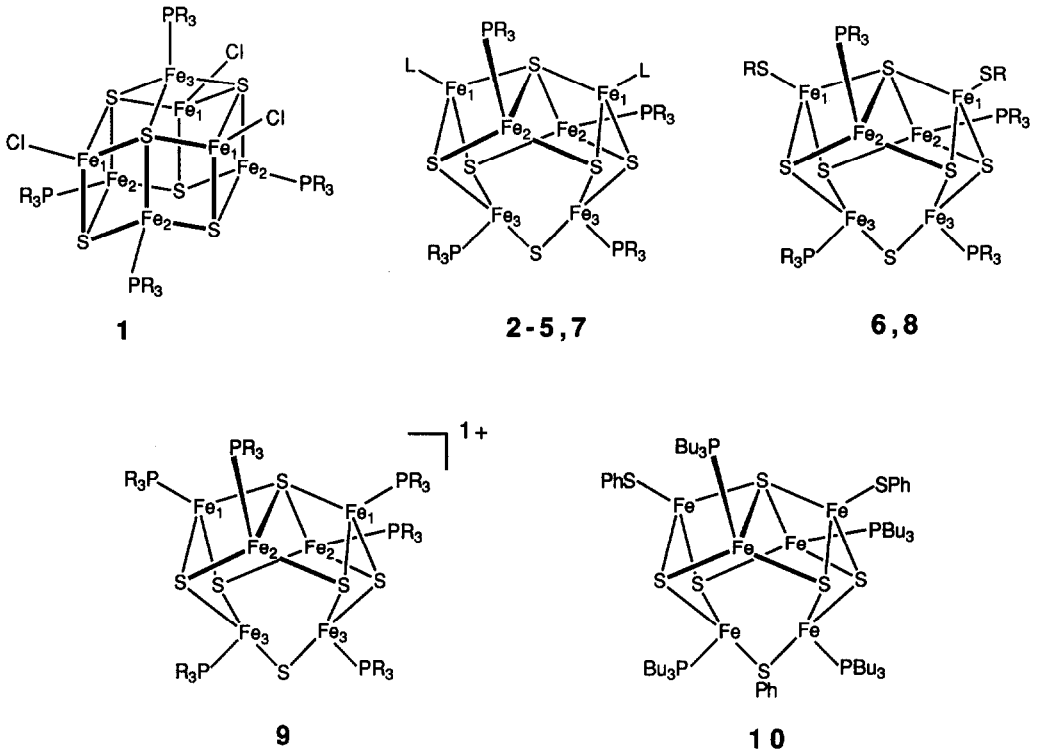

Fig. 1. Schematic structures of clusters **1–10** illustrating the monocapped prismane (**1**) and basket (**2–10**) topologies. Iron atoms are labelled so as to correspond to the site assignments in Table 2.

is not part of the aforementioned rhomb, serving as the handle. We designate these as "basket" clusters, as a means of distinguishing their $[Fe_6S_6]$ core topology from the idealized hexagonal prisms present in the "prismane" clusters, $[Fe_6S_6L_6]^{2-,3-}$.[13–16] The structures of $Fe_6S_6(PBu_3)_4Cl_2$,[11] $Fe_6S_6(PEt_3)_4(S\text{-}p\text{-}C_6H_4Br)_2$[3] and $[Fe_6S_6(PEt)_6]^{1+}$[12] define the basket topology, which is manifested in virtually isometric $[Fe(\mu_2\text{-}S)(\mu_3\text{-}S)_4(\mu_4\text{-}S)]^{2+,1+}$ core units. This unique topology is supported, in part, by the unusual coordination at the FeS_3P sites. Whereas FeS_3L sites in these and numerous other clusters have a distorted tetrahedral configuration, the phosphine-ligated sites exhibit a roughly trigonal pyramidal geometry, with the Fe atom closely approaching the S_3 plane. These species are also among the most reduced Fe—S clusters, with Fe mean oxidation states of +2.14 in $Fe_7S_6(PEt_3)_4Cl_3$, +2.17 in $[Fe_6S_6(PEt_3)_6]^{1+}$ and +2.33 in $Fe_6S_6(PEt_3)_4L_2$. As a result of their high nuclearities, unusual ligand sets and previously unencountered core structures, these molecules are of current interest as the newest additions to the extensive family of Fe—S clusters, which now encompasses seven nuclearities and 10 core structural types.[1–3] Most of these clusters exist in two or more oxidation levels, some of which have been isolated.

Their unique core structure suggests that the basket clusters may have unusual electronic features. Ground state properties, previously uninvestigated, have been examined by magnetic and Mössbauer techniques, and the leading results are reported here.

EXPERIMENTAL

Preparation of compounds

The compounds $Fe_7S_6(PEt_3)_4Cl_3$ (**1**),[9] $Fe_6S_6(PEt_3)_4Cl_2$ (**2**),[11] $Fe_6Se_6(PEt_3)_4Cl_2$ (**3**),[11] $Fe_6S_6(PEt_3)_4Br_2$ (**4**),[11] $Fe_6S_6(PEt_3)_4I_2$ (**5**),[11] $Fe_6S_6(PEt_3)_4(SPh)_2$ (**6**),[3] $Fe_6S_6(PEt_3)_4(S\text{-}p\text{-}C_6H_4Br)_2$ (**8**)[3] and $[Fe_6S_6(PEt_3)_6](BF_4)$ (**9**)[12] were prepared as previously described.

Physical measurements

All measurements were performed under strict anaerobic conditions. Magnetic susceptibility and magnetization measurements at applied fields of 10 kOe and up to 50 kOe, respectively, were carried out on a SHE 905 SQUID magnetometer operating between 1.8 and 300 K. Solid state measurements were made on finely ground polycrystalline samples (15–35 mg) loaded into precalibrated containers and

sealed with epoxy resin under a dinitrogen–helium atmosphere. Diamagnetic susceptibility corrections[17] were applied. Mössbauer spectra were determined with a constant-acceleration spectrometer equipped with a ^{57}Co source in a Rh matrix. Zero-field measurements were made between 4.2 and 300 K, with the spectrometer operating in the time mode and the source maintained at room temperature. Magnetically perturbed spectra were obtained in longitudinally applied fields up to 80 kOe, with the source and absorber at 4.2 K. Polycrystalline samples were dispersed in boron nitride powder and sealed with epoxy resin in plastic sample holders. Isomer shifts are reported relative to Fe metal at 4.2 K. EPR spectra were recorded at X-band frequencies at *ca* 19 K on a Varian E-109 spectrometer. Solution susceptibilities were determined by a NMR method.[18] Solvent susceptibilities were taken from the literature[19] and corrections for solution density changes with temperature were applied.

RESULTS AND DISCUSSION

The following clusters, **1–9**, are of primary interest in this investigation. The monocapped prismane structure of **1** has been crystallographically established.[9] The basket configurations are assigned to **2–6** on the basis of the crystal structures of **7** and **8**, and the correspondence of spectroscopic properties to those of the structurally defined clusters. All clusters are mixed-valence but individual Fe^{II} or Fe^{III} sites, if present, cannot be recognized unambiguously from crystallographic data. As will be seen, ^1H NMR spectra are consistent with retention of the basket structure of halide clusters in solution. $Fe_7S_6(PEt_3)_4Cl_3$ (**1**); $Fe_6S_6(PEt_3)_4Cl_2$ (**2**); $Fe_6Se_6(PEt_3)_4Cl_2$ (**3**); $Fe_6S_6(PEt_3)_4Br_2$ (**4**); $Fe_6S_6(PEt_3)_4I_2$ (**5**); $Fe_6S_6(PEt_3)_4(SPh)_2$ (**6**); $Fe_6S_6(PBu_3)_4Cl_2$ (**7**); $Fe_6S_6(PEt_3)_4(S\text{-}p\text{-}C_6H_4Br)_2$ (**8**); $[Fe_6S_6(PEt_3)_6]^{1+}$ (**9**).

Electronic properties

Ground spin states, other magnetic aspects and electronic distributions in clusters **1–7** have been examined using the methods of magnetic susceptibility, magnetization and ^{57}Fe Mössbauer spectroscopy. Related results for cluster **9** have been reported[12] and certain data are included here for comparison purposes. Before each measurement, the purity of a given compound was established from its distinctive, isotropically shifted ^1H NMR spectrum (*vide infra*) previously recorded on an analytical sample.[3,11,12] Magnetic and Mössbauer results are contained in Tables 1 and 2 respectively, and selected data are displayed in Figs 2–7. The numerical designation of Fe sites in Table 2 and Fig. 1 correspond. The Curie constant in the Curie–Weiss law, $\chi^M = C/(T-\theta)$, has the values $C = 0.375$, 1.000 and 1.875 emu K mol^{-1} for pure $S = 1/2$, $S = 1$ and $S = 3/2$ states, respectively, when $g_e = 2$.

Table 1. Magnetic properties of clusters **1–7**[a]

Cluster	T (K)[b]	C (emu K mol^{-1})	S	μ_{eff} (μ_B)	θ (K)	g_e	D (cm^{-1})	$\lvert E/D\rvert$
$Fe_7S_6(PEt_3)_4Cl_3$	6–45	0.581	1/2	2.16	−1.88	—	—	—
$CDCl_3$ soln	298	—		3.95[c,d]	—	—	—	—
$Fe_6S_6(PEt_3)_4Cl_2$	6–150	0.993	1	2.82	−4.49	1.89	−17.3	0.18
CD_2Cl_2 soln	190–302	—		2.74–2.81[c,e]	—	—	—	—
$Fe_6Se_6(PEt_3)_4Cl_2$	6–75	1.211	1	3.11	−1.28	2.06	−2.27	0.23
CD_2Cl_2 soln	190–302	—		3.30–3.44[c,f]	—	—	—	—
$Fe_6S_6(PEt_3)_4Br_2$	6–100	0.962	1	2.76	−8.80	1.80	−40.5	0.11
$Fe_6S_6(PEt_3)_4I_2$	6–75	1.174	1	3.07	−24.2	1.79	—	—
$Fe_6S_6(PEt_3)_4(SPh)_2$[g]	296	—	1	2.72	—	—	—	—
$[Fe_6S_6(PEt_3)_6]^{1+}$[h]	6–30	0.485	1/2	1.98	−0.85	—	—	—

[a] All data refer to the solid state unless otherwise indicated.
[b] Curie region.
[c] Calculated from the Curie law, $\mu_{eff} = 2.83(\chi^M T)^{1/2}$; moments increase monotonically with increasing temperature.
[d,e] Comparison solution/solid state moments at 300–302 K: [d]3.95/4.09; [e]2.81/3.04.
[f] $\mu_{eff} = 3.40\mu_B$ in solid state, 200 K.
[g] Toluene solution.
[h] Reference 12.

Table 2. Mössbauer spectroscopic results at 4.2 K

Cluster	Site	$\delta^{a,b}$ (mm s^{-1})	$\Delta E_Q{}^b$ (mm s^{-1})	$A_x{}^c$ (H_x)^d (mm s^{-1})	A_y (H_y) (mm s^{-1})	A_z (H_z) (mm s^{-1})	η^e
$Fe_7S_6(PEt_3)_4Cl_3$	1	0.67	0.51	0.005 (−0.37)	0.748 (−55.0)	0.649 (−47.7)	0.79
	2	0.36	0.87	−0.008 (0.59)	−0.161 (11.8)	−0.231 (17.0)	1.00
	3	0.36	0.28	−0.007 (0.52)	−0.001 (0.07)	−0.966 (73.2)	0.24
$Fe_6S_6(PEt_3)_4Cl_2$	1	0.63	0.60	−1.120 (88.7)	−0.397 (10.0)	−0.058 (7.7)	1.00
	2	0.34	0.87	0.440 (−34.9)	0.694 (−17.4)	0.939 (−125)	0.22
	3	0.32	1.10	0.448 (−35.5)	0.090 (−2.3)	0.023 (−3.1)	0.81
$Fe_6Se_6(PEt_3)_4Cl_2$	1	0.64	0.65	−1.013 (135)	−0.614 (78.3)	−0.318 (44.7)	0.00
	2	0.35	1.08	0.882 (−117)	0.567 (−72.3)	0.616 (−86.7)	0.40
	3	0.40	1.29	1.293 (−172)	0.843 (−107)	0.578 (−81.3)	1.00
$Fe_6S_6(PEt_3)_4Br_2$	1	0.61	0.56	−0.019 (0.77)	−0.017 (0.06)	−0.364 (44.3)	0.00
	2	0.33	0.79	0.426 (−17.4)	0.269 (−0.91)	0.121 (−14.7)	1.00
	3	0.29	1.04	0.450 (−18.3)	0.013 (−0.04)	0.096 (−11.7)	0.00
$Fe_6S_6(PEt_3)_4I_2$	1	0.60	0.53	−0.009 (0.21)	−0.007 (0.00)	−0.037 (3.05)	0.03
	2	0.38	0.84	0.665 (−15.4)	0.015 (0.00)	0.258 (−21.3)	0.47
	3	0.23	0.95	0.175 (−4.06)	0.008 (0.00)	0.120 (−9.90)	0.47
$Fe_6S_6(PEt_3)_4(SPh)_2$	1	0.43	0.61	—	—	—	
	2	0.39	0.86	—	—	—	
	3	0.37	1.15	—	—	—	
$[Fe_6S_6(PEt_3)_6](BF_4)$	1	0.41	0.53	0.564 (−41.5)	0.588 (−43.2)	0.459 (−33.7)	0.00
	2	0.41	0.88	0.440 (−32.3)	0.359 (−26.4)	0.418 (−30.7)	0.00
	3	0.38	1.25	0.027 (−1.98)	0.023 (−1.69)	0.018 (−1.32)	1.00
$FeCl_2(PEt_3)_2{}^f$	—	0.65	2.90	—	—	—	

[a] Relative to Fe metal at 4.2 K.
[b] Spectral fits made with line widths in the range 0.25–0.34 mm s^{-1} and $\eta = 0$.
[c] Magnetic hyperfine parameters for the 14.4 keV excited state of ^{57}Fe.
[d] Magnetic hyperfine field, kOe; negative hyperfine fields oppose applied field.
[e] Asymmetry parameters, $(V_{xx}-V_{yy})/V_{zz}$.
[f] 200 K.

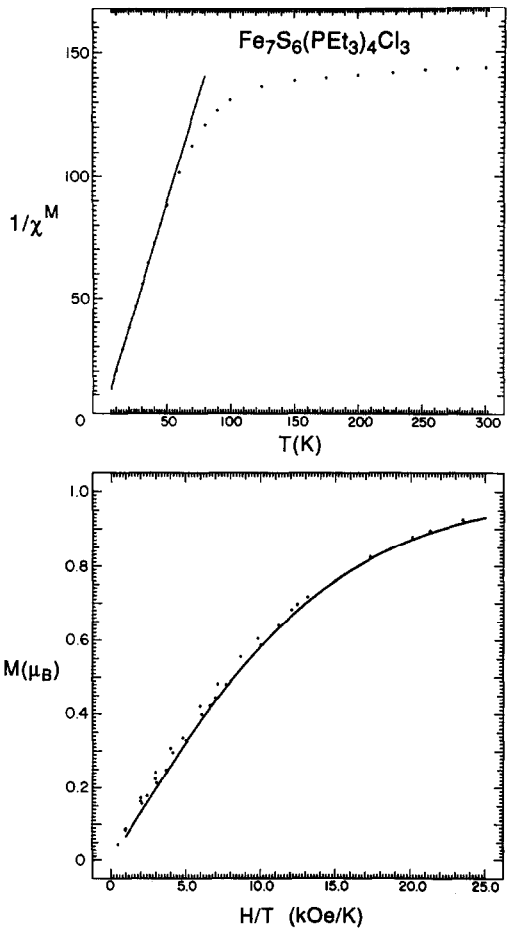

Fig. 2. Magnetic properties of cluster **1**. Upper: temperature dependence of the reciprocal molar magnetic susceptibility. Lower: magnetization at applied fields of 12.5, 25 and 50 kOe at $T = 1.8$–25 K. Solid lines are calculated Curie behaviour for $S = 1/2$ and theoretical fits to the magnetization data using the parameters in Table 1.

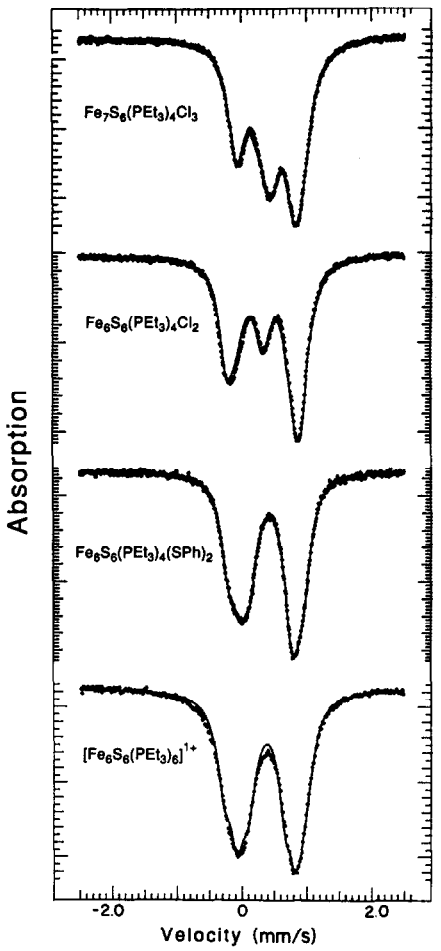

Fig. 3. Mössbauer spectra in zero applied magnetic field of clusters **1**, **2**, **6** and **9** (top to bottom). Solid lines are fits to the data using the parameters in Table 2.

(1) $Fe_7S_6(PEt_3)_4Cl_3$

(a) *Magnetism.* This odd-electron cluster formally contains $6Fe^{II} + Fe^{III}$. As shown in Fig. 2, cluster **1** obeys the Curie–Weiss law at 6–45 K, with $C = 0.581$ emu K mol^{-1}. The magnetization was found to be field-independent and to follow a $S = 1/2$ Brillouin function with saturation asymptotically approaching $g_e S\mu_B = 1\mu_B$. The EPR spectrum in frozen THF solution at 20 K (not shown) reveals a nearly isotropic signal at $g_e = 2.02$, consistent with a doublet state. Also present are weaker resonances at $g_e = 5.2$ and 5.5, which may be indicative of a small amount of the $S = 3/2$ state.[8] Physical mixtures of these spin states have been observed with Fe_4S_4 cubane-type clusters.[8] This situation could account (in part) for the positive deviation of the Curie constant from the $S = 1/2$ value and the small shift of magnetization data in the lower H/T region from the best fit for that state. The collective results support an $S = 1/2$ ground state. The negative deviation of the susceptibility from the Curie–Weiss law above 45 K indicates the population of excited levels with $S > 1/2$. At 298 K, the essentially equal solution and solid state magnetic moments of *ca* $4\mu_B$ show that the antiferromagnetic coupling (*vide infra*) is a molecular property.

(b) *Mössbauer spectra.* The monocapped prismane structure of **1** under idealized C_{3v} symmetry contains three Fe sites: Fe(1)(μ_3-S)(μ_4-S_2)$_2$Cl, Fe(2)(μ_3-S)$_2$(μ_4-S)P and Fe(3)(μ_4-S)$_3$P. The Fe(2,3) sites have approximate trigonal pyramidal geometry while the Fe(1) site is more nearly tetrahedral. The Mössbauer spectrum in zero field, shown in Fig. 3, was fit with a constrained site

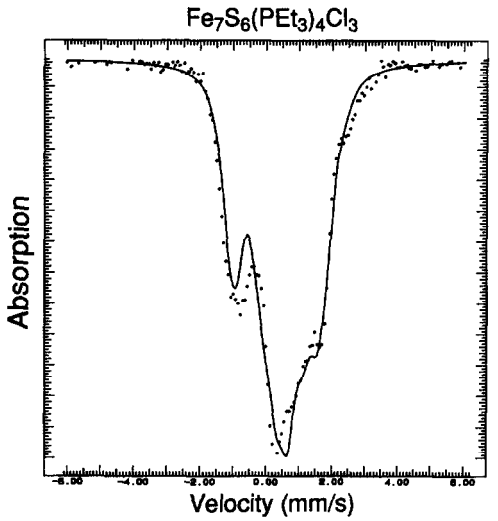

Fig. 4. Mössbauer spectrum of cluster **1** in an applied field of 60 kOe. The solid line is a theoretical fit to the data using the parameters in Table 2 with $S = 1/2$.

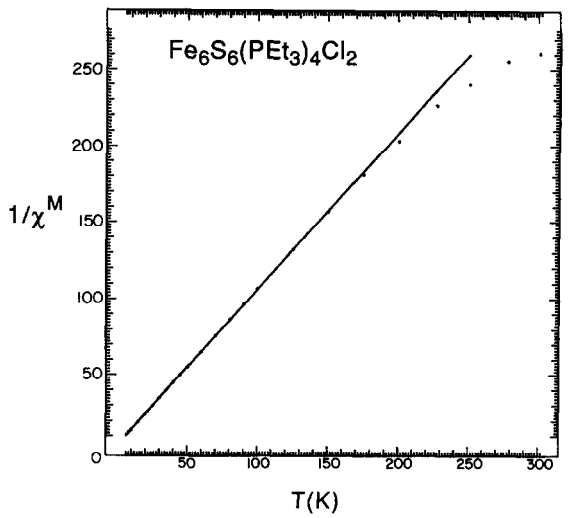

Fig. 5. Temperature dependence of the reciprocal molar susceptibility of cluster **2**. The solid line is a Curie–Weiss fit to the data using the parameters in Table 1.

population of 3:3:1. This allowed immediate identification of the Fe(3) site as that with isomer shift $\delta = 0.36$ mm s^{-1} and the (unusually) small quadrupole splitting $\Delta E_Q = 0.28$ mm s^{-1}. The Fe(2) site is common to **1** and to basket clusters **2–8**, where it also approaches trigonal pyramidal stereochemistry. On the basis of this commonality, the Fe(2) site is assigned the doublet with the same isomer shift as Fe(3), but a larger quadrupole splitting. This leaves the Fe(1) site, at which chloride is bound, as that with the largest isomer shift (0.67 mm s^{-1}). This assignment is consistent with data for the pairs $(Me_4N)_2[FeCl_4]^{20}/Fe(PEt_3)_2Cl_2$ (≈ 0.1 mm s^{-1}) and $(Me_4N)[FeCl_4]^{20}/Fe(PPh_3)Cl_3$[21] ($\approx 0.05$ mm s^{-1}), for which the indicated isomer shift differences correspond to a decrease in δ upon replacing chloride with phosphine.*

Magnetic Mössbauer spectra (not shown) exhibited movement of inner and outer features in opposite directions as the applied field was increased from 60 to 80 kOe, consistent with antiparallel spin coupling. The spectrum at 60 kOe is shown in Fig. 4, together with a theoretical fit obtained using the method described below for the basket clusters and the parameters in Table 2. In this way, the $S = 1/2$ ground state assignment was corroborated.

* Note, however, that the structure of $Fe(PPh_3)Cl_3$ has not been established.

(2) $Fe_6S_6(PEt_3)_4X_2$ (X = Cl^-, Br^-, I^-, PhS^-) *and* $Fe_6Se_6(PEt_3)_4Cl_2$

(a) *Magnetism.* This set consists of the even-electron basket clusters **2–6** which formally contain $4Fe^{II}+2Fe^{III}$. As will be evident, certain electronic aspects of these clusters are unusual and cannot be satisfactorily interpreted. Clusters **2–5** display Curie behaviour of magnetic susceptibilities over appreciable temperature intervals but in several cases with large Weiss constants (Table 1). Curie constants are fairly close to the value for a $S = 1$ state. The results for cluster **2**, which are fairly typical for compounds in this set, are shown in Fig. 5. Deviations from Curie behaviour are such as to indicate the population of higher spin states or a small TIP contribution.

Magnetization data for clusters **2–5** obtained at 1.8–100 K and at three applied fields are presented in Fig. 6. All show nested curves corresponding to different values of the applied field and indicating that the zero-field splitting parameter $D \neq 0$. The data were analysed under the simple spin Hamiltonian (1)

$$H = D[S_z^2 - S(S+1)/3] + E(S_x^2 - S_y^2) + g_e\mu_B\mathbf{H}\cdot\mathbf{S}, \quad (1)$$

with $S = 1$ by calculating the spin projection along the magnetic field direction; E is the rhombic splitting parameter and the other symbols have their usual meanings. The experimental data were simulated from the Curie to the saturation region by

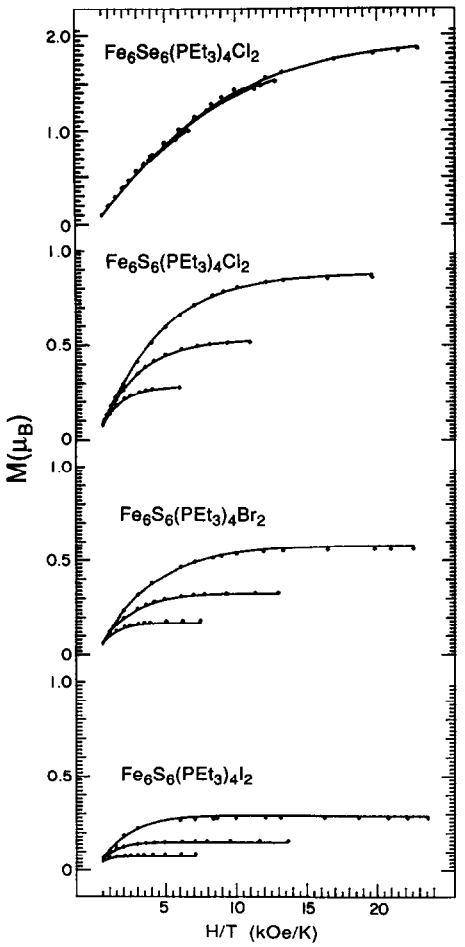

Fig. 6. Magnetization behaviour of clusters **3**, **2**, **4** and **5** (top to bottom). For each cluster, curves in ascending order refer to applied fields of 12.5, 25 and 50 kOe. The solid lines are theoretical fits to the data using the parameters in Table 1.

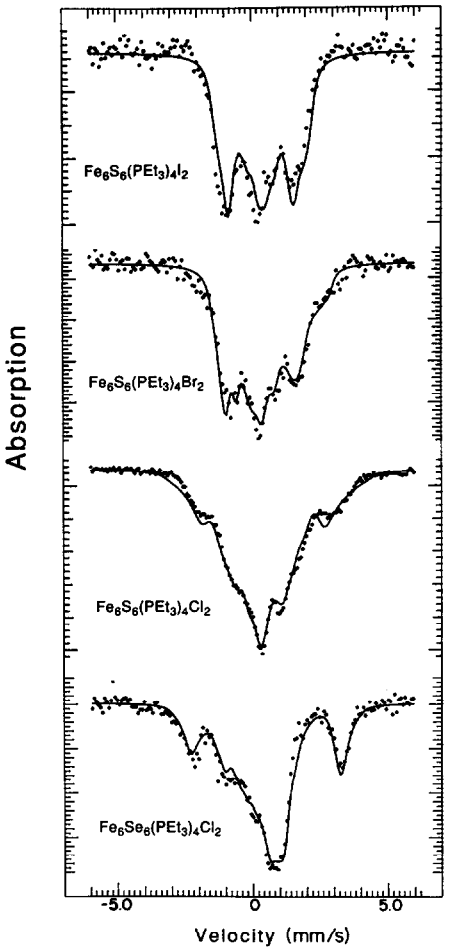

Fig. 7. Mössbauer spectra of clusters **5**, **4**, **2** and **3** (top to bottom) at 4.2 K in an applied field of 80 kOe. The solid lines are fits to the data using the parameters in Table 2 with $S = 1$.

least-squares fits, using a simplex algorithm and the parameters in Table 1. In order to obtain satisfactory fits, it was necessary to use $D < 0$ and $E/D > 0$ with inclusion of $g_e \neq 2$. The algorithm allowed for simultaneous fits of the data at the three applied fields.

The behaviour of cluster **3** is the simplest, in that the saturation magnetization of $2\mu_B$ is nearly reached and the data are well fit with unexceptional parameters for a spin-triplet, including a zero-field splitting (ZFS) of -2.27 cm^{-1}. However, the saturation magnetization of the remaining clusters (**2**, **4**, **5**) becomes increasingly and markedly suppressed in the order X = $Cl^- > Br^- > I^-$, reaching a minimum with cluster **5** ($0.29\mu_B$ at 50 kOe). Fits required increasing large negative D values, which are consistent with the respective Weiss constants. The suppression effect is intramolecular in origin because a magnetization measurement of a 41 mM solution of **4** in dichloromethane yielded essentially the same result as the polycrystalline sample.

While the foregoing treatment of magnetization is obviously phenomenological, it is presented as a means of comparing and contrasting the behaviours of clusters **2**–**5**. The large ZFS are not without precedent and are seemingly within physical reason for **2**–**4**. While no meaningful comparison can be made with other systems, owing to the uniqueness of the basket cluster topology, we note that apparent ZFS values of up to *ca* 20 cm^{-1} have been observed for certain $S = 5/2$ Fe^{III} porphyrins,[22,23] and that for two $S = 1$ planar Fe^{II} complexes values near 70 cm^{-1} have been obtained.[24,25] All of these are obviously *apparent* values, dependent on the theoretical formalism. (For a discussion of this point, cf. ref. 22.) In the present case, we are applying a spin

Hamiltonian formalism to a general case where it has not been otherwise tested; viz. to polynuclear spin-coupled systems with incompletely quenched orbital angular momentum and probable spin–orbit interactions at local metal sites.

Thiolate cluster **6** is the most anomalous member of the set. In the solid state it does not exhibit a Curie region (nor any indication of a Curie paramagnetic impurity), is very weakly paramagnetic at 6 K and shows nesting of magnetization curves with a nearly zero saturation magnetization ($0.1\mu_B$ at 50 kOe; data not shown). It is conceivable that this species represents an extension of the behaviour of **2–5**, but from the information available we are unable to demonstrate the ground state spin. Moreover, in toluene solution, $\mu_{eff} = 2.72\mu_B$, essentially the same as the solution moment for **2**, for which a triplet ground state has been established. On this limited evidence, the $S = 1$ ground state designation has been entered in Table 1. In the solid state the core structures of **8**, the magnetic properties of which are quite similar to those of **6**, and also of **7**, which bears a similar relationship to **2**, are virtually congruent.[3,11] It is unlikely, in either the solid or solution states, that the magnetic differences between **6** and other basket clusters arise from large core structural differences.

(b) *Solution properties.* In dichloromethane solutions at 190–302 K, magnetic moments of clusters **2** and **3** show a near-Curie dependence of magnetic susceptibilities with values consistent with an $S = 1$ ground state. Ranges in magnetic moments over the temperature range are given in Table 1. The larger magnetic moments of selenide cluster **3** vs sulphide cluster **2** in solution and in the solid state (Table 1) are consistent with an earlier observation of smaller antiferromagnetic coupling in Fe_4Se_4 than in Fe_4S_4 clusters.[26] The variable-temperature ^1H NMR spectra of clusters **2** and **3** are presented in Figs 8 and 9, respectively. The occurrence of two equally intense methylene and methyl resonances for **2**, from the inequivalent sites Fe(2,3), over the 190–300 K range, demonstrates retention of the solid state structure in solution. The spectra of **3** are similar but the methyl resonances are not well resolved. Line broadening at the lower temperatures is ascribed to the effect of increasing cluster paramagnetism rather than any dynamic process. The isotropic shifts of **3** are considerably larger than those of **2**, the difference being 32% at 300 K. The effect is qualitatively consistent with the magnetic susceptibilities and suggests that the isotropic shifts have a significant contact component. Other evidence for a contact contribution is the alternating phenyl proton shifts of cluster **6**.[3] However, the shifts of **2** and **3** do not scale linearly with the susceptibilities, as would be the case for pure contact shifts. This indicates the presence of dipolar

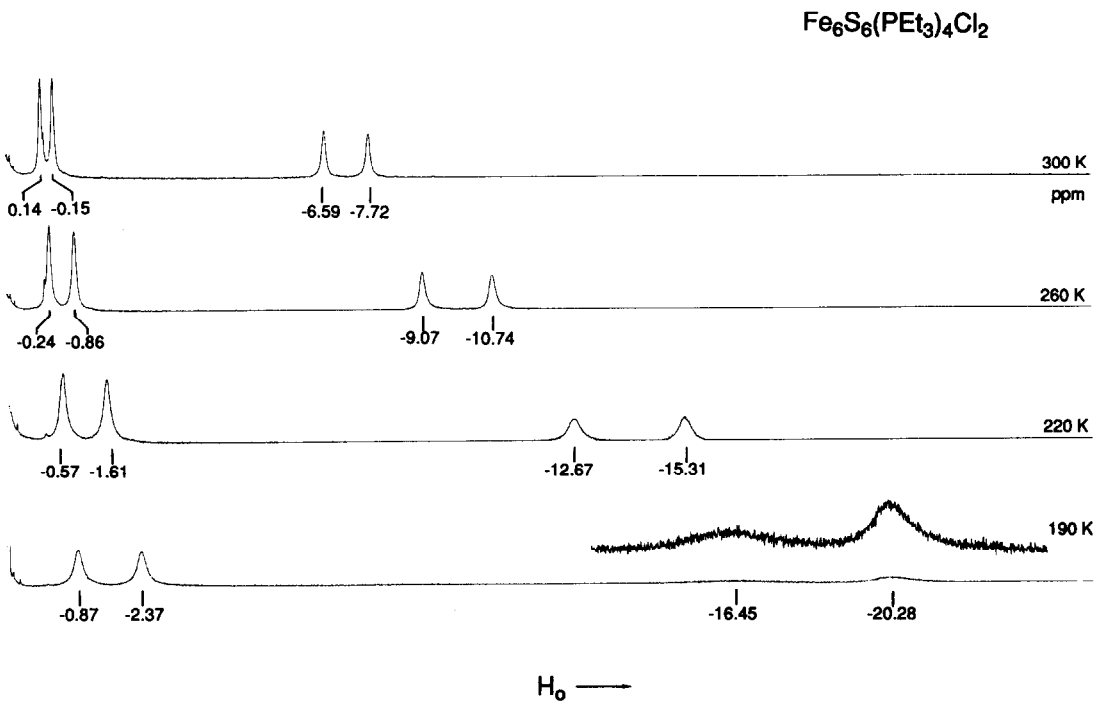

Fig. 8. Temperature dependence of the ^1H NMR spectra of cluster **2** in CD_2Cl_2 solution; chemical shifts are indicated.

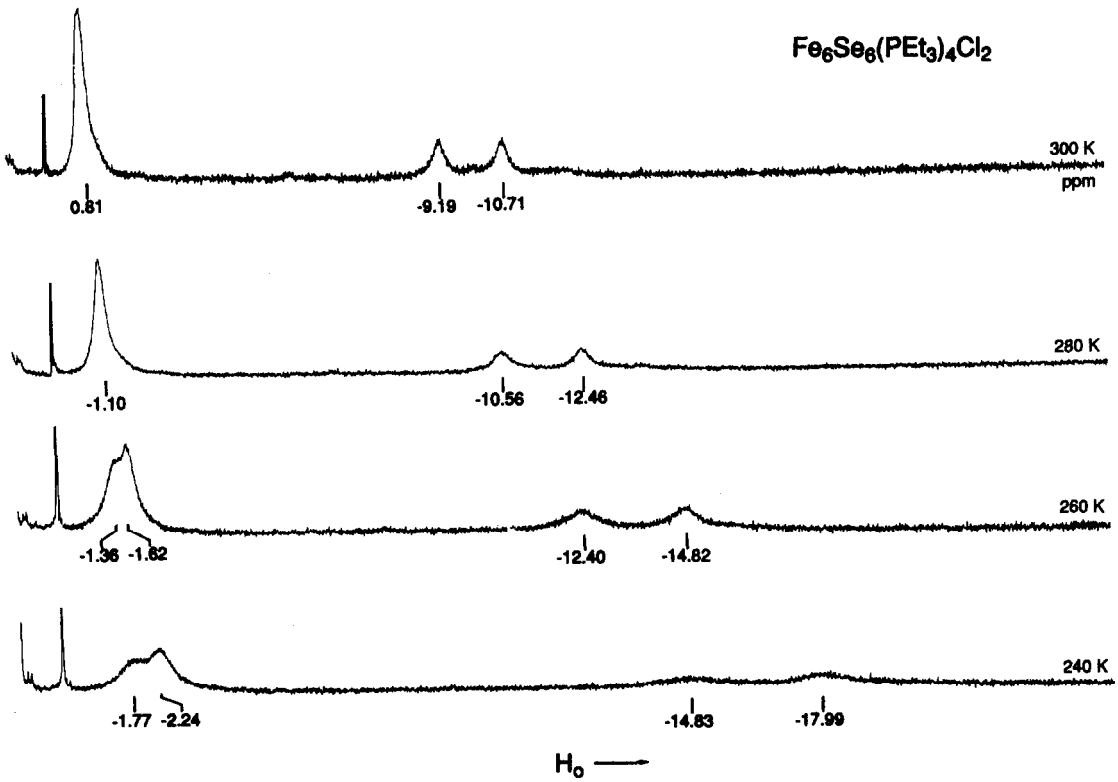

Fig. 9. Temperature dependence of the ^1H NMR spectra of cluster **3** in CD_2Cl_2 solution; chemical shifts are indicated.

shifts, a feature not unexpected in molecules with significant ZFS and magnetic anisotropies.

(c) *Mössbauer spectra.* Basket clusters contain three types of Fe sites (Fig. 1): Fe(1)(μ_3-S)$_2$(μ_4-S)L, Fe(2)(μ_3-S)$_2$(μ_4-S)P and Fe(3)(μ_2-S)(μ_3-S)$_2$P. The first of these is roughly tetrahedral, while the other two have distorted trigonal pyramidal geometry. The zero-field Mössbauer spectra of clusters **2** and **6** are displayed in Fig. 3; the spectrum of **2** closely resembles those of **3**–**5** (not shown), in containing three resolved features. All spectra were analysed with a 1:1:1 Fe site population. The assignment of the Fe(2) site has been discussed; that of the Fe(3) site in **6** is based on correlation of the largest quadrupole splitting (1.15 mm s^{-1}) with those in **2**–**5** (0.95–1.29 mm s^{-1}). This leaves the Fe(1) sites in **2**–**5** and in **6** as those with $\delta = 0.60$–0.64 and 0.43 mm s^{-1}, respectively. The relatively large isomer shift change (0.20 mm s^{-1}) upon replacing chloride (**2**) with thiolate (**6**), while the isomer shifts of the other sites change by no more than 0.05 mm s^{-1}, is another indication that the Fe(1) sites contain halide. Also, the small variation in isomer shift with halide is consistent with previous behaviour of FeS_3X sites in prismane clusters.[13–16] While we cannot insist on these site assignments, they are internally consistent within the cluster set **1**–**6** and we proceed on that basis.

Substitution of thiolate for chloride in tetrahedral FeS_3X units of prismane and cubane-type clusters has been found to cause a decrease of *ca* 0.05–0.11 mm s^{-1} in isomer shift.[13,27,28] In the basket clusters this results in the much larger change of 0.20 mm s^{-1}, as just noted. The smaller change in isomer shift in the cubane-type clusters has been previously considered in terms of a decrease in covalency of the Fe—L bond. In the case of the present clusters, however, the much larger change in δ values suggests that there is a detectable change in core charge delocalization upon ligand substitution. Earlier, it had been shown that in clusters containing well-defined Fe (mean) oxidation states, *s*, isomer shifts of tetrahedral FeS_4 sites follow the empirical linear relationship of eq. (2):[29]

$$\delta = 1.44\text{–}0.43s. \qquad (2)$$

Its application to **6** yields an oxidation state of 2.35+ at the Fe(1) sites, very close to the cluster mean oxidation state of 2.33+ and, therefore, consistent with a highly delocalized cluster. Based on structural results for $[Fe_4S_4(SR)_4]^{1-,2-,3-}$[1,7,8,30] the mean Fe—S terminal bond length of 2.255 Å in

8 is somewhat more consistent with 2.50+ than 2.33+, but not with 2.67+. No such δ/s relationship has been established for tetrahedral FeS_3Cl sites. We surmise that the chloride-bound sites Fe(1), on charge neutralization grounds, are biased toward iron(III) character, in which case the large isomer shifts result from the removal of electron density from orbitals with 4*s* character rather than an increase in the 3*d*-type orbitals. The isomer shift change of 0.05 mm s^{-1} at the Fe(2,3) sites is consistent with a marginal increase in iron(II) character, in apparent response to the effect of chloride at Fe(1). The mean Fe—Cl distance in **7** (2.193 Å), when compared with the value in $[Fe_4S_4Cl_4]^{2-}$ [2.216(2) Å],[31] is compatible with a mean oxidation state > 2.50+. In this argument, the site with the most ferric character has the largest, rather than the smallest, isomer shift. Whatever the merits of this interpretation it is certainly the case that, on the basis of structural[2,8–10] and spectroscopic evidence, clusters **1–6**, as all other mixed-valence synthetic and biological Fe—S clusters with a nuclearity of 3 or larger, are, electronically, largely delocalized systems. Note that for cluster **9**, which formally contains $5Fe^{II}+Fe^{III}$ and has only phosphine terminal ligands, isomer shifts are essentially identical.

Magnetically perturbed Mössbauer spectra of clusters **2–5** are presented in Fig. 7. For **2** and **3**, where the effect is the clearest, an increase in the applied field from 60 to 80 kOe caused features in the wings and in the central portions of the spectra to move in opposite directions, signifying antiferromagnetic coupling, which produces a $S = 1$ ground state. Solid lines are theoretical fits using the Hamiltonian (3) and a fitting program which is a modified version of the Lang–Dale minimizer.[32]

$$H = G_e\mu_B\mathbf{H}\cdot\mathbf{S}+\Sigma[A(i)\cdot\mathbf{I}_i\cdot\mathbf{S}-g_n\mu_n\mathbf{H}\cdot\mathbf{I}_i+H_Q(i)] \quad (3)$$

$$H_Q = (eQV_{zz}/12)[3I_z^2-15/4+\eta(I_x^2+I_y^2)] \quad (4)$$

Fits were performed in the fast relaxation regime with an imposed 1 : 1 : 1 site ratio, assumed random crystallite orientation, and otherwise as described for $[Fe_4S_4(SR)_4]^{3-}$ clusters.[7,8] The parameters for each site are the magnetic hyperfine coupling constants A_x, A_y and A_z, the EFG asymmetry parameter η, and the sign of the principal component of the EFG (V_{zz}). Values used in the spectral fits are listed in Table 2. Deviations of the theoretical fits from experimental points may arise from intermediate relaxation phenomena, as observed in related clusters,[6] and from the presence of crystallites. Theoretical fits of the magnetic spectra required progressively smaller values of hyperfine coupling constants along the halide series as the spectral width narrows, paralleling the monotonic decrease in the saturation magnetization for **2–5**. Inasmuch as these clusters all appear to have $S = 1$ ground states, they would be expected to have about the same A_i values at a given type of Fe site. That they do not, reflects differences in orbital states of the individual Fe sites. The spectrum of **6** (not shown) evidenced a small perturbation in an 80 kOe applied field (*ca* 2.8 mm s^{-1} spectral width) and resembled somewhat that of **5**. Owing to the uncertainty in the ground state, the spectrum was not analysed.

In the basket clusters **2–5**, phosphine-ligated sites Fe(2,3) show positive hyperfine coupling constants and correspondingly negative hyperfine fields. Site Fe(1), thought to be more ferric-like, has oppositely signed parameters while the sites Fe(1–3), in the all-phosphine basket cluster **9** have positive A_i and negative H_i parameters. These results are consistent with the same sign of the isotropic shifts of **2–5** and **9**,[12] so long as these are mainly contact in origin, as appears to be the case from other evidence. The spectra in Figs 8 and 9 show positive (upfield) shifts, when referred to Et_3P [δ 1.02 (CH_3), 1.36 (CH_2), CD_2Cl_2] as the diamagnetic reference.

All known basket clusters are schematically depicted in Fig. 1. A recent addition to this set is $Fe_6S_5(PBu_3)_4(SPh)_3$[33] (**10**), whose core structure is nearly identical to those of **7** and **8**. This molecule differs from clusters **2–9** in the handle of the basket is thiolate- rather than sulphide-bridged; it is isoelectronic with **9** and, therefore, has a probable $S = 1/2$ ground state. Cai *et al.*[33] consider that the atoms Fe(2,4) are more reduced in **10** than in **6** because of Fe—S distances in the handle which are 0.07 Å longer than in the latter cluster. As yet, no Mössbauer or other spectroscopic and magnetic data have been reported that would permit a comparison of electronic features with those of clusters **2–9**.

Acknowledgements—This research was supported by NIH Grant GM 28856 at Harvard University and by the Office of Naval Research program on Cluster Science and Dynamics under Contract No. N00014-89-J-1779 at MIT. The Francis Bitter National Laboratory is supported by the National Science Foundation.

REFERENCES

1. J. M. Berg and R. H. Holm, in *Iron–Sulfur Proteins* (Edited by T. G. Spiro), Ch. 1. Wiley-Interscience, New York (1982).
2. J.-F. You, B. S. Snyder, G. C. Papaefthymiou and R. H. Holm, *J. Am. Chem. Soc.* 1990, **112**, 1067.
3. M. S. Reynolds and R. H. Holm, *Inorg. Chem.* 1988, **27**, 4494.

4. A. Agresti, M. Bacci, F. Cecconi, C. A. Ghilardi and S. Midollini, *Inorg. Chem.* 1985, **24**, 689.
5. F. Cecconi, C. A. Ghilardi, S. Midollini, A. Orlandini and P. Zanello, *J. Chem. Soc., Dalton Trans.* 1987, 831.
6. V. Papefthymiou, M. Millar and E. Münck, *Inorg. Chem.* 1986, **25**, 3010.
7. M. J. Carney, G. C. Papaefthymiou, M. A. Whitener, K. Spartalian, R. B. Frankel and R. H. Holm, *Inorg. Chem.* 1988, **27**, 346.
8. M. J. Carney, G. C. Papaefthymiou, K. Spartalian, R. B. Frankel and R. H. Holm, *J. Am. Chem. Soc.* 1988, **110**, 6084.
9. I. Noda, B. S. Snyder and R. H. Holm, *Inorg. Chem.* 1986, **25**, 3851.
10. B. S. Snyder, M. S. Reynolds, I. Noda and R. H. Holm, *Inorg. Chem.* 1988, **27**, 595.
11. B. S. Snyder and R. H. Holm, *Inorg. Chem.* 1988, **27**, 2339.
12. B. S. Snyder and R. H. Holm, *Inorg. Chem.* 1990, **29**, 274.
13. M. G. Kanatzidis, N. C. Baenziger, D. Coucouvanis, A. Simopoulos and A. Kostikas, *J. Am. Chem. Soc.* 1984, **106**, 4500.
14. M. G. Kanatzidis, W. R. Hagen, W. R. Dunham, R. K. Lester and D. Coucouvanis, *J. Am. Chem. Soc.* 1985, **107**, 953.
15. M. G. Kanatzidis, A. Salifoglou and D. Coucouvanis, *Inorg. Chem.* 1986, **25**, 2460.
16. D. Coucouvanis, M. G. Kanatzidis, A. Salifoglou, W. R. Dunham, A. Simopoulos, J. R. Sams, V. Papaefthymiou, A. Kostikas and C. E. Strouse, *J. Am. Chem. Soc.* 1987, **109**, 6863.
17. C. J. O'Connor, *Prog. Inorg. Chem.* 1982, **29**, 203.
18. D. H. Live and S. I. Chan, *Anal. Chem.* 1970, **42**, 791.
19. W. Gerger, U. Mayer and V. Gutmann, *Mh. Chem.* 1977, **108**, 417.
20. N. N. Greenwood and T. C. Gibb, *Mössbauer Spectroscopy*, Ch. 6. Chapman and Hall, London (1971).
21. T. Birchall, *Can. J. Chem.* 1969, **47**, 1351.
22. S. Mitra, in *Iron Porphyrins* (Edited by A. B. P. Lever and H. B. Gray), Part 2, Ch. 1. Addison-Wesley, Reading, U.S.A. (1983).
23. V. R. Marathe and S. Mitra, *J. Chem. Phys.* 1983, **78**, 915.
24. C. G. Barraclough, R. L. Martin, S. Mitra and R. C. Sherwood, *J. Chem. Phys.* 1970, **53**, 1643.
25. P. D. W. Boyd, D. A. Buckingham, R. F. McMeeking and S. Mitra, *Inorg. Chem.* 1979, **18**, 3585.
26. M. A. Bobrik, E. J. Laskowski, R. W. Johnson, W. O. Gillum, J. M. Berg, K. O. Hodgson and R. H. Holm, *Inorg. Chem.* 1978, **17**, 1402.
27. M. J. Carney, J. A. Kovacs, Y. Zhang, G. C. Papaefthymiou, K. Spartalian, R. B. Frankel and R. H. Holm, *Inorg. Chem.* 1987, **26**, 719.
28. R. B. Frankel, B. A. Averill and R. H. Holm, *J. Phys. (Paris)* 1974, **35**, C6–107.
29. G. Christou, P. K. Mascharak, W. H. Armstrong, G. C. Papefthymiou, R. B. Frankel and R. H. Holm, *J. Am. Chem. Soc.* 1982, **104**, 2820.
30. T. O'Sullivan and M. M. Millar, *J. Am. Chem. Soc.* 1985, **107**, 4096.
31. M. A. Bobrik, K. O. Hodgson and R. H. Holm, *Inorg. Chem.* 1977, **16**, 1851.
32. G. Lang and B. W. Dale, *Nucl. Instrum. Meth.* 1986, **108**, 3541.
33. J.-H. Cai, C.-N. Chen, Q.-T. Liu, B.-T. Zhuang, B.-S. Kang and J.-X. Lu, *Jiegou Huaxue* (*J. Struct. Chem.*) 1989, **8**, 220.

Polyhedron Vol. 10, No. 2, pp. 215–219, 1991
Printed in Great Britain

0277–5387/91 $3.00 + .00
© 1991 Pergamon Press plc

SYNTHESIS OF ALKYLIDYNE TUNGSTEN COMPLEXES WITH HYDROTRIS(PYRAZOL-1-YL)BORATE LIGANDS

JOHN C. JEFFERY, F. GORDON A. STONE* and GEOFFREY K. WILLIAMS

Department of Inorganic Chemistry, The University of Bristol, Bristol BS8 1TS, U.K.

(*Received* 10 *August* 1990; *accepted* 12 *September* 1990)

Abstract—Treatment of the tungsten compounds $[W(\equiv CR)Br(CO)_4]$ (R = C_6H_4Me-4, C_6H_4OMe-2, or $C_6H_3Me_2$-2,6) in tetrahydrofuran with the salts $K[HB(3,5\text{-}Me_2pz)_3]$[$HB(3,5\text{-}Me_2pz)_3$ = hydrotris(3,5-dimethylpyrazol-1-yl)borate], $K[HB(3\text{-}Phpz)_3]$ [$HB(3\text{-}Phpz)_3$ = hydrotris(3-phenylpyrazol-1-yl)borate] and $K[HB(pz)_3]$ [$HB(pz)_3$ = hydrotris(pyrazol-1-yl) borate], affords, respectively, the complexes $[W(\equiv CC_6H_4Me\text{-}4)(CO)_2\{HB(3,5\text{-}Me_2pz)_3\}]$, $[W(\equiv C_6H_4Me\text{-}4)(CO)_2\{HB(3\text{-}Phpz)_3\}]$ and $[W(\equiv CR)(CO)_2\{HB(pz)_3\}]$ (R = $C_6H_3Me_2$-2,6 or C_6H_4OMe-2). Protonation of the compound $[W(\equiv CC_6H_4OMe\text{-}2)(CO)_2\{HB(pz)_3\}]$ with $HBF_4 \cdot Et_2O$ gives the salt $[W\{=C(H)C_6H_4OMe\text{-}2\}(CO)_2\{HB(pz)_3\}][BF_4]$. The NMR data for the new complexes are reported and discussed.

The ligating properties of the poly(pyrazol-1-yl)borato anions are well established, and these species have become important both in classical coordination chemistry and in organometallic chemistry.[1] In the latter area of study, metal complexes containing poly(pyrazol-1-yl)borate groups and alkylidyne ligands are rapidly increasing in number.[2–4] Our interest in this area stems from using the compound $[W(\equiv CC_6H_4Me\text{-}4)(CO)_2\{HB(pz)_3\}]$ (**1**)[4a] and related species as a reagent for preparing polynuclear metal complexes containing bonds between tungsten and other transition elements.[4] As part of our continuing studies, we describe herein the synthesis of some new mononuclear alkylidyne–tungsten reagents containing the anionic ligands $HB(pz)_3^-$ [hydrotris(pyrazol-1-yl)borato], $HB(3,5\text{-}Me_2pz)_3^-$ [hydrotris(3,5-dimethylpyrazol-1-yl)borato] and $HB(3\text{-}Phpz)_3^-$ [hydrotris(3-phenylpyrazol-1-yl)borato].

RESULTS AND DISCUSSION

Treatment of a THF (tetrahydrofuran) solution of the complex $[W(\equiv CC_6H_4Me\text{-}4)Br(CO)_4]$, prepared *in situ* from the alkylidene tungsten species $[W\{=C(OMe)C_6H_4Me\text{-}4\}(CO)_5]$, with the salt $K[HB(3,5\text{-}Me_2pz)_3]$ afforded the brown crystalline compound $[W(\equiv CC_6H_4Me\text{-}4)(CO)_2\{HB(3,5\text{-}Me_2pz)_3\}]$ (**2**). The complex $[W(\equiv CC_6H_4Me\text{-}4)(CO)_2\{HB(3\text{-}Phpz)_3\}]$ (**3**) was similarly obtained using the salt $K[HB(3\text{-}Phpz)_3]$. Data characterizing the species **2** and **3** are given in Tables 1 and 2. In the IR spectrum two CO bands are observed, at 1974 and 1888 cm^{-1} for **2** and at 1982 and 1897 cm^{-1} for **3**. These pairs of peaks are at somewhat lower frequencies than those observed in the spectrum of **1** (1986 and 1903 cm^{-1}).[4a] This might be expected since the donor ability of the hydrotris(pyrazol-1-yl)borato ligands should increase in the order $HB(pz)_3 < HB(3\text{-}Phpz)_3 < HB(3,5\text{-}Me_2pz)_3$.

The ^1H and $^{13}C\text{-}\{^1H\}$ NMR spectra of compounds **2** and **3** are informative and in agreement with static structures of the type shown. Both

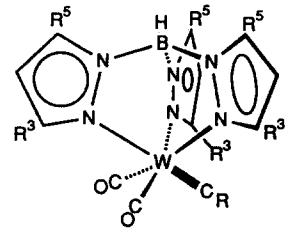

	R	R^3	R^5
(1)	C_6H_4Me-4	H	H
(2)	C_6H_4Me-4	Me	Me
(3)	C_6H_4Me-4	Ph	H
(4)	$C_6H_3Me_2$-2,6	H	H
(5)	C_6H_4OMe-2	H	H

* Author to whom correspondence should be addressed.

Table 1. Analytical[a] and physical data for the complexes

Compound	Colour	Yield (%)	ν(CO)[b] (cm^{-1})	Analysis (%) C	H	N
$[W(\equiv CC_6H_4Me\text{-}4)(CO)_2\{HB(3,5\text{-}Me_2pz)_3\}]$ (**2**)	Brown	80	1974m, 1888s	46.8(46.9)	4.6(4.5)	13.2(13.1)
$[W(\equiv CC_6H_4Me\text{-}4)(CO)_2\{HB(3\text{-}Phpz)_3\}]$ (**3**)	Brown	17[c]	1982m, 1897s	56.7(56.6)	3.7(3.7)	10.7(10.7)
$[W(\equiv CC_6H_3Me_2\text{-}2,6)(CO)_2\{HB(pz)_3\}]$ (**4**)	Brown	69	1984m, 1901s	42.2(42.1)	3.4(3.3)	14.8(14.7)
$[W(\equiv CC_6H_4OMe\text{-}2)(CO)_2\{HB(pz)_3\}]$ (**5**)	Pink	13[c]	1976m,[d] 1886s	39.8(39.9)	3.1(3.0)	14.4(14.7)
$[W\{=C(H)C_6H_4OMe\text{-}2\}(CO)_2\{HB(pz)_3\}][BF_4]$ (**6**)	Red	82	2032m, 1954s	34.4(34.6)	2.8(2.9)	12.6(12.7)

[a] Calculated values are given in parentheses.
[b] Measured in hexane, unless otherwise stated.
[c] Yield of crude product *ca* 80% prior to column chromatography.
[d] In CH_2Cl_2.

species display characteristic resonances for the ligated carbon atoms of the *p*-tolylmethylidyne groups at δ 279.6 (**2**) and 282.3 ppm (**3**). The signal for the $C{\equiv}W$ nucleus in the $^{13}C\text{-}\{^1H\}$ NMR spectrum of **1** is seen at δ 284.8 ppm.[4a]

The coordination environment of the tungsten atom in complexes **2** and **3** is essentially octahedral with the hydrotris(pyrazol-1-yl)borate group occupying three facial sites. Consequently one of the ligated nitrogen atoms is transoid to the CC_6H_4 Me-4 moiety, while the other two nitrogen atoms are transoid to CO groups. This arrangement generates a plane of symmetry through the tungsten atom, the alkylidyne-carbon and the pyrazol ring, which is transoid to the latter. The two CO groups and the remaining two pyrazol rings are, respectively, symmetrically related to each other on either side of the symmetry plane. Hence, the number of ^1H and $^{13}C\text{-}\{^1H\}$ resonances seen in the spectra is reduced from the number which would be anticipated if all three C_3N_2 rings and the two CO ligands were non-equivalent. Consequently, it was possible to make the peak assignments listed in Table 2 on the basis of the observed relative intensities of the various signals.

The two compounds $[W(\equiv CR)(CO)_2\{HB(pz)_3\}]$ (**4**, R = $C_6H_3Me_2$-2,6; **5**, R = C_6H_4 OMe-2) were prepared by treating the species $[W(\equiv CR)Br(CO)_4]$ in THF with $K[HB(pz)_3]$. Complexes **4** and **5** are closely related to the previously reported compound **1**,[4a] and some of the spectroscopic properties are very similar. Thus all three compounds display two CO stretching bands in their IR spectra as well as a diagnostic resonance for the carbon nuclei of the ligated alkylidyne groups in their $^{13}C\text{-}\{^1H\}$ NMR spectra. For **1** the signal occurs at 284.8 ppm, as mentioned above, while for **4** and **5** the peaks are at δ 288.6 and 280.5 ppm, respectively (Table 2). However, the ^1H and $^{13}C\text{-}\{^1H\}$ NMR data for **1**[4a] indicate that all three pyrazol rings are equivalent, as would be expected if the $HB(pz)_3$ group rotated on the NMR time scale. In contrast, the NMR data for **4** and **5** reveal a pattern of peaks corresponding to two equivalent and one non-equivalent pyrazol rings. This implies that the $HB(pz)_3$ ligand does not undergo dynamic behaviour, presumably because site exchange of the ligated nitrogen atoms is prevented by the presence of the *ortho* substituents on the phenyl rings of the alkylidyne groups which interact with the sterically demanding $HB(pz)_3$ moiety (see below).

We have previously shown that protonation of the compound $[W(\equiv CC_6H_4Me\text{-}4)(CO)_2(\eta\text{-}C_5H_5)]$ with $HBF_4 \cdot Et_2O$ affords the ditungsten salt $[W_2(\mu\text{-}H)\{\mu\text{-}C_2(C_6H_4Me\text{-}4)_2\}(CO)_4(\eta\text{-}C_5H_5)_2][BF_4]$.[5] Moreover, there is evidence that the latter is formed

Table 2. ^{1}H and ^{13}C NMR data[a] for the complexes

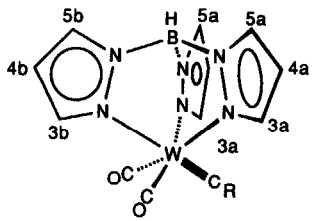

Compound	^{1}H (δ)	$^{13}C^{b}$ (δ)
2	2.29 (s, 3 H, Me-4), 2.35 (s, 3 H, $Me^{3b\text{ or }5b}$), 2.38 (s, 6 H, $Me^{3a\text{ or }5a}$), 2.44 (s, 3 H, $Me^{3b\text{ or }5b}$), 2.49 (s, 6 H, $Me^{3a\text{ or }5a}$), 5.83 (s, 1 H, H^{4b}), 5.93 (s, 2 H, H^{4a}), 7.11, 7.34 [$(AB)_2$, 4 H, C_6H_4, J(AB) 8]	279.6 (C≡W), 224.2 [CO, J(WC) 168], 152.8 (1 C, $C^{3b\text{ or }5b}$), 152.4 (2 C, $C^{3a\text{ or }5a}$), 148.1 [$C^{1}(C_6H_4)$], 145.9 (1 C, $C^{3b\text{ or }5b}$), 145.3 (2 C, $C^{3a\text{ or }5a}$), 138.4, 129.4. 129.0 (C_6H_4), 106.9 (1 C, C^{4b}), 106.6 (2 C, C^{4a}), 21.7 (Me-4), 16.5 (2 C, $Me^{3a\text{ or }5a}$), 15.3 (1 C, $Me^{3b\text{ or }5b}$), 12.7 (3 C, $Me^{3a\text{ or }5a}$ and $Me^{3b\text{ or }5b}$)
3	2.21 (s, 3 H, Me-4), 6.29 [d, 1 H, H^{4b}, $J(H^{4b}H^{5b})$ 2], 6.32, 6.78 [$(AB)_2$, 4 H, C_6H_4, J(AB) 8], 6.39 [d, 2 H, H^{4a}, $J(H^{4a}H^{5a})$ 2], 6.90–7.50 (m br, 15 H, Ph^{3}), 7.80 [d, 1 H, H^{5b}, $J(H^{5b}H^{4b})$ 2], 7.87 [d, 2 H, H^{5a}, $J(H^{5a}H^{4a})$ 2]	282.3 (C≡W), 221.5 (CO), 158.5 (1 C, C^{3b} or C^{5b}), 158.2 (2 C, $C^{3a\text{ or }5a}$), 146.2 [$C^{1}(C_6H_4)$], 137.8 (1 C, $C^{3b\text{ or }5b}$), 137.1 [3 C, $C^{3a\text{ or }5a}$ and $C^{4}(C_6H_4)$], 134.2–126.4 (Ph^{3}, C_6H_4), 107.5 (2 C, C^{4a}), 107.2 (1 C, C^{4b}), 21.7 (Me-4)
4	2.47 (s, 6 H, Me_2-2,6), 6.22 (s, 1 H, H^{4b}), 6.27 (s, 2 H, H^{4a}), 6.93 [(AB_2), 2 H, C_6H_3, J(AB) 7], 7.09 [(AB_2), 1 H, C_6H_3, J(AB) 7], 7.70 (s, 1H, $H^{3b\text{ or }5b}$), 7.71 (s, 1 H, $H^{3b\text{ or }5b}$), 7.73 (s, 2 H, $H^{3a\text{ or }5a}$), 8.03 (s, 2 H, $H^{3a\text{ or }5a}$)	288.6 (C≡W), 226.8 (CO), 147.7 [$C^{1}(C_6H_3)$], 145.6 (2 C, $C^{3a\text{ or }5a}$), 144.1 (1 C, $C^{3b\text{ or }5b}$), 140.8 (1 C, $C^{3b\text{ or }5b}$), 136.0 (2 C, $C^{3a\text{ or }5a}$), 143.7, 128.0, 127.6 (C_6H_3), 106.2 (1 C, C^{4b}), 106.1 (2 C, C^{4a}), 20.7 (Me_2-2,6)
5	3.90 (s, 3 H, OMe), 6.22 (s, 1 H, H^{4b}), 6.27 (s, 2 H, H^{4a}), 6.82–6.89 (m, 2 H, C_6H_4), 7.25–7.39 (m, 2 H, C_6H_4), 7.68–7.71 (m, 4 H, H^{3b}, H^{5b} and $H^{3a\text{ or }5a}$), 8.09 (s, 2 H, $H^{3a\text{ or }5a}$)	280.5 (C≡W), 225.1 (CO), 160.8 [$C^{1}(C_6H_4)$], 145.6 (2 C, $C^{3a\text{ or }5a}$), 144.3 (1 C, $C^{3b\text{ or }5b}$), 136.1 (1 C, $C^{3b\text{ or }5b}$), 135.9 (2 C, $C^{3a\text{ or }5a}$), 139.4, 131.6, 129.8, 120.3, 111.2 (C_6H_4), 106.2 (3 C, $C^{4a\text{ and }4b}$), 55.9 (OMe)
6	3.53 (s, 3 H, OMe), 6.57 (s, 3 H, $H^{4a\text{ and }4b}$), 7.42–7.60 (m, 6 H, C_6H_4 and $H^{3a\text{ or }5a}$), 7.99 (s, 1 H, $H^{3b\text{ or }5b}$), 8.08 (s, 2 H, $H^{3a\text{ or }5a}$), 8.15 (s, 1 H, $H^{3b\text{ or }5b}$), 12.69 [s, 1 H, C(*H*)C_6H_4OMe-2, J(WH) 27]	239.4 (C≡W), 217.3 (CO), 161.2 [$C^{1}(C_6H_4)$], 148.2 (1 C, $C^{3b\text{ or }5b}$), 143.8 (2 C, $C^{3a\text{ or }5a}$), 139.9 (1 C, $C^{3b\text{ or }5b}$), 138.7 (2 C, $C^{3a\text{ or }5a}$), 134.3 [C^{2}, C_6H_4], 133.6, 130.5, 125.8, 111.2 (C_6H_4), 109.6 (1 C, C^{4b}), 109.1 (2 C, C^{4a}), 64.6 (OMe)

[a] Chemical shifts (δ) in ppm, coupling constants in Hz, measurements at room temperature in CD_2Cl_2.
[b] ^{1}H decoupled, chemical shifts to high frequency of $SiMe_4$ (0.0 ppm).

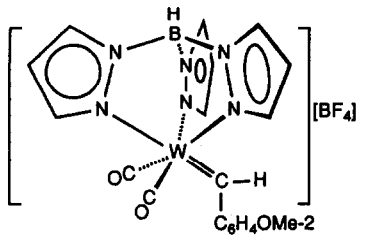

(6)

via the intermediacy of a transient mononuclear alkylidene tungsten species $[W\{{=}C(H)C_6H_4Me\text{-}4\}(CO)_2(\eta\text{-}C_5H_5)][BF_4]$, in which the tungsten atom with 16 electrons in its valence shell is electronically unsaturated, and therefore reacts further.[5,6] It was, therefore, of interest to protonate the species **1–5** which are isolobal with $[W(\equiv CC_6H_4Me\text{-}4)(CO)_2(\eta\text{-}C_5H_5)]$. In practice, only complex **5** on treatment with $HBF_4 \cdot Et_2O$ yielded a stable product, which was identified as the alkylidene tungsten salt $[W\{{=}C(H)C_6H_4OMe\text{-}2\}(CO)_2\{HB(pz)_3\}][BF_4]$ (**6**), data for which are given in Tables 1 and 2. Protonation of compound **1** or **2** with $HBF_4 \cdot Et_2O$ afforded salts similar to **6** based on IR and ^1H NMR measurements, but attempts to purify these products by crystallization from Et_2O or by column chromatography were unsuccessful, resulting in deprotonation and formation of the precursor **1** or **2**.

Although suitable crystals of complex **6** could not be grown for an X-ray diffraction study, the structure is well established by microanalysis and by the spectroscopic data. As expected, in the IR spectrum of **6** the two CO stretching bands at 2032 and 1954 cm^{-1} occur at appreciably higher frequency than the corresponding bands (1976 and 1886 cm^{-1}) in the spectrum of the neutral complex **5**. In the ^1H NMR spectrum of **6** there is a diagnostic resonance for the proton attached to the alkylidene-carbon at δ 12.69 and this signal displays ^{183}W satellite peaks [J(WH) 27 Hz]. In the $^{13}C\text{-}\{^1H\}$ NMR spectrum of the salt **6** the resonance for the ligated carbon of the alkylidene group $C(H)C_6H_4OMe\text{-}2$ is seen at δ 239.4 ppm. These ^1H and $^{13}C\text{-}\{^1H\}$ NMR chemical shifts are comparable with those previously reported for the compound $[W\{{=}C(H)C_6H_4Me\text{-}4\}I(CO)_2(\eta\text{-}C_5H_5)]$ [^1H, δ 13.08 for $C(H)C_6H_4Me\text{-}4$; $^{13}C\text{-}\{^1H\}$, δ 267.4 ppm for $C(H)C_6H_4Me\text{-}4$], the structure of which was established by X-ray diffraction.[5]

Our success in isolating a stable alkylidene tungsten complex by protonating compound **5** and our failure to obtain stable products by protonating the species **1–4** is probably related to the nature of the substituent groups attached to the alkylidyne-carbon atoms. In the alkylidene tungsten species produced by protonation, the metal atom has a 16 valence electron shell, a situation not conducive to stability. However, the presence of the OMe-2 group on the phenyl ring in **6**, with a lone pair of electrons on the oxygen atom, may exert a stabilizing influence. All the products of protonating compounds **1–5** would have six coordinate metal atoms. Nevertheless, tungsten can increase its coordination number beyond six. Hence, there is the possibility that the lone pair on the OMe-2 group in complex **6** interacts with the tungsten atom so as to give the latter a filled 18-electron valence shell. This could inhibit decomposition observed with the other species obtained by protonating **1–4**.

It is interesting to contrast the protonation of compounds **1–5** with $HBF_4 \cdot Et_2O$ with the formation of the ditungsten salt $[W_2(\mu\text{-}H)\{\mu\text{-}C_2(C_6H_4Me\text{-}4)_2\}(CO)_4(\eta\text{-}C_5H_5)_2][BF_4]$ on protonating $[W(\equiv CC_6H_4Me\text{-}4)(CO)_2(\eta\text{-}C_5H_5)]$, mentioned above. Formation of the ditungsten species requires a combination of an initially formed alkylidene complex $[W\{{=}C(H)C_6H_4Me\text{-}4\}(CO)_2(\eta\text{-}C_5H_5)]^+$ with a second molecule of $[W(\equiv CC_6H_4Me\text{-}4)(CO)_2(\eta\text{-}C_5H_5)]$, followed by C—C bond formation and migration of a hydrogen atom.[5] In the case of compounds **1–5** the presence of the hydrotris(pyrazol-1-yl)borate ligands would inhibit further reaction of an initially formed alkylidene species because of their steric bulk. The cone angles for the groups $HB\{3,5\text{-}Me_2(pz)_3\}$, $HB(pz)_3$ and $\eta\text{-}C_5H_5$ are 225, 180 and 100°, respectively.[1,7]

EXPERIMENTAL

All experiments were carried out under nitrogen using Schlenk tube techniques. Solvents were rigorously dried before use. The salts $K[HB(pz)_3]$, $K[HB(3,5\text{-}Me_2pz)_3]$ and $K[HB(3\text{-}Phpz)_3]$[7,8] and the compounds $[W(\equiv CR)Br(CO)_4]$ (R = C_6H_4Me-4, C_6H_4OMe-2 and $C_6H_3Me_2$-2,6)[9] were prepared by methods described previously. The reagent $HBF_4 \cdot Et_2O$ consisted of a 54% solution of HBF_4 in Et_2O. The NMR spectra were recorded with JEOL JNM GX270 and GX400 spectrometers, and the IR spectra were measured with a Perkin–Elmer FT1600 spectrophotometer. Analytical and physical data for the new compounds are given in Table 1.

Preparation of the alkylidyne tungsten compounds

(i) The complex $[W(\equiv CC_6H_4Me\text{-}4)Br(CO)_4]$ was first prepared by treating a hexane (80 cm^3) solution of $[W\{{=}C(OMe)C_6H_4Me\text{-}4\}(CO)_5]$ (3.03 g, 6.61 mmol) at −20°C with BBr_3 until an IR spectrum showed that none of the alkylidene tungsten reagent remained. The mixture was cooled to −30°C,

solvent was removed with a syringe, and the residue was washed with cold (*ca* −78°C) hexane (3 × 50 cm^3) to obtain [W(≡CC_6H_4Me-4)Br$(CO)_4$] (3.16 g, 6.61 mmol). The latter was dissolved in THF (100 cm^3) at −20°C and treated with the salt K[HB(3,5-Me_2pz)$_3$] (2.34 g, 6.96 mmol). Following this procedure, the mixture was stirred at *ca* −10°C for 24 h. Filtration through a Celite pad (*ca* 1 cm) at −20°C, followed by removal of solvent *in vacuo* gave brown *microcrystals* of [W(≡CC_6H_4Me-4)$(CO)_2${HB(3,5-Me_2pz)$_3$}] (**2**) (3.56 g) after crystallization from CH_2Cl_2–Et_2O (1 : 4).

(ii) The complex [W(≡CC_6H_4Me-4)$(CO)_2${HB(3-Phpz)$_3$}] (**3**) was similarly obtained, by stirring a mixture of [W(≡CC_6H_4Me-4)Br$(CO)_4$] (prepared *in situ* from [W{=C(OMe)C_6H_4Me-4}$(CO)_5$] (0.47 g, 1.02 mmol) and BBr_3) and K[HB(3-Phpz)$_3$] (0.48 g, 1.00 mmol) in THF for 4 days at *ca* −20°C. The mixture was filtered through a Celite pad (*ca* 1 cm) and solvent was removed *in vacuo*. The residue was dissolved in CH_2Cl_2–hexane (10 cm^3, 1 : 4) and chromatographed on silica gel (2 × 10 cm). Elution with the same solvent mixture, removal of solvent *in vacuo*, and recrystallization of the residue from CH_2Cl_2–Et_2O (1 : 5) gave brown *microcrystals* of compound **3** (0.13 g).

(iii) The alkylidene tungsten complex [W{=C(OMe)$C_6H_3Me_2$-2,6}$(CO)_5$] (3.10 g, 6.57 mmol) in hexane–CH_2Cl_2 (100 cm^3, 1 : 2) was converted to [W(≡$CC_6H_3Me_2$-2,6)Br$(CO)_4$] using BBr_3. After removal of solvent with a syringe, the residue was washed with cold (*ca* −50°C) hexane (3 × 50 cm^3) and dried *in vacuo*. The [W(≡$CC_6H_3Me_2$-2,6)Br$(CO)_4$] obtained in this manner was dissolved in THF (100 cm^3) and treated with K[HB$(pz)_3$] (1.71 g, 6.79 mmol). After stirring the mixture for 24 h at room temperature, it was filtered through a Celite pad (*ca* 1 cm). Solvent was removed *in vacuo*, and the residue was crystallized from CH_2Cl_2–Et_2O (1 : 5) to afford brown *microcrystals* of [W(≡$CC_6H_3Me_2$-2,6)$(CO)_2${HB$(pz)_3$}] (**4**) (2.60 g).

(iv) The complex [W(≡CC_6H_4OMe-2)$(CO)_2${HB$(pz)_3$}] (**5**) was obtained by converting [W{=C(OMe)C_6H_4OMe-2}$(CO)_5$] (3.01 g, 6.35 mmol) to [W(≡CC_6H_4OMe-2)Br$(CO)_4$] and treating the latter with K[HB$(pz)_3$] (1.71 g, 6.79 mmol) in THF (80 cm^3). The crude product was dried *in vacuo*, and then dissolved in CH_2Cl_2–hexane (10 cm^3, 1 : 2) and chromatographed at −10°C on alumina (Brockman activity III, 2 × 10 cm column), eluting with CH_2Cl_2–hexane (1. 2). After removal of solvent *in vacuo* from a pink fraction, complex **5** was obtained as dark pink *microcrystals* (0.45 g) after crystallization from CH_2Cl_2–hexane (1 : 4) at −78°C.

Protonation studies

A CH_2Cl_2 (20 cm^3) solution of complex **5** (0.10 g, 0.17 mmol) was treated with drops of $HBF_4 \cdot Et_2O$ solution (*ca* 0.1 cm^3), until the IR spectrum of the mixture showed that all of the starting compound had been consumed. Solvent was removed *in vacuo*, and the resulting residue was crystallized from CH_2Cl_2–Et_2O (1 : 3) to give deep red *crystals* of [W{=C(H)C_6H_4OMe-2}$(CO)_2${HB$(pz)_3$}][BF_4] (**6**) (0.094 g).

Acknowledgements—We thank BP Chemicals, Grangemouth Division, for the award of a CASE SERC Research Studentship to G.K.W.

REFERENCES

1. S. Trofimenko, *Acc. Chem. Res.* 1971, **4**, 17; *Chem. Rev.* 1972, **72**, 497; *Prog. Inorg. Chem.* 1986, **34**, 115.
2. T. Desmond, F. J. Lalor, G. Ferguson and M. Parvez, *J. Chem. Soc., Chem. Commun.* 1983 , 457; 1984, 75; S. Chaona, F. J. Lalor, G. Ferguson and M. M. Hunt, *J. Chem. Soc., Chem. Commun.* 1988, 1606.
3. H. P. Kim, S. Kim, R. A. Jacobson and R. J. Angelici, *Organometallics* 1984, **3**, 1124; H. P. Kim and R. J. Angelici, *Organometallics* 1986, **5**, 2489.
4. (a) M. Green, J. A. K. Howard, A. P. James, C. M. Nunn and F. G. A. Stone, *J. Chem. Soc., Dalton Trans.* 1986, 187; (b) M. Green, J. A. K. Howard, A. P. James, A. N. de M. Jelfs, C. M. Nunn and F. G. A. Stone, *J. Chem. Soc., Dalton Trans.* 1986, 1697; (c) S. H. F. Becke, M. D. Bermudez, N. H. Tran-Huy, J. A. K. Howard, O. Johnson and F. G. A. Stone, *J. Chem. Soc., Dalton Trans.* 1987, 1229; (d) M. D. Bermudez, E. Delgado, G. P. Elliott, N. H. Tran-Huy, F. Major-Real, F. G. A. Stone and M. J. Winter, *J. Chem. Soc., Dalton Trans.* 1987, 1235; (e) M. D. Bermudez, F. P. E. Brown and F. G. A. Stone, *J. Chem. Soc., Dalton Trans.* 1988, 1139; (f) I. J. Hart, A. F. Hill and F. G. A. Stone, *J. Chem. Soc., Dalton Trans.* 1989, 2261; (g) S. J. Davies, A. F. Hill, M. U. Pilotti and F. G. A. Stone, *Polyhedron* 1989, **8**, 2265; (h) R. A. Doyle, R. J. Angelici and F. G. A. Stone, *J. Organomet. Chem.* 1989, 378.
5. J. A. K. Howard, J. C. Jeffery, J. C. V. Laurie, I. Moore, F. G. A. Stone and A. Stringer, *Inorg. Chim. Acta* 1985, **100**, 23.
6. K. E. Garrett, J. B. Sheridan, D. B. Pourreau, W. C. Feng, G. L. Geoffroy, D. L. Staley and A. L. Rheingold, *J. Am. Chem. Soc.* 1989, **111**, 8383.
7. S. Trofimenko, J. C. Calabrese and J. S. Thompson, *Inorg. Chem.* 1987, **26**, 1507.
8. S. Trofimenko, *Inorg. Synth.* 1970, **12**, 99.
9. F.-E. Baumann, J. A. K. Howard, R. J. Musgrove, P. Sherwood and F. G. A. Stone, *J. Chem. Soc., Dalton Trans.* 1988, 1879; A. F. Hill, H. D. Hönig and F. G. A. Stone, *J. Chem. Soc., Dalton Trans.* 1988, 3031.

Polyhedron Vol. 10, No. 2, pp. 221–227, 1991
Printed in Great Britain

0277-5387/91 $3.00+.00
© 1991 Pergamon Press plc

COMPLEX FORMATION OF RUBIDIUM AND CAESIUM CATIONS WITH CROWN ETHERS IN ACETONITRILE: A ^{133}Cs COMPETITIVE NMR STUDY

ROBERT T. STREEPER* and SADEGH KHAZAELI†

Department of Chemistry, Southern Illinois University, Edwardsville, IL 62026, U.S.A.

(*Received* 16 *May* 1990; *accepted* 17 *September* 1990)

Abstract—Caesium-133 NMR measurements were used to study the complexation of rubidium and caesium cations by 13 different crown ethers in acetonitrile. The ^{133}Cs chemical shift data indicated that the caesium cation forms both 1:1 and 2:1 (crown ether/Cs^+) complexes with 18C6, DC21C7 and DC24C8 ligands. All other complexes were of the 1:1 stoichiometry. In general, Rb^+ complexes are more stable than the corresponding Cs^+ complexes. Formation constants of the 18C6 ligand series show the following trends. For Rb^+: 1,4DT18C6 < 1,10DT18C6 ≈ 1,10DA18C6 < DB18C6 < B18C6 < DC18C6 < 18C6. For Cs^+: 1,4DT18C6 < 1,10DT18C6 < B18C6 < DB18C6 < 1,10DA18C6 < DC18C6 < 18C6.

Nuclear magnetic resonances of ^{7}Li, ^{23}Na, ^{39}K and ^{133}Cs nuclei have been used rather extensively for the study of the thermodynamics of complexation of alkali cations with macrocyclic crown ethers in aqueous and non-aqueous solvents.[1] In contradiction, we have shown that ^{85}Rb or ^{87}Rb chemical shift measurements cannot be used for such studies.[2] The ^{87}Rb natural line-width of aqueous solutions of the rubidium cation is more than 100 Hz, due to the large Steinheimer antishielding factor of this nucleus.[3] Additions of macrocyclic ligands to Rb^+ aqueous solutions result in further broadening of the resonance lines. For example, at the (18-crown-6)/(Rb^+) molar ratios of 0.50, 0.98 and 1.20 the line-widths are in the order of 1800, 3600 and 3000 Hz, respectively.[2] The broadening of the resonance line is so large that the variation in the resonance frequency as a function of the mole ratio cannot be measured with reasonable precision. The situation is even worse in non-aqueous solvents.[2]

Cox *et al.*[4–7] have developed a competitive potentiometric technique for the determination of large formation constants of macrocyclic compounds. using a silver/silver ion electrode. This technique is useful for solvents in which the silver/silver ion electrode behaves reversibly. Zink and co-workers[8] reported the use of ^{205}Tl competitive NMR for the measurement of the formation constants of alkali cations with crown ethers. This method is limited to systems where the ligand : metal cation molar ratio is such that the ligand is predominantly in the complexed form, and where only complexes with 1:1 stoichiometry are formed.

Recently Boss and Popov[9] developed a competitive NMR technique for the determination of formation constants of metal ion complexes. Their technique allows the measurement of the formation constants of metal cations whose nuclear properties are not normally favourable for NMR measurements, and also allows the determination of formation constants that are too large to be measured by the conventional non-competitive metal NMR techniques.

It was of our interest to study the complexation of rubidium, magnesium and calcium ions with crown ethers in non-aqueous solvents using this NMR competitive method. Here we report the formation constants of rubidium cation complexes with various crown ethers in acetonitrile.

* Current address: Johns Hopkins University, Department of Pharmacology and Molecular Sciences, Baltimore, MD 21205, U.S.A.

† Author to whom correspondence should be addressed.

EXPERIMENTAL

Reagents

Caesium chloride, rubidium chloride (Alfa) and sodium tetraphenylborate (Aldrich) were dried at 110°C. Caesium tetraphenylborate ($CsBPh_4$) was prepared by reacting equimolar amounts of sodium tetraphenylborate and caesium chloride in tetrahydrofuran.[10] The mixture was heated to promote metathesis and then was allowed to cool. The product was precipitated by adding water (Baker, HPLC grade). Rubidium tetraphenylborate ($RbBPh_4$) was synthesized in a similar manner using rubidium chloride and sodium tetraphenylborate. The tetraphenylborate salts were thoroughly washed with water and dried at 150°C. The sodium content of these salts was measured by atomic emission (Varian–SpectrA A-10) and was found to be less than 0.005%.

Acetonitrile (Aldrich) was refluxed over calcium hydride and fractionally distilled onto freshly activated 3 Å molecular sieves (Aldrich). Samples were prepared in a dry box under nitrogen atmosphere. Water contents, determined by Karl Fischer titration, were found to be less than 100 ppm.

18-Crown-6 (18C6, Aldrich) was precipitated as the acetonitrile complex and vacuum dried at room temperature to remove the acetonitrile.[11] The following macrocyclic ligands were vacuum dried for 24 h but otherwise used as received: 15-crown-5 (15C5, Aldrich), benzo-18-crown-6 (B18C6, Parish), 1,4-dithia-18-crown-6 (1,4DT18C6, Parish), 1,10-dithia-18-crown-6 (1,10DT18C6, Parish), 1,10-diaza-18-crown-6 (1,10DA18C6, Matheson Coleman Bell), 21-crown-7 (21C7, Parish), 1,10-dicyclohexano-21-crown-7 (DC21C7, Parish) and 1,13-dicyclohexano-24-crown-8 (DC24C8, Aldrich). The ligands benzo-15-crown-5 (B15C5, Aldrich), dibenzo-18-crown-6 (DB18C6, Aldrich), dicyclohexano-18-crown-6 (DC18C6, Aldrich) and 1,13-dibenzo-24-crown-8 (DB24C8, Aldrich) were recrystallized from *n*-heptane (Fisher) and vacuum dried.

NMR measurements

Caesium-133 chemical shift measurements were carried out on a JEOL FX90Q multinuclear Fourier transform NMR instrument operating at a field strength of 21.14 kG. Caesium-133 resonates at 11.70 MHz at this field strength. The instrument was locked on an externally generated deuterium signal. Caesium-133 spectra were accumulated using a 100 Hz sweep width and 8 K data points. Signal to noise ratios were always greater than 10 and the uncertainties of the peak maxima were less than 0.02 ppm. Experiments were run in 10 mm O.D. NMR tubes (Wilmad) and at the probe temperature of 25 ± 1°C.

Caesium-133 chemical shifts were initially referred to an aqueous 0.7 M solution of caesium bromide. The chemical shifts were then corrected to refer to the aqueous solution at infinite dilution and were also corrected for the diamagnetic susceptibility of the solvent.[12] Changes in the diamagnetic susceptibilities of the solutions were assumed to be insignificant because of the low concentrations used. Downfield (paramagnetic) shifts are reported as positive.

Method

Complexation formation constants of the caesium cation with crown ethers were obtained by the conventional ^{133}Cs NMR method.[13] The formation constants of the 1 : 1 (crown ether/Cs^+) complexes were calculated by fitting the ^{133}Cs chemical shifts (δ_{obs}), at various (crown ether)/(Cs^+) mole ratios at the fixed concentration of the caesium salt (0.0050 M), to the following expression:

$$\delta_{obs} = \{\delta_0 + \delta_1[L]K_1\}/\{1 + K_1[L]\}. \quad (1)$$

Where δ_0 and δ_1 are the chemical shifts of the free solvated caesium cation and the limiting chemical shift of the 1 : 1 complex, respectively. K_1 is the formation constant of the 1 : 1 complex and [L] is the free ligand concentration. The value for [L] was obtained iteratively using the non-linear least-squares program KINFIT4,[14] according to the equation:

$$K_1[L]^2 + [K_1(C_L - C_{Cs}) + 1][L] - C_L = 0. \quad (2)$$

C_{Cs} and C_L are the analytical concentrations of the salt and the ligand, respectively.

In cases where both 1 : 1 and 2 : 1 caesium cation complexes were formed the corresponding equations are:[15]

$$K_1K_2[L]^3 + \{K_1K_2(2C_{Cs} - C_L) + K_1\}[L]^2 + \{K_1(C_{Cs} - C_L) + 1\}[L] - C_L = 0 \quad (3)$$

$$\delta_{obs} = \{\delta_0 + \delta_1K_1[L] + \delta_2K_1K_2[L]^2\}/\{1 + K_1[L] + K_1K_2[L]^2\}. \quad (4)$$

Where δ_1 and δ_2 are the limiting chemical shifts of the 1 : 1 and 2 : 1 complexes, respectively, and K_1 and K_2 are the formation constants of the 1 : 1 and 2 : 1 complexes, respectively.

The competitive complexation equilibria, where only 1 : 1 complexes are formed, are:

$$Cs^+ + L \rightleftarrows CsL^+ \quad K_{Cs} = [CsL^+]/[Cs^+][L] \quad (5)$$

$$Rb^+ + L \rightleftarrows RbL^+ \quad K_{Rb} = [RbL^+]/[Rb^+][L]. \quad (6)$$

The free ligand concentration is obtained from the following equation:

$$K_{Cs}K_{Rb}[L]^3 - \{K_{Cs}K_{Rb}(C_L - C_{Cs} - C_{Rb}) - K_{Cs} - K_{Rb}\}[L]^2 - \{K_{Cs}(C_L - C_{Cs}) + K_{Rb}(C_L - C_{Rb}) - 1\}[L] - C_L = 0. \quad (7)$$

The chemical shift data are fit to eq. (1).

In the case where Cs^+ ions form both 1:1 and 2:1 complexes the following equilibrium was considered along with equilibria (5) and (6):

$$CsL^+ + L \rightleftarrows CsL_2^+ \quad K_{Cs2} = [CsL_2^+]/[CsL^+][L]. \quad (8)$$

The free ligand concentration is then obtained from eq. (9) and the chemical shift data are fit to eq. (4).

$$K_{Cs}K_{Cs2}K_{Rb}(L)^4 + \{K_{Cs}K_{Cs2}K_{Rb}(2C_{Cs} + C_{Rb} - C_L) + K_{Cs}K_{Cs2} + K_{Cs}K_{Rb}\}[L]^3 + \{K_{Cs}K_{Cs2}(2C_{Cs} - C_L) + K_{Cs}K_{Rb}(C_{Cs} + C_{Rb} - C_L) + K_{Cs} + K_{Rb}\}[L]^2 + \{K_{Cs}(C_{Cs} - C_L) + K_{Rb}(C_{Rb} - C_L) + 1\}[L] - C_L = 0. \quad (9)$$

RESULTS AND DISCUSSION

In this study the ^{133}Cs nucleus was used as the probe nucleus. This nucleus was chosen because of its narrow resonance line, large chemical shift range and relatively high receptivity.

The use of the ^{133}Cs competitive NMR method for the evaluation of the complexation formation constants of the rubidium cation with crown ethers, K_{Rb}, requires that the formation constants of Cs^+ crown ether complexes, K_{Cs}, be known under similar experimental conditions.

Caesium cation complexes

We used the ^{133}Cs conventional NMR method to determine K_{Cs} values in acetonitrile, since in some cases such data were not available or since the literature values were obtained at significantly different experimental conditions.

Figures 1 and 2 show the variation of ^{133}Cs chemical shift as a function of the C_L/C_{Cs} molar ratio for the complexation of $CsBPh_4$ with crown ethers in acetonitrile. In all cases, except for 18C6, DC21C7 and DC24C8, only 1:1 (ligand/Cs^+) complexes were formed. The 1:1 complex formation constants, K_{Cs}, obtained from the fit of data to eqs (1) and (2) are given in Table 1 along with the corresponding literature values. The data for 18C6, DC21C7 and DC24C8 were fit to eqs (3) and (4). For these ligands the strong 1:1 complex formation is following by the formation of a weaker 2:1 complex as indicated by the change in the slope and/or the change in the direction of the chemical shift above mole ratio one.

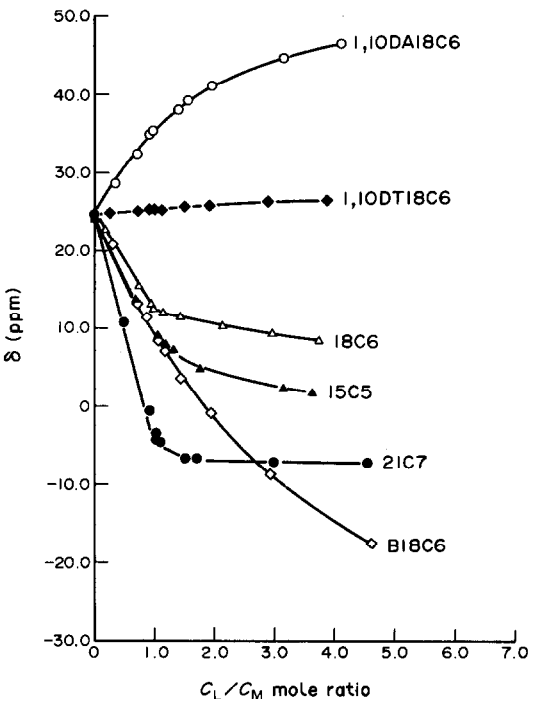

Fig. 1. Caesium-133 chemical shift vs crown ether/Cs^+ mole ratio for solutions containing 0.0050 M $CsBPh_4$ in acetonitrile, at 25°C. Solid lines are calculated curves.

The formation of the $Cs(18C6)_2^+$ "sandwich"

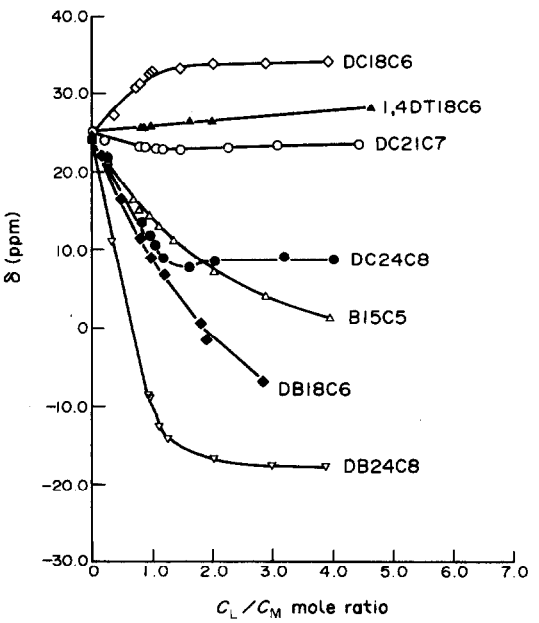

Fig. 2. Caesium-133 chemical shift vs crown ether/Cs^+ mole ratio for solutions containing 0.0050 M $CsBPh_4$ in acetonitrile, at 25°C. Solid lines are calculated curves.

Table 1. Logarithm for formation constants of complexes of caesium and rubidium cations with crown ethers in acetonitrile at 25°C

	Caesium cation		Rubidium cation	
Crown ether	This work	Literature value	This work	Literature value
15C5	2.88 ± 0.02[a]		3.51 ± 0.04[b]	
B15C5	2.11 ± 0.02	3.10[c]	2.91 ± 0.02	2.90[c]
18C6 (1 : 1)	> 4	> 4[d]	> 5	
(2 : 1)	1.37 ± 0.13	0.57 ± 0.07[d]	—[e]	
B18C6	1.80 ± 0.02	4.05[c] 3.8[f]	3.40 ± 0.06	4.40[c]
DB18C6	1.97 ± 0.06	1.54 ± 0.03[d] 3.50[c] 3.5$_9$[g]	3.32 ± 0.06	3.70[c]
DC18C6[h]	3.59 ± 0.09	> 4[d] 5.10[c]	4.47 ± 0.03	5.40[c]
1,10DA18C6	2.29 ± 0.01	2.48 ± 0.03[i]	3.26 ± 0.01	3.37 ± 0.05[i]
1,10DT18C6	1.75 ± 0.08	0.97 ± 0.27[j]	3.25 ± 0.75	
1,4DT18C6	0.98 ± 0.19		1.78 ± 0.14	
21C7	4.24 ± 0.04		4.40 ± 0.01	
DC21C7[h] (1 : 1)	> 4		> 5	
(2 : 1)	1.98 ± 0.08		—[e]	
DB24C8	3.68 ± 0.04	3.80[c] 3.94 ± 0.07[k]	3.94 ± 0.05	3.40[c]
DC24C8[h] (1 : 1)	> 4		> 5	
(2 : 1)	< 1		—[e]	

[a] The ESD of the last digit.
[b] The ESD when K_{Cs} is used as a constant. Overall ESDs are generally 1.5–2.5 times these SDs when the uncertainties of K_{Cs} are included.
[c] Reference 16, polarographic method, error estimates are not given.
[d] Reference 17, NMR method.
[e] No indication of 2 : 1 complex formation.
[f] Reference 18, conductance method, error estimates are not given.
[g] Reference 19, potentiometric method.
[h] Mixture of isomers.
[i] Reference 20, conductance method.
[j] Reference 21, NMR method.
[k] Reference 22, NMR method.

complexes are reported in many solvents.[1] The crystal ionic diameter of the Cs^+ cation is 3.38 Å[23] and the cavity diameter of 18C6 is about 2.70 Å.[24] This makes the formation of the 2 : 1 complexes possible. The cavity diameters of DC21C7 and DC24C8 are about 3.8 and 4.6 Å, respectively.[24] Since the ratio of the cavity diameter to the cationic diameter is greater than one in these cases, the formation of the 2 : 1 complexes should be unlikely. The formation of the 2 : 1 complexes of Cs^+ cation with dicyclohexano-substituted ligands might be due to the high degree of flexibility of both the large crown ether skeleton and the cyclohexano-groups. This high degree of flexibility makes the crown ether conformational changes easier. In the 2 : 1 "sandwich" complexes the cyclohexano-groups should stay far from each other. Then, in the 2 : 1 complex, the two crown ether molecules might bend outward to accommodate the cation. This situation decreases the effective cavity size as well as the degree of interaction between the cation and the oxygen donor atoms. Recently, Soong *et al.*[25] have

reported the formation of the 2:1 complexes of DC21C7 and DC24C8 with the caesium cation in amide solvents. Further studies are in progress in our laboratory to investigate the formation of the 2:1 complexes of large diameter crown ethers with alkali cations.

Even though the ratio of the cavity diameter of 15C5 to the cationic diameter is less than one, the fit of the chemical shift data was better with the 1:1 complexation equilibrium than with the simultaneous 1:1 and 2:1 equilibria. The simultaneous equilibria provided a 2:1 formation constant equal to zero, within the standard deviation estimate. At the same time, the standard deviation in K_1 increased by a factor of two. As can be seen in Table 1, the 1:1 complex is already rather unstable and the formation constant of the 2:1 complex is probably too small to be determined by our method.

The formation constants of caesium cation complexes in acetonitrile are in agreement with the criteria for selective complexation of alkali cations by macrocyclic crown ethers. The attachment of the benzo-group(s) to 15C5 or 18C6 causes a significant decrease in the formation constant. The value of log K_{Cs} falls about 0.8 units as a result of the attachment of the benzo-group to 15C5. The substitution of one or two benzo-groups to 18C6 results in the decrease of the formation constants by more than two orders of magnitude due to the electron-withdrawing nature of the substituents. The effect of the substitution of cyclohexano-groups is not as drastic as they are not as electron withdrawing as the benzo-groups. In addition, the higher rigidity of the benzo-groups compared with cyclohexano-groups inhibits the conformational changes of the crown ether molecules which are required for complex formation. A similar effect is observed for dibenzo- and dicyclohexano-substituted 24C8.

In the groups of 18C6 analogues studied, the 1:1 complex formation constants show the trend:

$$1,4DT18C6 < 1,10DT18C6 < B18C6 < DB18C6 < 1,10DA18C6 < DC18C6 < 18C6.$$

The complex formation constant of the Cs^+ cation with 1,10DA18C6 is smaller than those of 18C6 and DC18C6. This is expected since (1) the electron-donating ability of the nitrogen atoms is less than the electron-donating ability of the oxygen atoms; (2) the covalent diameter of nitrogen atom is smaller than that of the oxygen atom, which causes the 1,10DT18C6 ligand cavity to be smaller than that of 18C6 or DC18C6; and (3) the weak interaction between the relatively "hard" caesium cation and the relatively "soft" nitrogen atom.[26] Frensdorff[27] has shown that in methanol solution the complex formation constant of the K^+ ion with 1,10DA18C6 is four orders of magnitude smaller than with 18C6.

The sulphur substituted ligands, 1,4DT18C6 and 1,10DT18C6, have the smallest formation constants of all the 18-member crown ethers studied. This observation may result from at least two factors: (1) the smaller diameter of the ligand cavity due to the bulky sulphur atoms; and (2) the weak interaction between the relatively "hard" caesium cation and the relatively "soft" sulphur atoms.[26] Rounaghi and Popov[21] have determined the complex formation constant of caesium thiocyanate with 1,10DT18C6 in acetonitrile of log $K = 0.97 \pm 0.27$, compared with our result of 1.75 ± 0.08. The discrepancy probably arises from differences in the nature of the counter ion. The thiocyanate anion has a higher ion pair formation ability with the cation and/or the complexed cation as compared with the tetraphenylborate anion.[28] Since the ion pair formation competes with the complex formation, one would expect a less stable complex with the thiocyanate salt. The complex formation constant of Cs^+ is smaller with 1,4DT18C6 than with 1,10DT18C6. In 1,4DT18C6 the bulky sulphur atoms are close to each other and probably would exclude a portion of the cavity for the accommodation of the cation. Differences in the conformational mobilities of the 1,4- and 1,10-dithia-substituted ligands might also be responsible for the difference in the stability of their complexes.

Rubidium cation complexes

The similarity of the crystallographic diameters of the caesium cation (3.38 Å) and the rubidium cation (2.96 Å)[23] suggests the use of ^{133}Cs NMR to probe the complexation of the rubidium cation with crown ethers. Figures 3 and 4 depict the variation of the ^{133}Cs chemical shift as a function of C_L/C_{Cs} molar ratio ($C_{Cs} = 0.0050$ M) in the presence of rubidium tetraphenylborate ($C_{Rb} = 0.0050$ M) in acetonitrile. The data indicated the formation of only 1:1 rubidium complexes. The observed chemical shifts would fit to eqs (1) and (7) (where only 1:1 caesium complexes formed) or to eqs (4) and (9) (where both 1:1 and 2:1 caesium complexes formed). The formation constants of rubidium crown ether complexes are given in Table 1.

The chemical shift of the free solvated cation in the presence of rubidium salt is about 4 ppm downfield compared to the chemical shift in the absence of the rubidium cation, due to the difference in the ionic strengths of these solutions. For 18C6, DC21C7 and DC24C8, where K_{Cs} values are not known ($K_{Cs} > 10^4$), only the lower limits of K_{Rb} are reported.

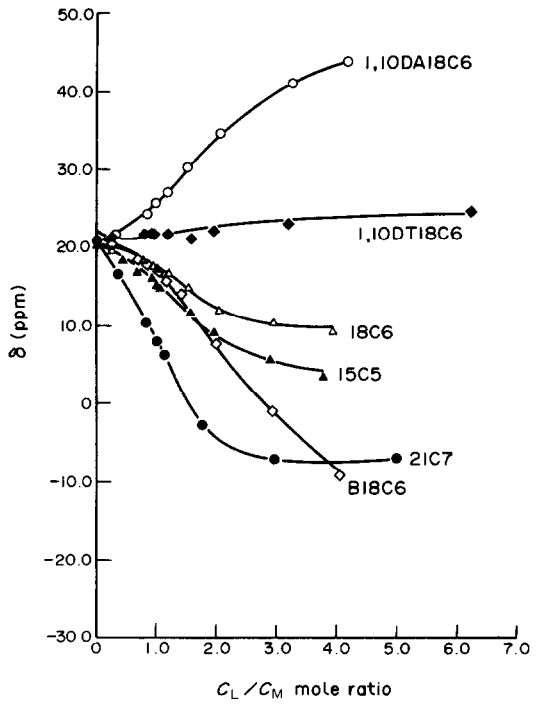

Fig. 3. Caesium-133 chemical shift vs crown ether/Cs^+ mole ratio for solutions containing 0.0050 M $CsBPh_4$ and 0.0050 M $RbBPh_4$ in acetonitrile, at 25°C. Solid lines are calculated curves.

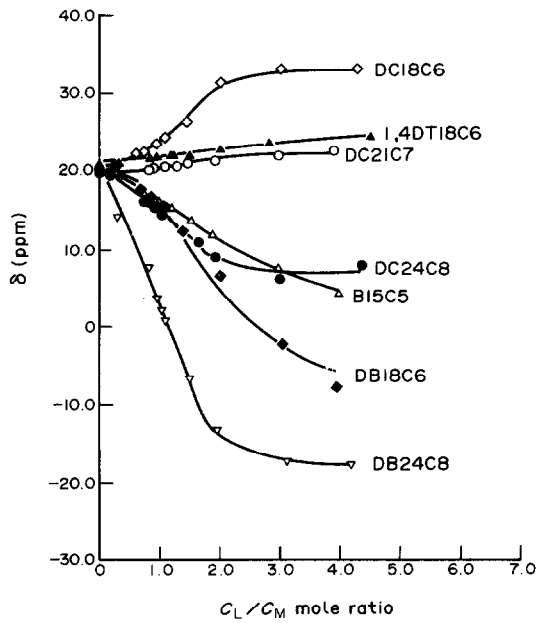

Fig. 4. Caesium-133 chemical shift vs crown ether/Cs^+ mole ratio for solutions containing 0.0050 M $CsBPh_4$ and 0.0050 M $RbBPh_4$ in acetonitrile, at 25°C. Solid lines are calculated curves.

In all cases rubidium complexes are more stable than the corresponding caesium complexes. The difference between the stability of the caesium and rubidium complexes are more pronounced with the smaller crown ethers than with the larger ligands. For smaller ligands the relative sizes of the macrocyclic cavity and the cation probably play the most important role with regard to the stability of the complexes. However, for larger crown ethers, other factors such as the flexibility of the ligand molecules can become more important.

The complex formation constants with the benzo-substituted crown ethers are smaller than with the corresponding non-substituted ligands, as expected from the electron-withdrawing ability of the benzene ring. The stability of the rubidium complexes with the benzo-substituted crown ethers increases in the order: B15C5 < DB18C6 ≈ B18C6 < DB24C8. This trend clearly shows the effect of the flexibility of the larger crown ethers on the stability of their complexes. Even though the rubidium cation is too small and its fit into the DB24C8 cavity ($d \approx 4.5$ Å) should be "loose", the crown ether molecules can wrap themselves around the cations as a result of their ability for conformational changes.

Rubidium cations form stronger complexes with the non-substituted crown ethers than with either the cyclohexano- or benzo-substituted crown ethers. This effect is similar to the caesium complexation discussed previously.

The substitution of two oxygen atoms by either two nitrogen or two sulphur atoms in the 18C6 ring decreases the stability of the rubidium complexes. This result should be interpreted with regard to the change in the crown cavity size and the interactions between relatively "hard acids" and "soft bases", as was discussed earlier. It should be mentioned that the error associated with the K_{Rb} of the $Rb^+ \cdot$ 1,10DT18C6 complex is very large due to the small chemical shift range. A more precise K_{Rb} value for this complex should be obtained before we can accurately compare this value with the other formation constants.

The above results show that the competitive ^{133}Cs NMR method can be successfully used to probe the thermodynamics of complexation of rubidium salts with macrocyclic crown ethers in non-aqueous solvents. The stability of the complexes depends not only on the relative sizes of the cation and the ligand cavity, but on other factors such as the nature of the substituents on the crown ether ring and the conformational changes of the macrocyclic ligand. Significantly, we have observed that large crown ethers may form 2 : 1 complexes with Cs^+ cation in addition to the more commonly known 1 : 1 complexes.

Acknowledgement—The authors gratefully acknowledge the support of this work by the Graduate School and the Department of Chemistry, Southern Illinois University, at Edwardsville.

REFERENCES

1. R. M. Izatt, J. S. Bradshaw, S. A. Nielson, J. D. Lamb and J. J. Christensen, *Chem. Rev.* 1985, **85**, 271 and refs cited therein.
2. S. Khazaeli, J. L. Dye and A. I. Popov, *Spectrochim. Acta* 1983, **39A**, 19.
3. B. Lindman and S. Forsén, *NMR and the Periodic Table* (Edited by R. K. Harris and B. E. Mann), pp. 130–131. Academic Press, New York (1978).
4. B. G. Cox and H. Schneider, *J. Am. Chem. Soc.* 1977, **99**, 2809.
5. B. G. Cox, H. Schneider and J. Stroka, *J. Am. Chem. Soc.* 1978, **100**, 4746.
6. B. G. Cox, D. Knop and H. Schneider, *J. Phys. Chem.* 1980, **84**, 320.
7. B. G. Cox, J. Garcia-Rosas and H. Schneider, *J. Am. Chem. Soc.* 1981, **103**, 1384.
8. C. Srivanavit, J. I. Zink and J. J. Dechter, *J. Am. Chem. Soc.* 1977, **99**, 5876.
9. R. D. Boss and A. I. Popov, *Inorg. Chem.* 1985, **24**, 3660.
10. W. J. Dewitte, L. Liu, E. Mei, J. L. Dye and A. I. Popov, *J. Solution Chem.* 1977, **6**, 337.
11. G. W. Gokel, D. J. Cram, C. L. Liotta, H. P. Harris and F. L. Cook, *J. Org. Chem.* 1974, **39**, 2445.
12. D. H. Live and S. I. Chan, *Anal. Chem.* 1970, **42**, 791.
13. E. T. Roach, P. R. Handy and A. I. Popov, *Inorg. Nucl. Chem. Lett.* 1973, **9**, 359.
14. J. L. Dye and V. A. Nicely, *J. Chem. Educ.* 1971, **48**, 443.
15. E. Mei, PhD thesis. Michigan State University, East Lansing, Michigan (1977).
16. A. Hofmanova, J. Koryta, M. Brenzina and M. L. Mittal, *Inorg. Chim. Acta* 1978, **28**, 73.
17. E. Mei, A. I. Popov and J. L. Dye, *J. Phys. Chem.* 1977, **81**, 1677.
18. Y. Takeda, Y. Ohyag and S. Akabori, *Bull. Chem. Soc. Japan* 1984, **57**, 3381.
19. I. M. Kolthoff and M. K. Chantooni Jr, *Anal. Chem.* 1980, **52**, 1039.
20. S. Kulstad and L. A. Malmsten, *J. Inorg. Nucl. Chem.* 1980, **42**, 537.
21. G. Rounaghi and A. I. Popov, *J. Inorg. Nucl. Chem.* 1981, **43**, 911.
22. M. Shamsipur, G. Rounaghi and A. I. Popov, *J. Solution Chem.* 1980, **9**, 701.
23. L. Pauling, *The Nature of the Chemical Bond.* Cornell University Press, Ithaca, New York (1960).
24. C. J. Pederson, *Angew. Chem., Int. Edn. Engl.* 1988, **27**, 1021.
25. L. Soong, G. E. Leroi and A. I. Popov, *Inorg. Chem.* 1990, **29**, 1366.
26. R. G. Pearson, *J. Am. Chem. Soc.* 1963, **85**, 3535.
27. H. K. Frensdorff, *J. Am. Chem. Soc.* 1971, **93**, 600.
28. S. Khazaeli, A. I. Popov and J. L. Dye, *J. Phys. Chem.* 1982, **86**, 4238.

Polyhedron Vol. 10, No. 2, pp. 229–235, 1991
Printed in Great Britain

0277–5387/91 $3.00+.00
© 1991 Pergamon Press plc

TRENDS IN $\delta \rightarrow \delta^*$ ENERGIES AND INTENSITIES IN BIS(ARYLIMINO)ISOINDOLINE COMPLEXES OF DIMOLYBDENUM

D. M. BAIRD† and K. Y. SHIH

Department of Chemistry, Florida Atlantic University, Boca Raton, FL 33431, U.S.A.

(*Received* 25 *June* 1990; *accepted* 17 *September* 1990)

Abstract—It has been found that the $\delta \rightarrow \delta^*$ band in the electronic absorption spectra of a series of bis(arylimino)isoindoline dimolybdenum complexes, $Mo_2(BAII)(OAc)_3$, follows three trends. First, as the energy of the band decreases across the series its intensity increases. Second, as electron-releasing groups are added to the aryl portion of the ligand the energy of the band increases, while addition of electron-releasing groups decreases its energy. Third, as the parent aryl group becomes a better π-acceptor the band's energy decreases. These three trends are taken to indicate that the energy of the $\delta \rightarrow \delta^*$ band in this series of compounds is determined by mixing of a ligand-to-metal charge-transfer transition with the original $\delta \rightarrow \delta^*$ transition.

The understanding of both the structural and reaction chemistry of multiple metal–metal bonds has matured greatly over the past 10 years or so. In particular, investigations concerning quadruply bonded dimolybdenum compounds have been numerous.[1] Only a few homologous series of dimolybdenum compounds have been studied, however, and these form the basis for our understanding of the physical and electronic properties of dimolybdenum species. The most extensive series of well studied and well understood dimolybdenum compounds are those with the general formulae $Mo_2X_4(PR_3)_4$ and $Mo_2X_4(PP)_2$, where X = halogen, NCS^-, NCO^-, etc., and PR_3 and PP refer to monodentate and bidentate phosphine ligands, respectively. Studies of these compounds have led to a greater understanding of the structural effects on the reactivities and properties of dimolybdenum compounds in general. In particular, a greater understanding of the relationship between the electronic absorption spectra and electronic structures of these compounds has recently been realized. The relationship between the energies and intensities of the so called "$\delta \rightarrow \delta^*$" band and the energies of ligand-to-metal charge-transfer transitions has, especially, been the topic of much discussion.[2–7] It is not clear whether the reasoning developed for the $Mo_2X_4(PR_3)_4$ series can be applied to other series of structurally related dimolybdenum compounds. In fact, there has been no other extensive series of structurally related compounds available which can be investigated in terms of their electronic structures.

We have recently synthesized[8] and studied a series of 11 dimolybdenum complexes which contain bis(arylimino)isoindoline (BAII) ligands which have the general structure shown below:

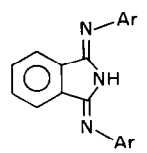

In the above structure aryl is substituted or unsubstituted pyridine, pyrazine, thiazole or pyrimidine. The complexes, $Mo_2(BAII)(OAc)_3$, have been shown by NMR spectroscopy to have structures analogous to the bis(pyridylimino)isoindoline derivative whose structure has been elucidated using X-ray crystallography.[9] These compounds contain the molybdenum–molybdenum quadruple bond bridged by three acetate groups. In addition, the BAII ligand, which is planar tridentate in mononuclear complexes, has been altered by rotation about one of the imino bonds prior to binding to the dimolybdenum unit (Scheme 1). Thus the BAII

† Author to whom correspondence should be addressed.

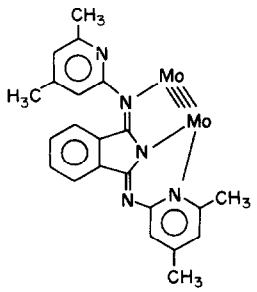

Structure 1. General structure of $Mo_2(BAII)(OAc)_3$. Bridging acetates have been removed for clarity. Note that the non-bonded aryl group is generally rotated out of the ligand plane.

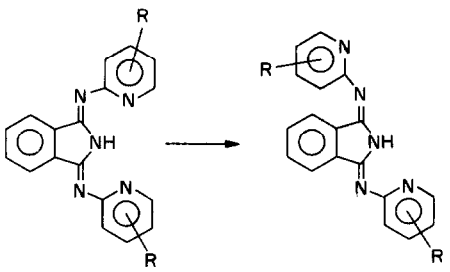

Scheme 1.

bridges the two molybdenum atoms by binding one metal with the isoindoline nitrogen and the other metal with the imino nitrogen about which rotation has occurred. This rotation places one pyridine in a position away from the dimetal unit. The other pyridine is bonded to one of the molybdenum atoms in a position co-axial with the metal–metal bond.

Since the compounds synthesized represented a large series of structurally similar dimolybdenum compounds, it was decided to subject them to a spectroscopic study. The results of this study are presented below.

EXPERIMENTAL

Materials and methods

All synthetic procedures were performed under an atmosphere of argon using standard Schlenk techniques or a glove box. Methylene chloride was dried by refluxing with calcium hydride or phosphorus pentoxide. Tetrahydrofuran was refluxed with Na–benzophenone, and methanol was refluxed with calcium sulphate. All solvents were distilled under argon just prior to use. Molybdenum acetate was prepared from $Mo(CO)_6$ using the method of Wilkinson and Dori.[10] The BAII ligands were prepared by the method of Siegl,[11] in which the appropriate aromatic amine was reacted with 1,2-dicyanobenzene in refluxing butanol in the presence of a small amount of anhydrous calcium chloride. The 2-aminoheterocyclic amines, except 5-iodopyridine, were purchased from Aldrich and used as received. 5-Iodopyridine was synthesized by the method of Caldwell *et al.*[12]

Spectroscopic samples were prepared as CH_2Cl_2 solutions in a glove box using cells equipped with a screw-on cap.

Spectra were obtained from 900 to 180 nm using a Shimadzu 2100 spectrophotometer.

Preparation of bis(pyrimidinylimino)isoindoline

It has been reported by other workers that the reaction between 1,2-dicyanobenzene and 2-aminopyrimidine does not occur.[11] We have successfully prepared this BAII derivative by the following procedure.

The reactants were heated in butanol at reflux temperature for 7 days. During this period the solution turned deep blue in colour while yellow and blue precipitates formed. After the mixture was cooled the solids were filtered and treated with $CHCl_3$. The undissolved blue–purple material was then filtered out. Addition of an equal volume of *n*-heptane to the filtrate and refrigeration produced the pale yellow bis(pyrimidinylimino)isoindoline as a precipitate (m.p. 222–224°C). This was filtered and dried *in vacuo*.

Syntheses of BAII *complexes of dimolybdenum,* $Mo_2(BAII)(OAC)_3$

$Mo_2(BAII)(OAc)_3$ (BAII = *bis(pyridylimino)isoindoline*).[9] $Mo_2(OAc)_4$ (1 g) was added as one portion to a solution of bis(pyridylimino)isoindoline in 35 cm^3 of dry, degassed methanol. The resulting yellow mixture slowly turned emerald green. After stirring overnight a green precipitate formed, which was filtered, washed with hexane and then dried *in vacuo*. This procedure resulted in about 75% yield after recrystallization from benzene–hexane.

Other BAII *complexes.* The same procedure was used for all other BAII complexes using *ca* 1 g of $Mo_2(OAc)_4$ with yields of 80% or above. In the case of the pyridine and 4-methylpyridine derivatives the yellow mixture slowly turned emerald green after stirring overnight.

The 4,6-dimethylpyridine derivative was stirred with $Mo_2(OAc)_4$ for 7 days before complete reaction was achieved. The reactions of the 5-halopyridines, the thiazole derivatives and the pyrazine

derivative were carried out overnight at reflux temperature.

RESULTS AND DISCUSSION

The $\delta \rightarrow \delta^*$ transition energies and intensities for the BAII dimolybdenum complexes are listed in Table 1 and typical spectra are shown in Fig. 1. Upon inspection of this data three trends become obvious. First, it is found that as the energy of this band decreases its intensity increases. Second, within a series of complexes derived from the same aromatic amine heterocycle the $\delta \rightarrow \delta^*$ band shifts to lower energy when electron-withdrawing substituents are added to the heterocyclic ring, and to higher energy upon addition of electron-releasing groups. Third, a large effect is observed for changes in the parent amine heterocycle. Each of these trends will be discussed below in detail.

Background

The majority of dimolybdenum complexes possess an eclipsed structure in which the donor atoms attached to one molybdenum eclipse the donor atoms on the other molybdenum when viewed along the metal–metal bond. This configuration maximizes the δ-overlap. In early reports it was thought that the energy of the $\delta \rightarrow \delta^*$ band may be a reflection of the extent of δ-overlap between the two metals.[3] Presumably then, a twist about the metal–metal bond would result in decreased δ-overlap and a lower energy $\delta \rightarrow \delta^*$ band due to a decrease in the separation of the δ and δ^* orbitals.

A series of diphosphine bridged dimolybdenum complexes, $Mo_2X_4(PP)_2$, have been reported by Cotton *et al.*,[13] in which a twist about the metal–metal bond exists due to ligand constraints imposed by the methylenes in its backbone. This work has shown that as the twist angle increases and δ-overlap decreases the energy of the $\delta \rightarrow \delta^*$ transition decreases. As would be expected, the intensity of the $\delta \rightarrow \delta^*$ band decreases as its energy decreases due to smaller δ-overlap. These results seem to confirm the notion that the energy of the $\delta \rightarrow \delta^*$ transition is related to the δ-overlap.

However, when the compounds in a series of complexes which all possess an eclipsed (twist angle = 0°) geometry are compared, it is found that the $\delta \rightarrow \delta^*$ band still varies over a fairly large range. For example, in the series $Mo_2Cl_4(PMe_3)_4$, $Mo_2Br_4(PMe_3)_4$, $Mo_2I_4(PMe_3)_4$ the $\delta \rightarrow \delta^*$ band, where δ-overlap has been theoretically estimated to change from 0.17 to 0.23,[5] red shifts by 1400 cm^{-1}. On the other hand, in the series $Mo_2X_4(PP)_2$, in which the halogen remains constant and the twist angle increases, a change of twist angle from 0 to 45° results in a red shift of the $\delta \rightarrow \delta^*$ band by 4640 cm^{-1}. It seems clear that the shift in the $\delta \rightarrow \delta^*$ band in the eclipsed series cannot be accounted for by change in δ-overlap since it is shifted more than one third that found in the twisted series, where the change in overlap should be about five times less in the most twisted case than in the eclipsed case.[6] In addition, the decrease in energy of the $\delta \rightarrow \delta^*$ transition in the eclipsed case is accompanied by an

Table 1. Spectroscopic data for $Mo_2(BAII)(OAc)_3$. Energies and intensities of the $\delta \rightarrow \delta^*$ band

BAII	$\delta \rightarrow \delta^*$ Wavelength (nm)	$\delta \rightarrow \delta^*$ Frequency (cm^{-1})	ε	f^a
4,6-$(CH_3)_2$-py (A)	653	15,300	1050	0.021
4-CH_3-py (B)	685	14,590	1700	0.034
H-py (C)	694	14,400	1980	0.036
5-I-py (D)	717	13,940	2140	0.038
5-Br-py (E)	717	13,940	2050	0.036
5-Cl-py (F)	713	14,030	2070	0.037
3,5-Cl_2-py[b] (G)	742	13,470	—	—
4-CH_3-thiazole[b] (H)	727	13,760	—	—
H-thiazole[b] (I)	742	13,470	—	—
H-pyrazine (J)	749	13,340	2940	0.054
H-pyrimidine (K)	789	12,680	3250	0.064

[a] f = oscillator strength $\approx (4.6 \times 10^{-9}) \times \varepsilon_{max} \times \nu_{1/2}$.
[b] Accurate intensity data could not be obtained due to persistent impurities.

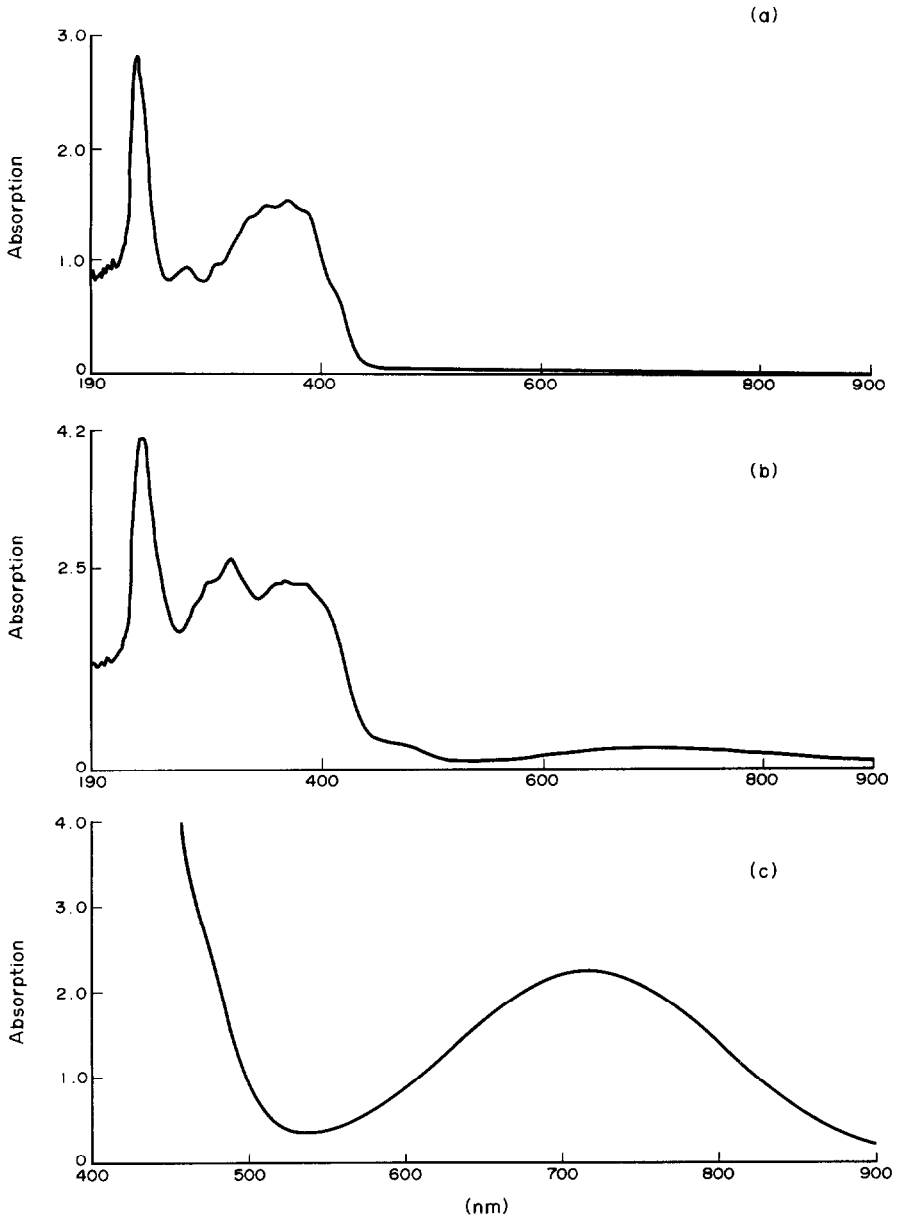

Fig. 1. Typical electronic absorption spectra of BAII ligands and complexes. (a) Spectrum of the 5-chloropyridine-derived BAII ligand; (b) spectrum of the 5-chloropyridine derivative of Mo_2(BAII)$(OAc)_3$; (c) close up of $\delta \rightarrow \delta^*$ band for the 5-chloropyridine derivative of Mo_2(BAII)-$(OAc)_3$.

increase in intensity. This is the opposite of the intensity trend observed for the twisted series where it is known that the δ-overlap decreases.

In order to explain the large energy shift and intensity increase across the eclipsed $Mo_2X_4(PR_3)_4$ series, Gray and co-workers have proposed that the original $\delta \rightarrow \delta^*$ transition mixes with a low energy ligand-to-metal charge-transfer (LMCT) transition.[7] The results of such mixing would be that the energy of the $\delta \rightarrow \delta^*$ transition would be lowered upon lowering of the LMCT transition. In addition, the band's intensity would be increased, rather than decreased, due to intensity borrowing.

Trends in the BAII *series*

Intensity trends. Inspection of the energies of the $\delta \rightarrow \delta^*$ band for the Mo_2(BAII)$(OAc)_3$ series reveals that the intensity increases as the energy decreases. In fact a plot of energy vs intensity yields a straight line (Fig. 2). The correlation coefficient for the line in Fig. 2 is 0.999. The halopyridine

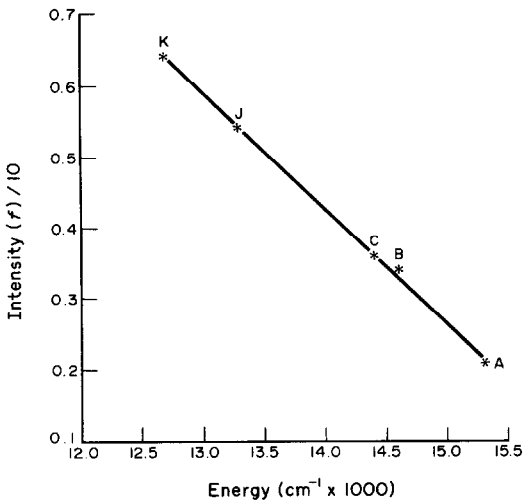

Fig. 2. Plot of energies vs intensities for the $\delta \rightarrow \delta^*$ band of Mo_2(BAII)$(OAc)_3$ complexes.

derivatives deviate slightly from the line but even when they are included the correlation is still 0.96. This would seem to suggest, based on the discussion above, that this band does not simply reflect the extent of δ-overlap between the two metal d_{xy} orbitals. This notion is further supported by the fact that the energy of this transition varies over a range of 2300 cm^{-1}. This would represent a rather large change in δ-overlap when compared with the twisted $Mo_2X_4(PP)_2$ series, where overlap is known to decrease by a factor of about five times and the band red shifts 4640 cm^{-1}. The trend of increasing intensity with decreasing energy seems to indicate that a low energy charge-transfer band may be mixing with the $\delta \rightarrow \delta^*$ band in a fashion analogous to that found in the $Mo_2X_4(PMe_3)_2$ series.

Effects of aryl substituents. The addition of electron-withdrawing substituents such as halogens to the aryl portion of the BAII ligand causes a red shift of the band relative to the unsubstituted aryl group derivative, while the addition of electron-releasing alkyl groups tends to cause a blue shift in this band. For example, inspection of the series made up of compounds derived from 3,5-dichloropyridine, 5-chloropyridine, pyridine, 4-methylpyridine and 4,6-dimethylpyridine demonstrates the trend clearly. A similar trend is observed for the thiazole and methylthiazole derivatives. This type of trend can also be observed in the compounds reported by Ewing and Shupack[14] which have the formula $Mo_2X_4(Py)_4$, where X is chloride or bromide and Py is pyridine, picoline or lutidine. If the series in which all complexes contain chlorine is examined it is discovered that addition of electron-releasing methyl groups tends to lower the energy of the $\delta \rightarrow \delta^*$ band. For example, for the series pyridine, 4-methylpyridine and 3,5-dimethylpyridine, the $\delta \rightarrow \delta^*$ band is reported at 16,667, 16,807 and 17,986 cm^{-1}, respectively. In the bromine series, the 3-methylpyridine derivative is reported to have a $\delta \rightarrow \delta^*$ band at 15,198 cm^{-1}, while the 3,4-dimethylpyridine derivative has this band at 17,904 cm^{-1}. This trend, however, is just the opposite of that expected for the mixing of a LMCT transition with the $\delta \rightarrow \delta^*$ transition such as has been observed in the $Mo_2X_4(PR_3)_4$ series. For example, an electron-releasing methyl would be expected to lower the energy of a LMCT transition. Thus after mixing, a lower energy $\delta \rightarrow \delta^*$ band would result. In the BAII series, addition of a methyl group causes a higher energy $\delta \rightarrow \delta^*$ band compared with the unsubstituted pyridine case. This apparent contradiction can be explained if the charge-transfer transition mixing with the $\delta \rightarrow \delta^*$ transition in the BAII series was a metal-to-ligand charge-transfer (MLCT) transition. In this case substitution of an electron-withdrawing chlorine onto the aryl group would result in a lowering of a MLCT transition which would then lower the energy of the $\delta \rightarrow \delta^*$ band through mixing. This is exactly what is observed in the BAII series. The idea that a MLCT transition of reasonably low energy is present in these complexes is consistent with the known π-accepting ability of aromatic nitrogen heterocycles such as the ones upon which the BAII ligands are based. In addition, the linearity of the energy vs intensity plot referred to earlier suggests that the changes in both the energy and the intensity of the $\delta \rightarrow \delta^*$ band are affected by the same phenomenon. That is, if the MLCT which is mixing with the $\delta \rightarrow \delta^*$ transition were a $\delta \rightarrow \pi^*$ transition, then lowering the ligand π^*-orbital energy would lower the MLCT transition. As a result lowering the energy of the $\delta \rightarrow \delta^*$ band. Simultaneously, the intensity of the band would increase due to more efficient intensity borrowing.

Effect of varying the parent heterocycle. If, in fact, the energy of the $\delta \rightarrow \delta^*$ band is related to the energy of a π^*-orbital on the ligand and, therefore, related to the π-accepting ability of the ligand, we would expect to find a trend which results from substituting the parent amine heterocycle portion of the BAII ligand. It can be seen that as the known π-accepting ability of the heterocycle increases (pyrazine > thiazole > pyridine) the energy of the $\delta \rightarrow \delta^*$ band decreases (pyrazine < thiazole < pyridine).

Unfortunately the role of the aryl group in these compounds is undoubtedly complex since the only

direct bond to the dimolybdenum unit from any aryl group is to the axial position at one end of the Mo—Mo bond. It seems reasonable at the outset to attribute changes in the energy of the $\delta \rightarrow \delta^*$ band to changes in the extent of axial bonding. Particularly in the case of the 4,6-dimethylpyridine derivative where steric interaction of the 6-methyl group may weaken axial bonding and shift the band towards that of the "bare" dimer. To answer this question it should be pointed out that the 3,5-dichloropyridine derivative, reported in Table 1, is shifted to an even greater extent (referenced to the unsubstituted pyridine case) than is the 4,6-dimethylpyridine case. Since there is no steric problem in the dichloropyridine case the Mo—N axial bond should be present. If axial bonding of the N-heterocycle had a significant effect on the energy of the $\delta \rightarrow \delta^*$ band it might be expected that the Mo—N axial bond in the dichloropyridine case should be weaker than in the unsubstituted pyridine case due to the electron-withdrawing groups. In this case then, the dichloro derivative should be closer to the "bare" dimer and would be expected to have a higher energy $\delta \rightarrow \delta^*$ band than the unsubstituted pyridine case. In fact, the energy in the dichloropyridine case is considerably lower than in the pyridine case. Based on this argument it must be concluded that the axial bond does not have a significant effect on the energy of the band in question. This is not unreasonable based on the long Mo—N axial bond distance in the crystal structure of the pyridine derivative. Small changes in the bond strength of the already weak bond upon addition of substituents should not have much impact. NMR spectra of the 4,6-dimethylpyridine-derived complex show that, at the very least, it has the same "inside–outside" arrangement of pyridine rings as the unsubstituted pyridine case. While it cannot be ruled out that steric interactions preclude axial Mo—N binding in this derivative, it is believed that, based on the above arguments, such bonding does not have a great impact on the energy of the $\delta \rightarrow \delta^*$ band.

Some further insight might be gained from consideration of the pyrimidine complex. In this case it is believed that, unlike the other BAII complexes, the aryl ring not bound to molybdenum is co-planar with the rest of the BAII ligand. Evidence for this notion has been gained from comparison of the ^{1}H NMR spectrum of the pyridimidine derivative with the spectra of the other BAII complexes. The spectra of the majority of BAII dimolybdenum complexes are characterized by an upfield shift of the α-proton resonance of the benzo portion of the isoindoline system closest to the non-co-planar aryl ring. This shift is apparently due to the proximity of this proton to the inside of the aryl group ring current. In the pyrimidine derivative both pyrimidine rings are co-planar with the isoindoline portion of the BAII system and the α-proton resonance is shifted downfield since it is on the outside of the ring current. The co-planarity of the second pyrimidine ring is apparently due to the fact that a nitrogen atom is in the 6-position of this ring. Since there is no hydrogen attached to this nitrogen the ring may remain co-planar without interacting with the α-proton of the benzo portion of the isoindoline group. In this case the $\delta \rightarrow \delta^*$ band is red shifted much more than would be expected based on the π-accepting ability of pyrimidine compared with the other heterocycles used in this study. Thus, it appears that the aryl rings simply act as electron-withdrawing or -releasing groups for the isoindoline portion of the ligand. In the pyrimidine case both rings may be conjugated with the isoindoline group resulting in a larger red shift of the band since the energy of the π-system of the isoindoline moiety would be lowered through increased conjugation.

CONCLUSION

In conclusion, the trend of increasing $\delta \rightarrow \delta^*$ intensity with decreasing energy indicates that this band is not simply a reflection of the extent of δ-overlap in these compounds and that there is mixing of a charge-transfer transition with the $\delta \rightarrow \delta^*$ transition. The substituent effects suggest that the charge-transfer involved is a MLCT transition, probably a $\delta \rightarrow \pi^*$ transition. The trend with respect to different heterocycles seems to confirm this idea. The possibility that the shift in the $\delta \rightarrow \delta^*$ band may be due to differences in base strength of the ligand seems to be ruled out by the range over which this band occurs in this series. Therefore, in dimolybdenum complexes of aromatic amine heterocycles the π-accepting ability of the ligand plays a role in determining the energy of the $\delta \rightarrow \delta^*$ band.

Acknowledgement—We would like to thank Research Corporation for a grant in support of this work.

REFERENCES

1. (a) F. A. Cotton and R. A. Walton, *Multiple Bonds Between Metal Atoms*. Wiley, New York (1982); (b) F. A. Cotton, *Polyhedron* 1986, **5**, 3.
2. B. E. Bursten and D. L. Clark, *Polyhedron* 1987, **6**, 695.
3. A. P. Stattelberger and J. P. Fackler, *J. Am. Chem. Soc.* 1977, **99**, 1258.
4. M. C. Manning and W. C. Trogler, *J. Am. Chem. Soc.* 1983, **103**, 5311.

5. W. C. Trogler and H. B. Gray, *Acc. Chem. Res.* 1978, **11**, 232.
6. (a) F. L. Campbell, F. A. Cotton and G. Powell, *Inorg. Chem.* 1984, **23**, 4222; (b) M. D. Hopkins, T. C. Zietlow, V. M. Miskowski and H. B. Gray, *J. Am. Chem. Soc.* 1985, **107**, 510.
7. (a) M. D. Hopkins, W. P. Schaefer, M. J. Bronikowski, W. H. Woodruff, V. M. Miskowski, R. F. Dallinger and H. B. Gray, *J. Am. Chem. Soc.* 1987, **109**, 408; (b) M. D. Hopkins, H. B. Gray and V. M. Miskowski, *Polyhedron* 1987, **6**, 705; (c) M. D. Hopkins, V. M. Miskowski and H. B. Gray, *J. Am. Chem. Soc.* 1988, **110**, 1787.
8. D. M. Baird and R. Hassan, *Inorg. Chim. Acta* 1987, **130**, 39.
9. D. M. Baird, K. Y. Shih, J. H. Welch and R. D. Bereman, *Polyhedron* 1989, **8**, 2359.
10. G. Wilkinson and Z. Dori, *Inorg. Synth.* 1969, 1872.
11. W. O. Siegl, *J. Org. Chem.* 1977, **42**, 1872.
12. W. T. Caldwell, F. T. Tyson and L. Lauer, *J. Chem. Soc.* 1944, **66**, 1479.
13. F. A. Cotton, K. R. Dunbar and M. Matusz, *Inorg. Chem.* 1986, **25**, 3641 and refs therein.
14. K. J. Ewing and S. I. Shupack, *Polyhedron* 1985, **4**, 2069.

Polyhedron Vol. 10, No. 2, pp. 237–242, 1991
Printed in Great Britain

0277–5387/91 $3.00+.00
© 1991 Pergamon Press plc

ACRYLAMIDE POLYMERIZATION PHOTO-INDUCED BY A CHROMIUM(VI)–COPPER(II) BICATIONIC SYSTEM IN AQUEOUS SOLUTION—I. STUDY OF COPPER INFLUENCE ON THE PRIMARY PHOTOPROCESS

GILLES MAILHOT and MICHÈLE BOLTE*

Laboratoire de Photochimie Moléculaire et Macromoléculaire, URA CNRS 433,
UFR de Recherche Scientifique et Technique, Université Blaise Pascal,
63177—Aubière Cedex, France

(*Received* 18 *April* 1990; *accepted* 26 *September* 1990)

Abstract—The polymerization of acrylamide photo-induced by a bicationic system was investigated. From the results of kinetic measurements, the couple chromium–copper was proved to be a suitable system to initiate and terminate the process of polymerization. $HCrO_4^-$ is the photo-initiator and $Cu(H_2O)_6^{2+}$, transparent at the excitation wavelength, only acts as a termination agent. At room temperature, the quantum yield remained unchanged when the concentration of copper(II) was varied from 5×10^{-5} to 5×10^{-3} mol dm^{-3}, whereas the rate of polymerization was strongly affected by the presence of copper(II) in the solution. By ESR spectroscopy measurements at low temperature, it was possible to assess that copper(II) was also involved in a reaction with chromium(V). Copper(II) is able to react with the two species, chromium(V) and R·, arising from the redox process between excited $HCrO_4^-$ and acrylamide.

The polymerization of a vinyl monomer, photo-initiated by coordination complexes, has received paticular interest. Iron(III) salts,[1,2] cobalt(III) salts[3–5] and manganese carbonyl complexes[6] have been proved to be efficient photo-initiators of the polymerization. Natarajan and Santappa[7] reported the photoredox phenomenon involved in acrylamide and acrylonitrile polymerization photo-initiated by diacidobis(ethylenediamine)cobalt(III) complexes. Delzenne[8] described the mechanism of acrylamide polymerization photo-initiated by penta-aminecobalt(III) complexes. Takemura and co-workers[9] more recently reported the acrylamide polymerization photo-initiated by $Ru(bipy)_3^{2+}$, excited with visible light in the presence of an electron donor.

In the series of previous papers, we reported the polymerization of vinyl monomers photo-initiated by chromium complexes in aqueous solution.[10–14] Chromium(VI) as $HCrO_4^-$ and/or chromium(III) as $Cr(H_2O)_6^{3+}$ appeared to be efficient photo-initiators of the polymerization of vinyl monomers. The initiation step, in any cases, is the redox process that takes place between the complex in the excited state and the monomer in the ground state, the final photoproducts being the polymer and chromium(III) (whatever the valence of the starting chromium complex). In the particular case of acrylamide (AA) polymerization photo-initiated by chromium(VI), two different domains were detected depending on the $[HCrO_4^-]$ concentration.[12] At low concentration, R_p (the rate of polymerization) increases with chromium concentration. A termination process of the polymerization occurring mainly by mutual annihilation of the macroradicals accounts for the experimental dependence of the polymerization rate. R_p was found to be proportional to $[AA]^{3/2}$ and $I_a^{1/2}$ (I_a being the absorbed light intensity). At higher concentrations of $HCrO_4^-$, R_p decreases with increasing chromium concentration. A process of oxidative termination of the radicals by chromium(VI) is involved, which corresponds to a different dependence of R_p; R_p appeared to be proportional to $[AA]^2$ and I_a. In this latter domain, $HCrO_4^-$ plays two roles: in the excited state, it reacts with acrylamide giving rise

* Author to whom correspondence should be addressed.

to chromium(V) and to a radical initiator of the polymerization ($HCrO_4^-$ acts as a photo-initiator). In the ground state, $HCrO_4^-$ reacts with the macroradicals yielding chromium(III) and the polymer ($HCrO_4^-$ also acts as a termination agent). Accordingly, we decided to separate these two roles: chromium(VI) as $HCrO_4^-$ would remain as the initiator agent and copper(II) as $Cu(H_2O)_6^{2+}$ would be the termination agent.

This paper deals with the primary process of the photopolymerization, a further paper will describe the kinetic parameters of the polymerization.

EXPERIMENTAL

Materials

$(NH_4)_2Cr_2O_7$ was of commercial origin (Fluka analytical grade) and used without further purification along with acrylamide (Fluka puriss product) and $CuCl_2$ (Fluka). The solutions were prepared with doubly-distilled water and deaerated by bubbling with argon for 30 min. Ionic strength was not controlled; the pH was adjusted with HCl or $HClO_4$ and was controlled to ± 0.02 pH unit.

Irradiation set-up

The monochromatic irradiations at 365 nm were performed with a high-pressure mercury lamp (Osram HBO 200 W), equipped with a grating monochromator (Bausch and Lomb). The beam was parallel and the reactor was a quartz cylindrical cell of 1 or 2 cm path length. The second set-up used was a cylinder made of stainless steel, built upon an elliptical basis. A high-pressure mercury lamp (Philips HPW type 125W), the emission of which at 365 nm was selected by an inner filter, was located at a focal axis of the elliptical cylinder, and the reactor, a water-jacketed Pyrex tube (diameter = 2.8 cm), was centred at the other focal axis. The reaction medium was stirred well. The incident light intensity was determined by ferri-oxalate actinometry. The averaged values were measured as:

$$I_o \approx 2.5 \times 10^{15} \text{ photons cm}^{-2}\text{s}^{-1}$$

$$I_o \approx 4 \times 10^{15} \text{ photons cm}^{-2}\text{s}^{-1}$$

for irradiation with the monochromator and in the elliptical system, respectively. To study the effect of the absorbed light intensity on the polymerization rate, the water surrounding the reactor in the elliptical system was replaced by a solution of CrO_4^{2-} (photostable species) used as a filter.

The UV–vis spectra were recorded on a double beam spectrophotometer (CARY 118 C). The percentage of acrylamide converted into polymer was calculated from the UV spectra based on the monomer absorption.[12] The polymer was also precipitated by pouring the irradiated solution into methanol and was then weighed. The values of monomer conversion obtained by the two methods were in good agreement. R_p, the rate of polymerization, was taken as the slope in the linear part of the curve giving the percentage of monomer conversion vs time.

ESR spectra were recorded on a Brucker ER-200D spectrometer at 9.30 GHz with a modulation field of 100 KHz. A xenon-mercury Hanovia lamp was used for irradiation in the ESR spectrometer cavity.

RESULTS

Chromium(VI) exists in three different forms, $HCrO_4^-$ and $Cr_2O_7^{2-}$ in acidic medium and CrO_4^{2-} in basic medium.[15] At pH = 3 and for the domain of concentration used, $HCrO_4^-$ was established to be the only absorbing species.[11] Under similar experimental conditions, $CuCl_2$ exists in solution as $Cu(H_2O)_6^{2+}$. The UV–vis spectra of both species are represented in Fig. 1. It appears that $Cu(H_2O)_6^{2+}$ does not absorb in the region where $HCrO_4^-$ is excited (365 or 436 nm). $Cu(H_2O)_6^{2+}$ is completely transparent over a wide range of wavelength, even at high concentration. When allowed to stand for a few days in the dark, a solution of chromium(VI), copper(II) and acrylamide was slightly unstable, therefore, the experiments were always performed with freshly prepared mixtures. In the presence of copper(II), the pH domain in which the study was performed was from 1.5 to 5. At pH values higher than 5, a precipitate

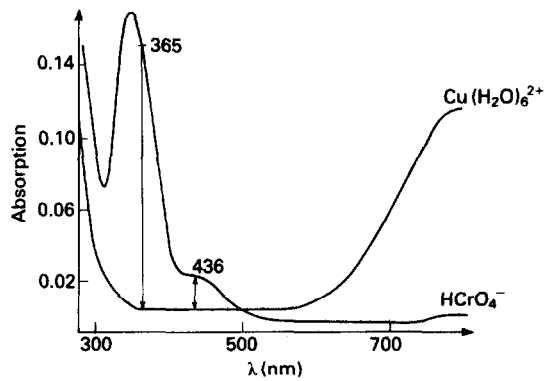

Fig. 1. UV–vis spectrum of aqueous solutions of $HCrO_4^-$ (10^{-4} mol dm^{-3}; pH = 2.5) and $Cu(H_2O)_6^{2+}$ (10^{-2} mol dm^{-3}; pH = 2.5).

was observed. We duplicated any experiment in the two domains of chromium(VI) concentration: when chromium(VI) acts only as a photo-initiator ($c < 7 \times 10^{-5}$ mol dm^{-3}) and when it plays two roles, as a photo-initiator and as a termination agent of polymerization ($c > 2 \times 10^{-4}$ mol dm^{-3}).

Photoredox phenomenon in the chromium(VI), *copper*(II)*–acrylamide system*

As shown in Fig. 2, upon irradiation at 365 nm, the absorbance at 350 and 440 nm characteristic of $HCrO_4^-$ decreased, the original yellow colour disappeared and for prolonged irradiations, the solution turned light blue. The absorbance at 700 nm due to $Cu(H_2O)_6^{2+}$ remains approximately constant and a very weak absorption at 575 nm ($\varepsilon \approx 15$ mol^{-1} dm^3 cm^{-1}) appeared together with an isosbestic point at 520 nm. The initial quantum yields of chromium(VI) to chromium(III) reduction were determined from the absorbance decrease at 350 nm vs irradiation time, neither the starting copper complex nor the final photoproducts absorb at that wavelength. We did not use any buffer to avoid the eventual complexation with the metallic cations. The quantum yields were measured with a 5% conversion at various values of pH. The ϕ values were only slightly affected by the presence of copper(II), a concentration of 10^{-2} mol dm^{-3} in copper(II) was necessary to induce a 20% decrease of the quantum yield:

$\phi = 1.6 \times 10^{-2}$ with $[CuCl_2] = 10^{-2}$ mol dm^{-3}

$\phi = 2.0 \times 10^{-2}$ in the absence of $CuCl_2$

pH = 3.

We determined that this result was not due to the change in ionic strength because the quantum yield of chromium(VI) reduction was constant in the presence or in the absence of a 1.5×10^{-2} mol dm^{-3} concentration of $NaClO_4$.

ESR spectroscopy upon irradiation ($\lambda > 335$ nm)

For a deaerated solution of $[HCrO_4^-]$, $[Cu(H_2O)_6^{2+}]$ and [AA] at room temperature ($\theta \approx 22$°C), two signals can be detected, the strong signal of copper(II) which decreased upon irradiation, and after long irradiations, the weak and broad signal of chromium(III). In a frozen solution ($\theta = -40$°C), an additional signal could be observed whose intensity increased, reached a maximum, then decreased (Fig. 3). As already described in our previous papers, the signal was assigned to chromium(V). For a given concentration of chromium(VI), the intensity of the chromium(V) signal was dependent on the copper(II) concentration; the higher the concentration, the lower the maximum intensity of the signal. The intensity maximum of the chromium(V) signal was divided by five when a 10^{-3} mol dm^{-3} concentration of copper(II) was added to the solution. This was true for both domains of chromium(VI) concentration but, at high concentrations of chromium(VI) a linear relationship occurred between the chromium(V) and copper(II) concentrations, which did not hold at lower concentration (Fig. 4).

The thermal decay of chromium(V) generated upon irradiation was, in the absence of copper(II), of first order at $[HCrO_4^-] = 5 \times 10^{-5}$ mol dm^{-3} and of second order at $[HCrO_4^-] = 5 \times 10^{-4}$ mol dm^{-3}. In the presence of increasing concentrations

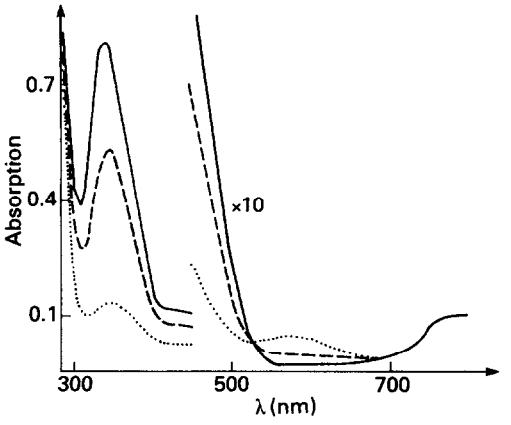

Fig. 2. Evolution of the UV–vis spectrum of a solution of $[HCrO_4^-] = 5 \times 10^{-4}$ mol dm^{-3}, $[Cu(H_2O)_6^{2+}] = 10^{-3}$ mol dm^{-3}, [AA] = 1 mol dm^{-3} and pH = 2.5, upon irradiation at 365 nm: (——) $t = 0$; (– – – –) $t =$ 1 h 40 min; (· · · ·) $t = 4$ h.

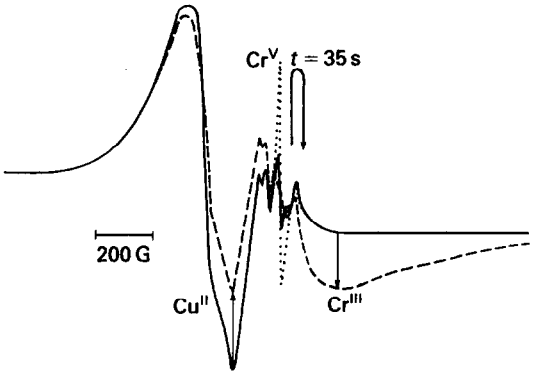

Fig. 3. ESR spectra of a frozen solution ($\theta = -40$°C) of $[HCrO_4^-] = 5 \times 10^{-4}$ mol dm^{-3}; $[Cu(H_2O)_6^{2+}] = 2 \times 10^{-4}$ mol dm^{-3}; [AA] = 2 mol dm^{-3} and pH = 2.5 upon polychromatic irradiation ($\lambda > 335$ nm); (——) $t = 0$; (· · · ·) $t = 35$ s; (– – – –) $t = 40$ min.

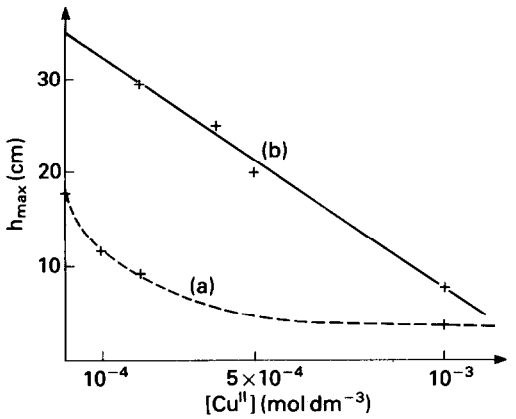

Fig. 4. Maximum intensity of the chromium(V) signal as a function of copper(II) concentration: (a) $[HCrO_4^-] = 5\times10^{-5}$ mol dm^{-3}; (b) $[HCrO_4^-] = 5\times10^{-4}$ mol dm^{-3}.

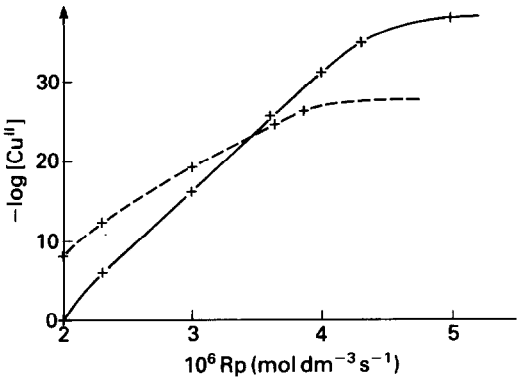

Fig. 5. R_p, the rate of polymerization, as a function of copper(II) concentration: (——) $[HCrO_4^-] = 5\times10^{-5}$ mol dm^{-3}; (– – –) $[HCrO_4^-] = 3\times10^{-4}$ mol dm^{-3}.

of copper(II), there was no more simple decay of the chromium(V) signal.

H^+ *consumption*

The photoreduction of chromium(VI) in the presence of a reductant consumes H^+ ions.[11,12] The pH measurements were performed during the photoredox process. The number of H^+ ions consumed by the redox reaction obviously depends on the number of chromium(VI) atoms reduced, therefore experiments were carried out with the same degree of conversion of chromium(VI) into chromium(III) using different concentrations of copper(II). We calculated, as a representative value, the ratio:

$$R = \frac{\text{Number of } H^+ \text{ consumed}}{\text{Number of } Cr^{VI} \text{ atoms reduced}}.$$

The values are summarized in Table 1. The effect of increasing concentration of copper(II) depends on the concentration of the photo-initiator. At low concentration of $HCrO_4^-$, where $HCrO_4^-$ played the role of initiator only, R decreased when the $CuCl_2$ concentration was increased. At higher concentrations of $HCrO_4^-$, chromium(VI) played two roles and R remained approximately constant whatever the concentration of copper(II).

Effect of copper(II) *on the polymerization rate of acrylamide*

The effect of copper(II) on R_p, the rate of polymerization, was studied at $[HCrO_4^-] = 5\times10^{-5}$ mol dm^{-3} and $[HCrO_4^-] = 3\times10^{-4}$ mol dm^{-3}. For both concentrations, the rate of polymerization decreased in the presence of copper(II) (Fig. 5).

When chromium(VI) did not interfere in the termination process ($c = 5\times10^{-5}$ mol dm^{-3}) and at $[Cu(H_2O)_6^{2+}] > 5\times10^{-4}$ M, the relationship between R_p, the monomer concentration [M] and I_a appeared to be $R_p \propto [M]^2$ and $R_p \propto [I_a]$. A 10^{-2} mol dm^{-3} concentration of copper(II) completely inhibited the polymerization.

At higher concentration of photo-initiator, in the absence or in the presence of copper(II), the rate of polymerization was proportional to I_a and to the square of the monomer concentration.

Table 1. H^+ uptake during the photoreduction of chromium(VI), pH = 3.6, λ = 365 nm

	$[HCrO_4^-] = 5\times10^{-5}$ mol dm^{-3}			$[HCrO_4^-] = 5\times10^{-4}$ mol dm^{-3}		
$CuCl_2$ (mol dm^{-3})	$Cr^{VI}\times10^5$ reduced	$H^+\times10^5$ consumed	$R = H^+/Cr^{VI}$	$Cr^{VI}\times10^5$ reduced	$H^+\times10^5$ consumed	$R = H^+/Cr^{VI}$
0	2	11	5.5	9	16	1.8
10^{-4}	2	9.3	4.7	10	20	2
5×10^{-4}	2	7.8	3.9			
10^{-3}	2.2	6.6	3	9	16	1.8

DISCUSSION

There is no complexation in the ground state between chromium(VI), copper(II) and acrylamide. Chromium(VI) as $HCrO_4^-$ is the only absorbing species. According to the general scheme we already described for acrylamide polymerization photo-initiated by $HCrO_4^-$,[12] the primary step is the formation of chromium(V) together with a radical initiator of polymerization ($AA^\cdot$) arising from acrylamide.

In a rigid matrix (the solution frozen at $-40°C$), the lifetime of chromium(V), the unstable species generated upon excitation of $HCrO_4^-$ in the presence of acrylamide, is long enough to enable its detection by ESR spectroscopy. Under these conditions and in the absence of copper(II), the first-order decay of the chromium(V) signal observed at low concentration of $HCrO_4^-$, reflects the reaction of chromium(V) with excess acrylamide present in the solution. At higher concentrations of $[HCrO_4^-]$, the second-order decay, already reported in the photoreaction between polyvinyl alcohol and dichromate,[16] is assigned to the disproportionation reaction

$$2\,Cr^{V} \longrightarrow Cr^{VI} + Cr^{IV}.$$

The decrease in chromium(V) concentration when copper(II) is added, reflects the reaction of copper(II) with chromium(V). The following equation can be written as

$$Cr^{V} + Cu^{II} \longrightarrow Cu^{I} + Cr^{VI}$$

which accounts for the experimental results.

At room temperature, when chromium(V) is short-lived, this reaction does not occur unless the concentration of copper(II) is very high. On the contrary, the rate of polymerization is very sensitive to the presence of copper(II): at low concentration of photo-initiator (pH = 3) and with a 10^{-2} mol dm^{-3} concentration of $Cu(H_2O)_6^{2+}$, the polymerization is totally inhibited, whereas the quantum yield of chromium(VI) reduction is only slightly affected. The kinetic expressions for the rate of polymerization photo-initiated by $HCrO_4^-$ were established as the following.[12]

If the termination occurs by mutual annihilation of two macroradicals, $[HCrO_4^-] < 7 \times 10^{-5}$ mol dm^{-3}:

$$M_n^\cdot + M_M^\cdot \longrightarrow \text{polymer}$$

$$R_p = k_p[AA]^{3/2} I_a^{1/2} \left[\frac{k_q}{2k_t k_d}\right]^{1/2}.$$

If the termination occurs by oxidative reaction with chromium(VI), $[HCrO_4^-] > 2 \times 10^{-4}$ mol dm^{-3}:

$$HCrO_4^- + M_n^\cdot \longrightarrow Cr^{III} + \text{polymer}$$

$$R_p = k_p[AA]^2 I_a \left[\frac{k_q}{k_{ot} k_d}\right] \frac{1}{[Cr^{VI}]}.$$

A process of oxidative termination by copper(II) would lead to the following expression:

$$R_p = k_p[AA]^2 I_a \left[\frac{k_q}{k'_{ot} k_d}\right] \frac{1}{[Cu^{II}]}.$$

The constants are defined in the general scheme.

The experimental dependence of R_p on I_a, M^2 and $1/[Cu^{II}]$, when chromium(VI) plays the role of initiator only, is in full agreement with this expression.

As far as the hydrogen consumption is concerned, the reduction of chromium(VI) into chromium(III) requires H^+ ions. For the same degree of chromium(VI) reduction, the number of H^+ ions consumed decreases with increasing concentration of copper(II) (Table 1), implying that the H^+ ions are supplied by an additional reaction. Simultaneously, the increasing copper(II) induces a decrease of the polymerization rate, which, therefore, means that the reaction between copper(II) and the macroradicals is more and more important. The following reaction accounts for the experimental observations:

$$Cu^{II} + M_n^\cdot + H_2O \longrightarrow Cu^{I} + M_nOH + H^+$$

and is assumed to be the source of H^+ ions necessary for the reduction of chromium(VI).

At high concentrations of chromium(VI), where the termination process always occurs by oxidative reaction with chromium(VI) and/or with copper(II), the ratio H^+/Cr^{VI} is lower and approximately constant, whatever the concentration of copper(II).

In conclusion, copper(II) as $Cu(H_2O)_6^{2+}$ is able to react with the two species generated upon irradiation of $HCrO_4^-$ in the presence of acrylamide according to the reactions:

$$Cu^{II} + M_n^\cdot \longrightarrow Cu^{I} + M_nOH + H^+ \qquad (1)$$

$$Cu^{II} + Cr^{V} \longrightarrow Cu^{I} + Cr^{VI}. \qquad (2)$$

At room temperature, chromium(V) is very short-lived which does not allow reaction with copper(II) to take place unless the concentration of copper(II) is very high. According to reaction (2), chromium(VI) is regenerated, resulting in a decrease of the quantum yield.

At low temperatures and in a rigid matrix chromium(V) is long-lived enough to react with copper(II), even at low concentrations of copper(II).

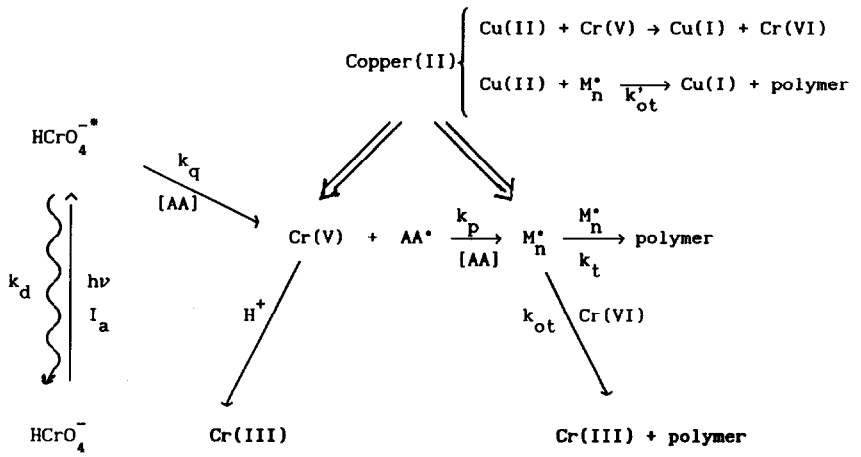

Scheme 1. General scheme of acrylamide polymerization photosensitized by $HCrO_4^-$, in the presence of copper(II).

Therefore, at room temperature, copper(II) mainly affects the polymerization rate. Copper(II) only acts as a termination agent of the polymerization, controlling the termination rate without interfering in the initiation process.

REFERENCES

1. T. Okimoto, Y. Inaki and K. Takemoto, *J. Macromolec. Sci., Chem.* 1973, **A7**, 1537.
2. A. Abbas and I. Tadjudin, *J. Photochem.* 1986, **35**, 87.
3. H. Kothandaraman and M. Santappa, *J. Polym. Sci. Chem. Ed.* 1971, **9**, 1351.
4. K. Kaeriyama and Y. Shimura, *Makromolec. Chem.* 1973, **167**, 129.
5. R. Bhaduri and S. Aditya, *Makromolec. Chem.* 1977, **178**, 1385.
6. C. H. Bamford and S. U. Mullik, *Polymer* 1973, **14**, 38.
7. L. V. Natarajan and M. Santappa, *J. Polym. Sci. Polym. Chem. Ed.* 1986, **6**, 3245.
8. G. A. Delzenne, *J. Polym. Sci.* 1967, **16C**, 1027.
9. K. Iwai, M. Uesugi and F. Takemura, *Polym. J.* 1987, **17**, 1005.
10. B. Robert, M. Bolte and J. Lemaire, *J. Chim. Phys.* 1985, **82**, 361.
11. P. Fageol, M. Bolte and J. Lemaire, *J. Phys. Chem.* 1988, **92**, 239.
12. P. Fageol and M. Bolte, *Makromolec. Chem.* 1989, **190**, 367.
13. P. Fageol and M. Bolte, *Makromolec. Chem., Rapid. Commun.* 1989, **10**, 533.
14. T. Galcera, X. Jouan and M. Bolte, *J. Photochem. Photobiol.* 1988, **45A**, 249.
15. M. Pourbaix, *Atlas d'equilibres Electrochimiques à 25°C*, p. 258. Gauthier-Villars, Paris (1963); *Handbook of Chemistry and Physics*, 64th edn, p. D169. CRC, Cleveland (1983–1984); H. G. Linge and A. L. Jones, *Aust. J. Chem.* 1968, **21**, 2189.
16. Lee Van Nice and R. Farlee, Proceedings of SPE Regional Technical Conferences Photopolymer Principles, Processes and Materials, NY, 53 (October 1976).

Polyhedron Vol. 10, No. 2, pp. 243–247, 1991
Printed in Great Britain

0277–5387/91 $3.00+.00
© 1991 Pergamon Press plc

COMPLEXES OF RHENIUM(V) WITH TRIDENTATE LIGANDS HAVING O, N AND P DONOR ATOMS. THE X-RAY CRYSTAL STRUCTURES OF $ReOCl_2[OC_6H_4\text{-}2\text{-}CH{=}N(CH_2)_3PPh_2]$ AND ITS REDUCED COUNTERPART $ReOCl_2[OC_6H_4\text{-}2\text{-}CH_2NH(CH_2)_3PPh_2]$

HILARY J. BANBERY, WASIF HUSSAIN, THOMAS A. HAMOR,* CHRISTOPHER J. JONES* and JON A. McCLEVERTY*

School of Chemistry, University of Birmingham, PO Box 363, Birmingham B15 2TT, U.K.

(*Received* 30 *May* 1990; *accepted* 27 *September* 1990)

Abstract—The tridentate ligand $HOC_6H_4\text{-}2\text{-}CH_2NH(CH_2)_3PPh_2$, which contains both "hard" and "soft" potential donor atoms, has been synthesized along with its rhenium(V) complex $ReOCl_2[OC_6H_4\text{-}2\text{-}CH_2NH(CH_2)_3PPh_2]$. Single crystal X-ray diffraction studies show that this molecule has a qualitatively similar structure to its Schiff base counterpart $ReOCl_2[OC_6H_4\text{-}2\text{-}CH{=}N(CH_2)_3PPh_2]$, despite the change in bonding at the central ligating nitrogen atom from sp^3 to sp^2. At a more detailed level, significant differences in structural parameters are found to occur. In both cases the coordination site *trans* to the Re=O oxygen [Re=O = 1.680(7) and 1.695(9) Å, respectively] is occupied by the phenolic oxygen [Re—O = 1.943(7) and 1.953(9) Å, respectively] and the rhenium atom has a distorted octahedral coordination environment. The Re—N distance lengthens on reduction of the ligand [Re—N(H)— = 2.224(8) Å, Re—N= = 2.111(11) Å] while the Re—N=C(sp^2) bond angle decreases by 12.7° on reduction.

In order to investigate the ways in which facultative polydentate ligands containing both "hard" and "soft" donor atoms might bind to the $\{ReO\}^{3+}$ moiety, we have been studying the reactions of $[ReOCl_4]^-$ with polydentate ligands which contain sulphur or phosphorus as "soft" donor atoms, in combination with aryloxo and amine or imine nitrogen as "hard" ligating sites. The potentially pentadentate ligand $(HOC_6H_4\text{-}2\text{-}CH{=}NCH_2CH_2)_2S$ has been found[1] to function as a tetradentate ligand in the complex $[ReO(OEt)\{OC_6H_4\text{-}2\text{-}CH{=}NCH_2CH_2\}_2S]$, the sulphur atom remaining uncoordinated as shown schematically in Fig. 1(a). Reduction of the —CH=N— moieties in this ligand results in the formation of a bimetallic complex in which all five ligand donor atoms are bound to rhenium, but not all to the same metal centre, as illustrated in Fig. 1(b). Thus it can be seen that a modest increase in the saturation of the ligand

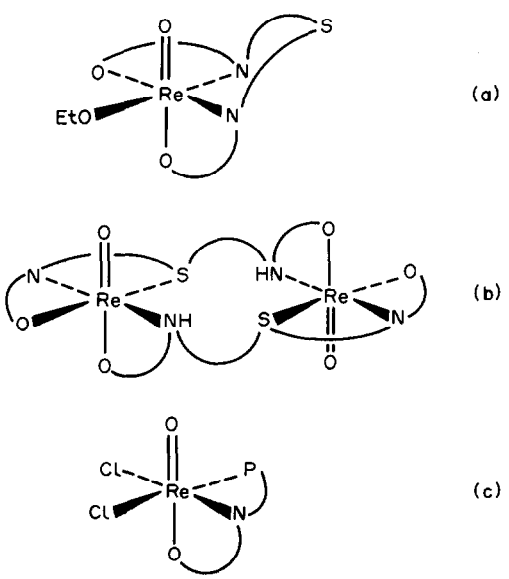

Fig. 1. Structural arrangements in some rhenium(V) complexes: (a) $[ReO(OEt)\{OC_6H_4\text{-}2\text{-}CH{=}NCH_2CH_2\}_2S]$;[1] (b) $[ReO\{(OC_6H_4\text{-}2\text{-}CH{=}NCH_2CH_2)_2S\}_2ReO]$;[1] (c) $ReOCl_2$(salimp).[2]

* Authors to whom correspondence should be addressed.

results in a profound structural change in the complex which is obtained.

The monobasic tridentate ligand, HOC_6H_4-2-$CH{=}N(CH_2)_3PPh_2$ (salimpH) coordinates to the $\{ReO\}^{3+}$ core through all three donor atoms in a mutually *fac* arrangement.[2] Octahedral coordination about rhenium is completed by two chloride ligands as shown in Fig. 1(c). In view of the large changes which followed reduction of the pentadentate ligand, we have now investigated the structural effect of reducing the tridentate ligand (salimpH) to HOC_6H_4-2-$[CH_2NH(CH_2)_3PPh_2]$ (salampH$_2$) to convert the sp^2 central ligating nitrogen atom to sp^3. The new complex, $ReOCl_2[OC_6H_4$-2-$CH_2NH(CH_2)_3PPh_2]$, was prepared and studied by X-ray diffraction methods. In order to provide a direct structural comparison the unsolvated complex, $ReOCl_2[OC_6H_4$-2-$CH{=}N(CH_2)_3PPh_2]$, was also prepared and studied by X-ray methods.

EXPERIMENTAL

Synthetic studies

Commercial reagents were used as supplied; HOC_6H_4-2-$CH{=}N(CH_2)_3PPh_2$[2] and $Bu^n{}_4N[ReOCl_4(H_2O)]$[3] were prepared according to previously described procedures. $ReOCl_2[OC_6H_4$-2-$CH{=}N(CH_2)_3PPh_2]\cdot CH_2Cl_2$ was prepared according to the previously described[2] method and recrystallized from Me_2SO to give the solvent-free complex, $ReOCl_2[OC_6H_4$-2-$CH{=}N(CH_2)_3PPh_2]$. Methanol and ethanol were dried over magnesium and redistilled before use, but other solvents were used as received without further purification.

IR spectra were recorded using a PE 297 instrument. ^{1}H NMR spectra were obtained using a Jeol GX 270 (270 MHz) instrument. Elemental analyses were performed by the Microanalytical Service of The School of Chemistry, University of Birmingham.

HOC_6H_4-2-$CH_2NH(CH_2)_3PPh_2$

To a solution of SalimpH (0.05 g, 1.43 mmol) in dry methanol (40 cm^3) was added $NaBH_4$ (0.31 g, 8.6 mmol). The mixture was stirred at room temperature for 1 h, after which time the solvent was removed to afford a colourless oil. The oil was triturated with n-pentane (2×15 cm^3). On standing at room temperature the pentane extract afforded the product as a white, crystalline solid. More product could be obtained by dissolving the trituration residues in dichloromethane, adding n-pentane and allowing the solution to stand at 0°C for 16 h to precipitate colourless needles of the product (total yield 0.18 g, 36%). Found: C, 75.4; H, 7.0; N, 3.7. Calc. for $C_{22}H_{24}NOP$: C, 75.6; H, 6.9; N, 4.0%.

$ReOCl_2[OC_6H_4$-2-$CH_2NH(CH_2)_3PPh_2]$

$Bu_4N[ReOCl_4(H_2O)]$ (0.25 g, 0.41 mmol) was added to a solution of SalampH$_2$ (0.15 g, 0.43 mmol) in dry methanol (10 cm^3) and the mixture stirred at room temperature for 2 h, then heated under reflux for 0.5 h. The green–brown solution which formed was allowed to cool and stand at 0°C for 16 h, during which time a green solid was deposited. This material was recrystallized from 1 : 1 dichloromethane–methanol to give bright green needles (26 mg, 10%). Found: C, 42.5; H, 3.7; N, 2.3. Calc. for $C_{22}H_{23}NO_2Cl_2PRe$: C, 43.0; H, 3.8; N, 2.4%.

Structural studies—X-ray analysis of $ReOCl_2[OC_6H_4$-2-$CH_2NH(CH_2)_3PPh_2]$ [$ReOCl_2$(salampH)] *and* $ReOCl_2[OC_6H_4$-2-$CH{=}N(CH_2)_3PPh_2]$ [$ReOCl_2$(salimp)]

Diffraction data were measured on an Enraf–Nonius CAD4 diffractometer operating in the ω–2θ mode with graphite monochromated Mo-K_α radiation ($\lambda = 0.71069$ Å) up to $\theta = 25°$ from crystals of size $0.2\times 0.3\times 0.3$ mm [$ReOCl_2$(salampH)] and $0.3\times 0.3\times 0.3$ mm [$ReOCl_2$(salimp)]. Three standard reflections were monitored periodically to check the stability of the system. 3882 unique reflections [$ReOCl_2$(salampH)] and 2498 reflections [$ReOCl_2$(salimp)] were scanned and 3254 and 1921, respectively, with $F > 5\sigma(F)$ were considered observed and used in the analyses.

Crystal data

$ReOCl_2$(salampH): $C_{22}H_{23}Cl_2NO_2PRe$, $M_r = 621.5$, monoclinic, $P2_1/c$, $a = 15.06(2)$, $b = 10.673(14)$, $c = 14.85(4)$ Å, $\beta = 111.5(2)°$, $V = 2201$ Å^3, $Z = 4$, $D_c = 1.859$ g cm^{-3}, μ(Mo-K_α) = 5.87 mm^{-1}.

$ReOCl_2$(salimp): $C_{22}H_{21}Cl_2NO_2PRe$, $M_r = 619.5$, orthorhombic $P2_12_12_1$, $a = 8.959(3)$, $b = 14.036(2)$, $c = 17.611(4)$ Å, $V = 2215$ Å^3, $Z = 4$, $D_c = 1.858$ g cm^{-3}, μ(Mo-K_α) = 5.89 mm^{-1}.

The structures were solved[4] using Patterson and Fourier methods and refined[5] by least-squares using weights, $w = 1/[\sigma^2(F)] + 0.0002F^2]$, for $ReOCl_2$(salampH) and unit weights for $ReOCl_2$(salimp), which resulted in satisfactory weighting analyses. Non-hydrogen atoms were allowed to vibrate anisotropically. Hydrogen atoms were included in calculated positions, riding on their respective

bonded atoms. Refinement was terminated when all shift/ESD ratios were < 0.1 and R, $Rw = 0.051$, 0.067 [$ReOCl_2$(salampH)] and $R = 0.034$ [$ReOCl_2$(salimp)] for 3254 and 1921 reflections, respectively. An empirical absorption correction[6] was applied to both data sets. Computations were carried out on the University of Birmingham's IBM 3090 computer. Additional material available from the Cambridge Crystallographic Data Centre comprises hydrogen atom coordinates, thermal parameters, and bond lengths and angles.

DISCUSSION

Synthetic studies

The ligand $SalampH_2$ may be prepared by the borohydride reduction of the Schiff base SalimpH. The IR spectrum of the white, crystalline solid obtained contains bands attributable to the presence of the phenyl and propyl groups, in addition to ν_{NH} at 3290 cm^{-1}. The ^1H NMR spectrum of the ligand contains two complex multiplets of total relative area 11 in the region δ_{TMS} 7.31–7.44 ppm, attributable to the phosphinophenyl protons and one of the salicylaldimine aryl protons. The remaining salicylaldimine aryl protons appear as two doublets at δ_{TMS} 6.95 ($^3J_{HH}$ 6 Hz) and 6.74 ppm ($^3J_{HH}$ 8 Hz) and a triplet at δ_{TMS} 7.11 ppm ($^3J_{HH}$ 7 Hz); each of relative area one. The protons of the 1,3-disubstituted-propyl and aryl-CH_2—N moieties appear as four signals each of relative area two at δ_{TMS} 3.91 (singlet), 2.73 (triplet, $^3J_{HH}$ 7 Hz), 2.05 (doublet of doublets, $^3J_{HH}$ 8 Hz, $^3J_{PH}$ *ca* 10 Hz) and 1.65 ppm (quintet, $^3J_{HH}$ *ca* 8 Hz).

The reaction between $Bu^n{}_4N[ReOCl_4(H_2O)]$ and $SalampH_2$ proceeded smoothly in methanol in the absence of air to produce a green complex. The IR spectrum of this material contains bands consistent with the presence of the ligand and includes ν_{NH} at 3150 cm^{-1} in addition to $\nu_{Re=O}$ at 978 cm^{-1}. The formulation of this complex as $ReOCl_2[OC_6H_4\text{-}2\text{-}CH_2NH(CH_2)_3PPh_2]$ was confirmed by the X-ray study described below.

Structural studies

The structures of the complexes $ReOCl_2$(salampH) and $ReOCl_2$(salimp) are shown in Figs 2 and 3,[7] respectively, and selected bond lengths and angles are compared in Table 1.* The X-ray analyses confirm that both complexes are neutral, monomeric compounds in which all three potential donor atoms of the ligand are coordinated to rhenium. The rhenium atom is in an approximately octahedral coordination environment with the binding of the ligands qualitatively the same in both complexes. It is note-worthy that the phenolic oxygen atom lies

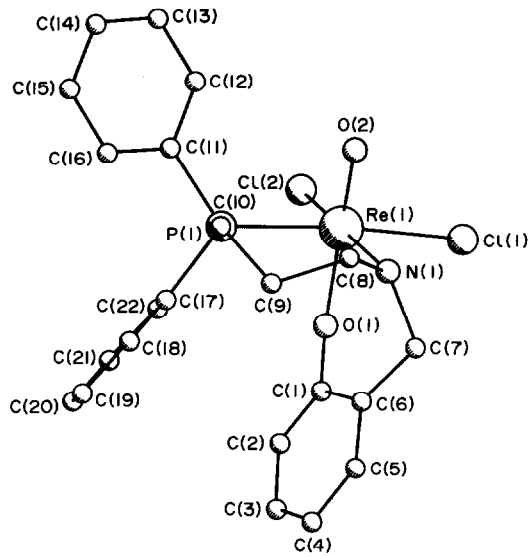

Fig. 2. A view of the complex $ReOCl_2$(salampH) along the C(10)—P bond showing the atom numbering. Hydrogen atoms have been omitted for clarity. The plotting routine is PLUTO.[7]

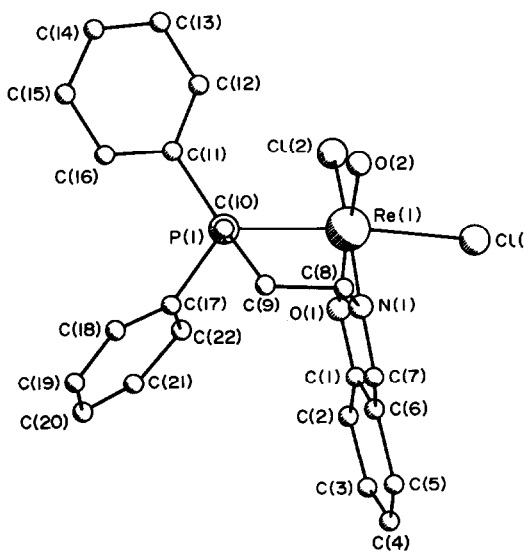

Fig. 3. A view of the complex $ReOCl_2$(salimp) along the C(10)—P bond showing the atom numbering. Hydrogen atoms have been omitted for clarity. The plotting routine is PLUTO.[7]

* Atomic coordinates, temperature factors and full lists of bond lengths and angles have been deposited with the Cambridge Crystallographic Data Centre.

Table 1. Selected bond lengths (Å) and angles (°) with ESDs in parentheses

	$ReOCl_2$(salampH)	$ReOCl_2$(salimp)	$ReOCl_2$(salimp)(solvate)[2]
Re—P	2.414(2)	2.433(4)	2.447[a]
Re—Cl(1)	2.454(3)	2.438(4)	2.438[a]
Re—Cl(2)	2.353(3)	2.376(4)	2.396[a]
Re—O(1)	1.943(7)	1.953(9)	1.960[a]
Re—O(2)	1.680(7)	1.695(9)	1.702[a]
Re—N(1)	2.224(8)	2.111(11)	2.123[a]
P—C(10)	1.817(10)	1.827(16)	1.850[a]
P—C(11)	1.808(11)	1.826(17)	1.826[a]
P—C(17)	1.799(10)	1.826(16)	1.820[a]
N(1)—C(7)	1.504(14)	1.350(21)	1.307[a]
N(1)—C(8)	1.503(11)	1.493(19)	1.493[a]
C(6)—C(7)	1.499(14)	1.469(23)	1.464[a]
P—Re—Cl(1)	175.1(1)	173.5(2)	172.3[a]
P—Re—Cl(2)	89.0(1)	94.6(2)	96.0[a]
P—Re—O(1)	87.3(2)	93.3(3)	90.7[a]
P—Re—O(2)	87.4(3)	86.9(4)	88.5[a]
P—Re—N(1)	95.4(2)	85.8(4)	84.7[a]
Cl(1)—Re—Cl(2)	90.2(1)	91.3(1)	91.1[a]
Cl(1)—Re—O(1)	87.9(2)	84.2(3)	86.5[a]
Cl(1)—Re—O(2)	97.5(3)	95.0(4)	93.8[a]
Cl(1)—Re—N(1)	85.0(2)	88.0(4)	87.8[a]
Cl(2)—Re—O(1)	91.5(2)	88.5(3)	87.6[a]
Cl(2)—Re—O(2)	101.9(3)	97.4(5)	98.1[a]
Cl(2)—Re—N(1)	173.6(2)	171.7(4)	170.4[a]
O(1)—Re—O(2)	165.4(3)	174.1(6)	174.4[a]
O(1)—Re—N(1)	84.0(3)	83.3(5)	82.9[a]
O(2)—Re—N(1)	83.0(3)	90.9(6)	91.6[a]
Re—P—C(10)	109.2(3)	104.5(5)	105.2[a]
Re—P—C(11)	114.1(4)	117.1(5)	118.0[a]
Re—P—C(17)	115.5(3)	117.3(6)	113.8[a]
C(10)—P—C(11)	104.6(5)	103.9(7)	104.2[a]
C(10)—P—C(17)	107.2(5)	107.0(8)	107.4[a]
C(11)—P—C(17)	105.5(5)	105.9(7)	107.3[a]
Re—N(1)—C(7)	114.8(6)	127.5(11)	126.9[a]
Re—N(1)—C(8)	118.4(6)	117.2(10)	116.3[a]
C(7)—N(1)—C(8)	113.3(9)	115.0(13)	116.6[a]
N(1)—C(7)—C(6)	116.2(8)	122.7(17)	126.2[a]

[a] Mean of values for two independent molecules.

trans to the oxo group, in accord with the well established tendency of oxygen donor atoms in polydentate ligands to coordinate at this site.[1,2,8–10]

There are, however, some significant differences in the structural parameters. Thus deviation from ideal octahedral coordination is greater in the reduced complex; $ReOCl_2$(salampH) maximum angular deviation 14.6°, mean deviation 5.2°; $ReOCl_2$(salimp) maximum angular deviation 8.3°, mean deviation 4.4°. This may well be a steric effect, the hydrogen atom linked to the nitrogen atom of the reduced ligand causing some additional distortion from ideal octahedral geometry, otherwise it might have been expected that the greater flexibility of the reduced form would allow a *closer* approach to octahedral geometry. That this is a systematic effect due to the difference in the nature of the N(1)—C(7) bond may be seen from a comparison of the rhenium coordination geometries in the present structures with that of rhenium in $ReOCl_2$(salimp) in crystals of the dichloromethane solvate.[2] Comparing equivalent angles at rhenium, the differences between the salimp and salampH complexes range from 0.7 to 9.6° with a mean difference of 4.0°, whereas the differences between the two salimp complexes are much smaller, 0.2–

2.6°, mean 1.1° [see Table 1, where pertinent parameters for $ReOCl_2(salimp)\cdot 0.25CH_2Cl_2$ are also listed]. With regard to bond lengths, the rhenium–sp^3-hybridized nitrogen distance is greater by 0.1 Å than the Re—N(sp^2) distances in the $ReOCl_2$(salimp) structures. As expected, significant differences occur also in the N(1)—C(7) bond length and in the valence angles at N(1) and C(7), clearly distinguishing between the different bonding states of these two atoms in the salampH and salimp complexes. The net effect of these differences may be gauged by comparing Figs 2 and 3 which show identical views of $ReOCl_2$(salampH) and $ReOCl_2$(salimp). The Re, N(1), C(7), C(6), C(1), O(1) chelate ring is planar to within ±0.12 Å in $ReOCl_2$(salimp), but is considerably more buckled in the reduced complex, atomic deviations from the mean plane ranging from 0.25 to −0.35 Å.

The phosphorus atom occupies a site *trans* to a chlorine and *cis* to the rhenyl oxo ligand in both complexes. The bond angles at phosphorus are essentially tetrahedral. As noted previously,[2] the Re—P—C(sp^3) angles are significantly smaller than those of type Re—P—C(sp^2). This was attributed[2] to an electronic effect. The P—C lengths, however, reflect the different hybridization states of the carbon atoms bonded to phosphorus only to a small extent. The orientations of the phenyl rings are somewhat different in the two complexes. Thus in $ReOCl_2$(salampH) the angles which the C(11)—C(16) and C(17)—C(22) phenyl rings make with the Re, C(11), C(17) plane, taken as the reference plane, are 36.5 and 85.2°, respectively, and the angle between the phenyl rings is 70.5°. The corresponding inter-planar angles in $ReOCl_2$(salimp) are 25.0, 65.8 and 81.8°. In the dichloromethane solvate of $ReOCl_2$(salimp) the angle between the phenyl rings is similar; 88.6 and 83.9° in the two independent molecules.[2]

In contrast to the finding that reduction of the imine linkage in the pentadentate ligand $[HOC_6H_4\text{-}2\text{-}CH{=}N(CH_2)_2]_2S$ leads to gross changes in its mode of coordination to the $\{ReO\}^{3+}$ moiety, the reduction of the imine linkage in salimpH does not produce gross geometric changes in the ligand binding arrangement. This occurs in spite of significant changes in more detailed aspects of the geometry of the coordinated ligand.

Acknowledgements—We are grateful to the SERC and Amersham International plc for their support (to H.B. and W.H.).

REFERENCES

1. H. J. Banbery, F. McQuillan, T. A. Hamor, C. J. Jones and J. A. McCleverty, *Polyhedron* 1989, **8**, 559.
2. W. Hussain, H. J. Banbery, T. A. Hamor, C. J. Jones and J. A. McCleverty, *J. Chem. Soc., Dalton Trans.* 1990, 657.
3. T. Lis and B. Jezowska-Trzebiatowska, *Acta Cryst.* 1976, **B33**, 1248.
4. G. M. Sheldrick, SHELX 86, Program for the solution of crystal structures. University of Gottingen (1987).
5. G. M. Sheldrick, SHELX 76, Program for Crystal Structure Determination. University of Cambridge (1976).
6. N. Walker and D. Stuart, *Acta Cryst.* 1983, **A39**, 158.
7. W. D. S. Motherwell and W. Clegg, PLUTO, Program for drawing crystal and molecular structures. University of Cambridge (1978).
8. H. J. Banbery, F. McQuillan, T. A. Hamor, C. J. Jones and J. A. McCleverty, *J. Chem. Soc., Dalton Trans.* 1989, 1405.
9. U. Mazzi, F. Refosco, G. Bandoli and M. Nicolini, *Transition Met. Chem.* 1985, **10**, 121.
10. F. Refosco, F. Tisato, U. Mazzi, G. Bandoli and M. Nicolini, *J. Chem. Soc., Dalton Trans.* 1988, 611.

Polyhedron Vol. 10, No. 2, pp. 249–253, 1991
Printed in Great Britain

0277–5387/91 $3.00+.00
© 1991 Pergamon Press plc

VANADIUM(V) EQUILIBRIA. SPECTROPHOTOMETRIC AND ENTHALPIMETRIC INVESTIGATION OF THE DIMERIZATION AND DEPROTONATION OF HVO_4^{2-}

J. J. CRUYWAGEN* and J. B. B. HEYNS

Department of Chemistry, University of Stellenbosch, Stellenbosch 7600, Republic of South Africa

(*Received* 25 *June* 1990; *accepted* 27 *September* 1990)

Abstract—The dimerization and deprotonation of HVO_4^{2-} have been investigated in 1 M Na(Cl) medium at 25°C. Spectrophotometric and calorimetric measurements were made at $[OH^-] \geqslant 0.05$ M, where all other vanadate(V) hydrolysis equilibria could be neglected. Equilibrium constants and other thermodynamic quantities have been determined: for the dimerization of HVO_4^{2-} $\log K_d = 0.83$, $\Delta H^0 = -28$ kJ mol^{-1} and $T\Delta S^0 = -24$ kJ mol^{-1}, and for the ionization $\log K = -13.29$, $\Delta H^0 = 24$ kJ mol^{-1} and $T\Delta S^0 = -52$ kJ mol^{-1}.

The hydrolysis of vanadate(V) leads to the formation of various mono- and polynuclear species, occurring in successive overlapping equilibria extending over the entire pH range.[1,2] Despite the complexity of the system, which comprises slow reactions in the pH range 4.5–7.5, great progress has been made in characterizing these equilibria, especially by potentiometric and NMR techniques.[3–7] Values for equilibrium constants have been reported for different ionic media, but the thermodynamic quantities ΔH^0 and ΔS^0 have not been determined for these equilibria. Only a non-specific value for the enthalpy of polymerization,[8] $\Delta H^0 = -21$ kJ mol^{-1} $H_2VO_4^-$, and another for the formation enthalpy of the polyanion, $HV_{10}O_{28}^{5-}$, have been reported,[9] which is not surprising in view of the speciation characteristics of the system.

The aim of the present investigation was to determine by spectrophotometric and calorimetric measurements the enthalpy and entropy changes for the first two hydrolysis reactions of VO_4^{3-}, i.e. for the formation of HVO_4^{2-} and $V_2O_7^{4-}$. These reactions take place in alkaline solution and by limiting the measurements to pH > 12.3, all other hydrolysis equilibria could be neglected, which brought about a considerable simplification in the interpretation and manipulation of the data. Because the interpretation of calorimetric data depends heavily on the values used for the equilibrium constants, a renewed attempt was made to obtain the best possible value for the dimerization equilibrium constant. The dimeric ion, $V_2O_7^{4-}$, attains its maximum concentration at pH ~ 12. Depending on the accuracy required, the useful range of a glass electrode in potentiometric investigations is limited to pH values less than 10 or 11. At these pH values, where several species co-exist and the percentage concentration of $V_2O_7^{4-}$ is rather small, very accurate determination of the dimerization constant is not possible. The value of the constant might also depend on the reaction model selected in the treatment of the data. Evaluation of this constant by some other method which is not based on direct pH measurements is therefore of interest, in addition to the need for an accurate value in calculating thermodynamic quantities. In the present investigation a flow-through cuvette of variable path length was used to measure the whole UV spectrum of solutions at various vanadium concentrations, from which a value for the dimerization constant was calculated. As a by-product the spectrum of $V_2O_7^{4-}$ was obtained for the first time.

EXPERIMENTAL

Reagents and solutions

Analytical grade reagents (Merck p.a. or BDH Analar) were used, and solutions were prepared

* Author to whom correspondence should be addressed.

with deionized water obtained from a Millipore Milli-Q system. A vanadate stock solution was prepared by dissolving $NaVO_3$ in hot water. The cooled solution was filtered through a porosity four sintered glass filter. Its concentration was determined by titrating a suitably diluted sample with ammonium ferrous sulphate that had been standardized by titration with potassium dichromate. Carbonate-free sodium hydroxide was standardized by titration with potassium hydrogen phthalate. The solution was kept in a polythene bottle and protected against carbon dioxide contamination with a soda lime guard tube. All vanadate solutions were prepared from the stock solution by appropriate dilution, with the addition of sodium hydroxide as required, and the further addition of sodium chloride such as to obtain a constant sodium ion concentration of 1.0 M. Solutions were left to stand for about 24 h to allow time for complete depolymerization of decavanadate ions present in the stock solution.

Spectrophotometric measurements

The measurements were made with a Varian Cary 210 spectrophotometer, and absorbance data collected by means of an Apple IIe computer. The dimerization equilibrium was studied by a titration procedure. A 0.05 M NaOH solution [1.0 M Na(Cl) medium] was titrated stepwise with a solution of 0.20 M $NaVO_3$ [0.25 M in NaOH and 1.00 M in Na(Cl)], to obtain in the titration cell the following series of vanadate(V) concentrations: 0.001980, 0.002956, 0.004305, 0.005825, 0.007692, 0.01025, 0.01343, 0.01818, 0.02456, 0.03333, 0.04375, 0.05507, 0.06667, 0.07805, 0.08889, 0.09474 M. The solution in the titration cell, which was set up in a thermostatted water bath, was circulated by means of a peristaltic pump to a variable path length flow-through cuvette. Purified and medium-conditioned nitrogen was bubbled through the solution throughout the experiment. Spectra were recorded vs air in the range 218–320 nm. The path length at each setting, which was obtained by calibration as described before,[10] was varied in this experiment from 0.1021 to 0.00386 cm. Blank absorbances were obtained by recording the spectrum of 0.0500 M NaOH [1.0 M in Na(Cl)] vs air at the corresponding path length settings.

The variation with temperature of the hydrolysis constant (K_h) of VO_4^{3-}, was studied by measuring the change in absorption of a solution of 2.002×10^{-4} M vanadate(V) [0.38 M in NaOH and 1.00 M in Na(Cl)]. After degassing with pure N_2, spectra of this solution were recorded from 240 to 320 nm, using a 0.50 cm cuvette against a degassed 0.38 M NaOH [1 M Na(Cl) medium] blank solution. By utilizing thermostatted cuvette holders, spectra were obtained at six different temperatures, viz. 11.1, 16.4, 20.1, 24.9, 29.3 and 34.75°C.

Calorimetric measurements

An isothermal titration calorimeter, Tronac model 550, described elsewhere[11,12] was used for the measurements. Vanadate solutions at three different concentrations, viz. 0.0800, 0.1144 and 0.1500 M, were titrated. Each solution was made up at least 24 h before the calorimetric titration was carried out with an accurately known concentration of NaOH, approximately equal to the vanadate(V) concentration and 1.0 M in Na(Cl). The solution (20 cm^3) was then titrated with 1.0 M NaOH from a Gilmont precision microburette at a constant speed (typically 0.05 $cm^3\ min^{-1}$) and the average number of heat pulses supplied by the control heater at fixed intervals (e.g. 100 s) recorded digitally. A blank titration of 1.0 M NaCl with 1.0 M NaOH was carried out to correct for the endothermic heat of dilution.

RESULTS AND DISCUSSION

Spectrophotometry

The dimerization equilibrium (1) has been investigated at a hydroxide ion concentration of 0.05 M, i.e. $pH_c = 12.40$ (where $pH_c = 13.70 - \log [OH^-]$ at 1 M NaCl[13])

$$2HVO_4^{2-} \overset{K_d}{\rightleftharpoons} V_2O_7^{4-} + H_2O. \quad (1)$$

At this pH_c all other protonation and condensation equilibria can be neglected. The bivanadate ion, HVO_4^{2-}, is the predominant mononuclear species; only about 10% is deprotonated to vanadate:[13]

$$HVO_4^{2-} + OH^- \overset{K_h^{-1}}{\rightleftharpoons} VO_4^{3-} + H_2O. \quad (2)$$

The vanadium concentration was varied from 0.002 to ~0.10 M and the absorption spectra measured in the wavelength range 218–320 nm. Very little dimerization takes place at concentrations < 0.002 M, whereas 0.10 M is about the upper limit which can be measured without having to forfeit accuracy because of the extremely short path length that would be required.

The computer program SPECFIT[14] was used to treat the absorbance data, taking into account equilibrium (2) and its effect on the free hydroxide ion concentration when dimerization increases. The spectra of HVO_4^{2-} and VO_4^{3-} as well as the equilibrium constant for reaction (2), pertaining to 1.0

M NaCl medium, are known with sufficient accuracy from previous work to be supplied to the program.[13] The dimerization constant, K_d, and the spectrum of $V_2O_7^{4-}$ were, therefore, the only unknown parameters to be calculated from the data. However, as a check on the consistency of the two sets of data the spectrum of HVO_4^{2-} was regarded as unknown and calculated together with K_d and the spectrum of $V_2O_7^{4-}$.

The dimerization constant, log $K_d = 0.83$, was computed with excellent agreement between experimental and calculated absorbances at all wavelengths. It is assumed that this value is more accurate than our previously reported value for 1.0 M Na(Cl) medium, i.e. log $K_d = 1.07$, which was determined from potentiometric[15] data in the pH range 7–10. In this pH range $V_2O_7^{4-}$ is one of several minor species which occur together in simultaneously overlapping equilibria and which might affect accurate characterization adversely. When the values determined for the dimerization constant in different ionic media are compared, namely log $K_d = 0.67$ (0.6 M NaCl),[4,15] log $K_d = 0.83$ (1.0 M NaCl), log $K_d = 1.24$ and 1.39 (2.0 M NaCl[7] and 2.0 M LiCl[3]) and log $K_d = 1.44$ and 1.69 (3.0 M $NaClO_4$),[6,16] and allowance is made for deviations, a rather strong dependence on ionic strength is indicated. A general stabilizing effect of high ionic medium on highly charged vanadate polyanions has also been reported by Pettersson *et al.*[6]

The spectrum now calculated for HVO_4^{2-} (Fig. 1) is practically identical to that previously obtained[13] in the determination of K_h from a series of measurements in the pH_c range 12–13.7. Also shown in Fig. 1 is the complete UV spectrum of $V_2O_7^{4-}$ which has been obtained for the first time. The spectrum of this ion, which has two strong absorption bands at 230 and 282 nm, is very similar to that of the tetrahedral[4] orthovanadate ion, VO_4^{3-}, which has absorption peaks at 226 and 270 nm. This similarity can be taken as strong evidence that the structure of $V_2O_7^{4-}$ in solution consists of two VO_4 tetrahedra sharing a vertex as is the case in the solid state.[17,18] Replacement of an oxygen atom of VO_4^{3-} by another orthovanadate group, to give $V_2O_7^{4-}$, causes a reversal in the intensity of the two charge-transfer bands and a slight shift of these bands to longer wavelengths. Similar changes in the spectra take place[19,20] when CrO_4^{2-} is protonated and dimerizes to form $Cr_2O_7^{2-}$, the only difference being that the absorption bands of $Cr_2O_7^{2-}$ appear at slightly shorter wavelengths than those of CrO_4^{2-}.

The enthalpy and entropy changes for reaction (2) were determined indirectly from the variation of the equilibrium constant with temperature. Because

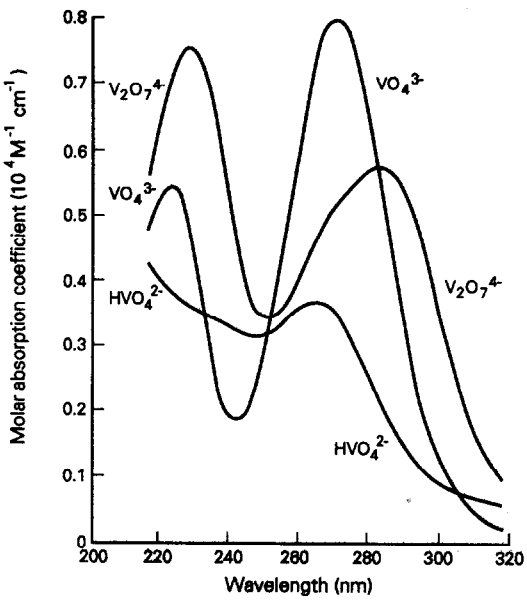

Fig. 1. Absorption spectra of VO_4^{3-}, HVO_4^{2-} and $V_2O_7^{4-}$. Molar absorption coefficients of $V_2O_7^{4-}$ have been divided by two in order to present comparable spectra.

of the great difference between the spectra of VO_4^{3-} and HVO_4^{2-} and the strong absorption bands of the latter species, the equilibrium constant can be determined quite accurately by spectrophotometry. The ΔH^0 and ΔS^0 values deduced from the straight line plot of log K_h vs $1/T$ (Fig. 2) by application of the relationship

$$-2.303RT \log K_h = \Delta G^0 = \Delta H^0 - T\Delta S^0$$

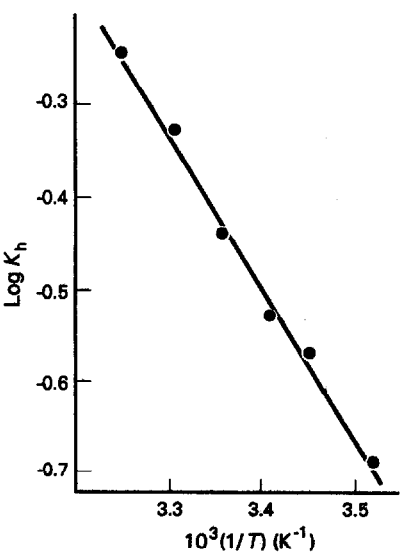

Fig. 2. Variation of logarithm of hydrolysis constant [equilibrium (2)] with reciprocal Kelvin temperature.

Table 1. Values for equilibrium constants and thermodynamic quantities for the reactions at 298.15 K in 1 M Na(Cl) medium

Reaction	log $K \pm 3\sigma$	ΔH^0 (kJ mol^{-1})	$T\Delta S^0$ (kJ mol^{-1})
$2HVO_4^{2-} \rightleftharpoons V_2O_7^{4-} + H_2O$	0.83 ± 0.02	-28	-24
$HVO_4^{2-} + OH^- \rightleftharpoons VO_4^{3-} + H_2O$	0.431 ± 0.014[13]	-32	-29
$HVO_4^{2-} \rightleftharpoons VO_4^{3-} + H^+$	-13.27 ± 0.02	$+24$	-52
$HPO_4^{2-} \rightleftharpoons PO_4^{3-} + H^+$	-12.35	$+15$	-56 ($I = 0$)[22]
$HAsO_4^{2-} \rightleftharpoons AsO_4^{3-} + H^+$	-11.5	$+18$	-47 ($I = 0$)[22]

are given in Table 1. By using the values $pK_w = 13.70$ and $\Delta H^0 = 56.1$ kJ mol^{-1} for the ionization of water in 1.0 M NaCl medium,[13,21] the corresponding thermodynamic quantities for the ionization of HVO_4^{2-} were calculated. It is seen that these values are comparable to those of similar ionization reactions[22] of the main group V species HPO_4^{2-} and $HAsO_4^{2-}$.

Calorimetry

The enthalpy change for the dimerization was determined directly from calorimetric measurements. Vanadate solutions were titrated with 1.0 M NaOH covering the pH_c range 12.3–13.0. A pH_c of 12.3 is the lower limit if one wishes to exclude all hydrolysis equilibria except the two in question and a pH_c of 13 is about the highest that can be reached when titrations are carried out with 1.0 M NaOH. Because of the great overlap between the two equilibria in this pH_c range and the comparatively small change in the concentrations of VO_4^{3-} and $V_2O_7^{4-}$, the calculation of ΔH^0 values for both reactions from these data is not justified. The spectrophotometrically determined values, $\Delta H_h^0 = -32$ kJ mol^{-1} was therefore used in the following equation to calculate a value for the enthalpy change for the dimerization from the measured heat (corrected for dilution effects):

$$Q = n_d \Delta H_d^0 + n_h \Delta H_h^0.$$

The values n_d and n_h are the number of moles formed, while ΔH_d^0 and ΔH_h^0 are the molar enthalpy changes for the formation of $V_2O_7^{4-}$ and VO_4^{3-}, respectively, at 25°C in 1.0 M Na(Cl) medium.

The enthalpy change obtained for the dimerization of HVO_4^{2-}, i.e. $\Delta H_d^0 = -28$ kJ mol^{-1}, can be compared with that reported for the dimerization of $HCrO_4^-$ at zero ionic strength (-20 kJ mol^{-1}).[22] The entropy change for dimerization of HVO_4^{2-} ($T\Delta S^0 = -24$ kJ mol^{-1}) is also comparable to that for $HCrO_4^-$ ($T\Delta S^0 = -11$ kJ mol^{-1}).

CONCLUSION

Values for the enthalpy and entropy changes for the ionization of VO_4^{2-}, as well as those for the formation of $V_2O_7^{4-}$, have been determined for the first time. A complete UV spectrum (220–320 nm) for $V_2O_7^{4-}$, which exhibits two strong absorption bands with maxima at wavelengths 230 and 282 nm, has been calculated from the spectrophotometric data. This spectrum should prove to be particularly useful in further spectrophotometric studies of vanadate equilibria at $pH_c < 12$, where $V_2O_7^{4-}$ overlaps with several other species, some of which have not yet been characterized unambiguously.

Acknowledgements—Financial support by the Foundation for Research Development and the University of Stellenbosch is gratefully acknowledged. We thank G. van Greunen for assistance with some of the experimental work.

REFERENCES

1. C. F. Baes and R. E. Mesmer, *The Hydrolysis of Cations*, p. 201 and refs cited therein. Wiley, New York (1976).
2. M. T. Pope, *Heteropoly and Isopoly Oxometalates*, p. 34 and refs cited therein. Springer, Berlin (1983).
3. E. Heath and D. W. Howard, *J. Chem. Soc., Dalton Trans.* 1981, 1105.
4. L. Pettersson, B. Hedman, I. Andersson and N. Ingri, *Chem. Scripta* 1983, **22**, 254.
5. K.-H. Tytko and J. Mehmke, *Z. Anorg. Allg. Chem.* 1983, **503**, 13.
6. L. Pettersson, I. Andersson and B. Hedman, *Chem. Scripta* 1985, **25**, 309.
7. A. A. Ivakin, L. D. Kurbatova, M. V. Kruchinina and N. I. Medvedeva, *Russ. J. Inorg. Chem.* 1986, **31**, 219.
8. P. H. Rieger, *Aust. J. Chem.* 1973, **26**, 1173.
9. V. K. Schiller and E. Thilo, *Z. Anorg. Allg. Chem.* 1961, **310**, 261.

10. T. C. Choat, J. J. Cruywagen and J. B. B. Heyns, *Anal. Chem.* 986, **58**, 2571.
11. J. J. Christensen, H. D. Johnston and R. M. Izatt, *Rev. Scient. Instrum.* 1968, **39**, 1356.
12. J. J. Christensen, J. W. Gardner, D. J. Eatough, P. J. Watts and R. M. Hart, *Rev. Scient. Instrum.* 1973, **44**, 481.
13. J. J. Cruywagen and J. B. B. Heyns, *Talanta* 1990, **37**, 741.
14. H. Gampp, M. Maeder, C. J. Meyer and A. D. Zuberbühler, *Talanta* 1985, **32**, 95.
15. J. J. Cruywagen, J. B. B. Heyns and J. L. Visagie, *Polyhedron* 1989, **8**, 1800.
16. L. Newman, W. J. La Fleur, F. J. Bronsaides and A. M. Ross, *J. Am. Chem. Soc.* 1958, **80**, 4491.
17. J. A. Konnert and H. T. Evans Jr, *Acta Cryst.* 1975, **B31**, 2688.
18. A. Björnberg, *Acta Chem. Scand.* 1979, **A33**, 539.
19. W. G. Davies and J. E. Prue, *Trans. Faraday Soc.* 1955, **51**, 1045.
20. Y. Sasaki, *Acta Chem. Scand.* 1962, **16**, 719.
21. J. J. Cruywagen and R. F. van de Water, *Polyhedron* 1986, **5**, 521.
22. A. E. Martell and R. B. Smith, *Critical Stability Constants*, Vol. 5, first supplement. Plenum Press, New York (1982).

Polyhedron Vol. 10, No. 2, pp. 255–260, 1991
Printed in Great Britain

0277–5387/91 $3.00+.00
© 1991 Pergamon Press plc

PALLADA- AND PLATINACYCLES—III.* SYNTHESIS OF 3,4-DIALKYLIDENE-PLATINACYCLOPENTANES AND THEIR METALLO-ENE TYPE REACTION WITH DIOXYGEN. X-RAY STRUCTURE OF A 2,3-DIOXA-PLATINACYCLOHEPTANE (dad)Pt—O—O—CMe_2—C(=CH_2)—C(=CMe_2)CH_2

H. TOM DIECK,† G. FENDESAK and C. MUNZ

Institute of Inorganic and Applied Chemistry, The University of Hamburg, Martin-Luther-King-Platz 6, D-2000 Hamburg 13, F.R.G.

(*Received* 9 *July* 1990; *accepted* 27 *September* 1990)

Abstract—The reaction of bis(dibenzylideneacetone)platinum with a diazadiene (dad = 2,6-Me_2-Ph-dad, 2,6-$^iPr_2$-Ph-dad) and 1,1-dimethylallene gives the 3,4-bis(isopropylidene)platinacyclopentanes (dad)Pt—CH_2—C(=CMe_2)—C(=CMe_2)CH_2 (**6**) and (**7**). The metallacyclopentane rings are non-planar and rigid. Under air or oxygen the violet complexes **6** and **7** are slowly and quantitatively converted to green complexes **8** and **9**, respectively. The dioxygen does not insert directly into the Pt—C bond but, instead, reacts in a metallo-ene type manner to give the dioxaplatinacycloheptanes (dad)Pt—O—O—CMe_2—C(=CH_2)—C(=CMe_2)—CH_2, as revealed by NMR and X-ray diffraction studies. In complex **8** the platinum atom shows square-planar coordination. The seven-membered ring (with an almost planar C_α—Pt—O—O fragment) is folded in such a way that the two *exo*-alkylidene groups are not in conjugation. The conformation is also rigid in solution. The disposition of the methyl groups proves the unexpected allylic inversion which occurs with the incorporation of dioxygen.

Bis(dibenzylideneacetone)palladium and -platinum[2] are good starting materials for numerous other complexes of these metals used in stoichiometric or catalytic reactions. In the presence of diazadienes (dad = R—N=CH—CH=N—R) and dialkyl acetylene dicarboxylate (E—C≡C—E) stable metallacyclopentadienes **1** and **2** are obtained, which can be used for further catalytic reactions.[1,3–5] The platinacycle **1** reacts slowly with some olefins to give insertion products. This reaction is much faster with the very reactive 1,1-dimethylallene (**3**) to yield the insertion product **4**, a platinacycloheptadiene.[6] We were interested to see whether the (dad)Pt^0 system would also interact with the allene in the absence of any ester (ECCE). The dimerization of allene via the central carbon atom to afford mononuclear or dinuclear complexes is known for numerous metals.[7] In the case of nickel[8] as well as platinum[9] 3,4-methylidene-metallacyclopentanes (**5**) are well characterized. With a (dad)Ni system similar to the one used in this work, allene has been reported to give an unexpected dinuclear nickel(II) complex.[10] We report here on rigid *exo*-dialkylidene platinacycles and their reaction with dioxygen as "ene" in a metallo-ene type reaction.[11,12]

EXPERIMENTAL

In contrast to other reactions of (dad)Pt^0 complexes the following synthesis of **6** and **7** must be performed under an atmosphere of dry nitrogen and with deaerated solvents. The silica gel column must also be prepared under nitrogen. NMR spectra were recorded with a Bruker AM 360 spectrometer. For ^1H and ^{13}C assignments H,H-COSY, C,H-COSY and APT experiments were performed. When broad ^1H(Pt) satellites result as a consequence of chemical shift anisotropy, additional 1D spectra at 80 MHz were recorded.

* For part II, see ref. 1.

† Author to whom correspondence should be addressed.

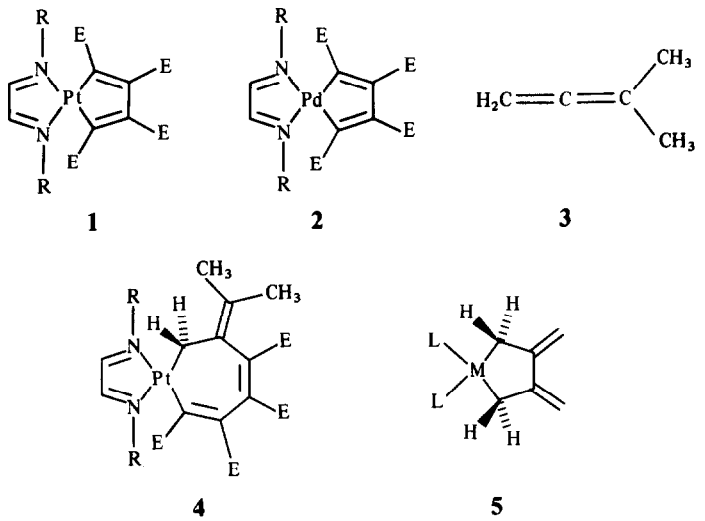

Scheme 1.

Glyoxalbis(2,6 - *dimethylphenylimine*) - 2,3 - *bis*(*isopropylidene*)*butane*-1,4-*diyl-platinum* (**6**)

Bis(dibenzylideneacetone)platinum [$Pt(dba)_2$:[2] 330 mg, 0.5 mmol] was stirred with glyoxalbis(2,6-dimethylphenylimine) (130 mg, 0.5 mmol) in 20 cm^3 of toluene. At ambient temperature a slight excess of 1,1-dimethylallene (130 mg, 1.9 mmol) was slowly added. The reaction was followed by thin-layer chromatography. After 10 h the $Pt(dba)_2$ was consumed and the new violet complex formed. After evaporating the toluene the residue was purified by column chromatography (on silica gel 60, eluent ether–hexane 1 : 1). The product **6** was a dark violet material, which unlike its solutions, is quite stable in air. Yield: 180 mg (55%). High quality crystals for an X-ray structure investigation could not be obtained.

^{1}H NMR (360 MHz, acetone-d_6): δ (ppm), J (Hz); 9.40 [s, HC=N, ^3J(PtH) = 36]; 7.17 (m, 6 H, CH_{arom}); 4.30 [d, H(1), ^2J(HH) = 12.4, ^2J(PtH) = 144, ^5J(HH) = 3]; 3.42 [d, H(1)′, ^2J(PtH) = 60]; 2.35, 2.26 (2 s, CH_{3arom}); 1.47, 1.28 (2 s, CH_3).

Glyoxalbis(2,6-*diisopropylphenylimine*)-2,3-*bis*(*isopropylidene*)*butane*-1,4-*diyl-platinum* (**7**)

In a procedure analogous to the one described for **6** with the corresponding dad, glyoxalbis(2,6-diisopropylphenylimine), a yield of 200 mg (52%) of **7** was obtained after purification.

^{1}H NMR (360 MHz; C_6D_6): δ (ppm), J (Hz); 8.79 [s, HC=N, ^3J(PtH) = 36]; 7.4 (m, CH_{arom}); 5.34 [d, H(1), ^2J(HH) = 12.4, ^5J(HH) = 3, ^2J(PtH) 155]; 4.33 [d, H(1)′, ^2J(PtH) = 90], 3.80, 3.55 (2 sept, CH_{ipr}); 2.09 (s, CH_3), 1.92 (br. s, CH_3); 1.68, 1.35 (double intensity); 1.23 (3d, CH_{3ipr}). ^{13}C NMR (90.5 MHz; $CDCl_3$): δ (ppm), J (Hz); 162.2 (CHN); 146.6 [C(2)]; 144.9 (C_{ipso}); 139.5, 139.2 (C_{ortho}); 127.0 (C_{para}); 123.0, 122.8 (C_{meta}); 113.4 [C(3); ^3J(PtC) = 72]; 27.5, 27.4 (CH_{ipr}); 25.1, 24.8, 23.2, 22.8 (CH_{3ipr}); 22.5, 19.7 (CH_{3ortho}); 14.5 [Cl, ^1J(PtC) = 745].

(*dad*)*platina*-3-*isopropylidene*-4-*methylene*-5,5-*dimethyl*-6,7-*dioxa*-*cycloheptanes* (**8** *and* **9**)

The (dad)platinacyclopentanes **6** or **7** were stirred for a few hours in toluene under an atmosphere of dioxygen. The colour changed from violet to green. The yield was quantitative. After evaporation of the toluene a green solid material was obtained, which crystallized from ether in the form of green needles.

8 (from **6**). Yield: 95%. ^{1}H NMR (360 MHz, $CDCl_3$): 9.77 [s, NCH, ^3J(PtH) = 84]; 8.69 [s, NCH, ^3J(PtH) = 42]; 7.2 (m, H_{arom}); 4.80 [d, H(8), ^2J(HH) = 2.4]; 4.65 [d, H(8)′]; 3.48 [d, H_α, ^2J(PtH) = 144]; 2.94 [d, $H_{\alpha'}$, ^2J(HH) 11.5, ^2J(PtH) = 60]; 2.36, 2.30, 2.21, 2.18 (4s, CH_{3ortho}), 1.54, 1.25, 1.17, 0.85 (4s, CH_3).

9 (from **7**). Yield: 98%. ^{1}H NMR (360 MHz, C_6D_6): 9.32 [s, NCH, ^3J(PtH) = 79], 7.99 [s, NCH, ^3J(PtH) = 40]; 7.4 (m, H_{arom}); 5.31, 5.18 [2 d, C=CH_2, ^2J(HH) = 2.5]; 4.50 [d, H_α, ^2J(HH) = 11.5, ^2J(PtH) = 144], 3.73 (m, $H_{\alpha'}$, and 2 CH_{ipr}); 3.57, 3.48 (2 sept. CH_{ipr}); 2.06, 1.75, 1.62, 1.38 (4s, C=CMe_2 and O—CMe_2); 1.76, 1.66, 1.55, 1.50, 1.31 (double intensity), 1.26, 1.22 (8d, CH_{3ipr}). ^{1}H NMR (360 Mhz, $CDCl_3$): 9.79 [s, ^3J(PtH) = 79], 8.64 [s, ^3J(PtH) = 35]; 7.35 (m, H_{arom});

4.83, 4.67 [2d, C=CH_2, ^2J(HH) = 2.3]; 3.73, 3.23 (2 sept, CH_{ipr}); 3.58 [d, H_α, ^2J(HH) = 11.5, ^2J(PtH) = 146]; 3.13 (m, $H_{\alpha'}$ and 2 CH_{ipr}); 1.50 [d, one CH_3-*exo*, $J(HH_\alpha)$ = 2 Hz]; 1.42 (double intensity), 1.31, 1.26, 1.20, 1.11, 1.04, 1.01 (8 d, CH_{3ipr}); 1.28, 1.06 (s, CH_3). ^{13}C NMR (90.5 MHz, $CDCl_3$): 164.4, 158.4 (HCN); 155.0 (C_β), 146.9, 146.5 (C_{ipso}); 140.8, 139.8, 139.1, 138.5 (C_{ortho}); 140.4 (C=CH_2); 127.9, 126.3 (C_{para}); 123.5, 123.4, 123.2, 122.7. (C_{meta}); 120.7 (C=CMe_2); 112.1 (CCH_2); 83.1 ($OCMe_2$); 28.0, 27.3 (CH_{iso}); 27.1, 25.1, 23.7, 19.5 (CH_3); 24.5, 24.0, 23.1, 22.9, 22.8, 22.6 (CH_{3iso}); 20.2 (C_α). UV–vis (CH_2Cl_2): max = 590, 388 nm.

X-ray diffraction study of **8**

Crystals were obtained from ethereal solutions, then transferred to a Lindemann tube and mounted on a Syntex $P2_1$ four-circle diffractometer. The crystals are orthorhombic, the space group is *Pcab* (No. 61),[13] the lattice constants were determined as a = 13.683(3), b = 14.058(5), c = 27.64(1) Å and V = 5316(4) Å^3. With Z = 8 and a molecular mass of 627.7 for the molecule $C_{28}H_{36}N_2O_2Pt$ the calculated density is 1.563 g cm^{-3}. The study was performed with Mo-K_α radiation (graphite monochromator, λ = 0.71069 Å). Of 5244 measured reflections and 4706 symmetry-independent reflections thereof, 2768 with $(F_o) > 3\sigma(F_o)$ were used. The number of refined parameters is 262. Linear absorption coefficient μ = 53.6 cm^{-1}. The 2θ range was 4.5–50°. The h, k, l range was 0–16; 0–16; 0–32. The position of the platinum atom was determined by a Patterson synthesis. In following difference Fourier maps the non-hydrogen atoms were located, the hydrogen atoms calculated in ideal positions.[14] All non-hydrogen atoms were refined anisotropically, the hydrogen atoms isotropically.[15] The R values converged to R = 0.0631 and R_w = 0.0764 (weight, w = 0.0005).

Further details on the crystal structure determination can be obtained from the Fachinformationszentrum Energie Physik Mathematik, D-75. Eggenstein-Leopoldshafen, on quoting the depository number CSD-54905, the authors, and the journal citation. Atomic coordinates have been deposited with the Cambridge Crystallographic Data Centre.

RESULTS AND DISCUSSION

Synthesis and spectra

When $Pt(dba)_2$ is stirred in toluene at ambient temperature with an equimolar amount of dad [R′ = H, R = 2,6-Me_2-C_6H_3 or 2,6-$(ipr)_2$-C_6H_3] and an excess of dimethylallene, the 3,4-bis(isopropylidene)platinacyclopentanes **6** and **7** are obtained as the only reaction products. Both complexes are fully characterized by ^{1}H and/or ^{13}C NMR. The ^{195}Pt satellites are helpful in determining the structure and the conformation.[5,16] The unsubstituted double bonds of two allene molecules combine to form the ring, the methylene group being directly bonded to the platinum. The α-CH_2 hydrogen atoms are diastereotopic and thus each appears as a doublet showing quite different Pt—H coupling constants (**6**: 144 and 60, **7**: 155 and 90 Hz). The lower field signal in both complexes is further structured by the coupling to one of the exocyclic isopropylidene methyl groups. This methyl signal has a larger width and a reduced height compared with the other. The spectra agree with the proposed C_2 structure. The steric demand of the isopropylidene groups makes the molecule very rigid and, of course, non-planar. The corresponding platinacyclopentane obtained by Green and coworkers from allene itself[9] does not show diastereotopic α-hydrogen atoms in the NMR. In **7** the ^{195}Pt–^{13}C coupling is easily detected for the α-carbon (^1J = 745 Hz) and the exocyclic sp^2-carbon (^3J = 72 Hz), but not for the β-carbon.

During the first preparation of **6** and **7** a second, green complex was observed when the reaction was followed by thin-layer chromatography. From the number of signals in the NMR an isomer with reduced symmetry appears to form. Repetition of the experiment with strict exclusion of oxygen did not show any such by-product. However, stirring solutions of pure **6** and **7** under an atmosphere of oxygen for some hours gave a virtually quantitative yield of the new green complexes **8** and **9**.

The ^{1}H NMR spectra, which are rather solvent dependent, give some information about the structure. The four methyl groups of the alkylidene substituents of the former **6**, **7** are now inequivalent. One α-CH_2 group seems to persist, while the other CH_2 group gives signals in the olefinic region with the typical small geminal coupling of a C=CH_2 fragment. The number of dad signals (**9**: eight methyl doublets, four CH_{iso} septets and two HC=N singlets; **8**: four methyl singlets, two imine proton signals) clearly shows a C_1 symmetry. A substantial rearrangement must have occurred in going from **6** and **7** to **8** and **9**. Therefore a crystal structure determination was performed for **8**.

Crystal structure of **8**

Suitable crystals were obtained from ethereal solutions. Selected bond lengths and angles are

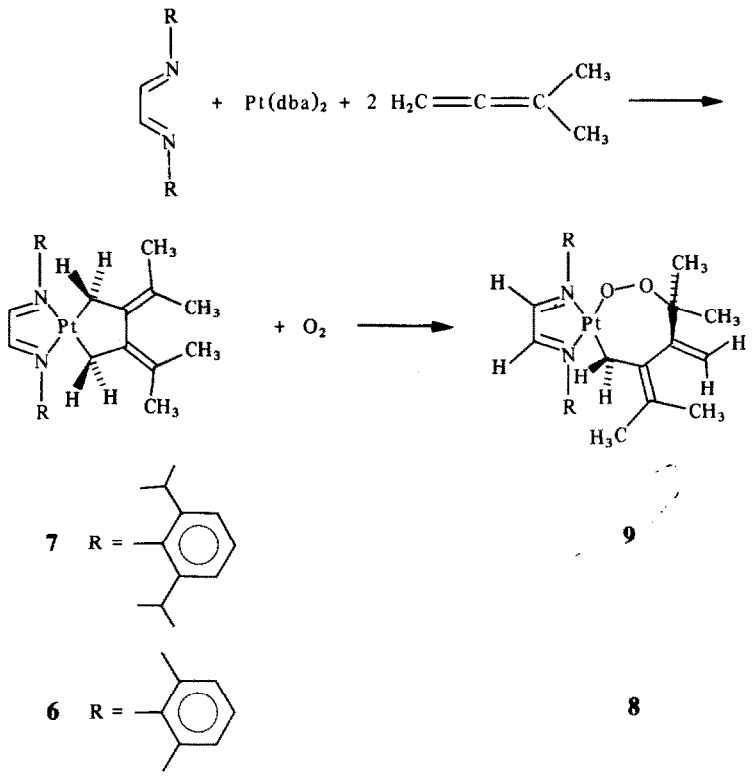

Scheme 2.

Table 1. Bond lengths (Å) and angles (°) of **8** (ESDs in parentheses)

Bond lengths (Å)			
Pt—O(6)	1.95(1)	Pt—N(1)	1.97(1)
Pt—N(2)	2.10(1)	Pt—C(3)	2.06(1)
O(6)—O(7)	1.49(1)	O(7)—C(8)	1.42(2)
N(1)—C(1)	1.32(2)	N(1)—C(11)	1.44(2)
N(2)—C(2)	1.24(2)	N(2)—C(21)	1.41(1)
C(1)—C(2)	1.48(3)	C(3)—C(4)	1.50(3)
C(4)—C(5)	1.35(2)	C(4)—C(9)	1.51(2)
C(5)—C(51)	1.47(3)	C(5)—C(52)	1.49(3)
C(8)—C(9)	1.53(2)	C(8)—C(81)	1.53(3)
C(8)—C(82)	1.54(3)	C(9)—C(91)	1.34(2)
Bond angles (°)			
O(6)—Pt—N(1)	170.4(5)	O(6)—Pt—N(2)	92.6(5)
O(6)—Pt—C(3)	90.5(5)	N(1)—Pt—N(2)	77.9(5)
N(1)—Pt—C(3)	99.0(5)	N(2)—Pt—C(3)	176.9(5)
Pt—O(6)—O(7)	117.1(8)	O(6)—O(7)—C(8)	111(1)
N(1)—C(1)—C(2)	112(1)	N(2)—C(2)—C(1)	118(1)
Pt—C(3)—C(4)	112(1)	C(3)—C(4)—C(5)	125(1)
C(3)—C(4)—C(9)	115(1)	C(5)—C(4)—C(9)	121(1)
O(7)—C(8)—C(9)	111(1)	C(4)—C(9)—C(8)	115(1)
C(4)—C(9)—C(91)	122(1)	C(8)—C(9)—C(91)	123(1)

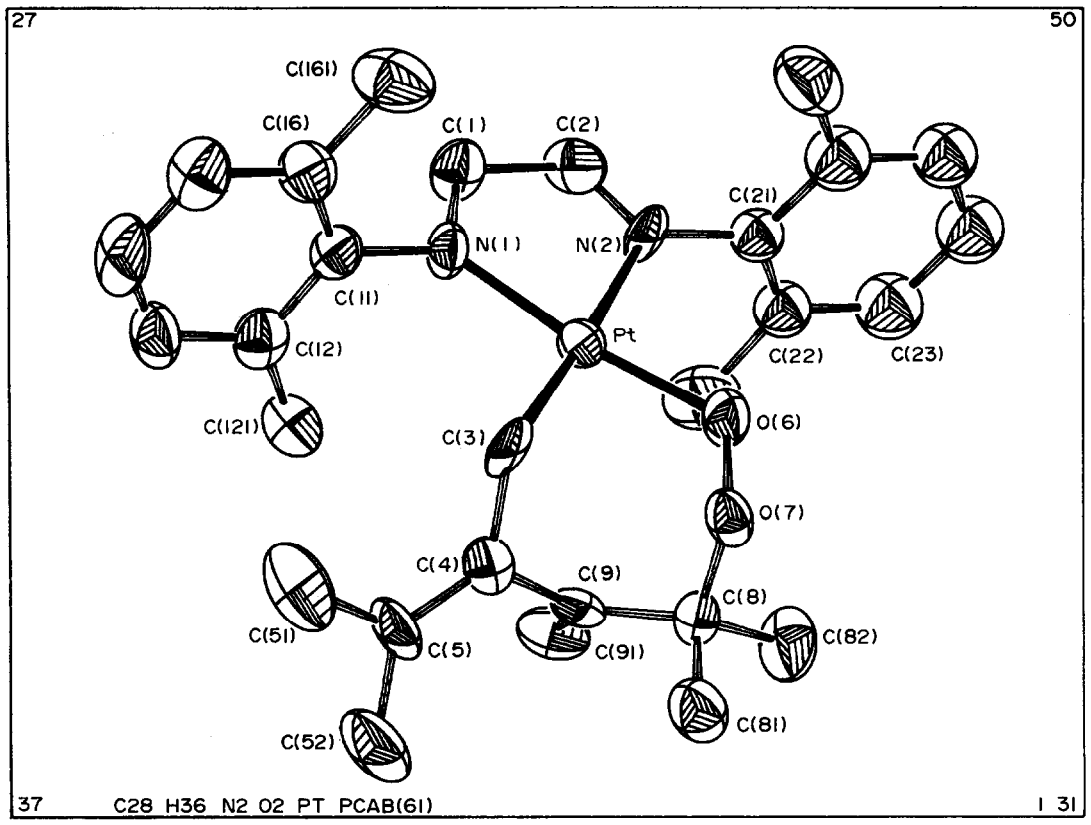

Fig. 1.

listed in Table 1 and Fig. 1 shows the molecule and the atomic numbering scheme

The molecule is a spiro compound with the platinum atom in the centre of a five-membered and a seven-membered ring. The coordination around platinum is square-planar, as expected. The dad system shows typical distances for a complex with the metal in a normal oxidation state, i.e. where backbonding does not play an important role. The standard deviations do not allow a detailed discussion, but it is obvious that the Pt—N(1) bond *trans* to oxygen is much shorter than the Pt—N(2) bond, reflecting the much stronger *trans* effect of a carbon ligand. Similar results are encountered for (dad)Ni and other (dad)Pt chelate complexes with carbon and halogen ligands.[17-19]

The interesting feature in the molecular structure is the incorporation of a dioxygen molecule. The disposition of the methyl groups, however, shows clearly that this does not occur via an insertion into the Pt—C_α bond of **6**. A metallo-ene type reaction,[11,12] as discussed below, can account for the regiochemistry.

The dihedral angle of the Pt—O—O—C fragment is 84(1)° and thus displays the typical orthogonal arrangement of hydrogen peroxide and its derivatives.[20] The *exo*-isopropylidene and the *exo*-methylene groups are not in conjugation, the dihedral angle C(5)—C(4)—C(9)—C(91) is 59(2)°. The Pt—C distance is in the expected region and slightly shorter than in the metallacycles with stronger *trans*-directing ligands than the sp^2-nitrogen.[21] As shown above, the molecule is rigid in solution. The conformation of the seven-membered ring is such that one of the α-hydrogen atoms [on C(3)] is equatorial, the other axial with respect to the plane defined by the platinum lignds. The platinum *s*-orbital is mainly engaged in the four σ-bonds, and therefore the coupling of the ^{195}Pt nuclear spin to the equatorial hydrogen is stronger (144 Hz) than to the axial one (60 Hz). Such values could give indications of the conformations of other compounds such as **6** and **7**. The equatorial hydrogen atoms on C_α in these compounds are coupled to one of the isopropylidene methyl groups and are deshielded with respect to the axial ones; structural models show that they are almost co-planar with the alkylidene substituent.

The reaction of the bis(alkylidene)platinacyclopentanes **6** and **7** with oxygen provided more information than anticipated. The structures of **8** and **9** show a direct link between oxygen and the former-

ly terminal carbon atom of one of the alkylidene groups, while the carbon atom, originally bonded to the metal, is now the terminal atom of an *exo*-methylene group. Such a reorientation is not unprecedented; there are many examples of the insertion of olefins into magnesium or zinc σ-allyl systems, with a concomitant inversion of the allyl group.[11] This work was extended to transition metals,[12] but in all cases C=C double bonds were inserted. Oppholzer called this a metallo-ene reaction,[11] and the stereochemistry of such processes invokes a six-membered cyclic transition state in a concerted process. Here, we have to consider a similar process with dioxygen as the "ene". The methyl substituents of the alkylidene groups in **6** and **7** are responsible for the strong deviation of the platinacyclopentane from planarity. This might facilitate the conformational change to the transition state. Catalytic reactions of this type are under investigation.

Acknowledgements—This work was supported by the Fonds der Chemischen Industrie, Frankfurt, and the Stiftung Volkswagenwerk, Hannover.

REFERENCES

1. H. tom Dieck, C. Munz and C. Müller, *J. Organomet. Chem.* 1990, **384**, 243.
2. P. Maitlis and K. Moseley, *J. Chem. Soc., Chem. Commun.* 1971, 982.
3. H. tom Dieck, C. Munz and J. Ehlers, in *Organometallics in Organic Synthesis 2* (Edited by H. Werner and G. Eker), pp. 22–43. Springer Verlag, Heidelberg (1989).
4. H. tom Dieck, C. Munz and C. Müller, *J. Organomet. Chem.* 1987, **326**, C1.
5. C. Munz, PhD thesis. University of Hamburg (1989).
6. H. tom Dieck, G. Fendesak and C. Munz, *J. Organomet. Chem.*, submitted.
7. C. G. Kreiter, M. Leyendecker and W. S. Sheldrick, *J. Organomet. Chem.* 1986, **302**, 35; A. Nakamura and N. Hagihara, *J. Organomet. Chem.* 1965, **3**, 480; A. S. Nakamura, *Bull. Chem. Soc. Japan* 1966, **39**, 543; W. Keim, *Angew. Chem. Int. Edn Engl.* 1968, **7**, 879; T. A. Peganova, L. S. Iseava, P. V. Petrovskii and D. N. Kravtsov, *J. Organomet. Chem.* 1990, **384**, 397.
8. P. W. Jolly, C. Krüger, R. Salz and J. C. Sekutowski, *J. Organomet. Chem.* 1979, **165**, C39.
9. G. K. Barker, M. Green, J. A. K. Howard, J. L. Spencer and F. G. A. Stone, *J. Chem. Soc., Dalton Trans.* 1978, 1839.
10. J. Sinnema, H. tom Dieck and G. Fendesak, *J. Organomet. Chem.* 1990, **397**, 261.
11. W. Oppholzer, *Angew. Chem.* 1989, **101**, 39. (Review: New Synthetic Methods, No. 75); *Angew. Chem. Int. Ed. Engl.* 1989, **28**, 38.
12. H. Lehmkuhl, *Pure Appl. Chem.* 1986, **58**, 495. (Review); H. Lehmkuhl, in *Organometallics in Organic Synthesis* (Edited by A. de Meijere and H. tom Dieck), pp. 185–202. Springer Verlag, Heidelberg (1987).
13. *International Tables for Crystallography* (Edited by T. Hahn), Vol. A. D. Reidel, Boston (1983).
14. G. M. Sheldrick, SHELXS-86, Programs for crystal structure determination. University of Göttingen (1986).
15. G. M. Sheldrick, SHELX-76, Programs for crystal structure determination. University of Cambridge (1976).
16. B. E. Mann and B. F. Taylor, ^{13}C *NMR Data for Organometallic Compounds.* Academic Press, London (1981).
17. H. tom Dieck and M. Svoboda, *Chem. Ber.* 1976, **109**, 1657.
18. H. G. von Schnering, K. Peters and E.-M. Peters, *Chem. Ber.* 1976, **109**, 1665.
19. L. Dahlenburg, S. Köhlbrandt, private communication: (dad)Pt(neopentyl)Cl (dad as in **8**) Pt—N1 1.88(2), Pt—N2 2.13(2), Pt—C 2.09(2) Å.
20. N. N. Greenwood and A. Earnshaw, *Chemie der Elemente.* VCH Publishers, Weinheim (1988).
21. G. C. Biefield, H. A. Eick and R. H. Grubbs, *Inorg. Chem.* 1973, **12**, 2166; M. Green, J. A. K. Howard, P. Mitrprachachon, M. Pfeffer, J. L. Spencer, F. G. A. Stone and P. Woodward, *J. Chem. Soc., Dalton Trans.* 1979, 306; coordinatively unsaturated platinum: N. Carr, B. J. Dunne, A. G. Orpen and J. L. Spencer, *J. Chem. Soc., Chem. Commun.* 1988, 926; for a (bipy)cyclo-PdC_4 system: P. Diversi, G. Ingrosso, A. Lucherini, T. Lumini, F. Marquetti, V. Adovasio and M. Nardelli, *J. Chem. Soc., Dalton Trans.* 1988, 133.

Note added in proof: After solving some severe local software problems an empirical absorption correction could be performed. The final R value now converged to 3.9%. Refined data are deposited.

Polyhedron Vol. 10, No. 2, pp. 261–265, 1991
Printed in Great Britain

0277–5387/91 $3.00+.00
© 1991 Pergamon Press plc

THE PREPARATION AND X-RAY CRYSTAL STRUCTURE OF $(PMe)_4Se_3$

STEPHEN W. HALL, MARK J. PILKINGTON, ALEXANDRA M. Z. SLAWIN, DAVID J. WILLIAMS and J. DEREK WOOLLINS*

Department of Chemistry, Imperial College of Science, Technology and Medicine, South Kensington, London SW7 2AY, U.K.

(*Received* 18 *July* 1990; *accepted* 27 *September* 1990)

Abstract—The reaction of $(PMe)_5$ with grey selenium in refluxing toluene has been studied with a range of P : Se ratios. With excess selenium, P : Se = 1 : 2, $(PMeSe_2)_2$ is obtained, whereas when the reaction is performed with P : Se ratios of between 4 : 1 and 1 : 1, complex mixtures are obtained. $(PMe)_4Se_3$ (**1**) has been isolated and crystallographically characterized, it has a folded five-membered P_4Se ring with the four phosphorus atoms coplanar. There are significant intermolecular non-bonded interactions between the exocyclic selenium atoms and the "vacant" tetrahedral site of the phosphorus(III) atoms.

Although phosphorus–sulphur rings are well known, there are only a few examples of P—Se heterocycles.[1] These compounds are potentially useful as selenating agents by analogy with the well known Lawessons reagent.[2,3] We have recently shown that reaction of $(PPh)_5$ with grey selenium gives four- and five-membered binary P—Se rings.[4–6] Here, we report on the reaction of $(PMe)_5$ with selenium, together with the X-ray crystal structure of $(PMe)_4Se_3$ (**1**).

EXPERIMENTAL

All manipulations were carried out under an atmosphere of argon or nitrogen; thf, ethoxyethane and diethyl ether were distilled from sodium–benzophenone and toluene was dried over sodium. $(PMe)_5$ was prepared by the literature method.[7] $^{31}P\{^1H\}$ NMR spectra were recorded at 101.4 and 202.8 MHz on Bruker-WM250 and AM500 instruments, respectively. IR spectra were obtained using a PE 1720X instrument. Mass spectra were obtained on a VG 2020 instrument operating in the electron impact mode.

Preparation of $(PMe)_xSe_y$

In a typical reaction grey selenium (1.33 g, 16.8 mmol) was added to 15 cm^3 of deoxygenated toluene. A solution of $(PMe)_5$ in hexane (7.8 cm^3, 0.653 M, 5.1 mmol) was added dropwise with stirring under a stream of oxygen-free nitrogen. The mixture was heated to reflux for 2.5 h. After cooling, the solvent was removed *in vacuo* to give a fine yellow powder. The solid was washed with 2×20 cm^3 cold, dry ethoxyethane and dried *in vacuo*. Yield: 1.7 g. NMR (toluene solution): see Fig. 1. IR (cm^{-1}): 2955 (m, br), 2386(w br), 1652(w br), 1405(m br), 1305(s), 1178(m br), 881(w), 849(w br), 734(m), 677(w), 491(s), 422(w), 361(w). Found: C, 11.8; H, 3.3. Calc. for $(PMe)_3Se_2$: C, 12.2; H, 3.1%. Mass spectrum: *m/z* 456 $(PMe)_3Se_4$, 424 $(PMe)_4Se_3$, 376 $(PMe)_3Se_3$, 330 $(PMe)_2Se_3$, 298 $(PMe)_3Se_2$, 252 $(PMe)_2Se_2$, 172 $(PMe)_2Se$, 126 PMeSe, 46 PMe.

Varying the phosphorus to selenium ratio of the starting materials (4P : 1Se and 1P : 1Se) gave products showing comparable NMR and IR spectra and identical mass spectra. Slow diffusion of hexane into toluene solutions of both the 1P : 1Se and 3P : 2Se reaction products gave rather poorly formed, slightly opaque crystals of $(PMe)_4Se_3$ which were just adequate for X-ray analysis.

A 1P : 2Se ratio resulted in a rust–orange powder insoluble in common solvents. Yield: 1.25 g, 66%. Found: C, 6.0; H, 2.1. Calc. for $(PMeSe_2)_2$: C, 5.9; H, 1.5%. IR (cm^{-1}): 2965(w), 2358(w), 1634(w br), 1385(w br), 844(vs), 725(m), 480(vs br), 418(w), 346(w), 303(w). Mass spectrum: *m/z* 492 $(PMe)_2Se_5$, 410 $(PMe)_2Se_4$, 330 $(PMe)_2Se_3$, 206 $PMeSe_2$, 126 PMeSe, 46 PMe.

Crystal data for $C_4H_{12}P_4Se_3$ (**1**). $M = 420.9$,

* Author to whom correspondence should be addressed.

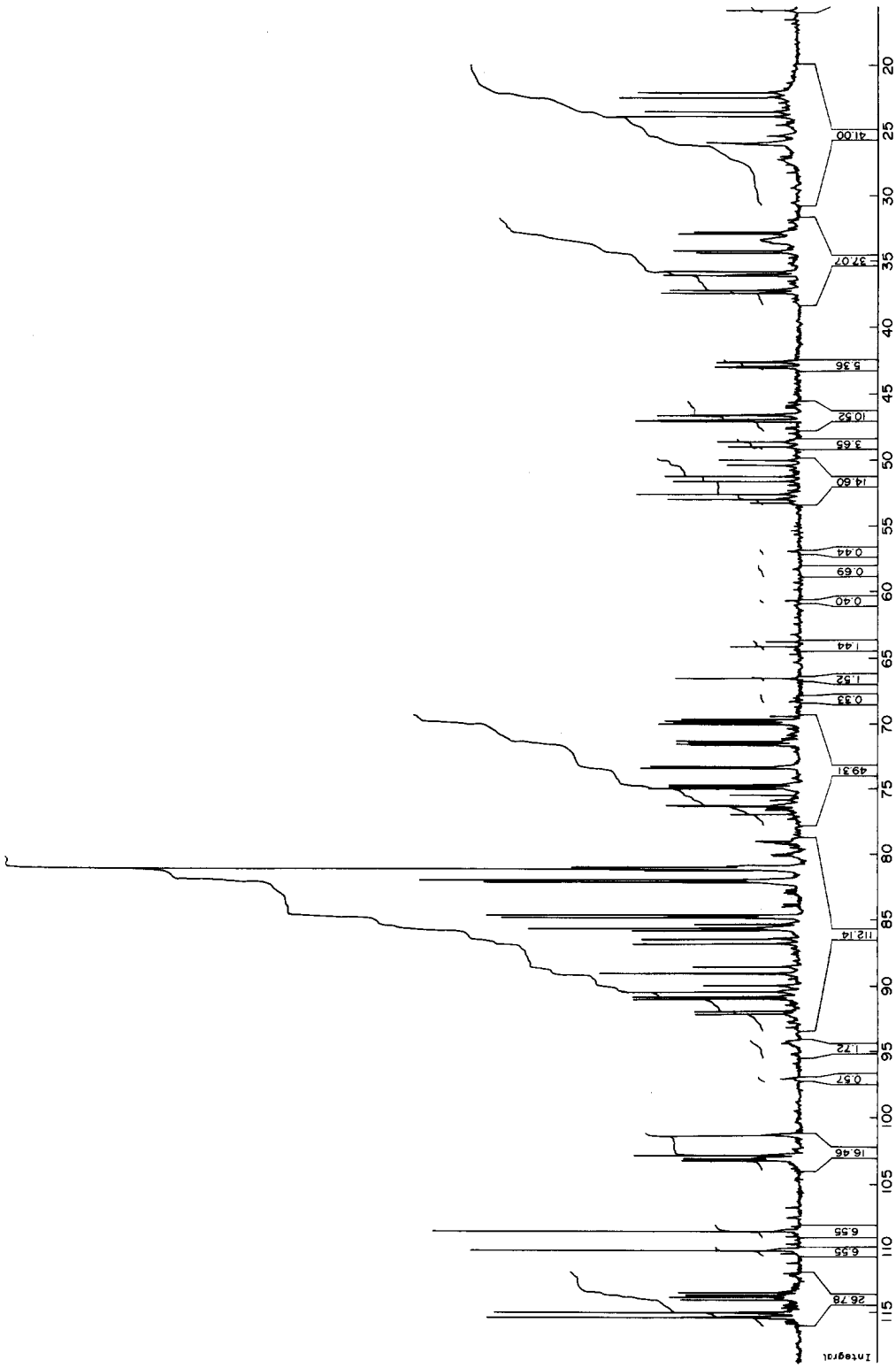

Fig. 1. $^{31}P\{^{1}H\}$ NMR (202.8 MHz) of the reaction between 3/5(PMe)$_5$ and 2Se.

monoclinic, $a = 13.225(41)$, $b = 10.586(26)$, $c = 18.493(22)$ Å, $\beta = 92.83(19)°$, $U = 2586$ Å^3, space group $I2/a$ (body-centred cell chosen because C face-centred cell had $\beta = 144°$), $Z = 8$, $D_c = 2.16$ g cm^{-3}. Crystal dimensions $0.67 \times 0.67 \times 0.40$ mm, μ(Cu-K_α) = 151 cm^{-1}, $\bar{\lambda} = 1.54178$ Å, $F(000) = 1584$. Due to the air sensitivity and instability of the compound the crystal was mounted in a Lindemann tube under liquid paraffin.

Data collection and processing. Nicolet R3m diffractometer, ω-scan method ($\theta \leqslant 58°$), graphite monochromated Cu-K_α radiation; 1427 independent measured reflections, 1298 observed [$|F_o| > 3\sigma(|F_o|)$], corrected for Lorentz and polarization factors; empirical absorption correction (ellipsoidal) based upon 312 azimuthal scans. Maximum and minimum transmission factors 0.068 and 0.008, respectively.

Structure analysis and refinement. The structure was solved by direct methods and all the non-hydrogen atoms refined anisotropically. The hydrogen atoms were idealized (C—H = 0.96 Å), assigned isotropic thermal parameters $U(H) = 1.2U\text{eq}(C)$ and allowed to ride on their parent carbons. The methyl groups were refined as rigid bodies. Refinement was by block-cascade, full-matrix least-squares to $R = 0.065$, $[R = \Sigma(|F_o| - |F_c|)/\Sigma|F_o|]$, $R_w = 0.077$ [$w^{-1} = \sigma^2(F) + 0.00085F^2$]. The maximum and minimum residual electron densities in the final ΔF map were 0.96 and -0.79 e Å^{-3} and the mean and maximum shifts/error in the final refinement cycle were 0.000 and 0.001, respectively. Computations were carried out on an Eclipse S140 computer using the SHELXTL program system.[8]

RESULTS AND DISCUSSION

We have previously reported[5,6] that reaction of $(PPh)_5$ with grey selenium gives, depending on the ratio of reactants, $(PhPSe_2)_2$ (**2**), $(PhP)_3Se_2$ (**3**), $(PhP)_4Se$ (**4**) and $(PhP)_3Se_3$ (**5**). These compounds were characterized by multi-element NMR, mass spectrometry, microanalyses and in the case of **4**, X-ray crystallography. Compound **4** consists of a puckered five-membered ring with all four phenyl substituents axial (average P—P and P—Se bond lengths are 2.194 and 2.271 Å, respectively). Karaghiosoff and Jochem have reported the structure of **5**.[9]

We have now studied the reaction of grey selenium with $(PMe)_5$ so as to probe the degree of steric control that the cyclophosphane substituents provide. Thus, refluxing $(PMe)_5$ with grey selenium using a variety of P : Se ratios was studied. During the course of the reaction the bulk of the selenium is consumed to give yellow solutions. The ^{31}P NMR (202.8 MHz) of a typical reaction is shown in Fig. 1. As can be seen, more than one compound is formed. Varying the P : Se ratio from 4 : 1 through to 1 : 1 had little effect on the spectrum [in contrast to the $(PPh)_5$ reactions]. Simple evaporation of solvent at this stage gave a solid containing a mixture of PSe rings. Attempts to separate this many component system by HPLC (silica gel and gel permeation) have been unsuccessful. However, addition of hexane to the crude reaction mixtures from the 1 : 1 and 3 : 2 ratio reactions gave crystalline **1**, the structure of which is discussed below. Redissolution of **1** into organic solvents resulted in complex NMR spectra similar to that in Fig. 1, suggesting that the system undergoes a number of rapid equilibria. It is not surprising that the methyl substituted compounds are more labile and air sensitive than their previously reported phenyl analogues.

Using increased amounts of selenium(1P : 2Se) gave a rust–orange solid (**6**) which is insoluble in most organic solvents [eq. (1)] and analyses correctly for $(PMeSe_2)_2$. Compound **6** has similar properties to **2**; both are red–orange insoluble solids, whereas all of the other (five-membered) rings that have been described are yellow, organic soluble solids. In **6** we assign the band at 480 cm^{-1} to ν(P=Se), cf. 508 cm^{-1} in **2**. We assume that both **2** and **6** have four-membered ring structures analogous to Lawessons reagent.

$$2/5(PMe)_5 + 4Se \longrightarrow (PMeSe_2)_2 \qquad (1)$$

The X-ray structure of **1** is shown in Fig. 2 with bond lengths and angles in Table 1. The molecule consists of a five-membered P_4Se ring with all of the phosphorus atoms having methyl substituents and two phosphorus atoms having P=Se groups, both of which lie on the same side of the ring. The phosphorus(V) and phosphorus(III) centres alter-

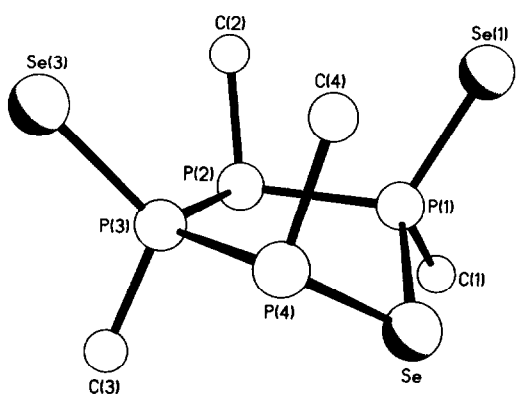

Fig. 2. The X-ray crystal structure of **1**.

Table 1. Bond lengths (Å) and angles (°) in **1**

P(1)—Se	2.267(4)	P(4)—Se	2.245(4)
P(1)—P(2)	2.216(4)	P(2)—P(3)	2.234(5)
P(3)—P(4)	2.201(5)	P(1)—Se(1)	2.104(4)
P(3)—Se(3)	2.105(3)	P(1)—C(1)	1.827(14)
P(2)—C(2)	1.814(16)	P(3)—C(3)	1.793(13)
P(4)—C(4)	1.844(15)		
P(1)—Se—P(4)	101.5(1)	Se—P(1)—P(2)	104.3(2)
P(1)—P(2)—P(3)	100.2(2)	P(2)—P(3)—P(4)	113.1(2)
P(3)—P(4)—Se	97.5(2)	Se—P(1)—Se(1)	116.9(2)
Se—P(1)—C(1)	112.8(5)	Se(1)—P(1)—C(1)	112.8(5)
Se(1)—P(1)—P(2)	116.4(2)	C(1)—P(1)—P(2)	102.8(4)
P(1)—P(2)—C(2)	101.0(6)	C(2)—P(2)—P(3)	99.5(5)
P(2)—P(3)—Se(3)	113.8(2)	P(2)—P(3)—C(3)	101.5(5)
Se(3)—P(3)—C(3)	114.3(4)	Se(3)—P(3)—P(4)	111.2(2)
C(3)—P(3)—P(4)	102.1(5)	Se—P(4)—C(4)	105.3(5)
P(3)—P(4)—C(4)	100.8(5)		

nate around the ring. This is the first example of a five-membered P—Se ring containing two phosphorus(V) atoms. The four phosphorus atoms in **1** are co-planar to within 0.01 Å. The ring is folded about the P(1)···P(4) direction with a dihedral angle of 47° between the P(1)—P(2)—P(3)—P(4) and P(1)—Se—P(4) planes. The ring selenium lies 1.83 Å from the plane of the phosphorus atoms, on the opposite side of the plane to the exocyclic selenium atoms. The bond lengths in **1** do not differ significantly from those in the related $(PhP)_4Se$ (**4**). However, although both methyl substituents on the phosphorus(III) atoms adopt axial geometries which are very similar to those of the phenyl substituents in **4**, the angles at these centres and at the ring selenium are significantly reduced in **1**, reflecting the oxidation of the P(1) and P(3) centres here. Furthermore, the puckering of the ring in **1**

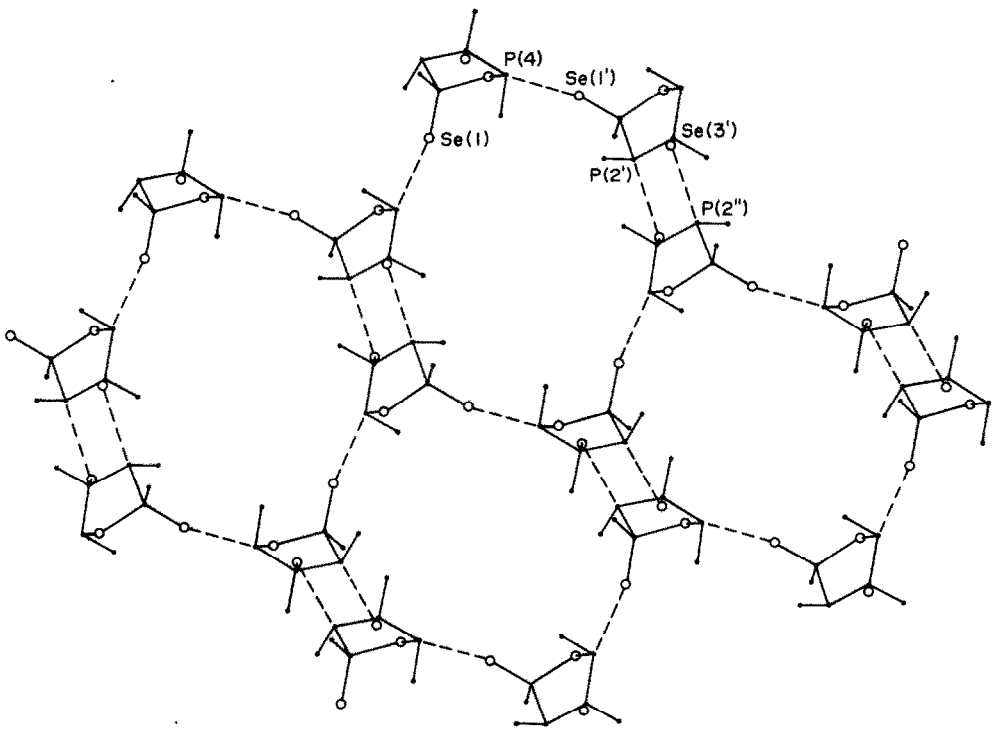

Fig. 3. Part of the contiguous hexagonal array of **1** in the crystal.

differs appreciably from that in **4** where the phosphorus atoms are significantly non-co-planar. The P=Se distances are similar to those reported for P=Se groups in organo-phosphorus–selenium compounds.[4] A study of the packing of **1** in the crystal (see Fig. 3) reveals important short, non-bonded intermolecular Se···P approaches between the exocyclic selenium atoms, Se(1),Se(3) and the phosphorus(III) atoms, P(2),P(4). There is a near tetrahedral approach of these exocyclic selenium atoms to the ring phosphorus atoms with P(4)···Se(1″) 3.43 Å (P—Se···P 165°) and P(2)···Se(3′) 3.77 Å (and vice versa about a crystallographic centre of symmetry, P—Se···P angle 116°). The combination of these interactions results in a contiguous network of loosely linked hexagonal arrays of molecules. These interactions, in particular the former, suggest possible reaction pathways for selenium transfer in these molecules. These interactions presumably involve overlap of sp^3 lone pairs on phosphorus and selenium with low-lying *d*-orbitals of the selenium and phosphorus, respectively.

Acknowledgements—We are grateful to the Wolfson Foundation and the SERC for financial support. J.D.W. is currently the Sir Edward Frankland Fellow of the Royal Society of Chemistry.

REFERENCES

1. For a review see: D. B. Sowerby, P—S and P—Se rings and cages, in *The Chemistry of Inorganic Homo and Heterocycles* (Edited by I. Haiduc and D. B. Sowerby). Academic Press, London (1987).
2. B. S. Pedersen, S. Scheibye, N. H. Nillsson and S. O. Lawesson, *Bull. Soc. Chim. Belg.* 1978, **87**, 22.
3. R. A. Cherkasov, G. A. Kutyrev and A. N. Pudovik, *Tetrahedron* 1985, **14**, 2588.
4. J. C. Fitzmaurice, D. J. Williams, P. T. Wood and J. D. Woollins, *J. Chem. Soc., Chem. Commun.* 1988, 741.
5. P. T. Wood and J. D. Woollins, *J. Chem. Soc., Chem. Commun.* 1988, 1191.
6. M. J. Pilkington, A. M. Z. Slawin, D. J. Williams, P. T. Wood and J. D. Woollins, *Heteroatom*, accepted for publication.
7. M. Baudler and K. Glinka, *Inorg. Synth.* 1989, **25**, 1.
8. G. M. Sheldrick, SHELXTL. An Integrated System for Solving, Refining and Displaying Crystal Structures from Diffraction Data. University of Göttingen (1978), Revision 4.1 (1983).
9. K. Karaghiosoff and G. Jochem, *Phosphorus and Sulphur* 1989, **41**, 460.

Polyhedron Vol. 10, No. 2, pp. 267–272, 1991
Printed in Great Britain

0277–5387/91 $3.00+.00
© 1991 Pergamon Press plc

THE CHEMISTRY OF CYCLOHEPTATRIENYL COMPLEXES OF MOLYBDENUM AND TUNGSTEN: LIGAND SUBSTITUTION VIA A RING SLIPPED INTERMEDIATE IN CATIONIC CARBONYLISONITRILE DERIVATIVES

JONATHAN R. HINCHLIFFE, ALLEN RICALTON and MARK W. WHITELEY*

Department of Chemistry, University of Manchester, Manchester M13 9PL, U.K.

(*Received* 25 *June* 1990; *accepted* 5 *October* 1990)

Abstract—Reaction of $[M(CO)_2(NCMe)(\eta^7\text{-}C_7H_7)]^+$ (M = Mo or W) with one equivalent of $CNBu^t$ affords $[M(CO)_2(CNBu^t)(\eta^7\text{-}C_7H_7)]^+$ (**1**, M = Mo; **2**, M = W), which react with further $CNBu^t$ to give the ring slipped products $[M(CO)_2(CNBu^t)_3(\eta^3\text{-}C_7H_7)]^+$ (**3**, M = Mo; **4**, M = W). At 20°C, **3** slowly converts to a mixture of $[Mo(CO)(CNBu^t)_2(\eta^7\text{-}C_7H_7)]^+$ (**5**) (the formal substitution product of **1** with $CNBu^t$) and $[Mo(CO)(CNBu^t)_4(\eta^3\text{-}C_7H_7)]^+$ (**7**). On heating to 50°C, **7** yields **5** and $[Mo(CNBu^t)_3(\eta^7\text{-}C_7H_7)]^+$ (**8**). Reflux of $[W(CO)_2(CNBu^t)_3(\eta^3\text{-}C_7H_7)]^+$ (**4**) in 2-butanone affords $[W(CO)(CNBu^t)_2(\eta^7\text{-}C_7H_7)]^+$ (**6**) as the major reaction product.

Much recent attention has been given to the ring slippage chemistry of transition metal cyclopentadienyl and indenyl complexes and the facilitation of substitution at the metal centre via ring slipped intermediates.[1] The cycloheptatrienyl ligand, C_7H_7, exhibits a wide range of hapticities (η^7, η^5, η^3 or σ)[2–5] in bonding to transition metals, so encouraging complementary studies on its ring slippage chemistry; our interest in this area centres on $\eta^7\text{-}C_7H_7 \rightarrow \eta^3\text{-}C_7H_7$ ring slip in complexes with molybdenum and tungsten.[6–8] Reports on $\eta^3\text{-}C_7H_7$ complexes of molybdenum and tungsten are quite scarce (see ref. 7 and refs therein) and moreover, with very few exceptions, synthesis involves addition of appropriate ligands to the metal centre of a very limited range of $\eta^7\text{-}C_7H_7$ precursors, $[MX(CO)_2(\eta^7\text{-}C_7H_7)]^{z+}$ (M = Mo or W; $z = 0$, X = halide; $z = +1$, X = NCMe). In general, $\eta^3\text{-}C_7H_7$ complexes of molybdenum and tungsten are sufficiently stable such that their intermediacy in ligand substitution processes at the metal centre, which proceed via ring slippage of the cycloheptatrienyl ligand, should be readily confirmed. However, prior to the current work only one established example of this substitution mechanism has been described,[9] namely the conversion of $[MoI(CO)_2(\eta^7\text{-}C_7H_7)]$ to $[MoI(dppe)(\eta^7\text{-}C_7H_7)]$ (dppe = $Ph_2PCH_2CH_2PPh_2$) which in fact proceeds via two successive intermediates, $[MoI(CO)_2(dppe)(\eta^3\text{-}C_7H_7)]$ and $[Mo(CO)(dppe)(\eta^7\text{-}C_7H_7)]I$.

We have previously reported the first example of $\eta^7 \rightarrow \eta^3$ ring slippage in cationic cycloheptatrienyl complexes:[8]

$$[M(CO)_2(NCMe)(\eta^7\text{-}C_7H_7)]^+ + 2NCMe \rightarrow$$
$$[M(CO)_2(NCMe)_3(\eta^3\text{-}C_7H_7)]^+ \text{ (M = Mo or W).}$$

This system does not lend itself to an investigation of substitution of CO by NCMe since NCMe is generally displaced from $[M(CO)_2(NCMe)_3(\eta^3\text{-}C_7H_7)]^+$ in preference to CO, resulting in reversion to $[M(CO)_2(NCMe)(\eta^7\text{-}C_7H_7)]^+$. However, we now describe the synthesis and reaction chemistry of some analogous cationic carbonylisonitrile complexes which provide a well defined example of ligand substitution at the metal centre proceeding via an isolated $\eta^3\text{-}C_7H_7$ intermediate.

RESULTS AND DISCUSSION

The application of the acetonitrile complexes $[M(CO)_2(NCMe)(\eta^7\text{-}C_7H_7)]^+$ (M = Mo or W) in the high yield synthesis of $[M(CO)_2L(\eta^7\text{-}C_7H_7)]^+$ (L = P-donor ligand) has been described in an earlier paper[8] and in the current work this method

* Author to whom correspondence should be addressed.

provided a convenient entry to the synthesis of a series of cationic isonitrile complexes. Treatment of a CH_2Cl_2 solution of $[M(CO)_2(NCMe)(\eta^7\text{-}C_7H_7)][BF_4]$ with one equivalent of $CNBu^t$ promoted a rapid colour change from green to red with the formation of $[M(CO)_2(CNBu^t)(\eta^7\text{-}C_7H_7)][BF_4]$ (**1**, M = Mo; **2**, M = W) (Scheme 1). Details of characterization by microanalysis, IR and FAB mass spectroscopy, ^1H and ^{13}C NMR spectroscopy are given in Tables 1–3.

The analogy between **1**, **2** and the nitrile complexes $[M(CO)_2(NCMe)(\eta^7\text{-}C_7H_7)]^+$ (M = Mo or W) prompted an examination of the susceptibility of **1** and **2** to undergo ring slip on addition of ligands (L) to give $[M(CO)_2(CNBu^t)L_2(\eta^3\text{-}C_7H_7)]^+$ (L = $CNBu^t$; L_2 = dppe, etc.). Reaction of **1** or **2** with $CNBu^t$ in an approximate 1:2 ratio, or alternatively, direct reaction of $[M(CO)_2(NCMe)(\eta^7\text{-}C_7H_7)][BF_4]$ with three equivalents of $CNBu^t$ in CH_2Cl_2 afforded red solutions of the trihaptocycloheptatrienyl complexes $[M(CO)_2(CNBu^t)_3(\eta^3\text{-}C_7H_7)][BF_4]$ (**3**, M = Mo; **4**, M = W) which were isolated as brown–red solids. The operation of $\eta^7\text{-}C_7H_7 \rightarrow \eta^3\text{-}C_7H_7$ ring slippage in the formation of **3** from **1** and of **4** from **2** is indicated by a characteristic shift to lower wavenumber of the IR active carbonyl stretching frequencies and, in the ^{13}C NMR spectra, by a shift of the C_7H_7 carbon signal to low field by *ca* 10 ppm. In both ^1H and ^{13}C NMR spectra of **3** and **4** the $\eta^3\text{-}C_7H_7$ ligand exhibits only a sharp singlet signal; this may be attributed to a low energy 1,2 shift process[10] which renders all the ring positions equivalent. In favourable cases,[7,10,11] limiting low temperature spectra have been obtained for complexes in which C_7H_7 is bonded trihapto to molybdenum or tungsten thus providing additional confirmation of the η^3 coordination mode of the ring. However, whilst the ^1H NMR spectra of **3** and **4** in CD_2Cl_2 exhibited some line broadening of the C_7H_7 singlet signal on cooling, the coalescence temperature was not approached, even at −90°C, and we conclude that **3** and **4** represent unfavourable subjects for the acquisition of limiting low temperature spectra. Assuming a pseudo octahedral geometry for **3** and **4**, three isomeric structures may be proposed; that shown in Scheme 1 with *cis* carbonyl ligands and a facial arrangement of $CNBu^t$ groups {analogous to the structure proposed for $[W(CO)_2(NCMe)_3(\eta^3\text{-}C_7H_7)][BF_4]$} is preferred on the basis of the observation of a single carbonyl carbon signal in the ^{13}C NMR spectrum and, in the IR spectrum, relative intensities of the two carbonyl bands typical of *cis* carbonyls. Also of note is the successful application of FAB mass spectroscopy in the characterization of **3** and **4**; our previous attempts to characterize

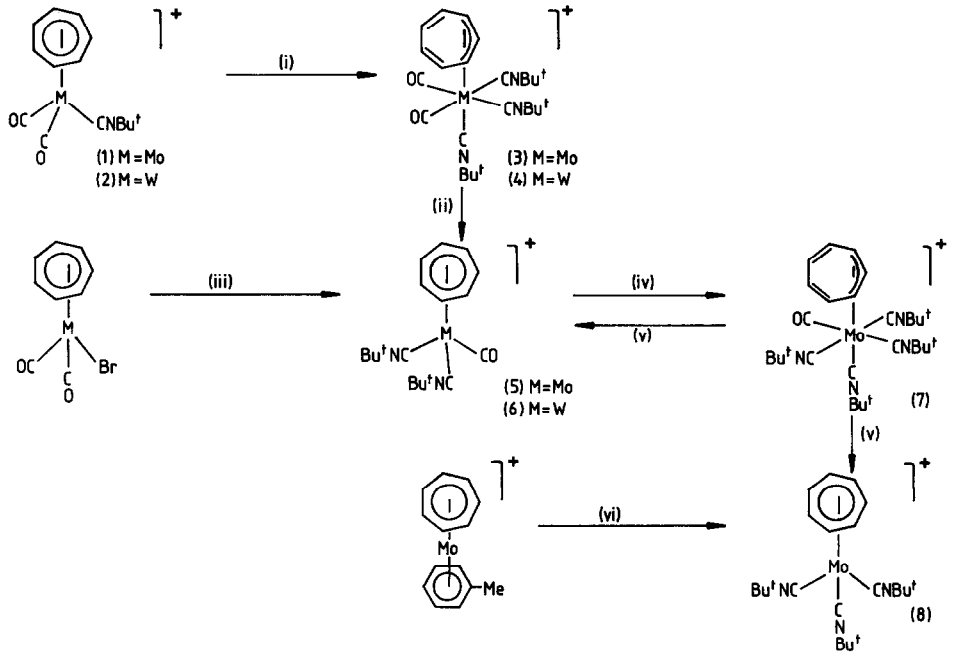

Scheme 1. (i) Stir with $CNBu^t$ in CH_2Cl_2; M = Mo, 0°C; M = W, 20°C; (ii) M = Mo, stir in CH_2Cl_2 at 20°C; M = W, reflux in 2-butanone; (iii) M = Mo only; reflux in acetone with $CNBu^t$, NH_4PF_6 (2:1); (iv) M = Mo, stir in CH_2Cl_2 at 20°C with excess $CNBu^t$; (v) M = Mo, heat to 50°C in $CDCl_3$; (vi) reflux in acetone with three equivalents of $CNBu^t$.

Table 1. IR and microanalytical data

Complex	Yield (%)	IR[a] ν(CO) (cm^{-1})	IR[a] ν(CN) (cm^{-1})	Analysis[b] (%) C	H	N
$[Mo(CO)_2(CNBu^t)(\eta^7\text{-}C_7H_7)][BF_4]$ (1)	94	2040, 2000	2176	40.1 (40.7)	3.8 (3.9)	3.3 (3.4)
$[W(CO)_2(CNBu^t)(\eta^7\text{-}C_7H_7)][BF_4]$ (2)	32	2028, 1981	2174	34.0 (33.6)	3.2 (3.2)	2.7 (2.8)
$[Mo(CO)_2(CNBu^t)_3(\eta^3\text{-}C_7H_7)][BF_4]$ (3)	54	1986, 1940	2180, 2164	49.6 (49.7)	6.0 (5.9)	6.9 (7.3)
$[W(CO)_2(CNBu^t)_3(\eta^3\text{-}C_7H_7)][BF_4]$ (4)	75	1981, 1935	2182, 2161	43.1 (43.2)	5.2 (5.1)	6.1 (6.3)
$[Mo(CO)(CNBu^t)_2(\eta^7\text{-}C_7H_7)][PF_6]$ (5)	70	1988	2167, 2152	41.1 (41.1)	4.8 (4.7)	5.4 (5.3)
$[W(CO)(CNBu^t)_2(\eta^7\text{-}C_7H_7)][BF_4]$ (6)	38	1972	2163, 2142	38.5 (38.8)	4.6 (4.5)	5.1 (5.0)
$[Mo(CO)(CNBu^t)_4(\eta^3\text{-}C_7H_7)][PF_6]$ (7)	84	1918	2172, 2126	48.1 (48.6)	6.4 (6.2)	7.9 (8.1)
$[Mo(CNBu^t)_3(\eta^7\text{-}C_7H_7)][PF_6]$ (8)	41		2154, 2125	45.0 (45.4)	5.9 (5.8)	7.0 (7.2)

[a] Solution spectra in CH_2Cl_2.
[b] Calculated values are given in parentheses.

any η^3-C_7H_7 complexes of molybdenum and tungsten by electron impact mass spectroscopy were unproductive.

Although **3** and **4** are close analogues of the acetonitrile complexes $[M(CO)_2(NCMe)_3(\eta^3\text{-}C_7H_7)]^+$ (M = Mo or W), $CNBu^t$ bonds more effectively to the metal centre than NCMe and therefore reversion of the C_7H_7 ring in **3** and **4** to η^7-hapticity resulted in loss of at least one carbonyl ligand and the formation of new substituted products. At

Table 2. FAB mass spectral and ^1H NMR data

Complex	FAB mass spectral data[a]	^1H NMR data[b] δ C_7H_7	δ $CNCMe_3$
1	328 M^+, 272 $[M-2CO]^+$	5.91 (7H)	1.53 (9H)
2	414 M^+, 386 $[M-CO]^+$, 358 $[M-2CO]^+$, 331 $[M-CNBu^t]^+$	5.86 (7H)	1.56 (9H)
3	494 M^+, 438 $[M-2CO]^+$, 383 $[M-CO-CNBu^t]^+$, 355 $[M-2CO-CNBu^t]^+$	5.72 (7H)	1.57 (27H)
4	580 M^+, 524 $[M-2CO]^+$, 469 $[M-CO-CNBu^t]^+$, 441 $[M-2CO-CNBu^t]^+$	5.46 (7H)	1.58 (27H)
5	383 M^+, 355 $[M-CO]^+$	5.51 (7H)	1.52 (18H)
6	469 M^+, 441 $[M-CO]^+$	5.48 (7H)	1.52 (18H)
7	549 M^+, 438 $[M-CO-CNBu^t]^+$, 383 $[M-2CNBu^t]^+$, 355 $[M-CO-2CNBu^t]^+$	5.30 (7H)	1.57, 1.56, 1.45 (36H)
8	438 M^+, 355 $[M-CNBu^t]^+$	5.14 (7H)	1.44 (27H)

[a] m/z values based on ^{98}Mo and ^{184}W isotopes, M = molecular ion.
[b] In $CDCl_3$, all signals singlets.

Table 3. ^{13}C NMR spectral data[a]

Complex	CO	*C*NCMe$_3$	C_7H_7	CN*C*Me$_3$	CNC*Me*$_3$
1	210.9	145.1	97.3	59.1	29.9
2	201.1	131.7	93.6	60.0	30.1
3	215.0	148.4, 146.8	107.3	58.8, 58.5	30.6, 30.3
4	204.6	137.4, 136.6	104.3	59.1, 58.7	30.5, 30.3
5	219.2	151.1	94.0	58.9	30.3
6	212.1	139.1	90.2	58.8	30.4
7	214.2	160.2, 153.9, 150.0	105.1	58.2, 58.0, 57.8	30.6, 30.5, 30.4
8		158.9	90.6	57.8	30.6

[a] In $CDCl_3$, chemical shifts in ppm downfield from $SiMe_4$.

ambient temperature the tungsten derivative **4** proved to be very stable but $[Mo(CO)_2(CNBu^t)_3(\eta^3\text{-}C_7H_7)][BF_4]$ (**3**) underwent slow conversion to new products; indeed the synthesis of **3** was best carried out at 0°C. The thermal decomposition of **3** was monitored spectroscopically at 30°C; in the ^1H NMR spectrum a decrease in the intensity of the C_7H_7 ring signal due to **3** at δ 5.72 ($CDCl_3$) was accompanied by the growth of two new signals in the C_7H_7 region of the spectrum at δ 5.51 and 5.30 and after 10 h, only these new signals remained with a respective integral ratio of 1.7 : 1. IR spectroscopy revealed two new carbonyl bands [ν(CO)(CH_2Cl_2) 1988, 1918 cm^{-1}] in addition to changes in the ν(CN) region of the spectrum. A preparative scale reaction starting with **3** led to the separation and isolation of two reaction products which were characterized by microanalysis, IR and FAB mass spectroscopy and by ^1H NMR spectroscopy.

The major reaction product was identified as $[Mo(CO)(CNBu^t)_2(\eta^7\text{-}C_7H_7)]^+$ (**5**), an authentic sample of which may be prepared more conveniently and in high yield via treatment of $[MoBr(CO)_2(\eta^7\text{-}C_7H_7)]$ with two equivalents of $CNBu^t$ and one equivalent of $NH_4[PF_6]$ in refluxing acetone; this latter reaction proceeds via the intermediate $[MoBr(CO)_2(CNBu^t)_2(\eta^3\text{-}C_7H_7)]$ which will be described in a subsequent report.

The reaction sequence **1** → **3** → **5**, demonstrates the formal substitution of CO by $CNBu^t$ via a ring slipped intermediate; it is very unlikely that **5** is formed directly from $[Mo(CO)_2(CNBu^t)(\eta^7\text{-}C_7H_7)]^+$ (**1**) since treatment of **1** with less than two equivalents of $CNBu^t$ initially leads to mixtures of **1** and **3**, moreover, monitoring by ^1H NMR spectroscopy provided no evidence for reversion of **3** to **1**. The formation of **5** from **3** is not however entirely straightforward. The minor product isolated from the thermal decomposition of $[Mo(CO)_2(CNBu^t)_3(\eta^3\text{-}C_7H_7)]^+$ (**3**) was identified as $[Mo(CO)(CNBu^t)_4(\eta^3\text{-}C_7H_7)]^+$ (**7**) and ^1H NMR experiments revealed that **7** can (in part) also be converted to $[Mo(CO)(CNBu^t)_2(\eta^7\text{-}C_7H_7)]^+$ (**5**). However, this reaction was very slow at 30°C and it seem improbable that **7** is a primary intermediate in the formation of **5** from **3**.

Complex **7** may be surmised to originate from a direct substitution of CO by $CNBu^t$ in **3** or alternatively via reaction of $[Mo(CO)(CNBu^t)_2(\eta^7\text{-}C_7H_7)]^+$ (**5**) with free $CNBu^t$ released in the conversion of **3** to **5**. To examine this latter possibility, the reaction of $[Mo(CO)(CNBu^t)_2(\eta^7\text{-}C_7H_7)][PF_6]$ with $CNBu^t$ was investigated. Prolonged reaction times and the use of a large excess of $CNBu^t$ led to the isolation of high yields of the $[PF_6]$ salt of **7**; note that the conversion of **5** to **7** is accompanied by changes in ν(CO) in the IR spectrum and δC_7H_7 in the ^{13}C NMR spectrum, characteristic of $\eta^7\text{-}C_7H_7 \rightarrow \eta^3\text{-}C_7H_7$ ring slip. On the basis of ^{13}C NMR data, **7** is assigned a structure in which $CNBu^t$ rather than CO lies *trans* to the C_7H_7 ring. The relatively strong, low field $CNBu^t$ donor carbon signal at 160.2 ppm in the ^{13}C NMR spectrum is tentatively assigned to the *trans* $CNBu^t$ ligands; in general, isocyanide donor carbons *trans* to isocyanides are deshielded with respect to isocyanide donor carbons *trans* to CO.[12] Variable temperature ^1H NMR studies on **7** in CD_2Cl_2 revealed some line broadening of the C_7H_7 signal on cooling to −90°C but, as with **3** and **4**, a limiting low temperature spectrum was not obtained.

Although the formation of **7** from **5** has been demonstrated and in fact provides the first example of ring slippage in a $\eta^7\text{-}C_7H_7$ complex not of the formulation $[MX(CO)_2(\eta^7\text{-}C_7H_7)]^{z+}$ (M = Mo or W; $z = 0$, X = halide; $z = +1$, X = NCMe), the direct formation of **7** from $[Mo(CO)_2(CNBu^t)_3(\eta^3\text{-}C_7H_7)]^+$ (**3**), excluding $[Mo(CO)(CNBu^t)_2(\eta^7\text{-}C_7H_7)]^+$ (**5**) as an intermediate, should not be discounted. Indeed the relatively large quantity of **7** formed from **3** after a few hours at 30°C, as determined by ^1H NMR, seems inconsistent with the

long reaction time and large excess of $CNBu^t$ required to effect conversion of **5** to **7**.

In principle, further substitution of CO by $CNBu^t$ in $[Mo(CO)(CNBu^t)_2(\eta^7\text{-}C_7H_7)]^+$ (**5**) might proceed via $[Mo(CO)(CNBu^t)_4(\eta^3\text{-}C_7H_7)]^+$ (**7**) to give $[Mo(CNBu^t)_3(\eta^7\text{-}C_7H_7)]^+$ (**8**) in an analogous manner to the reaction sequence **1** → **3** → **5**. Complex **8** has been reported previously[13] but, in view of the very limited characterization data given, was independently synthesized in the current work via reaction of $[Mo(\eta^6\text{-toluene})(\eta^7\text{-}C_7H_7)][PF_6]$ with three equivalents of $CNBu^t$ in refluxing acetone. Examination of ^1H NMR data reveals that an increase in the ratio of $CNBu^t$ to CO ligands along the sequence of complexes **1**, **3**, **5**, **7**, **8** produces a steady shift to high field of δ C_7H_7 in the ^1H NMR spectra. The proposed conversion of **7** to **8** was investigated by ^1H NMR spectroscopy in $CDCl_3$ at 50°C. After 6 h the major product of thermal decomposition of **7** was **5**, but a second minor product with δ C_7H_7 ($CDCl_3$) 5.14 was also observed and identified as **8**. At this point the approximate ratio of integrals for **5**:**7**:**8** was 3:1.5:1 but this was modified to 1:0.3:1 after a total reaction time of 6 days. A preparative scale reaction involving reflux of **5** with one equivalent of $CNBu^t$ in acetone was also attempted; the formation of **8** was confirmed by ^1H NMR spectroscopy and IR spectroscopy provided evidence for the presence of small quantities of **7**. However the reaction was very slow and neither complete conversion of **5** to **8** nor separation of the reaction mixture could be achieved. In conclusion, there is good evidence to support the feasibility of the reaction sequence **5** → **7** → **8** but it is not clear that **7** is an essential intermediate. The major problem is that reversion of **7** to products with a heptahapto-bonded C_7H_7 ring can involve either loss of one $CNBu^t$ and one CO ligand or alternatively two $CNBu^t$ groups; this is in contrast to the corresponding transformation of $[Mo(CO)_2(CNBu^t)_3(\eta^3\text{-}C_7H_7)]^+$ (**3**) which proceeds almost exclusively via loss of one $CNBu^t$ and one CO ligand.

The high thermal stability of $[W(CO)_2(CNBu^t)_3(\eta^3\text{-}C_7H_7)]^+$ (**4**) with respect to its molybdenum analogue **3** has already been noted. However, reflux of **4** for 5 h in 2-butanone resulted in complete conversion to new products with ν(CO)(CH_2Cl_2) at 1972 and 1910 cm^{-1}. Work-up of the reaction mixture afforded moderate yields of $[W(CO)(CNBu^t)_2(\eta^7\text{-}C_7H_7)]^+$ (**6**) which was fully characterized (Tables 1, 2 and 3), but attempts to isolate the minor reaction product [ν(CO)(CH_2Cl_2) 1910 cm^{-1}], suspected to be $[W(CO)(CNBu^t)_4(\eta^3\text{-}C_7H_7)]^+$, were unsuccessful.

The monoisonitrile complexes $[Mo(CO)_2(CNBu^t)(\eta^7\text{-}C_7H_7)]^+$ (M = Mo or W) also react with dppe to give ring slipped products formulated as $[M(CO)_2(CNBu^t)(dppe)(\eta^3\text{-}C_7H_7)]^+$. However definitive characterization of these species is not straightforward due either to facile chelate ring opening or the formation of isomeric mixtures.

EXPERIMENTAL

The preparation, purification and reactions of the complexes described were carried out under dry nitrogen. All solvents were dried by standard methods, distilled and deoxygenated before use. The complexes $[M(CO)_2(NCMe)(\eta^7\text{-}C_7H_7)][BF_4]$ (M = Mo or W)[8] and $[Mo(\eta^6\text{-}C_6H_5Me)(\eta^7\text{-}C_7H_7)][PF_6]$[13] were prepared by published procedures; Aldrich Chemical Co. supplied $CNBu^t$ and $NH_4[PF_6]$. ^1H NMR spectra were recorded on Brucker AC 300 E or AC 80 E instruments and ^{13}C NMR spectra at 75 MHz on a Varian Associates XL 300 spectrometer. IR spectra were obtained on a Perkin–Elmer FT 1710 spectrometer and FAB mass spectra using a Kratos Concept 1S instrument. Microanalyses were by the staff of the Microanalytical Service of the Department of Chemistry, University of Manchester.

Preparation of $[Mo(CO)_2(CNBu^t)(\eta^7\text{-}C_7H_7)][BF_4]$ (1)

Addition of $CNBu^t$ (0.513 g, 6.181 mmol) to a green, stirred solution of $[Mo(CO)_2(NCMe)(\eta^7\text{-}C_7H_7)][BF_4]$ (2.291 g, 6.175 mmol) in CH_2Cl_2 (50 cm^3) rapidly produced a red solution. After 20 min the solvent volume was reduced to *ca* 10 cm^3 and the product precipitated by addition of diethyl ether. Recrystallization from CH_2Cl_2–diethyl ether gave **1** as a red solid; yield 2.403 g (94%). An identical procedure was employed to prepare $[W(CO)_2(CNBu^t)(\eta^7\text{-}C_7H_7)][BF_4]$ (**2**) as a red solid in 32% yield from $[W(CO)_2(NCMe)(\eta^7\text{-}C_7H_7)][BF_4]$ (0.22 g, 0.48 mmol) and $CNBu^t$ (0.039 g, 0.47 mmol).

Preparation of $[Mo(CO)_2(CNBu^t)_3(\eta^3\text{-}C_7H_7)][BF_4]$ (3)

Method A. A solution of $[Mo(CO)_2(NCMe)(\eta^7\text{-}C_7H_7)][BF_4]$ (0.297 g, 0.80 mmol) in CH_2Cl_2 (60 cm^3) was cooled to 0°C and treated with $CNBu^t$ (0.20 g, 2.41 mmol). The solution was stirred and maintained at 0°C for 12 h, after which time solvent was removed and the residue recrystallized from CH_2Cl_2–diethyl ether to give **3** as a red–brown solid; yield 0.25 g (54%). The red–brown tungsten analogue $[W(CO)_2(CNBu^t)_3(\eta^3\text{-}C_7H_7)][BF_4]$ (**4**) was prepared in 75% yield from $[W(CO)_2(NCMe)$

(η^7-C_7H_7)][BF_4] (0.291 g, 0.63 mmol) and $CNBu^t$ (0.178 g, 2.14 mmol) by a similar procedure to **3**, except that reaction was complete after 4 h at 20°C.

Method B. A solution of [$Mo(CO)_2(CNBu^t)$(η^7-C_7H_7)][BF_4] (0.510 g, 1.24 mmol) in CH_2Cl_2 (30 cm^3) was cooled to 0°C, treated with $CNBu^t$ (0.227 g, 2.73 mmol), then stirred at 0°C for 12 h. A work-up procedure identical to method A gave **3**; yield 0.252 g (35%). Similarly, **4** was prepared in 39% yield from **2** (0.244 g, 0.487 mmol) and $CNBu^t$ (0.100 g, 1.20 mmol) in CH_2Cl_2 stirred at 20°C for 4 h.

Thermal decomposition of [$Mo(CO)_2(CNBu^t)_3$(η^3-C_7H_7)][BF_4] (**3**)

A solution of **3** (0.252 g, 0.435 mmol) in CH_2Cl_2 (30 cm^3) was stirred at 20°C for 24 h when IR spectroscopy indicated completion of the reaction. The solution was filtered, reduced in volume and diethyl ether added in small portions with constant stirring. The first precipitate so obtained was isolated and recrystallized from CH_2Cl_2–diethyl ether to give [$Mo(CO)(CNBu^t)_2$(η^7-C_7H_7)][BF_4] as an orange solid; yield 0.081 g (40%). Found: C, 46.5; H, 5.4; N, 6.1. Calc. for $C_{18}H_{25}N_2OMoBF_4$: C, 46.2; H, 5.3; N, 6.0%. Addition of further diethyl ether to the reaction solution afforded a deep red solid which was also isolated and recrystallized from CH_2Cl_2–diethyl ether to give [$Mo(CO)(CNBu^t)_4$(η^3-C_7H_7)][BF_4]; yield 0.045 g (16%). Found: C, 53.1; H, 6.8; N, 8.7. Calc. for $C_{28}H_{43}N_4OMoBF_4$: C, 53.0; H, 6.8; N, 8.8%.

Preparation of [$Mo(CO)(CNBu^t)_2$(η^7-C_7H_7)][PF_6] (**5**) *from* [$MoBr(CO)_2$(η^7-C_7H_7)]

A mixture of [$MoBr(CO)_2$(η^7-C_7H_7)] (0.317 g, 0.98 mmol), $CNBu^t$ (0.163 g, 1.96 mmol) and NH_4[PF_6] (0.161 g, 0.99 mmol) was dissolved in AR acetone (40 cm^3) and the solution refluxed for 3 h. Removal of acetone and recrystallization of the residue from CH_2Cl_2–diethyl ether gave [$Mo(CO)(CNBu^t)_2$(η^7-C_7H_7)][PF_6] as an orange solid; yield 0.36 g (70%).

Preparation of [$Mo(CO)(CNBu^t)_4$(η^3-C_7H_7)][PF_6] (**7**)

A solution of [$Mo(CO)(CNBu^t)_2$(η^7-C_7H_7)][PF_6] (0.49 g, 0.93 mmol) in CH_2Cl_2 (40 cm^3)was treated with $CNBu^t$ (0.405 g, 4.88 mmol) and stirred for 24 h. Solvent was removed and the residue recrystallized from CH_2Cl_2–diethyl ether, then acetone–diethyl ether to give **7** as a deep red solid; yield 0.542 g (84%).

Preparation of [$Mo(CNBu^t)_3$(η^7-C_7H_7)][PF_6] (**8**)

A solution of [$Mo(\eta^6$-$C_6H_5Me)$(η^7-C_7H_7)][PF_6] (0.30 g, 0.71 mmol) in AR acetone (50 cm^3) was refluxed for 0.5 h to give a red solution to which $CNBu^t$ (0.176 g, 2.12 mmol) was added. After continuing the reflux for a further 1 h, solvent was removed and the residue recrystallized from CH_2Cl_2–diethyl ether, then thf–diethyl ether to give **8** as a red pink solid; yield 0.168 g (41%).

Preparation of [$W(CO)(CNBu^t)_2$(η^7-C_7H_7)][BF_4] (**6**)

A solution of [$W(CO)_2(CNBu^t)_3$(η^3-C_7H_7)][BF_4] (**4**) (0.364 g, 0.55 mmol) in 2-butanone (70 cm^3) was refluxed with stirring for 5 h, after which time IR spectroscopy indicated complete conversion to products. Solvent was removed and the residue dissolved in CH_2Cl_2, filtered and treated with diethyl ether in small aliquots. The first precipitate thus obtained was isolated and recrystallized from CH_2Cl_2–diethyl ether to give **6** as a red–brown solid; yield 0.114 g (38%).

Acknowledgement—We thank the SERC for a Research Studentship (to J.R.H.).

REFERENCES

1. J. M. O'Connor and C. P. Casey, *Chem. Rev.* 1987, 307.
2. C. E. Davies, I. M. Gardiner, J. C. Green, M. L. H. Green, N. J. Hazel, P. D. Grebenik, V. S. B. Mtetwa and K. Prout, *J. Chem. Soc., Dalton Trans*, 1985, 669.
3. A. K. Campen, R. Narayanaswamy and A. J. Rest, *J. Chem. Soc., Dalton Trans.* 1990, 823.
4. F. Edelmann, G.-Y. Kiel, J. Takats, A. Vasudevamurthy and M.-Y. Yeung, *J. Chem. Soc., Chem. Commun.* 1988, 296.
5. D. M. Heinekey and W. A. G. Graham, *J. Am. Chem. Soc.* 1982, **104**, 915.
6. R. Breeze, S. Endud and M. W. Whiteley, *J. Organomet. Chem.* 1986, **302**, 371.
7. R. A. Brown, S. Endud, J. Friend, J. M. Hill and M. W. Whiteley, *J. Organomet. Chem.* 1988, **339**, 283.
8. R. Breeze, M. S. Plant, A. Ricalton, D. J. Sutton and M. W. Whiteley, *J. Organomet. Chem.* 1988, **356**, 343.
9. T. W. Beall and L. W. Houk, *Inorg. Chem.* 1973, **12**, 1979.
10. J. W. Faller, *Inorg. Chem.* 1969, **8**, 767.
11. M. L. H. Green, D. K. Siriwardene, D. O'Hare and L.-L. Wong, *J. Chem. Soc., Dalton Trans.* 1988, 2851.
12. M. Minelli and W. J. Maley, *Inorg. Chem.* 1989, **28**, 2954.
13. M. Bochmann, M. Cooke, M. Green, H. P. Kirsch, F. G. A. Stone and A. J. Welch, *J. Chem. Soc., Chem. Commun.* 1976, 381.

Polyhedron Vol. 10, No. 2, pp. 273–276, 1991
Printed in Great Britain

0277–5387/91 $3.00+.00
© 1991 Pergamon Press plc

COMMUNICATION

METAL–BETAINE INTERACTIONS—VI. CRYSTAL AND MOLECULAR STRUCTURE OF TETRAKIS(BETAINE)COPPER(II) NITRATE, $[Cu(Me_3NCH_2COO)_4](NO_3)_2$

XIAO-MING CHEN and THOMAS C. W. MAK*

Department of Chemistry, The Chinese University of Hong Kong, Shatin, New Territories, Hong Kong

(*Received* 27 *September* 1990; *accepted* 22 *October* 1990)

Abstract—The crystal and molecular structure of $[Cu(BET)_4]\cdot(NO_3)_2$ (BET = $Me_3N^+CH_2COO^-$) has been established by X-ray crystallography. The complex consists of discrete $[Cu(BET)_4]^{2+}$ and nitrate anions, with the copper(II) atom eight-coordinated by four short Cu—O(carboxy) bonds [1.948(3) Å] and four long Cu—O(carboxy) bonds [2.833(4) Å] in a distorted dodecahedral $\bar{4}2m$ (D_{2d}) environment.

Coordination numbers of seven and higher for copper in its carboxylates are rare even considering Cu—L distances up to 2.9 Å.[1] To our knowledge, hitherto only three examples of structurally characterized eight-coordinate complexes of copper(II) carboxylates have been reported, which are all double salts possessing polymeric structures in the solid state. The first example, $Ca[Cu(acetato)_4]\cdot 6H_2O$, was initially characterized by Langs and Hare[2] and later refined by Klop *et al.*[3] A study of the polarized single-crystal electronic spectrum and electron spin resonance spectrum of this double salt suggests that the long Cu—O contact of 2.788(2) Å reflects a significant, though weak, metal–ligand bonding.[4] The other two examples are $Rb_2[Cu(o\text{-phthalato})_2]\cdot 2H_2O$ (phthalato group abbreviated hereafter as pht) and $Li[Cu(pht)_2]\cdot 4H_2O$,[5] in which the long Cu—O contacts are *ca* 3.05 Å.

In the course of our systematic investigation on metal complexes of betaine ligands,[6] we have prepared and characterized the title copper(II) complex, namely tetrakis(betaine)copper(II) nitrate, $[Cu(BET)_4](NO_3)_2$ (BET = betaine, $Me_3N^+CH_2COO^-$; IUPAC name: 1-carboxy-N,N,N-trimethylmethanaminium hydroxide inner salt). Its structure has now been established by means of single-crystal X-ray diffraction.

* Author to whom correspondence should be addressed.

EXPERIMENTAL

Preparation and IR spectra

The complex was simply prepared by dissolving $Cu(NO_3)_2\cdot 3H_2O$ (0.242 g, 1.0 mmol) and betaine monohydrate (0.540 g, 4.0 mmol; Sigma) in hot water (3 cm^3, *ca* 60°C). After slow evaporation at room temperature for 2 days, violet–blue, cubic-like crystals suitable for X-ray work were obtained.

IR spectra (KBr pellets) were recorded on a Nicolet 20SXC FT–IR spectrometer in the range 4000–400 cm^{-1}. The complex exhibits the following IR carboxy absorption bands (v = very, s = strong, m = medium; cm^{-1}): ν(COO) at 1642vs, 1654vs and 1387vs, and δ(COO) at 727m. The average separation (Δ) between ν_{asym}(COO) and ν_{sym}(COO) is 267 cm^{-1}, which is significantly larger than that in anhydrous betaine [ν(COO) = 1624, 1388 cm^{-1}; Δ = 236 cm^{-1}],[7] hence indicative of the unidentate mode of carboxylato coordination in the present complex.[8]

X-ray crystallography

$Cu(Me_3NCH_2COO)_4 \cdot (NO_3)_2$, mol. wt 656.15, tetragonal, space group $I\bar{4}2m$ (No. 121), $a = 11.443(2)$, $b = 11.443(2)$, $c = 11.672$ (2) Å, $V = 1528.4(5)$ Å^3, $Z = 2$, $D_{exptl} = 1.427$ g cm^{-3} (flotation in CCl_4/*n*-hexane), $D_{calc} = 1.426$ g cm^{-3}, $F(000) = 694$, Mo-K_α radiation ($\lambda = 0.71073$ Å), $\mu = 0.78$ mm^{-1}.

Diffraction intensities (crystal size $0.26 \times 0.34 \times 0.40$ mm; $2\theta_{max} = 65°$, 832 unique data) were collected at 21°C on a Nicolet R3m/V diffractometer using the ω-scan (3.22–15.63°min^{-1}) mode.[9] Data processing, absorption corrections ($\mu r = 0.127$, transmission factors 0.514–0.533), structure solution and full-matrix least-squares refinement were performed with the SHELXTL-PLUS program package[10,11] on a DEC MicroVAX-II computer. The non-hydrogen atoms were refined anisotropically except the oxygen atoms of orientationally disordered nitrate groups, which were subjected to interatomic-distance constraints and assigned appropriate site occupancy factors in the refinement. Analytic expressions of neutral-atom scattering factors were employed, and anomalous dispersion corrections were incorporated.[12] The final residuals were $R_F = 0.052$ and $R_w = 0.065$ for 758 observed data with $I \geqslant 3\sigma(I)$.

Supplementary materials including non-hydrogen and hydrogen atomic coordinates and thermal parameters have been deposited at the Cambridge Crystallographic Data Centre, and observed and calculated structure factors are available upon request from the corresponding author.

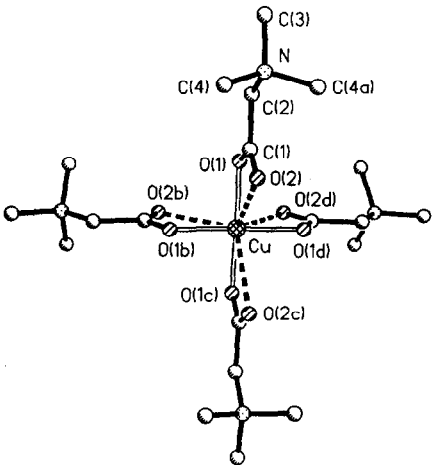

Fig. 1. Perspective view showing the molecular structure of the $[Cu(BET)_4]^{2+}$ cation and the atom numbering scheme. The short and long Cu—O(carboxy) bonds are represented by open and broken lines, respectively. Symmetry codes are given in Table 1.

RESULTS AND DISCUSSION

The crystal structure consists of a packing of discrete $[Cu(BET)_4]^{2+}$ cations and nitrate anions (Fig. 1). The copper(II) atom, occupying Wyckoff position 2(*a*) of site symmetry $\bar{4}2m$ (D_{2d}), is coordinated by four BET ligands with four short Cu—O(carboxy) bonds [Cu(1)—O(1) = 1.948(3) Å] in an approximately square-planar fashion, the most distorted angle being O(1)—Cu(1)—O(2c) at 173.2(4)° (Table 1). The coordination sphere of the

Table 1. Bond lengths (Å) and angles (°) for the $[Cu(BET)_4]^{2+}$ cation

Cu(1)—O(1)	1.948(3)	Cu(1)—O(2)	2.833(4)
O(1)—Cu(1)—O(1b)	90.2(1)	O(1)—Cu(1)—O(2)	51.3(3)
O(1)—Cu(1)—O(1c)	173.2(4)	O(2)—Cu(1)—O(2c)	84.1(4)
O(1)—Cu(1)—O(1d)	90.2(1)	Cu(1)—O(1)—C(1)	112.1(4)
O(1)—C(1)	1.270(8)	O(2)—C(1)	1.225(7)
C(1)—C(2)	1.520(7)	C(2)—N(1)	1.499(7)
N(1)—C(3)	1.489(8)	N(1)—C(4)	1.506(6)
O(1)—C(1)—O(2)	125.6(5)	O(1)—C(1)—C(2)	110.9(4)
O(2)—C(1)—C(2)	123.5(5)	C(1)—C(2)—N(1)	117.5(4)
C(2)—N(1)—C(3)	107.6(5)	C(2)—N(1)—C(4)	111.3(3)
C(3)—N(1)—C(4)	108.3(3)	C(4)—N(1)—C(4a)	110.0(5)

Symmetry codes: *a* y, x, z; *b* $-x, y, -z$; *c* $-x, -y, z$; *d* $x, -y, -z$.

Table 2. Structural parameters for some eight-coordinate tetrakis(carboxylato)copper(II) complexes

Compound	Chromophore and site symmetry	Cu—O(carboxy) short bond (Å)	Cu—O(carboxy) long bond (Å)	O—C—O angle (°)	Reference
$Ca[Cu(acetato)_4]\cdot 6H_2O$	$O_4O'_4$, S_4	1.969(1)	2.788(2)	122.0(2)	2, 3
$Rb_2[Cu(pht)_2]\cdot 2H_2O$	$O_4O'_4$, C_2	1.922(9)	2.792(8)	124.9(9)	5
	$(O_2O'_2O''_2O'''_2)$	1.965(9)	3.072(9)	125.0(8)	
$Li_2[Cu(pht)_2]\cdot 4H_2O$	$O_4O'_4$, C_i	1.942(3)	2.770(4)	122.8(5)	5
	$(O_2O'_2O''_2O'''_2)$	1.955(3)	3.033(4)	125.1(5)	
$[Cu(BET)_4](NO_3)_2$	$O_4O'_4$, D_{2d}	1.948(3)	2.833(4)	125.6(5)	This work

copper(II) atom is completed by the remaining four ligand O(2) atoms at much longer contacts of Cu(1)—O(2) = 2.833(4) Å. The BET ligands, as located at Wyckoff positions 8(*i*) of symmetry *m*, coordinate the copper(II) atom in an alternately up/down fashion, so that the cation may be considered to possess a (4+4*) distorted dodecahedral stereochemistry about the copper(II) atom.

Similar stereochemistry has been found in Ca[Cu(acetato)$_4$]·6H$_2$O,[2,3] in which the coordination geometry about the copper(II) atom has exact $\bar{4}$ (S_4) symmetry with four short and four long Cu—O(carboxy) bonds of lengths 1.969(1) and 2.788(2) Å, respectively. The enhanced extent of asymmetric chelation of the BET ligand to the copper(II) centre, as compared with the acetate ion, may be correlated with the fact that the O—C—O angle of the BET ligand is significantly larger in the present cation [125.6(5)°] than that of the acetato group in the calcium double salt [122.0(2)°]. The previous spectral study of the calcium double salt[4] has suggested that one of the filled sp^2 orbitals of the long-bonded carboxy oxygen weakly overlaps the d_{z^2} orbital of the copper(II) atom, and the p_z orbital of the long-bonded oxygen atom may also be involved in weak π-bonding to the metal d_{xz} and d_{yz} orbitals. The same type of metal–ligand interaction is expected to exist in the present cation. The main difference between the structures of the present complex and the calcium double salt is that the long-bonded carboxy oxygen in the latter also coordinates to the calcium(II) atom, thereby bridging the copper(II) and calcium(II) atoms into a one-dimensional polymeric structure.

As a neutral ligand, BET can form tetrakis-chelated carboxylate-like copper(II) complexes without the presence of other metal ions, thus eliminating their perturbation on the idealized geometry of the eight-coordinate copper(II) structure. The relevant structural parameters for some eight-coordinate tetrakis(carboxylato)copper(II) complexes are listed in Table 2. The calcium(II) ion has little influence on the structure of the tetrakis(carboxylato)copper(II) anion in the double salt,[2,3] which may be attributed to the fact that it has an appropriate ionic radius to coordinate the two long-bonded oxygen atoms of the upwards/downwards carboxy groups. In contrast, the geometries of the tetrakis(carboxylato)copper(II) anions in both $Rb_2[Cu(pht)_2]\cdot 2H_2O$ and $[Li_2Cu(pht)_2]\cdot 4H_2O$[5] are significantly distorted by the rubidium(I) and lithium(I) ions, which are either too large or too small, thus resulting in lowering of the symmetry of the copper(II) centres from S_4 to C_2 and C_i for the rubidium and lithium double salts, respectively, together with significantly greater differences (by more than 0.26 Å) between the pair of independent long-bonded Cu—O(carboxy) distances.

REFERENCES

1. B. J. Hathaway, in *Comprehensive Coordination Chemistry* (Edited by G. Wilkinson, R. D. Gillard and J. A. McCleverty), Vol. V, p. 612. Pergamon Press, Oxford (1987).
2. D. A. Langs and C. R. Hare, *J. Chem. Soc., Chem. Commun.* 1967, 890.
3. E. A. Klop, A. J. M. Duisenberg and A. L. Spek, *Acta Cryst.* 1983, **39C**, 1342.
4. D. E. Billing, B. J. Hathaway and P. Nicholls, *J. Chem. Soc. A* 1970, 1877.
5. M. B. Cingi, A. M. M. Lanfredi, A. Tiripicchio and M. Tiripicchio, *Acta Cryst.* 1977, **33B**, 659.
6. Z.-H. Zhuo, R.-J. Wang and T. C. W. Mak, *Inorg. Chim. Acta* 1990, submitted.
7. K. M. Harmon and G. F. Avci, *J. Molec. Struct.* 1984, **117**, 295.
8. G. B. Deacon and R. J. Philips, *Coord. Chem. Rev.* 1980, **33**, 227.
9. R. A. Sparks, in *Crystallographic Computing*

Techniques (Edited by F. R. Ahmed), p. 452. Munksgaard, Copenhagen (1976).
10. G. M. Sheldrick, in *Computational Crystallography* (Edited by D. Sayre), p. 506. Oxford University Press, New York (1982).
11. G. M. Sheldrick, in *Crystallographic Computing 3: Data Collection, Structure Determination, Proteins, and Databases* (Edited by G. M. Sheldrick, C. Krüger and R. Goddard), p. 175. Oxford University Press, New York (1982).
12. *International Tables for X-ray Crystallography*, Vol. IV, pp. 55, 99, 149. Kynoch Press, Birmingham. (Now distributed by Kluwer Academic Publishers, Dordrecht. The Netherlands.) (1974).

Polyhedron Vol. 10, No. 3, pp. 277–322, 1991
Printed in Great Britain

0277–5387/91 $3.00+.00
Pergamon Press plc

POLYHEDRON REPORT NUMBER 37

RUTHENIUM CLUSTERS CONTAINING *N*-DONOR LIGANDS

MICHAEL I. BRUCE, MARIE P. CIFUENTES* and MARK G. HUMPHREY*†

Jordan Laboratories, Department of Physical and Inorganic Chemistry,
The University of Adelaide, Adelaide, SA 5001, Australia

CONTENTS

1. INTRODUCTION 278
2. STRUCTURAL TYPES 278
3. ANIONIC LIGANDS 280
4. ORGANONITRILE DERIVATIVES 286
5. REACTIONS WITH AMINES 288
6. ALKYL- AND ARYL-IMIDO COMPLEXES 291
7. ENIMINES AND α,α′-DIIMINES (AZA- AND 1,4-DIAZABUTA-1,3-DIENES) . . . 298
8. *N*-HETEROCYCLES 302
9. NITROSYL COMPLEXES 309
10. NITRIDO CLUSTERS 311
11. CLUSTERS CONTAINING OTHER *N*-DONOR LIGANDS 312
12. REACTIONS OF ORGANO-NITROGEN COMPOUNDS GIVING MONO- OR BI-NUCLEAR PRODUCTS 314
13. REACTIONS OF ORGANO-NITROGEN COMPOUNDS CATALYSED BY RUTHENIUM CLUSTERS 317
14. CONCLUSION 317

ABBREVIATIONS

bipy 2,2′-bipyridyl
bipym 2,2′-bipyrimidine
biquin 2,2′-biquinoline
bqH benzo[*h*]quinoline
bzimH benzimidazole
bztzH benzotriazole
C-N chelating ligand with *C*- and *N*-donors
dppe 1,2-bis(diphenylphosphino)ethane
dppm bis(diphenylphosphino)methane
dppp 1,3-bis(diphenylphosphino)propane
napy 1,8-naphthyridine
pcH_2 phthalocyanine
phen 1,10-phenanthroline
ppn bis(triphenylphosphine)iminium, $[N(PPh_3)_2]^+$
ppyH 1*H*-pyrrolo[2,3-*b*]pyridine
py pyridine
pzH pyrazole
R-ape 1,2-bis(μ-alkylamido)-1,2-bis(2-pyridyl)-ethane, *N*-substituents R
R-dab 1,4-diaza-1,3-butadienes, *N*-substituents R
R-pyca pyridine-2-carbaldehyde-imines, *N*-substituents R
$salenH_2$ *N*,*N*′-ethylenebis(salicylidenimine)
thf tetrahydrofuran
$tppH_2$ tetraphenylporphyrin

* Present address: Department of Chemistry, University of New England, Armidale, NSW 2351, Australia.
† Author to whom correspondence should be addressed.

1. INTRODUCTION

The chemistry of triosmium clusters with nitrogen-donor ligands has been reviewed in some detail.[1,2] By comparison, relatively few derivatives of $Ru_3(CO)_{12}$ containing *N*-donor ligands had been described until recently. In most cases, this was the result of the use of harsh reaction conditions which leads to rapid break-up of the first-formed cluster complexes. The much greater tendency of triruthenium clusters, as opposed to triosmium clusters, to undergo cluster fragmentation is due to a greater M—M bond strength for the heavier metal; the M—M bond enthalpies of $Ru_3(CO)_{12}$ and $Os_3(CO)_{12}$ are 78 and 94 kJ mol^{-1}, respectively.[3] Although $Ru_3(CO)_{12}$ has been described as "more difficult to control"[2] than $Os_3(CO)_{12}$, its very reactivity leads not only to product types analogous to those obtained with its heavier transition metal congener, but also to novel modes of reactivity not observed with $Os_3(CO)_{12}$.

This literature survey of ruthenium cluster carbonyls containing *N*-donor ligands and their chemistry is classified according to the functional groups in the ligand, and extends the last such review[4] by incorporating results published between 1981 and mid-1990, although reference is made to earlier work if necessary. The fact that almost one half of the references are from 1986 or later testifies to the current strong interest in this field.

2. STRUCTURAL TYPES

Trinuclear ruthenium carbonyl clusters have been described containing *N*-donor ligands which may be attached to one, two or three metal atoms, and which may donate from two to eight electrons to the cluster. The main types of ligand are represented schematically in Fig. 1 and relevant bond parameters of structurally characterized examples of some of these types are collected in Table 1.

2e *Donors*

Complexes containing 2e donors (**A**) are known, but most readily undergo further intramolecular reactions which produce bridging (μ_2) or capping (μ_3) ligands. Examples include organic nitriles and pyridine. Simple anionic ligands containing nitrogen (CN^-, NCO^-) may bridge Ru—Ru bonds (**B**).

3e *Donors*

Several derivatives containing NO ligands have been described (Section 9). While clusters of other metals containing terminal NO groups are known, all the ruthenium complexes reported so far have this ligand bridging a Ru—Ru bond (**C**). The isoelectronic aryldiazo ligand forms similar derivatives (**D**).

Most complexes containing 3e donor ligands (including nitrosyls) also contain a second odd-electron ligand. In many cases, these ligands result from internal oxidative addition reactions across a Ru—Ru bond, the precursors often not being isolated. Examples include (a) H and NR_2 groups (**E**) and (b) H and N-C systems, such as 2-pyridyl (**F**).

4e *Donors*

Bidentate *N*-donor ligands may chelate one metal atom, such as found with 2,2′-bipyridyl (**G**), or bridge a Ru—Ru bond, such as 1,2-diazene (**H**). By contrast, the diazo (N=N) group acts as a 6e donor when it caps a triangular face (**I**); these complexes readily undergo N=N bond cleavage to give derivatives containing alkyl- or aryl-imido ligands (μ_3-NR) (**J**). Much chemistry has centred on these complexes which are also obtained from several other organo-nitrogen compounds.

In many cases, when one side of the Ru_3 cluster is capped by an NR group, a similar μ_3-ligand caps the opposite side; examples include μ_3-CO, μ_3-S. Where two μ_3-NR groups are present, one Ru—Ru bond is broken (**K**).

Other 4e ligands containing nitrogen include the metallated amido (**L**) and aryldiazo groups (**M**).

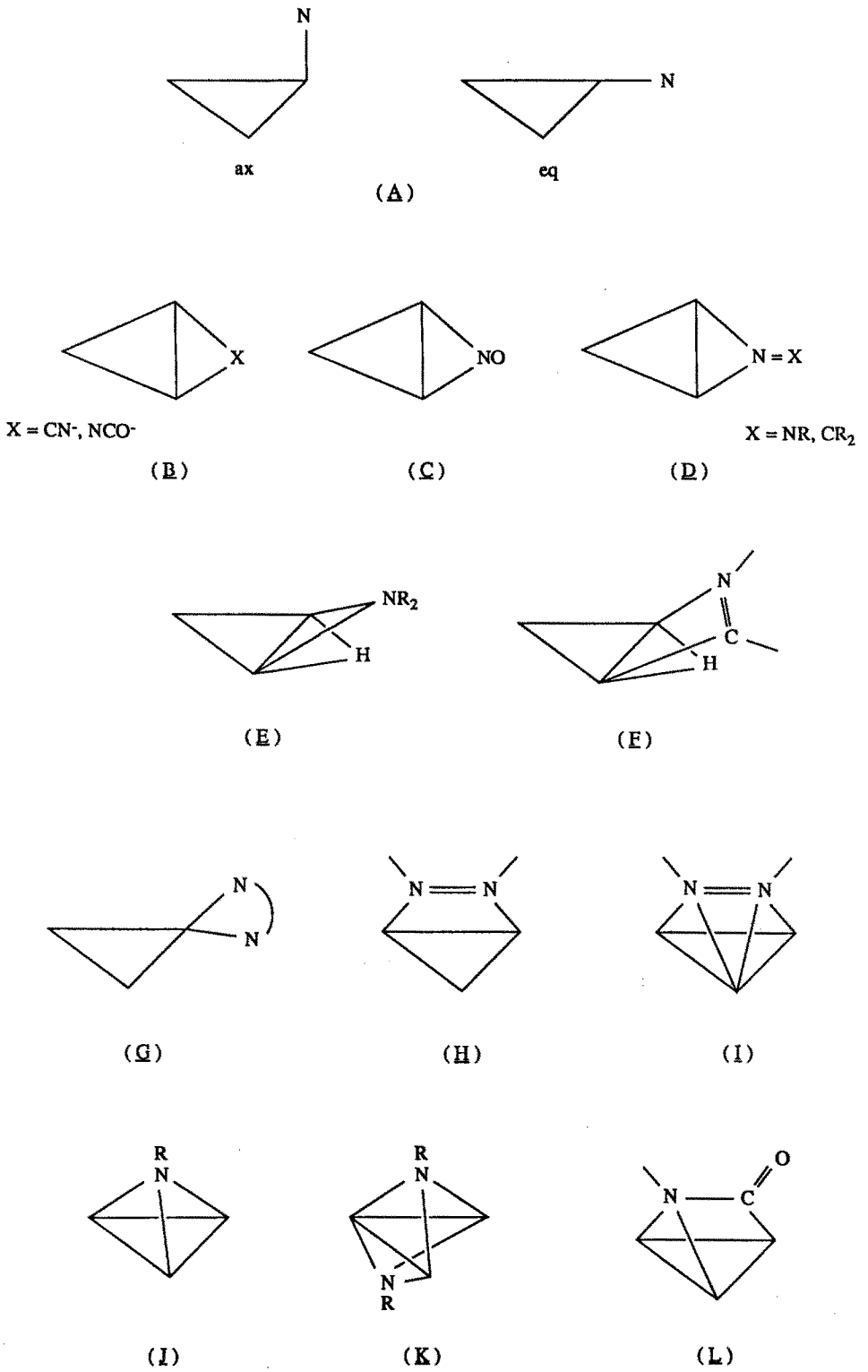

Fig. 1. Common structural types found in Ru_3 cluster complexes containing *N*-donor ligands.

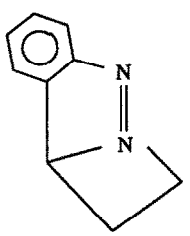

(M)

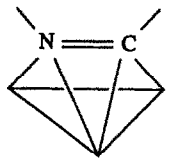

(N)

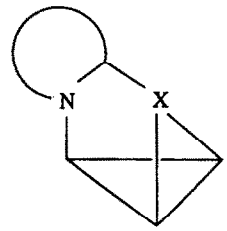

X = PR, NR, S

(O)

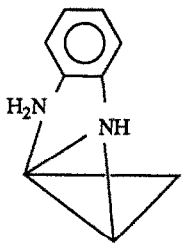

(P)

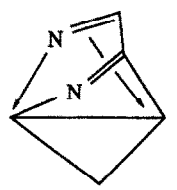

(Q)

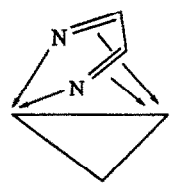

(R)

Fig. 1. (continued)

5e *Donors*

In the nitrido clusters (Section 10), the nitrogen atom acts as a 5e donor. Other 5e ligands include aldimines, μ_3-RC=NR (**N**) and those which contain a 3e bridging group and 2e donor atom in the same molecule, such as found in derivatives of 2-(diphenylphosphino)pyridine and thiazoles (**O**); mono-deprotonated arene-1,2-diamines also act as 5e donors, having both chelating and bridging functions (**P**).

6e *and* 8e *Donors*

Attachment of diazabutadiene ligands to Ru_3 clusters by both nitrogen atoms and the unsaturated system results in these ligands donating either 6e (**Q**) or 8e (**R**) to the cluster, although, interestingly, only two metal atoms are involved.

3. ANIONIC LIGANDS

The reaction between $Ru_3(CO)_{12}$ and [ppn][CN] proceeded by way of an intermediate formulated as $[Ru_3(CN)(CO)_{11}]^-$, which dimerized with loss of CO to give the hexanuclear dianion $[Ru_6(\mu\text{-}CN)_2(CO)_{20}]^{2-}$ (**1**), containing two parallel ruthenium triangles linked by two axial CN bridges.[5] Recently, Vahrenkamp has described the CN-bridged derivative **2** (R = C_5H_5), obtained from $[Mn(CN)(CO)_2(\eta\text{-}C_5H_5)]^-$;[6] use of $[Mn(CN)(CO)_2(\eta\text{-}C_5H_4Me)]^-$ afforded **3**, together with **2** (R = C_5H_4Me).[7]

Complexes containing isocyanate ligands have been obtained from the reaction between $Ru_3(CO)_{12}$ and [ppn][N_3], which initially afforded $[Ru_3(\mu\text{-}CO)_2(CO)_9(NCO)]^-$ (**4**); this lost CO to give $[Ru_3(\mu\text{-}NCO)(CO)_{10}]^-$ (**5**). Over several days, **5** was slowly converted to $[Ru_4(\mu\text{-}NCO)(\mu\text{-}$

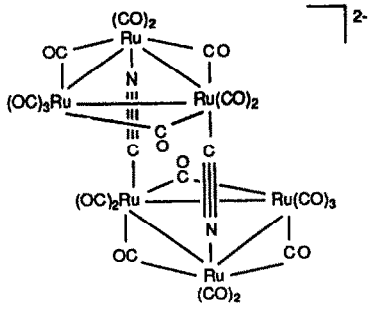

(1)

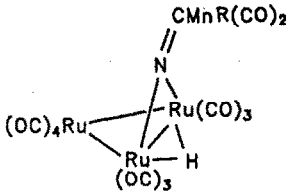

(2) R = C_5H_5, $C_5H_4CH_3$

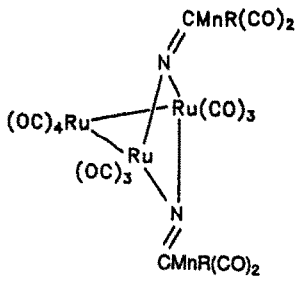

(3) R = $C_5H_4CH_3$

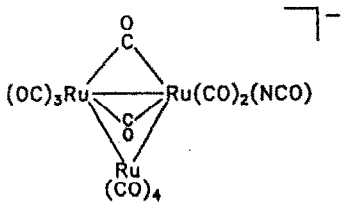

(4)

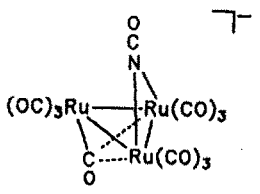

(5)

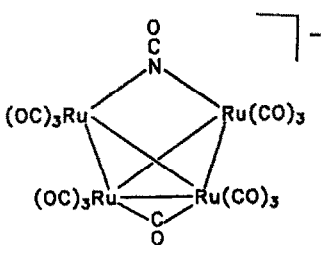

(6)

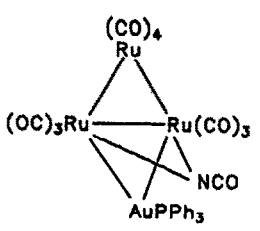

(7)

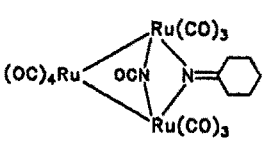

(8)

$CO)(CO)_{12}]^-$ (**6**).[8] The postulated structures for **4**, **5** and **6** were assigned on the basis of IR arguments.

Irradiation of a mixture of $Ru_3(CO)_{12}$ and $Au(N_3)(PPh_3)$ gave purple $AuRu_3(\mu\text{-NCO})(CO)_{10}(PPh_3)$ (**7**).[9] The $\overline{CN{=}N}$ ring in pentamethylenediazirine was cleaved during the reaction with $Ru_3(CO)_{12}$; the yellow product, **8**, contains μ-NCO and μ-ketenimine ligands.[10]

Table 1. Structural studies of Ru_3 cluster complexes with *N*-donor ligands

Complex	Structural type	Ru—N (Å)	Ru—Ru (Å)	Reference
$[ppn]_2[\{Ru_3(\mu\text{-}CN)(\mu\text{-}CO)_3(CO)_7\}_2]$	**A**	2.091, 2.113	2.870, 2.878, 2882	5
$Ru_3(\mu\text{-}H)(\mu\text{-}C{=}NMe_2)(CO)_9(py)$	**A**	2.250	2.802 (μ-H), 2.844, 2.855	39
$Ru_3(\mu\text{-}NCO)(\mu\text{-}N{=}C_6H_{10})(CO)_{10}$	**B, D**	2.089, 2.099 (NC_6H_{10}) 2.187, 2.187 (NCO)	Not reported	10
$Ru_3(\mu\text{-}H)(\mu\text{-}NO)(CO)_7\{P(OMe)_3\}_3$	**C**	2.17	2.773 (μ-H) 2.865, 2.871	145
$\{Ru_3(\mu\text{-}NO)(CO)_{10}\}_2Hg$	**C**	1.992, 1.998	2.832, 2.835, 2.861 (μ-Hg)	152
$Ru_3(\mu\text{-}NO)_2(CO)_{10}$	**C**	2.03, 2.04	2.861, 2.870	141
$Ru_3(\mu\text{-}H)(\mu\text{-}N{=}CHPh)(CO)_{10}$	**D**	2.02, 2.02	2.772 (μ-H), 2.819, 2.822	16
$Ru_3(\mu\text{-}H)(\mu\text{-}NH_2)(CO)_{10}$	**E**	2.101, 2.102	2.770 (μ-H), 2.820, 2.836	149
$Ru_3(\mu\text{-}H)(\mu\text{-}NHCH_2Ph)(CO)_{10}$	**E**	2.088, 2.105	2.746 (μ-H), 2.826, 2.830	17
$Ru_3(\mu\text{-}H)(\mu\text{-}bzim)(CO)_{10}$	**F**	2.10	2.858 (N), 2.880 (C), 2.949 (μ-H)	132
$Ru_3(\mu\text{-}CO)_2(CO)_8(bipy)$	**G**	2.188, 2.191	2.757 (μ-CO), 2.836, 2855	115, 119
$Ru_3(\mu\text{-}H)\{\mu\text{-}N_2C_3H(CF_3)_2\}(CO)_{10}$	**H**	2.137, 2.146	2.846, 2.849, 2.902 (μ-H)	115
$Ru_3(\mu\text{-}N_2C_4H_4)(\mu\text{-}CO)_3(CO)_7$	**H**	2.133, 2.136	2.744 (μ-N_2) 2.859, 2.861	129
$Ru_3(\mu\text{-napy})(\mu\text{-}CO)_3(CO)_7$	**H**	2.165, 2.199 (A) 2.187, 2.190 (B)	2.747 (A, μ-N_2) 2.838, 2.878 2.731 (B, μ-N_2) 2.848, 2.872	121
$Ru_3(\mu_3\text{-}NPh)(\mu_3\text{-}CO)(CO)_9$	**J**	2.054 (av) (A) 2.056 (av) (B)	2.735, 2.741, 2.750 (A) 2.734, 2.754, 2.760 (B)	56

$Ru_3(\mu_3\text{-NPh})(\mu_3\text{-CO})(CO)_6(\eta\text{-}C_6H_6)$	J	2.016, 2.043, 2.029 (C_6H_6)	2.695, 2.704, 2.726	59
$Ru_3(\mu_3\text{-NPh})(\mu_3\text{-CO})(\mu\text{-dppm})(CO)_7$	J	2.067, 2.068, 2.070	2.743, 2.743, 2.727 (μ-dppm)	80
$Ru_3(\mu_3\text{-NPh})\{\mu_3\text{-CORu}_2[\mu\text{-NPhCOC}(\eta\text{-Ph}){=}\text{CPh}](CO)_5\}(CO)_6$	J	2.021, 2.066, 2.074 (A) 2.035, 2.044, 2.065 (B)	2.699, 2.734, 2.742 (A) 2.716, 2.717, 2.753 (B)	89
$Ru_3(\mu\text{-H})(\mu_3\text{-NPh})(CO)_8(MeOC_6H_3N{=}NC_6H_4OMe\text{-}4)$	J	2.051, 2.072, 2.086 (NPh) 2.128 (N=)	2.669, 2.784, 2.865 (μ-H)	77
[Na(18-crown-6)][$Ru_3(\mu_3\text{-NPh})(I)(CO)_9$]	J	2.052, 2.056, 2.077	2.711, 2.740, 2.770	63, 76
$Ru_3(\mu\text{-H})_2(\mu_3\text{-NOMe})(\mu_3\text{-CO})(CO)_9$	J	2.006, 2.027, 2.027	2.740, 2.762, 2.762	151
$Ru_3(\mu\text{-H})_2(\mu_3\text{-NCH}_2C_6H_4OMe\text{-}4)(CO)_9$	J	2.030, 2.046, 2.056 (μ-H)	2.676, 2.799, 2.800	18
$Ru_3(\mu\text{-H})_2(\mu_3\text{-NPh})(CO)_9$	J	2.059, 2.072, 2.074 (μ-H)	2.680, 2.804, 2.806	78
$Ru_3\{\mu_3\text{-Au}_2(PPh_3)_2\}(\mu_3\text{-NPh})(CO)_9$	J	2.057, 2.063, 2.083	2.730, 2.821 2.909 (μ-Au_2)	91
$Ru_3(\mu_3\text{-NPh})_2(CO)_9$	K	2.052, 2.080, 2.061, 2.079 (outer) 2.110, 2.129 (inner)	2.626, 2.710	57
$Ru_3(\mu_3\text{-NPh})(\mu_3\text{-NC}_6H_4F\text{-}3)(CO)_9$	K	2.051, 2.098 (NPh, outer) 2.057, 2.082 (NC_6H_4F-3, outer) 2.127 (NPh, inner) 2.131 (NC_6H_4F-3, inner)	2.615, 2.702	70
$Ru_3(\mu_3\text{-NPh})_2(CO)_8(CNxy)$	K	2.064, 2.074, 2.067, 2.073 (outer) 2.119, 2.137 (inner)	2.620, 2.708	70

Table 1. (*continued*).

Complex	Structural type	Ru—N (Å)	Ru—Ru (Å)	Reference
$Ru_3(\mu_3\text{-NPh})_2(CO)_8(PPh_3)$	**K**	2.041, 2.208, 2.071, 2.097 (A, outer) 2.044, 2.110, 2.036, 2.141 (B, outer) 2.128, 2.145 (A, inner) 2.135, 2.152 (B, inner)	2.596, 2.717 (A) 2.619, 2.718 (B)	70
$Ru_3(\mu\text{-H})_2(\mu_3\text{-NC}_6H_4Cl\text{-}4)_2(CO)_8$	**K**	2.077, 2.093, 2.100	2.673, 2.686	79
[ppn][$Ru_3(\mu\text{-H})(\mu_3\text{-PhNCO})(CO)_{10}$]	**L**	2.139, 2.147	2.749, 2.753 2.773 (μ-H)	45
$Ru_3(\mu\text{-H})(\mu\text{-N=NC}_6H_4)(\mu_3\text{-AsPhCH}_2\text{AsPh}_2)(CO)_8$	**M**	2.065, 2.092	2.903, 3.055	169
$Ru_3(\mu\text{-H})(\mu_3\text{-NEt=CMe})(CO)_9$	**N**	2.086, 2.222	2.696 (μ-N) 2.720 (μ-C) 2.92 (μ-H)	43
$Ru_3(\mu\text{-H})(\mu\text{-NPh=CPh})(CO)_9$	**N**	2.081, 2.092	2.706, 2.716 2.931 (μ-H)	85
$Ru_3(\mu\text{-H})\{\mu_3\text{-NPh(C}_5H_4N)\}(CO)_9$	**O**	2.152 (py) 2.198, 2.201 (NPh)	2.7302, 2.7591 2.7531 (μ-N)	123

$[Ru_3(\mu\text{-}H)_2\{\mu_3\text{-}NH(C_5H_4N)\}(CO)_9][BF_4]$	**O**	2.098, 2.106 (NH) 2.177 (py)	2.7437 2.7855 (μ-N)	124
$Ru_3\{\mu_3\text{-}PPh(C_5H_4N)\}(\mu\text{-}PhCO)(CO)_9$	**O**	2.165	2.821, 2.877	136
$Ru_3\{\mu_3\text{-}PPh(C_5H_4N)\}(\mu\text{-}PhCO)(CO)_8(PPh_3)$	**O**	2.158	2.842, 2.883	137
$Ru_3\{\mu_3\text{-}PPh(C_5H_4N)\}(\mu\text{-}PCy_2)(\mu\text{-}CO)_2(CO)_6$	**O**	2.170	2.782, 2.830 2.864 (μ-PR_2)	138
$Ru_3\{\mu_3\text{-}PPh(C_5H_4N)\}(\mu\text{-}PPh_2)(CO)_9$	**O**	2.197	2.870 (μ_3-PPh) 2.916	138
$Ru_3\{\mu_3\text{-}PPh(C_5H_4N)\}(\mu\text{-}PPh_2)(\mu\text{-}CO)_2(CO)_5(PPh_3)$	**O**	2.212	2.754 2.824, 2.890 (μ-PR_2)	138
$Ru_3(\mu\text{-}H)(\mu_3\text{-mbt})(CO)_9$	**O**	2.177	2.786, 2.798 2.836 (μ-H)	139
$Ru_3(\mu\text{-}H)(\mu_3\text{-ppy})(CO)_9$	**O**	2.149 (N) 2.175, 2.177 (μ-N)	2.758, 2.761 2.764 (μ-N)	121
$Ru_3(\mu\text{-}H)\{\mu\text{-}(NH)(NH_2)C_6H_2Me_2\}(CO)_9$	**P**	2.093, 2.140 (μ-NH) 2.208 (NH_2)	2.777 (μ-L) 2.788, 2.816	46
$Ru_3\{\mu\text{-}(Bu^tCH_2)N{=}CHCH{=}N(CH_2Bu^t)\}(\mu\text{-}CH_2)(CO)_8$	**Q**	2.161, 2.163 (η^1-N) 2.215, 2.249 (η^2-N=CH)	2.8690 (μ-L) 2.9079	110
$[ppn][Ru_3(\mu\text{-}PhNCHO)(\mu\text{-}CO)_3(CO)_7]$		2.17	2.773 (μ-L) 2.865, 2.871	61
$Ru_3(\mu\text{-}NPr^i{=}CHCH{=}CMe)_2(CO)_6$		2.093 (η^1-N) 2.123 (η^2-N=CH)	2.704	97
$Ru_3(\mu\text{-}C_9H_6NO)_2(CO)_8$		2.142, 2.157	2.773, 2.774	128

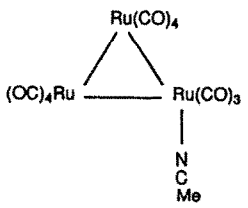

(9)

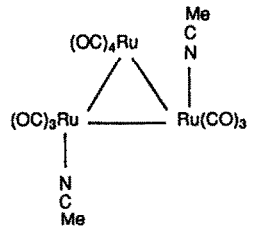

(10)

4. ORGANONITRILE DERIVATIVES

Triruthenium clusters with acetonitrile ligands have been made by the action of Me_3NO on $Ru_3(CO)_{12}$ in acetonitrile–dichloromethane mixtures: $Ru_3(CO)_{12-n}(NCMe)_n$ ($n = 1, 2$) (**9** and **10**) are formed.[11–13] The structures of these two complexes, featuring axial nitrile ligands, were assigned by comparison of their IR spectra with those of the analogous osmium complexes.[14,15] The acetonitrile ligands can be easily displaced by 2e donors (*vide infra*, Scheme 1), and these readily accessible

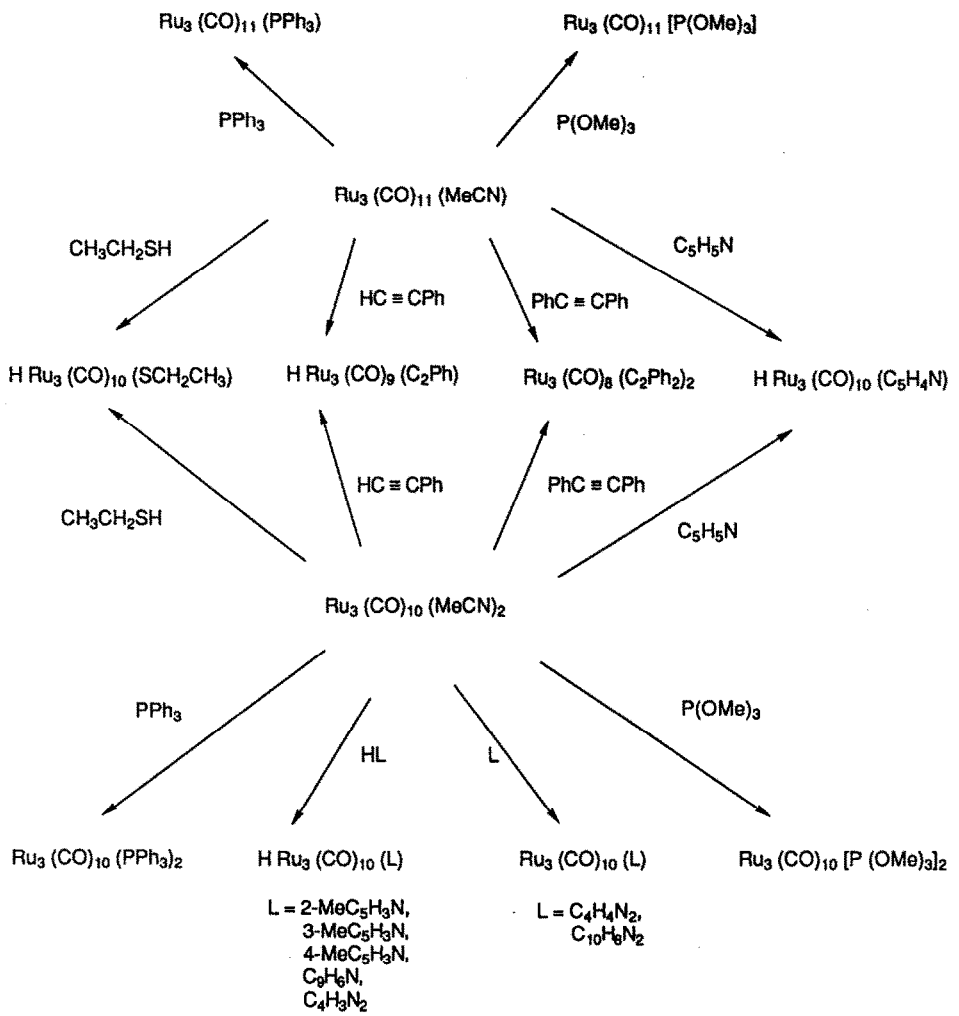

Scheme 1. Reactivity of $Ru_3(CO)_{12-n}(NCMe)_n$ ($n = 1, 2$).

precursors have been used to synthesize other triruthenium clusters incorporating *N*-donor ligands which are not obtained by a thermal route.

Other nitriles, such as benzonitrile, appear to form the capped clusters $Ru_3(\mu_3\text{-}NCR)(CO)_9$, which rapidly undergo further reaction. Early studies described reactions between $Ru_3(CO)_{12}$ and benzonitrile only in the presence of acetic acid or molecular hydrogen.[16] In the former case, the reaction afforded $Ru_4(\mu\text{-}H)_4(CO)_{12}$, $Ru_3(\mu\text{-}H)(\mu\text{-}N{=}CHPh)(CO)_{10}$ (**11**) and $Ru_3(\mu\text{-}H)(\mu\text{-}NHR)(CO)_{10}$ (**12**; R = CH_2Ph), the latter two containing ligands formed by reduction of a coordinated benzonitrile ligand.[17] Further work with substituted benzonitriles bearing electron-donating (OMe) or electron-withdrawing (NO_2) groups in the *para* position indicated that the formation of **12** was significantly enhanced by an electron-donating substituent; with an electron-withdrawing group, only decomposition occurred.[18] Recently, replacement of acetic acid by lauric acid has been shown to result in a higher yield of **12** (R = CH_2Ph, $CH_2C_6H_4NO_2$-4); the use of acetic acid gave higher conversion to **12** (R = $CH_2C_6H_4OCH_3$-4).[19] These results are consistent with a two-fold effect of the acid; activation of the substrate and proton donation. Reaction of $Ru_3(CO)_{12}$ with benzonitrile under 110 atm of H_2 gave mainly **12** (R = CH_2Ph), together with benzylamine, whereas reaction under H_2 at atmospheric pressure gave only **11**. Hydrogenation of **11** afforded $Ru_3(\mu\text{-}H)_2(\mu_3\text{-}NCH_2Ph)(CO)_9$ (**13**);[20] the imide–amide–nitrene transformations **11** ↔ **12** ↔ **13** have been shown to be reversible.[21,22]

The pentanuclear carbido cluster $Ru_5C(CO)_{15}$ reversibly takes up MeCN with an accompanying structural change from square pyramidal to distorted trigonal bipyramidal to afford **14**.[23,24]

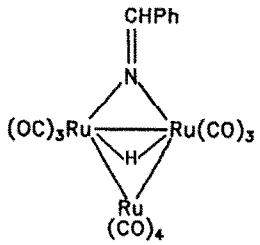

(11)

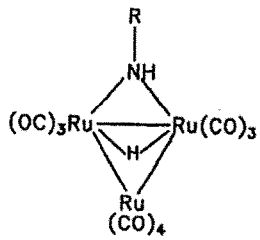

(12) R = Ph, CH_2Ph, $CH_2C_6H_4NO_2$-4, $CH_2C_6H_4OMe$-4

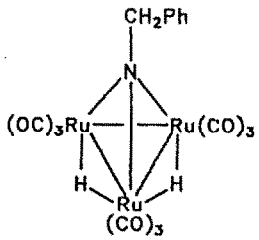

(13)

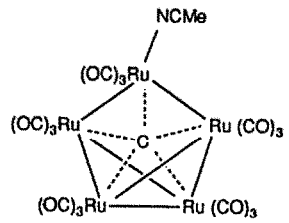

(14)

5. REACTIONS WITH AMINES

Aliphatic amines do not give complexes containing *N*-bonded ligands, reacting with $Ru_3(CO)_{12}$ by nucleophilic attack at a carbonyl group to give products incorporating the carbamoyl ligand. Thus, dimethylamine reacted with $Ru_3(CO)_{12}$ at $-30°C$ to afford $Ru_3(\mu\text{-H})\{\mu\text{-O=C(NMe}_2)\}(CO)_{10}$ (**15**; L = CO).[25-27] Reaction of $Ru_3(CO)_{12}$ with $C(NMe_2)_4$ gave the $[C(NMe_2)_3]^+$ salt of $[Ru_3\{\mu\text{-O=C(NMe}_2)\}(CO)_{10}]^-$, believed to contain bridging carbonyl groups.[28] Acidification and phosphite substitution afforded [**15**; L = $P(OR)_3$, R = Me, Et, Ph].[29] Addition of base to refluxing thf solution of **15** (L = CO) gave $[Ru_6H\{\mu\text{-O=C(NMe}_2)\}_2(\mu\text{-CO})_4(CO)_{14}]^-$ (**16**), which was isolated as its $[AsPh_4]^+$ salt.[30] Reaction of **15** (L = CO) with acetylenes has also been investigated; with dimethylacetylene, a mixture of **17**, **18** and **19** was obtained,[31,32] whereas reaction with arylacetylenes gave only dinuclear products.[33]

Recently, Süss-Fink *et al.* have synthesized chiral analogues of **15**, by reaction of $Ru_3(CO)_{12}$ with *S*-proline and *S*- and *R*-methoxymethylpyrrolidine; in the latter case, the μ_3-η^2-imino cluster, **20**, was formed as a byproduct.[34]

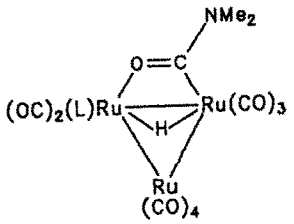

(15) L = CO, $P(OR)_3$
R = Me, Et, Ph

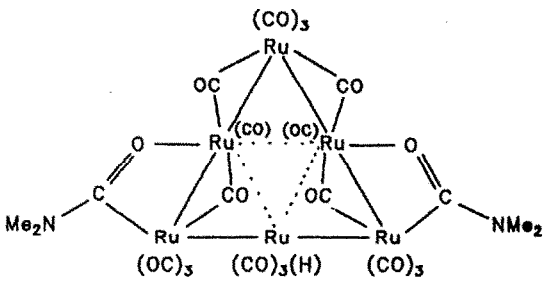

(16)

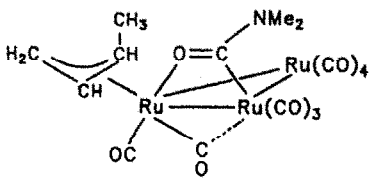

(17)

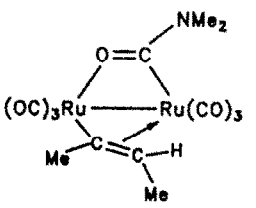

(18)

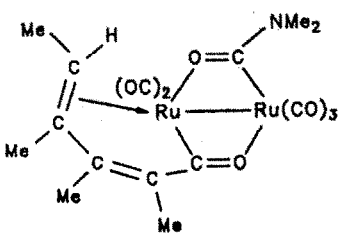

(19)

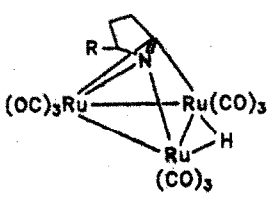

(20) R = CH_2OCH_3

Reaction of $Ru_3(\mu\text{-}H)(\mu\text{-}O{=}CMe)(CO)_{10}$ with $HNMe_2$, followed by alkylation with $EtSO_3CF_3$ gave $Ru_3(\mu\text{-}H)_2\{\mu_3\text{-}C(OEt)NMeCH\}(CO)_9$ (**21**).[35,36] The reaction of $Ru_3(\mu_3\text{-}S)_2(CO)_9$ with dimethylamine was followed spectroscopically and found to proceed by way of the substitution product **22** to the carbamoyl-bridged complex **23** and thence to the bis(carbamoyl)-bridged complex **24**.[37]

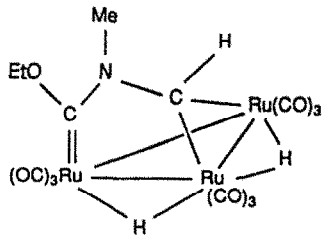

(21)

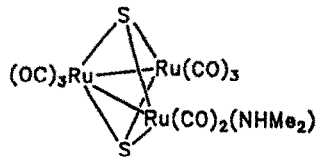

(22)

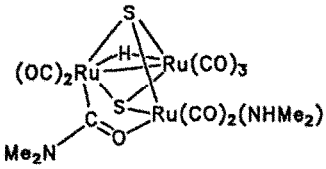

(23)

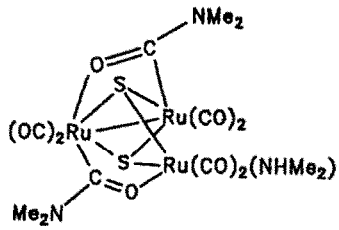

(24)

The halomethylidyne cluster $Ru_3(\mu\text{-}H)_3(\mu_3\text{-}CBr)(CO)_9$ reacted with diethylamine to give exclusively $Ru_3(\mu\text{-}H)(\mu\text{-}CNR_2)(CO)_{10}$ (**25**; R = Et), either in the presence or absence of carbon monoxide, by nucleophilic substitution at the methylidyne carbon and intermolecular CO transfer. It proved impossible to hydrogenate **25** (R = Et) to $Ru_3(\mu\text{-}H)_3(\mu_3\text{-}CNEt_2)(CO)_9$.[38] Pyridine- (R = Me) and triphenylphosphine- ($R = CH_2Ph$) substituted **25**, formed from acetonitrile-substituted **25**, have been structurally characterized;[39,40] in the former case, the pyridine occupies a "semiaxial" site on one of the dibridged ruthenium atoms and, in the latter case, the triphenylphosphine occupies an equatorial site on the non-bridged ruthenium atom.

Pyrolysis of **25** (R = Me) afforded three higher nuclearity clusters **26**, **27** and **28** in low yield; **26** could also be formed in high yield on reaction of **25** (R = Me) with $Ru(CO)_5$.[41] Further reaction

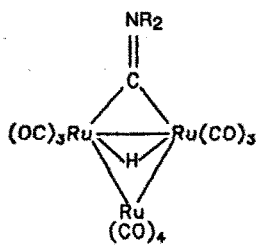

(25) R = Me, Et, CH_2Ph

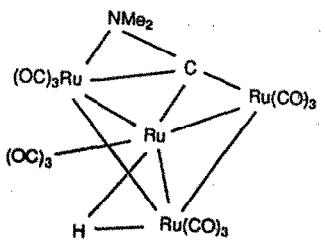

(26)

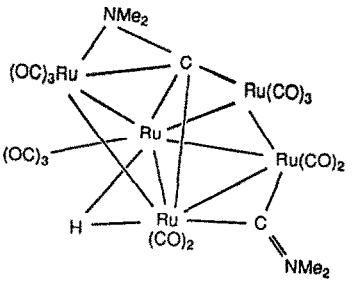

(27)

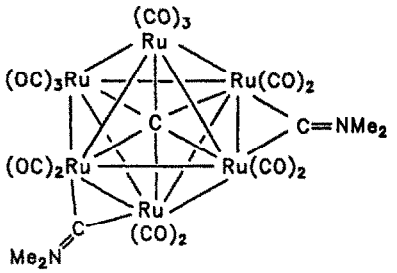

(28)

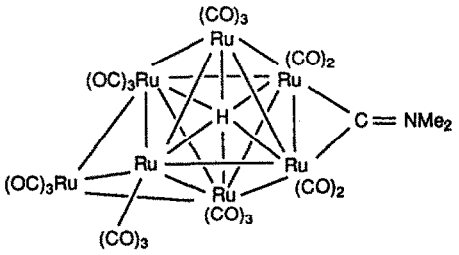

(29)

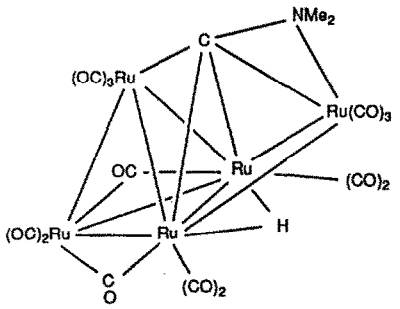

(30)

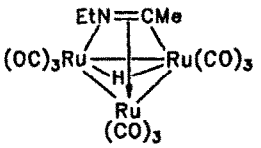

(31)

of **26** with $Ru(CO)_5$ afforded heptanuclear **29** and pentanuclear **30** in good yield, the former containing an interstitial hydride.[42]

In contrast with the above reactions, the $\{Fe(\mu\text{-SEt})(CO)_2(PPh_3)\}_2$-catalysed reaction between $Ru_3(CO)_{12}$ and NEt_3 in hexane gave $Ru_3(\mu\text{-H})(\mu_3\text{-EtN=CMe})(CO)_9$ (**31**) as the major product.[43]

The first product from the reaction between $Ru_3(CO)_{12}$ and aniline was $Ru_3(\mu\text{-H})(\mu\text{-NHPh})(CO)_{10}$ (**12**; R = Ph), formed by oxidative addition of the N—H bond across a Ru—Ru bond;[44] subsequent deprotonation with KOH afforded $[Ru_3(\mu\text{-H})\{\mu_3\text{-NPh(CO)}\}(CO)_9]^-$ (**32**) by intramolecular nucleophilic attack on CO.[45] Complex **32** lost CO irreversibly in solution at room temperature to give $[Ru_3(\mu\text{-H})(\mu_3\text{-NPh})(CO)_9]^-$.

1,2-Arenediamines reacted with $Ru_3(CO)_{12}$ under a CO atmosphere to give **33**, in which the deprotonated diamine chelates and bridges atoms on the cluster. In contrast, 1,8-diaminonaphthalene gave the binuclear complex $Ru_2\{\mu\text{-}(NH)_2C_{10}H_6\}(CO)_6$.[46]

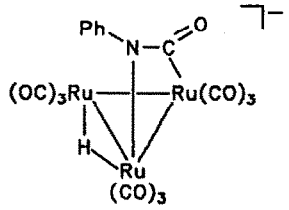

(32)

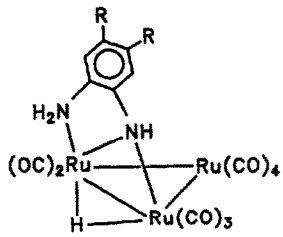

(33) R = H, Me

6. ALKYL- AND ARYL-IMIDO COMPLEXES

The metal carbonyl-catalysed reduction and, in some cases, carbonylation of nitrobenzenes to *N,N'*-disubstituted ureas,[47,48] anilines,[49–51] Schiff bases (in the presence of aldehydes),[51] carbamates (in alcohols)[52–54] and isocyanates[55] has prompted many studies on stoichiometric reactions involving these compounds. For example, nitrobenzene reacted with $Ru_3(CO)_{12}$ at elevated temperatures to afford $Ru_3(\mu_3\text{-NPh})(\mu_3\text{-CO})(CO)_9$ (**34**; R = Ph) and $Ru_3(\mu_3\text{-NPh})_2(CO)_9$ (**35**; R = R^1 = Ph).[44,56,57] Nitrene-containing species have been proposed as intermediates in the catalytic reduction of nitrobenzene to aniline[58] and isolation of polynuclear complexes with phenylnitrene groups such as **34** (R = Ph) can be taken as indirect evidence for the involvement of such species in the catalytic reaction. In the presence of $Co_2(CO)_8$, the same reaction gave **35** (R = R^1 = Ph) and $Ru_3(\mu_3\text{-NPh})(\mu_3\text{-CO})(CO)_6(\eta\text{-}C_6H_6)$ (**36**), but not **34** (R = Ph); small quantities of $Co_4(CO)_9(\eta\text{-}C_6H_6)$ were also isolated from the reaction system, and reaction of this complex with **34** (R = Ph) produced small amounts of **36**.[59]

The reductive carbonylation of nitrobenzene by $Ru_3(CO)_{12}$ with MeO^- as promoter and 2-methoxyethanol as solvent preferentially affords formanilide.[60] The carbonylation of **32** slowly formed $[Ru_3(\mu\text{-PhNCHO})(\mu\text{-CO})_3(CO)_7]^-$ (**37**) over a period of days. Furthermore, hydro-

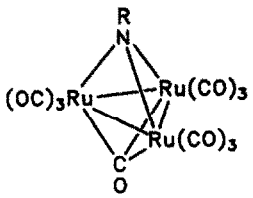

(34) R = Ph, $SiMe_3$

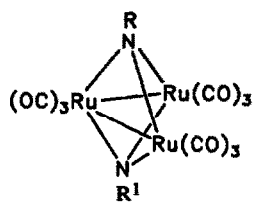

(35) R = R^1 = Ph, CF_2CHFCF_3, C_6H_4Me-4
R = Ph, R^1 = C_6H_4Cl-4, Bu^t, C_6H_4OMe-4

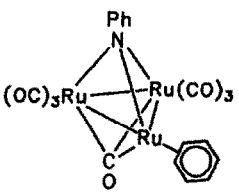

(36)

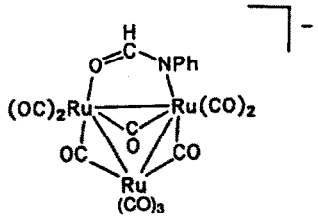

(37)

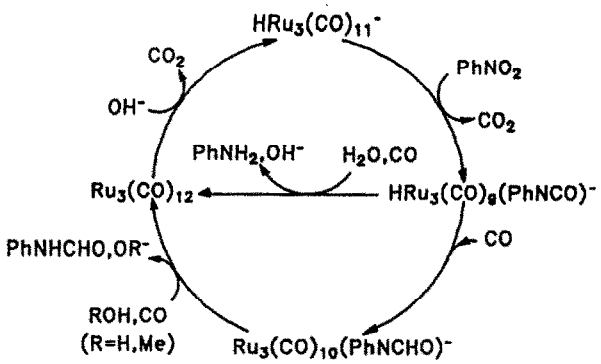

Scheme 2.

lysis of **32** and **37** gave aniline and formanilide, respectively, together with $Ru_3(CO)_{12}$, and reaction between $[Ru_3(\mu\text{-H})(CO)_{11}]^-$ and $PhNO_2$ afforded a small amount of **32**, lending support to the catalytic cycle shown in Scheme 2.[61]

Halide catalysis of the carbonylation of nitroarenes in the presence of alcohols has afforded carbamates with high selectivity;[62] this reaction has been modelled by the stoichiometric reaction between **34** (R = Ph) and $[Ru_3(\mu\text{-X})(CO)_{10}]^-$.[63,64] The presence of chelating ligands (dppm, dppe, dppp, bipy) also increases significantly the activity of $Ru_3(CO)_{12}$ in this reaction.[65]

Arylimido complexes have been obtained from several other precursors. For example, reactions of $Ru_3(CO)_{12}$ with *para*-substituted nitrosoarenes gave analogues of **34** (R = Ph) and **35** (R = R^1 = Ph); *p*-$ClC_6H_4NO_2$ reacted with **34** (R = Ph) to afford $Ru_3(\mu_3\text{-NPh})(\mu_3\text{-NC}_6H_4Cl\text{-4})(CO)_9$ (**35**; R = Ph, $R^1 = C_6H_4Cl$-4).[63] Significant promotion of this reaction by halide has been reported.[66] Reaction of $Ru_3(CO)_{12}$ with 2*H*-hexafluoropropyl azide afforded $Ru_3(\mu_3\text{-NCF}_2CHFCF_3)_2(CO)_9$ (**35**; R = R^1 = CF_2CHFCF_3);[67] the corresponding reaction with trimethylsilyl azide gave $Ru_3(\mu_3\text{-NSiMe}_3)(\mu_3\text{-CO})(CO)_9$ (**34**; R = $SiMe_3$).[68]

In 1971, Stone and co-workers reported that the reaction between $Ru_3(CO)_{12}$ and azobenzene afforded three complexes;[69] re-examination of this reaction recently showed that the products were **35** (R = R^1 = Ph), the mononuclear cyclometallated complex **38** (see below), and an as-yet unidentified black powder.[70] Azotoluene afforded **35** (R = R^1 = C_6H_4Me-4) and an analogue of **38**, while reactions of the asymmetric azoarenes PhN=NAr (Ar = C_6H_4F-3 and -4, $C_6H_4CF_3$-3, C_6F_5) gave the mixed complexes $Ru_3(\mu_3\text{-NPh})(\mu_3\text{-NAr})(CO)_9$, with no evidence for the formation of any cross product.

This result can be understood in terms of the formation of an intermediate $\mu_3\text{-}N_2Ar_2$ complex followed by an intramolecular cleavage of the N=N double and one Ru—Ru bond. Thermolysis of the iron–azoalkane complexes $Fe_3(\mu_3\text{-}N_2R_2)(CO)_9$ (R = Et, Pr) has given $Fe_3(\mu_3\text{-NR})_2(CO)_9$ in a reaction which is inhibited under CO.[6,71] The *o*-semidine derivative **39** was isolated from the reaction between iron carbonyl and azobenzene.[72,73]

The intermediacy of **A** in Scheme 3 has not been established in the ruthenium system, but in an

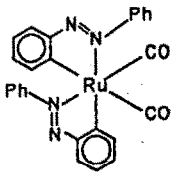

(38)

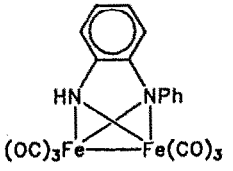

(39)

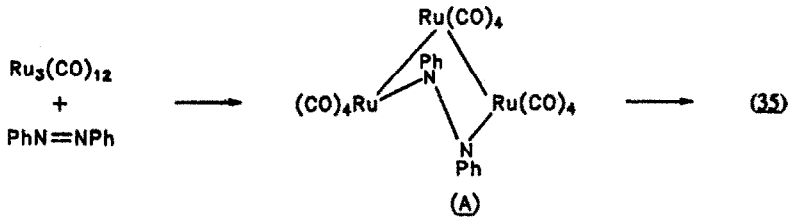

Scheme 3.

analogous reaction, $Os_3(CO)_{12-n}(MeCN)_n$ ($n = 1$ or 2) reacted with dimethyl azodicarboxylate to give $Os_3\{\mu\text{-}N(CO_2Me)NC(O)OMe\}(CO)_{11}$, which when heated in benzene afforded $Os_3\{\mu\text{-}N_2(C(O)OMe)_2\}(CO)_{10}$.[74,75] Stabilization of this intermediate is aided by coordination of the ester carbonyl oxygen atoms.

The catalysis of the carbonylation of nitrobenzene in MeOH to methyl *N*-phenylcarbamate, $PhNHCO_2Me$, is promoted by halide. Much work has been done on this reaction which is accelerated by halide ion. Scheme 4 summarizes many of the results obtained. Geoffroy's group has provided evidence for many of these postulated reactions and has clarified the role of the added halide. This chemistry has been reported in a seminal paper describing some reactions of cluster-bound imido ligands.[76]

Thus, halide does not promote deoxygenation of $PhNO_2$ to PhNO or PhN, but reactions between PhNO and $[Ru_3(\mu\text{-}X)(CO)_{10}]^-$ (X = Cl, Br, I) or $[Ru_3(CN)(CO)_{11}]^-$ rapidly gave quantitative yields of $[Ru_3(\mu_3\text{-}NPh)(\mu_3\text{-}CO)(X)(CO)_8]^-$ (X = Cl, Br, I, CN), with concomitant formation of CO_2; similarly, $[Ru_3(\mu\text{-}H)(CO)_{11}]^-$ gave $[Ru_3(\mu_3\text{-}H)(\mu_3\text{-}NPh)(CO)_9]^-$. The rates and yields of these reactions are significantly increased over those found for $Ru_3(CO)_{12}$; Cl^- and Br^- are the best promoters. A mechanism involving initial labilization of CO by halide to open up a binding site for PhNO was supported by the rapid high-yield formation of **34** (R = Ph) from PhNO and $Ru_3(CO)_{11}(NCMe)$. However, no evidence for the proposed PhNO complex was obtained, suggesting that once formed, rapid deoxygenation by CO occurred. Halides reacted with **35** ($R = R^1 = Ph$) to form $[Ru_3(\mu_3\text{-}NPh)_2(X)(CO)_8]^-$ quantitatively; addition of CO (1 atm, 22°C) reformed **35** ($R = R^1 = Ph$).[76]

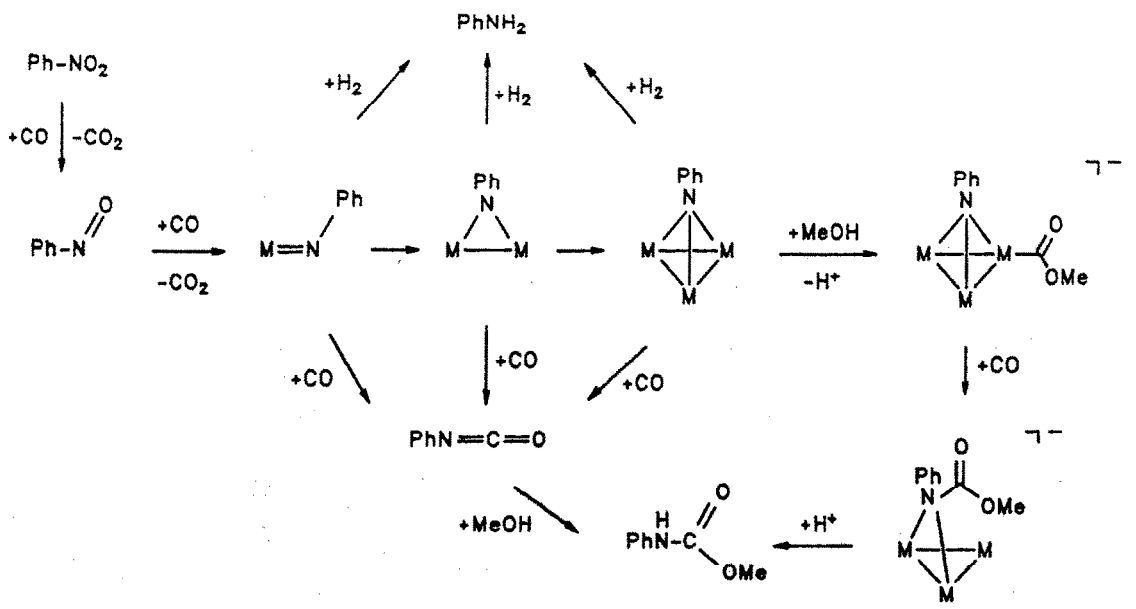

Scheme 4. Formation of methyl *N*-phenylcarbamate from nitrobenzene.

Introduction of a second NR group can be achieved by way of the complex $Ru_3(\mu_3\text{-NPh})(CO)_9(NCMe)$, obtained from **34** (R = Ph) and Me_3NO in acetonitrile; reactions with PhNO or Bu^tNO gave **35** (R = Ph, R^1 = Ph, Bu^t, respectively).[76]

Attempted carbonylation of **35** (R = R^1 = Ph) (120 atm, 150°C, 22 h) gave 69% recovery of starting material;[76] complex **34** (R = Ph) gave PhNO only after 6.5 h at 120°C under 170 atm. CO.[77] In contrast, the halide clusters $[Ru_3(\mu_3\text{-NPh})(X)(CO)_9]^-$ (X = Cl, Br) reacted with CO (1 atm., 22°C, 0.5–3 h) to give PhNCO (45% $PhNHCO_2Me$ isolated after addition of MeOH).[76]

Addition of $[Co(CO)_4]^-$ to **34** (R = Ph) resulted in metal exchange to give $[CoRu_2(\mu_3\text{-NPh})(CO)_9]^-$, which was protonated ($HBF_4$) to give $CoRu_2(\mu\text{-H})(\mu_3\text{-NPh})(CO)_9$; deprotonation with [ppn]Cl afforded pure $[ppn][CoRu_2(\mu_3\text{-NPh})(CO)_9]$. Carbonylation (6 atm., 100°C, 8 h) gave $Ru_3(CO)_{12}$, $[Co(CO)_4]^-$ and the phenyl isocyanate dimer, PhNC(O)NPhC(O).[76]

The acyl clusters $[Ru_3(\mu_3\text{-NPh})(\mu_3\text{-CO})\{C(O)R\}(CO)_8]^-$ (R = Me, Ph) were formed from **34** (R = Ph) and LiR; coupling of the acyl and imido ligands occurs under CO to give $[Ru_3\{\mu\text{-NPhC(O)R}\}(\mu\text{-CO})(CO)_7]^-$, which was readily protonated (HBF_4) to give $Ru_3(\mu\text{-H})\{\mu\text{-NPhC(O)R}\}(CO)_7$. The latter (R = Me) gave PhNHCOMe when treated with CO.[76]

The formation of isocyanate by coupling of NR and CO ligands probably proceeds according to Scheme 4. As mentioned above (Section 5), deprotonation of $Ru_3(\mu\text{-H})(\mu\text{-NHPh})(CO)_{10}$ gave the related μ_3-PhNCO complex, **32**.[45] Presumably, halide promotes the reaction by opening the μ_3-NR cap. Similar coupling of acyl and imido ligands occurred to give the anilido ligand.

Reactivity of **34** (R = Ph) *and* **35** (R^1 = R = Ph)

Hydrogenation of **34** (R = Ph) gave $Ru_3(\mu\text{-H})_2(\mu_3\text{-NPh})(CO)_9$ (**40**),[44,78] whereas the bis (arylimido) clusters afforded $Ru_3(\mu\text{-H})_2(\mu_3\text{-NAr})_2(CO)_8$ (**41**).[79] Substitution of CO by dppm has been studied; the product $Ru_3(\mu_3\text{-NPh})(CO)_8(dppm)$ could be carbonylated with great difficulty (60 atm. CO, 170°C, most of the starting material unreacted) to afford phenyl isocyanate and $Ru_3(CO)_{10}(dppm)$.[80]

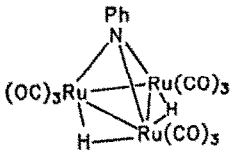

(40)

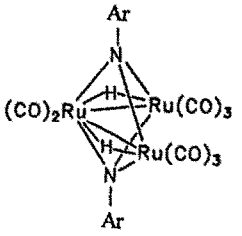

(41)

In **35** (R = R^1 = Ph), isocyanides substituted CO axially and tertiary phosphines equatorially, both on a terminal ruthenium atom, and bidentate tertiary phosphines span the non-bonded Ru···Ru vector. Carbonylation of **34** (R = Ph) or **35** (R = R^1 = Ph) in acetonitrile (20 atm., 140°C) gave quantitative yields of $Ru_3(CO)_{12}$.[81] Phenyl isocyanate is the sole organic product formed in these reactions.

Azoarenes reacted with **34** (R = Ph) and related aryl-substituted clusters under CO to give $Ru_3(\mu_3\text{-NAr})(\mu_3\text{-NAr}')(CO)_9$.[79]

The reaction of **35** (R = R^1 = Ph) with 4,4′-dimethoxyazobenzene afforded $Ru_3(\mu_3\text{-NPh})(\mu_3\text{-NC}_6H_4OMe\text{-}4)(CO)_9$ (**35**; R = Ph, $R^1 = C_6H_4OMe\text{-}4$) and $Ru_3(\mu\text{-H})(\mu_3\text{-NPh})(MeOC_6H_3N{=}NC_6H_4OMe)(CO)_8$ (**42**), with the latter incorporating a cyclometallated azoarene.[77] Pyrolysis of **42** under CO gave **35** (R = Ph, $R^1 = C_6H_4OMe\text{-}4$) and 4-$MeOC_6H_4NCO$. Reaction of **42** with excess 4,4′-dimethoxyazobenzene afforded **35** (R = Ph, $R^1 = C_6H_4OMe\text{-}4$) and **43**. The formation of a cyclometallated cluster was found to be dependent on the electronic character of the

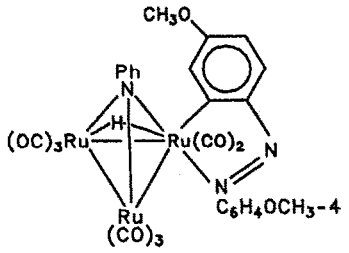

(42)

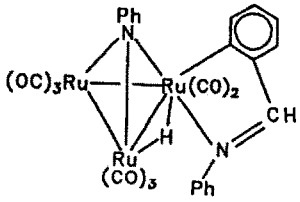

(44)

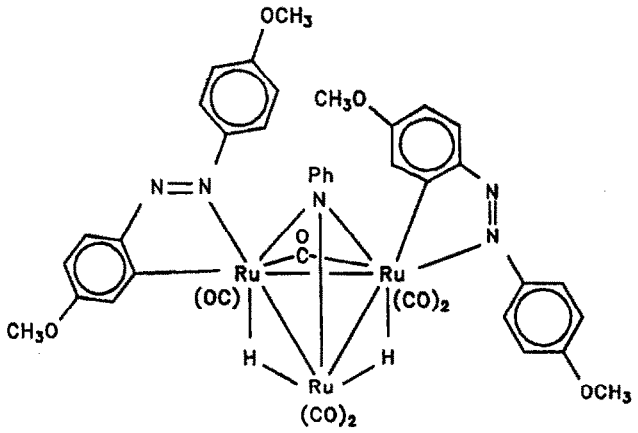

(43)

azoarene: with electron-poor aromatic rings (e.g. 4,4′-dinitroazobenzene), cyclometallation was never observed, while with electron-rich aromatic rings, N—N bond cleavage was preferred over cyclometallation only in the presence of CO. *N*-phenylbenzaldimine was cyclometallated by **35** (R = Ph) under CO to give **44**.[77]

The cyclic azoalkane 3,4-diazatricyclo[4.2.1.$0^{2,5}$]non-3-ene was found to react with $Ru_3(CO)_{12}$ to give a cluster containing an intact N_2R_2 ligand.[82,83] This compound is unstable, decomposing above room temperature in solution. The first simple azoalkane complexes were prepared recently from N_2R_2 (R = Et, Pr); further photochemical reaction with $Ru(CO)_5$ resulted in cluster expansion to give $Ru_4(\mu_4\text{-}N_2Et_2)(CO)_{12}$ (**45**) (65%), containing a Ru_4 butterfly bonded to a skewed N_2Et_2 moiety.[84]

The complex $Ru_3(\mu_3\text{-}H)(\mu_3\text{-}PhNCPh)(CO)_9$ (**46**) was isolated (45% yield) from $Ru_3(CO)_{12}$ and PhN=CHPh in Pr^iOH (as a H donor); the cyclometallated complex $Ru(C_6H_4CH{=}NPh)_2(CO)_2$ (**141**; R = Ph) was also formed in 30% yield.[85] The cluster complex is the only catalytically active species in transfer hydrogenation of ArCH=NPh to $ArCH_2NHPh$. With CO, **46** formed the decacarbonyl, which spontaneously decarbonylated on attempted isolation.

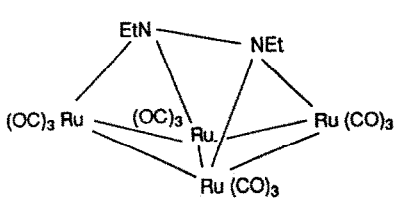

(45)

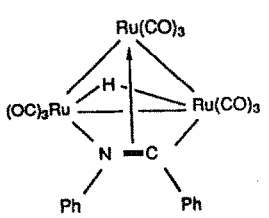

(46)

The reactions of **34** (R = Ph) with $W(C_2Ph)(CO)_3(\eta\text{-}C_5H_5)$ gave the dark red Ru_3W butterfly cluster, **47**, in which the NPh ligand asymmetrically bridges the hinge Ru—W bond, best described as a W=N(Ph) → Ru interaction; the acetylide ligand adopts a μ_4,η^2 bonding mode.[86] Hydrogenation of **47** gave $Ru_3W(\mu\text{-}H)_2(\mu\text{-}NPh)(\mu\text{-}CH{=}CHPh)(CO)_8(\eta\text{-}C_5H_5)$ (**48**), in which there is a tetrahedral metal core. Excess $C_2(tol)_2$ reacted with **47** to afford **49**, in which the alkyne takes up a μ_3,η^2-(‖) bonding mode to the WRu_2 face, while $C_2(CF_3)_2$ afforded **50**. In the latter, coupling of $C_2(CF_3)_2$ and C_2Ph moieties gave the $CPh{=}CC(CF_3){=}C(CF_3)$ ligand bridging an open Ru_2W system. In all reactions of **47**, the phenylimido ligand remains unchanged.

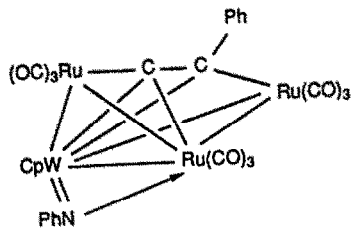

(47)

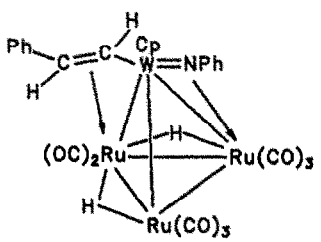

(48)

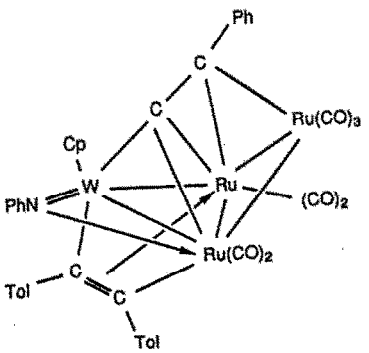

(49)

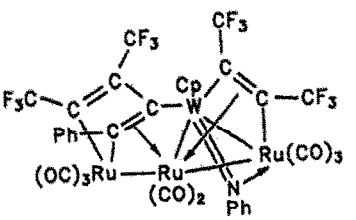

(50)

Thermolysis of **34** (R = Ph) gave the hexaruthenium cluster Ru_6 $(\mu_4\text{-}NPh)_2(CO)_{15}$ (**51**) in high yield;[87] the same complex was prepared from **35** (R = R^1 = Ph) and $Ru_3(CO)_{12}$. In the latter case, the heptaruthenium cluster $Ru_7(\mu_4\text{-}NPh)_2(CO)_{16}$ (**52**) was formed as a minor product.

Complex **34** (R = Ph) reacted with diphenylacetylene to give **53** (R = Ph), **54** and **55**, and with 1-phenylpropyne to give **53** (R = Me) by coupling of CO and the alkynes with the μ_3-nitrene. Complex **53** (R = Ph) reacted further with C_2Ph_2 and CO to form pentaphenylpyridone and 1,3,4-triphenylmaleimide, respectively.[88,89] $Ru_3(\mu_3\text{-}NPh)(dppm)(CO)_8$ (see above) reacted with phenylacetylene and diphenylacetylene to afford binuclear metallapyrrollidone complexes analogous to **53**.[90] Attempts to isolate the presumed trinuclear nitrene-alkyne intermediates were unsuccessful.

Reactions between **34** (R = Ph) or **35** (R = R^1 = Ph) and the trigoldoxonium cation $[O\{Au(PPh_3)_3\}]^+$ in the presence of $[Co(CO)_4]^-$ have given dark red $Au_2Ru_3(\mu_3\text{-}NPh)(CO)_9(PPh_3)_2$ (**56**) and orange–red $Au_2Ru_3(\mu_3\text{-}NPh)_2(CO)_8(PPh_3)_2$, respectively.[91] In **56**, the Au—Au bond is preserved, and the complex may model the approach of H_2 to **34** (R = Ph), which afforded Ru_3 $(\mu\text{-}H)_2(\mu_3\text{-}NPh)(\mu_3\text{-}CO)(CO)_8$ (**40**) as described above.

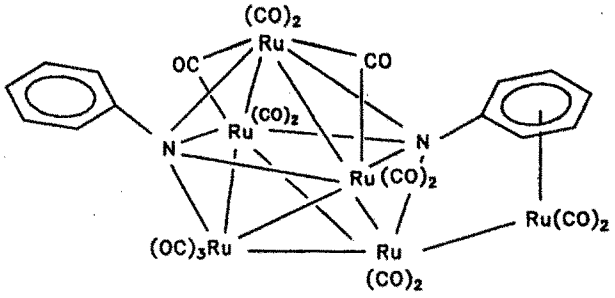

(51)

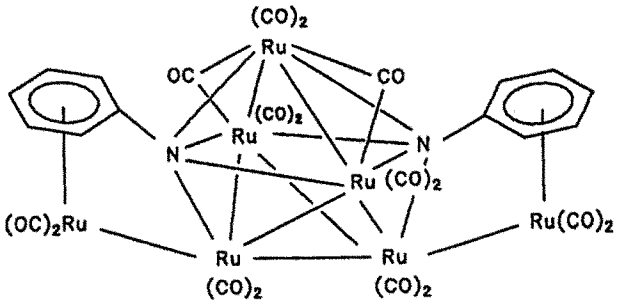

(52)

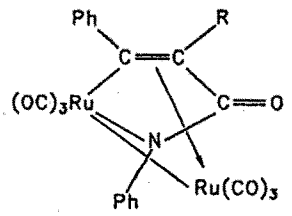

(53) R = Ph, Me

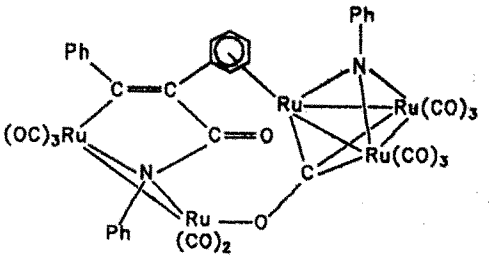

(54)

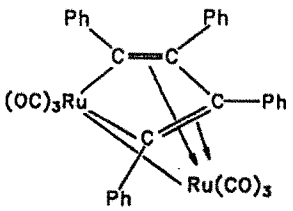

(55)

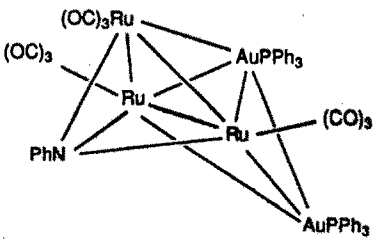

(56)

7. ENIMINES AND α,α′-DIIMINES (AZA- AND 1,4-DIAZABUTA-1,3-DIENES)

The work of the Dutch groups led by Vrieze and van Koten on the reactions of enimines and diazabutadienes with ruthenium carbonyls has recently been reviewed,[92–95] so this topic will not be surveyed exhaustively here.

Recently, attention has been focused on the reactivity of $Ru_3(CO)_{12}$ with monoazadienes. The enimines (*E*)-MeC(H)=C(H)C(H)=NR (R = Bu^t, Pr^i, cyclohexyl) reacted with $Ru_3(CO)_{12}$ to give mixtures of the linear tetraruthenium compounds $Ru_4(CO)_{10}\{MeC{=}CHCH{=}NR\}_2$ (**57**; R = Pr^i, cyclohexyl),[96] trinuclear $Ru_3(CO)_6(MeC{=}CHCH{=}NPr^i)_2$ (**58**),[97] and binuclear $Ru_2(CO)_6$ (μ-$CH_2CCHCH{=}NBu^t$) and $Ru_2(CO)_6(\mu$-EtCCHNBu^t).[98]

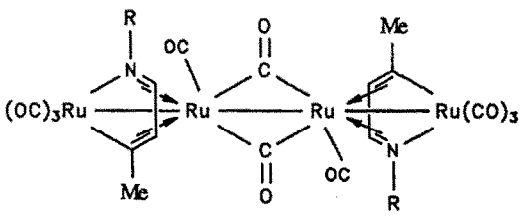

(57) R = Pr^i, cyclohexyl

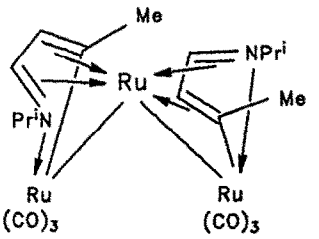

(58)

The diazadienes generally react with $Ru_3(CO)_{12}$ to give mono- or binuclear products, for which an extensive chemistry has been developed. Thus, reactions between $Ru_3(CO)_{12}$ and RN=CH CH=NR (R-dab) afforded $Ru(CO)_3$(R-dab) [**59**; R = 2,6-di(isopropyl)mesityl, mesityl and 2,6-xylyl].[92] For other R groups, the $Ru(CO)_3$(R-dab) intermediate reacted further with $Ru_3(CO)_{12}$ to give $Ru_2(CO)_6$(R-dab) (**60**; R = Pr^i, Bu^t, cyclohexyl).[99,100] Reversed phase HPLC was used to show that formation of an intermediate, postulated to be $Ru_3(CO)_{10}$(dab), is the rate-determining step in the former reaction, which is first order in $Ru_3(CO)_{12}$ and dab.[101] Reaction of **60** (R = Pr^i) with acetylenes has been examined in some detail.[102–106] Complex **61** was obtained from the reaction with acetylene.[102,103] By contrast, the reaction with HC_2CO_2Me was more complex. The first-formed product at room temperature was **62** after C—C coupling and Ru—Ru bond rupture. This subsequently lost CO to give **63** (R = H) with reformation of the Ru—Ru bond and the migration of a terminal CO ligand to adopt a bridging position. Reaction with $C_2(CO_2Me)_2$ proceeded likewise, but in this case **63** (R = CO_2Me) added a second equivalent of alkyne to give a mixture of **64** and $Ru_2(CO)_4\{Pr^iN{=}CHCH(NPr^i)C(CO_2Me){=}C(CO_2Me)\}$. Reaction with HC_2Ph afforded an inseparable mixture of two isomers of $Ru_2(CO)_4$(Pr^i-dab)(μ-PhC_2H);[104] the corresponding reaction with the internal acetylene MeC_2NEt_2 afforded **65** in the first reaction of this type with no C—C bond formation.[105]

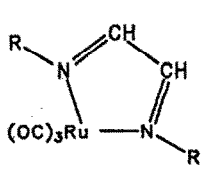

(59) R = 2,6-diisopropylmesityl, mesityl, 2,6-xylyl

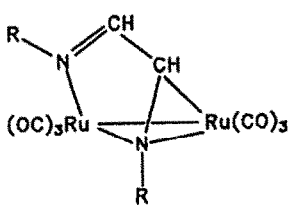

(60) R = Pr^i, Bu^t, cyclohexyl

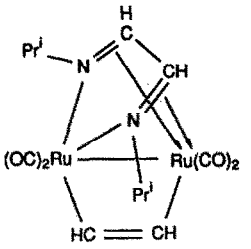

(61)

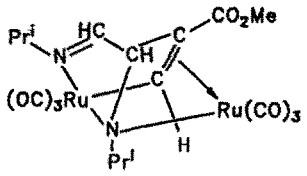

(62)

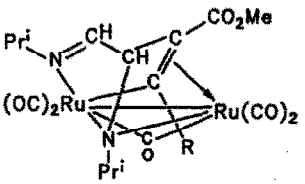

(63) R = H, CO_2Me

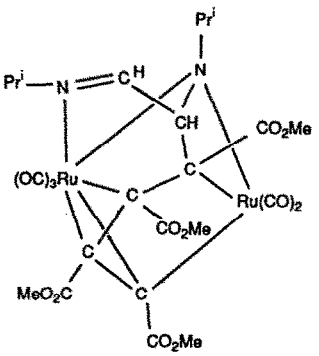

(64)

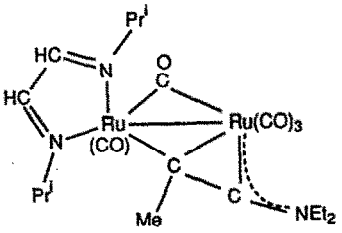

(65)

Reaction of **62** (R = Pr^i or cyclohexyl) with Me_3NO or reaction between $Ru_3(CO)_{12}$ and R-dab (R = CH_2Bu^t) afforded $Ru_2(CO)_5$(R-dab) (**66**; R = Pr^i, cyclohexyl, CH_2Bu^t).[107] Theoretical calculations indicate that there is no metal–metal bond in this complex, in contrast to the expectation from the metal–metal distance in **66** and qualitative electron counting methods.[108] When **67** (R = CH_2Bu^t, Bu^i, cyclohexyl) was heated with $Ru_3(CO)_{12}$, **67** and **68** were obtained.[109] In a "traffic light-like colour change", bright green **68** reversibly added CO to give bright red **67** and reacted with CH_2N_2 to afford **69** (R = CH_2Bu^t, Bu^i).[110] Treatment of **68** (R = CH_2Bu^t) with H_2 afforded **70**.[111]

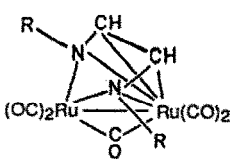

(66) R = neopentyl, Pr^i, cyclohexyl

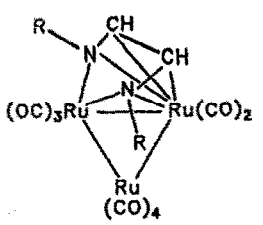

(67) R = neopentyl, Bu^i, cyclohexyl

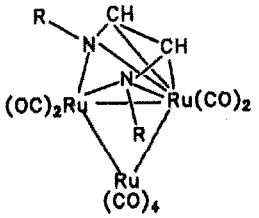

(68) R = neopentyl, Bu^i, cyclohexyl

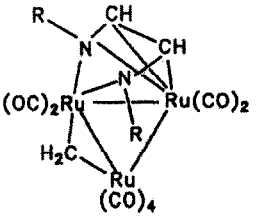

(69) R = neopentyl, Bu^i

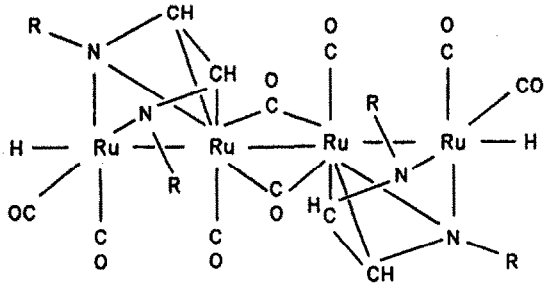

(70) R = neopentyl

The pyridine-2-carbaldehyde-imines, R^1-py-2-C(R^2)=NR (R-pyca) (R = Bu^t, Pr^i, cyclohexyl), reacted with $Ru_3(CO)_{12}$ to give $Ru_2(CO)_6$(R-pyca) (**71**); further reaction with R-pyca afforded $Ru_2(CO)_5$(R-ape) [R-ape = 1,2-bis(μ-alkylamido)-1,2-bis(2-pyridyl)ethane] (**72**) in which R-ape consists of the two C—C coupled R-pyca ligands.[112] Thermolysis of the latter gave $Ru_2(CO)_4$(R-ape) (**73**; R^1 = Me) or $Ru_2(CO)_4$(R-pyca)$_2$ (**74**; R^1 = H) after CO loss. Interestingly, CO addition to the products regenerated $Ru_2(CO)_5$(R-ape) (R = Pr^i) for both R^1 = H and Me, implying CO addition is concomitant with the formation of a C—C bond between the two imine carbons of two pyca ligands in $Ru_2(CO)_4$(Pr^i-pyca)$_2$.[113] The reactivity of **71** (R = Bu^t, Pr^i) toward alkynes is summarized in Scheme 5.[114] Some of this chemistry is analogous to the $Ru_2(CO)_6$(R-dab)/alkyne chemistry in that C—C coupling reactions of the alkyne with the coordinated diimine ligand are observed; more importantly, however, the C—C bond formed here seems to be significantly less stable leading to further reactions.

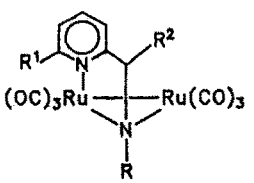

(71) R = Bu^t, Pr^i, R^1 = H, Me, R^2 = H
R = cyclohexyl, R^1 = R^2 = H
R = cyclohexyl, R^1 = H, R^2 = Me
R = cyclohexyl, R^1 = Me, R^2 = H

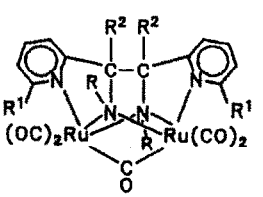

(72) R = Bu^t, Pr^i, R^1 = H, Me, R^2 = H
R = cyclohexyl, R^1 = R^2 = H

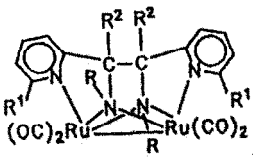

(73) R = Bu^t, Pr^i, cyclohexyl
R^1 = Me, R^2 = H

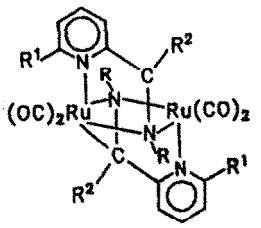

(74) R = Bu^t, Pr^i, R^1 = H, Me, R^2 = H
R = cyclohexyl, R^1 = R^2 = H

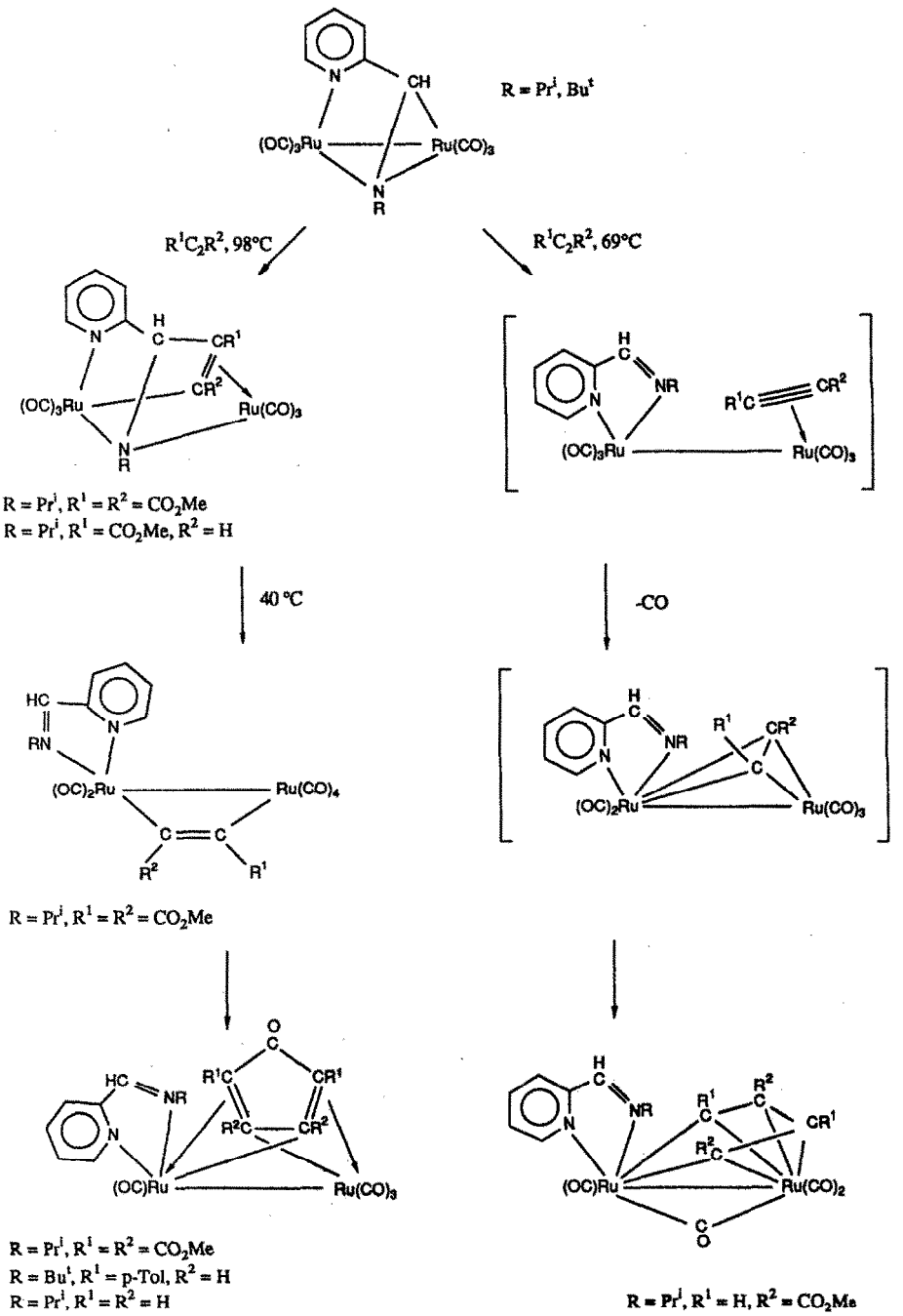

Scheme 5. Reactivity of $Ru_2(CO)_6$(R-pyca) towards alkynes.

8. *N*-HETEROCYCLES

The cyclometallated complex $Ru_3(\mu\text{-}H)(\mu\text{-}C_5H_4N)(CO)_{10}$ (**75**; R = R^1 = H) was obtained from pyridine and $Ru_3(CO)_{12}$;[115] the reaction is believed to occur by way of $Ru_3(CO)_{11}(py)$, but this intermediate was not detected either here or in the reactions of pyridine with $Ru_3(CO)_{12-n}(NCMe)_n$ (n = 1 or 2).[11] Reaction with excess pyridine afforded $Ru_3(\mu\text{-}H)_2(\mu\text{-}C_5H_4N)_2(CO)_8$ (**76**).[115,116] The 2-, 3- and 4-methyl-substituted pyridines reacted with the bis(acetonitrile) cluster complex to give analogous complexes, including two isomers of the product from 3-methylpyridine (**75**; R = Me, R′ = H; R = H, R′ = Me).[12]

An equimolar mixture of two isomers of $HRu_5C(CO)_{14}(C_5H_4N)$, **77** and **78**, differing only in the orientation of a bridging ligand, was obtained from reaction of $Ru_5C(CO)_{15}$ in excess pyridine. A third product, $HRu_5C(CO)_{13}(C_5H_4N)(C_5H_5N)$, was also obtained. Complexes **77** and **78** both underwent clean decarbonylation to give the same $HRu_5C(CO)_{13}(C_5H_4N)$, which could be re-carbonylated to a mixture of equal amounts of **77** and **78**.[117]

A $Ru_3(CO)_{12}$/2,2′-bipyridyl mixture has been reported to be a precursor for a highly active, low temperature catalyst for the water gas shift reaction.[118] The reaction between $Ru_3(CO)_{12}$ or $Ru_3(CO)_{10}(NCMe)_2$ and 2,2′-bipyridyl afforded a purple complex containing bridging CO groups, $Ru_3(bipy)(\mu\text{-}CO)_2(CO)_8$ (**79**);[12,115,119] this was shown to have a $Fe_3(CO)_{12}$-type structure with the bipy chelating one of the CO-bridged ruthenium atoms. Pyrolysis of **79** in refluxing toluene afforded

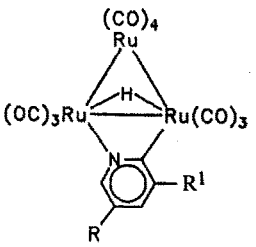

(**75**) R = R^1 = H
R = Me, R^1 = H
R = H, R^1 = Me

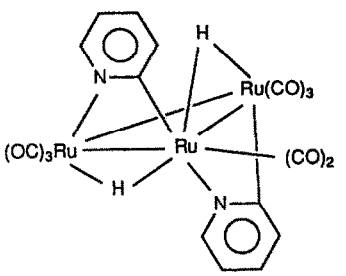

(**76**)

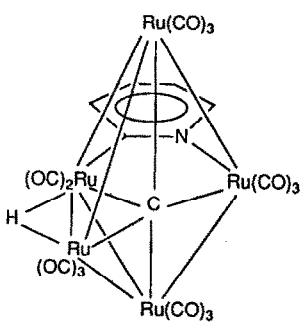

(**77**)

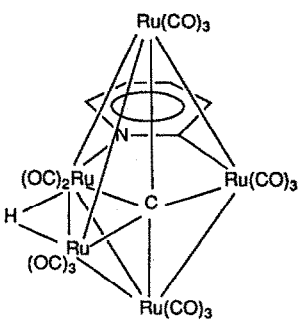

(**78**)

a cyclometallated complex for which structure **80** was postulated.[12] However, the structure of the pyrolysis product from the reaction between $Os_3(CO)_{12}$ and 2,2′-bipyridyl has been determined to be **81** (M = Os),[120] and structure **81** (M = Ru) seems more likely for the pyrolysis product from **79**.

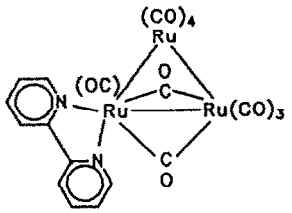

(79)

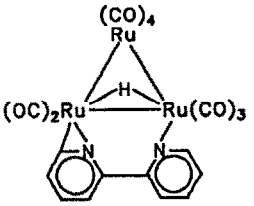

(80)

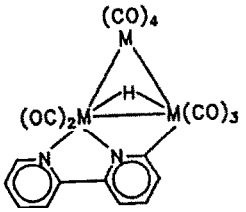

(81) M = Os, Ru

Reactions with 1,10-phenanthroline, 2,2′-biquinoline or 2,2′-bipyrimidine each gave $Ru_3(L\text{-}L)(\mu\text{-}CO)_2(CO)_8$ (L-L = phen, biquin or bipym, respectively), having the $Ru_3(bipy)(CO)_{10}$ structure.[121] 1,8-Naphthyridine reacted with $Ru_3(CO)_{12}$ to give the CO-bridged cluster $Ru_3(\mu\text{-napy})(\mu\text{-}CO)_3(CO)_7$ (**82**), which could be reversibly protonated to give $[Ru_3(\mu\text{-}H)(\mu\text{-napy})(CO)_{10}][BF_4]$ (**83**) containing only terminal carbonyls.

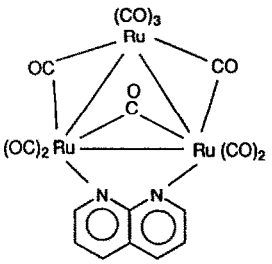

(82)

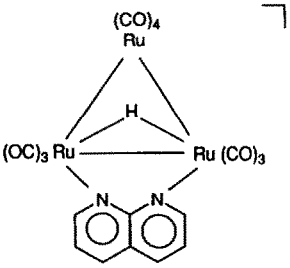

(83)

The considerably more reactive cluster $Ru_3(CO)_{10}(NCMe)_2$ cyclometallated quinoline to afford the trinuclear complex **84**; the corresponding reaction with isoquinoline afforded the two isomers **85** and **86**.[12] Reaction of quinoline with $Ru_3(CO)_{12}$ also afforded **84**;[117,122] in the presence of excess ligand, the bis(quinoline) product was obtained. Complex **84** afforded quinoline and Ru_4

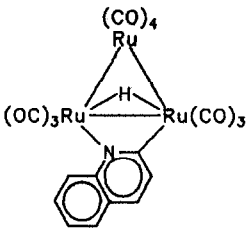

(84)

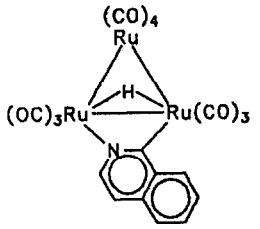

(85)

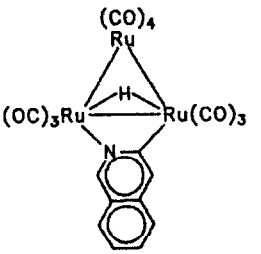

(86)

$(\mu\text{-H})_4(CO)_{12}$ on hydrogenation, but no reaction was observed with the hydridic reagents $Li[AlH_4]$ or $Li[BHEt_3]$.[122] As the carbon–nitrogen double bond is not reduced in the complex, but readily reduced in the free ligand, it seems the nitrogen ligand is not the site of reaction with H_2 or hydride reagents. Other heteroaromatic nitrogen compounds (1,2,3,4-tetrahydroquinoline, phenanthridine and 9,10-dihydrophenanthridine) also afforded oxidative addition products when reacted with $Ru_3(CO)_{12}$; the saturated nitrogen rings were dehydrogenated at the same time.

2-Aminopyridine reacted with $Ru_3(CO)_{12}$ to give orange–red $Ru_3(\mu\text{-H})(\mu\text{-NHpy})(CO)_9$ (**87**; R = R^1 = H); several substituted derivatives gave similar complexes, providing that there was at least one amino hydrogen atom present.[123] Substitution of equatorial CO groups *cis* to the μ-hydrogen and μ-amido fragments occurred in reactions of $Ru_3(\mu\text{-H})(\mu\text{-anpy})(CO)_9$ (**87**; R = Me, R^1 = H) (Hanpy = 2-amino-6-methylpyridine) with PPh_3 or dppm. The parent complex was readily protonated ($HBF_4 \cdot OEt_2$) to give $[Ru_3(\mu\text{-H})_2\{\mu_3\text{-NH}(C_5H_4N)\}(CO)_9]^+$; substitution of only those equatorial groups on the ruthenium bonded to one hydride occurred in similar reactions with tertiary phosphines.[124] The X-ray structure of the 2-anilinopyridyl complex **87** (R = H, R^1 = Ph) was determined, and is related to that of the 1*H*-pyrrolo[2,3-*b*]pyridine derivative.[121]

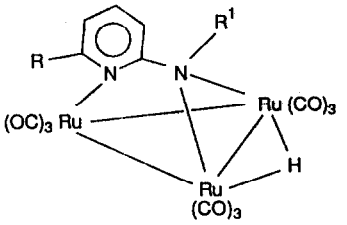

(87) R = R^1 = H
R = Me, R^1 = H
R = H, R^1 = Ph

In contrast, 2-dimethylaminopyridine gave black $Ru_3\{\mu\text{-Me}_2N(C_5H_4N)\}(\mu\text{-CO})_3(CO)_7$, whose structure resembles that of the naphthyridine complex (**82**).[121]

$Ru_3(CO)_{12}$ reacted with pyridine-2-thiol to afford $Ru_3(\mu\text{-H})(\mu_3\text{-pyS})(CO)_9$; this latter complex was successively converted into polymeric $[\{Ru(\mu_3\text{-pyS})(CO)_2\}_n]$ and $Ru(pyS)_2(CO)_2$. The cluster has the same structure as the analogous 2-anilinopyridyl (*vide supra*) and pyrrolo[2,3-*b*]pyridinate complexes, and reacted with *P*-donors PPh_3 and dppm by CO substitution; the capping μ_3-pyS group proved resilient to metal–element bond cleavage.[125] Heteronuclear clusters **88**–**91** were obtained on reaction of $Re_2(pyS)_2(CO)_6$ (py = pyridine-2-thionato) with $Ru_3(CO)_{12}$;[126] in related work, $Ru(pyS)_2(CO)_2$ reacted with $Ru_3(CO)_{12}$ to afford pentanuclear $Ru_5(\mu_4\text{-S})_2(\mu\text{-}C_5H_4N)_2(CO)_{11}$, containing a Ru_5S_2 pentagonal bipyramid.[127]

8-Quinolinol reacted with $Ru_3(CO)_{12}$ to give **92** and **93**, *O*-metallation being preferred over *C*-metallation.[128]

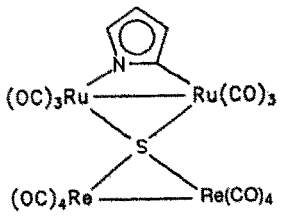

(88)

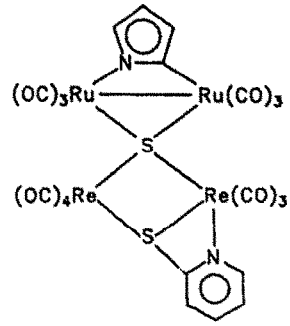

(89)

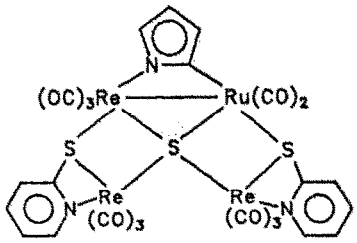

(90)

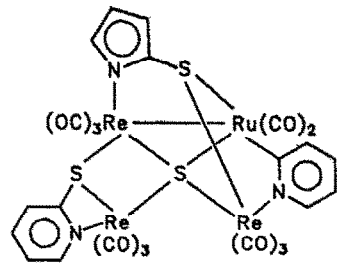

(91)

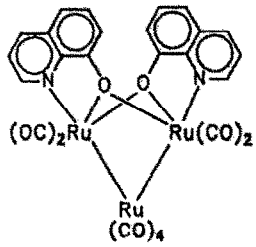

(92)

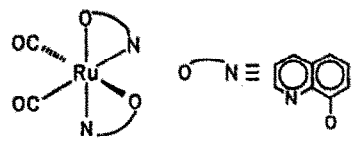

(93)

The reaction of 1,2-diazine with $Ru_3(CO)_{12}$ gave **94**;[129,130] the analogous reactions of two other 1,2-diazines afforded **95** and **96**.[131] Complex **94** can be considered to be derived from the supposed μ-CO intermediate for scrambling CO groups on $Ru_3(CO)_{12}$. The NMR spectrum at -156°C is in agreement with the solid-state structure. Between -156 and -86°C, the bridging and equatorial CO groups interchange by an exceptionally facile process ($E_a = 25.5$ kJ mol^{-1}). Between -117 and -86°C, the two axial CO groups on the unique ruthenium enter into the scrambling process, and all CO groups are equilibrated at ~ 75°C ($E_a = 58.1$ kJ mol^{-1}).

The complex $Ru_3(CO)_{10}(NCMe)_2$ reacted with 1,2-, 1,3- and 1,4-diazine to give **97**, isomeric **98** and **99**, and **100**, respectively;[12] as with pyridine, when *N*,*N*′-coordination is not possible, cyclometallation occurs.

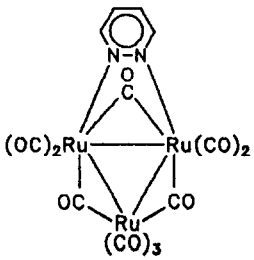

(94)

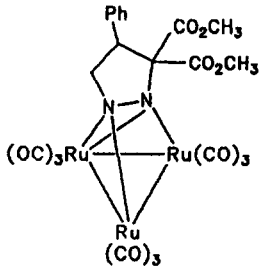

(95)

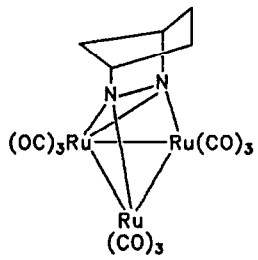

(96)

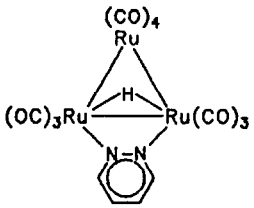

(97)

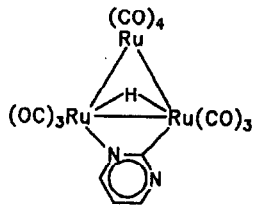

(98)

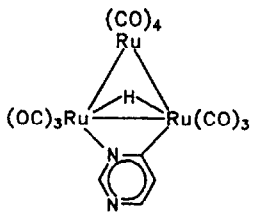

(99)

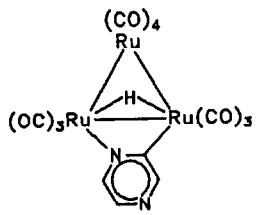

(100)

The 1 : 1 reaction between $Ru_3(CO)_{12}$ and pyrazoles in refluxing cyclohexane gave $Ru_3(\mu\text{-H})(\mu\text{-}N_2C_3HR_2)(CO)_{10}$ (**101**; R = H, Me or CF_3) by oxidative addition across a Ru—Ru bond.[115]

Thermal reactions between $Ru_3(CO)_{12}$ and the benzimidazole or benzotriazole gave $Ru_3(\mu\text{-H})(\mu\text{-bzim})(CO)_{10}$ (**103**) and $Ru_2(\mu\text{-bztz})_2(CO)_6$, respectively.[121] Reaction of **102** with PPh_3 gave a mixture of three isomers of $Ru_3(\mu\text{-H})(\mu\text{-bzim})(CO)_9(PPh_3)$ in the ratio 2.5 : 9 : 1 **103**:**104**:**105**.[132] The reaction between $Ru_3(CO)_{12}$ and 1*H*-pyrrolo-[2,3-*b*]pyridine afforded $Ru_3(\mu\text{-H})(\mu_3\text{-ppy})(CO)_9$ (**106**), the first example of a μ_3-pyrrolopyridine; the pyrrolic nitrogen is sp^3-hybridized, disrupting the ligand aromaticity.[121]

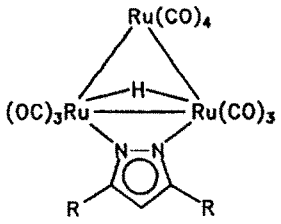

(101) R = H, Me, CF_3

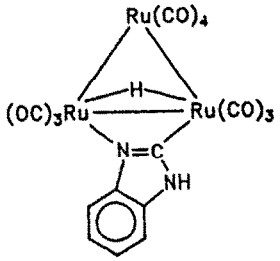

(102)

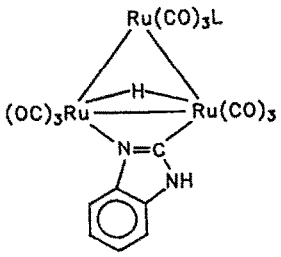

(103) L = PPh_3

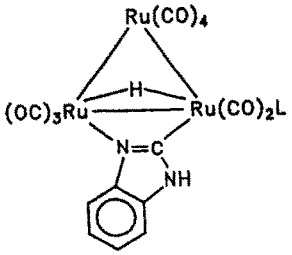

(104) L = PPh_3

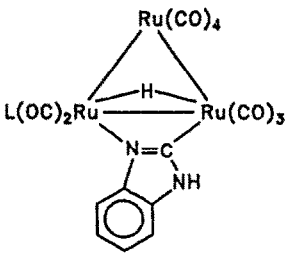

(105) L = PPh_3

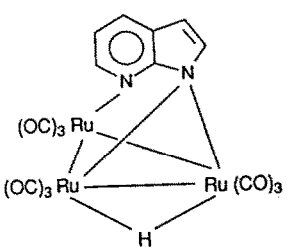

(106)

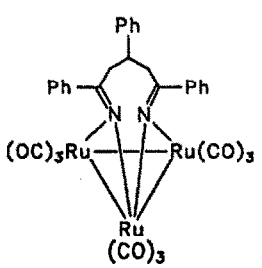

(107)

Even under very mild reaction conditions, $Ru_3(CO)_{12}$ and diazepines afforded mononuclear tricarbonyl complexes;[133,134] however, a small amount of **107** was isolated from the reaction with 4,5,6-trihydro-3,5,7-triphenyl-1,2-diazepine.[134]

The thermal reaction between $Ru_3(CO)_{12}$ and diphenyl(2-pyridyl)phosphine afforded $Ru_3(CO)_9\{PPh_2(py)\}_3$ and monomeric species.[135] The phosphine reacted with $Ru_3(CO)_{12}$ under catalytic substitution conditions {[ppn][OAc]} to give $Ru_3(CO)_{11}\{PPh_2(py)\}$; this was metastable at room temperature, yielding $Ru_3\{\mu_3\text{-}PPh(C_5H_4N)\}\{\mu\text{-}C(O)Ph\}(CO)_9$ (**108**; L = CO).[136] This complex undergoes carbonyl substitution stereospecifically at a site *cis* to the oxygen of the acyl group to afford $Ru_3\{\mu_3\text{-}PPh(C_5H_4N)\}\{\mu\text{-}C(O)Ph\}(CO)_8(L)$ (**108**; L = PPh_3, PPh_2H, PCy_2H).[137] The PhCO functionality in **108** (L = CO) was the site of further reaction; treatment with H_2 afforded **109** by loss of CO and benzene, and with [ppn][BH_4] gave **110** after loss of benzaldehyde.[138] Interconvertion of **109** and **110** was achieved using [ppn][BH_4] as base and CF_3CO_2H as acid. Mild thermolysis of **108** (L = PPh_2H, PCy_2H) gave **111** after benzaldehyde loss; its reactivity toward

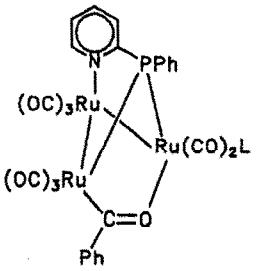

(108) L = CO, PPh_2H, PCy_2H

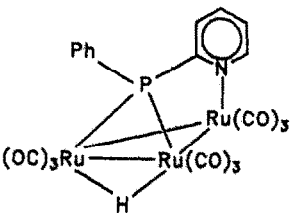

(109)

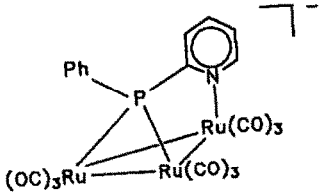

(110)

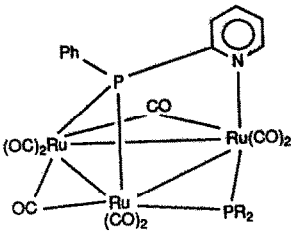

(111) R = Ph, cyclohexyl

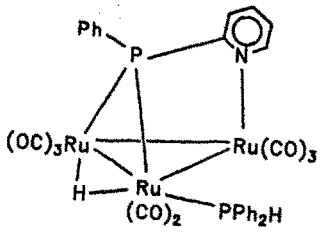

(112)

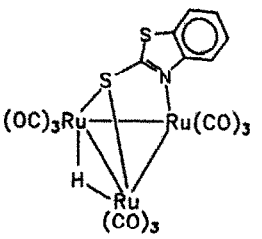

(113)

CO, PR_3 and H_2 was investigated. CO addition is reversible, and phosphines substitute at the non-phosphido-bridged ruthenium; hydrogenation afforded **112** as major product.

Coordination of the heterocyclic *N* atom was favoured over that of the *S* atom in the reaction between $Ru_3(CO)_{12}$ and the mercaptobenzothiazole (mbtH); oxidative addition of the thiol across a Ru—Ru bond gave **113**.[139] Addition of pyridine to the cluster afforded $\{Ru(\mu\text{-mbt})(CO)_2(py)\}_2$ and $Ru(mbt)_2(CO)_2(py)_2$.[140]

Reactions of many other *N*-heterocycles with $Ru_3(CO)_{12}$ have been studied and lead to mono- and binuclear products (Section 12).

9. NITROSYL COMPLEXES

Derivatives containing NO ligands have been obtained from reactions involving NO, NO^+ or NO_2^-. Direct reaction between $Ru_3(CO)_{12}$ and NO gave $Ru_3(\mu\text{-}NO)_2(CO)_{10}$ (**114**; X = NO), in which only two Ru—Ru bonds are present. Further reaction with NO gave a brown, insoluble, polymeric material,[141,142] while CO reacted with **114** (X = NO) to give a mixture of $Ru_3(CO)_{12}$, $Ru_3(\mu\text{-}NCO)(\mu\text{-}NO)(CO)_{10}$ (**114**; X = NCO) and $Ru_4(\mu_4\text{-}N)(\mu\text{-}X)(CO)_{12}$ (**115**; X = NO, NCO).[143] In the presence of triphenylphosphine, **114** (X = NO) underwent disubstitution to afford $Ru_3(\mu\text{-}NO)_2(CO)_8(PPh_3)_2$.[144]

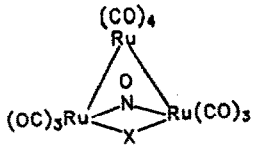

(114) X = NO, NCO

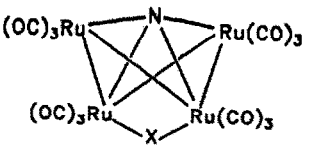

(115) X = NO, NCO

The cluster anion $[Ru_3(\mu\text{-}H)(CO)_{11}]^-$ reacted with $[NO][PF_6]$ to give $Ru_3(\mu\text{-}H)(\mu\text{-}NO)(CO)_{10}$ (**116**; L = CO); carbonyl substitution of this complex with $P(OMe)_3$ afforded **116** [L = $P(OMe)_3$].[145] The reaction between $Ru_3(CO)_{12}$ and $[ppn][NO_2]$ gave $[ppn][Ru_3(\mu\text{-}NO)(CO)_{10}]$ (**117**), which afforded **116** (L = CO) upon protonation with CF_3CO_2H.[146,147]

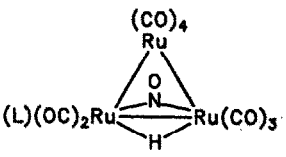

(116) L = CO, P(OMe)3

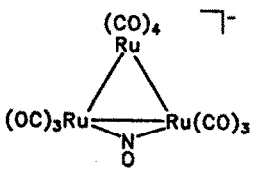

(117)

Hydrogenation of **116** gave $Ru_3(\mu\text{-}H)(\mu\text{-}NH_2)(CO)_{10}$ (**118**), $Ru_3(\mu\text{-}H)_2(\mu_3\text{-}NH)(CO)_9$ (**119**) and $Ru_4(\mu\text{-}H)_4(CO)_{12}$;[148] trace amounts of tetranuclear $Ru_4(\mu\text{-}H)_3(\mu\text{-}NH_2)(CO)_{12}$ (**120**) were also found.[149]

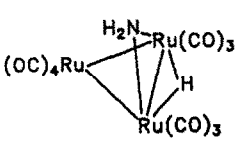

(118)

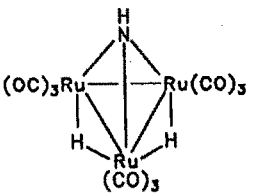

(119)

Protonation of **117** with CF_3SO_3H afforded **121** (R = H);[150] addition of the proton to the nitrosyl oxygen and subsequent capping by the face bridging NOH and CO is in contrast to the addition across a metal–metal bond found when CF_3CO_2H is used.[146] Photolysis of **121** (R = H)

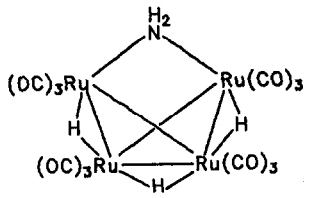

(120)

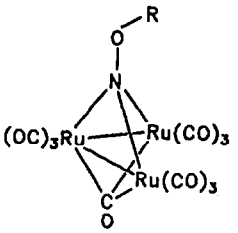

(121) R = H, Me

under CO generated $[Ru_3(NCO)(\mu\text{-}CO)_2(CO)_9]^-$ (**4**) quantitatively.[151] Methylation of **117** with CF_3SO_3Me gave **121** (R = Me), while reaction with [ppn][NO_2] under CO gave $[Ru(CO)_3(NO)]^-$.

The reaction of **117** with $HgCl_2$ afforded **122**, with the mercury atom bridging the same Ru—Ru bond in each Ru_3 triangular unit as the nitrosyl ligands.[152] The heteronuclear nitrosylcarbonyl cluster $[FeRu_3(CO)_{12}(NO)]^-$ (**123**) was obtained in good yield from the reaction between $Ru_3(CO)_{12}$ and $[Fe(CO)_3(NO)]^-$.[153]

Johnson, Lewis and co-workers synthesized hexaruthenium cluster nitrosyls by auration [AuCl(PPh_3)] (**124**), protonation (**125**) or nitrosylation {$[NO]^+$} (**126**) of $[Ru_6C(CO)_{15}(NO)]^-$, generated upon reaction of $Ru_6C(CO)_{17}$ with [ppn][NO_2].[154,155]

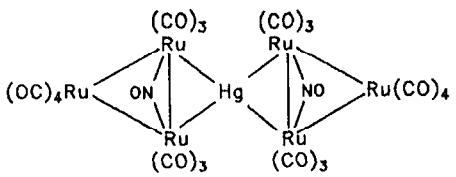

(122)

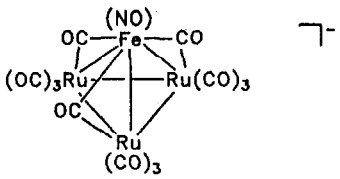

(123)

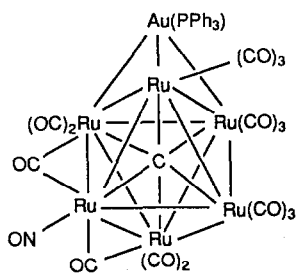

(124)

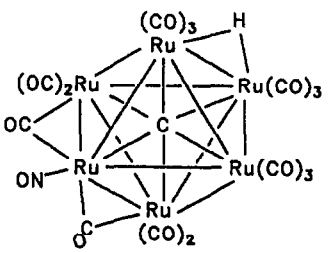

(125)

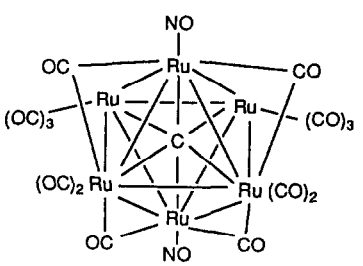

(126)

10. NITRIDO CLUSTERS

Gladfelter has surveyed the field of organometallic clusters containing nitrosyl or nitrido ligands,[156] and has summarized his earlier results in these areas with ruthenium clusters.[157]

Thermolysis of the μ-NCO complex **6** gave $[Ru_4(\mu_4\text{-}N)(CO)_{12}]^-$ (**127**) in high yield,[158] which on protonation with CF_3SO_3H gave a mixture containing $Ru_3(\mu_3\text{-}NH)(\mu_3\text{-}CO)(CO)_9$.[159] Reaction of either **4** or **9** with $Ru_3(CO)_{12}$ afforded the hexanuclear nitrido cluster $[Ru_6(\mu_6\text{-}N)(CO)_{16}]^-$ (**128**), which reacted rapidly with CO at room temperature to give $[Ru_5(\mu_5\text{-}N)(CO)_{14}]^-$ (**129**);[158] the pentanuclear complex was also obtained in low yield by thermolysis of **121** (R = H).[151]

Refluxing a mixture of $Ru_3(CO)_{12}$ and [ppn][N_3] in thf overnight gave **127** in addition to **6**;[160] formation of **127** involves the cleavage of a coordinated isocyanate into a coordinated nitrogen atom and carbon monoxide.

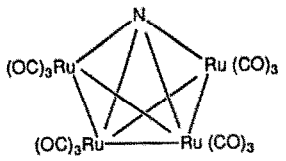

(127)

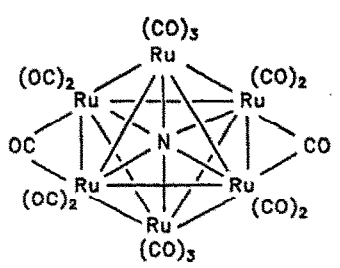

(128)

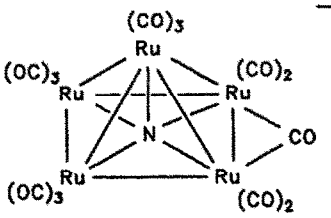

(129)

The anions $[M_4(\mu_4\text{-}N)(CO)_{12}]^-$ (M = Fe, Ru, Os) are isostructural; the *N* atom is approximately octahedral, with two *cis* coordination sites vacant. Its bonds to the hinge atoms are 0.13–0.16 Å longer than those to the wing-tip atoms.[161]

Fenske–Hall MO calculations of the electronic structures of $[M_4(\mu_4\text{-}N)(CO)_{12}]^-$ ($M_4 = Fe_4$, $FeRu_3$, Ru_4) have shown that the metal-based orbitals cover a wider energy range in the Ru_4 complex compared with Fe_4; metal–metal bonding is stronger in the former, with the bond between the hinge atoms being considerably stronger than those between the hinge and wing-tip atoms.[161] There is no significant difference in the M—N bond strengths. The metal–nitride stretching vibrations in $Ru_4(\mu\text{-}H)(\mu_4\text{-}N)(CO)_{12}$ have been assigned; however, no comparison could be made with similarly-bound nitrogen on a metal surface.[162]

The mixed-metal cluster exists as the two isomers (a) and (b), which interconvert in solution, in which the iron atom is in wing-tip or hinge positions. The metal–metal bonding is perturbed more in isomer (b). Protonation gives exclusively the hydride derived from (a), in which the hydrogen atom bridges the hinge bond, interacting with a localized hinge bonding MO found in (a) but not in (b). Auration using $AuCl(PPh_3)$ afforded an analogous product, with the $AuPPh_3$ fragment bridging the hinge and the iron atom exclusively in a wing-tip position.[163]

The mixed-metal nitrido cluster $CoRu_3(\mu_4\text{-}N)(CO)_{12}$, which is isoelectronic with the $[M_4(\mu_4\text{-}N)(CO)_{12}]^-$ anions discussed above, was isolated in low yield from the reaction between $[CoRu_3(CO)_{13}]^-$ and $[NO]^+$; the location of the cobalt atom was not determined.[164]

Protonation of both the Fe_4 and Ru_4 complexes appears to proceed by way of a μ-NH intermediate, which undergoes hydrogen migration to bridge the hinge atoms. In the Ru_4 system, the NH intermediate has been trapped by addition of diphenylacetylene, affording **130**;[165] an isostructural phenylnitrene has recently been prepared.[166]

Reaction of $[H_3Ru_4(CO)_{12}]^-$ with $[NO]^+$ afforded the nitrido cluster $Ru_4(\mu\text{-}H)(\mu_4\text{-}N)(CO)_{12}$, whose $P(OMe)_3$ derivative, **131**, was structurally characterized,[167] and **132**, amongst other products.[167,168]

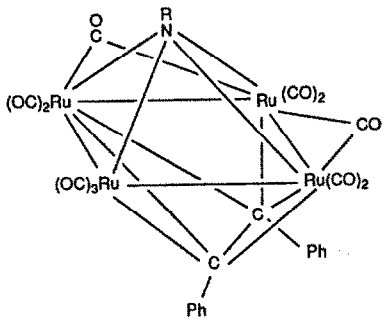

(130) R = H, Ph

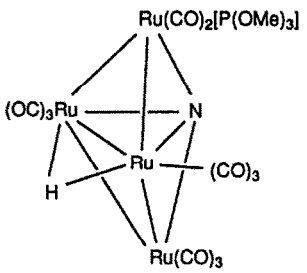

(131)

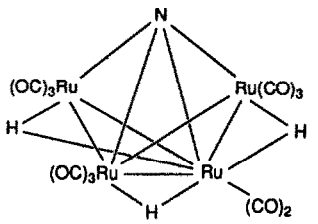

(132)

11. CLUSTERS CONTAINING OTHER *N*-DONOR LIGANDS

Given the large number of anionic Ru_3 clusters known, it is surprising that reactions with aryldiazonium cations have been little exploited in the synthesis of cluster carbonyl derivatives. One such reaction, between $[PhN_2][PF_6]$ and $[Ru_3(\mu_3\text{-}PhECH_2EPh_2)(CO)_9]^-$ (E = P, As), gave **133**, which on heating in cyclohexane underwent cyclometallation to give **134**.[169]

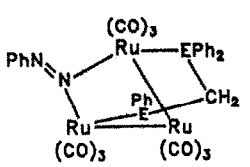

(133) E = P, As

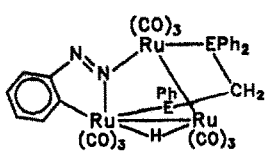

(134) E = P, As

Diphenyldiazomethane reacted with $Ru_5(CO)_{13}(\mu_4\text{-}\eta^2\text{-}C_2R)(\mu\text{-}PPh_2)$ (R = Ph, Pr^i) to afford **135**, which contains an intact μ_4-coordinated N_2CPh_2; CO inserted into the N—N bond of **135** to afford **136**.[170]

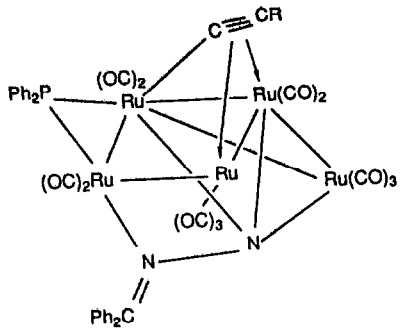

(135)

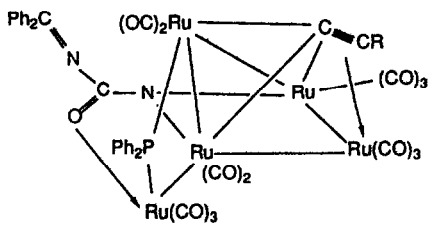

(136)

The reaction between $Ru_3(CO)_{12}$ and $S(NAsBu^t_2)_2$ afforded $Ru_3(\mu\text{-}H)(\mu_3\text{-}AsBu^t)(\mu\text{-}NSNAsBu^t_2)(CO)_8$ (**137**).[171]

Photogenerated $Ru_3(CO)_{11}$ reacted with N_2 at 110 K to yield axially substituted $Ru_3(N_2)(CO)_{11}$ (**138**); warming the matrix to 195 K led to quantitative regeneration of $Ru_3(CO)_{12}$.[172]

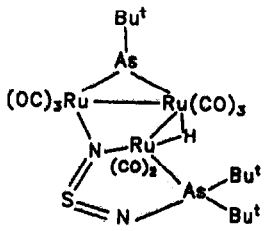

(137)

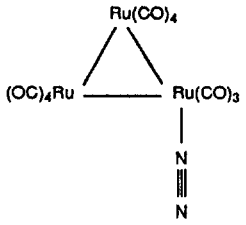

(138)

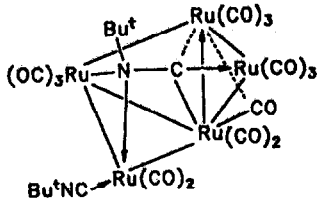

(139)

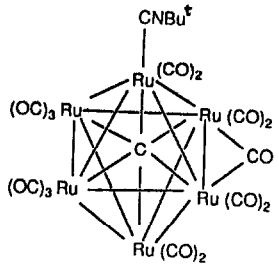

(140)

Moderate heating converted $Ru_3(CO)_{11}(CNBu^t)$ into $Ru_5(CO)_{14}(CNBu^t)_2$ (**139**), with an isocyanide ligand acting as a 6e donor bonded to all five metal atoms.[173] Pyrolysis of **139** in refluxing nonane afforded $Ru_6(\mu_6\text{-}C)(\mu\text{-}CO)(CO)_{15}(CNBu^t)$ (**140**); the carbide was shown by selective isotopic labelling to have been derived from the isonitrile ligand.[174]

12. REACTIONS OF ORGANO-NITROGEN COMPOUNDS GIVING MONO- OR BINUCLEAR PRODUCTS

(a) *Azoarenes*

One of the three complexes isolated from reactions between azobenzene and $Ru_3(CO)_{12}$ was characterized as $Ru(azb)_2(CO)_2$ (**38**), containing the cyclometallated 2-(phenylazo)phenyl ligand.[70,87] There are three possible isomers for $Ru(CO)_2(C\text{-}N)_2$, where (C-N) is a chelating ligand with *C* and *N* donors; a different isomer is found in the product obtained from $Ru_3(CO)_{12}$ and benzo[*h*]quinoline (*vide infra*).

(b) *Enimines and α,α′-diimines*

As described in Section 7, the usual products from reactions of compounds containing the N=C functionality are mono- or binuclear complexes. The reaction of $Ru_3(CO)_{12}$ with *N*-phenylsalicylidenimine afforded bis(*N*-phenylsalicylideniminato)dicarbonylruthenium(II); the corresponding reaction with *N,N′*-ethylenebis(salicylidenimine), $salenH_2$, gave a complex which analysed as Ru(CO)(salen) and was assigned a dimeric structure.[175] When this product was heated in pyridine, the monomer Ru(CO)(py)(salen) was obtained.[176] The reactions of other Schiff bases, PhCH=NR (R = Ph, Me), with $Ru_3(CO)_{12}$ also gave the yellow crystalline mononuclear complexes $Ru(C_6H_4CH{=}NR)_2(CO)_2$ (**141**; R = Ph, Me).[85,177]

(c) *Triazenes*

The ruthenium(I) triazenido complexes $\{Ru(ArNNNAr)(CO)_3\}_2$ (Ar = *p*-C_6H_4Me, *p*-C_6H_4Cl) were prepared by heating $Ru_3(CO)_{12}$ with free triazenes.[178] The bis(tolyl)triazenido complex reacted with bipy to afford the substitution product **142**.[179]

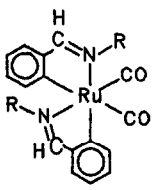

(141) R = Ph, Me

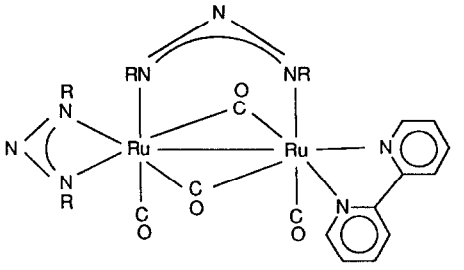

(142) R = C_6H_4Me-4

(d) N-*Heterocycles*

Reactions between $Ru_3(CO)_{12}$ and benzo[*h*]quinoline (bqH) gave the mononuclear complex $Ru(bq)_2(CO)_2$ (**143**),[180,181] together with $Ru_4(\mu\text{-}H)_4(CO)_{12}$.

The carbonyl reacted with three equivalents of pyrazoles to give the corresponding binuclear complexes **144** (R = H, Me) and **145**.[182–184] The indazole analogue was prepared similarly as a mixture of isomers. Complex **144** (R = H or Me) reacted with iodine to afford $[Ru_2(\mu\text{-}I)(\mu\text{-pyrazolyl})_2(CO)_6]I_3$ or $Ru_2I_2(\mu\text{-pyrazolyl})_2(CO)_6$, depending on the Ru : I ratio, and **144** (R = Me) reacted with excess of pyridine, acetonitrile, PPh_3, $P(C_6H_{11})_3$ or dppm at room temperature to afford monosubstituted $Ru_2(\mu\text{-dimethylpyrazolyl})(CO)_5(L)$; the pyridine product has C_s symmetry,

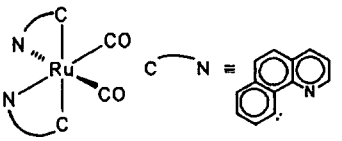

(143)

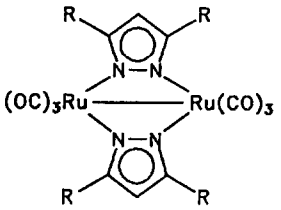

(144) R = H, Me

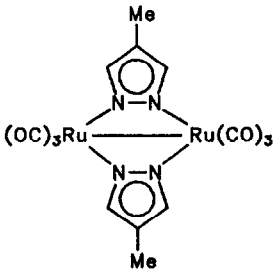

(145)

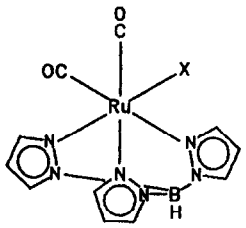

(146) X = Cl, Br, I

with the pyridine *trans* to the metal–metal bond, unlike all the others (C_1).[183] In refluxing thf, **144** (R = Me) could be disubstituted with dppm, to afford $Ru_2(CO)_4(\mu_2\text{-}\eta^2\text{-}Me_2pz)_2(\eta^1\text{-}dppm)_2$.[185] Complex **144** (R = H) reacted with dppe and (1*S*,2*S*)-(+)-1,2-bis(diphenylphosphinomethyl) cyclohexane (CYCLOP) to afford diphosphine-bridged $Ru_2(CO)_4(\mu_2\text{-}\eta^2\text{-}pz)(\mu_2\text{-}\eta^2\text{-}L_2)$ (L_2 = dppe, CYCLOP). In contrast, **144** (R = Me) reacted with dppe and CYCLOP by *ortho*-metallation of a phenyl group to afford $(\mu\text{-}H)Ru_2(CO)_3(\mu_2\text{-}\eta^2\text{-}3,5\text{-}Me_2pz)_2\{\eta^2\text{-}PPh_2XPPh_2(C_6H_4)\}$ (X = CH_2CH_2, $CH_2(C_6H_{10})CH_2$).[185] Complexes **144** (R = H or Me) reacted with carboxylic acids to give carboxylato-bridged dinuclear species, with displacement of the pyrazolato bridge to a monodenate position and concomitant protonation of the free nitrogen.[184] The reaction between $Ru_3(CO)_{12}$ and potassium tris(pyrazolyl)borate, K[HB(pz)$_3$], gave a deep red solution from which the compounds $RuX(CO)_2\{HB(pz)_3\}$ (**146**; X = Cl, Br, I) were obtained on treatment with the appropriate halogen.[186]

2-Pyridone reacted with $Ru_3(CO)_{12}$ to give the yellow polymeric $\{Ru_2(\mu\text{-}Opy)_2(CO)_4\}_n$, which reacted with ligands [L = CO, MeCN, $P(OPh)_3$, 2-pyridone] to give binuclear $Ru_2(\mu\text{-}Opy)_2(CO)_2(L)_2$. The cluster hydride $Ru_4(\mu\text{-}H)_4(CO)_{12}$ reacted with both 2-pyridone and $Ru_2(\mu\text{-}Opy)_2(CO)_2(L)_2$ to give the polymer.[123]

Porphyrins or phthalocyanines usually form mononuclear macrocyclic ligand complexes when reacted with $Ru_3(CO)_{12}$. The product of the reaction between $Ru_3(CO)_{12}$ and tetraphenylporphyrin (tpp) when recrystallized from chloroform–ethanol was eventually shown to be Ru(CO)(EtOH)(tpp),[187] after an earlier X-ray study had erroneously formulated it as the dicarbonyl, $Ru(CO)_2(tpp)$;[188] the unidentate ligands occupy axial sites. The *N*,*N*′-bridged tetraphenylporphyrin **147** afforded **148** and **149** from reaction with $Ru_3(CO)_{12}$, the former by insertion of the metal into the N—C(vinyl) bonds, the latter by insertion of the metal into a N—C(pyrrole) bond;[189,190] a small amount of the olefin-hydrogenated form of **149** was obtained also.[191] Heating a chlorobenzene solution of **149** cleanly afforded **148**.

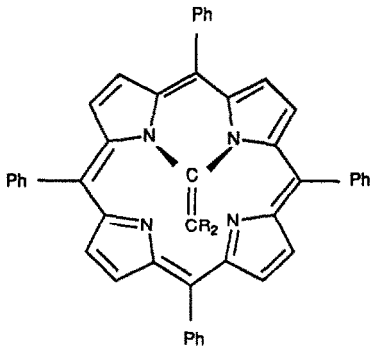

(147) R = C_6H_4Cl-4

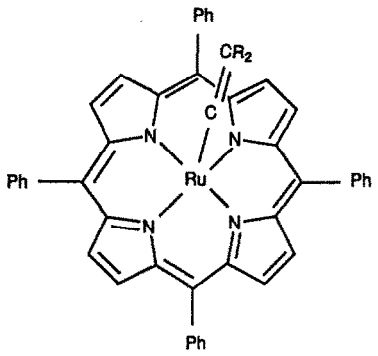

(148) R = C_6H_4Cl-4

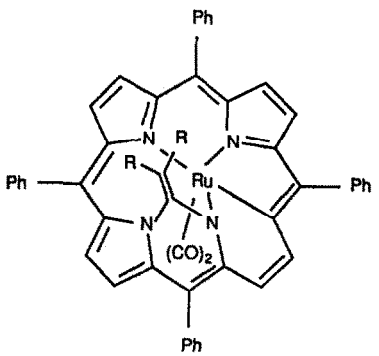

(149) R = C_6H_4Cl-4

Phthalocyanine (pcH_2) reacted with $Ru_3(CO)_{12}$ in refluxing benzonitrile to give a dark blue solid, probably Ru(CO)(pc); Soxhlet extraction with pyridine afforded $Ru(py)_2(pc)$.[192] The related complex Ru(CO)(py)(pc) was obtained from the reaction between $Ru_3(CO)_{12}$ and phthalonitrile when followed by pyridine work-up.[193]

High yields of binuclear compounds were obtained from reactions between $Ru_3(CO)_9(PPh_3)_3$ and *N*-donor ligands such as pyrazole, 2-pyridone, *N*-methyl-2-mercaptoimidazole and 1,8-diaminonaphthalene.[194]

(e) *Inorganic nitrogen ligands*

The binuclear complex $Ru_2(\mu\text{-}Me_3SiNSNCOSiMe_3)_2(CO)_4$ (**150**) was formed from the reaction of $Ru_3(CO)_{12}$ with $S(NSiMe_3)_2$.[195]

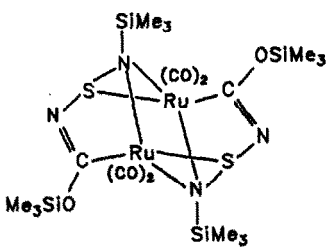

(150)

13. REACTIONS OF ORGANO-NITROGEN COMPOUNDS CATALYSED BY RUTHENIUM CLUSTERS

$Ru_3(CO)_{12}$ has been used as a catalyst for the carbonylation of amines to formamides;[196-198] carbomoyl complexes were proposed as intermediates.[198] Recently, Süss-Fink and co-workers have shown that $Ru_3(CO)_{12}$ and $Na[Ru_3(\mu\text{-}H)(CO)_{11}]$ catalyse the carbonylation of cyclic amines (piperidine, 3-methylpiperidine, pyrrolidine, heptamethylenimine and morpholine); in the case of $Ru_3(CO)_{12}$, carbamoyl clusters analogous to **15** were isolated.[199] The *ortho* positions of pyridines were acylated using olefins and carbon monoxide in the presence of $Ru_3(CO)_{12}$; the reaction is first order in pyridine and zero order in olefin and carbon monoxide, and most likely proceeds through a pyridyl hydrido intermediate such as **75**.[200]

Catalytic homogeneous double bond isomerization of 1,2-bis(ethoxycarbonyl)-1,2,3,6-tetrahydropyridazine with $Ru_4(\mu\text{-}H)_4(CO)_{12}$, but not with $Ru_4(\mu\text{-}H)_4(CO)_8(PBu_3)_4$,[201] conversion of dialkylcarbodiimides to trialkylguanidines under H_2 with several ruthenium-containing clusters,[202] and the hydro-coupling of alkyl isocyanates to carbamylformamides by $[Ru_4(\mu\text{-}H)_3(CO)_{12}]^-$[203] have been described; in the latter reaction, an intermediate containing a μ-NRCHO ligand was proposed.

$Ru_3(CO)_{12}$ has also been investigated as a catalyst for the reductive carbonylation of aromatic nitro compounds to give carbamates[52,54] and diphenylurea;[48] stoichiometric reactions aimed at elucidating the mechanism are discussed in Section 6.

$Ru_3(CO)_{12}$ catalysed the addition of *N*-substituted formamides to both terminal and internal olefins under carbon monoxide pressure,[204] and has been shown to catalyse the *N*-alkylation of amides, imides and lactams by alcohols.[205] It has also been shown to be an efficient catalyst for the transalkylation of amines.[206]

14. CONCLUSION

The chemistry of triruthenium clusters with *N*-donor ligands has expanded considerably since the former survey, due in some part to the use of milder reaction conditions involving activated triruthenium precursors. It is apparent that preferred reactivity patterns and modes of coordination of *N*-donor ligands with $Ru_3(CO)_{12}$ are becoming predictable; thus reaction types normally observed include oxidative addition across a Ru—Ru bond (benzonitriles, aromatic amines, *N*-heterocycles), reaction at a carbonyl ligand (aliphatic amines) and ligand fragmentation to give a μ_3-nitrene group (nitro-, nitroso- and azo-arenes, azides). The extensive chemistry developed with the diimines and enimines by the Vrieze–van Koten groups testifies to the potential richness of ruthenium carbonyl *N*-donor ligand chemistry and lends support to the suggestion that far from being "difficult to control", the reactivity of $Ru_3(CO)_{12}$ compared with its osmium analogue promises more chemical possibilities. The nitrosyl and nitrido chemistry, developed principally by Gladfelter and co-workers, is rather more fundamental in nature, and may model rearrangements involving nitrogen atoms occurring on metal surfaces.

Acknowledgements—We thank Dr J. A. Cabeza for sending us preprints. This review was written in Würzburg, F.R.G. and in Urbana, Illinois, and M.G.H. thanks Professors G. Erker and J. R. Shapley, respectively, for their hospitality; the Alexander von Humboldt-Stiftung is thanked for a Fellowship (M.G.H.).

REFERENCES

1. K. Burgess, *Polyhedron* 1984, **3**, 1175.
2. A. J. Deeming, *Adv. Organomet. Chem.* 1986, **26**, 1.
3. J. A. Connor, in *Transition Metal Clusters* (Edited by B. F. G. Johnson), p. 358. John Wiley, Chichester (1980).
4. M. I. Bruce, in *Comprehensive Organometallic Chemistry* (Edited by G. Wilkinson, F. G. A. Stone and E. W. Abel), Vol. 4, p. 843. Pergamon Press, Oxford (1982).
5. G. Lavigne, N. Lugan and J.-J. Bonnet, *J. Chem. Soc., Chem. Commun.* 1987, 957.
6. H. Vahrenkamp, *Pure Appl. Chem.* 1989, **61**, 1777.

7. B. Oswald, A. K. Powell, F. Rashwan, J. Heinze and H. Vahrenkamp, *Chem. Ber.* 1990, **123**, 243.
8. D. E. Fjare, J. A. Jensen and W. L. Gladfelter, *Inorg. Chem.* 1983, **22**, 1774.
9. G. Beuter and J. Strahle, *Z. Naturfor.* 1989, **44b**, 647.
10. P. Mastropasqua, A. Riemer, H. Kisch and C. Krüger, *J. Organomet. Chem.* 1978, **148**, C40.
11. G. A. Foulds, B. F. G. Johnson and J. Lewis, *J. Organomet. Chem.* 1985, **296**, 147.
12. G. A. Foulds, B. F. G. Johnson and J. Lewis, *J. Organomet. Chem.* 1985, **294**, 123.
13. S. R. Drake and R. Khattar, *Organomet. Synth.* 1988, **4**, 234.
14. B. F. G. Johnson, J. Lewis and D. A. Pippard, *J. Chem. Soc., Dalton Trans.* 1981, 407.
15. M. Tachikawa and J. Shapley, *J. Organomet. Chem.* 1977, **124**, C19.
16. P. M. Lausarot, M. Turini, G. A. Vaglio, M. Valle, A. Tiripicchio, M. T. Camellini and P. Garibaldi, *J. Organomet. Chem.* 1984, **273**, 239.
17. P. M. Lausarot, G. A. Vaglio, M. Valle, A. Tiripicchio and M. T. Camellini, *J. Chem. Soc., Chem. Commun.* 1983, 1391.
18. P. M. Lausarot, L. Operti, G. A. Vaglio, M. Valle, A. Tiripicchio, M. T. Camellini and P. Garibaldi, *Inorg. Chim. Acta* 1986, **122**, 103.
19. P. Benzi, P. M. Lausarot, L. Operti, G. A. Vaglio and M. Valle, *Gazz. Chim. Ital.* 1988, **118**, 837.
20. W. Bernhardt and H. Vahrenkamp, *Angew. Chem.* 1984, **96**, 362; *Angew. Chem., Int. Edn. Engl.* 1984, **23**, 381.
21. W. Bernhardt, C. von Schnering and H. Vahrenkamp, *Angew. Chem.* 1986, **98**, 285; *Angew. Chem., Int. Edn. Engl.* 1986, **25**, 279.
22. W. Bernhardt and H. Vahrenkamp, *Z. Naturfor.* 1988, **43b**, 643.
23. B. F. G. Johnson, J. Lewis, J. N. Nicholls, I. A. Oxton, P. R. Raithby and M. J. Rosales, *J. Chem. Soc., Chem. Commun.* 1982, 289.
24. B. F. G. Johnson, J. Lewis, J. N. Nicholls, J. Puga, P. R. Raithby, M. J. Rosales, M. McPartlin and W. Clegg, *J. Chem. Soc., Dalton Trans.* 1983, 277.
25. R. Szostak, C. E. Strouse and H. D. Kaesz, *J. Organomet. Chem.* 1980, **191**, 243.
26. H. D. Kaesz, C. B. Knobler, M. A. Andrews, G. van Buskirk, R. Szostak, C. E. Strouse, Y. C. Lin and A. Mayr, *Pure Appl. Chem.* 1982, **54**, 131.
27. H. D. Kaesz, *J. Organomet. Chem.* 1990, **383**, 413.
28. A. Mayr, Y. C. Lin, N. M. Boag and H. D. Kaesz, *Inorg. Chem.* 1982, **21**, 1704.
29. A. Mayr, Y. C. Lin, N. M. Boag, C. E. Kampe, C. B. Knobler and H. D. Kaesz, *Inorg. Chem.* 1984, **23**, 4640.
30. N. M. Boag, C. B. Knobler and H. D. Kaesz, *Angew. Chem.* 1983, **95**, 243; *Angew. Chem., Int. Edn. Engl.* 1983, **22**, 249.
31. N. M. Boag, W. J. Sieber, C. E. Kampe, C. B. Knobler and H. D. Kaesz, *J. Organomet. Chem.* 1988, **355**, 385.
32. H. D. Kaesz, U. Krone-Schmidt, U. Siber, N. M. Boag and S. B. Nobler, *Mezhdunar. Simp. Suyazi Gomogennym Geterog. Katal. 5th* 1986, **3**, 57; *Chem. Abstr.* 1988, **108**, 150669n.
33. H. D. Kaesz, Z. Xue, Y. Chen, C. B. Knobler, W. Krone-Schmidt, W. J. Sieber and N. M. Boag, *Pure Appl. Chem.* 1988, **60**, 1245.
34. G. Süss-Fink, T. Jenke, H. Heitz, M. A. Pellinghelli and A. Tiripicchio, *J. Organomet. Chem.* 1989, **379**, 311.
35. C. M. Jensen and H. D. Kaesz, *J. Organomet. Chem.* 1987, **330**, 133.
36. H. D. Kaesz and C. M. Jensen, *Polyhedron* 1988, **7**, 1035.
37. R. D. Adams and J. E. Babin, *Inorg. Chem.* 1986, **25**, 4010.
38. J. B. Keister and T. L. Horling, *Inorg. Chem.* 1980, **19**, 2304.
39. D. M. Dalton, D. J. Barnett, T. P. Duggan, J. B. Keister, P. T. Malik, S. P. Modi, M. R. Schaffer and S. A. Smesko, *Organometallics* 1985, **4**, 1854.
40. M. R. Churchill, J. C. Fettinger and J. B. Keister, *Organometallics* 1985, **4**, 1867.
41. R. D. Adams, J. E. Babin and J. Tanner, *Organometallics* 1988, **7**, 765.
42. R. D. Adams, J. E. Babin and J. T. Tanner, *Organometallics* 1988, **7**, 2027.
43. S. Aime, R. Gobetto, F. Padovan, M. Botta, E. Rosenberg and R. W. Gellert, *Organometallics* 1987, **6**, 2074.
44. E. Sappa and L. Milone, *J. Organomet. Chem.* 1973, **61**, 383.
45. S. Bhaduri, H. Khwaja and P. G. Jones, *J. Chem. Soc., Chem. Commun.* 1988, 194.
46. J. A. Cabeza, V. Riera, M. A. Pellinghelli and A. Tiripicchio, *J. Organomet. Chem.* 1989, **376**, C23.
47. M. Yamashita, K. Mizushima, Y. Watanabe, T.-A. Mitsudo and Y. Takegami, *J. Chem. Soc., Chem. Commun.* 1976, 670.
48. H. A. Dieck, R. N. Laine and R. F. Heck, *J. Org. Chem.* 1975, **40**, 2819.
49. H. Alper and H.-N. Paik, *Nouv. J. Chim.* 1978, **2**, 245.
50. H. des Abbayes and H. Alper, *J. Am. Chem. Soc.* 1977, **99**, 98.

51. A. F. M. Iqbal, *J. Org. Chem.* 1972, **37**, 2791.
52. S. Cenini, C. Crotti, M. Pizzotti and F. Porta, *J. Org. Chem.* 1988, **53**, 1243.
53. A. J. Kunin, M. D. Noirot and W. L. Gladfelter, *J. Am. Chem. Soc.* 1989, **111**, 2739.
54. S. Cenini, M. Pizzotti, C. Crotti, F. Porta and G. La Monica, *J. Chem. Soc., Chem. Commun.* 1984, 1286.
55. Yu. A. Belousov and T. A. Kolosova, *Polyhedron* 1987, **6**, 1959.
56. S. Bhaduri, K. S. Gopalkrishnan, G. M. Sheldrick, W. Clegg and D. Stalke, *J. Chem. Soc., Dalton Trans.* 1983, 2339.
57. W. Clegg, G. M. Sheldrick, D. Stalke, S. Bhaduri and K. S. Gopalkrishnan, *Acta Cryst.* 1984, **40C**, 927.
58. F. L'Eplattenier, P. Matthys and F. Calderazzo, *Inorg. Chem.* 1970, **9**, 342.
59. A. Basu, S. Bhaduri, H. Khwaja, P. Jones, K. Meyer-Bäse and G. M. Sheldrick, *J. Chem. Soc., Dalton Trans.* 1986, 2501.
60. H. Alper and K. E. Hashem, *J. Am. Chem. Soc.* 1981, **103**, 6514.
61. S. Bhaduri, H. Khwaja, K. Sharma and P. G. Jones, *J. Chem. Soc., Chem. Commun.* 1989, 515.
62. S. Cenini, M. Pizzotti, C. Crotti, F. Porta and G. La Monica, *J. Chem. Soc., Chem. Commun.* 1984, 1286.
63. S.-H. Han, G. L. Geoffroy and A. L. Rheingold, *Inorg. Chem.* 1987, **26**, 3426.
64. S.-H. Han and G. L. Geoffroy, *Polyhedron* 1988, **7**, 2331.
65. S. Cenini, M. Pizzotti, C. Crotti, F. Ragaini and F. Porta, *J. Molec. Catal.* 1988, **49**, 59.
66. J. A. Smieja and W. L. Gladfelter, *Inorg. Chem.* 1986, **25**, 2667.
67. M. J. McGlinchey and F. G. A. Stone, *J. Chem. Soc., Chem. Commun.* 1970, 1265.
68. E. W. Abel, T. Blackmore and R. J. Whitley, *Inorg. Nucl. Chem. Lett.* 1974, **10**, 941.
69. M. I. Bruce, M. Z. Iqbal and F. G. A. Stone, *J. Organomet. Chem.* 1971, **31**, 275.
70. M. I. Bruce, M. G. Humphrey, O. bin Shawkataly, M. R. Snow and E. R. T. Tiekink, *J. Organomet. Chem.* 1987, **336**, 199.
71. E. J. Wucherer, M. Tasi, B. Hansert, A. K. Powell, M.-T. Garland, J.-F. Halet, J.-Y. Saillard and H. Vahrenkamp, *Inorg. Chem.* 1989, **28**, 3564.
72. M. M. Bagga, P. L. Pauson, F. J. Preston and R. I. Reed, *J. Chem. Soc., Chem. Commun.* 1965, 543.
73. M. M. Bagga, W. T. Flannigan, G. R. Knox, P. L. Pauson, F. J. Preston and R. I. Reed, *J. Chem. Soc. C* 1968, 36.
74. F. W. B. Einstein, S. Nussbaum, D. Sutton and A. C. Willis, *Organometallics* 1983, **2**, 1259.
75. F. W. B. Einstein, S. Nussbaum, D. Sutton and A. C. Willis, *Organometallics* 1984, **3**, 568.
76. S.-H. Han, J.-S. Song, P. D. Macklin, S. T. Nguyen, G. L. Geoffroy and A. L. Rheingold, *Organometallics* 1989, **8**, 2127.
77. J. A. Smieja, J. E. Gozum and W. L. Gladfelter, *Organometallics* 1987, **6**, 1311.
78. S. Bhaduri, K. S. Gopalkrishnan, W. Clegg, P. G. Jones, G. M. Sheldrick and D. Stalke, *J. Chem. Soc., Dalton Trans.* 1984, 1765.
79. J. A. Smieja, J. E. Gozum and W. L. Gladfelter, *Organometallics* 1986, **5**, 2154.
80. M. Pizzotti, F. Porta, S. Cenini and F. Demartin, *J. Organomet. Chem.* 1988, **356**, 105.
81. A. Basu, S. Bhaduri and H. Khwaja, *J. Organomet. Chem.* 1987, **319**, C28.
82. P. Mastropasqua, P. Lahuerta, K. Hildenbrand and H. Kisch, *J. Organomet. Chem.* 1980, **172**, 57.
83. M. N. Ackerman, D. E. Adams, J. Pranate and C. F. Yamauchi, *J. Organomet. Chem.* 1989, **369**, 55.
84. H. Bantel, B. Hansert, A. K. Powell, M. Tasi and H. Vahrenkamp, *Angew. Chem.* 1989, **101**, 1084; *Angew. Chem., Int. Edn. Engl.* 1989, **28**, 1059.
85. A. Basu, S. Bhaduri, K. Sharma and P. G. Jones, *J. Chem. Soc., Chem. Commun.* 1987, 1126.
86. Y. Chi, D.-K. Hwang, S.-F. Chen and L.-K. Liu, *J. Chem. Soc., Chem. Commun.* 1989, 1540.
87. S.-H. Han, S. T. Nguyen, G. L. Geoffroy and A. L. Rheingold, *Organometallics* 1988, **7**, 2034.
88. S.-H. Han, G. L. Geoffroy and A. L. Rheingold, *Organometallics* 1986, **5**, 2561.
89. S.-H. Han, G. L. Geoffroy and A. L. Rheingold, *Organometallics* 1987, **6**, 2380.
90. M. Pizzoti, S. Cenini, C. Crotti and F. Demartin, *J. Organomet. Chem.* 1989, **375**, 123.
91. M. I. Bruce, P. A. Humphrey and E. R. T. Tiekink, unpublished results.
92. K. Vrieze and G. van Koten, *Inorg. Chim. Acta* 1985, **100**, 79.
93. K. Vrieze, *J. Organomet. Chem.* 1986, **300**, 307.
94. K. Vrieze, G. van Koten and L. H. Staal, *Inorg. Chim. Acta* 1982, **62**, 23.
95. G. van Koten and K. Vrieze, *Adv. Organomet. Chem.* 1982, **21**, 151.
96. L. H. Polm, W. P. Mul, C. J. Elsevier, K. Vrieze, M. J. N. Christophersen and C. H. Stam, *Organometallics* 1988, **7**, 423.
97. W. P. Mul, C. J. Elsevier, K. Vrieze, W. J. J. Smeets and A. L. Spek, *Recl. Trav. Chim. Pays-Bas* 1988, **107**, 297.
98. L. H. Polm, C. J. Elsevier, W. P. Mul, K. Vrieze, M. J. N. Christophersen, F. Muller and C. H. Stam, *Polyhedron* 1988, **7**, 2521.

99. L. H. Staal, L. H. Polm, R. W. Balk, G. van Koten, K. Vrieze and A. M. F. Brouwers, *Inorg. Chem.* 1980, **19**, 3343.
100. L. H. Staal, L. H. Polm, K. Vrieze, F. Ploeger and C. H. Stam, *Inorg. Chem.* 1981, **20**, 3590.
101. C. H. Gast, J. C. Kraak, L. H. Staal and K. Vrieze, *J. Organomet. Chem.* 1981, **208**, 225.
102. C. J. Elsevier, F. Muller, K. Vrieze and R. Zoet, *Nouv. J. Chim.* 1988, **12**, 571.
103. L. H. Staal, L. H. Polm, K. Vrieze, F. Ploeger and C. H. Stam, *J. Organomet. Chem.* 1980, **199**, C13.
104. F. Muller, G. van Koten, K. Vrieze and D. Heijdenrijk, *Inorg. Chim. Acta* 1989, **158**, 69.
105. F. Muller, G. van Koten, M. J. A. Kraakman, K. Vrieze, D. Heijdenrijk and M. C. Zoutberg, *Organometallics* 1989, **8**, 1331.
106. F. Muller, D. I. P. Dijkhuis, G. van Koten, K. Vrieze, D. Heijdenrijk, M. A. Rotteveel, C. H. Stam and M. C. Zoutberg, *Organometallics* 1989, **8**, 992.
107. J. Keijsper, L. Polm, G. van Koten, K. Vrieze, G. Abbel and C. H. Stam, *Inorg. Chem.* 1984, **23**, 2142.
108. M. Casarin, A. Vittadini, K. Vrieze, F. Muller, G. Granozzi and R. Bertoncello, *J. Am. Chem. Soc.* 1988, **110**, 1775.
109. J. Keijsper, L. H. Polm, G. van Koten, K. Vrieze, P. F. A. B. Seignette and C. H. Stam, *Inorg. Chem.* 1985, **24**, 518.
110. J. Keijsper, L. H. Polm, G. van Koten, K. Vrieze, K. Goubitz and C. H. Stam, *Organometallics* 1985, **4**, 1876.
111. J. Keijsper, L. H. Polm, G. van Koten, K. Vrieze, E. Nielsen and C. H. Stam, *Organometallics* 1985, **4**, 2006.
112. L. H. Polm, G. van Koten, C. J. Elsevier, K. Vrieze, B. F. K. van Sonten and C. H. Stam, *J. Organomet. Chem.* 1986, **304**, 353.
113. L. H. Polm, C. J. Elsevier, G. van Koten, J. M. Ernsting, D. J. Stufkens, K. Vrieze, R. R. Andréa and C. H. Stam, *Organometallics* 1987, **6**, 1096.
114. F. Muller, G. van Koten, L. H. Polm, K. Vrieze, M. C. Zoutberg, D. Heijdenrijk, E. Kragten and C. H. Stam, *Organometallics* 1989, **8**, 1340.
115. M. I. Bruce, M. G. Humphrey, M. R. Snow, E. R. T. Tiekink and R. C. Wallis, *J. Organomet. Chem.* 1986, **314**, 311.
116. A. Eisenstadt, C. M. Giandomenico, M. F. Frederick and R. M. Laine, *Organometallics* 1985, **4**, 2033.
117. G. Conole, M. McPartlin, H. R. Powell, T. Dutton, B. F. G. Johnson and J. Lewis, *J. Organomet. Chem.* 1989, **379**, C1.
118. T. Venäläinen, T. A. Pakkanen, T. T. Pakkanen and E. Iiskola, *J. Organomet. Chem.* 1986, **314**, C49.
119. T. Venäläinen, J. Pursiainen and T. Pakkanen, *J. Chem. Soc., Chem. Commun.* 1985, 1348.
120. A. J. Deeming, R. Peters, M. B. Hursthouse and J. D. J. Backer-Dirks, *J. Chem. Soc., Dalton Trans.* 1982, 787.
121. J. A. Cabeza, L. A. Oro, A. Tiripicchio and M. Tiripicchio Camellini, *J. Chem. Soc., Dalton Trans.* 1988, 1437.
122. R. H. Fish, T.-J. Kim, J. L. Stewart, J. H. Bushweller, R. K. Rosen and J. W. Dupon, *Organometallics* 1986, **5**, 2193.
123. P. L. Andreu, J. A. Cabeza, V. Riera, Y. Jeannin and D. Miguel, *J. Chem. Soc., Dalton Trans.* 1990, 2201.
124. P. L. Andreu, J. A. Cabeza, V. Riera, C. Bois and Y. Jeannin, *J. Organomet. Chem.* 1990, **384**, C25.
125. P. L. Andreu, J. A. Cabeza, J. M. Fernandez-Colinas and V. Riera, *J. Chem. Soc., Dalton Trans.* 1990, 2927.
126. A. J. Deeming, M. Karim, N. I. Powell and K. I. Hardcastle, *Polyhedron* 1990, **9**, 623.
127. A. J. Deeming, M. Karim and K. I. Hardcastle, unpublished results, cited in ref. 126.
128. J. A. van Doorn and P. W. N. M. van Leeuwen, *J. Organomet. Chem.* 1981, **222**, 299.
129. F. A. Cotton and J. D. Jamerson, *J. Am. Chem. Soc.* 1976, **98**, 5396.
130. F. A. Cotton, B. E. Hanson and J. D. Jamerson, *J. Am. Chem. Soc.* 1977, **99**, 6588.
131. P. Mastropasqua, P. Lahuerta, K. Hildenbrand and H. Kisch, *J. Organomet. Chem.* 1979, **172**, 57.
132. M. A. Pellinghelli, A. Tiripicchio, J. A. Cabeza and L. A. Oro, *J. Chem. Soc., Dalton Trans.* 1990, 1509.
133. A. J. Carty, G. Kan, D. P. Madden, V. Sniekus and M. Stanton, *J. Organomet. Chem.* 1971, **32**, 241.
134. D. P. Madden, A. J. Carty and T. Birchall, *Inorg. Chem.* 1972, **11**, 1453.
135. A. Maisonnat, J. P. Farr, M. M. Olmstead, C. T. Hunt and A. L. Balch, *Inorg. Chem.* 1982, **21**, 3961.
136. N. Lugan, G. Lavigne and J.-J. Bonnet, *Inorg. Chem.* 1986, **25**, 7.
137. N. Lugan, G. Lavigne and J.-J. Bonnet, *Inorg. Chem.* 1987, **26**, 585.
138. N. Lugan, G. Lavigne, J.-J. Bonnet, R. Réan, D. Neilbecker and I. Tkatchenko, *J. Am. Chem. Soc.* 1988, **110**, 5369.
139. S. Jeannin, Y. Jeannin and G. Lavigne, *Inorg. Chem.* 1978, **17**, 2103.
140. S. Jeannin, Y. Jeannin and G. Lavigne, *Transition Met. Chem.* 1976, **1**, 186, 192.
141. J. R. Norton, J. P. Collman, G. Dolcetti and W. T. Robinson, *Inorg. Chem.* 1972, **11**, 382.

142. J. R. Norton and G. Dolcetti, *Inorg. Synth.* 1976, **16**, 39.
143. J. P. Attard, B. F. G. Johnson, J. Lewis, J. M. Mace and P. R. Raithby, *J. Chem. Soc., Chem. Commun.* 1985, 1526.
144. J. R. Norton and J. P. Collman, *Inorg. Chem.* 1973, **12**, 476.
145. B. F. G. Johnson, P. R. Raithby and C. Zuccaro, *J. Chem. Soc., Dalton Trans.* 1980, 99.
146. R. E. Stevens, T. J. Yanta and W. L. Gladfelter, *J. Am. Chem. Soc.* 1981, **103**, 4981.
147. R. E. Stevens and W. L. Gladfelter, *Inorg. Chem.* 1983, **22**, 2034.
148. B. F. G. Johnson, J. Lewis and J. M. Mace, *J. Chem. Soc., Chem. Commun.* 1984, 186.
149. J. A. Smieja, R. E. Stevens, D. E. Fjare and W. L. Gladfelter, *Inorg. Chem.* 1985, **24**, 3206.
150. R. E. Stevens and W. L. Gladfelter, *J. Am. Chem. Soc.* 1982, **104**, 6454.
151. R. E. Stevens, D. E. Fjare and W. L. Gladfelter, *J. Organomet. Chem.* 1988, **347**, 373.
152. M. P. Gomez-Sal, B. F. G. Johnson, J. Lewis, P. R. Raithby and S. N. A. B. Syed-Mustaffa, *J. Organomet. Chem.* 1984, **272**, C21.
153. D. E. Fjare and W. L. Gladfelter, *J. Am. Chem. Soc.* 1984, **106**, 4799.
154. B. F. G. Johnson, J. Lewis, W. J. H. Nelson, J. Puga, P. R. Raithby, D. Braga, M. McPartlin and W. Clegg, *J. Organomet. Chem.* 1983, **243**, C13.
155. B. F. G. Johnson, J. Lewis, W. J. H. Nelson, J. Puga, M. McPartlin and A. Sironi, *J. Organomet. Chem.* 1983, **253**, C5.
156. W. L. Galdfelter, *Adv. Organomet. Chem.* 1985, **24**, 41.
157. W. L. Gladfelter, in *Organometallic Compounds* (Edited by B. L. Shapiro), p. 281. Texas A&M Press, U.S.A. (1983).
158. M. L. Blohm and W. L. Gladfelter, *Organometallics* 1985, **4**, 45.
159. M. L. Blohm, D. E. Fjare and W. L. Gladfelter, *J. Am. Chem. Soc.* 1986, **108**, 2301.
160. M. L. Blohm, D. E. Fjare and W. L. Gladfelter, *Inorg. Chem.* 1983, **22**, 1004.
161. S. Harris, M. L. Blohm and W. L. Gladfelter, *Inorg. Chem.* 1989, **28**, 2290.
162. C. E. Anson, J. P. Attard, B. F. G. Johnson, J. Lewis, J. M. Mace and D. B. Powell, *J. Chem. Soc., Chem. Commun.* 1986, 1715.
163. M. L. Blohm and W. L. Gladfelter, *Inorg. Chem.* 1987, **26**, 459.
164. D. E. Fjare, D. G. Keyes and W. L. Gladfelter, *J. Organomet. Chem.* 1983, **250**, 383.
165. M. L. Blohm and W. L. Gladfelter, *Organometallics* 1986, **5**, 1049.
166. A. L. Rheingold, D. L. Staley, S.-H. Han and G. L. Geoffroy, *Acta Cryst.* 1988, **44C**, 570.
167. D. Braga, B. F. G. Johnson, J. Lewis, J. M. Mace, M. McPartlin, J. Puga, W. J. H. Nelson, P. R. Raithby and K. H. Whitmire, *J. Chem. Soc., Chem. Commun.* 1982, 1081.
168. M. A. Collins, B. F. G. Johnson, J. Lewis, J. M. Mace, J. Morris, M. McPartlin, W. J. H. Nelson, J. Puga and P. R. Raithby, *J. Chem. Soc., Chem. Commun.* 1983, 689.
169. M. I. Bruce, M. L. Williams, B. W. Skelton and A. H. White, *J. Organomet. Chem.* 1986, **309**, 157.
170. D. Nucciarone, N. J. Taylor and A. J. Carty, *Organometallics* 1986, **5**, 2565.
171. M. Herberhold, K. Schamel, G. Hermann, A. Gieren, C. Ruiz-Perez and T. Hübner, *Z. Anorg. Allg. Chem.* 1988, **562**, 49.
172. J. G. Bentsen and M. S. Wrighton, *J. Am. Chem. Soc.* 1987, **109**, 4530.
173. M. I. Bruce, J. G. Matisons, J. R. Rodgers and R. C. Wallis, *J. Chem. Soc., Chem. Commun.* 1981, 1070.
174. R. D. Adams, P. Mathur and B. E. Segmüller, *Organometallics* 1983, **2**, 1258.
175. F. Calderazzo, C. Floriani, R. Henzi and F. L'Eplattenier, *J. Chem. Soc. A*, 1969, 1378.
176. N. Farrell, M. N. de Oliveira Bastus and A. A. Neves, *Polyhedron* 1983, **2**, 1243.
177. R. L. Bennett, M. I. Bruce, B. L. Goodall, M. Z. Iqbal and F. G. A. Stone, *J. Chem. Soc., Dalton Trans.* 1972, 1787.
178. S. F. Colsen, S. D. Robinson, M. Motevalli and M. B. Hursthouse, *Polyhedron* 1988, **7**, 1919.
179. S. F. Colson, S. D. Robinson and D. A. Tocher, *J. Chem. Soc., Dalton Trans.* 1990, 629.
180. M. I. Bruce, B. L. Goodall and F. G. A. Stone, *J. Organomet. Chem.* 1973, **60**, 343.
181. J. M. Patrick, A. H. White, M. I. Bruce, M. J. Beatson, D. St C. Black, G. B. Deacon and N. C. Thomas, *J. Chem. Soc., Dalton Trans.* 1983, 2121.
182. J. A. Cabeza, C. Landazuri, L. A. Oro, A. Tiripicchio and M. Tiripicchio Camellini, *J. Organomet. Chem.* 1987, **322**, C16.
183. J. A. Cabeza, C. Landazuri, L. A. Oro, D. Belletti, A. Tiripicchio and M. Tiripicchio Camellini, *J. Chem. Soc., Dalton Trans.* 1989, 1093.
184. F. Neumann and G. Süss-Fink, *J. Organomet. Chem.* 1989, **367**, 175.
185. F. Neumann, H. Stoeckli-Evans and G. Süss-Fink, *J. Organomet. Chem.* 1989, **379**, 151.
186. M. I. Bruce, D. N. Sharrocks and F. G. A. Stone, *J. Organomet. Chem.* 1971, **31**, 269.
187. J.-J. Bonnet, S. S. Eaton, G. R. Eaton, R. W. Holm and J. A. Ibers, *J. Am. Chem. Soc.* 1973, **95**, 2141.
188. D. Cullen, E. Meyer, T. Srivostava and M. Tsutsui, *J. Chem. Soc., Chem. Commun.* 1972, 584.
189. Y.-W. Chan, M. W. Renner and A. L. Balch, *Organometallics* 1983, **2**, 1888.

190. Y.-W. Chan, F. E. Wood, M. W. Renner, H. Hope and A. L. Balch, *J. Am. Chem. Soc.* 1984, **106**, 3380.
191. A. L. Balch, Y.-W. Chan, M. M. Olmstead, M. W. Renner and F. E. Wood, *J. Am. Chem. Soc.* 1988, **110**, 3897.
192. N. P. Farrell, A. J. Murray, J. R. Thornback, D. H. Dolphin and B. R. James, *Inorg. Chim. Acta* 1978, **28**, L144.
193. S. Omiya, M. Tsutsui, E. F. Meyer, I. Bernal and D. L. Cullen, *Inorg. Chem.* 1980, **19**, 134.
194. P. L. Andreu, J. A. Cabeza, V. Riera, F. Robert and Y. Jeannin, *J. Organomet. Chem.* 1989, **372**, C15.
195. A. Gieren, T. Hübner, J. Wu, M. Herberhold and W. Bühlmeyer, *J. Organomet. Chem.* 1987, **329**, 105.
196. T. J. Kealy and R. E. Benson, *J. Org. Chem.* 1961, **26**, 3126.
197. G. L. Rempel, W. K. Teo, B. R. James and D. V. Plackett, *Adv. Chem. Ser.* 1974, **132**, 166.
198. Y. Tsuji, T. Ohsumi, T. Kondo and Y. Watanabe, *J. Organomet. Chem.* 1986, **309**, 333.
199. G. Süss-Fink, M. Langenbahn and T. Jenke, *J. Organomet. Chem.* 1989, **368**, 103.
200. E. J. Moore, T. J. O'Connell and J. Harris, Amoco/University Poster Session, Amoco Research Center, Naperville, Illinois (October 1989); Poster C33.
201. G. Menchi, U. Matteoli, A. Scrivanti, S. Paganelli and C. Botteghi, *J. Organomet. Chem.* 1988, **354**, 215.
202. G. F. Schmidt and G. Süss-Fink, *J. Organomet. Chem.* 1988, **356**, 207.
203. G. Süss-Fink, G. Hermann and G. F. Schmidt, *Polyhedron* 1988, **7**, 2341.
204. Y. Tsuji, S. Yoshii, T. Ohsumi, T. Kondo and Y. Watanabe, *J. Organomet. Chem.* 1987, **331**, 379.
205. G. Jenner, *J. Molec. Catal.* 1989, **55**, 241.
206. R. M. Laine, *New. J. Chem.* 1987, **11**, 543.

Polyhedron Vol. 10, No. 3, pp. 323–324, 1991
Printed in Great Britain

0277–5387/91 $3.00+.00
© 1991 Pergamon Press plc

MOLYBDENUM(III) COMPLEXES WITH SOME IMIDAZOLES

K. M. PRASAD,* A. N. TRIPATHY and N. M. THAKUR

Department of Chemistry, H. D. Jain College, Arrah—802301, India

(*Received* 22 *August* 1989; *accepted after revision* 1 *August* 1990)

Abstract—The synthesis and characterization of complexes of stoichiometry $[MoL_3X_3]$ (L = imidazole, 2-methylimidazole, benzimidazole or 2-methylbenzimidazole and X = Cl^-, Br^- or NCS^-) are described. The effective magnetic moments (3.68–3.78 BM) are characteristic of octahedral molybdenum(III). The C=N stretching frequency of the ligands shift to higher frequency in the complexes, suggesting that tertiary nitrogen is the active site of coordination of the ligand (L). The ν(CN) and ν(CS) bands of thiocyanate complexes are diagnostic of N-bonded thiocyanate.

As part of a systematic investigation of the synthetic, structural and biological aspects of molybdenum(III) complexes,[1–4] we report here on the complexes of molybdenum(III) with imidazole and its substituted derivatives, as these ligands are common components of several biologically important molecules such as vitamin B_{12} and iron haem. The imidazole moiety plays an extremely crucial role in the structure and functioning of these molecules, generally by virtue of being coordinated to the metal ions. To discover whether the secondary (N_2H) nitrogen or the tertiary (N_3) nitrogen binds metal ions such as molybdenum(III), we investigated the molybdenum(III) complexes with imidazole (IzH), 2-methylimidazole (2-MeIzH), benzimidazole (BzH) and 2-methylbenzimidazole (2-MeBzH) by elemental analyses, conductance, magnetic moment, electronic and IR spectral measurement.

EXPERIMENTAL

Ammonium pentachloroaquomolybdate(III), pentabromoaquomolybdate(III) and ammonium hexaisothiocyanatomolybdate(III) were prepared by the electrolysis of ammonium molybdate in (8 N) HCl, 48% HBr and dil. H_2SO_4, respectively.[5–7] All the preparative work was carried out in a purified dry nitrogen atmosphere. Physicochemical measurements were made as reported in an earlier communication.[3]

Preparation of the complexes

$[Mo(IzH)_3Cl_3]$. $(NH_4)_2[MoCl_5H_2O]$ (approx. 1.0 g) was dissolved in a mixture of water (20 cm^3), HCl (10 cm^3) and methanol (10 cm^3), to which imidazole (0.63 g) dissolved in acetone was added. The pH of the mixture was adjusted to ~ 6 by adding ammonium acetate and the resulting brownish yellow solution was shaken with benzene and an oily layer separated. With the help of a separating funnel, the oily layer was placed in a conical flask, dissolved in methanol and then treated with excess acetone. After filtering, the filtrate was diluted with a large volume of air-free water and $[Mo(IzH)_3Cl_3]$ separated as a yellow compound. This was filtered, washed with 95% ethanol and dried *in vacuo* over KOH–$CaCl_2$.

The other tris-ligated chloro- and bromo-complexes were prepared by an analogous procedure. The complexes $[MoL_3(NCS)_3]$ (L = IzH, 2MeIzH, BzH or 2MeBzH) were prepared by the interaction of an ethanolic solution of the ligands (L) with an ethanolic solution of $(NH_4)_3[Mo(NCS)_6]$ in a 3:1 molar ratio under nitrogen. Analytical data are presented in Table 1.

RESULTS AND DISCUSSION

All the complexes $[MoL_3X_3]$ are stable in air and their methanolic solutions were almost non-

* Author to whom correspondence should be addressed.

Table 1. Analytical data[a]

Complex	Colour	μ_{eff} (BM) at *ca* 300 K	λ_{max} (cm^{-1})	Found (%)			Calculated (%)		
				Mo	N	Cl/Br	Mo	N	Cl/Br
$[Mo(IzH)_3Cl_3]$	Yellow	3.76	25,316 (25,641) (ε_{max} = 2790)	23.6	20.9	26.2	23.6	20.9	26.2
$[Mo(2\text{-}MeIzH)_3Cl_3]$	Yellow	3.78	24,390 — —	21.4	18.8	23.7	21.4	18.7	23.7
$[Mo(BzH)_3Cl_3]$	Yellow	3.75	25,773 — —	17.3	15.1	19.1	17.2	15.1	19.1
$[Mo(2\text{-}MeBzH)_3Cl_3]$	Yellow	3.74	26,316 — —	16.0	14.1	17.8	16.0	14.0	17.8
$[Mo(IzH)_3Br_3]$	Yellow	3.77	26,042 — —	17.8	15.6	44.6	17.7	15.5	44.4
$[Mo(2\text{-}MeIzH)_3Br_3]$	Yellow	3.76	25,063 (25,510) (ε_{max} = 3120)	16.5	14.4	41.3	16.5	14.4	41.3
$[Mo(BzH)_3Br_3]$	Yellow	3.68	26,247 — —	13.8	12.2	34.8	13.9	12.2	34.8
$[Mo(2\text{-}MeBzH)_3Br_3]$	Yellow	3.75	26,385 — —	13.2	11.5	33.1	13.1	11.5	32.8
$[Mo(IzH)_3(NCS)_3]$	Deep yellow	3.75	24,691 (24,390) (ε_{max} = 2980)	20.3	26.6	—	20.2	26.6	—
$[Mo(2\text{-}MeIzH)_3(NCS)_3]$	Deep yellow	3.78	24,510 — —	18.6	24.5	—	18.6	24.4	—
$[Mo(BzH)_3(NCS)_3]$	Deep yellow	3.69	24,390 (24,570) (ε_{max} = 2860)	15.4	20.2	—	15.4	20.2	—
$[Mo(2\text{-}MeBzH)_3(NCS)_3]$	Deep yellow	3.72	24,450 — —	14.4	18.8	—	14.4	18.9	—

[a] The band positions within parentheses are in chloroform.

conducting, indicating their non-ionic nature. The effective magnetic moment values of the complexes at room temperature are in the range 3.68–3.78 BM (Table 1), as expected for the spin-only value for a t^3_{2g} configuration,[8,9] suggesting an octahedral arrangement of the ligands around the molybdenum(III) ion. While the pentachloroaquomolybdate(III) and pentabromoaquomolybdate(III) exhibit three *d–d* transitions,[1] $[MoL_3X_3]$ complexes exhibit only one absorption band near 24,000–26,000 cm^{-1}. This has been attributed to the charge-transfer transition which masks the *d–d* transitions of molybdenum(III) in these complexes, as commonly observed with heterocyclic N-donor ligands.[2]

The IR spectra of ammonium hexaisothiocyanatomolybdate(III) has been reported in an earlier communication.[4] The $[MoL_3(NCS)_3]$ complexes exhibit only one strong C=N stretching band in the range 2070–2080 cm^{-1} and a weak CS stretching band near 810–815 cm^{-1}, which are diagnostic of N-bonded thiocyanate.[4,9] The C=N stretching band of IzH (~ 1580 cm^{-1}) and BzH (~ 1600 cm^{-1}) shift to higher frequency by 30 ± 15 suggesting that tertiary nitrogen is the bonding site of the ligands.[10–14]

Acknowledgement—The authors wish to thank U.G.C., New Delhi for the award of a research project to one of them (K.M.P.).

REFERENCES

1. S. P. Ghosh and K. M. Prasad, *J. Less-common Metals* 1974, **36**, 223.
2. S. P. Ghosh and K. M. Prasad, *Ind. J. Chem.* 1977, **15A**, 630.
3. S. P. Ghosh and K. M. Prasad, *J. Inorg. Nucl. Chem.* 1978, **40**, 1963.
4. S. P. Ghosh and K. M. Prasad, *J. Ind. Chem. Soc.* 1979, **56**, 660.
5. R. J. Irving and M. C. Steele, *Aust. J. Chem.* 1957, **10**, 490.
6. W. Wardlaw and A. J. I. Harding, *J. Chem. Soc.* 1926, 1592.
7. W. G. Palmer, *Experimental Inorganic Chemistry*, p. 415. Cambridge University Press, Cambridge (1962).
8. F. A. Cotton and G. Wilkinson, *Advanced Inorganic Chemistry*, p. 953. Interscience, New York (1966).
9. A. Sabatini and I. Bertini, *Inorg. Chem.* 1965, **4**, 959.
10. L. J. Boucher and J. C. Bailar Jr, *J. Inorg. Nucl. Chem.* 1965, **27**, 1093.
11. A. Mishra and J. P. Singh, *J. Inorg. Nucl. Chem.* 1979, **41**, 905.
12. D. M. L. Goodgame and M. Goodgame, *Inorg. Chem.* 1965, **4**, 139.
13. S. P. Ghosh and A. Mishra, *J. Inorg. Nucl. Chem.* 1971, **33**, 4199.
14. S. P. Ghosh, P. Bhattacharjee, L. Dubey and L. K. Mishra, *J. Ind. Chem. Soc.* 1977, **54**, 230.

Polyhedron Vol. 10, No. 3, pp. 325–332, 1991
Printed in Great Britain

0277-5387/91 $3.00+.00
© 1991 Pergamon Press plc

SYNTHESIS, CHARACTERIZATION, ^{113}Cd NMR AND DECOMPOSITION OF SOME CADMIUM THIOLATES

OMAR F. Z. KHAN* and PAUL O'BRIEN†

Department of Chemistry, Queen Mary and Westfield College,
Mile End Road, London E1 4NS, U.K.

(*Received* 18 *July* 1990; *accepted* 5 *September* 1990)

Abstract—The synthesis and characterization of a number of cadmium complexes with sulphur-containing ligands including: 2-mercaptopyridine, 2-mercaptobenzothiazole, 2-mercaptothiazoline, 1,4,8,11-tetrathiaundecane, 5-mercapto-1-methyltetrazole and dithiocarbamates are reported. ^{113}Cd solid-state NMR spectroscopy has been used to characterize several of the compounds and many of the complexes decompose to cadmium sulphide.

In this paper we report further studies of some thiolates of cadmium, work which is related to our recently published X-ray crystal structures[1] of the bis(mercaptobenzothioazole) and bis(2-mercaptopyridinato) complexes of cadmium. There is considerable current interest in thiolate complexes of cadmium[2–4] and other group 12 metals, which is in part due to the ability of thiolates, in combination with these metals, to form extended zeolitic and/or low-dimensional structures.[2–5] All of the complexes described in the present paper decompose to cadmium sulphide, which may make them of interest in the design of precursors for deposition of cadmium sulphide.

RESULTS AND DISCUSSION

Bis(2-mercaptopyridinato)cadmium(II)

There has been considerable interest in 2-mercaptopyridine (pySH) as a ligand.[6,7] The ligand exists in two tautomeric forms; the thione tautomer (**1**), which is thought to predominate when the ligand is dissolved in methanol or acetone,[8] and the thiol (**2**) tautomer in dilute cyclohexane solutions.[9] In the solid state the ligand exists as a hydrogen-bonded dimer.[10] The zinc complex of pyS^- has been synthesized but has not been fully characterized,[11] and a structure for the mercury complex was reported recently.[5] The cadmium complex $Cd(pyS)_2$ is a white, powdery solid which sublimes at 170°C/10^{-2} torr and is insoluble in most organic solvents, but does dissolve in pyridine and can be recrystallized. The crystal structure shows that coordination at each cadmium is close to octahedral (N_2S_4) with two different ligand coordination modes; one approximately parallel and the other perpendicular to the polymer chain, a packing diagram (not previously published) is shown in Fig. 1.

The compound is a genuine one-dimensional inorganic polymer, with the shorter Cd—S distances forming the chain as detailed in ref. 1. The mercury complex[5] shows a similar polymeric network, but

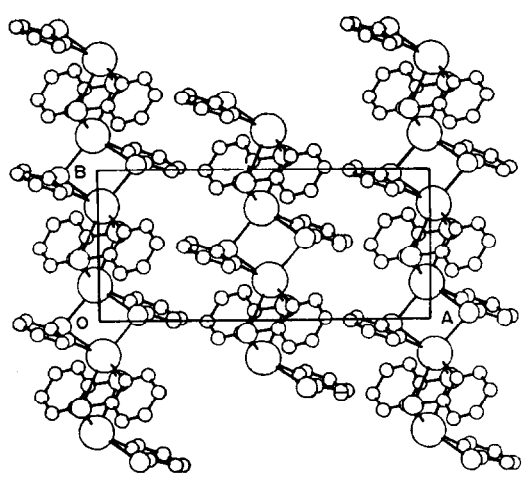

Fig. 1. The packing of the polymeric chains in the pyridine thiolate complex (viewed down *c*).

*Present address: Solid State Chemistry Group, Department of Chemistry, UMIST, PO Box 88, Manchester M60 1QD, U.K.

† Author to whom correspondence should be addressed.

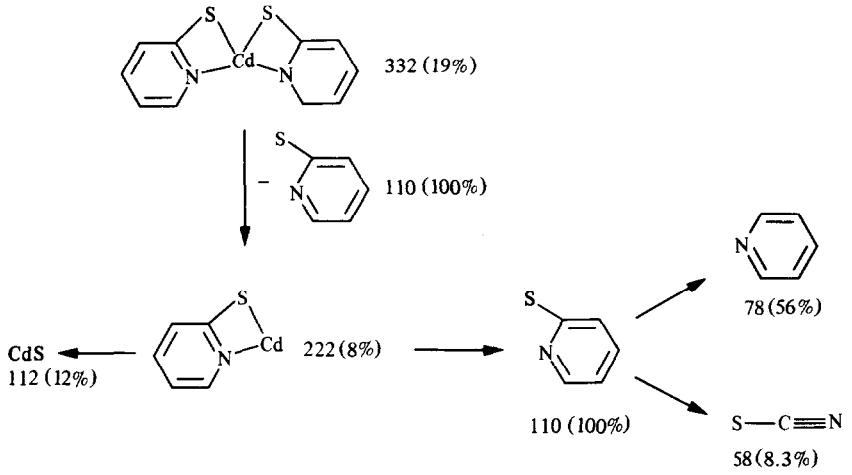

Scheme 1. Partial fragmentation pattern for bis(2-mercaptopyridinato)cadmium(II).

the nitrogen atoms are not coordinated to the metal; the mercury complex is able to coordinate metal ions and we are investigating such reactions of the cadmium complex.

Thermogravimetric analysis, in a stream of air, showed the compound to decompose cleanly to cadmium sulphide at a temperature of 230–500°C (theoretical, 43%; found, 42%). From the X-ray powder diffraction patterns, the cadmium sulphide was found to contain both cubic and hexagonal forms. The mass spectrum of bis(2-mercaptopyridinato)cadmium(II) included the fragmentation pattern shown in Scheme 1. Attempts to obtain a ^{133}Cd solid-state NMR spectrum of $Cd(pyS)_2$ were unsuccessful. This is probably due to the fact that the compound has a long proton relaxation time of *ca* 31 s.

Bis(2-mercaptobenzothiazolato)cadmium(II)

The crystal structure of $[^nBu_4N][Cd(C_7H_4NS_2)_3]$ has been described by McCleverty *et al.*[12] The cadmium atom is six-coordinate, with each $C_7H_4NS_2^-$ (MBZ^-) ligand (**3**) bonded through the exocyclic sulphur atom and the nitrogen atom. The bite angle of the ligand is 62°; the complex has strict C_3 symmetry distorted from trigonal prismatic towards octahedral.

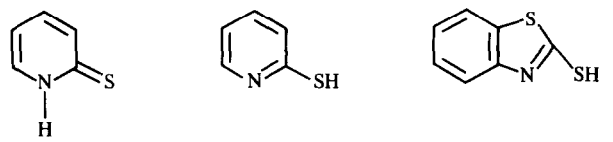

1 **2** **3**

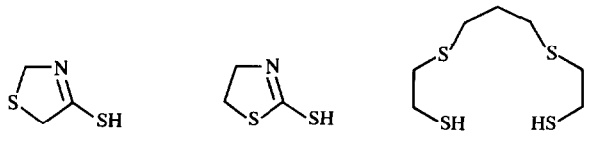

4 **5** **6**

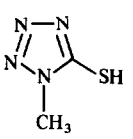

7

Ligands used in this study

(1) 2-Mercaptopyridine (pySH) thione tautomer
(2) 2-Mercaptopyridine (pySH) thiol tautomer
(3) 2-Mercaptobenzothiazole (MBT)
(4) 2-Mercaptothiazoline (MTZ)
(5) 2-Mercaptothiazolidine (TDZ)
(6) 1,4,8,11-tetrathiaundecanato (TTU)
(7) 5-Mercapto-1-methyltetrazole (MTTZ)

The bis-complex of **3** has been investigated using IR spectroscopy by Khullar and Argarwalla[13] and was assumed to be polymeric. It was postulated that the ligand was bound via the exo-sulphur and the endo-nitrogen, and that the endo-sulphur was not involved in coordination to the metal. The coordination at cadmium was thought to be tetrahedral (CdN_2S_2) with bridging ligands. The bis-complex is readily prepared from ethanolic solutions as described in the Experimental and is soluble only in polar solvents such as dimethylformamide.

The structure of the crystalline mercaptothiopyrazole complex[1] is similar to that of the mercaptopyridine complex, with short ligand-to-metal contacts (Cd—N and Cd—S) to different cadmium atoms. Again a genuine one-dimensional polymeric structure is developed, but in this case the ligands take up a helical pattern.[1] The two chelating Cd—S contacts are unusually long, and the cadmium atoms are separated by 3.77 Å, well outside the sum of the van der Waals' radii (3.2 Å). The mode of ligation is very different from the chelate mode shown in the anionic tris-complex.

The above results can be used to interpret spectroscopic studies of this complex and also to comment on the results of an earlier study. The IR spectra of the crystals and the powder are very similar. The strong band at 749 cm^{-1} (which has been assigned to the C=S stretch[13]) has a shoulder for the powder sample, as observed by Khullar and Argarwalla.[13] However, the IR spectrum of the crystalline sample contains a single peak. This small difference is the only change in the IR spectrum (4000–400 cm^{-1}) on recrystallization. The powder obtained on the initial precipitation of $Cd(MBZ)_2$ is microcrystalline and the X-ray powder diffraction pattern of the crude complex and recrystallized compound showed that the former contains many lines not observed for the latter.

The solid-state ^{113}Cd NMR spectrum of $Cd(MBZ)_2$ powder is shown in Fig. 2. The spectrum shows that there are two cadmium sites with chemical shifts of δ 340 and 329 from $Cd(ClO_4)_2$, presumably due to two phases being present in the sample, which is in agreement with the X-ray powder diffraction results (Table 1). The spinning sideband pattern is slightly different for each cadmium atom and the results are summarized in Table 2 and Fig. 3. The solid-state ^{113}Cd NMR spectrum of recrystallized $Cd(MBTZ)_2$ was obtained and is also shown in Fig. 2. A single ^{113}Cd resonance is observed with a chemical shift of δ 325. This is very close to the value of δ 329 obtained for Phase II of the powder. No complexes containing cadmium

Table 1. X-ray powder diffraction results for bis(2-mercaptobenzothiazolato)cadmium(II)

Powder		Crystals	
d-Spacing (Å)	Intensity	*d*-Spacing (Å)	Intensity
6.108	Strong	6.108	Strong
5.906	Medium	Absent	
5.215	Strong	5.215	Strong
4.928	Strong	Absent	
4.040	Medium	Absent	
3.708	Weak	Absent	
3.427	Very weak	Absent	
3.186	Weak	Absent	
3.079	Very weak	3.079	Very weak
2.978	Weak	2.978	Weak
2.796	Medium	Absent	
2.636	Strong	2.636	Strong
2.429	Weak	2.421	Weak
2.368	Weak	Absent	
2.309	Weak	2.338	Weak
2.201	Weak	2.211	Weak
2.151	Weak	2.151	Weak
2.103	Weak	2.112	Weak
2.080	Very weak	Absent	
2.023	Weak	2.014	Weak
1.859	Weak	Absent	
1.859	Weak	1.859	Weak

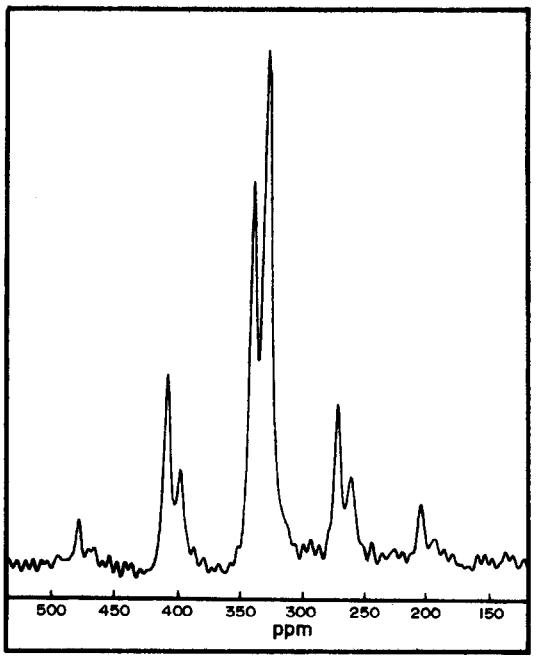

Fig. 2. High resolution solid-state ^{113}Cd NMR spectrum of the initial powder form of bis(2-mercaptobenzothiazolato)cadmium(II).

with the N_2S_4 coordination sphere have previously been studied by ^{113}Cd solid-state NMR spectroscopy.

The mass spectrum of $[Cd(MBZ)_2]_n$ (fw = 444 for monomer) consisted of many peaks, the M^+ peak observed had a mass greater than the parent ion mass. The following fragments were observed: $Cd(MBTZ)_2$, 444 (0.3%); Cd(MBTZ), 228 (0.2%); MBTZ, 116 (29%); C_6H_5NCS, 134 (14%); C_6H_5S, 109 (31%); CdS, 144 (1.9%); Cd, 112 (2.4%); CS_2, 76 (17%); SCN, 58 (24%). Thermogravimetric analysis of the complex in a stream of air showed the compound to decompose cleanly to give cadmium sulphide (theoretical yield: 32.4%; observed yield: 31.2%) at 250–500°C. X-ray powder diffraction of the cadmium sulphide obtained showed the presence of both hexagonal and cubic phases.

Bis(2-*mercaptothiazolinato*)*cadmium*(II)

The cadmium complex of 2-mercaptothiazoline (MTZ, **4**) has not been previously prepared. However, the cadmium complex of a related ligand, 2-mercaptothiazolidine (TDZ, **5**), has been synthesized and investigated by IR spectroscopy.[14] $Cd(MTZ)_2$ is a powdery white solid which is insoluble in common organic solvents; properties which are similar to those reported for $Cd(TDZ)_2$. Inspection of the IR spectrum of $Cd(MTZ)_2$ shows that shifts in the positions of the bands due to the thioamide group from those in the spectrum of the ligand are similar to the shifts reported for $Cd(TDZ)_2$. In particular, the band at 995 cm^{-1} [assigned to $\nu(C{=}N)+\nu(C{=}N)$] in the ligand appears at 976 cm^{-1}, probably indicating bonding through nitrogen and the exo-sulphur. The sulphur atom in the ring does not apparently take part in coordination. The band due to $\nu(C{-}S)$ appears at 650 cm^{-1} in the ligand and is shifted to a higher value of 677 cm^{-1} in the complex. This was also

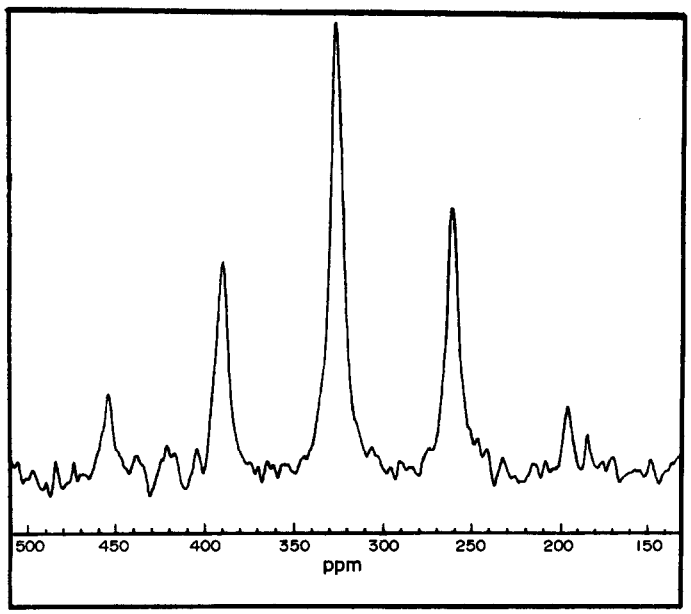

Fig. 3. High resolution solid-state ^{113}Cd NMR spectrum of recrystallized bis(mercaptobenzothiazolato)cadmium(II).

found to be the case with $Cd(TDZ)_2$.[14] The mass spectrum of $Cd(TDZ)_2$ gave a M^+ peak at 266 (3%) which is less than the mass of the parent molecule (fw = 348). The following fragments were also observed: TDZ, 118 (4%); CdS, 144 (19%); Cd, 112 (1%); CH_2CH_2SCN, 86 (23%); CS_2, 76 (24%); CH_3SCN, 73 (11%) 4.9.

1,4,8,11-*tetrathiaundecanatocadmium*(II)

The ligand 1,4,8,11-tetrathiaundecanato (TTU, **6**) was synthesized by following published procedures,[15] the complex CdTTU was prepared by the addition of $CdCl_2$ to a solution of Na_2TTU in ethanol. The elemental analysis showed that the ratio of Cd : TTU was 1 : 1, see Experimental. The cadmium complex is an involatile, white solid which decomposes at temperatures above *ca* 168°C and is insoluble in most common organic solvents. Thermogravimetric analysis showed the complex to decompose to cadmium sulphide and foul smelling products at *ca* 180°C.

The complex has not previously been synthesized. However, the reaction of zinc acetate with TTU in acetone has been reported by Roundhill[16] and yielded $Zn_3(TTU)_2(OAc)_2$.

Bis(5-*mercapto*-1-*methyltetrazolato*)*cadmium*(II)

The reaction, in aqueous solution, of cadmium chloride with the sodium salt of 5-mercapto-1-methyltetrazole (MTTZ, **7**) yields a white, powdery solid which is insoluble in most common organic solvents. Decomposition of the compound at 250–500°C in air yielded gaseous products (**CAUTION** this decomposition can be quite violent!) and a bright yellow solid which was found from X-ray powder diffraction to be a mixture of hexagonal and cubic cadmium sulphide. The ^{113}Cd solid-state NMR spectrum of $Cd(MTTZ)_2$ is detailed in Table 2 and shows a single chemical shift, δ 274 from $Cd(ClO_4)_2$, with spinning side bands; the spectrum is axial ($\sigma_{11} = \sigma_{22} = \sigma_\perp$ and $\sigma_{33} = \sigma_\parallel$) and the anisotropy is $\sigma = 235.5$, results are summarized in Table 2 and Fig. 4. This together with the chemical shift suggests coordination involving distorted S_4 tetrahedral geometry.

Cadmium dithiocarbamates

These are well known compounds and the solid-state ^{113}Cd NMR of bis(diethyldithiocarbamato) cadmium(II) (CdDTC) has been previously reported[17] (from a spectrometer with a 1.4 T magnet equivalent to 60 MHz proton frequency). A chemical shift of δ 377 was observed for the cadmium resonance, which is in good agreement with δ 357 obtained in this study. However, in an earlier paper the chemical shift principal components were not computed and, therefore, their relationship with the coordination at cadmium was not commented on. The structure of CdDTC is dimeric[18] with cadmium bonded to five sulphur atoms in a distorted trigonal bipyramid. The spectrum obtained in this study is shown in Fig. 5 and consists of a central band at δ 357 and a series of spinning side bands that are separated by the spinning frequency of 4.6 kHz. The chemical shift

Table 2. Summary of solid-state ^{113}Cd NMR results

Compound	δ (ppm)	σ_1	σ_2	σ_3	Coordination
Bis(2-*mercaptobenzothiazolato*)*cadmium*(II)					
Powder phase (I)	340	209	350	462	CdN_2S_4?
Phase (II)	329	230	349	408	CdN_2S_4?
Crystals	325	195	313	447	CdN_2S_4 (dist. oct.)
Bis(5-*mercapto*-1-*methyltetrazolato*)*cadmium*(II)					
	274	193	198	431	CdS_4 (tet.?)
Bis(*diethyldithiocarbamato*)*cadmium*(II)					
This work	377	63.4	426	766.7	CdS_5 dimer
Reference 17	357	67	318	745	(p.b.p.)
Bis(*pyrolidinethiocarbamato*)*cadmium*(II)					
	280, 211(imp.)	—	—	—	CdS_4 (reg. tet.)

Abbreviations: p.b.p., pentagonal bipyramidal; tet., tetrahedral; oct., octahedral; reg., regular; dist., distorted.

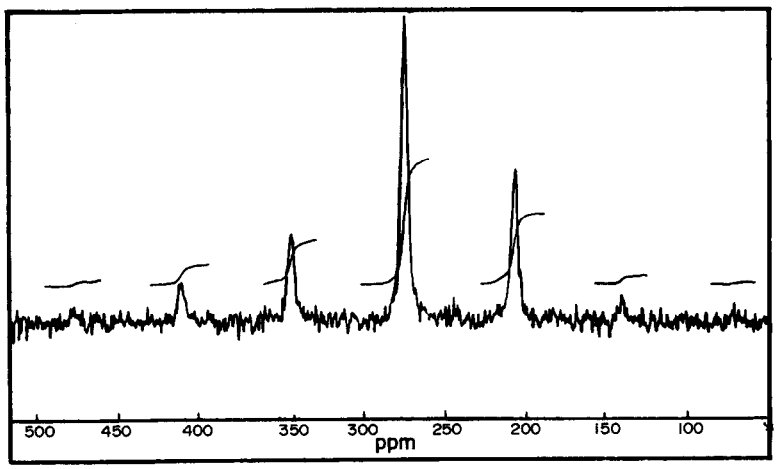

Fig. 4. High resolution solid-state ^{113}Cd NMR spectrum of bis(5-mercapto-1-methyltetrazolato) cadmium(II).

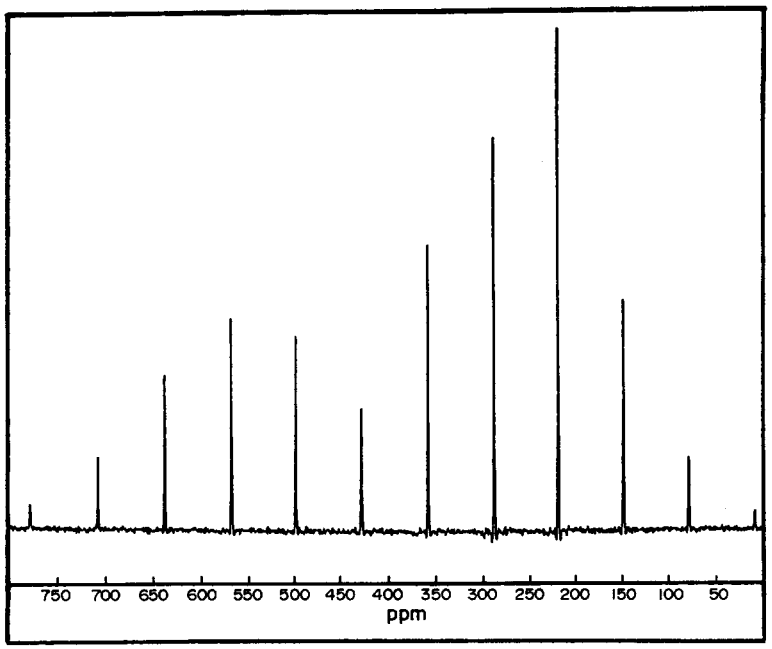

Fig. 5. High resolution solid-state ^{113}Cd NMR spectrum of bis(diethyldithiocarbamato)cadmium(II).

principal components were estimated and are given in Table 2, together with values computed from the line shapes of the spectrum given by Maciel and co-workers.[17] The signal-to-noise ratio in the earlier work was poor, our spectrum has an accuracy of *ca* 110 ppm for each value of the chemical shift component, and considering this there is good agreement between the two spectra.

The solid-state ^{113}Cd NMR spectrum of bis(pyrrolidinedithiocarbamato)cadmium(II), $Cd(PDTC)_2$, is very different from that of $Cd(DTC)_2$. The spectrum, which was obtained at a slower speed of 4.5 kHz, consists of a single peak at δ 280 and a very small peak (probably due to an impurity) at δ 211 (Table 2). The line shape indicates that the coordination around cadmium is highly symmetrical and is probably tetrahedral (S_4) since a trigonal bipyramid (S_5) geometry would lead to an axially symmetric line pattern.

Conclusions

A number of novel complexes of cadmium with sulphur-containing ligands have been prepared, and these complexes decompose to sulphide. ^{113}Cd solid-state NMR has been shown to be a sensitive

and powerful technique for characterizing such compounds.

EXPERIMENTAL

IR spectra in the region 400–200 cm^{-1} were measured using a Mattson Polaris Fourier transform IR spectrometer. Samples were prepared as mulls in Nujol (sodium dried), or as KBr or CsI discs. The following abbreviations are used in the assignment of IR bands: weak, w; medium, m; strong, s; broad, b; shoulder, sh. ^1H NMR spectra were obtained on a Bruker WP80 spectrometer. High resolution solid-state ^{113}Cd NMR were obtained on a Bruker MSL-300 NMR spectrometer with a 7.05 T magnet (equivalent to 300 MHz proton resonance frequency). Magic angle spinning (MAS), cross polarization (CP) and proton decoupling were used for signal enhancement and high resolution. ^{113}Cd chemical shifts were referenced to an external $Cd(ClO_4)_2$ reference. Mass spectra were recorded on an AEI MS902 mass spectrometer equipped with a MSS data system, and operating with an accelerating voltage of 70 eV. Thermogravimetric analysis was carried out with a Stanton Redcroft TG750 at 10°C min^{-1}, in an atmosphere of static air.

Preparation of the complexes

Bis(2-*mercaptopyridinato*)*cadmium*(II)

A solution of cadmium acetate (1 g, 0.037 mol) in water (15 cm^3) was added to a vigorously stirred solution of 2-mercaptopyridine (1.2 g, 0.0075 mol) in ethanol (40 cm^3). A white precipitate formed immediately on addition and was collected by filtration, washed with water and then ethanol, and finally air-dried. Yield obtained: 86%; dec. 324°C. Crystals were obtained by dissolving the complex in hot pyridine and slow evaporation of the hot solvent near its boiling point (*ca* 100°C). Found (Required for $C_{10}H_8N_2S_2Cd$): C, 36.0 (36.1); H, 2.3 (2.4); N, 8.4 (8.4); S, 19.2 (19.2)%. Major IR bands for the powder (Nujol mull) were as follows (cm^{-1}): 2950s, 2920s, 2850s, 1585s, 1542m, 1442s, 1415s, 1375w, 1260w, 1155w, 1135s, 1130s, 1080w, 1040w, 1000m, 770m, 750m, 750s, 720m.

Bis(2-*mercaptobenzothiazolato*)*cadmium*(II)

A solution of cadmium acetate (1 g, 0.037 mol) in water (15 cm^3) was added to a vigorously stirred solution of 2-mercaptobenzothiazole (1.2 g, 0.0075 mol) in ethanol (40 cm^3). A white precipitate formed immediately on addition and was filtered off, washed first with water and then with ethanol, and finally dried. X-ray quality crystals of the compound were obtained by dissolving the complex in hot dimethylformamide, and slow evaporation (*ca* 2 days) of the solvent near its boiling point (*ca* 140°C). Found (Required for $C_{14}H_8N_2S_4Cd$): C, 38.3 (37.8); H, 2.0 (1.8); N, 6.2 (6.3); S, 28.6 (28.8)%. Major IR bands (for the powder, Nujol mull) were as follows (cm^{-1}): 2953; 2924s, 2854s, 1560w, 1455s, 1385, 1312w, 1278w, 1247m, 1082m, 1026s, 1012s, 749s, 725m, 694m. These are in good agreement with those reported in the literature.

Bis(2-*mercaptothiazolinato*)*cadmium*(II)

A solution of cadmium acetate (1 g, 0.037 mol) in water (15 cm^3) was added to a vigorously stirred solution of 2-mercaptothiazoline (0.89 g, 0.0075 mol) in ethanol (40 cm^3). A white precipitate formed which was immediately filtered off. Yields were low, *ca* 23%; dec. 203°C. Found (Required for $C_6H_8N_2S_4Cd$): C, 20.7 (20.7); H, 2.5 (2.3); N, 8.2 (8.0); S, 37.3 (36.8)%. Major IR bands (Nujol mull) were as follows (cm^{-1}): 3139b, 3126b, 2953s, 2925s, 2854s, 1527s, 1502s, 1463s, 1444m, 1377m, 1303s, 1263w, 1198w, 1041s, 1023s, 976m, 936m, 677w.

1,4,8,11-*Tetrathiaundecanatocadmium*(II)

The ligand 1,4,8,11-tetrathiaundecane was prepared following published procedures.[5] Sodium (0.7 g, 0.03 mol) was dissolved in ethanol (150 cm^3) under nitrogen and 1,4,8,11-tetrathiaundecane (3.5 g, 0.0153 mol) was slowly added. The solution was stirred for 1 h and then added to a suspension of cadmium chloride (2.7 g, 0.0153 mol) in ethanol (150 cm^3), and the mixture stirred overnight. A white precipitate formed and was filtered, washed with water to remove any NaCl and then dried. Yield: 82%; dec. *ca* 168°C. Found (Required for $C_7H_{14}S_4Cd$): C, 26.5 (24.7); H, 4.4 (4.1); S, 38.08 (37.6)%. Major IR bands (Nujol mull) were as follows (cm^{-1}): 32,756, 32,106, 2954s, 2854s, 2825s, 1460s, 1377s, 1341m, 1298m, 1253s, 1197s, 1119m, 1050m, 721m, 694m.

Bis(5-*mercapto*-1-*methyltetrazolato*)*cadmium*(II)

A solution of cadmium chloride (1.6 g, 0.0087 mol) in water (100 km^3) was added to a stirred solution of sodium 5-mercapto-1-methyltetrazole (3 g, 0.017 mol) in water (100 cm^3). A white precipitate formed immediately and was filtered off, washed

with water, then with methanol and finally dried. Yield: 62%. Found (Required for $C_4H_6N_8S_2Cd$): C, 13.8 (14.0); H, 2.0 (1.8); N, 32.0 (32.7); S, 18.1 (18.7)%. The main IR bands (KBr disc) were (cm^{-1}): 3293br, 2959w, 1540w, 1522w, 1507w, 1466s, 1455s, 1414s, 1381s, 1281s, 1234w, 1175s, 1091m, 985s, 723s, 711s, 690s.

Bis(dithiocarbamato)cadmium(II)

A solution of cadmium chloride (1.2 g, 0.0066 mol) in water (80 cm^3) was added to a stirred solution of sodium diethyldithiocarbamate (3 g, 0.013 mol) in water. A white precipitate formed, which was filtered off and then dried. The compound was recrystallized from chloroform as large transparent crystals,[18] m.p. 248–250°C. Bis(pyrrolidinedithiocarbamato)cadmium(II) was prepared in an analogous manner.

Acknowledgements—We thank the SERC and Polaron equipment Ltd for a CASE award to O.F.Z.K., and Dr. C. J. Groombridge of the ULIRS solid-state NMR service at Royal Holloway and Bedford New College for ^{113}Cd NMR spectra.

REFERENCES

1. M. B. Hursthouse, O. F. Z. Khan, M. Mazid, M. Motevalli and P. O'Brien, *Polyhedron* 1990, **9**, 541.
2. I. G. Dance, R. G. Garbutt and D. C. Craig, *Inorg. Chem.* 1987, **26**, 3732.
3. (a) I. G. Dance, R. G. Garbutt, D. C. Craig and M. L. Scudder, *Inorg. Chem.* 1987, **26**, 4057; (b) I. G. Dance, R. G. Barbutt and M. L. Scudder, *Inorg. Chem.* 1990, **29**, 1571.
4. I. G. Dance, *Polyhedron* 1986, **5**, 1037.
5. (a) S. Wang and J. P. Fackler, *Inorg. Chem.* 1989, **28**, 2615.
6. E. Raper, *Coord. Chem. Rev.* 1985, **61**, 115.
7. A. J. Deeming, M. Karin, P. A. Bates and M. B. Hursthouse, *Polyhedron* 1988, **7**, 1401.
8. L. Stefanaik, *Org. Mag. Reson.* 1979, **12**, 379.
9. P. Beak, J. B. Covington, S. G. Smith, J. M. White and J. M. Ziegler, *J. Org. Chem.* 1980, **45**, 1534.
10. U. Ohms, H. Guth, A. Kutoglu and C. Sheringer, *Acta Cryst.* 1982, **B38**, 831.
11. S. Matsunami, S. Fujimura, K. Okimoto and M. Masaki, *Bull. Chem. Soc. Jpn* 1979, **52**, 536.
12. J. A. McCleverty, S. Gill, R. S. Z. Kowalski, N. A. Bailey, H. Adams, K. W. Lumbard and M. A. Murphy, *J. Chem. Soc., Dalton Trans.* 1982, 493.
13. I. P. Khullar and U. Agarwalla, *Can. J. Chem.* 1975, **53**, 1165.
14. C. Preti and G. Tosi, *Can. J. Chem.* 1976, **54**, 1558.
15. W. Rosen and D. H. Bush, *J. Am. Chem. Soc.* 1969, **91**, 4694.
16. D. M. Roundhill, *Inorg. Chem.* 1980, **19**, 557.
17. P. G. Mennit, M. P. Shatlock, V. J. Bartuska and G. E. Maciel, *J. Phys. Chem.* 1981, **85**, 2087.
18. M. Bonamico, G. Mazzone, A. Vaciago and L. Zambonelli, *Acta Cryst.* 1965, **19**, 898.

Polyhedron Vol. 10, No. 3, pp. 333–336, 1991
Printed in Great Britain

0277–5387/91 $3.00+.00
© 1991 Pergamon Press plc

AN INVESTIGATION ON THE INTERACTION BETWEEN PALLADIUM(II) AND L-CITRULLINE BY ^1H AND ^{13}C NMR SPECTROSCOPY AND POTENTIOMETRY

MARIA LUISA GANADU and VITTORIO LEONI

Dipartimento di Chimica, Università di Sassari, Via Vienna 2, 07100 Sassari, Italy

and

GUIDO CRISPONI* and VALERIA NURCHI

Dipartimento di Chimica e Tecnologie Inorganiche e Metallorganiche, Università di Cagliari, Via Ospedale 72, 09124 Cagliari, Italy

(*Received* 14 *May* 1990; *accepted* 26 *September* 1990)

Abstract—The palladium(II)–L-citrulline system has been studied in aqueous solution by potentiometric and ^1H and ^{13}C NMR spectroscopic methods. Evidence is given for the formation of a PdL_2 complex. A bonding scheme through the carboxylic and amine groups in the *trans* configuration is proposed, on the basis of NMR and IR spectra.

Metal ions play an important role in biological systems, often through coordination to proteins.[1] In order to obtain some insight into the behaviour of metal ions with L-citrulline,

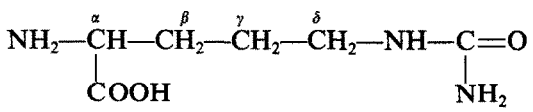

an amino acid involved in the urea cycle and of great biochemical interest, we have undertaken the present investigation on the palladium(II)–L-citrulline interaction. L-Citrulline contains, in addition to amino acid functions, a —NH—CO—NH_2 group in the side chain which can offer different coordination possibilities. Palladium was chosen to represent the behaviour of bivalent metal ions, which give square planar complexes, implied in biological systems;[3] in fact its exchange kinetics are sufficiently slow on the NMR time scale to allow the separate observation of free and complexed ligand molecules.[4]

This work is part of a study on complex formation between biological ligands and metal ions in aqueous solution.[5–8]

* Author to whom correspondence should be addressed.

EXPERIMENTAL

NMR studies

^{13}C NMR spectra were obtained in D_2O solution with a CFT-20 Varian spectrometer at a probe temperature of 37°C. Chemical shifts are expressed in ppm relative to external TMS. Typical Fourier transform conditions, under which the ^{13}C results were obtained, were the following: spectral width 6000 Hz, data points 8 K, pulse repetition times 0.8–4.0 s, number of accumulated transients 10,000–40,000. The ^{13}C spectra of L-citrulline and of the PdL_2 complex were obtained in the completely ^1H decoupled mode using 8 mm tubes.

^1H NMR spectra were recorded using D_2O solutions of 0.1 M L-citrulline and increasing palladium(II) concentration up to a [palladium(II)] : [L-citrulline] ratio of 1 : 2; above this ratio a white solid began to precipitate. The ^1H spectrum of pure L-citrulline was obtained on a VXR 300 Varian spectrometer.

Potentiometric studies

The titrations were performed on a pH-M-84 Radiometer pHmeter equipped with a Dosimat 655

Metrohm automatic titrator, at an ionic strength of 0.1 M (KNO_3) and 25°C. In all the titrations of the palladium(II)–L-citrulline solutions, the ligand concentration was 1×10^{-3} M (with added HCl, 2×10^{-3} M) and the palladium(II) concentration ranged from 0.25×10^{-3} to 2×10^{-3} M. The solutions (25 cm^3) were titrated with NaOH (0.1 M) at 25°C under a nitrogen atmosphere. The time delay between two consecutive base additions was 1200 s; 80 experimental points were collected for each titration. The standard potentials of the electrode and the slope were determined by titration of chloridic acid with NaOH, at an ionic strength of 0.1 M (KNO_3), before and after each palladium(II)–L-citrulline titration, which required about 27 h.

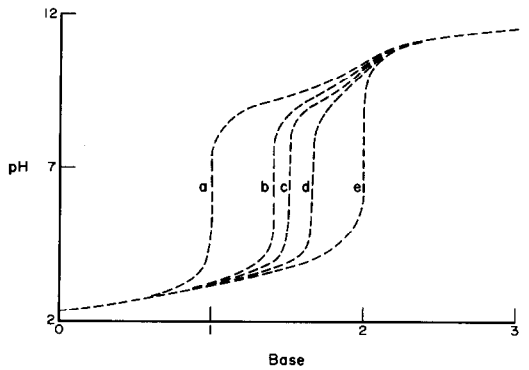

Fig. 1. The titration curves {$-\log [H^+]$ vs [titrant base]/[total L-citrulline]} of pure L-citrulline [curve (a)] and of various solutions with the same ligand concentration and increasing [palladium(II)]:[L-citrulline] ratios: (b) 1:5, (c) 1:4, (d) 1:3 and (e) 1:2.

IR spectra

Using a Perkin–Elmer 683B spectrophotometer at room temperature the IR spectra of L-citrulline and of the PdL_2 complex were obtained as KBr pellets in the range 4000–600 cm^{-1} and in Nujol on polyethylene disks in the range 600–200 cm^{-1}.

Calculations

Potentiometric data for the electrode standardization were analysed by the MAGEC program.[9] The ionization constants of L-citrulline and the formation constant of its adduct with palladium(II) were calculated by a slightly modified version of the PSEQUAD program.[11] The calculations were performed on a PS/2 50 IBM personal computer.

Materials

L-Citrulline was purchased from Sigma and used without further purification. $Na_2PdCl_4 \cdot 1/3H_2O$ was a JMC product. The complex PdL_2 (where L represents the completely deprotonated form of L-citrulline) was prepared by adding a solution of the ligand to a solution of Na_2PdCl_4, in slight excess of the ratio [palladium(II)]:[L-citrulline], 1:2. The complex was isolated as a solid by concentrating the yellow solution to a small volume *in vacuo*, at room temperature. The precipitate was washed with water and recrystallized from ethanol. Found: C, 31.6; H, 5.4; N, 18.5; Pd, 23.3. Calc. for PdL_2: C, 31.7; H, 5.3; N, 18.5; Pd, 23.4%. The value for Pd was determined by thermogravimetric analysis.

RESULTS AND DISCUSSION

The potentiometric titration of acidified L-citrulline [Fig. 1(a)] exhibits two distinct inflections; the corresponding calculated pK values are, respectively, $pK_1 = 2.275 \pm 0.005$ and $pK_2 = 9.349 \pm 0.002$, in close agreement with the pK values for carboxylic and amine groups in most amino acids. A delay of 20 min was given between the base additions in order to allow for the establishment of equilibrium; curves obtained with delay times less than 15 min were not reproducible, while no difference was noticed when 15 or 20 min delays were used. Titration curves of solutions at various [palladium(II)]:[L-citrulline] ratios are also reported in this figure. Since precipitation took place for ratios higher than 1:2, the analysis has been limited to the curves presented. They can be perfectly fitted by assuming only the formation of a PdL_2 complex with a formation constant, $\log \beta = 16.23 \pm 0.02$, which appears to be somewhat higher than those reported by Martell and Clarke[12] for 1:2 complexes of other bivalent cations with L-citrulline. The formation of PdL_2 involves the deprotonation of the amino groups of both L-citrulline molecules, which is lowered by about 6 pH units with respect to the deprotonation of free L-citrulline.

To obtain greater insight into the model of complexation we studied the palladium(II)–L-citrulline system by ^1H and ^{13}C NMR spectroscopy.

The proton 300 MHz spectra of the pure ligand shows two triplets centred at 3.65 and 3.03 ppm which can be attributed to the α-CH group and the δ-CH_2, respectively, on the basis of the signal intensities. The multiplets at 1.77 and 1.46 ppm were assigned to the β-CH_2 and γ-CH_2 groups on the basis of double resonance experiments.

^1H spectra (80 MHz) of palladium(II)–L-citrulline mixtures were collected for [palladium(II)]:[L-citrulline] ratios increasing up to 1:2, above which precipitation took place. These spectra, shown in

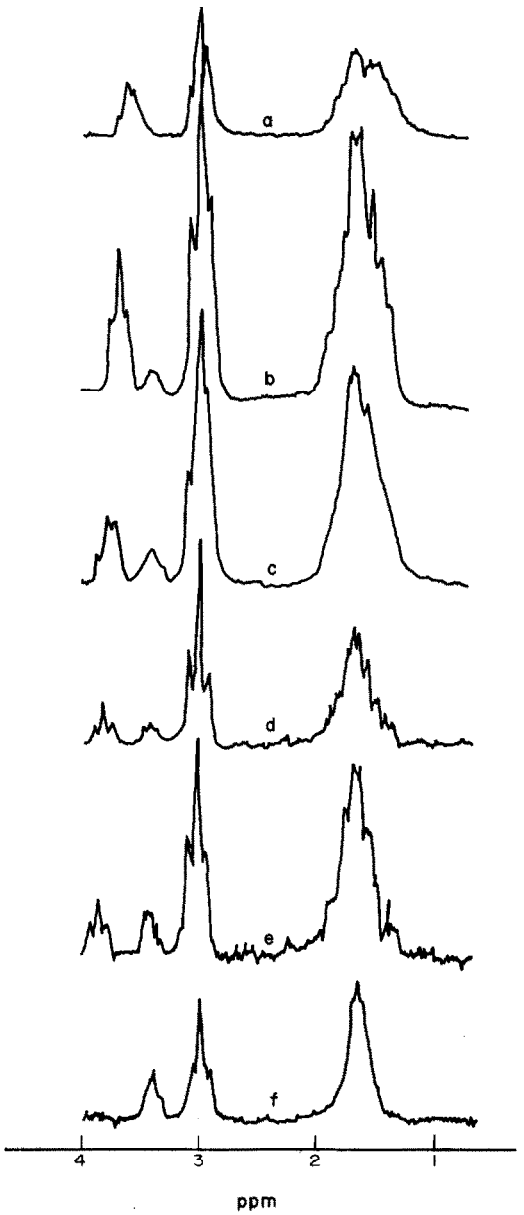

Fig. 2. ^{1}H NMR spectra (80 MHz) of pure L-citrulline (a) and various palladium(II)–L-citrulline solutions with increasing [palladium(II)]:[L-citrulline] ratios: (b) 1:10, (c) 1:8, (d) 1:6, (e) 1:4 and (f) 1:2.

Fig. 2, show some trends as a function of the added palladium(II):

(1) a small low-field shift and a decrease in intensity of the α-CH resonance, in addition to the appearance of a new signal at 3.4 ppm;

(2) the chemical shift of the δ-CH_2 triplet does not vary;

(3) the band of γ-CH_2 appears to converge towards the β-CH_2 band until at a ratio of 1:2 the two bands are superimposed;

(4) the signal from the α-CH of the free L-citrulline completely disappears for a 1:2 ratio, and a new band appears at 3.4 ppm.

A low-field shift of α-CH, also observed in solutions of pure L-citrulline when the pH is changed from neutral to acidic, can be ascribed to the deshielding of hydrogen atoms on formation of the unprotonated —COOH group. The shift in the spectra in Fig. 2 can therefore be attributed to the lowering of pH with palladium concentration, due to the release of protons when PdL_2 is formed.

The new band at 3.4 ppm (which appears as a single band in the resolution limits of the 80 MHz spectrometer used) is due to the α-CH in the PdL_2 complex undergoing slow exchange with the free L-citrulline; this band forms at the expense of the band at 3.65 ppm, which disappears when the 1:2 ratio is reached and PdL_2 is quantitatively formed. Analogous behaviour is shown by the γ-CH_2 signal, although less clearly due to overlap with the β-CH_2 signals. The signals of δ- and β-CH_2, however, seem completely unaffected by complex formation. It should be emphasized that the high-field shift of the α-CH in the complex ligand, with respect to that in the free ligand, is opposite to the behaviour of the γ-CH_2 shift.

The ^{13}C spectra of pure L-citrulline and the PdL_2 complex are reported in Fig. 3; the first spectrum exhibits six different signals, the assignments of which, reported on the same figure, were made on the basis of reports in the literature. The corresponding spectrum of the complex presents only four peaks: the resonances of the two quaternary carbons (the smallest in the spectra of pure ligand for relaxation reasons) cannot, in fact, be detected at all at the low concentration of the complex used due to its low solubility; this spectrum shows a high-field shift of the signals for the C(α) and C(β) carbon atoms.

On the basis of these observations, the involvement in complexation of the —COO^- and —NH_2 groups only can be assumed, the NH—CO—NH_2 moiety not being implicated at all. These remarks are in agreement with the results of potentiometric titration.

A planar complex such as PdL_2 can assume *cis* and *trans* configurations. In the actual situation of slow exchange between free and complexed ligand molecules, the *cis–trans* interconversion should be sufficiently slow to permit the observation of separate signals for the two isomers. The single signal exhibited by the complexed form leads to the assumption that only the *trans* isomer is present; in fact the two ligands in the *cis* configuration, being non-equivalent, should give separate signals. IR

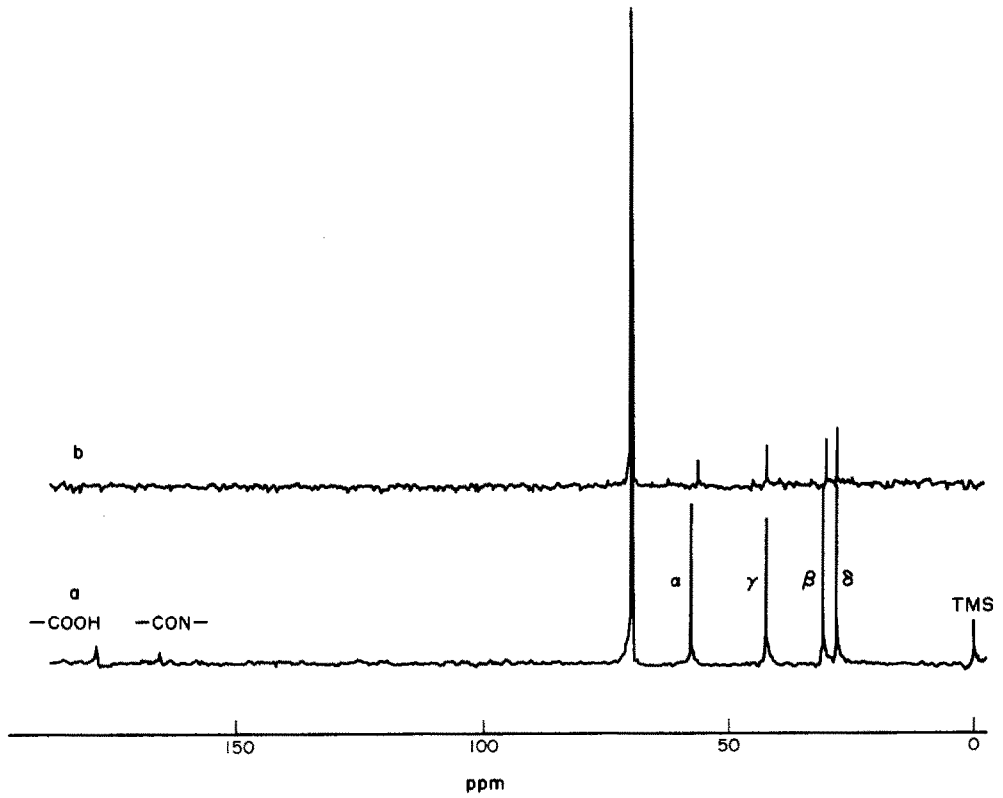

Fig. 3. ^{13}C NMR spectra of L-citrulline (a) and of PdL_2 (b) in aqueous solution.

spectra support such an assumption: in fact, while in the free ligand the NH_2 bands in the range 3450–3000 cm^{-1} are weak, due to the mixing of NH_2 and NH_3^+ signals, in the complexed form these bands are stronger due to the presence of two NH_2 groups. The shift of the ν(CO) from 1640 to 1655 cm^{-1} indicates that this group is probably involved in the binding of the metal ion; the presence of only one Pd—N band around 606 cm^{-1} moreover confirms the symmetric configuration of the complex.

Acknowledgements—This work has been supported by MPI and by Regione Sardegna.

REFERENCES

1. H. Sigel, *Metal Ions in Biological Systems*. Dekker, New York (1986).
2. H. R. Mahler and E. H. Cordes, *Biological Chemistry*. Harper and Row, New York (1967).
3. L. E. Erickson, J. W. McDonald, J. K. Howie and R. P. Clow, *J. Am. Chem. Soc.* 1968, **90**, 6371.
4. O. Yamauchi and A. Odani, *J. Am. Chem. Soc.* 1981, **103**, 391.
5. G. Crisponi, R. Caminiti, S. Biagini, M. Casu and A. Lai, *Polyhedron* 1984, **3**, 1105.
6. S. Biagini, M. Casu, A. Lai, R. Caminiti and G. Crisponi, *Chem. Phys.* 1985, **93**, 461.
7. R. Caminiti, G. Crisponi, V. Nurchi and A. Lai, *Z. Naturf.* 1984, **39a**, 1235.
8. G. Crisponi, A. Lai, M. Monduzzi and G. Saba, *Inorg. Chim. Acta* 1983, **80**, 85.
9. P. M. May, D. R. Williams, P. V. Linder and R. G. Torrington, *Talanta* 1982, **29f**, 249.
10. G. Crisponi, V. Nurchi, M. L. Ganadu and G. Lubinu, *Polyhedron* 1990, **9**, 789.
11. L. Zekany and J. Nagypal, *Computational methods for the Determination of Formation Constants* (Edited by D. J. Leggett), Ch. 11. Plenum Press, New York (1985).
12. E. R. Clarke and A. E. Martell, *J. Inorg. Nucl. Chem.* 1970, **32**, 911.

Polyhedron Vol. 10, No. 3, pp. 337–345, 1991
Printed in Great Britain

0277–5387/91 $3.00+.00
© 1991 Pergamon Press plc

SYNTHESIS AND X-RAY CRYSTAL STRUCTURES OF THE ONE-DIMENSIONAL RIBBON CHAINS $[MOBu^t \cdot Bu^tOH]_\infty$ AND THE CUBANE SPECIES $[MOBu^t]_4$ (M = K AND Rb)

MALCOLM H. CHISHOLM,* SIMON R. DRAKE, AHMAD A. NAIINI and WILLIAM E. STREIB

Department of Chemistry and the Molecular Structure Center, Indiana University, Bloomington, IN 47405, U.S.A.

(*Received* 5 *July* 1990; *accepted* 27 *September* 1990)

Abstract—The series $[MOBu^t \cdot Bu^tOH]_\infty$ (M = K, Rb and Cs) have been prepared by the reaction of M with Bu^tOH in THF. Single-crystal X-ray diffraction studies revealed for M = K or Rb that $[MOBu^t \cdot Bu^tOH]_\infty$ crystallizes from tetrahydrofuran–n-pentane at −20°C in the triclinic space group $P\bar{1}$, with unit cell dimensions [K, Rb]: a = 9.862(3), 9.886(2) Å; b = 9.929(4), 9.914(2) Å; c = 6.330(2), 6.640(1) Å; β = 90.66(2), 90.46(1)° and Z = 2, as a one-dimensional chain linked by hydrogen-bonding. The strong hydrogen-bonding within the chain O(2)—O(7) (2.46, 2.44 Å) also results in a near linear O(7)—H—O(2) angle (167.4, 172.61°) with the hydrogen atom closer to O(7) (1.22, 1.18 Å), than O(2) (1.24, 1.27 Å). These alcohol adducts may be readily converted into the compounds $[MOBu^t]_4$ (M = K, Rb and Cs) by sublimation. Single-crystal X-ray diffraction studies reveal for M = K or Rb, that $[MOBu^t]_4$ crystallizes from toluene at −20°C in the cubic space group $P\bar{4}3M$; with unit cell dimensions [K, Rb]; a = 8.372(1), 8.514(1) Å, and Z = 4, as cubane structures. Within the cubane-like structures the O—M—O angles are found to deviate only slightly from 90°, with O—M—O (90.18, 89.11°) and M—O—M (89.82, 90.89°) for M = K and Rb, respectively. The alcohol adducts undergo an alkoxide ligand exchange process that is rapid on the ^1H NMR time scale at room temperature.

The chemistry of main group metal alkoxides has received renewed attention as these materials are potential precursors to metal oxides.[1,2] The sol–gel technique takes advantage of the tendency of metal alkoxides to form polymeric structures upon hydrolysis.[3] Thermolysis of the resulting materials yields amorphous oxides that may be crystallized by heating to higher temperatures.[4]

Alkali metal oxides are involved in a vast range of advanced materials, such as superconductors ($Ba_{0.6}K_{0.4}BiO_3$),[5] optical modulators ($LiNbO_3$),[6] tungsten bronzes ($KSr_2Nb_5O_{15}$)[7] and ferro-electric materials ($KTa_xNb_{1-x}O_3$).[8] These materials are normally obtained by traditional high temperature solid-state routes. Molecular precursors of alkali metal oxides remain rather limited, although they have enormous value through either sol–gel or MOCVD techniques.

In this paper we report the synthesis and single-crystal X-ray structures of $[MOBu^t \cdot Bu^tOH]$ and $[MOBu^t]_4$, where M = K and Rb. The former are highly soluble compounds and in the solid-state are one-dimensional polymers, based on the mononuclear $[MOBu^t \cdot Bu^tOH]$ subunits.

EXPERIMENTAL

All manipulations were carried out under an atmosphere of dry (molecular sieves) argon, with rigorous exclusion of air and moisture. All hydrocarbon and etheral solvents were dried and distilled from sodium benzophenone ketyl. Alcohols were dried by distillation from magnesium turnings, activated by a crystal of iodine. NMR solvents were dried over 4 Å molecular sieves and stored under argon. Potassium, rubidium and caesium metals were purchased from the Aldrich Chemical Company, and stored in a dry box under an argon atmosphere. Elemental analyses were performed

* Author to whom correspondence should be addressed.

by Oneida Research Services. NMR data were recorded on a Bruker WM-500 NMR spectrometer, using the protio impurities of the deuterated solvents as reference for ^1H and the ^{13}C chemical shifts. IR spectra were recorded on a Nicolet 510P FTIR spectrometer as Nujol mulls between KBr plates.

Synthesis of $[KOBu^t \cdot Bu^tOH]_\infty$ **(1)**

Potassium metal balls (2.6 g, 66.5 mmol) were placed in a Schlenk tube under argon in a dry box. The tube was removed from the dry box, and to this was added tert-butanol (11.8 cm^3, 126.4 mmol). The solution was then heated to 70°C for 1 h, during which time all the metal dissolved to yield a colourless solution. The resulting solution was filtered and the solvent removed *in vacuo* to yield a white solid. A minimum amount of tetrahydrofuran (10 cm^3) was added to dissolve the solid, layered with n-pentane (15 cm^3) and the sample cooled to −25°C for 24 h. During this time, small, colourless crystals were formed. The solution was subsequently filtered, and the crystals dried carefully *in vacuo* to give $[KOBu^t \cdot Bu^tOH]$ (9.9 g, 53.2 mmol, 78.8%).

IR data: Nujol mull, cm^{-1} 3503 (br, OH). M.p.: slowly sublimes at 145–160°C, decomposes at 242–244°C. ^1H NMR data (500 MHz, toluene-d_8, 20°C): δ 2.12 (s, 18H, Me_3C), δ 6.67 (s, O*H*). Variable temperature ^1H NMR data (C_7D_8): no coalescence phenomena were observed when the sample was cooled to 220 K, but the resonances were broadened at this temperature: 220 K, δ 2.14 (s, br, 18H, Me_3C), δ 4.70 (s, *OH*). ^{13}C NMR data (126 MHz, 20°C, toluene-d_8): δ 50.41 (s, Me_3C), δ 66.88 (s, Me_3C). Found: C, 51.8; H, 10.4. Calc. for $C_8H_{19}O_2K$: C, 51.6; H, 10.2%. Molecular weights of 537 ± 41 and 569 ± 34 were measured at concentrations of 2.33×10^{-3} and 4.67×10^{-3} M, respectively. Calculated for $[KOBu^t \cdot Bu^tOH]_3 = 558.3$. Each value was determined by two measurements.

Synthesis of $[KOBu^t]_4$ **(2)**

Potassium metal balls (2.6 g, 66.5 mmol) were placed in a Schlenk tube under argon in a dry box. The tube was removed from the dry box, and to this was added tert-butanol (5.9 g, 63.2 mmol) and tetrahydrofuran (60 cm^3). The solution was heated at 70°C for 67 h, during which time the majority of the metal dissolved. The resulting solution was filtered and the solvent removed *in vacuo* to yield a white solid (5.9 g, 78.8%). The solid was then sublimed at 140–150°C (10^{-3} torr) to yield crystalline $[KOBu^t]_4$ (4.3 g, 38.4 mmol, 57.4%). M.p.: slowly sublimes at 170–190°C (10^{-2} torr), decomposes at 256–258°C. ^1H NMR data (500 MHz, 20°C, toluene-d_8): δ 1.08 (s, 9H, Me_3C), remains unchanged on cooling to 200 K. ^{13}C NMR data (126 MHz, 20°C, toluene-d_8): δ 37.66 (s, Me_3C), δ 66.57 (s, Me_3C). Found: C, 43.0; H, 8.3. Calc. for $C_4H_{90}K$: C, 42.8; H, 8.1%.

Synthesis of $[RbOBu^t \cdot Bu^tOH]_\infty$ **(3)**

Rubidium metal (5 g, 58.8 mmol) was placed in a Schlenk tube under helium in a dry box. The tube was removed from the dry box and to this was added tetrahydrofuran (60 cm^3) and tert-butanol (11.8 cm^3, 126.4 mmol). The solution was then heated to 70°C for 4 h, during which time all the metal dissolved to yield a colourless solution. The resulting solution was filtered and the solvent removed *in vacuo* to yield a white solid. A minimum amount of tetrahydrofuran (10 cm^3) was added to dissolve the solid, followed by filtration. The resulting solution was layered with n-pentane (156 cm^3) and the solution cooled to −25°C for 2 days. During this time, large, regular shaped, colourless crystals formed. The solution was subsequently filtered and the crystals dried carefully *in vacuo* to give $[RbOBu^t \cdot Bu^tOH]_\infty$ (9.4 g, 40.5 mmol, 68.9%).

IR data: Nujol mull, cm^{-1} 3179 (br, OH). M.p.: sublimes 170–200°C, decomposes at 272–274°C. ^1H NMR data (500 MHz, 20°C, toluene-d_8): δ 1.14 (s, 18H, Me_3C), δ 4.83 (s, OH). Variable temperature ^1H NMR data (toluene-d_8): no coalescence phenomena were observed when the sample was cooled to 220 K, but the resonances were broadened at this temperature: 220 K δ 1.16 (s, br, 18H, Me_3C), δ 4.86 (s, br, OH). ^{13}C NMR data (126 MHz, 20°C, toluene-d_8): δ 32.18 (s, Me_3C), δ 67.63 (s, Me_3C). Found: C, 41.4; H, 8.4. Calc. for $C_8H_{19}O_2Rb$: C, 41.3; H, 8.2%.

The molecular weights of 652 ± 88, 676 ± 71 and 712 ± 43 were measured at concentrations of 1.95×10^{-3}, 3.78×10^{-3} and 5.50×10^{-3} M, respectively. Calculated for $[RbOBu^t \cdot Bu^tOH]_3 = 694.5$. Each value was determined by two measurements.

Synthesis of $[RbOBu^t]_4$ **(4)**

Rubidium metal (2.5 g, 29.9 mmol) was placed in a Schlenk tube under helium in a dry box. The tube was removed from the dry box and to this was added tetrahydrofuran (60 cm^3) and tert-butanol (5.9 cm^3, 63.2 mmol). The solution was then heated to 70°C for 24 h, during which time the majority of the metal dissolved. The resulting solution was filtered and the solvent removed *in vacuo* to yield a

white solid. This was then dissolved in the minimum amount of tetrahydrofuran (10 cm^3), layered with n-pentane (15 cm^3) and the sample cooled to 25°C for 48 h. During this time small, colourless crystals were formed. The solution was subsequently filtered and the crystals dried carefully *in vacuo* to give $[RbOBu^t]_4$ (3.6 g, 22.8 mmol, 76.2%).

Alternatively $[RbOBu^t \cdot Bu^tOH]_\infty$ (2.4 g, 10.3 mmol) was placed in a sublimation vessel and heated at 140–150°C (10^{-3} torr) for 12 h. This yielded a white crystalline solid, $[RbOBu^t]_4$ (1.25 g, 7.9 mmol, 76.8%).

M.p.: 185–200°C (10^{-2} torr) sublimed with some decomposition, decomposes at 282–284°C. ^1H NMR data (500 MHz, 20°C, toluene-d_8): δ 1.09 (s, 9H, Me_3C), remains unchanged on cooling to 220 K. ^{13}C NMR data (126 MHz, 20°C, toluene-d_8): δ 37.72 (s, Me_3C), δ 66.40 (s, Me_3C). Found: C, 30.6; H, 5.9. Calc. for C_4H_9ORb: C, 30.3; H, 5.7%.

Synthesis of $[CsOBu^t \cdot Bu^tOH]_\infty$ **(5)**

Caesium metal (5 g, 37 mmol) was placed in a Schlenk tube under helium in a dry box. The tube was removed from the dry box and to this was added tetrahydrofuran (60 cm^3) and tert-butanol (6.2 cm^3, 83.3 mmol). The solution was then heated to 70°C for 90 min, during which time all the metal dissolved to yield a colourless solution. The resulting solution was filtered and the solvent removed *in vacuo* to yield a white solid. A minimum amount of tetrahydrofuran (10 cm^3) was added to dissolve the solid, which was then layered with n-pentane (15 cm^3) and the sample cooled to −25°C for 24 h. During this time long, colourless needles formed. The solution was subsequently filtered and the crystals dried carefully *in vacuo* to give $[CsOBu^t \cdot Bu^tOH]$ (8.0 g, 28.6 mmol, 77.2%).

IR data: Nujol mull, cm^{-1} 3177 (br, OH). M.p.: 165–190°C (10^{-2} torr) sublimes with some decomposition, decomposes at 282–284°C. ^1H NMR data (500 MHz, 20°C, toluene-d_8): δ 1.13 (s, 18H, Me_3C), δ 5.01 (s, OH). No coalescence phenomena were observed when the sample was cooled to 220 K, but the resonances were broadened at this temperature: 220 K, δ 1.15 (s, br, 18H, Me_3C), δ 5.02 (s, br, OH). ^{13}C NMR data (126 MHz, 20°C, toluene-d_8): δ 33.77 (s, Me_3C), δ 67.63 (s, Me_3C). Found: C, 34.6; H, 7.0. Calc. for $C_8H_{19}O_2Cs$: C, 34.3; H, 6.8%.

The molecular weights of 765 ± 100 and 802 ± 78 were measured at concentrations of 2.44×10^{-3} and 3.60×10^{-3} M, respectively. Calculated for $[CsOBu^t \cdot Bu^tOH]_3 = 840.3$. Each value was determined by two measurements.

Synthesis of $[CsOBu^t]_4$ **(6)**

Caesium metal (2.5 g, 18.5 mmol) was placed in a Schlenk tube under helium in a dry box. The tube was removed from the dry box and to this was added tetrahydrofuran (60 cm^3) and tert-butanol (1.45 cm^3, 19 mmol). The solution was then heated for 17 h, during which time the majority of the metal dissolved. The resulting solution was filtered and the solvent removed *in vacuo* to yield a white solid (3.6 g, 94.5%). The solid was then dissolved in tetrahydrofuran (10 cm^3), layered with n-pentane (18 cm^3) and the sample cooled to −25°C for 48 h. During this time small, colourless, cubic crystals were formed. The solution was subsequently filtered and the crystals dried carefully *in vacuo* to give $[CsOBu^t]_4$ (2.6 g, 12.6 mmol, 68.2%).

M.p.: > 350°C, no observable change in colour of the sample up to this temperature. ^1H NMR data (500 MHz, 20°C, toluene-d_8): δ 1.07 (s, 9H, Me_3C), remains unchanged on cooling to 220 K. ^{13}C NMR data (126 MHz, 20°C, toluene-d_8): δ 37.58 (s, Me_3C), δ 66.64 (s, Me_3C). Found: C, 23.6; H, 4.6. Calc. for C_4H_9OCs: C, 23.3; H, 4.4%.

X-ray diffraction studies

For each of the compounds **1–4**, a suitable crystal was chosen and transferred to the goniostat using standard inert atmosphere handling techniques. Data were collected in the usual manner,[9] using a continuous θ–2θ scan with fixed backgrounds. Data were reduced to a unique set of intensities and associated sigmas, and the structures were solved by a combination of direct methods (MULTAN78) and Fourier techniques.

X-ray crystal structure of $[MOBu^t \cdot Bu^tOH]_\infty$ **(1)**

M = K. Colourless crystals of $[KOBu^t \cdot Bu^tOH]_\infty$ (**1**) suitable for X-ray structure determination were grown from tetrahydrofuran–n-pentane and mounted, under a nitrogen atmosphere glove box using silicone grease, before transferring to a goniostat, where a single crystal was cooled to −171°C, for characterization and data collection.

A summary of crystal data and collection and refinement parameters is given in Table 1. A systematic search of a limited hemisphere of reciprocal space revealed no symmetry or systematic absences. Space group $P\bar{1}$ was determined by the successful solution of the structure.

The structure was solved using a combination of direct methods (MULTAN 78) and Fourier techniques. The potassium position was obtained from an E-map. The remainder of the atoms including

Table 1. Crystal parameters for $[MOBu^t \cdot Bu^tOH]_\infty$ (1) and (3) and $[MOBu^t]_4$ (2) and (4)

	1	2	3	4
Empirical formula	$C_8H_{19}O_2K$	$[C_4H_9OK]_4$	$C_8H_{19}O_2Rb$	$[C_4H_9ORb]_4$
Colour of crystal	Colourless	Colourless	Colourless	Colourless
Crystal dimensions (mm)	$0.1 \times 0.25 \times 0.35$	$0.2 \times 0.3 \times 0.4$	$0.24 \times 0.40 \times 0.40$	$0.32 \times 0.14 \times 0.32$
Space group	$P\bar{1}$	$P\bar{4}3M$	$P\bar{1}$	$P\bar{4}3M$
Cell dimensions:				
Temperature (°C)	−171	−156	−155	−157
a (Å)	9.862(3)	8.372(1)	9.886(2)	8.514(1)
b (Å)	9.929(4)	—	9.914(2)	—
c (Å)	6.330(2)	—	6.640(1)	—
α (°)	99.32(2)	90	98.90(1)	90
β (°)	90.66(2)	90	90.46(1)	90
γ (°)	66.80(1)	90	66.76(1)	90
Z	2	4	2	4
Volume (Å^3)	561.26	586.86	589.77	617.08
Calculated density (g cm^{-3})$^{-2}$	1.103	1.270	1.310	1.707
Wavelength (Å)	0.71069	0.71069	0.71069	0.71069
Molecular weight	186.33	112.21	232.70	158.58
Linear absorption coefficient (cm^{-1})	4.311	7.706	40.483	76.868
Detector to sample distance (cm)	22.5	22.5	22.5	22.5
Sample to source distance (cm)	23.5	23.5	23.5	23.5
Average omega scan width at half height	0.25	0.25	0.25	0.25
Scan speed (° min^{-1})	4.0	10.0	8.0	8.0
Scan width (° + dispersion)	2.0	1.8	2.0	2.0
Individual background (s)	8	4	4	4
Aperture size (mm)	3.0×4.0	3.0×4.0	3.0×4.0	3.0×4.0
2θ range (°)	6–45	6–55	6–45	6–55
Total number of reflections collected	1923	1585	2959	1659
Number of unique intensities	1476	176	1551	310
Number with $F\sigma$ 0.0	1390	175	1517	308
Number with $F\sigma$ 3.0(F)	1297	171	1481	307
$R(F)$	0.035	0.016	0.031	0.027
$Rw(F)$	0.037	0.018	0.031	0.027
Goodness of fit for the last cycle	1.043	0.708	1.610	1.210
Maximum δ/σ for last cycle	0.74	0.41	0.44	0.01

most of the hydrogen atoms were found in subsequent iterations of least-squares refinement and difference Fourier calculations. Most importantly, H(19), which hydrogen-bonds O(2) to O(7), was very evident. The positions of H(1)–H(18) were initially idealized.

In the final cycles of least-squares refinement, the non-hydrogen atoms were varied with anisotropic parameters and the hydrogen atoms were varied with isotropic thermal parameters to a final $R(F) = 0.035$. The final difference map was essentially featureless, the largest residual peak being 0.23 e Å^{-3}.

Selected bond distances and angles are collected in Table 2. Additional crystallographic data are available as supplementary material.

M = Rb. Colourless crystals of $[RbOBu^t \cdot Bu^tOH]_\infty$ (3) suitable for X-ray structure determination were also grown from tetrahydrofuran–n-pentane and mounted, under a nitrogen atmosphere glove box using silicone grease, before transferring to a goniostat, where a single crystal was cooled to −155°C, for characterization and data collection.

A summary of crystal data and collection and refinement parameters is given in Table 1. A systematic search of a limited hemisphere of reciprocal space revealed no symmetry or systematic absences. Space group $P\bar{1}$ was determined by the successful solution of the structure.

The structure was solved using a combination of direct methods (MULTAN 78) and Fourier techniques. The coordinates for the potassium atom in

Table 2. Listing of pertinent bond distances and angles for $[MOBu^t \cdot HOBu^t]_\infty$ compounds

	Distances (Å)	
	M = K (1)	M = Rb (3)
M—O(2)′	2.6200(20)	2.7667(27)
M—O(2)	2.7369(20)	2.8688(28)
M—O(7)′	2.6395(20)	2.7947(27)
M—O(7)	2.7055(2)	2.8352(28)
O(2)—O(7)	1.46(4)	1.44(6)
O—C(av.)	1.414(3)	1.415(5)
O(2)—H(19)	1.24(4)	1.27(6)
O(7)—H(19)	1.22(4)	1.17(6)
	Angles (°)	
	M = K (1)	M = Rb (3)
O(2)′—M(1)—O(2)	92.33(6)	91.76(8)
O(2)—M(1)—O(7)	52.26(6)	50.57(8)
O(2)—M(1)—O(7)′	109.18(6)	108.75(8)
O(2)′—M(1)—O(7)	106.77(6)	158.53(8)
O(2)′—M(1)—O(7)′	157.08(6)	105.90(8)
O(7)′—M(1)—O(7)	92.84(6)	92.43(8)
M(1)—O(2)′—H(19)′	109.1(18)	105.6(26)
M(1)—O(2)—H(19)	69.0(19)	67.3
M(1)—O(7)′—H(19)′	107.5(18)	111.3
M(1)—O(7)—H(19)	70.4(19)	69.3
O(2)—H(19)—O(7)	167.4	173.6

1 were used as a starting point for the rubidium atom in **3**. The remaining non-hydrogen atoms were obtained from subsequent iterations of least-squares refinement and difference Fourier calculations. As for **1**, H(19) hydrogen bonds O(2) to O(7). The positions of H(1)–H(18) were initially idealized.

In the final cycles of least-squares refinement, the non-hydrogen atoms were varied with anisotropic parameters and the hydrogen atoms were varied with isotropic thermal parameters to a final $R(F) = 0.031$. The final difference map was essentially featureless, with rubidium residual peaks of 0.57 to 0.64 e $Å^{-3}$ and all other residual peaks being 0.4 e $Å^{-3}$ or less. The structure of **3** is isostructural with that of **1**. Selected bond distances and angles are collected in Table 2.

X-ray crystal structure of $[MOBu^t]_4$ **(2)**

M = K. Colourless crystals of $[KOBu^t]_4$ (**2**) suitable for X-ray structure determination were grown from tetrahydrofuran–n-pentane and mounted under a nitrogen atmosphere glove box using silicone grease, before transferring to a goniostat, where a single crystal was cooled to −150°C, for characterization and data collection.

Crystal data collection and refinement parameters are given in Table 1. A systematic search of a limited hemisphere of reciprocal space revealed intensities with at least orthorhombic symmetry and possibly cubic symmetry. Following complete data collection and correction for absorption the cubic symmetry was more obvious. Space group $P\bar{4}3m$ was determined by the successful solution of the structure.

The coordinates in Weiss' powder diffraction study were used as a starting point for K(1), O(2), C(3) and C(4).[10] An initial least-squares refinement produced an unusually large thermal parameter for C(4). It was then removed, i.e. a difference Fourier was calculated, phased on the first three atoms only. This revealed that C(4) needs to be moved from a special position to a general position. The resulting structure was seen to have a well-defined disorder. Subsequent iterations of least-squares refinement and difference Fourier calculations revealed all remaining atoms including all of the hydrogen atoms. Because of this disorder, atoms C(4), H(2) and H(3) have half weight.

In the final cycles of refinement, the non-hydrogen atoms were varied with anisotropic thermal parameters and the hydrogen atoms were varied with thermal parameters to a final $R(F) = 0.016$. The final difference Fourier was featureless, the largest peak being 0.12 e $Å^{-3}$. Selected bond distances and angles are collected in Table 3.

M = Rb. Colourless plate-like crystals of $[RbOBu^t]_4$ (**4**) suitable for X-ray structure determination were grown from tetrahydrofuran–n-pentane. One crystal was mounted, under a nitrogen atmosphere glove bag using silicone grease and transferred to a goniostat, where it was cooled to −157°C, for characterization and data collection.

Table 3. Listing of pertinent bond distances and angles for $[MOBu^t]_4$ compounds

	Distances (Å)	
	M = K (2)	M = Rb (4)
M(1)—O(3)	2.6232(13)	2.757(4)
O(2)—C(3)	1.375(4)	1.387(13)
C—C(av.)	1.468(5)	1.472(4)
C—H(av.)	1.09(3)	1.091(1)
	Angles (°)	
	M = K (2)	M = Rb (4)
O—M—O	90.18(6)	89.11(17)
M—O—M	89.82(6)	90.89(16)
M—O—C	125.39(5)	124.64(12)
O(2)—C(3)—C(4)	111.00(16)	110.7(5)

Crystal data collection and refinement parameters are given in Table 1. A systematic search of a limited hemisphere of reciprocal space revealed intensities with at least orthorhombic or possibly cubic symmetry. Following complete data collection and correction for absorption the cubic symmetry was more obvious. Space group $P\bar{4}3m$ was determined by the successful solution of the structure.

The coordinates for the potassium atom in **2** were used as a starting point for the rubidium atom in **4**. The remaining non-hydrogen atoms were obtained from subsequent iterations of least-squares refinement and difference Fourier calculation. Hydrogen atoms were included in calculated positions to improve the refinement of the non-hydrogen atoms, however the hydrogens were not refined. Hydrogen thermal parameters were fixed at one, plus the isotropic thermal parameter of the atom to which they were bonded.

In the final cycles of refinement the non-hydrogen atoms were varied with anisotropic thermal parameters to a final $R(F) = 0.027$. The final difference map was essentially featureless, all residual peaks being 0.5 e $Å^{-3}$ or less.

This structure is isostructural with **2**, including the rather well-defined disorder. Because of this disorder, atoms C(4), H(2) and H(3) have half weight. Selected bond distances and angles are collected in Table 3.

RESULTS AND DISCUSSION

Synthesis

The Group I alkoxides reported herein were prepared according to the reactions summarized in Scheme 1 below. The isolated yields were in the range 58–78%, although spectroscopic data indicate that their formation is essentially quantitative. The compounds [MOBu^t] have been prepared previously, though no synthetic details are given in the literature.[1,10]

Solid-state structures

[MOBu^t · Bu^{t}OH]$_\infty$, *where* M = K (**1**) *and* Rb (**3**). The alkali metal alkoxide alcohol adducts [MOBu^t · Bu^{t}OH]$_\infty$ (**1**) and (**3**) form a one-dimensional chain in the solid state. Figure 1 shows an ORTEP view of the central skeleton of the potassium species with the atom numbering scheme, while Fig. 2 emphasizes the coordination environment in the asymmetric unit [MOBu^t · Bu^{t}OH]$_\infty$ of **1** and **3**. (See Table 2 for selected structural data on the potassium and rubidium alkoxides.)

The asymmetric unit contains two metal atoms having a distorted tetrahedral coordination provided by two μ_3-capping t-butoxide and two μ_3-capping t-butanol ligands. The chains are constructed around a series of distorted tetrahedral metal atoms. Within the asymmetric units, one can view the geometry as staggered MOBu^t · Bu^{t}OH units. The M—O distances fall into two sets; those within a triangular MOBu^t · Bu^{t}OH unit, [K, Rb] are the shorter distances, M—O(2) (2.62, 2.77 Å) and M—O(7) (2.64, 2.79 Å), while the longer M—O contacts are between such units and involve a square M_2O_2 unit, M—O(2) (2.74, 2.87 Å) and M—O(7) (2.706, 2.83 Å). Also noteworthy is the strong hydrogen-bonding interaction O(2)—O(7) of (2.46, 2.44 Å), with the proton more likely being associated with O(7) (1.22, 1.18 Å) than with O(2) (1.24, 1.27 Å).

There are crystallographic centres of symmetry at the centres of the squares bonded by M(1)—O(2)—M(1)—O(2) and M(1)—O(7)—M(1)—O(7). The strong hydrogen-bonding within one-dimensional chains also results in a near linear O(7)—H(19)—O(2) bond angle (167.4, 172.61°).

M = Cs. Attempts to prepare single-crystals of the corresponding caesium derivative **5** have, to date, not been successful.

[MOBu^t]$_4$ *where* M = K (**2**) *and* Rb (**4**). The alkali metal t-butoxide compounds [MOBu^t]$_4$ (**2**) and (**4**) have been shown by single-crystal X-ray diffraction to have cubane-type structures. Figure 3 shows an ORTEP view of the central skeleton of the cubane structure of the potassium (**2**) species with the atom numbering scheme. Previous studies have examined samples of the above compounds **2** and **4** by X-ray powder diffraction and a cubane structure was inferred.[10]

The asymmetric unit contains four metal atoms, each in an identical environment in the cubane structure. The t-butoxide ligands are all essentially equivalent, μ_3-bridging t-butoxide ligands. The

$$M + Bu^tOH_{(excess)} \xrightarrow{\Delta} \underset{\text{K (1), Rb (3) and Cs (5)}}{[MOBu^t \cdot Bu^tOH]_\infty} \underset{Bu^tOH}{\overset{\Delta/\text{sublimation}}{\rightleftharpoons}} \underset{\text{K (2), Rb (4) and Cs (6)}}{[MOBu^t]_4}$$

(M = K, Rb, Cs)

Scheme 1.

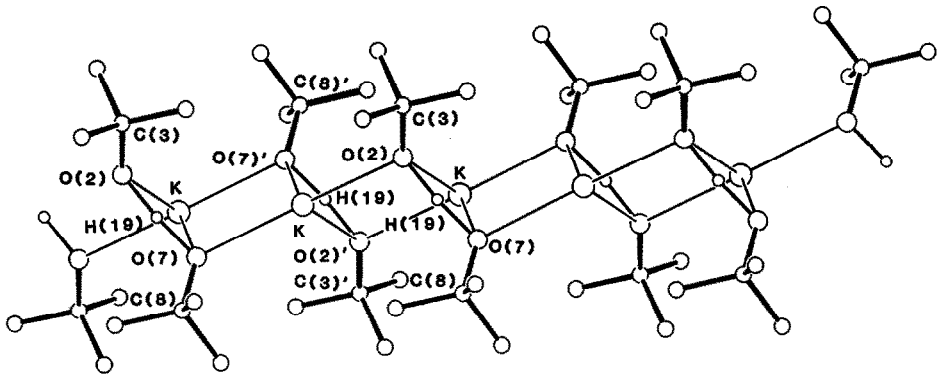

Fig. 1. A view of the $[KOBu^t]_4$ (**2**) central framework showing the cubane-like structure.

M—O distances may be compared, for **2** [2.6232(13)] and for **4** [2.757(4)]. The increase in distance expected on going from potassium to rubidium may be accounted for by the larger van der Waals' radius of rubidium. The M—O bond distances in **2** and **4** are comparable with those observed within the $MOBu^t \cdot Bu^tOH$ triangles.

Within the cubane-like structures, the O—M—O angles are found to deviate only slightly from 90°. For the angles O—M—O (90.18, 89.11°) and M—O—M (89.82, 90.89°), one may note a correlation with the ionic radii of the metal, the O—M—O angle being larger for potassium than rubidium, and likewise the M—O—M angle is larger for rubidium than potassium.

A summary of potassium and rubidium alkoxide and trialkylsiloxide structural parameters are given in Table 4. This table shows that these two metals are found in relatively low coordinative sites in these complexes, i.e. three and four.

Solution properties

In benzene-d_6 and toluene-d_8 $[MOBu^t \cdot Bu^tOH]_\infty$ compounds [M = K (**1**), Rb (**3**) and Cs (**5**)] exhibit only a single time-averaged type of t-butoxide ligand environment at room temperature, as shown by both ^1H and ^{13}C NMR spectroscopy. The ^1H NMR resonances gradually broadened upon cooling to 220 K, but the solution could not be cooled to a low enough temperature to observe coalescence. It is possible that the alcohol ligand is undergoing rapid exchange with the alkoxide ligand in solution. An intramolecular dynamic process is not surprising, given the possibility that potassium can have coordination numbers of three to eight. Likewise, ^{13}C NMR data provided no further insight, since only one type of t-butoxide ligand was observed for $[MOBu^t \cdot Bu^tOH]_\infty$, consistent with the ^1H NMR spectroscopic data. Cryoscopic molecular weight measurements for these species show

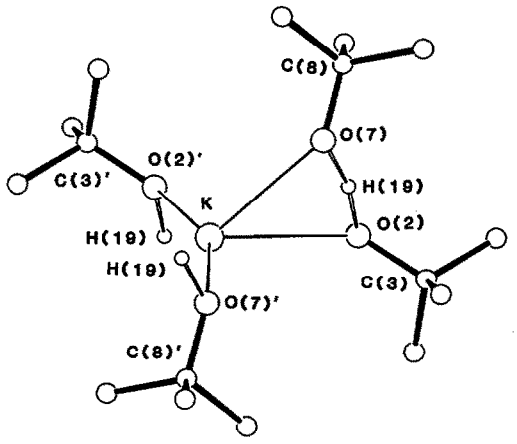

Fig. 2. A view of the asymmetric unit in the crystal structure of $[KOBu^t \cdot Bu^tOH]_\infty$ (**1**).

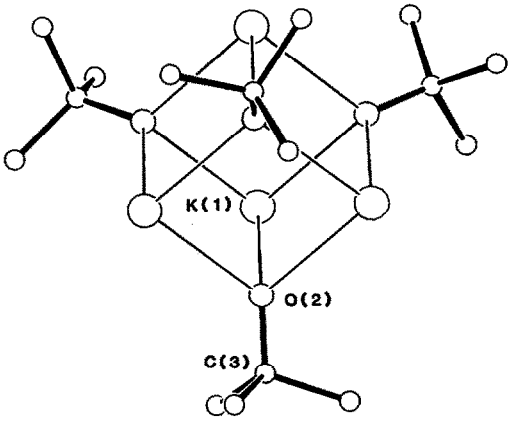

Fig. 3. A view of the $[KOBu^t \cdot Bu^tOH]_\infty$ (**1**) central skeleton from the crystal structure showing the one-dimensional connectivity.

Table 4. Selected X-ray structure data on potassium and rubidium alkoxides

Empirical formula	*n* in solid $(MOR)_n$	Coordination number of metal	M—O distance (Å) in plane	M—O distance (Å) between plane	O—C or O—Si distance (Å)	MOM angle (°)	OMO angle (°)	Reference
KOMe	∞	5	2.60	2.80	1.45	—	—	[a]
$KOSiMe_3$	4	3	2.61	—	1.60	92	88	[b]
$KOBu^t$ (2)	4	3	2.61	—	1.38	89.82	90.18	[c]
$KOBu^t \cdot Bu^tOH$ (1)	∞	4	2.62	2.74	1.41	87.67	92.33	
			2.64	2.71	1.41	87.16	92.84	
RbOMe	∞	5	2.72	2.95	1.38	—	—	[a]
$RbOSiMe_3$	4	3	2.74	—	1.61	93	87	[b]
$RbOBu^t$ (4)	4	3	2.757	—	1.39	90.89	89.11	[c]
$RbOBu^t \cdot Bu^tOH$ (3)	∞	4	2.767	2.87	1.41	88.24	91.76	[c]
			2.795	2.84	1.42	87.57	92.43	

[a] See ref. 16.
[b] See ref. 10.
[c] This work.

that in solution they exist as trimeric species, possibly as cyclic trimers.

The corresponding cubane species $[MOBu^t]_4$ (M = K, Rb and Cs) were also studied by both ^1H and ^{13}C NMR. In benzene and toluene solution these species exhibit a single, sharp line for the t-butoxide environment. On cooling to 220 K the lines remain sharp with no indication of broadening being observed. The ^{13}C NMR data are in accord with these observations.

Cryoscopic molecular weight measurements have been previously reported in a range of solvents, indicating that the tetramers remained intact in solution.[11] It is noteworthy that Lewis bases such as THF and Et_2O do not reduce the oligomerization or react with these species. This parallels the behaviour observed for $[Li(OCBu^t_3)(THF)]_2$ and $[Li(OCBu^t_3)]_2$.[12] Our observations on Group IIA alkoxides and aryloxides also have shown that metal geometries are strongly influenced by the type of Lewis base used.[13] This leads us to conclude that in weak donor media (Et_2O or THF), the solvent is bound more weakly than the alkoxide ligands and hence the cubane structure is retained. The interaction of an alkoxide with the solvent, and thus the degree of association of the alkoxide, is dependent not only on the composition and structure of the alkoxide, but also on the electron-donating properties and the structure of the solvent. Mass spectroscopic results on these materials have previously shown that even in the gas phase these cubane alkoxides remain tetrameric.[14] The related trimethylsilanolates $[MOSi(CH_3)_3]_4$ (M = K, Rb and Cs) have also been shown to exist in the vapour state as tetrameric units, by mass spectroscopy.[14] This surprising stability of alkali-metal alkoxides in the gas phase has allowed PES measurements on a variety of these species to be undertaken.[15] The results indicated that ionization of the alkoxides to their corresponding radical cations becomes easier as the electron density at the oxygen atom is increased.

CONCLUSIONS

The series of alkoxide–alcohol adducts $[MOBu^t \cdot Bu^tOH]_\infty$ (M = K, Rb and Cs) have been prepared from the reaction of alkali metals with tert-butanol–tetrahydrofuran and crystallized in good yields. For M = K or Rb, a one-dimensional ribbon-like chain is observed in the solid state. In benzene and toluene solution at room temperature, all of these complexes undergo a rapid dynamic exchange process on the ^1H NMR time scale, and in solution they exist as trimeric species.

The corresponding cubane alkoxides $[MOBu^t]_4$ (M = K, Rb or Cs) have been unambiguously characterized both in solution and by single-crystal X-ray studies. The interconversion of $[MOBu^t \cdot Bu^tOH]_\infty$ to $[MOBu^t]_4$ was accomplished by sublimation of the precursor in very good yield.

The excellent solubility of $[MOBu^t \cdot Bu^tOH]_\infty$ makes them very attractive for use as molecular precursors in sol–gel processes of mixed oxides. The coordinated alcohol may be an important feature of these molecules in reactions to form heterometallic

alkoxides, and further work along these lines is now in progress.

Acknowledgements—We thank the National Science Foundation for support. S.R.D. acknowledges St. John's College, Cambridge, for the award of a fellowship.

REFERENCES

1. D. C. Bradley, R. C. Mehrotra and D. P. Gaur, *Metal Alkoxides*. Academic Press, London (1978).
2. L. G. Hubert-Pfalzgraf, *Nouv. J. Chem.* 1987, **11**, 663.
3. J. D. Mackenzie, *J. Non-Cryst. Solids* 1988, **100**, 162.
4. K. S. Mazdiyashi, R. T. Dollof and J. S. Smith, *J. Am. Ceram. Soc.* 1969, **52**, 523; 1970, **53**, 91.
5. L. F. Schneemeyer, J. K. Thomas, T. Siegrist, B. Batlogg, L. W. Rupp, R. L. Opila, R. J. Cava and D. W. Murphy, *Nature* 1988, **335**, 421.
6. B. J. Curtis and H. R. Brunner, *Mater. Res. Bull.* 1975, **10**, 515.
7. See for example, D. C. Bradley, *Chem. Rev.* 1989, **89**, 1317.
8. E. Wu, K. C. Chen and J. D. Mackenzie, *Better Ceramics Through Chemistry* (Edited by C. J. Brinker, D. E. Clark and D. R. Ulrich), p. 169. North-Holland, New York (1984).
9. M. H. Chisholm, K. Folting, J. C. Huffman and C. C. Kirkpatrick, *Inorg. Chem.* 1984, **23**, 1021.
10. E. Weiss, H. Alsdorf and H. Kühr, *Angew. Chem. Intl. Ed. Engl.* 1967, **9**, 801; E. Weiss, H. Alsdorf, H. Kühr and H. Grützmacher, *Chem. Ber.* 1968, **101**, 3777.
11. P. Schmidt, L. Lochman and B. Schneider, *J. Molec. Struct.* 1971, **9**, 403; V. Halaska, L. Lochman and D. Lim, *Coll. Czech. Chem. Commun.* 1968, **33**, 3245.
12. J. Hvoslef, H. Hope, B. D. Murray and P. P. Power, *J. Chem. Soc., Chem. Commun.* 1983, 1438; G. Beck, P. B. Hitchcock, M. F. Lappert and I. A. MacKinnon, *J. Chem. Soc., Chem. Commun.* 1989, 1312.
13. K. G. Caulton, M. H. Chisholm, S. R. Drake and W. E. Streib, *Inorg. Chem.* 1990, **29**, 2707.
14. E. Weiss, K. Hoffmann and H.-F. Grützmacher, *Chem. Ber.* 1970, **103**, 1190.
15. M. Braun, D. Waldmüller and B. Mayer, *Angew. Chem. Intl. Ed. Engl.* 1989, **28**, 895.
16. E. Weiss and H. Alsdorf, *Z. Anorg. Allg. Chem.* 1970, **372**, 206.

Polyhedron Vol. 10, No. 3, pp. 347–350, 1991
Printed in Great Britain

0277–5387/91 $3.00+.00
© 1991 Pergamon Press plc

ANALYSIS OF COPPER(I) STABILITY IN THE CATIONIC $[Cu(CH_3CN)_{4-n}(Ph_3P)_n]^+$ SERIES OF COMPLEXES

ANA MARÍA LEIVA,* LEONARDO RIVERA and BÁRBARA LOEB*

Faculty of Chemistry, P. Catholic University of Chile, Casilla 6177, Santiago, Chile

(*Received* 9 *August* 1989; *accepted after revision* 5 *October* 1990)

Abstract—NMR and electrochemical studies on the stability of copper(I) complexes of the type $[Cu(CH_3CN)_{4-n}(Ph_3P)_n]^+$ ($n = 0$–4) were carried out to explore the effect of phosphine ligands on stabilization. The effect of phosphine ligands was demonstrated by cyclic voltammetry and ^{31}P NMR. A correlation between structural and electronic effects and the stability of the complexes was established.

Among the ligands known to stabilize copper(I), triphenylphosphine has been studied by several authors.[1,2] Different coordination geometries have been observed for copper(I)–triphenylphosphine complexes, but the tetrahedral geometry is dominant.[1] Triphenylphosphine complexes are expected to be more stable than those of acetonitrile for copper(I),[3,4] and CH_3CN should be displaced by PPh_3 in the equilibrium:

$$n PPh_3 + [Cu(CH_3CN)_4]^+ \rightleftharpoons [Cu(CH_3CN)_{4-n}(Ph_3P)_n]^+ + n CH_3CN. \quad (1)$$

Our work approaches the above problem by studying the electrochemical stability of the series of cationic complexes $[Cu(CH_3CN)_{4-n}(Ph_3P)_n]^+$ ($n = 0$–4). The related compound, $Cu(PPh_3)_3ClO_4$, was also studied and its behaviour compared to compounds of the above series.

EXPERIMENTAL

NMR spectra were obtained using a VARIAN XL 100 spectrometer with TMS and H_3PO_4[85% (external standard)] as references and $CDCl_3$ and $CHCl_3$ as solvents for ^1H and ^{31}P, respectively.

The voltammometric measurements were carried out with a Wenking HP72 potentiostat, a Wenking VSG72 signal generator and a Graphtex WX2300 XY recorder. For coulometric measurements a Wenking EVI80 voltage integrator was used. All electrochemical measurements were performed under Argon, purified by a Hydrox Purifier, model 8301. The working electrode was a platinum disc for cyclic voltammetry measurements, and a platinum mesh for coulometry. The counter electrode was a platinum wire and the reference a Ag/AgCl (in aqueous tetramethyl ammonium chloride) electrode, adjusted to the SCE potential.[5] All syntheses were carried out in dry solvents under nitrogen.

$[Cu(CH_3CN)_3(PPh_3)]PF_6$

PPh_3 (0.843 g, 3.21 mmol) was added to a solution of $Cu(CH_3CN)_4PF_6$[6] (1.198 g, 3.21 mmol) in dichloromethane (100 cm^3). The mixture was stirred at room temperature for 3 h and then concentrated to half its volume. The addition of diethyl ether (50 cm^3) to this mixture precipitated a white solid, which was separated by filtration under nitrogen. This product was recrystallized from a 3:1 mixture of dichloromethane–ether. Yield: 85%; ^1H NMR (TMS, $CDCl_3$): 2.16 ppm (s, 9H; CH_3), 7.37 ppm (m, 15H; C_6H_5); ^{31}P NMR (H_3PO_4 85%, $CHCl_3$): 1.23 ppm (s).

$[Cu(CH_3CN)(PPh_3)_3]ClO_4$

This product was synthesized by following a modification of the method of White and coworkers,[7b] with dichloromethane as the solvent; the solution was stirred over 3 h at room temperature.

* Authors to whom correspondence should be addressed.

$Cu(PPh_3)_3ClO_4$

Recrystallization of $[Cu(CH_3CN)(PPh_3)_3]ClO_4$ from boiling methanol gave white crystals of the product. X-ray diffraction showed[8a] the replacement of the coordinated acetonitrile by monodentate perchlorate, in agreement with literature reports.[8b]

All other complexes were synthesized following literature procedures: $Cu(CH_3CN)_4PF_6$,[6] $[Cu(CH_3CN)_2(PPh_3)_2]PF_6$[9] and $[Cu(PPh_3)_4]ClO_4$.[7a]

RESULTS AND DISCUSSION

(a) *Nuclear magnetic resonance*

The ^{31}P NMR spectra of the copper(I) complexes (Table 1) show a shift of the phosphorus atom signal toward lower field as the number of phosphine ligands in the complex increases, implying a smaller shielding of this nucleus.[10] This effect can be explained by a reduction in the π contribution to the Cu—P bond as the number of phosphine ligands increases. It is also corroborated by the Cu—P distances determined from X-ray structures of some copper complexes (Table 1),[7] which show that larger Cu—P distances occur with an increasing number of phosphine ligands in the complex.

The transformation of the $[Cu(CH_3CN)(PPh_3)_3]ClO_4$ complex into the $Cu(PPh_3)_3ClO_4$ monodentate perchlorate is shown by the displacement of the ^{31}P signal from 1.85 to 1.69 ppm, reflecting a shielding of the phosphorus nucleus due to a shortening of the Cu—P bond (from 233 to 231 ppm, as measured by X-ray diffraction[8]).

The ^1H NMR spectra of the complexes with acetonitrile ligands (Table 1) show a shift of the methyl group signal to higher field as the number of phosphine ligands in the complex increases, as expected for an increase in the electronic density around the methyl proton. This is corroborated by the X-ray data for complexes **I**, **III** and **IV** (Table 1) that indicate a lengthening of the Cu—N bond as the number of phosphine ligands increases.

(b) *Electrochemical results*

The voltammometric behaviour of triphenylphosphine has been extensively analysed and discussed;[11] in spite of some controversies,[12] it is now accepted that the phosphine undergoes an irreversible oxidation (at a potential > 1.0 V).[13] This process is ascribed to the one-electron oxidation of triphenylphosphine to the $PPh_3^{+\cdot}$ cationic radical.[14,15] The oxidation is followed by a chemical reaction in which the radical, $PPh_3^{+\cdot}$, reacts with nucleophilic components of the solution. In our system (DMF, TEAP 0.1 M, platinum disc working electrode) the oxidation of PPh_3 is observed at 1.38 V (vs SCE) and corresponds to a one-electron process (verified by coulometric measurements). The cyclic voltammograms for all the $[Cu(CH_3CN)_{4-n}(PPh_3)_n]^+$ ($n = 0$–4) compounds show an oxidation wave at potentials ranging from 0.6 to 0.92 V (Table 1), depending on the value of n. In addition, an oxidation process at the same potential (1.38 V) as free triphenylphosphine is observed for all the complexes (Fig. 1). The former wave is assigned to the oxidation of copper(I) to copper(II):

$$[Cu(CH_3CN)_{4-n}(PPh_3)_n]^+ \longrightarrow [Cu(CH_3CN)_{4-n}(PPh_3)_n]^{2+} + e. \quad (2)$$

Table 1. NMR chemical shifts, oxidation potentials and M—L distances for the $[Cu(CH_3CN)_{4-n}(PPh_3)_n]^+$ ($n = 0$–4) series of complexes

	δ ^{31}P (ppm)[a]	δ ^1H (ppm)[a,b]	E_p (vs SCE)[c]	$d_{P—Cu}$ (pm)	$d_{N—Cu}$ (pm)
$[Cu(CH_3CN)_4]^+$ (I)	—	2.14	0.6	—	199[d]
$[Cu(CH_3CN)_3(PPh_3)]^+$ (II)	1.27	2.16	0.6	—	—
$[Cu(CH_3CN)_2(PPh_3)_2]^+$ (III)	1.72	2.11	0.82	226[e]	200[e]
$[Cu(CH_3CN)(PPh_3)_3]^+$ (IV)	1.85	1.96	0.85	233[e]	210[e]
$[Cu(PPh_3)_4]^+$ (V)	2.716	—	0.92	252.4–260.5	—

[a] δ ^{31}P ref. H_3PO_4 85% (45, MHz); δ ^1H TMS (100 MHz); solvent $CDCl_3$.

[b] Methyl (CH_3CN) proton.

[c] ±20 mV; DMF (TEAP 0.1 M); under the same conditions E^0(ferrocene/ferricinium) = 0.4 V.

[d] Reference 7(c).

[e] Reference 7(b).

[f] Reference 7(a).

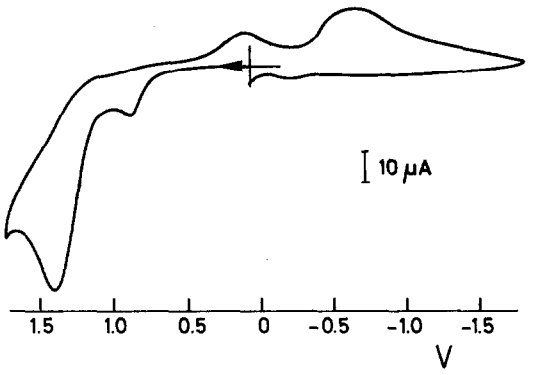

Fig. 1. Cyclic voltammetry for the $[Cu(CH_3CN)(PPh_3)_3]ClO_4$ complex (v = 200 mV s^{-1}) in DMF (TEAP 0.1 M) using a platinum disc as working electrode.

Controlled potential electrolysis corresponding to this oxidation generates, after the passage of one electron, a green coloured compound, probably a copper(II) complex. The current intensity does not manifestly decrease during the process, even after the passage of more than three electrons. The green colour quickly dissappears when the electrolysis is stopped. This behaviour suggests that the oxidation is complicated by a subsequent chemical reaction, probably the reduction of copper(II) by triphenylphosphine released during the electrochemical oxidation of the copper(I) complex [triphenylphosphine has a low affinity for copper(II)]. The ability of triphenylphosphine to reduce copper(II) is well known.[6] However, in this case, the subsequent chemical reduction is rather slow compared to the electrochemical oxidation, and therefore the copper(II) compound can be detected during the electrolysis. Similar behaviour has been shown for a series of rhenium(I) complexes of the type $[Re(CO)_2(PPh_3)_2\{(ArN)_2X\}]$ (X = N, CH; Ar = benzyl and substituted benzyl),[13] where the existence of subsequent chemical reactions was proven by several electrochemical criteria.

In the cyclic voltammetry of $Cu(PPh_3)_3ClO_4$ (**VI**) the oxidation wave appears at 0.6 V, i.e. at a considerably lower potential than the corresponding wave of $[Cu(CH_3CN)(PPh_3)_3]ClO_4$ (Table 1). Since the oxidation process for the related complex, $Cu(PPh_3)_3Cl$ (**VII**),[16] is also observed at 0.6 V, we conclude that **VI** and **VII** generate the same species in solution. An explanation for this behaviour could be the substitution of the solvent (DMF) for the perchlorate or chloride anion. The greater ease of oxidation of the solvated species reflects the greater affinity of DMF for copper(II).[17]

The electrochemical reduction of the complexes in the series was also investigated. A cathodic wave is observed for all of the complexes, the shape of it suggesting a metal deposit on the electrode. Indeed, controlled potential electrolysis for this process generated a copper deposit on the working electrode, after the passage of one electron. The voltammogram of the remaining solution corresponds to free triphenylphosphine, as would be expected for a $Cu^I \rightarrow Cu^0$ reduction.

CONCLUSIONS

The increase in the Cu—P and Cu—N bond lengths with the number of phosphine ligands in the $[Cu(CH_3CN)_{4-n}(PPh_3)_n]ClO_4$ (n = 0–4) complexes (Table 1) could be indicative of a corresponding decrease in stability. However, the greater crystal symmetry observed for the complexes with high values of n would suggest the opposite.* The actual stability tendency is clearly manifested by cyclic voltammetry, where the anodic wave related to the Cu^I/Cu^{II} oxidation moves to more positive potentials as the number of phosphine ligands in the complex increases.

In addition to the crystal symmetry effect, the enhanced stability can be ascribed to the M → L back-donation effect.[4] Since Cu^I-d^{10} is an electron-rich metal it can be regarded as a good π donor to phosphorus, which acts as a π base via its empty d orbitals. The electron density displacement is not possible with acetonitrile as the ligand since there are no energetically appropriate $d\pi$ orbitals on the nitrogen atom for this type of bond.

A comparison between the structure of the $Cu(PPh_3)_3ClO_4$ complex and that of $[Cu(CH_3CN)(PPh_3)_3]ClO_4$ reveals that the former belongs to a trigonal system,[8] while the latter belongs to an orthorhombic one.[7b] Therefore, the cyclic voltammetries should reflect the greater stability of $Cu(PPh_3)_3ClO_4$, but since the species in solution are different [due to the solvation of $Cu(PPh_3)_3ClO_4$] the oxidation of the latter complex is easier, given the greater affinity of DMF for copper(II).

It is concluded that, in this series of copper(I) complexes, a greater ordering of the structure increases the stability only if the species is not altered in solution, as seems to be the case for the $[Cu(CH_3CN)_{4-n}(PPh_3)_n]^+$ (n = 0–4) series of com-

* The $[Cu(CH_3CN)_2(PPh_3)_2]ClO_4$ complex belongs to a monoclinic system with marked distortion of the coordination polyhedra (P—Cu—P and N—Cu—N angles of 127.6 and 99.2°, respectively[7]), while the system for $Cu(PPh_3)_4ClO_4$ is rhombohedral with P—Cu—P angles of 109.6 and 109.3°.[7a]

plexes. On the other hand, the electronic effect on stability is reflected in the chemical shifts observed in the NMR spectra, as well as in the displacement of the electrochemical oxidation wave.

Acknowledgements—This work was supported by the Catholic University Research Office (DIUC) through Grant No. 206/86. We also thank the help given by Professor U. Müller (U. Marburg) to A.M.L. during her stay in his laboratory (through a project Fondecyt-DAAD) and to the Deutscher Akademischer Austauchsdienst (DAAD) that supported this stay. Helpful comments and suggestions from Dr G. Ferraudi (U. Notre Dame) and from Dr E. Roman (P. Catholic University) are also acknowledged.

REFERENCES

1. D. J. Fife, W. M. Moore and K. W. Morse, *Inorg. Chem.* 1984, **23**, 1684, and refs therein.
2. (a) V. G. Albano, P. L. Bellon, G. Ciani and M. Manassero, *J. Chem. Soc., Dalton Trans.* 1972, 171; (b) J. R. Kirchhoff, D. R. McMillin, W. R. Robinson, D. R. Powell, A. T. McKenzie and S. Chen, *Inorg. Chem.* 1985, **24**, 3928.
3. S. Ahrland, J. Chatt and N. R. Davies, *Quart. Rev.* 1958, **12**, 265.
4. (a) R. G. Pearson, *Chem. Britain* 1967, **3**, 103; (b) R. G. Pearson, *J. Am. Chem. Soc.* 1963, **85**, 3533.
5. D. T. Sawyer and J. Roberts, *Experimental Electrochemistry for Chemists*. Wiley Interscience, New York (1974).
6. G. J. Kubas, *Inorg. Synth.* 1970, **19**, 90.
7. (a) L. M. Engelhardt, C. Pakawatchai, A. H. White and P. C. Healy, *J. Chem. Soc., Dalton Trans.* 1985, 125; (b) P. F. Barron, J. C. Dyason, L. M. Engelhardt, P. C. Healy and A. H. White, *Aust. J. Chem.* 1985, **38**, 261; (c) I. Csöregh, P. Kierkegaard and R. Norrestam, *Acta Cryst.* 1975, **B31**, 314.
8. (a) A. M. Leiva and U. Müller, unpublished results; (b) J. C. Dyason, L. M. Engelhardt, P. C. Healy, H. L. Klich and A. H. White, *Aust. J. Chem.* 1986, **39**, 2003.
9. J. Diez, S. Falagán, P. Gamasa and J. Gimeno, *Polyhedron* 1988, **7**, 37.
10. (a) J. R. Van Wazer, *J. Am. Chem. Soc.* 1956, **78**, 5709; (b) J. R. Van Wazer, C. F. Callis, J. N. Schoolery and R. C. Jones, *J. Am. Chem. Soc.* 1956, **78**, 5715.
11. G. Schiavon, S. Zecchin, G. Cogoni and G. Bontempelli, *Electroanal. Chem. Interfacial Electrochem.* 1973, **48**, 425.
12. (a) J. A. Davies and V. Uma, *J. Electroanal. Chem.* 1984, **179**, 273; (b) J. A. Davies and V. Uma, *Inorg. Chim. Acta* 1983, **76**, L305; (c) G. Bontempelli and F. Magno, *Inorg. Chim. Acta* 1985, **99**, 19; (d) J. A. Davies and V. Uma, *J. Electroanal. Chem.* 1983, **158**, 13; (e) G. Mazzocchin, *J. Electroanal. Chem.* 1984, **179**, 269.
13. P. Zanello, A. Cinquantini and F. Laschi, *Polyhedron* 1988, **7**, 195.
14. A. S. Romakhin, E. V. Nikitin, O. V. Parakin, Y. A. Ignat'ev, B. S. Mironov and Y. M. Kargui, *Zh. Obshch. Khim.* 1986, **56**, 2597.
15. F. Pragst *et al.*, *J. Electroanal. Chem. Interfacial Electrochem.* 1986, **197**, 245.
16. J. P. Claude and B. Loeb, unpublished results.
17. V. Gutmann, *The Donor–Acceptor Approach to Molecular Interactions*. Plenum Press, New York (1978).

Polyhedron Vol. 10, No. 3, pp. 351–357, 1991
Printed in Great Britain

0277–5387/91 $3.00+.00
© 1991 Pergamon Press plc

MERCURY(II) HALIDE COMPLEXES WITH CARBONYL AND THIOCARBONYL DONORS

GIUSEPPINA FARAGLIA* and ZIJIAN GUO†

Dipartimento di Chimica Inorganica, Metallorganica ed Analitica dell'Università, via Loredan 4, 35100 Padova, Italy

and

SERGIO SITRAN

Istituto di Chimica e Tecnologia dei Radioelementi del C.N.R., corso Stati Uniti, 35020 Padova, Italy

(*Received* 24 *May* 1990; *accepted* 5 *October* 1990)

Abstract—Mercury(II) halides react with 2,6-dimethyl-4H-pyran-4-thione (DMTP) yielding complexes of general formulae $[Hg(DMTP)_2X_2]$ and $[Hg(DMTP)X_2]_n$ (X = Cl, Br or I), in which the ligand acts as a strong sulphur donor. With 2,6-dimethyl-4H-pyran-4-one (DMP) the complexes $[Hg(DMP)X_2]_n$ and $(HgX_2)_3(DMP)_2$ (X = Cl or Br) have been isolated, which easily release the weakly bound ligand molecules in common solvents. The compounds have been characterized by IR and NMR (^1H and ^{13}C) spectroscopy and by using thermogravimetric data. The adduct geometry is discussed on the basis of IR spectra, which suggest a tetrahedral arrangement for the 1:2 DMTP adducts. A halogen-bridged dimeric structure is proposed for the 1:1 DMTP adducts, whereas the $[Hg(DMP)X_2]_n$ adducts are probably chain polymers with halide–mercury contacts. The $(HgCl_2)_3(DMP)_2$ species should contain two types of mercury atoms with different coordination environments.

Mercury(II) halides form either 1:1 or 1:2 adducts with thiocarbonyl donors, the preferred geometry generally depending on the ligand substituents. Accordingly, benzenecarbothioamide yields 1:2 complexes, the IR spectra of which support a pseudo-tetrahedral structure,[1] whereas the N,N-dialkyl analogues preferentially display a 1:1 stoichiometry.[2,3] On the basis of X-ray structural data, the complex $[Hg\{PhC(S)NEt_2\}I_2]_2$ is dimeric with asymmetric iodine bridges, the mercury atom lying in a distorted tetrahedral environment.[3] As regards imidazolidine-2-thiones, the polymeric 1:1 complexes dichloro(N,N′-diethylimidazolidine-2-thione)mercury(II) and dibromo(5,5-dimethylimidazolidine-2-thione-4-one)mercury(II) have a *catena* structure held together by halide bridges, the tetrahedral coordination sphere of mercury being distorted to a trigonal pyramid.[4,5] In dichlorobis(N-ethylimidazolidine-2-thione)mercury(II) the metal assumes the usual pseudo-tetrahedral geometry.[4] Ethylene trithiocarbonate acts as a weak donor towards mercury(II) halides, the ligand being totally removed from 1:2 and 1:1 complexes in dimethylsulphoxide.[6] Weak sulphur–mercury bonds have been observed in thiocarbamic ester complexes of the type $[Hg(EtOSCNMe_2)X_2]_n$ and $[Hg(EtOSCNHMe)_2X_2]$ (X = halide), which easily release ligands in either benzene or acetone.[7,8] In $[Hg(EtOSCNMe_2)Cl_2]_n$ the mercury atom trigonally bonds ligand-sulphur and two chlorines. At the same time it forms elongated Hg···Cl contacts in a five-coordinated environment.[7] Recently, it has been observed that 2,6-dimethyl-4H-pyran-4-

* Author to whom correspondence should be addressed.
† On leave from the Department of Basic Courses, Agricultural University of Hebei, Baoding, P.R.C.

thione (DMTP) acts as a strong sulphur donor towards palladium(II) and platinum(II) halides, the related 2 : 1 adducts being unchanged in dimethyl sulphoxide, a solvent which easily removes ligand molecules from the thiocarbamic ester analogues.[9] It was therefore of interest to extend the study to the mercury halide complexes of this ligand, in which the aromatic character of the ring enhances the thiocarbonyl donor ability, and of the parent 2,6-dimethyl-4H-pyran-4-one (DMP), which accordingly should be a good carbonyl donor. Mercury halides generally form 1 : 1 adducts with monodentate oxygen donors. Thermochemical studies supported the presence of weak bonds in adducts with ureas, N,N-dimethylformamide and pyridine N-oxide.[10–14] Along with the 1 : 1 adducts, sulphoxides can give complexes with higher mercury halide to ligand ratios.[15,16] In particular, the complex $(HgCl_2)_3(Me_2SO)_2$ contains a dimeric unit in which two mercury chloride moieties are held together by two bridging Me_2SO molecules, the third mercury chloride molecule forming contacts with four chlorine atoms from adjacent dimers.[17]

EXPERIMENTAL

Materials

DMTP (C_7H_8OS, 2,6-dimethyl-4H-pyran-4-thione) was prepared by the method of Faraglia *et al.*[9] and DMP ($C_7H_8O_2$, 2,6-dimethyl-4H-pyran-4-one, Ega-Chemie) was used as supplied. Mercury halides were Merck products. Preparations of DMP complexes were carried out under nitrogen flux.

Preparation of $[Hg(DMTP)_2X_2]$

These complexes were prepared by reacting the apropriate metal salt with DMTP (molar ratio, 1 : 2.2; reaction time, *ca* 2 h) either in CH_2Cl_2 or in Me_2CO. As an example, $[Hg(DMTP)_2Cl_2]$ was prepared by adding DMTP (1.1 mmol) to a suspension of $HgCl_2$ in CH_2Cl_2 (0.5 mmol in 4 cm^3). The solid mixture gradually changed to orange and the reaction was complete within 3 h. The orange solid was filtered, washed with CH_2Cl_2 and n-pentane and dried *in vacuo* (yield, 85%). A further fraction of product separated by addition of n-pentane to the orange mother solution. The compound was also obtained by reaction of $HgCl_2$ and DMTP in Me_2CO (molar ratio 1 : 3; reaction time, 2 h). The product was washed with abundant Me_2CO and dried *in vacuo* (yield, 75%). All 1 : 2 adducts were slightly soluble in dichloromethane, acetone and methanol.

Preparation of $[Hg(DMTP)X_2]_n$

A solution of DMTP in Me_2CO (0.5 mmol in 2 cm^3) was added to a $HgCl_2$ suspension in the same solvent (0.5 mmol in 2 cm^3), with vigorous stirring. The pink solid was kept under stirring for 1 h and then was filtered, washed with abundant Me_2CO and dried *in vacuo*. The 1 : 1 chloro complex was also obtained by reaction of $HgCl_2$ and DMTP in CH_2Cl_2 (molar ratio 1 : 1; reaction time, 18 h). Bromo and iodo derivatives were prepared analogously. The complexes were generally insoluble in common solvents.

Preparation of $[Hg(DMP)X_2]_n$

The complex $[Hg(DMP)Cl_2]_n$ was prepared by dissolving $HgCl_2$ (0.5 mmol) in a solution of DMP in CH_2Cl_2 (2.1 mmol in 5 cm^3). White crystals separated out on addition of n-pentane, which were filtered, washed with C_6H_6 (1 cm^3) and n-pentane and dried *in vacuo* (yield, 80%). The same product was obtained by reaction of $HgCl_2$ and DMP in C_6H_6 (molar ratio 1 : 4; with stirring overnight). The white powder was washed with C_6H_6 and n-pentane and dried *in vacuo* (yield, 70%). If reactions were performed at lower molar ratios (1 : 3 or 1 : 2) the products were mixtures of the 1 : 1 adduct and $(HgCl_2)_3(DMP)_2$ complex. $[Hg(DMP)Br_2]_n$ was prepared in CH_2Cl_2 as for the chloro analogue (yield, 70%). Moreover, good crystals were isolated in low yield by dissolving $HgBr_2$ (1.0 mmol) and DMP (1.9 mmol) in MeOH (2 cm^3) by gentle heating. The crystals separated when the solution was left standing overnight at *ca* 4°C. They were filtered and washed with a few drops of chilled MeOH and dried *in vacuo*. Attempts to isolate the 1 : 1 iodo complexes were unsuccessful. Although HgI_2 dissolves in concentrated DMP solutions (in CH_2Cl_2 or Me_2CO) the complexes are unstable. The mercury salt is the main product when the solutions are either evaporated to dryness or treated with n-pentane.

Preparation of $(HgX_2)_3(DMP)_2$

A suspension of $HgCl_2$ (1.0 mmol) in a CH_2Cl_2 solution of DMP (1.0 mmol in 4 cm^3) was stirred overnight, obtaining a white solid which was discarded by filtration and a colourless solution which was treated with n-pentane until turbid. White needles separated slowly and were washed with n-pentane and dried *in vacuo* (yield, 50%). The bromo complex was prepared by dissolving $HgBr_2$ (1.0 mmol) and DMP (1.0 mmol) in warm Me_2CO. Addition of n-pentane until turbidity yielded white

needles which were washed with benzene and n-pentane and dried *in vacuo* (yield, 50%). The solids obtained by adding a large amount of n-pentane to the mother solution were generally mixtures of 1 : 1 and 3 : 2 species. For this reason sample homogeneity was tested by examining the crystalline products under a stereo-microscope. As for the 1 : 1 adducts, these complexes readily release DMP in common solvents.

Measurements

IR spectra were recorded by using either a Perkin–Elmer 580B spectrophotometer (4000–400 cm^{-1}) or a Bruker FT IR instrument (500–100 cm^{-1}) as Nujol mulls between KBr and polyethylene discs. In KBr pellets the spectra of the DMTP adducts were as those in Nujol whereas for the DMP adducts, partial ligand release was observed. ^1H and ^{13}C NMR spectra were obtained by a Jeol FX 90Q spectrometer. Thermogravimetric measurements were carried out on Netzsch STA 429 equipment either in air or in nitrogen (flux rate, 250 cm^3 min^{-1}; heating rate, 5°C min^{-1}; reference material, neutral Al_2O_3). Melting points (uncorrected) were determined using a Buchi apparatus.

RESULTS AND DISCUSSION

Mercury halide adducts with DMTP (Table 1) were prepared either in dichloromethane or in acetone by using reagents in stoichiometric ratios. The synthesis of the $[Hg(DMP)X_2]_n$ (X = Cl or Br) complexes required a large ligand excess (*ca* 1 : 4), otherwise mixtures of species with a lower ligand content were isolated. In particular, crystalline samples of

Table 1. Analytical data and selected IR frequencies for the mercury complexes

Compound	Colour	Melting point (°C)[a]	Found (Calc.) (%) C	H	IR frequencies (cm^{-1})		
$[Hg(DMTP)_2Cl_2]$[b]	Orange	215–217	30.5 (30.5)	3.0 (2.9)	1636, 1617s	1546m	1107m
$[Hg(DMTP)_2Br_2]$[b]	Reddish orange	210–211	26.2 (26.2)	2.4 (2.5)	1635, 1616s	1546m	1105m
$[Hg(DMTP)_2I_2]$[b]	Orange	172–174	22.7 (22.9)	2.1 (2.2)	1638, 1630s	1547m	1101m
$[Hg(DMTP)Cl_2]_n$[c]	Pink	176–179	20.5 (20.4)	2.0 (2.0)	1628s	1539m	1108m
$[Hg(DMTP)Br_2]_n$[c]	Pink	179–180	16.7 (16.8)	1.6 (1.6)	1627s	1539m	1104m
$[Hg(DMTP)I_2]_n$[c]	Pink	155–157	14.0 (14.1)	1.4 (1.4)	1626s	1541m	1103m
$[Hg(DMP)Cl_2]_n$[d]	White	140–143	21.2 (21.2)	2.0 (2.0)	1664s	1590sh 1568m 1554sh	
$[Hg(DMP)Br_2]_n$[d]	White	123–125	17.3 (17.3)	1.7 (1.7)	1668s	1590sh 1568m 1554sh	
$(HgCl_2)_3(DMP)_2$[e]	White	132–134	16.0 (15.8)	1.6 (1.5)	1668s	1593sh 1584m 1553sh	
$(HgBr_2)_3(DMP)_2$[e]	White	125–127	12.5 (12.6)	1.2 (1.2)	1667s	1592sh 1580m 1559sh	

[a] With decomposition.
[b] $C_{14}H_{16}X_2HgO_2S_2$ (X = Cl, Br or I).
[c] $C_7H_8X_2HgOS$ (X = Cl, Br or I).
[d] $C_7H_8X_2HgO_2$ (X = Cl or Br).
[e] $C_{14}H_{16}X_6Hg_3O_4$ (X = Cl or Br).

the $(HgX_2)_3(DMP)_2$ (X = Cl or Br) species were obtained by adding n-pentane to dichloromethane or acetone solutions containing HgX_2 and ligand in a 1 : 1 molar ratio.

Thermograms of all the adducts either in air or in nitrogen indicate that total sublimation of samples takes place beyond 600°C. As shown in Fig. 1(a), degradation of $[Hg(DMP)Cl_2]_n$ in air starts at *ca* 120°C, the melting endotherm being observed at 142°C. Weight loss occurs in two close steps (endotherms at 240 and 290°C), resulting in a *ca* 6% residue at 300°C which is slowly released up to 480°C. Apart from different melting temperatures, the thermograms of $[Hg(DMP)Br_2]_n$ and $(HgX_2)_3(DMP)_2$ (X = Cl or Br), in air, follow a similar trend, with a 100% weight loss at 480°C. Thermograms in nitrogen are like those in air up to 300°C, the following process ending at *ca* 550°C. The complex $[Hg(DMTP)Cl_2]_n$ [Fig. 1(b)] melts with decomposition at 175°C, the experimental weight loss in the first step (16.2%) being close to the calculated value for evolution of half a DMTP molecule (17%) to form $(HgCl_2)_2(DMTP)$ as an intermediate. The exothermic processes which follow (297 and 470°C) end at 560°C with a total sample release. The $[Hg(DMTP)Br_2]_n$ curves do not show the initial step due to partial ligand evolution, as with the iodo derivative [Fig. 1(c)]. Near melting, $[Hg(DMTP)I_2]_n$ presents two close endotherms at 155 and 161°C, respectively, followed by the two broad exotherms at *ca* 350 and 510°C. Melting of the 1 : 2 DMTP complexes occurs at temperatures higher than those of the corresponding 1 : 1 adducts. In particular, $[Hg(DMTP)_2Cl_2]$ [Fig. 1(d)] melts at 214°C with evolution of one DMTP molecule, the experimental weight loss being 24.2% against a calculated value of 25.4%. The degradation trend that follows resembles that of the 1 : 1 complex, two broad exotherms being observed at 330 and 475°C. The thermograms of the 1 : 2 adducts support formation of the corresponding 1 : 1 species as degradation intermediates. Accordingly, $[Hg(DMTP)_2Br_2]$ loses 20.8% of the initial weight (calculated for one DMTP molecule, 21.9%) in the first decomposition step, the related value for $[Hg(DMTP)_2I_2]$ being 18.5% (versus a calculated value of 19.2%).

In the 1700–1500 cm^{-1} range the IR spectrum of DMTP contains a strong absorption at 1641 cm^{-1}, assigned to $\nu(C{=}C)$, and a medium one at 1559 cm^{-1}, due to ring vibrations.[18] The corresponding bands in DMP are observed at 1669 and 1599 cm^{-1}, respectively, the latter appearing as a shoulder of the strong $\nu(C{=}O)$ absorption at 1611 cm^{-1}. On coordination, the ring absorptions of both ligands shift slightly to low energy ($\Delta\nu$ = 10–20 cm^{-1}).[9,19] Accordingly, the $[Hg(DMTP)X_2]_n$ adducts present (Table 1) a strong $\nu(C{=}C)$ absorption at *ca* 1627 cm^{-1} which splits in the $[Hg(DMTP)_2X_2]$ complexes, suggesting a different bonding situation in

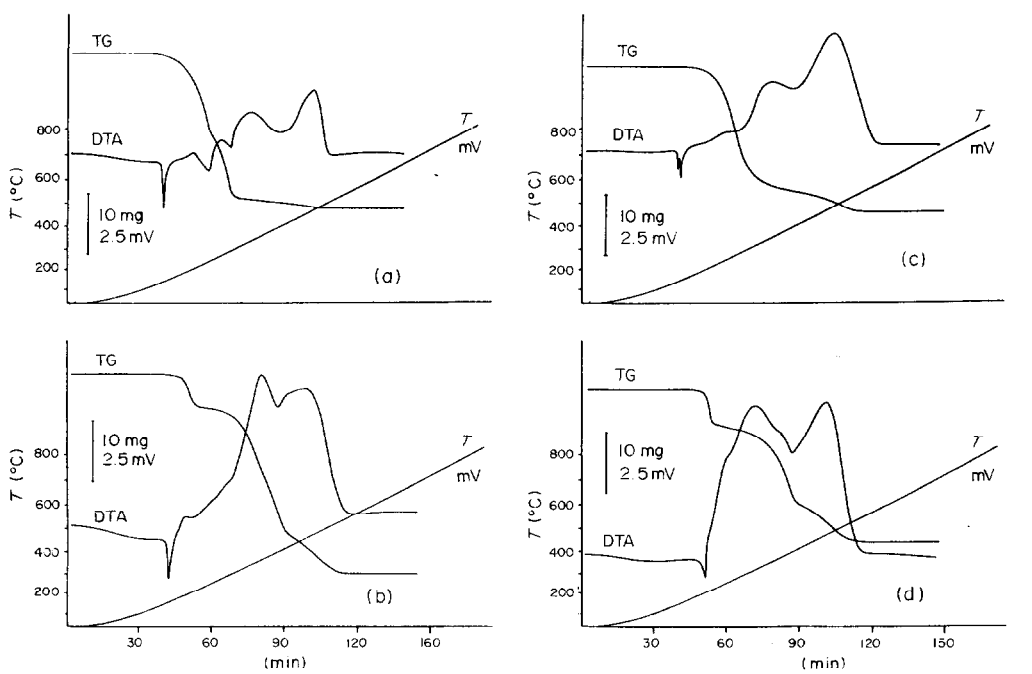

Fig. 1. Thermograms in air: (a) $[Hg(DMP)Cl_2]_n$ (25.60 mg); (b) $[Hg(DMTP)Cl_2]_n$ (32.39 mg); (c) $[Hg(DMTP)I_2]_n$ (24.11 mg); (d) $[Hg(DMTP)_2Cl_2]$ (24.56 mg).

the coordinated DMTP molecules. All DMTP adducts show the ring absorption at *ca* 1540 cm^{-1}, whereas the ν(C=S) band falls at *ca* 1105 cm^{-1} (versus 1095 cm^{-1} in free ligand). As expected, the IR spectra suggest that DMP is a weaker donor in mercury complexes than in lanthanide complexes.[19] In fact, the ring absorptions (Table 1; *ca* 1667 and 1592 cm^{-1}) are close to those of free DMP and the low energy shift of ν(C=O), of order 30 cm^{-1} for $(HgX_2)_3(DMP)_2$ (*ca* 1582 cm^{-1}) and 40 cm^{-1} for $[Hg(DMP)X_2]_n$ (1568 cm^{-1}), is smaller than in lanthanide complexes ($\Delta\nu$, 60–80 cm^{-1}).

Below 500 cm^{-1}, the IR spectra of the 1:2 DMTP adducts contain two bands assignable to mercury–halide bond vibrations (Table 2). When mercury is involved in a distorted tetrahedral arrangement with approximate C_{2v} symmetry, two mercury–halide stretching vibrations should be expected, due to symmetric and asymmetric modes. IR spectra of structurally similar 1:2 complexes sometimes show one (asymmetric) mercury–halide absorption, the symmetric vibration mode being Raman-active as for pyridine or phosphine adducts.[20,21] For a number of mercury chloride complexes there is a good correlation between the position of the high energy mercury–chloride band and the bond distance in such a way that the bond distance increases and consequently ν(Hg—Cl) decreases with the donor atom bond strength.[22] As is shown in Fig. 2, the $[Hg(DMTP)_2Cl_2]$ spectrum contains two strong ν(Hg—Cl) absorptions at 248 and 223 cm^{-1}, the strong $\delta(HgCl_2)$ absorption being observed at 94 cm^{-1}. The band at 223 cm^{-1} shows shoulders common to the iodo complex and due to ligand vibrations. In the $[Hg(DMTP)_2Br_2]$ spectrum a mercury–bromide stretching contribution to the medium band at 202 cm^{-1} can be ruled out owing to the presence of a band of similar shape and intensity in the spectra of platinum and palladium adducts. In the $[Hg(DMTP)_2I_2]$ spectrum the medium band at 123 cm^{-1} has been tentatively assigned to mercury–iodide stretching, because a smaller mercury–iodide band separation is usually observed in the spectra of 1:2 mercury iodide adducts with sulphur and phosphorus donors. The mercury–halogen bands observed in the IR spectra of 1:1 adducts are usually assigned to ν(Hg—X) modes associated with vibrations of terminal (high energy) and bridging (low energy) Hg—X bonds, the terminology used for halide-bridged dimers being extended to *catena* polymers. The separation of $\nu(Hg—X)_t$ and $\nu(Hg—X)_b$ bands is large, especially for chloro derivatives. In a series of 1:1 adducts with phosphines the $(Hg—Cl)_t$ absorptions are independent of the structure (dimeric or polymeric) and are observed in the 300–

Table 2. IR frequencies in the 450–100 cm^{-1} region [ν(Hg—X) in italics]

Compound	Frequencies (cm^{-1})											
$[Hg(DMTP)_2Cl_2]$		463vvw	418m	301vvw	285sh	278w	248s	223s	216sh	208sh	132vvw	125vvw	94vs
$[Hg(DMTP)_2Br_2]$		464vvw	420m	294sh	286mw	275m			202m	*171, 160*ms	130vw		88m
$[Hg(DMTP)_2I_2]$		464w	419m	293vw		277m			202m	197sh	*145*m	*123*m[b]	
$[Hg(DMTP)Cl_2]_n$		470vvw	416w	329w		[a]	278s		204sh	*195*sbr	166sh	152sh	126vvw	98s
$[Hg(DMTP)Br_2]_n$		469vvw	416m	322mw		278mw			205mw	*188*m	153sh	*136*mbr	122vvw	106vwbr
$[Hg(DMTP)I_2]_n$		466w	416m	307m		274mw			206m		159sh	*144*m	*117*m	81w
$[Hg(DMP)Cl_2]_n$			355vw	*337*s	296vvw	281vw				188m			123sh	95vs
$[Hg(DMP)Br_2]_n$			353m			280w	*240*s			188m			124vw	116sh
$(HgCl_2)_3(DMP)_2$			*358*ms	*327*s		277w			221vvw	195w	182sh		108sh	98vs
$(HgBr_2)_3(DMP)_2$			354m			280w	256ms	*233*s		195w	184sh		119vw	

[a] Obscured by the strong mercury–chloride absorption.
[b] Tentative assignment.

Table 3. NMR data (ppm: *T*, *ca* 25°C; solvent, d_6-Me_2SO)[a]

Compound	^1H NMR CH	^1H NMR CH_3	^{13}C NMR CS	^{13}C NMR COC	^{13}C NMR CH	^{13}C NMR CH_3
DMTP	6.96	2.23	200.7	159.8	123.6	18.5
DMTP[b]	6.93	2.18	201.8	158.9	124.5	19.2
$[Hg(DMTP)_2Cl_2]$	7.50	2.41	194.0	164.7	122.4	19.3
$[Hg(DMTP)_2Cl_2]$[b]	7.73	2.47				
$[Hg(DMTP)_2Br_2]$	7.49	2.40	193.8	164.8	122.2	19.3
$[Hg(DMTP)_2Br_2]$[b]	7.51	2.42				
$[Hg(DMTP)_2I_2]$	7.33	2.37	194.0	164.8	122.2	19.3
$[Hg(DMTP)_2I_2]$[b]	7.43	2.41	190.2	162.0	123.5	19.6
$[Hg(DMTP)Cl_2]_n$[c]	7.80	2.54	188.5	168.2	121.6	19.9
$[Hg(DMTP)Br_2]_n$[c]	7.73	2.51	190.1	167.3	121.7	19.7
$[Hg(DMTP)I_2]_n$	7.67	2.49	191.0	166.9	121.6	19.6
$[Hg(DMTP)I_2]_n$[b]	7.70	2.47				

[a] Spectra were recorded within 3 h of solution preparations.
[b] In $CDCl_3$.
[c] Almost insoluble in $CDCl_3$.

270 cm^{-1} range, whereas the position and the number of the bands arising from bridge vibrations vary with the adduct configuration.[23] The room temperature spectra of the $[Hg(DMTP)X_2]_n$ adducts (Table 2), which contain one absorption for either terminal or bridging mercury–halide bonds, could support a dimeric structure of the complexes. Conversely the coincidence of the high energy mercury–chloride absorption in $[Hg(DMTP)Cl_2]_n$ (278 cm^{-1}) with those of the polymeric $[Hg(EtOSCNMe_2)Cl_2]_n$ (280 cm^{-1}) and [Hg(N,N′-diethylimidazolidine-2-thione)$Cl_2]_n$ (280 cm^{-1}) complexes does not allow clarification of the bonding framework. Owing to the weak intereaction with oxygen donors, the mercury–halide molecules deviate slightly from linearity in complexes of the type $[Hg(L)X_2]_n$, in which L is Ph_2SO, 1,4-dioxane or tetrahydrofuran.[16,24] Consequently, the strong IR bands associated with the asymmetric ν(Hg—X) vibrations are close to those of free mercury halides[15,16,21,24] and are observed at 362 cm^{-1} for $[Hg(Ph_2SO)Cl_2]_n$, at 353 cm^{-1} for [Hg(1,4-dioxane)$Cl_2]_n$ and at 252 cm^{-1} for [Hg(tetrahydrofuran)$Br_2]_n$. Accordingly, the $[Hg(DMP)X_2]_n$ (X = Cl or Br) spectra (Table 2) show one strong ν_{as}(Hg—X) absorption (Cl, 337 cm^{-1}; Br, 240 cm^{-1}) at low energy with respect to the corresponding absorption in the above reported oxygen-bound adducts, suggesting a stronger Hg—O bond. The two strong mercury–halide bands, 20–30 cm^{-1} apart, in the $(HgX_2)_3(DMP)_2$ (X = Cl or Br) complex spectra could support a structural arrangement similar to that of $(HgCl_2)_3(Me_2SO)_2$.[17] The high energy bands (Cl, 358 cm^{-1}; Br, 256 cm^{-1}) should descend from ν_{as}(Hg—X) vibrations of the nearly linear HgX_2 molecules, whereas the low energy bands (Cl, 327 cm^{-1}; Br, 233 cm^{-1}) should be originated from the corresponding vibrations of the distorted HgX_2 molecules held by oxygen bridges to form dimeric units.

Owing to the presence of weak Hg—O bonds, the mercury halide DMP complexes readily release ligand molecules in solution. Proton NMR spectra of the complexes in deuterated chloroform and acetone contain the free DMP signals at *ca* 6.0 (ring CH) and 2.2 pm (CH_3). In contrast, the NMR spectra of the DMTP adducts (Table 3) are consistent with the coordinated ligand in either $CDCl_3$ or $(CD_3)_2SO$. On coordination both CH and CH_3 proton signals shift downfield, the effect being larger for the CH protons (0.4–0.8 ppm). Whereas $CDCl_3$ solutions of the complexes do not change over several days, $(CD_3)_2SO$ solutions begin to darken overnight. On standing for *ca* 1 week they form violet solutions and separate mixtures of unidentified violet and brown solids. For this reason the carbon spectra of Table 3 were recorded within 3 h of sample solubilization. As for the previously reported $[M(DMTP)_2X_2]$ (X = Pd or Pt) complexes, the CS carbon resonance appears upfield in the mercury complexes, with respect to free DMTP (Δppm, 4–11), whereas an opposite downfield shift is observed for the signal of the ring carbon atoms bound to oxygen (Δppm, 5–8). Carbon NMR spectra in dimethyl sulphoxide, recorded 1 day after sample solubilization, contain

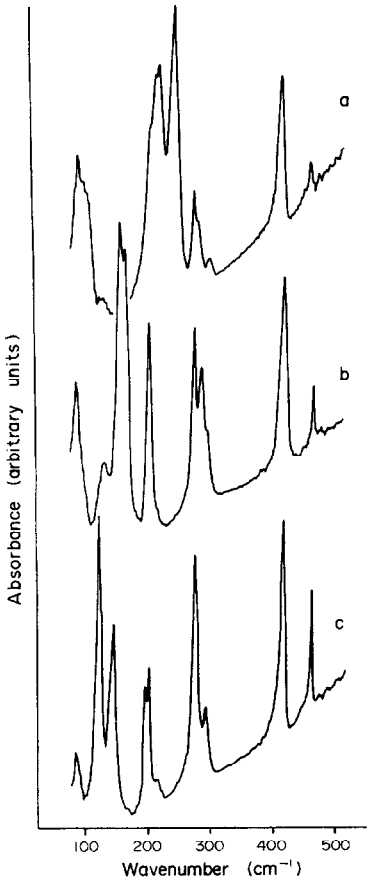

Fig. 2. IR spectra of $[Hg(DMTP)_2X_2]$: (a) X = Cl; (b) X = Br; (c) X = I.

a number of weak signals in addition to the strong resonances reported in Table 3. As an example, the $[Hg(DMTP)Br_2]_n$ spectrum displays weak signals at 185, 179 and 119 ppm, which do not coincide with free DMTP resonances.

Acknowledgements—The authors thank Mrs Franca Marzola for recording the far-IR spectra. One of us (Z.G.) thanks the Ministero degli Affari Esteri of Italy for an annual grant.

REFERENCES

1. A. Castiñeiras, A. Arquero and J. R. Masaguer, *Transition Met. Chem.* 1984, **9**, 273.
2. A. Arquero, J. R. Masaguer and A. Castiñeras, *Z. Anorg. Allg. Chem.* 1985, **531**, 183.
3. A. Castiñeiras, A. Arquero, J. R. Masaguer, S. Martinez-Carrera and S. Garcia-Blanco, *Z. Anorg. Allg. Chem.* 1986, **539**, 219.
4. M. Cannas, F. A. Devillanova, G. Morongiu and G. Verani, *J. Inorg. Nucl. Chem.* 1981, **43**, 2383.
5. P. L. Bellon, F. Demartin, F. A. Devillanova, F. Isaia and G. Verani, *J. Coord. Chem.* 1988, **18**, 253.
6. A. Castiñeiras, C. F. Vidal, R. Bastida, A. Macias and W. Hiller, *Polyhedron* 1988, **7**, 2503.
7. G. Faraglia, R. Graziani, L. Sindellari, E. Forsellini and U. Casellato, *Inorg. Chim. Acta* 1982, **58**, 167.
8. G. Faraglia, L. Sindellari and B. Zarli, *Inorg. Chim. Acta* 1981, **53**, L245.
9. G. Faraglia, F. Barbaro and S. Sitran, *Transition Met. Chem.* 1990, **15**, 242.
10. C. Airoldi, A. P. Chagas and F. P. Assunção, *J. Chem. Soc., Dalton Trans.* 1980, 1823.
11. C. Airoldi, A. P. Chagas and F. P. Assunção, *Can. J. Chem.* 1982, **60**, 2132.
12. F. P. Assunção, A. P. Chagas and C. Airoldi, *J. Chim. Phys.* 1982, **79**, 253.
13. O. A. De Oliveira, A. P. Chagas and C. Airoldi, *Inorg. Chem.* 1983, **22**, 136.
14. M. L. C. P. da Silva, A. P. Chagas and C. Airoldi, *J. Chem. Soc., Dalton Trans.* 1988, 2113.
15. P. Biscarini, L. Fusina and G. D. Nivellini, *J. Chem. Soc., Dalton Trans.* 1972, 1003.
16. P. Biscarini, L. Fusina, G. D. Nivellini, A. Mangia and G. Pelizzi, *J. Chem. Soc., Dalton Trans.* 1973, 159.
17. P. Biscarini, L. Fusina, G. D. Nivellini, A. Mangia and G. Pelizzi, *J. Chem. Soc., Dalton Trans.* 1974, 1846.
18. A. R. Katritzky and R. Alan Jones, *Spectrochim. Acta* 1961, **17**, 64.
19. S. Sitran, D. Fregona and G. Faraglia, *J. Coord. Chem.* 1989, **20**, 193.
20. I. Persson, M. Sandström, P. L. Goggin and A. Mosset, *J. Chem. Soc., Dalton Trans.* 1985, 1597.
21. N. A. Bell, T. D. Dee, P. L. Goggin, M. Goldstein, R. J. Goodfellow, T. Jones, K. Kessler, D. M. McEwan and I. W. Nowell, *J. Chem. Res. (S)* 1981, 2.
22. L. V. Konovalov and K. A. Davarski, *J. Coord. Chem.* 1986, **14**, 201.
23. N. A. Bell, M. Goldstein, T. Jones and I. W. Nowell, *Inorg. Chim. Acta* 1983, **69**, 155.
24. M. Kobayashi, M. Kohyama and H. Tadokoro, *J. Chem. Phys.* 1977, **66**, 4277.

Polyhedron Vol. 10, No. 3, pp. 359–364, 1991
Printed in Great Britain

0277–5387/91 $3.00+.00
© 1991 Pergamon Press plc

KINETICS OF THE REDOX REACTION BETWEEN $Mo_2O_4^{2+}$ AND VO_2^+ IN $HClO_4$ MEDIUM

D. O. MÁRTIRE, M. R. FÉLIZ* and A. L. CAPPARELLI†‡

Instituto de Investigaciones Fisicoquimicas Teóricas y Aplicadas (INIFTA), Facultad de Ciencias Exactas, Universidad Nacional de La Plata, Casilla de Correo 16, Sucursal 4, (1900) La Plata, Argentina

(*Received* 15 *June* 1990; *accepted* 5 *October* 1990)

Abstract—The kinetics of the oxidation of $Mo_2O_4^{2+}$ with VO_2^+ in $HClO_4$ medium at 25°C and ionic strength 2 M has been studied by the stopped-flow method. Under conditions of excess VO_2^+, the experimental rate constant is represented by the expression:

$$k_{app} = \frac{(1238[H^+]+811)}{(5.50\times10^{-4}+[H^+][VO_2^+])}[VO_2^+]^2.$$

This rate law can be interpreted by the following mechanism:

$$D \rightleftharpoons DOH + H^+ \quad \text{(I)}$$

$$D + VO_2^+ \underset{k_{-2}}{\overset{k_2}{\rightleftharpoons}} C + H^+ \quad \text{(II)}$$

$$DOH + VO_2^+ \underset{k_{-3}}{\overset{k_3}{\rightleftharpoons}} C \quad \text{(III)}$$

$$H^+ + C + VO_2^+ \xrightarrow{k_4} 2Mo^{VI} + 2V^{IV}, \quad \text{(IV)}$$

where D is $Mo_2O_4^{2+}$ and C an intermediate complex. For this mechanism, $k_2 = 1238$ $M^{-1}\,s^{-1}$, $k_3K_1 = 811\ s^{-1}$ and $k_{-3}/k_4 = 5.00\times10^{-4}\ M^2$. Limiting values for the individual constants can be estimated and the nature of the intermediate is discussed.

The kinetics of the oxidation of molybdenum(V) with different reactants has been the subject of several investigations.[1–9] The kinetics of the reaction between VO_2^+ and molybdenum(V) has already been studied by Issa *et al.*[10] in the highly complexing HCl medium via stopped-flow techniques. These authors worked in the proton concentration range 1–0.23 M HCl and ionic strength 1 M (NaCl). The pseudo first-order rate constant was found to be a function of the proton concentration but independent of the initial concentration of both reactants. They also reported very few results obtained in 1 M $HClO_4$ medium and also proposed that the effect of ClO_4^- would retard the reaction.

The present study was carried out in non-complexing perchloric medium in the concentration range 0.2–2 M ($HClO_4$) and ionic strength 2 M(Na ClO_4). Under our experimental conditions, molybdenum(V) is present as $Mo_2O_4(H_2O)_6^{2+}$. The experimental behaviour of the system and the measured rate law differ from those obtained in HCl. Therefore, the medium plays an important role in the kinetics and mechanism of this reaction.

EXPERIMENTAL

Aqueous solutions of $Mo_2O_4^{2+}$ were prepared according to Cayley and Sykes.[11] The $Mo_2O_4^{2+}$ concentration was determined at $\lambda = 384$ nm ($\varepsilon = 103\ M^{-1}\,cm^{-1}$).[12]

Reagent grade $NaClO_4\cdot H_2O$ (Merck), $HClO_4$ (Merck), $NaVO_3$ (Fluka), $VOCl_2$ (Carlo Erba) and

* Member of CICPBA.
† Member of CONICET.
‡ Author to whom correspondence should be addressed.

$Na_2MoO_4 \cdot 2H_2O$ (Merck) were used without further purification.

Absorption measurements were carried out by means of a Cary 14 spectrophotometer, while the kinetics of the reaction was followed spectrophotometrically using a Durrum-D110 stopped-flow apparatus. Most of the kinetic studies were carried out at $\lambda = 360$ nm and the ε values at this wavelength are (M^{-1} cm^{-1}) $Mo_2O_4^{2+}$, 92.5; VO_2^+, 73.5; Mo^{VI}, 14.2; and VO^{2+}, 2.0.

RESULTS AND DISCUSSION

Products and stoichiometry

The stoichiometry was determined by a spectrophotometric titration. The mole ratio of VO_2^+ to $Mo_2O_4^{2+}$ was 2.1 ± 0.1, in agreement with the oxidation of $Mo_2O_4^{2+}$ to molybdenum(VI) and the reduction of VO_2^+ to VO^{2+}. The formation of VO^{2+} was verified by comparison of the absorption spectra of the reaction mixture recorded on a Cary 14 spectrophotometer with that of a solution of $VOCl_2$ in the range 600–850 nm.

Kinetic results

The pseudo first-order rate constants (k_{app}) determined are presented in Table 1.

The experiments reported in Table 1 can be arranged into two groups:

(a) *Excess of* VO_2^+. The plots of apparent rate constants (k_{app}) against VO_2^+ initial concentrations at constant pH show a linear dependence. However, some of the straight lines obtained have negative intercepts. Therefore, a complex mechanism should be expected.

By plotting $[H^+][VO_2^+]^2/k_{app}$ against $[VO_2^+]$, a family of straight lines was found (their slopes are listed in Table 2). As shown in Fig. 1, a linear regression with proton concentration is found. In a similar way, $[VO_2^+]^2/k_{app}$ plotted against $[H^+][VO_2^+]$ appear to be linear but their slopes are reciprocal functions of $[H^+]$ (see Table 2).

An exhaustive analysis of the experimental data shows that the best fit is given by the following equation:

$$k_{app} = \frac{(1238[H^+]+811)}{(5.5\times10^{-4}+[H^+][VO_2^+])}[VO_2^+]^2. \quad (1)$$

(b) *Excess of dimer.* In an attempt to determine the reaction order with respect to the dimer, apparent rate constants were evaluated in excess dimer and are listed in Table 1. These rate constants were found to be proportional to the initial concentration of dimer.

Table 1. Apparent rate constants for the $Mo_2O_4^{2+}/VO_2^+$ reaction ($\mu = 2.0$ M $NaClO_4$, $t = 25°C$)

(a) Excess of VO_2^+ $[Mo_2O_4^{2+}] = 0.25$ mM, $\lambda = 360$ nm		
$[HClO_4]$ (M)	$[VO_2^+]$ (mM)	$k_{app} \pm \sigma$ (s^{-1})
0.2	1	1.33±0.05
0.2	2	4.5±0.35
0.2	3	9.4±0.72
0.2	4	13.6±1.95
0.2	5	15.8±1.28
0.3	1	1.49±0.08
0.3	2	4.7±0.12
0.3	3	9.1±1.34
0.3	4	14.3±1.10
0.3	5	15.4±2.70
0.4	1	1.28±0.07
0.4	2	3.4±0.15
0.4	3	6.0±0.41
0.4	4	7.7±0.11
0.4	5	11.3±0.85
0.5	1	1.72±0.05
0.5	2	3.86±0.04
0.5	3	4.9±0.11
0.5	4	7.0±0.14
0.5	5	8.3±0.29
0.5	10	15.2±0.70
1.5	1	2.38±0.07
1.5	3	6.7±0.23
1.5	4	8.0±0.43
1.5	5	9.7±0.94
1.5	10	17.8±1.51
2.0	1	1.76±0.15
2.0	2	4.1±1.13
2.0	3	5.9±0.26
2.0	4	7.4±0.41
2.0	5	7.1±0.35
2.0	6	10.9±0.52
(b) Excess of dimer $[VO_2^+] = 0.5$ mM, $\lambda = 0.36$ mm		
$[HClO_4]$ (M)	$[Mo_2O_4^{2+}]$ (mM)	$k_{app} \pm \sigma$ (s^{-1})
2.0	0.5	0.60±0.02
2.0	1.0	2.7±0.10
2.0	1.5	4.4±0.31
2.0	2.5	5.8±0.37

Analysis of the intermediate spectrum

Mixtures of solutions of $Mo_2O_4^{2+}$ and VO_2^+ were followed by means of the stopped-flow technique, at different wavelengths. The time resolution of the obtained spectra employing a computational program[13] allowed us to conclude that this reaction proceeds via the formation of an intermediate with

Table 2.

(a) Slopes from plotting $[VO_2^+]^2[H^+]/k_{app}$ against $[VO_2^+]$

$[H^+]$ (M)	slope (10^{-3} M^2 s)	r^a
0.2	0.04	0.95
0.3	0.12	0.94
0.4	0.15	0.99
0.5	0.34	0.99
1.5	0.88	0.99
2.0	1.15	0.94

(b) Slopes from plotting $[VO_2^+]^2/k_{app}$ against $[H^+][VO_2^+]$

$[H^+]$ (M)	slope (10^{-4} M s)	r^a
0.2	9.50	0.97
0.3	7.25	0.95
0.4	9.43	0.99
1.5	3.59	0.999
2.0	3.12	0.97

[a] Correlation coefficient.

an absorption maximum at around 330 nm. Its spectrum is shown in Fig. 2.

Efforts to detect an absorbing species different from VO^{2+} in the near-IR region (at about 750 nm), using the stopped-flow technique, were negative.

Influence of products

It was found that the addition of MoO_4^{2-} to the reaction mixtures did not affect the reaction kinetics.

The absorbances of solutions containing $Mo_2O_4^{2+}$ and VO^{2+} were measured. The mixtures of both species were found to be accompanied by changes in absorbance. However, if the only effect of VO^{2+} is the complexing of $Mo_2O_4^{2+}$, its influence on the kinetics should not be observed under conditions of excess VO_2^+. This was verified by addition of VO^{2+} to the mixtures of VO_2^+ and

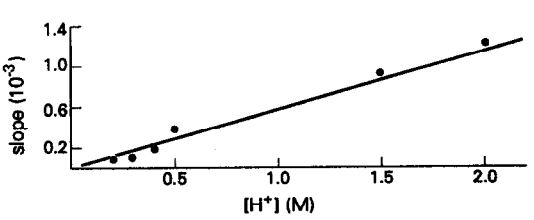

Fig. 1. Slopes obtained from the plots of $[H^+][VO_2^+]^2/k_{app}$ against $[H^+]$.

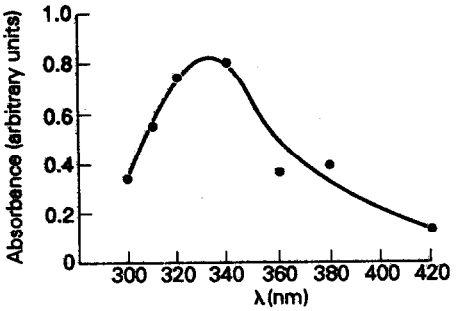

Fig. 2. Absorption spectrum for the intermediate, C, as obtained from the time-resolved stopped-flow traces.

$Mo_2O_4^{2+}$ in a series of stopped-flow experiments. The results are summarized in Table 3.

Mechanism

A dependence on VO_2^+ concentration similar to that represented by eq. (2) was observed for apparent rate constants in the oxidation of catechol, catechol derivatives and hydrazine[13] by VO_2^+.

To account for the observed rate law represented by eq. (1) and the linear dependence of k_{app} on dimer concentration under conditions of excess dimer, the following scheme is proposed:

$$D \overset{K_1}{\rightleftharpoons} DOH + H^+ \quad \text{(I)}$$

$$D + V \underset{k_{-2}}{\overset{k_2}{\rightleftharpoons}} C + H^+ \quad \text{(II)}$$

$$DOH + V \underset{k_{-3}}{\overset{k_3}{\rightleftharpoons}} C \quad \text{(III)}$$

$$H^+ + C + V \xrightarrow{k_4} \text{Products} \quad \text{(IV)}. \quad (2)$$

For the sake of simplicity D is $Mo_2O_4^{2+}$ and C, a complex intermediate.

Table 3. Effect of VO^{2+} on the kinetics of the reaction between $Mo_2O_4^{2+}$ and VO_2^+, $[VO_2^+]_0 = 2$ mM, $[Mo_2O_4^{2+}]_0 = 0.25$ mM and $[HClO_4] = 2$ M

$10[VO^{2+}]_0$ (mM)	$k_{app} \pm \sigma$ (s^{-1})
1	3.03±0.16
2	3.05±0.02
3	3.13±0.19
4	3.14±0.17
5	3.29±0.16
10	3.15±0.08
15	3.43±0.20
20	3.18±0.24

The formation of transient species prior to the electron-transfer process has been postulated for other oxidations by VO_2^+ in acidic media.[14-16] In other VO_2^+ oxidations[13,17-19] there is direct evidence for the formation of an intermediate complex.

An alternative pathway could involve $HOVO^{2+}$ as oxidant. This species has been postulated in solutions of high sulphuric acid concentrations (> 2 M), however no physical evidence has been provided to support its existence under our present conditions.[20-22]

A pathway similar to (IV) was proposed in the literature for the oxidation of catechol and catechol derivatives.[13]

As a consequence of the observed first-order rate law in the dimer, no dissociative pathway for $Mo_2O_4^{2+}$ was included in the present mechanism. Furthermore, no oxidant-independent term was observed. A similar behaviour has been observed in other redox reactions where the $Mo_2O_4^{2+}$ dimer participates.[7,8] The absence of an oxidant-independent term suggests the retention of at least one oxo-bridge during the oxidation process.

The equilibrium (I) involves the presence of $Mo_2O_4(H_2O)_5OH^+$, whose reactivity has been postulated in the literature.[5,9] The equilibrium constant for the substitution of H_2O by OH— was determined for the Mo_2O_4(Hedta) complex,[23] where a value of the order of 1×10^{-3} M has been reported. The expected value for that constant in the $Mo_2O_4(H_2O)_6^{2+}$ complex is approx. 1×10^{-2} M.[4,5]

By applying the steady-state condition to C and assuming that $k_{-2}[H^+] \ll k_{-3}+k_4[VO_2^+][H^+]$, the following expression for the apparent rate constant under excess of VO_2^+ is found:

$$k_{app} = \frac{(k_2[H^+]+K_1k_3)}{(k_{-3}/k_4+[VO_2^+][H^+])}[VO_2^+]^2. \quad (3)$$

By comparison with the experimental expression (1), we obtain

$$k_2 = 1238\ M^{-1}s^{-1}$$
$$k_3K_1 = 811\ s^{-1}$$
$$k_{-3}/k_4 = 5.5 \times 10^{-4} M^2. \quad (4)$$

The molar absorptivity of the intermediate (C) can be estimated from the analysis of the initial absorbance, A_0, as measured at $\lambda = 360$ nm for a series of experiments under conditions of excess VO_2^+ in 2 M $HClO_4$. Let us define ΔA_0 as the difference between A_0 and the absorbance value corresponding to a mixture of VO_2^+ and $Mo_2O_4^{2+}$ without interaction under the same experimental conditions. The ΔA_0 values are given in Table 4.

Table 4. ΔA_0 values for a series of stopped-flow experiments in excess of dimer

$[VO_2^+]_0 \times 10^2$ (M)	$[Mo_2O_4^{2+}]_0 \times 10^3$ (M)	ΔA_0
0.5	1.00	0.473
0.5	0.50	0.235
0.5	0.37	0.256
0.5	0.25	0.160
0.5	0.12	0.053
1.0	1.00	1.486
1.0	0.50	0.591
1.0	0.37	0.579
1.0	0.25	0.387
1.0	0.12	0.201
2.0	1.00	2.502
2.0	0.50	0.934
2.0	0.37	0.438
2.0	0.25	0.683
2.0	0.12	0.330

The C concentration can be easily calculated taking into account that for the experiments reported in Table 4, $[VO_2^+]_0 \gg [Mo_2O_4^{2+}]_0$. The following expression can be derived for ΔA_0

$$\Delta A_0 = \frac{(K[VO_2^+]_0)}{(1+K[VO_2^+]_0)}(\varepsilon_C-\varepsilon_D)l[Mo_2O_4^{2+}]_0, \quad (5)$$

where $K = K_2/[H^+]$; ε_C and ε_D are the molar absorptivities of the intermediate and $Mo_2O_4^{2+}$, respectively. The plots of ΔA_0 against $[VO_2^+]_0[Mo_0O_4^{2+}]_0$ are straight lines with an intercept at zero and a slope of 1.64×10^5. These results are consistent with $K[VO_2^+]_0 \ll 1$.

From the experimental conditions given in Table 4 (with $l = 2$ cm), we can estimate $K \ll 50$ and $K_2 \ll 100$. An extinction coefficient of the intermediate, $\varepsilon_C \gg 1.64 \times 10^3\ M^{-1}\ cm^{-1}$ at $\lambda = 360$ nm, can be obtained.

This value of ε_C could mean that the intermediate, C, may be treated as a charge-transfer complex.

From the values for $K_1(\sim 1 \times 10^{-2})$ and $K_2(\ll 100)$, limit values are obtained for the individual rate constants, i.e. $k_{-2} \gg 12\ M^{-1}\ s^{-1}$, $k_3 > 8 \times 10^4\ M^{-1}\ s^{-1}$. Since $k_3 < k_4$, then $k_4 \gg 8 \times 10^4\ M^{-1}\ s^{-1}$ and $k_{-3} > 44\ s^{-1}$.

Since k_2 is lower than k_3 it is assumed that reaction (II) involves the formation of a protonated complex species (CH), whose deprotonation is the rate-determining step. In the frame of the oxidation reactions by VO_2^+, the value for k_4 is in agreement with the large redox potential couple Mo^V/Mo^{VI}.[29] At this point, some comments as to whether the reaction proceeds via an inner- or outer-sphere mechanism are pertinent.

For reaction (III), using an estimated value of 0.078 M for the outer-sphere association constant (K_{1p}), the first-order rate constant for the outer-sphere precursor complex, $k = k_3/K_{1p}$, is 1.04×10^6 s^{-1}, which can be compared with k_0 for both reactants. The water exchange rate constant (k_0) for $Mo_2O_4^{2+}$ is 2.9×10^4 s^{-1} as evaluated from the complexation of $Mo_2O_4^+$ by SCN^-.[9] For VO_2^+, k_0 is unknown,[24–26] but a lower limit of 6×10^4 s^{-1} was estimated by Kustin *et al.*[27] This value is too high for substitution of $Mo_2O_4^{2+}$. Regarding VO_2^+, the k value also seems to be higher than that estimated by Kustin *et al.* and therefore, we could be tempted to assume that the reaction proceeds via an outer-sphere mechanism. Moreover, no examples of inner-sphere activated complexes with water as a bridging ligand are known.[30,31] Although this type of electron-transfer process has been proposed for different reactions where either $Mo_2O_4^{2+}$ or VO_2^+ participate,[5,13] both ions may also behave as inner-sphere reactants.[7,8,28]

Regarding the previous study,[10] the different behaviour observed can be attributed to the nature of the reactants involved and the intermediate species. In HCl medium, different chloro complexes of molybdenum(V) can exist in equilibrium,[30] $Mo_2O_4Cl_6^{4-}$ and $Mo_2O_3Cl_8^{4-}$ being the most important species. The intermediate spectrum reported by Issa *et al.* shows a maximum at around 440 nm which seems to be coincident with that observed for $Mo_2O_3Cl_8^{4-}$.[31] Moreover, flash photolysis studies performed on $Mo_2O_4Cl_6^{4-}$ reported the formation of a monobridged intermediate whose spectrum presents a maximum at 420 nm.[32]

The intermediate detected in the present paper has an absorption maximum at around 330 nm. Some polyoxometallates of molybdenum and vanadium also absorb in this region.[33] Moreover, mixed-valence complexes of Mo^V—Mo^{VI} are characterized by strong bands at around 306 nm with ε of 4×10^3 M^{-1} cm^{-1}. Therefore complex C could be considered as a mixed-valence successor complex. An OH or/and oxo-group could bridge both reactants. This assumption is supported by the ability of VO^{2+} to complex $Mo_2O_4^{2+}$.

The rate laws obtained in this present work and in the previous study are quite different; a consequence of the nature of the molybdenum(V) and intermediate species in non-complexing and highly complexing media.

Acknowledgements—This work was supported, in part, by the Consejo Nacional de Investigaciones Científicas y Técnicas de la República Argentina (CONICET) and Comisión de Investigaciones Científicas de la Provincia de Buenos Aires (CICPBA). Some of the equipment and chemicals used in the present work were provided by the cooperation agreement between the University of Mainz and the Universidad Nacional de La Plata. D.O.M. wishes to thank the CICPBA for a Research Studentship.

REFERENCES

1. E. P. Guymon and J. T. Spence, *J. Phys. Chem.* 1966, **70**, 1964.
2. E. P. Guymon and J. T. Spence, *J. Phys. Chem.* 1967, **71**, 1616.
3. R. K. Wharton, J. F. Ojo and A. G. Sykes, *J. Chem. Soc., Dalton Trans.* 1975, 1526.
4. Y. Sasaki, *Bull. Chem. Soc. Japan* 1977, **50**, 1939.
5. G. R. Cayley, R. S. Raylor, R. K. Wharton and A. G. Sykes, *Inorg. Chem.* 1977, **16**, 1377.
6. R. D. Taylor, P. G. Todd, N. D. Chasteen and J. T. Spence, *Inorg. Chem.* 1979, **18**, 44.
7. R. McAllister, K. W. Hicks, M. A. Hurless, S. T. Pittenger and R. W. Gedridge, *Inorg. Chem.* 1982, **21**, 4098.
8. G. A. Chappelle, A. MacStay, S. T. Pittenger, K. Ohashi and K. W. Hicks, *Inorg. Chem.* 1984, **23**, 2768.
9. H. Diebler and C. Millan, *Polyhedron* 1986, **5**, 5539.
10. F. A. Issa, K. Grzeskowiak, C. Halliday, A. Herry and S. T. Pittenger, *Inorg. Chem. Acta* 1987, **130**, 85.
11. G. R. Cayley and A. G. Sykes, *Inorg. Chem.* 1976, **15**, 2882.
12. N. H. Furman and W. M. Murray, *J. Am. Chem. Soc.* 1936, **15**, 1689.
13. K. Kustin, C. Nicolini and D. L. Tappen, *J. Am. Chem. Soc.* 1974, **96**, 7416.
14. G. V. Bakore and R. Shanker, *Can. J. Chem.* 1966, **44**, 1717.
15. J. R. Jones, W. A. Waters and J. S. Littler, *J. Chem. Soc.* 1961, 630.
16. G. V. Bakore and N. C. Bharga, *Z. Phys. Chem. (Leipzig)* 1966, **120**, 120.
17. G. A. Dean, *Can. J. Chem.* 1961, **39**, 1174.
18. J. S. Littler and W. A. Walters, *J. Chem. Soc.* 1959, 14046.
19. W. F. Pickering and A. McAuley, *J. Chem. Soc. A* 1968, 1173.
20. R. M. Adams, *Pure Appl. Chem.* 1972, **30**, 683.
21. M. R. Churchill, A. H. Reis Jr, J. W. Francis and M. W. Hawthorne, *J. Am. Chem. Soc.* 1970, **92**, 4993.
22. J. B. Ramsay, E. L. Colichman and L. C. Pack, *J. Am. Chem. Soc.* 1946, **68**, 1965.
23. Y. Sasaki and T. S. Morita, *Bull. Chem. Soc. Japan* 1977, **50**, 1637.
24. K. Wuthrich and R. E. Connick, *Inorg. Chem.* 1967, **6**, 583.
25. K. Wuthrich and R. E. Connick, *Inorg. Chem.* 1968, **7**, 1377.
26. D. R. Rosseinsky, *Chem. Rev.* 1972, **72**, 215.
27. K. Kustin, S. T. Liu, C. Nicolini and D. L. Toppen, *J. Am. Chem. Soc.* 1974, **96**, 7410.

28. K. Kustin and D. L. Topper, *Inorg. Chem.* 1973, **12**, 1404.
29. N. Stolica, *Standard Potentials in Aqueous Solution* (Edited by A. Bard, R. Parsons and J. Jordan), IUPAC. Dekker, New York (1985).
30. R. Colton and G. G. Rose, *Aust. J. Chem.* 1968, **21**, 883.
31. M. C. González, M. R. Féliz, E. San Román and A. L. Capparelli, *J. Photochem. Photobiol.* 1989, **A48**, 69.
32. P. Argitis and E. Papaconstantinou, *Inorg. Chem.* 1986, **25**, 4386. See also, E. Papaconstantinou, *Chem. Soc. Rev.* 1989, **18**, 1.
33. M. J. Chaudhury, *J. Chem. Soc., Dalton Trans.* 1984, 857.

Polyhedron Vol. 10, No. 3, pp. 365–371, 1991
Printed in Great Britain

0277–5387/91 $3.00+.00
© 1991 Pergamon Press plc

PREPARATION, CHARACTERIZATION, SPECTRAL AND THERMAL ANALYSES OF $(N_2H_5)_2MCl_4 \cdot 2H_2O$ (M = Fe, Co, Ni AND Cu); CRYSTAL STRUCTURE OF THE IRON COMPLEX

N. R. S. KUMAR, M. NETHAJI and K. C. PATIL*

Department of Inorganic and Physical Chemistry, Indian Institute of Science, Bangalore-560012, India

(*Received* 16 *July* 1990; *accepted* 5 *October* 1990)

Abstract—Hydrazinium metal chlorides, $(N_2H_5)_2MCl_4 \cdot 2H_2O$ (where M = Fe, Co, Ni and Cu), have been prepared from the aqueous solutions of the respective metal chlorides and hydrazine hydrochloride ($N_2H_4 \cdot HCl$ or $N_2H_4 \cdot 2HCl$) and investigated by spectral and thermal analyses. The crystal structure of the iron complex has been determined by direct methods and refined by full-matrix least-squares to an R of 0.023 and R_w of 0.031 for 1495 independent reflections. The structure shows ferrous ion in an octahedral environment bonded by two hydrazinium cations, two chloride anions and two water molecules. In the complex cation $[Fe(N_2H_5)_2(H_2O)_2Cl_2]^{2+}$, the coordinated groups are in *trans* positions.

The coordination chemistry of hydrazine is of interest because of its ability to serve as an electron-pair donor. The presence of two, free electron pairs, as in other polybasic ligands, offers the possibility of several different types of coordination behaviour toward transition metal ions.[1–3] It can function as a monodentate[4,5] and bridging bidentate[6–10] ligand. Numerous examples of monodentate and bridging hydrazine have been demonstrated crystallographically. Monoprotonated hydrazine, the hydrazinium cation $N_2H_5^+$, still retains a basic site and is capable of coordinating to the metal. Complexes containing positively-charged hydrazinium ions are of increasing interest.[11,12]

During the course of our studies on the chemistry of hydrazine derivatives[13–24] we have prepared a number of hydrazinium metal sulphates, e.g. $N_2H_5Ln(SO_4)_2 \cdot H_2O$ (where Ln = La, Ce, Pr, Nd or Sm);[23] oxalates, e.g. $(N_2H_5)_2M(C_2O_4)_2 \cdot nH_2O$ (where M = Co, Ni or Cu);[24] $(N_2H_5)_2UO_2(C_2O_4)_2 \cdot H_2O$[21] and $(N_2H_5)_6(UO_2)_2(C_2O_4)_5 \cdot 2H_2O$.[20] The crystal structures of hydrazinium neodymium sulphate,[23] hydrazinium copper oxalate[24] and the hydrazinium uranyl oxalates[20,21] have also been solved. In continuation of these studies, we now report the preparation, characterization, spectral and thermal studies of $(N_2H_5)_2MCl_4 \cdot 2H_2O$ (where M = Fe, Co, Ni and Cu) and the crystal structure of $(N_2H_5)_2FeCl_4 \cdot 2H_2O$.

RESULTS AND DISCUSSION

The reaction between aqueous solutions of metal chlorides and $N_2H_4 \cdot HCl$ or $N_2H_4 \cdot 2HCl$ yielded complexes of the general formula $(N_2H_5)_2MCl_4 \cdot 2H_2O$ (where M = Fe, Co, Ni and Cu). The results of chemical analysis (Table 1) are in good agreement with the proposed formulae. Hydrazine and its salts are strong reducing agents in aqueous solutions[3] and reduce iron(III) to iron(II), and copper salts to copper metal. Heating of the solution is required in the case of iron for the complete reduction of iron(III) to iron(II). In the case of copper, reduction to the metal can be prevented by employing $N_2H_4 \cdot 2HCl$ which is known to dissociate in water to form $N_2H_5^+$, H_3O^+ and Cl^- ions, providing the required acidic medium. This method of preparing $(N_2H_5)_2CuCl_4 \cdot 2H_2O$ from $N_2H_4 \cdot 2HCl$ and $CuCl_2 \cdot 2H_2O$ is much simpler compared with the procedure reported earlier.[11]

*Author to whom correspondence should be addressed.

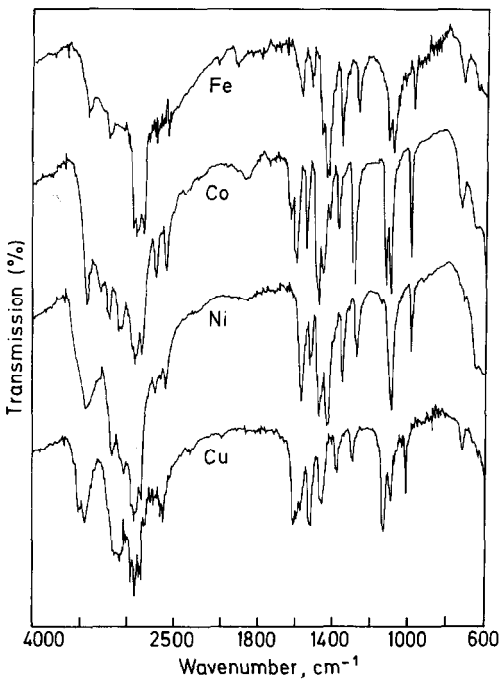

Fig. 1. IR spectra of $(N_2H_5)_2MCl_4 \cdot 2H_2O$.

IR spectra

IR spectra of all the complexes are similar (Fig. 1) and show characteristic absorption bands of $N_2H_5^+$: ~ 2650 cm^{-1} [ν(N—H) of —NH_3^+],[25] ~ 1100 cm^{-1} [ω(N—H) of —NH_3^+].[26] The N—N stretching of free $N_2H_5^+$ is known[27] to occur at 965 cm^{-1} and when it is coordinated, ν(N—N) invariably shifts to 1000 cm^{-1}. The observed ν(N—N) frequencies in the region 990–1015 cm^{-1} (Table 1) indicate the presence of coordinated $N_2H_5^+$ in all the complexes.

Electronic spectra and magnetic susceptibility measurements

The absorption bands of $(N_2H_5)_2MCl_4 \cdot 2H_2O$ in the visible region and the room temperature magnetic susceptibility values are included in Table 1. The electronic spectral data are comparable with those reported for octahedral cobalt(II), nickel(II) and copper(II).[28–31] Magnetic moment values correspond to spin-only values for cobalt(II), nickel(II) and copper(II) ions.

Thermal analysis

The results of TG–DTA studies of all hydrazinium metal chlorides are summarized in Table 2. The compositions of the intermediates proposed are those which best fit the observed weight loss. A typical TG–DTA curve of $(N_2H_5)_2CuCl_4 \cdot 2H_2O$ is shown in Fig. 2. The first step in the decomposition sequence corresponds to the loss of water molecules. The temperature range at which this decomposition occurs (60–85°C) indicates the possibility of non-coordination of water molecules to the metal. In the second step, the anhydrous compound decomposes, losing HCl and forming a hydrazine adduct. Evolution of HCl in this step has been confirmed by testing the evolved gases qualitatively. It is interesting to note that this intermediate further decomposes to form cuprous chloride, as evidenced by an endothermic DTA peak at 410°C corresponding to the melting of Cu_2Cl_2. This further decomposes to cuprous oxide at higher temperature.

The results of the other complexes show, more or less, a similar trend. They lose water in the first step followed by HCl and then form N_2H_4 adducts of different compositions. The temperature range at which the loss of water occurs (90–130°C) does not indicate conclusively whether water is bonded

Table 1. Analytical and spectral data for $(N_2H_5)_2MCl_4 \cdot 2H_2O$

M	Chemical analysis[a]			ν(N—N)	Electronic spectra	μ_{298}
	Metal (%)	Chloride (%)	Hydrazine (%)	(cm^{-1})	(cm^{-1})	(BM)
Fe	18.4(18.6)	22.2(22.0)	47.1(47.3)	1000	—	—
Co	19.2(19.4)	46.4(46.8)	21.0(21.1)	995	20,200 [$^4T_{1g}(F) \rightarrow {}^4T_{1g}(P)$] 18,800 [$^4T_{1g}(F) \rightarrow {}^4A_{2g}(F)$]	4.96
Ni	18.9(19.4)	46.9(46.9)	21.8(21.2)	1000	24,600 [$^3A_{2g}(F) \rightarrow {}^3T_{1g}(P)$] 14,900 [$^3A_{2g}(F) \rightarrow {}^3T_{1g}(F)$]	2.95
Cu	20.4(20.7)	45.9(46.1)	21.3(21.5)	1015	13,200 [$^2E_g \rightarrow {}^2T_{2g}$]	1.93

[a] Values in parentheses are theoretical values.

Table 2. Thermal analysis data for $(N_2H_5)_2MCl_4 \cdot 2H_2O$

M	Thermogravimetry: Step number	Thermogravimetry: Temperature range (°C)	Thermogravimetry: Weight loss[a] (%)	DTA peak temperature (°C) (−) = endo, (+) = exo	Solid product
Fe	1	60–120	12.0(12.0)	75(−)	$(N_2H_5)_2FeCl_4$
	2	205–240	34.0(33.6)	206(−)	$FeCl_2 \cdot 2N_2H_4$
	3	240–360	77.0(76.0)	260(+) 266(−) 350(+)	FeO
Co	1	90–110	12.0(11.9)	95(−) 105(+)	$(N_2H_5)_2CoCl_4$
	2	170–270	42.0(40.9)	210(−) 250(+)	$CoCl_2 \cdot 1.5N_2H_4$
	3	270–290	51.0(51.5)	280(+)	$CoCl_2 \cdot 0.5N_2H_4$
	4	290–385	57.0(57.1)	350(−)	$CoCl_2$
	5	390–530	73.0(73.5)	broad(−)	Co_3O_4
Ni	1	100–140	5.5(5.9)	125(−)	$(N_2H_5)_2NiCl_4 \cdot H_2O$
	2	140–175	22.0(23.9)	140(−)	$N_2H_5NiCl_3 \cdot N_2H_4$
	3	180–250	42.0(41.0)	235(−)	$NiCl_2 \cdot 1.5N_2H_4$
	4	275–350	58.5(57.2)	325(+)	$NiCl_2$
	5	370–555	75.0(75.3)	broad(−)	NiO
Cu	1	60–85	11.0(11.7)	75(−)	$(N_2H_5)_2CuCl_4$
	2	100–195	28.0(28.8)	130(−) 140(−)	$N_2H_5CuCl_3 \cdot 0.5N_2H_4$
	3	200–350	68.0(67.8)	235(+) 260(−)	$0.5Cu_2Cl_2$
	4	—	—	410(−)	—
	5	415—560	77.5(76.7)	broad(−)	$0.5Cu_2O$

[a] Theoretical values in parentheses.

to the metal or not. All the complexes decompose to their respective metal oxides via metal chlorides.

Coordination around the metal

The spectral and magnetic data coupled with thermal analysis suggest that the metal ions in iron, cobalt, nickel and copper complexes are octahedrally coordinated. IR spectra also suggest the coordination of $N_2H_5^+$ ions, but the nature of the coordination of other ligands is not clear. Furthermore, the relative positions of coordinated ligands cannot be determined from these data. For this reason, a single crystal X-ray analysis has been carried out.

Description of the structure of $(N_2H_5)_2FeCl_4 \cdot 2H_2O$

Crystal data for the complex are given in Table 3 and the bond lengths and angles are listed in Table 4. The structure of $(N_2H_5)_2FeCl_4 \cdot 2H_2O$ consists of chloride ions and the complex cation $[Fe(N_2H_5)_2(H_2O)_2Cl_2]^{2+}$. A perspective view of this complex cation showing its conformation and the atom numbering system is presented in Fig. 3.

The metal coordination site in the molecule is a distorted octahedron made up by two nitrogens (one from each $N_2H_5^+$ ion), two water oxygens and two chlorines. The cation $[Fe(N_2H_5)_2(H_2O)_2Cl_2]^{2+}$ possesses a pseudo-inversion centre as the coordinated atoms are *trans* to each other.

The observed metal–chlorine distances [2.441(1)

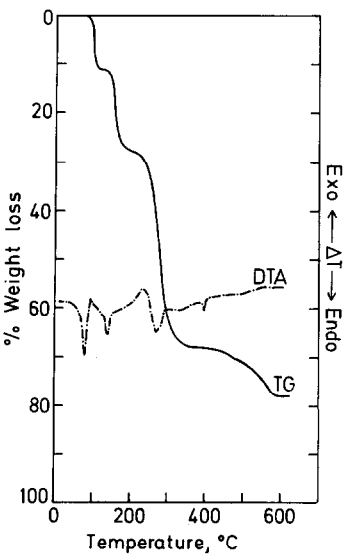

Fig. 2. Simultaneous TG–DTA curves for $(N_2H_5)_2CuCl_4 \cdot 2H_2O$.

Table 3. Details of the crystallographic analysis for the iron complex

Formula	$(N_2H_5)_2FeCl_4 \cdot 2H_2O$	D_m (g cm^{-3})	1.92
M_r	299.65	D_c (g cm^{-3})	1.91
Crystal system	Monoclinic	Scan mode	ω–2θ
Radiation (Å)	0.71069	2θ range (°)	60°
T (K)	293	Reflections measured	$\pm h, k, l$
Space group	*Pc*	Number of measured reflections	1759
a (Å)	8.027(1)	Number of unique data	1603
b (Å)	5.725(2)	Number of data used	1495
c (Å)	11.430(2)	Cut of criteria	$F > 3\sigma(F)$
β (°)	97.08(1)	Absolute coefficient (μ_{Mo}) (cm^{-1})	23.86
V (Å^3)	521.3	R_{int}	0.009
Z	2	Weights[a]	A, 0.002184
Crystal colour	Colourless	R	0.023
Crystal size (mm)	0.35 × 0.25 × 0.20	R_w	0.031

[a] Weighting scheme, $w = 1.0/[\sigma^2(F_o) + A|F_o|^2]$.

and 2.431(1) Å] are less than the distance of 2.526(1) Å found in the octahedral $[Fe(H_2O)_4Cl_2]$.[32,33] The metal–oxygen bonds in the present structure, with distances of 2.188(3) and 2.163(2) Å, are longer than the ones found in $[Fe(H_2O)_4Cl_2]$ [2.121(1) and 2.086(1) Å]. This indicates a relatively weaker metal–oxygen interaction which has been supported by thermal analysis.

The metal–nitrogen bond lengths [2.232(2) and 2.212(2) Å] are also larger than the estimated value of 2.15 Å for iron(II)–NH_3 complexes.[34] Comparison of metal–nitrogen bond lengths with metal–oxygen bond lengths reveal that the former are larger than the latter (Table 3). Such differences between metal–oxygen and metal–nitrogen bonds have not been observed in the complexes of neutral semicarbazide molecules, where the bonds in each of the two pairs are equal: Cu—O 1.97, Cu—N 1.99 Å; and Zn—O 2.06, Zn—N 2.07 Å.[35] The relatively longer Fe—N bonds compared with Fe—O bonds in the present structure thus indicate weaker Fe—N interaction.

The N—N distances found for the $N_2H_5^+$ ions are 1.480(4) and 1.429(2) Å. The difference in the N—N bond lengths, as well as the low temperature factors observed for these atoms, may be due to absorption effects. The average bond length of 1.452 Å is in good agreement with the value [1.457(7) Å] reported for $N_2H_5CuCl_3$.[11] The Fe—N—N′ angles in the present case are 122.5(2) and 120.2(2)°. A similar value has been reported for the copper complex [119.1(3)°].[11]

Table 4. Bond lengths (Å) and angles (°) in $(N_2H_5)_2FeCl_4 \cdot 2H_2O$

Fe—O(1)	2.188(3)	Fe—N(1)	2.232(2)
Fe—O(2)	2.163(2)	Fe—N(3)	2.212(2)
Fe—Cl(1)	2.441(1)	N(1)—N(2)	1.480(4)
Fe—Cl(2)	2.431(1)	N(3)—N(4)	1.424(3)
Fe—N(1)—N(2)	122.5(2)	O(2)—Fe—N(1)	93.4(1)
Fe—N(3)—N(4)	120.2(2)	O(2)—Fe—N(3)	87.8(1)
O(1)—Fe—O(2)	179.8(0)	Cl(1)—Fe—Cl(2)	179.5(0)
O(1)—Fe—Cl(1)	91.2(1)	Cl(1)—Fe—N(1)	93.5(1)
O(1)—Fe—Cl(2)	88.5(1)	Cl(1)—Fe—N(3)	85.5(1)
O(1)—Fe—N(1)	86.4(1)	Cl(2)—Fe—N(1)	86.0(1)
O(1)—Fe—N(3)	92.3(1)	Cl(2)—Fe—N(3)	95.0(1)
O(2)—Fe—Cl(1)	88.8(1)	N(1)—Fe—N(3)	178.4(1)
O(2)—Fe—Cl(2)	91.5(1)		

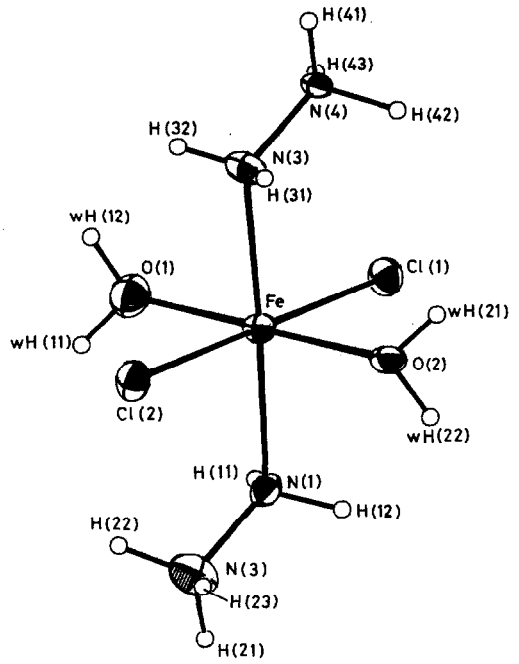

Fig. 3. ORTEP diagram and atom numbering scheme for $[Fe(N_2H_5)_2(H_2O)_2Cl_2]^{2-}$. Thermal ellipsoids are at the 50% probability level and hydrogen atoms are given arbitrary radii.

Structure of $(N_2H_5)_2CoCl_4 \cdot 2H_2O$

Preliminary studies on single crystals of the complex have been carried out. Unit cell dimensions and the space group were determined on a Weissenberg camera and were subsequently refined on a diffractometer. The systematic absences indicate the space group to be $P2_1/c$. These data are presented in Table 5.

As the space group is $P2_1/c$ and $Z = 2$, the centres of the molecules, namely the metal atoms, must lie in special positions which are inversion centres in the present case. This unequivocally shows that the coordinated atoms in the cobalt complex are also *trans* to each other as in the case of the iron complex. From these data we can infer that the most probable structure for the cobalt complex would be similar to that for the iron complex, viz. *trans*-$[Co(N_2H_5)_2(H_2O)_2Cl_2]Cl_2$.

Table 5. Preliminary data for $(N_2H_5)_2CoCl_4 \cdot 2H_2O$

M_r	298.7	a (Å)	7.999(1)
System	Monoclinic	b (Å)	5.703(2)
Space group	$P2_1/c$	c (Å)	11.405(2)
D_m (g cm^{-3})	1.95	β (°)	97.73(2)
D_c (g cm^{-3})	1.93	Z	2

Structure of $(N_2H_5)_2NiCl_4 \cdot 2H_2O$

Attempts to obtain single crystals of this complex were unsuccessful, but from the similarities of the spectral and thermal properties of this complex with those of the cobalt complex, it is possible to suggest that the structure of the nickel complex is similar to that of the iron and cobalt complexes.

Structure of $(N_2H_5)_2CuCl_4 \cdot 2H_2O$

From magnetic studies, Brown *et al.*[11] have assigned a *trans*-$[Cu(N_2H_5)_2Cl_4] \cdot 2H_2O$ structure to the copper complex. However, considering the similarities in spectral and thermal properties of this complex with the other complexes, it is probable that the structure would be *trans*-$[Cu(N_2H_5)_2(H_2O)_2Cl_2]Cl_2$.

EXPERIMENTAL

Preparations

The complexes were obtained from aqueous solutions of the respective metal chlorides and $N_2H_4 \cdot HCl$ or $N_2H_4 \cdot 2HCl$. Preparative methods for individual complexes vary and are described below.

$(N_2H_5)_2FeCl_4 \cdot 2H_2O$. The iron complex was prepared by refluxing an aqueous solution of $FeCl_3 \cdot 6H_2O$ (5.0 g) and $N_2H_4 \cdot HCl$ (7.6 g) in 200 cm^3 of water for 30 min. The resulting colourless solution was concentrated on a water bath and allowed to crystallize in a vacuum desiccator. Colourless plates which appeared after a week were removed from the solution, dried by pressing between filter paper and stored in an air-tight bottle.

$(N_2H_5)_2CoCl_4 \cdot 2H_2O$. The above complex was prepared by mixing aqueous saturated solutions of $CoCl_2 \cdot 6H_2O$ and $N_2H_4 \cdot HCl$ in a 1 : 2 mole ratio. The precipitate that initially formed was filtered off and the solution was left exposed to air for slow evaporation. Dark pink coloured crystals separated out from the solution, which were filtered, washed with alcohol and ether and stored in a desiccator.

Alternatively, the complex can be prepared by decomposing solid $N_2H_5Co(N_2H_3COO)_3 \cdot H_2O$[36] in dilute HCl (6 N) and keeping the solution for slow evaporation.

$(N_2H_5)_2NiCl_4 \cdot 2H_2O$. The nickel complex was prepared in a similar way, either from aqueous solu-

tions of nickel chloride and hydrazine hydrochloride or by decomposing $N_2H_5Ni(N_2H_3COO)_3 \cdot H_2O$[36] in dilute HCl. But in the present case a green crystalline product was obtained, which was found to be a hydrazine adduct, $(N_2H_5)_2NiCl_4 \cdot 2H_2O \cdot 0.5N_2H_4$. This green product was removed from the solution as and when it formed and later the hydrazinium nickel chloride complex separated out from the solution as a greenish-blue solid in small amounts.

$(N_2H_5)_2CuCl_4 \cdot 2H_2O$. The copper complex was prepared by adding a saturated solution of $CuCl_2 \cdot 4H_2O$ to a saturated solution of $N_2H_4 \cdot 2HCl$, in a 1 : 2 mole ratio, with vigorous stirring. The copper complex precipitated out as a blue crystalline mass in ~ 2 min, and was filtered off from the solution immediately and air-dried.

Physico-chemical techniques

The composition of the complexes was determined by chemical analysis.[37,38] Metal contents were estimated by titrating with EDTA, the hydrazine content by titrating with KIO_3 under Andrews conditions[3] and the chloride content by Volhard's method.

IR spectra of the complexes in the region 4000–600 cm^{-1} were recorded as Nujol mulls using a Perkin–Elmer 781 spectrophotometer. Electronic spectra in the visible region were recorded using a Hitachi U-3400 spectrophotometer. The spectra in the solid state were obtained by dispersing the samples in Nujol. Room temperature magnetic susceptibility measurements were made using a Faraday balance. Thermogravimetry (TG) and Differential Thermal Analysis (DTA) experiments were carried out using a simultaneous TG–DTG–DTA TA-1500 instrument (Ulvac Sinku Riko, Japan). All the experiments were carried out in air, using 6–8 mg of samples. Platinum cups were used as sample holders and alumina as reference. The heating rate employed was 10°C min^{-1}

X-ray work

A well-developed crystal of dimensions $0.35 \times 0.25 \times 0.20$ mm was mounted in a Lindeman capillary tube in order to prevent decomposition. Cell constants and corresponding standard deviations were obtained from a least-squares refinement of 25 reflections automatically centred on a Nonius CAD-4 diffractometer. The density of the crystal was measured by the flotation method using a chloroform–bromoform mixture.

Intensity data were collected in the usual manner.

Structure solution and refinement

The structure was solved by direct methods (SHELXS-86)[39] and refined by full-matrix least-squares procedures using the SHELX-76 system of programs.[40] Hydrogen atoms were located in the difference map and were included without refinement. Anisotropic thermal parameters were introduced for all non-hydrogen atoms. A further improvement was obtained after using weights. The final R and R_w values achieved in this way are 0.023 and 0.031, respectively.

All the details regarding the data collection and structural analysis are listed in Table 3. Major calculations were carried out on a DEC 1090 computer. The ORTEP-II program[41] was used to draw Fig. 3. Scattering factors for iron were taken from Ref. 42 and the values available in SHELX-76 were used for the other atoms.

REFERENCES

1. E. W. Schmidt, *Hydrazine and Its Derivatives*. John Wiley, New York (1984).
2. F. S. Bottomley, *Q. Rev. Chem. Soc.* 1970, **24**, 617.
3. L. F. Audrieth and B. A. Ogg, *The Chemistry of Hydrazine*. John Wiley, New York (1951).
4. A. Ferrari, A. Braibanti, G. Bigliardi and A. M. M. Lanfredi, *Z. Kristallogr. Kristallgeom.* 1965, **122**, 259.
5. E. N. Malsen, L. L. Raston, B. W. Skelton and A. H. White, *Aust. J. Chem.* 1975, **28**, 739.
6. A. Ferrari, A. Braibanti, G. Bigliardi and F. Dallavalle, *Z. Kristallogr. Kristallgeom.* 1963, **119**, 284.
7. A. Ferrari, A. Braibanti and G. Bigliardi, *Acta Cryst.* 1963, **16**, 498.
8. A. Ferrari, A. Braibanti and A. M. Lanfredi, *Acta Cryst.* 1964, **18**, 367.
9. A. Ferrari, A. Braibanti, G. Bigliardi and A. M. Lanfredi, *Acta Cryst.* 1965, **19**, 548.
10. D. T. Cromer, A. C. Larson and R. B. Roof, *Acta Cryst.* 1966, **20**, 279.
11. D. B. Brown, J. A. Donner, J. W. Hall, S. R. Wilson, R. B. Wilson, D. J. Hodgson and W. E. Hatfield, *Inorg. Chem.* 1979, **18**, 2635.
12. A. Nieuport and J. Reedijk, *Inorg. Chim. Acta* 1977, **7**, 323.
13. K. C. Patil, R. Soundararajan and V. R. Pai Verneker, *Inorg. Chem.* 1979, **18**, 1969.
14. K. C. Patil and J. P. Vittal, *J. Chem. Soc., Dalton Trans.* 1982, 2291.
15. K. C. Patil, C. Nesamani and V. R. Pai Verneker, *J. Chem. Soc., Dalton Trans.* 1983, 2047.
16. K. C. Patil, S. Govindarajan, R. Soundararajan and V. R. Pai Verneker, *Proc. Indian Acad. Sci. (Chem. Sci.)* 1981, **90**, 421.
17. S. Govindarajan and K. C. Patil, *Thermochim. Acta* 1982, **55**, 373.

18. K. C. Patil, R. Soundararajan and E. P. Goldberg, *Synth. React. Inorg. Metal-Org. Chem.* 1983, **13**, 29.
19. K. C. Patil, S. Govindarajan and H. Manohar, *Synth. React. Inorg. Metal-Org. Chem.* 1981, **11**, 245.
20. S. Govindarajan, K. C. Patil, M. D. Poojary and H. Manohar, *Inorg. Chim. Acta* 1986, **120**, 103.
21. M. D. Poojary and K. C. Patil, *Proc. Indian Acad. Sci. (Chem. Sci.)* 1987, **99**, 311.
22. P. Ravindranathan and K. C. Patil, *Proc. Indian Acad. Sci. (Chem. Sci.)* 1985, **95**, 354.
23. S. Govindarajan, K. C. Patil, H. Manohar and P. E. Werner, *J. Chem. Soc., Dalton Trans.* 1986, 119.
24. D. Gajapathy, S. Govindarajan, K. C. Patil and H. Manohar, *Polyhedron* 1983, **2**, 865.
25. L. Lindgren, J. De Villepin and A. Novak, *Chem. Phys. Lett.* 1969, **3**, 84.
26. V. Shettino and R. E. Salmon, *Spectrochim. Acta* 1974, **30A**, 1445.
27. A. Braibanti, F. Dallavalle, M. A. Pellinghelli and E. Laporti, *Inorg. Chem.* 1968, **7**, 1430.
28. C. J. Ballhausen and C. K. Jorgenson, *Acta Chem. Scand.* 1955, **9**, 397.
29. D. Nicholls and R. Swidells, *J. Inorg. Nucl. Chem.* 1968, **30**, 2211.
30. C. J. Ballhausen, *Introduction to Ligand Field Theory*. McGraw Hill, New York (1962).
31. A. B. P. Lever, *Inorganic Electronic Spectroscopy (Studies in Physical and Theoretical Chemistry No. 33)*, 2nd edn. Elsevier, Amsterdam (1984).
32. P. J. M. Piret and M. V. Meerssche, *Acta Cryst.* 1972, **B28**, 2329.
33. J. J. Verbist, W. C. Hamilton, T. F. Koetzle and M. S. Lehmann, *J. Chem. Phys.* 1972, **56**, 3257.
34. E. Kai, T. Misawa and K. Nishimoto, *Bull. Chem. Soc. Japan* 1980, **53**, 2481.
35. M. Nardelli, G. F. Gasparri, P. Boldrini and G. G. Battisini, *Acta Cryst.* 1965, **19**, 491.
36. A. Braibanti, G. Bigliardi, A. M. Lanfredi and A. Tiripicchio, *Nature (Lond.)* 1966, **211**, 1174.
37. A. I. Vogel, *A Text Book of Quantitative Inorganic Analysis*. Longman, London (1975).
38. T. S. West, *Complexometry with EDTA and Related Reagents*. BDH Chemicals Ltd, London (1969).
39. G. M. Sheldrick, *SHELXS-86 : A Program for Crystal Structure Solution*. University of Göttingen, Göttingen (1986).
40. G. M. Sheldrick, *SHELX-76, Program for Crystal Structure Determination*. University of Cambridge (1976).
41. C. K. Johnson, *ORTEP-II, A Program for Thermal Ellipsoid Plotting*. Oak Ridge National Laboratory, Oak Ridge, Tennessee (1976).
42. *International Tables for X-ray Crystallography*, Vol. IV. Kynoch Press, Birmingham (1974).

Polyhedron Vol. 10, No. 3, pp. 373–376, 1991
Printed in Great Britain

0277–5387/91 $3.00+.00
© 1991 Pergamon Press plc

PYROLYTIC REACTIONS OF AZIDOCHROMIUM(III) PORPHYRINS AND AZIDOIRON(III) PORPHYRINS IN THE SOLID STATE

HIROYUKI SUGAYA, JUNICHI TACHIBANA and TAIRA IMAMURA*

Department of Chemistry II, Faculty of Science, Hokkaido University, Sapporo 060, Japan

(*Received* 8 *August* 1990; *accepted* 5 *October* 1990)

Abstract—Azidochromium(III) tetraphenylporphyrin, $Cr^{III}(tpp)N_3$ (tpp = 5,10,15,20-tetraphenylporphyrinato), and azidoiron(III) tetraphenylporphyrin, $Fe^{III}(tpp)N_3$, in the solid state, were pyrolysed under 10^{-5}–10^{-6} torr at around 250°C, liberating nitrogen gas to afford $Cr^{II}(tpp)$ and $Fe^{II}(tpp)$ as final products, respectively. $Cr^{V}(tpp)N$ formed in the process of the $Cr^{III}(tpp)N_3$ pyrolysis is reduced to $Cr^{II}(tpp)$, although pure $Cr^{V}(tpp)N$ prepared independently is not pyrolysed under the same conditions. In the presence of dioxygen in the toluene solutions of these pyrolysed products, $Cr^{IV}(tpp)O$ or $[Fe(tpp)]_2O$ is formed. The mechanisms of these reactions in the solid state are discussed in comparison with those in solution.

The chemistry of azidometalloporphyrins is of great interest because these complexes undergo versatile reactions, forming either metal(II) porphyrins or nitridometal(V) porphyrins by their sensitive dependency on the conditions and the states of the reaction media. For example, both the pyrolysis of $Fe^{III}(tpp)N_3$ in xylene[1] and its photo-irradiation in THF afford the same complex; a μ-nitrido dimer of $[Fe(tpp)]_2N$.[2] However, in the presence of pyridine, the $Fe^{III}(tpp)N_3$ complex is photoreduced to form $Fe^{II}(tpp)(py)_2$,[2] suggesting that the μ-nitrido dimer of $[Fe(tpp)]_2N$ is formed by the reaction of unstable Fe(tpp)N with $Fe^{II}(tpp)$. On the other hand, the photo-irradiation of $Mn^{III}(P)N_3$ (P = porphyrinato) in organic solvents[2–4] or pyrolysis in the solid state,[5] gives the corresponding monomeric complex of $Mn^{V}(P)N$, causing cleavage of the N—N_2 bond of the axial ligand N_3. The photo-irradiation of $Mn^{III}(tpp)N_3$ in 2-methyltetrahydrofuran causes simultaneous oxidation and reduction of the central metal to produce $Mn^{V}(tpp)N$ and $Mn^{II}(tpp)$.[6] In the reaction processes of these azidometalloporphyrins, metal(II) porphyrins are indicative of playing a key role.

In the present paper, the pyrolyses of $Cr^{III}(tpp)N_3$ and $Fe^{III}(tpp)N_3$ in the solid state are reported in comparison with their reactions in solution. The study is especially focused on the mechanism of reaction in the solid state where the complexes having bulky porphyrinato ligands are supposed to be less mobile than they are in solution.

EXPERIMENTAL

Azidochromium(III) tetraphenylporphyrin† was prepared by the reaction of $Cr^{III}(tpp)Cl$ with HN_3,[8] dried at 120°C *in vacuo* and stored in the dark. Found: C, 74.3; H, 3.9; N, 13.8. Calc. for $C_{44}H_{28}N_7Cr$: C, 74.8; H, 4.0; N, 13.9%. Nitridochromium(V) tetraphenylporphyrin was prepared by the reaction of $Cr^{III}(tpp)Cl$ with NaOCl in the presence of NH_3, with reference to the reported method.[8] Found: C, 77.6; H, 4.3; N, 10.1. Calc. for $C_{44}H_{28}N_5Cr$: C, 77.9; H, 4.2; N, 10.3%. Azidoiron(III) tetraphenylporphyrin was prepared by the reaction of $Fe^{III}(tpp)Cl$ with NaN_3.[1] Found: C, 74.3; H, 4.0; N, 13.6. Calc. for $C_{44}H_{28}N_7Fe$: C, 74.4; H, 4.0; N, 13.8%.

Spectral grade toluene was purified and stored

* Author to whom correspondence should be addressed.

† In the preliminary study of the reactivity of $Cr(tpp)N_3$ we observed that this complex reacts with Mn(tpp)N in dichloromethane to produce Cr(tpp)N and $Mn(tpp)N_3$, as well as the nitrogen atom transfer reaction between Cr(tpp)Cl and Mn(tpp)N reported recently by Bottomley and Neely.[7]

with molecular sieves in the vessel on a vacuum line. Toluene must be purified, repeatedly and scrupulously, because when purification is insufficient $Cr^{III}(tpp)N_3$ changes to $Cr^{IV}(tpp)O$. The mechanism of the reaction is supposed to be that $Cr^{III}(tpp)N_3$ is first reduced by impurities such as thiophene to form $Cr^{II}(tpp)$, which is successively oxidized by dioxygen to form $Cr^{IV}(tpp)O$. Toluene was degassed rigorously by repeated freeze–thaw cycles, and vacuum-transferred into the vessel with an optical cell containing the pyrolysed products in the solid state. For preparations of the sample solutions, break–seal techniques were used to completely eliminate contamination by air. All samples in the solid state and in solution were manipulated in the dark, avoiding any photochemical reactions.

Electronic spectra were recorded on a Hitachi 808 spectrophotometer. ESR spectra were measured with a JES-FE1X spectrometer operating at 100 kHz modulation. Thermogravimetric analyses (TG) were carried out on a Cahn 2000 electrobalance. A Hitachi RMU-6 EI mass spectrometer was used to detect the gases evolved in the pyrolyses of $Cr^{III}(tpp)N_3$ and $Fe^{III}(tpp)N_3$.

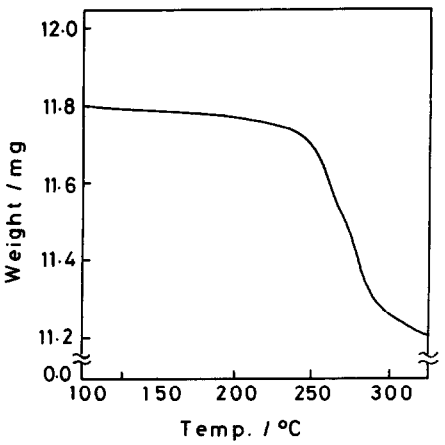

Fig. 1. Thermogravimetric analysis of $Cr^{III}(tpp)N_3$ under a 17 torr argon atmosphere.

RESULTS AND DISCUSSION

Pyrolysis of $Cr^{III}(tpp)N_3$

Our preliminary study showed that the pyrolysis of $Cr^{III}(tpp)N_3$ in the solid state yields some other complex in addition to $Cr^{V}(tpp)N$, depending on the conditions.[5] Thermogravimetric measurements showed that $Cr^{III}(tpp)N_3$ is pyrolysed at around 240°C under a 17 torr argon atmosphere (Fig. 1). The loss in weight was larger than the decrease expected by the formation of $Cr^{V}(tpp)N$. The pyrolysis was accompanied by the disappearance of the IR stretching frequency of the axial N_3 ligand observed at 2060 cm^{-1} (KBr pellet). Liberation of nitrogen gas in the pyrolysis was detected by mass spectral measurements. When the powder of the complex was pyrolysed for 30 min under 10^{-5}–10^{-6} torr at 250°C, after drying at 120°C, the products dissolved in toluene showed the spectrum with main absorption peaks at 421, 446 and 542 nm. The peak at 446 nm is due to the parent complex of $Cr^{III}(tpp)N_3$. The peaks at 421 and 542 nm almost agree with the peaks of $Cr^{V}(tpp)N$. ESR measurements of the toluene solution also confirmed that the products contained $Cr^{V}(tpp)N$, i.e. typical ESR signals ($\bar{g} = 1.98$) of ^{53}Cr ($I = 3/2$) coupled with five nitrogens with 11 lines were observed.[8,9] Usually $Cr^{V}(tpp)N$ is very resistant to pyrolysis. In practice, the $Cr^{V}(tpp)N$ complex prepared independently was not pyrolysed under the same conditions. However, the introduction of dry dioxygen or air to the above toluene solution of pyrolysed $Cr^{III}(tpp)N_3$ leads to a decrease in absorbance around 421 nm with the concomitant appearance of the absorption peak at 432 nm. The new peak is ascribed to $Cr^{IV}(tpp)O$.[10] The resulting absorption spectrum is composed of the absorption bands of $Cr^{V}(tpp)N$ (421 nm), $Cr^{IV}(tpp)O$ (432 nm) and the parent $Cr^{III}(tpp)N_3$ complex (446 nm) (Fig. 2).

The absorption spectrum of the toluene solution of the products, formed by 4 h pyrolysis of $Cr^{III}(tpp)N_3$, showed peaks at 423 and 542 nm. Introduction of dry dioxygen into the solution caused complete disappearance of these absorptions, with a simultaneous increase in the absorbances at 375, 432 and 544 nm due to the formation of $Cr^{IV}(tpp)O$ (Fig. 3). When a small amount of dioxygen was introduced into the solution prepared after pyrolysis, the μ-oxodimer of $[Cr(tpp)]_2O$ was formed. $Cr^{IV}(tpp)O$[11] and $[Cr(tpp)]_2O$[10,12] are formed by the reactions of $Cr^{II}(tpp)$ with dioxygen. These results indicate that only $Cr^{II}(tpp)$ was formed by 4 h pyrolysis, i.e. $Cr^{V}(tpp)N$ produced during the course of pyrolysis was reduced to $Cr^{II}(tpp)$ by the successive pyrolysis.* Namely, the pyrolysis of $Cr^{III}(tpp)N_3$ in the solid state affords $Cr^{II}(tpp)$ and $Cr^{V}(tpp)N$ simultaneously and the resulting $Cr^{V}(tpp)N$ is then reduced to $Cr^{II}(tpp)$.

$$2Cr(tpp)N_3 \longrightarrow 2Cr(tpp) + 3N_2. \quad (1)$$

When $Cr^{III}(tpp)N_3$ was refluxed for a few minutes

* When the pyrolysis was performed at 10^{-4}–10^{-5} torr for 4 h, relatively large amounts of $Cr^{V}(tpp)N$ were formed.

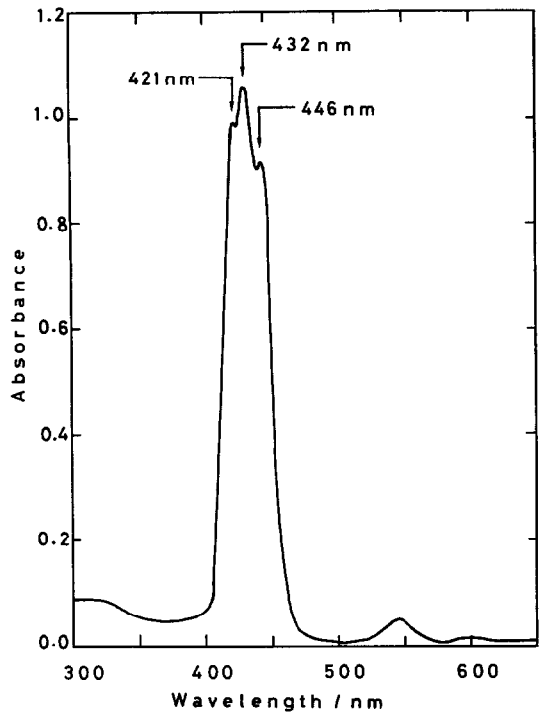

Fig. 2. Absorption spectrum, at 25°C, of the dioxygen-introduced toluene solution of the products formed by 30 min pyrolysis of $Cr^{III}(tpp)N_3$ in the solid state, at 250°C under 10^{-5}–10^{-6} torr.

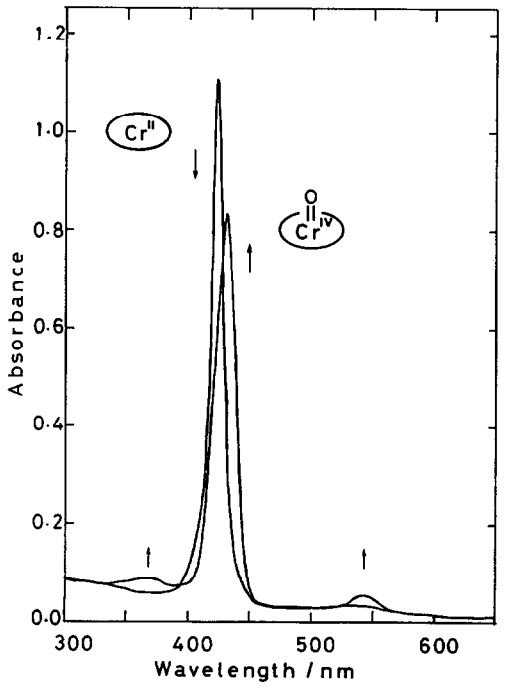

Fig. 3. Absorption spectra, at 25°C, of the toluene solution of $Cr^{II}(tpp)$ formed by 4 h pyrolysis of $Cr^{III}(tpp)N_3$ in the solid state and of $Cr^{IV}(tpp)O$ formed by the introduction of dioxygen into the solution.

in toluene or benzene in the dark, $Cr^{IV}(tpp)O$ was formed, suggesting the formation of $Cr^{II}(tpp)$ as the product in the absence of dioxygen. The formation of $Cr^{V}(tpp)N$ was not observed. The benzene solution of $Cr^{V}(tpp)N$ prepared separately was not reduced to form $Cr^{II}(tpp)$ or $Cr^{IV}(tpp)O$ in the presence of dioxygen by 3 h reflux. This suggests that the reduction path to $Cr^{II}(tpp)$ is advantageous in the pyrolytic reaction of $Cr^{III}(tpp)N_3$ in solution, compared with the pyrolytic reaction in the solid state. $Cr^{III}(tpp)Cl$ in benzene or toluene is not pyrolysed.

Pyrolysis of $Fe^{III}(tpp)N_3$

In contrast with the reported pyrolytic reaction of $Fe^{III}(tpp)N_3$ in xylene solution which afforded the μ-nitrido dimer of $[Fe(tpp)]_2N$,[1] the pyrolysis of the solid powder of $Fe^{III}(tpp)N_3$, under 10^{-5}–10^{-6} torr at 250°C for 4 h, gave $Fe^{II}(tpp)$ as the product. EI mass spectral measurements confirmed the liberation of nitrogen gas in the pyrolysis. The absorption spectrum of the product dissolved in toluene showed that no porphyrin complexes other than $Fe^{II}(tpp)$ were formed: only characteristic bands at 418, 444(sh) and 540 nm[13] were observed, as shown in Fig. 4.

$$2Fe^{III}(tpp)N_3 \longrightarrow 2Fe^{II}(tpp) + 3N_2 \qquad (2)$$

Introduction of dry dioxygen into the solution afforded $[Fe(tpp)]_2O$,[14] although $Fe^{III}(tpp)N_3$ was pyrolysed for a short time (30 min), no forma-

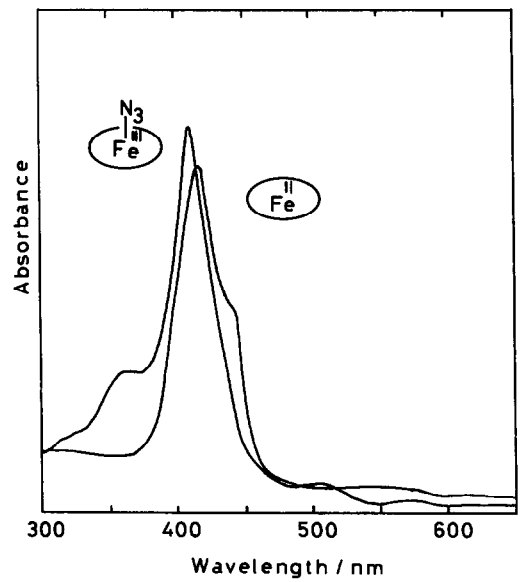

Fig. 4. Absorption spectra, at 25°C, of the toluene solutions of the parent $Fe^{III}(tpp)N_3$ and the pyrolysed product of $Fe^{II}(tpp)$.

tion of $[Fe(tpp)]_2N$ was observed. The following scheme for the pyrolysis of $Fe^{III}(tpp)N_3$ in xylene was one of those presented by Cohen and Summerville[1]:

$$Fe(tpp)N_3 \longrightarrow Fe(tpp)N + N_2 \quad (3)$$

$$Fe(tpp)N + Fe(tpp)N_3 \longrightarrow [Fe(tpp)]_2N_4 \quad (4)$$

$$[Fe(tpp)]_2N_4 \longrightarrow 2Fe(tpp)N_2 \quad (5)$$

$$2Fe(tpp)N_2 \longrightarrow Fe(tpp) + N_2 \quad (6)$$

$$Fe(tpp)N + Fe(tpp) \longrightarrow [Fe(tpp)]_2N. \quad (7)$$

The formation of $[Fe(tpp)]_2O$ in the pyrolysis with a low concentration of $Fe^{III}(tpp)N_3$ in xylene[1] suggests the presence of $Fe^{II}(tpp)$ as an intermediate in the solution pyrolysis. The photolysis of $Fe^{III}(tpp)N_3$ in THF also affords $Fe^{II}(tpp)(py)_2$ in the presence of pyridine, while in the absence of pyridine the product is $[Fe(tpp)]_2N$.[8] The formation of $Fe^{II}(tpp)(py)_2$ is not in conflict with the above steps (4)–(6) after photochemical fission of the N—N_2 bond of $Fe(tpp)N_3$. $Fe^{II}(tpp)$ formed in step (6) must be stabilized in the presence of pyridine or dioxygen by the formation of $Fe^{II}(tpp)(py)_2$ or $[Fe(tpp)]_2O$, the reaction in step (7) not occurring.

However, in the pyrolysis of the solid state, $Fe^{II}(tpp)$ only formed as the final product although there was no stabilizing ligand such as pyridine. This suggests that an intermediate complex of Fe(tpp)N is reduced by some agents to form $Fe^{II}(tpp)$, as in the $Cr^{III}(tpp)N_3$ system.

The following scheme reasonably represents the formation of metal(II) porphyrins in solid-state pyrolyses:

$$M(tpp)N_3 \longrightarrow M(tpp)N + N_2 \quad (M = Fe \text{ or } Cr) \quad (8)$$

$$M(tpp)N_3 \longrightarrow M(tpp) + {}^{\bullet}N_3 \quad (9)$$

$$M(tpp)N + {}^{\bullet}N_3 \longrightarrow M(tpp) + 2N_2 \quad (10)$$

$$2\,{}^{\bullet}N_3 \longrightarrow 3N_2. \quad (11)$$

The reactions of steps (8) and (9) proceed competitively. When the metal, M, is iron the unstable Fe(tpp)N formed by step (8) may react immediately with the ${}^{\bullet}N_3$ radical produced by the homolytic cleavage of the M—N_3 bond in step (9), affording $Fe^{II}(tpp)$ in step (10). The main difference between the two schemes for the solution system and for the solid-state system is that Fe(tpp)N dimerizes with $Fe^{II}(tpp)$ in the former system and Fe(tpp)N is reduced by ${}^{\bullet}N_3$ in the latter.* These differences may be caused by the greater mobility problems of bulky porphyrins in the solid state than in solution. The solid state may be disadvantageous to the collision between Fe(tpp)N and $Fe^{II}(tpp)$, as in step (7), but may favour the progress of step (10). This mechanism also reasonably explains the $Cr^{III}(tpp)N_3$ pyrolytic system in the solid state. In this system, $Cr^{V}(tpp)N$ was observed as an intermediate of the pyrolysis, which is unsurprising since $Cr^{V}(tpp)N$ has been stably isolated, while Fe(por)N is very unstable and was only detected recently by laser irradiation of thin films of the corresponding azido complexes at 30 K.[15] The homolytic cleavage of the Cr—N_3 bond in $Cr^{III}(tpp)N_3$ [step (9)] also seems feasible for pyrolysis in solution.

* Although the azide radical, ${}^{\bullet}N_3$, acts as an oxidizing agent for Fe(tpp)N, the metal centre of the iron atom is reduced to yield Fe(tpp).

REFERENCES

1. D. A. Summerville and I. A. Cohen, *J. Am. Chem. Soc.* 1976, **98**, 1747.
2. J. W. Buchler and C. Dreher, *Z. Naturf.* 1984, **39b**, 222.
3. J. T. Groves and T. Takahashi, *J. Am. Chem. Soc.* 1983, **105**, 2073.
4. T. Jin, T. Suzuki, T. Imamura and M. Fujimoto, *Inorg. Chem.* 1987, **26**, 1280.
5. Y. Yamamoto, T. Imamura, T. Suzuki and M. Fujimoto, *Chem. Lett.* 1988, 261.
6. T. Imamura, Y. Yamamoto, T. Suzuki and M. Fujimoto, *Chem. Lett.* 1987, 2185.
7. L. A. Bottomley and F. L. Neely, *J. Am. Chem. Soc.* 1989, **111**, 5955.
8. J. W. Buchler, C. Dreher, K.-L. Lay, A. Raap and K. Gersonde, *Inorg. Chem.* 1983, **22**, 879.
9. J. T. Groves, T. Takahashi and W. M. Butler, *Inorg. Chem.* 1983, **22**, 884.
10. J. R. Budge, B. M. K. Gatehouse, M. C. Nesbit and B. O. West, *J. Chem. Soc., Chem. Commun.* 1981, 370.
11. D. J. Liston and B. O. West, *Inorg. Chem.* 1985, **24**, 1568.
12. J. T. Groves, W. J. Kruper Jr, R. C. Haushalter and W. M. Butler, *Inorg. Chem.* 1982, **21**, 1363.
13. M. Momenteau, B. Loock, E. Bisagni and M. Rougee, *Can. J. Chem.* 1979, **57**, 1804.
14. For an example see: D.-H. Chin, G. N. La Mar and A. L. Balch, *J. Am. Chem. Soc.* 1980, **102**, 4344.
15. W.-D. Wagner and K. Nakamoto, *J. Am. Chem. Soc.* 1989, **111**, 1590.

Polyhedron Vol. 10, No. 3, pp. 377–387, 1991
Printed in Great Britain

0277–5387/91 $3.00+.00
Pergamon Press plc

SPECIATION STUDIES OF THE SOLUBILITY AND AQUEOUS SOLUTION CHEMISTRY OF TIN(II)– AND TIN(IV)–PYROPHOSPHATE COMPLEXES

JOHN R. DUFFIELD* and DAVID R. WILLIAMS†

School of Chemistry and Applied Chemistry, University of Wales College of Cardiff, P.O. Box 912, Cardiff CF1 3TB, U.K.

and

IVAN KRON

Institute of Experimental Medicine, UPJS, Kosice, Czechoslovakia

(*Received* 26 *June* 1990; *accepted* 17 *October* 1990)

Abstract—The chemical speciation of tin(II)– and tin(IV)–pyrophosphate systems have been researched by determining formation constants through pH potentiometry. Four protonation log constants for pyrophosphate were found (8.14, 14.01, 15.78 and 16.63) and seven constants are required to describe the tin(II) system and five constants for the tin(IV) system. The solubility product for $Sn_2P_2O_7$ was measured by both precipitation and dissolution approaches.

It has long been realized that the precise chemical form in which a trace element exists, i.e. its chemical speciation, has a most profound effect upon both the toxicology and bioavailability of that element. In fluids of physiological importance, for example, milk, blood plasma and saliva, the concentrations of the component metals and ligands are generally far below the levels analysable by standard laboratory procedures and, in such cases, computer modelling can identify the most abundant complexes and can provide a measure of their bioavailability.

In modelling the speciation of tin from dietary sources, it has been necessary to evaluate all possible metal–ligand interactions and, for this reason, the solubility product and stability constants of the tin–pyrophosphate systems were measured. The complexation of tin by the pyrophosphate ligand is of particular significance for the following reasons:

(i) Tin is present in food, medicine, healthcare agents, and our environment. The speciation of this element between organic and inorganic forms and between solid and aqueous solution phases of the latter determines whether the metal is a threat or a benefit and whether it is mobile in the geosphere or bioavailable from the gastrointestinal tract.[1,2]

(ii) Phosphates are widely distributed in nature and tin(II) is likely to encounter phosphates in ship-hull antifouling paints, in food and in biofluids. Thus, a knowledge of the solubility product of tin(II)–pyrophosphate is essential for modelling speciation.

(iii) Stannous pyrophosphate itself has found application in topical dental therapies for more than 15 years.[3–6] Since it is known that both stannous fluoride and stannous chloride function as bacteriostatic agents,[7] it seems likely that the efficacy of $Sn_2P_2O_7$ as an anticaries treatment and as an efficient plaque suppressor is related to the stannous ions rather than to the ligating moiety.

(iv) Pyrophosphate is a biological anion of some importance since many biosynthetic reactions are made irreversible by the hydrolysis of inorganic pyrophosphate. It is also instrumental in the synthesis of terpenes and steroids. Although tin is not recognized as an essential

* Present address: Department of Chemistry, Faculty of Science and Engineering, Manchester Polytechnic, John Dalton Building, Manchester M1 5DG, U.K.

† Author to whom correspondence should be addressed.

trace element in man, living cytoplasm functions as an efficient cation exchanger[8] and thus tin is often present in measurable amounts in the body. It is, therefore, not difficult to imagine complexation occurring *in vivo* between the essential ligand and the non-essential contaminating metal.

This paper compares values of stannous pyrophosphate formation constants obtained in this study with previously reported figures and presents a value for the $Sn_2P_2O_7$ solubility product determined from the cells in which titrations precipitate and also from dissolving the solid. Finally, the more difficult stannic pyrophosphate system was analysed by pH potentiometry and the "best" set of formation constants derived. This quantification of the tin pyrophosphate system will, thus, permit computer simulation models of the speciation chemistry under various conditions.

EXPERIMENTAL

Theory of measurement

Precipitation of tin complexes in the titration vessel during a potentiometric titration is a relatively common phenomenon. Usually when this occurs, the titration is terminated and the electrodes removed from the solution. However, provided that the composition of precipitated tin species is known and that the kinetics of precipitation is rapid, it is possible to calculate the solubility product (K_{sp}), and solubility (S_o) of the solid species and also the solution formation constants (β_{pqr}) from experimental data within the precipitation-free pH range. The detailed procedure is described later and refers to formation of tin pyrophosphate complexes at 25°C and ionic strength 150 mmol dm^{-3} chloride.

Materials

Tetrasodium pyrophosphate (Analar, BDH Ltd) was used without further purification. Sodium hydroxide and hydrochloric acid solutions were freshly prepared from concentrated stock solution ampoules (Convol, BDH Ltd). Stannous pyrophosphate was provided by Unilever Research, U.K.

A stock solution of tin was prepared by dissolving a weighed amount of stannous chloride dihydrate (Analar, BDH Ltd) in hydrochloric acid (100 mmol dm^{-3}). Any undissolved solid was removed by vacuum filtration and the solution made up to the mark with hydrochloric acid (100 mmol dm^{-3}). The tin concentration of these freshly prepared solutions was then determined by potassium iodate redox titrations using amaranth indicator.[9] The hydrogen ion concentration was measured using strong acid–strong base titrations.[10]

All solutions were prepared using distilled degassed doubly-deionized water and maintained at an ionic strength of 150 mmol dm^{-3} chloride by the addition of sodium chloride (Analar, BDH Ltd).

Method

Pyrophosphate (Pyr^{4-}) protonation constants and tin(II)–pyrophosphate formation constants were determined by glass electrode (Russell) potentiometric titration in a vessel thermostatted at 25.0 ± 0.1°C. The electrodes were calibrated with respect to the hydrogen ion by performing strong acid–strong base titrations.[10] A stream of pure nitrogen (with a $SnCl_2$ trap for oxygen followed by ionic background traps to prevent spray) was passed through the titration solutions in order to eliminate dissolved oxygen and carbon dioxide.

Protonation curves for the ligand were obtained at a variety of different total pyrophosphate concentrations (4–25 mmol dm^{-3}). Similarly, the metal complex formation curves were obtained at different pyrophosphate–tin ratios and for different total pyrophosphate (10–50 mmol dm^{-3}) and tin (3–25 mmol dm^{-3}) concentrations. Potentiometric titrimetry was carried out using three methods, namely:

(i) with both tin and pyrophosphate in the titration vessel;
(ii) tin in the vessel and pyrophosphate in the burette; and
(iii) pyrophosphate in the vessel and tin in the burette.

Titration data analysis

A general equilibrium involving Sn^{2+} cations (M), Pyr^{4-} anions (L) and H^+ ions and its overall formation constant can be expressed thus:

$$pM + qL + rH \rightleftharpoons M_pL_qH_r;$$

$$\beta_{pqr} = \frac{[M_pL_qH_r]}{[M]^p[L]^q[H]^r}, \qquad (1)$$

where square brackets indicate concentrations and charges have been omitted for simplicity.

Protonation and metal–ligand formation curves were generated using the ESTA suite of computer programs.[11] These are represented by $\bar{Z}_H$ [the average number of protons bound per ligand—ZBAR(H)] vs $-\log[H^+]$ for the pyrophosphate protonation; and $\bar{Z}_M$ [the average number of

ligands bound per metal–ZBAR(M)] vs −log [pyrophosphate] for the tin–pyrophosphate interactions. The formation constants for the selected models of species were refined using the optimization module of ESTA with a weighted least-squares objective function.

An average value for the dissociation constant of water ($\log K_w = -13.71$) determined in our research laboratories was used. Tin hydrolysis data were included, as these species could affect complexation with pyrophosphate.[12] The values used were:

Stannous:

$\log \beta_{10-1} = -4.2$; $\log \beta_{10-2} = -8.013$;
$\log \beta_{10-3} = -17.44$; $\log \beta_{20-2} = -4.161$;
$\log \beta_{40-3} = -9.555$.

Stannic:

$\log \beta^{10-1} = -1.937$ and
$\log \beta_{10-6} = -24.108$.

Table 1. Protonation constants of pyrophosphate (a) at 25°C, $I = 150$ mmol dm^{-3} chloride (seven titrations, 532 points) and (b) $\log \beta_{pqr}$ comparison with literature data for 25°C[13]

(a)

Species				Standard	Objective	
p	q	r	$\log \beta_{pqr}$	deviation	function	R factor
0	1	1	8.138	0.003		
0	1	2	14.014	0.005	2380	0.01519
0	1	3	15.779	0.017		
0	1	4	16.634	0.102		

(b)

			Ionic strength (mmol dm^{-3})				
p	q	r	0	100	150[a]	200	300
0	1	1	9.59	8.29	8.14	8.08	8.66
0	1	2	16.39	14.35	14.01	13.93	14.78
0	1	3	18.58		15.78		16.81
0	1	4	19.28		16.63		18.33

[a] Present study.

RESULTS AND DISCUSSION

Pyrophosphate protonation

The four protonation constants of pyrophosphate were measured (Table 1) optimizing simultaneously for electrode intercept and initial ligand concentration. The calculated values are in good agreement with literature data[13] for background electrolyte concentrations of 100 and 200 mmol dm^{-3}. The high standard deviation of the fourth protonation constant is due to the imprecision of the glass electrode at low pH and the spread of the protonation curve below pH = 1.5.

Tin(II)–pyrophosphate interactions

The shape and non-superimposibility of the experimental formation curves (Fig. 1) for the tin(II)–pyrophosphate interactions, which show the

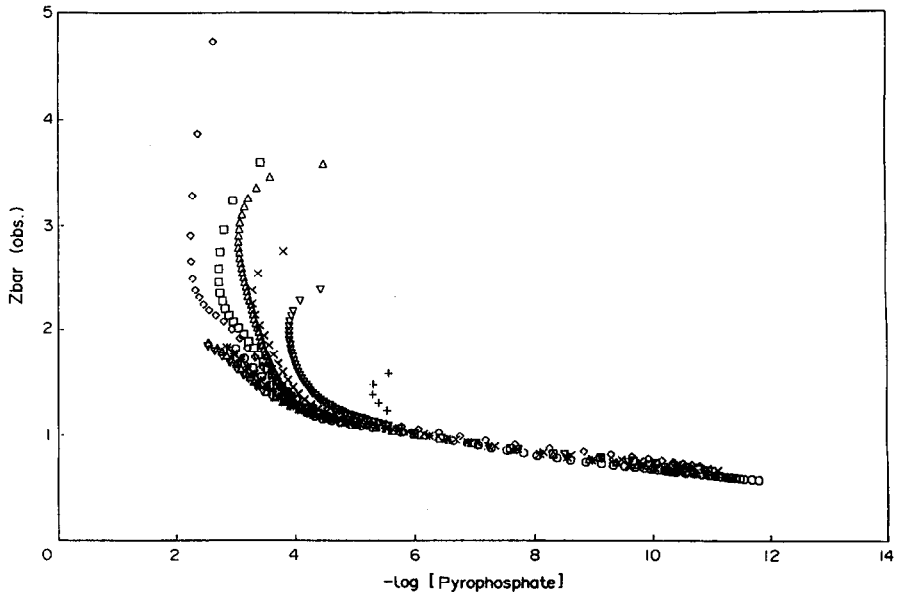

Fig. 1. Experimental metal complex formation curves for tin(II)–pyrophosphate; the different symbols indicate different titration concentrations.

results of 10 different titrations within the precipitation-free pH region from 2.2 to 11, indicate that a variety of species are present. Further, a white precipitate was observed at pH values below 2.6 when pyrophosphate was titrated with an acid solution of tin (seven titrations). Similarly, a precipitate formed on titration of an acid solution of tin(II) with pyrophosphate from pH 1.0 upwards. Initially, the composition with respect to the tin redox state of this white precipitate was uncertain as oxidation of tin(II) to tin(IV) is easily accomplished and tin(IV) salts are relatively insoluble. It was, thus, possible that the white precipitate observed in these tin(II)–pyrophosphate titrations was $SnP_2O_{7(s)}$, $Sn(OH)_{4(s)}$ or, indeed, a mixture of $SnP_2O_{7(s)}$ and $Sn_2P_2O_{7(s)}$ due to contamination of the tin(II) stock solutions with tin(IV). This perceived problem was further investigated by titrating tin(IV) solutions with pyrophosphate as described in the ensuing section(s).

The difficulties encountered in finding the "best" model to describe the experimental data are illustrated in Table 2. Most of the formation constants in model A are very close to literature values,[14–16] but this model was rejected because of poor statistical output and non-superimposibility of calculated and experimental titration curves. In model B, the overall statistics are good in comparison with the other models, but the high standard deviation of the ML_2 species (1.7028) precluded further consideration of this model. Therefore, the optimized formation constants of model C with relatively low standard deviations and objective function were considered to be the best model and were used to produce the simulated formation curves (Fig. 2). Comparison of this calculated formation curve with the experimental shows a good superimposibility.

Furthermore, comparison of the formation constants of tin(II)–pyrophosphate species with literature data revealed differences in values and species (Table 3).[14–16] This is probably due to the different experimental conditions used. Both Tur'yan *et al.*[14,15] and Orekhova *et al.*[16] worked at an ionic strength of 1 mol dm^{-3} and a lower overall concentration of tin ($\leqslant 1$ mmol dm^{-3}). For these reasons they probably did not observe precipitation at low pH values.

A knowledge of the species formed and their respective formation constants is crucial in the determination of the solubility product, K_{sp}, solubility, S_o, and formation constant, β_{pqr}, of the precipitated tin(II)–pyrophosphate species found at acid pH values.

Tin(IV)–*pyrophosphate interactions*

The potentiometric titrations were carried out using pyrophosphate solutions in the titration vessel

Table 2. Formation constants for the tin(II)–pyrophosphate interactions at 25°C, $I = 150$ mmol dm^{-3} chloride (10 titrations, 405 points)

Model	Species p	q	r	$\log \beta_{pqr}$	Standard deviation	Objective function	R factor
A	1	1	0	14.16	0.59	16,386	0.04662
	1	1	1	17.91	0.56		
	1	2	0	18.26	0.56		
	1	2	1	24.75	0.56		
	1	2	2	30.47	0.57		
	1	0	−2	−2.27	0.55		
B	1	1	0	11.81	0.09	12,358	0.05512
	1	2	0	13.96	1.70		
	1	2	1	21.79	0.19		
	1	2	2	27.40	0.25		
	1	2	3	31.54	0.13		
	1	1	−1	5.66	0.11		
C	1	1	0	12.04	0.11	9915	0.05006
	1	2	0	15.48	0.26		
	1	2	1	22.68	0.20		
	1	2	2	28.30	0.22		
	1	2	3	32.11	0.17		
	1	3	0	18.40	0.21		
	1	1	−1	5.97	0.15		

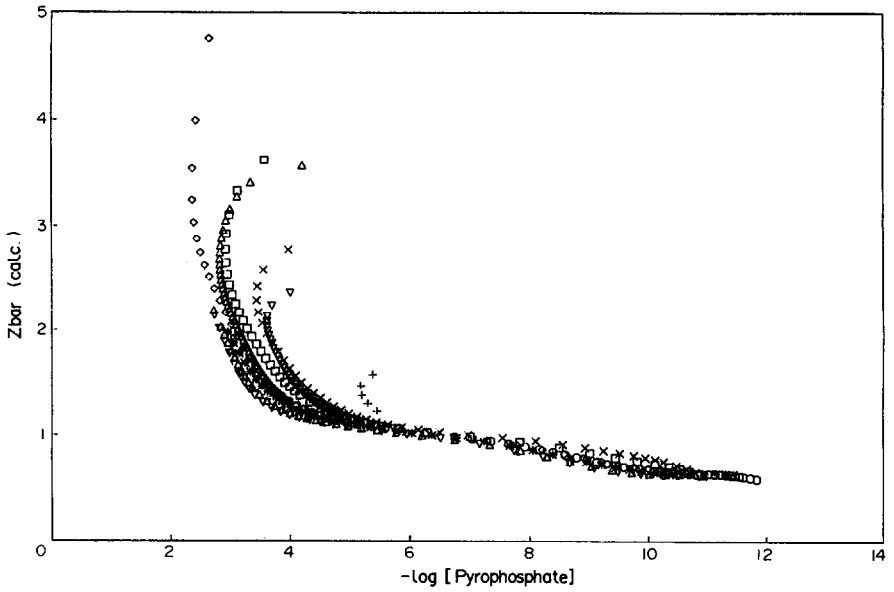

Fig. 2. Simulated metal complex formation curves using constants from model C.

Table 3. Comparison of formation constants ($\log \beta_{pqr}$) of tin(II)–pyrophosphate between literature data and the present study

Species	Tur'yan *et al.* (1986) 1 mol dm^{-3} $NaClO_4$, 25°C	Orekhova *et al.* (1980) 1 mol dm^{-3} K_2SO_4, 25°C	Present study 150 mmol dm^{-3} Cl^-, 25°C
ML	13.05±0.10	14.30	12.046±0.115
MLH	15.92±0.08		
MLH_2	17.47±0.06		
ML_2	16.27±0.02	16.47	15.48±0.286
ML_2H	22.31±0.03		22.66±0.205
ML_2H_2	26.79±0.06		28.31±0.225
ML_2H_3	30.07±0.08		32.11±0.178
ML_2H_4	31.58±0.08		
ML_3			18.40±0.210
ML(OH)	5.32±0.10		5.97±0.154
$ML(OH)_2$	−4.77±0.06		
$ML_2(OH)$	7.04±0.04		

as the titrand with tin(IV) solutions in the burette as the titrant. In this way, the point at which any precipitation of tin(IV)–pyrophosphate occurred in each titration could best be observed.

The shapes and non-superimposability of the experimental formation curves for the tin(IV)–pyrophosphate interactions, as with tin(II), indicated that a variety of species are present. It should be noted, however, that no precipitate was observed.

The difficulties encountered in finding the "best" models were similar to those for tin(II) but, by a process of elimination, the set of constants in Table 4 were preferred. Formation constants for tin(IV)–pyrophosphate species have not been previously reported in the literature.

Recently, Mathieu *et al.*[17] studied tin(IV)–pyrophosphate complexation by ^{119}Sn NMR spectroscopy and proposed a tin(IV)–pyrophosphate complex structure at a molar ratio of 1 : 1 [10 mmol dm^{-3} of tin(IV) solution and 100 mmol dm^{-3} of pyrophosphate solution] and pH 6.0 as ML_2. Figure 3 shows the tin(IV)–pyrophosphate distribution for a molar ratio of approximately 1 : 3 [15 mmol dm^{-3}

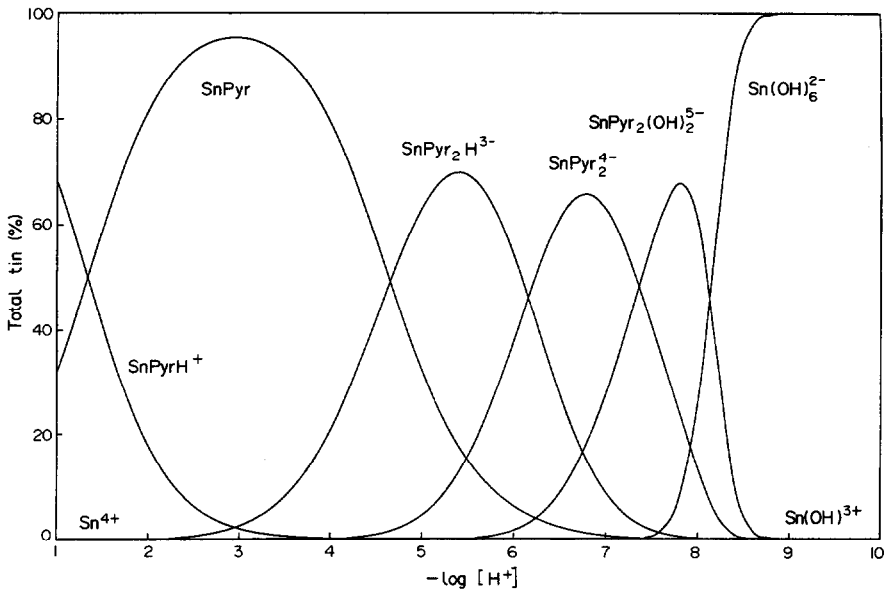

Fig. 3. The distribution of stannic pyrophosphate species calculated from the constants in Table 2 [Tin(IV) = 15 and pyrophosphate = 40 mmol dm^{-3}].

of tin(IV) solution and 40 mmol dm^{-3} of pyrophosphate solution] and the maximum of ML_2 species is at pH $\approx$ 7.0. However, one may expect a shift of the maximum to pH 6.0 and an increase of yield of the complex at a molar ratio of 1 : 10, which shows that the NMR studies support the validity of the determined formation constants.

Although the ML (stannic pyrophosphate) species predominates within the pH range 2–5 (Fig. 3), no precipitate occurred during the titrations. It follows that the precipitate of stannous pyrophosphate described next is not, therefore, contaminated with tin(IV) solids and its solubility product is not influenced by stannic pyrophosphate.

Determination of solubility product, K_{sp}, by titration

The titration of pyrophosphate with tin produced a white precipitate at pH values below 2.6. From the speciation profiles in Figs 4 and 5, it can be seen

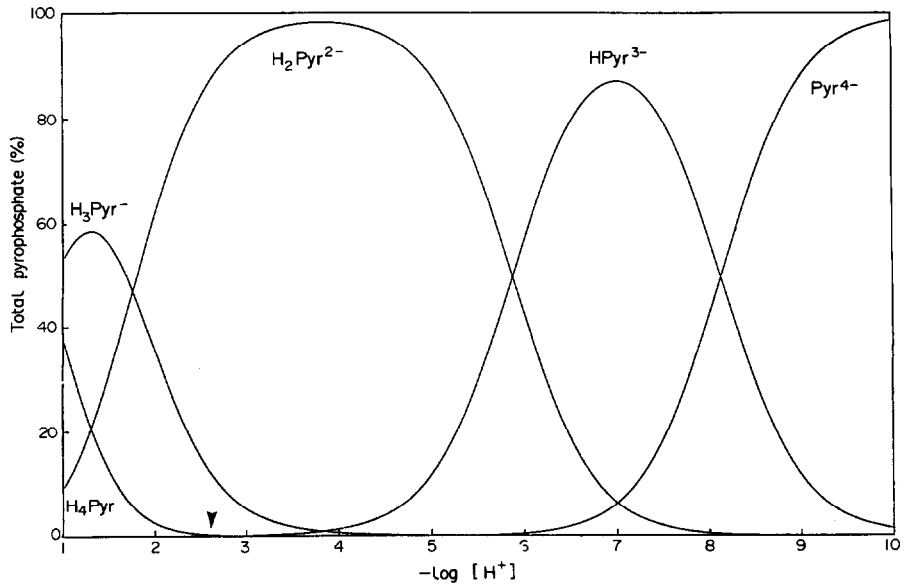

Fig. 4. Chemical species distribution plots for the proton–pyrophosphate system at $T_{Pyr^{4-}}$ = 20 mmol dm^{-3}. The arrowhead indicates pH = 2.6.

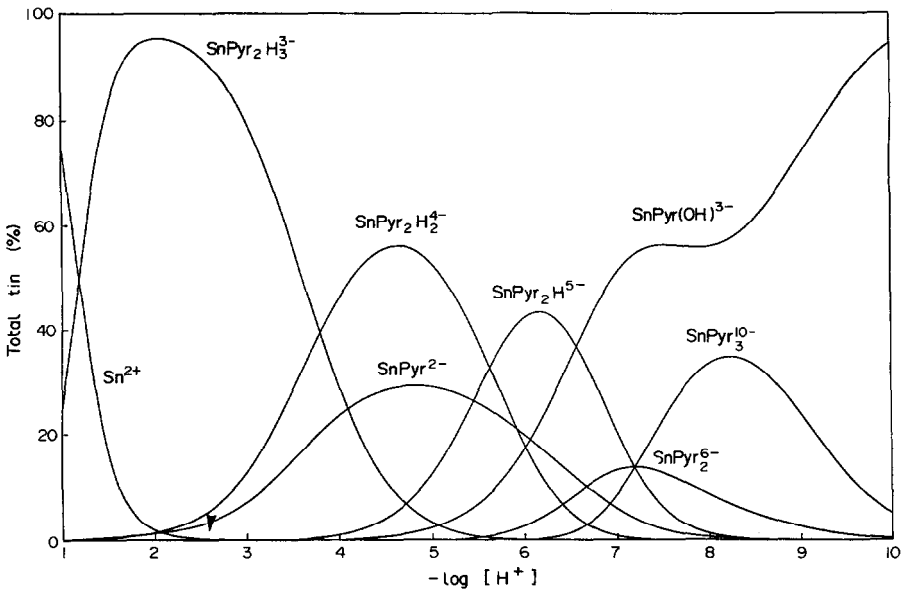

Fig. 5. Chemical species distribution plot for tin(II)–pyrophosphate. $T_{Sn^{2+}} = 5$ mmol dm^{-3}; $T_{Pyr^{4-}} = 20$ mmol dm^{-3}. The arrowhead indicates the precipitation point at pH = 2.6.

that a free metal ion and fully protonated ligand are present at approximately the same pH value. Thus, it is likely that the observed white precipitate in our experiments is stannous pyrophosphate, especially since it is known that stannous pyrophosphate can be prepared by adding tetrasodium pyrophosphate solution to a solution of stannous chloride in hydrochloric acid.[18]

The first appearance of a precipitate in the vessel indicates that saturation has been reached and the solubility product, K_{sp}, has been exceeded. This, solubility product, K_{sp}, can be expressed in the form of a general equilibrium, thus:

$$M_pL_q(s) \rightleftharpoons pM + qL; \quad K_{sp} = [M]^p[L]^q. \qquad (2)$$

The solubility product, K_{sp}, of a sparingly soluble salt can be calculated if the concentrations of free metal and ligand just before precipitation are known.

Generally, the concentrations of free metal and ligand are:

$$[M] = T_M - \sum p\beta_{pqr}[M]^p[L]^q[H]^r \qquad (3)$$

$$[L] = T_L - \sum q\beta_{pqr}[M]^p[L]^q[H]^r, \qquad (4)$$

where T_M and T_L are total concentrations of metal and ligand. Square brackets indicate free concentrations and charges have been omitted for simplicity.

Computer modelling programs permit the solution of such complex equilibria. Thus, the aqueous free ligand and free metal ion concentrations can be calculated at the point of precipitation if the ligand protonation and metal–ligand formation constants are known in addition to the free hydrogen ion concentration. Determination of the solubility product is then straightforward using eq. (2).

Table 4. Formation constants for the tin(IV)–pyrophosphate interactions at 25°C, $I = 150$ mmol dm^{-3} (four titrations, 244 points) using a stock solution of tin(IV) made from anhydrous stannic chloride

Model	Species p	q	r	$\log \beta_{pqr}$	Standard deviation	Objective function	R factor
	1	1	0	22.61	0.09		
	1	1	1	23.56	0.14		
A	1	2	0	27.08	0.03	1492	0.01352
	1	2	1	33.36	0.02		
	1	2	−1	19.84	0.04		

The solubility product can be used for the evaluation of stannous pyrophosphate solubility in water.[19] If S_o represents the solubility of stannous pyrophosphate in water (mol dm^{-3}), it follows that [Sn] = $2S_o$ and [L] = S_o, since each mole of stannous pyrophosphate that dissolves gives 2 moles of stannous ion and 1 mole of pyrophosphate ion. Hence,

$$[2S_o]^2[S_o] = K_{sp} \quad (5)$$

or

$$S_o = (K_{sp}/4)^{1/3} \quad (6)$$

or, in a negative logarithmic form,

$$pS_o = \tfrac{1}{3}pK_{sp} + 0.2. \quad (7)$$

Moreover, the same procedure can be used for calculating the formation constant, β_{210}, by substitution of eq. (5) into eq. (1). This gives eq. (6):

$$\log\beta_{210} = -\tfrac{2}{3}\log K_{sp} - 0.2 = \tfrac{2}{3}pK_{sp} - 0.2. \quad (8)$$

Solubility products calculated from the precipitation points of seven titrations are given in Table 5. The stated pH denotes the value at which precipitation was first observed. pL, pM, pK_{sp}, and pS_o are negative logarithmic values of free ligand and metal concentrations and for the solubility product, and solubility, respectively.

Variation of solubility product values may be due to (i) slower kinetics of precipitation than assumed; hence, creating an oversaturated solution in the titration vessel in spite of efficient stirring, and (ii) partial oxidation of tin(II) in the stock solution leading to the precipitate of stannous pyrophosphate becoming contaminated with stannic pyrophosphate which probably has a lower solubility product.

Literature values for the tin–pyrophosphate solubility product could not be found and, thus, the solubility product value for stannous pyrophosphate was verified as described below.

Determination of the solubility product, K_{sp}, by dissolution

The method involves dissolving to equilibrium pure samples of stannous pyrophosphate under carefully controlled pH conditions, separating solid from liquid phases, determining the total tin present in the aqueous phase and performing a speciation analysis in order to calculate the solubility product.

Tin solutions were analysed using a Varian graphite tube atomizer (GTA-95) in conjunction with a Varian atomic absorption spectrophotometer (AA 1275) and a printer (Epson LX 80). The light source was a Varian tin single-element hollow cathode lamp. The sample solutions were injected into a coated graphite tube by an automatic sampler.

The following instrumental parameters were used: lamp current 7 mA, spectral bandwidth 0.5 nm, wavelength 266.1 nm. Tin was measured from peak heights using read commands without background correction.

Standard solutions of tin (8 μg cm^{-3}) were prepared from solutions of stannous chloride (1 mg cm^{-3}) in hydrochloric acid (1 mol dm^{-3}) (Spectrosol, BDH Ltd) and by dilution with hydrochloric acid (50 mmol dm^{-3}) (Convol, BDH Ltd). These standard solutions were prepared daily. Hydrochloric acid (50 mmol dm^{-3}) and ascorbic acid (7%) were used as blanks and modifier, respectively.

Table 5. The determination of the solubility product (K_{sp}), solubility (S_o) and the formation constant (β_{210}) of stannous pyrophosphate at 25°C, I = 150 mmol dm^{-3} chloride

Titration number	pH	pA	pM	pK_{sp}	pS_o	log β_{210}
1	2.610	11.107	4.358	19.82	6.81	13.01
2	2.591	11.006	4.554	20.11	6.90	13.21
3	2.603	10.799	4.857	20.51	7.04	13.47
4	2.190	11.799	4.193	20.18	6.93	13.25
5	2.340	11.336	4.620	20.58	7.06	13.52
6	2.536	10.745	5.131	21.01	7.20	13.81
7	2.557	10.602	5.281	21.16	7.25	13.91
Average				20.48	7.03	13.45
Standard deviation				0.49	0.16	0.33

Method. Weighed amounts of stannous pyrophosphate (95.9–254.6 mg) were stirred, either with hydrochloric acid (50 cm^3) and sodium chloride (pH 1.07–3.32), or with water in a vessel thermostatted at 25.0±0.1°C, the ionic strength being maintained at 150 mmol dm^{-3} chloride. A stream of oxygen-free nitrogen was passed through the solutions in order to eliminate dissolved oxygen and carbon dioxide. The pH values of the solutions were determined after 3 h of stirring. Samples (2–3 cm^3) were taken usually at time intervals of 0.5, 1, 1.5, 2, 2.5, 3, 4, 5, 6 and 7 h from the commencement of stirring. The solid and liquid phases were separated by vacuum filtration through a Sartorius membrane filter (SM RS). The filtrate was diluted 1 : 10 with hydrochloric acid (50 mmol dm^{-3}) and analysed for tin content by atomic absorption spectrometry with electrothermal atomization. An injected volume of the samples varied from 0.002 to 0.01 cm^3 for the tin concentration and was topped up with blank (50 mmol dm^{-3} hydrochloric acid) to the total volume of 0.02 cm^3. Blanks were run after the standards and after each fifth sample. A plot of absorbance of the samples at 266.1 nm vs stirring time was produced for each solution. Values taken from the plateaus of the plots were expressed as total concentration of dissolved tin by reading the calibration curve and these were used for calculating solubility of stannous pyrophosphate. Measurements were repeated at each pH value.

Free concentrations of stannous and pyrophosphate ion were calculated using the ESTA program with the protonation constant, formation constant and pH as input.[11] This permitted the solubility product of stannous pyrophosphate to be calculated for each solution.

Atomizing conditions. Atomic absorption spectrometry using electrothermal atomization was chosen for determination because of simplicity of operation and its ability to analyse the suspected presence of very low concentrations. Simple samples containing just stannous, pyrophosphate, sodium and chloride ions required ≃ 45 s of drying time. However, chemical modifications of sample was necessary when analysing tin in sodium chloride matrices.[20] A range of concentrations and volumes for literature recommended modifiers such as diammonium hydrogen citrate, trisodium citrate, EDTA, citric and tartaric acids were examined, but the best results were obtained using ascorbic acid.[21] The addition of ascorbic acid (0.01 cm^3 of 7%) to the standards and samples containing up to 100 mmol dm^{-3} sodium chloride stabilizes the tin in solution and produces a single atomization peak. The optimal ash temperature was set at 700°C, and an atomizing temperature of 2600°C was retained.[20] A temperature of 3000°C was used for cleaning the tube of the remains of ascorbic acid ash. A new coated graphite tube was used for each set of measurements (i.e. to 70 injections). The wavelength chosen was 266.1 nm.[22]

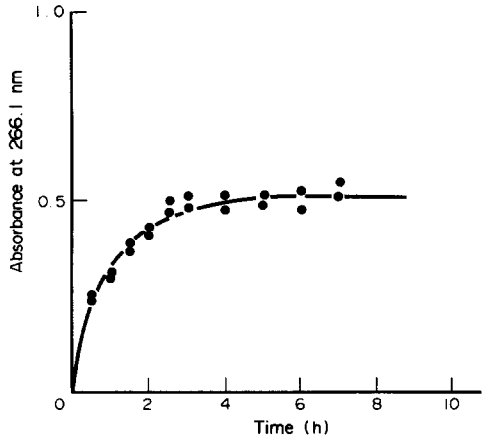

Fig. 6. Absorbance vs time for the dissolution of stannous pyrophosphate.

Dissolution. Centrifugation was replaced by vacuum filtration with a Sartorius membrane filter to separate phases. Tin concentrations in the samples were measured and a typical plot of absorbance with time of stirring is shown in Fig. 6, equilibrium being reached after 3–4 h.

Solubility of stannous pyrophosphate. The solubilities were calculated as being half of the total tin concentration on the plateau from the formula of $Sn_2P_2O_7$ (Fig. 6) and results are shown in Table 6.

Higher solubilities carry higher standard deviations because the samples are more highly diluted (see Method). Clearly, the solubility of stannous pyrophosphate decreases with increase in pH over the range 1.07–2.76. This confirms the report that stannous pyrophosphate is totally dissolved at pH 0.5.[23] Also, the solubility increased from pH 2.76

Table 6. Solubility of stannous pyrophosphate in water solutions at 25°C, I = 150 mmol dm^{-3} chloride

Composition of solutions (mmol dm^{-3})	pH	Number of points	Solubility ± SD (mmol dm^{-3})
100HCl + 50NaCl	1.07	9	2.04 ± 0.42
50HCl + 100NaCl	1.39	6	1.20 ± 0.21
10HCl + 140NaCl	1.86	10	0.51 ± 0.05
5HCl + 145NaCl	2.22	7	0.43 ± 0.04
1HCl + 149NaCl	2.76	6	0.36 ± 0.04
150NaCl	3.32	6	0.95 ± 0.07
Water	3.26	8	0.32 ± 0.03

Table 7. The solubility product (K_{sp}) for stannous pyrophosphate at 25°C, $I = 150$ mmol dm^{-3} chloride/or water

pH	Number of points	$-\log[Sn^{2+}]$	±SD	$-\log[P_2O_7^{4-}]$	±SD	pK_{sp}	SD
1.07	9	2.40	0.08	15.53	0.08	20.33	0.24
1.39	6	2.64	0.07	14.80	0.06	20.08	0.20
1.86	10	3.02	0.04	13.96	0.03	20.00	0.10
2.22	7	3.13	0.04	13.29	0.02	19.54	0.09
2.76	6	3.32	0.05	12.49	0.02	19.12	0.12
3.32	6	3.20	0.02	11.89	0.01	18.29	0.05
3.26	8	3.56	0.04	12.04	0.01	19.15	0.08

Free metal and ligand concentrations are in mol dm^{-3}. Compositions of the solutions are the same as in Table 1.

upwards and, as noted in the potentiometric data above, is totally dissolved by pH ≈ 6. Thus, minimum solubility is at pH 2.76, which matches the observations during the potentiometric study. The difference in solubilities between water and sodium chloride (150 mmol dm^{-3}) solution may be a result of interionic attraction.[24]

The solubility product of stannous pyrophosphate. The free concentrations of stannous and pyrophosphate ions were calculated by the ESTA program.[11] Input data used the total concentration of tin as determined by atomic absorption spectrometry and where the calculated total concentration of pyrophosphate was set equal to the solubility of stannous pyrophosphate. Output values of free concentrations of metal and ligand were used for calculating the solubility product of stannous pyrophosphate by eq. (9) (see Table 7).

$$K_{sp} = [Sn^{2+}]^2[P_2O_7^{4-}]. \quad (9)$$

The solubility product of stannous pyrophosphate decreases with increase in pH. The average values of $pK_{sp} = 19.65$, for ionic strength 150 mmol dm^{-3}, is not far removed from the potentiometric determined value (20.48). However, the former could be affected by kinetics of precipitation and possibly the presence of an oversaturated solution, but the agreement is quite good indicating that potentiometric titration can, indeed, be used for determining solubility products. The dissolution value was determined following equilibrium of stannous pyrophosphate dissolution and, therefore, is the best figure for speciation modelling studies.

Acknowledgement—One of us (I.K.) thanks the British Council for a scholarship to undertake this research.

REFERENCES

1. D. R. Williams, in *Introduction to the Principles of Drug Design* (Edited by H. J. Smith), pp. 159–190. J. Wright, London (1988).
2. J. R. Duffield and D. R. Williams, *Chemistry in Britain* 1989, 375.
3. R. A. Hiles, *Toxicol. Appl. Pharmacol.* 1974, **27**, 366.
4. M. Windholz (Ed.), *The Merck Index*, 9th edn, 8564–8568, Merck, Rahway, New Jersey (1976).
5. J. E. Ellingsen and J. Ekstrand, *J. Dent. Reks.* 1985, **64**, 1250.
6. A. Attramadal and B. Svatun, *Scand. J. Dent. Res.* 1984, **92**, 161.
7. K. G. Yost and P. J. Van Demark, *Appl. Environ. Microbiol.* 1978, **36**, 920.
8. H. J. M. Bowen, *Trace Elements in Biochemistry*. Academic Press, London/New York (1966).
9. A. I. Vogel, *A Textbook of Quantitative Inorganic Analysis*, 4th edn, p. 389. Longman Group, London (1981).
10. P. M. May and D. R. Williams, *Talanta* 1982, **29**, 249.
11. P. M. May, K. Murray and D. R. Williams, *Talanta* 1985, **32**, 483.
12. J. Kragten, *Atlas of Metal–Ligand Equilibria in Aqueous Solution*, p. 612. E. Horwood, Chichester (1978).
13. E. Högfeldt, *Stability Constants of Metal–Ion Complexes, Part A : Inorganic Ligands*, IUPAC Chemical Data Series, No. 21, p. 138. Pergamon Press, Oxford (1982).
14. I. Ya. Tur'yan, V. I. Kravtsov and V. V. Kondrat'ev, *Elektrokhimiya* 1986, **22**, 1388.
15. I. Ya. Tur'yan, V. I. Kravtsov and V. V. Kondrat'ev, *Elektrokhimiya* 1986, **22**, 1618.
16. V. V. Orekhova, F. K. Andryuschenko and N. D. Sakhnenko, *Elektrokhimiya* 1980, **16**, 1304.

17. L. Mathieu, P. Thivolle, J. C. Duplan and M. Berger, *J. Magn. Reson.* 1986, **69**, 362.
18. J. Vaid and T. L. Rama Char, *J. Electrochem. Soc.* 1957, **104**, 282.
19. T. Moeller and R. O'Connor, *Ions in Aqueous Systems. An Introduction to Chemical Equilibrium and Solution Chemistry*, p. 96. McGraw-Hill, New York (1972).

Polyhedron Vol. 10, No. 3, pp. 389-392, 1991
Printed in Great Britain

0277-5387/91 $3.00+.00
Pergamon Press plc

COMMUNICATION

NEW CYCLOHEPTATRIENE AND CYCLOHEPTATRIENYL DERIVATIVES OF NIOBIUM

MALCOLM L. H. GREEN,* PHILIP MOUNTFORD and PETER SCOTT

Inorganic Chemistry Laboratory, South Parks Road, Oxford OX1 3QR, U.K.

and

VICTOR S. B. MTETWA

University of Swaziland, P/B 4, Kwaluseni, Manzini, Swaziland

(*Received* 2 *October* 1990; *accepted* 22 *October* 1990)

Abstract—The one-pot syntheses of $[Nb(\eta^6\text{-}C_7H_8)(PMe_3)_2Cl_2]$ and $[Nb(\eta\text{-}C_7H_7)(\eta^4\text{-}C_7H_8)(PMe_3)]$ from $[NbCl_4(thf)_2]$ (thf = tetrahydrofuran) have provided a convenient route to the virtually unexplored η-cycloheptatrienyl niobium system. The X-ray crystal structures of the subsequent derivatives $[Nb(\eta\text{-}C_7H_7)(Me_2PCH_2CH_2PMe_2)CO]$ and 17-electron $[Nb(\eta\text{-}C_7H_7)(PMe_3)_2I]$ have been determined.

The organometallic chemistry of η-C_7R_7 ligands has been relatively little developed compared with that of the ubiquitous η-C_5R_5 ligands. However, since the functional group properties of the two classes of ligands differ markedly, it seems probable that there will be an extensive chemistry of C_7-ring–metal compounds which will differ significantly from that of the C_5-ring compounds. We believe the relative paucity of η^n-C_7-ring–metal compounds, where $n = 5$–7, is due primarily to the lack of synthetic routes to suitable starting materials. Therefore, we are developing the chemistry of C_7-ring compounds of the early transition metals. The early rather than later transition metals have been chosen since they have fewer valence electrons and hence require more electrons from the ligands to achieve a filled 18-electron shell.

We and others have developed the chemistry of η-C_7H_7 derivatives of molybdenum,[1] tungsten,[2] and titanium[3] and, more recently, we described convenient synthetic routes to a rich chemistry of C_7-complexes of zero- and divalent cycloheptatriene and cycloheptatrienyl zirconium[4–6] and hafnium.[6] We now describe the convenient synthesis of a variety of C_7-ring compounds of niobium.

Cycloheptatri-ene and -enyl complexes of niobium are rare. The compounds $[Nb(\eta\text{-}C_7H_7)(\eta\text{-}C_5H_5)]$[7] and $[Nb(\eta\text{-}C_5H_5)(\eta^4\text{-}C_7H_8)(CO)_2]$[8] have been described, and we recently reported the compounds $[Nb(\eta\text{-}C_6H_5Me)(\eta^5\text{-}C_7H_9)(PMe_3)]$ and $[Nb(\eta\text{-}C_7H_7)(\eta^4\text{-}C_7H_8)(PMe_3)]$, formed as a mixture from the reaction between $[Nb(\eta\text{-}C_6H_5Me)(PMe_3)_3H]$ and cycloheptatriene.[9] This route is inconvenient since it requires the precursor $[Nb(\eta\text{-}C_6H_5Me)_2]$ which is available only via metal vapour synthesis.[10]

Reduction of $[NbCl_4(thf)_2]$ (thf = tetrahydrofuran) with 2 equivalents of sodium amalgam in thf in the presence of cycloheptatriene and trimethylphosphine gives green, air-sensitive, paramagnetic crystals of $[Nb(\eta^6\text{-}C_7H_8)(PMe_3)_2Cl_2]$ (**1**). Selected data characterizing this and all the new compounds described are summarized in the foot-

* Author to whom correspondence should be addressed.

note.* In a typical experiment, 5 g of $[NbCl_4(thf)_2]$ gave 3 g of **1**. When the above reaction was carried out with an excess of sodium amalgam, the product (in low yield) was $[Nb(\eta\text{-}C_7H_7)(\eta^4\text{-}C_7H_8)(PMe_3)]$ (**2**), previously reported as a component in a mixture.[9] It appears that **1** is an intermediate in the formation of **2**, since stirring **1** with sodium amalgam in thf in the presence of cycloheptatriene gives **2**. We assume the structure **1** is analogous to that proposed for $[Zr(\eta^6\text{-}C_7H_8)(PMe_3)_2Cl_2]$.[5] Reduction of $[NbCl_4(thf)_2]$ with magnesium, in thf in the presence of cycloheptatriene and trimethylphosphine, gives air-sensitive, lime-green crystals of **2** directly and in good yield. Typically, 10 g of $[NbCl_4(thf)_2]$ gives 3.8 g of **2**. This clean and convenient route to **2** has allowed us to explore further the chemistry of the $Nb(\eta\text{-}C_7H_7)$ moiety.

Thus, treatment of **2** with ammonium hexafluorophosphate in thf yields orange microcrystals of $[Nb(\eta\text{-}C_7H_7)(\eta^5\text{-}C_7H_9)(PMe_3)][PF_6]$ (**3**). Also, **2** reacts with a mixture of dmpe and carbon monoxide (1 atm) giving scarlet crystals of $[Nb(\eta\text{-}C_7H_7)(dmpe)CO]$ (**4**). The X-ray crystal structure of this compound has been determined† (Fig. 1). The $[Nb(\eta\text{-}C_7H_7)(dmpe)]$ fragment is clearly electron-rich since the IR spectrum of **4** shows a strong band at 1785 cm^{-1} assignable to the $\nu(C{\equiv}O)$ mode for the terminal carbonyl ligand. Treatment of **2** with

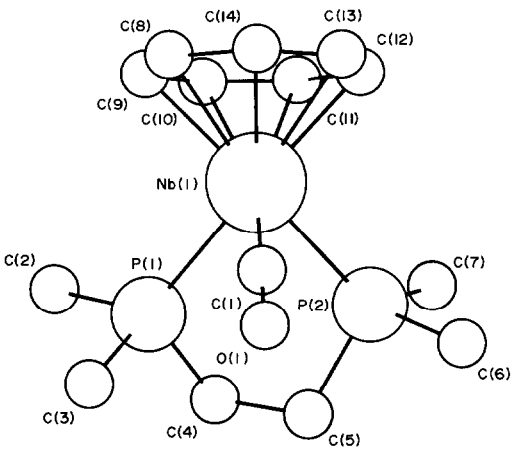

Fig. 1. Molecular structure of **4**. Hydrogen atoms omitted for clarity. Selected bond distances (Å): Nb(1)—C(1) 2.061(3), Nb(1)—P(1) 2.554(1), Nb(1)—P(2) 2.546(1), Nb(1)—C_7H_7(centroid) 1.707, Nb(1)—C(8–14, mean) 2.350(1). Selected bond angles (°): P(1)—Nb(1)—P(2) 78.15(3), P(1)—Nb(1)—C(1) 80.5(1), P(2)—Nb(1)—C(1) 80.2(1), P(1)—Nb(1)—C_7H_7(centroid) 131.14, P(2)—Nb(1)—C_7H_7(centroid) 125.6, Nb(1)—C(1)—O(1) 173.1(4).

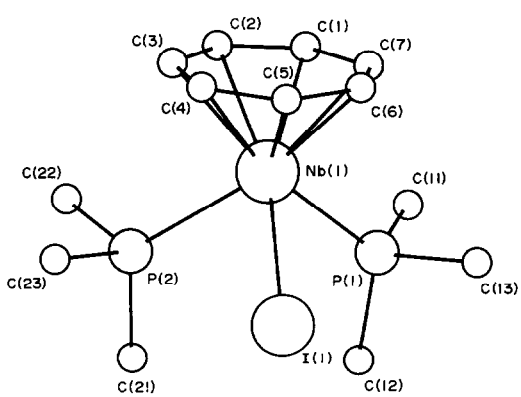

Fig. 2. Molecule structure of **5**. Hydrogen atoms omitted for clarity. Selected bond distances (Å): Nb(1)—I(1) 2.9130(8), Nb(1)—P(1) 2.658(2), Nb(1)—P(2) 2.660(2), Nb(1)—C_7H_7(centroid) 1.66, Nb(1)—C(1–7, mean) 2.324(1). Selected bond angles (°): P(1)—Nb(1)—P(2) 97.46(7), P(1)—Nb(1)—I(1) 81.11(5), P(2)—Nb(1)—I(1) 80.89(5), I(1)—Nb(1)—C_7H_7(centroid) 131.6, P(1)—Nb(1)—C_7H_7(centroid) 125.8, P(2)—Nb(1)—C_7H_7(centroid) 125.6.

* Selected data (^{1}H NMR at 300 MHz, coupling constants in Hz): Satisfactory elemental analysis has been obtained for all new compounds. Compound **1**: Found: C, 38.2; H, 6.4; Cl, 17.9. $C_{13}H_{26}Cl_2NbP_2$ requires: C, 38.2; H, 6.5; Cl, 17.4%. *m/z* (E.I.) 408. Compound **3**: ^{1}H NMR (dichloromethane-d_2) δ 5.96 [br d, 2H, J(H—H) 9.8, H_c or H_d], 5.17 (m, 1H, H_e), 5.12 [d, 7H, J(P—H) 5.01, η-C_7H_7], 5.01 (m, 2H, H_c or H_d), 2.23 (m, 4H, H_a and H_b), 1.34 [d, 9H, J(P—H) 7.2, PMe_3]. Compound **4**: ^{1}H NMR (benzene-d_6) δ 4.72 [t, 7H, J(P—H) 3.0, η-C_7H_7], 1.01 [d, 6H, J(P—H) 6.0, PMe_2], 0.92 [d, 6H, J(P—H) 6.0, PMe_2], 0.87 (m, 4H, PCH_2-CH_2P). Compound **6**: ^{1}H NMR (benzene-d_6) δ 4.64 (br s, 7H, η-C_7H_7), 3.88 (m, 2H, H_c), 2.79 [d, 2H, J(H—H) 7.9, H_i], 0.65 [br d, 2H, J(H—H) 10.2, H_b], 0.50 [d, 9H, J(P—H) 5.3, PMe_3]. Compound **8**: ^{1}H NMR (benzene-d_6) δ 4.91 (s, 5H, η-C_5H_5), 4.61 (s, 7H, η-C_7H_7).

† Crystal data for **4**: $C_{14}H_{23}ONbP_2$, $M = 362.19$, monoclinic, $P2_1/n$, $a = 7.013(1)$, $b = 13.903(3)$, $c = 16.829(3)$ Å, $\beta = 94.87(2)°$, $\theta_{max} = 26°$, $V = 1635.0$ Å^3, $Z = 4$, $D_c = 1.47$ g cm^{-3}, μ(Mo-K_α) 8.86, crystal size *ca* $0.20 \times 0.30 \times 0.5$ mm, $R = 0.025$, $R_w = 0.027$ from 2681 reflections [$I > 3\sigma(I)$] and 164 independent parameters. For **5**: $C_{13}H_{25}INbP_2$, $M = 463.09$, monoclinic, Pn, $a = 7.025(10)$, $b = 13.206(3)$, $c = 9.700(3)$ Å, $\beta = 92.60(8)°$, $\theta_{max} = 25°$, $V = 898.9$ Å^3, $Z = 2$, $D_c = 1.71$ g cm^{-3}, μ(Mo-K_α) 24.99, crystal size *ca* $0.35 \times 0.35 \times 0.40$ mm, $R = 0.039$, $R_w = 0.044$ from 1554 reflections [$I > 3\sigma(I)$] and 155 independent parameters. The data for both structures were collected on an Enraf–Nonius CAD4 diffractometer using graphite-monochromated Mo-K_α radiation. Empirical absorptions were applied and the structures solved using heavy atom methods and difference Fourier synthesis. Hydrogen atoms were placed in calculated positions (C—H = 0.96 Å).

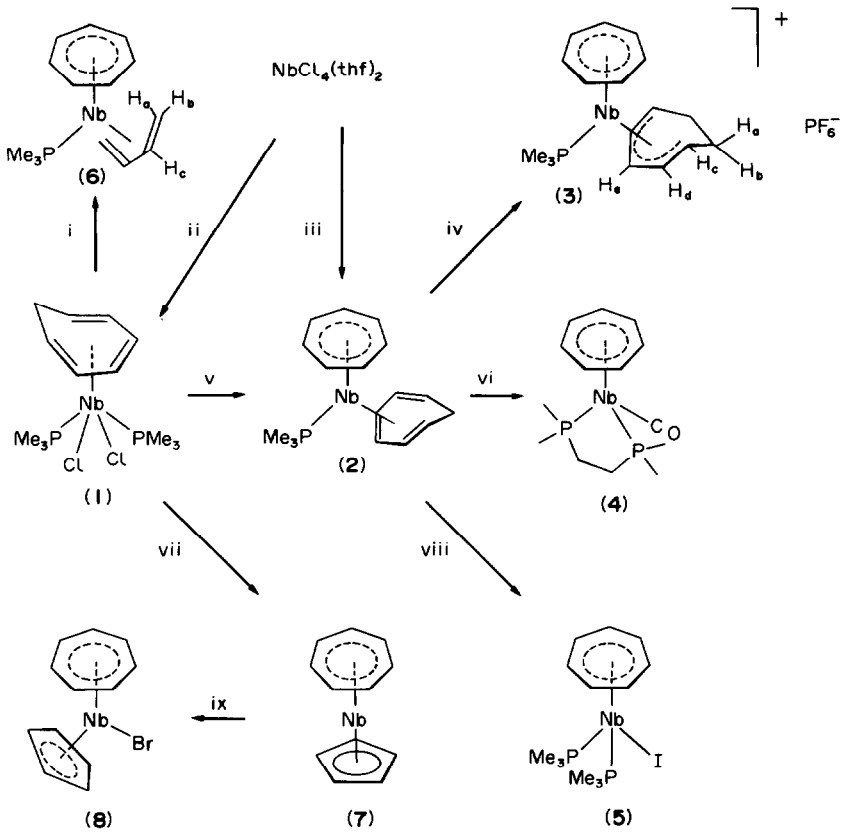

Scheme 1. Reagents and conditions: i, excess $[Mg(C_4H_6)\cdot 2(thf)]$ in thf at room temperature for 12 h (70%); ii, 2 Na/Hg, 2 PMe_3 and excess cycloheptatriene in thf at −80°C, warming slowly to room temperature, then stirring for 12 h (50%); iii, excess Mg, 2 PMe_3 and excess cycloheptatriene in thf at −80°C, warming slowly to room temperature then stirring for 12 h (40%); iv, NH_4PF_6 in thf at room temperature for 15 min (80%); v, excess Na/Hg and excess cycloheptatriene in thf at room temperature for 4 h (12%); vi, dmpe in toluene under CO (1 atm) at room temperature for 10 min (95%); vii, excess $Na(C_5H_5)$ in thf at room temperature for 3 h (80%); viii, MeI in toluene at −80°C warming to room temperature over 1 h (22%); ix, allyl bromide in toluene at −80°C warming to room temperature for 1 h (90%).

iodomethane in toluene gives low yields of the blue–green complex $[Nb(\eta\text{-}C_7H_7)(PMe_3)_2I]$ (**5**). A single crystal X-ray crystallographic study* (Fig. 2) on this 17-electron compound showed that it is isomorphous with the 16-electron zirconium analogue $[Zr(\eta\text{-}C_7H_7)(PMe_3)_2I]$.[5] This observation is in accord with our understanding of the bonding in $[Zr(\eta\text{-}C_7H_7)(PMe_3)_2I]$ such that the additional electron in **5** would be expected to occupy a largely non-bonding orbital and hence cause little perturbation of structural parameters.

Treatment of **1** with $[Mg(C_4H_6)\cdot 2(thf)]$[11] in thf gave lime-green crystals of $[Nb(\eta\text{-}C_7H_7)(\eta\text{-}C_4H_6)(PMe_3)]$ (**6**). Addition of an excess of sodium cyclopentadienide to **1** affords the previously reported sandwich complex $[Nb(\eta\text{-}C_7H_7)(\eta\text{-}C_5H_5)]$ (**7**) in good yield.[7] Typically, 3 g of **1** yielded 1.7 g of **7**.

We have initiated a study of the chemistry of this 17-electron compound and found that it reacts smoothly with allyl bromide to yield red crystals of the diamagnetic, bent-sandwich complex $[Nb(\eta\text{-}C_7H_7)(\eta\text{-}C_5H_5)Br]$ (**8**). This reaction is reminiscent of that between allyl bromide and $[Nb(\eta\text{-}C_6H_5Me)_2]$ giving $[Nb(\eta\text{-}C_6H_5Me)_2Br]$.[9]

The new compounds and reactions are shown in Scheme 1. We conclude that the ease of synthesis and stability of most of the compounds **1–8** shows there will be an extensive chemistry of the niobium–C_7-ring systems.

Acknowledgement—We thank the SERC for a Quota award (to P.S.).

REFERENCES

1. (a) J. S. Adams, C. Bitcon, J. R. Brown, D. Collison, M. Cunningham and M. W. Whitely, *J. Chem. Soc.*,

* See footnote † on previous page.

Dalton Trans. 1987, 3049; (b) M. L. H. Green, P. A. Newman and J. A. Bandy, *J. Chem. Soc., Dalton Trans.* 1989, 331.
2. (a) E. M. van Dam, W. N. Brend, M. P. Silvon and P. S. Skell, *J. Am. Chem. Soc.* 1975, **97**, 465; (b) M. L. H. Green, D. K. Siriwardene, D. O'Hare and L.-L. Wong, *J. Chem. Soc., Dalton Trans.* 1988, 2851.
3. C. E. Davies, I. M. Gardiner, J. C. Green, M. L. H. Green, N. J. Hazel, P. D. Grebenik, V. S. B. Mtetwa and K. Prout, *J. Chem. Soc., Dalton Trans.* 1985, 669.
4. M. L. H. Green and N. M. Walker, *J. Chem. Soc., Chem. Commun.* 1989, 850.
5. M. L. H. Green, P. Mountford and N. M. Walker, *J. Chem. Soc., Chem. Commun.* 1989, 908.
6. M. L. H. Green and N. M. Walker, *J. Chem. Soc., Chem. Commun.* 1989, 1865.
7. H. O. van Oven, C. J. Groenenboom and H. J. De Liefde Meijer, *J. Organomet. Chem.* 1975, **81**, 379.
8. R. B. King and C. D. Hoff, *J. Organomet. Chem.* 1982, **225**, 245.
9. M. L. H. Green, D. O'Hare and J. G. Watkin, *J. Chem. Soc., Chem. Commun.* 1989, 698.
10. F. G. N. Cloke, M. L. H. Green and D. H. Price, *J. Chem. Soc., Chem. Commun.* 1978, 431; F. G. N. Cloke and M. L. H. Green, *J. Chem. Soc., Dalton Trans.* 1981, 1938.
11. K. Fujita, Y. Ohnuma, H. Yasuda and H. Tani, *J. Organomet. Chem.* 1976, **113**, 201.

Polyhedron Vol. 10, No. 4/5, pp. 393–402, 1991
Printed in Great Britain

0277-5387/91 $3.00+.00
© 1991 Pergamon Press plc

EIGHT COORDINATION—I. EFFECT OF INTER-LIGAND REPULSION ON THE GEOMETRY OF EIGHT-COORDINATE COMPLEXES

I. G. SHTEREV

Institute of Food Industry, Plovdiv 4000, Bulgaria

and

G. ST. NIKOLOV* and N. TRENDAFILOVA

Institute of General and Inorganic Chemistry, Bulgarian Academy of Sciences, Sofia 1040, Bulgaria

and

R. KIROV

University of Plovdiv, Plovdiv 4000, Bulgaria

(*Received* 11 *September* 1989; *accepted after revision* 5 *October* 1990)

Abstract—The effect of non-bonded interactions (inter-ligand repulsion, ILR) on the geometry of eight-coordinate complexes was studied in the range of symmetry coordinates of the two highest symmetry structures, cube and hexagonal bipyramid (HBP). Only a few of the symmetry coordinates that convert the cube and the HBP into lower symmetry [dodecahedron (DD), square antiprism (SAP) and trigonal bicapped prism] were found to be important. ILR was demonstrated as the dominant factor in producing the lower symmetry structures for the closed-shell central atoms and it most certainly plays a very important role in helping or opposing the Jahn–Teller distortions for the orbitally degenerate complexes. The theoretical predictions were compared with a variety of structural data for ML_8. The predicted radial distortions were much larger than the experimental values and this was attributed to the electronic factors. Most of the angular distortions for ML_8 were explained in terms of a single e_u vibration.

The number of possible geometric structures sharply increases with increasing coordination number for the mononuclear ML_n complexes. Thus, for coordination number eight the following structures are possible in principle: cube, dodecahedron (DD), square prism (SP), square antiprism (SAP), bicapped (BCTP) or dishouldered (BSTP) trigonal prism, hexagonal bipyramid (HBP) and numerous intermediate structures[1–6] (see Fig. 1 for illustrations). In fact all intermediate and low symmetry structures may be obtained by symmetry descent from one of the two highest symmetry structures, namely the cube (O_h) and the hexagonal bipyramid (D_{6h}). These two structures form two distinct symmetry descent sequences that converge at C_{2v} and below.[7]

Previous studies on the shape of ML_8 complexes[1–6] have shown the predominance of two factors: (a) the electronic energy, given by electronic repulsion, central field attraction and Jahn–Teller distortion;[7] and (b) inter-ligand (non-bonded) repulsion.[3,4] These two factors can be assessed by semi-empirical methods, but the results obtained are dependent on the choice of M and L and they are not valid in general; the comparison is greatly

* Author to whom correspondence should be addressed.

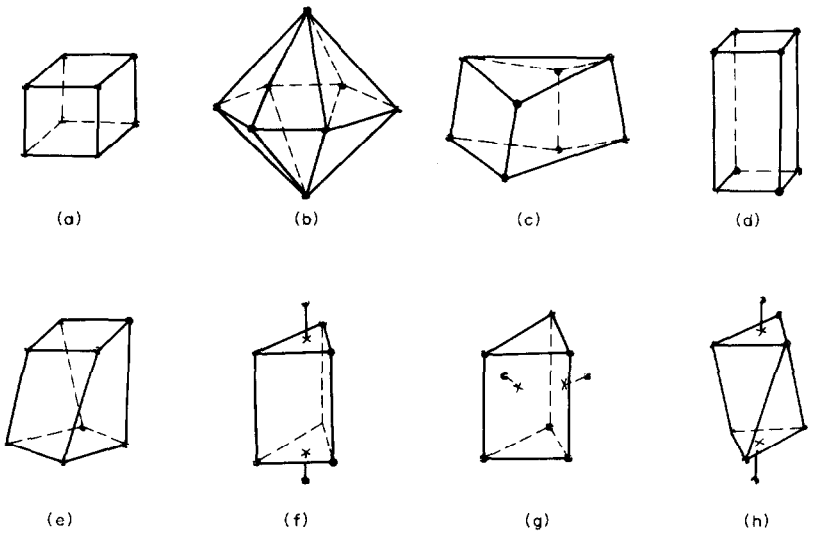

Fig. 1. Illustration of the main geometries occurring for the ML_8 complexes. Cube (a), hexagonal bipyramid (b), dodecahedron (c), square prism (d), square antiprism (e), bicapped (f), and bi-shouldered (g) trigonal prism, bicapped trigonal antiprism (h).

restricted by the initial choice. Highly sophisticated *ab initio* quantum mechanical methods can incorporate both factors (a) and (b), but for the higher coordination numbers these methods are not readily accessible even when the core potential version is used, and they give results of highly specific validity.

Studies on the shape of ML_8 complexes have shown that they form two series in order of increasing energy:[2]

$$\text{SAP} \sim \text{DD} < \text{cube} < \text{BCTP} \ll \text{BSTP} \quad \text{ILR} \quad (1)$$

$$\text{BCTP} < \text{BSTP} < \text{SAP} < \text{DD} \ll \text{cube} \sim \text{HBP} \quad \text{EH.} \quad (2)$$

The first series expresses the order in terms of the inter-ligand repulsion energy, while the second order was obtained by the Extended Huckel method[2] and involves both non-bonded repulsion and electronic factors, although the inter-electron repulsion is taken implicitly. The two structures DD and SAP are believed to be so close in ILR energy that they offer equal possibilities of forming M—L bonds; in such a case the choice of structure is governed by other factors such as the closest packing conditions in the crystal lattice.[5]

In the first paper of our series on eight-coordination we shall discuss the effect of inter-ligand repulsion on the molecular shape of ML_8. Subsequent papers will deal with the electronic factors, employing semi-empirical quantum chemical methods.

COMPUTATIONAL PROCEDURE

We shall study the inter-ligand repulsion energy as a function of the symmetry coordinates for the two highest symmetry structures, namely the cube and the hexagonal bipyramid. Thus, instead of varying one internal coordinate as previously[1,5] and missing what happens with the others, we shall separate, by symmetry, the $8 \times 3 = 24$-fold space of the L_8 cage structure, positioning M at the centre of our fixed coordinate system. Such an approach offers many advantages, the most important one being that the 24-dimensional L_8 coordinate space is reduced to:

$$a_{1g}, e_g, 2t_{2g}, a_{2u}, e_u, t_{1u}, t_{2u} \text{ for } O_h(\text{cube}) \quad (3)$$

$$2a_{1g}, b_{2g}, e_{1g}, 2e_{2g}, a_{2u}, b_{1u}, b_{2u}, 2e_{1u}, e_{2u} \text{ for } D_{6h}(\text{HBP}). \quad (4)$$

It can be readily seen that instead of groping in the 24-dimensional hyperspace we have reduced the problem to one six-dimensional ($2t_{2g}$), two three-dimensional (t_{1u} and t_{2u}), two two-dimensional (e_g and e_u) and two one-dimensional subspaces (a_{1g}, a_{2u}) for the cube. The highest dimensional subspaces for HBP are $2e_{2g}$ and $2e_{1u}$ (4), followed by e_{1g}, e_{2u} and $2a_{1g}$ (2), and the remaining b_{2g}, a_{2u}, b_{1u}, b_{2u} are one-dimensional.

Furthermore, we studied the variation of the ILR energy as a function of the symmetry coordinates listed above. These symmetry coordinates for L_8 in O_h and D_{6h} can be obtained in many ways, but in

this case were found by using projection operators.[8] The O_h symmetry coordinates were found first in D_{4h} and then by using the correlation analysis in its ascent of symmetry version they were grouped together to produce the cube's symmetry modes.[10] The final results are listed in Table 1. The projection operator technique was employed directly for D_{6h} (HBP).

Variations of the ILR energy were followed by calculating the so-called repulsion coefficient, X, as a function of the distances, d_{ij}, between each pair of non-bonded atoms, i and j, in the L_8 frame:[1]

$$X = \sum_{i<j} d_{ij}^{-6}. \qquad (5)$$

By inserting the incremental δr, $\delta\theta$ or $\delta\phi$ values in the position of atoms prescribed by the symmetry coordinates listed in Tables 1 and 2, the variation of X was found with the appropriate symmetry mode S, i.e. $X = f(S_i)$ where i numbers the symmetry species for L_8.

This simplest possible repulsion potential was widely used to explain the observed stereochemistry of many inorganic complexes,[1,4,5] and so we retain the generality of the results obtained. They would be independent of M and L and would (for the radial distortion) depend on the bond length in an explicit way.

When using eq. (5) to assess the ILR energy variations with S_i, in order to evaluate the softness or hardness of the potential energy surface near the energy minima, we have also calculated the derivatives $(\partial^2 X/\partial S_i^2)_{s_i=s_i^0}$. The numerical values thus obtained should be proportional to the Urey–Bradley force constants, reflecting the non-bonded interactions.[11,12] Our $(\partial^2 X/\partial S_i^2)_{s_i=s_i^0}$ values (Tables 3 and 4) obtained at the PES extrema could thus serve only for comparison's sake. They may be used to guess whether a certain motion over the PES is softer than another. In the same sense, the calculated changes in the repulsion coefficients, ΔX, along a certain symmetry coordinate, S_i, which convert one structure into another give a rough assessment of the barrier height of such a conversion, relative to changes in ILR energy.

In general, in order to find the pathways connecting different local minima we have used the gradients of X vs S_i.

Table 1. Symmetry coordinates for L_8 in O_h (cube), expressed as displacements of the ligand atoms in polar coordinates δr_i, $\delta\theta_i$, $\delta\phi_i$. R is the M—L distance with M placed at the cube centre. Normalization constant $(1/\sqrt{8})$

Symmetry species	Linear combinations of displacements	Distortion (IR)[a]
a_{1g}	$(\delta r_1+\delta r_2+\delta r_3+\delta r_4+\delta r_5+\delta r_6+\delta r_7+\delta r_8)$	$O_h\,(a_1)$
a_{2u}	$(\delta r_1-\delta r_2+\delta r_3-\delta r_4-\delta r_5+\delta r_6-\delta r_7+\delta r_8)$	$D_{2d}\,(b_1)$
	$(\delta r_1+\delta r_2+\delta r_3+\delta r_4-\delta r_5-\delta r_6-\delta r_7-\delta r_8)$	$C_{4v}\,(b_1)$
t_{1u}	$(\delta r_1+\delta r_2-\delta r_3-\delta r_4+\delta r_5+\delta r_6-\delta r_7-\delta r_8)$	$C_{4v}\,(e_a)$
	$(\delta r_1-\delta r_2-\delta r_3+\delta r_4+\delta r_5-\delta r_6-\delta r_7+\delta r_8)$	$C_{4v}\,(e_b)$
	$(\delta r_1-\delta r_2-\delta r_3+\delta r_4-\delta r_5+\delta r_6+\delta r_7-\delta r_8)$	$D_{2h}\,(b_{1g})$
t_{2g}	$(\delta r_1+\delta r_2-\delta r_3-\delta r_4-\delta r_5-\delta r_6+\delta r_7+\delta r_8)$	$D_{2h}\,(b_{3g})$
	$(\delta r_1-\delta r_2-\delta r_3+\delta r_4-\delta r_5+\delta r_6+\delta r_7-\delta r_8)$	$D_{2h}\,(b_{2g})$
	$R(\delta\theta_1+\delta\theta_2+\delta\theta_3+\delta\theta_4-\delta\theta_5-\delta\theta_6-\delta\theta_7-\delta\theta_8)$	$D_{4h}\,(a_{1g})$
e_g	$R(\delta\phi_1-\delta\phi_2+\delta\phi_3-\delta\phi_4+\delta\phi_5-\delta\phi_6+\delta\phi_7-\delta\phi_8)$	$D_{4h}\,(b_{1g})$
	$R(\delta\theta_1-\delta\theta_2+\delta\theta_3-\delta\theta_4-\delta\theta_5+\delta\theta_6-\delta\theta_7+\delta\theta_8)$	$D_{2h}\,(b_{1g})$
t_{2g}	$R(\delta\theta_1+\delta\theta_2-\delta\theta_3-\delta\theta_4+\delta\theta_5+\delta\theta_6-\delta\theta_7-\delta\theta_8)$	$D_{2h}\,(b_{3g})$
	$R(\delta\theta_1-\delta\theta_2-\delta\theta_3+\delta\theta_4+\delta\theta_5-\delta\theta_6-\delta\theta_7+\delta\theta_8)$	$D_{2h}\,(b_{2g})$
	$R(c_1\delta\phi_1+c_2\delta\phi_2+c_3\delta\phi_3+c_4\delta\phi_4-c_5\delta\phi_5-c_6\delta\phi_6-c_7\delta\phi_7-c_8\delta\phi_8)$	$D_2\,(a_1)$
e_u	$R(\delta\theta_1-\delta\theta_2+\delta\theta_3-\delta\theta_4+\delta\theta_5-\delta\theta_6+\delta\theta_7-\delta\theta_8)$	$D_{2d}\,(a_1)$
	$R(c_1\delta\phi_1-c_2\delta\phi_2+c_3\delta\phi_3-c_4\delta\phi_4-c_5\delta\phi_5+c_6\delta\phi_6-c_7\delta\phi_7+c_8\delta\phi_8)$	C_{2v}
t_{2u}	$R(\delta\theta_1+\delta\theta_2-\delta\theta_3-\delta\theta_4-\delta\theta_5-\delta\theta_6+\delta\theta_7+\delta\theta_8)$	$C_{2v}\,(a_1)$
	$R(\delta\theta_1-\delta\theta_2-\delta\theta_3+\delta\theta_4-\delta\theta_5+\delta\theta_6+\delta\theta_7-\delta\theta_8)$	$C_{2v}\,(a_1)$

[a] Irreducible representations to which the corresponding mode is reduced when the eight L are not in the cubic arrangement.

$c_1, \ldots, c_8$ are $\sin\theta_1, \ldots, \sin\theta_8$.

Table 2. Symmetry coordinates for L_8 in D_{6h} (hexagonal bipyramid), expressed as displacements of the ligand atoms in polar coordinates δr_i, $\delta\theta_i$, $\delta\phi_i$. R is the M—L distance with M placed at the HBP centre. Normalization constants are omitted

Symmetry	Linear combinations of displacements	Distortion[a]
a_{1g}	$(\delta r_1+\delta r_2+\delta r_3+\delta r_4+\delta r_5+\delta r_6)$	D_{6h}
a_{1g}	$(\delta r_7+\delta r_8)$	D_{6h}
a_{2u}	$(\delta r_7-\delta r_8)$	C_{6v}
b_{1u}	$(\delta r_1-\delta r_2+\delta r_3-\delta r_4+\delta r_5-\delta r_6)$	D_{3h}
$e_{1u}{}^s$	$(2\delta r_1+\delta r_2-\delta r_3-2\delta r_4-\delta r_5+\delta r_6)$	C_{2v}
	$(\quad\delta r_2+\delta r_3\quad-\delta r_5+\delta r_6)$	C_{2v}
$e_{2g}{}^s$	$(2\delta r_1-\delta r_2-\delta r_3+2\delta r_4-\delta r_5-\delta r_6)$	D_{2h}
	$(\quad\delta r_2-\delta r_3\quad+\delta r_5-\delta r_6)$	C_{2h}
b_{2g}	$R(\delta\theta_1-\delta\theta_2+\delta\theta_3-\delta\theta_4+\delta\theta_5-\delta\theta_6)$	C_{3v}
b_{2u}	$R(c_1\delta\phi_1-c_2\delta\phi_2+c_3\delta\phi_3-c_4\delta\phi_4+c_5\delta\phi_5-c_6\delta\phi_6)$	C_{2v}
e_{1g}	$R(2\delta\theta_1+\delta\theta_2-\delta\theta_3-2\delta\theta_4-\delta\theta_5+\delta\theta_6)$	C_s
	$R(\quad\delta\theta_2+\delta\theta_3\quad-\delta\theta_5-\delta\theta_6)$	C_s
$e_{1u}{}^b$	$R(2c_1\delta\phi_1+c_2\delta\phi_2-c_3\delta\phi_3-2c_4\delta\phi_4-c_5\delta\phi_5+c_6\delta\phi_6)$	C_{2v}
	$R(\quad c_2\delta\phi_2+c_3\delta\phi_3\quad-c_5\delta\phi_5-c_6\delta\phi_6)$	C_{2v}
$e_{2g}{}^b$	$R(2c_1\delta\phi_1-c_2\delta\phi_2-c_3\delta\phi_3+2c_4\delta\phi_4-c_5\delta\phi_5-c_6\delta\phi_6)$	C_s
	$R(\quad c_2\delta\phi_2-c_3\delta\phi_3\quad+c_5\delta\phi_5-c_6\delta\phi_6)$	D_{2h}
e_{2u}	$R(2\delta\theta_1-\delta\theta_2-\delta\theta_3+2\delta\theta_4-\delta\theta_5-\delta\theta_6)$	C_{2v}
	$R(\quad\delta\theta_2+\delta\theta_3\quad-\delta\theta_5-\delta\theta_6)$	C_s

[a] All a_1 distortions are irreducible representations.
$c_1, \ldots, c_6$ are $\sin\theta_1, \ldots, \sin\theta_6$.

The main advantage offered by the intended study of X vs S_i, which we shall call symmetry-constrained ILR energy variation, becomes evident when we begin to study the problem of mixing the electronic with the nuclear motion, i.e. when dealing with the so-called vibronic coupling.

RESULTS

Initial geometry cube

Leaving aside, for obvious reasons, the totally symmetric a_{1g} mode, we shall treat consecutively all the symmetry coordinates of L_8 with L's located at the vertices of a cube with O_h symmetry.

Symmetry coordinate a_{2u}. The variation of X with $S(a_{2u})$ is shown in Fig. 2. It can be readily seen from this figure that the cube is unstable with respect to this coordinate and that, depending on the distance to the cube centre (R in Å), the L_8 frame is easily taken into two ILR energy minima. This corresponds to two dodecahedral structures with non-equivalent A and B sites, respectively. The minima are located at

$$|\delta r| = 0.0117 + 0.1998\,R. \qquad (6)$$

This is a linear regression equation calculated from a 30 point set of local minima. $|\delta r|$ is the displacement involved in the a_{2u} symmetry coordinates at which mimum ILR energy is observed, and R is the distance to L from the cube centre in the initial octahedral geometry, both expressed in Å. Equation (6) holds for $\theta_A = \theta_B = 54.74°$. It may be used to obtain the ratio of the bond lengths for the two A and B sites in the dodecahedron, R being

Table 3. Curvature around the minima observed in the X vs S_i subspaces with initial geometry cube

Symmetry coordinate	$(\partial^2 X/\partial S_i^2)$ $(\times 10^2)$	Minimum X at:	Δx^a $(\times 10^3)$
a_{2u}	6.40	D_{2d} (DD)	3.2
t_{1u}	23.70	O_h (cube)	—
t_{2g}	7.70	O_h (cube)	—
e_g	0.11	O_h (cube)	—
t_{2g}	0.02	O_h (cube)	—
e_u	0.01	D_2 (DD)	4.6
	0.02	D_{4d} (SAP)[b]	3.9
t_{2u}	1.20	O_h (cube)	—

[a] X for the conversion of a cube (O_h) to the new geometry listed in Column 3.
[b] SAP is a local minimum.

Table 4. Curvature in the vicinity of the minima observed in the X vs S_i subspaces with initial geometry hexagonal bipyramid

Symmetry coordinate	$(\partial^2 X/\partial S_i^2)$	Minimum X at:	ΔX^a
a_{2u}	0.0255	D_{6h} (HBP)	—
e_{2g}	0.80	D_{2h}	0.0108
	0.16		
b_{1u}	0.12–6.58 ln R	D_{3h}	ln $X = 2.774 - 3.185\,R$
e_{1u}	0.65	D_{6h} (HBP)	—
	0.22		
b_{2g}	0.0617–0.00733 ln R	C_{3v}	ln $X = 2.951 - 3.187\,R$
e_{1g}	2.53×10^{-4}	D_{6h} (HBP)	—
	0.70×10^{-4}	D_{6h} (HBP)	—
e_{2u}	8.6	C_{2v}	0.00676
	2.5×10^{-4}	C_{2v}	—
e_{2g}	24.3×10^{-4}	D_{6h} (HBP)	—
	77.2×10^{-4}		
b_{2u}	48.7×10^{-4}	D_{6h} (HBP)	—
e_{1u}	22.5×10^{-4}	D_{6h} (HBP)	—
	7.7×10^{-4}	D_{6h}	—

[a] For conversion O_h—new geometry listed in Column 3.

the average ML bond length in a hypothetical cube:

$$R_A/R_B = (R+\delta r)/(R-\delta r) = 1.51\ \text{Å}. \quad (7)$$

This equation holds for $R = 1.5$–2.5 Å, $R_A = R+\delta r$, $R_B = R-\delta r$ and $\theta_A = 36.85°$ and $\theta_B = 69.46°$, as in the hard sphere model.[14] However, the ratios found in the literature for dodecahedral complexes exceed 1.1 Å in very few cases (see Table 5). When the condition $\theta_A = \theta_B = 54.74°$ in eq. (6) is relaxed ($\theta_A > 54.74°$, $\theta_B < 54.74°$ or vice versa), the minimum ILR energy occurs at even higher δr values, ILR being the lowest with the $\theta_A = \theta_B = 54.74°$ condition. Hence, it may be concluded that while $S(a_{2u})$ may aid the distortion of the cube to a dodecahedron, its action is strongly opposed by other factors (see Discussion).

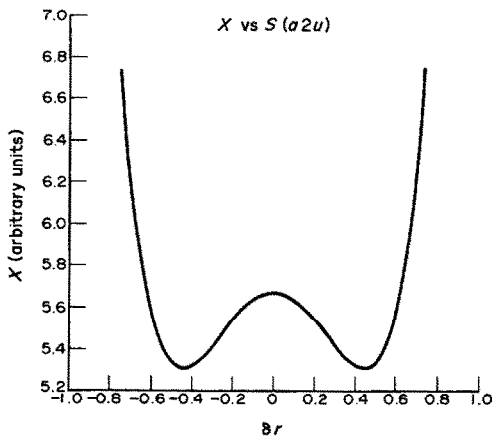

Fig. 2. The variation of the repulsion coefficient X [see eq. (5)] with the symmetry coordinate $S(a_{2u})$ in terms of δr for $R = 2.2$ Å. The distortions (δr) for minimum ILR energy as a function of R are given by eq. (6).

Table 5 contains the experimental results for the ML_8 complexes, only. No data on the chelate complexes are included since they reflect the constraints imposed by the rigid, multidentate ligands.[1]

The two differently shaped dodecahedra produced by $S(a_{2u})$ are separated by the barrier ΔX which is dependent on the distance of L to the cube centre, R, related by the equation

$$\ln(\Delta X) = 1.225 - 3.175\,R \quad (8)$$

(R is in Å). Once adopting the dodecahedron shape, the L_8 frame is very resistant (see Table 3) to possible further changes, since any attempt to take the structure out of the minima is met by a great energy loss.

Unfortunately there are no data on the interconversion of the two dodecahedra that could be compared with eq. (8).

Symmetry coordinate t_{1u}. This coordinate produces three truncated square-pyramids oriented with respect to the three coordinate axes x, y, z of the cube, each one related to the three t_{1u} components. However, the cube is the geometry of mini-

Table 5. A collection of structural data for ML_8. The numbering in the figures corresponds to the numbers in this table

Compound	Electronic configuration	R_A (Å)	R_B (Å)	θ_A (°)	θ_B (°)	ϕ (°)	Reference
Regular dodecahedron							
1. $K_4[Mo(CN)_8]\cdot 12H_2O$	d^2	2.16	2.16	36.0	73.5	94.3	17
2. $[Bu_4N]_3[Mo(CN)_8]$	d^1	2.12	2.12	37.2	72.3	87.7	18
3. $[Mo(CN)_4(CNMe)_4]$	d^2	2.18	2.15	35.7	75.7	90.0	19
4. $Rb_4[Mo(CN)_8]\cdot 3H_2O$	d^2	2.21	2.25	46.2	66.4	90.0	20
Distorted dodecahedron							
5. $(NH_4)_4[Mo(CN)_8]\cdot 1/2H_2O$[a]	d^2	2.16	2.13	38.1	65.8	89.0	20
6. $[Y(H_2O)_8]Cl_3$	f^0	2.35	2.40	35.5	71.0	108.5	21
Cube							
7. $La(bipyO_2)(ClO_4)_3$	f^0	2.50	—	56.2	—	87.3	22
Square antiprism							
8. $(NH_4)_4[Mo(CN)_8]\cdot 1/2H_2O$[a]	d^2	2.14	—	55.7	—	45.0	20
9. $H_4[W(CN)_8]\cdot 6H_2O$	d^2	2.18	—	57.6	—	44.6	23
10. $Na_3[W(CN)_8]\cdot 4H_2O$	d^1	2.14	—	59.1	—	29.6	24
11. $H_4[W(CN)_8]\cdot 4HCl\cdot 12H_2O$	d^2	2.26	2.08	56.1	—	40.3	25
12. $[ZrF_8]^{4-}$	d^0	2.10	—	57.1	—	30.0?	26
13. $Cs_4[U(NCS)_8]$	f^2	2.46	2.38	56.7	—	42.7	27
14. $Na_3[TaF_8]$	d^0	1.98	—	58.7	—	46.0	28
15. $[Sr(H_2O)_8][Bi_2Br_{10}]$	d^0	2.63	—	57.0	—	25.6	29
16. $[Y(H_2O)_8][TeCl_8]H_2O$	f^0	2.37	2.35	60.0	—	43.4	30
17. $[Lu(H_2O)_8][Na(crown\text{-}4)_2]Cl_4\cdot 2H_2O$	f^0	2.34	—	52.3	—	38.1	31
18. $K_5[Tb(HCOO)_8]$	f^8	2.41	—	53.0	—	42.1	32

[a] Different modifications.

mum ILR energy in this subspace and the three truncated square-pyramids appear as extrema on three rotationally symmetric troughs leading to the O_h minimum.

The t_{1u} symmetry mode is not stereochemically important since there are no ML_8 complexes with the structure of a truncated square-pyramid, possibly with expected unrecorded exceptions for $M(a\text{-}b)_4$ tetrakis-(bidentate) with asymmetric bidentate ligands, where the asymmetry of the ML_8 cage may arise from the different bonding provided by the bidentate ligands. Such cases, as mentioned previously, are outside the scope of the present study.

Symmetry coordinate t_{2u}. The three t_{2u} components take the L_8 frame into a D_{2h} structure. Such a structure is attained by elongation of the distances to four L from the cube centre, the four being located at two opposite edges connected with a body-diagonal of the cube. The ILR energy minimum for each pair of t_{2u} components was found for the cube structure. This minimum, however, is not related to rotationally symmetric troughs. The troughs that lead to the O_h minimum upon distancing from the cube centre split into two branches each without producing a new minimum, so that in the entire studied δr region (± 0.8 Å) the cube is the only ILR energy minimum. It should be noted, however, that the two branches from different troughs come so near to each other that the difference in δr becomes less than 0.1 Å, and the barrier separating these branches is solely $1\text{–}2 \times 10^{-2}$ units of X.

This symmetry coordinate, with the exception of the varieties of pathways leading to the cube, is again, not interesting stereochemically.

Symmetry coordinate e_g. The two e_g components produce different geometries when the L_8 frame is taken out of its equilibrium positions: (a) a square prism (D_{4h}) elongated along the x and y axes and compressed along z, (b) a square prism elongated along y, compressed along x and unchanged along z. The angle variation in the field of the two e_g components yields only one minimum for the cube (O_h). An interesting trough system is observed, the curvature along the troughs being equal and considerably less than for the stretching symmetry

coordinates. This coordinate, giving a single maximum for the cube, is also not interesting stereochemically. However, this coordinate is Jahn–Teller active for E and $T_{1(2)}$ ground-state molecules and hence it could be ultimately, vibronically active.

Symmetry coordinate t_{2g}. The cube is the geometry with least ILR energy in this subspace. The t_{2g} mode is Jahn–Teller active for $T_{1(2)}$ ground-state molecules and may produce distortions by the vibronic mechanism.

Symmetry coordinate e_u. Stereochemically this is the most interesting symmetry coordinate. Along e_u^a it leads to a DD structure, while e_u^b produces a square antiprism. The cubic structure located at $\delta\theta = 0$; $\delta\phi = 0$ is an ILR energy maximum (Fig. 3). Two regions, located symmetrically, indicate the existence of DD minima at $\delta\phi = 0$ and $\delta\theta = \pm 17.5°$, and there are two local minima for SAP at $\delta\theta = 0$ and $\delta\phi = \pm 22.5°$. The calculated $\delta\theta$ for DD corresponds to the hard sphere $\delta\theta$ value ($\delta\theta_A = +17.9°$ and $\delta\theta_B = -14.7°$) for $R_A/R_B = 1.50$, relative to the O_h value,[14] and they match nicely the angular distortions (Table 5 and Fig. 3).

The calculated X vs $\delta\theta$, $\delta\phi$ surface is shown in Fig. 4. The locations of the three structures (cube, DD, SAP) spanned in this subspace are easily recognized. One can also discern the trough leading from one DD over the SAP minima to the other DD minimum, which is an intricate motion involving both $\delta\theta$ and $\delta\phi$ variations.

Since any small deviations from the predicted

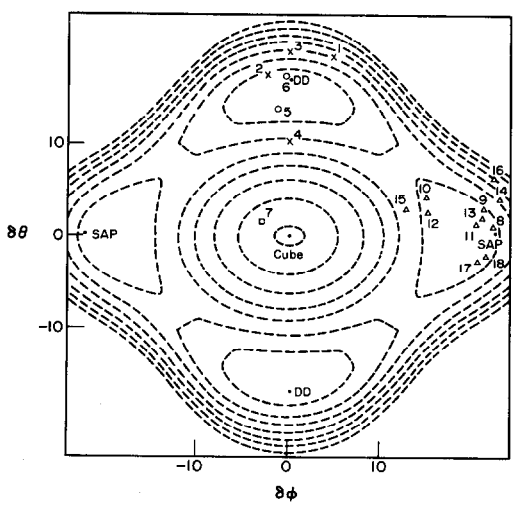

Fig. 3. The topographic surface of X vs $S(e_u^a)$ and $S(e_u^b)$. DD (dodecahedral minima), SAP (square antiprism local minima). The experimental points are: ×—regular DD; ▲—distorted DD; □—cube; ○—SAP. The lines are spaced at 0.015 units of X.

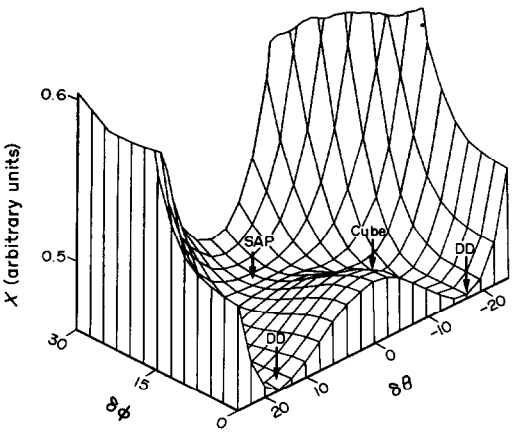

Fig. 4. The half-surface of X vs $S(e_u^a)$ and $S(e_u^b)$. The position of the three main geometries (cube, SAP, DD) are denoted.

regular structures (DD, SAP, cube) could be due to either crystal packing conditions or electronic factors we shall not discuss them at this stage. They will be discussed in the subsequent papers of this series.

Symmetry coordinate t_{2u}. The only existing minimum is for the cube. The curve is less steep with respect to $\delta\phi$, then to $\delta\theta$. This coordinate is not interesting stereochemically. Each t_{2u} component produces two troughs that split upon going away from the cube centre.

Mixing between the t_{2g} *coordinates.* We also studied possible combinations of the two t_{2g} modes, one stretching and one bending. All combinations produce an ILR energy minimum for the cube and highly distorted C_2 structures obtained by elongation along two body-diagonals and shortening along two other diagonals.

Initial geometry hexagonal bipyramid

Up to this point only a few of the possible structures for L_8 have been detected, the trigonally distorted structures lacking completely from our initial geometry cube treatment. Since any combination of the degenerate symmetry coordinates is a good starting mode, by combining some of the triply degenerate modes we could obtain coordinates that produce trigonally distorted structures. Thus for example, if a combination of the t_{2g} components in O_h are taken as operative, they produce a trigonal antiprism with two additional vertices. However, since no symmetry coordinate of the cube can generate a six-fold axis, such a conversion would be symmetry forbidden.[14c] Hence, instead of seeking the combination of symmetry coordinates for the

cube that produce trigonally distorted structures that may provide unrealistic conversion pathways, it may be more profitable to start a study of another genealogical tree, generated by the highest symmetry structure with a six-fold axis, namely the hexagonal bipyramid.

Symmetry coordinate a_{2u}. This reproduces the HBP, the resulting minimum being very soft (see Table 4), indicating that L_8 with HBP symmetry can easily leave this structure and acquire a new one.

Symmetry coordinate $e_{2g}{}^{s}$. With respect to this bond stretching coordinate, HBP is a maximum and cannot exist from the point of view of ILR. Three minima exist, comparatively shallow, rotated at 120° and they correspond to D_{2h} structures elongated along one of the diagonals of the common HBP base. Since this coordinate is Jahn–Teller active for $E_{1(2)}$ ground states the ILR energy would help the vibronic factor in distorting the HBP.

Symmetry coordinate b_{1u}. This coordinate causes ring puckering of the hexagonal base that removes the C_6 axis and makes it C_3. On the plots of X vs δr, HBP is a maximum at $\delta r = 0$. Two D_{3h} structures appear at:

$$\pm\delta r = 0.079 + 0.2635\,R, \qquad (9)$$

where R is the distance of a L to the pyramid centre. The two maxima are steeper for the shorter R:

$$(\partial^2 X/\partial S_i^2)_{s_i=s_i{}^0} = 5.12 - 6.58 \ln R. \qquad (10)$$

This dependence on R proves that the minima are not those of paraboloids.

The HBP maximum that separates the two D_{3h} structures decreases with increasing R:

$$\ln[\Delta X(D_{6h} \rightarrow D_{3h})] = 2.774 - 3.185\,R. \qquad (11)$$

It should be noted that the two D_{3h} structures are of lower ILR energy than HBP but they are energetically unfavourable even with respect to the cube, as predicted elsewhere.[2]

Symmetry coordinate $e_{1u}{}^{s}$. This bond stretching coordinate is not interesting from a real symmetry point of view. It lowers the symmetry down to C_{2v} (elongated or compressed HBP along one of the C_2 axes). The ILR energy minimum lies at HBP; the second e_{1u} component is softer than the first one (see Table 4).

Symmetry coordinate b_{2g}. The HBP structure is of maximum ILR energy. There are two C_{3v} ILR energy minima on both sides of HBP at $\delta\theta = \pm 19.6°$, irrespective of the R value.

$$\ln(\Delta X) = 2.951 - 3.187\,R \qquad (12)$$

$$10^3(\partial^2 X/\partial S_i^2)_{s_i=s_i{}^0} = 6.17 - 7.33 \ln R. \qquad (13)$$

It should be noted that the coefficients in the $\ln(\Delta X)$ vs R equations, (11) and (12), are practically the same. This can only imply that when HBP is the maximum, the D_{3h} and C_{3v} minima produced by the two coordinates e_{1u} and b_{2g} are equally deep and steep.

Symmetry coordinate e_{2u}. The e_{2u} subspace reveals that the initial HBP geometry is a maximum from which, along two troughs with $\delta\theta(e_{2u}{}^{b}) = 0°$, leads to two very shallow minima being reached at $\delta\theta(e_{2u}{}^{a}) = \pm 11°$. These minima correspond to a square bipyramidal structure with two additional shoulders and C_{2v} symmetry. The $\Delta X(C_{2v} \rightarrow D_{6h} \rightarrow C_{2v})$ barrier is very low and since the two structures differ in their orientation in space (see Fig. 3) this e_{2u} coordinate may bring about a fluxional behaviour of the C_{2v} structures. Further, the different softness of two e_{2u} components should be noted.

Symmetry coordinate $e_{2g}{}^{b}$. This bending coordinate and also the subsequent coordinates that include $\delta\phi$ variations with no changes in R and θ are not interesting in themselves: they yield changes in the HBP base with an exclusive ILR energy minimum at HBP. The e_{2g} mode components are very hard and the L_8 frame cannot easily escape the HBP minimum along these pathways. The $e_{2g}{}^{b}$ coordinate is Jahn–Teller active for $E_{1(2)}$ states in D_{6h}. Hence in this case, unlike for $e_{2g}{}^{s}$, the ILR and vibronic factors will oppose each other.

Symmetry coordinate b_{2u}. Similarly to e_{2g} this coordinate is very hard with a minimum at HBP. In combination with b_{2g}, however, it can produce a BCTP structure.

Symmetry coordinate e_{1g}. The effect of this coordinate is to produce a tilt of the hexagonal base with respect to the axial bonds, and the resulting symmetry is very low (C_s). The cube has minimum ILR energy. The coordinate e_{1g} is Jahn–Teller active and JT are opposite in direction.

Symmetry coordinate $e_{1u}{}^{b}$. This is a bending mode. The situation is analogous with the two preceding coordinates, involving changes in the HBP base. It should be noted that $e_{1u}{}^{b}$ is the softest coordinate with $\delta\phi$ variations.

Mixing between the two a_{1g} *coordinates.* The unconstrained variation of the two a_{1g} modes brings about a continuous rise away from the plane of the remaining six atoms. All combinations retain the D_{6h} symmetry.

Mixing the two e_{1u} *coordinates.* All resulting changes are in the L_6 molecular plane involving δr_i and $\delta\phi_i$ variations and the regular hexagon is the structure with the lowest ILR energy.

Mixing the two e_{2g} *coordinates.* They combine δr_i and $\delta\phi_i$ variations and the hexagon is the structure with the lowest ILR energy. The pathways away

from HBP lead to highly distorted structures with high ILR energy.

DISCUSSION

This work has shown that only a few symmetry coordinate modes are important with respect to the shape of the L_8 frame, governed by ILR: for the initial geometry cube they are the a_{2u} mode, producing regular dodecahedra, and the e_u mode, producing angularly distorted dodecahedra, SAP and intermediates. The trigonally distorted L_8 shapes can be obtained by combinations of the t_{2g} mode in O_h or by the e_{2g} and b_{2g} modes in D_{6h}. The experimental results can be seen to match the energy minima obtained in our theoretical treatment: the ML_8 structures, collected in Table 5, are mostly SAP and they cluster around the ILR-produced SAP local minima in the X vs $\delta\phi$, $\delta\theta$ surface. The fewer dodecahedral structures also take positions near the ILR-predicted minima (see Figs 3 and 4).

The main conclusion from this study is, however, that ILR cannot account for the very weak radial distortions ($|\delta r| < 0.1$ Å, see Table 5) away from the two highest symmetry structures that are observed experimentally. The ILR criterion predicts very large radial distortions ($|\delta r| > 0.4$ Å) that are not matched by experiment. This conclusion is reached on the basis of Fig. 2 for the a_{2u} mode in O_h and the R_A, R_B data from Table 5.

There is no discrepancy, however, with the unrestricted ILR predictions. In fact both the trigonal dodecahedron ($X = 5.245$) and the square antiprism ($X = 5.185$) are structures with lower ILR energy than the cube ($X = 5.758$).[1] Hence, the symmetry-constrained ILR version used here correctly predicts that the cube would be distorted to DD and SAP. There are some peculiarities as to the radial distortions which have to be explained in some detail in order to avoid confusion. In the unconstrained ILR version the DD structure is reached at $\theta_A = 36.85$, $\theta_B = 110.54°$ and $r_A/r_B = 1.50$ Å (see, for example, Wells for the hard sphere model[14a]). This means that the DD is formed by exerting both radial and angular distortions of the cube ($\theta_A = 54.74$ and $\theta_B = 125.26°$, $r_A/r_B = 1.000$). Our results [see eq. (7)] agree extremely well with the hard sphere model as to the r_A/r_B ratio. The much lower experimental r_A/r_B ratios ($\lesssim 1.1$) must be attributed to the stabilizing effect of the electronic energy, which is expected to be most favourable for the highest symmetry structure.[2a] Thus, the experimental r_A/r_B ratios reflect the compromise between the high radial distortions of the cube predicted by ILR to produce the lower repulsion shapes and no radial distortion governed by the electronic energy, with the predominance of the second factor. This compromise was discussed in detail by Burdett *et al.*[2a]. We should re-iterate that there are no discrepancies or inadequacies in the symmetry-constrained ILR method proposed here and its unrestricted version used by Kepert.[1] It was also stated by Kepert that the bond lengths are influenced to a high extent by the ability of the ligands to form π-bonds (electronic factors) and thus predictions of radial distortions are in disagreement with simple ILR theory (see ref. 1, ch. 12.3).

The angular distortions, which are softer (Tables 3 and 4), are covered better by the ILR treatment (this is a well known fact[1,2]). The two main structures (DD and SAP) are nicely reproduced by the e_u mode (Figs 3 and 4). This mode is exceptional since it mirrors most of the known ML_8 shapes.

For the open-shell central ions (d^1, d^2, f^2 in Table 5), the vibronic factors may complicate the picture based on ILR. Since for d^{1-9}, the ground state in O_h (cube), both E and $T_{1(2)}$ ground states may appear, the Jahn–Teller active vibrations are e_g (for E states) and $e_g + t_{2g}$ (for $T_{1(2)}$ states).[7] For the e_g coordinate the cube is with minimum energy. Hence, ILR (retains the cube) and JT (distorts the cube) would oppose each other in the e_g space. The same holds true for the t_{2g} coordinate. Hence, it may be concluded that for the Jahn–Teller ions the ILR and vibronic factors interfere and they are compensating each other to a certain extent. The real structures reflect this compromise.

In D_{6h} the orbitally degenerate electronic states can be E_1 and E_2 (both u and g). The Jahn–Teller active modes in D_{6h} (HBP) are e_{1g} and e_{2g}.[7] It can be seen from our ILR treatment that the ILR and JT factors interfere, and the observed shapes must be a subtle compromise between these two factors.

The vibronic factors for open shell central atoms will be discussed in detail in a subsequent paper of this series.

Acknowledgement—Partial financial support by the Bulgarian Council of Science under grant 152 is gratefully acknowledged.

REFERENCES

1. D. L. Kepert, *Inorganic Stereochemistry*. Springer Verlag, Berlin (1982) and refs therein.
2. (a) J. R. Burdett, R. Hoffmann and R. C. Fay, *Inorg. Chem.* 1987, **17**, 2443 and refs therein; (b) J. K. Burdett, *Molecular Shapes*. Wiley, New York (1980).
3. (a) M. G. B. Drew, *Coord. Chem. Rev.* 1977, **24**, 179; (b) R. B. King, *Inorg. Chem.* 1986, **25**, 506.
4. D. G. Blight and D. L. Kepert, *Theoret. Chim. Acta* 1963, **2**, 235.
5. D. L. Kepert, *Progr. Inorg. Chem.* 1978, **24**, 180.

6. K. G. Galton, D. L. Decock and R. F. Fenske, *J. Am. Chem. Soc.* 1970, **92**, 515.
7. R. Englman, *The Jahn–Teller Effect in Molecules and Crystals*. Wiley-Interscience, New York (1972).
8. (a) H. Poulet and J. P. Mathieu, *Spectre de Vibration et Symmetrie des Cristaux*. Gordon and Breach, Paris (1970); (b) D. Schonland, *Molecular Symmetry*. Van Nostrand, New York (1965).
9. E. B. Wilson, J. C. Decius and P. C. Cross, *Molecular Vibrations*. McGraw-Hill, New York (1955).
10. J. C. Decius and R. M. Hexer, *Molecular Vibrations in Crystals*. McGraw-Hill, New York (1981).
11. A. J. Barnes and W. J. Orville-Thomas (Eds), *Vibrational Spectroscopy*, Ch. 16. Elsevier, Amsterdam (1977).
12. C. R. Brubaker and D. W. Johnson, *Coord. Chem. Rev.* 1984, **53**, 1.
13. H. Kondo, H. H. Jaffe, H. Y. Lee and W. J. Welsh, *J. Comput. Chem.* 1984, **5**, 84.
14. (a) A. F. Wells, *Structural Inorganic Chemistry*, 5th edn. Clarendon Press, Oxford (1986); (b) R. Archer, R. O. Day and M. L. Illingsworth, *Inorg. Chem.* 1979, **18**, 2908; (c) R. Boča and P. Pelican, *Coord. Chem. Rev.* 1989, **71**, 83.
15. L. Hoard and J. V. Silverman, *Inorg. Chem.* 1963, **2**, 235.
16. W. D. Bonds, R. D. Archer and W. C. Hamilton, *Inorg. Chem.* 1971, **10**, 1764.
17. J. L. Hoard, T. A. Hamor and M. D. Glick, *J. Am. Chem. Soc.* 1968, **90**, 3177.
18. B. J. Corden, J. A. Cunningham and R. Eisenberg, *Inorg. Chem.* 1970, **9**, 356.
19. M. Novotny, D. F. Lewis and S. J. Lippard, *J. Am. Chem. Soc.* 1972, **94**, 6961.
20. D. I. Semenishin, T. Glowyak and M. G. Mys'kiv, *Koord. Khim.* 1985, **11**, 122.
21. R. G. Rogers and L. K. Kurihara, *Inorg. Chim. Acta* 1986, **116**, 171.
22. A. R. Al-Karaghouli, R. O. Day and J. S. Wood, *Inorg. Chem.* 1978, **17**, 3702.
23. S. S. Basson, L. D. C. Bok and J. G. Leipoldt, *Acta Cryst.* 1970, **B26**, 1209.
24. L. D. C. Bok, J. G. Leipoldt and S. S. Basson, *Acta Cryst.* 1970, **B26**, 684.
25. L. D. C. Bok, J. G. Leipoldt and S. S. Basson, *Z. Anorg. Chem.* 1972, **392**, 303.
26. J. Fischer, R. Elchinger and R. Weiss, *Acta Cryst.* 1973, **B29**, 1967.
27. G. Bombieri, P. T. Moseley and D. Brown, *J. Chem. Soc., Dalton Trans.* 1975, 1520.
28. J. L. Hoard, W. J. Martin, M. E. Smith and J. F. Whitney, *J. Am. Chem. Soc.* 1954, **76**, 3820.
29. F. Lazarini and I. Leban, *Acta Cryst.* 1980, **B36**, 2745.
30. F. A. Cotton, A. Davison, P. W. Day, M. F. Fredrich, C. Orvig and R. Swanson, *Inorg. Chem.* 1982, **21**, 1211.
31. R. D. Rogers and G. J. Voss, *Inorg. Chim. Acta* 1987, **133**, 181.
32. A. S. Antsishkina, M. A. Porai-Koshits and V. N. Ostrikova, *Koord. Khim.* 1988, **14**, 850.

Polyhedron Vol. 10, No. 4/5, pp. 405–407, 1991
Printed in Great Britain

0277–5387/91 $3.00+.00
Pergamon Press plc

X-RAY CRYSTAL STRUCTURE AND SPECTRAL STUDY OF $[Cu(C_{10}H_8N_2)_2(C_6H_4COSO_2N)]\cdot(C_6H_4COSO_2N)\cdot 3H_2O$

LI JIANMIN,* LIN WENBIN and ZHANG YUGENG

Department of Modern Chemistry, University of Science and Technology of China, Hefei, Anhui 230026, P.R.C.

and

LIU SHIXIONG and HUANG JINLING

Fuzhou University, Fuzhou, Fujian, P.R.C.

(*Received* 8 *January* 1990; *accepted* 9 *October* 1990)

Abstract—The title compound has been synthesized and its crystal structure determined at room temperature. The final R is 0.047 for 2216 independent observed reflections with $I \geqslant 3\sigma(I)$. The crystal structure consists of repeated $[Cu(bipy)_2(sacch)]^+$ cations, non-coordinated saccharin anions and three lattice water molecules. In the complex cation $[Cu(bipy)_2(sacch)]^+$, the Cu^{2+} is bonded to the five nitrogen atoms originating from two bipyridines and one saccharin with a distorted trigonal-bipyramidal stereochemistry. The *d–d* transition absorption and IR spectra of the title compound crystal are also reported and are explained perfectly by the scaling radial theory proposed by us.

Saccharin(*o*-sulphobenzoimide) has been used extensively as a food additive. Because of their potential effectiveness in biological systems, the structures of divalent transition metal complexes of saccharin have been determined[1,2] and the electronic spectra of these compounds have been interpreted.[3,4] The divalent transition metal ions were all found to be coordinated by the saccharin molecules and four water molecules to form an octahedral environment. In order to obtain more structural information on saccharin complexes we have used saccharin as a mixed ligand to study its complexes with transition metals. In particular, the mixed ligand copper(II) complex which has been synthesized is interesting because of its structure, which contains trigonal-bipyramidal five coordination stereochemistry.

EXPERIMENTAL

Synthesis

The title compound was obtained by a reaction between 2,2′-bipyridine and $[Cu(sacch)_2(H_2O)_4]\cdot 2H_2O$[5] in the molar ratio 2 : 1, in aqueous solution. The solution was heated in a water bath at 80–90°C with continuous stirring, and blue plate-like crystals were grown by repeated crystallization from water at room temperature. The results of elemental analysis correspond with its formula, $CuC_{32}H_{30}O_9N_6S_2$.

IR and d–d *transition spectra*

IR spectral measurements of $[Cu(sacch)(bipy)_2]\cdot(sacch)\cdot 3H_2O$ and $[Cu(sacch)_2(H_2O)_4]\cdot 2H_2O$ crystals were made as reflectance spectra, using KBr as the diluent on a FTIR instrument under standard operating conditions. The *d–d* transition spectrum was determined at room temperature in the region 4000–30,000 cm^{-1} using the absorption spectrograph for small crystals produced by the Geochemistry Institute of the Chinese Academy of Science.

Crystal structure

A crystal of approximate dimensions $0.06\times 0.60\times 0.57$ mm^3 was used. An AFC5R four-circle diffractometer with graphite-monochromatized

* Author to whom correspondence should be addressed.

Mo-K_α radiation, ω–2θ scan technique, was employed. 3774 independent reflections were collected for $\theta \leqslant 26°$ and corrected for Lorentz and polarization effects. An empirical absorption correction was also applied. 2216 independent observed reflections with intensity $I > 3\sigma(I)$ were used in the structure determination. The crystal structure was solved by direct-methods with the TEXSAN programs on a Micro VAXII computer. The structure was refined by the full-matrix least-squares method. 49 non-hydrogen atoms were refined anisotropically and the three oxygen atoms of the lattice water molecules refined isotropically. $R = 0.047$, $R_w = 0.064$. 25 hydrogen atoms (except for those of the three lattice water molecules) were located by difference Fourier synthesis and the HYDROGEN program. Hydrogen atom coordinates and isotropic temperature factors were used in the structure factor calculation but not in structure refinement. The final $R = 0.047$, $R_w = 0.054$.

Crystallographic data

$[Cu(C_{10}H_8N_2)_2(C_6H_4COSO_2N)] \cdot (C_6H_4COSO_2N) \cdot 3H_2O$, $Mr = 794.32$, orthorhombic, space group; $C222_1$, $a = 15.546(2)$, $b = 26.223(4)$, $c = 16.878(3)$ Å, $U = 6881$ Å^3, $Z = 8$, $D_{calc} = 1.535$ g cm^{-3}, $F(000) = 3272$, $R = 0.047$, $R_w = 0.054$, Mo-K_α: 0.71073 Å.

RESULTS AND DISCUSSION

The structure contains a $[Cu(bipy)_2(sacch)]^+$ complex cation, a $(sacch)^-$ anion and three lattice water molecules per asymmetric unit. In the complex cation, Cu^{2+} is bonded to five nitrogen atoms with trigonal-bipyramidal stereochemistry. The five nitrogen atoms originate from the coordinated saccharin [N(1)], the first bipyridine [N(2) and N(3)] and the second bipyridine [N(4) and N(5)]. N(1), N(2) and N(5) form a trigonal plane, the angles between these nitrogen atoms are: N(1)—N(2)—N(5), 63.5°; N(1)—N(5)—N(2), 63.2°; N(2)—N(1)—N(5), 53.3°. Cu^{2+} is 0.03 Å above the plane. N(4) and N(3), respectively, occupy the axial sites. (Bond lengths and angles are listed in Tables 1 and 2.) O(7), O(8) and O(9) are lattice water oxygen atoms, and O(4), O(5) and O(6) oxygen atoms from the other saccharin molecule are not coordinated to Cu^{2+} (see Fig. 1). The lattice water hydrogen atoms could not be located. However, since the O(7)—N(6) distance is 2.97(1) Å, the O(8)—O(4) and O(8)—O(4)′ distances are 2.64 and 2.94 Å, and the O(9)—O(6) and O(9)—O(6)′ distances are 2.82 Å and 2.89 Å, respectively, it is likely that O(7)—H···N(6), O(8)—H···O(4) and O(9)—H···O(6) hydrogen bonds exist in the crystal.

Table 1. Selected bond lengths (Å)

Cu—N(3)	1.963(6)	C(2)—H(3)	0.986
Cu—N(4)	1.972(7)	C(2)—C(3)	1.40(2)
Cu—N(1)	2.015(7)	C(3)—H(4)	0.971
Cu—N(2)	2.072(7)	C(3)—C(4)	1.40(2)
Cu—N(5)	2.095(8)	C(4)—H(5)	0.983
S(1)—O(3)	1.419(7)	C(4)—C(5)	1.37(1)
S(1)—O(2)	1.424(6)	C(5)—C(6)	1.37(1)
S(1)—N(1)	1.624(8)	C(6)—C(7)	1.49(1)
S(1)—C(5)	1.772(9)	C(11)—C(12)	1.38(1)
S(2)—O(5)	1.432(8)	C(12)—C(13)	1.37(1)
S(2)—O(6)	1.449(8)	C(13)—C(14)	1.35(1)
S(2)—N(6)	1.620(9)	C(14)—C(20)	1.38(1)
S(2)—C(35)	1.73(1)	C(16)—C(15)	1.37(1)
O(1)—C(7)	1.21(1)	C(15)—C(19)	1.41(1)
O(4)—C(37)	1.21(1)	C(16)—C(17)	1.35(1)
O(8)—O(8′)	0.46(4)	C(17)—C(18)	1.38(1)
O(9)—O(9′)	0.25(7)	C(19)—C(20)	1.48(1)
N(1)—C(7)	1.35(1)	C(21)—C(22)	1.37(1)
N(2)—C(11)	1.31(1)	C(22)—C(23)	1.35(1)
N(2)—C(20)	1.35(1)	C(23)—C(24)	1.37(1)
N(3)—C(18)	1.33(1)	C(24)—C(30)	1.38(1)
N(3)—C(19)	1.33(1)	C(25)—C(29)	1.36(1)
N(4)—C(21)	1.34(1)	C(25)—C(26)	1.37(1)
N(4)—C(30)	1.35(1)	C(26)—C(27)	1.32(1)
N(5)—C(28)	1.32(1)	C(27)—C(28)	1.40(1)
N(5)—C(29)	1.36(1)	C(29)—C(30)	1.47(1)
N(6)—H(1)	0.987	C(31)—C(36)	1.35(1)
N(6)—C(37)	1.33(1)	C(32)—C(33)	1.37(2)
C(1)—H(2)	0.992	C(33)—C(34)	1.39(2)
C(1)—C(2)	1.35(2)	C(34)—C(35)	1.39(1)
C(1)—C(6)	1.38(1)	C(35)—C(36)	1.41(1)
C(36)—C(37)	1.48(1)		

According to the above description, the structure of the title compound is roughly similar to the structure of $[Cu(C_{10}H_8N_2)_2(C_6H_5OPO_3)] \cdot (C_6H_5OPO_3) \cdot H_2O$[6] and $[Cu(bipy)_2(SCN)] \cdot (SCN)$[7] which also have distorted trigonal-bipyramidal configurations. This suggests that this type of geometry may easily arise if two bipyridine molecules coordinate with copper(II) in mixed ligand complexes.

The water molecule exhibits absorptions in the IR region 3200–3600 cm^{-1}, and the absorptions of coordinated water molecules show red transitions. As shown in Fig. 2(a), in the IR region near 3500 cm^{-1}, only one single, strong absorption exists at 3500 cm^{-1} for our compound. In Fig. 2(b) there are two strong absorptions in this IR region at 3500 and 3100 cm^{-1}. From this we can distinguish the various coordination modes of the water groups. In compound a, only uncoordinated water molecules exist, while compound b contains two types of water

Table 2. Selected bond angles (°)

N(3)—Cu—N(4)	174.5(3)	N(3)—Cu—N(1)	92.1(3)
N(3)—Cu—N(2)	80.0(3)	N(3)—Cu—N(5)	95.1(3)
N(4)—Cu—N(1)	92.6(3)	N(4)—Cu—N(2)	99.3(3)
N(4)—Cu—N(5)	79.8(3)	N(1)—Cu—N(2)	127.9(3)
N(1)—Cu—N(5)	127.4(3)	N(2)—Cu—N(5)	104.6(3)
O(3)—S(1)—O(2)	116.2(5)	O(3)—S(1)—N(1)	109.3(4)
O(3)—S(1)—O(5)	110.1(4)	O(2)—S(1)—N(1)	112.3(4)
O(2)—S(1)—C(5)	111.5(4)	N(1)—S(1)—C(5)	95.8(5)
O(5)—S(2)—O(6)	114.4(4)	O(5)—S(2)—N(6)	112.9(5)
O(5)—S(2)—C(35)	111.6(5)	O(6)—S(2)—N(6)	111.4(5)
O(6)—S(2)—C(35)	109.1(5)	N(6)—S(2)—C(35)	95.8(5)
C(7)—N(1)—S(1)	112.2(4)	C(7)—N(1)—Cu	124.2(6)
S(1)—N(1)—Cu	122.2(4)	C(11)—N(2)—C(20)	118.2(8)
C(11)—N(2)—Cu	128.0(6)	C(20)—N(2)—Cu	113.2(8)
C(18)—N(3)—C(19)	118.8(7)	C(18)—N(3)—Cu	124.2(6)
C(19)—N(3)—Cu	116.8(5)	C(21)—N(4)—C(30)	118.2(8)
C(21)—N(4)—Cu	124.6(7)	C(30)—N(4)—Cu	116.9(6)
C(28)—N(5)—C(29)	117.6(8)	C(28)—N(5)—Cu	128.8(7)
C(29)—N(5)—Cu	113.5(6)	C(37)—N(6)—S(2)	113.2(8)
C(2)—C(1)—C(6)	119(1)	C(1)—C(2)—C(3)	120(1)
C(2)—C(3)—C(4)	122(1)	C(5)—C(4)—C(3)	115(1)
C(4)—C(5)—C(6)	124(1)	C(4)—C(5)—S(1)	128.1(8)
C(6)—C(5)—S(1)	107.7(7)	C(5)—C(6)—C(1)	120(1)
C(5)—C(6)—C(7)	111.5(8)	C(1)—C(6)—C(7)	129(1)
O(1)—C(7)—N(1)	124(1)	O(1)—C(7)—C(6)	123(1)
N(1)—C(7)—C(6)	113.0(8)	N(2)—C(11)—C(12)	122.4(9)
C(13)—C(12)—C(11)	119.7(8)	C(14)—C(13)—C(12)	117.7(8)
C(13)—C(14)—C(20)	120.5(8)	C(16)—C(15)—C(19)	117.9(8)
C(17)—C(16)—C(15)	120.3(8)	C(16)—C(17)—C(18)	119.3(8)
N(3)—C(18)—C(17)	122.3(8)	N(3)—C(19)—C(15)	121.4(7)
N(3)—C(19)—C(20)	115.6(7)	C(15)—C(19)—C(20)	122.9(8)
N(2)—C(20)—C(14)	121.5(7)	N(2)—C(20)—C(19)	113.6(7)
C(14)—C(20)—C(19)	124.9(7)	N(4)—C(21)—C(22)	123(1)
C(23)—C(22)—C(21)	119(1)	C(22)—C(23)—C(24)	118.2(9)
C(23)—C(24)—C(30)	122(1)	C(29)—C(25)—C(26)	121(1)
C(27)—C(26)—C(25)	117(1)	C(26)—C(27)—C(28)	121(1)
N(5)—C(28)—C(27)	121(1)	N(5)—C(29)—C(25)	121(1)
N(5)—C(29)—C(30)	114.2(8)	C(25)—C(29)—C(30)	124.7(9)
N(4)—C(30)—C(24)	119.5(9)	N(4)—C(30)—C(29)	115.4(7)
C(24)—C(30)—C(29)	125(1)	C(36)—C(31)—C(32)	119(1)
C(33)—C(32)—C(31)	120(1)	C(32)—C(33)—C(34)	121(1)
C(35)—C(34)—C(33)	118(1)	C(34)—C(35)—C(36)	121(1)
C(34)—C(35)—S(2)	130.8(8)	C(36)—C(35)—S(2)	107.8(8)
C(31)—C(36)—C(35)	120(1)	C(31)—C(36)—C(37)	130(1)
C(35)—C(36)—C(37)	110.0(9)	O(4)—C(37)—N(6)	125(1)
O(4)—C(37)—C(36)	122(1)	N(6)—C(37)—C(36)	113.0(8)

molecule: coordinated and uncoordinated. This is confirmed by the X-ray crystal structure.

The X-ray crystal structure shows that one of the two saccharin groups is bonded to the copper(II) atom through one nitrogen in compound a, which is evidently different from compound b in which both saccharin groups are coordinated. The —CONH— group of saccharin absorbs in the IR region at 1550–1650 cm^{-1}. As shown in Fig. 2, compound b has two absorptions in this region with a small separation of about 25 cm^{-1}. These absorptions correspond to the crystal structure, which shows that the two coordinated saccharin groups are in slightly different environments. However, compound a has only one absorption in this region and the crystal structure shows that it con-

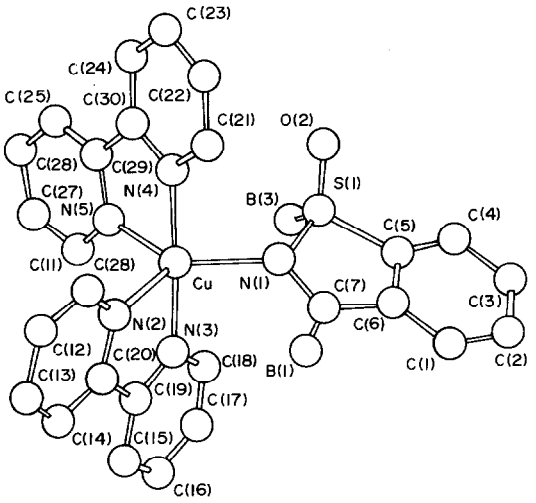

Fig. 1. Perspective view of $[Cu(C_{10}H_8N_2)_2(C_6H_4COSO_2N)]^+$.

tains an ionic saccharin group which would normally be expected to have a single absorption in this region with a small violet transition. However, in Fig. 2(a) such an absorption cannot be found in this IR region. According to the X-ray crystal structure, the ionic saccharin group is hydrated

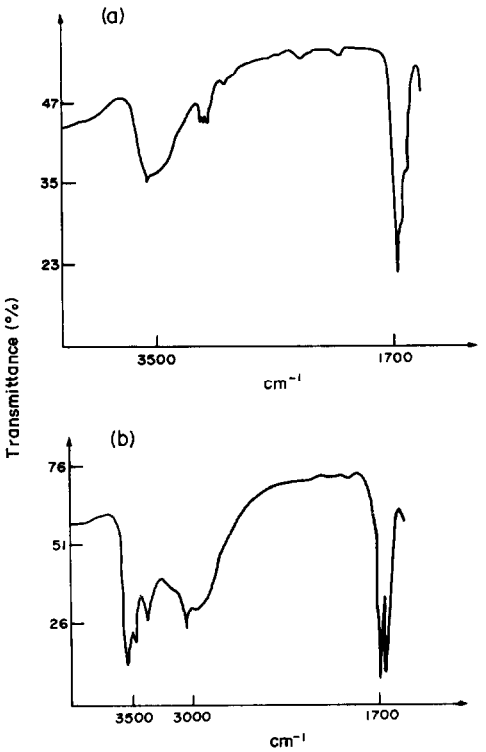

Fig. 2. IR absorptions in the 1500–3800 cm^{-1} region: (a) $[Cu(bipy)_2sacch)]\cdot(sacch)\cdot 3H_2O$ and (b) $[Cu(sacch)_2(H_2O)_4]\cdot 2H_2O$.

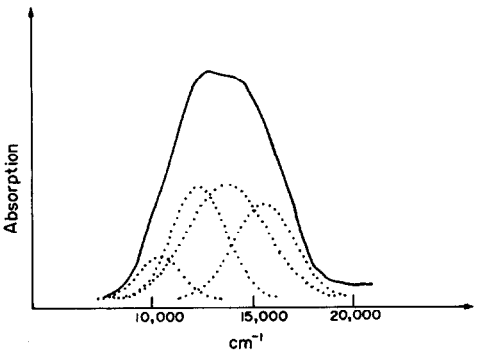

Fig. 3. The *d–d* transition spectrum of the title compound.

[O(4) and N(6) are from the ionic saccharin molecule —C(39)O(4)N(6)=] and it was suggested that extensive hydrogen bonding may be responsible,[8] explaining why the ionic saccharin group absorption is missing. In addition, Fig. 2(a) shows a multiply split, middle strong absorption in the IR region, 3000–3300 cm^{-1}, due to the vibrations of the C—H bonds of the 2,2′-bipyridine rings.

As shown in Fig. 3, the *d–d* transition spectrum of the title compound contains a strong, broad absorption band. The overlapping absorption band has been resolved using a computer program into absorption peaks at 10,474, 12,435, 13,814 and 15,627 cm^{-1}.

The wave function scaling radial theory of nonfree ions has been set up and the double-ξ radial wave functions of some transition metal ions have been proposed by our laboratory. We have discussed some coordination compounds and explained their electronic structure using this theory and results which agree perfectly with the experimental values have always been obtained.[9-11] Using the program package which calculates Ligand Field Theory (PLFT) and the crystal structure data, the crystal field parameters and the *d–d* transition energy levels of the title compound crystal were obtained and are listed in Tables 3 and 4. From the data in Table 4, the calculated results of the *d–d*

Table 3. The crystal parameters of the title compound

μ (Debye)	1.23600	a_1	0.58786
t	0.06363	a_2	0.64165
Ω (Hartree)	0.17920	$\langle r^2\rangle$ (a.u.)	2.13609
N	0.9850	$\langle r^4\rangle$ (a.u.)	12.55208
$P^{(2)}$	1.71349	$\langle r^{-3}\rangle$ (a.u.)	5.61996
$P^{(4)}$	2.23137	B (cm^{-1})	992
ξ^1	5.82642	C (cm^{-1})	3390
ξ^2	1.80946	ξ_{3d} (cm^{-1})	542

Table 4. The *d–d* transition energy levels of the title compound

$^2A(^2Eg_a, e)$	0	0
$^2A(^2T_2g_c, t)$	10,104	10,474
$^2A(^2Eg_b, e)$	12,735	12,435
$^2A(^2T_2g_b, t)$	13,569	13,814
$^2A(^2T_2g_a, t)$	15,123	15,627

transition energy levels appear to agree well with the experimental values.

REFERENCES

1. B. Kamenar and G. Jovanovski, *Cryst. Struct. Commun.* 1982, **11**, 257.
2. S. Z. Halder, K. M. A. Malik, K. J. Ahmed, H. Hess, H. Riffel and M. B. Hursthouse, *Inorg. Chim. Acta* 1983, **72**, 21.
3. J. M. Li and G. Q. Pan, *Cryst. Res. Technol.* 1986, **21**, 1327.
4. G. Q. Pan and J. M. Li, *Cryst. Res. Technol.* 1985, **20**, 71.
5. S. Z. Haider, K. M. A. Malik and K. J. Ahmed, *J. Bangladesh Acad. Sci.* 1981, **5**, 81.
6. T. Gloviak, A. W. Szemik and I. Wnek, *J. Cryst. Spect. Res.* 1986, **16**, 41.
7. D. Huang, J. L. Huang, Y. Zhang and J. Li, *J. Struct. Chem. Chinese* 1986, **2**, 138.
8. A. B. P. Lever, E. Mantovai and B. S. Ramaswamy, *Can. J. Chem.* 1971, **49**, 1957.
9. Zhang Yongfeng and Li Jianmin, *Inorg. Chim. Acta* 1984, **87**, L25.
10. J. Li and G. Pan, *Transition Met. Chem.* 1987, **12**, 525.
11. Li Jianmin and Zhang Yugeng, *Cryst. Res. Technol.* 1990, **25**, 977.

Polyhedron Vol. 10, No. 4/5, pp. 409–413, 1991
Printed in Great Britain

0277–5387/91 $3.00+.00
© 1991 Pergamon Press plc

POLYAMINE COMPLEXATION—I. STABILITY CONSTANTS FOR METAL ION COMPLEXATION OF 5-(4′-AMINO-2′-AZABUTANE)-5-METHYL-3,7-DIAZANONANE-1,9-DIAMINE

GARY K. HOLLINGSHED, GEOFFREY A. LAWRANCE, MARCEL MAEDER* and MONICA ROSSIGNOLI

Department of Chemistry, The University of Newcastle, New South Wales 2308, Australia

(*Received* 13 *June* 1990; *accepted* 9 *October* 1990)

Abstract—The protonation and metal complexation of the sexidentate N_6 ligand, sen [5-(4′-amino-2′-azabutane)-5-methyl-3,7-diazanonane-1,9-diamine], has been investigated using potentiometric pH titrations. The ligand forms relatively strong complexes with the small, first-row transition metals, Mn^{2+} ($\log K = 8.6$), Fe^{2+} ($\log K = 13.4$), Co^{2+} ($\log K = 18.0$), Cu^{2+} ($\log K = 26.2$), Zn^{2+} ($\log K = 17.0$) and weaker complexes with the larger, main-group elements Cd^{2+} ($\log K = 13.4$), Pb^{2+} ($\log K = 9.2$) and In^{3+} ($\log K = 15.1$). Compared with other N_6 ligands and first-row transition metals, these values are high; this fact is ascribed to the almost ideal "cage-like" geometry of the complexes.

Multidentate N_6 ligands are able to saturate the coordination sphere of most metal ions in 1 : 1 complexes. Surprisingly few of these ligands have been synthesized and their metal complexes characterized. Examples of N_6 ligands include linear polyamines such as pentaethylenehexamine (3,6,9,12-tetraazatetradecane-1,14-diamine, L^1),[1,2] edta-type branched ligands like N,N,N′,N′-tetrakis(2-aminoethyl)ethane-1,2-diamine (L^2)[3,4] and N,N,N′,N′ - tetrakis(2 - aminoethyl)propane - 1,3 - diamine (L^3),[5] the trigonal open ligands, sen [5-(4′-amino-2′ - azabutane) - 5 - methyl - 3,7 - diazanonane - 1,9-diamine, L^4][6] and e-sen [5-(4′-amino-2′-azabutane)-5-ethyl-3,7-diazanonane-1,9-diamine, L^5],[7] macromonocyclic ligands like diammac (6,13-dimethyl-1,4,8,11-tetraazacyclotetradecane-6,13-diamine, L^6)[8] and hexacyclen (1,4,7,10,13,16-hexaazacyclooctadecane, [18]ane N_6, L^7),[9] and the macrobicyclic cage-type ligands, sep (1,3,6,8,10,13,16,19-octaazabicyclo[6.6.6]eicosane, L^8)[10] and sar (1,3,6,10,13,19-hexaaza[6.6.6]eicosane, L^9).[11]

Due to their strong chelate effect these ligands are expected to form very thermodynamically stable complexes with many metal ions.[12] However, the relevant stability constants have only been determined for some of these ligands. In this contribution we report the stabilities of the complexes of sen (L^4) with the metal ions Mn^{2+}, Fe^{2+}, Co^{2+}, Cu^{2+}, Zn^{2+}, Cd^{2+}, Pb^{2+} and In^{3+}, using potentiometric pH titrations. Sen has a geometry which easily accommodates smaller ions, such as the first-row transition metal ions in their 2+ oxidation state and In^{3+}, to form favourable octahedral complexes. The larger ions, Cd^{2+} and Pb^{2+}, form weaker complexes.

EXPERIMENTAL

Synthesis of 5-(4′-*amino*-2′-*azabutane*)-5-*methyl*-3,7-*diazanonane*-1,9-*diamine hexahydrobromide* (sen·6HBr, L^4)

Sen was essentially synthesized as described.[6,7] For further purification, the perchlorate salt of the nickel complex of the crude ligand was made and recrystallized from water. (**CAUTION**: Perchlorate salts are potentially explosive, care should be taken in handling the dry salt.) Bubbling H_2S through an aqueous solution of the pure $Ni(sen)^{2+}$ complex resulted in the precipitation of NiS and the release of the free ligand which was further purified by ion exchange chromatography on a Dowex 50-WX2 (H^+ form) cation exchange column, eluting with 4 M HBr solution. Evaporation to dryness yielded

*Author to whom correspondence should be addressed.

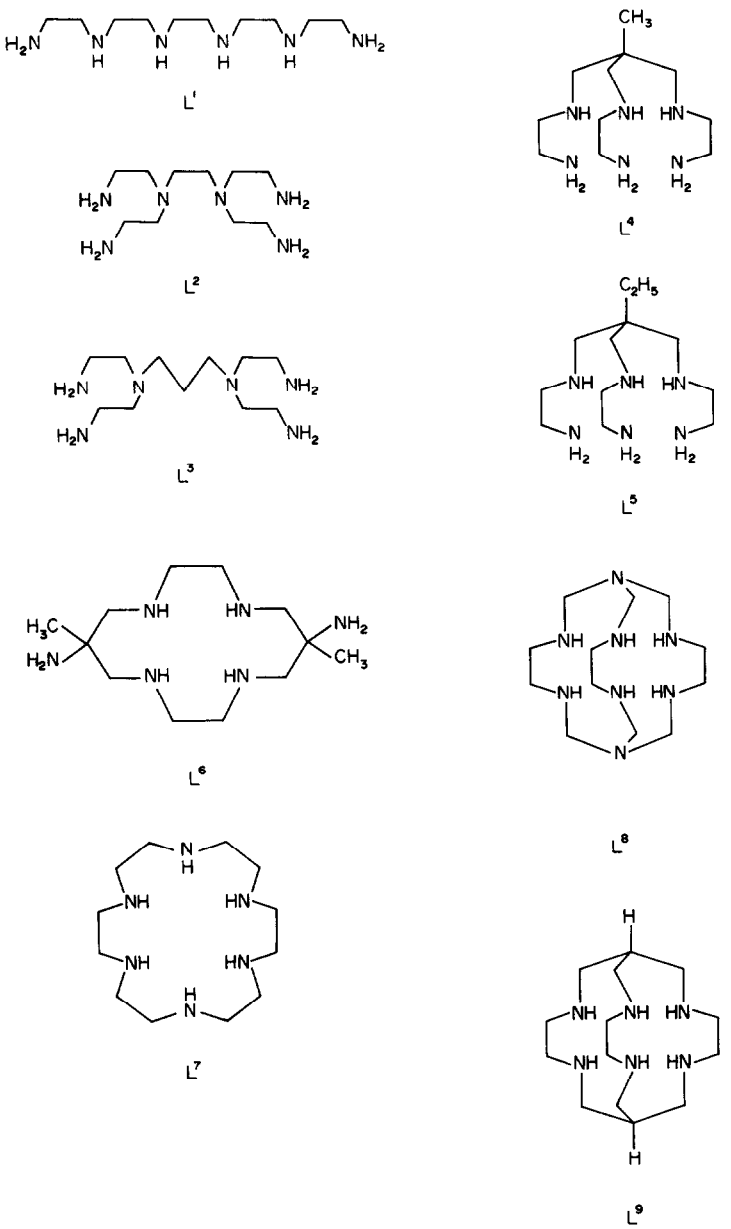

the hexahydrobromide, which was recrystallized from aqueous ethanol acidified with HBr solution.

Potentiometric titrations and data evaluation

Potentiometric titrations were obtained using a Metrohm 605 digital pH meter, a Metrohm 665 digital burette and Metrohm combined glass electrodes. All measurements were fully automated under computer control using an IBM clone computer.[13] NBS buffers pH 4 and pH 7 were used to calibrate the electrode, thus proton activities, 10^{-pH}, were used for $[H^+]$. All measurements were performed at 25°C and an ionic strength of 0.5 M KCl under nitrogen. Solutions of sen·6HBr (50 cm^3, 0.6 mM), alone and in the presence of 0.9 and 1.4 equivalents of metal ion, were titrated with 60 increments of NaOH (0.01 cm^3, 0.4 M). In the case of the copper ion, 0.1 mM of HCl was added to the solution prior to the titration. Data reduction was performed on an IBM AT clone computer using a TURBO BASIC version of TITFIT.[14]

RESULTS AND DISCUSSION

The protonation constants of the free ligand appear in Table 1 and are compared with some other N_6 ligands. The first three to four protonation constants are reasonably similar for all the listed ligands. The higher basicity of LH_4^{4+} and LH_5^{5+} in the case of sen can be ascribed to its branched

Table 1. The logarithms of the deprotonation constants and the stability constants of metal–ligand complexes with L^4 and other related N_6 ligands

	Complex	L^{4a}	L^1	L^{2b}	L^{3b}	L^{5c}	L^{7d}
H^+	HL/L·H	10.76		10.08	10.24	10.39	10.07
	H_2L/HL·H	10.08		9.58	9.56	9.56	9.11
	H_3L/H_2L·H	9.40		8.99	9.18	8.79	8.61
	H_4L/H_3L·H	7.20		8.42	8.44	6.54	3.97
	H_5L/H_4L·H	5.19		1.33	2.5	4.25	
	H_6L/H_5L·H	2.73				1.5	
Mn^{2+}	ML/M·L	8.6		9.3	5.3	8.2	
	MLH/ML·H	8.1					
Fe^{2+}	ML/M·L	13.4		11.1			
	MLH/ML·H	7.0					
Co^{2+}	ML/M·L	18.0		15.6	13.3	17.3	18.9[e]
	MLH/ML·H	5.9		6.8			
	MLH_2/MLH·H	5.6					
Cu^{2+}	ML/M·L	26.2	21.6[f]	22.1	21.1	22.7	25.1[g]
	MLH/ML·H	9.9		8.0	8.2		5.5
	MLH_2/MLH·H	5.6					
	M_2L/M·M·L	33.5					
	M_2LH_{-1}/M_2L·H^{-1}	7.8					
	M_2LH_{-2}/M_2LH·H^{-1}	10.7					
Zn^{2+}	ML/M·L	17.0		16.1	14.9	16.4	17.8
	MLH/ML·H	6.8		8.0	7.7		
	MLH_2/MLH·H	5.9					
Cd^{2+}	ML/M·L	13.4	17.9[h]	16.1	12.8	14.4	19.0
	MLH/ML·H	8.0					
	MLH_2/MLH·H	6.3					
Pb^{2+}	ML/M·L	9.2			10.5		14.1
	MLH/ML·H	9.1					
	MLH_2/MLH·H	7.5					
In^{3+}	ML/M·L	15.1					
	MLH/ML·H	9.7					
	MLH_2/MLH·H	6.7					
	MLH_{-1}/ML·H^{-1}	10.4					

[a] This work, standard errors of all values are 0.1 log units, with the exception of the value for CuL/Cu·L which is 0.3 log units. 25°C, $I = 0.5$ M.

[b] R. M. Smith and A. E. Martell (Eds), *Critical Stability Constants*, Vol. 2. Plenum Press, New York (1975); 25°C, $I = 0.1$ M.

[c] See ref. 7; 25°C, $I = 0.1$ M.

[d] R. M. Smith and A. E. Martell (Eds), *Critical Stability Constants*, Vol. 6. Plenum Press, New York (1975); 25°C, $I = 0.2$ M.

[e] 35°C, $I = 0.2$ M.

[f] See ref. 1.

[g] MLH/M·LH.

[h] See ref. 2.

and hence potentially more open structure, allowing a better spread of the high number of positive charges compared with the other ligands. The different complexation behaviour of the ligands, therefore, has to be associated with the steric properties rather than the basicities of the ligand coordination sites.

Furthermore, the metal–ligand complexation constants of sen with a variety of metal ions are compared with the ligands L^1, L^2, L^3, L^5 and L^7 in

Table 1. Confining consideration to the first-row transition metals, sen generally forms the strongest, or almost the strongest, complexes. Although sen can be considered as an open chain ligand, as a sexidentate it adopts a "hemi-cage" geometry, similar to the ligands L^8 and L^9, enhancing binding to most of the metal ions. Apparently this cage-like structure is superior to the geometries adapted by the edta-type ligands, L^2 and L^3. The stabilities of the complexes with L^4 and the very similar L^5 are in all cases higher than those with L^2 and L^3. The results for ligands L^4 and L^5 compare very well, apart from the stability of the copper complexes, where we found a value for L^4 3.5 orders of magnitude higher than the one for L^5. This discrepancy may arise from the difficulties in determining very high stability constants. The stability of the sen complexes compares very well with the macrocycle L^7 without having the extra macrocyclic effect. The exception is copper which forms the weaker protonated complex ML^7H only.

The larger main group cations Cd^{2+} and Pb^{2+} form relatively weak complexes with sen. This probably arises because the trigonal cap linking the secondary nitrogen donors limits separation of those donors in pseudo-octahedral geometries and therefore limits the size of the effective cavity, hence introducing a preference for the smaller cations. Free-ion radii of Cd^{2+} (0.97 Å) and Pb^{2+} (1.2 Å) are substantially higher than those of the first-row metal ions studied (range, 0.72–0.80 Å), suggesting that size does play an important role. The macrocyclic ligand L^7 forms significantly stronger complexes, a fact which is assigned in that case to the macrocyclic effect.

Only very few stabilities of In^{3+} complexes have been determined. However, recent interest in indium chemistry for medical applications[15,16] prompted us to include In^{3+} in the series. In^{3+}, like all elements in the third main group, strongly prefers oxygen donors and therefore the value of 10^{15} for the stability constant of the In^{3+} sen complex is surprisingly high. However, the ionic radius of free In^{3+} (0.81 Å) is not markedly different from that of first-row metal ions, suggesting the ligand allows good coordination of the ion and supporting the view that, as a sexidentate ligand, sen has a preferred cavity like macrocycles. The formation of the hydroxo species (pK 10.4) indicates that sen itself is not able to coordinatively saturate indium. One (or more) extra water ligand(s) are coordinated to the metal ion and at least one can be deprotonated. No further deprotonation has been detected and a seven-coordinate geometry might tentatively be ascribed to the complex. Figure 1 displays the species distribution curves of the species formed during the titration.

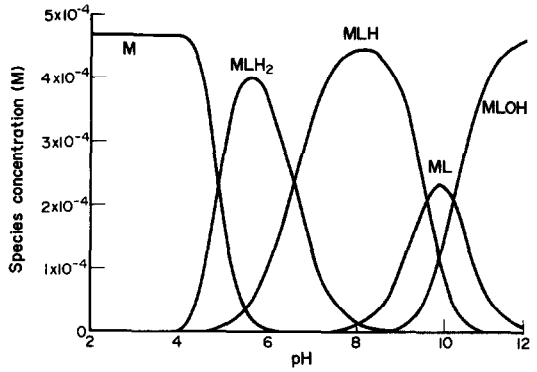

Fig. 1. Species distribution curves for the titration of L^4 (0.526 mM) with In^{3+} (0.475 mM).

Protonated complexes have been detected for all metals. The first protonation occurs at pH values between 5.9 (Co^{2+}) and 9.9 (Cu^{2+}) (see Table 1). With the exception of Mn^{2+} and Fe^{2+}, MLH_2 species have been detected at pH values between 5.6 (Co^{2+} and Cu^{2+}) and 7.5 (Pb^{2+}).

Titrations with an excess of 1.4 moles of metal with respect to ligand were performed to investigate the formation of multinuclear complexes. With the exception of copper, titrations with an excess of metal ion produced precipitates of the respective hydroxides. $Cu_2(sen)^{4+}$ has a stability of 33.5 log units, and hydroxo species $Cu_2(sen)(OH)^{3+}$ and $Cu_2(sen)(OH)_2{}^{2+}$ are formed with pK values of 7.8 and 10.7. Structural information about these multinuclear species must await spectroscopic studies.

REFERENCES

1. H. B. Jonassen, J. A. Bertrand, F. R. Groves Jr and R. I. Stearns, *J. Am. Chem. Soc.* 1957, **79**, 4279.
2. E. Jacobsen and K. Schrøder, *Acta Chem. Scand.* 1961, **16**, 1393.
3. G. Schwarzenbach and P. Moser, *Helv. Chim. Acta* 1953, **36**, 581.
4. L. Sacconi, P. Paoletti and M. Ciampolini, *J. Chem. Soc.* 1964, 5046.
5. P. Paoletti, R. Walser, A. Vacca and G. Schwarzenbach, *Helv. Chim. Acta* 1971, **54**, 243.
6. J. E. Sarneski and F. L. Urbach, *J. Am. Chem. Soc.* 1971, **93**, 884.
7. R. W. Green, K. W. Catchpole, A. T. Phillip and F. Lions, *Inorg. Chem.* 1963, **2**, 597.
8. P. Comba, N. F. Curtis, G. A. Lawrance, A. M. Sargeson, B. W. Skelton and A. H. White, *Inorg. Chem.* 1986, **25**, 4260.
9. M. Kodama, E. Kimura and S. Yamaguchi, *J. Chem. Soc., Dalton Trans.* 1980, 2536.

10. I. I. Creaser, R. J. Geue, J. M. Harrowfield, A. J. Herlt, A. M. Sargeson, M. R. Snow and I. Springborg, *J. Am. Chem. Soc.* 1982, **104**, 6016.
11. R. J. Geue, T. W. Hambley, J. M. Harrowfield, A. M. Sargeson and M. R. Snow, *J. Am. Chem. Soc.* 1984, **106**, 5478.
12. R. D. Hancock and A. E. Martell, *Chem. Rev.* 1989, **89**, 1875.
13. H. Gampp, D. Haspra, M. Maeder and A. D. Zuberbuehler, *Inorg. Chem.* 1984, **23**, 3724.
14. A. D. Zuberbuehler and T. A. Kaden, *Talanta* 1982, **29**, 201.
15. D. A. Scheinberg, M. Strand and O. A. Gansow, *Science* 1982, **215**, 1511.
16. A. Riesen, T. A. Kaden, W. Ritter and H. R. Maecke, *J. Chem. Soc., Chem. Commun.* 1989, 460.

Polyhedron Vol. 10, No. 4/5, pp. 415–419, 1991
Printed in Great Britain

0277–5387/91 $3.00+.00
© 1991 Pergamon Press plc

STRUCTURES OF PALLADIUM(II) AND NICKEL(II) COMPLEXES OF THE MESOCYCLIC DIPHOSPHINE, *CIS*-1,5-DIPHENYL-1,5-DIPHOSPHACYCLOOCTANE

BRIAN W. ARBUCKLE and W. KENNETH MUSKER*

Department of Chemistry, University of California, Davis, CA 95616, U.S.A.

(*Received* 13 *August* 1990; *accepted* 10 *October* 1990)

Abstract—The preparation and X-ray crystal structures of a planar mono complex of *cis*-1,5-diphenyl-1,5-diphosphacyclooctane with palladium(II) chloride and a pentacoordinated bis complex with nickel(II) chloride are reported. Dichloro(1,5-diphenyl-1,5-diphosphacyclooctane)palladium(II) crystallizes in the monoclinic space group $C2/c$ with cell constants $a = 26.647(6)$, $b = 7.884(1)$, $c = 13{,}053(3)$ Å, $\beta = 98.15(2)°$ and $Z = 4$ at $T = 130$ K. Chloro-bis(1,5-diphenyl-1,5-diphosphacyclooctane)nickel(II) chloride crystallizes in the monoclinic space group $P2_1/n$ with $a = 18.178(7)$, $b = 10.225(2)$, $c = 20.959(7)$ Å, $\beta = 111.77(2)°$ and $Z = 4$ at $T = 130$ K.

The synthesis and coordination chemistry of a number of 1,5-disubstituted cyclooctanes have been examined in detail over the past 20 years,[1–6] but one of the last members of that series was only characterized recently[7] and no examples of its complexes are known. Both the *cis* and *trans* diastereomers of 1,5-diphenyl-1,5-diphosphacyclooctane were prepared by $LiAlH_4$ reduction of the corresponding diphosphine oxides and separated by HPLC.[7] However, only the *cis* isomer can function as a chelating agent and it can be selectively removed from the *trans* isomer by coordination. Because these ligands are bidentate dialkylphenyl phosphines, they should be expected to form complexes which have different electronic and structural properties to acyclic mono- and diphosphines and macrocyclic polyphosphines. As a first step in the development of the chemistry of these ligands, we wish to report the preparation and X-ray crystal structures of a planar mono complex of *cis*-1,5-diphenyl-1,5-diphosphacyclooctane with palladium(II) chloride and a pentacoordinated bis complex with nickel(II) chloride.

EXPERIMENTAL

Dichloro(1,5-*diphenyl*-1,5-*diphosphacyclooctane*)*palladium*(II)

$PdCl_2(PhCN)_2$ (0.13 g, 0.34 mmol) was suspended in CH_2Cl_2 (5 cm^3). A mixture of *cis* and *trans*-1,5-diphenyl-1,5-diphosphacyclooctane (0.10 g, 0.33 mmol) was dissolved in CH_2Cl_2 (2 cm^3) and added dropwise to the solution of $PdCl_2(PhCN)_2$. After the addition was complete, the solution was stirred at reflux for 20 min. The solvent was removed to give an orange–yellow solid (yield: 0.12 g, 73%). Yellow crystals suitable for structural determination were grown by slow diffusion of diethyl ether into a methylene chloride solution of the complex. The crystallographic data for dichloro(1,5-diphenyl-1,5-diphosphacyclooctane) palladium(II) are given in Table 1.

Chloro-bis(1,5-*diphenyl*-1,5-*diphosphacyclooctane*)*nickel*(II) *chloride*

$NiCl_2 \cdot 6H_2O$ (0.030 g, 0.23 mmol) was dissolved in methanol (2 cm^3). A mixture of *cis* and *trans*-1,5-diphenyl-1,5-diphosphacyclooctane (0.063 g, 0.21 mmol) was dissolved in benzene (2 cm^3). The two reagents were added dropwise into a flask containing 2 cm^3 of benzene. The solution turned a deep purple colour and the solvent was removed to give a red solid. Thin layer analysis revealed two species in the crude product which was dissolved in 5% ethanol–$CHCl_3$ and run through a column of neutral alumina. The first component from the column was a purple complex (yield: 0.10 g, 62%). The second component from the column was an uncharacterized red–orange compound which could not be recrystallized. Purple crystals suitable for structural determination were grown by slow diffusion of hexane into an ethanol solution of the

* Author to whom correspondence should be addressed.

Table 1. Crystallographic data for dichloro(1,5-diphenyl-1,5-diphosphacyclooctane)palladium(II) and chloro-bis(1,5-diphenyl-1,5-diphosphacyclooctane)nickel(II) chloride

Formula	$PdCl_2(C_{18}H_{22}P_2)$	$[NiCl(C_{24}H_{22}P_2)_2]Cl$
Fw	773.3	874.39
Colour and habit	Yellow parallelepipeds	Purple parallelepipeds
Crystal system	Monoclinic	Monoclinic
Space group	$C2/c$	$P2_1/n$
a (Å)	26.647(6)	18.178(7)
b (Å)	7.884(1)	10.225(2)
c (Å)	13.053(3)	20.959(7)
β (°)	98.15(2)	111.77(2)
V (Å^3)	2714(1)	3618(2)
T (°)	130 K	130 K
Z	4	4
Crystal dimensions (mm)	$0.20 \times 0.50 \times 0.20$	$0.20 \times 0.35 \times 0.15$
d_{calc} (g cm^{-3})	1.89	1.61
Radiation (Å)	Mo-K_α ($\lambda = 0.71069$)	Mo-K_α ($\lambda = 0.71069$)
μ(Mo-K_α) (cm^{-1})	4.98	9.10
Range of transmission factors	0.63–0.85	0.54–0.79
Diffractometer	$P2_1$, graphite monochromator	
Scan method	ω, 1.3° range, 1.0° offset for background	
Scan speed (° min^{-1})	20	15
2θ range (°)	0–50	0–50
Octants collected	$h, k, \pm l$	$h, k, \pm l$
Number of data collected	2401	7057
Number of unique data	1422[R(merge) = 0.006]	4434[R(merge) = 0.005]
Number of data used in refinement	1392[$F > 4\sigma(F)$]	3876[$F > 6\sigma(F)$]
Number of parameters refined	130	415
R^1	0.057	0.044
$R_w{}^1$	0.065 [$w = 1/\sigma^2(F_o) + 0.00051F_o^2$]	0.044 [$w = 1/\sigma^2(F_o)$]
Goodness of fit	1.73	1.11

complex. The crystallographic data for chloro-bis(1,5-diphenyl-1,5-diphosphacyclooctane)nickel (II) chloride are also given in Table 1.

Structure determination and refinement

Crystals of the title complexes were coated with a hydrocarbon oil to retard decomposition, attached to a glass fibre with silicone grease and mounted in the cold stream of a Syntax $P2_1$ graphite monochromator diffractometer (Mo-K_α, $\lambda = 0.71069$) equipped with a locally modified LT-1 low temperature device ($T = 130$ K). The space groups were derived from observed extinctions. Crystals were obtained as explained in the Experimental. The 2θ range for all compounds was 0–50°. No decay in the intensity of standard reflections was observed during data collection. Solution of the structure was accomplished using the Patterson technique. All computing was carried out using the SHELXTL version 5 program installed on a Data General Eclipse computer. Atomic scattering factors and anomalous dispersion corrections were from common sources.[8] An absorption correction[9] was applied and structural refinement proceeded smoothly in the case of all compounds. All non-hydrogen atoms were assigned anisotropic thermal parameters, except in the palladium complex. Here, all non-hydrogen atoms and non-carbon atoms were assigned anisotropic thermal parameters except for three atoms in a disordered ethanol molecule, carbons C(10) and C(11) and oxygen O [O(a) and O(b)]. Oxygen (O) has partial occupancy of 50% in two positions [O(a) and O(b)]. Carbon C(2) has partial occupancy of 50% in two positions [C(2a) and C(2b)]. The hydrogen atoms were excluded from carbons C(2), C(10), C(11) and the atoms bonded to C(2) [C(1) and C(3)]. Five peaks were seen in the difference map with an electron density between 1.2 and 1.9, all due to the disordered ethanol molecule.

Hydrogen atoms were refined using a riding model in which an idealized C—H vector, 0.96 Å length, was recalculated with each cycle of refinement. Isotropic hydrogen thermal parameters were fixed at 1.2 times the equivalent isotropic thermal

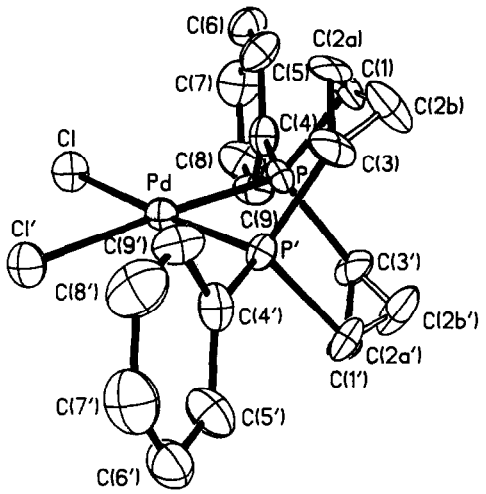

Fig. 1. Structure of dichloro(1,5-diphenyl-1,5-diphosphacyclooctane)palladium(II) showing 50% probability ellipsoids.

parameter of the bonded atom. Atomic coordinates for all compounds are given in the supplementary material.

DISCUSSION

Dichloro(1,5 - *diphenyl* - 1,5 - *diphosphacyclooctane*) *palladium*(II)

When a mixture of *cis* and *trans*-1,5-diphenyl-1,5-diphosphacyclooctane is treated with $PdCl_2(PhCN)_2$, a yellow precipitate containing yellow crystals forms. The X-ray crystal structure of the complex was carried out on a typical crystal recovered from the reaction flask. Figure 1 shows that *cis*-1,5-diphenyl-1,5-diphosphacyclooctane acts as a bidentate ligand by coordinating to the palladium atom through both phosphorus atoms. A crystallographic two-fold axis passes through the palladium and bisects the P—Pd—P angle. Selected bond lengths and bond angles are given in Tables 2 and 3. The final atomic coordinates are given in the supplementary material. The middle carbon in each methylene chain is disordered, having a partial occupancy of 50%. This shows that the ring is fluctional and the middle carbon on each trimethylene chain can either be pointing towards the palladium, C(2a), or pointing away from it, C(2b).

Table 2. Selected bond lengths (Å) for dichloro(1,5-diphenyl-1,5-diphosphacyclooctane)palladium(II)

Pd—C(1)	2.373(4)	Pd—P	2.234(4)
P—C(1)	1.840(13)	P—C(4)	1.835(13)
P—C(3a)	1.820(12)		

The four atoms, Cl, Cl(a), P, P(a), are in a planar arrangement about the palladium atom. The calculated distance from the best least-squares plane through these five atoms is as follows: Pd, 0.000; Cl, −0.017; P, 0.019; Cl(a), 0.017; P(a), −0.019 Å. The P—Pd—P bite angle of 83.3(2)° is smaller than that found in other diphosphine complexes, except when a four-membered ring is formed.[10] For example, in the following series of palladium thiocyanate complexes, $Pd(SCN)_2(Ph_2P(CH_2)_nPPh_2)$ (n = 1–3), the bite angle increases from 73.33(5) to 85.1(1) to 89.32(3)°, as n increases from 1 to 2 to 3.[10] The bite angle in the mesocycle is also much smaller than the bite angle [97.85(1)°] in the analogous acyclic bis-dialkylarylphosphine complex, *cis* - dichlorobis(dimethylphenyl)phosphinepalladium (II).[11]

The Pd—P bond length is 2.234(4) Å. This is in the lower range of the Pd—P bond lengths in the thiocyanate complexes shown above (2.24–2.28 Å)[10] and typical of complexes where the phosphine is *trans* to chloride; 2.260(2), [11] 2.232 and 2.237[12] and 2.220(4) Å.[13] The latter complex has a four-membered Pd—P—N—P ring. The Pd—Cl bond length of 2.373(4) Å is slightly longer than Pd—Cl bond lengths where the chloride is *trans* to a phosphine; typical values are 2.362(3),[11] and 2.357(2) and 2.352(1) Å.[12]

Table 3. Selected bond angles (°) for dichloro(1,5-diphenyl-1,5-diphosphacyclooctane)palladium(II)

Cl—Pd—P	92.3(1)	Cl—Pd—Cl(a)	92.2(2)
P—Pd—Cl(a)	175.5(1)	P—Pd—P(a)	83.3(2)
Pd—P—C(1)	113.2(5)	Pd—P—C(4)	117.7(4)
C(1)—P—C(4)	103.7(6)	Pd—P—C(3a)	111.4(4)
C(1)—P—C(3a)	106.7(6)	C(4)—P—C(3a)	103.1(6)

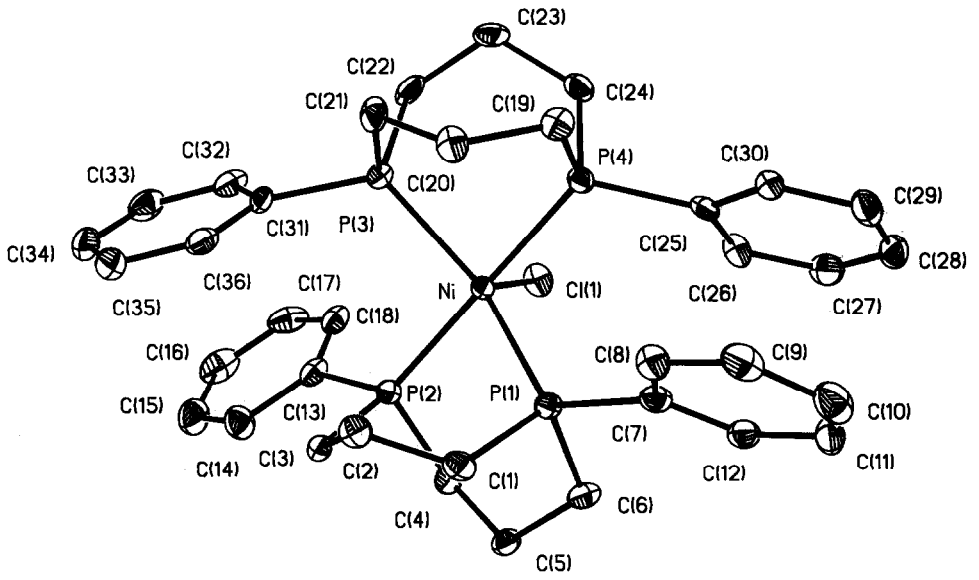

Fig. 2. Structure of chloro-bis(1,5-diphenyl-1,5-diphosphacyclooctane)nickel(II) chloride showing 50% probability ellipsoids.

Chloro - bis(1,5 - diphenyl - 1,5 - diphosphacyclooctane)nickel(II) chloride

When a mixture of *cis* and *trans*-1,5-diphenyl-1,5-diphosphacyclooctane is treated with $NiCl_2 \cdot 6H_2O$ a red solid is observed. Thin layer analysis reveals the solid to be a mixture of two components. After the solid was dissolved and chromatographed through a column of neutral alumina, two complexes were isolated; one is a reddish-orange colour and the other is a purple colour.

An X-ray structure determination of the purple compound revealed that it was a pentacoordinated nickel complex, Ni[Cl(*cis*-1,5-diphenyl-1,5-diphosphacyclooctane)$_2$]Cl as shown in Fig. 2. Selected bond lengths and bond angles are given in Tables 4 and 5.

The final atomic coordinates and a complete list of bond lengths and angles are given as sup-

Table 4. Selected bond lengths (Å) for chloro-bis(1,5-diphenyl-1,5-diphosphacyclooctane)nickel(II) chloride

Ni—Cl	2.410(1)	Ni—P(1)	2.237(1)
Ni—P(2)	2.215(1)	Ni—P(3)	2.228(2)
Ni—P(4)	2.202(4)	P(1)—C(1)	1.848(5)
P(1)—C(6)	1.842(6)	P(1)—C(7)	1.835(5)

Table 5. Selected bond angles (°) for chloro-bis(1,5-diphenyl-1,5-diphosphacyclooctane)nickel(II) chloride

Cl(1)—Ni—P(1)	111.8(1)	C(1)—Ni—P(2)	88.5(1)
P(1)—Ni—P(2)	84.1(1)	Cl(1)—Ni—P(3)	106.5(1)
P(1)—Ni—P(3)	141.7(1)	P(2)—Ni—p(3)	96.5(1)
Cl(1)—Ni—P(4)	91.1(1)	P(1)—Ni—P(4)	95.9(1)
P(2)—Ni—P(4)	179.7(1)	P(3)—Ni—P(4)	83.7(1)
Ni—P(1)—C(1)	110.2(2)	Ni—P(1)—C(6)	112.4(1)
C(1)—P(1)—C(6)	104.7(2)	Ni—P(1)—C(7)	125.3(2)
C(1)—P(1)—C(7)	101.2(2)	C(6)—P(1)—C(7)	100.8(2)
Ni—P(2)—C(3)	112.2(2)	Ni—P(2)—C(4)	111.5(2)
C(3)—P(2)—C(4)	105.9(2)	Ni—P(2)—C(13)	123.8(2)
C(3)—P(2)—C(13)	105.0(2)	C(4)—P(2)—C(13)	96.4(2)
Ni—P(3)—C(21)	112.8(2)	Ni—P(3)—C(22)	110.4(2)
C(21)—P(3)—C(22)	104.7(3)	Ni—P(3)—C(31)	120.4(2)
C(21)—P(3)—C(31)	102.8(3)	C(22)—P(3)—C(31)	104.2(2)
Ni—P(4)—C(19)	114.1(2)	Ni—P(4)—C(24)	111.8(2)
C(19)—P(4)—C(24)	105.2(3)	Ni—P(4)—C(25)	118.3(2)
C(19)—P(4)—C(25)	106.2(2)	C(24)—P(4)—C(25)	99.7(2)

plementary material. The molecule exhibits a distorted trigonal bipyramidal geometry with the chlorine atom occupying an equatorial position. Two phosphorus atoms [P(2) and P(4)] lie along the axis and are 179.7° apart. The Ni^{II}—P bond lengths range from 2.202(1) to 2.237(1) Å, values which are typical for trigonal bipyramidal nickel(II) complexes.[14,15] The Ni^{II}—Cl bond length is 2.410(1) Å, which is also typical.[16,17] The P—Pd—P bite angles for the chelated phosphines (83.7 and 84.1 Å) are similar to those observed in the palladium complex. The phenyl groups on the phosphorus atoms of different ligands are oriented in a near parallel fashion to each other and very similar to that observed in Pt(5-phenyl-1-thia-5-phosphacyclooctane)$_2$(BPh$_4$)$_2$.[6]

REFERENCES

1. W. K. Musker and M. S. Hussain, *J. Am. Chem. Soc.* 1969, **8**, 528.
2. W. K. Musker and N. L. Hill, *Inorg. Chem.* 1972, **11**, 710.
3. W. K. Musker, M. M. Olmstead and R. M. Kessler, *Inorg. Chem.* 1984, **23**, 1764.
4. K. Kanimori, W. E. Broderick, R. F. Jordan, R. E. Willett and J. I. Legg, *J. Am. Chem. Soc.* 1986, **108**, 7122.
5. M. M. Olmstead, R. M. Kessler, H. Hope, M. D. Yanuck and W. K. Musker, *Acta Cryst. C* 1987, **43**, 1890.
6. S. D. Toto, M. M. Olmstead, B. W. Arbuckle, P. K. Bharadwaj and W. K. Musker, *Inorg. Chem.* 1990, **29**, 691.
7. S. D. Toto, B. W. Arbuckle, P. K. Bharadwaj, J. T. Doi and W. K. Musker, *Phosphorus, Sulfur and Silicon*, in press.
8. *International Tables for X-Ray Crystallography*, Vol. IV. Kynoch Press, Birmingham, England (1976).
9. H. Hope and B. Moezzi, Program XABS. The program obtains an absorption tensor from the $F_o - F_c$ difference. B. Moezzi, PhD Dissertation, University of California, Davis (1987).
10. G. J. Palenik, M. Mathew, W. L. Steffen and G. Beran, *J. Am. Chem. Soc.* 1975, **97**, 1059.
11. L. L. Martin and R. A. Jacobson, *Inorg. Chem.* 1971, **10**, 1795.
12. S. J. Lippard, L. Wei, A. Bell, S. Warner and I. D. Williams, *J. Am. Chem. Soc.* 1986, **108**, 8302.
13. J. A. A. Mokuolu, D. S. Payne and J. C. Speakman, *J. Chem. Soc., Dalton Trans.* 1973, 1443.
14. E. P. Kyba, R. E. Davis, M. A. Fox, C. N. Clubb, S. T. Liu, G. Reitz, V. J. Scheuler and R. P. Kashyap, *Inorg. Chem.* 1987, **26**, 1647.
15. E. C. Alyea and D. W. Meek, *Inorg. Chem.* 1972, **11**, 1029.
16. B. Gramlich and C. H. Salmon, *J. Organomet. Chem.* 1979, **73**, C61.
17. P. K. Bernstein, G. A. Rodleg, R. March and H. B. Gray, *Inorg. Chem.* 1972, **11**, 3040.

Polyhedron Vol. 10, No. 4/5, pp. 421–427, 1991
Printed in Great Britain

0277–5387/91 $3.00+.00
© 1991 Pergamon Press plc

RUTHENIUM(II) ALKENYL COMPLEXES WITH SULPHUR CHELATED LIGANDS

HASSANE LOUMRHARI and JOSEP ROS*

Departament de Química, Universitat Autònoma de Barcelona, 08193-Bellaterra, Barcelona, Spain

and

M. ROSARIO TORRES

Instituto de Química-Física "Rocasolano" C.S.I.C., Serrano 119, 28006-Madrid, Spain

(*Received* 1 *August* 1990; *accepted* 10 *October* 1990)

Abstract—The reaction of $[Ru(CO)Cl(RC{=}CHR')(PPh_3)_2]$ complexes with $Na[S_2CNEt_2]$ and $K[S_2CO^iPr]$ gave the complexes, $Ru(S{-}S)(CO)(RC{=}CHR')(PPh_3)_2$, where S—S = S_2CNEt_2 and S_2CO^iPr, respectively, and in which the sulphur-containing ligands are η^2-coordinated to ruthenium. The structures of the synthesized products are proposed on the basis of spectroscopic data and they contain octahedral ruthenium(II) with the S—S, CO and —RC=CHR′ ligands in an equatorial plane and the two phosphines in the *trans* position. The chemical shifts (δ) of the terminal alkenyl-containing complexes have been compared with those of the related carboxylate complexes $[Ru(O_2CR'')(CO)(HC{=}CHR')(PPh_3)_2]$.

The unsaturated complexes $[Ru(CO)Cl(RC{=}CHR')(PPh_3)_2]$[1–3] are very reactive toward carboxylate anions, giving rise to complexes $[Ru(O_2CR'')(CO)(RC{=}CHR')(PPh_3)_2]$ in which the O_2CR'' ligand is η^2-coordinated to the metal.[4,5] The substitution of the chloride by the carboxylate group leaves the alkenyl ligand unchanged. The structures of the $[Ru(O_2CR'')(CO)(HC{=}CHR')(PPh_3)_2]$ complexes were established by X-ray crystallography which demonstrate the saturation of the metal centre by the ligands and the *trans* position of phosphines. At the same time, the donor strength of the carboxylate ligands induced changes in the chemical shifts of the alkenylic hydrogens in the ^1H NMR of complexes with respect to the signals of the same protons in the $[Ru(CO)Cl(RC{=}CHR')(PPh_3)_2]$ complexes.[4,5] In order to induce some transformation in the alkenyl ligand coordinated to ruthenium, we attempted to introduce strong chelating and very strong donor ligands containing sulphur atoms, for example diethyldithiocarbamate ($S_2CNEt_2^-$) and isopropylxanthate ($S_2CO^iPr^-$). These sulphur-containing ligands should induce π-interactions different from those produced by carboxylate ligands.

The literature on dithiocarbamate and xanthate ligands is very extensive[6] but information on their coordination chemistry with ruthenium(II)[7] is scarce and their catalytic applications unknown.[8] The dithiocarbamate ligand causes interesting reactivity in some organic fragments coordinated to transition metals. For example, the substitution of a halide by $S_2CNMe_2^-$ in the $[Mo(\eta^2\text{-}COR)X(CO)_n(PMe_3)_{4-n}]$ complexes yielded an unprecedented acetyl compound $[Mo(COCH_3)(S_2CNMe_2)(CO)(PMe_3)_2]$ in which the molybdenum atom interacts with a β-C—H bond to the acetyl group.[9] Another point of interest is the coupling of two alkynes η^2-coordinated to the same metal which is promoted by the action of HBF_4 upon the $[W(S_2CNEt_2)_2(PhC{\equiv}CPh)_2]$ complex producing a η^4-C_4Ph_4H ligand.[10] In this work we attempted to increase the reactivity of the alkenyl group by the introduction

* Author to whom correspondence should be addressed.

of sulphur-containing ligands, such as $S_2CNEt_2^-$ and $S_2CO^iPr^-$, into the Ru(CO)Cl(RC═CHR′)$(PPh_3)_2$ complexes. The results reflect no apparent changes in the alkenyl groups. The synthesized complexes were identified by C, H and N analyses and spectroscopic methods.

RESULTS AND DISCUSSION

When a CH_2Cl_2 solution of a [Ru(CO)Cl(RC═CHR′)$(PPh_3)_2$] complex (R = R′ = H, Me, Ph and CO_2Me; R = H and R′ = Ph, ^{t}Bu, $SiMe_3$, CO_2Me and CO_2Et) was reacted with a small excess of Na[S_2CNEt_2] or K[S_2CO^iPr], dissolved in MeOH, new yellow crystalline complexes were obtained in very good yields. The solubility and stability of these complexes were similar to those of the related carboxylate [Ru(O_2CR'')(CO)(RC═CHR′)$(PPh_3)_2$] complexes.[4] The C, N and H elemental analyses of the products were in accordance with the formulation [Ru(S—S)(CO)(RC═CHR′)$(PPh_3)_2$] (S—S = S_2CNEt_2 and S_2CO^iPr).

The IR and ^{1}H NMR data of the products are given in Tables 1 and 2. The solid IR spectra of these complexes display the characteristic bands of ligands coordinated to ruthenium. The [Ru(S_2CNEt_2)(CO)(RC═CHR′)$(PPh_3)_2$] derivatives show absorptions of the dithiocarbamate ligand at *ca* 1010 and 850 cm^{-1}, corresponding to $\nu(S_2C)$ vibrations.[11] The former is the $\nu(S_2C)_{asym}$ band which appears as a shoulder on one absorption which is also observed in [Ru(CO)Cl(RC═CHR′)$(PPh_3)_2$] complexes. The literature[11] does not assign any absorption to the dithiocarbamate ligand at *ca* 850 cm^{-1} but assuming that a medium band is observed in this position in all [Ru(S_2CNEt_2)(CO)(RC═CHR′)$(PPh_3)_2$] complexes and which is also displayed at higher energies in the IR spectrum of the sodium salt of the ligand, we assign the absorption to the $\nu(S_2C)_{sym}$ vibration. The vibration associated with ν(CN) is observed at *ca* 1548 cm^{-1}. The Ru(S_2CO^iPr)(CO)(RC═CHR′)$(PPh_3)_2$ complexes also present IR spectra with the $\nu(S_2C)$ bands at *ca* 1235 and 1049 cm^{-1} and the ν(C—O) at *ca* 1140 cm^{-1}. The strong ν(C≡O) absorptions of the sulphur derivatives[12] appear between 1909 and 1927 cm^{-1} in the dithiocarbamate complexes and at 1897–1943 cm^{-1} in the xanthate complexes. The general shift observed towards lower energies is indicative of the electron-releasing character of the ligands. The minimal ν(C≡O) values are displayed by complexes with terminal alkenyl groups containing alkyl or phenyl substituents. In complexes with an alkenyl ligand containing electron-withdrawing groups the ν(C≡O) band is observed at 1920–1943 cm^{-1}. The ν(C═C) band is often obscured by other intense absorptions but is located at *ca* 1540 cm^{-1}.

The ^{1}H NMR of two families of complexes {[Ru(S_2CNEt_2)(CO)(RC═CHR′)$(PPh_3)_2$] and [Ru(S_2CO^iPr)(CO)(RC═CHR′)$(PPh_3)_2$]} display signals due to the hydrogens of the coordinated ligands. In the complexes containing terminal alkenyl groups the signals of H_α and H_β appear as doublets with J_{H-H} = 16 Hz, indicating a *trans* disposition of the hydrogens.[4] The H_α signal is observed at 6.3–9.5 ppm and H_β at 4.5–5.5 ppm. In

Table 1. IR (ν in cm^{-1}) and ^{1}H NMR (δ in ppm) for the complexes [Ru(S_2CNEt_2)(CO)(RC═CHR′)$(PPh_3)_2$]

RC═CHR′	CO	C═C	SCS	CN	^{1}H NMR
HC═CH_2 (**1**)	1909	1547	1268 850	1458	0.59t, J = 8 Hz, 3H 0.76t, J = 8 Hz, 3H 2.78q, J = 8 Hz, 2H 3.13q, J = 8 Hz, 2H 4.57d, J = 16 Hz, 1H 5.23d, J = 8 Hz, 1H 7.29dd, J_1 = 8 Hz, 1H, J_2 = 16 Hz 7.4–7.7m, 30H
HC═CHPh (**2**)	1908	1544	1267 849	1457	0.70t, J = 8 Hz, 3H 0.78t, J = 8 Hz, 3H 2.90q, J = 8 Hz, 2H 3.17q, J = 8 Hz, 2H 5.62d, J = 16 Hz, 1H 6.5–7.5m, 35H 7.80d, J = 16 Hz, 1H

Table 1—*continued*

RC═CHR′	CO	C═C	SCS	CN	^{1}H NMR
HC═CHCMe$_3$ (**3**)	1905		1267 849	1458	0.39s, 9H 0.68t, J = 8 Hz, 3H 0.79t, J = 8 Hz, 3H 2.77q, J = 8 Hz, 2H 3.19q, J = 8 Hz, 2H 4.56d, J = 16 Hz, 1H 6.30d, J = 16 Hz, 1H 7.3–7.7m, 30H
HC═CHSiMe$_3$ (**4**)	1919		1269 851	1457	−0.50s, 9H 0.60t, J = 8 Hz, 3H 0.80t, J = 8 Hz, 3H 3.75q, J = 8 Hz, 3H 3.20q, J = 8 Hz, 2H 5.58d, J = 16 Hz, 1H 7.2–7.7m, 30H 7.68d, J = 16 Hz, 1H
MeC═CHMe (**5**)	1919		1270 848	1457	0.69t, J = 8 Hz, 3H 0.72t, J = 8 Hz, 3H 1.10d, J = 6 Hz, 3H 1.15s, 3H 2.88q, J = 8 Hz, 2H 3.06q, J = 8 Hz, 2H 5.94q, J = 6 Hz, 1H 7.2–7.7m, 30H
PhC═CHPh (**6**)	1928		1269	1459	0.67br, 3H 0.76br, 3H 2.90br, 2H 3.00br, 2H 5.80s, 1H 6.4–7.7m, 40H
HC═CHCO$_2$Me (**7**)	1920 1712	1533	1268 849	1458	0.65br, 3H 0.74br, 3H 2.83br, 2H 3.06br, 2H 3.38s, 3H 5.52d, J = 16 Hz, 1H 7.2–7.7m, 30H 9.54d, J = 16 Hz, 1H
HC═CHCO$_2$Et (**8**)	1920 1709	1534	1269 849	1457	0.62t, J = 6 Hz, 3H 0.70t, J = 6Hz, 3H 1.50t, J = 8 Hz, 3H 2.81q, J = 6 Hz, 2H 3.03q, J = 6 Hz, 2H 3.81q, J = 8 Hz, 2H 5.47d, J = 16Hz, 1H 7.2–7.7m, 30H 9.46d, J = 16 Hz, 1H
MeO$_2$CC═CHCO$_2$Me (**9**)	1927 1705	1559	1269 850	1458	0.51t, J = 6 Hz, 3H 0.68t, J = 6 Hz, 3H 2.65q, J = 6 Hz, 2H 3.00q, J = 6 Hz, 2H 3.35s, 3H 3.44s, 3H 5.10s, 1H 7.2–7.7m, 30H

Table 2. IR (ν in cm^{-1}) and ^1H NMR (δ in ppm) for the complexes $[Ru(S_2CO^iPr)(CO)(RC{=}CHR')(PPh_3)_2]$

RC=CHR′	CO	C=C	SCS	^1H NMR
HC=CH_2 (**10**)	1897	1546	1241 1049	0.81d, J = 6 Hz, 6H 4.35t, J = 6 Hz, 1H 4.59d, J = 17 Hz, 1H 5.24d, J = 8 Hz, 1H 7.2–7.6m, 30H 7.74dd, J_1 = 17 Hz. J_2 = 8 Hz, 1H
HC=$CHCMe_3$ (**11**)	1913		1238 1048	0.35s, 9H 0.71br, 6H 4.26br, 1H 4.57d, J = 16 Hz, 1H 6.17d, J = 16 Hz, 1H 7.2–7.5m, 30H
HC=$CHSiMe_3$ (**12**)	1921	1506	1233 1045	0.80d, J = 6 Hz, 6H 0.85s, 9H 4.49t, J = 6 Hz, 1H 5.59d, J = 15 Hz, 1H 7.2-7.7m, 30H
HC=CHPh (**13**)	1906	1548	1236 1047	0.87d, J = 6 Hz, 6H 4.47t, J = 6 Hz, 1H 5.64d, J = 15 Hz, 1H 6.5–7.6m, 35H 7.77d, J = 15 Hz, 1H
MeC=CHMe (**14**)	1917		1237 1047	0.83d, J = 6 Hz, 6H 1.11s, 3H 1.30s, 3H 4.39t, J = 6 Hz, 1H 4.49s, 1H 7.2–7.7m, 30H
PhC=CHPh (**15**)	1926	1545	1244 1045	0.71br, 6H 4.32br, 1H 5.30s, 1H 5.9–7.7m, 40H
HC=$CHCO_2Me$ (**16**)	1930 1669	1532	1238 1044	0.85d, J = 6 Hz, 6H 3.37s, 3H 4.46t, J = 6 Hz, 1H 5.88d, J = 16 Hz, 1H 7.2–7.7m, 30H 9.79d, J = 16 Hz, 1H
HC=$CHCO_2Et$ (**17**)	1926 1669	1534	1241 1045	0.71br, 6H 0.99br, 3H 3.72br, 2H 4.27br, 1H 5.37br, 1H 5.37d, J = 15 Hz, 1H 7.2–7.6m, 30H 9.31d, J = 15 Hz, 1H
MeO_2CC=$CHCO_2Me$ (**18**)	1943 1702	1564	1247 1056	0.74*d*, J = 6 Hz, 6H 3.40s, 3H 3.52s, 3H 4.35t, J = 6 Hz, 1H 5.09s, 1H 7.2–7.5m, 30H

Table 3. $[\Delta\delta = \delta(H_\alpha) - \delta(H_\beta)]$ in ppm of the complexes $[Ru(L—L)(CO)(HC{=}CHR')(PPh_3)_2]$

L—L	R′ = ^{t}Bu	R′ = CO_2Me	Reference
Cl	2.24	4.61	2,3
Cl and CO	1.63	3.44	Unpublished
O_2CH	1.33	4.11	15
O_2CMe	1.29	3.94	4
O_2CEt	1.27	4.01	4
$O_2CCH{=}CMe_2$	1.31	4.15	5
S_2CNEt_2	1.74	4.15	This work
S_2CO^iPr	1.60	3.91	This work

the complexes $[Ru(S—S)(CO)(HC{=}CH_2)(PPh_3)_2]$ (S—S = S_2CNEt_2 or S_2CO^iPr) the signals of the vinylic protons have values of $J_{H—H(trans)} = 16$ Hz and $J_{H—H(cis)} = 8$ Hz, whereas the geminal H—H coupling was too small to be resolved. The complexes containing a disubstituted alkenyl ligand display the alkenyl proton signals at 4.5–5.9 ppm.

As well as in related carboxylate complexes[4,5] the H_α and the H_β hydrogens are shifted in comparison with the same signals in the $Ru(CO)Cl(RC{=}CHR')(PPh_3)_2$ complexes. In Table 3 are shown the $[\Delta\delta = \delta(H_\alpha) - \delta(H_\beta)]$ values (in ppm) of some complexes synthesized by our group. It can be seen that the greater $\Delta\delta$ values are displayed by $[Ru(CO)Cl(HC{=}CHR')(PPh_3)_2]$ complexes. When L—L is a donor chelating ligand a general decrease in $\Delta\delta$ is observed which appears to be dependent on R′ and L—L. For R′ = ^{t}Bu, the greater $\Delta\delta$ values are displayed by complexes containing dithiocarbamate and xanthate ligands. The minimal $\Delta\delta$ values are displayed by the carboxylate-containing complexes. For complexes with R′ = CO_2Me, an electron-withdrawing group, the $\Delta\delta$ are higher, but carboxylate, dithiocarbamate and xanthate complexes show similar values. It appears that if R′ is an alkyl group (^{t}Bu), the σ-donor ability of the ligand induces a major approach of the H_α and H_β signals (carboxylates). If R′ is a strong electron-withdrawing group, the same effect is lower and not dependent on the donor characteristics of L—L. When L—L is CO and Cl $\{[Ru(CO)_2Cl(HC{=}CHR')(PPh_3)_2]\}$ the $\Delta\delta$ is similar to that of complexes containing dithiocarbamate and xanthate ligands. From these results it seems that CO and sulphur-containing ligands probably have similar electronic effects on the H_α and H_β hydrogens of terminal alkenyl ligands through π-interactions. Thus, the donor capabilities of the dithiocarbamate and xanthate ligands are combined with a π-acceptor character which is manifested in the ^{1}H NMR of the terminal alkenyl ligands coordinated to the same metal.

The stereochemistry of $[Ru(S_2CNEt_2)(CO)(RC{=}CHR')(PPh_3)_2]$ complexes can be deduced from ^{1}H NMR and ^{31}P NMR spectroscopies.[13] The planar configuration of the dithiocarbamate ligand and the high rotation energy[13] of the C—N bond allow us to distinguish between stereochemistries **I** and **II** with the ^{1}H NMR of complexes.

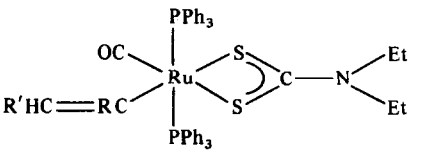

(I)

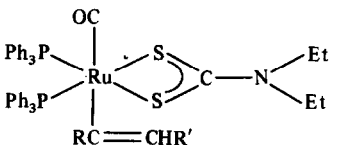

(II)

The ^{1}H NMR spectra of dithiocarbamate complexes at room temperature show different signals of the ethyl groups indicating structure **I** with the PPh_3 ligands in a *trans* position. This structure is supported by the ^{1}H-decoupled ^{31}P NMR spectra at room temperature of complexes $[Ru(S_2CNEt_2)(CO)(MeC{=}CHMe)(PPh_3)_2]$ and $[Ru(S_2CNEt_2)(CO)(HC{=}CHCO_2Me)(PPh_3)_2]$ which display signals at 34.32 and 39.77 ppm, respectively, characteristic of equivalent phosphorus atoms. The room temperature ^{1}H NMR spectra of xanthate complexes display one signal of the ^{i}Pr group revealing that the rotation around the C—O bond is fast on the NMR time-scale. The ^{1}H decoupled ^{31}P NMR spectra of $[Ru(S_2CO^iPr)(CO)(MeC{=}CHMe_2)(PPh_3)_2]$ and $[Ru(S_2CO^iPr)$

$(CO)(HC{=}CHPh)(PPh_3)_2]$, registered at room temperature, present singlets at 40.17 and 39.94 ppm, respectively, which are in accordance with an equivalence of phosphines and with a structure with the two PPh_3 in a *trans* position (**III**). Summarizing, the proposed structures for the complexes contain the two PPh_3 ligands in a *trans* position and the rest of the ligands in an equatorial plane, in accordance with the NMR data and with the structures of the related carboxylate complexes $[Ru(O_2CR'')(CO)(RC{=}CHR')(PPh_3)_2]$. The proposed structures for the dithiocarbamate and xanthate complexes are shown as **I** and **III**.

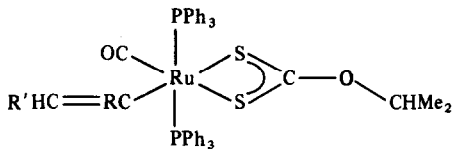

(III)

The synthesis of the complexes was performed by means of conventional Schlenk techniques. The starting materials $[Ru(CO)Cl(RC{=}CHR')(PPh_3)_2]$ were synthesized by published methods.[1-3] The compound $K[S_2CO^iPr]$ was prepared by the standard method from ^iPrOH, KOH and CS_2,[14] while $Na[S_2CNEt_2]$ was used as purchased. The IR spectra were recorded on a Perkin–Elmer 1710-FT apparatus using KBr disks. The ^1H NMR spectra were measured on a Bruker AM 400 spectrometer in $CDCl_3$ solutions and referenced to $SiMe_4$. The ^1H-decoupled ^{31}P NMR spectra were recorded on the same instrument in $CDCl_3$ solutions with aqueous 85% H_3PO_4 as external reference. The C, H and N elemental analyses were performed with a Perkin–Elmer 240-B analyser.

Synthesis of complexes

A small excess of $Na[S_2CNEt_2]$ or $K[S_2CO^iPr]$ dissolved in MeOH was added, with stirring, to a CH_2Cl_2 solution of $[Ru(CO)Cl(RC{=}CHR')(PPh_3)_2]$. The solution was stirred until the liquid turned yellow (30 min) and then the liquid was evaporated to dryness *in vacuo* and the residue extracted with CH_2Cl_2. The solution was concentrated and the products precipitated with petroleum ether. The crystalline products can be recrystallized with CH_2Cl_2–MeOH mixtures.

Complex **1**: $[Ru(S_2CNEt_2)(CO)(HC{=}CH_2)(PPh_3)_2]$. Found: C, 63.7; H, 5.0; N, 1.5. Calc. for $C_{44}H_{43}ONP_2S_2Ru$: C, 62.5; H, 5.1; N, 1.6%.

Complex **2**: $[Ru(S_2CNEt_2)(CO)(HC{=}CHPh)(PPh_3)_2]$. Found: C, 66.2; H, 5.3; N, 1.4. Calc. for $C_{50}H_{47}ONP_2S_2Ru$: C, 65.2; H, 5.2; N, 1.5%.

Complex **3**: $[Ru(S_2CNEt_2)(CO)(HC{=}CH^tBu)(PPh_3)_2]$. Found: C, 64.1; H, 5.7; N, 1.6. Calc. for $C_{48}H_{51}ONP_2S_2Ru$: C, 64.0; H, 5.7; N, 1.5%.

Complex **4**: $[Ru(S_2CNEt_2)(CO)(HC{=}CHSiMe_3)(PPh_3)_2]$. Found: C, 60.9; H, 5.9; N, 1.6. Calc. for $C_{47}H_{51}ONP_2SiS_2Ru$: C, 61.5; H, 5.6; N, 1.5%.

Complex **5**: $[Ru(S_2CNEt_2)(CO)(MeC{=}CHMe)(PPh_3)_2]$. Found: C, 63.1; H, 5.5; N, 1.5. Calc. for $C_{46}H_{47}ONP_2S_2Ru$: C, 63.3; H, 5.4; N, 1.6%. $\{^1H\}$ ^{31}P NMR: δ 34.32 ppm.

Complex **6**: $[Ru(S_2CNEt_2)(CO)(PhC{=}CHPh)(PPh_3)_2]$. Found: C, 66.7; H, 5.4; N, 1.4. Calc. for $C_{56}H_{51}ONP_2S_2Ru$: C, 67.4; H, 5.1; N, 1.4%.

Complex **7**: $[Ru(S_2CNEt_3)(CO)(HC{=}CHCO_2Me)(PPh_3)_2]$. Found: C, 61.0; H, 5.1; N, 1.5. Calc. for $C_{46}H_{45}O_3NP_2S_2Ru$: C, 61.2; H, 5.0; N, 1.5%. $\{^1H\}$ ^{31}P NMR: δ 39.77 ppm.

Complex **8**: $[Ru(S_2CNEt_2)(CO)(HC{=}CHCO_2Et)(PPh_3)_2]$. Found: C, 632.6; H, 5.2; N, 1.5. Calc. for $C_{47}H_{47}O_3NP_2S_2Ru$: C, 61.5; H, 5.2; N, 1.5%.

Complex **9**: $[Ru(S_2CNEt_2)(CO)(MeO_2CC{=}CHCO_2Me)(PPh_3)_2]$. Found: C, 61.2; H, 5.0; N, 1.6. Calc. for $C_{48}H_{47}O_5NP_2S_2Ru$: C, 60.0; H, 4.9; N, 1.5%.

Complex **10**: $[Ru(S_2CO^iPr)(CO)(HC{=}CH_2)(PPh_3)_2]$. Found: C, 63.6; H. 5.0. Calc. for $C_{42}H_{40}O_2P_2S_2Ru$: C, 62.7; H, 5.0%.

Complex **11**: $[Ru(S_2CO^iPr)(CO)(HC{=}CH^tBu)(PPh_3)_2]$. Found: C, 64.8; H, 5.6. Calc. for $C_{46}H_{48}O_2P_2S_2Ru$: C, 64.2; H, 5.6%.

Complex **12**: $[Ru(S_2CO^iPr)(CO)(HC{=}CHSiMe_3)(PPh_3)_2]$. Found: C, 62.3; H, 5.7. Calc. for $C_{45}H_{48}O_2P_2SiS_2Ru$: C, 61.7; H, 5.5%.

Complex **13**: $[Ru(S_{21}CO^iPr)(CO)(HC{=}CHPh)(PPh_3)_2]$. Found: C, 66.3; H, 5.6. Calc. for $C_{48}H_{44}O_2P_2S_2Ru$: C, 65.5; H, 5.0. $\{^1H\}$ ^{31}P NMR: δ 39.94 ppm.

Complex **14**: $[Ru(S_2CO^iPr)(CO)(MeC{=}CHMe)(PPh_3)_2]$. Found: C, 64.1; H. 5.2. Calc. for $C_{44}H_{44}O_2P_2S_2Ru$: C, 63.5; H, 5.3%. $\{^1H\}$ ^{31}P NMR: δ 40.17 ppm.

Complex **15**: $[Ru(S_2CO^iPr)(CO)(PhC{=}CHPh)(PPh_3)_2]$. Found: C, 67.0; H. 5.0. Calc. for $C_{54}H_{48}O_2P_2S_2Ru$: C, 67.8; H, 5.1%.

Complex **16**: $Ru(S_2CO^iPr)(CO)(HC{=}CHCO_2Me)(PPh_3)_2$: Found: C, 60.5; H, 4.8. Calc. for $C_{44}H_{42}O_4P_2Ru$: C, 61.3; H, 4.9%.

Complex **17**: $[Ru(S_2CO^iPr)(CO)(HC{=}CHCO_2Et)(PPh_3)_2]$. Found: C, 62.2; H, 4.9. Calc. for $C_{45}H_{44}O_4P_2S_2Ru$: C, 61.7; H, 5.1%.

Complex **18**: $[Ru(S_2CO^iPr)(CO)(MeO_2CC{=}CHCO_2Me)(PPh_3)_2]$. Found: C, 60.6; H, 4.7. Calc. for $C_{46}H_{44}O_6P_2S_2Ru$: C, 58.2; H, 4.5%.

Acknowledgements—Financial support of the DGICYT is acknowledged. H.L. thanks the Ministère de l'Education Nationale du Maroc for a fellowship.

REFERENCES

1. M. R. Torres, A. Vegas, A. Santos and J. Ros, *J. Organomet. Chem.* 1987, **326**, 413.
2. M. R. Torres, A. Vegas, A. Santos and J. Ros, *J. Organomet. Chem.* 1986, **309**, 169.
3. M. R. Torres, A. Santos, J. Ros and X. Solans, *Organometallics* 1987, **6**, 1091.
4. M. R. Torres, A. Perales, H. Loumrhari and J. Ros, *J. Organomet. Chem.* 1990, **385**, 379.
5. H. Loumrhari, J. Ros, M. R. Torres and A. Perales, *Polyhedron* 1990, **9**, 907.
6. G. Wilkinson, R. Gillard and J. A. McCleverty (Eds), *Comprehensive Coordination Chemistry*, Vol. 2, Ch. 16.4. Pergamon Press, Oxford (1987).
7. G. Wilkinson, F. G. A. Stone and E. Abel (Eds), *Comprehensive Organometallic Chemistry*, Vol. 4, Ch. 32.3. Pergamon Press, Oxford (1982).
8. G. Wilkinson, F. G. A. Stone and E. Abel (Eds), *Comprehensive Organometallic Chemistry*, Vol. 4, Ch. 32.9. Pergamon Press, Oxford (1982).
9. E. Carmona, L. Sanchez, J. M. Marin, M. L. Poveda, J. Atwood, R. Priester and R. D. Rogers, *J. Am. Chem. Soc.* 1984, **106**, 3214.
10. J. R. Morrow, T. L. Tonker and J. L. Templeton, *J. Am. Chem. Soc.* 1985, **107**, 5004.
11. K. Nakamoto, *Infrared and Raman Spectra of Inorganic Coordination Compounds*. Wiley Interscience, New York (1986).
12. M. F. Perpiñan, L. Ballester, M. E. Gonzalez-Caso and A. Santos, *J. Chem. Soc., Dalton Trans.* 1987, 281.
13. P. B. Critchlow and S. D. Robinson, *J. Chem. Soc., Dalton Trans.* 1975, 1367.
14. L. Ballester and M. F. Perpiñan, *J. Chem. Educ.* 1988, **65**, 362.

Polyhedron Vol. 10, No. 4/5, pp. 429–432, 1991
Printed in Great Britain

0277–5387/91 $3.00+.00
Pergamon Press plc

OXYGENATION OF NITRIC OXIDE IN THE PRESENCE OF A NITROSYL-BRIDGED COMPLEX OF MOLYBDENUM

JAN O. DZIĘGIELEWSKI* and KRZYSZTOF FILIPEK

Department of Inorganic and Radiation Chemistry, Institute of Chemistry, Silesian University, Szkolna 9, 40006 Katowice, Poland

and

BOGUSŁAWA JEŻOWSKA-TRZEBIATOWSKA

Institute of Chemistry, University of Wrocław, Wrocław, Poland

(*Received* 15 *August* 1990; *accepted* 10 *October* 1990)

Abstract—The binuclear, nitrosyl-bridged complex $Cs_2[Mo_2Cl_5H(NO)_2]$ was synthesized and employed in the oxygenation of nitric oxide, with insufficient oxygen. The mechanism of the oxygenation process is discussed and the "catalytic" activity of the complex in such a process described.

The goal of our work was to synthesize a molybdenum complex with nitrosyl bridges and examine the influence of such a complex on the process of nitric oxide oxygenation when oxygen is used in an insufficient amount.

The problems of treatment and utilization of nitrogen oxides as the components of exhaust gases have been known for many years[1] and there are many catalytic and non-catalytic methods involving either reduction[2] or oxygenation of NO_x.[3] The former reactions are much better known and applied more often, but the presence of oxygen, as an inseparable component of the gases, imposes serious difficulties on such processes.

Nitric oxide is hardly soluble in any alkaline solution, while the higher oxides of nitrogen are readily soluble.[4] In every case nitric oxide is present in the gases since the amount of air (oxygen) is insufficient to oxygenate it. Therefore, the methods of "extra oxygenation" of oxides of nitrogen followed by the absorption of the gases in alkaline solution have been widely applied.[1]

On the other hand, the reactivity of the nitrosyl complexes towards oxygen and nitric oxide has been indicated in the literature;[5] as a rule, these reactions are redox processes.[6] In our previous work[7] we described the possibility of such a reaction in the case of a molybdenum(II) complex with nitrosyl bridges and gaseous nitric oxide.

EXPERIMENTAL

The first stage of our work was to synthesize and characterize the nitrosyl molybdenum complex. The hydrido complex, $Cs_3[Mo_2Cl_8H]$, was prepared according to the literature[8] and the nitrosyl complex was obtained in the heterogeneous reaction with gaseous nitric oxide. Nitric oxide was formed in the reaction of $NaNO_2$ with $FeSO_4$ in H_2SO_4 solution and then purified by passing through a concentrated solution of KOH, and then over NaOH pellets. The reaction was carried out under strictly deoxygenated conditions and controlled by determination of the liberated NOCl, which was absorbed in 10% KOH, while the abstracted chlorides were determined using standard methods.[9] The solid-state mixture (complex + CsCl) was dissolved in THF and the CsCl was filtered off and dissolved in water to determine $[Cl^-]$ ions. The organic solution was evaporated and the residue was analysed using standard methods of elemental analysis. The results based on the formula $Cs_2Mo_2Cl_5HN_2O_2$ were as follows: Found: Mo,27.4; Cl, 25.8; N, 4.1 (or 3.9—from TG curve). Calc.: Mo. 27.6; Cl, 25.5; N, 4.0%. The complex was formed in the following reaction:

* Author to whom correspondence should be addressed.

$$Cs_3[Mo_2Cl_8H]+4NO \longrightarrow Cs_2[Mo_2Cl_5H(NO)_2]+CsCl+2NOCl.$$

The spectroscopic analysis of the complex was obtained with a Beckman 5240 spectrophotometer (absorption bands) and a Specord 75 IR spectrophotometer (IR measurements in KBr pellets). Magnetic susceptibility was measured using a Gouy balance and the thermogravimetric analysis was carried out with a Q-1500 D Paulik–Paulik system derivatograph.

The reactions of nitric oxide with oxygen in the presence of the complex were carried out in special tubes previously vented with argon. The mixtures of nitric oxide and oxygen (M : M = 10 : 1, 20 : 1, 30 : 1) were reacted with solid $Cs_2[Mo_2Cl_5H(NO)_2]$ several times using different amounts of the complex. In every case oxygen was added as the first component. The amounts of nitrogen oxides were determined spectrophotometrically[10] by dissolving in 2 M KOH and then determining as nitrites and nitrates. Since nitric oxide is almost insoluble in KOH (nevertheless the amounts of NO_2^- corresponding to nitric oxide were subtracted) the NO_2^- and NO_3^- formed are the products of the reaction of NO_2, N_2O_4 and N_2O_5 with KOH. The amounts of NO_2^- and NO_3^- could be easily converted into the quantities of the corresponding oxides. The reactions of similar compositions of the NO/O_2 mixtures were examined as references.

Table 1. IR vibrations of $Cs_2[Mo_2Cl_5H(NO)_2]$

Frequency (cm^{-1})	Assignment
1650(w)	ν_{as}(Mo—H—Mo)
1380(vs)	$\nu(NO_b)$
1250(w)	ν_{sym}(Mo—H—Mo)
620(m)	ν(Mo—N)
550(m)	δ(Mo—O—Mo, N)
540(w)	δ(Mo—H—Mo)
310(w), 295(m)	ν(Mo—Cl_t)
280(w)	ν(Mo—Cl_b)

RESULTS AND DISCUSSION

Characterization of the $Cs_2[Mo_2Cl_5H(NO)_2]$ *complex*

IR vibrations of the complex are presented in Table 1. The vibration at 1380 cm^{-1} is typical for a bridging nitrosyl group.[7,11] Dissolution of the complex in water is accompanied by the liberation of gaseous hydrogen and this fact, together with two weak intensity vibrations at 1650 and 1250 cm^{-1}, support the presence of the bridging hydrogen in the coordination sphere of the complex. The 60 cm^{-1} shift of ν_{as}(Mo—H—Mo) in comparison with the initial complex[12] is due to the presence in the coordination sphere of nitric oxide, a ligand with strong π-acceptor ability. The presence of the two suggested nitrosyl groups is supported by the thermal analysis results (see Fig. 1).

Two well-distinguished slopes in the mass loss curve (TG) between 400 and 600 K could be attributed to the two different nitrosyl groups abstracted from the complex in the form of gaseous dinitrogen.[13] These phenomena are accompanied by two peaks in the DTG and DTA curves due to the chemical reactions taking place during heating. The absorption bands of the complexes are presented in Table 2. The decay of the band attributed to the $\delta \rightarrow \delta^*$ transition in the initial complex is due to the cleavage of the Mo—Mo multiple bond. This is a typical effect of the multiple bond complex reactions with nitric oxide.[15] The complex formed is almost diamagnetic ($\mu_{eff.} = 0.3$ BM). Electrons from d_{xz} and d_{yz} orbitals could be effectively delocalized to the π^* orbitals of nitric oxide and then transferred to the lower unoccupied orbital (LUMO) of the central atom, i.e. b_2.[16] The transfer

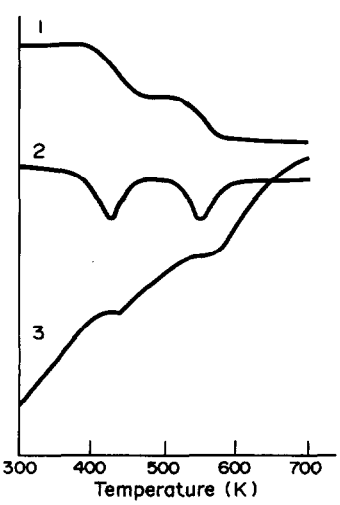

Fig. 1. Thermal analysis curves for the decomposition of $Cs_2[Mo_2Cl_5H(NO)_2]$ under nitrogen; heating rate 5 K min^{-1}. (1) TG—mass loss; (2) DTG—temperature derivative of the mass loss; (3) DTA—differential thermal analysis curve.

Table 2. Absorption bands and their characterization for $Cs_3[Mo_2Cl_8H]$ and $Cs_2[Mo_2Cl_5H(NO)_2]$ in 9 M HCl

Frequency (cm^{-1})	ε	Assignment
	$Cs_3[Mo_2Cl_8H]$[14]	
13,330	310	$e \rightarrow b_2$
28,570	2100	$e \rightarrow b_1$
32,790	12,500	$\pi \rightarrow \pi^*$
42,920	24,000	$e \rightarrow d_{x^2-y^2}$
45,450	22,000	$Cl \rightarrow b_2$
	$Cs_2[Mo_2Cl_5H(NO)_2]$	
18,690	330	$^2B_2(\pi^*_{NO}) \rightarrow \pi^*_{NO}$
23,810	1700	$^2A_1 \rightarrow {}^2B_2$
42,190	12,000	$^2A_1 \rightarrow \pi^*_{NO}$
47,600	16,500	$Cl \rightarrow {}^2B_2$

mentioned is the reason for a high activation of the bridged nitrosyl group.[17]

Reactions with oxygen and nitric oxide mixtures

It is worthy of note that the reactions of nitric oxide with oxygen in the absence of the complex have yields of about 3% (see Fig. 2). The results of similar reactions in the presence of the complex are presented in Fig. 3.

The process is not due to adsorption since the relation between the amount of oxygenated nitric oxide and the amount of the complex is curvilinear (see Fig. 4).

Consideration of the equilibrium constants of the possible reactions during the experiment[18] leads to the conclusion that the duration of the process could effect the composition of the higher nitrogen oxides formed. Since the applied method of analysis (see Experimental) enables simultaneous determination of both nitrites (as the products of the NO_2+OH^- reaction) and nitrates (N_2O_4 and $N_2O_5+OH^-$ reaction), we could estimate the amounts of NO_2 and N_2O_5 gases produced. It is clear (see Fig. 5) that the longer reaction time favours the higher contents of N_2O_5. Thus, the following reaction scheme could be proposed:

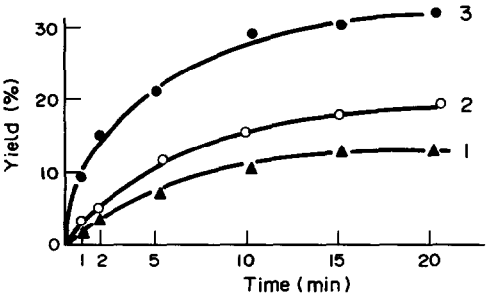

Fig. 3. Yields of the $NO+O_2$ reaction (%) vs time in the presence of $Cs_2[Mo_2Cl_5H(NO)_2]$. [Complex] = 0.5×10^{-4} M, [NO] = 4×10^{-3} M; [O_2] = 0.13×10^{-4} (1), 0.2×10^{-4} (2), 0.4×10^{-4} M (3).

(I) coordination of oxygen into the highly activated bridging NO group:

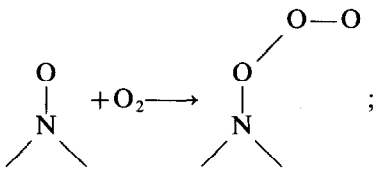

;

(II) abstraction of the very reactive NO_3 group from the coordination sphere;

(III) reaction of NO_3 with NO supplied into the system

$$NO_3 + NO \longrightarrow 2\,NO_2,$$

with the simultaneous reconstruction of the coordination sphere of the complex;

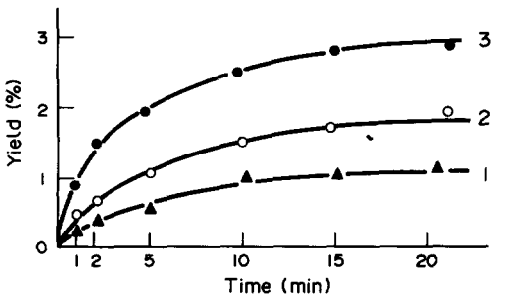

Fig. 2. Yields of the $NO+O_2$ reaction (%) vs time. [NO] = 4×10^{-3} M; [O_2] = 0.13×10^{-4} M (1), 0.2×10^{-4} M (2), 0.4×10^{-4} M (3).

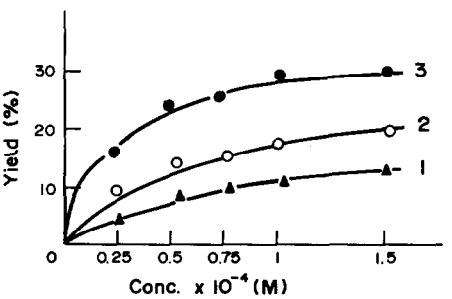

Fig. 4. Yields of the $NO+O_2$ reaction (%) vs the amount of complex, t = 15 min (Concentrations of the gases—as in Fig. 3.)

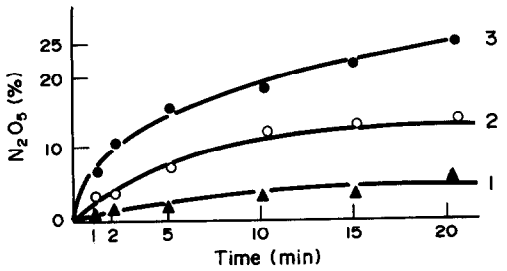

Fig. 5. The percentage of N_2O_5 in the gaseous products of the $NO+O_2$ reactions vs time. (Concentrations—as in Fig. 3.)

(IV) the slowest process,

$$NO_3 + NO_2 \longrightarrow N_2O_5.$$

The formation of the NO_3 group with the peroxo structure [reaction (I)] is a well known process,[19] while the lack of nitrite or nitro complexes on the solid surface (confirmed by recording an IR spectrum after each of the experiments) suggests the homolytic liberation of the NO_3 group[20] [reaction (II)]. The nitric oxide supplied readily reacts with NO_3, according to the corresponding rate constant,[18] while its excess reconstructs the coordination sphere of the complex [reaction (III)] and, as a consequence, the complex appears to behave as a catalyst. Kinetic factors contribute to the reaction of NO_3 with NO_2 [reaction (IV)] when sufficient time for the reaction is assured (see Fig. 5).

CONCLUSIONS

The oxygenation of nitric oxide is about 10 times more effective in the presence of the $Cs_2[Mo_2Cl_5H(NO)_2]$ complex in a system which is deficient in oxygen, due to the reactivity of the nitrosyl bridges.

REFERENCES

1. L. H. Yaverbaun, *Nitrogen Oxides Control and Removal: Recent Developments.* Noyes Data Company, New York (1979).
2. H. Bosch and F. J. J. G. Janssen, *Catalysis Today* 1988, **2**, 1.
3. H. T. Carlson and H. S. Rosenberg, *Indian Engng Chem. Process Design Develop.* 1984, **23**, 808.
4. H. Idemura, *Chem. Econ. Engng Rev.* 1974, **6**, 22.
5. (a) S. Bhaduri, J. Bratt, B. F. G. Johnson, A. Khair, J. A. Segal, R. Walters and C. Zuccaro, *J. Chem. Soc., Dalton Trans.* 1981, 234; (b) J. Backvall and A. Heumann, *J. Am. Chem. Soc.* 1986, **108**, 7107.
6. J. A. McCleverty, *Chem. Rev.* 1979, **79**, 53 and refs therein.
7. J. O. Dzięgielewski, K. Filipek and B. Jeżowska-Trzebiatowska, *Inorg. Chim. Acta* 1990, **171**, 89.
8. J. San Filippo Jr and H. J. Sniadoch, *Inorg. Synth.* 1979, **19**, 129.
9. G. H. Coleman and G. A. Lillis, *Inorg. Synth.* 1939, **1**, 55.
10. J. H. Wetters, *Anal. Chem.* 1970, **3**, 335.
11. R. C. Elder, F. A. Cotton and R. A. Schunn, *J. Am. Chem. Soc.* 1967, **89**, 3645.
12. K. Nakamoto, *Infrared and Raman Spectra of Inorganic and Coordination Compounds.* Wiley, New York (1970).
13. (a) B. Mohai, K. Gyoryova and L. Bencze, *J. Thermal Anal.* 1979, **17**, 159; (b) D. Dollimore, *Differential Thermal Analysis* (Edited by R. C. MacKenzie), p. 427. Academic Press, London (1970).
14. F. A. Cotton and R. A. Walton, *Multiple Bonds Between Metal Atoms.* Wiley, New York (1982).
15. M. H. Chisholm, F. A. Cotton, M. W. Extine and R. L. Kelly, *J. Am. Chem. Soc.* 1978, **100**, 3354.
16. (a) F. Bottomley, *Inorg. Chem.* 1983, **22**, 2656; (b) K. A. Kubat-Martin, M. E. Barr, B. Spencer and L. F. Dahl, *Organometallics* 1987, **6**, 2570.
17. (a) M. Kubota and D. A. Phillips, *J. Am. Chem. Soc.* 1975, **97**, 5637; (b) W. J. Bykov and A. P. Svytyn, *Metody razczeta parametrov aktywacji molekul*, p. 129. Nauka, Novosybirsk (1988).
18. F. Busi, M. D. D'Angelantonio, Q. G. Mulazzani, V. Rafaelli and O. Tubertini, *Radiat. Phys. Chem.* 1985, **25**, 47.
19. S. G. Clarkson and F. Basolo, *Inorg. Chem.* 1973, **12**, 1528.
20. B. S. Tovrog, F. Mares and S. E. Diamond, *J. Am. Chem. Soc.* 1980, **102**, 6616.

Polyhedron Vol. 10, No. 4/5, pp. 433–436, 1991
Printed in Great Britain

0277–5387/91 $3.00+.00
© 1991 Pergamon Press plc

SEVEN-COORDINATE ACETYLACETONATO, HEXAFLUOROACETYLACETONATO AND BENZOYLACETYLACETONATO COMPLEXES OF MOLYBDENUM(II) AND TUNGSTEN(II)

PAUL K. BAKER* and DAFYDD AP KENDRICK

Department of Chemistry, University of Wales, Bangor, Gwynedd LL57 2UW, U.K.

(*Received* 7 *September* 1990; *accepted* 11 *October* 1990)

Abstract—The complexes $[MI_2(CO)_3(NCMe)_2]$ (M = Mo or W) react in CH_2Cl_2 with one or two equivalents of PPh_3 to give $[MI_2(CO)_3(NCMe)(PPh_3)]$ or $[MI_2(CO)_3(PPh_3)_2]$, which when reacted, *in situ*, with one equivalent of Na[L⌒L] [L⌒L = acetylacetonato (acac), hexafluoroacetylacetonato (hfacac) or benzoylacetylacetonato (bzacac)] give the seven-coordinate complexes $[MI(CO)_3(PPh_3)(L⌒L)]$ and $[MI(CO)_2(PPh_3)_2(L⌒L)]$, respectively. The low temperature ^{13}C NMR spectra of selected complexes are interpreted to suggest the likely structures of these compounds.

Seven-coordinate complexes of molybdenum(II) and tungsten(II) containing bidentate anionic sulphur donor ligands such as dithiocarbamates and xanthates are numerous,[1–7] whereas analogous seven-coordinate compounds containing bidentate anionic oxygen donor ligands are relatively scarce. A series of seven-coordinate mono(chloro) compounds of the type $[MCl(CO)_2L'_2(L⌒L)]$ (M = Mo or W; L′ = PEt_3 or PPh_3; L⌒L = acac or hfacac) were prepared by the reaction of $[MCl_2(CO)_3(PPh_3)_2]$ with the sodium salts of either acetylacetone or hexafluoroacetylacetone.[8] The six-coordinate, 16-electron complex $[MoBr_2(CO)_2(PPh_3)_2]$ reacts with the sodium salts of a series of anionic bidentate oxygen and sulphur ligands to give the mono(bromo) compounds $[MoBr(CO)_2(PPh_3)_2(L⌒L)]$.[9]

In this paper we describe the synthesis and properties of some new mono(iodo) seven-coordinate complexes of molybdenum(II) and tungsten(II), containing anionic oxygen donor ligands derived from acetylacetone, hexafluoroacetylacetone or benzoylacetylacetone.

EXPERIMENTAL

All reactions were carried out under nitrogen using standard Schlenk techniques. The complexes $[MI_2(CO)_3(NCMe)(PPh_3)]$ (M = Mo or W)[10] and $[MI_2(CO)_3(PPh_3)_2]$[11] were prepared by the published methods. All chemicals were purchased from commercial sources. Dichloromethane was dried over P_4O_{10} and distilled, and all solvents were purged of oxygen before use. ^1H NMR spectra were recorded on a Bruker AC 250 CP/MAS NMR spectrometer and the low temperature ^{13}C NMR spectra were recorded on a Bruker WH 400 NMR spectrometer (all spectra were calibrated against tetramethylsilane). IR spectra were recorded on a Perkin–Elmer 1430 spectrophotometer. Elemental analyses for C, H and N were obtained using a Carlo Erba Elemental Analyser MOD 1106 (with helium as a carrier gas).

$[MoI(CO)_3(PPh_3)(acac)]$ (1)

To acetylacetone (0.097 g, 0.969 mmol) was added NaH (0.0466 g, 0.967 mmol, 50% by weight) and the mixture stirred in Et_2O (5 cm^3) for 5 min, with evolution of H_2 (g). The solvent was removed *in vacuo* and the resulting sodium salt resolvated in CH_2Cl_2 (5 cm^3) and MeOH (5 cm^3). To $[MoI_2(CO)_3(NCMe)_2]$ (0.500 g, 0.969 mmol) dissolved in CH_2Cl_2 (15 cm^3), with continuous stirring under a stream of dry nitrogen was added PPh_3 (0.254 g, 0.968 mmol). After stirring for 1 min, the previously prepared solution of Na[acac] was added and the mixture stirred for a further 18 h; after

* Author to whom correspondence should be addressed.

Table 1. Physical and analytical data[a] for the seven-coordinate complexes $[MI(CO)_3(PPh_3)(L\frown L)]$ and $[MI(CO)_2(PPh_3)_2(L\frown L)]$

Complex	Colour	Yield of pure product (%)	Analysis C (%)	Analysis H (%)
$[MoI(CO)_3(PPh_3)(acac)]$ (**1**)	Dark brown	76	46.3(46.7)	3.1(3.1)
$[WI(CO)_3(PPh_3)(acac)]$ (**2**)	Golden yellow	77	41.7(41.3)	2.9(2.9)
$[MoI(CO)_3(PPh_3)(hfacac)]$ (**3**)	Brown	60	40.8(40.2)	2.3(2.1)
$[WI(CO)_3(PPh_3)(hfacac)]$ (**4**)	Brown	80	36.0(36.1)	2.4(1.9)
$[MoI(CO)_3(PPh_3)(bzacac)]$ (**5**)	Brown	55	49.8(50.1)	3.2(3.3)
$[WI(CO)_3(PPh_3)(bzacac)]$ (**6**)	Olive green	81	45.3(45.5)	3.0(3.0)
$[MoI(CO)_2(PPh_3)_2(acac)]$ (**7**)	Dark brown	53	57.4(57.2)	4.2(4.1)
$[WI(CO)_2(PPh_3)_2(acac)]\cdot CH_2Cl_2$ (**8**)	Olive green	65	49.4(49.1)	3.5(3.7)
$[MoI(CO)_2(PPh_3)_2(hfacac)]$ (**9**)	Brown	42	51.9(51.1)	3.4(3.1)
$[WI(CO)_2(PPh_3)_2(hfacac)]$ (**10**)	Brown	75	47.5(47.0)	2.5(2.8)
$[MoI(CO)_2(PPh_3)_2(bzacac)]$ (**11**)	Brown	70	59.0(59.8)	4.2(4.1)
$[WI(CO)_2(PPh_3)_2(bzacac)]\cdot CH_2Cl_2$ (**12**)	Brown	79	51.7(51.8)	3.5(3.6)

[a] Calculated values in parentheses.

which the solvents were removed *in vacuo*. The product was resolvated in CH_2Cl_2 (15 cm^3) and filtered to remove NaI before the solvent was again removed *in vacuo* to give the dark brown crystalline complex $[MoI(CO)_3(PPh_3)(acac)]$ (**1**) (yield: 0.49 g, 76%), which was recrystallized from CH_2Cl_2.

Similar reactions of $[MI_2(CO)_3(NCMe)_2]$ (M = Mo or W) with one equivalent of PPh_3, followed by an *in situ* reaction with one equivalent of $Na[L\frown L]$ ($L\frown L$ = acac, hfacac or bzacac) gave the new complexes $[MI(CO)_3(PPh_3)(L\frown L)]$ (**2–6**). (See Table 1 for physical and analytical data.)

$[MoI(CO)_2(PPh_3)_2(acac)]$ (**7**)

To $[MoI_2(CO)_3(NCMe)_2]$ (0.500 g, 0.969 mmol) dissolved in CH_2Cl_2 (15 cm^3), with continuous stirring under a stream of dry nitrogen was added PPh_3 (0.508 g, 1.936 mmol). After stirring for 1 min, Na[acac] (0.118 g, 0.969 mmol) was added as a CH_2Cl_2–MeOH solution. The mixture was stirred for a further 18 h, after which the solvents were removed *in vacuo*. The product was resolvated in CH_2Cl_2 (15 cm^3) and filtered to remove NaI. The solvent was again removed *in vacuo* to give the dark brown complex $[MoI(CO)_2(PPh_3)_2(acac)]$ (**7**) (yield: 0.46 g, 53%), which was recrystallized from CH_2Cl_2.

Similar reactions of $[MI_2(CO)_3(NCMe)_2]$ (M = Mo or W) with two equivalents of PPh_3, followed by an *in situ* reaction with one equivalent of $Na[L\frown L]$ ($L\frown L$ = acac, hfacac or bzacac) gave the new complexes $[MI(CO)_2(PPh_3)_2(L\frown L)]$ (**8–12**). (See Table 1 for physical and analytical data.)

RESULTS AND DISCUSSION

The seven-coordinate complexes $[MI_2(CO)_3(NCMe)(PPh_3)]$[10] and $[MI_2(CO)_3(PPh_3)_2]$[11] react with one equivalent of the anionic bidentate oxygen donor ligands, $Na[L\frown L]$ ($L\frown L$ = acac, hfacac or bzacac), to give a series of new complexes, $[MI(CO)_3(PPh_3)(L\frown L)]$ (**1–6**) or $[MI(CO)_2(PPh_3)_2(L\frown L)]$ (**7–12**), respectively. Complexes **1–12** were characterized by elemental analyses (C, H and N) (Table 1), IR (Table 2) and ^1H NMR spectroscopy (Table 3). Compounds **8** and **12** were confirmed as CH_2Cl_2 solvates by repeated elemental

Table 2. IR data[a] for the seven-coordinate complexes $[MI(CO)_3(PPh_3)(L\frown L)]$ and $[MI(CO)_2(PPh_3)_2(L\frown L)]$

Complex	ν(C≡O) (cm^{-1})
1	2005(s), 1915(s) and 1890*
2	2000(s), 1920(s) and 1850(s)
3	2010(s), 1930(s) and 1890*
4	2005(s), 1950*, 1920(s) and 1855*
5	2000(s), 1930(s) and 1870*
6	2005(s), 1950*, 1915(s) and 1860(m)
7	2020(s) and 1904(s)
8	2005(s), 1940(s), 1895(s) and 1840(s)
9	2000(s) and 1900(s)
10	2000(s), 1920(s), 1900* and 1860(s)
11	2000(s) and 1895(s)
12	2005(s) and 1900(s)

[a] Spectra recorded as thin $CHCl_3$ films between NaCl plates: (s) = strong; (m) = medium; * = shoulder.

Table 3. ^{1}H NMR data[a] for the seven-coordinate complexes $[MI(CO)_3(PPh_3)(\widehat{L\ L})]$ and $[MI(CO)_2(PPh_3)_2(\widehat{L\ L})]$

Complex	^{1}H (δ, ppm)
1	7.5 (m, 15H, Ph); 5.5 (s, 1H, CH); 2.15 (s, 3H, CH_3), 2.05 (s, 3H, CH_3).
2	7.55 (m, 15H, Ph); 5.5 (s, 1H, CH); 2.15 (s, 3H, CH_3), 2.05 (s, 3H, CH_3).
3	7.6 (m, 15H, Ph); 5.85 (s, 1H, CH).
4	7.6 (m, 15H, Ph); 5.85 (s, 1H, CH).
5	7.65 (m, 20H, Ph); 5.88 (s, 1H, CH); 2.15 (s, 3H, CH_3).
6	7.55 (m, 20H, Ph); 6.18 (s, 1H, CH); 2.2 (s, 3H, CH_3).
7	7.55 (m, 30H, Ph); 5.5 (s, 1H, CH); 2.2 (s, 6H, CH_3).
8	7.6 (m, 30H, Ph); 5.5 (s, 1H, CH); 5.3 (s, 2H, CH_2Cl_2); 2.05 (s, 6H, CH_3).
9	7.5 (m, 30H, Ph); 5.9 (s, 1H, CH).
10	7.4 (m, 30H, Ph); 6.15 (s, 1H, CH).
11	7.6 (m, 35H, Ph); 6.2 (s, 1H, CH); 2.2 (s, 3H, CH_3).
12	7.5 (m, 35H, Ph); 6.2 (s, 1H, CH); 5.3 (s, 2H, CH_2Cl_2); 2.2 (s, 3H, CH_3).

[a] Spectra recorded in $CDCl_3$ (+25°C) and referenced to Me_4Si.

analyses and by ^{1}H NMR spectroscopy. Complexes **1–12** are soluble in polar solvents such as $CHCl_3$ and CH_2Cl_2, but only slightly soluble in Et_2O and hydrocarbon solvents. Compounds **1–12** are moderately air-sensitive in the solid state and should be stored under a nitrogen atmosphere.

The structure of these seven-coordinate complexes is likely to be capped octahedral, as most seven-coordinate compounds of molybdenum(II) and tungsten(II) have such a geometry.[12–19] From the work of Colton and Kevekordes,[20] the presence of a capping carbonyl ligand in a capped octahedral structure can be assigned from its particularly low field resonance. The low temperature ^{13}C NMR spectra (−70°C, CD_2Cl_2) of $[WI(CO)_3(PPh_3)(acac)]$, $[WI(CO)_3(PPh_3)(hfacac)]$ and $[MoI(CO)_3(PPh_3)(bzacac)]$ showed resonances at $\delta = 200.71$ and 228.24 ppm, $\delta = 200.61$ and 227.88 ppm, and $\delta = 207.79$ and 239.92 ppm, respectively, with intensity ratios of 2 : 1 (see Table 4). The spectrum in the carbonyl region of $[WI(CO)_3(PPh_3)(acac)]$ (**2**) is shown in Fig. 1. The very low field resonances at $\delta = 228.24$, 227.88 and 239.92 ppm, respectively, are likely to be due to a carbonyl in the unique capping position in these complexes,

Table 4. Low temperature ^{13}C NMR data[a] (δ, ppm) (C≡O) for selected complexes

Complex	^{13}C (δ, ppm)
2	200.71, 228.24
4	200.61, 227.88
5	207.79, 239.92
9	207.64, 239.73

[a] Spectra recorded in CD_2Cl_2 (−70°C) and referenced to Me_4Si.

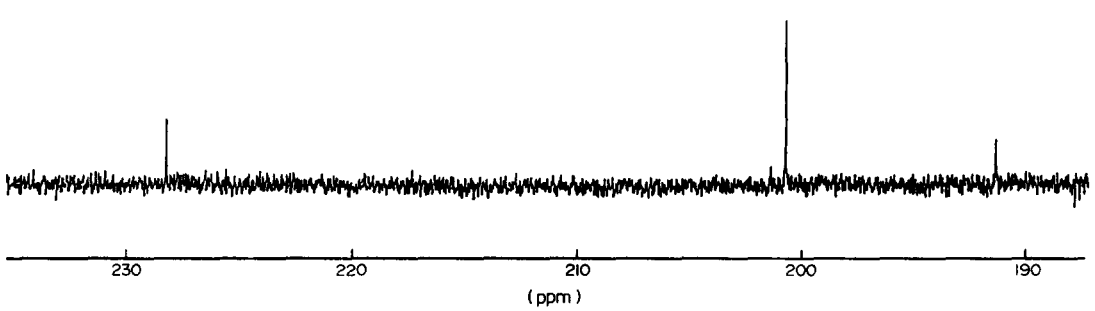

Fig. 1. Low temperature (−70°C, CD_2Cl_2) ^{13}C NMR spectrum (carbonyl region) of $[WI(CO)_3(PPh_3)(acac)]$ (**2**).

since Ganscow and Vernon[21] have suggested the low field resonances for carbonyl ligands in the capping position are due to π-back-donation, and the capping carbonyl resonance occurs at lower field compared with an octahedral carbonyl ligand. The low temperature ^{13}C NMR ($-70°C$, CD_2Cl_2) spectrum of $[MoI(CO)_2(PPh_3)_2(hfacac)]$ (**9**) shows resonances at $\delta = 207.64$ and 239.73 ppm with an intensity ratio of 2 : 1, suggesting[20,21] a capped octahedral structure with a carbonyl ligand in the capping position ($\delta = 239.73$ ppm).

Reactions of $[MI_2(CO)_3(NCMe)(PPh_3)]$ and $[MI_2(CO)_3(PPh_3)_2]$ with two equivalents of $Na[L\frown L]$ ($L\frown L$ = acac, hfacac or bzacac) were attempted. However, highly unstable reaction products and no satisfactory characterization of these products were obtained.

Acknowledgements—We wish to thank Dr O. W. Howarth for running the low temperature ^{13}C NMR spectra at the University of Warwick and the SERC for their support.

REFERENCES

1. R. Colton, G. R. Scollary and I. B. Tomkins, *Aust. J. Chem.* 1968, **21**, 15.
2. R. Colton and G. G. Rose, *Aust. J. Chem.* 1970, **23**, 1111.
3. G. J.-J. Chen, R. O. Yelton and J. W. McDonald, *Inorg. Chim. Acta* 1977, **22**, 249.
4. B. C. Ward and J. L. Templeton, *Inorg. Chem.* 1980, **19**, 1753.
5. J. A. Broomhead and C. G. Young, *Aust. J. Chem.* 1982, **35**, 277.
6. P. K. Baker and S. G. Fraser, *Transition Met. Chem.* 1986, **11**, 273.
7. P. K. Baker and K. R. Flower. *J. Coord. Chem.* 1987. **15**, 333.
8. D. C. Brower, P. B. Winston, T. L. Tonker and J. L. Templeton, *Inorg. Chem.* 1986, **25**, 2883.
9. V. Riera, F. J. Arnaiz and G. G. Herborsa, *J. Organomet. Chem.* 1986, **315**, 51.
10. P. K. Baker and S. G. Fraser, *Transition Met. Chem.* 1987, **12**, 560.
11. P. K. Baker and S. G. Fraser, *Inorg. Chim. Acta* 1986, **116**, L1.
12. A. Mawby and G. E. Pringle, *J. Inorg. Nucl. Chem.* 1972, **34**, 517.
13. M. G. B. Drew, *J. Chem. Soc., Dalton Trans.* 1972, 626.
14. M. G. B. Drew, *J. Chem. Soc., Dalton Trans.* 1972, 1329.
15. G. Schmid, R. Boese and E. Welz, *Chem. Ber.* 1975, **108**, 260.
16. M. G. B. Drew and C. J. Rix, *J. Organomet. Chem.* 1975, **102**, 467.
17. M. G. B. Drew and J. D. Wilkins, *J. Chem. Soc., Dalton Trans.* 1977, 194.
18. M. G. B. Drew and A. P. Wolters, *Acta Cryst.* 1977, **B33**, 205.
19. M. G. B. Drew, P. K. Baker, E. M. Armstrong and S. G. Fraser, *Polyhedron* 1988, **7**, 245.
20. R. Colton and J. Kevekordes, *Aust. J. Chem.* 1982, **35**, 895.
21. O. A. Ganscow and W. D. Vernon, *Top.* ^{13}C *NMR Spectrosc.* 1976, **2**, 270.

Polyhedron Vol. 10, No. 4/5, pp. 437–445, 1991
Printed in Great Britain

0277–5387/91 $3.00+.00
© 1991 Pergamon Press plc

MOLECULAR PRECURSORS OF BISMUTH OXIDES; β-DIKETONATES AND ALKOXIDES. MOLECULAR STRUCTURE OF $[Bi_2(\mu_2,\eta^1\text{-}OC_2H_4OMe)_4(\eta^1\text{-}OC_2H_4OMe)_2]_\infty$ AND OF $Bi(OSiPh_3)_3(THF)_3$

MARIE-CECILE MASSIANI, RENEE PAPIERNIK and LILIANE G. HUBERT-PFALZGRAF*

Laboratoire de Chimie Moléculaire, Associé au CNRS, Université de Nice, Parc Valrose, 06034 Nice, France

and

JEAN-CLAUDE DARAN

Laboratoire de Chimie des Métaux de Transition, URA 419, 4 Place Jussieu, 75203 Paris Cédex 05, France

(*Received* 23 *July* 1990; *accepted* 22 *October* 1990)

Abstract—Various routes to bismuth(III) alkoxides and β-diketonate derivatives have been investigated. Metathesis reactions of the halides and the appropriate sodium derivative offered $[Bi(O^tBu)_3]_\infty$ (**1**), $[Bi_2(OC_2H_4OMe)_6]_\infty$ (**2**), $[Bi(OSiPh_3)_3]_m$ and $Bi(dpm)_3$ (dpmH = dipivaloylmethane) in good yields. The alkoxides display different physical properties; **1** has good volatility, while **2** is highly soluble. Complex **2** and $Bi(OSiPh_3)_3(THF)_3$ (**3**) have been characterized by X-ray diffraction. Compound **2** shows a one-dimensional extended "skew" chain structure based on dimeric asymmetric $Bi_2(\mu_2,\eta^1\text{-}OC_2H_4OMe)_4(OC_2H_4OMe)_2$ units. The alkoxo functionality leads to a distorted pyramidal tetragonal surrounding, but the ether functionality of the bridging groups provides further oxygen donors, and thus coordination numbers of seven and even eight are reached. $Bi(OSiPh_3)_3(THF)_3$ is monomeric with a capped octahedron geometry around the metal. The thermal stability of the volatile precursors **1** and $Bi(dpm)_3$ is in favour of the alkoxide, while the high solubility of **2** is attractive for sol–gel purposes.

Bismuth(III) oxides are involved in various advanced materials such as superconductors,[1] photorefractive systems[2] or oxidation catalysis.[3] Molecular precursors of bismuth(III) oxides remain rather limited and most of these materials have been obtained by traditional high-temperature solid-state reactions. New precursors which could be of value for coatings, through either sol–gel or MOCVD techniques are thus desirable. Classical alkoxides $Bi(OR)_3$ (R = Me, Et, ^{i}Pr),[4] reported to form in high yield by metathesis reactions between the trichloride and alkali alkoxides, are poorly characterized, they display low solubility and are reported to sublime in low yield; although a compound of empirical formula $Bi(OEt)_3$ was used for access to Bi—Sr—Ca—Cu—O materials by MOCVD.[5] Siloxide derivatives are limited to $Me_2Bi(OSiMe_3)$.[6] β-Diketonates are often chosen as sources of oxide precursors for MOCVD applications, but surprisingly, no bismuth β-diketonate derivative has to the best of our knowledge been reported in the literature.[7]

We wish now to report the synthesis and characterization of various alkoxides, siloxides, as well as β-diketonates such as $Bi(O^tBu)_3$, $Bi(OC_2H_4OMe)_3$, $[Bi(OSiPh_3)_3]_m$, $Bi(OSiPh_3)_3(THF)_3$ and $Bi(dpm)_3$ (dpmH = dipivaloylmethane). $[Bi(O^tBu)_3]_\infty$ and

* Author to whom correspondence should be addressed.

$[Bi_2(OC_2H_4OMe)_6]_\infty$ are both polymeric solids but display different physical properties; $[Bi(O^tBu)_3]_\infty$ has good volatility, while $Bi(OC_2H_4OMe)_3$ is highly soluble; this makes them, respectively, attractive precursors for MOCVD and sol–gel processes. $Bi(OSiPh_3)_3(THF)_3$ as well as $[Bi_2(OC_2H_4OMe)_6]_\infty$ were characterized by X-ray diffraction; the characterization of the latter has been achieved and published quite independently by Buhro and his co-workers as a preliminary communication.[8]

EXPERIMENTAL

All manipulations were routinely performed under argon using Schlenk tubes and vacuum-line techniques with solvents purified by standard methods. $BiCl_3$ and $BiBr_3$ were sublimed before use, $Bi[N(SiMe_3)_2]_3$ was obtained according to the literature.[9] ^1H and ^{13}C NMR and IR spectra were run on Bruker WH-90, AC-200 and IR-FTS 45 spectrometers, respectively. IR spectra were obtained as Nujol mulls. Molecular weight measurements were obtained in benzene by using the Signer method.[10] Mass spectra were recorded on a R-10 Ribermag spectrometer by chemical ionization techniques. Analytical data were obtained from the Centre de Microanalyses du CNRS.

Synthesis of $Bi(OC_2H_4OMe)_3$

A solution of $NaOC_2H_4OMe$ (1.6 g, 0.07 mol) in 50 cm^3 of THF was added to $BiCl_3$ (7.4 g, 0.023 mol) dissolved in 50 cm^3 of THF. After 2 h, the medium was evaporated to dryness and extracted with hexane or diethyl ether. Concentration and cooling yielded 5.1 g (51%) of $Bi(OC_2H_4OMe)_3$, soluble in common organic solvents including aliphatic hydrocarbons. Found: C, 22.7; H, 4.7. Calc. for $C_{15}H_{21}O_6Bi$: C; 24.9; H, 4.5%. IR (cm^{-1}): 1273, 1236, 1194, 1123, 1070, 1010, 964, 995, 935, 740; 583, 524 [ν(Bi—O)]. ^1H NMR: ($CDCl_3$, ppm): 3.41s, 3.39s, 3.37s (CH_3); 3.50–3.54m, 3.7–3.77m (CH_2); $^{13}C\{^1H\}$ NMR (C_6D_6, 0.15 M, ppm): 58.4, 58.6 (CH_3); 62.6, 63.1, 63.5, 71.7, 71.9, 77.7 (CH_2).

The same product could also be obtained in ~ 60% yield by reaction of 2-methoxyethanol with $Bi[N(SiMe_3)_2]_3$ in hexane.

Synthesis of $Bi(O^tBu)_3$

A solution of $BiBr_3$ (4 g, 8.9 mmol) in 30 cm^3 of THF was added to a solution of NaO^tBu (26 mmol) in 50 cm^3 of THF. After 24 h, the reaction medium was evaporated to dryness, $Bi(O^tBu)_3$ was isolated by sublimation (80°C, 10^{-2} mm) (3.1 g, 80%). The compound is slightly soluble in aliphatic hydrocarbons, more soluble in aromatic hydrocarbons, dichloromethane or THF (m.p. 154°C). Found: C, 32.1; H, 5.8. Calc. for $C_{12}H_{27}O_3Bi$: C, 33.6; H, 6.3%. IR (cm^{-1}): 1232, 1182, 1022, 928, 758, 725; 572, 550, 459 (Bi—OR). ^1H NMR ($CDCl_3$, ppm): 1.39, SM: (m/z^+, IE) M = $Bi(O^tBu)_3$: M − CH_3 (24%), M − O^tBu (48%), $BiOH(O^tBu)$ (31%), BiC_4H_6 (49%), $BiOC_3H_2$ (40%), $BiOCH_3$ (29%), BiOH (15%), Bi (37%), C_4H_9 (100%).

Monocrystals were grown by sublimation in a sealed ampoule. Compound **1** crystallizes in the hexagonal 6/*mmm* system with unit cell parameters: $a = 9.955(2)$, $c = 9.887(6)$ Å, $V = 848.55$ Å^3, $D_c = 1.64$ g cm^{-3}, D_{exp}(F-decalin) ~ 1.9 g cm^{-3}, $Z = 2$. Data collection was made on a CAD-4 diffractometer with Mo-K_α radiation at room temperature. An empirical absorption correction was applied ($\mu = 98.7$ cm^{-1}). Patterson techniques were used to locate the metal atoms, which were found at 0,0,0 and 0,0,1/2. Systematic extinctions *hkl* for $l = 2n$ failed to allow a correct determination of the space group, and no atoms other than the metal atoms could be located.

Synthesis of $Bi(OEt)_3$

$Bi(OEt)_3$ was obtained quantitatively by alcoholysis of $Bi(O^tBu)_3$ in neat ethanol. It can be purified by sublimation (130°C, 10^{-2} mm Hg). It is poorly soluble in the usual organic solvents, but soluble in alcohols. Found: C, 20.8; H, 4.0. Calc. for $C_6H_{15}O_3Bi$: C, 20.9; H, 4.4%. IR (cm^{-1}): 1096, 1045, 885, 798, 729, 669, 557, 520 [ν(Bi—O)].

Synthesis of $[Bi(OSiPh_3)_3]_m$

A solution of $Bi[(N(SiMe_3)_2]_3$ (2.33 g, 3.38 mmol) in 30 cm^3 of Et_2O was added to a solution of $HOSiPh_3$ (2.86 g, 0.01 mol) in 40 cm^3 of Et_2O. Reflux was maintained for 24 h and a white precipitate formed. $Bi(OSiPh_3)_3$ was separated by filtration (2.16 g, 62%) and found to be poorly soluble. Found: C, 61.9; H, 4.3; Si, 8.3. Calc. for $C_{54}H_{45}O_3Si_3Bi$: C; 63.7; H, 4.3; Si, 8.1%. IR (cm^{-1}): 1111, 1020, 976, 916, 995, 864, 741, 708; 515, 509, 420 [ν(Bi—OR)].

Recrystallization in a mixture of THF and toluene (1:2) yielded the $Bi(OSiPh_3)_3(THF)_3$ adduct. IR (cm^{-1}): 1113, 1053, 1020, 939, 895, 741, 708; 511, 430 [ν(Bi—OR)]; 274, 215. ^1H NMR ($CDCl_3$, ppm): 7.6, 7.39 (m); 3.73(m), 1.84(m). ^{29}Si NMR (THF, ppm): −20.

Synthesis of $Bi(dpm)_3$

A solution of $BiCl_3$ (0.564 g, 1.8 mmol) in 20 cm^3 of THF was added to a solution of Nadpm (5.42 mmol) in 30 cm^3 of THF. Immediate formation of a white precipitate was observed. After 2 h, the reaction medium was evaporated to dryness. The β-diketonate derivatives were extracted by hexane or CH_2Cl_2. Separation of the unreacted Nadpm was achieved by sublimation (60°C, 4×10^{-4} mm Hg). Further sublimation (110°C, 4×10^{-4} mm Hg) gave microcrystals of $Bi(dpm)_3$ (0.55 g, 41%) (m.p. 78°C), soluble in toluene, CH_2Cl_2. Found: C, 53.0; H, 7.6. Calc. for $C_{33}H_{57}O_6Bi$: C, 52.2; H, 7.6%. IR (cm^{-1}): 1600, 1588, 1531 [ν(CO)], 1497, 1381, 1358, 1275, 1244, 1221, 1160, 1128, 1010, 951, 888, 793, 745, 735; 600, 476, 388, 274 [ν(Bi—O)]. ^1H NMR ($CDCl_3$): 1.18 (^{t}Bu), 5.74 (CH). SM: (m/z^+, %), $Bi(dpm)_2$ (100%), $Bi(dpm)(C_3H_5)$ (4%), Bi(dpm) (21%), $Bi(C_7H_{11}O_2)$ (41%), Bi (50%), $dpmH_2$ (7%), $C_7H_{11}O_2$ (50%).

Attempts to obtain monocrystals by slow sublimation (110°C) in an ampoule sealed under vacuum led to decomposition.

Crystallographic studies

The selected crystals of **2** and **3** were mounted onto an Enraf–Nonius CAD-4 automatic diffractometer. Accurate unit cell dimensions and crystal orientation matrices, together with their estimated standard deviations, were obtained from least-squares refinements of the setting angles of 25 reflections. Crystallographic data and other pertinent information are summarized in Table 1.

Table 1. Summary of crystallographic data of **2** and **3**

	2	**3**
Compound	$C_{18}H_{42}O_{12}Bi_2$	$C_{66}H_{69}O_6Si_3Bi$
Colour	White	White
Molecular weight	1251.5	1049.52
Crystal system	Monoclinic	Cubic
Space group	$P\bar{1}$	$Pa3$
a (Å)	10.726(3)	22.991(7)
b (A)	14.425(3)	22.991(7)
c (Å)	12.018(2)	22.991(7)
α (°)	93.44(2)	90
β (°)	113.66(2)	90
γ (°)	119.56(2)	90
V (Å^3)	1401	12152
Z	2	8
Density (calc) (g cm^{-3})	2.06	1.368
$F(000)$ (e^-)	334	569
Diffractometer	Nonius CAD-4	Nonius CAD-4
Temperature (°C)	−150	−93
Radiation	Mo-K_α	Mo-K_α
Linear absorption coefficient (cm^{-1})	125.7	29.97
Absorption correction	DIFABS[11]	DIFABS[11]
Scan type	ω–2θ	ω–2θ
Scan range (deg^{-1})	1.0–5.5	2–19
Scan width (deg^{-1})	$1.2+0.345 \tan\theta$	$1.2+0.345 \tan\theta$
hkl Limits	$\pm h, \pm k, l$	$+h, +k, +l$
Data collected	6415	5402
Unique data used [$F_o^2 > 3\sigma(F_o^2)$]	4070	640
Number of parameters refined	299	120
R	0.0372	0.0322
R_w	0.0432	0.0323
Ar coefficients	4.674	−1.587
	−2.338	7.595
	3.267	−2.412
		2.436
Quality-of-fit indicator	1.133	1.026

Corrections were made for Lorentz polarization and absorption[11] effects.

Computations were performed by using CRYSTALS[12] adapted on a Micro Vax II. Atomic form factors were taken from ref 13. Anomalous dispersion terms were used. For **2**, bismuth atoms were found using SHELXS,[14] whereas, the position of the bismuth atom in **3** was determined by Harker vector analysis of a three-dimensional Patterson map. All remaining non-hydrogen atoms were found by successive electron density map calculations. Hydrogen atoms were placed in calculated positions (H—C—H = 109°; H—C—C = 120°; C—H = 0.96 Å) and were not further refined but recalculated after each cycle. They were assigned isotropic thermal parameters 20% higher than those of the carbon atoms to which they were attached. Anisotropic temperature factors were introduced for all non-hydrogen atoms. Both structures were refined by least-squares techniques. The weighting scheme used in the last refinement cycles was $w = w'[1-(\Delta F/6\sigma(F))^2]^2$, with $w' = 1/\Sigma_{r=1,n}\mathrm{ArTr}(x)$ with n coefficients Ar for the Chebyshev polynomial $\mathrm{ArTr}(x)$ where x was $F_c/F_o(\max)$.[15] The models reached convergence with $R = \Sigma([F_o]-[F_c])/\Sigma[F_o]$ and $R_w = \{\Sigma w([F_o]-[F_c])^2/\Sigma w(F_o)^2\}^{1/2}$ having the values listed in Table 1. In complex **2**, one of the two terminal alkoxo groups is disordered. This disorder affects the oxygen atom of the ether functionality which is statistically distributed on two sites separated by 0.8 Å. The criteria for a satisfactory complete analysis were the ratios of the rms shift to standard deviation being less than 0.1 and no significant features in the final difference maps.

Positional parameters and equivalent isotropic thermal parameters are given as supplementary material.

RESULTS AND DISCUSSION

We have investigated various routes to bismuth(III) alkoxides and β-diketonates, including metathesis reactions of BiX_3 (X = Cl, Br), alcoholysis of $Bi[N(SiMe_3)_2]_3$ or alkoxide exchange reactions (Scheme 1). The various products were characterized by microanalysis and the usual spectroscopic methods: IR, NMR and mass spectroscopy. Complete structural characterization of $Bi(OC_2H_4OMe)_3$ and $Bi(OSiPh_3)_3(THF)_3$ was achieved by X-ray diffraction.

Synthesis and characterization

The homoleptic bismuth(III) alkoxides $Bi(O^tBu)_3$ (**1**) and $Bi(OC_2H_4OMe)_3$ (**2**) were obtained by reaction between $BiCl_3$ or $BiBr_3$ and the approximate sodium salt (ratio 1 : 3) in THF in 80% yield, while $Bi(OEt)_3$ was obtained quantitatively by alcoholysis of **1**. The good volatility of $Bi(O^tBu)_3$ allows its isolation and purification by sublimation (80–100°C, 10^{-2} mm), but although it is more soluble than the bismuth(III) alkoxides reported so far, it displays moderate solubility. The β-diketonate derivative $Bi(dpm)_3$ was isolated by sublimation as well, but is less volatile than $Bi(O^tBu)_3$. Functional alcohols are largely used as additives in the sol–gel process as a means of keeping a homogeneous medium.[16] Bismuth trismethoxyethanolate, $Bi(OC_2H_4OMe)_3$, is highly soluble (even in pentane) and was obtained by extraction of the reaction medium by diethyl ether. This alkoxide could also

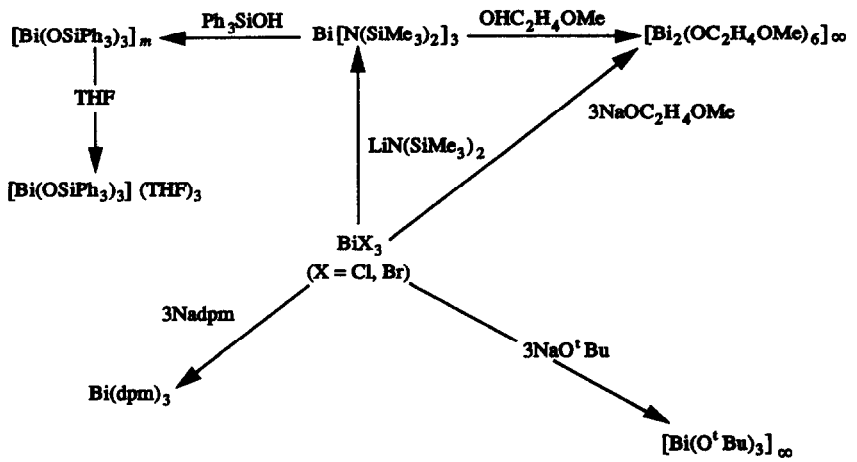

Scheme 1.

be obtained by alcoholysis of $Bi[N(SiMe_3)_2]_3$. The siloxide derivative $[Bi(OSiPh_3)_3]_m$ was obtained accordingly, but its poor solubility suggests a polymeric character. Solubilization could be achieved by Lewis bases and $Bi(OSiPh_3)_3(THF)_3$ was found to be monomeric by X-ray diffraction. Comparable behaviour was observed in the case of the yttrium[16] and copper triphenylsiloxides.[17]

The IR spectra of the various derivatives display essentially the absorption bands of the ligands. The tris-dipivaloylmethanide derivative, $Bi(dpm)_3$, is characterized by C—O stretching between 1600 and 1531 cm^{-1}.

The NMR spectra of the various derivatives offer limited structural information. The ^1H NMR spectra of $Bi(OSiPh_3)_3(THF)_3$ show a single set of THF resonances and rapid exchange is observed with free additional THF. The NMR spectra of $Bi(OC_2H_4OMe)_3$ were found to be a function of the dilution, and thus account for the presence of different molecular species in solution. Equilibrium between various oligomers and/or isomers involving η^1- and η^2-coordination modes of the functional alkoxo moiety is the most likely explanation. Molecular weight data measurements (0.1 M in benzene) are in favour of the formation of dimeric $Bi_2(OC_2H_4OMe)_6$ species ($M_{exp} = 811 \pm 80$, $M_{calc} = 434$) upon dissolution of the solid-state polymer.

Solid-state structure of $[Bi(\mu_2,\eta^1\text{-}OC_2H_4OMe)_4(\eta^1\text{-}OC_2H_4OMe)_2]_\infty$

Since bismuth can adopt numerous coordination numbers and the 2-methoxyethanol various coordination modes, X-ray diffraction studies were carried out on $Bi(OC_2H_4OMe)_3$. As for $[Bi(O^tBu)_3]_\infty$, whose structure could not be completely solved, a chain structure was found. The repeat unit of this chain is a dimer, $Bi_2(\mu_2,\eta^1\text{-}OC_2H_4OMe)_4(\eta^1\text{-}OC_2H_4OMe)_2$, which is shown in Fig. 1. Relevant bond lengths and angles are collected in Table 2.

At first approximation all bismuth atoms are pentacoordinated and display a distorted tetragonal pyramidal geometry. The bismuth alkoxo bond lengths vary from 2.071(6) to 2.573(6) Å, the terminal one being the shortest, as generally observed in alkoxide chemistry. The terminal alkoxo bond length is thus comparable to the value reported recently for $Bi(OC_6H_3Me_2\text{-}2,6)_3$.[18] The lone pair is directed opposite to the terminal OR and appears stereochemically active: the O(28)—Bi—O(basal) angles (av. 83.7°) are contracted as expected for an AB_5E compound, where E stands for the lone pair. The non-bonding distances between the Bi···Bi atoms along the chain are alternate: 3.6426(4) Å within the dimeric units [Bi(1)···Bi(2)] and 3.957 Å (av.) between such units. The Bi—O—C angles

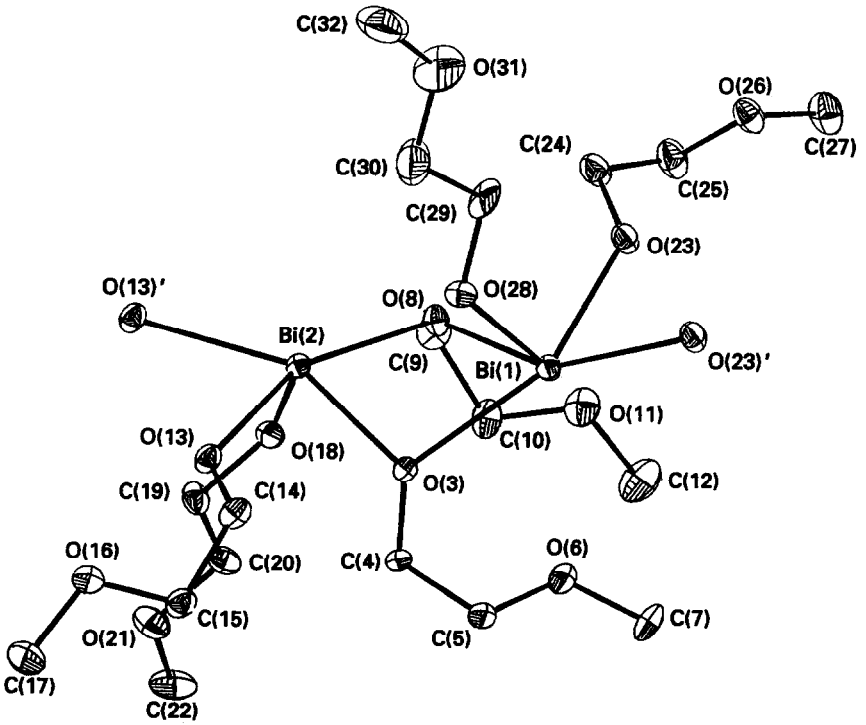

Fig. 1. ORTEP drawing of the asymmetric $[Bi_2(\mu_2,\eta^1\text{-}OC_2H_4OMe)_4(\eta^1\text{-}OC_2H_4OMe)_2]_\infty$ subunit showing the atom numbering scheme.

Table 2. Selected bond lengths (Å) and angles (°) of **2**[a] (standard deviations between parentheses)

Bond lengths			
Bi(1)—Bi(2)	3.6426(4)		
Bi(1)—Bi(1)′	3.9626(6)		
Bi(2)—Bi(2)′	3.9501(6)		
Bi(1)—O(3)	2.573(6)	Bi(2)—O(3)	2.230(6)
Bi(1)—O(8)	2.210(7)	Bi(2)—O(8)	2.526(7)
Bi(1)—O(23)	2.200(7)	Bi(2)—O(13)	2.224(7)
Bi(1)—O(23)′	2.513(7)	Bi(2)—O(13)′	2.523(6)
Bi(1)—O(28)	2.114(6)	Bi(2)—O(18)	2.071(6)
Angles (coordination polyhedron)			
O(8)—Bi(1)—O(3)	72.5(2)	O(8)—Bi(2)—O(3)	73.2(2)
O(23)—Bi(1)—O(3)	156.0(2)	O(13)—Bi(2)—O(3)	84.7(2)
O(23)—Bi(1)—O(8)	87.4(2)	O(13)—Bi(2)—O(8)	156.6(2)
O(23)′—Bi(1)—O(3)	130.6(2)	O(13)′—Bi(2)—O(3)	151.2(2)
O(23)′—Bi(1)—O(8)	151.6(2)	O(13)′—Bi(2)—O(8)	132.8(2)
O(23)′—Bi(1)—O(23)	65.7(3)	O(13)′—Bi(2)—O(13)	67.5(3)
O(28)—Bi(1)—O(3)	72.3(2)	O(18)—Bi(2)—O(3)	89.7(2)
O(28)—Bi(1)—O(8)	78.9(2)	O(18)—Bi(2)—O(8)	80.3(2)
O(28)—Bi(1)—O(23)	91.4(3)	O(18)—Bi(2)—O(13)	92.3(3)
O(28)—Bi(1)—O(23)	92.3(3)	O(18)—Bi(2)—O(13)	84.2(2)
Bi(2)—O(3)—Bi(1)	98.4(2)	Bi(2)—O(23)—Bi(1)	112.5(3)
Bi(2)—O(8)—Bi(1)	100.3(2)	Bi(1)—O(23)—Bi(1)	114.3(3)

[a] Atoms marked with ′ are related by the inversion centre.

range from 117.0(6) to 126.1(6)°; they are quite small and thus in agreement with the rather long bismuth alkoxo bonds.

In fact, additional neighbours led finally to a different surrounding for the two metals. Bi(1) is pseudo-octacoordinated, while Bi(2) is only hepta-coordinated. The terminal alkoxo moiety linked to Bi(1) interacts with Bi(2) in a semi-bridging way [Bi—O: 2.924(6) Å]. While the ether functionality of the bridging alkoxo groups is directed towards the "open" coordination of the pyramid and thus offers further oxygen neighbours for the metals [short contacts between O(16′) and Bi(2) and between O(6), O(11), O(26′) and Bi(1)]. Although these Bi—O(Me) distances (2.90–3.10 Å) are much longer than those observed for $[Y(OC_2H_4OMe)_3]_{10}$ or $Y_3(OC_2H_4OMe)_5(acac)_4$ (2.53–2.59 Å), in which the 2-methoxyethoxo groups act as authentic η^2-bridging–chelating ligands,[19] they are significantly shorter than the sum of the van der Waals' radii (3.47 Å). Most mixed bismuth(III) oxides have five or six oxygen atoms at distances ranging from 2.1 to 2.7 Å and a variable number of additional neighbours. The coordination polyhedron of bismuth in $GeBi_{12}O_{20}$ provides an example of such behaviour, which is also observed for bismuth derivatives, such as $BiCl_3$, for instance.[20]

The chains are thus built up from dimeric asymmetric $Bi_2(\mu_2,\eta^1\text{-}OC_2H_4OMe)_4(\eta^1\text{-}OC_2H_4OMe)_2$ units (Fig. 1). These repeat units are connected to each other through bridging alkoxo oxygens, O(13) and O(23), arranged around inversion centres 0,0,0 [Bi(1)···Bi(1′)] and 0,1/2,0 [Bi(2)···Bi(2′)]. The overall structure can also be viewed as a polymerization of the $Bi(OR)_3$ units to a chain of $Bi(OR)_5$ pyramids *trans*-fused as a basal edge. This is supported by the large differences observed for the alkoxo bridges: each bismuth atom has two *cis* Bi—O of 2.53 Å (av.), and two shorter ones of 2.21 Å (av.). This assembly with the lone pairs *trans* to each other leads to a skewed chain with bismuth atoms alternatively above and below the planes containing the oxygen atoms in bridging positions. Figure 2 shows the resulting "zigzag" chains extended along the *b* axis and the packing. The bridge within the dimeric unit is folded around the O(3)···O(8) edge with a dihedral angle of 142.5°. The bridges which ensure the extended chain structure are planar and as a result the bridging oxygens are of two types: pyramidal within the repeat unit [sum of

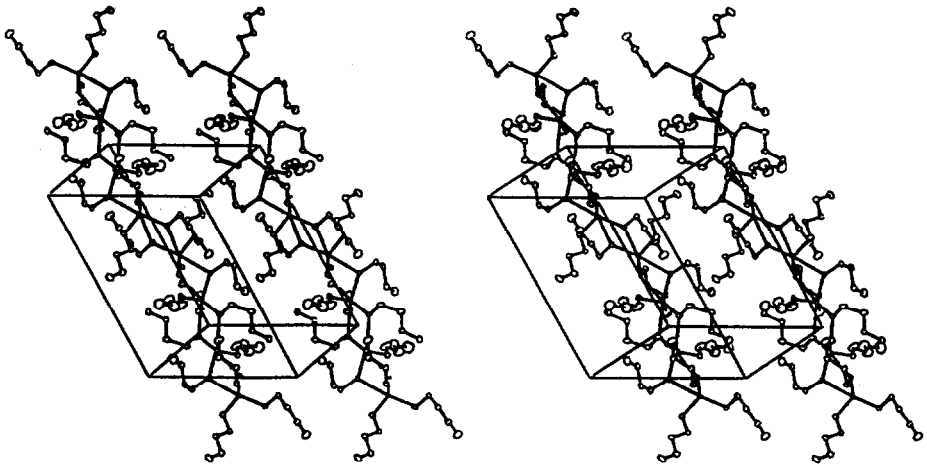

Fig. 2. Stereoview showing the extended "skew" chain structure of $[Bi_2(\mu_2,\eta^1\text{-}OC_2H_4OMe)_4(\eta^1\text{-}OC_2H_4OMe)_2]$ structure along the *b* axis. For clarity, only two chains have been represented.

the angles around O(3) and O(8), 339.4 and 344.8°, respectively], but nearly planar (Σ 359.8 and 355.5°) for O(23) and O(13) which connect the basic dimeric units. Strain in the bridge is evidenced by the reduction of the bridge angles at the metal from the ideal 90° value (72.8° in the repeat unit and 67.5° along the infinite chain). Structurally characterized polymeric alkoxides remain scarce; the overall structure of the bismuth derivative is somewhat related to that of $[VO(OMe)_3]_\infty$[21] or of $Mo_6O_{10}(O^iPr)_{12}$.[22] On the other hand, infinite "skew" chains appear as a common feature for the structures of bismuth halide derivatives such as $[BiX_4]^{n-}$ (X = Cl, Br), although the surrounding of the metal is generally octahedral.[23] The shortest contacts between two chains of $[Bi_2(OC_2H_4$

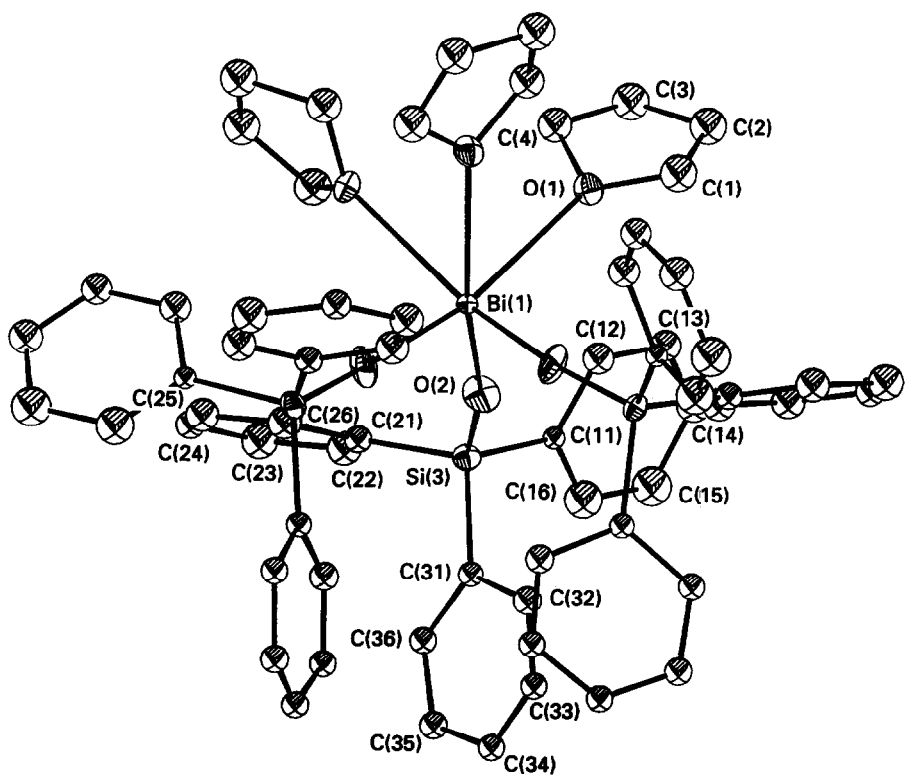

Fig. 3. ORTEP drawing of the $Bi(OSiPh_3)_3(THF)_3$ adduct indicating the atom numbering scheme.

$OMe)_6]_\infty$ are related to the carbon and oxygen atoms of the ether functionality of the terminal alkoxide (values ranging from 3.7 to 4.0 Å), the Bi···Bi distances between them being around 7.5 Å.

Structure of $Bi(OSiPh_3)_3(THF)_3$

The structure of the $Bi(OSiPh_3)_3(THF)_3$ complex is shown in Fig. 3 and selected bond distances and angles are given in Table 3. The complex is monomeric and the six oxygen-bound ligands roughly define a capped octahedron with the two sets of ligands oriented in a meridional arrangement. The overall geometry is thus greatly different from that of the lanthanide analogues $[Ln(OSiPh_3)_3(THF)_3]THF$ (Ln = Y,[16] Ce[24]) which have an octahedral facial arrangement and thus suggests a marked influence of the lone pair on the stereochemistry. The Bi—O(Si) distance is quite short [2.04(1) Å] as compared with the coordination bonds involving the THF ligands [2.95(1) Å]. These bismuth–siloxo bond distances are also quite short with respect to the values reported for other bismuth–alkoxo bonds [2.091(5) Å (av.) for $Bi(OC_6H_3Me_2\text{-}2,6)_3$] with an opening at the Bi—O—Si angles [164.8(8)°]. It appears, therefore, that although $OSiPh_3$ and $OC_6H_3Me_2$-2,6 may be interchangeable in size, the bonding mode might be different, at least in the case of bismuth. The angles involving the THF ligands, O(1)BiO(1′), are reduced to 78.9(3)°, compared with those involving the siloxo groups [∠O(2)—Bi—O(2)′ 93.0(5)°]. Distortion of the coordination polyhedron is also evidenced by the value of the angle involving THF and $OSiPh_3$ ligands *trans* to each other [168.5(4) Å].

$Bi(O^tBu)_3$, $Bi(OEt)_3$ and the β-dipivaloylmethanide derivative, $Bi(dpm)_3$, are volatile and monomeric in the vapour phase, as shown by mass spectrometry; however, by contrast with most elements, the thermal stability of the various bismuth(III) precursors is in favour of the alkoxides,[25] as shown by TGA analysis: $Bi(O^tBu)_3 > Bi(OEt)_3 > Bi(dpm)_3$.

Preliminary TGA analyses have shown a weight loss of ~ 15% for $Bi(dpm)_3$ (probably giving a polynuclear oxo species), but no further evolution between 250 and 450°C. These observations—tendency to lose some dipivaloylmethane—are in agreement with the air sensitivity of $Bi(dpm)_3$ and its poor thermal stability which precluded the obtaining of monocrystals by slow sublimation. $[Bi(O^tBu)_2(dpm)]_m$, obtained by adding one dpmH ligand to $Bi(OtBu)_3$, undergoes disproportionation reactions in the vapour phase.

Hydrolysis of $Bi(O^tBu)_3$ was performed in THF (0.2 M). Addition of small amounts of water (degree of hydrolysis, $h = 0.3$) leads to the immediate formation of a sol which transforms to a gel over a period of 12 h. Complete hydrolysis ($h = 3$) and thermal treatment at 550°C for 15 h of the amorphous powder offers cubic Bi_2O_3.[26] Hydrolysis of $Bi(OSiPh_3)_3(THF)_3$ in THF (0.06 M) with an excess of water in ethanol, and thermal treatment of the amorphous powder in air at 475°C, gives a black material corresponding to the oxohydroxocarbonate $(BiO)_4CO_3(OH)_2$.[27]

The solubility of $[Bi_2(\mu_2,\eta^1\text{-}OC_2H_4OMe)_4(\eta^1\text{-}OC_2H_4OMe)_2]_\infty$ appears attractive for obtaining Bi—Sr—Ca—Cu—O coatings via sol–gel or pyrosol techniques, and further experiments along this line are in progress.

Acknowledgements—We thank the CNRS–PIRMAT for financial support, Professor A. Gleizes (Toulouse) and D. Mercurio (Limoges) for the X-ray data of $Bi(O^tBu)_3$ and those of the hydrolysis products, respectively, and l'Air Liquide for obtaining the thermogravimetric data.

Table 3. Selected bond lengths and angles of 3[a]

Bond lengths	
Bi(1)—O(2)	2.04(1)
Bi(1)—O(1)	2.95(1)
Bond angles	
O(1)—Bi(1)—O(1)′	78.9(3)
O(2)—Bi(1)—O(1)	168.5(4)
O(2)—Bi(1)—O(1)′	98.1(4)
O(2)—Bi(1)—O(1)′	89.6(4)
O(2)—Bi(1)—O(2)′	93.0(5)

[a]The atoms quoted are related through a three-fold axis.

REFERENCES

1. H. Maeda, Y. Tamaka, M. Fukutoni and T. Asano, *Jpn J. Appl. Phys.* 1988, **27**, L209.
2. E. Moya, L. Contreras and C. Zaldo, *J. Opt. Soc. Am. B* 1988, **5**, 1737.
3. R. K. Graselli and J. D. Burrington, *Adv. Catal.* 1981, **30**, 133; R. K. Graselli, *J. Chem. Educ.* 1986, **63**, 216.
4. R. C. Mehrotra and A. K. Rai, *Ind. J. Chem.* 1966, **4**, 537.
5. T. Kobayashi, K. Nomura, F. Uchikawa, T. Masumi and Y. Uehara, *Jpn J. Appl. Phys.* 1988, **27**, L1880; H. Yamane, H. Kurzawa and T. Hirai, *Chem. Lett.* 1988, 1515.
6. H. Schmidbaur and M. Bergfeld, *Z. Anorg. Allg. Chem.* 1968, **363**, 84.

7. R. C. Mehrotra, R. Bohra and D. P. Gaur, *Metal β-Diketonates and Allied Derivatives*. Academic Press, New York (1978).
8. (a) M. C. Massiani, R. Papiernik, L. G. Hubert-Pfalzgraf and J. C. Daran, *J. Chem. Soc., Chem. Commun.* 1990, 301; (b) M. A. Matchett, M. Y. Chiang and W. E. Buhro, *Inorg. Chem.* 1990, **29**, 360.
9. M. S. Gunane, A. Hudson, M. F. Lappert, P. P. Power and H. Goldwhite, *J. Chem. Soc., Dalton Trans.* 1980, 2428.
10. R. Signer, *Ann* 1930, **478**, 246; E. P. Clark, *Ind. Engng Chem. Anal. Ed.* 1941, **13**, 820.
11. N. Walker and D. Stuart, *Acta Cryst.* 1983, **A39**, 158.
12. D. J. Watkin, J. R. Carruthers and P. W. Betteridge, CRYSTALS User Guide. Chemical Crystallography Laboratory, University of Oxford (1986); E. Prince, *Mathematical Techniques in Crystallography*. Springer-Verlag, Berlin (1982).
13. D. T. Cromer and W. Waber, *International Tables for X-ray Crystallography*, Vol. IV. Kynoch Press, Birmingham (1974).
14. G. M. Sheldrick, SHELXS 86, Program for Crystal Structure Solution. University of Gottingen, F.R.G. (1986).
15. D. J. Echorst and D. A. Payne, *Better Ceramics through Chemistry III, Proc. Material Research Soc. Symp.* 1988, **121**, 773; K. Jones, T. J. Davies, H. C. Winterton and N. N. Hughes, *Better Ceramics through Chemistry II, Proc. Material Research Soc. Symp.* 1986, **73**, 111.
16. M. J. McGeary, P. S. Coan, K. Folting, W. E. Streit and K. G. Caulton, *Inorg. Chem.* 1989, **28**, 3283.
17. N. El Khokh, Thesis (Nouveau Régime). Université de Nice, France (1990).
18. W. J. Evans, J. H. Hain and J. W. Ziller, *J. Chem. Soc., Chem. Commun.* 1989, 1628.
19. O. Poncelet, L. G. Hubert-Pfalzgraf, J. C. Daran and R. Astier, *J. Chem. Soc., Chem. Commun.* 1989, 1846; O. Poncelet, L. G. Hubert-Pfalzgraf and J. C. Daran, *Inorg. Chem.* 1990, **29**, 2883.
20. A. F. Wells, *Structural Inorganic Chemistry*, 5th edn. Clarendon Press, Oxford (1982).
21. C. N. Caughlan, H. M. Smith and K. Watenpaugh, *Inorg. Chem.* 1966, **5**, 2131.
22. M. H. Chisholm, K. Folting, J. C. Huffman and C. C. Kirkpatrick, *Inorg. Chem.* 1984, **23**, 1022.
23. B. K. Robertson, W. G. McPherson and E. A. Mayers, *J. Phys. Chem.* 1967, **71**, 3531.
24. P. S. Gradeff, K. Yunlu, T. J. Denning, J. M. Olofson, R. J. Doedens and W. J. Evans, *Inorg. Chem.* 1990, **29**, 420.
25. L. G. Hubert-Pfalzgraf, M. C. Massiani, R. Papiernik and O. Poncelet, *Proceed. Euro-CVD 7, J. Phys.* 1989, **50**, C-981.
26. ASTM File 27-0050.
27. ASTM File 38-0579.

Polyhedron Vol. 10, No. 4/5, pp. 447–454, 1991
Printed in Great Britain

0277–5387/91 $3.00+.00
© 1991 Pergamon Press plc

CLUSTER SYNTHESIS—XXIX. SYNTHESIS AND CHARACTERIZATION OF NEW SULPHUR-CONTAINING TUNGSTEN–RUTHENIUM CARBONYL CLUSTER COMPLEXES

RICHARD D. ADAMS,* THOMAS A. WOLFE and WENGAN WU

Department of Chemistry, University of South Carolina, Columbia, SC 29208, U.S.A.

(*Received* 9 *April* 1990; *accepted* 22 *October* 1990)

Abstract—The reaction of $Ru_3(CO)_9(\mu_3\text{-}S)_2$ (**4**) with $W(CO)_6$ under UV irradiation yielded the complex $Ru_3(CO)_9(\mu_3\text{-}S)(\mu_4\text{-}S)[W(CO)_5]$ (**5**) in 29% yield. Spectral data indicate that **5** has a structure similar to its osmium homologue in which a $W(CO)_5$ group is attached to one of the triply-bridging sulphido ligands in the cluster. The reaction of **4** with $W(CO)_5(PMe_2Ph)$ under UV irradiation yielded two isomeric cluster complexes, $WRu_3(CO)_{11}(PMe_2Ph)(\mu_4\text{-}S)_2$ (**6**) 16% and (**7**) 7%. Compounds **6** and **7** were characterized by single-crystal X-ray diffraction analyses. These complexes were found to contain approximately square-planar arrangements of the four metal atoms with quadruply-bridging sulphido ligands on each side of the cluster. Compound **6** contains a PMe_2Ph ligand on the tungsten atom. In compound **7** the PMe_2Ph ligand is coordinated to the ruthenium atom across the square from the tungsten atom. Crystal data for **6**: $WRu_3S_2O_{11}C_{19}H_{11}$, $M = 977.44$, orthorhombic, $P2_12_12_1$ (No. 19), $a = 13.794(2)$, $b = 16.616(2)$, $c = 11.780(2)$ Å, $V = 2700(1)$ Å^3, $D_c = 2.45$ g cm^{-3}, $Z = 4$, λ(Mo-K_α) = 0.71069 Å (graphite monochromator), $\mu = 62.1$ cm^{-1}. Methods: MITHRIL, difference Fourier, full-matrix least-squares. Refinement of 1960 reflections [$F^2 \geqslant 3\sigma(F^2)$], gave R and R_w values of 0.027 and 0.027, respectively. Crystal data for **7**: $WRu_3S_2O_{11}C_{19}H_{11}$, $M = 977.44$, monoclinic, $P2_1/n$ (No. 14), $a = 15.841(2)$, $b = 8.818(1)$, $c = 19.236(3)$ Å, $\beta = 98.04(1)°$, $V = 2660.5(6)$ Å^3, $D_c = 2.49$ g cm^{-1}, $Z = 4$, λ(Mo-K_α) = 0.17069 Å (graphite monochromator), $\mu = 63.1$ cm^{-1}. Methods: MITHRIL, difference Fourier, full-matrix least-squares. Refinement of 2880 reflections [$F^2 \geqslant 3\sigma(F^2)$], gave R and R_w values of 0.024 and 0.025, respectively.

In previous studies, we have investigated the reactions of the sulphur-containing cluster complexes $M_3(CO)_9(\mu_3\text{-}S)_3$ (M = Fe[1] and Os)[2,3] with $W(CO)_6$ and $W(CO)_5(PMe_2Ph)$ in the presence of UV irradiation. In both cases, the reactions with $W(CO)_6$ result in decarbonylation of the $W(CO)_6$ and the addition of a $W(CO)_5$ grouping to one of the sulphido ligands of the cluster to yield the adducts **1**. No metal–metal bonds were formed in the formation of **1**. Although small amounts of the phosphine-substituted adduct of **1** were obtained from the reaction of $Fe_3(CO)_9(\mu_3\text{-}S)_2$ with $W(CO)_5(PMe_2Ph)$, the principal product was the butterfly

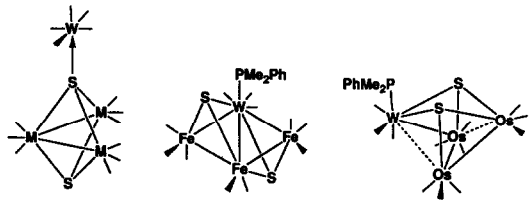

(1) (2) (3)

M = Fe, Os

cluster complex $WFe_3(CO)_{11}(PMe_2Ph)(\mu_3\text{-}S)_2$ (**2**), in which three tungsten–iron bonds were formed with the tungsten atom located in a "hinge" position.[1] In contrast, the reaction of $Os_3(CO)_9(\mu_3\text{-}S)_2$ with $W(CO)_5(PMe_2Ph)$ yielded the butterfly cluster complex $WOs_3(CO)_{12}(PMe_2Ph)(\mu_3\text{-}S)_2$ (**3**), in which two tungsten–osmium bonds were formed

* Author to whom correspondence should be addressed.

with the tungsten atom located in a "wing-tip" position.[3]

Recently, we have been developing the chemistry of sulphido–ruthenium carbonyl cluster complexes.[4] We have now investigated the reactions of $W(CO)_6$ and $W(CO)_5(PMe_2Ph)$ with $Ru_3(CO)_9(\mu_3\text{-}S)_2$ (**4**). The reaction of **4** with $W(CO)_6$ in the presence of UV irradiation yielded the complex $Ru_3(CO)_9(\mu_3\text{-}S)(\mu_4\text{-}S)[W(CO)_5]$ (**5**), that is believed to be structurally analogous to its iron and osmium homologues, **1**. However, the reaction of **4** with $W(CO)_5(PMe_2Ph)$ yielded two isomeric products with the formula $WRu_3(CO)_{11}(PMe_2Ph)(\mu_4\text{-}S)_2$ (**6**) and (**7**), whose structures are different from both the iron complex, **2**, and the osmium complex, **3**. Both compounds have been characterized crystallographically. The results of this study are described herein.

EXPERIMENTAL

All reactions were carried out under an atmosphere of nitrogen. Reagent grade solvents were stored over 4 Å molecular sieves. UV irradiations were performed in Pyrex glassware by using an externally positioned high-pressure mercury lamp. All TLC separations were performed in air on plates (Whatman 0.25 mm silica gel, 60 Å, F_{254}). ^1H NMR spectra were recorded on a Brüker AM-300 spectrometer operating at 300 MHz. IR spectra were recorded on a Nicolet 5DXB FT–IR spectrophotometer. Mass spectra were run on a VG Model 70SQ spectrometer by using electron impact ionization. $Ru_3(CO)_9(\mu_3\text{-}S)_2$ (**4**) was prepared by the previously reported procedure.[5]

Reaction of $Ru_3(CO)_9(\mu_3\text{-}S)_2$ (**4**) *with* $W(CO)_6$

A solution of **4** (30 mg, 0.048 mmol) and $W(CO)_6$ (85 mg, 2.42 mmol) in hexane (40 cm^3) was irradiated (UV) under a purge with nitrogen at 25°C for 30 min. The colour of the solution changed from yellow to dark red and some black precipitate formed. Most of the solvent was removed *in vacuo*; the remainder was decanted. The precipitate was washed five times with hexane (5 cm^3 portions), and the final residue was redissolved in 10 cm^3 of CH_2Cl_2 to give a red–brown solution that was filtered and crystallized to yield a dark brown powder of $Ru_3(CO)_9(\mu_3\text{-}S)(\mu_4\text{-}S)[W(CO)_5]$ (**5**), 13.2 mg (29%). IR[ν(CO) in CH_2Cl_2]: 2072(vs), 2067(sh), 2028(m), 1937(s) cm^{-1}.

Reaction of **4** *with* $W(CO)_5(PMe_2Ph)$

A solution of **4** (95 mg, 0.15 mmol) and $W(CO)_5(PMe_2Ph)$ (150 mg, 0.32 mmol) in 120 cm^3 of hexane was irradiated in the presence of a continuous purge of nitrogen for 30 min. The solvent was removed *in vacuo* and the residue was chromatographed on Florisil in a column. Two bands were collected. The first (yellow) was eluted with hexane–CH_2Cl_2, 9 : 1 and the second (brown) was eluted with hexane–CH_2Cl_2, 7 : 3. These bands were subsequently purified further by TLC. The first band yielded only unreacted **4**, 10.2 mg, and unreacted $W(CO)_5(PMe_2Ph)$, 40.5 mg. The second band yielded yellow $Ru_3(CO)_8(PMe_2Ph)(\mu_3\text{-}S)_2$, 4.5 mg (4%), $WRu_3(CO)_{11}(PMe_2Ph)(\mu_4\text{-}S)_2$ (**6**), 24.2 mg (16%), and its isomer **7**, 10.5 mg (7%). IR[ν(CO) in hexane] for **6**: 2074(m), 2041(vs), 2027(vs), 2010(s), 1997(m), 1971(m), 1935(w), 1885(w) 1859(w) cm^{-1}; for **7**: 2072(w), 2041(vs), 2027(m), 2014(s), 1998(m), 1971(w), 1934(m), 1874(w), 1864(w), 1831(w) cm^{-1}. ^1H NMR (δ in $CDCl_3$) for **6**: 7.47 (m, 5H), 2.24 (d, 6H, J_{P-H} = 9.6 Hz); for **7**: 7.42 (m, 5H), 1.80 (d, 6H, J_{P-H} = 10.5 Hz). Found: C, 22.8; H, 1.0. Calc. for **6**: C, 22.9; H, 1.1%. Found: C, 22.9; H, 0.98. Calc. for **7**. C, 22.9, H, 1.1%. $Ru_3(CO)_8(PMe_2Ph)(\mu_3\text{-}S)_2$ was characterized further by an independent synthesis, see below.

Reaction of **6** *with carbon monoxide*

A sample of **6** (20 mg, 0.020 mmol) in 30 cm^3 of hexane was refluxed for 1 h in the presence of a slow, purge of carbon monoxide. The solvent was removed *in vacuo*, and the residue was dissolved in a minimal amount of CH_2Cl_2 and transferred to TLC plates. Elution with a (hexane–CH_2Cl_2, 8 : 2) solvent mixture separated 2.1 mg of **4**, 17%; 22 mg of $W(CO)_5(PMe_2Ph)$, 24%; 2.6 mg of $Ru_3S_2(CO)_8(PMe_2Ph)$, 17%; and 3.4 mg of **7**, 17%.

Preparation of $Ru_3(CO)_8(PMe_2Ph)(\mu_3\text{-}S)_2$

Compound **4** (20 mg, 0.032 mmol) was dissolved in 10 cm^3 of hexane. PMe_2Ph (0.005 cm^3, 0.035 mmol) was added, and the solution was allowed to stir for 25 min at 25°C. The product, $Ru_3(CO)_8(PMe_2Ph)(\mu_3\text{-}S)_2$, was isolated in 72% yield by TLC using a hexane–CH_2Cl_2, 3 : 1, solvent mixture. IR [ν(CO) in hexane]: 2082(m), 2049(vs), 2031(m), 2027(sh), 2015(s), 1981(m) cm^{-1}. ^1H NMR (δ in $CDCl_3$): 7.59 (m, 5H, Ph), 2.28 (d, 6H, Me, J_{P-H} = 10.9 Hz). Mass spectrum [m/z = 731 − x(28), x = 1, 3–8; $M^+ - x$(CO)].

Crystallographic analyses

Crystals of **6** and **7** suitable for diffraction analyses were grown from solutions in hexane–CH_2Cl_2,

Table 1. Crystal data for the structural analyses of compounds **6** and **7**

	6	**7**
Empirical formula	$WRu_3S_2PO_{11}C_{19}H_{11}$	$WRu_3PS_2O_{11}C_{19}H_{11}$
Formula weight	997.44	997.44
Crystal system	Orthorhombic	Monoclinic
Lattice parameters	$a = 13.794(2)$ Å	$a = 15.841(2)$ Å
	$b = 16.616(2)$ Å	$b = 8.818(1)$ Å
	$c = 11.780(2)$ Å	$c = 19.236(3)$ Å
		$\beta = 98.04(1)°$
	$V = 2700(1)$ Å^3	$V = 2660.5(6)$ Å^3
Space group	$P2_12_12_1$ (No. 19)	$P2_1/n$ (No. 14)
Z value	4	4
D_{calc}	2.45 g cm^{-3}	2.49 g cm^{-3}
$\mu_{(Mo\text{-}K_\alpha)}$	62.14 cm^{-1}	63.06 cm^{-1}
Temperature	23°C	23°C
$2\theta_{max}$	48.0°	46.0°
Number of observations [$I > 3\ (I)$]	1960	2880
Number of variables	334	334
Residuals: R; R_w	0.027; 0.027	0.024; 0.025
Goodness-of-fit indicator	1.23	1.20
Maximum shift in final cycle	0.20	0.03
Largest peak in final difference map	0.58 (e$^-$/Å^3)	0.50 (e$^-$/Å^3)

1:9, solvent mixtures at 10°C. The data were collected on crystals mounted in thin-walled glass capillaries. Diffraction measurements were made on a Rigaku AFC6S automatic diffractometer by using graphite-monochromatized Mo-K_α radiation. The unit cells were determined from 15 randomly selected reflections obtained by using the AFC6 automatic search, centre, index and least-squares routines. Crystal data, data collection parameters and results of the analyses are listed in Table 1. All intensity measurements were made by using the standard ω-scan (moving crystal-stationary counter) technique. Background measurements were made by 1/4 additional scan at each end of the scan. All data processing was performed on a Digital Equipment Corp. MICROVAX II computer by using the TEXSAN structure solving program library (Version 2.0) obtained from the Molecular Structure Corp., The Woodlands, Texas. Neutral atom scattering factors were calculated by the standard procedures.[7a] Anomalous dispersion corrections were applied to all non-hydrogen atoms.[7b] Full-matrix least-squares refinements minimized the function: $\Sigma w(|F_{obs}| - |F_{calc}|)^2$, where $w = 1/\sigma(F)^2$, $\sigma(F) = \sigma(F_{obs}^2)/2F_{obs}$ and $\sigma(F_{obs}^2) = [\sigma(I_{raw})^2 + (0.02(F_{obs})^2)^2]^{1/2}/Lp$. Compound **6** crystallized in the orthorhombic crystal system. The space group $P2_12_12_1$ was established on the basis of the systematic absences observed during the collection of data. Compound **7** crystallized in the monoclinic crystal system. The space group $P2_1/n$ was established on the basis of the systematic absences observed during the collection of the data. Both structures were solved by a combination of direct methods (MITHRIL) and difference Fourier techniques. All non-hydrogen atoms were refined by using anisotropic thermal parameters. Hydrogen atom positions were calculated by assuming idealized geometries. Their scattering contributions were added to the structure factor calculations, but they were not refined. In the final stages of refinement of the structure of **6**, a test for enantiomorph was made by inverting the coordinates of all the atoms and refining again. This led to a significant improvement in the R-factor (0.038 vs 0.027). Thus, the second enantiomorph was deemed to be correct and is the one reported here.*

* Complete tables of bond angles, atomic coordinates, thermal parameters and observed and calculated structure factors have been deposited as supplementary material with the Editor, from whom copies are available upon request. Atomic coordinates have also been deposited with the Cambridge Crystallographic Data Centre.

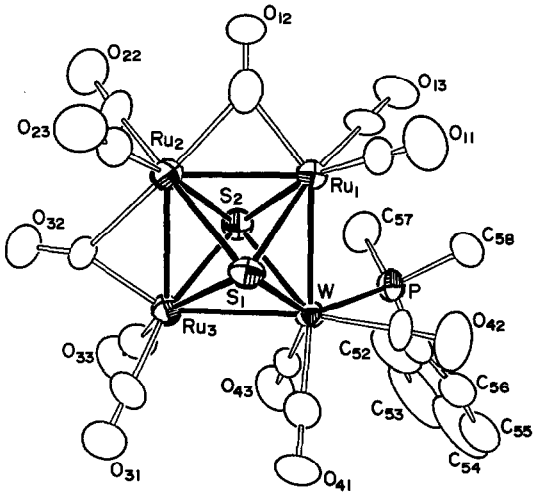

Fig. 1. An ORTEP drawing of **6** showing 50% probability thermal ellipsoids.

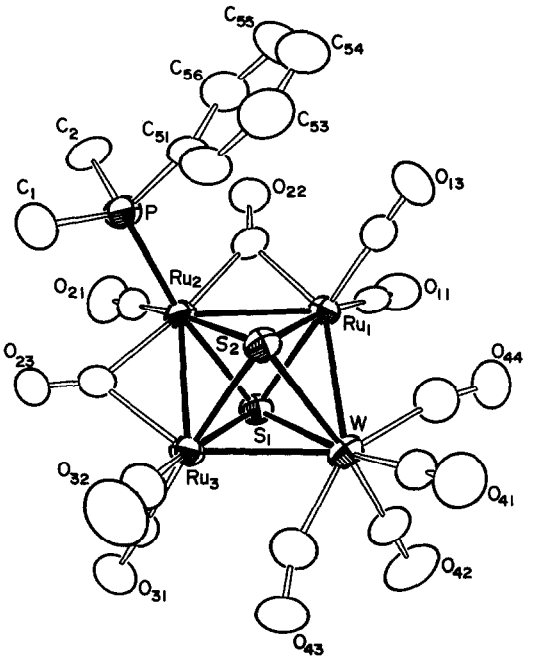

Fig. 2. An ORTEP drawing of **7** (an isomer of **6**) showing 50% probability thermal ellipsoids.

RESULTS AND DISCUSSION

From the reaction of **4** with $W(CO)_6$ in the presence of UV irradiation, the product **5** has been obtained in 29% yield. The IR spectrum of **5** is remarkably similar to those of its iron and osmium homologues. Thus, it is believed to possess an analogous structure. The osmium homologue has been characterized crystallographically.[2]

From the reaction of **4** with $W(CO)_5(PMe_2Ph)$ in the presence of UV irradiation we have isolated two new tungsten–ruthenium carbonyl complexes **6**, 16% and **7**, 7%, which have the same molecular formula, $WRu_3(CO)_{11}(PMe_2Ph)(\mu_4\text{-}S)_2$, and a small amount of the PMe_2Ph-substituted derivative of **4**, 4%. Compounds **6** and **7** are structural isomers and both have been characterized crystallographically.

ORTEP drawings of the structures of **6** and **7** are shown in Figs 1 and 2, respectively. Selected interatomic bond distances are listed in Tables 2 and 3, and selected interatomic angles are listed in Tables 4 and 5, respectively. Both molecules contain square arrangements of four metal atoms with quadruply-bridging sulphido ligands on opposite

Table 2. Intramolecular distances for **6**

W—C(41)	1.97(2)	Ru(2)—C(12)	2.17(2)
W—C(43)	2.00(1)	Ru(2)—C(32)	2.26(2)
W—C(42)	2.02(2)	Ru(2)—S(1)	2.536(3)
W—S(1)	2.497(3)	Ru(2)—S(2)	2.555(3)
W—S(2)	2.522(3)	Ru(2)—Ru(3)	2.749(2)
W—P(1)	2.524(5)	Ru(3)—C(33)	1.86(2)
W—Ru(3)	2.857(2)	Ru(3)—C(31)	1.91(2)
W—Ru(1)	2.884(2)	Ru(3)—C(32)	1.98(2)
Ru(1)—C(11)	1.83(2)	Ru(3)—S(1)	2.462(4)
Ru(1)—C(13)	1.87(2)	Ru(3)—S(2)	2.491(5)
Ru(1)—C(12)	2.05(2)	P(1)—C(57)	1.80(1)
Ru(1)—S(1)	2.461(4)	P(1)—C(58)	1.82(1)
Ru(1)—S(2)	2.487(5)	P(1)—C(51)	1.83(1)
Ru(1)—Ru(2)	2.747(2)	O—C(av.)	1.15(2)
Ru(2)—C(22)	1.85(1)	C—C(av.)	1.38(3)
Ru(2)—C(23)	1.87(1)		

Distances are in angstroms. Estimated standard deviations in the least significant figure are given in parentheses.

sides of the square plane. Similarly arranged $Ru_4(\mu_4\text{-}S)_2$ clusters were observed in the compounds $Ru_4(CO)_9(PMe_2Ph)_2(\mu_4\text{-}S)_2$ (**8**)[5] and $Ru_4(CO)_{10}[C(Ph)NMe_2](\mu_4\text{-}S)_2$ (**9**).[6] The principal difference between **6** and **7** is the location of the PMe_2Ph ligand. In **6** it is bonded to the tungsten atom, while in **7** it is bonded to the ruthenium atom opposite the tungsten atom, Ru(2). Both Ru—Ru bonds in **6** and **7** contain bridging carbonyl ligands. A similar arrangement was found in **8** and **9** and the Ru—Ru distances in all four molecules are very similar. The eight atoms bonded to the tungsten atom in **6** are arranged in a square antiprismatic coordination geometry. The three carbonyl ligands bonded to the tungsten atom are linear, and the Ru—W distances, 2.884(2) and 2.857(2) Å, are significantly longer than the Ru—Ru distances, 2.747(2) and 2.749(2) Å. In contrast, the eight atoms bonded to the tungsten atom in **7** are arranged in a square prismatic coordination geometry and two of the four carbonyl ligands have adopted semibridging coordinations along the Ru—W bonds, W—C(43)—O(43) = 162.1(8)° and W—C(44)—O(44) = 166.7(8)°. The Ru—W distances in **7** are similar to those in **6**, 2.8605(8) and 2.8347(7) Å. The Ru—S distances in **6**, **7**, **8** and **9** are very similar. Curiously, the W—S distances in **7** are significantly longer than those in **6**, 2.588(2) and 2.596(2) Å vs 2.522(3) and 2.524(5) Å. This may be related to the different coordination geometries about the tungsten atom in the two complexes. In **7**, a carbonyl ligand is positioned nearly opposite to each W—S bond. A structural *trans*-influence could thus be responsible for the comparative weakening of the W—S bonds in **7**.[8] In **6**, the carbonyl ligands are not positioned directly opposite to the M—S bonds.

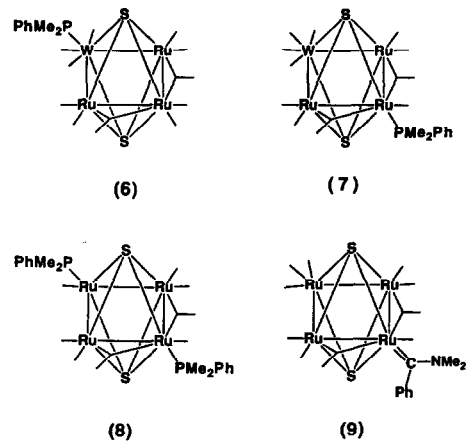

Compounds **6** and **7** contain 62 valence electrons. This is two electrons less than the number required by the 18-electron rule for a cluster with four M—M bonds. It is, however, in accord with the requirements of the Skeletal Electron Pair theory.[9] Interestingly, structure **2**, exhibited by the iron homologue of **6**, has five M—M bonds, and each of the metal atoms in **2** obeys the 18-electron rule. The reason why **2** adopts the electron precise structure and **6** and **7** the "unsaturated" structure is not obvious to us at this time. The reaction of $Os_3(CO)_9(\mu_3\text{-}S)_2$ with $W(CO)_5(PMe_2Ph)$ yielded compound **3**, *vide supra*. Compound **3** has one more carbonyl ligand than **2**, **6** and **7** and adopts yet another "butterfly" tetrahedral structure which is believed to adhere to the Skeletal Electron Pair theory. The

Table 3. Intramolecular distances for **7**

W—C(42)	1.964(8)	Ru(2)—C(22)	2.108(8)
W—C(41)	1.980(8)	Ru(2)—P(1)	2.335(2)
W—C(43)	2.031(9)	Ru(2)—S(2)	2.505(2)
W—C(44)	2.05(1)	Ru(2)—S(1)	2.521(2)
W—S(1)	2.588(2)	Ru(2)—Ru(3)	2.7364(9)
W—S(2)	2.596(2)	Ru(3)—C(32)	1.898(8)
W—Ru(3)	2.8347(7)	Ru(3)—C(31)	1.912(9)
W—Ru(1)	2.8605(8)	Ru(3)—C(23)	2.101(8)
Ru(1)—C(13)	1.887(9)	Ru(3)—S(2)	2.444(2)
Ru(1)—C(11)	1.892(8)	Ru(3)—S(1)	2.465(2)
Ru(1)—C(22)	2.073(8)	P(1)—C(2)	1.800(8)
Ru(1)—S(2)	2.443(2)	P(1)—C(1)	1.809(8)
Ru(1)—S(1)	2.462(2)	P(1)—C(51)	1.815(7)
Ru(1)—Ru(2)	2.7290(9)	O—C(av.)	1.142(9)
Ru(2)—C(21)	1.884(8)	C—C(av.)	1.38(1)
Ru(2)—C(23)	2.076(8)		

Distances are in angstroms. Estimated standard deviations in the least significant figure are given in parentheses.

Table 4. Intramolecular bond angles for **6**

C(41)—W—S(1)	90.1(6)	C(11)—Ru(1)—S(2)	167.0(6)
C(41)—W—S(2)	138.7(6)	C(11)—Ru(1)—Ru(2)	124.2(6)
C(41)—W—P(1)	120.3(6)	C(11)—Ru(1)—W	111.9(6)
C(41)—W—Ru(3)	85.0(6)	C(13)—Ru(1)—S(1)	168.7(6)
C(41)—W—Ru(1)	140.3(6)	C(13)—Ru(1)—S(2)	100.3(5)
C(43)—W—S(1)	136.5(4)	C(13)—Ru(1)—Ru(2)	129.1(6)
C(43)—W—S(2)	90.1(5)	C(13)—Ru(1)—W	113.9(5)
C(43)—W—P(1)	75.4(4)	C(12)—Ru(1)—S(1)	99.6(5)
C(43)—W—Ru(3)	83.4(4)	C(12)—Ru(1)—S(2)	94.5(6)
C(43)—W—Ru(1)	141.7(4)	C(12)—Ru(1)—Ru(2)	51.1(5)
C(42)—W—S(1)	91.3(6)	C(12)—Ru(1)—W	142.5(5)
C(42)—W—S(2)	139.8(6)	S(1)—Ru(1)—S(2)	75.8(1)
C(42)—W—P(1)	77.8(5)	S(1)—Ru(1)—Ru(2)	57.96(8)
C(42)—W—Ru(3)	141.2(5)	S(1)—Ru(1)—W	55.02(7)
C(42)—W—Ru(1)	86.8(6)	S(2)—Ru(1)—Ru(2)	58.18(8)
S(1)—W—S(2)	74.48(8)	S(2)—Ru(1)—W	55.42(7)
S(1)—W—P(1)	143.5(1)	Ru(2)—Ru(1)—W	91.66(5)
S(1)—W—Ru(3)	54.3(1)	C(22)—Ru(2)—S(1)	174.4(4)
S(1)—W—Ru(1)	53.8(1)	C(22)—Ru(2)—S(2)	101.1(4)
S(2)—W—P(1)	91.5(1)	C(22)—Ru(2)—Ru(1)	122.1(7)
S(2)—W—Ru(3)	54.7(1)	C(22)—Ru(2)—Ru(3)	121.3(7)
S(2)—W—Ru(1)	54.3(1)	C(23)—Ru(2)—S(1)	95.6(3)
P(1)—W—Ru(3)	140.2(1)	C(23)—Ru(2)—S(2)	168.8(3)
P(1)—W—Ru(1)	90.4(1)	C(23)—Ru(2)—Ru(1)	119.0(6)
Ru(3)—W—Ru(1)	85.66(3)	C(23)—Ru(2)—Ru(3)	117.0(6)
C(11)—Ru(1)—S(1)	94.8(6)	C(12)—Ru(2)—S(1)	94.4(6)
C(12)—Ru(2)—S(2)	90.0(6)	S(1)—Ru(3)—Ru(2)	57.92(8)
C(12)—Ru(2)—Ru(1)	47.6(6)	S(1)—Ru(3)—W	55.41(7)
C(12)—Ru(2)—Ru(3)	137.9(6)	S(2)—Ru(3)—Ru(2)	58.11(8)
C(32)—Ru(2)—S(1)	91.4(5)	S(2)—Ru(3)—W	55.78(7)
C(32)—Ru(2)—S(2)	89.3(5)	Ru(2)—Ru(3)—W	92.21(5)
C(32)—Ru(2)—Ru(1)	135.6(5)	Ru(1)—S(1)—Ru(3)	104.9(1)
C(32)—Ru(2)—Ru(3)	45.2(5)	Ru(1)—S(1)—W	71.1(1)
S(1)—Ru(2)—S(2)	73.27(8)	Ru(1)—S(1)—Ru(2)	66.7(1)
S(1)—Ru(2)—Ru(1)	55.3(1)	Ru(3)—S(1)—W	70.3(1)
S(1)—Ru(2)—Ru(3)	55.4(1)	Ru(3)—S(1)—Ru(2)	66.7(1)
S(2)—Ru(2)—Ru(1)	55.8(1)	W—S(1)—Ru(2)	106.8(1)
S(2)—Ru(2)—Ru(3)	55.9(1)	Ru(1)—S(2)—Ru(3)	103.3(1)
Ru(1)—Ru(2)—Ru(3)	90.47(4)	Ru(1)—S(2)—W	70.3(1)
C(33)—Ru(3)—S(1)	162.4(6)	Ru(1)—S(2)—Ru(2)	66.0(1)
C(33)—Ru(3)—S(2)	96.3(5)	Ru(3)—S(2)—W	69.5(1)
C(33)—Ru(3)—Ru(2)	131.0(6)	Ru(3)—S(2)—Ru(2)	66.0(1)
C(33)—Ru(3)—W	107.1(6)	W—S(2)—Ru(2)	105.5(1)
C(31)—Ru(3)—S(1)	95.2(5)	C(57)—P(1)—W	113.3(6)
C(31)—Ru(3)—S(2)	166.0(6)	C(58)—P(1)—W	117.6(5)
C(31)—Ru(3)—Ru(2)	125.9(7)	O(12)—C(12)—Ru(1)	142(2)
C(31)—Ru(3)—W	110.4(6)	O(12)—C(12)—Ru(2)	137(2)
C(32)—Ru(3)—S(1)	100.9(5)	Ru(1)—C(12)—Ru(2)	81.2(8)
C(32)—Ru(3)—S(2)	98.1(5)	O(32)—C(32)—Ru(3)	147(1)
C(32)—Ru(3)—Ru(2)	54.3(5)	O(32)—C(32)—Ru(2)	131(1)
C(32)—Ru(3)—W	146.4(5)	Ru(3)—C(32)—Ru(2)	80.5(6)
S(1)—Ru(3)—S(2)	75.7(1)	O—C—M(av.)	178(2)

Angles are in degrees. Estimated standard deviations in the least significant figure are given in parentheses.

Table 5. Intramolecular bond angles for **7**

C(42)—W—S(1)	96.6(2)	C(11)—Ru(1)—S(1)	98.5(2)
C(42)—W—S(2)	169.3(2)	C(11)—Ru(1)—Ru(2)	127.1(2)
C(42)—W—Ru(3)	118.7(2)	C(11)—Ru(1)—W	113.4(2)
C(42)—W—Ru(1)	122.9(2)	C(22)—Ru(1)—S(2)	97.0(2)
C(41)—W—S(1)	166.2(2)	C(22)—Ru(1)—S(1)	92.9(2)
C(41)—W—S(2)	93.3(2)	C(22)—Ru(1)—Ru(2)	49.8(2)
C(41)—W—Ru(3)	118.8(2)	C(22)—Ru(1)—W	143.0(2)
C(41)—W—Ru(1)	117.3(2)	S(2)—Ru(1)—Ru(2)	57.63(5)
C(43)—W—S(1)	101.7(2)	S(2)—Ru(1)—W	57.98(4)
C(43)—W—S(2)	100.4(2)	S(1)—Ru(1)—Ru(2)	57.84(5)
C(43)—W—Ru(3)	61.4(2)	S(1)—Ru(1)—W	57.60(4)
C(43)—W—Ru(1)	145.5(2)	Ru(2)—Ru(1)—W	93.39(2)
C(44)—W—S(1)	100.0(2)	C(21)—Ru(2)—P(1)	93.0(2)
C(44)—W—S(2)	105.3(3)	C(21)—Ru(2)—S(2)	172.6(2)
C(44)—W—Ru(3)	148.0(2)	C(21)—Ru(2)—S(1)	97.0(2)
C(44)—W—Ru(1)	64.1(2)	C(21)—Ru(2)—Ru(1)	121.2(2)
S(1)—W—Ru(3)	53.85(4)	C(21)—Ru(2)—Ru(3)	119.8(2)
S(1)—W—Ru(1)	53.44(4)	C(23)—Ru(2)—P(1)	90.4(2)
S(2)—W—Ru(3)	53.28(4)	C(23)—Ru(2)—S(2)	91.0(2)
S(2)—W—Ru(1)	52.93(4)	C(23)—Ru(2)—S(1)	94.8(2)
Ru(3)—W—Ru(1)	84.18(2)	C(23)—Ru(2)—Ru(1)	137.9(2)
C(13)—Ru(1)—S(2)	93.1(2)	C(23)—Ru(2)—Ru(3)	49.5(2)
C(13)—Ru(1)—S(1)	170.6(2)	C(22)—Ru(2)—P(1)	85.1(2)
C(13)—Ru(1)—Ru(2)	119.3(2)	C(22)—Ru(2)—S(2)	94.2(2)
C(13)—Ru(1)—W	115.4(2)	C(22)—Ru(2)—S(1)	90.4(2)
C(11)—Ru(1)—S(2)	171.3(2)	C(22)—Ru(2)—Ru(1)	48.7(2)
C(22)—Ru(2)—Ru(3)	137.2(2)	Ru(2)—Ru(3)—W	93.81(2)
P(1)—Ru(2)—S(2)	94.37(7)	Ru(1)—S(1)—Ru(3)	101.58(6)
P(1)—Ru(2)—S(1)	168.77(7)	Ru(1)—S(1)—Ru(2)	66.40(5)
P(1)—Ru(2)—Ru(1)	114.35(6)	Ru(1)—S(1)—W	68.96(5)
P(1)—Ru(2)—Ru(3)	122.65(5)	Ru(3)—S(1)—Ru(2)	66.55(5)
S(2)—Ru(2)—Ru(1)	55.45(5)	Ru(3)—S(1)—W	68.20(5)
S(2)—Ru(2)—Ru(3)	55.38(5)	Ru(2)—S(1)—W	105.57(6)
S(1)—Ru(2)—Ru(1)	55.75(4)	Ru(1)—S(2)—Ru(3)	102.72(6)
S(1)—Ru(2)—Ru(3)	55.74(4)	Ru(1)—S(2)—Ru(2)	66.92(5)
Ru(1)—Ru(2)—Ru(3)	88.61(2)	Ru(1)—S(2)—W	69.10(5)
C(32)—Ru(3)—S(2)	93.8(3)	Ru(3)—S(2)—Ru(2)	67.11(5)
C(32)—Ru(3)—S(1)	168.9(3)	Ru(3)—S(2)—W	68.37(4)
C(32)—Ru(3)—Ru(2)	123.7(2)	Ru(2)—S(2)—W	105.78(6)
C(32)—Ru(3)—W	111.4(3)	C(2)—P(1)—Ru(2)	115.0(3)
C(31)—Ru(3)—S(2)	173.9(2)	C(1)—P(1)—Ru(2)	116.7(3)
C(31)—Ru(3)—S(1)	97.2(2)	C(51)—P(1)—Ru(2)	112.0(2)
C(31)—Ru(3)—Ru(2)	122.7(2)	O(22)—C(22)—Ru(1)	137.6(6)
C(31)—Ru(3)—W	116.0(2)	O(22)—C(22)—Ru(2)	140.8(6)
C(23)—Ru(3)—S(2)	92.1(2)	Ru(1)—C(22)—Ru(2)	81.5(3)
C(23)—Ru(3)—S(1)	95.8(2)	O(23)—C(23)—Ru(2)	142.1(6)
C(23)—Ru(3)—Ru(2)	48.7(2)	O(23)—C(23)—Ru(3)	136.0(6)
C(23)—Ru(3)—W	142.3(2)	Ru(2)—C(23)—Ru(3)	81.9(3)
S(2)—Ru(3)—Ru(2)	57.51(5)	O(43)—C(43)—W	162.1(8)
S(2)—Ru(3)—W	58.35(4)	O(44)—C(44)—W	166.7(8)
S(1)—Ru(3)—Ru(2)	57.70(4)	O—C—M(av.)	178.0(8)
S(1)—Ru(3)—W	57.95(4)		

Angles are in degrees. Estimated standard deviations in the least significant figure are given in parentheses.

most important difference between compound **5** and the phosphine-containing complexes **6** and **7** is the existence of W—Ru bonds in the latter. This was also the most important distinction between the iron compounds, **1** and **2**, and the osmium compounds, **1** and **3**. We believe that this is directly attributable to the presence of the phosphine ligand. Since M—M bond formation occurred both in **6** and **7**, it indicates that the location of the phosphine ligand in the complex is not of major importance to the stability of the cluster. Comparison of the M—M bonds lengths of a few carbonyl cluster complexes and their phosphine-substituted derivatives has shown that they are shorter and presumably stronger in the derivatives.[10] It seems likely that this is related to increases in electron density on the metal atoms caused by the more strongly electron-donating phosphine ligand.

Under an atmosphere of carbon monoxide in refluxing hexane solvent, compound **6** is partially isomerized to **7**, but there is also considerable cluster degradation to yield **4**, $W(CO)_5(PMe_2Ph)$ and some $Ru_3(CO)_8(PMe_2Ph)(\mu_3\text{-}S)_2$. The transformation of **6** to **7** almost certainly involves a dissociation of the PMe_2Ph ligand from the tungsten atom, a rearrangement of the carbonyl ligands and a readdition of a PMe_2Ph ligand at the ruthenium atom, as found in **7**.

Acknowledgement—These studies were supported by the National Science Foundation under Grant CHE-8919786.

REFERENCES

1. R. D. Adams, J. E. Babin, J. G. Wang and W. Wu, *Inorg. Chem.* 1989, **28**, 703.
2. R. D. Adams, I. T. Horvath and S. Wang, *Inorg. Chem.* 1985, **24**, 1728.
3. R. D. Adams, I. T. Horvath and P. Mathur, *J. Am. Chem. Soc.* 1984, **106**, 6296.
4. R. D. Adams and M. Tasi, *J. Cluster Sci.*, in press.
5. R. D. Adams, J. E. Babin and M. Tasi, *Inorg. Chem.* 1986, **25**, 4515.
6. R. D. Adams, J. E. Babin and J. G. Wang, *Polyhedron* 1989, **8**, 2351.
7. *International Tables for X-ray Crystallography*, Vol. IV. Kynoch Press, Birmingham (1975): (a) Table 2.2B, pp. 99–101; (b) Table 2.3.1, pp. 149–150.
8. T. G. Appleton, H. C. Clark and L. E. Manzer, *Coord. Chem. Rev.* 1973, **10**, 335.
9. D. M. P. Mingos, *Accts Chem. Res.* 1984, **17**, 311.
10. R. D. Adams, J. E. Babin, P. Mathur, K. Natarajan and J. G. Wang, *Inorg. Chem.* 1989, **28**, 1440.

Polyhedron Vol. 10, No. 4/5, pp. 455–458, 1991
Printed in Great Britain

0277–5387/91 $3.00+.00
© 1991 Pergamon Press plc

COMPLEX COMPOUNDS OF DOXYCYCLINE WITH WO_4^{2-} AND MoO_4^{2-} IONS

M. JELIKIĆ-STANKOV* and D. MALEŠEV

Department of Analytical Chemistry, Faculty of Pharmacy, University of Belgrade, Yugoslavia

and

D. VESELINOVIĆ

Institute of Physical Chemistry, Faculty of Science, University of Belgrade, Yugoslavia

and

Z. RADOVIĆ

Institute of Physical Chemistry, Faculty of Pharmacy, University of Belgrade, Yugoslavia

(*Received* 28 *September* 1990; *accepted* 24 *October* 1990)

Abstract—By using the pH-metric method it has been found that antibiotic doxycycline (H_3DTC) reacts with tungstate and molybdate ions forming 1 : 1 and 2 : 1 (H_3DTC–WO_4^{2-} or H_3DTC–MoO_4^{2-}) complex compounds. The relative stability constants of these complexes were calculated from pH-metric measurements using Job's method.

Doxycycline is a tetracycline derivative which shows a very pronounced tendency to form complexes with different metal ions. Investigations on the complexes of tetracycline antibiotics are important since they demonstrate that attention should be paid to possible complexation reactions during parallel therapy with drugs such as antacide or iron preparations.

From the analytical standpoint many coloured tetracycline complexes have been applied to the assay of tetracycline antibiotics in different pharmaceutical preparations by spectrophotometric methods.

On the basis of our reported results[1] on the complexation reactions of tetracycline with WO_4^{2-} and MoO_4^{2-} ions, methods for the determination of tetracycline antibiotics in pharmaceutical preparations were proposed.[2–4]

The results of our investigations presented in this paper comprise the determination of the compositions and the stability constants of H_3DTC–WO_4^{2-} and H_3DTC–MoO_4^{2-} complexes. The data available in the literature refer to colour-forming reactions of tetracycline antibiotics with WO_4^{2-} and MoO_4^{2-} ions at elevated temperatures and under drastic conditions using Na_2CO_3 and H_2O_2, whereby degradations of the tetracycline molecule are possible.

EXPERIMENTAL

A Iskra Model MA 5705 pH-meter and VEB Prüfgeräte thermostat, precision ±0.02°C, were used. The pH-meter was calibrated using Radiometer buffer solutions, pH = 7.02 and pH = 4.00 at 20°C.

The reagents used were H_3DTC HCl standard (Sigma), $Na_2MoO_4 \cdot 2H_2O$ (Merck) and $Na_2WO_4 \cdot 2H_2O$ (Reanal), which were all of analytical grade. Solutions of H_3DTC were prepared by dissolving appropriate amounts of the H_3DTC standard in water, whereas solutions of Na_2MoO_4 and Na_2WO_4 were standardized gravimetrically.[5] For

* Author to whom correspondence should be addressed.

the preparation of solutions, fresh doubly-distilled water was used.

RESULTS AND DISCUSSION

Complexation equilibria in the WO_4^{2-}–H_3DTC *and* MoO_4^{2-} *systems*

The composition of complexes formed between H_3DTC and WO_4^{2-} and MoO_4^{2-} ions was determined by application of Job's method,[6,7] using the results of pH-metric measurements in a series of solutions:

(a) x cm^3 of H_3DTC and x cm^3 of Na_2WO_4 or Na_2MoO_4;

(b) x cm^3 of H_3DTC and $(10-x)$ cm^3 of water; and

(c) x cm^3 of Na_2WO_4 or Na_2MoO_4 and x cm^3 of water.

The concentrations of all solutions were 5×10^{-4} M. The pH measurements were performed after thermostatting for 10 min. It was evident that the pH of the mixed solution [H_3DTC and $Na_2WO_4^{2-}$ or Na_2MoO_4 solution (a)] was higher than that of the H_3DTC solution [solution (b)]. The decrease of H^+ ion concentration, due to complex formation, takes place according to the following possible reactions:

$$2H_3DTC+Na_2WO_4 \rightleftharpoons Na_2[WO_3(H_2DTC)_2]+H_2O \quad (1)$$

$$2H_3DTC+Na_2MoO_4 \rightleftharpoons Na_2[MoO_3(H_2DTC)_2]+H_2O \quad (2)$$

$$H_3DTC+Na_2WO_4 \rightleftharpoons Na_2[WO_3HDTC]+H_2O \quad (3)$$

$$H_3DTC+Na_2MoO_4 \rightleftharpoons Na_2[MoO_3HDTC]+H_2O. \quad (4)$$

In the case when no complexation according to reactions (1)–(4) occurs, the concentration of H^+ ions in the mixed solutions of Na_2WO_4 or Na_2MoO_4 and H_3DTC would be equivalent to the sum of H^+ ion concentrations in each separate solution [solution (b) and solution (c)]. The decrease of H^+ ions concentration was calculated using the equation:

$$[H^+] = [H^+]_a - \{[H^+]_b + [H^+]_c\}, \quad (5)$$

where $[H^+]_a$ denotes H^+ ions concentrations in solution (a), and $[H^+]_b$ and $[H^+]_c$ the concentrations in solutions (b) and (c), respectively. The results of pH measurements are given in Table 1.

The dependence of $\Delta[H^+]$ on the molar fraction, n, of WO_4^{2-} or MoO_4^{2-} [n = (mol of metal salt)/(mol of metal salt + mol of H_3DTC)] is shown in Figs 1 and 2. In the calculation of $[H^+]$ from the pH value, the activity factor of the H^+ ion was taken to be equal to unity. The curve obtained had maxima at molar fractions of $n = 0.5$ and $n = 0.33$, indicating the formation of WO_4^{2-} or MoO_4^{2-} complexes of 1 : 1 and 2 : 1 molar compositions.

Data in the literature indicate the possibility of colloidal tungstic acid formation[8] under the influence of H^+ ions, according to the reaction:

$$Na_2WO_4+2H^+ \rightleftharpoons H_2WO_4+2Na^+,$$

which would lead to an increase in the pH of the solution. Due to the presence of H^+ ions, polymerization of WO_4^{2-} or MoO_4^{2-} into polyanions may also take place according to the reaction:

$$6WO_4^{2-}+7HA \rightleftharpoons [HW_6O_{21}]^{5-}+7A^-+3H_2O,$$

which would also be followed by an increase in the

Table 1. pH values of solution mixtures of 5×10^{-4} M Na_2MoO_4 and H_3DTC

Na_2WO_4 or Na_2MoO_4 (cm^3)	Na_2WO_4[1] or Na_2MoO_4[2] + H_2O		Na_2WO_4[1] or Na_2MoO_4[2] + H_3DTC		H_3DTC[1], H_3DTC[2] + H_2O	
	pH[1]	pH[2]	pH[1]	pH[2]	pH[1]	pH[2]
1.00	5.58	5.94	3.47	3.63	3.42	3.41
2.00	5.60	5.88	3.74	3.81	3.40	3.40
3.35	5.61	5.81	4.00	4.26	3.50	3.50
3.50	5.64	5.95	4.14	4.33	3.52	3.51
4.50	5.69	5.96	4.58	4.53	3.59	3.57
5.00	5.70	5.76	4.98	4.72	3.70	3.70
6.00	5.76	5.73	5.23	4.87	3.74	3.72
8.00	5.80	5.73	5.65	5.12	4.09	4.08

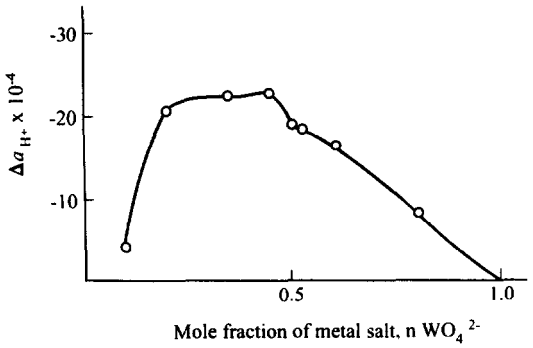

Fig. 1. Job's curve obtained by pH-metric measurements: $c_{H_3DTC} = 5 \times 10^{-4}$ M; $c_{NA_2WO_4} = 5 \times 10^{-4}$ M.

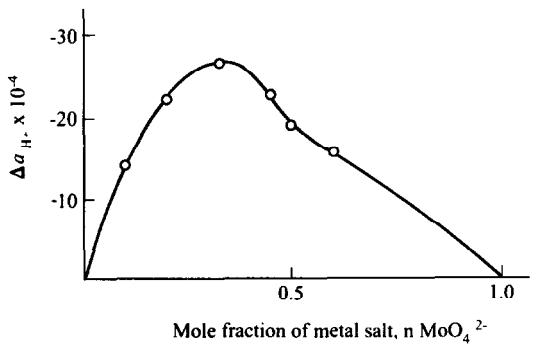

Fig. 2. Job's curve obtained by pH-metric measurements: $c_{H_3DTC} = 5 \times 10^{-4}$ M; $c_{NA_2MoO_4} = 5 \times 10^{-4}$ M.

pH of the solution.[9] However, the products of these reactions are colourless, whereas complexes formed between H_3DTC and WO_4^{2-} or MoO_4^{2-} ions are coloured.[10,11]

On the basis of the aforementioned data it may be concluded that the increase of the pH of the solution is due to the complexation reactions, not to colloidal acid formation.

Calculation of stability constants

The realtive stability constants of WO_3HDTC^{2-} and MoO_3HDTC complexes were calculated on the basis of pH-metric measurements, using the following equations:

$$[H_3DTC]^0 = [H_3DTC] + [H_2DTC^-] + [HDTC^{2-}] + [WO_3HDTC^{2-}] \quad (6)$$

$$[WO_4^{2-}]^0 = [WO_4^{2-}] + [WO_3HDTC^{2-}] \quad (7)$$

$$[H^+] = [H_2TC^-] + 2[HDTC^{2-}] \quad (8)$$

$$Kd_1 = \frac{[H^+][H_2DTC^-]}{[H_3DTC]};$$

$$Kd_2 = \frac{[H^+][HDTC^{2-}]}{[H_2DTC^-]}.$$

The relative stability constants of $WO_3(H_2DTC)_2^{2-}$ and $MoO_3(H_2DTC)_2^{2-}$ were calculated using the equations:

$$[H_3DTC]^0 = [H_3DTC] + [H_2DTC^-] + [HDTC^{2-}] + 2[WO_3(H_2DTC)_2^{2-}] \quad (9)$$

$$[WO_4^{2-}]^0 = [WO_4^{2-}] + [WO_3(H_2DTC)_2^{2-}]$$

$$\times [H^+] = [H_2DTC^-] + [HDTC^{2-}] \quad (10)$$

Kd_1 and Kd_2.

The calculations were carried out with the first and the second dissociation constants,[12] whereas the third dissociation constant was not taken into account, since the third proton dissociation takes place only in strongly basic media. The approximate concentrations of WO_4^{2-} and WO_3HDTC^{2-} were calculated from eqs (6)–(10) assuming that the activity coefficient of H^+ is equal to unity. By using the calculated approximate concentrations of these ions, the ionic strength of the solution and the activity factor were calculated. The correct H^+ ion concentration was calculated from the pH and the activity factor, and was used to calculate the concentrations of $HDTC^{2-}$, WO_4^{2-} and WO_3HDTC^{2-} ions. The relative stability constant of the complex was calculated by replacing the corresponding values into the equation:

$$K = \frac{[WO_3A]}{[WO_4^{2-}][A]}. \quad (11)$$

The results obtained are shown in Table 2.

The complexation reaction between H_3DTC and WO_4^{2-} or MoO_4^{2-} ions firstly involves the transformation of WO_4^{2-} into the oxide, which then reacts further with the ligand:

$$WO_4^{2-} + 2H^+ \rightleftharpoons WO_3 + H_2O \quad (12)$$

$$WO_3 + A \rightleftharpoons WO_3A. \quad (13)$$

Table 2. Stability constants of H_3DTC–WO_4^{2-} and H_3DTC–MoO_4^{2-} complexes

Complex	pH	I	$\log \beta_n$
WO_3HDTC^{2-}	4.98	9.03×10^{-4}	8.39
$WO_3(H_2DTC)_2^{2-}$	4.00	5.45×10^{-4}	8.26
MoO_3HDTC^{2-}	4.72	1.25×10^{-3}	7.99
$MoO_3(H_2DTC)_2^{2-}$	4.26	5.22×10^{-4}	9.21

The stability constant obtained on the basis of reaction (13) can be expressed as:

$$K = \frac{[WO_3A]}{[WO_3][A]}, \quad (14)$$

but it cannot be determined, since the equilibrium constant of reaction (12) is not known.

The stability constant calculated from eq. (11) represents a relative and specific stability constant. No data on the numerical values of the stability constants of doxycycline and WO_4^{2-} or MoO_4^{2-} complexes, determined by the pH-metric method, have so far been reported in the literature.

REFERENCES

1. D. Veselinović and K. Jelikić-Stankov, *Mikrochim. Acta* 1989, **I**, 329.
2. M. Jelikić-Stankov, D. Veselinović, D. Malešev and Z. Radović, *J. Pharm. Biomed. Anal.* 1989, **7**, 1565.
3. M. Jelikić-Stankov and D. Veselinović, *Analyst* 1989, **114**, 719.
4. D. Veselinović and M. Jelikić-Stankov, *Pharmazie* 1987, **42**, 199.
5. A. Vogel, *Quantitative Inorganic Analysis*, 3rd edn. Longmans, London (1961).
6. P. Job, *Annls Chim.* 1928, **9**, 113.
7. J. Inzedy, *Analytical Applications of Complex Equilibria.* Ellis Horwood and John Wiley, New York (1976).
8. G. S. Savčenko, *Him. Red. Elementov.* 1955, **2**, 68.
9. P. J. Bettinger and S. Y. Tyree, *J. Am. Chem. Soc.* 1957, **79**, 3355.
10. M. Jelikić-Stankov and D. Veselinović, *Vesnik Slovenskega Kemiksjega Društva* 1986, **33**, 199.
11. M. Jelikić-Stankov and D. Veselinović, *Pharmazie* 1988, **43**, 49.
12. G. S. Libinson, *Antibiotiki* 1977, **22**, 1093.

Polyhedron Vol. 10, No. 4/5, pp. 459–462, 1991
Printed in Great Britain

0277–5387/91 $3.00+.00
© 1991 Pergamon Press plc

η^3-ALLYL COMPLEXES OF TUNGSTEN—III. THE PREPARATION OF $(\eta^5\text{-}C_5H_5)(\eta^3\text{-}C_3H_5)_2(\eta^1\text{-}C_3H_5)W$ AND RELATED COMPOUNDS

M. C. AZEVEDO,* T. H. BROCK, P. W. JOLLY,† A. RUFIŃSKA and G. SCHROTH

Max-Planck-Institut für Kohlenforschung, D-4330 Mülheim a.d. Ruhr, F.R.G.

(*Received* 28 *September* 1990; *accepted* 24 *October* 1990)

Abstract—$[(\eta^3\text{-}C_3H_5)_3WCl]_2$ reacts with substituted cyclopentadienyl alkali metal derivatives to give $(\eta^5\text{-}RC_5H_4)(\eta^3\text{-}C_3H_5)_2(\eta^1\text{-}C_3H_5)W$ (where R is H, Me or t-C_4H_9). Analogous reactions involving indenyl- or fluorenyllithium produce $(\eta^5\text{-}L)(\eta^3\text{-}C_3H_5)_2W$ species.

Preceding publications in this short series have been concerned with the preparation of $[(\eta^3\text{-}C_3H_5)_3WCl]_2$ and its further reaction with alkylmagnesium halides to give $(\eta^3\text{-}C_3H_5)_3WR$ and $(\eta^3\text{-}C_3H_5)_3W(PR_3)R$ species.[1,2] Here we discuss the reactions with cyclopentadienylsodium and related compounds.

RESULTS AND DISCUSSION

$[(\eta^3\text{-}C_3H_5)_3WCl]_2$, prepared by reacting $(\eta^3\text{-}C_3H_5)_4W$ with HCl,[1] reacts with cyclopentadienylsodium at low temperatures to give a yellow compound (**1**) whose mass spectrum suggests that an exchange of the tungsten-bonded chlorine atom and the cyclopentadienyl group has occurred. The IR and ^{1}H NMR spectra indicate that complexation of an η^5-cyclopentadienyl group to the metal is accompanied by rearrangement of one of the η^3-allyl groups into the η^1-allyl form [eq. (1)]:

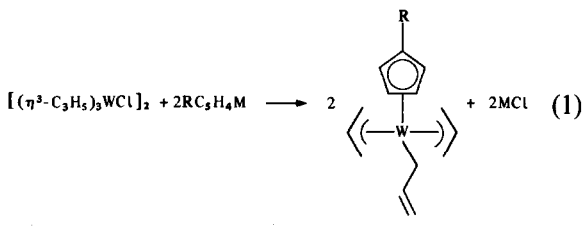

(1)

1 R = H **2** R = Me **3** R = t-C_4H_9

Related compounds (**2**, **3**) have been prepared by reacting methylcyclopentadienyllithium and t-butylcyclopentadienyllithium as well as 5,6-dimethoxyindenyllithium and 3-methyl-1-carbomethoxyindenyllithium, whereby in the last two cases the compounds have not been obtained analytically pure. Reactions with 2-phenyl-isopropylcyclopentadienyllithium and pentamethylcyclopentadienyllithium were unsuccessful. The stability of compounds **1**–**3** decreases with increasing size of the substituent, with **3** decomposing in solution at −20°C.

The structure follows from the IR and NMR spectroscopic data (Table 1). The stretching frequency of the uncomplexed double bond of the η^1-allyl group is assigned to an absorption at *ca* 1600 cm^{-1}. The ^{1}H NMR spectrum of **3** is shown in Fig. 1 : 10 signals are observed for the protons of the two η^3-allyl groups, indicating that they are inequivalent and suggesting that they are twisted with respect to each other about the allyl—W axis. In addition, **3** shows fluxional behaviour involving the η^3-allyl groups but not the η^1-allyl group between −48°C and the decomposition temperature of −20°C, which is possibly the result of an oscillation of the η^3-allyl groups about the metal axis of the type discussed for $(\eta^3\text{-allyl})_4M$ (M = Mo, W).[3]

The behaviour of the tungsten compounds should be contrasted with that of the molybdenum analogues: the final products of the reaction between $[(\eta^3\text{-}C_3H_5)_3MoCl]_2$ and the RC_5H_4Li derivatives are the 17-electron compounds $(\eta^5\text{-}RC_5H_4)(\eta^3\text{-}C_3H_5)_2Mo$. However, spectroscopic evidence suggests that here initially an $(\eta^5\text{-}RC_5H_4)(\eta^3\text{-}C_3H_5)_2(\eta^1\text{-}C_3H_5)Mo$ species is formed and that this reacts further with homolytic cleavage of the Mo—η^1-

*née Dias. Present address: Instituto Superior Técnico, Univ. Técnica de Lisboa, Portugal.

†Author to whom correspondence should be addressed.

Table 1. ^{1}H NMR spectroscopic data of the $(\eta^5\text{-L})(\eta^3\text{-}C_3H_5)_2(\eta^1\text{-}C_3H_5)W$ compounds[a]

	$(\eta^5\text{-}C_5H_5)$ $(\eta^3\text{-}C_3H_5)_2$ $(\eta^1\text{-}C_3H_5)W$ (**1**)[b]		$(\eta^5\text{-t-}C_4H_9C_5H_4)$ $(\eta^3\text{-}C_3H_5)_2$ $(\eta^1\text{-}C_3H_5)W$ (**3**)[c]		$(\eta^5\text{-}MeC_5H_4)$ $(\eta^3\text{-}C_3H_5)_2$ $(\eta^1\text{-}C_3H_5)W$ (**2**)[d]	$(\eta^5\text{-}(MeO)_2$indenyl$)$ $(\eta^3\text{-}C_3H_5)_2$ $(\eta^1\text{-}C_3H_5)W$ (**6**)[d]
	δ [e]H	$J(n,m)$	δ [e]H	$J(n,m)$	δ [e]H[e]	δ [e]H[e]
1	3.80	J(1,2) 8.3	4.71	J(1,2) 8.8	4.41	4.33
2	2.23	J(1,3) 8.6	2.40	J(1,3) 8.3	—	2.37
3	2.12	J(1,4) 12.5	2.36	J(1,4) 12.5	—	—
4	2.63	J(1,5) 11.1	2.28	J(1,5) 11.2	2.42	—
5	0.44	J(2,3) 2.4	0.25	J(2,3) ~2.1	0.30	−0.28
		J(2,4) 2.1		J(2,4) 2.3		
		J(3.5) 3.0		J(3,5) 1.7		
11	3.94	J(11,12) 6.5	3.76	J(11,12) 6.5	3.46	3.43
12	1.37	J(11,13) 6.5	2.02	J(11,13) 6.4	—	—
13	1.56	J(11,14) 8.8	0.96	J(11,14) 8.9	0.91	—
14	2.44	J(11,15) 8.0	2.58	J(11,15) 8.0	2.35	2.65
15	0.23	J(12,13) 4.1	−0.17	J(12,13) 4.0	−0.15	−0.06
				J(12,14) 0		
				J(13,15) 0		
21	5.78	J(21,22) 9.8	5.68	J(21,22) 9.8	5.68	(5.23)
22	4.72	J(21,23) 5.5	4.23	J(21,23) 5.2	4.18	4.15
23	2.02	J(21,24) 16.5	2.46	J(21,24) 16.9	2.02	—
24	4.80	J(21,25) 11.4	4.32	J(21,25) 11.7	4.30	4.26
25	1.70	J(22,23) 0	1.25	J(22,23) 0	1.27	—
		J(22,24) 2.9		J(22,24) 3.1		
		J(23,25) −11.0		J(23,25) −10.9		
	3.86 (C_5H_5)		1.25 (Me), 5.11/5.06/4.33 (C_5H_4)		1.85 (Me), 4.96/4.89/4.85/4.51 (C_5H_4)	3.75 (Me), 7.14/7.03/6.83/6.58/6.43 (indenyl)

[a] Numbering scheme

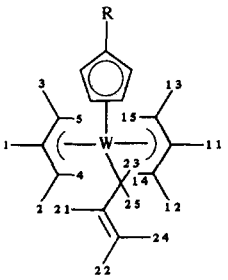

[b] d_8-toluene, −40°C.
[c] d_8-THF, −40°C.
[d] d_8-THF, −80°C.
[e] J (Hz) not determined.

allyl bond.[4,5] This difference in behaviour of the complexes of the two metals is presumably associated with the difference in stability of the M—C bonds involved: the W—C bond is significantly stronger than the Mo—C bond.[6,7]

Attempts to prepare $(\eta^5\text{-}C_5H_5)(\eta^3\text{-}C_3H_5)_2W$ by photochemical or thermal activation of the W—C bond in **1** were unsuccessful. However, the disappearance of the absorptions due to the η^1-allyl group and a broadening of the other signals above −20°C in the ^{1}H NMR spectrum of the least stable t-butylcyclopentadienyl derivative **3** suggest that a paramagnetic $(\eta^5\text{-t-}C_4H_9C_5H_4)(\eta^3\text{-}C_3H_5)_2W$ species is formed; although the compound could not be isolated analytically pure. Paramagnetic compounds (**4**, **5**) of this type were, however, the only

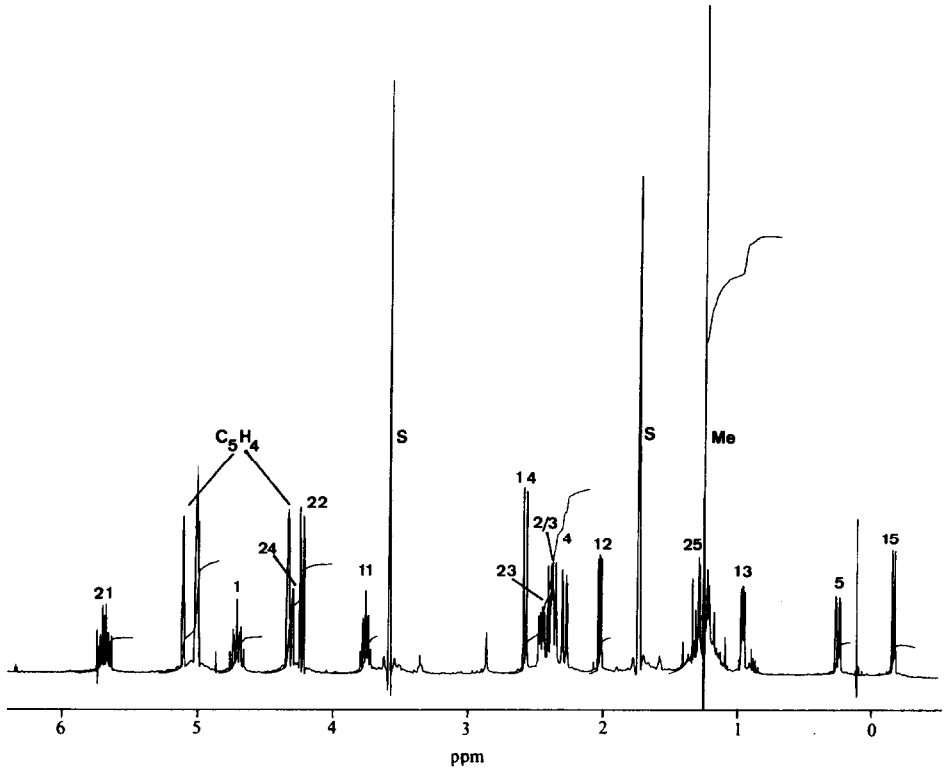

Fig. 1. The ^{1}H NMR spectrum of $(\eta^5$-t-$C_4H_9C_5H_4)(\eta^3$-$C_3H_5)_2(\eta^1$-$C_3H_5)W$ (3) (d_8-THF, −40°C; assignment see Table 1, footnote *a*; S = solvent).

tungsten-containing products which could be isolated from the reaction between $[(\eta^3C_3H_5)_3WCl]_2$ and indenyl- or fluorenyllithium [eq. (2)]:

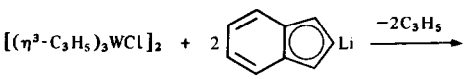

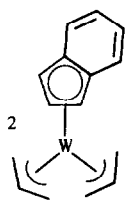

+ 2LiCl (2)

4

It is remarkable that the analogous reaction between fluorenyllithium and $[(\eta^3$-$C_3H_5)_3MoCl]_2$ leads to the tetrakis(η^3-allyl)molybdenum species, $(\eta^3$-$C_3H_5)_3(\eta^3$-fluorenyl)Mo.[4]

The compounds **1–3** are chemically relatively inert; protonolysis with HCl leads to cleavage of the W—C bond while no reaction is observed upon treatment with a variety of P-donor ligands.

EXPERIMENTAL

The experimental conditions and spectrometers used have been described earlier.[1] $[(\eta^3$-$C_3H_5)_3WCl]_2$ was prepared by treating $(\eta^3$-$C_3H_5)_4W$ with HCl in pentane at −78°C[1] and the substituted cyclopentadienylmetal species by reacting the appropriate cyclopentadiene compound with butyllithium or an alkali metal.[4]

$(\eta^5$-$C_5H_5)(\eta^3$-$C_3H_5)_2(\eta^1$-$C_3H_5)W$ (1)

C_5H_5Na (0.61 g, 6.90 mmol) was added to a solution of $[(\eta^3$-$C_3H_5)_3WCl]_2$ (1.45 g, 4.23 mmol) in THF (30 cm^3) at −40°C. The colour of the reaction mixture changed immediately from green to a dark salmon-pink. The reaction mixture was stirred for a further 30 min and the solvent removed under high vacuum at −40°C. Extraction of the solid residue with pentane (10 × 10 cm^3), concentration of the extract to 10 cm^3 and cooling to −70°C gave the compound as a yellow solid, which was recrystallized from pentane and dried at −40°C in a high vacuum. Yield 1.02 g (65% theory). Found: C, 45.1; H, 5.3; W, 49.2. Calc. for $C_{14}H_{20}W$: C, 45.2; H, 5.4; W, 49.4%.

IR (KBr, −40°C): ν 3040, 1465, 1021, 560 (η^3-C_3H_5); 1600 (η^1-C_3H_5); 3100, 1425, 1126, 1005, 830 (η^5-C_5H_5). MS *m/z* 372 (M^+), 342, 327, 287. ^{1}H NMR spectrum: see Table 1.

(η^5-MeC_5H_4)(η^3-C_3H_5)$_2$(η^1-C_3H_5)W (**2**)

MeC_5H_4Li (0.39 g, 4.53 mmol) was added over 5 min to a suspension of [(η^3-C_3H_5)$_3$WCl]$_2$ (1.44 g, 4.20 mmol) in THF (150 cm^3) at −30°C and the resulting solution stirred for a further 12 h. The solvent was removed under high vacuum at −30°C and the residue extracted with hexane (3 × 40 cm^3). The extract was treated three times with avicel and the concentrated solution cooled to −78°C to give the compound as a yellow solid. Yield 1.12 g (69% theory). Found: C, 46.5; H, 5.8; W, 47.8. Calc. for $C_{15}H_{22}W$: C, 46.7; H, 5.7; W 47.6%.

IR (KBr, −45°C): *v* 3080–3025, 1496, 1003, 570 (η^3-C_3H_5); 1602, 908 (η^1-C_3H_5); 3098, 1035, 860, 830 (η^5-RC_5H_4); 1375. MS: *m/z* 386 (M^+), 344, 340, 300. ^{1}H NMR spectrum: see Table 1.

(η^5-t-$C_4H_9C_5H_4$)(η^3-C_3H_5)$_2$(η^1-C_3H_5)W (**3**)

Prepared as above as a yellow solid from t-butylcyclopentadienyllithium and [(η^3-C_3H_5)$_3$ WCl]$_2$. Yield 69% theory. Found: C, 50.4; H, 6.6; W, 42.9. Calc. for $C_{18}H_{28}W$: C, 50.5; H, 6.6; W, 42.9%.

IR (KBr, −45°C): *v* 3080–3025, 1496, 1003, 570 (η^3-C_3H_5); 1602, 980 (η^1-C_3H_5); 3098, 1035, 860, 830 (η^5-RC_5H_4); 1365, 1375. MS: *m/z* 428 (M^+), 386, 182. ^{1}H NMR spectrum: see Table 1 and Fig. 1. ^{13}C NMR (d_8-THF, −50°C): δ 78.8 [C-1, *J*(C,H) 159], 38.4 [C-2, *J*(C,H) 156, *J*(C,W) 16.3], 41.9 [C-3, *J*(C,H) 156, *J*(C,W) 12.2], 111.6 [C-11, *J*(C,H) 155], 72.1 [C-12, *J*(C,H) 153, *J*(C,W) 14.1], 54.7 [C-13, *J*(C,H) 156, *J*(C,W) 12.2], 146.5 [C-21, *J* (C,H) 144], 103.2 [C-22, *J*(C,H) 153], 13.8 [C-23, *J*(C,H) 131, *J*(C,W) 46.8], 113.5 (C-31), 84.0 [C-32, *J*(C,H) 182], 92.4 [C-33, *J*(C,H) 176], 67.9 [C-34, *J*(C,H) 172], 81.0 [C-35, *J*(C,H) 179], 34.6 (C-41), 31.4 [C-42, *J*(C,H) 126]—numbering scheme shown above.

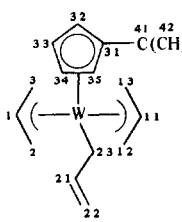

(η^5-Indenyl)(η^3-C_3H_5)$_2$W (**4**)

Prepared as above as a red solid from indenyllithium and [(η^3-C_3H_5)$_3$WCl]$_2$. Yield 58% theory. Found: C, 47.1; H, 4.5; W, 48.2%. Calc. for $C_{15}H_{16}W$: C, 47.2; H, 4.2; W, 48.2%.

IR (KBr, 25°C): *v* 3080–3025; 1485, 1000, 540 (η^3-C_3H_5); 3110, 1550, 850, 820, 750 (indenyl). MS: *m/z* 381 (M^+), 339, 299.

(η^5-Fluorenyl)(η^3-C_3H_5)$_2$W (**5**)

Prepared as above as a red solid from fluorenyllithium and [(η^3-C_3H_5)$_3$WCl]$_2$ whereby the reaction was warmed to 0°C for 10 min. Yield 32% theory. Found: C, 53.2; H, 4.3; W, 42.6%. Calc. for $C_{19}H_{19}W$: C, 52.9; H, 4.4; W, 42.6%.

IR (KBr, −35°C): *v* 3080–3015, 1478, 1000, 590 (η^3-C_3H_5); 3098, 1570, 860, 820, 740 (fluorenyl). MS: *m/z* 430 (M^+), 388, 348.

REFERENCES

1. R. Benn, T. H. Brock, M. C. F. B. Dias, P. W. Jolly, A. Rufińska, G. Schroth, K. Seevogel and B. Wassmuth, *Polyhedron* 1990, **9**, 11.
2. R. Benn, T. H. Brock, P. W. Jolly, A. Rufińska and G. Schroth, *Polyhedron* 1990, **9**, 23.
3. R. Benn, A. Rufińska and G. Schroth, *J. Organomet. Chem.* 1981, **217**, 91.
4. O. Andell, R. Goddard, S. Holle, P. W. Jolly, C. Krüger and Y. H. Tsay, *Polyhedron* 1989, **8**, 203.
5. P. W. Jolly, C. Krüger, C. C. Romão and M. J. Romão, *Organometallics* 1984, **3**, 936.
6. A. R. Dias, M. S. Salema and J. A. M. Simões, *J. Organomet. Chem.* 1981, **222**, 69.
7. H. A. Skinner and J. A. Connor, *Molec. Struct. Energetics* 1987, **2**, 233.

Polyhedron Vol. 10, No. 4/5, pp. 463–465, 1991
Printed in Great Britain

0277–5387/91 $3.00+.00
© 1991 Pergamon Press plc

UNUSUAL REACTIVITY OF ISOCYANATES WITH DIOXO- AND DIIMIDOMOLYBDENUM(VI) COMPLEXES

RICHARD LAI,* SYLVAIN MABILLE, ALAIN CROUX and SYLVIE LE BOT

ENSSPICAM, URA 1410, Université Aix-Marseille III, Marseille, France

(*Received* 4 *October* 1990; *accepted* 24 *October* 1990)

Abstract—Phenyl isocyanate reacts with dioxo- and diimidomolybdenum(VI) complexes such as $Mo(O)_2(mes)_2$ (**1**) (mes = mesityl = 2,4,6-$C_6H_2Me_3$), $Mo(mes)_2CH_2PBu_3(O)_2$ (**2**), $Mo(mes)\{CPBu_3(mes)\}(O)_2$ (**3**) and $Mo(NBu^t)_2(mes)_2$ (**4**), selectively affording phenyl mesityl amide. This reaction proceeds via insertion into the Mo—mesityl bond, leading to an unstable oxazamolydenacycle which has been identified by ^{13}C NMR. This intermediate is probably hydrolysed with generation of the amide during chromatographic work-up.

There are many reports in the literature of reactions involving heteroallenes such as isocyanates and transition metal complexes. The objectives of these studies were predominantly to better understand metal-promoted reactivity of CO_2-like molecules and also to develop reactions of synthetic utility.[1,2]

As part of our study of the synthesis and reactivity of multiple-bonded complexes,[3] it seemed appropriate to compare the reactivity of dioxodimesitylmolybdenum(VI), $Mo(O)_2(mes)_2$ (**1**) (where mes = mesityl = 2,4,6-$C_6H_2Me_3$), with the isoelectronic di(phenylimido)dimesitylmolybdenum(VI) complex. Therefore, we attempted to prepare this compound by reacting **1** with phenyl isocynate, a synthetic route which seems to have potential application to a wide variety of metals.[4] However, the reaction took an entirely different pathway and phenyl mesityl amide was found to be the sole identified product:

$$Mo(O)_2(mes)_2 + 2\,PhNCO \rightarrow \begin{cases} Mo(NPh)_2(mes)_2 + 2\,CO_2 \\ PhNHCO(mes). \end{cases}$$

We report here on the unusual reactivity of isocyanates with dioxo- and diimidomolybdenum(VI) complexes.

RESULTS AND DISCUSSION

When a yellow solution of $M(O)_2(mes)_2$ (**1**) in pyridine or tetrahydrofuran was treated with one equivalent of PhNCO, an instantaneous colour change occurred. After stirring for several hours, a brown solution was obtained. Analysis of the oily brown residue, obtained after vacuum evaporation of the solvent, did not reveal the presence of a diimido species, but column chromatography of the reaction mixture afforded an organic compound identified as phenyl mesityl amide by IR, NMR and mass spectrometry analysis. One equivalent of amide was obtained per mesityl group of the starting dioxo complex. Bu^tNCO reacted similarly affording $Bu^tNHCO(mes)$. However, only 0.6 equivalent of amide per mesityl group was isolated. The same behaviour was observed with the phosphorus ylide complex $Mo(mes)_2\ CH_2PBu_3(O)_2$ (**2**). However, in this case, elution of the amide from the column was only possible after on-column hydrolysis by dilute aqueous acid.

The dinitrene complex, $Mo(NBu^t)_2(mes)_2$ (**4**), obtained by an indirect method,[5] also reacted with PhNCO to give phenyl mesityl amide in good yield (92%). But in this case, the reaction was less selective since gas chromatographic analysis showed the presence of small amounts of other products. Two of them have been identified as tertiary butyl mesityl amide (1%) and a phenyl isocyanate trimer (5%). It is worth noting here that elimination of tertiary butyl mesityl amide has been observed upon treatment of $Cr(NBu^t)_2(mes)_2$ with CO.[5]

* Author to whom correspondence should be addressed.

When the dioxophosphinomethylidene complex, $Mo(mes)\{CPBu_3(mes)\}(O)_2$ (**3**), was reacted with PhNCO under the same conditions, no reaction was apparent after several hours at room temperature. Phenyl mesityl amide was detected only when the reaction was performed under more forcing conditions (70°C for 4 h) and no interaction with the Mo=C double bond was observed, in contrast with the results reported by Cramer *et al.* for $Cp_3U{=}CHPMe_2Ph$.[6]

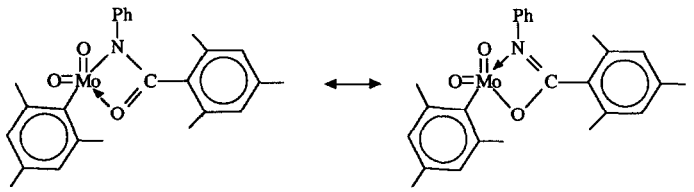

Scheme 1.

The generation of amides (or thioamides) from isocyanates (or isothiocyanates) and Grignard or organolithium reagents has been reported.[7,8] This type of reactivity with transition metal oxo and imido complexes is unprecedented, although the formation of cyclohexyl mesityl amide by reacting $C_6H_{11}NCO$ and a vanadium complex has been mentioned recently.[9] Generally, the interaction of transition metal complexes with isocyanates leads to stable compounds resulting from insertion of RNCO into M—C,[10] M—N,[11] M=C[6] or M≡C[12] bonds. As far as oxo complexes are concerned differences in reactivity have been reported depending on the starting compound. Thus, oxo complexes either give imido species in a "classical way", or adducts.[13] An oxo-imido complex has been reported from the reaction between $Mo(O)_2Cl_2(MeCN)_2$ and Bu^tNCO.[14] In contrast, $(\eta^5\text{-}C_5H_5)_2MoO$ reacts with PhNCO to form a cyclometallacarbamate, $Mo(\eta^5\text{-}C_5H_5)_2\{OC(O)N(Ph)\}$, resulting from a formal [2+2] cycloaddition of the C=N bond to the oxo linkage.[15]

In the present case, it is obvious that the reaction leading to the imido complex is very unfavourable, if not completely inoperative. Indeed, quantitative gas chromatography analysis of the atmosphere above the reaction mixture revealed the presence of CO_2 [less than 5% with a 10-fold excess of PhNCO vs **1**] and of CO (1%). Carbon monoxide formation could arise from the decomposition of PhNCO adducts, although this type of decomposition is very rare.[16] Even with an excess of phenyl isocyanate, a single isocyanate was inserted into the Mo—mesityl bond, as observed with other systems.[1c]

We believe that the amide is formed by hydrolysis of an unstable intermediate during the chromatographic work-up. We could neither isolate nor identify such an intermediate from **2** or from **4**. However, when **1** was reacted in a sealed NMR tube with one equivalent of PhNCO in dry C_5D_5N at 20°C, we were able to obtain good ^{13}C NMR evidence for a species tentatively described as an oxazamolybenacycle, represented here as two mesomeric forms:

Two low-field signals at 187.3 and 181.3 ppm are, respectively, assigned to the carbonyl carbon atom and to the *ipso*-carbon of the η^1-mesityl ligand. At higher field, four signals are observed at 27.95, 21.8, 20.80 and 18.70 ppm. The peaks at 27.95 and 20.80 ppm are associated with the signal at 181.3 ppm. They are assigned, by analogy with the ^{13}C NMR spectrum of **1**, to the *ortho*- and *para*-methyl groups of the η^1-mesityl ligand. The two other signals at 21.8 and 18.7 ppm are assigned to the *para*- and *ortho*-methyl groups, respectively, of the mesityl group in the η^2-amide ligand. The *ortho*-methyl group is shielded as in phenyl mesityl amide due to the proximity of the carbonyl group. The assignment of the signal at 187.3 ppm to the carbonyl group is, furthermore, consistent with the spectra of other complexes with related structures.[2b,12] Formation of such a species resulting from the insertion of the isocyanate into the Mo—C σ-bond is certainly favoured by the polarization of the Mo—C structure.[1c] This insertion occurs at the N=C bond rather than at the C=O bond, reflecting the difference in bond strength between these two bonds.[17] Depending on the structure of the starting complex, this reaction would be more or less easy as shown for the dioxophosphinomethylidene complex, **3**.

EXPERIMENTAL

General

Preparations of complexes **1**,[18] **2**,[19] **3**[20] and **4**[5] have been described earlier. PhNCO and Bu^tNCO were purchased from Janssen and distilled and stored under nitrogen. All operations were conducted under oxygen-free N_2 by standard Schlenk techniques and solvents were distilled before use from sodium/benzophenone, except for pyridine which was distilled from KOH under N_2. Anhy-

drous CH_2Cl_2 was kept on molecular sieves (4 Å) and degassed prior to use.

NMR spectra were recorded on a Bruker spectrometer AM-200 and GC/MS coupling experiments were performed on a Ribernag R.10.10.c. apparatus. IR spectra were obtained using a FT–IR Nicolet MX-S spectrometer.

Gas chromatography analyses were conducted on an Intersmat 1GC 120FB apparatus and an Intersmat ICR 1B integrator, on 5m × 1/8″ columns of 5% OV 17 on Chromosorb W. Gas chromatography of gases were carried out on an Intersmat 1GC 120MB using a thermal conductivity detector on 2m × 1/8″ columns of Prorapak N (CO_2) or of molecular sieves, 3 Å (CO). Benzamide was used as an internal standard for quantitative GLC analyses.

Description of a typical experiment with isocyanates

The complex (3.2×10^{-3} mol) was dissolved in tetrahydrofuran or pyridine (20 cm^3) and after cooling at −30°C, 0.36 cm^3 (3.2×10^{-3} mol) of PhNCO was added. The solution was allowed to warm slowly to room temperature and after 5 h stirring the reaction mixture was evaporated under reduced pressure to a small volume and passed down a silica gel column (0.063–0.2 mm, Merck). Elution of the amide was obtained with CH_2Cl_2. For complex **3**, after deposition of the reaction mixture on silica gel, 10 cm^3 of H_2SO_4 (5% v/v in H_2O) was passed down the column before CH_2Cl_2 elution.

Acknowledgement—We wish to express our thanks to Professor Sir Geoffrey Wilkinson for helpful discussions.

REFERENCES

1. (a) G. Fachinetti, C. Biran, C. Floriani, A. Chiesi-Villa and C. Guastini, *Inorg. Chem.* 1978, **17**, 2995; (b) S. Gambarotta, M. Pasquali, C. Floriani, A. Chiesi-Villa and C. Guastini, *Inorg. Chem.* 1981, **20**, 1173; (c) S. Gambarotta, S. Strologo, C. Floriani, A. Chiesi-Villa and C. Guastini, *Inorg. Chem.* 1985, **24**, 654.
2. (a) H. Hoberg, K. Radine and A. Milchereit, *J. Organomet. Chem.* 1985, **280**, C60; (b) H. Hoberg, K. Summerman and A. Milchereit, *J. Organomet. Chem.* 1985, **288**, 237.
3. R. Laï, *Advances in Metal Carbene Chemistry* (Edited by U. Schubert), Nato Asi Series, Series C, Vol. 269, p. 171. Kluwer Academic Publishers, Dordrecht (1989); R. Laï, S. Le Bot and R. Faure, *J. Organomet. Chem.* 1987, **336**, C5.
4. M. L. H. Green and K. J. Moynihan, *Polyhedron* 1986, **5**, 921; W. A. Nugent and B. L. Haymore, *Coord. Chem. Rev.* 1980, **31**, 123.
5. A. C. Sullivan, G. Wilkinson, M. Motavelli and M. B. Hursthouse, *J. Chem. Soc., Dalton Trans.* 1988, 53.
6. R. E. Cramer, J. H. Jeong and J. W. Gilje, *Organometallics* 1987, **6**, 2010.
7. Y. Zhang, J. Jiang and Y. Chen, *Tetrahedron Lett.* 1987, 3815; Y. Zhang, J. Jiang and Z. Zhang, *Tetrahedron Lett.* 1988, 651.
8. N. A. Lebel, R. M. Cherluck and E. A. Curtis, *Synthesis* 1973, 678.
9. M. Vivanco, J. Ruiz, C. Floriani, A. Chiesi-Villa and C. Guastini, *Organometallics* 1990, **9**, 2185.
10. I. Tkatchenko, *Comprehensive Organometallic Chemistry* (Edited by G. Wilkinson, F. G. A. Stone and E. W. Abel), p. 743. Pergamon Press, Oxford (1982); J. D. Wilkins, *J. Organomet. Chem.* 1974, **65**, 383.
11. Y. Takahashi, N. Onoyama, Y. Ishikawa, S. Motojima and K. Sugiyama, *Chem. Lett.* 1978, 525.
12. K. Weiss, U. Schubert and R. R. Schrock, *Organometallics* 1986, **5**, 397.
13. F. Bottomley and L. Sutin, *Adv. Organomet. Chem.* 1988, **28**, 1988; S. F. Pedersen and R. R. Schrock, *J. Am. Chem. Soc.* 1982, **104**, 7483.
14. D. Ehrenfeld, J. Kress, B. D. Moore, J. A. Osborn and G. Schoettel, *J. Chem. Soc., Chem. Commun.* 1987, 129.
15. P. Jernakoff, G. L. Geoffroy, A. L. Rheingold and S. J. Geib, *J. Chem. Soc., Chem. Commun.* 1987, 1610.
16. H. Hoberg, B. W. Oster, C. Kruger and Y. H. Tsay, *J. Organomet. Chem.* 1983, **252**, 365; J. G. Brennan and R. A. Andersen, *J. Am. Chem. Soc.* 1985, **107**, 514.
17. P. Jernakoff and N. J. Cooper, *J. Am. Chem. Soc.* 1987, **109**, 2173.
18. B. Heyn and R. Hoffmann, *Z. Chem.* 1976, **16**, 195.
19. R. Laï, S. Le Bot, A. Baldy, M. Pierrot and H. Arzoumanian, *J. Chem. Soc., Chem. Commun.* 1986, 1208.
20. H. Arzoumanian, A. Baldy, R. Laï, J. Metzger, M. L. Nkeng Peh and M. Pierrot, *J. Chem. Soc., Chem. Commun.* 1985, 1151.

Polyhedron Vol. 10, No. 4/5, pp. 467–470, 1991
Printed in Great Britain

0277-5387/91 $3.00+.00
© 1991 Pergamon Press plc

REACTIONS OF DINITROGEN AND HYDRAZIDO(2−) COMPLEXES OF MOLYBDENUM CONTAINING A TRIDENTATE LIGAND: THE EFFECT OF ADDING REDUCING AGENTS UPON AMMONIA FORMATION*

T. ADRIAN GEORGE,† MICHAEL A. JACKSON‡ and BHARAT B. KAUL

Department of Chemistry, University of Nebraska-Lincoln, Lincoln, NE 68588-0304, U.S.A.

(*Received* 6 *August* 1990; *accepted* 25 *October* 1990)

Abstract—The reaction of HBr with *trans*-[$Mo(N_2)_2$(dppee)(PR_3)] (**1**), where dppee = $O(CH_2CH_2PPh_2)_2$ and PR_3 = PPh_3, PPh_2Me, in CH_2Cl_2 yields a hydrazido(2−) complex which reacts further to form ammonia and hydrazine. During this reaction an intermediate can be isolated which upon hydrolysis produces hydrazine in almost quantitative yield. Addition of $SnCl_2$ (4 mol), a two-electron reducing agent, to the reaction mixture causes a doubling of the ammonia yield and concomitant decrease in the yield of N_2. The relationship to the electrochemical two-electron reduction of two different hydrazido(2−) complexes will be discussed.

The reactivity of N_2 is remarkably influenced by the metal to which it is bonded and the co-ligands.[3] In order to study the effects of changing the ligating atoms upon the reactivity of N_2 bonded to molybdenum, a series of complexes of the type *trans*-[$Mo(N_2)_2$(tri)(PR_3)], where tri = tridentate ligand, have been synthesized[4] and their reactions with acids studied. Reactions of acids with mono- and bis(N_2) complexes of molybdenum that contain a tridentate ligand afford ammonia and hydrazine.[5,6] Short-term reactions with acid lead to the formation of complexes containing the familiar hydrazido(2−) ligand.[7,8] The two-electron electrochemical reduction of hydrazido(2−) complexes has been successfully accomplished: for example, the conversion of $[W(OTs)(NNH_2)(dppe)_2]^+$, where OTs = tosylate, dppe = $Ph_2PCH_2CH_2PPh_2$, into ammonia {together with regeneration of *trans*-$[W(N_2)_2(dppe)_2]$[9]} and $[MoBr(N\overline{NCH_2(CH_2)_3CH_2})(dppe)_2]^+$ into piperidine and $[MoBr(NH)(dppe)_2]^+$ after treatment with acid.[10] We have attempted to achieve similar results by reacting **1** and its derivatives with reducing agents. In this paper we report (i) the reactions of acids with **1**, the corresponding hydrazido(2−) complexes and an uncharacterized intermediate, from which only hydrazine is formed, and (ii) the discovery of an external reducing agent that increases the yield of ammonia.[2] The reduction of bridging N_2 to ammonia in complexes such as [MCp* $Me_3]_2(\mu$-$N_2)$, where M = Mo or W, or mixed Mo/W, and Cp* = C_5Me_5, with excess acid in the presence of excess zinc amalgam has been reported recently.[11]

RESULTS AND DISCUSSION

Formation of hydrazido(2−) complexes

Reactions of *trans*-[$Mo(N_2)_2$(dppee)(PR_3)] (**1**), where dppee = $O(CH_2CH_2PPh_2)_2$, PR_3 = PPh_3 and $PMePh_2$, with HX (X = Br, Cl) afforded high yields of the corresponding hydrazido(2−) complexes of the form [$MoX(NNH_2)$(dppee)(PR_3)]X (**2**) with no evidence for dissociation of PR_3. Exchange of the counter ion with BPh_4^- revealed sharp absorptions in the FTIR spectrum between 3100 and 3350 cm^{-1} due to ν(NH).

Reactions of **1** (PPh_3) or **2** (Br-PPh_3) with HBr in THF produced little ammonia (0.10 mol/mol of

* For part XXVI, see ref. 1.

† Author to whom correspondence should be addressed.

‡ Based on PhD dissertation of Michael A. Jackson (see ref. 2).

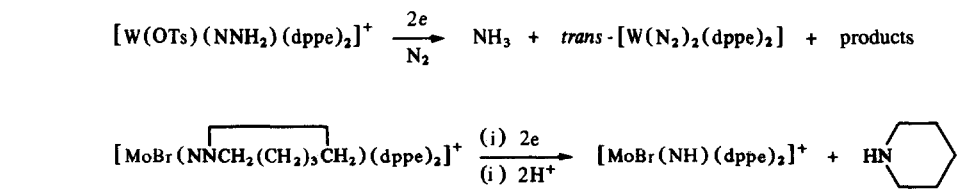

Scheme 1.

Mo), no hydrazine and 1.50 mol of N_2 for a 77% nitrogen-atom balance. On the other hand, in CH_2Cl_2, **1** (PPh_3) reacted with HBr to produce ammonia, hydrazine and N_2; 0.29, 0.44 and 1.27 mol/mol of Mo, respectively, for a 93% nitrogen-atom balance.

The hydrazido(2−) complexes formed from *trans*-[$Mo(N_2)_2$(tri)(PPh_3)], where tri = $S(CH_2CH_2CH_2PPh_2)_2$ and $PhP(CH_2CH_2CH_2PPh_2)_2$, were unstable losing PPh_3 in solution. The parent N_2 complexes displayed the same behaviour, which we attributed to steric effects associated with the propylene backbones in each tri ligand.[4]

Formation of intermediate

Reaction of [$MoBr(NNH_2)$(dppee)(PPh_3)]Br with excess HBr in CH_2Cl_2 led to the precipitation, within 1 h, of a solid **3** (*ca* 80% yield) whose colour varied from purple to purple–grey. The filtrate contained unreacted hydrazido(2−) but no free PPh_3. The latter forms the phosphonium salt under these experimental conditions. After exhaustive washing with CH_2Cl_2 and MeOH followed by drying *in vacuo*, hydrolysis of the solid with a H_2O/CH_2Cl_2 mixture produced *ca* 0.5 mol of hydrazine per mol of Mo and only a trace of ammonia. This is the first example in our work in which an intermediate produces only hydrazine. The yield of hydrazine is based upon the amount of **2** at the beginning of the reaction and results are reproducible. By the time precipitation of **3** was complete, *ca* 0.5 mol of N_2/mol of **2** had evolved. Thus beginning with **1**, *ca* 100% of the nitrogen was accounted for.

Elemental analyses of **3** were variable with Br > 40% and C:H:P ratios indicative of one dppee per Mo. The FTIR spectrum showed ν(NH) in the 2500–2800 region and ν(PH) at 2300 cm^{-1}, suggesting protonation of a pendant phosphine arm of dppee. The charge-compensating bromide ion associated with the phosphonium ion would contribute to the high per cent of bromine obtained. The solid was paramagnetic (Gouy method) and only dissolved in polar solvents such as DMF and DMSO in which is decomposed with evolution of N_2. Tests for the presence of hydrazine following decomposition were negative.

The role of external reducing agents

Dinitrogen complexes of molybdenum react with strong acids to produce ammonia or ammonia and hydrazine. The reaction involves a series of protonation and electronation steps. The initial phase entails protonation of the terminal nitrogen atom of N_2 and intramolecular electron reorganization which leads to the rapid formation of a hydrazido(2−) complex [eq. (1)]. The final phase, in THF solution, involves disproportionation[12]

$$\{Mo^0(N_2)\} + 2H^+ \longrightarrow \{Mo^{IV}(NNH_2)\}^{2+} \quad (1)$$

$$2\{Mo^{IV}(NNH_2)\}^{2+} + 4H^+ \longrightarrow 2\{Mo^{III}\} + 2NH_4^+ + N_2 \quad (2)$$

(intermolecular electron transfer) of the hydrazido(2−) complex to yield about one mol of ammonia and one-half mol of N_2 per mol of Mo, respectively [eq. (2)]. The interjection of electrons into the system would be an important step in the generation of a catalytic cycle for ammonia or hydrazine formation. This has been achieved by the two-electron electrochemical reduction of hydrazido(2−) complexes (see Introduction). We felt that the addition of a reducing agent might reduce the "purple" intermediate so that ammonia rather than hydrazine would be formed. Therefore, **1** and reducing agents were treated with HBr in CH_2Cl_2 and yields of nitrogen products determined.

Reducing agents such as cobaltocene, SmI_2 and amalgamated tin were unsuccessful, reacting with solvent or producing H_2. Tin(II) chloride, a two-electron reducing agent, provided the most satisfactory results (see Table 1). With a 1:4 ratio of **1** to $SnCl_2$, ammonia yields increased from 0.29 to 0.65 mol/mol of **1**, which corresponds almost exactly to the decrease in N_2 produced, 1.27 to 1.09. Thus, 0.18 mol of N_2 that would normally have been evolved have been converted into an extra 0.36 mol of ammonia. Hydrazine production was unaffected. The intermediate **3** was not observed in

Table 1. Yields[a] of nitrogen-containing products from reactions of **1** with HBr[b] in CH_2Cl_2 at 23°C for 46 h

Compound	Mol[a] $SnCl_2$	Yields[a] NH_3	N_2H_4	N_2	Per cent N[c] balance
1	0	0.29	0.44	1.27	93
1	4	0.65	0.43	1.09	92
1	10	0.50	0.18	—	—
1	20	0.16	0.03	—	—
1	4[d]	0.20	0.26	—	—
1	10[e]	0.15	0.22	1.06	68
3	0	Trace	0.55	—	—

[a] Mol/mol of Mo.
[b] 20 Mol/mol Mo.
[c] [(g Atoms N per mol Mo)/2] × 100.
[d] $[Et_4N][SnCl_3]$.
[e] VCl_3.

these reactions. It is hard to account for this increase without proposing that $SnCl_2$ is acting as a reducing agent.[13,14] VCl_3, a Lewis acid and potential reducing agent like $SnCl_2$, caused a decrease in the overall yields of nitrogen-containing products when used in similar reactions.

Similar reactions with 10 and 20 mol of $SnCl_2$/mol of **1** resulted in decreases in the amounts of ammonia and particularly hydrazine produced (see Table 1). $SnCl_2$ is not very soluble in CH_2Cl_2 and during the reaction it took more than 12 h before it dissolved completely. Addition of $[Et_4N][SnCl_3]$ (4 mol), which is very soluble in CH_2Cl_2, caused a decrease in ammonia and hydrazine yields.

In order to investigate the mechanism of these reactions, a number of experiments were carried out in an effort to incorporate tin-containing moieties[15] into the hydrazido(2−) and other intermediate stages of ammonia formation. (i) Compound **1** was reacted with $[HPPh_3][SnBr_3]$ to try and incorporate $SnBr_3^-$ as a ligand *trans* to NNH_2; the product was $[MoBr(NNH_2)(dppee)(PPh_3)][SnBr_3]$.* (ii) The reaction of $SnCl_2$ with $[MoBr(NNH_2)(dppee)(PPh_3)]Br$ produced the analogous $SnBrCl_2^-$ salt.† (iii) Similarly, the reaction of $[Et_4N][SnCl_3]$ with $[MoBr(NNH_2)(dppee)(PPh_3)]Br$ yielded the $SnCl_3^-$ salt.‡

Further work is underway to isolate (i) intermediates that incorporate tin(II) compounds and (ii) the tin(IV) product of these interesting redox reactions.

EXPERIMENTAL

General procedures

All reactions and manipulations were carried out under dry oxygen-free N_2 or *in vacuo*. All solvents were rigorously dried by heating at reflux over an appropriate drying agent followed by distillation under N_2. Solvents were saturated with N_2 immediately before use by bubbling N_2 through the solvent (*ca* 0.5 h). Solvents used in vacuum-line experiments were degassed through four to five freeze–pump–thaw cycles. Samples were weighed out in a Vacuum Atmospheres Corp. Dribox. Specific procedures for carrying out acid reactions with **1** and quantitative determination of yields of N_2, ammonia and hydrazine have been reported elsewhere.[5b] For reactions in which $SnCl_2$, $[Et_4N][SnCl_3]$ and VCl_3 were added, the reagent was weighed out with **1**.

Elemental analyses were performed by Galbraith Laboratories Inc., Knoxville, Tennessee.

Instrumentation

IR spectra were recorded with an Analect RFX-65 FTIR spectrometer. ^{31}P and ^1H NMR spectra were obtained at room temperature in CD_2Cl_2 with a Varian VXR-200 spectrometer operating at 80,984 and 200.050 MHz, respectively. Chemical shifts are referenced to PPh_3 (−5.8 ppm vs 85% H_3PO_4 = 0 ppm) and TMS. Mass spectral data were obtained on a Kratos MS50-TA mass spectrometer.

Reagents and chemicals

Details have been given elsewhere.[4,5b] Chemicals were purchased from commercial sources and used as obtained. The following complexes were prepared by published procedures: *trans*-$[Mo(N_2)_2(dpepp)(PR_3)]$ (**1**), where PR_3 = PPh_3 and PPh_2Me,[4] and $[Et_4N][SnCl_3]$.[16] $[HPPh_3][SnBr_3]$ was synthesized[17] by reacting $SnBr_2$ and $[HPPh_3]Br$[18] in anhydrous degassed methanol. The compound was characterized by FTIR [ν(PH) 2395 (vs) cm^{-1}] and mass spectrometry; the low resolution positive ion FAB mass spectrum contained the cation $[HPPh_3]^+$

* ^{31}P NMR: δ 48.40 (t, 1, $^2J_{P_aP_x}$ = 13.5 Hz, P_x), 26.75 (d, 2, P_a). FTIR (KBr disc): ν(NH) 3345 (m), 3220 (s), 3112 (w) cm^{-1}.

† ^{31}P NMR: δ 48.0 (t, 1, $^2J_{P_aP_x}$ = 13.6 Hz, P_x), 26.38 (d, 2, P_a). FTIR (KBr disc): ν(NH) 3341 (m), 3216 (s), 3120 (w) cm^{-1}.

‡ ^{31}P NMR: δ 47.7 (t, 1, $^2J_{P_aP_x}$ = 13.6 Hz, P_x), 25.89 (d, 2, P_a). ^1H NMR: δ 8.72 (m, 35, Ph), 5.64 (s, 2, NNH_2), 4.58 (m, 4, OCH_2), 2.85 (m, 4, PCH_2). FTIR (KBr disc): ν(NH) 3338 (m), 3213 (s), 3117 (w) cm^{-1}.

(m/z = 262) as the base peak, and the negative ion FAB spectrum contained an abundant $[SnBr_3]^-$ ion (m/z = 358 for the ion with the most abundant isotopes).

$[MoBr(NNH_2)(dppee)(PPh_3)]Br$

An excess of HBr (*ca* 2.55 mmol) was condensed onto **1** (0.15 g, 0.17 mmol) at −196°C. The mixture was allowed to warm to room temperature in a closed vessel with agitation as described previously. Volatiles (N_2 and HBr) were removed and the brown–green solid dried overnight *in vacuo*. The product was dissolved in THF, the solution filtered and ether added to precipitate a khaki-green microcrystalline solid (0.13 g, 0.13 mmol, 75%). Found: C, 55.6; H, 4.6; N, 2.5. Calc. for $C_{46}H_{45}Br_2MoN_2OP_3$: C, 55.7; H, 4.6; N, 2.8%. ^{31}P NMR: δ 49.6 (t, 1, $^2J_{P_aP_x}$ = 13.4 Hz, P_x), 29.0 (d, 2, P_a).

The following complexes were prepared similarly. $[MoCl(NNH_2)(dppee)(PPh_3)]Cl$; ^{31}P NMR: δ 23.7 (t, 1, $^2J_{P_aP_x}$ = 13 Hz, P_x), 1.8 (d, 2, P_a). $[MoCl(NNH_2)(dppee)(PPh_2Me)]Cl$; ^{31}P NMR: δ 32.4 (m, 1, $^2J_{P_aP_x}$ = 13 Hz, P_x), 31.8 (d, 2, P_a); Found: C, 58.1; H, 5.2. Calc. for $C_{41}H_{43}Cl_2MoN_2OP_3$: C, 58.6; H, 5.2%.

Intermediate 3

HBr (*ca* 2.20 mmol) and CH_2Cl_2 (10 cm^3) were condensed onto *trans*-$[Mo(N_2)_2(dppee)(PPh_3)]$ (100 mg, 0.11 mmol) at −196°C. The mixture was allowed to warm to room temperature and stirred. Within 1.5–2 h a precipitate began to form. After 4 h the grey–purple solid was filtered off, washed with 4×20 cm^3 CH_2Cl_2, 4×10 cm^3 methanol and dried *in vacuo*. Yield 0.08 g. FTIR (KBr disc): ν(NH) 3301, 3260, 2800; ν(PH) 2328 cm^{-1}.

Acknowledgements—We are grateful to the National Institutes of Health (Grant GM-38613) for support of this research. Further support was provided by the University of Nebraska Research Council and NIH Biomedical Research Support Fund RR-07055.

REFERENCES

1. T. A. George and B. B. Kaul, *Inorg. Chem.* 1990, **29**, 4969.
2. M. A. Jackson, PhD Dissertation, University of Nebraska (1988).
3. (a) J. Chatt, C. T. Kan, G. J. Leigh, C. J. Pickett and D. R. Stanley, *J. Chem. Soc., Dalton Trans.* 1980, 2032; (b) J. Chatt, J. R. Dilworth and R. L. Richards, *Chem. Rev.* 1978, **78**, 589; (c) R. A. Henderson, G. J. Leigh and C. J. Pickett, *Adv. Inorg. Chem. Radiochem.* 1983, **27**, 197.
4. T. A. George and M. A. Jackson, *Inorg. Chem.* 1988, **27**, 924.
5. (a) J. A. Baumann and T. A. George, *J. Am. Chem. Soc.* 1980, **102**, 6153; (b) J. A. Baumann, G. E. Bossard, T. A. George, D. B. Howell, L. M. Koczon, R. K. Lester and C. M. Noddings, *Inorg. Chem.* 1985, **24**, 3568.
6. (a) T. A. George and R. C. Tisdale, *J. Am. Chem. Soc.* 1985, **107**, 5157; (b) T. A. George and R. C. Tisdale, *Inorg. Chem.* 1988, **27**, 2909.
7. (a) J. Chatt, A. J. Pearman and R. L. Richards, *J. Chem. Soc., Dalton Trans.* 1978, 1766; (b) S. N. Anderson, M. E. Fakley, R. L. Richards and J. Chatt, *J. Chem. Soc., Dalton Trans.* 1981, 1973.
8. (a) K. Gebreyes, T. A. George, L. M. Koczon, R. C. Tisdale and J. Zubieta, *Inorg. Chem.* 1986, **25**, 405; (b) K. Gebreyes, T. A. George, L. M. Koczon, L. Ma, R. C. Tisdale, S. N. Shaikh and J. Zubieta, *Polyhedron* 1990, **9**, 545.
9. (a) C. J. Pickett and J. Talarmin, *Nature* (*Lond.*) 1985, **317**, 652; (b) C. J. Pickett, K. S. Ryder and J. Talarmin, *J. Chem. Soc., Dalton Trans.* 1986, 1453.
10. (a) W. Hussain, G. J. Leigh and C. J. Pickett, *J. Chem. Soc., Chem. Commun.* 1982, 747; (b) R. A. Henderson, G. J. Leigh and C. J. Pickett, *J. Chem. Soc., Dalton Trans.* 1989, 425.
11. R. R. Schrock, R. M. Kolodziej, A. H. Liu, W. M. Davis and M. G. Vale, *J. Am. Chem. Soc.* 1990, **112**, 4338.
12. B. B. Kaul, R. K. Hayes and T. A. George, *J. Am. Chem. Soc.* 1990, **112**, 2002.
13. More recent work based upon reactions of $SnCl_2$ and GeI_2 with resin-bound N_2 complexes of molybdenum (ref. 12) provide conclusive evidence of the redox behaviour of $SnCl_2$: T. A. George and B. B. Kaul, *Inorg. Chem.*, in press.
14. An unsuccessful attempt to employ $SnCl_2$ (and other reducing agents) to reduce hydrazido(2−) complexes has been noted: J. Chatt, G. A. Heath and R. L. Richards, *J. Chem. Soc., Dalton Trans.* 1974, 2074.
15. Many examples are known in which tin-containing species ligate to transition metal complexes: see M. S. Holt, W. L. Wilson and J. H. Nelson, *Chem. Rev.* 1989, **89**, 11.
16. G. W. Parshall, *Inorg. Synth.* 1974, **15**, 222.
17. For the general procedure see: (a) J. S. Morrison and H. M. Haendler, *J. Inorg. Nucl. Chem.* 1976, **29**, 393; (b) I. Wharf and D. F. Shaver, *Inorg. Chem.* 1969, **8**, 914.
18. D. Seyferth, S. O. Grimm and T. O. Read, *J. Am. Chem. Soc.* 1961, **83**, 1617.

Polyhedron Vol. 10, No. 4/5, pp. 471–476, 1991
Printed in Great Britain

0277–5387/91 $3.00+.00
© 1991 Pergamon Press plc

THE SYNTHESIS AND MOLECULAR STRUCTURE OF 3-PPh_3-4-SMe_2-3,1,2-*closo*-$CuC_2B_9H_{10}$: RELATIONSHIP OF ITS STRUCTURE TO THOSE OF 10,11-μ-H-9-SMe_2-7,8-*nido*-$C_2B_9H_{10}$ AND 10,11-μ-(PPh_3Au)-9-SMe_2-7,8-*nido*-$C_2B_9H_{10}$

EWAN J. M. HAMILTON and ALAN J. WELCH*

Department of Chemistry, University of Edinburgh, Edinburgh EH9 3JJ, U.K.

(*Received* 22 *August* 1990; *accepted* 1 *November* 1990)

Abstract—Stoichiometric reaction between Tl[9-SMe_2-7,8-*nido*-$C_2B_9H_{10}$] and $[Ph_3PCuBr]_4$ affords the title compound in good yield. Crystallographic analysis of this species shows that the copper atom is essentially symmetrically disposed above the five-atom ligand face, thus completing a *closo* 12 vertex polyhedron. In contrast, in the formally related species 10,11-μ-H-9-SMe_2-7,8-*nido*-$C_2B_9H_{10}$ and 10,11-μ-(PPh_3Au)-9-SMe_2-7,8-*nido*-$C_2B_9H_{10}$ the hydrogen atom and {Ph_3PAu} fragment occupy bridging positions on an open face, whereas in anionic non-SMe_2-substituted analogues of the last two the hydrogen atom and {Ph_3PAu} fragment adopt *endo*-terminal sites. These differences in respect to the SMe_2-substituted compounds are traced to the form of the HOMO of the [9-SMe_2-7,8-*nido*-$C_2B_9H_{10}$]$^-$ ligand. Inspection of the three occupied π-MOs of this ligand additionally yields a semi-quantitative understanding of patterns visible in the facial B—B, B—C and C—C distances of 3-PPh_3-4-SMe_2-3,1,2-*closo*-$CuC_2B_9H_{10}$, 10,11-μ-H-9-SMe_2-7,8-*nido*-$C_2B_9H_{10}$ and 10,11-μ-(PPh_3Au)-9-SMe_2-7,8-*nido*-$C_2B_9H_{10}$.

In a recent publication[1] we reported the synthesis and characterization of [10-*endo*-(Ph_3PAu)-7,8-*nido*-$C_2B_9H_{11}$]$^-$ ([$Ph_3PAucarb$]$^-$), the major structural feature of which is that the {Ph_3PAu} fragment is *endo*-σ-bonded to the central boron atom, B(10), of the open face of the *nido*-carbaborane ligand. This species is, therefore, structurally analogous to [7,8-*nido*-$C_2B_9H_{12}$]$^-$ ([carbH]$^-$) which has an *endo*-terminal hydrogen atom,[2] and distinct from [3-PPh_3-3,1,2-*closo*-$CuC_2B_9H_{11}$]$^-$ ([Ph_3PCucarb]$^-$) which shows an essentially closed icosahedral cage structure.[3] We rationalized observed patterns in the important molecular parameters for the series [carbH]$^-$, [$Ph_3PAucarb$]$^-$ and [Ph_3PCucarb]$^-$ in terms of differing degrees of depopulation of the occupied π-molecular orbitals (MOs) of [7,8-*nido*-$C_2B_9H_{11}$]$^{2-}$ by the fragments H^+, {Ph_3PAu}$^+$ and {Ph_3PCu},$^+$ respectively.

We are currently developing the *d*- and *f*-block metal chemistries of the monoanionic carbaborane ligand [9-SMe_2-7,8-*nido*-$C_2B_9H_{10}$]$^-$ ([carb′]$^-$),[4] and as part of these studies we have determined the molecular structures of the ligand precursor 10,11-μ-H-9-SMe_2-7,8-*nido*-$C_2B_9H_{10}$ (carb′H, **1**)[4a] and its isolobally substituted analogue 10,11-μ-(Ph_3PAu)-9-SMe_2-7,8-*nido*-$C_2B_9H_{10}$ ($Ph_3PAucarb'$, **2**).[4b] It was, therefore, of interest to similarly study the copper analogue $Ph_3PCucarb'$ to establish:

(i) If, as with [$Ph_3PCucarb$]$^-$, a *closo* icosahedral cluster geometry is observed.
(ii) If trends are also apparent in key molecular parameters for the series carb′H, Ph_3PAucarb′ and $Ph_3PCucarb'$, and further, if their origin can be traced to electronic effects.

Accordingly, this paper describes the synthesis, and the spectroscopic and structural characterization of $Ph_3PCucarb'$, and the results of a detailed comparison of its structure with those of **1** and **2**.

EXPERIMENTAL

Synthesis and characterization

Reactions were performed under dry N_2 using standard Schlenk-line techniques, with some sub-

* Author to whom correspondence should be addressed.

sequent manipulation in air. CH_2Cl_2 and n-hexane were dried and distilled under N_2 prior to use. NMR spectra were recorded on a Brucker WP200SY spectrometer as a CD_2Cl_2 solution at 298 K. Microanalyses were performed by the departmental service. The starting materials, 10,11-μ-H-9-SMe_2-7,8-*nido*-$C_2B_9H_{10}$[5] and $[Ph_3PCuBr]_4$,[6] were prepared by literature methods.

Synthesis of Tl[9-SMe_2-7,8-*nido*-$C_2B_9H_{10}$]

To a solution of 10,11-μ-H-9-SMe_2-7,8-*nido*-$C_2B_9H_{10}$ (**1**) (0.3006 g, 1.545 mmol) in dmso (8 cm^3) was added, dropwise with stirring, a solution of KOH (0.5268g, 9.37 mmol) in H_2O (8 cm^3). After 30 min a solution of thallium(I) acetate (0.4702 g, 1.78 mmol) in H_2O (10 cm^3) was added, affording a thick, dull yellow precipitate of Tl[9-SMe_2-7,8-*nido*-$C_2B_9H_{10}$] which was collected by filtration, washed with CH_2Cl_2 (5 cm^3) and Et_2O (2 × 5 cm^3), and stored in a foil-covered vessel. Yield: 0.5717 g, 93%. Found: C, 12.2; H, 3.9. Calc. for $C_4H_{16}B_9STl$: C, 12.1; H, 4.0%.

Synthesis of 3-PPh_3-4-SMe_2-3,1,2-*closo*-$CuC_2B_9H_{10}$ (**3**)

To a stirred suspension of Tl[9-SMe_2-7,8-*nido*-$C_2B_9H_{10}$] (0.4045 g, 1.12 mmol), in CH_2Cl_2 (5 cm^3) in a foil-covered reaction flask, was added a suspension of $[Ph_3PCuBr]_4$ (0.4545 g, 0.28 mmol) in CH_2Cl_2 (10 cm^3). The mixture was stirred overnight and filtered to afford a colourless filtrate, from which removal of solvent *in vacuo* gave an off-white solid. Colourless crystals of 3-PPh_3-4-SMe_2-3,1,2-*closo*-$CuC_2B_9H_{10}$ (**3**) were obtained by slow diffusion of n-hexane into a CH_2Cl_2 solution at −30°C. Yield: 0.4363 g, 75%. Found: C, 50.6; H, 6.1. Calc. for $C_{22}H_{31}B_9CuPS$: C, 50.9; H, 6.0%. NMR: ^1H δ 7.20–7.75 (multiplet, 20H, C_6H_5), 2.33 (s, 3H, CH_3), 2.24 (s, 3H, CH_3), 2.26 (br, s, 1H, $C_{cage}H$), 2.01 (br s, 1H, $C_{cage}H$) ppm; ^{11}B-{^1H} δ −15.37 (2B), −18.14 (1B), −19.54 (1B), −20.12 (1B), −21.71 (1B), −22.51 (2B), −33.66 (1B) ppm.

Crystallographic study

A single crystal (0.2 × 0.2 × 0.3 mm^3) of **3** was set on an Enraf–Nonius CAD4 diffractometer equipped with graphite-monochromated Mo-K_α X-radiation ($\bar{\lambda}$ = 0.71069 Å). The unit cell parameters and orientation matrix for data collection were determined from the least-squares refinement of the setting angles of 25 centred reflections ($10 < \theta < 11°$).

Crystal data. $C_{22}H_{31}B_9CuPS$, M = 519.36, triclinic, space group $P\bar{1}$ a = 9.100(8), b = 11.344(4), c = 14.171 Å, α = 66.85(3), β = 89.11(5), γ = 82.85(5)°, V = 1333.8 $Å^3$, Z = 2, D_c = 1.293 g cm^{-3}, μ(Mo-K_α) = 9.65 cm^{-1}, $F(000)$ = 536.

Data were collected by ω–2θ scans (ω scan width = 0.8 + 0.34 tan θ) in 96 steps for $+h$, $\pm k$, $\pm l$ and $1 \leqslant \theta \leqslant 25°$. No perceptible crystal decay or movement was noted. Of 5015 unique reflections measured, 3748 [$F \geqslant 2.0\sigma(F)$] were retained for structure solution and refinement.

The structure was solved by automatic direct methods (Cu, P, S atoms) (SHELX86[7]) and full-matrix least-squares refinement/ΔF syntheses (C, B, H_{cage}, H_{methyl}) (SHELX76[8]). Cage C atoms were identified by the usual combination of refined (as B) isotropic thermal parameters and internuclear distances. An empirical absorption correction (DIFABS[9]) was applied after isotropic convergence. Phenyl rings were modelled as regular, planar hexagons (C—C 1.395 Å, C—H 1.08 Å). All non-hydrogen atoms were allowed anisotropic thermal vibration and hydrogen atoms were refined with group isotropic thermal parameters [H_{cage}, H_{methyl} 0.062(3) $Å^2$, H_{phenyl} 0.110(4) $Å^2$ at convergence]. Weights were assigned according to $w^{-1} = [\sigma^2(F) + 0.000284F^2]$. R = 0.0410, R_w = 0.0419, S = 1.289. Maximum and minimum residues in ultimate ΔF synthesis were only 0.35 and −0.28 $eÅ^{-3}$, respectively. Atomic scattering factors for P, S, C, B and H were those inlaid in SHELX76; for Cu, values were taken from *International Tables for X-ray Crystallography*.[10]

Tables of final atomic positional and thermal parameters, a full list of interbond angles and tables of F_o/F_c values have been deposited with the Editor as supplementary material.

Theoretical study

An extended Huckel molecular orbital (EHMO) calculation was performed on [9-SMe_2-7,8-*nido*-$C_2B_9H_{10}]^-$ with charge iteration [$H_{ii} = H_{ii}^\circ$ + (sense) × (charge)]. The model was derived from the crystallographic coordinates of 3,3,3-$(CO)_3$-4-SMe_2-3,1,2-*closo*-$MnC_2B_9H_{10}$[4c] from which the {$Mn(CO)_3$} fragment was removed (note the differing numbering conventions for *closo* 12 vertex and *nido* 11 vertex polyhedra[11]). The calculation was made using the ICON8 program[12] and the weighted H_{ij} formula.[13] H_{ii}s and Slater exponents for S, C, B and H were those inlaid in ICON8.

RESULTS AND DISCUSSION

Stoichiometric reaction between suspensions of Tl[carb′] and $[Ph_3PCuBr]_4$ in CH_2Cl_2 affords the

target compound 3-PPh_3-4-SMe_2-3,1,2-*closo*-$CuC_2B_9H_{10}$ (Ph_3PCucarb′, **3**) in good yield, the crystalline product being characterized by microanalysis and by ^1H and ^{11}B NMR spectroscopy. In the ^1H NMR spectrum the methyl protons give rise to two singlets (2.33 and 2.24 ppm). This confirms the magnetic inequivalance of the two methyl groups of the SMe_2 function. The ^{11}B-{^1H} NMR spectrum diplays seven resonances of relative integral 2 : 1 : 1 : 1 : 1 : 2 : 1, consistent with a fully asymmetric carbametallaborane cage (two coincidences). On retention of proton coupling all resonances in the ^{11}B spectrum show doublet coupling (J_{BH} 120–150 ± 5 Hz) except for one of the components of the highest frequency resonance (δ −15.37 ppm), which may thus be assigned to B(4), the sulphur-bearing boron atom.

The structure of **3** was completely characterized by a single crystal X-ray diffraction study. Figure 1 presents a perspective view of a single molecule and demonstrates the atomic numbering scheme adopted.[11] Table 1 lists internuclear distances and key interbond angles determined.

Clearly, the essential structural feature of **3** is that the copper atom is η^5-bonded by the carbaborane ligand face, rendering the overall polyhedron a *closo* 12 vertex architecture. Thus the series carb′H,[4a] Ph_3PAucarb′[4b] and Ph_3PCucarb′ resembles the series [carbH]$^-$,[2] [Ph_3PAucarb]$^-$ [1] and [Ph_3PCucarb]$^-$ [3] in that the first two members are structurally similar to each other and involve a *nido* 11 vertex carbaborane supporting a non-vertex function (H and {Ph_3PAu} respectively, *endo* bonded in the carb series and bridging in the carb′ series), whereas in the final member of each series the {Ph_3PCu} fragment completes a *closo* 12 vertex (icosahedral) cluster. These findings are fully consistent with the available valence orbitals of H^+, $\{R_3PAu\}^+$ and $\{R_3PCu\}^+$,[14] and with the frontier orbitals of [carb]$^{2-}$ [1,15] and [carb′]$^-$ (see later for the last), to which more detailed reference will be subsequently made.

The carbacupraborane **3** represents an addition to the growing number of complexes of the carb′ ligand that have been structurally characterized. As in Ph_3PAucarb′,[4b] $(CO)_3$Mncarb′[4c] and carb′H itself,[4a] a preferred conformation about the B—S bond is apparent, the torsion angle* S(lone pair)—S—B(4)—C(1) being only 7.7(3)°. Moreover, S—B(4)—C(1) is considerably narrower than S—B(4)—B(8), 118.16(24) vs 128.85(4)°. These structural findings are fully consistent with an intra-

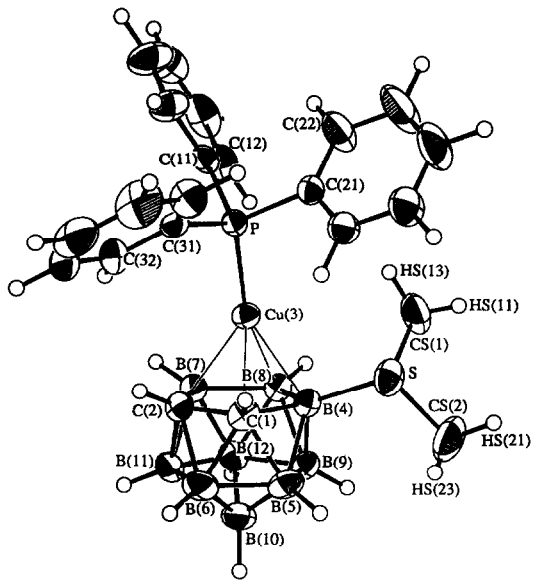

Fig. 1. Perspective view of **3**. Thermal ellipsoids are drawn at the 50% probability level, except for H atoms which have an artificial radius of 0.1 Å for clarity. Phenyl rings are numbered cyclically, C(*ij*) with i = 1–3, j = 1–6. H atoms not numbered carry the same number as the B or C to which they are attached. HS(12) and HS(22) are totally obscured by CS(1) and CS(2), respectively.

molecular electrostatic attraction between the sulphur lone pair of electrons and the (relatively protonic) H atom *exo* to C(1). It is of considerable interest that the preferred conformation about the B—S bond is retained in spite of steric crowding between the CS(1) methyl group and the C(21)—C(26) phenyl ring [HS(13)···C(21) 2.97(4) Å, HS(13)···C(26) 2.93(4)Å]. Rather than adopt an alternative B—S torsion, which would presumably relieve this crowding, it appears preferable for the SMe_2 groups to undergo a depression of *ca* 5° from its idealized 26° angle of inclination to the metallabonded C_2B_3 face. Similar intramolecular crowding was noted in the structure of Ph_3PAucarb′.[4b]

In **3** the copper atom is 1.721 Å from the C_2B_3 ligand face. The latter is measurably non-planar, being folded into an envelope conformation about the B(4)···B(7) vector, and subtending fold angles[15,16] of θ, 2.11° and ϕ, 1.15°. Moreover, the copper atom is consistently closer to the facial boron atoms than the cage carbon atoms, resulting in a slip parameter,[15,16] Δ, of +0.34 Å. As expected,[15] this slip distortion can be traced to localization of the frontier orbitals of the [carb′]$^-$ ligand onto the boron atoms of the ligand face.

The occupied π-MOs of [carb′]$^-$, as given by EHMO calculation, are sketched in Fig. 2 from a

*Calculated from the directly measurable angles CS(1)—S—B(4)—C(1) and CS(2)—S—B(4)—C(1).

Table 1. Internuclear distances (Å) and selected interbond angles (°) for **3**

Cu(3)—P	2.1681(9)	B(4)—B(5)	1.783(6)
Cu(3)—C(1)	2.394(3)	B(4)—B(8)	1.787(5)
Cu(3)—C(2)	2.369(3)	B(4)—B(9)	1.761(5)
Cu(3)—B(4)	2.212(4)	B(5)—B(6)	1.747(6)
Cu(3)—B(7)	2.187(4)	B(5)—B(9)	1.788(6)
Cu(3)—B(8)	2.130(4)	B(5)—B(10)	1.752(6)
P—C(11)	1.8192(24)	B(5)—H(5)	1.13(4)
P—C(21)	1.8179(25)	B(6)—B(10)	1.748(6)
P—C(31)	1.8178(25)	B(6)—B(11)	1.756(6)
S—CS(1)	1.784(5)	B(6)—H(6)	1.06(4)
S—CS(2)	1.800(6)	B(7)—B(8)	1.791(5)
S—B(4)	1.911(4)	B(7)—B(11)	1.792(6)
CS(1)—HS(11)	0.95(4)	B(7)—B(12)	1.784(6)
CS(1)—HS(12)	0.93(4)	B(7)—H(7)	1.13(4)
CS(1)—HS(13)	0.85(4)	B(8)—B(9)	1.789(5)
CS(2)—HS(21)	1.02(4)	B(8)—B(12)	1.781(5)
CS(2)—HS(22)	0.96(4)	B(8)—H(8)	1.11(4)
CS(2)—HS(23)	0.85(4)	B(9)—B(10)	1.792(6)
C(1)—C(2)	1.555(5)	B(9)—B(12)	1.779(6)
C(1)—B(4)	1.643(5)	B(9)—H(9)	1.11(4)
C(1)—B(5)	1.710(5)	B(10)—B(11)	1.770(6)
C(1)—B(6)	1.718(6)	B(10)—B(12)	1.801(6)
C(1)—H(1)	0.93(4)	B(10)—H(10)	1.15(4)
C(2)—B(6)	1.721(5)	B(11)—B(12)	1.764(6)
C(2)—B(7)	1.670(5)	B(11)—H(11)	1.00(4)
C(2)—B(11)	1.695(5)	B(12)—H(12)	1.17(4)
C(2)—H(2)	0.94(4)		

P—Cu(3)—C(1)	119.33(8)	C(1)—B(6)—B(5)	59.15(23)
P—Cu(3)—C(2)	122.48(8)	C(2)—B(6)—B(11)	58.35(23)
P—Cu(3)—B(4)	135.38(10)	B(5)—B(6)—B(10)	60.16(25)
P—Cu(3)—B(7)	142.18(10)	B(10)—B(6)—B(11)	60.7(3)
P—Cu(3)—B(8)	161.74(10)	Cu(3)—B(7)—C(2)	74.44(18)
C(1)—Cu(3)—C(2)	38.11(11)	Cu(3)—B(7)—B(8)	63.86(17)
C(1)—Cu(3)—B(4)	41.56(12)	C(2)—B(7)—B(11)	58.50(22)
C(2)—Cu(3)—B(7)	42.78(13)	B(8)—B(7)—B(12)	59.76(21)
B(4)—Cu(3)—B(8)	48.55(14)	B(11)—B(7)—B(12)	59.11(23)
B(7)—Cu(3)—B(8)	48.99(14)	Cu(3)—B(8)—B(4)	68.12(17)
Cu(3)—P—C(11)	115.67(8)	Cu(3)—B(8)—B(7)	67.15(17)
Cu(3)—P—C(21)	113.77(8)	B(4)—B(8)—B(9)	59.00(21)
Cu(3)—P—C(31)	111.81(8)	B(7)—B(8)—B(12)	59.94(21)
C(11)—P—C(21)	104.86(11)	B(9)—B(8)—B(12)	59.78(22)
C(11)—P—C(31)	105.05(11)	B(4)—B(9)—B(5)	60.31(22)
C(21)—P—C(31)	104.67(11)	B(4)—B(9)—B(8)	60.44(21)
CS(1)—S—CS(2)	98.6(3)	B(5)—B(9)—B(10)	58.59(23)
CS(1)—S—B(4)	104.49(21)	B(8)—B(9)—B(12)	59.88(22)
CS(2)—S—B(4)	108.47(22)	B(10)—B(9)—B(12)	60.58(23)
Cu(3)—C(1)—C(2)	70.08(17)	B(5)—B(10)—B(6)	59.87(25)
Cu(3)—C(1)—B(4)	63.29(17)	B(5)—B(10)—B(9)	60.61(24)
C(2)—C(1)—B(6)	63.23(23)	B(6)—B(10)—B(11)	59.86(25)
B(4)—C(1)—B(5)	64.21(23)	B(9)—B(10)—B(12)	59.36(23)
B(5)—C(1)—B(6)	61.27(24)	B(11)—B(10)—B(12)	59.20(24)
Cu(3)—C(2)—C(1)	71.81(18)	C(2)—B(11)—B(6)	59.81(23)
Cu(3)—C(2)—B(7)	62.78(17)	C(2)—B(11)—B(7)	57.15(21)
C(1)—C(2)—B(6)	62.99(23)	B(6)—B(11)—B(10)	59.46(25)
B(6)—C(2)—B(11)	61.83(24)	B(7)—B(11)—B(12)	60.22(23)
B(7)—C(2)—B(11)	64.35(23)	B(10)—B(11)—B(12)	61.27(24)
Cu(3)—B(4)—C(1)	75.15(18)	B(7)—B(12)—B(8)	60.31(21)
Cu(3)—B(4)—B(8)	63.33(16)	B(7)—B(12)—B(11)	60.67(23)

C(1)—B(4)—B(5)	59.71(22)	B(8)—B(12)—B(9)	60.33(22)
B(5)—B(4)—B(9)	60.60(22)	B(9)—B(12)—B(10)	60.06(23)
B(8)—B(4)—B(9)	60.56(21)	B(10)—B(12)—B(11)	59.52(24)
C(1)—B(5)—B(4)	56.07(21)	P—C(11)—C(12)	118.37(17)
C(1)—B(5)—B(6)	59.58(23)	P—C(11)—C(16)	121.61(17)
B(4)—B(5)—B(9)	59.08(22)	P—C(21)—C(22)	122.21(18)
B(6)—B(5)—B(10)	59.97(25)	P—C(21)—C(26)	117.68(18)
B(9)—B(5)—B(10)	60.80(24)	P—C(31)—C(32)	117.45(18)
C(1)—B(6)—C(2)	53.78(21)	P—C(31)—C(36)	122.49(18)
S—B(4)—C(1)	118.16(24)	S—B(4)—B(8)	128.85(24)
S—B(4)—B(5)	110.24(23)	S—B(4)—B(9)	119.60(24)

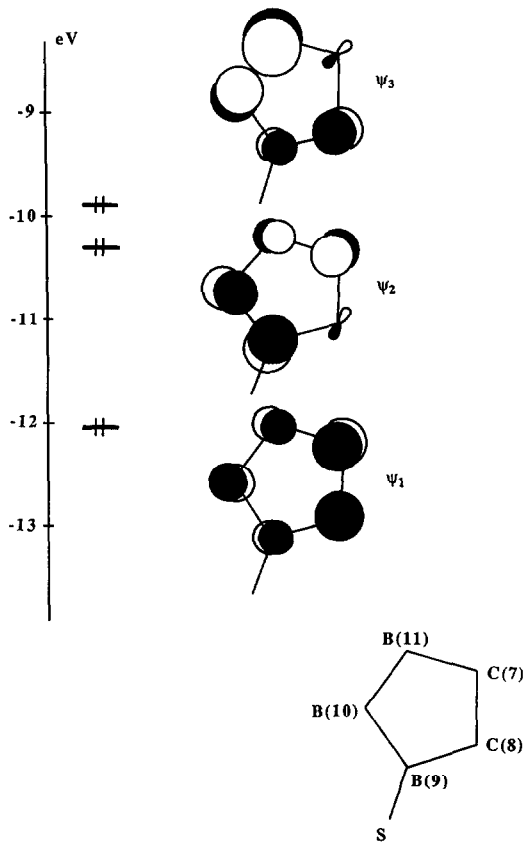

Fig. 2. The occupied π-molecular orbitals of [carb′]$^-$.

position above the centre of the C_2B_3 face. As with the series[1] [carbH]$^-$, [Ph$_3$PAucarb]$^-$ and [Ph$_3$PCucarb]$^-$, we have attempted to analyse the essential structural features of **1**, **2** and **3** by consideration of the forms of these ligand orbitals.

ψ_1 is fully analogous to the third highest occupied MO (HOMO) of [7,8-*nido*-$C_2B_9H_{11}$]$^{2-}$, being fully in phase and localized on the cage carbon atoms. ψ_2 and ψ_3 are localized on boron atoms and have near-orthogonal perpendicular nodal planes (as expected for orbitals analogous to the degenerate HOMOs of [C_5H_5]$^-$), but since [carb′]$^-$ lacks symmetry these nodal planes are not required to lie in any special direction; in fact, they appear to be rotated *ca* 36° with respect to those of [carb]$^{2-}$, the nodal plane of ψ_3, the HOMO of [carb′]$^-$, running from C(7) to the approximate mid-point of B(9)—B(10). ψ_3 is predominantly localized between B(10) and B(11), c.f. the HOMO of [carb]$^{2-}$ localized on B(10), explaining why H$^+$ and {Ph$_3$PAu}$^+$ fragments assume bridging sites in **1** and **2** but *endo*-terminal sites in [carbH]$^-$ and [Ph$_3$PAucarb]$^-$.

In Table 2 we list intrafacial distances for the carb′ ligand in **1**, **2** and **3**. Note that the accepted polyhedral numbering scheme[11] differs between *nido* **1** and **2**; and *closo* **3**, and for ready comparison the facial atoms in Table 2 are refered to the [9-SMe$_2$-7,8-*nido*-C_2B_9] framework typified by **1**.

The essential trends that are apparent in Table 2 as we more from **1** → **2** → **3** may be summarized as follows:

(i) The B—B distances, initially quite different, converge towards a common value.
(ii) Both C—B connectivities lengthen.
(iii) The C—C distance increases.

The general pattern of these trends is readily understandable by considering the depopulation of ψ_1–ψ_3 by the appropriate acceptor orbitals of H$^+$, {Ph$_3$PAu}$^+$ and {Ph$_3$PCu}$^+$, in a manner anal-

Table 2. Comparison of intrafacial distances (Å) for compounds **1**–**3**

	1[4a]	**2**[4b]	**3**
B(9)—B(10)	1.774(4)	1.772(8)	1.787(5)
B(10)—B(11)	1.847(5)	1.844(8)	1.791(5)
C(7)—B(11)	1.618(4)	1.636(8)	1.670(5)
C(8)—B(9)	1.577(5)	1.594(8)	1.643(5)
C(7)—C(8)	1.525(4)	1.558(8)	1.555(5)

ogous to our previous analysis[1] of the structures of $[carbH]^-$, $[Ph_3PAucarb]^-$ and $[Ph_3PCucarb]^-$. Briefly, as the acceptor fragment moves from bridging across B(10)—B(11) (H^+ and $\{Ph_3PAu\}^+$ fragments) to a much more central position above the five-atom face ($\{Ph_3PCu\}^+$ fragment), ψ_3 is depopulated less, and ψ_2 and ψ_1 are depopulated more. This is expected to result in the following structural changes:

(i) The changes in occupation of all three ligand orbitals will cause B(9)—B(10) to lengthen, and such lengthening is clearly apparent in **3** relative to **1** and **2**. B(10)—B(11) is expected to shorten as a consequence of the changes in occupation of ψ_3 and ψ_2, but lengthen due to the change in occupation of ψ_1. Clearly the former is the dominant effect, particularly as ψ_3 is heavily localized on these boron atoms.

(ii) C(7)—B(11) shows the anticipated lengthening as a result of increased deoccupation of both ψ_1 and ψ_2, being essentially unaffected by changes in ψ_3 since the nodal plane of the last passes close to C(7). Equally, the nodal plane of ψ_2 is close to C(8), and thus changes in the C(8)—B(9) distance are expected to reflect changes in the populations of, predominantly, ψ_1 and ψ_3. These are predicted to alter the C(8)—B(9) distance in opposite directions, but ψ_1 is much more carbon based, and thus it is quite reasonable that the change in its population, giving rise to a longer C(8)—B(9) connectivity, apparently dominates.

(iii) The length of C(7)—C(8) is influenced almost exclusively by changes in ψ_1. Increased deoccupation of this ligand orbital explains the longer C—C distance in **3** than in **1**. Less clear, however, is the cause of the apparently long C—C connectivity in **2**.

In summary, this kind of simple analysis goes a long way towards explaining structural patterns in the carb′ complexes carb′H, $Ph_3PAucarb'$ and $Ph_3PCucarb'$, and it is particularly rewarding that trends in the two independent facial B—C distances (which alter in the same direction) and two independent B—B distances (which alter in opposite directions) may be understood.

Acknowledgement—We thank the SERC for support (E.J.M.H.).

REFERENCES

1. E. J. M. Hamilton and A. J. Welch, *Polyhedron* 1990, **9**, 2407.
2. J. Buchanan, E. J. M. Hamilton, D. Reed and A. J. Welch, *J. Chem. Soc., Dalton Trans.* 1990, 677.
3. Y. Do, H. C. Kang, C. B. Knobler and M. F. Hawthorne, *Inorg. Chem.* 1987, **26**, 2348.
4. (a) J. Cowie, E. J. M. Hamilton, J. C. V. Laurie and A. J. Welch, *Acta Cryst.* 1988, **C44**, 1648; (b) E. J. M. Hamilton and A. J. Welch, *Acta Cryst.* 1990, **C46**, 1228; (c) J. Cowie, E. J. M. Hamilton, J. C. V. Laurie and A. J. Welch, *J. Organomet. Chem.* 1990, **394**, 1.
5. J. Plesek, Z. Janousek and S. Hermanek, *Collect. Czech. Chem. Commun.* 1978, **43**, 2862.
6. G. Costa, E. Reisenhover and L. Stefani, *J. Inorg. Nucl. Chem.* 1965, **27**, 2581.
7. G. M. Sheldrick, SHELX86. University of Göttingen (1986).
8. G. M. Sheldrick, SHELX76. University of Cambridge (1976).
9. N. G. Walker and D. Stuart, *Acta Cryst.* 1983, **A39**, 158.
10. *International Tables for X-ray Crystallography*, Vol. 4, Kynoch Press, Birmingham (1974).
11. J. B. Casey, W. J. Evans and W. H. Powell, *Inorg. Chem.* 1983, **22**, 2228.
12. J. Howell, A. Rossi, D. Wallace, K. Haraki and R. Hoffmann, *Quantum Chemistry Program Exchange*, No. 344. Univeristy of Indiana (1977).
13. J. H. Ammeter, H.-B. Burgi, J. C. Thibeault and R. Hoffmann, *J. Am. Chem. Soc.* 1982, **100**, 3686.
14. D. G. Evans and D. M. P. Mingos, *J. Organomet. Chem.* 1982, **232**, 171.
15. D. M. P. Mingos, M. I. Forsyth and A. J. Welch, *J. Chem. Soc., Dalton Trans.* 1978, 1363.
16. D. E. Smith and A. J. Welch, *Acta Cryst.* 1986, **C42**, 1717.

Polyhedron Vol. 10, No. 4/5, pp. 477–482, 1991
Printed in Great Britain

0277–5387/91 $3.00+.00
© 1991 Pergamon Press plc

THE PREPARATION AND PROPERTIES OF SOME TERTBUTYLIMIDOTUNGSTEN(VI) COMPLEXES. THE X-RAY CRYSTAL STRUCTURE OF $[W(NBu^t)(OBu^t)_3Cl(NH_2Bu^t)]$

DONALD C. BRADLEY,* ANDREW J. HOWES, MICHAEL B. HURSTHOUSE* and JOHN D. RUNNACLES

Department of Chemistry, Queen Mary and Westfield College, Mile End Road, London E1 4NS, U.K.

(*Received* 26 *September* 1990; *accepted* 1 *November* 1990)

Abstract—Reactions of $[W(NBu^t)_2(NHBu^t)_2]$ (**1**) with ROH (R = Pr^i, Bu^t, CPh_3) gave $[W(NBu^t)(OPr^i)_4]$ (**2**), $[W(NBu^t)(OBu^t)_4]$ (**3**) and $[W(NBu^t)_2(OCPh_3)_2]$ (**4**). Reaction of $WOCl_4$ with $Bu^t(Me_3Si)NH$ gave $[WO(NBu^t)(NHBu^t)Cl(NH_2Bu^t)]$ (**5**) which was converted to $[WO(NBu^t)(OBu^t)_2(NH_2Bu^t)]$ (**6**) with trace amounts of $[W(NBu^t)(OBu^t)_3Cl(NH_2Bu^t)]$ (**7**) by reaction with Bu^tOH. Compound **7** was structurally characterized by single crystal X-ray crystallography. It has a distorted octahedral structure with the tertbutylimido (WN = 1.740 Å) and tertbutylamine (WN = 2.429 Å) *trans* to each other, with the three tertbutoxy (WO = 1.897, 1.864, 1.892 Å) and chloride (WCl = 2.503 Å) ligands in the equatorial plane. Compound **5** reacted with PMe_3 to give $[WO(NBu^t)_2(PMe_3)]$ (**8**).

The bis-tertbutylimido-bis-tertbutylamido tungsten(VI) compound $[W(NBu^t)_2(NHBu^t)_2]$ (**1**) was isolated by Nugent and Harlow from the reaction of WCl_6 with excess Bu^tNH_2.[1] Compound **1** was found to react with tertbutyl alcohol or triphenylsilanol to give the derivatives $W(NBu^t)_2(OR)_2$ (R = Bu^t, Ph_3Si).[1] More recently, Chan *et al.*[2] have shown that with pinacols ($HOCR_2CR_2OH$) the nature of the product of the reaction with **1** depends on group R.

$$W(NBu^t)_2(NHBu^t)_2 + HOC(CF_3)_2C(CF_3)_2OH \longrightarrow Bu^tNH_2 \longrightarrow W(NBu^t)_2\{OC(CF_3)_2C(CF_3)_2O\}(Bu^tNH_2) \quad (1)$$

$$W(NBu^t)_2(NHBu^t)_2 + HOC(Ph)_2C(Ph)_2OH \longrightarrow W(NBu^t)(NHBu^t)_2\{OC(Ph)_2C(Ph)_2O\} + 2Bu^tNH_2. \quad (2)$$

Although a single isomer was present in the crystalline state, ^1H and ^{13}C NMR studies showed that in solution a dynamic equilibrium between the isomeric forms, **I** and **II**, occurred (R = Me, CF_3, Ph).

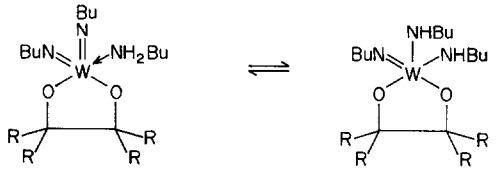

(I) (II)

We now report some results on the reactions of **1** with Pr^iOH and Bu^tOH.

In addition, we have studied the reaction of $WOCl_4$ with $Bu^t(Me_3Si)NH$ as a means of synthesizing oxo-organoimido complexes of tungsten(VI).

RESULTS AND DISCUSSION

Reaction of **1** with four equivalents of Pr^iOH gave $[W(NBu^t)(OPr^i)_4]$ as a volatile (sublimes 50–60°C/10^{-3} torr), colourless, crystalline compound, **2**:

$$W(NBu^t)_2(NHBu^t)_2 + 4Pr^iOH \longrightarrow [W(NBu^t)(OPr^i)_4] + 3Bu^tNH_2. \quad (3)$$

The highest mass peak in the mass spectrum of **2** corresponded to the fragment ion $[W(NBu^t)(OPr^i)_3]^+$

* Authors to whom correspondence should be addressed.

and the ^{1}H NMR spectrum showed the presence of two types of isopropoxide in the ratio of 3 : 1 which suggests that it might be a mononuclear complex with a trigonal bipyramidal configuration with three isopropoxo groups equatorial and one axial. It is noteworthy that the analogous complex $[W_2(NC_6H_4Me\text{-}p)_2(\mu\text{-}OPr^i)_2(OPr^i)_6]$ has been structurally characterized as a dimer by single crystal X-ray diffraction.[3]

Reaction of **1** with four equivalents of tertbutanol gave $[W(NBu^t)(OBu^t)_4]$ (**3**) as a volatile (sublimes 70–80°C/10^{-3} torr), colourless, crystalline compound which was very soluble in hydrocarbon solvents. Its mass spectrum gave a highest mass fragment ion corresponding to $[W(NBu^t)(OBu^t)_3]^+$. The ^{1}H and ^{13}C NMR spectra showed the presence of one type of tertbutoxy ligand suggesting that **3** is monomeric in solution. Steric hindrance of the tertbutoxo groups prevents dimerization. Although a single crystal was grown from CS_2 at −30°C it was not possible to solve the structure fully due to disorder, but the presence of a four-fold axis suggests a tetragonal, pyramidal structure with the tertbutoxo groups at the base. The presence of the tertbutyl imido group in the apical position probably caused the problems in solving the structure due to its three-fold symmetry.

In contrast to $W(NBu^t)(OPr^i)_4$ which readily reacts with more Pr^iOH to form $W(OPr^i)_6$, compound **3** did not react further with excess Bu^tOH. Interestingly, it was not possible to isolate an intermediate complex, $[W(NBu^t)(NHBu^t)(OBu^t)_3]$, by the reaction of **1** with three equivalents of Bu^tOH; instead an equimolecular mixture of $W(NBu^t)_2(OBu^t)_2$ and $W(NBu^t)(OBu^t)_4$ was obtained suggesting that $W(NBu^t)(NHBu^t)(OBu^t)_3$ reacts faster with Bu^tOH than does $W(NBu^t)_2(OBu^t)_2$.

Reaction of **1** with two equivalents of triphenylcarbinol gave $[W(NBu^t)_2(OCPh_3)_2]$ (**4**) as a colourless solid.

We have explored the synthesis of tungsten oxo tertbutylimido complexes by using $WOCl_4$ as starting material. When either Bu^tNH_2 or Bu^tLiNH were used an intractable mixture of products was obtained but from the reaction of $WOCl_4$ and $Bu^t(Me_3Si)NH$ we obtained $[WO(NBu^t)(NHBu^t)Cl(NH_2Bu^t)]$ (**5**) as a pale yellow solid which was characterized by ^{1}H and ^{13}C NMR and IR spectra:

$$WOCl_4 + 3Bu^t(Me_3Si)NH \longrightarrow [WO(NBu^t)(NHBu^t)Cl(NH_2Bu^t)] + 3Me_3SiCl. \quad (4)$$

The IR spectrum of **5** gave a strong band at 970 cm^{-1} due to the terminal W=O stretching vibration and bands at 3250, 3190 and 3130 cm^{-1} due to NH_2 and NH stretching vibrations. Broad peaks in the ^{1}H NMR (C_6D_6 solution at δ 7.56 and 11.57) were assigned to NH_2 and NH protons, respectively. Although a parent molecular ion was not observed in the mass spectrum a fragment ion was observed (*m/z*, 395) corresponding to the species $(\mathbf{5}-C_4H_8)^+$. Unfortunately we were unable to grow a single crystal for X-ray crystallographic studies and the structure of **5** is a matter for conjecture.

If the oxo- and tertbutylimido ligands in **5** are both acting as four-electron donors then the tungsten(VI) attains an 18-electron configuration as a mononuclear five-coordinated complex. A trigonal pyramidal structure seems likely with the tertbutylimido and tertbutylamine ligands *trans* to one another in the axial positions and the chloro, tertbutylamido and oxo ligands in the equatorial plane. By placing the four-electron donors *cis* to one another they are able to maximize their π-bonding involving the vacant metal *d*-orbitals. A plausible alternative would place the oxo and chloro ligands *trans* to each other in the axial positions and the three bulky tertbutyl-containing ligands in the equatorial plane.

Also a matter for conjecture is the origin of the tertbutylamine which could be formed either by an intramolecular α-hydrogen transfer in an intermediate: $WO(NHBu^t)_3Cl \rightarrow [WO(NBu^t)(NHBu^t)Cl(NH_2Bu^t)]$; or by reaction of $Bu^t(Me_3Si)NH$ with HCl to give Me_3SiCl and Bu^tNH_2. Previous work[4] has shown that Bu^tNH_2 is formed in the reactions of $[W(NR)Cl_4]_2$ (R = Ph, C_6H_4Me-*p*) with $Bu^t(Me_3Si)NH$ which gave the dimeric complexes $[W(NR)(NBu^t)Cl_2(NH_2Bu^t)]_2$, which were structurally characterized by X-ray diffraction.

Compound **5** is interesting in containing tertbutylimido, tertbutylamido and tertbutylamine ligands bonded to tungsten, and may be compared with the vanadium[5] and tantalum[6] complexes, $[M(NBu^t)(NHBu^t)Cl_2(NH_2Bu^t)]_2$ (M = V, Ta).

Compound **5** was treated with one equivalent of Bu^tOH in an attempt to replace the tertbutylamido group by the tertbutoxo, but $[WO(NBu^t)(OBu^t)_2(NH_2Bu^t)]$ (**6**) was obtained in small yield instead of $[WO(NBu^t)(OBu^t)Cl(NH_2Bu^t)]$. Also, treatment of **5** with one equivalent of Bu^tLiO gave a small yield of **6** instead of the expected $[WO(NBu^t)(NHBu^t)(OBu^t)(NH_2Bu^t)]$. The best yield of **6** was obtained by treating **5** with two equivalents of Bu^tOH in the presence of tertbutylamine:

$$[WO(NBu^t)(NHBu^t)Cl(NH_2Bu^t)] + 2Bu^tOH \longrightarrow [WO(NBu^t)(OBu^t)_2(NH_2Bu^t)] + Bu^tNH_3Cl. \quad (5)$$

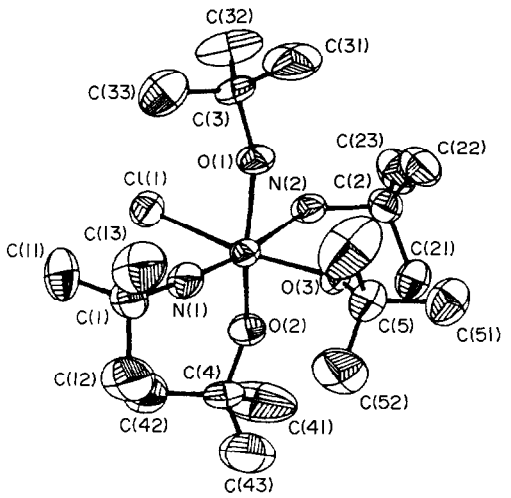

Fig. 1. ORTEP plot of $[W(NBu^t)(OBu^t)_3Cl(NH_2Bu^t)]$ (**7**): organoimido nitrogen, N(1); amine nitrogen, N(2).

Compound **6** was crystallized from pentane at −30°C as colourless crystals and its high volatility (sublimes 45–66°C/10^{-3} torr) suggests a mononuclear complex with five-coordinated tungsten(VI). Attempts to grow single crystals from solution or by sublimation suitable for X-ray diffraction were unsuccessful. The IR spectrum showed two sharp N—H stretching vibrations (3326, 3317 cm^{-1}) and a terminal W=O stretching vibration (970 cm^{-1}). In the course of recrystallizing **6**, a single crystal was obtained which was shown by X-ray crystallography to be the complex $[W(NBu^t)(OBu^t)_3Cl(NH_2Bu^t)]$ (**7**) which contains no oxo ligand. The structure of **7** is depicted in Fig. 1 and some bond lengths and bond angles are given in Table 1. The octahedral tungsten(VI) atom has the tertbutylimido group (W ≡ N = 1.74 Å) *trans* to the tertbutylamine (W ← N = 2.429 Å), and the three tertbutoxo (W—O = 1.897, 1.892, 1.864 Å) and chloro ligands in the equatorial plane. This structure is entirely analogous to that of $[W(NPh)(OBu^t)_3Cl(NH_2Bu^t)]$ obtained from the reaction of $[W(NPh)Cl_4]_2$ with Bu^tOH and Bu^tNH_2.[7] The formation of **7** apparently as a minor product of the reaction of $[WO(NBu^t)(NHBu^t)Cl(NH_2Bu^t)]$ with Bu^tOH is puzzling especially as the reaction of either compound **5** or **6** with excess Bu^tOH gave the tungsten oxo tetratertbutoxide $WO(OBu^t)_4$ without loss of the oxo ligand. Loss of the oxo ligand might have occurred in the genesis of compound **5** from the reaction of $WOCl_4$ with $Bu^t(Me_3Si)NH$ due to attack of the Si—N bond by the W=O oxygen, viz.

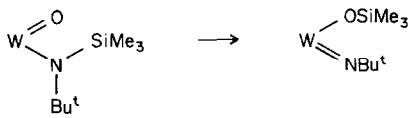

(6)

Exchange of the trimethylsiloxo ligand by tertbutanol would complete the removal of the oxo ligand.

Finally, we report one other interesting reaction of compound **5**. In an attempt to replace the coordinated Bu^tNH_2 by another Lewis base, **5** was treated with PMe_3. The tungsten product isolated was $[WO(NBu^t)_2(PMe_3)]$ (**8**) after separation from tertbutylamine hydrochloride [eq. (7)]:

$$[WO(NBu^t)(NHBu^t)Cl(NH_2Bu^t)] + PMe_3 \longrightarrow Bu^tNH_3Cl + [WO(NBu^t)_2(PMe_3)]. \quad (7)$$

Compound **8** was characterized by ^1H NMR [80 MHz, C_6D_6; δ, 1.21 (PMe_3); 1.23 (NBu^t)] and IR [ν(W=O), 970 cm^{-1}; absence of NH_2 or NH stretching vibrations] spectroscopy. The PMe_3 protons gave a doublet ($^2J_{HP}$ = 10 Hz) with ^{183}W satellites ($^3J_{HW}$ = 2 Hz). Although no molecular ion was detected in the mass spectrum a number of fragment ions were observed.

Table 1. Selected bond lengths (Å) and bond angles (°) in $[W(NBu^t)Cl(OBu^t)_3(NH_2Bu^t)]$ (**7**)

W—N(1)	1.740(9)	W—O(1)	1.897(7)
W—N(2)	2.429(5)	W—O(2)	1.864(8)
W—Cl	2.503(5)	W—O(3)	1.892(6)

W—N(1)—C(1)	171.9(5)	O(1)—W—Cl	84.4(2)
W—N(2)—C(2)	130.8(4)	O(1)—W—O(2)	155.6(3)
N(1)—W—N(2)	168.6(2)	O(1)—W—O(3)	91.8(3)
N(1)—W—Cl	91.7(3)	O(1)—W—N(2)	78.3(3)
N(1)—W—O(1)	100.8(4)	O(2)—W—N(2)	77.8(3)
N(1)—W—O(2)	101.7(4)	O(3)—W—N(2)	87.6(3)
N(1)—W—O(3)	103.8(3)	Cl—W—N(2)	76.8(2)

EXPERIMENTAL

Preparations and manipulations were carried out under dry, oxygen-free nitrogen using standard Schlenk tube techniques. Solvents were distilled from the sodium ketyl of benzophenone and stored over molecular sieve (4 Å). $WOCl_4$ was prepared from WO_3 and $SOCl_2$ and sublimed[8] and $[W(NBu^t)_2(NHBu^t)_2]$ (**1**) was prepared from WCl_6 and Bu^tNH_2 by the literature method.[1] NMR spectra were obtained using Bruker WP-80 or WM-250 instruments and IR spectra using a Perkin–Elmer 577 spectrophotometer between 4000 and 200 cm^{-1} using Nujol mulls between CsI plates. Mass spectra were obtained by direct insertion using an AEI MS-902 spectrometer operating at 70 eV. Elemental analyses were obtained from the Microanalytical Laboratory, University College, London.

Preparation of $[W(NBu^t)_2(OCPh_3)_2]$ (**4**)

A solution of Ph_3COH (1.27 g, 4.9 mmol) in THF (30 cm^3) was added to a solution of $W(NBu^t)_2(NHBu^t)_2$ (1.15 g, 2.45 mmol) in benzene (30 cm^3) and the mixture stirred for 18 h. Solvents were evaporated off *in vacuo* and the residue crystallized from toluene–heptane (1 : 3) giving colourless needles (0.82 g) which were supplemented by another crop (0.56 g) obtained by concentrating the mother liquor, adding more heptane and cooling to −25°C. The combined batches were washed with pentane and dried *in vacuo* (1.38 g, 71% yield). Found: C, 66.2; H, 5.8; N, 3.1. $C_{38}H_{48}O_2N_2W$ requires: C, 65.5; H, 5.7; N, 3.3%. ^{1}H NMR (80 MHz, C_6D_6): δ, 1.18 (18H, s, =NBu^t), 7.05–7.60 (30H, m, aromatic CHs). ^{13}C NMR (20.1 MHz, $CDCl_3$): δ, 32.85 [NC(CH_3)$_3$], 66.19 [NC(CH$_3$)$_3$] 90.91 (OCPh$_3$), 126.99 (OCPh$_3$, *para*-C), 127.59, 128.56 (OCPh$_3$, *ortho*- and *meta*-C), 147.81 (OCPh$_3$, *ipso*-C). IR spectrum: 1595m, 1490m, 1445s, 1355m, 1295m, 1238s, 1215m, 1152m, 1086m, 1048s, 998s, 942m, 920m, 900m, 845w, 818s, 798s, 764s, 755m, 735m, 698s, 670w, 625m cm^{-1}.

Preparation of $[W(NBu^t)(OBu^t)_4]$ (**3**)

Bu^tOH (3.06 cm^3, 32.4 mmol) was added dropwise to a solution of $W(NBu^t)_2(NHBu^t)_2$ (3.82 g, 8.1 mmol) in pentane (20 cm^3) and the mixture stirred for 18 h followed by removal of solvent *in vacuo*. The colourless viscous residue was heated at 40–50°C/10^{-3} torr to remove the small amount of $W(NBu^t)_2(OBu^t)_2$ present, followed by sublimation at 70–80°C/10^{-3} torr. The sublimate was contaminated with a trace of $W(NBu^t)_2(OBu^t)_2$ which was removed by crystallization from pentane at −78°C (1.55 g, 34% yield). The low yield was caused by the very high solubility of **3** in pentane. Found: C, 41.9; H, 7.9; N, 2.6. $C_{20}H_{45}O_4NW$ requires: C, 43.9; H, 8.2; N, 2.6%. ^{1}H NMR (80 MHz, C_6D_6): δ, 1.34 (9H, s, NBu^t), 1.52 (36H, s, OBu^t). ^{13}C NMR (20.1 MHz, C_6D_6): δ, 32.17 (OBu^t, CH_3), 32.83 (NBu^t, CH_3), 69.12 (NBu^t, CMe$_3$), 80.48 (OBu^t, CMe$_3$). IR spectrum: 1469m, 1382m, 1360s, 1280m, 1235m, 1175vs, 1025w, 955vs, 782s, 550m, 520w, 480m, 368m, 282w cm^{-1}. Mass spectrum (m/z): 472 [W(NBu^t)(OBu^t)$_3$], 416 [W(NBu^t)$_2$(OH)], 360 [W(OBu^t)$_2$O$_2$], 304 [W(OBu^t)(OH)O$_2$], 288 [W(OBu^t)(OH)O], 248 [W(OH)$_2$O$_2$], 59 (C_3H_7O), 58 (C_3H_6O), 57 (C_4H_9).

Preparation of $[W(NBu^t)(OPr^i)_4]$ (**2**)

Compound **2** was obtained by adding Pr^iOH (4 mol) to $W(NBu^t)_2(NHBu^t)_2$ (1 mol) in a similar manner to the previous experiment and was obtained as colourless crystals (50% yield) after sublimation at 50–60°C/10^{-3} torr. ^{1}H NMR (250 MHz, C_6D_6): δ, 1.31 (9H, s, NBu^t), 1.36 [18H, d (^3J = 6 Hz), OCH(CH_3)$_2$], 1.52 [6H, d (^3J = 6.2 Hz), OCH (CH_3)$_2$], 4.95 [3H, sept. (^3J = 6.0 Hz), OCHMe$_2$], 5.14 [1H, sept. (^3J = 6.2 Hz), OCHMe$_2$]. IR spectrum: 1370s, 1355s, 1319s, 1275vs, 1212m, 1160s, 1110s, 970vs, 842vs, 805w, 770m, 665s, 605s, 578s, 528s, 448s, 422m, 375w, 340m, 300 cm^{-1}. Mass spectrum (m/z): 430 [W(NBu^t)(OPr^i)$_3$], 388 [W(NBu^t)(OPr^i)$_2$(OH)], 371 [W(NBu^t)(OPr^i)$_2$], 346 [W(NBu^t)(OPr^i)(OH)$_2$], 304 [W(NBu^t)(OH)$_3$], 248 [W(NH)(OH)$_3$], 59 (C_3H_7O), 58 (C_3H_6O), 57 (C_4H_9), 56 (C_4H_8).

Preparation of $[WO(NBu^t)(NHBu^t)Cl(NH_2Bu^t)]$ (**5**)

$Bu^t(Me_3Si)NH$ (2.43 cm^3, 12.5 mmol) was added dropwise to a suspension of $WOCl_4$ (1.95 g, 5.70 mmol) in benzene (50 cm^3) and the mixture, which quickly changed colour from dark red to pale orange, was stirred for 48 h. The pale yellow solution was filtered and the filtrate evaporated *in vacuo* leaving a pale yellow gum which was treated with pentane (3 × 30 cm^3) until a pale yellow powder (1.57 g, 61% yield) was obtained. Satisfactory elemental analyses were not obtained. ^{1}H NMR (80 MHz, C_6D_6): δ, 1.35 (9H, s, NH$_2$Bu^t), 1.44 (9H, s, NHBu^t), 1.56 (9H, s, =NBu^t), 7.56 (2H, broad s, $\Delta\omega_{1/2}$ = 20 Hz, NH_2Bu^t), 11.57 (1H, broad s, $\Delta\omega_{1/2}$ = 8 Hz, NHBu^t). ^{13}C NMR (20.1 MHz, C_6D_6): δ, 26.68 [NH$_2$C(CH_3)$_3$], 28.62 [NHC (CH_3)$_3$], 30.93 [=NC(CH_3)$_3$], 52.92 (NH$_2$$CMe_3$), 60.99 (NH$CMe_3$), 70.99 (=N$CMe_3$). IR spectrum. 3250m, 3190sh, 3130s, 1605m, 1582w, 1481s,

1402m, 1362s, 1345m, 1292m, 1255vs, 1215s, 1195s, 970m, 845m, 802m, 792m, 708m, 580w, 450w, 325s cm^{-1}. Mass spectrum (*m/z*): 395 (**5**−C_4H_8), 380 (**5**−C_4H_8−CH_3), 324 (**5**−$2C_4H_8$−CH_3), 58 (C_4H_{10}), 57 (C_4H_9).

Preparation of [$WO(NBu^t)(OBu^t)_2(NH_2Bu^t)$] (**6**)

Compound **5** (1.15 g, 2.55 mmol) was suspended in pentane (50 cm^3) and Bu^tOH (0.75 cm^3, 7.65 mmol) was added. The tungsten starting material dissolved and a white solid (identified as Bu^tNH_3Cl) was precipitated over a period of 8 h. After filtration, the filtrate was concentrated to *ca* 4 cm^3 and cooled to −78°C giving colourless crystals (0.42 g, 33% yield). The low yield resulted from the high solubility of **6** in pentane. The compound was sublimed at 45–60°C/10^{-3} torr with loss due to decomposition. Found: C, 39.7; H, 7.8; N, 4.7. $C_{16}H_{38}O_3N_2W$ requires: C, 39.2; H, 7.8; N, 4.9%. ^1H NMR (80 MHz, C_6D_6): δ, 1.14 (9H, s, NH_2Bu^t), 1.42 (18H, s, OBu^t), 1.56 (9H, s, NBu^t), 3.11 (2 H, broad s, $\Delta\omega_{1/2}$ = 10 Hz, NH_2Bu^t). ^{13}C NMR (20.1 MHz, C_6D_6): δ, 31.21 [$NH_2C(CH_3)_3$], 31.46 [large broad peak, overlapping $NC(CH_3)_3$ and $OC(CH_3)_3$], 52.34 (NH_2CMe_3), 71.74 ($NCMe_3$), 84.83 ($OCMe_3$). IR spectrum: 3326m, 3167m, 1560m, 1382vs, 1374sh, 1361vs, 1260vs, 1250vs, 1235, 1150vs, 1118s, 1019s, 970vs, 931vs, 911vs, 845w, 805m, 790s, 748m, 708m, 632m, 600m, 568s, 482sh, 469m, 452sh, 376m, 367m, 282vs, 255sh cm^{-1}. Mass spectrum (*m/z*): 400 (**6**−CH_3−Bu^tNH_2), 344 (**6**−Bu^tNH_2−Bu^tN), 342 (**6**−Bu^tNH_2−Bu^tO), 327 (**6**−Bu^tNH_2−Bu^tO−CH_3), 269 (**6**−$2Bu^tO$−Bu^tNH_2), 59 (C_3H_7O), 58 (C_4H_{10}), 57 (C_4H_9).

Preparation of [$WO(NBu^t)_2(PMe_3)$] (**8**)

Compound **6** (0.35 g, 0.78 mmol), dissolved in benzene (10 cm^3), was treated with PMe_3 (0.07 cm^3, 0.78 mmol) which caused a colour change from pale yellow to orange. The mixture was stirred for 18 h and the solvent evaporated off *in vacuo* and the off-white solid washed with pentane (10 cm^3). The residue contained some Bu^tNH_3Cl (IR spectrum) which was removed by dissolving the product in benzene and filtering. Evaporation of the filtrate *in vacuo* left the solid product (0.17 g, 53% yield). ^1H NMR (80 MHz, C_6D_6): δ, 1.21 [9H, *d* ($^2J_{HP}$ = 10 Hz), PMe_3], 1.23 (18H, s, NBu^t). IR spectrum: 1420m, 1376m, 1358s, 1289m, 1276s, 1261m, 1238s, 1210s, 1140m, 970s, 955sh, 805m, 760w, 750m, 680w, 583m, 499w, 320s, 282m cm^{-1}. Mass spectrum (*m/z*): 284 (**8**−C_4H_8−PMe_3), 283 (**8**−C_4H_9−PMe_3), 269 (**8**−C_4H_8−PMe_3−CH_3), 268 (**8**−C_4H_9−PMe_3−CH_3), 267 (**8**−C_4H_9−$OPMe_3$), 76 (PMe_3), 61 (PMe_2), 57 (C_4H_9).

X-ray crystallography

Structure determination of compound **7**. All X-ray measurements were made on a crystal of dimensions 0.45 × 0.40 × 0.25 mm^3 sealed under argon in a thin-walled glass capillary. Following preliminary X-ray photography, unit cell dimensions and intensities were obtained using standard procedures and a CAD4 diffractometer, operating in the ω–2θ scan mode with graphite monochromated Mo-K_α radiation (λ = 0.71069 Å). The intensity data were corrected for absorption using psi-scan profiles. The structure was solved via the heavy atom method and refined by full-matrix least-squares. Non-hydrogen atoms were assigned anisotropic displacement factor coefficients, hydrogen atoms were included in idealized positions and refined as components of rigid groups with group N_{iso} values. Experimental details are as follows. Crystal data: $C_{20}H_{47}ClN_2O_3W$, *Mr* = 582.95, monoclinic, *a* = 17.714(2), *b* = 10.647(4), *c* = 15.328(3) Å, β = 108.13(1)°, *V* = 2747.2 $Å^3$, space group $P2_1/a$, *Z* = 4, D_c = 1.41 g cm^{-3}, μ = 44.1 cm^{-1}.

Data collection: $1.5 \leqslant \theta \leqslant 25.0°$, *T* = 265 K, total data measured 5271, total unique 4821, observed [$F_o > 3\sigma(F_o)$] 3581.

Refinement: 432 parameters, weights = $[\sigma^2(F_o)+0.0001F_o^2]^{-1}$, *R* = 0.038, R_ω = 0.034.

Scattering factor data were as included in the SHELX program or obtained from ref. 9, and calculations were made on a VAX11/750 using SHELX80[10] and associated programs.

Acknowledgements—We thank the SERC for financial support (research studentships to A.J.H. and J.D.R.). We are grateful to Mr Greg Coumbarides for obtaining the 250 MHz NMR spectra and to Mr Peter Cook for obtaining the mass spectra.

REFERENCES

1. W. A. Nugent and R. L. Harlow, *Inorg. Chem.* 1980, **19**, 777.
2. D. M. T. Chan, W. C. Fultz, W. A. Nugent, D. C. Roe and T. H. Tulip, *J. Am. Chem. Soc.* 1985, **107**, 251.
3. W. Clegg, R. J. Errington and C. Redshaw, personal communication.
4. D. C. Bradley, R. J. Errington, M. B. Hursthouse,

A. J. Nielson and R. L. Short, *Polyhedron* 1983, **2**, 483; B. R. Ashcroft, A. J. Nielson, D. C. Bradley, R. J. Errington, M. B. Hursthouse and R. L. Short, *J. Chem. Soc., Dalton Trans.* 1987, 2059.
5. F. Pruess, E. Fuchslocher and W. Sheldrick, *Z. Naturfor.* 1985, **40B**, 363.
6. A. C. Jones, A. J. Nielson and C. E. F. Rickard, *J. Chem. Soc., Chem. Commun.* 1984, 205.
7. A. J. Nielson, J. M. Waters and D. C. Bradley, *Polyhedron* 1985, **4**, 285.
8. R. Colton and I. B. Tomkins, *Aust. J. Chem.* 1965, **18**, 447.
9. *International Tables for X-ray Crystallography.* Kynoch Press, Birmingham (1974).
10. G. M. Sheldrick, SHELX80: Enlarged version of SHELX76. University of Cambridge (1976).

Polyhedron Vol. 10, No. 4/5, pp. 483–489, 1991
Printed in Great Britain

0277–5387/91 $3.00+.00
Pergamon Press plc

REACTION OF 1,1′-DIACETYLFERROCENE WITH HYDRAZINE HYDRATE: SYNTHESIS AND X-RAY CRYSTAL STRUCTURES OF BIS(HYDRAZINE)BIS(HYDRAZINECARBOXYLATO-N′,O)IRON(II), $[Fe(N_2H_4)_2(O_2CNHNH_2)_2]$, AND THE CYCLIC BIFERROCENE DIAZINE, $[—N(Me)CC_5H_4FeC_5H_4C(Me)N—]_2$

REV. MICHAEL T. CASEY,* PAULINE GUINAN, ANGELA CANAVAN and MALACHY McCANN*

Chemistry Department, St. Patrick's College, Maynooth, Co. Kildare, Ireland

and

CHRISTINE CARDIN* and NORAH B. KELLY

Chemistry Department, Trinity College, Dublin, Ireland

(*Received* 10 *July* 1990; *accepted* 2 *November* 1990)

Abstract—1,1′-Diacetylferrocene reacts with neat hydrate over a period of 72 h at 20°C to give the dihydrazone $[H_2NN(Me)CC_5H_4FeC_5H_4C(Me)NNH_2]$ (**6**) in almost quantitative yield. Either prolonging the reaction time or reacting **6** with fresh hydrazine causes the iron to be stripped from the metallocene and bis(hydrazine)bis(hydrazinecarboxylato-N′,O) iron(II), $[Fe(N_2H_4)_2(OOCNHNH_2)_2]$ (**11**), crystallizes. In the presence of Ba^{2+} or Mo^{2+} ions two molecules of complex **6** react to give the cyclic diazine $[—N(Me)CC_5H_4FeC_5H_4C(Me)N—]_2$ (**7**) in high yield. Hydrazine is liberated in this reaction. Complexes **6** and **11** have been characterized crystallographically. The cyclic voltammograms of complexes **6** and **7** contain essentially non-reversible oxidation peaks.

In 1973 Gol'din *et al.*[1] found that formyl- and acetylferrocene reacted with hydrazine to give the azines **1** and **2**, respectively (Scheme 1). The same paper described the synthesis of the hydrazones **3** and **4** from formylferrocene and the respective disubstituted hydrazine. Furthermore, the authors found that a warm ethanolic solution of 1,1′-diacetylferrocene (0.02 mol) reacted with hydrazine (0.05 mol) to give the monohydrazone of the azine **5** in 26% yield (Scheme 2).[1]

We have discovered that when 1,1′-diacetylferrocene is stirred with a large excess of neat hydrazine hydrate at room temperature for *ca* 72 h (see later) the dihydrazone **6** precipitates in almost quantitative yield (Scheme 2). Similar double Schiff-base condensation reactions are known to occur when 1,1′-diacetylferrocene is treated with solutions of thiocarbonhydrazide, semicarbazide, benzoic acid hydrazide and *p*-nitrobenzoic acid hydrazide.[2]

Complex **6** reacts with an alcoholic solution of $Ba(ClO_4)_2$ {or $[Mo_2(\mu\text{-}O_2CCH_3)_2(MeCN)_6][BF_4]_2$}[3] to give the cyclic diazine **7** in high yield (Scheme 2). The X-ray crystal structure of complex **7** (Fig. 1 and Table 1) contains staggered ferrocene rings and therefore a slightly twisted macrocycle, in keeping with the chirality found in the solid state (space group is the non-centrosymmetric $P2_1$). The nitrogen lone pairs are directed away from the centre of the macrocycle.

The cyclization reaction leading to the formation of complex **7** possibly proceeds via the metal-ion-catalysed transamination (amine exchange) route outlined in Scheme 3. Coordination of the NH_2 groups to the Ba^{2+} ion as in species **8** makes the C=N groups more susceptible to intermolecular

* Authors to whom correspondence should be addressed.

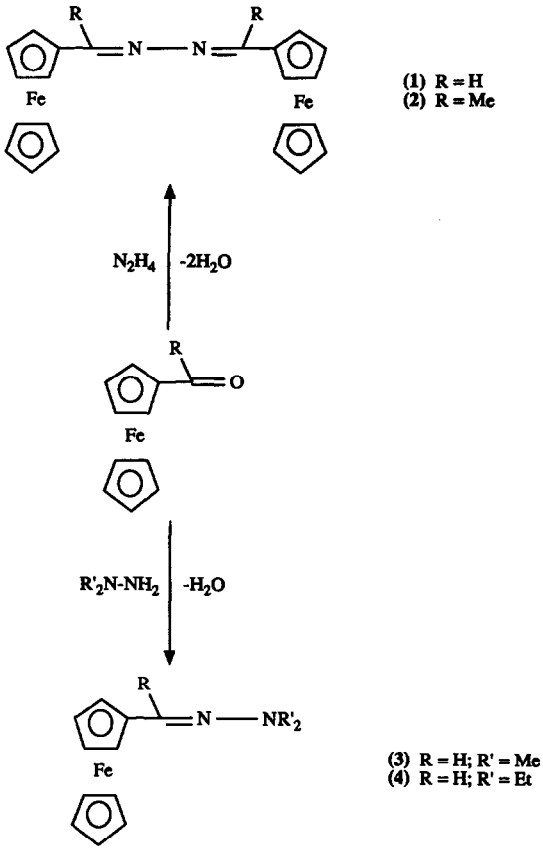

Scheme 1.

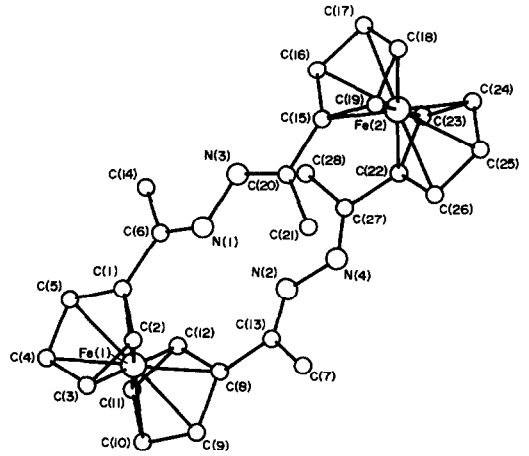

Fig. 1. Structure of complex **7**.

nucleophilic attack by **6**, thus leading to the formation of the *gem*-diamine addition compound **9**. Elimination of one molecule of hydrazine would then give the azinedihydrazone **10**. Ring closure is effected by intramolecular nucleophilic attack on the second imine, followed by the elimination of a second hydrazine molecule. The liberated N_2H_4 was detected by adding one drop of Nessler's reagent[4] to the reaction filtrate after the removal of complex **7** (immediate formation of a black precipitate).

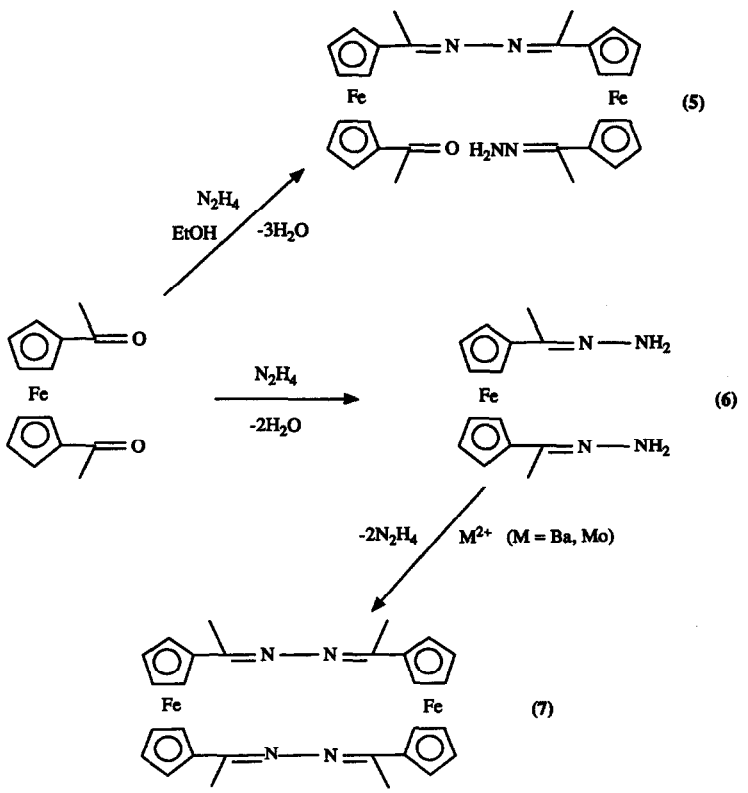

Scheme 2.

Table 1. Bond lengths (Å) and angles (°) for complex **7**

C(1)—Fe(1)	2.065(13)	C(2)—Fe(1)	2.074(15)
C(3)—Fe(1)	2.085(15)	C(4)—Fe(1)	2.052(14)
C(5)—Fe(1)	2.053(14)	C(8)—Fe(1)	2.047(12)
C(9)—Fe(1)	2.054(13)	C(10)—Fe(1)	2.038(14)
C(11)—Fe(1)	2.029(16)	C(12)—Fe(1)	2.059(14)
N(3)—N(1)	1.406(12)	C(6)—N(1)	1.294(14)
C(20)—N(3)	1.302(14)	N(4)—N(2)	1.394(13)
C(13)—N(2)	1.259(14)	C(27)—N(4)	1.235(14)
C(2)—C(1)	1.449(17)	C(5)—C(1)	1.418(17)
C(6)—C(1)	1.458(15)	C(3)—C(2)	1.417(17)
C(4)—C(3)	1.492(18)	C(5)—C(4)	1.400(17)
C(14)—C(6)	1.476(17)	C(13)—C(7)	1.513(18)
C(13)—C(8)	1.471(15)	C(20)—C(15)	1.451(15)
C(21)—C(20)	1.493(16)	C(27)—C(22)	1.506(16)
C(28)—C(27)	1.519(18)		
C(6)—N(1)—N(3)	114.2(10)	C(20)—N(3)—N(1)	113.6(10)
C(13)—N(2)—N(4)	115.2(10)	C(27)—N(4)—N(2)	114.1(10)
C(6)—C(1)—C(2)	127.4(11)	C(6)—C(1)—C(5)	126.3(11)
C(1)—C(6)—N(1)	115.9(11)	C(14)—C(6)—N(1)	126.0(11)
C(14)—C(6)—C(1)	118.1(11)	C(7)—C(13)—N(2)	125.9(11)
C(8)—C(13)—N(2)	117.1(11)	C(8)—C(13)—C(7)	116.9(10)
C(15)—C(20)—N(3)	116.3(10)	C(21)—C(20)—N(3)	125.7(10)
C(21)—C(20)—C(15)	118.0(10)	C(22)—C(27)—N(4)	117.2(10)
C(28)—C(27)—N(4)	127.2(11)	C(28)—C(27)—C(22)	115.5(10)

Table 2. Bond lengths (Å) and angles (°) for complex **11**

O(1)—Fe	2.069(5)	N(1)—Fe	2.241(5)
N(3)—Fe	2.224(5)	C(1)—O(1)	1.281(5)
C(1)—O(2)	1.230(6)	N(2)—C(1)	1.378(6)
N(2)—N(1)	1.408(6)	H(1)—N(1)	0.890(49)
H(4)—N(1)	0.862(48)	H(5)—N(2)	0.779(48)
N(4)—N(3)	1.453(6)	H(2)—N(3)	1.093(49)
H(7)—N(3)	0.688(47)	H(3)—N(4)	0.889(52)
H(6)—N(4)	0.862(48)		
N(1)—Fe—O(1)	75.7(2)	N(3)—Fe—O(1)	88.2(2)
N(3)—Fe—N(1)	86.8(2)	C(1)—O(1)—Fe	118.1(3)
O(2)—C(1)—O(1)	125.4(4)	N(2)—C(1)—O(1)	116.4(4)
N(2)—C(1)—O(2)	118.2(4)	N(2)—N(1)—Fe	104.8(3)
H(1)—N(1)—Fe	117.8(30)	H(1)—N(1)—N(2)	107.4(31)
H(4)—N(1)—Fe	113.3(30)	H(4)—N(1)—N(2)	98.9(32)
H(4)—N(1)—H(1)	112.3(41)	N(1)—N(2)—C(1)	119.1(4)
H(5)—N(2)—C(1)	115.0(36)	H(5)—N(2)—N(1)	122.6(37)
N(4)—N(3)—Fe	118.3(4)	H(2)—N(3)—Fe	113.6(24)
H(2)—N(3)—N(4)	107.1(24)	H(7)—N(3)—Fe	106.6(44)
H(7)—N(3)—N(4)	114.2(43)	H(7)—N(3)—H(2)	94.6(49)
H(3)—N(4)—N(3)	106.8(30)	H(6)—N(4)—N(3)	112.9(32)
H(6)—N(4)—H(3)	102.7(44)		

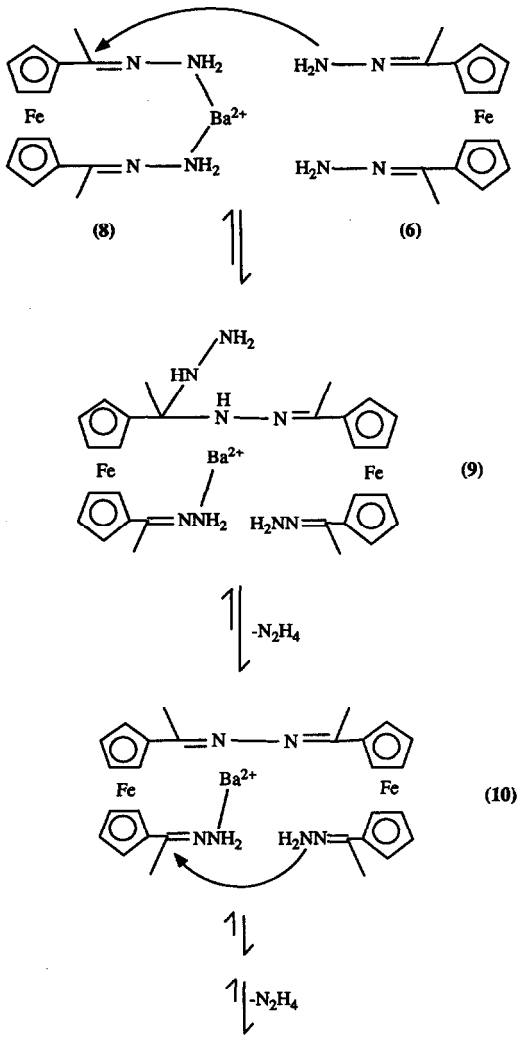

Scheme 3.

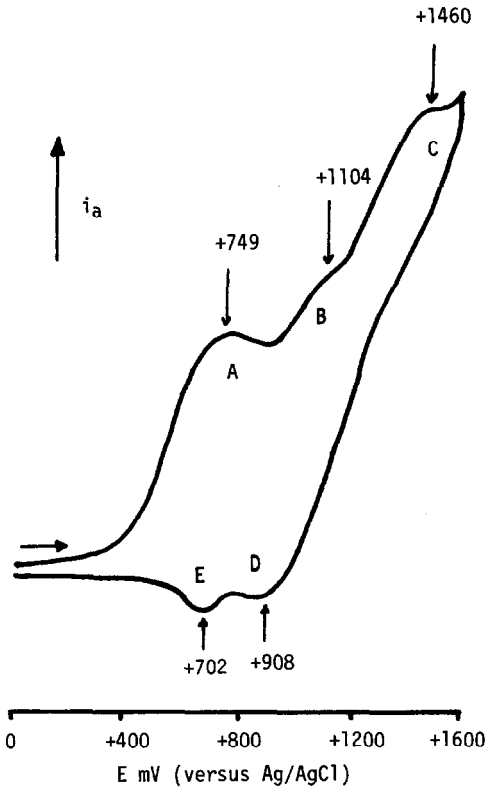

Fig. 2. Cyclic voltammogram of complex **6**. (Scan rate = 50 mV s^{-1}.)

Similar transamination reactions leading to the formation of macrocyclic Schiff-base complexes have been reported by Nelson *et al.*[5] Attempts to reduce the four imine (C=N) functions of **7** with $Na[BH_4]$ and $Li[AlH_4]$ failed, and only the unreacted diazine was recovered.

The cyclic voltammogram of complex **6** (Fig. 2) shows an irreversible oxidation peak (A) and two further quasi-reversible oxidations (BE and CD) in the region 500–1600 mV (vs Ag/AgCl). This behaviour differs markedly to that reported for other 1,1′-disubstituted ferrocenes, which are generally found to exhibit only a single, reversible, one-electron oxidation wave.[6]

The voltammogram of the diazine **7** (Fig. 3) has two irreversible oxidation peaks at 781 (F) and 1032 mV (G), and a strong reduction peak (H) at 268 mV. The electrochemical behaviour of complex **7** is very different to that reported for the closely related mono-azine **2** (Scheme 1) which showed only two, one-electron oxidations at 604 and 1002 mV (vs SCE) corresponding to the formation of $[Fe^{II}Fe^{III}]^+$ and $[Fe^{III}Fe^{III}]^{2+}$ species, respectively.[7] In addition, the large separation between the two oxidation potentials for complex **2** (ΔE = 398 mV) inferred that there was some degree of electronic interaction between the two halves of the mixed-valence complex. This difference in the redox behaviour of complexes **2** and **7** may be attributed to the presence in the molecules of one and two bridging ligands, respectively. Studies on various biferrocene complexes have, indeed, shown that both the nature and the number of bridging ligands in the molecule have a dramatic effect on its redox properties.[8,9]

When the orange dihydrazone **6** is stirred in fresh hydrazine hydrate at 40°C for *ca* 1 week the solid slowly dissolves and the solution gradually changes from orange to a pale straw colour. On cooling the solution to 4°C pale green (almost colourless) crystals of bis(hydrazine)bis(hydrazinecarboxylato-N′,O)iron(II), $[Fe(N_2H_4)_2(OOCNHNH_2)_2]$ (**11**), form in high yield (Scheme 4). Furthermore, during

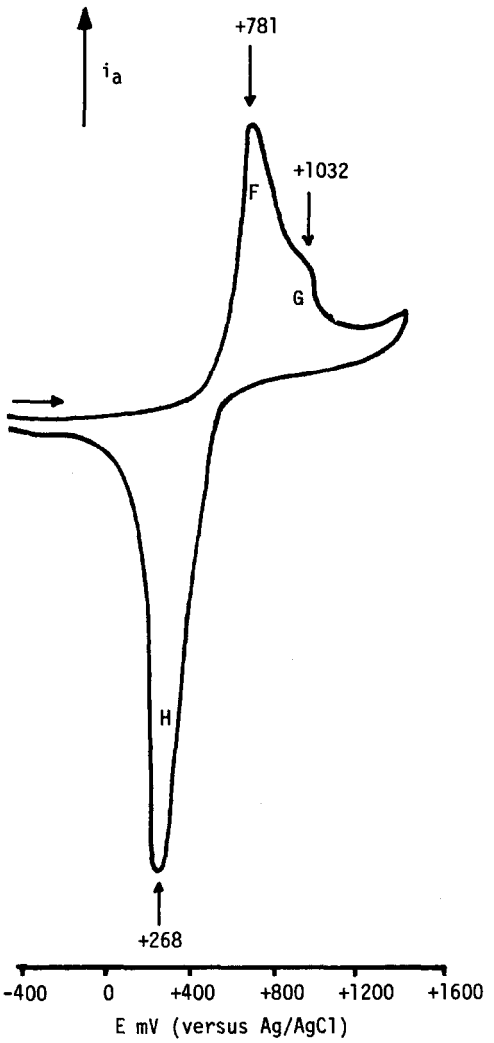

Fig. 3. Cyclic voltammogram of complex **7**. (Scan rate = 50 mV s^{-1}.)

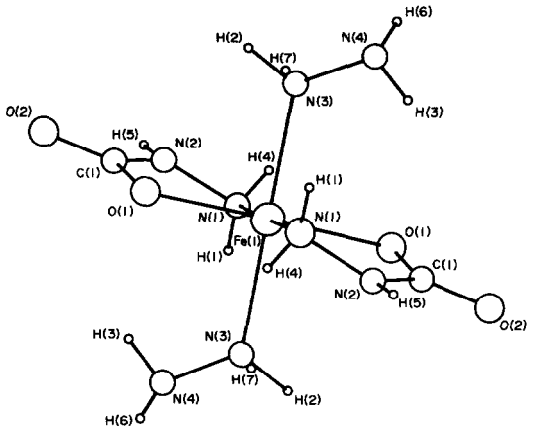

Fig. 4. Structure of complex **11**.

the preparation of complex **6** care must be taken not to greatly exceed the 72 h reaction period. When the reaction time is prolonged, complex **6** slowly redissolves and **11** gradually precipitates. The formation of complex **11** involves the abstraction of the Fe^{2+} ion from the metallocene **6** and its subsequent complexation with hydrazine and the hydrazinecarboxylate anion.* The conventional methods used for the preparation of complex **11** are the reactions of aqueous Fe^{2+} solutions with (i) hydrazinium hydrazinecarboxylate[11] and, (ii) a 5% solution of hydrazinecarboxylic acid in hydrazine hydrate.[12,13]

The availability of high quality crystals together with the interest in the coordination properties of the hydrazinecarboxylato ligand (which has a similar structure to the glycinato ligand[14]) prompted us to investigate the X-ray crystal structure of complex **11**. The structure of the complex is shown in Fig. 4 (see Table 2), and it is seen to be isostructural with the previously characterized zinc(II)[15] and cobalt (II)[16] complexes. The iron atom lies on a centre of symmetry; it is six-coordinate, being surrounded by two monodentate hydrazines and two bidentate

*$N_2H_4 \cdot H_2O$ absorbs atmospheric CO_2 to form hydrazinecarboxylic acid ($N_2H_3CO_2H$) metathetically,[10] and this reacts further with hydrazine to give $N_2H_5^+$ $N_2H_3CO_2^-$.

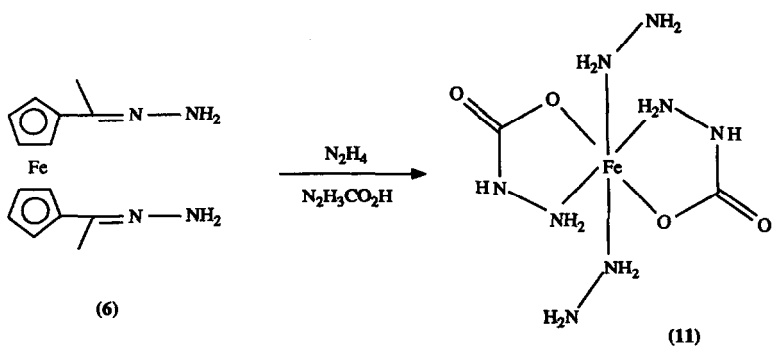

Scheme 4.

Table 3. Main interatomic bond distances (Å) for structurally characterized $[M(N_2H_4)_2(OOCNHNH_2)_2]$ complexes (M = Fe, Co,[16] Zn[15])

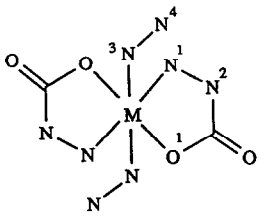

Metal	M—O^1	M—N^1	M—N^3	N^1—N^2	N^3—N^4
Fe	2.069	2.241	2.224	1.408	1.453
Co	2.064	2.198	2.178	1.425	1.454
Zn	2.05	2.25	2.17	1.39	1.46

hydrazinecarboxylato(N′,O) ligands. Table 3 shows that the main interatomic distances in the iron, cobalt and zinc complexes are very similar.

EXPERIMENTAL

All chemicals were reagent grade and were used without further purification. $[Mo_2(\mu\text{-}O_2CCH_3)_2(MeCN)_6][BF_4]_2$ was prepared using the literature method.[3] Elemental analyses were performed by the Microanalytical Laboratory, University College Cork, Ireland. ^{1}H NMR spectra were run on a Bruker AC 80 spectrometer, and mass spectra were obtained using an AEI MS30 instrument equipped with a MSS Data System. IR spectra (KBr disc) were recorded in the region 4000–200 cm^{-1} on a Perkin–Elmer 783 grating spectrometer, and UV–vis spectra were run on a Milton Roy Spectronic 3000 Array. Cyclic voltammograms (*ca* 20°C and under N_2) were recorded using an EG&G Model 264A polarographic analyser in combination with an EG&G PARC Model 303 electrode assembly. A glassy carbon disc and a platinum wire were used as the working counter electrodes, respectively. Potentials (mV) were recorded with respect to a silver–silver chloride reference electrode (*i*Ru compensation not used). Tetrabutylammonium perchlorate in dry THF (0.2 M) was used as the supporting electrolyte/solvent system.

$[H_2NN(Me)CC_5H_4FeC_5H_4C(Me)NNH_2]$ (**6**)

A red suspension of 1,1′-diacetylferrocene (1.0 g, 3.7 mmol) in hydrazine hydrate (20 cm^3) was stirred for *ca* 72 h at 20°C under N_2. The orange product which formed was removed by filtration, washed with ice-cold ethanol and then dried *in vacuo*. Yield: 1.04 g (94%). Found: C, 56.4; H, 6.1; N, 18.2. Calc: C, 56.4; H, 6.1; N, 18.8%; m.p. 182–185°C; MS: *m/z* 298 (M^+); IR: 3340, 3205 (—NH_2), 1590 cm^{-1} (—C=N); UV–vis (EtOH): $\lambda_{max.}$ 452 nm, $\varepsilon_{max.}$ 574 dm^3 mol^{-1} cm^{-1}; ^{1}H NMR (ppm):* 1.20 (s, 6H, CH_3), 4.27 (t, 4H, Fc ring), 4.54 (t, 4H, Fc ring), 5.10 (br-s, 4H, NH_2).

$[—N(Me)CC_5H_4FeC_5H_4C(Me)N—]_2$ (**7**)

Method (a). **6** (0.40 g, 1.34 mmol) and anhydrous barium perchlorate (0.45 g, 1.34 mmol) were refluxed together in ethanol (50 cm^3) for 15 h. When the red–orange solution was reduced to *ca* 5 cm^3 the red product precipitated. The solid was washed with ice-cold ethanol and then dried *in vacuo*. The product was recrystallized from chloroform. Yield: 0.31 g (87%).

Method (b). Complex **7** was also prepared by reacting a methanolic solution of $[Mo_2(\mu\text{-}O_2CCH_3)_2(MeCN)_6][BF_4]_2$ with **6** in a 1:3 molar ratio at 20°C under N_2. Found: C, 63.5; H, 5.2; N, 10.95. Calc.: C, 63.2; H, 5.3; N, 10.5%; m.p. 250°C (dec); MS: *m/z* 532 (M^+); IR: 1597 cm^{-1} (—C=N); UV–vis ($CHCl_3$): $\lambda_{max.}$ 475 nm, $\varepsilon_{max.}$ 2252 dm^3 mol^{-1} cm^{-1}; ^{1}H NMR (ppm):* 2.51 (s, 12H, CH_3), 4.25 (sx, 4H, Fc ring), 4.57 (sx, 4H, Fc ring), 4.73 (q, 4H, Fc ring), 5.13 (q, 4H, Fc ring).

$[Fe(N_2H_4)_2(OOCNHNH_2)_2]$ (**11**)

A mixture comprising complex **6** (0.20 g, 0.67 mmol) and hydrazine hydrate (10 cm^3) was shaken at 40°C under N_2 for 1 week. The solution gradually changed from red to a pale straw colour. On standing for 2 weeks at 4°C the product formed as light green (almost colourless) crystals. After centrifugation the solid was washed with several portions of cold ethanol and then dried *in vacuo*. Yield: 0.14 g (77%). The solid is somewhat air-sensitive and the crystals take on a light brown coloration after a few days. Found: C, 9.0; H, 5.3; N, 40.7. Calc: C, 8.9; H, 5.2; N, 41.5%; IR:[11,17] 3260, 3160 (—NH_2), 1470 (sym. —OCO), 990 (—N—N of $N_2H_3CO_2$), 950 (—N—N of N_2H_4), 418 cm^{-1} (—Fe—N).

* br = broad, s = singlet, t = triplet (dd), q = quintet (ddd), sx = sextet (ddd), dd = doublet of doublets, ddd = doublet of doublets of doublets.

Crystallography

For complex **7** a red, needle-shaped crystal of approximate size $0.5 \times 0.5 \times 0.1$ mm^3 was used, and for complex **11** a colourless, rhombic crystal of approximate size $0.1 \times 0.1 \times 0.3$ mm^3 was used. X-ray reflections were measured using an Enraf–Nonius CAD4 diffractometer, and the intensities of the reflections in the range $1 < \theta < 20°$ were measured using Mo-K_α radiation with a graphite monochromator. For complex **7** the data were corrected for decay and absorption, and reduced to give 2215 reflections (merging $R = 1.3\%$) of which 2052 had $|F_{obs}| > 4\sigma(F_{obs})$ and were used in structure solution and refinement. For complex **11** the data were corrected for decay and absorption, and reduced to give 660 reflections (merging $R = 1.4\%$) of which 637 had $|F_{obs}| > 4\sigma(F_{obs})$ and were used in structure solution and refinement. The structures were solved by the direct method (SHELXS) and refined by full-matrix least-squares to a conventional R-factor of 6.2% for **7** (2.97% for **11**). Unit weights were used with hydrogen atoms in calculated positions. Heavy atoms were given anisotropic temperature factors. The programs SHELXS and SHELX-76 were used by kind permission of Professor G. F. Sheldrick (University of Gottingen). The data have been deposited with the Cambridge Crystallographic Data Centre. Crystal data for complex **7**: $C_{28}H_{28}Fe_2N_4$, $M_r = 532.250$, monoclinic, space group $P2_1$, $a = 9.747(1)$, $b = 10.219(1)$, $c = 12.228(2)$ Å; $\beta = 102.95(1)$, $U = 1186.93$ Å^3. $D_c = 1.49$ g cm^{-3}, $Z = 2$; $F(000) = 551.96$, $\lambda = 0.71069$ Å, μ(Mo-K_α) = 11.78 cm^{-1}. Crystal data for complex **11**: $C_2H_{14}FeN_8O_4$, $M_r = 270.032$, monoclinic, space group $P2_1/n$, $a = 8.144(5)$, $b = 7.378(2)$, $c = 8.651(5)$ Å; $\beta = 110.51(3)$, $U = 486.86(42)$ Å^3. $D_c = 1.842$ g cm^{-3}, $Z = 2$; $F(000) = 280$, $\lambda = 0.71069$ Å, μ(Mo-K_α) = 14.90 cm^{-1}.

Acknowledgements—We wish to thank Dr D. G. Gilheany for assistance with NMR interpretations, and also EOLAS for a postgraduate grant (to P.G.).

REFERENCES

1. G. S. Gol'din, T. A. Balabina, T. V. Trynkina and A. N. Ushakova, *Zh. Obshch. Khim.* 1973, **43**, 1271.
2. K. Iyanar, S. Prema and K. Kishore, *J. Chem. Eng. Data* 1988, **33**, 220.
3. W. Clegg, G. Pimplett and C. D. Garner, *Polyhedron* 1986, **5**, 31.
4. A. I. Vogel, *A Text-book of Quantitative Inorganic Analysis*, 3rd edn, p. 783. Longmans, London (1968).
5. S. M. Nelson, C. V. Knox, M. McCann and M. G. B. Drew, *J. Chem. Soc., Dalton Trans.* 1981, 1669 and refs therein.
6. W. F. Little, C. N. Reilley, J. D. Johnson and A. P. Sanders, *J. Am. Chem. Soc.* 1964, **86**, 1382; D. W. Hall and C. D. Russell, *J. Am. Chem. Soc.* 1967, **89**, 2316.
7. H. H. Wei, C. Y. Lin and S. J. Chang, *Proc. Natl. Sci. Counc. Repub. China B* 1983, **7**, 35.
8. W. F. Morrison Jr, S. Krogsrud and D. N. Hendrickson, *Inorg. Chem.* 1973, **12**, 1998.
9. J. E. Gorton, H. L. Lentzner and W. E. Watts, *Tetrahedron* 1971, **27**, 4353.
10. R. Stolle and K. A. Hofmann, *Ber. Deut. Chem. Ges.* 1904, **37**, 4523.
11. K. C. Patil, R. Soundararajan and E. P. Goldberg, *Synth. React. Inorg. Met.-Org. Chem.* 1983, **13**, 29.
12. P. Ravindranathan and K. C. Patil, *Proc. Indian Acad. Sci. (Chem. Sci.)* 1985, **95**, 345.
13. K. C. Patil, R. Soundararajan and V. R. Pai Verneker, *Proc. Indian Acad. Sci.* 1979, **88A**, 211.
14. C. K. Jorgenson, *Inorganic Complexes*. Academic Press, London (1963).
15. A. Ferrari, G. Bigliardi and A. M. Lanfredi, *Z. Krist.* 1965, **122**, 259.
16. E. N. Maslen, C. L. Raston, B. W. Skelton and A. W. White, *Aust. J. Chem.* 1975, **28**, 739; E. N. Maslen and S. C. Ridout, *Acta Cryst.* 1987, **B43**, 352.
17. A. Braibanti, F. Dallavalle, M. A. Pellinghelli and E. Leporati, *Inorg. Chem.* 1968, **7**, 1430.

Polyhedron Vol. 10, No. 4/5, pp. 491–494, 1991
Printed in Great Britain

0277–5387/91 $3.00+.00
© 1991 Pergamon Press plc

THE FIRST STRUCTURALLY CHARACTERIZED DIRUTHENIUM(II,III) COMPLEX WITH FOUR BRIDGING ARYLCARBOXYLATO LIGANDS

BIRINCHI K. DAS and AKHIL R. CHAKRAVARTY*

Department of Inorganic and Physical Chemistry, Indian Institute of Science, Bangalore 560 012, India

(*Received* 4 *July* 1990; *accepted* 2 *November* 1990)

Abstract—The diruthenium(II,III) compound $[Ru_2Cl(O_2CC_6H_4\text{-}p\text{-}OMe)_4](H_2O)_{0.25}$ (**1**) has been prepared and its crystal structure determined by X-ray studies. The crystals belong to the triclinic space group, $P\bar{1}$, and the asymmetric unit consists of one full dimer and two half dimers. The $\{Ru_2(O_2CC_6H_4\text{-}p\text{-}OMe)_4^+\}$ units are bridged by chloride ions into an infinite zigzag chain, with an average Ru—Cl distance and Ru—Cl—Ru angle of 2.567(2) Å and 121.0(1)°, respectively. The average Ru—Ru distance of 2.286(1) Å in **1** is comparable with that in analogous tetra-alkylcarboxylates, $Ru_2Cl(O_2CR)_4$ and tetra-amidates, $Ru_2Cl(ArCONH)_4$.

An interesting feature[1] in the chemistry of diruthenium compounds with four three-atom bridging ligands and a Ru—Ru multiple bond is the unusual stability of the Ru_2^{5+} mixed-valance state. The tetra-alkylcarboxylates, $Ru_2Cl(O_2CR)_4$, which constitute an important class of compounds in this chemistry were the first to be discovered,[2] structurally characterized[3–7] and subjected to various physico-chemical studies.[8–16] The chemistry of analogous tetra-arylcarboxylato compounds has, however, remained virtually unexplored.[17–19]

Recent work from our laboratory has shown[18,20,21] that $Ru_2Cl(O_2CAr)_4$ could be a better precursor for studying the reactivity of the diruthenium(II,III) core towards phosphine- and nitrogen-donor bases. While our earlier attempts[18] to crystallize the sparingly soluble tetra-alkylcarboxylates were unsuccessful, we have now succeeded in isolating $[Ru_2Cl(O_2CC_6H_4\text{-}p\text{-}OMe)_4](H_2O)_{0.25}$ (**1**) in crystalline form. The results of the X-ray study carried out on **1** are presented here. The structural data are of importance in developing the chemistry of the hitherto unknown series of tetra-arylcarboxylatodiruthenium(II,III) complexes.

* Author to whom correspondence should be addressed.

EXPERIMENTAL

Compound **1** was isolated as a homogeneous crystalline mass by using a diffusion technique in which a methanolic solution of *p*-methoxybenzoic acid was layered carefully on a saturated methanolic solution of $Ru_2Cl(O_2CMe)_4$. The crystals obtained from this reaction were found to be suitable for X-ray studies.

Crystal data for **1**

$[Ru_2Cl(O_2CC_6H_4\text{-}p\text{-}OMe)_4](H_2O)_{0.25}$, M = 842.12, triclinic, $P\bar{1}$, a = 12.765(2), b = 12.879(4), c = 23.855(4) Å, α = 80.55(2), β = 98.61(1), γ = 116.58(2)°, V = 3447 Å^3, Z = 4, d_c = 1.631 g cm^{-3}, λ = 0.7107 Å, μ(Mo-K_α) = 8.26 cm^{-1}.

Structure solution and refinement[21]

12,094 unique data were collected on an Enraf–Nonius range CAD-4 diffractometer using the ω–2θ scan method in the range $4° \leqslant 2\theta \leqslant 50°$, out of which 9478 reflections had $I \geqslant 2.5\sigma(I)$. Lorentz and polarization corrections were made on the data but no absorption correction was made. No decay of the crystal was noticed during data collection. The

structure was solved by the direct method part of SHELX-86 and refined by SHELX-76.[22] Atoms in the coordination sphere along with the carbon atoms in the carboxylate groups were refined anisotropically leaving out the remaining atoms at the isotropic stage. Residuals: $R = 0.0653$ ($R_w = 0.0738$ for $w = k/[\sigma^2(F_o)+gF_o^2]$), $g = 0.000000$; overall scale factor 1.39; lowest shift/ESD = 0.10; highest peak in the final difference Fourier map = 1.94 e/Å^3 situated 0.96 Å away from the Ru(4) atom; number of parameters in the final stage of least-squares refinement was 531.

The probable source of water as solvent of crystallization in **1** could be methanol which was used as a reaction medium. The water molecule which refined with a site occupancy factor of 0.5 for oxygen does not have any interaction with the atoms of the metal complex. Complete tables of structure factors, anisotropic thermal parameters and complete lists of bond distances and angles (59 pages) have been deposited with the Editor at Queen Mary and Westfield College. Positional parameters and isotropic thermal parameters have been forwarded to the Director, Cambridge Crystallographic Data Centre.

RESULTS AND DISCUSSION

The structure of **1**, obtained by X-ray crystallography,[22] is shown in Fig. 1. The asymmetric unit of the unit cell consists of one full dimer and two half dimers. The presence of three different dimeric units in the unit cell could be due to packing effects in the presence of bulky aryl groups. The dimeric $\{Ru_2(\mu\text{-}O_2CC_6H_4\text{-}p\text{-}OMe)_4^+\}$ cores are linked by chloride bridges in a zigzag fashion forming an infinite chain. A similar sort of bridging is known to occur in tetra-alkylcarboxylates[3-7] and in tetra-amidates[23,24] with two exceptions[4] in which the Ru—Cl—Ru bridge is linear.

The essential bond distances and angles in **1** are presented in Table 1. A comparison of the Ru—Ru and Ru—Cl distances in **1** and in other related complexes is given in Table 2. In **1**, the average Ru—Ru distance is 2.286(1) Å, the geometry of each ruthenium centre is near octahedral and the Ru—Ru—Cl angles are essentially linear. The presence of a relatively weak Ru—Cl bond in **1** is observed from the structural data, which is also consistent for a Ru—Ru bond order of 2.5 with a $\sigma^2\pi^4\delta^2(\delta^*\pi^*)^3$ ground electronic configuration. From the data in Table 2, we infer that while linear and/or zigzag Ru—Cl—Ru bridges are observed in the tetra-alkylcarboxylato compounds containing small alkyl groups like methyl or ethyl, the presence of a bulky alkyl or an aryl group in the carboxylato or amidato ligands, bonded to the diruthenium(II,III) core, makes the Ru—Cl—Ru bridge non-linear with an angle of *ca* 120° in forming an infinite zigzag chain.

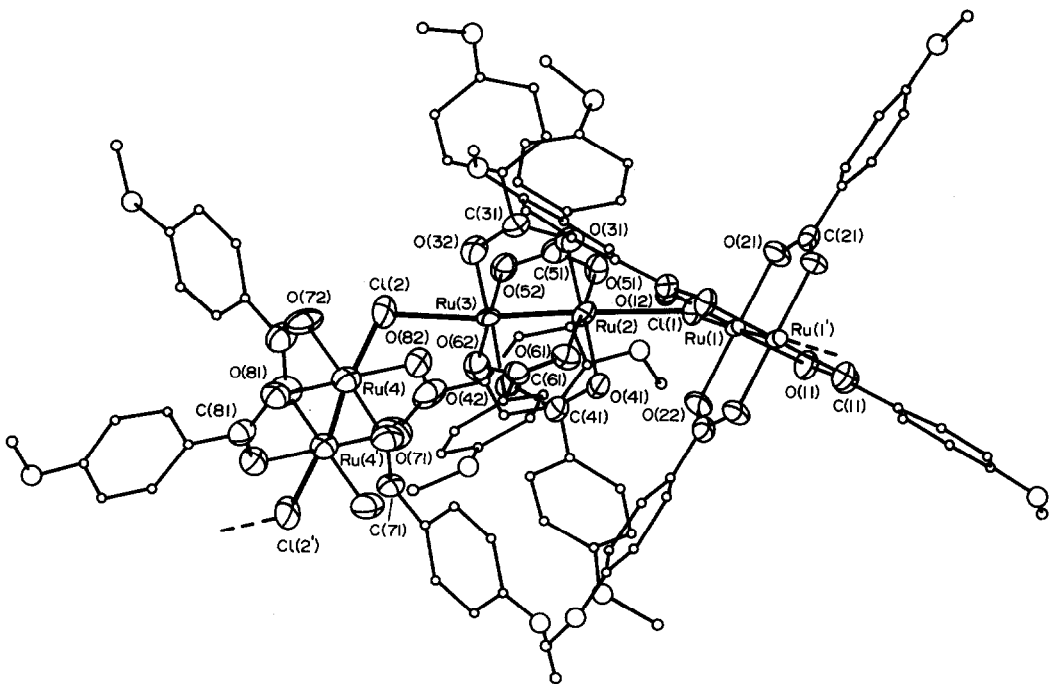

Fig. 1. An ORTEP drawing of the complex $Ru_2Cl(O_2CC_6H_4\text{-}p\text{-}OMe)_4$ with the atom-labelling scheme of the coordination sphere. The sizes of the atoms in the aryl groups are reduced for clarity.

Table 1. Selected bond distances and angles in $Ru_2Cl(O_2CC_6H_4\text{-}p\text{-}OMe)_4$

Bond distances (Å)			
Ru(1)—Ru(1)′	2.284(1)	Ru(2)—O(41)	2.009(7)
Ru(2)—Ru(3)	2.290(1)	Ru(2)—O(51)	2.012(5)
Ru(4)—Ru(4)′	2.283(2)	Ru(2)—O(61)	2.017(5)
Ru(1)—Cl(1)	2.554(2)	Ru(3)—O(32)	2.014(7)
Ru(2)—Cl(1)	2.583(2)	Ru(3)—O(42)	2.006(7)
Ru(3)—Cl(2)	2.563(2)	Ru(3)—O(52)	2.005(5)
Ru(4)—Cl(2)	2.568(3)	Ru(3)—O(62)	2.020(5)
Ru(1)—O(11)	2.024(5)	Ru(4)—O(71)	2.018(7)
Ru(1)—O(12)	2.014(5)	Ru(4)—O(72)	2.034(7)
Ru(1)—O(21)	2.024(5)	Ru(4)—O(81)	2.023(5)
Ru(1)—O(22)	2.025(5)	Ru(4)—O(82)	2.011(5)
Ru(2)—O(31)	2.031(7)		

Bond angles (°)			
Ru(1)—Cl(1)—Ru(2)	124.2(1)	Cl(1)—Ru(2)—Ru(3)	175.3(1)
Ru(3)—Cl(2)—Ru(4)	117.8(1)	Cl(1)—Ru(1)—O(11)	91.7(1)
Cl(1)—Ru(1)—O(12)	90.0(1)	Cl(1)—Ru(1)—O(21)	89.1(1)
Cl(1)—Ru(1)—O(22)	92.8(1)	O(11)—Ru(1)—O(12)	178.3(2)
O(11)—Ru(1)—O(21)	88.1(2)	O(11)—Ru(1)—O(22)	91.0(2)
O(12)—Ru(1)—O(21)	91.7(2)	O(12)—Ru(1)—O(22)	89.2(2)
O(21)—Ru(1)—O(22)	177.9(2)	Cl(1)—Ru(2)—O(31)	94.7(2)
Cl(1)—Ru(2)—O(41)	87.2(2)	Cl(1)—Ru(2)—O(51)	88.3(2)
Cl(1)—Ru(2)—O(61)	92.8(2)	O(31)—Ru(2)—Ru(3)	89.4(1)
O(31)—Ru(2)—O(41)	178.0(2)	O(31)—Ru(2)—O(51)	88.0(2)
O(31)—Ru(2)—O(61)	89.9(2)	O(41)—Ru(2)—O(51)	91.8(2)
O(41)—Ru(2)—Ru(3)	88.7(1)	O(41)—Ru(2)—O(61)	90.3(2)
O(51)—Ru(2)—Ru(3)	89.6(1)	O(51)—Ru(2)—O(61)	177.7(3)
O(61)—Ru(2)—Ru(3)	89.4(1)	Ru(2)—Ru(3)—O(32)	89.2(1)
Ru(2)—Ru(3)—O(42)	89.9(1)	Ru(2)—Ru(3)—O(52)	88.9(1)
Ru(2)—Ru(3)—O(62)	88.9(1)	Cl(2)—Ru(3)—O(32)	85.1(2)
Cl(2)—Ru(3)—O(42)	96.1(2)	Cl(2)—Ru(3)—O(52)	88.7(2)
Cl(2)—Ru(3)—O(62)	93.2(2)	O(32)—Ru(3)—O(42)	178.9(2)
O(32)—Ru(3)—O(52)	88.4(3)	O(32)—Ru(3)—O(62)	89.8(2)
O(42)—Ru(3)—O(52)	91.2(3)	O(42)—Ru(3)—O(62)	90.5(2)
O(52)—Ru(3)—O(62)	177.3(2)	Cl(2)—Ru(4)—O(71)	83.6(2)
Cl(2)—Ru(4)—O(72)	97.9(2)	Cl(2)—Ru(4)—O(81)	93.4(2)
Cl(2)—Ru(4)—O(82)	88.4(2)	O(71)—Ru(4)—O(72)	177.9(2)
O(71)—Ru(4)—O(81)	89.7(2)	O(71)—Ru(4)—O(82)	91.5(2)
O(72)—Ru(4)—O(81)	88.7(2)	O(72)—Ru(4)—O(82)	90.0(2)
O(81)—Ru(4)—O(82)	177.9(2)		

Table 2. Structural data on polymeric diruthenium(II,III) complexes

Complex	Ru—Ru (Å)	Ru—X (Å) (X = Cl, Br)	Ru—X—Ru chain	References
$Ru_2Cl(O_2CCH_3)_4 \cdot 2H_2O$	2.267(1)	2.556(1)	Linear	4
$Ru_2Cl(O_2CCH_3)_4$	2.281(3)	2.571(1)	Zigzag	5
$Ru_2Cl(O_2CCH_3)_4$	2.287(2)	2.577(1)	Zigzag	6
$Ru_2Cl(O_2CC_2H_5)_4$	2.292(7)	2.566(4)	Linear	4
$Ru_2Cl(O_2CC_3H_7)_4$	2.281(4)	2.587(5)	Zigzag	3
$Ru_2Br(O_2CH)_4$	2.2899(7)	2.7242(9)	Zigzag	7
$[Ru_2Cl(O_2CC_6H_4\text{-}p\text{-}OMe)](H_2O)_{0.25}$	2.286(1)	2.567(2)	Zigzag	This work
$Ru_2Cl(PhCONH)_4$	2.293(2)	2.592(3)	Zigzag	24
$Ru_2Cl(p\text{-}Cl\text{-}C_6H_4CONH)_4 \cdot MeOH$	2.296(1)	2.583(2)	Zigzag	23

Acknowledgement—We thank CSIR (New Delhi) for financial support.

REFERENCES

1. J. G. Norman Jr, G. E. Renzoni and D. A. Case, *J. Am. Chem. Soc.* 1979, **101**, 5256.
2. T. A. Stephenson and G. Wilkinson, *J. Inorg. Nucl. Chem.* 1966, **28**, 2285.
3. M. J. Bennett, K. G. Kaulton and F. A. Cotton, *Inorg. Chem.* 1969, **8**, 1.
4. A. Bino, F. A. Cotton and T. R. Felthouse, *Inorg. Chem.* 1979, **18**, 2599.
5. D. S. Martin, R. A. Newman and L. M. Vlasnik, *Inorg. Chem.* 1980, **19**, 3404.
6. T. Togano, M. Mukaida and T. Nomura, *Bull. Chem. Soc. Japan* 1980, **53**, 2085.
7. T. Kimura, T. Sakurai, M. Shima, T. Togano, M. Mukaida and T. Nomura, *Bull. Chem. Soc. Japan* 1982, **55**, 3927.
8. F. A. Cotton and R. A. Walton, *Multiple Bonds Between Metal Atoms.* John Wiley, New York (1982); *Structure Bond.* 1985, **62**, 1.
9. R. P. Tooze, M. Motevalli, M. B. Hursthouse and G. Wilkinson, *J. Chem. Soc., Chem. Commun.* 1984, 799; R. P. Tooze, G. Wilkinson, M. Motevalli and M. B. Hursthouse, *J. Chem. Soc., Dalton Trans.* 1986, 2711.
10. V. M. Miskowski and H. B. Gray, *Inorg. Chem.* 1988, **27**, 2501.
11. F. A. Cotton, M. Matusz and B. Zhong, *Inorg. Chem.* 1988, **27**, 4368.
12. F. A. Cotton, V. M. Miskowski and B. Zhong, *J. Am. Chem. Soc.* 1989, **111**, 6177.
13. E. C. Royer, C. Ruiz-Valero, F. A. Urbanos, E. G. Puebla and A. Monge, *Polyhedron* 1989, **8**, 2571.
14. A. Carvill, P. Higgins, G. M. McCann, H. Ryan and A. Shields, *J. Chem. Soc., Dalton Trans.* 1989, 2435.
15. M. Schröder and T. A. Stephenson, *Comprehensive Coordination Chemistry* (Edited by G. Wilkinson, R. D. Gillard and J. A. McCleverty), Vol. 4, pp. 425–429. Pergamon Press, Oxford (1987).
16. A. R. Chakravarty, *Proc. Indian Natl. Sci. Acad.* 1986, **52A**, 749.
17. M. Mukaida, T. Nomura and T. Ishimori, *Bull. Chem. Soc. Japan* 1972, **45**, 2143.
18. B. K. Das and A. R. Chakravarty, *Polyhedron* 1988, **7**, 685.
19. P. Higgins and G. M. McCann, *J. Chem. Soc., Dalton Trans.* 1988, 661.
20. S. K. Mandal and A. R. Chakravarty, *Inorg. Chim. Acta* 1987, **132**, 157.
21. B. K. Das and A. R. Chakravarty, *Inorg. Chem.* 1990, **29**, 1783, 2078.
22. G. M. Sheldrick, SHELX-76. A Program for Crystal Structure Determination. Cambridge University Press, Cambridge (1976).
23. A. R. Chakravarty, F. A. Cotton and D. A. Tocher, *Polyhedron* 1985, **4**, 1097.
24. A. R. Chakravarty and F. A. Cotton, *Polyhedron* 1985, **4**, 1957.

Polyhedron Vol. 10, No. 4/5, pp. 495–500, 1991
Printed in Great Britain

0277–5387/91 $3.00+.00
© 1991 Pergamon Press plc

CRYSTAL STRUCTURE AND SPECTROSCOPIC PROPERTIES OF A COPPER(II) COMPLEX WITH A CHAIN ARRANGEMENT: [Cu(pymep)Cl(H_2O)](PF_6)

M. I. ARRIORTUA,*† J. VIA,* J. I. R. LARRAMENDI, B. DIAZ, L. LEZAMA and T. ROJO

Departamentos de Mineralogía-Petrología* y Química Inorgánica, Universidad del Pais Vasco, Aptdo. 644, 48080 Bilbao, Spain

(*Received* 19 *July* 1990; *accepted* 2 *November* 1990)

Abstract—A novel complex of copper(II) with the tridentate ligand N-[2′-(6-methyl)pyridyl]methylene-2-(2′-pyridyl)ethylamine (pymep), of formula [Cu(pymep)Cl(H_2O)](PF_6), has been synthesized and its X-ray crystal structure determined. The structure consists of [Cu(pymep)Cl(H_2O)]$^+$ cations and hexafluorophosphate anions. The copper complex is stacked to make a chain arrangement orientated in the |010| direction. The geometry of the coordination polyhedron around the copper(II) ion is close to tetrahedrally distorted square pyramidal (SP_{th}). One broad, unresolved band centred at 13,800 cm^{-1} is observed in the diffuse reflectance spectrum. The X-band ESR powder spectrum shows an orthorhombic signal with $g_1 = 2.219$, $g_2 = 2.210$ and $g_3 = 2.047$.

Continual study is devoted to low dimensional systems, by both physicists and chemists, because of their interesting properties (magnetic, optic, electric, . . .).[1–3] In this context, we have reported the synthesis and magnetic characterization of a wide set of one-dimensional pentacoordinated copper(II) compounds containing the entity [$CuL_{III}X$], where L_{III} is a tridentate rigid "quasi-planar" ligand, such as terpy (2,2′ : 6′,2″-terpyridine), paphy (pyridine-2-carboxaldehyde 2-pyridylhydrazone), and X is a halide or pseudohalide anion.[4–7] The precursors of these condensed systems are the monomeric [$CuL_{III}X_2$] complexes.[8–11] When an X ligand is extruded from the monomer, the planarity of the tridentate ligands favours the stacking of the resulting planar [$CuL_{III}X$] moieties to give dimers[4,12–14] or more extended systems (linear or ladder-like chains).[6,15]

The rigidity of the tridentate ligands plays an important role in determining the final arrangement of the copper(II) ions. Binuclear species have been obtained with the rigid ligand, terpy,[4–5] whereas dimers and linear and ladder-like chains were obtained with the less rigid tridentate ligand, paphy.[6–7] In order to improve our knowledge of the rigidity effects, we have studied a series of compounds with the Schiff base N-[2′-(6-methyl) pyridyl]methylene-2-(2′-pyridyl)ethylamine (hereafter called pymep), a tridentate ligand with less rigidity than those mentioned above.

In this work, the crystal structure and spectroscopic properties of the [Cu(pymep)Cl(H_2O)](PF_6) complex are reported. Unlike the related [Cu(paphy)Cl](PF_6)(H_2O) (linear chain)[6] and [Cu(terpy)Cl]$_2$(PF_6)$_2$ (dimer)[4] compounds, the title compound exhibits a chain arrangement via hydrogen bonds.

EXPERIMENTAL

Synthesis

Analytical grade copper(II) chloride, N-[2′-(6-methyl)pyridyl]methylene-2-(2′-pyridyl)ethylamine, and potassium hexafluorophosphate were employed to prepare samples of [Cu(pymep)Cl(H_2O)](PF_6). An excess of a saturated KPF_6 aqueous solution was added to a warm aqueous solution containing the simple Cu(pymep)Cl_2 complex previously prepared.[16] The resulting solution was evaporated to obtain microcrystalline

† Author to whom correspondence should be addressed.

powder. Crystallization from a saturated aqueous solution of the latter precipitate gave blue prismatic crystals of relatively good quality. Found: Cu, 13.2; C, 34.3; H, 3.4; N, 8.6. Calc. for $CuC_{14}H_{17}N_2ClOPF_6$: Cu, 13.0; C, 34.5; H, 3.5; N, 8.6%.

X-ray and structure determination

Preliminary cell dimensions and space group symmetry were determined from Weissenberg and oscillation photographs. A prismatic crystal ($0.25 \times 0.20 \times 0.05$ mm) was selected and mounted on an Enraf–Nonius CAD-4 diffractometer with its long dimension roughly parallel to the ϕ axis of the goniometer. Accurate cell parameters and orientation matrix were obtained by a least-squares refinement of the setting angles of 25 reflections with $10 \leqslant 2\theta \leqslant 34°$, recorded using graphite-monochromatized Mo-K_{α_1} radiation.

Crystal data. $[Cu(C_{14}H_{15}N_6)Cl(H_2O)](PF_6)$, $M = 487.3$ g mol^{-1}, orthorhombic system, space group *Pbca*, $a = 7.9222(4)$, $b = 15.7633(5)$, $c = 29.623(1)$ Å; $V = 3699.3(3)$ Å^3; $Z = 8$; $D_x = 1.75$ g cm^{-3}; λ(Mo-K_{α_1}) = 0.7107 Å, μ(Mo-K_{α_1}) = 14.73 cm^{-1}, $F(000) = 1944$, $T = 292$ K. Density was measured by flotation in a bromoform–ethanol solution [$D_m = 1.75(6)$ g cm^{-3}].

A total of 5368 reflections were recorded in the range $2 \leqslant 2\theta \leqslant 60°$, with h: $0 \rightarrow 11$, k: $0 \rightarrow 22$, l: $0 \rightarrow 41$, ω–2θ scan technique. Orientation (every 150 reflections) and intensity control (every 3600 s) by means of three standard reflections showed no significant changes during the data collection. The intensity data were corrected for Lorentz polarization factors; absorption effects were neglected. 1763 reflections with $I \geqslant 3\sigma(I)$ were taken into account to solve the structure via direct methods (MULTAN 84 system),[17] and for refinement by successive least-squares and Fourier synthesis cycles (SHELX 76 program).[18] The function minimized was $\Sigma w[|F_o| - |F_c|]$, were $w = [\sigma^2(F_o) + 0.0024(F_o)]^{-1}$. Anisotropic thermal parameters were introduced for all atoms except hydrogen atoms whose thermal parameters were isotropic. The hydrogen positions could be derived from a difference Fourier map. Final difference maps revealed no significant regions of electron density with max. 0.65 and min. -0.32 eÅ^{-3}. The final value of the discrepancy indice is $R = 4.31$ ($R_w = 4.78$).

Scattering factors were taken from the *International Tables for X-Ray Crystallography*.[19] All calculations were carried out on a MicroVAX computer at the computer centre of the Basque University. The geometric calculations were performed with XANADU[20] and molecular illustrations were drawn with SCHAKAL 88.[21] Further details are presented as Supplementary Data, together with final atomic coordinates, thermal parameters, bond lengths and angles, mean average planes and structure factors.

Physical measurements

Water was determined thermogravimetrically using a Perkin–Elmer TSG-1 thermobalance. IR spectra were obtained with KBr pellets in the 4000–250 cm^{-1} region, using a Perkin–Elmer 1430 spectrophotometer. Visible reflectance spectra on solid powdered samples were recorded at room temperature using a Perkin–Elmer Lamba-9 UV-vis/NIR spectrophotometer. A Bruker 200 tt spectrometer equipped with a standard low-temperature device, operating at X-band calibrated by a NMR probe for the magnetic field and a HP 5342A frequency counter for the microwave frequency, was used to record the ESR powder spectra of the complex at different temperatures.

RESULTS AND DISCUSSION

The structure of the title compound consists of cationic $[Cu(pymep)Cl(H_2O)]^+$ units and hexafluorophosphate anions. The copper complex, presented with labelling in Fig. 1, is stacked to make a chain arrangement orientated in the |010| direction.

The main interatomic distances and angles of this compound are listed in Table 1.

The coordination sphere of the copper(II) ion can be described as a distorted square pyramid. The basal positions are occupied by the three nitrogen atoms of the tridentate ligand [Cu—N(1), N(2), N(3); 2.010(6), 1.964(5), 2.046(6) Å, respectively] and the chlorine atom [Cu—Cl, 2.240(2) Å]. The fifth coordination site (at the apical position) is occupied by the oxygen atom from the water molecule [Cu—O_w, 2.439(7) Å].

The $[Cu(pymep)Cl(H_2O)]^+$ units are linked by hydrogen bonds between the water molecules and the $(PF_6)^-$ ions (see Fig. 2). The $O_w \cdots F(4)$ and $F(5) \cdots O_w^i$ [$i = -x+3/2, y+1/2, z$] distances are 3.091(10) and 3.190(10) Å, respectively. An helicoidal binary axis serves to propagate the chain along the b axis. The chains are isolated with the shorter interchain distance Cu—Cu^{ii} being 7.922(1) Å [$ii = x+1, y, z$].

The hexafluorophosphate anion exhibits a geometry close to regular octahedron. The average P—F distance is 1.55(3) Å, while the average *cis*- and *trans*-F—P—F angles are 90(2) and 178(2)°, respectively.

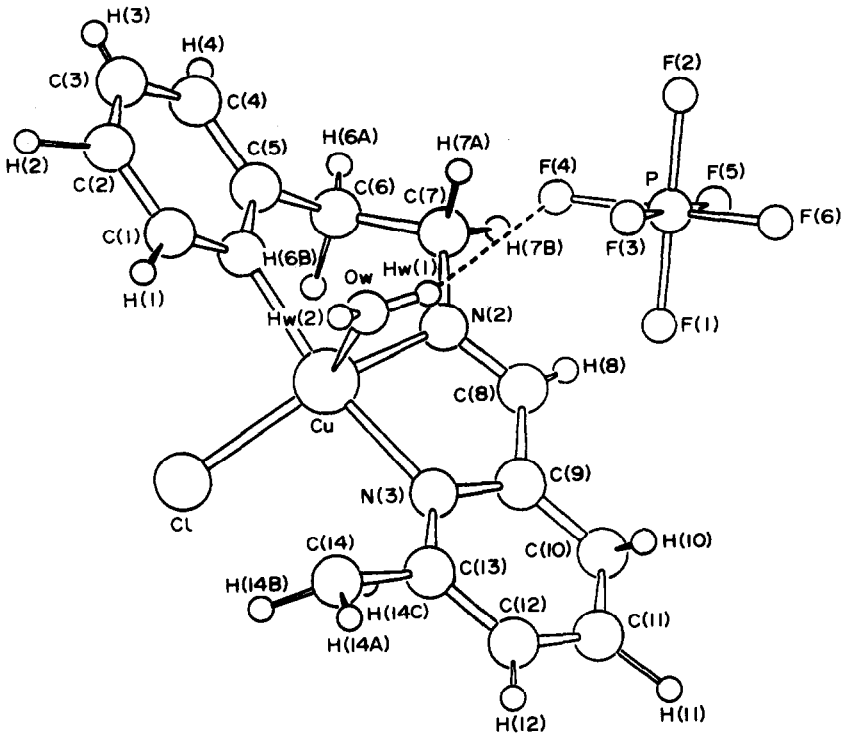

Fig. 1. Molecular structure of the $[Cu(pymep)Cl(H_2O)](PF_6)$ complex.

Table 1. Selected bond distances (Å) and angles (°) in the $[Cu(C_{14}H_{15}N_3)Cl(H_2O)](PF_6)$ complex

Distance/angle		Distance/angle	
	Copper coordination sphere		
Cu—N(1)	2.010(6)	Cu—N(2)	1.964(5)
Cu—N(3)	2.046(6)	Cu—Cl	2.240(2)
Cu—O_w	2.439(7)		
N(1)—Cu—N(2)	92.3(3)	N(1)—Cu—N(3)	167.6(2)
N(1)—Cu—Cl	92.2(2)	N(1)—Cu—O_w	86.1(2)
N(2)—Cu—N(3)	81.5(2)	N(2)—Cu—Cl	143.4(2)
N(2)—Cu—O_w	100.2(2)	N(3)—Cu—Cl	99.2(2)
N(3)—Cu—O_w	84.4(2)	Cl—Cu—O_w	116.3(2)
	Average values in the pymep ligand		
C—N	1.35(6)	C—C	1.41(6)
C—C—C	120(2)	C—N—C	119.7(6)
	Hexafluorophosphate anion and water molecule		
P—F(1)	1.558(7)	P—F(2)	1.560(7)
P—F(3)	1.553(8)	P—F(4)	1.545(9)
P—F(5)	1.520(9)	P—F(6)	1.504(12)
cis-F—P—F	90(2)	*trans*-F—P—F	178(2)
O_w—F(4)	3.091(10)	O_w—F(5)^i	3.190(10)
$H_w(1)$—O_w—$H_w(2)$	124(9)		

$i = -x+3/2, y+1/2, z.$

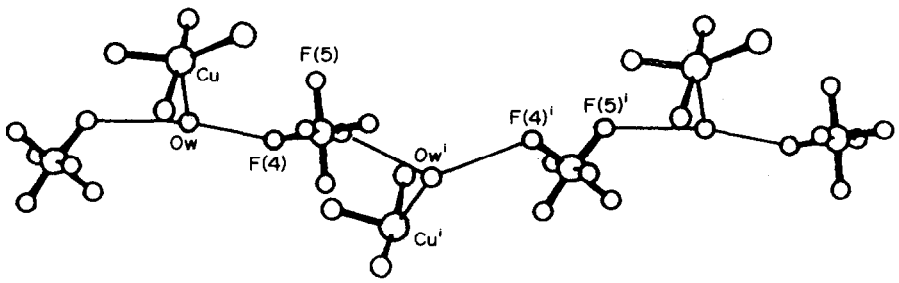

Fig. 2. Perspective view of the catenation of the [Cu(pymep)Cl(H_2O)](PF_6) complex in the |010| direction.

The coordination polyhedron around the copper atom in this type of compound has been described as "distorted square pyramidal" or "distorted trigonal bipyramidal". However, these geometries are better described as "regular square pyramidal" (SP_r) and "tetrahedral or trigonal distorted square pyramidal" (SP_{th} and SP_{tr}, respectively) as Hathaway[22] has pointed out. We have quantified the distortion of the coordination polyhedron of the title compound using the Muetterties and Guggenberger[23] description and by considering the regular square pyramid (SP_r) and the ideal trigonal bipyramid (TBP) as the limiting geometries. The dihedral angles and the deviation (Δ) from TBP for the ideal geometries and the title compound are given in Table 2. The value obtained for this compound ($\Delta = 0.24$) shows a topology close to the tetrahedral distorted square pyramidal (SP_{th}).

In the IR spectrum, the characteristic vibrations of the H_2O and PF_6 groups can be observed. For the water molecule, the stretching and bending vibrations appear at 3660–3580 and 1665 cm^{-1}, respectively. The rotation modes are masked by the pymep ligand bands and cannot be observed. The F_{1u} active modes of the PF_6 group are observed at 545 and 840 cm^{-1}. The band at 840 cm^{-1} appears slightly split due to the hydrogen bonds between the F(4) [F(5)] and O_w [O_w'] atoms.

The X-band room temperature spectrum of a powdered sample of the title compound is given in Fig. 3. The spectrum exhibits the characteristics of an orthorhombic g tensor [$g_1 = 2.219$, $g_2 = 2.120$, $g_3 = 2.047$] and remains unchanged over the temperature range 4.2–298 K. On the other hand, the diffuse reflectance spectrum of the [Cu(pymep)Cl(H_2O)](PF_6) complex, recorded at room tem-

Table 2. Dihedral angles (°) and distortion (Δ) of the [CuN_3ClO] polyhedron in the [Cu($C_{14}H_{15}N_3$)Cl(H_2O)](PF_6) complex

Dihedral angle	TBP (°)	SP_{th} (°)	[CuN_3ClO]	SP_{tr} (°)	SP_r (°)
δa_1	101.5	106.4	97.6 [O_w—N(1)—N(2)—Cl]	109.9	121.8
δa_3	101.5	106.4	109.6 [O_w—N(1)—Cl—N(2)]	109.9	121.8
δa_4	101.5	106.4	100.7 [O_w—N(2)—N(3)—Cl]	109.9	121.8
δa_6	101.5	106.4	105.8 [O_w—N(3)—Cl—N(2)]	109.9	121.8
δa_2	101.5	93.0	92.6 [Cl—N(1)—O_w—N(2)]	88.0	73.9
δa_5	101.5	93.0	92.2 [N(2)—O_w—N(3)—Cl]	88.0	73.9
δe_1	53.1	55.5	60.5 [N(1)—N(2)—O_w—N(3)]	64.1	73.9
δe_2	53.1	55.5	64.5 [N(1)—Cl—O_w—N(3)]	64.1	73.9
δe_3	53.1	46.6	43.2 [N(1)—N(2)—Cl—N(3)]	28.7	0
Δ	0	0.22	0.24	0.46	1

Δ is calculated using the following formula:

$$\Delta = \Sigma\left|\frac{(\delta a_1+\delta a_3+\delta a_4+\delta a_6)-406.0}{182.7}\right| + \left|\frac{(\delta a_2+\delta a_5)-203.0}{248.4}\right| + \left|\frac{(\delta e_1+\delta e_2)-106.2}{187.2}\right| + \left|\frac{(\delta e_3)-53.1}{477.9}\right|.$$

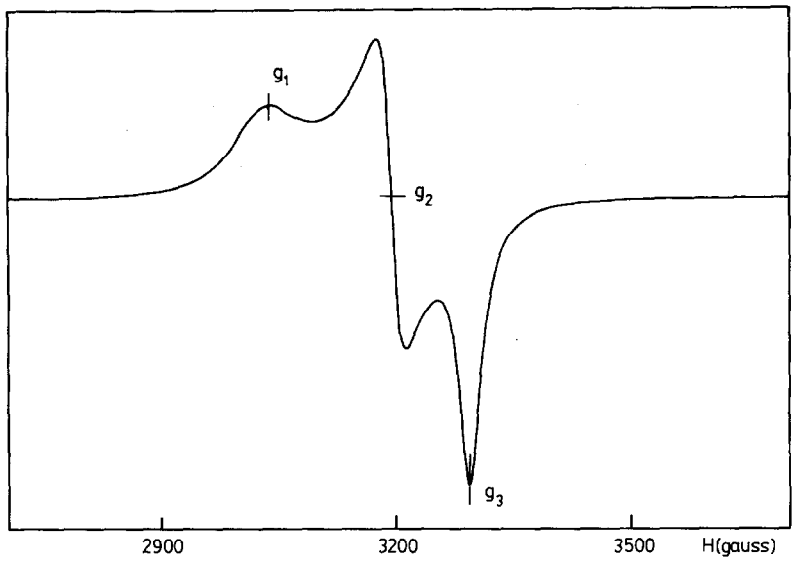

Fig. 3. X-band ESR spectrum of a powdered sample of the $[Cu(pymep)Cl(H_2O)](PF_6)$ complex, recorded at room temperature.

perature, shows one broad, unresolved band centred at about 13,800 cm^{-1}. These results are in good agreement with a geometry near to SP_{th} for the $[CuN_3ClO]$ chromophore.[24-26]

In the $[Cu(pymep)Cl(H_2O)](PF_6)$ compound, magnetic interactions could be propagated by a super-exchange path through the water molecules and PF_6^- ions connected by hydrogen bonds (see Fig. 2). Considering the Cu—Cu^i distance through that extended bridging network [14.2 Å] and the experimentally determined function for long-range magnetic super-exchange proposed by Coffman and Buettner,[27] the expected $|J|$ value is less than 10^{-3} cm^{-1}. Likewise, a dipolar magnetic interaction cannot be assumed negligible in this compound ($D_d = 2 \times 10^{-3}$ cm^{-1} from the Cu—Cu^{ii} shorter interchains distances). Thus, magnetic measurements at temperatures lower than 1 K should be performed to detect these magnetic interactions.

Acknowledgement—This work was financially supported in part by the Universidad del Pais Vasco (grant UPV 130.310.0014/88), which we gratefully acknowledge.

REFERENCES

1. L. J. Alcacer, *The Physics and Chemistry of Low Dimensional Solids*. Reidel, Dordrecht, Holland (1980).
2. J. Bernasconi and T. Schneider, *Physics in One Dimension*. Springer-Verlag, Berlin (1981).
3. J. S. Miller, *Extended Linear Chain Compounds*. Plenum Press, New York (1983).
4. T. Rojo, M. I. Arriortua, J. Ruiz, J. Darriet, G. Villeneuve and D. Beltrán, *J. Chem. Soc., Dalton Trans.* 1987, 285.
5. T. Rojo, M. I. Arriortua, J. L. Mesa, R. Cortés, G. Villeneuve and D. Beltrán, *Inorg. Chim. Acta* 1987, **134**, 59.
6. T. Rojo, J. L. Mesa, M. I. Arriortua, J. M. Savariault, J. Galy, G. Villeneuve and D. Beltrán, *Inorg. Chem.* 1988, **27**, 3904.
7. J. L. Mesa, T. Rojo, M. I. Arriortua, G. Villeneuve, J. V. Folgado, A. Beltrán and D. Beltrán, *J. Chem. Soc., Dalton Trans.* 1989, 53.
8. W. Henke, S. Kramer and D. Reinen, *Inorg. Chem.* 1983, **22**, 2858.
9. M. I. Arriortua, J. L. Mesa, T. Rojo, T. Debaerdemaeker, D. Beltrán, H. Stratemeier and D. Reinen, *Inorg. Chem.* 1988, **27**, 2976.
10. T. Rojo, A. García, J. L. Mesa, J. Vía and M. I. Arriortua, *Inorg. Chim. Acta* 1988, **149**, 159.
11. J. L. Mesa, M. I. Arriortua, L. Lezama, J. L. Pizarro, T. Rojo and D. Beltrán, *Polyhedron* 1988, **7**, 1383.
12. J. V. Folgado, E. Escrivá, A. Beltrán and D. Beltrán, *Trans. Met. Chem.* 1986, **11**, 485.
13. J. V. Folgado, E. Coronado and D. Beltrán, *J. Chem. Soc., Dalton Trans.* 1988, 1061.
14. J. V. Folgado, R. Ibañez, E. Coronado, D. Beltrán, J. M. Savariault and J. Galy, *Inorg. Chem.* 1988, **27**, 19.
15. D. Beltrán, J. V. Folgado, R. Ibañez, E. Coronado, J. L. Mesa, T. Rojo and G. Villeneuve, *Organic and Inorganic Low Dimensional Crystalline Materials*, NATO-ARW Series. Plenum Press, New York (1987).
16. Y. Nakao, *Inorg. Chim. Acta* 1983, **74**, 159.
17. P. Main. G. Germain and M. M. Woolfson, MULTAN84. *A System of Computer Programs for the Automatic Solution of Crystal Structures from X-ray*

Diffraction Data. University of York, England, and Louvain, Belgium, (1984).
18. G. M. Sheldrick, SHELX76, *Program for Crystal Structure Determination*. University of Cambridge, England (1976).
19. *International Tables for X-ray Crystallography*, Vol. 4, pp. 72–99. Kynoch Press, Birmingham (1974).
20. P. Roberts and G. M. Sheldrick, XANADU, *Program for Torsion Angle, Mean Plane and Libration Correction Calculations*. University of Cambridge, England (1975).
21. E. Ketler, SCHAKAL 88. *A Fortran Program for the Graphic Representation of Molecular and Crystallographic Models*. University of Freiburg (1988).
22. B. J. Hathaway, *Coord. Chem. Rev.* 1982, **41**, 423.
23. E. L. Muetterties and L. J. Guggenberger, *J. Am. Chem. Soc.* 1974, 1748.
24. R. C. Slade, A. A. G. Tomlinson, B. J. Hathaway and D. E. Billing, *J. Chem. Soc.* (*A*) 1968, 61.
25. B. J. Hathaway and D. E. Billing, *Coord. Chem. Rev.* 1970, **5**, 143.
26. B. J. Hathaway, *Struct. and Bonding* 1984, **57**, 55 and refs therein.
27. R. Coffman, G. R. Buettner, *J. Chem. Phys.* 1979, **83**, 2387.

Polyhedron Vol. 10, No. 4/5, pp. 501–507, 1991
Printed in Great Britain

0277–5387/91 $3.00+.00
© 1991 Pergamon Press plc

METAL COMPLEXES OF FUNCTIONALIZED PHOSPHINES—I. SYNTHESIS AND CHARACTERIZATION OF 2-DIPHENYLPHOSPHINOETHYLAMINES AND SOME OF THEIR COMPLEXES WITH PLATINUM. X-RAY STRUCTURE OF $[Pt(Ph_2PCH_2CH_2NHBu^t)(Ph_2PCH_2CH_2NHBu^t \cdot HCl)Cl]Cl \cdot H_2O$

MANDY BASSETT, DAVID L. DAVIES,* JULIE NEILD, LESLEY J. S. PROUSE and DAVID R. RUSSELL

Department of Chemistry, University of Leicester, Leicester LE1 7RH, U.K.

(*Received* 15 *August* 1990; *accepted* 5 *November* 1990)

Abstract—The new bidentate ligands $Ph_2PCH_2CH_2NHR$ [R = Bu^t, CH_2Ph, CH(Me)Ph] and $Ph_2PCH_2CH_2N(CH_2Ph)_2$ and their corresponding hydrochloride salts have been synthesized and were characterized by ^1H, $^{31}P\{^1H\}$ and $^{13}C\{^1H\}$ NMR spectroscopy. The ligand $Ph_2PCH_2CH_2NHBu^t$ reacts with K_2PtCl_4 or $(COD)PtCl_2$ to form $[Pt(Ph_2PCH_2CH_2NHBu^t)(Ph_2PCH_2CH_2NHBu^t \cdot HCl)Cl]Cl$, whose structure has been determined by X-ray diffraction. Treatment of this complex with HCl gas gives $[Pt(Ph_2PCH_2CH_2NHBu^t \cdot HCl)_2Cl_2]$ which can also be synthesized from $Ph_2PCH_2CH_2NHBu^t \cdot HCl$ and K_2PtCl_4.

Recently we have studied a range of amino-alkyl and hydroxy-alkyl substituted phosphines. In this paper we report the synthesis of a number of diphenylphosphinoethylamines and some of their complexes with platinum metals.

Bidentate ligands with one hard nitrogen donor and one soft phosphorus donor have been the subject of many recent reports.[1–9] These ligands can act as chelating ligands or as bridging ligands, and the enhanced stability provided by chelation has been used to examine platinum metal amides and N—H activation by these metals. Though early transition metal amides are well known, such complexes of the platinum metals are still quite rare.[10,11] However, such species have been implicated in many catalytic processes such as the rhodium catalysed synthesis of β-lactams by carbonylation of aziridines.[12] Platinum metal amides have also been proposed as key intermediates in a possible route to the catalytic amination of alkenes.[13–15] To date, most of the studies have used phosphines having a phenyl backbone connecting the phosphorus and the nitrogen centres, we are examining ligands with an alkyl backbone which should be more flexible. During the course of this work some related work using the ligand diphenylphosphinoethyl-benzylamine has been published.[16] We have synthesized this phosphine by a different route and have found some differences to the published data which were discussed below.

RESULTS AND DISCUSSION

Base-catalysed addition of amines to vinyldiphenylphosphine has been reported, using methyl lithium as the base catalyst.[17] Using primary amines the products were usually bis(diphenylphosphinoethyl)amines, though it was stated that the intermediate diphenylphosphinoethyl secondary amine could be isolated in certain cases. We have found that sodium amide is a convenient catalyst for this reaction, its low solubility in THF means that it is only present in small concentrations. Thus, refluxing vinyldiphenylphosphine with an excess of amine in THF with sodium amide as catalyst gives diphenylphosphinoethylamines $Ph_2PCH_2CH_2NHR$ [R = Bu^t, CH_2Ph, CH(Me)Ph] (**1a–c**) in good yields. The ligand **1a** is isolated as a crystalline solid, however **1b** and **1c** are oils. An excess of

* Author to whom correspondence should be addressed.

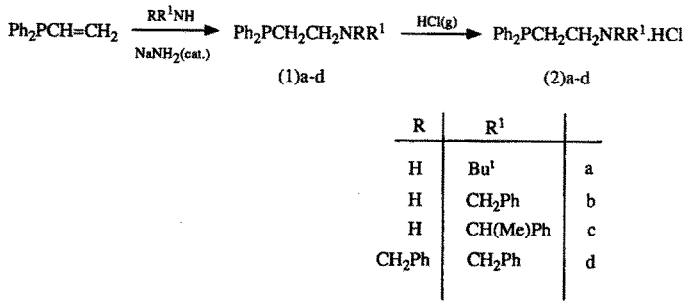

Scheme 1.

amine is used to minimize the formation of bis(diphenylphosphinoethyl)amines. If the secondary amine dibenzylamine is used instead of a primary amine, then the product is $Ph_2PCH_2CH_2N(CH_2Ph)_2$ (**1d**) (see Scheme 1).

The ligands have been characterized by their ^1H, ^{13}C-$\{^1H\}$ and ^{31}P-$\{^1H\}$ NMR spectra (Table 1). All the ligands show a single resonance in the ^{31}P-$\{^1H\}$ NMR spectrum at around δ −20. The ^{13}C-$\{^1H\}$ NMR spectra each show two doublets between δ 29 and 46 due to the C_2H_4 backbone, as well as signals due to the phenyl groups and the R substituent on the nitrogen. There is some confusion in the literature about the assignment of these signals

Table 1. ^1H, ^{13}C-$\{^1H\}$ and ^{31}P-$\{^1H\}$ NMR data for new ligands[a]

Compound	$\delta(^{31}P)$[b]	$\delta(^1H)$	$\delta(^{13}C)$[c]
1a	−20.6	1.25 (s, 9H, But), 2.24 [t, 2H, CH_2, *J*(HH) 7.5], 2.70 [td, 2H, CH_2, *J*(HH) 7.5, *J*(PH) 8.5], 7.35 (m, 10H, Ph)	28.9 (CMe_3), 29.9 [d, C_1, ^1J(PC) 12], 39.4 [d, C_2, ^2J(PC) 21], 50.4 (CMe_3), 128–139 (Ph)
2a	−19.9	1.25 (s, 9H, But), 2.84 (m, 2H, CH_2), 2.94 (m, 2H, CH_2), 7.55 (m, 10H, Ph), 9.4 (br, 2H, NH_2)	24.9 [d, C_1, ^1J(PC) 14], 26.0 (CMe_3), 39.4 [d, C_2, ^2J(PC) 28], 128–136 (Ph)
1b	−20.6	1.60 (br, 1H, NH), 2.29 [t, 2H, CH_2, *J*(HH) 7.5], 2.78 [td, 2H, CH_2, *J*(HH) 7.5, *J*(PH) 8.5], 3.7 (s, 2H, CH_2Ph), 7.3 (m, 15H, Ph)	29.0 [d, C_1, ^1J(PC) 12], 46.0 [d, C_2, ^2J(PC) 20], 53.6 (CH_2Ph), 125–140 (Ph)
2b	−20.4	2.62 (m, 2H, CH_2), 2.85 (m, 2H, CH_2), 3.95 (s, 2H, CH_2Ph), 7.35 (m, 15H, Ph), 10.1 (br, 2H, NH_2)	24.1 [d, C_1, ^1J(PC) 16], 43.2 [d, C_2, ^2J(PC) 26], 50.1 (CH_2Ph), 128–136 (Ph)
1c	−20.8	1.28 [d, 3H, Me, *J*(HH) 6.5], 2.22 (m, 2H, CH_2), 2.61 (m, 2H, CH_2), 3.70 [q, 1H, CH, *J*(HH) 6.5], 7.3 (m, 15H, Ph)	24.2 (Me), 29.1 [d, C_1, ^1J(PC) 12], 44.1 [d, C_2, ^2J(PC) 19.6], 57.8 (CH), 126–145 (Ph)
2c	−20.8	1.69 [d, 3H, Me, *J*(HH) 6.6], 2.75 (m, 4H, CH_2), 4.13 (m, 1H, CH), 7.3 (m, 15H, Ph), 9.99 (Br, 1H, NH), 10.38 (br, 1H, NH)	20.7 (Me), 24.2 (br, C_1) 43.0 [d, C_2, ^2J(PC) 22], 58.5 (CH), 127–136 (Ph)
1d	−20.4	2.25 (m, 2H, CH_2), 2.61 (m, 2H, CH_2), 3.55 (s, 4H, CH_2Ph), 7.29 (m, 20H, Ph)	25.6 [d, C_1, ^1J(PC) 13], 49.7 [d, C_2, ^2J(PC) 22], 57.8 (CH_2Ph), 126–140 (Ph)
2d	−19.8	1.70 (br, 1H, MeO*H*), 2.65 (m, 2H, CH_2), 2.94 (m, 2H, CH_2), 3.46 (s, 3H, *M*eOH), 4.05 [dd, 2H, CH, *J*(HH) 5, 13], 4.30 [dd, 2H, CH, *J*(HH) 2, 13], 7.4 (m, 20H, Ph), 12.5 (br, 1H, NH)	22.5 [d, C_1, ^1J(PC) 17], 47.4 [d, C_2, ^2J(PC) 29], 50.6 (MeOH), 56.7 (CH_2Ph), 128–136 (Ph)

[a] Chemical shifts (δ) in ppm, coupling constants in Hz. Measurements at room temperature in $CDCl_3$.
[b] Chemical shifts are positive to high frequency of 85% H_3PO_4 (external) (0.0 ppm).
[c] The carbon atoms of the ethyl backbone of the ligands are numbered as follows $Ph_2PC_1C_2NRR^1$.

which has been based on the relative magnitudes of ^1J(PC) and ^2J(PC).[9,16] Since we have made a series of these ligands which vary only in the nature of the groups attached to nitrogen we have been able to base our assignments on chemical shift arguments as well as on coupling constants. The signal at δ 29 does not vary by more than 1 ppm for each different R group, whereas the other doublet at around δ 40 varies by about 7 ppm depending on the nature of R thus, we assign the signals at approx. δ 29 to the CH_2 next to the phosphorus atom and those at approx. δ 40 to the CH_2 next to the nitrogen. The greater electronegativity of nitrogen compared to phosphorus leads to the signal being more down field. With these assignments we find that ^2J(PC) is bigger than ^1J(PC) for all these phosphines, as was suggested for $Ph_2PCH_2CH_2NMe_2$.[9] A previous study of tertiary phosphines concluded that ^1J(PC) and ^2J(PC) for alkyl side chains are approximately equal in magnitude.[18] This contrasts with the assignment made recently for the ligand $Ph_2PCH_2CH_2NHR \cdot HCl$ (R = CH_2Ph) where the assignments were made on the basis that ^1J(PC) is larger than ^2J(PC).[16] The ^{1}H NMR spectra show two multiplets in the region δ 2–3 due to the CH_2CH_2 backbone, as well as signals due to the phenyl groups and the R substituent attached to nitrogen. We assume the multiplet to lower field is due to the CH_2 next to nitrogen, with that to higher field being the one next to phosphorus as suggested for the $^{13}C\{^1H\}$ spectra.

Reaction of the ligands **1a–d**, as a solution in diethyl ether, with HCl gas readily yields the hydrochloride salts, **2a–d**, which may be recrystallized from methanol, in certain cases with incorporation of methanol into the crystal. It is this presence of methanol of crystallization which we feel confused previous workers in their reported isolation of $Ph_2PCH_2CH_2NHCH_2Ph \cdot HCl$ (**2b**). The ^{1}H NMR spectrum of this salt (Table 1) shows two multiplets at δ 2.6 and 2.85 assigned to the PCH_2CH_2N backbone, as well as a singlet δ 3.95 due to the CH_2 of the benzyl. This contrasts with the reported values of multiplets at δ 4.2 and 2.7 assigned to the PCH_2CH_2N backbone, and a singlet at δ 3.5 due to the CH_2 of the benzyl. We believe that the ligand previously formulated as $Ph_2PCH_2CH_2NHCH_2Ph \cdot HCl$[16] (**2b**) is in fact $Ph_2PCH_2CH_2N(CH_2Ph)_2 \cdot HCl \cdot (MeOH)$ (**2d**), which we have prepared independently from vinyldiphenylphosphine and dibenzylamine followed by treatment with gaseous HCl as described above. On examining the ^{1}H NMR spectrum of $Ph_2PCH_2CH_2N(CH_2Ph)_2 \cdot HCl \cdot (MeOH)$ (**2d**) at high field (300 MHz) (Table 1), the signal at δ 2.7 can be seen to consist of two multiplets at δ 2.65 and 2.95 which we assign to the PCH_2CH_2N backbone, while the multiplet at δ 4.2 is actually two doublets of doublets at δ 4.3 and 4.15 which we now assign to the CH_2 of the benzyl groups, each CH_2 consisting of two diastereotopic protons which couple to each other and to the hydrogen on the nitrogen. The singlet at δ 3.5 is due to methanol of crystallization and can be observed in the $^{13}C\{^1H\}$ NMR spectrum at δ 50.

We have attempted to repeat the synthesis of $Ph_2PCH_2CH_2NHCH_2Ph$ as reported by Khan and Reddy[16] starting from 2-aminoethanol and benzyl chloride. However, we find that this gives dibenzylaminoethanol as the major product even when only one equivalent of benzyl chloride is used. This could explain their isolation of $Ph_2PCH_2CH_2N(CH_2Ph)_2$ which, as explained above, we believe to be their final product.

The ligand **1a** (R = Bu^t) reacts with K_2PtCl_4 or with $(COD)PtCl_2$ to give the salt **3** (Scheme 2) in which one ligand coordinates through just the phosphorus atom while the other forms a five-membered ring coordinating through both the phosphorus and nitrogen atoms. This is easily seen in the $^{31}P\{^1H\}$ NMR spectrum which shows two inequivalent phosphorus atoms at δ +32.67 and −2.22, respectively. The signal to lower field being the phosphorus in the five-membered ring.[19] The P—Pt coupling constants are 3765 and 3203 Hz as expected for phosphorus *trans* to chloride and amine, respectively. Similar complexes have been obtained from $Ph_2PCH_2CH_2NMe_2$[9] and $Ph_2PCH_2CH_2NHR$ (R = CH_2Ph),[16] though as discussed above the latter actually contains $Ph_2PCH_2CH_2N(CH_2Ph)_2$. Using the related hydroxyalkylphosphine, $Ph_2PCH_2CH_2OH$, Pringle *et al.* showed that the species formed was solvent dependent.[20] We observe some broadness in the $^{31}P\{^1H\}$ NMR spectrum of **3** in $CDCl_3$ which may be indicative of an exchange process, but do not observe the species with both chlorides coordinated and the ligands coordinated only through the phosphorus. This is consistent with an amine being a better donor than an alcohol and thus competing more effectively with chloride for one coordination site.

We have carried out an X-ray crystal structure determination of complex **3** which actually crystallized as the hydrochloride salt, i.e. the uncoordinated nitrogen had been protonated by traces of acid possibly from the dichloromethane solvent, and with a molecule of water of crystallization. The structure of the cation and the principal bond lengths and angles are shown in Fig. 1. The structure clearly shows the presence of one monodentate phosphine and one bidentate ligand. The chelating ligand spans an angle of 85.9(3)° and has Pt—P and

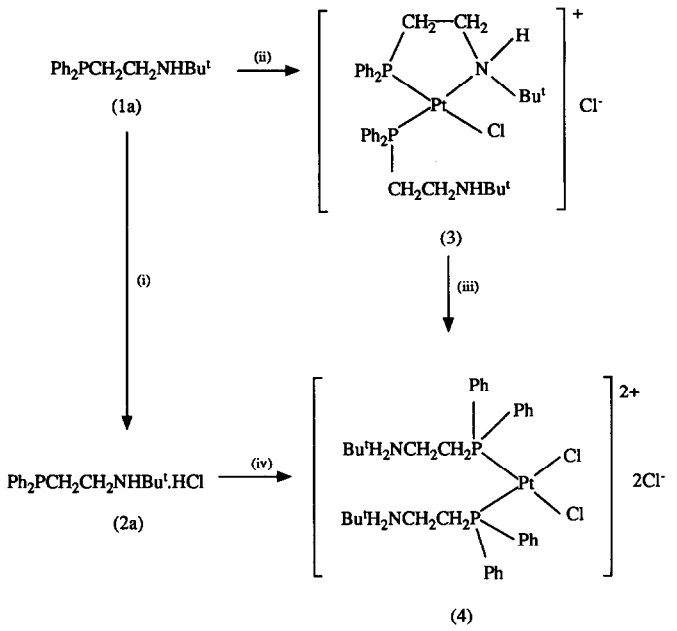

Scheme 2. (i) HCl(g); (ii) K_2PtCl_4 or $(COD)PtCl_2$; (iii) HCl(g); (iv) K_2PtCl_4.

Pt—N bond lengths of 2.226(3) and 2.139(8) Å, respectively, which are similar to those of 86.4°, 2.245 and 2.12 Å, respectively, found for the *o*-diphenylphosphinoaniline ligand in the dication *cis*-$[Pt(o\text{-}Ph_2PC_6H_4NH_2)_2]^{2+}$.[4b]

Treatment of complex **3** with HCl gas gives complex **4** (Scheme 2) in which both the ligands are coordinated through the phosphorus atom only, the amine substituents having been protonated to the hydrochloride salts. This complex may be prepared independently from the ligand hydrochloride salt and K_2PtCl_4. Complex **4** shows the expected $^{31}P\{^1H\}$ NMR spectrum (δ +3.63) with platinum satellites [J(Pt—P) = 3623 Hz] consistent with phosphorus coordinated *trans* to chloride.

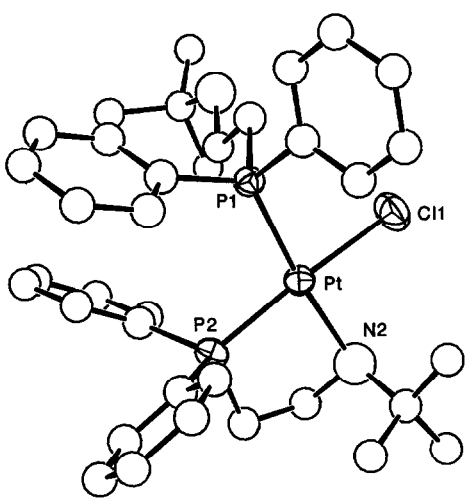

Fig. 1. Molecular structures of the cation $[Pt(Ph_2PCH_2CH_2NHBu^t)(Ph_2PCH_2CH_2NH_2Bu^t)Cl]^{2+}$. Selected bond lengths (Å) and bond angles (°): P(1)—Pt 2.260(2), Pt—Cl(1) 2.367(3), P(2)—Pt 2.226(3), N(2)—Pt 2.139(8); P(2)—Pt—P(1) 100.4(1), P(2)—Pt—N(2) 85.9(3), P(1)—Pt—Cl(1) 87.0(1), N(2)—Pt—Cl(1) 86.6(3).

In conclusion, we have shown that sodium amide-catalysed addition of amines to vinyldiphenylphosphine can be used to produce a series of ligands $Ph_2PCH_2CH_2NHR$. Our evidence suggests that a previous report[16] of $Ph_2PCH_2CH_2NH(CH_2Ph)$ and some of its complexes is wrong, and that they should be reformulated as containing $Ph_2PCH_2CH_2N(CH_2Ph)_2$. The ligand $Ph_2PCH_2CH_2NHBu^t$ reacts with K_2PtCl_4 or $(COD)PtCl_2$ to form a complex in which one ligand is chelated and the other is bound only through phosphorus. Further studies to examine the reactivity of this complex and the effect of changing the Bu^t group are in progress.

EXPERIMENTAL

Petroleum ether, diethyl ether, toluene and THF were all dried by refluxing over purple sodium/benzophenone in a nitrogen atmosphere. Dichloromethane was purified by refluxing over calcium hydride. The compounds vinyldiphenylphosphine[21] and $(COD)PtCl_2$[22] were prepared by the literature methods. Chlorodiphenylphosphine and L-(−)-1-phenylethylamine (Lancaster Synthesis), t-butylamine, benzylamine and sodium amide suspension in toluene (Aldrich) were all used as

supplied. The syntheses of phosphorus-containing compounds were carried out in deoxygenated solvents under a nitrogen atmosphere. Once isolated as pure solids, all new phosphine compounds are relatively air-stable and precautions for their storage are unnecessary.

^1H and ^{13}C-$\{^1H\}$ NMR spectra were recorded on a Bruker AM300 spectrometer as $CDCl_3$ solutions with internal $SiMe_4$ as reference. ^{31}P-$\{^1H\}$ NMR spectra were recorded on a Jeol FX60 instrument at 24.15 MHz in $CDCl_3$ solution and were referenced to external 85% H_3PO_4 with shifts to high frequency being positive. Microanalyses were performed by Butterworth Laboratories Ltd, Middlesex.

Preparation of $Ph_2PCH_2CH_2NHBu^t$ (**1a**)

An excess of t-butylamine (3.38 g, 46.12 mmol) and sodium amide (two spatulas full from a suspension in toluene) were added to a solution of vinyldiphenylphosphine (2.46 g, 11.53 mmol) in THF (30 cm^3). The solution was refluxed under a nitrogen atmosphere for 1.5 h. The sodium amide was destroyed by addition of aqueous ammonium chloride solution (15 cm^3 of a 10% solution). The phosphine was extracted from the aqueous layer with dichloromethane and dried with anhydrous magnesium sulphate. The dichloromethane was removed under reduced pressure and the product was dissolved in petroleum ether and filtered to remove any insoluble impurities. Recrystallization from petroleum ether gave $Ph_2PCH_2CH_2NHBu^t$ as a cream solid (2.80 g, 85%). Found: C, 75.2; H, 8.3; N, 4.3. $C_{18}H_{24}NP$ requires: C, 75.8; H, 8.5; N, 4.9%.

Preparation of $Ph_2PCH_2CH_2NHCH_2Ph$ (**1b**)

This was prepared in a similar manner to $Ph_2PCH_2CH_2NBu^t$ above from vinyldiphenylphosphine (5.34 g, 25.2 mmol), though after refluxing for 1.5 h the solution had become purple. Excess benzylamine was removed from the product by heating at 60°C *in vacuo*. The product, $Ph_2PCH_2CH_2NHCH_2Ph$ (5.84 g, 73%), was isolated as a yellow oil.

Preparation of $Ph_2PCH_2CH_2NHCH(Me)Ph$ (**1c**)

$Ph_2PCH_2CH_2NHCH(Me)Ph$ was prepared as above, and was isolated as a colourless oil in 84% yield.

Preparation of $Ph_2PCH_2CH_2N(CH_2Ph)_2$ (**1d**)

This was prepared in a similar way except that only a slight excess of dibenzylamine was used (1.1 equiv.). Excess amine was removed by heating at 150°C *in vacuo* and $Ph_2PCH_2CH_2N(CH_2Ph)_2$ was isolated as a pale yellow oil in 79% yield.

Preparation of $Ph_2PCH_2CH_2NHBu^t \cdot HCl$ (**2a**)

Hydrogen chloride gas was bubbled through a solution of $Ph_2PCH_2CH_2NHBu^t$ (3.0 g, 10.51 mmol) in diethyl ether (50 cm^3). After a few seconds a white solid precipitated, the diethyl ether was removed *in vacuo* and the product was recrystallized from methanol giving $Ph_2PCH_2CH_2NHBu^t \cdot HCl$ (2.78 g, 82%) as white crystals. Found: C, 66.0; H, 7.4; N, 4.4. $C_{18}H_{25}ClNP$ requires: C, 67.2; H; 7.8; N, 4.3%.

The other hydrochloride salts were prepared in the same way; $Ph_2PCH_2CH_2NH(CH_2Ph) \cdot HCl$ (**2b**) (80%); Found: C, 69.6; H, 6.7; N, 4.0. $C_{21}H_{23}ClNP$ requires: C, 70.9; H, 6.5; N, 3.9%. $Ph_2PCH_2CH_2NHCH(Me)Ph \cdot HCl$ (**2c**) (75%); Found: C, 70.1; H, 7.0; N, 3.9. $C_{22}H_{25}ClNP$ requires: C, 71.4; H, 6.8; N, 3.8%. $Ph_2PCH_2CH_2N(CH_2Ph)_2 \cdot HCl \cdot (MeOH)$ (**2d**) (64%); Found: C, 72.6; H, 6.9; N, 3.1. $C_{29}H_{33}ClNOP$ requires: C, 72.9; H, 7.0; N, 2.9%.

Reaction of K_2PtCl_4 *with* $Ph_2PCH_2CH_2NHBu^t$

A solution of $Ph_2PCH_2CH_2NHBu^t$ (700 mg, 2.45 mmol) in acetone (25 cm^3) was added to a solution of K_2PtCl_4 (500 mg, 1.2 mmol) in water (8 cm^3). The solution changed from red to yellow on addition of the phosphine and was stirred for 0.5 h at room temperature. The solvent was removed *in vacuo* and the residue was dissolved in dichloromethane and filtered to remove potassium chloride. Evaporation of the dichloromethane gave $[\overline{Pt(Ph_2PCH_2CH_2NHBu^t)}(Ph_2PCH_2CH_2NHBu^t)Cl]Cl$ (**3**) as a yellow solid (915 mg, 91%). Recrystallization gave the hydrochloride salt with one molecule of water of crystallization. Found: C, 47.9; H, 5.9; N, 2.6. $C_{36}H_{51}Cl_3N_2OP_2Pt$ requires: C, 48.5; H, 5.8; N, 3.1%. ^1H NMR: δ 1.35 (s, 9H, Bu^t), 1.45 (s, 9H, Bu^t), 2.6–3.5 (br m, 8H, CH_2), 7.5 (m, 20H, Ph). ^{31}P-$\{^1H\}$ NMR: δ −2.2 [d, J(PP) 20, J(PtP) 3203 Hz], +32.7 [d, J(PP) 20, J(PtP) 3765 Hz].

Reaction of $(COD)PtCl_2$ *with* $Ph_2PCH_2CH_2NHBu^t$

A solution of $(COD)PtCl_2$ (300 mg, 0.80 mmol) and $Ph_2PCH_2CH_2NHBu^t$ (480 mg, 1.68 mmol) in dichloromethane (50 cm^3) was stirred for 30 min,

the solution was reduced in volume and petroleum ether was added to precipitate [Pt($Ph_2PCH_2CH_2NHBu^t$)($Ph_2PCH_2CH_2NHBu^t$)Cl]Cl (**3**) (506 mg, 75%) as a yellow solid.

Reaction of K_2PtCl_4 *with* $Ph_2PCH_2CH_2NHBu^t \cdot HCl$

A solution of $Ph_2PCH_2CH_2NHBu^t \cdot HCl$ (404 mg, 1.26 mmol) in methanol (30 cm^3) was added to a solution of K_2PtCl_4 (260 mg, 0.63 mmol) in water (5 cm^3). The solution was stirred for 2 h after which time the solvent was removed and the residue was dissolved in dichloromethane and filtered. Evaporation of the dichloromethane gave [Pt($Ph_2PCH_2CH_2NHBu^t \cdot HCl)_2Cl_2$] (**4**) as a white solid (360 mg, 68%). Found: C; 46.9; H, 6.0; N, 2.8. $C_{36}H_{50}Cl_4N_2P_2Pt$ requires: C, 47.5; H, 5.5; N, 3.1%. ^1H NMR: δ 1.40 (s, 18H, Bu^t), 3.40 (br, 8H, CH_2), 7.30 (br m, 20H, Ph), 9.50 (br, 4H, NH_2). ^{31}P-{^1H} NMR: δ 3.63 [J(PtP) 3623 Hz].

Reaction of [Pt($Ph_2PCH_2CH_2NHBu^t$)($Ph_2PCH_2CH_2NHBu^t$)Cl]Cl (**3**) *with* HCl

Hydrogen chloride gas was bubbled through a solution of [Pt($Ph_2PCH_2CH_2NHBu^t$)($Ph_2PCH_2CH_2NHBu^t$)Cl]Cl in methanol for 5 min, after which time the ^{31}P-{^1H} NMR spectrum showed complete conversion to [Pt($Ph_2PCH_2CH_2NHBu^t \cdot HCl)_2Cl_2$] (**4**).

Crystal structure determination

Crystals of complex **3** were obtained from methanol–dichloromethane. The unit cell parameters were determined by least squares refinement of ω-measurements of different layers.[23] Data were collected on a Stoë STADI-2 diffractometer with an ω-scan technique in the range $7 < 2\theta < 50°$. The intensities of 8135 reflections were measured and these data were corrected for Lorentz and polarization effects to give 4958 unique reflections with $I > 3\sigma(I)$. Subsequent calculations were carried out with the computer program SHELX-76.[24]

Crystal data for [$C_{36}H_{51}Cl_3N_2OP_2Pt$] (**3**): M = 891.16, monoclinic, a = 11.430(14), b = 14.726(9), c = 24.129(6) Å, β = 104.46(4)°, U = 3932.69 $Å^3$, Z = 4, D_c = 1.50 g cm^{-3}, $F(000)$ = 1792. Space group $P2_1/c$, λ(Mo-K_α) = 0.71069 Å, μ(Mo-K_α) = 36.41 cm^{-1}.

The molecular structure was solved by conventional Patterson and Fourier difference techniques. Scattering factors were taken from ref. 25. An absorption correction[23] was applied to the data with the maximum and minimum transmission factors of 0.712 and 0.604, respectively. Phenyl rings were included as rigid groups with D_{6h} symmetry and C—C distances of 1.395 Å. The hydrogen atoms of the phenyl and the CH_2 groups were included in calculated positions (C—H = 1.08 Å). All non-hydrogen atoms were refined anisotropically. Final cycles of refinement employed a weighting factor w calculated from $w = k/(\sigma^2F + gF^2)$, where k = 1.6096 and g = 0.000826, and gave final values of R = 0.0534 and R_w = 0.0535.

Acknowledgements—We thank the SERC for a studentship (J.N.), the Nuffield Foundation for an award to newly appointed science lecturers (D.L.D.), Johnson Matthey for a loan of platinum salts, and Leicester University Computer Centre who provided support and facilities for X-ray single crystal calculations.

REFERENCES

1. M. K. Cooper and J. M. Downes, *Inorg. Chem.* 1978, **17**, 880.
2. T. B. Rauchfuss, F. T. Patino and D. M. Roundhill, *Inorg. Chem.* 1975, **14**, 652.
3. D. M. Roundhill, R. A. Bechtold and S. G. N. Roundhill, *Inorg. Chem.* 1980, **19**, 284.
4. (a) M. K. Cooper, J. M. Downes, K. Henrick, H. J. Goodwin and M. McPartlin, *Inorg. Chim. Acta* 1983, **76**, L159; (b) M. K. Cooper, J. M. Downes, K. Henrick, H. J. Goodwin and M. McPartlin, *Inorg. Chim. Acta* 1983, **76**, L157.
5. D. Hedden and D. M. Roundhill, *Inorg. Chem.* 1985, **24**, 4152.
6. D. Hedden, D. M. Roundhill, W. C. Fultz and A. L. Rheingold, *Organometallics* 1986, **5**, 336.
7. S. Park, D. Hedden, A. L. Rheingold and D. M. Roundhill, *Organometallics* 1986, **5**, 1305.
8. S. Park, M. P. Johnson and D. M. Roundhill, *Organometallics* 1989, **8**, 1700.
9. G. K. Anderson and R. Kumar, *Inorg. Chem.* 1984, **23**, 4064.
10. M. F. Lappert, P. P. Power, R. A. Sanger and R. C. Srivastava, *Metal and Metalloid Amides*. Ellis Horwood, Chichester, U.K. (1980).
11. H. E. Bryndza and W. Tam, *Chem. Rev.* 1988, **88**, 1163.
12. S. Calet, F. Urso and H. Alper, *J. Am. Chem. Soc.* 1989, **111**, 931.
13. A. L. Casalnuovo, J. C. Calabrese and D. Milstein, *Inorg. Chem.* 1987, **26**, 971.
14. R. L. Cowan and W. C. Trogler, *Organometallics* 1987, **6**, 2451.
15. A. L. Casalnuovo, J. C. Calabrese and D. Milstein, *J. Am. Chem. Soc.* 1988, **110**, 6738.
16. M. M. T. Khan and A. P. Reddy, *Polyhedron* 1987, **6**, 2009.
17. Von G. Markl and B. Merkl, *Tetrahedron Letts* 1981, **22**, 4459.
18. B. E. Mann, *J. Chem. Soc., Perkin Trans 2* 1972, 30.

19. P. E. Garrou, *Chem. Rev.* 1981, **81**, 229.
20. N. W. Alcock, A. W. G. Platt and P. Pringle, *J. Chem. Soc., Dalton Trans.* 1987, 2273.
21. K. D. Berlin and G. B. Butler, *J. Org. Chem.* 1961, **26**, 2537.
22. J. X. McDermott, J. F. White and G. M. Whitesides, *J. Am. Chem. Soc.* 1976, **98**, 6521.
23. W. Clegg and G. M. Sheldrick, *Z. Krist.* 1984, **167**, 23.
24. G. M. Sheldrick, SHELX-76, Program for Crystal Structure Determination. University of Cambridge, U.K. (1976).
25. *International Tables for X-ray Crystallography*, Vol. 4. Kynoch Press, Birmingham (1975).

Polyhedron Vol. 10, No. 4/5, pp. 509–516, 1991
Printed in Great Britain

0277–5387/91 $3.00+.00
© 1991 Pergamon Press plc

TIN(IV) PORPHYRIN COMPLEXES—IV.* CRYSTAL STRUCTURES OF *MESO*-TETRAPHENYLPORPHYRINATOTIN(IV) COMPLEXES WITH HYDROXIDE, WATER, BENZOATE, SALICYLATE AND ACETYLSALICYLATE AS AXIAL LIGANDS

GRAHAM SMITH and DENNIS P. ARNOLD†

Department of Chemistry, Queensland University of Technology, Brisbane 4001, Australia

and

COLIN H. L. KENNARD

Department of Chemistry, University of Queensland, Brisbane 4072, Australia

and

THOMAS C. W. MAK

Department of Chemistry, Chinese University of Hong Kong, Shatin, New Territories, Hong Kong

(*Received* 21 *August* 1990; *accepted* 5 *November* 1990)

Abstract—A series of five complexes of tin(IV) with 5,10,15,20-tetraphenylporphyrin (H_2tpp) of the type [SnX_2(tpp)] has been prepared and characterized using NMR and single crystal X-ray diffraction techniques. The complexes are [$Sn(OH)_2$(tpp)] (**1**), [$Sn(OH_2)_2$(tpp)] $(CF_3SO_3)_2$ (**2**), [$Sn(C_6H_5CO_2)_2$(tpp)] (**3**), [$Sn(2\text{-}OH\text{-}C_6H_4CO_2)_2$(tpp)] (**4**) and [$Sn(2\text{-}OCOCH_3\text{-}C_6H_4CO_2)_2$(tpp)] (**5**). All complexes are monomeric with little structural variation within the Sn(tpp) framework. All axial substituents act as unidentate ligands with the Sn—O bond lengths varying from 2.017(4) Å (X = OH) (**1**) through 2.055(5) Å (**3**), 2.06(3) Å (mean) (**5**), 2.09(1) Å (**4**) (the substituted benzoates) to 2.16(1) Å (mean) ($X = OH_2$) (**2**).

The octahedral tin(IV) complexes of porphyrins and related ligands have attracted interest in recent years in a variety of fields. Tin(IV) proto- and meso-porphyrin show promise as therapeutic agents for neonatal jaundice, as they are potent inhibitors of haem oxygenases.[2] Morgan *et al.* have reported studies of photodynamic cancer treatment using the tin complexes of the porphyrin-derived purpurins and verdins.[3] Water-soluble complexes such as tetrakis(N-methyl-4-pyridyl)porphyrinatotin(IV) have been used as photosensitizers for energy transfer to water and other molecules for hydrogen generation.[4] Most recently, Meyerhoff and co-workers[5] reported the use of dichloro-5,10,15,20-tetraphenylporphyrinatotin(IV) {[$SnCl_2$(tpp)]} in polymer membrane anion-selective electrodes. These electrodes displayed surprising selectivity for salicylate over benzoate, and excellent selectivity for salicylate over chloride. It was proposed that the order of anion selectivities reflects strength of binding of anions to a cationic tin porphyrin centre in the membrane.[5]

One of us has studied a wide range of Sn(tpp) complexes by NMR and visible absorption spectroscopy. The favourable chemical and NMR properties of these complexes have enabled the gen-

* For part III, see ref. 1.

† Author to whom correspondence should be addressed.

eration of spectroscopic *cis*- and *trans*-influence series for oxygen-bound axial ligands of widely differing base strengths, and for various other ligands.[1,6] Others have investigated the electrochemical behaviour of some tetra(aryl)porphyrin tin(IV) complexes,[7] although some of their spectroscopic data are in conflict with an earlier communication.[6b] It therefore appeared worthwhile to study the solid-state structures of some Sn(tpp) complexes with various axial ligands, to see if salicylate displayed any unusual coordination behaviour, and to complement the spectroscopic studies.

Tin(IV) porphyrins have not been extensively studied by crystallography. The dichloro complexes $[SnCl_2(tpp)]$[8] and $[SnCl_2(oep)]$ (H_2oep = 2,3,7,8, 12,13,17,18-octaethylporphyrin),[9] and a partially disordered example of the dihydroxo complex $[Sn(OH)_2(tpp)]$ [as a bis(chloroform), bis(carbon tetrachloride) solvate][10] are the only published structures containing simple electronegative axial ligands. As the dihydroxo species is the normal starting material for most tin(IV) tpp bis(acido) complexes, we felt it was important to determine its structure more precisely, for comparison with other complexes. We report herein the structures of five Sn(tpp) complexes which are relevant to several of the above-mentioned studies, namely $[SnX_2(tpp)]$ (X = hydroxide, water, benzoate, salicylate and acetylsalicylate).

EXPERIMENTAL

General

IR spectra were recorded in KBr discs on a Perkin–Elmer 881 spectrometer, and visible spectra in $CHCl_3$ solutions (unless otherwise stated) on a Varian DMS100 spectrometer. NMR spectra were recorded in $CDCl_3$ on the Bruker CXP300 instrument at the Brisbane NMR Centre, Griffith University. Spectra were accumulated with 16K data points and zero filled to 32K, using spectral widths of 3500–5500 Hz. The individual satellites due to coupling of β-pyrrole protons with ^{117}Sn and ^{119}Sn were not resolved. Coupling constants are therefore averaged values determined from the top of the peak as assigned by the spectrometer computer, so are $\pm$*ca* 0.5 Hz at the digital resolution obtainable. Microanalyses were carried out by the Microanalytical Service, University of Queensland. Chloroform was distilled from anhydrous potassium carbonate and tetrahydrofuran (THF) from sodium under nitrogen. All other solvents were Ajax A.R. grade. Organic acids were Merck "zur Synthese" grade. Silver trifluoromethanesulphonate (triflate) was obtained from Aldrich.

Preparation of complexes

(a) $[Sn(OH)_2(tpp)]$ (**1**). This complex was prepared as previously reported,[6c] and crystals were grown by diffusion of pentane vapour into a $CHCl_3$ solution.

(b) $[Sn(CF_3SO_3)_2(tpp)]$ *or* $[Sn(OH_2)_2(tpp)](CF_3SO_3)_2$ (**2**). Silver triflate (160 mg, 0.63 mmol) was placed in a Schlenk flask and dried *in vacuo*. Nitrogen was admitted, then THF (*ca* 15 cm^3) was distilled from sodium into the flask. Solid $[SnCl_2(tpp)]$ (250 mg, 0.31 mmol) was added, and the mixture was stirred under nitrogen for 20 min. The solution was removed from the silver chloride by decantation through a cannula with attached filter paper, and concentrated *in vacuo* to a volume of *ca* 5 cm^3. Hexane (30 cm^3) was slowly added with stirring, to yield a fine, dark red powder. Recrystallization from THF–pentane gave maroon microcrystals (233 mg, 73%). Crystals for X-ray analysis were grown by layering pentane over a concentrated THF solution, and leaving in a refrigerator for several weeks. Elemental analysis and the crystal structure showed these to be the diaqua complex. We have subsequently prepared **2** by reaction of triflic acid with $[Sn(OH)_2(tpp)]$ in CH_2Cl_2 solution[1] (Found: C, 52.0; H, 3.0; N, 5.2. $C_{46}H_{32}F_6N_4O_8S_2Sn$ requires: C, 51.8; H, 3.0; N, 5.25%); ν_{max} (Nujol) 1295s and 1022s (SO_3), 1225vs and 1180m cm^{-1} (CF_3); δ_H *ca* 7.8 (m, 3′, 4′ and 5′), *ca* 8.3 (m, 2′ and 6′) and 9.36 [s, ^4J(SnH) 20 Hz] (see text for discussion); λ_{max} (THF) 512, 550 and 590 nm (log ε 3.49, 4.32 and 3.83), ($CHCl_3$) 420, 511, 549 and 588 nm (log ε 5.75, 3.48, 4.37 and 3.85).

(c) $[Sn(C_6H_5CO_2)_2(tpp)]$ (**3**). Solid benzoic acid (30 mg, 0.25 mmol) was added to a solution of $[Sn(OH)_2(tpp)]$ (77 mg, 0.1 mmol) in $CHCl_3$ (5 cm^3), and the mixture was stirred at room temperature for 30 min. The solution was filtered through anhydrous sodium sulphate and evaporated to dryness *in vacuo*. The residue was recrystallized from chloroform–hexane to yield violet prisms (83 mg, 86%). Crystals for X-ray analysis were grown by diffusion of pentane vapour into a CH_2Cl_2 solution (Found: C, 71.8; H, 3.9; N, 5.75. $C_{58}H_{38}N_4O_4Sn$ requires: C, 71.55; H, 3.9; N, 5.75%); ν_{max} 1649, 1314 and 1298 cm^{-1} (carboxylate); δ_H 4.90 (4H, dd, 2″ and 6″), 6.32 (4H, dt, 3″ and 5″), 6.65 (2H, dt, 4″), *ca* 7.8 (12H, m, 3′, 4′ and 5′), *ca* 8.2 (8H, m, 2′ and 6′) and 9.18 [8H, s, ^4J(SnH) 15 Hz, β-pyrrole]; λ_{max} 423, 517, 556 and 596 nm (log ε 5.78, 3.53, 4.33 and 3.98).

(d) $[Sn(2\text{-}OH\text{-}C_6H_4CO_2)_2(tpp)]$ (**4**). This complex

(94 mg, 94%) was prepared and purified as for **3** above, using salicylic acid (30 mg, 0.22 mmol) and [Sn(OH)$_2$(tpp)] (77 mg, 0.1 mmol) (Found: C, 69.2; H, 3.7; N, 5.6. $C_{58}H_{38}N_4O_6Sn$ requires: C, 69.3; H, 3.8; N, 5.6%); ν_{max} 1667, 1634 and 1307 (carboxylate) and 1363 cm^{-1} (phenol C—O); δ_H 3.96 (2H; br d, 6″), 5.67 (2H, dt, 5″), 5.97 (2H, dd, 3″), 6.57 (2H, dt, 4″), *ca* 7.8 (12H, m, 3′, 4′ and 5′), *ca* 8.2 (8H, m, 2′ and 6′), 9.21 [8H, s, ^4J(SnH) 16 Hz, β-pyrrole] and 9.3 (2H, br s, OH); λ_{max} 423, 517, 556 and 595 nm (log ε 5.76, 3.53, 4.34 and 3.98).

(e) [Sn(2-OCOCH$_3$-C$_6$H$_4$CO$_2$)$_2$(tpp)] (**5**). This complex (97 mg, 89%) was prepared as for **3** above, using acetylsalicylic acid (42 mg, 0.23 mmol) and [Sn(OH)$_2$(tpp)] (77 mg, 0.1 mmol). Crystals were grown by diffusion of pentane vapour into a $CHCl_3$ solution (Found: C, 68.0; H, 3.9; N, 5.0. $C_{62}H_{42}N_4O_8Sn$ requires: C, 68.3; H, 3.9; N, 5.1%); ν_{max} 1766, 1750 and 1363 (acetate), 1654 and 1313 cm^{-1} (carboxylate); δ_H 1.19 (6H, s, CH_3), 4.18 (2H, dd, 6″), 6.01 (2H, dd, 3″), 6.08 (2H, dt, 5″), 6.61 (2H, dt, 4″), *ca* 7.8 (12H, m, 3′, 4′ and 5′), *ca* 8.3 (8H, m, 2′ and 6′), and 9.15 [8H, s, ^4J(SnH) 15 Hz, β-pyrrole]; λ_{max} 424, 518, 557 and 596 nm (log ε 5.77, 3.53, 4.32 and 3.95).

X-ray data collection, structure solution and refinement

Data for complexes **1**–**5** were collected on Nicolet R3m diffractometers, **3**, **4** and **5** at normal temperature (293 K), **1** and **2** at low temperature (163 K). Data were corrected for absorption. Structures were solved using SHELXS 86[11] and refined using SHELX 76.[12] Disorder problems were resolved using partial site occupancies for atoms in structures **2** (in the $CF_3SO_3^-$ groups) and **5** (the peripheral phenyl rings and acetylsalicylate groups). This accounts for the rather high refinement residuals for these structures. Anisotropic thermal parameters were used for all non-hydrogen atoms in structures **1**, **3** and **4**, while for **2** and **5** isotropic factors were used. Hydrogens were incorporated only in the structures showing no disorder. These were located by difference methods and were included with refinement of both positional and thermal parameters. Neutral atom scattering factors were used,[13] while the heavy atoms were corrected for the effects of anomalous dispersion.[13]

Atomic coordinates, thermal parameters, and observed and calculated structure factors have been

Table 1. Crystal data for **1**–**5**

	1	**2**	**3**	**4**	**5**
Formula	$C_{44}H_{30}N_4O_2Sn$	$C_{46}H_{32}F_6N_4O_8S_2Sn$	$C_{58}H_{38}N_4O_4Sn$	$C_{58}H_{38}N_4O_6Sn$	$C_{62}H_{42}N_4O_8Sn$
M_r	765.4	1065.6	973.7	1005.7	1089.7
a (Å)	13.463(2)	20.250(5)	10.228(2)	10.597(3)	11.14(1)
b (Å)	13.463(2)	8.964(3)	11.312(2)	11.198(2)	12.59(1)
c (Å)	9.669(2)	27.926(9)	11.537(2)	11.621(3)	19.06(1)
α (°)	90	90	65.95(2)	65.29(2)	84.87(6)
β (°)	90	118.01(2)	68.61(2)	66.99(2)	88.97(7)
γ (°)	90	90	76.05(1)	74.93(2)	68.58(7)
V (Å^3)	1752.6(6)	4476(2)	1128.3(4)	1145.4(5)	2478(3)
Z	2	4	1	1	2
D_c	1.446	1.581	1.432	1.457	1.460
Space group	$I4/m$	Cc	$P\bar{1}$	$P\bar{1}$	$P\bar{1}$
F(000)	776	2144	496	512	1112
μ (cm^{-1})	7.8	7.5	6.3	6.3	5.9
R^a	0.039	0.071	0.055	0.077	0.156[b]
R_w[c]	0.040	0.074	0.058	0.081	
A[c]	1.30	1.00	0.83	1.02	
B[c]	5.3×10^{-3}	9.0×10^{-3}	2.5×10^{-3}	4.7×10^{-3}	
Crystal size (mm)	$0.32\times0.15\times0.14$	$0.25\times0.08\times0.08$	$0.06\times0.16\times0.20$	$0.12\times0.16\times0.20$	$0.22\times0.30\times0.50$
Data collected	1495	3010	2945	2145	6493
$2\theta_{max}$	45	45	45	40	45
Temperature (K)	163	163	293	293	293
Data used	1256	1771	2389	1711	3822
Discrimination	$I > 2.5\sigma(I)$	$I > 2.5\sigma(I)$	$I > 2.5\sigma(I)$	$I > 2.5\sigma(I)$	$I > 2.5\sigma(I)$

[a] $R = [\Sigma||F_o|-|F_c||/|F_o|]$.
[b] Unit weights.
[c] $R_w = [(\Sigma w(||F_o|-|F_c||^2/\Sigma w|F_o|^2)^{1/2}]$; $w = A/(\sigma^2F_o+BF_o^2)$.

Table 2. Bond distances (Å) and angles (°) about the coordination polyhedra for complexes **1–5**

	1	**2**	**3**	**4**	**5** Molecule A	**5** Molecule B
(a) Distances						
Sn—N(1)	2.106(3)	2.04(2)	2.088(5)	2.09(1)	2.10(3)	2.08(3)
Sn—N(1)′	2.106(3)	2.09(2)	2.088(5)	2.09(1)	2.10(3)	2.08(3)
Sn—N(8)	2.106(3)	2.07(2)	2.085(5)	2.08(1)	2.09(3)	2.12(3)
Sn—N(8)′	2.106(3)	2.04(2)	2.085(5)	2.08(1)	2.09(3)	2.12(3)
Sn—O	2.017(4)	2.14(1)	2.055(5)	2.08(1)	2.05(3)	2.06(3)
Sn—O′	2.017(4)	2.18(1)	2.055(5)	2.08(1)	2.05(3)	2.06(3)
(b) Angles						
N(1)—Sn—N(8)	90.0(2)	93(1)	90.2(2)	90.6(4)	91(1)	90(1)
N(1)—Sn—N(8)′	90.0(2)	91(1)	90.2(2)	90.6(4)	89(1)	90(1)
N(1)—Sn—O	90.0(2)	91(1)	86.2(2)	91.1(4)	92(1)	85(1)
N(1)—Sn—O′	90.0(2)	87(1)	86.2(2)	91.1(4)	88(1)	95(1)
N(1)—Sn—N(1)′	180.0(2)	178(1)	180.0(4)	180.0(4)	180(1)	180(1)
N(8)—Sn—N(1)′	90.0(2)	88(1)	89.8(2)	89.4(4)	89(1)	90(1)
N(8)—Sn—N(8)′	180.0(2)	175(1)	180.0(4)	180.0(4)	180(1)	180(1)
N(8)—Sn—O	90.0(2)	91(1)	88.2(2)	92.7(4)	88(1)	87(1)
N(8)—Sn—O′	90.0(2)	85(1)	91.8(2)	87.3(4)	92(1)	93(1)
N(8)′—Sn—O′	90.0(2)	87(1)	91.8(2)	92.7(4)	91(1)	87(1)
N(8)′—Sn—O	90.0(2)	86(1)	91.8(2)	87.3(4)	92(1)	93(1)
N(8)′—Sn—N(1)′	90.0(2)	88(1)	90.2(2)	90.6(4)	91(1)	90(1)
O—Sn—O′	180.0(2)	175(1)	180.0(2)	180.0(4)	180(1)	180(1)
O—Sn—N(1)′	90.0(2)	89(1)	93.8(2)	88.9(4)	88(1)	95(1)
N(1)′—Sn—O′	90.0(2)	94(1)	86.2(2)	91.1(4)	92(1)	85(1)

deposited with the Editor as supplementary material; copies are available on request. Table 1 lists crystal data for the five compounds. Bond distances and angles for the coordination polyhedra are given in Table 2. Intraligand bond distances and angles and hydrogen atom coordinates are available from the authors.

RESULTS AND DISCUSSION

The complexes **1** and **3–5** were prepared and purified by standard methods.[1,6] The diaqua complex **2** was isolated as a result of attempts to extend the previously studied *cis*-influence series[6a] to complexes of weakly basic anions. The complex was prepared either by abstraction of chloride from $[SnCl_2(tpp)]$ with silver triflate in THF or by protonation of $[Sn(OH)_2(tpp)]$ with anhydrous triflic acid in dichloromethane. It is very insoluble in $CDCl_3$, in contrast to all other known members of the family of $[SnX_2(tpp)]$ complexes, with the exception of $X = ClO_4$. Moreover, solutions of **2** in $CDCl_3$ which initially show one major β-pyrrole signal [δ 9.36, ^4J(SnH) 20 Hz] and a minor, broader one at slightly higher field, slowly deposit solid, with diminution of the former signal. This behaviour is similar to that reported for $[Sn(ClO_4)_2(tpp)]$,[6a] and is explicable in terms of equilibria involving the covalent bis(triflate), and mono- and bis(solvento) ionic forms. Kadish *et al.*[7] recently reported similar findings for $[Sn(ClO_4)_2L]$ complexes [H_2L = tetrakis(*m*- and *p*-tolyl)porphyrin]. The earlier conclusion of a possible intermolecular aggregation[6a] is probably erroneous. In any case, the species which crystallized from THF/pentane was shown by elemental and crystal structure analyses to be the diaqua complex **2**.

The structures of the five tpp complexes have been determined with varying degrees of precision. Complex **1** (Fig. 1) has crystallographically imposed 4/*m* symmetry and exhibits none of the disorder evident in the other complexes. Because of the fourfold rotational symmetry, the hydroxyl protons are delocalized over four quarter sites and are therefore not located in the determination. The complex is isomorphous with the dichloro analogue.[8] Its ease of crystallization free from solvent molecules contrasts with the previously reported and considerably disordered structure for $[Sn(OH)_2(tpp)]$.[10] Importantly, for comparison with complexes of less basic

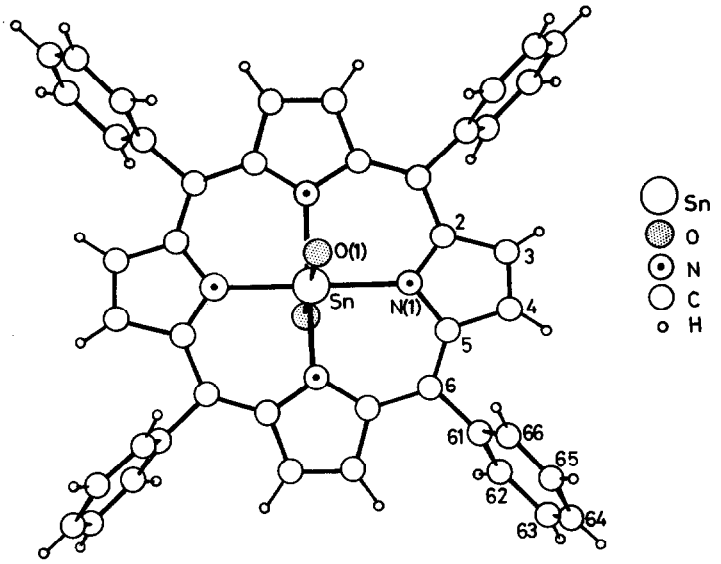

Fig. 1. Molecular configuration and atom naming scheme for **1**. The molecule has four-fold rotational symmetry down the O(1)—Sn—O(1)′ bond, while primed atoms are generated by mirror symmetry. Unless otherwise indicated, atoms are carbons.

axial ligands, the Sn—N and Sn—O bond distances [2.106(3) and 2.017(4) Å, respectively] have been determined to a higher precision than before [averages 2.09(5) and 2.02(4) Å].[10]

In crystals of compounds **2**–**5**, approximate or exact inversion symmetry is found for the [SnX_2(tpp)] species. With **2** (Fig. 2), only pseudo-inversion symmetry is present, while **3**, **4** and **5** have crystallographic inversion centres. In the case of **5**, the two independent molecules (A and B) are located about inversion centres at (0,0,0) and $(0,\frac{1}{2},\frac{1}{2})$, respectively. With these examples (**2**–**5**), various degrees of disorder were found in the peripheral substituents. However, bond distances and angles within the coordination polyhedra are considered precise enough to allow a meaningful comparison for the series. The tin(IV) ion is amongst the largest which can be accommodated within a planar tpp moiety. The Sn—N bond distances in complexes **1**–**5**, and in [$SnCl_2$(tpp)], vary only slightly, as expected for such a situation. While the core size is constrained, variation is certainly evident in the axial Sn—O distances. These increase in the order hydroxide < benzoate ≈ acetylsalicylate < salicylate < water, and so broadly follow the trend expected for mutually *trans* ligands of decreasing basicity. To complement our spectroscopic studies of the *cis*- and *trans*-influences in [Sn(tpp)] complexes, it would be interesting to determine the structures of some unsymmetrical derivatives [SnXY(tpp)]. Such studies would most likely be frustrated by redistribution equilibria, which prevent crystallization of pure complexes.[1]

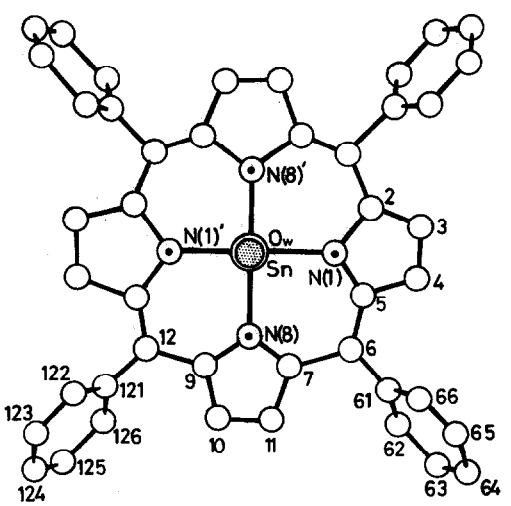

Fig. 2. Molecular configuration and atom naming scheme for **2**. Primed atoms are generated by pseudo-inversion symmetry.

The benzoate and salicylate structures are very similar (Figs 3 and 4). This is apparent not only from cell data (Table 1), but also from structural features, e.g. the conformations of the phenyl rings and the disposition of the axial ligands. The comparative C(5)—C(6)—C(61)—C(62) and C(9)—C(12)—C(121)—C(122) torsion angles for the phenyl rings are +79, −74° (**3**) and −82, +75°

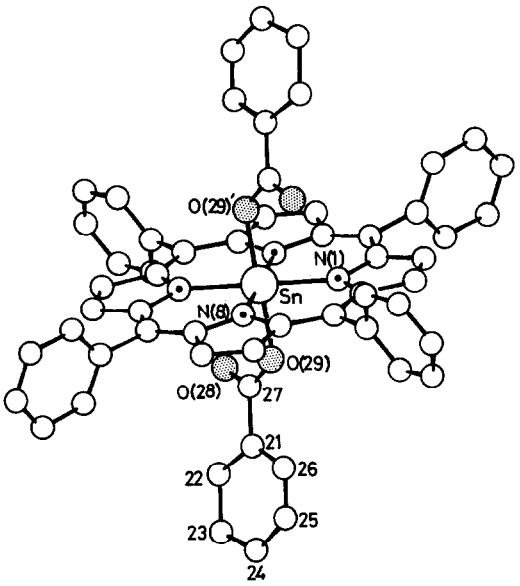

Fig. 3. Molecular configuration and atom naming scheme for **3**. Primed atoms are generated by inversion symmetry. For the tpp moiety, naming follows the convention used in **2**.

(**4**), which compare with 90° in **1**, which has mirror symmetry. The maximum deviation from 90° is found in **2** (−61°). In all carboxylate examples, the interaction with the metal is purely unidentate, the second carboxylate oxygen being 3.356(5) Å (**3**), 3.44(1) Å (**4**) and 3.28, 3.36(3) Å (**5**) from the tin atom. This further confirms the IR spectroscopic method of assigning bonding type in metalloporphyrin carboxylates,[14] since the present series shows frequency differences for the two carboxylate bands of *ca* 330 cm^{-1}. Ionic/bidentate carboxylates exhibit frequency differences of $\leqslant 150$ cm^{-1}. Furthermore, the *ortho*-hydroxy group in **3** does not interact in any way with either the tin or any atoms from adjacent molecules. However, it is clearly instrumental in maintaining the planar conformation of the whole axial ligand via intramolecular hydrogen-bonding, leading to an O—O distance of 2.50(2) Å to the non-coordinated carboxylate oxygen. In this respect it is similar to the parent salicylic acid[15] (O—O, 2.62 Å). The comparative torsion angles [C(22)—C(21)—C(27)—O(29)] for **3**, **4** and salicylic acid are +166, +174 and 180°, respectively. For the acetylsalicylate derivative **5** (Fig. 5), the complex molecule not showing disorder in the axial substituent (Molecule B), is also found to be conformationally similar to the parent acid.[16] The carboxylate group is approximately co-planar with the phenyl ring [C(22)—C(21)—C(27)—O(29), +172°] while the acetyl group is synclinally related to the ring [C(21)—C(22)—O(22)—C(30), +73°]. These compare with +178 and −85°, respectively, for acetylsalicylic acid. The packing of all complexes in their respective unit cells involves few intermolecular associations. This may be seen in Fig. 6 for **1**. The aquated porphyrin cation in **2** shows O—O contacts with the disordered triflate anions $O_w(2)$—O(3)A (2.64 Å) and $O_w(2)$—O(5)A (2.86 Å) (Fig. 7).

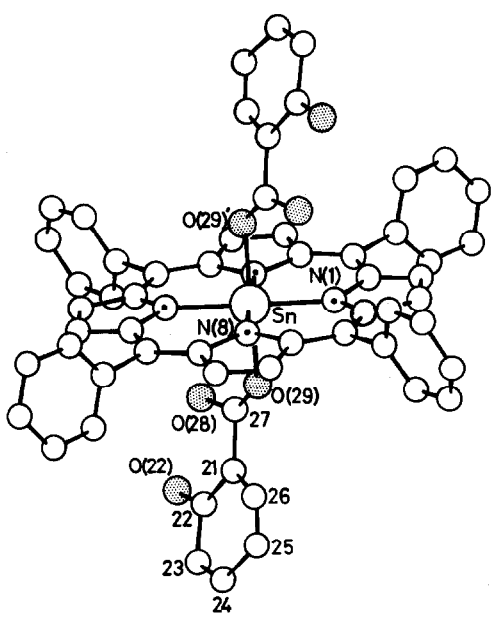

Fig. 4. Molecular configuration and atom naming scheme for **4**.

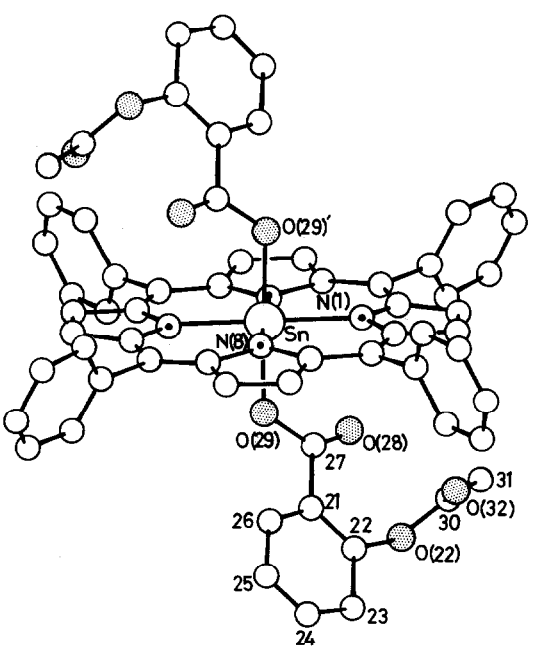

Fig. 5. Molecular configuration and atom naming scheme for **5** (Molecule B).

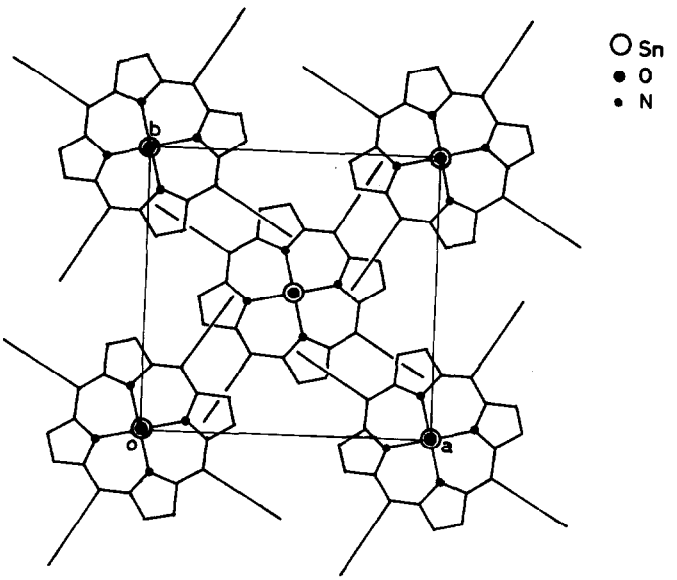

Fig. 6. Packing of **1** in the cell viewed down the four-fold axis.

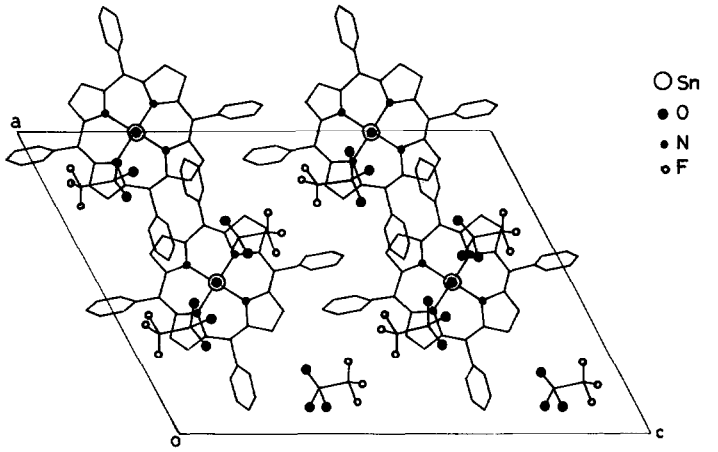

Fig. 7. Packing of **2** in the unit cell viewed down the *b* axis.

Finally, do these structures indicate any specific structural reasons for the salicylate selectivity of the [Sn(tpp)] based membrane electrode?[5] With the obvious caveat regarding comparisons of solution and solid-state structures, there appear to be no such special factors in operation. Likewise, the NMR data for **3**, **4** and **5** are unexceptional, although in this series only *cis*-influences can be studied. Even in the complexes $[Sn(HCO_2)(X)(tpp)]$, where *trans*-influences are observable, the ligands benzoate and salicylate are well-behaved within a series of oxygen-bound ligands.[1] The ion-selectivity displayed by the electrodes appears to have its origin in factors other than simply relative binding strengths of anions.

Acknowledgements—The authors thank Associate Professor Ward Robinson of the Chemistry Department, University of Canterbury, New Zealand for low temperature data collection on compounds **1** and **2**. The Chinese University of Hong Kong is thanked for the use of data collection facilities, while the Queensland University of Technology Research and Development Scheme and the University of Queensland are also thanked for financial support.

REFERENCES

1. D. P. Arnold, E. A. Morrison and J. V. Hanna, *Polyhedron* 1990, **9**, 1331.
2. G. S. Drummond, R. A. Galbraith, M. K. Sardana and A. Kappas, *Arch. Biochem. Biophys.* 1989, **255**,

64; G. S. Drummond and A. Kappas, *J. Clin. Invest.* 1989, **77**, 971.
3. A. R. Morgan, G. M. Garbo, R. W. Keck and S. H. Selman, *Cancer Res.* 1988, **48**, 194.
4. J. Handman, A. Harriman and G. Porter, *Nature* 1984, **307**, 537; A. Harriman, G. Porter and P. Walters, *J. Chem. Soc., Faraday Trans. 1* 1983, **79**, 1335.
5. N. A. Chaniotakis, S. B. Park and M. E. Meyerhoff, *Analyt. Chem.* 1989, **61**, 566; S. C. Ma, N. A. Chaniotakis and M. E. Meyerhoff, *Analyt. Chem.* 1988, **60**, 2293.
6. (a) D. P. Arnold, *Polyhedron* 1986, **5**, 1957; (b) D. P. Arnold, *Polyhedron* 1988, **7**, 2225; (c) D. P. Arnold, *J. Chem. Educ.* 1988, **65**, 1111.
7. K. M. Kadish, Q. Y. Y. Xu, G. B. Maiya, J.-M. Barbe and R. Guilard, *J. Chem. Soc., Dalton Trans.* 1989, 1531.
8. D. M. Collins, W. R. Scheidt and J. L. Hoard, *J. Am. Chem. Soc.* 1972, **94**, 6689.
9. D. L. Cullen and E. L. Meyer, *Acta Cryst.* 1973, **29B**, 2507.
10. P. G. Harrison, K. Molloy and E. W. Thornton, *Inorg. Chim. Acta* 1979, **33**, 137.
11. G. M. Sheldrick, SHELXS 86, Program for Crystal Structure Determination. University of Göttingen, F.R.G. (1986).
12. G. M. Sheldrick, SHELX 76, Program for Crystal Structure Determination. University of Cambridge, U.K. (1976).
13. *International Tables for X-ray Crystallography* (Edited by J. A. Ibers and W. C. Hamilton), Vol. 4. Kynoch Press, Birmingham (1974).
14. J. W. Buchler, in *Porphyrins and Metalloporphyrins* (Edited by K. M. Smith). Elsevier, Amsterdam (1975).
15. M. Sundaralingam and L. H. Jensen, *Acta Cryst.* 1965, **18**, 1053.
16. P. J. Wheatley, *J. Chem. Soc.* 1964, 6036.

Polyhedron Vol. 10, No. 4/5, pp. 517–521, 1991
Printed in Great Britain

0277–5387/91 $3.00+.00
© 1991 Pergamon Press plc

COMMUNICATION

POTENTIOMETRIC INVESTIGATION OF THE COMPLEXATION OF DIMETHYLTHALLIUM(III) BY 2-THIOBARBITURATE IN AQUEOUS SOLUTION

M. S. GARCÍA-TASENDE and M. GARCÍA BUGARÍN

Departamento de Química Inorgánica, Universidad de Santiago de Compostela, 15076 Santiago de Compostela, Spain

and

M. FILELLA*

Département de Chimie Minérale, Analytique et Appliquée, Université de Genève, Quai Ernest Ansermet 30, 1211 Genève 4, Switzerland

(*Received* 18 *May* 1990; *accepted* 26 *November* 1990)

Abstract—The system formed by dimethylthallium(III), 2-thiobarbiturate (TBA) and hydrogen ions in aqueous solution at 20°C and $I = 100$ mmol dm^{-3} (nitrate) has been characterized by means of glass-electrode potentiometry. Protonation constants for 2-thiobarbiturate and the formation constant for the complex $[(Me_2Tl)(TBA)]^-$ were found to be $\log \beta_{LH} = 10.531$, $\log \beta_{LH_2} = 12.634$ and $\log \beta_{ML} = 2.343$, respectively.

Concern about the environmental and toxicological effects of the biomethylation of heavy metals[1] has led to increasing research on the coordination chemistry of methylated metal species. Like mercury and lead, inorganic thallium can be biomethylated by anaerobic organisms in sediments.[2] But, unlike other organometallic compounds generated by biological systems, e.g. methylmercury(II), dimethylthallium(III) appears to be less toxic than other chemical forms of the metal.[3] The observed behaviour of dimethylthallium(III), probably related to its binding properties, has prompted us to study its coordination chemistry in solution with ligands offering a variety of forms of bonding.

A literature search regarding the solution chemistry of dimethylthallium(III) shows that this field is largely unexplored. Only one reference concerning equilibria with β-diketones[4] could be found in the literature. Our first study[5] on the complexation of dimethylthallium(III) by some sulphur-containing amino acids revealed that dimethylthallium(III) weakly binds with amino and thiol groups, their logarithmic stability constants being 1.2 and 2.6, respectively. The presence of both groups in the same chelating ring did not exhibit any additional effect.

Since a deeper understanding of the coordinating behaviour of dimethylthallium(III) *vis-à-vis* ligands containing nitrogen, sulphur and oxygen appeared to be desirable, the study of its complexation by 2-thiobarbiturate was chosen as a model system for studying its complexation properties. 2-Thiobarbiturate contains thioenolic, enolic and imine groups in a benzenoid heterocyclic ring (Fig. 1) and therefore can act as a multidentate ligand. A number of solid metal complexes of 2-thiobarbiturate have been characterized[6–13] and formation constants for some metal complexes in solution have been reported.[14–18] Because of its complexing properties, 2-thiobarbiturate has been used as an analytical reagent for the determination of metal ions.[19–28]

* Author to whom correspondence should be addressed.

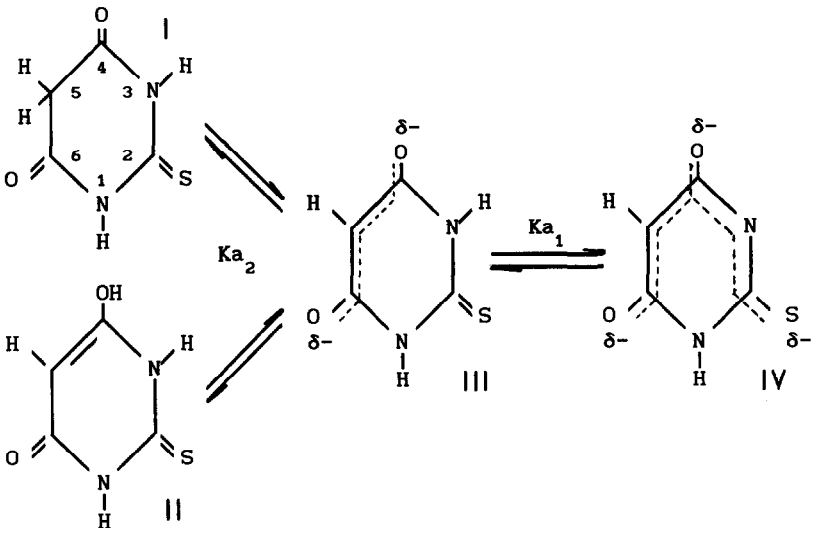

Fig. 1. Acid–base equilibria of 2-thiobarbiturate.

EXPERIMENTAL

Analytical grade reagents were used throughout. All solutions were prepared using demineralized water (Millipore system), boiled and cooled under nitrogen.

2-Thiobarbituric acid was supplied by Ega-Chemie as a biochemical grade product. Its purity was tested potentiometrically and was found to be sufficiently pure and therefore did not need further purification. Freshly prepared solutions were used for each titration and were thoroughly flushed with nitrogen before use. The poor water solubility of the ligand limited the range of ligand concentrations that could be used, i.e. 2-thiobarbiturate solutions having concentrations greater than 5 mmol dm^{-3} could not be prepared.

Stock solutions of dimethylthallium(III) nitrate, obtained as described previously,[5] were slightly acidified by adding nitric acid to prevent hydrolysis and absorption of carbon dioxide. Its mineral acid concentration was determined by titrating it with standard alkali (Gran plots).

Potassium hydroxide solutions and nitric acid solutions were prepared and standardized as previously described.[29] The ionic strength of the solution was maintained at 100 mmol dm^{-3} by the addition of potassium nitrate.

Formation constants were determined by performing potentiometric titrations at 20°C. The equipment and procedures used have already been described in detail.[29] The electrode system was calibrated in terms of hydrogen ion concentration by performing strong acid versus strong base titrations.[30] The logarithmic product of water under the same experimental conditions was found to be −13.88. The data used for the calculation of the formation constants are summarized in Table 1.

Protonation constants of 2-thiobarbiturate and formation constants of the complexes formed with dimethylthallium(III) were calculated using the latest version of the computer program library ESTA.[31–34] The approach followed in the selection of the possible species formed is discussed in detail in ref. 35. The ESTA objective function can be minimized with respect to either EMF or total ion concentration. The objective functions quoted in Table 2 are based on unweighted total ion concentration residuals (OBJT) and on weighted EMF residuals (OBJE). The weighting scheme proposed by May and Murray[33] was applied throughout the OBJE calculations. The weight at each titration point was based on errors of 0.2% in analytical concentrations, 0.01 cm^3 in titre and 0.1 mV in EMF.

Computations were done on a VAX 8700 computer and on a COMPAQ DESKPRO 386/20e microcomputer.

RESULTS AND DISCUSSION

The TBA–H^+ *system**

TBA protonation curves obtained for five protonation titrations carried out with ligand concentrations in the range 2.5–5 mmol dm^{-3} (and the conditions given in Table 1) revealed two separate buffer zones from which two protonation constants

* TBA = L^{2-} = deprotonated 2-thiobarbituric acid.

Table 1. Summary of titration data used in formation constant calculations. Number of titration points, initial total concentrations of dimethylthallium(III) (C_M), 2-thiobarbiturate (C_L) and nitric acid (C_H), and $-\log$ [H] range investigated. All concentrations are expressed in mmol dm^{-3}

System	Titration	Number of points	C_M	C_L	C_H	$-\log$[H] range
TBA–H$^+$	1	27		2.500	5.025	2.46–11.07
	2	29		5.000	5.025	2.11–11.08
	3	29		5.000	10.050	2.05–11.52
	4	42		5.000	10.050	1.91–11.85
	5	36		5.000	20.100	1.67–11.39
Me_2Tl^+–TBA–H$^+$	1	27	2.000	4.970	10.050	3.04–11.39
	2	31	2.000	4.890	10.060	3.10–10.95
	3	28	2.500	4.975	10.050	3.01–11.34
	4	29	2.500	4.975	10.060	3.04–11.09
	5	25	5.000	2.500	5.025	3.06–11.38
	6	21	5.000	5.000	10.050	3.07–10.64
	7	25	10.000	5.000	10.050	3.07–11.07
	8	28	10.000	5.050	10.050	2.84–11.34
	9	27	12.500	5.000	10.050	3.09–11.44
	10	21	15.000	5.000	10.050	2.94–10.67

were calculated. Values found are presented in Table 2. A satisfactory fit between the calculated parameters and the experimental data is indicated by reasonable values obtained for the ESTA objective functions (Table 2). Nevertheless, it should be mentioned that the experimental data do not cover all the jump corresponding to the second protonation constant (the highest $\bar{Z}_H$ values varied between 1.26 in titration 1 and 1.73 in titration 5) because of the acidic value (2.10) of the constant. This experimental limitation is reflected by the higher standard deviation associated with the corresponding calculated value.

The protonation constants found in this study are in reasonable agreement with those previously reported under similar conditions (2.10, 10.55 at 18°C in 100 mmol dm^{-3} $NaClO_4$)[16] (1.97, 10.54 at 25°C in 100 mmol dm^{-3} KCl).[36] Unfortunately, most of the data published[15,37–43] could not be considered for comparison purpose due either to the non-specification of the experimental conditions used or to the use of aqueous ethanolic mixtures to dissolve the ligand.

Assignment of the macroscopic, calculated protonation constants to the functional groups present in the molecule has been extensively discussed but

Table 2. Formation constants determined in this study at 20°C and I = 100 mmol dm^{-3} NO_3^-. ($\beta_{pqr} = [M_pL_qH_r]/[M]^p[L]^q[H]^r$)

System		p	q	r	$\log \beta_{pqr}$	SD[a]	OF[b]	R[c]	n[d]
TBA–H$^+$	OBJE	0	1	1	10.531	0.003	1.58	0.003	306
		0	1	2	12.634	0.006			
	OBJT	0	1	1	10.534	0.004	4.03E-09	0.010	
		0	1	2	12.608	0.005			
Me_2Tl^+–TBA–H$^+$	OBJE	1	1	0	2.343	0.005	2.10	0.006	262
	OBJT	1	1	0	2.343	0.005	4.07E-09	0.018	

[a] Standard deviations given by the programs.

[b] OF, in OBJE output = $[\Sigma w(EMF^o - EMF^c)^2]/(N-n_p)$; in OBJT output = $[(T_i^o - T_i^c)^2]/(N-n_p)$, where N = number of points, n_p = number of refined parameters, T_i = total concentrations.

[c] R = Hamilton R factor.

[d] Number of points used in the calculations.

inconclusive results have been obtained up until now. In fact, this problem is directly linked to the problem of determining the predominant tautomeric forms present in aqueous solution. The answer to this still remains open with regard to thiobarbiturate derivatives.

The second stepwise protonation constant (2.10) has been associated either with the ionization of the methylene hydrogen at the 5-position[37,41,42] in the tautomeric dioxothione form I or with the ionization of the phenolic group in the hydroxy-oxothione form II[38,42] (Fig. 1). Probably, both equilibria co-exist at a certain degree in solution since aqueous solutions of 2-thiobarbituric acid have been found to contain both tautomeric forms,[42,44] although the hydroxy-oxo-thione II and its zwitterion seem to predominate over the dioxothione I when the dielectric constant of the solvent increases.[44] The tentative assignment of the second protonation constant to the protonation of a nitrogen by some authors[40] seems highly improbable. A more general consensus seems to exist on the assignment of the first protonation constant (10.53) to the ionization of the HNCS group[37,41,42] (Fig. 1).

The possibility of a hydrolytic process taking place instead of the HNCS deprotonation has been carefully considered in the present work; but, although the alkaline hydrolysis of barbitals is well-documented[45] and the alkali-catalysed opening of the 1–6 bond of the pyrimidine ring has been reported in the case of 2-thiobarbituric acid,[46] no indication of ligand hydrolysis could be obtained under the experimental conditions used: all the protonation titration curves obtained at different initial ligand concentrations are fully superimposable.

The dimethylthallium(III)–TBA–H^+ *system*

The system Me_2Tl^+–TBA–H^+ was studied by performing 10 titrations with initial metal concentrations of 2.0–15.0 mmol dm^{-3}. As mentioned earlier, the upper concentrations used were limited by the poor solubility of the ligand in water. The individual metal complexation curves yielded overlapping formation curves, the maximum $\bar{Z}_M$ values found depended on the metal–ligand ratio. These maximum values never exceeded one. Thus, the experimental formation curves suggest that mononuclear binary complexes with a maximum metal–ligand ratio of one predominate. This working hypothesis was fully confirmed by applying our usual data reduction approach:[35] as expected, polynuclear (i.e. M_2L, M_2L_2), hydroxo (i.e. MLOH, $ML(OH)_2$) and high ratio ligand–metal species were systematically rejected by the computer program.

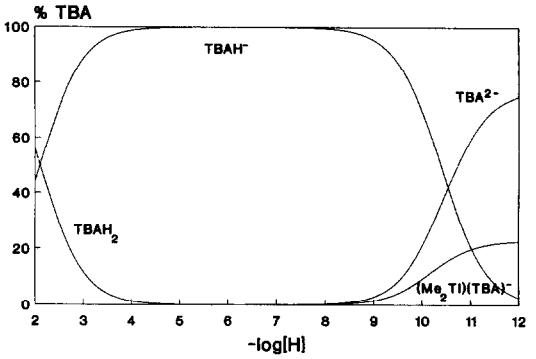

Fig. 2. Simulated species distribution of TBA: free, protonated and dimethylthallium(III)-complexed species as a function of $-\log[H]$, for TBA concentration = 5 mmol dm^{-3} and dimethylthallium(III) concentration = 2.5 mmol dm^{-3}.

A value for the MLH formation constant (12.0) was calculated by the program, but this species was discarded because the estimated error in its formation constant was unacceptable, the percentage of the complex formation negligible and its inclusion did not improve the goodness of the fit. Finally in the model chosen, only the ML complex was included and the results found for the numerical and graphical fitting (Table 2) were satisfactory.

Figure 2 shows the species distribution for this system, computed from the constants reported in Table 2, for total concentration of TBA equal to 5.0 mmol dm^{-3} and total concentration of dimethylthallium(III) equal to 2.5 mmol dm^{-3}. It can be seen that ML formation begins at $-\log[H] = 8$, when the ligand starts losing its second proton, thus implying that for coordination to occur the ionization of the NCS group is necessary. A simultaneous coordination of thallium by the N and S of the NCS group can be suggested on the basis that a similar type of coordination has been reported for the dimethyl(pyridine-2-thiolato)thallium(III) crystal structure from X-ray measurement.[47] Participation of the thiol group in the coordination is indicated by the fact that the value of the ML formation constant (2.34) is of the same order of magnitude as that of the estimated stability constant of the dimethylthallium(III) complexes formed with a deprotonated thiol group as the donor centre (2.6).[5]

The MLH species has been isolated in the solid form from an equimolar mixture of Me_2TlOH and TBA.[48] Its negligible formation in aqueous solution may be explained by its high degree of ionization, derived from the hard nature[49,50] of the coordinating atoms present in the monoanionic form of the ligand. As MLH is highly ionized in DMSO,[48] it

could be fully ionized in a solvent with a higher dielectric constant such as water.

Acknowledgements—Financial support of this work by CAYCIT (PR84-0624) and DGICYT (PB87-0482) (Spain) is gratefully acknowledged.

REFERENCES

1. P. J. Craig, *The Handbook of Environmental Chemistry* (Edited by O. Hutzinger), Vol. 1, Part A, p. 169. Springer, Berlin (1980).
2. F. Huber and H. Kirchmann, *Inorg. Chim. Acta* 1978, **29**, L249.
3. J. M. Morgan, PhD Thesis, University of Mississippi (1980), University Microfilms Int, London (1982).
4. J. R. Cook and D. F. Martin, *J. Inorg. Nucl. Chem.* 1964, **26**, 1249.
5. M. García Bugarín, M. E. García, G. Berthon, J. S. Casas and J. Sordo, *Polyhedron* 1988, **7**, 2487.
6. V. Nikolasev, J. Szabo and J. Morvay, *Glas. Hem. Drus., Beograd* 1971, **36**, 161; *Chem. Abstr.* **77**, 158289a.
7. R. Basosi, E. Gaggelli, E. Tiezzi and G. Valensin, *J. Chem. Soc., Perkin Trans. II* 1975, 423.
8. K. S. Siddiqi, P. Khan, S. Khan and S. A. A. Zaidi, *Synth. React. Inorg. Met.-Org. Chem.* 1982, **12**, 681.
9. M. S. Masoud, A. M. Heiba and F. M. Ashmawy, *Transition Met. Chem. (Weinheim, Ger.)* 1983, **8**, 124.
10. A. Jimenez, H. Jimenez and J. Borras, *Synth. React. Inorg. Met.-Org. Chem.* 1987, **17**, 159.
11. M. I. Leon Palomino, B. E. Zaitsev, R. K. Gridasova and T. M. Ivanova, *Zh. Neorg. Khim.* 1988, **33**, 2347; *Chem. Abstr.* **109**, 243001z.
12. R. Weiss and H. Venner, *Hoppe-Seyler's Z. Physiol. Chem.* 1969, **350**, 1188.
13. F. Popea and C. Marculescu, *Rev. Roum. Chim.* 1973, **18**, 425.
14. R. J. Murphy and G. Svehla, *Anal. Chim. Acta* 1978, **99**, 115.
15. W. O. Foye and C.-C. Chao, *J. Pharm. Sci.* 1984, **73**, 1284.
16. B. R. Singh, R. K. Jain, M. K. Jain and R. Ghosh, *Thermochim. Acta* 1984, **78**, 175.
17. S. Krzewska and H. Podsiadly, *Polyhedron* 1986, **5**, 937.
18. S. Tabassum, K. S. Siddiqi, N. H. Khan, R. I. Kureshy and S. A. A. Zaidi, *Indian J. Chem.* 1987, **26A**, 489.
19. H. Sikorska-Tomicka, *Fresenius' Z. Anal. Chem.* 1968, **234**, 414.
20. H. Sikorska-Tomicka, *Mikrochim. Acta* 1969, 715.
21. H. Sikorska-Tomicka, *Mikrochim. Acta* 1969, 718.
22. B. Morelli, *Analyst (Lond.)* 1982, **107**, 282.
23. B. Morelli, *Analyst (Lond.)* 1983, **108**, 386.
24. B. Morelli, *Analyst (Lond.)* 1983, **108**, 870.
25. B. Morelli, *Analyst (Lond.)* 1983, **108**, 959.
26. B. Morelli, *Analyst (Lond.)* 1983, **108**, 1506.
27. B. Morelli, *Analyst (Lond.)* 1984, **109**, 47.
28. B. Morelli, *Analyst (Lond.)* 1987, **112**, 1395.
29. M. García Bugarín, J. S. Casas, J. Sordo and M. Filella, *J. Inorg. Biochem.* 1989, **35**, 95.
30. P. W. Linder, R. G. Torrington and D. R. Williams, *Analysis using Glass Electrodes*. Open University Press, Milton Keynes (1984).
31. P. M. May, K. Murray and D. R. Williams, *Talanta* 1985, **32**, 483.
32. P. M. May, K. Murray and D. R. Williams, *Talanta* 1988, **35**, 825.
33. P. M. May and K. Murray, *Talanta* 1988, **35**, 927.
34. P. M. May and K. Murray, *Talanta* 1988, **35**, 933.
35. M. Filella, N. Garriga and A. Izquierdo, *Talanta* 1987, **34**, 971.
36. E. Bosch, J. Guiteras, A. Izquierdo and M. D. Prat, *Anal. Lett.* 1988, **21**, 1273.
37. Y. Sato, *Nippon Kagaku Zasshi* 1957, **78**, 921; *Chem. Abstr.* **54**, 4598b.
38. H. G. Mautner and E. M. Clayton, *J. Am. Chem. Soc.* 1959, **81**, 6270.
39. B. Stanovnik and M. Tigler, *Arzneim.-Forsch.* 1964, 1004.
40. W. F. Smyth, G. Svehla and P. Zuman, *Anal. Chim. Acta* 1970, **52**, 129.
41. Z. Kazimierczuk, A. Psoda and D. Shugar, *Acta Biochim. Pol.* 1973, **20**, 83.
42. B. A. Ivin, V. I. Slesarev and N. A. Smorygo, *J. Org. Chem. USSR* 1974, **10**, 1977.
43. R. N. Nacheva, B. V. Chemishev, Z. D. Raikov and D. N. Mihailova, *Dokl. Bolg. Akad. Nauk.* 1981, **34**, 283.
44. M. V. Jovanovic and E. R. Biehl, *J. Heterocycl. Chem.* 1987, **24**, 191.
45. E. R. Garrett, J. T. Bujarski and G. J. Yakatan, *J. Pharm. Sci.* 1971, **60**, 1145.
46. M. Niyaz Khan and A. Aziz Khan, *Ind. J. Chem.* 1982, **21A**, 365.
47. M. V. Castaño, A. Macías, A. Castiñeiras, A. Sánchez González, E. García Martínez, J. S. Casas, J. Sordo, W. Hiller and E. E. Castellano, *J. Chem. Soc., Dalton Trans.* 1990, 1001.
48. M. S. García-Tasende, M. I. Suárez Gimeno, A. Sánchez, J. S. Casas, J. Sordo and E. E. Castellano, *J. Organomet. Chem.* 1990, **19**, 384.
49. R. G. Pearson, *J. Am. Chem. Soc.* 1963, **85**, 3533.
50. R. G. Pearson, *Coord. Chem. Rev.* 1990, **100**, 403.

Polyhedron Vol. 10, No. 6, pp. 523–533, 1991
Printed in Great Britain

0277–5387/91 $3.00+.00
© 1991 Pergamon Press plc

NEW COPPER(II)–TETRAAZAANNULENE COMPLEXES. POTENTIAL BUILDING BLOCKS FOR MIXED VALENCE, CONDUCTING, MOLECULAR CRYSTALS: SYNTHESIS, EXPERIMENTAL AND THEORETICAL CHARACTERIZATION

FRANCESCO LELJ,* GIANCARLO MORELLI, GIAMPAOLO RICCIARDI and ANGELA ROSA

Dipartimento di Chimica, Università della Basilicata, Via N. Sauro 85, 85100 Potenza, Italy

(*Received* 23 *April* 1990; *accepted* 26 *September* 1990)

Abstract—Copper(II)–tetraaza[14]annulene complexes: Cu(dibenzo[b,i][1,4,8,11]tetraaza [14]annulene), Cu(dbTAA); Cu(dinaphtho[b,i][1,4,8,11]tetraaza[14]annulene), Cu(dnTAA) and Cu(diphenanthro[b,i][1,4,8,11]tetraaza[14]annulene), Cu(dpTAA) have been synthesized and studied by UV–vis spectroscopy, static magnetic susceptibility, ESR and cyclic voltammetry. UV–vis spectral evidence for Cu(dbTAA) and Cu(dnTAA) association was found in low donor ability solvents. The ground state electronic structure of Cu(dbTAA) has been investigated by very accurate SCF–LCAO calculations in the local-density approximation. According to the ESR and magnetic susceptibility data, the theoretical results indicate that the unpaired electron is shared in almost equal amounts by metal $3d_{xy}$ and ligand nitrogen orbitals. The optical transitions in the case of Cu(dbTAA) have been calculated by a ΔSCF procedure and compared with experimental spectra obtained in highly diluted solution. Cyclic voltammetry, UV–vis and theoretical calculations suggest that the dpTAA ligand both in the free state as well as in the complex strongly deviates from planarity.

Since the end of the past decade it has been known[1,2] that partial iodine oxidation of tetraazaannulene complexes of various transition metals provides an interesting class of molecular conductors. The interest in these compounds is due to the anisotropic conducting properties associated with their one-dimensionality.[3] Although the effect on their properties of the nature of the ligand and the degree of oxidation has not been systematically investigated, some studies on metal(II) (M = Ni, Cu, Co, Pd) complexes of the dianionic ligands: dibenzo [b,i][1,4,8,11]tetraaza[14]annulene^{2-} (dbTAA);[1,3–6] 5,7,12,14-tetramethyldibenzo[b,i][1,4,8,11]tetraaza [14]annulene^{2-} (dbTMTAA)[1,7–9] and other variously substituted dibenzo[b,i][1,4,8,11]tetraaza[14] annulenes^{2-},[1,3] have been undertaken. Among these, the non-substituted dbTAA ligand gave rise to the most conductive materials and showed very promising transport parameters, slightly smaller than those of "molecular metals" like (NiPc)I (Pc = phthalocyanine).[10,11]

The lack of studies on these systems is probably due to the difficulty in obtaining single crystals of the oxidized materials suitable for structural and anisotropic investigation.

In this paper we present the preparation and an experimental characterization of complexes of copper(II) with new tetraaza[14]annulene macrocyclic dianionic ligands with increasing aromatic moiety, i.e. dinaphtho[b,i][1,4,8,11]tetraaza[14] annulene^{2-} (dnTAA)$^{2-}$ and diphenanthro[b,i][1,4, 8,11]tetraaza[14]annulene^{2-} (dpTAA), as well as a detailed discussion of the influence of the ligand structure and conformation on the properties of the complexes in view of their potential

* Author to whom correspondence should be addressed.

use as starting compounds for new conducting materials. Furthermore, the results concerning these compounds are compared with new data and a very accurate theoretical characterization for the analogous copper(II)dibenzo [b,i][1,4,8,11]tetraaza[14]annulene complex, Cu (dbTAA). Metal tetraazaannulene complexes have not been theoretically investigated and their chemical behaviour has been interpreted by analogy with related system metalloporphyrins and metallophthalocyanins. The little data available in the literature[1] are in agreement with our results. We compare these new compounds with substituted phthalocyanine, which has been synthesized[12] by the same philosophy suggested by us in the case of aromatic diimine ligands.[13(b)]

EXPERIMENTAL

Reagents

1,2-Diaminobenzene, 2,3-diaminenaphthalene and 9,10-diaminephenanthrene were obtained commercially (Aldrich) and purified by sublimation (10^{-2} mm Hg). Propiolaldehyde was obtained by oxidation of propargyl alcohol.[14] Crystals of I_2, 99.8% A.C.S. reagent grade, were used after resublimation. Solvents were of analytical reagent or spectrograde quality. Dimethylformamide (DMF) was dried by the standard method when used for cyclic voltammetric measurements. Elemental analyses were performed by the Analytical Laboratory, Faculty of Engineering, Potenza.

Synthesis of the compounds

The three ligands H_2dbTAA, H_2dnTAA and H_2dpTAA were obtained as previously reported for H_2dbTAA,[14] by condensation of propiolaldehyde with the appropriate diamine in a refluxing DMF–methanol (9 : 1) solution. Prolonged refluxing time, 8 h and 5 d for H_2dnTAA and H_2dpTAA, respectively, was needed.

H_2dnTAA was obtained in 60% yield as a blue–purple microcrystalline powder. Found: C, 81.3; H, 4.9; N, 14.2. Calc. for $C_{26}H_{20}N_4$: C, 80.5; H, 5.1; N, 14.5%. ^{1}H NMR signals ($CDCl_3$ solution, TMS as internal standard) at: 7.1–6.8 multiplets (aromatic protons, 12 H), 5.03 triplet (C—C*H*=C, 2 H), 7.66 multiplet (=C*H*—NH, triplet, superimposed to —C*H*=N, doublet, 4 H), 13.60 triplet (—N*H*, 2 H). UV–vis (DMF, 4×10^{-5} M): 484(3809)sh, 412(17,619), 390(20,000), 288(30,000)sh nm (mol cm^{-1}).

H_2dpTAA was obtained in 90% yield as a blue–purple microcrystalline powder. Found: C, 84.1; H, 5.3; N, 11.1%. Calc. for $C_{34}H_{28}N_4$: C, 83.0; H, 5.7; N, 11.4%. ^{1}H NMR signals ($CDCl_3$ solution, TMS as internal standard) at: 7.1–6.8 multiplets (aromatic protons, 12 H), 5.05 triplet (C—C*H*=C, 2 H), 7.69 multiplet (=C*H*—NH, triplet, superimposed to —C*H*=N, doublet, 4 H), 13.60 triplet (—N*H*, 2 H). UV–vis (acetone, 3×10^{-5} M): 412(2243)sh, 380(5128)sh, 296(23,076)sh, 276(48,076)sh nm (mol cm^{-1}).

Copper complexes of the three ligands (Fig. 1) were obtained according to the procedure used for the Cu(dbTAA) complex[15] by reaction of equimolar solutions of $Cu(CH_3COO)_2 \cdot H_2O$ and of the appropriate annulene ligand in boiling DMF.

Cu(dnTAA) was obtained as dark-red crystals in 95% yield. Found: C, 69.8; H, 4.3; N, 12.6. Calc. for $C_{26}H_{18}CuN_4$: C, 69.4; H, 4.0; N, 12.4%.

Cu(dpTAA) was obtained as yellow needle crystals in 70% yield. Found: C, 74.4; H, 4.1; N, 10.5. Calc. for $C_{34}H_{28}CuN_4$: C, 74.2; H, 4.0; N, 10.2%.

Methods

Spectroscopy and cyclic voltammetry. IR spectra were recorded on Nujol mulls with a Perkin–Elmer Model 883 spectrophotometer. Solution (DMF or CH_2Cl_2, 10 cm path length cells) UV–vis spectra

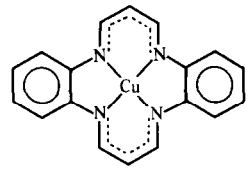

Copper(II) – dibenzo[b,i][1,4,8,11] tetraaza[14]annulene
[Cu(dbTAA)]

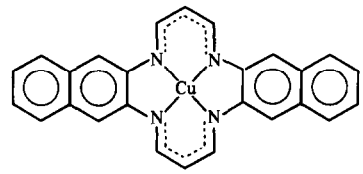

Copper(II) – dinaphto[b,i][1,4,8,11] tetraaza[14]annulene
[Cu(dnTAA)]

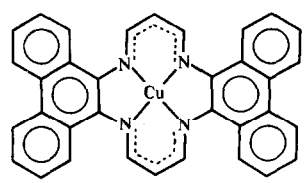

Copper(II) – diphenanthro[b,i][1,4,8,11]tetraaza[14]annulene
[Cu(dp AA)]

Fig. 1. Structures of the three complexes.

were run by using a Cary 2300 spectrophotometer. ^{1}H NMR spectra were obtained with a Bruker 300 MHz spectrometer in $CDCl_3$ solutions at room temperature. The ESR spectra were recorded with a Bruker 200D spectrometer operating at the X band and equipped with an Aspect 2000 computer for spectra accumulation and magnetic parameter calculation. Susceptibility measurements were carried out by an AZTEC-DSM5 susceptometer operating at 13,500 G equipped with a Bruker BE15 electromagnet.

D.C. cyclic voltammograms were performed by using a G&G PAR model 273 Potentiostat–Galvanostat coupled to a computerized data acquisition system. A two-compartment, three-electrode locally built cell was used. The compartment of the working electrode (Pt disk, 0.07 cm^2 of area) was separated from that of the counter electrode (Pt wire) by a very fine porosity frit glass set. As reference we used an aqueous Ag/AgCl electrode. The solutions were typically 1.5×10^{-4} M in the electroactive species and contained 0.1 M [TBA][BF_4] as supporting electrolyte in DMF. The reversible couple ferrocene–ferrocenium ion was used as an internal standard to eliminate the interference of contact potentials. Scans were run at 0.100 V s^{-1} where not stated otherwise. The scan range was 0.00 to +1.40 to 0.00 V (vs NHE) in DMF. The solutions were degassed with purified Nitrogen for 10 min before measurements and trace contamination by oxygen was avoided. All the data are reported vs NHE.

Theoretical calculations. All calculations were based on the newest vectorized version of the HFS program system[16,17] with minor modifications to allow for Becke's[18] non-local exchange correction, as well as the correlation between electrons of different spins in the formulation by Stoll *et al.*[19] based on parametrization from electron gas data, Vosko *et al.*[20] Ionization and excitation energies were obtained from the ΔSCF procedure employing the scheme for total energy differences developed by Ziegler and Rauk.[21] Relaxation effects were thus fully incorporated. The Slater type basis[22] used was of double quality for the valence shells except for the 3*d* copper orbital where a triple basis was used. A 4*p* STO polarization function for copper was added. The total molecular electron density was fitted in each SCF iteration by an auxiliary basis of *s*, *p*, *d*, *f* and *g* STOs[23] centred on the different atoms in order to represent the Coulomb and exchange potentials accurately. Use was made of the frozen core approximation.[24] In absence of experimental structural data we assumed for Cu(dbTAA) the idealized D_{2h} geometry of the planar Ni(dbTAA)[5] as standard, with the nitrogen atoms moved out from the centre to a distance of 1.90 Å, according to preliminary studies of spin-echo ESR[24] and molecular mechanics calculations.[25]

RESULTS AND DISCUSSION

UV–vis characterization

Electronic spectra of Cu(dbTAA), Cu(dnTAA) and Cu(dpTAA) were recorded using solvents with different polarity and coordination power. In Fig. 2 the spectra of the three complexes in the range 250–800 nm in DMF are reported. The absorptions for the three complexes are observed in the same spectral wavelength range as the respective free ligands (see Experimental for the absorption maxima of free ligands). The main spectroscopic behaviour of Cu(dpTAA) does not appear to be affected by the coordinating power or polarity of the solvents; conversely the electronic spectra of Cu(dbTAA) and Cu(dnTAA), when recorded in CH_2Cl_2 solutions at low concentrations (10^{-5} M), show new bands at 720 nm [Cu(dbTAA)] and 740 nm [Cu(dnTAA)]. Furthermore, an isosbestic point at 475 nm for Cu(dbTAA) and at 520 nm for Cu(dnTAA) was observed: the colour of the two solutions changes from yellow to pale green on going to lower concentration values (from 10^{-4} to 10^{-6} M). Contextually, a large deviation from the Lambert–Beer law is observed for both complexes as the concentration of Cu(dbTAA) and Cu(dnTAA) reaches 2×10^{-6} and 1.2×10^{-6} M, respectively. This behaviour can be interpreted assuming that an equilibrium exists in non-coordinating solvents, between a monomeric and a dimeric (or oligomeric) form, as previously observed for square-planar nickel(II) complexes with aromatic diimine.[13] The solubility of Cu (dpTAA) in dichloromethane was negligible.

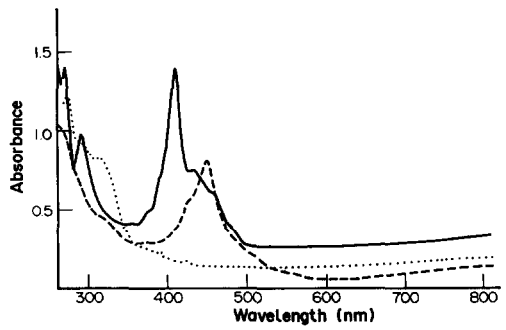

Fig. 2. UV–vis spectra of Cu(dbTAA) (solid line); Cu(dnTAA) (dashed line) and Cu(dpTAA) (dotted line) in DMF 1.8×10^{-5} M at room temperature.

Moreover, a comparative examination of the three UV–vis spectra in DMF solution (see Fig. 2) shows a bathochromic effect on going from Cu(dbTAA) to Cu(dnTAA), while Cu(dpTAA) does not follow this trend. This behaviour parallels that found for the free ligands.

In Table 1 the calculated optical transitions (*in vacuo*) are reported for Cu(dbTAA) and compared with experimental values obtained in very diluted CH_2Cl_2, since this solvent shows very low complexing ability and simulates the vacuum conditions better than DMF. There is fair agreement between the main features of the excitation spectrum; in particular, the intense absorption Soret band at 405(CH_2Cl_2), 408(DMF), 390(theoretical) can be assigned to a π–π^* transition between $4b_{2g}$ and $3a_u$ ligand-centred orbitals, whereas the α band is assigned to transitions from the $4b_{3g}$ to $3a_u$ orbital. Two further considerations suggest this assignment: (i) there is no significant shift of this band as compared with the analogous band in the free ligand spectrum; (ii) a red shift is observed in Cu(dnTAA), where the degree of delocalization increases. The pronounced shoulder of the Soret band at 385 nm is due to a charge-transfer transition from the $10b_{1g}$ HOMO orbital into the b_{1u} π ligand orbital. Moreover, transitions into the half-filled $10b_{1g}$ level span the region 486–250 nm and in the same region fall the remaining π–π^* transitions. The calculated HOMO–LUMO transition falls at too low energy (893 nm) compared with the experimental band (724 nm), so we believe that this assignment is ambiguous. In the case of complex Cu(dnTAA) a shift of 20 nm towards higher wavelengths, without an appreciable change in the shape of the spectrum, can be noted for the Soret band and its π–π^* bands. The spectrum of Cu(dpTAA) exhibits a totally different shape, being dominated by highly intense bands centred at 280, 304 and 310(sh) nm, related to the aromatic ligand moiety (as can be deduced by comparing the data of the free ligand) and probably to a charge-transfer transition. Furthermore, a band at 415 nm is observed. The spectra of all three complexes showing strong absorptions in the low wavelength region are consistent with a square-planar coordination of copper(II),[26] as also shown for Cu(dbTAA) from the theoretical results.

Table 1. Comparison of theoretical and experimental optical transitions in Cu(dbTAA)[a]

Experimental values[b]	Calculated values	Transition
724	893	$10b_{1g} \rightarrow 3a_u$
480	495	$5b_{1u} \rightarrow 5b_{2g}$
	486	$5b_{1u} \rightarrow 10b_{1g}$
	486	$4b_{3g} \rightarrow 10b_{1g}$
460	474	$4b_{3g} \rightarrow 3a_u$
427	429[c]	$4b_{3g} \rightarrow 5b_{2g}$
405[d]	390	$4b_{2g} \rightarrow 3a_u$
385	386	$10b_{1g} \rightarrow 6b_{1u}$
367	341[c]	$4b_{2g} \rightarrow 5b_{2g}$
295	309	$10b_{1g} \rightarrow 4a_u$
	295	$5b_{1u} \rightarrow 5b_{3g}$
275	264	$3b_{2g} \rightarrow 3a_u$
250	255	$2a_u \rightarrow 10b_{1g}$
	230	$12b_{3u} \rightarrow 10b_{1g}$

[a] Values in nm.
[b] Absorption spectra in 1.2×10^{-6} M CH_2Cl_2 solution.
[c] Electronically forbidden transition.
[d] Soret band.

Cyclic voltammetry studies

The three complexes, Cu(dbTAA), Cu(dnTAA) and Cu(dpTAA), exhibit two anodic ($E_{pa,1}$; $E_{pa,2}$), totally irreversible, monoelectronic waves centred at (0.44; 0.88), (0.40; 0.70) and (0.60; 0.82) V, respectively (Fig. 3). The Cu(dbTAA) data are in good agreement with already[27,28] published data. In the case of the $E_{pa,1}$ value of Cu(dpTAA) the process becomes reversible if the sample is swept with a speed greater than 0.50 V s^{-1}. The free ligands have oxidation waves (totally irreversible) at $E_{pa,1}$ and $E_{pa,2}$ values about 0.020 V more anodic than the respective copper complexes. For all three complexes $E_{pa,2}$ shifts towards more anodic values

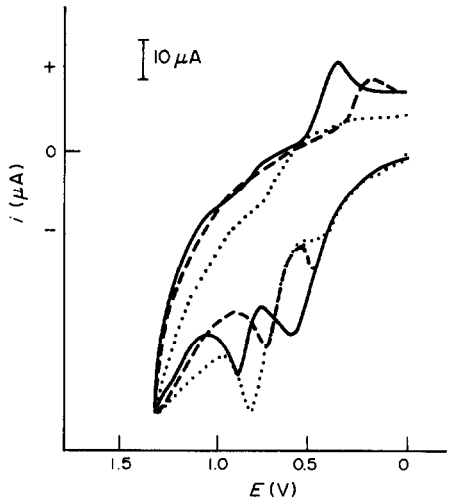

Fig. 3. Voltammograms of: Cu(dbTAA) (dotted line), Cu(dnTAA) (dashed line) and Cu(dpTAA) (solid line) in DMF solutions; scan range 0–1.300 V (potentials reported vs NHE); scan rate: 0.200 V s^{-1}; [TBA][BF4] as supporting electrolyte.

(about 0.035 V) as the scan rate is increased 10-fold on going from 0.010 to 0.200 V s^{-1}; in the same scan rate range $i_{pa}2/v^{1/2}$ is independent of v, as found for EC processes.[29] The two oxidative processes mimic the behaviour of similar tetraazaannulene complexes of various transition metals[27,28,30] and porphyrin complexes.[12] The first process generates a radical cation which undergoes further oxidation followed by homogeneous reaction. It has been noted[12] that expansion of the π system of the porphyrins by peripheral substitution of the ligand results in a lowering of the first oxidation potential of the macrocycle; this is indeed the case on going from Cu(dbTAA) to Cu(dnTAA), but the first oxidative potential of Cu(dpTAA) is higher than that found for Cu(dbTAA).

IR spectroscopy

The three complexes as well as the free ligands were investigated by IR spectroscopy in the range 200–4000 cm^{-1}. The most important features of the spectra concern the position and the intensity of the sharp and strong absorption attributable to the stretching of the C=N group bonded to the aromatic rings. We found that this band occurred for the free ligands at 1665 (H_2dbTAA), 1685 (H_2dnTAA) and 1665 cm^{-1} (H_2dpTAA), respectively; considerable shifts towards lower frequencies were observed in the copper complexes: these showed intense bands localized at 1550 (CudbTAA), 1560 (CudnTAA) and 1550 cm^{-1} (CudpTAA); the free ligands also showed a strong absorption at 3200 cm^{-1} due to N—H stretching that obviously disappeared when the complexes were formed.

Magnetic susceptibility

The static paramagnetic susceptibility (χ^S_M) of Cu(dbTAA), Cu(dnTAA) and Cu(dpTAA), measured at 290 K and corrected for the diamagnetism of the tetraazaannulene ring and the metal, at 1.32×10^{-3}, 1.33×10^{-3} and 1.28×10^{-3} emu mol^{-1}, respectively. These values correspond to 1.0 unpaired electron spin ($S = 1/2$, assuming $g = 2$) for each metallomacrocycle and are coherent with an appreciable localization of the unpaired electron on the copper atom, as shown by ESR data (*vide infra*), as well as with susceptibility data reported[31] for Cu(dbTAA).

ESR results

The ESR spectra of powders of Cu(dbTAA) (Fig. 4) exhibited a single line at $H \approx 3377$ G ($g \approx 2.065$).

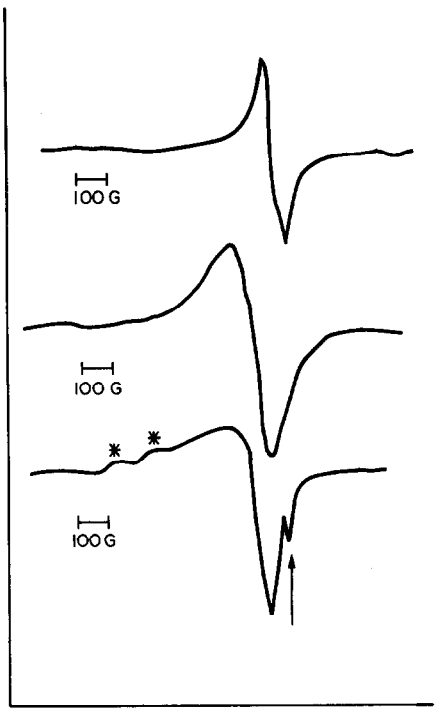

Fig. 4. Room temperature ESR powder spectra of: (a) Cu(dbTAA) (field modulation intensity: 0.25 Gpp; gain: 5.103); (b) Cu(dnTAA) (field modulation intensity: 0.25 Gpp; gain: 1.6.104); and (c) Cu(dpTAA) (field modulation intensity: 1.0 Gpp; gain: 5.104). All the spectra were recorded with a central field $H = 3200$ G and scan range 1500 G.

To our knowledge only the $A_\parallel$ 218 cm^{-1} has been determined for this complex when diluted in the metal-free ligand;[4] thus one can set this value as a lower limit for the exchange strength. The derivative absorption line shape of Cu(dnTAA) is still determined by spin–spin interactions; the signal is centred at $g \approx 2.067$, very close to the value found in the Cu(dbTAA); however the line width is $\delta H \approx 150$ G, whereas in the Cu(dbTAA) $\delta H \approx 90$ G; this indicates a lower exchange interaction. Finally the spectrum of Cu(dpTAA) can be interpreted as the superposition of two signals; the two low-field bands can be identified as slightly resolved parallel hyperfine lines with $m = 3/2, 1/2$ (asterisked in Fig. 4) due to a copper species in a relatively diluted environment; approximated evaluation of $g_\parallel$ and $g_\perp$ gives 2.30 and 2.07. The superimposed signal is a broadened line centred at $g \approx 2.08$ with a $\delta H \approx 190$ G, assignable to a copper species undergoing spin–spin exchange,[32] weakened with respect to that of Cu(dnTAA). The position ($g \approx 2.00$) and narrowness of the very low amplitude signal at $H \approx 3490$ G (arrow in Fig. 4) are similar to those

of the absorption found by other authors in systems involving phthalocyanines[33] and diamagnetic metal–phthalocyanines complexes.[34] They are attributed by Assour and Harrison[35] to a radical formed by reversible absorption of oxygen by phthalocyanines. We found that ESR spectra of our ligands showed a quite similar signal. On this basis, the partial resolution of a copper spectrum can be due to the dilution exerted by metal-free ligand molecules present as impurities.

The spectral behaviour indicates that the exchange interaction between the metallic electrons decreases by increasing the number of rings in the copper(II) complexes. This effect denotes an increased distance among the molecules in the crystal going from Cu(dbTAA) to Cu(dpTAA). In all cases the suggested arrangement of the four nitrogen atoms around the metal is planar with a little tetragonal distortion to take into account the anisotropy of the g tensor.

Ligand conformation

Both the UV–vis and cyclic voltammetry results seem to suggest that the behaviour of the dpTAA ligand does not follow the trend indicated by dpTAA and dnTAA. At present structures of the 5,7,12,14-tetramethyldibenzo[b,i][1,4,8,11]tetraaza[14]annulene (tmdbTAA) free ligand and of M(tmdbTAA) complexes (M = Ni, Co, Fe, Mn, Pd, Pt) are known[36–39] as well as the M(dbTAA) complexes (M = Ni, Pd, Cu)[3,40] [although only cell parameters and interplanar spacing have been published in the case of the mixed valence solid obtained by iodine oxidation of Cu(dbTAA)] which seem to indicate that in the case of dbTAA the free ligand in the complex is substantially planar, whereas in the case of tmdbTAA the ligand, both free and in the complex, strongly deviates from planarity. In order to check the behaviour of the whole series of our studied compounds, we have performed some molecular mechanics computations on the free ligand using the force-field of Allinger and Burkert[41] in connection with the MM2[42] program which includes the explicit treatment of π electrons by means of a Huckel–VESPR approach.[41]

Full geometry optimization (i.e. bond length, valence angles and dihedral angles) in the case of H_2(tmdbTAA) results in fairly good agreement with the X-ray experimental data of the free ligand[38] (all bond distance and valence angles within 0.02 nm and 1.1°, respectively) with the only exception being the C_{aryl}—N bond which is predicted to be 0.07 nm shorter than the X-ray data value. As regards the molecular shape, the computations indicate that the molecule also has a non-planar structure *in vacuo*. The deviation from planarity measured as the dihedral angle between both the mean phenanthrene plane and the mean pentadiiminato plane, with respect to the four nitrogen atoms, is 20.1° and 32.2°, in good agreement with the values found[38] of (25.1°, 24.1°) and (32.0°, 36.5°) for the benzene and diiminato planes, respectively. The same procedure applied in the case of H_2(dbTAA) gives a planar structure that compares well with the ligand geometry in the nickel and palladium complexes.[3]

For the H_2(dnTTA) and H_2(dpTAA) molecules the same procedure gives a different trend. In fact, while the former has the same behaviour as the H_2(dbTAA) molecule (i.e. the molecule is planar) the latter shows a fairly large deviation from planarity, as can be seen in Fig. 5. The deviation from planarity, previously defined, is 8.5° and 36.2°. The molecular distortion for tmdbTAA is due to the interaction between the methyl groups on the pentadiiminate moieties and the hydrogen atoms on the benzo moieties. On the other hand, for the dnTAA ligand the most important interaction is between the hydrogen atoms on the pentadiiminato and the phenanthrene moieties. Because the two phenanthrene moieties and pentadiiminate moieties bend out from the molecule plane, a non-negligible breaking of the molecular π conjugation results: this may well account for the different spectroscopic behaviour of the molecules and their complexes.

Electronic structure

In Fig. 6 we show the calculated ground-state level ordering of Cu(dbTAA) in terms of the copper atom and the dbTAA ligand fragment. The splitting between $10b_{1g}$ HOMO and $5b_{1u}$ SHOMO is 1.56 eV and the ground state of this complex is quite unambiguously $^2B_{1g}$.

The ground-state one-electron energies and composition of the orbitals are given in Table 2. For the Mulliken population analysis, on which the table is based, we have transformed the primitive basis set to a basis of SCF orbitals of the macrocycle and copper atom. The HOMO, shown in Fig. 7, is found to be an anti-bonding mixture (we found a Cu–dbTAA overlap population of −0.128) of almost equal amounts of Cu-$3d_{xy}$ and dbTAA-$2b_{1g}$ which, within the dbTAA ligand, is mainly localized (75.4%) on the nitrogen atoms. In fact Fig. 7(b) shows the large peaks corresponding to the Cu-d_{xy} orbital and the related N-"lone pairs" originated from the $2s$, $2p_x$ and $2p_y$ nitrogen orbitals, and the not negligible peaks due to the amplitude around the C—N—C moieties whose intensity is far larger than those of other carbon and hydrogen orbitals. Furthermore,

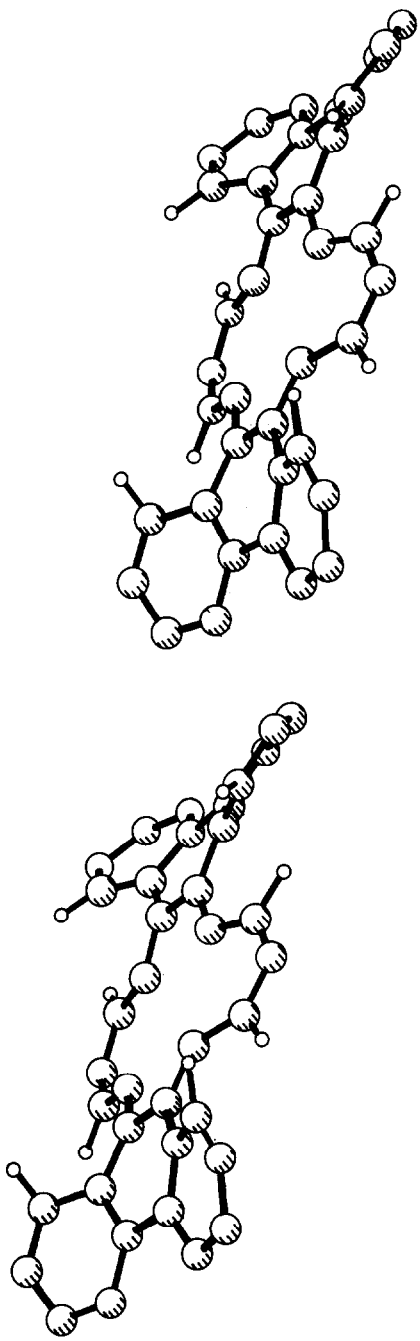

Fig. 5. Stick and ball stereo plot of the computed structure by the molecular mechanics approach to H_2dpTAA. Only strongly interacting hydrogen atoms are reported. Small ball H; medium ball C; large ball N.

as can be seen from Table 2, the HOMO is an antibonding mixture of the Cu-d_{xy} and dbTAA-$2b_{1g}$ orbitals and this is well pointed out by Fig. 7(a) which clearly shows the out-of-phase mixing of the Cu-d_{xy} and the N-"lone pairs". The bonding partner of the $10b_{1g}$ HOMO is the $9b_{1g}$ orbital which lies 5 eV below.

The σ interactions are by far the most important ones and account for the metal–macrocycle bond in the complex. The charge rearrangement due to the bond may be inferred by the Mulliken gross population given in Table 3 for each symmetry. We should note that two electrons are transferred from the copper to the B_{1u} symmetry in Cu(dbTAA), so the reference copper configuration is $3d^9 4s^0$. The $4s$ population in copper is mainly provided by the macrocycle σ-orbitals, although a small amount is due to the admixture of $4s$ into $3d_{z^2}$ orbital occurring in $15a_g$. The $4p_x$ and $4p_y$ copper orbitals are also involved to a small extent in the σ bond as it comes out from their population. From the populations given in Table 3 for B_{1g} symmetry it is immediately apparent how strong the mixing of $3d_{xy}$ is with the dbTAA-σ ($2b_{1g}$).

The large energy gap between copper-$3d$ and the ligand empty orbitals does not allow for a back-donation in the complex, as is clearly shown in the gross populations relative to B_{3g} and B_{2g} symmetry which remain substantially unchanged.

As found for metal–porphyrins,[23,43(a,b)] this complex shows a large polarity, even though the calculated copper charge (+0.75) indicates that the metal does not achieve the ionicity corresponding to its formal valence (+2). Furthermore, the charge distribution we found in the complex suggests that the delocalization in the ligand moiety only slightly involves the "1,2-diaminobenzene" five-membered chelate rings, while it is confined in benzene and to a lesser extent in diiminato rings. In particular, the calculated overlap population is 0.29 for a C—N bond in five-membered rings against the values 0.38, 0.43 and 0.43 relative to the three C—C bonds in benzene rings and 0.32 and 0.41 relative to the C—N and C—C bonds of diiminato rings, respectively. These results are in agreement with X-ray data available[5] for M(dbTAA) complexes which show a lengthening of the C_{aryl}—N bond.

CONCLUSIONS

Comparison of spectroscopic results for Cu (dbTAA), Cu(dnTAA) and Cu(dpTAA) coupled with very accurate theoretical investigations on Cu(dbTAA) allows us to consider all the compounds as complexes with the copper atom in an N_4 planar environment. Little tetragonal distortion of the metal can occur in the solid state [as also suggested by our own, and previous, ESR studies[4] on Cu(dbTAA)] to take into account the values of anisotropy for the g tensor. For Cu(dpTAA), as well as for the free ligand, appreciable deviation of the phenanthrene rings from plan-

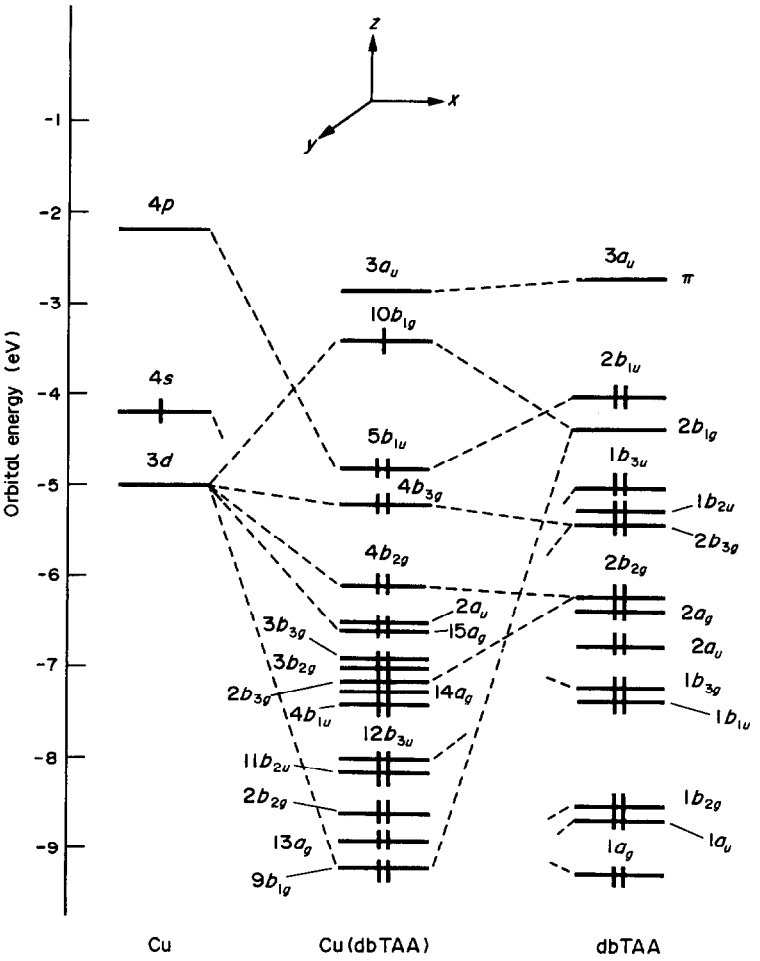

Fig. 6. Energy level diagram for Cu(dbTAA). Only some correlations are reported. The 4*p* copper atomic level does not correspond to the calculated one electron energy.

Table 2. Energies and composition of Cu(dbTAA) orbitals

Orbital	$-\varepsilon i$ (eV)	Character	Percentage copper atomic orbital				Percentage L fragment orbital L = dbTAA
			$d\sigma$	$d\pi$	4*s*	4*p*	
$6b_{1u}$	1.28	L π n.b.					100.0 ($3b_{1u}$)
$5b_{2g}$	2.51	L π n.b.		2.5			97.5 ($3b_{2g}$)
$3a_u$	2.87	L π					100.0 ($3a_u$)
$10b_{1g}$ (HOMO)	3.24	$d\sigma$L σ a.b.	46.5				53.5 ($2b_{1g}$)
$5b_{1u}$	4.80	L π n.b.				2.6	97.4 ($2b_{1u}$)
$4b_{3g}$	5.15	L $\pi(+d\pi)$ a.b.		15.1			84.9 ($2b_{3g}$)
$4b_{2g}$	6.09	L $\pi(+d\pi)$ a.b.		8.0			92.0 ($2b_{2g}$)
$2a_u$	6.47	L π					100.0 ($2a_u$)
$15a_g$	6.49	$d\pi$(+4s, L σ)		85.0	8.3		6.7 ($2a_g$)
$3b_{3g}$	6.87	L π-$d\pi$ a.b.		36.4			63.6 ($1b_{3g}$)
$3b_{2g}$	6.89	L π-$d\pi$ a.b.		73.8			26.2 ($1b_{2g}$)
$2b_{3g}$	7.15	L π-$d\pi$ b.		41.4			58.6 ($1b_{3g}$)
$14a_g$	7.20	$d\sigma$(+L σ)	93.2				6.8 ($1a_g$)
$4b_{1u}$	7.35	L π n.b.					100.0 ($1b_{1u}$)
$12b_{3u}$	7.79	L $\pi(+4p_y)$				5.9	94.1 ($1b_{3u}$)

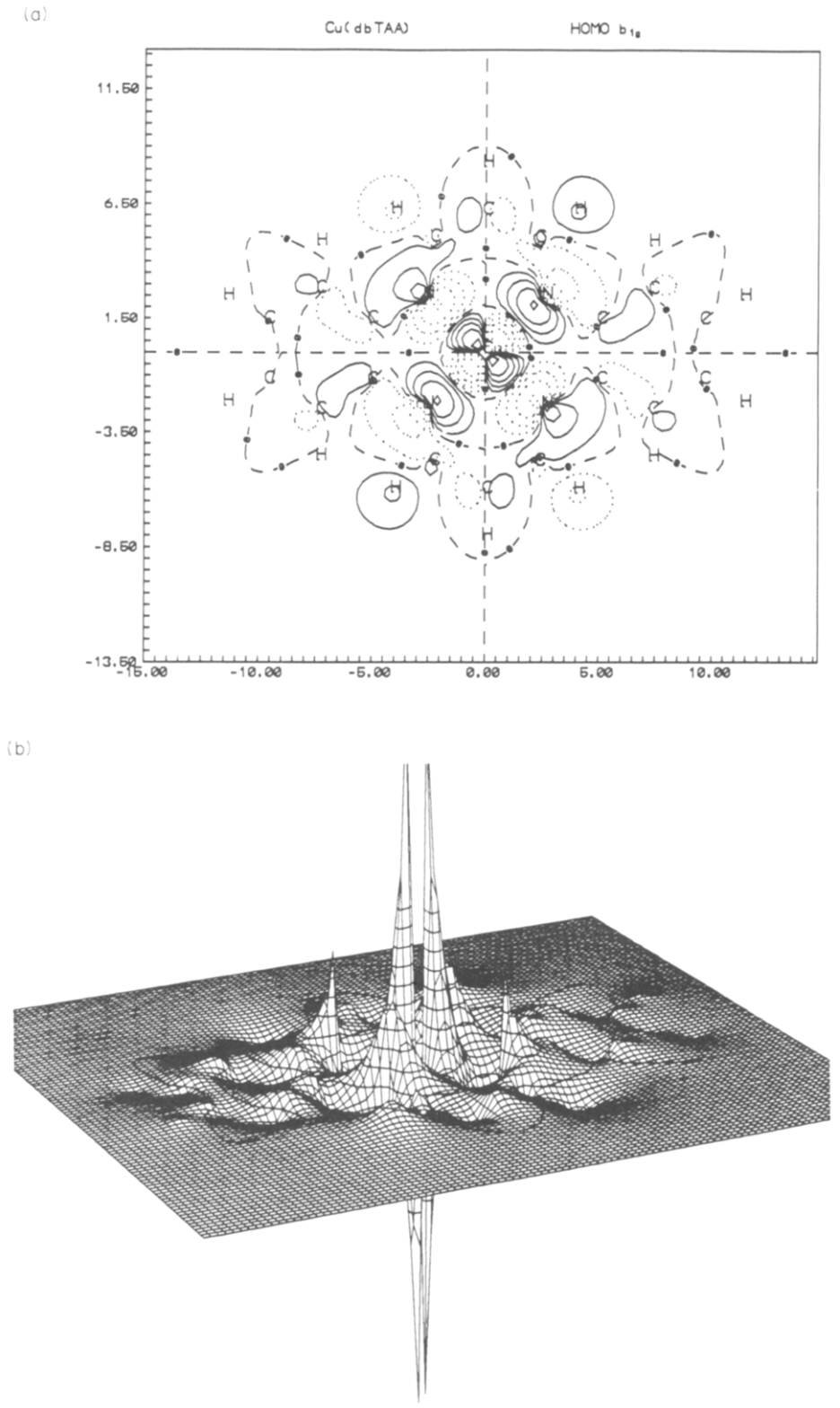

Fig. 7. (a) Two-dimensional plot of the HOMO b_{1g} in the molecular plane. Contour levels are -0.4, -0.2, -0.1, -0.04, -0.02, 0.0, 0.02, 0.04, 0.1, 0.2, 0.4 (electrons a.u.$^{-3}$)$^{1/2}$. Dotted, dashed dot and full lines refer to negative, zero and positive function values, respectively. x and y units are in a.u. (b) Three-dimensional view of (a).

Table 3. Gross population of SCF orbitals of copper and dbTAA in Cu(dbTAA)

A_g	Cu	$3s$	1.994	B_{1g}	Cu	$3d_{xy}$	1.541	B_{2g}	Cu	$3d_{xz}$	1.930
		$3d_{z^2}$	1.942			$4d_{xy}$	0.034		dbTAA	$1b_{2g}$	2.001
		$3d_{x^2-y^2}$	1.976		dbTAA	$1b_{1g}$	2.000			$2b_{2g}$	1.999
		$4s$	0.405			$2b_{1g}$	1.390			$3b_{2g}$	0.044
	dbTAA	$1a_g$	1.998								
		$2a_g$	1.521								
B_{3g}	Cu	$3d_{yz}$	1.984	B_{1u}	Cu	$3p_z$	1.999	B_{2u}	Cu	$3p_y$	1.955
	dbTAA	$1b_{3g}$	1.999			$4p_z$	0.068			$4p_y$	0.179
		$2b_{3g}$	1.999		dbTAA	$1b_{1u}$	1.996		dbTAA	$1b_{2u}$	1.825
						$2b_{1u}$	1.915				
B_{3u}	Cu	$3p_x$	1.994	A_u	dbTAA	$1a_u$	1.993				
		$4p_x$	0.192			$2a_u$	1.997				
	dbTAA	$1b_{3u}$	1.819			$3a_u$	0.003				

arity with respect to the macrocyclic framework can be predicted on the basis of the observed trend in the case of UV spectra. The deviation from planarity can be explained on the basis of the steric repulsion between hydrogen atoms of the diiminic carbon and the opposite hydrogen bonded to the phenanthrene ring, as supported by molecular mechanics calculations.[25] Furthermore, the distortion of the phenanthrene moiety explains well the increased distance between the copper centres in the solid state as pointed out by ESR results.

The paramagnetism of the Cu(dbTAA) complex is in agreement with the HOMO composition which indicates that the unpaired electron is shared, in almost equal amounts, by the metal-centred d_{xy} orbital and a combination of s and p orbitals of the nitrogen atoms of the ligand. Owing to the substantial structural similarity of all three complexes and on the basis of the susceptibility values and ESR measurements, it is reasonable to assume that the unpaired electron in Cu(dnTAA) and Cu(dpTAA) is similar in character to that of Cu(dbTAA).

Acknowledgements—We thank Professor E. J. Baerends for a copy of the newest version of the HFS-program system. We are indebted to Professor M. Romanelli (University of Basilicata) and Dr M. F. Ottaviani (University of Firenze) for ESR measurements and helpful discussions, Dr C. Caneschi (University of Firenze) for magnetic susceptibility measurements, Dr M. Latronico (University of Basilicata) for elemental analyses and C. Barlabà for technical support. We would like to thank Cineca of Bologna for the access to the Cray Y-MP 8/432 computer and C.I.S.I.T. of Università della Basilicata for a generous gift of computer time. This work was partially supported by the Italian National Research Council (CNR) (Progetto Finalizzato: Materiali Speciali per Tecnologie Avanzate).

REFERENCES

1. T. J. Marks and D. W. Kalina, *Extended Linear Chain Compounds* (Edited by J. S. Miller), Vol. 1, pp. 271–278. Plenum Press, New York (1982) and refs therein.
2. T. J. Marks, *Science* 1985, **227**, 881.
3. (a) M. Hunziker, B. Hilti and G. Rihs, *Helv. Chim. Acta* 1981, **64**, 82; (b) Y. M. Wuu, S. M. Peng and H. Chang, *J. Inorg. Nucl. Chem.* 1980, **42**, 839.
4. K. Sakata, M. Hashimoto, N. Tagami and Y. Murakami, *Bull. Chem. Soc. Japan* 1980, **53**, 2262.
5. M. C. Weiss, G. Gordon and V. l. Goedken, *Inorg. Chem.* 1977, **16**, 305.
6. L. S. Lin, T. J. Marks, C. R. Kannewurf, J. W. Lyding, M. S. McClure, M. T. Ratajack and T. C. Whang, *J. Chem. Soc., Chem. Commun.* 1980, 954.
7. M. Tsutsui, R. L. Bobsein and R. Pettersen, *Inorg. Chem.* 1979, **18**, 758.
8. M. Hunziker, H. Loeliger, G. Rihs and B. Hilti, *Helv. Chim. Acta* 1981, **64**, 2544.
9. F. Adams, R. Gompper and E. Kujath, *Angew. Chem. Int. Edn Engl.* 1989, **28**, 1060.
10. C. J. Schramm, D. R. Stojakovic, B. M. Hoffman and T. J. Marks, *Science* 1978, **200**, 47.
11. J. Martinsen, S. M. Palmer, J. Tanaka, R. C. Greene and B. M. Hoffman, *Phys. Rev.* 1984, **30B**, 6269.
12. J. H. Fuhrhop, K. M. Kadish and D. G. Davis, *J. Am. Chem. Soc.* 1973, **95**, 5140.
13. (a) F. Lelj, G. Morelli, G. Ricciardi, M. F. Brigatti and A. Rosa, *Polyhedron* 1989, **8**, 2603; (b) F. Lelj, A. Rosa, G. P. Ricciardi, M. Casarin, P. L. Cristinziano and G. Morelli, *Chem. Phys. Lett.* 1989, **160**, 139.
14. M. G. Veliev and M. M. Guselnov, *Syntheses* 1980, 461.
15. C. L. Honeybourne, *Inorg. Synth.* 1978, **18**, 44.
16. E. J. Baerends, D. E. Ellis and P. Ros, *Chem. Phys.* 1973, **2**, 71.
17. E. J. Baerends and P. Ros, *Int. J. Quant. Chem.* 1978, **S12**, 169.

18. A. J. Becke, *J. Chem. Phys.* 1986, **84**, 4524.
19. H. Stoll, E. Golka and H. Preuss, *Theor. Chim. Acta* 1980, **55**, 29.
20. S. H. Vosko, L. Wilk and M. Nusair, *Can. J. Phys.* 1980, **58**, 102.
21. T. Ziegler and A. Rauk, *Theor. Chim. Acta* 1977, **46**, 1.
22. P. Vernooijs, G. J. Snijders and E. J. Baerends, Slater type basis functions for the whole periodic system. Internal report, Free University, Amsterdam, The Netherlands (1981).
23. J. Krijn and E. J. Baerends, Fit functions in the HFS-method. Internal report, Free University, Amsterdam, The Netherlands (1984).
24. R. Romanelli, M. F. Ottaviani, F. Lelj, G. Morelli, G. Ricciardi and A. Rosa, preliminary results.
25. F. Lelj, G. Morelli, R. Ricciardi and A. Rosa, *Polyhedron*, submitted.
26. A. B. P. Lever, *Inorganic Electronic Spectroscopy*. Elsevier, Amsterdam (1984).
27. A. Belleira and F. Walsh, *Electrochim. Acta* 1986, **13**, 113.
28. K. M. Kadish, D. Schaeper, L. A. Bottomley, M. Tsutsui and R. L. Bobsein, *J. Inorg. Nucl. Chem.* 1980, **42**, 469.
29. W. E. Geiger, *Inorganic Reactions and Methods*, Vol. 15, Ch. 12. VCH Publishers (1986) and references therein.
30. C. L. Bailey, R. D. Bereman and D. P. Rillema, *Inorg. Chem.* 1986, **25**, 3149.
31. C. L. Honeybourne and P. Burchill, *Inorg. Nucl. Chem. Lett.* 1974, **10**, 715.
32. A. Abragam and B. Bleaney, *Electron Paramagnetic Resonance of Transition Ions*, Ch. I and IX. Oxford University Press. New York (1970).
33. (a) J. M. Assour and W. K. Kahn, *J. Am. Chem. Soc.* 1965, **87**, 207; (b) C. M. Guzy, J. B. Raynor and M. C. R. Symons, *In. Chem. Soc. A* 1969, 2299.
34. R. Neiman and D. Kivelson, *J. Chem. Phys.* 1961, **35**, 162.
35. J. M. Assour and S. E. Harrison, *J. Chem. Phys.* 1964, **68**, 872.
36. V. Goedken, S. Peng and Y. Park, *J. Am. Chem. Soc.* 1975, **96**, 281.
37. Y. Wang, S. Peng, Y. Lee, M. Chuang, C. Tang and C. Wang, *J. Chinese Chem. Soc.* 1982, **29**, 217.
38. V. Goedken, S. Peng, J. Molin-Norris and Y. Park, *J. Am. Chem. Soc.* 1976, **98**, 8391.
39. M. Tutsui, R. L. Bobsen, G. Cash and R. Pettersen, *Inorg. Chem.* 1979, **18**, 758.
40. M. Hunziker and G. Rihs, *Inorg. Chim. Acta* 1985, **102**, 39.
41. U. Burkert and N. L. Allinger, *Molecular Mechanics*. ACS Monograph 177, American Chemical Society, Washington, D.C. (1982).
42. MM2, program number 395. Available from Quantum Chemistry Program Exchange, Indiana University, Bloomington, Indiana, U.S.A.
43. (a) D. E. Ellis and Z. Berkovitch-Yellin, *J. Chem. Phys.* 1981, **74**, 2427; (b) A. M. Schaffer, M. Gouterman and E. R. Davidson, *Ther. Chim. Acta* 1973, **30**, 9.

Polyhedron Vol. 10, No. 6, pp. 535–542, 1991
Printed in Great Britain

0277–5387/91 $3.00+.00
© 1991 Pergamon Press plc

SYNTHESIS, DEMETALLATION, REMETALLATION AND TRANSMETALLATION OF NEW MONO- AND BINUCLEAR SCHIFF BASE COMPLEXES

AHMED EL-TOUKHY

Department of Chemistry, Faculty of Science, University of Qatar, P.O. Box 2713, Doha, Qatar

(*Received* 23 *April* 1990; *accepted* 9 *October* 1990)

Abstract—New mono- and binuclear nickel(II) complexes [PyNi(ONS-COPh)] and [PyNi(ONS-CO)]$_2$-C_6H_4 have been prepared by a nucleophilic substitution reaction of the C—H methine-containing complex, mono-pyridine-S-methyl-N-acetylacetonehydrazinecarbodithioate nickel(II) [PyNi(HONS)], with benzoyl chloride and phthaloyl dichloride, respectively. Reaction of phenylisocyanate and *m*-xylene diisocyanate to [PyNi(HONS)] also gave new mono- and binuclear nickel(II) complexes, [PyNi(ONS-CONHPh)] and [PyNi(ONS-CONH)]$_2$-*m*-xyl, respectively. The demetallation and transmetallation of the prepared nickel(II) complexes with Na_2EDTA and copper(II) acetate monohydrate afford the corresponding mono- and binucleating ligands and mono- and binuclear copper(II) complexes, respectively. The conditions of the reliable demetallation and transmetallation reactions are described. The copper(II) complexes are also synthesized from the reaction of copper(II) acetate with the free ligands. All new compounds are characterized by various physical techniques. The mono- and binuclear nickel(II) and copper(II) complexes display magnetic and spectroscopic behaviour characteristic of square planar complexes. The ESR spectra of the mono- and binuclear copper(II) complexes are similar, indicating the absence of any magnetic coupling between the metal centres.

There has been considerable interest in the synthesis, characterization and reactivity of binuclear complexes which contain ligands capable of holding two metal ions in close proximity.[1–4] Homo- and hetero-dinuclear complexes are of interest in studies related to metalloenzymes[5,6] and bioinorganic chemistry,[7] homogeneous catalysis and the activation of small molecules (N_2, O_2, CO, CO_2, H_2),[5,8–11] multi-electron transfer processes,[12,13] redox catalysis,[14] and magnetic exchange phenomena.[15,16] Many Schiff base ligands have been synthesized which exhibit some or all of the features specified above.[1,4,17,18]

In this paper, interest has been focused upon the reactivity of the nickel(II) complex, **I**, containing a C—H methine group in a metallo-organic ring. The complex is capable, in principle, of undergoing addition–insertion reactions[4] with phenylisocyanate and *m*-xylenediisocyanate and nucleophilic substitution reactions[19–23] with benzoyl chloride and isophthaloyl dichloride according to the reaction scheme shown in Fig. 1. Demetallation of the prepared mono- and binuclear nickel(II) complexes and remetallation of the isolated ligands with copper(II) are also reported. By applying the recently discovered transmetallation procedure,[24,25] the replacement of nickel by copper (Fig. 1) is possible and the usually laborious, multistep synthesis can be avoided.

EXPERIMENTAL

Materials

All solvents used were reagent grade and were dried using standard literature procedures. The parent complex, **I**, was prepared according to the method of Iskander *et al.*[26] and recrystallized from dichloromethane. Na_2EDTA, benzoyl chloride, isophthaloyl dichloride, phenylisocyanate and *m*-xylenediisocyanate were purchased from Aldrich and used without further purification.

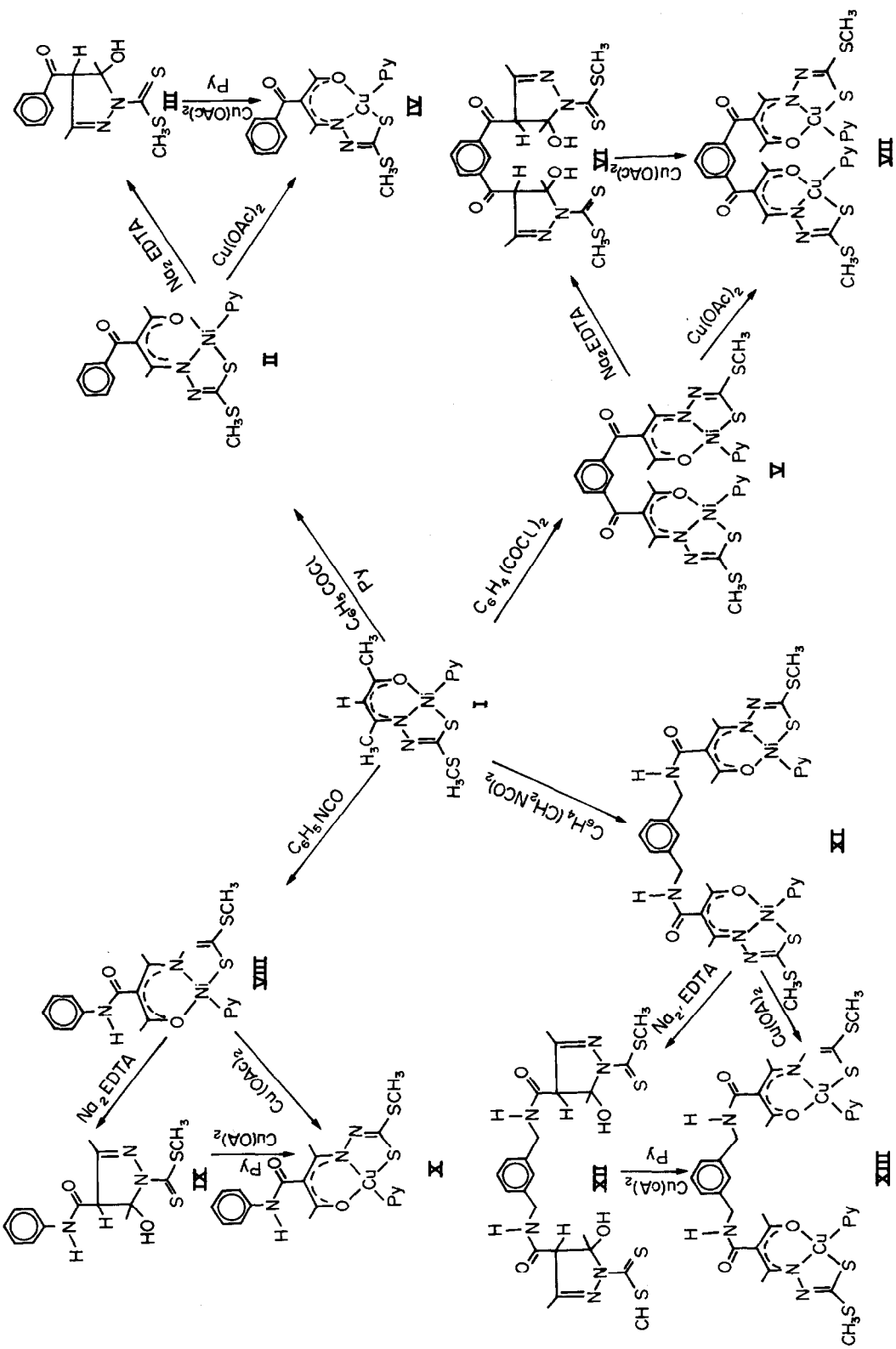

Fig. 1.

Preparation of [PyNi(ONS-COPh)] (**II**)

A clear solution of **I** (0.01 mol) in dry benzene (30 cm^3) was treated with benzoyl chloride (0.01 mol) in the presence of pyridine (0.01 mol). The reaction mixture was refluxed for 6 h with stirring, evaporated to half its volume and left to cool. A crystalline precipitate consisting of the benzoylation product and pyridine hydrochloride was filtered off, dried and treated with hot water with stirring. The brown, crystalline material was collected, washed with hot water and alcohol and recrystallized from benzene–petroleum ether (40–60°C).

Preparation of [PyNi(ONS-CO)]$_2$-*m*-xyl (**V**)

The reaction of **I** with isophthaloyl dichloride in a 2 : 1 molar ratio was performed by a procedure similar to that described above for the preparation of the title compound.

Preparation of [PyNi(ONS-CONHPh)] (**VIII**)

The title mononuclear complex was prepared by mixing a stirred solution of **I** and phenylisocyanate (1 : 1 molar ratio) in dichloromethane at room temperature for 6 h. The reaction mixture was evaporated under reduced pressure to a small volume and diluted with n-hexane. A brown solid material was collected, dried and then recrystallized from dichloromethane–hexane.

Preparation of [PyNi(ONS-CONH)]$_2$-*m*-xyl (**XI**)

This binuclear nickel(II) complex was prepared according to a method similar to that for the mononuclear nickel(II) complex, **VIII**, except that **I** and *m*-xylenedi-isocyanate were reacted in a 2 : 1 molar ratio.

Preparation of the metal free ligands: (H_2ONS-COPh) (**III**), (H_2ONS-CONHPh) (**IX**), (H_2ONS-CO)$_2$-*m*-xyl (**VI**) *and* (H_2ONS-CONH)$_2$-*m*-xyl (**XII**)

General procedure. The demetallation of the nickel(II) complexes was carried out by treating the suspended complex (0.5 g) in water (50 cm^3), with a 0.05 M Na_2EDTA solution (25 cm^3). The reaction mixture was stirred for 3 h at room temperature. The metal-free ligand was deposited as an insoluble solid, filtered off, washed with water and recrystallized from ethanol.

Preparation of copper(II) *complexes:* [PyCu(ONS-COPh)] (**IV**), [PyCu(ONS-CONHPh)] (**X**), [PyCu(ONS-CO)]$_2$-*m*-xyl (**VII**) *and* [PyCu(ONS-CONH)]$_2$-*m*-xyl (**XIII**)

(a) *Direct method.* A clear solution of the ligand, **III**, **VI**, **IX** or **XII**, in ethanol, was treated with a methanol solution of copper(II) acetate monohydrate in the appropriate molar ratio in the presence of pyridine. The reaction mixture was refluxed for 1 h, evaporated to half its volume and left to cool. The precipitated complex was filtered off, washed with ethanol and diethyl ether and dried *in vacuo*.

(b) *Transmetallation method.* A clear solution of the nickel(II) complex (0.01 mol) in methylene chloride (50 cm^3) was treated with copper(II) acetate monohydrate [0.01 mol for the mononuclear nickel(II) complexes **II** and **VIII**, and 0.02 mol for the binuclear nickel(II) complexes **V** and **XI**] in methanol (30 cm^3). The reaction mixture was stirred for 6 h at room temperature. The solvent was removed using a rotary evaporator. The copper(II) complex was extracted with methylene chloride, reprecipitated with hexane, isolated by filtration, washed with hexane and dried *in vacuo*.

Physical measurements

Nickel and copper analyses were performed on a Leeman Labs Plasma Spec inductively coupled plasma emission spectrometer. Nitrogen and sulphur analyses were performed by Mic Anal. Organic Microanalysis, Tucson, U.S.A. Cryoscopic molecular weight measurements of products were made by measuring the freezing point depression of nitrobenzene solutions containing a known amount of solute. The freezing point depression constant ($K_f = 7.00$°C mol^{-1}) for nitrobenzene was determined using benzil as a standard (see Table 1).

Solution electronic spectral measurements were made with a Perkin–Elmer 552 spectrophotometer in matched quartz cells at room temperature. The solvent, dichloromethane, was used as reference. IR spectra (KBr disks) were obtained with a Pye Unicam SP2000 spectrophotometer calibrated with the 906.5 or 3026.3 cm^{-1} absorption of polystyrene. ^{1}H NMR spectra were recorded with a Varian EM-390-90 MHz NMR spectrometer; the magnet temperature was adjusted to 38°C. A tetramethylsilane (TMS) signal ($\delta = 0$) was employed as internal standard and deutero-chloroform (Aldrich) was used as the solvent. ESR spectra were recorded at 100 kHz modulation and 10 G modulation amplitude on a Varian E-9 spectrometer. An incident power of 10 mW was used and resonance conditions were *ca* 9.75 GHz (X-band) at room temperature and *ca*

Table 1. Elemental analysis, cryoscopic data, electronic spectra and magnetic moments of the organic ligands and their nickel(II) and copper(II) complexes

Compound	Elemental analysis[a] N (%)	S (%)	M (%)	Molecular weight[b]	Band maxima (nm), (log ε, mol dm^3 cm^{-1})					μ_{eff} (BM)
II	9.1	14.1	13.0	428±20	255,	310,	400,	475,	590sh	—
	(9.5)	(14.4)	(13.3)	(444)	(4.32)	(3.97)	(4.11)	(3.45)	(2.08)	
III	9.2	20.7	—	300±20	250,	300sh,	370sh			—
	(9.1)	(20.8)		(308)	(4.17)	(3.92)	(3.06)			
IV	9.3	14.0	13.9	430±20	265,	335,	400sh,	590		1.83
	(9.4)	(14.3)	(14.2)	(448.5)	(4.38)	(4.10)	(3.87)	(2.48)		
V	10.5	16.1	14.9	770±20	260,	315,	400sh,	480,	605sh	—
	(10.7)	(16.3)	(15.0)	(786)	(418)	(4.06)	(4.16)	(3.65)	(2.50)	
VI	10.8	24.8	—	510±20	255,	310sh,	335,	375sh		—
	(10.9)	(24.9)		(514)	(4.41)	(4.05)	(3.93)	(3.26)		
VII	10.2	15.8	15.8	785±20	265,	330,	410sh,	600		1.80
	(10.6)	(16.1)	(16.0)	(795)	(4.27)	(4.18)	(3.92)	(2.37)		
VIII	12.1	13.6	12.6	465±20	260,	310,	410sh,	480,	585sh	—
	(12.2)	(13.9)	(12.8)	(459)	(4.41)	(4.05)	(4.22)	(3.39),	(2.04)	
IX	12.8	19.8	—	330±20	255,	305sh,	325,	385sh		—
	(13.0)	(19.8)		(323)	(4.11)	(3.99)	(4.21)	(3.04)		
X	11.9	13.5	13.6	455±20	260,	335,	390,	570sh		1.79
	(12.0)	(13.8)	(13.7)	(463.5)	(4.41)	(4.02)	(3.97)	(2.59)		
XI	13.1	15.4	13.7	835±20	255,	310sh,	405,	470,	580sh	—
	(13.3)	(15.2)	(14.0)	(849)	(4.31)	(4.10)	(4.25)	(3.44)	(2.47)	
XII	14.3	22.1	—	558±20	245,	300sh,	320,	380sh		—
	(14.7)	(22.4)		(572)	(4.23)	(3.87)	(4.18)	(3.26)		
XIII	13.2	15.3	14.7	820±20	265,	325,	405,	590sh		1.77
	(14.1)	(15.0)	(14.9)	(853)	(4.19)	(4.05)	(3.98)	(2.49)		

[a] Analytical methods are described in the text; calculated values are given in parentheses.
[b] In nitrobenzene: typical molar concentration, 2×10^{-2}.

9.10 GHz at 11 K. Spectra at low temperature were obtained with an Air Products LTD-3-100 Heli-Tran liquid helium transfer refrigerator; the field being calibrated with a powder sample of DPPH (g = 2.0037).[27] Magnetic susceptibilities were measured by the Gouy method using $HgCo(SCN)_4$ for calibration, and Pascal constants were used to correct all data for diamagnetism.[28]

RESULTS AND DISCUSSION

The starting mononuclear, square planar nickel (II) complex, **I**, (Fig. 1) has been prepared following the previously reported procedure.[26] The presence of a C—H methine group in the metallo-organic ring in **I** greatly assists nucleophilic substitution reactions on that centre.[19] According to the reaction procedure shown in Fig. 1, the γ-substituted mono- and binuclear nickel(II) complexes **II** and **V** were obtained by reaction of a solution of **I** in benzene with benzoyl chloride and isophthaloyl dichloride, respectively, in a 1:1 and 2:1 molar ratio in the presence of pyridine (see Experimental). Also, the mono- and binuclear nickel(II) complexes **VIII** and **XI** were obtained by reaction of **I** with phenylisocyanate and *m*-xylenediisocyanate, respectively, in a 1:1 and 2:1 molar ratio in methylene chloride at room temperature. These addition–insertion reactions were carried out almost quantitatively because the starting nickel(II) complex, **I**, and the isocyanate-containing compounds possess nucleophilic and electrophilic centres, respectively.[4]

The mononucleating (**III**, **IX**) and the binucleating (**VI**, **XII**) ligands can be obtained by the demetallation reaction of the corresponding nickel(II) complexes with aqueous Na_2EDTA,[29] (Fig. 1). These ligands can be formulated either as a cyclic pyrazoline, **XIV**, or an open chain hydrozone, **XVa**[26] (Fig. 2).

The ^1H NMR spectra of the isolated ligands in $CDCl_3$ (Table 2) show that these products exist mainly as the 5-hydroxy-2-pyrazolin-1-(S-methyl-carbodithioate), **XIV**, rather than the open chain

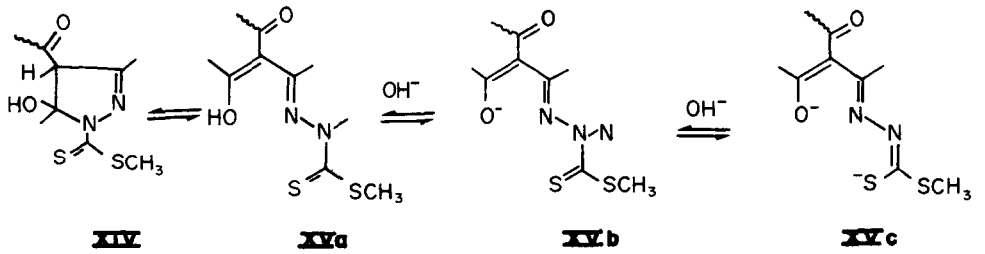

Fig. 2.

Schiff base, **XV**.[26] The electronic spectra of **III** at different values of pH provide evidence for the existence of an equilibrium between the cyclic, **XIV**, and open chain, **XV**, tautomers. By increasing the pH of the medium the equilibrium is shifted towards the formation of the dinegative anion **XVc**[26] (Fig. 2).

Remetallation of these ligands with copper(II) can be easily performed by reaction of **IV**, **IX** and **VI**, **XII** ligands with copper(II) acetate monohydrate in 1 : 1 and 1 : 2 molar ratios, respectively, in the presence of pyridine. The high affinity of such sulphur–nitrogen-containing ligands to copper, relative to nickel,[20] stimulates an interest to apply the transmetallation phenomenon[24,25] for the preparation of the mono- and binuclear copper(II) complexes **IV**, **VII**, **X** and **XIII**, to avoid the multi-step demetallation–remetallation route. The transmetallation reactions were carried out by mixing a stirred methylene chloride solution of the nickel(II) complexes with a methanolic solution of copper(II) acetate monohydrate* for 6 h at room temperature (see Experimental). The elemental analyses for the prepared ligands and complexes are given in Table 1. All the organic ligands and the nickel(II) and copper(II) complexes are quite stable at room temperature and do not show any sign of decomposition over long periods of time. All of the ligands and complexes do not possess sharp melting points but they decompose above 200°C.

Crystals suitable for X-ray crystallographic analysis have not been obtained to date. Cryoscopic measurements in nitrobenzene (Table 1) indicate that **VI** and **XII** are binucleating ligands and that **V**, **VII**, **XI** and **XIII** are all binuclear complexes.

The diffuse reflectance IR spectra of the reaction products of **I** with isocyanates, **VIII–XIII**, differ from those of the starting compounds, most notably in the absence of the intense band at 2250 cm^{-1} assignable to the ν(C=N) stretching mode of isocyanate. The IR spectra of all products, **II–XIII**, exhibit new strong broad absorptions either at *ca* 1700 cm^{-1} or *ca* 1640 cm^{-1} due to the ν(C=O) stretch of the carbonyl group in compounds **II–VII** and the amide NHCO group in compounds **VIII–**

* The metal(II) acetate is insoluble in methylene chloride which necessitated the use of methanol as the solvent in the transmetallation reaction.

Table 2. ^{1}H NMR spectra of mono- and binucleating ligands and their nickel(II) complexes in $CDCl_3$

	δ (ppm)							
Compound	SCH_3	CH_3C—O	CH_3C—N	C—H	N—H	O—H	CH_2	Aromatic H
I	2.43	2.20	1.90	5.08[a]	—	—	—	7.31–8.73
II	2.47	2.26	1.97	—	—	—	—	7.42–8.96
III	2.40	2.07	1.72	3.58	—	4.38	—	7.72–8.37
V	2.51	2.25	1.93	—	—	—	—	7.25–8.88
VI	2.38	2.11	1.78	3.52	—	4.35	—	7.64–8.52
VIII	2.54	2.28	1.94	—	9.62s	—	—	7.58–8.93
IX	2.43	2.09	1.80	3.55	9.48s	4.32	—	7.66–8.35
XI	2.53	2.27	1.96	—	9.67t[b]	—	4.30d[b]	7.39–8.86
XII	2.41	2.08	1.79	3.52	9.46t[b]	4.31	4.15d[b]	7.91–8.49

[a] Vinylic proton, s = singlet, d = doublet, t = triplet.
[b] J = 7 Hz.

XIII, respectively. The IR spectra of both **III** and **VI** ligands lack any absorption which can be attributed to N—H vibration modes. This gives further evidence for the formation of the 5-hydroxy-2-pyrazoline-1-(S-methylcarbodithioate) and excludes the possible formation of the open chain, **XV**, in the solid state. Based on the analogue of the reaction products of N,N-diacetylacetoneethylenediiminocopper(II) with isocyanates,[31] the weak sharp absorption in the IR spectra of compounds **VIII**–**XIII** at *ca* 3230 cm^{-1} can be assigned to the amide N—H stretch of the molecules. The IR spectra of metal(II) complexes show two strong but broad absorptions at *ca* 1570 and 1510 cm^{-1} which are attributed to the C⋯O and C⋯N stretching modes of the molecules. Similar spectral properties have been reported for other metal(II) Schiff base macrocycles.[2,4,32] In the far-IR region, all the metal(II) complexes show bands at *ca* 430, 390 and 280 cm^{-1} which are assigned to ν(M—O), ν(M—N) and ν(M—S) vibrations, respectively.[33,34]

The isolated nickel(II) complexes, **II**, **V**, **VIII** and **XI**, are diamagnetic in the solid state and in $CDCl_3$ solution (^{1}H NMR detectable) implying an $^1A_{1g}$ ground state.[35] The methylene chloride solution electronic spectra of these complexes (Table 1) exhibit *d–d* transitions at *ca* 400, 480 and 600 nm. No absorption was observed beyond 700 nm. Both magnetic and spectral data are consistent with a square planar arrangement of the N_2OS donor atoms around the nickel(II) ion.[26,36] The bands at *ca* 400 and 480 nm are assigned as ν_3 and ν_2, respectively.[35] The band at *ca* 600 nm is not always present in the spectra of square planar nickel(II) complexes, however, it is usually observed with complexes of sulphur ligands.[36] Indeed, the spectra of the Schiff base complexes (Table 1) are very similar to those of the nickel(II) complexes of sulphur ligands, the parent compound, **I**,[26] diethyl dithiophosphate, diethyl dithiocarbamate and ethylxanthate.[37] In fact, the spectra of the binuclear nickel(II) complexes **V** and **XI**, resemble those of the mononuclear complexes **II** and **VIII** and the parent nickel(II) complex **I**, so that the effects due to substitution and the formation of the binuclear species were not observed in the electronic spectra. The same observation was seen in the spectra of the binuclear copper(II) complexes **VII** and **XIII** and those of the mononuclear copper(II) complexes **IV** and **X** (Table 1).

The copper(II) complexes, **IV**, **VII**, **X** and **XIII**, are paramagnetic in the solid state and in solution. The room temperature effective magnetic moment of these complexes as a solid is $\simeq$ 1.85 BM/Cu centre (normal magnetic moment), which is consistent with other square planar copper(II) complexes.[38,39] The methylene chloride solution electronic spectra of these copper(II) complexes (Table 1) are typical of square planar copper(II) complexes and show a λ_{max} at *ca* 590 nm with a shoulder at *ca* 400 nm. These bands are assignable to *d–d* transitions and several bands in the UV region are assignable to L–L and charge-transfer bands. The solid-state spectra agree with the results obtained in solution, indicating that there is no change in coordination geometry as a result of solvent interactions.[40]

The ^{1}H NMR spectra of the **III**, **VI**, **IX** and **XII** ligands as well as their corresponding diamagnetic nickel(II) complexes, **II**, **V**, **VIII** and **XI**, were recorded in $CDCl_3$. Table 2 contains the ^{1}H NMR data and their respective assignments. The methine proton resonance of the acetylacetonato residue at δ 5.08 ppm appeared in the spectrum of the unsubstituted nickel(II) complexes, **I**, but disappeared in those of mononuclear **II** and **VIII** and in those of binuclear **V** and **XI** nickel(II) complexes and their demetallated products, **III**, **VI**, **IX** and **XII**, indicative of substitution. It was noted that the ^{1}H NMR spectra of all ligands and their nickel(II) complexes shows the —SCH_3 signal at δ 2.46 $\pm$ 0.08, which is essentially constant and independent of the rest of the molecule.[41,42] Two distinct singlets are observed for the free ligands, **III**, **VI**, **IX** and **XII**, and the nickel(II) complexes, **I**, **II**, **V**, **VIII** and **XI**, δ 2.07–2.28 and 1.72–1.97 ppm, which are assigned to the two inequivalent sets of methyl protons, CH_3C—O and CH_3C—N, respectively.

It is of interest to note that the chemical shifts of these methyl protons in the spectra of all nickel(II) complexes show a downfield shift compared with the corresponding organic ligands. This can be attributed to a quasi-aromatic character of the chelate ring and the resulting ring current could cause deshielding of the groups attached to the chelate ring. Similar deshielding effects were previously observed for many nickel(II) and palladium(II) chelates with sulphur-containing ligands.[41,43]

The ^{1}H NMR spectra of **XI** and **XII** show the resonance of the methylene protons of the *m*-xylene dicarbamoyl, as a bridging group, and the —SCH_3 protons at δ 4.15–4.30 ppm and δ 2.41–2.53 ppm, respectively. The ratio of the integrated intensities is 2 : 3, consistent with the formation of the binuclear species.

The N—H resonance, which disappeared on deuteration, is observed as a singlet at δ 9.62 and 9.48 ppm for **VIII** and **IX**, respectively, while in **XI** and **XII** it is observed as a triplet centred at δ 9.67 and 9.46 ppm, respectively. The chemical shifts of aromatic and pyridine protons appear as a series of multiplets at δ 6.9–8.9 ppm.

Table 3. ESR spectra of mono- and binuclear copper(II) complexes in methylene chloride

Compound	Temperature (K)	ESR parameters g_0 (A_0)[a]	$g_\parallel$ ($A_\parallel$)[a]	$g_\perp$	$\langle g \rangle$[b]	G[c]	Ground state
IV	298	2.09 (100)					
	11		2.21 (155)	2.05	2.10	4.20	$d_{x^2-y^2}$
VII	300	2.11 (95)					
	11		2.19 (140)	2.04	2.09	4.75	$d_{x^2-y^2}$
X	300	2.08 (97)					
	11		2.22 (150)	2.05	2.11	4.40	$d_{x^2-y^2}$
XIII	298	2.12 (94)					
	11		2.18 (135)	2.03	2.08	6.00	$d_{x^2-y^2}$

[a] Units are in 10^{-4} cm^{-1}.
[b] $\langle g \rangle = 1/3g_\parallel + 2/3g_\perp$.
[c] $G = (g_\parallel - 2)/(g_\perp - 2)$.

The X-band ESR spectra of mono- and binuclear copper(II) complexes, **IV**, **X**, **VII** and **XIII**, were measured in methylene chloride solution at ambient and liquid helium temperatures. The ESR spectral data are collected in Table 3. The room temperature ESR spectra of **IV**, **X**, **VII** and **XIII** are isotropic spectra with a four-line pattern ($g_0 \simeq 2.10$ and $A_0 \simeq 95 \times 10^{-4}$ cm^{-1}) observed for planar mononuclear copper(II) complexes and indicative of an electron interacting with only one copper nucleus. There are also no observable $\Delta M_s = 2$ transitions and no ligand hyperfine structure. Apparently, complexes **VII** and **XIII** exist as magnetic, noncoupled dimers in methylene chloride at room temperature. Even at 11 K the ESR spectra are consistent with a monomeric environment around each copper centre. The spectra are of axial symmetry with $g_\parallel > g_\perp$, small exchange coupling (G in the range of 4–6) and $d_{x^2-y^2}$ ground state (Table 3). This indicates square planar geometry around the copper(II) centre.[44] The rather low g values (Table 3) are typical of copper(II) chromophores containing sulphur ligands.[45] Five lines are clearly resolved on the perpendicular component, with an average spacing of 7×10^{-4} cm^{-1} indicating that the unpaired electron is interacting with two nitrogen nuclei.

CONCLUSIONS

Two new mononucleating, **III** and **IX**, and two new binucleating, **VI** and **XII**, ligands have been prepared and characterized. The four ligands form stable nickel(II) and copper(II) complexes. The spectral and magnetic properties of nickel(II) and copper(II) complexes are characteristic of a square planar ligand environment. No magnetic exchange was observed between the copper(II) centres in the solid state or in solution at room or liquid helium temperatures, indicating that the metal centres are magnetically isolated. Attempts to determine the flexibility of the binuclear system through the formation of adducts bridging both metal centres in these and other similar binuclear Schiff base complexes are in progress.

Acknowledgements—The author would like to thank Dr K. Z. Ismaiel for useful discussions, Dr M. Nelson for experimental assistance in obtaining ESR spectra and Dr T. R. Gilbert for performing the nickel and copper analysis at Northeastern University, Boston (U.S.A.).

REFERENCES

1. M. S. Mashuta, R. M. Buchanan and W. Pierce, *Inorg. Chim. Acta* 1989, **158**, 227.

2. M. S. Mashuta, T. N. Doman, W. Pierce and R. M. Buchanan, *Inorg. Chim. Acta* 1988, **145**, 21.
3. G. Davies, N. El-Kady, M. A. El-Sayed and A. El-Toukhy, *Inorg. Chim. Acta* 1985, **104**, 131.
4. N. Matsumoto, M. Asakawa, H. Nogami and A. Ohyoshi, *Inorg. Chim. Acta* 1985, **96**, 87.
5. T. N. Sorell, Binuclear Copper Complexes: Synthetic Models for the Active Site of Type III Copper Proteins, in *Biological and Inorganic Copper Chemistry* (Edited by K. D. Karlin and J. A. Zubieta), Vol. 2, p. 41. Academic Press, Guilderland, New York (1986): J. S. Thompson, Copper–Dioxygen Chemistry. Synthesis, Properties and Reactions of Cu(II)–Superoxide and –Peroxide Complexes, in *Biological and Inorganic Copper Chemistry*, Vol. 2, p. 1. Academic Press, Guilderland, New York (1986).
6. N. Herron, W. P. Schammel, S. C. Jackels, J. J. Grybowski, L. L. Zimmer and D. H. Busch, *Inorg. Chem.* 1983, **22**, 1433; J. E. Bulkowski, M. F. Ludmann and J. A. Osborn, *J. Chem. Soc., Chem. Commun.* 1977, 498; M. Suzuki, H. Kanatomi and I. Murase, *Chem. Lett.* 1981, 1745.
7. N. E. Kagan, D. Mauzerall and R. B. Merrifield, *J. Am. Chem. Soc.* 1977, **99**, 5484; M. R. Wasielewski, W. A. Svec and B. T. Cope, *J. Am. Chem. Soc.* 1978, **100**, 1961; E. I. Solomon, K. W. Penfield and D. E. Wilcox, *Struct. Bonding (Berlin)* 1983, **53**, 1.
8. M. Pasquale, C. Floriani, G. Venturi, A. G. Manfredotti and A. Chiesi-Villa, *J. Am. Chem. Soc.* 1982, **104**, 4092.
9. K. G. Caulton, G. V. Goeden, T. H. Lemmen, L. F. Rhodes and J. C. Huffman, Rational Syntheses of Copper Polyhydride Complexes (see ref. 5, p. 259).
10. M. G. Simmons, C. L. Merrill, L. J. Wilson, L. A. Bottomley and K. M. Kadish, *J. Chem. Soc., Dalton Trans.* 1980, 1827.
11. M. A. El-Sayed, A. El-Toukhy and G. Davies, *Inorg. Chem.* 1985, **24**, 3387.
12. R. R. Durand, C. S. Bencosme, J. P. Collman and F. C. Anson, *J. Am. Chem. Soc.* 1983, **105**, 2710.
13. J. P. Gisselbrecht, M. Gross, A. H. Alberts and J. M. Lehn, *Inorg. Chem.* 1980, **19**, 1386.
14. M. M. Rogic and T. R. Demmin, *J. Am. Chem. Soc.* 1978, **100**, 5472.
15. W. E. Hatfield, *Comments Inorg. Chem.* 1981, **1**, 105.
16. Melnik, *Coord. Chem. Rev.* 1982, **42**, 259.
17. D. E. Fenton, Copper(II) Complexes of Schiff Base Ligands Derived from Pyrrole-2,5-dicarboxyaldehyde and from 2-acetoacetylpyrrole (see ref 5, p. 179).
18. E. Sinn, Structures and Properties of Homo- and Hetero-binuclear and Polynuclear Complexes Containing Copper (see ref. 5, p. 195).
19. J. Eilmes, *Polyhedron* 1985, **4**, 943.
20. K. Kasuga, H. Kuramitsu, M. Kadowaki, T. Nagahara and Y. Yamamoto, *Bull. Chem. Soc. Japan* 1986, **59**, 1467.
21. M. Cusumano and A. Giannetto, *Inorg. Chim. Acta* 1988, **142**, 85.
22. B. Corain, E. Scanagatta, M. Basato, G. Valle, S. Sitran and A. C. Veronese, *Inorg. Chim. Acta* 1988, **148**, 105.
23. M. Basato, B. Corain, G. Favero, G. Valle and J. Eilmes, *Inorg. Chim. Acta* 1989, **159**, 59.
24. A. El-Toukhy, G. Z. Cai, G. Davies, T. R. Gilbert, K. D. Onan and M. Veidis, *J. Am. Chem. Soc.* 1984, **106**, 4596.
25. G. Davies, M. A. El-Sayed and A. El-Toukhy, *Comments Inorg. Chem.* 1989, **8**, 203.
26. M. F. Iskander, L. El-Sayed, A. El-Toukhy and M. Tawfik, *Transition Met. Chem.* 1982, **7**, 135.
27. J. E. Wertz and J. R. Bolton, *Electron Spin Resonance*. McGraw Hill, New York (1972).
28. R. S. Drago, *Physical Methods in Chemistry*. W. B. Saunders, Philadelphia (1977).
29. L. El-Sayed, A. El-Toukhy, N. El-Kady and M. F. Iskander, *Transition Met. Chem.* 1080, **5**, 293.
30. G. Davies, M. A. El-Sayed, A. El-Toukhy, M. Henary, T. S. Kasem and C. A. Martin, *Inorg. Chem.* 1986, **25**, 3904.
31. P. N. Howells, J. W. Kenney, J. H. Nelson and R. A. Henry, *Inorg. Chem.* 1976, **15**, 124.
32. E. Sinn and C. M. Harris, *Coord. Chem. Rev.* 1969, **4**, 391.
33. D. M. Adams, *Metal–Ligand and Related Vibrations*. Edward Arnold, London (1979).
34. K. Nakamoto, *Infrared and Raman Spectra of Inorganic and Coordination Compounds*, 3rd edn. Wiley-Interscience, New York (1978).
35. A. B. P. Lever, *Inorganic Electronic Spectroscopy*, pp. 318, 333. Elsevier, Amsterdam (1968).
36. (a) S. E. Livingston and J. E. Oluka, *Transition Met. Chem.* 1977, **2**, 163; (b) *Transition Met. Chem.* 1977, **2**, 190.
37. C. K. Jorgensen, *J. Inorg. Nucl. Chem.* 1962, **24**, 1571.
38. Y. Nishida and S. Kida, *Coord. Chem. Rev.* 1979, **27**, 275.
39. M. F. Iskander, L. El-Sayed and A. El-Toukhy, *J. Inorg. Nucl. Chem.* 1980, **42**, 1145.
40. (a) K. Ueno and A. E. Martell, *J. Phys. Chem.* 1955, **59**, 998; (b) A. E. Martell, R. L. Belford and M. Calvin, *Inorg. Chem.* 1958, **5**, 170.
41. M. F. Iskander, M. M. Mishrikey, L. El-Sayed and A. El-Toukhy, *J. Inorg. Nucl. Chem.* 1979, **41**, 815.
42. D. Gattegno and A. M. Giuliani, *J. Inorg. Nucl. Chem.* 1974, **36**, 1553.
43. A. R. Hendricks and R. L. Martin, *Inorg. Chem.* 1975, **14**, 914.
44. B. J. Hathaway and A. A. G. Tomlinson, *Coord. Chem. Rev.* 1970, **5**, 1.
45. A. W. Addison, T. N. Rao and E. Sinn, *Inorg. Chem.* 1984, **23**, 1957; L. Casella, M. Gullotti and R. Vigano, *Inorg. Chim. Acta* 1986, **124**, 121.

Polyhedron Vol. 10, No. 6, pp. 543–551, 1991
Printed in Great Britain

0277–5387/91 $3.00+.00
© 1991 Pergamon Press plc

SYNTHESIS OF PHOSPHIDO-BRIDGED MULTINUCLEAR COMPLEXES VIA A MONONUCLEAR RHODIUM(I) COMPOUND: X-RAY STRUCTURES OF $Rh_3H(COD)_2(\mu\text{-}CO)_2\{\mu\text{-}P(t\text{-}Bu)_2\}_2$ AND $[Fe(CO_3)](\mu\text{-}CO)\{\mu\text{-}P(t\text{-}Bu)_2\}[Rh(CO)\{HP(t\text{-}Bu)_2\}]$ (COD = 1,5-CYCLOOCTADIENE)

ATTA M. ARIF, DUANE E. HEATON and RICHARD A. JONES*

Department of Chemistry, The University of Texas at Austin, Austin, TX 78712, U.S.A.

(*Received* 19 *July* 1990; *accepted* 22 *October* 1990)

Abstract—The mononuclear rhodium(I) complex *trans*-$RhCl(CO)\{HP(t\text{-}Bu)_2\}_2$ (**1**) was used to form multinuclear complexes with $P(t\text{-}Bu)_2$ bridges. Reaction of **1** with n-BuLi in THF yields yellow–orange crystalline $[Rh(CO)\{HP(t\text{-}Bu)_2\}]_2(\mu\text{-}H)\{\mu\text{-}P(t\text{-}Bu)_2\}$ (**2**) (74%). Reaction of a mixture of **1** and $[Rh(COD)Cl]_2$ (COD = 1,5-cyclooctadiene) with n-BuLi in THF produces orange $[Rh(COD)](\mu\text{-}H)\{\mu\text{-}P(t\text{-}Bu)_2\}[Rh(CO)\{HP(t\text{-}Bu)_2\}]$ (**3**) (46%) and dark red $Rh_3H(COD)_2(\mu\text{-}CO)_2\{\mu\text{-}P(t\text{-}Bu)_2\}_2$ (**4**) (25%). Reaction of **1** with $Fe(CO)_5$ in refluxing toluene yields orange crystalline $[Fe(CO)_3](\mu\text{-}CO)\{\mu\text{-}P(t\text{-}Bu)_2\}[Rh(CO)\{HP(t\text{-}Bu)_2\}]$ (**5**) (85%). The structures of **4** and **5** have been determined by X-ray crystallography. Complex **2** has been described elsewhere. The proposed structure of **3** has a planar core with a $P(t\text{-}Bu)_2$ unit and a hydride bridging a metal–metal bond. One rhodium atom is further coordinated by a COD (1,5-cyclooctadiene) ligand, while the other rhodium atom bears a CO group and an $HP(t\text{-}Bu)_2$ ligand. The molecular structure of **4** consists of a linear arrangement of three rhodium atoms with single metal–metal bonds bridged by $P(t\text{-}Bu)_2$ and CO groups. The terminal rhodium atoms are coordinated by COD ligands. The molecular structure of **5** consists of a mixed metal dinuclear complex with a single Fe—Rh bond bridged by a $P(t\text{-}Bu)_2$ unit and a CO group in a butterfly configuration. The rhodium atom is further coordinated by a CO and an $HP(t\text{-}Bu)_2$ ligand. The iron atom bears three terminal CO groups.

There has been increased interest in the synthesis of multinuclear transition metal complexes because of their potential as homogeneous catalysts, as models for heterogeneous catalysts, and as reagents for specific stoichiometric transformations.[1–3] Much attention has recently been focused on the potential of the phosphide (R_2P^-) ligand as a building block for multinuclear complexes due to its tendency to act as a bridging ligand and its ability to tolerate a wide range of metals and bonding situations.[4]

One method for preparing multinuclear complexes from mononuclear species involves deprotonation of a coordinated secondary phosphine followed by reaction with a transition metal halide.

$$L_nMPR_2H + \text{n-BuLi} \longrightarrow L_nMPR_2Li + \text{n-BuH}$$

$$L_nMPR_2Li + L_nM'X \longrightarrow L_nM(\mu\text{-}PR_2)M'L_n + LiX$$

L = ancilliary ligands; X = halide.

This approach has proven particularly useful in the synthesis of heterobimetallic complexes. For example, Geoffroy and co-workers, using $W(CO)_4(PPh_2H)_2$, have prepared a series of mixed metal complexes of the general formula $(CO)_4W(\mu\text{-}PPh_2)_2ML_x$ [$ML_x = Re(CO)_3CH_3$, $RhH(CO)(PPh_3)$, $IrH(CO)(PPh_3)$, IrH(COD), $Pt(PPh_3)$, $ZrCp_2$, $Os(CO)_3$], many of which have displayed unusual reaction chemistry.[5] Similarly, $Fe(CO)_3\{HP(t\text{-}Bu)_2\}_2$ may be used to prepare a series of novel Fe—Rh complexes of formula $[Fe(CO)_2L](\mu\text{-}CO)\{\mu\text{-}P(t\text{-}Bu)_2\}[RhL'L'']$ [$L = HP(t\text{-}Bu)_2$,

* Author to whom correspondence should be addressed.

Scheme

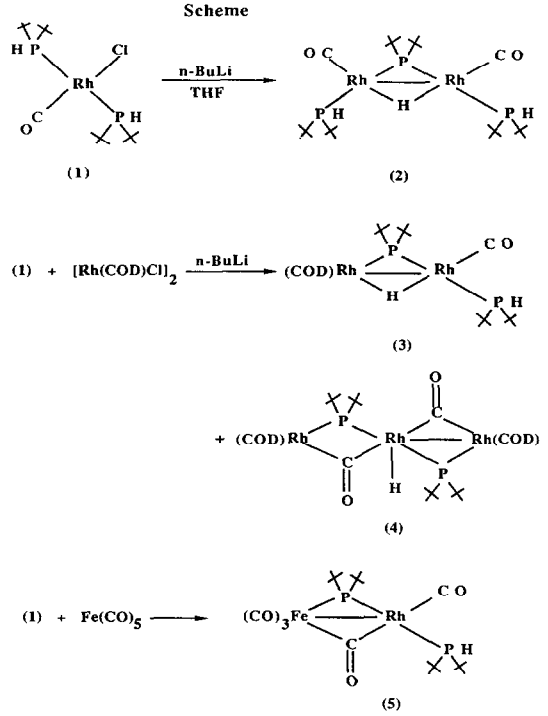

Scheme 1.

L′L″ = COD (1,5-cyclooctadiene), $(CO)_2$; L = PMe_3, L′ = PMe_3, L″ = PMe_3, CO].[6,7]

As part of a programme to investigate steric and electronic effects in transition metal phosphides (R_2P^-) we have studied multinuclear complexes containing the sterically demanding μ-P(t-Bu)$_2$ ligand. In this paper we describe studies of the mononuclear, late transition metal rhodium(I) complex *trans*-RhCl(CO){HP(t-Bu)$_2$}$_2$ (**1**)[8] (see Scheme 1). The reaction of n-BuLi with **1** produces the dirhodium complex [Rh(CO){HP(t-Bu)$_2$}]$_2$(μ-H){μ-P(t-Bu)$_2$} (**2**), which was previously synthesized via a different route.[9] A mixture of **1** and [Rh(COD)Cl]$_2$ reacts with n-BuLi to produce the asymmetric dinuclear complex [Rh(COD)](μ-H){μ-P(t-Bu)$_2$}[Rh(CO){HP(t-Bu)$_2$}] (**3**) and the unusual linear trinuclear complex $Rh_3H(COD)_2(\mu\text{-}CO)_2\{\mu\text{-}P(t\text{-}Bu)_2\}_2$ (**4**). The reaction of **1** with $Fe(CO)_5$ in boiling toluene produces the mixed metal complex [Fe(CO)$_3$](μ-CO){μ-P(t-Bu)$_2$}[Rh(CO){HP(t-Bu)$_2$}] (**5**). This paper describes the synthesis and characterization of **2**–**5**, and the X-ray crystal structures of **4** and **5**.

RESULTS AND DISCUSSION

Synthesis of [Rh(CO){HP(t-Bu)$_2$}]$_2$(μ-H){μ-P(t-Bu)$_2$} (**2**)

Reaction of *trans*-RhCl(CO){HP(t-Bu)$_2$}$_2$ (**1**) with n-BuLi in THF at 25°C produces an orange solution from which the dinuclear complex [Rh(CO){HP(t-Bu)$_2$}]$_2$(μ-H){μ-P(t-Bu)$_2$} (**2**) can be isolated following chromatography as yellow–orange solvent-dependent crystals in *ca* 71% yield. This complex has been previously described and is formed as a product of the reaction of $Rh_4(CO)_{12}$ with HP(t-Bu)$_2$ in refluxing toluene.[9] Spectroscopic data for **2** were in accord with those previously described.[9]

Although the actual mechanistic pathway by which **2** is formed is not clear, it must involve removal of chloride as well as the loss of hydrogen from a phosphine HP(t-Bu)$_2$ unit. In an effort to prepare complexes of higher nuclearity, the use of n-BuLi was investigated with a mixture of **1** and [Rh(COD)Cl]$_2$.

Synthesis of [Rh(COD)](μ-H){μ-P(t-Bu)$_2$}[Rh(CO){HP(t-Bu)$_2$}] (**3**) *and* $Rh_3H(COD)_2(\mu\text{-}CO)_2\{\mu\text{-}P(t\text{-}Bu)_2\}_2$ (**4**)

Reaction of a mixture of **1** and [Rh(COD)Cl]$_2$ (COD = 1,5-cyclooctadiene) with n-BuLi in THF at 25°C produces a deep red solution from which the dinuclear complex [Rh(COD)](μ-H){μ-P(t-Bu)$_2$}[Rh(CO){HP(t-Bu)$_2$}] (**3**) and the linear trinuclear complex $Rh_3H(COD)_2(\mu\text{-}CO)_2\{\mu\text{-}P(t\text{-}Bu)_2\}_2$ (**4**) can be isolated as orange and red crystals following chromatography. Complex **3** represents one in a series of isostructural complexes of rhodium and iridium recently characterized, with the general formula [MLL′](μ-H){μ-P(t-Bu)$_2$}[ML″L‴] (M = Rh, Ir; L,L′,L″,L‴ = two-electron donor ligand). Other complexes in this series include [Ir(CO){HP(t-Bu)$_2$}]$_2$(μ-H){μ-P(t-Bu)$_2$},[10] [Ir(CO)$_2$](μ-H){μ-P(t-Bu)$_2$}[Ir(CO){HP(t-Bu)$_2$}][10] and complex **2**. These complexes generally consist of a central metal–phosphorus core with a metal–metal bond bridged by a P(t-Bu)$_2$ ligand and a hydride; the metal atoms are further coordinated by two two-electron donor ligands producing square-planar geometry about each metal. Unfortunately, crystals of **3** were unsuitable for X-ray crystallographic studies.

The structure of **3** is assigned on the basis of spectroscopic data and the IR spectrum contains a terminal ν(CO) absorption (1944 cm^{-1}) in addition to weak ν(P—H) and ν(Rh—H) peaks at 2305 and 1891 cm^{-1}, respectively. The ^{1}H NMR spectrum contains a signal assigned to the *H*P(t-Bu)$_2$ proton [δ 4.57, ^1J(P—H) = 306 Hz] and an upfield multiplet indicative of a μ-*H* proton (δ −10.85). The $^{31}P\{^1H\}$ NMR spectrum consists of a doublet of doublets in the region expected for a coordinated phosphine [δ 56.2, ^2J(P—P) = 196 Hz, ^1J(Rh—P) = 121 Hz] and a doublet of doublets of

doublets in the region expected for a phosphido group bridging a metal–metal bond [δ 226.0, ^2J(P—P) = 196 Hz, ^1J(Rh—P) = 140 Hz, ^1J(Rh—P) = 110 Hz].[11] Both signals show coupling to each other as well as the appropriate number of rhodium atoms. Unfortunately, crystals of **3** were unsuitable for X-ray crystallographic studies.

For complex **4**, spectroscopic data are in accord with the structure as determined by X-ray crystallography and the IR spectrum exhibits bands in the regions expected for a terminal hydride (1947 cm^{-1}) and bridging carbonyl groups (1832 cm^{-1}). The ^1H NMR of **4** exhibits a multiplet shifted upfield in the region expected for a hydride (δ −8.35). The $^{31}P\{^1H\}$ NMR of **4** in C_6D_6 (ambient temperature) shows a broad multiplet shifted well down field (δ 228.2) indicative of phosphido groups bridging metal–metal bonds.[12]

Table 1. Selected bond lengths (Å) for complex **4**

Rh(1)—Rh(2)	2.818(2)	P(1)—C(10)	1.87(2)
Rh(1)—P(1)	2.296(5)	P(1)—C(14)	1.92(3)
Rh(1)—C(1)	2.19(5)	O(1)—C(1)	1.35(7)
Rh(2)—P(1)	2.275(5)		
Rh(2)—C(1)	1.94(5)		
Rh(2)—C(2)	2.24(3)		
Rh(2)—C(3)	2.25(2)		
Rh(2)—C(6)	2.10(2)		
Rh(2)—C(7)	2.16(2)		

Numbers in parentheses are ESDs in the least significant digits.

X-ray structure of **4**

Molecules of **4** crystallize in the monoclinic space group $P2_1/n$ with two molecules in the unit cell. Figure 1 shows the molecular geometry and atom numbering scheme and selected bond lengths and angles are given in Tables 1 and 2, respectively. The structure of **4** was successfully solved with each molecule possessing a centre of inversion at Rh(1).

The core of **4** contains a precisely linear arrangement of three singly-bonded rhodium atoms with each bond bridged by a μ-P(t-Bu)$_2$ unit and a carbonyl ligand. Due to the centre of inversion, the μ-P(t-Bu)$_2$ groups are *trans* to each other through Rh(1), as are the μ-CO groups. The two terminal rhodium atoms are each coordinated to a 1,5-cyclooctadiene ligand and the molecule thus has a planar core consisting of the three rhodium atoms, the two phosphorus atoms and the two carbonyl groups. Hydrogen atoms were not located in the structure and so the location of the single hydride ligand cannot be determined unequivocally. A model involving crystals of **4** which contain equal amounts of the hydride bridging Rh(1)—Rh(2) as well as Rh(1)—Rh(2)′ would be consistent with the crystallographically imposed symmetry of the molecule. Although simple electron counting procedures are often misleading, if one arbitrarily assigns the single Rh—H to Rh(1) then each rhodium atom is formally rhodium(I); the terminal rhodium atoms, Rh(2) and Rh(2)′, would then have electron counts of 16, while Rh(1) would have 18 electrons. The two Rh—Rh bond distances

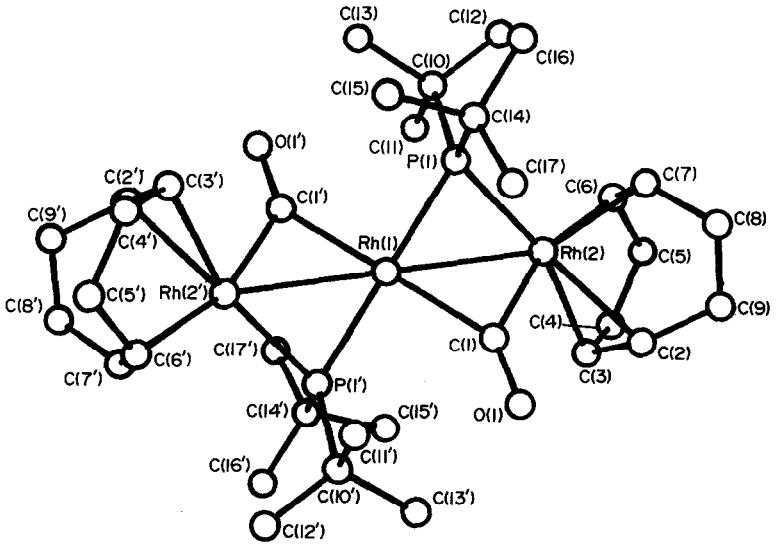

Fig. 1. View of **4** showing the atom numbering scheme.

Table 2. Selected bond angles (°) for complex **4**

Rh(2)—Rh(1)—P(1)	51.6(1)	C(1)—Rh(2)—C(7)	144.(2)
Rh(2)—Rh(1)—C(1)	43.(1)	C(2)—Rh(2)—C(3)	37.(1)
P(1)—Rh(1)—C(1)	89.(1)	C(2)—Rh(2)—C(6)	88.(1)
Rh(1)—Rh(2)—P(1)	52.3(1)	C(2)—Rh(2)—C(7)	80.(1)
Rh(1)—Rh(2)—C(1)	51.(2)	C(3)—Rh(2)—C(6)	83.2(9)
Rh(1)—Rh(2)—C(2)	124.5(8)	C(3)—Rh(2)—C(7)	98.9(9)
Rh(1)—Rh(2)—C(3)	109.1(7)	C(6)—Rh(2)—C(7)	38.8(9)
Rh(1)—Rh(2)—C(6)	141.5(6)	Rh(1)—P(1)—Rh(2)	76.1(2)
Rh(1)—Rh(2)—C(7)	151.9(6)	Rh(1)—P(1)—C(10)	120.1(8)
P(1)—Rh(2)—C(1)	97.(2)	Rh(1)—P(1)—C(14)	112.0(8)
P(1)—Rh(2)—C(2)	160.7(8)	Rh(2)—P(1)—C(10)	118.9(7)
P(1)—Rh(2)—C(3)	157.3(7)	Rh(2)—P(1)—C(14)	112.4(7)
P(1)—Rh(2)—C(6)	104.2(6)	C(10)—P(1)—C(14)	113.(1)
P(1)—Rh(2)—C(7)	100.0(6)	Rh(1)—C(1)—Rh(2)	86.(2)
C(1)—Rh(2)—C(2)	74.(2)	Rh(1)—C(1)—O(1)	137.(4)
C(1)—Rh(2)—C(3)	75.(2)	Rh(2)—C(1)—O(1)	137.(4)
C(1)—Rh(2)—C(6)	158.(2)		

Numbers in parentheses are ESDs in the least significant digits.

[2.818(2) Å] are within normal limits for a Rh—Rh single bond. The Rh—P distances [2.296(5) and 2.275(5) Å] and the Rh—C(1) distances [2.19(5) and 1.94(5) Å] are also typical of those for phosphido and carbonyl groups bridging a Rh—Rh bond, and all other structural parameters for the molecule fall within reasonable limits.

There are few structurally characterized examples of open phosphido-bridged trinuclear complexes and, to the best of our knowledge, **4** represents the first with an accurately linear metal core. Some other examples of such compounds and the angle between the three metal atoms are as follows: $[Rh\{Fe(\mu\text{-}PPh_2)(\mu\text{-}CO)_2(\eta^5\text{-}C_5H_4Me)\}_2]^+$ [145.03(5)°],[13] $Fe_3(\mu\text{-}PMe_2)_3(CO)_4(NO)_3$ [160.1(3)°],[11] $Fe_2Co(\mu\text{-}PMe_2)_3(CO)_5(NO)_2$ [161.1(2)°][11] and $PtMn_2(\mu\text{-}PPh_2)_2(CO)_9$ [159.56(4)°].[14]

Synthesis of $[Fe(CO)_3](\mu\text{-}CO)\{\mu\text{-}P(t\text{-}Bu)_2\}[Rh(CO)\{HP(t\text{-}Bu)_2\}]$ (**5**)

Reaction of **1** with $Fe(CO)_5$ in boiling toluene produces a red–black solution from which the mixed metal dinuclear complex $[Fe(CO)_3](\mu\text{-}CO)\{\mu\text{-}P(t\text{-}Bu)_2\}[Rh(CO)\{HP(t\text{-}Bu)_2\}]$ (**5**) can be isolated as red–orange crystals following chromatography in *ca* 85% yield. Spectroscopic data for **5** are in accord with the structure as determined by X-ray crystallography, and the IR spectrum exhibits bands in the regions expected for terminal carbonyl groups, a bridging carbonyl group (1843 cm^{-1}) and a P—H unit (2310 cm^{-1}). The ^1H NMR of **5** exhibits a signal corresponding to the proton on the coordinated phosphine [δ 4.398, $^1J(P—H) = 312$ Hz]. The $^{31}P\{^1H\}$ NMR of **5** shows two doublets of doublets one of which is shifted well down field (δ 220.9) indicative of a phosphido group bridging a metal–metal bond.[12] The other multiplet (δ 62.6) is in the region expected for a coordinated phosphine ligand.

This complex represents one in a series of μ-P(t-Bu)$_2$ bridged Fe—Rh dinuclear complexes which include $[Fe(CO)_2(HP(t\text{-}Bu)_2)](\mu\text{-}CO)\{\mu\text{-}P(t\text{-}Bu)_2\}[Rh(COD)]$ (COD = η^4-1,5-cyclooctadiene),[6] $[Fe(CO)_2\{HP(t\text{-}Bu)_2\}](\mu\text{-}CO)\{\mu\text{-}P(t\text{-}Bu)_2\}[Rh(CO)_2]$,[7] $[Fe(CO)_2(PMe_3)](\mu\text{-}CO)\{\mu\text{-}P(t\text{-}Bu)_2\}[Rh(PMe_3)_2]$[7] and $[Fe(CO)_2(PMe_3)](\mu\text{-}CO)\{\mu\text{-}P(t\text{-}Bu)_2\}[Rh(CO)(PMe_3)]$[7] and these compounds appear to be isostructural with **5**.

X-ray structure of **5**

Molecules of **5** crystallize in the monoclinic space group $P2_1/a$ with four molecules in the unit cell. Figure 2 shows the molecular geometry and atom numbering scheme of complex **5**, and selected bond lengths and angles are given in Tables 3 and 4, respectively. The overall molecular geometry contains a single Fe—Rh bond [Fe—Rh = 2.670(1) Å] which is bridged by a μ-P(t-Bu)$_2$ group and a semibridging CO ligand [C(4)—O(4)] in a butterfly configuration. The Fe(1)—C(4)—O(4) angle of 157.5(8)° and the Fe(1)—C(4) distance of 1.840(9) Å indicate only a slight degree of bonding to the rhodium atom. Thus, the Rh(1)—C(4) distance is relatively long [2.268(9) Å] and the Rh(1)—C(4)—O(4) angle relatively acute [121.5(7)°]. The

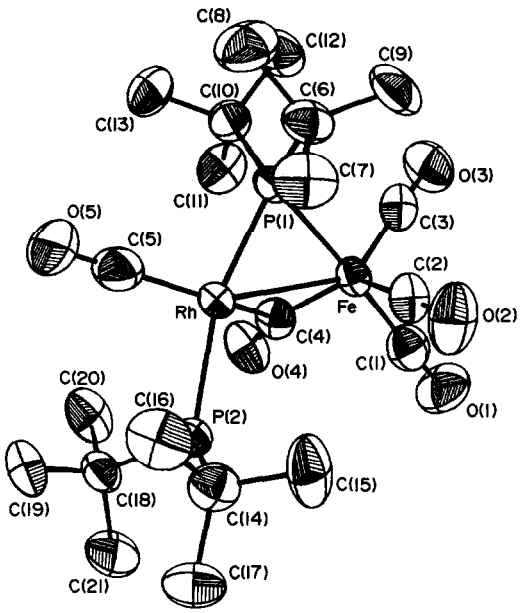

Fig. 2. ORTEP view of **5** showing the atom numbering scheme.

Table 3. Selected bond lengths (Å) for complex **5**

Rh(1)—Fe(1)	2.670(1)	P(1)—C(6)	1.921(10)
Rh(1)—P(1)	2.262(2)	P(1)—C(10)	1.915(9)
Rh(1)—P(2)	2.355(2)	P(2)—C(14)	1.877(10)
Rh(1)—C(4)	2.268(9)	P(2)—C(18)	1.874(9)
Rh(1)—C(5)	1.815(10)	O(1)—C(1)	1.134(12)
Fe(1)—P(1)	2.301(3)	O(2)—C(2)	1.136(13)
Fe(1)—C(1)	1.795(10)	O(4)—C(4)	1.165(11)
Fe(1)—C(2)	1.807(10)	O(5)—C(5)	1.147(13)
Fe(1)—C(3)	1.779(10)		
Fe(1)—C(4)	1.840(9)		

Numbers in parentheses are ESDs in the least significant digits.

coordination geometry about iron, ignoring the Fe—Rh bond, is roughly trigonal bipyramidal and the μ-P(t-Bu)$_2$ group occupies an axial position *trans* to a terminal carbonyl ligand [C(1)—O(1); P(1)—Fe(1)—C(1) = 175.3(3)°]. The two remaining terminal carbonyl groups and the semi-bridging CO ligand are virtually co-planar and occupy the equatorial positions around the iron atom with the sum of the angles subtended about iron = 359.7°. The rhodium atom of **5** has a roughly square-planar coordination geometry with the μ-P(t-Bu)$_2$ group and the HP(t-Bu)$_2$ ligand *trans* to each other [P(1)—Rh(1)—P(2) = 164.32(8)°]. The Fe(1)—Rh(1) distance as well as the Fe(1)—P(1) and Rh(1)—P(1) distances are normal [Fe(1)—P(1) = 2.301(3) Å, Rh(1)—P(1) = 2.262(2) Å] and can be compared along with all other structural parameters to those found in similar complexes.[6,7]

EXPERIMENTAL

All reactions were performed under oxygen-free nitrogen or *in vacuo*. Hexane, THF and toluene

Table 4. Selected bond angles (°) for complex **5**

Fe(1)—Rh(1)—P(1)	54.86(7)	C(1)—Fe(1)—C(3)	92.1(5)
Fe(1)—Rh(1)—P(2)	110.53(7)	C(1)—Fe(1)—C(4)	85.2(4)
Fe(1)—Rh(1)—C(4)	42.8(2)	C(2)—Fe(1)—C(3)	110.7(4)
Fe(1)—Rh(1)—C(5)	153.6(4)	C(2)—Fe(1)—C(4)	134.1(4)
P(1)—Rh(1)—P(2)	164.32(8)	C(3)—Fe(1)—C(4)	114.9(4)
P(1)—Rh(1)—C(4)	81.3(2)	Rh(1)—P(1)—Fe(1)	71.65(8)
P(1)—Rh(1)—C(5)	99.4(4)	Rh(1)—P(1)—C(6)	117.7(3)
P(2)—Rh(1)—C(4)	90.7(2)	Rh(1)—P(1)—C(10)	117.9(3)
P(2)—Rh(1)—C(5)	95.6(4)	Fe(1)—P(1)—C(6)	117.0(3)
C(4)—Rh(1)—C(5)	137.3(4)	Fe(1)—P(1)—C(10)	116.6(3)
Rh(1)—Fe(1)—P(1)	53.49(6)	C(6)—P(1)—C(10)	111.0(4)
Rh(1)—Fe(1)—C(1)	124.1(3)	Rh(1)—P(2)—C(14)	112.0(3)
Rh(1)—Fe(1)—C(2)	91.7(3)	Rh(1)—P(2)—C(18)	118.1(3)
Rh(1)—Fe(1)—C(3)	138.7(3)	C(14)—P(2)—C(18)	112.9(4)
Rh(1)—Fe(1)—C(4)	56.8(3)	Fe(1)—C(1)—O(1)	176.(1)
P(1)—Fe(1)—C(1)	175.3(3)	Fe(1)—C(2)—O(2)	172.7(9)
P(1)—Fe(1)—C(2)	96.2(3)	Rh(1)—C(4)—Fe(1)	80.4(3)
P(1)—Fe(1)—C(3)	88.8(3)	Rh(1)—C(4)—O(4)	121.5(7)
P(1)—Fe(1)—C(4)	90.2(3)	Fe(1)—C(4)—O(4)	157.5(8)
C(1)—Fe(1)—C(2)	87.8(5)	Rh(1)—C(5)—O(5)	175.(1)

Numbers in parentheses are ESDs in the least significant digits.

were dried over sodium and distilled from sodium–benzophenone under nitrogen before use. Instruments: IR, Perkin–Elmer 1330, Digilab FTS-40; NMR, Varian EM-390 (^{1}H 90 MHz), Nicolet NT 360 (^{1}H), FT-80 (^{31}P, 32.384 MHz), GE QE-300 (^{1}H, ^{31}P). IR spectra were run as Nujol mulls by using NaCl disks or in solution (matched KBr cells). NMR spectra were recorded in C_6D_6 at ambient temperature unless otherwise stated and are in ppm referenced to Me_4Si (δ 0.0, ^{1}H) and 85% H_3PO_4(aq.) (δ 0.0, ^{31}P). Melting points were obtained in sealed capillaries under nitrogen (1 atm) and are uncorrected. Complex **1**[8] and $[Rh(COD)Cl]_2$[15] were prepared as previously described.

Synthesis of $[Rh(CO)\{HP(t\text{-}Bu)_2\}]_2(\mu\text{-}H)\{\mu\text{-}P(t\text{-}Bu)_2\}$ **(2)**

To a solution of *trans*-$RhCl(CO)\{HP(t\text{-}Bu)_2\}_2$ **(1)** (0.23 g, 0.50 mmol) in THF (40 cm^3) at room temperature was added n-BuLi (0.42 cm^3 of a 2.4 M hexane solution, 1.0 mmol) dropwise with a syringe. The solution darkened immediately and was left to stir for 1 h. Volatile materials were removed *in vacuo* and the residue was extracted with hexane (2×15 cm^3). The filtered combined extracts were concentrated *in vacuo* (*ca* 15 cm^3) and passed down a column of alumina (4 cm × 3 cm) using hexane as the eluent, giving a yellow–orange band which was collected. The solution was concentrated *in vacuo* (*ca* 10 cm^3) and cooled (−40°C), producing yellow–orange, solvent-dependent crystals of **2** which were collected and dried *in vacuo*. Yield 0.13 g, 74.0%, based on rhodium.

Synthesis of $[Rh(COD)](\mu\text{-}H)\{\mu\text{-}P(t\text{-}Bu)_2\}[Rh(CO)\{HP(t\text{-}Bu)_2\}]$ **(3)** *and* $Rh_3H(COD)_2(\mu\text{-}CO)_2\{\mu\text{-}P(t\text{-}Bu)_2\}_2$ **(4)**

To a mixture of *trans*-$RhCl(CO)\{HP(t\text{-}Bu)_2\}_2$ **(1)** (0.19 g, 0.41 mmol) and $[Rh(COD)Cl]_2$ (0.30 g, 0.61 mmol) in THF (40 cm^3) at room temperature was added n-BuLi (0.49 cm^3 of a 3.3 M hexane solution, 1.63 mmol) dropwise with a syringe. The solution immediately darkened to deep red and was left to stir for 1 h. Volatile materials were removed *in vacuo* and the residue was extracted with hexane (2×25 cm^3). The filtered combined extracts were concentrated *in vacuo* (*ca* 15 cm^3) and passed down a column of alumina (15 cm × 3 cm) using hexane as the eluent. This resulted in three fractions (orange, purple and red) which were collected. The first and third fractions were concentrated *in vacuo* (*ca* 10 and 5 cm^3, respectively) and cooled (−40°C) producing orange crystals of **3** and red crystals of **4**, respectively, which were collected and dried *in vacuo*. The second fraction is still under investigation. For **3**: Yield 0.12 g, 45.7%, based on **1**. M.p.: 163–168°C (dec.). IR (Nujol mull): 2304m, 1944s, 1891w,sh, 1510w, 1435m, 1379w, 1358m, 1331w, 1304w, 1171m, 1025m, 1017m, 848m, 810m (cm^{-1}). ^{1}H NMR (300.152 MHz): δ 5.49 (br. mult., 2H, COD), 5.10 (br. mult., 2H, COD), 4.57 [d, 1H, ^1J(P—H) = 306 Hz, *H*P(t-Bu)$_2$], 1.95 (br. mult., 8H, COD), 1.46 [d, 18H, ^3J(P—H) = 13 Hz, μ-P(t-*Bu*)$_2$], 1.20 [d, 18H, ^3J(P—H) = 15 Hz, HP(t-*Bu*)$_2$], −10.85 (mult., 1H, μ-*H*). ^{31}P{^{1}H} NMR (121.503 MHz): δ 225.7 [ddd, ^2J(P—P) = 196 Hz, ^1J(Rh—P) = 140 Hz, ^1J(Rh—P) = 110 Hz, μ-*P*(t-Bu)$_2$], 56.2 [dd, ^2J(P—P) = 196 Hz, ^1J(Rh—P) = 121 Hz, H*P*(t-Bu)$_2$]. For **4**: Yield 0.09 g, 24.9%, based on **1**. M.p.: 155–158°C (dec.). IR (Nujol mull, NaCl plates): 1947m, 1832s, 1353m, 1347m,sh, 1324w, 1298w, 1168m, 1069w, 1012m, 942w, 928w, 860w, 839w, 807m (cm^{-1}); (hexane solution, KBr cells): 1949w, 1851m (cm^{-1}). ^{1}H NMR (361.084 MHz): δ 5.62 (br. mult., 4H, COD), 5.09 (br. mult., 4H, COD), 2.06 (br. mult., 16H, COD), 1.45 [t, 36H, μ-P(t-*Bu*)$_2$], −8.35 [dtt, 1H, ^1J(Rh(1)—H) = 25 Hz, ^2J(P—H) = 13 Hz, ^2J(Rh(2)—H) = 9 Hz, Rh—*H*]. ^{31}P{^{1}H} NMR (32.384 MHz): δ 228.2 [br. mult., μ-P(t-Bu)$_2$].

Synthesis of $[Fe(CO)_3](\mu\text{-}CO)\{\mu\text{-}P(t\text{-}Bu)_2\}[Rh(CO)\{HP(t\text{-}Bu)_2\}]$ **(5)**

$Fe(CO)_5$ (1.0 cm^3) was added to a solution of **1** (0.41 g, 0.90 mmol) in toluene (40 cm^3) and the resulting mixture was refluxed (4 h) during which time the solution gradually turned black–green with the formation of considerable black precipitate. The mixture was filtered and the black residue was washed with toluene (15 cm^3). The resulting solution was passed down an alumina column (3 cm × 3 cm) giving a yellow–orange band which was collected. Volatile materials were removed *in vacuo* and the residue was dissolved in hexane (10 cm^3) and cooled (−40°C), producing orange crystals of **5** which were collected and dried *in vacuo*. Yield: 0.45 g, 85%, based on rhodium. M.p.: 138–139°C (dec.). IR (Nujol mull, NaCl plates): 2310w, 2024s, 1962s, 1950s, 1905w,sh, 1843br, 1362m, 1168s, 1023m, 930m, 887m, 825m, 803s, 624m, 605m (cm^{-1}); (hexane solution, KBr cells): 2025s, 1965s, 1952s, 1921w, 1855br (cm^{-1}). ^{1}H NMR (361.084 MHz): δ 4.40 [d, 1H, ^1J(P—H) = 312 Hz, *H*P(t-Bu)$_2$], 1.37 [d, 18H, ^3J(P—H) = 14 Hz, μ-P(t-*Bu*)$_2$], 1.17 (d, 18H, ^3J(P—H) = 14 Hz, HP(t-*Bu*)$_2$]. ^{31}P{^{1}H} NMR (32.384 MHz): δ 220.9 [dd, ^1J(Rh—P) = 97 Hz, ^2J(P—P) = 189 Hz, μ-*P*(t-Bu)$_2$], 62.6 [dd, ^1J(Rh—P) = 126 Hz, ^2J(P—P) = 189 Hz, H*P*(t-Bu)$_2$].

X-ray experimental data

Details of crystal data and a summary of intensity data collection parameters for **4** and **5** are given in Table 5. Data were collected on an Enraf–Nonius CAD-4 diffractometer at 23±2°C using graphite monochromated Mo-K_α radiation. All calculations were performed on a PDP 11/44 computer using the Enraf–Nonius software package "SDP-PLUS".[16] For each structure, the data were corrected for Lorentz and polarization effects. The structures were solved by direct methods (MULTAN)[17] and suc-

Table 5. Crystal data and collection parameters for complexes **4** and **5**

Description of crystal	**4**	**5**
Colour	Dark red	Orange
Habit	Plate	Prism
Maximum crystal dimensions (mm)	0.38 × 0.24 × 0.15	0.35 × 0.30 × 0.12
Unit cell		
Crystal system	Monoclinic	Monoclinic
Space group	$P2_1/n$	$P2_1/a$
Unit cell parameters:		
a (Å)	10.868(6)	13.622(2)
b (Å)	14.332(4)	11.724(1)
c (Å)	11.503(4)	16.805(2)
α (°)	90	90
β (°)	96.98(4)	91.51(1)
γ (°)	90	90
U (Å^3)	1778.4(5)	2682.9(5)
Molecules per unit cell	2	4
Formula	$C_{34}H_{61}O_2P_2Rh_3$	$C_{21}H_{37}FeO_5P_2Rh$
Molecular weight (g mol^{-1})	872.53	590.23
Calculated density (g cm^{-3})	1.627	1.461
μ(Mo-K_α)$_{calc}$ (cm^{-1})	14.72	12.89
Data collection		
Radiation (Å)	Mo-K_α (0.71073)	Mo-K_α (0.71073)
Scan width (°)	0.8+0.35 (tan θ)	0.8+0.35 (tan θ)
Range of indices h, k, l	+12, +16, ±13	+15, +13, ±14
2θ range (°)	3–48	3–48
Number of reflections measured	3078	4637
Standard reflections:		
intensity	4 4 2, 1 6 $\bar{3}$	3 4 6, 2 $\bar{6}$ 2
orientation	1 6 5, 4 $\bar{5}$ 1	4 7 2, 7 1 $\bar{3}$
Decay of standards	< 1%	1.4%
Minimum % transmission	—	75.32
Maximum % transmission	—	99.78
Average % transmission	—	87.68
Agreement factor for averaged reflections		
F_o	0.056	0.022
intensity	0.055	0.018
Structure determination		
Number of reflections used [$I > 3\sigma(I)$]	1261	2810
Number of parameters varied	175	271
Data/parameter ratio	7.206	10.369
Shift to error ratio	4.164	0.083
ESD of an observation of unit weight	4.114	3.960
R^a	0.0739	0.0422
$R_w{}^b$	0.0789	0.0542

[a] $R = \Sigma|F_o| - |F_c|/\Sigma|F_o|$.

[b] $R_w = [\Sigma\omega(|F_o| - |F_c|)^2/\Sigma\omega(|F_o|)^2]^{1/2}$. The function minimized in the least-squares refinement was $\Sigma\omega(|F_o| - |F_c|)^2$, $\omega = 1/\sigma^2(|F_o|)$.

cessive cycles of difference Fourier maps followed by least-squares refinement.

Complex **4**. Crystals suitable for X-ray diffraction were grown by cooling a hexane solution (−35°C). The crystals were mounted in thin walled glass capillaries and sealed under nitrogen. Unit cell parameters were obtained by centring 25 reflections having 2θ values between 20 and 26°. The monoclinic space group $P2_1/n$ was uniquely determined by the systematic absences $h01$, $h+1=2n+1$, $0k0$, $k=2n+1$ and data were collected in the $+h+k\pm l$ quadrant between 2θ values of 3 and 48°. The check reflections indicated < 1% decrease in intensity over the course of data collection, and hence no correction was applied. A ψ scan of four reflections having χ values between 80 and 90° showed that no absorption correction was necessary and none was applied. The observed structure factors of equivalent reflections were averaged. Hydrogen atoms were not located, but their contributions were included in the final refinements, while all non-hydrogen atoms except for O(1), C(1) and C(2) were refined anisotropically. Data with intensities less than $3.0\sigma(I)$, $(\sin\theta)/\lambda$ greater than 0.55 and $(\sin\theta)/\lambda$ less than 0.05 were excluded, and a non-Poisson contribution weighting scheme with an experimental instability factor of $P=0.06$ was used in the final stages of refinement.* The maximum peak in the final difference Fourier map had a height of 1.468 e/Å^3 and was located 0.657 Å from Rh(1).

Complex **5**. Crystals suitable for X-ray diffraction were grown by cooling a hexane solution (−35°C). The crystals were mounted in thin walled glass capillaries and sealed under nitrogen. Unit cell parameters were obtained by centring 25 reflections having 2θ values between 22 and 26°. The monoclinic space group $P2_1/a$ was uniquely determined by the systematic absences $h01$, $h=2n+1$, $0k0$, $k=2n+1$. Data were collected in the $+h+k\pm l$ quadrant between 2θ values of 3 and 48°. The check reflections indicated a 1.4% decrease in intensity over the course of data collection, and hence no correction was applied. A ψ scan of four reflections having χ values between 80 and 90° showed a minimum transmission of 75.3% and a maximum transmission of 99.8%. An empirical absorption correction was applied. The observed structure factors of equivalent reflections were averaged. Hydrogen atoms were not located, but their contributions were included in the final refinements. Data with intensities less than $3.0\sigma(I)$ and $(\sin\theta/\lambda)$ less than 0.10 were excluded, and a non-Poisson contribution weighting scheme with an experimental instability factor of $P=0.06$ was used in the final stages of refinement.* The maximum peak in the final difference Fourier map had a height of 1.303 e/Å^3 and was located 0.660 Å from Rh(1).

Acknowledgements—We thank the National Science Foundation (CHE-8818984) and the Robert A. Welch Foundation (F-816) for support.

* P is used in the calculation of $\sigma(I)$ to downweight intense reflections in the least square refinement. The function minimized was $\Sigma\omega(|F_o|-|F_c|)^2$, where $\omega=4(F_o)^2/[\Sigma(F_o)^2]^2$, in which $[\Sigma(F_o)^2]^2=[S^2(C+R^2B)+\{P(|F_o|)^2\}^2]/(L_p)^2$ (S is the scan rate, C is the total integrated peak count, R is the ratio of scan time to background counting time, B is the total background count and L_p is the Lorentz-polarization factor).

REFERENCES

1. B. F. G. Johnson, *Transition Metal Clusters*. John Wiley, New York (1980).
2. F. A. Cotton and G. Wilkinson, *Advanced Inorganic Chemistry*, 5th edn, Ch. 23. John Wiley, New York (1988).
3. D. A. Roberts and G. L. Geoffroy, *Comprehensive Organometallic Chemistry* (Edited by G. Wilkinson, F. G. A. Stone and E. W. Abel), 4th edn, Ch. 40. Pergamon Press, Oxford (1984) and refs therein.
4. H. Vahrenkamp, *Transition Metal Chemistry* (Edited by A. Muller and D. Diemann). Verlag Chemie, Weinheim (1980).
5. See for examples: (a) W. C. Mercer and G. L. Geoffroy, *Organometallics* 1985, **4**, 1418; (b) P. M. Shulman, E. D. Burkhardt, E. G. Lundquist, R. S. Pilato, G. L. Geoffroy and A. L. Rheingold, *Organometallics* 1987, **6**, 101; (c) M. J. Breen, P. M. Shulman, G. L. Geoffroy, A. L. Rheingold and W. C. Fultz, *Organometallics* 1984, **3**, 782; (d) S. Rosenberg, W. S. Mahoney, J. M. Hayes, G. L. Geoffroy and A. L. Rheingold, *Organometallics* 1986, **5**, 1065; (e) E. D. Morrison, A. D. Harley, M. A. Marcelli, G. L. Geoffroy, A. L. Rheingold and W. C. Fultz, *Organometallics* 1984, **3**, 1407; (f) T. S. Targos, R. P. Rosen, R. R. Whittle and G. L. Geoffroy, *Inorg. Chem.* 1985, **24**, 1375; (g) S. Rosenberg, R. R. Whittle and G. L. Geoffroy, *J. Am. Chem. Soc.* 1984, **106**, 5934.
6. A. M. Arif, D. J. Chandler and R. A. Jones, *Organometallics* 1987, **6**, 506.
7. R. D. Moulton, D. J. Chandler, A. M. Arif, R. A. Jones and A. J. Bard, *J. Am. Chem. Soc.* 1988, **110**, 5714.
8. R. G. Goel, R. G. Montemayor and W. O. Ogini, *J. Am. Chem. Soc.* 1978, **100**, 3629.
9. A. M. Arif, R. A. Jones, M. H. Seeberger, B. R. Whittlesey and T. C. Wright, *Inorg. Chem.* 1986, **25**, 3943.
10. A. M. Arif, D. E. Heaton, R. A. Jones, K. B. Kidd,

T. C. Wright, B. R. Whittlesey, J. L. Atwood, W. E. Hunter and H. Zhang, *Inorg. Chem.* 1987, **26**, 4065.

11. E. Keller and H. Vahrenkamp, *Chem. Ber.* 1979, **112**, 2347.
12. Down field shifts in the ^{31}P NMR of the Ph_2P groups bridging metal–metal bonds have been noted by several groups of workers. See for example: P. E. Garrou, *Chem. Rev.* 1981, **81**, 229; A. J. Carty, *Adv. Chem. Ser.* 1982, **196**, 163 and refs 1–5 therein; A. J. Carty, S. A. MacLaughlin and D. Nucciarone, in *Phosphorus-31 NMR Spectroscopy in Stereochemical Analysis* (Edited by J. G. Verkade and L. D. Quin), Ch. 16, p. 559. VCH, Weinheim (1987). Similar down field shifts have been noted for μ-P(t-Bu)$_2$ complexes; see refs 6, 7, 12 and 13.
13. R. Mason and J. A. Zubieta, *J. Organomet. Chem.* 1974, **66**, 279.
14. P. Braunstein, D. Matt, O. Bars and D. Grandjean, *Angew. Chem. Int. Ed. Engl.* 1979, **18**, 797.
15. G. Giordano and R. H. Crabtree, *Inorg. Synth.* 1979, **19**, 218.
16. "SDP Plus", 4th edn. B. A. Frenz and Associates, College Station, Texas (1981).
17. G. Germain, P. Main and M. M. Wolfson, *Acta. Cryst.* 1971, **A27**, 368.

Polyhedron Vol. 10, No. 6, pp. 553–560, 1991
Printed in Great Britain

0277–5387/91 $3.00+.00
© 1991 Pergamon Press plc

SYNTHESES AND STEREOCHEMISTRY OF DICOBALT(II) COMPLEXES $[Co_2(dppm)(\mu\text{-}SR)_2(SR)_2]$ (dppm = $Ph_2PCH_2PPh_2$; R = C_6H_5, *m*-$C_6H_4CH_3$, *p*-$C_6H_4CH_3$ AND *p*-C_6H_4-$^tC_4H_9$) AND $[Co_2(dppe)(\mu\text{-}SPh)_3(SPh)]$ (dppe = $Ph_2PCH_2CH_2PPh_2$)

GUOWEI WEI, HANQIN LIU,* ZHIYING HUANG, MAOCHUN HONG, LIANGREN HUANG and BEISHENG KANG

Fuzhou Laboratory of Structural Chemistry and Fujian Institute of Research on the Structure of Matter, Chinese Academy of Sciences, Fuzhou, Fujian 350002, P.R.C.

(*Received* 3 *April* 1990; *accepted* 31 *October* 1990)

Abstract—From reactions of $Co(dppm)_2Cl_2$ or $Co(dppm)Cl_2$ with thiolate and elemental selenium or sulphur in DMF, the following complexes were prepared in good yields: $[Co_2(dppm)(\mu\text{-}SR)_2(SR)_2]$ (R = C_6H_5, **1**; *m*-$C_6H_4CH_3$, **2**; *p*-$C_6H_4CH_3$, **3**; and *p*-C_6H_4-$^tC_4H_9$, **4**). Compound **1** crystallizes in two different isomeric crystals, **1A** and **1S**, containing three stereoisomers of molecular conformations: **1aa**, **1sa** and **1ss**. The two different crystal structures of compound **1** were confirmed by thermal analysis and IR spectra. Compound **2** crystallizes with molecules of type **ss**. Compound $[Co_2(dppe)(\mu\text{-}SPh)_3(SPh)]$ (**5**) is an asymmetric molecule with one five-coordinate cobalt atom and one four-coordinate cobalt atom. From the EPR spectra and magnetic susceptibility data, it is deduced that there is antiferromagnetic coupling between the two paramagnetic cobalt(II) atoms in compounds **1**–**5**.

Tertiary phosphine ligands have played a major role in modern coordination chemistry.[1] Ditertiary phosphine complexes of transition metals have been studied extensively recently, not only due to their variation of structures and properties, but also because of their application as homogeneous or heterogeneous catalytic functions.[2] Metal thiolato complexes are known as ubiquitous biological electron-transfer mediators,[3,4] yet complexes containing both diphosphine and thiolato ligands have received relatively little attention and only a few reports have been found in this area.[5]

We have explored the coordination chemistry and the reactivity of metal complexes combining both ditertiary phosphine and thiolate ligands. Herein we report the syntheses and stereochemistry of two types of dicobalt complexes: $[Co_2(dppm)(\mu\text{-}SR)_2(SR)_2]$ (R = Ph, **1**; *m*-tol, **2**; *p*-tol, **3**; and *p*-tbb, **4**)† and $[Co_2(dppe)(\mu\text{-}SPh)_3(SPh)]$ (**5**) with a mole ratio of 2:1 for metal–diphosphine. A preliminary account of the asymmetrical dicobalt(II) complex **5** has been communicated elsewhere.[6]

EXPERIMENTAL

All operations were carried out under a dinitrogen atmosphere. The reagent dppm was purchased from Aldrich, thiols from Merck, solvents and $CoCl_2 \cdot 6H_2O$ from the Shanghai Factory of Chemical Reagents. Solvents were dried, distilled and gassed prior to use. $Co(dppm)Cl_2$ and $Co(dppm)_2Cl_2$ were prepared according to the literature method.[7]

Preparation of $[Co_2(dppm)(\mu\text{-}SPh)_2(SPh)_2]$ (1)

(i) *From* $Co(dppm)Cl_2$ *and elemental sulphur.* A mixture of NaSPh (0.264 g, 2 mmol) and elemental sulphur (0.032 g, 1 mmol) in DMF (20 cm^3) formed an orange solution after stirring for 30 min. The

* Author to whom correspondence should be addressed.

† Abbreviations: Ph, C_6H_5; tol, $C_6H_4CH_3$; tbb, tert-butylbenzyl (C_6H_4-$^tC_4H_9$); dppm, bis(diphenylphosphino)methane; dppe, 1,2-bis(diphenylphosphino) ethane; dppp, 1,3,-bis(diphenylphosphino)propane; b for bridge; t for terminal; IR, infrared; EPR, electron paramagnetic resonance.

solution turned crimson–black after addition of $Co(dppm)Cl_2$ (0.514 g, 1 mmol) and stirring for 30 min. Part of the solvent was removed under reduced pressure at 40°C to yield a sticky liquid.

(ii) *From* $Co(dppm)_2Cl_2$ *and elemental selenium.* The procedure is similar to that of (i) except 1.5 mmol of elemental selenium (0.118 g) was used and $Co(dppm)Cl_2$ was replaced by $Co(dppm)_2Cl_2$. A sticky liquid was also obtained after concentrating the solution at 40°C.

(iii) *Crystallization of* **1A**. Ethanol (10 cm^3) was added to either of the above sticky liquids from (i) or (ii) and the mixture was stirred for 15 min. After standing overnight at room temperature, the precipitate was removed by filtration. The solution was kept at 5°C for 3 weeks and the black, octahedral-shaped crystals were collected, washed with ethanol and ether, and dried *in vacuo* to afford 0.39 g (83%) of crystal **1A**. Found: C; 62.2; H, 4.5; Co, 12.4; P, 6.6; S, 13.5. Calc. for $C_{49}H_{42}Co_2P_2S_4$: C, 62.3; H, 4.5; Co, 12.6; P, 6.6; S, 13.7%. IR data and magnetic moment values are summarized in Table 1. The solution was sensitive to both air and water, but the crystal was stable in dry air for weeks.

(iv) *Crystallization of* **1S**. Ethanol (40 cm^3) was added to either of the above sticky liquids from (i) or (ii). After stirring slowly for 5 min, the precipitate was removed by filtration. The filtrate was kept at 0°C for 4 days. Black, rhombic, plate-shaped crystals were collected and washed with ethanol and ether to afford 0.35 g (74%) of **1S**. Found: C, 62.4; H, 4.7; Co, 12.5; P, 6.1; S, 13.2. Calc. for $C_{49}H_{42}Co_2P_2S_4$: C, 62.3; H, 4.5; Co, 12.6; P, 6.6; S, 13.7%. The remaining filtrate which was kept at 0°C for a month yielded a small amount of **1A**.

Preparation of $[Co_2(dppm)(\mu\text{-S-}m\text{-tol})_2(\text{S-}m\text{-tol})_2]$ (**2**)

Compound **2** was prepared from either $Co(dppm)Cl_2$ and sulphur or $Co(dppm)_2Cl_2$ and selenium following procedures similar to those for the preparation of **1**. Na(S-*m*-tol) (0.298 g, 2 mmol), elemental selenium (0.118 g, 1.5 mmol), $Co(dppm)_2Cl_2$ (0.899 g, 1 mmol) and DMF (25 cm^3) were used, and the volume of the mixture was reduced to one-fourth by low pressure evaporation. Ethanol (10 cm^3) was added and the precipitate was removed after the solution was kept overnight at room temperature. After standing at room temperature for 2 weeks, black, plate-like crystals (0.27 g, 54%) were collected and washed with ethanol and ether. Found: C, 64.6; H, 5.8; Co, 11.6; S, 13.3. Calc. for $C_{53}H_{50}Co_2P_2S_4$: C, 64.0; H; 5.1; Co, 11.9; S, 12.9%. Attempts to grow isomeric crystals similar to **1** were not successful.

Preparation of $[Co_2(dppm)(\mu\text{-S-}p\text{-tol})_2(\text{S-}p\text{-tol})_2]$ (**3**) *and* $[Co_2(dppm)\text{-}(\mu\text{-S-}p\text{-tbb})_2(\text{S-}p\text{-tbb})_2]$ (**4**)

The procedures were similar to those for the preparation of **1**. The yields were between 50 and 70%.

Preparation of $[Co_2(dppe)(\mu\text{-SPh})_3(\text{SPh})]$ (**5**)

This has been described elsewhere.[6]

X-ray structures

A suitable single crystal of **1A**, **1S** or **2** was mounted on a glass fibre and data collections were performed at ambient temperature on an Enraf–Nonius CAD4 diffractometer using graphite-monochromatized Mo-K_α radiation ($\lambda = 0.71073$ Å). The crystallographic and machine parameters are summarized in Table 2. The cell parameters were obtained from the least-squares refinement, using 25 high-angle reflections. All intensity data were corrected for standard decay, since the three standard reflections monitored periodically during data collection showed small fluctuations of intensity. The data were corrected for Lorentz and polariz-

Table 1. IR absorption and magnetic moments at ambient temperature

Compound	IR (cm^{-1})	μ_{eff}[a] (μ_B)
1A	359(s) 332(s) 320(sh) 305(m) 262(m) 226(m) 195(m) 172(m)	1.64
1S	361(s) 336(m) 316(m) 283(m) 259(m) 253(m) 216(m) 198(m)	1.65
2	363(m) 355(m) 347(m) 338(s) 322(m) 208(m) 183(m)	1.73
3	359(m) 349(m) 338(s) 287(m) 232(w)	1.57
4	374(s) 353(s) 337(s) 212(m) 193(m)	1.76
5	367(s) 355(s) 337(m) 284(m) 216(m) 179(m)	3.69

[a] Effective magnetic moment, $\mu_{eff} = 2.834[(\chi_{mol} - \chi_{dia}) \times T]^{1/2}$, where χ_{mol} and χ_{dia} are measured and diamagnetic molar susceptibilities, respectively.

Table 2. Summary of crystal data and data collection parameters

	1A	1S	2
Formula	$Co_2S_4P_2C_{49}H_{42}$	$Co_2S_4P_2C_{49}H_{42}$	$Co_2S_4P_2C_{53}H_{50}$
Molecular weight	938.95	938.95	995.06
Space group	$P2_1/n$	$P2/n$	$Pbca$
Systematic absences	$h0l$ $h+l=2n$ $0k0$ $k=2n$	$h0l$ $h+l=2n$	$hk0$ $h=2n$ $h0l$ $l=2n$ $0kl$ $k=2n$
a (Å)	13.330(2)	19.011(6)	18.109(9)
b (Å)	15.150(1)	13.608(8)	20.15(1)
c (Å)	22.155(3)	35.36(1)	27.200(4)
β (°)	95.66(1)	102.15(2)	
V (Å^3)	4452.2(1.8)	8952.4(12.3)	9924.2(11.2)
Z	4	8	8
d_{calc} (g cm^{-3})	1.401	1.395	1.332
Crystal dimensions (mm)	$0.25\times0.26\times0.32$	$0.22\times0.30\times0.40$	$0.20\times0.33\times0.34$
Temperature (°C)	23	23	23
Radiation (wavelength)	Mo-K_α (0.71073 Å)	Mo-K_α (0.71073 Å)	Mo-K_α (0.71073 Å)
Monochromator	Graphite	Graphite	Graphite
Linear absorbance coefficient (cm^{-1})	10.275	10.230	9.258
Scan method	θ–2θ	θ–2θ	θ–2θ
h, limits	−15 to 15	−20 to 0	0 to 21
k, limits	−18 to 0	0 to 14	0 to 24
l, limits	−26 to 0	−38 to 38	0 to 32
2θ range (°)	50.0	46.0	50.0
Scan width (°)	$0.50+0.35\tan\theta$	$0.70+0.35\tan\theta$	$0.45+0.35\tan\theta$
F(000)	1936	3872	4128
Number of reflections collected	7803	12,686	9511
Number of data for refinement[a]	5818	5082	4812
Number of variables	515	992	550
Largest residue (e/Å^3)	0.232	0.566	0.922
R	0.034	0.066	0.059
R_w	0.046	0.078	0.084

[a] $I > 3\sigma(I)$ for **1A** or **1S**, $I > 4\sigma(I)$ for **2**.

ation effects. Absorption corrections for crystals of **1A** and **1S** were based on empirical psi-scan and DIFABS techniques, respectively. Both empirical psi-scan absorption and DIFABS were applied for the crystal of **2**.

Calculations were performed on a VAX-11/785 computer with the SDP program package.[8] The structures were solved by direct methods and subsequently by difference Fourier maps. Anisotropic thermal refinements were applied[9] to all non-hydrogen atoms, except for seven carbon atoms in crystal **1S**. In the last stage of refinement, contributions were included for hydrogen atoms with fixed "idealized" positions of C—H = 0.95 Å and a group of isotropic thermal parameters varied according to the average thermal parameters of the carbon atoms in the corresponding benzene ring. Atomic positional and thermal parameters, and listings of interatomic distances and bond angles for **1A**, **1S** and **2** are available as supplementary material from the Editor or the Authors.

Spectral measurements

IR spectra were recorded on a Digilab FTS-20E/D spectrometer. Magnetic susceptibilities were measured with a powdered sample at room temperature on a home-made Gouy–Faraday magnetic balance using the Faraday method.[4] The magnetic moment (μ_{eff}) was calculated after diamagnetic molar correction (χ_{dia}) of the ligands: $\mu_{eff}^2 = 3kT(fw\chi_g - \chi_{dia})$. EPR spectra were obtained on a Bruker ER-420 spectrometer at both 295 and 77 K. NMR spectra were recorded on a Varian FT-80A spectrometer. Elemental analyses were performed by the Analytical Chemistry Group of this Institute.

RESULTS AND DISCUSSION

Syntheses of $[Co_2(dppm)(\mu\text{-}SR)_2(SR)_2]$

The synthetic reaction of the dppe complexes consists of the formation of the by-product $dppeX_2$ (X = S or Se) as described by eq. (1):

$$[2NaSR + (2n-1)X] + Co(dppe)_nCl_2 \longrightarrow 1/2[Co_2(dppe)(SR)_4] + (n-1/2)dppeX_2 + 2NaCl \quad (n = 1 \text{ or } 2). \quad (1)$$

Equation (1) is applicable for $dppmS_2$, but not for $dppmSe_2$. ^{31}P NMR spectra revealed that selenium reacts with dppm to form the monoselenium compound dppmSe, while elemental sulphur reacts with dppm to form the disulphide compound $dppmS_2$, while elemental sulphur reacts with dppm to form the disulphide compound $dppmS_2$. Carr and Colton observed a similar result in reacting $SeCN^-$ and SCN^- with dppm.[10] Therefore, the mole ratio of the reagents is altered according to the following equation in order to prepare compound **1**:

$$[2NaSR + 3/2Se] + Co(dppm)_2Cl_2 \longrightarrow 1/2[Co_2(dppm)(SR)_4] + 3/2dppmSe + 2NaCl. \quad (2)$$

Attempts to prepare compound **1** or **2** by direct interaction of NaSR with $Co(dppm)Cl_2$ or with $CoCl_2$ and dppm in the absence of elemental sulphur or selenium did not succeed.

General structural features of $[Co_2(dppm)(SR)_4]$

The structures of the two neutral dicobalt compounds containing dppm were determined. The two cobalt atoms in compound **1** or **2** are bridged by two SR ligands and joined by a dppm ligand through the two phosphorus atoms. The core $Co_2(\mu\text{-}S)_2$ is decidedly non-planar, but slightly puckered with cobalt(II) and S_b atoms on the opposite sides of the weighted least-squares plane. The phenyl rings of the two bridging SPh and the plane of CoPCPCo are perpendicular to and on opposite sides of the above Co_2S_2 "plane", as seen in Figs 1–3.

There are three different molecular conformations of the compound $[Co_2(dppm)(\mu\text{-}SPh)_2(SPh)_2]$ in the two isomeric crystals **1A** and **1S**: **1aa**, **1sa** and **1ss** as shown in Figs 1, 2 and 3, respectively. Selected interatomic distances and bond angles of **1aa**, **1sa** and **1ss** are collected in Table 3. The corresponding atomic distances in the three conformations do not differ considerably from each other. The main difference between the three stereoisomers is the geometry of the terminal

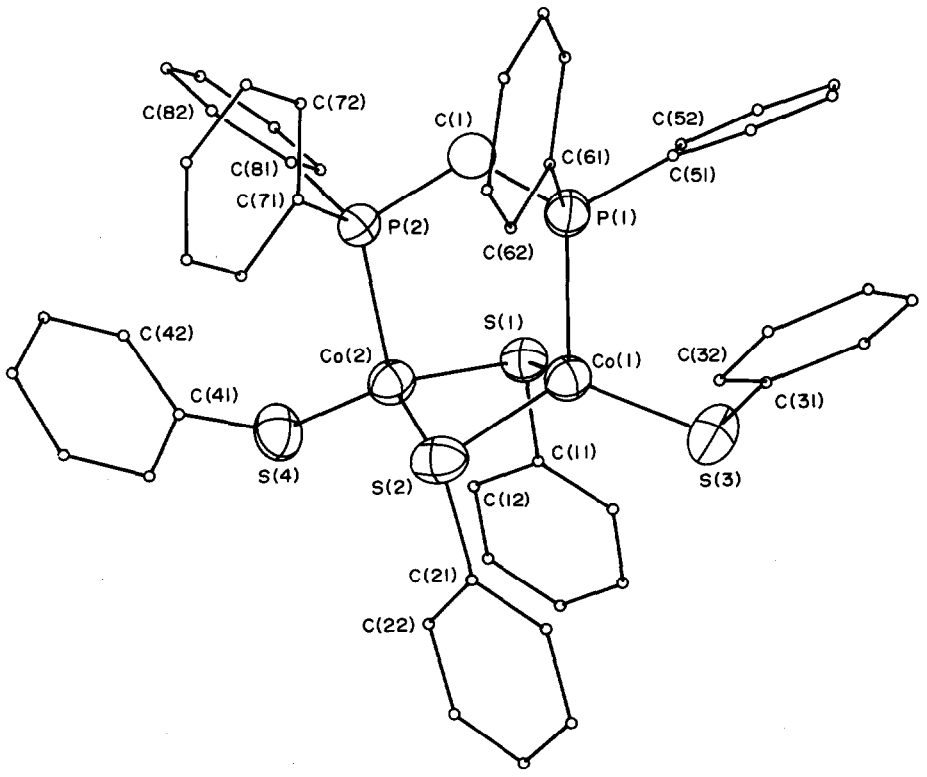

Fig. 1. Perspective view of the structure of the molecular conformation **1aa**.

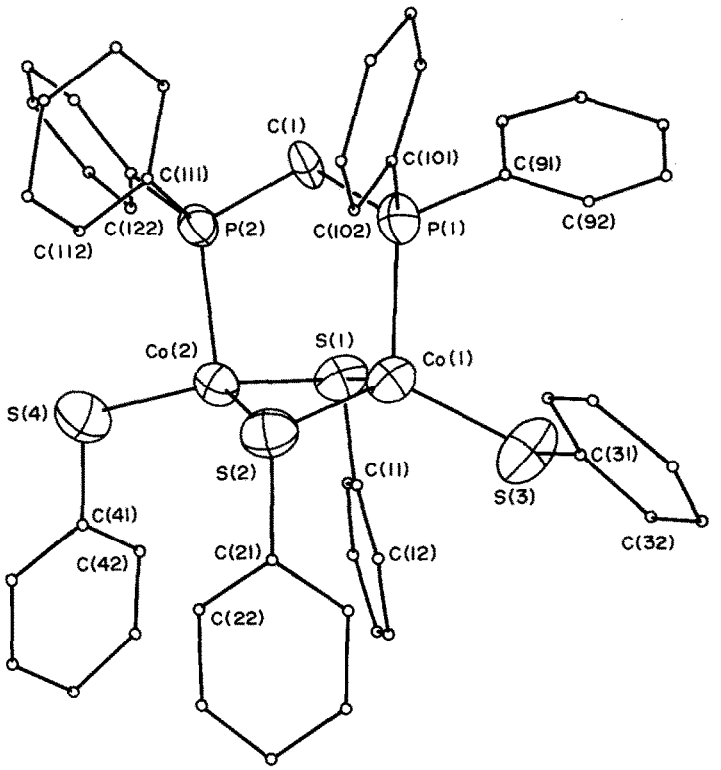

Fig. 2. Perspective view of the structure of the molecular conformation **1sa**.

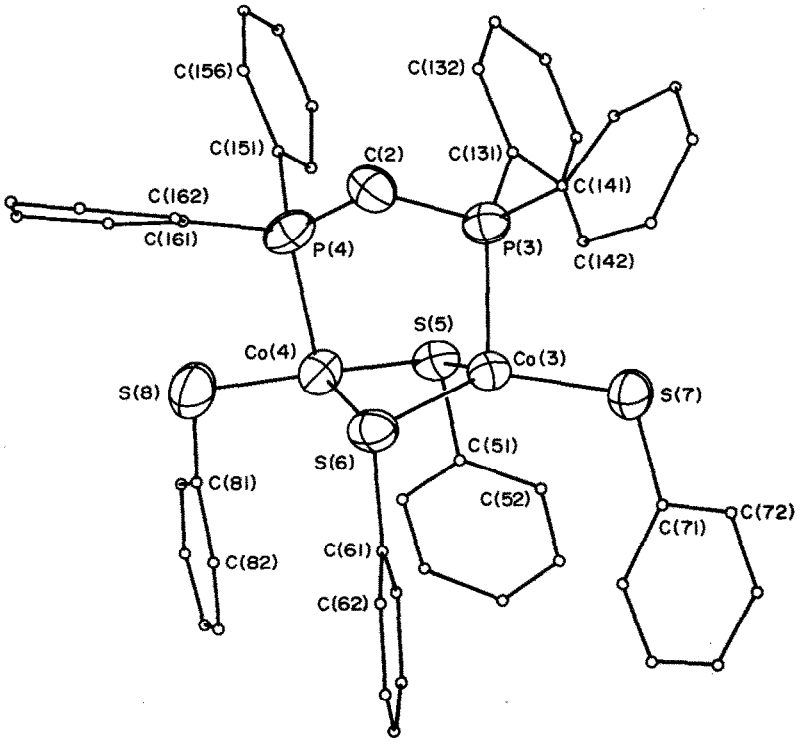

Fig. 3. Perspective view of the structure of the molecular conformation **1ss**.

Table 3. A comparison of selected atomic distances (Å) and bond angles (°) for all compounds[a]

	1aa	**1sa**	**1ss**	**2**	**5**	**6s**[b]
Co—Co	2.6832(6)	2.655(3)	2.670(3)	2.634(2)	2.632(2)	3.02
Co—S_b	2.266(7)	2.256(10)	2.265(56)	2.261(14)	2.312(35)	2.36
Co—S_t	2.211(9)	2.198(9)	2.197(14)	2.185(4)	2.215(4)	2.27
Co—P	2.337(4)	2.343(7)	2.349(4)	2.342(6)	2.210(16)	
Co—Co—S_t	156.5(3)	148.8				
		168.4	170.5(2)	169.0(23)	169.0	
S_b—Co—S_t	118.0(35)	115.2(50)				110.1
		123.4(21)	123.9(24)	123.3(33)		
P—Co—S_t	108.6(9)	114.3(1)				
		98.0	95.3(4)	95.8(14)		
P—Co—S_b	103.3(57)	102.0(52)				
		100.9(21)	101.5(34)	100.1(19)		
S_b—Co—S_b	103.2(1)	105.2(5)	104.9(0)	106.7(3)	90.7(41)	97.1
Co—S_b—Co	72.6(2)	72.0(6)	72.2(1)	71.3(5)	69.4(5)	79.5

[a] Numbers in parentheses are ESDs of SDs for several equivalent values; $s = [\text{sum}\,\chi_i^2 - n\bar{\chi}^2]^{1/2}n$, $\bar{\chi} = [\text{sum}\,\chi_i]/n$.

[b] Average values of *syn*-$[Co_2(SEt)_6]^{2-}$.

SPh ligand with respect to the central core. Relative to the "spine" S—Co—S—S—Co—S, the phenyl groups of the bridging and terminal —SPh can be arranged in the *anti* or *syn* form, and therefore the molecular conformations could be one of the three forms: *anti–anti* (**aa**), *syn–anti* (**sa**) or *syn–syn* (**ss**). The S—Co—Co—S spine is noticeably straightened in going from **1aa** to **1ss**. Different molecular

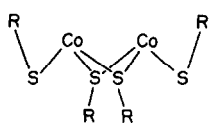

anti-anti
aa

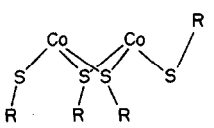

syn-anti
sa

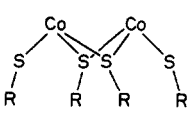

syn-syn
ss

structure arrangements also occur in other cobalt thiolate compounds, for example for $[Co_2(SEt)_6]^{2-}$ (**6**) with *anti* and *syn* bridged forms.[11] The *syn* conformation (**6s**) is closely related to compound **1** because their central Co_2S_2 cores are puckered to the butterfly form. The atomic distances Co—S_t and Co—S_b in **1** are 0.06–0.10 Å shorter than those of **6s**, and the Co—Co distance in **1** is much shorter than that of **6s**, 2.67 vs 3.02 Å. The ditertiary phosphine ligand dppm plays an important role in stabilizing the dicobalt complex **1** and locks together two metal atoms in close proximity, and consequently reduces the bridge angle Co—S_b—Co, from 79.5(2)° in **6s** to 72.3(3)° in **1** The usual order of distances between the cobalt atom and bridging or terminal ligands, Co—S_b > Co—S_t, prevails in both compounds.

There are four molecules of **1aa** in a unit cell of **1A** and four molecules each of **1as** and **1ss** in a unit cell of **1S**. In our experiment, the crystals of **1A** grow in a solution having a lower ratio of EtOH–DMF and at a lower rate than those of **1S**. The difference in structure of **1A** and **1S** is confirmed by IR spectra (presented in Table 1) and by differential thermal analyses.[12] The Co—S—Ph bond rotates freely in solution, but there are energy wells with respect to the —PPh_2 group and to the crystal lattice, and therefore it is possible to have different stereoisomers in the solid state.

Compound **2** crystallizes in the orthorhombic space group *Pbca* with eight molecules of type **ss** in a unit cell. Since the perspective view of **3** is very similar to that of **1ss** (Fig. 3), its ORTEP drawing is given in the supplementary material. Selected interatomic distances and bond angles of **2** are also listed in Table 3 for comparison.

Comparison of the molecular structures

Ditertiary phosphine reacts with cobalt(II) and thiolate to form disparate molecular structures:

dppm acts as a bridge to connect two cobalt atoms forming a symmetric dicobalt compound **1**; dppe acts as a bidentate ligand chelating to a cobalt atom forming an asymmetric dicobalt compound **5** (Fig. 4); dppp also acts as a bidentate ligand chelating to one cobalt atom forming a mono-cobalt complex, $Co(dppp)(SR)_2$.[13]

The coordination geometry of the core $P_2Co_2S_4$ in structure type **1** can be viewed as two edge-shared trigonal pyramids. Although there is no imposed symmetry for compounds **1** or **2**, inspection of the structure of **1aa** and **1ss** shown in Figs 1 and 3 and their geometric data reveals that the entire neutral molecules of **1aa**, **1ss** or **2** approach C_2 symmetry. Atoms Co(1), Co(2), P(1), P(2), S(3) and S(4) are in a plane. The bidentate phosphine ligand bridges two cobalt atoms and provides additional stability to the structure in the sense of locking two cobalt atoms together.

The role of the thiolate ligands, —SR, as a μ_2-bridge in transition-element compounds has been extensively documented by X-ray structure determination.[11] Acting as a μ_2-bridge, —SPh forms a di-bridge in compound **1** and tri-bridge in compound **5**. The structure of compound **5** is totally different from that of **1**. The molecule of **5** is asymmetric with one five-coordinate and one four-coordinate cobalt atom. The atomic distances between cobalt and the bridging sulphur atom vary moderately in structure type **1**, but dramatically in compound **5**, which range from 2.215(4) to 2.376(3) Å. The mean bond length, Co—S_t, of 2.197(22) Å in type **1** is close to the Co(2)—S(4) distance [2.215(4) Å] in structure **5** but is shorter than the mean Co—S_t bond length of 2.245(4) Å in the five-coordinate cobalt complex $Co[(C_6H_5)_2PC_2H_4]_2PC_6H_5(SPh)_2$,[13] and much shorter than that of 2.33(1) Å found in the tetrahedral complex $[Co(SPh)_4]^{2-}$.[14] The mean Co—P bond lengths ot type **1**, ranging from 2.337(1) Å in **1aa** to 2.349(9) Å in structure **1ss**, is significantly longer than that of 2.210(6) Å in structure **5**. No dramatic variation can be observed in the corresponding cobalt–ligand bond lengths among the three conformations of **1**. However, the cobalt–cobalt distances vary considerably even among the three conformations of the same complex [from 2.683 to 2.655(2) Å]. This cannot be explained by the individual cobalt–ligand coordination mode, but should take into account the whole structure. Structure **2** might benefit from both a favourable steric conformation and electronic effects of the methyl groups in phenyl-thiols acting on the cobalt atoms, which consequently enable the molecule to possess the shortest cobalt–

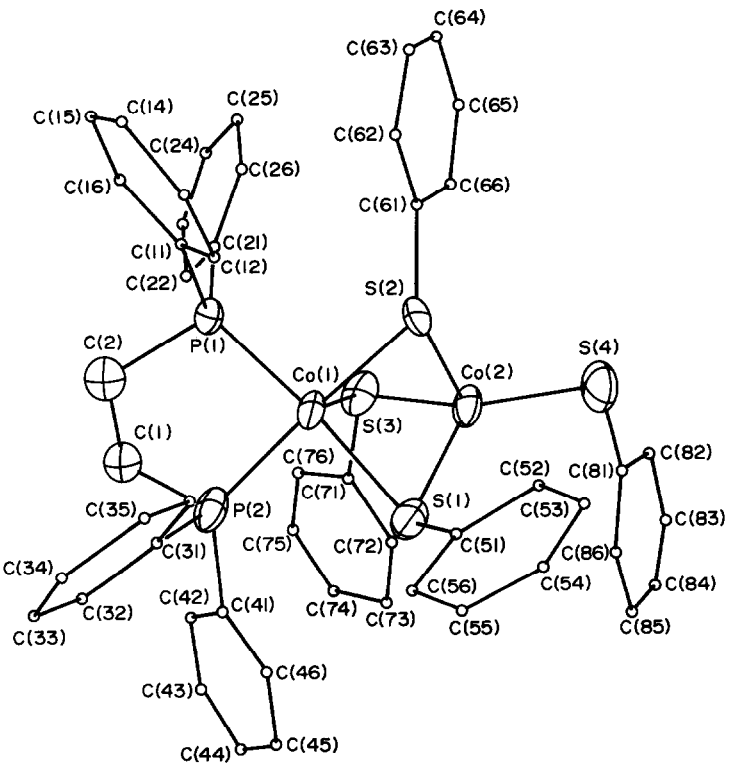

Fig. 4. Perspective view of the structure of $[Co_2(dppe)(SPh)_4]$ (**5**).

cobalt distance [2.634(1) Å] of the four structures.

Cobalt(II) (d^7) can assume either a low- ($S = 1/2$) or a high- ($S = 3/2$) spin configuration when the energy separation (ΔE) between the two highest orbitals is higher or lower than the spin-pairing energy. Five-coordinate complexes with "soft" donor atoms such as phosphorus have the low-spin configuration.[15] Making assumptions of spin-only, high-temperature approximation and no magnetic interaction between paramagnetic centres, the magnetic moment of the complex can be calculated as $\mu_{calc} = \Sigma[g_i S_i(S_i+1)]^{1/2}/N$. For the complex containing two low-spin cobalt(II), $\mu_{ll} = 2.45\ \mu_B$, and for the complex with one high-spin and one low-spin cobalt(II) atoms, $\mu_{hl} = 4.24\ \mu_B$. The observed magnetic moments of complexes with dppm (**1–4**, $1.67 \pm 0.05\ \mu_B$) and with dppe (**5**, $3.69\ \mu_B$) are slightly smaller than the calculated values of μ_{ll} and μ_{hl}, respectively. Therefore, it is sensible to assume that the former complexes (**1–4**) consist of two low-spin cobalt(II) atoms, while **5** consists of one high- and one low-spin cobalt(II) atom with antiferromagnetic coupling between the two cobalt(II) atoms within a molecule in any one of the complexes **1–5**. The EPR spectra showed coherent signals for complex **5**, but there is no EPR signal for the dppm complexes (**1–4**). The g features of **5** are similar to those of five-coordinate mono-cobalt(II) complexes in the literature.[16]

Acknowledgement—This work was partly supported by a National Natural Science Foundation Grant.

REFERENCES

1. C. A. McAuliffe and W. Levason, *Phosphine, Arsine and Stibine Complexes of the Transition Elements*. Elsevier, Amsterdam (1979).
2. R. J. Puddephatt, *Chem. Soc. Rev.* 1983, **12**, 99; F. A. Cotton, K. R. Dunbar and M. G. Verbruggen, *J. Am. Chem. Soc.* 1987, **109**, 5498; A. L. Balch, in *Reactivity of Metal–Metal Bonds* (Edited by M. H. Chisholm). ACS Symposium Series, 1981, **155**, 167; M. Atoh, I. Kinoshita, K. Kashiwabara and J. Fujita, *Bull. Chem. Soc. Japan* 1982, **55**, 3179; R. U. Kirss and R. Eisenberg, *Inorg. Chem.* 1989, **28**, 3372.
3. P. J. Blower and J. R. Dilworth, *Coord. Chem. Rev.* 1987, **76**, 121; I. G. Dance, *Polyhedron* 1986, **5**, 1037; T. E. Wolff, J. N. Berg, P. P. Power, K. O. Hodgson and R. H. Holm, *Inorg. Chem.* 1980, **19**, 430.
4. H. Q. Liu, Q. T. Liu, B. S. Kang, L. J. He, C. N. Chen, K. Zhao, M. C. Hong, L. R. Huang, J. Zhuang and J. X. Lu, *Scientia Sin.* 1988, **31B**, 10; B. S. Kang, L. H. Weng, D. X. Wu, F. Wang, Z. Guo, L. R. Huang, Z. Y. Huang and H. Q. Liu, *Inorg. Chem.* 1988, **27**, 1128.
5. P. S. Braterman, V. A. Wilson and K. K. Joshi, *J. Organomet. Chem.* 1971, **31**, 123; D. C. Povey, R. L. Richards and C. Shortman, *Polyhedron* 1986, **5**, 369; J. A. M. Canich, F. A. Cotton, K. R. Dunbar and L. R. Falvello, *Inorg. Chem.* 1988, **27**, 804; C. T. Hunt and A. L. Balch, *Inorg. Chem.* 1981, **20**, 2267.
6. G. W. Wei, H. Q. Liu, Z. Y. Huang, L. R. Huang and B. S. Kang, *J. Chem. Soc., Chem. Commun.* 1989, 1839.
7. K. K. Chow and C. A. McAuliffe, *Inorg. Chim. Acta* 1975, **14**, 121.
8. B. A. Frenz, *Computing in Crystallography* (Edited by H. Schenk, R. Olthof-Hazekamp, H. Van Koningsveld and G. C. Bassi), p. 64. Delft University Press, Delft, The Netherlands (1978).
9. The full-matrix least-squares program was revised to be suitable for 210 atoms and 996 parameters; difference Fourier map program and ATOMS program were revised correspondingly.
10. S. W. Carr and R. Colton, *Aust. J. Chem.* 1981, **34**, 35.
11. K. S. Hagen and R. H. Holm, *Inorg. Chem.* 1984, **23**, 418.
12. G. W. Wei and Q. Z. Huang, unpublished work.
13. G. W. Wei, Z. Y. Huang, M. C. Hong, L. R. Huang and H. Q. Liu, submitted.
14. D. Swenson, N. C. Baenziger and D. Coucouvanis, *J. Am. Chem. Soc.* 1978, **100**, 1932.
15. L. Sacconi, *J. Chem. Soc. A* 1970, 248.
16. G. Labauze and J. B. Raynor, *J. Chem. Soc., Dalton Trans.* 1981, 590.

Polyhedron Vol. 10, No. 6, pp. 561–566, 1991
Printed in Great Britain

0277-5387/91 $3.00+.00
© 1991 Pergamon Press plc

SYNTHESIS AND CHARACTERIZATION OF PALLADIUM COMPLEXES WITH BIS(BENZYLTHIO)METHANE

YOSHIO FUCHITA* and HIROYUKI MARUYAMA

Laboratory of Chemistry, College of General Education, Kyushu University, Ropponmatsu, Chuo-Ku, Fukuoka 810, Japan

and

MASANORI KAWATANI and KATSUMA HIRAKI

Department of Industrial Chemistry, Faculty of Engineering, Nagasaki University, Bunkyo-machi, Nagasaki 852, Japan

(*Received* 8 *August* 1990; *accepted* 31 *October* 1990)

Abstract—Reactions of $Na_2[PdCl_4]$ with one equivalent and two equivalents of bis(benzylthio)methane (btm) yield *trans*-$[PdCl_2(\mu\text{-btm})]_n$ (**1**) and *trans*-$[PdCl_2(\text{btm-}S)_2]$ (**2**), respectively. Treatment of **2** with $[PdCl_2(NCMe)_2]$ gives the face-to-face type palladium(II) complex, *trans*-$[Pd_2Cl_4(\mu\text{-btm})_2]$ (**3**), whereas the reaction of **2** with $[Pd(dba)_2]$ (dba = dibenzylideneacetone) produces the side-by-side type palladium(I) complex, $[Pd_2Cl_2(\mu\text{-btm})_2]$ (**4**). Treatment of **4** with dimethyl acetylenedicarboxylate gives the A-frame type complex $[Pd_2Cl_2\{\mu\text{-}C_2(CO_2Me)_2\}(\mu\text{-btm})_2]\cdot 1/2CH_2Cl_2$ (**5**). The complexes obtained in this study were characterized by elemental analysis, IR and NMR spectroscopy.

There has been interest recently in binuclear complexes containing the "short-bite" ligands such as bis(diphenylphosphino)methane[1] and 2-(diphenylphosphino)pyridine,[2] etc. In our previous papers, we have reported the synthesis of mono- and bimetallic complexes of palladium[3] and rhodium[4] containing the unsymmetrical "short-bite" ligand, (benzylthiomethyl)diphenylphosphine. Syntheses have also been reported of various metal complexes with symmetrical "short-bite" sulphur donor ligands; specifically thioether ligands, $RSCH_2SR$ (R = Me, Ph).[5–12] These dithioether ligands are mostly coordinated in unidentate or bidentate chelating modes in metal complexes. As for the bidentate bridging coordination mode of dithioether ligands, few have been reported: the platinum complexes of $[(PtXMe_3)_2(\mu\text{-MeSCH}_2\text{SMe})]$[8,9] and the rhodium complex of $[Rh_2Cl_2(\mu\text{-CO})(\mu\text{-PhSCH}_2\text{SPh})_2]$[10] are two examples.

Here, we wish to report the synthesis of palladium complexes with a dithioether ligand, bis(benzylthio)methane (btm), including the side-by-side type bimetallic complex of $[Pd_2Cl_2(\mu\text{-btm})_2]$, the face-to-face type complex of $[Pd_2Cl_4(\mu\text{-btm})_2]$ and the A-frame type complex of $[Pd_2Cl_2\{\mu\text{-}C_2(CO_2Me)_2\}(\mu\text{-btm})_2]$.

RESULTS AND DISCUSSION

The new reactions of bis(benzylthio)methane are summarized in Scheme 1. Yields, melting points and analytical data are listed in Table 1, while ^1H and ^{13}C NMR data are summarized in Table 2.

Reactions of $Na_2[PdCl_4]$ *with* btm

Treatment of btm with one or a half equivalent of $Na_2[PdCl_4]$ yielded *trans*-$[PdCl_2(\mu\text{-btm})]_n$ (**1**) and *trans*-$[PdCl_2(\text{btm-}S)_2]$ (**2**), respectively. The ^1H NMR spectrum of **1** was not obtained due to its poor solubility in common solvents. However, the far-IR spectrum showed a single band at 361 cm^{-1} assigned to ν(Pd—Cl), suggesting a *trans* con-

* Author to whom correspondence should be addressed.

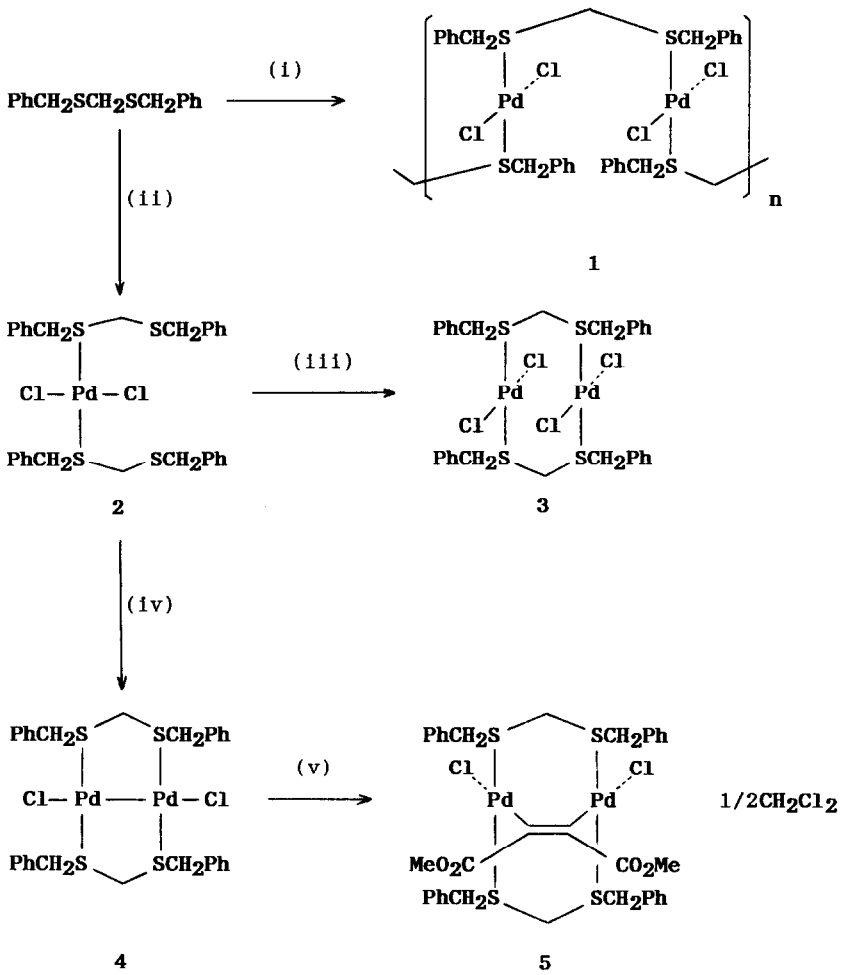

Scheme 1. Formation and reactions of btm complexes of palladium: (i) one equivalent of $Na_2[PdCl_4]$; (ii) a half equivalent of $Na_2[PdCl_4]$; (iii) $[PdCl_2(NCMe)_2]$; (iv) $[Pd(dba)_2]$; (v) $MeO_2CC{\equiv}CCO_2Me$.

figuration of the chloro ligands. On the basis of these results and the elemental analysis, **1** was assigned an oligomeric structure in which btm acts as a bidentate bridging ligand, as shown in Scheme 1.

As for **2**, the elemental analysis supported the formulation of $[PdCl_2(btm\text{-}S)_2]$ and the far-IR spectrum indicated a *trans* configuration of the chloro ligands [ν(Pd—Cl) 362 cm^{-1}]. Complex **2** showed temperature-dependent ^1H NMR spectra, as shown in Fig. 1. At 50°C, two singlets appeared at δ 4.11 and 3.81 due to CH_2Ph and SCH_2S, respectively. The former singlet broadened at 25°C and then at −10°C separated into two broad resonances at δ 4.25 and 3.95. Furthermore, at −50°C the resonance at δ 4.25 became sharp (δ 4.28), whereas the signal at δ 3.95 separated into two resonances at δ 3.95 and 3.90. In contrast, the SCH_2S resonance, observed at δ 3.81 at 50°C, broadened at −10°C and then at −50°C separated into two humps at δ 3.8 and 3.6. These phenomena could be explained in terms of 1,3-intramolecular metal shifts between the four ligand sulphur atoms and the pyramidal inversions of the ligated sulphur atoms, as illustrated in Fig. 2. At 50°C, the 1,3-metal shifts and the

Table 1. Yields, melting points and analytical data

Complex	Yield (%)	Melting point (°C)	Analysis (%)[b] C	H
1	87	166	40.8(41.2)	3.6(3.7)
2	75	100	51.1(51.6)	4.6(4.6)
3	80	105	41.0(41.2)	3.7(3.7)
4	50	128	44.3(44.8)	3.9(4.0)
5	50	165	44.6(44.3)	4.1(4.0)

[a] With decomposition.
[b] Calculated values in parentheses.

Table 2. NMR spectral data

Complex	^{1}H NMR[a]	^{13}C{^{1}H} NMR[a]
2	3.81 (s, SCH_2S); 4.11 (s, CH_2Ph); 7.2–7.4 (m, Ph)	37.93 (SCH_2S); 38.45 (CH_2Ph); 128.03 (*para*-Cs); 128.92 (*meta*-Cs); 129.77 (*ortho*-Cs)[b]
3	3.9 (br s, SCH_2S); 4.35 (br s, CH_2Ph); 7.1–7.5 (m, Ph)	—[c]
4	3.96 (s, SCH_2S); 4.29 (s, CH_2Ph); 7.1–7.4 (m, Ph)	38.12 (SCH_2S); 42.89 (CH_2Ph); 128.89 (*para*-Cs); 129.14 (*meta*-Cs); 129.55 (*ortho*-Cs); 133.60 (*ipso*-Cs)
5	2.73 [d, ^2J(HH) 12.1 Hz, SCH_2S]; 3.43 [d, ^2J(HH) 12.1 Hz, SCH_2S]; 3.69 [s, OCH_3]; 4.38 [d, ^2J(HH) 13.9 Hz, CH_2Ph]; 4.45 [d, ^2J(HH) 13.9 Hz, CH_2Ph]; 5.28 (s, CH_2Cl$_2$)	31.51 (SCH_2S); 41.31 (CH_2Ph); 52.23 (CO_2CH_3); 128.61 (*para*-Cs); 129.22 (*meta*-Cs); 129.65 (*ortho*-Cs); 133.65 (*ipso*-Cs); 163.47 (CO_2CH_3)[d]

[a] Spectra obtained in $CDCl_3$ at 50°C. s = singlet, d = doublet, m = multiplet and br = broad.
[b] *Ipso*-Cs could not be detected.
[c] Not measured (see text).
[d] Olefinic carbons could not be detected.

pyramidal inversions were supposed to take place rapidly, and these motions caused two differential sited CH_2Ph groups to resonate as one singlet at δ 4.11. At −10°C, the 1,3-metal shifts seem to be quenched, while the pyramidal inversions are still occurring. Accordingly, at this temperature two different environmental CH_2Ph groups appeared as two signals. Finally, at −50°C, when the pyramidal inversions were nearly quenched, the CH_2Ph groups directly attached to the ligated sulphur atoms further split into two signals owing to the presence of diastereomers, DL and *meso* (Fig. 2). Corresponding to this fact, at −50°C SCH_2S separated into two humps. Further measurements below −50°C were

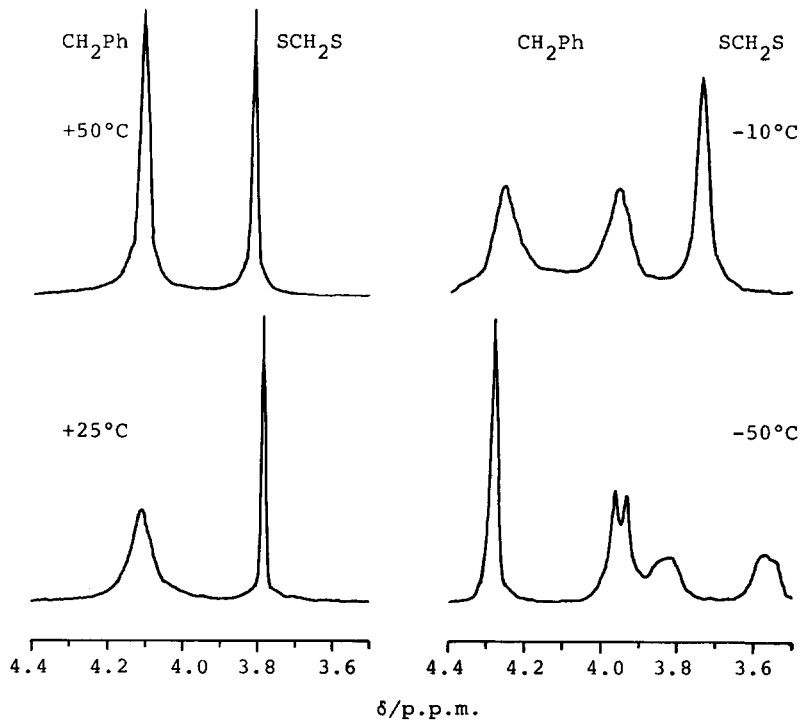

Fig. 1. Temperature-dependent ^{1}H NMR spectra of [$PdCl_2$(btm-*S*)$_2$] (**2**) in $CDCl_3$.

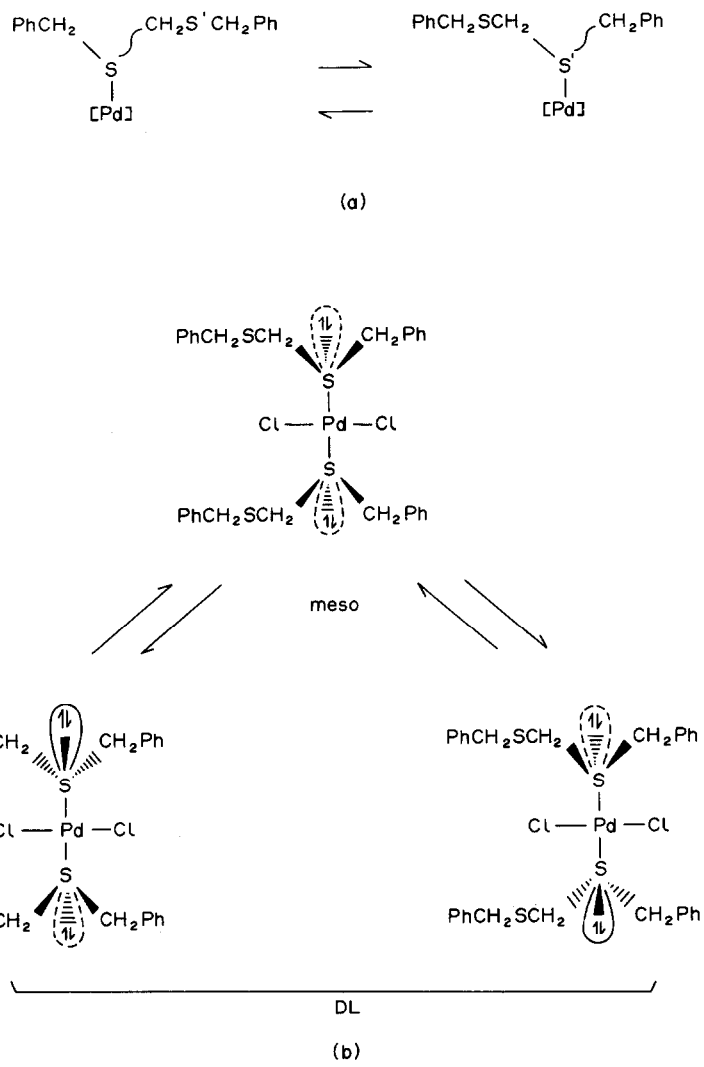

Fig. 2. (a) The 1,3-intramolecular metal shifts and (b) the pyramidal inversions of ligated sulphur atoms and invertomers of $[PdCl_2(btm\text{-}S)_2]$ (**2**).

unsuccessful due to precipitation of solids from the NMR sample solution. Precise studies on the 1,3-intramolecular metal shifts between the ligand sulphur atoms and the pyramidal inversions of the sulphur atoms have been reported by the groups of Abel[5] and Kuhn.[11] In the $^{13}C\{^1H\}$ NMR spectrum at 50°C, two methylene carbons due to CH_2Ph and SCH_2S were observed at δ 38.45 and 37.93, respectively.

On the basis of the results mentioned above, together with the molar conductance (Λ_M 2.4 S cm^2 mol^{-1} in acetone), **2** was assigned to *trans*-$[PdCl_2(btm\text{-}S)_2]$ in which two btm ligands are coordinated in a unidentate fashion. Two sulphur atoms in each btm ligand in **2** are coordinatively free, and **2** reacted to form bimetallic complexes (see below).

The face-to-face type complexes $[Pd_2Cl_4(\mu\text{-btm})_2]$ (**3**)

Treatment of **2** with one equivalent of $[PdCl_2(NCMe)_2]$ afforded **3** which had the same composition as **1** by elemental analysis. However, the molecular weight of **3** was 804.5 (determined by osmometry in benzene at 42°C; calc. for $C_{30}H_{32}Cl_4Pd_2S_4$: 875.5). In contrast with **1**, **3** is soluble in benzene, chloroform and dichloromethane, but is not as stable under conditions of prolonged standing or heating in solution due to gradual conversion back to **1**. For this reason, the ^{13}C NMR spectrum could not be measured. Temperature-dependent ^1H NMR spectra were observed for **3**. At 50°C, **3** showed a nearly high-

temperature limiting spectrum exhibiting two kinds of methylene proton due to CH_2Ph and SCH_2S moieties. These occurred as slightly broad singlets at δ 4.35 and 3.9, respectively. However, the low-temperature limiting spectra were very complicated owing to a number of conformers caused by the pyramidal inversions of the ligated sulphur atoms. Complete analysis of the temperature-dependent spectra will be reported elsewhere in due course. The ^1H NMR spectra of **4** and **5**, showed similar situations to **3**, but only high-temperature limiting spectra are described in this paper (see below).

On the basis of these results and the far-IR spectrum [ν(Pd—Cl) 357 cm^{-1}], **3** was assigned to the face-to-face type palladium(II) complex, $[Pd_2Cl_4(\mu\text{-btm})_2]$, as illustrated in Scheme 1.

The side-by-side type complex $[Pd_2Cl_2(\mu\text{-btm})_2]$ **(4)**

Treatment of **2** with one equivalent of $[Pd(bda)_2]$ (dba = dibenzylideneacetone) afforded **4** as orange–brown microcrystals. The high-temperature limiting ^1H NMR spectrum at 50°C exhibited singlets at δ 4.29 and 3.96 due to CH_2Ph and SCH_2S, respectively. The $^{13}C\{^1H\}$ NMR spectrum at 50°C exhibited two methylene carbon signals at δ 42.89 (CH_2Ph) and 38.12 (SCH_2S). On the basis of these results, elemental analysis, its deep colour and the reactivity towards dimethyl acetylenedicarboxylate (see below), **4** was assigned to the side-by-side type palladium(I) complex $[Pd_2Cl_2(\mu\text{-btm})_2]$.

The A-frame type complex $[Pd_2Cl_2\{\mu\text{-}C_2(CO_2Me)_2\}(\mu\text{-btm})_2]$ **(5)**

The reaction of **4** with dimethyl acetylenedicarboxylate yielded the A-frame type complex **5**. The IR spectrum showed a ν(C=O) band at 1700 cm^{-1} and a ν(C=C) band at 1580 cm^{-1}. The ^1H NMR spectrum was measured at 50°C, a temperature at which the pyramidal inversions occurred rapidly. Together with the OCH_3 resonance at δ 3.69, CH_2Ph and SCH_2S appeared as AB quartets at δ 4.45 (d) and 4.38 (d), and δ 3.43 (d) and 2.73 (d), respectively. As this complex is an A-frame type, the two protons of the SCH_2S moieties are originally non-equivalent and CH_2Ph are diastereotopic even when rapid pyramidal inversions of the ligated sulphur atoms occur, and they were observed as AB quartets. In the $^{13}C\{^1H\}$ NMR spectrum at 50°C, all carbons except for the olefinic carbons formed by the insertion of the acetylene were clearly detected (Table 2).

Conclusions

The dithioether ligand, btm, was found to coordinate to palladium complexes in a unidentate manner in **2**, and a bidentate bridging fashion in **1** to form an oligomeric compound, or in **3** and **4** to produce bimetallic complexes. Complexes **2**–**4** are fairly stable in the solid state, but gradually decomposed in solution under prolonged heating or standing in air, which precluded the growing of suitable crystals for X-ray structural analysis. The ^{13}C NMR spectra could be successfully measured at 50°C. ^1H NMR spectra were all temperature-dependent mainly owing to the pyramidal inversions of the ligated sulphur atoms, and therefore in this paper only high-temperature limiting spectra have been described.

EXPERIMENTAL

General methods were as previously described in a recent paper from our laboratory.[3] Bis(benzylthio)methane was prepared according to a literature method.[13]

Preparation of trans-$[PdCl_2(\mu\text{-btm})]_n$ **(1)**

A solution of btm (0.097 g, 0.36 mmol) in MeOH (5 cm^3) was added to a solution of $Na_2[PdCl_4]$ (0.100 g, 0.34 mmol) in MeOH (15 cm^3). A yellow precipitate was formed immediately. The resulting suspension was stirred at room temperature for 2 h and filtered to yield **1**.

Synthesis of trans-$[PdCl_2(btm\text{-}S)_2]$ **(2)**

A solution of btm (0.186 g, 0.71 mmol) in MeOH (10 cm^3) was added to a solution of $Na_2[PdCl_4]$ (0.100 g, 0.34 mmol) in MeOH (15 cm^3). A yellow precipitate which initially formed was dissolved and then a yellow precipitate reappeared. Stirring was continued for at least 1 day at room temperature, and the precipitate was collected to give **2**.

Preparation of $[Pd_2Cl_4(\mu\text{-btm})_2]$ **(3)**

Solid $[PdCl_2(NCMe)_2]$ (0.037 g, 0.14 mmol) was added to a solution of **2** (0.100 g, 0.14 mmol) in CH_2Cl_2 (10 cm^3). The resulting solution was stirred at room temperature for 2 h, and the volatile materials were removed under reduced pressure. The residue was recrystallized from CH_2Cl_2–Et_2O–hexane to afford **3** as yellow crystals.

Synthesis of $[Pd_2Cl_2(\mu\text{-btm})_2]$ (**4**)

Solid $[Pd(dba)_2]$ (0.300 g, 0.52 mmol) was added to a solution of **3** (0.363 g, 0.52 mmol) in CH_2Cl_2 (15 cm^3), and the mixture was refluxed for 30 min. After the reaction mixture was evaporated to dryness, the residue was chromatographed on a silica gel column (200 mesh, 200 × 10 mm). The red fraction eluted by CH_2Cl_2 was concentrated and diluted with hexane to give **4** as orange–brown microcrystals.

Preparation of $[Pd_2Cl_2\{\mu\text{-}C_2(CO_2Me)_2\}(\mu\text{-btm})_2]\cdot 1/2CH_2Cl_2$ (**5**).

An excess of dimethyl acetylenedicarboxylate (0.233 g, 1.57 mmol) was added to a stirred solution of **4** (0.315 g, 0.39 mmol) in CH_2Cl_2 (20 cm^3). The resulting solution was stirred for 1 day, during which time the colour changed from orange–brown to yellow–orange. After the reaction mixture was evaporated to dryness, the residue was chromatographed on a silica gel column (200 mesh, 180 × 10 mm). The yellow–orange fraction eluted by CH_2Cl_2–Et_2O (10 : 1) was collected and recrystallized from CH_2Cl_2–hexane to afford **5**.

REFERENCES

1. R. J. Puddephatt, *Chem. Soc. Rev.* 1983, **12**, 99 and refs therein.
2. A. L. Balch, *Homogeneous Catalysis with Metal Phosphine Complexes* (Edited by L. H. Pignolet), Ch. 5, p. 167. Plenum Press, London (1983).
3. Y. Fuchita, K. I. Hardcastle, K. Hiraki and M. Kawatani, *Bull. Chem. Soc. Japan* 1990, **63**, 1961.
4. Y. Fuchita, Y. Ohta, K. Hiraki, M. Kawatani nd N. Nishiyama, *J. Chem. Soc., Dalton Trans.* 1990, 3767.
5. E. W. Abel, T. E. Mackenzie, K. G. Orrell and V. Sik, *Polyhedron* 1987, **6**, 1785.
6. S. G. Murray, W. Levason and H. E. Tuttlebee, *Inorg. Chim. Acta* 1981, **51**, 185.
7. A. R. Sanger and J. E. Weiner-Fedorak, *Inorg. Chim. Acta* 1980, **42**, 101.
8. E. W. Abel, A. R. Khan, K. Kite, K. G. Orrell and V. Sik, *J. Chem. Soc., Dalton Trans.* 1980, 1169.
9. E. W. Abel, A. R. Khan, K. K. Kite, K. G. Orrell and V. Sik, *J. Chem. Soc., Dalton Trans.* 1980, 2208.
10. A. R. Sanger, C. G. Lobe and J. E. Weiner-Fedorak, *Inorg. Chim. Acta* 1981, **53**, L123.
11. N. Kuhn, W. Adams and P. Sartori, *Chem. Z.* 1984, **108**, 224.
12. A. R. Sanger, *Can. J. Chem.* 1984, **62**, 822.
13. K. Brodersen and W. Rolz, *Chem. Ber.* 1977, **110**, 1042.

Polyhedron Vol. 10, No. 6, pp. 567–574, 1991
Printed in Great Britain

0277–5387/91 $3.00+.00
© 1991 Pergamon Press plc

A STUDY OF THE INTERACTION OF METHYL SALICYLATE WITH SMECTITE CLAYS

PAUL O'BRIEN* and COLIN J. WILLIAMSON

Department of Chemistry, Queen Mary and Westfield College, Mile End Road, London, E1 4NS, U.K.

(*Received* 17 *July* 1990; *accepted* 2 *November* 1990)

Abstract—The binding of methyl salicylate to smectite clays has been studied using a wide range of techniques. The work encompasses studies by classical methods (thermal analysis and adsorption isotherms) and by ^{13}C solid-state NMR, electronic and FTIR spectroscopies. Mobile and static phases have been identified within the clay matrix in MAS and CP/MAS solid-state NMR experiments. Pillaring of the clay substantially modifies the mode of interaction of methyl salicylate with the clay; NMR evidence is again particularly useful.

Smectite clays are widely used as adsorbents/absorbants in a variety of industrial applications, including waste disposal and catalysis.[1,2] Fuller's Earth, calcium montmorillonite, is a common, cheap clay widely utilized for organic/inorganic absorption. Molecules can bind to clays in many ways depending on the properties of the molecule (e.g. polarity, size, charge) and the clay (e.g. interlamellar cation, hydration state, surface charge). Accommodation of organic molecules by the clay is mainly, but not exclusively, within the interlamellar regions.

The binding of organic molecules to clays saturated with inorganic cations can occur in a variety of ways. These include: direct coordination to the interlamellar metal ion(s), coordination via water bridges, van der Waals' attraction between molecules and the clay surfaces, protonation of organic bases and hydrogen bonding to surface oxygens.[3] In the present work, the sorption of methyl salicylate by montmorillonites has been studied using solid-state ^{13}C NMR, thermogravimetric analysis (TGA), Fourier transform IR (FTIR) and diffuse reflectance electronic spectroscopy. Results from these studies complement an earlier study in which X-ray diffraction (XRD) and differential thermal analysis (DTA) were used to investigate various clay, methyl salicylate systems.[4]

In the present paper, the sorption of methyl salicylate by various cation-exchanged smectite clays, calcium montmorillonite, Westonite (a magnesium montmorillonite especially suitable for NMR work) and Westonite pillared with hydroxyaluminium ions, has been studied. Previous studies of methyl salicylate binding to smectite clays have shown that Fuller's Earth and Westonite adsorb/absorb 26% and 22% w/w methyl salicylate, respectively, before free liquid is observed by thermal methods.[4] However, ^{1}H solid-state NMR spectra provide unequivocal evidence of mobile species even at low loadings.[5] Such observations may be important for a proper understanding of the mobility of organic molecules both in soil and within clay matrices used for waste disposal.

RESULTS AND DISCUSSION

Adsorption isotherms for methyl salicylate

The uptake of methyl salicylate (MS) from hexane, by the various clay samples, was monitored by electronic spectroscopy using the absorption band of methyl salicylate centred on 307 nm (n to π^* of C=O, $\varepsilon = 33{,}980\ mol^{-1}\ cm^{-1}\ dm^3$). Hexane, being non-polar, has little or no affinity for the clay, an assumption which was tested by immersing a small quantity of the clay in hexane and leaving the sample to stand for some hours. After the removal

* Author to whom correspondence should be addressed.

of the hexane, by filtration, and air drying, the FTIR spectrum of the clay showed no evidence for sorbed hexane.

A typical set of adsorption isotherms for the methyl salicylate/calcium montmorillonite system are shown in Fig. 1. As the concentration of methyl salicylate in solution is increased the quantity absorbed by the clay increases to a limiting value. The isotherms are close to hyperbolic, and of several adsorption isotherms[6] considered, the Langmuir isotherm provided the best fit, especially at the lower temperatures. The absorption characteristics of the various clay samples, in a range of hydration states, have been investigated and these results are summarized in Figs 1 and 2 and Table 1.

The effect of temperature on the absorption of methyl salicylate is interesting. At higher temperatures the maximum amount of methyl salicylate adsorbed decreases (Fig. 1). However, consistent isosteric heats of adsorption can be calculated using the Clausius–Clapeyron equation (see Table 1). The fact that such plots give excellent straight lines and consistent values for H suggests that similar sites are responsible for absorption at each temperature. The variation in equilibrium coverage with temperature (Fig. 1) can be explained in terms of the equilibrium position of the reaction shifting in favour of desorption as temperature increases; the expected result for an exothermic process. The values obtained for the heat of adsorption by expanded clays, 3–30 kJ mol^{-1}, are in the range

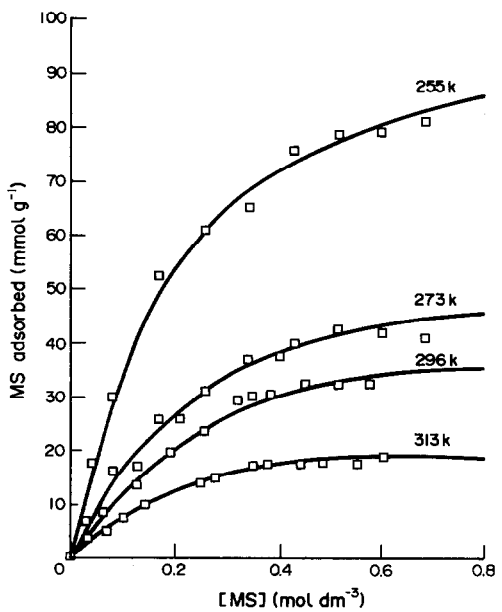

Fig. 1. Adsorption isotherms: the solid lines are fits to the experimental data using the Langmuir isotherm by the Marquard method.

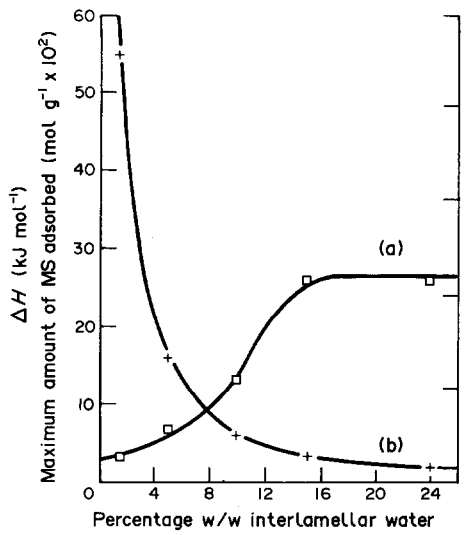

Fig. 2. Variation of maximum observed surface coverage (b) and enthalpy of absorption (a) with hydration state (at 296 K).

generally taken as being typical of the physisorption to a surface. However, in this case some other form of weak interaction, such as hydrogen bonding to interlamellar water, provides a more likely explanation *vide infra*.

The adsorption of methyl salicylate from solution in hexane is also influenced by the state of hydration of the clay. Clays with a decreased water content, in the interlamellar region, have an increased maximum affinity for methyl salicylate at room temperature, but a lower isosteric enthalpy of absorption (see Fig. 2 and Table 1). These results suggest that water has a crucial role in determining the absorption/adsorption of methyl salicylate by smectite clays.

The nearly totally dehydrated clay (1.5% w/w water) is effectively "collapsed" and failed to re-expand (confirmed by XRD) on exposure to methyl salicylate. In this case only external surfaces are available for adsorption of methyl salicylate.

The change in the interlamellar cation, Ca^{2+} to Mg^{2+} (Fuller's Earth to Westonite), causes a slight increase in the amount of methyl salicylate adsorbed, and a decrease in the enthalpy of absorption. This may be due to an effect of the greater charge density of magnesium on either, methyl salicylate directly, or on methyl salicylate via a water bridge. The latter appears to be a more likely explanation; water is not displaced from the interlamellar region on the intercalation of methyl salicylate (see IR results) at the same hydration state. The pillared clay has a much higher heat of absorption for methyl salicylate than any of the other clays studied (Table 1), an observation which may

Table 1. Equilibrium studies of the sorption of methyl salicylate from hexane by various clays[a]

Clay	$10^2\theta_{max}$ (mol g^{-1})	$10^3\beta$ (mol g^{-1})	ΔH_{ads} (kJ mol^{-1})	Average
FE(1.5%)	55(±4)	1.0	4.3	
		2.0	3.1	3.4
		3.0	2.9	
FE(5%)	10(±2)	0.4	7.6	
		0.8	6.9	6.8
		1.1	6.7	
FE(10%)	6(±0.6)	0.3	13.4	
		0.5	13.7	13.3
		0.7	12.8	
FE(15%)	3.5(±0.2)	0.1	26.6	
		0.2	28.1	26.0
		0.3	23.4	
FE(24%)	2.0(±0.2)	0.05	29.5	
		0.13	23.8	26.1
		0.2	25.1	
WEST(15%)	4.0(±0.2)	0.1	15.2	
		0.2	17.2	16.1
		0.3	16.0	
PILW(9%)	3.0(±0.2)	0.1	29.4	
		0.2	27.6	28.5

[a] FE—Fuller's Earth, WEST—Westonite, PILW—pillared interlamellar Westonite. The figures in parentheses represent the percentage w/w interlamellar water.

θ, Maximum coverage, as measured experimentally at 296 K.

β, Surface coverage used in enthalpy estimation.

suggest a different site of interaction for this clay. This suggestion is supported by the NMR spectroscopic studies.

Thermogravimetric analysis of clay/methyl salicylate samples

Thermogravimetric traces for the Fuller's Earth, 5% and 12% interlamellar water, and the same samples loaded with 10% w/w methyl salicylate, are shown in Fig. 3. The results for the clays show that interlamellar water desorbs from the clay and is completely removed by *ca* 80°C (10°C min^{-1}, static air).

The samples doped with methyl salicylate show two distinct steps in their decomposition. The nature of the species in the vapour phase above such samples was investigated by FTIR spectroscopy, methyl salicylate was found to be present in the vapour at all temperatures.

The "two-step" nature of the desorption of methyl salicylate suggests that there are two types of loss of it from the clay. Methyl salicylate lost concurrently with the loss of interlamellar water, and a second, subsequent loss predominantly of methyl salicylate alone. A possible explanation for these observations is as follows. At lower temperatures, methyl salicylate is coordinated to the hydrated silicate layers and hydrated metal cations, loss of methyl salicylate occurs concurrently with the loss of coordinated water molecules. However, methyl salicylate is less volatile than water (the temperatures for saturated vapour pressures of 40 torr are 126 and 34.1°C, respectively[7]) and once the interlamellar water is removed, the methyl salicylate remaining in the sample re-orientates and binds to the dehydrated layers/cations and is only removed at elevated temperatures. Lower dopings were tested (*ca* 5%) but the same pattern of traces occurred.

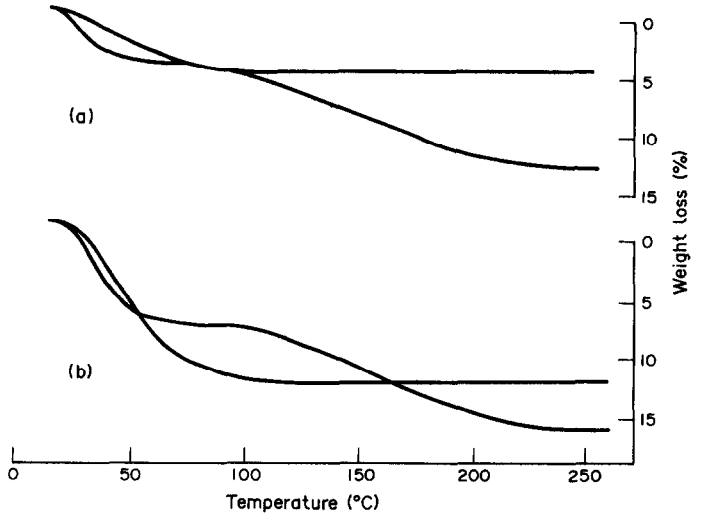

Fig. 3. Typical thermal analysis results. Traces are for clay in the presence and absence of methyl salicylate. (a) 10% methyl salicylate on Fuller's Earth (5% w/w water); (b) 10% methyl salicylate on Fuller's Earth (10% w/w/ water).

Solid-state NMR and FTIR spectra of methyl salicylate/clay samples

Westonite was chosen as a substitute for Fuller's Earth when recording solid-state NMR due to the very small quantities of paramagnetic ions, mainly iron(III) and manganese(II), within the clay. ESR and EDAX measurements were able to establish the quantity of paramagnetics and hence assess the suitability for solid-state NMR.[8] Two kinds of solid-state NMR experiments have been carried out: magic-angle spinning (MAS) decoupled spectra and cross-polarized CP/MAS spectra. The methods are detailed in the Experimental; CP/MAS spectra are only observed for immobile phases, whereas MAS spectra will occur predominantly for mobile and to a lesser extent for immobile phases. Static ^{1}H NMR spectra could not be observed for Westonite/methyl salicylate samples, presumably due to the presence of some paramagnetic material in the clay sample.

A typical ^{13}C NMR CP/MAS spectrum of methyl salicylate adsorbed on Westonite is shown in Fig. 4. The spectrum is unusual when compared with the ^{13}C solution or solid-state (frozen MS) NMR spectrum of methyl salicylate in that the resonances associated with the two carbons adjacent to the ester function (7 and 1) are absent. The signal for the carbon adjacent to the phenolic group (2) is also affected and is weakened in the CP/MAS spectrum. However, the signal due to the methyl group of the ester function (8) is still observed. Similar results are obtained for other salicylate esters. However, related systems containing a quaternary carbon atom, such as the Westonite complex of methyl-2-hydroxyisobutyric acid, have peaks for the quaternary carbon atoms in the CP/MAS spectrum.

The explanation for the disappearance of peaks in the CP/MAS spectrum of the Westonite/methyl

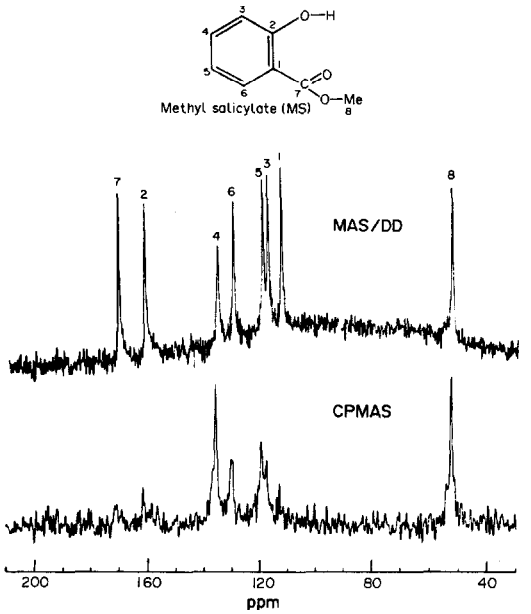

Fig. 4. Typical ^{13}C solid-state NMR spectra of Westonite/methyl salicylate samples. Spectra of methyl salicylate/Westonite (23% w/w). The ^{13}C NMR spectrum of liquid methyl salicylate is identical with the MAS/DD spectrum above and the major peaks in the CP/MAS spectrum, see Table 1.

salicylate system is probably that traces of paramagnetics in the clay relax the nuclei of the carbon atoms closest to the point of attachment too rapidly for these nuclei to be observed. The CP/MAS experiment is particularly sensitive to such effects. These observations may suggest that the protons which are not observed lie close to the clay sheets, as these contain the paramagnetic ions.

It was also possible to observe a MAS/decoupled spectrum of methyl salicylate associated with a clay sample. Such spectra were essentially identical to the high resolution spectrum of liquid or solid methyl salicylate (Fig. 4, Table 2). Solid-state ^1H MAS NMR also provides evidence for mobile species of methyl salicylate associated with the clay at low dopings; sharp peaks associated with the organic are observed.[5]

Taken together, the results suggest that methyl salicylate exists as two phases within the clay matrix, a fluid phase (giving rise to the MAS/decoupled spectrum) and an immobile phase (associated with the CP/MAS spectrum). As might be expected, the signal due to the fluid phase was relatively more intense at the higher dopings of methyl salicylate onto the clay.

It is interesting to contrast the major changes in the solid-state NMR spectrum with the relatively small shifts observed in the IR spectrum of methyl salicylate adsorbed by such clays. In the conventional IR region of the spectrum the frequency of the carbonyl peak at 1678 cm^{-1} increases by 2–4 cm^{-1} on intercalation (spectra as Nujol mulls or in KBr/CsI discs), and although a new peak associated with the —OH stretch of methyl salicylate can be observed, this is only possible after spectral subtraction. Other changes occur in the far-IR spectrum (Fig. 5, Table 3), but are more difficult to measure. The IR changes are all associated with the ester and phenolic functions, suggesting that these groups are involved in the bonding of the methyl salicylate to the clay. IR spectra of various samples of the clays with methyl salicylate show no evidence for the displacement of water from the interlamellar space of the clay, as has recently been reported for the intercalation of phosphate esters.[9] In contrast, the peaks associated with both the ester function and the carbon adjacent to the phenolic group are greatly modified in the CP/MAS spectrum, and provide clear evidence that these are influenced by sorption. The NMR spectra also provide evidence for two separate phases of methyl salicylate within the clay, fluid and immobile.

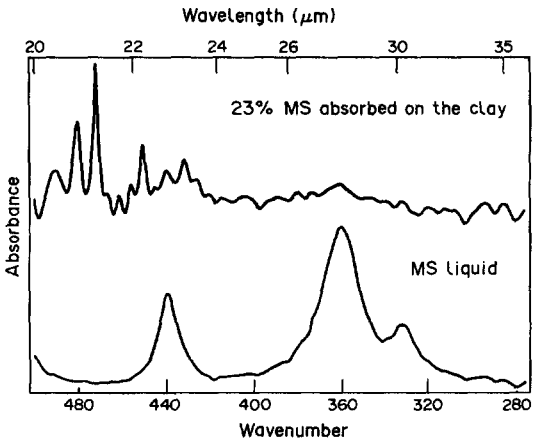

Fig. 5. Far IR spectrum (clay subtracted) of sorbed methyl salicylate compared with a thin film of methyl salicylate.

Typical CP/MAS and MAS/DD spectra of 20% w/w methyl salicylate adsorbed on the pillared Westonite clay are shown in Fig. 6. The CP/MAS spectra of methyl salicylate adsorbed on Westonite and

Table 2. Chemical shift values for the various Westonite/methyl salicylate samples

Carbon	Methyl salicylate liquid	16% w/w MAS/DD	16% w/w CP/MAS	59% w/w MAS/DD	59% w/w CP/MAS
1	112.1	112.9	—	112.7	—
2	161.4	161.8	—	162.1	—
3	117.2	117.8	117.8	117.7	117.6
4	135.3	136.2	136.2	135.8	135.8
5	118.8	119.8	119.5	119.3	119.3
6	129.6	130.7	130.5	130.3	130.2
7	170.3	171.2	—	170.8	—
8	51.6	52.6	52.8	52.1	52.1

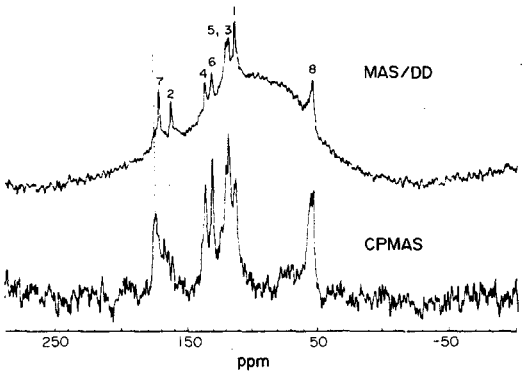

Fig. 6. Typical ^{13}C solid-state NMR spectrum of pillared Westonite/methyl salicylate samples. Spectra of methyl salicylate/Westonite (23% w/w).

the pillared Westonite are different. All eight peaks of methyl salicylate are present in the CP/MAS spectrum of pillared interlamellar Westonite compared with only five in the CP/MAS of methyl salicylate on Westonite (MS/W). The appearance of resonances 1, 2 and 7 of methyl salicylate in the spectrum of pillared interlamellar Westonite may suggest a different point of attachment of the organic molecule to the clay. One explanation for this observation is that the adsorption sites are removed from any paramagnetic impurities (in the clay matrix), which in the parent clay (Westonite) system caused relaxation of the appropriate carbons. Conversely, the fact that all the characteristic signals of methyl salicylate can be observed in the CP/MAS for the pillared interlamellar Westonite sample supports the suggestion that the point of attachment is responsible for the disappearance of these resonances in the parent system. Specifically this observation tends to rule out explanations for the non-appearance of the resonances based on their quaternary nature. The MAS/DD spectrum is identical to that of the parent system, suggesting a fluid phase within the clay.

There are other important features of the CP/MAS spectrum of the pillared interlamellar Westonite/methyl salicylate samples. Significant shifts in the carbonyl and phenolic carbon resonances (2 ppm for the latter case) occur. This observation may indicate binding to the pillar adjacent to these carbon atoms; no such shifts were found for the parent system. There is also splitting of the resonances due to carbons 1, 2, 7 and 8 in the CP/MAS spectrum, suggesting two immobile or motion-restricted phases of methyl salicylate within the pillared clay sample. The remaining four phenolic carbons may be too far away from the point of attachment to be significantly affected. There appears to be three types of methyl salicylate molecule associated with pillared interlamellar Westonite, two motion-restricted species and a mobile species.

Electronic spectroscopy

Various ion-exchanged samples of Westonite and Westonite/methyl salicylate were investigated using UV diffuse reflectance spectroscopy. The results of this work are summarized in Table 4. Varying the interlamellar cation within the clay produces little or no change in the dominant UV absorption at *ca* 257 nm. This transition is difficult to assign, but charge-transfer behaviour involving the intercalated metal ion can be ruled out on the basis of this observation.

In the presence of 10% methyl salicylate, this peak shifts to lower wavelength (higher energy) by about 15 nm— a blue, hypochromic shift. The shift appears to be independent of the cation, with the exception of NBu_4^+, for which the shift is only 7 nm. Higher dopings were assessed but no further changes were apparent. The absorption at 307 nm, due to methyl salicylate, is unaffected by the in clay/methyl salicylate samples.

Table 3. IR peaks (cm^{-1}) associated with the sorption of methyl salicylate by montmorillonites

MS	Westonite 10/20% w/w	Fuller's Earth 10–20% w/w	
360	Absent	Absent	COO rock
440	Absent	Absent	Out-of-plane ring deformation
1678	1682	1684	C=O stretch
3200	3200	3200	OH stretch
	3400	3400	OH stretch

Table 4. Diffuse reflectance electronic spectroscopy results (λ_{max}) for various ion-exchanged Westonite clays

Cation	Clay (nm)	10% Methyl salicylate (nm)
Ca^{2+}	257	242
Mg^{2+}	257	245
Al^{3+}	257	244
NBu_4^+	257	250
PILW	255	245

CONCLUSIONS

As detected by solid-state ^1H and ^{13}C NMR spectroscopy there are mobile organic species associated with the clay at a range of dopings. These species are unlike the liquid state. The Westonite/methyl salicylate samples also contain a restricted-motion species which tends to be associated with the small amount of paramagnetics within the clay.

The adsorption is probably best described as binding via "water bridges" within the clay interlamellar spacing, particularly evident in the FTIR spectrum. The isosteric enthalpy of adsorption and the maximum surface coverage is also strongly dependent upon the state of hydration of the clay.

It can be assumed that water bridge formation is the most likely type of adsorption of methyl salicylate to the clay in its normal state of hydration. This type of binding has been suggested for a variety of montmorillonite–organic clay complexes. Molecules of study have included benzonitrile,[10] benzoic acid and nitrobenzene,[11] pyridine,[12] ketones,[13] pyridine-N-oxide,[14] aniline and its derivatives,[15] nitriles[16] and phenol.[17] All such cases tend to be associated with the benzene rings coupled to an electronegative group.

EXPERIMENTAL

Materials

Fuller's Earth (calcium montmorillonite, unknown type location) was obtained from the British Drug Houses (Poole, Dorset, U.K.) and used in various hydration states. Westonite is a naturally-occurring magnesium montmorillonite, low in paramagnetic iron, and was a gift from English China Clays, St Austell, Cornwall (of unknown type location). This clay has been used as a substitute for Fuller's Earth in obtaining NMR spectra and used in its natural hydration state. Westonite has also been studied after "pillaring" with a hydroxy-aluminium ion by a literature method.[18] Each of the clays was characterized as a smectite by XRD and the water content was determined by TGA. Their properties were as follows.

Fuller's Earth (used in various states of hydration) had interlamellar water contents ranging from 2 to 24% (w/w) and corresponding $d(001)$ values from 10.2 to 18.6 Å.

Westonite had a water content of 13% w/w and a $d(001)$ value of 14.7 Å, characteristic of two layers of intercalated water. Pillared interlamellar Westonite had a water content of 9% w/w and a $d(001)$ value of 18.4 Å.

Methyl salicylate was distilled under reduced pressure and dried over molecular sieves before use. Clay samples were prepared by direct mixing of known weights of methyl salicylate and the clay followed by gentle mixing in a pestle and mortar. For the adsorption isotherms, 1 g of clay was added to 10 cm^3 of the appropriate methyl salicylate solution and allowed to equilibrate, with shaking, at the appropriate temperature, for 2 h. A small portion of the solution was extracted and the concentration of methyl salicylate remaining in the solution evaluated spectrophotometrically.

Instrumentation

Solid-state NMR spectra were recorded with a Bruker MSL-300 Instrument (equivalent proton frequency, 300 MHz). ^{13}C NMR shifts are in ppm relative to external TMS. The rotor used was a Kelrin type and the spinning frequency was in the range 4–4.5 kHz. All measurements were made at room temperature. ^{13}C NMR spectra were recorded in single pulse magic-angle spinning experiments (MAS/DD), typically: 400 scans, with a 10 s delay, 34 ms acquisition time. Cross-polarization magic-angle spinning experiments (CP/MAS) were typically: 2000 scans, with a 2 s delay, an acquisition time of 34 ms and a contact time of 1 ms. In both cases the sweep width was close to 30,000 Hz with 70 kHz proton decoupling. FTIR spectra were recorded on a Mattson Polaris Instrument in the range 50–4000 cm^{-1}, using KBr or CsI discs (typically 2 mg of sample to 200 mg of KBr/CsI), 4 cm^{-1} resolution and 32 scans. Electronic spectra were recorded on a Perkin–Elmer 330 spectrophotometer. TGA results were obtained on a Stanton Redcroft TG-750 apparatus in a static air atmosphere using a heating rate of 10° min^{-1}, sample weights were of the order of 5 mg.

Acknowledgements—We thank the Procurement Executive of the Ministry of Defence for their support of this

project and Dr C. J. Groombridge of the University of London Intercollegiate Solid-state NMR Service at Royal Holloway and Bedford New College for enthusiastic help with the solid-state NMR spectroscopy.

REFERENCES

1. P. L. Hall, in *A Handbook of Determinative Methods in Clay Mineralogy* (Edited by M. J. Wilson), Ch. 1, p. 1. Blackie, Glasgow and London (1987).
2. J. M. Adams, S. E. Davies, S. H. Graham and J. M. Thomas, *J. Catal.* 1982, **78**, 197.
3. J. A. Raussell-Colom and J. M. Serratosa, *Chemistry of Clays and Clay Minerals* (Edited by A. C. D. Newman), pp. 385–396. Wiley-Interscience, New York (1987).
4. P. O'Brien and C. J. Williamson, *Clays Clay Miner.* 1990, **38**, 322.
5. P. O'Brien and C. J. Williamson, *Chem. Ind.* 1990, 752.
6. Y. Soma and M. Soma, *Environ. Health Perspect.* 1989, **83**, 205.
7. *C.R.C. Handbook of Chemistry and Physics*, 55th edn, D178. C.R.C. Press, Cleveland (1974).
8. P. O'Brien, C. J. Williamson and C. J. Groombridge, *Chem. Mater.* 1991, in press.
9. J. M. Bowen, C. R. Powers, A. E. Ratcliffe, M. G. Rockley and A. W. Hounslow, *Environ. Sci. Technol.* 1988, **22**, 1178.
10. J. M. Serratosa, *Am. Miner.* 1968, **53**, 1244.
11. S. Yariv, J. D. Russell and V. C. Farmer, *Israel J. Chem.* 1966, **4**, 210.
12. V. C. Farmer and M. M. Mortland, *J. Chem. Soc. A* 1966, 344.
13. R. L. Parfitt and M. M. Mortland, *Soil Sci. Soc. Am. Proc.* 1968, **32**, 355.
14. S. Olejnik, A. M. Posner and J. P. Quirk, *Clays Clay Miner.* 1973, **21**, 191.
15. S. Yariv, L. Heller and N. Kaufher, *Clays Clay Miner.* 1969, **17**, 310.
16. A. Sanchez, A. Hidalgo and J. M. Serratosa, *Proc. Int. Clay Conf. 1972, Madrid*, pp. 617–626. Division de Ciencias, C.S.I.C., Madrid (1973).
17. D. B. Fenn and M. M. Mortland, *Proc. Int. Clay Conf. 1972, Madrid*, pp. 591–603. Division de Ciencias, C.S.I.C., Madrid (1973).
18. G. W. Brindley and R. E. Sempels, *Clay Miner.* 1977, **12**, 229.

Polyhedron Vol. 10, No. 6, pp. 575–577, 1991
Printed in Great Britain

0277–5387/91 $3.00+.00
© 1991 Pergamon Press plc

ON THE CIRCULAR DICHROISM OF TRIS(S-ALANINATO)CHROMIUM: ABSOLUTE CONFIGURATIONS AND EVIDENCE FOR UNEXPECTED LABILITY

JULIO PEDROSA DE JESUS* and TERESA M. DOS SANTOS

Department of Chemistry, Universidade de Aveiro, Aveiro, 3800, Portugal

and

PAUL O'BRIEN*

Department of Chemistry, Queen Mary and Westfield College, University of London, Mile End Road, London E1 4NS, U.K.

(*Received* 1 *November* 1990; *accepted* 10 *December* 1990)

Abstract—Pink tris(S-alaninato)chromium(III) has been prepared and characterized. The compound is found to have sufficient solubility in water for the circular dichroism to be measured, moreover the circular dichroism in water is identical to that of the complex dissolved in DMSO or in the solid state (KBr disc). These results are used to comment on the work of earlier workers and can be used to clarify the assignments of the dominant bands in the visible circular dichroism of tris-aminoacidates of chromium(III).

The tris-aminoacidates of chromium(III) have been studied on a number of occasions.[1–6] Despite the large number of studies of such complexes, there is a remarkable variation both in the nature of the chiroptic spectra reported and their assignment. In this work we report a detailed study of the pink form of the tris-chelate of S-alanine with chromium(III) and clarify this confusion.

The synthesis of a complex of chromium(III) with alanine was first reported by Ley and Winkler in 1912.[1] However, it is only more recently that detailed studies of such complexes have been reported. Such work has tended to point to the formation of a single, or very significantly dominant, isomer. The complex which forms stereospecifically is usually assigned, for the S-alanine complex, as the Λ-*fac*(+) or β-(+) isomer.[2–6] This compound has generally been considered to be insoluble in water. To our knowledge, Green and Ang[2] are the only workers to suggest slight solubility of the tris complex in water, and they only reported electronic spectra. However, they did note some instability of the complex, in aqueous solution, with time. A similar observation was later reported by Minor *et al.*,[3] but these authors suggested the presence of two different species in the solid. The first soluble in water and the second insoluble.

RESULTS AND DISCUSSION

The compound studied in the present work was prepared by a variety of methods, as reported in the earlier literature,[2–5] and in all cases each sample had the same spectroscopic properties. The solid has slight solubility in water and it was possible to dissolve a complete sample by successive extractions with separate aliquots of water, all fractions having identical circular dichroism. A typical spectrum of the complex dissolved in water is shown in Fig. 1 and detailed in Table 1. The solid complex is much more soluble in DMSO or acidic aqueous solutions. Freshly prepared acidic solutions† are pink and

* Authors to whom correspondence should be addressed.

† Slight colour changes from red–pink to purple have been noted for the reactions discussed in this paper. However the changes in the electronic spectra are very slight, very small shifts in the maxima of broad bands and changes in half-widths, results of such studies have been uninformative and for the sake of brevity are not detailed here.

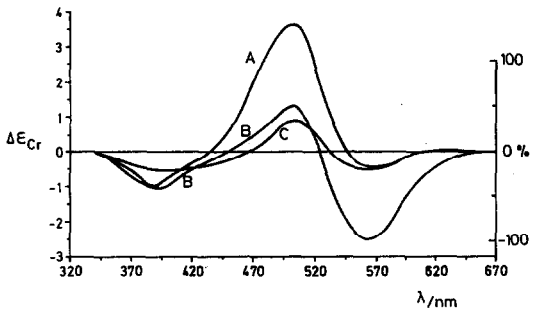

Fig. 1. The circular dichroism of tris(S-alaninato) chromium(III): (A) In water; (B) As 1% KBr pellet; (C) In DMSO.

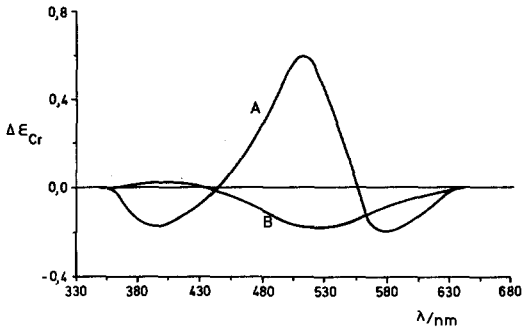

Fig. 2. The circular dichroism of tris(S-alaninato) chromium(III) in acidic solution. The compound was dissolved in 4 M perchloric acid and the spectrum recorded as soon as possible after mixing; (A) and (B) 30 min later.

have a circular dichroism spectrum which resembles that of a solution in water or DMSO. However, on standing, the spectra of acidic solutions soon change, over a period of minutes, in the way shown in Fig. 2. The instability of the complex in acidic solution does not appear to have been appreciated by earlier workers.[4] Another interesting observation is that the spectrum in acidic solution can be reversed to that of the aqueous solution by neutralization with sodium hydroxide. The fact that the reaction in acid occurs over a period of minutes suggests a genuine chemical reaction, such as ring opening, rather than the formation of an outer-sphere complex.

The solid complex dispersed in a KBr disc has the same circular dichroism sign pattern as the complex in aqueous solution, Table 1. The spectrum of the tris complex, as determined in the present study, either in the solid, aqueous or DMSO solution, shows the same sign pattern, strongly suggesting that the same complex is present in each of these situations.

There has been considerable debate concerning the assignment of the lowest energy ligand-field transitions in tris-chelates of chromium(III) (T_{2g}

Table 1. Typical circular dichroism results

Complex	Solvent	Circular dichroism maxima/nm $\Delta\varepsilon_{max}$[a-c]			Reference
Λ-(+)-β-[Cr(L-ala)$_3$]	$HClO_4$ 50%		522(+0.1)[a]	400(+0.13)[a]	4
[Cr(L-ala)$_3$][b]	Acid	606(+0.02)[c]	526(−0.10)[c]	408(+0.05)[c]	3
[Cr(L-ala)$_3$]	$HClO_4$ 20%	580(−0.19)[d]	510(+0.61)[d]	400(−0.17)[d]	This work[e]
[Cr(L-ala)$_3$]	$HClO_4$ 20%		530(−0.19)[d]	410(+0.03)[d]	This work[f]
[Cr(L-ala)$_3$][g]	H_2O	565(−0.15)[c]	505(+0.22)[c]	400(−0.12)[c]	3
[Cr(L-ala)$_3$]	H_2O	570(−0.53)[d]	505(+3.64)[d]	385(−0.96)[d]	This work[h]
Λ-(+)-β-[Cr(L-ala)$_3$]	Solid state[i]	546(−0.80)[a]	478(+1.00)[a]		4
[Cr(L-ala)$_3$]	Solid state[i]	560(−0.77)[a]	500(+1.00)[a]	385(−0.51)[a]	This work[j]
[Cr(L-ala)$_3$]	Solid state[i]	566(−1.00)[a]	500(+0.80)[a]	385(−0.50)[a]	This work[k]
[Cr(L-ala)$_3$]	Solid state[i]	560(−1.00)[a]	500(+0.47)[a]	388(−0.40)[a]	This work
[Cr(L-ala)$_3$]	DMSO	570(−0.54)[d]	505(+0.86)[d]	395(−0.56)[d]	This work

[a] Sign and relative intensity in parentheses.
[b] Insoluble isomer (ref. 3).
[c] Sign and intensity ($\Delta\varepsilon_M$) from ref. 3 (Fig. 4).
[d] $\Delta\varepsilon_{Cr}$ calculated per chromium atom.
[e] Circular dichroism spectrum taken as soon as possible after the dissolution of the complex.
[f] Circular dichroism spectrum taken about 30 min after the previous spectrum.
[g] Soluble isomer (ref. 3).
[h] Circular dichrosim spectrum taken as soon as possible.
[i] KBr disk.
[j] Solid prepared according to ref. 4.
[k] Solid prepared according to the insoluble isomer in ref. 3.

parentage in O_h, the A and E terms.[7,8] The argument was eventually settled by X-ray crystallographic studies.[9] The ordering of the A and E terms is different in the tris(ethylenediamine) and tris (oxalato) complexes of chromium(III).[8] Consequently, the sign of the E component, which can be correlated with the absolute configuration of the complex[4,8] must be determined with care. However, the dominant tris(S-alanine) complexes of cobalt (III) and chromium(III) are isomorphous,[4] suggesting that they are both lambda-β isomers. Our work, in addition, allows us to observe that the circular dichroism of the chromium complex (Fig. 1) is fully consistent with the ordering of the terms A followed by E, as in the corresponding lambda-tris(oxalato)chromium(III).[8,9] The simple correlation of the spectrum of the tris complex with absolute configuration had been overlooked in earlier work because of a lack of sensitivity of circular dichroism equipment and a failure to realize the reactivity of such compounds in aqueous and acidic solutions. The lability of the chromium(III) complexes in acidic solution is perhaps surprising. The corresponding cobalt complexes have identical spectra in acidic and neutral solution. Relatively labile complexes of chromium(III) are rare[10] and the kinetics of these reactions are under further investigation.

EXPERIMENTAL

Materials and method

Chromium nitrate nonahydrate was obtained from Fluka, S-alanine, dimethylsulphoxide and perchloric acid from Merck and sodium hydroxide from Pronolab.

Circular dichroism spectra were recorded with a Jobin-Yvon Auto-Dichrographie Mk.IV at the Universidade Aveiro; essentially similar results were obtained using a JASCO C.D. instrument at the University of London Intercollegiate Service at University College. X-ray powder diffraction results were obtained from the Department of Earth Sciences at Queen Mary and Westfield College.

Preparation of the complex

The method was either, essentially as described by Minor *et al.*[3] or Gillard *et al.*[4] and involved the reaction of hot aqueous solution of S-alanine with chromium nitrate, followed by neutralization with sodium hydroxide, or by the "solid-state" method of Oki.[5,11] A pink compound with identical spectroscopic properties to those described in this paper was obtained on all occasions. The compound was isomorphous with the pink insoluble phase described by Minor *et al.*[3] and had satisfactory microanalysis (CHN) for the anhydrous tris complex.

Acknowledgements—We are grateful to INIC, Cento de Quimica do Meio Aquatico da Universidade de Aveiro and to the British Council for the support of our collaborative work. We also thank the Calouste Gulbenkian Foundation for a grant to purchase C.D. equipment for the Universidade da Aveiro and Dr A. Drake of the University of London Intercollegiate C.D. service for assistance in obtaining confirmatory circular dichroism spectra.

REFERENCES

1. H. Ley and H. Winkler, *Berichte* 1909, **42**, 3894.
2. R. W. Green and K. P. Ang, *J. Am. Chem. Soc.* 1955, **77**, 5482.
3. S. S. Minor, G. Witte and G. W. Everett Jr, *Inorg. Chem.* 1976, **15**, 2052.
4. R. D. Gillard, S. H. Laurie, D. C. Price, D. A. Phipps and C. F. Weick, *J. Chem. Soc., Dalton Trans.* 1974, 1385.
5. H. Oki, *Bull. Chem. Soc. Japan* 1977, **50**, 680.
6. H. Mizuochi, A. Uehara, E. Kyuno and R. Tsuchiya, *Bull. Chem. Soc. Japan* 1971, **44**, 1555.
7. See for example L. F. Larkworthy, K. B. Nolan and P. O'Brien, Chromium, in *Comprehensive Coordination Chemistry* (Edited by R. D. Gillard and J. A. McCleverty), Ch. 35, pp. 699–969. Pergamon Press, Oxford (1986).
8. A. J. McCaffery, S. F. Mason and R. E. Ballard, *J. Chem. Soc.* 1965, 2883.
9. K. R. Butler and M. R. Snow, *J. Chem. Soc., Chem. Commun.* 1971, 550.
10. P. O'Brien, J. Pedrosa de Jesus and T. M. dos Santos, *Inorg. Chim. Acta* 1987, **131**, 5.
11. P. O'Brien and N. B. Sellers, *Polyhedron* 1990, **9**, 119.

Polyhedron Vol. 10, No. 6, pp. 579–582, 1991
Printed in Great Britain

0277–5387/91 $3.00+.00
© 1991 Pergamon Press plc

SYNTHESIS, SPECTRAL AND STRUCTURAL STUDIES ON $(N_2H_5)_2MCl_4(H_2O)_2$ (M = Pt AND Pd); CRYSTAL STRUCTURE OF THE PLATINUM COMPLEX

N. R. SREENIVASA KUMAR, I. I. MATHEWS and K. C. PATIL*

Department of Inorganic and Physical Chemistry, Indian Institute of Science, Bangalore-560012, India

(*Received* 2 *August* 1990; *accepted* 5 *November* 1990)

Abstract—Hydrazinium complexes of platinum and palladium, viz. $(N_2H_5)_2MCl_4(H_2O)_2$ (where M = Pt and Pd), have been prepared and characterized. The structure of the platinum complex has been determined by single crystal X-ray crystallography. The platinum atoms lie on inversion centres and are coordinated by two chlorines and two $N_2H_5^+$ ions through *trans* positions.

In continuation of our studies on metal complexes containing the hydrazinium cation, e.g. $N_2H_5Ln(SO_4)_2(H_2O)$ (Ln = La, Ce, Pr, Nd and Sm),[1] $(N_2H_5)_2M(C_2O_4)_2(H_2O)_n$ (M = Co, Ni and Cu),[2] $(N_2H_5)_2UO_2(C_2O_4)_2(H_2O)$,[3] $N_2H_5M(N_2H_3COO)_3(H_2O)$ (M = Fe, Co, Ni and Zn),[4] $(N_2H_5)_6(UO_2)_2(C_2O_4)_5(H_2O)_2$[5] and $(N_2H_5)_2MCl_4(H_2O)_2$ (M = Fe, CO, Ni and Cu),[6] we now report the synthesis of $(N_2H_5)_2MCl_4(H_2O)_2$ (M = Pt and Pd) and also the crystal structure of the platinum complex.

RESULTS AND DISCUSSION

The reaction between the metal chlorides of platinum and palladium [K_2PtCl_4 or $H_2PtCl_6(H_2O)_2$ Na_2PdCl_4] and hydrazinium dihydrochloride [$N_2H_4(HCl)_2$] yields $(N_2H_5)_2PtCl_4(H_2O)_2$ and $(N_2H_5)_2PdCl_4(H_2O)_2$ complexes instantaneously. It is essential to use $N_2H_4(HCl)_2$ rather than N_2H_4HCl in order to prevent the reduction of platinum and palladium salts to the metals. The compositions of the complexes have been fixed by chemical analysis (Table 1). IR spectra of the complexes show ν(N—N) of $N_2H_5^+$ at around 1000 cm^{-1} indicating coordination of $N_2H_5^+$ to the metal.[7] The observed absorptions in the visible region (24,800 and 26,400 cm^{-1}) are characteristic of $^1A_{1g} \rightarrow {}^1B_{1g}$ transitions of square-planar complexes.[8]

Hydrazine, which can be visualized as the amino derivative of ammonia, is a weaker base than ammonia because of the electronegative character of the amino group. Monoprotonated hydrazine, the hydrazinium cation, has a lone pair like in the ammine and its basicity is very much lowered due to the presence of a positive charge immediately adjacent to the donor atom.[9]

It is well known that the reaction between K_2PtCl_4 and NH_4Cl leads to the formation of *cis*-$[Pt(NH_3)_2Cl_2]$. Because of the similarities between $:NH_3$ and $:N_2H_5^+$, a similar *cis* structure was proposed for the corresponding hydrazinium complex.[10] Further, from IR studies, Stetsenko *et al.* have assigned the *cis* structure to $[Pt(N_2H_5)_2Cl_2]Cl_2(H_2O)_2$.[11] However, single crystal X-ray studies have shown that the complex has a *trans* structure.

Description of the structure

The structure of $(N_2H_5)_2PtCl_4(H_2O)_2$ consists of $[Pt(N_2H_5)_2Cl_2]^{2+}$, Cl^- ions and water molecules. The platinum atom has a square-planar coordination, bonded by two chlorine atoms and two nitrogen atoms from the $N_2H_5^+$ ions. The structure of the cation, $[Pt(N_2H_5)_2Cl_2]^{2+}$, is illustrated in Fig. 1.

The Pt—Cl distance [2.296(1) Å] is equal to the value of 2.30(2) Å found in *trans*-$[Pt(NH_3)_2Cl_2]$[12] and also in a variety of other chloroplatinum(II) complexes. The Pt—N bond length [2.044(5) Å] observed in the present structure is unusually

* Author to whom correspondence should be addressed.

Table 1. Analytical and spectral data for $(N_2H_5)_2MCl_4(H_2O)_2$

M	Chemical analysis[a] Metal (%)[b]	Chloride (%)	Hydrazine (%)	ν(N—N) (cm^{-1})	Electronic spectra (cm^{-1})
Pd	31.0(30.4)	40.5(40.5)	18.0(18.2)	1000	24,800 [$^1A_{1g} \rightarrow {}^1B_{1g}$]
Pt	45.0(44.4)	32.0(32.3)	14.8(15.0)	1010	26,400 [$^1A_{1g} \rightarrow {}^1B_{1g}$]

[a] Theoretical values in parentheses.
[b] From TG weight loss.

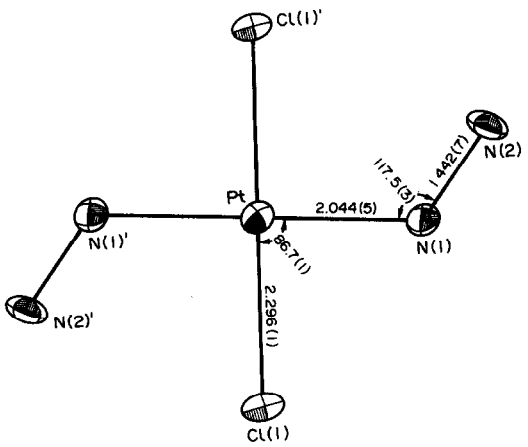

Fig. 1. ORTEP diagram of the $[Pt(N_2H_5)_2Cl_2]^{2+}$ ion with bond lengths (Å) and angles (°). Thermal ellipsoids are drawn at the 50% probability level and symmetry related atoms are shown by primes (′).

shorter than in the corresponding ammine complexes, e.g. 2.17(4) Å in *trans*-$[Pt(NH_3)_2Cl_2]$. The observed short metal–nitrogen distance in the present case is surprising as $N_2H_5^+$ is a poorer σ-donor compared to NH_3 and known to form weak metal–nitrogen bonds. The N—N bond length [1.443(7) Å] in the present structure is not significantly different from the one observed in N_2H_5Cl (1.45 Å).[13] The Pt—N(1)—N(2) angle is 117.5(3)°, larger than the value of 110° observed in $(N_2H_5)_2Zn(SO_4)_2$,[14] but comparable to 119.1(3)° found in $N_2H_5CuCl_3$.[15]

The N(2) atom is 0.476 Å away from the plane of Pt—N(1)—Cl(1). The water molecules are in the vicinity of $—NH_3^+$ of $N_2H_5^+$, bonded by N—H---O type hydrogen bonds. The distance of 2.755(1) Å observed for N(2)—O(w) indicates strong hydrogen bonding. The angle observed for N(1)—N(2)—O(w) is 104.5(1)°.

NH_3 *vs* $N_2H_5^+$

Ammines complex to platinum(II) ion by donation of an electron pair from an sp^3 hybrid on nitrogen to an empty orbital of correct symmetry on platinum. Since there are no low-energy empty orbitals on nitrogen suitable for π-back donation, the Pt—N bond can be considered to be a pure σ-bond. The $N_2H_5^+$ cation is similar to ammine in this aspect. Further, the ammine ligands are low in the *trans* effect and the *trans* influence series, low in the nephalauxetic series and high in the spectrochemical series.[16] This feature is evidenced where the singlet→singlet absorption is at 29,800 cm^{-1} in *cis*-$[Pt(NH_3)_2Cl_2]$, at 26,600 cm^{-1} in *trans*-$[Pt(NH_3)_2Cl_2]$, but at 21,000 cm^{-1} in K_2PtCl_4.[17] Surprisingly, the electronic spectrum of *trans*-$[Pt(N_2H_5)_2Cl_2]Cl_2(H_2O)_2$ (Table 1) shows the absorption at 26,400 cm^{-1}, indicating the similar bonding nature of the $N_2H_5^+$ ion with respect to NH_3, even though the basicity of the $N_2H_5^+$ ion is significantly lower than the ammine.[9] Being a poorer σ donor, formation of the *trans* isomer in the case of $N_2H_5^+$ compared with NH_3 is rather puzzling.

Although the *trans* effect is concerned only with kinetics, reference is sometimes made to a static *trans* influence which affects physical properties such as bond lengths, vibrational frequencies, etc.[18,19] Moreover, investigations on the thermal stabilities of platinum(II) ammines indicate that *trans* isomers are generally more stable than the corresponding *cis* isomers.[20] This difference in stabilities was explained on the basis that the *trans* effect of Cl^- is greater than that of NH_3, and also that the Pt—Cl bond strength is less than that of Pt—N. Thus, in the *cis* isomer, the Pt—N bond is weaker than in the *trans* form because of the greater bond-weakening effect of Cl^- compared with NH_3. For the same reason, the reverse is true for the Pt—Cl bond. Since the Pt—Cl bond strength is less than that of Pt—N, the overall stability of the complex will be affected more by changes in the Pt—N than Pt—Cl bond strengths. This explanation supports the view that the *trans* effect order $Cl^- > NH_3$ is a consequence of Pt—Cl bond weakening. In this connection it is of interest to recall that the intermediate $[Pt(NH_3)Cl_3]$ reacts to yield *cis*-

$[Pt(NH_3)_2Cl_2]$, meaning that the less stable isomer is formed as the kinetic product. Since the Pt—N bond in the hydrazinium complex is shorter than the corresponding ammine complex, the same *cis* product can be expected, though experiments show the formation of the *trans* isomer. Thus the formation of the *trans* product in the case of $N_2H_5^+$, in contrast to NH_3, can be attributed to the reduced repulsion between the two $N_2H_5^+$ cations in the resulting complex due to the larger separation in the *trans* arrangement.

Structure of $(N_2H_5)_2PdCl_4(H_2O)_2$

Since the IR and electronic spectral data for the above complex are similar to those observed for the platinum complex (Table 1), the same structure, viz. *trans*-$[Pd(N_2H_5)_2Cl_2]Cl_2(H_2O)_2$ can be assigned to the palladium complex.

EXPERIMENTAL

Preparation

$(N_2H_5)_2PtCl_4(H_2O)_2$. The platinum complex was obtained by adding K_2PtCl_4 (or H_2PtCl_6) solution (0.5 g in a minimum amount of water) to a saturated solution of $N_2H_4(HCl)_2$ (10 cm^3). Golden yellow crystals of the complex formed in a day. The crystals were filtered from the solution and air dried.

$(N_2H_5)_2PdCl_4(H_2O)_2$. The palladium complex was prepared in the same way by starting either with Na_2PdCl_4 or $PdCl_2$ (in HCl) and $N_2H_4(HCl)_2$.

Physico-chemical methods

The composition of the complexes was determined by chemical analysis:[21] hydrazine by titrating with KIO_3 under Andrews conditions, metals from TG weight loss, and chloride by Volhard's method.

IR spectra of the complexes in the region 4000–600 cm^{-1} were recorded using a Perkin–Elmer 781 spectrophotometer as Nujol mulls. Electronic spectra in the solid state were obtained using a Hitachi U-3400 spectrophotometer by dispersing the samples in Nujol.

X-ray analysis

A crystal of dimensions $0.40 \times 0.30 \times 0.15$ mm was used in the present work. The cell dimensions

Table 2. Details of crystallographic analysis for the platinum complex

Formula	$(N_2H_5)_2PtCl_4(H_2O)_2$
M_r	439.0
Crystal system	Monoclinic
Radiation (Å)	0.71069
T (K)	293
Space group	$P2_1/c$
a (Å)	7.427(1)
b (Å)	7.717(1)
c (Å)	9.629(1)
β (°)	101.40(1)
V (Å^3)	540.9
Z	2
Crystal colour	Golden yellow
Crystal size (mm)	$0.40 \times 0.30 \times 0.15$
d_m (g cm^{-3})	2.69
d_c (g cm^{-3})	2.70
Scan mode	ω–2θ
$2\theta_{max}$ (°)	64
Reflections measured	$\pm h, k, l$
Number of measured reflections	2458
Number of unique data	2158
Number of data used	1617
Cut-off criteria	$F > 3.0\sigma(F)$
Absorbance coefficient (μ_{Mo})	145.5 cm^{-1}
R_{int}	0.048
Weights[a]	A, 0.00578
R	0.045
wR	0.053

[a] Weighting scheme $w = 1/[\sigma^2(F_o) + A|F_o|^2]$.

and space group were determined on a Weissenberg camera and the cell constants were subsequently refined on a CAD-4 diffractometer. Intensity data were collected in the usual manner.

Structure solution and refinement

The structure was solved by conventional Patterson function and refined by full-matrix least-squares techniques using SHELX-76 system of programs.[22] Hydrogen atoms could not be located in the difference Fourier map. Further refinement of the structure was carried out by introducing anisotropic thermal parameters, followed by the sigma weighting scheme and absorption corrections. The ORTEP-II program[23] was used for the diagram. All the details regarding the data collection and structural analysis are given in Table 2.

Acknowledgements—The authors are grateful to Professor H. Manohar and Dr M. D. Poojary for valuable discussions and interest.

REFERENCES

1. S. Govindarajan, K. C. Patil, H. Manohar and P. E. Werner, *J. Chem. Soc., Dalton Trans.* 1986, 119.
2. D. Gajapathy, S. Govindarajan, K. C. Patil and H. Manohar, *Polyhedron* 1983, **2**, 865.
3. M. D. Poojary and K. C. Patil, *Proc. Ind. Acad. Sci. (Chem. Sci.)* 1987, **99**, 311.
4. P. Ravindranathan and K. C. Patil, *Proc. Ind. Acad. Sci. (Chem. Sci.)* 1985, **95**, 354.
5. S. Govindarajan, K. C. Patil, M. D. Poojary and H. Manohar, *Inorg. Chim. Acta* 1986, **120**, 103.
6. N. R. S. Kumar, M. Nethaji and K. C. Patil, *Polyhedron* 1991, **10**, 365.
7. A. Braibanti, F. Dallavalle, M. A. Pellinghelli and E. Laporati, *Inorg. Chem.* 1968, **7**, 1430.
8. C. J. Ballhausen, *Introduction to Ligand Field Theory*. McGraw-Hill, New York (1962).
9. G. Schwarzenbach, *Helv. Chim. Acta* 1936, **19**, 178.
10. F. Audrieth and B. A. Ogg, *The Chemistry of Hydrazine*, p. 188. John Wiley, New York (1951).
11. A. I. Stetsenko, L. S. Tikhonova, L. I. Shigina and I. M. Ginzburg, *Russ. J. Inorg. Chem.* 1978, **23**, 1029.
12. A. J. C. Wilson, *Structure Reports*, Vol. 18, p. 537. International Union of Crystallography, Netherlands (1961).
13. K. Sakurai and Y. Tomiie, *Acta Cryst.* 1952, **5**, 293.
14. C. K. Prout and Powell, *J. Chem. Soc. A.* 1961, 4177.
15. D. B. Brown, J. A. Donner, J. W. Hall, S. R. Wilson, R. B. Wilson, D. J. Hodgson and W. E. Hatfield, *Inorg. Chem.* 1979, **18**, 2635.
16. C. K. Jorgenson, *Absorption Spectra and Chemical Bonding in Complexes*. Pergamon Press, Oxford (1962).
17. A. V. Babaeva and R. I. Rudy, *J. Inorg. Chem. (USSR)* 1956, **1**, 52.
18. F. Basolo and R. G. Pearson, *Prog. Inorg. Chem.* 1962, **4**, 381.
19. F. Basolo and R. G. Pearson, *Mechanisms of Inorganic Reactions*. John Wiley, New York (1967).
20. I. I. Chernyaev, V. A. Palkin, R. A. Baranova and N. N. Kuzmina, *Russ. J. Inorg. Chem. (Engl. Transl.)* 1960, **5**, 1428.
21. A. I. Vogel, *A Text Book of Quantitative Inorganic Analysis*. Longman, London (1961).
22. G. M. Sheldrick, SHELX-76, Program for Crystal Structure Determination. University of Cambridge, Cambridge, U.K. (1976).
23. C. K. Johnson, ORTEP-II, A Program for Thermal Ellipsoid Plotting. Oak Ridge National Laboratory, Oak Ridge, Tennessee (1976).

Polyhedron Vol. 10, No. 6, pp. 591–594, 1991
Printed in Great Britain

0277–5387/91 $3.00+.00
© 1991 Pergamon Press plc

ISOLATION OF $Cp_2Cr_2(CO)_4Se_2$ FROM THE INTERACTION OF $Cp_2Cr_2(CO)_4Se$ WITH MOLECULAR OXYGEN. ESR EVIDENCE FOR PARAMAGNETIC INTERMEDIATES

LAI YOONG GOH* and S. K. KHOO

Department of Chemistry, University of Malaya, 59100 Kuala Lumpur, Malaysia

(*Received* 27 *April* 1990; *accepted* 16 *November* 1990)

Abstract—The interaction of $Cp_2Cr_2(CO)_4Se$ with molecular oxygen at ambient temperature led to the isolation of *ca* 30% yield of $Cp_2Cr_2(CO)_4Se_2$ from a product mixture also containing $Cp_4Cr_4Se_4$ and other CpCr diamagnetic species. $CpCr(CO)_2(O_2)$ was one of the paramagnetic intermediates detected at −70°C in the ESR spectrum.

The degradation of organometallic compounds by molecular oxygen is a well-known, though little-understood phenomenon.[1] In the last two decades, the interaction of dioxygen with organic and organometallic compounds has received increasing attention because of their relevance to organic synthesis and biological processes.[2–6] Literature reports include the air-oxidation of $[CpMo(CO)_3]_2$,[7] the $CpMo(CO)_3^-$ anion,[8] and lately of $[(C_5Me_5)Mo(\mu\text{-Br})(Me)NO]_2$,[9] the photo-oxidation of $Mn_2(CO)_{10}$ and related complexes,[10] the unusual hydrogen atom abstraction by O_2 from one of the CH_3 groups of $CpFe(\eta^6\text{-}C_6Me_6)$,[11] oxygenation reactions of $[CpMn(CO)_2]_2S$,[12] $CpM(NO)R_2$ (M = Mo, W),[13] $Cp_2Cr_2(CO)_6$,[14] $Cp_2Mo_2S_4$[15] and more recently of $[CpMo(\mu\text{-S})(\mu\text{-SH})]_2$,[16] $(C_5Me_5)_2Ta(=CH_2)H$[17] and $(C_5Me_5)_2W{=}O$,[18] and alkyliron(III) porphyrins.[19] In this paper, we describe the interaction of $Cp_2Cr_2(CO)_4Se$ (**1**) with O_2. This study was prompted by the facile insertion of sulphur[20] and selenium,[21] the heavier congeners of oxygen in Group 16, into the Cr≡Se≡Cr bond of **1**.

RESULTS AND DISCUSSION

Reaction with oxygen

Products. The reaction of the triply-bonded Cr≡Se≡Cr complex, $Cp_2Cr_2(CO)_4Se$ (**1**), with O_2 led to the isolation of crystalline $Cp_2Cr_2(CO)_4Se_2$ (**2**) in *ca* 30% yield, which could be increased to *ca* 50% with a controlled supply of O_2, together with impure solids of $Cp_4Cr_4Se_4$ [eq. (1)],

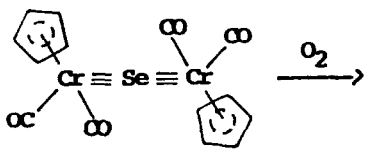

(1)

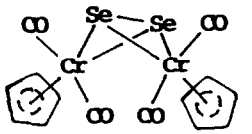

(2)

$$+ Cp_4Cr_4Se_4 + \cdots \quad (1)$$

and minor amounts of some unidentified CpCr species detectable in solution in the NMR spectrum. Complex **2** was characterized by its elemental analysis and the identical resemblance of its spectral features to those of the structurally determined $\mu\text{-}\eta^2\text{-}Se_2$ bonded dichromium complex.[21] On a comparative note, it may be pointed out that this complex was also the major product from the interaction of **1** with elemental sulphur[20] and selenium.[21]

Paramagnetic intermediates

A solution of **1** in toluene was ESR-inactive under an inert atmosphere. However, in the presence of a trace amount of air or O_2 at −70°C, two weak

* Author to whom correspondence should be addressed.

signals rapidly developed, viz. X ($g = 2.021$) and Y ($g = 1.996$). Signal Y was observed to be stronger and broader. As more air or O_2 was admitted, signal X was observed to sharpen and intensify, while signal Y gradually diminished and eventually disappeared. This was accompanied by the emergence of a third signal Z which was observed as a sextet ($a = 0.12$ mT) with clearly visible quartet satellites ($a = 1.72$ mT) centred at $g = 1.987$. The resulting ESR spectrum is illustrated in Fig. 1. The signal intensity of X and Z persisted for several hours at $-70°C$ but showed signs of decomposition when the temperature was raised above $-45°C$.

The sextet characteristics of Z, arising from the hyperfine interactions of the five ^1H nuclei in the Cp ring, together with its quartet satellites, assignable to coupling with the central ^{53}Cr nucleus ($I = 3/2$, 9.5% natural abundance), conform exactly to those reported for the chromium dioxygen complex **3A**.[14] The latter species has been generated from the interaction of $[CpCr(CO)_3]_2$ in toluene at $-70°C$ with O_2 or air, pressurized at 100–300 torr, or from photo-oxygenation of Hg $[CpCr(CO)_3]_2$ and $CpCr(CO)_3Cu(phen)_n$.[14]

The close proximity of the g value (2.021) of the X signal to those observed for CO-substituted derivatives, $CpCr(CO)_2L$, of the radical $CpCr(CO)_3$, e.g. $g = 2.025$ for $L = C_6H_5CN$,[22] $g = 2.030$ (broad doublet) for $L = PPh_3$,[23] and $g = 1.996$ for $L = P(OMe)_3$,[24] suggests that it is derived from an analogous radical, where L = Se, as represented by **3B**. It is conceivable that **1** interacts with O_2 to form a peroxo complex (**3**), as shown in Scheme 1. Subsequent homolytic dissociation of **3** will generate the 17-electron paramagnetic species **3A** and **3B**, which are substantiated by our ESR observations.

The proposal of an intermediate peroxo radical species (**3**) is in agreement with the observation of the transient ESR signal Y which diminishes with the growth of two signals, Z ascribed to **3A** as discussed above, and X attributed to **3B**. Initially, only signals X and Y were observed without Z. This is due to the broad character of signal Y and the close proximity of the g values of Y and Z, resulting in the weak signal Z being obscurred under the broad envelope of Y. The assignment of **3** as a peroxo radical finds precedent in similar species isolated or ESR-detected in the photo-oxidation of $Mn_2(CO)_{10}$, $[CpFe(CO)_2]_2$ and related dimeric species,[10] in the insertion of O_2 into the M—C bond of alkylcobaloximes[25] and alkyliron(III) porphyrins,[19] and in the interaction of the dirhodium(II) aquo cation $\{Rh_2(aq)^{4+}\}$ with O_2.[26] Indeed, there is ample evidence indicating that the reaction of organometallic compounds with O_2 involves primarily the initial coordination of O_2 to the central M atom, leading to the eventual formation of peroxo complexes or radicals which may be organic or organometallic in nature.[4] Hence, probable for-

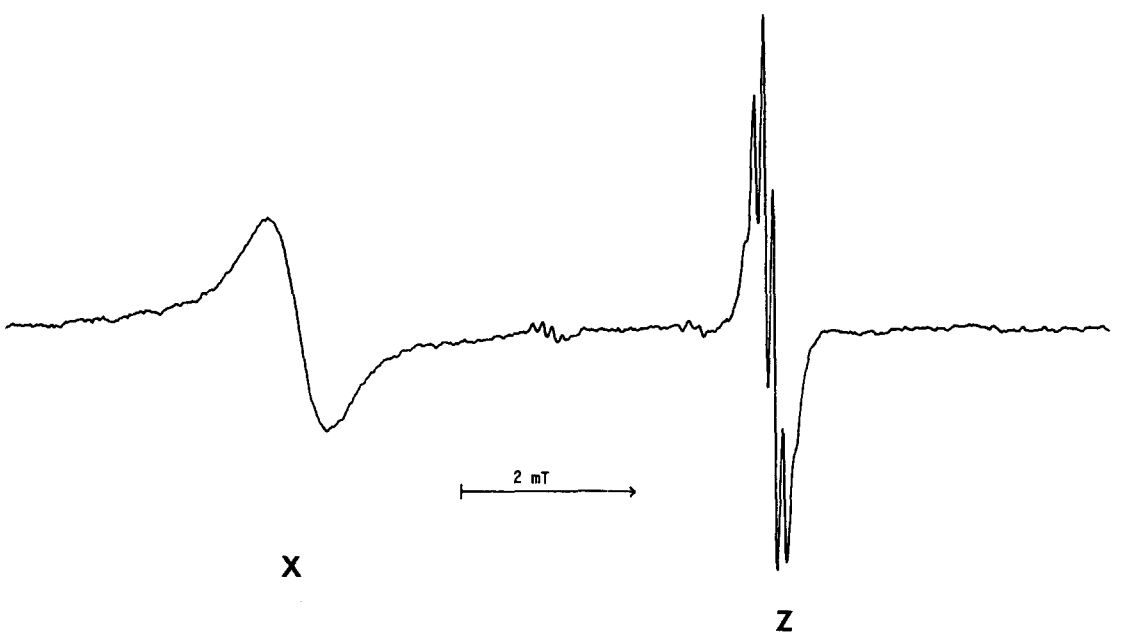

Fig. 1. ESR spectrum of a solution of **1** in toluene at $-70°C$ in the presence of air or O_2.

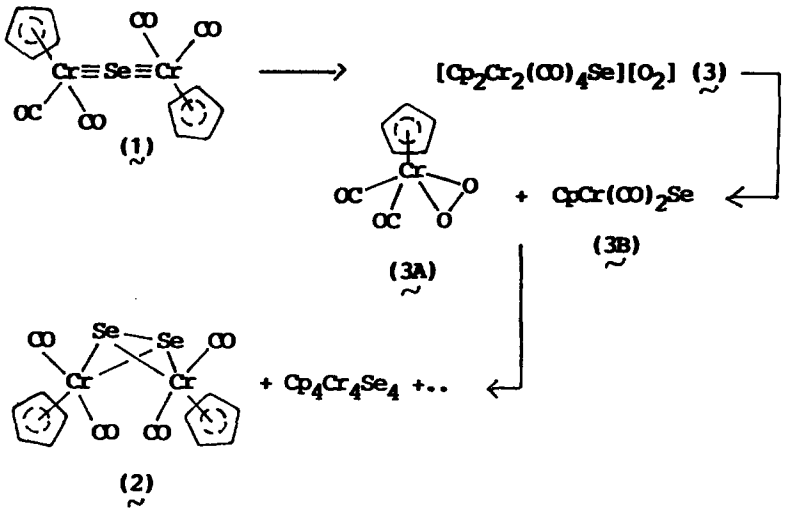

Scheme 1.

mulations for **3** may be represented by structures **4A–4C**, but are beyond the scope of this study.

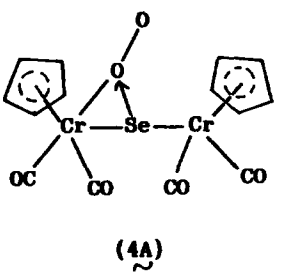

(4A)

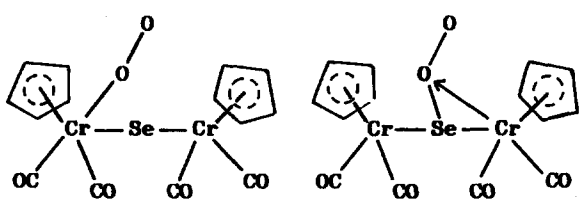

(4B) (4C)

EXPERIMENTAL

General procedures and physical measurements

Inert atmospheric manipulation techniques, sources and preparation of reagents and solvents were as described previously.[20,21] ^{1}H NMR spectra were measured on a JEOL FX100 100 MHz spectrometer, and chemical shifts are relative to residual C_6H_6 in C_6D_6. ESR spectra were measured on a Bruker B-R 70 spectrometer (23 cm magnet) equipped with a variable temperature accessory and the field determined with the aid of a NMR oscillator; the g value was calibrated using DPPH. IR spectra were measured on a Perkin–Elmer 1330 instrument. Elemental analyses were performed by the Analytical Unit of the Research School of Chemistry, Australian National University, except for chromium, which we analysed as CrO_4^{2-}.[27]

Reaction of $Cp_2Cr_2(CO)_4Se$ (**1**) *with* O_2

A filtered solution of **1**, prepared *in situ* from $Cp_2Cr_2(CO)_6$ (400 mg, 1.0 mmol) and Se_8 (80 mg, 1.0 mmol)[21] in toluene (*ca* 10 cm^3) was stirred under an atmosphere of dried O_2 at ambient temperature for 3 h, until the original orange–brown colour had turned to dark greenish-brown. IR monitoring of the carbonyl stretching frequency indicated that the reaction was almost complete. Filtration removed fine, dark, sparingly soluble solids (*ca* 200 mg). IR (Nujol): ν(CO) 1925 and 1855 cm^{-1}. ^{1}H NMR (C_6D_6): δ 4.08, 5.13 and 5.88 pertaining to **2**, $Cp_4Cr_4Se_4$ and an unidentified species, respectively. The dark brown filtrate possessed Cp resonances at δ 4.36 and 4.08 belonging to **1** and $Cp_2Cr_2(CO)_4Se_2$ **2**, respectively, with a relative intensity of 1 : 7. On concentration to *ca* 1 cm^3 and addition of n-hexane (*ca* 1 cm^3), followed by cooling at −30°C, dark brown needles of **2** were obtained (146 mg, 0.29 mmol, 29% yield). (Found: C, 32.45; H, 1.97; Cr, 20.57; Se, 30.70. $(C_5H_5)_2Cr_2(CO)_4Se_2$ requires: C, 33.35; H, 2.00; Cr, 20.63; Se, 31.32%.) A small amount remained in the mother liquor together with traces of other unidentified cp-containing species. The above reaction with a controlled amount of O_2 [**1**, 41 mg, 0.096 mmol, in toluene (4 cm^3) and O_2 (6 cm^3, *ca* 0.3 mmol)] for 4 h led to a 33% conversion to **2**, as indicated in the ^{1}H NMR spectrum of the resultant solution. Approx-

imately 50% conversion was achieved after a further 3 h of reaction with a fresh quantity (10 cm^3) of O_2.

ESR spectra

ESR experiments were carried out on a *ca* 0.06 mol dm^{-3} solution of **1**, prepared in toluene in a 2-mm serum-capped quartz tube under argon. Air or O_2 was admitted when required via a needle puncture in the serum cap. X-band ESR spectra were recorded at $-70°C$ and higher temperatures.

Acknowledgements—The authors acknowledge, with thanks, financial support from the University of Malaya and IRPA Grant No. 04-07-04-127.

REFERENCES

1. J. K. Kochi, *Organometallic Mechanisms and Catalysis*, pp. 517–522. Academic Press, New York (1978).
2. L. Vaska, *Accts Chem. Res.* 1976, **9**, 175.
3. G. McLendon and A. E. Martell, *Coord. Chem. Rev.* 1976, **19**, 1.
4. G. A. Razuvaeu and T. G. Brilkina, *Russ. Chem. Rev.* 1976, **45**, 1135 and refs therein.
5. R. D. Jones, D. A. Summerville and F. Basolo, *Chem. Rev.* 1979, **79**, 138.
6. S. J. Lippard, *Angew. Chem. Int. Ed. Engl.* 1988,**27**, 344.
7. M. Cousins and M. L. H. Green, *J. Chem. Soc.* 1964, 1567; *J. Chem. Soc. A* 1969, 16.
8. M. D. Curtis and K. R. Han, *Inorg. Chem.* 1985, **24**, 378.
9. P. Gomez-Sal, E. de Jesus, P. Royo, A. V. de Miguel, S. Martinez-Carrera and S. Garcia-Blanco, *J. Organomet. Chem.* 1988, **353**, 191.
10. W. E. Lindsell and P. N. Preston, *J. Chem. Soc., Dalton Trans.* 1979, 1105.
11. D. Astruc, J.-R. Hamon, E. Roman and P. Michaud, *J. Am. Chem. Soc.* 1981, **103**, 7502.
12. M. Hofler and A. Baitz, *Chem. Ber.* 1976, **109**, 3147.
13. (a) P. Legzdins, S. J. Rettig and L. Sanchez, *Organometallics* 1985, **4**, 1470; (b) P. Legzdins, E. C. Phillips and L. Sanchez, *Organometallics* 1989, **8**, 940.
14. L. Carlton, W. E. Lindsell and P. N. Preston, *J. Chem. Soc., Chem. Commun.* 1981, 531; *J. Chem. Soc., Dalton Trans.* 1982, 1483.
15. H. Brunner, H. Kauermann, J. Pfauntsch, J. Wachter, J. H. Enemark and C. G. Young, *J. Organomet. Chem.* 1987, **331**, 45.
16. (a) L. D. Tanner, R. C. Haltiwanger, J. Noordik and M. R. DuBois, *Inorg. Chem.* 1988, **27**, 1736; (b) L. D. Tanner, R. C. Haltiwanger and M. R. DuBois, *Inorg. Chem.* 1988, **27**, 1741.
17. A. Van Asselt, M. S. Trimmer, L. M. Henling and J. E. Bercaw, *J. Am. Chem. Soc.* 1988, **110**, 8254.
18. G. Parkin and J. E. Bercaw, *J. Am. Chem. Soc.* 1989, **111**, 391.
19. R. D. Arasasingham, A. L. Balch, C. R. Cornman and L. Latos-Grazynski, *J. Am. Chem. Soc.* 1989, **111**, 4357.
20. L. Y. Goh, *J. Chem. Soc., Dalton Trans.* 1989, 431.
21. L. Y. Goh, C. Wei and E. Sinn, *J. Chem. Soc., Chem. Commun.* 1985, 462; *Organometallics* 1988, **7**, 2020.
22. J. R. Morton, K. F. Preson, N. A. Cooley, M. C. Baird, P. J. Krusic and S. J. McLain, *J. Chem. Soc., Faraday Trans. 1* 1987, **83**, 3535.
23. N. A. Cooley, M. C. Baird, J. R. Morton, K. F. Preston and Y. L. Page, *J. Mag. Reson.* 1988, **76**, 325.
24. L. Y. Goh and Y. Y. Lim, unpublished result.
25. (a) C. Fontaine, K. N. V. Duong, C. Merienne, A. Gaudemer and C. Giannotti, *J. Organomet. Chem.* 1972, **38**, 167 and refs therein; (b) F. R. Jensen and R. C. Kiskis, *J. Am. Chem. Soc.* 1975, **97**, 5825; (c) C. Bied-Charreton and A. Gaudemer, *J. Am. Chem. Soc.* 1976, **98**, 3997; (d) A. Nishinaga, K. Nishizawa, Y. Nakayama and T. Masuura, *Tetrahedron Lett.* 1977, 85; (e) P. J. Toscano and L. G. Marzilli, *Prog. Inorg. Chem.* 1984, **31**, 105.
26. M. Moszner and J. J. Ziolkowski, *Inorg. Chim. Acta* 1988, **145**, 299.
27. G. W. Haupt, *J. Res. Nat. Bur. Stand.* 1952, **48**, 414.

Polyhedron Vol. 10, No. 6, pp. 595–603, 1991
Printed in Great Britain

0277–5387/91 $3.00+.00
© 1991 Pergamon Press plc

BIS[1,2-BIS(DIMETHYLPHOSPHINO)ETHANE] DICHLOROTUNGSTEN(II) AND ITS REACTIONS. X-RAY CRYSTAL STRUCTURES OF BIS[1,2-BIS(DIMETHYLPHOSPHINO) ETHANE]TETRACHLOROTUNGSTEN(V) HEXACHLOROANTIMONATE(V) AND BIS{BIS[1,2-BIS(DIMETHYLPHOSPHINO)ETHANE] TETRAHYDROALUMINATOHYDRIDOMOLYBDENUM(II)}

VAHÉ SABOONCHIAN and GEOFFREY WILKINSON*

Johnson Matthey Laboratory, Chemistry Department, Imperial College, London SW7 2AY, U.K.

and

BILQUIS HUSSAIN-BATES and MICHAEL B. HURSTHOUSE*

Chemistry Department, Queen Mary and Westfield College, London, E1 4NS, U.K.

(*Received* 15 *October* 1990; *accepted* 16 *November* 1990)

Abstract—The reduction of $WCl_4(THF)_2$ by sodium naphthalenide in the presence of 1,2-bis(dimethylphosphino)ethane (DMPE) in tetrahydrofuran affords *trans*-$WCl_2(DMPE)_2$. Interaction of this complex with $NaBPh_4$ in MeCN gives $[WCl(\eta^2\text{-MeCN})(DMPE)_2]BPh_4$ and with $SbCl_5$ the tungsten(V) complex $[WCl_4(DMPE)_2]SbCl_6$. The X-ray crystal structure of the latter shows the cation to have dodecahedral geometry with equatorial chlorine atoms. Interaction of *trans*-$MCl_2(DMPE)_2$ (M = Mo and W) with $LiAlH_4$ gives the hydrido aluminohydrides, $[MH(AlH_4)(DMPE)_2]_2$, and the X-ray crystal structure of the molybdenum compound has been determined. Methanolysis of the tungsten compound gives $WH_4(DMPE)_2$.

The compounds of the Group 6 elements, *trans*-$MCl_2(DMPE)_2$ (M = Cr[1] and Mo[2]) and reactions of the chromium[3a,b] and molybdenum[4] halides with acetonitrile have been described. The proposal of a η^2-MeCN intermediate in the reactions of $[Cr(MeCN)_2(DMPE)_2]^{2+}$ and $[CrCl(MeCN)(DMPE)_2]^+$ with methanol[3b] was supported by the isolation and X-ray crystal structure determination of *trans*-$[MoCl(\eta^2\text{-MeCN})(DMPE)_2]BPh_4$.[4]

The hydridoaluminohydrido complex of chromium(II), $[(DMPE)_2HCr(\mu\text{-H})_2Al(H)(\mu\text{-H})]_2$, and for molybdenum and tungsten the similar PMe_3 complexes $[(Me_3P)_4HM(\mu\text{-H})_2Al(H)(\mu\text{-H})]_2$ were obtained.[5] The tetrahydrides $MH_4(DMPE)_2$ (M = Cr[6a] and Mo[6b]) have also been described.

We now describe the synthesis of *trans*-$WCl_2(DMPE)_2$, its oxidation by $SbCl_5$ to $[WCl_4(DMPE)_2]SbCl_6$ and the synthesis of the aluminohydrides $[MH(AlH_4)(DMPE)_2]_2$ (M = Mo and W) and of $WH_4(DMPE)_2$.

RESULTS AND DISCUSSION

The interaction of $WCl_4(THF)_2$ with two equivalents of sodium naphthalenide in THF containing excess DMPE gives *trans*-$WCl_2(DMPE)_2$ in about 35% yield. On a small scale Na/Hg can be used as reductant. The compound crystallizes from hexane as large, deep red crystals that are soluble in toluene, THF, CH_2Cl_2 and MeCN but sparingly soluble in Et_2O and hexane. In addition to DMPE bands, the IR spectrum shows a single band at 324 cm^{-1} that can be assigned as the W—Cl stretch of

* Authors to whom correspondence should be addressed.

the *trans*-ClWCl moiety. Although paramagnetic with the magnetic moment, $\mu_{eff} = 2.2$ BM, implying a low spin d^4 configuration with two unpaired electrons [cf. $MoCl_2(DMPE)_2$, $\mu_{eff} = 2.65$ BM[2]], the compound is EPR silent at both 293 and 77 K. As for the molybdenum compound,[2] NMR spectra can be obtained for this and other tungsten(II) complexes; the CH_2 and CH_3 resonances of DMPE are, however, shifted compared with diamagnetic species.

Reaction with acetonitrile

In refluxing MeCN in the presence of $NaBPh_4$ the compound reacts to give a green solution from which the monosubstituted complex $[WCl(\eta^2\text{-MeCN})(DMPE)_2]BPh_4$, similar to its molybdenum analogue,[4] can be isolated. This complex is a 1:1 electrolyte in MeCN; the IR spectrum shows no band attributable to MeCN—a phenomenon[7] not uncommon.

The ^1H NMR spectrum shows the methyl resonance of MeCN at 3.4 ppm, which is close to the values for similar η^2-MeCN species,[4] while the $^{31}P\{^1H\}$ spectrum has a singlet (14.92 ppm) showing ^{183}W satellites ($J_{W-P} = 118$ Hz).

Reaction with antimony pentachloride

Although bis-acetonitrile complexes, $[M(DMPE)_2(MeCN)_2]^{2+}$, were obtained for chromium[3] and vanadium,[4] neither the molybdenum[4] nor tungsten analogues but only the cations $[MCl(\eta^2\text{-MeCN})(DMPE)_2]^+$, were formed. In an attempt to remove the second chloride we treated $WCl_2(DMPE)_2$ with $SbCl_5$ in refluxing MeCN. This led, however, to chlorination by $SbCl_5$ and the isolation in high yield of the unusual tungsten(V) salt, $[WCl_4(DMPE)_2]SbCl_6$. It may be noted that $MoCl_2(DMPE)_2$ could be oxidized only to the molybdenum(III) cation $[MoCl_2(DMPE)_2]^+$.[2]

The magnetic moments for tungsten(V) compounds d^1, are known to be low[8-10] and no shift in MeCN solutions of the salt by Evans' NMR method were observed. In CH_2Cl_2 solution at 293 K, the X-band EPR spectrum showed a single sharp resonance with $g = 1.90$.

Cationic tungsten(V) species are not well known. Some poorly characterized complexes have been considered[8-10] to be of the type $[WX_4L_2]X$, which include the green WCl_5dppe[9] [dppe = 1,2-bis(diphenyl)phosphinoethane]. Apart from compounds containing oxo, sulphido, η^5-cyclopentadienyl, etc., groups, established tungsten(V) compounds are the halides and alkoxohalides[10] and octahedral WX_6^- and eight-coordinate $[W(CN)_8]^{3-}$ anions.[10,11] Recently, aryloxides, notably the Et_4N^+ and Li^+ salts of the octahedral $[W(OC_6H_5)_6]^-$ ion,[12] and the aryloxohalides with bulky OAr groups, $WCl_3(OC_6H_3\text{-}2,6\text{-}Ph_2)_2L$ (L = THF and PMe_2Ph),[13a] and $W(O\text{-}C_6H_3\text{-}2,6\text{-}Cl_2)_4Cl(Et_2O)$[13b] have had their X-ray structures determined.

The $[WCl_4(DMPE)_2]^+$ cation has a dodecahedral structure with the four chlorines occupying the equatorial, **B**, sites and the phosphorus atoms the **A** sites. A diagram of the crystal structure, which also contains two independent centrosymmetric $SbCl_6^-$ anions, is shown in Fig. 1(a), the cation in Fig. 1(b); bond lengths and angles are given in Table 1.

The dodecahedral geometry is analogous to that found in the chromium(IV) complex $CrH_4(DMPE)_2$,[6a] in which the anionic ligands, the hydrides, are also equatorial. Dodecahedral geometry also almost certainly occurs in the tungsten(IV) phosphine hydride and aluminohydride complexes,[14,15a] but in these structures the monodentate phosphines occupy both types of site. It is pertinent to note that the W—P bonds in the present tungsten(V) complex are longer than any of those in the tungsten(IV) complexes *and* also longer than the W—Cl bonds. This feature is a reflection of the weakness of the W—P interactions in the absence of any W—P π-back bonding.

Aluminohydride complexes

As noted above, interaction of $CrCl_2(DMPE)_2$ with $LiAlH_4$ gave a chromium(II) hydrido aluminohydride $[CrH(AlH_4)(DMPE)_2]_2$,[5] which was characterized by X-ray diffraction.

For both tungsten and molybdenum, interaction of excess $LiAlH_4$ on $MCl_2(DMPE)_2$ in Et_2O gives the metal(II) aluminohydride species, $[MH(AlH_4)(DMPE)_2]_2$, as yellow air- and moisture-sensitive crystals. Due to twinning, X-ray quality crystals of the tungsten compound could not be obtained but suitable crystals of the molybdenum compound were found.

The structure of the molybdenum complex as $[(DMPE)_2HMo(\mu\text{-}H)_2Al(H)(\mu\text{-}H)]_2$ has been confirmed by X-ray crystallography. A diagram of the dimeric molecule is shown in Fig. 2; selected bond lengths and angles are given in Table 2.

Although we were not able to reliably locate any hydrogens except for the two in the $Al(\mu\text{-}H)_2Al$ bridge, the structure is similar in most respects to those for other hydridoaluminohydride complexes.[15a] The relative position of the molybdenum

Table 1. Bond lengths (Å) and angles (°) for $[WCl_4(DMPE)_2]SbCl_6$

		Bond lengths	
Cl(4)—Sb(1)	2.357(7)	Cl(5)—Sb(1)	2.352(7)
Cl(6)—Sb(1)	2.349(8)	Cl(1)—Sb(2)	2.374(6)
Cl(2)—Sb(2)	2.350(7)	Cl(3)—Sb(2)	2.352(6)
Cl(11)—W(1)	2.432(5)	Cl(12)—W(1)	2.432(5)
Cl(13)—W(1)	2.431(5)	Cl(14)—W(1)	2.421(5)
P(1)—W(1)	2.588(7)	P(2)—W(1)	2.575(7)
P(3)—W(1)	2.590(7)	P(4)—W(1)	2.581(7)
C(11)—P(1)	1.838(18)	C(12)—P(1)	1.833(20)
C(13)—P(1)	1.866(19)	C(22)—P(2)	1.865(20)
C(23)—P(2)	1.817(19)	C(32)—P(2)	1.814(22)
C(21)—P(3)	1.842(20)	C(31)—P(3)	1.839(20)
C(33)—P(3)	1.857(23)	C(41)—P(4)	1.820(22)
C(42)—P(4)	1.805(21)	C(43)—P(4)	1.803(22)
C(23)—C(13)	1.454(27)	C(43)—C(33)	1.466(30)
		Bond angles	
Cl(12)—W(1)—Cl(11)	146.0(1)	Cl(13)—W(1)—Cl(11)	89.7(2)
Cl(13)—W(1)—Cl(12)	100.2(2)	Cl(14)—W(1)—Cl(11)	100.4(2)
Cl(14)—W(1)—Cl(12)	89.3(2)	Cl(14)—W(1)—Cl(13)	146.1(1)
P(1)—W(1)—Cl(11)	78.0(2)	P(1)—W(1)—Cl(12)	75.2(2)
P(1)—W(1)—Cl(13)	69.9(2)	P(1)—W(1)—Cl(14)	143.7(1)
P(2)—W(1)—Cl(11)	75.2(2)	P(2)—W(1)—Cl(12)	78.0(3)
P(2)—W(1)—Cl(13)	143.9(1)	P(2)—W(1)—Cl(14)	69.8(2)
P(2)—W(1)—P(1)	75.0(2)	P(3)—W(1)—Cl(11)	70.3(2)
P(3)—W(1)—Cl(12)	143.4(1)	P(3)—W(1)—Cl(13)	78.3(2)
P(3)—W(1)—Cl(14)	75.0(2)	P(3)—W(1)—P(1)	134.7(1)
P(3)—W(1)—P(2)	124.2(2)	P(4)—W(1)—Cl(11)	143.6(1)
P(4)—W(1)—Cl(12)	70.0(2)	P(4)—W(1)—Cl(13)	74.0(2)
P(4)—W(1)—Cl(14)	79.1(2)	P(4)—W(1)—P(1)	123.3(2)
P(4)—W(1)—P(2)	135.1(1)	P(4)—W(1)—P(3)	74.6(2)
C(11)—P(1)—W(1)	116.1(7)	C(12)—P(1)—W(1)	115.9(8)
C(12)—P(1)—C(11)	105.1(10)	C(13)—P(1)—W(1)	109.4(7)
C(13)—P(1)—C(11)	105.7(10)	C(13)—P(1)—C(12)	103.5(10)
C(22)—P(2)—W(1)	116.0(7)	C(23)—P(2)—W(1)	111.7(7)
C(23)—P(2)—C(22)	105.8(10)	C(32)—P(2)—W(1)	117.1(8)
C(32)—P(2)—C(22)	102.2(10)	C(32)—P(2)—C(23)	102.5(10)
C(21)—P(3)—W(1)	115.7(7)	C(31)—P(3)—W(1)	116.3(7)
C(31)—P(3)—C(21)	103.5(10)	C(33)—P(3)—W(1)	109.8(7)
C(33)—P(3)—C(21)	106.5(10)	C(33)—P(3)—C(31)	103.9(11)
C(41)—P(4)—W(1)	116.9(8)	C(42)—P(4)—W(1)	115.4(8)
C(42)—P(4)—C(41)	104.7(10)	C(43)—P(4)—W(1)	111.0(7)
C(43)—P(4)—C(41)	101.2(11)	C(43)—P(4)—C(42)	106.2(12)
C(23)—C(13)—P(1)	110.8(13)	C(13)—C(23)—P(2)	109.1(14)
C(43)—C(33)—P(3)	109.1(13)	C(33)—C(43)—P(4)	109.3(14)
Cl(5)—Sb(1)—Cl(4)	89.8(3)	Cl(6)—Sb(1)—Cl(4)	89.5(3)
Cl(6)—Sb(1)—Cl(5)	90.0(4)	Cl(2)—Sb(2)—Cl(1)	90.2(3)
Cl(3)—Sb(2)—Cl(1)	90.1(3)	Cl(3)—Sb(2)—Cl(2)	89.9(3)
Cl(4)—Sb(1)—Cl(4B)	180.0(2)	Cl(5)—Sb(1)—Cl(4B)	90.2(3)
Cl(5)—Sb(1)—Cl(5B)	180.0(3)	Cl(6)—Sb(2)—Cl(5B)	90.0(3)
Cl(4)—Sb(2)—Cl(6B)	90.5(3)	Cl(6)—Sb(2)—Cl(6B)	180.0(2)
Cl(1)—Sb(1)—Cl(1B)	180.0(2)	Cl(2)—Sb(1)—Cl(1B)	89.8(3)
Cl(2)—Sb(1)—Cl(2B)	180.0(3)	Cl(3)—Sb(2)—Cl(1B)	90.0(3)
Cl(3)—Sb(2)—Cl(3B)	180.0(2)	Cl(2)—Sb(2)—Cl(3B)	90.1(3)

Key to symmetry operations relating designated atoms to reference atoms at (x, y, z): (B) $1.0+x$, $1.0+y$, z.

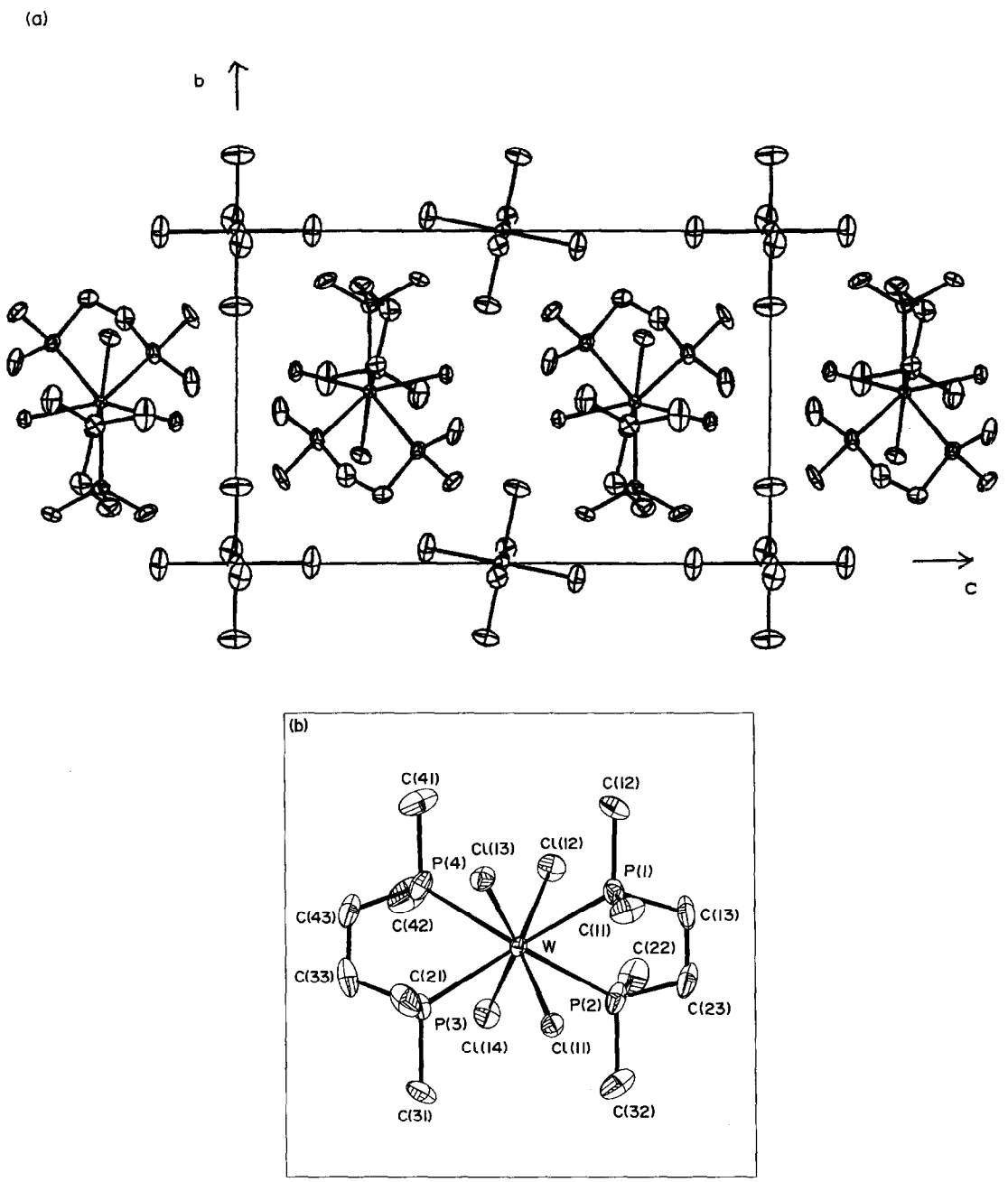

Fig. 1. (a) The crystal structure of $[WCl_4(DMPE)_2]^+[SbCl_6]^-$ and (b) the structure of the $[WCl_4(DMPE)_2]^+$ cation.

atom to the plane of the $Al(\mu\text{-}H)_2Al$ bridge strongly suggests that if, as is likely, the Mo···Al links are also via $Mo(\mu\text{-}H)_2Al$ bridges, then a terminal hydrogen is also present on the aluminium atom. That this is the case is shown by the ^{27}Al NMR spectra which fall in the region for five-coordinate aluminium.[5,15]

The four phosphorus atoms coordinate in an approximately planar manner and we presume the single hydrogen on molybdenum occupies the apparent vacant site "*trans*" to the coordination of the two bridging hydrogens. The molybdenum is thus seven-coordinate as in the similar molybdenum(II) and tungsten(II) trimethylphosphine complexes.[5] In view of the approximate planarity of the MoP_4 unit with *trans* P—Mo—P angles of 149 and 169°, a distorted mono-capped octahedral structure is a possibility. The absence of confirmed positions for the hydrides makes it difficult to have much confidence in this assignment, however.

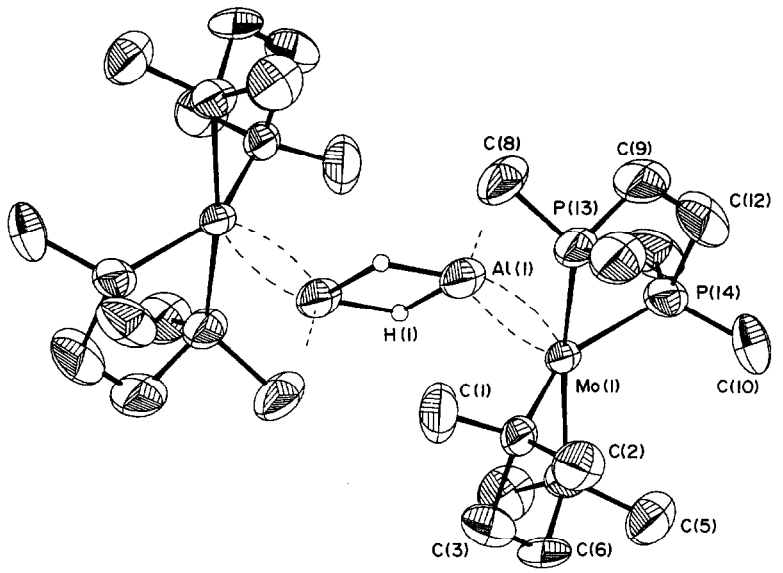

Fig. 2. The structure of one of the two indendent molecules of $[MoH(AlH_4)(DMPE)_2]_2$. Bonds to presumed hydrogen atoms are shown by dashed lines.

The ^1H NMR spectra are not very useful since the bands are broad as a result of the ^{27}Al quadrupole phosphorus couplings and the paramagnetism; also the molecules are doubtless non-rigid as in similar species.[5] The bands, though poorly resolved, are in similar positions to those in the PMe_3 compounds,[5] with terminal Al—H and $Al(\mu\text{-}H)_2Al$ bands at *ca* 4.1 ppm, the CH_2 and CH_3 resonances of DMPE around 1.58 ppm and the $Al(\mu\text{-}H)_2M$ bands around −5.5 ppm. For the tungsten compound there is a band at −8.3 ppm which is due to the terminal W—H.

Interaction of the tungsten complex with methanol allows the isolation of the *tetrahydride*, $WH_4(DMPE)_2$, as pale yellow crystals [cf. methanolysis of the PMe_3 analogues to give $MH_4(PMe_3)_4$[5]]. The molybdenum tetrahydride, $MoH_4(DMPE)_2$, which was made[6b] by sodium reduction of $MoCl_2(DMPE)_2$ under hydrogen, can also be obtained by methanolysis of the aluminohydride. The IR and NMR spectra of the tungsten tetrahydride are similar to those of the molybdenum and chromium[6a] analogues. Thus the IR spectrum has W—H bands at 1745 and 1720 cm^{-1}, while the ^1H NMR spectrum has a quintet at −5.46 ppm (333 K) with $J_{P-H} = 29.2$ Hz (cf. Cr, −6.91 ppm, $J_{P-H} = 56.1$; Mo −5.51 ppm, $J_{P-H} = 31.5$ Hz). Unlike the rigid chromium analogue, $WH_4(DMPE)_2$ is non-rigid from the fast exchange limit (333 K) down to 273 K, similar to $MH_4(PMe_3)_4$ (M = Mo and W).[16] No comment is made [6b] concerning non-rigidity of $MoH_4(DMPE)_2$, but presumably it is.

EXPERIMENTAL

The general techniques and instrumentation used have been described.[17] $WCl_4(THF)_2$ was prepared by adding excess THF to $WCl_4(SEt_2)_2$[18] and stirring for a few minutes, when the THF complex precipitates as an orange powder which was collected, washed with THF and dried. IR spectra are in Nujol mulls in cm^{-1}; NMR spectra, δ values in ppm in C_6D_6 unless otherwise stated and referenced to Me_4Si (^1H), external H_3PO_4 (^{31}P) and external $[Al(H_2O)_6]^{3+}$ (^{27}Al). All operations were carried out under nitrogen, argon or *in vacuo*.

(1) Trans-*bis*[1,2-*bis*(*dimethylphosphino*)*ethane*] *dichlorotungsten*(II)

To a suspension of $WCl(THF)_2$ (6 g, 13 mmol) in THF (100 cm^3) at 0°C was added DMPE (4.5 cm^3 27 mmol) and sodium naphthalenide (92 cm^3 of a 0.28 M solution in THF, 26 mmol). The solution was stirred at room temperature for about 18 h, filtered and evaporated to dryness. The naphthalene was removed by sublimation *in vacuo* and the residue was extracted into warm hexane (4 × 50 cm^3). The extract was filtered, concentrated to about 100 cm^3 and cooled at −20°C to give 2.1 g of dark red crystals of $WCl_2(DMPE)_2$. Further crops of crystals may be obtained from the supernatant. Combined yield: 2.5 g (35%); m.p. *ca* 310°C. (Found: C, 25.1; H, 5.8. $C_{16}H_{32}P_4W$ requires: C, 26.0; H, 5.8%.) Magnetic moment (Evans' NMR method), 2.2 BM. IR: 1418s, 1291m, 1277s, 1227s, 1227w, 1112m,

Table 2. Bond lengths (Å) and angles (°) for $[MoH(AlH_4)(DMPE)_2]_2$

Bond lengths			
P(11)—Mo(1)	2.414(6)	P(12)—Mo(1)	2.417(7)
P(13)—Mo(1)	2.398(8)	P(14)—Mo(1)	2.410(6)
C(1)—P(11)	1.844(24)	C(2)—P(11)	1.799(18)
C(3)—P(11)	1.837(27)	C(4)—P(12)	1.797(25)
C(5)—P(12)	1.840(21)	C(6)—P(12)	1.920(17)
C(7)—P(13)	1.824(23)	C(8)—P(13)	1.847(23)
C(9)—P(13)	1.822(22)	C(10)—P(14)	1.813(22)
C(11)—P(14)	1.815(20)	C(12)—P(14)	1.859(29)
C(6)—C(3)	1.420(29)	C(12)—C(9)	1.469(31)
P(21)—Mo(2)	2.417(7)	P(22)—Mo(2)	2.409(7)
P(23)—Mo(2)	2.390(7)	P(24)—Mo(2)	2.419(6)
C(1B)—P(21)	1.814(17)	C(2B)—P(21)	1.814(27)
C(3B)—P(21)	1.821(22)	C(4B)—P(22)	1.796(22)
C(5B)—P(22)	1.831(28)	C(6B)—P(22)	1.836(24)
C(10B)—P(23)	1.838(23)	C(11B)—P(23)	1.832(19)
C(12B)—P(23)	1.882(20)	C(7B)—P(24)	1.841(20)
C(8B)—P(24)	1.831(24)	C(9B)—P(24)	1.841(24)
C(6B)—C(3B)	1.524(23)	C(12B)—C(9B)	1.534(26)
Al(1)—Mo(1)	2.578(9)	Al(2)—Mo(2)	2.565(9)
Al(1)—Al(1a)	2.661(15)	Al(2)—Al(2b)	2.644(14)
H(1)—Al(1)	1.64(23)	H(2)—Al(2)	1.77(28)
H(1)—Al(1a)	1.66(26)	H(2)—Al(2a)	1.73(26)
Bond angles			
P(11)—Mo(1)—Al(1)	113.1(3)	P(12)—Mo(1)—Al(1)	109.1(3)
P(12)—Mo(1)—P(11)	79.3(2)	P(13)—Mo(1)—Al(1)	82.1(3)
P(13)—Mo(1)—P(11)	95.0(3)	P(13)—Mo(1)—P(12)	168.7(2)
P(14)—Mo(1)—Al(1)	97.3(3)	P(14)—Mo(1)—P(11)	148.3(2)
P(14)—Mo(1)—P(12)	99.6(3)	P(14)—Mo(1)—P(13)	80.1(3)
C(1)—P(11)—Mo(1)	121.9(7)	C(2)—P(11)—Mo(1)	121.6(8)
C(2)—P(11)—C(1)	99.0(10)	C(3)—P(11)—Mo(1)	109.3(6)
C(3)—P(11)—C(1)	102.4(11)	C(3)—P(11)—C(2)	98.9(12)
C(4)—P(12)—Mo(1)	117.7(9)	C(5)—P(12)—Mo(1)	123.8(9)
C(5)—P(12)—C(4)	98.9(11)	C(6)—P(12)—Mo(1)	108.5(8)
C(6)—P(12)—C(4)	106.2(12)	C(6)—P(12)—C(5)	99.3(10)
C(7)—P(13)—Mo(1)	117.9(9)	C(8)—P(13)—Mo(1)	125.9(10)
C(8)—P(13)—C(7)	99.3(11)	C(9)—P(13)—Mo(1)	111.0(8)
C(9)—P(13)—C(7)	99.1(12)	C(9)—P(13)—C(8)	99.1(11)
C(10)—P(14)—Mo(1)	124.1(8)	C(11)—P(14)—Mo(1)	120.3(10)
C(11)—P(14)—C(10)	97.5(11)	C(12)—P(14)—Mo(1)	110.1(7)
C(12)—P(14)—C(10)	98.0(13)	C(12)—P(14)—C(11)	102.8(11)
C(6)—C(3)—P(11)	108.0(18)	C(3)—C(6)—P(12)	108.5(14)
C(12)—C(9)—P(13)	112.3(17)	C(9)—C(12)—P(14)	110.3(19)
P(21)—Mo(2)—Al(2)	114.5(3)	P(22)—Mo(2)—Al(2)	110.3(3)
P(22)—Mo(2)—P(21)	79.8(2)	P(23)—Mo(2)—Al(2)	79.6(3)
P(23)—Mo(2)—P(21)	95.1(3)	P(23)—Mo(2)—P(22)	170.0(2)
P(24)—Mo(2)—Al(2)	96.9(3)	P(24)—Mo(2)—P(21)	147.0(2)
P(24)—Mo(2)—P(22)	99.2(2)	P(24)—Mo(2)—P(23)	80.3(2)
C(1B)—P(21)—Mo(2)	120.3(8)	C(2B)—P(21)—Mo(2)	119.0(8)
C(2B)—P(21)—C(1B)	102.3(10)	C(3B)—P(21)—Mo(2)	111.7(7)
C(3B)—P(21)—C(1B)	100.5(9)	C(3B)—P(21)—C(2B)	99.8(11)
C(4B)—P(22)—Mo(2)	124.4(11)	C(5B)—P(22)—Mo(2)	118.2(10)
C(5B)—P(22)—C(4B)	100.5(15)	C(6B)—P(22)—Mo(2)	111.1(7)
C(6B)—P(22)—C(4B)	99.7(12)	C(6B)—P(22)—C(5B)	98.7(12)
C(10B)—P(23)—Mo(2)	118.0(8)	C(11B)—P(23)—Mo(2)	126.8(9)
C(11B)—P(23)—C(10B)	97.8(11)	C(12B)—P(23)—Mo(2)	111.1(7)
C(12B)—P(23)—C(10B)	99.4(11)	C(12B)—P(23)—C(11B)	99.1(10)
C(7B)—P(24)—Mo(2)	121.3(7)	C(8B)—P(24)—Mo(2)	117.7(8)
C(8B)—P(24)—C(7B)	100.1(10)	C(9B)—P(24)—Mo(2B)	110.6(6)
C(9B)—P(24)—C(7B)	101.3(11)	C(9B)—P(24)—C(8B)	103.2(11)
C(6B)—C(3B)—P(21)	110.4(14)	C(3B)—C(6B)—P(22)	111.1(15)
C(12B)—C(9B)—P(24)	111.1(16)	C(9B)—C(12B)—P(23)	107.1(15)
H(1)—Al(1)—H(1a)	72.5(12)	Al(1)—H(1)—Al(1b)	107.6(13)
H(2)—Al(2)—H(2a)	81.7(15)	Al(2)—H(2)—Al(2b)	98.3(14)

Key to symmetry operations relating designated atoms to reference atoms at (x, y, z): (a) $2.0-x, -y, 2.0-z$; (*b*) $1.0-x, 1.0-y, 1.0-z$.

1073m, 989m, 927vs, 921vs, 888s, 859s, 832s, 784s, 730s, 698s, 630s, 452m, 324s. ^{1}H NMR: 19.55 (s, PCH_2); −3.99 (s, PMe_2).

(2) Trans-(*η^2-acetonitrile*)(*chloro*)*bis*[1,2-*bis*(*dimethylphosphino*)*ethane*]*tungsten*(II) *tetraphenylborate*

To $WCl_2(DMPE)_2$ (0.31 g, 0.56 mmol) in MeCN (50 cm^3) was added an excess of $NaBPh_4$ (0.4 g, 1.17 mmol). The solution was refluxed for 24 h, cooled and the yellow–green solution filtered. After evaporation, the residue was extracted with CH_2Cl_2 (30 cm^3) and the extract evaporated to dryness; the residue was crystallized from MeCN. Yield: 0.35 g (71%); m.p. 190°C. (Found: C, 51.1; H, 6.2; N, 1.4. $WC_{38}H_{55}P_4BClN$ requires: C, 51.9; H, 6.3; N, 1.6%.) IR: 3050s, 3032s, 1945w, 1881w, 1814w, 1580m, 1428s, 1416s, 1299m, 1288m, 1267w, 1182w, 1149w, 1033w, 944s, 930s, 891m, 865w, 851w, 793w, 745s, 710s, 703s, 976m, 649m, 625w, 615m, 604s, 485w, 452w. Conductivity (MeCN): $\Lambda_M = 86\ \Omega^{-1}$ cm^2 mol^{-1}. ^{1}H NMR (CD_3CN): 7.31–6.96 (20, m, BPh_4); 3.4 (3, s, CH_3CN); 1.57–1.35 (32, m, DMPE). ^{31}P-{^{1}H} NMR: 14.92s; $J_{W-P} = 118$ Hz.

(3) Trans-*bis*[1,2-*bis*(*dimethylphosphino*)*ethane*] *tetrachlorotungsten*(V) *hexachloroantimonate*

To $WCl_2(DMPE)_2$ (0.3 g, 0.54 mmol) in MeCN (50 cm^3) was added $SbCl_5$ (1.2 cm^3 of a 1 M solution in CH_2Cl_2, 1.2 mmol). The initial red solution was refluxed for 12 h, after which the colour was green. The solution was filtered, concentrated (15 cm^3) and cooled at −20°C to give dark green crystals. Yield: 0.33 g (73%); m.p. 230°C. (Found: C, 15.3; H, 3.4; P, 12.5. $C_{12}H_{32}Cl_{10}P_4SbW$ requires: C, 15.0; H, 3.4; P, 12.9%.) IR: 1413s, 1295m, 1284s, 1247w, 1132w, 1086w, 1001w, 938vs, 901s, 853w, 794w, 749m, 717s, 659m, 643w, 433m. Conductivity (MeCN): $\Lambda_M = 90\ \Omega^{-1}$ cm^2 mol^{-1}.

(4) *Bis*[1,2-*bis*(*dimethylphosphino*)*ethane*](*tetrahydridoaluminato*)*hydridotungsten*(II) *dimer*

To $WCl_2(DMPE)_2$ (0.22 g, 0.40 mmol) in Et_2O (50 cm^3) at −78°C was added a suspension of $LiAlH_4$ (0.12 g, 3.20 mmol) in Et_2O (30 cm^3). Upon warming to room temperature the solution turned orange and gas was evolved. After stirring for 12 h; the solution was filtered, concentrated (*ca* 50 cm^3) and cooled to −20°C to give yellow crystals. Further crops of crystals may be obtained from the supernatant. Combined yield: 0.29 g (72%); m.p. 215°C (decomp). (Found: C, 28.0; H, 7.2; P, 23.8. $W_2C_{24}H_{72}P_8Al_2$ requires: C, 28.0; H, 7.0; P, 24.0%.) IR: 1618s (AlH), 1650s, [W(μ-H)$_2$Al]; other bands 1420s, 1336s, 1291m, 1275s, 1228w, 1118w, 1077w, 936vs, 922vs, 886s, 836s, 787m, 696s, 636s, 575m, 535s, 461m. ^{1}H NMR: 4.1 (m, terminal Al—H and Al—H—Al); 1.58 (m, DMPE); −5.5 (m, W—H—Al); −8.3 (m, W—H-terminal). ^{31}P-{^{1}H} NMR: 20.84, s; $J_{W-P} = 108.55$ Hz. ^{27}Al-{^{1}H} NMR: 99 ("t", $w_{1/2} = 4500$ Hz).

The *molybdenum* analogue was obtained similarly from $MoCl_2(DMPE)_2$;[2] X-ray quality crystals were grown from diethyl ether. The IR and NMR spectra closely resemble those of the tungsten compound except that the Mo—H band is probably mixed in with the Mo—H—Al resonances as in other cases.[5]

(5) *Bis*[1,2-*bis*(*dimethylphosphino*)*ethane*]*tetrahydridotungsten*(IV)

To a solution of $[WH(AlH_4)(DMPE)_2]_2$ (0.42 g, 0.41 mmol) in hexane (30 cm^3) was added MeOH dropwise until gas evolution ceased. The solution was filtered, evaporated to dryness and the residue extracted with hexane. The filtered extract was concentrated (to *ca* 10 cm^3) and cooled to −20°C to give pale yellow crystals (0.11 g). Further crops of crystals may be obtained from the supernatant. Combined yield: 0.14 g (70%); m.p. 152°C. (Found: C, 29.5; H, 7.4; P, 25.4. $WC_{12}H_{36}P_4$ requires: C, 29.5; H, 7.4; P, 25.4%.) IR: 1745m, 1720s, (W—H); other bands 1415m, 1283m, 1270s, 1230w, 1115w, 1080w, 923vs, 885s, 835s, 787s, 700s, 639s, 549w, 456m. ^{1}H NMR: 1.56–1.43 (m, 32, DMPE); −5.46 (m, 4, W—H), $J_{P-H} = 29.2$ Hz. ^{31}P-{^{1}H} NMR: 22.92 (s, DMPE), $J_{W-P} = 82$ Hz.

X-ray crystallography

Crystals of the two complexes were sealed under argon in glass capillaries. Following preliminary photography, unit cell and intensity data were obtained using an Enraf–Nonius CAD4 diffractometer and graphite monochromatized Mo-K_α radiation ($\lambda = 0.71069$ Å) by following standard procedures.[19]

The structures were solved via the heavy atom method and refined by full-matrix least-squares. Non-hydrogen atoms were refined in the anisotropic approximation; hydrogen atoms on the ligands (in idealized positions) plus the two in the Al(μ-H)$_2$Al bridge were included only for the molybdenum complex and refined in the isotropic approximation. Crystallographic data are given in Table 3. Atomic coordinates, temperature factor

Table 3. Crystal data, details of intensity measurements and structure refinement

Molecular formula	$[WCl_4(DMPE)_2]SbCl_6$	$[MoH(AlH_4)(DMPE)_2]_2$
Molecular weight	960.408	852.453
Crystal system	Triclinic	Triclinic
a (Å)	9.258(4)	12.785(8)
b (Å)	10.104(6)	20.283(11)
c (Å)	16.416(3)	9.572(5)
α (°)	89.76(4)	98.34(5)
β (°)	91.13(2)	103.58(5)
γ (°)	86.39(5)	108.15(5)
Volume (Å^3)	1532.23	2228.54
Space group	$P\bar{1}$	$P\bar{1}$
Z	2	2[a]
D_c (g cm^{-3})	2.08	1.270
μ (cm^{-1})	58.13	8.852
$F(000)$	918	888
h, k, l range	$-11 \rightarrow 11$	$-13 \rightarrow 13$
	$-12 \rightarrow 12$	$-21 \rightarrow 21$
	$0 \rightarrow 19$	$0 \rightarrow 10$
Total number of reflections	5559	5862
Number of unique reflections	5357	5455
Number of reflections used [$F > 3\sigma(F)$]	4766	3029
Number of parameters	256	382
Weighting scheme parameter g in $w = 1/[\sigma^2(F)+gF_0^2]$	0.0002	0.00075
Final R	0.0636	0.0649
Final Rw	0.0659	0.0654

[a] The structure contains two independent centrosymmetric dimers.

coefficients and full lists of bond lengths and angles have been deposited as supplementary material.

Acknowledgement—We thank the SERC for a studentship (V.S.) and provision of X-ray facilities.

REFERENCES

1. G. S. Girolami, G. Wilkinson, A. M. R. Galas, M. Thornton-Pett and M. B. Hursthouse, *J. Chem. Soc., Dalton Trans.* 1985, 1339.
2. L. K. Fong, J. R. Fox, B. M. Foxman and N. J. Cooper, *Inorg. Chem.* 1986, **25**, 1880.
3. (a) J. E. Salt, G. Wilkinson, M. Motevalli and M. B. Hursthouse, *J. Chem. Soc., Dalton Trans.* 1986, 1141; (b) A. R. Barron, J. E. Salt, G. Wilkinson, M. Motevalli and M. B. Hursthouse, *J. Chem. Soc., Dalton Trans.* 1987, 2947.
4. S. J. Anderson, F. J. Wells, G. Wilkinson, B. Hussain and M. B. Hursthouse, *Polyhedron* 1988, **7**, 2615.
5. A. R. Barron, J. E. Salt and G. Wilkinson, *J. Chem. Soc., Dalton Trans.* 1986, 1329.
6. (a) J. E. Salt, G. S. Girolami, G. Wilkinson, M. Motevalli, M. Thornton-Pett and M. B. Hursthouse, *J. Chem. Soc., Dalton Trans.* 1985, 685; (b) L. K. Fong, J. R. Fox and N. J. Cooper, *Organometallics* 1987, **6**, 223.
7. G. Rouschias and G. Wilkinson, *J. Chem. Soc. A* 1968, 449.
8. T. M. Brown and B. Ruble, *Inorg. Chem.* 1967, **7**, 1335.
9. P. M. Boorman, N. N. Greenwood, M. A. Hildon and R. V. Parish, *J. Chem. Soc. A* 1968, 2002.
10. Z. Dori, in *Comprehensive Coordination Chemistry* (Edited by G. Wilkinson, R. D. Gillard and J. A. McCleverty), Vol. 3, Sect. 37.4.1., p. 894. Pergamon Press, Oxford (1987).
11. F. A. Cotton and G. Wilkinson, *Advanced Inorganic Chemistry*, 5th edn, Ch. 19C. John Wiley, New York (1988).
12. J. I. Davies, J. F. Gibson, A. C. Skapski, G. Wilkinson and W. K. Wong, *Polyhedron* 1982, **1**, 641.
13. (a) J. L. Kerschner, P. E. Fanwick, I. P. Rothwell and J. C. Huffman, *Inorg. Chem.* 1989, **28**, 780; (b) R. M. Kolodziej, R. R. Schrock and J. C. Dewan, *Inorg. Chem.* 1989, **28**, 1243.
14. A. R. Barron, G. Wilkinson, M. Motevalli and M. B. Hursthouse, *J. Chem. Soc., Dalton Trans.* 1987, 837.
15. For reviews see (a) A. R. Barron and G. Wilkinson, *Polyhedron* 1986, **5**, 1897; (b) B. M. Bulchev, *Polyhedron* 1990, **9**, 387.

16. D. Lyons and G. Wilkinson, *J. Chem. Soc., Dalton Trans.* 1985, 587, and refs quoted.
17. A. A. Danopoulos, C. J. Longley, G. Wilkinson, B. Hussain-Bates and M. B. Hursthouse, *Polyhedron* 1989, **8**, 2657.
18. M. A. Schaefer King and R. E. McCarley, *Inorg. Chem.* 1973, **12**, 1972.
19. M. B. Hursthouse, R. A. Jones, K. M. A. Malik and G. Wilkinson, *J. Am. Chem. Soc.* 1979, **101**, 4128.

Polyhedron Vol. 10, No. 6, pp. 605–611, 1991
Printed in Great Britain

0277–5387/91 $3.00+.00
© 1991 Pergamon Press plc

SELECTIVE PROTONATION OF TERMINALLY BOUND η^3-ALLYLS ON $(\eta^3$-ALLYL$)_2(\mu_2$-η^3-ALLYL$)_2$DIMOLYBDENUM(II) BY β-DIKETONES FORMING $(\mu_2$-η^3-ALLYL$)_2(\eta^2$-β-DIKETONATE$)_2$ DIMOLYBDENUM(II) COMPLEXES

REED J. BLAU,* MARY S. GOETZ and RONG-JER TSAY

Department of Chemistry, University of Texas at Arlington, Arlington, TX 76019, U.S.A.

(*Received* 20 *August* 1990; *accepted* 20 *November* 1990)

Abstract—The β-diketones, R(C=O)CH$_2$(C=O)R′ [where R = R′ = Me (acac); R = Me, R′ = CF$_3$ (tfac); or R = R′ = CF$_3$ (hfac)] selectively protonate the terminally bound η^3-allyls on $Mo_2(\mu_2$-η^3-allyl$)_2(\eta^3$-allyl$)_2$ (**A**) leaving the $Mo_2(\mu_2$-η^3-allyl$)_2$ core intact. The molybdenum(II) dimers, $Mo_2(\mu_2$-η^3-allyl$)_2(\eta^2$-L$)_2$ [where L = acac (**B**), tfac (**C**) or hfac (**D**)] are formed from this reaction. From ^{1}H, ^{13}C and ^{19}F NMR data, it is evident that the two bridging allyls in each complex, **B**–**D**, are bound in a *cis* arrangement with endo and exo conformations, respectively. Thus, a plane of symmetry bisects the Mo—Mo bond axis and the two bridging allyls in **B** and **D**, but is absent parallel to the Mo—Mo bond axis and bisecting each of the chelating β-diketonate ligands. The complex, **C**, exists primarily as the isomer in which the bulky trifluoromethyl groups on the two tfac ligands are as far apart as possible from each other. As the electron-donating ability of the terminally bound ligands in **A**–**D** decreases, allyl > acac > tfac > hfac, an upfield shift in the proton resonances of the bridging allyls is observed.

Allyl complexes of the group VI transition metals, W(η^3-allyl)$_4$, Mo(η^3-allyl)$_4$, $Mo_2(\mu_2$-η^3-allyl$)_2(\eta^3$-allyl$)_2$, Cr(η^3-allyl)$_3$ and $Cr_2(\mu_2$-η^3-allyl$)_2(\eta^3$-allyl$)_2$ were first characterized at the dawn of the modern era of organotransition metal chemistry.[1] They have been utilized extensively as precursors in the formulation of catalysts for olefin[2] and alkyne metathesis,[3] propene and ethanol oxidation,[4] olefin and thiophene hydrogenation,[5] and the polymerization of a variety of olefins including butadiene,[6] methyl methacrylate,[7] alicyclic dienes and trienes.[8] Most recently, catalysts have been prepared by chemisorption of these allyl complexes on inorganic oxide support surfaces. Many of these catalysts have been characterized stoichiometrically and spectroscopically and much is known about the structure and function of their active sites.[4,9]

Our initial interest in this area was stimulated by reports that $Mo_2(\mu_2$-η^3-allyl$)_2(\eta^3$-allyl$)_2$[10] forms discrete surface structures when allowed to react with hydroxyl groups on silica or alumina surfaces.[4] These surface species were found to be efficient olefin metathesis catalysts[11] as well as precursors to several other functional surface structures.[12,13] The species resulting from $Mo_2(\mu_2$-η^3-allyl$)_2(\eta^3$-allyl$)_2$ chemisorption on silica were assigned to be molybdenum(III) or molybdenum(IV) dimers depending on the type of silica, with two or four allylic ligands, respectively, still intact. In an effort to better understand the chemisorption process and what factors control the variability in structure and oxidation state of the surface species thus formed, we are investigating homogeneously the reactions of $Mo_2(\mu_2$-η^3-allyl$)_2(\eta^3$-allyl$)_2$ with a variety of proton donors. We report herein results from the reactions of a series of β-diketones with $Mo_2(\mu_2$-η^3-allyl$)_2(\eta^3$-allyl$)_2$.

$Mo_2(\mu_2$-η^3-allyl$)_2(\eta^3$-allyl$)_2$ (**A**) is unique in that its four allylic ligands are coordinated through two different bonding modes: two π-allyls are bridging the Mo—Mo quadruple bond in a *cis* arrangement, with each π-allyl in the remaining pair binding to a single molybdenum atom.[14] Exchange of allyls between bridging and terminal positions is not observed even at 80°C.[15] In solution, **A** is reported to exist as a mixture of two isomers differing only

* Author to whom correspondence should be addressed.

in the relative conformation of the terminal ligands:

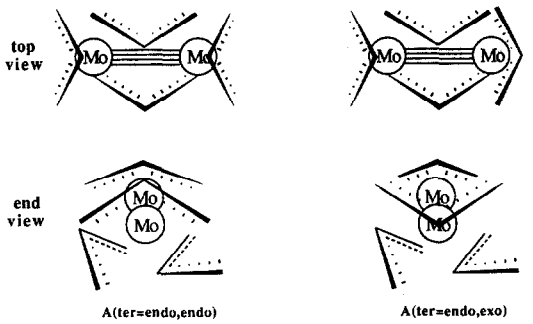

These isomers were observed in a nine to one ratio of $Mo_2(\mu_2\text{-}\eta^3\text{-endo-allyl})(\mu_2\text{-}\eta^3\text{-exo-allyl})(\eta^3\text{-endo-allyl})_2$ **[A(ter = endo,endo)]** to $Mo_2(\mu_2\text{-}\eta^3\text{-endo-allyl})(\mu_2\text{-}\eta^3\text{-exo-allyl})(\eta^3\text{-endo-allyl})(\eta^3\text{-exo-allyl})$ **[A(ter = endo,exo)]**. Interconversion of these two isomers was detected at 80°C by way of ^{1}H NMR magnetization transfer.[15] The investigation into the reactions of proton donors and other reagents with **A** has led to a better understanding of structure/reactivity relationships as they deal with the synergy between the bridging allyls, the Mo—Mo quadruple bond and the terminally coordinated ligands in **A** and related complexes.

RESULTS AND DISCUSSION

Synthesis of $Mo_2(allyl)_2(\beta\text{-diketonate})_2$ *complexes*

The reaction of green $Mo_2(\mu_2\text{-}\eta^3\text{-allyl})_2(\eta^3\text{-allyl})_2$ **(A)**[10] with two equiv. of acetylacetone (acacH) at 0°C in pentane yields a pink precipitate with concurrent, ^{1}H NMR verifiable evolution of propene. Similarly, violet and brown products are formed from the reaction of **A** with two equiv. of trifluoroacetylacetone (tfacH) and hexafluoroacetylacetone (hfacH), respectively. The latter two products are considerably more soluble in pentane and related solvents than the acac derivative. Empirical observations suggest that rates of product formation parallel the inherent acidity of the diketone: $k_{hfacH} > k_{tfacH} > k_{acacH}$.

Elemental analyses of these derivatives are consistent with the empirical formula $Mo_n(allyl)_n(diketonate)_n$. Intense molecular ion peaks are observed via electron impact mass spectrometry which correspond to dimeric species, $Mo_2(allyl)_2(diketonate)_2$. Thus, protonation of two allylic ligands on **A** by β-diketones to form propene occurs concurrently with coordination of the two resulting β-diketonate anions:

$$Mo_2(C_3H_5)_4 + 2R\text{-}CO\text{-}CH_2\text{-}CO\text{-}R' \longrightarrow Mo_2(C_3H_5)_2(R\text{-}CO\text{-}CH\text{-}CO\text{-}R')_2 + 2C_3H_6.$$

Additional products form upon addition of more than two equiv. of β-diketone to **A** with further evolution of propene. In most cases, these products have not been characterized, however, $Mo(hfac)_3$ is formed in significant yields in the reaction of **A** with hfacH.

Molecular structure of $Mo_2(\mu_2\text{-}\eta^3\text{-allyl})_2(\eta^2\text{-diketonate})_2$ *complexes*

There are two common modes of diketonate binding to metal centres:

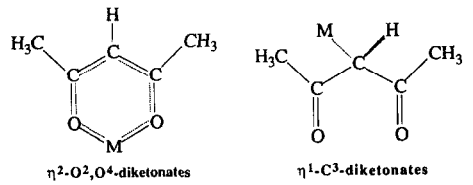

Sharp bands are observed in the IR spectra of $Mo_2(allyl)_2(diketonate)_2$ at 1570, 1615 and 1630 cm^{-1} for the acac, tfac and hfac derivatives, respectively. These bands are in the range normally observed for C=O stretches of complexes containing η^2-O^2,O^4-diketonates.[16] The C=O stretch for platinum(II) complexes containing η^1-C^3-diketonates is observed at higher frequency, i.e. near 1670 cm^{-1}.[17] Thus, the diketonate ligands in these dimolybdenum(II) complexes are acting as bidentate, four electron donors binding through the two carbonyl oxygens.

The NMR spectra for this series of molybdenum dimers are rich in information and were invaluable in selecting the most probable structural type. The spectral characterization of the acac and hfac derivatives will be discussed initially due to their higher symmetry.

Through various ^{1}H NMR homodecoupling techniques, it was determined that both $Mo_2(allyl)_2(acac)_2$ **(B)** and $Mo_2(allyl)_2(hfac)_2$ **(D)** contain two π-allyls unrelated by symmetry. Two allylic AMM′XX′ coupling patterns are observed for **B** whereas one AMM′XX′ pattern and a more complicated ABB′XX′ pattern are observed for **D** (see Table 1). This suggests that the two *syn* and *anti* protons in each allyl are related symmetrically. The ^{13}C NMR data are supportive of these propositions: two methine and two methylene carbons are observed in the allylic region of each spectrum.

In **B** and **D**, the β-diketonate ligands are symmetrically related because only one type of methine hydrogen is observed in the ^{1}H NMR, however, each diketonate is coordinated asymmetrically since two types of methyl or trifluoromethyl resonances are observed in their ^{1}H or ^{19}F NMR spectra, respectively.

Table 1. Proton chemical shifts and coupling constants for $Mo_2(\mu_2\text{-}\eta^3\text{-allyl})_2L_2$ complexes in benzene-d_6

Derivative	Exo-allyl Chemical shifts (ppm)			Exo-allyl J(H–H) (Hz)		Endo-allyl Chemical shifts (ppm)			Endo-allyl J(H–H) (Hz)	
	meso	*syn*	*anti*	(*m*–*s*)	(*m*–*a*)	*meso*	*syn*	*anti*	*J*(*m*–*s*)	*J*(*m*–*a*)
Terminal allyls in **A**[a,b]	3.99	3.49	0.70	8.3	14.4		3.87[b]	1.44[b]	8.3[b]	15.1[b]
Bridging allyls in **A**[a]	6.42	3.38	0.77	7.0	11.7	2.72	1.31	3.10	6.4	9.4
B, L = acac	4.11	3.35	0.50	6.9	12.0	2.23	3.02	2.05	6.6	11.2
C, L = tfac	4.12	3.21	0.29	7.2	12.0	2.03	2.82	1.89	6.8	11.0
D, L = hfac	4.13	3.13	0.10	7.1	11.8	1.80	2.67	1.84	3.4	12.4

[a] Values are for $Mo_2(\mu_2\text{-}\eta^3\text{-endo-allyl})(\mu_2\text{-}\eta^3\text{-exo-allyl})(\eta^3\text{-endo-allyl})_2$ **[A(ter = endo,endo)]** in benzene-d_6 from ref. 15.

[b] The two *syn* and two *anti* protons of these terminal allyls are not related by symmetry. Thus, the second set of *syn* and *anti* chemical shifts and coupling constants are found in the second column.

Given the metal to ligand ratios, the molecular weights and the spectroscopic data for these complexes, two structures are possible. Structure **I** may be derived from both reported isomers of $Mo_2(\mu_2\text{-}\eta^3\text{-allyl})_2(\eta^3\text{-allyl})_2$ **[A(ter = endo,endo)]** and **A(ter = endo,exo)**,[15] by replacing the two allyls bound terminally by chelating diketonate ligands. Structure **II** has two β-diketonates bridging the dimolybdenum centre. It is closely related to **A(ter = endo,exo)**, since both structures contain an endo,exo arrangement of terminal allyl ligands. Although **A(ter = endo,exo)** is found in 10% abundance relative to **A(ter = endo,endo)** in solution, interconversion is observed at 80°C which occurs via rotation of a terminal allyl about its Mo–allyl bond axis.[15] This allows a potential pathway for the formation of Structure **II** from **A(ter = endo,endo)**.

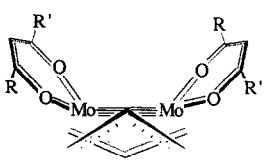

Structure I

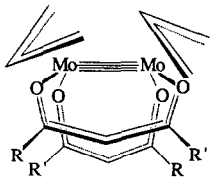

Structure II

Literature precedence suggests that Structure **I** is most plausible for this series of complexes. For instance, the two acac ligands in the molybdenum(II) dimer, $Mo_2(\eta^2\text{-}\mu_2\text{-acetate})_2(\eta^2\text{-acac})_2$, bind preferentially at terminal positions with the two bridging acetates binding *cis* to each other.[18] Again, in the platinum(II) dimer, $Pt_2(\eta^2\text{-}Pt^1,\sigma\text{-}Pt^2\text{-allyl})(\sigma\text{-}Pt^1,\eta^2\text{-}Pt^2\text{-allyl})(\eta^2\text{-acac})_2$,[19] the acetylacetonate ligands chelate a single platinum atom whereas the allylic ligands bridge two metal atoms.[20] Bridging β-diketonates such as those in Structure **II** form seven-membered rings which are strained relative to the six-membered rings formed upon chelation of one molybdenum as in Structure **I**. Furthermore, aromatic resonance may enhance the stability of chelating versus bridging diketonates.[21]

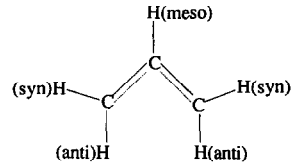

Comparison of the proton chemical shifts (discussed below) and ^1H–^1H coupling constants of **B**, **C** and **D** with those for **A** (see Table 1) suggests that the two allylic ligands in each of the β-diketonate derivatives are in bridging positions. This is supportive of **I** as the most likely structure. The $^1H_{meso}$–$^1H_{syn}$ and $^1H_{meso}$–$^1H_{anti}$ coupling constants[22] in **A** are consistently smaller for the bridging allyls than they are for those at terminal positions. Both types of coupling constants in **B**, **C** and **D** are similar in magnitude with those observed for the bridging allyls in **A(ter = endo,endo)** (see Table 1). Thus, β-diketonates have replaced the terminal η^3-allyls structurally in **A** leaving the $Mo_2(\mu_2\text{-}\eta^3\text{-endo-allyl})(\mu_2\text{-}\eta^3\text{-exo-allyl})$ core intact.

$Mo_2(\mu_2\text{-}\eta^3\text{-endo-allyl})(\mu_2\text{-}\eta^3\text{-exo-allyl})(tfac)_2$ (**C**) (R = Me, R′ = CF_3 in Structure **I**) exists predominantly as the isomer in which the bulkier CF_3 groups of the two tfac ligands are as far apart as possible. NMR spectra include a pair each of well-separated methyl and trifluoromethyl resonances. Thus, the two tfac ligands in **C** are not symmetry related as the β-diketonate ligands are in **B** and **D**. This is supported by the fact that two predominant tfac methine resonances are observed in the ^1H NMR of **C**. Also, the two methylene groups in each bridging allyl are not related symmetrically since we observe six allylic resonances in the ^{13}C NMR spectrum of $Mo_2(\mu_2\text{-}\eta^3\text{-endo-allyl})(\mu_2\text{-}\eta^3\text{-exo-allyl})(tfac)_2$ due to the central and two unique ter-

minal carbons in each allyl.[23] Because this geometric isomer lacks a plane of symmetry, it should exist as a racemic mixture of two optical isomers.

If the above-mentioned, major isomer of **C** is designated as *trans*, there will be two *cis* isomers: one with the two CF_3 groups closest to the μ_2-η^3-exo-allyl and the other with the CF_3 groups closest to the μ_2-η^3-endo-allyl. Both *cis* isomers will exhibit only one type of methyl or CF_3 resonance each and indeed, two low intensity CF_3 resonances with near equal intensity are observed in the reaction mixture resulting from the reaction of **A** with tfacH. The *trans* isomer can be isolated from the mixture of isomers by fractional crystallization.

Trends in proton chemical shifts on bridging allyls as a function of terminal ligand, L, *in* $Mo_2(\mu_2\text{-}\eta^3\text{-allyl})_2L_2$

There is a general shift upfield for the μ_2-η^3-allylic ^1H NMR resonances of $Mo_2(\mu_2\text{-}\eta^3\text{-allyl})_2(\eta^2\text{-}\beta\text{-diketonate})_2$ as the electron donor ability of the terminal ligand decreases: acac > tfac > hfac (Table 1). The change in chemical shift over this series of complexes is greatest for the *anti* protons of the μ_2-η^3-exo-allyls and the *meso* protons of the μ_2-η^3-endo-allyls (Table 1):[24]

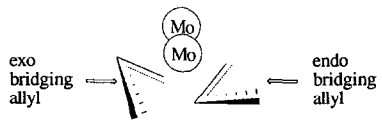

These particular protons are on the opposite side of the Mo—Mo quadruple bond and thus insensitive to anisotropic effects of the terminal ligands. Because of this, their electronic and steric environment is similar not only in the η^2-β-diketonate-containing series **B–D** but also in **A(ter = endo,endo)**. Thus, the trend in decreasing chemical shifts for the *anti* protons of the μ_2-η^3-exo-allyls and the *meso* protons of the μ_2-η^3-endo-allyls can be expanded in the series $Mo_2(\mu_2\text{-}\eta^3\text{-endo-allyl})(\mu_2\text{-}\eta^3\text{-exo-allyl})(L)_2$ to include L = allyl: allyl > acac > tfac > hfac. These allylic protons are not only tangential to the electron cloud of the Mo—Mo quadruple bond, but may also be affected by the π-electron cloud of the adjacent bridging allyl.

This upfield trend in chemical shifts parallels an increase in the electron-accepting ability of the corresponding terminally bound ligands: allyl ≪ acac < tfac < hfac. Supporting evidence for the latter trend comes, for example, from the highest energy CO stretching frequencies in $(CO)_4ReL$: allyl (2083 cm^{-1}), acac (2105 cm^{-1}), tfac (2110 cm^{-1}) and hfac (2120 cm^{-1}).[25,26] A similar trend is observed in $(CO)_2RhL$: allyl (2060 cm^{-1}), acac (2085 cm^{-1}), tfac (2094 cm^{-1}) and hfac (2103 cm^{-1}).[27,28] Thus, the allyl ligand may be considered a poor electron acceptor, whereas hfac resembles chlorophosphines or phosphites in their ability to accept electrons.[25] We postulate that the increased electron accepting ability of the terminal ligands increases the positive charge on the Mo_2 centre which, in turn, should promote enhanced bonding to the strongly π-electron donating μ_2-η^3-allyls. Thus, the μ_2-η^3-allylic Mo—C bonds are predicted to be shorter. This, in turn, should force the accompanying allylic protons to be closer to the Mo_2 electron cloud resulting in an increased anisotropic shift of the respective proton resonances upfield.

Reactivity of $Mo_2(\mu_2\text{-}\eta^3\text{-allyl})_2(L)_2$ *complexes*

The electron-withdrawing ability of the terminal ligands, L, not only effects the chemical shifts of the μ_2-η^3-allylic protons as described, but also the oxygen sensitivity for this series of molybdenum dimers: allyl ≫ acac > tfac ≈ hfac. Thus, the greater electron-withdrawing ability of the terminal tfac and hfac ligands stabilizes the $Mo_2(\mu_2\text{-}\eta^3\text{-allyl})_2$ fragment towards oxidation.

Carbon monoxide does not react with complexes where L = β-diketone under ambient conditions, whereas it readily promotes cleavage of the Mo—Mo quadruple bond in $Mo_2(\mu_2\text{-}\eta^3\text{-allyl})_2(\eta^3\text{-allyl})_2$ forming $Mo(CO)_6$ and 1,5-hexadiene as the ultimate products.[29]

$Mo_2(\mu_2\text{-}\eta^3\text{-allyl})_2(\eta^2\text{-diketonate})_2$ complexes do react with allylMgX reforming $Mo_2(\mu_2\text{-}\eta^3\text{-allyl})_2(\eta^3\text{-allyl})_2$. Similar reactions with allylMgX in which the allyl is substituted or deuterated may allow formation of $Mo_2(\mu_2\text{-}\eta^3\text{-allyl})_2(\eta^3\text{-substituted allyl})_2$. Such complexes may be synthetically or mechanistically useful, e.g. in probing the mechanism of the carbon monoxide-induced allyl coupling from $Mo_2(\mu_2\text{-}\eta^3\text{-allyl})_2(\eta^3\text{-allyl})_2$.[29]

The pronounced selectivity exhibited by β-diketones for protonation of the terminally bound allyls relative to their bridging counterparts in **A** suggests that a variety of complexes, $Mo_2(\mu_2\text{-}\eta^3\text{-allyl})_2(L)_2$, may be synthesized. The terminal ligand(s), L, may be a variety of anionic four-electron donors or a combination of two two-electron donors: one anionic and one neutral, e.g. t-BuO^- and pyridine in $Mo_2(\mu_2\text{-}\eta^3\text{-allyl})_2(O\text{-t-Bu})_2(py)_2$.[30] Thus, the reactivity may be fine tuned over a broad range for the organometallic fragment, $Mo_2(\mu_2\text{-}\eta^3\text{-allyl})_2$, containing allylic ligands in the rare symmetrically bridging mode of bonding.[31]

A determination of the general reactivity of this series of complexes is ongoing.

EXPERIMENTAL

Physical techniques

Elemental analyses were performed by Texas Analytical Laboratories, Tallahassee, Florida. IR spectra were recorded on a Perkin–Elmer 599B spectrophotometer as Nujol mulls between NaCl plates. NMR spectra were recorded on a Nicolet NT-200WB spectrometer at 200, 50 and 188 MHz for ^{1}H, ^{13}C and ^{19}F, respectively, using C_6D_6 as the solvent. Occasional ^{13}C and ^{19}F spectra were obtained on a Bruker MSL-300 NMR spectrometer. All ^{1}H NMR chemical shifts are in ppm relative to the C_6D_5H singlet set at 7.13 ppm. The ^{13}C chemical shifts are relative to the C_6D_6 triplet at 128.0 ppm, whereas ^{19}F chemical shifts are relative to an external perfluorobenzene standard (−163.0 ppm). Difference homodecoupling spectroscopy was utilized to resolve ^{1}H–^{1}H coupling for more complicated spectra with overlapping multiplets.[32] Mass spectra were obtained on a Finnigan MAT TSQ-70 mass spectrometer in the electron-impact ionization (EI) mode. The samples were introduced quickly on a direct exposure solid probe before insertion into the source vacuum lock.

General synthetic techniques

All the reactions were carried out under a dry and oxygen-free atmosphere of nitrogen using standard Schlenk techniques. Samples were handled in a Vacuum Atmospheres Co. Dry Lab System. Pentane and hexane were refluxed over a Na–K alloy for at least 16 h before use. Diethyl ether was dried over sodium benzophenone ketyl. All solvents were collected and stored over 3-A molecular sieves. Organic reagents were procured commercially and deoxygenated by bubbling nitrogen through them for about 20 min. Molybdenum hexacarbonyl was purchased from Pressure Chemical. Tetrakis(acetato)dimolybdenum[33] and allylmagnesium chloride[34] were prepared according to literature procedures. The latter may be stored as a solid in the dry box after removal of the diethyl ether in which it was synthesized. Tetraallyldimolybdenum can be synthesized utilizing $MoCl_5$,[14] $MoCl_3$[35] or $Mo_2(OOCCH_3)_4$[9] as the molybdenum source. The latter method was found to be most suitable for this application.

Bis(μ_2-η^3-allyl)bis(acetylacetonato)dimolybdenum (**B**)

2,4-Pentanedione (0.150 cm^3, 1.46 mmol) was added by a syringe at a rate of 0.025 cm^3 every 5 min to 0.4 g (1.1 mmol) of $Mo_2(\mu_2$-η^3-allyl)$_2(\eta^3$-allyl)$_2$ dissolved in 150 cm^3 of pentane at 0°C in a 250-cm^3 round bottom flask. The colour of the solution changed from green to violet. The pink precipitate which formed was allowed to settle to the bottom of the flask over a period of 1 h at room temperature. The supernatant liquid was decanted. The pink solid was washed with two 10 cm^3 portions of pentane, dried *in vacuo* and 0.25 g (0.53 mmol) of analytically pure product were collected. The yield was 47%. Found: C, 40.4; H, 5.2. Calc.: C, 40.7; H, 5.1%. IR (cm^{-1}): 1570(s), 1525(s), 1275(s), 1090(sh), 1020(m), 860(m), 825(s), 770(m), 676(s). Mass spectrum (*m/z* for $^{100}Mo_2$): 388 [Mo_2(acac)$_2$], 430 [Mo_2(acac)$_2$(allyl)], 480 [Mo_2(acac)$_2$(allyl)$_2$]. ^{13}C NMR (ppm): $CH_3(C{=}O)CH(C{=}O)CH_3$ 189.9, 189.0; $CH_3(C{=}O)CH(C{=}O)CH_3$ 100.2; CH_2CHCH_2 91.7, 84.8; CH_2CHCH_2 57.9, 55.3; $CH_3(C{=}O)CH(C{=}O)CH_3$ 27.5, 26.7. ^{1}H NMR (ppm): $CH_3(C{=}O)CH(C{=}O)CH_3$ 5.06; for allyl resonances, see Table 1; $CH_3(C{=}O)CH(C{=}O)CH_3$ 1.84, 1.74.

Bis (μ_2 - η^3 - allyl)bis(1,1,1 - *trifluoroacetylacetonato)dimolybdenum* (**C**)

1,1,1-Trifluoro-2,4-pentanedione (0.341 cm^3, 2.8 mmol) was added by a syringe to an ether solution of 0.5 g (1.4 mmol) of $Mo_2(\mu_2$-η^3-allyl)$_2(\eta^3$-allyl)$_2$ at 0°C and stirred for 6 h. The solvent was then removed *in vacuo* and the purple–red solid was extracted with hexane. The solution was then filtered through celite and hexane was removed *in vacuo*, leaving a purple–red solid. The yield was 75–80%. Analytically pure microcrystalline solid can be obtained via crystallization from pentane. Found: C, 32.5; H, 3.6. Calc.: C, 33.1; H, 3.1%. IR (cm^{-1}): 1615(s), 1525(s), 1300(s), 1225(s), 1180(s), 1138(s), 1020(m), 880(m), 840(s), 790(s), 731(s). Mass spectrum (*m/z* for $^{100}Mo_2$): 436 [Mo_2(tfac)$_2$], 498 [Mo_2(tfac)(allyl)$_2$], 588 [Mo_2(tfac)$_2$(allyl)$_2$]. ^{13}C NMR (ppm): $CH_3(C{=}O)CH(C{=}O)CF_3$ 198.4, 198.3; $CH_3(C{=}O)CH(C{=}O)CF_3$ 169.7, 169.5; $CH_3(C{=}O)CH(C{=}O)CF_3$ 113.6, 113.6, $^1J(^{13}C$–$^{19}F)$ = 285 Hz, $^2J(^{13}C$–$^{19}F)$ = 33 Hz; $CH_3(C{=}O)CH(C{=}O)CF_3$ 95.9, 95.7; CH_2CHCH_2 91.8, 86.3; CH_2CHCH_2 59.3, 59.1, 51.7, 51.5; $CH_3(C{=}O)CH(C{=}O)CF_3$ 28.6, 27.7. ^{1}H NMR (ppm): $CH_3(C{=}O)CH(C{=}O)CF_3$ 5.52, 5.51; for allyl resonances, see Table 1; $CH_3(C{=}O)CH(C{=}O)CF_3$ 1.77, 1.67 (minor isomers: 1.61, 1.51).

^{19}F NMR (ppm): −77.9, −78.0 (minor isomers −78.1, −78.2).

Bis (μ_2 - η^3 - *allyl*)*bis*(1,1,1,5,5,5 - *hexafluoroacetylacetonato*)*dimolybdenum* (**D**)

1,1,1,5,5,5-Hexafluoro-2,4-pentanedione (0.397 cm^3, 2.8 mmol) was added by a syringe to an ether solution containing 0.5 g (1.4 mmol) of $Mo_2(\mu_2\text{-}\eta^3\text{-allyl})_2(\eta^3\text{-allyl})_2$ at 0°C and stirred overnight. The ether was removed *in vacuo* and the brown–red solid was extracted with pentane. The solution was filtered through celite and the pentane was evaporated, leaving a brown–red solid. The yield was 65–70%. Analytically pure microcrystalline solid can be obtained via crystallization from pentane. Found: C, 27.8; H, 1.7. Calc.: C, 27.9; H, 1.8%. IR (cm^{-1}): 1630(s), 1605(s), 1560(s), 1530(m), 1259(s), 1220(s), 1145(s), 1112(m), 1020(m), 900(m), 850(s), 809(s), 740(m), 665(s). Mass spectrum (*m/z* for $^{100}Mo_2$): 438 [Mo_2(hfac)(allyl)], 604 [$Mo_2(hfac)_2$], 696 [$Mo_2(hfac)_2(allyl)_2$]. ^{13}C NMR (ppm): $CF_3(C{=}O)CH(C{=}O)CF_3$ 177.8; $CF_3(C{=}O)CH(C{=}O)CF_3$ 117.6, $^1J(^{13}C\text{–}^{19}F) = 282$ Hz, $^2J(^{13}C\text{–}^{19}F) = 21$ Hz; $CF_3(C{=}O)CH(C{=}O)CF_3$ 90.7; CH_2CHCH_2 91.3, 87.1; CH_2CHCH_2 61.2, 52.8. ^1H NMR (ppm): $CF_3(C{=}O)CH(C{=}O)CF_3$ 5.97; for allyl resonances, see Table 1. ^{19}F NMR (ppm): −73.9, −74.1.

Reaction of **B**, **C** *or* **D** *with allylmagnesium chloride*

$Mo_2(\mu_2\text{-}\eta^3\text{-allyl})_2(acac)_2$, $Mo_2(\mu_2\text{-}\eta^3\text{-allyl}_2(tfac)_2$ or $Mo_2(\mu_2\text{-}\eta^3\text{-allyl})_2(hfac)_2$ (0.3 g) were added to an ether solution containing three equiv. of C_3H_5MgCl at 0°C and then stirred for 3 h. The ether was evaporated at room temperature and the solid was extracted with pentane. The resulting green solution was filtered through celite and pentane was removed *in vacuo*, yielding a green solid. The yield was 50–60%. The NMR spectrum of the green solid was found to be exactly identical with that of $Mo_2(\mu_2\text{-}\eta^3\text{-allyl})_2(\eta^3\text{-allyl})_2$.[15]

Acknowledgements—This work was supported by grants from the Robert A. Welch Foundation (Y-1076), and the donors of the Petroleum Research Fund, administered by the American Chemical Society (19493-G3). Purchase of the Bruker MSL-300 NMR spectrometer through a grant from the Defense Advanced Research Projects Agency monitored by the Office of Naval Research is gratefully acknowledged.

REFERENCES

1. G. Wilke, B. Bogdanović, P. Hardt, P. Heimbach, W. Keim, M. Kröner, W. Oberkirch, K. Tanaka, E. Steinrucke, W. Walter and H. Zimmerman, *Angew. Chem., Int. Ed. Engl.* 1966, **5**, 151.
2. Y. I. Ermakov, B. N. Kuznetsov, Y. P. Grabovskii, A. N. Startzev, A. M. Lazutkin, V. A. Zakharov and A. I. Lazutkina, *J. Molec. Catal.* 1976, **1**, 93.
3. A. Mortreux, F. Petit and M. Blanchard, *J. Molec. Catal.* 1980, **8**, 97.
4. Y. Iwasawa, *Tailored Metal Catalysts* (Edited by Y. Iwasawa), Ch. 1. Reidel, Member of Kluwer Academic Publishers Group, Boston (1986).
5. Y. I. Ermakov, A. N. Startsev, V. A. Burmistrov and B. N. Kuznetsov, *Kinet. Catal. Lett.* 1980, **14**, 155.
6. V. I. Skoblikova, S. S. Passova, B. D. Babitskii and V. A. Kormer, *Vysokomol. Soedin Ser. B* 1968, **10**, 590.
7. D. G. H. Ballard, W. H. Janes and T. Medinger, *J. Chem. Soc. B* 1968, 1168.
8. T. L. Jufa, I. A. Poleteava, V. A. Kormer, B. D. Babitsky, M. I. Lobech, V. V. Markova and L. A. Churlyaeva, *Brit. Pat. 1* 338, 155 (21 November 1973).
9. J. P. Candlin and H. Thomas, *Homogeneous Catalysis-II* (*Advances in Chemistry Series No. 132*) (Edited by D. Forster and J. F. Roth), Ch. 15. American Chemical Society, Washington, D.C. (1974).
10. W. Oberkirch, Ph.D. Thesis, Technische Hochschule Aachen (1963).
11. Y. Iwasawa, H. Kubo and H. Hamamura, *J. Molec. Catal.* 1985, **28**, 191.
12. Y. Iwasawa and Y. Yamagishi, *J. Catal.* 1983, **82**, 373.
13. Y. Iwasawa, S. Yoshiharu and H. Kuroda, *J. Catal.* 1983, **82**, 289.
14. F. A. Cotton and J. R. Pipal, *J. Am. Chem. Soc.* 1971, **93**, 5441.
15. R. Benn, A. Rufinska and G. Schroth, *J. Organomet. Chem.* 1981, **217**, 91.
16. R. D. Hancock and D. A. Thornton, *J. Molec. Struct.* 1969, **4**, 377.
17. G. T. Behnke and K. Nakamoto, *Inorg. Chem.* 1967, **6**, 440.
18. G. C. Garner, S. Parkes, I. B. Walton and W. Clegg, *Inorg. Chim. Acta* 1978, **31**, L451.
19. G. Raper and W. S. McDonald, *J. Chem. Soc., Dalton Trans.* 1972, 265.
20. In **A**, the allyl ligands bridge the two molybdenums in a symmetrical η^3-mode, whereas the allyls bridge the platinum(II) dimer in the unusual σ,π-mode.
21. J. P. Collman, *Angew. Chem. Int. Ed. Engl.* 1965, **4**, 132.
22. H. C. Clark, M. J. Hampden-Smith and H. Ruegger, *Organometallics* 1988, **7**, 2085.
23. The two types of *syn* and *anti* proton resonances for each allylic ligand in **C** are not properly resolved.
24. The $\mu_2\text{-}\eta^3$-endo-allyls and the $\mu_2\text{-}\eta^3$-exo-allyls of **A** were assigned on the basis of an NOE effect between the *meso* proton of the former and the *anti* protons of the latter (see ref. 14). There is a large disparity in the chemical shifts corresponding to the *meso* protons of the two $\mu_2\text{-}\eta^3$-allyls in **A**–**D**. Since the *meso*

protons of the μ_2-η^3-endo-allyls of both types of complexes, $Mo_2(allyl)_4$ and $Mo_2(allyl)_2(diketonate)_2$, have very similar environments and since **B–D** each have *meso* resonances in the same chemical shift range as that of the μ_2-η^3-endo-allyl of **A(ter = endo,exo)** and **A(ter = endo,endo)**, the most upfield *meso* resonance in each complex was assigned to the μ_2-η^3-endo-allyl.

25. M. Moll, H. Behrens, H.-J. Seibold and P. Merbach, *J. Organomet. Chem.* 1983, **248**, 329.
26. M. C. Fredette and C. J. L. Lock, *Can. J. Chem.* 1975, **53**, 2481.
27. G. S. McNulty, K. Cannon and J. Schwartz, *Inorg. Chem.* 1986, **25**, 2919.
28. F. Bonati and G. J. Wilkinson, *J. Chem. Soc.* 1965, 3156.
29. R. J. Blau and U. Siriwardane, *Organometallics*, in press.
30. R. J. Blau, P. R. Hill, C. J. Smith, R.-J. Tsay and H. M. Zhang, manuscript in preparation.
31. M. H. Chisholm, M. J. Hampden-Smith, J. C. Huffman and K. G. Moodley, *J. Am. Chem. Soc.* 1988, **110**, 4070.
32. J. K. M. Sanders and B. K. Hunter, *Modern NMR Spectroscopy: A Guide for Chemists*, pp. 540–557, 138–150. Oxford University Press, New York (1987).
33. A. B. Brignole and F. A. Cotton, *Inorg. Synth.* 1972, **13**, 87.
34. O. Grummitt, E. P. Budewitz and C. C. Chudd, *Org. Synth.* 1963, **4**, 751.
35. R. J. Blau, O. V. Papadopoulou and R.-J. Tsay, unpublished results.

Polyhedron Vol. 10, No. 6, pp. 613–618, 1991
Printed in Great Britain

0277–5387/91 $3.00+.00
© 1991 Pergamon Press plc

BORIC ACID COMPLEXES OF PHENOLIC ACIDS

COLIN F. BELL,* BERNADETTE C. GALLAGHER, KENNETH A. K. LOTT, ERIC L. SHORT and LESLEY WALTON

Department of Chemistry, Brunel University, Uxbridge UB8 3PH, U.K.

(*Received* 25 *June* 1990; *accepted* 26 *November* 1990)

Abstract—The complexation between boric acid and the three phenolic carboxylic acids, 3,4-dihydroxybenzoic, caffeic and chlorogenic acids, has been examined spectroscopically and this has established that a 1 : 1 complex is formed in each case. With the first two acids, there is also evidence of a 2 : 1 complex being formed at high acid to B ratios. Equilibrium constants have been calculated from ^{11}B NMR spectra of mixtures for the equation for the formation of the 1 : 1 complex: $B+H_2A^- = BA^{2-}+H_3O^+$. Conditions in which aerial oxidation of the organic acids occurs have been studied by ESR and UV spectroscopy. The presence of boron stabilizes the acids towards oxidation to free radicals and also retards the rate at which the radicals, when formed, are oxidized further to semiquinones.

Boron is an essential trace element in higher plants and in some algae and diatoms. It is believed to be multifunctional and to be involved in processes as diverse as growth and differentiation, the control of membrane permeability, sugar translocation, and the control of enzymes involved in the metabolism of carbohydrates, auxins, nucleic acids and polyphenols.

Boron deficiency in the plant appears to lead to an accumulation of phenolic compounds and a decrease in lignin levels. Lignin precursors such as caffeic (3,4-dihydroxycinnamic acid) and chlorogenic acids accumulate at the same time. Necrosis of tissue due to boron deficiency may be related to increased levels of caffeic acid.[1]

Caffeic and chlorogenic acids are derivatives of catechol and they should form borato complexes by reaction of the *ortho*-hydroxy groups with boric acid or borate.[2–4] With catechol, the formation of a mono and a spirocyclic complex (in which the molar ratios of acid to boron are respectively 1 : 1 and 2 : 1) has been shown.

We have studied complexation in aqueous solution between boron and 3,4-dihydroxybenzoic acid, caffeic acid and chlorogenic acid using UV, NMR and ESR spectroscopy, and evaluated formation constants for the species observed. The acids are easily oxidized in alkaline media to produce semiquinone radicals and we report on the effect of added borate or boric acid on the oxidation process.

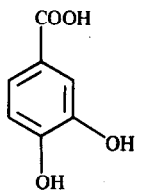

I

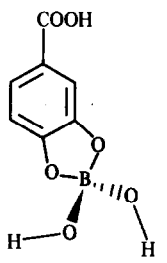

II

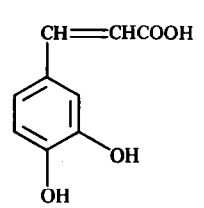

III

* Author to whom correspondence should be addressed.

Table 1. UV absorption spectra of aqueous solutions of phenolic acids at 25°C

3,4-Dihydroxybenzoic acid
Experimental λ_{max} (nm) and relative absorbance (in parentheses)
pH 2.0: 203.4(1.52), 217.3(1.33), 260.4(0.76), 293.4(0.39)
pH 6.5: 203.7(3.0), 227.0(1.80), 280.0(1.23), 290.0(1.40)
pH 8.5: 203.6(2.94), 226.7(1.82), 281.0(1.3), 301.2(1.49)
Theoretical λ_{max} (nm) and oscillator strength (in parentheses)
For H_2A^-: 195.6(0.72), 200.8(0.75), 205.7(0.32), 236.7(0.36)
For HA^{2-}: 197.1(0.81), 210.0(0.28), 277.2(0.61), 317.5(0.14)

Caffeic acid
pH 2.0: 193.7(1.54), 217.7(1.21), 234.8(0.96), 300.0(1.22), 321.7(1.38)
pH 6.5: 215.0(1.72), 232.0(1.23), 286.2(1.35), 309.8(1.22)
pH 8.5: 216.4(1.86), 240.0(1.15), 288.4(1.37), 315.5(1.38)
For H_2A^{2-}: 193.6(0.42), 217.6(0.18), 227.0(0.27), 286.2(0.71), 293.0(0.22)
For HA^{2-}: 191.6(0.61), 200.1(0.41), 215.5(0.23), 239.5(0.23), 325.8(0.19), 327.4(0.37), 336.8(0.59)

Chlorogenic acid
pH 2.0: 190.0(1.62), 217.1(0.88), 240.0(0.59), 299.8(0.85), 325.0(1.01)
pH 6.0: 218.5(0.85), 240.4(0.62), 200.2(0.92), 324.8(1.10)
pH 8.5: 225.2(0.59), 257.7(0.48), 310.4(0.44), 367.4(1.27)
For HA^{2-}: 194.2(0.40), 216.4(0.12), 226.0(0.16), 236.9(0.60), 286.8(0.33)

RESULTS

3,4-*Dihydroxybenzoic acids* (I)

This is tribasic ($pK_1 = 4.25$, $pK_2 = 8.64$, $pK_3 = 13.12$[5]). UV spectra of aqueous solutions of pH 2, 6.5 and 8.5 show four maxima between 190 and 310 nm (Table 1). At pH 2, the spectrum is that of the undissociated acid, H_3A; at pH 6.5, H_2A^-, formed by the loss of the carboxyl group proton predominates; and at pH 8.5, H_2A^- and HA^{2-}, formed by the deprotonation of one phenolic OH, are present in nearly equal amounts. Above pH 9.5, absorbance in the above wavelength range decreases rapidly with time as aerial oxidation occurs. Oscillator strengths and λ_{max} values for H_2A^- and HA^{2-}, calculated by the PPP Semi-empirical Theory of Electronic Spectra,[6–8] are also given in Table 1. The general agreement between experimental and calculated values confirms the ionization scheme for H_3A.

^{11}B NMR spectra of boric acid/3,4-dihydroxybenzoic acid mixtures show the presence of a mono complex (**II**) (δ 7.55–7.82 ppm over the range pH 6.0–12.0). In the pH range 7–11 the resonance peak due to uncomplexed boron moves from 18.9 to 1.56 ppm as the boric acid/borate ratio changes with pH. At pH 7.0, the extent of formation of the complex varies with acid/B molar ratio as shown in Table 2. Complexation is maximal between pH 8.0 and 10.0 and little complexation takes place at pH 12.0 even with ratios of 10 or above. However, the presence of boron evidently has a stabilizing effect on the ligand at this high pH for it to be possible to observe complexation at all. At pH 8.0 with a ratio of 16, a small second peak (δ 13.1 ppm) shows the formation of a spirocyclic complex.

Table 2. Complexation of boric acid by phenolic acids[a]

[Acid]:[B] Ratio	$\%B_{free}$	$\%BA^{2-}$	pH
3,4-Dihydroxybenzoic acid			
4.0	75.8	24.2	6.0
4.0	23.3	76.7	8.0
5.0	62.5	37.5	6.2
5.0	14.8	85.2	8.0
Caffeic acid			
0.5	87.4	12.6	8.0
1.0	71.2	28.8	8.0
1.0	76.0	24.0	8.4
2.0	53.5	46.5	8.0
4.0	19.4	80.6	8.0
5.0	15.5	84.5	8.4
Chlorogenic acid			
1.0	70.3	29.7	8.0
2.0	50.0	50.0	8.0
3.0	39.5	60.5	8.0
5.0	17.1	82.9	8.0

[a] Note that many spectra were measured but this table includes only the data used in calculating equilibrium constants.

When 3,4-dihydroxybenzoic acid is aerially oxidized in water–ethanol solutions of high nominal pH, the primary semiquinone radical is produced. The ESR spectrum has the structure expected from the splitting effect of the three non-equivalent ring protons, namely a $2\times2\times2$ pattern.[9,10] Coupling constants were measured and their values refined by simulation until the best possible match between experimental and simulated spectra was reached. Values (mT) found, $a_2 = 0.07$, $a_5 = 0.12$ and $a_6 = 0.31$, are in good agreement with those reported earlier.[9]

For 3,4-dihydroxybenzoic acid in water/ethanol (1 : 1 by vol.) radical formation is first observed at pH 10.06. At pH 11.6, the radical is stable for at least 5 min: at pH 12.5, slow decay is observed and this becomes rapid ($t_{1/2} = 2.5$ min) at pH 13.0. When boron is present, with a boron/ligand molar ratio of 3, no ESR spectrum is observed below pH 10.2. Above this, a stable radical is produced up to pH 12.6. The spectrum is very similar to that when borate is absent, although there are small decreases in coupling constants ($a_1 = 0.070$, $a_5 = 0.12$, $a_6 = 0.307$).

The first peak in the ESR spectrum is prominent and well-resolved with a constant line width as we have assumed its height to be a reliable measure of radical concentration. This is found to be less at a given pH when boron is present rather than when it is absent (Fig. 1). We may therefore conclude that boric acid stabilizes the phenolic acid at a given pH with respect to oxidation and that the radical, once formed, decays more slowly when boron is also present.

3,4-*Dihydroxycinnamic acid* (*caffeic acid*) (III)

This is tribasic ($pK_1 = 4.45$, $pK_2 = 8.66$, $pK_3 = 11.8$[11]). UV absorption spectra of aqueous solutions of caffeic acid are similar to those of 3,4-dihydroxybenzoic acid and four maxima are observed between 195 and 325 nm. Table 1 gives λ_{max} and relative absorbance values for solutions of pH 2.0, 6.5 and 8.5. As before, theoretically calculated values for H_2A^- and HA^{2-} are included. At pH 8.5, these forms are present in approximately equal amounts. Above pH 9.5, absorbance in the given wavelength range decreases with time, accompanied by a broadening of bands until only one, λ_{max} *ca* 290 nm, remains. These changes are due to oxidation. When boric acid is added to solutions of caffeic acid of pH 6 and above, λ_{max} values do not change significantly but there are small increases in relative absorbance for each band as a result of complexation.

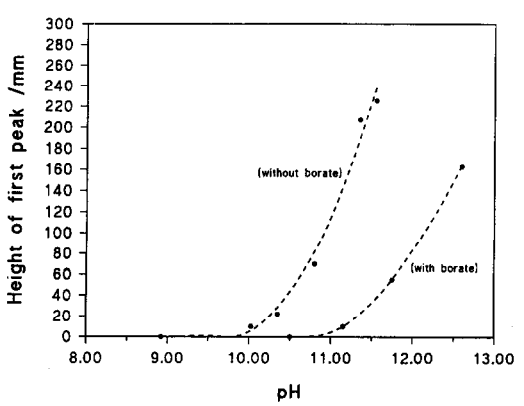

Fig. 1. 3,4-Dihydroxybenzoic acid ESR spectra; effect of pH on peak height.

From ^{11}B NMR spectroscopy, we have identified a mono complex at various acid/B ratios between pH 6 and 12 (δ 7.5 ppm). Table 2 shows how the proportion of mono complex changes with composition at pH 7. The presence of boron stabilizes caffeic acid towards oxidation at higher pHs. With large (>10) acid/B ratios, a small amount of spirocyclic complex (δ 13.3 ppm) is also observed.

ESR spectroscopy of oxidized caffeic acid in water/ethanol mixtures demonstrates primary semiquinone radical formation. Coupling constants (mT) were $a_\alpha = 0.12$, $a_\beta = 0.12$, $a_2 = 0.025$, $a_5 = 0.227$, $a_6 = 0.268$ (α and β are side-chain protons in H_2A^- and a_2, a_5 and a_6 are ring protons). Refinement by simulation proved difficult in this case because the central spectral region showed evidence of secondary radical formation, but our values are close to those reported by Ashworth.[10] At pH < 9, the acid is stable to oxidation. Above pH 9, oxidation produces the semiquinone radical which decays rapidly at pH > 11. Borate stabilizes the acid towards radical formation up to pH 10.7. From pH 11.5 to 12.1, the primary radical is formed. At pH > 12.4, this decays with increasing rate the higher the pH. The presence of boron therefore has exactly the same kind of stabilization effect as it does on 3,4-dihydroxybenzoic acid. There are slight changes in coupling constants due to the presence of boron (a_α 0.12, a_β 0.11, a_2 0.019, a_5 0.238, a_6 0.272). There is no evidence of hyperfine structure due to boron coupling.

Chlorogenic acid (IV)

This is tribasic ($pK_1 = 3.37$, $pK_2 = 8.27$, $pK_3 = 11.5$[11]). UV absorption spectra data are given in Table 1 for aqeuous solutions at three pH values. At pH 8.5, the strongest absorbance is at 367 nm and this is believed to indicate partial decomposition. The onset of this occurs at a lower pH

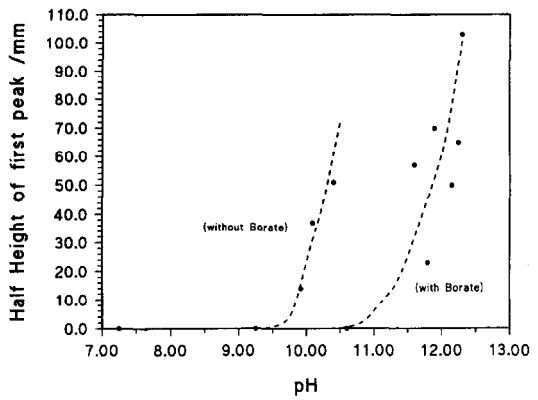

Fig. 2. Caffeic acid ESR spectra; effect of pH on peak height.

than with caffeic or 3,4-dihydroxybenzoic acids. Theoretical PPP values for λ_{max} and oscillator strength for HA^{2-} were found by making the simplifying assumption that there was no effect on the π-electron system of the cinnamic acid moiety from the attached trihydroxycyclohexane carboxylate moiety. This could be another reason for the lack of good agreement between experimental and theoretical values in addition to a discrepancy arising from acid degeneration.

A mono complex (δ 7.70 ppm) is indicated by ^{11}B NMR spectroscopy. It does not form below pH 6.5 and reaches optimum concentration between pH 8.0 and 9.0. At pH 8, a 10-fold excess of chlorogenic acid is sufficient to complex all the boron present as the mono species but there is no sign of a spirocyclic form. Table 2 shows how the composition of mixtures at pH 8 varies with molar proportions of the components. Difficulty was experienced in measuring the ESR spectra of radicals formed in solution by chlorogenic acid. Dissolution in ethanol gave solutions which immedially darkened due to decomposition. Aqueous solution study was limited because of the low solubility of the acid. Oxidation in aqueous solution was noticeably more rapid than for the other two acids studied.

Initially, the spectrum of the primary radical was produced but this decayed in a short time to a secondary species, as observed for other substituted catechols.[9] It was possible, however, to establish that the presence of boron in solution increased the stability of the primary radical and decreased the rate at which this decayed at a given pH.

DISCUSSION

Aqueous solutions of boric acid and one of the phenolic acids studied at pH < 8.0 contain $B(OH)_3$ and H_2A^- as the predominant species [as the pK_a of boric acid is 8.98, possible complexation involving $B(OH)_4^-$ need not be considered[12]]. 1 : 1 Complex formation proceeds according to:

$$B + H_2A^- = BA^{2-} + H_3O^+ \qquad (1)$$

where B is $B(OH)_3$.

At a pH of 7 or 8, a carboxylic acid with a pK_a value of ~4 will be virtually completely dissociated and it is therefore assumed that $[H_3A] \approx 0$.

(a) $B + OH^- \overset{K_b}{\rightleftharpoons} B^-$ and, hence, $[B^-] = K_b[B][OH^-]$,

where $B \equiv B(OH)_3$

(b) $[H_3A]_t = [H_2A^-] + [HA^{2-}] + [BA^{2-}]$ and $K_2 = [H^+][HA^{2-}]/[H_2A^-]$, where $BA^{2-} \equiv (OH)_2BA^{2-}$.

Therefore

$$[H_3A]_t = [H_2A^-] + \frac{K_2[H_2A^-]}{[H^+]} + [BA^{2-}]$$

$$= [H_2A^-]\left\{1 + \frac{K_2}{[H^+]}\right\} + [BA^{2-}]. \quad (i)$$

Now consider the equilibrium

$$B + H_2A^- \overset{K_1}{\rightleftharpoons} BA^{2-} + H_3O^+ :$$

therefore

$$[BA^{2-}] = K_1[B][H_2A^-]/[H^+].$$

By substituting the latter expression into (i), we obtain

$$[H_3A]_t = [H_2A^-]\left\{1 + \frac{K_2}{[H^+]} + \frac{K_1[B]}{[H^+]}\right\}.$$

Also,

$$[B]_t = [B]\left\{1 + K_b[OH^-] + \frac{K_1[H_2A^-]}{[H^+]}\right\}$$

or

$$[B] = \frac{[B]_t}{(1 + K_b[OH^-] + K_1[H_2A^-]/[H^+])}. \quad (ii)$$

By substituting (ii) into (i), we obtain

$$[H_3A]_t = [H_2A^-]\left\{1 + \frac{K_2}{[H^+]} + \frac{K_1[B]_t}{\{[H^+] + K_bK_w + K_1[H_2A^-]\}}\right\}.$$

This equation is now solved for $[H_2A^-]$.

After some manipulation, it is represented as a quadratic equation in $[H_2A^-]$:

$$A[H_2A^-]^2 + B[H_2A^-] + C = 0,$$

where

$$A = K_1 \times X \times [H_3A]_t;$$

$$B = [H_3A]_t\{X[H^+] + X \times K_bK_w - K_1\} + K_1[B]_t;$$

$$C = -[H_3A]_t\{[H^+] + K_bK_w\}$$

$$X = \{1/[H_3A]_t\} + \{K_2/([H_3A]_t[H^+])\}.$$

Once $[H_2A^-]$ has been found, the equilibrium concentrations of all the other species present can be easily calculated.

The procedure is started with a trial value of K_1 and this is subsequently modified until the sum of the squares of the differences between the calculated and experimental concentrations is minimized. K_1 values for the 1 : 1 complexes are found to be: 3,4-dihydroxybenzoic acid, 4.3×10^{-6}; caffeic acid, 7.2×10^{-7}; and chlorogenic acid, 1.06×10^{-6}.

These constants are a measure of the stabilities of the respective 1 : 1 complexes; they are several orders of magnitude less than K_1 for boric acid/lactic acid complexation (1.8×10^{-3}).[13] The difference shows the much greater stability of the chelate of lactic acid (using the carboxyl and the adjacent OH group) compared with that formed by a 1,2-*cis*-diol grouping.

The significance of the K_1 values for caffeic and chlorogenic acids is that they point to maximum complexation with boric acid close to the pH levels believed to exist in plant tissues. Our results also show that only a very small amount of 2 : 1 complex is formed in the case of 3,4-dihydroxybenzoic and caffeic acids and then only with a large excess of organic acid present. We would expect K_2 to be very small because complexation of a second H_2A^- ion by BA^{2-} is most improbable on steric grounds.

One of the most common pathways for lignin synthesis is from shikimic acid, produced by biosynthesis from D-glucose[14]. Shikimic acid is converted to either L-phenylalanine or L-tyrosine. The biosynthetic route from L-phenylalanine to coniferyl alcohol (**V**), the immediate precursor of lignin, proceeds thus:

L-phenylalanine → *trans*-cinnamic acid
→ *p*-coumaric acid → caffeic acid
→ ferulic acid → coniferyl alcohol.

Caffeic acid is the only one of these compounds that contains the 1,2-diol grouping for boron coordination. If boric acid is present, *in vivo* complexation at physiological pHs would be expected to occur, as indicated by our NMR results. This is thus likely to influence the methylation of caffeic acid to give ferulic acid (**VI**). Phenolic acids are reported to accumulate in boron-deficient plants beyond levels found in healthy plants. It appears

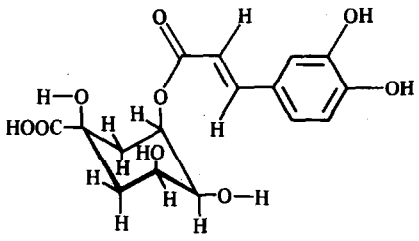

IV

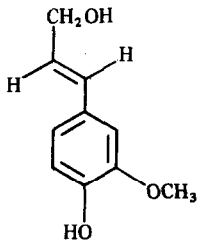

V

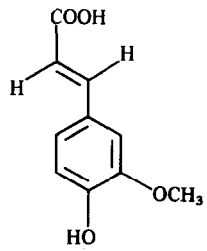

VI

therefore that the presence of boron in some way favours the synthesis of ferulic acid.

It has been shown[15] that ferulate is formed from caffeate at pH 7 by methylation with S-adenosylmethionine catalysed by catechol O-methyltransferase isolated from plant tissue. If this type of enzyme is responsible for the methylation of caffeate *in vivo*, boron complexation with the catechol component would be another factor to consider. It is intriguing to also note that S-adenosylmethionine itself has a 1,2-*cis*-diol grouping in the adenosyl moiety which could also chelate boron under appropriate conditions.

Boron evidently has a stabilizing influence on the oxidation of caffeic and chlorogenic acids to a free radical and retards the further oxidation of this to a quinone. Aluminium also stabilizes *o*-semiquinone radicals in aqueous solution and is believed to influence the manner in which these polymerize.[16]

EXPERIMENTAL

Sodium tetraborate (98%) and boric acid (99.5%) were obtained from BDH Chemicals Ltd and 3,4-dihydroxybenzoic acid (97%), 3,4-dihydroxycinnamic acid (99%) and chlorogenic acid (predominantly *trans*) were obtained from

Aldrich Chemical Co Ltd. Solutions, except where specified, were made up in deaerated, distilled water and the pH adjusted using either dilute hydrochloric acid or sodium hydroxide solutions. UV spectra were recorded at 25°C on a Cecil Series 5000 Computing Double Beam spectrometer. ^{11}B NMR spectra were recorded at 33°C on a Joel JNM FX 200 Multinuclear NMR spectrometer operating at 63.95 MHz, using $(C_2H_5)_2O \cdot BF_3$ as external reference. Solutions were prepared by mixing different molar ratios of borax to phenolic acid in aqueous solution, so that in each case the resulting solution was 0.01 mol dm^{-3} with respect to boron. Where small quantities of acid were used and the pH of the borax solution would have been high enough to cause oxidation, dilute hydrochloric acid was added to ensure the pH stayed below 9. Equilibrium in solution was rapidly attained and the spectra were measured as soon as possible after mixing to eliminate the possibility of decomposition. ESR spectra were recorded on a Varian E-3 EPR spectrometer. In the case of 3,4-dihydroxybenzoic and 3,4-dihydroxycinnamic acids, mixtures were made up of 25 cm^3 of a solution of the phenolic acid in ethanol (0.02 mol dm^{-3}) and 25 cm^3 of an aqueous solution of the required amounts of boric acid and sodium hydroxide. The phenolic acid/boron molar ratio was three in each case and the pH was adjusted with sodium hydroxide solution (0.1 mol dm^{-3}). Chlorogenic acid solutions were prepared in water because of the rapid aerial oxidation observed for this acid in ethanol solution. ESR spectra were run using a mixture of 10 cm^3 of chlorogenic acid solution and 25 cm^3 of boric acid/sodium hydroxide solution.

REFERENCES

1. J. Dean and S. Aronoff, *Plant Physiol.* 1965, **40**, 458.
2. K. Yoshino, M. Kotaka, M. Okamoto and H. Kakihana, *Bull. Chem. Soc. Japan* 1979, **52**, 3005.
3. R. Pizer and L. Babcock, *Inorg. Chem.* 1977, **16**, 1677.
4. L. Babcock and R. Pizer, *Inorg. Chem.* 1983, **22**, 174.
5. P. K. Migal and V. A. Ivanov, *Zh. Neorg. Khim.* 1973, **18**, 1019.
6. I. Levine, *Quantum Chemistry, Vol. 2 Molecular Spectroscopy*, pp. 83–84. Allyn and Bacon, Boston (1970).
7. R. Pariser and R. Parr, *J. Chem. Phys.* 1953, **21**, 466.
8. R. Pariser and R. Parr, *J. Chem. Phys.* 1956, **24**, 250.
9. T. J. Stone and W. A. Waters, *J. Chem. Soc.* 1965, 1488.
10. P. Ashworth, *J. Org. Chem.* 1976, **41**, 2920.
11. I. Lamy, M. Stewart, M. Cromer and J.-P. Scharff, *Analyt. Chim. Acta* 1985, **176**, 201.
12. N. Ingri, *Acta Chem. Scand.* 1962, **16**, 439.
13. R. Pizer and R. Selzer, *Inorg. Chem.* 1984, **23**, 3023.
14. K. Freudenberg and A. C. Neish, *Constitution and Biosynthesis of Lignin*, pp. 6–9. Springer-Verlag, Berlin (1968).
15. B. J. Finkle and R. F. Nelson, *Biochim. Biophys. Acta* 1963, **78**, 747.
16. M. B. McBride, F. J. Sikora and L. G. Wesselink, *Soil Sci. Soc. Am. J.* 1988, **52**, 985.

Polyhedron Vol. 10, No. 6, pp. 619–628, 1991
Printed in Great Britain

0277-5387/91 $3.00+.00
© 1991 Pergamon Press plc

EARLY STAGES OF THE HYDROLYSIS OF CHROMIUM(III) IN AQUEOUS SOLUTION—VI.† KINETICS OF INTRAMOLECULAR INTERCONVERSION BETWEEN SINGLY- AND DOUBLY-BRIDGED HYDROLYTIC DIMERS

LEONE SPICCIA‡

Department of Chemistry, Monash University, Clayton, Victoria, 3168 Australia

and

WERNER MARTY§

Institut de Chimie, Université de Neuchâtel, Av. de Bellevaux, 51, CH-2000 Neuchâtel,

(*Received* 12 *September* 1990; *accepted* 26 *November* 1990)

Abstract—The singly-bridged hydrolytic dimer $[(H_2O)_5Cr(\mu\text{-}OH)Cr(OH_2)_5]^{5+}$ (SBD), undergoes a ring closure reaction which transforms it into the doubly-bridged dimer, $[(H_2O)_4Cr(\mu\text{-}OH)_2Cr(OH_2)_4]^{4+}$ (DBD). The kinetics of this conversion have been studied over the pH range 0–4.93, temperature range 288.15–313.35 K and $I = 1.0$ M (adjusted with either $LiClO_4$ or $NaClO_4$). The pH dependence of the first-order rate constant, k_{obs}, was interpreted in terms of three distinct pathways involving ring closure within fully protonated, mono- and doubly-deprotonated SBD and two pathways accounting for acid-catalysed and uncatalysed cleavage of DBD which are important at low pH. Least-squares analysis of the data permitted the determination of rate constants for each of these pathways and the first two acid dissociation constants of the SBD. A reactivity increase of *ca* four-fold observed on monodeprotonation of SBD was suggested to reflect, at least in part, the greater nucleophilicity of coordinated OH^-, cf. coordinated H_2O. The more substantial rate enhancement of 25-fold resulting from double deprotonation of SBD was concluded to be due to an increase in the lability of the chromium(III) centre at which substitution occurs. The activation parameters for all pathways are consistent with an associative substitution mechanism, either *A* or I_a.

In the hydrolytic polymerization of metal ions in aqueous solution, *deprotonation* and *substitution*, either intermolecular or intramolecular, are two fundamental processes that are involved in the formation and rearrangement of polynuclear species. As part of our continuing work on the hydrolytic polymerization of chromium(III), several reactions which feature both of these processes have been studied: viz. the dimerization of Cr^{3+} to give the doubly-bridged dimer (DBD),[2] the dimerization of DBD to give the tetramer,[3] and the interconversion between the open and closed form of tetramer.[4]

The dimerization studies[2,3] have highlighted the importance of deprotonation in promoting the substitution processes that ultimately result in the propagation of polymerization. In both cases, pairs of conjugate bases of the reactant were found to undergo dimerization at a much faster rate than the aqua ions alone, or in combination with a conjugate base. For Cr^{3+},[2] each additional deprotonation corresponds to rate enhancement of 50–200-fold and the measured rates were much faster than H_2O

† For part V, see ref. 1.

‡ Author to whom correspondence should be addressed.
§ Deceased 20 September 1986.

exchange on Cr^{3+}.[5] These rate accelerations were consistent with the increase in rate of H_2O exchange on $CrOH^{2+}$ compared with Cr^{3+} [5] and were attributed to increases in the lability of the chromium(III) centres on deprotonation. This facilitated substitution by H_2O from the solvent or by a nucleophile such as OH^- coordinated to chromium.[2]

Formation of the dimer from conjugate bases of Cr^{3+} is believed to involve two consecutive substitution processes, intermolecular substitution to form a singly-bridged dimer (SBD), followed by intramolecular ring closure to a doubly-bridged form, eq. (1):[2]

$$2Cr(OH)_r^{(3-r)+} \underset{k_{-d}}{\overset{k_d}{\rightleftharpoons}} Cr(\mu\text{-}OH)Cr(OH)_s^{(5-s)+} \underset{k_{-c}}{\overset{k_c}{\rightleftharpoons}} Cr(\mu\text{-}OH)_2Cr(OH)_t^{(4-t)+}. \quad (1)$$

Supporting this proposal was evidence that SBD was an intermediate in the cleavage of DBD in acidic solution (pH $\leqslant$ 1).[6] This arises because the rates of interconversion between SBD and DBD (k_c and k_{-c}) are much faster than cleavage of SBD (k_{-d}).[6] Thus, an equilibrium [eq. (2)] is established between the two forms of dimer prior to slow cleavage of SBD into Cr^{3+}:

$$Cr(\mu\text{-}OH)Cr^{5+} \underset{}{\overset{K_{eq}}{\rightleftharpoons}} Cr(\mu\text{-}OH)_2Cr^{4+} + H^+. \quad (2)$$

This behaviour parallels that of related tetramine complexes of the type, $A_4M(\mu\text{-}OH)_2MA_4^{4+}$, where M = Cr, Rh or Ir and $A_4 = (en)_2$ or $(NH_3)_4$, whose properties have been reviewed recently.[7]

Early estimates of K_{eq} (1.24 M at 25°C), obtained from kinetic studies of the SBD–DBD interconversion in the pH range 0–2.3, indicated that SBD is favoured at high $[H^+]$ and DBD at low $[H^+]$. Note that this conclusion is supported by recent direct determinations of K_{eq} (1.83 M at 25°C and I = 1.0 M) which were made possible by the successful use of low temperature (0–5°C) ion-exchange chromatography to quantitatively separate SBD forms from DBD present in dimer solutions at equilibrium.[1] Combining these results with the observation that k_d was slower than either k_c or k_{-c}, intermolecular formation of SBD was concluded to be rate determining in the dimerization of Cr^{3+}.[2]

The interconversion between SBD and DBD [eq. (2)] is sufficiently slow to measure using conventional kinetic techniques and has been previously investigated at low pH ($\leqslant$ 2.3),[6] where small variations in rate were found. The present study has focussed attention on the conversion of SBD into DBD in the pH range 0–5, but in addition, information about the conversion of DBD into SBD has been obtained. The major aims of this work were:

(1) to probe the effect of deprotonation on the rate of an intramolecular hydrolytic process. The SBD is ideal for such a study since, in principle, the rate of ring closure could be measured over several deprotonations of the reactant and compared with the rate enhancements observed for intermolecular processes such as the dimerization of Cr^{3+};
(2) to determine whether dimerization of Cr^{3+} is rate determined by SBD formation throughout the accessible pH range. Previous conclusions (see above) are based on rate constants measured over different pH ranges, 3.5–5.0 for Cr^{3+} [2] dimerization and 0–2.3 for SBD–DBD interconversion.[6]

In this context, the work is not intended to duplicate existing data. However, it was necessary to measure rates over the pH range 0–5 in order to obtain a complete set of rate constants under identical experimental conditions.

RESULTS

The conversion of SBD into DBD was studied using conventional techniques in the pH range 0–4.93, temperature range 288.15–313.35 K and I = 1.0 M. Reaction mixtures were prepared by adding small volumes of standardized SBD stock solutions to thermally equilibrated solution of either $HClO_4$ or a buffer depending on the desired pH value (see Experimental) and the reaction followed using UV–vis spectrophotometry.

At low pH ($\leqslant$ 2), conversion of SBD into DBD resulted in increases in absorbance in the UV region (λ < 300 nm) which were much larger than spectral changes observed at higher λ. The reaction was followed at 250 nm where for $[SBD]_0 = 2.72 \times 10^{-3}$ M the absorbance increased by 0.25–0.5 units. Buffering of the reaction mixtures was necessary at pH > 2 because firstly, the overall reaction involves the liberation of H^+ and secondly, the two dimer forms differ in their acidity. The choice of buffers was restricted to those which do not react with or bind to either form of dimer, at least during the time scale of the reaction. However, all of the buffers which satisfied this requirement and whose pK_a was in the correct range were found to absorb strongly in the UV and the reaction could no longer be followed in this region. Fortunately, the visible spectrum of SBD changes appreciably upon deprotonation (pK_{a1} = 0.74 at 298.15 K was reported recently[1] and is similar to the value deter-

mined here) making it considerably different from that of DBD. The reaction was followed at 440 nm where absorbance decreases of between 0.2 and 0.3 units were observed for $[SBD]_0 = 6.81 \times 10^{-3}$ M.

The observed rate constants (k_{obs}) were determined by non-linear least-squares fitting of the absorbance data, taken over at least four half-lives, to expression (3).

$$A_t = (A_0 - A_\infty)\, e^{-k_{obs}t} + A_\infty. \quad (3)$$

Excellent fits were obtained for each run ($\sigma_{k_{obs}} \leqslant 0.015\, k_{obs}$) indicating that the reaction is first order with respect to SBD over the whole pH range. A table of the dependence of k_{obs} on $[H^+]$ and T is available as supplementary material. As a check for specific cation effects, duplicate measurements were made in $LiClO_4$ and $NaClO_4$. However, k_{obs} values determined with different electrolytes agreed within experimental error. For example, at pH = 0.22 and $T = 298.15$ K, $k_{obs} = 1.94(\pm 0.02) \times 10^{-4}$ s^{-1} in $LiClO_4$ and $1.97(\pm 0.02) \times 10^{-4}$ s^{-1} in $NaClO_4$.

Reaction mechanism and rate law

The pH dependence of k_{obs} (Fig. 1) shows the presence of two regions in which increases in rate are evident, one in the pH range 0.5–2 and the other at pH $\leqslant$ 3. In addition, a small decrease in rate with pH is found at the lowest pH values and temperatures. This kinetic data can be interpreted in terms of the three reaction pathways given in Scheme 1. These pathways involve fully protonated (SBD), mono-deprotonated (SBD − H) and doubly-deprotonated (SBD − 2H) singly-bridged dimer. This interpretation is in keeping with conclusions reached in previous kinetic[6] and thermodynamic[1] studies of the SBD–DBD interconversion at low pH ($\leqslant$ 2). Thompson[6] attributed variations in the rate of interconversion between SBD and DBD to the existence of pathways involving SBD and SBD − H, with both forward and back reactions being significant. This proposal is strongly supported by recent measurements of the SBD–DBD equilibrium[1] at pH < 2. These experiments have established that the relative amounts of SBD species and DBD present at equilibrium vary with $[H^+]$ in a manner consistent with the view that deprotonation of SBD occurs as pH increases, to generate SBD − H. Furthermore, the values of K_1K_{a1}, K_1 and K_{a1}, determined from this work, suggest that at pH < 2, SBD, SBD − H and DBD are present in significant concentrations at equilibrium. In contrast, very little HDBD, formed by protonation of DBD (Scheme 1), is expected at these acid concentrations since $K_{p3} \ll 0.1$ M^{-1} is predicted from information on analogous systems.[7] In summary, this information strongly supports the proposal that for the SBD and SDB − H pathways both forward and back reactions contribute to the overall rate. This is clear at the lowest pH values where decreases in k_{obs} are observed as pH increases (Fig. 1). Although the SBD and SBD − H pathways can rationalize rate variations at low pH they cannot account for the large accelerations in rate

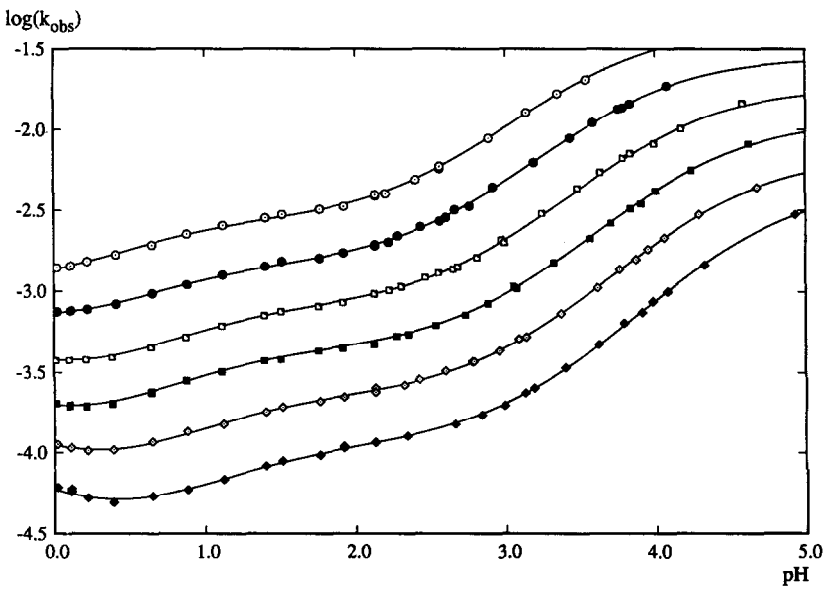

Fig. 1. pH and temperature dependence of the observed rate constant (k_{obs}) for the SBD–DBD interconversion at $I = 1.0$ M. Solid lines are the calculated values of k_{obs} obtained from eq. (6): (◆) 288.15 K; (◇) 293.35 K; (■) 298.15 K; (□) 303.05 K; (●) 308.15 K; (○) 313.35 K.

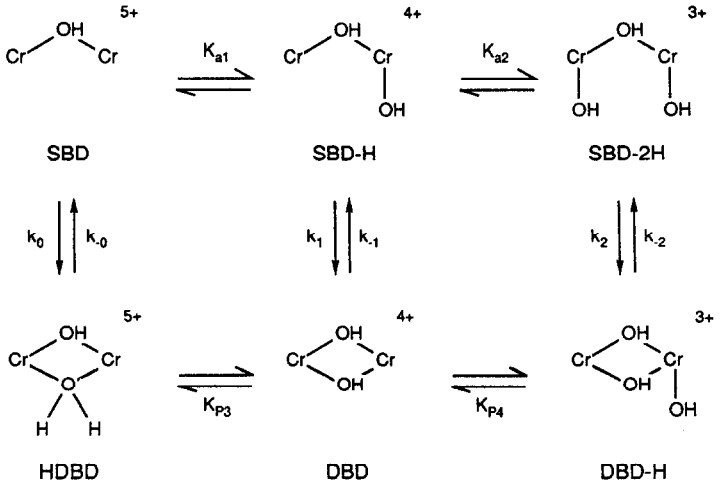

Scheme 1.

observed at pH $\geqslant$ 3. We attribute this to the formation of SBD−2H, which undergoes ring closure at a faster rate than either SBD or SBD−H. Note that in principle the reaction could be followed over several further deprotonations of SBD, but that this is precluded in practice by the precipitation of the "active" dimer hydroxide which forms from DBD at pH $\geqslant$ 5.

From the rate law for conversion of SBD into DBD [eq. (4)]

$$\frac{d[DBD]_T}{dt} = k_0[SBD]+k_1[SBD-H] + k_2[SBD-2H]-k_{-0}[HDBD]-k_{-1}(DBD] -k_{-2}[DBD-H] \quad (4)$$

and appropriate expressions for the various acid–base equilibria, the following expressions for k_{obs} may be derived:

$$k_{obs} = \left[\frac{k_0[H^+]^2+k_1K_{a1}[H^+]+k_2K_{a1}K_{a2}}{[H^+]^2+K_{a1}[H^+]+K_{a1}K_{a2}}\right] + \left[\frac{k_{-0}K_{p3}[H^+]+k_{-1}+k_{-2}/(K_{p4}[H^+])}{K_{p3}[H^+]+1+1/(K_{p4}[H^+])}\right]. \quad (5)$$

The following independent experiments show that some of the terms in eq. (5) are small and that a number of simplifications to the expression for k_{obs} are justified:

(i) Previous work on the closely related $[A_4Cr(\mu\text{-}OH)_2CrA_4]^{4+}$ systems [$A_4 = (NH_3)_4$ or $(en)_2$] has concluded that $K_{p3} \ll 0.1$ M^{-1}.[7] Consequently, at the concentrations of H^+ in our study (< 1 M), $K_{p3}[H^+]$ is small and need not be included in the denominator of the back reaction term in eq. (5).

(ii) Chromatographic analysis (procedure outlined elsewhere[1]) of dimer solutions after the interconversion reaction had reached completion at pH−4.10 and $T = 298.15$ [substantial proportions of DBD−H would be present at this pH since pK_a (DBD) = 3.68], showed that the amount of SBD present was below the limit of detection of *ca* 2–3%. This means that at this and higher pH the contribution of the back reactions (k_{-0}, k_{-1}, k_{-2} pathways), either individually or in total, is less than 3%. Since the contribution of the k_{-2} pathway (Scheme 1) is small under these conditions and it is expected to be even smaller at lower pH, where even less DBD−H is present in solution, it may be concluded that the k_{-2} pathway will make only very minor contributions to the reaction rate over the whole pH range. The inclusion of this term in the expression for k_{obs} [eq. (5)] is not warranted. The term $1/(K_{p4}[H^+])$ which appears in the denominator of the second half of eq. (5) can also be neglected since it would become important at pH > 3 ($K_{p4} = 10^{3.68}$ M^{-1},[8] where we have shown that the back reaction is not significant and in any case its effect would be to reduce the contribution of the back reaction to the overall rate.

Modification of eq. (5) to incorporate the above information and substitution of k_{-0} K_{p3} and k_{-1} by k_0/K_1K_{a1} and k_1K_{a1}/K_1K_{a1}, respectively, gives the following expression for k_{obs}:

$$k_{obs} = \left[\frac{k_0[H^+]^2+k_1K_{a1}[H^+]+k_2K_{a1}K_{a2}}{[H^+]^2+K_{a1}[H^+]+K_{a1}K_{a2}}\right] + \left[\frac{k_0[H^+]+k_1K_{a1}}{K_1K_{a1}}\right]. \quad (6)$$

Table 1. Rate and equilibrium constants describing the SBD–DBD interconversion at $I = 1.0$ M

T (K)	$10^4 k_0$ (s^{-1})	$10^4 k_1$ (s^{-1})	$10^4 k_2$ (s^{-1})	K_{a1} (M)	$10^5 K_{a2}$ (M)	$10^4 k_{-1}$[a] (s^{-1})	$10^4 k_{-0}K_{p3}$[b] ($M\ s^{-1}$)	K_1[c]
288.15	0.290(±0.008)	1.10(±0.02)	46(±1)	0.052(±0.003)	2.10(±0.08)	0.043(±0.004)	0.22(±0.01)	26(±3)
293.35	0.55(±0.02)	2.22(±0.03)	68(±2)	0.074(±0.005)	3.6(±0.1)	0.10(±0.01)	0.35(±0.02)	21(±3)
298.15	0.88(±0.06)	4.26(±0.08)	114(±4)	0.11(±0.01)	5.0(±0.2)	0.27(±0.03)	0.48(±0.04)	16(±2)
303.05	1.9(±0.1)	7.9(±0.2)	183(±4)	0.12(±0.01)	7.9(±0.3)	0.41(±0.06)	0.83(±0.07)	19(±3)
308.15	3.7(±0.3)	14.3(±0.3)	282(±8)	0.18(±0.02)	14.1(±0.7)	0.85(±0.16)	1.2(±0.2)	17(±4)
313.35	5.4(±0.7)	26.1(±0.7)	440(±20)	0.29(±0.04)	22(±2)	2.1(±0.4)	1.5(±0.3)	12(±3)

[a] Calculated from $k_{-1} = k_1 K_{a1}/K_1 K_{a1}$, using K_{a1} and k_1 from this work and $K_1 K_{aa}$ from ref. 1.
[b] Calculated using $k_{-0}K_{p3} = k_0/K_1 K_{a1}$ and using k_0 from this work and $K_1 K_{a1}$ from ref. 1.
[c] $K_1 = k_1/k_{-1}$.

(Note that $K_1 K_{a1}$ corresponds to the equilibrium constant for interconversion between SBD and DBD.)[1]

In fitting the data to eq. (6), published values at $K_1 K_{a1}$ were used.[1]† These were obtained over the same range of temperature and $I = 1.00$ M.[1] The data were fitted using a weighted least-squares analysis procedure minimizing the function, $\Sigma_i w_i[k_{obs,i} - k_{calc,i}]^2$, where $w_i = 1/\sigma^2_{k_{obs,i}}$ and $k_{obs,i}$, $k_{calc,i}$, w_i and $\sigma^2_{k_{obs,i}}$ are the observed rate constants, calculated rate constants, weighting factors and standard errors in each k_{obs} value, respectively. The difference between measured and calculated k_{obs} values were always $\leqslant 5\%$ and were unsystematically scattered around the fitted curve throughout the pH range and for all temperatures studied (see also Fig. 1). This observation provides strong support for the model chosen to describe the conversion of SBD into DBD (Scheme 1). All of the parameters in the expression for k_{obs}, i.e. k_0, k_1, k_2, K_{a1} and K_{a2}, were evaluated simultaneously. Their values are listed in Table 1 together with previously published values of $K_1 K_{a1}$[1] and values of $k_{-0}K_{p3}$, k_{-1} and K_1 which were calculated from k_0, k_1, K_{a1} and $K_1 K_{a1}$ using the expressions $k_{-0}K_{p3} = k_0/K_1 K_{a1}$, $k_{-1} = k_1 K_{a1}/K_1 K_{a1}$, and $K_1 = k_1/k_{-1} = K_1 K_{a1}/K_{a1}$, respectively.

Activation parameters for k_0, k_1, k_2, k_{-1} and $k_{-0}K_{p3}$, and thermodynamic constants for K_{a1}, K_{a2} and K_1 were determined from the temperature dependence of each constant by weighted non-linear least-squares analysis. They are listed in Table 2.

† Further reduction in the number of parameters to four was possible by using values of K_1 and K_{a1} determined in the same work[1] but these values were of lower accuracy and more importantly their use in fitting the data led to systematic variations between measured and calculated k_{obs} values.

DISCUSSION

The kinetic data for the conversion of SBD into DBD can be rationalized in terms of the reaction pathways described in Scheme 1. The pH dependence of k_{obs} has been successfully fitted to an expression [eq. (6)] which allows for contributions to the overall rate from both forward (k_0, k_1 and k_2) and back (k_{-0} and k_{-1}) reactions and for the effect of K_{a1} and K_{a2} on the distribution of SBD species in solution.

The values of pK_{a1} (1.00 at 298.15 K) and related thermodynamic constants (Table 2) are in good agreement with those obtained from direct measurements on the SBD–DBD equilibrium made using ion-exchange chromatography.[1] The constants (K_1, ΔH^0 and ΔS^0; Tables 1 and 2) describing the equilibrium between SBD−H and DBD also match those from this previous work.[1] These results have been rationalized by invoking the participation of SBD−H in hydrogen-bond stabilization.[1] Hydrogen-bond stabilization is widely believed to be responsible for the high acidity of related tetraamine mono-ols.[7] Direct measurements of pK_{a2} for SBD have been precluded by the fast rate of conversion of SBD into DBD in the pH range where this deprotonation takes place. The value of pK_{a2} (4.30 at 298.15 K) determined from this kinetic study is similar to pK_{a1} for other chromium(III) hydrolytic oligomers[8] [for example, pK_{a1}(DBD) = 3.68 and pK_{a1}(Trimer) = 4.30], but smaller than pK_{a2} for the tetraammine mono-ols.[7] Double deprotonation of the tetraammine mono-ols requires disruption of the hydrogen-bonding network of the monodeprotonated form, giving rise to the high pK_{a2} values, while for SBD, double deprotonation may occur without hydrogen-bond disruption. For SBD, a comparison of the thermodynamic constants of K_{a1} and K_{a2} reveals that ΔS^0 is essentially the same and that an increase in ΔH^0 for K_{a2} of *ca* 20 kJ mol^{-1} is predominantly

Table 2. Activation parameters and thermodynamic constants for the interconversion between SBD and DBD

Parameter	k/K^a (at 298.15 K)	$\Delta H^{*/0}$ (kJ mol^{-1})	$\Delta S^{*/0}$ (J K^{-1} mol^{-1})
k_0	$1.01(\pm0.04)\times10^{-4}$	$88.0(\pm3.2)^b$	$-26(\pm11)^b$
k_1	$4.17(\pm0.03)\times10^{-4}$	$92.24(\pm0.64)^b$	$-0.3(\pm2.2)$
k_2	$1.14(\pm0.02)\times10^{-2}$	$67.0(\pm1.8)^b$	$-57.5(6.1)^b$
K_{a1}	$0.101(\pm0.004)^b$	$47.6(\pm3.6)^b$	$141(\pm12)^b$
		$42.6(\pm4.1)^c$	$128(\pm13)^c$
K_{a2}	$5.4(\pm0.2)\times10^{-5}$	$68.2(\pm2.8)^b$	$147(\pm10)^b$
k_{-1}	$2.2(\pm0.1)\times10^{-5}$	$110.2(\pm4.6)^b$	$35(\pm16)^b$
		$110.3(\pm5.8)^d$	$36(\pm19)^d$
		$102.6(\pm3.3)^e$	$15(\pm11)^e$
$k_{-0}K_{p3}$	$5.2(\pm0.1)\times10^{-5}$	$58.6(\pm2.4)^b$	$-130(\pm8)^b$
	$5.5(\pm0.3)\times10^{-5}$	$58.5(\pm4.3)^f$	$-130(\pm20)^f$
K_1	$19(\pm1)$	$-19.6(\pm5.0)^b$	$-41(\pm17)^b$
	$10.1(\pm0.6)$	$-10.4(\pm2.7)^c$	$-15.1(\pm8.9)^c$
$k_{ex}(Cr^{3+})^g$	2.4×10^{-6}	$108.6(\pm2.7)$	$11.6(\pm8.6)$
$k_{ex}(CrOH^{2+})$	1.8×10^{-4}	$111.0(\pm2.5)$	$55.6(\pm8.1)$

[a] Units: s^{-1} for k_0, k_1, k_2, k_{-1}, k_{ex}; M^{-1} s^{-1} for $k_{-0}K_{p3}$; M^{-1} for K_{a1} and K_{a2}.

[b] Calculated from the data in Table 2.

[c] From ref. 1.

[d] Calculated from parameters for k_1, K_{a1} and K_1K_{a1} (ref. 1) assuming $k_{-1} = k_1K_{a1}/K_1K_{a1}$.

[e] Calculated from parameters for k_1 and K_1 (ref. 1) assuming $k_{-1} = k_1/K_1$.

[f] Calculated from parameters for k_0 and K_1K_{a1} (ref. 1) assuming $k_{-0}K_{p3} = k_0/K_1K_{a1}$.

[g] Data for solvent exchange on Cr^{3+} and $CrOH^{2+}$ taken from ref. 5.

responsible for the difference in the values of K_{a1} and K_{a2}. For $[(H_2O)(en)_2Ir(\mu\text{-}OH)Ir(en)_2(OH_2)]^{5+}$ the difference between $\Delta H^0(K_{a2})$ and $\Delta H^0(K_{a1})$ is about 40 kJ mol^{-1} and is coupled with little change in ΔS^0. This difference has been attributed to the need for hydrogen-bond disruption prior to double deprotonation.[9]

Previous work in this area has analysed the effect of deprotonation on the rate of dimerization of Cr^{3+}.[2] It has been proposed that the reaction involves intermolecular formation of SBD followed by conversion to DBD [eq. (1)]. Although intermolecular substitution was concluded to be rate determining, the rate of the two steps [eq. (1)] could not be compared in the pH range of dimerization studies because of a lack of information on the conversion of SBD into DBD. The data presented here, determined under identical experimental conditions, strongly support this earlier conclusion. Since the two processes differ in molecularity (uni- and bimolecular), overall rates rather than rate constants will be compared for $[Cr]_T = 0.02$ M (concentration used in both studies). The bimolecular rate constant for conversion of $CrOH^{2+}$ into $[Cr(\mu\text{-}OH)_2Cr]^{4+}$, $k_{11} = 2\times10^{-4}$ M^{-1} s^{-1},[2] corresponds to a rate of 8×10^{-8} M s^{-1} ($R = k_{11}[CrOH^{2+}]^2$ where $[CrOH^{2+}] = 0.02$ M) which is considerably slower than the rate of ring closure within $[Cr(\mu\text{-}OH)Cr(OH)]^{4+}$ (SBD−H) of 4.2×10^{-6} M s^{-1} ($R = k_1$[SBD−H], where [SBD−H] = 0.01 M and $k_1 = 4.2\times10^{-4}$ s^{-1}). Similarly, the bimolecular rate constant for the reaction of $CrOH^{2+}$ with $Cr(OH)_2^+$ to give $[Cr(\mu\text{-}OH)_2(Cr(OH)]^{3+}$ (DBD−H), 3.8×10^{-2} M^{-1} s^{-1},[2] converts to a rate of 3.8×10^{-6} M s^{-1} ($R = k_{21}$ $[CrOH^{2+}](Cr(OH)_2^+]$, where $[CrOH^{2+}] = [Cr(OH)_2^+] = 0.01$ M) which is once again slower than the rate of ring closure within $[(HO)Cr(\mu\text{-}OH)Cr(OH)]^{3+}$ (SBD−2H) of 1.14×10^{-4} M s^{-1} ($R = k_2$[SBD−2H], where [SBD−2H] = 0.01 M and $k_2 = 1.14\times10^{-2}$ s^{-1}). These simple comparisons indicate that an assessment of the effect of deprotonation on the rate of both intra- and intermolecular processes can be made by comparing results of the current work with those from previous dimerization studies.[2]

The *most important feature of the reaction mechanism is the pathway involving SBD−2H* which is proposed to account for large accelerations in rate

at pH $\geqslant 3$. Previous work on this system[6] concentrated on measurements at low pH ($\leqslant 2$) where this pathway makes little contribution. The mechanism for conversion of SBD into DBD at low pH is the same as reported for ring closure within a range of related mono-ols, $[A_4(H_2O)M(\mu\text{-}OH)M(OH_2)A_4]^{5+}$ [M = Cr, Rh or Ir and $A_4 = (NH_3)_4$ or $(en)_2$].[7] For these systems, kinetic studies concentrated on the pH range 0–5 where only one coordinated H_2O is deprotonated. Deprotonation of the remaining H_2O does occur at higher pH but ring closure is then expected to be more difficult (slower) since it requires substitution of OH^- rather than H_2O. Hydrolytic systems, such as SBD, are distinctly different from tetraamine complexes in that the presence of many H_2O ligands allows the reaction to proceed via the more facile substitution of H_2O even when the reactant has been deprotonated several times.

The rate constants for conversion of SBD and SBD−H into DBD ($k_0 = 1.01 \times 10^{-4}$ s^{-1} and $k_1 = 4.17 \times 10^{-4}$ s^{-1} at 298.15 K) determined in this study are in agreement with those obtained from early studies on this system[6] ($k_0 = 1.2 \times 10^{-4}$ s^{-1} and $k_1 = 8.1 \times 10^{-4}$ s^{-1} at 298.15 K and $I = 2.0$ M). The rate enhancement of about four-fold resulting from monodeprotonation reflects to some extent the greater nucleophilicity of coordinated OH^-, cf. coordinated H_2O.† Springborg and coworkers have proposed the order of nucleophilicity Cr—OH > H_2O > Cr—OH_2 from studies on the $[(H_2O)(NH_3)_4Cr(\mu\text{-}OH)Cr(NH_3)_4(OH_2)]^{5+}$ system.[7,10,11] However, the net effect of nucleophilicity is masked by hydrogen-bond stabilization of the monodeprotonated mono-ols.[7,10,11] This may also be the case for SBD−H (Scheme 2). It is important to note that in the case of the en mono-ols of iridium and rhodium, $k_0 > k_1$, that is, deprotonation leads to a slower rate of ring closure.

The much larger rate increase of *ca* 25-fold observed on double deprotonation of SBD ($k_2 = 1.14 \times 10^{-2}$ s^{-1}) is interpretable in terms of the labilization introduced at one chromium(III) centre which facilitates nucleophilic attack by an OH^- coordinated to the other chromium(III) centre. This rate enhancement is in excellent agreement with the 20-fold increase in the rate of dimerization of DBD for each additional deprotonation of DBD.[3] However, it is somewhat smaller than those observed in the dimerization of Cr^{3+}, where each additional deprotonation results in rate increases of 50–200-fold[3] and the increase in the rate of H_2O exchange on $CrOH^{2+}$ compared with Cr^{3+} (75-fold).[5] The current work demonstrates that the effect of deprotonation on the rate of hydrolytic substitution reactions is not restricted to intermolecular processes but it is also important in intramolecular processes.

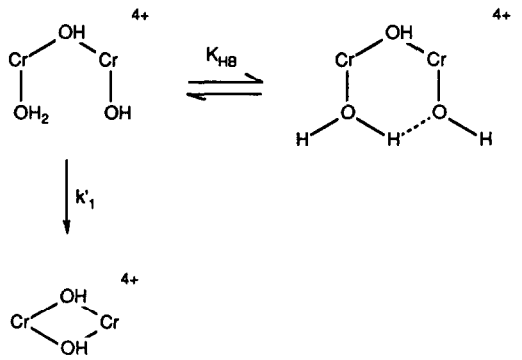

Scheme 2.

ΔH^* for ring closure within SBD is in good agreement with that for the SBD−H pathways, while ΔS^* is more positive for the latter (Table 2). Assuming coordinated OH^- is a better nucleophile than coordinated H_2O, $\Delta H^*(k_1)$ would be lower than $\Delta H^*(k_0)$ for an associative mechanism and close to equal for a dissociative mechanism.[11] Thus, ring closure appears to occur via a dissociative mechanism. However, this straightforward interpretation does not take into account the effect of hydrogen-bonding within SBD−H, which is disrupted prior to diol formation and would result in artificially high values of $\Delta H^*(k_1)$ and $\Delta S^*(k_1)$. In reality, ΔH^* and ΔS^* for k'_1 (true rate constant for ring closure within SBD−H) are probably lower than $\Delta H^*(k_1)$ and $\Delta S^*(k_1)$. This means that $\Delta H^*(k'_1)$ is also lower than $\Delta H^*(k_0)$ which would suggest an associative mechanism of substitution. The parameters for k_2 (Table 2) are consistent with this interpretation. In addition, the much lower value of $\Delta H^*(k_2)$ is consistent with the proposal that the much faster rate of ring closure is due to labilization of the chromium(III) coordination sphere. The values of ΔS^* are probably all negative and in the range −20 to −60 J K^{-1} mol^{-1}, after allowance for hydrogen-bonding stabilization is made. This is also in keeping with an associative mode of substitution.

The back reactions involving acid-catalysed ($k_{-0}K_{a3}$) and uncatalysed cleavage (k_{-1}) of DBD

† We favour this interpretation because it is consistent with data from previous work.[7] An alternative interpretation can be based on the proposal that the introduction of a coordinated OH^- at one of the chromium(III) centres, by deprotonation of an H_2O ligand, labilizes its coordinated H_2O, and, as is the case for SBD, the ring closure reaction could occur by attack of coordinated H_2O at the more labile chromium(III) centre and H_2O displacement from that centre.

are another important feature of the SBD–DBD system. The values of these rate constants (Table 1), determined from k_0, k_1 and K_{a1} of this work and K_1K_{a1} from previous work on the SBD–DBD equilibrium[1] compare favourably with those determined previously[6] ($k_{-0}K_{p3} = 9.4 \times 10^{-5}$ M^{-1} s^{-1} and $k_{-1} = 1.5 \times 10^{-5}$ s^{-1}) under different reaction conditions, such as $I = 2.0$ M. At low pH in particular, these pathways represent a significant proportion of the overall rate. For example, they account for 37 and 10% of k_{obs} at pH = 0 and 1, respectively. A major proportion of the difference in activation parameters for $k_{-0}K_{p3}$ and k_{-1} (Table 2) is attributable to contributions from the K_{p3} term. Assuming as a very rough approximation that protonation of bridging and terminal OH^- are energetically similar, i.e. $\Delta H^0 = -45$ kJ mol^{-1} and $\Delta S^0 = -130$ J K^{-1} mol^{-1} for protonation of SBD−H, then it may be concluded that for the acid-catalysed cleavage of DBD, $\Delta H^*(k_{-0}) \simeq 104$ kJ mol^{-1} and $\Delta S^*(k_{-0}) \simeq 0$ J K^{-1} mol^{-1}. These estimates and the experimentally determined values for k_{-1} are very similar to those for H_2O exchange on Cr^{3+} (Table 2),[5] which has been estabished to occur via an associative mechanism (note that these reactions are similar in the sense that they all involve substitution by H_2O from the bulk solvent). Thus, it would seem reasonable to suggest that both bridge cleavage reactions occur via associative substitution. This may be less important for the acid-catalysed pathway where protonation of a bridging OH^- occurs prior to substitution.

In the preceding discussion the experimental data for the SBD–DBD system has been rationalized by invoking an associative substitution mechanism at chromium(III) for both ring closure within SBD forms and cleavage of DBD which is essentially unaffected by the degree of protonation or deprotonation of the reactants. However, recent measurements of ΔV^* for H_2O exchange on Fe^{3+} [12] and Cr^{3+} [5] suggest that deprotonation causes changes in mechanism for associative (A or I_a) to dissociative (probably I_d). ΔV^* was negative for exchange of M^{3+} and positive for exchange on MOH^{2+}. These changes in mechanism could not be ascertained from temperature dependence studies because the faster rate of H_2O exchange on MOH^{2+} originates from ΔS^* for $CrOH^{2+}$ [5] and ΔH^* for $FeOH^{2+}$.[13]

Mechanistic information concerning H_2O exchange of aqueous metal ions, M^{3+}, cannot be directly related to hydrolytic processes such as the interconversion between SBD and DBD because of several differences between these systems: (i) for ring closure within SBD, the nucleophilicity of coordinated OH^- and H_2O is probably different from that of free H_2O;[7,11] (ii) for cleavage of DBD the leaving group is either an OH^- or H_2O coordinated to chromium(III) and not H_2O alone, as is the case for H_2O exchange; (iii) bridging OH^- may introduce steric constraints which may affect the mechanism; and (iv) both SBD and DBD contain OH^- bridges which might give rise to more dissociative substitution, as is the case for H_2O exchange on $CrOH^{2+}$ [5] and $FeOH^{2+}$.[12] Thus, there is a need for detailed investigations of the pressure dependence of these ring closure and bridge cleavage reactions to assist with the assignment of mechanisms. This could be nicely complemented with mechanistic studies of H_2O exchange on SBD and DBD, and other related systems.

In conclusion, the singly-bridged hydrolytic dimer of chromium(III) may be considered as a model system which has allowed us to probe the effect of successive deprotonations on the rate of intramolecular ring closure. Our data indicate that deprotonation leads to substantial rate enhancements, in keeping with observations for the intermolecular dimerization processes of Cr^{3+} [2] and DBD,[3] and for H_2O exchange on Cr^{3+}.[5] Collectively, these investigations demonstrate that deprotonation plays a major role in the polymerization of metal ions in aqueous solution, by facilitating the substitution processes involved in the formation of polynuclear species.

EXPERIMENTAL

Materials

Solutions of $[Cr(OH_2)_6](ClO_4)_3$ and $[Cr_2(\mu\text{-}OH)_2(OH_2)_8](ClO_4)_4$ were prepared and standardized as described previously.[8] Lithium perchloriate (Fluka, puriss), sodium perchlorate (Merck, p.a.), 70% perchloric acid (Fluka, puriss), Titrisol standard solutions of NaOH and HCl (Merck), 4-sulphanilic acid (Fluka, puriss), isonicotinamide (Fluka, purum) and 2,6-dimethylpyridine 3-sulphonic acid (Merck, p.a.) were all used as received. Water was deionized and distilled prior to use.

Sodium perchlorate solutions of accurately known concentrations were prepared by neutralization of standardized NaOH solutions with perchloric acid. All solutions were filtered through Sartorius SM11307 cellulose nitrate membrane filters (0.2. μm median pore size) prior to use.

Solutions of the hydrolytic DBD, free of $NaClO_4$, were prepared by elution of the DBD from a Sephadex SP C25 cation exchange column with $HClO_4$ (0.2–0.5 M). Rapid elution (*ca* 30 min) minimized the acid hydrolysis of the resin. Evaporation of the eluted dimer solution gave concentrated solu-

tions of the SBD since this form is favoured at high $[H^+]$. Typically, 600 cm^3 of 0.02 M dimer ($[HClO_4] \sim 0.25$ M) was reduced in volume at 25°C to *ca* 25 cm^3 to give [dimer] ~ 0.45 M and $[HClO_4] \sim 6$ M. This solution was equilibrated at room temperature (20°C) for 120 min, to ensure conversion to the SBD, and then stored at −18°C until required. The preparation was complete in 4 h. This procedure minimized the acid-induced cleavage of the dimer into Cr^{3+} ($t_{1/2} \sim 7$ days in 1 M $HClO_4$ at 25°C).[8] Indeed, chromatographic analysis of the stock SBD solution showed that only small amounts of Cr^{3+} had formed (< 2%), in agreement with the cleavage information. In any case, Cr^{3+} is not expected to interfere with the study of the SBD conversion to DBD since its concentration will remain constant throughout the reaction.

Instruments

UV–vis spectra were recorded using a Uvikon 820 spectrophotometer fitted with a multiple cell compartment. This accessory allowed the simultaneous measurement of six kinetic runs. Within the cell compartment constant temperature (±0.1 K) was maintained by circulating water from a Haake N3 thermostat. Calibrated thermometers were used to accurately measure the temperatures of the reaction mixtures directly in the cell compartment.

pH measurements

The pH values of the reaction mixture were measured using a Ross glass electrode (Orion) connected to a Metroohm 605 pH meter. These measurements were made at constant temperature in a jacketed vessel connected to a Haake N3 thermostat. Since the acidity (or basicity) constants of the buffers may vary with temperature it was necessary to measure the pH of the reaction mixtures at each temperature. This involved standardization of the electrode at each temperature by titration of a 0.01 M $HClO_4$ solution with 0.1 M Titrisol, both at $I = 1.00$ M ($NaClO_4$). As a consequence of this calibration, the pH values measured for the reaction mixtures are in concentration units which is convenient for the treatment of kinetic data.

Kinetic measurements

(*a*) *Experiments at low* pH (≤ 2). Reaction mixtures for kinetic studies in the pH range 0–2 were prepared by adding 3×10^{-2} cm^3 of concentrated SBD stock ([SBD] = 0.454 M and $[H^+] = 6.48$ M) to 5 cm^3 of (Na, H)ClO_4 mixtures at thermal equilibrium in a spectrophotometer cell, 2 cm path length. This gave $[SBD] = 2.72 \times 10^{-3}$ M and $I = 1.0$ M. The reaction was followed in the region 240–300 nm where substantial increases in absorbance are observed; much greater than the corresponding changes in the visible region. In some experiments, $LiClO_4$ was substituted for $NaClO_4$ to check on whether the reaction rate was affected by the counter-cation.

(b) *Experiments at higher* pH (≥ 2). In the pH range 2–4.9, reaction mixtures were buffered to minimize changes in $[H^+]$ during the reaction. Reaction mixtures containing 4-sulphanilic acid/NaOH and 2,6-dimethylpyridine 3-sulphonic acid/NaOH were prepared by mixing 7.5×10^{-2} cm^3 of SBD stock [concentration as in (a) above] with 5 cm^3 of each buffer equilibrated at the desired temperature. This gave $[SBD] = 6.81 \times 10^{-3}$ M at the commencement of the reaction. Mixtures containing isonicotinamide were made by mixing 0.1 cm^3 of SBD stock ([SBD] = 0.404 M, $[H^+] = 5.86$ M) with 5 cm^3 of the buffers, giving $[SBD] = 7.9 \times 10^{-3}$ M. The buffer solutions contained sufficient $NaClO_4$ to give $I = 1.0$ M in the reaction mixture. Since all of these buffers absorb strongly in the UV region, it was necessary to follow the reaction in the visible region (440 nm) where the absorbance of deprotonated forms of SBD is greater than that of DBD (see Results).

At the highest pH values, the dimer has been shown to undergo polymerization (initially producing tetramer) and it was necessary to check whether the extent of this polymerization reaction was sufficient to interfere with measurements of the rate of conversion of SBD into DBD. A reaction mixture was prepared from SBD and 0.14 M 2,6-dimethylpyridine 3-sulphonic acid/NaOH (pH = 4.65) and reacted until conversion of SBD into DBD was complete. The mixture was quenched with 0.5 cm^3 of 70% $HClO_4$, after a reaction time of 25 min at 298.15 K (*ca* 18 $t_{1/2}$), diluted to *ca* 100 cm^3 and absorbed onto a Sephadex SP C25 ion exchange column. The oligomers present, eluted in turn with increasing $[NaClO_4]$, were monomer ≈ 1%; dimer 93.7%; and tetramer, 3.2%. [After $5 \times t_{1/2}$ of the SBD–DBD reaction, the amounts of monomer (≈ 1%) and tetramer (< 1%) are too small to have a significant effect on the spectra and are, therefore, unlikely to influence k_{obs}.]

Supplementary material. Table of k_{obs} values for the SBD–DBD interconversion is available from the authors (L.S.).

Acknowledgements—This work was supported by the Swiss National Foundation and Australian Research Council. We are grateful to Dr M. Grace for valuable comments.

REFERENCES

1. T. Merakis and L. Spiccia, *Aust. J. Chem.* 1989, **42**, 1579.
2. F. P. Rotzinger, H. Stünzi and W. Marty, *Inorg. Chem.* 1986, **25**, 489.
3. C. Besso, Travail de diplomé, Université de Neuchâtel (1984).
4. H. Stünzi, F. P. Rotzinger and W. Marty, *Inorg. Chem.* 1984, **23**, 2160.
5. F.-C. Xu, R. Krouse and T. W. Swaddle, *Inorg. Chem.* 1985, **24**, 267.
6. G. Thompson, PhD thesis, University of California, Berkeley, Lawrence Livermore Laboratory Report UCRL-11410 (1964).
7. J. Springborg, *Adv. Inorg. Chem.* 1988, **32**, 55.
8. H. Stünzi and W. Marty, *Inorg. Chem.* 1983, **22**, 2145.
9. F. Galsbol, S. Larsen, B. Rasmussen and J. Springborg, *Inorg. Chem.* 1986, **25**, 290.
10. M. Hancock, B. Nielsen and J. Springborg, *Acta Chem. Scand.* 1982, **A36**, 313.
11. G. Christensson and J. Springborg, *Inorg. Chem.* 1985, **24**, 2129.
12. T. W. Swaddle and A. E. Merbach, *Inorg. Chem.* 1981, **20**, 4212.
13. M. W. Grant and R. B. Jordan, *Inorg. Chem.* 1981, **20**, 55.

Polyhedron Vol. 10, No. 6, pp. 629–632, 1991
Printed in Great Britain

0277–5387/91 $3.00+.00
© 1991 Pergamon Press plc

LANTHANIDE PERCHLORATE COMPLEXES OF BIS(PHENYLSULPHINYL)ETHANE

RUO-HUA ZHANG,* QUN-YING LIU and JING-TANG CHEN

Department of Chemistry, Nankai University, Tianjin, 300071, China

(*Received* 23 *July* 1990; *accepted* 28 *November* 1990)

Abstract—Lanthanide perchlorate complexes with *rac*-bis(phenylsulphinyl)ethane: $[Ln_2(L)_7(ClO_4)_2](ClO_4)_4 \cdot nH_2O$ (where Ln = La–Nd, Sm, Gd–Er, Yb; $n = 0, 4$) have been prepared by the reaction of the corresponding lanthanide perchlorate with *rac*-bis(phenylsulphinyl)ethane and characterized by elemental analysis, electrical conductance, magnetic susceptibility, IR and electronic spectra and thermal analysis.

Disulphoxide complexes with trivalent lanthanides have been reported over the last few years.[1,2] They have been shown to produce lanthanide complexes with different stoichiometries.[2,3] While there is some information about transition metal complexes with bis(phenylsulphinyl)ethane,[4,5] little is known about lanthanide complexes with this ligand.[3] We recently reported lanthanide complexes with *meso*-bis(phenylsulphinyl)ethane of the ratio 1 : 3.[6] In this paper, the synthesis and characterization of lanthanide complexes of *rac*-bis(phenylsulphinyl) ethane of the ratio 1 : 3.5 are reported.

EXPERIMENTAL

Physical and analytical measurements

IR spectra were obtained on KBr pellets using a Nicolet DX V4 spectrometer in the 400–4000 cm^{-1} region. Electronic spectra were recorded on a UV-240 spectrophotometer in the regions 340–900 nm (solid) and 190–330 nm (solution). Conductivity measurements were carried out using a 10^{-3} M solution in methanol and methyl cyanide on a DDS-11A conductometer at 25°C. Magnetic susceptibility measurements were carried out using Gouy's method. Thermal characterization studies were undertaken using a standard TG-DTA analyser and MP-500 melting point meter. Metal analyses were determined by titration with EDTA after decomposition of the sample with $HClO_4$. Carbon and hydrogen analyses were obtained on a Perkin–Elmer 240C elemental analyser, and sulphur was determined by the literature method.[7]

Materials and methods

The lanthanide perchlorates were prepared by dissolving the respective oxide (99.95%) in $HClO_4$. The ligand, *rac*-bis(phenylsulphinyl)ethane, was prepared according to the literature method.[4] The other chemicals were analytical reagent grade.

The complexes were prepared as follows. A solution of metal perchlorate (0.5 mmol) in anhydrous ethanol (5 cm^3) was added dropwise to a 10 cm^3 solution of the ligand (2 mmol) in chloroform containing 2 cm^3 of triethylorthoformate. The reaction mixture was stirred and refluxed for 6 h, to give the complex as a precipitate. The complex was filtered, washed several times with chloroform, ethanol and ether, and dried *in vacuo* over P_4O_{10} at room temperature.

RESULTS AND DISCUSSION

Elemental analyses (Table 1) show that the metal-to-ligand ratio in the complexes is 1 : 3.5. The complexes are air-stable at room temperature, soluble in DMF, DMSO and CH_3CN, slightly soluble in CH_3OH and C_2H_5OH, and insoluble in water.

The electrical conductance data in CH_3OH and CH_3CN (Table 2) indicate that they behave as 2 : 1 electrolytes in these solvents.[8] Thermal analyses of the ligand and its complexes show that decomposition occurs when they are heated above 150°C. The TGA data of Nd and Ho complexes (Table 1)

* Author to whom correspondence should be addressed.

Table 1. Elemental analyses and some physical properties of complexes

Complex	Calculated/(Found) (%) C	H	S	M	Decomposition point (°C)	TGA weight lost (%)	Assignment
$LaL_{3.5}(ClO_4)_3$	41.9	3.4	15.9	9.8	159		
	(41.7	3.5	16.0	9.6)			
$CeL_{3.5}(ClO_4)_3$	41.6	3.5	15.9	9.6	155		
	(41.3	3.5	15.6	9.5)			
$PrL_{3.5}(ClO_4)_3 \cdot 2H_2O$	40.6	3.7	15.5	9.7	166		
	(40.1	3.5	15.8	9.6)			
$NdL_{3.5}(ClO_4)_3 \cdot 2H_2O$	40.5	3.6	15.5	9.9	150	2.36	$2H_2O$
	(40.4	3.5	15.6	9.6)			
$SmL_{3.5}(ClO_4)_3 \cdot 2H_2O$	40.3	3.6	15.4	10.3	157		
	(40.2	3.4	15.6	10.3)			
$GdL_{3.5}(ClO_4)_3 \cdot 2H_2O$	40.1	3.6	15.3	10.7	157		
	(39.9	3.5	15.7	10.6)			
$TbL_{3.5}(ClO_4)_3 \cdot 2H_2O$	40.1	3.6	15.3	10.8	151		
	(40.5	3.6	15.5	10.5)			
$DyL_{3.5}(ClO_4)_3$	41.0	3.4	15.6	11.3			
	(40.6	3.6	15.3	11.0)			
$HoL_{3.5}(ClO_4)_3 \cdot 2H_2O$	39.9	3.6	15.2	11.2	154	3.01	$2H_2O$
	(39.5	3.3	15.6	11.0)			
$ErL_{3.5}(ClO_4)_3 \cdot 2H_2O$	39.9	3.6	15.2	11.3	152		
	(39.5	3.2	15.4	11.5)			
$YbL_{3.5}(ClO_4)_3 \cdot 2H_2O$	39.7	3.6	15.2	11.8	150		
	(39.5	3.2	15.4	11.7)			

Table 2. Molar conductance and magnetic moments

Complex $LnL_{3.5}(ClO_4)_3 \cdot nH_2O$	Λ_m (s cm^2 mol^{-1}) CH_3OH	CH_3CN	μ_{eff} (BM)
La	165	276	Diamagnetic
Ce	159	276	
Pr	163	269	3.27
Nd	168	298	3.44
Sm	160	259	1.57
Gd	169	295	7.10
Tb	165	254	9.38
Dy	160	275	10.26
Ho	166	307	10.12
Er	171	292	9.47
Yb	169	339	4.44

show that the complex $NdL_{3.5}(ClO_4)_3 \cdot 2H_2O$ loses about 2.36% of its weight, which corresponds to the loss of two crystal water molecules (calc. for $2H_2O$, 2.48%) at 50–100°C. Similarly, $HoL_{3.5}(ClO_4)_3 \cdot 2H_2O$ loses 3.01% of its weight (calc. for $2H_2O$, 2.44%) at 50–100°C which apparently is also crystal water. Thus, based on the analytical data, electrical conductance and thermal studies, the empirical formula $[Ln_2L_7(ClO_4)_2](ClO_4)_4 \cdot nH_2O$ ($n = 0, 4$) may tentatively be assigned to the complexes.

IR spectra

The IR spectra of all the complexes (Table 3) indicate that the ligand binds the metal through the oxygen atoms of the disulphoxide moieties: the S—O bond stretching frequencies of the complexes are lower than the corresponding ones in the free ligand. Investigation of a wide variety of sulphoxide complexes strongly suggests that the IR shift of the S—O bond on coordination reflects the nature of the donor atom, i.e. sulphur or oxygen. An increase in ν(S—O) is diagnostic for sulphur coordination, and a decrease for oxygen coordination.[9] Thus the ligand acts as a neutral, bidentate ligand in the complexes, coordinating through the oxygen atoms of disulphoxide moieties forming a seven-membered chelate ring. IR data for the complexes also show the Cl—O vibrational band of ClO_4^- (*Td*) and ClO_4^- (C_{2v}) (Table 3), which suggests the existence of ClO_4^- which is coordinated bidentately.[10]

Magnetic susceptibility

The observed magnetic moments of the complexes are close to those given by Van Vleck, indi-

Table 3. Important IR frequencies (cm^{-1}) of the complexes

Complex	ν(S—O)	ν^c(Cl—O)					ν^f(Cl—O)
		ν_8	ν_6	ν_1	ν_2	ν_7	ν_3
La	994.3	1145.7	1115.7	1013.1	926.0	628.6	1087.7
Ce	992.3	1143.3	1092.9	1007.9	939.5	625.2	1089.2
Pr	990.5	1144.2	1102.4	1007.9	926.8	624.8	1089.0
Nd	988.7	1144.8	1111.3	1009.3	921.3	625.9	1086.9
Sm	988.0	1143.8	1107.1	1008.8	922.0	625.5	1086.8
Gd	989.5	1145.4	1112.6	1010.2	943.3	626.6	1088.1
Tb	986.9	1143.4	1124.9	1006.9	931.3	624.3	1089.4
Dy	989.0	1145.7	1113.9	1010.7	938.6	627.6	1086.8
Ho	991.8	1146.3	1116.7	1014.0	942.3	629.5	1085.4
Er	991.5	1146.7	1115.4	1014.1	942.7	629.3	1085.6
Yb	988.1	1145.2	1111.6	1009.9	927.5	626.2	1087.7

cating that the lanthanides in the complexes remain in the +3 oxidation state and the 4*f* electrons are little influenced by the ligand bis(phenylsulphinyl)ethane.

Electronic spectra

The electronic spectra of Pr, Nd, Ho and Er complexes have been determined in the solids in the 340–900 nm region. The nephelauxetic parameter (β) was calculated from the spectroscopic data, in comparison with the corresponding values of the aquoions.[11] The nephelauxetic parameter (β), the bonding parameter ($b^{1/2}$)[12] and Sinha's covalence parameter (δ)[13] for the complexes of Pr^{3+}, Nd^{3+}, Ho^{3+} and Er^{3+} are presented in Table 4. The parameters suggest a weak covalent nature of the M—O bonds formed between the metal ion and ligand. The values of $b^{1/2}$ and δ in the complexes are in the order Pr, Nd > Ho, Er which reveals that for the same ligand covalency in the lighter lanthanides is greater than in the heavier lanthanides.

Table 4. Covalence parameters

Complex	β	$b^{1/2}$	δ
$PrL_{3.5}(ClO_4)_3 \cdot 2H_2O$	0.9965	0.0418	0.3512
$NdL_{3.5}(ClO_4)_3 \cdot 2H_2O$	0.9930	0.0592	0.7050
$HoL_{3.5}(ClO_4)_3 \cdot 2H_2O$	0.9985	0.0274	0.1502
$ErL_{3.5}(ClO_4)_3 \cdot 2H_2O$	0.9997	0.0122	0.0300

The UV spectral data of the ligand and its complexes in methanol are shown in Table 5. It can

Table 5. UV spectra

Ligand and its complex	λ_{max} (nm) (ε, $dm^3\ mol^{-1}\ cm^{-1}$) π–π^*		λ_{max} (nm) (ε, $dm^3\ mol^{-1}\ cm^{-1}$) n–π^*
	B	*K*	
L	269.6 (1155)	241.0 (7006)	219.6 (4407)
La	270.0 (1538)	240.0 (9691)	215.0 (10,720)
Ce	269.8 (2051)	240.4 (9720)	217.2 (9731)
Pr	270.0 (1600)	240.8 (9406)	218.4 (9149)
Nd	270.0 (1662)	240.8 (9043)	218.2 (9014)
Sm	268.8 (1914)	240.8 (9951)	217.2 (9763)
Gd	269.8 (1745)	240.6 (9163)	217.6 (9126)
Tb	269.2 (1866)	240.0 (9689)	217.0 (9911)
Dy	270.0 (1863)	241.0 (9966)	217.8 (10,246)
Ho	269.2 (1611)	241.0 (9957)	217.6 (9171)
Er	269.2 (1727)	241.0 (9034)	217.2 (9097)
Yb	270.6 (1447)	240.0 (9846)	219.6 (12,591)

be seen that the UV spectra of the ligand and its complexes are similar, and show characteristic bands at 240 and 270 nm arising from the *K* and *B* bands (π–π^*) of the benzene ring.[14] The characteristic band at about 218 nm is attributed to an n–π^* transition of the S=O group.

Conclusion

Lanthanide perchlorates with *rac*-bis(phenylsulphinyl)ethane form complexes which may be formulated as $[Ln_2L_7(ClO_4)_2](ClO_4)_4 \cdot nH_2O$ (where Ln = La–Nd, Sm, Gd–Er, Yb; $n = 0$, 4). The ligand is bidentate in these complexes, coordinating through the oxygen atoms of the disulphoxide moieties. The coordination number is nine.

REFERENCES

1. A. P. Zipp and S. G. Zipp, *J. Inorg. Nucl. Chem.* 1980, **42**, 395.
2. R. H. Zhang, F. H. Zhu, Q. S. Xue and Z. H. Huang, *Zhongguo Xitu Xuebao* 1987, **5**, 7.
3. R. H. Zhang and Q. S. Xue, *Gaodeng Xuexiao Huaxue Xuebao* 1987, **8**, 204.
4. T. R. Musgrave and G. D. Kent, *J. Coord. Chem.* 1972, **2**, 23.
5. L. Cattalini and G. Michelon, *J. Chem. Soc., Dalton Trans.* 1979, 96.
6. R. H. Zhang, Q. W. Zhang and D. L. Kong, *Zhongguo Xitu Xuebao*, in press.
7. M. M. Zulu and S. R. Madan, *Inorg. Chim. Acta* 1988, **142**, 315.
8. W. J. Geary, *Coord. Chem. Rev.* 1971, **7**, 81.
9. J. A. Davies, *Adv. Inorg. Chem. Radiochem.* 1981, **24**, 116.
10. K. Nakamoto, *Infrared and Raman Spectra of Inorganic and Coordination Compounds*, Ch. 3. John Wiley, New York (1978).
11. W. T. Carnall, P. R. Fields and K. Rajnak, *J. Chem. Phys.* 1968, **49**, 4412.
12. D. E. Henrie and G. R. Choppin, *J. Chem. Phys.* 1968, **49**, 477.
13. S. P. Sinha, *Spectrochim. Acta* 1966, **22**, 57.
14. R. M. Silverstein, G. C. Bassler and T. C. Morrill, *Spectrometric Identification of Organic Compounds*, p. 320. John Wiley, New York (1981).

Polyhedron Vol. 10, No. 6, pp. 633–643, 1991
Printed in Great Britain

0277–5387/91 $3.00+.00
© 1991 Pergamon Press plc

THE ULTRAVIOLET–VISIBLE ABSORPTION SPECTRUM OF DIMERIC GOLD(III) CHLORIDE IN THE GAS PHASE. AN EQUILIBRIUM STUDY OF VAPOURS FORMED BY GOLD–CHLORINE–WATER MIXTURES

D. S. RUSTAD

Department of Chemistry, Sonoma State University, Rohnert Park, CA 94928, U.S.A.

and

N. W. GREGORY*

Department of Chemistry, University of Washington, Seattle, WA 98195, U.S.A.

(*Received* 21 *May* 1990; *accepted* 4 *December* 1990)

Abstract—The UV–vis absorption spectrum of $Au_2Cl_6(g)$ is reported. Maxima are observed at 222, 244 and 460 nm. Spectral data are used to derive equilibrium and thermodynamic constants for vaporization reactions in the gold–chlorine system. In gold–chlorine–water mixtures, no evidence is found for the presence of complexes of gold(III) chloride and water in the vapour phase.

Recently, we have reported spectral evidence for the formation of iron(III) halide hydrate molecules, $Fe(H_2O)X_3$, in the vapour phase;[1,2] a similar study of other transition metal halide systems is of interest. We now report a spectrophotometric study of vapours formed by gold–chlorine and gold–chlorine–water mixtures. No previous report of the UV–vis absorption spectrum of gold(III) chloride vapour has been found. Like iron(III) chloride, gold(III) chloride is appreciably volatile[3–11] around 500 K and is known to form stable complexes with water in aqueous solutions at room temperature.[12] However, gold(III) chloride is less stable than iron(III) chloride, and thermally decomposes at relatively low temperatures to gold(I) chloride or gold and chlorine. The observed spectral data have also been used to derive enthalpy and entropy changes for the reactions

$$Au_2Cl_6(s) = Au_2Cl_6(g) \quad (1)$$

$$2Au(s)+3Cl_2(g) = Au_2Cl_6(g) \quad (2)$$

$$2AuCl(s)+2Cl_2(g) = Au_2Cl_6(g) \quad (3)$$

$$0.5Au_2Cl_6(s) = AuCl(s)+Cl_2(g). \quad (4)$$

The results are compared with those of other workers who used different methods.[3–11] The spectra provide no evidence, however, that the addition of water leads to the formation of appreciable concentrations of gold chloride hydrate molecules in the vapour phase.

EXPERIMENTAL

The procedures for preparing and isolating mixtures in quartz absorption cells, heating and measuring temperatures, and recording of spectra with a Cary 14H spectrophotometer were similar to those described in the previous iron halide studies.[1,2] The gold (Morgan, Hastings and Co., "pure" gold) was examined with an ICP atomic emission spectrometer (Model 955, Plasmo Atomcorp); no significant impurities were found. For the samples used to determine the molar absorptivity of $Au_2Cl_6(g)$ the small quantities of gold necessary were weighed on a Cahn 21 automatic electrobalance. A Mettler analytical balance was used for larger quantities. As before, chlorine was prepared by heating $CuCl_2(s)$. Cell path lengths, b, volumes, V, and initial amounts of reactants for the nine mixtures studied are listed in Table 1. Only gold and chlorine were present in samples 1–5. Water

* Author to whom correspondence should be addressed.

Table 1. Samples; initial amounts

Sample number	b (cm)[a]	V (cm^3)[b]	m_{Au} (μmol)[c]	Cl_2 (μmol)[d]	H_2O (μmol)[e]
1	1	3.581	22	87.4	0
2	10	31.51	0.167	87.9	0
3	1	3.171	0.249	69.5	0
4	1	3.510	61.4	73.4	0
5	10	30.68	64.4	82.8	0
6	10	30.65	13	60.7	831
7	10	30.46	0.167	87.9	55.6
8[f]	5	15.50	0.308	88.0	280
9	10	30.93	14	61.2	275

[a] Path length ± 0.001, certified by Pyrocell Mfg. Co., Westwood, New Jersey.
[b] Determined from mass of water necessary to fill cell.
[c] Values <1 μmol and >1 μmol have estimated uncertainties of ± 0.003 and ± 1 μmol, respectively.
[d] Estimated uncertainties of $\pm 1\%$.
[e] Estimated uncertainties of $\pm <1\%$.
[f] HCl, 37.8 ± 0.4 μmol, present.

was also introduced[1,2] in samples 6, 7 and 9; water and hydrogen chloride were introduced in sample 8.

After isolation in a cell, a given mixture was held at a selected temperature until equilibrium was reached, i.e. until the absorbance no longer changed with time. Temperatures were measured with calibrated chromel–alumel thermocouples. The temperature of the gas was taken as that of the cell body, T(g). The temperature of any solid phase, T(s), was measured at the place where the solid condensed, usually in the cell sidearm. A day, or in some cases several days, was usually required for equilibration when a solid phase was present; a few minutes were sufficient for the all vapour samples.

RESULTS AND DISCUSSION

The gold–chlorine system has been studied and reviewed by a number of investigators.[3–12] Hager and Hill[7] give a summary of work prior to 1970. At temperatures of interest in the present work, 450–650 K, only three solid phases, Au, AuCl and Au_2Cl_6 have been observed; only Cl_2 and Au_2Cl_6 have been found at significant concentrations in the vapour phase. Recent workers have used static pressure,[6] transpiration,[3,8] effusion[6,8] and mass spectrometric measurements[3,6–8] to characterize the various vaporization reactions.

The UV–vis absorption spectrum of Au_2Cl_6(g)

Chlorine gas has a temperature-dependent, vibronic, absorption spectrum between 250 and 480 nm, with λ_{max} at 330 nm.[13] The chlorine absorbances must be subtracted from the total absorbances to derive the spectrum of Au_2Cl_6(g). In an unreported study, we have derived equations for the temperature dependence of the chlorine molar absorptivity, $\varepsilon_{C,\lambda}$, at various wavelengths λ. For example, $\varepsilon_{C,330} = 82.0 - 0.0529T + 1.427 \times 10^{-5}T^2$ dm^3 mol^{-1} cm^{-1} (T in Kelvin). The concentration of chlorine, before and after reaction with the gold to form gold(III) chloride, was determined at room temperature from the measured absorbance at 330 nm and $\varepsilon_{C,330}$. The chlorine concentration, together with the appropriate molar absorptivity–temperature equation, was then used to derive the chlorine absorbances at the various wavelengths and temperatures of the equilibrium mixtures. These values were subtracted from the total observed absorbances between 250 and 480 nm to obtain the absorbances of Au_2Cl_6(g), $A_{D,\lambda}$ (subscript D designates dimer); at other wavelengths the total absorbance was attributed to Au_2Cl_6(g).

Samples 2, 3, 7 and 8 contained small enough amounts of gold and sufficient amounts of chlorine so that complete vaporization of gold, as Au_2Cl_6(g), could be achieved. Consequently, molar absorptivities of Au_2Cl_6(g), $\varepsilon_{D,\lambda}$, were determined at various wavelengths and temperatures from $A_{D,\lambda}$, using the relationship: $\varepsilon_{D,\lambda} = 2A_{D,\lambda}V/bm_{Au}$ dm^3 mol^{-1} cm^{-1}, where m_{Au} is the number of moles of gold in the cell of volume V and path length b. To derive absorptivities from absorbances measured when part of the gold was in a condensed phase, the least-squared molar absorptivity–temperature equation for $\varepsilon_{D,244}$, based on 23 observations for fully vaporized samples, see Table 2(a), was used

Table 2. Absorbance data for various equilibrium mixtures

(a) Gold completely vaporized (as Au_2Cl_6); $Q = A_{244}V/bm_{Au} = 0.5\varepsilon_{D,244}$

Sample number	T(g) (K)	A_{244}	A_{330}	P_C(atm)	Q
2	468.8	0.856	1.710	0.1070	0.1615E+05
2	469.8	0.855	1.705	0.1072	0.1613E+05
2	470.5	0.866	1.720	0.1074	0.1634E+05
2	473.2	0.866	1.719	0.1080	0.1634E+05
2	474.8	0.854	1.706	0.1084	0.1611E+05
2	476.0	0.841	1.694	0.1087	0.1587E+05
2	476.5	0.865	1.708	0.1088	0.1632E+05
2	478.5	0.853	1.694	0.1092	0.1609E+05
2	484.8	0.857	1.694	0.1107	0.1617E+05
7	467.8	0.871	1.761	0.1105	0.1589E+05
7	475.5	0.876	1.756	0.1123	0.1598E+05
7	477.5	0.887	1.750	0.1128	0.1618E+05
8	487.0	1.602	1.754	0.2257	0.1612E+05
8	497.5	1.584	1.732	0.2306	0.1594E+05
8	501.2	1.579	1.732	0.2323	0.1589E+05
8	514.0	1.562	1.707	0.2382	0.1572E+05
3	516.0	1.233	1.320	0.9235	0.1570E+05
3	530.4	1.218	1.306	0.9492	0.1551E+05
3	561.8	1.199	1.288	1.0054	0.1527E+05
3	549.2	1.211	1.301	0.9829	0.1542E+05
3	534.5	1.231	1.311	0.9566	0.1568E+05
3	519.0	1.240	1.324	0.9288	0.1579E+05
3	576.0	1.186	1.281	1.0308	0.1510E+05

Least-squares gives $\varepsilon_{D,244} = 41399.1 - 19.23T$.

(b) Vapour in equilibrium with Au_2Cl_6(s) at T(s). $Q = P_D$

Sample number	T(g) (K)	T(s) (K)	A_{244}	A_{330}	P_C(atm)	Q
1	466.0	462.8	0.129	0.899	0.5652	0.1520E−03
1	478.0	471.0	0.185	0.889	0.5761	0.2252E−03
1	485.8	480.8	0.362	0.903	0.5926	0.4500E−03
1	504.8	498.0	0.875	0.906	0.6093	0.1143E−02
1	506.8	499.6	0.975	0.905	0.6086	0.1280E−02
1	509.5	504.0	1.171	0.926	0.6215	0.1549E−02
1	520.5	513.0	2.060	1.173	0.7907	0.2802E−02
1	520.0	515.0	2.158	1.198	0.8047	0.2931E−02
2	449.5	441.3	0.279	1.705	0.1026	0.3141E−04
2	461.2	449.0	0.508	1.699	0.1053	0.5908E−04
2	469.5	452.8	0.607	1.696	0.1072	0.7221E−04
2	465.2	457.0	0.825	1.712	0.1062	0.9700E−04
4	483.0	467.8	0.155	0.192	0.1228	0.1912E−03
4	489.0	478.3	0.277	0.284	0.1831	0.3472E−03
4	511.2	500.6	1.079	0.742	0.4957	0.1433E−02
4	516.0	505.8	1.315	0.870	0.5867	0.1768E−02
4	477.8	466.3	0.155	0.189	0.1191	0.1886E−03
4	489.0	477.0	0.285	0.291	0.1876	0.3573E−03
4	507.5	495.8	0.683	0.547	0.3655	0.8986E−03
4	513.5	505.3	1.150	0.784	0.5265	0.1536E−02
4	513.5	505.6	1.211	0.822	0.5519	0.1618E−02
4	502.2	495.6	0.893	0.646	0.4231	0.1159E−02
4	500.0	496.0	0.845	0.611	0.3979	0.1090E−02
4	515.8	506.8	1.338	0.874	0.5886	0.1798E−02
4	516.0	506.6	1.369	0.892	0.6009	0.1841E−02
5	443.8	432.3	0.175	0.444	0.0259	0.1938E−04
5	454.2	441.0	0.247	0.545	0.0327	0.2817E−04

$\ln P_D = -13744(0.93\%)/T(s) + 20.835(1.3\%)$; variance = 0.0050.

Table 2—*continued*

(c) Vapour in equilibrium with Au(s) at T(s). $Q = P_D/P_C^3$

Sample number	T(g) (K)	T(s) (K)	A_{244}	A_{330}	P_C(atm)	Q
3	588.8	590.6	0.530	1.234	1.0569	0.7208E−03
3	573.8	575.4	0.917	1.263	1.0282	0.1307E−02
3	580.4	582.7	0.713	1.248	1.0410	0.9951E−03
3	590.8	592.6	0.492	1.229	1.0607	0.6651E−03
3	608.6	611.1	0.277	1.207	1.0937	0.3559E−03
4	556.8	565.2	1.320	1.278	0.9760	0.2112E−02
4	564.2	573.7	0.970	1.258	0.9905	0.1512E−02
4	571.2	579.7	0.789	1.243	1.0018	0.1209E−02
4	575.5	585.4	0.663	1.234	1.0095	0.1003E−02
4	584.5	593.0	0.522	1.223	1.0273	0.7652E−03
4	589.2	599.4	0.426	1.212	1.0331	0.6209E−03
4	596.0	605.0	0.360	1.208	1.0488	0.5095E−03
4	601.8	612.4	0.294	1.200	1.0586	0.4101E−03
4	607.8	617.0	0.260	1.192	1.0675	0.3586E−03
4	614.0	624.7	0.210	1.187	1.0802	0.2835E−03
4	623.8	634.7	0.165	1.176	1.0961	0.2180E−03
4	557.2	565.2	1.188	1.219	0.9345	0.2168E−02
4	569.0	576.7	0.848	1.242	0.9934	0.1325E−02
4	579.5	587.2	0.649	1.249	1.0323	0.9267E−03
4	596.0	604.2	0.381	1.194	1.0356	0.5601E−03
4	554.5	562.7	1.408	1.274	0.9642	0.2324E−02
5	520.2	520.2	0.218	1.576	0.1146	0.1969E−01
5	506.8	506.8	0.357	1.560	0.1091	0.3610E−01
5	463.5	467.0	0.578	1.026	0.0629	0.2722E+00
5	456.0	461.0	0.389	0.812	0.0489	0.3814E+00
5	450.5	454.2	0.204	0.554	0.0330	0.6405E+00
5	470.5	470.5	0.624	1.150	0.0719	0.2001E+00
5	486.0	486.0	0.817	1.652	0.1080	0.8062E−01
5	490.8	490.8	0.659	1.692	0.1126	0.5814E−01
6	503.8	514.0	0.100	1.162	0.0812	0.2438E−01
6	492.0	502.7	0.156	1.184	0.0800	0.3854E−01
6	485.8	495.4	0.231	1.181	0.0782	0.5999E−01
6	479.8	489.4	0.319	1.226	0.0797	0.7719E−01
7	497.5	497.5	0.670	1.721	0.1176	0.5287E−01
7	504.2	504.2	0.491	1.704	0.1192	0.3781E−01
7	506.5	506.5	0.431	1.700	0.1198	0.3292E−01
7	512.0	512.0	0.346	1.695	0.1211	0.2593E−01
7	525.0	525.0	0.194	1.684	0.1242	0.1391E−01
7	529.2	529.2	0.161	1.681	0.1252	0.1139E−01
7	536.5	536.5	0.119	1.672	0.1270	0.8225E−02
7	545.8	545.8	0.064	1.654	0.1292	0.4297E−02
8	528.2	528.2	0.512	1.672	0.2457	0.9578E−02
8	534.5	534.5	0.390	1.662	0.2487	0.7144E−02
8	539.0	545.4	0.319	1.654	0.2508	0.5758E−02
8	543.2	550.4	0.265	1.647	0.2528	0.4719E−02
8	549.5	556.4	0.209	1.637	0.2558	0.3649E−02
8	552.5	560.0	0.177	1.631	0.2572	0.3062E−02
8	564.0	571.4	0.111	1.614	0.2627	0.1855E−02
8	569.5	577.0	0.089	1.609	0.2652	0.1463E−02
8	575.5	575.5	0.104	1.612	0.2667	0.1706E−02
8	564.5	564.5	0.149	1.635	0.2616	0.2523E−02
8	556.2	556.2	0.209	1.643	0.2578	0.3626E−02
8	543.5	543.5	0.345	1.662	0.2519	0.6219E−02
8	533.8	533.8	0.495	1.675	0.2474	0.9195E−02
8	523.0	523.0	0.778	1.708	0.2424	0.1496E−01
9	504.8	512.7	0.106	1.142	0.0799	0.2711E−01

Table 2(c)—*continued*

Sample number	T(g) (K)	T(s) (K)	A_{244}	A_{330}	P_C(atm)	Q
9	492.5	500.2	0.162	1.151	0.0778	0.4350E−01
9	487.5	497.0	0.210	1.169	0.0778	0.5559E−01
9	481.0	490.2	0.316	1.174	0.0765	0.8662E−01
9	479.8	489.0	0.330	1.177	0.0764	0.9050E−01
9	477.5	486.4	0.366	1.176	0.0758	0.1023E+00

$\ln P_D/P_C^3 = 12959(0.64\%)/T(s) - 29.011(0.53\%)$; variance = 0.010.

(d) Vapour in equilibrium with AuCl(s) at T(s). $Q = P_D/P_C^2$

Sample number	T(g) (K)	T(s) (K)	A_{244}	A_{330}	P_C(atm)	Q
4	511.2	514.7	1.079	0.742	0.4957	0.5832E−02
4	516.0	519.4	1.315	0.870	0.5867	0.5136E−02
4	551.5	560.0	0.783	0.876	0.6649	0.2601E−02
4	545.8	554.0	0.840	0.870	0.6490	0.2889E−02
4	531.0	540.6	1.010	0.881	0.6281	0.3576E−02
4	530.0	538.2	1.070	0.898	0.6372	0.3671E−02
4	545.0	553.0	1.300	1.093	0.8050	0.2900E−02
4	539.0	546.7	1.423	1.098	0.7927	0.3226E−02
4	537.5	546.2	1.427	1.093	0.7858	0.3280E−02
4	536.0	543.4	1.445	1.074	0.7678	0.3466E−02
4	530.0	537.2	1.533	1.078	0.7564	0.3732E−02
4	534.8	542.0	1.585	1.123	0.7979	0.3510E−02
4	527.0	533.7	1.640	1.090	0.7561	0.3966E−02
4	523.8	531.4	1.663	1.072	0.7360	0.4211E−02
4	522.5	529.2	1.703	1.078	0.7366	0.4290E−02
4	529.2	537.0	1.780	1.158	0.8064	0.3805E−02
4	517.5	524.2	1.900	1.103	0.7391	0.4695E−02
4	522.8	530.6	2.015	1.188	0.8078	0.4224E−02
4	477.8	480.7	0.155	0.189	0.1191	0.1330E−01
4	489.0	492.2	0.285	0.291	0.1876	0.1015E−01
4	507.5	511.2	0.683	0.547	0.3655	0.6725E−02
4	513.5	517.7	1.150	0.784	0.5265	0.5542E−02
4	513.5	518.2	1.211	0.822	0.5519	0.5312E−02
4	502.2	506.6	0.893	0.646	0.4231	0.6474E−02
4	500.0	505.0	0.845	0.611	0.3979	0.6888E−02
4	515.8	519.7	1.338	0.874	0.5886	0.5190E−02
4	516.0	520.6	1.369	0.892	0.6009	0.5098E−00
4	512.0	515.4	1.073	0.761	0.5105	0.5479E−02
4	511.8	515.7	1.078	0.754	0.5051	0.5621E−02
4	498.8	503.5	0.774	0.544	0.3525	0.8014E−02
4	485.2	489.4	0.384	0.327	0.2068	0.1115E−01
4	471.5	470.4	0.217	0.209	0.1281	0.1581E−01
5	443.8	443.8	0.175	0.444	0.0259	0.2886E−01
5	462.8	466.0	0.887	1.304	0.0793	0.1646E−01
5	463.5	467.0	0.578	1.026	0.0629	0.1711E−01
5	458.0	462.7	0.565	0.984	0.0593	0.1849E−01
5	456.0	461.0	0.389	0.812	0.0489	0.1865E−01
5	450.5	454.0	0.328	0.713	0.0423	0.2069E−01
5	450.5	454.2	0.204	0.554	0.0330	0.2114E−01
5	470.5	477.0	0.624	1.150	0.0719	0.1439E−01
5	460.0	460.0	0.376	0.772	0.0470	0.1973E−01

$\ln P_D/P_C^2 = 5250(1.1\%)/T(s) - 15.341(0.74\%)$; variance = 0.0022.

Table 2—*continued*

(e) Vapour in equilibrium with AuCl(s) and Au_2Cl_6(s) at T(s). $Q = P_C$

Sample number	T(g) (K)	T(s) (K)	A_{244}	A_{330}	P_C(atm)
4	474.5	453.8	0.080	0.118	0.0742
4	476.8	457.6	0.095	0.131	0.0827
4	483.0	467.8	0.155	0.192	0.1228
4	489.0	478.3	0.277	0.284	0.1831
4	511.2	500.6	1.079	0.742	0.4957
4	516.0	505.8	1.315	0.870	0.5867
4	477.8	466.3	0.155	0.189	0.1191
4	489.0	477.0	0.285	0.291	0.1876
4	507.5	495.8	0.683	0.547	0.3655
4	513.5	505.3	1.150	0.784	0.5265
4	513.5	505.6	1.211	0.822	0.5519
4	502.2	495.6	0.893	0.646	0.4231
4	500.0	496.0	0.845	0.611	0.3979
4	515.8	506.8	1.338	0.874	0.5886
4	516.0	506.6	1.369	0.892	0.6009
4	512.0	498.8	1.073	0.761	0.5105
4	511.8	501.0	1.078	0.754	0.5051
4	498.8	490.8	0.774	0.544	0.3525
4	485.2	478.0	0.384	0.327	0.2068
4	471.5	465.3	0.217	0.209	0.1281
5	443.8	432.3	0.175	0.444	0.0259

$\ln P_C = -9258(1.6\%)/T(s) + 17.760(1.7\%)$; variance = 0.0035.

to calculate the concentration of Au_2Cl_6(g), C_D: $C_D = A_{D,244}/b\varepsilon_{D,244}$. $\varepsilon_{D,\lambda}$ Values at other wavelengths were then calculated for these samples from C_D and $A_{D,\lambda}$, $\varepsilon_{D,\lambda} = A_{D,\lambda}/bC_D$. Using all data, the variation of the molar absorptivity with temperature at each wavelength was approximated by a least-squares fit to the empirical equation $\varepsilon_{D,\lambda} = A + BT$. The derived constants, A and B, and the relative standard deviations of the means are listed in Table 3. Within the experimental uncertainties, samples with and without the various condensed phases present, and with and without water, or water and hydrogen chloride, gave identical spectra. Hence we conclude that, under the conditions of our study, complexes of gold(III) chloride with water or hydrogen chloride are not present in the vapour at concentrations which can be detected by the Cary 14H spectrophotometer.

Evidence that photolysis of Au_2Cl_6(g) occurs was observed with samples 2 and 7. While light was passing through the cell, a decrease in absorbance with time and formation of condensate on the windows were detected; the absorbance returned to its initially observed value after the cell was allowed to stand in the dark for a short time. Photolytic effects were not observed with the other samples. In these other cases the concentrations of the other gases were apparently high enough to decrease the rate of diffusion and thus the photolysis products recombined before condensation occured; also no changes with time were observed when vapour concentrations were fixed by equilibrium with a solid phase. This photolytic behaviour is similar to that observed for Fe_2Cl_6(g).[14] $[AuCl_4]^-$ ions in solution are also reported to photolyse readily.[15] For samples 2 and 7 light was not passed through the vapour except for the brief period necessary to record an absorbance reading at a preset wavelength.

The Au_2Cl_6(g) spectrum is significantly different from that reported by others for the square-planar $[AuCl_4]^-$ ion in solution and that of solid gold(III) chloride in a film. For example, spectra[16] of $[(n\text{-}C_4H_9)_4N][AuCl_4]$ in different solvents at 300 and 70 K show transitions in the following ranges of wavelengths in nm (molar absorptivities in M^{-1} cm^{-1}): 226 (44,250), 322 (5020)–329 (6500), 400 (304)–380 (267) and 460 (15). The first and second transitions are distinct peaks with quite different molar absorptivities, whereas the third and fourth transitions are seen as very weak shoulders. In solid gold(III) chloride, square-planar Au_2Cl_6 molecular units are observed.[17] The spectrum[18] of solid gold(III) chloride film shows four distinct peaks at 293 K—230, 320, 358 and 438 nm—and three distinct peaks at 83 K—230, 320 and 438 nm. For the solid the molar absorptivities for the 358 and

Table 3. Molar absorptivity–temperature equations ($\varepsilon_{D,\lambda} = A + BT$ dm^3 mol^{-1} cm^{-1}, for $Au_2Cl_6(g)$ in the range 464–576 K[a])

λ (nm)	$10^{-3}A$	B	Percentage[b]	λ (nm)	$10^{-3}A$	B	Percentage[b]
200	7.97		1.1	400	0.54		5.6
210	26.73	−18.29	0.7	410	0.83		1.2
222	29.95	−8.79	0.2	420	1.10		1.8
230	24.79		0.2	430	2.29	−1.65	1.0
240	44.27	−26.89	0.3	440	4.05	−4.42	1.5
244	41.40	−19.23	0.6	450	3.45	−3.01	1.0
250	28.17		0.4	460	3.79	−3.37	1.0
260	6.44	21.30	0.6	470	1.82		1.6
270	−0.01	18.31	0.4	480	1.71		1.2
280	1.32	9.27	1.6	490	1.70		2.4
290	2.02	4.98	0.7	500	1.32		1.5
300	3.61		2.8	510	−0.08	2.18	1.2
310	2.73		2.2	520	−0.56	2.60	2.4
320	1.93		2.6	530	−0.39	1.92	2.6
330	1.42		2.4	540	−0.93	2.65	3.5
340	1.00		4.0	550	−0.89	2.25	4.6
350	0.60		6.7	560	0.21		14
360	0.30		17	570	0.15		20
370	0.31		6.5	580	0.13		15
380	0.40		5.0	590	0.07		14
390	0.43		4.7				

[a] Based on 10–23 observations at each wavelength.
[b] $[\Sigma\{(\varepsilon_{D,\lambda}(\text{obs}) - \varepsilon_{D,\lambda}(\text{calc}))/\varepsilon_{D,\lambda}(\text{obs})\}^2]^{0.5} \times 100/(\text{No. obs})$.

438 nm peaks are relatively larger than those for the $[AuCl_4]^-$ ion. In contrast, $Au_2Cl_6(g)$ has three distinct peaks—222, 244 and 460 nm—see Fig. 1. The first two have similar large molar absorptivities; the third is much weaker but has a much larger molar absorptivity than the corresponding peak for the $[AuCl_4]^-$ ion. These spectral differences are being studied further.

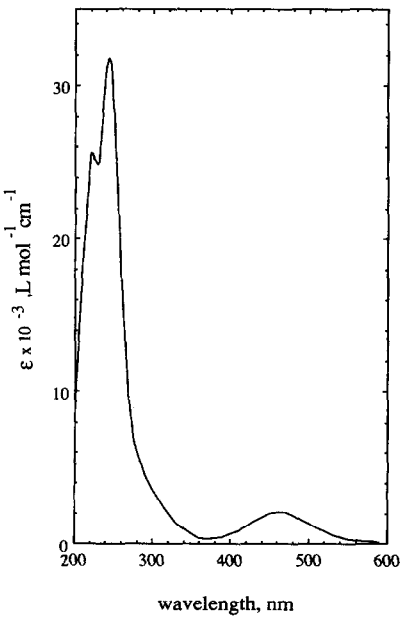

Fig. 1. Absorption spectrum for $Au_2Cl_6(g)$, derived from equations in Table 3 at 500 K.

Vaporization equilibria

Values of the total observed absorbance, A, at 244 nm, A_{244}, and 330 nm, A_{330}, the temperatures, the partial pressures of chlorine, derived using the perfect gas law, and equilibrium quotients are listed in Table 2. In cases where the concentration of chlorine could not be determined in the manner described above, due to the decomposition of gold(III) chloride, chlorine partial pressures, P_C, were derived from the expression $P_C(\text{atm}) = [A_{330} - (A_{244}\varepsilon_{D,330}/\varepsilon_{D,244})] \times 0.08205 \times T(\text{g})/b\varepsilon_{C,330}$. Values of $\varepsilon_{D,\lambda}$ were taken from the results in Table 3. Chlorine does not absorb significantly at 244 nm. Partial pressures of $Au_2Cl_6(g)$, P_D, were calculated from the equation $P_D(\text{atm}) = A_{244} \times 0.08205 \times T(\text{g})/b\varepsilon_{D,244}$.

Equilibrium constants[19] for the reaction $Cl_2(g) + H_2O(g) = 2HCl(g) + 0.5O_2(g)$ are *ca* 1.6×10^{-3} atm$^{0.5}$ in the temperature range in which samples 6, 7 and 9 were studied, 480–580 K. Hence, one expects that for these samples chlorine will react with

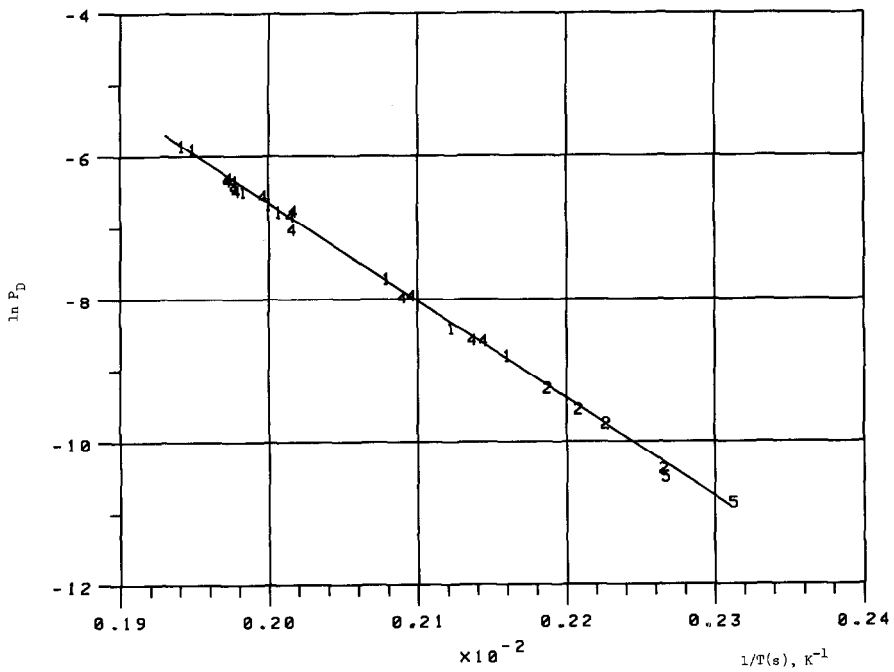

Fig. 2. ln P_D vs $1/T$(s) for equilibrium 1. Points identified by sample numbers. [See Tables 1 and 2(b).] Solid line corresponds to least-squares fit.

water to form appreciable amounts of hydrogen chloride and oxygen. We did not, however, observe the changes in the chlorine absorbance expected from this reaction and conclude, consistent with the observations of others,[20] that the chlorine–water reaction is kinetically inhibited under the conditions of our experiments.

Equilibrium 1

At 432–515 K, samples 1, 2, 4 and 5 have vapour in equilibrium with Au_2Cl_6(s). The A_{244} values correlate with T(s), the temperature of the cell sidearm tip where the solid was observed to condense. Data are listed in Table 2(b) and are shown, plotted as ln P_D vs $1/T$(s), in Fig. 2. The line drawn represents the least-squares fit of 27 observations: ln $P_D = -13744(0.93\%)/T(s)+20.835(1.3\%)$; variance 0.0050.* At low temperatures, absorbances of samples with water present were less than values expected for equilibrium with Au_2Cl_6(s) and condensed liquid solutions were visible. In such cases, absorbance values were not used.

Equilibrium 2

At higher temperatures, up to 635 K, the exact range depending on composition, vapours are in equilibrium with Au(s). Because reaction 2 is exothermic, gold crystals deposited in the section of the cell at the highest temperature. Generally this was in the sidearm close to the cell body, at a point where the sidearm passed close to the heating element of the cell body furnace. For samples 3–9 a thermocouple placed at this point was used to measure T(s).† For some of the samples with large amounts of gold, measurements were sometimes made before all the gold had been transported from the cell body to the hot spot, occasionally confirmed by visual observation; in these cases T(g) was taken as T(s). The 60 observations are tabulated in Table 2(c); a plot of ln $P_D/P_C{}^3$ vs $1/T$(s) is shown in Fig. 3. Samples with and without water show a similar behaviour. A least-squares treatment gave ln $P_D/P_C{}^3 = 12959(0.64\%)/T(s)-29.011(0.53\%)$; variance 0.010.

Equilibrium 3

In the ranges 470–560 K for sample 4 and 444–477 K for sample 5, Au_2Cl_6(s) is not present; Cl_2(g)

* The numbers in parentheses, in this and in similar equations to follow, are least-squares per cent standard deviations for slope and intercept, respectively. The variance represents the value of $[\Sigma(\ln Q(\text{obs})-\ln Q(\text{calc}))^2]/n-1$; Q is the equilibrium quotient for the particular reaction and n is the number of observations.

† T(s) was not measured for samples 1 and 2; these samples were excluded from consideration of equilibrium 2.

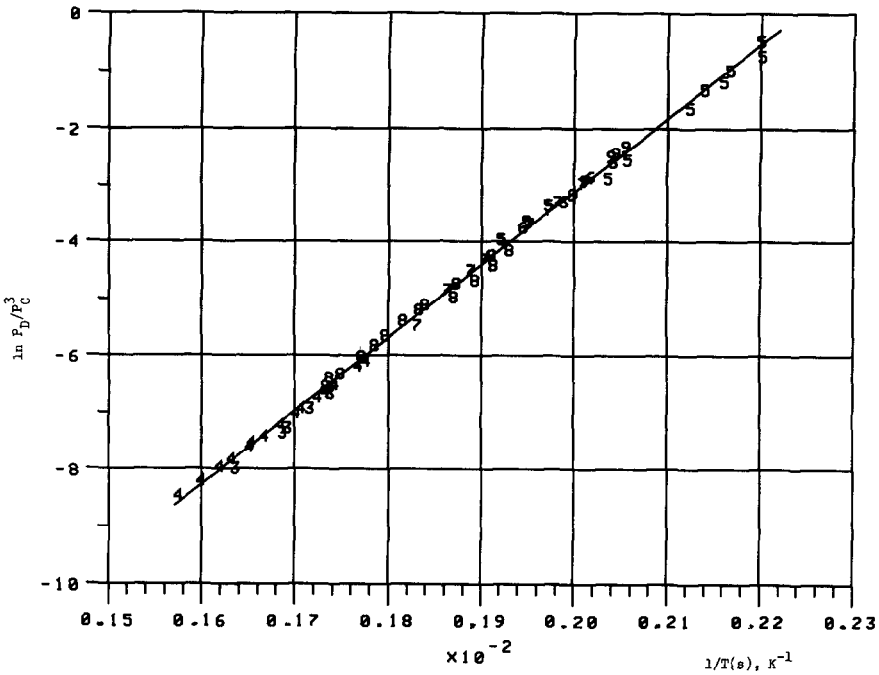

Fig. 3. ln $P_D/P_C{}^3$ vs $1/T$(s) for equilibrium 2. Points identified by sample numbers. [See Tables 1 and 2(c).] Solid line corresponds to least-squares fit.

and Au_2Cl_6(g) are in equilibrium with AuCl(s). The 41 observed absorbances are listed in Table 2(d). In some of these mixtures solid gold is also present. As observed by other workers,[3–11] the reaction between crystalline gold and chlorine is slow. Equilibration between Cl_2(g), Au_2Cl_6(g) and AuCl(s) was faster, however, and even though Cl_2(g) pressures changed very slowly as Au(s) and AuCl(s) were interconverted, the ratios $P_D/P_C{}^2$ measured during the change were found to correlate well with those measured when equilibrium had been fully established. Results are shown graphically in Fig. 4,

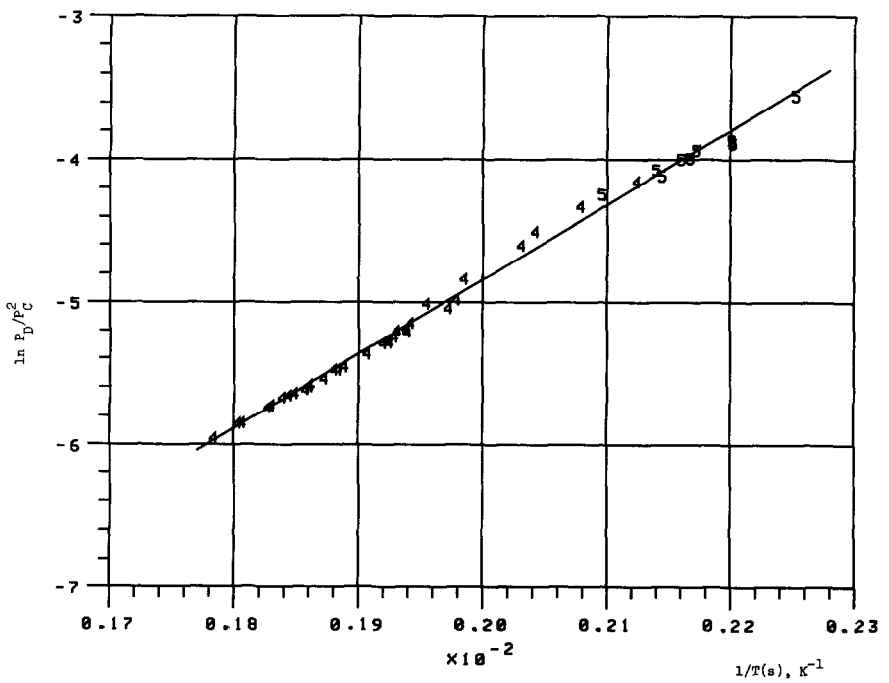

Fig. 4. ln $P_D/P_C{}^2$ vs $1/T$(s) for equilibrium 3. Points identified by sample numbers. [See Tables 1 and 2(d).] Solid line corresponds to least-squares fit.

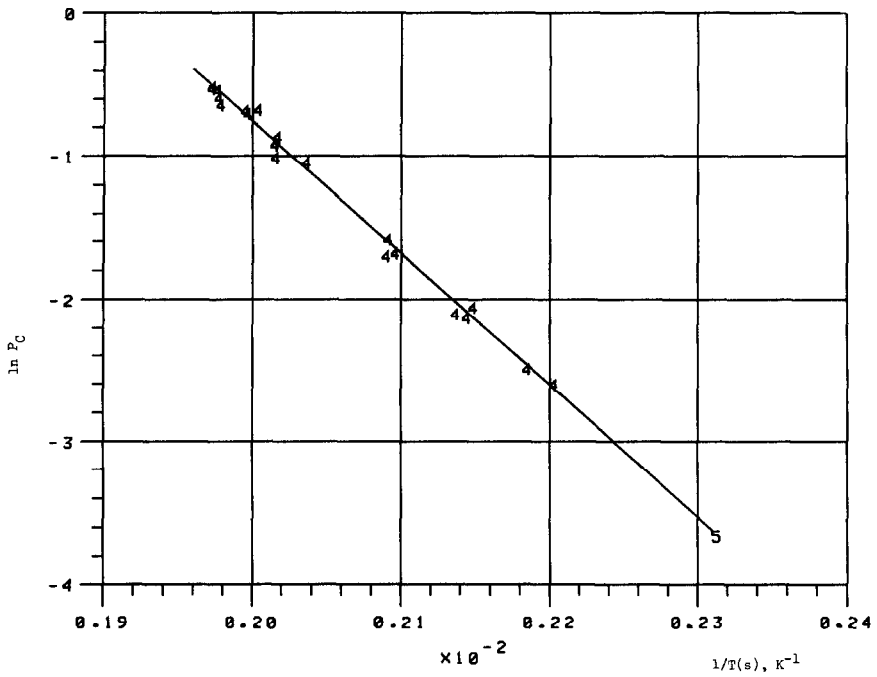

Fig. 5. ln P_C vs $1/T$(s) for equilibrium 4. Points identified by sample numbers. [See Tables 1 and 2(e).] Solid line corresponds to least-squares fit.

along with the least-squares solution line, ln $P_D/P_C^2 = 5250(1.1\%)/T(s) - 15.341(0.74\%)$; variance 0.0022.

Equilibrium 4

Equilibrium constants for reaction 4 correspond to the Cl_2(g) partial pressures when both AuCl(s) and Au_2Cl_6(s) are present. Values were observed for samples 4 and 5 in the range 432–507 K. The 20 observations, mainly from sample 4, are listed in Table 2(e) and are shown graphically in Fig. 5. The least-squares line corresponds to the equation ln $P_C = -9258(1.6\%)/T(s) + 17.760(1.7\%)$; variance 0.0035.

Only three of these four reactions are independent, and, for example, the thermodynamic constants derived for reaction 4 may be compared with

Table 4. Thermodynamic constants, vicinity 500 K

Reaction	ΔH (kJ mol^{-1})	ΔS (J K^{-1} mol^{-1})	T(K) range	Reference
1	113.2	168.0	470–520	3, 9
	117.6		*ca* 390	6
	110.9	167.1	340–515	8, 10
	114.3	173.2	432–515	This work
2	−102.9	−250.2	530–560	7
	−102.1	−234.2	580–650	3
	−103.9	−236.0	585–725	3, 10
	−120.5	−264.5	490–725	8, 9
	−99.2		*ca* 390	6
	−107.7	−241.2	454–635	This work
3	−51.4	−140.3	470–555	8, 9
	−43.6	−127.5	444–560	This work
4	75.7	144.8	460–525	6
	79.7	153.0	360–525	3, 7, 11
	81.1	153.7	405–520	8, 11
	77.0	147.6	432–507	This work
0.5(1–3)	78.9	150.4		This work

those calculated from the constants derived for reactions 1 and 3, 0.5(1–3). In Table 4 the various constants, derived from the least-squares equations presented above, are compared with those reported by other workers. The general accord supports our belief that the absorbance data have been interpreted correctly.

Several differences in the properties of iron(III) chloride and gold(III) chloride appear related to the lack of formation of detectable concentrations of a volatile hydrate in the gold chloride system. Around 500 K, the saturation vapour pressure of iron(III) chloride is *ca* 10 times larger than that of gold(III) chloride. Hence, higher vapour concentrations of iron(III) chloride can be produced at lower temperatures. And, importantly, the dissociation of $Fe_2Cl_6(g)$ to $FeCl_3(g)$ is substantial at low concentrations in the temperature ranges of interest here. In the iron system, only the vapour hydrate of the monomer was observed. In contrast, the monomer $AuCl_3(g)$ has not been detected in gold(III) chloride vapours. At higher temperatures, at which dissociation of the dimer to monomer might be expected, gold(III) chloride is unstable relative to chlorine and gold. Furthermore one would expect the gold–oxygen bond energy in a hydrate linkage to be appreciably less than the similar interaction for iron.

REFERENCES

1. D. S. Rustad and N. W. Gregory, *Inorg. Chem.* 1988, **27**, 2840.
2. N. W. Gregory, *Inorg. Chem.* 1988, **27**, 4264.
3. S. E. James and J. P. Hager, *Metall. Trans.* 1978, **9B**, 501.
4. E. M. W. Janssen. F. Pohlmann and G. A. Wiegers. *J. Less-Common Met.* 1976, **45**, 261.
5. E. M. W. Janssen, J. C. Folmer and G. A. Wiegers, *J. Less-Common Met.* 1974, **38**, 71.
6. A. Visnapuu, B. C. Marek and J. W. Jensen, *U.S. Bur. Mines, Rept. Invest.* 1971, **7513**, Washington, DC.
7. J. P. Hager and R. B. Hill, *Metall. Trans.* 1970, **1**, 2723.
8. A. Landsberg and C. L. Hoatson, *J. Less-Common Met.* 1970, **22**, 327.
9. W. Biltz, W. Fischer and R. Juza, *Z. Anorg. Allg. Chem.* 1928, **176**, 121.
10. W. Fischer and W. Biltz, *Z. Anorg. Allg. Chem.* 1928, **176**, 81.
11. A. A. Shchkukarev, M. R. Oranskaya and V. M. Tsintsius, *Russ. J. Inorg. Chem.* 1956, **1**, 881.
12. R. J. Puddephatt, *The Chemistry of Gold.* Elsevier, New York (1978).
13. D. J. Seery and D. Britton, *J. Phys. Chem.* 1964, **68**, 2266; G. Burns and R. G. W. Norrish, *Proc. R. Soc. (Lond.), Ser. A* 1963, **271**, 289; G. E. Gibson and N. S. Bayliss, *Phys. Rev.* 1933, **44**, 188.
14. D. S. Rustad and N. W. Gregory, *Inorg. Nucl. Chem. Letts* 1980, **16**, 521.
15. V. Balzani and V. Carassiti, *Photochemistry of Coordination Compounds.* Academic Press, New York (1970).
16. W. R. Mason and H. B. Gray, *Inorg. Chem.* 1968, **7**, 55.
17. E. S. Clark and D. H. Templeton, *Acta Cryst.* 1958, **11**, 284.
18. T. N. Silukova, P. A. Babin and S. F. Voropaev, *Fiz. Kondensiv. Sostoyaniya Veshchestva, Khabarovsk* 1978, 14.
19. M. W. Chase Jr, C. A. Davies, J. R. Downey, D. J. Frurip, R. A. McDonald and A. N. Syverud, *JANAF Thermochemical Tables*, 3rd edn. American Chemical Society and American Institute of Physics, New York (1986).
20. G. N. Lewis, *J. Am. Chem. Soc.* 1906, **28**, 1380.

Polyhedron Vol. 10, No. 6, pp. 645–647, 1991
Printed in Great Britain

0277–5387/91 $3.00+.00
© 1991 Pergamon Press plc

COMMUNICATION

PREPARATION OF VOLATILE, MONOMERIC COPPER(I) β-DIKETONATE COMPLEXES

H.-K. SHIN, M. J. HAMPDEN-SMITH* and E. N. DUESLER

Department of Chemistry, Center for Micro-Engineered Ceramics, University of New Mexico, Albuquerque, NM 87131, U.S.A.

and

T. T. KODAS

Department of Chemical Engineering, Center for Micro-Engineered Ceramics, University of New Mexico, Albuquerque, NM 87131, U.S.A.

(*Received* 9 *July* 1990; *accepted* 9 *November* 1990)

Abstract—A series of (β-diketonate)Cu(PMe_3), where β-diketonate = acetylacetonate (acac) (**1**), trifluoroacetylacetonate (**2**) and hexafluoroacetylacetonate (**3**), compounds have been prepared by the reaction of β-diketones with (η^5-C_5H_5)CuPMe_3. A single crystal X-ray diffraction study of (tfa)CuPMe_3 reveals that it is monomeric in the solid state with a trigonal planar copper coordination environment. All three new compounds are volatile and soluble in hydrocarbon solvents.

The metal–organic chemistry of copper is currently receiving renewed interest due to new applications including Chemical Vapour Deposition (CVD) of copper metal for microelectronic applications and copper oxide for superconducting ceramics. These applications have driven the development of molecular routes to copper-containing materials. The synthesis of multi-component metal oxide phases containing copper is being investigated by using either volatile precursors to copper oxide for CVD[1] or soluble precursors for hydrolytic condensation.[2] The deposition of copper metal films by CVD also requires molecular precursors that are volatile.[3] There is, however, a distinct paucity of volatile and soluble copper(I) and copper(II) compounds, due to their tendency to oligomerize.[4] Copper(II) β-diketonates[3,5] and $[Cu(O\text{-}t\text{-}Bu)]_4$[6] have been used as precursors to copper metal films, but have low volatility (e.g. $[Cu(O\text{-}t\text{-}Bu)]_4$ sublimes slowly at 100°C and 10^{-5} torr). It has recently been demonstrated that copper(I) species, such as cyclopentadienyl copper(I) phosphine complexes, have higher volatility and are suitable precursors for deposition of copper.[7] Here we report the synthesis and characterization of a series of monomeric copper(I) β-diketonate complexes, which are both volatile and soluble in hydrocarbon solvents. Although copper(II) β-diketonates are well known, there are few reports of copper(I) β-diketonate compounds,[8] and their solubility and volatility is much lower than that of the title compounds.

The reaction of cyclopentadienyl copper(I) trimethylphosphine, (η^5-C_5H_5)CuPMe_3, with β-di-

* Author to whom correspondence should be addressed.

ketones results in the displacement of cyclopentadiene, according to the reaction of eq. (1) below.*

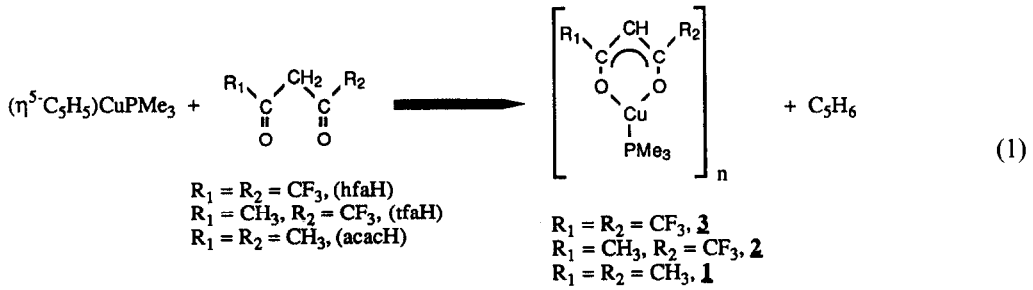

(1)

Upon work-up, **1** is isolated as a yellow liquid, while **2** and **3** are isolated as pale yellow and orange solids, respectively. All three reactions result in high yields of the respective products that can be crystallized from n-pentane at low temperatures. All three compounds can be sublimed *in vacuo* at relatively low temperatures and pressures (~35°C and 0.01 torr). However, while **2** and **3** sublime unchanged, **1** decomposes upon sublimation to yield (acac)Cu(PMe_3)$_2$ (**4**).†

The high volatility of these species is consistent with a low degree of molecular aggregation. In benzene solution, **2** and **3** are monomeric, as determined by cryoscopic molecular weight determination. However, positive ion mass spectral data (electron impact) of **1–3** exhibit ions of higher molecular mass than those expected for monomeric species.‡ For example, the highest masses observed for both **2** and **3** correspond to [(β-diketonate)$Cu_2(PMe_3)_2$]$^{+\cdot}$ with isotope distribution patterns characteristic of the presence of two copper atoms.

To unambiguously establish the degree of oligomerization in the solid state, a single crystal X-ray diffraction study of **2** was carried out.§ The molecular structure of **2** is shown in Fig. 1, together with relevant bond lengths and angles. These data show that **2** is monomeric in the solid state, with a trigonal planar copper(I) coordination environment.[9] The β-diketonate ligand is chelated to copper through oxygen ligands,[10] as expected, but distinction cannot be made between the Cu—O(1) and Cu—O(2) distances within the limits of error on the data. The Cu—P distance is slightly longer than the value we have recently observed in the structure of (η^5-C_5H_5)$CuPMe_3$.[7b] The O(1)—Cu—O(2) angle is small [91.9(2)°], as expected from the bite angle of

* Compounds **1–3** were prepared by a similar method. The preparation of **2** is described here. (η^5-C_5H_5)$CuPMe_3$ (3.40 g, 16.6 mmol) was placed in a 100 cm^3 Schlenk flask and 10 cm^3 of dry n-pentane were added. The suspension was cooled to 0°C and 4.04 cm^3 (33.2 mmol) of trifluoroacetylacetone (tfaH) were added while stirring. The (η^5-C_5H_5)$CuPMe_3$ started to dissolve to give a yellow solution. After stirring for 0.75 h, all the starting material had dissolved and the volatile components were removed *in vacuo* to give a yellow–green oily residue. The residue was sublimed at 35°C/10^{-2} torr to give 4.86 g of (tfa)$CuPMe_3$, a yield of 96.3%. This compound is soluble in n-pentane and can be crystallized from this solvent at −30°C. Compounds **1** and **3** were obtained in yields of 87.8 and 98.5%, respectively, from reactions conducted on a similar scale. Characterization data: m.p. (sealed tube, uncorrected): **1** = 27°C, **2** = 48°C, **3** = 67°C. ^{1}H NMR data (C_6D_6, 23°C, 250.13 MHz): **1**: 5.41 ppm, s, 1H; 1.98 ppm, s, 6H; 0.68 ppm, d, 6.7 Hz, 9H. **2**: 5.88 ppm, s, 1H; 1.83 ppm, s, 3H; 0.51 ppm, d, 7.4 Hz, 9H. **3**: 6.33 ppm, s, 1H; 0.38 ppm, d, 8.0 Hz, 9H. ^{31}P NMR data (C_6D_6, 23°C, 101.22 MHz): **1**: −44.1 ppm, s, br. **2**: −43.7 ppm, s, br. **3**: −42.7 ppm, s, br. Elemental analysis: **2**: Found: C, 33.2; H, 4.5. Calc.: C, 32.8; H, 4.5%. **3**: Found: C, 28.3; H, 2.8. Calc.: C, 27.7; H, 2.9%. Molecular weight data (cryoscopic, C_6H_6): **3**, measured 340 (+/−14) (0.040 M); 338 (±7) (0.078 M); calculated for (hfa)$CuPMe_3$ 347: **2**, measured 286 (±13) (0.040 M); calculated for (tfa)$CuPMe_3$ 293.

† Characterization data for **4**. ^{1}H NMR data (C_6D_6, 23°C, 250.13 MHz): 5.35 ppm, s, 1H; 2.03 ppm, s, 6H; 0.86 ppm, d, 5.3 Hz, 18H. ^{31}P NMR data (C_6D_6, 23°C, 101.22 MHz): s, br, −48.2. Elemental analysis: Found: C, 42.0; H, 7.6. Calc.: C, 41.7; H, 8.0%.

‡ Summary of mass spectral data for **1–3** (70 eV) at high *m/z*: **1**, 379, 5%; 324, 2%; 261, 52%; 246, 28%; 238, 58%; base mass = 139; **2**, 428, 1%; 369, 8%; 327, 2.5%; 300, 2.7%; 292, 25%; base mass = 139; **3**, 487, 1.5%; 346, 20%; base mass = 139.

§ Crystal structure data for **2**: orthorhombic, space group *Pbca*, a = 10.317(4), b = 11.630(3), c = 18.295(4) Å, V = 2554.8(14) Å^3, Q_{calc} = 1.522 g cm^{-3}, Z = 8, 1484 unique reflections collected from 2θ = 2.0–50.0° with $F_o > 3.0\sigma(F)$. Nicolet R3M/V diffractometer, Mo-K_α radiation, λ = 0.71073 Å, T = 20°C. Solution by Patterson Map Interpretation using Siemers SHELXTL PLUS (MicroVAX II), refined by full-matrix least-squares, R_w = 3.91%. Further details are available as supplementary material. Atomic positional parameters have been deposited with the Director, Cambridge Crystallographic Data Centre.

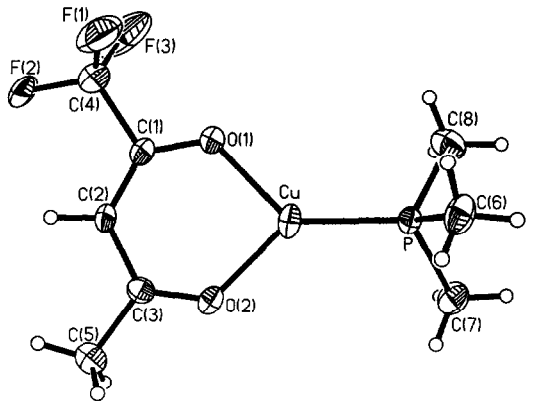

Fig. 1. Ortep plot of **2**, emphasizing the coordination environment of copper. Relevant bond lengths (Å): Cu—P = 2.133(2), Cu—O(2) = 1.982(4), Cu—O(1) = 1.990(4), C(1)—O(1) = 1.257(7), C(1)—C(2) = 1.362(9), C(2)—C(3) = 1.406(8), C(3)—O(2) = 1.249(7), C(1)—C(4) = 1.539(12), C(3)—C(5) = 1.496(8). Relevant bond angles (°): O(2)—Cu—O(1) = 91.9(2), P—Cu—O(1) = 132.4(1), P—Cu—O(2) = 135.6(1), Cu—O(2)—C(3) = 126.5(4), O(2)—C(3)—C(2) = 124.4(s), C(3)—C(2)—C(1) = 124.4(s), C(2)—C(1)—O(1) = 128.6(s), C(1)—O(1)—Cu = 123.1(4).

this chelating ligand, resulting in enlarged O(1)—Cu—P and O(2)—Cu—P angles. Other angles and distances within the ligands are unremarkable, and there is no evidence for intermolecular interactions.

The apparent discrepancy between the mass spectral data and the X-ray diffraction data probably results from the high volatility of these species. However, variation in the mass spectral parameters, such as reducing the ionization potential and decreasing the sample size, did not result in a significant reduction of the ions of higher mass than the monomeric molecular ion. Finally, we note that the solid state, solution phase and gas phase IR data for **2** are virtually identical, and it is likely that **2** is monomeric in the gas phase, although this remains to be established unambiguously.

In conclusion, some examples of a new family of copper(I) β-diketonate compounds have been prepared and characterized that are both volatile and soluble in hydrocarbon solvents. This family of compounds has the potential to be substituted either at the metal centre, or at the β-diketonate ligand to produce copper(I) species with a variety of physical properties.

Acknowledgements—We thank Spectrum CVD, Phoenix, Arizona, for an equipment donation, NSF for an NMR instrumentation grant, and Eva Quesnell for typing this manuscript.

REFERENCES

1. A. D. Berry, R. T. Holm, M. Fateni and D. K. Gaskill, *J. Mater. Res.* 1990, **5**, 1109.
2. (a) S. G. Goel, K. S. Kramer, P. C. Gibbons and E. W. Buhro, *Inorg. Chem.* 1989, **28**, 3619; (b) H. S. Horowitz, S. J. McLain, A. W. Sleight, J. D. Druliner, P. L. Gai, M. J. Vankavelaar, J. L. Wagner, B. D. Briggs and S. J. Poon, *Science* 1989, **243**, 66.
3. F. A. Houle, C. R. Jones, T. H. Baum, C. Pieu and C. A. Kovac, *Appl. Phys. Lett.* 1985, **46**, 204.
4. F. A. Colton and G. Wilkinson, in *Advanced Inorganic Chemistry*, 5th edn, pp. 477–478, 755–775. John Wiley, New York (1988).
5. (a) C. Oehr and H. Suhr, *Appl. Phys. A.* 1988, **45**, 151; (b) D. Temple and A. Reisman, Technical report Number 4. Microelectronic Center of North Carolina (28 July 1988).
6. P. M. Jeffries and G. S. Girolami, *Chem. Mat.* 1989, **1**, 8.
7. (a) G. C. Dupuy, D. B. Beach, J. E. Hurst and J. M. Jasinski, *Chem. Mat.* 1989, **1**, 16; (b) M. J. Hampden-Smith, T. T. Kodas, M. Paffett, J. D. Farr and H. K. Shin, *Chem. Mat.* 1990, **2**, 636.
8. B. Emmert, H. Grott-Schneider and H. Starger, *Chem. Ber.* 1936, **69B**, 1319. (β-diketonate)Cu $(PPh_3)_2$ species have previously been prepared: T. Yamamoto, M. Kubota, A. Miyoshita and A. Yamamoto, *Bull. Chem. Soc. Japan* 1978, **51**, 1835; and more recently complexes of the type $[Cu(\beta\text{-diketonate})]_nL_m$, where L = CO, alkene or diene: G. Doyle, K. A. Eriksen and D. Van Engen, *Organometallics* 1985, **4**, 830.
9. A. F. Wells, in *Structural Inorganic Chemistry*, 4th edn, p. 884. Clarendon Press, Oxford (1975).
10. S. Kawaguchi, in *Variety in Coordination Modes of Ligands in Metal Complexes*, Inorganic Chemistry Concepts, Vol. II. Springer-Verlag, Berlin (1988).

Polyhedron Vol. 10, No. 6, pp. 649–651, 1991
Printed in Great Britain

0277–5387/91 $3.00+.00
© 1991 Pergamon Press plc

COMMUNICATION

PREPARATION AND X-RAY CRYSTAL STRUCTURE OF $[N(CH_3)_4]_4[\{H(SO_4)W_3O_7(O_2)_2\}_2O]$

MASATO HASHIMOTO and TOSCHITAKE IWAMOTO*

Department of Chemistry, College of Arts and Sciences, The University of Tokyo, Komaba, Meguro, Tokyo 153, Japan

and

HIKARU ICHIDA and YUKIYOSHI SASAKI

Department of Chemistry, Faculty of Science, The University of Tokyo, Hongo, Bunkyo, Tokyo 113, Japan

(*Received* 13 *November* 1990; *accepted* 7 *January* 1991)

Abstract—The title peroxotungstosulphate as the first example of a polytungstosulphate has been prepared and its structure determined. The salt crystallizes under the conditions: $[WO_4^{2-}] = 0.3$–1.0 mol dm^{-3}, $[WO_4^{2-}]/[SO_4^{2-}] = 1$–$1/4$, $[WO_4^{2-}]/[H_2O_2] = 1/2$–$1/4$ and pH < 1. The SO_4^{2-} tetrahedron shares its three vertices with two $WO_5(O_2)_2$ decahedra and one WO_6 octahedron to form a diperoxotritungstosulphate moiety; the polyanion is made of the two moieties bridged with three μ-oxo groups.

In the course of our investigations on peroxopolytungstates, the title compound was obtained from X^+–H^+–WO_4^{2-}–H_2O_2 systems, and its structure was determined by single crystal X-ray diffraction. As far as polyoxometallosulphates are concerned, three structures have been reported;[1–3] this is the first example of a structure being analysed for a polytungstosulphate.

EXPERIMENTAL

Preparation

To prepare the mother solution of this compound, two methods were available.

(1) To a solution of $Na_2WO_4 \cdot 2H_2O$ (5.0 g) in 17 cm^3 of H_2O, 3.0 cm^3 of H_2O_2 was added and the pH promptly adjusted to *ca* 0.5 with 60% nitric acid. Then tetramethylammonium hydrogensulphate (5.0 g) in 10 cm^3 of H_2O was added.

(2) WS_2 powder (5.0 g) was dissolved in 50 cm^3 of 30% H_2O_2 (Note: the reaction is very vigorous). After evaporating the solution to *ca* 12 cm^3, it was mixed with an equivolume aqueous solution of $N(CH_3)_4HSO_4$ (8.0 g).

In each case pale yellow, tabular crystals were obtained within a few days at room temperature. A single crystal for X-ray diffraction measurements was prepared by method (1).

This compound crystallizes in wide ranges of $[WO_4^{2-}]$, $[WO_4^{2-}]/[SO_4^{2-}]$ and $[WO_4^{2-}]/[H_2O_2]$ at pH < 1. Appropriate conditions are $[WO_4^{2-}] = 0.3$–1.0 mol dm^{-3}, $[WO_4^{2-}]/[SO_4^{2-}] = 1$–$1/4$ and $[WO_4^{2-}]/[H_2O_2] = 1/2$–$1/4$.

Intensity collection and structure determination

A single crystal with dimensions $0.22 \times 0.31 \times 0.45$ mm^3 was mounted on a RIGAKU AFC-5R automated four-circle diffractometer at the Department of Chemistry, Faculty of Science, The University of Tokyo, using graphite-monochromated Mo-K_α radiation (50 kV, 200 mA, $\lambda = 0.71069$ Å) at 25°C.

* Author to whom correspondence should be addressed.

Crystallographic data: formula $C_{16}H_{50}N_4O_{31}S_2W_6$, FW = 1961.81, monoclinic, $C2/c$, $a = 20.87(1)$, $b = 10.611(2)$, $c = 20.077(8)$ Å, $\beta = 103.13(3)°$, $V = 4330$ Å^3, $D_m = 2.98$, $D_x = 3.01$ g cm^{-3} and $Z = 4$.

Calculations were carried out on HITAC M-680H/682H systems at the Computer Centre, The University of Tokyo, using UNICS III programs[4] including ORTEP.[5] Atomic scattering factors including real and imaginary dispersion corrections were cited from the *International Tables for X-Ray Crystallography*.[6] Positions of three independent tungsten atoms were determined from Patterson functions and the remaining non-hydrogen atoms were located by successive Fourier and difference Fourier syntheses. Tungsten, sulphur and oxygen atoms were refined anisotropically and nitrogen and carbon atoms isotropically using the block-diagonal least-squares method with the absorption correction based on psi-scans.

The final R value, 0.0655, was obtained for 3176 independent reflections with $4.0° \leqslant 2\theta \leqslant 55°$, $|F_o| > 5.5\sigma(F_o)$ and $|F_o| > 10.0$ from 5548 measured reflections.

STRUCTURE DESCRIPTION AND DISCUSSION

An ORTEP view of the polyanion together with the atomic numbering is shown in Fig. 1, and a polyhedra model in Fig. 2. Two $[H(SO_4)W_3O_8(O_2)_2]$ units related by a two-fold axis passing through O(12) are linked by three μ-oxo groups, and the anion has C_2 symmetry. The SO_4^{2-} groups behave as a tripod ligand sharing three oxygen atoms with respective independent tungsten atoms. Each of two peroxo groups in the asymmetric unit coordinates to W(2) and W(3); O(7)—O(8) to W(2) and O(9)—O(10) to W(3), respectively. Thus seven oxygen atoms ligate to these two tungsten atoms constructing decahedral (pentagonal bi-

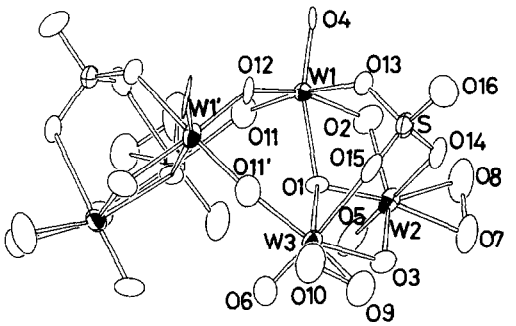

Fig. 1. An ORTEP view of $[\{H(SO_4)W_3O_7(O_2)_2\}_2O]^{4-}$ together with the atomic numbering.

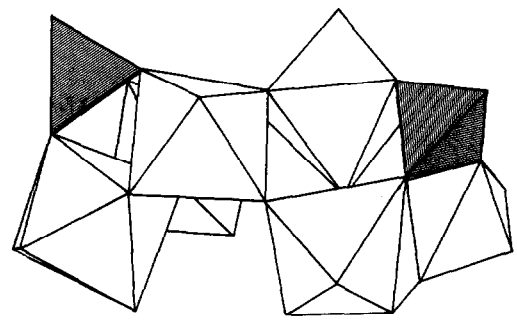

Fig. 2. The anion structure in the polyhedra model (the SO_4^{2-} groups are shaded).

pyramid) coordination spheres. W(1) has no O_2^{2-} ligand and shares two vertices of its octahedral (square bipyramid) sphere with the other half of the polyanion. A dihedral angle of *ca* 100° is found between W(1)—W(2)—W(3) and W(1')—W(2')—W(3') (the primed atoms are generated by rotation of original atoms about the two-fold axis through the polyanion) planes. Hence the shape of the polyanion looks like a twisted boomerang. The sulphate group is only slightly distorted from the regular tetrahedral structure. The tripod ligation of SO_4^{2-} makes each axis of the three tungsten polyhedra recline about 20°, and an apparently trigonal pyramid is formed with O(16) at the top and O(5)—O(6)—O(11) at the bottom. The result of bond valence calculations[7] shows that the acidity of O(2) is lower (1.46) than the other oxygen atoms, suggesting that this position is protonated.

In the IR spectrum, as shown in Fig. 3, the bands due to the S—O stretch mode (ν_1)[8] and the deformation mode (ν_2) are observed at *ca* 970 and 450 cm^{-1} with shoulders, respectively. Both mode types

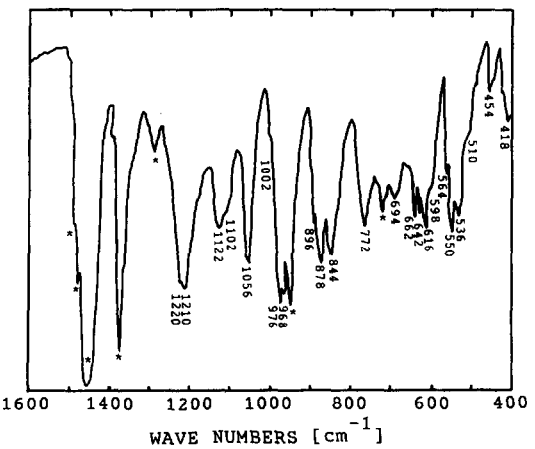

Fig. 3. IR spectrum of the salt in Nujol (signals due to Nujol and tetramethylammonium are marked with asterisks).

are IR-inactive in T_d symmetry, but become active in the approximate C_{3v} symmetry of the tripod coordination. Two deformation modes, ν_3 and ν_4, are also observed in the regions 1200 and 640 cm^{-1}, respectively, with splittings.

REFERENCES

1. J. Fuchs, H.-U. Kreusler and A. Förster, *Z. Naturfor.* 1979, **34b**, 1683.
2. A. Boter and J. Fuchs, *Z. Naturfor.* 1982, **37b**, 806.
3. T. Hori, O. Tamada and S. Himeno, *J. Chem. Soc., Dalton Trans.* 1989, 1491.
4. T. Sakurai and K. Kobayashi, *Rep. Inst. Phys. Chem. Res.* 1977, **55**, 69.
5. C. K. Johnson, ORTEP, Report ORNL—3794. Oak Ridge National Laboratory, Tennessee, U.S.A. (1965).
6. *International Tables for X-ray Crystallography*, Vol. 4. Kynoch Press, Birmingham (1974).
7. I. D. Brown and D. Altermatt, *Acta Cryst.* 1985, **41B**, 244.
8. K. Nakamoto, *Infrared Spectra of Inorganic and Coordination Compounds*, 2nd edn. Wiley-Interscience, New York (1970).

Polyhedron Vol. 10, No. 7, pp. 653–657, 1991
Printed in Great Britain

0277–5387/91 $3.00+.00
Pergamon Press plc

MONONUCLEAR AND BINUCLEAR 4-CYANOPYRIDINE COMPLEXES OF BIS(2,2′-BIPYRIDINE) (PYRIDINE)RUTHENIUM(II)*

EDGARDO H. CUTIN† and NESTOR E. KATZ†‡

Instituto de Química Fisica, Facultad de Bioquímica, Química y Farmacia, Universidad Nacional de Tucumán, Ayacucho 491 (4000), San Miguel de Tucumán, República Argentina

(*Received* 17 *September* 1990; *accepted* 22 *October* 1990)

Abstract—New complexes derived from the $Ru(bpy)_2(py)^{2+}$ moiety (bpy = 2,2′-bipyridine, py = pyridine) were synthesized and characterized by spectroscopic techniques. The mononuclear complex $[Ru(bpy)_2(py)(4\text{-}CNpy)]^{2+}$ (4-CNpy = 4-cyanopyridine) seems to be the pyridine-bonded isomer of 4-CNpy, as disclosed by IR and UV–vis data ($\nu_{CN(nitrile)}$ = 2240 cm^{-1}, λ_{max} = 434 nm in CH_3CN). The binuclear complexes $[Ru(bpy)_2(py)(4\text{-}CNpy)Ru(NH_3)_5]^{4+}$ and $[Ru(bpy)_2(py)(4\text{-}CNpy)Fe(CN)_5]^{-}$ were also prepared; they showed new absorptions in the visible region at λ_{max} *ca* 450 nm ascribable to MLCT (metal-to-ligand charge-transfer) transition from d_π orbitals of ruthenium or iron to π^* orbitals of 4-CNpy. The former dimer was obtained as a PF_6^- salt, which presented $\nu_{CN(nitrile)}$ = 2178 cm^{-1}, as expected from an ammineruthenium(II) moiety bonded to 4-CNpy through the nitrile group. Oxidation of this species with cerium(IV) yielded the mixed-valence complex $[Ru^{II}(bpy)_2(py)(4\text{-}CNpy)Ru^{III}(NH_3)_5]^{5+}$, with concomitant disappearance of the MLCT band of lowest energy.

4-Cyanopyridine (4-CNpy) is an ambidentate ligand which can coordinate to transition metals through its pyridine nitrogen or its nitrile nitrogen, giving rise to stable isomeric forms of mononuclear and binuclear complexes. We are particularly interested in the properties of 4-CNpy as an effective electronic conductor,[1,2] and thus we report in this work the preparation and spectroscopic properties of new complexes derived from the $Ru(bpy)_2(py)^{2+}$ moiety (bpy = 2,2′-bipyridine, py = pyridine) which can have 4-CNpy as a bridging ligand. The $Ru^{II}(bpy)_2$ group is a well-known photosensitizer,[3] while bridged binuclear complexes are systems under intense scrutiny due to their importance in electron (or energy) transfer reactions that may eventually lead to conversion of light energy into chemical energy.[4,5]

*Presented, in part, at the VI Argentine Congress on Physical Chemistry, Termas de Río Hondo, Santiago del Estero, República Argentina (1989).

† Members of the Research Career, CONICET, República Argentina.

‡ Author to whom correspondence should be addressed.

EXPERIMENTAL

Syntheses

Analytical reagent compounds were used for all experiments reported in this work. Doubly distilled water was redistilled from alkaline permanganate in all-glass apparatus.

$[Ru(bpy)_2(py)(4\text{-}CNpy)](PF_6)_2 \cdot 8H_2O$ (A)

A mixture of $[Ru(bpy)_2(py)Cl]Cl$ (0.3 g, 0.5 mmol, prepared as in ref. 6) and 4-cyanopyridine (2 g, 19 mmol) was refluxed for 1 h in a solution of water (10 cm^3) and methanol (5 cm^3). The resulting dark red solution was filtered, evaporated to a volume of 5 cm^3 and precipitated with an aqueous saturated solution of NH_4PF_6. The solid was collected on a sintered-glass filter, washed with cold water and recrystallized from hot methanol by the addition of ether. It was dried in a vacuum desiccator over KOH. Yield: 0.27 g, 52% (Found: C, 36.1; H, 4.2; N, 10.9. Calc.: C, 36.1; H, 4.0; N, 9.5%).

$[Ru(bpy)_2(py)(4\text{-}CNpy)Ru(NH_3)_5](PF_6)_4 \cdot 8H_2O$ (**B**)

$[Ru(bpy)_2(py)(4\text{-}CNpy)](PF_6)_2 \cdot 8H_2O$ (100 mg, 0.097 mmol) and $[Ru(NH_3)_5(H_2O)](PF_6)_2$ (51 mg, 0.1 mmol, prepared as in ref. 7) were dissolved in distilled acetone (8 cm^3) under argon and the mixture was stirred for 5 h with continuous argon bubbling. Ether was added and after 1 h at 0°C, the solid was collected and washed with dichloromethane. It was then dissolved in acetone, reprecipitated with ether, filtrated and dried *in vacuo* over KOH (Found: C, 24.6; H, 3.2; N, 10.1. Calc.: C, 24.7; H, 3.7; N, 11.1%.)

$[Ru(bpy)_2(py)(4\text{-}CNpy)Fe(CN)_5]^-$ (**C**)

Compound **A** (0.5 g) was dissolved in 10 cm^3 of argon-deoxygenated water and mixed with a slight excess of $Na_3[Fe(CN)_5(NH_3)] \cdot 3H_2O$, obtained as in ref. 8. The mixture was stirred under argon for 30 min, and then visible spectra were recorded.

Instrumentation and techniques

IR spectra were obtained as KBr pellets on a Perkin-Elmer Model 983G spectrophotometer. Electronic spectra were recorded on a Perkin–Elmer Coleman 124 spectrophotometer. C, H and N microanalyses were performed at UMYMFOR, Universidad de Buenos Aires, Argentina. Oxidation experiments were carried out on the binuclear ruthenium complex (**B**) by adding stoichiometric amounts of cerium(IV) to a solution of **B** in CH_3CN (with a few added drops of HNO_3) and then recording the visible spectra.

RESULTS AND DISCUSSION

IR spectra

The wavenumbers of the IR absorptions, together with their relative intensities and description of the modes, are presented in Table 1 for complexes **A** and **B**. Assignments are tentative and made by comparison with the spectra of the free ligands py,[9] bpy[10] and 4-CNpy[11] and with those of similar complexes derived from ruthenium ammines[1,12] and polypyridines.[2,13] For the mononuclear complex **A**, the stretching frequency of the nitrile group (2240 cm^{-1}) is nearly equal to the value for the free ligand (2243 cm^{-1}),[14] suggesting coordination to the pyridine nitrogen. In the dimer **B**, the value of this frequency (2178 cm^{-1}) is shifted 65 cm^{-1} below the free ligand value, a lowering already observed in similar complexes,[1,14,15] and which can be attributed to the π-backbonding ability of the $Ru(NH_3)_5^{2+}$ moiety. The vibration corresponding to the ammonia symmetric deformation appears at 1301 cm^{-1} in the spectrum of **B** and is characteristic of ruthenium(II) ammines.[16] The IR data thus indicate that 4-CNpy bonds through its pyridine nitrogen to the polypyridine ruthenium and through its nitrile nitrogen to the ammine ruthenium. This result is in contrast to that found in ref. 2, which

Table 1. IR spectra of $[Ru(bpy)_2(py)(4\text{-}CNpy)](PF_6)_2 \cdot 8H_2O$ (**A**) and $[Ru(bpy)_2(py)(4\text{-}CNpy)Ru(NH_3)_5](PF_6)_4 \cdot 8H_2O$ (**B**) (as KBr pellets). Wavenumbers are in cm^{-1}

A	B	Description of modes
3605 sh	3619 sh	
3452 vw	3450 w	$\nu(H_2O)$, ν(NH)
3385 vw	3383 w	
	3198 br,m	
3134 vw		ν(CH)
3046 vw		
2926 vw	2940 br,m	
2860 vw	2850 vw	
2240 w	2178 w	ν(C≡N)
1692 w	1681 m	
1620 sh	1621 w	$\delta(H_2O)$
1605 w	1604 m	ν(C=C)
1553 vw	1549 vw	
1493 vw	1489 vw	ν(C=N)
1468 w	1468 w	
1447 w	1446 m	
1416 w	1423 w	δ(CCH)(bpy)
1394 br,w	1394 vw	ν(ring)
1320 sh	1320 sh	ν(C=N)(bpy)
	1301 w	$\delta(NH_3)$
1296 vw	1297 vw	ν(CC)
1272 sh		
1219 vw	1230 vw	
1164 vw	1162 vw	δ(CCH) in-plane
1120 sh	1124 vw	
1057 w	1071 vw	
1033 w		Ring breathing
	1008 vw	
839 vs	841 vs	ν(PF)
762 m	765 m	δ(CCH) out-of-plane
734 w	734 w	
708 vw	712 br,m	δ(CC)
631 sh	628 vw	δ(CCC) inter-ring
557 m	558 m	δ(CC)
506 vw		ν(Ru—N)
435 vw	422 vw	
353 vw		

Abbreviations: vs, very strong; s, strong; m, medium; w, weak; vw, very weak; sh, shoulder; br, broad; ν, stretching; δ, deformation.

may be due to different synthetic conditions and/or different steric effects.

UV–vis spectra

Figure 1 shows the UV–vis spectrum of a 2×10^{-5} mol dm^{-3} solution of complex **A** in CH_3CN at room temperature. Values of λ_{max} and ε_{max}, together with the corresponding assignments (done by comparison with similar complexes),[2] are shown in Table 2. When comparing the spectrum of $[Ru(bpy)_2(py)(4\text{-}CNpy)]^{2+}$ ($\lambda_{max} = 434$ nm in CH_3CN) to that of $[Ru(bpy)_2(py)_2]^{2+}$ ($\lambda_{max} = 460$ nm in methanol),[17] a shift of the MLCT transition $d_\pi(Ru) \rightarrow \pi^*(bpy)$ to higher energy occurs, in agreement with the higher π-acceptor ability of 4-CNpy with respect to pyridine. In addition, the band at 382 nm, attributed to a $d_\pi(Ru) \rightarrow \pi^*(4\text{-}CNpy)$MLCT, is shifted to lower energies when compared with the corresponding band in $[Ru(bpy)_2(4\text{-}CNpy)_2]^{2+}$ ($\lambda_{max} \sim 360$ nm),[2] as expected for a pyridine-bonded isomer of 4-CNpy. Indeed, λ_{max} for these MLCT visible bands are unchanged in 0.1 M HCl and 1 M HCl for complex **A**, indicating the following structure:

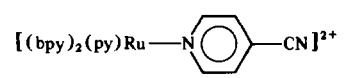

in agreement with the IR results. The nitrile-bonded isomer must have a spectrum sensitive to pH.[2]

Figure 2 shows the obtained visible spectra for complexes **B** and **C** in CH_3CN and water, respectively, at room temperature. Both species present new absorption bands at λ_{max} *ca* 450 nm (454 nm for **B** and 452 nm for **C**) which can be assigned to MLCT transitions from d_π orbitals of ruthenium or iron [of the $Ru^{II}(NH_3)_5$ or $Fe^{II}(CN)_5$ groups] to π^* orbitals of 4-CNpy. Actually, these bands seem to be composed of superimposed polypyridine Ru → bpy and ammine Ru (or Fe) → 4-CNpy MLCT bands (cf. ref. 2). Complex **B** also has greater absorption at higher wavelengths than complex **C**; this result agrees with the higher π-backbonding capability of the $Ru(NH_3)_5^{2+}$ moiety compared with the $Fe(CN)_5^{3-}$ moiety.[18] When analysing data of visible absorption maxima of $[(CN)_5Fe^{II}L]$ complexes, as shown in Table 3, or of $[(NH_3)_5Ru^{II}L]$ derivatives, as shown in Table 4, where L = nitrile bonded 4-CNpy (with its free nitrogen coordinated to different moieties), complexes **B** and **C** fall within the correlation of λ_{max} (of the Ru or Fe → 4-CNpy MLCT band) with the inductive effect of the pyridine-bonded centres. Thus, the following structures

Table 2. Electronic spectrum of the mononuclear complex $[Ru(bpy)_2(py)(4\text{-}CNpy)]^{2+}$ in CH_3CN

λ_{max} (nm)[a]	$10^{-3}\,\varepsilon_{max}$ (dm^3 mol^{-1} cm^{-1})[b]	Assignments
434	9.1	$d_\pi(Ru) \rightarrow \pi^*(bpy)$
382	7.7	$d_\pi(Ru) \rightarrow \pi^*(4\text{-}CNpy)$
342	7.5	$d_\pi(Ru) \rightarrow \pi^*(py)$
288	49	$\pi \rightarrow \pi^*(bpy)$
254 sh	17	$\pi \rightarrow \pi^*$(bpy, 4-CNpy, py)
245	21	
218 sh	27	

[a] Error = ±2 nm.
[b] Error = ±5%.
sh, Shoulder.

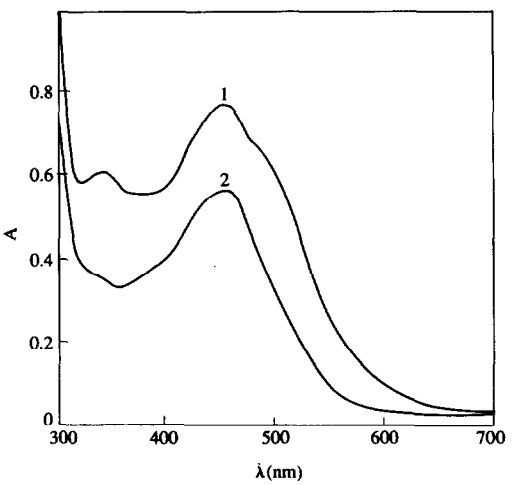

Fig. 2. Visible spectra of: (1) 6.6×10^{-5} mol dm^{-3} solution of $[Ru(bpy)_2(py)(4\text{-}CNpy)Ru(NH_3)_5]^{4+}$ (**B**), in CH_3CN; (2) 4.8×10^{-5} mol dm^{-3} solution of $[Ru(bpy)_2(py)(4\text{-}CNpy)Fe(CN)_5]^-$ (**C**), in water.

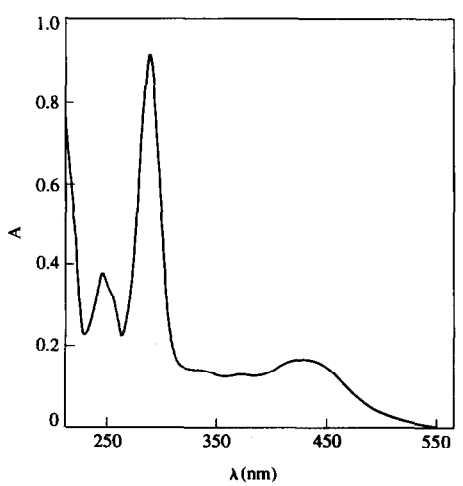

Fig. 1. UV–vis spectrum of a 2×10^{-5} mol dm^{-3} solution of $[Ru(bpy)_2(py)(4\text{-}CNpy)]^{2+}$ in CH_3CN.

Table 3. Electronic spectra of $[(CN)_5Fe^{II}L]$ complexes in aqueous solutions

L	λ_{max} (nm)	$10^{-3}\,\varepsilon_{max}$ ($dm^3\,mol^{-1}\,cm^{-1}$)	Reference
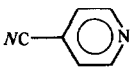	405	7.4	19
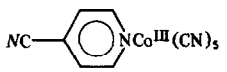	429	~ 3	20
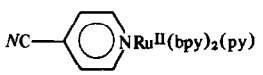	452	11	This work
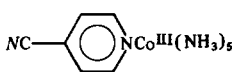	490	7.0	21
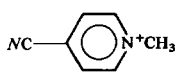	555	2.4	22

Table 4. Electronic spectra of $[(NH_3)_5Ru^{II}L]$ complexes[a]

L	λ_{max} (nm)	$10^{-3}\,\varepsilon_{max}$ ($dm^3\,mol^{-1}\,cm^{-1}$)	Reference
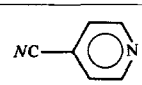	425	5.4	14
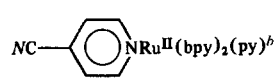	454	12	This work
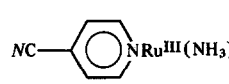	488	13	23
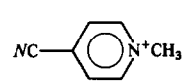	532	—	24

[a] In water, unless otherwise noted.
[b] In CH_3CN.

are disclosed:

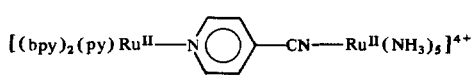

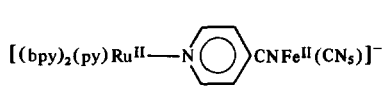

Oxidation of complex **B** with cerium(IV) in CH_3CN (with added HNO_3) causes the disappearance of the MLCT band at 454 nm. The obtained mixed valence complex,

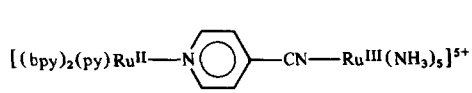

has an absorption band with $\lambda_{max} = 424$ nm, attributed to $d_\pi(Ru^{II}) \rightarrow \pi^*$(bpy)MLCT. No MMCT (metal-to-metal charge-transfer) transitions were detected up to 800 nm.

CONCLUSIONS

4-CNpy can effectively bridge the $Ru(bpy)_2(py)^{2+}$ moiety with $Ru(NH_3)_5^{2+/3+}$ or $Fe(CN)_5^{3-}$ groups. In the binuclear complex, 4-CNpy coordinates through its pyridine nitrogen to polypyridineruthenium(II) and through its nitrile nitrogen to ammineruthenium(II) and (III) or cyanoferrate(II) moieties, as deduced from spectroscopic measurements, both in the solid state and in solution. These systems may be used as models for the study of intramolecular electron (or energy) transfer processes.

Acknowledgements—We thank CONICET and CIUNT for financial support.

REFERENCES

1. E. H. Cutin and N. E. Katz, *Polyhedron* 1987, **6**, 159.
2. N. E. Katz, C. Creutz and N. Sutin, *Inorg. Chem.* 1988, **27**, 1687.
3. J. V. Caspar and T. J. Meyer, *Inorg. Chem.* 1983, **22**, 2444.
4. F. Scandola, C. A. Bignozzi and V. Balzani, in *Homogeneous and Heterogeneous Photocatalysis* (Edited by E. Pelizzetti and N. Serpone), p. 29. Reidel, Dordrecht (1986).
5. J. D. Petersen, W. R. Murphy Jr, R. Sahai, K. J. Brewer and R. R. Ruminski, *Coord. Chem. Rev.* 1985, **64**, 261.
6. B. Bosnich and F. P. Dwyer, *Aust. J. Chem.* 1966, **19**, 2229.
7. J. E. Sutton and H. Taube, *Inorg. Chem.* 1981, **20**, 3125.
8. D. J. Kenney, T. P. Flynn and J. G. Gallini, *J. Inorg. Nucl. Chem.* 1961, **20**, 75.
9. L. Corrsin, B. J. Fax and R. C. Lord, *J. Chem. Phys.* 1953, **21**, 1170.
10. R. G. Inskeep, *J. Inorg. Nucl. Chem.* 1962, **24**, 763.
11. J. H. S. Green and D. J. Harrison, *Spectrochim. Acta* 1977, **33A**, 75.
12. S. K. Doorn and J. T. Hupp, *J. Am. Chem. Soc.* 1989, **111**, 4704.
13. P. K. Mallick, G. D. Danzer, D. P. Strommen and J. R. Kincaid, *J. Phys. Chem.* 1988, **92**, 5628.
14. R. E. Clarke and P. C. Ford, *Inorg. Chem.* 1970, **9**, 495.
15. D. E. Richardson and H. Taube, *J. Am. Chem. Soc.* 1983, **105**, 40.
16. A. Yeh, A. Haim, M. Tanner and A. Ludi, *Inorg. Chim. Acta* 1979, **33**, 51.
17. G. M. Bryant, J. E. Fergusson and H. K. J. Powell, *Aust. J. Chem.* 1971, **24**, 257.
18. C. R. Johnson and R. E. Shepherd, *Inorg. Chem.* 1983, **22**, 2439.
19. A. P. Szecsy, S. S. Miller and A. Haim, *Inorg. Chim. Acta* 1978, **29**, 189.
20. K. J. Pfenning, L. Lee, H. D. Wolhers and J. D. Petersen, *Inorg. Chem.* 1982, **21**, 2477.
21. A. P. Szecsy and A. Haim, *J. Am. Chem. Soc.* 1982, **104**, 3063.
22. J. E. Figard, J. V. Paukstelis, E. F. Byrne and J. D. Petersen, *J. Am. Chem. Soc.* 1977, **99**, 8417.
23. K. J. Moore, L. Lee, J. E. Figard, J. A. Gelroth, A. J. Stinson, H. D. Wohlers and J. D. Petersen, *J. Am. Chem. Soc.* 1983, **105**, 2274.
24. K. J. Moore, L. Lee, G. A. Mabbott and J. D. Petersen, *Inorg. Chem.* 1983, **22**, 1108.

Polyhedron Vol. 10, No. 7, pp. 659–664, 1991
Printed in Great Britain

0277–5387/91 $3.00+.00
Pergamon Press plc

^{31}P NMR AND RAMAN SPECTROSCOPIC STUDIES ON BINDING ISOMERISM AND ISOMERIZATION EQUILIBRIUM OF ALUMINIUM COMPLEXES OF MONOMERIC PHOSPHORUS OXOANIONS IN SOLUTION

QI FENG and HIROHIKO WAKI*

Department of Chemistry, Faculty of Science, Kyushu University, Higashiku, Fukuoka, Japan

(*Received* 14 *March* 1990; *accepted* 31 *October* 1990)

Abstract—The binding isomerism of Al^{3+}–phosphinate, –phosphite and –phosphate complexes was investigated by using ^{31}P NMR and Raman spectroscopies in solution. It was found that there are two types of binding mode in the complexes: a non-chelate binding mode in which the monomeric phosphorus oxoanions coordinate to the aluminium ion as monodentate ligands, and a chelate binding mode in which the monomeric phosphorus oxoanions coordinate to the aluminium ion as bidentate ligands. Furthermore, an isomerization equilibrium analysis was made on the chelate and the non-chelate isomers. The isomerization constants, $K^{chel}_{non\text{-}chel}$, for formation of the chelate isomer from the non-chelate one, were evaluated to be 2.8 for the $AlPH_2O_2^{2+}$ complex, 3.7 for the $AlPHO_3^{+}$ complex and 3.9 for the $AlPO_4$ complex.

In the coordination of a monomeric oxoanion to a metal ion in solution, non-chelate binding in which the oxoanion ligand coordinates as monodentate has been considered to be common, and there have been very few reports[1–4] on four-membered ring formation in which the ligand coordinates as bidentate. Recently we clarified the equilibrium co-existence of these two types of binding for chromium(III)–phosphinate complexes by a ^{31}P NMR study of the solution.[5] It was found that the saturated inner-sphere complex $Cr(PH_2O_2)_6^{3-}$ contained only non-chelate species, whereas the lower complexes $Cr(PH_2O_2)_5^{2-}$ and $Cr(PH_2O_2)_4^{-}$ contained both the non-chelate and chelate species. The equilibrium between these two types can also be expected for other metal–oxoanion complex systems.

In this work, a distinction between the chelate and non-chelate binding modes for more labile complexes such as aluminium–phosphinate, –phosphite and –phosphate complexes, and their isomerization equilibrium has been investigated by ^{31}P NMR and Raman spectroscopies.

* Author to whom correspondence should be addressed.

EXPERIMENTAL

Reagents

Aluminium nitrate, aluminium chloride, sodium phosphinate, sodium phosphite and potassium phosphate were of commercially available reagent grade. The acidity of stock solutions of aluminium nitrate and aluminium chloride were maintained at 0.1 M with nitric acid or hydrochloric acid to avoid the formation of the hydroxo complexes.

NMR measurements

In the NMR study, the sample solutions were adjusted to pH 2 with nitric acid or sodium hydroxide. The ^{31}P NMR spectra were recorded on a JEOL spectrometer JNM-GX 400 operating at 161.86 MHz at 20°C, using a 10 mm i.d. spinning sample tube. The phosphorus chemical shift was recorded relative to an external standard of 85% H_3PO_4, a positive shift being down field. The experimental conditions were as follows: spectral width, 30,000 Hz; data points, 16 K; pulse width, 20 μs (45°); repetition time, 3.0 s. It was experimentally confirmed that quantitative data can be obtained at these conditions. The signal ratio of the complex

species to the free ligand was determined by measuring the paper weight corresponding to each signal area recorded.

Measurement of Raman spectra

In the Raman spectroscopic study, the sample solution containing aluminium chloride and the salt of the phosphorus oxoanion was adjusted to pH 2 with hydrochloric acid or sodium hydroxide. The Raman spectra were recorded at 20°C on a JASCO NR-1100 laser Raman spectrophotometer equipped with a double monochromator and a control microcomputer. The excitation beam wavelength was 514.5 nm, which was obtained from a NEC GLG 3200 argon gas laser. The spectrum for the complex was obtained by subtracting the Raman band of the free ligand from that of the corresponding sample using the datum treatment system of the Raman spectrophotometer.

RESULTS AND DISCUSSION

^{31}P NMR study of the one-to-one complexes

The ^{31}P NMR spectra of a series of solutions in which the total concentration ratio of aluminium to phosphinate was unity were measured and an example is shown in Fig. 1(a). Triplet A is from the free phosphinate and resonances B, C and D can be assigned to the complexes. The dependence of the peak area ratios of B to C and D to C on the total aluminium concentration or phosphinate are given in Fig. 2. In the lower concentration range, only triplets C and D were observed for the complexes with a nearly constant area ratio. Since under these conditions only one-to-one complexes are expected to be formed, these two peaks may have different structures to each other. We assigned them to the binding isomers in which the phosphinate ions are bound as monodentate (**I**) and bidentate (**II**), as found for the chromium–phosphinate complexes.[5] Since the interaction between the central metal ion and the ligand is stronger for chelate binding than for non-chelate binding, a larger shift from the position of the free ligand should occur for the chelate structure. Therefore, it was concluded that resonance C was due to the chelate isomer and resonance D to the non-chelate isomer. The further upfield resonance B may be due to a binuclear complex $Al_2(PH_2O_2)_2^{4+}$ (**III**). This assignment may be reasonable from its high chemical shift value and due to the fact that the intensity of peak B increased with increasing aluminium or phosphinate concentration.

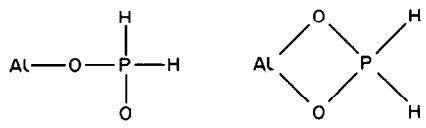

(I) (II)

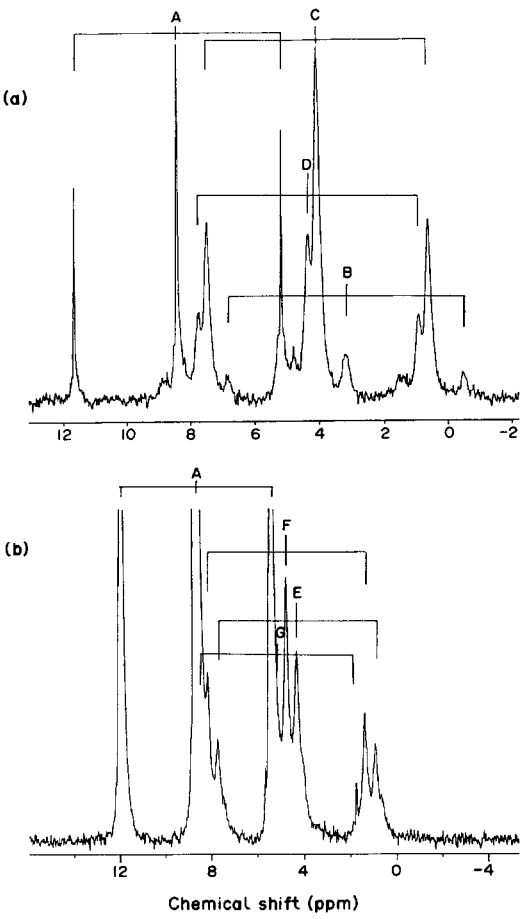

Fig. 1. ^{31}P NMR spectra of aluminium–phosphinate complexes at pH 2 and 20°C. (a) 0.1 M $Al(NO_3)_3$–0.1 M $NaPH_2O_2$ solution and (b) 0.025 M $Al(NO_3)_3$–0.25 M $NaPH_2O_2$ solution.

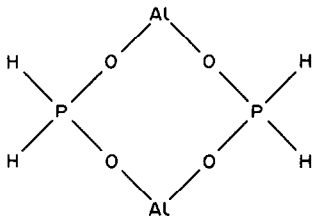

(III)

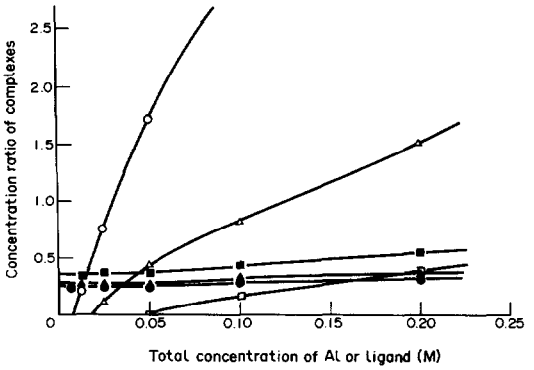

Fig. 2. The concentration dependence of the complex concentration ratio at $C_{Al}/C_P = 1$, pH 2 and 20°C. ■, □: C_D/C_C, C_B/C_C for Al^{3+}–$PH_2O_2^-$ complexes; ▲, △: C_D/C_C, C_B/C_C for Al^{3+}–PHO_3^{2-} complexes; ●, ○: C_D/C_C, C_B/C_C for Al^{3+}–PO_4^{3-} complexes.

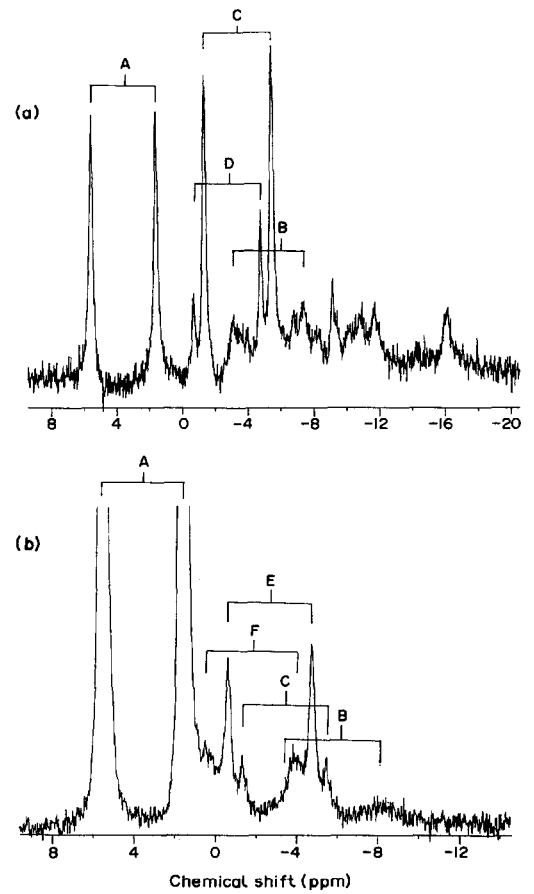

Fig. 3. ^{31}P NMR spectra of aluminium–phosphite complexes at pH 2 and 20°C. (a) 0.05 M $Al(NO_3)_3$–0.05 M Na_2PHO_3 solution and (b) 0.025 M $Al(NO_3)_3$–0.25 M Na_2PHO_3 solution.

In Fig. 3(a), doublets A, B, C and D may be assigned to the free phosphite ion, the binuclear complex $Al_2(PHO_3)_2^{2+}$, the chelate $AlPHO_3^+$ and the non-chelate $AlPHO_3^+$, respectively, using the above

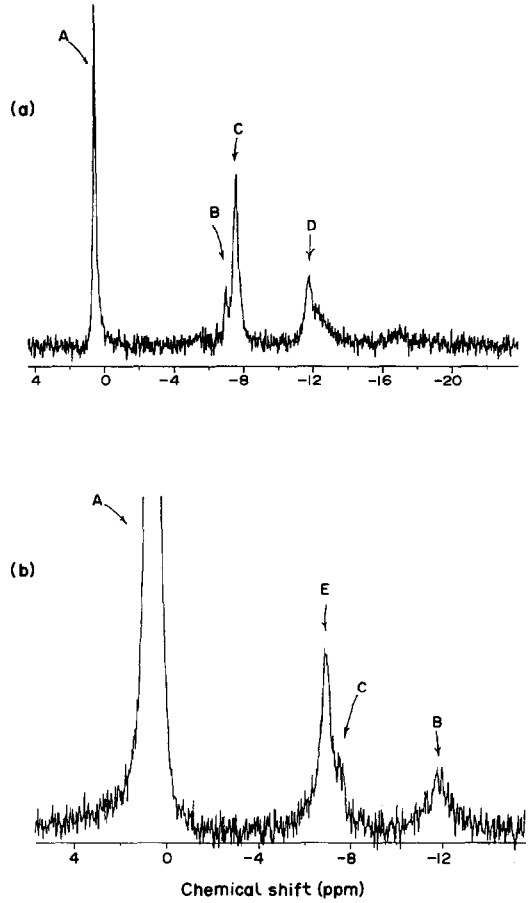

Fig. 4. ^{31}P NMR spectra of aluminium–phosphate complexes at pH 2 and 20°C. (a) 0.025 M $Al(NO_3)_3$–0.025 M KH_2PO_4 solution and (b) 0.025 M $Al(NO_3)_3$–0.25 M KH_2PO_4 solution.

reasoning. The concentration ratios of the non-chelate to the chelate isomer and of the binuclear complex to the chelate isomer are plotted against the concentration of aluminium or phosphite in Fig. 2. The concentration ratio of the non-chelate to the chelate isomer was almost unchanged, whereas that of the binuclear complex to the chelate isomer was greatly altered. The resonances observed further upfield than those of the binuclear complex are probably due to $Al_2PHO_3^{4+}$ and/or more polymeric complexes, although further studies were not carried out.

Similarly, singlets A, B, C and D in Fig. 4(a) are assigned to the free phosphate ion, the binuclear complex $Al_2(PO_4)_2$, the chelate $AlPO_4$ isomer and the non-chelate $AlPO_4$ isomer, respectively. The concentration ratio behaviour for these complexes is analogous to that of the aluminium–phosphinate and aluminium–phosphite complexes described above (Fig. 2).

^{31}P NMR study of complexes with a greater number of ligands

^{31}P NMR spectra of a series of solutions containing 0.025 M $Al(NO_3)_3$, and $NaPH_2O_2$, Na_2PHO_3 and KH_2PO_4 of differing excess concentrations were measured. Figure 1(b) shows an example of the ^{31}P NMR spectrum for aluminium–phosphinate complexes at 10 times excess ligand concentration. A signal from the one-to-one chelate complex appeared as a shoulder C, and a set of triplets E, F and G appeared with increasing ligand concentration. The E, F and G peaks may be assigned to $Al(PH_2O_2)_2^+$, $Al(PH_2O_2)_3$ and $Al(PH_2O_2)_4^-$, respectively, from the order of the chemical shifts and the increasing–decreasing behaviour with ligand concentration. Similar to the one-to-one complex, these complexes should consist of several isomers due to the chelate and non-chelate binding ligands. However, the complexes did not reveal two separate peaks in the spectrum. These chelate and non-chelate peaks are closer together than in one-to-one complexes and may overlap with peaks of complexes containing a different number of ligands. For example, peak E may be the chelate $Al(PH_2O_2)_2^+$ which overlaps the non-chelate $AlPH_2O_2^{2+}$. The sharpness of peak G may be due to the saturated tetrahedral complex with four non-chelated $PH_2O_2^-$ ligands, and the large difference in chemical shift between peaks E and F may presumably be due to the conversion of octahedral $Al(PH_2O_2)_2^+$ into tetrahedral $Al(PH_2O_2)_3$ or to a large change in the non-chelate/chelate ligand abundance in these two complexes, each peak indicating the predominance of one form.

An example of the ^{31}P NMR spectrum for the aluminium–phosphite complex system containing a large excess of phosphite is given in Fig. 3(b). Here peak C is the chelated $AlPHO_3^+$, and a broader peak F may presumably be $Al(PHO_3)_3^{3-}$, containing both chelate and non-chelate ligands or a mixture of tetrahedral and octahedral forms of the same composition. A binuclear signal B was also observed in the spectrum.

In the aluminium–phosphate complex system with a large excess of phosphate ligand [Fig. 4(b)], except for peak C (chelate $AlPO_4$), only one large peak E was revealed, which can be assigned to chelate $Al(PO_4)_2^{3-}$ overlapping with the non-chelated $AlPO_4$. A binuclear peak B was also observed under these conditions.

The chemical shift values for the aluminium–phosphinate, –phosphite and –phosphate stepwise complexes are tabulated in Table 1. It was found that the coordination ^{31}P NMR chemical shift in the corresponding aluminium complexes increases in the order $PO_4^{3-} > PHO_3^{2-} > PH_2O_2^-$, in agreement with increasing ligand charge.

Raman spectroscopic study of the aluminium–phosphinate complexes

The chelate and non-chelate binding of phosphinate ligands can also be distinguished by their Raman spectra. Figure 5 shows a Raman spectrum for a $NaPH_2O_2$ solution and for a 1 : 1 mixture of $NaPH_2O_2$ and $AlCl_3$ in the 700–1400 cm^{-1} region, where the stretching vibration band of the PO_2 group is expected to appear. In order to obtain a pure spectrum for the complexes, the free $PH_2O_2^-$ bands were eliminated by datum treatment in Fig. 5(c). In the figure, the bands at 935 and 1158 cm^{-1} are assigned to the twisting and the scissoring vibrations of the PH_2 group in the coordinated ligands, respectively. The bands at 1083, 1107 and 1191 cm^{-1} are assigned to the stretching vibration modes of the PO_2 group in the coordinated ligand. The concentration dependence of intensity ratio for the three bands at a 1 : 1 molar ratio of $AlCl_3$–$NaPH_2O_2$ is presented in Fig. 6. The intensity ratio 1191 cm^{-1}/1083 cm^{-1} was almost constant, independent of the concentration of aluminium or phosphinate, and the intensity ratio 1107 cm^{-1}/1083 cm^{-1} was constant only in the low concentration

Table 1. ^{31}P NMR chemical shift data of the complexes, relative to the corresponding fully deprotonated free ligand

	Chemical shift (ppm)					
	1 : 1					
	Chelating	Non-chelating	1 : 2	1 : 3	1 : 4 Non-chelating	2 : 2 Bridging
Al^{3+}–$PH_2O_2^-$	−3.77	−3.50	−3.48	−3.00	−2.64	−4.60
Al^{3+}–PHO_3^{2-}	−7.12	−6.43	−6.41	−5.51		−9.02
Al^{3+}–PO_4^{3-}	−13.27	−12.70	−12.66			−17.03

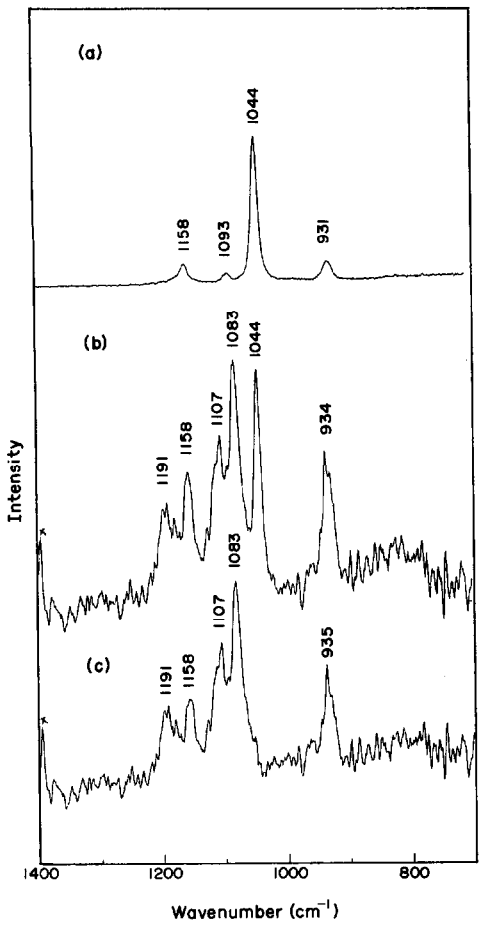

Fig. 5. Raman spectra of phosphinate and aluminium–phosphinate complexes at pH 2 and 20°C. (a) 0.2 M $NaPH_2O_2$ solution, (b) 0.075 M $AlCl_3$–0.075 M $NaPH_2O_2$ solution and (c) net complex spectrum obtained by eliminating vibration bands of the free $PH_2O_2^-$ anion from (b).

range, $C_{Al} < 0.05$ M, where binuclear complexes are negligible. The bands at 1083 and 1191 cm^{-1} may be assigned to symmetric and antisymmetric stretching vibrations of the PO_2 group of the non-chelating

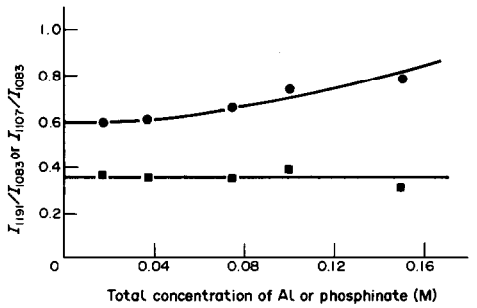

Fig. 6. The concentration dependence of vibration band intensity ratios for Al^{3+}–$PH_2O_2^-$ complex system at $C_{Al}/C_P = 1$, pH 2 and 20°C. ■: I_{1191}/I_{1083}, ●: I_{1107}/I_{1083}.

ligand, respectively, because of the constant intensity ratio. The band at 1107 cm^{-1} may be assigned to the symmetric stretching vibration of the PO_2 group of the chelating ligand. The increase in the 1107 cm^{-1}/1083 cm^{-1} ratio at high concentrations of $AlCl_3$ may be ascribed to the formation of a binuclear complex that has a PO_2 symmetric stretching vibration of the bridged $PH_2O_2^-$ ligand at 1118 cm^{-1} which overlaps with the 1107 cm^{-1} band.

The observed wave numbers of the free ligand and the complexes with their assignments are summarized in Table 2. It can be seen that all the stretching bands of the PO_2 group of the coordinated ligand shift to a higher wave number than that of the free ligand. The magnitude of the symmetric stretching band shift was 39 cm^{-1} for the non-chelating ligand, 63 cm^{-1} for the chelating ligand and 74 cm^{-1} for the bridging ligand, respectively. This behaviour agrees with the expected change in interaction between the central metal and ligand in the different types of binding.

Raman spectra of aluminium–phosphinate complexes at different ligand concentrations were also measured. The wave numbers for the complexes did

Table 2. Raman spectrum data and assignments of the free $PH_2O_2^-$ anion and Al^{3+}–$PH_2O_2^-$ complexes

Assignment	Frequency (cm^{-1})			
	Free[a]	Non-chelating	Chelating	Bridging
A_2 PH_2 twist	931	935	935	935
A_1 PO_2 symmetric stretch	1044	1083	1107	1118
B_2 PH_2 wag	1093			
A_1 PH_2 scissor	1158	1158	1158	1158
B_2 PO_2 antisymmetric stretch	1180[b]	1191		

[a] Only the assignment of the free ion is referred to in the literature.[6,7]
[b] IR spectrum datum.[6]

not appreciably change with increasing ligand concentration. This indicates that the Raman band depends only on the binding mode but is independent of the coordinated ligand number. The band intensity for the non-chelating ligand at 1083 cm^{-1} increased and that for chelating ligand at 1107 cm^{-1} decreased with increasing ligand concentration. This indicates that the abundance of chelating ligand in the complex decreases with increasing ligand number of the complex, which is in accordance with the observation in the ^{31}P NMR study.

Isomerization equilibrium of the chelating and non-chelating isomers

In the complex of composition AlL_x, where L denotes a bidentate ligand like phosphinate anion, a series of binding isomers $Al(L_{chel})_n(L_{non\text{-}chel})_{x-n}$ can, in general, be formed. In the simplest case of the one-to-one aluminium–phosphinate complex, the complexation process can be represented by the reactions

$$Al(H_2O)_6^{3+} \underset{K_{non\text{-}chel}}{\overset{-H_2O,\ +PH_2O_2^-}{\rightleftharpoons}} \underset{\text{(non-chelate complex)}}{Al(OPH_2O)(H_2O)_5^{2+}} \quad (1)$$

$$\underset{K^{chel}_{non\text{-}chel}}{\overset{-H_2O}{\rightleftharpoons}} \underset{\text{(chelate complex)}}{Al(O_2PH_2)(H_2O)_4^{2+}}. \quad (2)$$

The equilibrium constants are

$$K_{non\text{-}chel} = \frac{[Al(OPH_2O)(H_2O)_5^{2+}]}{[Al(H_2O)_6^{3+}][PH_2O_2^-]} \quad (3)$$

$$K^{chel}_{non\text{-}chel} = \frac{[Al(O_2PH_2)(H_2O)_4^{2+}]}{[Al(OPH_2O)(H_2O)_5^{2+}]}. \quad (4)$$

Since reaction (2) for the formation of the chelate from the non-chelate binding is clearly a *pseudo*-intramolecular reaction, the concentration ratio of the two isomers may be constant even at different concentrations of free Al^{3+} ion or ligand. Similar equations may be written for each step forming aluminium complexes of higher ligand number, and also for the complexes of other oxoanion ligands.

In order to provide quantitative information on the distribution of chelate and non-chelate isomers, we evaluated $K^{chel}_{non\text{-}chel}$ and $K_{non\text{-}chel}$ for the one-to-one aluminium complexes of phosphinate, phosphite and phosphate from the peak area ratios in the ^{31}P NMR spectra (Table 3). For evaluation of $K_{non\text{-}chel}$, protonation constants of the free ligands from the literature[8] were used. The conventional stability constants, K_1, were also calculated and are presented in the table for comparison. As can be seen from the table, the $K^{chel}_{non\text{-}chel}$ values occur in increasing order aluminium–phosphinate < –phosphite < –phosphate, reflecting a higher probability of oxygen binding in oxygen-rich ligands. However, this tendency did not seem very remarkable, in comparison with the difference in stability constants for these three ligands. This may be due to the fact that much more energy is required to remove water molecules from oxygen-rich ligands of higher charge coordinated to a metal ion.

Table 3. Stability constants of 1 : 1 complexes at $I = 0.1$, pH 2 and 20°C

	$K^{chel}_{non\text{-}chel}$	$K_{non\text{-}chel}$	K_1
Al^{3+}–$PH_2O_2^-$	2.8	63	2.4×10^2
Al^{3+}–PHO_3^{2-}	3.7	2.8×10^5	1.3×10^6
Al^{3+}–PO_4^{3-}	3.9	3.7×10^{16}	1.8×10^{17}

REFERENCES

1. D. L. Nelson and D. E. Irish, *J. Chem. Phys.* 1971, **54**, 4479; J. T. Miller and D. E. Irish, *Can. J. Chem.* 1967, **45**, 147.
2. J. Podlaha and M. Ebert, *Nature* 1960, **188**, 657; *Russ. J. Inorg. Chem.* 1962, **17**, 1130.
3. C. C. Addison, P. M. Boorman and N. Logan, *J. Chem. Soc. A* 1966, 1434.
4. S. K. Ramalingan and S. Soundararajan, *J. Inorg. Nucl. Chem.* 1967, **29**, 1763; S. S. Krishnamurthy and S. Soundararajan, *J. Inorg. Nucl. Chem.* 1966, **28**, 1689.
5. Q. Feng and H. Waki, *Polyhedron* 1990, **9**, 1555.
6. M. Tsuboi, *J. Am. Chem. Soc.* 1957, **79**, 1351.
7. T. J. Hanwick and P. O. Hoffman, *J. Chem. Phys.* 1949, **17**, 1166.
8. E. Hogfeldt (Ed.), *Stability Constants of Metal-ion Complexes, Part A: Inorganic ligands.* Pergamon Press, Oxford (1982).

Polyhedron Vol. 10, No. 7, pp. 665–671, 1991
Printed in Great Britain

0277–5387/91 $3.00+.00
© 1991 Pergamon Press plc

^{95}Mo NMR INVESTIGATION ON CATIONIC $[C_5H_5Mo(CO)_2L_2]BF_4$ COMPLEXES (L = GROUP 15 DONOR LIGANDS*

HANS SCHUMANN†‡

Department of Chemistry, University of Utah, Salt Lake City, UT 84112, U.S.A.

and

JOHN H. ENEMARK† and MICHAEL J. LABARRE

Department of Chemistry, University of Arizona, Tucson, AZ 85721, U.S.A.

and

MICHAEL BRUCK and PAMELA WEXLER

Molecular Structure Laboratory, University of Arizona, Tucson, AZ 85721, U.S.A.

(*Received* 19 *July* 1990; *accepted* 2 *November* 1990)

Abstract—Photochemically-initiated oxidative fission of the Mo—Mo bond in $[C_5H_5Mo(CO)_3]_2$ by the ferricenium salt $[(C_5H_5)_2Fe]BF_4$ in the presence of four equivalents of L affords a good yield of $[C_5H_5Mo(CO)_2L_2]BF_4$ (L = group 15 donor ligands). ^{95}Mo NMR data are reported and discussed together with the NMR and IR data of new complexes. Decomposition of the title cations in polar solvents affords low yields of the corresponding $[C_5H_5Mo(CO)_3L]BF_4$ complexes. The X-ray crystal structure of $[C_5H_5Mo(CO)_3\{P(C_6H_5)_3\}]BF_4$ is reported. The cation has the $CpML_4$ piano-stool geometry.

In contrast to the well investigated cationic iron complexes $[C_5H_5Fe(CO)_{3-n}L_n]X$,[2] cationic molybdenum complexes of the type $[C_5H_5Mo(CO)_{4-n}L_n]X$ have attracted much less interest.[3] Known complexes of the type $[C_5H_5Mo(CO)_2L_2]X$ with L = group 15 donor ligands have been obtained by different methods: by photochemically-initiated disproportionation of $[C_5H_5Mo(CO)_3]_2$ in the presence of L ($X = [C_5H_5Mo(CO)_3]^-$) followed by anion exchange in some cases;[4] from the protonation of $C_5H_5Mo(CO)_3CH_3$ with HBF_4·ether in the presence of L = $NCCH_3$ (X = BF_4);[5] from $C_5H_5Mo(CO)_3X$ (X = halide) and two equivalents of L in refluxing non-polar solvents;[6] or from the oxidative fission of the Mo—Mo bond in $[C_5H_5Mo(CO)_3]_2$ by AgX salts (X = BF_4 or PF_6) in the presence of L.[7] All these methods have the major disadvantage that they are not normally generally applicable because of special conditions, requirements for L or the price of anhydrous AgX salts. However, during our attempts to develop new routes to cationic organometallic complexes,[8] we found a new, more general preparation of the title complexes by photochemically-initiated oxidative fission of the Mo—Mo bond in $[C_5H_5Mo(CO)_3]_2$; by ferricenium cations in the presence of L. This method makes $[C_5H_5Mo(CO)_2L_2]X$ (X = BF_4, PF_6 or SbF_6) complexes and their chemistry accessible[9] and we now report results from a ^{95}Mo NMR investigation of these complexes.

EXPERIMENTAL

Materials

$[C_5H_5Mo(CO)_3]_2$ [I (Strem)], $E(C_6H_5)_3$ [II, E = P, As, Sb (Aldrich) and E = Bi (Alfa)], PR_3

* See ref. 1.

† Authors to whom correspondence should be addressed.

‡ Present address: Bensberger Str. 15A, D-5064 Rösrath, F.R.G.

[**II**, R = CH_3, C_2H_5, i-C_3H_7, t-C_4H_9 (Strem), OCH_3 (Aldrich)] and $[(C_6H_5)_2PCH_2]_2$ [**II** (Aldrich)] were obtained from commercial sources and used without further purification. $[(C_5H_5)_2Fe]BF_4$ (**IV**)[10] was prepared and purified as described in the literature. All reactions were conducted in oven-dried Schlenk tubes using dried and degassed solvents under nitrogen.

Instrumentation

^1H, $^{13}C\{^1H\}$ and $^{31}P\{^1H\}$ NMR spectra were recorded on Varian XL-300 spectrometers as *ca* 5% solutions in dried and degassed acetone-d_6 vs internal TMS (^1H and ^{13}C) or external 85% H_3PO_4 (^{31}P) as reference. ^{95}Mo NMR spectra were obtained at room temperature on a Bruker AM-500 spectrometer equipped with a broad band tunable probe (^{95}Mo: 32.6 MHz, 90° pulse width 35 μs and using an aquisition delay of 34 μs to reduce probe ringing) in $CDCl_3$–CH_2Cl_2 solutions (*ca* 0.04 M). The external standard was 2 M Na_2MoO_4 at pH 11. IR spectra, ν(CO), were recorded in 1,2-$Cl_2C_2H_4$ solution on a Perkin–Elmer 298 IR spectrometer in 0.1 mm CaF_2 cells and were calibrated against a polystyrene standard. Microanalysis for all new complexes were carried out by Dornis und Kolbe, Mülheim (F.R.G.).

Synthesis

All $[C_5H_5Mo(CO)_2L_2]BF_4$ complexes [**VI(a)**–**VI(j)**] were obtained from the following general method. To a solution of 1.0 g (2.0 mmol) $[C_5H_5Mo(CO)_3]_2$ (**I**) in 40 cm^3 1,2-$Cl_2C_2H_4$ were added 5.0 mmol (1.25 equivalents) of **II** (for L = $[(C_6H_5)_2PCH_2]_2$ only 2.5 mmol) and 1.1 g (4.0 mmol) $[(C_5H_5)_2Fe]BF_4$ (**IV**). The resulting solution was then UV irradiated until the colour changed from red (**I**) to yellow–brown (**VI**; about 0.5 to 1.5 h). Filtration followed by concentration to 1/3 *in vacuo* and addition of excess ether precipitated the cationic complexes **VI** with yields > 90%. For further purification, the solids were washed several times with ether to remove any remaining free ligand and recrystallized from CH_2Cl_2–ether (1/2 to 1/4) at 0°C.

Spectroscopic and analytical data for all new complexes

$[C_5H_5Mo(CO)_2\{P(C_2H_5)_3\}_2]BF_4$ [**VI(b)**]. ^1H NMR: δ 5.68 [br t, C_5H_5; J(P, H) = 1.4 Hz], 2.19 [5 line m, PCH_2; J(H, H) = J(P, H) = 7.6 Hz], 1.22 [5 line m, CH_3 on PC_2H_5; J(H, H) = 7.6 Hz] ppm. $^{13}C\{^1H\}$ NMR: δ 236.13 [t, MoCO; J(P, C) = 26 Hz], 94.14 (s, C_5H_5), 23.15 [pseudo t, PCH_2; J(P, C) = 14.7 Hz], 7.08 [d, CH_3 on PC_2H_5; J(P, C) = 4.7 Hz] ppm. $^{31}P\{^1H\}$ NMR: δ 40.0 (s) ppm. IR spectrum: 1964, 1885, ν(CO), cm^{-1}. Found: C, 42.5; H, 6.6. Calc. for $C_{19}H_{35}BF_4MoO_2P_2$: C, 42.3; H, 6.5%.

$[C_5H_5Mo(CO)_2\{P(CH_3)_2C_6H_5\}_2]BF_4$ [**VI(c)**]. ^1H NMR: δ 7.74, 7.57 (m, PC_6H_5), 5.48 [t, C_5H_5; J(P, H) = 1.3 Hz], 2.16 [pseudo d, PCH_3; J(P, H) = 9.9 Hz] ppm. $^{13}C\{^1H\}$ NMR: δ 234.48 [t, MoCO; J(P, C) = 27.0 Hz], 138.4 (br m, C-1), 131.45 (s, p-C), 130.41 [t, o-C; J(P, C) = 4.5 Hz], 129.58 [t, m-C; J(P, C) = 5.2 Hz], 94.60 (s, C_5H_5), 19.58 [pseudo t, PCH_3; J(P, C) = 17.7 Hz] ppm. $^{31}P\{^1H\}$ NMR: δ 22.2 (s) ppm. IR spectrum: 1968, 1887, ν(CO), cm^{-1}. Found: C, 47.8; H, 4.6. Calc. for $C_{23}H_{27}BF_4MoO_2P_2$: C; 47.7; H, 4.7%.

$[C_5H_5Mo(CO)_2\{P(C_6H_5)_2CH_3\}_2]BF_4$ [**VI(d)**]. ^1H NMR: δ 7.61 to 7.51 (m, 10H, PC_6H_5), 5.51 [t, C_5H_5; J(P, H) = 1.3 Hz], 2.49 [pseudo d, PCH_3; J(P, H) = 8.9 Hz] ppm. $^{13}C\{^1H\}$ NMR: δ 234.16 [t, MoCO; J(P, C) = 28 Hz], 135.1 (br m, C-1), 132.35 [t, o-C; J(P, C) = 4.8 Hz], 131.85 (s, p-C), 129.57 [t, m-C; J(P, C) = 5.3 Hz], 95.41 (s, C_5H_5), 20.2 (br s, PCH_3) ppm. $^{31}P\{^1H\}$ NMR: δ 38.7 (s) ppm. IR spectrum: 1975, 1896, ν(CO) cm^{-1} Found: C, 56.7; H, 4.6. Calc. for $C_{33}H_{31}BF_4MoO_2P_2$: C, 56.4; H, 4.4%.

$[C_5H_5Mo(CO)_2\{P(OCH_3)_3\}_2]BF_4$ [**VI(i)**]. ^1H NMR: δ 5.80 (br s, C_5H_5), 3.77 (br s, 9H, $POCH_3$) ppm. $^{13}C\{^1H\}$ NMR: δ 230.66 [t, MoCO, J(P, Cl = 40.1 Hz], 93.87 (s, C_5H_5), 54.99 (br s, $POCH_3$) ppm. $^{31}P\{^1H\}$ NMR: δ 177.0 (s) ppm. IR spectrum: 1929 [br, ν(CO)] cm^{-1}. Found: C, 29.0; H, 4.4. Calc. for $C_{13}H_{23}BF_4MoO_8P_2$: C, 28.3; H, 4.2%.

$[C_5H_5Mo(CO)_2\{(C_6H_5)_2PCH_2\}_2]BF_4$ [**VI(g)**]. NMR data were remeasured in acetone-d_6; for analytical data see the literature.[9] ^1H NMR: δ 7.83 to 7.48 (m, 20H, PC_6H_5), 5.01 (s, C_5H_5), 2.42, 3.31 (each br m, 2 H, PCH_2) ppm. $^{13}C\{^1H\}$ NMR: δ 238.44 [t, MoCO; J(P, C) = 13.7 Hz], 137.29, 132.22 [both t, inequivalent C-1; J(P, C) = 24.3, 25.0 Hz], 132.23, 131.53 (both s, inequivalent p-C), 133.67, 131.02 [both t, inequivalent o-C; J(P, C) = 5.2, 5.1 Hz], 130.02, 129.52 [both t, inequivalent m-C; J(P, C) = 5.3, 4.9 Hz], 95.57 (s, C_5H_5), 29.92 [t, PCH_2; J(P, C) = 21.5 Hz] ppm. $^{31}P\{^1H\}$ NMR: δ 76.6 (s) ppm. IR spectrum (1,2-$Cl_2C_2H_4$): 1987, 1921, ν(CO), cm^{-1}.

For complete analytical and spectroscopical data for all other complexes of **VI** see the literature.[8,9]

Crystal structure determination

A brown block-like crystal of $[C_5H_5Mo(CO)_3\{P(C_6H_5)_3\}]BF_4$ (**VII**) suitable for X-ray crystallo-

graphy with the approximate dimensions $0.50 \times 0.33 \times 0.25$ mm was obtained from the repeated recrystallization of $[C_5H_5Mo(CO)_2\{P(C_6H_5)_3\}_2]BF_4$ from acetone–CH_2Cl_2–ether (see text).

Crystal data

$C_{26}H_{20}BF_4MoO_3P$, monoclinic, $a = 12.798(1)$, $b = 10.302(2)$, $c = 19.598(3)$ Å, $\beta = 96.55(1)°$, $U = 2567.1$ Å^3, space group $P2_1/c-C^5_{2h}$ (no. 14), $Z = 4$, $M = 594.17$, $D_c = 1.54$ g cm^{-3}, $\mu = 6.1$ cm^{-1}, $F(000) = 1192$.

Measurements

Refined unit cell parameters were obtained by centring 25 reflections on a Syntex $P2_1$ diffractometer. Using the θ–2θ scan measuring routine, 6287 independent reflections (up to $2\theta = 55°$) were measured with Mo-K_α radiation (graphite crystal monochromator).

Structure analysis

The structure was solved by the Patterson heavy-atom method which revealed the position of the molybdenum atom. The remaining atoms were located in succeeding difference Fourier syntheses. The structure was refined by full-matrix least-squares. Hydrogen atoms were included but constrained to ride on the carbon atom to which they are bonded. Only the 4044 reflections which had $F_o^1 > 3\sigma(F_o^2)$ were used in the refinements, which converged to give $R = 0.041$ and $R_w = 0.051$. Computations were carried out on a VAX computer using SDP/VAX programs.[11]

Final atomic and thermal parameters, structure factors together with F_o and F_c data have been deposited with the Editor as supplementary material. Atomic coordinates have also been deposited with the Cambridge Crystallographic Data Centre.

RESULTS AND DISCUSSION

Preparative and spectroscopic

The results show that the preparation of cationic $[C_5H_5Mo(CO)_2L_2]BF_4$ complexes with group 15 ligands (L) is readily achieved in high yields by oxidative fission of the Mo—Mo bond in $[C_5H_5Mo(CO)_3]_2$ by the ferricenium ion. As indicated in Scheme 1, the reaction clearly depends on the donor/acceptor properties of L: with strong donor ligands, **II** and **I** react directly to form the spectroscopically observed intermediate $[C_5H_5Mo(CO)_2L]_2$ (**III**)[9] while weaker donor ligands need photochemical irradiation to form **III**. Oxidation of **III** with two equivalents of $[(C_5H_5)_2Fe]^+$ (**IV**) may first afford the suggested intermediate **V**. For **V**, two different structures are possible: the unsaturated 16e complex may be stabilized either by coor-

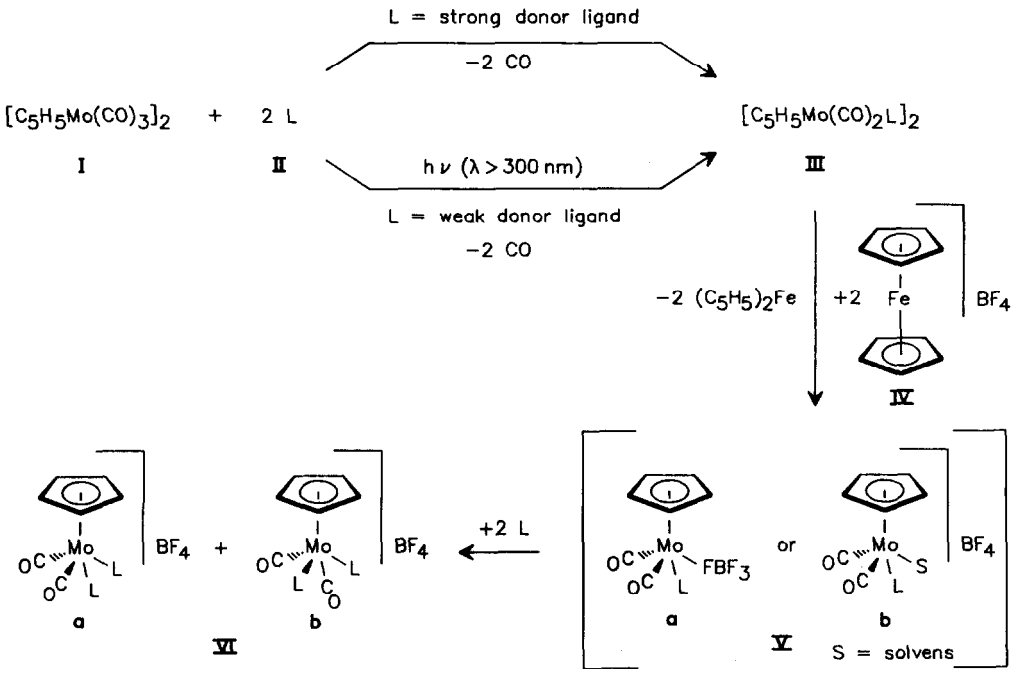

Scheme 1.

dination of the BF_4 anion [structure **V(a)**];[12] or by coordination of a solvent molecule, S [structure **V(b)**], e.g. S = CH_2Cl_2 or acetone.[13] Both structures should be quite reactive and therefore react rapidly with the still present second equivalent of ligand to form *cis*- and/or *trans*-$[C_5H_5Mo(CO)_2L_2]^+$ [**V(a)** and **V(b)**]. The observed mixture of *cis*/*trans* isomers may arise from the intermediary of a cationic six-coordinated intermediate $[C_5H_5Mo(CO)_2L]^+$ (under the assumption that C_5H_5 occupies three coordination sites)[14] prior to the formation of seven-coordinated **V** (only the *cis* form is shown). "Small" ligands (L) such as alkyl-substituted phosphanes and phosphites afford exclusively *cis*-disubstituted complexes of **VI** while sterically more demanding ligands such as aryl-substituted ligands afford mixtures of both, with a dominance of the *cis* isomers.[15]

All complexes of **VI** were obtained in > 90% yield as yellow–brown powders which afford yellow air stable crystals after recrystallization. The complexes are very soluble in common polar solvents such as methylene chloride, acetone or nitromethane but prolonged stirring in the weak donor solvents acetone, nitromethane or dimethylsulphoxide causes decomposition with formation of the related $[C_5H_5Mo(CO)_3(L)]BF_4$ complexes in low yield. The preparation method failed for L = $P(C_3H_7\text{-i})_3$, $P(C_4H_9\text{-t})_3$ and $P[N(CH_3)_2]_3$. In all these cases, only unidentified C_5H_5- and CO-free decomposition products were obtained which can be explained by their strong donor/weak acceptor properties together with their increasing size.

The spectroscopic data obtained for all new complexes of **VI** (see Experimental) are unexceptional and in agreement with their structure. More informative are the ^{95}Mo NMR data given in Table 1 (for a general introduction to ^{95}Mo NMR spectroscopy see reference 16).

All observed ^{95}Mo NMR data are found within a relatively small range between −1687 and −1470 ppm as expected for mononuclear molybdenum(II) complexes with line widths ($H_{1/2}$) between 165 Hz [**VI(b)**] and 650 Hz [**VI(d)**, see Figs 1 and 2]. Due to the comparable small values of $^1J(^{95}Mo, ^{31}P)$ = 133–220 Hz, these couplings are only resolved in complexes **VI(b)** (*ca* 100 Hz) and **VI(i)** (170 Hz). In general, all complexes except **VI(j)** (shift *ca* 300 ppm) are shifted down field by *ca* 150 ppm with respect to the related molybdenum complexes *cis*-$Mo(CO)_4L_2$ and the coupling constants $^1J(^{95}Mo, ^{31}P)$ are of comparable size.[16] Due to the lower symmetry of complexes of **VI** with respect to *cis*-$Mo(CO)_4L_2$ and the known influence of symmetry on the line width,[16] the unresolved coupling $^1J(^{95}Mo, ^{31}P)$ for **VI** may be explained. Comparison of the chemical shift values for complexes of **VI** with data of other $C_5H_5Mo^{II}(CO)_2(L,L)$ complexes containing chelating carbon–nitrogen, dinitrogen or disulphur ligands (δ ^{95}Mo *ca* −560 to −130 ppm and $H_{1/2}$ = 70–160 Hz)[17] show that the title cations are shielded by well over 1000 ppm. This large difference may be explained at least in part by the

Table 1. Comparison of ^{95}Mo NMR data with selected other spectroscopic data for $[C_5H_5Mo(CO)_2L_2]BF_4$ (**VI**)

Complex	Ligand	δ ^{13}CCO[a] (ppm)	δ ^{95}Mo($H_{1/2}$)[b] (ppm) (Hz)	ν(CO)[c] (cm^{-1})
VI(a)	$P(CH_3)_3$	234.8	−1580 (365)	1958
VI(b)	$P(C_2H_5)_3$	236.1	−1563 (165)	1964
VI(c)	$P(CH_3)_2C_6H_5$	234.5	−1508 (590)	1968
VI(d)	$P(C_6H_5)_2CH_3$	234.2	−1467 (650)	1975
VI(e)	$P(C_6H_5)_3$	226.1	−1481 (250)	1977
VI(f)	$As(C_6H_5)_3$	225.0	−1479 (285)	1976
VI(g)	$Sb(C_6H_5)_3$	225.3	−1687 (355)	1968
VI(h)	$Bi(C_6H_5)_3$	224.3	—[d]	1967
VI(i)	$P(OCH_3)_3$	230.7	−1642 (195)[e]	(1929)
VI(j)	$[(C_6H_5)_2PCH_2]_2$	238.4	−1470 (325)	1987

[a] Data measured in acetone-d_6; ±0.1 ppm.
[b] Data measured in $CDCl_3$–CH_2Cl_2; ±5 ppm.
[c] Only absorption at higher wavenumbers given; ±2 cm^{-1}.
[d] No spectrum observed due to rapid decomposition and limited solubility.
[e] $^1J(^{95}Mo, ^{31}P)$ = 170 Hz.

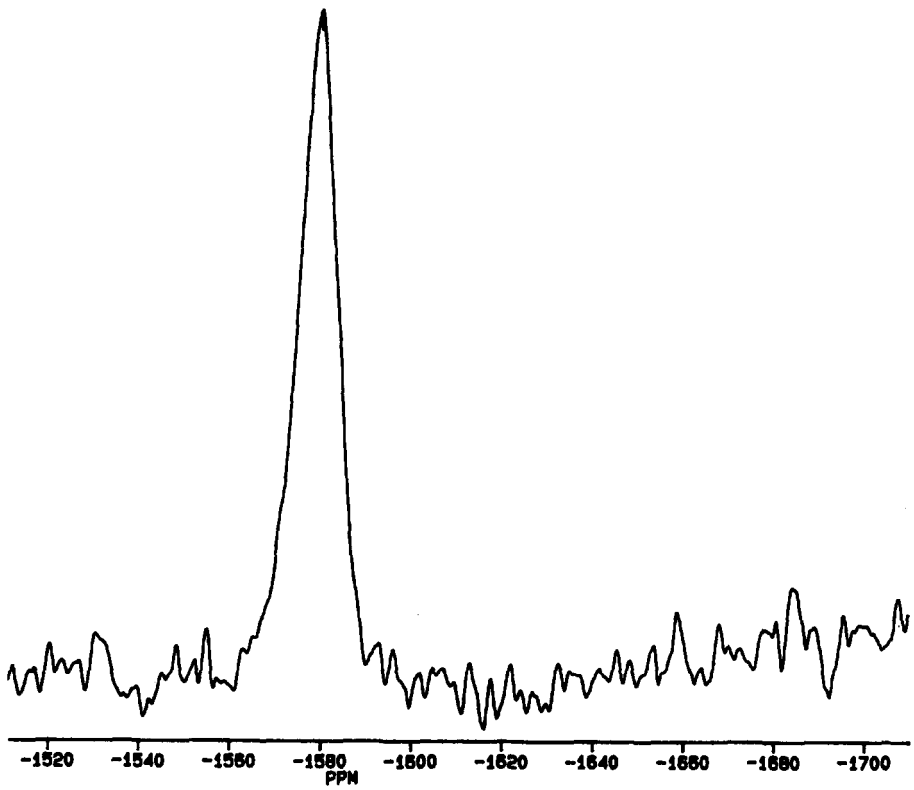

Fig. 1. ^{95}Mo NMR spectrum of $[C_5H_5Mo(CO)_2\{P(CH_3)_3\}_2]BF_4$ [VI(a)].

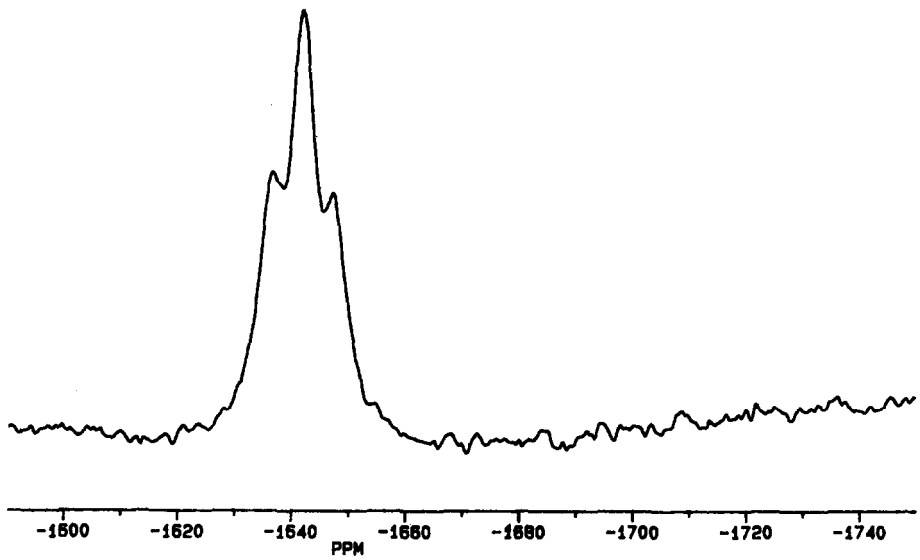

Fig. 2. ^{95}Mo NMR spectrum of $[C_5H_5Mo(CO)_2\{P(OCH_3)_3\}_2]BF_4$ [VI(i)].

better acceptor properties of the ligands used in this work.

Further comparison of ^{95}Mo NMR data with other spectroscopic data which are also regarded as indicative for the bonding situation Mo—L[15] indicate no overall correlation with respect to a general application of ^{95}Mo NMR as a probe for ligand properties.

During attempts to obtain single crystals of complex **VI(e)** suitable for X-ray structure determination for comparison with the known structure of cation **VI(a)**[18] by repeated crystallization from CH_2Cl_2–acetone–ether mixtures, yellow crystals were obtained. The following structure determination identified these crystals subsequently as $[C_5H_5Mo(CO)_3\{P(C_6H_5)_3\}]BF_4$ (**VII**). The formation of **VII** may be rationalized as the result of the labile Mo—L bond in polar solvents under partial ligand replacement [possibly via a complex such as **V(b)**] followed by decomposition under CO release. Part of the released CO substitutes the coordinated solvent under formation of **VII**. Control experiments reveal the general nature of this observation; stirring of complexes **VI(c)**–**VI(i)** in acetone or acetonitrile solution for a prolonged period of time caused extensive decomposition of complexes related to **VII** to be observed.

The structure of $[C_5H_5Mo(CO)_3\{P(C_6H_5)_3\}]BF_4$ **(VII)**

As shown in Fig. 3, this cation belongs to the class of $C_5H_5MoL_4$ complexes with a four-legged piano-stool geometry around molybdenum for which a wide series of structural determinations were performed[19] and theoretical aspects discussed in detail.[20] For comparison, selected bond lengths and bond angles are given in Table 2 together with those for the related pentamethylcyclopentadienyl complex $[C_5(CH_3)_5Mo(CO)_3\{P(C_6H_5)_3\}]^+$.[21]

The data indicate a very close resemblance of both complexes in all major bond distances and angles within the standard deviation, and need no further discussion. As noted before,[21] the Mo—P

Table 2. Comparison of selected bond lengths (Å) and bond angles (°) for $[C_5H_5Mo(CO)_3\{P(C_6H_5)_3\}]BF_4$ (**VII**) and $[C_5(CH_3)_5Mo(CO)_3\{P(C_6H_5)_3\}]BF_4 \cdot 0.5CH_3OH$[a]

	$[C_5H_5Mo(CO)_3\{P(C_6H_5)_3\}]^+$	$[C_5(CH_3)_5Mo(CO)_3\{P(C_6H_5)_3\}]^+$
Mo—P(9)	2.5314(8)	2.562(2)
Mo—C(1)	2.300(3)	2.408(7)
Mo—C(2)	2.296(3)	2.333(8)
Mo—C(3)	2.325(3)	2.305(8)
Mo—C(4)	2.344(3)	2.292(7)
Mo—C(5)	2.343(3)	2.347(10)
Mo—C(6)	2.017(3)	1.991(11)
Mo—C(7)	2.007(4)	1.975(10)
Mo—C(8)	2.010(4)	1.995(10)
C(6)—O(6)	1.130(4)	1.138(10)
C(7)—O(7)	1.135(4)	1.170(10)
C(8)—O(8)	1.135(4)	1.134(10)
P(9)—C(11)	1.833(3)	1.812(5)
P(9)—C(21)	1.831(3)	1.821(5)
P(9)—C(31)	1.818(3)	1.819(5)
P(9)—Mo—C(6)	129.00(9)	122.5(3)
P(9)—Mo—C(7)	77.5(1)	76.4(2)
P(9)—Mo—C(8)	75.43(9)	77.5(2)
C(6)—Mo—C(7)	77.5(1)	76.9(4)
C(6)—Mo—C(8)	76.9(1)	74.4(4)
C(7)—Mo—C(8)	116.1(1)	121.1(4)
Mo—C(6)—O(6)	179.0(3)	176.5(8)
Mo—C(7)—O(7)	176.7(3)	176.9(9)
Mo—C(8)—O(8)	179.2(3)	174.9(9)
Mo—P(9)—C(11)	113.0(1)	114.1(2)
Mo—P(9)—C(21)	116.0(1)	115.2(2)
Mo—P(9)—C(31)	113.3(1)	114.3(2)

[a] Data from ref. 21 using the atom numbering from Fig. 3.

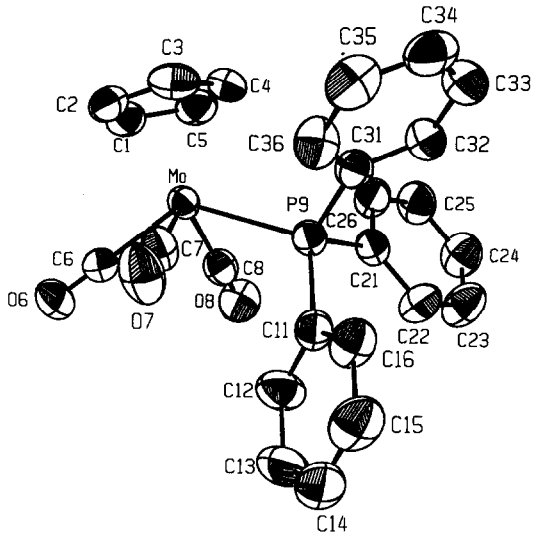

Fig. 3. ORTEP presentation of the cation $[C_5H_5Mo(CO)_3\{P(C_6H_5)_3\}]BF_4$ (**VII**) showing 50% probability ellipsoids.

bond is slightly longer than in the comparable neutral $C_5H_5Mo(CO)_2P(C_6H_5)_3$ complexes (2.48–2.52 Å)[22] which may be attributed to the cationic nature of both complexes.

Acknowledgements—One of us (H.S.) would like to thank Professors R. W. Parry and T. G. Richmond (Department of Chemistry, University of Utah) for their kind interest and support during his stay (1987–1988) and sincerely appreciates a scholarship of Studienstiftung Des Deutschen Volkes, Bonn (F.R.G.).

REFERENCES

1. Presented at the IV European Symposium on Inorganic Chemistry, Freiburg (F.R.G.), September 1988, Abstract D23.
2. For a review see: *Gmelin Handbook of Inorganic Chemistry*, Vols B11, B12, B15, 8th edn, Organoiron Series. Springer-Verlag, Berlin (1983, 1984, 1989).
3. For reviews consult: R. Davies and L. A. P. Kane-Maguire, Molybdenum Compounds with η^2 to η^8 Carbon Ligands, in *Comprehensive Organometallic Chemistry* (Edited by G. Wilkinson, F. G. A. Stone and E. W. Abel), Vol. 3. Pergamon Press, Oxford (1982); H. Schumann, in *Gmelin Handbook of Inorganic Chemistry*, Vols 6–8. 8th edn. Organomolybdenum Series. Springer-Verlag, Berlin, in press.
4. R. J. Haines, R. S. Nyholm and M. H. B. Stiddard, *J. Chem. Soc.* (*A*) 1968, **43**; A. E. Stiegman, M. Stieglitz and D. R. Tyler, *J. Am. Chem. Soc.* 1983, **105**, 6032.
5. S. R. Allen, P. G. Beevor, M. Green, A. G. Orpen, K. E. Paddick and I. D. Williams, *J. Chem. Soc., Dalton Trans.* 1987, 591.
6. A. R. Manning, *J. Chem. Soc.* (*A*) 1967, 1984; P. M. Treichel, K. W. Barnett and R. L. Shubkin, *J. Organomet. Chem.* 1967, **7**, 449.
7. M. Bottrill and M. Green, *J. Chem. Soc., Dalton Trans.* 1977, 2365.
8. H. Schumann, *J. Organomet. Chem.* 1986, **304**, 341.
9. H. Schumann, *J. Organomet. Chem.* 1987, **323**, 193.
10. H. Schumann, *Chemiker-Ztg.* 1987, **111**, 111.
11. For details see: B. A. Frenz, The Enraf–Nonius CAD 4 SDP—A Real-time System for Concurent X-Ray Data Collection and Crystal Structure Determination, in *Computing in Crystallography* (Edited by H. Schenk, R. Olthof-Hazelkamp, H. van Konigsveld and G. C. Basel), pp. 64–71. Delft University Press, Delft, Holland (1978).
12. M. Appel and W. Beck, *J. Organomet. Chem.* 1987, **319**, C1. For a review see: W. Beck and K. Sünkel, *Chem. Rev.* 1988, **88**, 1405.
13. For examples on related complexes with solvent molecules as weak donor ligands see T. S. Piper, F. A. Cotton and G. Wilkinson, *J. Inorg. Nucl. Chem.* 1955, **1**, 165 ($[C_5H_5Fe(CO)_2(L)]^+$, L = H_2O); D. L. Reger and C. Coleman, *J. Organomet. Chem.* 1977, **131**, 153 ($[C_5H_5Fe(CO)_2(L)]^+$, L = THF); W. E. Williams and F. J. Lalor, *J. Chem. Soc., Dalton Trans.* 1973, 1329 ($[C_5H_5Fe(CO)_2(L)]^+$, L = $CH_3C(=O)CH_3$) or J. M. Fernandez and J. A. Gladysz, *Organometallics* 1989, **8**, 207 ($[C_5H_5Re(NO)\{P(C_6H_5)_2\}(L)]^+$, L = CH_2Cl_2).
14. A. Asdar, M.-J. Tudoret and C. Lapinte, *J. Organomet. Chem.* 1988, **349**, 353 (related work on the more stable $[C_5(CH_3)_5Mo(CO)_2LL']^+$ complexes).
15. See C. A. Tolman, *Chem. Rev.* 1977, **77**, 313 for steric factors and U. Bertholdt, E. Wenschuh and J. Reinhold, *Z. Anorg. Allg. Chem.* 1989, **577**, 59 for bonding properties of L.
16. M. Minelli, J. H. Enemark, R. C. Brownlee, M. J. O'Connor and A. G. Wedd, *Coord. Chem. Rev.* 1985, **68**, 169.
17. J. Y. LeGall, M. M. Kubicki and F. Y. Petillon, *J. Organomet. Chem.* 1981, **221**, 287; H. Brunner, P. Beier, E. Frauendorfer, M. Muschiol, D. K. Rastogi, J. Wachter, M. Minelli and J. H. Enemark, *Inorg. Chim. Acta* 1985, **96**, L5.
18. U. Schubert, K. Ackermann, R. Janta, S. Vosan and W. Malisch, *Chem. Ber.* 1982, **115**, 2003.
19. For an overview see: M. I. Bruce, Index of Structures Determined by Diffraction Methods, in *Comprehensive Organometallic Chemistry* (Edited by G. Wilkinson, F. G. A. Stone and E. W. Abel), Vol. 9. Pergamon Press, Oxford (1982).
20. P. Kubaceck, R. Hoffmann and Z. Havlas, *Organometallics* 1982, **1**, 180; T. A. Albright, J. K. Burdett and M.-H. Whangbo, *Orbital Interactions in Chemistry*. Wiley-Interscience, New York (1985).
21. P. Leoni, E. Aquilini, M. Pasquali, F. Marchetti and M. Sabat, *J. Chem. Soc., Dalton Trans.* 1988, 329.
22. M. A. Busch, A. D. V. Hardy, L. Manoilovic-Muir and G. A. Sim, *J. Chem. Soc.* (*A*) 1971, 1003; M. R. Churchill and S.W.-Y. Chang, *Inorg. Chem.* 1975, **14**, 98.

Polyhedron Vol. 10, No. 7, pp. 673–681, 1991
Printed in Great Britain

0277-5387/91 $3.00+.00
© 1991 Pergamon Press plc

FTIR STUDY OF NOVEL PALLADIUM TRIMETHYLPHOSPHINECARBONYL CLUSTERS ENCAGED IN ZEOLITE Y

ZONGCHAO ZHANG and WOLFGANG M. H. SACHTLER*

Ipatieff Laboratory, Center for Catalysis and Surface Science, Northwestern University, Evanston, IL 60208, U.S.A.

(*Received* 24 *September* 1990; *accepted* 7 *November* 1990)

Abstract—Green palladium trimethylphosphinecarbonyl (TMPC) clusters in zeolite Y have been prepared using a "ship-in-a-bottle" method. Trimethylphosphine (TMP) ligands stabilize palladium clusters of small nuclearity; they preferentially coordinate to the corner palladium atoms. Absorption bands of triply-bonded carbonyl (1886 cm^{-1}) are observed only for samples with initially large palladium nuclearity ($n > 4$). Bands at 1960 and 1950 cm^{-1}, attributed to doubly-bonded carbonyl in a butterfly configuration, dominate the IR spectra. The palladium core in palladium TMPC clusters is electron-rich, in comparison to palladium single crystals, due to electron donation from phosphorus to the palladium. The spectra of the zeolite encaged clusters differ from those reported for Pd TAPC (A = alkyl such as ethyl and butyl) clusters in solution with nuclearity varying from 4 to 38. Zeolite encaged Pd TMPC clusters are stable at 200°C in a flow of H_2+CO. At 300°C, the TMP ligands decompose and poison the palladium particles.

Palladium carbonyl clusters are known to be unstable under normal conditions.[1] They have never been prepared from solution, but Pd_nCO and $Pd_n(CO)_2$ have been detected in molecular beams.[2] In solids, their stabilization strictly requires inert isolation matrices, such as frozen inert gases at 20 K[1] or in zeolites.[3–5] Using EXAFS and FTIR, we recently discovered that the size of the palladium carbonyl clusters is determined by the diameter of the supercage in zeolite Y, the α-cage in zeolite A, and also by the dimensions of the windows in both zeolites.[6,7] Palladium particles of nuclearity 1–6 atoms have been found for unligated clusters after mild reduction procedures. The stabilization of the extremely small palladium metal particles has been attributed to the strong metal zeolite interaction (SMZI).[6,7] However, palladium carbonyl clusters have invariably been found to have a nuclearity of at least 13 atoms in NaY, irrespective of the original particle size prior to admission of CO at room temperature. The mobility and instability of the primary palladium carbonyl clusters cause them to coalesce in the supercages of zeolite Y. Apparently, further migration of $Pd_{13}(CO)_x$ is restricted by the diameter of the supercage windows.[3–5] Thermal expansion of this window at a higher temperature leads to further particle growth, up to an average nuclearity of about 40 atoms per palladium cluster.[6,7] By selecting a zeolite of comparable cage size, but of smaller window diameter than zeolite Y, for example zeolite 5A, six-atom palladium carbonyl clusters have been stabilized by introducing CO at room temperature to pre-reduced palladium in zeolite 5A.[8]

In catalytic reactions, the large dimensions of the supercage and window diameters are desired for the passage of molecules of moderate size. Stabilization of palladium clusters with cores that are smaller than the cage windows can conceivably be achieved by introducing large and strong-bonding ligands, such as trialkylphosphines (TAP), to the primary metal particles which have been previously reduced inside the zeolite. The examination of this concept forms the main incentive for the work described in the present paper. In addition, the unique catalytic performance of rhodium triphenylphosphine (TMP) complexes in hydrogenation and hydroformylation reactions[9,10] motivates experimental work on TAP addition to reduced PdNaY, in the hope that this

*Author to whom correspondence should be addressed.

might lead to superior palladium catalysts for hydroformylation or related CO-conversion reactions.

In organic solvents, Pd_n^0 trialkylphosphinecarbonyl (TAPC) complexes of $n = 4$–38 have been prepared.[11–14] The preparation generally involves reduction of Pd^{2+} precursor compounds under a CO atmosphere and in the presence of TAP. In addition, the palladium nuclearity in the Pd TAPC complexes varies with the phosphine/carbonyl ligand ratio. In zeolites, however, palladium ionic precursors can be reduced to Pd^0 by hydrogen, prior to the admission of TAP and CO. As mentioned, unlike organic solvents, rigid zeolite cages can stabilize clusters of low nuclearity. The entrapment of Pd TAPC clusters in the zeolite framework provides a means of manufacturing a heterogeneous catalyst that avoids the need of reaction product and catalyst separation.

In the present study, faujasite type zeolite NaY is used as the stabilizing matrix. Palladium trimethylphosphinecarbonyl (TMPC) clusters are generated by the "ship-in-a-bottle" method, after prereducing the palladium ionic precursor with hydrogen.

EXPERIMENTAL

PdNaY samples (5 wt% Pd) were prepared using ion exchange techniques. A solution containing 0.01 M $Pd(NH_3)_4^{2+}$ ions [AESAR, $Pd(NH_3)_4(NO_3)_2$] was added dropwise into a slurry of NaY [200 cm^3 of doubly-distilled water (DDW) per gram of zeolite] at room temperature. Ion exchange was allowed to proceed for 24 h. The sample was filtered and washed with DDW to remove the NO_3^- ions. After drying in air, the sample was stored in a desiccator over a saturated NH_4Cl solution.

Samples were made into self-supporting wafers of 20 mg cm^{-2}. Sample wafers were supported on a quartz holder inside a pretreatment chamber. They were calcined to specified temperatures (T_c) in a flow of 200 cm^3 min^{-1} O_2 and at a heating rate of 0.5°C min^{-1}, followed by purging with Ar at T_c for 20 min. After cooling to room temperature, reduction in flowing H_2 was performed by heating at a rate of 8°C min^{-1} from room temperature to a specified temperature (T_R), followed by holding at T_R for 20 min at a flow rate of 60 cm^3 min^{-1}. Following reduction, Ar was introduced at T_R for 20 min to purge adsorbed hydrogen. The samples were then cooled to room temperature and kept under the Ar stream, unless other pretreatment conditions are specified in the text.

Specially designed glassware was used in the admission of $P(CH_3)_3$ after reduction. The Ar flow used to purge the system was switched to flow through a tube containing solid trimethylphosphine (TMP) silver iodide. The TMP silver iodide/Ar system was then slowly heated to 150–200°C to sufficiently saturate the PdNaY wafer. The tube with TMP silver iodide was then closed and the Ar gas was switched back to purge excess TMP in the reactor for 20 min at room temperature. Subsequently, a stream of CO at 1 atm was passed through the system for a specific length of time, as seen in our IR spectra. Each FTIR spectrum was collected after purging the excess CO with Ar for 10 min, using a Nicolet 60SX single-beam Fourier transform IR spectrometer (resolution: 1 cm^{-1}).

RESULTS

Samples are labelled $T_c/T_R/P$, where T_c is the calcination temperature, T_R the reduction temperature and P stands for the TMP treatment. For the samples that are further treated under a mixed flow of H_2 and CO at various reaction temperatures, T_{RXN}, the notation $T_C/T_R/P/T_{RXN}$ will be used. FTIR spectra of CO absorption were obtained by subtracting the background spectrum of the palladium zeolite sample after adsorption of TMP, followed by Ar purge from the spectra, obtained after introducing CO at various lengths of time. The FTIR spectra of sample 500/250/P after CO admission for various lengths of time on stream are shown in Fig. 1. It is evident from the spectra

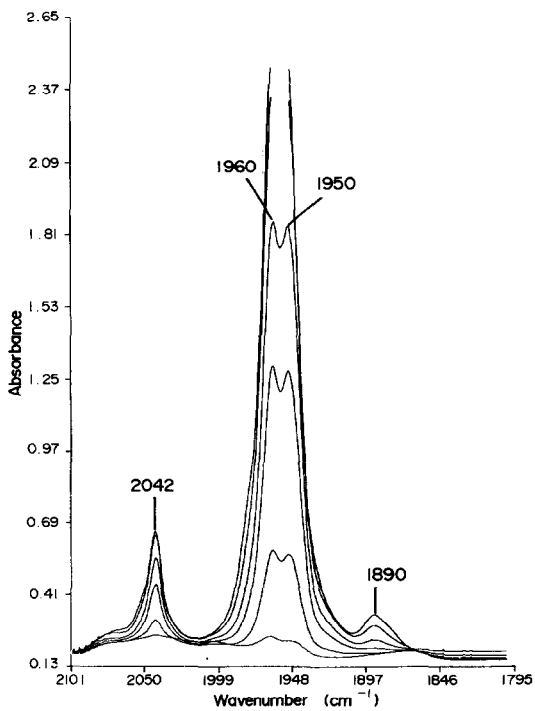

Fig. 1. CO FTIR spectra of sample 500/250/P after time on stream in CO for 1, 11, 41, 71, 131 and 191 min (from bottom to top).

that the CO absorption intensity increases with time during constant CO flow at 1 atm. The prominent peaks are the twin bands at 1960 and 1950 cm^{-1}. Two much less intense bands at 1890 and 2042 cm^{-1} are observed after extended exposure to CO. The twin bands at 1960 and 1950 cm^{-1} are off scale after 131 and 191 min, respectively, during CO exposure.

To determine the thermal stability of the Pd TMPC clusters in zeolite Y, sample 500/250/*P* was heated at 200°C for 5 min in a flow of H_2/CO (about 30 cm^3 min^{-1} each). This was followed by an Ar purge at the same temperature for an additional 5 min before cooling to room temperature under Ar. The spectrum of this sample (500/250/*P*/200) is shown in Fig. 2(A). The twin bands are off scale, but the bands at 2042 and 1890 cm^{-1} have increased slightly. The samples 500/250/*P*/250 and 500/250/*P*/300 were treated similarly to sample 500/250/*P*/200, and their FTIR spectra are shown in Fig. 2 as traces B and C, respectively. The band intensities for 500/250/*P*/250 have dropped significantly and for 500/250/*P*/300 all bands have completely disappeared. A series of colour changes were observed in the following sequence: The colour of the sample is orange after calcination to 500°C. After reduction, the catalyst turns grey. Introduction of TMP to the reduced sample does not change the colour. However, after CO admission, the colour of the sample gradually changes to green. When the sample is heated under a flow of CO and H_2 at 200°C, the same sample turns bright green, at 250°C it turns dark green, and at 300°C it turns black.

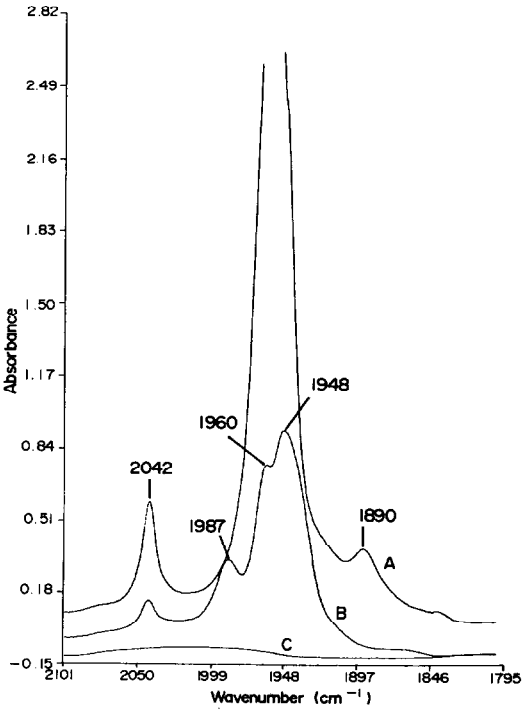

Fig. 2. CO FTIR spectra of samples 500/250/*P*/200 (A), 500/250/*P*/250 (B) and 500/250/*P*/300 (C).

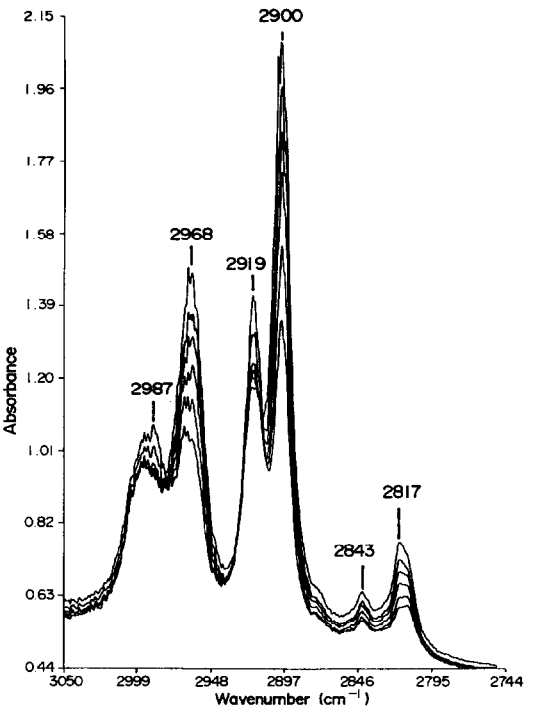

Fig. 3. CH FTIR spectra of sample 500/250/*P* after time on stream in CO for 1, 11, 41, 71, 131 and 191 min.

Figure 3 shows the absorption bands for the C—H vibration of $P(CH_3)_3$ in sample 500/250/*P*. There are six major bands at 2987, 2968, 2919, 2900, 2843 and 2817 cm^{-1}. With increasing time on stream in CO at room temperature, the bands at 2900, 2968, 2843 and 2817 cm^{-1} decrease, while the bands at 2919 and 2987 cm^{-1} increase.

The spectrum in Fig. 4(A) was recorded for sample 500/250/*P* after 191 min on stream in CO at room temperature. Figure 4(B), (C) and (D) are the spectra of 500/250/*P*/200, 500/250/*P*/250 and 500/250/*P*/300, respectively. The bands at 2900 and 2968 cm^{-1} decrease rapidly and shift to higher wavenumbers (2905 and 2973 cm^{-1}) as the reaction temperature increases. By 300°C, the C—H absorption bands disappeared altogether, concomitant with the disappearance of the CO absorption bands as shown in Fig. 2. The spectra of the C—H vibration for samples at a variety of T_c and T_R values are very similar to those displayed in Figs 3 and 4; therefore they are not included.

The CO absorption spectra for the sample 250/250/*P* are shown in Fig. 5. Again, the twin bands appear at 1960 and 1951 cm^{-1} and their intensities increase with time on stream in CO. A linear band appears at 2042 cm^{-1}. In addition, one

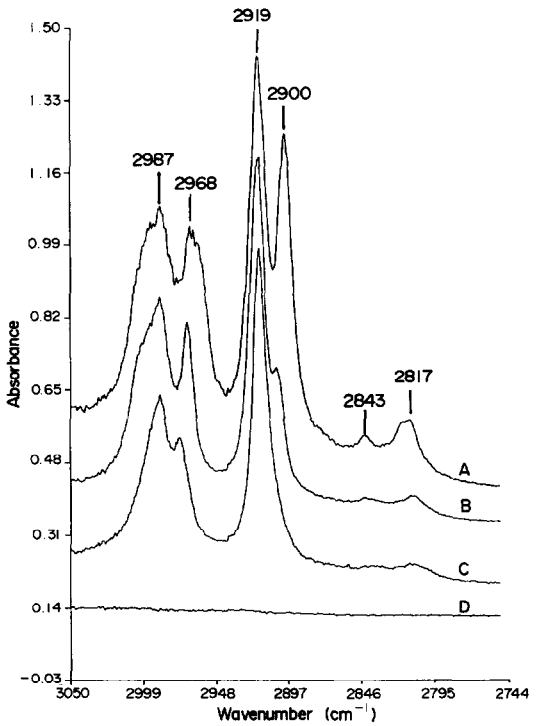

Fig. 4. CH FTIR spectra of samples 500/250/*P* (A), 500/250/*P*/200 (B), 500/250/*P*/250 (C) and 500/250/*P*/300 (D).

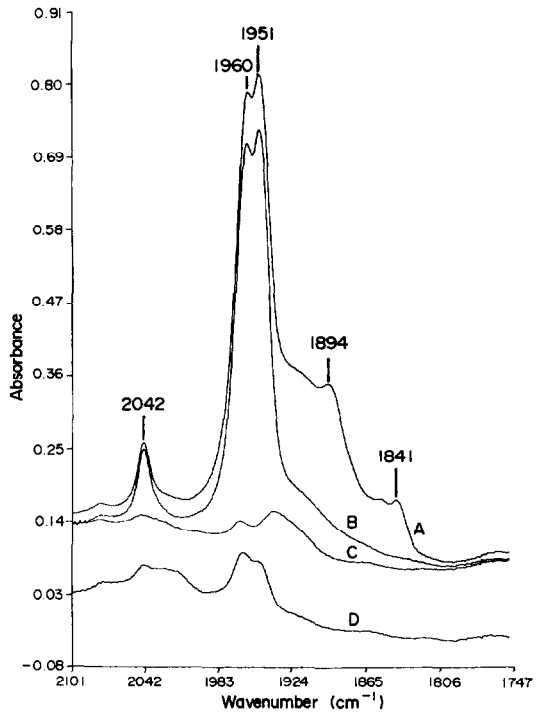

Fig. 6. CO FTIR spectra of sample 250/250/*P*/200 (i) in H_2 and CO (A), (ii) in H_2 only after i (C), and (iii) in H_2 and CO after ii (B); and CO FTIR of 250/250/*P*/250.

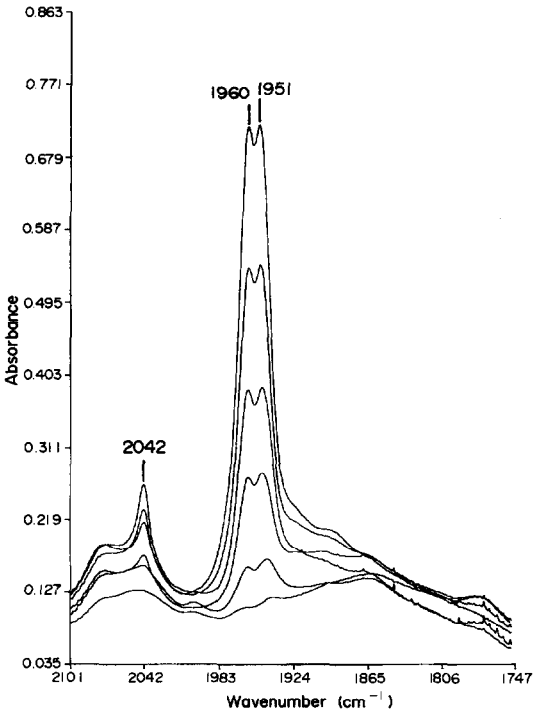

Fig. 5. CO FTIR spectra of sample 250/250/*P* after time on stream in CO for 1, 11, 41, 71, 131 and 191 min (from bottom to top).

band due to linearly-bonded CO and one very broad band, due to triply-bonded CO, were observed as soon as CO was introduced. At 200°C under H_2 and CO flow, the intensities of the twin bands reached a maximum value [Fig. 6(A)], but all the bands could be removed at 200°C by H_2 alone, as shown in Fig. 6(C). The linear and the twin CO bands were restored by introducing CO at 200°C [Fig. 6(B)]. However, the intensity of the bands (1894 and 1841 cm^{-1}) at the triply-bonded region decreased tremendously. The CO band intensities had decreased remarkably at 250°C under CO and H_2 flow. This was also observed for the sample 500/250/*P*.

The difference spectra displayed in Figs 7 and 8 for sample 250/250/*P* were obtained by subtracting the background of the reduced palladium zeolite sample before admission of TMP from those obtained at various lengths of time on stream in CO. A band at 2481 cm^{-1} appears after adsorption of $P(CH_3)_3$. This band remains even after extended time on stream (191 min) during CO purge at room temperature [Fig. 7(A)]. FIgure 8 is the difference spectra due to O—H vibration after admission of TMP. The negative peak in Fig. 8 shows that the O—H band at 3650 cm^{-1} immediately decreased after $P(CH_3)_3$ admission. In fact, before background subtraction, the strong O—H band before

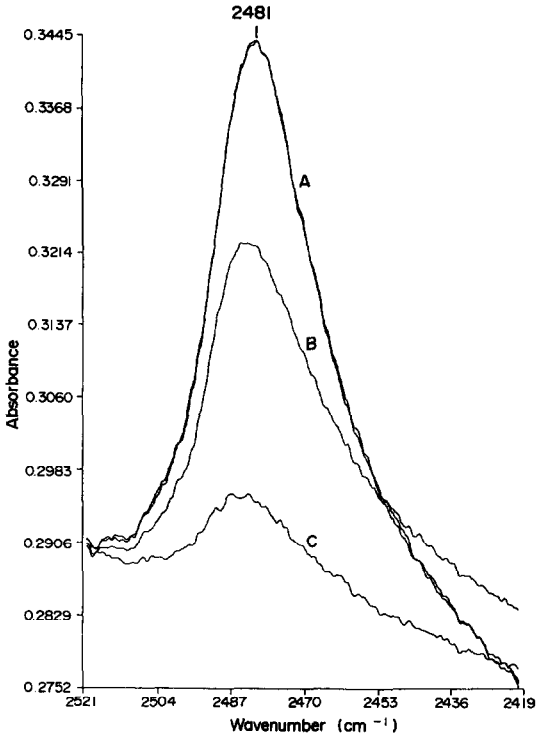

Fig. 7. PH FTIR spectra of 250/250/*P* (A), 250/250/*P*/200 (also A), 250/250/*P*/250 (B) and 250/250/*P*/300 (C).

admission of TMP completely disappeared as soon as TMP was introduced to the system. This indicates total neutralization of the protons in the sample by TMP molecules. Further treatment at both 200 and 250°C under CO and H_2 flow led to a decrease of the P—H band at 2481 cm^{-1}. However, the intensity of the negative band in Fig. 8 did not change. Similar absorption behaviour was observed for all other samples (not shown) except that the intensities differ. For example, samples that were reduced at 500°C have much lower band intensities at 2481 and 3650 cm^{-1}.

Figure 9 shows the IR absorption of the CO ligands in sample 500/500/*P*. The linear CO band at 2042 cm^{-1} and the twin bands at 1960 and 1949 cm^{-1} follow the same trends as those bands observed for samples 500/250/*P* and 250/250/*P*. In sample 500/500/*P*, a broad band is observed near the triply-bonded CO region (1848 cm^{-1}) immediately after the admission of TMP. With time on stream in CO flow, a band (at 1885 cm^{-1}) appears on top of the broad band. The reaction temperature effect is shown in Fig. 10. The intensities of the linear CO band and the doubly-bridged CO twin bands again reached a maximum at 200°C, and then decreased at 250°C, remaining consistent with all other samples previously run. The two low frequency bands after treatment at 200°C are located

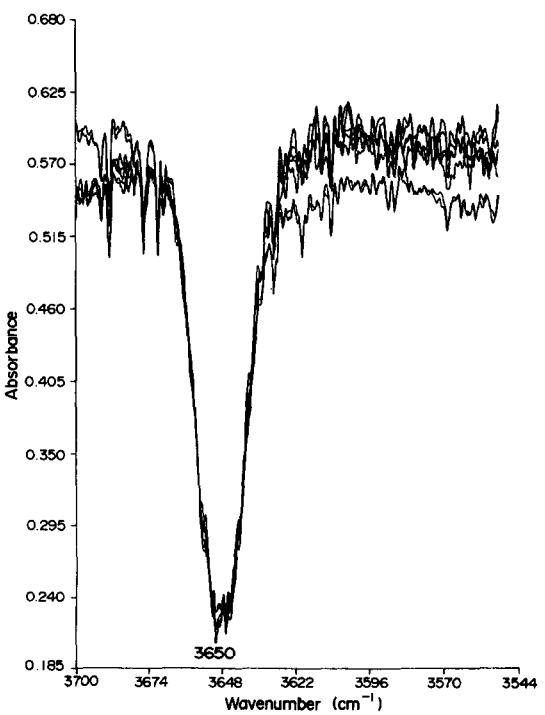

Fig. 8. OH difference FTIR spectra of 250/250/*P* after time on stream in CO for 1, 41, 71, 131 and 191 min; 250/250/*P*/200, 250/250/*P*/250 and 250/250/*P*/300.

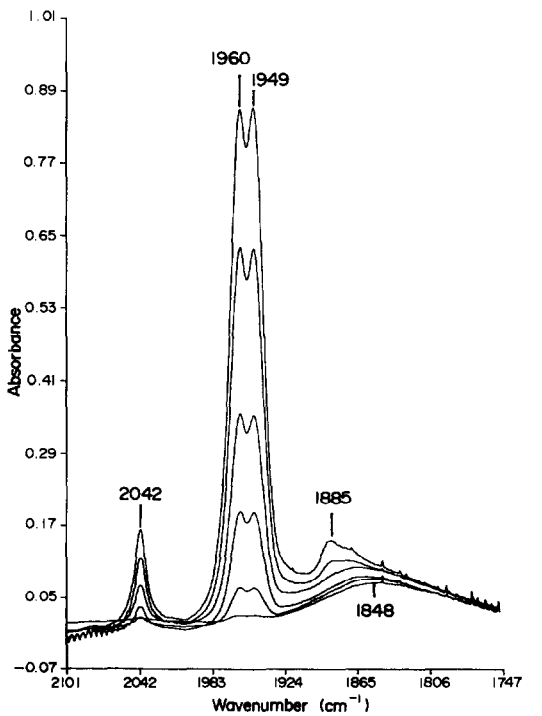

Fig. 9. CO FTIR spectra of 500/500/*P* after time on stream in CO for 1, 11, 41, 71, 131 and 191 min (from bottom to top).

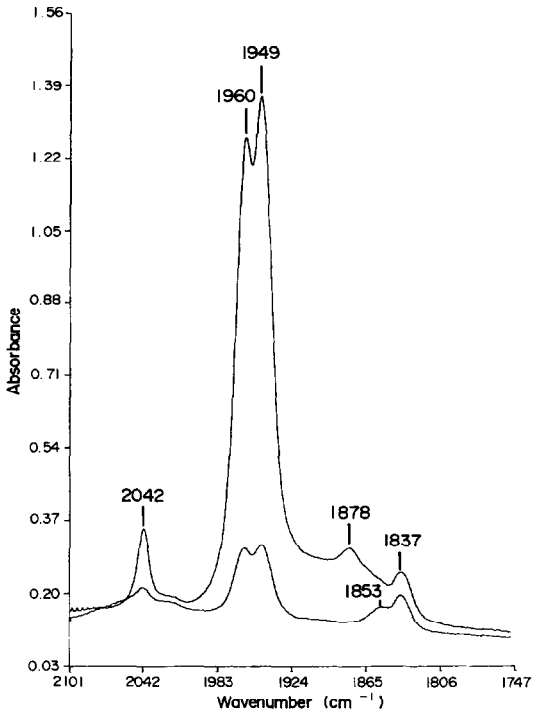

Fig. 10. CO FTIR spectra of 500/500/*P*/200 and 500/500/*P*/250.

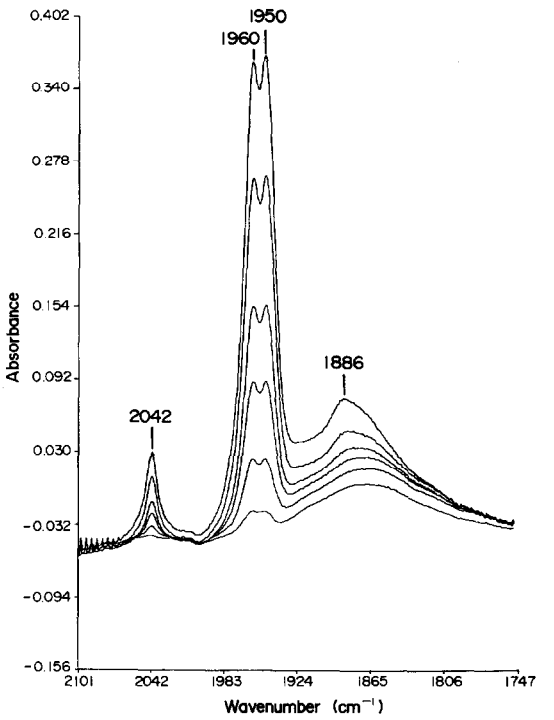

Fig. 11. CO FTIR spectra of 250/500/*P* after time on stream in CO for 1, 11, 41, 71, 131 and 191 min (from bottom to top).

at 1878 and 1837 cm^{-1} but at 250°C the bands are observed at 1853 and 1837 cm^{-1}, respectively.

The CO absorption spectra of 250/500/*P* are shown in Fig. 11. Again, they are similar to those spectra of 500/500/*P*. After high temperature reaction, spectra are similar to the ones presented above and are, therefore, not shown.

An unreduced sample was exposed to TMP after calcination and Ar purge at 500°C. This sample is referred to as 500/*P*. The spectra of CO absorption recorded at various times on stream are shown in Fig. 12. The sample mainly shows the doubly-bridged CO twin peaks with very weak linear and triply-bound CO absorption. The reaction products of CO and H_2 at high temperature were not analysed in this IR study. It will be the subject of future research.

DISCUSSION

IR and NMR studies have been reported on the characterization of zeolite acidity using TMP as a probe molecule.[15-18] The IR absorption in the region between 2800 and 3000 cm^{-1} is generally attributed to the C—H vibration in $P(CH_3)_3$.[15] Even though the total absorption decreases with time on stream in CO, the fact that the bands at 2968 and 2900 cm^{-1} decrease concomitant with the increase of the bands at 2987 and 2918 cm^{-1} (Fig

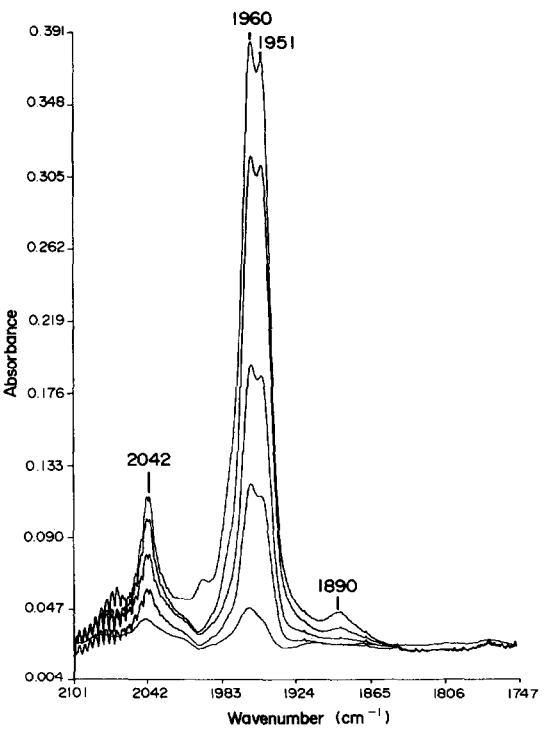

Fig. 12. CO FTIR spectra of 500/*P* after time on stream in CO for 10, 40, 70, 130 and 190 min (from bottom to top).

3 and 4) suggests that there are two main types of C—H bond. The monotonically decreasing bands at 2843 and 2817 cm^{-1} may correspond to another minor portion of $P(CH_3)_3$, which interacts with the zeolite differently from the other two.

The studies by Lunsford and co-workers[16–18] and Schoonheydt *et al.*[15] have revealed the existence of several TMP adducts: phosphonium ions, such as $[(CH_3)_3PH]^+$, $[(CH_3)_3PNa]^+$ and (Si—)(Al—)O—$P(CH_3)_3$, along with TMP oxide, $(CH_3)_3PO$. In the present study, the Pd—$P(CH_3)_3$ interaction also exists. Unfortunately, the present data do not allow for a clear assignment of the C—H absorption associated with the Pd—$P(CH_3)_3$ adducts. We will pursue this issue in our future study using ^{31}P NMR. From the spectra shown in Figs 7 and 8, we conclude that the zeolitic protons are completely consumed in the formation of the trimethylphosphonium ions. The phosphonium ions with a characteristic P—H absorption band at 2481 cm^{-1} are stable at room temperature in CO flow for an extended period. If these catalysts are heated above 250°C, the trimethylphosphonium ions are partially destroyed, but the zeolitic protons are not restored.

Previous characterization studies of palladium exchanged faujasite zeolites with X-ray diffraction;[19–21] temperature programmed oxidation, reduction and desorption;[22,23] UV–vis diffuse reflectance and EXAFS;[24–26] and FTIR[3–5] have shown that the location and size of the palladium particles are determined by the pretreatment conditions. Palladium ionic precursors are located in the supercages after calcination at temperatures below 250°C. At calcination temperatures (T_c) above 300°C, they migrate swiftly into the sodalite cages. For samples calcined at 250°C and reduced at low temperature, the palladium particles are located in the supercages. For the sample reduced at $T_R = 200$°C, the coordination number determined by EXAFS was 2.4, corresponding to Pd_3 and Pd_4 particles. When the reduction temperature is increased to $T_R = 500$°C, larger palladium particles are generated for samples calcined either at $T_c = 250$ or 500°C. On the other hand, reduced monometallic palladium located in the sodalite cages can be obtained by calcination at $T_c = 500$°C, followed by reduction at $T_R = 200$°C. Above $T_R = 350$°C, the palladium atoms will migrate out of the sodalite cages and coalesce in the supercages. A very interesting phenomenon recently observed is that the admission of CO at room temperature to reduced palladium zeolite samples induces the migration and coalescence of the primary palladium particles to an average of 13 atoms, within wide limits, independent of the sample preparation history.[6,7] The FTIR spectra after CO adsorption on all the above prereduced samples, therefore, results in identical spectra.[3–5]

In the present study, sample 500/250 is expected to have predominantly isolated palladium atoms inside the sodalite cages. The results indicate that, after introduction of TMP, palladium atoms migrate to the supercages, where they become strongly coordinated to the TMP ligands. A migration of palladium atoms from the sodalite cages at room temperature after CO admission has been previously observed.[7] The bond between palladium and phosphorus in Pd—$P(CH_3)_3$ is much stronger than the Pd—CO bond. This follows from the slow replacement of TMP by CO at room temperature under CO flow, as shown in the CO spectra (e.g. Fig. 1). Conversely, when CO was introduced to prereduced samples first, the replacement of CO by subsequently introduced TMP was found to be instantaneous. The large molecular size of the TMP ligand, in combination with the strong Pd—P bond, impede the migration of the primary Pd TMP clusters out of the supercages. Sample 500/250/*P* is, therefore, expected to contain clusters of small palladium nuclearity. In fact, the absence of triply-bonded CO bands in Fig. 1 suggests that the palladium nuclearity is, indeed, extremely small. On the basis of the absence of the linear CO bands in all CO absorption IR spectra, it is evident that TMP preferentially occupies corner positions in the clusters. However, TMP ligands do not limit the adsorption of CO on the Pd(111) sites when large palladium particles are present before the introduction of TMP. This can be rationalized on the basis of the large molecular size of TMP in comparison to CO molecules. In samples 500/500/*P* and 250/500/*P* (Figs 9 and 11), large palladium particles prevail after reduction. After introduction of TMP, the corner palladium atoms are bonded to phosphorus. However, intense CO absorption bands in the triply-bonded region are immediately observed after admission of CO to these samples. For sample 250/250, the nuclearity of palladium is estimated to be close to a tetrahedron on the basis of our previous EXAFS evaluation.[6,7] A triply-bonded CO band is also observed for sample 250/250/*P* (Fig. 5). The increase in intensity for the doubly-bridged CO twin bands with extended CO purge is likely due to purging off some of the physisorbed TMP molecules, which block the cage window, as well as purging off some of the TMP molecules on the palladium cluster. In comparison to the Pd_{13} carbonyl clusters, it is remarkable that the Pd TMPC clusters in zeolite indeed reflect the history of sample preparation.

At 200°C, the maximum intensity of CO absorption and the maintenance of the C—H bands at 2987 and 2918 cm^{-1} (Fig. 4) suggest that the Pd TMPC clusters remain stable at this reaction temperature. At $T_{RXN} = 250°C$, the decrease of the CO absorption bands' intensity and the C—H stretch clearly show the clusters degrading. At 300°C, the total disappearance of the C—H (Fig. 4) and CO absorption bands [Fig. 2(C)] clearly indicates that TMP decomposes and the palladium particles are completely poisoned by the P and CH_x fragments. A colour change was observed which can be directly related to the change of the ligand structure. Pd TMPC clusters in zeolites are green, but the poisoned samples, after destruction of TMP at elevated temperature, are black in colour. It is noted that most reported Pd TAPC clusters in organic solvents show a red colour.[11-14] It has been reported for some $Pd_4(CO)_5(PR_3)_4$ (R = alkyl group) and $Pd_4(CO)_3(PPhMe_2)_4$ in organic solvents that CO ligands are coordinated in butterfly configuration.[11,27] Based on our CO absorption spectra, the butterfly configuration prevails in the present zeolite encaged Pd TMPC clusters. Since there are no other Pd TAPC clusters known to which the present cluster can be compared, the wavenumber (cm^{-1}) of the absorption bands of CO in the closest comparable phosphine system, $Pd_4(CO)_5(PEt_3)_4$, are listed as follows:[28] 2018 v.w., 1889 m, 1874 w, 1844 s, and 1797 sh. This reported cluster has completely different IR identity from our cluster shown in Fig. 1. Only a weak band at 1890 cm^{-1} in Fig. 1 is reminiscent of the 1889 cm^{-1} band of $Pd_4(CO)_5(PEt_3)_4$; while strong triply-bonded bands appear only when the palladium nuclearity is quite large. These striking differences in IR spectra could be due to differences of the environment (organic liquid vs solid zeolite) or of the alkyl groups (Et vs Me). Furthermore, in our sample, the size of the palladium clusters is presumably smaller than those prepared in organic solvents, due to the limited dimension of the zeolite cage structure. The cluster size of our zeolite encaged Pd TMPC will be determined in our future study with EXAFS.

Our previous FTIR studies in palladium zeolite systems have shown that the linear CO absorption on electron-deficient palladium carbonyl clusters is shifted to higher wavenumbers with respect to the CO absorption band on palladium single crystals.[5,29] The terminal CO absorption on palladium single crystals has been reported to vary between 2090 and 2112 cm^{-1}, depending on the type of crystal face.[30,31] The position of the weak linear CO absorption band at 2042 cm^{-1} in the Pd TMPC clusters shows that palladium has become electron-rich in comparison to palladium single crystals. We attribute this to electron donation from phosphorus to palladium. In addition, chemical bonding of palladium clusters with zeolite protons is destroyed by the interaction of acid protons with TMP molecules acting as Lewis bases.

In the preparation of the Pd^0 TAPC clusters in organic solvents, the general strategy involves reduction of Pd^{2+} in various solvents with PR_3 under a CO atmosphere.[11-14] Figure 12 shows that Pd^0 carbonyl TMP clusters in a zeolite can also be prepared using a similar strategy. The spectra shown in Fig. 12 are essentially the same as those in Fig. 1, except the intensity is lower. It is very likely that the coalescence of the palladium cluster via this route is also limited. However, reduction with phosphine may result in undesirable destruction byproducts of phosphines, which may poison the palladium cluster. This may be the cause of the significantly lower intensity in Fig. 12 in comparison to Fig. 1.

Conclusion

Novel Pd TMPC clusters in zeolite Y are prepared using the ship-in-bottle method. TMP molecules stabilize palladium cores of small nuclearity. The FTIR spectra of the clusters, therefore, reflect the sample preparation history. TMP ligands preferentially coordinate to the corner palladium atoms. The absorption bands of triply-bonded CO are observed only for samples with initially large nuclearity ($n > 4$). Butterfly configurations of double-bonded CO prevail for all the CO absorption spectra in IR region. The Pd TMPC clusters are stable at 200°C in a flow of H_2 and CO mixture. At 300°C, the TMP ligands decompose and completely poison the palladium particles.

Acknowledgements—Support from the U.S. National Science Foundation under contract CTS-8911184 and a grant in aid from the Engelhard Co. are gratefully acknowledged.

REFERENCES

1. F. A. Cotton and G. Wilkinson, *Adv. Inorg. Chem.* 1988, 1024.
2. D. M. Cox, K. C. Reichmann, D. J. Trevor and A. Kaldor, *J. Chem. Phys.* 1988, **88**, 111.
3. L. L. Sheu, H. Knözinger and W. M. H. Sachtler, *Catal. Lett.* 1989, **2**, 129.
4. L. L. Sheu, H. Knözinger and W. M. H. Sachtler, *J. Molec. Catal.* 1989, **57**, 61.
5. L. L. Sheu, H. Knözinger and W. M. H. Sachtler, *J. Am. Chem. Soc.* 1989, **111**, 8125.
6. Z. Zhang, H. Chen, L. L. Sheu and W. M. H. Sachtler, *J. Catal.* 1991, **127**, 213.

7. Z. Zhang, H. Chen and W. M. H. Sachtler, *J. Chem. Soc., Faraday Trans.*, in press.
8. Z. Zhang and W. M. H. Sachtler, *J. Molec. Catal.*, in press.
9. J. A. Osborne, F. H. Jardine, J. F. Young and G. Wilkinson, *J. Chem. Soc. A* 1966, 1711.
10. *Chemical and Engineering News* (26 April 1976).
11. E. G. Mednikov, N. K. Eremenko, S. P. Gubin, Yu. L. Slovokhtov and Yu. T. Struchkov, *J. Organomet. Chem.* 1982, **239**, 401.
12. E. G. Mednikov, N. K. Eremenko, V. A. Mikhailov, S. P. Gubin, Yu. L. Slovokhotov and Yu. T. Strichkov, *J. Chem. Soc., Chem. Commun.* 1981, 989.
13. E. G. Mednikov, N. K. Eremenko, Yu. L. Slovokhotov and Yu. T. Struchkov, *J. Organomet. Chem.* 1986, **301**, C35.
14. E. G. Mednikov, N. K. Eremenko, Yu. L. Slovokhotov and Yu. T. Struchkov, *J. Chem. Soc., Chem. Commun.* 1987, 218.
15. R. A. Schoonheydt, D. Van Wouwe and H. Leerman, *Zeolites* 1982, **2**, 109.
16. W. P. Rothwell, W. Shen and J. H. Lunsford, *J. Am. Chem. Soc.* 1984, **106**, 2452.
17. J. H. Lunsford, W. P. Rothwell and W. Shen, *J. Am. Chem. Soc.* 1985, **107**, 1540.
18. J. H. Lunsford, P. N. Tutunjian, P. Chu, E. B. Yeh and D. J. Zalewski, *J. Phys. Chem.* 1989, **93**, 2590.
19. P. Gallezot and B. Imelik, *Molec. Sieve, Avd. Chem. Ser.* 1973, **121**, 66.
20. G. Bergeret, T. M. Tri and P. Gallezot, *J. Phys. Chem.* 1983, **87**, 1160.
21. G. Bergeret, P. Gallezot and B. Imelik, *J. Phys. Chem.* 1981, **85**, 411.
22. S. T. Homeyer and W. M. H. Sachtler, *J. Catal.* 1989, **117**, 91.
23. S. T. Homeyer and W. M. H. Sachtler, *J. Catal.* 1989, **118**, 266.
24. Z. Zhang, W. M. H. Sachtler and H. Chen, *Zeolites* 1990, **10**, 784.
25. K. Möller and T. Bein, *J. Phys.* 1986, **C8-231**.
26. K. Möller, D. C. Koningsberger and T. Bein, *J. Phys. Chem.* 1989, **93**, 6116.
27. J. Dubrawskii, J. C. Kriege-Simondson and R. D. Feltham, *J. Am. Chem. Soc.* 1980, **102**, 2089.
28. E. G. Mednikov and N. K. Eremenko, *Izvestiya Akademii Nauk SSSR, Seriya Khimicheskaya* 1981, **10**, 2400.
29. Z. Zhang, T. Wong and W. M. H. Sachtler, *J. Catal.*, in press.
30. A. M. Bradshaw and F. Hoffmann, *Surf. Sci.* 1975, **52**, 449.
31. A. Palazov, C. C. Chang and R. J. Kokes, *J. Catal.* 1975, **36**, 338.

Polyhedron Vol. 10, No. 7, pp. 683–685, 1991
Printed in Great Britain

0277–5387/91 $3.00+.00
© 1991 Pergamon Press plc

THE TEMPLATE SYNTHESIS AND CHARACTERIZATION OF NEW HEXADENTATE N_4O_2 ACYCLIC SCHIFF BASE COMPLEXES OF LANTHANUM, PRASEODYMIUM AND NEODYMIUM NITRATES

WANDA RADECKA-PARYZEK* and VIOLETTA PATRONIAK

Faculty of Chemistry, Adam Mickiewicz University, 60-780 Poznań, Poland

(*Received* 4 *July* 1990; *accepted* 26 *November* 1990)

Abstract—The partial Schiff base condensation reactions between 2,6-diacetylpyridine and 1,8-diaminonaphthalene in the presence of lanthanum(III), praseodymium(III) and neodymium(III) nitrates produced the new hexadentate N_4O_2-open chain complexes, which were characterized by IR, UV–vis, ^1H NMR and MS data, in addition to elemental and thermogravimetric analyses.

Interest in exploring the metal ion complexes with Schiff base ligands has continually increased, since it has been recognized that many of these complexes may serve as models for biologically important, naturally occurring ionophores. These synthetic model complexes are divided into macrocyclic (coronates and cryptates) and acyclic (podates) ionophores. The investigations concerning lanthanide complexes with Schiff bases have been devoted to their synthesis and structural studies and biological application of metal–enzyme or protein bindings.[1–6]

As part of our studies on the effectiveness of the metal ions of varying radius and electron configuration in the synthesis of Schiff base ligands, we have found that different experimental conditions (the type of metal, counterion, ratio of starting material) lead to the isolation of the macrocyclic (coronate) or ring-opened (podate) complexes.[7–9] The present paper is concerned with the preparation and characterization of Schiff base complexes of the podate type, formed in the reaction of early lanthanide nitrates with 2,6-diacetylpyridine and 1,8-diaminonaphthalene.

EXPERIMENTAL

The hydrated lanthanum, praseodymium and neodymium nitrates were prepared by dissolving the appropriate 99.99% oxide in nitric acid. The solutions were evaporated and precipitates recrystallized from methanol. 2,6-Diacetylpyridine was purchased from Aldrich Chemical Company and 1,8-diaminonaphthalene from Merck, and were used without further purification.

Preparation of the complexes. General procedure

To a solution of appropriate metal nitrate (0.1 mmol) in methanol (5 cm^3), 2,6-diacetylpyridine (0.33 g, 0.2 mmol) in methanol (10 cm^3) and 1,8-diaminonaphthalene (0.16 or 0.32 g, 0.1 or 0.2 mmol) in methanol (15 cm^3) were added dropwise with stirring. The reaction was continued for 8 h. The solution volume was then reduced to 10 cm^3 by roto-evaporation, and a dark violet precipitate formed on addition of a small amount of anhydrous diethyl ether. This was filtered off, washed with ether and dried *in vacuo*. Yields: 73–79%. The results of elemental analysis of the complexes are listed in Table 1.

Measurements

IR spectra were recorded using CsI pellets in the range 4000–200 cm^{-1} on a Perkin–Elmer 580 spectrophotometer. Electronic absorption spectra were measured on a Beckman 25 spectrophotometer. ^1H NMR spectra were run on a Varian EM-360 60 MHz spectrometer for DMSO-d_6 solutions using TMS as internal standard. Mass spectra were obtained on a Jeol–JMS mass spectrometer. Thermogravimetric measurements were

* Author to whom correspondence should be addressed.

Table 1. Analytical data for lanthanum, praseodymium and neodymium complexes of L

Compound	Calculated (%) C	H	N	Found (%) C	H	N
$[LaL(NO_3)_3]\cdot 2H_2O$	41.5	3.5	12.1	41.7	3.7	12.4
$[PrL(H_2O)_2](NO_3)_3$	41.4	3.5	12.1	41.1	3.4	12.1
$[NdL(H_2O)_2](NO_3)_3\cdot 2H_2O$	39.5	3.8	11.5	39.2	3.8	11.8

performed using the Derivatograph OD-102, MOM.

RESULTS AND DISCUSSION

The reaction of 2,6-diacetylpyridine with 1,8-diaminonaphthalene with the use of lanthanum, praseodymium and neodymium nitrates as template agents gave the new complexes of stoichiometry $[LaL(NO_3)_3]\cdot 2H_2O$, $[PrL(H_2O)_2](NO_3)_3$ and $[NdL(H_2O)_2](NO_3)_3\cdot 2H_2O$, where L is the acyclic product of a Schiff base condensation of two molecules of diketone with one molecule of diamine.

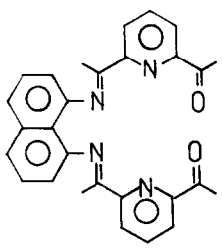

L

The complexes appear to be dark violet, air-stable solids, soluble in common polar solvents. The formulations of these complexes follow from spectral and thermal analyses, as discussed below, and elemental analysis.

The IR spectra of these three complexes are all very similar except for the anion and water vibrational modes. The most diagnostic band is the C=N stretching mode at 1625 cm^{-1} which indicates the Schiff base condensation. There is no absorption at 3050 and 3350 cm^{-1}, which would occur if residual amine groups were present. The appearance of the band at 1680 cm^{-1}, assigned to the C=O stretching vibration, indicates the formation of the open-chain product containing terminal acetylpyridyl groups. The shift of this band from 1705 cm^{-1} in uncomplexed diacetylpyridine is evidence that the carbonyl groups are coordinated to the metal. The profile of the pyridine ring vibrations observed in the 1600–1400 cm^{-1} region and the band at *ca* 1000 cm^{-1} are typical for metal bonding at the pyridine nitrogen atom.[10] The hexadentate nature of the ligand is further confirmed by the appearance of weak bands around 470–480 and 330–360 cm^{-1}, which can be assigned to ν(M—N) and ν(M—O) vibrations, respectively.[11]

The IR spectrum of the lanthanum complex demonstrates the presence of coordinated nitrates. The two bands associated with the asymmetric stretch appear near 1320 and 1470 cm^{-1}. The magnitude of the separation in addition to the appearance of the band at 1040 and 820 cm^{-1} are indicative of the interaction of the nitrate oxygen atoms with the metal ion, and provide evidence for chelating bidentate behaviour of the nitrate groups in this complex.[12,13]

In the IR spectra of praseodymium and neodymium nitrate complexes, a strong absorption band at 1380 cm^{-1} and medium band at 825 cm^{-1} occur which are typical for uncoordinated nitrate ions.

The broad, diffuse band centred at 3400 cm^{-1} is observed for all three complexes and is assigned to the symmetric and antisymmetric O—H stretching modes for water. Furthermore, the IR spectra of praseodymium and neodymium complexes exhibit weak bands at 840–870 cm^{-1} attributable to the coordinated water molecules. The presence of water bound in different ways is supported by the results of the thermogravimetric analysis. In the case of the lanthanum complex, the loss of two water molecules is observed below 100°C, whereas the praseodymium complex loses two water molecules at 150–170°C. The complex of neodymium indicates the loss of two water molecules per mol of metal ion in the temperature range 160–180°C, and the loss of two molecules at 50–70°C.

The electronic spectra of all the complexes recorded in methanol show similar features, containing three intense and medium bands with maxima at 228, 292–293 and 331–333 nm, which may be assigned to the transition of the $\pi \rightarrow \pi^*$ type located on the C=N groups and to the $n \rightarrow \pi^*$ transition of the carbonyl groups, respectively.[14]

The ^1H NMR spectrum of the diamagnetic complex of lanthanum obtained in DMSO-d_6 solution

shows the presence of pyridine (6H) and naphthalene protons (6H) at δ 8.6–8.2 and 7.2–6.4, respectively. The methyl protons of the two CH_3CO and two CH_3CN groups are observed at δ 2.98 and 2.28. The integrated intensities for all the protons are in the ratio 1 : 1 : 1 : 1, consistent with the proposed formulation of this complex. A downfield shift of the CH_3CO methyl proton resonances from δ 2.72 in the free 2,6-diacetylpyridine is assumed to be a consequence of coordination of the carbonyl oxygen atoms to the metal ion.

The mass spectrum of this complex provides strong evidence for the formation of an open-chain compound, showing the highest fragment at m/z 449 corresponding to the uncoordinated ligand.

On the basis of available evidence it can be concluded that the lanthanum, praseodymium and neodymium ions are effective templates for the synthesis of Schiff base complexes of the podate type, in which the podand acts as the hexadentate N_4O_2 ligand.

In the lanthanum complex, the metal ion is presumably coordinated to the four nitrogen atoms and to the two oxygen atoms of the open-chain ligand and to the six oxygen atoms of the bidentate chelating nitrate groups.

In the complexes of the slightly smaller praseodymium and neodymium ions, the bidentate nitrate groups are replaced by the less hindering water molecules and the coordination sphere is filled by one molecule of the N_4O_2 ligand and two water molecules.

Acknowledgement—Financial support from the Polish Academy of Science (Project CPBP 01.12.4.18) is gratefully acknowledged.

REFERENCES

1. J.-C. Bünzli, in *Handbook on the Physics and Chemistry of Rare Earths* (Edited by K. A. Gschneidner Jr and L. Eyring), Vol. 9. Elsevier, Amsterdam (1987).
2. D. E. Fenton, U. Casellato, P. A. Vigato and M. Vidali, *Inorg. Chim. Acta* 1984, **95**, 187.
3. P. A. Vigato and D. E. Fenton, *Inorg. Chim. Acta* 1987, **139**, 39.
4. G. Bombieri, *Inorg. Chim. Acta* 1987, **139**, 21.
5. D. E. Fenton and P. A. Vigato, *Chem. Soc. Rev.* 1988, **17**, 69.
6. L. M. Vallarino, *J. Less-Common Met.* 1989, **149**, 121.
7. W. Radecka-Paryzek, *Inorg. Chim. Acta* 1981, **52**, 261.
8. W. Radecka-Paryzek, *Polyhedron* 1989, **8**, 1217.
9. W. Radecka-Paryzek and E. Luks, *Polyhedron* 1990, **9**, 475.
10. E. Baraniak, R. S. L. Bruce, H. C. Freeman, N. J. Hair and J. James, *Inorg. Chim. Acta* 1976, **15**, 2226.
11. K. Nakamoto, *Infrared and Raman Spectra of Inorganic and Coordination Compounds*, 3rd edn. Wiley Interscience, New York (1978).
12. J.-C. Bünzli and D. Wessner, *Inorg. Chim. Acta* 1980, **44**, L55.
13. W. Radecka-Paryzek and E. Jankowska, *Inorg. Chim. Acta* 1987, **134**, 179.
14. I. A. Tossidis, C. A. Bolos, P. N. Aslanidis and G. A. Katsoulos, *Inorg. Chim. Acta* 1987, **133**, 275.

Polyhedron Vol. 10, No. 7, pp. 687–695, 1991
Printed in Great Britain

0277–5387/91 $3.00+.00
© 1991 Pergamon Press plc

A NEW π DONOR–ACCEPTOR COMPOUND DERIVED FROM TETRAPHENYLDITHIAPYRANYLIDENE AND BIS-(1,3-DITHIA-2-THIONE-4,5-DITHIOLATO)-NICKELATE: CRYSTAL STRUCTURE AND EPR STUDY

H. STRZELECKA

Chimie et Electrochimie des Matériaux Moléculaires, UA 429 du CNRS, ESPCI, 10 rue Vauquelin, 75231 Paris, France

R. VICENTE and J. RIBAS

Departament de Quimica Inorganica, Facultat de Quimica, Universitat de Barcelona, Diagonal 647, 08028 Barcelona, Spain

J.-P. LEGROS and P. CASSOUX*

Laboratoire de Chimie de Coordination du CNRS, UPR 8241 liée par conventions à l'Université Paul Sabatier et l'Institut National Polytechnique de Toulouse, 205 route de Narbonne, 31077 Toulouse Cédex, France

and

P. PETIT and J.-J. ANDRE

GRIMM, Institut C. Sadron, 6 rue Boussingault, 67083 Strasbourg Cédex, France

(*Received* 16 *July* 1990; *accepted* 26 *November* 1990)

Abstract—The electrosynthesis, X-ray crystal structure and EPR study of the 1 : 1 adduct between tetraphenyldithiapyranylidene and bis-(1,3-dithia-2-thione-4,5-dithiolato)-nickelate, (DIPSΦ$_4$)[Ni(dmit)$_2$], are reported. The triclinic unit cell contains one Ni(dmit)$_2$ and one DIPSΦ$_4$ entity, the molecular centre of each lying on a crystallographic centre of symmetry. The structure is characterized by a loose stacking (> 10 Å) of Ni(dmit)$_2$ units along [001], with no strong intermolecular interaction, consistent with the low electrical conductivity. Single-crystal EPR spectra show a single, broad line for any orientation. The angular dependences of the line width and of the *g*-factors have been determined, as well as the principal *g*-values and directions. The temperature-dependences of the susceptibility, the line width and the *g*-factor have been measured in the range 4–300 K. Analysis of these results indicates that dipolar spin–spin interaction takes place in this highly electron-correlated semiconducting system with complete charge transfer between the donor DIPSΦ$_4$ and the acceptor Ni(dmit)$_2$.

π Donor–acceptor compounds derived from [M(dmit)$_2$]$^{n-}$ complexes (M = Ni, Pd, Pt; dmit^{2-} = 1,3-dithia-2-thione-4,5-dithiolato; Fig. 1) exhibit interesting structural and electrical properties.[1–5] For example, TTF[Ni(dmit)$_2$]$_2$ (TTF = 1,4,5,8-tetrathiafulvalene) undergoes a superconducting transition under pressure.[2]

On the other hand, the heterocyclic π donor tetraphenyldithiapyranylidene (DIPSΦ$_4$ = 4-H-thiopyran, 4(2,6-diphenyl,4H-thiopyran-4-ylidene)-2,6-diphenyl; Fig. 1) is a useful precursor of organic one-dimensional conductors.[6–11] A charge-transfer complex of DIPSΦ$_4$ with TCNQ (TCNQ =

* Author to whom correspondence should be addressed.

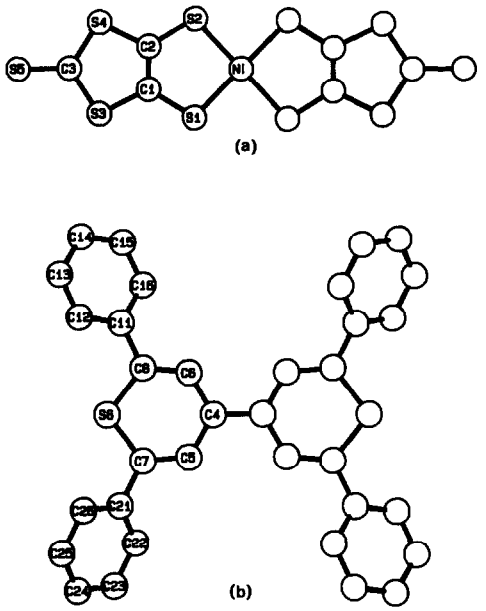

Fig. 1. Atomic numbering scheme for (a) the $Ni(dmit)_2$ centrosymmetric unit and (b) the $DIPS\Phi_4$ centrosymmetric unit.

7,7,8,8-tetracyano-*p*-quinodimethane) exhibits a high conductivity (250 S cm^{-1} at room temperature).[6,7] Mixed-valence radical cation salts have been obtained by oxidation with iodine. The composition of these salts depends on the ratio of the initial reagents. Particular attention has been devoted to the highly conducting tri-iodide salt $(DIPS\Phi_4)0.76(I_3^-)$.[8-10] The oxidation of $DIPS\Phi_4$ (in CH_2Cl_2 or CH_3CN) proceeds in two well-defined electron waves[10b] corresponding to the successive formation of the radical cation and dication:

$$DIPS\Phi_4 - e^- \rightleftharpoons (DIPS\Phi_4)^+ - e^- \rightleftharpoons (DIPS\Phi_4)^{2+}.$$

It was thus tempting to explore the use of the donor $DIPS\Phi_4$ molecule and the acceptor $[M(dmit)_2]^{n-}$ complexes for preparing new donor–acceptor compounds which would possibly exhibit novel solid-state properties. We report here the synthesis and electrocrystallization, the X-ray structure determination and the EPR study of $(DIPS\Phi_4)[Ni(dmit)_2]$. The presence of a nickel complex in this system introduces a strong contribution to spin orbit coupling of the unpaired electron. This gives an opportunity to study the local environment of the charge transferred.

EXPERIMENTAL

Synthesis and electrocrystallization

The starting materials, $(n\text{-}Bu_4N)[Ni(dmit)_2]$ and $DIPS\Phi_4$, have been prepared following the procedures described by Steimecke *et al.*[12] and Fabre *et al.*,[13] respectively.

Crystals of $(DIPS\Phi_4)[Ni(dmit)_2]$ have been obtained by galvanostatic electrolysis of a $CHCl_3$ solution containing $(n\text{-}Bu_4N)[Ni(dmit)_2]$ (10^{-3} M) and $DIPS\Phi_4$ (2×10^{-3} M). This solution was placed in the anodic compartment of a nitrogen flushed U-type cell where the anode and the cathode (platinum wires) are separated by a medium-porosity glass frit. The cathodic compartment contained a $CHCl_3$ solution of $(n\text{-}Bu_4N)[Ni(dmit)_2]$ (10^{-3} M) as supporting electrolyte. The cell was thermostated (20°C) and the current ($I = 1.5$ μA; current density = 1×10^{-5} A cm^2) was held constant for periods as long as 1 month. A mixture of different crystals, formed on the anode, was collected on a glass frit by filtration, washed with ethanol and vacuum dried. This mixture contained two kinds of crystals: green needles which were characterized by IR spectroscopy as unreacted $DIPS\Phi_4$, and blue parallelepipedic crystals (typically $0.8 \times 0.4 \times 0.2$ mm^3) which were characterized by single-crystal X-ray diffraction studies as the 1:1 adduct $(DIPS\Phi_4)[Ni(dmit)_2]$.

Electrochemical measurements

Half-wave redox potentials were measured as described in refs 14 and 15 by linear and cyclic voltammetry. Deaerated CH_2Cl_2 (Merck) was used as a solvent and $(n\text{-}Bu_4N)PF_6$ (0.1 M) as supporting electrolyte. Potentials were referred vs an Ag/AgCl (0.1 M KCl) electrode.

The radical cation salts $(DIPS\Phi_4)X$ ($X = ClO_4^-$, BF_4^-, SCN^-, PF_6^-, ...) are more soluble than the starting $DIPS\Phi_4$ donor. Consequently, we were not able to isolate these salts. $(DIPS\Phi_4)^+$ species were generated in a $CH_2Cl_2/(n\text{-}Bu_4N)PF_6$ (0.1 M) solution of $DIPS\Phi_4$ (2×10^{-3} M) by controlled potential electrolyses and coulometric determination. Electrolyses were carried out at 0.25 V on a platinum gauze electrode. The resulting solution was frozen at 100 K and used for EPR measurements.

X-ray structure determination

Crystal data are reported in Table 1, together with relevant details of the intensity data collection. Data collection and reduction were conducted following standard procedures previously described.[16] The structure was determined by direct methods and refined using usual full-matrix least-squares procedure and Fourier synthesis, as previously described.[16] The centrosymmetric space group $P\bar{1}$ was assumed on the basis of $N(Z)$ statistics. Phenyl

Table 1. Crystallographic data for $(DIPS\Phi_4)[Ni(dmit)_2]$

Crystal data	
Formula	$C_{40}H_{24}NiS_{12}$
Formula weight	948.1
Crystal system	triclinic
Space group	$P\bar{1}$
a (Å)	10.065(3)
b (Å)	11.322(2)
c (Å)	10.030(5)
α (°)	94.70(3)
β (°)	119.39(3)
γ (°)	92.01(2)
V (Å^3)	989
Z	1
$F(000)$	484
ρ_m (g cm^{-3})	1.58(2)
ρ_c (g cm^{-3})	1.59
μ(Mo-K_α) (cm^{-1})	10.8
Crystal size (mm^3)	$0.22\times0.12\times0.60$
Data collection and reduction	
T	293 K
Diffractometer	CAD4 Enraf–Nonius
Radiation	Mo-K_α, λ = 0.71069 Å, graphite monochromator
Scan mode	ω–2θ, maximum Bragg angle = 30°
Scan width	$(0.8+0.35\tan\theta)$° for ω angle
Max. and min. transmission coefficients	0.874 and 0.785
Number of reflections for the refinement of cell dimensions	25
Number of unique reflections	5763
Number of utilized reflections (NO)	3674 [$I > 2\sigma(I)$]
Number of refined parameters (NV)	217
Final reliability factors:	
$R = \Sigma\|k\|F_o\|-\|F_c\|\|/\Sigma k\|F_o\|$	0.040
$Rw = [\Sigma w(k\|F_o\|-\|F_c\|)^2/\Sigma w k^2 F_o^2]^{1/2}$	0.045
$S = [\Sigma w(k\|F_o\|-\|F_c\|)^2/(NO-NV)]^{1/2}$	0.93
Unit weights	

rings were treated as idealized rigid groups, with individual isotropic temperature factors for each carbon atom and fixed arbitrary temperature factors (U = 0.07 Å^2) for hydrogen atoms. All other atoms were given anisotropic thermal parameters. Final agreement factor values are given in Table 1. Atoms are labelled according to Fig. 1; bond lengths and angles are listed in Table 2.*

EPR measurements

The X-band EPR spectrum of a CH_2Cl_2 frozen (100 K) solution of $(DIPS\Phi_4)^+$ species generated by electrolysis (see above) was obtained on a Brucker 200 TT spectrometer equipped as previously described.[17]

The single-crystal EPR experiments have been carried out using a Bruker ESP 300 X-band spectrometer provided with a NMR gaussmeter, a frequency meter and a HP900-330 computer for data handling facilities. A one-axis goniometer has been used for the rotating experiments. A single crystal was fixed on a cubic sample holder in order to perform rotations in orthogonal planes chosen in view of the crystal morphology (Fig. 2).

* Supplementary material. Positional parameters and equivalent isotropic temperature factors for non-hydrogen atoms, components of the anisotropic temperature factors, hydrogen atom positional parameters, and observed and calculated structure factor amplitudes have been deposited with the Editor.

RESULTS AND DISCUSSION

π Donor–acceptor compounds, such as the typical TTF·TCNQ, have aroused a strong interest because of their unusual solid-state properties, and

Table 2. Bond lengths (Å) and bond angles (°) with ESDs in parentheses

Bond lengths (Å)		Bond angles (°)	
Ni—S(1)	2.138(1)	S(1)—Ni—S(2)	93.1(1)
Ni—S(2)	2.159(1)	Ni—S(1)—C(1)	102.8(1)
S(1)—C(1)	1.705(4)	Ni—S(2)—C(2)	102.1(1)
S(2)—C(2)	1.717(4)	C(1)—S(3)—C(3)	97.3(2)
S(3)—C(1)	1.740(4)	C(2)—S(4)—C(3)	97.4(2)
S(3)—C(3)	1.720(4)	S(1)—C(1)—S(3)	122.5(2)
S(4)—C(2)	1.736(4)	S(1)—C(1)—C(2)	121.3(3)
S(4)—C(3)	1.730(4)	S(3)—C(1)—C(2)	116.1(3)
S(5)—C(3)	1.642(4)	S(2)—C(2)—S(4)	123.5(2)
C(1)—C(2)	1.357(5)	S(2)—C(2)—C(1)	120.7(3)
		S(4)—C(2)—C(1)	115.9(3)
		S(3)—C(3)—S(4)	113.3(2)
		S(3)—C(3)—S(5)	122.7(3)
		S(4)—C(3)—S(5)	124.0(2)
S(6)—C(7)	1.720(4)	C(7)—S(6)—C(8)	103.4(2)
S(6)—C(8)	1.723(4)	C(5)—C(4)—C(6)	118.9(3)
C(4)—C(4)^{i}	1.451(6)	C(4)—C(5)—C(7)	125.8(3)
C(4)—C(5)	1.420(4)	C(4)—C(6)—C(8)	126.3(3)
C(4)—C(6)	1.412(4)	C(5)—C(7)—S(6)	122.8(3)
C(5)—C(7)	1.370(5)	S(6)—C(7)—C(21)	114.5(2)
C(6)—C(8)	1.365(5)	C(5)—C(7)—C(6)	122.7(3)
C(7)—C(21)	1.463(4)	S(6)—C(8)—C(6)	122.6(3)
C(8)—C(11)	1.476(4)	S(6)—C(8)—C(11)	115.3(2)
		C(6)—C(8)—C(11)	122.1(3)
		C(4)^{i}—C(4)—C(5)	120.9(3)
		C(4)^{i}—C(4)—C(6)	120.2(3)

Superscript i indicates inversion through a centre of symmetry.
In phenyl rings C—C = 1.395 Å, C—C—C = 120.0°.

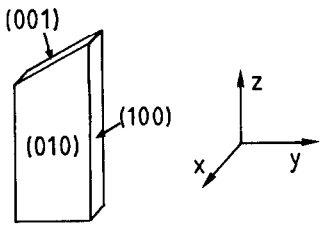

Fig. 2. Description of the single crystal used for the EPR experiments and the axes used for the discussion. The z axis is parallel to c; the x axis is parallel to $a \wedge c$ (i.e. parallel to b^*); the y axis is parallel to $c \wedge (a \wedge c)$.

especially their high conductivity. In such compounds, partial charge transfer between separately stacked donor and acceptor molecules leads to one-dimensionally delocalized systems. Among the many criteria suggested for the formation of these partial charge-transfer compounds, the relationship $E_{1/2}(D \rightarrow D^+ + e^-) - E_{1/2}(A + e^- \rightarrow A^-) = 0.1$–$0.4$ V between the half-wave redox potentials of the donor and the acceptor has been used for the selection of appropriate donor–acceptor pairs.[18–20]

On the basis of the redox potentials [$E_{1/2}$ ($DIPS\Phi_4 \rightarrow DIPS\Phi_4^+ + e^-$) ~ 0.20 (0.28 V[10b]) and $E_{1/2}(Ni(dmit)_2 + e^- \rightarrow [Ni(dmit)_2]^-)$ ~ 0.21 V, vs Ag/AgCl], the charge transfer between the $DIPS\Phi_4$ and $Ni(dmit)_2$ moieties in $(DIPS\Phi_4)[Ni(dmit)_2]$ should be close to one, leading to $(DIPS\Phi_4)^+$ and $[Ni(dmit)_2]^-$ ionic species. This result would be consistent with the low compaction-powder conductivity (lower than 10^{-5} S cm^{-1} at room temperature) of this compound and its 1 : 1 stoichiometry.

The 1 : 1 stoichiometry of $(DIPS\Phi_4)[Ni(dmit)_2]$ has been estimated by elemental analysis, and confirmed by the X-ray structural determination.

The unit cell contains one $Ni(dmit)_2$ and one $DIPS\Phi_4$, the molecular centre of each lying on a crystallographic centre of symmetry (Fig. 3); the proposed 1 : 1 stoichiometry is thus confirmed. As usual, the $Ni(dmit)_2$ unit is fairly close to planarity. However, in the dmit ligand the outermost atoms, C(3) and S(5), deviate significantly from the plane of the inner atoms (Table 3). The planes of the inner atoms of the two dmit moieties of a $Ni(dmit)_2$ unit

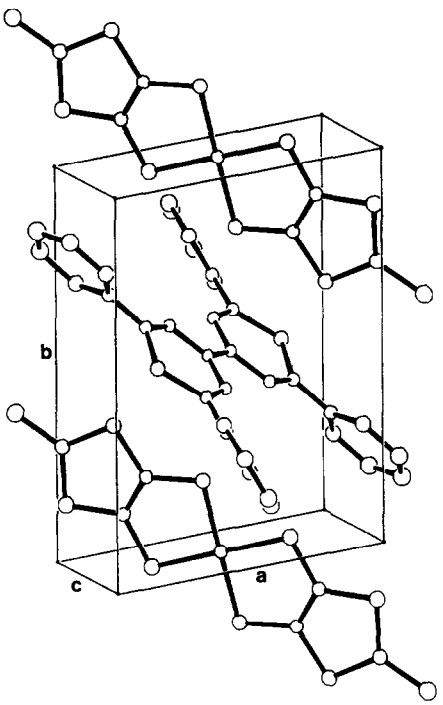

Fig. 3. Perspective view of the unit cell content.

are parallel by symmetry but apart by 0.04 Å; when a plane is fitted to all the atoms of a $Ni(dmit)_2$ unit the maximum deviation is 0.05 Å for S(5). A similar analysis of planarity can be made for the heterocyclic ring of $DIPS\Phi_4$. In each ring, the S(6) atom is well off the plane of the carbon atoms (Table 3); the ring can be considered as folded by 5° about a line between S(6) and C(4). Planes fitted to the rings are parallel by symmetry but apart by 0.15 Å; when a plane is fitted to all the atoms of the heterocyclic ring the maximum deviation is 0.07 Å for C(7). The deviation from planarity is similar, though less important, to that observed for the neutral $DIPS\Phi_4$.[21] In the polyiodides $(DIPS\Phi_4)I_x$ the two thiapyranylidene rings are not parallel but twisted by ~ 20° relative to each other.[10a,11]

Table 3. Deviations (Å) of atoms from their least-squares planes and dihedral angles (°)

Plane I		Plane II	
Atoms	Deviations	Atoms	Deviations
Ni*	−0.021	C(4)*	0.013
S(1)*	0.004	C(5)*	−0.003
S(2)*	−0.005	C(6)*	−0.019
S(3)*	−0.005	C(7)*	−0.003
S(4)*	0.005	C(8)*	0.011
S(5)	−0.068	S(6)	0.097
C(1)*	0.002		
C(2)*	−0.006		
C(3)*	−0.029		

Dihedral angles: I–II: 87.8; II–Φ(1): 30.4; II–Φ(2): 43.3; Φ(1)–Φ(2): 27.0.

Starred atoms have been used to define the plane.

Luss and Smith[21] have compared the bond lengths in the dithiapyranylidene double ring for the neutral and oxidized $DIPS\Phi_4$ species. It is worthy to extend this comparison to $(DIPS\Phi_4)[Ni(dmit)_2]$ since it has been shown that, in some cases, bond lengths in radical ions can be related to the amount of charge transfer.[22] From Table 4, it seems that the central C(4)—C(4)′ bond is the most sensitive to charge transfer as in the case of TTF.[23] Whatever the case, Table 4 clearly shows that bond lengths in $(DIPS\Phi_4)[Ni(dmit)_2]$ are close to those observed in the more oxidized species and consistent with the high charge transfer previously suggested. It would have been useful to ascertain this observation using bond lengths in the $Ni(dmit)_2$ unit. Unfortunately, as pointed out before,[1] the poor accuracy and dispersion of available results prevent drawing reliable conclusions from such a comparison.

The crystal structure can be described as being composed of stacks of $Ni(dmit)_2$ units along [001]. These stacks are arranged in layers parallel to (010) alternating with layers of $DIPS\Phi_4$. However, the stacking of the $Ni(dmit)_2$ units is very loose since the repeat parameters are more than 10 Å in both the [001] and [100] directions. This is reflected in the low density of the material (1.58 g cm^{-3}). As a result, there is no strong intermolecular interaction between the $Ni(dmit)_2$ units: the shortest intermolecular S···S distance is 3.69 Å. As a matter of fact, the "stacking" of the $Ni(dmit)_2$ units is governed by the spatial arrangement of the large $DIPS\Phi_4$ units. The central plane of the $DIPS\Phi_4$ units is perpendicular to the molecular plane of the $Ni(dmit)_2$ units (Table 3), so that they can be considered arranged side by side with almost no overlap in-between. The shortest S(6)···S distance is 4.11 Å, and thus no significant intermolecular interaction is observed between the $DIPS\Phi_4$ and the $Ni(dmit)_2$ units.

Although donor and acceptor molecules are arranged in segregated layers, the looseness of stacking of $Ni(dmit)_2$, the side by side arrangement of $DIPS\Phi_4$ and the absence of intermolecular interaction are consistent with the electrical behaviour of this material.

Since the $(DIPS\Phi_4)^+$ and $[Ni(dmit)_2]^-$ species should each carry a single unpaired electron, two single unpaired spins should be observed in the EPR spectrum of $(DIPS\Phi_4)[Ni(dmit)_2]$. In apparent contradiction with the small intermolecular inter-

Table 4. Comparison of bond lengths in neutral and oxidized $DIPS\Phi_4$. For convenience, atoms have been numbered according to Fig. 1

Bond References	$DIPS\Phi_4$ 22	$(DIPS\Phi_4)(I_3)_{0.72}$ 11	$(DIPS\Phi_4)(I_3)_{0.76}$ 10a	$(DIPS\Phi_4)(I_3)_{0.36}(I_5)_{0.40}$ 11	$(DIPS\Phi_4)$3.3–3.45I 10a	$(DIPS\Phi_4)[Ni(dmit)_2]$ This work
S(6)—C(8)	1.742	1.715	~ 1.716[a]	1.729	[b]	1.723
S(6)—C(7)	1.747		~ 1.713[a]			1.720
C(6)—C(8)	1.341	1.366	~ 1.331[a]	1.360	[b]	1.365
C(5)—C(7)	1.337		~ 1.340[a]			1.370
C(4)—C(4)[i]	1.389	1.442	~ 1.424[a]	1.447	[b]	1.451
C(4)—C(6)	1.442	1.422	~ 1.444[a]	1.417	[b]	1.412
C(4)—C(5)	1.439		~ 1.472[a]			1.420
C(8)—C(11)	1.477	1.482	~ 1.418[a]	1.465	[b]	1.476
C(7)—C(21)	1.482		~ 1.433[a]			1.463
Charge transfer	0	0.72	0.76	0.76	0.9–1	~ 1

[a] Averaged bond lengths for a disordered model refined in the orthorhombic space group *Pbam*.

[b] Bond lengths in $(DIPS\Phi_4)$3.3–3.45I cannot be determined from partial two-dimensional crystallographic data.[10a] However, the cell parameters of this salt are almost identical to those of $(DIPS\Phi_4)(I_3)_{0.36}(I_5)_{0.40}$.[11]

Table 5. Principal values of the g-tensor. Capitals refer to the principal axes of the g-tensor; minuscules refer to the crystal geometric axes (Fig. 2)

$g_{XX} = 2.0033$	$(X,x) = 35°$	$(X,y) = 123°$	$(X,z) = 100°$
$g_{YY} = 2.0353$	$(Y,x) = 102°$	$(Y,y) = 90°$	$(Y,z) = 168°$
$g_{ZZ} = 2.0462$	$(Z,x) = 58°$	$(Z,y) = 33°$	$(Z,z) = 97°$

action expected, only one signal was observed in the entire range of temperature investigated (300–4 K). It is noteworthy that the average g-value of this signal, 2.028 (determined on a single crystal; see below and Table 5) is intermediate between that of $(DIPS\Phi_4)^+$ species generated in solution by electrolysis, 2.007 (determined on a CH_2Cl_2 frozen solution) and that of a $[Ni(dmit)_2]^-$ salt, 2.049 (determined on a single crystal of $(n\text{-}Bu_4N)[Ni(dmit)_2]$[24]). This observation alone suggests some kind of spin-exchange coupling between both the $(DIPS\Phi_4)^+$ and $[Ni(dmit)_2]^-$ moieties in $(DIPS\Phi_4)[Ni(dmit)_2]$.

At room temperature, the single-crystal EPR spectra of $(DIPS\Phi_4)[Ni(dmit)_2]$ show a single broad line for any orientation. The g-factor differs from that of the free electron, indicating a strong spin–orbit coupling. Such a high value ($g \sim 2.03$) is in favour of a contribution of the nickel atom to the spin–orbit coupling, the two heteroatoms involved in $DIPS\Phi_4$ could not alone assume this coupling. This point has already been reported for similar complexes.[25,26] The broad line width (of the order of 25 G) confirms the role of the magnetic moment of the metal on the properties of this complex. The anisotropy of the g-factor is strong (Fig. 4; Table 5). One of the principal axis is in the xOz plane. The lowest eigenvalue corresponding to nearly the free

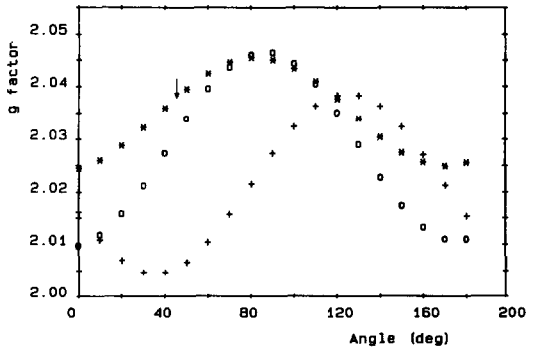

Fig. 4. Angular variation of the g-factor of a single crystal of $(DIPS\Phi_4)[Ni(dmit)_2]$ in three orthogonal planes. ○: rotation in the xOz plane, with $H_0 \| Oz$, for $\theta = 0$; +: rotation in the yOz plane, with $H_0 \| Oz$, for $\theta = 0$; *: rotation in the xOy plane with $H_0 \| Oy$, for $\theta = 0$.

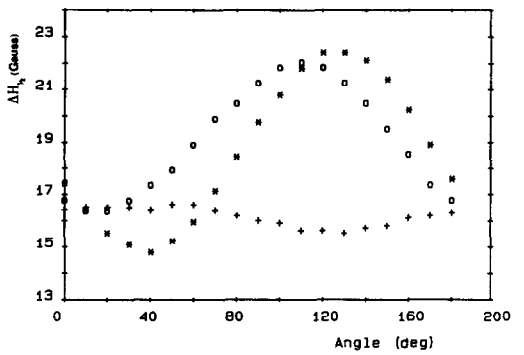

Fig. 5. Angular variation of the half width at half power, $\Delta H_{1/2}$, of a single crystal of $(DIPS\Phi_4)[Ni(dmit)_2]$ in three orthogonal planes. See Fig. 4 for orientation conventions.

electron g-factor ($g_{xx} = 2.0033$) is related to the lowest spin–orbit coupling which is mainly due to the $[Ni(dmit)_2]$ complex moiety. The associated direction should be then nearly perpendicular to the plane of this molecule. Projection in the (010) plane of both the lowest g-factor direction and the perpendicular to the plane of the $[Ni(dmit)_2]$ complex show an angle with the z or c axis of 33 and 19°, respectively.

The angular variation of the EPR line width of this system (Fig. 5) is driven by the dipolar electronic spin–spin interaction; its anisotropy, when rotating the crystal in the applied magnetic field, shows a $(1+\cos^2\theta)$ dependence, characteristic of a three-dimensional spin diffusion.[27] The directions of the extremal values of the line width are not indentified to the principal axes of the g-tensor. The important dipolar coupling (broad line) confirms the partial molecular delocalization of the π electrons' spin nearby the nickel atoms. Both types of molecule are clearly implied in the magnetic properties; the single line indicates interstack spin exchange.

The variation of the susceptibility as a function of the temperature has been measured on one single crystal in the range 4–300 K (Fig. 6). A Curie–Weiss law is observed for temperatures higher than 30 K with a Curie–Weiss constant of $\theta_{cw} \sim 30$–50 K, confirming the antiferromagnetic spin exchange. In the same temperature range, and for a particular orientation, the line width continuously decreases (from 17 G down to 5 G; Fig. 7), whereas the g-factor increases (Fig. 8). When the temperature is lowered, the susceptibility deviates from the linear fit; the line width goes through a minimum and increases, while the g-factor strongly increases from the room temperature value, 2.036, up to 2.063 at liquid helium temperature.

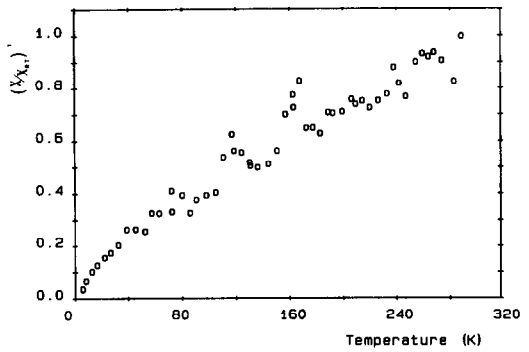

Fig. 6. Inverse of the normalized susceptibility as a function of the temperature of a single crystal of $(DIPS\Phi_4)[Ni(dmit)_2]$. The noisy signal linked to the small size of the crystal explains the spread-over of the points of the susceptibility obtained by double integration of the EPR spectra.

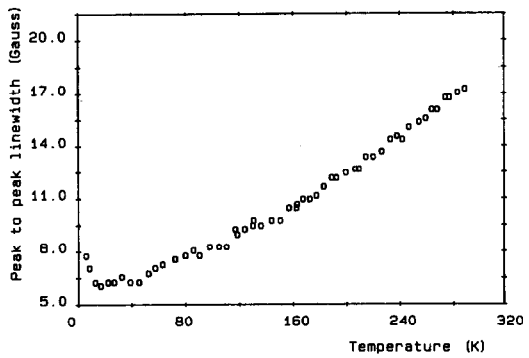

Fig. 7. Temperature dependence of the peak-to-peak line width of a single crystal of $(DIPS\Phi_4)[Ni(dmit)_2]$ for a peculiar orientation (indicated by an arrow in Fig. 4).

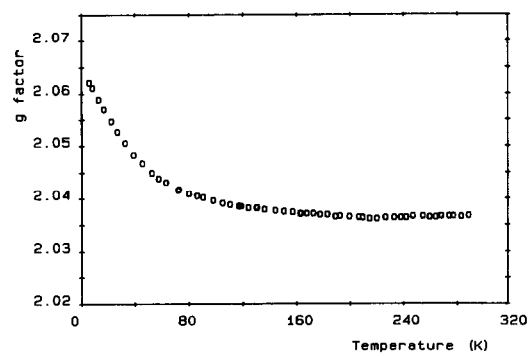

Fig. 8. Temperature dependence of the g-factor of a single crystal of $(DIPS\Phi_4)[Ni(dmit)_2]$ in the same orientation as in Fig. 7.

The decrease of the line width with decreasing temperature is very similar to that observed in the family of organic conductors, $(TMTSeF)_2X$, for example.[28] The simultaneous increase of the g-factor is also similar to that observed in these latter systems, but the susceptibility behaviour of both systems is very different. For $(DIPS\Phi_4)[Ni(dmit)_2]$, this temperature-dependence of the susceptibility, associated with the low value of the conductivity observed on a compressed powder and with the absence of any Dysonian EPR line shape, discarded a metallic behaviour; this system is likely to be a semiconductor. As no low-dimensional spin diffusion occurs in this system, and in view of the crystal structure, the gap should not be related to a Peierls distortion; this complex probably is, as previously inferred from the redox potential values, a highly electron-correlated system with a complete charge transfer from the donor to the acceptor.

In a situation of three-dimensional exchange narrowing limit, the line width is described by the model of Anderson and Weiss,[29] in which the line width is governed by the ratio $\omega_e/\omega_p{}^2$, where ω_e is the spin exchange frequency and ω_p is the characteristic frequency of the dipolar couplings. When the temperature is lowered, both interactions vary. The g-factor and the dipolar coupling increases are due to the nickel atoms (EPR silent), whereas the decrease of the line width reflects the stronger exchange between both π systems. The two phenomena may be simply related to lattice contraction which affect more efficiently the spin–spin exchange than the long range dipolar interactions.

Acknowledgements—Financial assistance from the CICYT (Grant No. PB88/0197) and from a "France-Spain Integrated Action" (Grant No. 048; 1989) is acknowledged. We thank D. de Montauzon and C. Faulmann for electrochemical measurements.

REFERENCES

1. M. Bousseau, L. Valade, J.-P. Legros, P. Cassoux, M. Garbauskas and L. V. Interrante, *J. Am. Chem. Soc.* 1986, **108**, 1908.
2. L. Brossard, M. Ribault, L. Valade and P. Cassoux, *Physica B&C.* 1986, **143B**, 378.
3. A. Kobayashi, H. Kim, Y. Sasaki, R. Kato and H. Kobayashi, *Solid State Commun.* 1987, **62**, 57.
4. H. Kobayashi, R. Kato, A. Kobayashi and Y. Sasaki, *Chem. Lett.* 1985, 535.
5. R. Kato, H. Kobayashi, A. Kobayashi and Y. Sasaki, *Chem. Lett.* 1985, 131.
6. J. Alizon, J.-P. Blanc, J. Galice, H. Robert, C. Fabre, H. Strzelecka, J. Rivory and C. Weyl, *Lecture Notes Phys.* 1977, **65**, 563.
7. H. Strzelecka, J. Rivory and W. Schönfelder, *Molec. Cryst. Liq. Cryst.* 1979, **52**, 307.
8. (a) H. Strazelecka, C. Weyl and J. Rivory, *Int. Conf. on Quasi One-Dimensional Conductors, Dubrovnick, Yugoslavia.* 4–8 September 1978; *Lecture Note Phys.* 1979, **96**, 348; (b) H. Strzelecka and J. Rivory, *Mater. Res. Bull.* 1980, **15**, 897; (c) P. A. Albouy,

J. P. Pouget and H. Strzelecka, *Phys. Rev. B* 1987, **35**, 173 (and refs therein).
9. L. C. Isett, G. A. Reynolds, E. M. Schneider and J. H. Perlstein, *Solid State Commun.* 1979, **30**, 1.
10. (a) D. Chasseau, J. Gaultier, C. Hauw, S. Lefrant, J. Rivory, E. Rzepka and H. Strzelecka, *Solid State Commun.* 1980, **34**, 873; (b) V. Gionis, R. Fugnitto, G. Mayer, H. Strzelecka and J. C. Dubois, *Molec. Cryst. Liq. Cryst.* 1982, **90**, 153 (and refs therein).
11. H. R. Luss and D. L. Smith, *Acta Cryst.* 1980, **B36**, 1580.
12. G. Steimecke, H. J. Sieler, R. Kirmse and E. Hoyer, *Phosphorus and Sulfur* 1979, **7**, 49.
13. C. Fabre, R. Fugnitto and H. Strzelecka, *C. R. Acad. Sci. Paris, Série C.* 1976, **282**, 175.
14. L. Valade, J.-P. Legros, D. de Montauzon, P. Cassoux and L. V. Interrante, *Israel J. Chem.* 1986, **27**, 353.
15. P. Cassoux, R. Dartiguepeyron, P. L. Fabre and D. de Montauzon, *Electrochim. Acta* 1985, **30**, 1485.
16. R. Vicente, J. Ribas, C. Zanchini, D. Gatteschi, J.-P. Legros, C. Faulmann and P. Cassoux, *Z. Naturfor.* 1988, **43b**, 1137.
17. B. Mabad, P. Cassoux, J.-P. Tuchagues and D. N. Hendrickson, *Inorg. Chem.* 1986, **25**, 1420.
18. R. C. Wheland, *J. Am. Chem. Soc.* 1976, **98**, 3926.
19. L. Interrante, J. Bray, H. Hart Jr., J. Kasper and P. Piacente, *Ann. N.Y. Acad. Soc.* 1978, **313**, 407.
20. J. B. Torrance, *Accts Chem. Res.* 1979, **12**, 79.
21. H. R. Luss and D. L. Smith, *Acta Cryst.* 1980, **B36**, 986.
22. S. Flandrois and D. Chasseau, *Acta Cryst.* 1977, **B33**, 2744.
23. J.-P. Legros, M. Bousseau, L. Valade and P. Cassoux, *Molec. Cryst. Liq. Cryst.* 1983, **100**, 181.
24. R. Kirmse, J. Stach, W. Dietzsch, G. Steimecke and E. Hoyer, *Inorg. Chem.* 1980, **19**, 2679.
25. M. Weber, PhD thesis, p. 57. Paris (1987).
26. G. A. Bowmaker, P. D. W. Boyd and G. K. Campbell, *Inorg. Chem.* 1983, **22**, 1208.
27. D. L. Huber, *Phys. Rev.* 1972, **B6**, 3180.
28. H. J. Pedersen, J. C. Scott and K. Bechgaard, *Phys. Rev.* 1981, **B24**, 5014.
29. P. W. Anderson and P. R. Weiss, *Rev. Mod. Phys.* 1953, **25**, 269.

Polyhedron Vol. 10, No. 7, pp. 697–702, 1991
Printed in Great Britain

0277–5387/91 $3.00+.00
© 1991 Pergamon Press plc

HYDROLYSIS OF CYCLOPENTA-, CYCLOHEPTA-, LINEAR PENTA- AND HEPTAPHOSPHATE IN AQUEOUS SOLUTION

GENICHIRO KURA

Department of Chemistry, Fukuoka University of Education,
Akama, Munakata, Fukuoka 811-41, Japan

(*Received* 16 *July* 1990; *accepted* 26 *November* 1990)

Abstract—The hydrolysis rates and activation energies of cyclopenta- and cycloheptaphosphate, which were isolated by the use of a QAE-Sephadex A-25 column, have been measured in both acidic and alkaline solutions. The rate data for the linear pentamer and heptamer have also been determined. The reaction mechanism of the hydrolysis of these condensed phosphates is discussed by comparing the rate data with those for other polyphosphates.

Condensed phosphates are useful materials as inorganic polyvalent electrolytes.[1] We have studied various chemical properties of cyclopolyphosphates with a polymerization degree smaller than eight.[2–5] Research into the hydrolysis reactions of cyclopoly- and linear polyphosphates with polymerization degrees 3, 4, 6 and 8 in aqueous solutions has recently been undertaken using the automated liquid chromatographic system.[6] Cyclopolyphosphates with polymerization degrees 3, 4, 6 and 8 can be relatively easily prepared,[7,8] as can linear tri- and tetraphosphate.[9] Sample solutions containing sufficient quantities of linear hexa- or octaphosphate for the hydrolysis study were prepared by partial hydrolysis of cyclohexa- or cyclooctaphosphate, respectively. However, preparation of cyclopenta- and cycloheptaphosphate in sufficient quantities is difficult and therefore their chemical properties have not been investigated. These two cyclopolyphosphates are known to be minor components of Graham's salt and their isolation from the salt was first achieved by Kura and Ohashi[2] using a QAE-Sephadex A-25 column.

In this study, the hydrolysis rates and activation energies of cyclopenta- and cycloheptaphosphate, isolated from the column, in 0.1 M HCl and 0.5 M NaOH were determined by automated liquid chromatography. The data thus obtained were compared with those for other cyclopolyphosphates. Hydrolysis reactions of linear penta- and heptaphosphate were similarly investigated and analysed.

In the figures and tables in this paper, cyclopolyphosphates and linear polyphosphates are abbreviated as P_{nm} and P_n, respectivly, where n is the polymerization degree.

EXPERIMENTAL

Graham's salt, $(NaPO_3)_n$, was synthesized by heating monosodium dihydrogen orthophosphate at 1000°C for approx. 2 h and rapidly cooling on an aluminium plate. A cyclopolyphosphate mixture was obtained from Graham's salt by acetone fractionation.[2] Cyclopenta- and cycloheptaphosphate were isolated from the mixture using a QAE-Sephadex A-25 column (85 cm in length and 1.5 cm in diameter).[2] As an eluting reagent, 0.3 M potassium chloride was used. Details of the hydrolysis procedure and the analytical system have been described in my previous paper.[6]

The mixture of cyclopolyphosphates contained in Graham's salt was concentrated by acetone fractionation[10] and cyclopenta- and cycloheptaphosphate in the mixture were isolated by the use of a QAE-Sephadex A-25 column. On partial hydrolysis of cyclopenta- and cycloheptaphosphate in 0.5 M LiOH for about 8 h at 40°C, the sample solutions containing the respective linear penta- and heptaphosphate to be hydrolysed were obtained. Using these samples, the hydrolysis rates of cyclic and linear phosphates with polymerization degrees 5 and 7 were determined in 0.1 M HCl and 0.5 M NaOH.

RESULTS AND DISCUSSION

The concentration of cyclopoly- and linear phosphates with the same polymerization degree at time t are denoted as x and y, and the first-order hydrolysis rate constants are defined as k_m and k_n, respectively. The following rate equations can be derived:

$$-dx/dt = k_m x \quad (1)$$

$$-dy/dt = -k_m x + k_n y. \quad (2)$$

The concentrations of cyclopolyphosphates at time t, which were experimentally determined, were substituted in a modified version of eq. (1) and k_m values were determined. The chromatograms of the hydrolysis samples of cyclopenta- and cycloheptaphosphate in 0.1 M HCl are shown as examples in Fig. 1(a) and (b). The cyclotriphosphate peak is observed in the chromatograms. The phosphate is known to be formed during the hydrolysis reactions of linear polyphosphates. The reaction rates of cyclopenta- and cycloheptaphosphate at various temperatures are shown in Fig. 2(a) and (b). The phosphate concentration at time 0 and t are defined as $[P]_0$ and $[P]_t$, respectively, and the good linear relationship between $\log([P]_t/[P]_0)$ vs t [as shown in Fig. 2(a) and (b)] reveals that the hydrolysis reaction of both phosphates is strictly first-order.

Employing k_m calculated from the slope of the straight lines in Fig. 2 and using eq. (2), the rate constants for linear penta- and heptaphosphate, k_n, were determined simultaneously from the data obtained by the analysis of the same chromatograms. Thus the obtained values k_m and k_n reproduce the experimental data. Figure 3(a) and (b) show the time dependence of the concentration of penta- and heptaphosphate during the course of hydrolysis, where the full lines represent the calculation of substituting k_m and k_n into eq. (2) and the circles indicate the experimental points. In a similar manner, the hydrolysis rates of the cyclic and linear pentamer and heptamer in 0.5 M NaOH were determined. Since these phosphates are comparatively stable in alkaline solution, taking into account the experimental error, the rates at higher temperatures, 70, 80 and 90°C, were measured. Hydrolysis rates of cyclopenta- and cycloheptaphosphate are shown in Fig. 4(a) and (b), and those of linear penta- and heptaphosphate are schematically shown in Fig. 5(a) and (b). The Arrhenius activation energies of the four phosphates in 0.1 M HCl and 0.5 M NaOH were obtained from the temperature dependence of log k_m or log k_n. The Arrhenius plots are shown in Figs 6 and 7. The hydrolysis rate constants in 0.1 M HCl and 0.5 M NaOH at various temperatures are shown in Tables 1 and 2. The rate constants in 0.5 M NaOH at 50°C are predicted values obtained by the extrapolation of the Arrhenius plots. The activation energies, E_a, are presented in Tables 1 and 2, along with the rate

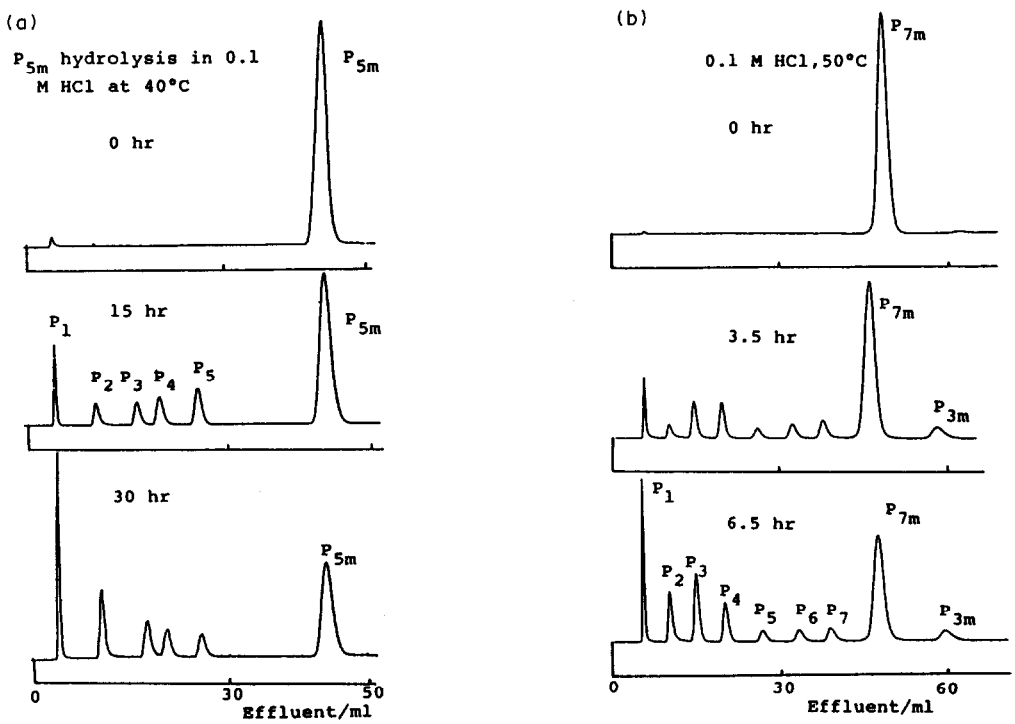

Fig. 1. Chromatograms of the hydrolysis samples in 0.1 M HCl.

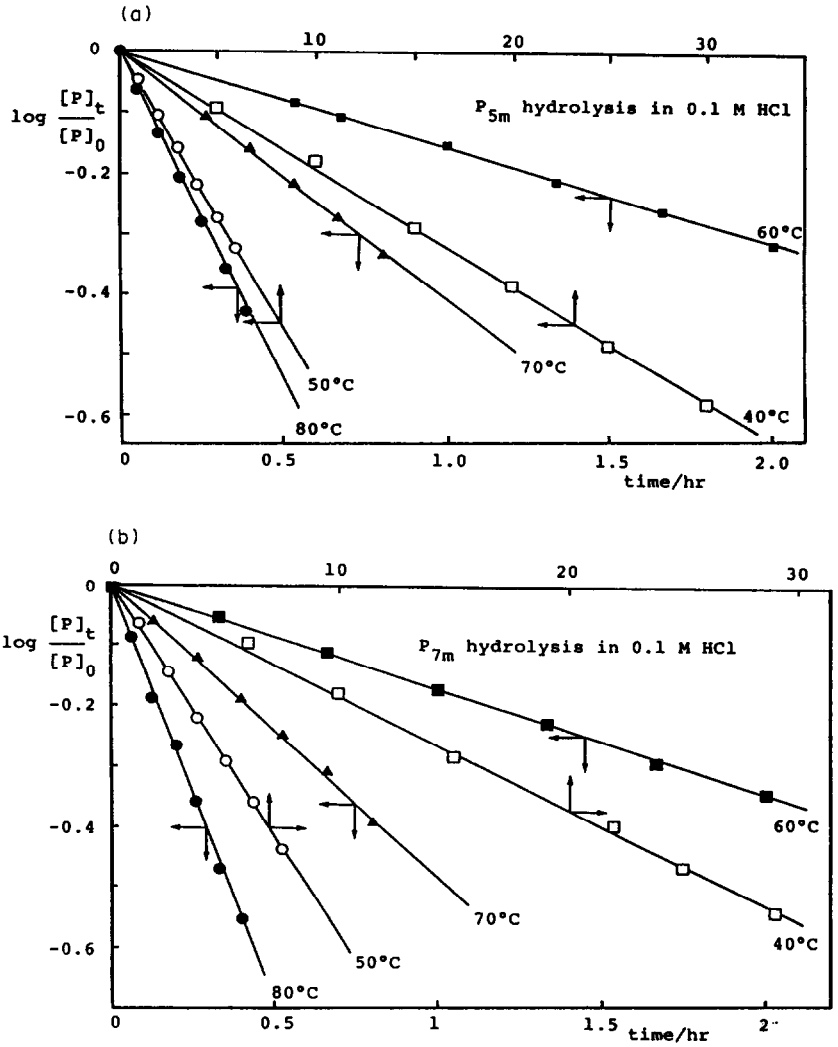

Fig. 2. Hydrolysis of cyclopenta- and cycloheptaphosphate in 0.1 M HCl.

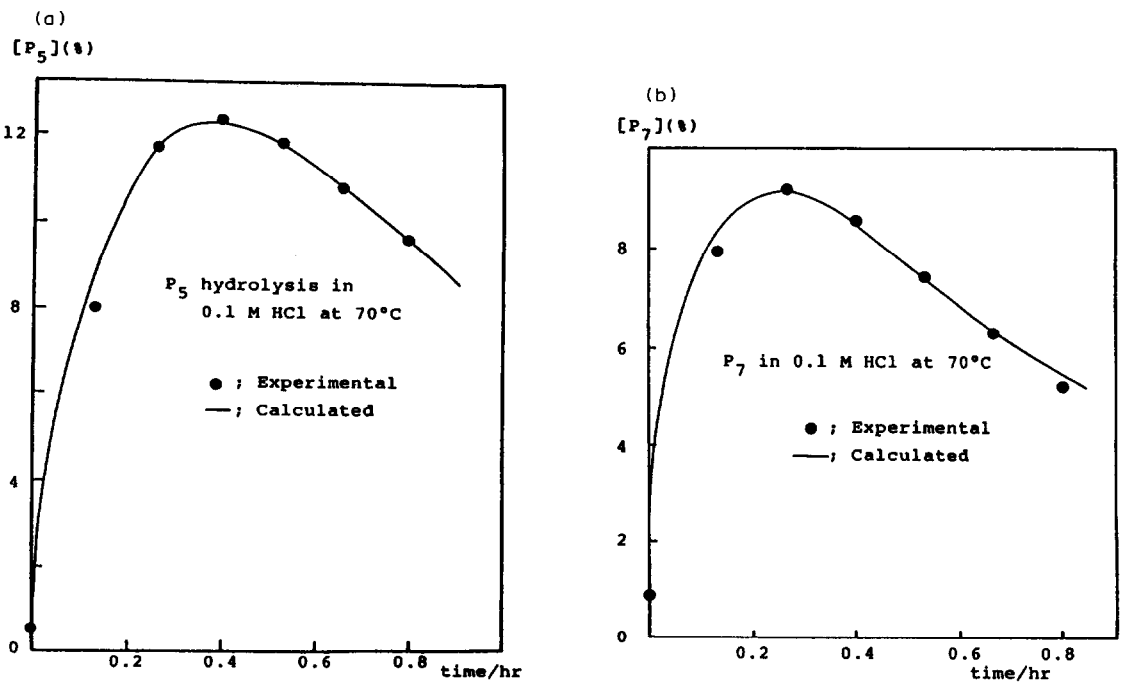

Fig. 3. Hydrolysis of linear penta- and heptaphosphate in 0.1 M HCl at 70°C.

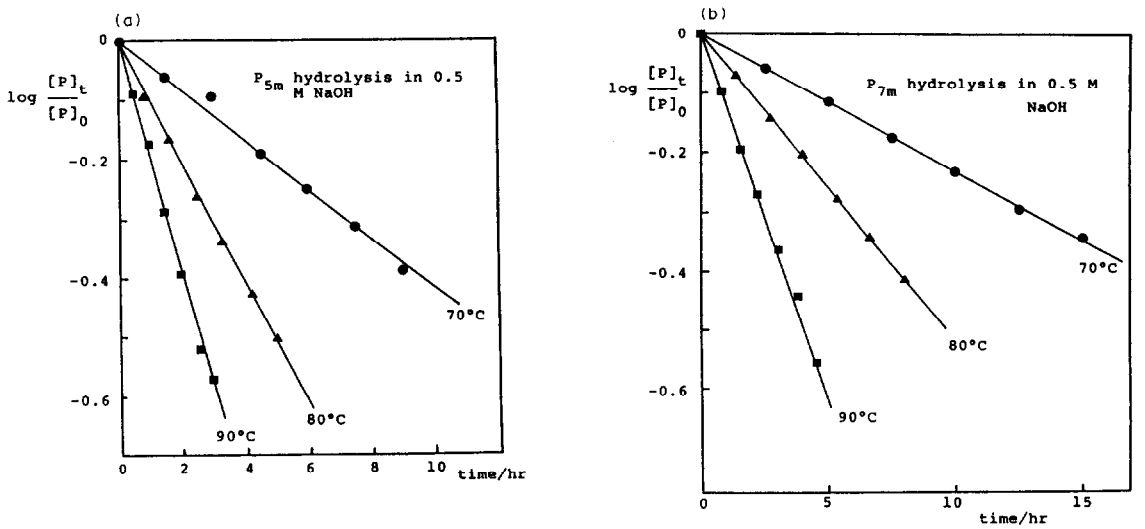

Fig. 4. Hydrolysis of cyclopenta- and cycloheptaphosphate in 0.5 M NaOH.

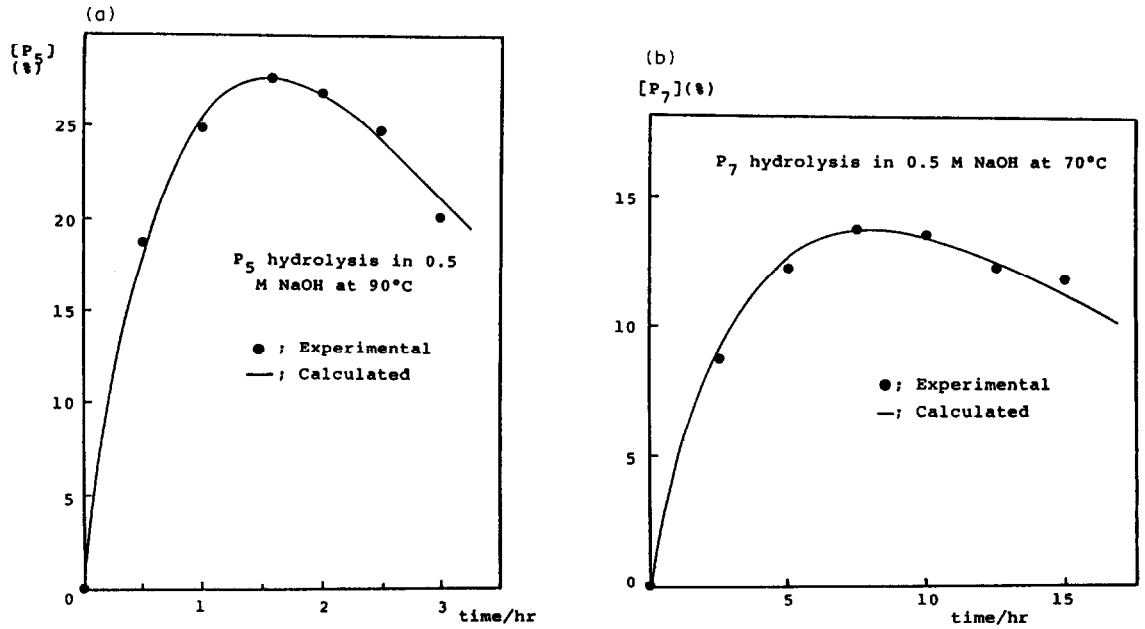

Fig. 5. Hydrolysis of linear penta- and heptaphosphate in 0.5 M NaOH at 90 and 70°C, respectively.

Table 1. Rate constants and activation energies in 0.1 M HCl

	k_m or k_n (h^{-1})			
	P_{5m}	P_5	P_{7m}	P_7
40°C	0.0432	0.265	0.0429	0.475
50°C	0.128	0.764	0.136	1.54
60°C	0.367	2.07	0.411	3.83
70°C	0.948	5.31	1.13	9.29
80°C	2.32	12.8	3.05	23.2
E_a (kcal mol^{-1})	22.0	21.4	23.3	21.0

Table 2. Rate constants and activation energies in 0.5 M NaOH

	k_m or k_n (h^{-1})			
	P_{5m}	P_5	P_{7m}	P_7
(50°C)	(0.0166)	(6.76×10^{-3})	(7.41×10^{-3})	(0.0234)
70°C	0.0944	0.0783	0.0520	0.242
80°C	0.219	0.271	0.121	0.654
90°C	0.472	0.799	0.283	1.83
E_a (kcal mol^{-1})	18.9	27.1	21.0	25.1

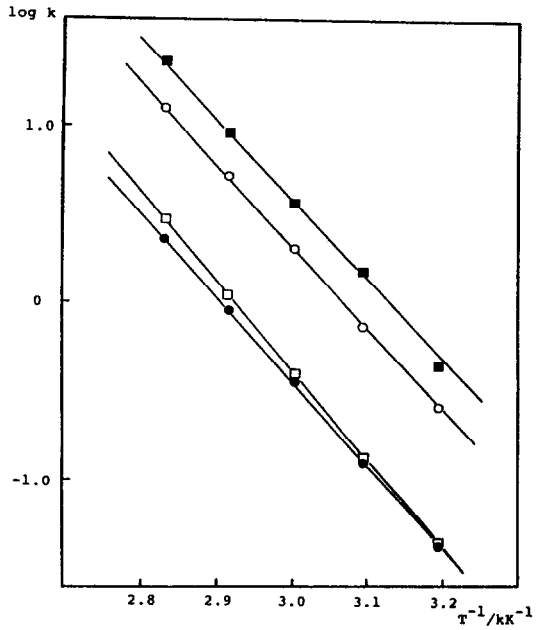

Fig. 6. Arrhenius plots for cyclopenta-, cyclohepta-, linear penta- and heptaphosphate in 0.1 M HCl: ●—●, P_{5m}; ○—○, P_5; ■—■, P_{7m}; □—□, P_7.

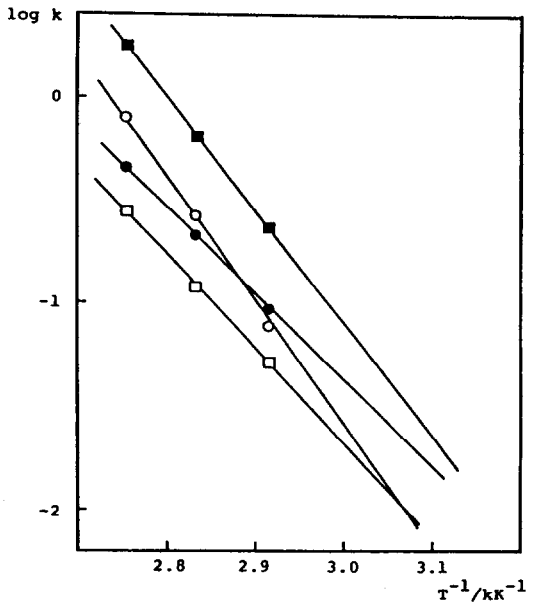

Fig. 7. Arrhenius plots for cyclopenta-, cyclohepta-, linear penta- and heptaphosphate in 0.5 M NaOH: ●—●, P_{5m}; ○—○, P_5; ■—■, P_{7m}; □—□, P_7.

constants. Four of the phosphates are hydrolysed faster in acidic solution than in alkaline solution. Linear oligophosphates contain terminal PO^- groups which are very strong Brønsted bases and combine with the H^+ ions in acidic solution. These bond formations accelerate the P—O—P bond cleavage by nucleophilic attack of H_2O on the P atoms. For the cyclopolyphosphates, as the polymerization degree becomes higher, 5 or 7, the binding to a proton becomes stronger.[3] The fast cleavage of the cyclic oligomer in acidic solution may be interpreted in the same manner as for the linear phosphates. For both pentamer and heptamer, the hydrolysis rates of the linear oligomers in acidic solution are faster. This fact is attributable to the basic strength of the terminal PO^- group in the linear oligomers.

In alkaline solution at 50°C, the rate of cleavage of the cyclic pentamer is faster than that of the linear pentamer, and on the contrary, for the heptamer the linear phosphate is hydrolysed faster.

There are no large differences between the activation energies of both linear and cyclic oligomers in acidic solution, whereas in alkaline solution, the activation energies of the linear pentamer and heptamer are higher by about 4–8 kcal mol^{-1}. The nucleophilic attack of OH^- on the P atoms in alkaline solution occurs more easily in the hydrolysis of the cyclic oligomers. The electrostatic repulsion of OH^- and PO^- groups in the linear oligomers is predicted to be stronger.

For comparison sake, the rate data for the pentamers and heptamers in 0.1 M HCl and 0.5 M NaOH are illustrated in Figs 8 and 9, along with the data for the cyclic and linear oligomers with

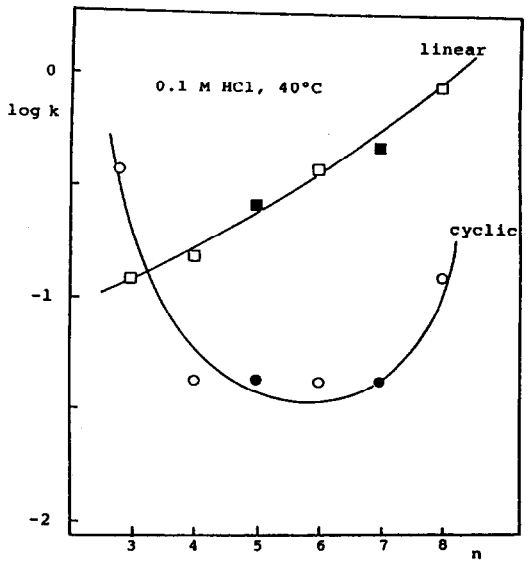

Fig. 8. Rate constants for cyclic and linear oligophosphates in 0.1 M HCl at 40°C.

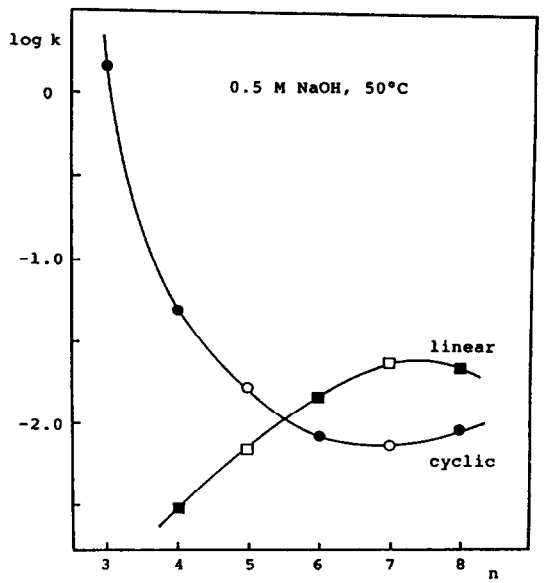

Fig. 9. Rate constants for cyclic and linear oligophosphates in 0.5 M NaOH at 50°C.

polymerization degrees 3, 4, 6 and 8.[11,12] In acidic solution, linear oligomers are hydrolysed faster than cyclic oligomers, except for cyclotriphosphate. For the linear phosphates, the rate gradually increases with increasing degree of polymerization. For the cyclic oligomers, the hydrolysis rate of the octamer becomes faster, which has been explained by greater interactions with the hydrogen ions due to the increased flexibility of the anion structure.[3] In alkaline solution, large differences are observed between the rates for cyclic and linear oligomers. However, with increasing polymerization degree the differences become smaller. For higher linear and cyclic oligomers, structural resemblance in the aqueous state is supposed. The faster rates for the lower cyclopolyphosphates are speculated to be ascribed to the ease of nucleophilic attack of OH^- on the P atoms on their strongly bending cyclic structures. During this research, the hydrolysis features in 0.1 M HCl and 0.5 M NaOH for all cyclic and linear oligomers with polymerization degrees of 3–8 have been elucidated.

Acknowledgements—The author expresses his deep gratitude to Miss Chie Osoegawa and Miss Miho Yano for their technical assistance.

REFERENCES

1. J. R. Van Wazer, *Phosphorus and its Compounds*. Interscience, New York (1958).
2. G. Kura and S. Ohashi, *J. Chromatogr.* 1971, **56**, 111.
3. G. Kura and S. Ohashi, *J. Inorg. Nucl. Chem.* 1976, **38**, 1151.
4. S. Ohashi, G. Kura, Y. Shimada and M. Hara, *J. Inorg. Nucl. Chem.* 1977, **39**, 1457.
5. G. Kura, *Polyhedron* 1986, **5**, 2097.
6. G. Kura, *J. Chromatogr.* 1988, **447**, 91.
7. E. J. Griffith and R. L. Buxton, *Inorg. Chem.* 1965, **4**, 549.
8. U. Schülke, *Z. Anorg. Allg. Chem.* 1968, **360**, 231.
9. E. J. Griffith, *J. Inorg. Nucl. Chem.* 1964, **26**, 1381.
10. E. Thilo and U. Schülke, *Z. Anorg. Allg. Chem.* 1965, **341**, 293.
11. G. Kura, *Bull. Chem. Soc. Japan* 1983, **56**, 3769.
12. G. Kura, *Bull. Chem. Soc. Japan* 1987, **60**, 2857.

Polyhedron Vol. 10, No. 7, pp. 703–709, 1991
Printed in Great Britain

0277–5387/91 $3.00+.00
© 1991 Pergamon Press plc

VOLUMES OF ACTIVATION FOR DISSOCIATION OF THE CATIONS OF [TRIS-2,2′-BIPYRIDYL]IRON(II), [TRIS-1,10-PHENANTHROLINE]IRON(II) AND OF OTHER DIIMINE IRON(II) COMPLEXES IN AQUEOUS SOLUTION

JOHN BURGESS and SASKIA A. GALEMA†

Department of Chemistry, University of Leicester, Leicester LE1 7RH, U.K.

and

COLIN D. HUBBARD‡

University of New Hampshire, Durham, NH 03824-3598, U.S.A.

(*Received* 1 *October* 1990; *accepted* 4 *December* 1990)

Abstract—The kinetics of dissociation of several iron(II) diimine complexes by aqueous hydroxide ions have been studied spectrophotometrically at atmospheric pressure and elevated pressures, at 298.2 K. Values of ΔV^* are between +10 and +16 $cm^3\ mol^{-1}$, and are interpreted as arising from a significant loss of electrostricted water from the hydroxide ion as it reacts with the iron(II) complex associatively. Dissociation of the $[Fe(5NO_2phen)_3]^{2+}$ and $[Fe(5Brphen)_3]^{2+}$ complexes in the presence of aqueous EDTA is reported. For both, ΔV^* is +22 $cm^3\ mol^{-1}$. These values can be understood by considering the reaction as a process comparable to aquation in acidic medium, a dissociative process. Activation enthalpy data support this idea.

Markedly positive activation volumes (ΔV^*) have been found for hydroxide and/or cyanide attack at low-spin iron(II) tris-diimine cations, $[Fe(bpy)_3]^{2+}$ (bpy = 2.2′-bipyridyl), $[Fe(phen)_3]^{2+}$ (phen = 1,10-phenanthroline)[1] and $[Fe(4Mephen)_3]^{2+}$ [2] in aqueous solutions. For a bimolecular reaction a value of about −10 $cm^3\ mol^{-1}$ is expected for ΔV^*.[3] For the former two ions, Stranks and co-workers,[1] although recognizing the possibility of a dominant role for desolvation of the attacking ion on forming the transition state, argued that the values of +19 to +22 $cm^3\ mol^{-1}$ pointed to a dissociative mode of activation. This interpretation was also proposed for cyanide ion displacement of ligand from $[Fe(CN)_5L]^{3-}$,[4,5] where L is 3,5-dimethylpyridine, imidazole or pyrazine, and was based upon a combination of analysis of atmospheric pressure kinetics results, and volume of activation data (ΔV^* is $\cong$ +20 $cm^3\ mol^{-1}$ and independent of departing ligand). The dissociative mechanism has been reiterated recently for base hydrolysis of several iron(II) complexes.[6] However, various features of some of these reactions are not yet resolved unambiguously and require further study and discussion.

On the basis of thorough kinetic studies of nucleophilic dissociation of $[Fe(phen)_3]^{2+}$, Margerum and Morgenthaler[7] concluded that the mechanism was associative. Except at very high nucleophile concentrations the rate law reduces to a two-term expression; one is for the aquation step and the second contains a first-order term in, for example, hydroxide ion concentration. Under typical reaction conditions, using a large excess of hydroxide ion over metal complex ion, the rate is dominated by the latter term, and thus the rate-determining step is second-order, and considered to be bimolecular and the mechanism associative. Dissociation of the complex ion can also occur in the presence of an acid or other reagents, for example, EDTA.[8,9] In these cases the reaction rate is independent of the concentration of the dissociating agent, and a ligand

† Permanent address: Department of Organic Chemistry, University of Groningen, Groningen, The Netherlands.

‡ Author to whom correspondence should be addressed.

molecule which has begun to separate from the ion is prevented from resuming coordination by being scavenged rapidly by a proton, in the presence of acid, or when EDTA is present the iron is scavenged. Dissociation by aquation is considered to be a dissociative mechanism.

Because of our interest in these reactions we have also proceeded to study the kinetics in selected cases, over a range of pressure, with the objective of gaining additional insight into reaction mechanism. Aquation in the presence of sulphuric acid of $[Fe(phen)_3]^{2+}$ and the 5-nitro and 4,7-dimethyl analogues yielded, at 308.2 K, ΔV^* values of +15.4, +17.9 and +11.6 $cm^3\ mol^{-1}$, respectively.[10] These results were rationalized in terms of a dissociative activation mode which consists of a two-ended partial dissociation of a phen bidentate ring, with different degrees of bond extension explaining the variation in ΔV^* values. The D mechanism for cyanide replacement of ligand in $[Fe(CN)_5L]^{3-}$ is predicated on the virtually constant degree of stretching of the Fe—N bond which gives rise to an invariant ΔV^*.[5] The hydrophilic cyanide ion has an unchanged state of solvation in the rate-determining step and the intrinsic component of ΔV^* completely dominates.

In considering bimolecular nucleophilic dissociation, the contribution of solvation effects to ΔV^* must be included and this will be especially significant for charged nucleophiles. This was illuminated by high pressure studies[11] on the reactions between $[Fe(ppsa)_3]^{4-}$ and OH^- (ppsa = **1**), and between $[Mo(CO)_4(bpy)]$ and CN^-,[3] the latter in dimethylsulphoxide. For the former case, ΔV^* is approximately zero, and ΔV^* is $-9\ cm^3\ mol^{-1}$ for the reaction of the molybdenum complex. The latter value was explained as a consequence of an associative process in which there is little or no desolvation contribution because the cyanide ion is very poorly solvated in DMSO. The reaction of the tris-iron(II) complex of **1**, which has a minus four charge, with OH^- is characterized overall, by a modest degree of desolvation as the transition state is reached, since the intrinsic volume change for the associative process is negative. Dissociation of $[Fe(4Mephen)_3]^{2+}$ by aqueous cyanide ions yields a ΔV^* value of $+10\ cm^3\ mol^{-1}$. These early examples indicate desolvation contributions ranging from zero to about $+20\ cm^3\ mol^{-1}$.

We also measured ΔV^* for attack by hydroxide ion for several closely related iron(II) complex cations, $[Fe(gmi)_3]^{2+}$,[12] $[Fe(Me_2bsb)_3]^{2+}$[13] and $[Fe(hxsb)]^{2+}$[13] (gmi = **2**, Me_2bsb = **3**, hxsb = **4**). The values of ΔV^* were +16, +11 and +13 $cm^3\ mol^{-1}$, respectively, decidedly positive, but lower than those determined for nucleophilic dissociation earlier. Because of this we measured activation volumes for hydroxide attack at two closely related Schiff base complexes, the iron(II) complexes of 3Mebsb (**5**) and 4MeObsb (**6**). Again values in the range +10 to +15 $cm^3\ mol^{-1}$ were obtained (*vide infra*).

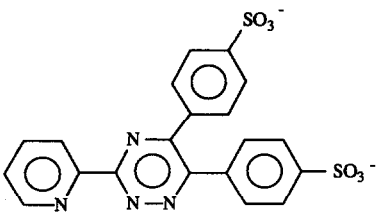

ppsa 1

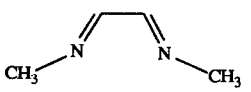

gmi 2

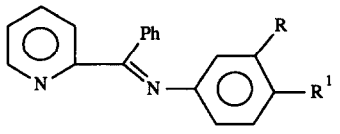

R=R¹=CH₃ Me₂bsb 3
R=CH₃, R¹=H 3Mebsb 5
R=H, R¹=OCH₃ 4MeObsb 6

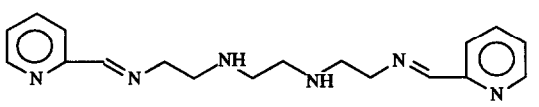

hxsb 4

A dissociative mechanism for a given complex would, in principle, have a constant ΔV^*, independent of the subsequent attack of the nucleophile. Since the rate-limiting step involves only lengthening of a ligand–metal bond, nucleophile solvation change is not relevant. For different complexes reacting with the same nucleophile, ΔV^* could vary, reflecting the difference in partial molar volume of the departing ligand and different degrees of stretching in the transition state. For a bimolecular reaction a negative value of ΔV^* is expected in the absence of solvation.[3] However, significant changes in the solvation of both the metal complex ion and the nucleophile can occur for an associatively formed activated complex. For a small anionic nucleophile, loss of electrostricted solvent is larger than for a positively-charged complex ion (of much lower charge density). Added co-solvent will, it may be predicted, change solvation of both species giving rise to changes in ΔV^* for a particular reactant pair. Such changes have been observed[13–15] and explanations sought in terms of solvation variation both of the nucleophile, and as a consequence of the hydrophobic/hydrophilic complex ion being compatible or not, with the co-solvent. The focus in this paper is on aqueous solution, but these earlier results[13–15] should be borne in mind as they provide a framework of explanation of ΔV^* variation. Aquation reactions for similar systems, *vide supra*, yielded variations in ΔV^*. Consequently, variations or constancy of ΔV^*, alone, are of no particular assistance necessarily in an attempt to assign a mechanism unambiguously.

However, because values of ΔV^* established for nucleophilic dissociation of several iron(II) diimine complexes were in the range +10 to +16 cm^3 mol^{-1}, it seemed incumbent on us to remeasure ΔV^* for hydroxide attack at $[Fe(phen)_3]^{2+}$ and $[Fe(bpy)_3]^{2+}$ as one step in an attempt to clarify the situation. In addition, because of our general interest in dissociation and other properties of iron(II) diimine complexes, we have examined the kinetics of dissociation of two substituted trisphen complexes, $[Fe(5Brphen)_3]^{2+}$ and $[Fe(5NO_2phen)_3]^{2+}$, in aqueous EDTA solution at elevated pressures. Thus we can compare ΔV^* values with those obtained for aquation in acid medium.

EXPERIMENTAL

Materials

Solutions of $[Fe(bpy)_3]^{2+}$ and $[Fe(phen)_3]^{2+}$ were prepared by dissolving appropriate amounts of their perchlorate salts in water. The solutions of the $[Fe(5Brphen)_3]^{2+}$ and $[Fe(5NO_2phen)_3]^{2+}$ cations were obtained by adding a small excess of ligand to an aqueous solution of iron(II) ammonium sulphate. Concentrations of these solutions were checked spectrophotometrically via published molar extinction coefficients: $[Fe(bpy)_3]^{2+}$ has ε (522 nm) = 8700 mol^{-1} dm^3 cm^{-1},[16] $[Fe(phen)_3]^{2+}$ has ε (510 nm) = 11,000 mol^{-1} dm^3 cm^{-1},[17,18] $[Fe(5NO_2phen)_3]^{2+}$ has ε (512 nm) = 12,100 mol^{-1} dm^3 cm^{-1}[17] and $[Fe(5Brphen)_3]^{2+}$ has ε (510 nm) = 11,500 mol^{-1} dm^3 cm^{-1}.[19] Iron(II) complexes of the Schiff base ligands, 3Mebsb (**5**) and 4MeOBsb (**6**), were prepared according to published procedure[20] in the form of their chloride salts, which were subsequently dissolved in water to give solutions of appropriate concentration. Solutions of iron(II) cations were made up immediately prior to use in kinetic experiments. Sodium hydroxide, sodium chloride, potassium hydroxide, potassium chloride and Na_2EDTA were Analar materials.

Methods

The experimental techniques and apparatus used were those described in detail in earlier publications.[13,21]

RESULTS

All kinetic runs were carried out at 298.2 K in the presence of a large excess of hydroxide ion, or of EDTA, and all followed first-order kinetics for at least three half lives. The experimental results are presented in the form of logarithms of ratios of rate constants under pressure to those for an aliquot of the same reactions at atmospheric pressure in Table 1. For each complex, plots of these ratios against pressure were linear within experimental uncertainty. Examples are shown for OH^- + $[Fe(phen)_3]^{2+}$ and EDTA + $[Fe(5NO_2phen)_3]^{2+}$ in Fig. 1 and OH^- + $[Fe(bpy)_3]^{2+}$ and EDTA + [Fe

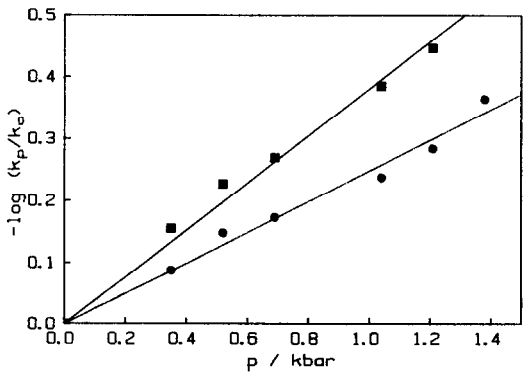

Fig. 1. Plots of $-\log(k_p/k_0)$ against pressure for dissociation of $[Fe(phen)_3]^{2+}$ in 0.0050 mol dm^{-3} NaOH (●), and for dissociation of $[Fe(5NO_2phen)_3]^{2+}$ in the presence of 0.010 mol dm^{-3} EDTA (■), at 298.2 K.

Table 1. Dissociation of iron(II)–diimine complexes at 298.2 K;[a] $-\log(k_p/k_0)$ at specified pressures in aqueous solution

Complex	p (kbar) 0.17	0.34	0.51	0.68	0.85	1.01	1.18	1.35
$[Fe(bpy)_3]^{2+}$ [b,c]		0.080	0.149	0.157	0.186	0.245		0.305
$[Fe(phen)_3]^{2+}$ [b,d]		0.088	0.149	0.173		0.238	0.284	0.364
$[Fe(3Mebsb)_3]^{2+}$ [b,e,f]		0.110		0.178			0.278	
$[Fe(4MeObsb)_3]^{2+}$ [b,e,f]		0.0825		0.159	0.173	0.206		
$[Fe(5Brphen)_3]^{2+}$ [g]	0.070	0.146	0.229	0.288	0.313	0.396		
$[Fe(5NO_2phen)_3]^{2+}$ [g]		0.155	0.227	0.269		0.385	0.446	

[a] Ionic strength, I, for each reaction due to the dissociating agent except as in [f].
[b] Nucleophilic attack.
[c] $[OH^-] = 0.010$ mol dm^{-3}.
[d] $[OH^-] = 0.0050$ mol dm^{-3}.
[e] $[OH^-] = 0.073$ mol dm^{-3}.
[f] $I = 0.33$ mol dm^{-3} (KCl).
[g] Aquation, in 0.010 mol dm^{-3} EDTA.

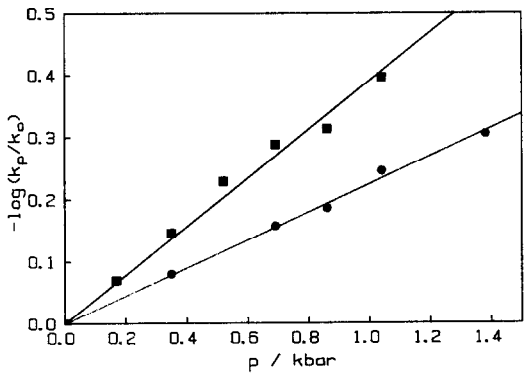

Fig. 2. Plots of $-\log(k_p/k_0)$ against pressure for dissociation of $[Fe(bpy)_3]^{2+}$ in 0.010 mol dm^{-3} NaOH (●) and for dissociation of $[Fe(5Brphen)_3]^{2+}$ in the presence of 0.010 mol dm^{-3} EDTA (■), at 298.2 K.

$(5Brphen)_3]^{2+}$ in Fig. 2. Activation volumes obtained from the slopes are reported in Table 2, together with published data for other iron(II) diimine complexes. The results are separately grouped for dissociation by nucleophilic attack and for aquation in acidic medium[10] or in the presence of EDTA. No correction was made for the contribution of aquation in the nucleophilic-dependent dissociation reaction as the former represents a very minor contribution to the observed rate constant. For dissociation by nucleophile most systems were studied at an ionic strength of 0.33 mol dm^{-3}. This and other conditions chosen reflect the need for data comparison in aqueous solvent mixtures (not reported in this communication) and practical considerations regarding solubility and rate ranges for accurate and convenient measurement.

DISCUSSION

Dissociation by hydroxide ion

All ΔV^* results for nucleophilic attack on iron(II) complexes, except those reported earlier,[1] are within the range +10 to +16 cm^3 mol^{-1}. Our results for the reaction of hydroxide on $[Fe(bpy)_3]^{2+}$ and $[Fe(phen)_3]^{2+}$, +13 and +14 cm^3 mol^{-1}, respectively, are in the centre of the small range. The earlier ΔV^* values obtained for both hydroxide and cyanide ion reaction with these two complexes are +19 to +22 cm^3 mol^{-1}, and clearly much higher than those reported here. The measurement temperature for the two studies differed by 5°C; this would give rise to a very small difference in ΔV^* values. There is a difference of about 0.10 mol dm^{-3} in the ionic strength of the solutions of the two sets of experiments, but again this would probably not account for the whole difference in ΔV^* values. Accordingly, since our values are within the range of +10 to +16 cm^3 mol^{-1} found for six other diimine complexes of iron(II), we conclude that the differences in ΔV^* remain unexplained and beyond experimental error. It is our position that the rate law for the reaction[7,10,11] indicates that the reaction is associative, and that ΔV^* can be attributed to the common domination of release of electrostricted solvent from hydroxide upon reaction with the complex ion in achieving the transition state. Since hydroxide desolvation predominates, the solvation changes at the complex ion may well be minor. Values of ΔV^* differ by only ±2 to 3 cm^3 mol^{-1}, which is not much greater than experimental error

Table 2. Activation volumes for dissociation of iron(II) diimine cations in aqueous solution

Complex[a]	Reactant	I (mol dm^{-3})	ΔV^* (cm^3 mol^{-1})	T (K)	Reference
$[Fe(bpy)_3]^{2+}$	NaCN	0.10	20.9±1.6	293.2	1
	NaOH	0.10	21.5±0.4	293.2	1
	NaOH	0.010	12.8±0.4	298.2	This study
$[Fe(phen)_3]^{2+}$	NaCN	0.10	19.8±1.0	293.2	1
	NaOH	0.10	19.7±0.3	293.2	1
	NaOH	0.0050	14.2±0.8	298.2	This study
$[Fe(4Mephen)_3]^{2+}$	KCN	0.033	10±2	298.2	2
$[Fe(Me_2bsb)_3]^{2+}$	KOH[b]	0.33	11.1±1.6	298.2	13
$[Fe(3Mebsb)_3]^{2+}$	KOH[b]	0.33	13.6±1.8	298.2	This study
$[Fe(4MeObsb)_3]^{2+}$	KOH[b]	0.33	12.0±2.1	298.2	This study
$[Fe(hxsb)]^{2+}$	NaOH[c]	0.33	13.4±1.9	298.2	13
$[Fe(gmi)_3]^{2+}$	NaOH[c]	0.33	16.7	298.2	12
$[Fe(5Brphen)_3]^{2+}$[d]	EDTA	0.030	22.3±1.0	298.2	This study
$[Fe(5NO_2phen)_3]^{2+}$[d]	EDTA	0.030	21.7±1.0	298.2	This study
$[Fe(5NO_2phen)_3]^{2+}$[e]	H_2SO_4	3.0	17.9±0.3	308.2	10
$[Fe(phen)_3]^{2+}$[f]	H_2SO_4	3.0	15.4	308.2	10
$[Fe(4,7Me_2phen)_3]^{2+}$[e]	H_2SO_4	3.0	11.6	308.2	8

[a] Ligands and abbreviations defined in text and formulae **1**–**6**.
[b] KCl was used to maintain the ionic strength.
[c] NaCl was used to maintain the ionic strength.
[d] Aquation in the presence of 0.010 mol dm^{-3} EDTA.
[e] Aquation in the presence of 1.0 mol dm^{-3} H_2SO_4.

and an attempt at an explanation is therefore not warranted. If the changes are not minor they are quite common to each iron(II) complex cation. This situation is dramatically different for dissociation in aqueous alcohol mixtures of complexes **2**, **3** and **4**,[12,13] illustrating therein significant ligand influence upon solvation changes. Preliminary findings for dissociation by hydroxide of $[Fe(phen)_3]^{2+}$ and $[Fe(bpy)_3]^{2+}$ in aqueous alcohol mixtures at high pressures indicate a significant participation by the hydrophobic ligands, more so for $[Fe(phen)_3]^{2+}$ than for $[Fe(bpy)_3]^{2+}$, in the solvation contribution to ΔV^*.

Activation parameters from temperature dependence studies provide support for different mechanisms for the aquation and nucleophilic attack routes of dissociation of $[Fe(phen)_3]^{2+}$. Aquation, discussed in more detail below, in the presence of 1.0 mol dm^{-3} H_2SO_4 is characterized[10] by a ΔH^* value of 122.4±0.8 kJ mol^{-1}, while dissociation by 0.1 mol dm^{-3} OH^- has a ΔH^* value of 96.3±0.5 kJ mol^{-1}. The values of ΔS^* are 88±3 and 18±3 J mol^{-1} K^{-1} for aquation and dissociation by OH^-, respectively. In the present work, we have measured the temperature dependence of the dissociation of $[Fe(5Brphen)_3]^{2+}$ in the presence of 0.10 mol dm^{-3} HCl and 0.010 mol dm^{-3} EDTA at five temperatures and find ΔH^* values of 115.6 and 119.0 kJ mol^{-1}, and ΔS^* values of 74.7 and 86.4 J mol^{-1} K^{-1}, in the two media. (Table 3 and references therein.) In contrast, the dissociation in the presence of OH^- yields $\Delta H^* = 84.2$ kJ mol^{-1} and $\Delta S^* = 37.8$ J mol^{-1} K^{-1}. Such results argue against a common mode of dissociative release of diimine ligand.

In summary, the interpretation of a dissociative process based only on ΔV^* values of ref. 2 is not unreasonable; however, the nature of the rate law, and other considerations outlined above, yield a preponderance of support for an associative process for nucleophilic attack.

Aquation

During aquation of $[Fe(phen)_3]^{2+}$ one ligand becomes extended to a certain distance from the central ion thus permitting protons to prevent reattachment of a phen ligand and causing the subsequent complete complex dissociation. It has been shown previously,[8] and in this study, that EDTA can perform an equivalent function to H^+ in the aquation process. Both can prevent the partly dissociated phen ligand reattaching itself completely to the central iron; EDTA can react with the cation, and the acid can protonate a phenanthroline nitrogen. The rate constants at atmospheric pressure for

Table 3. Activation parameters for dissociation of iron(II) tris-phen complexes

	ΔH^* (kJ mol^{-1})	ΔS^* (J mol^{-1} K^{-1})	Reference
Base hydrolysis			
$[Fe(phen)_3]^{2+}$ [a]	96.3	18	Cited in ref. 10
$[Fe(5Brphen)_3]^{2+}$ [b]	84.2	37.8	This study
Aquation			
$[Fe(phen)_3]^{2+}$ [c]	122.4	88	Cited in ref. 10
$[Fe(5Brphen)_3]^{2+}$ [d]	115.6	74.7	This study
$[Fe(5Brphen)_3]^{2+}$ [e]	119.0	86.4	This study

[a] 0.1 mol dm^{-3} NaOH.
[b] Parameters derived from second-order rate constants.
[c] 1.0 mol dm^{-3} H_2SO_4.
[d] 0.1 mol dm^{-3} HCl.
[e] 0.01 mol dm^{-3} Na_2 EDTA.

aquation in the presence of acid and EDTA are the same and virtually independent of concentration. The associated enthalpies of activation for these two reactions are the same,[9] as discussed earlier, confirming the idea of a scavenging function. Aquation occurs through a dissociative mode of activation giving rise to similar ΔV^* values for similar ligands. The differences found[10] for $[Fe(5NO_2phen)_3]^{2+}$, $[Fe(4,7diMephen)_3]^{2+}$ and $[Fe(phen)_3]^{2+}$, +17.9, +11.6 and +15.4 cm^3 mol^{-1}, respectively, can be rationalized in terms of a spin-state change of the iron(II),[10,22] but also with differing degrees of bond lengthening (Fe—N bonds) in the transition state. The value of ΔV^* for aquation of $[Fe(5Brphen)_3]^{2+}$, $+22.3 \pm 1.0$ cm^3 mol^{-1} (Table 2) is consistent with the variation in ΔV^*, caused by ligand substituent, that was found earlier[10] (Table 2). However, practical reasons ruled out study of the aquation kinetics at high pressure in the directly comparable acidic medium (1.0 mol dm^{-3} H_2SO_4). Where a parallel study was possible, we report ΔV^* values of $+21.7 \pm 1.0$ cm^3 mol^{-1} in the presence of EDTA at 298.2 K, and 17.9 ± 0.3 cm^3 mol^{-1} [10] for aquation of $[Fe(5NO_2phen)_3]^{2+}$ in 1.0 mol dm^{-3} H_2SO_4 at 308.2 K. This difference is larger than could be explained by experimental uncertainty or the different temperature of measurement. At present we are unable to examine the generality (or not) of this result. However, it would appear that in addition to differences in bond extension within complexes containing similar ligands, solvation effects by virtue of reaction in very different media may yield a significant difference in ΔV^* for aquation with the same ligand;[23-25] the ionic strength is 3.0 mol dm^{-3} in the acid aquation study, much higher than in the presence of 0.010 mol dm^{-3} EDTA. This gives rise to different structural characteristics of water in general and in the vicinity of the activated complex in the two reactions. Exactly how this gives rise to the particular solvation difference, and whether ionic strength effects are as significant as in redox reactions[23-25] remain to be explained. The complicated dependence upon $[H^+]$ for dissociation of $[Fe(bpy)_3]^{2+}$ [26-28] precludes a parallel proton/EDTA aquation investigation.

Dissociation of $[Fe(phen)_3]^{2+}$ in the presence of 0.1 M CF_3SO_3H in anhydrous methanol yields[22c] an activation volume of +14.1 cm^3 mol^{-1}, close to the value for aquation in aqueous acid solution (+15.4 cm^3 mol^{-1}). But both are well below the reported values for dissociation in the presence of the nucleophiles, OH^- ($\Delta V^* = +19.7$ cm^3 mol^{-1}) and CN^- ($\Delta V^* = +19.8$ cm^3 mol^{-1}). The closeness of the two ΔV^* values for the aquation is perhaps surprising in view of the pronounced differences in the reaction media, and bearing in mind the possibility that ionic strength variation may cause different volume changes upon achieving the transition state. However, it has been suggested[10,22] that ΔV^* for a dissociative reaction of this type is dominated by the spin-change preequilibrium and is only modestly sensitive to aromatic substitution, and therefore perhaps also to medium changes. It is almost ironical that ΔV^* for dissociation of $[Fe(phen)_3]^{2+}$ by OH^- according to the new results reported here and for aquation are numerically the same, although we have argued that the mechanisms are different. Therefore, based upon the interpretation presented here, the agreement is fortuitous.

Acknowledgements—We thank Royal Dutch Shell Oil Company, H. J. Backer fund, the Henriëtte Beck Fund and the University of Groningen fund for support (S.A.G.), the University of New Hampshire for a sabbatical leave during which some of the research was conducted in Leicester (C.D.H.) and the National Science Foundation for a grant towards the purchase of the Cary 219 spectrophotometer (CHE-7908399).

REFERENCES

1. G. A. Lawrance, D. R. Stranks and S. Suvachittanont, *Inorg. Chem.* 1979, **18**, 82.
2. J. Burgess, A. J. Duffield and R. Sherry, *J. Chem. Soc., Chem. Commun.* 1980, 350.
3. T. Asano and W. J. LeNoble, *Chem. Rev.* 1978, **73**, 407.
4. M. J. Blandamer, J. Burgess and R. I. Haines, *J. Chem. Soc., Dalton Trans.* 1976, 1203.
5. T. R. Sullivan, D. R. Stranks, J. Burgess and R. I. Haines, *J. Chem. Soc., Dalton Trans.* 1977, 1460.
6. R. van Eldik, T. Asano and W. J. LeNoble, *Chem. Rev.* 1989, **88**, 549.
7. D. W. Margerum and L. P. Morgenthaler, *J. Am. Chem. Soc.* 1962, **84**, 706.
8. J. Burgess and M. V. Twigg, *Transition Met. Chem.* 1978, **3**, 88.
9. S. A. Galema, Research Report. University of Leicester, Leicester, U.K. (1988).
10. J. M. Lucie, D. R. Stranks and J. Burgess, *J. Chem. Soc., Dalton Trans.* 1975, 245.
11. M. J. Blandamer, J. Burgess, P. P. Duce, K. S. Payne, R. Sherry, P. Wellings and M. V. Twigg, *Transition Met. Chem.* 1984, **9**, 163.
12. M. J. Blandamer, J. Burgess, P. Guardado, C. D. Hubbard, S. Nuttall, L. J. S. Prouse, S. Radulovic and D. R. Russell, *Inorg. Chem.*, to be submitted.
13. J. Burgess and C. D. Hubbard, *J. Am. Chem. Soc.* 1984, **106**, 1717.
14. J. Burgess and C. D. Hubbard, *J. Chem. Soc., Chem. Commun.* 1983, 1482.
15. J. Burgess and C. D. Hubbard, *Inorg. Chem.* 1988, **27**, 2548.
16. W. M. Banick and G. F. Smith, *Anal. Chim. Acta.* 1958, **19**, 304.
17. M. L. Moss, M. G. Mellon and G. F. Smith, *Analyt. Chem.* 1942, **14**, 931.
18. D. H. Wilkins and G. F. Smith, *Anal. Chim. Acta.* 1953, **9**, 538.
19. G. F. Smith and F. P. Richter, *Phenanthroline and Substituted Phenanthroline Indicators.* G. F. Smith Chemical Co., Columbus, Ohio (1942).
20. P. Krumholz, *Inorg. Chem.* 1965, **4**, 609; J. Burgess, *J. Chem. Soc.* 1968, 497.
21. N. Hallinan, P. McArdle, J. Burgess and P. Guardado, *J. Organomet. Chem.* 1987, **333**, 77.
22. (a) G. A. Lawrance and D. R. Stranks, *Inorg. Chem.* 1978, **17**, 1804; (b) G. A. Lawrance, D. R. Stranks and T. R. Sullivan, *Aust. J. Chem.* 1981, **34**, 1763; (c) G. A. Lawrance, *Aust. J. Chem.* 1985, **38**, 1117.
23. S. Wherland, *Inorg. Chem.* 1983, **17**, 2349.
24. L. Spiccia and T. W. Swaddle, *Inorg. Chem.* 1987, **26**, 2265.
25. R. van Eldik, T. Asano and W. J. LeNoble, p. 591, ref. 7.
26. P. Krumholz, *Nature* 1949, **163**, 724.
27. J. H. Baxendale and P. George, *Trans. Faraday Soc.* 1950, **46**, 736.
28. F. Basolo, J. C. Hayes and H. M. Neumann, *J. Am. Chem. Soc.* 1954, **76**, 3808.

Polyhedron Vol. 10, No. 7, pp. 711–716, 1991
Printed in Great Britain

0277–5387/91 $3.00+.00
© 1991 Pergamon Press plc

THE SYNTHESIS AND SPECTRAL PROPERTIES OF THE NEW BIS(BUT-2-YNE) AND MONO(BUT-2-YNE) COMPLEXES $[W(CO)L(S_2CNC_4H_8)(\eta^2\text{-}MeC_2Me)_2][BPh_4]$ AND $[W(CO)L_2(S_2CNC_4H_8)(\eta^2\text{-}MeC_2Me)][BPh_4]$ (WHERE L = IMIDAZOLE, 2-METHYLIMIDAZOLE AND 4-METHYLIMIDAZOLE)

PAUL K. BAKER* and KEVIN R. FLOWER

Department of Chemistry, University of Wales, Bangor, Gwynedd LL57 2UW, Wales, U.K.

(*Received* 23 *August* 1990; *accepted* 5 *December* 1990)

Abstract—Reactions of the complex $[W(CO)(NCMe)(S_2CNC_4H_8)(\eta^2\text{-}MeC_2Me)_2][BPh_4]$ with one equivalent of L (L = imidazole, 2-methylimidazole or 4-methylimidazole) in the presence of excess but-2-yne at room temperature in CH_2Cl_2 affords good yields of the bis(but-2-yne) complexes $[W(CO)L(S_2CNC_4H_8)(\eta^2\text{-}MeC_2Me)_2][BPh_4]$ (**1–3**). Whereas, reaction of $[W(CO)(NCMe)(S_2CNC_4H_8)(\eta^2\text{-}MeC_2Me)_2][BPh_4]$ with two equivalents of L (L = imidazole, 2-methylimidazole or 4-methylimidazole) affords high yields of the new mono(but-2-yne) complexes $[W(CO)L_2(S_2CNC_4H_8)(\eta^2\text{-}MeC_2Me)][BPh_4]$ (**4–6**). ^{13}C NMR spectroscopy indicates that the but-2-yne ligands in **1** are donating a total of six electrons to the tungsten, whereas in **4–6** the but-2-yne is donating four electrons to the tungsten. Variable-temperature ^1H NMR studies have been carried out on **4–6** in order to calculate the barrier to but-2-yne rotation.

In recent years considerable attention has been paid to cationic alkyne complexes of molybdenum(II) and tungsten(II). The cationic cyclopentadienyl- or indenyl-containing bis(alkyne) complexes of the type $[Mo(CO)(\eta^2\text{-}RC_2R')_2(\eta^5\text{-}C_5H_5$ or $C_9H_7)][BF_4]$[1] have been shown to be useful precursors for a diverse range of chemistry.[2–8] Templeton and co-workers[9] have reported the preparation of the cationic mono(alkyne) complex $[W(CO)(S_2CNEt_2)(dppe)(\eta^2\text{-}HOC_2CH_2Ph)][BF_4]$; more recently, we reported the synthesis of the cationic bis(but-2-yne) complex $[W(CO)(NCMe)(S_2CNC_4H_8)(\eta^2\text{-}MeC_2Me)_2][BPh_4]$[10] and described its reactions with monodentate phosphines.[11] To date, however, there have been no reports of cationic bis(alkyne) dithiocarbamate complexes of tungsten(II) containing coordinated imidazole or substituted imidazole ligands. In this paper we report on the reaction of the bis(but-2-yne) complex $[W(CO)(NCMe)(S_2CNC_4H_8)(\eta^2\text{-}MeC_2Me)_2][BPh_4]$ with one and two equivalents of imidazole and substituted imidazoles.

EXPERIMENTAL

The complex $[W(CO)(NCMe)(S_2CNC_4H_8)(\eta^2\text{-}MeC_2Me)_2][BPh_4]$ was prepared according to the published method.[10] All other chemicals were purchased from commercial sources.

Elemental analyses for carbon, hydrogen and nitrogen were determined using a Carlo Erba Elemental Analyser MOD 1106 (using helium as a carrier gas). IR spectra were recorded on a Perkin–Elmer 1430 ratio recording IR spectrophotometer as thin films in $CHCl_3$ between NaCl plates. ^1H and ^{13}C NMR spectra were recorded on a Bruker AC 250 CP/MAS NMR spectrometer and calibrated against tetramethylsilane.

$[W(CO)(N_2C_3H_4)(S_2CNC_4H_8)(\eta^2\text{-}MeC_2Me)_2][BPh_4]\cdot 0.5CH_2Cl_2$ (1)

To $[W(CO)(NCMe)(S_2CNC_4H_8)(\eta^2\text{-}MeC_2Me)_2][BPh_4]$ (0.4 g, 0.484 mmol) dissolved in CH_2Cl_2 (15 cm^3) containing but-2-yne (0.2 cm^3), with continuous stirring under a stream of dry N_2, was

* Author to whom correspondence should be addressed.

Table 1. Physical and analytical data[a] for the complexes $[W(CO)L(S_2CNC_4H_8)(\eta^2\text{-}MeC_2Me)_2][BPh_4]$ and $[W(CO)L_2(S_2CNC_4H_8)(\eta^2\text{-}MeC_2Me)][BPh_4]$

Compound	Colour	Yield	C (%)	H (%)	N (%)
$[W(CO)(N_2C_3H_4)(S_2CNC_4H_8)(\eta^2\text{-}MeC_2Me)_2][BPh_4]\cdot 0.5CH_2Cl_2$ (1)	Yellow	75	55.6 (55.6)	5.1 (5.1)	4.2 (4.7)
$[W(CO)(N_2C_3H_3\text{-}2Me)(S_2CNC_4H_8)(\eta^2\text{-}MeC_2Me)_2][BPh_4]\cdot 0.5CH_2Cl_2$ (2)	Yellow	77	56.4 (56.1)	5.5 (5.2)	4.2 (4.6)
$[W(CO)(N_2C_3H_3\text{-}4Me)(S_2CNC_4H_8)(\eta^2\text{-}MeC_2Me)_2][BPh_4]$ (3)	Yellow	84	58.5 (58.1)	5.6 (5.3)	4.4 (4.8)
$[W(CO)(N_2C_3H_4)_2(S_2CNC_4H_8)(\eta^2\text{-}MeC_2Me)][BPh_4]\cdot 0.5CH_2Cl_2$ (4)	Purple	74	53.7 (53.4)	4.9 (4.8)	7.6 (7.7)
$[W(CO)(N_2C_3H_3\text{-}2Me)_2(S_2CNC_4H_8)(\eta^2\text{-}MeC_2Me)][BPh_4]$ (5)	Purple	72	56.8 (56.3)	6.0 (6.1)	8.0 (7.8)
$[W(CO)(N_2C_3H_3\text{-}4Me)_2(S_2CNC_4H_8)(\eta^2\text{-}MeC_2Me)][BPh_4]$ (6)	Purple	75	56.6 (56.3)	6.0 (6.1)	8.3 (7.8)

[a] Calculated values in parentheses.

added $N_2C_3H_4$ (imidazole) (0.033 g, 0.484 mmol). After stirring for 20 h the solution was filtered and the solvent volume reduced to 1 cm^3 *in vacuo*. Dropwise addition of diethyl ether precipitated the yellow cationic complex $[W(CO)(N_2C_3H_4)(S_2CNC_4H_8)(\eta^2\text{-}MeC_2Me)_2][BPh_4]\cdot 0.5CH_2Cl_2$ (**1**), which on recrystallization from CH_2Cl_2/Et_2O afforded 0.33 g, 75% of pure product.

Similar reactions of $[W(CO)(NCMe)(S_2CNC_4H_8)(\eta^2\text{-}MeC_2Me)_2][BPh_4]$ with one equivalent of $N_2C_3H_3$-2Me and $N_2C_3H_3$-4Me in CH_2Cl_2 afforded the analogous cationic bis(but-2-yne) complexes $[W(CO)L(S_2CNC_4H_8)(\eta^2\text{-}MeC_2Me)_2][BPh_4]$ (**2** and **3**) (see Table 1 for physical and analytical data).

$[W(CO)(N_2C_3H_4)_2(S_2CNC_4H_8)(\eta^2\text{-}MeC_2Me)][BPh_4]\cdot 0.5CH_2Cl_2$ (**4**)

To $[W(CO)(NCMe)(S_2CNC_4H_8)(\eta^2\text{-}MeC_2Me)_2][BPh_4]$ (0.4 g, 0.484 mmol) dissolved in CH_2Cl_2 (15 cm^3), with continuous stirring under a stream of dry N_2, was added $N_2C_3H_4$ (0.066 g, 0.968 mmol). After stirring for 3 days the solution was filtered and the solvent reduced to 0.5 cm^3 *in vacuo*. Dropwise addition of diethyl ether precipitated the purple cationic complex $[W(CO)(N_2C_3H_4)_2(S_2CNC_4H_8)(\eta^2\text{-}MeC_2Me)][BPh_4]\cdot 0.5CH_2Cl_2$ (**4**) which on recrystallization from CH_2Cl_2/Et_2O yielded 0.31 g, 74% of pure product.

Similar reactions of $[W(CO)(NCMe)(S_2CNC_4H_8)(\eta^2\text{-}MeC_2Me)_2][BPh_4]$ with two equivalents of $N_2C_3H_3$-2Me and $N_2C_3H_3$-4Me in CH_2Cl_2 afforded the analogous cationic compounds $[W(CO)L_2(S_2CNC_4H_8)(\eta^2\text{-}MeC_2Me)][BPh_4]$ (**5** and **6**) (see Table 1 for physical and analytical data).

RESULTS AND DISCUSSION

Equimolar quantities of the complex $[W(CO)(NCMe)(S_2CNC_4H_8)(\eta^2\text{-}MeC_2Me)_2][BPh_4]$ and L (L = imidazole, 2-methylimidazole or 4-methylimidazole) react in the presence of but-2-yne in CH_2Cl_2 at room temperature to afford a high yield of the cationic bis(but-2-yne) complexes $[W(CO)L(S_2CNC_4H_8)(\eta^2\text{-}MeC_2Me)_2][BPh_4]$ (**1–3**). Reactions of $[W(CO)(NCMe)(S_2CNC_4H_8)(\eta^2\text{-}MeC_2Me)_2][BPh_4]$ with two equivalents of L (L = imidazole, 2-methylimidazole or 4-methylimidazole) afford high yields of the mono(but-2-yne) complexes $[W(CO)L_2(S_2CNC_4H_8)(\eta^2\text{-}MeC_2Me)][BPh_4]$ (**4–6**). Complexes **1–6** are stable when stored under nitrogen for prolonged periods, however, they slowly decompose when exposed to air in solution. Compounds **1–6** are all soluble in CH_2Cl_2, $CHCl_3$, $OC(CH_3)_2$ and NCMe, but are totally insoluble in Et_2O and hydrocarbon solvents. All of the compounds have been fully characterized by elemental analysis (C, H and N, Table 1), IR (Table 2), ^1H and selected cases ^{13}C NMR spectroscopy (Tables 3 and 4). Compounds **1**, **2** and **4** have been confirmed as $0.5CH_2Cl_2$ solvates by repeated elemental analysis and ^1H NMR spectroscopy.

When the complex $[W(CO)(NCMe)(S_2CNC_4H_8)(\eta^2\text{-}MeC_2Me)_2][BPh_4]$ is reacted with one equivalent of $N_2C_3H_4$, $N_2C_3H_3$-2Me or $N_2C_3H_3$-4Me

Table 2. IR data[a] for the compounds [W(CO)L($S_2CNC_4H_8$)(η^2-MeC_2Me)$_2$][BPh_4] and [W(CO)L_2($S_2CNC_4H_8$)(η^2-MeC_2Me)][BPh_4]

Compound	ν(NH) cm^{-1}	ν(C≡O) cm^{-1}	ν(C≡C) cm^{-1}
1	3320m 3150m	2050s	1850w
2	3310m 3160m	2055s	1840w
3	3310m 3160m	2055s	1840w
4	3325m 3200m	1900s	[b]
5	3300m 3220m	1905s	[b]
6	3330m 3220m	1900s	[b]

[a] Spectra recorded as thin films in $CHCl_3$ between NaCl plates: m = medium, s = strong, w = weak.
[b] ν(C≡C) was not observed for these complexes.

in CH_2Cl_2, IR spectroscopy shows the formation of the expected bis(alkyne) complexes [W(CO)L($S_2CNC_4H_8$)(η^2-MeC_2Me)$_2$][BPh_4]; however, there is also evidence for the formation of the 2:1 adducts [W(CO)L_2($S_2CNC_4H_8$)(η^2-MeC_2Me)][BPh_4] [see eq. (1)]:

$$[W(CO)(NCMe)(S_2CNC_4H_8)(\eta^2\text{-}MeC_2Me)_2][BPh_4] + L \longrightarrow [W(CO)L(S_2CNC_4H_8)(\eta^2\text{-}MeC_2Me)_2][BPh_4] \underset{MeC_2Me}{\overset{L}{\rightleftharpoons}} [W(CO)L_2(S_2CNC_4H_8)(\eta^2\text{-}MeC_2Me)][BPh_4] \quad (1)$$

The addition of the second imidazole or substituted imidazole can be suppressed by the addition of free but-2-yne to the reaction mixture thus, allowing isolation of the bis(but-2-yne) complexes (**1–3**) without contamination from the bis-substituted mono-(but-2-yne) compounds.

The formation of the compounds [W(CO)L_2($S_2CNC_4H_8$)(η^2-MeC_2Me)][BPh_4] (**4–6**) takes approximately 3 days, even when an excess of imidazole or substituted imidazoles was added. The most likely reason for this slow alkyne substitution is due to the ability of free but-2-yne generated preventing the second substitution taking place.

The IR spectra of compounds **1–3** all show an intense carbonyl stretching band around 2055 cm^{-1}, whereas compounds **4–6** show a single intense carbonyl band around 1900 cm^{-1}. The lower value for complexes **4–6** is due to the loss of a strong π-accepting but-2-yne ligand which allows more electron density to be back donated into the π^*

Table 3. ^{1}H NMR data[a] for the compounds [W(CO)L($S_2CNC_4H_8$)(η^2-MeC_2Me)$_2$][BPh_4] and [W(CO)L_2($S_2CNC_4H_8$)(η^2-MeC_2Me)][BPh_4]

Compound	^{1}H (δ dppm)
1	11.25 (s, 1H, N=C*H*); 10.47 (d, 2H, C=C*H*, J_{H-H} = 12 Hz); 7.35–6.78 (m, 20H, Ph); 6.12 (s, 1H, N*H*); 5.30 (s, 1H, CH_2Cl_2); 3.75 (m, 2H, NCH_2); 3.42 (m, 2H, NCH_2); 3.11, 2.96, 2.82, 2.73 (4s, 12H, ≡C*Me*); 1.98 (m, 4H, CH_2).
2	10.32 (d, 2H, C=C*H*, J_{H-H} = 9 Hz); 7.45–6.8 (m, 20H, Ph); 5.85 (s, 1H, N*H*); 5.29 (s, 1H, CH_2Cl_2); 3.62 (bm, 4H, CH_2); 3.25, 3.13, 2.96, 2.78 (4s, 12H, ≡C*Me*); 2.23 (s, 3H, CH_3); 1.99 (m, 4H, CH_2).
3	11.25 (s, 1H, N=C*H*); 10.42 (s, 1H, C=C*H*); 7.55–6.82 (m, 20H, Ph); 5.98 (s, 1H, N*H*); 3.75 (m, 2H, NCH_2); 3.38 (m, 2H, NCH_2); 2.98, 2.83, 2.73, 2.70 (4s, 12H, ≡C*Me*); 1.97 (bm, 4H, CH_2); 1.78 (s, 3H, CH_3).
4	11.21–10.71 (m, 6H, HC=C and N=CH); 7.49–6.8 (m, 20H, Ph); 6.38 (s, 1H, N*H*); 6.18 (s, 1H, N*H*); 5.29 (s, 1H, CH_2Cl_2); 3.78 (t, 2H, NCH_2, J_{H-H} = 6.72 Hz); 3.5 (t, 2H, NCH_2, J_{H-H} = 6.72 Hz); 3.21 (s, 6H, ≡C*Me*); 2.05 (m, 4H, CH_2).
5	11.31–10.62 (m, 4H, HC=C); 7.49–6.75 (m, 20H, Ph); 6.52 (s, 1H, N*H*); 6.36 (s, 1H, N*H*); 3.75 (t, 2H, NCH_2, J_{H-H} = 6.74 Hz); 3.53 (s, 2H, NCH_2, J_{H-H} = 6.72 Hz); 3.28 (s, 6H, ≡C*Me*); 2.06 (m, 4H, CH_2); 1.83 (s, 3H, CH_3); 1.79 (s, 3H, CH_3).
6	11.34–10.41 (m, 4H, HC=C and N=CH—N); 7.52–6.74 (m, 20H, Ph); 6.37 (s, 1H, N*H*); 6.02 (s, 1H, N*H*); 3.76 (t, 2H, NCH_2, J_{H-H} = 6.82 Hz); 3.48 (t, 2H, NCH_2, J_{H-H} = 6.79 Hz); 3.27 (s, 6H, ≡C*Me*); 2.31 (s, 3H, CH_3); 2.25 (s, 3H, CH_3); 2.04 (m, 4H, CH_2).

[a] Spectra recorded in $CDCl_3$ (+25°C) referenced to $SiMe_4$; s = singlet, t = triplet, m = multiplet.

Table 4. ^{13}C NMR data[a] for the compounds $[W(CO)L(S_2CNC_4H_8)(\eta^2\text{-}MeC_2Me)_2][BPh_4]$ and $[W(CO)L_2(S_2CNC_4H_8)(\eta^2\text{-}MeC_2Me)][BPh_4]$

Compound	^{13}C (δ ppm)
1	202.46 (s, CS_2); 188.05, 183.59, 179.29, 174.0 (4s, $C{\equiv}C$); 165.03, 164.24, 163.46, 162.68 (q, B—C, J_{B-C} = 49.5 Hz); 135.84, (s, N=C—N); 134.45, 126.1, 122.31 (3s, BPh_4); 116.9 (s, $C{=}C$); 53.1 (s, CH_2Cl_2); 50.6 (s, CH_2N); 49.62 (s, NCH_2); 24.79 (s, CH_2); 24.59 (s, CH_2); 20.37, 18.49, 17.84, 16.79 (4s, ≡C*Me*).
4	230.7 (s, C≡O); 208.42 (s, CS_2); 164.74, 164.25, 163.75, 163.26 (q, B—C, J_{B-C} = 49.5 Hz); 142.5 (s, N—C=N); 138.30 (s, N—C=N); 135.96, 126.13, 122.44 (3s, BPh_4); 129.54, 128.20 (2s, $C{=}C$); 53.4 (s, CH_2Cl_2); 51.17 (s, NCH_2); 50.20 (s, NCH_2); 24.76 (s, CH_2); 24.52 (s, CH_2); 21.5 (s, ≡C*Me*).
5	231.47 (s, C≡O); 208.69 (s, CS_2); 164.5, 164.01, 163.5, 163.03 (q, B—C, J_{B-C} = 49.5 Hz); 141.36, 137.59 (2s, N=C—N); 135.84, 126.03, 122.18 (3s, BPh_4); 128.34, 126.75 (2s, $C{=}C$); 51.2, 50.16 (2s, NCH_2); 24.61 (s, CH_2); 24.23 (s, CH_2); 20.51 (s, ≡C*Me*); 9.56, 9.25 (s, CH_3).
6	232.09 (s, C≡O); 212.05 (bs, $C{\equiv}C$); 207.91 (s, CS_2); 164.4, 163.91, 163.42, 162.93 (q, B—C, J_{B-C} = 49.5 Hz); 150.52, 148.32 (2s, N—C=N); 135.77, 126.06, 122.07 (3s, BPh_4); 131.43, 129.18 ($C{=}C$); 118.01, 117.15 (2s, C≡C); 51.08, 50.80 (2s, NCH_2); 24.72, 24.49 (2s, CH_2); 20.35 (s, ≡C*Me*); 14.42, 12.78 (2s, CH_3).

[a] Spectra recorded in $CDCl_3$ (+25°C) referenced to $SiMe_4$; s = singlet, q = quarter, b = broad.

antibonding molecular orbitals of the coordinated carbon monoxide. A weak band around 1850 cm^{-1} has been assigned to the alkyne $\nu(C{\equiv}C)$ in compounds **1–3**, this band was not observed in complexes **4–6**.

The ^1H NMR spectra of compounds **1–3** all show four but-2-yne methyl resonances which is indicative of an asymmetric isomer present in solution, Fig. 1. Considering the solid-state geometry of $[W(CO)(NCMe)(S_2CNC_4H_8)(\eta^2\text{-}MeC_2Me)_2][BPh_4]$ determined by Drew and co-workers,[10] as displayed in Fig. 2, and the fluctional properties of these molecules the rearrangement in geometry can be explained in terms of a trigonal twist rearrangement, as shown in Scheme 1. The room temperature ^1H NMR spectra of compounds **4–6** display one coordinated but-2-yne methyl resonance, which is indicative of the ligated but-2-yne undergoing rapid propeller-like rotation. In order to show that the fluxional process is intramolecular and not intermolecular for $[W(CO)(N_2C_3H_3\text{-}2Me)_2(S_2CNC_4H_8)(\eta^2\text{-}MeC_2Me)][BF_4]$ (**5**), the ^1H NMR spectrum of this complex was obtained in $CDCl_3$ solution above its coalescence temperature in the presence of an equimolar quantity of but-2-yne. This spectrum clearly showed two singlets at chemical shifts corresponding to those of free but-2-yne (δ 1.8 ppm) and of complex **5** (δ 3.28 ppm) rather than one signal at an averaged chemical shift. This indicates that the fluxional process observed for this complex is intramolecular. The ^1H NMR spectra for the but-2-yne methyl protons of $[W(CO)(N_2C_3H_4)_2(S_2CNC_4H_8)(\eta^2\text{-}MeC_2Me)][BPh_4]\cdot 0.5CH_2Cl_2$ (**4**) are shown in Fig. 3. The barriers to but-2-yne rotation in complexes **4–6** have been calculated using the Gutowsky–

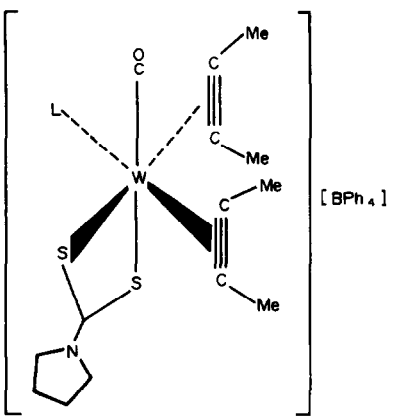

Fig. 1. Proposed coordination geometry for **1–3** in solution.

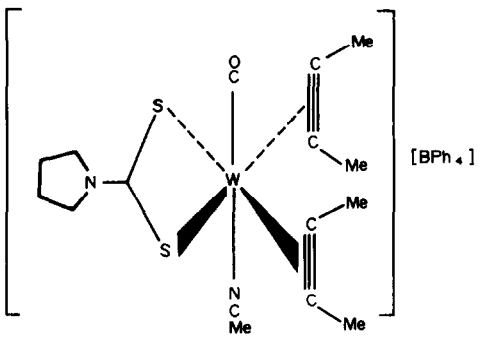

Fig. 2. X-ray crystallographically found geometry of $[W(CO)(NCMe)(S_2CNC_4H_8)(\eta^2\text{-}MeC_2Me)_2][BPh_4]$.[10]

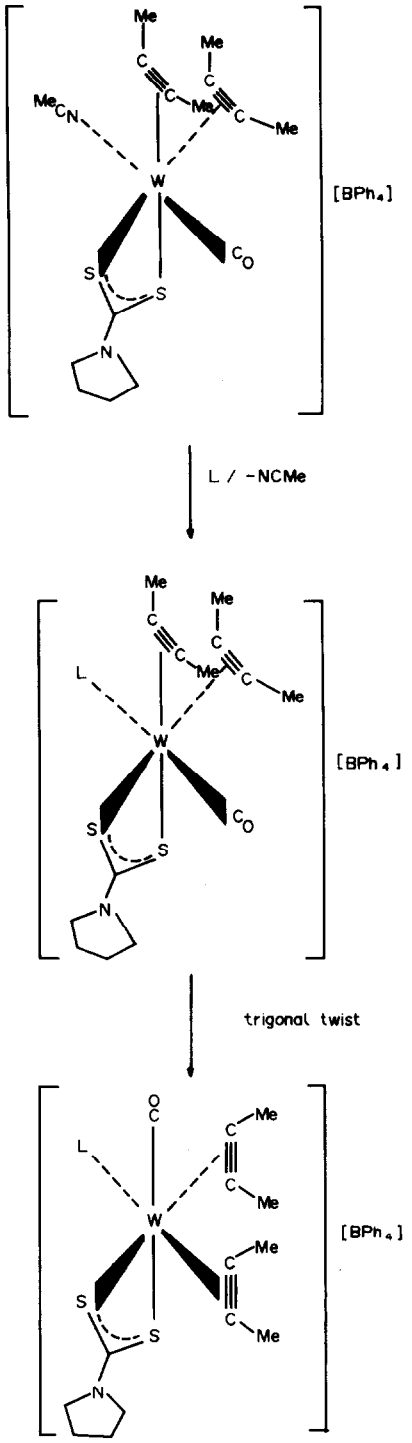

Scheme 1. Trigonal twist rearrangement to explain the solution state geometry of [W(CO)L(S$_2$CNC$_4$H$_8$)(η^2-MeC$_2$Me)$_2$][BPh$_4$].

Holm equation[13,14] [$\Delta G^{\ddagger} = -RT_c \ln(\pi\Delta\nu h/\sqrt{2}K_B T_c)$], see Table 5 for coalescence temperatures and barriers for but-2-yne rotation. All three complexes have the same value for but-2-yne rotation, within the experimental errors of the method, $\Delta G^{\ddagger} \sim 56$ kJ mol^{-1}.

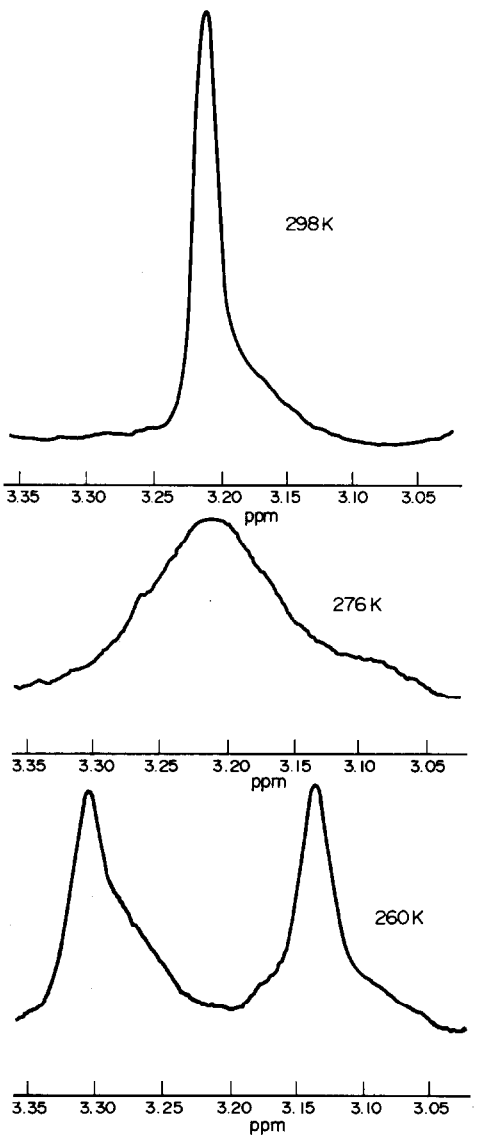

Fig. 3. ^{1}H NMR spectra of the but-2-yne methyl protons of [W(CO)(N$_2$C$_3$H$_4$)$_2$(S$_2$CNC$_4$H$_8$)(η^2-MeC$_2$Me)][BPh$_4$]·0.5CH$_2$Cl$_2$ (**4**) at three different temperatures.

The addition of the methyl groups in the 2 or 4 position seems to have little effect on the barrier to but-2-yne rotation. The other resonances in the ^{1}H NMR spectra are indicative of the coordinated imi-

Table 5. Calculated barriers to but-2-yne rotation for the compounds [W(CO)L$_2$(S$_2$CNC$_4$H$_8$)(η^2-MeC$_2$Me)][BPh$_4$]

Compound	T_c (K)	$\Delta\nu$ (Hz)	$\Delta G^{\ddagger}$ (kJ mol^{-1})
4	276	42.92	56
5	270	45.78	56
6	275	64.14	56

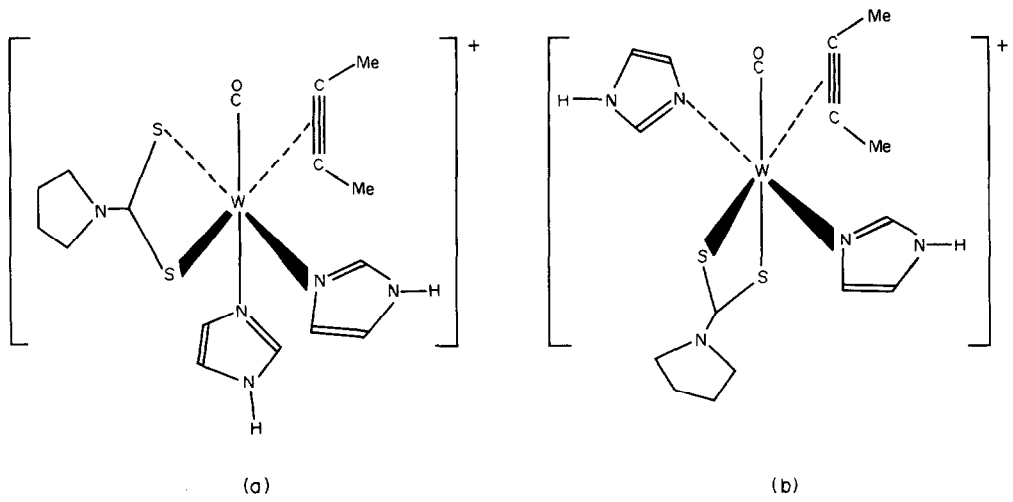

(a) (b)

Fig. 4. Possible coordination geometries for complexes **4–6**.

dazoles being *cis* within the coordination sphere, Fig. 4(a). However, on careful consideration there is a possibility of the imidazoles being coordinated *trans*, Fig. 4(b). If the two imidazoles are not undergoing rapid rotation about the (W—N) bond they may take different orientations which would explain the observation of two resonances for each imidazole proton. The *trans* orientation of monodentate ligands within this system has been observed before in the bis(phosphine) complexes $[W(CO)L_2(S_2CNC_4H_8)(\eta^2\text{-}MeC_2Me)][BPh_4]$.[11] It is, therefore, difficult to distinguish between these two possible isomers.

The ^{13}C NMR spectrum of compound **1** shows alkyne contact carbon resonances between 188.05 and 174.0 ppm, which is indicative[14] of the but-2-yne ligands donating a total of six electrons to the tungsten. Whereas, for compounds **4–6** the alkyne contact carbon resonances are above 200 ppm which suggests[14] the coordinated but-2-yne is using both sets of $p\pi$ orbitals in bonding with the tungsten, thus behaving as a four-electron donor. The quartet around 165 ppm is indicative of the $[BPh_4]^-$ counteranion and confirms the cationic nature of these complexes.

Acknowledgements—K.R.F. thanks the SERC for a studentship, and we thank Dr M. A. Beckett for useful discussions.

REFERENCES

1. M. Bottrill and M. Green, *J. Chem. Soc., Dalton Trans.* 1977, 2365.
2. S. R. Allen, P. K. Baker, S. G. Barnes, M. Green, L. Trollope, L. M. Muir and K. W. Muir, *J. Chem. Soc., Dalton Trans.* 1981, 873.
3. M. Green, N. C. Norman, A. G. Orpen and C. J. Schaverien, *J. Chem. Soc., Dalton Trans.* 1984, 2455.
4. P. G. Bourner, L. Brammer, M. Green, S. Moran, A. G. Orpen, C. Reeve and C. J. Schaverien, *J. Chem. Soc., Chem. Commun.* 1985, 409.
5. L. Brammer, M. Green, A. G. Orpen, K. E. Paddick and D. R. Saunders, *J. Chem. Soc., Dalton Trans.* 1986, 657.
6. M. Green, *J. Organomet. Chem.* 1986, **300**, 93.
7. M. Green, *Polyhedron* 1986, **5**, 427.
8. M. Green, N. K. Jetha, R. J. Mercer, N. C. Norman and A. G. Orpen, *J. Chem. Soc., Dalton Trans.* 1988, 1843.
9. K. R. Birdwhistell, T. L. Tonker and J. L. Templeton, *J. Am. Chem. Soc.* 1985, **107**, 4474.
10. P. K. Baker, M. G. B. Drew and K. R. Flower, *J. Organomet. Chem.* 1990, **391**, C12.
11. P. K. Baker and K. R. Flower, *J. Organomet. Chem.*, in press.
12. H. S. Gutowsky and C. H. Holm, *J. Chem. Phys.* 1956, **25**, 1228.
13. A. Allerhand, H. S. Gutowsky, J. Jones and R. A. Meinzer, *J. Am. Chem. Soc.* 1966, **88**, 3185.
14. B. C. Ward and J. L. Templeton, *J. Am. Chem. Soc.* 1980, **102**, 3288.

Polyhedron Vol. 10, No. 7, pp. 717–723, 1991
Printed in Great Britain

0277–5387/91 $3.00+.00
© 1991 Pergamon Press plc

THE SYNTHESIS AND REACTIVITY OF SOME μ-PHTHALOYL AND μ-PHENYLENE COMPLEXES

SELWYN F. MAPOLIE and JOHN R. MOSS†

Department of Chemistry, University of Cape Town, Rondebosch 7700, South Africa

(*Received* 24 *September* 1990; *accepted* 5 *December* 1990)

Abstract—The binuclear μ-phthaloyl compounds 1,4-$C_6H_4(COM)_2$, where M = $Re(CO)_5$, $Mn(CO)_5$, η^5-$C_5H_5Fe(CO)_2$, η^5-$C_5H_5Mo(CO)_3$, $Rh(PPh_3)_2Cl_2$ or $Co(CO)_3(PPh_3)$, have been prepared and converted to the μ-phenylene compounds 1,4-$C_6H_4M_2$, where M = $Re(CO)_5$, $Mn(CO)_5$ or η^5-$C_5H_5Fe(CO)_2$. The reactions of the μ-phthaloyl compounds with halogens, reducing agents and PPh_3 are reported, as are the reactions of the μ-phenylene complexes with CO, synthesis gas, SO_2, halogens and tertiary phosphines.

Mononuclear aryl complexes L_nM-Ar are well known. These complexes can be models for metal aryl species in catalytic reactions which give monofunctional aryl products, ArX.[1] Difunctional aryl compounds such as the phthalic acids $C_6H_4(COOH)_2$ are of great commercial importance.[2] Potential precursors of 1,4-$C_6H_4X_2$ compounds in a catalytic cycle would be the binuclear μ-phenylene or μ-phthaloyl complexes 1,4-$C_6H_4(ML_n)_2$ or 1,4-$C_6H_4(COML_n)_2$. When we started our investigations, very few binuclear compounds of these types were known. The compounds where ML_n = $Mn(CO)_5$ or $Re(CO)_5$ had been briefly mentioned,[3] as had 1,4-$C_6H_4(Cp^*_2Lu)_2$ (Cp^* = η^5-C_5Me_5).[4] The compound 1,4-$C_6H_4[Ni(PPh_3)_2Br]_2$ is known[5] and 1,4-C_6H_4[Fe(porphyrin)]$_2$ has recently been reported.[6] While our work was in progress, Hunter and co-workers reported some μ-phthaloyl and μ-phenylene complexes[7–10] which we had independently prepared. We now report some examples of these complexes, some new data on previously prepared compounds, as well as the results of some reactivity studies on these compounds.

EXPERIMENTAL

All reactions were performed under an atmosphere of high purity nitrogen using standard Schlenk tube techniques. Solvents were purified by standard procedures. The compounds $Mn_2(CO)_{10}$, $Re_2(CO)_{10}$, $[CpFe(CO)_2]_2$, $[CpMo(CO)_3]_2$ and $Co_2(CO)_8$ were purchased from Strem; K-Selectride (potassium tri-*sec*-butylborohydride) was purchased from Aldrich. These and other reagents were used as received. The compounds $RhCl(PPh_3)_3$[11] and $[Co(CO)_3(PPh_3)]_2$[12] were prepared by standard procedures. IR spectra were recorded on a Perkin–Elmer 983 spectrophotometer and NMR spectra on either a Varian XL 100 or VXR 200 or a Bruker WH 90 instrument. Tetramethylsilane was used as an internal standard (δ 0.00 ppm) for NMR spectra. Mass spectra were recorded on a V.G. Micromass 16 F spectrometer operating at 70 eV and using an accelerating voltage of 4 kV. Melting points were determined on a Reichert Thermovar hotstage microscope. Microanalyses were performed in the microanalytical laboratory at the University of Cape Town. Photochemical reactions were carried out in a Hanovia photochemical reactor (125 W) and high pressure reactions in a 250 cm^3 Berghoff autoclave.

μ-Phthaloyl complexes

Preparation of 1,4-$C_6H_4[COCpMo(CO)_3]_2$ (**1**)

A solution of $Na[CpMo(CO)_3]$ (2.04 mmol) was added to a solution of 1,4-$C_6H_4(COCl)_2$ (0.21 g, 1.02 mmol) in THF (2 cm^3) at −78°C. The reaction mixture was then stirred at −78°C for 30 min and then allowed to warm up to room temperature over 30 min. The solvent was removed to give a brown residue which was extracted with CH_2Cl_2

† Author to whom correspondence should be addressed.

($50\ cm^3$) and filtered. The filtrate was evaporated, resulting in an orange–red residue which was dissolved in benzene and chromatographed on an alumina column. A red band was eluted with benzene which gave $[CpMo(CO)_3]_2$ (78%). An orange band was eluted with 20% CH_2Cl_2/benzene which produced an orange–yellow solid on evaporation. The solid was recrystallized from CH_2Cl_2/hexane to yield the required product. The yield, m.p., elemental analysis and spectral data for this and other new complexes are given in Table 1. The compounds 1,4-$C_6H_4(COM)_2$ [where M = $Mn(CO)_5$ (**2**) or $CpFe(CO)_2$ (**3**)] were prepared in a similar way, as has been described by Hunter and Szigety.[9]

Preparation of 1,4-$C_6H_4[CORe(CO)_5]_2$ (**4**)

A solution of the sodium salt $Na[Re(CO)_5]$ (2 mmol) in THF ($30\ cm^3$) was added dropwise to a solution of 1,4-terephthaloyl dichloride (1 mmol) in THF ($5\ cm^3$) with rapid stirring. The reaction mixture was stirred for 3 h after which the solvent was removed and the residue triturated with water ($4 \times 30\ cm^3$). The solid product was filtered off, washed with diethyl ether ($5 \times 30\ cm^3$) and dried *in vacuo*.

Preparation of 1,4-$C_6H_4[COCo(CO)_3(PPh_3)]_2$ (**5**)

The compound $[Co(CO)_3(PPh_3)]_2$ (0.50 g, 0.62 mmol) as a suspension in THF ($20\ cm^3$) was stirred

Table 1. Data for μ-phthaloyl and μ-phenylene compounds

Compound number	Yield (%)	Melting point (°C)	Microanalysis[a] (%)		IR ν(CO)[b] (cm^{-1})		NMR[c]	δ (ppm)
1	7	131–138	C 46.0	(46.3)	2024 m	1938 s	7.44	(4H, C_6H_4)
			H 2.2	(2.3)	1607 m		5.54	(10H, C_5H_5)
4	44	210–218	C 27.8	(27.6)	2133 w	2060 m		
					2018 sh	2002 s		[e]
			H 0.7	(0.5)	1976 vs	1566 m		
5	23	204–212	C 63.3	(63.7)	2051 w	1983 s	7.72	(4H, C_6H_4)
			H 3.8	(3.6)	1966 s	1622 m	7.44	(30H, C_6H_5)
6	74	206–211	C 62.5	(62.9)	1701 m	1665 w[d]		[e]
			H 4.6	(4.2)				
7	56	210–215	C 26.5	(26.4)	2128 w		7.26	(4H, C_6H_4)[f]
			H 0.70	(0.55)	2020 s	1986 sh	183.4	(CO)
							181.5	(CO)
							134.3	(Re—C of C_6H_4)
							146.1	(other C of C_6H_4)
10	18	166–173	C 32.0	(32.3)	2137 m	2985 w		[e]
			H 0.68	(0.68)	2051 s	2022 m		
11	33	198–210	C 22.0	(22.4)	2158 w	2045 vs		[e]
			H 0.49	(0.47)				
12	77	174–181	C 42.7	(43.0)	2054 s	2011 vs	7.38	(s, 4H, C_6H_4)
			H 2.4	(2.5)			5.10	(s, 10H, C_5H_5)
13	65	161–164	C 58.5	(59.1)	2065 m	1988 s	7.38	(m, 20H, C_6H_5)
			H 3.8	(4.0)	1969 vs	1946 s	6.90	(s, 4H, C_6H_4)
							1.67	(d, 6H, $J = 9$ Hz)
15	11	98–107	C 72.5	(72.2)	1913 s		7.34	(m, 30H, C_6H_5)
			H 4.8	(4.9)			6.54	(s, 4H, C_6H_4)
							4.36	(d, 10H, C_5H_5)

[a] Calculated values in parentheses.
[b] CH_2Cl_2 solution unless otherwise stated; s = strong, m = medium, w = weak.
[c] $CDCl_3$ solution unless otherwise stated.
[d] Nujol mull.
[e] Not recorded due to insolubility of sample.
[f] CD_2Cl_2.

with a sodium amalgam (0.1 g Na in 2 cm^3 Hg) for 18 h. The resulting green solution of $Na[Co(CO)_3(PPh_3)]$ (1.24 mmol) was added to a solution of 1,4-$C_6H_4(COCl)_2$ (0.13 g, 0.62 mmol) in THF (2 cm^3) and the mixture stirred for 18 h at room temperature. The solvent was removed leaving a green residue which was extracted with CH_2Cl_2 (60 cm^3) and filtered. The volume of the filtrate was reduced to *ca* 10 cm^3 and chromatographed on a Florisil column. A pale yellow band containing 1,4-$C_6H_4(COCl)_2$ and 1,4-$C_6H_4(COOH)_2$ was eluted initially using CH_2Cl_2. A bright yellow band was then eluted with CH_2Cl_2/ethanol (1 : 1) which gave a solid on evaporation. This was recrystallized from CH_2Cl_2/hexane to give microcrystals of the product. The same compound is obtained, in lower yield, from the reaction of $Na[Co(CO)_4]$ with 1,4-$C_6H_4(COCl)_2$ followed by the addition of PPh_3 to the reaction mixture.

Preparation of 1,4-$C_6H_4[CORhCl_2(PPh_3)_2]_2$ (**6**)

To a solution of $RhCl(PPh_3)_3$ (0.50 g, 0.54 mmol) in CH_2Cl_2 (10 cm^3) was added a solution of 1,4-$C_6H_4(COCl)_2$ (0.055 g, 0.27 mmol) in CH_2Cl_2 (2 cm^3) and the reaction mixture was stirred for 6.5 h at room temperature. During this time, the solution changed colour from red to yellow and a fine precipitate formed. Hexane (100 cm^3) was added and the resulting precipitate was filtered and washed with CH_2Cl_2 (4 × 10 cm^3) to give the product as yellow microcrystals. IR (Nujol): ν(RhCl) 356 and 324 cm^{-1}.

μ-Phenylene complexes

Preparation of 1,4-$C_6H_4[Re(CO)_5]_2$ (**7**)

The compound **3** (0.050 g, 0.064 mmol), as a suspension in methyl isobutyl ketone (5 cm^3), was refluxed for 35 min then filtered hot. The solvent was reduced and the resulting mixture cooled to −15°C to give the product as white microcrystals.

The compound 1,4-$C_6H_4[Mn(CO)_5]_2$ (**8**) was prepared in 74% yield by refluxing the corresponding μ-phthaloyl compound in toluene and 1,4-$C_6H_4[CpFe(CO)_2]_2$ (**9**) was obtained in 26% yield on UV irradiation of a toluene solution of the μ-phthaloyl compound **4**; the data obtained for the manganese and iron compounds agreed well with that reported by Hunter and Szigety.[9]

Reactions of the μ-phthaloyl compounds

(a) *With halogens*

1,4-$C_6H_4[COMnCO)_5]_2$ (**2**) *with* Br_2 *or* I_2. A suspension of **2** (0.19 mmol) in THF (7 cm^3) was stirred at room temperature for *ca* 70 h with the halogen (0.76 mmol). Unreacted starting material (48%) was filtered off and 1,4-$C_6H_4(COOH)_2$ (48%) and $Mn(CO)_5X$ [where X = Br (44%), I (32%)] were isolated from the filtrate and identified by their IR spectra.

1,4-$C_6H_4[COCpFe(CO)_2]_2$ (**3**) *with* Br_2 *or* I_2. In a similar way, **4** (0.21 mmol) was reacted with the halogen (0.42 mmol) in THF (7 cm^3) for 20 min to give 1,4-$C_6H_4(COOH)_2$ (94%) and $CpFe(CO)_2X$ [where X = Br (85%), I (77%)], the latter compounds were identified by IR and ^1H NMR.

1,4-$C_6H_4[CORe(CO)_5]_2$ (**4**) *with* Br_2 *or* I_2. In a similar way, **3** (0.13 mmol) was reacted with the halogen (0.26 mmol) in THF (7 cm^3) for 2 h to give 1,4-$C_6H_4(COOH)_2$ (83%) and $Re(CO)_5X$ [where X = Br (74%), I (69%)].

(b) *With tertiary phosphines*

1,4-$C_6H_4[COCpFe(CO)_2]_2$ (**3**) *with* PPh_3. A mixture of **4** (0.41 mmol) and PPh_3 (0.82 mmol) in toluene (200 cm^3) was irradiated in a photochemical reactor for 4 h. The solvent was removed and a benzene solution of the residue was chromatographed on an alumina column. An orange band was eluted with benzene which, after evaporation and recrystallization gave 1,4-$C_6H_4[CpFe(CO)(PPh_3)]_2$ (**15**) as orange microcrystals. Elution with CH_2Cl_2/benzene (1 : 9) gave **9** (6%).

(c) *With reducing agents*

1,4-$C_6H_4[COMn(CO)_5]_2$ (**2**) *with* K–*Selectride*. K–Selectride (0.76 cm^3 of a 1 M THF) solution was added to a suspension of **2** (0.38 mmol) in THF (5 cm^3) at −78°C. The reaction mixture immediately changed colour from yellow to orange and the IR showed new bands at 1886 and 1557 cm^{-1} which are assigned to $Mn(CO)_5^-$ and an unstable formyl complex. The only product isolated after work-up of the reaction mixture was $Mn_2(CO)_{10}$ (61%).

1,4-$C_6H_4[COCpFe(CO)_2]_2$ (**3**) *with* K–*Selectride or* $LiAlH_4$. Similarly, the reaction of **4** with K–Selectride gave $[CpFe(CO)_2]_2$ (65%), whereas the corresponding reaction with $LiAlH_4$ gave $[CpFe(CO)_2]_2$ (67%) and starting material (29%).

1,4-$C_6H_4[COMn(CO)_5]_2$ (**2**) *with* $LiBEt_3H$. The reaction was carried out in THF at room temperature and monitored by IR. New bands were observed at 1880 and 1560 cm^{-1} but the only product isolated was $Mn_2(CO)_{10}$ (54%).

1,4-$C_6H_4(COM)_2$ [M = $Mn(CO)_5$ $CpFe(CO)_2$ *or* $Re(CO)_5$] *with* BH_3·THF. No reaction of these μ-phthaloyl compounds was observed with BH_3·THF at room temperature in THF.

Reactions of μ-phenylene compounds

(a) *With* CO

1,4-$C_6H_4[Mn(CO)_5]_2$ (**8**) *with* CO. The autoclave was charged with **8** (0.11 mmol), THF (10 cm^3) and CO (30 atm). The mixture was then stirred at room temperature for 22 h, after which time the autoclave was vented and the solvent removed under reduced pressure from the reaction solution to give a white solid. The solid was washed with ether and identified as **2** (84%).

1,4-$C_6H_4M_2$ *with* CO. Similarly, reaction of 1,4-$C_6H_4[Re(CO)_5]_2$ (**7**) with CO (30 atm) on stirring at room temperature for 48 h gave **3** (20%) and unreacted starting material. Compound **9** showed no reaction with CO under these conditions.

(b) *With synthesis gas*

1,4-$C_6H_4[Mn(CO)_5]_2$ (**8**) *with* CO/H_2 (1 : 1). The autoclave was charged with **8** (0.21 mmol), THF (10 cm^3) and CO/H_2 (1 : 1) (40 atm) and the mixture heated at 70°C for 3.5 h. The autoclave was cooled and the gases vented. The resulting yellow solution was filtered and the solvent removed under reduced pressure. Addition of hexane gave a white solid which was filtered off and identified as 1,4-$C_6H_4(CH_2OH)_2$ (69%) by ^1H NMR, IR and mass spectra. The solvent was removed from the yellow filtrate to give $Mn_2(CO)_{10}$ (71%).

1,4-$C_6H_4M_2$ *with* CO/H_2 (1 : 1), *where* M = $Re(CO)_5$ *or* $CpFe(CO)_2$. Under similar conditions to the above, **7** gave a mixture of products containing unreacted starting material, **3**, 1,4-$C_6H_4(CH_2OH)_2$ and an unidentified aldehyde species, which could not be separated. Similarly, **9**, after 8 h, gave unreacted starting material (58%) and $[CpFe(CO)_2]_2$ (37%).

(c) *With* SO_2

1,4-$C_6H_4[Re(CO)_5]_2$ (**7**) *with* SO_2. A Carius tube was charged with **7** (0.07 mmol) and liquid SO_2 (10 cm^3) was condensed onto the solid and the tube was sealed with its Teflon tap. The tube was then treated at 80°C for 48 h. The SO_2 was evaporated to give a cream coloured residue which was extracted with CH_2Cl_2, filtered and the solvent removed. The resulting solid was recrystallized from hot $CHCl_3$/hexane to give 1,4-$C_6H_4[SO_2Re(CO)_5]_2$ (**11**) as a white microcrystalline solid; IR (Nujol): ν(SO) 1186s, 1048s cm^{-1}.

1,4-$C_6H_4[Mn(CO)_5]_2$ (**8**) *with* SO_2. Similarly, this reaction was carried out with **8** (0.21 mmol) and SO_2 (10 cm^3) at 80°C for 60 h, after which time the SO_2 was allowed to evaporate. The pale yellow residue was extracted with ethanol (3 × 20 cm^3), filtered and the solvent removed. The resulting solid was washed with CH_2Cl_2 (4 × 10 cm^3) to give 1,4-$C_6H_4[SO_2Mn(CO)_5]_2$ (**10**) as a yellow microcrystalline solid; IR (Nujol): ν(SO) 1190s, 1030m cm^{-1}.

1,4-$C_6H_4[CpFe(CO)_2]_2$ (**9**) *with* SO_2. Similarly, a Carius tube was charged with **9** (0.07 mmol) and liquid SO_2 (10 cm^3). The mixture was then stirred at room temperature for 38 h. The excess SO_2 was evaporated and the resulting residue recrystallized from CH_2Cl_2/hexane to give 1,4-$C_6H_4[SO_2CpFe(CO)_2]_2$ (**12**) as a yellow solid; IR (Nujol): ν(SO) 1193m, 1045m cm^{-1}.

(d) *With halogens*

1,4-$C_6H_4[CpFe(CO)_2]_2$ (**9**) *with* Br_2 *or* I_2. A solution of **9** (0.23 mmol) in THF (12 cm^3) was treated with Br_2 (0.46 mmol) and the brown mixture stirred for 30 min at room temperature. The solvent was removed leaving a red–brown residue. This was taken up in CH_2Cl_2 and chromatographed on an alumina column. Elution with CH_2Cl_2/hexane (1 : 9) resulted in 1,4-$C_6H_4Br_2$ (84%). Elution with CH_2Cl_2/hexane (1 : 1) gave $CpFe(CO)_2Br$ (82%).

Similarly, the reaction of **9** with I_2 gave 1,4-$C_6H_4I_2$ (60%) and $CpFe(CO)_2I$ (62%).

1,4-$C_6H_4[Re(CO)_5]_2$ (**7**) *with* Br_2. A similar reaction with **7** (0.28 mmol) in THF (12 cm^3) gave 1,4-$C_6H_4Br_2$ (76%) and $Re(CO)_5Br$ (81%).

(e) *With tertiary phosphines*

1,4-$C_6H_4[Mn(CO)_5]_2$ (**8**) *with* $PMePh_2$. A solution of **8** (0.13 mmol) and $PMePh_2$ (0.26 mmol) in CH_2Cl_2 (10 cm^3) was treated with $Me_3NO \cdot 2H_2O$ (0.26 mmol) and the solution stirred at room temperature until no starting material remained, as judged by the IR spectrum. The solution was concentrated and chromatographed on an alumina column. Elution with CH_2Cl_2/hexane (1 : 1) gave a yellow solid from which 1,4-$C_6H_4[Mn(CO)_4(PMePh_2)]_2$ (**13**) was isolated. A similar reaction of **7** with PPh_3 gave 1,4-$C_6H_4[Mn(CO)_4(PPh_3)]_2$ (**14**) (76%).

1,4-$C_6H_4[CpFe(CO)_2]_2$ (**9**) *with* PPh_3. Compound **9** (0.23 mmol) and PPh_3 (0.46 mmol) in benzene (150 cm^3) was irradiated for 2 h. The solution was concentrated, chromatographed on an alumina column and eluted with benzene to give 1,4-$C_6H_4[CpFe(CO)(PPh_3)]_2$ (**15**) (11%).

DISCUSSION

The μ-phthaloyl compounds of molybdenum, manganese, rhenium, iron and cobalt were prepared by the following route

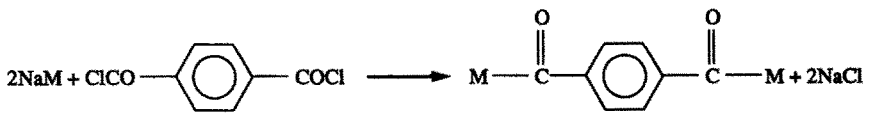

(1)

1 M = $CpMo(CO)_3$
2 M = $Mn(CO)_5$
3 M = $CpFe(CO)_2$
4 M = $Re(CO)_5$
5 M = $Co(CO)_3(PPh_3)$

The rhodium complex, $1,4\text{-}C_6H_4[CORhCl_2(PPh_3)_2]_2$ (**6**), was prepared by the oxidative addition reaction of $RhCl(PPh_3)_3$ to $1,4\text{-}C_6H_4(COCl)_2$. Characterization data for the new μ-phthaloyl compounds are given in Table 1. Data for compounds **2** and **3** have recently been reported by Hunter and Szigety.[9] Like the manganese and iron compounds (**2** and **3**) the rhenium and rhodium compounds (**4** and **6**) are air-stable in contrast to the molybdenum and cobalt compounds (**1** and **5**). With the exception of the cobalt compound, all the μ-phthaloyl compounds are rather insoluble. The ν(CO) bands in the IR spectra for **1**, **2** and **4** are in similar positions to those reported for the respective mononuclear analogues $CpMo(CO)_3(COPh)$[13] and $M(CO)_5(COPh)$ (where M = Mn or Re).[14] The IR spectrum of **6** is similar to that reported for $RhCl_2(PPh_3)_2(COR)$,[15] suggesting that the PPh_3 groups in both compounds may be *trans* to each other.

The μ-phenylene compounds of manganese, rhenium and iron were prepared by decarbonylation of the μ-phthaloyl precursors:

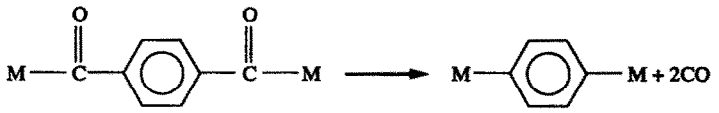

(2)

1 M = $Re(CO)_5$
2 M = $Mn(CO)_5$
3 M = $CpFe(CO)_2$

We obtained the rhenium and manganese compounds (**7** and **8**) by refluxing the appropriate μ-phthaloyl compounds in toluene or methyl isobutyl ketone. For compound **9**, decarbonylation was effected by either UV irradiation or chemical decarbonylation using $RhCl(PPh_3)_3$. The characterization data obtained for compounds **8** and **9** agreed well with that reported by Hunter and Szigety.[9] An attempt to synthesize **9** from $Na[CpFe(CO)_2]$ and $1,4\text{-}C_6H_4I_2$ in refluxing THF gave $1,4\text{-}C_6H_4I[CpFe(CO)_2]$ in 4% yield. We were not able to efficiently decarbonylate compounds **1**, **5** and **6** to give μ-phenylene products.

Mass spectra of the μ-phthaloyl compounds **2**–**4** did not show parent ions and the highest mass peaks we observed correspond to $[M-2CO]^+$; in fact, the spectra are identical to those of the corresponding μ-phenylene complexes **7**–**9**.

As reported by Hunter and Szigety,[9] we observe parent ions in the mass spectra for compounds **7**–**9**. We have also identified the main fragmentation pathways for these compounds which can be summarized as follows:

For compound **8**:
(1) Loss of 10 CO's from parent to give $M_2(C_6H_4)$
(2) Loss of $M(CO)_5$ from parent then 5 CO's

For compound **7**:
(1) and (2) above but also
(3) Loss of C_6H_4 from parent followed by 10 CO's

For compound **9**:
(1) Loss of 4 CO's from parent to give $Cp_2Fe_2(C_6H_4)$
(2) Loss of $CpFe(CO)_2$ from parent then 2 CO's.

Reactivity of the μ-phthaloyl complexes

Most of the reactions outlined below were carried out on the μ-phthaloyl compounds (**2–4**).

(a) *Reactivity of the μ-phthaloyl complexes* **2–4** *with halogens*

Although there are many reports of electrophilic cleavage of transition metal–carbon bonds of alkyl compounds, there are few reports of similar reactions of metal aroyl compounds and none that we are aware of on binuclear μ-phthaloyl compounds.[1] We have investigated the reactions of the μ-phthaloyl compounds of manganese, rhenium and iron with Br_2 and I_2 in THF at room temperature. In each case the metal halide and terephthalic acid were produced

$$1,4\text{-}C_6H_4(COM)_2 + 2X_2 \longrightarrow 2M\text{-}X$$

$$+ [1,4\text{-}C_6H_4(COX)_2] \longrightarrow 1,4\text{-}C_6H_4(COOH)_2$$
Not observed

[where M = $Mn(CO)_5$, $Re(CO)_5$ or $CpFe(CO)_2$; X = Br or I]; the terephthalic acid may result from hydrolysis of aroyl halide intermediates.

Even though the same type of products were obtained for the three complexes $1,4\text{-}C_6H_4(COM)_2$, the rates of the reactions were significantly different and followed the order $CpFe(CO)_2 > Re(CO)_5 > Mn(CO)_5$. This may be explained on the basis that metal–carbon bond cleavage is an electrophilic process. This is borne out by the reactivity order following decreasing electron density on the metal and that the reactions with iodine appear slower than those with bromine.

(b) *The reaction of* $1,4\text{-}C_6H_4[COCpFe(CO)_2]_2$ *with* PPh_3

Substitution of CO by PPh_3 is difficult in this complex since no reaction of compound **3** with PPh_3 occurred after refluxing in xylene for 3 days. UV irradiation in toluene for 4 h produced a 9% yield of the substituted phenylene complex, viz. $1,4\text{-}C_6H_4[CpFe(CO)(PPh_3)]_2$ (**15**).

(c) *Reactions of μ-phthaloyl complexes with reducing agents*

Attempts to reduce the aroyl CO groups in compounds **2** and **3** were made using K–Selectride, $LiAlH_4$, $LiBEt_3H$ or $BH_3 \cdot THF$ as reducing agents. Compounds **2** and **3** reacted with K–Selectride to give anionic intermediates, however, no new products could be isolated. Reaction of **3** with $LiAlH_4$ was slow and $[CpFe(CO)_2]_2$ was the only product identified, whereas $[Mn(CO)_5]^-$ was the only product identified from the reaction of **2** with $LiBEt_3H$. No reactions of **2–4** with $BH_3 \cdot THF$ were observed.

Reactivity of the μ-phenylene complexes

(a) *With* CO

Compound **8** gave 85% conversion to the μ-phthaloyl compound **2** after 22 h with CO (30 atm) in THF. There was no reaction of **8** with CO (1 atm) after 48 h. Compound **8** undergoes CO insertion much less readily than its mononuclear analogue $Mn(CO)_5Ph$.[16] The rhenium compound is less readily carbonylated than the manganese complex and only 20% of the μ-phthaloyl compound **4** was isolated after 48 h reaction time with CO (30 atm) at room temperature. The iron complex **9** showed no CO insertion under similar conditions.

(b) *With synthesis gas* (CO/H_2, 1 : 1)

The reaction of $1,4\text{-}C_6H_4[Mn(CO)_5]_2$ (**8**) gave $1,4\text{-}C_6H_4(CH_2OH)_2$ as the only isolable organic product and $Mn_2(CO)_{10}$. The reaction appears to be similar to that reported for $(CO)_5Mn(CH_2)_4Mn(CO)_5$ with synthesis gas.[17] In both these cases, the reaction with synthesis gas leads, via initial CO insertion, to a diol. No evidence for any further carbon chain growth is observed. This may be a general result in catalytic reactions, also that CO insertion leads to termination, with alcohol and aldehyde formation but not to carbon chain growth.

Compounds **7** and **9** were found to be less reactive towards synthesis gas.

(c) *With* SO_2

Since some mononuclear aryl complexes are known to react with SO_2 to form the corresponding S-sulphinates,[18,19] we were interested to investigate similar reactions with μ-phenylene complexes. Thus, we find that compounds **7–9** react with liquid SO_2 according to the following equation

$$1,4\text{-}C_6H_4M_2 + 2SO_2 \longrightarrow 1,4\text{-}C_6H_4(SO_2M)_2 \qquad (3)$$

10 M = $Mn(CO)_5$
11 M = $Re(CO)_5$
12 M = $CpFe(CO)_2$.

Data for compounds **1–12** are given in Table 1. In general, the reactions of the binuclear μ-phenylene complexes with SO_2 are significantly slower than analogous reactions with mononuclear phenyl compounds.

(d) *With halogens*

Compared to the corresponding μ-phthaloyl compounds, the μ-phenylene compounds **7–9** react more readily with the halogens Br_2 or I_2 in THF to yield the corresponding metal carbonyl halides and 1,4-dihalobenzenes [eq. (4)]:

$$1,4\text{-}C_6H_4M_2 + 2X_2 \longrightarrow 1,4\text{-}C_6H_4X_2 + 2MX \quad (4)$$

[M = $Mn(CO)_5$, $Re(CO)_5$ or $CpFe(CO)_2$; X = Br or I].

Similar results have been found for the reactions of the manganese and iron compounds.[9] We find the rate of metal–carbon cleavage by halogen in $1,4\text{-}C_6H_4M_2$ to be $CpFe(CO)_2$ > $Re(CO)_5$ > $Mn(CO)_5$; exactly the same order as we found for the μ-phthaloyl compounds.

(e) *With tertiary phosphines*

The reactions of **8** and **9** with PPh_3 or $PMePh_2$ were carried out under various conditions and gave substitution products according to eq. (5):

$$1,4\text{-}C_6H_4[M(CO)]_2 + 2PR_3 \longrightarrow 1,4\text{-}C_6H_4[M(PR_3)]_2 + 2CO \quad (5)$$

13 M = $Mn(CO)_4$, PR_3 = $PMePh_2$

14 M = $Mn(CO)_4$, PR_3 = PPh_3

15 M = CpFe(CO), PR_3 = PPh_3.

This CO substitution reaction is analogous to that reported for $Mn(CO)_5Ph$ with PPh_3, although the rate of reaction of the μ-phenylene complex **8** with PPh_3 is slower than that for $Mn(CO)_5Ph$.[20] Products resulting from aryl migration were not observed. Our results agree well with those reported by others for the reaction of **8** with PPh_3.[9] In the presence of Me_3NO, the reactions to give **13** and **14** in eq. (5) proceded much faster. Similar rate enhancement has been found for the substitution of CO by PPh_3 in $Mn(CO)_5Ph$.[21] On the basis of IR spectra in the ν(CO) region, compounds **13** and **14** adopt a *cis*-configuration at manganese.

CONCLUSIONS

The reactivity of the μ-phthaloyl and μ-phenylene complexes of several metals give similar products to analogous reactions of mononuclear compounds, although the rates of some of the reactions are different. We are at present obtaining quantitative data on these rate differences. These findings may have significance in catalytic reactions that yield difunctional aryl products.

Acknowledgements—We thank the University of Cape Town and FRD for support, Johnson Matthey for a generous loan of rhodium trichloride and Nazir Ahmed for help with the manuscript.

REFERENCES

1. J. P. Collman, L. S. Hegedus, J. R. Norton and R. G. Finke, *Principles and Applications of Organotransition Metal Chemistry*, 2nd edn, p. 433. University Science Books, Mill Valley, California (1987).
2. F. A. Cotton and G. Wilkinson, *Advanced Inorganic Chemistry*, 4th edn, p. 1267. Wiley, New York (1980).
3. A. N. Nesmeyanov, K. N. Anisimov and N. E. Kolobova, *Akad. Nauk SSSR, Ser. Khim.* 1963, 1348.
4. P. L. Watson and G. W. Parshall, *Accts Chem. Res.* 1985, **18**, 51.
5. B. Hipler, E. Uhlig and J. Vogel, *J. Organomet. Chem.* 1981, **218**, C1.
6. K. Shin, B.-S. Yu and H. M. Goff, *Inorg. Chem.* 1990, **29**, 889.
7. A. D. Hunter, *Organometallics* 1989, **8**, 1118.
8. G. B. Richter-Addo and A. D. Hunter, *Inorg. Chem.* 1989, **28**, 4065.
9. A. D. Hunter and A. B. Szigety, *Organometallics* 1989, **8**, 2670.
10. A. D. Hunter and J. L. McLernon, *Organometallics* 1989, **8**, 2679.
11. J. A. Osborn, F. H. Jardine, J. F. Young and G. Wilkinson, *J. Chem. Soc. A* 1966, 1711.
12. A. R. Manning, *J. Chem. Soc. A* 1968, 1135.
13. A. N. Nesmeyanov, L. G. Makarova, N. A. Ustynyuk and L. V. Boyatyreva, *J. Organomet. Chem.* 1972, **42**, 105.
14. W. Beck, W. Hieber and H. Tengler, *Chem. Ber.* 1961, **94**, 862.
15. D. L. Egglestone, M. C. Baird, C. J. L. Lock and G. Turner, *J. Chem. Soc., Dalton Trans.* 1977, 1576.
16. F. Calderazzo, *Angew. Chem. Int. Ed.* 1977, **16**, 299.
17. S. F. Mapolie and J. R. Moss, *J. Chem. Soc., Dalton Trans.* 1990, 299.
18. F. A. Hartman and A. Wojcicki, *Inorg. Chem.* 1968, **8**, 1504.
19. S. E. Jacobsen and A. Wojcicki, *J. Am. Chem. Soc.* 1973, **95**, 6962.
20. W. D. Bannister, B. L. Booth, M. Green and R. N. Hazeldine, *J. Chem. Soc. A* 1969, 698.
21. D. J. Blumer, K. W. Barnett and T. L. Brown, *J. Organomet. Chem.* 1979, **173**, 71.

Polyhedron Vol. 10, No. 7, pp. 725–729, 1991
Printed in Great Britain

0277–5387/91 $3.00+.00
© 1991 Pergamon Press plc

CARBONYL SUBSTITUTION REACTIONS OF CYCLOPENTADIENYLDICARBONYL COBALT(I) AND ACETYLCYCLOPENTADIENYLDICARBONYL COBALT(I) WITH BIS(1,3-DIMETHYLIMIDAZOLIN-2-YLIDENE). A KINETIC AND MECHANISTIC STUDY

S. DELGADO,* C. MORENO and M^{a}J. MACAZAGA

Departamento de Química (Inorgánica), Universidad Autónoma de Madrid, Cantoblanco, 28049 Madrid, Spain

(*Received* 27 *July* 1990; *accepted* 5 *December* 1990)

Abstract—The reaction of $(\eta^5\text{-Cp}')\text{Co(CO)}_2$ (Cp′ = C_5H_5, C_5H_4COMe) with bis(1,3-dimethylimidazolin-2-ylidene) gives the monosubstituted products $(\eta^5\text{-Cp}')\text{Co(CO)}[\dot{C}(NMe)CH_2CH_2(\dot{N}Me)]$. The reaction proceeds by first order in metal complex and first order in olefin. The rate of replacement of CO by the carbene fragment for $(\eta^5\text{-}C_5H_4COMe)Co(CO)_2$ in toluene at 95°C is 15 times faster than for the reaction of $(\eta^5\text{-}C_5H_5)Co(CO)_2$. The reasons for this difference are discussed in mechanistic terms.

Since the discovery of the first transition metal carbene complex, $(CO)_5W[C(OCH_3)CH_3]$, by Fischer and Maasböl,[1] there has been an ever increasing interest in the preparation, structure and reactivity of new transition metal carbene complexes.[2]

Carbene complexes derived from electron-rich olefins have been obtained by Lappert and coworkers,[3–5] exhibiting the nucleophilic character of the carbene fragment. The first mononuclear cobalt carbene complex derived from $(\eta^5\text{-}C_5H_5)Co(CO)_2$ has been reported recently[6] and the carbene fragment in $(\eta^5\text{-}C_5H_5)Co(CO)[\dot{C}(NMe)CH_2CH_2(\dot{N}Me)]$ is an extremely strong σ-donor ligand.

Substitution reactions of cyclopentadienyl metal compounds have been of special interest ever since Schuster-Woldan and Basolo[7] studied the reactions of $(\eta^5\text{-}C_5H_5)Rh(CO)_2$ and proposed that the cyclopentadienyl ligand promoted an associative pathway for carbonyl substitution reactions, due to the ability of the cyclopentadienyl ligand to accept an electron pair from the metal, thus creating a vacant orbital susceptible to nucleophilic attack.

If this mechanism is valid, then a complex with an electron-withdrawing group on the cyclopentadienyl ring should react faster than the parent complex. This is shown by the rate of replacement of C_2H_4 in the series $(\eta^5\text{-}C_5H_4CN)Rh(C_2H_4)_2$ > $(\eta^5\text{-}C_5H_5)Rh(C_2H_4)_2$ > $(\eta^5\text{-}C_5Me_5)Rh(C_2H_4)_2$,[8] and in the rate of replacement of CO in $(\eta^5\text{-}C_5H_4CO_2Me)Co(CO)_2$ > $(\eta^5\text{-}C_5Me_5)Co(CO)_2$ with phosphines and phosphites.[9,10]

Due to the relevance of carbene complexes in catalytic reactions, an understanding of how coordinatively saturated organometallic compounds react by associative mechanisms is significant for these catalytic transformations.

We now report a kinetic and mechanistic study of the formation of the transition metal carbene complexes from an electron-rich olefin. The reaction of $(\eta^5\text{-}C_5H_4COMe)Co(CO)[\dot{C}(NMe)CH_2CH_2(\dot{N}Me)]$ with TCNE is reported. This olefin can act as a π-acceptor ligand or as a σ-donor ligand bonding to the metal through a nitrile nitrogen. Examples of the latter are the previously reported complexes $(\eta^5\text{-}C_5H_4Me)Co(CO)L$ [L = CO, PPh_3, $P(OMe)_3$, py][11] in which TCNE acts as an oxidizing agent and coordinates to the metal through a nitrogen atom.

RESULTS AND DISCUSSION

Table 1 lists the carbonyl stretching frequencies of $Cp'Co(CO)_2$ and $Cp'Co(CO)[\dot{C}(NMe)CH_2CH_2(\dot{N}Me)]$ (Cp′ = C_5H_5, C_5H_4COMe).

Evidently the addition of the electron-withdrawing acetyl group to the cyclopentadienyl ring

* Author to whom correspondence should be addressed.

Table 1. Carbonyl stretching frequencies in toluene solution

Complex	ν(CO) (cm^{-1})
$C_5H_5Co(CO)_2$	2023.2, 1959.8
$(C_5H_4COMe)Co(CO)_2$	2033.0, 1973.4
$C_5H_5Co(CO)[\overline{C(NMe)CH_2CH_2(NMe)}]$	1902.1
$(C_5H_4COMe)Co(CO)[\overline{C(NMe_4)CH_2CH_2(NMe)}]$	1916.8

results in a shift of ν(CO) to higher frequency, relative to $(\eta^5\text{-}C_5H_5)Co(CO)_2$. This is attributed to the reduced amount of backbonding between cobalt and carbon, making the CO bond closer to the triple bond in free CO, and indicates that the cobalt is less electron-rich in the acetylcyclopentadienyl complex.

Thus, substitution reaction (1) was expected to proceed faster for the acetylcyclopentadienyl compound than for the corresponding cyclopentadienyl compound.

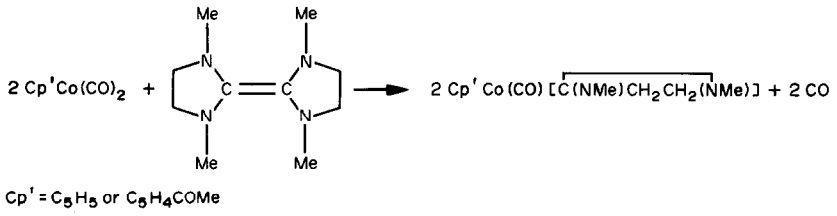

(1)

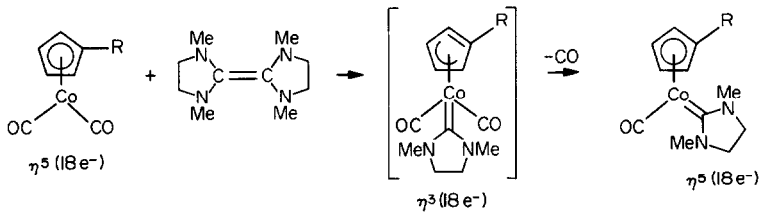

(2)

This was observed experimentally; Table 2 contains the rate constant for reaction (1), $(\eta^5\text{-}C_5H_4COMe)Co(CO)_2$ reacts approximately 15 times faster than $(\eta^5\text{-}C_5H_5)Co(CO)_2$ in toluene at 95°C.

The rate of reaction (1) is directly proportional to the concentration of the incoming ligand. Figure 1 shows that for $(\eta^5\text{-}C_5H_4COMe)Co(CO)_2$, a straight line with a zero intercept is obtained indicating no detectable contribution from a ligand-independent (first-order) process under these experimental conditions.

Small enthalpies and especially large negative entropies of activation (Table 2) provide further evidence for an associative mechanism (S_N2). All of these results are consistent with a S_N2 mechanism similar to the mechanism first proposed for $(\eta^5\text{-}C_5H_5)Rh(CO)_2$ with PPh_3.[7]

The mechanism can be represented by eq. (2) involving a transition state in which a rearrangement of the ring from a delocalized structure to an allyl-ene structure occurs, the cobalt being bound only to the allyl portion. Several reports[8,12,13] have established a good deal of support for the η^5-to-η^3 slippage mechanism for associative substitution reactions of cyclopentadienyl compounds. An η^3-cyclopentadienyl ring has been observed during the

Table 2. Rate constants and activation parameters (in toluene) for the reaction $Cp'Co(CO)+L \rightarrow Cp'Co(CO)L+Co$

Complex	L	Temperature (°C)	10^4K_{obs} (s^{-1})	$\Delta H^{\ddagger}$ (kcal mol^{-1})	$\Delta S^{\ddagger}$ (eu)
$C_5H_5Co(CO)_2$	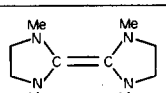	80	0.268		
		90	0.541		
		95	0.698	16.7±0.5	−32.5±1.8
$(C_5H_4COMe)Co(CO)_2$	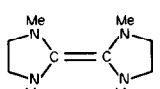	80	3.826		
		90	7.341		
		95	10.018	16.5±0.2	−27.6±0.6

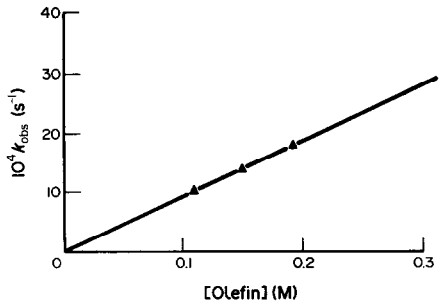

Fig. 1. Plot of k_{obs} (s^{-1}) vs olefin concentration (M) for reaction (1) (Cp′ = C_5H_4COMe; T = 95°C). The uncertainty of the derived rate constants are ±3%.

matrix photolysis of $(\eta^5\text{-}C_5H_5)Fe(CO)_2CH_3$[14] and Hüttner and co-workers[15] have isolated an η^3-cyclopentadienyl compound $(\eta^5\text{-}C_5H_5)W(\eta^3\text{-}C_5H_5)(CO)_2$. The increase in the rate constant observed for the acetylcyclopentadienyl complex is in accord with this mechanism and may be ascribed to a resonance stabilization of the transition state owing to the presence of the electron-withdrawing acetyl group on the ring, relative to the parent cyclopentadienyl compound, eq. (3).

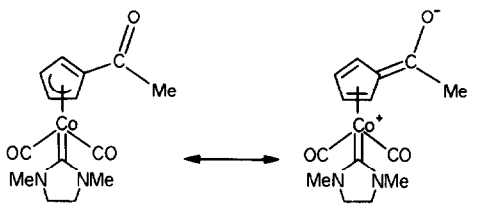

(3)

Addition under nitrogen of a toluene solution of TCNE to a solution of $(\eta^5\text{-}C_5H_4COMe)Co(CO)[\dot{C}(NMe)CH_2CH_2(\dot{N}Me)]$ in the same solvent results in loss of CO and precipitation of a brown–black solid with the stoichiometry $(\eta^5\text{-}C_5H_4COMe)Co(TCNE)[\dot{C}(NMe)CH_2CH_2(\dot{N}Me)]$. Their IR spectra were obtained from Nujol mulls and tetrahydrofuran (THF) and dimethylsulphoxide (DMSO) solutions. The $\nu(C{\equiv}N)$ frequencies are listed in Table 3. In Nujol mulls these spectra show three bands. The one at lower frequency is broad but is resolved in solution, the resolution becoming better as the polarity of the solvent is increased (Fig. 2). The $\nu(C{\equiv}N)$ value is lowered with respect to that in free TCNE (2260, 2225 cm^{-1}). The multiplicity of $\nu(C{\equiv}N)$ bands is consistent with low (local) symmetry of the coordinated TCNE, indicating that TCNE is σ-bonded to cobalt through a nitrogen nitrile[16,17] atom.

The ^{13}C NMR spectrum shows two doublets at 91.05 and 116.94 ppm assigned to CN and C=C, respectively; this is also in accordance with coordination to cobalt through a nitrile nitrogen atom.

The electronic spectra were obtained in these same solvents. A broad band was observed at λ_{max} *ca* 550 nm. In the 360–490 nm region hyperfine structure (363, 388, 407, 423, 437, 456, 486 nm) characteristic of the TCNE anion radical is observed.[18]

The ESR spectra was obtained at room temperature in acetone, DMF and DMSO solutions. The spectra in the first two solvents show a broad signal; however, in DMSO solution the ESR spectra display a strong signal characteristic of the TCNE anion radical (nine lines, a_N 1.60 G, g = 1.998).[19] All the data obtained for the complex $(\eta^5\text{-}C_5H_4COMe)Co(TCNE)[\dot{C}(NMe)CH_2CH_2(\dot{N}Me)]$ indicate that TCNE is reduced to $TCNE^-$ and coordinates to cobalt through one of the nitrile nitrogen atoms. Thus the complex can be regarded formally as $(\eta^5\text{-}C_5H_4COMe)Co[\dot{C}(NMe)CH_2CH_2(\dot{N}Me)]^+ \cdot TCNE^-$, in which the cation has accepted σ-electron density from a nitrile nitrogen atom of $TCNE^-$.

These results are similar to those obtained for analogous complexes[11] containing phosphorus-donor ligands such as $(\eta^5\text{-}C_5H_4Me)Co(TCNE)(L)$ [L = PPh_3, $P(OMe)_3$].

Table 3. $\nu(C{\equiv}N)$ stretching frequencies for the complexes (in cm^{-1})

	Nujol	THF	Acetone	DMSO
$(\eta^5\text{-}C_5H_4COMe)Co(TCNE)$ $[\dot{C}(NMe)CH_2CH_2(\dot{N}Me)]$	2212 vs	2220 vs	2219 vs, sh	2219 vs, sh
	2199 vs	2213 vs	2213 vs	2212 vs
	2133 s, br	2200 vs	2201 vs	2199 vs
		2129 m, br	2167 vw	2189 s
			2149 m	2167 m
			2126 m	2147 s
				2121 m
				2118 m

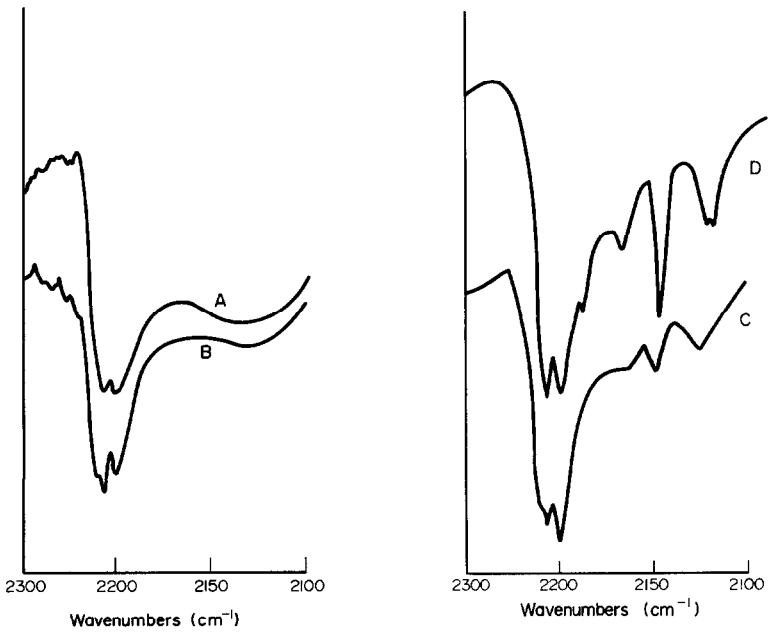

Fig. 2. $\nu(C{\equiv}N)$ stretching frequencies for the complex (η^5-C_5H_4COMe)Co(TCNE)[$\overline{C(NMe)CH_2CH_2(NMe)}$] in (A) Nujol mulls, (B) THF, (C) acetone and (D) DMSO solution.

EXPERIMENTAL

All manipulations were carried out by using standard Schlenk techniques under an atmosphere of oxygen-free nitrogen. Toluene, hexane and THF were dried over and distilled from sodium benzophenone ketyl under a nitrogen atmosphere, then bubbled with nitrogen for 1 h and stored under nitrogen. DMSO was dried over and distilled from BaO.

The reagent TCNE was obtained from Fluka and was used without further purification. Bis (1,3-dimethylimidazolin-2-ylidene)[20] was prepared according to a literature method and distilled in a stream of nitrogen at reduced pressure immediately prior to use. The compounds (η^5-C_5H_5)$Co(CO)_2$,[21] (η^5-C_5H_4COMe)$Co(CO)_2$[22] and (η^5-C_5H_5)Co(CO)[$\overline{C(NMe)CH_2CH_2(NMe)}$][6] were prepared by methods described in the literature and characterized by their IR and NMR spectra.

The microanalyses were performed by the Microanalytical Laboratory of this Department. The cobalt was determined by titration of the cobalt–EDTA complex in the presence of NET as indicator.

Instruments

The IR spectra were recorded in the range 4000–200 cm^{-1} on a Nicolet 5DX FT–IR spectrometer using Nujol and hexachlorobutadiene mulls between CsI windows or in THF and DMSO solution. $^1H^{13}C$ NMR spectra were obtained on a Bruker WH-200-SY instrument, chemical shifts are relative to TMS. The electronic spectrum was recorded on a Pye Unicam SP8-100 spectrophotometer. The ESR spectra were recorded at a microwave frequency of 9 GHz (*X*-band) on a Varian E-12 spectrometer equipped with a HP 5342 A frequency-meter and a Bruker NMR Gaussmeter.

Kinetic studies

Solutions of both the ligand and the compound (η^5-Cp′)$Co(CO)_2$ (Cp′ = C_5H_5, C_5H_4COMe) were placed under nitrogen in an aluminium foil-wrapped Schlenk flask and thermostatted in a constant temperature bath (±0.2°C). At zero time the solution of olefin was added via syringe to the cobalt compound to give exactly 8 cm^3 of reaction mixture. Aliquots were subsequently withdrawn through a rubber septum with the use of a syringe at intervals to obtain 5–10 readings during 2–3 half-lives of reaction and transferred to a 0.5 mm NaCl cell. The IR cell was flushed with nitrogen and sealed with a rubber septum before use.

Reactions were followed by monitoring the disappearance of the highest frequency carbonyl

stretching band of the complexes (η^5-Cp′)Co(CO)$_2$ (Cp′ = C_5H_5 or C_5H_4COMe) with a Nicolet 5DX FT-IR spectrophotometer, using the absorbance mode.

Approximately 8.5×10^{-3} M solutions of complex were used, and all kinetic experiments were carried out under pseudo-first-order conditions with at least a ten-fold excess of ligand. All reactions went to completion to give the corresponding monocarbonyl product (η^5-Cp′)Co(CO)[$\overline{C(NMe)CH_2CH_2(NMe)}$] (Cp′ = C_5H_5, C_5H_4COMe).

The plot of log A (absorbance, of the highest carbonyl band of the complexes) vs time were linear for more than three half-lives and k_{obs} was determined from the slope of this line by the least-squares methods. The correlation of the least-squares line ($R^2 > 0.996$) was very good.

Preparation of (η^5-C_5H_4COMe)Co(CO)[$\overline{C(NMe)CH_2CH_2(NMe)}$]

To a solution of (η^5-C_5H_4COMe)Co(CO)$_2$ (2 g, 9.01 mmol) in toluene (30 cm^3) in a nitrogen-filled 100 cm^3 Schlenck flask was slowly added, by ampoule transfer, a solution of bis(1,3-dimethylimidazolin-2-ylidene) (0.88 g, 4.51 mmol). The mixture was refluxed for 22 h, then the solution was allowed to cool to 25°C, filtered, and the solvent removed *in vacuo*. The product was recrystallized from toluene–hexane in a 1 : 1 ratio to give a brown–red powder. The yield was 1.87 g (71%) (Found: C, 53.3; H, 5.9; N, 9.5; Co, 20.1. Calc. for $C_{13}H_{17}N_2O_2Co$: C, 53.4; H, 5.8; N, 9.6; Co, 20.0%). ^{1}H NMR ($CDCl_3$): δ 2.33 (s, 3H, CH_3); 2.71 (s, 4H, CH_2); 3.29 (s, 6H, CH_3); 5.05 [s, br, 2H, H(3,4)]; 5.22 [s, br, 2H, H(2,5)].

Preparation of (η^5-C_5H_4COMe)Co(TCNE)[$\overline{C(NMe)CH_2CH_2(NMe)}$]

A solution of TCNE (0.44 g, 3.42 mmol) in toluene (30 cm^3) was slowly added, with stirring at room temperature, to a solution of (η^5-C_5H_4COMe)Co(CO)[$\overline{C(NMe)CH_2CH_2(NMe)}$] (1 g, 3.42 mmol) in toluene (15 cm^3). A brown–black solid immediately appeared and evolution of carbon monoxide was observed. The product was filtered, washed with hexane–toluene (1 : 1) and dried *in vacuo*. The yield was quantitative (Found: C, 55.0; H, 4.3; N, 21.3; Co, 15.0. Calc. for $C_{18}H_{17}N_6OCo$: C, 55.1; H; 4.3; N, 21.4; Co, 15.0%). ^{1}H NMR ($CDCl_3$): 2.34 (s, 3H, CH_3); 2.55 (s, 4H, CH_2); 3.47 (s, 6H, CH_3); 5.14 [t, 2H, H(3,4)], 5.29 [t, 2H, H(2,5)]. ^{13}C NMR ($CDCl_3$): 39.37, 38.64, 52.47, 91.05 (d, J = 66.7 Hz), 116.94 (d, J = 74.96 Hz), 128.21 m, 158.75, 175.00.

REFERENCES

1. E. O. Fischer and A. Maasböl, *Angew. Chem. Int. Edn. Engl.* 1964, **3**, 580.
2. *Advances in Metal Carbene Chemistry* (Edited by U. Schubert). Kluwer, The Netherlands (1989).
3. M. F. Lappert, *J. Organomet. Chem.* 1975, **100**, 139.
4. M. F. Lappert, P. L. Pye and G. M. McLaughlin, *J. Chem. Soc., Dalton Trans.* 1977, 1272.
5. M. F. Lappert, *J. Organomet. Chem.* 1988, **358**, 185.
6. D. W. Macomber and R. D. Rogers, *Organometallics* 1985, **4**, 1485.
7. H. G. Schuster-Woldan and F. Basolo, *J. Am. Chem. Soc.* 1966, **88**, 1657.
8. R. Cramer and L. P. Seiwell, *J. Organomet. Chem.* 1975, **92**, 245.
9. C. Moreno, M. J. Macazaga and S. Delgado, *Organometallics*, in press.
10. M. E. Rerek and F. Basolo, *Organometallics* 1983, **2**, 372.
11. M. J. Macazaga, M. S. Delgado and J. R. Masaguer, *J. Organomet. Chem.* 1986, **310**, 249.
12. C. P. Casey, J. M. O'Conner, W. D. Jones and K. J. Haller, *Organometallics* 1983, **28**, 535.
13. M. E. Rerek and F. Basolo, *J. Am. Chem. Soc.* 1984, **106**, 5908.
14. D. J. Feltes, R. Narayanaswamy and A. J. Rest, *J. Chem. Soc., Dalton Trans.* 1981, 2311.
15. G. Hüttner, H. H. Brintzinger, L. G. Bell, P. Friedlich, V. Bejenke and D. Nengebauer, *J. Organomet. Chem.* 1978, **159**, 189.
16. M. F. Rettig and R. M. Wing, *Inorg. Chem.* 1969, **8**, 2685.
17. D. Ittel, C. A. Tolman, P. J. Krusic, A. D. English and J. P. Jesson, *Inorg. Chem.* 1978, **17**, 3432.
18. O. W. Webster, W. Mahler and R. E. Benson, *J. Am. Chem. Soc.* 1962, **84**, 3678.
19. W. P. Phillips, J. C. Rowell and S. I. Weissman, *J. Chem. Phys.* 1960, **33**, 626.
20. H. E. Winberg, *Chem. Abstr.* 1966, **164**, 15854h.
21. M. D. Rausch and R. A. Genetti, *J. Org. Chem.* 1970, **35**, 3888.
22. R. D. Rogers, J. L. Atwood, M. D. Rausch, D. W. Macomber and W. P. Hart, *J. Organomet. Chem.* 1982, **238**, 79.

Polyhedron Vol. 10, No. 7, pp. 731–736, 1991
Printed in Great Britain

0277-5387/91 $3.00+.00
© 1991 Pergamon Press plc

CATALYTIC AND MAGNETIC PROPERTIES OF A NEW SERIES OF BINUCLEAR COPPER(II) COMPLEXES

B. SRINIVAS, N. ARULSAMY and P. S. ZACHARIAS*

School of Chemistry, University of Hyderabad, Hyderabad 500 134, India

(*Received* 3 *May* 1990; *accepted* 5 *December* 1990)

Abstract—Binuclear copper(II) complexes of ligands derived from condensation of 2,6-diformyl-4-methylphenol with various aromatic mono- and diamines have been synthesized. Complexes derived from monoamines have the Cu_2LCl_3 composition and those from diamines have the $Cu_2L'Cl_2$ composition, where L and L′ represent the ligands. Analytical data, conductance and spectral studies support these formulations. Cu_2LCl_3 complexes are chloro-bridged, as evidenced by two intense IR bands centred around 300 and 320 cm^{-1}. Magnetic susceptibility measurements show that Cu_2LCl_3 complexes have low μ_{eff} values indicating magnetically interacting copper(II) centres and $Cu_2L'Cl_2$ complexes have non-interacting copper(II) centres. Cu_2LCl_3 complexes undergo single-step quasi-reversible reduction at −0.62 V vs SCE. Catalysis of Cu_2LCl_3 complexes for the oxidation of 3,5-di-t-butylcatechol (3,5-DTBC) and ascorbic acid by dioxygen is studied.

Investigations on binuclear complexes of transition metals are of contemporary relevance due to their interesting magnetic, catalytic and electron-transfer properties and as models of bioinorganic chemistry.[1–7] They belong to two major classes: (i) where the metal centres are close enough to have metal–metal interaction either directly or through a bridge system,[8–10] and (ii) where the metal centres are isolated and have no significant interaction.[11–13] A number of magnetically interacting binuclear copper(II) complexes are shown to be catalytically active in the oxidation of substrates like 3,5-di-t-butylcatechol (3,5-DTBC)[4,14] or N,N,N′,N′-tetramethyl-*p*-phenylenediamine (TMPD)[15,16] by oxygen. While planar mononuclear copper(II) complexes have little or no catalytic activity, binuclear copper(II) complexes are catalytically efficient. In addition, many of the binuclear copper(II) complexes undergo facile reduction to copper(I) in the presence of two-electron donors such as ascorbic acid, etc.[14] To investigate the interdependence of magnetic interaction, reduction potentials and catalytic properties, a number of new binuclear copper(II) complexes have been synthesized from ligands obtained from the condensation of 2,6-diformyl-4-methylphenol and aromatic mono- and diamines.

* Author to whom correspondence should be addressed.

EXPERIMENTAL

All amines were either distilled or recrystallized prior to use. The ligands L and L′ were synthesized by the condensation of 2,6-diformyl-4-methylphenol[17] with the appropriate aromatic monoamines (aniline, *o*-anisidine, *o*-toluidine, 2-chloroaniline, 2-aminopyridine) and aromatic diamines (*o*-dianisidine, *o*-tolidine, 4,4′-diaminodiphenylmethane and 4,4′-diaminodiphenylethane), respectively. In a typical condensation reaction, 2,6-diformyl-4-methylphenol (10 mM) was refluxed with the respective monoamine (25 mM) in methanol for 4 h. Reducing the volume of the reaction mixture and cooling yielded red crystalline Schiff bases (L), which were recrystallized from methanol. The macrocyclic ligands, L′, were obtained using a 1:1 stoichiometric ratio of 2,6-diformyl-4-methylphenol and diamine. The crude product was recrystallized from chloroform.

Cu_2LCl_3 *complexes*

To a methanolic solution (20 cm^3) of ligand L (1 mM) was added a drop of ammonia solution and cupric chloride dihydrate (0.425 g, 2.5 mM) in methanol (20 cm^3). The resultant green microcrystalline product was recrystallized from either acetone or a dichloromethane–hexane (1:1) mixture.

$Cu_2L'Cl_2$ complexes

To a solution of the ligand (1 mM) in chloroform (100 cm^3) was added cupric chloride dihydrate (0.425 g, 2.5 mM) in methanol (20 cm^3). The resultant brown coloured product was filtered, washed thoroughly with chloroform and diethyl ether and dried *in vacuo* at 80°C for 12 h.

Physical measurements

The C, H and N analyses were carried out on a Perkin–Elmer 240C elemental analyser. Metal estimations were done on an inductively coupled plasma spectrometer (Labtem, Australia). Molecular weight measurements were carried out on a Dumfdruck Knauer osmometer in chloroform solvent using benzil as standard. Conductivity measurements were carried out on an Elico Model CM-82T conductivity meter at 25°C in dichloromethane. Melting points were recorded on a Buchi 510 melting point apparatus and are uncorrected. IR spectra were recorded on a Perkin–Elmer 283 model in the range 4000–200 cm^{-1}. Electronic spectra (Nujol mull) were recorded on a Cary 17D spectrophotometer in the range 1600–200 nm and in chloroform solution (10^{-5} M) on a Shimadzu UV 200S double beam spectrophotometer. ESR spectra were recorded on a JEOL JES FE-3X spectrometer. The room temperature magnetic susceptibility measurements were carried out on a Bruker BM-6 magnetic susceptibility set-up consisting of a Sartorius digital balance. Other measurements (77–298 K) used a Princeton Applied Research magnetometer Model-155 calibrated using a standard nickel pellet and cross checked against $[HgCo(CNS)_4]$. The resultant susceptibilities were corrected for diamagnetism and temperature independent paramagnetism (TIP). Cyclic voltammetric (CV) and differential pulse voltammetric (DPV) experiments were carried out using a three-electrode cell assembly with a PAR 175 universal programmer and PAR RE 0074 XY recorder. The cell consisted of an E410 hanging mercury drop electrode (HMDE) as the working electrode and a platinum wire auxiliary electrode. Tetraethylammonium perchlorate (TEAP) in 0.1 M concentration was used as the supporting electrolyte. All the potentials reported here are referred to the saturated calomel electrode (SCE) and are uncorrected for liquid junction potentials.

Catalysis experiments were carried out on a Shimadzu UV-200S double beam spectrophotometer using methanol as solvent. A methanol solution of 3,5-DTBC (0.3 mmol dm^{-3}) and copper(II) complex (0.003 mmol dm^{-3}) in a 25 cm^3 standard flask was kept under nitrogen. 3,5-DTBQ has a characteristic absorbance at 400 nm which was taken as a measure of the quinone formation [ε (mol^{-1} dm^3 cm^{-1}) = 1900 in methanol].[18] Absorbance was measured at intervals of 10 min immediately after exposing the solution to air. A similar procedure was used for the ascorbic acid oxidations by using 1 : 5 and 1 : 1 stoichiometric ratios of the complex and ascorbic acid.

RESULTS AND DISCUSSION

All the ligands have been characterized by analytical, IR and spectral methods. The binuclear complexes obtained from the ligands, L, can have either a 1 : 1 or 1 : 2 ligand-to-metal ratio, as shown in structures **1** and **2** (Fig. 1), respectively. Structure **2** has been identified to be correct on the basis of the following experimental observations. (i) For structure **1** the average molecular weight is *ca* 850 while for **2** it is *ca* 500. Molecular weight determinations in chloroform solution give values in the range 450–600 (Table 1), therefore excluding the structure **1**. (ii) Conductivity values of the complexes in dichloromethane are low indicating that

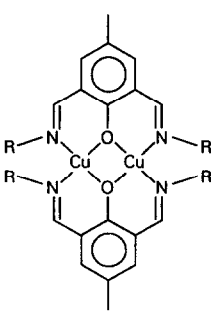

1 $Cu_2L_2^{2+}$

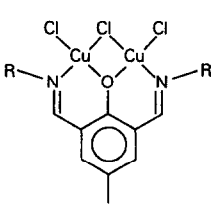

2 Cu_2LCl_3

$Cu_2L^1Cl_3$: R = C_6H_5
$Cu_2L^2Cl_3$: R = *o*-$CH_3C_6H_4$
$Cu_2L^3Cl_3$: R = *o*-$OCH_3C_6H_4$
$Cu_2L^4Cl_3$: R = *o*-ClC_6H_4
$Cu_2L^5Cl_3$: R = *o*-C_6H_4N

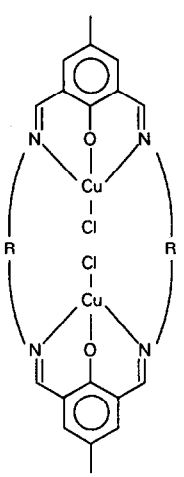

3 $Cu_2L'Cl_2$

$Cu_2L'^1Cl_2$: R =
$Cu_2L'^2Cl_2$: R =
$Cu_2L'^3Cl_2$: R = 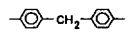
$Cu_2L'^4Cl_2$: R = 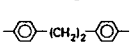

Fig. 1. Structures of binuclear copper(II) complexes.

Table 1. Analytical and magnetic data for binuclear copper(II) complexes

Complex	Analysis (%)[a] C	H	N	Cu	Molecular[a] weight	μ_{eff}[b] (BM)
$Cu_2L^1Cl_3$	46.8(46.2)	3.1(3.1)	5.0(5.1)	23.2(22.8)	448(546)	1.30
$Cu_2L^2Cl_3$	48.3(48.0)	3.7(3.7)	4.8(4.8)	22.1(22.0)	487(574)	0.83
$Cu_2L^3Cl_3$	45.2(45.5)	3.7(3.5)	4.5(4.6)	20.9(20.5)	566(606)	0.93
$Cu_2L^4Cl_3$	41.9(41.0)	2.7(2.5)	4.4(4.5)	20.6(20.2)	592(615)	0.95
$Cu_2L^5Cl_3$	41.8(41.6)	2.8(2.7)	10.1(10.2)	23.2(23.0)	454(548)	1.00
$Cu_2L'^1Cl_2 \cdot 5H_2O$	56.7(57.0)	4.6(4.9)	6.0(5.8)	12.9(13.1)	[c]	1.79
$Cu_2L'^2Cl_2 \cdot 7H_2O$	51.1(51.7)	4.6(4.8)	5.3(5.2)	12.0(11.9)	[c]	1.80
$Cu_2L'^3Cl_2 \cdot 5H_2O$	56.0(56.2)	4.5(4.7)	5.7(5.9)	13.3(13.5)	[c]	2.01
$Cu_2L'^4Cl_2 \cdot 5H_2O$	57.2(57.7)	4.9(5.0)	5.6(5.8)	13.4(13.3)	[c]	1.84

[a] Values in parentheses are calculated.
[b] Per copper atom.
[c] Measurement not made due to poor solubility.

the complexes are non-electrolytes. (iii) The presence of a chloro bridge is evident from the observation of two IR peaks at 320 and 300 cm^{-1}, which is characteristic of chloro-bridged binuclear copper(II) complexes.[19] (iv) The analytical data (C, H, N) presented in Table 1 conclusively support structure **2**.

Structure **3**, formulated for the complexes of L′, is supported by analytical and other experimental data. The mode of coordination shown in structures **2** and **3** are further supported by IR data. The broad band at *ca* 3000 cm^{-1}, due to the free —OH group of the ligand, disappears on complex formation indicating oxygen–metal bond formation. C=N stretching vibrations of the ligands are found at 1635–1650 cm^{-1}. The band at 1550–1570 cm^{-1} is indicative of a binuclear structure bridged by phenolic oxygen.

Spectral and magnetic data

Electronic spectra of the Cu_2LCl_3 complexes in dichloromethane exhibit the *d–d* band around 720 nm. The exact positions of this band for various complexes are given in Table 2. The two prominent bands observed in the UV region at *ca* 390 and 270 nm are of ligand origin. It is known that binuclear copper(II) complexes with chloro bridges produce a *d–d* transition around 725 nm[20,21] and are of planar geometry. Hence, a similar geometry is suggested for the Cu_2LCl_3 complexes. Solution electronic spectra for $Cu_2L'Cl_2$ complexes could not be recorded due to their insolubility in various solvents. Solid spectra did not provide any resolved bands.

Powder ESR spectra of the Cu_2LCl_3 complexes show a broad band centred at *ca* 3300 gauss. For $Cu_2L^1Cl_3$ and $Cu_2L^2Cl_3$ complexes, another signal at 1600 gauss was also observed resulting from the $\Delta M_s = 2$ transition. In general, chloro-bridged binuclear copper(II) complexes give broad ESR signals[22] and is taken as further evidence for chloro-bridged structures. The $Cu_2L'Cl_2$ complexes in the solid phase give a single line ESR absorption band centred at *ca* 3200 gauss. Such spectra are characteristic of non-interacting copper(II) centres; since the two copper centres are separated by at least ~10 Å no Cu—Cu interaction is expected.

Room temperature magnetic moment values for the Cu_2LCl_3 complexes are in the range 0.8–1.2 BM. At *ca* 200 K, the μ_{eff} values are in the range 0.4–0.5 BM. At temperatures lower than 200 K these complexes showed diamagnetic behaviour resulting from a high degree of demagnetization by spin pairing. The μ_{eff} values for various complexes are given in Table 1. The spin exchange interaction is caused by the super-exchange mechanism rather than direct overlapping of the metal *d* orbitals. The $Cu_2L'Cl_2$ complexes have μ_{eff} values in the range 1.8–2.0 BM per copper centre indicating the absence of antiferromagnetic interactions. Such interactions are not expected since the two copper centres are separated by a large distance and interaction through the bridging ligands is not expected to be substantial.

Relative catalytic activity of the copper(II) complexes is partly attributable to their reduction potentials.[15] The more positive the reduction potential is, the higher the catalytic activity becomes. Binuclear complexes can undergo two-electron

Table 2. Spectral, conductance and cyclic voltammetric data of binuclear copper(II) complexes

Complex	$\lambda^a(\varepsilon)$ nm ($dm^3\ mol^{-1}\ cm^{-1}$)	Conductance[a] (μ Mhos cm^{-1})	Characteristic IR bands (cm^{-1}) C=N	C—O	Cl / \ Cu Cu	Cyclic voltammetry Scan rate ($V\ s^{-1}$)	E_{Pc} (V)	E_{Pa} (V)	ΔE_p (V)
$Cu_2L^1Cl_3$	737(330)	51.5	1620	1340	300, 320	0.01	−0.57	[b]	—
						0.02	−0.59	[b]	—
						0.05	−0.60	−0.45	0.15
						0.10	−0.63	−0.45	0.18
$Cu_2L^2Cl_3$	727(279)	54.0	1630	1560	300, 320	0.01	[b]	[b]	—
						0.02	−0.67	−0.48	0.19
						0.05	−0.68	−0.52	0.16
						0.10	−0.68	−0.52	0.16
$Cu_2L^3Cl_3$	742(310)	66.5	1620	1350	300, 325	0.01	−0.64	−0.50	0.14
						0.02	−0.68	−0.50	0.18
						0.05	−0.65	−0.50	0.15
						0.10	−0.65	−0.48	0.17
$Cu_2L^4Cl_3$	724(267)	67.0	1620	1330	290, 330	0.01	−0.63	−0.50	0.13
						0.02	−0.65	−0.50	0.15
						0.05	−0.64	−0.49	0.15
						0.10	−0.62	−0.48	0.14
$Cu_2L^5Cl_3$	745(267)	37.0	1620	1325	300, 320	0.01	−0.60	0.51	0.11
						0.02	−0.61	−0.50	0.11
						0.05	−0.60	−0.50	0.15
						0.10	−0.60	−0.48	0.12

[a] In dichloromethane solution.
[b] Peak absent.

reduction involving both copper centres at the same potential or have two successive one-electron reduction steps.[17,23] To identify the pattern of reduction steps and to correlate the reduction potential with the catalytic activity of the complexes, reduction characteristics of the Cu_2LCl_3 complexes are examined by cyclic voltammetric methods in dimethylformamide. They show single quasi-reversible redox peaks with an E_p value of *ca* 150 mV. The reduction peak occurs at *ca* −0.65 V and the oxidation peak at *ca* −0.50 V. CV data are collected in Table 2. The influence of reduction potential on catalytic activity is discussed in the next section. The $Cu_2L'Cl_2$ complexes could not be investigated by cyclic voltammetric methods due to their poor solubility.

Catalysis

Binuclear planar copper(II) complexes show catalytic activity for oxidation of 3,5-DTBC to quinone by dioxygen, while square-planar mononuclear complexes have little or no catalytic activity.[14] In binuclear copper(II) complexes, larger magnetic exchange interaction is observed when the planarity of the metal centre increases.[22] Binuclear systems with larger magnetic interaction (lower μ_{eff} values) should therefore exhibit greater catalytic activity. This has been found to be true in the case of some binuclear complexes of 1,3,5-triketones.[4] Catalytic activity of the Cu_2LCl_3 binuclear copper(II) complexes was examined for the oxidation of 3,5-DTBC to quinone by dioxygen. The activity for the methanolic solution of a 1 : 100 complex-to-DTBC ratio, was discovered by measuring the absorbance of the 400 nm band which is characteristic of 3,5-DTBQ. The conversion of 3,5-DTBC to 3,5-DTBQ was complete in about 90 min in the presence of various binuclear copper(II) complexes investigated here. Figure 2 shows the time-dependent growth of 3,5-DTBQ in the presence of $Cu_2L^1Cl_3$, and also the absorption profile of 3,5-DTBC with a binuclear complex under nitrogen atmosphere. In this case, the absorption at 400 nm is totally absent confirming the influence of dioxygen. The catalytic efficiency of the binuclear complexes under similar conditions is compared in Fig. 3. To a general approximation, it becomes apparent that

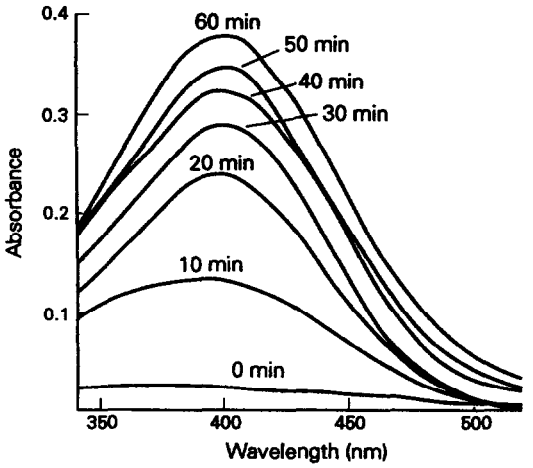

Fig. 2. Oxidation of 3,5-DTBC by a binuclear copper(II) complex ($Cu_2L^1Cl_3$).

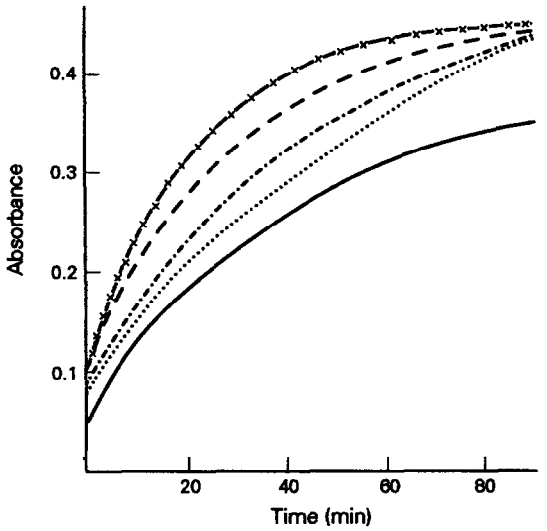

Fig. 3. Time-dependent formation of 3,5-DTBQ in the presence of $Cu_2L^1Cl_3$ (——), $Cu_2L^2Cl_3$ (---), $Cu_2L^3Cl_3$ (— · —), $Cu_2L^4Cl_3$ (— × —) and $Cu_2L^5Cl_3$ (· · · ·).

the catalytic efficiency is greater for the binuclear system which has a lower magnetic moment. The influence of the reduction potential on the catalytic efficiency of binuclear complexes is not well understood. The electron-transfer reaction between two-electron donors like ascorbic acid and the binuclear copper(II) complexes was also investigated by the same method in methanol, the *d–d* band of the complex at *ca* 14,000 cm^{-1} (720 nm) being monitored during the experiment. This *d–d* band disappears upon addition of ascorbic acid under nitrogen atmosphere and reappears when the solution is exposed to air, as shown in Fig. 4 for a representative complex $Cu_2L^1Cl_3$. These experiments clearly show that copper(II) is easily reduced to copper(I) by ascorbic acid. The proposed pathway for the electron-transfer reaction between ascorbic acid and a binuclear copper(II) complex involves a "steric match" between a donor and an acceptor.[14] A similar intermediate between the complexes and ascorbic acid is envisaged in the present case also. The $Cu_2L'Cl_2$ complexes are not expected to show any catalytic activity because of the lack of donor–acceptor interactions due to the large internuclear distance.

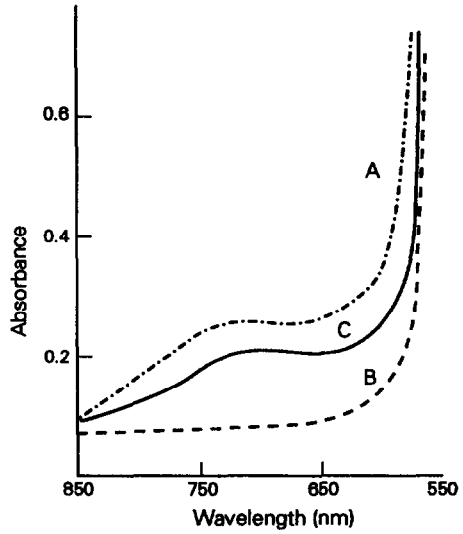

Fig. 4. Absorption spectra of $Cu_2L^1Cl_3$ (in methanol at 25°C) in presence of ascorbic acid. (A) $Cu_2L^1Cl_3$ alone, (B) $Cu_2L^1Cl_3$+ascorbic acid (under nitrogen) and (C) solution (B) in air.

Acknowledgements—Financial assistance from the University Grants Commission and the Council of Scientific and Industrial Research, New Delhi, is gratefully acknowledged by B.S. and N.A.

REFERENCES

1. S. L. Lambert and D. N. Hendrickson, *Inorg. Chem.* 1979, **18**, 2683.
2. S. K. Mandal, L. K. Thompson, K. Nag, J. P. Charland and E. J. Gabe, *Can. J. Chem.* 1987, **65**, 2815.
3. P. Lacroix, O. Kahn, F. Theobald, J. Leroy and C. Wakselman, *Inorg. Chim. Acta* 1988, **142**, 129.
4. U. Casellato, S. Tamburini, P. A. Vigato, A. Destefani, M. Vidali and D. E. Fenton, *Inorg. Chim. Acta* 1983, **69**, 45.
5. S. K. Mandal, L. K. Thompson, M. J. Newlands and E. J. Gabe, *Inorg. Chem.* 1989, **28**, 3707.
6. E. I. Solomon, *Copper Proteins* (Edited by T. G. Spiro), Ch. 2. Wiley, New York (1981).
7. K. D. Karlin and J. Zubeta (Eds), *Copper Coordination Chemistry, Biochemical and Inorganic Per-*

spectives, pp. 259, 456. Adenine Press, Gilderland, New York (1983).
8. S. K. Mandal, L. K. Thompson, K. Nag, J. P. Charland and E. J. Gabe, *Inorg. Chem.* 1987, **26**, 1391.
9. R. R. Gagne, C. A. Koval, T. J. Smith and M. C. Cimolino, *J. Am. Chem. Soc.* 1979, **101**, 4571.
10. R. C. Long and D. N. Hendrickson, *J. Am. Chem. Soc.* 1983, **105**, 1513.
11. E. F. Hasty, L. J. Wilson and D. N. Hendrickson, *Inorg. Chem.* 1978, **17**, 1834.
12. E. F. Hasty, T. J. Colburn and D. N. Hendrickson, *Inorg. Chem.* 1973, **12**, 2414.
13. P. S. Zacharias and A. Ramachandraiah, *Polyhedron* 1985, **4**, 1013.
14. N. Oishio, Y. Nishida, K. Ida and S. Kida, *Bull. Chem. Soc. Japan* 1980, **53**, 2847.
15. Y. Nishida, N. Oishio, H. Kuramoto and S. Kida, *Inorg. Chim. Acta* 1982, **57**, 253.
16. Y. Nishida, N. Oishio and S. Kida, *Inorg. Chim. Acta* 1980, **46**, L69–L70.
17. R. R. Gagne, C. L. Spiro, T. J. Smith, C. A. Hamann, W. R. Thies and A. K. Shiemke, *J. Am. Chem. Soc.* 1981, **103**, 4073.
18. W. Flaig, Th. Ploetz and A. Kullmer, *Z. Naturfor.* 1955, **10b**, 668.
19. W. E. Estes, J. R. Wasson, J. W. Hall and W. E. Hatfield, *Inorg. Chem.* 1978, **17**, 3657.
20. I. E. Dickson and R. Robson, *Inorg. Chem.* 1974, **13**, 1301.
21. R. B. Coles, C. M. Harris and E. Sinn, *Inorg. Chem.* 1969, **12**, 2608.
22. H. Okawa, T. Tokh, Y. Nonaka, Y. Muto and S. Kida, *Bull. Chem. Soc. Japan* 1973, **46**, 1462.
23. D. E. Fenton and R. L. Lintvedt, *J. Am. Chem. Soc.* 1978, **100**, 6367.

Polyhedron Vol. 10, No. 7, pp. 737–739, 1991
Printed in Great Britain

0277–5387/91 $3.00+.00
Pergamon Press plc

SYNTHESIS AND X-RAY CRYSTAL STRUCTURE OF TETRAKIS[BIS(1,2-DIMETHYLPHOSPHINO)ETHANE] DISILVER(I)BIS(TETRAPHENYLBORATE)

VÁHE SABOONCHIAN and GEOFFREY WILKINSON*

Johnson Matthey Laboratory, Chemistry Department, Imperial College, London SW7 2AY, U.K.

and

BILQUIS HUSSAIN-BATES and MICHAEL B. HURSTHOUSE*

Chemistry Department, Queen Mary and Westfield College, Mile End Road, London E1 4NS, U.K.

(*Received* 30 *October* 1990; *accepted* 10 *December* 1990)

Abstract—The interaction of silver trifluoromethanesulphonate and 1,2-bis(dimethylphosphino)ethane (DMPE) in acetonitrile in the presence of sodium tetraphenylborate gives the dimeric complex $[Ag_2(DMPE)_4](BPh_4)_2$. In the cation, each silver atom is four-coordinate with one chelating diphosphine and two phosphorus atoms from the two bridging DMPE ligands. The Ag—P distances are 2.465–2.557(6) Å and the AgP_4 unit has distorted tetrahedral geometry.

There are a number of monomeric, dimeric and tetrameric phosphine complexes of silver(I);[1,2] most of the diphosphine (P⌒P) compounds are of the type $[XAg(\mu\text{-P⌒P})]_2$. We now describe a new type with 1,2-bis(dimethylphosphino)ethane as ligand.

RESULTS AND DISCUSSION

The interaction of AgO_3SCF_3 with two equivalents of DMPE and of sodium tetraphenylborate in acetonitrile allows isolation of the colourless crystalline complex $[Ag_2(DMPE)_4](BPh_4)_2$. The crystal structure contains dimeric $[Ag(DMPE)_2]_2^{2+}$ cations and BPh_4^- anions. A diagram of the cation which lies on a centre of symmetry is shown in Fig. 1, whilst selected bond lengths and angles are given in Table 1.

In the dication, each silver ion is coordinated by two phosphorus atoms from a chelating DMPE ligand and then by one phosphorus from each of two bridging DMPE ligands. The AgP_4 geometry is distorted tetrahedral, the largest distortion arising from the restricted bite of the chelating DMPE [P—Ag—P = 83.5(2)°]. The Ag—P distances vary considerably, over a range of almost 0.1°, with those in the chelate ring the larger. Distances in other four-coordinate silver phosphine complexes vary from 2.42 to 2.50 Å.[3]

The ^1H and ^{31}P NMR spectra are consistent for the structure. Attempts to oxidize the cation to a silver(II) species, chemically or electrochemically, were unsuccessful; cyclic voltammetry in MeCN showed no oxidation wave.

EXPERIMENTAL

Analyses by Pascher, Remagen and Imperial College Laboratories.

Tetrakis[bis(1,2 - *dimethylphosphino)ethane]disilver*(I) *bis(tetraphenylborate)*

To $AgCF_3SO_3$ (0.20 g, 0.78 mmol) in MeCN (30 cm^3) was added DMPE (0.3 cm^3, 1.8 mmol) and $NaBPh_4$ (0.59 g, 1.7 mmol). The solution was stirred for 12 h when the solvent was removed, the white residue washed with diethyl ether (2 × 15 cm^3) and

* Authors to whom correspondence should be addressed.

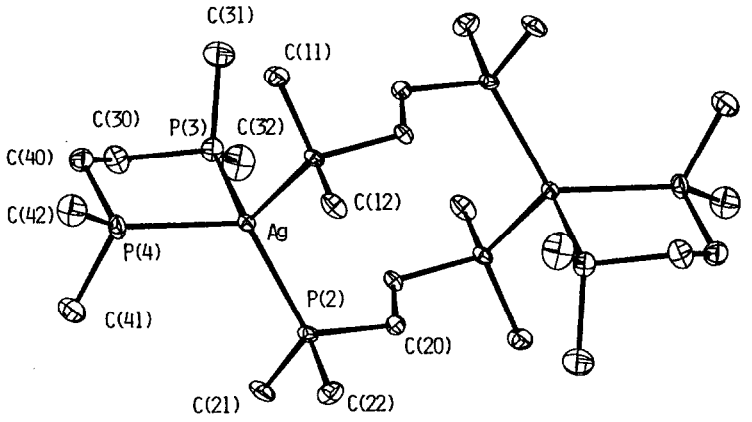

Fig. 1. The structure of the cation $[(DMPE)Ag(\mu\text{-}DMPE)]_2^{2+}$.

Table 1. Selected bond lengths (Å) and angles (°)

Bond lengths			
P(1)—Ag(1)	2.471(4)	P(2)—Ag(1)	2.465(4)
P(3)—Ag(1)	2.557(6)	P(4)—Ag(1)	2.491(4)
C(10)—P(1)	1.840(11)	C(11)—P(1)	1.842(12)
C(12)—P(1)	1.829(14)	C(20)—P(2)	1.827(10)
C(21)—P(2)	1.856(12)	C(22)—P(2)	1.850(13)
C(30)—P(3)	1.837(14)	C(31)—P(3)	1.860(19)
C(32)—P(3)	1.856(19)	C(40)—P(4)	1.864(13)
C(41)—P(4)	1.906(17)	C(42)—P(4)	1.791(18)
C(10)—C(20′)	1.551(16)	C(40)—C(30)	1.446(19)
Bond angles			
P(2)—Ag(1)—P(1)	109.6(2)	P(3)—Ag(1)—P(1)	114.1(2)
P(3)—Ag(1)—P(2)	144.4(2)	P(4)—Ag(1)—P(1)	115.6(2)
P(4)—Ag(1)—P(2)	117.6(2)	P(4)—Ag(1)—P(3)	83.5(2)
C(10)—P(1)—Ag(1)	113.8(4)	C(11)—P(1)—Ag(1)	117.7(4)
C(11)—P(1)—C(10)	103.6(5)	C(12)—P(1)—Ag(1)	116.1(5)
C(12)—P(1)—C(10)	101.2(5)	C(12)—P(1)—C(11)	102.2(6)
C(20)—P(2)—Ag(1)	115.3(4)	C(21)—P(2)—Ag(1)	115.3(4)
C(21)—P(2)—C(20)	102.7(6)	C(22)—P(2)—Ag(1)	117.8(5)
C(22)—P(2)—C(20)	99.2(5)	C(22)—P(2)—C(21)	104.1(7)
C(30)—P(3)—Ag(1)	102.9(5)	C(31)—P(3)—Ag(1)	118.0(6)
C(31)—P(3)—C(30)	99.8(7)	C(32)—P(3)—Ag(1)	128.0(5)
C(32)—P(3)—C(30)	101.9(7)	C(32)—P(3)—C(31)	101.6(9)
C(40)—P(4)—Ag(1)	103.9(5)	C(41)—P(4)—Ag(1)	115.3(5)
C(41)—P(4)—C(40)	100.5(7)	C(42)—P(4)—Ag(1)	126.4(6)
C(42)—P(4)—C(40)	105.0(7)	C(42)—P(4)—C(41)	102.4(8)
P(2)—C(20)—C(10′)	111.7(9)	P(1)—C(10)—C(20′)	111.4(9)
C(40)—C(30)—P(3)	115.4(10)	C(30)—C(40)—P(4)	114.4(8)

extracted into CH_2Cl_2 (3×30 cm^3). Reduction in volume and cooling (−20°C) gave 0.45 g of a white powder. Further crops of the compound may be obtained from the supernatant. Combined yield, 0.87 g (77%); m.p. 205–207°C. Crystals for X-ray structure determination were obtained by slow evaporation of an acetonitrile solution. (Found: C, 59.6; H, 7.3. $C_{72}H_{104}Ag_2B_2P_8$ requires: C, 59.9; H, 7.2%.) The compound is readily soluble in MeCN but sparingly soluble in CH_2Cl_2 and THF. The conductivity in MeCN gives $\Lambda_M = 175\ \Omega^{-1}$ cm^2 mol^{-1}. NMR (δ ppm in CD_3CN): ^{1}H: 7.2–6.9 (m, B*Ph*$_4$); 1.7 (s, CH_2); 1.2 (s, CH_3). ^{31}P-{^{1}H}: −19.5, −26.3 both s.

Crystallography

A crystal of dimensions $0.375 \times 0.45 \times 0.53$ mm^3 was sealed in a thin-walled glass capillary and used for all X-ray measurements. Following preliminary photography, unit cell dimensions and intensity data were obtained following standard procedures using a CAD4 diffractometer and graphite monochromated Mo-K_α radiation ($\lambda = 0.71069$ Å) operating in the ω–2θ scan mode. The structure was solved via the heavy-atom method and refined by full-matrix least-squares. Non-hydrogen atoms were refined with anisotropic displacement factor coefficients; hydrogens were included in idealized positions with group U_{iso} values for the phenyl groups on the BPh_4 anion which were themselves treated as idealised rigid bodies. Experimental details are as follows.

Crystal data. $[C_{24}H_{64}P_8Ag_2][C_{24}H_{20}B]_2$ $M_r = 1454.77$, monoclinic, $a = 11.173(3)$, $b = 21.819(4)$, $c = 16.565(5)$ Å, $\beta = 103.85(3)°$, $V = 3920.9$ Å^3, space group $P2_1/n$, $Z = 4$, $D_c = 1.32$ g cm^{-3}, μ(Mo-K_α) = 6.21 cm^{-1}, $F(000) = 1356$.

Data collection. $1.5 \leqslant \theta \leqslant 25°$, $-13 \leqslant h \leqslant 13$, $0 \leqslant k \leqslant 26$, $0 \leqslant l \leqslant 19$; 7456 reflections measured, 7368 unique, 3809 observed [$F_o > 6\sigma(F_o)$]. Lp and empirical absorption correction based on psi-scans.

Refinement. Two blocks [half cation (158 parameters) and anion (182 parameters)]. Final R, $R_w = 0.056$, 0.062, respectively, weights = $1.9/[\sigma^2(F_o) + 0.0020F_o^2]$. All calculations were made using SHELX-80 installed on a T800 transputer hosted by an IBM/AT clone.

Acknowledgement—We thank the SERC for a studentship (V.S.) and X-ray facilities.

REFERENCES

1. R. J. Lancashire, in *Comprehensive Coordination Chemistry* (Edited by G. Wilkinson, R. D. Gillard and J. A. McCleverty), Vol. 5, p. 798. Pergamon Press, Oxford (1987).
2. F. A. Cotton and G. Wilkinson, *Advanced Inorganic Chemistry*, p. 944. John Wiley, New York (1988).
3. See for example: M. Barrow, H. B. Burgi, M. Cainelli, F. Caruso, E. Fischer, L. M. Venanzi and L. Zambonelli, *Inorg. Chem.* 1983, **22**, 2356; D. M. Ho and R. Bau, *Inorg. Chem.* 1983, **22**, 4073; A. Cassel, *Acta Cryst.* 1976, **32B**, 2521.

Polyhedron Vol. 10, No. 7, pp. 741–745, 1991
Printed in Great Britain

0277-5387/91 $3.00+.00
© 1991 Pergamon Press plc

ELECTROCHEMICAL REDUCTION OF Re_3Cl_9 IN AQUEOUS ACIDIC SOLUTIONS. ISOLATION AND CRYSTAL STRUCTURE CHARACTERIZATION OF THE ONE-ELECTRON REDUCED PRODUCT AS THE TRICAESIUM-μ_3-SULPHATO-HEXACHLORO-TRI-μ-CHLORO-TRIANGULO-TRIRHENIUM COMPLEX, $Cs_3[Re_3Cl_9(SO_4)]$

CONSTANTINOS MERTIS* and NICOS PSAROUDAKIS

University of Athens, Inorganic Chemistry Laboratory, Panepistimiopolis, Kouponia, 15701 Athens, Greece

and

A. TERZIS and A. HOUNDAS

NRC Democritos, Institute of Materials Science, Ag. Paraskevi 15310, Athens, Greece

(*Received* 8 *June* 1990; *accepted* 10 *December* 1990)

Abstract—Electrochemical reduction of the cluster chloride Re_3Cl_9 (**1**) containing the Re_3^{9+} core, in aqueous hydrochloric acid, gives a purple, oxygen-sensitive but thermally stable solution, from which the singly reduced Re_3^{8+} anion, $[Re_3Cl_{12-n}]^{(4-n)-}$ (**4**), has been isolated and structurally characterized as the capped triply-bridging sulphato derivative $Cs_3[Re_3(\mu\text{-}Cl)_3Cl_6(\mu_3\text{-}SO_4)]$ (**5**).

The rhenium(III) cluster chloride Re_3Cl_9 (**1**) contains Re≡Re double bonds and is of interest both for historic and fundamental reasons.[1] Addition of many Lewis bases along the vacant sites of the $[Re_3(\mu\text{-}Cl)_3]^{6+}$ plane gives an extensive class of coordination compounds, for example the adducts $Re_3Cl_9(L)_n$ ($n = 1$, 2 or 3) or the salts $[Re_3Cl_{12-n}(H_2O)_n]^{(3-n)-}$ ($n = 1$, 2 or 3), depending on the conditions and the nature of the cation present.[1]

In contrast, pyridine and various aromatic amines of different basicity induce one-, two- or three-electron reduction[2] producing the complexes $[Re_3Cl_{9-n}(L)_n]_x$ ($n = 1$, 2 or 3), which while still derivatives of the $Re_3^{(9-n)+}$ ($n = 1$, 2 or 3) core are of special interest because they are the only known binary chloroanions having the rhenium atom(s) formally in an oxidation state of two.

Their structure, despite the efforts, has not been determined, but on the basis of ESCA and electronic spectra, magnetic and conductivity studies and the facile conversion to the rhenium(III) salts (amine $H)_2Re_3Cl_{11}$ on treatment with methanolic HCl, are believed to possess a halogen bridge "polymer of trimer structure"[2] except in the case of acridine where the salt $(AcrH)_2Re_3Cl_8$ is formed[3] rather than the adduct $[Re_3Cl_6(Acr)_3]$. The stepwise three-electron reduction of the Re_3^{9+} cluster unit to give Re_3^{6+} is in accordance with current ideas[4] concerning the electronic structure of these species.

The chloride **1**, in its complexed form[5] as the anion $[Re_3Cl_{12}]^{3-}$ (**2**), has been reduced electrochemically in aqueous hydrochloric acid at a DME[6] and in a eutectic, basic chloroaluminate melt ($AlCl_3$-MeEtimCl) at a glassy-carbon electrode.[7] In both media, purple species having the same electronic spectra are formed, but there is ambiguity concerning their spectroelectrochemically assigned identity. In aqueous hydrochloric acid, a single six-electron reduction wave is observed, and it has been proposed that one chloride ion is lost from the axial position on each rhenium atom during the reaction

* Author to whom correspondence should be addressed.

process to give **3** [eq. (1)],

$$\underset{(2)}{[ReCl_{12}]^{3-}} + 6e^- \rightleftharpoons \underset{(3)}{[Re_3Cl_9]^{6-}} + 3Cl^-, \quad (1)$$

whereas in the melt, a reversible one-electron reaction occurs attributable to the formation of species **4** [eq. (2)] for which n may be 1:

$$\underset{(2)}{[Re_3Cl_{12}]^{3-}} + e^- \rightleftharpoons \underset{(4)}{[Re_3Cl_{12-n}]^{(4-n)-}} + nCl^-. \quad (2)$$

Here, we report the isolation of the above-mentioned purple compound and the structure determination of the product from its reaction with sulphuric acid.

EXPERIMENTAL

Re_3Cl_9 has been prepared from rhenium metal according to the literature procedures[8,9] and $Cs_3Re_3Cl_{12}$ by dissolution of the trichloride in aqueous hydrochloric acid (6 M) containing caesium chloride.[1,5] All reagents were of analytical grade, thoroughly purified and carefully deoxygenated. Demineralized by ion exchange and doubly distilled water was used. Sulphuric acid was also doubly distilled. All reactions including the electroreduction in an appropriate[10] modified cell were carried out under strictly anaerobic conditions (Argon). Microanalyses were performed in this Laboratory. Electronic spectra were recorded with a Hitachi U-2000.

Crystal structure solution

$Cs_3[Re_3Cl_9SO_4]$, space group *Pmcn* (No. 62), absences $hk0$, $h+k=2n$ and $h0l$, $l=2n$, $a = 11.665(1)$, $b = 12.339(1)$, $c = 14.265(2)$ Å, $V = 2053.3(3)$ Å^3, $Z = 4$, $d_c = 4.44$ g cm^{-3}. Unit cell dimensions were derived from a least-squares refinement of the setting angles of 32 automatically centred reflections in the range $11 < 2\theta < 23°$ on a Syntex P_{21} diffractometer controlled by the Crystal Logic software and using niobium-filtered Mo-K_α radiation. The crystal was mounted in a capillary under argon. Lorentz and Ψ-scan absorption corrections were applied to the data. Three standard reflections measured every 100 reflections showed < 3.5% intensity fluctuations. The data set consisted of 2086 reflections of which 1218 with $I_o > 3\sigma(I_o)$ were used during the refinement. The structure was solved using SIR[11] and refined with SHELX76,[12] using the full-matrix least-squares method and a weighting scheme of $1/w = \sigma^2(F_o) + 0.001(F_o)$.[12] All atoms were refined anisotropically and the number of refined parameters was 103. Final $R = 0.037$ and $\Delta\rho_{max}/\Delta\rho_{min} = 1.6/-1.4$ e Å^{-3}, with all the large peaks in the final difference Fourier map being around the rhenium positions.

Electrolytic reduction of the nonachloro-tri-μ-chloro-triangulo-trirhenium(III,III,III) *trianion and reaction with sulphuric acid*

A solution of Re_3Cl_9 (0.0412 g, 0.0469 mmol) in aqueous 6 M HCl (50 cm^3) was exhaustively electrolysed using a mercury cathode and platinum wire anode with 15 cm^3 of 0.5 M HCl as anode solution, at a steady potential of −0.400 V (relative to SCE). The dark red solution of Re_3Cl_9 slowly changed to deep purple.

To a portion of the above solution (9 cm^3) was added H_2SO_4 (1 cm^3) and the mixture was heated at 80°C for *ca* 1 h. Caesium chloride was subsequently added (0.1 g) and the solution was kept at −10°C for a week. Black crystals were precipitated which were filtered, washed with small portions of iced ethanol, and dried *in vacuo* to give 0.0547 g of a compound identified by elemental analysis and crystallography to be $Cs_3Re_3Cl_9SO_4$; yield 85% based on Re_3Cl_9. Found: Re, 40.5; Cs, 28.7; Cl, 23.4; S, 2.2. Calc.: Re, 40.7; Cs, 29.0; Cl, 23.2; S, 2.3%.

RESULTS AND DISCUSSION

The dark red coloration of an aqueous HCl (6 M) solution of **1** changes slowly to deep purple upon exhaustive reduction at −0.400 V at room temperature. The reaction can be followed by visible spectroscopy and the spectrum of the final product is shown in Fig. 1. The characteristic peaks of **2**[5,13] at 763 and 513 nm slowly diminish and absorptions at 1072, 883 and 554 nm appear which are similar to those reported.[6,7]

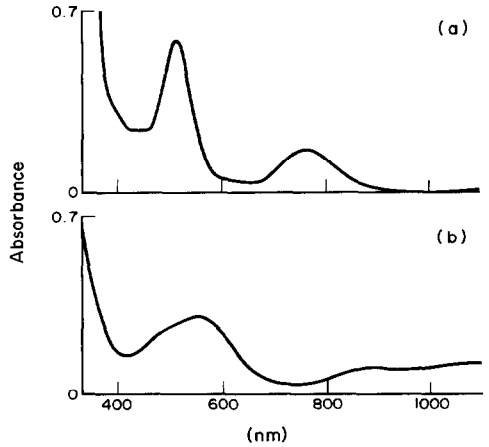

Fig. 1. Absorption spectra of: (i) a solution of Re_3Cl_9 (3.4×10^{-4} M) in aqueous HCl (6 M); (ii) after exhaustive electrolysis at room temperature.

The purple solution obtained is susceptible to oxidation by traces of oxygen, but is stable for longer periods at room temperature. By using different cations and mixtures of solvents, red–black solids precipitate upon cooling the solutions, but analytical results were not reproducible. This is due both to contamination by the co-crystallizing salt(s) of the countercation(s) and the presence of other species as indicated from examination of the electronic absorption spectra.

However, addition of sulphuric acid to the initially obtained purple solution followed by heating, causes precipitation of an oxygen-sensitive black solid, which when redissolved in HCl (6 M) gives the anion **2**.

Analytical data are consistent with its formulation as $Cs_3[Re_3Cl_9(SO_4)]$ **5** and X-ray crystallography showed that the sulphate oxyanion has displaced three labile chlorides$_{to}$[14] and functions as a tridentate triply bridging ligand capping the trirhenium unit in the same fashion as in the analogous Re_3^{9+} derivative $[N(CH_3)_4]_2[Re_3Cl_9(SO_4)]$ (**6**).[15] Such trimetal clusters, containing tridentate capping μ_3-$O_3S{=}O$ ligands, are rare[14–16] and of importance because they are considered as models for the interaction of metal clusters and oxide supports[17] or are related to oxyanion species identified when absorbed on platinum electrodes.[18] The possibility that the reduction is a multielectron process and **5** is the end oxidation product of more highly reduced species by the sulphuric acid can not be excluded. Also, the stability of **3** or **4** in HCl (6 M) and of **5** in a hot mixture of HCl/H_2SO_4 is intriguing when compared with the facile oxidation to the Re_3^{9+} cluster of the corresponding rhenium(II) derivatives, $[Re_3Cl_6 \cdot Ln]_x$ (n = 1, 2 or 3; L = aromatic amine) and makes it challenging to establish the exact nature of the latter species. The characterization of the reduction product(s) and their reactivity is under investigation.

Crystal structure

The anion structure and packing arrangement of **5** is shown in Figs 2 and 3; bond lengths and angles are given in Table 1. The triangle of the rhenium

Table 1. Bond lengths and angles for $Cs_3[Re_3Cl_9(SO_4)]$

Bond lengths (Å)			
Re(1)—Re(1)	2.4667(8)	Re(2)—Cl(1)	2.402(4)
Re(1)—Re(2)	2.4657(11)	Re(2)—Cl(5)	2.472(7)
Re(1)—Cl(1)	2.408(5)	Re(2)—Cl(6)	2.331(8)
Re(1)—Cl(2)	2.384(6)	Re(2)—O(3)	2.106(17)
Re(1)—Cl(3)	2.319(4)	S—O(1)	1.512(11)
Re(1)—Cl(4)	2.491(4)	S—O(2)	1.432(18)
Re(1)—O(1)	2.096(11)	S—O(3)	1.525(16)
Bond angles (°)			
Cl(4)—Re(1)—Re(1)	147.3(1)	Cl(5)—Re(2)—Re(1)	147.6(2)
Cl(4)—Re(1)—Re(2)	149.1(1)	Cl(5)—Re(2)—Cl(1)	90.3(1)
Cl(4)—Re(1)—Cl(1)	91.6(1)	Cl(5)—Re(2)—Cl(6)	88.8(3)
Cl(4)—Re(1)—Cl(2)	89.9(1)	Cl(5)—Re(2)—O(3)	77.0(5)
Cl(4)—Re(1)—Cl(3)	86.3(2)	Re(1)—Re(2)—Re(1)	60.03(5)
Cl(4)—Re(1)—O(1)	79.7(3)	Re(1)—Re(2)—Cl(1)	59.3(1)
Re(1)—Re(1)—Re(2)	59.99(3)	Re(1)—Re(2)—Cl(1)	119.3(1)
Re(1)—Re(1)—Cl(1)	119.0(1)	Re(1)—Re(2)—Cl(6)	102.1(2)
Re(1)—Re(1)—Cl(2)	58.85(8)	Re(1)—Re(2)—O(3)	90.2(3)
Re(1)—Re(1)—Cl(3)	103.4(1)	Cl(1)—Re(2)—Cl(1)	176.2(2)
Re(1)—Re(1)—O(1)	89.0(3)	Cl(1)—Re(2)—Cl(6)	91.9(1)
Re(2)—Re(1)—Cl(1)	59.0(1)	Cl(1)—Re(2)—O(3)	88.2(1)
Re(2)—Re(1)—Cl(2)	118.8(2)	Cl(6)—Re(2)—O(3)	165.8(7)
Re(2)—Re(1)—Cl(3)	102.1(1)	Re(1)—Cl(1)—Re(2)	61.7(2)
Re(2)—Re(1)—O(1)	89.6(3)	Re(1)—Cl(2)—Re(1)	62.3(3)
Cl(1)—Re(1)—Cl(2)	175.8(2)	O(3)—S—O(1)	108.1(6)
Cl(1)—Re(1)—Cl(3)	90.7(2)	O(3)—S—O(2)	112(1)
Cl(1)—Re(1)—O(1)	88.8(3)	O(1)—S—O(1)	104.7(6)
Cl(2)—Re(1)—Cl(3)	93.3(2)	O(1)—S—O(2)	111.8(7)
Cl(2)—Re(1)—O(1)	87.6(3)	Re(1)—O(1)—S	112.8(5)
Cl(3)—Re(1)—O(1)	166.0(5)	Re(2)—O(3)—S	111.3(7)

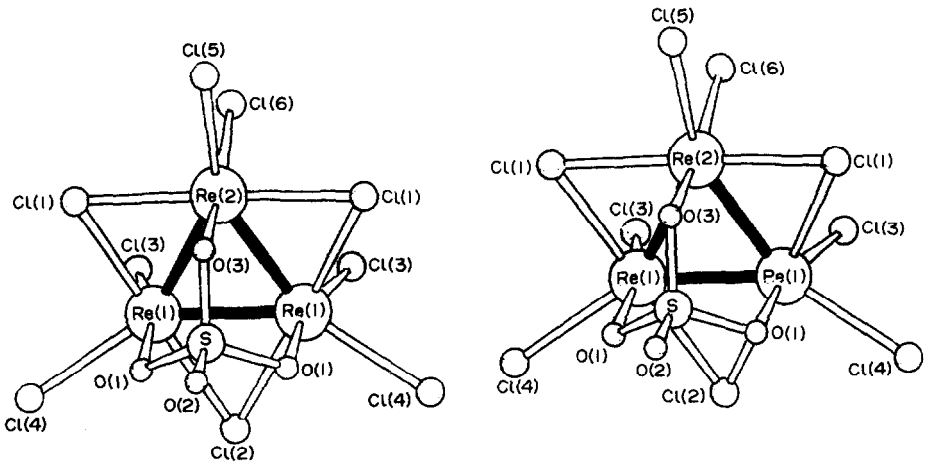

Fig. 2. The structure of $[Re_3Cl_9(SO_4)]^{3-}$.

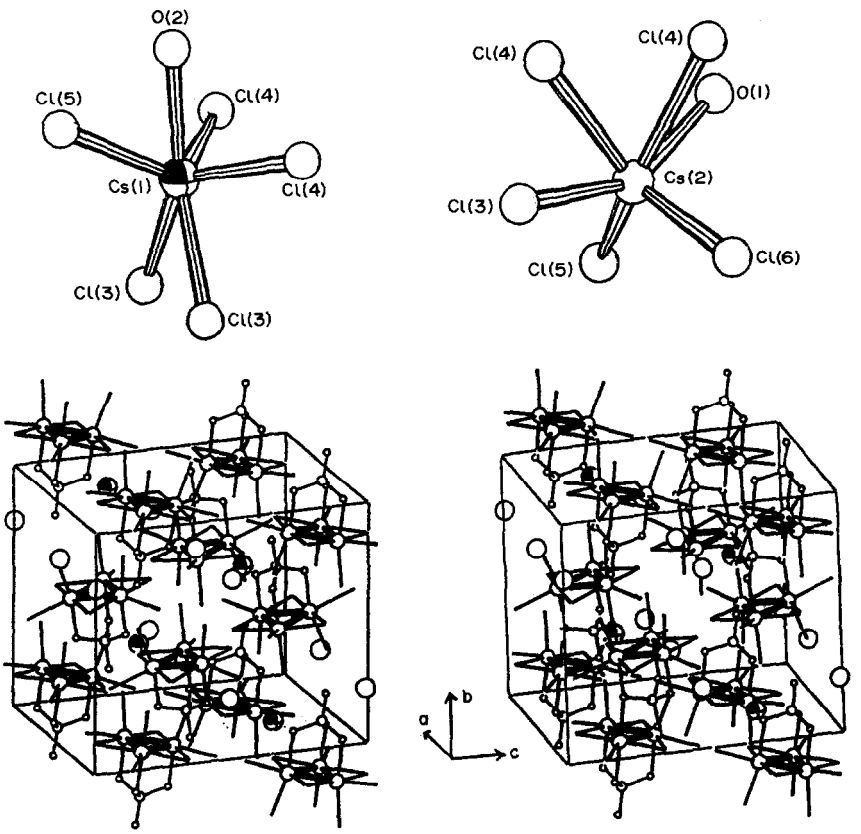

Fig. 3. ORTEP packing diagram and contact spheres of the caesium ions; Cs(1) which occupies a special position is shaded.

atoms remains equilateral [2.466(1) Å av.] with the sulphato ligand capping the trimetal unit (O—O distances are 2.43 Å av.). The three Re—O_c bonds are equidistant [2.10(1) Å av.], almost vertical to the Re_3 plane (mean Re—Re—O_c angle = 89.6° av.). Structural changes occur in the sulphato moiety relative to the free tetrahedral ion (S—O distance 1.49 Å).[19] The S—O_c distances are longer [1.51(1) Å av.] than the S—O_t distance [1.43(2) Å] and the interior O_c—S—O_c angles average 107.0°, whereas the exterior O_c—S—O_t angles average 111°. The one-electron reduction does not cause any significant changes and the structure of **5** overall is very similar to its unreduced counterpart **6**.[15]

In the crystal structure the anions are arranged in layers with the sulphate ligands pointing in opposite directions in consecutive layers. One caesium ion (the one in a special position) lies on the layers, the other one lies between the layers. The anion is situated on a crystallographic mirror plane which goes through the atoms Re(2), Cl(2), Cl(5), Cl(6), S, O(2) and O(3). Both caesium ions form six close contacts, five with chlorine and one with oxygen atoms. Cs(1) is held tightly and Cs(2) more loosely. The range in which the five Cs···Cl contacts lie is 3.310–3.398(4) Å for Cs(1) and 3.482–3.651(5) Å for Cs(2), while the Cs···O contacts are 3.04(2) Å for Cs(1) and 3.21(1) Å for Cs(2).

Acknowledgement—We thank the Greek General Secretariat of Research and Technology for previous support to establish part of this Laboratory.

REFERENCES

1. F. A. Cotton and R. A. Walton, *Multiple Bonds between Metal Atoms*. Wiley, New York (1982).
2. D. G. Tisley and R. A. Walton, *Inorg. Chem.* 1973, **12**, 373.
3. D. G. Tisley and R. A. Walton, *J. Inorg. Nucl. Chem.* 1973, **35**, 1905.
4. B. E. Bursten, F. A. Cotton, J. C. Green, E. A. Seddon and G. G. Stanley, *J. Am. Chem. Soc.* 1980, **102**, 955.
5. W. Geilmann and F. W. Wrigge, *Z. Anorg. Allg. Chem.* 1935, **223**, 144.
6. R. Z. Munze, *Phys. Chem. (Leipzig)* 1964, **226**, 415; R. Z. Munze, *Phys. Chem. (Leipzig)* 1969, **240**, 135.
7. S. K. D. Strubinger, I. W. Sun, W. E. Cleland Jr and C. L. Hussey, *Inorg. Chem.* 1990, **29**, 993.
8. R. Lincoln and G. Wilkinson, *Inorg. Synth.* 1980, **20**, 44.
9. D. A. Edwards and R. T. Ward, *J. Chem. Soc. A* 1970, 1617.
10. J. B. Heatridge, *Electrochemical Techniques for Inorganic Chemists*, p. 58. Academic Press, London and New York (1969).
11. C. Ciacovazzo and G. Cascavano, SIR, Program for Crystal Structure Determination, University of Bari, Italy (1988).
12. G. Sheldrick, *SHELX76. Program for Crystal Structure Determination*. University of Cambridge, U.K.
13. R. A. Bailey and J. A. McIntyre, *Inorg. Chem.* 1966, **5**, 1940; F. A. Cotton and J. T. Mague, *Inorg. Chem.* 1964, **3**, 1402.
14. B. H. Robinson and J. E. Fergusson, *J. Chem. Soc.* 1964, 5683.
15. M. Irmler and G. Meyer, *Naturwissenschaften* 1988, **75**, 308.
16. R. L. Keiter, D. S. Strickland, S. R. Wilson and J. R. Shapley, *J. Am. Chem. Soc.* 1986, **108**, 3846.
17. J. S. Tanster, C. S. Fung and R. L. Garten, *J. Am. Chem. Soc.* 1978, **100**, 170; J. S. Rieck and A. T. Bell, *J. Catal.* 1985, **95**, 88 and refs therein.
18. P. Zelenay, M. A. Habib and J. O'M. Bockris, *J. Electrochem. Soc.* 1984, **131**, 2464; M. A. Habib and J. O'M. Bockris, *J. Electrochem. Soc.* 1983, **130**, 2510.
19. A. F. Wells, *Structural Inorganic Chemistry*, pp. 584–587. Clarendon Press, Oxford (1975).

Polyhedron Vol. 10, No. 7, pp. 747–751, 1991
Printed in Great Britain

0277–5387/91 $3.00+.00
© 1991 Pergamon Press plc

ORGANOAMIDOMETALLICS—IV.* SYNTHESES OF N,N′-BIS(POLYFLUOROPHENYL)ETHANE-1,2-DIAMINATO(2−)PLATINUM(II) COMPLEXES WITH TWO DIFFERENT FLUOROCARBON GROUPS

D. P. BUXTON and G. B. DEACON†

Chemistry Department, Monash University, Clayton, Victoria 3168, Australia

(*Received* 9 *November* 1990; *accepted* 11 *December* 1990)

Abstract—The N,N′-bis(polyfluorophenyl)ethane-1,2-diaminato(2−)platinum(II) complexes [Pt(N(*p*-HC_6F_4)CH_2CH_2NR)$(py)_2$] (R = *p*-HC_6F_4, *p*-BrC_6F_4, C_6F_5 or *p*-MeC_6F_4; py = pyridine) have been prepared by decarboxylation reactions between [PtI_2(*p*-$HC_6F_4NHCH_2CH_2NH_2$)], thallium(I) 2,3,5,6-tetrafluorobenzoate and a suitable polyfluorobenzene, RF, in hot dry pyridine. When R ≠ *p*-HC_6F_4, the two different polyfluorophenyl groups can be distinguished by different F3,5 resonances in the ^{19}F NMR spectra. The reactant and analogous complexes [PtX_2($RNHCH_2CH_2NH_2$)](R = *p*-HC_6F_4, X = I or Cl; R = C_6F_5, X = I) were prepared by treatment of K_2PtX_4 (X = I or Cl) with the appropriate N-polyfluorophenylethane-1,2-diamine.

Novel N,N-bis(polyfluorophenyl)ethane-1,2-diaminato-(2−)platinum(II) complexes, [$Pt(NRCH_2)_2(py)_2$] (py = pyridine), have been prepared by decarboxylation reactions between $PtCl_2$(en) (en = ethane-1,2-diamine) and thallium(I) pentafluorobenzoate or thallium(I) 2,3,5,6-tetrafluorobenzoate and a suitable reactive polyfluorobenzene in hot pyridine.[2,3] The synthetic path is completely new in organoamidometallic chemistry.[4–6] The products are moisture-stable, by contrast with simple platinum(II) organoamides, e.g. [$Pt(NRCH_2)_2$(bpy)] (R = H or Me, bpy = 2,2′-bipyridyl),[7,8] and have appreciable antitumour activity.[9] Of necessity, the decarboxylation syntheses result in substitution of the same polyfluorophenyl group on each nitrogen of the ethane-1,2-diaminate ligand. We now report a preparative route to analogous complexes with two different polyfluorophenyl groups.

RESULTS AND DISCUSSION

The synthetic strategy required the initial preparation of platinum(II) halide complexes of N-polyfluorophenylethane-1,2-diamines. The ligands $RNHCH_2CH_2NH_2$ [R = *p*-HC_6F_4 (**1a**) or C_6F_5 (**1b**)] were obtained by nucleophilic substitution reactions between ethane-1,2-diamine and the appropriate polyfluorobenzene with (R = *p*-HC_6F_4) or without (R = C_6F_5) an added base. Compound **1b** has previously been prepared in higher yield in a pyridine medium,[10] with characterization by F, N analyses and ^{19}F NMR spectroscopy.[10,11] Although the melting point of **1b** was well below the reported value,[10] identification was unequivocal on the basis of microanalyses (C, H, F, N), ^1H and ^{19}F NMR spectra and the mass spectrum. Reaction of **1a** and **1b** with the appropriate potassium tetrahalogenoplatinate(II) complex gave [PtX_2($RNHCH_2CH_2NH_2$)] [R = *p*-HC_6F_4, X = I (**2a**) or Cl (**2b**); R = C_6F_5, X = I (**2c**)]. Considerable variation in yield was observed, depending on the solvent system used (see Experimental).

Syntheses of N,N′-bis(polyfluorophenyl)ethane-1,2-diaminato(2−)platinum(II) complexes, [Pt(N(*p*-HC_6F_4)CH_2CH_2NR)$(py)_2$] (**3**), were effected by heating **2a** with thallium(I) 2,3,5,6-tetrafluorobenzoate and a polyfluoroaromatic compound, RF, in hot pyridine. Details of the reactions are given in Table 1. The method was initially validated by synthesis of the known[2,3] symmetrical organoamide **3a** before application to complexes

* For Part III, see ref. 1.

† Author to whom correspondence should be addressed.

with two different polyfluorophenyl groups, **3b–3d**.

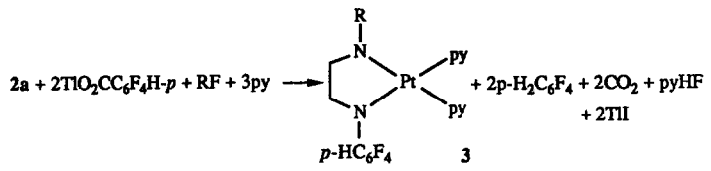

(1)

3a R=*p*-HC_6F_4
3b R=*p*-BrC_6F_4
3c R=C_6F_5
3d R=*p*-MeC_6F_4

On the basis of the reaction path to the symmetrical complexes $[Pt(NRCH_2)_2(py)_2]$,[3] reaction (1) can be envisaged as occurring by deprotonation to give the nucleophilic species, $[Pt(N(p\text{-}HC_6F_4)CH_2CH_2NH)(py)_2]$, which attacks the polyfluoroarene, RF, giving **3**. Deprotonation is effected by highly carbanionic *p*-HC_6F_4 groups, generated by decarboxylation, and the resulting 1,2,4,5-tetrafluorobenzene is relatively unreactive to nucleophilic substitution.[12]

Yields of pure complexes were low, despite near quantitative decarboxylation, owing to formation of dark coloured impurities which could be difficult to remove. Two complexes, **3b** and **3c**, were isolated as ether solvates, the composition being indicated by both duplicate microanalyses and ^1H NMR integrations. Parent ions were observed in the spectra of the unsymmetrical complexes **3b–3d**. However, only a single CH_2N resonance and a single set of pyridine resonances were observed, despite the presence of two different polyfluorophenyl groups. The (average) ^3J[PtH(py)] and ^3J[PtH(CH_2)] coupling constants (Table 2) are of similar magnitude to those of the symmetrical complexes, $[Pt(NRCH_2)_2(py)_2]$,[3] e.g. **3a** (Table 2). Clear differentiation between the two different polyfluorophenyl groups was observed in the F3,5 resonances (Table 2). The F3,5 chemical shifts of the individual polyfluorophenyl groups of **3b–3d** are in close agreement with those of the corresponding symmetrical complexes (Table 2). On the other hand, little differentiation was observed in the F2,6 resonances, since the dominant influence on the chemical shift is the amido nitrogen, which is *ortho* to F2,6 in each case.

The synthesis method, reaction (1), developed for organoamides **3b–3d** with two different polyfluorophenyl groups could presumably be extended to other similar complexes, for example, by use of **2c** as a reactant, or by preparation and use of other reactants **2** incorporating different fluorocarbon groups.

EXPERIMENTAL

General

Microanalyses were by the Australian Microanalytical Service, Melbourne. Carbon dioxide was determined gravimetrically as barium carbonate. Decarboxylation was monitored using a small volume barium hydroxide trap additional to the main trap and reactions were terminated when carbon dioxide evolution ceased. Spectroscopic methods are as for Part I.[3] Listed IR bands of compounds examined as Nujol and hexachlorobutadiene mulls are restricted to those of medium or greater intensity, except for N—H and Pt—halogen stretching frequencies. Proton chemical shifts are in ppm downfield from internal Me_4Si and fluorine chemical shifts in ppm from internal $CFCl_3$. For platinum-containing ions in the mass spectra, only the most intense peak [containing ^{195}Pt or ^{275}(PtBr)] of

Table 1. Synthesis of N,N′-bis(polyfluorophenyl)ethane-1,2-diaminato(2−)platinum(II) complexes[a]

2a (mmol)	Reagents $TlO_2CC_6F_4H$-*p* (mmol)	RF	mmol	Reaction Temperature (°C)	Time (min)	Product	Yield (%)
1.00	2.00	C_6F_5H	18.0	105–107	25	**3a**	30
1.00	2.00	C_6F_5Br	16.0	105–110	22	**3b** $0.5C_4H_{10}O$	15
1.00	2.00	C_6F_6	17.4	100–110	15	**3c** $0.4C_4H_{10}O$	19
0.30	0.60	C_6F_5Me	4.3	115	25	**3d**	17

[a] Reactions were carried out in pyridine (10 cm^3) and gave 85–100% CO_2.

Table 2. Some NMR data for [Pt(N(*p*-HC_6F_4)CH_2CH_2NR)$(py)_2$] complexes

Complex	δ(F3,5)[a]	δ(F3,5)[b]		^3J[PtH(py)]	^3J[PtH(CH_2)]
3a	−144.8	−144.8		34	29
3b	−144.5	−140.8	(−141.0)[c]	31	[f]
3c	−144.6	−168.7	(−168.9)[d]	30	[f]
3d	−144.9	−150.0	(−150.1)[e]	35	30

[a] For *p*-HC_6F_4.
[b] For R.
[c] δ(F3,5) of [Pt(N(*p*-BrC_6F_4)CH_2)$_2$$(py)_2$].[3]
[d] δ(F3,5) of [Pt(N(C_6F_5)CH_2)$_2$$(py)_2$].[3]
[e] δ(F3,5) of [Pt(N(*p*-MeC_6F_4)CH_2)$_2$$(py)_2$].[3]
[f] Not resolved.

the cluster is given. For bromine-containing ions without platinum, the listed peak is for the ^{79}Br ion. Visible spectra are for solutions in 95% ethanol in the range 350–700 nm.

Solvents and reagents

Petrol refers to the fraction b.p. 60–85°C unless indicated otherwise. Pentafluorobenzene and hexafluorobenzene (Bristol Organics) and ethane-1,2-diamine were dried over molecular sieves (Grade 4A) before use. Triethylamine was refluxed over and distilled from acetic anhydride under nitrogen. Purification of other solvents and sources or preparations of other reagents have been given in earlier papers.[3,13]

Synthesis of N-(polyfluorophenyl)ethane-1,2-diamines

N-(2,3,5,6-Tetrafluorophenyl)ethane-1,2-diamine (**1a**). Pentafluorobenzene (170 mmol) and ethane-1,2-diamine (84 mmol) were refluxed over anhydrous K_2CO_3 for 7 h under nitrogen. Evaporating the mixture to dryness under high vacuum gave a solid which was partitioned between ether and water. Repeated ether extraction and evaporation of the ether *in vacuo* gave a light yellow oil which crystallized upon cooling. The solid was twice recrystallized from ether–petrol giving colourless crystals (yield, 32%), m.p. 44–45°C (Found: C, 45.7; H, 3.7; F, 36.3; N, 13.8. $C_8H_8F_4N_2$ requires: C, 46.2; H, 3.9; F, 36.5; N, 13.5%). ^{19}F NMR ($CDCl_3$): −142.1, m, 2F, F3,5; −160.7, m, 2F, F2,6. ^1H NMR ($CDCl_3$): 1.15, s, 2H, NH_2; 2.91, t, ^3J(HH) 6 Hz, 2H, CH_2NH_2; 3.37, qt, ^3J[HH(CH_2)] 6 Hz, ^3J[HH(NH)] 6 Hz, ^5J(HF) 1 Hz, 2H, $CH_2N(H)C_6F_4H$; 4.40, br, 1H, N(**H**)C_6F_4H; 6.36, tt, ^3J(HF) 10 Hz, ^4J(HF) 7 Hz, 1H, HC_6F_4. IR: 3474w, 3381w and 3285(br) ν(NH), 2943m, 1650s, 1526vs, 1509vs, 1470s, 1358m, 1156s, 1142s, 924m cm^{-1}. Mass spectrum: *m/z* 208 [17%, M^+], 179 [78, $C_7H_5F_4N^+$], 178 [100, HC_6F_4NH CH_2^+]. Similarly, reaction of pentafluorobenzene (79 mmol) and ethane-1,2-diamine (26 mmol) in refluxing triethylamine (9 cm^3, 65 mmol) for 19 h under anhydrous conditions gave **1a** (21%) (IR identification).

Hydrochloride derivative. Hydrogen chloride and nitrogen were bubbled through a stirred ether solution of **1a** (9.6 mmol). The precipitated white solid (**1a**·HCl) was refluxed in acetone–petrol for a few minutes, collected and dried (yield, 70%), m.p. 275–280°C (dec.) (Found: C, 39.4; H, 3.6; N, 11.2. $C_8H_9ClF_4N_2$ requires: C, 39.3; H, 3.7; N, 11.5%). ^{19}F NMR [$(CD_3)_2SO$]: −141.2, m, 2F, F3,5; −158.8, m, 2F, F2,6. ^1H NMR [$(CD_3)_2SO$]: 3.00, t, ^3J(HH) 6 Hz, 2H, $CH_2NH_3^+$; 3.59, m, 2H, $CH_2N(H)C_6F_4H$; 6.20, m(br), 1H, N(**H**)C_6F_4H; 7.00, tt, ^3J(HF) 11 Hz, ^4J(HF) 7 Hz, 1H, HC_6F_4; 8.29, s(br), 3H, NH_3^+. IR: 3318s and 3058s(br) ν(NH), 2909m, 1651m, 1602m, 1544s(br), 1513s(br), 1471s, 1457s, 1448s, 1365s, 1282m, 1157s(br), 1110s, 1037s, 1028s, 958m, 925s, 862m, 829s, 801s, 710s, 692m, 550m(br) cm^{-1}.

N-(Pentafluorophenyl)ethane-1,2-diamine (**1b**). Stirring hexafluorobenzene (170 mmol) and ethane-1,2-diamine (170 mmol) under nitrogen with gentle heating promoted a vigorous exothermic reaction. After 10 min, the near solid mixture was dissolved in ethanol (50 cm^3) which was refluxed for 2 h. Filtration and evaporation of the solution to dryness *in vacuo* gave a dark brown solid. Recrystallization from ether–petrol at 0°C gave colourless crystals (yield, 30%), m.p. 46°C, ref. 10 m.p. 70–71°C (Found: C, 42.8; H, 3.0; F, 41.7; N,12.7. Calc. for $C_8H_7F_5N_2$: C, 42.5; H, 3.1; F, 42.0; N, 12.4%). ^{19}F NMR ($CDCl_3$): −160.2, m, 2F, F2,6; −165.2, m, 2F, F3,5; −172.7, m, 1F, F4, in satisfactory agreement with values[10,11] using CCl_4 as

solvent. ^{1}H NMR ($CDCl_3$): 1.16, s, 2H, NH_2; 2.91, m, ^3J(HH) 6 Hz, 2H, CH_2NH_2; 3.31, qt, ^3J[HH(CH_2)] 6 Hz, ^3J[HH(NH)] 6 Hz, ^5J(HF) 1 Hz, 2H, $CH_2N(H)C_6F_5$; 4.17, br, 1H, N(H) C_6F_5. IR: 3473w, 3392w, 3326w and 3212w ν(NH), 2945m, 2867m, 1518vs, 1488vs, 1470s, 1356m, 1021m, 990m, 976m, 954m cm^{-1}. Mass spectrum: *m/z* 226 [22%, M^+], 197 [68, $C_7H_4F_5N^+$], 196 [100, $C_6F_5NHCH_2^+$].

Synthesis of N-(polyfluorophenyl)ethane-1,2-diamineplatinum(II) complexes

Bis - iodo[N - (2,3,5,6 - *tetrafluorophenyl)ethane-1,2-diamine*]*platinum*(II) (**2a**). K_2PtCl_4 (1.2 mmol) and KI (5.3 mmol) were stirred in water (50 cm^3) with gentle heating for 0.5 h. Addition of a solution of **1a** (1.3 mmol) in ethanol (10 cm^3) and stirring overnight gave an orange precipitate, which was washed with a minimum of ethanol and then ether, recrystallized twice from acetone–petrol (b.p. 80–100°C), and refluxed in ether for 2 h giving an orange solid (yield, 16%), m.p. 188–189°C (Found: C; 14.3; H; 1.5; F, 11.3; N, 4.3. $C_8H_8F_4I_2N_2Pt$ requires: C, 14.6; H, 1.2; F, 11.6; N, 4.3%). UV–vis spectrum [λ_{max} (ε)]: 321 (750), 379 (820) nm. IR: 3249m and 3189s ν(NH), 3128m, 3103m, 3070m, 1562m, 1526vs, 1500m, 1473s, 1460m, 1445m, 1429m, 1257m, 1208m, 1175s, 1150m, 1062m, 1038m, 1011m, 930s, 845s, 711m, 687m, 650m, 541m, 193w and 178w ν(Pt—I) cm^{-1}. Mass spectrum: *m/z* 254 [43%, I_2^+], 208 [12, $C_8H_8F_4N_2^+$], 179 [81, $C_7H_5F_4N^+$], 178 [100, $HC_6F_4NHCH_2^+$]. A similarly prepared solution of K_2PtI_4 (0.60 mmol) in water (50 cm^3) was treated with **1a** (0.63 mmol) in acetone (10 cm^3) giving a brown oil that dissolved upon addition of more acetone (60 cm^3). After stirring for 0.5 h, the solution was evaporated to dryness *in vacuo* leaving an orange solid. The solid was extracted with acetone, the solution was filtered and again evaporated to dryness. Dissolution in ethanol and precipitation by petrol gave an orange precipitate of **2a** (yield, 73%) (IR identification). An analogous preparation in aqueous t-butanol gave crude **2a** in 86% yield (IR identification).

Dichloro[*N* - (2,3,5,6 - *tetrafluorophenyl)ethane-1,2-diamine*]*platinum*(II) (**2b**). A solution of K_2PtCl_4 (1.2 mmol) in water (15 cm^3) was stirred for 2 days with **1a** (1.5 mmol) in t-butanol (15 cm^3) giving a cream precipitate which was collected, washed with water then petrol, and dried (yield, 88%), m.p. > 250°C (dec.) (Found: C, 20.6; H, 1.5; N, 6.2. $C_8H_8Cl_2F_4N_2Pt$ requires: C, 20.3; H, 1.7; N, 5.9%). UV–vis spectrum [λ_{max} (ε)]: 313 (380), 378 (87) nm. IR: 3277m and 3202s ν(NH), 3125m, 3076m, 1648m, 1566m, 1531 and 1527vs, 1505m, 1477m, 1352m, 1288m, 1261m, 1220m, 1178s, 1170s, 1062m, 1038m, 1029m, 932vs, 846s, 713m, 690m, 658m, 337m and 331m ν(Pt—Cl) cm^{-1}. Mass spectrum: *m/z* 208 [12%, $C_8H_8F_4N_2^+$], 188 [11, $C_8H_7F_3N_2^+$], 178 [100, $HC_6F_4NHCH_2^+$].

Bis - iodo[*N* - (*pentafluorophenyl)ethane* - 1,2-*diamine*]*platinum*(II) (**2c**). K_2PtCl_4 (1.2 mmol) and KI (5.1 mmol) in water (50 cm^3) were stirred for 0.5 h and then **1b** (1.3 mmol) in acetone (25 cm^3) was added. After stirring overnight, the mixture was evaporated to dryness *in vacuo*. The solid was recrystallized from ethanol–petrol (b.p. < 40°C) to give the title compound (yield, 20%), m.p. 183–184°C (dec.) (Found: C, 14.7; H, 1.0; F, 14.3; N, 4.3. $C_8H_7F_5I_2N_2Pt$ requires: C, 14.2; H, 1.0; F, 14.1; N, 4.2%). UV–vis spectrum [λ_{max} (ε)]: 321 (880) 380 (960) nm. IR: 3246m ν(NH), 3182m, 3127m, 3110m, 1530s, 1523vs, 1456s, 1352m, 1206m, 1138m, 1131m, 1051m, 1012m, 996s, 982s, 669m, 190w and 172w ν(Pt—I) cm^{-1}. Mass spectrum: *m/z* 254 [11%, I_2^+], 226 [26, $C_8H_7F_5N_2^+$], 206 [13, $C_8HF_5N^+$], 197 [94, $C_7H_4F_5N^+$], 196 [100, $C_6F_5NHCH_2^+$].

Synthesis of N,N'-bis(polyfluorophenyl)ethane-1,2-diaminato(2−)platinum(II) *complexes*

Amounts of reagents, reaction conditions and yields of products are given in Table 1. In each case bis-iodo[N-(2,3,5,6-tetrafluorophenyl)ethane-1,2-diamine]platinum(II), thallium(I) 2,3,5,6-tetrafluorobenzoate, dry pyridine (10 cm^3) and the appropriate polyfluorobenzene were heated with stirring under purified nitrogen. After reaction, the mixture was evaporated to dryness *in vacuo* and the residue washed with petrol (2 × 20 cm^3) and extracted with ether or acetone. The resulting solution was filtered, evaporated to dryness and the residue was washed with a minimum of ethanol (2 × 2 cm^3) on a glass sinter, and recrystallized as indicated below. ^3J(PtH) values are given in Table 2.

[*N,N' -bis*(2,3,5,6 -*tetrafluorophenyl)ethane* - 1,2-*diaminato*(2−)]*dipyridineplatinum*(II) (**3a**). Extraction with acetone and recrystallization from ether–petrol gave the yellow title compound, m.p. 188–190°C (dec.), ref. 3 m.p. 173°C (dec.). ^{1}H and ^{19}F NMR, IR and mass spectra of the solid were identical with those of the authentic compound.

[*N* - (4 - *bromo* - 2,3,5,6 - *tetrafluorophenyl*) - *N'*-(2,3,5,6 - *tetrafluorophenyl)ethane* - 1,2 - *diaminato*(2−)]*dipyridineplatinum*(II)–*ether* (1:0.5) (**3b**·$0.5Et_2O$). Extraction with acetone and recrystallization from ether–petrol gave the title compound, m.p. 178–182°C (dec.) (Found: C, 38.1; 37.8; H, 2.2, 2.3; N, 6.7, 7.0. $C_{24}H_{15}BrF_8N_4Pt$·$0.5C_4H_{10}O$ requires: C, 37.9; H, 2.5; N, 6.8%).

^{19}F NMR [$(CD_3)_2CO$]: −140.8, m, 2F, F3,5 (C_6F_4Br); −144.5, m, 2F, F3,5 (C_6F_4H); −148.9, m, 2F, F2,6 (C_6F_4Br); −150.5, m, 2F, F2,6 (C_6F_4H). ^{1}H NMR [$(CD_3)_2CO$]: 1.10, t, 3H, Me; 3.16, br, 4H, CH_2N; 3.39, q, 2H, CH_2O; 6.26, tt, ^3J(HF) 10 Hz, ^4J(HF) 7 Hz, 1H, HC_6F_4; 7.27, m, 4H, H3,5(py); 7.85, m, 2H, H4(py); 8.61, m, 4H, H2,6(py). UV–vis spectrum [λ_{max} (ε)]: 364 (9300) nm. IR: 2892m, 2836m, 1642s, 1619s, 1604s, 1578m, 1493vs, 1479vs(sh), 1470vs, 1448s, 1438s, 1333m, 1277m, 1160m, 1151m, 1128s, 1089m, 1068m, 940s, 908m, 829m, 761m, 694m cm^{-1}. Mass spectrum: *m/z* 786 [0.7%, M^+], 706 [0.6, Pt($C_{14}H_4BrF_8N_2$)py$^+$], 625 [0.3, Pt($C_{14}H_2BrF_8N_2$)$^+$], 528 [0.5, Pt(BrC_6F_4NC)py$^+$], 434 [11, $HC_6F_4NH(CH_2)_2NHC_6F_4Br^+$], 432 [8, $HC_6F_4N(CH_2)_2NC_6F_4Br^+$], 256 [28, $BrC_6F_4NHCH_2^+$], 178 [100, $HC_6F_4NHCH_2^+$].

[*N*-(*pentafluorophenyl*)-*N'*-(2,3,5,6-*tetrafluorophenyl*)*ethane* - 1,2 - *diaminato*(2−)]*dipyridineplatinum*(II)–*ether* (1:0.4) (**3c**·0.4Et_2O). Extraction with acetone and recrystallization twice from ether–petrol gave the title compound, m.p. 192–196°C (dec.) (Found: C, 40.8, 40.6; H, 2.5, 2.6; N, 7.9, 7.7. $C_{24}H_{15}F_9N_4Pt \cdot 0.4C_4H_{10}O$ requires: C, 40.7; H, 2.5; N, 7.4%). ^{19}F NMR [$(CD_3)_2CO$]: −144.6, m, 2F, F3,5 (C_6F_4H); −150.8, complex m, 4F, F2,6 (C_6F_4H and C_6F_5); −168.7, m, 2F, F3,5 (C_6F_5); −177.1, m, 1F, F4 (C_6F_5). In $CDCl_3$, two F2,6 resonances were observed: −150.6, m, *p*-HC_6F_4; −151.0, m, C_6F_5. ^{1}H NMR ($CDCl_3$): 1.21, t, 2.4H, Me; 3.11, br m, 2H, $CH_2NC_6F_5$; 3.23, br m, 2H, $CH_2NC_6F_4H$; 3.48, q, 1.6H, CH_2O; 6.06, tt, ^3J(HF) 10 Hz, ^4J(HF) 7 Hz, 1H, HC_6F_4; 7.09, m, 4H, H3,5(py); 7.66, m, 2H, H4(py); 8.54, m, 4H, H2,6(py). UV–vis spectrum [λ_{max} (ε)]: 358 (6100) nm. IR: 2898m, 2843m, 1631s, 1605m, 1581m, 1504vs, 1494vs, 1468s, 1449vs, 1440vs, 1333m, 1162m, 1132s, 1113m, 1093m, 1062s, 1011s, 990m, 950s, 906s, 873s, 760s, 694s, 570m, 487m cm^{-1}. Mass spectrum: *m/z* 725 [0.3%, M^+], 644 [0.2, Pt($C_{14}H_3F_9N_2$)py$^+$], 564 [0.2, Pt($C_{14}H_2F_9N_2$)$^+$], 467 [0.7, Pt(C_6F_5NC)py$^+$], 449 [0.8, Pt(HC_6F_4NC)py$^+$], 372 [11, $HC_6F_4N(CH_2)_2NC_6F_5^+$], 370 [8, $HC_6F_4(CH)_2C_6F_5^+$], 196 [31, $C_6F_5NHCH_2^+$], 178 [49, $HC_6F_4NHCH_2^+$], 79 [100, py$^+$].

[*N* - (2,3,5,6 - *tetrafluoro* - 4 - *methylphenyl*) - *N'*-(2,3,5,6 - *tetrafluorophenyl*)*ethane* - 1,2 - *diaminato*(2−)]*dipyridineplatinum*(II) (**3d**). Ether extraction and recrystallization from ether–petrol gave **3d**, m.p. 183–184°C (dec.) (Found: C, 41.5; H, 2.3; F, 20.6; N, 7.8. $C_{25}H_{18}F_8N_4Pt$ requires: C, 41.6; H, 2.5; F, 21.1; N, 7.8%). ^{19}F NMR [$(CD_3)_2CO$]: −144.9, m, 2F, F3,5 (C_6F_4H); −150.0, m, 2F, F3,5 (C_6F_4Me); −151.1, br m, 4F, F2,6 (HC_6F_4 and C_6F_4Me). ^{1}H NMR [$(CD_3)_2CO$]: 1.94, m, 3H, Me; 3.14, m, 4H, CH_2; 6.22, m, 1H, HC_6F_4; 7.25, m, 4H, H3,5(py); 7.84, m, 2H, H4(py); 8.58, m, 4H, H2,6(py). UV–vis spectrum [λ_{max} (ε)]: 356 (5200) nm. IR: 1648m, 1630s, 1606m, 1578m, 1494 and 1483vs, 1448vs, 1426m, 1379m, 1332m, 1274m, 1168m, 1131s, 1092m, 1057m, 920s, 872s, 760s, 694s cm^{-1}. Mass spectrum: *m/z* 721 [0.4%, M^+], 463 [1.0, Pt(MeC_6F_4NC)py$^+$], 449 [0.7, Pt(HC_6F_4NC)py$^+$], 368 [32, $MeC_6F_4N(CH_2)_2NC_6F_4H^+$], 366 [23, $MeC_6F_4N(CH)_2NC_6F_4H^+$], 192 [92, $MeC_6F_4NHCH_2^+$], 178 [53, $HC_6F_4NHCH_2^+$], 79 [100, py$^+$].

Acknowledgements—This work was carried out during the tenure of a grant from the Anti-Cancer Council of Victoria, and was further assisted by a loan of platinum from Johnson Matthey.

REFERENCES

1. D. P. Buxton, G. B. Deacon and D. St. C. Black, *Polyhedron* 1989, **8**, 143.
2. G. B. Deacon, B. M. Gatehouse, I. L. Grayson and M. C. Nesbit, *Polyhedron* 1984, **3**, 753.
3. D. P. Buxton, G. B. Deacon, B. M. Gatehouse, I. L. Grayson, R. J. Thomson and D. St. C. Black, *Aust. J. Chem.* 1986, **39**, 2013.
4. D. C. Bradley and M. H. Chisholm, *Accts Chem. Res.* 1976, **9**, 273.
5. M. F. Lappert, P. P. Power, A. R. Sanger and R. C. Srivastava, *Metal and Metalloid Amides*. Ellis-Horwood, Chichester (1980).
6. M. D. Fryzuk and C. D. Montgomery, *Coord. Chem. Rev.* 1989, **95**, 1.
7. G. W. Watt and D. G. Upchurch, *J. Am. Chem. Soc.* 1968, **90**, 914.
8. G. W. Watt and D. G. Upchurch, *J. Am. Chem. Soc.* 1967, **89**, 177.
9. Cancer Institute Board, Anti-Cancer Council of Victoria and Monash University, "Composition and methods for tumour treatment", Australian Provisional Patent Specification, 1988 P1 9505/88; G. B. Deacon, Paper A9, *Conference on Metal Complexes in the Detection and Treatment of Cancer*, Marysville, Victoria (1989).
10. F. I. Abezgauz and A. V. Sokolov, *J. Gen. Chem. U.S.S.R.* 1968, **38**, 2418.
11. L. N. Pushkina, A. P. Stepanov, V. S. Zhukov and A. D. Naumov, *Org. Mag. Reson.* 1972, **4**, 607.
12. R. D. Chambers, W. K. R. Musgrave, J. S. Waterhouse, D. L. H. Williams, J. Burdon, W. B. Hollyhead and J. C. Tatlow, *J. Chem. Soc., Chem. Commun.* 1974, 239.
13. D. P. Buxton, G. B. Deacon, B. M. Gatehouse, I. L. Grayson and D. St. C. Black, *Aust. J. Chem.* 1988, **41**, 943.

Polyhedron Vol. 10, No. 7, pp. 753–762, 1991
Printed in Great Britain

0277–5387/91 $3.00+.00
© 1991 Pergamon Press plc

CHROMIUM(VI)–THIOESTER FORMATION IN N,N-DIMETHYLFORMAMIDE

WALDEMAR MAZUREK

Materials Research Laboratory, Defence Science and Technology Organization, P.O. Box 50, Ascot Vale, Victoria 3032, Australia

and

PETER J. NICHOLS and BRUCE O. WEST*

Department of Chemistry, Monash University, Clayton, Victoria 3168, Australia

(*Received* 19 *October* 1990; *accepted* 13 *December* 1990)

Abstract—The interaction of thiols (RSH; R = n-butyl, t-butyl, *p*-bromophenyl, *p*-nitrophenyl and phenyl) with dichromate in dimethylformamide (DMF) has been studied and found to involve the formation of chromium(VI) thioester anions ($[RSCrO_3]^-$) followed by much slower redox reactions resulting in the formation of chromium(III) and disulphide species. The chromium(VI) thioesters can be precipitated from DMF/ether solutions as tetraphenylarsonium or bis(triphenylphosphine)iminium salts. They show characteristic visible absorptions around 420 nm (extinction coefficients *ca* 2000 mol^{-1} dm^3 cm^{-1}) and IR absorptions at *ca* 945 cm^{-1} [$\nu(Cr—O)_{asym}$] and 890 cm^{-1} [$\nu(Cr—O)_{sym}$]. The initial interaction between thiols and dichromate in DMF is an acid-catalysed hydrolysis of dichromate followed by the substitution of protonated chromate by the thiol. Arylthiols catalyse the hydrolysis more effectively, and substitute chromate more rapidly, than alkylthiols. Chromium(VI) arylthioesters decompose more rapidly than the alkyl thiol derivatives with chromium(V) intermediates being involved in the process.

The reduction of dichromate anions by thiols has been studied almost exclusively in aqueous solution, in part influenced by the interest in understanding the carcinogenic and mutagenic properties of chromium(VI).[1,2] The presence of chromium(VI) thioesters as transient intermediates in such redox processes has been suggested by UV–vis spectroscopy and other intermediates involving chromium(V) and chromium(IV) have been proposed from an analysis of kinetic data.[1,2] Recent work on the aqueous chromate/glutathione system indeed indicates a relatively stable chromium(V) intermediate.[3] The observed kinetic profile and relative stabilities of the intermediates vary with pH and nature of buffers used.[1,2]

Reactions in organic solvents have been little studied but the understanding of the use of dichromate as a "curing" agent for polysulphide prepolymers, used as sealants, requires knowledge of the redox reaction in non-aqueous media.[4] One such study by Averko-Antonovich *et al.*[5] used polarography to examine the reaction of a polysulphide oligomer with $Na_2[Cr_2O_7]$ in alcoholic KOH and DMF. It showed that thiol groups were oxidized to disulphides and chromium(VI) reduced to chromium(III). A mechanism was proposed which, as in aqueous solution, involved the initial formation of a chromium(VI) thioester followed by successive reductions to chromium(III). No study of the intermediate steps was reported.

This paper reports studies of the kinetics of reactions between dichromate anions and various aryl and alkyl thiols using spectroscopic techniques together with the isolation of further examples of chromium(VI) thioester intermediates. The structural characterization of one such compound, $[Ph_4As][p\text{-}BrPhSCrO_3]$, by a single crystal X-ray diffraction study has been reported separately.[6]

*Author to whom correspondence should be addressed.

The overall reduction of dichromates by thiols results in the formation of water [eq. (1)]

$$[Cr_2O_7]^{2-} + 2RSH \rightleftharpoons 2[RSCrO_3]^- + H_2O \quad (1)$$

and hence such reactions cannot be carried out under completely anhydrous conditions. This means that $[Cr_2O_7]^{2-}$ anions can undergo hydrolysis as water is formed and an examination of the kinetics of hydrolysis of the dichromate anion in DMF has been made.

RESULTS AND DISCUSSION

The conversion of dichromate into the chromium(VI) thioesters involves an intermediate species as evident from the absence of isosbestic points in the plots of visible spectra of reacting solutions with time (Fig. 1). This results from the accompanying hydrolysis of dichromate to give the protonated chromate anion, $[HOCrO_3]^-$ (Fig. 2; Table 1). An examination of the hydrolysis of dichromate in DMF was therefore undertaken to aid the interpretation of the chromium(VI) thioester formation results.

Hydrolysis of dichromate

The hydrolysis of dichromate in aqueous solution has been the subject of several investigations.[11–15] The reaction is catalysed by acids[12] and bases,[11,13,14] as well as being affected by a number of "inert"

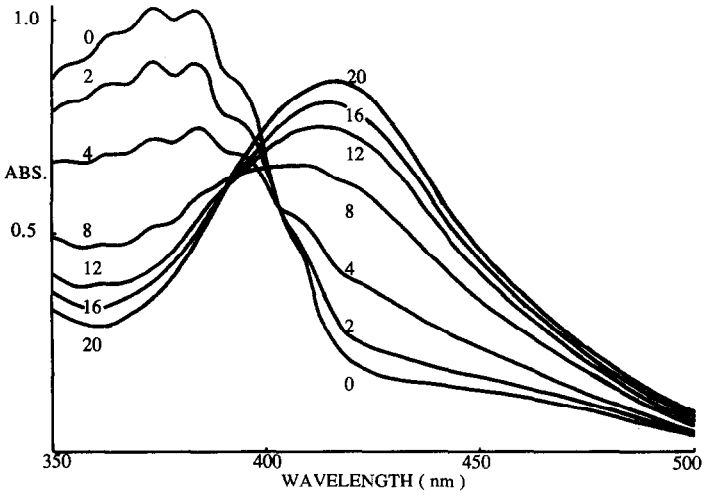

Fig. 1. Change in visible spectrum with chromium(VI) n-butyl thioester formation in DMF at 47.3°C in the presence of 1 mol dm^{-3} $NaNO_3$. Spectra recorded at the times (min) indicated (0.0108 mol dm^{-3} n-BuSH, 2.33×10^{-4} mol dm^{-3} $Na_2[Cr_2O_7]$).

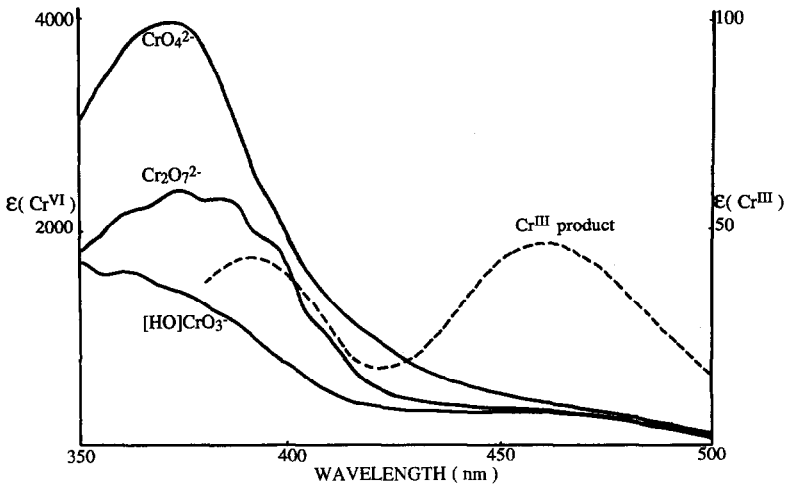

Fig. 2. Visible absorption spectra of chromium species in DMF.

Table 1. Visible absorption data for chromium(VI) species in DMF and H_2O

Complex	DMF[a] λ_{max} (nm)	DMF[a] ε (per Cr) (mol^{-1} dm^3 cm^{-1})	H_2O λ_{max} (nm)	H_2O ε (per Cr) (mol^{-1} dm^3 cm^{-1})	Reference
$[Cr_2O_7]^{2-}$	374	2250	370	1990	7
	371[b]	2300[b]			
$[CrO_4]^{2-}$	372	3950	372	4810	9
$[HOCrO_3]^-$	355	1620	350	1563	10
$[n\text{-}BuSCrO_3]^-$	416	1890			
$[t\text{-}BuSCrO_3]^-$	420	1800			
$[PhSCrO_3]^-$	420	2080			
$[p\text{-}BrPhSCrO_3]^-$	412	2000			
	414[c]	2440[c]			

[a] This work.
[b] Reference 8.
[c] This work, solutions prepared from $[Ph_4As][p\text{-}BrPhSCrO_3]$ or $[PPN][p\text{-}BrPhSCrO_3]$; similarly $\lambda_{max} = 410$ nm and $\varepsilon = 2170$ mol^{-1} dm^3 cm^{-1} in THF.

salts.[14,15] Nucleophiles can substitute directly onto dichromate forming reactive intermediates [eqs (2)–(4)],

$$B + [Cr_2O_7]^{2-} \xrightarrow{\text{slow}, k_B} [BCrO_3] + [CrO_4]^{2-} \quad (2)$$

$$[BCrO_3] + H_2O \xrightarrow{\text{rapid}} [HOCrO_3]^- + BH^+ \quad (3)$$

$$[HOCrO_3]^- + B \xrightarrow{\text{rapid}} [CrO_4]^{2-} + BH^+ \quad (4)$$

whereas acid catalysis most likely results from protonation of the μ-oxo bond of dichromate with subsequent heterolytic fission [eqs. (5)–(7)]:

$$HA + [Cr_2O_7]^{2-} \xrightarrow{\text{slow}, k_A} [HOCrO_3]^- + CrO_3 + A^- \quad (5)$$

$$CrO_3 + H_2O \xrightarrow{\text{rapid}} [HOCrO_3]^- + H^+ \quad (6)$$

$$H^+ + A \xrightarrow{\text{rapid}} HA. \quad (7)$$

The reaction of $[Cr_2O_7]^{2-}$ (*ca* 10^{-4} mol dm^{-3}) with excess thiol results in the formation of H_2O (*ca* 10^{-4} mol dm^{-3}) [eq. (1)]. The HPLC-grade DMF employed in this study contained < 0.03% H_2O (i.e. $< 10^{-2}$ mol dm^{-3} H_2O). Drying the DMF and/or deliberately adding up to 5% H_2O (3.1 mol dm^{-3}) had little effect on the rates or degree of chromium(VI) thioester formation. We measured the effect of both acids and bases on the rate of hydrolysis of dichromate in DMF solution containing 3.1 mol dm^{-3} H_2O ($\approx$ 5% by volume). In the absence of any catalyst the dichromate anion slowly hydrolysed ($t_{1/2} \approx 4$ h at 43°C) with $[HOCrO_3]^-$ being the final product (Fig. 2).

Catalysis by acids and bases

The addition of 3,5-lutidine resulted in an increased rate of hydrolysis which was found to vary linearly with the concentration of 3,5-lutidine (Fig. 3). Surprisingly the final product was still $[HOCrO_3]^-$ indicating that 3,5-lutidine was not a strong enough base to deprotonate this species in DMF solution thus reflecting a significant change in the relative pK_a's of these species from H_2O to DMF (cf. pK_a ($[CrO_4]^{2-}$) = 5.74[16] and pK_a (3,5-lutidine) = 6.15[17] in H_2O at 25°C).

The addition of aqueous NaOH to DMF solutions of dichromate (such that the final water content was 5%) resulted in the rapid hydrolysis to $[CrO_4]^{2-}$ (Fig. 2). The first-order rate constants observed varied linearly with $[OH^-]$ and the calculated second-order rate constant is given in Table 2. Et_3N (0.02 mol dm^{-3}) had no measurable effect on the rate of hydrolysis of dichromate in DMF.

Thus nucleophilic substitution on dichromate anion in DMF appears to be similar, albeit somewhat slower than, such reactions in aqueous solution. The relative abilities of bases to catalyse the hydrolysis of dichromate also appear to be similar (OH^- > 3,5-lutidine > H_2O > Et_3N). The poor catalytic ability of Et_3N is presumably a consequence of steric hindrance.

NH_4^+ effectively catalyses the hydrolysis of dichromate to give $[HOCrO_3]^-$ in DMF at 43°C. The variation in rate of hydrolysis with the concentration of NH_4^+ was not linear (Fig. 3) and is consistent with the catalytic species being NH_3. A half-order dependence of the first-order rate constant, k_{obs}, on the concentration of NH_4^+ is consistent with an initial dissociation into NH_3. The slope of this plot gives $k_B(K_a)^{1/2} = 0.022(2)$ mol$^{-1/2}$ dm$^{3/2}$ s^{-1}. Owing to difficulties in arranging solutions containing known concentrations of H^+ and/or NH_3 without adding competing catalysts, it was not possible to determine separate values of k_B and K_a.

Formic acid also proved to be an effective catalyst for the hydrolysis of dichromate, again resulting in the formation of $[HOCrO_3]^-$. The observed first-order rate constant varied linearly with the concentration of HCOOH over the range studied (2×10^{-4}–10^{-3} mol dm^{-3}). The mode of catalysis may again be via dissociation of the acid to give an active base ($HCOO^-$) but in view of the results, obtained for the effect of acetic acid[12] in aqueous solution, acid catalysis is most likely. HCOOH or H^+ may be the reactive species depending on the degree of dissociation in DMF ($pK_a = 3.75$[17] in H_2O at 20°C but a higher value would be expected in DMF). In Table 2, k_A represents the value obtained on dividing the observed first-order rate constants by the concentration of HCOOH.

Kinetics of chromium(VI) *thioester formation*

The observed visible absorption changes accompanying chromium(VI) thioester formation could be accurately simulated using eqs (8) and (9). For the conditions of a large excess of thiol, the scheme represents coupled pseudo first-order reactions:

$$H_2O + [Cr_2O_7]^{2-} \xrightarrow{k_A, \text{"RSH"}} 2[HOCrO_3]^- \quad (8)$$

$$RSH + [HOCrO_3]^- \xrightarrow{k_4} [RSCrO_3]^- + H_2O \quad (9)$$

* The rate equations derived from eqs (8) and (9) [where eq. (8) represents the thiol-catalysed hydrolysis of $[Cr_2O_7]^{2-}$, i.e. eqs (5)–(7)] were solved numerically by third-order Taylor expansion. Initial estimates of k_A and k_4 were used to generate concentrations of $[Cr_2O_7]^{2-}$, $[HOCrO_3]^-$ and $[RSCrO_3]^-$. Absorbance as a function of time could then be calculated from these concentrations and the known extinction coefficients for the species. The estimates of k_A and k_4 were varied and the calculated absorbance vs time data compared to the experimental data.

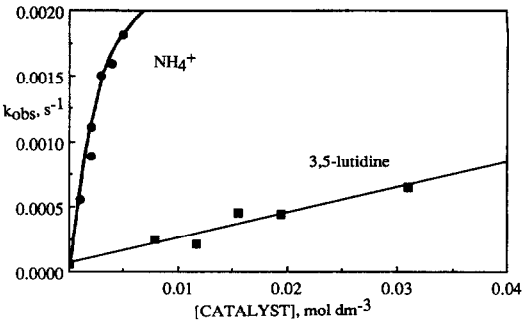

Fig. 3. Variation in first-order rate constants for dichromate hydrolysis in DMF as a function of catalyst concentration (1 mol dm^{-3} $NaNO_3$, 43°C).

$$[RSCrO_3]^- \xrightarrow{\text{"RSH"}} \text{final products.} \quad (10)$$

The calculated* visible spectrum for the intermediate substitution species {$[HOCrO_3]^-$, eq. (8)} is very similar to that of the final product of the hydrolysis of dichromate in DMF, $[HOCrO_3]^-$ (Fig. 2).

The initial step in the biphasic formation of chromium(VI) thioesters in DMF is the thiol-catalysed hydrolysis of dichromate to yield $[HOCrO_3]^-$ and estimates for k_A are given in Table 2. The thiol-catalysed hydrolysis of dichromate presumably does not involve the interaction of the sulphur atom with chromium since this would essentially give us the final product, the chromium(VI) thioester. Acid-catalysed hydrolysis may be a more precise description of this initial step. Neither thiol would be expected to dissociate to a significant amount in DMF at concentrations $> 10^{-3}$ mol dm^{-3} (aque-

Table 2. Second-order rate constants for the catalysed hydrolysis of dichromate

Additive	k_B DMF[a] (mol^{-1} dm^3 s^{-1})	k_B H_2O[b] (mol^{-1} dm^3 s^{-1})
NH_3		1250
OH^-	17(1)	670
3,5-Lutidine	0.019(0.003)	
2,6-Lutidine		0.6
Et_3N	$< 10^{-4}$	
H_2O	$1.6(0.3) \times 10^{-5}$	1.2×10^{-3}
	k_A DMF[a] (mol^{-1} dm^3 s^{-1})	
HCOOH	26(1)	
p-BrPhSH	2.0(0.5)	
n-BuSH	0.16(0.04)	

[a] This work; 1 M $NaNO_3$, 43°C.

[b] 0.1 M KNO_3, values calculated for 43°C from ΔH^*, ΔS^* given in ref. 12.

Errors indicated are estimates of standard deviations.

ous solution; pK_a (n-BuSH) = 10.65,[18] pK_a (*p*-BrPhSH) = 6.02[19]).

The results for the acid-catalysed hydrolysis of dichromate in DMF by the three acids studied (HCOOH, *p*-BrPhSH, n-BuSH) appear consistent with the conclusions drawn for reaction in aqueous solution,[12] i.e. that acid catalysis is general rather than specific with the catalytic constant increasing with increasing acid strength.

Chromium(VI) thioester formation results from thiol substitution onto $[HOCrO_3]^-$ [eq. (4)] and estimates for k_4 place *p*-BrPhSH ($k_4 \approx 4$ mol^{-1} dm^3 s^{-1}) as more reactive than n-BuSH ($k_4 \approx 0.2$ mol^{-1} dm^3 s^{-1}). There was no evidence for the direct attack on $[Cr_2O_7]^{2-}$, hence this process must be much slower than substitution on $[HOCrO_3]^-$.

Catalysis of chromium(VI) *thioester formation*

The addition of HCOOH, a possible contaminant in DMF, catalysed the formation of the thioester. HCOOH catalyses the hydrolysis of dichromate in DMF (*vide infra*). The addition of n-BuSH to solutions of $[HOCrO_3]^-$ generated by HCOOH catalysed hydrolysis of $[Cr_2O_7]^{2-}$ resulted in the rapid formation of the chromium(VI) thioester which increased non-linearly with the concentration of HCOOH and appeared independent of n-BuSH at a given HCOOH concentration.

Ammonium cations were found to catalyse the reaction relative to Na^+. The rate of formation of thioesters in the presence of NH_4^+ depended on how the experiment was performed. The addition of a small aliquot of concentrated n-BuSH solution to a solution of $[NH_4]_2[Cr_2O_7]$ in 1 mol dm^{-3} NH_4NO_3 held at 35°C, resulted in variable rates of reaction, with rates faster for "older" $[Cr_2O_7]^{2-}$/NH_4^+ solutions (Fig. 4). The addition of fresh $[NH_4]_2[Cr_2O_7]$ solution to solutions of n-BuSH/1 mol dm^{-3} NH_4NO_3 (at 35°C), however, resulted in a reproducible formation of thioester at rates independent of the concentration of n-BuSH (Fig. 4). The formation kinetics in both cases appeared first-order with no sign of the intermediate observed for the reaction in the presence of Na^+. The second-order rate constant for the apparent thiol-dependent reaction in the presence of 1 mol dm^{-3} NH_4^+ is approximately 100 times that in the presence of Na^+.

The catalysis of chromium(VI) thioester formation by HCOOH or NH_4^+ appears to result from the formation of $[HOCrO_3]^-$ which is more susceptible to substitution by thiols than $[Cr_2O_7]^{2-}$. The presence of ammine or formate complexes may also provide catalytic pathways to chromium(VI) thioester formation.

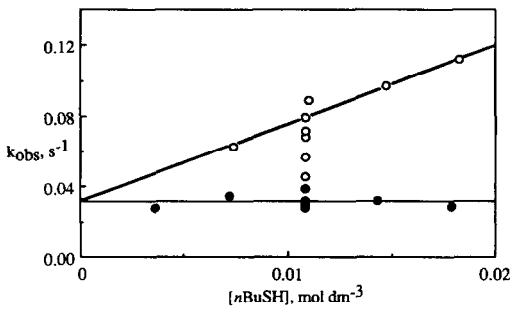

Fig. 4. Change in first-order rate constant, k_{obs}, with concentration of n-BuSH for thioester formation in DMF at 35°C in the presence of 1 mol dm^{-3} NH_4NO_3: ● $[Cr_2O_7]^{2-}$ added to n-BuSH in NH_4NO_3 solution; ○ n-BuSH added to $[Cr_2O_7]^{2-}$ in NH_4NO_3 solution.

Et_3N greatly retards the formation of the chromium(VI) n-BuS-thioester. The addition of *p*-BrPhSH to $Et_3N/[Cr_2O_7]^{2-}$ solutions results in deprotonation of *p*-BrPhSH (as evident from the immediate increase in absorbance around 360 nm) followed by chromium(VI) *p*-BrPhS-thioester formation. The rate of formation is slower than in the absence of Et_3N and does not reach completion before redox processes begin to consume chromium(VI) (as evident from the decrease in absorbance over the range 350–550 nm). The effect of Et_3N could then be explained as due to a reduction in active H^+ in the systems. Et_3N, itself, is a poor catalyst for dichromate hydrolysis.

Characterization of chromium(VI) *thioester salts*

Bis(triphenylphosphine)iminium and tetraphenylphosphonium salts of chromium(VI) thioesters can be isolated from DMF/ether solutions and Table 3 lists microanalytical data obtained for a range of such salts. The substituted thiophenol derivatives were prepared at 0°C so as to limit contamination of the products by paramagnetic material generated by redox decomposition of the chromium(VI) thioesters. The butylthiol derivatives were prepared at room temperature with much longer reaction times owing to the slow substitution onto chromium(VI). Redox reactions involving the butylthiol derivatives are also much slower than for the arylthiol species. The tetraphenylarsonium salt of the chromium(VI) *p*-bromophenylthioester, $[Ph_4As][p\text{-}BrPhSCrO_3]$, has been the subject of an X-ray structural study.[6]

The chromium thioester salts dissolve readily in most polar organic solvents. Visible absorption spectra were similar for DMF, THF and $CHCl_3$ solutions. The thioesters were sensitive to acid impurities in $CHCl_3$ but otherwise showed similar stabilities in the three solvents, slowly undergoing

Table 3. Microanalytical and IR data for chromium(VI) thioester salts

Thioester salts	Analysis [Found % (Calc. %)] C	H	N	S	P	Br	ν(Cr—O)[a] (cm^{-1}) asym.	sym.
$[Ph_4As][p\text{-}BrPhSCrO_3]$	53.6(53.7)	3.5(3.6)		4.6(4.8)		12.0(11.9)	946	891
$[Ph_4P][p\text{-}BrPhSCrO_3]$	57.3(57.4)	4.2(3.9)		5.4(5.1)	5.2(4.9)	12.8(12.7)	946	889
$[PPN][p\text{-}BrPhSCrO_3]$	61.0(61.0)	4.1(4.2)	1.8(1.7)	3.7(3.9)	7.9(7.5)	9.5(9.7)	945	890
$[PPN][PhSCrO_3]$	67.1(67.5)	5.0(4.7)	2.2(1.9)	4.2(4.3)	8.1(8.3)		946	891
$[PPN][p\text{-}NO_2PhSCrO_3]$	63.9(63.6)	4.5(4.3)	3.7(3.5)	3.8(4.0)	7.8(7.8)		947	893
[PPN][n-BuSCrO$_3$]	66.3(66.0)	5.8(5.4)	2.1(1.9)	4.2(4.4)	8.8(8.5)		940	888
[PPN][t-BuSCrO$_3$]	66.2(66.0)	5.2(5.4)	2.2(1.9)	4.2(4.4)	8.2(8.5)		942	888

[a] Samples prepared as Nujol mulls.

hydrolysis and/or redox decomposition over the course of many hours at room temperature.

^1H and ^{13}C NMR spectra were recorded for [PPN][n-BuSCrO$_3$] in $CDCl_3$ (atom positions as in $^{\delta}CH_3{}^{\gamma}CH_2{}^{\beta}CH_2{}^{\alpha}CH_2S$). The ^1H NMR spectrum consisted of a multiplet at 7.500 ppm, relative to internal TMS, due to the aromatic protons of the PPN^+ cation and multiplets at; 0.823 ppm ($^{\delta}H$), 1.354 ppm ($^{\gamma}H$), 1.653 ppm ($^{\beta}H$) and 3.006 ppm ($^{\alpha}H$). Integration of the peaks supported the assignments. Some broadening of the resonances due to paramagnetic decomposition products prevented complete resolution of the multiplets. Reported[20] values for n-BuSH in $CDCl_3$ are 0.92 ppm ($^{\delta}H$), 1.53 ppm ($^{\gamma}H$ and $^{\beta}H$), and 2.52 ppm ($^{\alpha}H$).

Similarly, the broad band decoupled ^{13}C NMR spectrum consisted of peaks due to the aromatic carbons of PPN^+ (nine peaks, includes ^{31}P coupling, *ca* 130 ppm relative to internal TMS) and the n-butylthio group: 13.831 ppm ($^{\delta}C$), 22.201 ppm ($^{\gamma}C$), 35.149 ppm ($^{\alpha}C$) and 35.983 ppm ($^{\beta}C$). Assignment was based on the reported[21] values for ^{13}C NMR spectra ($CDCl_3$, TMS internal standard) for n-BuSH ($^{\delta}C$, 13.5; $^{\gamma}C$, 21.5; $^{\alpha}C$, 24.3; $^{\beta}C$, 36.2) and the thioester, n-BuS-C(O)CH_3 ($^{\delta}C$, 13.6; $^{\gamma}C$, 22.1; $^{\alpha}C$, 28.9; $^{\beta}C$, 31.8).

IR spectral absorptions arising from the cations (PPN^+ bands at *ca* 695, 725, 745 and 998 cm^{-1}) and thiols (*p*-BrPhS bands at *ca* 815 and 1008 cm^{-1}; *p*-NO_2PhS bands at *ca* 845 and 852 cm^{-1}) can be identified. The chromium(VI) thioesters are characterized by two strong bands at *ca* 945 and 890 cm^{-1}, with the band at 945 cm^{-1} often having added structure (Table 3). $[ClCrO_3]^-$ also gives rise to similar bands at 954 and 907 cm^{-1} which have been assigned to $\nu(Cr—O)_{asym}$ and $\nu(Cr—O)_{sym}$ stretches, respectively.[22] A notable difference from the IR spectra of dichromates is the loss of a band at *ca* 780 cm^{-1} which has been assigned to asymmetric vibrations of the Cr—O—Cr feature.[23]

The IR spectra of DMF solutions of $Na_2[Cr_2O_7]$ with and without added *p*-BrPhSH clearly demonstrates the loss of the μ-oxo bond on thioester formation (Fig. 5). The Cr—O bands of the chromium(VI) thioester anion generated by mixing $Na_2[Cr_2O_7]$ and *p*-BrPhSH in DMF are in the same position as those observed in the IR spectrum of DMF solutions of the isolated salts, viz. 949 and 892 cm^{-1}. Nujol mulls of the solids show slight shifts in the positions of these bands (Table 3). Coupled with a similar coincidence of the visible spectra of chromium(VI) thioester anions prepared *in situ* by reaction of dichromate and thiol and on dissolution of the isolated salts (Table 1), the data strongly suggests the same structure exists in solution as in the solid state.

Thermodynamics of chromium(VI) *thioester formation*

The addition of H_2O (up to 3.1 mol dm^{-3}; $\approx$5.5% v/v) had no apparent effect on chromium(VI) thioester formation. There was no evidence for dissociation of the chromium(VI) thioester in the presence of excess thiol ($> 5\times10^{-4}$ mol dm^{-3}) even under the conditions where 3.1 mol dm^{-3} H_2O was present. $[Ph_4As][p\text{-}BrPhSCrO_3]$ (10^{-4} mol dm^{-3}) dissolved in DMF at 43°C in the presence of 3.1 mol dm^{-3} H_2O and 1 mol dm^{-3} $NaNO_3$ slowly hydrolysed into $[HOCrO_3]^-$. The process followed first-order kinetics with a half-life of 3.6 h.

The reaction corresponds to the reverse step of eq. (9), and assuming overall second-order kinetics, the implied chromium(VI) thioester hydrolysis rate constant is $k_{-4} \approx 2\times10^{-5}$ mol^{-1} dm^3 s^{-1}. The equilibrium constant for chromium(VI) thioester formation in DMF (43°C, 1 mol dm^{-3} $NaNO_3$) can then be calculated from the estimated formation and hydrolysis rate constants as $K = k_4/k_{-4} = 2\times10^4$. This value is consistent with the observa-

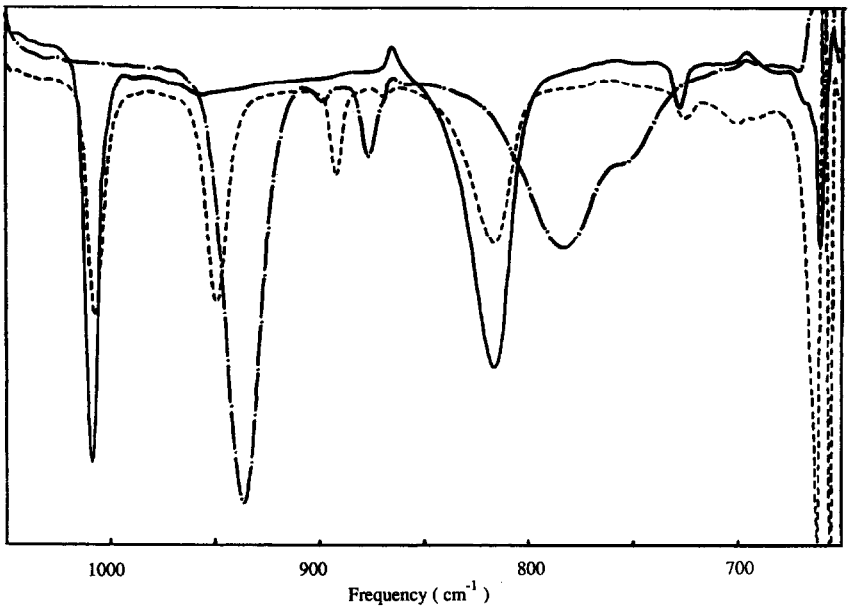

Fig. 5. IR spectra of 10^{-2} mol dm^{-3} $Na_2[Cr_2O_7]$ (– · – –), 0.25 mol dm^{-3} *p*-BrPhSH (——) in DMF and a 15 min old 50 : 50 mixture of the two solutions (– – – –).

tions of essentially complete formation of the chromium(VI) thioester in the presence of excess *p*-BrPhSH and the substantial hydrolysis in the absence of any added *p*-BrPhSH.

[PPN][n-BuSCrO$_3$] (10^{-4} mol dm^{-3}) hydrolysed in DMF in the presence of 3.1 mol dm^{-3} H_2O (43°C, 1 mol dm^{-3} $NaNO_3$) at a much slower rate ($t_{1/2} \approx 40$ h, $k_{-4} \approx 2 \times 10^{-6}$ mol^{-1} dm^3 s^{-1}). The chromium(VI) n-BuS-thioester formation equilibrium constant, $K = k_4/k_{-4} \approx 10^5$, is similar to that calculated for the *p*-BrPhSH derivative.

In aqueous solution,[1,2] chromium(VI) thioester formation constants have been found to be of the order of 1000 mol^{-1} dm^3. Inclusion of the water concentration term to establish the same constants described above, results in $K \approx 5 \times 10^4$.

Decomposition of chromium(VI) *thioesters*

Hydrolysis of the chromium(VI) thioesters has been discussed above. The chromium(VI) thioesters were also found to react with excess thiol resulting in the eventual formation of chromium(III) and disulphide. EPR spectroscopic studies have indicated the presence of chromium(V) intermediate species.[3,24–27] Thiophenol added to $K_2[Cr_2O_7]$ in DMF is reported to result in the appearance of two signals with g values at 1.996 and 1.982.[24] Likewise the reaction of chromates with glutathione in aqueous solution generates chromium(V) complexes characterized by EPR signals at $g = 1.996$ and $g = 1.985$,[3,25–27] with the $g = 1.996$ peak dominating at high concentrations of glutathione. The species with $g = 1.996$ has been isolated although not structurally characterized as yet.[26] The generation of glutathione radicals has also been indicated from EPR experiments.[27] Thus the decomposition of [*p*-BrPhSCrO$_3$]$^-$ in the presence of excess *p*-BrPhSH showed evidence for such an intermediate step.

In the presence of larger excesses of *p*-BrPhSH, $Na_2[Cr_2O_7]$ reacts to form unstable solutions of the chromium(VI) thioester anion. A general increase in absorbance over the range 550–350 nm and the development of a new band at 750 nm, was observed for several minutes after mixing the reagents, followed by a general decrease in absorption over the entire spectral range. This was consistent with conversion to chromium(III) species. The latter process followed first-order kinetics ($t_{1/2} \approx 1$ h; 0.016 mol dm^{-3} *p*-BrPhSH, 10^{-4} mol dm^{-3} $Na_2[Cr_2O_7]$, DMF, 43°C, 1 mol dm^{-3} $NaNO_3$).

EPR experiments indicated that on mixing [Ph_4As][*p*-BrPhSCrO$_3$] (10^{-3} mol dm^{-3}) in DMF with a five-fold excess of *p*-BrPhSH at room temperature, two signals ($g = 1.997$ and $g = 1.983$) appeared and increased in intensity over $\approx 1/2$ h. The relative proportion of the two species changed with time with the $g = 1.983$ peak dominating as time progressed.

Solution IR studies showed little change in the position of the Cr—O bands on reaction of [Ph_4As][*p*-BrPhSCrO$_3$] in the presence of excess *p*-BrPhSH, possibly indicating that the intermediate

species evident from the UV–vis and EPR spectral changes represent a small percentage of the total chromium.

During attempts to isolate the chromium(VI) thioesters, longer reaction times led to the formation of paramagnetic materials. The products ranged from apparently polymeric chromium(III) species (as judged by their low solubility, magnetic moments and visible absorption spectra) of uncertain constitution to a paramagnetic black solid which analysed as the chromium(V) salt, $[Ph_4As][p\text{-}BrPhSCr(O)_2(OH)]$.

The magnetic moment for this latter sample was found to be $\mu_{eff} = 1.78$ BM, consistent with the chromium(V) assignment. The product dissolved in DMF to give a UV–vis spectrum similar to that of the chromium(VI) thioester but was quite unstable, decomposing back to a mixture of $[(HO)CrO_3]^-$ and $[p\text{-}BrPhSCrO_3]^-$. The IR spectrum of a Nujol mull of the product was very similar to that of the chromium(VI) thioester, $[Ph_4As][p\text{-}BrPhSCrO_3]$, with absorptions corresponding to the cation and p-$BrPhS^-$ anion. Absorptions due to Cr—O bonds were present at 948 and 891 cm^{-1}, as well as a new absorption band at 985 cm^{-1}. A band at 3300 cm^{-1} indicated the presence of an OH group. The solid decomposed with time as evident by its change in solubility, eventually becoming insoluble in all common solvents.

Further attempts at improving the preparation of the compound have proven unsuccessful. Dark olive-green plates have been collected in samples containing chromium(VI) thioester and precipitated salts, but it has not proved possible to collect pure samples of the material.

The half-life for the disappearance of the chromium(VI) thioester generated from the reaction between n-BuSH (0.018 mol dm^{-3}) and $[Cr_2O_7]^{2-}$ (2×10^{-4} mol dm^{-3}), in DMF at 43°C in the presence of $NaNO_3$ (1 mol dm^{-3}), is approximately 2 days (cf. $t_{1/2}$ for substitution of *ca* 15 min). The spectrum of the final product is typical of an octahedral chromium(III) species (Fig. 2). Di-n-butyldisulphide could be extracted from the final solution. No intermediate chromium(V) species were apparent in the decomposition process. Much lower concentrations of chromium(V) species may result from a less favourable one-electron oxidation of the alkylthiol by chromium(VI) [eq. (10)]

$$[RSCrO_3]^- + RSH \rightleftharpoons [RSCr(O)_2(OH)]^- + RS^{\bullet} \quad (10)$$

as a result of the higher redox potential for the alkylthiol/alkylthio radical couple relative to that of the arylthiol.[28] This is the same step as proposed for the generation of the chromium(V) glutathione complex.[27]

EXPERIMENTAL

Visible spectra were recorded on a Varian Super Scan 3 spectrophotometer fitted with cell holders connected to a constant temperature bath (Haake D8 immersion circulator and Haake EK12 immersion cooler). IR spectra were recorded on a Perkin–Elmer Model 1600 FT-IR spectrophotometer. ^1H and ^{13}C NMR spectra were recorded on a Bruker AC-200 spectrometer with alkali-washed $CDCl_3$ as solvent and TMS as an internal reference. EPR spectra were recorded on a Varian E-line EPR spectrometer (X-band) using a flat solution cell. Magnetic moments were determined by the Faraday technique. Microanalyses were carried out by the Australian Microanalytical Service.

HPLC grade DMF (Aldrich) and AR grade anhydrous diethyl ether (Univar) were used as received. Thiophenol (PhSH; Aldrich), n-butylthiol (n-BuSH; Koch-Light Lab.) and t-butylthiol (t-BuSH; Aldrich) were dried over molecular sieves (4A; BDH) and then distilled under reduced pressure and stored under nitrogen. [PPN]Cl (PPN^+ = bis[triphenylphosphine]iminium cation; Aldrich), p-bromothiophenol (p-BrPhSH; Aldrich) and p-nitrothiophenol (p-NO_2PhSH; Aldrich) were used as received. Sodium dichromate dihydrate (May & Baker Pty. Ltd.) was dehydrated by heating at 110°C for 48 h and was stored in a desiccator. Other high purity reagents were used as received.

Solutions were freshly prepared by standard volumetric techniques. Solutions of dichromate in DMF deteriorate rapidly (noticeable colour change within hours, orange–brown powder deposited over several days) if exposed to the light, but are much more stable if kept in the dark. Reactions were generally initiated by adding small aliquots of one reagent via microlitre syringe (SGE) to much larger volumes of solutions of the second reagent in the spectrophotometric cells fitted with *Suba seal* septa and held at constant temperature in the compartment of the spectrophotometer which automatically recorded spectra at set time intervals. Much slower reactions were followed by sampling techniques whereby the reaction solutions were kept at the desired temperature in the water bath with aliquots being systematically removed for spectrophotometric examination.

Preparation of chromium(VI) *thioester salts*

Bis(triphenylphosphine)iminium thiophenolatochromate(VI), [PPN][$PhSCrO_3$]. $Na_2[Cr_2O_7]$ (0.2 g,

0.8 mmol) was stirred with thiophenol (0.34 g, 3.2 mmol) in DMF (20 cm^3) at 0°C for 15 min. Bis [triphenylphosphine]iminium chloride ([PPN]Cl, 0.9 g, 1.6 mmol) in DMF (10 cm^3) was added and the solution stirred at 0°C for a further 2 h. The addition of ether (150 cm^3) precipitated an orange powder (0.6 g). The product was dissolved in cold DMF (15 cm^3), ether (20 cm^3) added and the solution filtered. Further ether (150 cm^3) was layered onto the filtrate and after standing overnight at −5°C, orange needles (*ca* 0.4 g) of [PPN][$PhSCrO_3$] were collected and washed with ether.

Similar methods of preparation were used to obtain the PPN^+ salts of the *p*-bromothiophenol, *p*-nitrothiophenol t-butylthiol and n-butylthiol derivatives. For the butylthiol derivatives the reactions were carried out at room temperature and generally left overnight. The products were more soluble and could be separated from unreacted chromates by recrystallization as described above.

Tetraphenylarsonium and tetraphenylphosphonium salts could also be obtained (microanalytical data are given in Table 3), whereas Na^+, NH_4^+, $[n\text{-}Bu_4N]^+$ and $[MePh_3P]^+$ salts could not be isolated from DMF/ether solutions.

Isolation of a chromium(V) *thioester salt*

Tetraphenylarsonium(p - *bromothiophenolato)hydrogenchromate*(V), [Ph_4As][*p*-$BrPhSCr(O)_2(OH)$]. Although the method of preparation was essentially the same in each attempt at isolation, the composition of the products obtained was variable from one experiment to another. The reasons for this irreproducibility are not clear. A typical experimental procedure was as follows:

$Na_2[Cr_2O_7]$ (0.4 g, 1.6 mmol) in DMF (5 cm^3) was added to *p*-bromothiophenol (1.2 g, 6.4 mmol) in DMF (5 cm^3) at room temperature and the resulting dark solution was stirred for 15 min. The solution was cooled to 0°C and [Ph_4As]Br (0.75 g, 1.6 mmol) in DMF (5 cm^3) was added. After 2 h at 0°C, ether (200 cm^3) was added and an oil separated. The bulk of the solution was separated from the oil and left to stand overnight at 0°C, after which time a dark solid precipitated (yield ≈ 0.1 g).

Microprobe analysis was consistent with the sample being a homogeneous product containing equimolar amounts of As, Br, Cr and S. Microanalysis was consistent with the formulation [Ph_4As][*p*-$BrPhSCr(O)_2(OH)$]. Found: C, 53.8; H, 3.9; Br, 12.1; S, 5.2; Cr, 8.1. $C_{30}H_{25}AsBrCrO_3S$ requires: C, 53.6; H, 3.7; Br, 11.9; S, 4.8; Cr, 7.7%.

The chromium content was determined spectrophotometrically after dissolution of the complex in HCl and conversion of any chromium to $[CrO_4]^{2-}$ by H_2O_2/NaOH treatment. It was noted that di(*p*-bromophenyl)disulphide was precipitated in the acid dissolution step.

Other attempts at synthesizing the complex tended to produce small amounts contaminated with chromium(VI) thioester or other $[Ph_4As]^+$ salts. Varying the ratios of precipitating cation to chromate, the ratios of thiol to chromate, the thiol, temperature control and solvent composition did not establish reproducible conditions for obtaining pure samples of the chromium(V) species.

Acknowledgements—This work was supported by contract number CDS 12/87 with the Materials Research Laboratory, Australian Defence Science and Technology Organization (B.O.W., P.J.N.) and by an Australian Research Committee Grant (B.O.W.).

REFERENCES

1. P. H. Connett and K. E. Wetterhahn, *Struct. Bond.* 1983, **54**, 93.
2. P. H. Connett and K. E. Wetterhahn, *J. Am. Chem. Soc.* 1986, **108**, 1842.
3. P. O'Brien and Z. Ozolins, *Inorg. Chim. Acta* 1989, **161**, 261.
4. N. D. Ghatge, S. O. Vernekar and S. V. Lonikar, *Rubber Chem. Tech.* 1981, **54**, 198.
5. L. A. Averko-Antonovich, V. Y. Rubanov and L. I. Klimova, *Polymer Sci. USSR* 1977, **19**, 1826.
6. W. Mazurek, G. D. Fallon, P. J. Nichols and B. O. West, *Polyhedron* 1990, **9**, 777.
7. W. G. Davies and J. F. Prue, *Trans. Faraday Soc.* 1955, **51**, 1045.
8. A. Bartecki, L. Liberacka and M. Cieslak-Golonka, *Polish J. Chem.* 1978, **52**, 247.
9. K. A. Muirhead and G. P. Haight Jr, *Inorg. Chem.* 1973, **12**, 1116.
10. K. A. Muirhead, G. P. Haight Jr and J. K. Beattie, *J. Am. Chem. Soc.* 1972, **94**, 3006.
11. P. Moore, Y. Ducommun, P. J. Nichols and A. E. Merbach, *Helv. Chim. Acta* 1983, **66**, 2445.
12. R. Baharad, B. Perlmutter-Hayman and M. A. Wolff, *J. Phys. Chem.* 1969, **73**, 4391.
13. B. Perlmutter-Hayman and M. A. Wolff, *J. Phys. Chem.* 1967, **71**, 1416.
14. B. Perlmutter-Hayman and Y. Weissmanni, *J. Phys. Chem.* 1967, **71**, 1409.
15. B. W. Clare, D. M. Druskovich, D. L. Kepert and J. H. Kyle, *Aust. J. Chem.* 1977, **30**, 2116.
16. T. Shen-yang and L. Ke-an, *Talanta* 1986, **33**, 775.
17. R. C. Weast (Ed.), *C.R.C. Handbook of Chemistry and Physics*, pp. D-165, D-167. CRC Press, Cleveland (1983).
18. D. L. Yabroff, *Ind. Engng Chem.* 1940, **32**, 257.
19. P. DeMaria, A. Fini and F. M. Hall, *J. Chem. Soc., Perkin Trans. II* 1973, 1969.

20. H. A. Szymanski and R. E. Yelin, *NMR Band Handbook*, p. 141. IFI/Plenum, New York (1968).
21. C. M. Hall and J. Wemple, *J. Org. Chem.* 1977, **42**, 2118.
22. H. Stammreich, O. Sala and K. Kawai, *Spectrochim. Acta* 1961, **17**, 226.
23. H. Stammreich, D. Bassi, O. Sala and H. Siebert, *Spectrochim. Acta* 1958, **13**, 192.
24. A. M. Galeev and G. A. Chmutova, *Izv. Akad. Nauk SSSR, Ser. Khim.* 1974, 715.
25. S. Kitagawa, H. Seki, F. Kametani and H. Sakurai, *Inorg. Chim. Acta* 1988, **152**, 251.
26. P. O'Brien and Z. Ozolins, *Recl. Trav. Chem. Pays-Bas* 1987, **106**, 423; P. O'Brien, J. Pratt, F. J. Swanson, P. Thornton and G. Wang, *Inorg. Chim. Acta* 1990, **169**, 265.
27. X. Shi and N. S. Dalal, *Biochem. Biophys. Res. Commun.* 1988, **156**, 137.
28. P. J. Nichols and M. W. Grant, *Aust. J. Chem.* 1989, **42**, 1085.

Polyhedron Vol. 10, No. 7, pp. 763–767, 1991
Printed in Great Britain

0277–5387/91 $3.00+.00
© 1991 Pergamon Press plc

A NEW IRON(II) COMPLEX WITH THE N_6-MACROCYCLIC LIGAND HEXACYCLEN WITH A THERMALLY DEPENDENT STRUCTURE

M. MITEWA and P. R. BONTCHEV*

Department of Chemistry, University of Sofia, 1126 Sofia, Bulgaria

and

V. RUSSANOV

Department of Physics, University of Sofia, 1126 Sofia, Bulgaria

and

E. ZHECHEVA and D. MECHANDJIEV

Institute of General and Inorganic Chemistry, Bulgarian, Academy of Sciences, 1040 Sofia, Bulgaria

and

K. KABASSANOV

Institute of Solid State Physics, Bulgarian Academy of Sciences, 1113 Sofia, Bulgaria

(*Received* 23 *August* 1989; *accepted* 13 *December* 1990)

Abstract—A new complex of iron(II) with the N_6-macrocyclic ligand hexacyclen (N-analogue of 18-Crown-6) has been synthesized. Using Mössbauer, EPR and magnetochemical measurements, a thermally controlled intramolecular reverse electron transfer was proved for the complex

Intermediate-spin iron(II) (IS) ($S = 1$) $\rightleftharpoons$ High-spin iron(III) (HS) ($S = 5/2$).

Recently we have studied the coordination and extraction ability of the N_6-macrocyclic ligand hexacyclen (Hex) (N-analogue of 18-Crown-6)[1,2] and the structure of its complexes with cobalt(II), nickel(II) and copper(II).[3–5] It was found that complexes with different structures are formed: the structure of Co(Hex)·2TPB is of the "phthalocyanine" type, e.g. planar,[3] while for Cu(Hex)·2TPB and Ni(Hex)·2TPB temperature-dependent structures were proved,[4,5] due most probably to the flexibility of the hexacyclen molecule (TBP = tetraphenylborate).

Taking into account the ability of polydentate N-containing ligands to stabilize iron(II) and, on the other hand, the ability of hexacyclen to form complexes with different structures, we have studied the magnetic properties of the iron(II) hexacyclen complex using magnetochemical, ^{57}Fe Mössbauer, EPR and IR spectroscopic methods in the temperature range 70–300 K.

EXPERIMENTAL

Apparatus

The electronic and IR spectra (KBr discs) were obtained on Specord UV–vis and Perkin-Elmer 580 spectrometers, respectively.

* Author to whom correspondence should be addressed.

The ^{57}Fe Mössbauer spectra were recorded in transmission geometry using a ^{57}Co[Pd] source (activity ~40 mC; kept at room temperature) on a Hungarian conventional spectrometer operating in the constant-acceleration mode. All isomer shifts are referred to the ^{57}Co[Pd] source as zero shift. The samples were pressed with polyvinyl alcohol (PVA) (the iron surface density being 5 mg cm^{-2}) and mounted in a nitrogen bath cryostat equipped with a calibration thermodiode and temperature controller (±0.5 K). The temperature changes were performed with a velocity of 3 K min^{-1}. The spectra were recorded in the range 77–298 K and fitted to Lorentzian lines by means of a least-squares fitting program.

Magnetic susceptibility measurements were performed over the temperature range 130–300 K in argon atmosphere according to the Faraday method and the EPR spectra were obtained on an *X*-band EPR spectrometer ERS-220 (F.R.G.) in the range 90–420 K as already described.[3,4] The *g*-values were determined according to the relation $g_1 = g_2(H_2/H_1)$, DPPH being used as the *g*-marker.

Procedures and materials

Fe(Hex)·2TPB was obtained as described elsewhere,[1] using Hex·3H_2SO_4 (Aldrich) as starting material. All other reagents used were of AR grade.

RESULTS AND DISCUSSION

The iron(II)–hexacyclen complexation is associated with an intense red coloration of the solution (λ_{max} ~ 500 nm) most probably due to a charge-transfer band. In the IR spectrum of Fe(Hex)·2TPB two ν(NH) bands are observed (3210 and 3270 cm^{-1}) similar to the Cu(Hex)·2TPB spectrum.[4]

The magnetochemical data obtained for Fe(Hex)·2TPB in the range 130–300 K (Fig. 1) show that on the μ_{eff}/T curve a knee is observed as in the corresponding Cu(Hex)·2TPB dependence.[4] These data indicate the presence of different structures at different temperatures.

The value of μ_{eff} (~5 BM) observed at ambient temperature may be ascribed either to d^6 high-spin ($S = 2$) or to d^5 high-spin ($S = 5/2$) octahedral structures.[6] On the other hand, the magnetic moment was found to be temperature dependent (Fig. 1), while the μ_{eff} values for high-spin iron(II) and iron(III) octahedral complexes should be temperature independent.[6] Hence, the data obtained indicate that at low temperatures (below 200 K) a further paramagnetic structure exists, thus ruling out the possibility of realizing a low-spin ($S = 0$) iron(II) species.

In order to obtain additional information concerning the complex, Mössbauer and EPR investigations were performed.

The ^{57}Fe Mössbauer spectra of Fe(Hex)·2TPB were recorded in the range 77–298 K. The data obtained showed that all the observed spectra are superpositions of two quadrupole doublets. The Mössbauer spectra at 77 and 298 K are represented in Fig. 2.

It is evident that in the temperature range studied two iron complexes with different spin-states are present simultaneously. One of them ($\delta = 0.18 \pm 0.03$ mm s^{-1}; $\Delta = 0.75 \pm 0.03$ mm s^{-1}

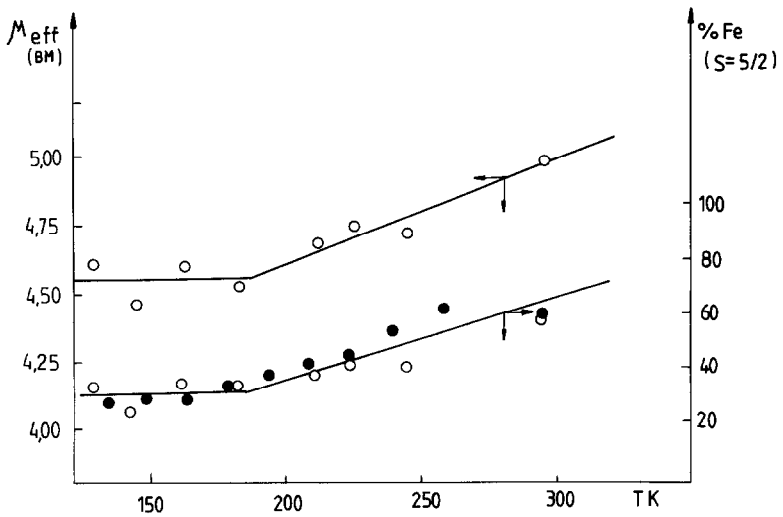

Fig. 1. Temperature dependence of μ_{eff} of Fe(Hex)·2TPB and of the molar fraction of HS ($S = 5/2$) species; ● molar fractions obtained from Mössbauer spectra and ○ molar fractions obtained from magnetochemical data.

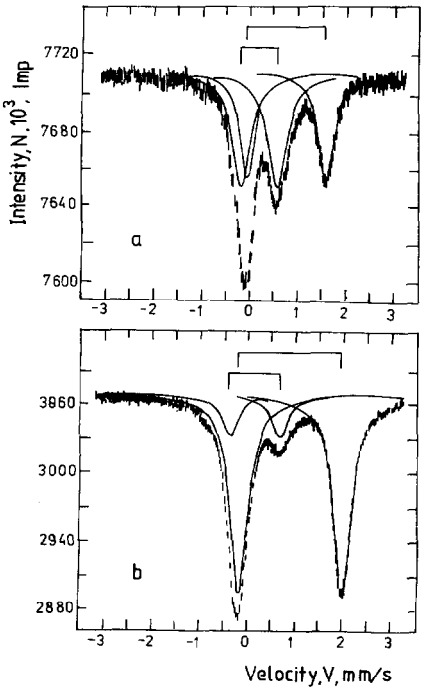

Fig. 2. Mössbauer spectra of Fe(Hex)·2TPB at different temperatures: (a) 298 K and (b) 77 K.

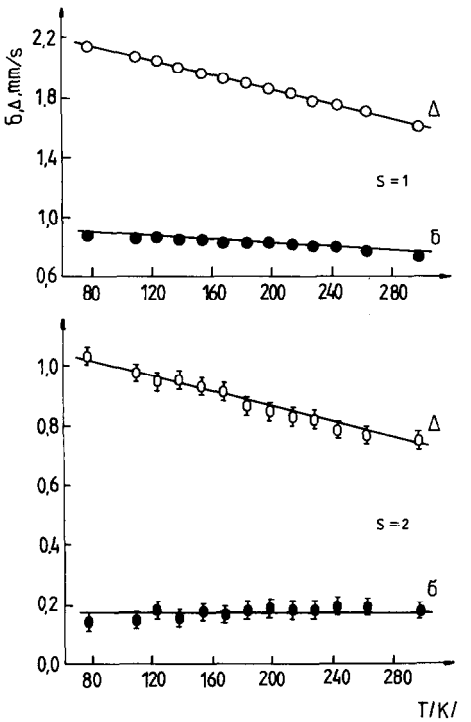

Fig. 3. Temperature dependence of isomer shifts (δ) and quadrupole splittings (Δ) of both Mössbauer doublets.

at 298 K) might be ascribed to a high-spin (HS) ($S = 5/2$) iron(III) species.[7-9] The other species ($\delta = 0.74 \pm 0.01$ mm s^{-1}; $\Delta = 1.61 \pm 0.01$ mm s^{-1} at 298 K) is likely to be due to the intermediate (IS) ($S = 1$) spin-state, typical for four-coordinated iron(II) porphyrins.[10,11]

The temperature dependence of Mössbauer parameters of both species are shown in Fig. 3. It should be noted that the Δ values of both spin-states are strongly temperature dependent and no hysteresis effects are observed in the course of Mössbauer and magnetochemical studies.

Table 1. Molar fractions (± 0.04) of IS and HS Fe(Hex)·2TPB at different temperatures

Temperature (K)	IS ($S = 1$)	HS ($S = 5/2$)
77	0.85	0.15
108	0.77	0.23
122	0.72	0.28
138	0.72	0.28
154	0.72	0.28
168	0.72	0.28
184	0.64	0.35
198	0.62	0.37
212	0.58	0.42
228	0.54	0.46
242	0.45	0.54
262	0.37	0.63
298	0.40	0.58

The molar fractions of IS iron(II) and HS iron(III) at different temperatures were calculated and the data obtained are represented in Table 1.

The Mössbauer data thus obtained are in agreement with the magnetochemical measurements. Taking into account that for the iron(II) phthalocyanine complex ($S = 1$) the μ_{eff} value was found to be 3.96 BM at 293 K,[6] it might be assumed that the IS Fe(Hex)·2TPB exhibits a similar effective magnetic moment (3.9 BM). According to the literature, μ_{eff} values for the HS iron(III) complexes in the range 5.2–5.9 BM would be expected[6] thus allowing an approximation to 5.5 BM. On the basis of these suppositions, the increase in the HS molar fraction with temperature explains the increase in the magnetic moment of the system above 200 K, while in the range 130–200 K the magnetic moment is constant as the molar fractions of both spin-states also remain constant (Fig. 1 and Table 1).

Therefore, a reversible intramolecular electron transfer with temperature might be assumed to take place in Fe(Hex)·2TPB. The latter should be connected with a free radical formation:

$$\underset{\text{IS}\ (S=1)}{[\text{Fe}^{\text{II}}\text{—L}]} \rightleftharpoons \underset{\text{HS}\ (S=5/2),}{[\text{Fe}^{\text{III}}\text{—L}^{\cdot}]}$$

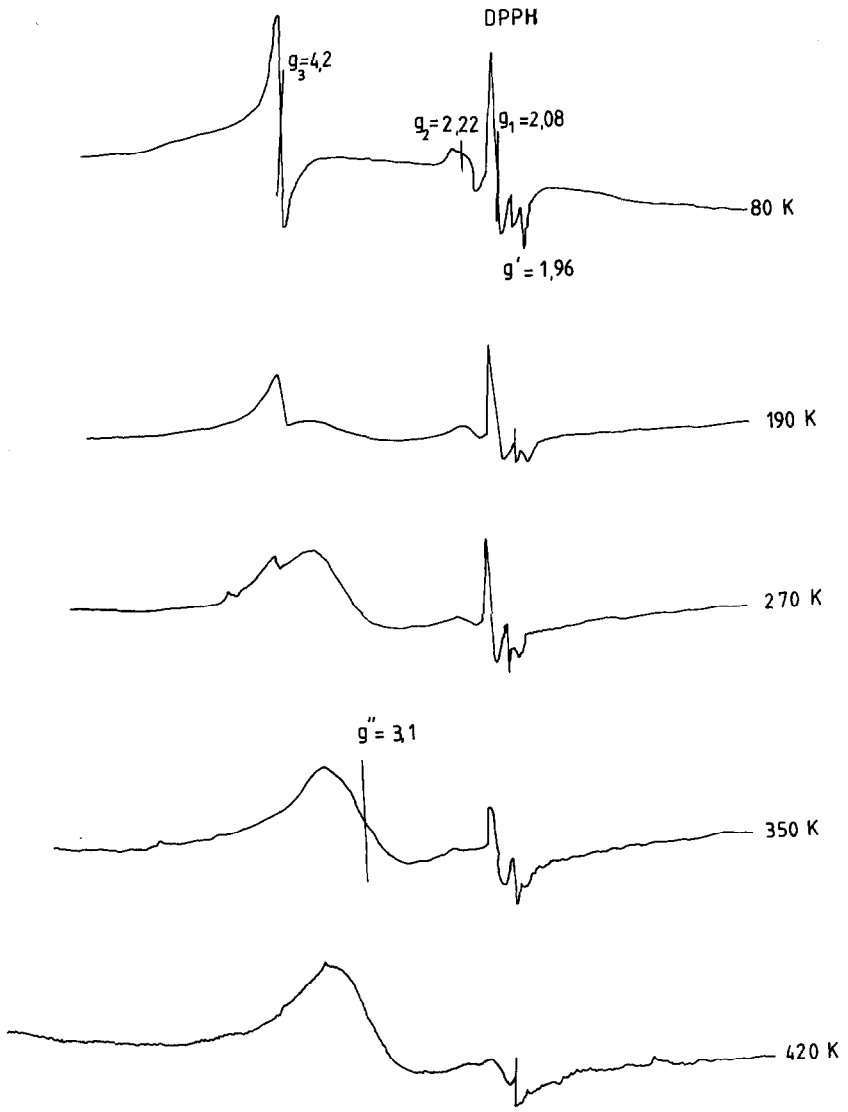

Fig. 4. EPR spectra of Fe(Hex)·2TPB at different temperatures.

where L = hexacyclen and L˙ = the free radical obtained from it. It should be noted that a reversible electron transfer with temperature was observed for Ni(Hex)·2TPB also.[5]

Using the above mentioned μ_{eff} values for both spin-states the percentage of HS iron(III) species was calculated and was found to be in a good agreement with the Mössbauer data (Fig. 1).

The existence of two different iron complex species is supported also by the presence of two bands assigned to ν(NH) in the IR spectrum of Fe(Hex)·2TPB.

Additional information was obtained by studying their EPR spectra at different temperatures; the data obtained are represented in Fig. 4. At low temperatures four different EPR signals are observed (80–200 K); a doublet with $g' \sim 2.00$ and three other EPR signals with $g_1 = 2.08$, $g_2 = 2.22$ and $g_3 = 4.2$. The intensities of g_1, g_2 and g_3 decrease with increasing temperature and therefore they might be ascribed to IS iron(II) species. The presence of more than one signal in the g-range 2.0–2.2 might be explained by dimer formation, and it seems likely that the signal with $g_3 = 4.2$ is due to the $M = 2$ dimer absorption.[12]

It might be expected that the existence of iron(II) dimers at low temperature would lead with a temperature increase to the formation of iron(III) couples also. For the latter, symmetrical Mössbauer doublets are typical and in our case also a symmetrical doublet was observed (Fig. 2). The antiferromagnetic coupling, however, evidently is not

strong, so that the resulting effective magnetic moment of the system is increasing with the temperature.

On the other hand, with increasing temperature, in addition to g', a further EPR signal with $g'' \sim 3.1$ appears with increasing intensity, and at high temperature (above 350 K) only g_1 of low intensity and g' and g'' are observed. The latter may be ascribed to the HS [Fe^{III}—L] species.

By taking into account all the available experimental data it may be assumed that iron(II) hexacyclen complex formation is accompanied by thermally controlled intramolecular electron transfer.

Acknowledgements—This study was carried out as a part of Contract 138/1988–89 sponsored by the Bulgarian Committee of Science. The authors are grateful to the referee for some helpful discussions.

REFERENCES

1. M. Mitewa, P. R. Bontchev, E. Zhecheva, D. Mechandjiev, K. Kabassanov and D. Vassileva, *Proc. 11th Conf. Coord. Chem.*, p. 235. Smolenice, ČSSR (1987).
2. S. Arpadjian, M. Mitewa and P. R. Bontchev, *Talanta* 1987, **34**, 953.
3. M. Mitewa, P. R. Bontchev, E. Zhecheva, D. Mechandjiev, K. Kabassanov and D. Vassileva, *Inorg. Chim. Acta* 1987, **134**, 17.
4. M. Mitewa, P. R. Bontchev, K. Kabassanov, D. Vassileva, E. Zhecheva and D. Mechandjiev, *J. Coord. Chem.* 1988, **17**, 287.
5. M. Mitewa, P. R. Bontchev, G. Gencheva, E. Zhecheva and K. Kabassanov, *Inorg. Chim. Acta* 1990, **170**, 137.
6. B. N. Figgis and J. Levis, *Progress in Inorganic Chemistry* Vol. 6, pp. 169 and 176. John Wiley, New York (1964).
7. A. S. Brar, S. Brar and S. S. Sandhu, *Ind. J. Chem.* 1986, **25A**, 23.
8. H. Abu-Soud and J. Silver, *Inorg. Chim. Acta* 1988, **153**, 139.
9. H. Abu-Soud and J. Silver, *Inorg. Chim. Acta* 1989, **161**, 139.
10. J. Silver, G. Al-Jaff and J. Al-Taies, *Inorg. Chim. Acta* 1987, **135**, 151.
11. B. R. McGarvey, *Inorg. Chem.* 1988, **27**, 4691.
12. T. Yoshimura, *Inorg. Chim. Acta* 1986, **125**, L27.

Polyhedron Vol. 10, No. 7, pp. 769–770, 1991
Printed in Great Britain

0277-5387/91 $3.00+.00
© 1991 Pergamon Press plc

COMMUNICATION

THE SYNTHESIS OF BIS(HEXAMETHYLDISILYLAMIDO)BARIUM(II)

J. M. BONCELLA,* C. J. COSTON and J. K. CAMMACK

Department of Chemistry, University of Florida, Gainesville, FL 32611, U.S.A.

(*Received* 30 *November* 1990; *accepted* 7 *January* 1991)

Abstract—Bis(hexamethyldisilylamido)barium(II) (**1**) was synthesized in the reaction between $BaCl_2$ and 2 equivalents of $NaN(SiMe_3)_2$. Compound **1** forms adducts with a variety of Lewis bases and can be used as a precursor to $YBa_2Cu_3O_{7-x}$.

The discovery of the $YBa_2Cu_3O_{7-x}$ family of superconductive ceramics in 1987[1,2] has led to a considerable research effort directed toward the use of soluble or volatile precursor compounds that can be used in sol–gel or chemical vapour deposition methods for the synthesis of this material.

In searching for novel precursors for the $YBa_2Cu_3O_{7-x}$ family of superconductors our attention was focused on the possible use of hexamethyldisilylamido complexes of the constituent metals. Such compounds are pontential precursors since they readily hydrolyse giving hexamethyldisilazane and the metal hydroxide (or oxide).[3b] Moreover, the hexamethyldisilazane is susceptible to further hydrolysis to give ammonia and hexamethyldisiloxane as products, as shown in eq. (1):

$$M[N(SiMe_3)_2]_x + xH_2O \longrightarrow M(OH)_x + xHN(SiMe_3)_2$$
$$HN(SiMe_3)_2 + H_2O \longrightarrow NH_3 + (Me_3Si)_2O. \quad (1)$$

The compounds $\{Cu[N(SiMe_3)_2]\}_4$ and $Y[N(SiMe_3)_2]_3$ have been previously reported.[3,4] However, it appears as though $Ba[N(SiMe_3)_2]_2$ has not been prepared until now. What follows is a brief account of the synthesis of this compound and some of its base adducts.

When anhydrous $BaCl_2$ was allowed to react with 2 equivalents of $NaN(SiMe_3)_2$ at room temperature in diethyl ether, the $BaCl_2$ slowly dissolved and a fine precipitate of NaCl formed over 24 h [eq. (2)]:

$$BaCl_2 + 2NaN(SiMe_3)_2 \longrightarrow \{Ba[N(SiMe_3)_2]_2\}_x \quad (2)$$
(1)

Filtration and removal of the ether under reduced pressure followed by crystallization from toluene at −20°C gives an 80% yield of $Ba[N(SiMe_3)_2]_2$ (**1**) as white crystals which become opaque when exposed to a vacuum or upon standing under an argon atmosphere at room temperature. Both the ^1H and ^{13}C NMR spectra† of **1** in toluene-d_8 show only one line down to −60°C, suggesting a highly fluxional associated structure or a monomeric structure. We assume that the former possibility is more likely since the manganese and ytterbium compounds have been shown to exist as dimers in the solid state.[5,6] Furthermore, even though **1** readily reacts with a variety of Lewis bases, there is no evidence of coordinated diethyl ether in the NMR spectra of **1** or its hydrolysis products, suggesting that diethyl ether is so weakly bound that it is removed during the isolation procedure.

Compound **1** is soluble in toluene and ether and only sparingly soluble in aliphatic hydrocarbons. It is extremely sensitive to hydrolysis in both the solid state and solution. It readily undergoes reaction with a variety of Lewis bases to give white, crys-

* Author to whom correspondence should be addressed.

† Compound **1**: ^1H NMR (300 MHz, C_6D_6, 22°C) δ 0.108 (S); $^{13}C\{^1H\}$NMR (74.4 MHz, C_6D_6, 22°C) δ 6.92.

talline adducts as shown in eq. (3):

$$\{Ba[N(SiMe_3)_2]_2\}_x + 2L \longrightarrow [(Me_3Si)_2N]_2BaL_2 \quad (2)$$

2a: L= 1/2 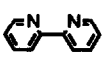 **2b**: L= 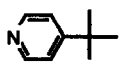

2c: L= 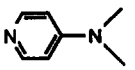 (3)

Compounds **2a–c** are all sparingly soluble in aliphatic hydrocarbons and soluble in aromatic hydrocarbons. Additionally, they may be recrystallized from THF without displacement of the amine bases from the compound. These compounds were characterized using ^{1}H NMR spectroscopy as well as by elemental analysis.* Attempts to grow single crystals suitable for an X-ray diffraction study have been frustrated by the fact that **1** and **2a–c** lose crystallinity and crumble when dried under vacuum or a stream of inert gas.

When THF solutions containing **1**, $Y[N(SiMe_3)_2]_3$ and $\{Cu[N(SiMe_3)_2)]\}_4$ in the correct stoichiometry are hydrolysed by the dropwise addition of water, an orange precipitate forms which may be processed by heating, grinding and annealing to give powders which have been shown to contain up to 80% of the superconducting phase, $YBa_2Cu_3O_{7-x}$, via X-ray diffraction techniques.[7] We are continuing to test the suitability of these compounds as precursors to superconducting ceramics.

Acknowledgement—This work was supported by DARPA as a part of the Florida S.U.S. initiative.

REFERENCES

1. J. G. Bednorz, K. A. Muller and M. Takashige, *Science* (Washington, D.C.) 1987, **236**, 73.
2. R. J. Cova, B. Batlogg, R. B. VanDover, P. W. Murphy, S. Sunshine, T. Siegrist, J. P. Remeika, E. A. Reitman, S. Zahvrak and G. P. Espinosa, *Phys. Rev. Lett.* 1987, **58**, 1676.
3. (a) H. Burger and U. Wannagat, *Monatsh. Chem.* 1964, **95**, 1099; (b) D. C. Bradley, unpublished results cited in M. F. Lappert, P. P. Power, A. R. Sanger and R. C. Srivastava, *Metal and Metaloid Amides*. John Wiley, New York (1980).
4. D. C. Bradley, J. S. Gohtra and F. A. Hart, *J. Chem. Soc., Dalton Trans.* 1973, 1021.
5. D. C. Bradley, M. B. Hursthouse, K. M. A. Malik and R. Moseler, *Transition Met. Chem.* 1978, **3**, 253.
6. (a) J. M. Boncella and R. A. Andersen, *Organometallics* 1985, **4**, 205; (b) A. G. Avent, M. A. Edelman, M. F. Lappert and G. A. Lawless, *J. Am. Chem. Soc.* 1988, **111**, 3423; (c) J. M. Boncella, PhD thesis, University of California, Berkeley, California (1984).
7. D. E. Clark, personal communication.

* Compound **2a**: ^{1}H NMR (300 MHz, C_6D_6, 22°C) δ 8.85 (d, J = 6.5 Hz, 2H, ring), δ 7.56 (Br, m, 2H, ring), δ 7.04 (t, J = 8.1 Hz, 2H, ring), δ 6.70 (t, J = 6.5 Hz, 2H, ring), δ 0.232 (s, 36H, Si-*Me*). Compound **2b**: ^{1}H NMR (300 MHz, C_6D_6, 22°C) δ 8.48 (aa′bb′ d of d, 4H, ring), δ 6.77 (aa′bb′ d of d, 4H, ring), δ 0.903 (S, 18H, t-Bu), δ 0.438 (S, Si*Me*$_3$). Compound **2c**: ^{1}H NMR (300 MHz, C_6D_6, 22°C), δ 8.28 (aa′bb′ d of d, 4H, ring), δ 5.89 (aa′bb′ d of d, 4H, ring), δ 2.05 (S, 12H, N*Me*$_2$), δ 0.469 (S, 36H, Si*Me*$_3$). Satisfactory elemental analyses have been obtained for compounds **2a–c**. We have been unable to obtain consistent results for compound **1** which always analyses 2–3% low in carbon.

Polyhedron Vol. 10, No. 8, pp. 771–778, 1991
Printed in Great Britain

0277-5387/91 $3.00+.00
© 1991 Pergamon Press plc

STEREODYNAMICAL INTERCONVERSION OF BIS(N-ARYL-α-ISOPROPYL-β-AMINOVINYLTHIONATO)ZINC(II) AND -CADMIUM(II)

L. E. KONSTANTINOVSKII, R. YA. OLEKHNOVITCH, M. S. KOROBOV, L. E. NIVOROZHKIN and V. I. MINKIN*

Institute of Physical and Organic Chemistry, Rostov State University, 344711 Rostov-on-Don, U.S.S.R.

(*Received* 3 *January* 1990; *accepted* 13 *August* 1990)

Abstract—Bis N-aryl(α-isopropyl-β-aminovinylthionato)zinc(II) and -cadmium(II) complexes [**I(a,b)**] have been prepared in order to investigate their stereochemical non-rigidity and conformational interconversion. For the zinc(II) complexes [**I(a,b)**], two types of energy barrier were observed by the use of dynamic ^1H and ^{13}C NMR spectroscopy. The lower barrier ($\Delta G^{\ddagger}_{298} \sim 60$ kJ mol^{-1}) measured by averaging anisochronous *o,o'*-carbons (C-aryl ring A) is assigned to the hindered rotation of the β-phenyl ring. The higher energy barrier ($\Delta G^{\ddagger}_{298} = 77$–$78$ kJ mol^{-1}) was calculated for the interchange of the diastereotopic methyls of the α-isopropyl group for complexes **I(a,b)** and the anisochronous methyls of the N-aryl ring B in complexes **I(a)** during the $(R) \rightleftharpoons (S)$ inversion. Whereas, the tetrahedral $(R) \rightleftharpoons (S)$ inversion in the cadmium(II) complexes, **I(a,b)**, is faster ($\Delta G^{\ddagger}_{298} = 51$–$53$ kJ mol^{-1}) compared with the zinc(II) complexes. In this case, the *o,o'*-carbons in the C-aryl ring manifest the $(R) \rightleftharpoons (S)$ inversion process ($\Delta G^{\ddagger}_{298} = 47.5$–$49$ kJ mol^{-1}). The anisochronous *o,o'*-methyls of the N-aryl ring B may thus be used for studying the tetrahedral inversion at the metal centre along with the diastereotopic methyl groups in the type **I** complexes. The energy barrier for the intermolecular ligand degenerate exchange reaction ($\Delta G^{\ddagger}_{298} = 64.4$ kJ mol^{-1}) is higher than for the intramolecular $(R) \rightleftharpoons (S)$ inversion at the metal centre.

The stereochemical non-rigidity of tetrahedral bis-N-alkyl,aryl(α-isopropyl-β-aminovinylthionato) zinc(II) and -cadmium(II) (**I**) has been extensively investigated in recent years by means of the total line-shape analysis of variable-temperature NMR spectroscopic data.[1–4]

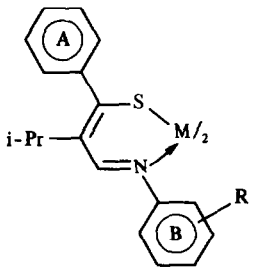

M = Zn, Cd
R = 2,4,6-CH_3 (Mes) (**a**); n-$N(CH_3)_2$ (**b**)
A = β-phenyl ring
B = N-phenyl ring.

I

* Author to whom correspondence should be addressed.

These studies have been focused on the investigation of the inversion of the tetrahedral configuration $(R) \rightleftharpoons (S)$ (**1**) at the metal centre of the complexes

(1)

R *S*

The basic condition for the successful recording of the interconversion of enantiomers (*R*) and (*S*) (**1**), occurring on the NMR time scale, without their prior separation, was the presence of a prochiral α-isopropyl group within the dissymmetric system (**I**). By varying the substituent R, attached to the ligating atom N, it was found that the energy barriers to the enantiomerization of N-aryl,alkyl substituted complexes of type **I** essentially depend on the nature

of the metal centre atom being higher for the zinc(II) complexes than for those of cadmium(II).[1-4]

While studying the stereochemical non-rigidity of complexes **1** we have investigated their spectral behaviour caused by rotation of the two rings (A and B) about the C—N and the C—C bond, respectively. Kinetic data on the $(R) \rightleftharpoons (S)$ inversion and rotation of aryl rings have also been obtained in order to estimate the barriers of these processes. It was of particular interest to compare the data, calculated by using two independent indicator groups (i-Pr and Mes).

RESULTS AND DISCUSSION

Zinc(II) *complexes*

In the ^{1}H DNMR spectra of zinc(II) complexes **I(a)** below +50°C, anisochronous 2,6-methyls of the B-ring (doublet) are observed along with anisochronous methyls of the C-isopropyl group (a pair of overlapping doublets), Fig. 1. This anisochronicity stems from a coplanarity of the B-ring with respect to the chelate ring.

As the temperature of the solution is raised, the signals of the methyl groups of the isopropyl are substantially broadened and coalesce to a six-proton singlet. Such a dynamic picture can be produced both by inversion of configuration $(R) \rightleftharpoons (S)$ at the central atom and by increasing the velocity of the N-mesityl ring rotation about the C—N bond (Scheme 1).

It has been found that kinetic parameters for the averaging of signals of anisochronous *o,o'*-methyls in the N-aryl ring and methyls of the prochiral i-Pr group do in fact coincide within experimental accuracy (Table 1). This suggests that the inversion at

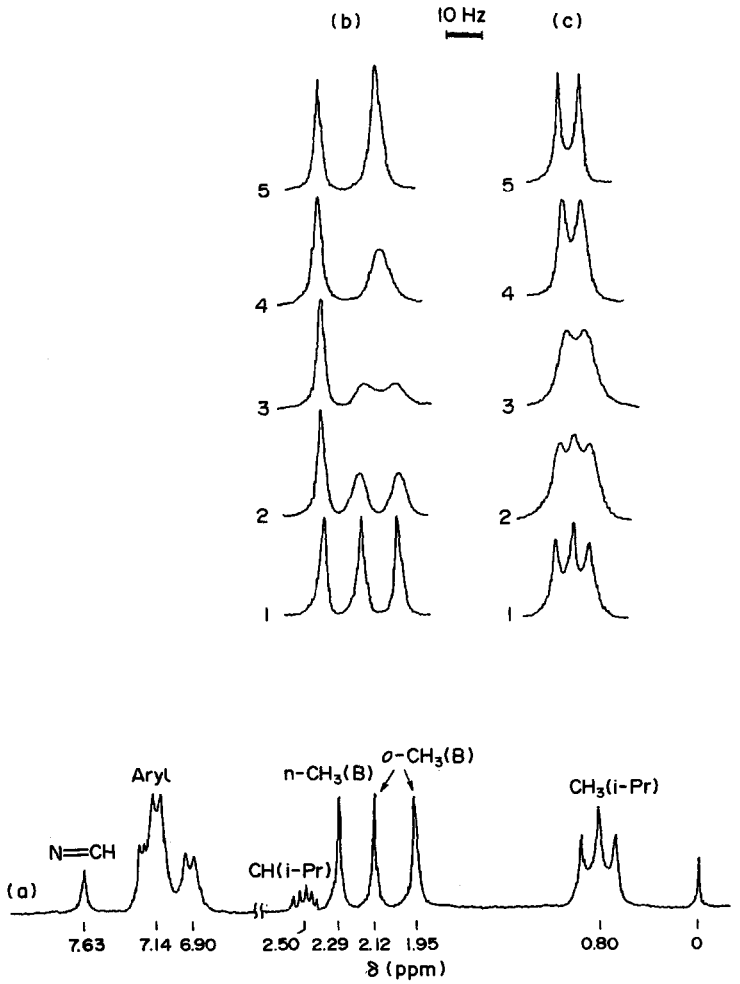

Fig. 1. 100-MHz ^{1}H NMR spectrum of complex **I(a)** (M = Zn) at 25°C in $CDCl_3$ (a); variable-temperature NMR spectra of the *o,o'*-CH_3 groups (B-ring) (b): (1) 50°, 3.25 s^{-1}; (2) 70°, 20 s^{-1}; (3) 75°, 33 s^{-1}; (4) 80°, 50 s^{-1}; (5) 110°, 541 s^{-1}; and the CH_3 groups (i-Pr) (c): (1) 40°, 0.8 s^{-1}; (2) 60°, 10 s^{-1}; (3) 65°, 17 s^{-1}; (4) 70°, 32 s^{-1}; (5) 80°, 96 s^{-1}.

Table 1. Kinetic and activation parameters for inversion of the conformation at cadmium and zinc of complexes **I(a,b)** in $CDCl_3$

N	M	R	Process	Indicator group	$\Delta H^{\ddagger}$ (kJ mol^{-1})	$\Delta S^{\ddagger}$ (J mol^{-1} K^{-1})	$\Delta G^{\ddagger}_{298}$ (kJ mol^{-1})	k_{298} (s^{-1})
1	Zn	2,4,6-$(CH_3)_3C_6H_2$	$R \rightleftharpoons S$	$CH(CH_3)_2$	107.1±2.4	28.5±4.2	78.6±0.1[a]	1×10^{-1}
2			$R \rightleftharpoons S$	*o,o'*-$(CH_3)_2$ (B)	85.4±1.3	94.9±0.4	77.0±0.2[a]	2×10^{-1}
3			Hindered rotation	*o,o'*-C (A)	54.0±0.8	−20.1±2.9	60.0±0.1	1.9×10^{2}
4		n-$N(CH_3)_2C_6H_4$	$R \rightleftharpoons S$	$CH(CH_3)_2$	80.4±1.9	12.5±5.6	76.6±0.1	2×10^{-1}
5			Hindered rotation	*o,o'*-C (A)	47.7±1.5	−40.7±5.5	59.8±0.1	2×10^{2}
6	Cd	2,4,6-$(CH_3)_3C_6H_2$	$R \rightleftharpoons S$	$CH(CH_3)_2$	43.9±1	−26.9±4.2	51.8±0.3	5.4×10^{3}
7			$R \rightleftharpoons S$	$CH(^{13}CH_3)_2$	39.8±1.4	−45.6±5.9	53.3±0.4	2.7×10^{3}
8			$R \rightleftharpoons S$	*o,o'*-CH_3 (B)	40.6±0.7	−37.2±2.7	51.6±0.1	5.4×10^{3}
9			$R \rightleftharpoons S$	*o,o'*-$^{13}CH_3$ (B)	45.4±1.4	−19±6.3	51.1±0.4	6.7×10^{3}
10			Hindered rotation	*o,o'*-C (A)	35.6±0.8	−39.9±3.3	47.5±0.1	2.9×10^{4}
11			Hindered rotation	*m,m'*-C (B)	—	—	45.4[b] (218 K)	6×10 (218 K)
12	Cd	n-$N(CH_3)_2C_6H_4$	$R \rightleftharpoons S$	$CH(CH_3)_2$	28.3±1.5	−70±2	49.2±0.1	1.5×10^{4}
13			Hindered rotation	*o,o'*-C (A)	37.2±1.0	−37.8±4.2	48.5±1	2×10^{4}
14	^{111}Cd	2,4,6-$(CH_3)_3C_6H_2$	Ligand exchange	$^{3}J_{^{111}Cd-N=CH}$	47.7±0.8	−56.0±3	64.4±0.1	3.4×10

[a] In $C_2H_2Cl_4$.
[b] Coalescence point.

the metal centre rather than a hindered rotation of the N-mesityl group makes a predominant contribution to the kinetics of the averaging process, which is recorded by the temperature evolution of *o,o'*-CH_3 (B-ring) signals.

The variable-temperature ^{13}C NMR spectra of complex **I(a)** have also indicated the anisochronicity of *o,o'*-carbons of the C-aryl ring (δ 125.6 and 129.3 ppm) below $-20°C$. They have collapsed and transformed to a singlet peak upon raising the temperature to $+60°C$. Such a dynamic ^{13}C NMR pattern should be interpreted as a result of the rotational process (Scheme 1), since the energy barrier of such a process is lower than that for the $(R) \rightleftharpoons (S)$ inversion (Table 1). The energy barrier thus found agrees with the known data[5] on C-aryl rotations. For complex **I(b)** the inversion barrier is also higher than the rotational barrier in the case of the C-aryl ring, and its magnitude is comparable with that of **I(a)** (Table 1).

Cadmium(II) *complexes*

In the temperature-dependent ^1H NMR spectra of complexes **I(a,b)** (M = Cd) the dynamic process manifesting itself in the averaging of the signals of the diastereotopic CH_3 groups (α-i-Pr) and the anisochronous *o,o'*-CH_3 groups (B-ring) occurs at a lower temperature ($-60°$ to $-10°C$) than in the case of the zinc(II) analogues. This indicates rapid $(R) \rightleftharpoons (S)$ inversion at cadmium. Calculated barriers (Table 1) have typical values for this kind of bischelate complex[3] and are 30–40 kJ mol^{-1} lower than those for analogous zinc(II) complexes.

The methyl region of the ^{13}C NMR spectrum of **I(a)** (M = Cd) is illustrated in Fig. 2. The energy barrier calculated from line-shape changes of anisochronous methyls (i-Pr and Mes) at $-47°C$ and above this temperature, associated with the $(R) \rightleftharpoons (S)$ inversion, agrees well with the magnitude obtained from the ^1H DNMR spectrum (Table 1).

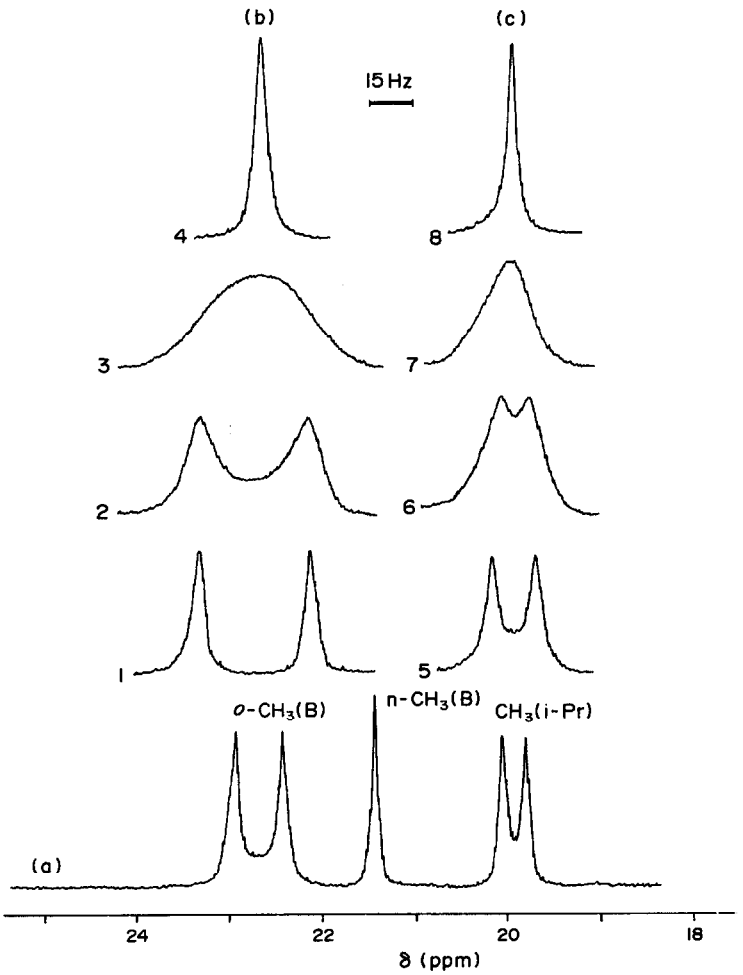

Fig. 2. 3100.58-MHz ^{13}C NMR spectrum (methyl region) of complex **I(a)** (M = Cd) at $-88°C$ in $CDCl_3$ (a); variable-temperature NMR spectra of the *o,o'*-CH_3 (B-ring) (b) and the CH_3 (i-Pr) (c) groups corresponding to: (1,5) $-47°$, 19.3 and 14.3 s^{-1}; (2,6) $-42°$, 31.3 and 21.1 s^{-1}; (3,7) $-36°$, 69 and 46.4 s^{-1}; (4,8) $-15°$, 380 and 223 s^{-1}.

Thus, the study of the $(R) \rightleftharpoons (S)$ inversion of the tetrahedral bis-chelate complexes **I(a)** (M = Cd) and **I(a)** (M = Zn), based on the temperature-dependent spectral behaviour of two different indicator groups (α-i-Pr and N-Mes), has given similar magnitudes for the energy barriers. This provides a basis for the utilization of *o,o'*-CH_3 in the N-aryl ring B as a diastereotopic probe in the ^1H and ^{13}C NMR spectra of bis-chelate complexes of type **I**.

In the ^{13}C NMR spectra of **I(a,b)** (M = Cd) (Fig. 3) at −68°C, as well as for their zinc analogues, anisochronous *o,o'*-carbons of the C-aryl ring A (δ 125.13 and 127.47 ppm) were also observed. The increase in the barrier of the hindered rotation linked to the chelate ring makes it possible to observe the process of rotation about the C—C bond on the NMR time scale.

Because the averaging of the signals of all various anisochronous groups including methyls (i-Pr), *o,o'*-methyls (Mes), *o,o*-carbons (A) and *m,m*-carbons (B) proceeded with barriers which were very close in value (Table 1), it can be inferred that the $(R) \rightleftharpoons (S)$ inversion barrier in cadmium(II) complexes is lower than the rotational one, or their values coincide accidentally.

It may be, therefore, concluded that the processes of $(R) \rightleftharpoons (S)$ inversion and of hindered rotation of phenyl rings in zinc(II) and cadmium(II) complexes [**I(a,b)**] proceed in accordance with Scheme 1, where four interconverting forms are shown. For zinc(II) complexes the lower energy barrier ($\Delta G^{\ddagger}_{rot}$) is associated with the C-aryl ring (A) rotation process, $R(r,s) \rightleftharpoons R(s,r)$ or $S(r,s) \rightleftharpoons S(s,r)$, observed in ^1H and ^{13}C DNMR spectra at lower temperatures, and the higher energy barrier ($\Delta G^{\ddagger}_{inv}$) is associated with the $R(r,s) \rightleftharpoons S(s,r)$ or $R(s,r) \rightleftharpoons S(r,s)$ interconversion at higher temperatures. Whereas for cadmium(II) complexes the energy barrier for the inversion process is lower than that of the C-aryl ring rotation. Therefore, both processes in temperature-variable NMR spectra are observed simultaneously.

To provide some information on the mechanism of these reactions, the dependence of energy barriers on the concentration of solutions was studied. The 10-fold dilution of the solutions of complexes **I(a)** (M = Zn, Cd) does not lead to any detectable changes in the activation energies (within the usual experimental accuracy). This corroborates the intramolecular character of the inversion process.

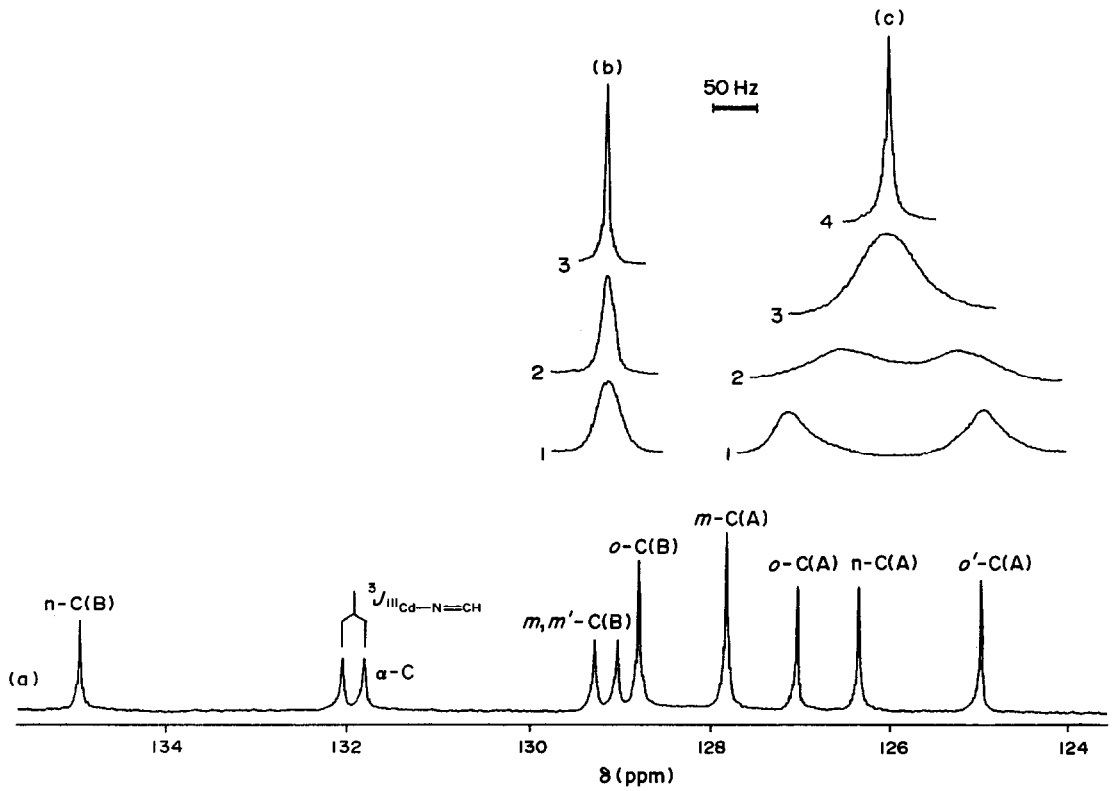

Fig. 3. 400-MHz ^{13}C NMR spectrum (aryl region) of complex **I(a)** (M = ^{111}Cd) at −68°C in $CDCl_3$ (a); variable temperature NMR spectra of the *m,m*-carbons (B-ring) (b): (1) 55°, 60 s^{-1}; (2) −45°; (3) −20°; and the *o,o'*-C groups (A-ring) (c): (1) −58°, 94 s^{-1}; (2) −33°, 370 s^{-1}; (3) −29°, 997 s^{-1}; (4) −6°, 4800 s^{-1}.

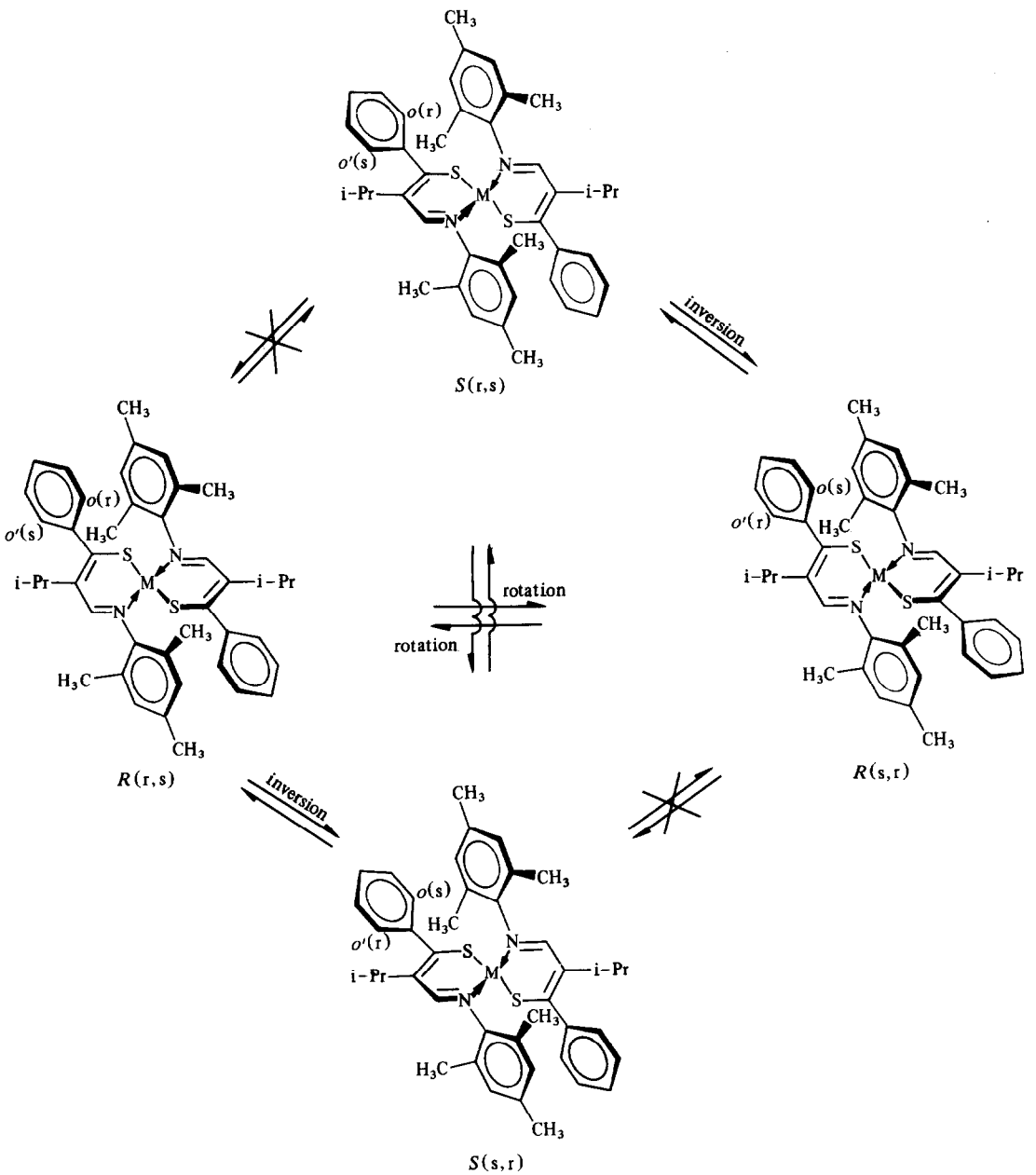

Scheme 1. General scheme of the stereodynamics of complexes **I(a,b)**. For the zinc complexes, $\Delta G^{\ddagger}_{inv} > \Delta G^{\ddagger}_{rot}$. The processes of inversion and rotation may be, therefore, independently observed. For the cadmium complexes, $G^{\ddagger}_{inv} \leqslant G^{\ddagger}_{rot}$; simultaneous averaging of all the diastereotopic groups is observed.

The intermolecular degenerate ligand exchange process was found to take place in solutions of bis-chelate cadmium(II) complexes with energy barriers 10–15 kJ mol^{-1} higher than those for the intramolecular inversion.[1]

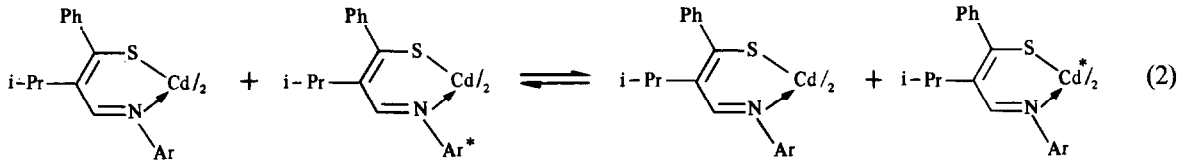

(2)

The reaction, second-order in kinetics, is conveniently monitored by studying the temperature dependence of the $^3J(^{111}Cd—N=CH)$ spin–spin coupling. For complexes **I(a,b)** (M = Cd), 95% enriched in ^{111}Cd, the energy barrier of the ligand exchange reaction ($\Delta G^{\ddagger}_{298} = 64.4$ kJ mol^{-1}) thus obtained is higher than those of the inversion and C-alkyl ring rotation. This value agreed well with the data obtained earlier[1,3] for intermolecular ligand exchanges in solutions of N-aryl(α-isopropyl-β-aminovinylthionato)^{111}cadmium(II). The earlier suggested mechanism[1] for the ligand exchange reaction includes an intermediate dimer with trigonal bipyramidal coordinated cadmium. The rates of reaction (2), as well as of the intramolecular inversion (1), are not affected by the addition of equimolar amounts of free ligands.

EXPERIMENTAL

NMR spectroscopy

^1H and ^{13}C DNMR spectra were recorded using Tesla BS 567A (100 MHz) and Varian VXR (400 MHz) NMR spectrometers, equipped with a variable-temperature probe. The temperature of the samples was controlled with an accuracy of ±1 K. ^1H and ^{13}C chemical shifts were measured with respect to hexamethyldisiloxane as internal standard. Computer simulated spectra were calculated using the total line-shape analysis technique as described in ref. 6. The spectral parameters of indicator groups, for example δ—chemical shift, Δν—limit expansion and $\Delta\nu_0^{1/2}$—line width at half height, necessary for kinetic analysis, are given in Table 2. Activation parameters were obtained from least-square Eyring plots [$\ln(kT)$ vs $1/T$], where $k = 1/\tau$ (τ—life-time of a site). For kinetic studies, the commercially available solvents CD_2Cl_2 and

Table 2. Spectral parameters of indicator groups

N	Observable nucleus	Indicator group	δ (ppm)	Δν (Hz)	$\Delta\nu_0^{1/2}$ (Hz)
1	^1H	$(CH_3)_2CH$	0.81[a]	9.0	2.0
2	^1H	*o,o'*-CH_3 (B)	1.95, 2.12	17.5	2.0
3	^{13}C	*o,o'*-C (A)	125.6, 127.9	23.0	4.0
4	^1H	$(CH_3)_2CH$	1.05[a]	9.5	2.0
5	^{13}C	*o,o'*-C (A)	125.6, 126.5	23.0	4.1
6	^1H	$(CH_3)_2CH$	0.9[a]	21.6	2.5
7	^{13}C	$(CH_3)_2CH$	19.8, 20.0	16.9	4.5
8	^1H	*o,o'*-CH_3 (B)	1.9, 2.3	30.3	2.2
9	^{13}C	*o,o'*-CH_3 (B)	22.4, 22.8	37.5	6.3
10	^{13}C	*o,o'*-C (A)	125.1, 127.5	231.5	4.1
11	^{13}C	*m,m'*-C (B)	129.5, 129.9	40.5	4.0
12	^1H	$(CH_3)_2CH$	0.92[a]	15.6	1.5
13	^{13}C	*o,o'*-C (A)	125.7, 127.9	217.6	4.0
14	^1H	$^3J_{^{111}Cd—N=CH}$	7.5[b]	25.3	2.5

[a] Double doublet with $^1J_{CH—CH_3} = 6.5$–7 Hz.
[b] Doublet.

$CDCl_3$, exposed for 24 h over 4 Å molecular sieves, were used.

Synthesis

The ligands for type **I** complexes were synthesized in 70–80% yields by reflushing equimolar amounts of amine and ether solutions of α-isopropyl-β-thiocinnamic aldehyde in ethanol solutions. The following compounds were synthesized from α-isopropyl-β-chlorcinnamic aldehyde and Na_2S in DMSO according to an earlier described procedure.[2] Complexes **I** were prepared by coupling ligands and the respective metal acetate in absolute methanol (heating: 10 min; yields: 80%).[7] After crystallization from benzene, melting points were: **I(a)** (Zn), 240–242°C; **I(a)** (Cd), 259–260°C. Elemental analyses for all the complexes were satisfactory.

REFERENCES

1. L. E. Nivorozhkin, V. I. Minkin, N. I. Borisenko, L. E. Konstantinovskii, M. S. Korobov and R. Ya. Olekhnovich, *Dokl. Akad. Nauk SSSR* 1981, **266**, 1176.
2. L. E. Nivorozhkin, R. Ya. Olekhnovich, M. S. Korobov, L. E. Konstantinovskii and V. I. Minkin, *Koord. Khim.* 1982, **8**, 1080.
3. L. E. Nivorozhkin, R. Ya. Olekhnovich, M. S. Korobov, L. E. Konstantinovskii and V. I. Minkin, *Koord. Khim.* 1986, **12**, 899.
4. L. E. Nivorozhkin, R. Ya. Olekhnovich, M. S. Korobov, N. I. Borisenko, L. E. Konstantinovskii and V. I. Minkin, *Koord. Khim.* 1987, **13**, 466.
5. L. M. Jackman, in *Dynamic Nuclear Magnetic Resonance Spectroscopy*, p. 203. Academic Press, New York (1975).
6. N. I. Borisenko, L. P. Olekhnovich and V. I. Minkin, *Teor. Eksper. Khim.* 1976, **12**, 813.
7. V. I. Minkin, L. E. Nivorozhkin, L. E. Konstantinovskii and M. S. Korobov, *Koord. Khim.* 1977, **3**, 174.

Polyhedron Vol. 10, No. 8, pp. 779–788, 1991
Printed in Great Britain

0277–5387/91 $3.00+.00
© 1991 Pergamon Press plc

SYNTHETIC AND SPECTROSCOPIC INVESTIGATIONS OF SOME DIOXOURANIUM(VI) COMPLEXES OF MULTIDENTATE DISALICYLALDEHYDE ADIPOYLDIHYDRAZONE

M. HUSAIN, S. S. BHATTACHARJEE, K. B. SINGH and R. A. LAL*

Chemistry Department, Pachhuga University College, North-Eastern Hill University, Aizawl-796001, Mizoram, India

(*Received* 15 *January* 1990; *accepted* 22 *October* 1990)

Abstract—Reactions of disalicylaldehyde adipoyldihydrazone with uranyl acetate dihydrate and uranyl nitrate hexahydrate in aqueous and ethanolic media under different experimental conditions were studied and the resulting complexes with the compositions $[UO_2(H_2L_2)(H_2O)]_n$, $[UO_2(H_2L_2)]_n3nH_2O$, $[UO_2(H_3L_2)(CH_3COO)]_n3nH_2O$, $[UO_2Zn(L_2)(H_2O)_2]_n2nH_2O$, $[(UO_2)_2(H_2L_2)(C_2O_4)]_n2nH_2O$ and $[(UO_2)_2(L_2)(py)_2(H_2O)_4]$ were characterized on the basis of elemental analyses, EDAX and thermoanalytical data. The structural assessment of the complexes was carried out by using molar conductance, magnetic moment and ESR data and IR, electronic and ^1H NMR spectroscopy. In the complexes, the ligand functions as a bridging monobasic tetradentate, dibasic hexadentate and tetrabasic hexadentate ligand, and exhibits keto–enol tautomerism. The acetate and oxalate groups act as chelating bidentate and bridging tetradentate ligands. The complexes are considered to involve seven, eight, nine and ten coordinated uranium atoms with ligand atoms arranged in the equatorial plane around the linear uranyl group and in the heterobimetallic complex $[UO_2Zn(L_2)(H_2O)_2]_n2nH_2O$ the zinc atom is considered to have tetrahedral stereochemistry.

Due to the diverse properties of acyl- and pyridoylhydrazones and their application in many fields (pharmacological, analytical, technological, etc.) the literature indicates an increased interest in the study of their complexing affinities towards different transition metal ions.[1,2] The dihydrazones derived from condensation of *o*-hydroxyaromatic aldehydes and ketones, and acyl- and pyridoyldihydrazines, are similar to monoacyl-, aroyl-, pyridoylhydrazones in all respects except that they possess two hydrazone groupings (which are separated from each other by methylene chains of varying length or by phenyl or pyridyl groups) and two —OH groups. Therefore, depending upon the preferred stereochemical disposition of the metal valencies and nature of the bonds formed in the coordination process, these complexes may offer several alternate modes of bonding and are capable of giving rise to condensed systems, i.e. bi- and polynuclear complexes involving ligand and phenolic oxygen bridging. Disalicylaldehyde adipoyldihydrazone is an example of a novel ligand capable of exhibiting multidentate behaviour by virtue of having a greater number of donor atoms and more flexibility in three-dimensional space. This is in contrast to aroyl- and pyridoyldihydrazones in which the phenyl or pyridyl rings between the two hydrazone groupings impose planarity on them. Disalicylaldehyde adipoyldihydrazone is capable of binding two or more similar or different metal atoms in close proximity to one another and the synthesis and study of such complexes have been the subjects of active research over the past few years because the redox properties of such homometallic and heterodimetallic transition metal complexes may be related to the multinuclear metal sites in metalloenzymes.[3,4] The present paper reports the results of an investigation into the reactions of uranyl salts with disalicylaldehyde adipoyldihydrazone, capable of existing in the keto (**I**), keto–enol (**II**) and enol (**III**) forms under different

* Author to whom correspondence should be addressed.

experimental conditions. Characterization and structural assessment of the resulting monometallic, homodimetallic and heterobimetallic complexes containing uranium and zinc were made by using molar conductance, magnetic moment and ESR data, and IR, electronic and ^{1}H NMR spectroscopy.

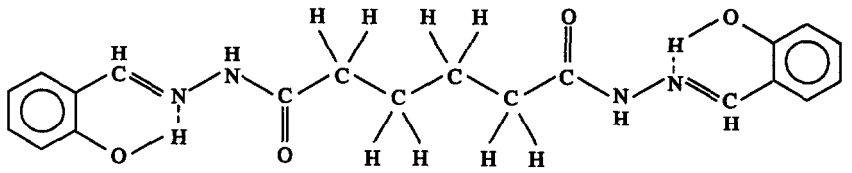

(I)

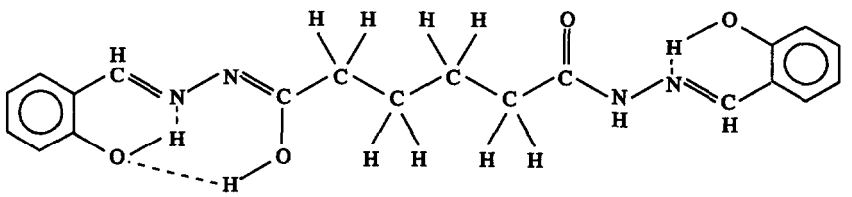

(II)

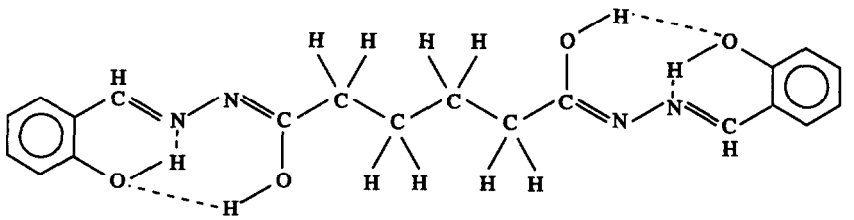

(III)

RESULTS AND DISCUSSION

Disalicylaldehyde adipoyldihydrazone (H_4L_2) is an octadentate ligand which may function as a mono- and dibasic ligand in the keto form and tri- and tetrabasic ligand in the enol form under suitable experimental and preparation conditions. However, simultaneous involvement of all the donor atoms in coordination is an unlikely possibility. In the present study, the reaction of uranyl acetate dihydrate with H_4L_2 in a 1 : 1 molar ratio in ethanol medium results in the precipitation of the complex $[UO_2(H_3L_2)(CH_3COO)]_n3nH_2O$; this signifies the loss of only one proton from the phenolic —OH group of half of the ligand. The reaction of the product of uranyl acetate dihydrate with ligand in a 3 : 1 molar ratio in 95% ethanol medium with excess of pyridine yields a complex of the composition $[(UO_2)_2(L_2)(py)_2(H_2O)_4]$, signifying a loss of four protons. When the ligand is allowed to react with uranyl nitrate hexahydrate in aqueous medium in a 1 : 3 molar ratio (ligand = uranyl nitrate hexahydrate), a complex of composition $[UO_2(H_2L_2)]_n3nH_2O$ is obtained in which the ligand functions as a dibasic species. The reaction of uranyl nitrate hexahydrate with ligand in a 2 : 1 molar ratio and subsequent reaction of the reaction mixture with oxalic acid in a molar ratio of 2 : 1 : 2 yields a complex of composition $[(UO_2)_2(H_2L_2)(C_2O_4)]_n2nH_2O$, which again shows that the ligand behaves as a dibasic ligand. This indicates that the nature of the reaction medium and metal salt plays an important role in the determination of the composition of the complexes, and basicity of the ligand. In order to synthesize the heterobimetallic complexes, the complex $[UO_2(H_3L_2)(CH_3COO)]_n3nH_2O$ was allowed to react with zinc acetate dihydrate in aqueous medium and with copper nitrate tetrahydrate, in slight excess of the 1 : 1 molar ratio. This led to the successful precipitation of the zinc complex $[UO_2Zn(L_2)(H_2O)_2]_n2nH_2O$, while the reaction with copper nitrate tetrahydrate led to complete displacement of the uranyl ion from the resultant precipitate (evident from its green colour). This was further confirmed by the IR spectrum of the compound which showed the absence of a strong absorption band in the region 950–890 cm^{-1}, characteristic of the uranyl ion due to its asymmetric stretching frequency. The initial reaction between uranyl acetate dihydrate and adipoyldihydrazine in a 1 : 1 molar ratio yielded the complex $[UO_2(CH_2CH_2C(O)NNH_2)_2]2H_2O$. This compound, on reaction with excess salicylaldehyde, precipitated a complex of composition $[UO_2(H_2L_2)(H_2O)]_n$ in which H_2L_2 refers to the loss of a proton from the enolized carbonyl oxygen.

The complexes isolated in the present study together with their colour, analyses, decomposition point and molar conductivity data are summarized in Table 1. The results of elemental analyses are consistent with the suggested formulation of the complexes. The study of the heterobimetallic complex (**4**) by EDAX[34] has shown that uranium and zinc are in the ratio of 1 : 1 and thus confirmed its formulation based on the elemental analysis. This ruled out the possibility of formation of mixed species in this case. All complexes are amorphous powders and are either dark red, orange, dark orange or brownish-orange. All complexes are insoluble in common organic solvents and dissolve in coordinating solvents like DMF and DMSO except for complex **4** which does not even dissolve in DMF and gives a suspension in DMSO. Due to their insolubility in common organic solvents, the complexes could not be recrystallized. The DMSO solutions of the compounds are coloured without showing any sign of colour change on dissolution, ruling out the possibility of displacement of the ligands in the coordination sphere by solvent molecules. All complexes decompose without melting above 300°C. The DMSO solutions of all the complexes (except that of the heterobimetallic complex **4** whose insolubility in DMSO excluded the possibility of its study by TLC) show a uniform spot on a TLC plate covered with silica gel and developed using a mixture of petroleum ether, ether and methanol in the ratio 2:2:1. The water contents were determined by heating the compounds at ~ 110 and ~ 180°C, respectively, for 4 h in an electric oven and passing the vapours through a trap containing anhydrous copper sulphate which turned blue. Complex **3** showed weight loss corresponding to three water molecules at ~110°C, while in complexes **2**, **4** and **5**, the weight loss corresponded to two water molecules only. The water molecules lost at ~ 110°C indicate that they are present in the lattice structure of the complexes. Complexes **1** and **2** showed weight loss corresponding to one water molecule while in **6** the weight loss corresponded to four water molecules at ~ 180°C. The water molecules lost at ~ 180°C in these complexes suggest that they are present in the coordination sphere around the metal centre. The IR spectra of **4** and **6** show a new band at 650 and 630 cm^{-1}, characteristic of coordinated water molecules[5,6] while that of complex **2** does not show any such band. This suggests that lone water lost at ~ 180°C in complex **2** is, most probably, embedded in the lattice structure of the complex in the strongly hydrogen-bonded form. The high decomposition temperature of the complexes suggest that they are polymeric materials in the solid state. The molar conductances of all the complexes except that of the heterobimetallic complex **4** lie in the range 20.5–0.5 Ω^{-1} cm^2 mol^{-1} in DMSO, indicating that these complexes are non-electrolytes in this solvent.[33]

Thermal analyses of the complex $[UO_2(H_2L_2)]_n$ $3nH_2O$ have been carried out as a representative sample up to 600°C. The final product of decomposition is U_3O_8. The decomposition of the complex occurs in three prominent steps, i.e. 80–120, 200–220 and 300–460°C. The complex loses

Table 1. Analysis, decomposition point, molar conductance data and per cent yield of dioxouranium(VI) complexes of disalicylaldehyde adipoyldihydrazone

Complex and colour	Decomposition point (°C)	Yield (%)	Analysis: found (calc.) % U	C	H	N	Molar conductance M M (Ω^{-1} cm^2 mol^{-1})
$[UO_2(H_2L_2)(H_2O)]_n$ (**1**) Orange	> 300	65	35.2 (35.6)	36.4 (35.9)	3.3 (3.3)	8.1 (8.4)	1.2
$[UO_2(H_2L_2)]_n3nH_2O$ (**2**) Orange	> 300	85	34.3 (33.8)	33.6 (34.1)	3.6 (3.7)	7.9 (8.0)	0.7
$[UO_2(H_3L_2)(CH_3COO)]_n3nH_2O$ (**3**) Brownish-orange	> 300	99	31.2 (31.7)	34.1 (34.6)	4.0 (3.9)	7.6 (7.3)	0.5
$[UO_2Zn(L_2)(H_2O)_2]_n2nH_2O^a$ (**4**) Orange	> 300	85	29.9 (30.3)	30.9 (30.6)	3.3 (3.3)	6.9 (7.1)	—
$[(UO_2)_2(H_2L_2)(C_2O_4)]_n2nH_2O^b$ (**5**) Dark red	> 300	65	45.1 (45.6)	25.7 (25.3)	2.3 (2.3)	5.5 (5.4)	20.5
$[(UO_2)_2(L_2)(py)_2(H_2O)_4]$ (**6**) Dark orange	> 300	60	41.1 (41.5)	31.7 (31.4)	3.2 (3.1)	6.9 (7.3)	2.8

[a] Zn = 8.6 (8.4) %.
[b] C_2O_4 = 8.2 (8.5) %.

mass in the temperature range 80–120°C and the mass loss corresponds to two water molecules, indicating that they are part of the lattice. Beyond 120°C, the complex is stable up to 200°C as the average mass loss is about 0.25% per 20°C interval. The complex shows mass loss corresponding to one water molecule in the temperature range 200–200°C. Although the loss of one water molecule at such high temperatures may indicate its presence in the coordination sphere around the uranium centre,[5] the IR spectrum of the complex does not show any new band around $\sim 630\ cm^{-1}$ characteristic of the coordination of water.[6] This suggests that the third water molecule in this complex is also present in the structural unit of the complex in the strongly hydrogen-bonded form with the coordinated anion.[7] The most significant decomposition of the complex occurs in the temperature range 300–460°C, the average mass loss being 8.7% per 20°C interval. The mass loss in this temperature range corresponds to two phenyl groups, two hydrazine groupings and one —C—$(CH_2)_4$—C— group. The loss of ligand starts at 300°C, occurs simultaneously in a single step, and is complete at 420°C. Beyond this temperature the complex shows negligible mass loss and the weight becomes constant at a temperature > 460°C, corresponding to U_3O_8. Such thermal behaviour of the complex indicates the symmetrical attachment of the ligand to the uranyl ion.

IR spectral data are given in Table 2. The essential features are medium–strong, broad bands in the IR spectrum of the uncoordinated ligand in the regions 3500–3250 and 3200–3000 cm^{-1}, having multiplet structure with maximum absorption at 3423 and 3186 cm^{-1} attributed to the composite nature due to ν(OH) and ν(NH) stretching vibrations of the ligand, which are altered on complex formation. The IR spectra of complexes **1**, **4** and **6** show a single, strong, broad band in the region 3650–3100 cm^{-1} with maximum absorption in the region 3438–3420 cm^{-1}. This band arises from ν(OH) of the phenolic —OH group of the ligand or ν(OH) of the lattice or coordinaed water molecules (**4**, **6**). The bands present in the regions 3500–3250 and 3200–3000 cm^{-1} in the IR spectrum of the uncoordinated ligand undergo splitting in the IR spectra of **2**, **3** and **5** and show maximum absorptions in the regions 3580–3537, 3420–3352 and 3200–3186 cm^{-1}. The bands in the region 3580–3557 cm^{-1} are due to the ν(OH) of either the uncoordinated phenolic —OH group or of the lattice water molecules, while the band in the region 3200–3186 cm^{-1} is due to the ν(NH) of the secondary amine group of the ligand. The band in the region 3420–3352 cm^{-1} may have a composite nature due to ν(OH) and ν(NH) stretching vibrations. The band present in the region 3200–3186 cm^{-1} in the IR spectra of the complexes, which is either at the same or higher position compared with the position of ν(NH) (3186 cm^{-1}) of the —CONH— group of the uncoordinated dihydrazone, rules out the possibility of coordination of the ligand through the secondary amine nitrogen atom. The essential features of the IR spectra of **1**, **4** and **6** in the region 3650–3100 cm^{-1} compared to those in the IR spectra of **2**, **3** and **5** suggest that the ligand coordinates to the uranyl ion in the enol form in the former complexes and in the keto form in the latter.

The band present at 1666 cm^{-1}, due to ν(C=O) in the IR spectrum of the uncoordinated ligand, disappears in the IR spectra of **1**, **4** and **6** suggesting the enolization of the ligand in these complexes and its subsequent coordination to the uranyl ion through the enolized carbonyl oxygen atom. The IR spectra of **2**, **3** and **5** show single, medium to strong bands in the region 1659–1639 cm^{-1} except in the case of complex **3** in which ν(C=O) splits into two bands which appear at 1675 and 1650 cm^{-1}. The appearance of only one band in the IR spectra of **2** and **5** suggests the coordination of the ligand to the uranyl ion through both of the carbonyl oxygen atoms, and that the two uranium–oxygen bonds are of equal strength. The splitting of the ν(C=O) band in the IR spectrum of complex **3** and its appearance at higher as well as lower positions compared to the position of the ν(C=O) band in the IR spectrum of the uncoordinated ligand, suggests the coordination of the ligand through only one $>C=O$ group while the other $>C=O$ group remains unbonded. When **3** is allowed to react with zinc acetate dihydrate in a 1 : 1 molar ratio in aqueous medium, the IR spectrum of the resulting compound $[UO_2Zn(L_2)(H_2O)_2]_n 2nH_2O$ does not show any band characteristic of a $>C=O$ group suggesting the enolization of the ligand in the complex.[8]

The band at 1555 cm^{-1} attributed to amide II and the ν(C—O) (phenolic) group of the uncoordinated ligand appears at 1542 cm^{-1} in the IR spectrum of complex **1**, indicating non-involvement of the phenolic oxygen atom in bonding. The band at 1542 cm^{-1} may be due to the ν(NCO) vibration of the newly created NCO group, produced as a result of enolization of the ligand. In the remaining complexes (**2** and **6**) this band undergoes splitting into two bands. The bands present in the region 1575–1564 cm^{-1} in the IR spectra of the complexes indicate the involvement of the phenolic —OH group in bonding. Such a high shift of the ν(C—O) stretching vibration indicates the involvement of the phenolic

Table 2. Important IR spectral bands of disalicylaldehyde adipoyldihydrazone and its dioxouranium(VI) complexes

Complex	ν(OH) + ν(NH)	ν(C=O)	ν(C=N)	Amide II + ν(C—O) (phenolic)	ν(NCO)	ν(C—O)	ν(N—N)	ν_3	ν_2	ν(U—O) (phenolic)	ν(U—O) (carbonyl)	ν(U—N)	Anion vibrations
H_4L_2	3423m 3186s	1666s	1623s 1612s	1555s	—	1278s 1261m	1035w	—	—	—	—	—	—
$[UO_2(H_2L_2)(H_2O)]_n$ (1)	3600–3300mbr	—	1603vs	1558msh	1542m	1275w	1034w	903vs	239s	—	477w 434w	396w 331w	—
$[UO_2(H_2L_2)]_n 3nH_2O$ (2)	3580s 3636–3300vsbr	1639s	1606s	1573s 1564s	—	1279s	1030w	903s	263m	594w 512w	416w 383w	368msh 318w	—
$[UO_2(H_3L_2)(CH_3COO)]_n$ (3)	3650–3300vsbr	1675s 1650s	1615vs	1565s 1555s 1510s[a]	—	1315s 1282m	1035w	905vs	255s	550w	430w	390s 345w	1510s[a] 1410m
$[UO_2Zn(L_2)(H_2O)_2]2nH_2O$ (4)	3600–3100sbr	—	1610vs	1575ssh	1545s	1307s 1280msh	1049w	905s 890s	255m	600m 545m	450m 405m	350w 320w	—
$[(UO_2)_2(H_2L_2)(C_2O_4)]_n 2nH_2O$ (5)	3557s 3417s 3199s	1659s[b]	1603s	1585s 1547s	—	1299s	1035w	911s	264s	603m 521m	495w 413w	379w	ν_{as}(C=O) 1659s ν_s(C=O) 1394s 1329m
$[(UO_2)_2(L_2)(py)_2(H_2O)_4]$ (6)	3650–3100sbr	—	1607vs	1550s	1545s	1304m	1035w	905s	250s	595s 520m	410s 395s	323s 313s	ν(U—N) (pyridine) 270s

[a] Mixed contribution due to the amide II (ligand) and ν_{as}(OCO) of the coordinated acetato group.
[b] ν_{as}(C=O) (oxalate) and ν(C=O) (dihydrazone) mixed.

oxygen atom in the bridge formation.[9,10] The band present in the region 1547–1510 cm^{-1} indicated the coordination of the carbonyl oxygen atom to the uranyl ion in **2**, **3** and **5**. The band at 1545 cm^{-1} in complexes **4** and **6** is due to the newly created NCO group as a result of enolization,[11] while ν(C—O) (phenolic) appears at 1550 cm^{-1} in complex **6**. The position of ν(C—O) (phenolic) in this complex rules out the possibility of the existence of oxo-bridging. In complex **3** the IR spectrum contains a band at 1555 cm^{-1} indicating that only one $\rangle C{=}O$ group takes part in coordination while the other $\rangle C{=}O$ group remains unbonded.[12]

The IR spectrum of the ligand shows absorption bands at 1623 and 1612 cm^{-1} which are assigned to a ν(C=N) stretching vibration. These bands lose their doublet character on complexation and are considerably lower in energy, appearing in the region 1615–1603 cm^{-1} in the IR spectra of the complexes. This suggests the involvement of the azomethine nitrogen atoms in bonding.[13,14] The loss of the doublet character of bands due to $\rangle C{=}N$ groups in the IR spectra of the complexes suggests that the two azomethine nitrogen atoms are coordinated to the uranium centre and the two uranium–nitrogen bonds are of equal strength. On examining the spectra of the ligand and its uranyl complexes in the low frequency IR spectral region, the new bands appearing in the ranges 603–510, 495–383 and 396–313 cm^{-1} are tentatively assigned to ν(U—O) (phenolic),[15] ν(U—O) (carbonyl)[16] and ν(U—N),[17] respectively. Complex **6** shows a strong absorption band at 270 cm^{-1} in the low frequency IR spectral region which is observed neither in the ligand nor in the remaining complexes. This band is tentatively assigned as an IR active uranium–nitrogen stretching mode due to the coordinated pyridine group.[18]

Complex **3** shows additional bands at 1510 and 1410 cm^{-1} in its IR spectrum, which are observed neither in the IR spectrum of the uncoordinated ligand nor in those of the other complexes. Hence, these bands are identified as ν_{as}(CO) and ν_s(CO) of the coordinated acetate groups. The IR frequencies associated with ν_{as}(CO) and ν_s(CO) stretching vibrations of the coordinated acetate groups in these complexes are in the same region in which the bidentate chelating acetate group has been established to absorb by X-ray[19] and IR spectroscopy.[20] The oxalato complex (**5**) shows bands at 1659, 1394 and 1329 cm^{-1}. The band at 1659 cm^{-1} has a composite nature due to the amide I band of the coordinated ligand and ν_{as}(C=O) of the coordinated oxalate group. In view of the absence of isotopic substitution studies it is difficult, at present, to assign unambiguously the bands due to ν_{as}(CO) of the coordinated oxalate group and ν(C=O) of the coordinated ligand. The absence of any band at 1750–1680 cm^{-1} which is regarded as typical of chelated and bridging bidentate oxalato groups is consistent with the bridging tetradentate nature of the oxalato group in the complex.[21]

The IR spectra of all the uranyl complexes studied here show strong absorption in the 911–890 cm^{-1} region, masking weak ligand bands occurring in this region. This band is assigned to a ν_3 asymmetric stretching vibration of the uranyl group. ν_1 Symmetric stretching vibration of the linear uranyl group is IR forbidden. The IR spectra of the complexes do not show any band around 860 cm^{-1} except for complex **1** in which a medium intensity band is observed at 861 cm^{-1}. This band appears to have its origin due to a weak intensity band at 864 cm^{-1} in the IR spectrum of the uncoordinated ligand which appears to be activated on complex formation. This double degenerate bending mode is observed as a medium to strong band in the 264–239 cm^{-1} region.

The ligand H_4L_2 shows absorption bands at 245, 290, 300 and 344 nm due to $n \rightarrow \pi^*$ and $\pi \rightarrow \pi^*$ transitions[22,23] within the ligand molecule. The absorption spectra of the complexes $[(UO_2)_2(L_2)(py)_2(H_2O)_4]$ and $[UO_2Zn(L_2)(H_2O)_2]_n 2nH_2O$ were recorded in the solid state in the region 300–800 nm as representative samples which show rather strong and easily detectable absorption bands at 370, 415, 500 and 375, 500 nm, respectively. The ligand band at 344 nm shifts to longer wavelength and appears at 370 and 375 nm in the electronic spectra of the complexes. This longer shift of the 344 nm absorption band on complexation shows that uranium–ligand interaction is strong in these complexes. The absorption band at 415 nm in the complex $[(UO_2)_2(L_2)(py)(H_2O)_4]$ may arise by strong absorption, corresponding to the charge-transfer from equatorial ligands to the uranium atom. The band at 500 nm arises from the electronic transitions from apical oxygen to *f* orbitals of the uranyl moiety.[24] Although the electronic spectrum of **4** does not exhibit any additional band in the region 375–500 nm, due to the transfer of charge from the completely filled 3*d* orbital of zinc to the completely vacant 5*f* orbital of the uranium atom, the possibility of the existence of a $3d^{10} \rightarrow 5f^0$ transition in these complexes cannot be eliminated. This band is either merged with the strong band around 375 nm or with the absorption band at around 500 nm due to the electronic transition from apical oxygen to the *f* orbital of the uranyl moiety. Thus the possibility of the existence of a metal–metal

Table 3. ^{1}H NMR spectral data for disalicylaldehyde adipoyldihydrazone and some of its dioxouranium(VI) complexes

Complex	—$(CH_2)_4$—	Phenyl	—NH—	Azomethine	—OH
H_4L_2	1.65 2.28	6.6–7.7(m)	11.17	8.34–8.42	11.57
$[UO_2(H_2L_2)(H_2O)]_n$ (1)	2.13–2.70(m)	6.71–7.87(m)	—	9.27	10.49
$[UO_2(H_2L_2)]_n 3nH_2O$ (2)	2.05–2.72(m)	6.69–7.85(m)	11.38	9.19	—
$[(UO_2)_2(H_2L_2)(C_2O_4)]_n 2nH_2O$ (5)	2.00–2.70(m)	6.73–7.69(m)	11.31	9.19	—
$[(UO_2)_2(L_2)(py)_2(H_2O)_4]$ (6)	2.05–2.63(m)	6.57–7.77(m)	—	9.07	—

m, multiplets.

interaction in this complex cannot be ruled out.[25]

^{1}H NMR spectral data are given in Table 3. In complexes **2**, **5** and **6** the signal due to phenolic-OH protons appearing at 11.57 ppm in the ^{1}H NMR spectrum of uncoordinated dihydrazone disappears, indicating deprotonation of the phenolic-OH group on complex formation. However, this signal is observed at 10.49 ppm in the ^{1}H NMR spectrum of $[UO_2(H_2L_2)(H_2O)]$, indicating the presence of the phenolic-OH group in the complex. The presence of phenolic-OH at the higher field suggests that the phenolic-OH group is free from strong intramolecular hydrogen-bonding, but the possibility of the existence of weak intramolecular hydrogen-bonding cannot be dismissed. This, alternatively, suggests the bonding of the ligand to the uranyl ion through the enolized carbonyl oxygen atom. The signal due to the azomethine proton appears as a singlet in the region 9.07–9.27 ppm in the ^{1}H NMR spectra of these complexes. The azomethine protons appear as a doublet resonance (8.34, 8.42 ppm) in the ^{1}H NMR spectrum of the uncoordinated dihydrazone. This downfield shift is due to the deshielding caused by the coordination of azomethine nitrogen to the uranyl ion.[26,27] The signal due to —NH protons in free ligands at 11.17 ppm disappears in **1** and **6** and appears at 11.28 and 11.31 ppm in **2** and **5**. The disappearance of the —NH signal in **1** and **6** indicates that the ligand is present in the complex in the enolic form while in **2** and **5** the downfield shift of —NH signals on complexation in ^{1}H NMR spectra is due to deshielding caused by the drainage of electrons of carbonyl oxygen to the uranyl group as a result of coordination. The multiplet resonances due to the phenyl ring protons of the ligand are altered in position on complexation and appear as multiplets in the ^{1}H NMR spectra of the complexes, indicating involvement of the ligand in coordination to the uranyl ion. The signals due to pyridine are merged with the signals of phenyl protons in the ^{1}H NMR spectrum of complex **6**. The methylene proton signals in the ligand are shifted downfield on complexation, indicating coordination of the ligand through the >C=O group either in the keto or enol form. The signals due to methylene protons of the free ligand at 1.65 and 2.28 ppm appear in the region 1.92–2.72 ppm in the ^{1}H NMR spectra of the complexes.

Based on the physico-chemical evidence presented and discussed above, complexes **5** and **6** may be suggested to involve eight-coordinated uranium[28] while **1–3** may be suggested to involve seven-,[28] nine-[29] and ten-[30]coordinated uranium, respectively. The position of $\nu_3(UO_2^{2+})$ in the IR spectrum of **4**, compared with its position in the IR spectra of the remaining complexes, and the equatorial coordination number of the uranium atom may indicate that the equatorial coordination number of uranium in this complex should be between five and eight. This therefore demands the coordination of water molecules to the uranium centre in the complex. The coordination of two water molecules to the uranium centre raises the equatorial coordination number of the complex to six. The phenolic-oxygen atom, enolized carbonyl-oxygen atom, azomethine-nitrogen atom and oxo-bridged oxygen atom occupy the vertices of a tetrahedron around the zinc atom.

EXPERIMENTAL

Materials and measurements

Uranyl acetate dihydrate, uranyl nitrate hexahydrate, diethyl adipate, hydrazine hydrate and salicylaldehyde were of BDH, AR or equivalent grade. Adipoyldihydrazine was prepared by reacting the diethyladipate (1 mol) with hydrazine hydrate (2 mol). The disalicylaldehyde adipoyldihydrazone was prepared by reacting a warm dilute ethanol solution of adipoyldihydrazine (1 mol) with salicylaldehyde (2 mol) and was suction filtered, washed with water and ethanol and dried at 70°C in an electric oven; it was characterized as described elsewhere.[31]

Uranium and zinc in the complexes were determined by the standard literature procedure.[32] Carbon, hydrogen and nitrogen were determined by microanalyses. The EDAX spectrum was recorded using the Energy Dispersive X-ray spectrometer (AN 10000, Link-Analytical). The sample was coated with carbon in a JEOL vacuum evaporator and placed into the specimen chamber of the microscope column (scanning electron microscope, JSM-3SCF) operating at 20 kV. Water molecules were determined by heating the sample in an electric oven at 110 and 180°C, respectively, and passing the vapours through a trap containing copper sulphate, which turned blue, and estimating the weight loss. IR spectra were recorded on a Perkin–Elmer 983 spectrophotometer using KBr pellets in the 4000–180 cm^{-1} region. The molar conductance of the complexes at 10^{-3} M dilution in DMSO was measured using an Elico-conductivity bridge, model CM-82T, with a dip-type conductivity cell. Electronic spectra of the complexes were recorded on a Cary-14 model in the region 300–800 nm. Magnetic measurements were made on powders using a Gouy balance with MTTCC as calibrant. The ESR spectra were recorded on a Varian spectrometer in the solid state using DPPH as reference. The ^1H NMR spectra were run on a EM-390 90 MHz spectrometer using DMSO-d_6 solutions.

Preparation of the complexes

The complexes were prepared by the following procedures.

$[UO_2(H_2L_2)(H_2O)]_n$ (**1**). An aqueous solution of adipoyldihydrazine (0.1 M, 50 cm^3) was added to the uranyl acetate dihydrate (0.11 M, 50 cm^3) solution and stirred for about 10 min, which produced a turbid mixture. The reaction mixture was refluxed for 2 h and yielded a coloured compound. This was removed by filtration, washed with water containing a drop of acetic acid, water, ethanol and ether and dried before suspending in ethanol (20 cm^2), followed by addition of salicylaldehyde (100 cm^3). The resulting mixture was refluxed for 2 h giving a dark coloured solution, which on cooling yielded a precipitate. This was removed by filtration, washed with ethanol and dried over anhydrous calcium chloride.

$[UO_2(H_2L_2)]_n3nH_2O$ (**2**). H_4L_2 (1.0 g), powdered using an agate mortar, was placed in a beaker containing 60 cm^3 of water and stirred well to give a homogeneous slurry. Uranyl nitrate hexahydrate (0.1 M) in water was added to the ligand slurry with gentle stirring, maintaining the molar ratio at 3 : 1. The complex precipitated on refluxing the reaction mixture for 3 h and was again refluxed for 15 min in benzene. It was then filtered by suction, washed twice with hot benzene and twice with water containing a drop of acetic acid, three times with hot alcohol and finally with ether and was collected as above.

$[UO_2(H_3L_2)(CH_3COO)]_n3nH_2O$ (**3**). Uranyl acetate dihydrate (1.8 g) was dissolved in warm ethanol (100 cm^3) containing a drop of acetic acid by gentle stirring. To this solution salicylaldehyde (47 cm^3, 0.1 M) in ethanol was added, accompanied by stirring, and refluxed for 15 min. Adipoyldihydrazine (42.5 cm^3, 0.1 M) in hot ethanol was added with vigorous stirring and the resulting solution was refluxed for 2 h. The complex which precipitated was filtered while hot and again refluxed for an additional 30 min in benzene and hot filtered. The complex was washed with hot benzene, ethanol and ether, and collected as above.

$[UO_2Zn(L_2)(H_2O)_2]_n2nH_2O$ (**4**). The complex $[UO_2(H_3L_2)(CH_3COO)]_n3nH_2O$ (1.0 g) was suspended in water (50 cm^3). To this suspension, zinc acetate dihydrate (0.05 M, 35 cm^3) was added and the resulting reaction mixture was refluxed for 3 h. The compound was filtered by suction, and washed three times with ethanol containing a drop of acetic acid, pure ethanol, benzene and ether, and collected as above.

$[(UO_2)_2(H_2L_2)(C_2O_4)]_n2nH_2O$ (**5**). Method 1: H_4L_2, powdered using an agate mortar, was placed in a beaker containing ethanol and stirred well to give a homogeneous slurry (0.05 M, 50 cm^3). An ethanolic solution of uranyl nitrate hexahydrate (0.05 M, 150 cm^3) was added to the ligand slurry with gentle stirring. The resulting mixture was refluxed for 3 h and produced a clear solution. Any undissolved impurities at this stage were removed by filtration. The solution, on concentration (70 cm^3) followed by addition of ether, precipitated a semi-solid. This was extracted with benzene, stirred well for about 1 h, and kept overnight. The precipitate so obtained was washed with an ethanol–benzene mixture, suspended in ethanol (100 cm^3) and heated again to give a solution. To this solution, oxalic acid solution (0.05 M, 150 cm^3) was added, maintaining the molar ratio of uranyl nitrate hexahydrate : H_4L_2 : oxalic acid at 3 : 1 : 3. The reaction mixture was refluxed for an additional 30 min which precipitated the complex. The complex was filtered while hot, washed several times with ethanol, benzene and ether, and collected as above.

Method 2: H_4L_2, powdered using an agate mortar, was placed in a beaker containing ethanol and stirred well to give a homogeneous slurry (0.05 M, 50 cm^3). Uranyl nitrate hexahydrate in ethanol was added to the ligand slurry with continuous stirring, maintaining the molar ratio at 2 : 1, and the resulting mixture was refluxed for 2 h. To this

reaction mixture, oxalic acid was added in slight excess of the required 2 : 1 : 1 molar ratio of uranyl nitrate hexahydrate : H_4L_2 : oxalic acid. The reaction mixture was refluxed for an additional 30 min followed by concentration, washing with ethanol and benzene and finally with ether, and collected as above.

$[(UO_2)_2(L_2)(py)_2(H_2O)_4]$ (**6**). Uranyl acetate dihydrate was dissolved in water solution. A slurry of the ligand (1.0 g) was prepared in the usual way in a 50 cm^3 water–ethanol mixture (4 : 1). Uranyl acetate solution was added to this slurry maintaining the uranyl acetate dihydrate : H_4L_2 ratio at 3 : 1. This reaction mixture was refluxed for 1 h and the precipitated complex was filtered, washed with a water–ethanol mixture and then suspended in excess pyridine (50 cm^3) and refluxed for 2 h. The precipitate dissolved completely, resulting in a clear solution. The solution was concentrated to 30 cm^3 by evaporation and cooled to room temperature. To this solution, benzene (150 cm^3) was added which precipitated the complex. The reaction mixture was stirred for 10 min and the precipitated complex was removed by filtration, washed with benzene, ethanol and ether, and collected in the usual manner.

Acknowledgements—The authors are thankful to Professor M. K. Chaudhuri for helpful discussion. Furthermore, they thank Dr D. T. Khathing, Head, Regional Sophisticated Instrumentation Centre, Shillong, for recording IR, NMR and EDAX spectra of the complexes.

REFERENCES

1. J. R. Dilworth, *Coord. Chem. Rev.* 1976, **12**, 29; M. Katyal and Y. Dutt, *Talanta* 1975, **22**, 150.
2. R. L. Dutta and Md. M. Hossain, *J. Sci. Indian Res.* 1985, **44**, 635; R. P. Singh, R. B. Singh and P. Jain, *Talanta* 1982, **29**, 77.
3. P. J. Sadler, *Inorg. Perspect. Biol. Med.* 1978, **1**, 233; A. M. Bond, M. Haga, I. S. Greece, R. Robson and J. C. Wilson, *Inorg. Chem.* 1988, **27**, 712.
4. I. Margenstern-Badaran, D. Cocco, A. Desideri, G. Rotilio, J. Jordanov and N. Dupre, *J. Am. Chem. Soc.* 1986, **108**, 300; Y. Pei, Y. Journaux and O. Khan, *Inorg. Chem.* 1988, **27**, 399.
5. A. C. Fabretti, C. G. Franchini, C. P. Preti and G. Tosi, *Can. J. Chem.* 1980, **19A**, 137.
6. A. R. Nicholson and G. J. Sutton, *Aust. J. Chem.* 1969, **22**, 273; B. Singh, B. P. Yadava and R. C. Aggarwal, *Indian J. Chem.* 1984, **23A**, 33.
7. A. V. Nikolov, V. A. Logvinenko and L. I. Myachina, *Thermal Analysis*, Vol. 2. Academic Press, New York (1969).
8. V. M. Leovac, L. J. Bjelica, L. S. Jovanovic and S. Y. Chandak, *Polyhedron* 1986, **5**, 983; V. M. Leovac, L. J. Bjelica and L. J. Jovanovic, *Polyhedron* 1985, **4**, 233; S. Yu. Chundsk, N. V. Gerbeleu and S. S. Butsko, *Zh. Neorg. Khim.* 1984, **29**, 1481.
9. R. J. Butcher, J. Jasinki, G. M. Mockler and E. Sinn, *J. Chem. Soc., Dalton Trans.* 1976, 1099.
10. J. O. Miners, E. Sinn, R. B. Coles and C. M. Harris, *J. Chem. Soc., Dalton Trans.* 1972, 1149 and refs therein.
11. H. Yamada, *Bull. Chem. Soc. Japan* 1959, **32**, 1051.
12. L. El-Sayed, M. F. Iskander and A. El-Toukhy, *J. Inorg. Nucl. Chem.* 1976, **38**, 2209.
13. S. A. Pardhy, K. Joseph, S. Gopinathan and C. Gopinathan, *Polyhedron* 1985, **4**, 307; N. S. Navaneetham, R. Kalyasundaram and S. Soundaranjan, *Inorg. Chim. Acta* 1985, **110**, 169; T. M. Aminabhavi, N. S. Biradar, C. S. Patil and W. E. Rudzinski, *Inorg. Chim. Acta* 1983, **78**, 107.
14. W. E. Rudzinski, T. M. Aminabhavi, N. S. Biradar and C. S. Patil, *Inorg. Chim. Acta* 1982, **67**, 177; 1983, **69**, 83; 1983, **78**, 51.
15. G. C. Percy and D. A. Thornton, *J. Inorg. Nucl. Chem.* 1973, **34**, 3351; 3369; 1973, **35**, 2719; G. C. Percy, *J. Inorg. Nucl. Chem.* 1975, **37**, 2071.
16. M. Mikami, I. Nakagawa and T. Shimanouchi, *Spectrochim. Acta* 1967, **23A**, 1037.
17. R. J. H. Clark, *J. Chem. Soc.* 1962, 1377; R. J. H. Clark and C. S. Williams, *Chem. Ind.* 1964, 1317; *Inorg. Chem.* 1965, **4**, 350.
18. J. R. Ferraro, *Low Frequency Vibrations of Inorganic and Coordination Compounds*, Chaps 5 and 7. Plenum Press, New York (1971).
19. W. H. Zachariasen and H. A. Plettinger, *Acta. Cryst.* 1959, **12**, 526.
20. K. Nakamoto, J. Fujita, S. Tanaka and M. Kobayashi, *J. Am. Chem. Soc.* 1957, **79**, 4904.
21. K. Nakamoto, *Infrared Spectra of Inorganic and Coordination Compounds*, 2nd edn. Wiley-Interscience, New York (1970).
22. A. A. T. Hsieh, R. M. Sheahan and B. O. West, *Aust. J. Chem.* 1975, **28**, 885; A. Syamal and M. R. Maurya, *Indian J. Chem.* 1985, **24A**, 836.
23. R. L. Dutta and A. K. Pal, *Indian. J. Chem.* 1985, **24A**, 76.
24. B. I. Kim Bong, C. Miyake and S. Imoto, *J. Inorg. Nucl. Chem.* 1975, **37**, 763; I. S. Ahuja, C. L. Yadava and S. Tripathi, *Indian. J. Chem.* 1988, **27A**, 171.
25. D. W. Stephan and T. A. Wark, *Inorg. Chem.* 1987, **26**, 363 and refs therein.
26. S. A. Patil and V. H. Kulkarni, *Inorg. Chim. Acta* 1984, **95**, 195.
27. M. Vidali, P. A. Vigato and U. Casellato, *J. Inorg. Nucl. Chem.* 1975, **37**, 955; G. Paolucci, G. Marangoni, G. Bandoli and D. A. Clemente, *J. Chem. Soc., Dalton Trans.* 1980, 1304.
28. A. F. Wells, *Structural Inorganic Chemistry*, 3rd edn. Oxford University Press, Oxford (1966); W. H. Zachariasen, *Acta Cryst.* 1954, **7**, 795; C. Cattalini, U. Croatto, S. Degetto and E. Tandello, *Inorg. Chim. Acta Rev.* 1971, **5**, 19.
29. I. S. Ahuja and R. Singh, *J. Inorg. Nucl. Chem.* 1973, **35**, 561.

30. I. S. Ahuja and R. Singh, *Transition Met. Chem.* 1977, **2**, 32.
31. R. A. Lal, K. N. Srivastava and S. Das, *Synth. React. Inorg. Met.-Org. Chem.* 1988, **17**, 837.
32. A. I. Vogel, *A Text Book of Quantitative Inorganic Analysis*. The English Language Book Socicty, Longmans, London (1973).
33. W. J. Geary, *Coord. Chem. Rev.* 1971, 7, 81.
34. P. Guerriero, P. A. Vigato and B. Burtet-Fabris, *Inorg. Chim. Acta* 1989, **165**, 155; T. J. Hopen, B. G. Wortmen, L. D. Detter, J. M. Redstock and T. B. Vander, *International Laboratory* 1989, 14.

Polyhedron Vol. 10, No. 8, pp. 789–791, 1991
Printed in Great Britain

0277–5387/91 $3.00+.00
© 1991 Pergamon Press plc

SYNTHESIS AND CHARACTERIZATION OF ARYLOXY DERIVATIVES OF TRIORGANOARSENIC(V)

NEERAJ SHARMA,* B. S. GOLEN, R. K. MAHAJAN and S. C. CHAUDHRY

Department of Chemistry, Himachal Pradesh University,
Summer Hill, Shimla-171005, India

(*Received* 20 *June* 1990; *accepted* 16 *November* 1990)

Abstract—Triorganoarsenic(V) aryloxides of composition $Ph_3AsCl_{2-n}(OAr)_n$ (where Ar = *p*-ClC_6H_4, *p*-$(CH_3)_3CC_6H_4$, *p*-$NO_2C_6H_4$, *p*-$CH_3OC_6H_4$) have been obtained by the reaction of triphenylarsenic dichloride with the respective phenols in appropriate molar ratios in tetrahydrofuran in the presence of triethylamine. They have been characterized on the basis of elemental analysis, conductance, IR and NMR spectral studies.

A survey of the literature reveals that the role of pentacoordination of main group elements in reaction mechanisms[1–5] is potentially one of the best methods to explore the possibility of conformations extended from the ideal trigonal bipyramid to the square or rectangular pyramid. The compounds of pentacoordinated phosphorus,[6,7] arsenic and antimony[8] are probably the most interesting. Compared with pentacoordinated phosphorus and antimony compounds containing P—O and Sb—O bonds, only a limited number of analogous arsenic compounds are known. A few acyclic compounds of the type $As(OR)_5$ (R = Me, Et), $R_2As(OMe)_3$ (R = Me, Ph) and $R_3As(OMe)_2$ (R = Ph) have been reported[9,10] to be formed by the reaction of the corresponding halides of trivalent arsenic with bromine and sodium methoxide in bromine solution. In an effort to extend this chemistry, we have synthesized aryloxy derivatives of triorganoarsenic(V) by a facile and high yield synthetic route.

EXPERIMENTAL

Triphenylarsenic dichloride was prepared by the reported method, employing the reaction of triphenylarsine oxide with 2 mol of acetyl chloride. Phenols used were purified by recrystallization from carbon tetrachloride, and all the reactions were carried out under strictly anhydrous conditions. The arsenic content in isolated compounds was determined as silver arsenate. The IR spectra in the 4000–200 cm^{-1} region were scanned using KBr pellets with Perkin–Elmer 337 and 621 spectrophotometers. ^1H NMR spectra were recorded on a JEOL JNM-DMX60 spectrometer in $CDCl_3$ solutions using TMS as internal standard.

Preparation of $Ph_3AsCl(OAr)$ *and* $Ph_3As(OAr)_2$

Compounds of composition $Ph_3AsCl(OAr)$ and $Ph_3As(OAr)_2$ were prepared by reacting Ph_3AsCl_2 with the corresponding phenols in 1:1 and 1:2 molar ratios in THF in the presence of triethylamine at 0°C. The reaction mixture was slowly brought to room temperature and stirred for 3 h. Triethylamine hydrogen chloride which formed as a white solid was removed by filtration. The excess solvent from the filtrate was removed under reduced pressure at 30°C. The remaining solution was concentrated *in vacuo* to give a colourless liquid.

^1H NMR and IR spectra of the liquid compounds were recorded immediately. Brief exposure to moisture or work-up of the liquid compounds to obtain their solid analogues gave a hydrolysed product, triphenylarsenic hydroxy chloride or triphenylarsenic oxide, confirmed from the melting points reported in the literature.

RESULTS AND DISCUSSION

The compounds isolated in the present study are listed in Table 1 and can be considered to be formed as follows:

* Author to whom correspondence should be addressed.

Table 1. Physicochemical data of phenoxides of triorganoarsenic(V)

Compounds	Boiling point (°C)	Elemental analysis: % Arsenic found (calc)	Elemental analysis: % Chlorine found (calc)	Molar conductance in nitrobenzene ($\Omega^{-1}cm^2mol^{-1}$)	IR: C—O	IR: As—O	IR: As—Cl	^{1}H NMR phenoxy protons as As—OC_6H_4: H_o	H_m	—$C(CH_3)_3$	—OCH_3
$Ph_3AsCl[OC_6H_4C(CH_3)_3$-*p*]	124	15.3 (15.2)	7.2 (7.2)	16.6	1190	775	365	6.85–6.95	7.15–7.25	1.25	—
$Ph_3AsCl(OC_6H_4NO_2$-*p*)	148	16.0 (15.9)	7.4 (7.4)	18.7	1234	782	372	7.1–7.15	7.9–8.0	—	—
$Ph_3AsCl(OC_6H_4OCH_3$-*p*)	138–140	16.2 (16.1)	7.6 (7.6)	17.9	1188	778	370	6.8–6.9	6.6–6.7	—	3.67
$Ph_3AsCl(OC_6H_4Cl$-*p*)	169	16.0 (15.9)	14.9 (15.1)	16.9	1210	780	375	6.7–6.9	7.15–7.25	—	—
$Ph_3As[OC_6H_4C(CH_3)_3$-*p*]$_2$	105	12.1 (12.2)	—	15.2	1192	770	—	6.8–6.9	7.1–7.2	1.25	—
$Ph_3As(OC_6H_4NO_2$-*p*)$_2$	129	12.8 (12.8)	—	16.6	1240	786	—	7.15–7.2	8.05–8.15	—	—
$Ph_3As(OC_6H_4OCH_3$-*p*)$_2$	112	13.5 (13.5)	—	16.0	1195	782	—	6.9–6.95	6.75	—	3.60
$Ph_3As(OC_6H_4Cl$-*p*)$_2$	132	13.3 (13.3)	—	15.5	1212	784	—	6.8–6.85	7.2	—	—

$$Ph_3AsCl_2 + ArOH \xrightarrow[THF]{Et_3N} Ph_3AsCl(OAr) + Et_3NHCl$$

$$Ph_3AsCl_2 + 2ArOH \xrightarrow[THF]{Et_3N} Ph_3As(OAr)_2 + 2Et_3NHCl.$$

The elemental analyses of the compounds revealed that their stoichiometric composition was $Ph_3AsCl(OAr)$ and $Ph_3As(OAr)_2$. The magnitude of molar conductance values of the compounds in nitrobenzene, acetonitrile and acetone suggest they are weak electrolytes.

The formation of triorganoarsenic(V) aryloxides is clearly indicated by the absence of phenolic OH protons in the ^1H NMR and the disappearance of bands in the region 3500–3200 cm^{-1} in the IR spectra. A significant lowering of the ν(C—O) band by 30–40 cm^{-1} and the appearance of new bands in the region 760–780 cm^{-1} attributed to ν(As—O) was observed, together with bands in the region 390–360 cm^{-1} in some of the above compounds which may be assigned to ν(As—Cl).

The aromatic protons of As—Ph appear at δ 7.6–7.7, and the positions of the protons *ortho* and *meta* to the aryloxy oxygen and those of *para* substituents also support the formation of the above compounds. All the important bands in the IR and NMR spectra are presented in Table 1. The data available do not conflict with the proposition of a trigonal bipyramidal structure for the new compounds.

REFERENCES

1. R. R. Holmes, *Pentacoordinated Phosphorus Reaction Mechanisms*, Vol. III, ACS Monogr. 176. Washington, DC (1980).
2. R. R. Holmes, *J. Am. Chem. Soc.* 1978, **100**, 433.
3. D. L. Keppert, *Inorganic Stereochemistry*. Springer-Verlag, Berlin (1982).
4. A. C. Sau and R. R. Holmes, *J. Organomet. Chem.* 1981, **217**, 157.
5. J. S. Wood, *Prog. Inorg. Chem.* 1972, **16**, 227.
6. R. R. Holmes, *Pentacoordinated Phosphorus Structure and Spectroscopy*, Vol. 1, ACS Monogr. 175. Washington, DC (1980).
7. R. Luckenbach, *Dynamic Stereochemistry of Pentacoordinated Phosphorus and Related Elements*. Thieme, Stuggart (1973).
8. V. K. Jain, R. Bohra and R. C. Mehrotra, *Struct. Bond.* 1982, **52**, 147.
9. A. S. Dale and P. Froyen, *Acta Chem. Scand.* 1975, **B29**, 362.
10. H. Preiss, *Z. Anorg. Allg. Chem.* 1975, **175**, 404.

Polyhedron Vol. 10, No. 8, pp. 793–797, 1991
Printed in Great Britain

0277–5387/91 $3.00+.00
© 1991 Pergamon Press plc

MONOMER AND DIMER COMPLEXES OF COPPER(II) ACETATE WITH PYRIDINE AND PICOLINES—II.* SOLUTION EQUILIBRIA BY SPECTROPHOTOMETRIC AND NMR MAGNETIC MEASUREMENTS

A. LATIF ABUHIJLEH†

Chemistry Department, Birzeit University, P.O. Box 14, West Bank—Via Israel

and

I. Y. AHMED

Chemistry Department, The University of Mississippi, University, MS 38677, U.S.A.

(*Received* 3 *May* 1990; *accepted* 10 *December* 1990)

Abstract—Equilibrium constants (K) for the reaction:

$$[Cu(OAc)_2 \cdot L]_2 + 2L \rightleftharpoons 2[Cu(OAc)_2 \cdot L_2],$$

where OAc is the acetate anion and L = pyridine (py), β-picoline (β-pic) or γ-picoline (γ-pic), were determined from spectrophotometric and variable-temperature magnetic measurements in chloroform solutions. Good agreement was found between the two methods. The small K values (0.01–0.45) found for the equilibria are consistent with the observed instability of the monomers in chloroform, and increase in the order: py < β-pic < γ-pic. The position of the β-picoline system, for which no crystalline monomer could be isolated, and the anomalous behaviour of α-picoline within this series are discussed in terms of crystal-packing requirements arising from the steric properties of these ligands. Thermodynamic parameters for the equilibria were obtained from the temperature dependence of K. The values of $\Delta H^{\ominus}$ and $\Delta S^{\ominus}$ are in close agreement with those found for adduct formation of related copper(II) chelates with these ligands, and are discussed in terms of contributions from electronics and structural reorganization, bond formation and solvation effects.

Copper(II) carboxylate adducts with a large variety of ligands have been extensively investigated, and the results have been summarized in several reports.[1–4] Attention has been directed primarily at understanding the structural basis for the special magnetic and spectral properties of the dimeric mono-adducts. Some copper(II) carboxylates, on the other hand, tend to form monomeric bis- and tetrakis-adducts with these ligands.[5–9] There have been many studies to investigate the factors which influence dimer formation over monomer formation in copper(II) carboxylate solvate complexes.[3,6–8] It has been found, generally, that increasing acidity of the carboxylate groups and/or the basicity of the ligands increases the tendency towards formation of a monomeric adduct which is related to the electronic effects of the carboxylate groups and of the ligands.[6–8]

Previously,[9] we reported the preparation and characterization of some monomeric bis-adducts as well as the dimeric mono-adducts of copper(II) acetate with pyridine and picolines. Although the four dimeric adducts are converted to the monomeric complexes in solutions of their respective ligands, only in the cases of pyridine and α-picoline were crystalline monomeric bis-adducts isolated. In an effort to shed some light on the role of the addend in stabilizing either of the two structural types, we report herein the results of equilibrium measurements for the monomer–dimer interconversion.

* For Part I, see ref. 9.

† Author to whom correspondence should be addressed.

Because the two adducts have distinctly different spectral and magnetic properties and as a result of the relative instability of the monomers in most solvents, these systems are well suited for detailed examination by electronic and NMR spectral method. The utility of NMR spectroscopy to measure temperature-dependent magnetic properties and solution equilibria, where structural changes with concomitant changes in magnetic moments occur, has been amply demonstrated for several types of equilibria exhibited in solutions of transition metal complexes.[10-13] Solution magnetic studies of structural equilibria have the advantage of providing reliable thermodynamic parameters which are free from unpredictable lattice effects. The availability of a variable-temperature NMR probe permits the equilibrium constant to be determined over a wide range of temperatures and the thermodynamic parameters to be ascertained.

EXPERIMENTAL

Apparatus and measurements

Preparation of the complexes and characteristics of their solutions have been described previously.[9] Solution mixtures for equilibrium constant determination were prepared by the addition of varying amounts of the ligand to portions of a known fixed concentration of the dimer in chloroform solution. For NMR measurements, the latter solution contained 6% (v/v) cyclohexane as internal reference and 4% TMS for signal-locking. The ^{1}H NMR spectral measurements were recorded at 90 MHz on a Perkin–Elmer R-32 spectrometer in Wilmad co-axial tubes with movable glass spacers. The temperature calibration was monitored by methanol or ethylene glycol samples. The signal separation of the reference at each temperature was the average of at least four consecutive recordings which were further checked by comparison with the separation of chloroform signals averaged in the same manner. All other measurements and apparatus were as described previously.[9]

Procedure

According to the NMR technique proposed by Evans,[14] the corrected molar magnetic susceptibility, χ'_m, is related to the shift of the reference signal, $\delta\nu$, by the equation:

$$\chi'_m = \frac{3\delta\nu}{2\pi\nu C}, \qquad (1)$$

where ν is the oscillator frequency and C is the concentration of the paramagnetic material in mol cm^{-3}. For a solution containing an equilibrium mixture of monomer (M) and dimer (D), the observed molar susceptibility per copper is the weighted average of contributions from the monomer and dimer magnetic susceptibility.[10]

It can be shown that the observed shift for a solution mixture is given by:

$$\delta\nu = [M]\Delta\nu_{(M)} + 2[D]\Delta\nu_{(D)}, \qquad (2)$$

where $\Delta\nu$ is the "molar shift" ($\delta\nu/c$) for pure monomer or pure dimer and can be determined separately from their respective solutions at various temperatures. The concentration of the monomer and dimer for each solution can then be determined from eq. (2) and also the known total copper concentration for each mixture.

RESULTS

Spectrophotometric measurements

Representative electronic spectra of equilibrium mixtures in chloroform of copper(II) acetate-γ-picoline complexes are presented in Fig. 1. Spectra of the mixtures show two isosbestic points, consistent with an equilibrium which involves two

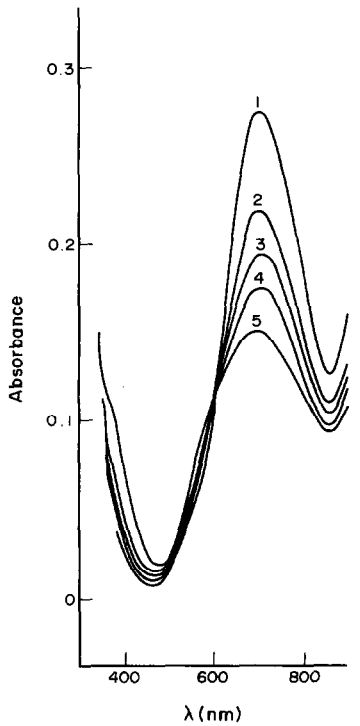

Fig. 1. Visible spectra of equilibrium mixtures in chloroform of copper(II) acetate-γ-picoline complexes, $[Cu^{2+}] = 1.916 \times 10^{-3}$ M, and γ-pic/Cu^{2+} = 25 (1), 50 (2), 76 (3), 101 (4), 239 (5), where the number in parentheses refers to the absorption curve in the figure.

absorbing species. The constant for the equilibrium:

$$[Cu(OAc)_2 \cdot L]_2 + 2L \rightleftharpoons 2[Cu(OAc)_2 \cdot 2L] \quad (3)$$
$$(D) \qquad\qquad (M)$$

was evaluated from absorptivities at the two wavelengths[9] (at the pure dimer maximum around 700 nm and at the pure monomer maximum around 650 nm), by common procedures[15] with the aid of a computer program. To further assess the degree of ligand participation in the equilibrium, the data were analysed graphically in terms of the equilibrium: $D + nL \rightleftharpoons 2M$, for which the equilibrium constant is given by:

$$K = \frac{[M]^2}{[D][L]^n}. \quad (4)$$

This can be rearranged in the form:

$$\log [M]^2/[D] = n \log [L] + \log K. \quad (5)$$

Plots of $\log [M]^2/[D]$ vs $\log [L]$ produced straight lines which are shown in Fig. 2. The value of n can be obtained from the slope, and was found to be two in all cases. The equilibrium constant values were found to be: $(1.2 \pm 0.2) \times 10^{-2}$, $(7.0 \pm 0.3) \times 10^{-2}$ and $(39 \pm 3) \times 10^{-2}$ for pyridine, β-picoline and γ-picoline, respectively. It should be pointed out that measurements of the β-picoline system were carried out at about 20°C to ensure complete conversion to the monomer in the neat ligand solutions, whereas data for the other two systems were obtained conveniently at room temperature (30°C). For comparison, the K value for the pyridine system at 20°C was found to be 3.0×10^{-2}. It was not possible to evaluate an analogous equilibrium constant for the α-picoline system since traces of dimer persist even in its solutions in the neat ligand cooled to 0°C.[9] In addition, the electronic spectra of equilibrium mixtures of the α-picoline complexes show an anomalous shift to lower energies as the ligand concentration is increased. This is in contrast to the behaviour observed in the other systems, and makes evaluation of equilibrium constants from such data questionable.

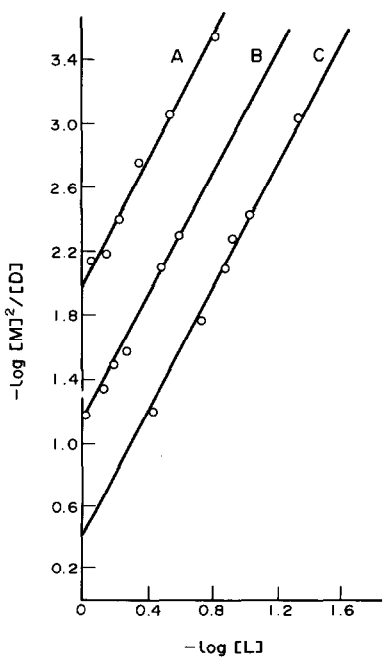

Fig. 2. Graphic determination of K and n from eq. (5): (A) py, (B) β-pic and (C) γ-pic.

NMR measurements

The effect of incremental addition of pyridine upon the NMR shift of the reference in chloroform solutions of the dimer at various temperatures is shown in Fig. 3. Similar behaviour was found at other concentrations and for the other systems. The plots demonstrate the exothermic nature of reaction (3) and the effect of the ligand on the equilibrium position. The equilibrium constant at each temperature was evaluated by solution of eq. (2). The temperature dependence of the equilibrium constants for the three systems is shown in Fig. 4. Analysis of the data by the least-squares method yielded the thermodynamic parameters for the equilibrium, which are summarized in Table 1.

DISCUSSION

The results of this study are interesting in many respects. Equilibrium constant values, at room

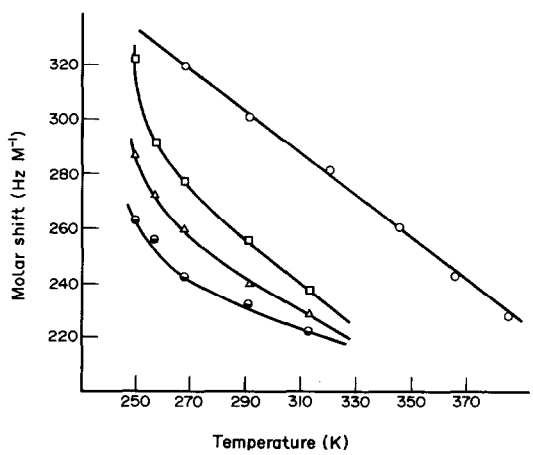

Fig. 3. Effects of temperature and pyridine concentration, 1.82 M (□), 1.27 M (△), 1.02 M (◒), on the NMR molar shift of the reference in the equilibrium mixtures; ○ represents the molar shift in solution of the pure monomer, $[Cu^{2+}] = 3.07 \times 10^{-2}$ M.

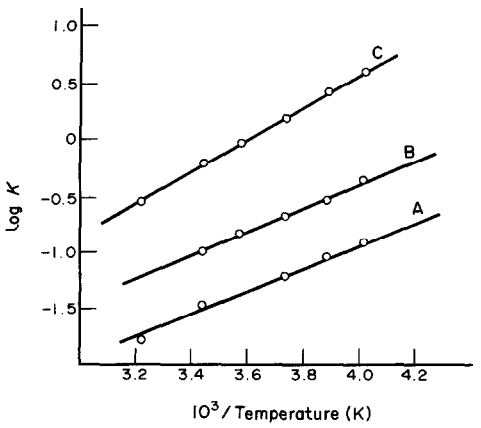

Fig. 4. Temperature dependence of the equilibrium constants: (A) py, (B) β-pic and (C) γ-pic.

temperature, measured by the NMR method agree reasonably well with those obtained spectrophotometrically, despite the inherent differences and experimental uncertainties associated with the two techniques. This confirms the validity of the equilibrium stoichiometry and the reliability of the NMR method for studying structural equilibria in solution. The small K values for the dimer–monomer conversion are consistent with the observed instability of the monomers in chloroform solutions.[9] The most obvious result, however, is that the relative formation constants of the monomeric complexes with these bases increase in the order: py < β-pic < γ-pic. This is the order of increased base strength and the order observed for the formation constants of their complexes with a large variety of Lewis acids.[16-19]

This study, on the other hand, demonstrates that the pyridine bis-adduct shows exceptional stability in spite of the smaller value of its formation constant in solution, whereas the β-picoline bis-adduct, with a higher formation constant in solution, could not be isolated as a crystalline solid. The apparent contradiction can be reconciled if one recognized that the thermal stability of the solid may have little relationship with the solution formation constants. Factors related to crystal packing requirements which stem from symmetry properties of the ligand may account for the thermal instability of the β-picoline bis-adduct. This is further demonstrated in the case of α-picoline which has the same base strength as γ-picoline but fails to form a monomeric bis-adduct either in the crystalline state or in solution. The tendency to attain six-coordination with this ligand is suppressed by crowding around the central metal ion.[9,19] Steric interactions undoubtedly play a significant role in destabilizing the monomeric complex in the case of the α- and β-picolines.

Table 1. Thermodynamic values at 298 K for the equilibrium:

$$\text{Dimer} + 2\text{L} \rightleftharpoons 2 \text{ monomer}$$

L	$K \times 10^{2a}$	$-\Delta H^{\ominus} \pm 0.5$ (kJ mol^{-1})	$-\Delta S^{\ominus} \pm 1$ (J mol^{-1} K^{-1})
Pyridine	2.5 ± 0.2 (1.2)	20.8	100
β-Picoline	8.4 ± 0.3 (7.0)	20.5	89
γ-Picoline	45 ± 2 (39)	27.6	98

[a] Values in parentheses are from spectrophotometric measurements at ~30°C.

The enthalpy and entropy values obtained for the equilibrium are not significantly different for the three systems, and are in close agreement with those found for adduct formation of related copper(II) chelates with these ligands.[16-19] The $\Delta H^{\ominus}$ values are in the range expected for copper–nitrogen bond formation[19] and increase in the order: py ≃ β-pic < γ-pic. Negative $\Delta S^{\ominus}$ values of the observed order of magnitude are to be expected in a system in which there is a net loss of translational freedom of two reactant species.

The observed thermodynamic values represent changes occurring in the total energy of the system upon monomer formation, and can be interpreted as the net result of contributions from electronic and structural reorganization, metal–ligand bond formation and solvation energy effects. However, the absence of thermochemical data for these systems does not allow a quantitative analysis of the various terms, but the significance of these contributions can be qualitatively assessed. Contribution from electronic rearrangement which accompanies monomer formation is evidenced by the fairly significant shift to higher energy in the electronic spectra (from around 700 nm in the dimer to around 650 nm in the monomer).[9] Structural reorganization within the dimer, whereby the four bridging acetate groups act as an essentially monodentate or asymmetric chelating ligand in the monomer, is expected to be extensive. The energy contribution of this term is expected to inhibit monomer formation by making a positive contribution to the enthalpy. However, the contribution of this term should be constant, or nearly so, in the three systems and is balanced by the negative contribution to the enthalpy as a result of formation of comparable copper–oxygen bonds in the monomer.

Formation of the additional copper–nitrogen bond should make a negative contribution to the enthalpy. In the absence of any steric effects, the

contribution due to bond formation depends on the availability of the electron pair on the nitrogen atom and, within a related series of ligands, is reflected by the relative order of their dipole moments, ionization energies and pK_a values.[17] On this basis the sequence of donor ability is well established to be: py < β-pic < α-pic < γ-pic.

That contribution to the observed thermodynamic parameters from solvation effects must be significant is clearly manifested in the instability of the monomer in chloroform solution where it is quantitatively converted to the dimer. Whether the dimers are solvated to any extent in these solutions is not clear, but no large variations in the degree of solvation are expected among the four complexes. On the other hand, pyridine bases are known to interact strongly with chloroform, presumably via hydrogen bonding.[17,19,20] This interaction contributes a large exothermic ΔH(soln) term, which increases in the order: py < β-pic < α-pic < γ-pic. Variations in the actual values of $\Delta H^{\ominus}$ and $\Delta S^{\ominus}$ are affected, no doubt, by differences in the solvation effects which may account for the lower than expected values found for the β-picoline system.

The thermodynamic parameters found for these systems are, in general, in accord with this analysis. While the electronic properties of the carboxylate group may be significant in affecting the stabilization of a particular structural type,[1] the steric and electronic properties of the addend also play an important role in this respect.[6–8] This view is supported by the structural results of the copper(II) acetate bis-adduct with collidine[6] in which, despite prohibitive steric crowding resulting from the two α-methyl groups, the superior donor ability of this ligand allows copper–nitrogen bond formation at the expense of disrupting the copper–acetate bonding. In addition, the importance of electronic properties of the addend are also demonstrated when basic ligands such as ammonia and imidazoles react with copper(II) acetate in which only monomeric adducts are formed.[5,21]

REFERENCES

1. R. J. Doedens, *Prog. Inorg. Chem.* 1976, **21**, 209.
2. R. W. Jotham, S. F. A. Kettle and J. A. Marks, *J. Chem. Soc., Dalton Trans.* 1972, 428.
3. M. Melnik, *Coord. Chem. Rev.* 1981, **36**, 1.
4. M. Kato and Y. Muto, *Coord. Chem. Rev.* 1988, **92**, 45.
5. H. A. Henriksson, *Acta Cryst.* 1977, **B33**, 1947.
6. N. E. Heimer and I. Y. Ahmed, *Inorg. Chim. Acta* 1982, **64**, L65.
7. F. T. Greenaway, A. Pezeshk, A. W. Cordes, M. C. Noble and J. R. J. Sorenson, *Inorg. Chim. Acta* 1984, **93**, 67.
8. A. Latif Abuhijleh, *Polyhedron* 1989, **8**, 2777.
9. I. Y. Ahmed and A. L. Abuhijleh, *Inorg. Chim. Acta* 1982, **61**, 241.
10. T. H. Crawford and J. Swanson, *J. Chem. Educ.* 1971, **48**, 382.
11. D. F. Evans and T. A. James, *J. Chem. Soc., Dalton Trans.* 1979, 723.
12. R. H. Petty, E. V. Dose, M. F. Tweedle and L. J. Wilson, *Inorg. Chem.* 1978, **17**, 1064.
13. L. Rusnak and R. B. Jordan, *Inorg. Chem.* 1971, **10**, 2199.
14. D. F. Evans, *J. Chem. Soc.* 1959, 2003.
15. R. S. Drago, *Physical Methods in Chemistry*, pp. 88–93. Saunders, Philadelphia (1977).
16. J. J. Christensen, D. J. Eatough and R. M. Izatt, *Handbook of Metal Ligand Heats*, 2nd edn, pp. 306–338. Marcel Dekker, New York (1975).
17. B. L. Libutti, B. B. Wayland and A. F. Garito, *Inorg. Chem.* 1969, **8**, 1510; A. F. Garito and B. B. Wayland, *J. Am. Chem. Soc.* 1969, **91**, 866.
18. F. G. Herring and R. L. Tapping, *J. Phys. Chem.* 1974, **78**, 316.
19. D. P. Graddon, *Coord. Chem. Rev.* 1969, **4**, 1.
20. W. Libus, S. K. Hoffman, M. Kluczkowski and H. Twardowska, *Inorg. Chem.* 1980, **19**, 1625.
21. Y. A. Simonoo, A. U. Abloo and T. I. Molmoski, *Kristallografiya* 1963, **8**, 205.

Polyhedron Vol. 10, No. 8, pp. 799–803, 1991
Printed in Great Britain

0277–5387/91 $3.00+.00
© 1991 Pergamon Press plc

PLATINUM CREATININE BLUES: REACTION OF *CIS*-DIAMMINEDIAQUAPLATINUM(II) WITH CREATININE STUDIED BY ^{195}Pt AND ^{13}C NMR

C. F. G. C. GERALDES*

Departamento de Quimica, Universidade de Coimbra, 3000 Coimbra, Portugal

and

M. ARAGON-SALGADO and J. MARTIN-GIL

E.T.S.I.I., Universidad de Valladolid, 47011 Valladolid, Spain

(*Received* 15 *June* 1990; *accepted* 10 *December* 1990)

Abstract—Using ^{195}Pt NMR spectroscopy, several products formed in the 1 : 1 reaction at pH = 6–7 of *cis*-$[Pt(NH_3)_2(H_2O)_2]^{2+}$ with creatinine ($C_4H_7N_3O$) have been identified at pH 4 in aqueous solution. The following products have been found: the head-to-head and head-to-tail creatinine-bridged dimers $[Pt_2(NH_3)_4(C_4H_7N_3O)_2]^{2+}$, assigned at −1341 ppm, −2452 ppm and −1908 ppm, respectively; the known hydroxo-bridged dimer $[(NH_3)_2Pt(OH)_2Pt(NH_3)_2]^{2+}$ at −1153 ppm; the creatinine monomer *cis*-$[Pt(NH_3)_2(N_d$-creatinine)] at −2222 ppm. They are closely related to the products that are obtained in analogous reactions of free and substituted pyrimidines. ^{13}C NMR spectra of the complexes indicate large shifts for the C(3) and C(4) nuclei relative to the free ligand, indicating that the NH moiety within the creatinine ring, rather than the exocyclic one, is directly coordinated to the metal ion.

The field of aqueous platinum(II) chemistry is currently of great interest mainly due to the discovery and exploration of the antitumour properties of *cis*-diamminedichloroplatinum(II) (*cis*-DDP or cisplatin) which led to its widespread success in the clinical treatment of human cancer.[1] The reactions of the drug with nucleic acids and their constituents have been thoroughly studied[2–9] in an attempt to understand the inhibition of cellular replication induced by the interaction of *cis*-DDP with DNA.[10]

The reaction of *cis*-DDP or the aquated form of the complex, *cis*-$[Pt(NH_3)_2(H_2O)_2]^{2+}$, with free or substituted pyrimidine bases, leads to a variety of products[11–25] containing different numbers of platinum atoms. A variety of simple mononuclear and dinuclear platinum complexes of free and substituted pyrimidine bases have been isolated and studied by ^1H NMR.[12–25] In these compounds the platinum binding sites were clearly identified. In mononuclear complexes they are one of the heterocyclic nitrogens [N(1) or N(3)] of the pyrimidine base, whereas in pyrimidine-bridged dinuclear complexes they are a combination of N(1) or N(3) and one of the exocyclic atoms [O(2), O(4) or N(4)]. However, polynuclear species produced in many of the reactions of platinum with pyrimidines have been far more difficult to characterize.[11–22] This is due to the multiplicity and interconversion of the binding sites of both reactants, ligand exchange reactions which interconvert the various products, and valence instability, which may lead to the formation of partially oxidized materials collectively known as the "platinum pyrimidine blues".

In recent years, great interest has been shown in platinum blues, especially on their potential antitumour activity and low nephrotoxicity compared with the anticancer drug cisplatin. We are working on the synthesis and characterization of new crystalline platinum creatinine complexes, particularly

* Author to whom correspondence should be addressed.

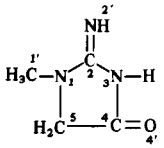

Fig. 1. Chemical structure and IUPAC numbering scheme of creatinine.

their coloured derivatives. 2-Imino-1-methyl-4-imidazolidinone, commonly known as creatinine [H_3C-N-C(NH)-NH-CO-CH_2, see Fig. 1 for structure and numbering], has been chosen as a ligand because as the final catabolic product of the important metabolite creatine its level in serum and urine is a very sensitive index of renal function (Creatinine Clearance Test). It has been suggested that the study of the metal–creatinine complexes can lead to an understanding of some biological aspects of creatinine metabolism.[26] Creatinine is also similar to 2-pyrrolidone, which forms a structurally well characterized family of compounds known as platinum tans, and has been chosen as a ligand because of its importance in clinical chemistry and its similarity to 2-pyrrolidone, which is structurally characterized in platinum tans.[27] Although creatinine is quite similar to the nucleotide bases in relation to its metal ion coordination potentialities,[28] so far only the crystal structures of creatininium tetrachlorocuprate(II),[29] bis(creatinine)silver(I) perchlorate and bis(creatinine)diiodoplatinum(II) trihydrate [binding at N(3)][30] have been determined.

In this paper we describe a ^{195}Pt and ^{13}C NMR characterization of the reaction products of *cis*-$[Pt(NH_3)_2(H_2O)_2]^{2+}$ with creatinine (pH = 4.0) in aqueous solution. These results are compared with previous ^{195}Pt NMR studies of the hydrolysis reactions of *cis*-$[Pt(NH_3)_2(H_2O)_2]^{2+}$.[31–36]

EXPERIMENTAL

Preparation of the platinum creatinine blues

The standard procedure for the preparation of blue complexes which was followed in this work arises from previous work on the reaction between the aquated products of cisplatin ligands such as uracil, thymine, uridine or other related pyrimidines. A second preparation procedure, involving the reaction between the tetrachloroplatinate(II) anion and primary amides, orotic acid or creatinine, has also been described.[37]

A 0.15 M solution of the *cis*-diamminediaquaplatinum(II) hydrolysis products was prepared by mixing 0.3 g of *cis*-$[(NH_3)_2PtCl_2]$ (prepared according to a published method[38]) and 0.34 g of $AgNO_3$ (from Merck) in approximately 7 cm^3 of water. After stirring in the dark at room temperature overnight, the solution was centrifuged twice to remove the AgCl precipitate. One equivalent of creatinine (from Merck), dissolved in a minimum amount of water and adjusted to pH 10 with 0.1 M NaOH, was then added to the *cis*-diamminediaquaplatinum(II) solution and the reaction mixture was adjusted to neutral pH (pH = 6–7) with 0.1 M NaOH. The solution was then kept in the dark at 37–40°C for approx. 24 h, until a deep blue–green colour appeared. Following incubation, a few drops of concentrated nitric acid and 0.75 g of sodium nitrate were added to the blue–green solution, pH = 1. This solution immediately turned very dark blue in colour and was allowed to stand for 12 h at 0°C. Dark blue crystalline needles, unsuitable for X-ray analysis, were collected.

Spectral measurements

NMR spectra of solutions of creatinine and of the products obtained from the reaction of equivalent amounts (1 : 1) of *cis*-DDP hydrolysis products and creatinine, were obtained at room temperature in D_2O (99.8% isotopic purity, from Sigma Chemical Co.). The pH was adjusted using 0.1 M solutions of DCl and NaOD (obtained from Sigma). pH values were measured on a Metrohm E250 pH meter, equipped with an Ingold 405-M3A glass electrode.

Broad-band ^1H decoupled ^{13}C NMR spectra were recorded on a Bruker WP-80 spectrometer. All ^{13}C chemical shifts were measured relative to TSP as external reference and were referenced to TMS. Natural abundance ^{195}Pt NMR spectra were obtained at 64.5 MHz on a Varian XL-200 spectrometer with a broad-band (10 mm) probe. Spectral data were typically acquired with a 26-μs pulse (90° flip angle), 160-ms acquisition time and a spectral width of either 83 or 100 kHz. ^{195}Pt shifts were measured relative to 0.2 M K_2PtCl_4 (in 0.4 M KCl/D_2O) used as external reference, with a shift of −1631 ppm relative to K_2PtCl_6.[39]

RESULTS AND DISCUSSION

The reaction of the *cis*-DDP hydrolysis products with one equivalent of creatinine in aqueous solution at pH = 6–7 were examined using natural abundance ^{195}Pt NMR spectroscopy at pH 4. This technique proved to be a feasible method to monitor the formation of reaction products, as in our instrumentation good quality spectra could be obtained within 18–20 h on samples that were 0.1 M in platinum. The large ^{195}Pt chemical shift range (15,000

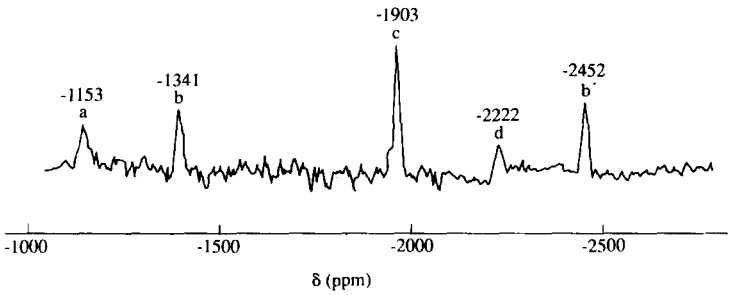

Fig. 2. ^{195}Pt NMR spectrum of the products obtained from the reaction of a 0.15 M solution of *cis*-DDP hydrolysis products with 1 equiv. of creatinine after 24 h. The chemical shifts are referenced to K_2PtCl_6 with negative values indicating a low frequency position relative to the reference. The pH of the solution was kept at 4.0, and the number of transients 50,000. The spectral assignments are described in the text.

ppm) and the predictable dependence of the shifts upon ligand substitution[39] provide an excellent means of product identification in the aqueous solution reactions of *cis*-diammineplatinum(II) complexes.[31] For example, the ^{195}Pt chemical shifts of the complexes of the form *cis*-$[Pt(NH_3)_2L_2]^{n+}$, where L is either a neutral or anionic nitrogen donor (N_d) or oxygen donor (O_d), covering a range of over 1300 ppm, are correlated in a nearly linear fashion with the electronegativity of the donor ligands L, and are found to increase in the order, *cis*-$Pt(NH_3)_2(N_d)_2$ < *cis*-$Pt(NH_3)_2(N_d)(O_d)$ < *cis*-$Pt(NH_3)_2(O_d)_2$. While other important factors also influence the ^{195}Pt chemical shifts,[39] this order holds for the complexes that are relevant to the present investigation.

The ^{195}Pt NMR spectrum of the reaction mixture of an aqueous solution of *cis*-DDP with one equivalent of creatinine, taken after 24 h of reaction at pH 6.0 and 40°C, and with the pH adjusted afterwards to 4.0, is shown in Fig. 2. At this stage in the reaction the major spectral components are peak c (at −1908 ppm) and the two peaks of equal intensity, b and b′ (at −1341 and −2452 ppm, respectively). Two other signals, of smaller but nearly equivalent intensities, are also present. These are peaks a at −1153 and d at −2222 ppm.

Assignment of the ^{195}Pt signals provides the identification of the reaction products. Some of these assignments are based on previous ^{195}Pt NMR studies of the pH dependent chemical behaviour of *cis*-$[Pt(NH_3)_2(H_2O)_2]^{2+}$ in aqueous media,[32] especially its condensation reactions following removal of acidic protons of the coordinated water molecules at pH values above 2.[31,40] Among others, the hydroxide-bridged dimer $[(NH_3)_2Pt(OH)_2Pt(NH_3)_2][(NO_3)_2]$ and a distribution of monomeric hydroxyaqua complexes *cis*-$[Pt(NH_3)_2XY]^{n+}$ (where X,Y = OH or H_2O) have been identified.[31,32] A number of these products have been isolated and fully characterized by X-ray diffraction methods.[32] Comparison of the chemical shifts of the spectral signals of Fig. 2 with the literature data[31,41] allows the assignments of peak a to the hydroxide-bridged dimer. However, the trimer, $[Pt(NH_3)_2(OH)_2]_3^{3+}$, and the monomeric hydroxyaqua complexes are not detected at this stage of the reaction, as opposed to what has been observed in a similar study with α-pyridone.[41]

The identification of the remaining signals was undertaken by comparison of their chemical shifts with the data available for the α-pyridone reaction[41] and also using the signal intensities. Thus, peak d was assigned to the mono-creatinine complex *cis*-$[Pt(NH_3)_2\{creatinine\text{-}N(3)\}(H_2O)]^{2+}$, peak c to the head-to-tail dimer and peaks b and b′ to the two signals of the head-to-head dimer. The two signals in this isomer result from the non-equivalent platinum centres: Pt(1) is bound to four nitrogen donors (peak b′), and Pt(2) is bound to two oxygen and two nitrogen donors (peak b) (Fig. 3). From the relative intensity of the signals both isomers are estimated to be present in nearly equal amounts.

The results of this experiment strongly suggest that, at the point of acidification in the preparation of the platinum creatinine blue, the head-to-head platinum(II) dimer is a major component in solution. However, when the pH of the solution is lowered from 4.0 to 1.0 with nitric acid, the solution rapidly changes colour from deep blue–green to deep blue. No ^{195}Pt NMR spectrum could be obtained from this solution, even after 50,000 transients, indicating the presence of residual paramagnetism in these samples. In fact, EPR signals of various platinum blues have been detected and interpreted in terms of partially oxidized mixed-valent complexes.[42,43] Electrochemical studies of α-pyridonate complexes[44] suggest that electron exchange reactions between the head-to-head platinum(II) and platinum(III) dimers may be involved

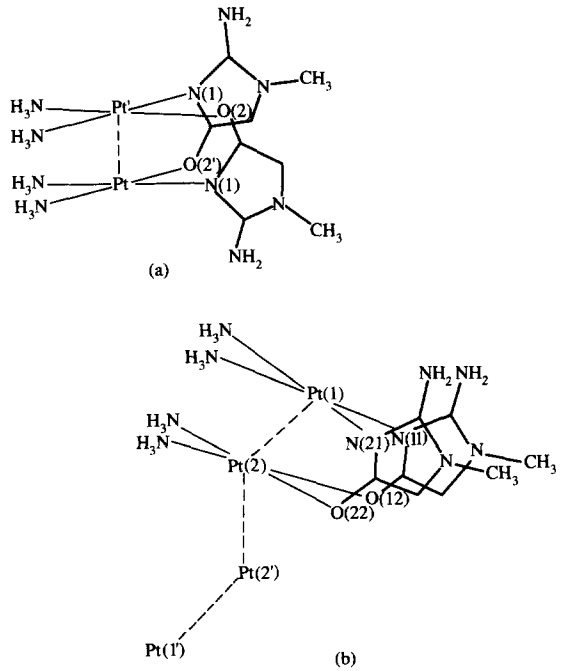

Fig. 3. Proposed structures of the creatinine-bridged complexes of *cis*-DDP: $[Pt_2(NH_3)_4(C_4H_7N_3O)_2]^{2+}$ (a) the platinum(II) dimer head-to-tail (peak c) and (b) head-to-head (peaks b and b').

in the formation of the partially oxidized tetramer.

In a similar fashion to what has been observed previously with other ligands,[41] the chemical shifts of the dinuclear creatinine complexes are shifted to high frequency relative to the corresponding mononuclear analogues. Comparing two platinum atoms with similar primary coordination sphere chemical environments, it is found that the average chemical shift difference between the head-to-tail dimer and the mononuclear creatinine complex, *cis*-$[Pt(NH_3)_2\{creatinine\text{-}N(3)\}(H_2O)]^{2+}$, is 314 ppm. This difference, too large to be attributed to charge effects, has been interpreted using a molecular orbital formulation of a metal–metal interaction in the dinuclear complexes.[45] Although the quantitative dependence of the ^{195}Pt chemical shifts upon the strength of the metal–metal interaction in binuclear platinum(II) complexes is not established, it is worth noting that the high frequency chemical shift effect observed for the head-to-tail dimer of creatinine (+314 ppm) is substantially larger than the value of +220 ppm observed for the α-pyridone complex.[41]

Creatinine is a cyclic compound containing cyclic [N(3)] and exocyclic imine [N(2'), bound to C(2)] nitrogen atoms (Fig. 1) capable, in principle, of coordinating the platinum ions. The ^{13}C complexation shifts of creatinine were, therefore, used to investigate the nitrogen coordination of creatinine. The ^{13}C NMR spectra of D_2O solutions of creatinine and of *cis*-DDP with creatinine, obtained at pH 6.0, were compared. The resonances of the C(2), C(4), C(5) and C(1') carbons of a 0.15 M solution of creatinine in D_2O occur[46] at 166.4, 184.9, 57.3 and 33.5 ppm. The products obtained from the reaction of a 0.15 M solution of *cis*-DDP hydrolysis products with one equivalent of creatinine, in D_2O at the same pH value, yield the same four intense signals at the corresponding chemical shift values of 171.7, 191.0, 58.7 and 32.5 ppm. Therefore, these ^{13}C NMR studies indicate that there are large shifts in C(2) and C(4), pointing towards coordination of creatinine occurring through the cyclic N(3) nitrogen, in agreement with the structures of the complexes proposed in Fig. 3.

This conclusion about the creatinine coordination is supported by ^1H and ^{13}C NMR data on creatinine complexation by zinc(II), cadmium(II) and mercury(II) in DMSO-d_6. The ^1H NMR spectrum of creatinine in this solvent exhibits resonances at 7.3, 3.6, 3.2 and 2.8 ppm (relative to TMS), which are due to the cyclic NH, imine NH, $—CH_2—$ and $—NCH_3$ protons, respectively.[26] The assignments were made upon comparison with the substituted guanidines.[47] Comparison of the spectra of the zinc(II), cadmium(II) and mercury(II) complexes with that of creatinine revealed that there is a large shift of the cyclic N(3)H proton (resonance at 8.4 ppm), while the positions of the other protons are unaltered.[48] ^{13}C complexation shifts, induced by those ions, of the carbonyl C(4) and imine C(2) carbons also support metal binding at N(3).[26]

CONCLUSIONS

The following platinum(II) complexes are obtained in the reactions of *cis*-$[Pt(NH_3)_2(H_2O)_2]^{2+}$ with creatinine: the mono-creatinine complex *cis*-$[Pt(NH_3)_2\{creatinineN(3)\}(H_2O)]^{2+}$, as well as the head-to-head and head-to-tail isomeric dinuclear complexes of formula $[Pt_2(NH_3)_4(creatinine)_2]$ which both contain a metal–metal bond; they are closely related to the products that are obtained in analogous reactions of free and substituted pyrimidines.

Both head-to-head and head-to-tail dinuclear species have been found from ^{195}Pt NMR studies to form in equal proportions in the reaction that leads to complex formation. ^{13}C complexation shifts indicate that platinum coordination occurs through the pyrrole-type nitrogen N(3) and the carbonyl O(4') of creatinine. Addition of nitric acid (pH = 1) to these solutions converts the head-to-

head platinum(II) complex into the platinum blue analogue while leaving the head-to-tail complex in the platinum(II) oxidation state. The importance of pH in controlling the oxidation state in the creatinine complexes of platinum has therefore, once more, been established and could possibly be used in the synthesis of related amidato-bridged complexes.

Acknowledgements—C.F.G.C.G. acknowledges support from INIC, of the Portuguese Ministry of Education. We thank Professor J. Reedijk for useful suggestions.

REFERENCES

1. B. Rosenberg and L. Van Camp, *Cancer Res.* 1970, **30**, 1799.
2. J. P. Davidson, P. J. Faber, R. J. Fischer Jr, S. Mansy, H. J. Peresie, B. Rosenberg and L. Van Camp, *Cancer Chemother. Rep.* 1975, **59**, 287.
3. J. Reedijk, *Pure Appl. Chem.* 1987, **59**, 181.
4. A. Pasini and F. Zunino, *Angew. Chem.* 1987, **26**, 615.
5. J. Reedijk, A. M. J. Fichtinger-Schepman, A. T. van Oosterom and P. van de Putte, *Struct. Bond.* 1987, **67**, 53.
6. S. E. Sherman and S. J. Lippard, *Chem. Rev.* 1987, **87**, 1153.
7. B. Lippert, *Prog. Inorg. Chem.* 1989, **37**, 1.
8. N. Farrell, *Transition Metal Complexes as Drugs and Chemotherapeutic Agents*. Kluwer Academic Publishers, Dordrecht (1989).
9. W. I. Sundquist and S. J. Lippard, *Coord. Chem. Rev.* 1990, **100**, 293.
10. J. J. Roberts and A. J. Thompson, *Prog. Nucleic Acid Res. Molec. Biol.* 1979, **22**, 71.
11. B. Lippert, *J. Clin. Hematol. Oncol.* 1977, **7**, 26.
12. R. Pfab, P. Jandik and B. Lippert, *Inorg. Chim. Acta* 1982, **66**, 193.
13. T. V. O'Halloran, P. K. Mascharak, I. D. Williams, M. M. Roberts and S. J. Lippard, *Inorg. Chem.* 1987, **26**, 1261.
14. T. V. O'Halloran and S. J. Lippard, *Inorg. Chem.* 1986, **25**, 957.
15. K. Sakaai and K. Matsumoto, *J. Am. Chem. Soc.* 1989, **111**, 3074.
16. K. Matsumoto, H. H. Miyamae and H. Moriyama, *Inorg. Chem.* 1989, **28**, 2959.
17. K. Matsumoto and N. Matoba, *Inorg. Chim. Acta* 1986, **120**, L1–L3.
18. R. Faggiani, B. Lippert and C. J. L. Lock, *Inorg. Chem.* 1980, **19**, 295.
19. R. Faggiani, C. J. L. Lock, R. J. Pollock, B. Rosenberg and G. Turner, *Inorg. Chem.* 1981, **20**, 804.
20. R. Faggiani, B. Lippert, C. J. L. Lock and R. A. Speranzini, *J. Am. Chem. Soc.* 1981, **103**, 1111.
21. B. Lippert, D. Neugebauer and U. Schubert, *Inorg. Chim. Acta* 1980, **46**, L11.
22. B. Lippert, *Inorg. Chem.* 1981, **20**, 4326.
23. F. J. Dijt, G. W. Canters, J. H. J. den Hartog, A. T. M. Marcelis and J. Reedijk, *J. Am. Chem. Soc.* 1984, **106**, 3644.
24. A. T. M. Marcelis, H. J. Korte, B. Krebs and J. Reedijk, *Inorg. Chem.* 1982, **106**, 3644.
25. C. G. van Kralingen, J. Reedijk and A. L. Spek, *Inorg. Chem.* 1980, **19**, 1481.
26. S. Muralidharan, K. S. Nagaraja and M. R. Udupa, *Polyhedron* 1984, **3**, 619.
27. K. Matsumoto and K. Fuwa, *J. Am. Chem. Soc.* 1982, **104**, 897.
28. D. J. Hodgson, *Prog. Inorg. Chem.* 1977, **23**, 211.
29. M. D. Udupa and B. Krebs, *Inorg. Chim. Acta* 1979, **33**, 241.
30. P. T. Beurskens, A. Perales, F. J. Martin-Gil and J. Martin-Gil, *Monatsch. Chem.* 1988, **119**, 1189.
31. S. J. S. Kerrison and P. J. Sadler, *J. Chem. Soc., Chem. Commun.* 1981, 61.
32. R. Faggiani and B. Lippert, *Inorg. Chem.* 1977, **16**, 1192.
33. S. E. Miller and D. A. House, *Inorg. Chim. Acta* 1989, **166**, 189.
34. T. G. Appleton, J. R. Hall, S. F. Ralph and C. S. M. Thompson, *Inorg. Chem.* 1989, **28**, 1989.
35. S. A. Miller and D. A. House, *Inorg. Chim. Acta* 1989, **166**, 189; 1990, **173**, 53.
36. R. B. Martin, in *Platinum, Gold and Other Metal Chemotherapeutic Agents* (Edited by S. J. Lippard), p. 231. ACS Symposium Series 209, Washington, D.C. (1983).
37. F. J. Martin-Gil and J. Martin-Gil, *Inorg. Chim. Acta* 1987, **137**, 131.
38. S. Dhara, *Ind. J. Chem.* 1970, **8**, 193.
39. S. J. S. Kerrison and P. J. Sadler, *J. Magn. Reson.* 1978, **31**, 321.
40. J. R. Perumareddi and A. W. Adamson, *J. Phys. Chem.* 1968, **72**, 414.
41. L. S. Hollis and S. J. Lippard, *J. Am. Chem. Soc.* 1983, **105**, 3494.
42. J. K. Barton, C. Caravana and S. J. Lippard, *J. Am. Chem. Soc.* 1979, **101**, 7269.
43. P. Arrizabalaga, P. Castan, M. Geoffroy and J. P. Laurent, *Inorg. Chem.* 1985, **24**, 3656.
44. L. S. Hollis and S. J. Lippard, *J. Am. Chem. Soc.* 1981, **103**, 6761.
45. K. R. Mann, N. S. Lewis, R. M. Williams and H. B. Gray, *Inorg. Chem.* 1978, **17**, 828.
46. R. F. Dietrich, M. A. Marletta and G. L. Kenyon, *Org. Magn. Reson.* 1980, **13**, 79.
47. V. N. Shafranskii, A. A. Stratulat and I. V. Dranka, *Russ. J. Inorg. Chem.* 1981, **26**, 975.
48. G. Gencheva, J. Macicek, O. Angelova and V. I. Nefedov, *Procs 11th Conf. Coord. Chem.*, Smolenice, Bratislava, CSSR (2–5 June 1987).

Polyhedron Vol. 10, No. 8, pp. 805–810, 1991
Printed in Great Britain

0277-5387/91 $3.00+.00
Pergamon Press plc

THE SYNTHESIS AND CHARACTERIZATION OF VOLATILE LITHIUM ALKOXIDES, AND THE SINGLE CRYSTAL X-RAY STRUCTURE OF $[LiOCMe_2Ph]_6$

MALCOLM H. CHISHOLM,* SIMON R. DRAKE, AHMAD A. NAIINI and WILLIAM E. STREIB

Department of Chemistry and Molecular Structure Center, Indiana University, Bloomington, IN 47405, U.S.A.

(*Received* 31 *July* 1990; *accepted* 10 *December* 1990)

Abstract—The lithium alkoxides, $[LiOR]_n$ [R = Bu^t (**1**) and $PhMe_2C$ (**2**)], have been prepared and fully characterized in solution by IR, ^1H, ^{13}C and ^7Li NMR, and cryoscopy in benzene, which gave a value of $n = 6$. Single-crystal X-ray diffraction studies on $[LiOCMe_2Ph]_6$ (**2**) at $-169°C$ revealed that this molecule crystallizes in the monoclinic space group $P2_1/n$, with unit cell dimensions, $a = 12.555(2)$, $b = 12.010(2)$, $c = 16.405(3)$ Å; $\beta = 99.44(1)°$, $Z = 2$, $d_{calc} = 1.161$ g cm^{-3}, as a hexagonal prism. The oxygen and lithium atoms in the hexameric species are arranged into two Li_3O_3 planes.

The solution and solid-state structures of lithiated organic compounds is an area of burgeoning interest,[1] both from a purely synthetic and also a theoretical standpoint.[2] In the vast majority of these complexes, lithium is found to be in a four-coordinate environment,[3] although coordination members of five have also recently been observed in macrocyclic complexes.[4] Lower coordination numbers, e.g. two[5] and three,[6] are still comparatively rare (see Table 3), although recent examples have included lithium alkoxides and boroxides.

These materials find wide usage in organic chemistry, e.g. anionic polymerization is initiated by LiOR,[7] and it has been previously noted that organolithium (LiR) compounds are less stable in the presence of LiOR.[8] Recent studies have demonstrated that the super-base $[Bu^tLi \cdot LiOBu^t]_n$ is a tetramer of unusual structure.[9]

Previous studies have shown that $[LiOBu^t]_n$ (**1**) is in fact a hexamer in benzene (degree of aggregation, $n = 6.0$).[10] In this paper we report the synthesis of $[LiOR]_6$ (R = Bu^t and CMe_2Ph), their solution properties, and a single crystal X-ray structure of $[LiOCMe_2Ph]_6$ (**2**).

* Author to whom correspondence should be addressed.

RESULTS AND DISCUSSION

Attempts to prepare single crystals of $[LiOBu^t]_6$ have been successful, but it appears that the molecule is disordered.[11] We have found similar problems, and have instead used the ligand $PhMe_2COH$. Lithiation of this molecule in tetrahydrofuran yields $[LiOCMe_2Ph]_n$ (**2**). The elucidation of the single-crystal X-ray structure was of interest in its own right, and also because the solid-state structure of **2** would be most likely related to that of **1**.

Both **1** and **2** are air-sensitive and must be handled in dry and oxygen-free atmospheres.

Solid-state and molecular structure of $[LiOCMe_2Ph]_6$ (**2**)

A ball-and-stick drawing of the molecule is given in Fig. 1 and selected bond distances and bond angles are given in Table 2. The atom numbering scheme used in Table 2 is shown in Fig. 2.

The molecule has a centre of symmetry and has a skeleton related to $[NaOBu^t]_6$,[12] with the oxygen and ligand atoms alternating at the corners of a hexagonal prism. The atoms in this hexameric species are thus arranged into two near-parallel planes. In **2** the Li—O distances are 1.91(5) Å (av.), which

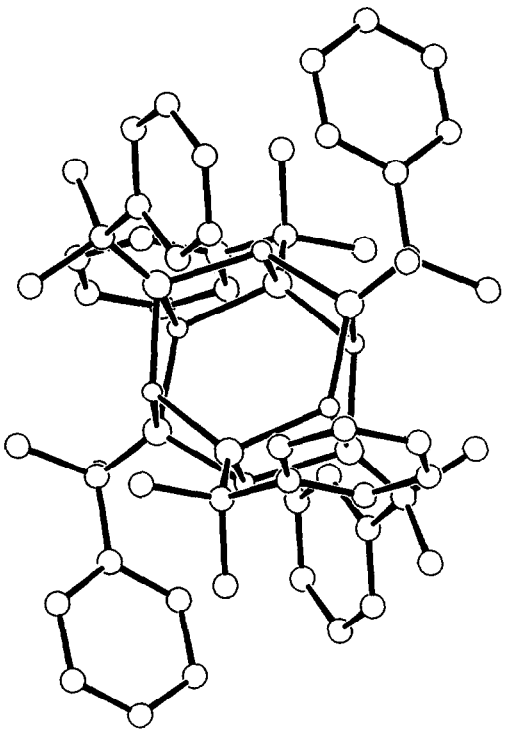

Fig. 1. Molecular structure of $[LiOCMe_2Ph]_6$ (hydrogen atoms omitted).

may be compared to those in $[NaOBu^t]_6$, 2.24(1) Å (av.),[12] the difference being accounted for by the larger ionic radii of Na^+ with respect to Li^+.

There are several features worthy of comment in this structure. The inter-lithium distances in the isosceles triangle, are 2.46 ± 0.01 Å, with the third side being longer, 2.528(14) Å (see Table 2). These features are also observed in the Li(1)—Li(3)—Li(2) angle of 77.0°. The lithium atoms in this molecule are three coordinate (see Table 3), the distances of Li(1) to O(4) and O(14) in the same plane are nearly identical, 1.88 ± 0.01 Å, while the distance between Li_3O_3 layers, Li(1)—O(24), is slightly longer, 1.92(1) Å. Similar features are also observed for Li(2) and Li(3) in relation to the Li—O distances. It may also be noted that the distances in the Li_3O_3 hexagon are not regular and span the range 1.87–1.98 Å.

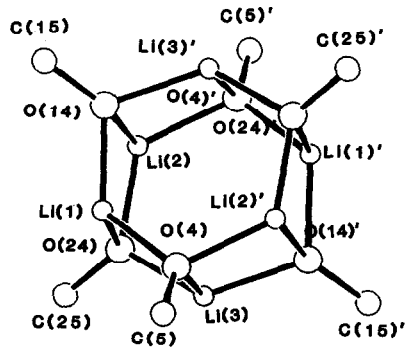

Fig. 2. A ball-and-stick drawing of the central $[LiOC]_6$ framework showing the hexagonal prismatic geometry.

Within the hexagonal prismatic structure, the O—M—O angles are found to vary over a wide range, 97.75(12)–126.277(12)°, with the most extreme being O(4)′—Li(2)—O(14) and O(4)—Li(1)—O(14). The 2-phenyl-2-propoxide ligands are essentially equivalent, being μ_3-bridging ligands.

Solution properties of **1** *and* **2**

In d_6-benzene and d_8-toluene, **1** and **2** exhibit only a single signal for the methyl groups at room temperature, as shown by ^1H and ^{13}C NMR spectroscopy. The spectra do *not* change on cooling to 220 K. As judged by the simple pattern of resonances observed for the phenyl ring (i.e. only one type of phenyl ring environment) in both ^1H and ^{13}C NMR spectra, the molecular structure is retained in solution. In solution, ^1H and ^{13}C NMR variable temperature spectroscopic studies show that the ^tBuO groups in **1** are equivalent.

In contrast, the behaviour in weak Lewis base media (e.g. THF) is more complex. The ^7Li NMR of **1** in C_7D_8 at 298 K shows only one resonance (δ −1.73), as would be expected if all the lithium environments are equivalent as observed in the solid-state structure. The behaviour of **1** in d_8-THF was markedly different, with not only a large chemical shift of 5 ppm (^7Li has a small chemical shift range), but also the observation of another peak. The two peaks are found in a ratio of 4:1 at 193 K.

Related behaviour is also observed for **2**, which exhibits a singlet at δ 4.06 in C_7D_8 at 293 K, which remains unchanged down to 253 K, and below this temperature the sample precipitates from solution. When **2** is dissolved in d_8-THF, two resonances are observed at δ 4.29 and 4.47 in a ratio of 9:1. The more sterically hindered CMe_2Ph group reducing the amount of $[LiOCMe_2Ph \cdot THF]_n$ that formed in solution, e.g.

$$[LiOR]_6 \underset{\text{toluene}}{\overset{\text{THF}}{\rightleftharpoons}} [LiOR \cdot THF]_4.$$

Removal of the d_8-THF from either **1** or **2**, and redissolution in d_8-toluene, regenerates the parent non-solvated materials. Previous studies on alkali-metal alkoxides (Li, Na and K) in a range of solvents, demonstrated that the degree of aggregation was affected by different aprotic

Table 1. X-ray data for the structural determination of **2**

Empirical formula	$C_8H_{11}OLi$
Colour of crystal	Colourless
Crystal dimensions (mm)	$0.65 \times 0.70 \times 0.80$
Space group	$P2_1/n$
Cell dimensions	
Temperature (°C)	−169
a (Å)	12.555(2)
b (Å)	12.010(2)
c (Å)	16.405(2)
β (°)	99.44(1)
Z (molecules/cell)	2
Volume (Å^3)	2439.94
Calculated density (g cm^{-3})	1.161
Wavelength (Å)	0.71069
Molecular weight	852.76
Linear absorption coefficient (cm^{-1})	0.667
Detector-to-sample distance (cm)	22.5
Sample-to-source distance (cm)	23.5
Average omega scan width at half height	0.25
Scan speed (° min^{-1})	10.0
Scan width (° + dispersion)	2.0
Individual background (s)	4
Aperture size (mm)	3.0×4.0
Two-theta range (°)	6–55
Total number of reflections collected	7938
Number of unique intensities	5640
Number with $F\sigma 3.0(F)$	4974
$R(F)$	0.0486
$Rw(F)$	0.0533
Goodness-of-fit for the last cycle	1.598
Maximum delta/sigma for last cycle	0.24

Table 2. Listing of selected bond distances and angles for **2**

Distances (Å)			
Li(1)—Li(2)	2.457(4)	Li(2)—O(14)	1.9795(27)
Li(1)—Li(3)	2.467(3)	Li(2)—O(24)	1.8771(26)
Li(2)—Li(3)′	2.528(4)	Li(3)—O(4)	1.9514(27)
Li(1)—O(4)	1.8742(1)	Li(3)—O(14)′	1.9118(26)
Li(1)—O(14)	1.8985(18)	Li(3)—O(24)	1.9069(26)
Li(1)—O(24)	1.9185(16)	O—C(av.)	1.4136(16)
Li(2)—O(4)′	1.9158(26)		

Angle (°)			
Li(2)—Li(1)—Li(3)	79.35	Li(2)′—O(4)—C(5)	115.95(11)
Li(1)—Li(2)—Li(3)′	78.24	Li(3)—O(4)—C(5)	128.65(11)
Li(1)—Li(3)—Li(2)′	77.00	Li(1)—O(14)—Li(2)	78.60
O(4)—Li(1)—O(14)	126.277(12)	Li(1)—O(14)—Li(3)′	111.30(8)
O(4)—Li(1)—O(24)	100.41(7)	Li(1)—O(14)—C(15)	116.67(9)
O(14)—Li(1)—O(24)	100.55(7)	Li(2)—O(14)—Li(3)′	81.00(11)
O(4)′—Li(2)—O(14)	97.75(12)	Li(2)—O(14)—C(15)	139.93(11)
O(4)′—Li(2)—O(24)	126.06(14)	Li(3)—O(14)—C(15)	120.65(11)
O(14)—Li(2)—O(24)	99.11(12)	Li(1)—O(24)—Li(2)	80.67(9)
O(4)—Li(3)—O(14)′	98.86(12)	Li(1)—O(24)—Li(3)	80.32(8)
O(4)—Li(3)—O(24)	98.10(12)	Li(1)—O(24)—C(25)	121.66(8)
O(14)′—Li(3)—O(24)	123.85(13)	Li(2)—O(24)—Li(3)	112.36(11)
Li(1)—O(4)—Li(2)′	110.26(9)	Li(2)—O(24)—C(25)	127.51(11)
Li(1)—O(4)—Li(3)	80.29(9)	Li(3)—O(24)—C(25)	117.68(10)
Li(1)—O(4)—C(5)	127.61(9)	O(4)—C(5)—C(av.)	109.17(11)
Li(2)′—O(4)—Li(3)	81.63(11)		

Table 3. Selected X-ray structure data on lithium alkoxides

Empirical formula	n in solid $(MoR)_n$	Coordination number of metal	⟨M—O⟩ (Å)	⟨O—C⟩ (Å)	⟨LiOLi⟩ (°)	⟨OLiO⟩ (°)	Reference
LiOMe	∞	4	1.95	1.42	80.3	101.7, 131.1	3
$LiOCMe_2Ph$ (**2**)	6	3	1.91(5)	1.414(1)	90.72(1)	107.94(9)	This work
$LiOCBu^t_3$	2	2	1.75(8)	1.387(13)	77(3)	103(3)	5
$LiOCBu^t_3(THF)$	2	3	1.84(1)	1.392(7)	79.3(5)	98.7(4)	13
$LiOAr(OEt_2)$	2	3	1.86(1)	1.34(1)	83.8(4)	96.2(4)	14

solvents.[10,15] It was demonstrated that solvation of lithium alkoxides could occur to a considerable extent in tetrahydrofuran, with crystalline coordination compounds, containing 1 mol of THF per mole of alkoxide being obtained. Thermoelectric molecular weight measurements showed that tetrameric aggregates are formed. One can visualize, for example, that these species would be related to the cubane alkoxides, $[MOBu^t]_4$ (M = K, Rb or Cs).[12] Hence in THF an equilibrium between hexamer and tetramer is proposed, with the coordination number of lithium remaining unchanged.

Cryoscopic molecular weight measurements for **1** and **2** in benzene are in accord with the NMR, yielding values for aggregations of six.[16] One may note that the substitution of a methyl group by phenyl in **2** increases the sublimation temperature by 60°C (at 10^{-2} torr), thereby decreasing the volatility of this species.

Electron impact mass spectrometer studies have recently been used to study the gas-phase compositions of a wide variety of lithium alkoxides (LiOR, R = Et, Pr^i, Bu^n, s-amyl, Bu^t and others).[17] The most abundant ions corresponding to tetramers, hexamers and even the observation of larger aggregates. The larger lithium clusters were stabilized by hydroxide ligands, presumably via water contamination of the materials.

Mass spectra of gas-phase lithium alkoxides share many features with those of the alkyl lithiums, yet it is clear that the higher coordination number of oxygen allows very stable and potentially larger alkoxide aggregates to form.

Mass spectroscopic results have revealed that $[LiOBu^t]_6$ (**1**) is extremely volatile, exhibiting not only a molecular ion (M^+ 480), but also the corresponding $[LiOBu^t]_n$ (n = 1–5) fragments. These mass spectral results are in accord with those of Schleyer and co-workers,[17] and Hartwell and Brown[18] who also demonstrated that **1** is a hexamer in the vapour phase. The related lithium alkyloxide $[LiOCMe_2Ph]_6$ (**2**), also yields a molecular ion in electron impact mass spectroscopy.

Concluding remarks

The lithium alkoxides $[LiOR]_n$ (R = Bu^t and CMe_2Ph) (**1**) and (**2**) have been characterized in solution, the solid-state and the vapour phase. It has been shown that the hexameric nature of these complexes remains intact in all three phases.

In deutero-benzene and toluene solutions these species show only one type of tert-butoxide environment for **1**, and one 2-phenyl-2-propoxide environment for **2** according to ^1H, ^{13}C and ^7Li NMR. The latter is in accord with the single-crystal X-ray structure, where a hexagonal prismatic geometry is observed.

Whereas in Lewis-base media more complex situations arise, in THF both **1** and **2** are solvated to a small extent (20%) to yield the corresponding $[LiOR \cdot THF]_n$ adducts, as shown by ^1H, ^{13}C and ^7Li NMR. It is highly probable that these hexameric species are in equilibrium in solution in THF with tetrameric species such as $[LiOBu^t \cdot THF]_4$.

EXPERIMENTAL

All manipulations were carried out under an atmosphere of dry (molecular sieves) argon (using standard dry-box and Schlenk techniques). All hydrocarbon and ethereal solvents were dried and distilled from sodium benzophenone ketyl. Alcohols were dried by distillation from magnesium turnings, activated by a crystal of iodine. NMR solvents were dried over 4 Å molecular sieves and stored under argon. Lithium sand was purchased from the Aldrich Chemical Company and stored in a dry-box, under an argon atmosphere. Elemental analyses were performed by Oneida Research Services. NMR data were recorded on a Bruker WM-500 NMR spectrometer, using the protio impurities of the deuterated solvents as reference for ^1H spectra and the ^{13}C resonance of the solvent as a reference for ^{13}C spectra. The ^7Li NMR data were recorded at 194.36 MHz, using a 1.0 M LiCl solution in D_2O as a reference. IR spectra were recorded on a FTIR

spectrometer. All of these experiments were carried out in either [$^2H_8$] toluene or [$^2H_8$] tetrahydrofuran solutions prepared in a glove-box under argon. All chemical shifts are positive to high frequency of the standard. At least two solutions of each compound, at a range of concentrations (0.05–0.25 M), were used.

Relative molecular mass measurements were carried out using a thermistor-type apparatus, fitted with vacuum tubing and high pressure taps to allow prior repeated evacuation/argon-filling and to allow a slow argon stream through it during the determination. The measurements were carried out with variable concentrations in benzene as solvent, typically spanning the range 50–600 mg of sample in 25 cm^3 of benzene. Each value was determined by three measurements.[16]

Mass spectroscopic studies were performed on a Kratos MS80RFQQ, operating in electron impact mode, using a direct insertion probe (to alleviate decomposition of samples), and operating over the temperature range 50–100°C.

Synthesis of [$LiOBu^t$]$_6$ (**1**)

A Schlenk flask was charged with lithium sand (0.70 g, 100.8 mmol) and suspended in toluene (45 cm^3). The Schlenk flask was then cooled to 0°C using an ice-bath and tert-butyl alcohol (8.6 cm^3, 90.8 mmol) added via syringe. After stirring for 24 h at ambient temperature, the solution was filtered to remove the excess metal, and the solvent removed *in vacuo* to yield a white solid. The product was purified by sublimation at 110–120°C (10^{-1} torr), as colourless crystals, to give 4.4 g, 54.97 mmol of [$LiOBu^t$]$_6$, a yield of 60.6% (based on Bu^tOH consumed). Found: C, 59.9; H, 11.2. Calc. for $LiOC_4H_9$: C, 60.0; H, 11.3%. Melting point: sublimes over the range 170–205°C (760 torr), > 250°C decomposes.

IR data (cm^{-1}): 1354(m), 1250(m), 1205(s), 1106(m), 962(s), 885(w), 833(m), 777(m), 754(m), 688(m).

NMR data: ^{1}H, 298 K, C_7D_8: δ 1.26 (s), spectrum remains unchanged on cooling to 220 K; ^{13}C, 298 K, C_7D_8: δ 35.67 (s, CMe_3), δ 64.96 (s, $OCMe_3$), also remains unchanged on cooling to 220 K; ^{7}Li, 233 K, C_7D_8: δ 2.83 (s), lower temperature limit; d_8-THF, 233 K: δ 3.15 (s), δ 3.67 (s) in a ratio of 4 : 1.

The molecular weights of 451 ± 46 and 468 ± 30 were measured at concentrations of 4.15×10^{-4} and 7.26×10^{-4} M, respectively. Calculated for [$LiOBu^t$]$_6$ = 480. Each value was determined by three measurements.

Mass spectroscopy shows M^+ 480 with clearly defined species, $[Li_3(OBu^t)_5]^+$ 420, $[Li_4(OBu^t)_4]^+$ 360, $[Li_3(OBu^t)_3]^+$ 300, $[Li_2(OBu^t)_2]^+$ 240 and $[LiOBu^t]^+$ 180.

Synthesis of [$LiOCMe_2Ph$]$_6$ (**2**)

A Schlenk flask was charged with lithium sand (0.14 g, 20 mmol) and 2-phenyl-2-propanol (2.73 g, 20 mmol) and tetrahydrofuran (30 cm^3). The reaction mixture was refluxed for 36 h during which time all the lithium metal was consumed. The solution was filtered to remove any unreacted metal, and the solvent removed *in vacuo* to yield a white solid. The product was then dissolved in the minimum amount of toluene (10 cm^3) and layered with n-pentane (25 cm^3), and the sample cooled to 5°C for 24 h. During this time large, regular shaped, colourless crystals of the product were deposited. The solution was subsequently filtered, and the crystals dried carefully *in vacuo* to give 2.41 g, 15.86 mmol of [$LiOCMe_2Ph$]$_6$, a yield of 79.2%. Melting point: 120–122°C, sublimes over the range 170–185°C (10^{-3} torr). Found: C, 71.2; H, 7.4. Calc. for $LiOC_9H_{11}$: C, 71.0; H, 7.2%.

IR data (cm^{-1}): 3040(m), 3020(m), 1244(s), 1161(s), 976(s), 868(s), 765(s), 592(s), 534(s).

NMR data: ^{1}H, 298 K, C_6D_6: δ 1.34 (s, Bu^t), δ 7.02 (m, Ph), δ 7.12 (m, Ph), δ 7.47 (m, Ph), spectrum remains unchanged on cooling to 220 K in C_7D_8; ^{13}C, 298 K, C_6D_6: δ 34.89 (s, CH_3), δ 70.92 (s, CMe_2), δ 124.74 (s, *para*-C), δ 126.25 (s, *meta*-C), δ 129.015 (s, *ortho*-C), δ 154.89 (s, *ipso*-C), also remains unchanged on cooling to 220 K in C_7D_8; ^{7}Li, 233 K, C_7D_8: δ 4.06 (s), lower temperature limit; d_8-THF, 233 K: δ 4.29 (s), δ 4.47 (s) in a ratio of 9 : 1.

The molecular weights of 793 ± 69 and 821 ± 44 were measured at concentrations of 3.63 ± 10^{-4} and 7.96×10^{-4} M, respectively. Calculated for [$LiOCMe_2Ph$]$_6$ = 853. Each value was determined by three measurements.

Mass spectroscopy shows M^+ 853 with clearly defined envelopes for $[Li_5(OR)_5]^+$ 710.83, $[Li_4(OR)_4]^+$ 586.67, $[Li_3(OR)_3]^+$ 426.5 and $[Li_2(OR)_2]^+$ 284.33.

X-ray diffraction studies

General operating procedures and a listing of programs have been given previously.[19] A summary of crystal data is given in Table 1. A suitable crystal was located and transferred to the goniostat using standard inert atmosphere handling techniques employed by the Indiana University Molecular

Structure Center and cooled to −169°C for characterization and data collection.

A systematic search of a limited hemisphere of reciprocal space located a set of diffraction maxima with symmetry and systematic absences corresponding to the unique monoclinic space group $P2_1/n$. Subsequent solution and refinement of the structure confirmed this choice.

Data were collected in the usual manner using a continuous θ–2θ scan with fixed backgrounds. The data were reduced to a unique set of intensities and associated sigmas in the usual manner. The structure was solved by a combination of direct methods (MULTAN78) and Fourier techniques. Refinement progressed smoothly, with a difference Fourier phased on the non-hydrogen atoms revealing the positions of most of the hydrogen atoms. The positions of the latter were fixed in their idealized positions for the remainder of the refinement.

In the final cycles of least-squares refinement, the non-hydrogen atoms were varied with anisotropic parameters and the hydrogen atoms were varied with isotropic thermal parameters to a final $R(F) = 0.0486$ and $Rw(F) = 0.0533$. The final difference was essentially featureless, the larger residual peak being 0.24 e/Å^3.

Selected bond distances and angles are collected in Table 2. Atomic positional parameters have been deposited with the Director, Cambridge Crystallographic Centre.

Acknowledgements—We thank the National Science Foundation for support. S.R.D. acknowledges St. John's College, Cambridge, for the award of a fellowship.

REFERENCES

1. W. N. Setzer and P. V. R. Schleyer, *Adv. Organomet. Chem.* 1985, **24**, 353.
2. B. J. Wakefield, *Best Synthetic Methods: Organolithium Methods*. Academic Press, London (1988); D. Seebach, *Angew. Chem. Intl. Ed. Engl.* 1988, **27**, 1624.
3. P. G. Williard and G. J. MacEwan, *J. Am. Chem. Soc.* 1989, **111**, 7671; P. J. Wheatley, *J. Chem. Soc.* 1960, 4270.
4. E. C. Constable, M. J. Doyle, J. Healy and P. R. Raithby, *J. Chem. Soc., Chem. Commun.* 1988, 1262.
5. G. Beck, P. B. Hitchcock, M. F. Lappert and I. A. MacKinnon, *J. Chem. Soc., Chem. Commun.* 1989, 1312.
6. L. M. Engelhardt, J. M. Harrowfield, M. F. Lappert, I. A. MacKinnon, B. H. Newton, C. L. Rashon, B. W. Skelher and A. H. White, *J. Chem. Soc., Chem. Commun.* 1986, 846.
7. L. Lochmann, M. Rodova and J. Trekoval, *J. Polymer Sci. Polym. Chem. Ed.* 1974, **12**, 2091; H. L. Hsieh, *J. Polymer Sci.* 1970, **A18**, 533.
8. W. H. Glaze and G. M. Adams, *J. Am. Chem. Soc.* 1966, **88**, 4653.
9. M. Marsch, K. Harms, L. Lochmann and G. Boche, *Angew. Chem. Intl. Ed. Engl.* 1990, **29**, 308.
10. H. Huml, *Czech. J. Phys.* 1965, **B15**, 699; V. Halaska, L. Lochmann and D. Lim, *Collect. Czech. Chem. Commun.* 1968, **33**, 3245.
11. See, M. Braun, D. Waldmüller and B. Mayer, *Angew. Chem. Intl. Ed. Engl.* 1989, **28**, 895, ref. 4.
12. T. Greiser and E. Weiss, *Chem. Ber.* 1977, **110**, 3388; J. E. Davies, J. Kopf and E. Weiss, *Acta. Cryst.* 1982, **B28**, 2251 and refs therein; E. Weiss, H. Alsdorf, H. Kühr and H-F. Grützmacher, *Chem. Ber.* 1968, **101**, 3777.
13. J. Hvoslef, H. Hope, B. D. Murray and P. P. Power, *J. Chem. Soc., Chem. Commun.* 1983, 1438.
14. B. Cetinkaya, I. Gümrükcü, M. F. Lappert, J. L. Atwood and R. Shakir, *J. Am. Chem. Soc.* 1980, **102**, 2088.
15. J. H. Exner and E. C. Steiner, *J. Am. Chem. Soc.* 1974, **96**, 1782.
16. D. P. Shoemaker, C. W. Garland and J. I. Steinfield, *Experiments in Physical Chemistry*, 3rd edn, pp. 174–185. McGraw-Hill, New York (1974).
17. J. D. Kahn, A. Haag and P. von R. Schleyer, *J. Phys. Chem.* 1988, **92**, 212.
18. G. E. Hartwell and T. L. Brown, *Inorg. Chem.* 1966, **5**, 1257.
19. M. H. Chisholm, K. Folting, J. C. Huffman and C. C. Kirkpatrick, *Inorg. Chem.* 1984, **23**, 1021.

Polyhedron Vol. 10, No. 8, pp. 811–818, 1991
Printed in Great Britain

0277–5387/91 $3.00+.00
© 1991 Pergamon Press plc

STERIC EFFECTS AND GEOMETRICAL DISTORTIONS ON A NEW SERIES OF COBALT(II) ENTWINED COMPLEXES: STABILIZATION OF LOW VALENT OXIDATION STATES, COBALT(I) AND COBALT(0) COMPLEX SPECIES

MD. ATHAR MASOOD and P. S. ZACHARIAS*

School of Chemistry, University of Hyderabad, Hyderabad-500 134, India

(*Received* 13 *August* 1990; *accepted* 10 *December* 1990)

Abstract—Cobalt(II) complexes of 2,9-disubstituted and 2-monosubstituted 1,10-phenanthrolines by phenyl moieties containing *ortho* substituents were prepared and investigated by electronic spectral and electrochemical methods. Larger *ortho* substituents are found to cause more tetrahedral distortions, while the absence of substitution at the 9-position of the phenanthroline leads to smaller distortions. The tetrahedral distortion imposed by the bulkiness of the ligands and the weakly interacting forces mediated through the *ortho* substituents of the phenyl with the central metal ion influences the electrochemical reductions and also leads to stabilized cobalt(I) and cobalt(0) complex species.

Ligands such as 1,10-phenanthroline (phen) and its substituted derivatives are known to form stable complexes with transition metal ions in their normal valencies and low valence states. The 2,9-disubstitution imposes a strain in the molecule due to steric crowding. Due to this the complexes will be constrained to form a pseudo-tetrahedral/tetrahedral geometry with a $M(N—N)_2$ chromophore environment. Recently, it has been reported that catenands derived from 2,9-di(*p*-methoxyphenyl)-1,10-phen are more suited to stabilize low oxidation states, and nearly perfect electrochemical reversibility could be achieved for the redox couples. This is attributed to the topography (two entwined units) and the topology (interlocked rings) of the ligand system. On the other hand, copper(I) complexes of 2,9-di(*p*-methoxyphenyl)-1,10-phen undergo electrochemical reduction followed by rapid dissociation to copper metal and free ligand.[1] Electrochemically these complexes are irreversible.

It was reported earlier from our laboratory that copper(I) complexes of 2,9-di(*o*-substituted phenyl)-1,10-phen show electrochemical reversibility for the Cu^{1+}/Cu^0 redox process[2] comparable with the electrochemical reversibility of the copper(I) catenate. The ligands which are soft (π-acceptors) assist in the stabilization of lower valent oxidation states, while the entwining nature of the ligands, together with the large geometrical distortions arising from the *ortho* substituents of the phenyl ring (of the ligand system), are responsible for the electrochemical reversibility of the Cu^+/Cu^0 redox couple, in which the copper(0) complex species obtained was still found to be entrapped without undergoing any dissociation into the metal atom and free ligand. Furthermore, we have also investigated the relationship between the common ligand environment and the different valence states of the copper metal and the geometrical distortions in the context of the electron transfer. Encouraged by the results on copper(I) and copper(II) complexes, it seemed appropriate to investigate the stability and electrochemical response of cobalt(II) complexes of these ligands. The results of our investigation on these complexes are presented and discussed in the following sections.

EXPERIMENTAL

Materials

All the solvents were of reagent grade and distilled either over CaH_2 or Na-wire and stored over molecular sieves prior to use. 1,10-Phenanthroline

* Author to whom correspondence should be addressed.

(E. Merck), 2-bromoanisole, 2-bromotoluene and *o*-phenetidine were obtained from Fluka and used as supplied. *o*-Phenetidine was converted to 2-bromoethoxybenzene by the usual method of diazotization followed by coupling with cuprous bromide.

Preparation of the ligands

The ligands were prepared according to a procedure described earlier.[2] These ligands are 2,9-di(*o*-tolyl)-1,10-phen (dtphen), 2,9-di(2-methoxyphenyl)-1,10-phen (dmophen), 2,9-di(2-ethoxyphenyl)-1,10-phen (deophen), 2-(2-tolyl)-1,10-phen (tphen) and 2-(2-ethoxyphenyl)-1,10-phen (eophen).

Preparation of the complexes

The $[Co(L)_2](ClO_4)_2$ and $[Co(L')_2](ClO_4)_2]$ type complexes (where L and L′ are disubstituted and monosubstituted phen ligands, respectively) were prepared by the following general procedure:

To the respective ligands (2.1 mmol) dissolved in CH_2Cl_2 (5 cm^3), an acetone solution (5 cm^3) of $Co(ClO_4)_2 \cdot 6H_2O$ (1 mmol) was added while stirring. In the case of the dtphen ligand, a violet solution with green fluorescence was obtained, and for all other ligands yellow solutions were obtained. These solutions were reduced in volume when precipitation occurred. The $[Co(dtphen)_2]^{2+}$ complex was recrystallized from hexane–benzene (4 : 1 volume ratio) and obtained as beautiful violet–green crystals. The other complexes were recrystallized from hexane–CH_2Cl_2 (4 : 1) and obtained as yellow powders. The generalized structure of these types of complexes are shown in Fig. 1.

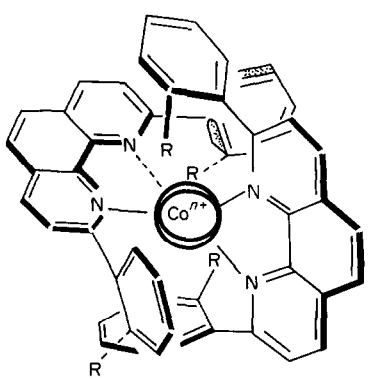

Fig. 1. Generalized structure of the bis[2,9-di(*o*-substituted phenyl)-1,10-phenanthroline] cobalt(II) complexes.

Preparation of $[CoLCl_2]$ *and* $[CoL'Cl_2]$ *complexes*

To the respective ligands (1.1 mmol) in CH_2Cl_2–EtOH (1 : 4, 5 cm^3) was added an ethanolic solution (5 cm^3) of $CoCl_2 \cdot 6H_2O$ (1 mmol) and this was stirred for 30 min. A large proportion of the solvent was allowed to evaporate at room temperature and then acetone (10 cm^3) was added and stirred vigorously, and thereby the complexes precipitated out. These were crystallized from CH_2Cl_2–hexane (1 : 4) and obtained as dark blue or dark green powder to crystalline compounds.

Physical measurements

The C, H and N analyses were carried out on a Perkin–Elmer 240C elemental analyser. Conductivity measurements were carried out on a CM 82 T Elico Model conductivity meter at 25°C in nitromethane. Vibrational spectra were recorded as KBr discs in the range 4000–200 cm^{-1} on a Perkin–Elmer 283 IR spectrophotometer. Electronic spectra were recorded with a Perkin–Elmer Lambda 3B UV–vis spectrophotometer in acetonitrile using 1×10^{-3} M solutions for the visible range and 1×10^{-5} M solutions for the UV range. Magnetic susceptibilities were measured on a Bruker BM 6 magnet with a Faraday magnetic balance. $HgCo(NCS)_4$ was used as calibrant. Cyclic voltammetric (CV) and differential pulse voltammetric (DPV) studies were carried out on a PAR electrochemistry system consisting of a 174 A polarographic analyser and a single compartment cell. Solutions of the complexes were 1×10^{-3} M in acetonitrile. In all the experiments the supporting electrolyte was 0.1 M tetraethylammonium perchlorate (TEAP) which was prepared as previously described,[3] recrystallized twice from a H_2O–MeOH mixture and dried *in vacuo* at 40°C. All experiments were carried out under dry nitrogen at 27 ± 1°C in a three-electrode configuration with a hanging mercury drop electrode (HMDE) as the working electrode, a platinum wire as the auxiliary electrode and a standard calomel electrode (SCE) as the reference electrode. All potentials are referred to vs the SCE and are uncorrected for liquid junction potential.

RESULTS AND DISCUSSION

Complexes of the types $[Co(L)_2]^{2+}$, $[Co(L')_2]^{2+}$, $[CoLCl_2]$ and $[CoL'Cl_2]$, where L = 2,9-di(*o*-substituted phenyl)-1,10-phen and L′ = 2-mono(*o*-substituted phenyl)-1,10-phen ligands, were prepared and investigated. These complexes have been characterized by elemental analyses and spectral

methods. Ligands L and L′ are abbreviated depending on the *ortho* substitution of the phenyl moiety and details are given in the Experimental. $[Co(L)_2]^{2+}$ and $[Co(L')_2]^{2+}$ type complexes show conductivity in nitromethane in the range 130–160 Ω^{-1} cm^2 mol^{-1}. These values are typical for 1 : 2 electrolyte.[4] Their IR spectra show a strong absorption band at about 1090 cm^{-1}, characteristic of an ionic perchlorate group.[5] The covalently bonded perchlorate group, on the other hand, shows two distinct IR peaks at *ca* 1030 and 1310 cm^{-1}. These bands are not observed in the complexes, therefore supporting the ionic nature of the perchlorate group. The C=N stretching band appears in the region 1490–1505 cm^{-1}. This is characteristic of the nitrogen atoms of the phen coordinating to the metal. The halide complexes of cobalt(II) do not show any electrical conductance, thus exhibiting the non-ionic nature of these complexes in conformity with their structures.

It was earlier reported that Co—$(Cl)_2$ stretches in the 300–350 cm^{-1} region for $[CoLCl_2]$ complexes.[6] All the cobalt(II) halide complexes exhibit a sharp band in that region. The analytical and spectral data are tabulated in Table 1.

The $[Co(dtphen)_2]^{2+}$ complex is found to exhibit electronic absorption bands in the visible region. In the spectra, a broad band at 590 nm with a shoulder at *ca* 575 nm and a small band at 534 nm occur, which are characteristic of distorted tetrahedral geometry with the bands decreasing in intensity in that order. Likewise, $[Co(tphen)_2]^{2+}$ exhibits bands at 543, 510 and 482 nm thus indicating less tetrahedral distortion. The absence of similar absorption bands in $[Co(dmophen)_2]^{2+}$, $[Co(deophen)_2]^{2+}$ and $[Co(eophen)]^{2+}$, which are expected to have distorted tetrahedral geometry, is due to the intramolecular charge-transfer interaction (methoxy or ethoxy phenanthrolines) to the low energy bands found in the absorption spectra.[7] Similar interactions and the consequent absence of visible absorption bands of tetrahedral geometry have been reported in the case of $[Co(dap)_2](ClO_4)_2$, where dap = 2,9-di(*p*-methoxyphenyl)-1,10-phen.

$[CoLCl_2]$ and $[CoL'Cl_2]$ complexes show absorption bands in the visible region characteristic of tetrahedral geometry. The spectra contain a broad band with two components at about 670 and 640 nm and a sharp band at 570 nm. The intensity is greater for the 670 nm band than the 570 nm band. Similar spectral features were observed for $[Co(dmp)Cl_2]$, where dmp = 2,9-dimethyl-1,10-phen, which has a tetrahedral geometry.[8] Effective magnetic moment values of cobalt(II) complexes at room temperature are in the range 4.5–5.0 μ_B,* which is as expected for complexes of tetrahedral/pseudo-tetrahedral geometry and is due to the orbital contribution to the spin-only value.

Electrochemical, CV and DPV data were obtained in acetonitrile solvent. Both positive and negative potential ranges were examined. All ligands are found to be electrochemically inactive up to −1.90 V. CV profiles at various scan rates and repeated scans were also investigated. All the cobalt(II) complexes of the type $[Co(L)_2]^{2+}$ and $[Co(L')_2]^{2+}$ show two perfectly reversible, one-electron reduction steps in the negative potential range. For the $[Co(dtphen)_2]^{2+}$ complex the successive reductions occur at −0.58 (Co^{2+}/Co^{1+}) and −1.26 V (Co^{1+}/Co^0). For the $[Co(dmophen)_2]^{2+}$ and $[Co(deophen)_2]^{2+}$ complexes the values are at more negative potentials. The ΔE_p values are *ca* 60 mV and the $-i_c/i_a$ ratio is *ca* 1 for both sets of redox peaks. Potential values do not show any shift at various scan rates. DPV technique was also used to determine the E_p values, which were in good agreement with the CV data. Similar comparisons can be drawn between $[Co(tphen)_2]^{2+}$ and $[Co(eophen)_2]^{2+}$, but the Co^{2+}/Co^{1+} couple is found at more negative potentials and the ΔE_p values are about 70–80 mV. The relevant electrochemical data is collected in Tables 2 and 3 and the CV profiles of the representative complexes are shown in Fig. 2.

Cobalt(II) catenate, obtained from interlocking catenands derived from dap units, have successive redox couples at −0.60 and −1.30 V. For $[Co(dap)_2]^{2+}$ these couples occur at −0.60 and −1.27 V. The only significant difference between catenate and its open analogue is a slightly wider potential stability range for the monovalent cobalt species. This difference is explained on the basis of the topography and the topology of the catenate. It is also a well established fact that $E_{1/2}$ moves towards more positive potentials with an increase in tetrahedral distortion for the copper(II) complexes.[9] Extending this argument, it can also be pointed out that the octahedral cobalt(II) complexes will have more negative reduction potentials than the tetrahedral complexes.[10,11] The redox potential for the Co^{2+}/Co^{1+} couples in the complex $[Co(dtphen)_2]^{2+}$ is more positive by *ca* 50 mV than that of the corresponding redox peak of the cobalt (II) catenate. This is to be expected since this complex is less distorted and not as stabilized as the catenate complex. However, for $[Co(dmophen)_2]^{2+}$ and $[Co(deophen)_2]^{2+}$ the corresponding values are more negative than the catenate complex. Thus the

* One BM signifies 9.27×10^{-24} A m^2.

Table 1. Analytical, spectral and magnetic data for the cobalt(II) complexes

Complex	Elemental analyses[a] C (%)	H (%)	N (%)	IR absorption (cm^{-1}) (Co-x)	$(ClO_4)^-$	(C=N)	Conductance ($\Omega^{-1}\,cm^2\,mol^{-1}$)	Absorption[b] λ_{max} (nm) [log ε]	Magnetic moment (μ_B)
$[Co(dtphen)_2](ClO_4)_2$	63.8 (63.7)	4.1 (4.1)	5.7 (5.7)	—	1087	1491	130	590[2.42], 575[2.34] 534[2.19]	5.05
$[Co(dmophen)_2](ClO_4)_2$	59.9 (59.3)	3.9 (3.7)	5.4 (5.2)	—	1090	1492	145	330sh[4.71], 299[4.86]	4.31
$[Co(deophen)_2](ClO_4)_2$	63.2 (63.0)	4.4 (4.3)	5.1 (4.9)	—	1095	1505	150	337[4.57], 303[4.68]	4.96
$[Co(tphen)_2](ClO_4)_2$	57.1 (57.0)	3.5 (3.5)	7.0 (7.0)	—	1090	1491	140	543[2.39], 510[2.30] 482[2.18]	4.57
$[Co(eophen)_2](ClO_4)_2$	53.9 (53.8)	3.7 (3.7)	6.5 (6.5)	—	1092	1501	160	277[4.76], 233[4.86]	4.53
$[Co(dtphen)Cl_2]$	63.7 (63.0)	4.1 (4.0)	4.7 (4.7)	352	—	1491	—	675[2.54], 64sh[2.38] 576[2.84]	4.72
$[Co(dmophen)Cl_2]$	59.8 (58.2)	3.9 (3.7)	5.4 (5.0)	352	—	1490	—	672[2.5], 639sh[2.81], 574[2.76]	4.89
$[Co(deophen)Cl_2]$	63.2 (63.0)	4.4 (4.3)	5.1 (5.0)	352	—	1491	—	673[2.55], 643sh[2.42] 574[2.38]	4.95
$[Co(tphen)Cl_2]$	57.0 (55.8)	3.5 (3.5)	7.0 (7.0)	349	—	1491	—	669[2.62], 640sh[2.51] 572[2.40]	4.69
$[Co(eophen)Cl_2]$	55.8 (54.7)	3.8 (3.7)	6.5 (6.4)	350	—	1490	—	667[2.53], 643sh[2.42] 573[2.78]	4.84

[a] Numbers in parentheses correspond to theoretical values.
[b] Whenever bands are not observed in visible region, the higher energy bands are given.

Table 2. Cyclic voltammetric data for the cobalt(II) complexes

Complex	Scan rate ($V\ s^{-1}$)	Co^{2+}/Co^{1+}					Co^{1+}/Co^{0}				
		E_p, c (V)	E_p, a (V)	ΔE_p (V)	$E_{1/2}$ (V)	$-i_c/i_a$	E_p, c (V)	E_p, a (V)	ΔE_p (V)	$E_{1/2}$ (V)	$-i_c/i_a$
$[Co(dtphen)_2]^{2+}$	0.02	−0.58	−0.52	0.06	−0.55	0.93	−1.26	−1.20	0.06	−1.23	1.08
	0.05	−0.58	−0.52	0.06	−0.55	0.94	−1.27	−1.21	0.06	−1.24	1.14
	0.10	−0.58	−0.51	0.07	−0.55	0.97	−1.26	−1.20	0.06	−1.23	0.94
$[Co(dmophen)_2]^{2+}$	0.02	−0.84	−0.77	0.07	−0.81	1.00	−1.39	−1.32	0.07	−1.36	1.07
	0.05	−0.84	−0.79	0.06	−0.82	1.00	−1.39	−1.33	0.06	−1.36	1.19
	0.10	−0.84	−0.78	0.06	−0.81	1.00	−1.40	−1.34	0.06	−1.37	1.00
$[Co(deophen)_2]^{2+}$	0.02	−0.78	−0.72	0.06	−0.75	1.15	−1.38	−1.32	0.06	−1.35	1.15
	0.05	−0.78	−0.72	0.06	−0.75	1.00	−1.39	−1.33	0.06	−1.36	0.96
	0.10	−0.79	−0.72	0.06	−0.76	1.00	−1.39	−1.33	0.06	−1.36	0.97
$[Co(tphen)_2]^{2+}$	0.02	−1.05	−0.98	0.07	−1.03	1.20	−1.25	−1.18	0.07	−1.21	0.95
	0.05	−1.05	−0.98	0.07	−1.02	1.12	−1.26	−1.20	0.06	−1.23	0.96
	0.10	−1.07	−0.99	0.08	−1.03	1.18	−1.26	−1.20	0.06	−1.23	1.06
$[Co(eophen)_2]^{2+}$	0.02	−1.14	−1.06	0.08	−1.10	1.08	−1.36	−1.28	0.08	−1.32	1.07
	0.05	−1.13	−1.06	0.07	−1.10	1.05	−1.36	−1.28	0.08	−1.32	1.12
	0.10	−1.13	−1.05	0.08	−1.09	1.08	−1.36	−1.28	0.08	−1.32	1.10
$[Co(dtphen)Cl_2]$	0.02	−1.07[a]	—				−1.55[b]	—			
	0.05	−1.07	—				−1.56[b]	—			
	0.10	−1.05	—				−1.57	—			
$[Co(dmophen)Cl_2]$	0.02	−0.83[c]	−0.77	0.06	−0.8	1.12	−1.40	—			
	0.05	−0.83	−0.77	0.06	−0.8	1.09	−1.43	—			
	0.10	−0.83	−0.78	0.06	−0.8	1.14	−1.44	—			
$[Co(deophen)Cl_2]$	0.02	−0.79[c]	−0.73	0.06	−0.76	1.05	−1.35[b]	—			
	0.05	−0.80	−0.74	0.06	−0.77	1.09	−1.38	—			
	0.10	−0.78	−0.72	0.06	−0.75	1.12	−1.42	—			

[a] The peak is very ill-defined.
[b] The peaks are very ill-defined.
[c] The peaks are well-defined and found to be reversible because of the bulkiness of the dmophen and deophen ligands.
Note: $[Co(tphen)Cl_2]$ and $[Co(eophen)Cl_2]$ exhibit no peaks.

Table 3. Differential pulse voltammetric data for the cobalt(II) complexes at a scan rate of 0.02 V s^{-1}

Complex	Co^{2+}/Co^{1+}						Co^{1+}/Co^{0}					
	E_p, c (V)	E_p, a (V)	$W_{1/2}$ cathodic	$W_{1/2}$ anodic	n^a cathodic	n^a anodic	E_p, c (V)	E_p, a (V)	$W_{1/2}$ cathodic	$W_{1/2}$ anodic	n^a cathodic	n^a anodic
$[Co(dtphen)_2]^{2+}$	−0.57	−0.50	0.110	0.110	0.82	0.82	−1.26	−1.19	0.100	0.100	0.90	0.90
$[Co(dmophen)_2]^{2+}$	−0.84	−0.76	0.110	0.115	0.82	0.79	−1.38	−1.32	0.100	0.110	0.90	0.82
$[Co(deophen)_2]^{2+}$	−0.76	−0.70	0.100	0.100	0.91	0.91	−1.37	−1.31	0.100	0.100	0.90	0.90
$[Co(tphen)_2]^{2+}$	−1.06	−1.00	0.105	0.100	0.86	0.91	−1.26	−1.19	0.110	0.115	0.82	0.79
$[Co(eophen)_2]^{2+}$	−1.13	−1.05	0.120	0.130	0.75	0.70	−1.36	−1.27	0.120	0.120	0.75	0.75

[a] $n = 90.4/W_{1/2}$.

potential stability range for cobalt(I) complex species has decreased in the two complexes. These two complexes should be tetrahedrally more distorted because of the presence of bulky *ortho* substituents, and hence should show a less negative potential. The shift of the potential to more negative values thus indicates the stabilization of the cobalt(II) oxidation state, which is related to the weak interaction of the methoxy or ethoxy of the *ortho* substituent of the phenyl ring of the substituted phen with the cobalt metal ion. This weak interaction has already been explored for the iron(II) and copper(II) complexes of the above ligands. It has also been pointed out that the approach of —OMe towards the central metal ion is less hindered than that of —OEt, and that the tetrahedral distortion in the complexes involving deophen is comparable with that of catenate. Hence cobalt(II) in $[Co(dmophen)_2]^{2+}$ is more stabilized than in $[Co(deophen)_2]^{2+}$, though tetrahedrally less distorted than the latter.

Furthermore, it can be seen from the electrochemical data that the redox potential values for the Co^{1+}/Co^{0} couple have not changed in comparison with cobalt(II) catenate, still, there is a slight negative potential shift for $[Co(dmophen)_2]^{1+}$ and $[Co(deophen)_2]^{1+}$ complex species. Although the stabilization range for cobalt(I) has narrowed, the cobalt(I) species is nevertheless highly stabilized and can either revert back to cobalt(II) on oxidation at the electrode surface or can further reduce to form the cobalt(0) complex species which itself it found to be stabilized. This effect can be seen clearly in CV profiles where two perfectly reversible one-electron processes with ΔE_p values of *ca* 65 mV are observed, for any of the scan rates, and there is no decomposition of either of the species as the current cathodic and anodic peaks remain the same in multiple scans. The term "stabilized species" infers that the reduced ion or the metal species is still bound to the $(N—N)_2$ chromophore and does not dissociate into the free ligand and the metal species. Again it can be said that the —OMe at the *para* position (as in the dap ligand) will not interact with the central metal ion. Furthermore, as can be seen from the reversibility of the reduction processes, the electron transfer is not accompanied by any structural reorganization either before or after the reduction and it is reasonable to infer that all the oxidation states of cobalt, viz. (II), (I), (0), involve the tetrahedral disposition of the ligand.

Also, comparison of the electrochemical properties with the previously reported data for the cobalt bipyridyl or phen complexes[10–14] shows here, a strong stabilization of all the reduced states. Other sterically constrained polyimine cobalt compounds also lead to stabilized monovalent complexes.[15–17]

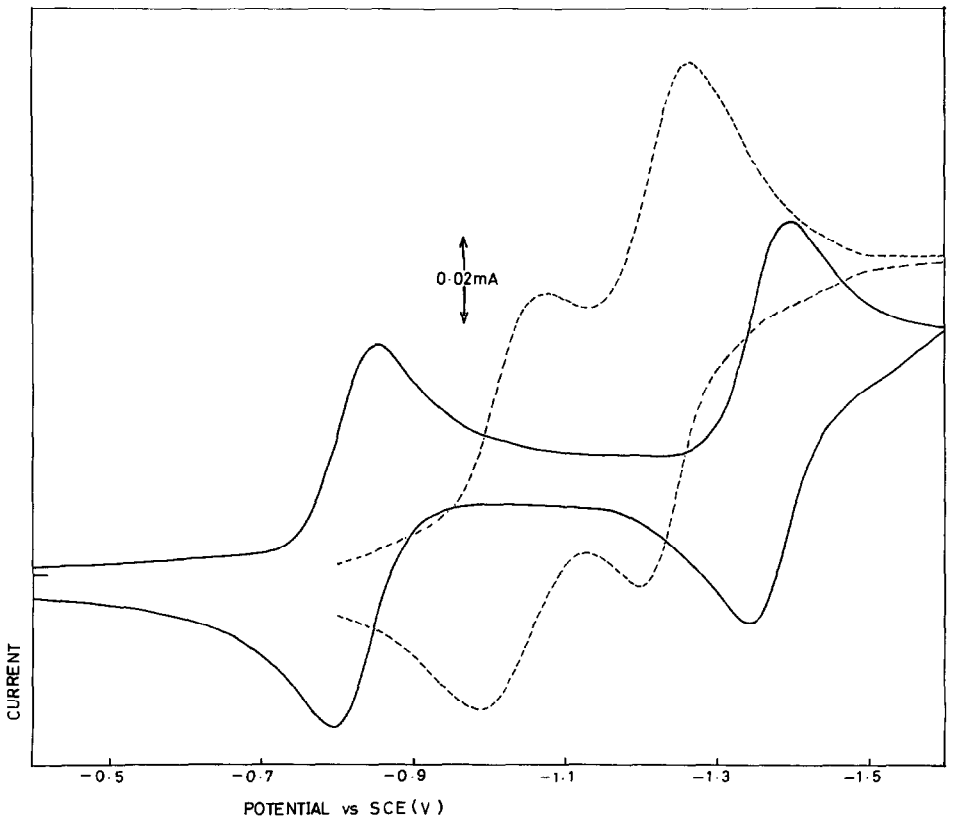

Fig. 2. Cyclic voltammetric profiles of $[Co(dmophen)_2]^{2+}$ (——) and $[Co(tphen)_2]^{2+}$ (– – – –) at a scan rate of 0.10 V s^{-1}.

For instance, the redox potential of the $Co(dmbp)_2^{2+/1+}$ couple (dmbp = 6,6′-dimethyl-2,2′-bipy) is −0.63 V, showing that in the above case of the complexes although there is no particular topography effect, stabilization is the consequence of —OMe, —OEt mediated interactions and geometrical distortions.

Remarkable also is the drastic structural effect of the ligands on the Co^{3+}/Co^{2+} redox potential, whereas bipy or phen complexes of cobalt(II) can very easily be electrochemically oxidized to octahedral cobalt(III),[18,19] the redox potential value of the Co^{3+}/Co^{2+} couple being close to 0.00 V, no oxidation peak is observed for the present complexes. The destabilization effect on this couple due to entwined ligands and *ortho* substituents, as well as due to a poor ligand field of tetrahedral geometry, is thus very large.

The monosubstituted cobalt(II) phen complexes show similarly two reversible peaks, but the peak positions for the Co^{2+}/Co^{1+} couple have moved towards higher negative potentials, *ca* −1.10 V, which, as was described earlier, is a result of less tetrahedral distortion due to the absence of substitution at the 9-position of phen. Between $[Co(eophen)_2]^{2+}$ and $[Co(tphen)_2]^{2+}$ cobalt(II) is stabilized by about 80 mV and is consistent with the interpretation of a weak intramolecular interaction of the *ortho* substituent of the phenyl of 1,10-phen with the central metal ion. Comparing this stabilization difference of 80 mV with the difference obtained between the disubstituted complexes, *ca* 270 mV, clearly demonstrates the extent of stabilization which occurs due to disubstituted ligands containing electron donor sites as *ortho* substituents in the form of alkoxy groups.

The $[CoLCl_2]$ and $[CoL'Cl_2]$ complexes are found to give either quasi-reversible or totally irreversible peaks and are thus not significant in the stabilization of the lower valent oxidation states. This also signifies that electrochemical reversibility depends on a type of chromophore environment where the central metal ion is enveloped.

Thus electrochemical reversibility, hence the stabilization of various valence states of cobalt, viz. 2, 1, 0, can invariably be accounted for as due to the π^*-nature of the ligands, the steric impositions which lead to tetrahedral disposition of the ligands around the central metal ion, the same stereochemistry in all the reduced states, and largely to

the weak interaction of the *ortho* substituents of the phenyl of 1,10-phen.

Acknowledgement—M.A.M. thanks the CSIR for financial support.

REFERENCES

1. C. O. Dietrich-Buchecker and J. P. Sauvage, *J. Am. Chem. Soc.* 1984, **106**, 3043.
2. Md. Athar Masood and P. S. Zacharias, *J. Chem. Soc., Dalton Trans.* 1991, 111.
3. H. O. House, E. Feng and N. Peet, *J. Org. Chem.* 1971, **36**, 2371.
4. W. J. Geary, *Coord. Chem. Rev.* 1971, **7**, 81.
5. B. J. Hathaway and A. E. Underhill, *J. Chem. Soc.* 1961, 3091.
6. Chan-Cheng Su and Shiou-Mei Huong, *Transition Met. Chem.* 1984, **9**, 220.
7. C. O. Dietrich-Buchecker, J. P. Sauvage and J. M. Kern, *J. Am. Chem. Soc.* 1989, **111**, 7791.
8. D. B. Fox, J. R. Hall and R. A. Plowman, *Aust. J. Chem.* 1965, **18**, 691.
9. H. Yokoi and A. W. Addison, *Inorg. Chem.* 1977, **16**, 1341.
10. G. Arena, R. P. Bonoma, S. Musumeci and E. Rizzarelli, *Z. Anorg. Allg. Chem.* 1975, **412**, 161.
11. R. R. Ruminski and J. D. Peterson, *Inorg. Chim. Acta* 1984, **88**, 63.
12. A. A. Vlcek, *Nature* 1957, **180**, 753.
13. N. Maki, T. Hirano and S. Musha, *Bull. Chem. Soc. Japan* 1963, **36**, 756.
14. N. Tanaka and Y. Sato, *Bull. Chem. Soc. Japan* 1968, **41**, 2059.
15. C. W. G. Ansell, J. Lewis, M. C. Liptrot, P. R. Raithby and M. Schroder, *J. Chem. Soc., Dalton Trans.* 1982, 1593.
16. A. M. Tait, F. V. Lovecchio and D. H. Busch, *Inorg. Chem.* 1977, **16**, 2206.
17. S. Musumeci, E. Rizzarelli, S. Sammartano and R. P. J. Bonomo, *Electroanal. Chem.* 1973, **46**, 109.
18. B. C. Willet and F. C. Anson, *J. Electrochem. Soc.* 1982, **129**, 1260.
19. Y. W. D. Chen, K. S. V. Santhanam and A. J. Bard, *J. Electrochem. Soc.* 1982, **129**, 61.

Polyhedron Vol. 10, No. 8, pp. 819–822, 1991
Printed in Great Britain

0277–5387/91 $3.00+.00
© 1991 Pergamon Press plc

PEROXO COMPLEXES OF ZIRCONIUM(IV), THORIUM(IV), MOLYBDENUM(VI), TUNGSTEN(VI) AND URANIUM(VI) CONTAINING TWO QUADRIDENTATE ONNO SCHIFF BASES

M. T. H. TARAFDER* and A. R. KHAN

Department of Chemistry, University of Rajshahi, Rajshahi, Bangladesh

(*Received* 29 *October* 1990; *accepted* 10 *December* 1990)

Abstract—Some new peroxo complexes of molybdenum, tungsten, uranium, zirconium and thorium containing quadridentate, dinegative Schiff base ligands have been synthesized and characterized. The Schiff bases $C_{20}H_{14}N_2O_2H_2$ and $C_{14}H_{10}N_2O_2H_2$ were derived from the condensation of *o*-phenylenediamine or hydrazine hydrate with salicylaldehyde, respectively. The Schiff bases undergo deprotonation, while complexation having ONNO donor sequences producing complexes of compositions $[M(O)(O_2)(ONNO)]$ and $[M'(O_2)(ONNO)]$ [M = Mo^{VI}, W^{VI} and U^{VI}; M′ = Zr^{IV} and Th^{IV}; ONNO = $C_{20}H_{14}N_2O_2^{2-}$ and $C_{14}H_{10}N_2O_2^{2-}$]. The chelate effect of the quadridentate ligands stabilizes the metal–peroxo moiety which prevents oxygen transfer reactions to both organic and inorganic substrates. The σ-donor nature of the quadridentate ligands influences the mode of coordination of the peroxo moiety. The frequency of the ν_1 mode of the $M(O_2)$ grouping decreases with an increase in the atomic number of the metals in a particular group.

The incorporation of ancillary ligands with different donor properties into metal peroxides gives complexes which exhibit intriguing lability differences. The chemistry of the peroxo complexes has received considerable attention in recent years,[1–12] mainly because they are sources of active oxygen atoms and can be used as stoichiometric, as well as catalytic, oxidants for organic and inorganic substrates.[5–12] We have successfully employed peroxo complexes to generate glycerine from allyl alcohol which is, indeed, an industrial aspect of this project.[8] However, the metal–peroxo moiety is greatly stabilized when tridentate or quadridentate auxiliary ligands are used.[9–12] To examine this further, we have extended our study to peroxo complexes of different elements of Groups 4A and 6A containing two quadridentate, dinegative ligands. We report here the synthesis of these complexes and studies on their potential as oxygen transfer reagents. An attempt has also been made to study the effect of the size of the metal ion and the electronic nature of the quadridentate ligands on the ν_1(O—O) modes of the complexes in their IR spectra.

* Author to whom correspondence should be addressed.

EXPERIMENTAL

IR spectra (as KBr discs) were recorded with a Pye–Unicam SP3-300 IR spectrophotometer. Conductivities of 10^{-3} M solutions of the complexes in dimethyl sulphoxide (DMSO) were measured at 25°C using a WPA CM35 conductivity meter and dip-type cell with platinized electrodes.

Reagents

All chemicals used were reagent grade and were used as supplied by E. Merck.

Analyses

Carbon, hydrogen and nitrogen analyses were carried out by Microanalytical Services at the University of St. Andrews, Scotland.

Preparation of ligands

Preparation of $C_{20}H_{14}N_2O_2H_2$. Salicylaldehyde (1.22 g, 0.01 mol) in absolute ethanol (30 cm^3) was added to a solution of *o*-phenylenediamine (0.54 g, 0.005 mol) in the same solvent (20 cm^3). The mixture

was boiled down to *ca* 25 cm^3 and cooled to room temperature. The orange–red crystals which separated were washed with ethanol. Melting point 142–144°C. (Found: C, 75.8; H, 4.9; N, 8.8. Calc. for $C_{20}H_{14}N_2O_2H_2$: C, 75.9; H, 5.1; N, 8.9%.)

Preparation of $C_{14}H_{10}N_2O_2H_2$. Salicylaldehyde (1.22 g, 0.01 mol) in absolute ethanol (30 cm^3) was added to a solution of hydrazine hydrate (0.25 g, 0.005 mol) in the same solvent (15 cm^3). The mixture was heated on a water bath to reduce the volume to *ca* 20 cm^3 and cooled to room temperature. The yellow crystals were separated and washed with ethanol. Melting point 209–211°C. (Found: C, 69.9; H, 4.9; N, 11.7. Calc. for $C_{14}H_{10}N_2O_2H_2$: C, 70.0; H, 5.0; N, 11.7%.)

Preparation of complexes

General method for the preparation of complexes **1**, **3** *and* **4**: $[M(O)(O_2)L]$ ($M = Mo^{VI}$ *and* W^{VI}; $L = C_{20}H_{14}N_2O_2^{2-}$ *or* $C_{14}H_{10}N_2O_2^{2-}$). A suspension of MO_3 (0.017 mol) in 30% H_2O_2 (60 cm^3) was stirred overnight at 45–50°C. This was filtered and to the clear filtrate was added a solution of L (0.017 mol) in hot ethanol (150 cm^3). The mixture was stirred whilst cooling at the same time in an ice–salt bath. A yellow precipitate appeared, which was washed successively with water and ether and dried *in vacuo* over P_4O_{10}.

Preparation of **2** *and* **5**: $[U(O)(O_2)L]$ (L = $C_{20}H_{14}N_2O_2^{2-}$ *and* $C_{14}H_{10}N_2O_2^{2-}$). To a solution of $UO_2(NO_3)_2 \cdot 6H_2O$ (0.006 mol) in ethanol (35 cm^3), a solution of L (0.006 mol) in the same solvent (100 cm^3) and then 30% H_2O_2 (35 cm^3) were added. The product was separated and stored as above.

Preparation of complexes **6** *and* **7**: $[M(O_2)(C_{20}H_{14}N_2O_2)]$ ($M = Zr^{IV}$ *and* Th^{IV}). A solution of $M(NO_3)_4 \cdot 6H_2O$ (0.005 mol) in water (40 cm^3) was added to a solution of $C_{20}H_{14}N_2O_2H_2$ (0.005 mol) in ethanol (100 cm^3), followed by the addition of 30% H_2O_2 (30 cm^3). The product was separated and stored as above.

Attempted reactions of **1** *and* **4** *with allyl alcohol and* **5–7** *with triphenylphosphine and triphenylarsine, respectively*

Refluxing of **1** with allyl alcohol in a 1 : 1 molar ratio in tetrahydrofuran (THF) medium for 48 h failed to produce any reaction; **1** was recovered unchanged.

Refluxing of **4** with allyl alcohol in the presence of a large excess of 30% H_2O_2 in dioxane medium for 48 h at 90°C also failed to produce any reaction; **2** was recovered unchanged.

Refluxing of **5–7** with equimolar quantities of triphenylphosphine and triphenylarsine, respectively in THF for 48 h also failed to produce any reaction; **5–7** were recovered unchanged.

RESULTS AND DISCUSSION

The analytical data are presented in Table 1. The molar conductance values show that all of the com-

Table 1. Analytical data and other physical properties of the peroxo complexes[a]

Compound	Colour	Carbon (%) Calc.	Carbon (%) Found	Hydrogen (%) Calc.	Hydrogen (%) Found	Nitrogen (%) Calc.	Nitrogen (%) Found	Molar conductance (Ω^{-1} cm^2 mol^{-1})
$[Mo(O)(O_2)C_{20}H_{14}N_2O_2]$ (**1**)	Yellow	52.41	52.36	3.06	3.04	6.11	6.10	2
$[U(O)(O_2)C_{20}H_{14}N_2O_2]$ (**2**)	Yellow	40.00	39.89	2.33	2.31	4.67	4.52	0
$[Mo(O)(O_2)C_{14}H_{10}N_2O_2]$ (**3**)	Yellow	43.98	43.92	2.62	2.56	7.33	7.18	5
$[W(O)(O_2)C_{14}H_{10}N_2O_2]$ (**4**)	Yellow	35.76	35.72	2.13	2.10	5.96	5.93	1
$[U(O)(O_2)C_{14}H_{10}N_2O_2]$ (**5**)	Yellow	32.06	32.00	1.91	1.89	5.34	5.32	0
$[Zr(O_2)C_{20}H_{14}N_2O_2]$ (**6**)	Colourless	54.89	54.78	3.20	3.20	6.40	5.99	3
$[Th(O_2)C_{20}H_{14}N_2O_2]$ (**7**)	Colourless	51.52	51.50	2.42	2.41	4.84	4.81	0

[a]The organic moieties for the compounds are:

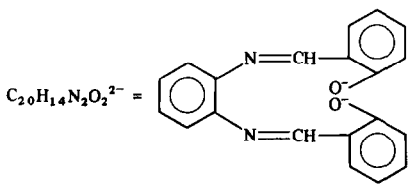

1, **2**, **6** and **7**

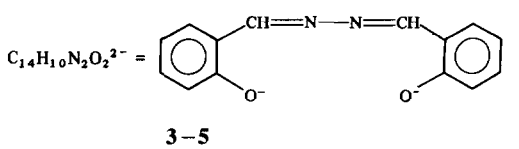

3–5

Table 2. IR spectral data for the Mo^{VI}, U^{VI}, W^{VI}, Zr^{IV} and Th^{IV} complexes[a] [band maxima (cm^{-1})]

Compound	ν(O—H)	ν(C=N)	ν(N—N)	ν(M=O)	ν_1(O—O)	ν_3(M<O,O>)	ν_2(M<O,O>)	ν(M—O′)	ν(M—N)
$C_{20}H_{14}N_2O_2H_2$	3600–3300br	1560vs							
1		1510vs		920vs	840vs	615vs	525vs	365s	352m
2		1520vs		910vs	790vs	610s	520vs	420s	260s
$C_{14}H_{10}N_2O_2H_2$	3600–3400br	1570s	985vs						
3		1515vs	960s	925	845s	615s	528s	360s	350m
4		1525vs	965s	930	825vs	615s	525s	375s	295m
5		1530vs	970s	910	795vs	615s	525m	435s	270m
6		1520vs			820vs	670m	560m	420s	310w
7		1530s			805s	602vs	520m	400m	300m

[a] Relative band intensities are denoted by vs, s, m, w and br, representing very strong, strong, medium, weak and broad, respectively.

plexes are non-electrolytes in DMSO indicating that the chelate anions are covalently bonded in all the cases. These data are consistent with seven-fold coordination of molybdenum(VI), tungsten(VI) and uranium(VI) complexes, while the zirconium(IV) and thorium(IV) analogues are hexacoordinated.

IR spectral data are presented in Table 2. The ligands $C_{20}H_{14}N_2O_2H_2$ and $C_{14}H_{10}N_2O_2H_2$ are potentially quadridentate, coordinating via the two methine nitrogen atoms and oxo anions generated during complexation. The free Schiff bases produce ν(OH) bands (Table 2) which disappear in the complexes indicating deprotonation at the —OH end, thus providing an oxo coordination. This is also apparent from the non-electrolytic nature of the complexes. That the ligands deprotonate at the —OH end is also evident from the appearance of ν(M—O′) (O′ = oxygen in organic ligands) modes at 360–435 cm^{-1} (Table 2) in the far-IR spectra of the complexes.[4–11] The ν(C=N) bands observed at 1560 and 1570 cm^{-1} for $C_{20}H_{14}N_2O_2H_2$ and $C_{14}H_{10}N_2O_2H_2$, respectively, are shifted to lower frequencies (Table 2) upon complexation, indicating coordination by the methine nitrogen atoms. This is also apparent from the ν(M—N) modes at 260–350 cm^{-1} in the far-IR spectra of the complexes.[4–11] The ν(N—N) band[13] observed at 985 cm^{-1} for free $C_{14}H_{10}N_2O_2H_2$ is shifted to lower frequencies in **3–5**, indicating that both the azo methine nitrogen atoms are coordinated. Complexes **1–5** show diagnostic bands at 910–925 cm^{-1} attributable to ν(M=O) modes.[4,10,11] The metal–peroxo grouping (local C_{2v} symmetry) gives rise to three IR and Raman-active vibrational modes. These are predominantly O—O stretching (ν_1), the symmetric M—O stretch (ν_2) and the antisymmetric M—O stretch (ν_3). The characteristic ν_1(O—O) modes of **1–7** appear at 795–840 cm^{-1} (Table 2). In particular, the ν_1 mode decreases upon passing from molybdenum complexes (**1** and **3**) (840 and 845 cm^{-1}) to the corresponding tungsten complex (**4**) (825 cm^{-1}), which is then further decreased in the uranium peroxo complexes (**2** and **5**) (790 and 795 cm^{-1}). The ν_1 mode of the thorium peroxo complex (**7**) (805 cm^{-1}) appears at a lower frequency than the zirconium analogue (**6**) (820 cm^{-1}). The present study thus clearly reveals that for the $M(O_2)$ grouping, the ν_1(O—O) modes decrease with an increase in the atomic number of metals in a particular group. Again in the present examples, it is discernible that the ν_1 modes of molybdenum, tungsten, uranium, zirconium and thorium complexes appear at lower frequencies than the peroxo complexes of these metals containing monodentate, bidentate and tridentate auxiliary ligands.[3–11] This is presumably due to a greater charge cancellation of the metal centres by the quadridentate σ-donor ligands, thereby causing a weaker coulombic interaction in the M^{n+}—O_2^{2-} ($n = 4$ or 6) moiety in the present examples. The present peroxo complexes display ν_3 and ν_2 modes at 602–670 and 520–560 cm^{-1}, respectively (Table 2).

Reactivity

The present peroxo complexes were found to be inert towards oxidation of olefin and other substrates. Complexes **1** and **4** failed to oxidize allyl alcohol even when refluxing at 90°C was continued for 48 h. Compounds **5–7** were also unreactive towards phosphine and arsine. These negative results outline the enhanced stability of the metal–

peroxo moiety in the presence of quadridentate, dinegative chelating ligands which precludes oxygen transfer reactions. We also observed a similar stabilizing effect of the peroxo complexes containing various multidentate organic ligands.[4–6, 9–11]

Acknowledgements—We are indebted to the Department of Chemistry, Rajshahi University, Bangladesh, for the financial support and for the provision of laboratory facilities. One of us (M.T.H.T.) gratefully acknowledges the assistance provided by the Microanalytical Services, University of St. Andrews, Scotland.

REFERENCES

1. H. Mimoum, *J. Molec. Catal.* 1980, **7**, 1.
2. S. E. Jacobson, R. Tang and F. Mares, *Inorg. Chem.* 1978, **17**, 3055.
3. A. D. Westland, F. Haque and J. M. Bouchard, *Inorg. Chem.* 1980, **19**, 225.
4. A. D. Westland and M. T. H. Tarafder, *Inorg. Chem.* 1981, **20**, 3992.
5. A. D. Westland and M. T. H. Tarafder, *Inorg. Chem.* 1982, **21**, 3228.
6. M. T. H. Tarafder and M. A. L. Miah, *Inorg. Chem.* 1986, **25**, 2265.
7. M. T. H. Tarafder and A. Ahmed, *Indian J. Chem.* 1986, **25A**, 729.
8. M. T. H. Tarafder and A. R. Khan, *Polyhedron* 1987, **6**, 275.
9. M. T. H. Tarafder, *Indian J. Chem.* 1987, **26A**, 874.
10. M. T. H. Tarafder and A. A. M. A. Islam, *Polyhedron* 1989, **8**, 109.
11. M. T. H. Tarafder, M. B. H. Howlader, B. Nath, R. Khan and A. A. M. A. Islam, *Polyhedron* 1989, **8**, 1371.
12. A. C. Dengel and W. P. Griffith, *Polyhedron* 1989, **8**, 1371.
13. M. A. Ali, G. Hossain, S. M. H. Majumder, M. N. Uddin and M. T. H. Tarafder, *Polyhedron* 1987, **6**, 1653.

Polyhedron Vol. 10, No. 8, pp. 823–827, 1991
Printed in Great Britain

0277–5387/91 $3.00+.00
© 1991 Pergamon Press plc

SYNTHESIS AND CHARACTERIZATION OF SOME METAL COMPLEXES CONTAINING A QUADRIDENTATE NSSN AND A SEXIDENTATE ONSSNO LIGAND

M. RAHMAN, M. AKBAR ALI,* P. BHATTACHARJEE and M. NAZIMUDDIN

Department of Chemistry, Chittagong University, Bangladesh

(*Received* 16 *July* 1990, *accepted* 13 *December* 1990)

Abstract—New metal complexes of general formulae $M(NSSN)X_2 \cdot xH_2O$ (M = Ni, Cu; NSSN = quadridentate sulphur–nitrogen ligand; X = Cl, Br, NCS or I; $x = 0$ or 2) and M(ONSSNO) [M = Ni, Cu, Zn, Cd; $ONSSNO^{2-}$ = anion of sexidentate ligand formed from salicylaldehyde and α,α′-xylene-bis(N-methyldithiocarbazate)] have been prepared and characterized by conductance, magnetic and spectroscopic measurements. The nickel(II) complexes of both the ligands are high-spin and octahedral. Tetragonally distorted octahedral structures are assigned to the copper(II) complexes. In the presence of the sexidentate ligand, cobalt(II) is readily air-oxidized to form a cobalt(III) complex, Co(ONSSNO)Cl, which is spin-paired and octahedral.

There is continuing interest in the coordination chemistry of both open-chain and macrocyclic quadridentate ligands containing the N_2S_2 donor set.[1–4] Copper(II) complexes of these types of ligands have attracted considerable interest because of the occurrence of the CuN_2S_2 chromophore in blue copper proteins such as plastocyanin.[5,6] In this paper we report the synthesis and characterization of some complexes of two new multidentate sulphur–nitrogen chelating agents containing the N_2S_2 and $O_2N_2S_2$ donor sets.

EXPERIMENTAL

Physical measurements

All physical measurements and analytical procedures were similar to those described previously.[7]

Preparation of the N_2S_2 *ligand, α,α′-xylene-bis(N-methyldithiocarbazate)*

An ice-cold solution of methylhydrazine (1.84 g) in ethanol (25 cm^3) was added slowly and with constant stirring to a solution of potassium hydroxide (2.24 g) in a 9:1 mixture of ethanol and water (100 cm^3). Carbon disulphide (3.04 g) was added dropwise with vigorous stirring of the reaction mixture. The temperature of the reaction mixture was kept below 10°C during the entire period of addition of carbon disulphide. A solution of α,α′-xylene-dibromide (5.28 g) in ethanol (100 cm^3) was added with stirring over a period of 40 min, during which time a white product appeared which was filtered off, washed with water and recrystallized from ethanol. Yield, 3.5 g; m.p. 164–165°C. Found: C, 41.6; H, 5.4; N, 16.3. $C_{12}H_{18}N_4S_4$ requires: C, 41.6; H, 5.2; N, 16.2%. Mass spectrum; $m/z = 346$ (M^+); ^1H NMR ($CDCl_3$): 3.40, 3.65 (N—CH_3), 4.30, 4.52 (S—CH_2—), 5.55 (—NH_2), 7.20–7.40 (aromatic).

Preparation of the sexidentate $O_2N_2S_2$ *ligand*

A solution of α,α′-xylene-bis(N-methyldithiocarbazate) (3.46 g) in dry ethanol (250 cm^3) was added to a solution of salicylaldehyde (2.40 g) in the same solvent (50 cm^3). The mixture was heated under reflux for a period of 4 h and thereafter left to cool. The product which had formed was collected by filtration and recrystallized from acetone. Yield, 4.5 g; m.p. 217°C. Found: C, 56.3; H, 4.6; N, 10.2. $C_{26}H_{26}N_4S_4$ requires: C, 56.2; H,

* Author to whom correspondence should be addressed. Present address: Department of Chemistry, University of Brunei Darussalam, Gadong 3186, Brunei Darussalam.

4.7; N, 10.1%. ^{1}H NMR ($CDCl_3$): 10.28 (—OH), 3.64 (—NCH_3), 8.01 (—CH=N), 7.25–7.47 (aromatic), 4.41 (—SCH_2—).

General method for the preparation of $M(N_2S_2)X_2 \cdot xH_2O$ (M = Ni, Cu; X = NCS, I; $x = 0, 2$)

These were prepared by heating solutions of the appropriate metal salts with the ligand in ethanol in a 1 : 1 molar ratio and filtering out the precipitated complexes.

General method of preparation of $M(O_2N_2S_2)$ *and* $Co(O_2N_2S_2)Cl$

The ligand (1 mmol) dissolved in boiling acetone (50 cm^3) was mixed with the appropriate metal acetate (chloride in the case of cobalt) (1 mmol) in methanol (30 cm^3) and the mixture heated under reflux for *ca* 12 h. The volume of the reaction mixture was reduced to *ca* 30 cm^3, whereupon the product which had deposited was filtered off, washed several times with methanol followed by acetone.

RESULTS AND DISCUSSION

The ligand obtained by reacting α,α′-xylenedibromide with the potassium salt of N-methyldithiocarbazate can be structurally formulated as shown in Fig. 1. This formulation is supported by ^{1}H NMR, mass and IR spectroscopic data. The ligand can exhibit conformational isomerism due to hindered rotation about the partially double SC—N and SC—S bonds.[8] The ^{1}H NMR spectrum of the N_2S_2 ligand shows two signals for each —NCH_3 and —SCH_2— proton. Their 1 : 2 relative intensities suggest the presence of two conformers.

Although the signal due to the —NH_2 protons is not split, its broadness is in keeping with the presence of two isomers. The appearance of two signals for the —NCH_3— protons can tentatively be ascribed to the *cis–cis* and *trans–cis* conformers, by analogy, with similar compounds like N-methyl-S-methyldithiocarbazate,[8] thioureas[9] and thiocarbamate esters.[10]

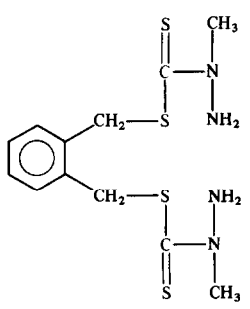

Fig. 1.

Reaction of nickel(II) salts with the ligand was found to be dependent on the nature of the anion being used. Thus, with nickel(II) nitrate, chloride and perchlorate salts the ligand failed to yield any complexes even after prolonged heating of the reaction mixture. However, reactions of nickel(II) iodide and thiocyanate with the ligand afforded stable complexes of general formula $M(N_2S_2)X_2$. This behaviour may be attributed to the symbiosis phenomenon.[11] According to the Ahrland–Chatt–Davies classification of metal complexes, the nickel(II) ion is termed as a fairly hard ion with a limited tendency to form bonds with soft thioether donors present in the ligand. However, in the presence of softer anions such as the iodide and thiocyanate, the hard nickel(II) is probably symbiotically motivated to act as a soft acceptor, thereby forming complexes with the present ligand. The hard Cl^-, ClO_4^- and NO_3^- ions cannot act in a similar manner and, therefore, no complexes are formed. With copper(II) salts, the ligand readily reacted giving complexes of formula $Cu(N_2S_2)X_2 \cdot 2H_2O$, which are non-electrolytes in DMF, indicating that the halide ions are coordinated to the copper(II) ion. The molar conductivity data of the nickel(II) complexes (Table 1) indicate that they are appreciably dissociated in DMF, but the conductance values are less than those found for 1 : 1 electrolytes. The IR spectrum of the thiocyanato complex, $Ni(N_2S_2)(NCS)_2$, shows a strong unsplit band at 2100 cm^{-1} indicating that the thiocyanate ions are coordinated to the nickel(II) ion as an N-bonded ligand.[12] The IR data in Table 2 also show that the $\nu_s(NH_2)$ and $\nu_{as}(NH_2)$ bands of the free ligand are shifted to lower frequencies in the spectra of metal complexes, indicating that the ligand is coordinated to the nickel(II) and copper(II) ions via the amino nitrogen atoms. The presence of ν(M—S) bands around 320 cm^{-1} in the spectra of the complexes suggests metal–sulphur bonding. The facts stated above indicate that the present ligand behaves as an N_2S_2 quadridentate chelating agent coordinating nickel(II) and copper(II) ions via the amino nitrogen and the two thioether sulphur atoms.

The nickel(II) complexes, $Ni(N_2S_2)X_2$ (X = NCS, I), are high-spin with room-temperature magnetic moments of 2.93 BM. Their electronic spectra (Table 2) show *d–d* bands which are typical of octa-

Table 1. Colour, decomposition temperatures, conductivities, magnetic moments and analytical data for the complexes

Compound	Colour	Decomposition temperature	Λ^a (Ω^{-1} cm^2 mol^{-1})	μ (BM)	Analytical data[b] C	H	N	M
$Ni(NSSN)(NCS)_2$	Pale blue	177–179	47.0	2.90	32.0 (32.2)	3.7 (3.5)	15.9 (16.1)	11.5 (11.2)
$Ni(NSSN)I_2$	Pale blue	181–183	68.0	2.93	22.3 (21.9)	3.4 (2.7)	8.1 (8.3)	9.0 (8.9)
$Cu(NSSN)Cl_2 \cdot 2H_2O$	Green	176–177	30.0	1.81	27.7 (27.8)	3.7 (4.3)	10.5 (10.8)	12.5 (12.3)
$Cu(NSSN)Br_2 \cdot 2H_2O$	Deep green	150–153	38.0	1.87	23.5 (23.8)	3.45 (3.6)	8.9 (9.2)	11.1 (10.6)
Ni(ONSSNO)	Brown	180–182	0.8	2.88	50.8 (51.1)	4.2 (4.0)	8.7 (9.2)	9.5 (9.6)
Cu(ONSSNO)	Brown	151–153	0.5	1.81	50.4 (50.7)	4.1 (3.9)	8.7 (9.1)	10.0 (10.3)
Co(ONSSNO)Cl	Brown	171–172	1.3	Diamagnetic	48.0 (48.3)	4.0 (3.6)	8.6 (8.7)	8.8 (9.1)
Zn(ONSSNO)	Yellow	206–208	1.2	Diamagnetic	50.0 (50.5)	4.2 (3.9)	8.7 (9.1)	10.3 (10.6)
Cd(ONSSNO)	Yellow	214–216	0.9	Diamagnetic	45.3 (45.7)	4.3 (4.0)	6.1 (6.6)	16.9 (17.4)

[a]Molar conductance of *ca* 10^{-3}M solutions in DMSO.
[b]Calculated values are given in parentheses.

Table 2. Selected IR absorption frequencies and electronic spectral data for the ligands and their complexes

Compound	IR absorption bands $\nu(NH_2)$	ν(C=N)	ν(N—N)	ν(C=S)	ν(M—S)	Vis–UV bands, λ_{max}, (nm)
NSSN	3320s 3250m	—	932s	780s	—	
$H_2ONSSNO$	—	1610s	985s	790s	—	
$Ni(NSSN)(NCS)_2$	3220m 3140m	—	1000s	780s	320w	854, 590, 366
$Ni(NSSN)I_2$	3120s 3140m	—	995s	778s	325w	850, 530, 390
$Cu(NSSN)Cl_2 \cdot 2H_2O$	3200w 3060sh	—	1000s	782s	380w	720, 380, 298
$Cu(NSSN)Br_2 \cdot 2H_2O$	3200w,br 3095s,br	—	1008s	790s	380w	750, 370, 298
Ni(ONSSNO)	—	1598s	1048s	790m	310s	874, 461, 429, 300
Cu(ONSSNO)	—	1607s	1013s	770m	315w	*ca* 600, 425, 300
Cd(ONSSNO)	—	1600s	1008s	777s	310w	404, 300
Zn(ONSSNO)	—	1600s	1006s	778s	315w	394, 299
Co(ONSSNO)Cl	—	1604m	1020m	780s	320m	600, 492, 300

hedral or pseudo-octahedral nickel(II).[13] Unfortunately, the first band corresponding to the $^3A_{2g} \rightarrow {}^3T_{2g}(F)$ transition could not be measured due to the limitation of the spectrophotometer. However, the colour, magnetism and electronic spectra are consistent with their octahedral geometries.

The room-temperature magnetic moments of the copper(II) complexes, $Cu(N_2S_2)X_2 \cdot 2H_2O$ (1.81–1.87 BM), are normal for a $3d^9$ ion and their electronic spectra display a broad *d–d* band which probably contains all the transitions expected for a copper(II) ion in a tetragonal complex.

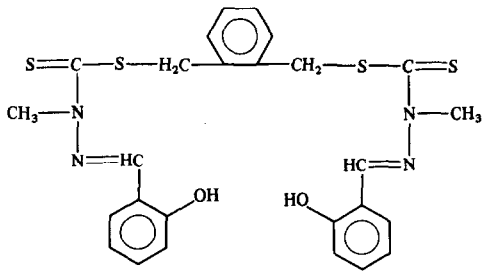

Fig. 2. $H_2ONSSNO$.

Complexes of the sexidentate ligand

The Schiff base obtained by condensation of α,α′-xylene-bis(N-methyldithiocarbazate) with salicylaldehyde may be represented by the structural formula shown in Fig. 2.

The structural formula shown in Fig. 2 is consistent with analytical and IR and ^1H NMR spectroscopic data. The electron impact mass spectrum of the compound does not display any peak due to the molecular ion, presumably due to its decomposition in the inlet tube of the spectrometer, but peaks at $m/z = 104$, 168 and 256 in the spectrum may be assigned to the $C_6H_4CH_2CH_2^{\cdot}$, $C_6H_4CH_2CH_2SS^{\cdot}$ and $C_6H_4CH_2CH_2SSCSCS^{\cdot}$ fragments, respectively, in agreement with the structure shown in Fig. 2.

Reaction of metal acetate salts with the Schiff base afforded microcrystalline compounds of empirical formula M(ONSSNO), which were found to be insoluble in most of the common non-polar solvents. They were, however, soluble in DMF, in which conductivity measurements were made. The conductivity data in Table 1 suggest that the complexes behave essentially as non-electrolytes. The Schiff base, therefore, must be coordinated to the metal ions as a dianionic ligand, which is also supported by the IR data. The IR spectrum of the free ligand shows the phenolic ν(OH) at 3420 cm^{-1} which is absent in the spectra of the complexes, supporting deprotonation of the ligand during complex formation. The ν(C=N) bands of the free ligand at 1620 cm^{-1} are lowered in the spectra of complexes indicating coordination by the azomethine nitrogen atoms.[14] The presence of ν(M—S)[15] in the range 310–320 cm^{-1} in the spectra of the complexes supports coordination by the sulphur atoms. However, since the ν(C=S) bands[16] of the free ligand at 790 cm^{-1} are not affected in the spectra of the complexes, it is assumed that the thione sulphur atoms do not participate in coordination.

The nickel(II) complex, Ni(ONSSNO), is high-spin with a room-temperature magnetic moment of 2.89 BM. Its solid-state electronic spectrum in the range 1000–200 nm shows bands at 874, 461, 429 and 300 nm. Of these, the bands at 874 and 461 nm may be assigned to the $^3A_{2g} \rightarrow {}^3T_{1g}(F)$ and $^3A_{2g} \rightarrow {}^3T_{1g}(P)$ transitions, respectively, of octahedral nickel(II).[13] The copper(II) complex is brown in colour with a room-temperature magnetic moment of 1.81 BM, normal for a copper(II) ion in a magnetically dilute environment. Its electronic spectrum shows a broad *d–d* band at 600 nm which can be assigned to all the transitions expected for a tetragonal copper(II). Reaction of cobalt(II) chloride with the ligand yields a cobalt complex of composition $Co(O_2N_2S_2)Cl \cdot H_2O$, which behaves as a non-electrolyte in DMF. Its diamagnetic nature (Table 1) suggests that it is a cobalt(III) complex. The ready oxidation of cobalt(II) salts in the presence of sulphur-containing ligands to yield cobalt(III) complexes has been well documented in the literature.[17] In the cobalt complex the ligand is most probably coordinated to the cobalt(III) ion in a pentadentate fashion with the chloride ion occupying the sixth coordination position. Its solid-state electronic spectrum contains bands at 600, 492 and 300 nm. Of these three bands, the first two may be assigned to the $^1A_{1g} \rightarrow {}^1T_{1g}$ and $^1A_{1g} \rightarrow {}^1T_{2g}$ transitions, respectively, of octahedral cobalt(III). Because of its insoluble nature in most of the common polar and non-polar organic solvents, crystals suitable for X-ray crystallographic examination could not be obtained. The zinc and cadmium complexes are yellow in colour, probably due to charge-transfer transitions of the type M → S. Their IR spectra are very similar to the nickel(II) complex indicating that they probably have octahedral geometries.

Acknowledgements—We acknowledge with thanks the assistance provided for this work by the IOCD. We also thank Professor M. S. Tempesta of the Chemistry Department, University of Missouri-Columbia, U.S.A., for the NMR and mass spectroscopic data and Professor S. Matlin of the Chemistry Department, City University of London, U.K., for the microanalytical data.

REFERENCES

1. E. C. Constable, J. Lewis, V. E. Marquiz and P. R. Raithby, *J. Chem. Soc., Dalton Trans.* 1986, 1717.
2. R. W. Hay, N. Govan and M. P. Pujari, *J. Chem. Soc., Dalton Trans.* 1987, 963.
3. M. Akbar Ali, S. M. G. Hossain, S. M. M. H. Majumder, M. Nazimuddin and M. T. H. Tarafder, *Polyhedron* 1987, **6**, 1653.
4. H. G. Petering, H. H. Buskirk and G. E. Underwood, *Cancer Res.* 1964, **24**, 367.
5. K. D. Karlin and J. Zubeita (Eds), *Copper Coordination Chemistry, Biochemical and Inorganic Perspectives*. Adenine Press, New York (1983).

6. R. W. Hay, *Bio-inorganic Chemistry*. Ellis-Horwood, Chichester (1984).
7. S. M. M. H. Majumder, M. Akbar Ali, F. E. Smith and M. A. U. Mridha, *Polyhedron* 1988, **7**, 2183.
8. D. Gattegno and A. M. Giuliani, *Tetrahedron* 1974, **30**, 701.
9. A. M. Giuliani, *J. Chem. Soc., Dalton Trans.* 1972, 492 and refs therein.
10. R. A. Bauman, *J. Org. Chem.* 1967, **32**, 4129.
11. M. Akbar Ali, *Can. J. Chem.* 1980, **58**, 727.
12. R. A. Bailey, S. L. Kozak, T. W. Michelson and M. N. Mills, *Coord. Chem. Rev.* 1971, **6**, 1407.
13. A. B. P. Lever, *Inorganic Electronic Spectroscopy*, Elsevier, New York (1967).
14. J. E. Kovacic, *Spectrochim. Acta* 1967, **23A**, 183; K. Ueno and A. E. Martell, *J. Am. Chem. Soc.* 1955, **59**, 998.
15. D. M. Adams, *Metal–Ligand and Related Vibrations*, p. 319. Arnold, London (1967).
16. M. Mashima, *Bull. Chem. Soc. (Japan)* 1974, **37**, 974.
17. M. Akbar Ali, S. E. Livingstone and D. J. Phillips, *Inorg. Chim. Acta*, 1971, **5**, 119; 1973, **7**, 179; 1972, **6**, 532.

Polyhedron Vol. 10, No. 8, pp. 829–835, 1991
Printed in Great Britain

0277–5387/91 $3.00+.00
© 1991 Pergamon Press plc

REDUCTION OF $Ru_2(CH_3COO)_4^+$ AND $Co(C_2O_4)_3^{3-}$ BY OXALATOTITANIUM(III) COMPLEXES IN AQUEOUS ACIDIC SOLUTION

A. OLAYINKA OYETUNJI,* OLUSEGUN OLUBUYIDE and J. FOLORUNSO OJO

Department of Chemistry, Obafemi Awolowo University, Ile-Ife, Nigeria

and

JOSEPH E. EARLEY*

Department of Chemistry, Georgetown University, Washington, DC 20057, U.S.A.

(*Received* 25 *September* 1990; *accepted* 19 *December* 1990)

Abstract—Reductions of $Ru_2(CH_3COO)_4^+$ and $Co(C_2O_4)_3^{3-}$ by oxalato complexes of titanium(III) have been studied in $LiCF_3SO_3$ media of 1.0 mol dm^{-3} ionic strength. At 25°C and $[H^+]_f = 0.150$ mol dm^{-3}, $Ru_2(CH_3COO)_4^+$ and $Co(C_2O_4)_3^{3-}$ are reduced by $Ti(C_2O_4)_2^-$ with second-order rate constants of $(4.17 \pm 0.08) \times 10^3$ and $(3.20 \pm 0.05) \times 10^3$ dm^3 mol^{-1} s^{-1}, respectively. Both oxidants show no detectable reactivity towards $Ti(C_2O_4)^+$. Both reactions are base-catalysed. The magnitude of the rate constant for reduction of $Ru_2(CH_3COO)_4^+$ establishes an outer-sphere mechanism; the magnitude of the rate constant for $Co(C_2O_4)_3^{3-}$ indicates a substitution-limited inner-sphere mechanism.

The oxalate ion is often an efficient bridging ligand in ruthenium(III)–titanium(III)[1] and cobalt(III)–titanium(III)[2,3] electron-transfer (ET) reactions. In many of these cases the rate-determining step in the overall redox process is formation of the precursor complex.[4,5] The ET process for a dimeric ruthenium(II,III) oxidant containing an unusual orientation of the bridging oxalate ion[8] involves a more complicated mechanism.[6] Addition of the oxalate ion as a non-bridging ligand on titanium(III) accelerates Ti^{III}—Co^{III} ET reactions[3] and also Ti^{III}—Ru^{III} redox reactions.[7] The present study explores the effect of non-bridging oxalate (on both oxidant and reductant) on ET between titanium(III) and cobalt (III) and investigates the effect of non-bridging oxalate (on the reductant) on ET between a dimeric ruthenium(II,III) complex and titanium(III).

EXPERIMENTAL

Tetrakis(μ-acetato)diruthenium(II,III) chloride, $Ru_2(CH_3COO)_4Cl$, was synthesized as previously described.[8] Elemental analysis[9] and molar extinction coefficient ($\varepsilon = 695$ dm^3 mol^{-1} cm^{-1} at 425 nm) agreed with expectations.[8] Potassium tris-oxalatocobaltate(III), $K_3Co(C_2O_4)_3$, was prepared according to the method of Bailar and Jones.[10] Its molar extinction coefficients at 425 and 285 nm ($\varepsilon = 232$ and 1440 dm^3 mol^{-1} cm^{-1}, respectively) are in reasonable agreement with literature values.[11] Emerald green needles were stored in a bottle wrapped with aluminium foil.

Titanium(III) solutions were prepared under nitrogen as described.[1,12,13] The absorbance maximum of Ti^{3+} at 504 nm in CF_3SO_3H solutions ($\varepsilon = 3.87$ dm^3 mol^{-1} cm^{-1}) agrees with the literature.[12] Concentrations determined by titration of aliquot solutions with dichromate ion and those determined spectrophotometrically agreed within 5%. Standardized solutions were kept under nitrogen in a refrigerator. Oxalato complexes of titanium(III) were prepared immediately before reaction by the method of Chaudhuri and Diebler,[14] adding oxalic acid solution to aqueous solutions of titanium(III). Addition of oxalic acid to a solution of Ti^{3+} changed the colour of the solution from purple to yellowish-brown. UV–vis spectra showed peaks at

* Authors to whom correspondence should be addressed.

382 nm and 400 nm at low and high oxalate concentrations, respectively. These agree well with literature values[14] for the formation of $Ti(C_2O_4)^+$ (380 nm, $\varepsilon = 86\ dm^3\ mol^{-1}\ cm^{-1}$) and $Ti(C_2O_4)_2^-$ (400 nm, $\varepsilon = 490\ dm^3\ mol^{-1}\ cm^{-1}$).

Rate measurements were made by following absorbance changes on a computer-linked Durrum stopped-flow spectrophotometer. All reactions were monitored under pseudo first-order conditions; titanium(III) was in at least 10-fold excess over the oxidants. Kinetic measurements were made at ionic strength 1.0 mol dm^{-3} ($LiCF_3SO_3$) and at $(25.0 \pm 0.1)°C$ in a thermostated water bath. Reactions were studied in a nitrogen atmosphere to avoid air-oxidation of titanium(III).

RESULTS

The stoichiometry of each reaction was determined by spectrophotometric titration: 1.0 mole of oxidant was consumed per mole of reductant in all cases.

Pseudo first-order rate plots obtained for both systems were linear for at least three half-times. The pseudo first-order rate constants, k_s, obtained from such plots were generally reproducible within 10%. The observed second-order rate constants, k_{obs}, were obtained by dividing k_s by the total titanium(III) concentration. These rate constants, listed in Tables 1 and 2, were found to increase with increasing free oxalate ion concentration, [L].

When oxalic acid, H_2L, is added to a Ti^{3+} solution of concentration [M], several equilibria occur:

$$H_2C_2O_4 \rightleftharpoons HC_2O_4^- + H^+ \quad K_1 = \frac{[H^+][HL]}{[H_2L]} \tag{1}$$

$$HC_2O_4^- \rightleftharpoons C_2O_4^{2-} + H^+ \quad K_2 = \frac{[H^+][L]}{[HL]} \tag{2}$$

$$Ti^{3+} + C_2O_4^{2-} \rightleftharpoons TiC_2O_4^+ \quad K_3 = \frac{[ML]}{[M][L]} \tag{3}$$

$$Ti(C_2O_4)^+ + C_2O_4^{2-} \rightleftharpoons Ti(C_2O_4)_2^-$$
$$K_4 = \frac{[ML_2]}{[ML][L]} \tag{4}$$

$$Ti(C_2O_4)_2^- + C_2O_4^{2-} \rightleftharpoons Ti(C_2O_4)_3^{3-}$$
$$K_5 = \frac{[ML_3]}{[ML_2][L]} \tag{5}$$

$$Ti^{3+} + HC_2O_4^- \rightleftharpoons Ti(HC_2O_4)^{2+}$$
$$K_6 = \frac{[MHL]}{[M][HL]}. \tag{6}$$

Table 1. Kinetic data for titanium(III) reduction of $Ru_2(CH_3COO)_4^+$ in the presence of added oxalate ions[a]

$10^3[H^+]_T$ (mol dm^{-3})	$10^3[H^+]_f$ (mol dm^{-3})	$10^3[Ox^{2-}]_T$ (mol dm^{-3})	$10^6[Ox^{2-}]_f$ (mol dm^{-3})	$10^5[Ti^{3+}]_f$ (mol dm^{-3})	$10^4[Ti(Ox)^+]$ (mol dm^{-3})	$10^4[Ti(Ox)_2^-]$ (mol dm^{-3})	k_s (s^{-1})	k_{obs}[b] ($dm^3\ mol^{-1}\ s^{-1}$)
102.0	99.8	2.5	2.8	10.9	9.0	0.7	0.30	278
105.0	99.3	5.0	7.2	4.0	8.6	1.9	0.49	454
109.0	99.6	7.5	11.7	2.2	7.8	2.8	0.69	639
112.0	99.0	10.0	16.5	1.4	7.1	3.5	0.97	898
116.0	99.2	12.5	21.1	1.0	6.6	4.1	1.34	1241
120.0	99.5	15.0	25.7	0.8	6.1	4.7	1.55	1435
153.0	150.5	2.5	1.6	18.4	8.6	0.4	0.26	241
156.0	149.7	5.0	3.9	7.7	9.0	1.1	0.40	370
160.0	149.8	7.5	6.3	4.6	8.7	1.7	0.64	593
163.0	148.8	10.0	8.8	3.1	8.3	2.2	0.89	824
167.0	148.9	12.5	11.3	2.3	7.9	2.7	1.10	1019
171.0	148.9	15.0	13.8	1.8	7.5	3.1	1.25	1157

[a] Conditions: in 1.0 mol dm^{-3} CF_3SO_3Li; $T = (25.0 \pm 0.1)°C$; $[Ru_2^{II,III}] = 1.03 \times 10^{-4}$ mol dm^{-3}; $[Ti^{III}]_T = 1.08 \times 10^{-3}$ mol dm^{-3}.
[b] $k_{obs} = k_s/[Ti^{III}]_T$; $[Ti^{III}]_T = [Ti^{3+}]_f + [TiOH^{2+}] + [TiOx^+] + [TiOx_2^-]$; $Ox^{2-} = C_2O_4^{2-}$.

Table 2. Kinetic data for titanium(III) reduction of $Co(C_2O_4)_3^{3-}$ in the presence of added oxalate ions[a]

$10^3[H^+]_T$ (mol dm^{-3})	$10^3[H^+]_f$ (mol dm^{-3})	$10^3[Ox^{2-}]_T$ (mol dm^{-3})	$10^6[Ox^{2-}]_f$ (mol dm^{-3})	$10^5[Ti^{3+}]_f$ (mol dm^{-3})	$10^4[Ti(Ox)^+]$ (mol dm^{-3})	$10^4[Ti(Ox)_2^-]$ (mol dm^{-3})	k_s (s^{-1})	k_{obs}[b] ($dm^3\ mol^{-1}\ s^{-1}$)
153.0	151.1	2.5	1.8	35.0	12.3	0.4	0.20	124
155.6	150.1	5.0	3.4	13.3	13.5	1.4	0.36	222
158.5	149.2	7.5	5.8	7.6	13.2	2.3	0.58	358
162.0	148.8	10.0	8.2	5.1	12.6	3.1	0.79	488
165.5	148.4	12.5	10.7	3.7	12.0	3.8	1.00	617
169.5	148.5	15.0	13.2	2.9	11.4	4.5	1.22	753
126.8	125.1	2.5	1.5	28.7	12.8	0.6	0.23	142
130.4	125.2	5.0	4.4	10.1	13.4	1.8	0.51	315
134.0	125.1	7.5	7.6	5.6	12.8	2.9	0.63	389
137.5	124.8	10.0	10.8	3.7	12.0	3.9	0.88	543
141.3	124.8	12.5	14.0	2.7	11.2	4.7	1.12	691
145.2	124.9	15.0	17.2	2.0	10.6	5.5	1.36	840
153.0	125.0	20.0	23.7	1.3	9.4	6.7	1.84	1136
160.6	124.9	25.0	30.3	0.9	8.4	7.7	2.24	1393
102.0	100.4	2.5	1.9	22.7	1.5	0.8	0.28	173
104.0	99.1	5.0	6.2	7.1	1.3	2.4	0.74	457
107.0	98.6	7.5	10.7	3.7	1.2	3.8	0.96	592
111.0	99.0	10.0	15.2	2.4	1.1	5.0	1.45	895
114.5	98.8	12.5	19.8	1.7	1.0	6.0	1.84	1136
118.0	98.7	15.0	24.5	1.3	0.9	6.8	2.11	1303
76.5	75.1	2.5	2.7	16.6	13.5	1.1	0.43	265
78.5	74.0	5.0	9.1	4.5	12.4	3.4	0.58	358
81.5	73.7	7.5	16.0	2.3	10.8	5.2	1.07	661
85.0	73.8	10.0	23.0	1.4	9.5	6.6	1.43	882
88.5	73.9	12.5	30.0	0.9	8.5	7.6	2.03	1253
92.2	74.1	15.0	37.0	0.7	7.6	8.5	2.61	1611
52.0	50.9	2.5	4.1	10.9	13.5	1.7	0.38	235
54.0	50.1	5.0	14.9	2.5	11.0	4.9	0.85	525
57.0	50.0	7.5	26.5	1.1	9.0	7.1	1.59	982
60.0	49.9	10.0	38.6	0.7	7.5	8.7	2.07	1278
63.5	50.1	12.5	50.6	0.4	6.4	9.7	3.04	1877
66.5	49.9	15.0	63.3	0.3	5.6	10.6	3.65	2253

[a] Conditions: in 1.0 mol dm^{-3} CF_3SO_3Li; $T = (25.0 \pm 0.1)$°C; $[Co^{III}]_T = 1.60 \times 10^{-4}$ mol dm^{-3}; $[Ti^{III}]_T = 1.62 \times 10^{-3}$ mol dm^{-3}.
[b] $k_{obs} = k_s/[Ti^{III}]_T$; $[Ti^{III}]_T = [Ti^{3+}]_f + [TiOH^{2+}] + [TiOx^+] + [TiOx_2^-]$, $Ox = C_2O_4^{2-}$.

Ti^{3+} undergoes hydrolysis as

$$Ti^{3+} + H_2O \rightleftharpoons TiOH^{2+} + H^+$$

$$K_A = \frac{[MOH][H^+]}{[M]}. \quad (7)$$

$TiOH^{2+}$ reacts with oxidant, Ox [Ox—$Co(C_2O_4)_3^{3-}$ or $Ru_2(CH_3COO)_4^{+}$] according to the equation

$$TiOH^{2-} + Ox \xrightarrow{k} \text{products}. \quad (8)$$

A large number of such reactions have been studied and the rate constants, k, determined.[1-7] Chaudhuri and Diebler,[14] as well as Pecsok,[15] sought, but did not find, evidence to show that $Ti(C_2O_4)_3^{3-}$ exists; the formation constant K_5 is, therefore, small. Under our conditions, contributions by $Ti(HC_2O_4)^{2+}$ and $Ti(C_2O_4)_3^{3-}$ are negligible.[16] The major species formed in the presence of added oxalate ions are $Ti(C_2O_4^{+})$ and $Ti(C_2O_4)_2^{-}$ and $TiOH^{2+}$ [eqs (3), (4) and (7)].

$$Ti(C_2O_4)^{+} + Ox \xrightarrow{k'} \text{products} \quad (9)$$

$$Ti(C_2O_4)_2^{-} + Ox \xrightarrow{k''} \text{products}. \quad (10)$$

Moorehead and Sutin[17] have determined values of K_1 and K_2 as 0.09 and 4×10^{-4} mol dm^{-3} under our conditions. Values of K_3 and K_4 have been given[16] as 8.5×10^5 and 2.5×10^5 dm^3 mol^{-1} under conditions similar to ours. Combination of eqs. (1)–(4) with (7)–(10) results in an overall equation of the form:

$$B = k' + k''K_4[C_2O_4^{2-}]_f, \quad (11)$$

where

$$B = \frac{k_{obs}\left[1 + \frac{K_A}{[H^+]_f} + K_3[C_2O_4^{2-}]_f + K_3K_4[C_2O_4^{2-}]_f^2\right] - \frac{kK_A}{[H^+]_f}}{K_3[C_2O_4^{2-}]_f} \quad (12)$$

can be calculated (see Table 3) from the known or calculated values of the parameters (k, K_A, K_3 and K_4) and calculated values of the final concentrations for each experiment in eq. (12). A plot of B vs $[C_2O_4^{2-}]_f$ should therefore be linear with an intercept of k' and a slope $k''K_4$. Such plots were linear with no detectable intercepts (within experimental error) and gave slopes of 9.63×10^7 and 1.19×10^8 dm^6 mol^{-2} s^{-1} for reductions of $Co(C_2O_4)_3^{3-}$ and $Ru_2(CH_3COO)_4^{+}$, respectively. These results indicate that k' for each of the two oxidants is less than 1.0 dm^3 mol^{-1} s^{-1}, while $k'' = 3.2 \times 10^3$ and 4.2×10^3 dm^3 mol^{-1} s^{-1} for $Co(C_2O_4)_3^{3-}$ and $Ru_2(CH_3COO)_4^{+}$, respectively.

DISCUSSION

Titanium(III) has been shown to reduce $Ru_2(CH_3COO)_4^{+}$ [12] and $Co(C_2O_4)_3^{3-}$ [2] by outer-sphere and inner-sphere mechanisms, respectively. At a constant free acid concentration, the increase in rate constant with increasing free oxalate ion concentration observed here is similar to the result obtained in earlier studies.[3,7,16] The rate constant of 4.17×10^3 dm^3 mol^{-1} s^{-1} with which $Ti(C_2O_4)_2^{-}$ reduces $Ru_2(CH_3COO)_4^{+}$ is greater than that obtained for either the Ti^{3+} or $TiOH^{2+}$ reduction of the same oxidant.[12] Also, $Ti(C_2O_4)_2^{-}$ reduces $Co(C_2O_4)_3^{3-}$ ($k = 3.21 \times 10^3$ dm^3 mol^{-1} s^{-1}) at a faster rate than does $Ti(C_2O_4)^{+}$, Ti^{3+} or $TiOH^{2+}$. The enhanced rate of reduction of $Ru_2(CH_3COO)_4^{+}$ by $Ti(C_2O_4)_2^{+}$, as compared with reduction by Ti^{3+} or $TiOH^{2+}$, may be understood to involve coulombic effects which increase the stability of the precursor complexes of outer-sphere ET reactions. However, $Co(C_2O_4)_3^{3-}$, an anionic complex, is also reduced by $Ti(C_2O_4)_2^{-}$ at a faster rate than either $Ti(C_2O_4)^{+}$ or $TiOH^{2+}$.

Olubuyide and Earley[3] based the derivation of eq. (11) on the assumption that reaction paths involving oxalatotitanium(III) complexes are base-catalysed. The results of the present study are consistent with that assumption. At constant total oxalate concentration, the rate constant increased with decreasing acidity (Tables 1 and 2).

It has been concluded[16] that the formation constants of the trinuclear intermediate involving titanium(III) and $Ru_2(CH_3COO)_2(C_2O_4)_2^{-}$ decreases as non-bridging oxalate ligands are added. We expected a similar trend with the $Ru_2(CH_3COO)_4^{+}$ oxidant, consistent with the following mechanism:

$$Ru_2(CH_3COO)_4^{+} + Ti^{3+} \rightleftharpoons Ru_2(CH_3COO)_4Ti^{4+} \quad (13)$$

$$Ru_2(CH_3COO)_4Ti^{4+} \longrightarrow \text{products} \quad (14)$$

$$Ru_2(CH_3COO)_4^{+} + Ti(C_2O_4)^{+} \rightleftharpoons Ru_2(CH_3COO)_4Ti(C_2O_4)^{2+} \quad (15)$$

$$Ru_2(CH_3COO)_4Ti(C_2O_4)^{2+} \longrightarrow \text{products} \quad (16)$$

$$Ru_2(CH_3COO)_4^{+} + Ti(C_2O_4)_2^{-} \rightleftharpoons Ru_2(CH_3COO)_4Ti(C_2O_4)_2 \quad (17)$$

$$Ru_2(CH_3COO)_4Ti(C_2O_4)_2 \longrightarrow \text{products}, \quad (18)$$

where the species produced in eqs (15) and (17) are outer-sphere complexes.

As observed from a plot of B against $[C_2O_4^{2-}]_f$

Table 3. Dependence of B [calculated using eq. (12)] on free oxalate concentration, at 25°C and $[H^+]_f = 0.150$ mol dm^{-3}

$10^6[Ox^{2-}]_f$ (dm^3 mol^{-1} s^{-1})	k_{obs} (dm^3 mol^{-1} s^{-1})	$B_{Ru_2(OAc)_4^+}$ (dm^3 mol^{-1} s^{-1})	$B_{Co(Ox)_3^{3-}}$ (dm mol^{-1} s^{-1})
1.6	240.7	284.9	—
3.4	222.2	—	156
3.9	370.4	438.5	—
5.8	358.2	—	381
6.3	592.6	732.0	—
8.2	487.7	—	589
8.8	824.1	1070.3	—
10.7	617.3	—	808
11.3	1018.5	1391.9	—
13.2	753.1	—	1051
13.8	1157.1	1662.7	—

in eq. (11), the first added non-bridging oxalate does not have a significant effect on the redox rate constant, but the addition of the second non-bridging oxalate increases the rate constant for reactions involving both oxidants. Similar non-bridging ligand effects have been observed in inner-sphere titanium(III) reductions of $Co(NH_3)_4C_2O_4^+$,[3] $Ru(C_2O_4)_3^{3-}$ [7] and $Ru_2(CH_3COO)_2(C_2O_4)_2^-$.[16]

The rate constant for $Ti(C_2O_4)_2^-$ reduction of $Ru_2(CH_3COO)_4^+$ falls in the linear free energy relationship for outer-sphere Ru^{III}—Ti^{III} reactions (Fig. 1), suggesting that this diruthenium(II,III) complex is reduced by an outer-sphere mechanism of the usual kind. Even though reduction of $Ru_2(CH_3COO)_4^+$ by $Ti(C_2O_4)_2^-$ occurs at a faster rate than reduction by Ti^{3+} or $TiOH^{2+}$, all three ET reactions occur at rates that are consistent with outer-sphere mechanisms. $Ru_2(CH_3COO)_4^+$ is capable of adding one or more ligands in axial positions, replacing solvent molecules (omitted in the formulae used in this paper) that are weakly bound at those sites. Since the data give no indication that the ET reactions studied here involve any species in which oxalate occupies such a site, we may conclude that either such a species does not form or, more likely, that it forms but does not provide a sufficiently favourable pathway for ET to compete with the outer-sphere path. This in turn suggests that the attack of the reductant is roughly perpendicular to the Ru—Ru bond axis, between the acetate CH_3 groups. The rate enhancement by non-bridging oxalate can be understood to be an effect of changes in the reaction driving force.

Normally, reductions of ruthenium(III) oxidants by a given reductant are faster than reductions of the corresponding cobalt(III) oxidants by the same reductant (Table 5). The rate constant for the reaction of $Ru(C_2O_4)_3^{3-}$ with Ti^{3+} is larger than the rate constant for the reduction of $Co(C_2O_4)_3^{3-}$, but the difference is quite small. The rate constant for reduction of $Ru(C_2O_4)_3^{3-}$ by $Ti(C_2O_4)_2^-$, reported here, and also in ref. 7, is the same, within experimental error, as the rate constant for reduction of $Co(C_2O_4)_3^{3-}$ by $Ti(C_2O_4)_2^-$. The only consistent interpretations of the data are that both ruthe-

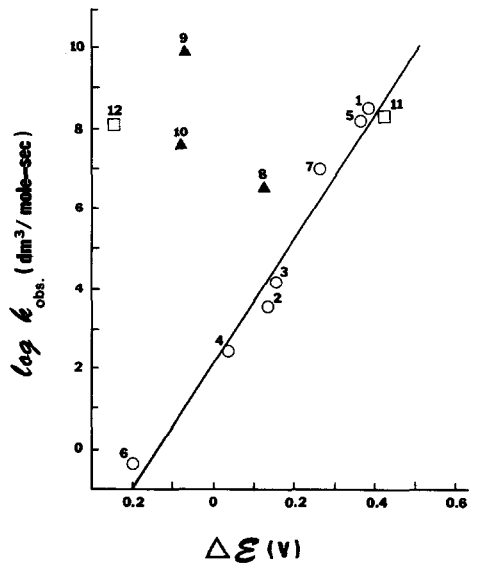

Fig. 1. Variation of the second-order rate constant with redox potential of the oxidant for reduction of certain ruthenium(III) complexes by $TiOH^{2+}$. The numbering of the points is as given in Table 4. Point 11 is the reduction of $Ru_2(OAc)_4^+$ by $TiOH^{2+}$. Point 12 is the reduction of $Co(C_2O_4)_3^{3-}$ by $TiOH^{2+}$, included with the Ru^{III}—Ti^{III} reactions for comparison purposes only.

Table 4. Second-order rate constants (25°C, 1 M non-complexing media) for inner-sphere oxidations of titanium(III) by some carboxalato complexes

Oxidant	k (dm^3 mol^{-1} s^{-1})			
	M = Co	Reference	M = Ru	Reference
$M(NH_3)_4(C_2O_4)^+$	75	18	3.6×10^4	1
$M(NH_3)_5(C_2O_4)^+$	8.6×10^4	19	2.5×10^4	1
$M(NH_3)_5CH_3COO^{2+}$	3	19	7×10^2	1
$M(NH_3)_5SalH^{2+}$	1×10^2	20	6.3×10^2	4
$Ru_2(CH_3COO)_2(C_2O_4)_2^-$	—	—	1.5×10^5	16
$Co_2(OH)_2(NH_3)_6(C_2O_4)^{2+}$	4.8	18	—	—
$M(C_2O_4)_3^{3-}$	1.9×10^3	2	5.3×10^2	7
$M(C_2O_4)_3^{3-a}$	3.2×10^3	This work	3.2×10^3	7

[a] Reductant is $Ti(C_2O_4)_2^-$.

Table 5. Variation of the second-order rate constant (25°C, 1 M non-complexing aqueous media) with reaction driving force for titanium(III)[a] reduction of certain ruthenium(III) and titanium(III) oxidants

Oxidant[b]	ΔE (mV)	k_{obs} (dm^3 mol^{-1} s^{-1})	$\ln k_{obs}$	Mechanism[c]	Reference
1. $Ru(NH_3)_5py^{3+}$	385	4.2×10^3	8.34	o.s.	21
2. $Ru(NH_3)_6^{3+}$	131	35	3.56	o.s.	22
3. $Ru(NH_3)_5H_2O^{3+}$	146	66	4.19	o.s.	21
4. $Ru(NH_3)_5Cl^{2+}$	38	12	2.48	o.s.	22
5. $Ru_2(OAc)_4^+$	370	3.5×10^3	8.16	o.s.	12
6. $Ru(pd)_3$	−198	0.7	−0.36	o.s.	12
7. $Ru(en)_3^{3+}$	262	1×10^3	6.91	o.s.	23
8. $Ru(NH_3)_5(OAc)^{2+}$	124	700	6.55	i.s.	1
9. $Ru_2(OAc)_3(C_2O_4H)^+$	−70	2×10^4	9.90	i.s.	24
10. $Ru(pd)_2(fpd)$	−80	2×10^3	7.60	i.s.	25
11. $Ru_2(OAc)_4^+$	410	4.0×10^3	8.29	o.s.	This work
12. $Co(C_2O_4)_3^{3-}$	−250	3.2×10^3	8.07	i.s.	This work

[a] Reductant for oxidants 1–7 is $TiOH^{2+}$, for oxidants 8–10 the reductant is Ti^{3+}, and for oxidants 11 and 12 the reductant is $Ti(C_2O_4)_2^-$.

[b] py = pyridine; OAc = acetate; pd = anion of 2,4-pentanedione; en = ethylenediamine: fpd = anion of 3-formyl-2,4-pentanedione.

[c] o.s. = outer-sphere mechanism; i.s. = inner-sphere mechanism.

nium(III) and cobalt(III) reactions involve inner-sphere ET and that the rate-limiting feature is formation of the binuclear complex through substitution on titanium(III).

It seems likely that the reactions between $Co(C_2O_4)_3^{3-}$, $Ru(C_2O_4)_3^{3-}$ and Ti^{3+} are also substitution-controlled, or nearly so. The small difference between the two rates may be due to partial rate control by the ET step in the case of the cobalt(III) oxidant. The reason why non-bridging oxalate increases the rate of the redox reaction is that addition of the non-bridging ligand increases the rate of substitution on titanium(III) and formation of the binuclear complex.[5] Using this interpretation, the similarity between the magnitudes of the effects of the non-bridging ligand in the two cases is fortuitous.

Acknowledgements—We are grateful to the National Science Foundation (INT-8319177) and the Research Corporation for partial support, and to the referee for helpful suggestions.

REFERENCES

1. A. Adegite, J. E. Earley and J. F. Ojo, *Inorg. Chem.* 1979, **18**, 1535.
2. N. Akinyugha, J. Ige, J. F. Ojo, O. Olubuyide and R. Simoyi, *Inorg. Chem.* 1978, **17**, 218.
3. O. Olubuyide and J. E. Earley, *Inorg. Chem.* 1981, **20**, 3569.
4. R. N. Bose and J. E. Earley, *Inorg. Chem.* 1981, **20**, 2739.
5. R. A. Lee and J. E. Earley, *Inorg. Chem.* 1981, **20**, 1739.
6. R. N. Bose, P. A. Wagner and J. E. Earley, *Inorg. Chem.* 1984, **23**, 1132.
7. O. Olubuyide, K. Lu, A. O. Oyetunji and J. E. Earley, *Inorg. Chem.* 1986, **25**, 4798.
8. R. W. Mitchell, A. Spencer and G. Wilkinson, *J. Chem. Soc., Dalton Trans.* 1973, 846.
9. Galbraith Laboratory, Knoxville, Tennessee, U.S.A.
10. J. C. Bailer Jr and E. M. Jones, *Inorg. Synth.* 1939, **1**, 37.
11. A. W. Adamson, H. Ogata, J. Grossman and R. Newbury, *J. Inorg. Nucl. Chem.* 1958, **6**, 319.
12. J. E. Earley, R. N. Bose and B. H. Berrie, *Inorg. Chem.* 1983, **22**, 1836.
13. P. Barone and J. E. Earley, *Inorg. Chem.* 1988, **27**, 1378.
14. P. Chaudhuri and H. Diebler, *J. Chem. Soc., Dalton Trans.* 1977, 596.
15. R. L. Pecsok, *J. Am. Chem. Soc.* 1951, **73**, 1304.
16. K. Lu, J. F. Ojo and J. E. Earley, *Inorg. Chem.* 1988, **27**, 2325.
17. E. G. Moorehead and N. Sutin, *Inorg. Chem.* 1966, **5**, 1866.
18. M. Hery and K. Wieghardt, *Inorg. Chem.* 1978, **17**, 1130.
19. A. H. Martin and E. S. Gould, *Inorg. Chem.* 1975, **14**, 873.
20. A. H. Martin and E. S. Gould, *Inorg. Chem.* 1976, **15**, 1934.
21. K. M. Davies and J. E. Earley, *Inorg. Chem.* 1978, **17**, 3350.
22. P. Chalilpoyil, K. M. Davies and J. E. Earley, *Inorg. Chem.* 1977, **16**, 3344.
23. R. Iadevia and J. E. Earley, *Inorg. Chim. Acta* 1981, **53**, L143.
24. J. E. Earley, B. Berrie, P. Barone, R. N. Bose and R. A. Lee, *IUPAC, Coord. Chem.* 1980, **20**, 65.
25. B. H. Berrie and J. E. Earley, *J. Chem. Soc., Chem. Commun.* 1982, 471.

Polyhedron Vol. 10, No. 8, pp. 837–840, 1991
Printed in Great Britain

0277–5387/91 $3.00+.00
© 1991 Pergamon Press plc

MONONUCLEAR PYRIDINE-2-THIONATO COMPLEXES FORMED DIRECTLY FROM RUTHENIUM TRICHLORIDE

ANTONY J. DEEMING* and MANZURUL KARIM

Department of Chemistry, University College London, 20 Gordon Street, London WC1H 0AJ, U.K.

(*Received* 21 *August* 1990; *accepted* 4 *January* 1991)

Abstract—Reductive carbonylation of ruthenium trichloride in refluxing 2-methoxyethanol leads to a chlorocarbonyl complex of ruthenium(II) which reacts directly with pyridine-2-thione (pySH) to give high yields of $[Ru(pyS)_2(CO)_2]$, and the 6-methylpyridine-2-thionato analogue is prepared similarly but in much lower yield. Quinoline-2-thione (quinSH) gives high yields of the compound $[RuCl_2(quinSH)_2(CO)_2]$ and only low yields of the dehydrochlorination compound $[Ru(quinS)_2(CO)_2]$. The more crowded thione, 4,8-dimethylquinoline-2-thione, gives only the chloro complexes and no dehydrochlorination.

Ruthenium(II) chlorocarbonyl complexes are easily synthesized by treating ruthenium trichloride with carbon monoxide in refluxing alcoholic solvents, followed by the addition of a neutral ligand.[1] For example, tertiary phosphine complexes such as $[RuCl_2(CO)_2L_2]$ are readily synthesized in this way.[1,2] We wished to synthesize mononuclear pyridine-2-thionato complexes of ruthenium as starting materials for the synthesis of cluster and cage compounds, for example, we have synthesized the 2-pyridyl clusters $[Ru_5(S)_2(C_5H_4N)_2(CO)_{11}]$ and $[Ru_6(S)_2(C_5H_4N)_2(CO)_{18}]$ from $[Ru(pyS)_2(CO)_2]$ and $[Ru_3(CO)_{12}]$,[3] and these results will be reported later. We originally synthesized $[Ru(pyS)_2(CO)_2]$ from $[Ru_3(CO)_{12}]$ and an excess of pySH under vigorous conditions[4] but we sought a good easy route from $RuCl_3 \cdot 3H_2O$ and this method is described herein.

RESULTS AND DISCUSSION

It is well known that bubbling carbon monoxide through a refluxing solution of ruthenium trichloride in 2-methoxyethanol gives a yellow solution containing reactive ruthenium(II) chlorocarbonyl species.[1] Probably the major one present is *fac*-$[RuCl_3(CO)_3]^-$. These solutions are valuable in the synthesis of ruthenium(II) species and tertiary phosphines, arsines, amines, pyridine (L), etc., give $[RuCl_2(CO)_2L_2]$ or $[RuCl_2(CO)L_3]$ in different stereochemistries.[1,2]

Ruthenium(II) pyridine-2-thione (pySH) or thionato (pyS) complexes have been prepared previously from tertiary phosphine-containing precursors and all contain tertiary phosphines, e.g. $[Ru(pyS)_2(CO)(PPh_3)]$, $[RuH(pyS)(CO)(PPh_3)_2]$, $[Ru(pyS)_2(CO)_2(PPh_3)]$, $[RuHCl(pySH)(CO)(PPh_3)]$, or $[RuCl(pyS)(pySH)(CO)(PPh_3)_2]$.[5–7] These complexes contain pyS as a monodentate S-bonded or chelating ligand or pySH as a S-bonded neutral thione ligand.

In looking for a straightforward route to $[Ru(pyS)_2(CO)_2]$ from $RuCl_3 \cdot 3H_2O$, we found that treatment of the 2-methoxyethanol solution containing ruthenium(II) chlorocarbonyl species with pySH, followed by thermal dehydrochlorination, provides a one-pot synthesis of $[Ru(pyS)_2(CO)_2]$ in high yield (89%). Earlier we had prepared this dicarbonyl from $[Ru_3(CO)_{12}]$ with an excess of pySH.[4] Initially the reaction of pySH with $[Ru_3(CO)_{12}]$ gives the trinuclear compound $[Ru_3H(\mu\text{-pyS})(CO)_9]$, but this reacts easily with an excess of pySH to give the mononuclear compound. This is a satisfactory synthesis but more expensive than that from $RuCl_3 \cdot 3H_2O$ and is less convenient even though the yields are good in both cases.

The compound $[Ru(pyS)_2(CO)_2]$ was obtained as yellow, air-stable crystals which were simply characterized by IR and NMR spectra (Table 1). It is closely related to the corresponding osmium com-

* Author to whom correspondence should be addressed.

Table 1. Selected spectroscopic data for the new compounds

Compound	ν(CO)[a] (cm^{-1})	^{1}H NMR[b]	
$[Ru(pyS)_2(CO)_2]$	2046vs	8.13(ddd,H^6)	J_{35} 1.3
	1988s	7.38(ddd,H^4)	J_{34} 8.3
		6.86(ddd,H^3)	J_{46} 1.3
		6.75(ddd,H^5)	J_{45} 7.9
			J_{56} 5.5
$[Ru(pyS)_2(pySH)(CO)]$	1934vs	13.3(s,br,N*H*)	
		8.30(ddd,H^6,pyS)	*J* 0.9, 1.8, 5.4
		8.12(ddd,H^6,pyS)	*J* 0.9, 1.7, 5.5
		7.63(ddd,H^3,pySH)	
		7.60(d,br,H^6,pySH)	
		7.28(m,3H^4)	
		6.88(ddd,H^3,pyS)	
		6.84(ddd,H^3,pyS)	
		6.6–6.8(m,3H^5)	
$[Ru(MepyS)_2(CO)_2]$	2048s	7.23(t,H^4)	*J* 8.0
	1987s	6.68(d,H^3)	
		6.50(d,H^5)	
		2.62(s,Me)	
$[Ru(quinS)_2(CO)_2]$	2051s	8.85(d,H^8)	*J* 8.0
	1991s	7.66(d,H^4)	*J* 8.8
		7.53(m,H^5,H^6)	
		7.26(m,H^7)	
		6.29(d,H^3)	*J* 8.8
$[RuCl_2(quinSH)_2(CO)_2]$	2061s	14.5(s,br,N*H*)	
	1998s	7.75(d,H^8)	*J* 9.0
		7.55–7.65(m,H^{4-6})	
		7.28–7.40(m,H^3,H^7)	
$[RuCl_2(4,8\text{-}Me_2quinSH)_2(CO)_2]$	2055s	13.3(s,br,N*H*)	
	1988s	7.65(d,H^6)	*J* 7.2
		7.45(m,H^5,H^7)	
		7.25(m,H^3)	
		2.91(s,Me)	
		2.58(s,Me)	

[a] In cyclohexane except for dichloro compounds which were in dichloromethane.
[b] In $CDCl_3$ at 200 MHz.

pound, which we have synthesized indirectly from $[Os_3(CO)_{12}]$.[8] The reaction of trifluoroactic acid with the dodecacarbonyl gives $[Os(CF_3CO_2)_2(CO)_4]$ and this can be converted with pySH into $[Os(pyS)_2(CO)_2]$, which has been structurally characterized by XRD. The pyS ligands are equivalent, the carbonyl *cis* and the S-atoms *trans*, and the ruthenium compound is almost certainly isostructural with it. The minor product analyses as $[Ru(pyS)_2(pySH)(CO)]$ and contains non-equivalent chelating pyS ligands and a S-bonded pySH thione ligand (^{1}H NMR evidence, Table 1). The N*H* proton in the ^{1}H NMR spectrum appears as a broad singlet at δ 13.3. We cannot be sure of the structure based on spectra but simple carbonyl substitution without rearrangement is likely since the compound would then have a structure related to those established for $[Ru(pyS)_2(CO)(PPh_3)]$[5] and $[Ru(pyS)_2(PPh_3)_2]$.[9]

Directly comparable reactions of $RuCl_3 \cdot 3H_2O$ with other thiones have been examined: 6-methylpyridine-2-thione (MepySH), quinoline-2-thione (quinSH) and 4,8-dimethylquinoline-2-thione (4,8-MequinSH). The only product from MepySH is $[Ru(MepyS)_2(CO)_2]$, which is directly analogous to the parent pyS compound but is formed in much lower yield. We have not accounted for the different yield but most of the material from the reaction does not elute on the TLC plate and we have been unable to characterize it. The other two thiones give good yields but mainly of the chloro complexes $[RuCl_2(CO)_2L_2]$ (L = quinSH or 4,8-Me_2quinSH),

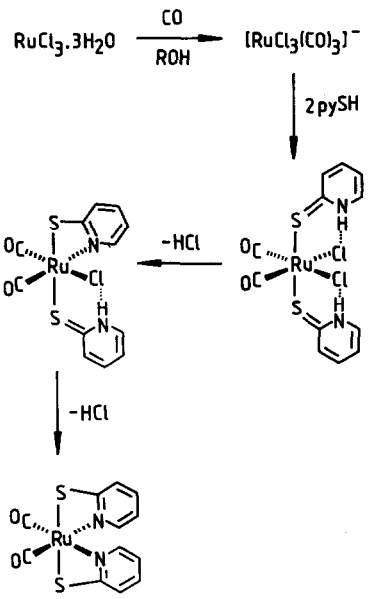

Scheme 1.

which correspond to the products expected from neutral ligands. The ligand quinSH also gives a minor amount of the dehydrochlorination product $[Ru(quinS)_2(CO)_2]$. We propose the reaction route given in Scheme 1. The initial reaction leads to the adducts $[RuCl_2(CO)_2L_2]$ which are isolable for the more sterically demanding thiones and the only product for 4,8-MequinSH. Deprotonation of these thione complexes would give thionato species but it would seem that the thionato ligands, quinS and 4,8-Me_2quinS, do not easily form chelate rings with the displacement of a *cis*-chloride ligand. Certainly with 4,8-Me_2quinS there would be a serious clash of the 8-methyl group with an adjacent *cis* ligand if a chelate ring were formed. When chelate ring formation creates no such problem, it occurs readily as in the formation of $[Ru(pyS)_2(CO)_2]$ and in this case the chloro species are not observed.

EXPERIMENTAL

Reaction of $RuCl_3 \cdot 3H_2O$ *with carbon monoxide followed by pyridine-2-thione*

Carbon monoxide gas was bubbled through a refluxing dark red–brown solution of ruthenium trichloride (0.100 g, 0.38 mmol) in 2-methoxyethanol (40 cm^3) for 3 h to give a yellow solution. Pyridine-2-thione (0.106 g, 0.95 mmol) was added and the reflux without carbon monoxide gas was continued for 2 h. Water was added and the mixture extracted with dichloromethane. The dichloromethane was removed to give a yellow oil which was separated by TLC [SiO_2; light petroleum (b.p. $<40°C$)–dichloromethane (1 : 1 v/v)] to give one main yellow band yielding $[Ru(pyS)_2(CO)_2]$ as yellow crystals (0.129 g, 89%) from a dichloromethane and hexane mixture (Found: C, 38.1, H, 2.0; N, 7.25; S, 16.75. $C_{12}H_8N_2O_2RuS_2$ requires: C, 38.2; H, 2.15; N, 7.4; S, 17.0%). A minor band yielded a monocarbonyl species as an orange solid, shown by its spectra to be $[Ru(pyS)_2(pySH)(CO)]$ (0.006 g, 3%) (see alternative synthesis below).

Reaction of $[Ru_3(CO)_{12}]$ *with an excess of pyridine-2-thione*

A solution of $[Ru_3(CO)_{12}]$ (0.200 g, 0.31 mmol) and pySH (0.208 g, 1.19 mmol) in *m*-xylene was refluxed under nitrogen for 2 h. The deep yellow residue after removal of the solvent *in vacuo* was separated by TLC [SiO_2: light petroleum (b.p. $<40°C$)–dichloromethane (1 : 1 v/v)]. The major band gave $[Ru(pyS)_2(CO)_2]$ as yellow crystals (0.317 g, 89%) (Found: C, 38.1; H, 2.25; N, 7.35; S, 16.75%) and a minor band gave $[Ru(pyS)_2(pySH)(CO)]$ as orange needles (0.008 g, 2%) from a dichloromethane–hexane mixture (Found: C, 41.25; H, 2.8; N, 8.9; S, 20.85. $C_{16}H_{13}N_3ORuS_3$ requires: C, 41.7; H, 2.85; N, 9.1; S, 20.9%). Both were spectroscopically identical to the products from the previous synthesis.

Reaction of $RuCl_3 \cdot 3H_2O$ *with carbon monoxide followed by 6-methylpyridine-2-thione*

Carbon monoxide was bubbled through a refluxing solution of ruthenium trichloride (0.200 g, 0.76 mmol) in 2-methoxyethanol (40 cm^3) for 3 h. The bubbling was stopped, MepySH (0.239 g, 1.90 mmol) was added and the solution refluxed for 2 h. TLC work-up as above gave $[Ru(MepyS)_2(CO)_2]$ as yellow crystals (0.0207 g, 7%) (Found: C, 41.2; H, 2.85; N, 6.7; S, 15.1. $C_{14}H_{12}N_2O_2RuS_2$ requires: C, 41.45; H, 3.0; N, 6.9; S, 15.8%). There were other low-yield and uncharacterized products but most of the material did not elute and was not studied further.

Reaction of $RuCl_3 \cdot 3H_2O$ *with carbon monoxide followed by quinoline-2-thione*

Carbon monoxide was bubbled through a refluxing solution of ruthenium trichloride (0.300 g, 1.15 mmol) in 2-methoxyethanol (40 cm^3) for 3 h. Quinoline-2-thione (0.462 g, 2.87 mmol) was added and the solution refluxed for 15 min. Brick-red crystals,

which deposited on cooling for 1 h, were collected, washed with light petroleum (b.p. $<40°C$) and characterized as $[RuCl_2(quinSH)_2(CO)_2]$ (0.595 g, 94%) (Found: C, 43.65; H, 2.7; Cl, 12.8; N, 4.95; S, 11.25. $C_{20}H_{14}N_2O_2Cl_2RuS_2$ requires: C, 43.65; H, 2.55; Cl, 12.9; N, 5.1; S, 11.65%). Removal of the solvent from the mother liquor and TLC of the residue [SiO_2; light petroleum (b.p. $<40°C$)–methanol (19 : 1 v/v)] gave $[Ru(quinS)_2(CO)_2]$ as yellow crystals (0.010 g, 2%) from a dichloromethane–methanol mixture (Found: C, 49.45; H, 2.45; N, 5.5. $C_{20}H_{12}N_2O_2RuS_2$ requires: C, 50.3; H, 2.55; N, 5.85%).

Reaction of $RuCl_3 \cdot 3H_2O$ *with carbon monoxide followed by* 4,8-*dimethylquinoline-2-thione*

Treatment of ruthenium trichloride (0.200 g, 0.76 mmol) in 2-methoxyethanol (40 cm^3) with carbon monoxide as above, followed by treatment with the thione (0.285 g, 1.51 mmol) and further reflux for 2 h gave a solution which deposited brick-red crystals (0.272 g) on cooling for 1 h. Removal of the solvent from the mother liquor and recrystallization of the residue from a dichloromethane–methanol mixture gave more brick-red crystals (0.125 g). The total yield of $[RuCl_2(4,8\text{-}Me_2quinSH)_2(CO)_2]$ was 0.342 g (74%) (Found: C, 47.2; H, 3.65; Cl, 11.5; N, 4.6; S, 10.5. $C_{24}H_{22}Cl_2N_2O_2RuS_2$ requires: C, 47.5; H, 3.65; Cl, 11.4; N, 4.6; S, 10.5%).

Acknowledgements—We thank the Association of Commonwealth Universities for a studentship (for M.K.) and Johnson–Matthey for a loan of $RuCl_3 \cdot 3H_2O$.

REFERENCES

1. J. Chatt, B. L. Shaw and A. E. Field, *J. Chem. Soc.* 1964, 3466; M. L. Berch and A. Davison, *J. Inorg. Nucl. Chem.* 1973, **35**, 3763.
2. W. Manchot and J. König, *Berichte* 1924, **57**, 2130; A. T. Stephenson and G. Wilkinson, *J. Inorg. Nucl. Chem.* 1966, **28**, 945; J. V. Kingston and G. R. Scollary, *J. Inorg. Nucl. Chem.* 1972, **34**, 227; J. P. Collman and W. R. Roper, *J. Am. Chem. Soc.* 1965, **87**, 4008; J. M. Jenkins, M. S. Lupin and B. L. Shaw, *J. Chem. Soc. A* 1966, 1787; M. S. Lupin and B. L. Shaw, *J. Chem. Soc. A* 1968, 741; D. F. Gill, B. E. Mann and B. L. Shaw, *J. Chem. Soc., Dalton Trans.* 1973, 311.
3. B. Cockerton, A. J. Deeming, K. I. Hardcastle and M. Karim, unpublished results.
4. A. J. Deeming and M. Karim, unpublished results.
5. P. Mura, B. G. Olby and S. D. Robinson, *J. Chem. Soc., Dalton Trans.* 1985, 2101.
6. N. Ahmed, S. D. Robinson and M. F. Uttley, *J. Chem. Soc., Dalton Trans.* 1972, 843.
7. N. Ahmed, S. D. Robinson, J. J. Levison and M. F. Uttley, *Inorg. Chem.* 1975, **15**, 45.
8. A. J. Deeming, M. N. Meah, N. P. Randle and K. I. Hardcastle, *J. Chem. Soc., Dalton Trans.* 1989, 2211.
9. S. R. Fletcher and A. C. Skapski, *J. Chem. Soc., Dalton Trans.* 1972, 635.

Polyhedron Vol. 10, No. 8, pp. 841–849, 1991
Printed in Great Britain

0277–5387/91 $3.00+.00
© 1991 Pergamon Press plc

VARIABLE TEMPERATURE ^{13}C NMR STUDY OF SOME $L(CO)_3FeH(SiR_3)$ (L = CO, $P(OPh)_3$; R = Ph, Me, Cl) SPECIES. X-RAY CRYSTAL STRUCTURE OF $P(OPh)_3(CO)_3Fe(H)SiPh_3$

JOHN W. CONNOLLY* and MICHAEL J. HATLEE†

Department of Chemistry, University of Missouri-Kansas City, Kansas City, MO 64110, U.S.A.

and

ALAN H. COWLEY

Department of Chemistry, University of Texas at Austin, Austin, TX 78741, U.S.A.

and

PAUL R. SHARP

Department of Chemistry, University of Missouri-Columbia, Columbia, MO 65211, U.S.A.

(*Received* 24 *April* 1990; *accepted* 4 *January* 1991)

Abstract—Intramolecular rearrangement of $(CO)_4FeH(SiPh_3)$ (**I**), $(CO)_4FeH(SiMe_3)$ (**II**), $(CO)_4FeH(SiCl_3)$ (**III**) and $P(OPh)_3(CO)_3Fe(H)SiPh_3$ (**IV**), as studied by variable temperature ^{13}C NMR spectroscopy, yielded activation enthalpies (kcal mol^{-1}): 10.3 ± 0.1, 10.4 ± 0.4, 17.4 ± 0.1 and 10.9 ± 0.03, respectively, and activation entropies (cal deg^{-1} mol^{-1}): -1.8 ± 0.5, -2.21 ± 0.1, 0.7 ± 0.5 and -2.2 ± 0.2, respectively. Crystal structure data for **IV**: $C_{39}H_{31}FeO_6PSi$, OC-6-23-tricarbonylhydrido(triphenylphosphite)(triphenylphosphine)iron(II), triclinic, $P\bar{1}$, $a = 11.509(2)$, $b = 14.403(3)$, $c = 11.153(4)$ Å, $\alpha = 108.04(2)$, $\beta = 95.10(2)$, $\gamma = 92.55(2)°$, $Z = 2$, $V = 1746(1)$ Å^3, final R factor 0.030. The structure is a highly distorted octahedron.

Intramolecular rearrangements of organometallic compounds have been studied using variable temperature NMR spectroscopy for some time. Using ^1H and ^{31}P spectroscopy, Muetterties and co-workers studied a series of $H_2Fe(PR_3)_4$ (and analogous ruthenium) compounds. In addition to obtaining the activation parameters they proposed a tetrahedral hopping mechanism as a pathway for the rearrangement process.[1] Using ^{13}C NMR spectroscopy, Graham and co-workers studied a series of $(CO)_4M(ER_3)_2$ (M = Fe, Ru, Os; E = Si, Ge, Sn, Pb) compounds. In their studies, observation of the *trans* intermediate leads to the conclusion that the rearrangement process proceeds by a *cis–trans* equilibrium process.[2] In both of these elegant studies structural details obtained crystallographically were correlated with the proposed rearrangement mechanisms. There are other possible rearrangement mechanisms for octahedral complexes and Butler demonstrated recently that *mer*-$Cr(CO)_2(CX)[(MeO)_3P]_3$ undergoes intramolecular rearrangement by a trigonal twist mechanism.[3] A calculated study by Hansen and Marynick gives evidence that the trigonal prismatic configuration is the transition state for intramolecular rearrangement by the Bailer twist, the Ray and Dutt twist and the bicapped tetrahedral mechanism in $Cr(CO)_5PH_3$.[4] There have been several other reports on the room temperature fluxional behav-

* Author to whom correspondence should be addressed.
† Present address: Department of Chemistry, Briarcliff College, Sioux City, IA 51104, U.S.A.

iour of hydrido-silyl iron carbonyl compounds but they have not been studied in detail.[5] In this paper we report variable temperature ^{13}C NMR spectra of $(CO)_4Fe(H)(SiR_3)$ (R = Ph, **I**; Me, **II**; Cl, **III**) and $P(OPh)_3(CO)_3Fe(H)SiPh_3$ (**IV**).

EXPERIMENTAL

Materials

The NMR solvents, perdeuterotoluene and hexane, were dried over calcium hydride and de-aerated with argon. Compounds **I–III** were prepared by literature[6] methods and enriched by exposure to ^{13}CO in solution for 12 h or longer. Enriched samples of **IV** were prepared from enriched **I** and triphenylphosphite.[7] The crystallographic sample of **IV** was prepared photochemically from triphenylsilane and $P(OPh)_3Fe(CO)_4$;[8] X-ray quality crystals were grown from a 90 : 10 hexane–toluene solution at −15°C.

NMR experiments/simulation

NMR measurements on **I–III** were carried out using a GE QE300 spectrometer at the University of Texas; measurements on **IV** were carried out using a Varian XL300 spectrometer at the University of Kansas; measurements on deuterated **III** were carried out on a Varian VXR 300 at the Midwest Research Institute, K.C. MO. Spectrometer probe temperatures were calibrated using the chemical shift differences in methanol or ethylene glycol.[9] A mixed solvent of hexane and C_7D_8 was used in the variable temperature spectra of **I** and **II**, pure C_7D_8 was used for **III** and **IV**. Simulation was carried out using the DNMRH program obtained from QCPE. Input parameters (chemical shifts, coupling constants and line widths) were obtained from the lowest temperature spectrum. The experimental spectra in Fig. 3 were prepared by reading the raw NMR data into a VAX computer at UMKC and processing it with the FTNMR program available from Hare Research, Inc.

Structure determination

A large crystal of **IV** was cut to size and mounted on the end of a glass fibre. Cell dimensions were based upon a Delaunay reduction of a cell obtained from the centring of 25 reflections on the diffractometer (Enraf–Nonius CAD4). Intensity data were measured (298 K) with Mo-K_α radiation using a graphite monochronometer (w-2 scan, 96 steps/scan, 16 steps/side background). The intensities of three standard reflections were measured after each 7200 s exposure to the X-rays and showed a 15.2% intensity decay during the experiment. The correction factors for this decay ranged from 0.97 to 1.24. No absorption correction was needed based on scans and the low absorption coefficient. A total of 4822 reflections were measured and averaged ($R = 0.011$, on intensity) to give 4549 independent reflections. The Enraf–Nonius SDP program package was used for calculations. The structure was resolved by Patterson methods followed by successive applications of Fourier methods. Two orientations (rings 2 and 2′) for one of the phosphite phenyl groups were found with an occupancy of 80 and 20%. Occupancy values were set so that reasonable and equivalent thermal parameters for both ring orientations were obtained. The *para*-carbon [C(24)] position of the major ring orientation of an adjacent molecule overlaps with the *para*-carbon position of the minor orientation. The overlap is not exact and leads to a distorted minor ring. The peak identified as the iron hydrogen was the largest peak in the difference map. It refined correctly as hydrogen, its location in a gap between equatorial carbonyls is intuitively correct, and the Fe—C bond opposite it shows a modest *trans* influence. Phenyl hydrogen atoms were placed in calculated positions and not refined. Full matrix least-squares refinement minimizing $\Sigma w(|F_o| - |F_c|)^2$ converged to the R values given in Table 1. No extinction correction was applied. The final difference Fourier had the largest peak (0.21 e/Å^3) in the vicinity of the iron atom. The ORTEP diagram for compound **IV** is shown in Fig. 1.*

RESULTS

In Table 2 are listed the low-temperature limiting chemical shifts and coupling constants for the compounds under study, while the rate data and activation parameters for intramolecular carbonyl exchange are listed in Table 3. The line widths used in the simulation are a consequence of the ^{13}C–^{13}C coupling in the enriched samples used in the NMR studies. Figure 2 shows two high resolution spectra (0.13 Hz/data point) of an enriched sample of **III**, one at 270 K, where the compound is rigid, and the other at 298 K, where the rate constant is about 1 Hz. As the compound becomes fluxional the individual lines of the isotopomers are no longer resolved. Since this is the case, there is no advantage

* Atomic coordinates, thermal parameters, additional bond angles and bond distances, and torsional angles have been deposited with the Director, Cambridge Crystallographic Data Centre.

Table 1. Summary of crystallographic data

Formula	$FeSiPO_6C_{39}H_{31}$
Formula weight	710.59
Crystal size (mm)	$0.33 \times 0.30 \times 0.17$
Crystal system	Triclinic
Space group	$P\bar{1}$
Cell parameters	
a (Å)	11.509(2)
b (Å)	14.403(3)
c (Å)	11.153(4)
α (°)	108.04(2)
β (°)	95.10(2)
γ (°)	92.55(2)
Cell volume (Å^3)	1746(1)
Z	2
Calculated density (g cm^{-3})	1.352
Absorption coefficient (cm^{-1})	5.53
Radiation Mo-K_α (Å)	0.71073
Variation in Ψ	< 3%
2θ range (°)	4–45
Data rejected if $I <$	3σ
Total reflections	4549
Observed reflections	3300
Number of variables	457
Data to variable ratio	7.22
Largest peak in final difference Fourier (e/Å)	0.21
R	0.030
R_w	0.041

in obtaining all the data under high resolution conditions. Therefore the data were obtained using instrument settings of about 1 Hz/data point and the experimentally observed line width of 4.5 Hz was used.

Figures 3(a) and (b) show the experimental and simulated NMR spectra of **III** and **IV**, respectively. Figure 3(a) is typical of the results obtained for **I**–**III**. Using the temperatures and rate constants (Hz) in Table 3, Eyring plots yielded straight lines with correlation coefficients greater than 0.99 in each case. The spectra shown in Fig. 3 are proton decoupled. Separate room temperature measurements made with the decoupler off for **I** and **II** showed spin coupling between the iron hydrogen and the carbonyl carbon atoms, which indicates that these processes are intramolecular. The limiting fast exchange spectrum for **III** was not observed due to the high temperature required. In the case of **IV**, phosphorus–carbon spin coupling can be observed in the low temperature and high temperature regions of the spectra.

DISCUSSION

Variable temperature NMR studies yield activation parameters for the intramolecular processes which cause the fluxionality and, if the compounds

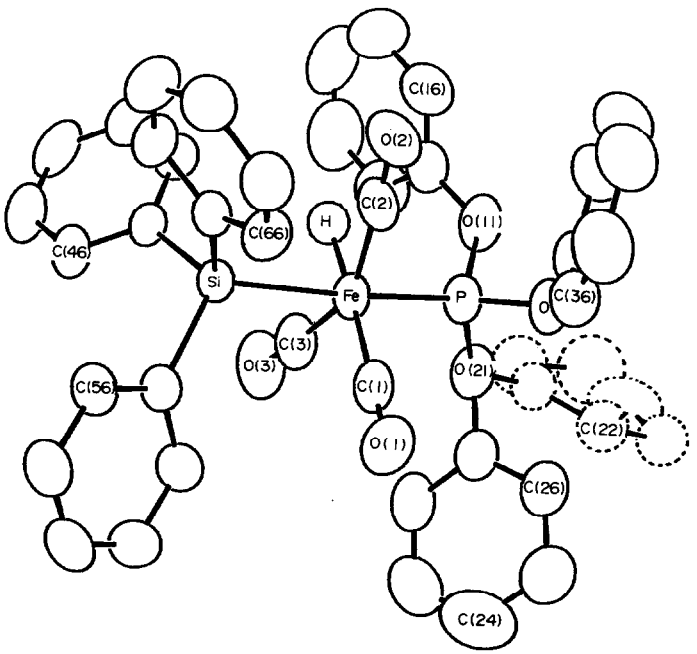

Fig. 1. ORTEP diagram of **IV**. Phenyl carbons are numbered sequentially about the ring [e.g. ring 1 : C(11), C(12), C(13), C(14), C(15), C(16)]. The dashed atoms of ring 2′ represent a second minor position for ring 2—see Experimental.

Table 2. Low temperature limiting NMR data

Compound	^{13}CO δ values Axial	Equatorial	$^2J_{C-P}$
I	206.2	206.6, 204.2	
II	207.4	206.6, 203.9	
III	201.7	200.1, 199.5	
IV	208.9	210.3	19.5, 12.7

are sufficiently asymmetric, mechanistic information about the intramolecular process. Input parameters for the simulation program include exchange vectors, which indicate which nuclei are actually exchanging. The best experimental results were obtained with **III** (Fig. 3a). Exchange vectors were chosen which best fit these data and the same exchange vectors were used for compounds **I–III**. For compound **IV** an equivalent set of exchange vectors was used except that phosphorus was substituted for carbon atom 4 and was kept in the same position throughout the exchange process. It was given a chemical shift outside the simulation range.

Figure 4 shows an idealized structure of compounds **I–IV**, and the carbonyl numbering system. The best fit of the experimental spectra was obtained by the following four exchange processes: simultaneous pairwise exchange between carbonyls 1 and 3 and 2 and 4, simultaneous pairwise exchange between 1 and 4 and 2 and 3, and pairwise exchange between 3 and 4 (counted twice). (The exchange vectors which accomplish these exchanges are 3412, 4312, 1243 and 2143, respectively.) Of course any mechanism which yields these exchange vectors is consistent with the experimental results. We have been unable to find a mechanism which yields these exchange vectors without editing. For example, the *cis–trans* mechanism proposed by Graham does not account for the 3–4 exchange being twice as fast as the other two processes. The twist mechanisms mentioned above give sets of exchange vectors which include the above four, but they also include processes which exchange carbonyls 1 and 3 (for example) faster than the data indicate.

Figure 5 shows another possible mechanism in which an incipient Si—H bond forms to produce a five-coordinate intermediate. That intermediate can rearrange to one observed product by rotation about the three-centre Fe—H—Si bond, it can also undergo a Berry pseudo-rotation which makes the other products accessible. This latter mechanism has the advantage that the activation energy pattern fits the known propensities of these compounds to eliminate the silane ligands, probably by passing through such an intermediate.[4] However, a significant deuterium isotope effect might be expected

Table 3. (a) Rate data and (b) activation parameters

(a)

I		**II**		**III**		**IV**	
T (K)	Rate (Hz)	T (K)	Rate (Hz)	T (K)	Rate (Hz)	T (K)	Rate (Hz)
193	3	183	0.5	298	1	213	10
203	12	193	2	308	3	233	90
213	40	203	10	318	8	253	700
223	150	233	150	328	25		
233	350	243	1200	338	45		
				348	100		
				373	500		

(b)

Compound	$\Delta G^{\ddagger}$ (kcal mol^{-1})	$\Delta H^{\ddagger}$ (kcal mol^{-1})	$\Delta S^{\ddagger}$ (cal deg^{-1} mol^{-1})	Reference
I	10.8	10.3±0.1	−1.8±0.5	This work
II	11.0	10.4±0.4	−2.1±1	This work
$(CO)_4Fe(SiMe_3)_2$	10.7			2
$(CO)_4Fe(SiMe_2Cl)_2$	13.2			2
$(CO)_4Fe(SiMeCl_2)_2$	16.5			2
$(CO)_4Fe(SiCl_3)_2$	17.5			2
III	17.2	17.4±0.1	0.7±0.5	This work
IV	11.6	10.9±0.03	−2.2±0.2	This work

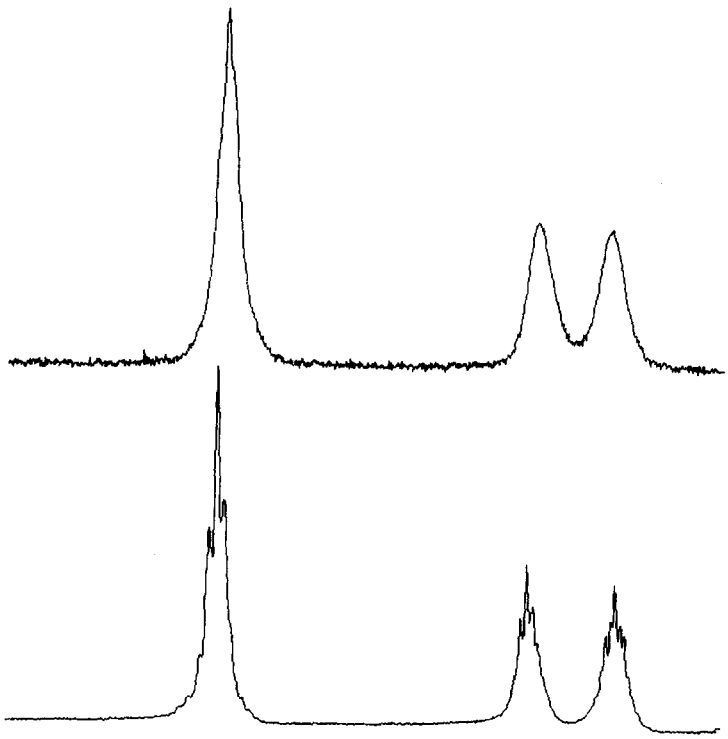

Fig. 2. High resolution ^{13}C NMR spectrum of **III** at 298 K (top) and 270 K (bottom).

for this mechanism and it appears from Fig. 6 that such is not the case. [The line widths in $(CO)_4FeD$ $Si(Cl)_3$ in Fig. 6 are broader due to deuterium-carbon coupling.] It has already been observed that substitution of deuterium for hydrogen in $HRh(PF_3)_4$ has very little effect on the rate of rearrangement.[10]

In Table 3(b) are listed the activation parameters for the compounds studied here, together with the literature data for similar compounds. Steric factors have surprisingly little effect on molecular rigidity. That is, replacement of one SiR_3 group by a hydrogen atom has essentially no effect on the activation energy, nor does the replacement of carbonyl by $P(OPh_3)$. This may be due to the fact that these are all highly distorted structures.

The magnitude of the observed activation free energies is dominated by the electronegativity of the silyl substituent, both in our results and in the previous study on bis-silyl iron carbonyls.[2] It is possible that the electron-withdrawing power of the silyl substituent simply makes the structure more rigid or it may be that the ground-state structure of the trichlorosilyl-containing compounds are further from the structure of the transition state. The only structural information obtained so far has been on the more rapidly exchanging compounds. The crystal structure of $(CO)_4Fe(SiMe_3)_2$ shows it to be close to a bicapped tetrahedron.[2] Table 4 lists the important bond lengths and angles for compounds **I** and **IV**. These structures are very similar to several other compounds of this type that have been reported.[12] In all cases there is significant distortion from octahedral geometry. The major distortion is the CO(2)—Fe—CO(3) bond angle which is closer to 150° than to the ideal value of 180°. On the other hand, the crystal structure of $(CO)_4Ru(GeCl_3)_2$[13] shows it to be nearly perfectly octahedral, but it is known that hexacoordinated ruthenium compounds are more nearly octahedral than hexacoordinated iron compounds.[12a]

The properties of **III** do not lend themselves to crystallographic study. Since the trichlorosilyl analogue of **IV**[14] is nearly rigid in solution at room temperature we attempted to determine its structure. We were unable to grow crystals of sufficient regularity to get a publishable crystallographic data set, although there appears to be a CO—Fe—CO bond angle of 147° in the structure. A calculational effort is underway in an attempt to explain the effect of silyl substituents on the molecular rigidity of the compounds studied here.

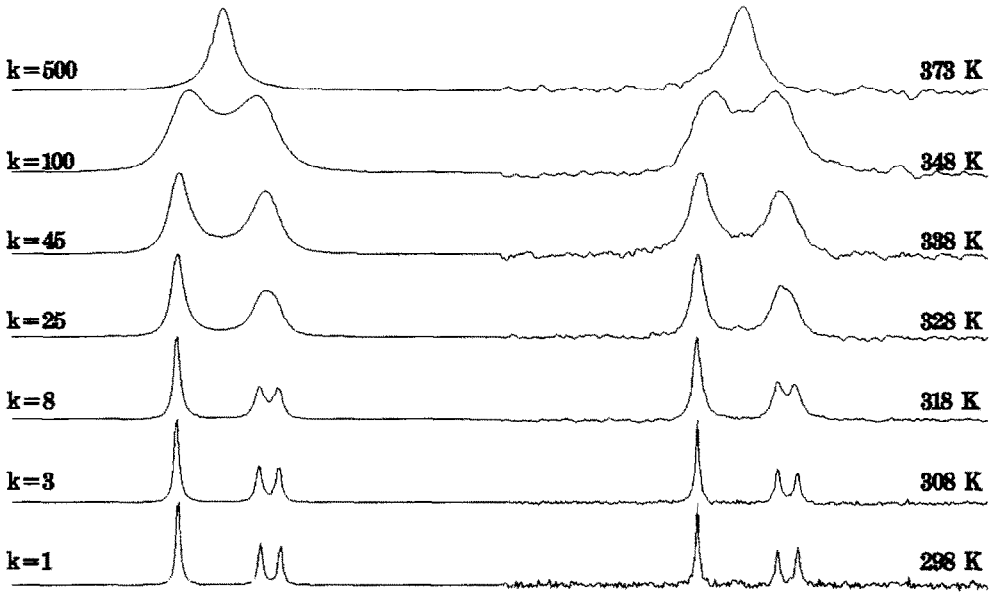

Fig. 3(a). ^{13}C NMR spectrum of **III**, simulated (left) and experimental (right).

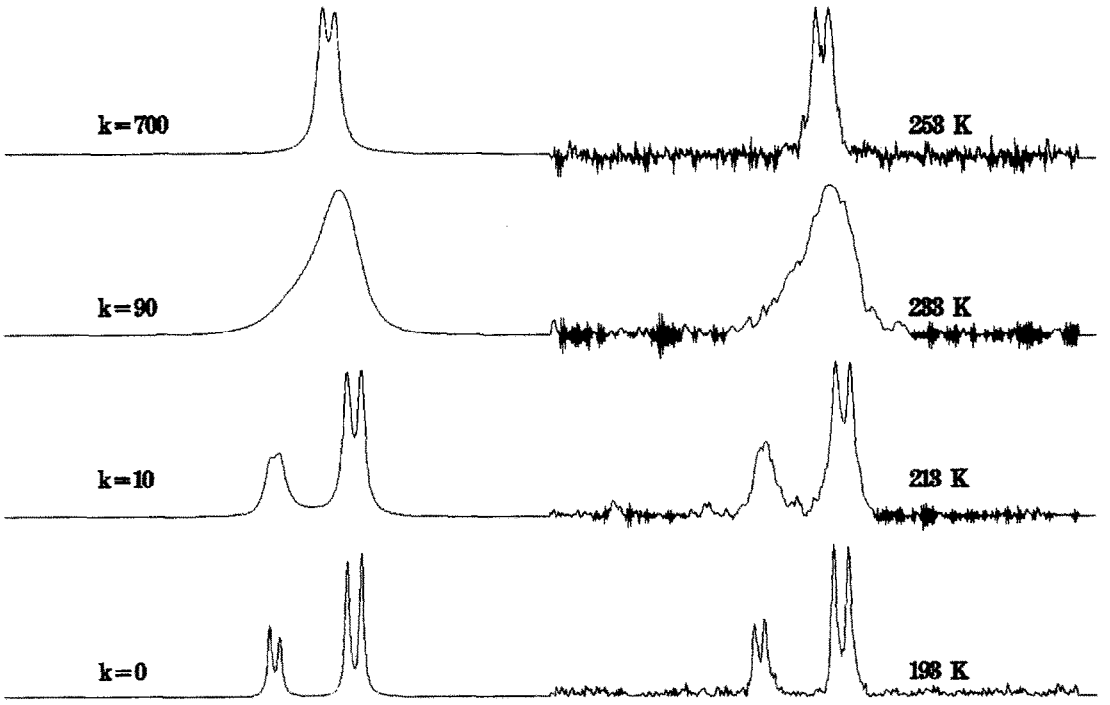

Fig. 3(b). ^{13}C NMR spectrum of **IV**, simulated (left) and experimental (right).

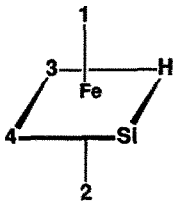

Fig. 4. Idealized structure of compounds I–IV.

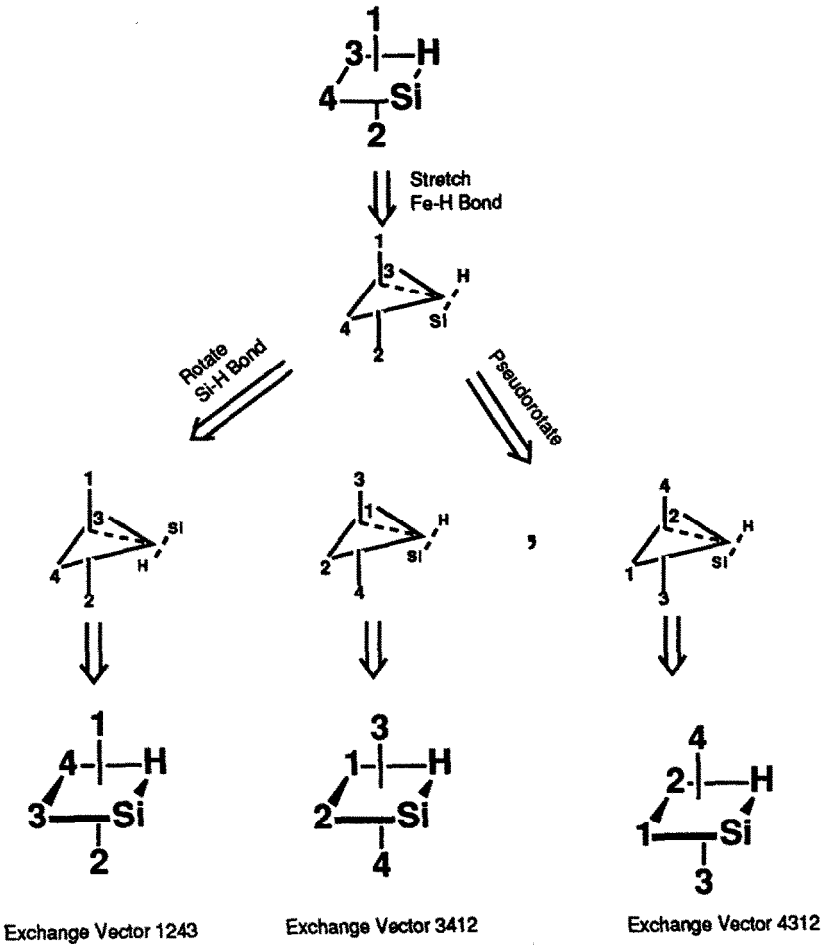

Fig. 5. Mechanism showing intramolecular exchange through pseudorotation.

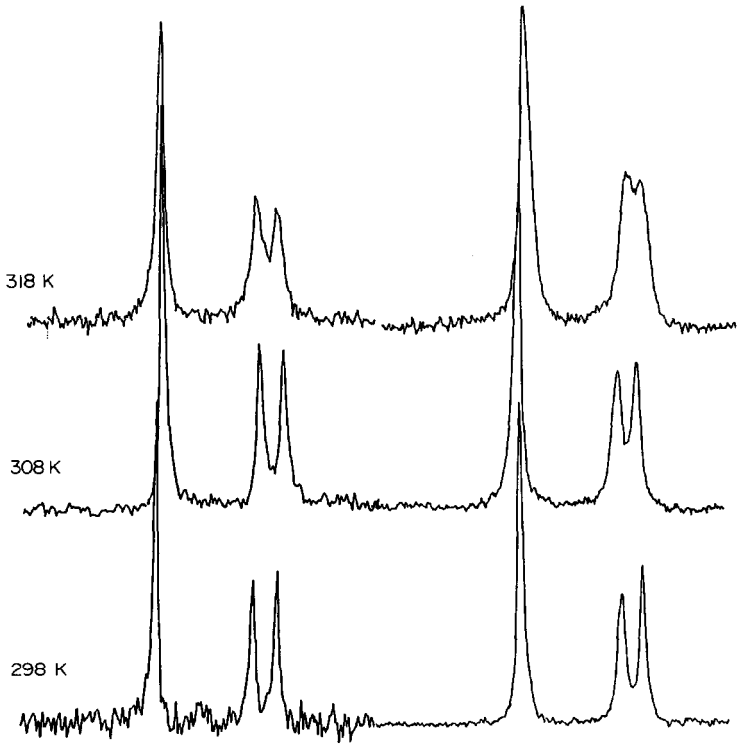

Fig. 6. Comparison of ^{13}C NMR spectra of **III** (left) and $(CO)_4FeDSi(Cl)_3$ (right).

Table 4. Selected bond lengths and angles for compounds **I** and **IV**

	I	**IV**
Fe—H	1.64(10)	1.46(3)
Fe—P		2.163(1)
Fe—Si	2.357(3)	2.380(1)
Fe—C(4)	1.821(10)	
Fe—C(1)	1.754(8)	1.794(3)
Fe—C(2)	1.775(7)	1.775(3)
Fe—C(3)	1.753(7)	1.756(3)
H—Fe—P	96(3)[a]	88(1)
H—Fe—Si	82(3)	85(1)
H—Fe—C(1)	168(3)	174(1)
H—Fe—C(2)	75(3)	74(1)
H—Fe—C(3)	76(3)	78(1)
P—Fe—Si	178.0(4)[a]	172.65(3)
P—Fe—C(1)	96.3(4)[a]	96.67(8)
P—Fe—C(2)	94.3(4)[a]	94.85(9)
P—Fe—C(3)	95.4(5)[a]	94.49(9)
Si—Fe—C(1)	85.6(3)	90.43(8)
Si—Fe—C(2)	85.6(3)	85.42(9)
Si—Fe—C(3)	83.9(3)	81.96(9)
C(1)—Fe—C(2)	104.9(5)	102.4(1)
C(1)—Fe—C(3)	102.4(4)	103.7(1)
C(2)—Fe—C(3)	149.8(4)	151.0(1)

[a] C(4) replaces P.

Acknowledgements—J.W.C. gratefully acknowledges financial support of this work by UMKC, including a research leave and a grant funded by the Weldon Springs Foundation. He also acknowledges the help of Dr David Vander Velde, Department of Medicinal Chemistry, University of Kansas, and of Dr Evelyn Murrill, Midwest Research Institute, for valuable assistance in obtaining NMR spectra, as well as the help of his son, Daniel Connolly, in conversion of the QE-300 NMR data files to a VAX-readable format.

REFERENCES

1. P. Meakin, E. Muetterties, F. Tebbe and J. Jesson, *J. Am. Chem. Soc.* 1971, **93**, 4701.
2. L. Vancea, R. Pomeroy and W. A. G. Graham, *J. Am. Chem. Soc.* 1971, **98**, 1407.
3. A. Ismall, J. Sauriol and I. Butler, *Organometallics* 1985, **4**, 1914.
4. L. H. Hansen and D. S. Marynick, *Inorg. Chem.* 1990, **29**, 2482.
5. M. Knorr, J. Muller and U. Schubert, *Chem. Ber.* 1987, **120**, 879.
6. W. Jetz and W. A. G. Graham, *Inorg. Chem.* 1971, **10**, 4.
7. D. Liu, C. Brinkley and M. Wrighton, *Organometallics* 1984, **3**, 1449.
8. G. Bellachiome, G. Cardaci, E. Colomer and R. Corriu, *Organometallics* 1989, **28**, 519.

9. A. Von Geet, *Anal. Chem.* 1968, **40**, 2227.
10. P. Meakin, E. Muetterties and J. Jesson, *J. Am. Chem. Soc.* 1972, **94**, 5271.
11. K. Simpson, PhD thesis, University of Alberta (1973).
12. (a) C. Brinkley, J. Dewan and M. Wrighton, *Inorg. Chim. Acta* 1986, **12**, 119; (b) U. Schubert, E. Kunz, M. Knorr and J. Muller, *Chem. Ber.* 1987, **120**, 1079.
13. L. Vancea, E. Bennet, C. Jones, R. Smith and W. A. G. Graham, *Inorg. Chem.* 1977, **16**, 897.
14. J. W. Connolly, A. H. Cowley and C. M. Nunn, *Polyhedron* 1990, **9**, 1337.

Polyhedron Vol. 10, No. 8, pp. 851–857, 1991
Printed in Great Britain

0277–5387/91 $3.00+.00
© 1991 Pergamon Press plc

DINUCLEAR PLATINUM(II) COMPLEXES WITH A BRIDGING MERCAPTO GROUP: X-RAY CRYSTAL STRUCTURE OF A CHLORO/MERCAPTO-BRIDGED DIMER

V. K. JAIN* and R. P. PATEL

Chemistry Division, Bhabha Atomic Research Centre, Trombay, Bombay-400 085, India

and

K. VENKATASUBRAMANIAN

Discipline of Coordination Chemistry and Homogeneous Catalysis, Central Salt & Marine Chemicals Research Institute, Bhavnagar-364 002, India

(*Received* 30 *March* 1989; *accepted* 4 *January* 1991)

Abstract—$[Pt_2Cl_2(\mu\text{-}X)(\mu\text{-}Y)(PR_3)_2]$ complexes [X = Cl, SPh; X = Y = SPh, Pr^i; PR_3 = PBu_3, PMe_2Ph, PPh_3, $P(p\text{-tol})_3$] have been prepared and characterized by elemental analysis, ^1H and ^{31}P NMR spectroscopy. Bridge cleavage reactions with various donor ligands have been investigated by $^{31}P\{^1H\}$ NMR. The X-ray crystal structure of $[Pt_2Cl_2(\mu\text{-}Cl)(\mu\text{-}SEt)(PMe_2Ph)_2]$ is reported.

Coordination geometries of dinuclear platinum(II) complexes of the type $[Pt_2(\mu\text{-}X)(\mu\text{-}Y)Z_2L_2]$ depend on the method of preparation and on the nature of the X, Y, Z and L ligands which also influence the chemical reactivity of such complexes. The dimercapto-bridged complexes[1–10] (X = Y = SR) usually prefer a *cis* configuration when R = alkyl, but when R = aryl and L = PPr_3, only the *trans* isomer exists. The monothio-bridged complexes[1,2,9] (X = Z = Cl) adopt a *cis* configuration, however, for Z = $SnCl_3$ the *sym trans* isomer forms.[9] The *cis* and *trans* configurations can readily be identified on the basis of ^3J(Pt—P) and ^4J(P—P) values.[8–10] In continuation of our previous work, we now report the phenyl and isopropyl mercapto-bridged complexes wherein L determines the geometry of the complex, together with the X-ray structure of $[Pt_2Cl_2(\mu\text{-}Cl)(\mu\text{-}SEt)(PMe_2Ph)_2]$.

RESULTS AND DISCUSSION

Treatment of $[Pt_2Cl_2(\mu\text{-}Cl)_2(PR_3)_2]$ with thiophenol in 1:2 stoichiometry, in the presence or absence of pyridine, affords the phenylthio-bridged complexes. A similar reaction, in the absence of pyridine, in 1:1 stoichiometry in dichloromethane yields the μ-chloro-μ-phenylthio complexes. These can also be obtained by reacting the tetrachloro complex with the dimercapto-bridged compound in dichloromethane. The tetrachloro complex reacts with excess isopropylmercaptan in acetone to give di-μ-isopropylthio complexes. Physical and analytical data of these complexes are given in Table 1.

The ^{31}P NMR data for $[Pt_2Cl_2(\mu\text{-}SPh)_2(PR_3)_2]$ (Table 2) suggest that these complexes adopt a *sym trans* configuration [^3J(Pt—P) = ~50 Hz and ^4J(P—P) = ~12 Hz][8,9] except tris(*p*-tolyl)phosphine which is a mixture of *cis* and *trans* isomers. The latter is in contrast to the observation of Chatt and Hart[1] that with the arylthio ligand the *trans* configuration is preferred. The existence of the *cis* isomer for $P(p\text{-tol})_3$ suggests that phosphine ligands also play a role in determining the geometry of the complex. The magnitude of ^1J(Pt—P) reflects that the chloro/mercapto-bridged complexes adopt a *sym cis* configuration in which the phosphine ligand is *trans* to the bridging chlorine.

The ^1H NMR spectra of the complex $[Pt_2Cl_2(\mu\text{-}Cl)(\mu\text{-}SPh)(PMe_2Ph)_2]$ displayed two doublets for

* Author to whom correspondence should be addressed.

Table 1. Physical and analytical data for $[Pt_2Cl_2(\mu\text{-}X)(\mu\text{-}SR)(PR_3)_2]$ complexes

Complex	Recrystallization solvent (per cent yield)	Melting point (°C)	Per cent analyses: Found (Calc.) C	H	S
$[Pt_2Cl_2(\mu\text{-}SPh)_2(PBu_3)_2]$	Benzene–hexane (61)	137	39.0 (39.9)	5.6 (5.9)	—
$[Pt_2Cl_2(\mu\text{-}Cl)(\mu\text{-}SPh)(PBu_3)_2]$	Benzene–hexane (90)	135	35.2 (35.7)	5.8 (5.9)	3.4 (3.2)
$[Pt_2Cl_2(\mu\text{-}SPh)_2(PMe_2Ph)_2]$	CH_2Cl_2–methanol (90)	224	34.5 (35.2)	3.1 (3.4)	6.8 (6.7)
$[Pt_2Cl_2(\mu\text{-}Cl)(\mu\text{-}SPh)(PMe_2Ph)_2]$	CH_2Cl_2–methanol (97)	219–220	29.3 (30.0)	3.0 (3.1)	3.7 (3.6)
$[Pt_2Cl_2(\mu\text{-}SPh)_2(P\text{-}tol_3)_2]$	Benzene–hexane (63)	271–273	50.0 (50.3)	3.8 (4.1)	5.5 (5.0)
$[Pt_2Cl_2(\mu\text{-}SPr^i)_2(P\text{-}tol_3)_2]$	Benzene (43)	253–255	46.9 (47.2)	4.6 (4.6)	5.5 (5.3)
$[Pt_2Cl_2(\mu\text{-}SPr^i)_2(PPh_3)_2]$	Chloroform (65)	264–265	43.9 (44.4)	3.9 (3.9)	—

the methyl protons indicating non-equivalence of the methyl groups on phosphine. The corresponding di-μ-phenylthio complex exhibited only one doublet for the P—Me protons.

Structure of $[Pt_2Cl_2(\mu\text{-}Cl)(\mu\text{-}SEt)(PMe_2Ph)_2]$

A single-crystal X-ray analysis of $[Pt_2Cl_2(\mu\text{-}Cl)(\mu\text{-}SEt)(PPhMe_2)_2]$ has confirmed that complexes of this type have a *sym cis* configuration. An ORTEP[11] plot of the molecule, together with the numbering of non-hydrogen atoms, is shown in Fig. 1. Table 3 lists the bond lengths and bond angles in the molecule with their estimated standard deviations. The bond lengths, as shown below, are in good agreement with those reported in the literature.[3,6]

Table 2. ^1H and $^{31}P\{^1H\}$ NMR data for mercapto-bridged dinuclear platinum(II) complexes in $CDCl_3$

Complex	$^{31}P\{^1H\}$ NMR data δ(Pt—P) (ppm)	^1J(Pt—P) (in Hz)	^3J(Pt—P) (in Hz)	^4J(P—P) (in Hz)	^1H NMR data
$[Pt_2Cl_2(\mu\text{-}SPh)_2(PBu^n_3)_2]$	3.1	3160	53	11.5	
$[Pt_2Cl_2(\mu\text{-}Cl)(\mu\text{-}SPh)(PBu^n_3)_2]$	0.5	3937	—	—	
$[Pt_2Cl_2(\mu\text{-}SPh)_2(PMe_2Ph)_2]$	−12.1	3200	52	14	P—Me_2 1.57 (d, 11 Hz)[a] ^3J(Pt—H) 33 Hz
$[Pt_2Cl_2(\mu\text{-}Cl)(\mu\text{-}SPh)(PMe_2Ph)_2]$	−17.2	4075	—	—	P—Me_2[a] 1.78 (d, 13.7 Hz); 1.66 (d, 13.7 Hz); Ph = 6.99–7.46 (m)
$[Pt_2Cl_2(\mu\text{-}SPh)_2(P\text{-}tol_3)_2]$	12.6 14.9	3325 3276	7.5 42	— 13	P—C_6H_4Me 2.29 s(br)[b]
$[Pt_2Cl_2(\mu\text{-}SPr^i)_2(P\text{-}tol_3)_2]$	14.4	3249	40	12	$SCMe_2$ 1.35 (d, 6 Hz)[b] PC_6H_4Me 2.32 (s)
$[Pt_2Cl_2(\mu\text{-}SPr^i)_2(PPh_3)_2]$	9.7	3255	36	12	$SCMe_2$ 1.40 (d, 6 Hz)[b] SCH 2.35 (m)

[a] Recorded on a Varian VXR 300 S.
[b] Recorded on a Varian FT-80A.

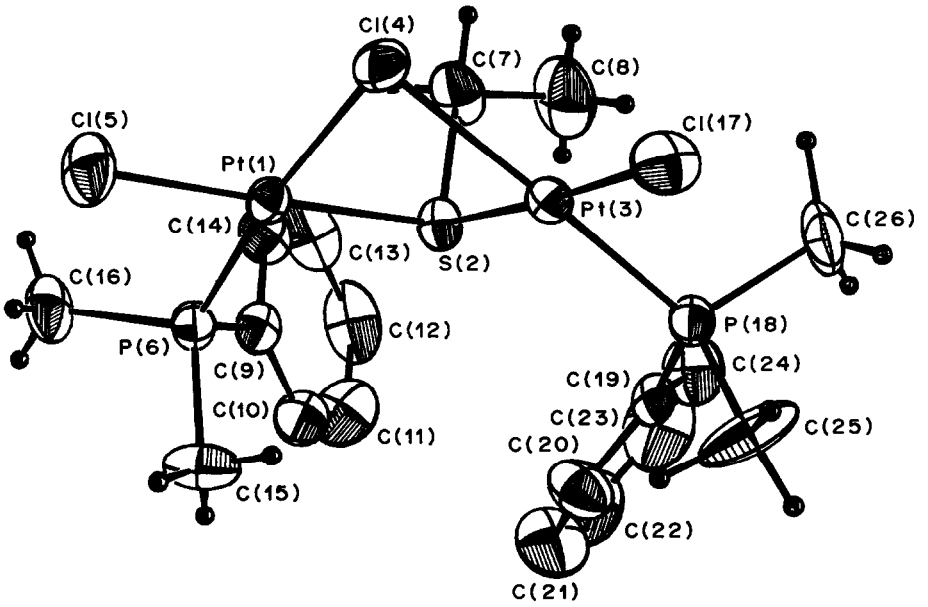

Fig. 1. ORTEP view of $[Pt_2Cl_2(\mu\text{-}Cl)(\mu\text{-}SEt)(PMe_2Ph)_2]$.

Bond	*trans* group	Bond length (Å) Expected[3,6]	⟨observed⟩$_{av}$
⟨Pt—P⟩	Cl	2.23	2.222(4)
⟨Pt—S⟩	Cl	2.27	2.271(4)
⟨Pt—Cl⟩$_{terminal}$	SR	2.34	2.334(5)
⟨Pt—Cl⟩$_{bridging}$	PR_3	2.43	2.452(5)

The terminal Pt—Cl distances are shorter than the bridging distances. The Pt—P and Pt—S distances are considerably shorter than their radius sum of 2.42 and 2.36 Å, respectively. The bond lengths are thus in keeping with the usual *trans* influence order P ≫ S > Cl. The shortening of the Pt—S bond has been attributed to a strong π-bond character.[3] The possibility of forming two strong bonds at sulphur, as suggested by Hall *et al.*,[3] results in a P—Pt—S—Pt—P chain and stabilizes the *cis* configuration. The *trans* configuration would lead to weakening of one of the Pt—S bonds due to the strong *trans* influence of the phosphine ligand, thereby destabilizing the bridge framework. The Pt···Pt distance [3.299(1) Å] lies within the expected[6,12] range, 3.18–3.48 Å.

The angles around both the platinum atoms are normal and fall within the expected range. The S—Pt—P angle is larger than the ideal 90° [91.8(2) and 95.9(2)°, respectively], which results in minimization of the crowding of the alkyl and aryl groups on the sulphur and phosphorus atoms, respectively. Further, the Pt—Cl—Pt angle which lies in the range 94–96° in di-μ-chloro-bridged complexes[12–16] shows a significantly smaller value of 84.5(2)° in the present case. The angle around the bridging sulphur atom [Pt(1)—S(2)—Pt(3)] is significantly larger [93.1(2)°] than that reported for any sulphur-bridged dinuclear platinum(II) complex[6] [85.5–92.0°]. Although a wide variation in the angle at the bridging sulphur (79–98°)[17,18a] has been observed with different metal ions, the reason for this, except due to the ionic radii variation, is not clear.

The conformations of the two PMe_2Ph ligands are different. The methyl carbon [C(15)] attached to P(6) nearly lies in the plane defined by C(9), C(10), C(11), C(12), C(13), C(14) [deviation ~ 0.16(2) Å], and in the plane defined by P(6), C(9), C(10), C(11), C(12), C(13), C(14) [deviation ~ 0.11(2) Å], while deviations of −1.63(2) and −1.59(2) Å occur for C(16). The respective values for C(25) and C(26) from the planes defined by C(19), C(20), C(21), C(22), C(23), C(24), and P(18), C(19), C(20), C(21), C(22), C(23), C(24) in the other phosphine ligand are −1.31(2), −1.35(2) Å and −0.46(3), −0.50(3) Å, respectively. These deviations are also reflected in the corresponding torsion angles C(15)—P(6)—C(9)—C(10) [0.7 (2.0)°], C(15)—P(6)—C(9)—C(14) [−176.7 (1.7)°], C(16)—P(6)—C(9)—C(10) [109.6 (1.8)°], C(16)—P(6)—C(9)—C(14) [72.9 (1.8)°], C(25)—P(18)—C(19)—C(20) [53.3 (2.0)°], C(25)—P(18)—C(19)—C(24) [−127.6 (1.9)°], C(26)—

Table 3. Selected bond lengths (Å) and angles (°)

Pt(1)—Cl(4)	2.442(5)	P(6)—C(9)	1.797(16)
Pt(1)—Cl(5)	2.332(5)	P(6)—C(15)	1.815(25)
Pt(1)—S(2)	2.275(4)	P(6)—C(16)	1.818(27)
Pt(1)—P(6)	2.214(5)	P(18)—C(19)	1.802(17)
Pt(3)—Cl(4)	2.463(4)	P(18)—C(25)	1.779(14)
Pt(3)—Cl(17)	2.334(5)	P(18)—C(26)	1.809(27)
Pt(3)—S(2)	2.267(4)	S(2)—C(7)	1.823(18)
Pt(3)—P(18)	2.230(4)	C(7)—C(8)	1.517(37)
Pt(1)—Pt(3)	3.299(1)		

Cl(4)—Pt(1)—S(2)	83.0(2)	Cl(4)—Pt(3)—S(2)	82.7(2)
Cl(5)—Pt(1)—P(6)	92.5(2)	Cl(17)—Pt(3)—P(18)	88.5(2)
S(2)—Pt(1)—P(6)	91.8(2)	S(2)—Pt(3)—P(18)	95.9(2)
Cl(4)—Pt(1)—Cl(5)	92.5(5)	Cl(4)—Pt(3)—Cl(17)	93.0(2)
Pt(1)—P(6)—C(9)	114.0(7)	Pt(3)—P(18)—C(19)	115.5(7)
Pt(1)—P(6)—C(15)	109.1(8)	Pt(3)—P(18)—C(25)	116.1(9)
Pt(1)—P(6)—C(16)	116.8(8)	Pt(3)—P(18)—C(26)	110.2(9)
C(9)—P(6)—C(15)	107.4(9)	C(19)—P(18)—C(25)	103.6(10)
C(9)—P(6)—C(16)	104.3(9)	C(19)—P(18)—C(26)	107.1(10)
C(15)—P(6)—C(16)	104.6(10)	C(25)—P(18)—C(26)	103.2(12)
Pt(1)—S(2)—C(7)	102.4(8)	Pt(3)—S(2)—C(7)	103.3(8)
Pt(1)—Cl(4)—Pt(3)	84.5(2)	Pt(1)—S(2)—Pt(3)	93.1(2)
S(2)—C(7)—C(8)	108.1(16)		

$\langle C—C \rangle_{av}$ bond length in phenyl rings 1.370(33) Å.

P(18)—C(19)—C(20) [162.8 (1.7)°] and C(26)—P(18)—C(19)—C(24) [−18.1 (2.0)°]. A similar conformation has been reported for di-μ-chlorodi(propionyl) bis (dimethylphenylphosphine)diplatinum (II).[16] These values show that the deviations of one of the methyl groups from the PPh plane are different at the two ends of the molecule, one end being distinctly more planar than the other. The two phenyl rings are inclined to each other at 129.6(9)°. The ethyl group on S(2) adopts the axial position relative to the mean plane through the Pt(1), Cl(4), S(2), Pt(3) atoms with the methylene carbon [C(7)] staggered with respect to Pt(3), as reflected by the values of the torsion angles. The Pt—S—Cl—Pt bridge is non-planar with an interplanar angle between the two platinum coordination planes of 135.6(5)°. This is in agreement with the value observed for $[Pt_2Cl_2(\mu\text{-}SEt)_2(PPr_3)_2]$ where the corresponding angle[3] is 130°. An ORTEP view of the unit cell contents is shown in Fig. 2. Most of the aforementioned results are analogous to those of the palladium derivative[18b] and the two structures appear to be isomorphous.

A few bridge cleavage reactions of phenylthio-bridged complexes have been carried out and monitored by $^{31}P\{^1H\}$ NMR spectroscopy. The products formed were identified by comparison of the observed chemical shifts and coupling constants with those reported previously.[8,9,15] The phenylthio-bridged complexes undergo bridge cleavage reactions more readily than the corresponding alkylthio complexes. Pyridine cleaves the μ-chloro-μ-phenylthio bridge readily. The $^{31}P\{^1H\}$ NMR spectra of the reactions of pyridine with $[Pt_2Cl_2(\mu\text{-}Cl)(\mu\text{-}SPh)(PR_3)_2]$ ($PR_3 = PBu_3$, PMe_2Ph) in $CDCl_3$, obtained immediately after mixing, showed resonances assignable to three molecular species, viz. $[Pt_2Cl_2(\mu\text{-}SPh)_2(PR_3)_2]$, *trans*-$[PtCl_2(py)(PR_3)]$ and $[PtCl(SPh)(py)(PR_3)]$. The concentration of *trans*-$[PtCl_2(py)(PR_3)]$ did not change with time, but the mononuclear complex $[PtCl(SPh)(py)(PR_3)]$, phosphine *trans* to pyridine [PBu_3: δ −4.6 ppm, ^1J(Pt—P) 3502 Hz; PMe_2Ph: δ −20.8 ppm, ^1J(Pt—P) 3580 Hz], established equilibrium within 10–15 h with the di-μ-phenylthio complex, since even after a week no change in their concentrations was noticed. The relative ratio of the three species from ^{31}P NMR integration was approximately 2.7 : 1.7 : 1.0 (PBu_3) and 2.5 : 1.1 : 1.2 (PMe_2Ph).

A similar bridge cleavage reaction of $[Pt_2Cl_2(\mu\text{-}SPh)_2(PBu_3)_2]$ with 2 mole equivalents of $AsPh_3$ in $CDCl_3$ gave four products, *trans*- and *cis*-$[PtCl_2(AsPh_3)(PBu_3)]$ [δ 3.4 ppm, ^1J(Pt—P) 3054 Hz; δ −3.3 ppm, ^1J(Pt—P) 3341 Hz], [PtCl(SPh)

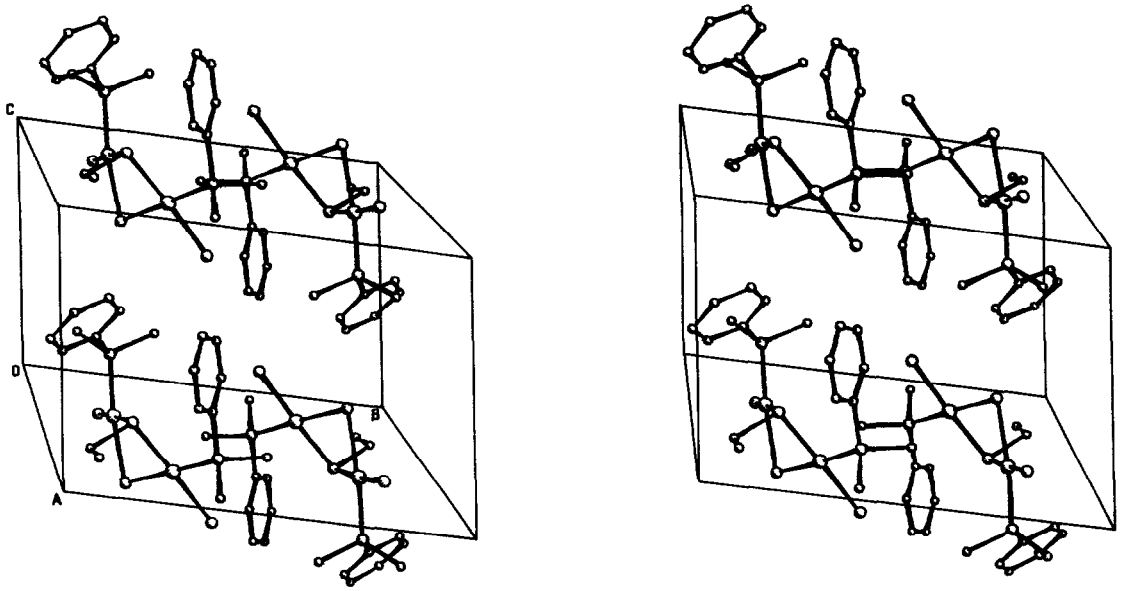

Fig. 2. ORTEP view of the unit cell contents.

$(AsPh_3)(PBu_3)]$ [δ 6.6; 0.4 ppm, ^1J(Pt—P) 3937 Hz]. After 20 h only three products, the former two and *sym trans*-$[Pt_2Cl_2(\mu\text{-}SPh)_2(PBu_3)_2]$, existed in solution and no further change was noticed even after 3 days.

A ^{31}P NMR spectrum obtained immediately after mixing an excess of pyridine with a $CDCl_3$ solution of $[Pt_2Cl_2(\mu\text{-}SPh)_2(PBu_3)_2]$ showed the formation of $[PtCl(SPh)(py)(PBu_3)]$ [δ −4.6 ppm, ^1J(Pt—P) 3504 Hz] and within a few hours (4–6) an equilibrium was established, the two being in an approximately 1:2.8 ratio, as no change was observed even after 4 days. Removal of pyridine *in vacuo* gave the parent complex quantitatively. This is in contrast to the alkylthio-bridged dinuclear platinum(II) compounds which are inert to such ligands.[1,8,9]

EXPERIMENTAL

The complexes $[Pt_2Cl_2(\mu\text{-}Cl)_2(PR_3)_2]$ [PR_3 = PBu_3, PMe_2Ph, PPh_3, $P(p\text{-tol})_3$] were prepared according to literature methods.[19–21] Methods and spectroscopic techniques are similar to those described previously.[9,10]

Preparation of $[Pt_2Cl_2(\mu\text{-}SPh)_2(PR_3)_2]$

(a) To a benzene solution of $[Pt_2Cl_2(\mu\text{-}Cl)_2(PBu_3)_2]$ (406 mg, 0.43 mmol), excess pyridine (0.2 cm^3) was added and the reaction mixture was stirred at room temperature for 30 min. To this, a benzene solution (~ 5 cm^3) of benzenethiol (95 mg, 0.86 mmol) was added and the mixture was heated at ~ 60°C with stirring for 2 h. After cooling, the solvents were stripped off *in vacuo* leaving a pasty mass which was extracted from benzene, and recrystallized from benzene–hexane in 62% yield (289 mg).

(b) To a dichloromethane solution (20 cm^3) of $[Pt_2Cl_2(\mu\text{-}Cl)_2(PMe_2Ph)_2]$ (142 mg, 0.17 mmol), benzenethiol (39 mg, 0.35 mmol) was added and the reactants were stirred at room temperature for 2 h. The solvent was reduced to 5 cm^3, and an equal amount of methanol was added to give pale yellow crystals (141 mg, 84%).

Similar reactions in 1:1 stoichiometry gave chloro/phenylthio-bridged complexes. The di-μ-SPr^i complexes were prepared by a method similar to the one described previously.[8,9]

Preparation of $[Pt_2Cl_2(\mu\text{-}Cl)(\mu\text{-}SPh)(PBu_3)_2]$

Benzene solutions containing $[Pt_2Cl_2(\mu\text{-}SPh)_2(PBu_3)_2]$ (120 mg, 0.11 mmol) and $[Pt_2Cl_2(\mu\text{-}Cl)_2(PBu_3)_2]$ (106 mg, 0.11 mmol) were mixed and heated under reflux for 3 h. Concentrating to 5 cm^3 under reduced pressure and addition of 10 cm^3 of hexane gave pale yellow crystals in 90% yield (205 mg). Similarly, the complex $[Pt_2Cl_2(\mu\text{-}Cl)(\mu\text{-}SEt)(PMe_2Ph)_2]$ was prepared and characterizing data are reported elsewhere.[9]

Bridge cleavage reactions

Pyridine (0.5 cm^3) or a $CDCl_3$ solution of 2 mole equivalents of $AsPh_3$ was added to a $CDCl_3$ solu-

tion of dinuclear platinum(II) complexes (90–120 mg) in an NMR tube and the progress of the reaction was monitored by $^{31}P\{^{1}H\}$ NMR spectroscopy.

Crystal data

$C_{18}H_{27}Cl_3P_2SPt_2$, Mol. wt 833.4, triclinic, space group $P\bar{1}$, $a = 10.412(1)$, $b = 13.782(1)$, $c = 9.325(1)$ Å, $\alpha = 98.00(1)$, $\beta = 112.26(2)$, $\gamma = 80.29(1)°$, $V = 1219.2$ Å^3, $Z = 2$, $D_c = 2.264$ g cm^{-3}, $D_m = 2.273$ g cm^{-3} (flotation technique, solvents: $CHBr_3$ and CH_3I), $\mu = 126.9$ cm^{-1}, $F(000) = 767.9$.

Data collection

Intensity data for 4290 reflections (crystal size: $0.3 \times 0.32 \times 0.34$ mm) were collected on an Enraf–Nonius CAD-4 diffractometer using graphite monochromatized Mo-K_α ($\lambda = 0.71068$ Å) radiation in the range $3 < 2\theta < 53°$ employing zigzag mode of data collection. Three control reflections were monitored after every 200 reflections (maximum decay = 0.70% during data collection which was corrected during data reduction). Data were corrected for Lorentz, polarization and absorption effects. The unit cell dimensions were refined using 25 arbitrarily chosen higher order reflections around θ of 15–16°.

Structure solution and refinement

A three-dimensional sharpened origin removed Patterson map yielded the positions of the platinum atoms. The least-squares method alternated with difference Fourier synthesis gave the positions of all the non-hydrogen atoms. A weighted anisotropic refinement of all the non-hydrogen atoms using BLOKLS, while keeping the hydrogen atoms in stereochemically acceptable positions, with a unit weighting scheme modified by the Dunitz–Seiler weighting scheme, gave final R and R_w values of 0.055 and 0.067, respectively. The refinement was deemed to be over when the shift-to-error ratio in scale and, positional and thermal parameters of non-hydrogen atoms reached 0.01. The final difference map has ripples of 1.68–1.00 Å around the heavy atoms. The scattering factors for platinum, phosphorus, sulphur and chlorine were taken from Vol. IV of the *International Tables for X-ray Crystallography*,[22] while those of hydrogen were taken from Stewart *et al.*[23] All the computations were carried out using the SDP package available for PDP-11/73.[24]*

Acknowledgements—Thanks are expressed to Dr J. P. Mittal, Head, Chemistry Division, BARC and Professor M. M. Taqui Khan, Director, CSMCRI, Bhavnagar for their interest in this work and the Analytical Chemistry Division, BARC for the microanalysis. Thanks are also expressed to Mr V. S. Jakkal and Mr K. V. Muralidharan of the Applied Chemistry Division for helpful discussions.

REFERENCES

1. J. Chatt and F. A. Hart, *J. Chem. Soc.* 1953, 2363; 1960, 2807; J. Chatt and J. M. Davidson, *J. Chem. Soc.* 1964, 2433.
2. P. L. Goggin, R. J. Goodfellow and F. J. S. Reed, *J. Chem. Soc. A* 1971, 2031.
3. M. C. Hall, J. A. S. Jarvis, B. T. Kilbourn and P. G. Owston, *J. Chem. Soc., Dalton Trans.* 1972, 1544.
4. P. H. Bird, U. Siriwardane, R. D. Lai and A. Shaver, *Can. J. Chem.* 1982, **60**, 2075; J. Soulie, J. Y. Lallemand and R. C. Rao, *Org. Magn. Res.* 1979, **12**, 67.
5. K. R. Dixon, K. C. Moss and M. A. R. Smith, *J. Chem. Soc., Dalton Trans.* 1974, 971.
6. C. E. Briant, C. J. Gardner, T. S. A. Hor, N. D. Howells and D. M. P. Mingos, *J. Chem. Soc., Dalton Trans.* 1984, 2645.
7. M. P. Brown, R. J. Puddephatt and C. E. E. Upton, *J. Chem. Soc., Dalton Trans.* 1976, 2490.
8. H. C. Clark, V. K. Jain and G. S. Rao, *J. Organomet. Chem.* 1985, **279**, 181.
9. V. K. Jain and G. S. Rao, *Inorg. Chim. Acta* 1987, **127**, 161.
10. V. K. Jain, *Inorg. Chim. Acta* 1987, **133**, 261.
11. C. K. Johnson, ORTEP II, Report ORNL-3794. Oak Ridge National Laboratory, Tennessee (1970).
12. S. F. Watkins, *J. Chem. Soc. A* 1970, 168.
13. M. Black, R. H. B. Mais and P. G. Owston, *Acta Cryst.* 1969, **B25**, 1760.
14. R. Mason, M. Textor, N. Al-Saleem and B. L. Shaw, *J. Chem. Soc., Chem. Commun.* 1976, 292; A. B. Goel, S. Goel and D. Vanderveer, *Inorg. Chim. Acta* 1981, **51**, 1267.
15. H. C. Clark, G. Ferguson, V. K. Jain and M. Parvez, *Inorg. Chem.* 1981, **24**, 1477.
16. G. K. Anderson, R. J. Cross, L. Manojlovic-Muir, K. W. Muir and T. Solomun, *J. Organomet. Chem.* 1979, **170**, 385.
17. D. L. Sales, J. Stokes and P. Weedward, *J. Chem. Soc. A* 1968, 1858.
18. (a) A. T. McPhail and G. A. Sim, *J. Chem. Soc. A* 1968, 1858; (b) V. K. Jain, R. P. Patel, K. V. Muralidharan and R. Bohra, *Polyhedron* 1989, **8**, 2151.

* Tables of fractional coordinates, anisotropic thermal parameters, hydrogen atom parameters, torsion angles, planes and F_o/F_c data have been deposited with the Editor.

19. R. J. Goodfellow and L. M. Venanzi, *J. Chem. Soc.* 1965, 7533.
20. A. C. Smithies, M. Rycheck and M. Orchin, *J. Organomet. Chem.* 1968, **12**, 199.
21. F. R. Hartley and G. W. Searle, *Inorg. Chem.* 1973, **12**, 1949.
22. *International Tables for X-ray Crystallography*, Vol. IV. Kynoch Press, Birmingham (1974). (Present Distributor: D. Reidel, Dordrecht.)
23. R. F. Stewart, E. R. Davidson and W. T. Simpson, *J. Chem. Phys.* 1965, **42**, 3175.
24. Enraf–Nonius, Structure Determination Package. Enraf-Nonius, Delft, The Netherlands (1983).

Polyhedron Vol. 10, No. 8, pp. 859–865, 1991
Printed in Great Britain

0277–5387/91 $3.00+.00
© 1991 Pergamon Press plc

PREPARATION AND CHARACTERIZATION OF A $[Ni(en)_2]^{2+}$ COMPLEX OF PERMETHYLPOLYAZINE

WILLIAM B. EULER

Department of Chemistry, University of Rhode Island, Kingston, RI 02881, U.S.A.

(*Received* 2 *November* 1990; *accepted* 4 *January* 1991)

Abstract—The bis(ethylenediamine)nickel(II) complex of permethylpolyazine is reported. The synthetic method used gives a polymer with alternate di-imine sites complexed to the metal ion. IR spectra of the monomer and polymer metal complexes are similar and demonstrate that interaction with the metal has changed the polymer geometry from all-*trans* to a mixture of *cis* and *trans* bonds. ^{1}H NMR spectra show that the ethylenediamine chelate rings attain several conformations in the monomer metal complex, but that one ring conformation dominates in the polymer. The UV–vis spectrum of the monomer metal complex shows *d–d*, π–π^* and MLCT bands, but in the polymer complex the *d–d* transitions are lost in the tails of the MLCT bands. This is consistent with band formation in the polyazine ligand.

Polyazines, $[N{=}C(R){-}C(R){=}N]_x$ (PAZ), are conjugated polymers that can be doped with iodine into highly conducting materials.[1] This is not especially surprising since polyazines are formally isoelectronic to the prototype conducting polymer, polyacetylene.[2] However, unlike polyacetylene, polyazine (with any R group) is environmentally stable.

Polyazine is amenable to a variety of chemical modifications. Like typical organic polymers, variation of the substituent groups at the carbon sites leads to polymers with different characteristics.[3–6] Long alkyl (propyl) groups can be used to give the polymer solubility in organic solvents,[4] thereby allowing films to be cast. Methyl substituents lead to polymers with the best conductivity,[1] while the completely unsubstituted polyazine is laden with saturated defects[5–7] leading to materials with low conductivity.

Use of the nitrogen atom in the polymer chain as a site of chemical modification has not been previously reported. Although the imine nitrogens are not useful as points of organic substitution, chelation of metal ions to di-imines is well known.[8] The repeat unit in polyazine is indeed a di-imine and thus should be usable as a ligand for the metal ions. However, direct reaction of a metal ion with polyazine is unsuccessful because the polymer is in the all-*trans* conformation (double bonds *E* and single bonds s-*trans*) which is unacceptable for formation of the five-membered chelate ring. Rather, a metal complex with the appropriate monomer ligand must be prepared and this is then polymerized to give the metal-containing polyazine.

The presence of the metal ion may have a number of effects on the polyazine. Certainly, the electronic structure of the conjugated π system must be perturbed which should effect the spectroscopic, oxidative and conductivity properties of the material. If a magnetic metal is used, long range interactions may lead to either antiferromagnetism or ferromagnetism (and perhaps these may be adjustable properties). Finally, a polymer-bound metal complex may be useful for catalysis purposes.

This paper reports the preparation and characterization of a bis(ethylenediamine)nickel(II) complex bound to permethylpolyazine. To achieve this polymer, the bis(ethylenediamine)mono(2,3-butanedionedihydrazone)nickel(II) complex is prepared and then this is polymerized to give the product. Dihydrazones are good ligands and are known to form bis and tris complexes with a number of metal ions.[9,10] However, a monohydrazone complex is required so that a linear, non-crosslinked polyazine can be formed. The permethyl derivative of polyazine is chosen so that a defect free linear π system will be formed. The IR, ^{1}H NMR and UV–vis spectroscopies are discussed in this paper.

EXPERIMENTAL

All starting materials were reagent grade and used as received. Hydrazine hydrate and 2,3-butanedione were obtained from Aldrich and nickel chloride hexahydrate was obtained from Allied Chemical. Elemental analyses were determined by M–H–W Laboratories, Phoenix, Arizona.

$[Ni(en)_2(BDDH)]Cl_2 \cdot 2.5H_2O$

Bis(ethylenediamine)nickel(II) chloride dihydrate[11] and 2,3-butanedionedihydrazone[1] (BDDH) were prepared by literature procedures. The nickel complex (2.00 g, 7.00 mmol) was dissolved in methanol (50 cm^3); water (1 cm^3) was added to ensure complete dissolution. To this was added freshly recrystallized BDDH (0.80 g, 7.0 mmol). The mixture was brought to the boil for *ca* 10 min, and then the solvent was removed *in vacuo* at room temperature to quantitatively give a red–brown, slightly hygroscopic, water-soluble powder. Found: C, 23.7; H, 7.2; N, 27.3; Cl, 17.1. Calc. for $NiC_8H_{26}N_8Cl_2 \cdot 2.5H_2O$: C, 23.5; H, 7.6; N, 27.4; Cl, 17.3%. Magnetic susceptibility: $\mu = 3.18$ BM at 20°C.

$[Ni(en)_2(C_8H_{12}N_4)Cl_2 \cdot 4H_2O]_x$

$[Ni(en)_2(BDDH)]Cl_2 \cdot 2.5H_2O$ (1.00 g, 2.44 mmol) was dissolved in methanol (10 cm^3) and brought to reflux. A solution of 2,3-butanedione (0.20 cm^3, 2.3 mmol) in methanol (5 cm^3) was added dropwise to the refluxing nickel solution over the course of *ca* 10 min. This caused the solution to change from purple to green and eventually to red. The reaction was heated and stirred for an additional 24 h. The solvent was removed *in vacuo* until the product was dry. The black, water-soluble powder is very hygroscopic and must be kept under desiccant. The yield is quantitative. Found: C, 30.7; H, 6.8; N, 22.8; Cl, 14.2. Calc. for $CH_3C(O)[NiC_{12}H_{26}N_8Cl_2 \cdot 4H_2O]_{6.2}C(O)CH_3$: C, 30.4; H, 7.3; N, 22.4; Cl, 14.2%. Magnetic susceptibility: $\mu = 3.10$ BM at 26°C.

Instrumentation

IR spectra were run as KBr pellets between 300 and 4000 cm^{-1} on a Perkin–Elmer 1430 Ratio Recording Infrared spectrophotometer. NMR spectra were run in D_2O at room temperature on a Bruker AM300 spectrometer at 300 MHz. Magnetic susceptibilities were measured on a home-built Gouy balance at room temperature using $HgCo(SCN)_4$ as a reference. UV–vis spectra were run between 200 and 1100 nm on a Perkin–Elmer Lambda 2 spectrophotometer.

Extended Hückel calculations

Standard parameters were used for carbon and nitrogen[12] atoms, while the values for nickel were taken from Whangbo and Stewart.[13] Bond lengths were estimated as follows:[14,15] C=N, 1.30 Å; C—C, 1.50 Å; N—N, 1.45 Å; and Ni—N, 1.84 Å. Only nearest neighbour overlaps were considered, so that the issue of *cis* and *trans* geometry is avoided. Orbitals are labelled in the C_{2v} point group as is appropriate for these complexes.

RESULTS AND DISCUSSION

Synthesis

Preparation of the nickel-containing polymer can not be accomplished using the uncomplexed polyazine as a reactant (all attempts using nickel salts with uncomplexed permethylpolyazine gave no reaction). This is because the free polymer is in the all-*trans* conformation, which is not amenable to chelation, and the complexation reaction does not provide sufficient driving energy to rotate large chain segments as would be required in this polymer. Rather, a monohydrazone metal complex is prepared that can then be condensed in the usual fashion with a diketone to form the complexed polyazine. In this manner, a nickel ion is placed at every other potential chelating position along the polyazine chain.

The monohydrazone complex is prepared by reacting one equivalent of BDDH with one equivalent of *trans*-dichlorobis(ethylenediamine) nickel(II):

$$\textit{trans}\text{-}[Ni(en)_2Cl_2] + BDDH \rightarrow [Ni(en)_2(BDDH)]Cl_2.$$

Although the nickel complex is in the *trans* conformation, the coordination sphere is sufficiently labile for the necessary ligand exchange to occur [the bis(ethylenediamine)nickel(II) chloride is prepared by ligand exchange between tris(ethylenediamine)nickel(II) and hexa-aquanickel(II)[11].] The product complex can form in a number of geometrical and optical isomers, several of which are observed in the ^1H NMR.

Polymerization of the monohydrazone nickel complex results via a condensation with 2,3-butanedione. The terminal amino groups of the dihydrazone ligand which are not involved in bonding to the metal are free to react with the diketone

similar to any other condensation that forms a polyazine:[1]

$$[Ni(en)_2(BDDH)]Cl_2 + CH_3C(O)C(O)CH_3 \rightarrow [Ni(en)_2(C_8H_{12}N_4)Cl_2]_x + H_2O.$$

This leads to a polymer with half of the N=C—C=N units acting as chelates bound to a nickel ion forcing a s-*cis* C—C bond. These nickel-bound di-imine sites alternate with free di-imine units. Elemental analysis (using an end group analysis, with carbonyl end groups indicated) suggests an average chain length of about 12.5 di-imine repeat units, shorter than the degree of polymerization (about 45 repeat units) found in the uncomplexed polymer.

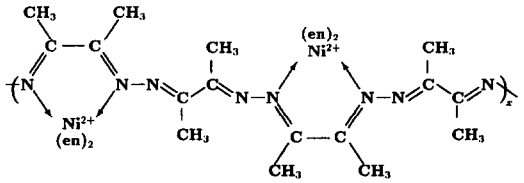

The binding of a metal ion to polyazine should cause a drastic change in the geometry of the polymer chain. In the uncomplexed polymer the chain is found in the all-*trans* conformation. Upon complexation to the metal ion several of the bonds along the chain rotate to *cis* (all the double bonds are still *E* but the C—C in the chelate ring and the N—N are s-*cis* while the C—C not involved in complexation probably remains s-*trans*), as shown above. The N—N bonds at uncomplexed imine sites attain s-*cis* conformation because of repulsion between the substituent methyl group and ethylenediamine (en) ligands bound to the nickel ion (as indicated by molecular models).

IR spectroscopy

The major assigned IR bands are summarized in Table 1 for the materials reported here, as well as relevant comparison compounds. The N—H stretching region is diagnostic of the various species. The s-*trans* BDDH has two sharp bands in this region, while $[Ni(BDDH)_3]Cl_2$, which has s-*cis* BDDH ligands, has three sharp bands. In contrast, $[Ni(en)_2(BDDH)]Cl_2 \cdot 2.5H_2O$ has a broad band in this spectral area with five distinct peaks that are poorly resolved. This is a reflection of the different types of N—H bonds found in the en and BDDH ligands. Finally, the metal polymer complex only has a single, broad peak at these energies, consistent with the multiple sites expected in polymeric material.

The C—CH_3 deformation is especially useful in assessing the geometric characteristics of these materials. The C—CH_3 deformation is found at 1355 cm^{-1} for both BDDH and the uncomplexed polyazine; this shows that the local geometry about the H_3C—C—C—CH_3 bonds are the same in both compounds, i.e. s-*trans*.[1] In contrast, $[Ni(BDDH)_3]Cl_2$, which must have the C—C bond in the s-*cis* conformation, has two peaks at higher energy than the uncomplexed ligand. Finally, the polymer has bands attributable to both s-*cis* (1380 cm^{-1}) and s-*trans* conformations (1350 cm^{-1}), consistent with the conformations suggested previously.

Table 1. Major IR absorptions; values given in cm^{-1}

	NH_2 stretch	NH_2 int. deformation	C=N stretch	C—CH_3 deformation
BDDH	3185 3325	1630	1560	1355
$[Ni(BDDH)_3]Cl_2$[a]	3180 3395 3460	1655	1610	1365sh 1375
$[Ni(en)_2(BDDH)]Cl_2 \cdot 2.5H_2O$	3180 3255 3300 3350 3500	1595 1620 1650	1610	1375
$[Ni(en)_2(C_8H_{12}N_4)Cl_2 \cdot 4H_2O]_x$	3300br	1600br		1350sh 1380
$(C_4H_6N_2)_x$			1585	1355

[a] In agreement with ref. 10.
sh = shoulder, br = broad.

The assignments of the NH_2 internal deformation and the C=N stretch for $[Ni(en)_2(BDDH)]Cl_2 \cdot 2.5H_2O$ are ambiguous: complete deuteriation of the amino protons could not be achieved in this complex so that an unambiguous assignment of the C=N band is not possible. $[Ni(en)_3]Cl_2$ has a pair of bands centred around 1600 cm,$^{-1}$ so the assignments in Table 1 are tentatively given. The polymer complex has a single broad band centred at 1600 cm^{-1} that originates from both NH_2 and C=N vibrations.

Several absorptions that are characteristic of the chelated en ring can also be identified. $[Ni(en)_3]Cl_2$ has peaks at 2895, 2950 and 2970 cm^{-1} due to C—H stretches, a peak at 1465 cm^{-1} due to CH_2 scissoring, and peaks at 500 and 530 cm^{-1} due to chelate ring deformation.[16] Similar absorptions can be found in $[Ni(en)_2(BDDH)]Cl_2$ and the polymer complex also. The monomer has peaks characteristic of C—H stretches at 2900, 2960 and 2980 cm,$^{-1}$ a strong peak at 1455 cm^{-1} associated with the CH_2 scissor, and the chelate ring deformation peaks are found at 505 and 530 cm^{-1}. The polymer complex is slightly different because of the long chain nature of the material. The sharp peak at 2895 cm^{-1} is still present in the polymer but the characteristic doublet at higher energy in the monomer is found as a single broad peak centred at 2960 cm.$^{-1}$ These are the C—H stretching vibrations. The peak due to the CH_2 scissoring motion is found at 1450 cm,$^{-1}$ and has a similar line shape as the monomer. Finally, a peak at 520 cm^{-1} is accompanied by only a very weak shoulder at 500 cm^{-1}; these are attributed to the chelate ring deformation. Although some differences occur, vibrations due to chelated en are still observed in the polymer complex indicating that the polymerization condensation indeed occurred with BDDH amino groups and not with en amino groups.

^1H *NMR*

All of the compounds studied here have chemical shifts and line widths typical of paramagnetic nickel complexes.[17,18] Two well separated types of protons are found in these materials, either due to CH_3 substituents on the BDDH ligand, observed upfield of TMS, or CH_2 groups found in the en ligand, detected downfield of TMS. The amino protons from either en or BDDH are not observed, probably because of large line widths arising from a combination of exchange and paramagnetic effects. The chemical shifts are reported in Table 2. Multiple resonances are seen in some cases, reflecting the existence of different ring conformations that exist for these complexes in solution.

Table 2. Chemical shifts for ^1H NMR reported vs TMS. All spectra were run at room temperature at 300 MHz in D_2O

	CH_3	CH_2
$[Ni(en)_3]^{2+}$ [a]		78.2
		118.4
$[Ni(en)_2Cl_2]$ [a]		99.0
$[Ni(BDDH)_3]^{2+}$	−10.3	
$[Ni(en)_2(BDDH)]^{2+}$	−1.1	103.2
	−2.6	
	−4.7	
	−6.4	
$[Ni(en)_2(C_8H_{12}N_8)^{2+}]_x$	−8.0	95.7

[a] In agreement with ref. 18.

The model compounds, $[Ni(en)_3]Cl_2$, $[Ni(en)_2Cl_2]$ and $[Ni(BDDH)_3]Cl_2$, all have simple spectra in D_2O solution. The tris-en complex has two resonances due to CH_2 protons, interpreted as arising from two different geometrical isomers.[18] The bis-en complex (which is undoubtedly a *trans*-diaqua species in solution) has a single CH_2 resonance.[19] The tris-BDDH complex also displays a single peak, due to the CH_3 groups. The resonances from the two optical isomers are not resolved. The mixed ligand complex, $[Ni(en)_2(BDDH)]Cl_2$, has several peaks in the CH_3 region but a single peak due to CH_2 protons. The peak due to the CH_2 groups is similar to the previous examples, but the resonances from the CH_3 groups are shifted 4–9 ppm downfield relative to the tris-BDDH complex. Clearly, several conformations exist in solution and the CH_3 protons are excellent remote probes of these geometries. Finally, the polymer complex has a relatively simple NMR spectrum: a single, broad peak in both the CH_2 and CH_3 region. It is reasonable that a single conformation of the en chelate rings is found in the polymer, since interactions with the main chain backbone restrict access to the other ring conformations.

UV–vis spectroscopy

The nickel complexes all have two distinct spectral regions. Low intensity *d–d* transitions are observed in the visible and near-IR. In the UV, intense π–π^* and MLCT bands are seen. Each of these spectral regions will be discussed separately.

The visible and near-IR transitions for $[Ni(en)_2(BDDH)]^{2+}$ and $[Ni(en)_2(C_8H_{12}N_4)]_x^{2+}$ are

Table 3. *d–d* Transitions given in cm^{-1} (molar extinction coefficients are given in parentheses) using the O_h notation

	$^3T_{2g}$	$^3A_{2g}$ ^1E_g	$^3T_{1g}(F)$	*Dq*	*B*
$[Ni(en)_3]^{2+}$ [a]	11,300 (6)	12,800sh (3)	18,300 (6)	1180	790
$[Ni(BDDH)_3]^{2+}$ [b]	12,800 (9)	11,800sh (7)	20,200 (21)	1250	1070
$[Ni(en)_2(BDDH)]^{2+}$	11,300 (8)	12,500sh (4)	18,900 (10	1170	1000
$[Ni(en)_2(C_8H_{12}N_4)]_x^{2+}$	11,100sh (13)			1110	

[a] In agreement with ref. 19.
[b] In agreement with ref. 20.

summarized in Table 3. For comparison purposes, the *d–d* transitions for $[Ni(en)_3]^{2+}$[19] and $[Ni(BDDH)_3]^{2+}$[20] are also given in Table 3. The Racah *B* parameter is found using the equations of Dou.[21] The values for *Dq* are found using the procedure of Jorgensen,[19] where $10Dq$ is found from the weighted average of the two lowest energy transitions. This weighting procedure was found necessary in order to obtain a reasonable value of *B* for the $[Ni(en)_2(BDDH)]^{2+}$ complex. For the polymer complex, the lowest energy transition is seen only as a broad shoulder on the tail of the intense UV band, and therefore a rather large error is associated with the value of *Dq*.

The UV spectra of BDDH and the metal complexes $[Ni(BDDH)_3]$,$^{2+}$ $[Ni(en)_2(BDDH)]^{2+}$ and $[Ni(en)_2(C_8H_{12}N_4)]_x^{2+}$ are shown in Fig. 1. In water, the ligand has a single transition at 38,200 cm^{-1} ($\varepsilon = 14{,}000$ dm^3 mol^{-1} cm^{-1}) (similar to the spectrum in chloroform reported earlier[4]). Complexation of Ni^{2+} with three BDDH ligands to form $[Ni(BDDH)_3]^{2+}$ gives a spectrum with a strong band at about the same energy as the ligand, 38,000 cm^{-1} ($\varepsilon = 22{,}000$ dm^3 mol^{-1} cm^{-1}), and a shoulder at 33,300 cm^{-1} ($\varepsilon = 12{,}000$ dm^3 mol^{-1} cm^{-1}). $[Ni(en)_2(BDDH)]^{2+}$ shows similar features [a peak at 37,900 cm^{-1} ($\varepsilon = 8800$ dm^3 mol^{-1} cm^{-1}) and a shoulder at 33,300 cm^{-1} ($\varepsilon = 8400$ dm^3 mol^{-1} cm^{-1})], although the relative intensity of the shoulder is nearly as great as the main peak. The polymer complex, $[Ni(en)_2(C_8H_{12}N_4)]_x^{2+}$, is similar to the monomer but with extra shoulders and a much longer tail in the visible [a peak at 38,100 cm^{-1} ($\varepsilon = 8400$ dm^3 mol^{-1} cm^{-1}) and shoulders at 33,300 cm^{-1} ($\varepsilon = 7000$ dm^3 mol^{-1} cm^{-1}) and 27,800 cm^{-1} ($\varepsilon = 2400$ dm^3 mol^{-1} cm^{-1})].

The assignment of these peaks is made using the energy level diagrams shown in Fig. 2. These energy levels were found by using Extended Hückel calculations on the orbitals of π symmetry on the fragments shown in Fig. 2. The effects of the ethylene-

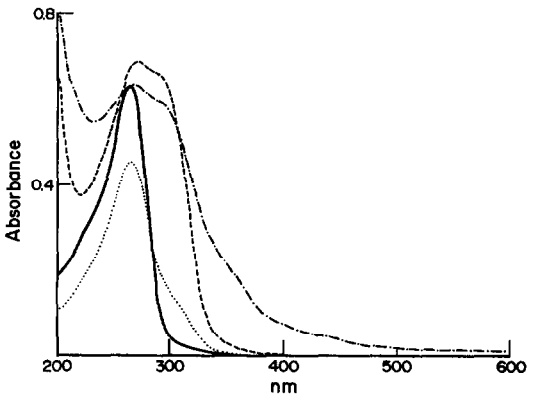

Fig. 1. UV spectra of aqueous solutions of BDDH (solid), $[Ni(BDDH)_3]^{2+}$ (dotted), $[Ni(en)_2(BDDH)]^{2+}$ (dashed) and $[Ni^{2+}(en)_2(C_8H_{12}N_4)]_x$ (dot–dash).

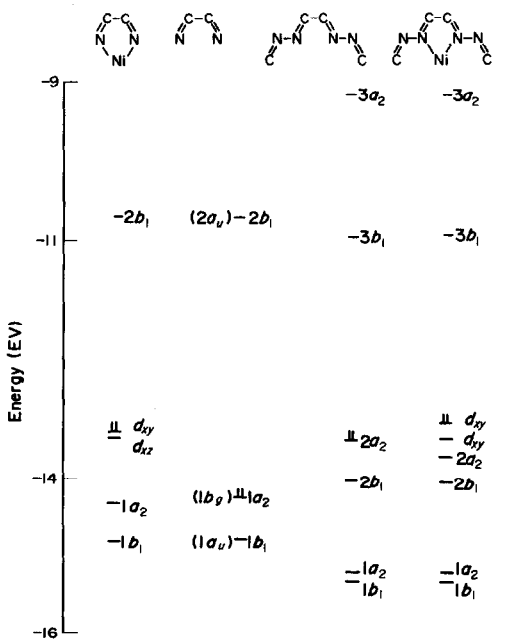

Fig. 2. Energy level diagram of the π systems for di-imine and nickel di-imine fragments.

diamine ligands and methyl groups on BDDH were ignored. The energy level diagram for the ligands is as reported previously,[14,15] while the inclusion of the metal orbitals only causes minor perturbations.

In the solid state BDDH has a s-*trans* conformation (point group C_{2h}), as determined X-ray crystallographically,[1] and the UV spectrum suggests that this geometry is retained in solution. The only allowed π–π^* transition for the C_{2h} structure is $^1A_g \rightarrow {}^1B_u$ ($1b_g^2 \rightarrow 1b_g^1 2a_u^1$), while for the s-*cis* (C_{2v}) structure both the $^1A_1 \rightarrow {}^1B_1$ ($1a_2^2 \rightarrow 1a_2^1 2b_1^1$) and $^1A_1 \rightarrow {}^1A_1$ ($1b_1^2 \rightarrow 1b_1^1 2b_1^1$) transitions are allowed. Since only a single π–π^* transition is observed, the C_{2h} structure is maintained in solution and the 38,200 cm^{-1} transition is assigned to $^1A_g \rightarrow {}^1B_u$.

Coordination of three BDDH molecules to Ni^{2+} gives the D_3 $[Ni(BDDH)_3]^{2+}$ but, as evidenced by the analysis of the *d–d* transitions, the O_h point group is an adequate approximation for this complex. In O_h, the group orbitals analogous to the highest occupied $1a_2$ transform as t_{2g}, while the lowest unoccupied π^* orbitals transform as t_{1u}. This leads to one allowed π–π^* transition, $^1A_{1g} \rightarrow {}^1T_{1u}$ ($t_{2g}^6 \rightarrow t_{2g}^5 t_{1u}^1$), which should be at nearly the same energy as the π–π^* transition in the uncomplexed molecule. A MLCT transition from the metal e_g orbitals to the empty ligand π^* orbitals is also possible. An allowed transition, $^3A_{2g} \rightarrow {}^3T_{2u}$ ($e_g^2 \rightarrow e_g^1 t_{1u}^1$), is expected at lower energy than the π–π^* transition since the metal e_g orbitals are expected to be higher in energy than the ligand π orbitals (although the relative energy of the $^3T_{2u}$ and $^1T_{1u}$ states is unknown). Thus, the peak at 38,000 cm^{-1} is assigned as a $^1A_{1g} \rightarrow {}^1T_{1u}$ ligand π–π^* transition and the shoulder at 33,300 cm^{-1} is assigned as a $^3A_{2g} \rightarrow {}^3T_{2u}$ MLCT transition.

The UV spectrum of $[Ni(en)_2(BDDH)]^{2+}$ is similar to the spectrum of $[Ni(BDDH)_3]^{2+}$, but must be interpreted in the C_{2v} point group. Thus, the peak at 37,900 cm^{-1} is assigned to the $^1A_1 \rightarrow {}^1B_2$ ($1a_2^2 \rightarrow 1a_2^1 2b_1^1$) ligand-centred π–π^* transition and the shoulder at 33,300 cm^{-1} to the $^3A_2 \rightarrow {}^3B_2$ ($d_{xy}^2 \rightarrow d_{xy}^1 2b_1^1$) MLCT transition. The π–π^* transition $1b_1^2 \rightarrow 1b_1^1 2b_1^1$ is also allowed in this complex and may be responsible for the high energy band seen at 200 nm and below in Fig. 1. The MLCT $d_{xz}^2 \rightarrow d_{xz}^1 2b_1^1$ ($^3A_2 \rightarrow {}^3A_1$) is *not* allowed for this complex.

$[Ni(en)_2(BDDH)]^{2+}$ and $[Ni(en)_2(C_8H_{12}N_4)]_x^{2+}$ have similar UV spectra, but the polymer spectrum has additional low energy shoulders and a considerably more intense tail throughout the visible region. This is consistent with band formation in the π system of the ligand. The features of the polymer at 38,100 and 33,300 cm^{-1} have the same assignments as $[Ni(en)_2(BDDH)]^{2+}$ while the visible shoulders and tail are absorptions into the delocalized band of the polymer.

CONCLUSIONS

The nickel-containing polyazine reported here indicates a different method to modify the properties of conducting polymer systems. Permethylpolyazine is a yellow, insoluble material; complexation to nickel changes this to a black, water-soluble complex. IR spectroscopy demonstrates that the desired complex has been attained, but the chain geometry is quite different from the uncomplexed polyazine. ^1H NMR spectra reveal that the monomer precursor complex has a number of conformations available, but only one of these is found with any abundance in the polymer. Presumably, this is due to steric repulsions between the en ligands on the metal ion and the bulk of the polymer chain. The dark colour of the polymer complex is due to MLCT bands that have significant tails into the visible region. The breadth of these absorptions is typical of spectral transitions associated with delocalized electronic bands.

Acknowledgement—Acknowledgement is made to the donors of the Petroleum Research Fund, administered by the American Chemical Society, for support of this work.

REFERENCES

1. C. R. Hauer, G. S. King, E. L. McCool, W. B. Euler, J. D. Ferrara and W. J. Youngs, *J. Am. Chem. Soc.* 1987, **109**, 5760.
2. T. A. Skotheim (Ed.), *Handbook of Conducting Polymers*. Marcel Dekker, New York (1986).
3. W. B. Euler and G. S. King, *Macromolecules* 1989, **22**, 4664.
4. W. B. Euler, *Chem. Mater.* 1990, **2**, 209.
5. W. B. Euler and B. C. Gill, Advanced organic solid state materials, *Materials Research Society Symposium Proceedings* (Edited by L. Y. Chiang, P. M. Chaikin and D. O. Cowan) 1990, **173**, 375.
6. B. Chaloner-Gill, C. J. Cheer, J. E. Roberts and W. B. Euler, *Macromolecules* 1990, **23**, 4597.
7. Y. Cao and S. Li, *J. Chem. Soc., Chem. Commun.* 1988, 937.
8. K. Vrieze, *J. Organomet. Chem.* 1986, **300**, 307.
9. R. C. Stoufer and D. H. Busch, *J. Am. Chem. Soc.* 1956, **78**, 6016.
10. R. C. Stoufer and D. H. Busch, *J. Am. Chem. Soc.* 1960, **82**, 3491.
11. H. M. State, *Inorganic Synthesis* (Edited by E. G. Rochow), Vol. VI, p. 109. McGraw-Hill, New York (1960).
12. R. Hoffmann, *J. Chem. Phys.* 1963, **39**, 1397.
13. M.-H. Whangbo and K. R. Stewart, *Isr. J. Chem.* 1983, **23**, 133.

14. W. B. Euler and C. R. Hauer, *Solid State Commun.* 1984, **51**, 473.
15. W. B. Euler, *J. Phys. Chem.* 1987, **91**, 5795.
16. Z. Gabelica, *Spectrochim. Acta* 1976, **32A**, 327.
17. R. J. Fitzgerald and R. S. Drago, *J. Am. Chem. Soc.* 1968, **90**, 2523.
18. F. F.-L. Ho and C. N. Reilley, *Analyt. Chem.* 1970, **42**, 600.
19. C. K. Jorgensen, *Acta Chem. Scand.* 1955, **9**, 1362.
20. M. A. Robinson, J. D. Curry and D. H. Busch, *Inorg. Chem.* 1963, **2**, 1178.
21. Y. Dou, *J. Chem. Educ.* 1990, **67**, 135.

Polyhedron Vol. 10, No. 8, pp. 867–872, 1991
Printed in Great Britain

0277-5387/91 $3.00+.00
© 1991 Pergamon Press plc

SYNTHESIS AND X-RAY STRUCTURAL INVESTIGATION OF *CIS*-HYDRIDO(TRIPHENYLSILYL)-1,4-BUTANEDIYL-*BIS*-(DICYCLOHEXYLPHOSPHINE)PLATINUM(II)

D. F. MULLICA* and E. L. SAPPENFIELD

Department of Chemistry, Baylor University, Waco, TX 76798, U.S.A.

and

M. J. HAMPDEN-SMITH

Department of Chemistry, University of New Mexico, Albuquerque, NM 87131, U.S.A.

(*Received* 12 *November* 1990; *accepted* 7 *January* 1991)

Abstract—The title compound was prepared by the oxidative addition of triphenylsilane to $Pt^0[1,4\text{-}(Cy_2P(CH_2)_4PCy_2)]$ (where Cy = cyclohexyl) generated *in situ*. The crystal structure of *cis*-$H(Ph_3Si)Pt[Cy_2P(CH_2)_4PCy_2]$ (**2**) has been determined by single-crystal X-ray diffraction techniques. The square planar geometry about the platinum atom is angularly distorted with a bite angle between the diphosphine ligands (P—Pt—P) of 102.3(1)°. Details of the structural content and selected bond lengths and angles are discussed and presented. The phenyl rings are planar and the cyclohexyl rings are in chair conformations. The enlarged tetrahedral angles at the phosphorus and silicon atoms are probably due to the steric bulk of the ligands. "Ligand profile" calculations ($\theta/2$ vs ϕ) have been performed to probe the steric interaction about the diphosphine and triphenylsilyl ligands.

The chemical significance of control over steric demands of substituents in stabilizing kinetically labile species is well known in all aspects of synthetic chemistry. In particular, the effects of the steric demands of phosphine ligands have been extensively studied in zero-valent complexes of the group 10 metals.[1,2] The steric demands of these ligands have been described by a number of different methods. Tolman characterized the steric bulk of a phosphine group by introducing the cone angle (θ) concept which was extended by Alyea *et al.*[3] and Richardson and Payne.[4] A new angle, ϕ, was defined as the angle of rotation about the metal–phosphorus bond. A plot of $\theta/2$ vs ϕ resulted in a "ligand profile". This profile, which resembles a silhouette of the orientated ligands, was improved by Smith and Oliver[5] by presenting a ligand profile defined by atomic coordinates from a structural analysis. The improved method is flexible enough to calculate ligand profiles for other stabilizing ligands such as AsR_3 and SiR_3.[6]

The reactivity of low coordination number, bulky phosphine-stabilized platinum(0) complexes towards oxidative addition has also been the subject of many studies. $Pt(PCy_3)_2$ was shown to undergo oxidative addition with polar C—H bonds,[7] but more recently, the highly reactive species $Pt^0(Cy_2P(CH_2)_2PCy_2)$, generated *in situ*, was established as the first example of activation of unactivated C—H bonds at a platinum(0) centre.[8] This is presumably the result of the small bite angle of the 1,2-$(Cy_2P(CH_2)_2PCy_2)$ ligand. We have previously reported the reactivity of similar *cis*-bis-phosphine and chelating diphosphine supported platinum(0) centres towards oxidative addition,[9–13] particularly with respect to correlation of chelate ligand backbone chain length with solution dynamic behaviour and reactivity.[11,14] Here we describe the synthesis and structural characterization of *cis*-$H(Ph_3Si)Pt[Cy_2P(CH_2)_4PCy_2]$ (**2**) together with ligand profiles for both the phosphine and silyl ligands.

* Author to whom correspondence should be addressed.

EXPERIMENTAL

All manipulations were carried out under an atmosphere of dry (4 Å molecular sieves) and deoxygenated (MnO) nitrogen.[15] Hydrocarbon solvents were dried and distilled from sodium benzophenone ketyl and stored under nitrogen over 4 Å molecular sieves prior to use. Deuterated NMR solvents were dried over 4 Å molecular sieves and stored under nitrogen. NMR spectra were recorded on a Bruker AC-250 NMR spectrometer. ^{1}H NMR chemical shifts were referenced to the protio impurity in the deuterated solvent. ^{31}P NMR chemical shifts were referenced to external phosphoric acid and are quoted using the downfield positive sign convention. Temperatures were calibrated using methanol and ethylene glycol standards.

Synthesis of cis-H(Ph_3Si)Pt[$Cy_2P(CH_2)_4PCy_2$] (**2**)

To Cl_2Pt[1,4-($Cy_2P(CH_2)_4PCy_2$)] (**1**) (0.95 g, 1.33 mmol) suspended in 8 cm^3 of THF in a 50 cm^3 Schlenk flask at 0°C was added a slight excess of two equivalents of a 0.5 M solution of sodium naphthalenide in THF until the colour of the solution just remained green.[16] The reaction mixture was stirred for 3 h during which time it warmed to room temperature. The volatile components were removed *in vacuo* and the residue extracted with three 10 cm^3 portions of warm n-pentane to give a pale yellow solution believed to contain Pt^0[1,4-($Cy_2P(CH_2)_4PCy_2$)]. [The presence of the platinum(0) species was confirmed by removal of a small (0.5 cm^3) aliquot of the solution and exposure to air, which immediately resulted in the formation of a white precipitate.] To this solution was added a slight excess of Ph_3SiH (0.40 g, 1.54 mmol) which caused immediate formation of a white precipitate. The reaction mixture was stirred for 1 h, filtered and the white solid washed three times with 5 cm^3 of n-pentane to remove the excess Ph_3SiH and naphthalene. The white solid, 0.82 g (0.91 mmol) analysed correctly for **2** and was obtained in a yield of 68.1%. ^{1}H NMR data (20°C, 250 MHz, C_6D_6): −2.51 ppm, d × d, $^2J_{H-P_{cis}}$ = 19 Hz, $^2J_{H-P_{trans}}$ = 149 Hz, $^2J_{H-Pt}$ = 867 Hz, Pt—*H*; 1.0–1.3 ppm, multiplets, $Cy_2P(CH_2)_4PCy_2$; 7.20 ppm, m, Si*Ph*$_3$; 7.41 ppm, m, Si*Ph*$_3$; 8.24 ppm, m, Si*Ph*$_3$. ^{31}P NMR data (20°C, 101.2 MHz, C_6D_6): 33.9 ppm, d, J_{P-P} = 20 Hz, J_{P-Pt} = 1607 Hz, J_{P-Si} = 162 Hz, J_{P-H} = 18 Hz, P *trans* to Si; 39.4 ppm, d, J_{P-Pt} = 2471 Hz, J_{P-H} = 146 Hz, P *trans* to H. Found: C, 60.6; H, 7.3. Calc.: C, 61.0; H, 7.5%. Melting point, 172–174°C.

Crystallographic data

Crystal data. $C_{46}H_{68}P_2PtSi$, Mr = 906.16, monoclinic, space group $P2_1/n$, a = 14.142(4), b = 16.160(4), c = 20.120(6) Å, β = 109.16(2)°, V = 4343(3) Å^3, Z = 4, D_c = 1.386 Mg m^{-3}, D_m = 1.40(1) Mg m^{-3} (flotation), $F(000)$ = 1864, Mo-$K_{\bar{\alpha}}$ (λ = 0.71073 Å), μ = 3.36 mm^{-1}, T = 295 K, 6068 reflections were measured on a CAD-4F diffractometer ($2\theta_{max}$ = 45.0°); 5636 were unique and 3606 had $I > 3\sigma(I)$. Lorentz, polarization and empirical absorption corrections (transmission range, 0.9395–0.9995) were made.

Unit cell parameters were determined by employing a Debye–Scherrer cylindrical camera (114.6 mm, 295 K using Cu-$K_{\bar{\alpha}}$ radiation, λ_{mean} = 1.54184 Å). Crystals of **2** were finely ground and placed into a 0.2 mm capillary. Characterization was based on 54 lines. "Figures-of-merit" values are $F(30)$ = 46(0.005, 137)[17] and M_{20} = 20.9.[18]

Solution and refinement. The structure solution was solved by direct methods (SHELX-86)[19] and refined by block full-matrix least-squares using the SHELX-76 computer program.[20] The function minimized was $\Sigma w(|F_o| - |F_c|)^2$, where $w = (\sigma^2(F_o) + 0.0058|F_o|^2)^{-1}$. All non-hydrogen atoms were refined anisotropically. The hydrogen atom positions were computed and were not refined. The final reliability factors are R = 0.056 and R_w = 0.058 for all observed reflections.* An extinction correction was also refined. The final cycle of block refinement had 408 variables and maximum shift/error of 0.00058. In the final D-map, the highest peak density was 0.71 e$^-$ Å^{-3} and the deepest hole showed a density of −0.99 e$^-$ Å^{-3}, both in the vicinity of the platinum atom. Elsewhere, only a random fluctuating background was observed. Weights based on counting statistics were used throughout. Atomic scattering factors and anomalous dispersion correction factors were taken from the usual source.[21]

RESULTS AND DISCUSSION

The synthesis of **2** was carried out via oxidative addition of triphenylsilane to the platinum(0) species Pt^0[1,4-($Cy_2P(CH_2)_4PCy_2$)] generated *in situ* as previously reported in the literature.[14] In contrast to a number of *cis*-H[SiR_3]Pt(PR'_3)$_2$ derivatives (where R = variously substituted phenyl and

* Atomic coordinates, thermal parameters and a list of F_o/F_c values have been deposited as supplementary data with the Editor, from whom copies are available on request. Atomic coordinates have also been deposited with the Cambridge Crystallographic Data Centre.

R′ = variously substituted phenyl and cyclohexyl), **2**, does not undergo rapid intramolecular ligand position exchange in solution.[11,14,22] This dynamic process is most easily characterized by monitoring the temperature variation of the intensity of certain resonances of the hydride ligand by ^{1}H NMR spectroscopy which are selectively broadened due to retention of spin correlation during the transition state.[23] The variable temperature ^{1}H NMR data for **2** over the range +60 to −70°C are completely temperature invariant. A close analogue of **2**, *cis*-H(SiPh$_3$)Pt[1,4-(Ph$_2$P(CH$_2$)$_4$PPh$_2$)] (**3**), which has recently been structurally characterized,[24] also does not undergo the intramolecular ligand position exchange process describd above. In order to shed more light on this observation, a single crystal X-ray diffraction study of **2** has been carried out to examine the bite angle in the 1,4-(Cy$_2$P(CH$_2$)$_4$PCy$_2$) ligand.

The title compound crystallizes in the monoclinic space group $P2_1/n$ and contains four molecules per unit cell. The platinum atom has angularly distorted square-planar geometry and is bonded to a hydrogen atom, two phosphorus atoms and a silicon atom. The molecular structure of **2** is shown in Fig. 1 and selected bond lengths and angles are given in Table 1. The atoms of the platinum first coordination sphere display only minor deviations from planarity (mean deviation of 0.035 Å) probably as a result of the minimal space requirement for the hydrogen atom compared with the more sterically demanding triphenylsilyl and diphosphine ligands. The "bite" angle of the two phosphorus atoms [P(1)—Pt—P(2) is 102.3(1)°] brought about by the bridging hydrocarbon chain, also contributes to the angular distortion. In contrast, the bite angle of *cis*-H[Ph$_3$Si(Ph$_2$P(CH$_2$)$_4$PPh$_2$)] is 103.5(1)°, which is slightly larger probably as a result of the less sterically demanding substituents on the phosphorus atoms. Due to the established higher *trans* influence of the triphenylsilyl group compared with hydride, the Pt—P(2) bond length is longer than the Pt—P(1) bond.[25] The Pt—Si distance is reasonable when compared with published values in *BIDICS*.[26] The mean P—C length of 1.864(14) Å and the mean Si—C length of 1.901(13) Å, which are bonded to the cyclohexyl and the phenyl rings, respectively, are quite normal as well as the P(1)—C(1) and

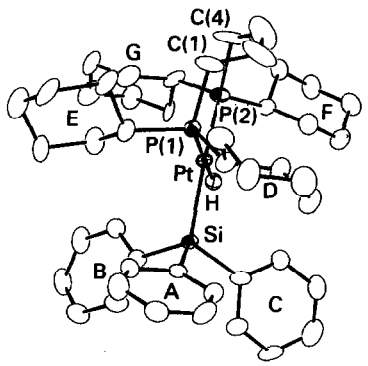

a

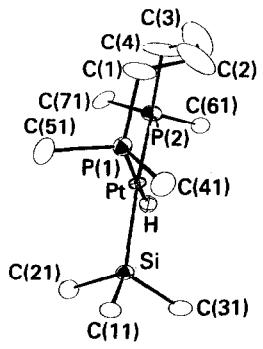

b

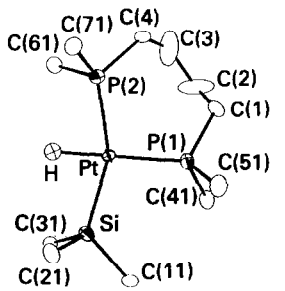

c

Fig. 1. (a) Perspective drawing of **2** displaying ellipsoids of 50% probability. The idealized hydrogen atom has been added for descriptive clarity. (b) and (c) Partial molecular drawings without the triphenyl and dicyclohexyl ligands showing the structure of the four carbon bridge and the coordinated phosphorous, silicon and hydrogen atoms about the platinum atom.

Table 1. Selected bond lengths (Å) and angles (°)

Pt—Si	2.363(4)	Si—Pt—P(1)	102.2(1)
Pt—P(1)	2.313(4)	Si—Pt—P(2)	155.4(1)
Pt—P(2)	2.338(4)	P(1)—Pt—P(2)	102.3(1)
Si—C(11)	1.883(14)	Pt—Si—C(11)	121.5(4)
Si—C(21)	1.907(14)	Pt—Si—C(21)	110.6(4)
Si—C(31)	1.914(15)	Pt—Si—C(31)	112.1(5)
P(1)—C(1)	1.827(16)	C(11)—Si—C(21)	102.1(7)
P(1)—C(41)	1.863(13)	C(11)—Si—C(31)	101.8(6)
P(1)—C(51)	1.887(16)	C(21)—Si—C(31)	107.6(6)
P(2)—C(4)	1.812(17)	Pt—P(1)—C(1)	115.2(6)
P(2)—C(61)	1.848(16)	Pt—P(1)—C(41)	114.5(5)
P(2)—C(71)	1.859(14)	Pt—P(1)—C(51)	113.8(5)
C(1)—C(2)	1.51(3)	C(1)—P(1)—C(41)	105.2(7)
C(2)—C(3)	1.50(3)	C(1)—P(1)—C(51)	104.1(8)
C(3)—C(4)	1.38(3)	C(41)—P(1)—C(51)	102.8(7)
		Pt—P(2)—C(4)	122.8(7)
		Pt—P(2)—C(61)	110.6(5)
		Pt—P(2)—C(71)	113.6(6)
		C(4)—P(2)—C(61)	106.3(11)
		C(4)—P(2)—C(71)	97.6(8)
		C(61)—P(2)—C(71)	103.8(7)
		P(1)—C(1)—C(2)	112.1(13)
		C(1)—C(2)—C(3)	118.8(16)
		C(2)—C(3)—C(4)	122.5(23)
		C(3)—C(4)—P(2)	117.4(14)

	Ring	Distance Mean	Distance Range	Angles Mean	Angles Range
A	C(11)—C(16)	1.392(40)	1.340–1.443	120.0(23)	115.4–122.0
B	C(21)—C(26)	1.378(31)	1.319–1.418	120.0(28)	114.7–122.7
C	C(31)—C(36)	1.375(14)	1.359–1.397	119.9(36)	114.1–124.9
D	C(41)—C(46)	1.521(32)	1.460–1.555	111.5(14)	109.2–112.2
E	C(51)—C(56)	1.517(57)	1.393–1.569	111.0(38)	106.0–118.5
F	C(61)—C(66)	1.513(15)	1.486–1.533	110.9(24)	108.4–114.7
G	C(71)—C(76)	1.502(25)	1.474–1.546	111.4(22)	108.0–115.3

the P(2)—C(4) bond distances. Distortions are observed in the angles around the two ligating phosphorus atoms, with a maximum deviation from an ideal tetrahedral angle of 13.3°. However, the mean angles about atoms P(1) and P(2) are 109.3 and 109.2°, respectively. This type of distortion has been previously observed in tricyclohexylphosphine platinum complexes.[9–11] A similar distorted

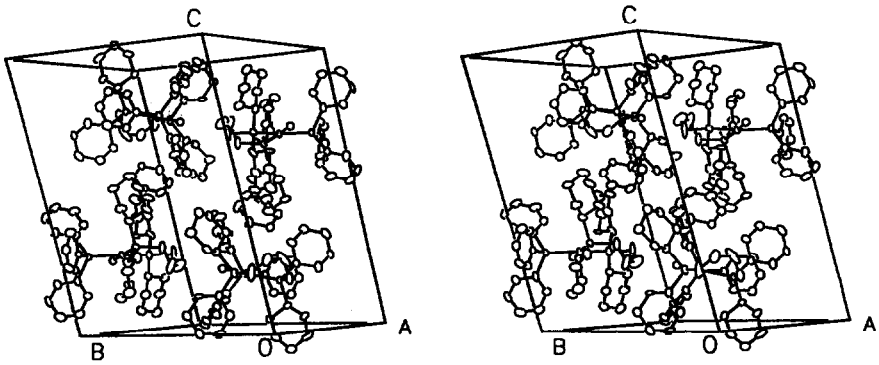

Fig. 2. Stereoscopic packing diagram of the unit cell of **2**.

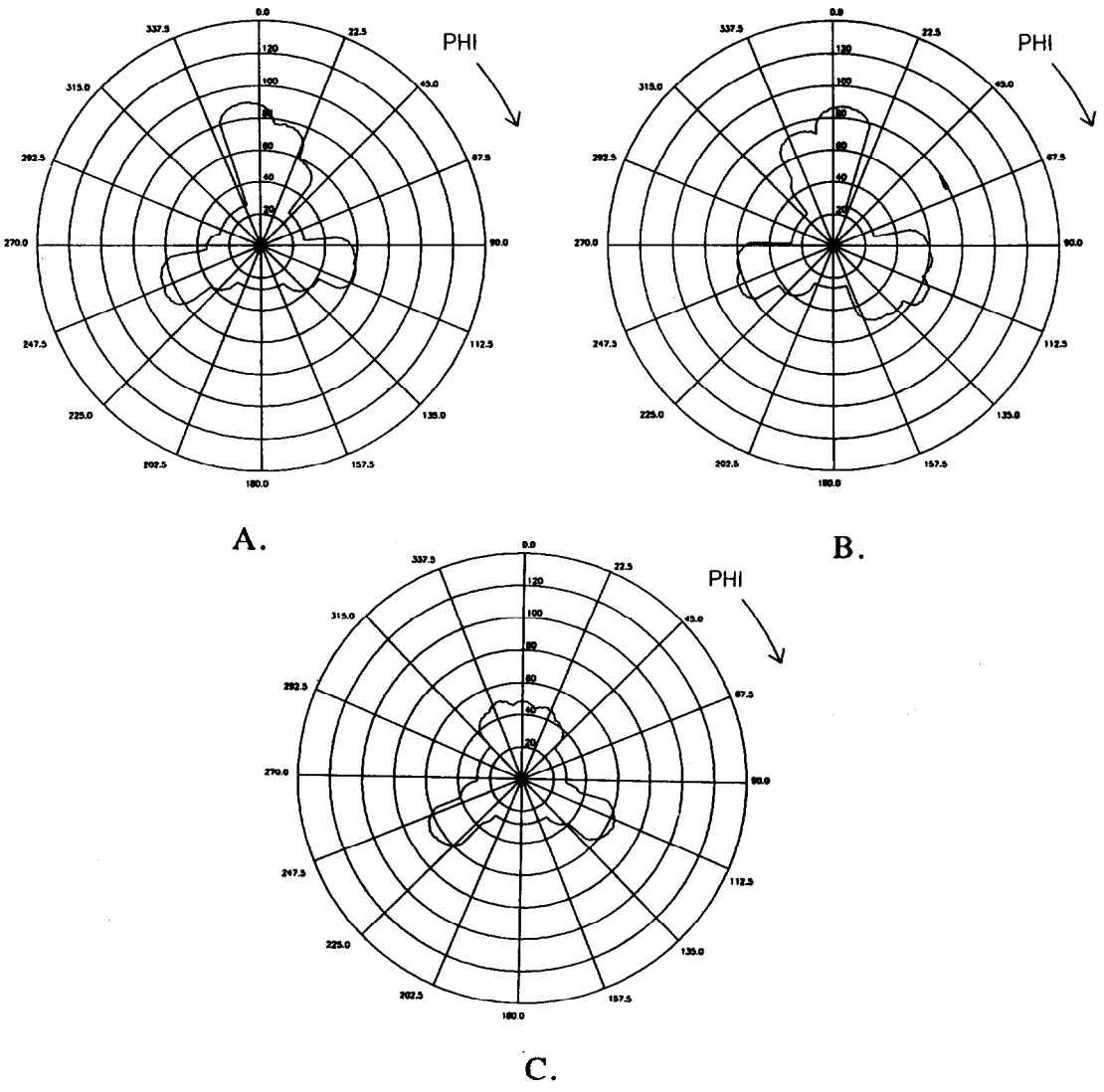

Fig. 3. Ligand profiles ($\theta/2$ vs ϕ) of **2** looking down (A) the Pt—P(1) bond, (B) the Pt—P(2) bond and (C) the Pt—Si bond.

arrangement is seen about the central silicon atom in the $SiPh_3$ ligand. The largest deviation from ideality is 12.0° (mean angle about the Si atom, 109.3°). The C—C bond distances and C—C—C bond angles within each ring system varied considerably, see Table 1. The platinum, two phosphorus and four bridging carbon atoms make up a seven-membered ring with distinct puckering. The puckering involves the virtual eclipsing of the substituents of carbons C(2) and C(3) in the seven-membered ring. This eclipsing is more severe than commonly encountered in seven-membered cycloalkane rings[27] and probably is a result of the small P(1)—Pt—P(2) angle and the planarity of these atoms. The bond lengths and angles associated with the hydrocarbon chain bridging the phosphorus atoms is further evidence of considerable ring strain.

Ligand profiles for the two phosphine ligands and the triphenylsilyl group are shown in Fig. 3. The steric bulk about the two phosphorus atoms is viewed down the platinum–phosphorus bonds: (A) for the Pt—P(1) and (B) for Pt—P(2). Note that even though both phosphorus atoms have the same type of bonded lignds and basically similar silhouettes, one of the lobes of the Pt—P(2) profile reveals more steric bulk, which further evidences the extended bond distance of Pt—P(2). This added bulk to the profile is related to the distinct ring strain puckering in the seven-membered ring, compare Pt—P(2)—C(4,61,71) angle variances to the uniformity of Pt—P(1)—C(1,41,51) angles, see Table 1. The concept of the half cone angle ($\theta/2$) and the rotational angle (ϕ)[3,4] coupled with the experimental polar ligand profile obtained from cry-

stallographic data, has also been used to evaluate steric demand in phosphine ligands. For **2**, the maximum (minimum) half-cone angle calculations about the diphosphine and triphenylsilyl ligands are: $Cy_2P(1)(CH_2)_4 = 90(61)°$, $Cy_2P(2)(CH_2)_4 = 87(62)°$ and $SiPh_3 = 66(50)°$, ESDs for each, $\pm 1.0°$. This profile is very similar to that of $H(Ph_3Si)Pt[Ph_2P(CH_2)_4PPh_2]$.[24]

Further studies of the chemical significance of sterically demanding substituents at platinum centres are in progress.

Acknowledgements—D.F.M. and E.L.S. thank The Robert A. Welch Foundation (Grant No. AA-668) for financial support of this work and Baylor University. M.H.-S. thanks the NSF chemical instrumentation program for the purchase of a low-field NMR spectrometer, Johnson Matthey for loan of precious metals, and Professor H. C. Clark for a post-doctoral fellowship, under whom this work was initiated.

REFERENCES

1. C. A. Tolman, *J. Am. Chem. Soc.* 1970, **92**, 2956.
2. H. C. Clark, *Israel J. Chem.* 1977, **15**, 210.
3. E. C. Alyea, S. A. Dias, G. Ferguson and R. J. Restivo, *Inorg. Chem.* 1977, **16**, 2329.
4. J. F. Richardson and N. C. Payne, *Can. J. Chem.* 1977, **55**, 3203.
5. J. D. Smith and J. D. Oliver, *Inorg. Chem.* 1978, **17**, 2585.
6. D. H. Leschnitzer, Thesis. Baylor University, Waco, Texas (1989).
7. J. Forries, M. Green, J. L. Spencer and F. G. A. Stone, *J. Chem. Soc., Dalton Trans.* 1977, 1006.
8. M. Hackett and G. M. Whitesides, *J. Am. Chem. Soc.* 1988, **110**, 1449; M. Hackett, J. A. Ibers and G. M. Whitesides, *J. Am. Chem. Soc.* 1988, **110**, 1436.
9. D. F. Mullica, J. D. Oliver, E. L. Sappenfield and D. A. Grossie, *Acta Cryst.* 1986, **C42**, 1695.
10. D. F. Mullica, J. D. Oliver and D. A. Grossie, *Acta Cryst.* 1987, **C43**, 591.
11. H. C. Clark and M. J. Hampden-Smith, *Coord. Chem. Rev.* 1987, **79**, 229.
12. H. C. Clark, G. Ferguson, M. J. Hampden-Smith, B. Kaitner and H. Ruegger, *Polyhedron* 1988, **7**, 1349.
13. G. Ferguson, M. J. Hampden-Smith and B. L. Ruhl, *Acta Cryst.* 1987, **C43**, 788.
14. H. C. Clark and M. J. Hampden-Smith, *J. Am. Chem. Soc.* 1986, **108**, 3829.
15. D. F. Schriver and M. A. Dreydon, *The Manipulation of Air-Sensitive Compounds*, 2nd edn, pp. 78–79. Wiley-Interscience, New York (1986).
16. T. Yoshida and S. Otsuka, *Inorg. Synth.* 1979, **19**, 101.
17. G. S. Smith and R. L. Synder, *J. Appl. Cryst.* 1979, **23**, 60.
18. P. M. deWolff, *J. Appl. Cryst.* 1968, **1**, 108.
19. G. M. Sheldrick, SHELXS-86, Program for Crystal Structure Determination. University of Göttingen, F.R.G. (1986).
20. G. M. Sheldrick, SHELX-76, Program for Crystal Structure Determination. University of Cambridge, U.K. (1976).
21. J. A. Ibers and W. C. Hamilton, *International Tables for X-ray Crystallography*, Vol. IV. Kynoch Press, Birmingham (1974).
22. H. Azizian, K. R. Dixon, C. Eaborn, A. Pidcock, N. M. Shuaib and J. Vinaixa, *J. Chem. Soc., Chem. Commun.* 1982, 1020.
23. M. J. Hampden-Smith and H. Ruegger, *Mag. Res. Chem.* 1989, **27**, 1107.
24. A. Chow, H. C. Clark, D. A. Grossie, M. J. Hampden-Smith, D. F. Mullica and H. Ruegger, *Organometallics*, submitted for publication.
25. T. G. Appleton, H. C. Clark and L. E. Manzer, *Coord. Chem. Rev.* 1973, **10**, 335.
26. *Bond Index of the Determination of Inorganic Crystal Structure*. Institute for Material Research, Hamilton, Canada (1969–1981).
27. A. Streitwieser and C. H. Heathcock, *Introduction to Organic Chemistry*, Ch. 23. Macmillan, New York (1976).

Polyhedron Vol. 10, No. 8, pp. 873–876, 1991
Printed in Great Britain

0277-5387/91 $3.00+.00
© 1991 Pergamon Press plc

THE PREPARATION AND CRYSTAL STRUCTURE DETERMINATION OF A POLYMERIC ADDUCT OF COPPER(II) ACETATE WITH 2-AMINOPYRIMIDINE

GRAHAM SMITH*

School of Chemistry, Queensland University of Technology, Brisbane 4000, Australia

and

COLIN H. L. KENNARD and KARL A. BYRIEL

Department of Chemistry, The University of Queensland, Brisbane 4072, Australia

(*Received* 24 *September* 1990; *accepted* 7 *January* 1991)

Abstract—The adduct of copper(II) acetate with 2-aminopyrimidine, *catena*-[(2-aminopyrimidine-*N*,*N*′)-tetrakis-μ-(ethanoato-*O*,*O*′)-dicopper(II)], has been prepared and its structure determined using X-ray diffraction. The structure is based on a tetracarboxylate-bridged dimer unit of the copper(II) acetate hydrate type [Cu---Cu, 2.633(2) Å] but is extended into an infinite zigzag polymer via the *meta*-related nitrogen atoms of bridging 2-aminopyrimidine molecules [Cu—N, 2.218(5) Å].

Since the first tetracarboxylate-bridged copper(II) dimer structure (**1**) was reported for copper(II) acetate hydrate by van Niekerk and Schoening[1] in 1953, a number of nitrogen base and oxygen donor group adducts of copper(II) with unsubstituted acetate have been reported. These include urea,[2] α-picoline,[3] benzimidazole,[4] dimethylformamide,[5] methyl nicotinamide,[6] 2-aminopyridine,[7] isatin-3-phenylhydrazone,[8] acetic acid,[5] methanol,[9,5] N,N-diethylnicotinamide,[10] hexamethylenetetramine,[11] 1,4-diazabicyclo(2.2.2)octane,[12] pyrazine,[12] pyridine,[13] quinoline[14] and thiocyanate.[15] The majority of examples involve a discrete dimer with terminal adducted molecules (replacing water in **1**), while in only isolated cases, adducted molecules with bifunctional donor groups extend the dimers into linear polymers (**2**).[5,11,12]

With 2-aminopyrimidine (2-ampym), the *meta*-related ring nitrogen atoms have potential for the formation of an analogous but zigzag polymer chain structure, although only one such example of this has been reported, the copper(II) (2-chlorophenoxy)ethanoate-2-aminopyrimidine adduct.[16] In contrast, the adduct with copper(4-fluorophenoxy)ethanoate[17] is a discrete dimer. The chemically stable, dark green adduct formed between 2-aminopyrimidine and copper(II) acetate in ethanol gave an analysis consistent with [$Cu_2(RCO_2)_4$(2-ampym)$_1$], and suggested a polymer structure, which was confirmed in the single crystal structure determination.

EXPERIMENTAL

Preparation

The complex was prepared by dropwise addition of a 1:1 stoichiometric amount of 2-aminopyrimidine in ethanol to a stirred ethanolic solution of copper(II) acetate hydrate, maintained at 70°C. An immediate colour change was followed by rapid growth of small, dark green, prismatic crystals from the cooling solution. (Found: C, 31.0; H, 3.7; N, 8.9. Calc. for $C_{12}H_{17}Cu_2N_3O_8$: C, 31.4; H, 3.73; N, 9.2%.)

Crystal data

$C_{12}H_{17}Cu_2N_3O_8$, $M = 458.4$, monoclinic, $a = 15.126(3)$, $b = 13.709(1)$, $c = 8.659(2)$ Å, $\beta =$

* Author to whom correspondence should be addressed.

93.79(1)°, $U = 1791.7(6)$ Å^3, $D_m = 1.71$, $D_c = 1.698$ g cm^{-3}, $Z = 4$, Mo-K_α radiation, $\lambda = 0.71073$ Å, μ(Mo-K_α) = 25.1 cm^{-1}, $F(000) = 928$, space group $C2/c$, $t = 296$ K.

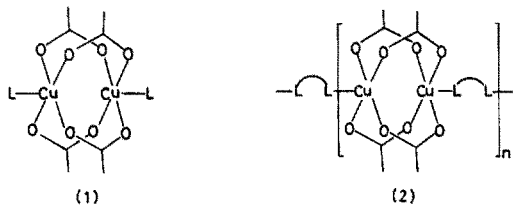

Data collecion, structure solution and refinement

Data were collected from a specimen measuring 0.12 × 0.05 × 0.04 mm on an Enraf–Nonius CAD-4 diffractometer. 2352 reflections were collected ($2\theta_{max} = 50°$; *hkl* range: $h = \pm 18$, $k = 0$–16, $l = 0$–10), giving 1377 unique, of which 889 with $I > 3.0\sigma(I)$ were used in structure refinement. Crystal monochromatized Mo-K_α radiation ($\lambda = 0.71073$ Å) was used, with empirical absorption corrections applied to the data. A total loss of *ca* 1% in the intensities of three standards monitored during the collection period indicated negligible crystal decay. The structure was solved using the Patterson method (SHELXS 86[18]) and refined using SHELX 76.[19] Neutral atom scattering factors and f', f'' terms for anomalous dispersion were taken from ref. 20. Full-matrix least-squares refinement with anisotropic thermal parameters on all non-hydrogen atoms gave R* and R_w† of 0.042 and 0.044, respectively, with a value of $w = 0.4/(\sigma^2 F_o + 5.9 \times 10^{-3} F_o^2)$ being used. Hydrogen atoms were located by difference methods and their positional and isotropic thermal parameters refined. The maximum peak in the final difference-Fourier analysis was *ca* 0.7 eÅ^{-3}.

Bond distances and angles are given in Table 1. Atomic fractional coordinates, anisotropic thermal parameters, observed and calculated structure factors and intraligand bond distances and angles are deposited with the Editor as supplementary material, from whom copies are available on request. Atomic coordinates have also been deposited with the Cambridge Crystallographic Data Centre.

DISCUSSION

The structure comprises centrosymmetric tetracarboxylate-bridged dimers of the copper(II) acetate hydrate type (Fig. 1), with a Cu···Cu separation of 2.633(2) Å and a mean Cu—O (equatorial) distance of 1.966(5) Å. These values compare with 2.616(2) and 1.969(3) Å, respectively, in the re-refined copper(II) acetate hydrate structure.[21] In the axial sites of the dimers, the 2-aminopyrimidine molecules extend the structure into a zigzag chain polymer with *ca* 120° offsets through the *meta*-related hetero nitrogen atoms. The Cu—N distance [2.218(5)Å] compares with 2.243 and 2.248(9) Å in the analogous 2-aminopyrimidine adduct of copper(II) (2-chlorophenoxy)ethanoate.[16] The slight extension probably results from the greater steric imposition of the larger phenoxyalkanoate residues. The 2-aminopyrimidine molecules also lie on crystallographic two-fold rotation axes at

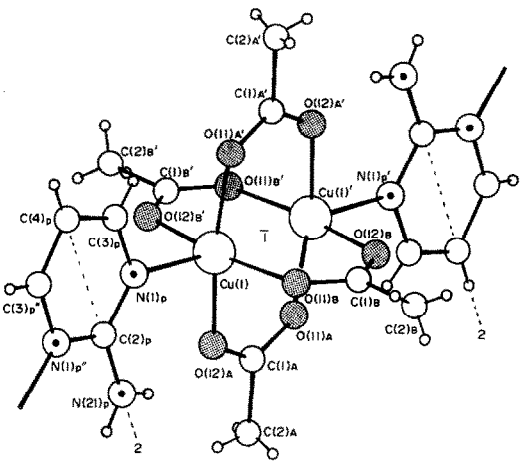

Fig. 1. Molecular configuration and atom naming scheme. Primed atoms are generated by inversion symmetry, double primes by a two-fold rotation axis.

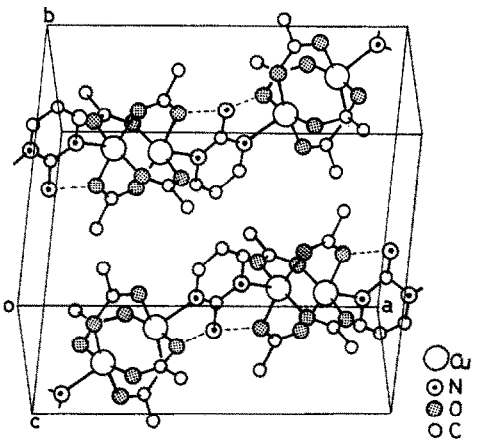

Fig. 2. Perspective view of the packing in the unit cell.

* $R = \Sigma||F_o|-|F_c||/\Sigma|F_o|$.

† $R_w = [\Sigma w(||F_o|-|F_c||)^2/\Sigma w(|F_o|)^2]^{1/2}$.

Table 1. Bond distances (Å) and angles (°)

		Distances	
Cu(1)—O(11)A	1.983(5)	C(1)A—C(2)A	1.502(13)
Cu(1)—O(12)A	1.979(5)	C(1)B—O(11)B	1.262(9)
Cu(1)—O(11)B	1.950(6)	C(1)B—O(12)B	1.242(9)
Cu(1)—O(12)B	1.954(5)	C(1)B—C(2)B	1.482(12)
Cu(1)—N(1)p	2.218(5)	N(1)p—C(2)p	1.348(6)
Cu(1)—Cu(1)′	2.633(2)	N(1)p—C(3)p	1.325(10)
C(1)A—O(11)A	1.240(8)	C(2)p—N(21)p	1.328(14)
C(1)A—O(12)A	1.268(8)	C(3)p—C(4)p	1.371(10)
		Angles	
O(11)A′—Cu(1)—O(12)A	167.9(2)	O(11)A—C(1)A—O(12)A	124.1(8)
O(11)A′—Cu(1)—O(11)B	89.1(3)	O(11)A—C(1)A—C(2)A	118.1(8)
O(11)A′—Cu(1)—O(12)B′	89.3(3)	O(12)A—C(1)A—C(2)A	117.7(8)
O(11)A′—Cu(1)—N(1)p	93.3(2)	O(11)B—C(1)B—O(12)B	124.1(8)
O(12)A—Cu(1)—O(11)B	89.4(2)	O(11)B—C(1)B—C(2)B	117.5(8)
O(12)A—Cu(1)—O(12)B′	89.6(2)	O(12)B—C(1)B—C(2)B	118.3(8)
O(12)A—Cu(1)—N(1)p	98.8(2)	N(1)p—C(2)p—N(1)p″	125.0(5)
O(11)B—Cu(1)—O(12)B′	167.6(2)	N(1)p—C(2)p—N(21)p	117.5(4)
O(11)B—Cu(1)—N(1)p	96.1(2)	C(2)p—N(1)p—C(3)p	115.7(6)
O(12)B′—Cu(1)—N(1)p	96.2(2)	N(1)p—C(3)p—C(4)p	124.3(8)
Cu(1)—O(12)A—C(1)A	122.3(4)	C(3)p—C(4)p—C(3)p″	114.9(7)
Cu(1)—O(11)A′—C(1)A′	125.6(4)		
Cu(1)—O(11)B—C(1)B	123.9(4)		
Cu(1)—O(12)B′—C(1)B′	124.4(4)		
Cu(1)—N(1)p—C(2)p	129.4(5)		
Cu(1)—N(1)p—C(3)p	114.8(5)		

′Related by inversion $(1/2-x, 1/2-y, -z)$.
″Related by two-fold symmetry.

$x = 0, 1/2$ in the cell (Fig. 2). Bond distances and angles within these residues are similar to those found for the free base.[22] There are no significant inter-chain hydrogen bonding interactions, although intra-chain associations between the amine nitrogen of the 2-aminopyrimidine and the carboxyl oxygens of the dimer [N(21)p---O(12)A, 2.89 Å] give rigidity to the polymer.

Acknowledgements—The authors thank the Australian Research Council, The University of Queensland and the Queensland University of Technology for financial assistance.

REFERENCES

1. J. N. van Niekerk and F. R. L. Schoening, *Acta Cryst.* 1953, **6**, 227.
2. Yu A. Simonov, V. I. Ivanov, T. I. Malinovskii and L. I. Landa, *Izv. Akad. Nauk. Mold. SSR* 1976, 33.
3. F. Pavelcik and F. Hanic, *J. Cryst. Molec. Struct.* 1978, **8**, 59.
4. M. Bukowska-Stryzewska, J. Skoweranda and A. Tosik, *Acta Cryst.* 1982, **38B**, 2904.
5. V. M. Rao, D. N. Sathyanarayana and H. Manohar, *J. Chem. Soc., Dalton Trans.* 1983, 2167.
6. G. R. Newkome, K. J. Theriot, V. K. Gupta, R. N. Balz and F. R. Fonczek, *Inorg. Chim. Acta* 1986, **114**, 21.
7. A. S. Antsyshkina, M. A. Porai-Koshits, V. M. Ostrikova, D. A. Garnovskii, A. P. Sadimenko and O. A. Osipov, *Koord. Khim.* 1987, **13**, 838.
8. A. Coda, G. Gatti, A. C. Coda, G. Desimona, P. P. Righetti and G. Tacconi, *Gazz. Chim. Ital.* 1985, **115**, 549.
9. V. M. Rao and H. Manohar, *Inorg. Chim. Acta* 1979, **34**, L213.
10. L. Kh. Minacheva, T. S. Khodashova, M. A. Porai-Koshits and A. Yu. Tsivadze, *Koord. Khim.* 1981, **7**, 455.
11. J. Pickardt, *Acta Cryst.* 1981, **37B**, 1753.
12. B. Morosin, R. C. Hughes and Z. G. Soos, *Acta Cryst.* 1975, **31B**, 762.
13. F. Hanic, D. Stempelova and K. Hanikova, *Acta Cryst.* 1964, **17**, 1963; G. A. Barclay and C. H. L. Kennard, *J. Chem. Soc.* 1961, 5244.
14. Yu. A. Simonov, V. I. Ivanov, A. B. Ablov, A. L. Mikova and T. I. Malinovskii, *J. Struct. Chem.* 1976, **17**, 444.

15. D. M. L. Goodgame, N. J. Hill, D. F. Marsham, A. C. Skapski, M. L. Smart and P. G. H. Troughton, *J. Chem. Soc., Chem. Commun.* 1969, 629.
16. G. Smith, E. J. O'Reilly, C. H. L. Kennard and A. H. White, *J. Chem. Soc., Dalton Trans.* 1985, 243.
17. E. J. O'Reilly, G. Smith and C. H. L. Kennard, *Inorg. Chim. Acta* 1984, **90**, 63.
18. G. M. Sheldrick, SHELXS 86, Program for Crystal Structure Solution. University of Göttingen, F.R.G.
19. G. M. Sheldrick, SHELX 76, Program for Crystal Structure Determination. University of Cambridge, U.K.
20. *International Tables for X-ray Crystallography* (Edited by J. A. Ibers and W. C. Hamilton), Vol. 4. Kynoch Press, Birmingham (1974).
21. P. de Meester, S. R. Fletcher and A. C. Skapski, *J. Chem. Soc., Dalton Trans.* 1973, 2575.
22. J. Scheinbein and E. Schempp, *Acta Cryst.* 1976, **32B**, 607.

Polyhedron Vol. 10, No. 8, pp. 877–880, 1991
Printed in Great Britain

0277–5387/91 $3.00+.00
© 1991 Pergamon Press plc

PHOTOCHEMISTRY OF $(\eta^5\text{-}C_5Me_5)Re(CO)_2Br_2$ ON Si(III) SURFACES AT LOW TEMPERATURE

BENTLEY J. PALMER, ANNA BECALSKA, RAMZI HADER and ROSS H. HILL*

Department of Chemistry, Simon Fraser University, Burnaby, British Columbia, Canada, V5A 1S6

(*Received* 29 *October* 1990; *accepted* 14 *January* 1991)

Abstract—The photolysis of $(\eta^5\text{-}C_5Me_5)Re(CO)_2Br_2$ on Si(III) surfaces at 77 K results in *cis* to *trans* isomerism. The mechanism of the photoreaction involves CO loss to generate an isomer of $(\eta^5\text{-}C_5Me_5)Re(CO)Br_2$ which, upon warming, reacts thermally with CO to generate only *trans*-$(\eta^5\text{-}C_5Me_5)Re(CO)_2Br_2$. The first isomer of $(\eta^5\text{-}C_5Me_5)Re(CO)Br_2$ is photosensitive and converts to a second isomer which upon reaction with CO yields exclusively *cis*-$(\eta^5\text{-}C_5Me_5)Re(CO)_2Br_2$.

We report here on the photoisomerism reactions of a film of $(\eta^5\text{-}C_5Me_5)Re(CO)_2Br_2$ deposited on a silicon surface. Previously, we demonstrated that $(\eta^5\text{-}C_5Me_5)Re(CO)_2Br_2$, in low temperature glasses, underwent efficient CO loss to generate $(\eta^5\text{-}C_5Me_5)Re(CO)Br_2$.[1] This product could be generated by photolysis of either *cis*- or *trans*-$(\eta^5\text{-}C_5Me_5)Re(CO)_2Br_2$ although, upon warming, only the *trans* isomer formed in a thermal reaction with CO. This observation explained why the solution isomerism occurred only in the *cis* to *trans* direction.[2]

As part of the program underway in our group[3] to examine the different photochemistry observable in solid films we have re-examined the photochemistry of *cis*-$(\eta^5\text{-}C_5Me_5)Re(CO)_2Br_2$ on a Si(III) surface. Here we report our observations concerning the photoreactivity of *cis*-$(\eta^5\text{-}C_5Me_5)Re(CO)_2Br_2$ on the surface of a single crystal of silicon.

EXPERIMENTAL

The complexes, *cis*- and *trans*-$(\eta^5\text{-}C_5Me_5)Re(CO)_2Br_2$, were prepared by literature[4] methods. The Si(III) wafers were obtained from Pacific Microelectronics Center, Canada. The wafers were *p*-type silicon with tolerances and specifications as per SEMI Standard M1.1.STD.5. The wafers were cut to the approximate dimensions of 1 cm × 1.5 cm in house.

The FTIR spectra were obtained with 4 cm^{-1} resolution using a BOMEM Michelson MB-120 FTIR spectrophotometer. The samples were held in a high conductivity copper sample mount within a CaF_2 faced vacuum Dewar.

The photolysis beam was a 100 W high pressure mercury lamp in an Oriel housing equipped with quartz condenser lenses.

Calibration of absorption of $(\eta^5\text{-}C_5Me_5)Re(CO)_2Br_2$ *on a surface*

A stock solution of $(\eta^5\text{-}C_5Me_5)Re(CO)_2Br_2$ was prepared in dichloromethane (1.4 mM). A drop (3.1×10^{-3} cm^3) of this solution was deposited on the surface of a silicon wafer, allowed to evaporate, and the absorbance measured. The area of the drop was found to be 0.5 cm^2. This process was repeated several times yielding the data shown in Fig. 1.

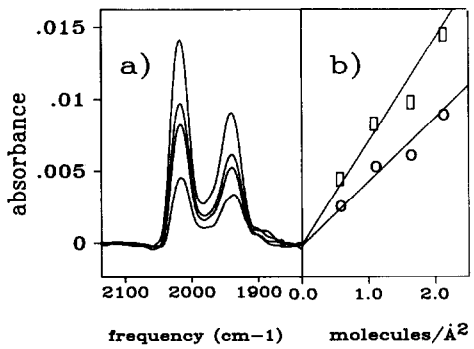

Fig. 1. (a) FTIR spectra associated with 0.5, 1.1, 1.6 and 2.2 molecules of *cis*-$(\eta^5\text{-}C_5Me_5)Re(CO)_2Br_2$ per $Å^2$ on a silicon surface. (b) Plot of absorbance of the symmetric (□) and antisymmetric (○) CO stretches of *cis*-$(\eta^5\text{-}C_5Me_5)Re(CO)_2Br_2$ vs coverage, data from Fig. 1(a).

* Author to whom correspondence should be addressed.

A similar experiment was conducted with the *trans* isomer yielding slopes of 0.0060 and 0.0073 molec $Å^{-2}$ for the high and low energy bands, respectively.

Photolysis of $(\eta^5\text{-}C_5Me_5)Re(CO)_2Br_2$ *on silicon surfaces*

Five drops of a dichloromethane solution containing $(\eta^5\text{-}C_5Me_5)Re(CO)_2Br_2$ were deposited on a silicon surface and the solvent allowed to evaporate. The silicon crystal was then mounted in the copper holder and transferred to the vacuum Dewar. This was then cooled to 77 K with liquid nitrogen and photolysed for 80 s. Spectral changes are summarized in Fig. 2.

In a similar experiment, a cut-off filter (band pass > 420 nm) and a 10 cm water filter with Pyrex optics were interposed between the light source and the sample. Spectral changes are summarized in Fig. 3.

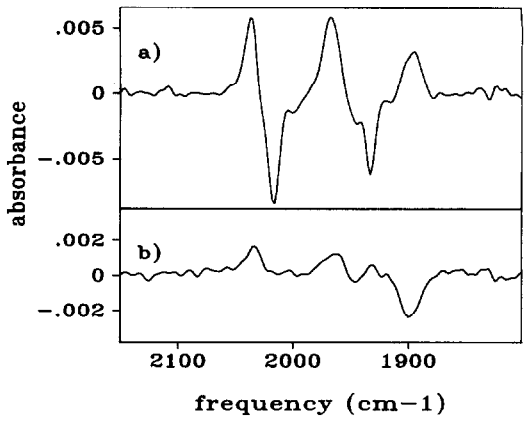

Fig. 2. FTIR spectral changes associated with (a) the photolysis of a film of *cis*-$(\eta^5\text{-}C_5Me_5)Re(CO)_2Br_2$ on a silicon surface for 80 s followed by (b) the spectral changes associated with warming this sample to 150 K and recooling to 77 K.

RESULTS AND DISCUSSION

From the curve of absorbance vs coverage, Fig. 1, we can see that the surface film is composed of many monolayers of *cis*-$(\eta^5\text{-}C_5Me_5)Re(CO)_2Br_2$. The photochemistry reported here is occurring in the film and is not expected to be reflective of the silicon surface environment. For example, if we assume that the average footprint of a molecule is 100 $Å^2$ then an absorbance of 0.02 would correspond to more than 300 monolayers. The FTIR of *cis*-$(\eta^5\text{-}C_5Me_5)Re(CO)_2Br_2$ on a surface consists of two absorptions in the metal carbonyl region. These are assigned as the symmetric and antisymmetric stretches at 2017 and 1938 cm^{-1}, respectively. Both the positions and relative ratio of the two CO stretching absorptions are in good agreement with the results from a low temperature glass, Table 1. Similar results are found for the deposition

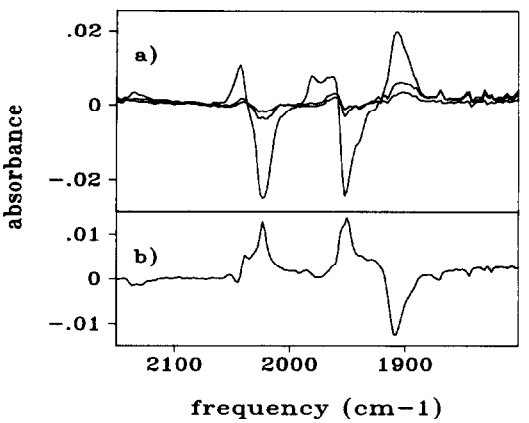

Fig. 3. FTIR spectral changes associated with (a) the photolysis of a film of *cis*-$(\eta^5\text{-}C_5Me_5)Re(CO)_2Br_2$ on a silicon surface for 100 and 220 min using filtered light (band pass > 420 nm) and 5 min using unfiltered light followed by (b) the spectral changes associated with warming this sample to 150 K and recooling to 77 K.

Table 1. FTIR spectral data for relevant complexes

Complex	Medium[a]	ν(CO) cm^{-1} (relative intensity)
cis-$(\eta^5\text{-}C_5Me_5)Re(CO)_2Br_2$	Si(III)	2017 (1.6), 1938 (1.0)
	Glass	2028 (1.5), 1935 (1.0)
trans-$(\eta^5\text{-}C_5Me_5)Re(CO)_2Br_2$	Si(III)	2040 (1.0), 1967 (1.2)
	Glass	2039 (1.0), 1963 (2.5)
Isomer 1 $(\eta^5\text{-}C_5Me_5)Re(CO)_2Br_2$	Si(III)	1900
Isomer 2	Si(III)	1909
	Glass	1910

[a] Data in glass are at 13 K in 1,2-epoxyethylbenzene, data on Si(III) are at 77 K.

of the *trans* isomer on Si(III), although the relative intensities differ considerably. The relative intensity of the antisymmetric stretch is reduced. If we use these data to calculate the angles between the CO ligands[5] we find angles of 115° in the glass and 95° on the surface. The angle observed in the crystal structure[2] is 104°. This change may be due to an orientation effect of the surface.

Photolysis of *cis*-$(\eta^5\text{-}C_5Me_5)Re(CO)_2Br_2$, at 77 K, into the lowest energy *d–d* absorption (band pass > 420 nm) leads to the spectral changes shown in Fig. 2(a). Loss of intensity due to the starting material at 2017 and 1938 cm^{-1} and the appearance of three new bands at 2042, 1970 and 1900 cm^{-1} is observed. The two at highest energy may be shown to be due to *trans*-$(\eta^5\text{-}C_5Me_5)Re(CO)_2Br_2$ by its independent synthesis and deposition on the surface. The latter is associated with the unsaturated complex $(\eta^5\text{-}C_5Me_5)Re(CO)Br_2$. We do not observe CO to be produced due to the low extinction coefficient. Upon warming the surface to 150 K reaction occurs consuming $(\eta^5\text{-}C_5Me_5)Re(CO)Br_2$ and presumably free CO to generate *trans*-$(\eta^5\text{-}C_5Me_5)Re(CO)_2Br_2$, Fig. 2(b). This overall process is shown in Scheme 1, pathways (i) and (ii). This photoreaction is entirely analogous to that reported earlier in 1,2-epoxyethylbenzene glass. A similar result is found if we irradiate with higher energy photons.

The observation of $(\eta^5\text{-}C_5Me_5)Re(CO)Br_2$ and free CO establishes that CO loss is one primary photochemical event. This result explains the observed *cis* → *trans* isomerism. The unsaturated species is however photosensitive. The spectral changes are illustrated in Fig. 3(a). Initially, photolysis results in the appearance of both *trans*-$(\eta^5\text{-}C_5Me_5)Re(CO)_2Br_2$ and the unsaturated species at 1900 cm^{-1}. Continued photolysis results in the growth of an absorption at 1909 cm^{-1} which we associate with a second isomer of $(\eta^5\text{-}C_5Me_5)Re(CO)Br_2$. At these higher conversions free CO is observed in the film at 2132 cm^{-1}. This photochemical step and likely geometries for each isomer of the unsaturated species are shown in the scheme. This second isomer upon warming reacts with CO to generate only *cis*-$(\eta^5\text{-}C_5Me_5)Re(CO)_2Br_2$ as indicated by the spectral changes in Fig. 3(b). This result is insensitive to irradiation wavelength.

In a 1,2-epoxyethylbenzene glass only one isomer of $(\eta^5\text{-}C_5Me_5)Re(CO)Br_2$ was observed and reaction with CO resulted in the formation of *trans*-$(\eta^5\text{-}C_5Me_5)Re(CO)_2Br_2$. On a silicon surface we find that photolysis of this isomer leads to the photoproduction of a second isomer of $(\eta^5\text{-}C_5Me_5)Re(CO)Br_2$. The two isomers are found to react thermally with CO to yield the two different isomers of $(\eta^5\text{-}C_5Me_5)Re(CO)_2Br_2$.

The probable structures of the two observed isomers are shown in Scheme 1. Each isomer is pre-

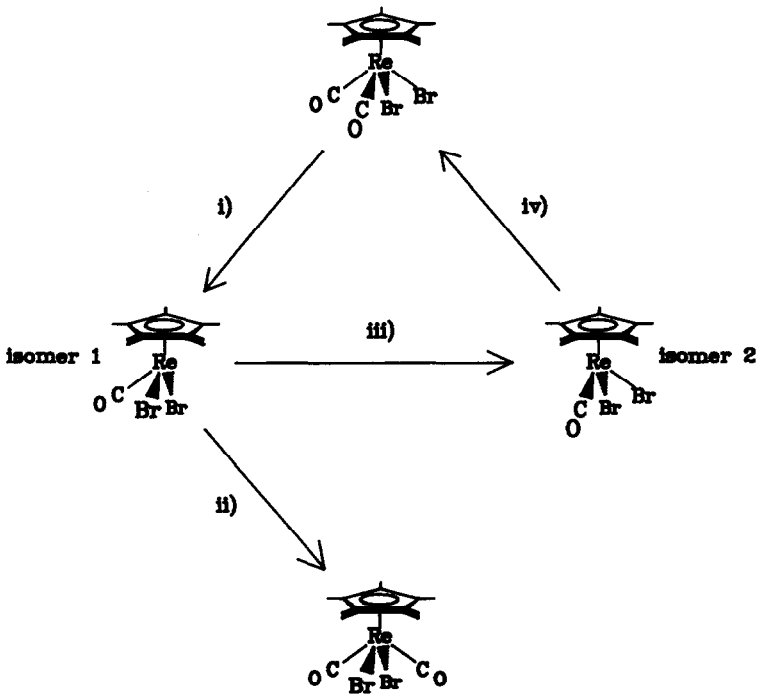

Scheme 1. (i) Photolysis in a glass at either 77 or 20 K, or photolysis in a film at 77 K; (ii) warming either a surface film or glass; (iii) photolysis in a film at 77 K; and (iv) warming photogenerated in a surface film.

sumably a result of the molecule retaining a four-legged piano stool geometry. The assignment of the structure of the two isomers is tentative. It does, however, seem most likely that the geometry of the basal ligands would be retained throughout the thermal reactions. The reaction of isomer 1 with CO results in a *trans* product. For this reason we assign isomer 1 as having CO *trans* to a vacant coordination site. Since the thermal reaction of isomer 2 with CO results in the *cis* product, we assign it as containing CO *cis* to the vacant site.

Interestingly, in glasses we have observed[6] two isomers for the unsaturated species derived from the isoelectronic molecules $(\eta^5\text{-}C_5H_5)Mo(CO)_2PR_3X$. In each case reaction of $(\eta^5\text{-}C_5H_5)Mo(CO)PR_3X$ with CO resulted in the specific generation of an isomer of $(\eta^5\text{-}C_5H_5)Mo(CO)_2PR_3X$.

Deposition and photolysis of *trans*-$(\eta^5\text{-}C_5Me_5)Re(CO)_2Br_2$ results in no change in the spectral features of this sample. This result is apparently independent of photolysis wavelength. In contrast with this is the photochemistry of *trans*-$(\eta^5\text{-}C_5Me_5)Re(CO)_2Br_2$ in a low temperature glass where CO loss was observed.[1]

We have demonstrated here that the photochemistry of *trans*-$(\eta^5\text{-}C_5Me_5)Re(CO)_2Br_2$ is altered upon the change of the medium from a low temperature glass to a surface film. Additionally, we have shown that in a film photoisomerism of $(\eta^5\text{-}C_5Me_5)Re(CO)Br_2$ is observable. The results obtained, both in a film and in a low temperature glass, are summarized in Scheme 1.

Acknowledgements—We wish to thank D. Sutton for valuable encouragement and NSERC(Canada) for generous financial support.

REFERENCES

1. R. H. Hill and B. J. Palmer, *Organometallics* 1989, **8**, 1651.
2. F. W. B. Einstein, A. H. Klahn-Oliva, D. Sutton and K. G. Tyers, *Organometallics* 1986, **5**, 53.
3. B. J. Palmer, A. Becalska and R. H. Hill, *J. Photochem. Photobiol.*, in press.
4. G. Diaz, A. H. Klahn-Oliva and C. Manzur, *Polyhedron* 1988, **7**, 2743.
5. R. B. King and R. H. Reimann, *Inorg. Chem.* 1976, **15**, 183.
6. J. Debad and R. H. Hill, *Can. J. Chem.* 1990, **68**, 2216.

Polyhedron Vol. 10, No. 8, pp. 883–884, 1991
Printed in Great Britain

0277-5387/91 $3.00+.00
Pergamon Press plc

COMMUNICATION

THE EFFECT OF RING SIZE UPON THE STABILITY OF COPPER(II) COMPLEXES OF DIAMINODIAMIDO LIGANDS

GRAHAM E. JACKSON,* PETER W. LINDER and ALEXANDER VOYÉ
Department of Chemistry, University of Cape Town, Rondebosch 7700, South Africa

(*Received* 10 *December* 1990; *accepted* 5 *February* 1991)

Abstract—A novel copper(II) diaminodiamido complex is presented in which the 5,5,5-membered chelate is more stable than the 5,6,5-membered chelate analogue.

Over the years the effect of ring size upon the thermodynamic stability of copper(II) complexes has received considerable attention.[1-3] More recently, diaminodiamido ligands of the type L6–L9, shown in Fig. 1, have proved interesting.[2-4] Upon loss of the amide protons, these ligands can coordinate to a metal ion via the four nitrogen atoms, giving rise to three chelate rings. So far, copper(II) complexes of ligands which give rise to a five-, a six- and a five-(5,6,5) membered chelate system have proved more stable than their 5,5,5 chelate analogues. Although, in general, five-membered chelate rings tend to be more stable than six-membered chelate rings, the lower stability of the 5,5,5 ligands results from steric constraints of three contiguous, small rings.

Recently we have had cause to study the thermodynamic stability of copper(II) complexes of L1–L3, the results of which are given in Table 1. The results for the MLH_{-2} species show, for the first time, a system in which the 5,5,5 chelate (L1) complex is more stable than the 5,6,5 complex (L2). In order to explain this result, molecular mechanics (MM2) calculations[6] were performed on these complexes and their tetraamine analogues. The results indicate a difference of 11.3 kJ mol^{-1} in strain energy between L1 and L2 when they adopt the conformation necessary for complexation of copper(II) to all four nitrogen atoms, the 5,5,5 chelate system being more stable. On the other hand, as

Table 1. Thermodynamic stability, β_{pqr}, of copper(II) complexes ($M_pL_qH_r$) of L1–L3 measured at 25°C and $\mu = 0.15$ mol dm^{-3} NaCl. For comparison, results for related ligands are also given

Ligand	p	q	r	$\log \beta_{pqr}$
L1	0	1	1	8.72
	0	1	2	16.62
	1	1	0	8.33
	1	1	−1	1.06
	1	1	−2	−7.06
	2	1	−2	0.79
	2	1	−3	−6.89
L2	0	1	1	8.84
	0	1	2	16.87
	1	1	0	6.85
	1	1	−1	−1.11
	1	1	−2	−8.50
L3	0	1	1	8.84
	0	1	2	16.87
	1	1	0	8.39
	1	1	−1	−0.27
	1	1	−2	−9.82
	2	1	−2	−1.26
	1	2	0	10.93
L(555)[5]	1	1	−2	−6.44
L(565)[5]	1	1	−2	−3.08
triene[a]	1	1	0	20.2
2,3,2-tet[b]	1	1	0	23.9

[a] trien = *N*,*N*′-bis(2-aminoethyl)ethylenediamine.[5]
[b] 2,3,2-tet = *N*,*N*′-bis(2-aminoethyl)propanediamine.[5]

* Author to whom correspondence should be addressed.

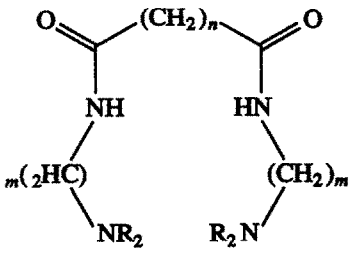

L1: $n = 0$; $m = 2$; R = Me
L2: $n = 1$; $m = 2$; R = Me
L3: $n = 0$; $m = 3$; R = Me
L4: $n = 0$; $m = 2$; R = H
L5: $n = 1$; $m = 2$; R = H

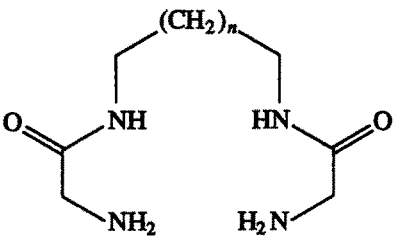

L6: $n = 0$
L7: $n = 1$

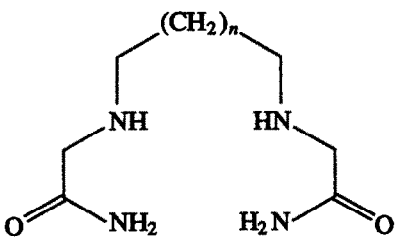

L8: $n = 0$
L9: $n = 1$

Fig. 1. Structural formulae of ligands.

expected, MM2 calculations on the tetraamine analogues showed that there was less strain in the 5,6,5 chelate than the 5,5,5 chelate. In the case of L2, it is difficult for the two amide groups to maintain their planarity and to coordinate to the metal ion. This destabilizes the central malonamide system relative to the oxamide system. At the same time the extra methylene group in the L_2 complex forces the terminal methyl groups together, further destabilizing the complex.

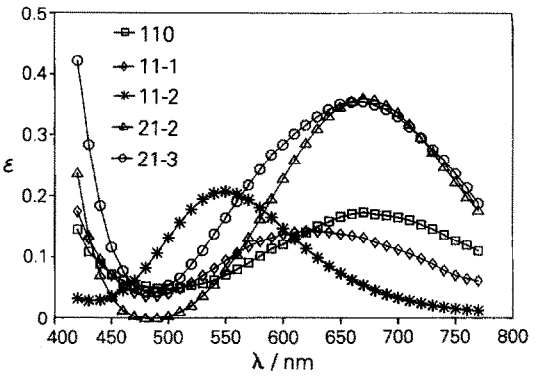

Fig. 2. Calculated electronic spectra of copper/L1 species in aqueous solution: ML (□), MLH_{-1} (◇), MLH_{-2} (*), M_2LH_{-2} (△) and M_2LH_{-3} (○).

Desseyn[7] has shown that, in the solid state, the structure of the MLH_{-2} complex (where L = L4) involves coordination of all four nitrogen atoms to the central metal ion. In order to confirm that the same structure applies to the MLH_{-2} complex of L1 and L2 in solution, the electronic spectra of these species were determined. This was achieved by calculating the individual species' contributions to the measured spectrum. The results for the Cu^{II}/L1 system are shown in Fig. 2. A λ_{max} of 540 nm for the MLH_{-2} species is consistent with coordination by two amide and two amine nitrogen atoms.[8]

In conclusion, we present evidence, for the first time, of a copper(II) chelate complex, in which a 5,5,5 chelate ligand forms more stable complexes than the 5,6,5 analogue.

REFERENCES

1. J. Burgess, *Ions in Solution*. Ellis Horwood, Chichester (1988).
2. C.-H. Len and C.-S. Chung, *J. Chem. Soc., Dalton Trans.* 1990, 1755.
3. M.-S. Chao and C.-S. Chung, *J. Chem. Soc., Dalton Trans.* 1981, 683.
4. A. Zuberbühler and S. Fallab, *Helv. Chim. Acta* 1967, **50**, 889.
5. D. Weatherburn, E. Billo, J. Jones and D. Margerum, *Inorg. Chem.* 1970, **9**, 1557.
6. U. Burkert and N. Allinger, *Molecular Mechanics*. A.C.S. Monograph 177, American Chemical Society, Washington D.C. (1982).
7. H. O. Desseyn, personal communication.
8. A. Zuberbühler and T. Kaden, *Helv. Chim. Acta* 1968, **51**, 1805.

Polyhedron Vol. 10, No. 9, pp. 885–892, 1991
Printed in Great Britain

0277-5387/91 $3.00+.00
© 1991 Pergamon Press plc

SYNTHESIS AND PROPERTIES OF FLUOROTHALLIUM(III) PORPHYRINS. X-RAY CRYSTAL STRUCTURE OF FLUORO-(5,10,15,20-TETRAPHENYLPORPHYRINATO) THALLIUM(III)

ATHANASSIOS G. COUTSOLELOS* and MICHAEL ORFANOPOULOS

Department of Chemistry, Inorganic Chemistry Laboratory, University of Crete, P.O. Box 1470, Heraklion GR-714 09, Crete, Greece

and

DONALD L. WARD

Department of Chemistry, Michigan State University, East Lansing, MI 48824–1322, U.S.A.

(*Received* 27 *July* 1990; *accepted* 2 *November* 1990)

Abstract—The action of sodium fluoride on chlorothallium(III) porphyrins, Tl(Por)Cl, produces the corresponding fluoroporphyrins, Tl(Por)F. These complexes were characterized by their ^{1}H-NMR, UV–vis and IR data. The crystal structures of the title compound [Tl(TPP)F] has been determined by X-ray diffraction. It crystallizes in the monoclinic space group $P2_1/n$ with $Z = 4$ and lattice dimensions $a = 10.118(3)$, $b = 16.236(5)$, $c = 21.189(6)$ Å, $\beta = 90.86(2)°$, $V = 3480(2)$ Å^3. $C_{44}H_{28}FN_4Tl$, $F_w = 836.11$ g, $\rho = 1.60$ g cm^{-3}, $\mu = 47.3$ cm^{-1}, $F(000) = 1640$, temperature 23(1)°C, $R(F) = 0.045$, $Rw(F) = 0.050$ for 2135 observed reflections. The thallium–fluorine distance is 2.441(6) Å with the thallium atom situated 0.741(1) Å above the porphyrin ring.

Much interest has been recently directed towards the synthesis and characterization of one-dimensional inorganic–organic polymeric systems in which a metallic or pseudometallic element alternates along the chain direction with a bridging element such as oxygen or fluorine.[1–6] The metallic or pseudometallic element is usually the central atom of a phthalocyanine or a porphyrin system, resulting in a rigid bridge-stacked polymeric structure. These derivatives become electrical conductors upon iodine oxidation.[7–13] We have recently initiated a search for similar low-dimensional systems in which the central atom of the porphyrin ring is a group III_B element, in which the large phthalocyanine ring is replaced by a porphyrin ligand.[14] Difference Fourier analysis of the EXAFS spectra of the hydroxo- and fluorogallium(III)-2,3,7,8,12,13,17,18-octamethylporphyrins [Ga(OMP)OH and Ga(OMP)F] has afforded some evidence for the polymeric structure of the latter complex.[14]

In this paper, the synthesis and properties of Tl(Por)F complexes are described, the metallic ion of the porphyrin centre, gallium, having been replaced by thallium. No evidence for polymer formation is found and we present a description of the crystal structure of Tl(TPP)F which is, as far as we know, the first X-ray study of a fluorothallium(III) porphyrin.

EXPERIMENTAL

Preparation of complexes

The chloro and fluoro complexes were synthesized following the general procedure described below.

* Author to whom correspondence should be addressed.

Abbreviations. Por: unspecified porphyrinate (2^-); OEP: 2,3,7,8,12,13,17,18-octaethyl porphyrinate (2^-); TPP: 5,10,15,20-tetraphenyl porphyrinate (2^-); OMP: 2,3,7,8,12,13,17,18-octamethyl porphyrinate (2^-).

Chloro-(porphyrinato)thallium(III). $Tl(CH_3COO)_3 \cdot 3/2H_2O$ (37.7 mmol) was added to a solution of porphyrin (9.35 mmol) and tetrahydrofuran (200 cm^3) and the mixture was refluxed for 4 h. Evaporation of the reaction mixture under reduced pressure and extraction of the residue with CH_2Cl_2–H_2O, followed by drying of the organic phase and evaporation *in vacuo* gave a precipitate which was chromatographed (CH_2Cl_2, Al_2O_3). Traces of the free base were eluted first, with the chloro complex as the second fraction. After evaporation of the solvent, the precipitate was recrystallized by slow diffusion of hexane or pentane into a saturated CH_2Cl_2 solution of the porphyrinic complex.

Fluoro-(porphyrinato)thallium(III). Chloro-(porphyrinato)thallium(III) (80 mmol) was dissolved in 100 cm^3 of dichloromethane. After the addition of sodium fluoride (240 mmol) and 2 cm^3 of distilled water, the mixture was stirred for 16 h. The excess of sodium fluoride was removed by washing the organic phase with water. After drying with magnesium sulphate, the solvent was removed under reduced pressure and the residual precipitate was dried at 80°C under 15 mm Hg and recrystallized as described above for the chloro complexes.

Physical measurements

^1H NMR spectra were recorded on a Varian FT-80. Spectra were measured for complex (5 mg) solutions in 0.6 cm^3 of $CDCl_3$ with tetramethylsilane as internal reference. IR spectra were recorded on a Perkin–Elmer 298 spectrophotometer. Samples were prepared as 1% dispersions in CsI pellets or Nujol mulls. Electronic absorption spectra were recorded on a Perkin–Elmer 330 spectrophotometer using 5×10^{-3} mol dm^{-3} dichloromethane solutions or a ORIEL diode-array visible spectrometer.

Crystal and molecular structure determination

A suitable crystal of Tl(TPP)F was obtained by slow diffusion of pentane into a dichloromethane solution of the compound. All data were collected on a Nicolet P3F diffractometer with Mo-K_α radiation ($\lambda = 0.71073$ Å). The crystal data and data collection parameters are summarized in Table 1.

Preliminary Weissenberg photographs along the *b* axis revealed a two-fold symmetry, and from the reflection conditions of $h0l$, $h+l = 2n$ and $0k0$, $k = 2n$ reflections and the subsequent least-squares refinement, the space group was determined to be $P2_1/n$. Experimental conditions and details of the calculations are also included in Table 1. The structure was solved using the Patterson heavy-atom method which revealed the position of the thallium atom. The remaining atoms were located in succeeding difference Fourier syntheses with the hydrogen atoms included in the refinement, but restrained to ride on the atom to which they are bonded. Full-matrix least-squares refinement minimizing $\Sigma w(|F_o| - |F_c|)^2$, with the weight w defined as $4F_o^2/\sigma(F_o^2)^2$, converged to the agreement factors shown in Table 1. The scattering factors were taken from Cromer and Waber.[15] Anomalous dispersion effects were included in F_c;[16] the values for $\Delta f'$ and $\Delta f''$ were those of Cromer.[17] Only the 2135 reflections having intensities greater than three times their standard deviations were used in the refinements. A selection of bond distances and bond angles is given in Table 2.*

RESULTS AND DISCUSSION

During the last two decades, a number of thallium(III) porphyrin complexes possessing different axial ligands have been reported.[18,19] In general, "soft" bases like Cl, I and CN tend to favour five-coordination of the thallium atom in the Tl(Por)X complexes, while a higher coordination number is achieved with hard bases like the acetate ligand.[20] Six-coordination for thallium is also known in the aquohydroxythallium(III) derivatives, Tl(Por)OH(H_2O).[19] The synthesis of metal–carbon complexes from thallium(III) porphyrins was studied first by Henrick *et al.*[21]

We have prepared the chlorothallium(III) porphyrins by the action of $Tl(CH_3COO)_3 \cdot 3/2H_2O$ on free bases in boiling tetrahydrofuran. These complexes were obtained in yields varying from 70 to 90%. Treatment of Tl(Por)Cl with sodium fluoride in dichloromethane led to Tl(Por)F derivatives, whose yields varied with the nature of the axial and equatorial ligands (57–80%).

Tl(Por)X compounds exhibit electronic absorption spectra belonging to the "normal" class[22] (Table 3). They show an intense band in the 418–436 nm region and two bands between 500 and 600 nm (α- and β-bands). One extra band [$Q(2,0)$] observed in the visible region appears blue shifted compared to the Soret band (see Fig. 1). As previously reported by Gouterman *et al.*[23,24] for tin octaethylporphyrin dihalides (with halide = F, Cl, Br, or I), the shifts in the transition energies and relative intensities of the α- and β-bands depend on

* Fractional atomic coordinates, anisotropic thermal parameters and a list of structure factors have been deposited as supplementary data with the Editor, from whom copies are available on request.

Table 1. Experimental details (crystal data, intensity measurements, structure solution and refinement)

Formula	$C_{44}H_{28}FN_4Tl$
Formula weight	836.11
Space group	Monoclinic, $P2_1/n$
a (Å)	10.118(3)
b (Å)	16.236(5)
c (Å)	21.189(6)
β (°)	90.86(2)
V (Å^3)	3480(2)
Z	4
C (g cm^{-3})	1.60
μ (cm^{-1})	47.3
$F(000)$	1640
Temperature (°C)	23(1)
Crystal dimensions (mm)	$0.08 \times 0.20 \times 0.26$
Maximum 2θ (°)	45
Number of reflections measured	5250 total, 4568 unique
Solution	Patterson method
Refinement	Full-matrix least squares
Minimization function	$\Sigma w(\|F_o\| - \|F_c\|)^2$
Least-squares weights	$4F_o^2/\sigma(F_o^2)^2$
Anomalous dispersion	All non-hydrogen atoms
Reflections included	2135 with $I > 3\sigma(I)$
Parameters refined	446
Unweighted agreement factor	0.045
Weighted agreement factor	0.050
Factor including unobserved data	0.045
ESD of observed data of unit weight	1.41
High peak in final difference map	1.15(14)e/Å^3
Low peak in final difference map	−0.62(14)e/Å^3
Computer hardware	VAX 11/750
Computer software	SDP/VAX (Enraf–Nonius & B.A. Frenz & Associates, Inc.)

the charge and polarizability of the axial ligand and correlate with changes in the electron density in the porphyrin ring.

The IR spectra of the isolated chloro complexes show a band in the region 275–290 cm^{-1}, assigned to the Tl—Cl stretching. This characteristic band is found between 415–485 cm^{-1} for the fluoro derivatives (415 and 485 cm^{-1} for TPP and OEP, respectively).

Table 4 summarizes ^{1}H NMR data for each Tl(Por)Cl and Tl(Por)F complex. No dramatic changes in the porphyrin chemical shifts as a func-

Table 2. Selection of bond distances (Å) and angles (°)

Bond distances (Å)			
Tl(1)—F(1)	2.441(6)	Tl(1)—N(23)	2.181(12)
Tl(1)—N(21)	2.221(12)	Tl(1)—N(24)	2.225(14)
Tl(1)—N(22)	2.223(14)		

Bond angles (°)			
F(1)—Tl(1)—N(21)	108.3(4)	N(21)—Tl(1)—N(23)	140.2(5)
F(1)—Tl(1)—N(22)	110.5(4)	N(21)—Tl(1)—N(24)	83.5(5)
F(1)—Tl(1)—N(23)	111.5(4)	N(22)—Tl(1)—N(23)	83.4(5)
F(1)—Tl(1)—N(24)	107.9(4)	N(22)—Tl(1)—N(24)	141.6(5)
N(21)—Tl(1)—N(22)	82.8(5)	N(23)—Tl(1)—N(24)	84.5(5)

Table 3. UV–vis data (λ/nm)[a]

Compound	B(1,0)	B(0,0)	Q(2,0)	Q(1,0) (or α)	Q(0,0) (or β)
Tl(OEP)Cl[b]	sh	418	498	545	582
	—	(225.7)	(2.1)	(11.8)	(10.5)
Tl(OEP)F[c]	sh	421	501	549	583
	—	(296.8)	(2.3)	(19.3)	(14.5)
Tl(TPP)Cl[b]	sh	434	520	566	608
	—	(360.5)	(2.7)	(13.6)	(8.5)
Tl(TPP)F[c]	sh	436	522	569	609
	—	(445.9)	(3.1)	(22.6)	(11.3)

[a] 10^{-3} ε/dm^3 mol^{-1} cm^{-1} given in parentheses.
[b] Reference 26.
[c] This work.

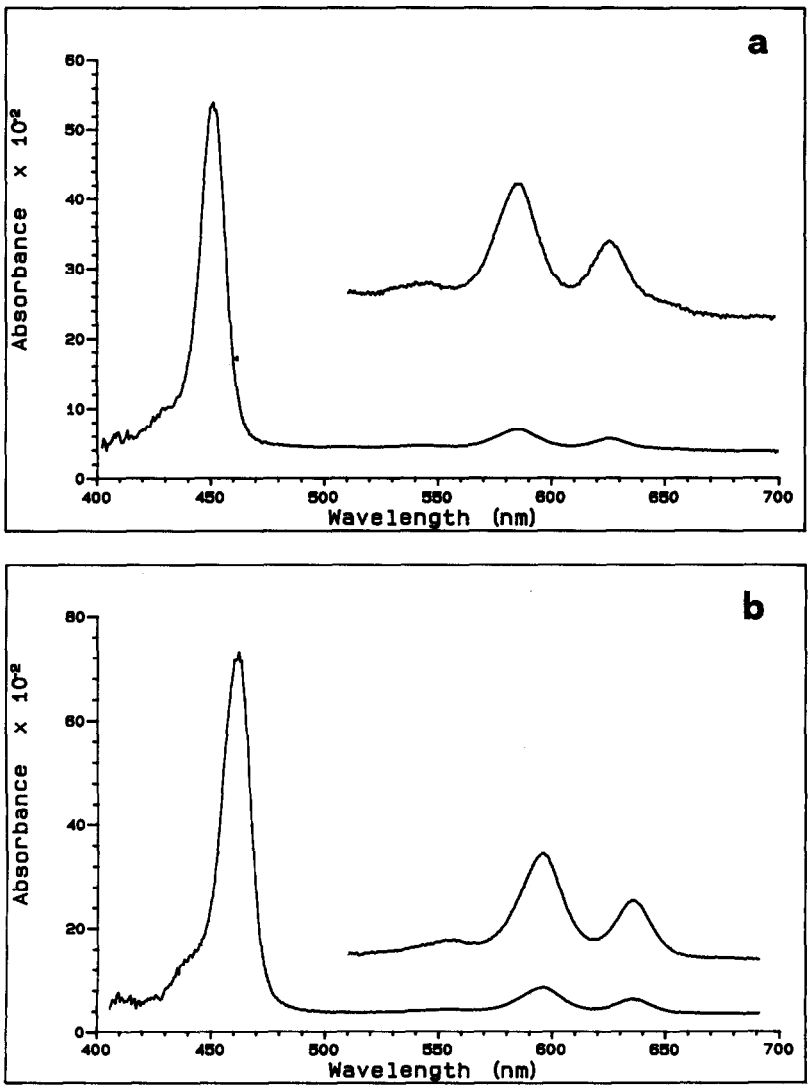

Fig. 1. UV–vis spectra of (a) Tl(TPP)F and (b) Tl(TPP)Cl complexes.

Table 4. ^{1}H NMR[a] data

Compound	R^1	R^2	Protons of R^1	Protons of R^2
Tl(OEP)Cl[b]	H	Et	d/4 10.33(39)[c]	t,24 1.79 m,16 3.87
Tl(OEP)F[d]	H	Et	d/4 10.25(44)[c]	t,24 1.86 m/16 4.06
Tl(TPP)Cl[b]	Ph	H	*o*-H, m/8 7.98	d/8 9.03(63) *m,p*-H m/12 7.42
Tl(TPP)F[c]	Ph	H	*o*-H, m/8 7.83	d/8 9.01(64) *m,p*-H m/12 7.73

[a] Spectra recorded on $CDCl_3$. Data given as multiplicity, intensity, δ/ppm.
[b] Reference 26.
[c] Values in parentheses are ^1H–$^{203,205}Tl$ coupling constants in Hz.
[d] This work.

tion of the axial ligand are observed. More positively charged central metal ions reduce the electron density on the porphyrin macrocycle and thus deshield the porphyrin protons.[25] The porphyrin electron density is also dependent on the electron-withdrawing properties of the axial ligand,[26] and the *meso* proton chemical shift of Tl(OEP)X varies with the axial ligand X, as Cl < F (Fig. 2 with some ^{1}H NMR spectra). The central metal of Tl(Por)R is a heavy metal and this fact appears to be more important in influencing deshielding than the electron-donor or acceptor properties of the axial ligand. For comparison, the porphyrin proton resonances of Ga(Por)R do not depend upon the electron-donor ability of the axial ligand.[27]

As reported[28,29] in the literature, ^{1}H–^{203,205}Tl

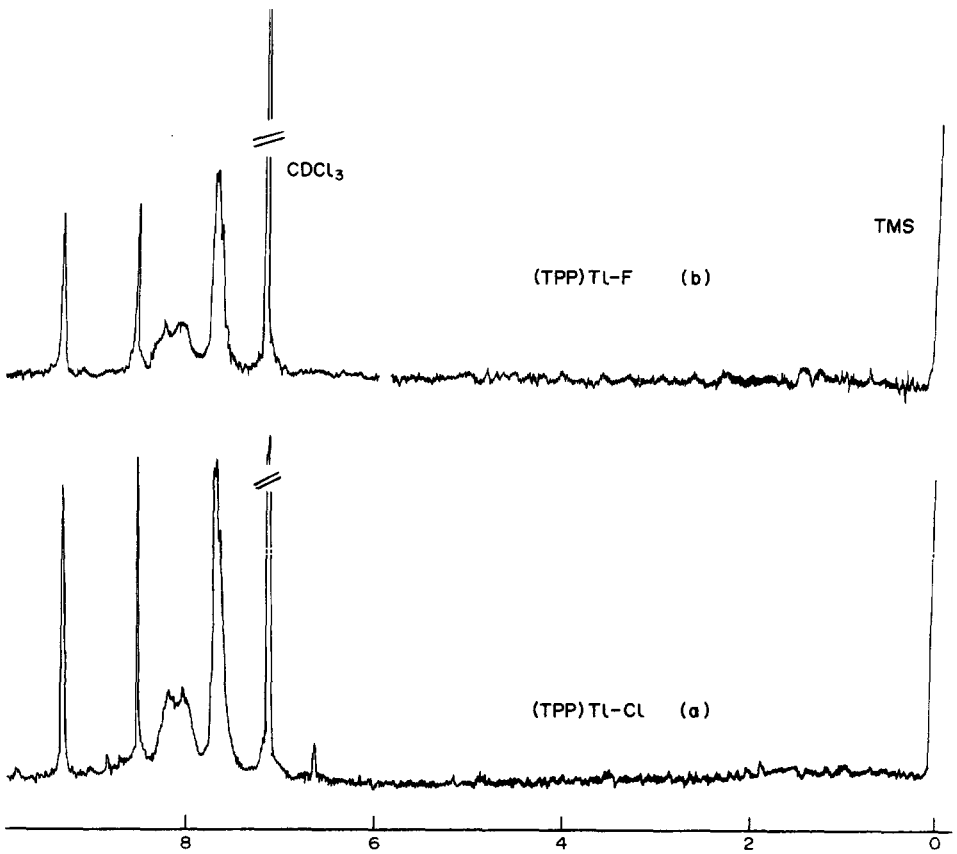

Fig. 2. ^{1}H NMR spectra of (a) Tl(TPP)Cl and (b) Tl(TPP)F complexes.

couplings are observed, but only between thallium(III) and *meso* or pyrrole protons of the porphyrin macrocycle, and the axial ligand proton. The magnitude of the coupling varies with the proton–thallium distance. The signals of octaethylporphyrin complexes show a multiplet for the methylene protons as the AB part of the ABX_3 system. This is similar to the case for complexes in the gallium or indium series and agrees with pentacoordination of the thallium(III) metal as well as an out-of-plane metal atom. The specific chemical shifts for each of Tl(OEP)X and Tl(TPP)X are given in Table 4. As seen in this table, only small and insignificant variations of the chemical shifts occur. The resonances of the methine protons or *meso* protons depend on the electron-donating ability of the axial ligands, which is a conclusion reached by comparison with other five-coordinated thallium porphyrins, where X = —CN, —SCN and $—N_3$.[30]

As no structure of a fluorothallium porphyrin has been reported before, and in order to provide a comparison with the case of gallium and indium fluoroporphyrins, the crystal structure of Tl(TPP)F has been determined (Fig. 3). The ORTEP drawing of the molecule reveals the five-coordination geometry of the thallium atom to the four nitrogen atoms (N_p) of the porphyrinato group and the fluorine atom; the coordination polyhedron is very close to a square pyramid with a Tl—F bond distance of 2.441(6) Å, and a mean Tl—N_p bond of 2.21(1) Å; the thallium atom lies 0.741(1) Å above the plane defined by the porphyrinato nitrogen atoms, resulting in a mean F—Tl—N_p bond angle of 109.6(6)°. The above values are very similar to the ones encountered in Tl(TPP)Cl and $Tl(TPP)CH_3$, where, for example, the bond distances to the axial ligands are 2.420(4) and 2.147(12) Å, respectively. From these data, the reason for the adoption of five-coordinate geometry by thallium becomes apparent: in order to minimize radial strain, the approach of a second axial ligand would require either a major distortion from planarity of the N_4 donor set, or a significant shortening of the Tl—N bonds from the average of 2.21 Å to a value of 2.01 Å. In Table 5, are collected the M—L and the average M—N_p distances for a number of metalloporphyrins of group III_B with various axial ligands. It is apparent that these distances correlate well with the increase in ionic radii from Ga^{3+} to Tl^{3+}, with the absolute values depending on the axial ligand also. Nevertheless, even though the size of the cation plays a major role in the resulting geometry of the metalloporphyrin complex, the case of the $[In(TPP)OSO_2CH_3]_n$ polymeric system clearly demonstrates that this rule is not always

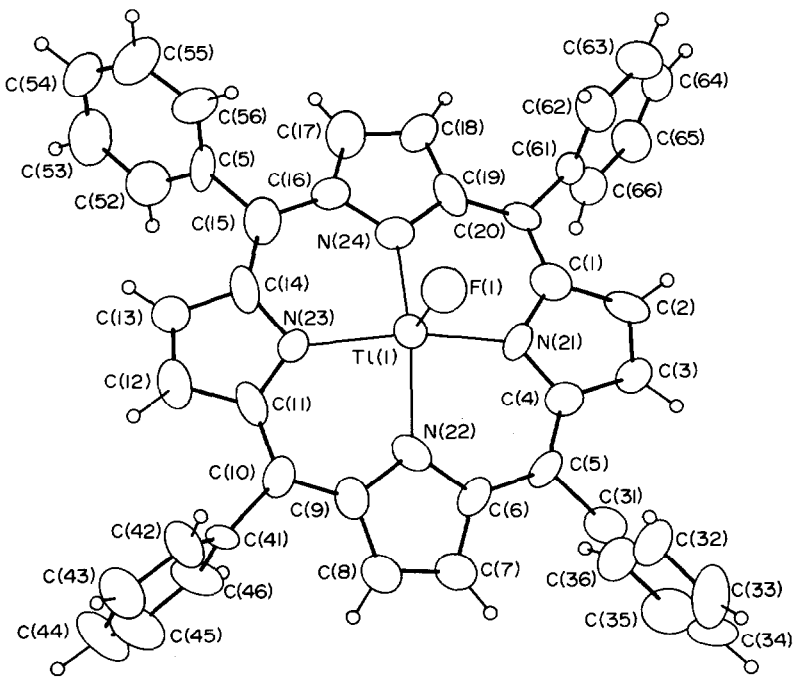

Fig. 3. ORTEP view of the Tl(TPP)F complex.

Table 5. Comparative X-ray data for metalloporphyrins of group III_B

Compound	M—L (Å)	M—4N_n (Å)	Reference
$Ga(OEP)OSO_2CH_3$	1.908(6)	2.013(5)	38
$Ga(OEP)N_3$	1.955(2)	2.034(3)	39
Ga(OMP)F	1.97(3)	2.04	14
Ga(TPP)Cl	2.196(2)	2.021	37
Ga(TPP)Cl,py	2.33 and 2.27	2.01	30
In(TPP)Cl	2.369(2)	2.156(6)	35
$In(TPP)CH_3$	2.132(15)	2.205(10)	21
In(TPP)[$(N_4C)R$]	2.183(5)	2.128(4)	36
$In(TPP)CO_2CH_3$	2.15 and 2.60	2.16	33
$[In(TPP)OSO_2CH_3]_n$	2.352(12), 2.357(11)	2.13, 2.08	40
$Tl(TPP)CH_3$	2.147(6)	2.229	21
Tl(TPP)Cl	2.420(4)	2.21(1)	21
Tl(TPP)F	2.441	2.213	This work

obeyed. We are continuing our systematic exploration of the metalloporphyrin complexes of group III_B.

Acknowledgements—This work was supported by a grant from the Greek General Secretariat of Research and Technology (No. 87 ΠΣ 64). We thank Hourdakis Corporation for partial support. Special thanks are due to Professor G. J. Karabatsos for the continuous scientific encouragement over the past 3 years. The X-ray diffractometer was provided, in part, by the National Science Foundation Grant (CHE 84-03823).

REFERENCES

1. R. S. Nohr and K. J. Kalina, *J. Chem. Soc., Chem. Commun.* 1981, 1210.
2. P. Brandt, D. C. Weber, S. G. Haupt, R. S. Nohr and K. J. Wynne, *J. Chem. Soc., Dalton Trans.* 1985, 269.
3. T. J. Marks, *J. Coatings Technol.* 1976, **48**, 53.
4. T. J. Marks and D. W. Kalina, in *Extended Linear Chain Compounds* (Edited by J. S. Miller), Vol. 1, Ch. 6, p. 197. Plenum Press, New York (1982).
5. C. W. Dirk and T. J. Marks, *Inorg. Chem.* 1984, **43**, 4325.
6. E. Ciliberto, K. A. Doris, W. J. Pietro, G. M. Reisner, D. E. Ellis, I. Fragala, F. H. Herbstein, M. A. Ratner and T. J. Marks, *J. Am. Chem. Soc.* 1984, **106**, 7748.
7. T. E. Phillips and B. M. Hoffman, *J. Am. Chem. Soc.* 1977, **99**, 7734.
8. C. J. Schramm, D. R. Stojakovic, B. M. Hoffman and T. J. Marks, *Science* 1978, **200**, 47.
9. M. Cowie, A. Gleizes, G. W. Grynkewich, D. W. Kalina, M. S. McClure, R. P. Scaringe, R. C. Teitelbaum, S. L. Ruby, J. A. Ibers, C. R. Kannewurf and T. J. Marks, *J. Am. Chem. Soc.* 1979, **101**, 7071.
10. K. F. Schoch Jr, B. R. Kundalkar and T. J. Marks, *J. Am. Chem. Soc.* 1979, **101**, 7071.
11. P. M. Kuznesof, K. J. Wynne, R. S. Nohr and M. E. Kenney, *J. Chem. Soc., Chem. Commun.* 1980, 121.
12. (a) B. M. Hoffman, T. E. Phillips, C. J. Schramm and S. K. Wright, in *Molecular Metals* (Edited by W. E. Hatfield), p. 393. Plenum Press, New York (1979); (b) J. P. Collman, G. E. Barnes and L. K. Woo, *Proc. Natl. Acad. Sc. USA* 7684, **80**, 1983.
13. R. S. Nohr, P. M. Kuznesof, K. J. Wynne, M. E. Kenney and P. G. Siebenman, *J. Am. Chem. Soc.* 1981, **103**, 4371.
14. J. Goulon, P. Friant, C. Goulon-Ginet, A. Coutsolelos and R. Guilard, *Chem. Phys.* 1984, **83**, 367.
15. D. T. Cromer and J. T. Waber, *International Tables for X-ray Crystallography*, Vol. IV, Table 2. 2B. Kynoch Press, Birmingham, U.K. (1974).
16. J. A. Ibers and W. C. Hamilton, *Acta Cryst.* 1964, **17**, 781.
17. D. T. Cromer, *International Tables for X-ray Crystallography*, Vol. IV, Table 2. 2B. Kynoch Press, Birmingham, U.K. (1974).
18. R. J. Abraham, G. H. Barnett and K. M. Smith, *J. Chem. Soc., Perkin Trans.* 1975, **1**, 2142.
19. K. Henrick, R. W. Mattwes and P. A. Tasker, *Inorg. Chem.* 3293, **16**, 1977.
20. R. G. Pearson, *Science* 1966, **151**, 172.
21. K. Henrick, R. W. Matthews and P. A. Tasker, *Inorg. Chem.* 1977, **12**, 3293.
22. M. Gouterman, in *The Porphyrins* (Edited by D. Dolphin), Vol. 3, p. 1. Academic Press, New York (1978).
23. M. Gouterman, F. P. Schwarz and P. D. Smith, *J. Chem. Soc.* 1973, **59**, 676.
24. M. Gouterman, F. P. Schwarz and P. D. Smith, *J. Chem. Soc.* 1974, **61**, 3491.
25. H. Sheer and J. J. Katz, in *Porphyrins and Metalloporphyrins* (Edited by K. M. Smith), Ch. 10. Elsevier, Amsterdam (1975).

26. K. M. Kadish, A. Tabard, A. Zrineh, M. Ferhat and R. Guilard, *Inorg. Chem.* 1987, **26**, 2459.
27. K. M. Kadish, B. Boisselier-Cocolios, A. Coutsolelos, P. Mitaine and R. Guilard, *Inorg. Chem.* 1985, **24**, 4521.
28. T. R. Janson and J. J. Katz, in *The Porphyrins* (Edited by D. Dolphin), Vol. IV, Ch. 1, and refs therein. Academic Press, New York (1978).
29. R. J. Abraham, G. E. Hawkwes, M. F. Hudson and K. M. Smith, *J. Chem. Soc., Perkin Trans. 2* 1975, 204, and preceding papers cited therein.
30. A. Coutsolelos, unpublished results.
31. D. M. Collins and J. L. Hoard, *J. Am. Chem. Soc.* 1970, **92**, 3761.
32. P. Cocolios, P. Fournari, R. Guilard, C. Lecomte, J. Protas and J. C. Boudel, *J. Chem. Soc., Dalton Trans.* 1980, 2081.
33. P. Cocolios, D. Bayeul and C. Lecomte, *Inorg. Chem.* 1985, **24**, 2058.
34. A. Coutsolelos, *Thèse d'Etat.* Université de Dijon (1985).
35. R. G. Ball, K. M. Lee, A. G. Marshall and J. Trotter, *Inorg. Chem.* 1980, **19**, 1463.
36. R. Guilard, S. S. Gerges, A. Tabard, P. Richard, M. A. El Borai and C. Lecomte, *J. Am. Chem. Soc.* 1987, **109**, 7228.
37. A. Coutsolelos, R. Guilard, A. Bayeul and C. Lecomte, *Polyhedron* 1986, **6**, 1157.
38. A. Boukhris, C. Lecomte, A. Coutsolelos and R. Guilard, *J. Organomet. Chem.* 1986, **303**, 151.
39. A. Coutsolelos, R. Guilard, A. Boukhris and C. Lecomte, *J. Chem. Soc., Dalton Trans.* 1986, 1779.
40. P. Cocolios, P. Fournari, R. Guilard, C. Lecomte, J. Protas and J. C. Boudel, *J. Chem. Soc., Dalton Trans.* 1980, 2081.

Polyhedron Vol. 10, No. 9, pp. 893–898, 1991
Printed in Great Britain

0277–5387/91 $3.00+.00
© 1991 Pergamon Press plc

COORDINATION GEOMETRIES AND COOPERATIVE ORDERING EFFECTS IN COPPER(II) COMPLEXES WITH TRIDENTATE SCHIFF BASE DIANIONS—II. EPR STUDY ON N-SALICYLIDENEGLYCINATOCOPPER(II) COMPLEXES WITH IMIDAZOLE DERIVATIVES*

G. PLESCH†

Institute of Inorganic Chemistry, Slovak Academy of Sciences, CS-842 36 Bratislava, Czechoslovakia

and

C. FRIEBEL†

Fachbereich Chemie der Philipps-Universität, DW-3550 Marburg, F.R.G.

and

O. ŠVAJLENOVÁ and J. KRÄTSMÁR-ŠMOGROVIČ

Department of Inorganic and Organic Chemistry, Faculty of Pharmacy, Comenius University, CS-832 32 Bratislava, Czechoslovakia

(*Received* 7 *February* 1990; *accepted* 5 *December* 1990)

Abstract—N-salicylideneglycinatocopper(II) complexes of the composition Cu(salgly)(L)$(H_2O)_x$ were synthesized with L = 1-methylimidazole, 2-methylimidazole, 2-ethylimidazole, 2-ethyl-4-methylimidazole, 2-phenylimidazole, benzimidazole; and $x = 0$, 1 or 2. According to the results of ligand-field and EPR spectra, the coordination polyhedra around copper(II) exhibit geometries ranging from square-pyramidal to square-planar. The water of crystallization and the substituents on the imidazole ligand, moreover, remarkably influence cooperative ordering effects. A variety of coupling patterns between ferrodistortive and antiferrodistortive is observed. In some cases enhancement of the EPR measuring frequency from 9 to 35 GHz results in partial decoupling of the systems.

N-salicylideneglycinatocopper(II) complexes are of much interest as model compounds for the intermediates in the non-enzymatic transamination reaction.[1] Much attention has been devoted to structural and spectroscopic studies on these compounds in the solid state. As proven by X-ray structural analysis most N-salicylideneglycinatocopper(II) complexes adopt square-pyramidal copper(II) coordination with three donor atoms of the tridentate Schiff base dianion and one of the additional neutral ligands in the basal plane.[2,3] The apex of the pyramid is occupied by an oxygen atom (O′) from a neighbouring molecule or from water. For N-salicylideneglycinato(4-methylpyridine) copper(II) hexahydrate, however, square-planar copper(II) coordination has been reported recently.[4]

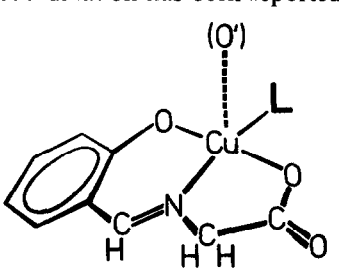

(I)

* For part I, see ref. 9.

† Authors to whom correspondence should be addressed.

A number of N-salicylideneglycinatocopper(II) adducts (**I**) with various neutral monodentate ligands (L) involving O, N, S donor atoms has been prepared.[4-6] According to EPR and electronic spectral data most of these complexes are square-pyramidal. The substitution of the neutral ligand and variation of the number of crystal water molecules, however, remarkably influence cooperative ordering effects in the crystal structure. A variety of coupling patterns between ferrodistortive and antiferrodistortive has been observed.

In order to gain further insight into the influence of the neutral ligand on the structure of these complexes, we prepared a series of N-salicylideneglycinatocopper(II) adducts with variously substituted imidazole. Their EPR and ligand-field spectra were studied. In particular, the EPR spectroscopy is a valuable tool for investigating the coordination geometry and cooperative coupling effects in the solid state of these copper(II) complexes.

EXPERIMENTAL

Preparation of the complexes

N-salicylideneglycinato(aqua)copper(II) hemihydrate (**A**) was prepared according to ref. 7.

The N-salicylideneglycinatocopper(II) adducts with 1-methylimidazole(→ monohydrate), 2-methylimidazole(→ dihydrate), 2-ethylimidazole, 2-ethyl-4-methylimidazole, 2-phenylimidazole(→ dihydrate) and benzimidazole were synthesized in diluted ethanol (ethanol–water = 3 : 1). Each time, 1.34 g (5 mmol) of **A** was dissolved in 140 cm^3 of the solvent (in the case of 1-methylimidazole in 100 cm^3), heated to boiling and the neutral ligand was added in excess: 10 mmol were used of 1- and 2-methylimidazole (0.82 g), of 2-ethylimidazole (0.96 g) and of 2-ethyl-4-methylimidazole (1.10 g), respectively, but 7.5 mmol of 2-phenylimidazole (1.08 g) and of benzimidazole (0.90 g); the last one was in the form of a 7 cm^3 aqueous solution. The resulting solutions were heated to boiling, filtered and allowed to cool. The green or bluish-green crystals which deposited, were washed with cool solvent and dried in air.

Dehydrated N-salicylideneglycinato(2-methylimidazole)copper(II) was prepared in an analogous way using 100 cm^3 of diluted methanol (methanol–water = 3 : 1), 1.34 g of **A** and 10 mmol (0.82 g) of 2-methylimidazole.

The analytical data of the obtained complexes are given in Table 1.

Spectral measurements

The EPR spectra of powdered solids were measured at room temperature in X band (9.1 GHz) with a Varian E-4 spectrometer and in Q band (35 GHz) with a Varian E-15 device. DPPH was used as an internal standard.

The electronic spectra of finely powdered samples were recorded in the range 11,000–30,000 cm^{-1} with a Specord M-40 spectrometer (C. Zeiss, Jena) and also with a Zeiss DMR-21 spectrometer equipped with a low-temperature accessory. MgO was used as standard.

RESULTS AND DISCUSSION

The reaction of N-salicylideneglycinato(aqua)copper(II) hemihydrate with imidazole derivatives (L) led to adducts of the general formula Cu(salgly)(L)$(H_2O)_x$, where $x = 0$, 1 or 2. The preparation and spectral properties of the complexes with L = imidazole, $x = 0$, and L = 2-propylimidazole, $x = 1$, respectively, were reported in our previous paper.[5] The electronic spectra containing an asymmetric ligand-field band (maximum in the range 14,400–16,700 cm^{-1}) with a broad shoulder of about the same intensity but higher energy (Table 2) indicate square-pyramidal copper(II) coordina-

Table 1. Analytical data for N-salicylideneglycinatocopper(II) complexes, Cu(salgly)(L)$(H_2O)_x$

L[a]	x	Formula	Elemental analysis (%)—Found (Calc.) C	H	N
1-MeIm	1	$C_{13}H_{15}CuN_3O_4$	46.0 (45.8)	4.6 (4.4)	12.4 (12.3)
2-MeIm	0	$C_{13}H_{13}CuN_3O_3$	48.4 (48.4)	4.2 (4.1)	13.0 (13.0)
2-MeIm	2	$C_{13}H_{17}CuN_3O_5$	43.4 (43.5)	4.8 (4.8)	11.6 (11.7)
2-EtIm	0	$C_{14}H_{15}CuN_3O_3$	49.8 (49.9)	4.6 (4.5)	12.4 (12.5)
2-Et-4-MeIm	0	$C_{15}H_{17}CuN_3O_3$	50.8 (51.3)	4.9 (4.9)	12.0 (12.0)
2-PhIm	2	$C_{18}H_{19}CuN_3O_5$	51.6 (51.4)	4.6 (4.6)	10.0 (10.0)
benzIm	0	$C_{16}H_{13}CuN_3O_3$	53.1 (53.6)	3.7 (3.7)	11.6 (11.7)

[a] Im = imidazole; Me = methyl; Et = ethyl; Ph = phenyl.

Table 2. Ligand-field and EPR spectral data of N-salicylideneglycinatocopper(II) complexes, Cu(salgly)(L)$(H_2O)_x$, aranged in order of increasing elongation of the copper(II) coordination pyramids

Neutral donor ligand (L) and crystal water content (x)		Observed band positions ($\times 10^3$ cm^{-1})		EPR parameters							
				g_z / $g_\parallel$		g_y		g_x / $g_\perp$			
					g_1^c		g_2^c		g_3^c		
L	x	Δ_{max}	Δ_{sh}	g_{av}		$g_\perp^c$		$g_\parallel^c$			
2-PhIm	2	14.4	≈ 16.6	2.126	2.262			2.062		2.054	
2-MeIm[a]	0	14.6	≈ 16.4	2.126		2.176		2.146		2.056	
2-PrIm[b,c]	1	15.3	≈ 17.8	2.125		2.188		2.131		2.057	
2-EtIm	0	15.0	≈ 17.5	≃2.122		≈ 2.15$_5$				2.055	
				2.122		2.145		2.138		2.082	
benzIm	0	15.2	≈ 17.0	2.119	2.247					2.055	
				2.119		2.195		2.108		2.054	
1-MeIm	1	15.2	≈ 17.0	2.118	2.245					2.055	
Im[c]	0	15.5	≈ 17.8	2.117		2.152		2.145		2.053	
2-Et-4-MeIm	0	16.4	—	2.108	2.227			2.052			2.044
2-MeIm	2	16.7	—[d]	2.107	2.228					2.046	

[a] Reference 9.
[b] Pr = propyl.
[c] Reference 5.
[d] Band positions at 5 K: Δ_{max} = 15.3/17.1; $\Delta_{sh} \approx 20.0$.

tion.[5,6,8] We tentatively assign the maximum to a superposition of the $d_{x^2-y^2} \leftarrow d_{z^2}$ and $d_{x^2-y^2} \leftarrow d_{xy}$ transitions. According to this, the shoulder may be correlated with the $d_{x^2-y^2} \leftarrow d_{xz,yz}$ transition. Apart from this, the last two examples in Table 2 deviate by a pronounced blue-shift of the absorption bands, confirmed by a low-temperature measurement in the case of [Cu(salgly)(2-MeIm)]·$2H_2O$.

The EPR spectra, however, show a great variety of patterns (Figs 1 and 2, Table 2). The g_{av} values lie, with the exception of the complexes [Cu(salgly)(2-Et-4-MeIm)] and [Cu(salgly)(2-MeIm)]·$2H_2O$, in the range 2.126–2.117. Such g factors were found for square-pyramidal N-salicylideneglycinato- or N-pyruvideneglycinatocopper(II) complexes with additional N donor ligands.[5,6,8]

The molecular g components for a system of tetragonal symmetry with the $d_{x^2-y^2}$ ground state are defined by the expressions

$$g_\parallel = 2.0023 - 8k_\parallel{}^2\lambda_0/\Delta E_{xy}$$
$$g_\perp = 2.0023 - 2k_\perp{}^2\lambda_0/\Delta E_{xz,yz} \qquad (1)$$

where $\lambda_0 = -830$ cm^{-1} is the spin–orbit coupling constant for the free Cu^{2+} ion, $k_\parallel$ and $k_\perp$ are the orbital

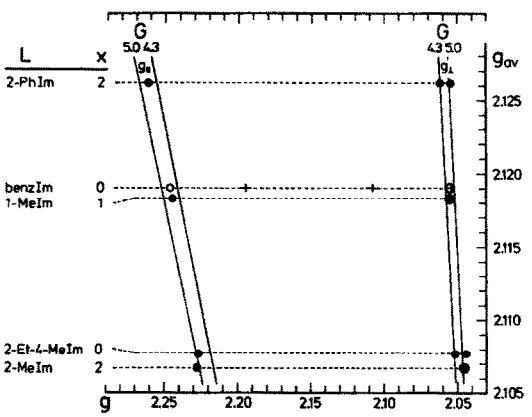

Fig. 1. Diagram showing the g values of N-salicylideneglycinatocopper(II) complexes, Cu(salgly)(L)$(H_2O)_x$: coupled components in the case of ferrodistortively ordered complex molecules, corresponding to molecular g factors. (For the benzimidazole adduct superimposed g components of a disturbed antiferrodistortive pattern are marked by crosses, see text.)

reduction factors, and ΔE the ligand-field splitting energies. Significant contribution to these energies comes from the $4\delta_1 = \Delta E(d_{x^2-y^2} \leftarrow d_{z^2})$ splitting of the cubic ^2E_g ground state of Cu^{2+} ions. This split-

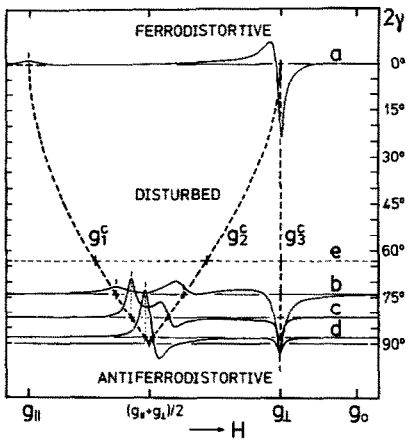

Fig. 2. EPR powder spectra of Cu(salgly)(L)$(H_2O)_x$ resulting from coupled molecular g components ($g_{\parallel}$, $g_{\perp}$) according to eq. (2); ferrodistortive pattern: L = 1-MeIm, $x = 1$ (a); disturbed antiferrodistortive patterns: L = 2-PrIm, $x = 1$ (b); L = 2-MeIm, $x = 0$ (c); L = Im, $x = 0$ (d); L = benzIm, $x = 0$ (e).

ting is proportional to the axial ligand-field component. From recently performed X-ray structural analysis of [Cu(salgly)(2-MeIm)] it is known that the highest $g_{av} = 2.126$ corresponds to an apical Cu—O′ distance of 248 pm.[9] Hence, we assume that the smaller g_{av} value of < 2.11 in both [Cu(salgly)(2-Et-4-MeIm)] and of [Cu(salgly)(2-MeIm)]·$2H_2O$ reflects a remarkably weaker axial ligand-field component in these complexes, corresponding to square-planar coordination geometry. It is in accordance with the observed blue-shift in the electronic spectra (Table 2) and identical with the g_{av} value, which was observed for the square-planar copper(II) coordination in [Cu(salgly)(4-MePy)]·$6H_2O$.[4]

The different EPR spectra give evidence for a variety of cooperative ordering effects in these solid N-salicylideneglycinatocopper(II) complexes. When the unit cell contains coordination polyhedra, the Cu^{2+} centres of which are coupled by directed sufficiently strong dipolar interactions, cooperative effects influence the EPR spectra.[10] In the case of two sets of axial complex molecules, where the g_z axes are canted by an angle 2γ ($0° \leqslant 2\gamma \leqslant 90°$), the following crystal g values are observed:[11]

$$g_1^c = \cos^2\gamma g_{\parallel} + \sin^2\gamma g_{\perp}$$
$$g_2^c = \sin^2\gamma g_{\parallel} + \cos^2\gamma g_{\perp}$$
$$g_3^c = g_{\perp}. \qquad (2)$$

If all $g_{\parallel}$ axes are aligned parallel ($2\gamma = 0°$, ferrodistortive ordering) the experimental g^c factors correspond to molecular ones. These g values, according to eq. (1), directly reflect the geometry of the coordination polyhedra. The value of the parameter $G = (g_{\parallel} - g_0)/(g_{\perp} - g_0)$ usually lies in the range 4.5–4.9 [for g tensors with small orthorhombic splitting we take $g_{\perp} = (g_x + g_y)/2$].[12] Values of the G parameter which are smaller than 4.4 indicate the presence of coupling of Cu^{2+} ions in coordination polyhedra with mutually non-parallel g_z axes. The g components are then given by both coordination geometry and cooperative ordering effects.

Four of the complexes, Cu(salgly)(L)$(H_2O)_x$, of the imidazole series with L = 2-PhIm, $x = 2$; L = 2-MeIm, $x = 2$; L = 1-MeIm, $x = 1$; and L = 2-Et-4-MeIm, $x = 0$, respectively, show molecular g values (in Fig. 1 indicated by full circles). The exchange-narrowed EPR spectral lines [see Fig. 3(a,b)] provide evidence for coupling effects between ferrodistortively ordered complex units in the structure. The g tensor of [Cu(salgly)(2-PhIm)]·$2H_2O$, where position 2 of the imidazole group adjacent to the donor nitrogen atoms is occupied by the bulky phenyl substituent, shows some orthorhombic splitting (Table 2, Fig. 1). A comparable splitting is observed for the 2-ethyl-4-methylimidazole adduct [Figs 1 and 3(a)]. The other complexes appear to be of axial symmetry. The g parameters of the compound [Cu(salgly)(2-MeIm)]·$2H_2O$ yield $G = 5.1$ (Fig. 1). High G values have been reported to arise from out-of-plane π bonding.[13] We have no reasonable explanation for this value in our complex, however.

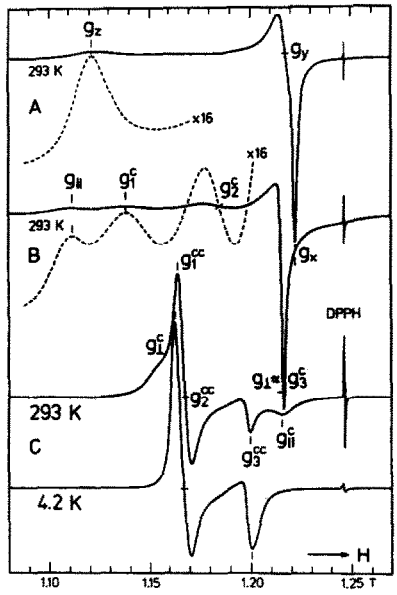

Fig. 3. A selection of EPR powder spectra (34.95 GHz) summarizing all the characteristics of local and cooperative symmetry effects in adducts of N-salicylideneglycinatocopper(II) with imidazole derivatives: (a) [Cu(salgly)(2-Et-4-MeIm)], (b) [Cu(salgly)(benzIm)] and (c) [Cu(salgly)(2-EtIm)].

When the highest experimental g component lies lower than the $g_\parallel$ area in Fig. 1, then the g tensor is influenced by coupling of the Cu^{2+} ions in crystallographically equivalent sites generated by glide-reflection planes parallel (010) to the monoclinic unit-cells, corresponding to canting angles, $20° < 2\gamma \leqslant 90°$, between the 3-ring planes of the Cu(salgly) complex molecules.* Separation of the contributions of coordination geometry and cooperative ordering effects to the experimentally determined g tensor is here of interest. From eq. (2) follows for the canting angle, 2γ:

$$\cos 2\gamma = (g_1^c - g_2^c)/(g_1^c + g_2^c - 2g^c). \qquad (3)$$

For the full interpretation, however, the complete structural data from X-ray diffraction and EPR measurements on monocrystals are necessary.[14,15]

The EPR spectra of N-salicylideneglycinatocopper(II) adducts with imidazole [Fig. 2(d)] and 2-propylimidazole [Fig. 2(b)] were interpreted in terms of two coupled copper(II) coordination polyhedra of axial symmetry canted by an angle of $2\gamma = 88°$ and 74°, respectively.[5] In the case of [Cu(salgly)(2-MeIm)] [Fig. 2(c)], from a detailed EPR investigation of a monocrystal combined with the crystallographic data from a X-ray structure analysis,[9] a canting angle of $2\gamma = 81.5°$ was deduced, resulting in an orthorhombic molecular g tensor with the components $g_z = 2.263$, $g_y = 2.063$, $g_x = 2.052$. Therefore the assumption of axial symmetry in the preceding examples was arbitrary and strictly speaking not compulsory. Changing from tetragonal to moderately orthorhombic symmetry of the estimated molecular g tensor, however, in the disturbed antiferrodistortive range, has negligible influence on the resulting canting angle, 2γ, which would become uncertain by less than 1°. Structural determinations on [Cu(salgy)(2-MeIm)] as well as on $[Cu(salgy)(OH_2)]\cdot 0.5H_2O$ gave evidence that the Cu(salgly) units are connected by carboxylate oxygen atoms from adjacent molecules to zigzag chains, where the canting angles, 2γ (82 and 58°, respectively),[2,9] are very different. As the estimated canting angles of the investigated adducts are spread over this range, we assume a comparable chain-like bridging of the complex molecules as the structural principle in this series.

Some compounds exhibit particularly interesting coupling patterns depending on the frequency of the measurement. The Q band EPR spectrum of [Cu(salgly)(benzIm)] [Fig. 3(b)] shows a superposition of two differently coupled g tensors. In addition to ferrodistortively coupled Cu^{2+} ions (Fig. 1, open circles), lines corresponding to disturbed antiferrodistortive ordering are also observed [Figs 1, crosses; 2(e)]. Using eq. (2) we calculate for the disturbed antiferrodistortively coupled complexes the molecular g values of $g_\parallel = 2.249$, $g_\perp = 2.054$, which are nearly equal to the ferrodistortive g components (Table 2). The canting angle results in $2\gamma = 63.5°$ [Fig. 2(e)]. The additional lines from the disturbed antiferrodistortive coupling of the molecular g tensors were not detected at X band frequency due to poor resolution. We assume in this compound a partly decoupled system of two disturbed antiferrodistortively ordered ferrodistortive sublattices. The compound [Cu(salgly)(2-EtIm)] shows an exchange-coupled EPR spectrum (with $g_\perp^{cc} = 2.143$ and $g_\parallel^{cc} = 2.081$) at 9 GHz. At a higher measuring frequency (35 GHz) the system is partly decoupled, and the EPR powder spectrum consists of a superposition of two differently coupled g tensors. In addition to the aforementioned coupled g^{cc} tensor ($g_1^{cc} = 2.145$, $g_2^{cc} = 2.138$, $g_3^{cc} = 2.082$), lines with $g_\perp^c \approx 2.15_5$ and $g_\parallel^c = 2.055$ are observed, which also disappear on lowering the temperature to 4.2 K [Fig. 3(c)]. Such spectral behaviour provides evidence for a coupled system, containing Cu^{2+} ions in four differently orientated coordination pyramids, which is partly decoupled at Q band frequency and higher temperatures. In this case, however, the system seems to consist of two disturbed antiferrodistortively ordered *anti*ferrodistortive sublattices. A striking angular dependence of line widths ranging between 0.5 mT and about 100 times this value was found in measurements on monocrystals.[16] This provides evidence for specific directions within the structure, where the exchange coupling becomes highly effective.[10] Further investigations in this field are in progress.

CONCLUSIONS

The spectral data provide evidence for square-pyramidal and in two cases also for square-planar coordination of the Cu^{2+} ions in the complexes under investigation. The substitutions on the imidazole ligand exhibit rather weak but distinct effects on the local environment around the Cu^{2+} ions. Some differences in axial ligand-field strength and distortions in the basal xy plane are observed. The cooperative ordering effects, however, are strongly influenced by water of crystallization and by sub-

* In the case of canting angles, 2γ, below $\approx 20°$ it is difficult to estimate whether a small orthorhombic splitting of the EPR pattern is caused by orthorhombic molecular components or by canting of axial g tensors, as can be seen from Fig. 2.

stituents on imidazole. The change from ferrodistortive to disturbed antiferrodistortive g tensors on going from N-salicylideneglycinato(2-methylimidazole)copper(II) dihydrate to the anhydrous compound is assumed to result from coupling of two disturbed antiferrodistortively ordered ferrodistortive sublattices. Analogical effects were observed in N-salicylideneglycinatocopper(II) adducts with pyridine and 4-methylpyridine.[4,6] The coupled system, at least, is confirmed in the structure of [Cu(salgly)(2-MeIm)], where the complex molecules are aligned in zigzag chains.[9] In the imidazole series, however, examples with an EPR frequency-dependent exchange coupling effect characteristic for a unit cell with four coupled Cu^{2+} ions were also detected. The substituents on the imidazole influence the hydrogen bonding system, which probably plays a considerable role in stabilizing the cooperative ordering effects in solid N-salicylideneglycinatocopper(II) complexes. Furthermore, the formation of dimers by analogy to those of [Cu(salgly)(thiouria)] noted by Pavelčik *et al.*[3] might be realized in compounds with ferrodistortively ordered square-pyramidal copper(II) coordination polyhedra.

Acknowledgements—The authors wish to thank Mr B. Schreiner (Marburg) for his experimental assistance and the German Research Association for financial support. One of the authors (G.P.) gratefully acknowledges the German Academic Exchange Organisation (DAAD) and the Slovak Literary Fund for support.

REFERENCES

1. D. E. Metzler, M. Ikawa and E. E. Snell, *J. Am. Chem. Soc.* 1954, **76**, 648.
2. T. Ueki, T. Ashida, Y. Sasada and M. Kakudo, *Acta Cryst.* 1967, **22**, 870; 1969, **B25**, 328.
3. F. Pavelčík, J. Krätsmar-Šmogrovič, O. Švajlenová and J. Majer, *Collect. Czech. Chem. Commun.* 1981, **46**, 3186.
4. C. Friebel, W. Massa, D. Nußhär, U. Dietz and U. Oppermann, *Proc. 12th Conf. Coord. Chem.*, p. 91. Smolenice, Bratislava (1989).
5. G. Plesch, C. Friebel, O. Švajlenová and J. Krätsmár-Šmogrovič, *Inorg. Chim. Acta* 1987, **129**, 81.
6. C. Friebel, G. Plesch, O. Švajlenová and J. Krätsmár-Šmogrovič, *Proc. 11th. Conf. Coord. Chem.*, p. 71. Smolenice, Bratislava (1987).
7. M. Kishita, A. Nakahara and M. Kubo, *Aust. J. Chem.* 1964, **17**, 810.
8. G. Plesch, C. Friebel, O. Švajlenová, J. Krätsmár-Šmogrovič and D. Mlynarčík, *Inorg. Chim. Acta* 1988, **151**, 139.
9. J. Sivý, V. Kettmann, J. Krätsmár-Šmogrović, O. Švajlenová, C. Friebel and G. Plesch, *Z. Anorg. Allg. Chem.* 1990, **583**, 55.
10. C. Friebel and M. J. Gonzalez-Garmendia, *Z. Naturfor.* 1975, **30b**, 883.
11. D. Reinen and C. Friebel, *Struct. Bonding (Berlin)* 1979, **37**, 1.
12. B. J. Hathaway and D. Billing, *Coord. Chem. Rev.* 1970, **5**, 143.
13. C. Friebel, *Z. Naturfor.* 1974, **29b**, 295.
14. C. Friebel, *Z. Naturfor.* 1974, **29b**, 634.
15. K. Dyrek, J. Goslar, S. A. Hodorowicz, S. K. Hoffmann, B. J. Oleksyn and A. Weselucha-Birczynska, *Inorg. Chem.* 1987, **26**, 1481.
16. C. Friebel and G. Plesch, unpublished results.

Polyhedron Vol. 10, No. 9, pp. 899–908, 1991
Printed in Great Britain

0277–5387/91 $3.00+.00
© 1991 Pergamon Press plc

ELECTROCHEMICAL REDUCTION OF PLATINUM(II) COMPLEXES CONTAINING BIDENTATE TERTIARY PHOSPHINE LIGANDS: EVIDENCE FOR THE GENERATION OF NON-LINEAR TWO-COORDINATE COMPLEXES

JULIAN A. DAVIES† and RICHARD J. STAPLES‡

Departments of Chemistry and Medicinal and Biological Chemistry,
The University of Toledo, Toledo, OH 43606, U.S.A.

(*Received* 6 *August* 1990; *accepted* 4 *January* 1991)

Abstract—The electrochemical reduction of $[PtCl_2L_2]+L_2^*$ (L_2 and L_2^* = $Ph_2PCH_2CH_2PPh_2$, dppe; $Cy_2PCH_2CH_2PCy_2$, dcpe; $^nBu_2PCH_2CH_2P^nBu_2$, dbpe) systems may proceed via two different routes. Path 1 involves reduction of $[PtCl_2L_2]$ to produce $[PtL_2]$ which is trapped by L_2^* to form $[PtL_2L_2^*]$. Path 2 involves prior reaction of $[PtCl_2L_2]$ with L_2^* to form $[PtL_2L_2^*]^{2+}$ which is reduced to form $[PtL_2L_2^*]$. The extent of prior reaction of $[PtCl_2L_2]$ with L_2^* has been monitored by both cyclic voltammetry, which detects only the electroactive components in solution, and by $^{31}P\{^1H\}$ NMR spectroscopy, which allows structural assignments to be made. Bulk electrolyses have been performed at potentials sufficient to reduce both $[PtCl_2L_2]$ and $[PtL_2L_2^*]^{2+}$ and also at potentials sufficient to reduce $[PtL_2L_2^*]^{2+}$ but not to reduce $[PtCl_2L_2]$. Product analyses by $^{31}P\{^1H\}$ NMR spectroscopy show that path 1 is operative in sterically congested systems, path 2 is operative in uncongested systems, and both pathways may be operative in systems with intermediate steric congestion. Reactions via path 2 produce $[PtL_2L_2^*]$ efficiently, whereas reactions via path 1 are complicated by alternative trapping reactions of $[PtL_2]$ with the solvent/electrolyte system which compete with trapping by L_2^*.

Recently we have shown that two-coordinate platinum(0) complexes containing either triphenylphosphine or triethylphosphine as ligands may be generated by electrochemical reduction of the corresponding *cis*-$[PtCl_2L_2]$ complexes,[1–3] eq. (1):

$$cis\text{-}[PtCl_2L_2]+2e^- \longrightarrow [PtL_2]+2Cl^- . \quad (1)$$

These relatively unhindered $[PtL_2]$ compounds exhibit enhanced reactivity in comparison with their better-known, more sterically crowded analogues, such as $[Pt(PCy_3)_2]$ (Cy = cyclohexyl).[4] The electrochemical method of generation appears complementary to the previously reported photochemical[5] [e.g. eq. (2)] or thermal[4] [e.g. eq. (3)] techniques and the better-known chemical approaches[6] to the generation of $[PtL_2]$ complexes:

$$[Pt(C_2O_4)(PEt_3)_2] \xrightarrow{h\nu} [Pt(PEt_3)_2]+2CO_2 \quad (2)$$

$$trans\text{-}[PtH_2(PCy_3)_2] \xrightarrow{\Delta} [Pt(PCy_3)_2]+H_2. \quad (3)$$

Interest in the chemistry of $[PtL_2]$ complexes was recently spurred by Whitesides and co-workers' reports[7–9] that the C_{2v} intermediate $[Pt(Cy_2PCH_2CH_2PCy_2)]$, generated by thermolysis of an alkylhydride, reacts with alkanes and a variety of other organic substrates by C—H oxidative addition.[10] Here we describe an initial investigation into the utility of electrochemical reductive strategies for the generation of such non-linear $[PtL_2]$ compounds from simple $[PtCl_2L_2]$ precursors.

RESULTS AND DISCUSSION

In a preparative scale electrochemical experiment both a relatively polar solvent and a background

† Author to whom correspondence should be addressed.
‡ Present address: Department of Chemistry, Texas A&M University, College Station, TX 77843, U.S.A.

electrolyte are required and we felt that generation of a non-linear $[PtL_2]$ compound in such a system might lead to indiscriminate reaction with these components. An experiment involving the bulk reductive electrolysis of $[PtCl_2(dppe)]$ (dppe = $Ph_2PCH_2CH_2PPh_2$) in CH_3CN/C_6H_6 (1/1, v/v) containing tetra(n-butyl)ammonium perchlorate (TBAP, 0.08 M) at a mercury pool electrode employing a potential of −1.75 V (vs Ag/AgCl; −35 mV vs SCE) confirms this expectation. The $^{31}P\{^1H\}$ NMR spectrum of the product mixture showed that multiple products were formed, none of which could be identified by comparison of spectroscopic data with literature values. Data from this experiment are included in the Experimental for completeness. Given this situation, we felt that a trapping agent was necessary which would effectively compete for any non-linear $[PtL_2]$ intermediate that might be generated. Such a trapping agent has to survive the very negative potentials required to reduce $[PtCl_2L_2]$ complexes and bind strongly to any $[PtL_2]$ fragment generated. Accordingly we sought to use bidentate ligands as traps for potential $[PtL_2]$ fragments since the resulting $[PtL_2L_2*]$ complexes are quite robust species.[11] The choice of such a set of trapping agents is not without inherent problems since it allows two possible reaction pathways, as illustrated in Scheme 1. The first path involves reduction of $[PtCl_2L_2]$ to generate $[PtL_2]$ which is subsequently trapped by L_2* to produce $[PtL_2L_2*]$. The second path involves prior reaction of $[PtCl_2L_2]$ with L_2* to generate $[PtL_2L_2*]^{2+}$ which is subsequently reduced to produce $[PtL_2L_2*]$. Thus, the pathway of the reaction will in part be controlled by the extent to which the well-known halide displacement[12] of $[PtCl_2L_2]$ by L_2* occurs prior to electrolysis. In order to investigate this question, $^{31}P\{^1H\}$ NMR measurements (see Experimental) were made on $[PtCl_2L_2]+L_2*$ mixtures in CH_3CN/C_6D_6 which was 0.1 M in TBAP. In every case dication formation (Table 1) was detected, although it was clear that in cases where L_2 and L_2* are both sterically demanding, the reaction does not proceed to completion in the time scale of these NMR experiments (typically 1–3 h). For example, although addition of $Cy_2PCH_2CH_2PCy_2$ (dcpe) to $[PtCl_2(dcpe)]$ did indeed produce $[Pt(dcpe)_2]^{2+}$, both free dcpe and unreacted $[PtCl_2(dcpe)]$ were still present after several hours in solution. Thus, in every $[PtCl_2L_2]+L_2*$ system we have investigated, both $[PtCl_2L_2]$ and $[PtL_2L_2*]^{2+}$ could potentially participate in an electrochemical reduction and so any differentiation between the possible pathways indicated in Scheme 1 must rely heavily on differences in the electrochemical behaviour of these components. Cyclic voltammetry (CV)[13–16] gives some insight into these differences.

Figure 1(a) shows the cyclic voltammogram of $[PtCl_2(dppe)]$ in CH_3CN (0.1 M in TBAP) at a Hg/Au amalgam electrode measured at a scan rate of 200 mV s^{-1} over the potential range −0.50 to −2.20 V vs Ag/AgCl. On the basis of chemical evidence (*vide infra*) we assign peak A (−1.71 V) to the irreversible reduction of $[PtCl_2(dppe)]$, eq. (4):

$$[PtCl_2(dppe)]+2e^- \longrightarrow [Pt(dppe)]+2Cl^- \quad (4)$$

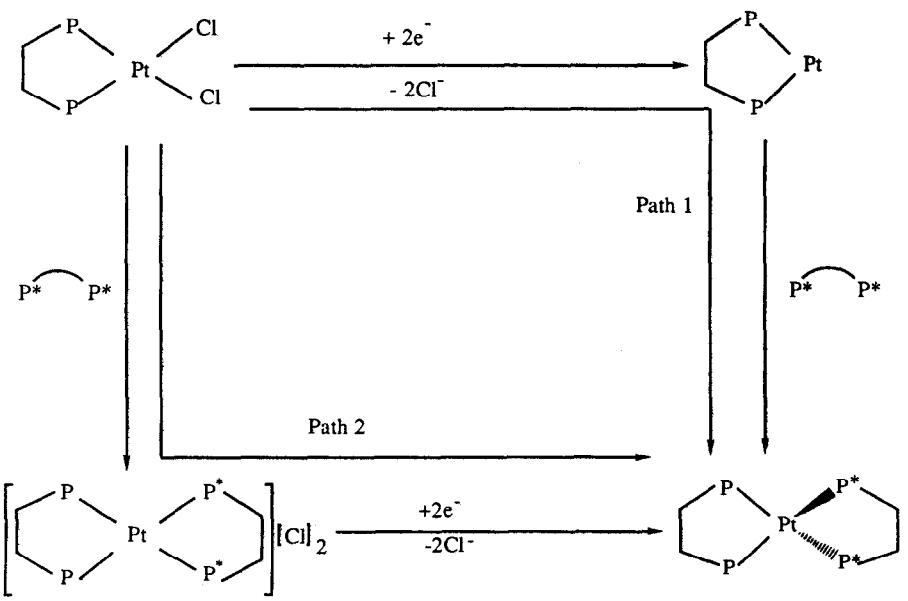

Scheme 1.

Table 1. $^{31}P\{^1H\}$ NMR data for platinum(II) dications[a]

Dication	Compound number[b]	δP_1 (ppm)	δP_2 (ppm)	$J(Pt,P_1)$ (Hz)	$J(Pt,P_2)$ (Hz)	$J(P_1,P_{1'})$ (Hz)	$J(P_2,P_{2'})$ (Hz)	$J(P_1,P_2)$ (Hz)	$J(P_1,P_{2'})$ (Hz)
$[Pt(dppe)_2]^{2+}$	**1**	47.0		2375					
$[Pt(dcpe)(dppe)]^{2+}$	**2**	71.4	46.8	2256	2184	3	1.5	−15	277
$[Pt(dcpe)_2]^{2+}$	**3**	61.3		2187					
$[Pt(dcpe)(dbpe)]^{2+}$	**4**	67.7	49.3	2187	2155	6	−9	−20	278
$[Pt(dppe)(dbpe)]^{2+}$	**5**	49.5	46.1	2359	2290	12	12	−23	300
$[Pt(dbpe)_2]^{2+}$	**6**	45.0		2248					

[a] Recorded in C_6D_6 and referenced to external 85% H_3PO_4 with more positive values of the chemical shifts representing deshielding. Spectra of compounds **1**, **3** and **6** measured at 36.2 MHz; spectra of compounds **2**, **4** and **5** measured at 161.0 MHz.

[b] For **2**, $\widehat{P_1P_{1'}}$ = dcpe, $\widehat{P_2P_{2'}}$ = dcppe; for **4**, $\widehat{P_1P_{1'}}$ = dcpe, $\widehat{P_2P_{2'}}$ = dbpe; for **5**, $\widehat{P_1P_{1'}}$ = dppe, $\widehat{P_2P_2}$ = dbpe; for **1**, **3** and **6**, $P_1 = P_{1'} = P_2 = P_{2'}$.

Addition of one equivalent of dppe to the solution of $[PtCl_2(dppe)]$ followed by immediate measurement of a cyclic voltammogram produces the result shown in Fig. 1(b). Sweeping to negative potential now generates peak B, which we assign to the reduction of the dication $[Pt(dppe)_2]^{2+}$, with peak A, due to reduction of $[PtCl_2(dppe)]$, now barely visible. This interpretation is in accord with our $^{31}P\{^1H\}$ NMR results (see Experimental) and with CV on independently prepared samples of both $[Pt(dppe)_2]Cl_2$ and $[Pt(dppe)_2]$.[17] The reverse sweep

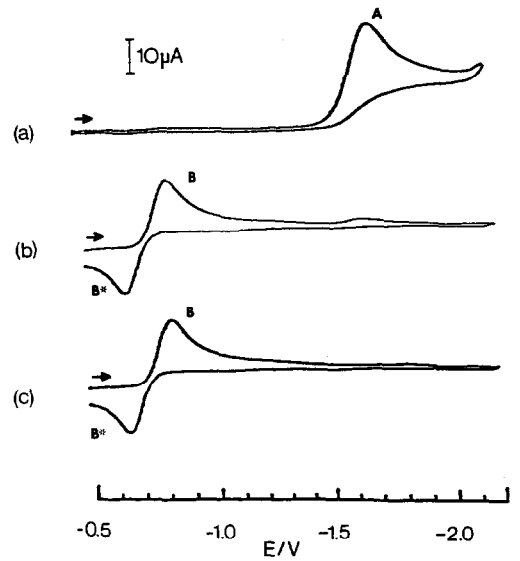

Fig. 1. Cyclic voltammograms measured in CH_3CN (10^{-1} M TBAP) at a Au/Hg amalgam working electrode (1.77 mm^2) using a scan rate of 200 mV s^{-1}. (a) 10^{-3} M solution of $[PtCl_2(dppe)]$; (b) 10^{-3} M solution of $[PtCl_2(dppe)]$ immediately after adding one equivalent of dppe; (c) 10^{-3} M solution of $[PtCl_2(dppe)]$ 1 h after adding one equivalent of dppe.

of the cyclic voltammogram shown in Fig. 1(b) produces peak B* which we assign to re-oxidation of $[Pt(dppe)_2]$. The question of reversibility of the processes generating peaks B and B* is redundant since the platinum(II)/platinum(0) interconversion is accompanied by a structural change between square-planar and tetrahedral geometries, and hence this reaction is perhaps best described as an EC process. In the absence of a structural change we would ideally anticipate a peak separation of 29.5 mV for the two-electron process. The actual separation of peaks B and B* in Fig. 1(b) is 150 mV. After standing for 1 h, the solution of $[PtCl_2(dppe)]$ + dppe produced the cyclic voltammogram shown in Fig. 1(c), i.e. no $[PtCl_2(dppe)]$ was detected and the only electroactive component found in solution was $[Pt(dppe)_2]^{2+}$.

Based on the $^{31}P\{^1H\}$ NMR and CV results, it is not surprising that controlled potential bulk reductive electrolysis of $[PtCl_2(dppe)]$ in the presence of one equivalent of dppe at a potential of −1.75 V (i.e. just negative of peak A) produces $[Pt(dppe)_2]$ efficiently. As is common in bulk electrolyses of the type described here,[1-3] separation of the products from the background electrolyte, which is present in large excess, can be exceedingly difficult. Since we are primarily interested in the solution chemistry we have not typically performed such separations. In the present case, $^{31}P\{^1H\}$ NMR spectroscopy showed $[Pt(dppe)_2]$ (83% estimated by peak heights in the spectrum) and traces of dppe, dppe oxide (dppeO) and dppe dioxide ($dppeO_2$) to be present after electrolysis. The traces of phosphine oxides were present in approximately the same amount as impurities in the original dppe added to the reaction mixture (see Experimental).

Figure 2 shows a series of cyclic voltammograms

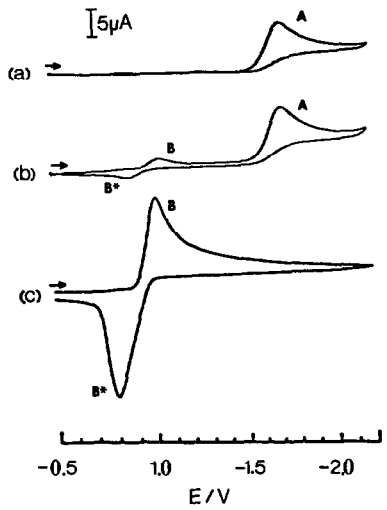

Fig. 2. Cyclic voltammograms measured in CH_3CN (10^{-1} M TBAP) at a Au/Hg amalgam working electrode (1.77 mm^2) using a scan rate of 200 mV s^{-1}. (a) 10^{-3} M solution of $[PtCl_2(dppe)]$; (b) 10^{-3} M solution of $[PtCl_2(dppe)]$ immediately after adding one equivalent of dcpe; (c) 10^{-3} M solution of $[PtCl_2(dppe)]$ 1 h after adding one equivalent of dcpe.

illustrating the effect of adding one equivalent of dcpe to $[PtCl_2(dppe)]$. Immediately after addition the sterically demanding dcpe ligand has generated only a small amount of dication and significant $[PtCl_2(dppe)]$ remains. After 1 h [Fig. 2(c)], no $[PtCl_2(dppe)]$ is detected and only the dication is observed. In the voltammogram shown in Fig. 2(c) the peak current for the reduction of $[Pt(dppe)(dcpe)]^{2+}$ is less than the peak current for the associated re-oxidation (i.e. B < B*). This effect arises since reduction of $[Pt(dppe)(dcpe)]^{2+}$ occurs at all potentials more negative than B and the reduced species, which apparently adsorbs on the electrode, is then stripped off by re-oxidation at one potential (B*) on the reverse sweep. The CV results for the $[PtCl_2(dppe)]$+dcpe system are in agreement with the $^{31}P\{^1H\}$ NMR results, where $[Pt(dppe)(dcpe)]^{2+}$ was identified as the major species in solution (Table 1). Also detected was some $[PtCl_2(dcpe)]$ formed by displacement of dppe by the stronger σ-donor dcpe, but this minor component is not detected in the cyclic voltammograms shown in Fig. 2. Given these results, the controlled potential bulk reductive electrolysis of $[PtCl_2(dppe)]$+dcpe at −1.75 V might be anticipated to produce [Pt(dppe)(dcpe)] as a major product and this is indeed the case (Table 2). In addition to this product (54% by peak heights), some $[Pt(dppe)_2]$ was also detected (8.5%), along with unreduced $[PtCl_2(dcpe)]$ (8.5%) and trace ligand impurities.

The reaction of dppe with $[PtCl_2(dcpe)]$ proceeds in a different manner to the reaction of dcpe with $[PtCl_2(dppe)]$ (*vide supra*). Thus, addition of dppe to $[PtCl_2(dcpe)]$ followed by immediate measurement of a cyclic voltammogram [Fig. 3(b)] shows some formation of a dication (peak B), but considerable $[PtCl_2(dcpe)]$ remains. Interestingly, after scanning through peak A, the reverse scan gives rise to peak B* with a larger current than peak B. We interpret this as being due to the fact that traversing peak A generates [Pt(dcpe)], some of which is trapped by dppe to produce [Pt(dcpe)(dppe)]. On the reverse scan, the oxidation of [Pt(dcpe)(dppe)] thus produces an enhanced current for peak B*. After 1 h in solution the $[PtCl_2(dcpe)]$+dppe system produces the voltammogram shown in Fig. 3(c). On the forward scan, peak B, corresponding to dication reduction, shows that significant amounts of this species are present. Peak A shows that some $[PtCl_2(dcpe)]$ remains also. On the reverse scan, no

Table 2. $^{31}P\{^1H\}$ NMR data for platinum(0) phosphine complexes[a]

Platinum(0) complex	Compound number[b]	P_1 (ppm)	P_2 (ppm)	$J_{Pt-P(1)}$ (Hz)	$J_{Pt-P(2)}$ (Hz)	$J_{P(1)-P(2)}$ (Hz)	References
$[Pt(dppe)_2]$	**7**	29.8		3729			11
[Pt(dcpe)(dppe)]	**8**	43.3	21.0	3610	3665	60	11
$[Pt(dcpe)_2]$	**9**	30.7		3589			8
[Pt(dcpe)(dbpe)]	**10**	44.9	5.7	3613	3610	59	
[Pt(dbpe)(dppe)]	**11**	29.1	18.2	3710	3629	61	
$[Pt(dbpe)_2]$	**12**	18.2		3629			

[a] Recorded in C_6D_6 and referenced to external 85% H_3PO_4 with more positive values of the chemical shifts representing deshielding. Spectra of compounds **7**, **8**, **9**, **10** and **12** measured at 36.2 MHz; spectrum of **11** measured at 161.0 MHz.

[b] For **8**, $\widehat{P_1P_1}$ = dcpe, $\widehat{P_2P_2}$ = dppe; for **10**, $\widehat{P_1P_1}$ = dcpe, $\widehat{P_2P_2}$ = dbpe; for **11**, $\widehat{P_1P_1}$ = dppe, $\widehat{P_2P_2}$ = dbpe; for **7**, **9** and **12**, $P_1 = P_2$.

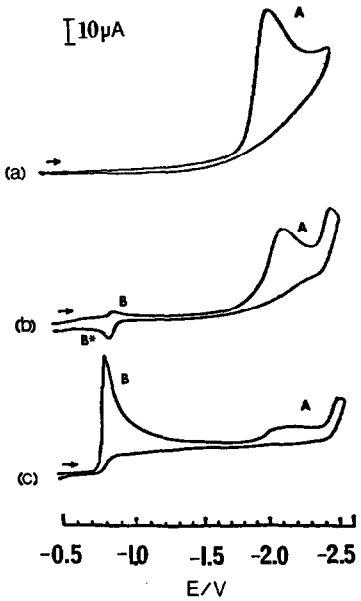

Fig. 3. Cyclic voltammograms measured in CH_3CN (10^{-1} M TBAP) at a Au/Hg amalgam working electrode (1.77 mm^2) using a scan rate of 200 mV s^{-1}. (a) 10^{-3} M solution of $[PtCl_2(dcpe)]$; (b) 10^{-3} M solution of $[PtCl_2(dcpe)]$ immediately after adding one equivalent of dppe; (c) 10^{-3} M solution of $[PtCl_2(dcpe)]$ 1 h after adding one equivalent of dppe.

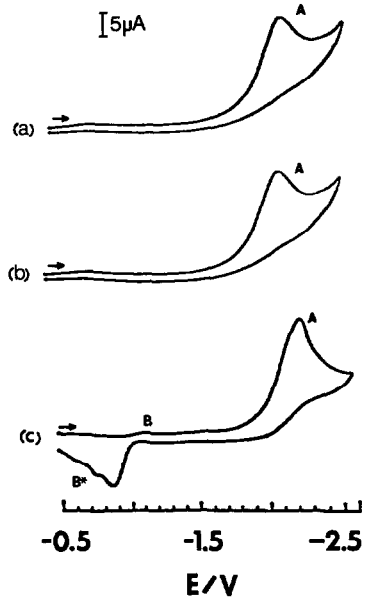

Fig. 4. Cyclic voltammograms measured in CH_3CN (10^{-1} M TBAP) at a Au/Hg amalgam working electrode (1.77 mm^2) using a scan rate of 200 mV s^{-1}. (a) 10^{-3} M solution of $[PtCl_2(dcpe)]$; (b) 10^{-3} M solution of $[PtCl_2(dcpe)]$ immediately after adding one equivalent of dcpe; (c) 10^{-3} M solution of $[PtCl_2(dcpe)]$ 1 h after adding one equivalent of dcpe.

peak for the oxidation of [Pt(dcpe)(dppe)] is seen, an occurrence for which we have no explanation. The $^{31}P\{^1H\}$ NMR results on this system show only $[Pt(dcpe)(dppe)]^{2+}$ and trace ligand impurities in solution after *ca* 1 h. Controlled potential bulk reductive electrolysis at −2.2 V (i.e. just negative of peak A) produced [Pt(dcpe)(dppe)] in 50.4% spectroscopic yield, with some $[Pt(dppe)_2]$ and trace ligand impurities also detected. The unusual CV results thus remain unexplained.

The addition of one equivalent of dcpe to $[PtCl_2(dcpe)]$ followed by immediate measurement of a cyclic voltammogram produced the result shown in Fig. 4(b). Clearly, no dication is detected. After 1 h in solution, the cyclic voltammogram shown in Fig. 4(c) is obtained. On the sweep to negative potential, peak B is barely visible with a very small current, consistent with $^{31}P\{^1H\}$ NMR measurements which show only low levels of $[Pt(dcpe)_2]^{2+}$ in solution. Square wave voltammetry unambiguously shows the presence of peak B despite its low current. Sweeping through peak A then produces peak B* in the cyclic voltammogram with a large current on the reverse sweep. Peak B* does not appear unless peak A is first traversed. This is clear evidence that traversing peak A produces [Pt(dcpe)], some of which is trapped by dcpe to generate $[Pt(dcpe)_2]$, and it is this species that is re-oxidized at peak B*. This interpretation is supported by the results of controlled potential bulk reductive electrolysis experiments. Thus, attempted electrolysis at −1.20 V (i.e. just negative of the small peak B) resulted in essentially no current flow since hardly any $[Pt(dcpe)_2]^{2+}$ was present. Electrolysis at −2.25 V (i.e. just negative of peak A), however, results in significant generation of $[Pt(dcpe)_2]$ (39% by peak heights) via initial formation of [Pt(dcpe)] and subsequent trapping by dcpe. Consistent with this interpretation is the observation of a second, unidentified product [δ = 51.6 ppm, J(Pt,P) = 3133 Hz] which we feel must originate from reaction of [Pt(dcpe)] with components of the solvent/electrolyte system. These results suggest that electrochemical reduction of the $[PtCl_2(dcpe)]$+dcpe system follows path 1 (Scheme 1) rather than path 2, which appears to dominate for the other systems described so far. It is also noteworthy that peak B* in the cyclic voltammogram shown in Fig. 4(c) may contain more than one component (*vide infra*). This may be due to the oxidation of transient platinum(0) species other than $[Pt(dcpe)_2]$. Species such as [Pt(dcpe)(solvent)$_x$] or [Pt(dcpe)(η^1-dcpe)] may be likely candidates, although, whatever the nature of this species, it is too short-lived for detection by $^{31}P\{^1H\}$ NMR methods.

Addition of dppe to $[PtCl_2(dbpe)]$ (where dbpe = $^nBu_2PCH_2CH_2P^nBu_2$) gave rise to the cyclic

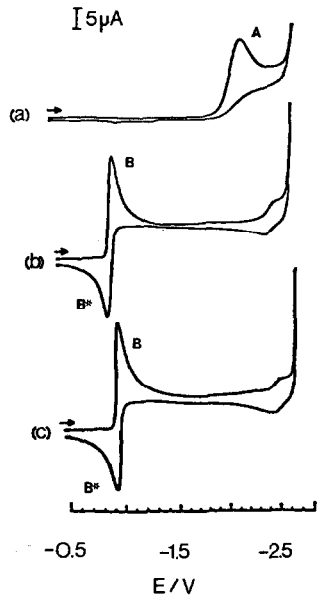

Fig. 5. Cyclic voltammograms measured in CH_3CN (10^{-1} M TBAP) at a Au/Hg amalgam working electrode (1.77 mm^2) using a scan rate of 200 mV s^{-1}. (a) 10^{-3} M solution of $[PtCl_2(dbpe)]$; (b) 10^{-3} M solution of $[PtCl_2(dbpe)]$ immediately after adding one equivalent of dppe; (c) 10^{-3} M solution of $[PtCl_2(dbpe)]$ 1 h after adding one equivalent of dbpe.

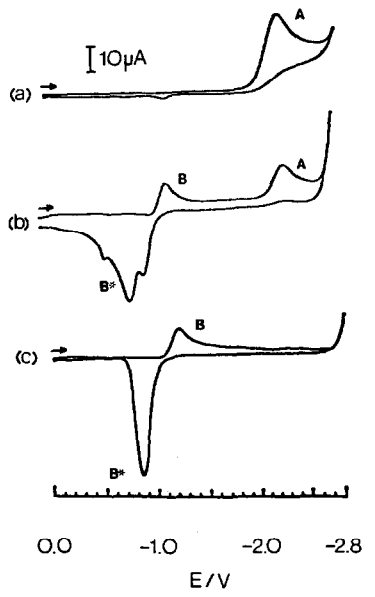

Fig. 6. Cyclic voltammograms measured in CH_3CN (10^{-1} M TBAP) at a Au/Hg amalgam working electrode (1.77 mm^2) using a scan rate of 200 mV s^{-1}. (a) 10^{-3} M solution of $[PtCl_2(dbpe)]$; (b) 10^{-3} M solution of $[PtCl_2(dbpe)]$ immediately after adding one equivalent of dcpe; (c) 10^{-3} M solution of $[PtCl_2(dbpe)]$ 1 h after adding one equivalent of dcpe.

voltammograms shown in Fig. 5. Immediately after the addition, substantial $[Pt(dbpe)(dppe)]^{2+}$ is formed while some $[PtCl_2(dbpe)]$ persists. This situation is essentially unchanged after 1 h [Fig. 5(c)]. The $^{31}P\{^1H\}$ NMR spectrum agrees with this assignment exactly (see Experimental). Controlled potential bulk reductive electrolysis at −2.40 V (i.e. just negative of peak A) produces largely [Pt(dbpe)(dppe)], as expected (63% by peak heights), but small amounts of $[Pt(dppe)_2]$ and an unidentified product [δ = 44.2 ppm, J(Pt,P) = 2245 Hz] are also formed. The latter component presumably has its origins in a reaction of [Pt(dbpe)], produced by reduction of $[PtCl_2(dbpe)]$, with components of the solvent/electrolyte system.

We find that addition of the more sterically demanding dcpe to $[PtCl_2(dbpe)]$ proceeds in a different manner to the reaction of dppe with $[PtCl_2(dbpe)]$. Thus, Fig. 6 shows the CV results for the addition of one equivalent of dcpe to $[PtCl_2(dbpe)]$. Immediately after addition, a sweep to negative potential reveals the reduction of $[Pt(dbpe)(dcpe)]^{2+}$ (peak B) followed by reduction of $[PtCl_2(dbpe)]$ (peak A). The latter process generates [Pt(dbpe)] which we might anticipate leads to the formation of additional [Pt(dbpe)(dcpe)] via possible intermediates such as $[Pt(dbpe)(solvent)_x]$ and/or $[Pt(dbpe)(\eta^1\text{-dcpe})]$. Thus, the reverse sweep reveals peak B* with a larger current than peak B and containing several components for oxidation of the different platinum(0) species present. Consistent with this interpretation, we find that after 1 h in solution [Fig. 6(c)], the reaction of $[PtCl_2(dbpe)]$ with dcpe has proceeded to completion and only $[Pt(dbpe)(dcpe)]^{2+}$ is detected on the scan to negative potential. Since reduction of the cation occurs at all potentials more negative than peak B, the reverse sweep causes stripping of adsorbed platinum(0) at the potential of peak B*, which now corresponds to the re-oxidation of just one species, [Pt(dbpe)(dcpe)]. Controlled potential bulk reductive electrolysis results support these conclusions. Thus electrolysis at −1.25 V (i.e. just negative of peak B) produces [Pt(dbpe)(dcpe)] essentially quantitatively. However, electrolysis at −2.40 V (i.e. just negative of peak A) produces not only [Pt(dbpe)(dcpe)] (49% by peak heights) but also the disproportionation products $[Pt(dbpe)_2]$ and $[Pt(dcpe)_2]$ as well as several unidentified species, formed in low yield, presumably by reaction of [Pt(dbpe)] with components of the solvent/electrolyte system. $^{31}P\{H\}$ NMR data for these unidentified minor components are listed in the Experimental for completeness.

Interestingly, we found that controlled potential electrolysis of an independently synthesized sample of $[Pt(dbpe)_2]Cl_2$, performed at a potential of −1.50 V, generated not only $[Pt(dbpe)_2]$ but also

an unidentified complex (see Experimental), suggesting that the reduction of four-coordinate dbpe complexes may involve ligand dissociation, producing reactive fragments.

CONCLUSIONS

The work described here shows that non-linear $[PtL_2]$ intermediates can be generated by electrochemical reduction of readily available $[PtCl_2L_2]$ precursors. In the absence of a specific trapping agent, [Pt(dppe)] was found to react indiscriminately with the components of the solvent/electrolyte system, but in the presence of another bidentate ligand as a trapping agent some selectivity for formation of $[PtL_2L_2^*]$ was achieved. The existence of two competing pathways (Scheme 1) caused us to investigate a series of $[PtCl_2L_2]$ precursors and L_2^* trapping agents, and this work shows how the steric and electronic effects of L_2 and L_2^* modify reactivity. Based upon these results, we are currently examining the electrochemical generation and reactivity of non-linear $[PtL_2]$ complexes containing ligands other than dppe in order to achieve more selective reactions with organic substrates.[18]

EXPERIMENTAL

General procedures

Acetonitrile (Fisher, ACS grade) was stirred with CaH_2 for 48 h, decanted and distilled from P_4O_{10}. The first 15% of the distillate was discarded as was the last 15%. The middle 70% (b.p. 83.0°C) was refluxed with CaH_2 and then fractionally distilled. Again the first and last 15% of the distillate was discarded and the middle 70% was stored under argon over Al_2O_3, activated at 110°C for 24 h. Benzene (Fisher, ACS grade) was freshly distilled from sodium wire under nitrogen prior to use. Benzene-d_6 was purchased from Aldrich and deoxygenated prior to use. Tetra(n-butyl)ammonium perchlorate (TBAP, G.F.S.) was recrystallized five times from absolute ethanol and dried *in vacuo* for 48 h at room temperature. The phosphines, bis(dicyclohexylphosphino)ethane and bis(di{n-butyl}phosphino)ethane were purchased from Strem and bis(diphenylphosphino)ethane was prepared by literature methods.[19] Commercial bis(dicyclohexylphosphino)ethane was purified by recrystallization from tetrahydrofuran prior to use, which removed several impurities although small amounts of dcpeO and $dcpeO_2$ remained. The complexes $[PtCl_2(dppe)]$ and $[PtCl_2(dcpe)]$ were prepared by displacement of 1,5-cyclooctadiene from $[PtCl_2(cod)]$[20] in methylene chloride. The complex $[PtCl_2(dbpe)]$ was synthesized by the displacement of acetonitrile from $[PtCl_2(CH_3CN)_2]$[21] in acetonitrile and was recrystallized from THF. The preparation of the dication $[Pt(dbpe)_2]Cl_2$ was accomplished by reaction of the bis-acetonitrile complex with two equivalents of phosphine.[12]

$^{31}P\{^1H\}$ (36.2 MHz) NMR spectra were measured on a Jeol FX 90Q spectrometer operating in the Fourier transform mode or were recorded on a Varian VXR 400 (161 MHz) spectrometer when second-order effects were seen at the lower field of the FX 90Q spectrometer. $^{31}P\{^1H\}$ NMR chemical shifts were measured using 85% H_3PO_4 as an external standard, with positive values of the chemical shift representing deshielding. Yields were estimated from peak heights in the $^{31}P\{^1H\}$ NMR spectra unless cited as isolated yields.

The mixed ligand platinum(II) dications gave rise to $^{31}P\{^1H\}$ NMR spectra which could be interpreted in terms of AA′BB′ or AA′XX′ spin systems (ignoring the effects of ^{195}Pt). Each spectrum was simulated using Varian's 6.2 software package to within an error of ± 5 Hz of the expected line positions, with the majority of the lines simulated to less than ± 1 Hz of the positions in the original spectra.

Cyclic voltammograms were obtained using a Bioanalytical Systems 100 control unit. Typically, 2.0×10^{-3} M solutions of the complexes in acetonitrile (10 cm^3), which was 0.08 M in TBAP, were employed. In this solvent system the ferrocene/ferrocenium couple appears at +0.760 V with a peak separation of 90 mV. The cobaltocene/cobaltocenium couple appears at −0.570 V with a peak separation of 82 mV.

A single compartment cell, thermostatted to 25 ± 1°C, equipped with a Ag/AgCl reference electrode (−35 mV vs SCE), a platinum wire auxiliary electrode and a mercury/gold amalgam working electrode was used. We have discussed CV of platinum(II) complexes using similar techniques previously.[13–16] Controlled potential bulk reductive electrolyses[1–3] were performed using a Bioanalytical Systems SP-2 synthetic potentiostat. A three-compartment cell was employed which was constructed in-house. The working electrode compartment contained the Ag/AgCl reference electrode and 18 cm^3 of mercury connected to the potentiostat by a platinum wire. The auxiliary electrode compartment contained a platinum spiral wire electrode. The compartments were separated by two medium porosity frits. The cell was equipped with

a number of fitted openings to allow inert atmosphere operation and manipulation of solutions.

$^{31}P\{^{1}H\}$ *NMR measurements*

The reactions of $[PtCl_2L_2]$ with L_2* were monitored by $^{31}P\{^{1}H\}$ NMR spectroscopy. Solutions were prepared in acetonitrile/benzene-d_6 and in acetonitrile/benzene-d_6 which was 0.1 M in TBAP. Essentially identical results were obtained for the two solvent systems.

(i) $[PtCl_2(dppe)]$ + dppe. $[Pt(dppe)_2]^{2+}$ and dppe were identified in solution. Also present were small amounts of dppeO and $dppeO_2$ which were initially present as trace impurities in the dppe employed in the reaction. No insoluble material was formed.

(ii) $[PtCl_2(dppe)]$ + dcpe. $[Pt(dppe)(dcpe)]^{2+}$ and $[PtCl_2(dcpe)]$ were identified in solution along with $dcpeO_2$, originally present as an impurity in the dcpe employed in the reaction. Some insoluble material {perhaps $[PtCl_2(dppe)]$} was also formed.

(iii) $[PtCl_2(dcpe)]$ + dppe. $[Pt(dcpe)(dppe)]^{2+}$ and dppe were identified in solution along with the ligand impurities dppeO and $dppeO_2$.

(iv) $[PtCl_2(dcpe)]$ + dcpe. $[Pt(dcpe)_2]^{2+}$, $[PtCl_2(dcpe)]$ and dcpe were identified in solution along with the ligand impurity $dcpeO_2$.

(v) $[PtCl_2(dbpe)]$ + dppe. $[Pt(dbpe)(dppe)]^{2+}$ and $[PtCl_2(dbpe)]$ were identified in solution. Trace amounts of unidentified compounds which did not appear to contain platinum were identified at very high signal-to-noise ratios. No insoluble material was formed.

(vi) $[PtCl_2(dbpe)]$ + dcpe. $[Pt(dbpe)(dcpe)]^{2+}$, $[PtCl_2(dcpe)]$ and $[Pt(dbpe)_2]^{2+}$ were identified in solution along with the trace ligand impurity $dcpeO_2$.

Controlled potential electrolyses (CPE)

Each CPE described below was repeated at least twice with consistent results.

(i) *CPE of* $[PtCl_2(dppe)]$ *in the presence of* dppe. Twenty-four hours prior to an experiment, the controlled potential electrolysis cell was charged with alumina (1.0 g) and dried at 110°C. From this point on all manipulations of the cell were done under an argon atmosphere at room temperature unless otherwise noted. At the time of the experiment, mercury (25 cm^3) was extracted with dry benzene (10 cm^3) and then the mercury (18 cm^3) and a small magnetic stirrer bar were added to the cell which was cooled under argon. A 0.1 M solution of TBAP in acetonitrile/benzene (60 cm^3, 1 : 1, v/v) was introduced into the cell under an argon stream. This was allowed to outgas for 1 h. The solution was then stirred and pre-electrolysed to approximately zero current at a potential of −1.75 V.

To the pre-electrolysed solution was added $[PtCl_2(dppe)]$ (*ca* 30 mg) and one equivalent of dppe (*ca* 18 mg) which was purged with argon for 1 h. This was then electrolysed to essentially zero current at a potential of −1.75 V. This usually required 30 min to 1 h and coulometry indicated approximately a 2-electrons/equivalent reduction, with integrations in the range of 1.9–2.1 electrons/equivalent. When the electrolysis was complete, the solution was transferred (using inert atmosphere techniques) to a Schlenk tube and evaporated. The yellowish solid was extracted with benzene (2×10 cm^3) and evaporated to give a yellow solid which was dissolved in C_6D_6 and transferred to an NMR tube. $^{31}P\{^{1}H\}$ NMR spectroscopy showed $[Pt(dppe)_2]$, $\delta_P = 29.8$ ppm, $J_{Pt-P} = 3729$ Hz (82.9%); dppe, $\delta = -13.4$ ppm (4.6%); dppeO, $\delta_{P(1)} = 26.8$ ppm, $\delta_{P(2)} = -12.5$ ppm, $J_{P-P} = 34$ Hz (5.6%); $dppeO_2$, $\delta = 28.1$ ppm (5.9%).

(ii) *CPE of* $[PtCl_2(dppe)]$ *in the presence of* dcpe. To the pre-electrolysed (−1.75 V, CH_3CN) solution was added $[PtCl_2(dppe)]$ (*ca* 30 mg) and one equivalent of dcpe (*ca* 20 mg) which was then purged with argon for 1 h and electrolysed to essentially zero current at −1.75 V. This usually required 30 min to 1 h and coulometry indicated approximately a 2-electrons/equivalent reduction, with integrations in the range of 2.0–2.1 electrons/equivalent. After work-up as previously described, $^{31}P\{^{1}H\}$ NMR spectroscopy showed [Pt(dppe)(dcpe)] (54.0%), $[Pt(dppe)_2]$ (8.5%); $[PtCl_2(dcpe)]$ (7.5%); dcpe, $\delta = 0.36$; dcpeO, $\delta_{P(1)} = 45.8$, $\delta_{P(2)} = 1.2$ ppm, $J_{P-P} = 37$ Hz; $dcpeO_2$, $\delta = 47.7$ ppm.

(iii) *CPE of* $[PtCl_2(dcpe)]$ *in the presence of* dppe. To the pre-electrolysed solution (−2.20 V, CH_3CN) was added $[PtCl_2(dcpe)]$ (*ca* 30 mg) with one equivalent of dppe (*ca* 18 mg) which was purged with argon for 1 h and electrolysed to zero current flow (1–1.5 h) with coulometry indicating a 2-electrons/equivalent reduction (range 1.9–2.1 electrons/equivalent). Collection of a yellow solid which precipitated from the acetonitrile yielded [Pt(dcppe)(dppe)] (50.4% isolated yield). A trace of $dppeO_2$ was seen by $^{31}P\{^{1}H\}$ NMR. In the solution, which was worked-up as previously described, remained $[Pt(dppe)_2]$ (17.0%); $dppeO_2$ (25.1%), dppeO (28.0%); dppe (11.4%); and $dcpeO_2$ (18.5%).

(iv) *CPE of* $[PtCl_2(dcpe)]$ *in the presence of* dcpe. (a) To the pre-electrolysed solution (−2.20 V, CH_3CN) was added $[PtCl_2(dcpe)]$ (*ca* 30 mg) and one equivalent of dcpe (*ca* 19 mg) which was purged with argon for 1 h and electrolysed to zero current flow (1.5–2.5 h) with coulometry indicating a 2-

electrons/equivalent reduction (range 1.9–2.3 electrons/equivalent). After work-up, $^{31}P\{^1H\}$ NMR (C_6D_6) showed [Pt(dcpe)$_2$] (39.2%); dcpeO$_2$ (18.2%); dcpeO (10.2%); dcpe (25.5%); and a platinum complex with the data: $\delta = 51.6$ ppm, $J_{Pt-P} = 3133$ Hz (6.9%).

(b) To a pre-electrolysed solution (−1.20 V, CH_3CN) was added [PtCl$_2$(dcpe)] (*ca* 30 mg) and one equivalent of dcpe (*ca* 19 mg) which was purged with argon for 1 h and electrolysed to near zero current flow (1–2 h). The current flow was very low and coulometry indicated that only 0.15 electrons/equivalent were consumed. After the usual work-up, $^{31}P\{^1H\}$ NMR (C_6D_6) showed [PtCl$_2$(dcpe)] (20.0%); dcpe (52.8%); dcpeO (9.1%); and dcpeO$_2$ (18.1%).

(v) *CPE of* [PtCl$_2$(dbpe)] *in the presence of* dppe. To the pre-electrolysed solution (2.40 V, CH_3CN) was added [PtCl$_2$(dbpe)] (*ca* 30 mg) with one equivalent of dppe (*ca* 20 mg) and purged with argon for 1 h. This solution was electrolysed until approximately 2 electrons/equivalent were consumed and then the electrolysis was terminated (30 min to 1 h). The formation of a precipitate occurred as the acetonitrile was concentrated and this precipitate was isolated: [Pt(dbpe)(dppe)] (52.6% isolated yield). [Pt(dbpe)(dppe)] was identified by its 161 MHz $^{31}P\{^1H\}$ NMR spectrum due to the second-order nature of the spectrum obtained at 36.2 MHz. The remaining solution contained several compounds including [Pt(dbpe)(dppe)] (66.6%); [Pt(dppe)$_2$] (10.3%) along with traces of dbpeO$_2$, dppeO$_2$ and dppeO. The only component unidentified had the data: $\delta = 44.2$ ppm, $J_{Pt-P} = 2243$ Hz.

(vi) *CPE of* [PtCl$_2$(dbpe)] *in the presence of* dcpe. (a) To the pre-electrolysed solution (−2.40 V, CH_3CN) was added [PtCl$_2$(dbpe)] (*ca* 30 mg) with one equivalent of dcpe (*ca* 22 mg). This was electrolysed until 2-electrons/equivalent were consumed (30 min to 1 h). A precipitate formed which was collected. $^{31}P\{^1H\}$ NMR data of this dark yellow solid (in C_6D_6 solution) revealed [Pt(dbpe)(dcpe)] (48.8%); [Pt(dcpe)$_2$] (11.2%); and dcpe (33.6%). In the remaining solution was seen five platinum phosphine complexes. The data for these unidentified complexes are as follows: $\delta = 46.6$ ppm, $J_{Pt-P} = 2270$ Hz (29.2%); $\delta_P = 49.8$ ppm, $J_{Pt-P} = 2020$ Hz (12.9%); $\delta_P = 39.6$ ppm, $J_{Pt-P} = 2619$ Hz (13.7%); $\delta_P = 65.0$ ppm, $J_{Pt-P} = 2430$ Hz (11.8%); $\delta_P = 68.0$ ppm, $J_{Pt-P} = 2064$ Hz (6.4%). The remaining peaks were attributed to dcpe, dbpe and the corresponding oxides.

(b) To the pre-electrolysed solution (1.50 V, CH_3CN) was added [PtCl$_2$(dbpe)] (*ca* 30 mg) with one equivalent of dcpe (*ca* 22 mg). This was electrolysed to near zero current at which point 2.2 electrons/equivalent were consumed and a white precipitate was collected. $^{31}P\{^1H\}$ NMR data of this white solid revealed [Pt(dbpe)(dcpe)] as the only phosphorus-containing product. The remaining solution contained no significant phosphorus-containing material and only traces of dcpe and dbpeO$_2$ were observed spectroscopically.

(vii) *CPE of* [Pt(dbpe)$_2$]Cl$_2$. To a pre-electrolysed solution (−1.50 V, CH_3CN/C_6H_6, 1:1 v/v) the complex [Pt(dbpe)$_2$]Cl$_2$ (*ca* 30 mg) was added and then purged with argon for 1 h. The solution was electrolysed to near zero current with coulometry indicating approximately 2-electrons/equivalent consumed (range 2.0–2.2 electrons/equivalent). After work-up as previously described the $^{31}P\{H\}$ NMR spectrum revealed three platinum complexes in addition to peaks for the free phosphine (dbpe) and its oxides. Of the three platinum complexes two were identified as [Pt(dbpe)$_2$] (48.9%) and [Pt(dbpe)$_2$]$^{2+}$ (19.2%). The remaining complex, $\delta_P = 36.7$ ppm, $J_{2Pt-P} = 3090$ Hz (11.5%) remains unidentified.

(vii) *CPE of* [PtCl$_2$(dppe)] *in the absence of a trapping agent*. To the pre-electrolysed solution (−1.75 V, CH_3CN/C_6H_6, 1:1 v/v) the complex [PtCl$_2$(dppe)] (*ca* 30 mg) was added and the solution was purged with argon for 1 h. The solution was electrolysed to near zero current with coulometry indicating consumption of 1.4 electrons/equivalent. After work-up as previously described, the $^{31}P\{^1H\}$ NMR spectrum revealed the presence of the following compounds: $\delta_P = 38.3$ ppm, $J_{Pt-P} = 1626$ Hz; $\delta_P = 40.4$ ppm, $J_{Pt-P} = 3587$ Hz; $\delta_P = 33.4$ ppm, $J_{Pt-P} = 4592$ Hz; $\delta_P = 35.2$ ppm, $J_{Pt-P} = 3592$ Hz, $J_{P-P} = 8$ Hz. The ^1H NMR spectrum of this mixture did not reveal any resonances attributable to hydrides.

Acknowledgement—Thanks are expressed to the Petroleum Research Fund, administered by the American Chemical Society, for support of this work.

REFERENCES

1. J. A. Davies, C. T. Eagle, D. E. Otis and U. Venkataraman, *Organometallics* 1986, **5**, 1264.
2. J. A. Davies and C. T. Eagle, *Organometallics* 1986, **5**, 2149.
3. J. A. Davies, C. T. Eagle, D. E. Otis and U. Venkataraman, *Organometallics* 1989, **8**, 1080.
4. G. K. Anderson, H. C. Clark and J. A. Davies, *Organometallics* 1982, **1**, 550.
5. R. S. Paonessa, A. L. Priganano and W. C. Trogler, *Organometallics* 1985, **4**, 647.
6. B. E. Mann and A. Musco, *J. Chem. Soc., Dalton Trans.* 1980, 775.

7. M. Hackett and G. M. Whitesides, *J. Am. Chem. Soc.* 1988, **110**, 1449.
8. M. Hackett, J. A. Ibers, P. Jernakoff and G. M. Whitesides, *J. Am. Chem. Soc.* 1986, **108**, 8094.
9. M. Hackett, J. A. Ibers and G. M. Whitesides, *J. Am. Chem. Soc.* 1988, **110**, 1436.
10. J. A. Davies, P. L. Watson, A. Greenberg and J. F. Liebman (Eds), *Selective Hydrocarbon Activation: Principles and Progress.* VCH, New York (1990).
11. H. C. Clark, P. M. Kapoor and I. J. McMahon, *J. Organomet. Chem.* 1984, **265**, 107.
12. G. K. Anderson, J. A. Davies and D. J. Schoeck, *Inorg. Chim. Acta* 1983, **76**, L251.
13. J. A. Davies and V. Uma, *Inorg. Chim. Acta* 1983, **76**, L305.
14. J. A. Davies and V. Uma, *J. Electroanalyt. Chem.* 1983, **158**, 13.
15. J. A. Davies and V. Uma, *J. Electroanalyt. Chem.* 1984, **179**, 273.
16. J. A. Davies, V. Uma and J. G. Mierzwiak, *J. Electroanalyt. Chem.* 1985, **196**, 329.
17. M. Martelli, G. Pilloni, G. Zotti and S. Daolio, *Inorg. Chim. Acta* 1974, **11**, 155.
18. J. A. Davies and R. J. Staples, unpublished results.
19. M. Hewertson and H. R. Watson, *J. Chem. Soc.* 1962, 1490.
20. D. Drew, J. R. Doyle and A. G. Shaver, *Inorg. Synth.* 1972, **13**, 47.
21. F. R. Hartley, S. G. Murray and C. A. McAuliffe, *Inorg. Chem.* 1979, **18**, 1394.

Polyhedron Vol. 10, No. 9, pp. 909–917, 1991
Printed in Great Britain

0277–5387/91 $3.00+.00
© 1991 Pergamon Press plc

C—X AND C—H CLEAVAGE BY ELECTROCHEMICALLY GENERATED NON-LINEAR [PtL_2] COMPLEXES

JULIAN A. DAVIES† and RICHARD J. STAPLES‡

Departments of Chemistry and Medicinal and Biological Chemistry,
The University of Toledo, Toledo, OH 43606, U.S.A.

(*Received* 6 *August* 1990; *accepted* 4 *January* 1991)

Abstract—The electrochemical reduction of [PtX_2L_2] (X = halide, L_2 = bidentate diphosphine: $Ph_2PCH_2CH_2PPh_2$, dppe; $Cy_2PCH_2CH_2PCy_2$, dcpe; $Cy_2P\{CH_2\}_3PCy_2$, dcpp) has been used as a method of generating non-linear [PtL_2] compounds whose reactivity with substrates Ar—X (X = Cl, Br, CN, H, C≡CPh) has been examined. Generation of [PtL_2] (L_2 = dppe or dcpe) in the presence of excess Ph—X (X = Cl, Br) produces [PtXPhL_2] efficiently. Similarly, generation of [PtL_2] (L_2 = dppe or dcpe) in the presence of PhC≡CPh results in trapping to form [PtL_2(PhC≡CPh)]. Generation of [PtL_2] (L_2 = dppe or dcpe) in the presence of PhCN or PhH results in indiscriminate reactions that do not produce tractable products. In contrast, reduction of [$PtCl_2$(dcpp)] in $CH_3CN/C_6H_6/Bu_4NClO_4$ produces [PtHPh(dcpp)] with considerable selectivity via aromatic C—H activation by [Pt(dcpp)]. At room temperature the complex [PtHPh(dcpp)] undergoes exchange with C_6D_6 to generate [PtD(C_6D_5)(dcpp)].

In a recent series of papers Whitesides and coworkers[1–3] have shown that C_{2v} [PtL_2] complexes can react with hydrocarbon substrates, including alkanes, by C—H oxidative addition. Thus, thermolysis of the alkylhydride [PtH(CH_2CMe_3)($Cy_2PCH_2CH_2PCy_2$)] (Me = methyl, Cy = cyclohexyl) was shown to result in reductive elimination of neopentane and reaction of the resulting non-linear [PtL_2] fragment with an organic substrate present in excess. We have demonstrated[4–7] that electrochemical reduction of *cis*-[$PtCl_2L_2$] complexes generates [PtL_2] equivalents and that in the case where L_2 is a bidentate tertiary phosphine ligand[7] the non-linear intermediate may be trapped by other bidentate ligands to produce [PtL_2L_2*]. Here we report on the reactions of non-linear [PtL_2] equivalents, generated by electrochemical reduction, with organic substrates including examples where C—X (X = halogen) and C—H oxidative additions are observed.

Initially we believed that the electrochemical generation of non-linear [PtL_2] equivalents by reduction of [PtX_2L_2] might prove to be problematic since the electrochemical method requires the use of a relatively polar solvent and a background electrolyte, both of which might participate in indiscriminate reactions with the C_{2v} intermediate. However, work with bidentate ligands as trapping agents[7] showed that unselective reactions with the solvent/electrolyte could largely be avoided provided a suitable trap was already present in solution as the [PtL_2] intermediate was generated. Thus, in order to probe the reactions of non-linear [PtL_2] complexes with organic substrates we sought suitable compounds to act as trapping agents. The requirements are quite stringent since the trapping agent must survive the very negative potentials required to reduce the [PtX_2L_2] precursors (typically[4–7] *ca* −1.50 to −2.40 V vs Ag/AgCl). Additionally, we sought trapping agents that would not react with the [PtX_2L_2] precursors, a problem that we had previously encountered in using bidentate ligands as trapping agents.[7] Based upon these requirements we examined compounds of the type Ph—X (where X = Cl, Br, CN, H, C≡CPh) which could either be used as solvents for electrochemical reduction or added to a solvent/electrolyte system of acetonitrile/TBAP [TBAP = tetra(n-butyl)ammonium perchlorate]. In order to probe ligand effects on the reactivity of non-linear [PtL_2] com-

† Author to whom correspondence should be addressed.
‡ Present address: Department of Chemistry, Texas A&M University, College Station, TX 77843, U.S.A.

pounds we have examined complexes of dppe ($PhPCH_2CH_2PPh_2$) and dcpe ($Ph_2PCH_2CH_2PPh_2$) with each trapping agent. Some experiments have also been performed with complexes of dcpp ($Cy_2P\{CH_2\}_3PCy_2$).

RESULTS AND DISCUSSION

Our initial experiments utilized PhX (X = Cl, Br, CN) as both solvent and trapping agent for the electrochemical reduction of $[PtX_2(dppe)]$ and $[PtX_2(dcpe)]$. None of these solvents is truly suitable for electroanalytical work since each has a low dielectric constant[8] (PhCl: 5.62; PhBr: 5.40; PhCN: 25.20; cf. CH_3CN: 37.50) and this is manifested in the cyclic voltammograms of $[PtI_2(dppe)]$ shown in Fig. 1. Based on these and similar measurements for other complexes we selected appropriate potentials for controlled potential bulk reductive electrolysis experiments. Each electrolysis experiment was performed utilizing the three-compartment cell, equipped with a mercury pool working electrode, a Ag/AgCl reference electrode and a platinum auxiliary electrode that we have described previously.[6] In many of the experiments described here we found that the low dielectric constant solvents led to low current flow resulting in long electrolysis times which made coulometry unreliable as a guide to determining the extent of reaction. Accordingly, many experiments were terminated at an arbitrary point where the starting material had not been fully consumed.

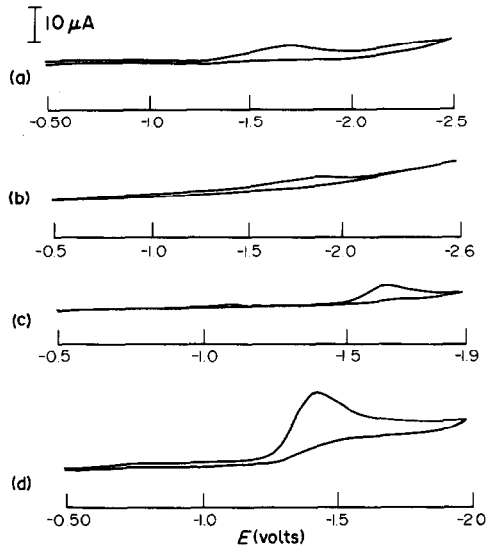

Fig. 1. Cyclic voltammograms of $[PtI_2(dppe)]$ as a 10^{-4} M solution in a solvent that is 0.08 M in TBAP, measured using a Hg/Au amalgam working electrode (1.77 mm^2) at a scan rate of 200 mV s^{-1} with a Ag/AgCl reference electrode. Solvents used were: (a) chlorobenzene, (b) bromobenzene, (c) benzonitrile and (d) acetonitrile.

Electrolysis of $[PtCl_2(dppe)]$ in chlorobenzene at −2.0 V was followed by a standard work-up (see Experimental) and examination by $^{31}P\{^1H\}$ NMR spectroscopy which showed the exclusive formation of [PtClPh(dppe)] and the presence of some residual starting material. Formation of the chlorophenyl complexes suggests electrochemical generation of the non-linear intermediate, [Pt(dppe)], followed by C—Cl oxidative addition. A similar reduction of $[PtI_2(dppe)]$ in chlorobenzene at −1.80 V was complicated by the fact that in this case generation of [Pt(dppe)] liberates iodide ions, which can engage in metathesis reactions with the starting material or product. Thus, $^{31}P\{^1H\}$ NMR spectroscopy indicates the formation of [PtIPh(dppe)], together with the presence of starting material and its metathesis products {i.e. $[PtI_2(dppe)]$, [PtICl(dppe)] and $[PtCl_2(dppe)]$}. Additionally, a trace amount of an unidentified compound (δ_P = 36.7 ppm, J_{Pt-P} = 4165 Hz) was detected. The electrochemical reduction of $[PtI_2(dcpe)]$, containing the bulky σ-donor $Cy_2PCH_2CH_2PCy_2$ ligand, in chlorobenzene at −2.0 V produced [PtClPh(dcpe)] and its metathesis product, [PtIPh(dcpe)]. Some unreacted $[PtI_2(dcpe)]$ was also detected in solution. With the dcpe ligand, no unidentified species were generated (cf. the analogous dppe reaction).

Reactions in bromobenzene were found to proceed similarly. Thus, reduction of $[PtCl_2(dppe)]$ in C_6H_5Br/CH_3CN (5:1) at −2.0 V produced [PtBrPh(dppe)] and its metathesis product, [PtClPh (dppe)]. Some residual starting material was found to be metathesized to [PtClBr(dppe)] and $[PtBr_2$ (dppe)]. The electrochemical reduction of $[PtI_2$ (dcpe)] in bromobenzene at −1.80 V produced both [PtBrPh(dcpe)] and [PtIPh(dcpe)] with some $[PtI_2(dcpe)]$ remaining.

In each of the above experiments the compounds $[PtXPhL_2]$ (X = Cl, Br, I; L_2 = dppe, dcpe), formed by Ph—X oxidative addition, and the mixed halide complexes, $[PtXYL_2]$ (X = Cl; Y = Br, I; L_2 = dppe), formed by halide metathesis, were identified by comparison of their spectroscopic data with data obtained for independently synthesized materials. Details of these syntheses are given in the Experimental and spectroscopic data, along with pertinent literature references, are collected in Tables 1 and 2.

Electrochemical reductions of both $[PtI_2(dppe)]$ and $[PtCl_2(dcpe)]$ in benzonitrile proved to be very complex. Although our earlier work[5,6] on the electrochemical reduction of *cis*-$[PtCl_2(PEt_3)_2]$ in PhCN had shown that *trans*-$[PtCN(Ph)(PEt_3)_2]$ could be effectively generated, neither of the present

Table 1. $^{31}P\{^1H\}$ NMR data of phenylplatinum(II) complexes[a]

	Solvent	δP_A (ppm)	δP_B (ppm)	J_{Pt-P_A} (Hz)	J_{Pt-P_B} (Hz)
[PtClPh(dppe)][b]	C_6D_6	37.7	37.6	1608	4092
	$CDCl_3$	38.7	37.9	1640	4098
[PtBrPh(dppe)]	C_6D_6	38.7	39.0	1615	4083
[PtIPh(dppe)]	C_6D_6	39.2	39.0	1654	3999
[PtClPh(dcpe)]	C_6D_6	60.7	50.7	1692	3956
	$CDCl_3$	62.0	51.8	1718	4062
[PtBrPh(dcpe)]	C_6D_6	59.4	51.7	1689	3969
	$CDCl_3$	60.7	53.1	1710	4059
[PtIPh(dcpe)]	C_6D_6	57.8	50.7	1686	3850
	$CDCl_3$	59.0	52.7	1702	3922

[a] P_A is the phosphorus *trans* to the halide, P_B is the phosphorus *trans* to the phenyl group. Data for independently synthesized samples (see Experimental).

[b] Literature data (ref. 9), δP_A 38.7; δP_B 36.9 ppm; J_{Pt-P_A} 1638; J_{Pt-P_B} 4192 Hz.

Table 2. $^{31}P\{^1H\}$ NMR data of mixed haloplatinum(II) complexes[a]

	δP_A (ppm)	δP_B (ppm)	J_{Pt-P_A} (Hz)	J_{Pt-P_B} (Hz)	J_{P-P} (Hz)
[PtClI(dppe)]	42.6	43.7	3550	3428	0.7
[PtBrCl(dppe)]	43.5	42.6	3562	3542	0.8
[PtIBr(dppe)]	45.2	45.0	3394	3523	1.0
[PtClI(dcpe)]	66.5	65.8	3379	3523	4.9
[PtBrCl(dcpe)]	66.4	64.9	3547	3550	5.1
[PtIBr(dcpe)]	66.3	67.5	3394	3502	5.3

[a] P_A refers to the phosphorus *trans* to the first named halide, P_B refers to the phosphorus *trans* to the second named halide. Data for independently synthesized samples (see Experimental).

systems produced tractable products. Indeed, current flow in these experiments continued past the anticipated 2 electrons/equivalent, perhaps indicating that any *cis*-phenylcyano complexes generated were unstable under the reaction conditions. In this regard it is noteworthy that our attempts to independently synthesize [PtCN(Ph)(dppe)] by treatment of [PtClPh(dppe)] with cyanide ion (see Experimental) invariably led to decomposition.

Diphenylacetylene proved to be an effective trapping agent for non-linear [PtL_2] equivalents. Thus, electrochemical reduction of [PtX_2(dppe)] in CH_3CN/C_6H_6 containing one equivalent of PhC≡CPh produced [Pt(PhC≡CPh)(dppe)] in high yield (X = Cl: 93.5%; X = Br: 94.5%; X = I: 87.0%; estimated from peak heights in the $^{31}P\{^1H\}$ NMR spectra). A similar reduction of [PtI_2(dcpe)] in the presence of PhC≡CPh generated [Pt(PhC≡CPh)(dcpe)] but here the yield was reduced to 56% with other, unidentified by-products also present. The complex [Pt(PhC≡CPh)(dppe)] was identified by comparison of its spectroscopic data with those of a sample independently synthesized by $NaBH_4$ reduction of [PtI_2(dppe)] in the presence of PhC≡CPh (see Experimental). The dcpe analogue was identified by comparison of its spectroscopic data with those extant in the literature.[1]

The results in the preceding paragraphs show that electrochemical reduction of [PtX_2L_2] precursors containing bidentate ligands produces non-linear [PtL_2] equivalents which can be trapped by Ph—X (X = Cl, Br) oxidative addition or by coordination to PhC≡CPh. As mentioned in the introductory paragraphs, we thought that reduction of

$[PtX_2L_2]$ in the absence of a trapping agent but in the presence of a relatively polar solvent (e.g. CH_3CN or CH_3CN/C_6H_6) containing a background electrolyte (e.g. TBAP) might lead to indiscriminate reaction of the non-linear $[PtL_2]$ intermediate. Indeed, reduction of $[PtCl_2(dppe)]$ (at -1.75 V) or $[PtBr_2(dppe)]$ (at -1.60 V) in CH_3CN/C_6H_6 (1 : 1, v/v, 0.1 M TBAP) produced product mixtures containing many components (see Experimental), none of which could be identified by comparison of $^{31}P\{^1H\}$ NMR data with literature values. However, reduction of $[PtI_2(dppe)]$ (at -1.40 V) in CH_3CN/C_6H_6 (1 : 2, v/v, 0.1 M TBAP) gave an indication that some meaningful chemistry might evolve from this area since the $^{31}P\{^1H\}$ NMR spectrum of the complicated product mixture contained resonances attributable to [PtIPh(dppe)], suggesting that C—H cleavage of the benzene component of the solvent mixture might have occurred, although ligand cleavage might also serve as a source of phenyl groups.

Similar indications of aromatic C—H activation were found in experiments using $[PtCl_2(dcpe)]$. Thus, although reduction in CH_3CN (0.1 M TBAP) at -2.25 V produced only unidentifiable products, reduction in CH_3CN/C_6H_6 (1 : 2, v/v, 0.1 M TBAP) at -2.25 V generated a product mixture whose ^1H NMR spectrum showed the presence of a component with a Pt—H bond and a component with a Pt—Ph bond (by the characteristic pattern[1] for the *ortho* protons). The $^{31}P\{^1H\}$ NMR spectrum of this product mixture showed that several platinum phosphine complexes were formed but no resonances attributable to the known compound [PtHPh(dcpe)][1] could be identified. Thus, it seems likely that the Pt—H and Pt—Ph groups observed in the ^1H NMR spectrum are present in different compounds. In this case ligand cleavage cannot be a source of phenyl groups and so C—H activation of benzene seems likely.

After examining several precursors, we found that electrochemical reduction of $[PtCl_2(dcpp)]$ (where dcpp = $Cy_2P\{CH_2\}_3PCy_2$) in CH_3CN/C_6H_6 (1 : 1, v/v, 0.1 M TBAP), followed by a standard work-up (see Experimental) and examination of a C_6D_6 solution by $^{31}P\{^1H\}$ NMR spectroscopy, produced the spectrum shown in Fig. 2(a). The presence of two doublets and the magnitudes of the couplings to platinum[1] suggested the compound formed was [PtHPh(dcpp)]. However,

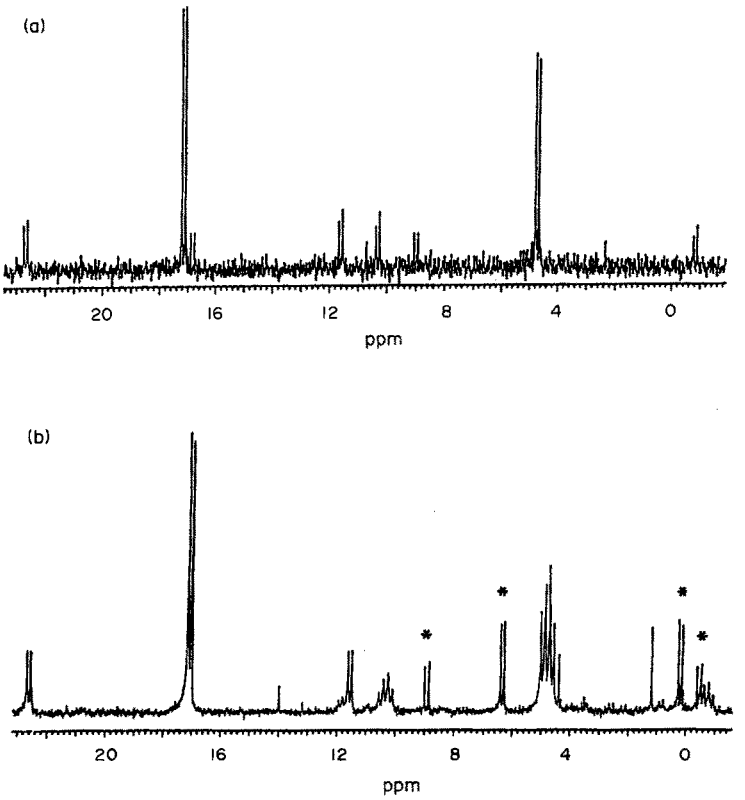

Fig. 2. $^{31}P\{^1H\}$ NMR spectra (C_6D_6 solution) of the product mixture arising from the electrochemical reduction of $[PtCl_2(dcpp)]$ in CH_3CN/C_6H_6 (1 : 1, v/v, 0.1 M TBAP): (a) immediately after work-up and (b) after 6 h in solution.

after 6 h in solution the $^{31}P\{^1H\}$ NMR spectrum had changed to that shown in Fig. 2(b). From this spectrum it is clear that both a new compound is being formed (indicated by *) and that one of the two doublets assigned to [PtHPh(dcpp)] has been transformed into a more complex multiplet while the other doublet has remained unchanged. A 2D-$^{31}P\{^1H\}$-COSY spectrum of the solution demonstrated unambiguously that the doublet at 17.1 ppm is coupled to the new multiplet at 4.7 ppm and that no other coupling to phosphorus is involved in generating this multiplet. Accompanying these changes in the $^{31}P\{^1H\}$ NMR spectrum over time are changes in the ^1H NMR spectrum. The initial ^1H NMR spectrum shows characteristic resonances for Pt—H and Pt—Ph with coupling constants entirely in accord[1] with the proposed structure, [PtHPh(dcpp)]. Six hours later, the hydride and Pt—Ph resonances are no longer present and only resonances attributable to coordinated dcpp are observed.

In order to account for these observations, we postulated that the electrochemical reduction of [PtCl$_2$(dcpp)] produces a non-linear intermediate, [Pt(dcpp)], which reacts selectively with benzene by C—H oxidative addition, despite the presence of both CH_3CN and TBAP. The complex [PtHPh(dcpp)] when dissolved in C_6D_6 undergoes two competing processes: one is decomposition to generate an unknown species [indicated by * in Fig. 2(b)] and the other is a more rapid reaction with the C_6D_6 solvent to generate [PtD(C_6D_5)(dcpp)]. In order to test this postulate, we measured the 2D $^{31}P\{^1H\}$ *J*-resolved NMR spectrum of the solution after it had stood for several hours and then generated the $^{31}P\{^1H, ^{31}P\}$ NMR spectrum. From these data we deduced that the multiplet shown at 4.7 ppm in Fig. 2(b) arose from coupling to the phosphorus observed at 17.1 ppm (*vide supra*) and coupling to a second nucleus (not ^1H or ^{31}P) which generated a 1 : 1 : 1 pattern. This pattern is entirely as expected for coupling of ^{31}P to deuterium and the magnitude of the observed coupling, $^2J(^{31}P, ^2H) = 28$ Hz, agrees well with the analogous value of $^2J(^{31}P, ^1H) = 179$ Hz for the larger of the two ^{31}P–^1H couplings observed in the ^1H NMR spectrum of [PtHPh(dcpp)]. Thus, the magnitudes of the magnetogyric ratios of ^1H and ^2H determine that a coupling of 28 ± 1 Hz involving deuterium will lead to a coupling of 182 ± 6 Hz for the analogous protio compound.

In order to confirm this exchange process, the solution which gave rise to the $^{31}P\{^1H\}$ NMR spectrum shown in Fig. 2(a), i.e. largely [PtHPh(dcpp)], was rapidly evaporated *in vacuo* and an IR spectrum of a KBr pellet of the resulting material was obtained. The spectrum showed the presence of Pt—H with ν(Pt—H) = 1995 cm^{-1}. Similar treatment of a sample giving rise to the $^{31}P\{^1H\}$ NMR spectrum shown in Fig. 2(b), i.e. largely [PtD(C_6D_6)(dcpp)], produced an IR spectrum in which the absorption at 1995 cm^{-1} was absent and a new absorption at 1419 cm^{-1} was present. This value agrees well with the calculated value of 1418 cm^{-1} for replacement of hydrogen by deuterium.

The results that we describe here show interesting similarities and differences to the results of Whitesides and co-workers.[1-3] Thus, Whitesides demonstrated that thermal generation of [Pt(dcpe)] led to selective reactions with substrates present in excess, typically as the solvent. We found that the same intermediate could be generated electrochemically by reduction of [PtX$_2$(dcpe)], but that unless specific trapping agents (e.g. PhCl, PhBr) were present, indiscriminate reaction with the C_6H_6/CH_3CN/TBAP solvent/electrolyte system occurred. Similar statements can be made for the electrochemical generation of the analogous dppe intermediate, whose thermal generation has not been described. However, use of the dcpp ligand allowed electrochemical generation of an intermediate which showed considerable selectivity in producing [PtHPh(dcpp)] via C—H oxidative addition of benzene even in the presence of reactive materials such as CH_3CN and TBAP. Whitesides and co-workers[1-3] observed that [PtHPh(dcpe)] could be induced to undergo exchange with C_6D_6 at $\geqslant 79$°C and have reported a detailed mechanistic investigation. We found that [PtHPh(dcpp)] undergoes the same exchange process at room temperature. Presumably the difference in behaviour of the dcpe and dcpp systems relates to the degree to which the non-linear [PtL$_2$] intermediate can approach linearity. Thus, in our electrochemical system we find that the presumably linear [Pt(PEt$_3$)$_2$] does not react with unactivated C—H bonds, the non-linear [Pt(dcpe)] with a dimethylene ligand backbone reacts indiscriminately, while the [Pt(dcpp)] intermediate with a trimethylene ligand backbone reacts quite selectively.[10]

EXPERIMENTAL

General procedures

The solvents, bromobenzene, chlorobenzene and benzonitrile were purified by first refluxing with anhydrous $MgSO_4$ (10 g dm^{-3}) for 24 h, followed by distillation under argon to a dry flask containing activated alumina (25 g dm^{-3}), where the first 20% of the distillate and the last 20% were discarded.

Collection temperatures were: bromobenzene 154–155°C, chlorobenzene 131–132°C and benzonitrile 190–192°C. Acetonitrile was purified as previously described.[6] Benzene (Fisher, ACS grade) was freshly distilled from sodium wire under nitrogen prior to use. Benzene-d_6 (Aldrich) and chloroform-d (Norell) were stored over molecular sieves (3 Å) and deoxygenated prior to use. Tetra(n-butyl)ammonium perchlorate (TBAP, G.F.S) was purified by recrystallization from absolute ethanol (200 g in 75 cm^3) at room temperature, followed by vacuum drying for 48 h. Diphenylacetylene (Aldrich) was vacuum dried prior to use.

The ligands dppe and dcpe were purchaed from Strem Chemicals and dcpp was prepared by a literature route.[11] The complexes [$PtCl_2$(dppe)], [$PtCl_2$(dcpe)] and [$PtCl_2$(dcpp)] were prepared by displacement of 1,5-cyclooctadiene (cod) from [$PtCl_2$(cod)]. [PtI_2(dppe)] and [PtI_2(dcpe)] were similarly prepared from [PtI_2(cod)]. [$PtBr_2$(dppe)] was prepared by NaBr metathesis of [$PtCl_2$(dppe)] in CH_2Cl_2/acetone. The complexes [PtXPhL_2] (X = Cl, Br, I; L_2 = dppe, dcpe) were prepared (X = Cl) by displacement of 1,5-cyclooctadiene from [PtClPh(cod)] and by NaX metathesis (X = Br, I) of [PtClPhL_2].

$^{31}P\{^1H\}$ (36.2 MHz) NMR spectra were measured on a JEOL FX 90Q spectrometer operating in the Fourier transform mode or were recorded on a Varian VXR 400 (162 MHz) spectrometer. $^{31}P\{^1H\}$ NMR chemical shifts were measured using 85% H_3PO_4 as an external standard with positive values of the chemical shift representing deshielding. Yields were estimated from peak heights in the $^{31}P\{^1H\}$ NMR spectra. The 2D NMR experiments were performed using the standard software on the Varian VXR 400 spectrometer. The COSY experiments were performed using the standard COSY pulse sequence with 128 × 128 fid (free induction decay) collected at 162 MHz with the 2K × 2K processed using pseudo-echo shaped weighting to give the best resolution. The homonuclear 2D *J*-resolved spectrum was recorded using a fid grid with the 1K × 1K processed using pseudo-echo shaped weighting to give the best resolution. ^1H NMR spectra were recorded on a Varian VXR 400 spectrometer and IR spectra were recorded using a Nicolet 5DX FTIR spectrometer with samples pressed as KBr pellets.

Cyclic voltammograms were obtained using a Bioanalytical Systems 100 control unit. Typically, 2.0×10^{-3} M solutions of the complexes in the appropriate solvent (10 cm^3), which was 0.08 M in TBAP, were employed. A single compartment cell, controlled to a temperature of 25 ± 1°C, equipped with a Ag/AgCl reference electrode (−35 mV vs S.C.E.), a platinum wire auxiliary electrode and a mercury/gold amalgam (Hg/Au) working electrode were used. We have discussed cyclic voltammetry of platinum(II) complexes using similar techniques previously.[12–15] Controlled potential bulk reductive electrolyses (CPRE) were performed using a Bioanalytical Systems SP-2 synthetic potentiostat. A three-compartment cell was employed which was constructed in-house. The working electrode compartment contained the Ag/AgCl reference electrode and 18 cm^3 of mercury connected to the potentiostat by a platinum wire. The auxiliary electrode compartment contained a platinum spiral wire electrode. The two compartments were separated by two medium porosity frits. The cell was equipped with a number of fitted openings to allow inert atmosphere operation and manipulation of solutions.

CPRE of [$PtCl_2$(dppe)] *in chlorobenzene*

Twenty-four hours prior to an experiment, the controlled potential electrolysis cell was charged with alumina (1.0 g) and a stir bar, and dried at 100°C. From this point on, all manipulations of the cell were performed under an argon atmosphere at room temperature unless otherwise noted. At the time of the experiment, mercury (25 cm^3) was extracted with dry chlorobenzene (10 cm^3) and then mercury (18 cm^3) was added to the cell which was cooled under argon. A 0.1 M solution of TBAP in chlorobenzene (60 cm^3) was introduced into the cell under an argon stream. This was allowed to outgas for 1 h. The solution was then stirred and pre-electrolysed for 20 min at a potential of −1.75 V.

To the pre-electrolysed solution was added [$PtCl_2$(dppe)] (*ca* 33.1 mg) which was purged with argon for 1 h. This was electrolysed for 2 h 45 min by which time the solution was yellow. The solution was then transferred to a Schlenk tube. Evaporation of the solvent (8 h) resulted in a white solid. This solid was extracted with benzene (2 × 10 cm^3), filtered and evaporated to give a white solid which was dissolved in C_6D_6 (1 cm^3) and transferred to a dry NMR tube under argon. The $^{31}P\{^1H\}$ NMR spectrum showed [PtClPh(dppe)] (88.%) $\delta_{P(1)}$ = 37.7 ppm, $J_{Pt-P(1)}$ = 1608 Hz, $\delta_{P(2)}$ = 37.6 ppm, $J_{Pt-P(2)}$ = 4092 Hz; and [$PtCl_2$(dppe)] (11.9%) δ_P = 41.2 ppm, J_{Pt-P} = 3620 Hz.

CPRE of [PtI_2(dppe)] *in chlorobenzene*

To the pre-electrolysed solution (−1.8 V, PhCl) was added [PtI_2(dppe)] (*ca* 30.0 mg) which was purged with argon for 1 h. This was electrolysed for 3 h with a low current flow (*ca* 0.6 electrons/

molecule) and worked-up as described above. The $^{31}P\{^1H\}$ NMR spectrum of a C_6D_6 solution showed [PtI_2(dppe)] (33.4%) $\delta_P = 45.8$ ppm, $J_{Pt-P} = 3384$ Hz; [PtIPh(dppe)] (45.3%) $\delta_{P(1)} = 39.2$ ppm, $J_{Pt-P(1)} = 1654$ Hz, $\delta_{P(2)} = 39.0$ ppm, $J_{Pt-P(2)} = 3999$ Hz; [$PtCl_2$(dppe)] (2.1%) δ_P 41.2 ppm, $J_{pt-P} = 3621$ Hz; [PtClI(dppe)] (14.9%) $\delta_{P(1)} = 42.2$ ppm, $J_{Pt-P(1)} = 3550$ Hz, $\delta_{P(2)} = 44.2$ ppm, $J_{Pt-P(2)} = 3446$ Hz; $dppeO_2$ (1.1%) $\delta_P = 30.4$ ppm; and a minor component (3.2%) $\delta_P = 36.7$ ppm, $J_{Pt-P} = 4165$ Hz.

CPRE of [PtI_2(dcpe)] *in chlorobenzene*

To the pre-electrolysed solution (−2.0 V, PhCl) was added [PtI_2(dcpe)] (*ca* 34.6 mg) which was then purged with argon for 1 h. Electrolysis resulted in a low current flow and was stopped after 3 h 10 min, after which the clear solution was evaporated (10 h 15 min) and worked-up as described above. The $^{31}P\{^1H\}$ NMR spectrum of a $CDCl_3$ solution showed [PtIPh(dcpe)] (68.9%) $\delta_{P(1)} = 59.0$ ppm, $J_{Pt-P(1)} = 1702$ Hz, $\delta_{P(2)} = 52.7$ ppm, $J_{P(1)-P(2)} = 3922$ Hz; [PtI_2(dcpe)] (16.0%) $\delta_P = 66.9$ ppm, $J_{Pt-P} = 3373$ Hz; [PtClPh(dcpe)] (15.1%) $\delta_{P(1)} = 62.0$ ppm, $J_{Pt-P(1)} = 1718$ Hz, $\delta_{P(2)} = 51.8$ ppm, $J_{Pt-P(2)} = 4062$ Hz.

CPRE of [$PtCl_2$(dppe)] *in bromobenzene/acetonitrile*

To the pre-electrolysed solution (−1.8 V, $PhBr/CH_3CN$, 5:1, v/v) was added [$PtCl_2$(dppe)] (*ca* 30.2 mg) which was then purged with argon for 1 h. Electrolysis resulted in a large current flow. A dark orange solution was produced in the oxidation compartment which began to travel to the reduction compartment. Accordingly, electrolysis was stopped after 1 h 20 min. Evaporation of the solvent required 8 h and resulted in a brown solid. The $^{31}P\{^1H\}$ NMR spectrum of a C_6D_6 extract (which leaves a white precipitate) gave the following data: [PtClBr(dppe)] (26.5%), [PtBrPh(dppe)] (20.2%), [$PtBr_2$(dppe)] (10.8%), [PtClBr(dppe)] (11.1%) and $dppeO_2$ (18.4%), with one complex undefined with data: $\delta_P = 42.3$ ppm, $J_{Pt-P} = 2310$ Hz (12.5%). A $CDCl_3$ solution of the white precipitate left from the extraction showed only [PtClPh(dppe)].

CPRE of [PtI_2(dcpe)] *in bromobenzene*

To the pre-electrolysed solution (−1.8 V, PhBr) was added [PtI_2(dcpe)] (*ca* 33.4 mg) which was then purged with argon for 1 h. Electrolysis resulted in a small current flow and was continued for 2 h 50 min. Work-up produced a light yellow solid and the $^{31}P\{^1H\}$ NMR spectrum of a $CDCl_3$ solution showed only [PtI_2(dcpe)]. This electrolysis was repeated with an electrolysis time of 6 h, with the current remaining at a low level. Evaporation of the solvent (11 h) and work-up produced a light yellow solid. The $^{31}P\{^1H\}$ NMR spectrum of a $CDCl_3$ solution showed the presence of [PtI_2(dcpe)] (50.0%), [PtIPh(dcpe)] (30.0%) and [PtIBr(dcpe)] (20%).

CPRE of [PtI_2(dppe)] *in benzonitrile*

To the pre-electrolysed solution (−1.7 V, PhCN) was added [PtI_2(dppe)] (*ca* 31.8 mg) which was then purged with argon for 1 h. Electrolysis resulted in a very large current flow and after 16 min coulometry indicated consumption of 2.25 electrons/molecule. The resulting orange solution turned yellow by the time the evaporation of the solvent *in vacuo* was complete (10 h, warm water bath). After the work-up, the $^{31}P\{^1H\}$ NMR spectrum of a C_6D_6 solution showed only the presence of [PtI_2(dppe)].

CPRE of [$PtCl_2$(dcpe)] *in benzonitrile*

To the pre-electrolysed solution (−1.5 V, PhCN) was added [$PtCl_2$(dcpe)] (*ca* 27.0 mg) which was then purged for 1 h with argon. Electrolysis resulted in a large current flow and was halted after 2.1 electrons/molecule had been consumed. The dark yellow solution was evaporated (20 h) and after work-up the $^{31}P\{^1H\}$ NMR spectrum of a C_6D_6 solution showed approximately 68 peaks including one set of resonances identifiable as a platinum complex: $\delta_P = 71.5$ ppm, $J_{Pt-P} = 3024$ Hz. ^1H NMR data: $\delta_H = -1.14$ ppm, $J_{P(1)-H} = 179.6$ Hz, $J_{P(2)-H} = 14$ Hz, J_{Pt-H} was not observed. No strong ν(C≡N) was observed in the IR spectrum.

CPRE of [$PtCl_2$(dppe)] *in the presence of* Ph—C≡C—Ph

To the pre-electrolysed solution (−1.7 V, CH_3CN/C_6H_6, 1:1, v/v) which contained Ph—C≡C—Ph (0.1804 g) was added [$PtCl_2$(dppe)] (*ca* 27.7 mg) which was purged for 1 h with argon. The electrolysis to essentially zero current was performed at −1.7 V for 1 h. Coulometry indicated 1.85 electrons/molecule were consumed. After work-up the $^{31}P\{^1H\}$ NMR spectrum of a C_6D_6 solution showed [Pt(Ph—C≡C—Ph)(dppe)] (93.5%) $\delta_P = 49.1$ ppm, $J_{Pt-P} = 3143$ Hz and peaks at $\delta_P = 38.9$ ppm (4.0%); $\delta_P = 40.2$ ppm (2.5%) of unknown origin.

CPRE of $[PtBr_2(dppe)]$ *in the presence of* Ph—C≡C—Ph

To the pre-electrolysed solution (−1.6 V, CH_3CN/C_6H_6, 1:1, v/v) which contained Ph—C≡C—Ph (0.1513 g) was added $[PtBr_2(dppe)]$ (28.5 mg in one experiment and 26.7 mg in a second experiment) which was purged for 1 h with argon. This was electrolysed to essentially zero current for 1 h 20 min. Coulometry indicated 1.8 electrons/molecule consumed. After work-up, the $^{31}P\{^1H\}$ NMR spectrum of a C_6D_6 solution showed [Pt(Ph—C≡C—Ph)(dppe)] (94.5%) $\delta_P = 49.1$ ppm, $J_{Pt-P} = 3146$ Hz and a peak at $\delta_P = 38.9$ ppm (5.5%) of unknown origin.

CPRE of $[PtI_2(dppe)]$ *in the presence of* Ph—C≡C—Ph

To the pre-electrolysed solution (−1.4 V, CH_3CN/C_6H_6, 1:1, v/v) which contained Ph—C≡C—Ph (0.1371 g) was added $[PtI_2(dppe)]$ (29.8 mg in one experiment and 28.4 mg in a second experiment) which was then degassed for 1 h with argon. Electrolysis to essentially zero current at −1.4 V took 1 h 20 min. Coulometry indicated 2.1 electrons/molecule consumed. After work-up the $^{31}P\{^1H\}$ NMR spectrum of a C_6D_6 solution showed [Pt(Ph—C≡C—Ph)(dppe)] (87%) $\delta_P = 49.1$ ppm, $J_{Pt-P} = 3146$ Hz and the following peaks of unknown origin: $\delta_P = 38.9$ ppm (7.7%), $\delta_P = 48.5$ ppm (1.5%), $\delta_P = 37.8$ ppm (3.8%).

CPRE of $[PtI_2(dcpe)]$ *in the presence of* Ph—C≡C—Ph

To the pre-electrolysed solution (−1.95 V, CH_3CN/C_6H_6, 1:1, v/v) which contained Ph—C≡C—Ph (0.1616 g) was added $[PtI_2(dcpe)]$ (28.1 mg in one experiment and 26.7 mg in a second experiment) which was purged for 1 h with argon. Electrolysis was performed at −1.7 V for 33 min, at which time coulometry indicated that 2.1 electrons/molecule were consumed. After work-up the $^{31}P\{^1H\}$ NMR spectrum of a C_6D_6 solution showed [Pt(Ph—C≡C—Ph)(dcpe)] (55.9%) $\delta_P = 66.9$ ppm, $J_{Pt-P} = 3010$ Hz; with two unknown complexes $\delta_P = 74.2$ ppm, $J_{Pt-P} = 1753$ (27.8%) and $\delta_{P(1)} = 60.7$ ppm, $J_{Pt-P(1)} = 1803$ Hz, $\delta_{P(2)} = 60.6$ ppm, $J_{Pt-P(2)} = 1750$ Hz (16.3%). ^1H NMR spectroscopy revealed a hydride signal $\delta_H = -0.34$ ppm, $J_{P-H} = 17.6$ Hz, $J_{P-H} = 189$ Hz, $J_{Pt-H} = 1230$ Hz.

CPRE of $[PtI_2(dppe)]$ *in* CH_3CN/C_6H_6/TBAP

To the pre-electrolysed solution (−1.5 V, CH_3CN/C_6H_6, 2:4 v/v) was added $[PtI_2(dppe)]$ (*ca* 32.5 mg) which was purged with argon for 1 h and electrolysed to essentially zero current at −1.4 V. This required 2 h and coulometry indicated 1.8 electrons/molecule consumed. After work-up the dark orange solution generated a brown solid. The $^{31}P\{^1H\}$ NMR spectrum of a C_6D_6 solution was obtained which gave the following data: $\delta_{P(1)} = 51.1$ ppm, $J_{Pt-P(1)} = 3700$ Hz; $\delta_{P(2)} = 50.1$ ppm, $J_{Pt-P(2)} = 2875$ Hz, $J_{P(1)-P(2)} = 60$ Hz; [PtIPh(dppe)]: $\delta_{P(1)} = 39.2$ ppm, $J_{Pt-P(1)} = 3959$ Hz; $\delta_{P(2)} = 39.3$ ppm, $J_{Pt-P(2)} = 1656$ Hz. In a similar manner to this experiment, electrolyses of $[PtCl_2(dppe)]$ (−1.75 V), $[PtBr_2(dppe)]$ (−1.60 V) and $[PtCl_2(dcpe)]$ (−2.25 V) were performed. In none of these experiments were any identifiable components present in the complex product mixtures.

CPRE of $[PtCl_2(dcpp)]$ *in acetonitrile/benzene* (1:1, v/v)

Twenty-four hours prior to an experiment, the controlled potential electrolysis cell was charged with alumina (1.0 g) and dried at 110°C. From this point on, all manipulations of the cell were carried out under an argon atmosphere at room temperature unless otherwise noted. At the time of the experiment, mercury (25 cm^3) was extracted with dry benzene (10 cm^3) and then 18 cm^3 of mercury and a small magnetic stir bar was added to the cell which was cooled under argon. A 0.1 M solution of TBAP in acetonitrile/benzene (60 cm^3, 1:1, v/v) was introduced into the cell under an argon stream. This was allowed to outgas for 1 h. The solution was then stirred and pre-electrolysed to approximately zero current at a potential of −2.10 V.

To the pre-electrolysed solution was added $[PtCl_2(dcpp)]$ (*ca* 30 mg) which was purged with argon for 1 h and then electrolysed to essentially zero current at a potential of −2.1 V. This usually required 75 min to 2 h and coulometry indicated approximately a 2 electrons/molecule reduction, with integrations in the range of 1.9–2.0 electrons/molecule. When the electrolysis was complete, the solution was transferred (using inert atmosphere techniques) to a Schlenk tube and evaporated. The brownish solid was extraced with benzene (2 × 10 cm^3) and evaporated to give a brown solid which was dissolved in C_6D_6 and transferred to an NMR tube. The $^{31}P\{^1H\}$ NMR spectrum measured immediately [Fig. 2(a)] showed [PtHPh(dcpp)] (87.4%). $^{31}P\{^1H\}$ NMR: $\delta_{P(1)} = 17.1$ ppm, $J_{Pt-P(1)} = 1793$ Hz; $\delta_{P(2)} = 4.7$ ppm, $J_{Pt-P(2)} = 1809$

Hz; $J_{P(1)-P(2)} = 21$ Hz. ^1H NMR: δ(hydride) = -1.58 ppm, $J_{P-H} = 21$ Hz, $J_{P-H} = 179$ Hz, $J_{Pt-H} = 1152$ Hz; δ(*o*-phenyl protons) = 7.86 ppm, $J_{H-H} = 13$ Hz, $J_{Pt-H} = 59$ Hz. IR (KBr pellet): ν(Pt—H) = 1995 cm^{-1}. After several hours, the spectrum began to change and when 6 h had elapsed, the $^{31}P\{^1H\}$ NMR spectrum showed [PtD(Ph-d_5)dcpp] (56.7%) and other components [Fig. 2(b)]: $\delta_P = 6.3$ ppm, $\delta_P = 0.18$ ppm, $J_{P-P} =$ 21 Hz (19.5%); $\delta_P = 8.9$ ppm, $\delta_P = -0.47$ ppm, $J_{P-P} = 24$ Hz (12.6%); $\delta_P = 47.6$ ppm (2.2%); $\delta_P = 23.7$ ppm (1.7%); $\delta_P = 4.37$ ppm (3.1%); $\delta_P = 1.18$ ppm (4.2%).

Preparation of [Pt(Ph—C≡C—Ph)(dppe)]

To a Schlenk flask containing 20 cm^3 of degassed ethanol was added [PtI_2(dppe)] (51.4 mg, 6.07×10^{-5} mol) and Ph—C≡C—Ph (10.6 mg, 5.95×10^{-5} mol). This was heated to reflux for 30 min, then allowed to cool, and $NaBH_4$ (5.1 mg, 1.42×10^{-4} mol) dissolved in H_2O (3 cm^3) was added and stirred. A precipitate appeared and the mixture was stirred for 3 h. This was then filtered quickly and vacuum dried to yield 25.1 mg (49.6%) of light yellow solid. The $^{31}P\{^1H\}$ NMR spectrum of this solid in 1 cm^3 of C_6D_6 showed [Pt(PhC≡CPh)(dppe)] exclusively: $\delta_P = 49.1$ ppm, $J_{Pt-P} = 3146$ Hz.

Generation of mixed haloplatinum(II) *complexes*

In order to obtain spectroscopic data for comparison purposes, mixed halo complexes were generated *in situ* using the following general method cited here for the specific case of [PtClL(dppe)] as an example. [$PtCl_2$(dppe)] (15.1 mg, 2.27×10^{-5} mol) and NaI (4.0 mg, 2.73×10^{-5} mol) were suspended in acetonitrile (1 cm^3) and then dichloromethane was added until all the solid was dissolved. After 10 min, the solution was evaporated *in vacuo* to a white solid and the soluble material was dissolved in 1 cm^3 of $CDCl_3$. The $^{31}P\{^1H\}$ NMR spectrum shows [PtI_2(dppe)] ($\delta_P = 46.0$ ppm, $J_{Pt-P} = 3337$ Hz), [$PtCl_2$(dppe)] ($\delta_P = 41.2$ ppm, $J_{Pt-P} = 3621$ Hz) and [PtClI(dppe)] ($\delta_{P(1)} = 42.6$ ppm, $J_{Pt-P(1)} = 3550$, $\delta_{P(2)} = 43.7$ ppm, $J_{Pt-P(2)} = 3428$ Hz, $J_{P-P} = 0.7$ Hz).

Reaction of [PtClPh(dppe)] *with* NaCN

To [PtClPh(dppe)] (15.2 mg) dissolved in CH_2Cl_2 (15 cm^3, dry, under argon) was added excess NaCN. This was stirred for 1 h then evaporated on a vacuum line to a white solid. A C_6D_6 (1 cm^3) extract produced a $^{31}P\{^1H\}$ NMR spectrum that showed only dppe ($\delta_P = -13.5$ ppm) present. Extraction with $CDCl_3$ also showed only dppe in the $^{31}P\{^1H\}$ NMR spectrum.

Acknowledgement—Thanks are expressed to the Petroleum Research Fund administered by the American Chemical Society for support of this work.

REFERENCES

1. M. Hackett and G. M. Whitesides, *J. Am. Chem. Soc.* 1985, **86**, 159.
2. M. Hackett, J. A. Ibers, P. Jernakoff and G. M. Whitesides, *J. Am. Chem. Soc.* 1988, **108**, 8094.
3. M. Hackett, J. A. Ibers and G. M. Whitesides, *J. Am. Chem. Soc.* 1988, **110**, 1436.
4. J. A. Davies, C. T. Eagle, D. E. Otis and U. Venkataraman, *Organometallics* 1988, **5**, 1264.
5. J. A. Davies and C. T. Eagle, *Organometallics* 1986, **5**, 2149.
6. J. A. Davies, C. T. Eagle, D. E. Otis and U. Venkataraman, *Organometallics* 1989, **8**, 1080.
7. J. A. Davies and R. J. Staples, *Polyhedron*, 899.
8. J. A. Dean (Ed.), *Lange's Handbook of Chemistry*, 13th edn. McGraw-Hill, New York (1985).
9. G. K. Anderson, H. C. Clark and J. A. Davies, *Inorg. Chem.* 1981, **20**, 3607.
10. J. A. Davies and R. J. Staples, in *Selective Hydrocarbon Activation: Principles and Progress* (Edited by J. A. Davies, P. L. Watson, J. F. Liebman and A. Greenberg). VCH, New York (1990).
11. M. Hewertson and H. R. Watson, *J. Chem. Soc.* 1962, 1490.
12. J. A. Davies and V. Uma, *Inorg. Chim. Acta* 1983, **76**, L305.
13. J. A. Davies and V. Uma, *J. Electroanalyt. Chem.* 1983, **158**, 13.
14. J. A. Davies and V. Uma, *J. Electroanalyt. Chem.* 1984, **179**, 273.
15. J. A. Davies, V. Uma and J. G. Mierzwiak, *J. Electroanalyt. Chem.* 1985, **196**, 329.

Polyhedron Vol. 10, No. 9, pp. 919–926, 1991
Printed in Great Britain

0277–5387/91 $3.00+.00
© 1991 Pergamon Press plc

SOLVENT EXTRACTION OF 1-PHENYL-1,2-PROPANEDIONE-2-OXIME AND OF ITS COPPER(II) AND NICKEL(II) COMPLEXES INTO CHLOROFORM

A. IZQUIERDO,* R. COMPAÑÓ* and M. GRANADOS

Departament de Química Analítica, Universitat de Barcelona, Diagonal 647, 08028 Barcelona, Spain

(*Received* 23 *March* 1990; *accepted* 7 *January* 1991)

Abstract—The distribution equilibria of 1-phenyl-1,2-propanedione-2-oxime (PPO) and of the copper(II)–PPO and nickel(II)–PPO complexes in the water–chloroform system have been studied at 25°C. From the graphical treatment of the equilibrium data it has been deduced that PPO dimerizes in the organic phase, copper is extracted as the $CuL_2(HL)$ and $CuL_2(HL)_2$ complexes and nickel as NiL_2 and $NiL_2(HL)$. These models have been checked by treating the data with the LETAGROP-DISTR program and the following equilibrium constants have been obtained: PPO, $pK_a = 9.25 \pm 0.03$, $\log K_{DR} = 1.60 \pm 0.02$, $\log K_2 = 0.60 \pm 0.06$; copper(II)–PPO, $\log \beta_1 = 5.9 \pm 0.1$, $\log \beta_2 = 11.56 \pm 0.05$, $\log K_{DC} K_{m,1} = 2.7 \pm 0.1$, $\log K_{m,2} = 1.0 \pm 0.1$; nickel(II)–PPO, $NiL_2 \log K_{ex} = -13.57 \pm 0.05$, $NiL_2(HL)$, $\log K_{ex} = -12.6 \pm 0.1$.

α-Oxooximes act as bidentate ligands, via carbonyl and oximic nitrogen, forming chelating five-membered rings.

These compounds have been proposed as spectrophotometric reagents for the determination of iron(II), nickel(II), palladium(II), cobalt(II), iridium(III), rhodium(III) and platinum(IV).[1] Since the complexes formed are scarcely soluble in water, a previous extraction into an organic solvent is necessary, usually chloroform.

In spite of their analytical usefulness, very few studies on the formation and distribution equilibria of the metal complexes of this class of reagents have been carried out.[2–4] On the other hand, several studies on the composition and structure of the solid metal complexes of different α-oxooximes have been performed.[5–7]

In the present paper we report the study of the distribution equilibria of 1-phenyl-1,2-propanedione-2-oxime (PPO) and of its copper(II) and nickel(II) complexes in the water–chloroform system. In a previous paper[8] we reported the results of a similar study carried out with N-ethylglyoxylanilide oxime.

* Authors to whom correspondence should be addressed.

EXPERIMENTAL

Reagents

1-Phenyl-1,2-propanedione-2-oxime was supplied by Aldrich and used without further purification. Stock solutions of copper and nickel (1 g dm^{-3}) were prepared and standardized as described earlier.[8] The other chemicals used were all of analytical reagent grade.

Apparatus

A Beckman DU-7 spectrophotometer with 1 cm quartz cells, a Perkin–Elmer 1100B atomic absorption spectrophotometer with an air–acetylene flame and a Perkin–Elmer 4000 atomic absorption spectrophotometer with a graphite furnace (Perkin–Elmer HGA 500) and an auto-sampler (Perkin–Elmer AS-40) were used. The volumes injected into the graphite furnace were 0.02 cm^3. A Radiometer pH-meter PHM64, equipped with a Ross combination pH electrode, standardized with buffer solutions at pH 4.008 and 6.865 (25°C) prepared from Merck salts according to DIN 19266, was also used.

Procedure

The procedures followed to study the distribution of PPO and of its copper(II) and nickel(II) complexes were analogous to those used in a previous study.[8] The pH of the aqueous phase was adjusted with a potassium dihydrogen phosphate–potassium hydroxide buffer for the study of the distribution of copper(II), and with a boric acid–potassium hydroxide buffer in the case of the nickel(II) study.

In order to determine the concentration of PPO in the aqueous phase, absorbance measurements were carried out at 294 nm.

Data treatment

The experimental data were treated with graphical methods (slope analysis and curve-fitting methods) and with the LETAGROP-DISTR program.[9]

RESULTS AND DISCUSSION

Distribution of PPO *in the water–chloroform system*

The distribution ratio values obtained at pH 4.05 and 9.42 show that 5 min of shaking is enough to attain the distribution equilibrium. In subsequent experiments, an extraction time of 15 min was adopted. The influence of the reagent concentration on the distribution ratio values (Fig. 1) shows that, in the concentration range studied, molecular association in the organic phase should be taken into account. Figure 2 shows the plots of $\log D$ vs pH obtained with 10^{-1} and 10^{-2} M PPO solutions in chloroform.

Calculation of the equilibrium constants

Assuming that only the monomeric PPO is capable of distributing into the aqueous phase, and

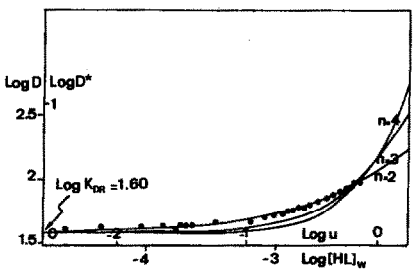

Fig. 1. Influence of reagent concentration on the distribution ratio of PPO. The full lines are the normalized curves $\log D^*$ vs $\log u$; $D^* = 1 + nu^{(n-1)}$.

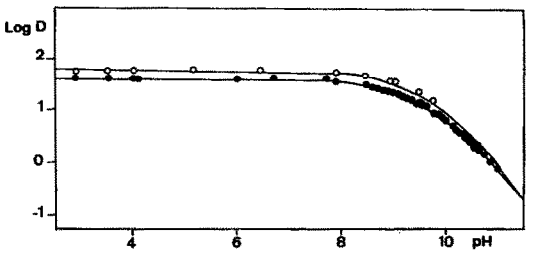

Fig. 2. Influence of pH on the distribution ratio of PPO. ○, $C_{HL} = 10^{-1}$ M; ●, $C_{HL} = 10^{-2}$ M. The full curves are calculated with the HALTAFALL program[21] using the constants given in Table 1.

that only one polymeric species exists in the organic phase, the distribution ratio of PPO is given as

$$D = \frac{[HL]_o + n[(HL)_n]_o}{[HL]_w + [L^-]} = \frac{K_{DR}[HL]_w + nK_nK_{DR}^n[HL]_w^n}{[HL]_w + K_a[H^+]^{-1}[HL]_w}, \quad (1)$$

where HL represents PPO, and K_{DR}, K_a and K_n are, respectively, the distribution, dissociation and polymerization constants of the reagent. The subscripts o and w denote the organic and the aqueous phase, respectively. When $[H^+] \gg K_a$ the following equation is obtained

$$D = K_{DR} + nK_nK_{DR}^n[HL]_w^{n-1}. \quad (2)$$

Graphical treatment

Curve-fitting methods[10,11] were applied to the experimental data in order to determine n, K_n, K_{DR} and K_a. The normalized variables and curves were defined as in a previous paper.[8] In Fig. 1 these curves are superimposed on the experimental points, $\log D$ vs $\log [HL]_w$, in the conditions of best fit. The experimental points fit the curve corresponding to $n = 2$, which means that the polymeric species is a dimer. The values obtained for $\log K_{DR}$ and $\log K_2$ are shown in Table 1.

In order to determine K_a, and because there is an increase in D due to the formation of dimers in the organic phase, corrected values of D have been calculated $\{D_{cor} = [HL]_o/([HL]_w + [L^-])\}$. In Fig. 3 the experimental curve, $\log D_{cor}$ vs pH, and the normalized curve, $\log D^*$ vs $\log u$, in the conditions of best fit are shown. The value obtained for pK_a is shown in Table 1.

Numerical treatment

The final values of the constants and their standard deviations are given in Table 1. The calculated

Table 1. Dissociation constant of PPO and its distribution and dimerization constants in the water–chloroform system

Method	pK_a	$\log K_{DR}$	$\log K_2$	$\sigma(\log D)$
Graphical	9.25	1.60	0.55	
LETAGROP-DISTR[a]	9.25±0.03	1.60±0.02	0.60±0.06	0.026

[a] The limits given for the constants correspond to $\log[K \pm 3\sigma(K)]$; $\sigma(\log D) = [\Sigma(\log D_{exp} - \log D_{calc})^2/N]^{1/2}$.

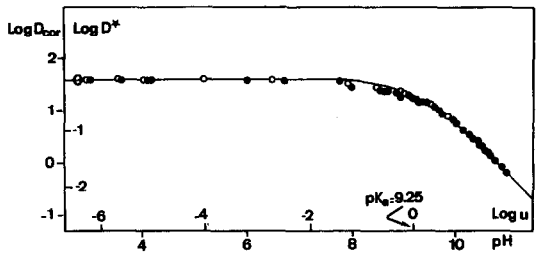

Fig. 3. $\log D_{cor}$ vs pH superimposed on the normalized curve $\log D^*$ vs $\log u$; $D^* = 1/(1+u)$.

$\log D$ values superimposed on the experimental points are plotted in Fig. 2. The good agreement between them confirms the proposed model.

Distribution of the copper complex

In studying the distribution of the copper complex, the appearance of green precipitates at the interface was observed depending on the metal and reagent concentrations, and pH. As the metal/reagent ratio increased, the pH at which the precipitation took place was lower. Thus, in order to avoid the formation of solid phases, PPO concentrations of 8×10^{-2} M or higher were used throughout the study.

A shaking time of 15 min was adopted. The buffer concentration (potassium dihydrogenphosphate–potassium hydroxide) was 2.5×10^{-3} M and the ionic strength of the aqueous phases was adjusted to 0.1 M with potassium nitrate. For details of the influence of these parameters on the distribution ratio see Table 2.

The influence of metal concentration was studied by varying it between 3.15×10^{-5} and 3.15×10^{-4} M at PPO concentrations of 0.4 and 0.1 M. In both cases the distribution ratio is independent of the metal concentration, which suggests that only mononuclear species are extracted.

The influence of pH on the distribution ratio was studied at six different ligand concentrations ranging from 8.0×10^{-2} to 4.0×10^{-1} M. The results are shown in Fig. 4. To examine the influence of PPO concentration on the distribution ratio, at constant pH, the values of $\log D$ corresponding to each reagent concentration were calculated from the curves shown in Fig. 4 at pH 5.20, 5.30, 5.40 and 5.50. These values, plotted against $\log[HL]_o$, are shown in Fig. 5.

Finally, the influence of a second ligand on the distribution equilibrium was studied. Sometimes the addition of a second ligand increases the distribution ratio or inhibits the appearance of insoluble species via the formation of mixed complexes. Of the substances commonly used, 4-methylpyridine was chosen because in studies with similar

Table 2. Effect of shaking time, buffer concentration and nitrate concentration on the distribution ratio of the copper system

Shaking time		Buffer concentration		Nitrate concentration	
t (min)	$\log D^a$	$C_{PO_4^{3-}}$ (M)	$\log D^b$	$[NO_3^-]$ (M)	$\log D^c$
5	−0.42	1.0×10^{-3}	0.87	2.0×10^{-2}	0.20
10	−0.42	2.5×10^{-3}	0.89	5.0×10^{-2}	0.19
15	−0.42	5.0×10^{-3}	0.89	1.0×10^{-1}	0.21
30	−0.44	1.0×10^{-2}	0.71	2.0×10^{-1}	0.20
60	−0.42			4.0×10^{-1}	0.21

[a] pH = 5.30, [PPO] = 1.0×10^{-1} M.
[b] pH = 6.00, [PPO] = 1.0×10^{-1} M.
[c] pH = 5.40, [PPO] = 1.40×10^{-1} M.

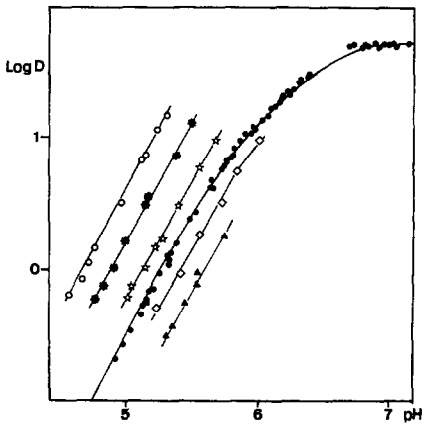

Fig. 4. Influence of pH on the distribution ratio of copper(II). C_{Cu} 6.29×10^{-5} M; C_{PPO}, ▲ = 8.0×10^{-2} M; ◇ = 1.0×10^{-1} M; ● = 1.4×10^{-1} M; ☆ = 2.0×10^{-1} M; * = 3.0×10^{-1} M; ○ = 4.0×10^{-1} M. The full curve is calculated with the HALTAFALL program[21] using the constants given in Tables 1 and 4.

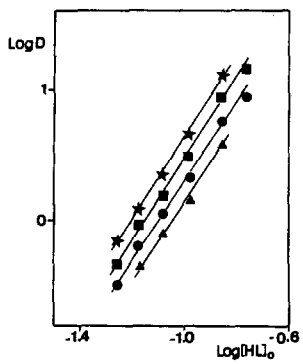

Fig. 5. Influence of reagent concentration on the distribution ratio of copper(II). $C_{Cu} = 6.29\times10^{-5}$ M. pH: ▲ = 5.20; ● = 5.30; ■ = 5.40; ★ = 5.50.

copper–oxime complexes[2] it was the optimum synergic agent. Six different 4-methylpyridine concentrations in the range 0.01–0.50 M were studied. The results are plotted in Fig. 6. In order to take into account the formation of copper(II)–4-methylpyridine complexes in the aqueous phase, $\log D + \log \alpha_{Cu}$ has been plotted against pH. The side reaction coefficient for copper(II) is given by

$$\alpha_{Cu} = 1+\beta_1[P]+\beta_2[P]^2+\beta_3[P]^3+\beta_4[P]^4,$$

where [P] represents the equilibrium concentration of 4-methylpyridine in the aqueous phase and the values of β_i were taken from the references.[12] The fact that the points obtained with different 4-methylpyridine concentrations fall on the same curve, shows that this substance does not participate in the distribution equilibria.

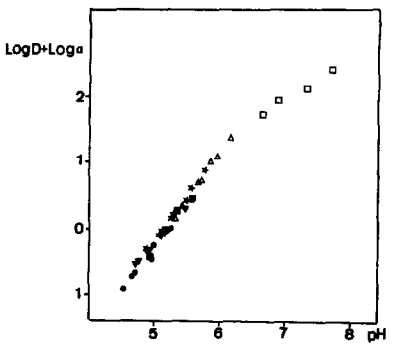

Fig. 6. Influence of 4-methylpyridine (P) concentration on the distribution ratio of copper(II). $\alpha_{Cu} = 1+\beta_1[P]+\beta_2[P]^2+\beta_3[P]^3+\beta_4[P]^4$. $C_{Cu} = 6.29\times10^{-5}$ M. $C_{PPO} = 1.4\times10^{-1}$ M. $C_{4\text{-Pic}}$: ● = 1.0×10^{-2} M; ▲ = 2.0×10^{-2} M; ★ = 3.0×10^{-2} M; ■ = 5.0×10^{-2} M; △ = 1.0×10^{-1} M; □ = 5.0×10^{-1} M.

Composition of the extracted species and calculation of the equilibrium constants

Since under the experimental conditions only mononuclear species are extracted, and complexes with nitrate, phosphate, borate and hydroxide[13] ions can be neglected in the aqueous phase, the metal distribution ratio is given by

$$D = \frac{\sum_n \sum_m [ML_n(HL)_m]_o}{[M]_w + \sum_p [ML_p]_w}, \qquad (3)$$

where M represents the metal and HL the extracting agent. The subscripts o and w denote the organic and the aqueous phase, respectively. Charges have been omitted for simplicity. If only the species $ML_n(HL)_m$ is extracted and the metal is present in the aqueous phase predominantly as the cation M^{n+}, the following equation can be obtained

$$\log D = \log K_{ex} + n\,\mathrm{pH} + (n+m)\log[HL]_o, \qquad (4)$$

where K_{ex}, the extraction constant of $ML_n(HL)_m$, is $K_m K_{DC} \beta_n K_a^n / K_{DR}^m$ (β_n, formation constant of ML_n; K_{DC}, distribution constant of ML_n; K_m, adduct formation constant in the organic phase; K_a and K_{DR}, dissociation and distribution constants of the reagent, respectively).

When species other than ML_n can be neglected in the aqueous phase, a plot of $\log D$ vs pH will give a straight line with a slope of zero; in which case the following equation is valid

$$\log D = \log(K_m K_{DC}) + m \log[HL]_o. \qquad (5)$$

Graphical treatment

The plots $\log D$ vs pH (Fig. 4) corresponding to $\log D < 1$ are straight lines with slopes 1.8–1.9. As

Table 3. Survey of the equilibrium constants for the extraction of copper(II) with PPO into chloroform

Method	$\log\beta_1$	$\log\beta_2$	$\log K_{DC}K_{m1}$	$\log K_{m2}$	$\sigma(\log D)$
Graphical	5.80	11.60	2.83		
LETAGROP-DISTR	5.9±0.1	11.56±0.05	2.7±0.1	1.0±0.1	0.043

$\log D$ increases the slope of the curve decreases progressively to zero at pH above 6.7. On the other hand, the values of $\log D$ vs $\log[HL]_o$ give straight lines with slopes 2.9–3.2. According to eqs (4) and (5) this suggests that the adduct $CuL_2(HL)$ is the extracted species.

Since under the experimental conditions the simple chelate CuL_2 is never present in the organic phase in appreciable amounts, its distribution constant could not be calculated. To calculate the product $K_{DC}K_m$, as well as the stability constants of CuL^+ and CuL_2 in the aqueous phase, Sillén's curve-fitting method was applied to the data. The normalized curves are given by $D^* = u^2/(1+pu+u^2)$, where the normalized variables and the parameter, p, are defined by $D^* = D/K_{DC}K_m[HL]_o$, $u = \beta_2^{1/2}[L^-]$ and $p = \beta_1/\beta_2^{1/2}$. The values of the constants calculated by this method are given in Table 3.

Numerical treatment

Several calculations were performed in order to ascertain the best set of complexes which would fit the experimental data. The results are given in Table 4. They show that the inclusion of the species $CuL_{2(o)}$ in the proposed model does not improve the fit with the experimental data. On the other hand, the complex $CuL_2(HL)_{2(o)}$ was tried because the slopes of the curves $\log D$ vs $\log[HL]_o$ are slightly higher than three, and its inclusion in the model considerably reduces the value of u. The values of the constants obtained with the proposed model are given in Table 3. The calculated $\log D$ values superimposed on the experimental points are plotted in Fig. 4; the good agreement between them confirms the proposed model.

Table 4. Values of u and $\sigma(\log D)$ for the different combinations of copper(II)–PPO complexes tried

Species	u	$\sigma(\log D)$
CuA^+ CuA_2 $CuA_2(HA)_o$	0.437	0.070
CuA^+ CuA_2 $CuA_{2,o}$ $CuA_2(HA)_o$	0.437	0.071
CuA^+ CuA_2 $CuA_2(HA)_o$ $CuA_2(HA)_{2,o}$	0.162	0.043

EPR absorption spectra

In order to determine the ligand atoms involved in the bonding and the structure of the extracted complexes, EPR experiments have been performed on chloroform solutions, obtained under the conditions used in the extraction study.

The EPR spectra of room temperature solutions consist of the characteristic four bands, with $g = 2.111$ and $A = 70$ G, due to coupling between the unpaired electron and copper(II) nucleus ($I = 3/2$). The high field band shows additional superhyperfine structure, consisting of five bands, with $A = 15$ G. This additional splitting is consistent with the interaction of the copper unpaired electron with two equivalent nitrogen nuclei of two PPO molecules. This assumption agrees with the proposed structures for the α-oxooximes–divalent ion complexes,[3] where these reagents act as bidentate ligands, via carbonyl and oximic nitrogen.

Besides the four main bands, at higher field values another band appears partially overlapped with the nearest one. Splitting of the fifth band is hardly observed and only three peaks can be seen, although a five peak splitting is expected. This fifth band can be attributed to the fact that two complexes, $CuL_2(HL)$ and $CuL_2(HL)_2$, are extracted, and only at higher field values, when more resolution is attained, can their respective spectra be partially resolved.

The EPR spectra of the frozen solutions at 150 K are poorly resolved. They show only two series of bands due to anisotropic electron–spin interactions ($g_\parallel \simeq 2.22$ and $g_\perp \simeq 2.01$).

All the results obtained are consistent with an octahedrically distorted geometry with a very strong in-plane interaction.

Distribution of the nickel complex

A shaking time of 15 min was adopted. The buffer concentration (boric acid–potassium hydroxide) was 5×10^{-3} M and the ionic strength of the aqueous phases was adjusted to 0.1 M with potassium nitrate. For details of the influence of these parameters on the distribution ratio, see Table 5.

At nickel concentrations below 1.0×10^{-4} M the metal concentration has no effect on the distribution. For nickel concentrations greater than 1.0×10^{-4} M the distribution ratio increases with the metal concentration, suggesting that polynuclear species are extracted under these conditions. In subsequent experiments, a nickel concentration of 6.3×10^{-5} M was used.

The influence of pH on the distribution ratio was studied for seven different ligand concentrations, ranging between 2.0×10^{-2} and 2.0×10^{-1} M. The results of these experiments are plotted in Fig. 7.

To examine the influence of PPO concentration on the distribution ratio, at constant pH, the values of $\log D$ corresponding to each reagent concentration were calculated from the curves in Fig. 7 at pH 7.6, 7.8, 8.0, 8.2 and 8.4. These values, plotted against $\log [HL]_o$ are given in Fig. 8.

Composition of the extracted species and calculation of the equilibrium constants

Graphical treatment. The curves $\log D$ vs pH (Fig. 7) are straight lines with slopes between 1.9 and 2.1. In accordance with eq. (4), this suggests that $n = 2$. The values of $\log D$ plotted vs $\log [HL]_o$ give straight lines with slopes between 2.5 and 2.9, which according to eq. (4) suggests the presence of a mixture of NiL_2 and $NiL_2(HL)$ in the organic phase, $NiL_2(HL)$ being the predominant species.

To calculate the extraction constants of the species $NiL_2(K_{1,2})$ and $NiL_2(HL)(K_{1,3})$ a curve

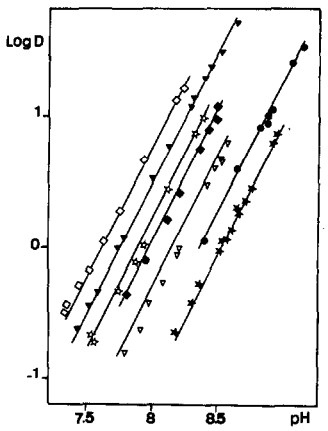

Fig. 7. Influence of pH on the distribution ratio of nickel(II). $C_{Ni} = 6.82 \times 10^{-5}$. C_{PPO}: ★ = 2.0×10^{-2} M; ● = 3.0×10^{-2} M; △ = 5.0×10^{-2} M; ◆ = 8.0×10^{-2} M; ☆ = 1.0×10^{-1} M; ▲ = 1.4×10^{-1} M; ◇ = 2.0×10^{-1} M. The full curves are calculated with the HALTAFALL program[21] using the constants given in Tables 1 and 6.

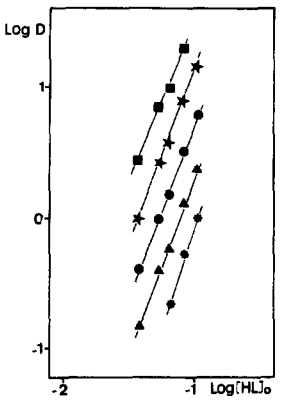

Fig. 8. Influence of the reagent concentration on the distribution of nickel(II). $C_{Ni} = 6.82 \times 10^{-5}$ M. pH: * = 7.60; ▲ = 7.80; ● = 8.00; ★ = 8.20; ◆ = 8.40.

Table 5. Effect of shaking time, buffer concentration and nitrate concentration on the distribution ratio of the nickel system

Shaking time		Buffer concentration		Nitrate concentration	
t (min)	$\log D^a$	$C_{BO_2^-}$ (M)	$\log D^b$	$[NO_3^-]$ (M)	$\log D^c$
5	0.19	2.5×10^{-3}	0.44	2.0×10^{-2}	−0.01
10	0.18	5.0×10^{-3}	0.43	5.0×10^{-2}	0.01
15	0.18	7.5×10^{-3}	0.44	1.0×10^{-1}	−0.01
30	0.19	1.0×10^{-2}	0.33	2.0×10^{-1}	0.01
60	0.18			4.0×10^{-1}	0.01

[a] pH = 8.45, [PPO] = 3.0×10^{-2} M.
[b] pH = 8.50, [PPO] = 3.0×10^{-2} M.
[c] pH = 8.20, [PPO] = 5.0×10^{-2} M.

Table 6. Survey of the equilibrium constants for the extraction of nickel(II) with PPO into chloroform

Method	$\log K_{1,2}$	$\log K_{1,3}$	$\sigma(\log D)$
Graphical	-13.54	-12.58	
LETAGROP-DISTR	-13.57 ± 0.05	-12.6 ± 0.1	0.053

fitting method analogous to that used in a previous paper[8] was applied. The values obtained in the conditions of best fit are given in Table 6.

Numerical treatment. The final values of the constants are also given in Table 6. Theoretical $\log D$ values superimposed on the experimental points are plotted in Fig. 7; the good agreement between them confirms the proposed model.

The coordination between the metal ion and PPO may take place through the oximic nitrogen and carbonyl oxygen, as has been reported for nickel(II)–α-oxooximes complexes.[3,6] Usually these complexes show a square-planar geometry.

CONCLUSIONS

Despite the fact that PPO and phenylglyoxal aldoxime (PGA) have a very similar structure, the pK_a of PPO, 9.25 ± 0.03, is higher than that of PGA, which is 8.55 ± 0.08,[2] both values determined from solvent extraction data. The dissociation constants of these substances, determined by glass electrode potentiometry in a water–ethanol medium (50% v/v),[14] still show a great difference. Since both compounds are the *E* isomers, the differences between their acidities cannot be explained in terms of *E* and *Z* isomery. On the other hand, the greater acidity of aldoximes compared with that of ketoximes, although it has not been explained theoretically, has been observed in many cases.[15–17]

The pK_a values of PPO and N-ethylglyoxylanilide oxime (NEG)[8] are similar. This can be attributed to the presence of the amido group in NEG, which diminishes the acidity of its aldoxime function.

The $\log K_{DR}$ of PPO is 0.7 units higher than that of PGA.[2] Very similar increments have been observed owing to the introduction of a methyl group into other organic reagents.[18] These results agree with the increase by a factor of four observed by Dyrssen[19] in the K_{DR} values of homologous series of organic reagents when an additional carbon atom is attached to the molecule.

PPO as NEG dimerizes in the organic phase, which was not observed by Peshkova *et al.*[2] in the case of PGA. This may be due to the lower reagent concentration used in that work.

The green precipitates obtained in the extraction of copper(II) with PPO, with low PPO/copper(II) ratios, were analogous to those appearing during the potentiometric study of the copper(II)–PPO system in a water–ethanol medium (50% v/v).[20] They may consist of mixed polynuclear complexes $\{CuL(OH)\}_n$ which are very insoluble in the common solvents.[5] The high reagent concentrations used in order to avoid the formation of precipitates favour the formation of self-adduct complexes, which were not detected with other α-oxooximes studied at lower concentration ranges.[2,8]

The stoichiometry of the extracted nickel(II)–PPO complexes are analogous to those obtained with NEG,[8] although the extraction constants are lower in the case of PPO. This causes the displacement of the extraction curves by more than two pH units towards the basic region.

Acknowledgements—The authors gratefully acknowledge Dr Anna Izquierdo-Ridorsa and Dr Romà Tauler for helpful discussions about ERR spectra.

REFERENCES

1. R. B. Singh, B. S. Garg and R. P. Singh, *Talanta* 1979, **26**, 425.
2. V. M. Peshkova, Yu. A. Barbalat, T. V. Polenova and N. A. Plekhanov, *Zh. Anal. Khim.* 1973, **28**, 902.
3. M. Tyagi and P. P. Bhargava, *Indian J. Chem.* 1986, **25A**, 193.
4. C. G. S. Manku, *Z. Anorg. Allg. Chem.* 1971, **382**, 202.
5. J. C. Danilewicz, R. D. Gillard and R. Wootton, *Inorg. Chim. Acta* 1975, **15**, L5.
6. N. V. Thakkar and B. C. Haldar, *J. Inorg. Nucl. Chem.* 1980, **42**, 843.
7. Ch. Natarajan and A. N. Hussain, *Transition Met. Chem.* 1982, **7**, 252.
8. A. Izquierdo, R. Compañó, M. Granados and X. Duarri, *Polyhedron* 1989, **8**, 1957.
9. D. Hay Liem, *Acta Chem. Scand.* 1971, **25**, 1521.
10. L. G. Sillén, *Acta Chem. Scand.* 1956, **10**, 186.
11. D. Dyrssen and L. G. Sillén, *Acta Chem. Scand.* 1953, **7**, 663.
12. *R. M. Smith and A. E. Martell, Critical Stability Constants*, Vol. 2. Plenum Press, New York (1976).

13. C. F. Baes and R. E. Mesmer Jr, *The Hydrolysis of Cations*. Wiley, New York (1976).
14. A. Izquierdo, J. L. Beltran, J. Guiteras and M. Granados, *Mikrochim. Acta* 1990, **III**, 129.
15. J. Armand and J. P. Guetté, *Bull. Soc. Chim.* 1969, 2849.
16. C. Pigenet, J. Armand and H. Lumbroso, *Bull. Soc. Chim.* 1970, 2124.
17. A. L. Green and B. Saville, *J. Chem. Soc.* 1956, 3887.
18. A. Izquierdo and R. Compaño, *Mikrochim. Acta* 1983, **I**, 371.
19. D. Dyrssen, Division of Analytical Chemistry, ACS Summer Symposium, Tucson, Arizona (1963).
20. M. Granados, unpublished data.
21. N. Ingri, W. Kakolowicz, L. G. Sillén and B. Warnquist, *Talanta* 1967, **14**, 1261.

Polyhedron Vol. 10, No. 9, pp. 927–934, 1991
Printed in Great Britain

0277–5387/91 $3.00+.00
© 1991 Pergamon Press plc

SYNTHESES, PROPERTIES AND X-RAY CRYSTAL STRUCTURES OF HEXANUCLEAR COBALT–CHALCOGEN CLUSTERS $Co_6S_8(PPh_3)_6$ AND $Co_6Se_8(PPh_3)_6 \cdot THF$

MAOCHUN HONG,* ZHIYING HUANG, XINJIAN LEI, GUOWEI WEI, BEISHENG KANG and HANQIN LIU

Fuzhou Laboratory of Structural Chemistry and Fujian Institute of Research on the Structure of Matter, Chinese Academy of Sciences, Fuzhou, Fujian 350002, China

(*Received* 25 *April* 1990; *accepted* 7 *January* 1991)

Abstract—The reaction of Na_2X_x (X = S or Se) with $CoBr_2$ and triphenylphosphine in DMF gave rise to the clusters $Co_6X_8(PPh_3)_6$ [X = S (**I**), X = Se (**II**)] in high yields. The molecular structures of **I** and **II** have been determined by single-crystal X-ray diffraction. Both structures were solved by direct methods and refined by full-matrix least-squares techniques to converge with $R = 0.053$ for **I** and 0.048 for **II** on the basis of 5488 and 8175 reflections with $I > 3\sigma(I)$, respectively. The two clusters are isostructural with the inner core consisting of a slightly distorted Co_6 octahedron. The Co—Co distances fall in the ranges of 2.848–2.894 Å for **I** and 2.955–3.037 Å for **II**. Electrochemistry in dichloromethane shows the electron-transfer sequence for **I**:

$$Co_6S_8(PPh_3)_6 \rightleftharpoons [Co_6S_8(PPh_3)_6]^+$$

and for **II**:

$$Co_6Se_8(PPh_3)_6 \rightleftharpoons [Co_6Se_8(PPh_3)_6]^+ \rightleftharpoons [Co_6Se_8(PPh_3)_6]^{2+}.$$

Metal–sulphur cluster compounds have greatly attracted the attention of chemists because they play a prominent role as synthetic analogues of the active sites of biological function.[1] Recently polynuclear metal–chalcogen cluster compounds have become even more interesting owing to their novel structural features and potential uses as heterogeneous catalysts,[2] except as synthetic biological analogues. Structural characterization of polynuclear clusters was deemed to be exceedingly important in establishing a relevance between geometry and electronic structure. Moreover, polynuclear cluster compounds can undergo electron-transfer reaction. Therefore, it is important to understand their redox behaviours, as well as relevant structural effects.

In the studies of transition metal cluster compounds, we have successively synthesized and characterized a series of electron-rich, polynuclear metal clusters, $[M_2Cu_5S_6X_2(R_2dtc)_3]^{2-}$ (M = Mo, W; X = O, S; R = Me, Et),[3] $Co_6Se_8(PEt_3)_6$,[4] $[Au_{13}Ag_{12}(\mu\text{-}Cl)_6(PPh_3)_{10}Cl_2]^{+}$ [5] and $Ni_{15}(\mu_3\text{-}S)_6(\mu_4\text{-}S)_9(PPh_3)_6$.[6] These clusters are interesting for the following reasons. Firstly, the skeletons of these clusters may not be changed by the addition or removal of valence electrons, yet the metal–metal bonds are sensitive to the total electron count. Secondly, recognition of the polynuclear clusters suggests that they may provide a bridge for understanding the relevance of molecular compounds to infinite lattices in metal and metal sulphide, and that they may pave the way for the discovery of novel materials with unusual physical or chemical properties. Thirdly, these clusters can act as multi-electron carriers because of their ability to store unpaired electrons. Recently, several clusters with a regular octahedral Co_6 core have been characterized.[7] For a better understanding of the relevance between bonding and electron structure in Co_6X_8 (X = S, Se) clusters, we have preliminarily reported three cluster compounds, $Co_6Se_8(PEt_3)_6$,[4] $Co_6S_8(PPh_3)_6$ and $Co_6Se_8(PPh_3)_6 \cdot THF$,[8] with the

* Author to whom correspondence should be addressed.

distorted octahedral Co_6 core. This paper presents the syntheses and electrochemical properties, together with the results of X-ray diffraction analysis of the two polynuclear cobalt–chalcogen clusters, $Co_6S_8(PPh_3)_6$ (**I**) and $Co_6Se_8(PPh_3)_6 \cdot THF$ (**II**).

EXPERIMENTAL

Synthesis of $Co_6S_8(PPh_3)_6$ (I)

This compound was synthesized according to our previous report,[8] but with improvements. To a stirred solution of $(Ph_3P)_2CoBr_2$, obtained from anhydrous $CoBr_2$ (1.10 g, 5 mmol) and triphenylphosphine (5.25 g, 20 mmol), in 40 cm^3 of DMF was added a solution of $Na_2S \cdot 9H_2O$ (1.60 g, 6.7 mmol) in 20 cm^3 of DMF. On mixing, the blue–green solution immediately turned dark brown and a black precipitate gradually formed. After stirring for 2 days the black solid was collected, washed with water, acetone and THF–hexane (1 : 1, v/v). The black solid which contained a small amount of binary cobalt sulphide was treated with 100 cm^3 of CH_2Cl_2 : THF (1 : 1, v/v). The resulting solution was filtered and the filtrate was covered with a layer of hexane. On standing at room temperature for several weeks, large dark brown crystals were formed which were collected, washed with THF : hexane (1 : 1, v/v) and then with dimethyl ether to give 1.26 g of **I** (69%). Found: C, 59.5; H, 4.2; Co, 16.0; P, 8.3. Calc. for $C_{108}H_{90}Co_6P_6S_8$: C, 59.4; H, 4.2; Co, 16.2; P, 8.5%.

Synthesis of $Co_6Se_8(PPh_3)_6 \cdot THF$ (II)

To a deoxygenated, stirred solution of $(Ph_3P)_2CoBr_2$, obtained from anhydrous $CoBr_2$(1.10 g, 5 mmol) and triphenylphosphine (5.25 g, 20 mmol), in 40 cm^3 of DMF was added a solution of Na_2Se_x, obtained from heating sodium (0.35 g, 15 mmol) and selenium (1.08 g, 13.5 mmol), in 20 cm^3 of DMF under nitrogen. On mixing, the blue–green solution turned immediately dark brown and microcrystals gradually precipitated. After stirring for 2 days the black solid was collected, washed with water, acetone and THF : hexane (1 : 1, v/v). The black solid which contained a small amount of binary cobalt selenide was treated with 100 cm^3 of CH_2Cl_2 : THF (1 : 1, v/v). The resulting solution was filtered and the filtrate was covered with a layer of hexane. On standing at room temperature for several weeks, large dark brown crystals formed which were collected, washed with THF : hexane (1 : 1, v/v) and then with dimethyl ether to give 1.63 g of **II** (74%). Found: C, 51.6; H, 3.8; Co, 13.5; P, 7.0. Calc. for $C_{112}H_{98}OCo_6P_6Se_8$: C, 51.1; H, 3.7; Co, 13.5; P, 7.1%.

X-ray data collection and structure determination

Diffraction data were collected at room temperature on a RIGAKU AFC5R four-circle diffractometer for **I** and an Enraf–Nonius CAD4 four-circle diffractometer for **II**. The crystal of compound **II** was mounted in a capillary with mother liquid to prevent solvent loss during the data collection. Crystal data and data collection parameters are presented in Table 1. All the calculations were performed on a VAX/VMS computer by using the SDP program package. Intensity data used in structure determination and refinement were corrected for Lorentz and polarization effects and empirically for absorption. Both structures were determined by direct methods. Several Fourier maps successively revealed all non-hydrogen atoms. Refinements were based on F_0 and weight $w = 1/\sigma^2(F_0)$. The structures were refined by full-matrix least-squares techniques with anisotropic temperature factors for all non-hydrogen atoms of the molecule and with isotropic factors for all solvent atoms. The final refinement converged at R and R_w factor values of 0.053 and 0.065 for **I** and 0.048 and 0.059 for **II**.* Final difference Fourier maps contained residual peaks ranging from 1.03 to 0.10 eA^{-3} for **I** and 0.95 to 0.13 eA^{-3} for **II**.

Physical measurements

In case the compounds in solution may be oxidized by air, all manipulation and measurement were carried out under a pure nitrogen atmosphere. Dichloromethane was dried before use. Electromeasurements were carried out with a DHZ-1 electrochemical multipurpose instrument and *X–Y* recorder. The cell was of the standard three-electrode design containing a platinum auxiliary electrode, a SCE reference electrode and a platinum working electrode. The solution contained 0.05 M Bu_4NBF_4 as supporting electrolyte and *ca* 10^{-3} M samples. Bu_4NBF_4 was dried *in vacuo* and used without further purification.

RESULTS AND DISCUSSION

Syntheses

The reaction of $(Ph_3P)_2CoBr_2$ with Na_2X_x (X = S or Se) at room temperature affords the clus-

*Atomic coordinates and thermal parameters have been deposited at the Cambridge Crystallographic Data Centre.

Table 1. Crystal data and data collection parameters

Compound	I	II
Molecular formula	$Co_6S_8P_6C_{108}H_{90}$	$Co_6Se_8P_6C_{112}OH_{98}$
Molecular weight	2181.9	2629.1
a (Å)	15.052(4)	15.165(4)
b (Å)	15.219(4)	16.522(4)
c (Å)	14.201(3)	21.274(5)
α (°)	114.80(3)	92.75(2)
β (°)	92.59(3)	90.56(2)
γ (°)	117.90(2)	102.47(2)
V (Å^3)	2488.5	5197.4
Z	1	2
Space group	$P\bar{1}$	$P\bar{1}$
D_c (g cm^{-3})	1.457	1.680
Dimensions (mm)	$0.32 \times 0.38 \times 0.46$	$0.29 \times 0.36 \times 0.50$
Linear absorbance coefficient (cm^{-1})	12.787	38.470
Radiation	Mo-K_α	Mo-K_α
2θ limits (°)	$2 < 2\theta < 48$	$2 < 2\theta < 44$
Number of total data	8776	13001
Number of data used [$I > 3\sigma(I)$]	5488	8175
Final number of variables	577	1173
R	0.053	0.048
R_w	0.065	0.059

ter compounds $Co_6X_8(PPh_3)_6$ [X = S (**I**), X = Se (**II**)]. Compound **I** can be synthesized in air, but compound **II** must be prepared with the exclusion of air in the initial stage of the reaction to prevent oxidation of Na_2Se_x. If a large excess of PPh_3 was used, the yield can be increased because precipitation of CoX_2 during the reactions can be avoided. At the end of the reactions the metal atoms in both clusters are oxidized to a mean oxidation state of +2.67 per cobalt atom. A similar oxidation was observed during the formation of the clusters $[Co_6S_8(PEt_3)_6]^{n+}$ ($n = 0, 1$),[7] with mean oxidation states of +2.67 ($n = 0$) and +2.83 ($n = 1$). If reactions were carried out under nitrogen, S_x^{2-} (or Se_x^{2-}) can be used as either oxidant or bridging ligand. However, S^{2-} must be used if the reaction was to be carried out in air. Compounds are air-stable both in the solid state and in solution. They are very soluble in polar organic solvents such as tetrahydrofuran, dichloromethane and benzene.

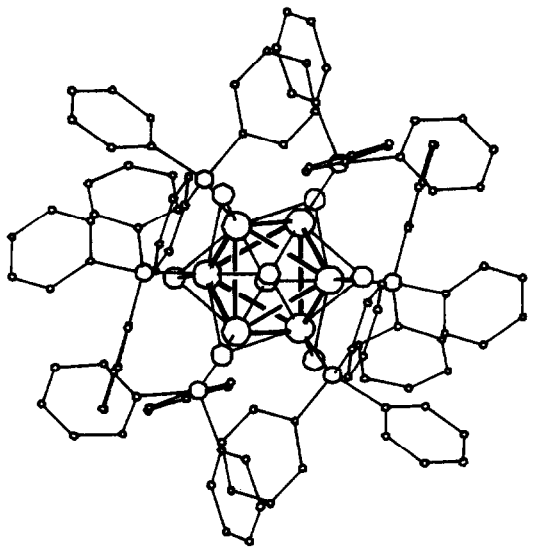

Fig. 1. Molecular structure of $Co_6S_8(PPh_3)_6$.

Description of the structures

Figure 1 shows a perspective view of the molecular structure of **I**, and Figs 2 and 3 show the inner cores of compounds **I** and **II**, respectively. Selected bond lengths and bond angles of compound **I** are presented in Tables 2 and 3, respectively. Tables 4 and 5 list selected bond lengths and bond angles of compound **II**. Compound **II** consists of two discrete cluster units (A and B), located on (1/2, 1/2, 1/2) and (0, 0, 0), with an interpenetrating molecule of tetrahydrofuran in a unit cell. The two cluster compounds, **I** and **II**, possess analogous structures. The inner Co_6 core consists of a slightly distorted octahedron of cobalt atoms. The eight Co_3 faces of the octahedral Co_6 core are each triply-bridged by one sulphur (**I**) or selenium (**II**) atom. Moreover, each cobalt atom is terminally coordinated by a triphenylphosphino ligand. Therefore, each cobalt atom is surrounded by four sulphur (selenium)

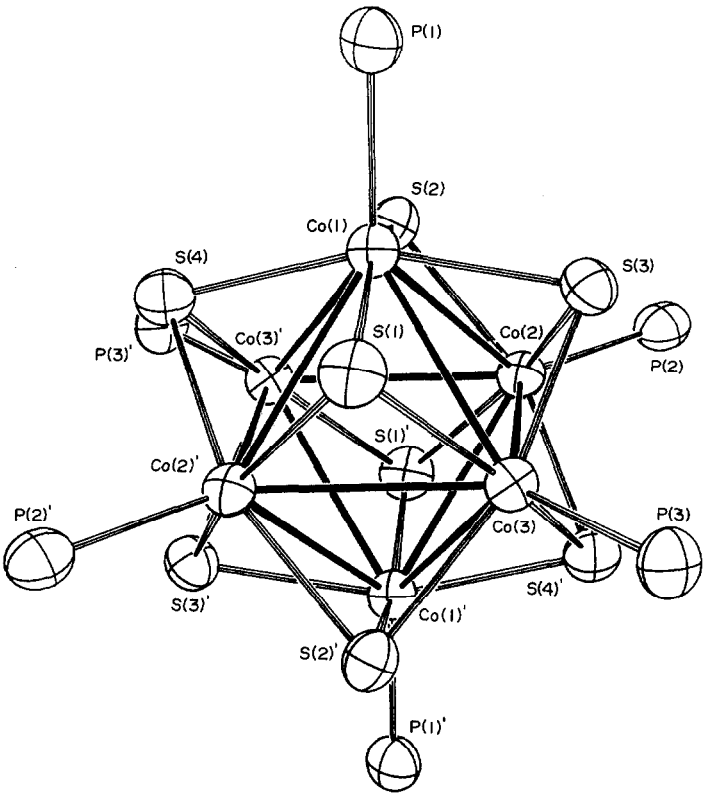

Fig. 2. Inner core of the cluster compound $Co_6S_8(PPh_3)_6$.

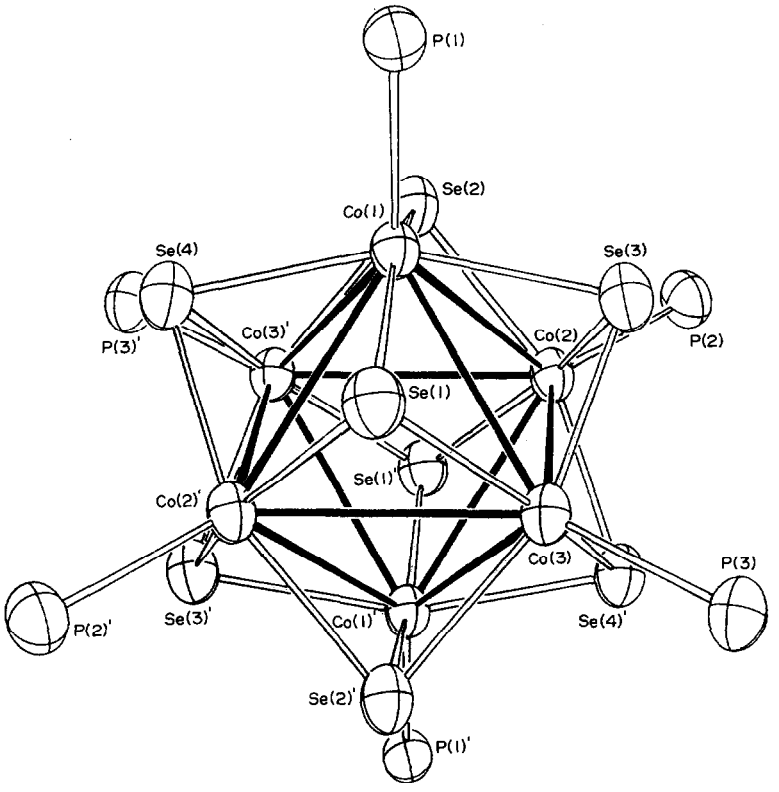

Fig. 3. Inner core of the cluster compound $Co_6Se_8(PPh_3)_6$.

Table 2. Selected bond lengths (Å) for $Co_6S_8(PPh_3)_6$

Co(1)—Co(2)	2.891(1)	Co(1)—Co(3)	2.894(1)
Co(1)—Co(2)′	2.851(1)	Co(1)—Co(3)′	2.848(1)
Co(2)—Co(3)	2.855(1)	Co(2)—Co(3)′	2.868(1)
Co(1)—S(1)	2.232(2)	Co(1)—S(2)	2.210(2)
Co(1)—S(3)	2.271(2)	Co(1)—S(4)	2.218(3)
Co(2)—S(1)′	2.216(3)	Co(2)—S(2)	2.243(2)
Co(2)—S(3)	2.297(2)	Co(2)—S(4)′	2.201(2)
Co(3)—S(1)	2.228(2)	Co(3)—S(2)′	2.223(3)
Co(3)—S(3)	2.269(2)	Co(3)—S(4)′	2.218(2)
Co(1)—P(1)	2.169(2)	Co(2)—P(2)	2.154(3)
Co(3)—P(3)	2.164(3)		

Table 3. Selected bond angles (°) for $Co_6S_8(PPh_3)_6$

Co(2)—Co(1)—Co(3)	59.11(6)	Co(2)—Co(1)—Co(2)′	89.62(6)
Co(2)—Co(1)—Co(3)′	59.91(6)	Co(3)—Co(1)—Co(2)′	59.93(6)
Co(3)—Co(1)—Co(3)′	89.62(6)	Co(2)′—Co(1)—Co(3)′	60.07(6)
Co(1)—Co(2)—Co(3)	60.51(6)	Co(1)—Co(2)—Co(1)′	90.43(6)
Co(1)—Co(2)—Co(3)′	59.30(6)	Co(3)—Co(2)—Co(1)′	59.91(5)
Co(1)—Co(3)—Co(2)	60.41(5)	Co(2)—Co(3)—Co(1)′	59.90(5)
Co(1)—Co(3)—Co(1)′	90.38(6)	Co(1)—Co(3)—Co(2)′	59.30(5)
Co(1)—S(1)—Co(3)′	80.92(5)	Co(1)—S(1)—Co(2)′	79.77(5)
Co(3)—S(1)—Co(2)′	80.42(6)	Co(1)—S(2)—Co(2)	81.00(5)
Co(1)—S(2)—Co(3)′	80.02(5)	Co(2)—S(2)—Co(3)′	79.90(5)
Co(1)—S(3)—Co(2)	78.51(5)	Co(1)—S(3)—Co(3)	79.21(5)
Co(2)—S(3)—Co(3)	77.41(5)	Co(1)—S(4)—Co(2)′	80.34(5)
Co(1)—S(4)—Co(3)′	79.91(5)	Co(2)′—S(4)—Co(3)′	80.53(5)
Co(2)—Co(1)—P(1)	128.93(5)	Co(3)—Co(1)—P(1)	142.60(6)
Co(1)—Co(2)—P(2)	142.01(5)	Co(3)—Co(2)—P(2)	139.10(6)
Co(1)—Co(3)—P(3)	131.55(6)	Co(2)—Co(3)—P(3)	130.95(5)

Table 4. Selected bond lengths (Å) for $Co_6Se_8(PPh_3)_6 \cdot THF$

A		B	
Co(1)—Co(2)	3.037(1)	Co(4)—Co(5)	2.987(1)
Co(1)—Co(3)	2.986(1)	Co(4)—Co(5)	3.010(1)
Co(1)—Co(2)′	2.969(1)	Co(4)—Co(5)′	3.019(1)
Co(1)—Co(3)′	3.015(1)	Co(4)—Co(6)′	2.955(1)
Co(2)—Co(3)	3.018(1)	Co(5)—Co(6)	2.975(1)
Co(2)—Co(3)′	3.004(1)	Co(5)—Co(6)′	3.109(1)
Co(1)—Se(1)	2.322(2)	Co(4)—Se(5)	2.332(2)
Co(1)—Se(2)	2.343(2)	Co(4)—Se(6)	2.328(2)
Co(1)—Se(3)	2.363(2)	Co(4)—Se(7)	2.369(2)
Co(1)—Se(4)	2.365(4)	Co(4)—Se(8)	2.337(3)
Co(2)—Se(1)′	2.344(3)	Co(5)—Se(5)′	2.337(3)
Co(2)—Se(2)	2.325(2)	Co(5)—Se(6)	2.329(2)
Co(2)—Se(3)	2.333(2)	Co(5)—Se(7)	2.361(2)
Co(2)—Se(4)′	2.368(2)	Co(5)—Se(8)′	2.373(2)
Co(3)—Se(1)	2.358(2)	Co(6)—Se(5)	2.349(2)
Co(3)—Se(2)′	2.360(3)	Co(6)—Se(6)′	2.326(3)
Co(3)—Se(3)	2.365(2)	Co(6)—Se(7)	2.328(2)
Co(3)—Se(4)′	2.360(2)	Co(6)—Se(8)′	2.373(2)
Co(1)—P(1)	2.146(2)	Co(4)—P(4)	2.169(2)
Co(2)—P(2)	2.154(3)	Co(5)—P(5)	2.154(3)
Co(3)—P(3)	2.140(3)	Co(5)—P(6)	2.164(3)

Table 5. Selected bond angles (°) for $Co_6Se_8(PPh_3)_6 \cdot THF$

Co(2)—Co(1)—Co(3)	60.41(6)	Co(5)—Co(4)—Co(6)	59.31(6)
Co(2)—Co(2)—Co(2)′	90.32(5)	Co(5)—Co(4)—Co(5)′	90.62(5)
Co(2)—Co(1)—Co(3)′	59.71(6)	Co(5)—Co(4)—Co(6)′	61.31(6)
Co(3)—Co(1)—Co(2)′	60.53(6)	Co(6)—Co(4)—Co(5)′	60.23(5)
Co(3)—Co(1)—Co(3)′	90.82(5)	Co(6)—Co(4)—Co(6)′	89.62(6)
Co(2)′—Co(1)—Co(3)′	60.07(6)	Co(5)′—Co(4)—Co(6)′	60.17(6)
Co(1)—Co(2)—Co(3)	59.51(5)	Co(4)—Co(5)—Co(6)	60.51(5)
Co(1)—Co(2)—Co(1)′	89.73(6)	Co(4)—Co(5)—Co(4)′	90.43(6)
Co(1)—Co(2)—Co(3)′	60.10(5)	Co(4)—Co(5)—Co(6)′	59.30(5)
Co(3)—Co(2)—Co(1)′	60.51(5)	Co(6)—Co(5)—Co(4)′	59.91(5)
Co(1)—Co(3)—Co(2)	60.41(6)	Co(4)—Co(6)—Co(5)	60.01(5)
Co(2)—Co(3)—Co(1)′	58.90(5)	Co(5)—Co(6)—Co(4)′	59.90(5)
Co(1)—Co(3)—Co(1)′	89.22(6)	Co(4)—Co(6)—Co(4)′	90.38(6)
Co(1)—Co(3)—Co(2)′	59.30(5)	Co(4)—Co(6)—Co(5)′	59.30(5)
Co(1)—Se(1)—Co(3)	80.82(6)	Co(4)—Se(5)—Co(6)′	80.92(5)
Co(1)—Se(1)—Co(2)′	79.52(5)	Co(4)—Se(5)—Co(5)′	79.77(5)
Co(3)—Se(1)—Co(2)′	80.50(6)	Co(6)—Se(5)—Co(5)′	79.02(6)
Co(1)—Se(2)—Co(2)	81.00(5)	Co(4)—Se(6)—Co(5)	81.00(6)
Co(1)—Se(2)—Co(3)′	79.52(6)	Co(4)—Se(6)—Co(6)′	81.52(5)
Co(2)—Se(2)—Co(3)′	80.80(5)	Co(5)—Se(6)—Co(6)′	79.40(5)
Co(1)—Se(3)—Co(2)	80.41(6)	Co(4)—Se(7)—Co(5)	79.01(5)
Co(1)—Se(3)—Co(3)	79.81(6)	Co(4)—Se(7)—Co(6)	79.99(6)
Co(2)—Se(3)—Co(3)	80.01(5)	Co(5)—Se(7)—Co(6)	80.41(5)
Co(1)—Se(4)—Co(2)′	78.11(5)	Co(4)—Se(8)—Co(5)′	79.04(6)
Co(1)—Se(4)—Co(3)′	79.11(6)	Co(4)—Se(8)—Co(6)′	77.91(5)
Co(2)′—Se(4)—Co(3)′	80.00(5)	Co(5)′—Se(8)—Co(6)′	79.63(5)
Co(2)—Co(1)—P(1)	132.93(5)	Co(5)—Co(4)—P(4)	136.53(6)
Co(3)—Co(1)—P(1)	139.70(6)	Co(6)—Co(4)—P(4)	137.90(6)
Co(1)—Co(2)—P(2)	137.81(5)	Co(4)—Co(5)—P(5)	138.81(5)
Co(3)—Co(2)—P(2)	133.10(6)	Co(6)—Co(5)—P(5)	140.80(6)
Co(1)—Co(3)—P(3)	129.05(6)	Co(4)—Co(6)—P(6)	129.05(6)
Co(2)—Co(3)—P(3)	125.45(5)	Co(5)—Co(6)—P(6)	126.65(6)

atoms and one phosphorus atom in a distorted square pyramidal environment and is linked to another four cobalt atoms.

Both clusters possess crystallographic *Ci*-$\bar{1}$ symmetry. The octahedron in **I** is slightly elongated along the three-fold axis through the Co(1)′—Co(2)—Co(3) face, while no systematic distortion is present in **II**. The Co—Co distances of compounds **I** and **II** fall in the ranges 2.848–2.894 and 2.955–3.037 Å, respectively. The distances of Co—S (or Se) and Co—P are in the ranges 2.201–2.297 Å (**I**), 2.322–2.373 Å (**II**) and 2.154–2.169 Å (**I**), 2.152–2.164 Å (**II**), respectively. The average Co—S and Co—Se bond lengths in the title clusters are 2.235 and 2.344 Å, respectively, in good agreement with those reported in other clusters with Co_6S_8 and Co_6Se_8 cores.[7] The Co—P bond lengths in the two clusters are nearly equal within experimental error, and are slightly longer than that in $[Co_6S_8(PEt_3)_6]$ (2.138 Å).[7d]

The Co—Co—Co angles of compound **I** fall within the ranges 59.1(1)–61.4(1) and 89.6(1)–91.4(1)° and are very similar to the values in cluster **II** [59.3(1)–61.3(1)° and 89.2(1)–90.8(1)°], both are very close to the values of 60.0 and 90.0° for a regular octahedron, despite the slight elongation in **I**.

Alternatively, the clusters can also be described as a slightly distorted X_8 (X = S or Se) cube, and each X_4 face is topped by a cobalt atom. The distances from metal atom to the X_4 plane in the two clusters are quite similar, ranging from 0.49 to 0.51 Å. The X—X distances are in the ranges 3.094–3.110 Å (**I**) and 3.180–3.266 Å (**II**). In comparison with X—X distances in other compounds, the S—S distances can be considered to be non-bonding, while Se—Se distances are more or less bonding. The Co—X—Co angles of 77.4(1)–81.0(1)° for **I** and 77.9(1)–81.5(1)° for **II** agree well with those in other Co_6X_8 clusters.

The clusters contain 98 valence electrons which is 14 electrons more than the 18-electron rule[9] and one electron more than in the cluster $[Co_6S_8(PEt_3)_6]^{+}$ [7e] with an almost regular Co_6 octa-

hedron. The average Co—Co bond length of 3.007 Å in compound **II** is slightly longer than that in compound **I** (2.868 Å) and is distinctly longer than any length in $[Co_6S_8(PPh_3)_6]^+$ (2.810 Å, 97e),[7b] or $[Co_6S_8(PEt_3)_6]^+$ (2.798 Å, 97e).[7e] This lengthening of the Co—Co distance indicates that metal–metal bonding does exist and that extra electrons from the selenium atoms occupy the antibonding orbitals.

Electrochemistry

The electrochemical behaviour of the two hexamers has been studied. The cyclic voltammograms of compounds **I** and **II** at a platinum electrode in CH_2Cl_2 solution are shown in Fig. 4. Compound **I** gives rise to one reversible one-electron redox wave at +0.60 V ($i_{pa}/i_{pc} = 1$), which indicates the existence of the monocationic cluster $[Co_6S_8(PPh_3)_6]^+$. In fact, this monocationic compound has already been prepared by Fenske and co-workers.[7b] However, compound **II** gives rise to two waves at +0.58 V ($i_{pa}/i_{pc} = 1$) and +1.23 V ($i_{pa}/i_{pc} < 1$). As it can be seen in Fig. 4(b), the former ($i_{pa}/i_{pc} = 1$) can be considered as a one-electron reversible charge-transfer. However, the latter ($i_{pa}/i_{pc} < 1$) is somewhat complicated, and can be considered as a one-electron reversible charge-transfer by following chemical reactions. The electrochemical data of compound **II** show the existence of three discrete species: the neutral cluster, $Co_6Se_8(PPh_3)_6$; the monocationic cluster, $[Co_6Se_8(PPh_3)_6]^+$; and the bicationic cluster, $[Co_6Se_8(PPh_3)_6]^{2+}$, of which the bicationic one is not stable for long, and the monocation has already been reported by Fenske.[7c] The electrochemistry in dichloromethane shows the electron-transfer sequence (1) for **I**:

$$Co_6S_8(PPh_3)_6 \rightleftharpoons [Co_6S_8(PPh_3)_6]^+ \quad (1)$$

and (2) for **II**:

$$[Co_6Se_8(PPh_3)_6] \rightleftharpoons [Co_6Se_8(PPh_3)_6]^+ \rightleftharpoons [Co_6Se_8(PPh_3)_6]^{2+}. \quad (2)$$

Moreover, it also indicates that the removal of one or two electrons from the antibonding orbitals of $[Co_6Se_8(PPh_3)_6]$ or the addition of one or two electrons to the antibonding orbitals of $[Co_6Se_8(PPh_3)_6]^{n+}$ ($n = 1, 2$), or the removal of one electron from the antibonding orbital of $Co_6S_8(PPh_3)_6$ or the addition of one electron to the antibonding orbital of $[Co_6S_8(PPh_3)_6]^+$ is feasible.

Acknowledgements—The authors are grateful to Professors Qianjin Wu and Shixiong Liu and co-workers for the X-ray data collections and to the National Natural Sciences Foundation of China for financial support.

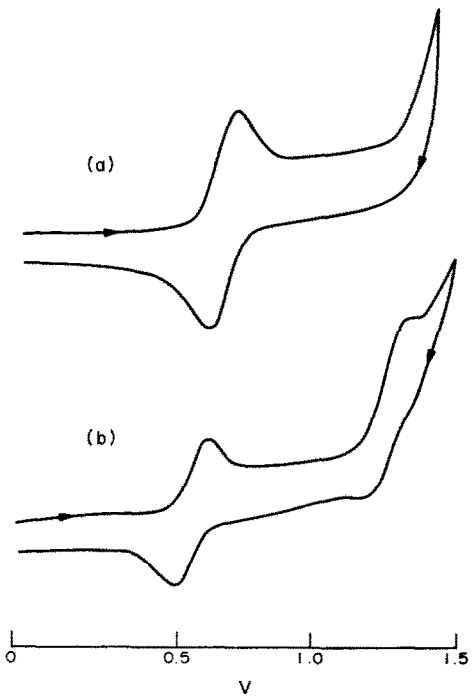

Fig. 4. Cyclic voltammogram of (a) $Co_6S_8(PPh_3)_6$ and (b) $Co_6Se_8(PPh_3)_6 \cdot THF$ in 0.05 M Bu_4NBF_4 dichloromethane with a scan rate of 100 mV s^{-1}.

REFERENCES

1. S. Kuwabata, K. Tanak and T. Tanak, *Inorg. Chim. Acta* 1986, **25**, 1691; A. Müller, *Polyhedron* 1986, **5**, 323.
2. H. Topsoe and B. S. Clausen, *Catal. Rev.* 1984, **26**, 395; B. Bogdanovich, P. Gottsch and M. Rubach, *J. Molec. Catal.* 1981, **11**, 135.
3. Xinjian Lei, Zhiying Huang, Maochun Hong, Qiutian Liu and Hanqin Liu, *Inorg. Chim. Acta* 1989, **164**, 119; Xinjian Lei, Zhiying Huang, Qiutian Liu, Maochun Hong and Hanqin Liu, *Inorg. Chem.* 1989, **28**, 4302; Hanqin Liu, Rong Cao, Xinjian Lei, Daxu Wu, Guowei Wei, Zhiying Huang, Maochun Hong and Beisheng Kang, *J. Chem. Soc., Dalton Trans.* 1990, 1023.
4. Maochun Hong, Zhiying Huang, Xinjian Lei, Guowei Wei Beisheng Kang and Hanqin Liu, *Clin. Chem.*, in press.
5. Maochun Hong, Zhiying Huang, Xinjian Lei, Beisheng Kang and Hanqin Liu, *Inorg. Chim. Acta* 1990, **168**, 163.
6. Maochun Hong, Zhiying Huang and Hanqin Liu, *J. Chem. Soc. Chem. Commun.* 1990, 1210.
7. (a) D. Fenske and J. Ohmer, *Angew. Chem., Int. Edn Engl.* 1987, **26**, 148; (b) D. Fenske, J. Ohmer and J. Hachgenei, *Angew. Chem., Int. Edn Engl.* 1985, **24**, 993; (c) D. Fenske, J. Ohmer and K. Merzweiler, *Z. Naturfor.* 1987, **B42**, 803; (d) F. Cecconi, C. A. Ghilardi, S. Midollini and A. Orlandini, *Inorg. Chim.*

Acta 1983, **76**, L183; (e) F. Cecconi, C. A. Ghilardi and S. Midollini, *Inorg. Chim. Acta* 1981, **64**, L47; (f) F. Cecconi, C. A. Ghilardi, S. Midollini and A. Orlandini, *Polyhedron* 1986, **5**, 2021.

8. Maochun Hong, Zhiying Huang, Xinjian Lei, Guowei Wei Beisheng Kang and Hanqin Liu, *Inorg. Chim. Acta* 1989, **159**, 1; Maochun Hong, Zhiying Huang, Xinjian Lei, Guowei Wei, Beisheng Kang and Hanqin Liu, *J. Struct. Chem.* 1990, **9**, 47.
9. F. A. Cotton and E. Haas, *Inorg. Chem.* 1964, **3**, 10.

Polyhedron Vol. 10, No. 9, pp. 935–940, 1991
Printed in Great Britain

0277–5387/91 $3.00+.00
© 1991 Pergamon Press plc

SYNTHESIS AND PHOTOLYSIS OF MIXED COPPER(I) COMPLEXES WITH THIONES AND TRI-*p*-TOLYLPHOSPHINE OR TRIPHENYLPHOSPHINE; X-RAY CRYSTAL STRUCTURE OF BIS[COPPER(I)(1,3-THIAZOLIDINE-2-THIONE) (TRI-*p*-TOLYLPHOSPHINE)CHLORIDE]

S. K. HADJIKAKOU, P. ASLANIDIS and P. KARAGIANNIDIS*

University of Thessaloniki, Faculty of Chemistry, General and Inorganic Chemistry Department, P.O. Box 135, GR-540 06 Thessaloniki, Greece

and

D. MENTZAFOS and A. TERZIS

X-ray Laboratory, NCR 'Democritos', Athens, Greece

(*Received* 13 *August* 1990; *accepted* 7 *January* 1991)

Abstract—Reaction of $[Cu(PR_3)Cl]_4$ [where PR_3 = tri-*p*-tolylphosphine (tptp), or triphenylphosphine(tpp)] with several heterocyclic thiones (L) yields binuclear complexes of the general formula $[Cu(PR_3)(L)Cl]_2$ [L = 1,3-thiazolidine-2-thione (tzdtH), benz-1,3-thiazoline-2-thione (bztztH), dithiouracil (dtu), purine-6-thione (pur6SH) and thiourea (tu)]. Irradition of the complexes, in chloroform, methanol and acetonitrile solutions, caused phosphine evolution while the Cu_2S_2 core remained intact. The crystal structure of $[Cu(tptp)(tzdtH)Cl]_2$ has been established by single-crystal X-ray diffraction methods. In the Cu_2S_2 core the Cu—S bond lengths are 2.386(1) and 2.470(1) Å. The Cu—P and Cu—Cl distances are 2.222(1) and 2.283(1) Å, respectively.

Copper complexes have received considerable attention since they provide suitable models for the representation of several enzyme sites[1,2] as well as active intermediates in organic synthetic reactions,[3] in particular photocatalytic isomerizations.[4,5]

Recently we have been engaged with the experimentation of a series of mixed copper(I) complexes with heterocyclic thiones and phosphines or arsines[6–8] as ligands. A study of the photoreactivity of these complexes ensued the observation of a darkening of their chloroform solution.

In an attempt to gain better understanding of the role of heterocyclic thione as well as triphenylphosphine and their derivatives as ligands, the above mentioned mixed ligand complexes have been prepared and studied.

* Author to whom correspondence should be addressed.

EXPERIMENTAL

Material and instruments

Copper(I) chloride, tri-*p*-tolylphosphine (Merck) and triphenylphosphine (B.D.H.) were used as obtained, while all thiones (Merck or Aldrich) were recrystallized from hot ethanol prior to their use. The solvents used were of reagent grade and the preparations were carried out without any precautions for moisture or oxygen.

The IR spectra were obtained in KBr discs with a Perkin–Elmer 1430 spectrophotometer, while a Shimadzu UV 160 spectrophotometer was used to obtain the electronic absorption spectra. The ^1H NMR spectra were recorded in $CDCl_3$ solutions with a Brucker AW 80 spectrometer. Mass spectra were obtained on a Finigan mass spectrometer. Conductivity measurements were performed with a Wheatstone bridge Model RC 216

B2 using 10^{-3} M chloroform solutions. Melting points are uncorrected upon tube measurements. Elemental analyses for C, N and H were carried out with a Perkin–Elmer 240 elemental analyser.

For the photolyses, an Osram high pressure HBO 200 W/4 lamp was used.

Preparation of complexes

$[Cu(tptp)Cl]_4$ was prepared by refluxing equimolar quantities of CuCl and tptp in acetonitrile, for approximately 2 h,[9] while $[Cu(tpp)Cl]_4$ was prepared as described in the literature[10].

The complexes of formula $[Cu(PR_3)(L)Cl]_2$ were prepared according to the following general procedure. A solution of 0.4 mmol of the appropriate thione in 20 cm^3 of methanol was added to a solution of 0.1 mmol of $[Cu(PR_3)Cl]_4$ in 20 cm^3 of acetonitrile and the resulting solution was moderately heated. The solution was allowed to cool and the microcrystalline products were isolated. The compounds were identified by elemental analyses and by their spectral data.[9,11]

Collection and reduction of intensity data

Complete crystal data and parameters for data collection are reported in Table 1. Unit cell dimen-

Table 1. Summary of crystal and intensity collection data

Formula	$Cu_2Cl_2(C_3H_5NS_2)_2(PC_{21}H_{21})_2$
fw	1044.12
a (Å)	9.5184(4)
b (Å)	10.2654(5)
c (Å)	14.5138(6)
α (°)	83.549(1)
β (°)	74.527(1)
γ (°)	63.088(1)
V (Å^3)	1218.7(1)
Z	1
D_{calc} (Mg m^{-3})	1.418
D_{meas} (Mg cm^{-3})	1.40
Space group	$P\bar{1}$
Crystal dimensions (mm)	$0.24 \times 0.15 \times 0.15$
Radiation	Cu-K_α ($\lambda = 1.5418$)
μ (cm^{-1})	44.54
Transmission factors	0.4272–0.6570
Scan speed (° min^{-1})	4.5
Scan range (°)	2.0 plus $\alpha1$–$\alpha2$
2θ limit (°)	130.0
Data collected	4370
Data unique	4102
Data used	3832
$F_o >$	$4.0\sigma(F_o)$
R_{int}	0.0181
Range of $h\ k\ l$	0 to 11, −10 to 10, −16 to 16
Weighting scheme	$1/w = \sigma^2(F_o)+0.0018\|F_o\|^2$
$F(000)$	536
Nr[a]	375
$[\Delta/\sigma]$max	0.166
$(\Delta\rho)$max (e Å^{-3})	0.301
$(\Delta\rho)$min (e Å^{-3})	−0.518
S[b]	2.09
R (obs)[c]	0.0335
R (all data)[c]	0.0355
R_w (obs)[d]	0.0565
R_w (all data)[d]	0.0571

[a] Nr = Number of refined parameters.

[b] $S = [\Sigma w(\Delta F)^2/(N-P)]^{1/2}$; P = number of parameters, N = number of reflections.

[c] $R = \Sigma|\Delta F||/\Sigma|F_o|$.

[d] $R_w = [\Sigma w(\Delta F)^2/\Sigma w|F_o|^2]^{1/2}$.

sions were derived from a least-squares refinement of the setting angles of 48 automatically centred reflections on a Syntex $P2_1$ diffractometer upgraded with CRYSTAL LOGIC with nickel-filtered Cu-K_α radiation. Three standard reflections measured every 97 reflections showed less than 3% intensity fluctuation. Lp and absorption corrections were applied. Scattering factors were taken from the *International Tables for X-ray Crystallography*.[12] The refinement was carried out by blocked full-matrix least-squares, in which $\Sigma w\Delta^2$ was minimized using SHELX 76.[13] The non-hydrogen atoms were refined using anisotropic temperature factors. One reflection which showed poor agreement was given zero weight during final refinement cycles.

The fractional atomic coordinates, lists of observed and calculated structure factors, anisotropic thermal parameters of the non-hydrogen atoms and thermal parameters of hydrogen atoms have been deposited.

RESULTS AND DISCUSSION

All the complexes prepared are microcrystalline solids, soluble in chloroform, acetonitrile, ethanol, methanol and acetone. Their conductivity measurements indicate their non-electrolytic nature. The most relevant physical properties of the compounds along with their analyses are reported in Table 2.

Spectroscopy

Copper(I) complexes containing heteroaromatic thiones exhibit a low-lying metal to ligand charge-transfer band (MLCT) in the near-UV spectral region.[14]

The UV–vis spectra in chloroform are dominated by two main absorptions at 250–260 and 280–310 nm, respectively. The corresponding bands in methanol or acetonitrile occur at 200–230 and 250–280 nm, respectively. The first band is ascribed to the intraligand transitions of the phosphine ligand, since the spectrum of the free phosphine reveals bands at 245, 215 and 210 nm for the chloroform, acetonitrile or methanol solutions, with log ε values similar to those observed in the complexes. Furthermore, it is readily seen[15,16] that arylphosphines do not shift their intraligand bands upon coordination to copper(I). The second band expresses a small red shift (10–20 nm) with respect to the corresponding one in the spectra of the free thiones. Therefore, it could be suggested that this band contains some MLCT character also.[16] The electronic spectra were also recorded in toluene and tetrahydrofuran; the absorption bands originating from the thione express a small blue shift (no more than 10 nm) on going to more polar solvents.

IR spectra in the region 4000–250 cm^{-1} provide information concerning the thione ligand coordination mode. The predominance of the thione form of the ligands is confirmed by the presence of ν(NH) bands at 3200–3130 cm^{-1},[17–19] the absence of ν(SH) bands in the region 2500–2600 cm^{-1}[20,21] and the occurrence of characteristic "thioamide bands"[20] as well as the ν(Cu—S) bands at 370–340 cm^{-1}.[22]

The ^1H NMR spectra of the compounds in $CDCl_3$ solution at ambient temperature display, apart from the signals expected for the phosphine and thione ligands, a single resonance at $\delta \sim 11$–14 ppm attributed to the NH protons, indicating the prevalence of the thione tautomer in solution also.

Table 2. Analytical data and relevant physical properties of the studied complexes

Complex	Melting point (°C)	Molecular weight	Elemental analysis[a] N(%)	C(%)	H(%)	Colour
$[Cu(tptp)(tzdtH)Cl]_2$	190	1044	3.3(2.7)	55.0(55.2)	5.0(5.0)	Yellow
$[Cu(tptp)(bztztH)Cl]_2$	146	1140	2.4(2.4)	60.9(58.9)	5.3(4.9)	Yellow
$[Cu(tptp)(dtu)Cl]_2$	200[b]	1086	5.3(5.1)	54.8(54.8)	4.5(4.6)	Orange
$[Cu(tptp)(pur6tH)Cl]_2$	> 250	1146	9.8(9.8)	53.4(54.5)	4.4(4.4)	Orange
$[Cu(tptp)(tu)Cl]_2$	204	958	5.7(5.8)	55.4(55.2)	5.1(5.2)	White
$[Cu(tpp)(tzdtH)Cl]_2$	211	960	3.1(2.9)	53.6(52.5)	4.4(4.2)	Yellow
$[Cu(tpp)(bztztH)Cl]_2$	162	1056	2.9(2.7)	57.6(56.8)	4.2(3.8)	Yellow
$[Cu(tpp)(dtu)Cl]_2$	220[b]	1010	5.7(5.5)	52.5(52.3)	4.1(3.8)	Red
$[Cu(tpp)(pur6tH)Cl]_2$	> 250	1062	11.3(10.5)	53.0(52.0)	2.8(3.2)	Red
$[Cu(tpp)(tu)Cl]_2$	194[b]	874	5.6(6.4)	51.0(52.2)	4.3(4.3)	White

[a] Observed values with calculated values in parentheses.
[b] Decomposition.

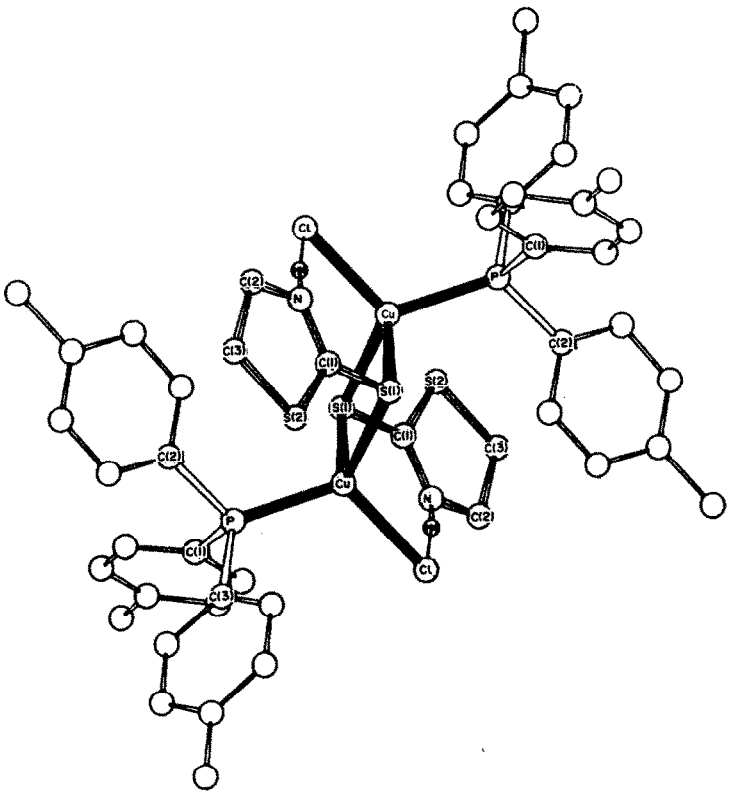

Fig. 1. A view of the complex. The thin lines denote N—H···Cl hydrogen bonds.

Photolysis

UV irradiation of the complexes in chloroform, methanol and acetonitrile solutions at room temperature causes decomposition of the complexes within minutes, without the appearance of new bands in the UV–vis spectrum. The decomposition of the complexes, which can be summarized in the following equation, yields two photoproducts, as we can estimate following Coleman's method[23] (Fig. 2)

$$[Cu(PR_3)(L)Cl]_2 \underset{\text{heat}}{\overset{h\nu}{\rightleftharpoons}} [Cu(L)Cl]_2 + 2PR_3.$$

In every case solid products were deposited and their constitution was corroborated by elemental analyses and by their physical and spectroscopic properties. TLC of the soluble photoproducts indicates that in every case it is phosphine. To ascertain the above mechanism and to verify the reversibility, the solid photoproducts were treated with equimolar amounts of phosphine, affording the initial complexes.

Description of the crystal structure

An ORTEP[24] view of the molecule is given in Fig. 1. The complex consists of dimeric $[Cu(tptp)(L)Cl]_2$ units which are well separated from each other. The molecule is centrosymmetric. The copper(I) atoms display a distorted tetrahedral coordination surrounded by a phosphorus, a chloride and two sulphur atoms. The sulphur atoms of the thione ligands serve as bridges between two copper(I) centres.

Selected bond lengths and angles are given in Table 3. It should be pointed out that the Cu^I—P and Cu^I—S distances observed are similar to those in $[Cu(tptp)(pymtH)Cl]_2$[9] for equivalent bonds. The only significant difference is the slight shortening of the Cu^I—Cl bond in this complex, which is comparable with that in $[Cu(tptp)(pmtH)Cl]_2$ [2.283(1) and 2.300(1) Å].

The Cu^I—P and Cu^I—Cl bond lengths in the Cu/P = 1 : 1 molecule (2.22 and 2.29 Å) are comparably shorter than those found for Cu/P = 1 : 2 molecules. In contrast to this, there is no significant difference in the Cu^I—S distance of both series of complexes (2.37 Å). The copper and bridging sulphur atoms form a planar Cu_2S_2 core. The angles within the central Cu_2S_2 unit [S—Cu—S′ = 92.48(2)° and Cu—S—Cu′ = 87.52(3)°] are similar to those found in $[Cu(tptp)(pmtH)Cl]_2$ [93.24(2) and 86.72(3)°] and

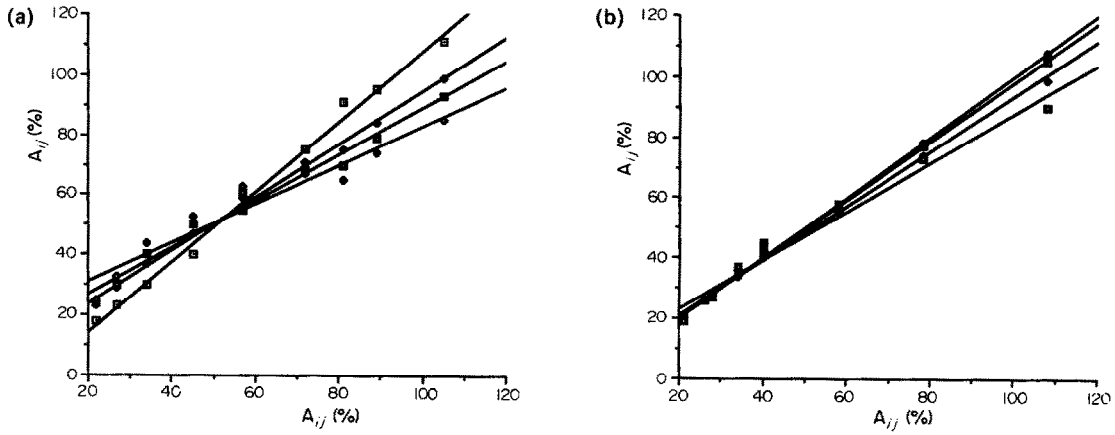

Fig. 2. Plots of the graphical matrix method test for two species in the $[Cu(tptp)(tzdtH)Cl]_2$ system during irradiation in chloroform (a) and methanol (b) solutions. A_{ij} is the absorbance of the jth (400–200 nm) wavelength after i seconds (0, 15, 30, 45, 60) of irradiation.

Table 3. Interatomic distances (Å) and angles (°)[a] for $[Cu(tptp)(tzdtH)Cl]_2$

Cu—P	2.222(1)	C(14)—C(17)	1.151(4)
Cu—Cl	2.283(1)	C(14)—C(15)	1.389(3)
Cu—S(1)	2.386(1)	C(15)—C(16)	1.391(3)
P—C(11)	1.834(2)	C(21)—C(22)	1.388(3)
P—C(21)	1.826(2)	C(21)—C(26)	1.385(3)
P—C(31)	1.824(2)	C(22)—C(23)	1.383(3)
S—C(1)	1.698(2)	C(23)—C(24)	1.378(3)
N—C(1)	1.310(3)	C(24)—C(27)	1.517(3)
S(2)—C(1)	1.730(2)	C(24)—C(25)	1.371(3)
N—C(2)	1.462(3)	C(25)—C(26)	1.401(3)
C(2)—C(3)	1.484(5)	C(31)—C(32)	1.379(3)
C(3)—S(2)	1.814(3)	C(31)—C(36)	1.391(3)
C(11)—C(12)	1.387(3)	C(32)—C(33)	1.399(4)
C(11)—C(16)	1.397(3)	C(33)—C(34)	1.373(4)
C(12)—C(13)	1.386(3)	C(34)—C(37)	1.521(4)
C(13)—C(14)	1.386(3)	C(34)—C(35)	1.382(4)
		C(35)—C(36)	1.390(3)

S(1)—Cu—Cl	110.0(0)	C(15)—C(14)—C(17)	120.3(3)
P—Cu—Cl	115.9(0)	C(14)—C(15)—C(16)	120.9(2)
P—Cu—S(1)	119.7(0)	C(11)—C(16)—C(15)	120.4(2)
Cu—S(1)—C(1)	110.2(1)	P—C(21)—C(22)	117.3(2)
S(1)—C(1)—N	125.2(2)	P—C(21)—C(26)	124.5(2)
S(1)—C(1)—S(2)	121.9(1)	C(22)—C(21)—C(26)	118.1(2)
N—C(1)—S(2)	112.8(2)	C(21)—C(22)—C(23)	121.0(2)
C(1)—N—C(2)	117.6(2)	C(22)—C(23)—C(24)	121.1(2)
N—C(3)—C(2)	108.2(2)	C(23)—C(24)—C(25)	118.2(2)
C(2)—C(3)—S(2)	108.1(2)	C(23)—C(24)—C(27)	120.7(2)
C(1)—S(2)—C(3)	92.2(1)	C(25)—C(24)—C(27)	121.2(2)
Cu—P—C(11)	110.3(1)	C(24)—C(25)—C(26)	121.5(2)
Cu—P—C(21)	117.4(1)	C(21)—C(26)—C(275)	120.0(2)
C(11)—P—C(21)	103.1(1)	P—C(31)—C(32)	118.8(2)
Cu—P—C(31)	115.7(1)	P—C(31)—C(36)	122.5(2)
C(11)—P—C(31)	104.1(1)	C(36)—C(31)—C(32)	118.7(2)
C(21)—P—C(21)	104.8(1)	C(31)—C(32)—C(33)	120.3(2)
P—C(11)—C(21)	124.0(2)	C(32)—C(33)—C(34)	121.1(2)
P—C(11)—C(16)	117.3(2)	C(33)—C(34)—C(35)	118.6(2)
C(12)—C(11)—C(16)	118.6(2)	C(33)—C(34)—C(37)	121.4(3)
C(11)—C(12)—C(13)	120.5(2)	C(35)—C(34)—C(37)	120.0(3)
C(12)—C(13)—C(14)	121.3(2)	C(34)—C(35)—C(36)	120.9(2)
C(13)—C(14)—C(15)	118.2(2)	C(31)—C(36)—C(35)	120.4(2)
C(13)—C(14)—C(17)	121.4(3)		

[a] ESDs are given in parentheses.

[Cu(purinium-6-thione)Cl]$_2$[25] [92.9° and 87.5°]. The geometric arrangement of the Cu_2S_2 core is also in agreement with the prediction made by Summerville and Hoffmann[26] for $Y_2MX_2MY_2$ dimers, as well as the observations reported by Raper *et al.*[27] in a series of centrosymmetric dimers, and is attributed to the concerted steric effects of the ligands.

The S···S distance is equal to 3.508(1) Å, while the Cu···Cu separation of 3.359(1) Å is too long to represent metal–metal interaction.[28] In analogy with similar compounds already investigated[9] the nitrogen-bonded hydrogen atom participates in an intramolecular Cl···H—N hydrogen bond, Cl···N = 3.182(3) Å, N—H = 0.92(3) Å, H(N)···Cl = 2.35(2) Å and N—H···Cl = 150(2)°.*

*Supplementary material: lists of observed and calculated structure factors and positional thermal parameters.

REFERENCES

1. T. G. Spiro (Ed.), *Copper Proteins*. Wiley Interscience, New York (1981).
2. R. Lontie, *Copper Proteins and Copper Enzymes*, Vols I–III. CRC Press, Boca Raton, Florida (1984).
3. S. Sakaki, G. Koga, S. Hinokuma, S. Hashimoto and K. Ohkubo, *Inorg. Chem.* 1987, **26**, 1817.
4. G. Spritchnik, H. W. Spritchnik, P. P. Kirch and D. G. Whitten, *J. Am. Chem. Soc.* 1986, **98**, 2337.
5. M. Wrighton, *Chem. Rev.* 1984, **74**, 401.
6. P. Karagiannidis, P. Aslanidis, S. Papastefanou, D. Mentzafos, A. Hountas and A. Terzis, *Inorg. Chim. Acta* 1989, **156**, 265.
7. C. Lecomte, S. Skoulika, P. Aslanidis, P. Karagiannidis and S. Papastefanou, *Polyhedron* 1988, **7**, 1103.
8. P. Karagiannidis, P. D. Akrivos, D. Mentzafos and A. Terzis, *Inorg. Chim. Acta* 1991, **181**, 263.
9. P. Karagiannidis, S. K. Hadjikakou, P. Aslanidis and A. Hountas, *Inorg. Chim. Acta* 1990, **178**, 27.
10. G. Costa, E. Reisenhofer and L. Stefani, *J. Inorg. Nucl. Chem.* 1965, **27**, 2581.
11. P. Karagiannidis, P. Aslanidis, D. P. Kessissoglou, B. Krebs and M. Dartmann, *Inorg. Chim. Acta* 1989, **156**, 47.
12. *International Tables for X-ray Crystallography*, Vol. IV. Kynoch Press, Birmingham (1974).
13. G. M. Sheldrick, SHELX 76, Program for Crystal Structure Determination. University of Cambridge (1976).
14. A. A. Del Paggio and D. R. McMillin, *Inorg. Chem.* 1983, **22**, 691.
15. S. W. Orchard and C. Kutal, *Inorg. Chem.* 1982, **21**, 538.
16. C. Kutal, *Coord. Chem. Rev.* 1990, **99**, 213.
17. A. W. McLellan and G. A. Melson, *J. Chem. Soc. A* 1967, 137.
18. P. P. Singh and R. Rivest, *Can. J. Chem.* 1968, **46**, 2361.
19. B. Singh, M. M. Rukhaivar and R. J. Sinha, *J. Inorg. Nucl. Chem.* 1977, **39**, 29.
20. C. N. R. Rao and P. Vankataraghavan, *Spectrochim. Acta* 1962, **18**, 541.
21. E. S. Raper and J. L. Brooks, *J. Inorg. Nucl. Chem.* 1977, **39**, 2163.
22. L. J. Bellamy, *The Infrared Spectra of Complex Molecules*. John Wiley, New York (1966).
23. J. S. Coleman, L. P. Varga and S. H. Mastin, *Inorg. Chem.* 1970, **9**, 1015.
24. G. M. Sheldrick, in *Crystallographic Computing* (Edited by G. M. Sheldrick, C. Kruger and R. Goddard), pp. 175–189. Oxford University Press, Oxford (1985).
25. A. C. Shoemaker, P. Singh and D. J. Hodgson, *Acta Cryst. B.* 1976, **32**, 979.
26. R. H. Summerville and R. Hoffmann, *J. Am. Chem. Soc.* 1976, **98**, 7240.
27. J. R. Creighton, D. J. Gardiner, A. C. Gorvin, C. Gutteridge, A. R. W. Jackson, E. S. Raper and P. M. A. Sherwood, *Inorg. Chim. Acta* 1985, **103**, 195.
28. P. K. Mehrotra and R. Hoffmann, *Inorg. Chem.* 1978, **17**, 2187.

Polyhedron Vol. 10, No. 9, pp. 941–944, 1991
Printed in Great Britain

0277–5387/91 $3.00+.00
© 1991 Pergamon Press plc

SYNTHESIS, CRYSTAL STRUCTURE AND MAGNETIC PROPERTIES OF DIBROMO(1,13-DIOXA-4,7,10,16,19,22-HEXAAZACYCLOTETRACOSANE)DICOPPER(II) BROMIDE

ZONG-HUI JIANG,* DAI-ZHENG LIAO, SONG-QI HAO,† JIN-LING HAO, ZHI-YONG ZHANG‡ and GENG-LIN WANG

Department of Chemistry, Nankai University, Tianjin, China

(*Received* 16 *August* 1990; *accepted* 7 *January* 1991)

Abstract—A new dinuclear copper(II) complex with the macrocyclic ligand (1,13-dioxa-4,7,10,16,19,22-hexaazacyclotetracosane), [24]-N_6O_2, has been prepared and its crystal structure has been determined. The two copper ions are contained inside the molecular cavity and are bound to the NNN chelating subunits situated at the two poles of the macrocycles. Each copper(II) centre displays square-pyramidal coordination. The Cu^{II}—Cu^{II} distance is 5.16 Å, and the macrocycle has an *S*-type conformation. The molecule has a symmetry centre. The temperature dependence of the magnetic susceptibility for the title complex was studied in the range 4–300 K, giving an exchange integral of $J = 19.1$ cm^{-1}. This indicates a ferromagnetic interaction between the metal ions. The ESR spectra are also discussed.

Recently attention has been directed towards cyclic polyaza complexes.[1–5] The interest in the dinuclear macrocyclic complexes is in the unusual physical properties that they may possess, in their significance as models of biological dimetallic sites,[6,7] and in their potential chemical reactivity as dinuclear catalysts.

We describe here the synthesis, the crystal structure and the magnetic properties of the dibromo dicopper(II) bromide complex with the macrocyclic ligand (1,13-dioxa-4,7,10,16,19,22-hexaazacyclotetracosane), [24]-N_6O_2.

EXPERIMENTAL

Materials

The commercially available chemicals used were of reagent grade. 2-(2-Chloroethoxy)ethanol was prepared using the literature method.[8]

Syntheses

The ligand [24]-$N_6O_2 \cdot 6HBr \cdot 4H_2O$ was synthesized using the literature method.[5]

Preparation of the title complex. [24]-$N_6O_2 \cdot 6HBr \cdot 4H_2O$ (90 mg) was dissolved in water and passed over an anion-exchange column in the hydroxide form (Dowex 50). The effluent was added to an aqueous solution of 45 mg of $CuBr_2$ and the colour of the solution changed from green to blue. After evaporation of the blue solution, blue crystals were obtained. Found: C, 21.2; H, 5.3; N, 9.3; Cu, 14.0. Calc. for $[C_{16}H_{38}N_6O_2]Cu_2Br_4 \cdot 6H_2O$: C, 21.3; H, 5.5; N, 9.3, Cu, 14.1%.

Measurements

Analyses for C, H and N were carried out on a Perkin–Elmer analyser Model 240 and metal contents were determined by EDTA titration. The electronic spectra were measured on a Perkin–Elmer Hitachi-240 spectrophotometer. Variable-temperature magnetic susceptibility was measured on a vibrating-sample magnetometer Model CF-1. Diamagnetic corrections were made using Pascal's constants[9] for all the constituent atoms, and the magnetic moments were calculated by the equation $\mu_{eff} = 2.828\ (XT)^{1/2}$.

* Author to whom correspondence should be addressed.
† Visiting Scholar, Tianjin Second Medical College, Tianjin, China.
‡ Visiting Scholar, Changsha Railway College, Changsha, Huan, China.

X-ray structure determination

A single crystal of the title complex having approximate dimensions $0.3 \times 0.3 \times 0.1$ mm^3 was mounted on a glass fibre. Examination was performed with Mo-K_α radiation ($\lambda = 0.71073$ Å) on a CAD4 diffractometer equipped with a graphite monochromator. A total of 3158 independent reflections was collected by the ω–2θ scan technique in the range $2 \leqslant \theta \leqslant 25°$, in which 1424 reflections [$I > 3\sigma(I)$] were considered to be observed. Intensity data were corrected for LP factors and empirical absorption.

The locations of the copper and bromine atoms were determined by direct methods. The coordinates of the remaining non-hydrogen atoms were found in succeeding difference Fourier syntheses. The final refinement by the full-matrix least-squares method with positional and anisotropic thermal parameters for the non-hydrogen atoms was converged with the unweighted and weighted agreement factors of 0.044 and 0.051 (unit weights for all observed reflections). The highest peak in the final difference Fourier map had a height of 0.713 e/Å^3 and was 0.9 Å away from the Br(1) atom. All calculations were performed on a PDP11/44 computer.

RESULTS AND DISCUSSION

Elemental analyses have indicated that the reaction of the macrocyclic ligand [24]-N_6O_2 with $CuBr_2$ yielded the binuclear copper(II) macrocyclic complex [24]-$N_6O_2Cu_2Br_4 \cdot 6H_2O$. In the electronic absorption spectra of aqueous solutions of the complex, a strong absorption at 267 nm ($\varepsilon = 4 \times 10^3$ M^{-1} cm^{-1}) and a broad absorption at 640 nm ($\varepsilon = 2 \times 10^2$ M^{-1} cm^{-1}) were observed. The former may be attributed to the charge-transfer absorption bands and the latter to the *d*–*d* transition. Features of the optical spectra are consistent with the expected five-coordinate binuclear complex.[10] It was reported[11] that the coordination environment around the copper(II) ion can affect the frequency of the *d*–*d* transition and as the distortion from planarity increases, a lowering in the transition frequency occurs. In this complex there is no significant difference between the planarity of the copper(II) ion basal planes, hence two bands of the *d*–*d* transition may be superimposed and a broad band is observed.

The crystal structure of the complex

The complex crystallizes in the monoclinic space group $P2_1/C$, with $a = 12.702(3)$, $b = 7.885(1)$, $c = 17.316(2)$ Å, $\beta = 112.00(1)°$, $V = 1608.0$ Å^3, Mr = 895.28, $Z = 2$, $D_x = 1.848$ g cm^{-3}, $\mu = 62.936$ cm^{-1}, $F(000) = 888$.

The molecular structure of the complex is shown in Fig. 1. The macrocyclic ligand, [24]-N_6O_2, contains two sets of diethylenetriamine units which coordinate with two copper(II) ions respectively. The two copper ions are contained inside the molecular cavity bound to the NNN chelating subunits situated at the two poles of the macrocycles. The molecule has a centre symmetry. Each of the two copper atoms has a square-pyramidal coordination environment; the basal plane is defined by three nitrogen atoms and one bromide ligand. The basal planes of the two square-pyramidal CuN_3Br moieties are parallel to each other with Cu^{II}—Cu^{II} = 5.16 Å. The copper–nitrogen distances are almost equivalent [Cu—N(1) = 2.059(5) Å, Cu—N(2) = 2.044(5) Å, Cu—N(3) = 2.016(5) Å] and are shorter than the copper–bromide and

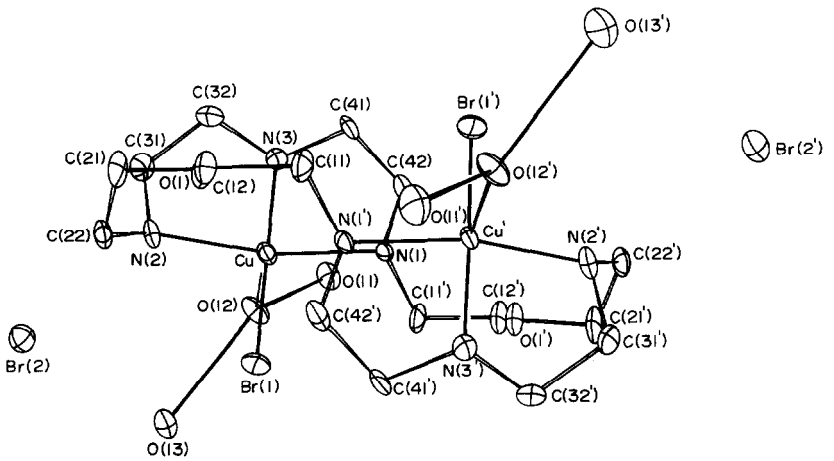

Fig. 1. A perspective view of the complex molecule.

Table 1. Main bond lengths (Å) and bond angles (°)

Cu—Br(1)	2.384(2)	N(1)—Cu—N(2)	166.5
Cu—N(1)	2.059(5)	N(3)—Cu—Br(1)	172.6(2)
Cu—N(2)	2.044(5)	O(12)—Cu—N(1)	96.1
Cu—N(3)	2.016(5)	O(12)—Cu—N(2)	90.3
Cu—O(12)	2.342	O(12)—Cu—N(3)	90.7
O(11)—O(12)	2.798	O(12)—Cu—Br(1)	96.8
O(12)—O(13)	2.776		
Cu---Cu′	5.16		
Cu---Br(2)	4.976		

copper–oxygen distances [Cu—Br(1) = 2.384(2) Å, Cu—O(12) = 2.342 Å]. Selected bond distances and angles are collected in Table 1. The coordinated water molecule acts as the apical ligand and links with two water molecules via hydrogen bonds. The axial copper–oxygen distance [Cu—O(12)] is 2.342 Å. Each copper(II) ion coordinates only one bromide ion and the other bromide ion [Br(2)] is outside the coordination sphere [Cu—Br(2) = 4.97 Å]; the Cu—Br(1)′ distance is 4.856 Å.

Compared with the molecular structure of uncomplexed [24]-N_6O_2[12] there is an obvious difference in conformation between the coordinated and uncoordinated [24]-N_6O_2. Coordinated [24]-N_6O_2 has an *S*-type conformation which may be stabilized by the formation of four pentamembered rings.

ESR spectra and magnetic properties

The X-band powder ESR spectra at room temperature for the complex are given in Fig. 2. The principal values of the g tensor are $g_1 = 2.197$, $g_2 = 2.121$ and $g_3 = 2.060$. The average g value is equal to 2.126, in agreement with the value determined from the magnetic data. No resonance is detected in the $\Delta M_s = 2$ region at 77 K, which could be due to the very weak zero-field splitting.

Fig. 2. Powder X-band ESR spectra of the complex.

Variable-temperature (4–300 K) magnetic susceptibility for the complex is shown in Fig. 3. The magnetic moment, μ_{eff}, increases slightly on cooling and appears to reach a maximum equal to 2.65 BM at *ca* 77 K, and then remains almost constant down to 47 K. This behaviour is characteristic of ferromagnetic coupling[13] between the copper(II) ions stabilizing the triplet state with respect to the singlet state. Furthermore, since the decrease in the magnetic moment below 47 K suggests that a very weak antiferromagnetic intermolecular interaction superimposes itself on the intramolecular ferromagnetic coupling, one can account for this intermolecular effect by using a θ Weiss correction. To determine J, the singlet–triplet energy gap, we may correct the Bleaney–Bowers equation based on the Heisenberg operator using the Weiss parameter, θ, as shown in eq. (1)

$$X_M = \frac{2N\beta^2 g^2}{K(T-\theta)}[3+\exp(-J/KT)]^{-1}, \qquad (1)$$

where X_M denotes the susceptibility per binuclear complex and the remaining symbols have their usual meaning. As shown in Fig. 3, good fits to the experimental data are obtained with eq. (1) by the least-squares procedure. Magnetic parameters thus determined are $J = 19.1$ cm^{-1}, $g = 2.16$ and $\theta = -5.84$ K. The agreement factor defined by $F = \Sigma_i (X_i^{obs} - X_i^{calc})^2 (X_i^{obs})^{-1}$ is equal to 3×10^{-4}. $J > 0$ indicates that there is a ferromagnetic exchange interaction between Cu^{II}—Cu^{II} and smaller $|J|$ values suggest that the interaction is weaker. Also, $\theta < 0$ and $|\theta|$ is smaller. This indicates a very weak antiferromagnetic intermolecular interaction.

Further investigation on this and similar systems is still required in order to explain the mechanism of the exchange interaction for the binuclear complexes in which there is no bridging ligand between the two metal ions.

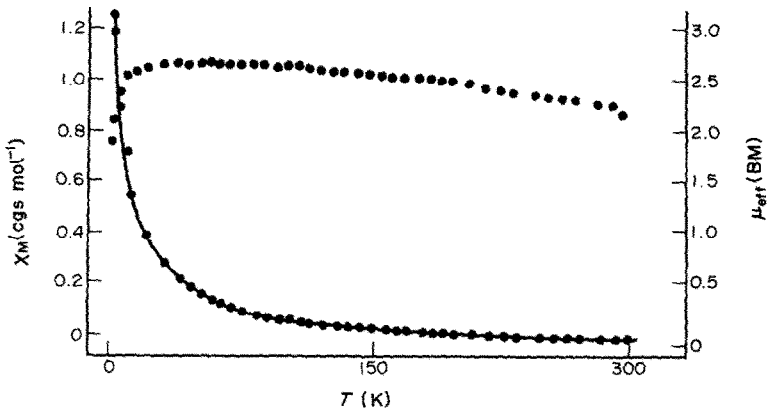

Fig. 3. Molar paramagnetic susceptibility, X_M, and effective magnetic moment per molecule, μ_{eff}, vs temperature curves for the complex. The solid lines represent the best fit of the data of the theoretical equation given in the text.

Acknowledgement—This project was supported by the National Natural Science Foundation of China.

REFERENCES

1. R. M. Izatt and J. J. Christenes, *Synthetic Multidentate Macrocyclic Compounds*. Academic Press, New York (1978).
2. G. A. Melson, *Coordination Chemistry of Macrocyclic Compounds*. Plenum Press, New York (1979).
3. P. K. Coughlin, J. C. Pewan, S. J. Lippard, E. I. Watanabe and J.-M. Lehn, *J. Am. Chem. Soc.* 1979, **101**, 265.
4. P. K. Coughlin and S. J. Lippard, *J. Am. Chem. Soc.* 1981, **103**, 3228.
5. J. Comarmond, P. Plumere, J.-M. Lehn, Y. Aguus, R. Louis, R. Weiss, O. Kahn and I. M. Badarau, *J. Am. Chem. Soc.* 1982, **104**, 6330.
6. E. I. Solomon, in *Copper Proteins, Metal Ions in Biology* (Edited by T. G. Spiro), Vol. 3, pp. 41–108. Wiley, New York (1981).
7. H. Jahansouz, Z.-H. Jiang, R. H. Himes, M. P. Mertes and K. B. Mertes, *J. Am. Chem. Soc.* 1989, **111**, 1049.
8. C. G. Krespau, *J. Org. Chem.* 1975, **40**, 1207.
9. P. W. Selwood, *Magnetochemistry*, p. 48. Interscience, New York (1965).
10. E. D. McKenzie, *J. Chem. Soc. A* 1970, 3095.
11. P. K. Bhattacharya, *J. Indian Chem. Soc.* 1982, **59**, 505.
12. Z.-H. Jiang and G.-L. Wang, *Chem. J. Chin. Univ.* 1990, **6**, 660.
13. O. Kahn, J. Galy, P. Tola and M. Coudanne, *J. Am. Chem. Soc.* 1978, **100**, 3931.

Polyhedron Vol. 10, No. 9, pp. 945–947, 1991
Printed in Great Britain

0277–5387/91 $3.00+.00
© 1991 Pergamon Press plc

CADMIUM COMPLEXES WITH THE TRIDENTATE AMINO-KETOENAMINES DERIVED FROM PENTANE-2,4-DIONE AND ALIPHATIC DIAMINES

MAREK KWIATKOWSKI,* EDMUND KWIATKOWSKI, ALEKSANDRA OLECHNOWICZ and BOŻENA KOŚCIUSZKO

Institute of Chemistry, University of Gdańsk, Sobieskiego 18, 80-952 Gdańsk, Poland

(*Received* 6 *June* 1990; *accepted* 9 *January* 1991)

Abstract—Two new cadmium complexes with the tridentate amino-ketoenamine ligands, obtained by 1 : 1 condensation of pentane-2,4-dione with 1,2-diaminoethane and 1,3-diaminopropane, respectively, exhibit an unusual coordination type, wherein the cadmium ion is coordinated by two non-deprotonated, neutral ligand molecules, in spite of the acidic properties of the enamine hydrogen atom.

An enamine hydrogen atom *f* in the mono-condensation products of pentane-2,4-dione and 1,2-diaminoethane or 1,3-diaminopropane (HL^1 and HL^2, respectively, Fig. 1) is fairly acidic and, therefore, dissociates readily upon the complexation of the metal ion.[1] All metal complexes with HL^1 and HL^2 described up to date[2–9] share a common structural feature; roughly planar ML^1 or ML^2 subunits, wherein one metal(II) ion is bound by one singly-deprotonated tridentate ligand molecule. In this paper, we report the first example of the entirely different coordination type exhibited by HL^1 and HL^2, observed in their cadmium complexes $[Cd(HL^1)_2]I_2$ and $[Cd(HL^2)_2]I_2$. In these complexes, two non-deprotonated ligand molecules are bound to one, presumably hexacoordinated cadmium ion.

RESULTS AND DISCUSSION

When HL^1 and HL^2 ligands are allowed to react with cadmium iodide at room temperature in methanol, white, microcrystalline solids separate slowly from the reaction medium. Elemental analysis shows that the products can be formulated as $[Cd(HL^1)_2]I_2$ and $[Cd(HL^2)_2]I_2$, respectively, wherein the cadmium ion is bound by two neutral tridentate amino-ketoenamine ligand molecules, forming a dipositive complex cation neutralized by two iodide counterions. FAB mass spectra of the products (Table 1) support this formulation: although the peaks of the $Cd(HL)_2I_2$ aggregate are not present, the fragments $Cd(HL)_2I$, $Cd(HL)_2$, Cd(HL)I, and Cd(HL) give rise to the most abundant fragmentation ions in the spectra of both cadmium complexes.

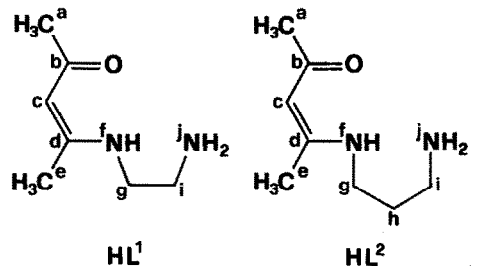

Fig. 1. Line drawings of the amino-ketoenamine ligands including the labelling scheme (indexes *a–j*) used in the discussion of the NMR spectra.

^1H NMR spectra of the cadmium complexes bear a close resemblance to the spectra of the free ligands.[1,2,5,10] Only minor shifts (up to 0.2 ppm) of proton resonances are observed upon the complexation of HL^1 and HL^2 with cadmium, except for the primary amino hydrogen atoms *j* experiencing a shift of *ca* 1 ppm. The most conspicuous similarity is the presence of a broadened resonance at 10.6 ppm in the spectra of both the free ligands and their cadmium complexes. As this resonance is attributed to the enamine proton *f* coupled to the adjacent methylene group *g* with J_{fg} *ca* 7 Hz, its presence in the spectra of cadmium compounds pro-

* Author to whom correspondence should be addressed.

Table 1. Spectroscopic data for the cadmium complexes

Compound	FAB Mass spectra[a]		^{1}H NMR spectra[b]	^{13}C NMR spectra[c]
$[Cd(HL^1)_2]I_2$	$[Cd(HL^1)_2I]^+$	525(7)	*a, e* 1.858s, 1.917s (1.98s, 2.05s)	*a, e* 18.56, 28.54
	$[Cd(HL^1)_2]^+$	398(28)	*g*[d] 3.336br(3.48m)	*g, i* 41.97, 43.85
	$[Cd(HL^1)I]^+$	383(100)	*i* 2.721t(3.02br)	*c* 94.94
	$[Cd(HL^1)]^+$	256(74)	*c* 4.955s(5.05s)	*b* 193.11
			f 10.647br(10.90br)	*d* 162.86
			j 3.194br(ov.)	
$[Cd(HL^2)_2]I_2$	$[CD(HL^2)_2I]^+$	553(2)	*a, e* 1.850s, 1.918s (1.93s, 1.96s)	*a, e* 18.30, 28.40
	$[Cd(HL^2)_2]^+$	426(12)	*g* 3.266q(3.33q)	*g, i* ov.[h]
	$[Cd(HL^2)I]^+$	397(88)	*i* 2.656t(2.95t)	*h* 32.10
	$[Cd(HL^2)]^+$	270(100)	*h* 1.710k(ov.[e])	*c* 94.44
			c 4.936s(4.91s)	*b* 192.63
			f 1.671t[f](10.62br)	*d* 162.93
			j 3.3br[g]	

[a] *m/z* (% relative abundance) for the most abundant cadmium isotope ^{114}Cd (28.8%).

[b] 300 MHz in d_6-DMSO solution with TMS as internal reference, δ(ppm); the chemical shifts for $CDCl_3$ solution (100 MHz) vs TMS are given in parentheses; s: singlet, t: triplet, q: quartet, k: quintet, m: multiplet, br: broadened band, ov.: overlapped by other resonances.

[c] Noise-decoupled spectra in DMSO solution with TMS as internal reference, δ(ppm).

[d] Quartet in d_5-pyridine at $\delta = 3.14$ ppm.

[e] Partially, by methyl *a* and *e* singlets.

[f] Triplet of broadened components.

[g] Partially overlapping with quartet of *g*.

[h] Entirely overlapped by the solvent multiplet. The explanation of *a–j* is the same as in Fig. 1.

vides additional evidence for the $[Cd(HL^1)_2]I_2$ and $[Cd(HL^2)_2]I_2$ formulation. A perceptible broadening of the methylene *g* and *i* resonances in the $[Cd(HL^1)_2]I_2$ spectrum implies some restriction of pseudo-rotary motion within the —CH_2—CH_2— moiety when compared with a more flexible —CH_2—CH_2—CH_2— fragment in $[Cd(HL^2)_2]I_2$, giving rise to narrower signals.

^{13}C NMR spectra of the cadmium complexes are almost identical (Table 1) and very close to the spectrum reported for the ligand HL^1 (the largest discrepancy being 1.6 ppm).[5,10] As the deprotonation of HL^1 results normally in much more substantial shifts (e.g. 17 ppm upfield for carbonyl carbon atom *b* and 9 ppm downfield for the methylene carbon atom *g* resonances[5,10]), this again indicates the unusual behaviour of HL^1 and HL^2 coordinating the cadmium(II) ion as neutral molecules.

EXPERIMENTAL

Cadmium complexes

The appropriate ligand, HL^1 or HL^2 (0.02 mol), in 150 cm^3 of methanol was added to cadmium(II) iodide (0.01 mol) dissolved in 150 cm^3 of methanol. The resulting solution was stirred for 15 min at room temperature and filtered. Cadmium complexes separated slowly from the solution in the form of white solids. These were removed by filtration, washed with methanol and dried *in vacuo* at room temperature. Bis(1-amino-3-aza-4-methyl-4-heptene-6-one)cadmium(II) diiodide, $[Cd(HL^1)_2]I_2$, was obtained in the form of small needles, yield 65%, m.p. 130°C. Found: C, 25.8; H, 4.3; I, 39.0; N, 8.6. $C_{14}CdH_{28}I_2N_4O_2$ requires: C, 25.9; H, 4.3; I, 39.0; N, 8.6%. Bis(1-amino-4-aza-5-methyl-5-octene-7-one)cadmium(II) diiodide, $[Cd(HL^2)_2]I_2$, was obtained as a white, microcrystalline powder, yield 45%, m.p. 120°C. Found: C, 28.6; H, 4.8; I, 37.5; N, 8.3. $C_{16}CdH_{32}I_2N_4O_2$ requires: C, 28.3; H, 4.8; I, 37.4; N, 8.3%.

Physical measurements

Elemental analyses were performed on a Carlo Erba MOD 1106 elemental analyser (C, H, N). Iodine content was determined by potentiometric titration of acidified solution with silver nitrate. Melting points were obtained as endothermic peaks on thermogravimetric curves recorded on a Paulik–Paulik type OD 103 derivatograph. FAB (Fast

Atom Bombardment) mass spectra of cadmium complexes in DMSO solution were recorded using a glycerol matrix on a VG 30–250 spectrometer at the probe temperature; xenon was used as the primary beam gas and the ion gun was operated at 8 kV and 100 μA. ^{1}H and ^{13}C NMR spectra were run on 300 MHz Nicolet and 100 MHz Tesla FT spectrometers.

Acknowledgements—This research was supported by Grant DS-5-530-7-016-1 from the kBN and Instrumentation Grant CHE 8102974 from NSF. The authors are grateful to Dr Edward Deutsch for his help in NMR and FAB mass studies.

REFERENCES

1. E. Kwiatkowski and M. Kwiatkowski, *Inorg. Chim. Acta* 1984, **82**, 101.
2. M. Kwiatkowski, E. Kwiatkowski, A. Olechnowicz, D. M. Ho and E. Deutsch, *Inorg. Chim. Acta* 1988, **150**, 65.
3. E. Kwiatkowski, M. Kwiatkowski, A. Olechnowicz, J. Mrozinski, D. M. Ho and E. Deutsch, *Inorg. Chim. Acta* 1989, **158**, 37.
4. J. P. Costes, F. Dahan and J. P. Laurent, *J. Coord. Chem.* 1984, **13**, 355.
5. J. P. Costes, *Transition Met. Chem.* 1985, **10**, 185.
6. J. P. Costes, F. Dahan and J. P. Laurent, *Inorg. Chem.* 1986, **25**, 413.
7. J. P. Costes, J. F. Serra, F. Dahan and J. P. Laurent, *Inorg. Chem.* 1986, **25**, 2790.
8. J. P. Costes, G. Commenges and J. P. Laurent, *Inorg. Chim. Acta* 1987, **134**, 237.
9. J. P. Costes and J. P. Laurent, *Inorg. Chim. Acta* 1987, **134**, 245.
10. G. Cros and J. P. Costes, *C.R. Acad. Sci. Paris* 1982, **294–II**, 173.

Polyhedron Vol. 10, No. 9, pp. 949–954, 1991
Printed in Great Britain

0277–5387/91 $3.00+.00
© 1991 Pergamon Press plc

SYNTHESIS AND CHARACTERIZATION OF SOME HETEROBIMETALLIC ISOPROPOXIDES OF LANTHANUM WITH ZIRCONIUM

UPENDRA M. TRIPATHI, A. SINGH and R. C. MEHROTRA*

Department of Chemistry, University of Rajasthan, Jaipur 302004, India

(*Received* 22 *October* 1990; *accepted* 9 *January* 1991)

Abstract—Seven heterobimetallic isopropoxide derivatives of lanthanum have been synthesized by the reaction of $LaCl_3 \cdot 3Pr^iOH$ with $K\{Zr_2(OPr^i)_9\}$ in different molar ratios (1 : 1, 1 : 2, 1 : 3) to yield hydrocarbon-soluble derivatives of the types $[Cl_{3-n}La\{Zr_2(OPr^i)_9\}_n]$ (n = 1, 2 or 3). The reactions of the above bimetallic chloride isopropoxides with the appropriate potassium alkoxides yield derivatives of the types $[(OR)_{3-n}La\{Zr_2(OPr^i)_9\}_n]$ (n = 1 or 2; R = Pr^i and Bu^t). All these have been characterized by elemental analyses and spectroscopic (IR and NMR) studies.

The synthesis and characterization of a large number of heterometal alkoxides[1–5] which are soluble in organic solvents and generally volatile under reduced pressure have added a new dimension to the variety of known heterometal coordination compounds. A conjecture[6] about the formation of such derivatives in a solution of a number of metal alkoxides used as precursors for ceramic materials was made in 1971 on the basis of the extraordinary homogeneity of the final products obtained by the solution–sol–gel (S–G) process. Recently, heterometal alkoxides[7–12] have attracted considerable attention as precursors for ceramics in the S–G process.

There has been of late an unprecedented upsurge in metal alkoxide chemistry[13,14] particularly for yttrium and the lanthanides.[15–19] It is interesting to note that attempts to prepare homoleptic isopropoxide of yttrium (by the reaction of the metal with isopropanol) and neodymium (by the reaction of $NdCl_3$ with $NaOPr^i$ in a 1 : 3 molar ratio) appear to result in the formation of oxide[16] or chloride alkoxides,[15] respectively. By contrast, addition of $Al(OPr^i)_3$ to the yttrium oxide–alkoxide species *in situ* results[16] in the formation of heterobimetallic isopropoxide,[1,19] $Y\{Al(OPr^i)_4\}_3$, indicating a higher stability of the heterometallic in comparison with the homoleptic alkoxides.

Despite extensive work in the field of bimetallic alkoxides of transition metals[2–5] containing different types of alkoxometallate ligands, only the tetraalkoxyaluminate(gallate) complexes of lanthanons have been described.[20,21] Observations[20,21] regarding the volatility of bimetallic isopropoxides of lanthanum with ligands like $\{Al(OPr^i)_4\}^-$ and $\{Ga(OPr^i)_4\}^-$ prompted us to synthesize new tris-bimetallic alkoxides of lanthanum with some more complex alkoxometallate ligands like $\{Zr_2(OPr^i)_9\}^-$ and extend the work to the synthesis of bimetallic chloride alkoxides of lanthanum, as such heteroleptic complexes of lanthanons do not appear to have been reported so far.

We therefore describe herein (Table 1) the synthesis and characterization of some novel heterobimetallic isopropoxide derivatives of lanthanum with zirconium of the types $[Cl_{3-n}La\{Zr_2(OPr^i)_9\}_n]$ and $[(OR)_{3-n}La\{Zr_2(OPr^i)_9\}_n]$ (where n = 1, 2 or 3).

EXPERIMENTAL

Stringent precautions were taken to exclude moisture throughout the experimental procedure. All reactions were carried out with glass apparatus which was oven-dried (130–140°C) thoroughly and cooled under a moisture-free atmosphere prior to use.

Toluene, benzene and n-hexane were dried by refluxing over sodium/benzophenone, followed by distillation. Isopropanol was dried by refluxing

* Author to whom correspondence should be addressed.

Table 1. Preparative, analytical and some physical data for new heterometal isopropoxide of lanthanum

Reactants (g, mmol)	Products (g)	Properties	Yield (%)	Analysis(%) Found(Calc.)			
				La	Zr	OPr^i	Cl
$LaCl_3 \cdot 3Pr^iOH$ + $3K\{Zr_2(OPr^i)_9\}$ (0.885, 2.00) {K(0.236, 6.03) + $Zr(OPr^i)_4 \cdot Pr^iOH$ (4.673, 12.05)}	$[La\{Zr_2(OPr^i)_9\}_3]$ (4.105)	White solid	91	5.9 (6.0)	24.5 (24.0)	69.7 (69.9)	—
$LaCl_3 \cdot 3Pr^iOH$ + $2K\{Zr_2(OPr^i)_9\}$ (1.878, 4.41) {K(0.344, 8.79) + $Zr(OPr^i)_4 \cdot Pr^iOH$ (6.820, 17.59)}	$[ClLa\{Zr_2(OPr^i)_9\}_2]$ (6.895)	White, crystalline solid	98	8.2 (8.6)	23.1 (22.8)	66.1 (66.3)	2.5 (2.2)
$LaCl_3 \cdot 3Pr^iOH$ + $K\{Zr_2(OPr^i)_9\}$ (2.747, 6.45) {K(0.252, 6.46) + $Zr(OPr^i)_4 \cdot Pr^iOH$ (5.008, 12.91)}	$[Cl_2La\{Zr_2(OPr^i)_9\}]$ (3.908)	White, crystalline solid	99	14.9 (15.0)	20.1 (19.7)	57.3 (57.5)	7.7 (7.7)
$[ClLa\{Zr_2(OPr^i)_9\}_2]$ + $KOPr^i$ (2.885, 1.77) K(0.070, 1.79)	$[(OPr^i)La\{Zr_2(OPr^i)_9\}_2]$ (2.803)	White solid	96	8.3 (8.5)	22.8 (22.4)	68.7 (69.0)	—
$[ClLa\{Zr_2(OPr^i)_9\}_2]$ + $KOBu^t$ (2.815, 1.75) K(0.068, 1.73)	$[(OBu^t)La\{Zr_2(OPr^i)_9\}_2]$ (2.482)	Colourless, pasty mass	87	8.2 (8.4)	22.5 (22.2)	64.2 (64.8)	—
$[Cl_2La\{Zr_2(OPr^i)_9\}]$ + $2KOPr^i$ (2.366, 2.56) K(0.200, 5.11)	$[(OPr^i)_2La\{Zr_2(OPr^i)_9\}]$ (2.376)	White solid	96	14.4 (14.3)	19.0 (18.8)	66.6 (66.9)	—
$[Cl_2La\{Zr_2(OPr^i)_9\}]$ + $2KOBu^t$ (2.386, 2.58) K(0.202, 5.16)	$[(OBu^t)_2La\{Zr_2(OPr^i)_9\}]$ (2.483)	White solid	96	13.7 (13.9)	18.3 (18.2)	52.9 (53.2)	—

over aluminium isopropoxide or calcium hydride, followed by distillation. Both benzene and isopropanol were finally dried by azeotropic distillation in the presence of dry isopropanol or benzene, respectively. Tert-butanol was fractionated over sodium tert-butoxide.

Anhydrous lanthanum trichloride was obtained by heating a mixture of hydrated lanthanum trichloride and ammonium chloride in a current of dry chlorine and hydrogen chloride gas; the temperature had to be carefully regulated in the above procedure to avoid the formation of fusible oxychloride (LaOCl).

Zirconium isopropoxide isopropanolate, $Zr(OPr^i)_4 \cdot Pr^iOH$, was prepared by the literature procedure.[22]

Zirconium was estimated as ZrO_2 after precipitation as mandelate and ignition to the oxide. Lanthanum was estimated as La_2O_3 after ignition of precipitated oxalate.

Isopropoxy contents were estimated by the oxidimetric method[23] using a N-$K_2Cr_2O_7$ solution in 12.5% H_2SO_4. Chloride was estimated by Volhard's method.

IR spectra (4000–200 cm^{-1}) were recorded as Nujol mulls on Perkin–Elmer 557 and Carl Zeiss Specord M80 spectrophotometers using CsI optics. ^1H (89.55 MHz) and ^{13}C (22.49 MHz) NMR spectra were recorded on a JEOL FX 90Q FT NMR spectrometer in $CDCl_3$ or C_6H_6, respectively. Chemical shifts were referenced internally to *protio* solvent impurities (δ 7.25, $CDCl_3$) and solvent ^{13}C references (δ 128.5, C_6H_6; δ 77.0, $CDCl_3$) and have been reported in ppm downfield of tetramethylsilane (TMS).

Preparation of $[La\{Zr_2(OPr^i)_9\}_3]$

A freshly prepared solution of $K\{Zr_2(OPr^i)_9\}$, prepared by dissolving potassium (0.236 g, 6.03 mmol) and $Zr(OPr^i)_4 \cdot Pr^iOH$ (4.673 g, 12.05 mmol) in the presence of dry isopropanol (~ 5 cm^3) and benzene (~ 25 cm^3), was added slowly to a suspension of $LaCl_3 \cdot 3Pr^iOH$ (0.855 g, 2.00 mmol) in benzene (~ 15 cm^3). The reaction mixture was refluxed for 3 h. Excess isopropanol was then distilled off and after addition of benzene (~ 60 cm^3), the reaction mixture was again refluxed for ~ 4 h. The precipitated KCl (0.441 g, 5.91 mmol) was filtered off. After removal of volatiles from the filtrate under reduced pressure, and finally drying the resulting mass at 50°C/0.8 torr for 2 h, a white, sticky, solid product of the composition $[La\{Zr_2(OPr^i)_9\}_3]$ (4.105 g, 91%) was obtained. The compound was purified by sublimation (~ 90% yield) at 217°C/0.5 torr.

Preparation of bimetallic chloride isopropoxide $[ClLa\{Zr_2(OPr^i)_9\}_2]$

Initial efforts to prepare $[ClLa\{Zr_2(OPr^i)_9\}_2]$ by the reaction of $LaCl_3 \cdot 3Pr^iOH$ and $K\{Zr_2(OPr^i)_9\}$ (1:2 molar ratio) in the presence of excess isopropanol tended to crystallize out the isopropanolate, $Zr(OPr^i)_4 \cdot Pr^iOH$. The derivative could finally be obtained by exclusion of free isopropanol in the reaction mixture.

A solution of the reagent $K\{Zr_2(OPr^i)_9\}$ in an isopropanol–benzene mixture was first prepared by the interaction of $KOPr^i$ [synthesized by dissolving 0.344 g (8.79 mmol) of potassium in a mixture of isopropanol (~ 5 cm^3) and benzene (~ 10 cm^3)] with $Zr(OPr^i)_4 \cdot Pr^iOH$ (6.820 g, 17.59 mmol) in benzene (~ 10 cm^3). This solution was evaporated to dryness and then dissolved in benzene.

A benzene solution of the reagent was added slowly to the suspension of $LaCl_3 \cdot 3Pr^iOH$ (1.878 g, 4.41 mmol) in benzene (~ 15 cm^3) with continuous stirring. The reaction mixture was stirred for 2 h with heating at ~ 65°C, followed by further stirring at room temperature for ~ 10 h. The precipitated KCl (0.621 g, 8.33 mmol) was filtered off and the volatiles were removed from the filtrate under reduced pressure (0.8 torr) at room temperature (~ 27°C) to obtain $[ClLa\{Zr_2(OPr^i)_9\}_2]$ (6.895 g, 98% yield) as a white, crystalline solid. The compound was purified by crystallization from n-hexane.

$[Cl_2La\{Zr_2(OPr^i)_9\}]$ was prepared similarly as a white, crystalline solid by the interaction of $K\{Zr_2(OPr^i)_9\}$ (4.865 g, 6.45 mmol) with $LaCl_3 \cdot 3Pr^iOH$ (2.747 g, 6.45 mmol); the product could be recrystallized from n-hexane and toluene.

Reaction of $[ClLa\{Zr_2(OPr^i)_9\}_2]$ *with* $KOPr^i$

A benzene suspension of $KOPr^i$, prepared from potassium (0.070 g, 1.79 mmol) in isopropanol (~ 2 cm^3) containing benzene (~ 20 cm^3), was added dropwise to a solution of $[ClLa\{Zr_2(OPr^i)_9\}_2]$ (2.885 g, 1.77 mmol) in benzene (~ 15 cm^3). The reaction mixture was stirred at room temperature for *ca* 8 h. The precipitated KCl (0.113 g, 1.51 mmol) was removed by filtration. After removal of the volatiles from the filtrate under reduced pressure, a white solid of the composition $[(OPr^i)La\{Zr_2(OPr^i)_9\}_2]$ (2.803 g, 96% yield) was obtained.

In a similar procedure, the reaction of $[ClLa\{Zr_2(OPr^i)_9\}_2]$ with $KOBu^t$ in an equimolar ratio afforded $[(OBu^t)La\{Zr_2(OPr^i)_9\}_2]$ in 87% yield.

Reaction of $[Cl_2La\{Zr_2(OPr^i)_9\}]$ *with* $KOPr^i$ *in a* 1 : 2 *molar ratio*

Interaction of $KOPr^i$, prepared from potassium (0.200 g, 5.11 mmol) and isopropanol (~ 5 cm^3), with a benzene solution of $[Cl_2La\{Zr_2(OPr^i)_9\}]$ (2.366 g, 2.56 mmol), followed by stirring at room temperature for a few hours resulted in the precipitation of KCl (0.373 g, 5.00 mmol), which was filtered off. The filtrate was dried under reduced pressure (0.8 torr) at room temperature to obtain the white, solid product of composition $[(OPr^i)_2La\{Zr_2(OPr^i)_9\}]$ (2.376 g, 96%).

By the same procedure, the reaction of $[Cl_2La\{Zr_2(OPr^i)_9\}]$ with $KOBu^t$ in a 1:2 molar ratio afforded a white solid, $[(OBu^t)_2La\{Zr_2(OPr^i)_9\}]$, in 96% yield.

RESULTS AND DISCUSSION

Interaction of $LaCl_3 \cdot 3Pr^iOH$ and $K\{Zr_2(OPr^i)_9\}$ in different molar ratios in benzene can be represented by the following equation:

$$LaCl_3 \cdot 3Pr^iOH + nK\{Zr_2(OPr^i)_9\} \longrightarrow [Cl_{3-n}La\{Zr_2(OPr^i)_9\}_n] + 3KCl\downarrow + 3Pr^iOH. \quad (n = 1\text{–}3)$$

Replacement of chloride in $[Cl_2La\{Zr_2(OPr^i)_9\}]$ and $[ClLa\{Zr_2(OPr^i)_9\}_2]$ with alkoxy groups produced derivatives of the types, $[(OR)_2La\{Zr_2(OPr^i)_9\}]$ and $[(OR)La\{La_2(OPr^i)_9\}_2]$:

$$[Cl_nLa\{Zr_2(OPr^i)_9\}_{3-n}] + 2KOR \longrightarrow [(OR)_nLa\{Zr_2(OPr^i)_9\}_{3-n}] + 2KCl\downarrow. \quad (R = Pr^i, Bu^t;\ n = 1, 2)$$

All these new heterobimetallic derivatives are colourless products which are highly moisture-sensitive and soluble in common, organic solvents.

The identity of the tris-product, $[La\{Zr_2(OPr^i)_9\}_3]$, has been corroborated by its sublimation in 90% yield. Similarly, the identity of the dichloride product is supported by its recrystallization from n-hexane/toluene in ~ 64% yield.

In view of $LaCl_3$ forming a stable isopropanolate, $LaCl_3 \cdot 3Pr^iOH$, an attempt was made to prepare isopropanol adducts of the chloride products by refluxing these derivatives with isopropanol. From the yields, as well as the analysis of the products, it appears that these complexes do not form any adduct(s) with isopropanol which tends to indicate that the lanthanum must be attaining a higher stable coordination state by internal chloride and isopropoxy bridges. Although final proof will emerge only after X-ray structure determination (efforts of which are in progress), non-crystallization of the zirconium tetraisopropoxide adduct, $Zr(OPr^i)_4 \cdot Pr^iOH$, tends to corroborate that these complexes are stable coordination entities which do not tend to dissociate into the component lanthanum and zirconium isopropoxide or chloride isopropoxides.

IR spectra of these newly synthesized heterobimetallic isopropoxides are being interpreted on the basis of earlier characterization of C—O and M—O stretching frequencies[1,24,25] as well as deformation and skeletal vibrations[1,26,27] due to the *gem*-dimethyl group in the spectra of metal isopropoxides.

The spectra of heterobimetallic isopropoxides of lanthanum show C—H deformation stretching frequencies due to $(CH_3)_2C<$ groups in the ranges 1370–1365 and 1360–1355 cm^{-1}, while skeletal vibrations have been observed in the ranges 1160–1115 and 1120–1115 cm^{-1}. In mixed (t-butoxide) isopropoxide derivatives, the presence of the t-butoxide group is indicated by the absorption in the ranges 1382–1378 and 1260–1200 cm^{-1} due to C—H deformation and skeletal vibrations, respectively.

The ν(C—O) band which occurs at 1070 cm^{-1} in free isopropyl alcohol is observed in the ranges 1085–960 cm^{-1} (terminal) and 945–910 cm^{-1} (bridging) in these new heterometal isopropoxide derivatives.

The medium to strong broad absorptions displayed in the range 560–410 cm^{-1} may be related to ν(Zr—O) (560–535 cm^{-1}) and ν(La—O) (460–410 cm^{-1}). The heterobimetallic chloride isopropoxide derivatives exhibited absorptions in the range 294–210 cm^{-1}, which may be tentatively assigned to La—Cl stretching frequencies.[28,29]

The room temperature ^1H NMR spectrum (in $CDCl_3$) of freshly prepared $[Cl_2La\{Zr_2(OPr^i)_9\}]$ displays (i) a multiplet at δ 4.44 ppm arising from overlapping septets due to methine protons and (ii) three doublets at δ 1.67, 1.61; 1.49, 1.43; and 1.34, 1.27 ppm due to *gem*-dimethyl protons, in the approximate intensity ratio 3:2:4 which correspond to two triply (μ_3-OPr^i), three doubly (μ_2-OPr^i) bridged, and four terminal isopropoxy groups, respectively.

In view of the large size (1.15 Å), La^{3+} should generally prefer to attain a coordination higher than six in isopropoxide derivatives. Thus the ^1H NMR spectrum could, therefore, be interpreted in terms of a tentative structure **A**; this suggestion is corroborated by ^{13}C NMR data [δ 72.03, 71.14, 70.60 ppm (α-carbons); 25.25 and 24.27 ppm (β-carbons)] and the crystal structures of $KU_2(OBu^t)_9$[30] and $ClCd\{Zr_2(OPr^i)_9\}$.[31]

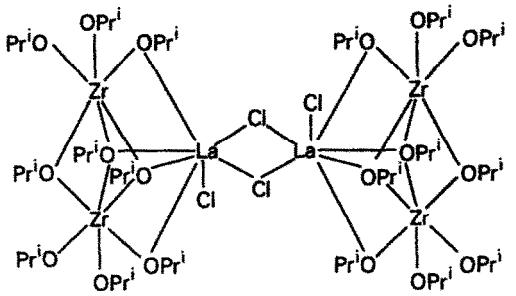

(A)

A noteworthy feature of the NMR spectrum of the complex, $[Cl_2La\{Zr_2(OPr^i)_9\}]$, is the appearance of new, minor peaks in the form of doublets on ageing the sample, which may be ascribed to structural changes from further association of the molecule.

The ^1H NMR spectra of $[X_2La\{Zr_2(OPr^i)_9\}]$ ($X = OPr^i$, OBu^t) in $CDCl_3$ at room temperature are less informative because of the broad and complex nature of observed signals due to methine and *gem*-dimethyl protons, but these could be expected to exhibit structures similar to that suggested for the parent chloro derivative, $[Cl_2La\{Zr_2(OPr^i)_9\}]$.

The derivative $[ClLa\{Zr_2(OPr^i)_9\}_2]$ exhibits an averaged septet and doublet (δ 1.29, 1.20 ppm) centred at δ 4.38 and 1.245 ppm, respectively, due to methine and *gem*-dimethyl protons, indicating fast exchange (on the NMR time scale) between bridging and terminal isopropoxy groups. The ^{13}C NMR spectrum (in benzene) for the same sample exhibits a single peak for both the α- and β-carbon atoms, respectively, at δ 69.67 and 26.49 ppm, which may be ascribed to a rapid exchange between bridging and terminal isopropoxy groups on the NMR time scale. On the basis of these observations, one can tentatively speculate structure **B** for the complex $[ClLa\{Zr_2(OPr^i)_9\}_2]$.

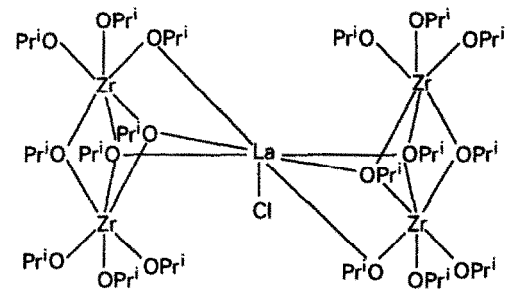

(B)

The ^1H NMR spectra of $[(Pr^iO)La\{Zr_2(OPr^i)_9\}_2]$ and $[(OBu^t)La\{Zr_2(OPr^i)_9\}_2]$ in $CDCl_3$ showed, as expected, an averaged septet and doublet due to α- and β-protons of the isopropoxy groups, respectively. Thus they may be expected to adopt structures similar to the one proposed for the precursor chloro complex (structure **B**).

The ^1H NMR spectrum of $[La\{Zr_2(OPr^i)_9\}_3]$ in $CDCl_3$ exhibits a broad peak centred at δ 4.37 ppm due to methine protons and two pairs of doublets centred at δ 1.34 and 1.21 ppm due to *gem*-dimethyl protons. The integration between the two sets of methyl protons appears to be an approximately 1 : 2 ratio. In the ^{13}C NMR spectrum, $[La\{Zr_2(OPr^i)_9\}_3]$ in $CDCl_3$ shows only two peaks at δ 26.63 and 70.19 ppm due to the *gem*-dimethyl (β) and methine (α) carbon atoms, respectively.

Although a definitive structure has to await X-ray studies, on the basis of spectroscopic data and known structures of similar compounds, a plausible structure (**C**) could be suggested with the possibilities of lanthanum attaining higher coordination state(s) by further bridging through suitably situated isopropoxy group(s).

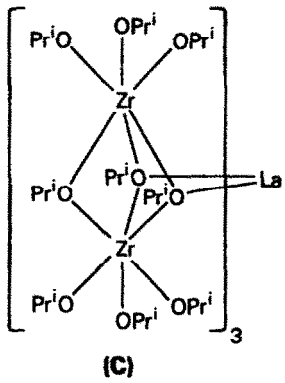

(C)

Acknowledgements—The authors are grateful to the State Government of Rajasthan, the DST and the U.G.C., New Delhi, for financial support under the Special Assistance Programme, and to Mr Suman Gupta for recording all the NMR spectra.

REFERENCES

1. D. C. Bradley, R. C. Mehrotra and D. P. Gaur, *Metal Alkoxides*. Academic Press, London (1978).
2. R. C. Mehrotra and A. Mehrotra, *Inorg. Chim. Acta Rev.* 1972, **5**, 127.
3. R. C. Mehrotra, *Adv. Inorg. Chem. Radiochem.* 1983, **26**, 269.
4. R. C. Mehrotra, in *Sol–Gel Science and Technology* (Edited by M. A. Aegerter, M. Jafelicce, D. F. Souza and E. D. Zanotto), pp. 17–39. World Scientific, Singapore (1989).
5. R. C. Mehrotra, A. Singh and U. M. Tripathi, *Chem. Rev.*, submitted.
6. H. Dislich, *Angew. Chem., Int. Edn Engl.* 1971, **10**, 363.
7. R. C. Mehrotra, *Mater. Res. Soc. Symp. Proc.* 1988, **121**, 81.

8. K. Jones, T. J. Davies, H. G. Emblem and P. Parks, *Mater. Res. Soc. Symp. Proc.* 1986, **73**, 111.
9. R. C. Mehrotra, *Chemtracts* 1990, **2**, 143.
10. S. Hirano, T. Hayashi, K. Nasaki and K. Kato, *J. Am. Chem. Soc.* 1989, **72**, 707.
11. D. J. Eichorst, D. A. Payne, S. R. Wilson and K. E. Howard, *Inorg. Chem.* 1990, **29**, 1458.
12. R. C. Mehrotra, *J. Non-Cryst. Solids* 1990, **121**, 1.
13. D. C. Bradley, H. Chudzynska, D. M. Frigo, M. B. Hursthouse and M. A. Mazid, *J. Chem. Soc., Chem. Commun.* 1988, 1258.
14. D. C. Bradley, *Chem. Rev.* 1989, **89**, 1317.
15. R. A. Anderson, D. H. Templeton and A. Zalkin, *Inorg. Chem.* 1978, **17**, 1962.
16. O. Poncelet, W. J. Sortain, L. G. Hubert-Pfalzgraf, K. Folting and K. G. Caulton, *Inorg. Chem.* 1989, **28**, 263.
17. O. Poncelet, L. G. Hubert-Pfalzgraf, J. C. Daran and R. Astier, *J. Chem. Soc., Chem. Commun.* 1989, 1846.
18. W. J. Evans, J. M. Olofson and J. W. Ziller, *J. Am. Chem. Soc.* 1990, **112**, 2308 and refs therein.
19. P. B. Hitchcock, M. F. Lappert and I. A. MacKinnon, *J. Chem. Soc., Chem. Commun.* 1988, 1557.
20. R. C. Mehrotra, M. M. Agarwal and A. Mehrotra, *Synth. React. Inorg. Met.-Org. Chem.* 1973, **3**, 181.
21. R. C. Mehrotra, M. M. Agarwal and A. Mehrotra, *Synth. React. Inorg. Met.-Org. Chem.* 1973, **3**, 407.
22. D. C. Bradley, R. C. Mehrotra and W. Wardlaw, *J. Chem. Soc.* 1952, 2027.
23. R. C. Mehrotra, *J. Ind. Chem. Soc.* 1953, **30**, 585.
24. C. N. R. Rao, *Chemical Applications of Infrared Spectroscopy*. Academic Press, New York (1963).
25. C. G. Barraclough, D. C. Bradley, J. Lewis and I. Thomas, *J. Chem. Soc*, 1961, 2601.
26. L. J. Bellamy, *The Infrared Spectra of Complex Molecules*. Methuen, London (1958).
27. L. J. Bellamy, *Advances in Infrared Group Frequencies*. Methuen, London (1968).
28. J. Murphy, H. H. Caspers and R. A. Buchanan, *J. Chem. Phys.* 1964, **40**, 743.
29. M. D. Taylor, T. T. Cheung and M. A. Hussein, *J. Inorg. Nucl. Chem.* 1972, **34**, 3073.
30. F. A. Cotton, D. O. Marler and W. Schwotzer, *Inorg. Chem.* 1984, **23**, 4211.
31. S. Sogani, A. Singh and R. C. Mehrotra, *J. Chem. Soc., Chem. Commun.*, submitted.

Polyhedron Vol. 10, No. 9, pp. 955–961, 1991
Printed in Great Britain

0277–5387/91 $3.00+.00
© 1991 Pergamon Press plc

ON THE SYNTHESIS AND CHARACTERIZATION OF $Cu[C_6H_4(NH)_2]_2$ [$C_6H_4(NH)_2$ = SEMI-BENZOQUINONEDIIMINATE] AS A DONOR PRECURSOR OF THE SEMICONDUCTING AND FERROMAGNETIC $Cu[C_6H_4(NH)_2]_2(I_3)_{1.66}$ CHARGE-TRANSFER COMPLEX

GIAMPAOLO RICCIARDI, ANGELA ROSA, GIANCARLO MORELLI and FRANCESCO LELJ*

Department of Chemistry, University of Basilicata, via N. Sauro, 85–85100 Potenza, Italy

(*Received* 5 *November* 1990; *accepted* 9 *January* 1991)

Abstract—The synthesis and characterization of $Cu[C_6H_4(NH)_2]_2$ [$C_6H_4(NH)_2$ = semi-benzoquinonediiminate, abbreviated s-bqdi] are described and its relevant properties are compared with those of the known d^8 and d^6 metal bis- or tris-benzoquinonediiminate. The complex is paramagnetic in the solid state with μ_{eff} = 1.86 BM. The dominant form of Cu(s-bqdi)$_2$ in aliphatic alcohols like methanol, ethanol and n-butanol or in THF is dimeric or oligomeric, but monomeric in acetonitrile, DMSO and DMF, as proved by UV–vis and ESR spectra. The stability of Cu(s-bqdi)$_2$ to oxygen exposure in different solvents parallels the association behaviour and follows the order: ethanol ≫ DMF ≫ acetonitrile. The electrochemical (voltammetric) response of the $[Cu—N_4]^z$ system ($z = 0, \pm1, \pm2$) in acetonitrile consists of two $0 \rightleftharpoons +1$ ($E_{1/2} = -0.10$ V vs SCE) and $+1 \rightleftharpoons +2$ ($E_{1/2} = +0.98$ V vs SCE) reversible electron transfers and an irreversible process at $E_{p,c} = -1.87$ V attributed to $0 \rightarrow -1$ reduction. Iodination of an ethanolic solution of Cu(s-bqdi)$_2$ led to the isolation of polycrystalline Cu(s-bqdi)$_2$I$_5$ which is formulated as Cu(s-bqdi)$_2$(I$_3$)$_{1.66}$ on the basis of IR, Raman and thermogravimetric analysis. The new material exhibits high, room-temperature conductivity ($\sigma = 6.6 \cdot 10^{-2}$ S cm^{-1}) and semiconducting behaviour in the temperature range 70–300 K, with a sharp transition at 215 K. Static magnetic susceptibility measurements provide μ_{eff} = 1.23 BM for Cu(s-bqdi)$_2$(I$_3$)$_{1.66}$ at 295 K [calculated from $\mu_{eff} = 2.83(\chi T)^{1/2}$] which is found to obey the Curie–Weiss law between 70 and 295 K. The electrical and magnetic behaviour of Cu(s-bqdi)$_2$(I$_3$)$_{1.66}$ is interpreted as being due to strong homomolecular intra- and interstack interactions between donor molecules with radical cationic character.

Considerable efforts are still being carried out to build up new charge-transfer complexes whose stacked packing at the molecular level is the origin of peculiar, low-dimensional, cooperative phenomena. This has been recently carried out by exploring the potential of organometallic donors like decamethylferrocene, $Fe(C_5Me_5)_2$,[1] or by introducing chemical modifications on MPc[2] (Pc = phtalocyanine, M = Cu), or on classical organic donors like tetrathiofulvalene, TTF.[3]

It has been seen that the coupling of new donors with a wide variety of counterions in the oxidized species leads to a fine tunability of the phenomenological properties of these materials.[4–6] In this respect, the [M—N$_4$] open systems like M(s-bqdi)$_2$ (s-bqdi = semi-benzoquinonediiminate, M = transition metals) have not been extensively investigated, due to the difficulties in growing pure crystals both of the starting compounds and of the oxidized species. In some cases, as in Cu(s-bqdi)$_2$, the practical impossibility to extend the synthetic procedure used in the d^8 analogues prevented any investigation in this direction.

Nevertheless, the recent acquisition of more suitable syntheses for the preparation of the α-diiminate

* Author to whom correspondence should be addressed.

complexes[7,8] and our discovery that suitable substitutions on the benzene ring can enhance the electrical conductivity in Ni(s-bqdi)$_2$I$_x$[9] to the values shown by NiPcI$_x$,[10] encouraged us to continue the study of this class of compounds.

The first aim was to verify the effects produced by a d^9 metallic centre in a partially oxidized bis-semi-benzoquinonediiminate context and we successfully attempted a new and reproducible synthetic approach for the title compound. Moreover, we were able to isolate its highly iodinated counterpart Cu(s-bqdi)$_2$I$_5$.

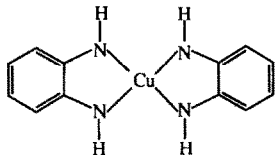

Thus we report here on these results together with the first spectroscopical and electrochemical characterization of Cu(s-bqdi)$_2$ and an overview of the interesting electrical and magnetic properties of Cu(s-bqdi)$_2$I$_5$. These are discussed with respect to the analogous behaviour of charge-transfer complexes in which donors and/or acceptors exhibit radical ionic character.

EXPERIMENTAL

Materials

All chemicals necessary for the syntheses were of reagent grade (Aldrich) and used without further purification. Absolute ethanol was purchased from BDH (Italy) and was kept over 4 Å activated molecular sieves for 24 h before use. Acetonitrile, tetrahydrofuran (THF), N,N′-dimethylformamide (DMF) and dimethylsulphoxide (DMSO) were HPLC or spectroscopic grade and were purified by standard techniques when used for voltammetric studies.

Synthesis of Cu(s-bqdi)$_2$

o-Phenylenediammine (0.50 g, 4.5 mmol) was gently refluxed in 30 cm^3 of absolute ethanol with an equimolar amount of copper acetate monohydrate (0.95 g) under argon. After 1 h, the colour of the solution turned from deep green to deep blue and a dark precipitate rapidly formed. After 3 h, the solution was cooled and filtered. The black–green solid, washed in successive steps with 20 cm^3 of water, methanol and low boiling (40–60°C) petroleum ether, respectively, and again with absolute ethanol, until a colourless washing liquid was obtained, was air-dried at 80°C. Extraction by infusion followed by accurate filtration of the black precipitate in absolute ethanol led to a deep blue–purple solution. Concentration by evaporation under a stream of nitrogen, followed by filtration, afforded green–brown, microcrystalline powders, which were vacuum-dried. Yield, calculated on *o*-phenylenediamine, 30%. Found: C, 52.4; H, 4.3; N, 20.8. Calc: C, 52.3; H, 4.4; N, 20.3%.

The most relevant spectroscopic data are: (a) UV-vis, λ in nm (log ε), ethanol as solvent, sh = shoulder, 652(4.21), 650sh(4.17), 632sh(4.07), 480sh(3.60), 460(3.47), 300sh(3.69), 285sh(3.84), 260sh(3.84), 240sh(4.30), 205sh(4.81); (b) IR, KBr pellets, vs = very strong, m = medium intensity, w = weak, 3320, 3325, 3340 cm^{-1} vs triplet of N—H stretch.; 1590, 1582 cm^{-1}, m, doublet of C=C aromatic stretch.; 1495 cm^{-1}, vs, C=N stretch.; 765 cm^{-1}, vs, out-of-plane bending of aromatic C—H; 452, 475 cm^{-1}, s, doublet of Cu—N stretch.

Synthesis of Cu(s-bqdi)$_2$I$_5$

Cu[C$_6$H$_4$(NH)$_2$]$_2$ (0.200 g) was dissolved in anhydrous ethanol; a 10^{-2} M solution of iodine in the same solvent was slowly added under magnetic stirring to the deep blue solution, until the colour turned to dark red and brilliant crystals started to form; these were collected by filtration and washed with low boiling petroleum ether. Yield, 70%. Found: C, 15.7; H, 1.3; N, 6.0. Calc: C, 15.8; H, 1.3; N, 6.2%.

The most relevant IR data are: 3276 cm^{-1}, vs, N—H stretch.; 1589, m, 1548, 1538 cm^{-1}, s, aromatic C=C stretch.; 1442 cm^{-1}, s, C=N stretch.; 868 cm^{-1}, vs, out-of-plane arom. C—H bend.; 452 cm^{-1}, s, Cu—N stretch.

Physical measurements

Electronic absorption and vibrational spectra were recorded on Cary 2300 and Perkin–Elmer 283B spectrophotometers, respectively. Elemental analyses were performed by H. Malissa and G. Roiter GmbH Analytische Laboratorien, Gummersbach, F.R.G. and by the Engineering Faculty of the Basilicata University. Magnetic susceptibility was determined by the Faraday method using an AZTEC-DSM5 susceptometer operating at 13.5 kG equipped with a Bruker BE15 electromagnet. Four probe dc electrical conductivity measurements at variable temperatures, thermogravimetric analysis and differential thermal analysis were performed as previously described.[9] ESR spectra were recorded with a Bruker 200D spectrometer operating at X-band. Voltammetry recorded at 200 mV s^{-1}

scan rate was performed using a standard H cell and an AMEL 5000 SYSTEM potentiostat galvanostat coupled to a microcomputer. The working electrode was a platinum disc (0.07 cm^2) and a saturated potassium chloride calomel electrode was used as reference. The solutions for spectroelectrochemistry were transferred in ESR capillaries under argon.

RESULTS AND DISCUSSION

Synthesis and spectroelectrochemical characterization of $Cu(s\text{-}bqdi)_2$

It is known that *o*-phenylenediamine (opda) can be deprotonated and oxidized to form the anionic-radical s-bqdi or the neutral diimine molecules o-benzoquinonediimine (bqdi) according to the following scheme:

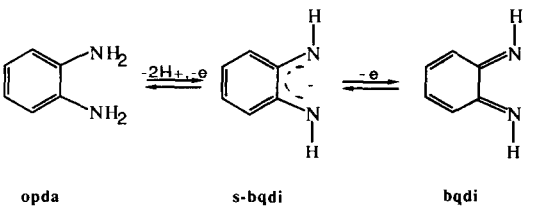

Scheme 1.

The s-bqdi ligand provides square-planar, diamagnetic complexes of d^8 metal ions, with molecular orbitals well delocalized over the entire system.[11,12] These compounds, together with bqdi tris-α-diiminate complexes of d^6 metal ions have been the object of a number of investigations.[13-20] Nevertheless, since the first unambiguous spectroelectrochemical characterization of $M(s\text{-}bqdi)_2$ (M = Co, Ni, Pd, Pt),[13] the synthesis of $Cu(s\text{-}bqdi)_2$ which involves a d^9 metal ion, has been a challenge for many researchers. Yet recently Peng and Liaw[21] believed that $Cu(s\text{-}bqdi)_2$ could be an intermediate of the air oxidation of an acetonitrile solution of $Cu(opda)_2(ClO_4)_2$. To date, only one report concerning the title complex is available.[21] Here, the synthesis of $Cu(s\text{-}bqdi)_2$ is briefly described using the same procedure as used for the nickel analogue. Characterization data for the complex was not reported. Our findings, in accord with those of Balch and Holm[13] show that this method is ineffective. We used the Cu^{2+}/Cu^0 couple as an oxidizing agent for opda in place of oxygen, which is the usual oxidant in the synthesis of $M(s\text{-}bqdi)_2$ complexes. In fact, our results show that oxygen largely affects the stability of $Cu(s\text{-}bqdi)_2$. As a result, black powders of copper and acetic acid, the latter being due to the deprotonating action of the acetate ion on opda, were secondary reaction products. The high electronic affinity of the copper(II) ion has been observed in the oxidation of the cyanide ion to cyanogen[22] and is considered to be the origin of the instability of the $Cu(s\text{-}disn)_2$ complex[8] (s-disn = semi-diiminosuccinonitrile). It is noteworthy that Balch and Holm used the Co^{III}/Co^{II} electron-withdrawing couple to oxidize opda in synthesizing $Co(s\text{-}bqdi)_2$.[13] The solubility, stability and electronic spectra of $Cu(s\text{-}bqdi)_2$ are strongly dependent on the solvent and conditions. $Cu(s\text{-}bqdi)_2$ is easily dissolved in highly boiling solvents like DMSO, DMF and acetonitrile yielding deep green solutions (10^{-2} M). These slowly turn brown and decompose, although to a lesser extent in DMSO and DMF, when air-exposed. The lower solubility of the complex (10^{-3} M) in aliphatic alcohols is coupled to an appreciable stability (approximately 1 week in ethanol). After this time period, open-air evaporation of ethanolic solutions affords a grey precipitate, characterized by microanalysis as 2,3-diaminophenazine, as already found in the disproportionation of $Ni(s\text{-}bqdi)_2^+$.[7,8,14] Comparable stability is found in THF, but solubility in this solvent is scarce ($< 10^{-4}$ M). The electronic spectra of $Cu(s\text{-}bqdi)_2$ in ethanol and in acetonitrile are shown in Fig. 1 as examples of two limiting situations. $Cu(s\text{-}bqdi)_2$ in ethanol displays an intense band at 660 nm, which lies in the wavelength range characteristic of metal–semi-benzoquinonediiminate complexes. Nevertheless, the absorption exhibits shoulders of comparable intensity at 650 and 632 nm. The ethanolic solutions of $Cu(s\text{-}bqdi)_2$ being ESR silent, while the powders are paramagnetic, with $\mu_{eff} = 1.86$ BM consistent with a $S = 1/2$ ground state, may undergo dimerization or oligomerization in this solvent. Similar behaviour has been found in $Co(s\text{-}bqdi)_2$[13] and in $Ni(s\text{-}bqdi)_2$.[12] The multiple

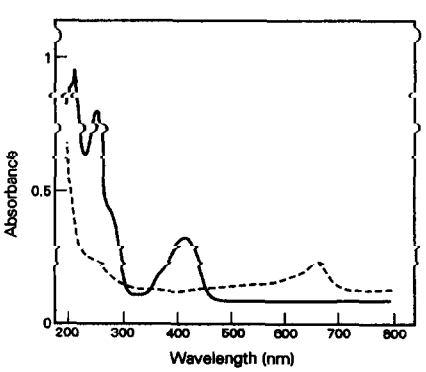

Fig. 1. Electronic absorption spectra of $Cu(s\text{-}bqdi)_2$ in acetonitrile (——) and in ethanol (– – –) at 22±1°C. *Concentrations are* 2.2×10^{-5} *M and* 2.6×10^{-5} *M*, respectively.

absorptions around 650 nm might be attributable to oligomers built with different numbers of monomers. The electronic spectrum of Cu(s-bqdi)$_2$ in acetonitrile displays an intense absorption at 420 nm whose shape appears to be reminiscent of that found at 660 nm in ethanol and is dominated in the UV region by highly intense charge-transfer bands. We note that the electronic spectrum of Cu(s-bqdi)$_2$ in its associated form looks like that of Ni(s-bqdi)$_2$ in acetone and, similarly, the region above 500 nm flattens as the complexes become monomeric, while the UV and the near-UV region is enriched by intense charge-transfer transitions.[12]

This behaviour strengthens the idea that Cu(s-bqdi)$_2$ is in a dimeric form in alcohols and THF, unlike Co(s-bqdi)$_2$ which was found to dimerize both in solution and in polycrystalline powders.[13] Room temperature X-band ESR spectra in DMF show a persistent, although not strong, signal at $g_{iso} = 2.085$. The absorption is further split by hyperfine splittings from ^{63}Cu, with $A_{iso} = 70$ G. The low value of A_{iso} compared with that of other [Cu—N$_4$] systems[23] suggests a large delocalization of the unpaired electron.

The voltammogram of Cu(s-bqdi)$_2$ in acetonitrile, as shown in Fig. 2, exhibits two, fully reversible and monoelectronic waves at $E_{1/2}(1) = -0.10$ V ($i_{p,a}/i_{p,c} = 0.98$, $\Delta E_p = 0.062$ V), $E_{1/2}(2) = 0.98$ V ($i_{p,a}/i_{p,c} = 0.95$, $\Delta E_p = 0.060$ V) vs SCE $\pm$ 0.01 V and a totally irreversible wave with $E_{p,c} = -1.87 \pm 0.01$ V vs SCE. The electrochemical behaviour of the complex in DMSO and DMF retain the same essential features as in acetonitrile. However, some changes, indicative of the strong interactions between the complex and solvents, are noticeable. In DMSO and DMF, the second oxidative process shows a complete loss of its cathodic counterpart, while its position is coincident with that found in acetonitrile [$E_{p,a}(2)$ is 0.94 and 0.90, respectively]. The first oxidation, while becoming quasi-reversible in DMSO and DMF ($\Delta E_p = 0.095$ V), shifts markedly towards positive potentials. The value of $E_{p,a}(1)$ is found to be 0.180 V in DMSO and 0.350 V (vs SCE) in DMF. The considerable influence of the nature of the solvent on the energetics of the first anodic process might be interpreted as due to the strong destabilization of the HOMO orbital in the complex. In this hypothesis, the high donating capability of acetonitrile could be responsible for the lowering of the potential for the removal of the first electron in Cu(s-bqdi)$_2$. The similar donating ability is probably the origin of the stabilization of the cations produced after the first and second oxidation in the voltammetric time scale used. Most likely, the easy oxidizability of the complex when exposed to oxygen in strong donor solvents and the tendency to dimerize in less powerful donors solvents have to be reconciled to the same cause.

ESR characterization of the oxidized species of Cu(s-bqdi)$_2$ was carried out after controlled potential electrolysis of a 10^{-3} M solution in 0.1 M [n-Bu$_4$N][BF$_4$] acetonitrile, 150 mV beyond $E_{1/2}(1)$ and $E_{1/2}(2)$, respectively. For the sake of completeness, we should report that ESR and UV–vis spectra of the final products of a bulk controlled potential electrolysis in DMF or in ethanol looked like that found in acetonitrile. The one-electron removal produced an ESR silent solution, while the

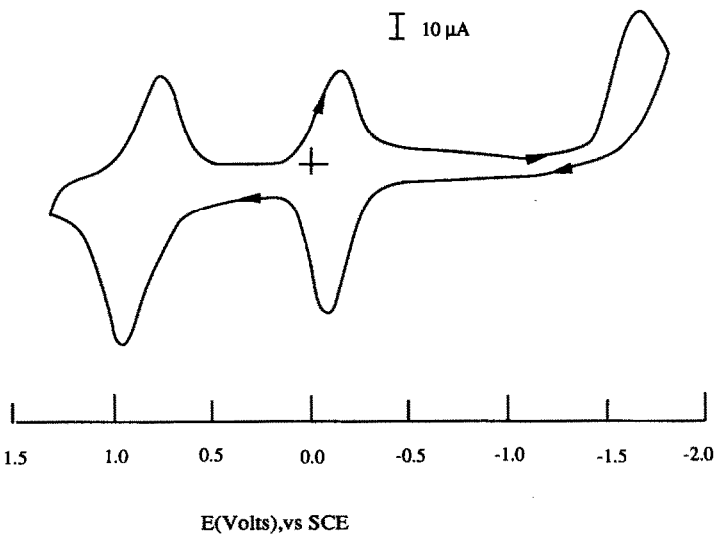

Fig. 2. DC cyclic voltammogram of a 5.0×10^{-4} M solution of Cu(s-bqdi)$_2$; $v = 200$ mV/s; 0.1 M [n-Bu$_4$N][BF$_4$]/CH$_3$CN; Pt disc, E vs SCE.

species resulting from the second oxidation showed a large absorption ($\Delta H = 180$ G) centred at $g = 2.150$. This spectroscopic evidence led us to believe that the first oxidation is essentially centred on copper, while the second one produces a complete rearrangement of the electronic structure of the molecule. As a result, the formation of $Cu(bqdi)_2(BF_4)_2$ can be taken into account. The irreversibility of the reduction at $E_{p,c} = -1.87$ V (vs SCE) can be attributed to the formation of a very reactive and geometrically distorted copper(I) species: due to the high cathodic potential of formation its characterization was impossible. Unlike found in d^8 metal ion s-bqdi complexes, Cu(s-bqdi)$_2$ does not show the complete charge-transfer $[M—N_4]^z$ series, where $z = \pm 2, \pm 1, 0$.

Synthesis, conductivity and magnetic data for Cu(s-bqdi)$_2$I$_5$

As expected, the response of Cu(s-bqdi)$_2$ to iodine was quite dependent on the solvent. Oxidation in acetonitrile, DMF or DMSO afforded red–brown microcrystals that were characterized as $Cu(bqdi)_2I_3$. This compound was found to be diamagnetic and electrically non-conducting ($\sigma_{295K} = 1.8 \times 10^{-9}$ S cm^{-1}). In anhydrous ethanol, very thin, gold, lustrous platelets with almost uniform dimensions ($0.13 \times 0.09 \times 0.005$ mm^3) were isolated. Their composition, checked by microanalysis and DTGA, was found to be $Cu(s\text{-}bqdi)_2I_5$ regardless of the preparative conditions. Polycrystalline samples diffracted very well, but single crystals were not suitable for structural, magnetic and electrical determinations. TGA and DTGA curves of $Cu(s\text{-}bqdi)_2I_5$ in the range 20–300°C are shown in Fig. 3. Two, sharp, almost equivalent iodine losses with maxima at 170 and 245°C were observed. This shaped thermogram was found in highly iodinated $NiPcI_x$,[10] in $(SiOPc)_nI_x$[24] and $Ni(s\text{-}bqdi)_2I_x$,[9] and was interpreted as due to the successive decomposition of I_5^- and I_3^- polyiodide, respectively. Raman spectra of $Cu(s\text{-}bqdi)_2I_5$ showed the intense absorption at 108 cm^{-1} and the superior harmonics of the symmetric I_3^- stretching, but did not reveal the presence of I_5^- or I_2 in the range 150–220 cm^{-1}. Therefore, the two consecutive iodine losses are due to decomposition of structurally distinguishable I_3^- species. In the mixed-valence notation, $Cu(s\text{-}bqdi)_2I_5$ can be written as $Cu(s\text{-}bqdi)_2(I_3)_{1.66}$: this evidences the incomplete oxidation of the starting complex. Surprisingly, the room temperature conductivity of $Cu(s\text{-}bqdi)_2I_5$ (6.6×10^{-2} S cm^{-1}) is 10^3–10^4 times greater than that found for $Ni(s\text{-}bqdi)_2I_x$ powders.[9,16] The conductivity is activated in the range 80–300 K and the values fit the Arrhenius-like relation $\sigma = \sigma^0 e^{-E_a/kT}$, where k = Boltzmann constant and $E_a = 0.10$ eV from 300 to ~215 K; at this temperature, as shown in Fig. 4, a transition is observed, indicating a slower diminution of the conductivity. This could be due to the creation of defects by cracking processes on crystals at lower temperatures. In fact, while the conductivity data in the range 300–215 K, obtained by cooling the sample, are reproduced on warming, the same does not occur in the range 200–70 K. On the other hand, at the same temperature we did not find similar magnetic behaviour (*vide infra*). Static magnetic susceptibility measurements on $Cu(s\text{-}bqdi)_2I_5$ gave

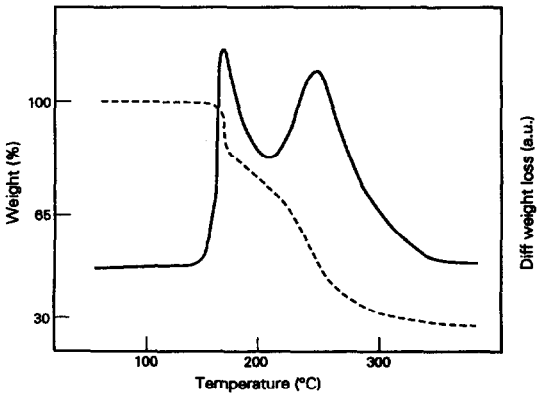

Fig. 3. TGA (– – –) and DTGA (——) of $Cu(s\text{-}bqdi)_2I_5$. Initial weight = 8.7 mg; heating rate = 20° min^{-1}.

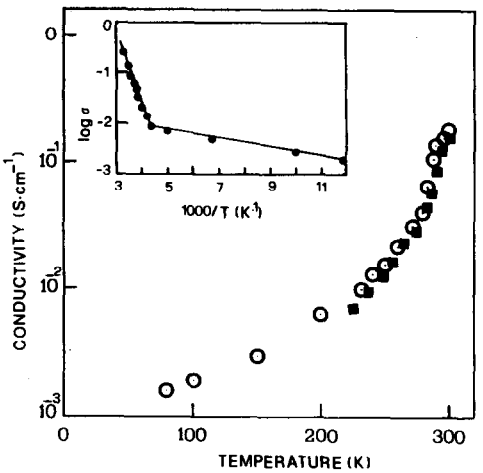

Fig. 4. Four probe DC electrical conductivity of $Cu(s\text{-}bqdi)_2I_5$ plotted vs temperature (○) obtained by cooling the sample from 300 to 70 K. The reversible values of the conductivity obtained by warming the sample in the range 200–300 K are also shown (■). Inset: log σ is reported as a function of $1000/T$.

$\mu_{eff} = 1.23$ BM at 295 K [calculated from $\mu_{eff} = 2.83(\chi T)^{1/2}$], which is consistent with 2/3 unpaired electrons per Cu(s-bqdi)$_2^{1.66+}$ molecular unit in the spin-only approximation. This value is coincident with that calculated on the basis of the ionic formula.

A similar distribution of the unpaired electrons, owing to the electrochemical behaviour of the complex, might imply the formation of alternate diamagnetic [Cu(s-bqdi)$_2$]$^+$ and radical [Cu(s-bqdi)$_2$]$^{+\cdot}$ cationic species. The radical character of [Cu(s-bqdi)$_2$]$^{+\cdot}$ implies that a formal oxidation state of +3 can be assumed for the copper centre and the ligand localization of the unpaired electron. The ESR spectrum of Cu(s-bqdi)$_2$I$_5$ shows a unique signal centred at $g = 2.064$. This value seems to suggest that there is a strong interaction between hypothetical copper(II) centres and unpaired electrons located on the α-diiminate frame. This could be achieved by an internal redox process between adjacent donor molecules. Cu(s-bqdi)$_2$I$_5$ is ferromagnetic given that, as shown in Fig. 5, χT increases as T decreases. Attempts to fit the experimental data show that the compound obeys the Curie–Weiss law between 70 and 295 K with $\theta = 28 \pm 5$ K. The value of θ is indicative of relatively strong coupling in this temperature range. Since the first elaboration of a physical model for ferromagnetism in charge-transfer complexes by McConnell in 1963,[25] only a limited number of experimental situations have been well characterized. Dominant ferromagnetic interactions have been found in tetrathiofulvalene platinum bis(*cis*-1,2-ditrifluoromethylene-1,2-dithienate) (TTF)[Pt(S$_2$C$_2$(CF$_3$)$_2$],[26] between 270 and 40 K, and more recently in decamethylferrocenium tetracyanoethenide, [(C$_5$Me$_5$)]$^+$[TCNE]$^{-\cdot}$.[1] Both these compounds have paramagnetic donors (D) and acceptors (A) stacked in a ...DADA... sequence and show strong intra- and interchain interactions.

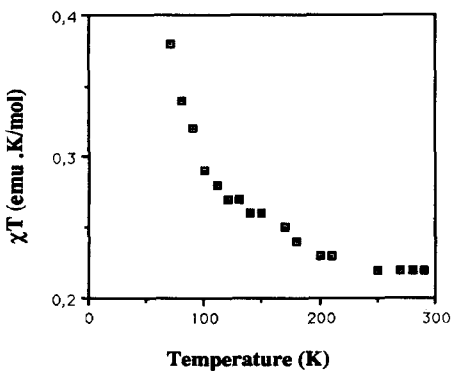

Fig. 5. Experimental values of χT plotted vs temperature for Cu(s-bqdi)$_2$I$_5$.

Owing to the diamagnetism of I_3^-, the magnetic behaviour of Cu(s-bqdi)$_2$I$_5$ is similar to that of ditetrabutylammonium copper maleonitride, [n-Bu$_4$N]$_2$[Cu(mnt)$_2$],[27] where stacks of paramagnetic, square-planar [Cu(mnt)$_2$]$^{2-}$ units are separated by [n-Bu$_4$N]$^+$ cations. However, the ferromagnetic coupling in Cu(s-bqdi)$_2$I$_5$ suggests that interactions between Cu(s-bqdi)$_2^{1.66+}$ radical cations are considerably stronger and, probably, not negligible in bidimensional directions, as supported by the strongly exchange-coupled ESR signal ($\Delta H = 70$ G) and by the partial loss of resolution of the most important IR absorptions. On the other hand, homomolecular ferromagnetic coupling due to disproportion of the donor molecules, is not excluded by McConnell, and this model has been found to rationalize ferromagnetism in [(C$_5$Me$_5$)]$^{\cdot+}$ [TCNE]$^{-\cdot}$ also.

Summarizing, the results allow us to conclude that:

(i) the first complete characterization data set on Cu(s-bqdi)$_2$ shows unambiguously that it belongs to the metal ion semi-benzoquinonediiminate complexes that, from an electrochemical point of view, are confirmed to be the counterparts of metal dithiolenes in the oxidative field; however the insertion of a d^9 metal centre into the diiminate square-planar environment enriches the properties of this class of compounds;

(ii) chemical oxidation of Cu(s-bqdi)$_2$ provides a compound with extremely promising electrical and magnetic properties.

Furthermore, electrical conductivity and magnetical data for Cu(s-bqdi)$_2$I$_5$ show that [M—N$_4$] open systems can be compared at least with [M—S$_4$] charge-transfer complexes. Nevertheless, structural order and stoichiometries, though basic requirements, are very far from their optimization. Attempts to grow crystals of Cu(s-bqdi)$_2$I$_5$ suitable for structural investigations and the characterization of similar charge-transfer complexes using paramagnetic counteranions are currently in progress in our laboratory.

Acknowledgements—This work was partially supported by the Italian National Research Council (CNR), "Progetto Finalizzato: Materiali Speciali per Tecnologie Avanzate". We would like to thank Mr Claudio Barlaba' for technical support.

REFERENCES

1. J. S. Miller, J. C. Calabrese, H. Rommelmann, S. R. Chittipeddi, J. H. Zhang, W. M. Reiff and A. J. Epstein, *J. Am. Chem. Soc.* 1987, **109**, 769.
2. K. Liou, M. Y. Ogawa, T. P. Newcomb, G. Quirion,

M. Lee, M. Poirier, W. P. Halperin, B. M. Hoffman and J. Ibers, *Inorg. Chem.* 1989, **28**, 3889.
3. M. A. Beno, H. H. Wang, A. M. Kini, K. D. Carlson, U. Geiser, W. K. Kwok, J. E. Thompson, J. M. Williams, J. Ren and M. H. Whangbo, *Inorg. Chem.* 1990, **29**, 1601.
4. D. B. Morse, *Chem. Mater.* 1990, **2**, 33.
5. A. Pénicaud, P. Batail, P. Davidson, A. M. Levelut, C. Coulon and C. Perrin, *Chem. Mater.* 1990, **2**, 117.
6. A. Pénicaud, P. Batail, C. Coulon, E. Canadell and C. Perrin, *Chem. Mater.* 1990, **2**, 123.
7. S. M. Peng and D. S. Liaw, *Inorg. Chim. Acta* 1986, **113**, L11.
8. P. H. Cheng, H. Y. Cheng, C. C. Lin and S. M. Peng, *Inorg. Chim. Acta* 1990, **169**, 19.
9. F. Lelj, G. Morelli, G. Ricciardi, M. F. Brigatti and A. Rosa, *Polyhedron* 1989, **8**, 2603.
10. C. J. Schramm, R. P. Scaringe, D. R. Stojakovic, B. M. Hoffman, J. A. Ibers and T. J. Marks, *J. Am. Chem. Soc.* 1980, **102**, 6702.
11. J. Weber, C. Daul, A. von Zelewsky, A. Goursot and E. Pennigault, *Chem. Phys. Lett.* 1982, **88**, 78.
12. F. Lelj, A. Rosa, G. P. Ricciardi, M. Casarin, P. L. Cristinziano and G. Morelli, *Chem. Phys. Lett.* 1989, **160**, 39.
13. A. L. Balch and R. H. Holm, *J. Am. Chem. Soc.* 1966, **88**, 5201.
14. M. G. Miles and J. D. Wilson, *Inorg. Chem.* 1975, **14**, 2357.
15. G. S. Hall and R. Soderberg, *Inorg. Chem.* 1968, **7**, 2300.
16. Y. M. Wuu and S. M. Peng, *J. Inorg. Nucl. Chem.* 1980, **42**, 205.
17. M. L. Hsieh, M. C. Cheng and S. M. Peng, *Inorg. Chim. Acta* 1988, **145**, 1.
18. M. Zehnder and H. Loliger, *Helv. Chim. Acta* 1980, **63**, 754.
19. P. Belser, A. von Zelewsky and M. Zehnder, *Inorg. Chem.* 1981, **20**, 3098.
20. L. Warren, *Inorg. Chem.* 1977, **16**, 2814 and refs therein.
21. H. Hara, K. Nakamura and Y. Suzuki, *Belg. Pat.* 872,002 (Cl. 09K) (1 March 1979).
22. F. A. Cotton and G. Wilkinson, in *Advanced Inorganic Chemistry*. Wiley, New York (1980).
23. K. Sakata, M. Hashimoto, N. Tagami and Y. Murakami, *Bull. Chem. Soc. Jpn* 1980, **53**, 2262 and refs therein.
24. B. N. Diel, T. Inabe, J. W. Lyding, K. F. Schoch Jr, C. R. Kannewurf and T. J. Marks, *J. Am. Chem. Soc.* 1983, **105**, 1551.
25. H. M. McConnell, *J. Phys. Chem.* 1963, **39**, 1910.
26. I. S. Jacobs, L. V. Interrante and H. R. Hart Jr, AIP *Conf. Proc.* 1974, **24**, 355.
27. L. Alcacer and H. Novais, in *Extended Linear Chain Compounds* (Edited by J. S. Miller), Vol. 3, Ch. 6. Plenum Press, New York (1983) and refs therein.

Polyhedron Vol. 10, No. 9, pp. 963–972, 1991
Printed in Great Britain

0277–5387/91 $3.00+.00
© 1991 Pergamon Press plc

A COMPARATIVE STUDY OF THE REACTIVITY OF SOME DINUCLEAR ALKANEDIYL COMPLEXES OF THE TYPE $[L(CO)_2M(CH_2)_nM(CO)_2L]$ (WHERE M = Fe AND L = η^5-C_5H_5, η^5-C_5H_4Me OR η^5-C_5Me_5 AND n = 4–6 OR M = Ru AND L = η^5-C_5H_5 AND n = 5)

KAROL P. FINCH, MANSOOR A. GAFOOR, SELWYN F. MAPOLIE and JOHN R. MOSS†

Chemistry Department, University of Cape Town, Rondebosch 7700, South Africa

(*Received* 27 *November* 1990; *accepted* 9 *January* 1991)

Abstract—Some reactions of the μ-(α,ω)alkanediyl complexes of the type $[L(CO)_2M(CH_2)_nM(CO)_2L]$ with both nucleophiles and electrophiles have been investigated. Reaction of the di-iron compounds $[L(CO)_2Fe(CH_2)_nFe(CO)_2L]$ with neutral donor ligands (D) gives $[LD(CO)FeC(O)(CH_2)_nC(O)Fe(CO)DL]$ [where L = η^5-C_5H_4Me (Cp′), D = $PMePh_2$, PMe_2Ph or t-BuNC and n = 4 or 6; L = η^5-C_5Me_5 (Cp*), D = CO and n = 4]. Reactions of the di-iron compounds with SO_2 yield disulphinato derivatives $[L(CO)_2Fe(SO_2)(CH_2)_4(SO_2)Fe(CO)_2L]$ (L = Cp′ or Cp*). Halogens cause cleavage of the M—C bonds to give $LM(CO)_2X$ and $X(CH_2)_nX$ (M = Fe, L = Cp′ or Cp*, X = Br or I and n = 4–6; M = Ru, L = Cp, X = Br or I and n = 5). Reactions of the di-iron or diruthenium compounds with Ph_3CPF_6 yield the cationic alkene, alkyl complexes $[L(CO)_2M\{\mu$-$(C_nH_{2n-1})\}M(CO)_2L]PF_6$ (M = Fe, L = Cp or Cp* and n = 4 or 6; M = Ru, L = Cp and n = 5). The diruthenium complex $[Cp(CO)_2Ru(CH_2)_5Ru(CO)_2Cp]$ reacts with ligands (D) to give the monosubstituted monoacyl compound $[Cp(CO)_2Ru(CH_2)_5C(O)Ru(CO)DCp]$ and the disubstituted diacyl compound $[CpD(CO)RuC(O)(CH_2)_5C(O)Ru(CO)DCp]$ (D = PPh_3, $PMePh_2$ or PMe_2Ph). The reactions are compared with those found for the di-iron compounds $[Cp(CO)_2Fe(CH_2)_nFe(CO)_2Cp]$ as well as mononuclear alkyl analogues.

There is currently much interest in hydrocarbon-bridged dinuclear metal complexes.[1–4] We are particularly interested in trying to determine the factors that can affect the reactivity of complexes of the type $[L_mM(CH_2)_nML_m]$ (where L_mM is a metal with its associated ligands). A particular class of compounds of this type are the bis(cyclopentadienyl metal dicarbonyl) alkanediyl compounds $[L(CO)_2M(CH_2)_nM(CO)_2L]$. Here there is the opportunity to vary the metal (M), the cyclopentadienyl ligand (L) and the length of the polymethylene chain (n) and to see what effect changing these parameters has on the reactivity of the complexes.

We have previously reported the synthesis,[5] structure[6] and reactivity[7] of some of the complexes $[Cp(CO)_2Fe(CH_2)_nFe(CO)_2Cp]$ [where Cp = η^5-C_5H_5, η^5-C_5H_4Me (Cp′) and η^5-C_5Me_5 (Cp*)] as well as the ruthenium compounds $[Cp(CO)_2Ru(CH_2)_nRu(CO)_2Cp]$ (n = 5–10).[8] We now report results of our reactivity studies on some of these alkanediylbridged dinuclear complexes.

EXPERIMENTAL

All reactions were carried out in Schlenk tubes under an atmosphere of nitrogen. General experimental methods have been described previously.[7] IR spectra were recorded on a Perkin–Elmer 983 spectrophotometer and NMR spectra on a Brucker WH 90 or a Varian VXR 200 spectrometer using tetramethylsilane as standard (δ 0.00 ppm). The compound $[CpRu(CO)_2]_2$ was prepared by the method of Doherty and Knox.[9] $[Cp'Fe(CO)_2]_2$ and $[Cp^*Fe(CO)_2]_2$ were obtained from Strem. The alkanediyl compounds $[L(CO)_2Fe(CH_2)_n(CO)_2L]$

† Author to whom correspondence should be addressed.

(L = Cp,[5] Cp′[10] or Cp*[10]) and $[Cp(CO)_2Ru(CH_2)_nRu(CO)_2Cp]$[8] were prepared as previously described. Yields and characterization data for the new compounds are given in Table 1.

Reactions with neutral donor ligands

(i) $[Cp'(CO)_2Fe(CH_2)_4Fe(CO)_2Cp']$ (**1**) *with tertiary phosphines.* A solution containing **1** (0.46 mmol) and PR_3 (0.92 mmol) in THF (15 cm^3) was heated under reflux (17 h for $PMePh_2$, 12 h for PMe_2Ph) until no further change was observed in the IR spectrum in the ν(CO) region. The solvent was removed under reduced pressure and the resulting residue extracted with hexane (30 cm^3), filtered, concentrated and cooled to give yellow–orange solids $[Cp'(CO)(PR_3)FeC(O)(CH_2)_4C(O)Fe(CO)$

Table 1. Yields and characterization data for new compounds

Compound	Yield (%)	Melting point (°C)	Elemental[a] analysis	IR[b] ν(CO)	NMR[c] ($CDCl_3$)
2	73	142–148	C, 65.7 (65.9) H, 5.4 (5.8)	1905s 1590m	7.32(20H, br m, P—Ph) 4.15(8H, br s, C_5H_4—Me) 2.47(4H, br m, CH_2CO) 1.85(6H, d, P—Me, J_{PH} = 9 Hz) 1.31(6H, s, *Me*—C_5H_4) 1.02(4H, br m, CH_2)
3	80	97–102	C, 60.3 (60.5) H, 5.9 (6.2)	1905s 1590m	7.38(10H, br m, P—Ph) 4.13(8H, br s, C_5H_4—Me) 2.72(4H, br m, CH_2CO) 1.78(12H, d, P—Me, J_{PH} = 9 Hz) 1.44(6H, s, *Me*—C_5H_4) 1.31(4H, br m, CH_2)
5	25	71-76	C, 59.7 (59.4) H, 6.2 (6.3)	2001s 1943vs	2.77(4H, t, CH_2—CO) 1.76(30H, s, Me) 1.48(4H, m, CH_2)
6	79	Oil	C, 59.2 (59.6) H, 6.6 (6.7) N, 4.6 (4.6)	1937vs 1610m 2125s[d] 2076sh[d]	4.35(8H, m, C_5H_4—Me) 2.74(4H, t, CH_2CO) 1.86(6H, s, *Me*—C_5H_4) 1.42(18H, s, t-BuNC) 1.40(4H, m, CH_2)
8	53	Oil	C, 60.4 (60.8) H, 6.2 (7.0) N, 4.7 (4.4)	1936vs 1608m 2128s[d] 2080sh[d]	4.42(8H, m, C_5H_4—Me) 2.74(4H, t, CH_2CO) 1.86(6H, s, *Me*—C_5H_4) 1.44(18H, s, t-BuNC) 1.30(4H, m, CH_2CH_2CO) 0.86(4H, m, $CH_2CH_2CH_2CO$)
10	91	Oil	C, 59.0 (59.0) H, 6.1 (6.5) N, 4.7 (4.7)	1945s[e] 1636m[e] 2114m[d,e] 2080sh[d,e]	4.59(5H, s, C_5H_5) 2.78(4H, t, CH_2CO) 1.46(18H, s, t-BuNC) 1.40(4H, m, CH_2CH_2CO) 1.14(2H, m, CH_2) 269.6(CO) 218.6($COCH_2$) 166.4(Fe—CN) 84.6(C_5H_5) 64.9($COCH_2$) 57.4(t-BuNC) 30.9(t-*Bu*NC) 28.9(CH_2) 25.1(CH_2CH_2CO)

Table 1—*continued*

Compound	Yield (%)	Melting point (°C)	Elemental[a] analysis	IR[b] ν(CO)	NMR[c] ($CDCl_3$)
12	46	42–48	C, 57.1 (57.2) H, 4.6 (4.5)	2010m 1943m 1922m 1600m	7.47(15H, PPh_3) 5.14[5H, C_5H_5—$Ru(CO)_2$] 4.90[5H, C_5H_5—$Ru(CO)(PPh_3)$] 2.43(1H, H_A)[f] 2.16(1H, $H_{A'}$)[f] 1.19(2H, $H_B/H_{B'}$) 0.82(6H, $CH_2CH_2CH_2Fe$) 256.2(d, $COCH_2$) 205.6(d, CO) 135.3(d, PPh_3)[g] 133.0(d, PPh_3)[g] 129.4(s, PPh_3)[g] 127.5(d, PPh_3)[g] 88.5[C_5H_5—$Ru(CO)_2$] 88.3[C_5H_5—$Ru(CO)(PPh_3)$] 65.6(CH_2CO) 39.4(CH_2CH_2Ru) 29.4(CH_2CH_2CO) 24.3($CH_2CH_2CH_2CO$) −3.5(CH_2—Ru)
13	77	95–102	C, 63.0 (63.6) H, 4.8 (4.9)	1922s 1603m	7.43(30H, PPh_3) 4.94(10H, C_5H_5) 2.44(2H, H_A)[f] 2.10(2H, $H_{A'}$)[f] 1.09(2H, H_B)[f] 0.75(2H, $H_{B'}$)[f] 0.67(2H, H_C)[f] 255.8(d, $COCH_2$) 205.6(d, CO) 135.8(d, PPh_3)[g] 132.9(d, PPh_3)[g] 129.4(s, PPh_3)[g] 127.5(d, PPh_3)[g] 88.3(C_5H_5) 65.5(CH_2Ru) 24.5(CH_2CH_2Ru) 28.3($CH_2CH_2CH_2Ru$)
14	9		*	2017m[e] 1959s[e] 1933m[e] 1600m[e]	*
15	67	50–56	C, 58.9 (59.1) H, 5.1 (5.1)	1920vs 1592m	7.36(20H, $PMePh_2$) 4.94(10H, C_5H_5) 2.29(2H, H_A)[f] 1.95(2H, $H_{A'}$)[f] 1.15(2H, H_B)[f] 0.98(2H, $H_{B'}$)[f] 0.69(2H, H_C)[f] 2.00(6H, Me) 257.2(d, $COCH_2$) 204.9(d, CO) 138.3(d, $PMePh_2$)[g] 137.3(d, $PMePh_2$)[g] 131.9(d, $PMePh_2$)[g]

Table 1—*continued*

Compound	Yield (%)	Melting point (°C)	Elemental[a] analysis	IR[b] ν(CO)	NMR[c] ($CDCl_3$)
					131.0(d, $PMePh_2$)[g] 129.5(s, $PMePh_2$) 129.1(s, $PMePh_2$) 127.8(d, $PMePh_2$)[g] 127.6(d, $PMePh_2$)[g] 87.6(C_5H_5) 65.1(CH_2Ru) 24.7(CH_2CH_2Ru) 28.4($CH_2CH_2CH_2Ru$) 17.5(d, Me)[g]
16	90	Oil	C, 53.7 (53.5) H, 5.6 (5.4)	1922s 1605m	7.52(10H, PMe_2Ph) 4.93(10H, C_5H_5) 2.65(2H, H_A)[f] 2.48(2H, $H_{A'}$)[f] 1.36(4H, H_B)[f] 1.07(2H, H_C)[f] 1.55(6H, Me) 1.77(6H, Me) 258.1(d, $COCH_2$) 205.2(d, CO) 139.8(d, PMe_2Ph)[g] 129.4(d, PMe_2Ph)[g] 128.4(s, PMe_2Ph) 128.0(d, PMe_2Ph)[g] 87.1(C_5H_5) 65.9(CH_2Ru) 24.9(CH_2CH_2Ru) 28.6($CH_2CH_2CH_2Ru$) 19.2(d, Me)[g] 18.2(d, Me)[g]
17	53	169–173	C, 41.9 (42.4) H, 3.7 (3.9)	2054vs[h] 2005s[h] 1996m[ij] 1040m[ij]	5.12(4H, br s, C_5H_4—Me) 4.86(4H, br s, C_5H_4—Me) 3.06(4H, br t, CH_2SO_2) 2.00(6H, s, Me) 1.96(4H, br m, CH_2)
18	52	203–211	C, 49.2 (49.6) H, 5.6 (5.6)	2024s 1975s 1882m[j] 1038m[j]	2.96(4H, br t, CH_2SO_2) 1.86(30H, s, Me) 1.68–1.26(4H, br m, CH_2)
19	43	115–123 decomp.	C, 41.1 (41.3) H, 3.3 (3.6)	2068s 2030s 1997s 1937s	5.37(4H, br d, C_5H_4—Me) 5.26(1H, br m, =CH) 5.58(4H, br d, C_5H_4—Me) 3.62(1H, d, $=CH_2$, J = 7.5 Hz) 3.06(1H, d, $=CH_2$, J = 14 Hz) 2.32(2H, m, CH_2) 2.03(3H, s, Me) 1.86(3H, s, Me) 1.17(2H, m, CH_2Fe)
20	53	108–113 decomp.	C, 42.9 (43.3) H, 3.9 (4.1)	2070s 2032s 1997vs 1936vs	5.36(4H, br s, C_5H_4—Me) 5.27(1H, br m, =CH) 4.52(4H, br d, C_5H_4—Me) 3.64(1H, d, $=CH_2$, J = 8 Hz) 3.22(1H, d, $=CH_2$, J = 14 hz)

Table 1—*continued*

Compound	Yield (%)	Melting point (°C)	Elemental[a] analysis	IR[b] ν(CO)	NMR[c] ($CDCl_3$)
					2.36(2H, br m, CH_2—CH=CH_2) 1.36(4H, br m, CH_2) 0.90(2H, br m, CH_2Fe)
21	53	158–164 decomp.	C, 48.7 (48.4) H, 5.4 (5.4)	2052vs 2013s 1983s 1925vs	3.98(1H, br m, =CH) 3.08(1H, d, =CH_2, J = 8 hz) 2.76(1H, d, =CH_2, J = 14 Hz) 1.88(15H, s, C_5Me_5—Fe^+) 1.70(15H, s, C_5Me_5—Fe) 2.14(2H, br m, CH_2—CH=CH_2) 1.15(2H, br m, CH_2Fe)
22	70	141–145	C, 34.3 (34.7) H, 2.9 (2.9)	2082s 2039s 2012s 1948s	6.15(5H, s, C_5H_5—Ru^+)[k] 5.43(5H, s, C_5H_5—Ru) 4.00(1H, d, =CH_2, J_{cis} = 8 Hz) 3.93(1H, d, =CH_2, J_{trans} = 14 hz) 2.8–1.7(6H, m, CH_2) the resonance due to =CH was not resolved 92.2(C_5H_5—Ru^+)[k] 89.8(C_5H_5—Ru) 86.5(=CH) 51.6(=CH_2) 43.7(=CHCH_2) 43.0(CH_2CH_2Ru) −4.7(CH_2Ru) the CO resonances were not resolved
23	68	ref. 11	ref. 11	2073s 2037s 2003s 1943s	5.87(5H, s, C_5H_5—Fe^+)[k] 5.29(1H, m, =CH) 4.92(5H, s, C_5H_5—Fe) 4.00(1H, br d, =CH_2, J_{cis} = 7 Hz) 3.56(1H, br d, =CH_2, J_{trans} = 13 Hz) 1.51(4H, m, $CH_2CH_2CH_2Fe$) 1.10(2H, m, CH_2Fe) 92.1(C_5H_5—Fe^+)[k] 89.1(=CH_2) 86.7(C_5H_5—Fe) 54.7(=CH_2) 42.4(=CHCH_2) 42.2(CH_2CH_2Fe) 2.6(CH_2Fe) the CO resonances were not resolved.

[a] Calculated values in parentheses.
[b] Measured in CH_2Cl_2 unless otherwise stated.
[c] Measured in $CDCl_3$.
[d] Due to ν(CN).
[e] Measured in hexane.
[f] $H_A/H_{A'}$, $H_B/H_{B'}$ and H_C represent the geminal methylene protons of the alkyl chain.
[g] Signals occur as doublets due to ^{31}P coupling.
[h] Measured in $CHCl_3$.
[i] Measured in Nujol.
[j] Due to ν(SO)
[k] Measured in acetone-d_6.
* Data not obtained.

$(PR_3)Cp']$ (**2**) ($PR_3 = PMePh_2$) and (**3**) ($PR_3 = PMe_2Ph$).

(ii) $[Cp^*(CO)_2Fe(CH_2)_4Fe(CO)_2Cp^*]$ (**4**) *with* CO. A solution of **4** (0.05 g) in THF (6 cm^3) was placed in an autoclave which was then charged with CO (30 atm). The reaction mixture was stirred at room temperature for 23 h, after which time the gases were vented and the reaction mixture evaporated to dryness. The resulting solid was dissolved in CH_2Cl_2 and chromatographed on an alumina column. The first yellow band was identified as **4** (70%) and a second, bright yellow band gave the yellow solid diacyl compound **5**.

(iii) *Compound* **1** *with* t-BuNC. A solution containing **1** (0.10 g, 0.23 mmol) and t-BuNC (0.038 g, 0.46 mmol) in THF (10 cm^3) was heated under reflux until no further change occurred in the IR spectrum (43 h). The solvent was removed under reduced pressure and the residue extracted with hexane, filtered and the filtrate cooled to $-78°C$. A yellow–orange precipitate of **6** formed which melted to an oil below room temperature.

(iv) $[Cp'(CO)_2Fe(CH_2)_6Fe(CO)_2Cp']$ (**7**) *with* t-BuNC. In a similar way, the reaction of **7** (0.11 g, 0.24 mmol) with t-BuNC (0.04 g, 0.48 mmol) in THF (10 cm^3) gave **8** as an orange–yellow oil.

(v) $[Cp(CO)_2Fe(CH_2)_5Fe(CO)_2Cp]$ (**9**) *with* t-BuNC. In a similar way, the reaction of **9** (0.19 g, 0.45 mmol) with t-BuNC (0.074 g, 0.89 mmol) in THF (20 cm^3) (after 22 h) gave **10** as an orange–yellow oil.

Reaction of $Cp(CO)_2Ru(CH_2)_5Ru(CO)_2Cp]$ (**11**) with t-BuNC in refluxing xylene for 21 h gave $[Cp(CO)(t\text{-BuNC})Ru(CH_2)_5Ru(t\text{-BuNC})(CO)Cp]$ (20%), identified by its IR only; ν(CN) 2156 m and 2117 m, ν(CO) 1969 m cm^{-1}.

(vi) *Compound* **11** *with* PPh_3. Compound **11** (0.17, 0.33 mmol) and PPh_3 (0.17 g, 0.66 mmol) in xylene (15 cm^3) were heated under reflux for 165 h. The solvent was removed under reduced pressure and the residue taken up in CH_2Cl_2 and chromatographed on a Florisil column. Elution with CH_2Cl_2/hexane (1 : 1) gave a pale yellow band from which yellow microcrystals of $[Cp(CO)_2Ru(CH_2)_5C(O)Ru(CO)(PPh_3)Cp]$ (**12**) (0.07 g, 23%) were obtained. [Compound **12** was obtained in yields up to 46% on using shorter reaction times (17 h) with a 1 : 1 molar ratio of compound **11** : PPh_3]. Elution with CH_3OH gave a yellow band from which **13** was isolated as pale yellow crystals. Compounds **12** (31%) and **13** (14%) were obtained on refluxing **11** with PPh_3 (1 : 2) in CH_3CN for 10 days.

(vii) *Compound* **11** *with* $PMePh_2$. Similarly, from the reaction of **11** (0.25 g, 0.49 mmol) with $PMePh_2$ (0.20 g, 1.0 mmol) on refluxing in xylene (20 cm^3) for 92 h were isolated orange $[Cp(CO)_2Ru(CH_2)_5C(O)Ru(CO)(PMePh_2)Cp]$ (**14**) (0.03 g, 9%) and pale yellow microcrystals of **15**.

(viii) *Compound* **11** *with* PMe_2Ph. Similarly, the reaction of **11** (0.17 g, 0.32 mmol) with PMe_2Ph (0.10 g, 0.23 mmol) on refluxing in xylene (15 cm^3) for 21 h gave **16** as a yellow oil.

Reactions with sulphur dioxide

(i) *Compound* **1** *with* SO_2. A Carius tube was charged with **1** (0.10 g, 0.23 mmol) and liquid SO_2 (10 cm^3), sealed with its Teflon tap and the mixture stirred at room temperature for 21 h. The tube was opened and the SO_2 allowed to evaporate leaving a red–brown residue. This was extracted with $CHCl_3$, filtered and the filtrate cooled to $-15°C$ to give **17** as a yellow, microcrystalline solid.

(ii) *Compound* **4** *with* SO_2. In a similar way, reaction of **4** (0.06 g, 0.12 mmol) with liquid SO_2 (10 cm^3) gave, after 8 h at room temperature, compound **18** as yellow microcrystals.

Reactions with halogens

(i) *Compound* **1** *with* X_2 (X = Br *or* I). A solution of Br_2 (0.26 mmol) in THF (2 cm^3) was added to a solution of **1** (0.13 mmol) in THF (5 cm^3) and the red–brown reaction mixture was stirred at room temperature for 10 min. The solvent was removed under reduced pressure leaving a brown residue which was dissolved in CH_2Cl_2 and chromatographed on an alumina column made up with hexane. Elution with hexane gave a pale yellow band which resulted in an almost colourless oil on removal of the solvent. This was identified as $Br(CH_2)_4Br$ by comparison of its IR and ^1H NMR spectra with that of an authentic sample. Elution with CH_2Cl_2 gave a red band which yielded a dark red solid on removal of solvent, this solid showed identifical IR and ^1H NMR spectra to an authentic sample of $Cp'Fe(CO)_2Br$ (85%). Similar reactions of $[Cp'(CO)_2Fe(CH_2)_5Fe(CO)_2Cp']$ with X_2 yielded $X(CH_2)_5X$ and $Cp'Fe(CO)_2Br$ (76%) or $Cp'Fe(CO)_2I$ (69%), where X = Br or I, respectively.

(ii) *Compound* **4** *with* X_2 (X = Br *or* I). In a similar way, reaction of **4** with X_2 gave $X(CH_2)_4X$ and $Cp^*Fe(CO)_2Br$ (93%) and $Cp^*Fe(CO)_2I$ (80%), where X = Br or I, respectively. Similar reactions of $[Cp^*(CO)_2Fe(CH_2)_6Fe(CO)_2Cp^*]$ with X_2 gave $X(CH_2)_6X$ and $Cp^*Fe(CO)_2Br$ (73%) and $Cp^*Fe(CO)_2I$ (69%), where X = Br or I, respectively.

(iii) *Compound* **11** *with* X_2 (X = Br *or* I). In a similar way, reaction of **11** with X_2 gave $X(CH_2)_5X$ (> 90%) and $CpRu(CO)_2Br$ (91%) and $CpRu(CO)_2I$ (86%), where X = Br or I, respectively.

Reactions with trityl salt

(i) *Compound* **1** *with* Ph_3CPF_6. A solution of **1** (0.11 g, 0.24 mmol) in CH_2Cl_2 (5 cm^3) was added to a solution of Ph_3CPF_6 (0.093 g, 0.24 mmol) in dichloromethane (2 cm^3). The reaction mixture was stirred for 12 h at room temperature, the solution filtered and the filtrate concentrated. Addition of diethyl ether and cooling gave a fine, yellow solid which was filtered and washed with diethyl ether (3×5 cm^3) and dried to give $[Cp'(CO)_2Fe(CH_2CHCH_2CH_2)Fe(CO)_2Cp']^+PF_6^-$ (**19**) as yellow microcrystals.

(ii) *Compound* **7** *with* Ph_3CPF_6. Similarly, reaction of **7** (0.10 g, 0.21 mmol) with Ph_3CPF_6 (0.08 g, 0.21 mmol) in CH_2Cl_2 (7 cm^3) gave **20** as yellow microcrystals.

(iii) *Compound* **4** *with* Ph_3CPF_6. Similarly, reaction of **4** (0.07 g, 0.13 mmol) with Ph_3CPF_6 (0.05 g, 0.13 mmol) in CH_2Cl_2 (7 cm^3), after 3 h at room temperature, gave **21** as yellow microcrystals.

(iv) *Compound* **11** *with* Ph_3CPF_6. Ph_3CPF_6 (0.057 g, 0.147 mol) was added to a solution of **11** (0.05 g, 0.097 mmol) in CH_2Cl_2 (8 cm^3) and the solution stirred for 10 min at room temperature. The solvent was removed and the residue dissolved in a minimum of CH_2Cl_2. Addition of hexane to the solution gave fine, white microcrystals which were filtered, washed with hexane and dried to give $[Cp(CO)_2Ru(CH_2CHCH_2CH_2CH_2)Ru(CO)_2Cp]^+PF_6^-$ (**22**).

(v) *Compound* **9** *with* Ph_3CPF_6. Similarly, reaction of **9** (0.40 g, 0.94 mmol) with Ph_3CPF_6 (0.55 g, 1.42 mmol) in CH_2Cl_2 (10 cm^3), after 10 min at room temperature, gave **23** as yellow microcrystals. This is an improved procedure to that reported previously for this compound.[11]

RESULTS AND DISCUSSION

The reactions of the alkanediyl compounds with the neutral donor ligands (D) gave, in most cases, disubstituted diacyl compounds [eq. (1)]:

$$[L(CO)_2M(CH_2)_nM(CO)_2L] + 2D \longrightarrow \left[L(CO)DMC(=O)(CH_2)_nC(=O)MD(CO)L \right] \quad (1)$$

2 M = Fe, L = Cp′, D = $PMePh_2$, $n = 4$
3 M = Fe, L = Cp′, D = PMe_2Ph, $n = 4$
5 M = Fe, L = Cp*, D = CO, $n = 4$
6 M = Fe, L = Cp′, D = t-BuNC, $n = 4$
8 M = Fe, L = Cp′, D = t-BuNC, $n = 6$
10 M = Fe, L = Cp, D = t-BuNC, $n = 5$
13 M = Ru, L = Cp, D = PPh_3, $n = 5$
15 M = Ru, L = Cp, D = $PMePh_2$, $n = 5$
16 M = Ru, L = Cp, D = PMe_2Ph, $n = 5$.

From the reactions of $[Cp(CO)_2Ru(CH_2)_5Ru(CO)_2Cp]$ (**11**) with some ligands, the monosubstituted monoacyl compounds $[Cp(CO)_2Ru(CH_2)_5C(O)Ru(CO)DCp]$ (**12**, D = PPh_3 and **14**, D = $PMePh_2$) could also be isolated. The reaction of **11** with t-BuNC in refluxing xylene for 21 h gave a product which was partially characterized as $[Cp(CO)(t\text{-}BuNC)Ru(CH_2)_5Ru(t\text{-}BuNC)(CO)Cp]$; this disubstituted alkanediyl compound may be formed by decarbonylation of the diacyl species under the reaction conditions.

From these reactions of the alkanediyl complexes several general conclusions can be drawn:

(1) the reactions with neutral donor ligands usually lead to disubstituted, diacyl compounds;
(2) the reactions of the diruthenium compounds are much slower than their iron analogues;
(3) increasing the methyl substitution in the Cp ring decreases the reaction rate for steric and electronic reasons thus $C_5H_5 > C_5H_4Me \gg C_5Me_3$;
(4) stronger nucleophiles react faster.

From previous studies,[7] it has also been shown that the rates of similar ligand-induced migrating insertion reactions of $[Cp(CO)_2Fe(CH_2)_4Fe(CO)_2Cp]$ with PPh_3 increased with increasing polymethylene chain, presumably mainly due to the relief of steric crowding. However, this is not always the case since the reaction of $[Cp'(CO)_2Fe(CH_2)_4Fe(CO)_2Cp']$ with t-BuNC is slower for $n = 6$ than $n = 4$. It is also interesting to note that compounds $[L(CO)_2FeC(O)(CH_2)_4C(O)Fe(CO)_2L]$ (L = Cp or Cp*) are extremely reluctant to undergo decarbonylation; this may be, in part, for steric reasons since decarbonylation would place the two metals closer together. Similarly, it has previously been found that decarbonylation of $[(CO)_5MnC(O)(CH_2)_4C(O)Mn(CO)_5]$ is *slower* than for mononuclear $RMn(CO)_5$ (R = CH_3 or C_2H_5) but that reaction of $(CO)_5Mn(CH_2)_4Mn(CO)_5$ with PPh_3 is *faster* than for $RMn(CO)_5$

($R = CH_3$ or C_2H_5).[12] We also find that the rate of the reaction of $[Cp(CO)_2Ru(CH_2)_5Ru(CO)_2Cp]$ with PPh_3 is faster if the ligand concentration is higher; this may be a general result for $L_mM(CO)R$ and $[L_m(CO)M(CH_2)_nM(CO)L_m]$.

We also note that the reaction of $[Cp(CO)_2Ru(CH_2)_5Ru(CO)_2Cp]$ with PPh_3 to give CO insertion products occurs *faster* than for the mononuclear analogues $CpRu(CO)_2R$, with a five times excess of PPh_3 under similar conditions. It is interesting to note that the monosubstituted monoacyl products (e.g. **12**) have one chiral metal centre and the disubstituted diacyl products (e.g. **2**) have two. It has been shown that the chiral auxiliary $CpFe(CO)(PPh_3)$, in mononuclear complexes, is useful to effect stereospecific transformations.[13] It may be that complexes such as **2** will be useful for the synthesis of molecules with two chiral centres. The chirality of **13**, **15** and **16** is reflected in their ^1H and ^{13}C NMR spectra.

Since the insertion reaction into a metal–alkyl bond is a fundamental step in many catalytic reactions and because we have shown in the previous section that CO insertion can occur at both ends of the alkanediyl complexes, we were interested to see if SO_2 would also insert in these binuclear systems.[14] We thus investigated the reactions shown in eq. (2):

$$[L(CO)_2Fe(CH_2)_4Fe(CO)_2L] + 2SO_2 \longrightarrow [L(CO)_2Fe(SO_2)(CH_2)_4(SO_2)Fe(CO)_2L] \quad (2)$$

17 L = Cp′
18 L = Cp*.

The disulphinato products **17** and **18**, where SO_2 has inserted into both $Fe—CH_2$ bonds, were isolated as yellow, microcrystalline solids and characterized by the usual techniques (see Table 1). This reaction is similar to that reported for the complex $[Cp(CO)_2Fe(CH_2)_3Fe(CO)_2Cp]$ with SO_2.[15] All these reactions give the disulphinato complexes containing the group

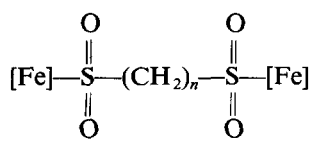

(where [Fe] = metal and associated ligands). It is interesting to note that although the same *types* of products are obtained with Cp, Cp′ or Cp*, the rates of reactions with SO_2 follow the order Cp* > Cp′ > Cp, which is the same order as found for SO_2 insertion reactions of the mononuclear iron alkyl compound $[LFe(CO)_2CH_2Ph]$ (where L = Cp, Cp′ or Cp*).[16] Thus the rates of these reactions with SO_2 increase with increasing electron density on the iron.

The electrophilic cleavage reaction of metal–carbon bonds in mononuclear alkyl compounds is well-known.[17] We were interested to see how the binuclear alkanediyl compounds would react with halogens and particularly to see what effects, if any, there would be in changing the metal, the substituents on the cyclopentadienyl ring and the nature of the halogen.

The diruthenium compound $[Cp(CO)_2Ru(CH_2)_5Ru(CO)_2Cp]$ reacts with bromine or iodine according to eq. (3):

$$[L(CO)_2M(CH_2)_nM(CO)_2L] + 2X_2 \longrightarrow 2LM(CO)_2X + X(CH_2)_nX \quad (3)$$

M = Ru, L = Cp, $n = 5$, X = Br or I
M = Fe, L = Cp′, $n = 4$ or 5, X = Br or I
M = Fe, L = Cp*, $n = 4$ or 6, X = Br or I.

The diruthenium compound reacted rapidly at room temperature to give the cleavage products in high yield. No evidence was obtained for the intermediacy of any cationic intermediate as had been observed in the reactions of the similar di-iron compounds.[7]

The reactions of the Cp′ di-iron compounds similarly proceed rapidly at room temperature to give the cleavage products in high yields. These reactions appear to be independent of alkanediyl chain length. No haloalkyl intermediates were observed as was found with the Cp di-iron compounds, this may be a consequence of the Cp′ compounds reacting faster with halogens due to increased electron density on the metal. In agreement with this, the reactions of the Cp* di-iron alkanediyl compounds appear to proceed slightly faster than the Cp′ or Cp analogues.

The reactions of mononuclear $[CpFe(CO)_2R]$ with trityl salts (such as Ph_3CPF_6) are known to give cationic alkene species $[CpFe(CO)_2(alkene)]^+$[18,19] and binuclear compounds $[Cp(CO)_2Fe(CH_2)_nFe(CO)_2Cp]$ also give cationic species; $[Cp(CO)_2Fe(C_nH_{2n-1})Fe(CO)_2Cp]^+$ by hydride abstraction.[11,20,21] The di-iron alkene, alkyl cations

are thought to be good models for 1-alkene formation in the Fischer Tropsch reaction.[22] We were thus interested to see the effect of changing the metal, the substituents on the cyclopentadienyl rings, as well as the chain length.

The reactions investigated here all proceeded according to eq. (4) to give moderate to good yields of the dinuclear cationic alkene, alkyl complexes as air-stable, crystalline solids.

electrophiles follow the reverse order, thus the reactions with halogens are all fast but follow the order Cp* > Cp′ > Cp. Also, the reactions of the dinuclear ruthenium compounds with electrophiles are at least as fast, if not faster than their iron counterparts. Further experiments are underway to obtain quantitative information on these reactions.

$$[L(CO)_2M(CH_2)_nM(CO)_2L] + Ph_3CPF_6 \longrightarrow [L(CO)_2M(=CH_2)CH{-}(CH_2)_{n-2}M(CO)_2L]PF_6 \quad (4)$$

19 M = Fe, L = Cp′, $n = 4$
20 M = Fe, L = Cp′, $n = 6$.
21 M = Fe, L = Cp*, $n = 4$
22 M = Ru, L = Cp, $n = 5$
23 M = Fe, L = Cp, $n = 5$.

The di-iron complexes ***19***, ***20*** and ***23*** are pale yellow, **21** is yellow–orange and the diruthenium complex **22** is white. All these alkene, alkyl compounds show four strong ν(CO) bands in their IR spectra with the two high frequency bands corresponding to the cationic metal alkene end of the molecule and the two lower ν(CO) bands are due to the alkyl end of the complex. The reactions of the di-iron Cp* compounds appear to react faster with Ph_3CPF_6 than the Cp′ or Cp analogues.

CONCLUSIONS

From the reactions of the alkanediyl complexes that have been studied it is possible to make several generalizations:

(1) Changing the metal from iron to ruthenium and changing the ligands from Cp to Cp′ to Cp* in most cases does not change the *type* of products formed but it does significantly change the rates at which these products are formed. Similarly, the types of products are often analogous to those obtained for mononuclear alkyl compounds but again, the rates of the reactions, on a qualitative basis, are different.
(2) For the ligand induced migrating insertion reactions, the di-iron complexes react much faster than the diruthenium analogues. Also, increasing the methyl substitution of the cyclopentadienyl rings decreases the rates of these reactions with nucleophiles, thus the reactivity order is Cp > Cp′ ≫ Cp*.
(3) Reactions of the alkanediyl complexes with

Acknowledgements—We thank the University of Cape Town, FRD and Mobil for support, Johnson Matthey for a generous loan of ruthenium trichloride and SAR Knox for a kind donation of some $Ru_3(CO)_{12}$. We also thank Nazir Ahmed for synthesizing some of the $[CpRu(CO)_2]_2$.

REFERENCES

1. M. H. Chisholm, *Polyhedron* 1988, **7**, 757.
2. Polyhedron Symposium in Print No. 5, *Polyhedron* 1988, **7**, No. 10/11.
3. C. P. Casey and J. Audett, *Chem. Rev.* 1986, **86**, 339.
4. J. R. Moss and L. G. Scott, *Coord. Chem. Rev.* 1984, **60**, 171.
5. L. G. Scott, J. R. Moss, M. E. Brown and K. J. Hindson, *J. Organomet. Chem.* 1985, **282**, 255.
6. L. Pope, P. Sommerville, M. Laing, K. J. Hindson and J. R. Moss, *J. Organomet. Chem.* 1976, **112**, 309.
7. J. R. Moss and L. G. Scott, *J. Organomet. Chem.* 1989, **363**, 351.
8. K. P. Finch, J. R. Moss and M. L. Niven, *Inorg. Chim. Acta* 1989, **166**, 181.
9. N. M. Doherty and S. A. R. Knox, *Inorg. Synth.* 1989, **25**, 179.
10. S. F. Mapolie and J. R. Moss, *S. Afr. J. Chem.* 1987, **40**, 12.
11. J. W. Johnson and J. R. Moss, *Polyhedron* 1985, **4**, 563.
12. M. A. Bothma, G. E. Jackson and J. R. Moss, unpublished results reported in S. F. Mapolie and J. R. Moss, *J. Chem. Soc., Dalton Trans.* 1990, 299.
13. S. G. Davies, I. M. Dorder-Hedgecock, K. H. Sutton and M. Whittaker, *J. Am. Chem. Soc.* 1987, **109**, 5711.
14. C. Lindsay, E. Cesarotti, H. Adams, N. A. Bailey and C. White, *Organometallics* 1990, **9**, 2594.
15. J. P. Bibler and A. Wojcicki, *J. Am. Chem. Soc.* 1966, **88**, 4862.

16. S. E. Jacobson and A. Wojcicki, *J. Am. Chem. Soc.* 1973, **95**, 6962.
17. J. P. Collman, L. S. Hegedus, J. R. Norton and R. G. Finke, *Principles and Applications of Organotransition Metal Chemistry*, 2nd edn, p. 433. University Science Books, Mill Valley, California (1987).
18. M. L. H. Green and P. L. I. Nagy, *J. Organomet. Chem.* 1963, **1**, 58.
19. D. E. Laycock, J. Hartgerink and M. C. Baird, *J. Org. Chem.* 1980, **45**, 291.
20. R. B. King and M. B. Bisnette, *J. Organomet. Chem.* 1967, **7**, 311.
21. M. Laing, J. R. Moss and J. Johnson, *J. Chem. Soc., Chem. Commun.* 1977, 656.
22. M. A. Gafoor and J. R. Moss, submitted for publication.

Polyhedron Vol. 10, No. 9, pp. 973–976, 1991
Printed in Great Britain

0277–5387/91 $3.00+.00
© 1991 Pergamon Press plc

PEROXO COMPLEXES OF ZIRCONIUM(IV), THORIUM(IV), MOLYBDENUM(VI), TUNGSTEN(VI) and URANIUM(VI) IONS CONTAINING A QUADRIDENTATE SNNS SCHIFF BASE

M. T. H. TARAFDER* and A. R. KHAN

Department of Chemistry, University of Rajshahi, Rajshahi, Bangladesh

(*Received* 14 *November* 1990; *accepted* 9 *January* 1991)

Abstract—New peroxo complexes of zirconium(IV), thorium(IV), molybdenum(VI), tungsten(VI) and uranium(VI) containing a quadridentate Schiff base, formed by the condensation of S-benzyldithiocarbazate and benzil, have been synthesized and characterized. The complexes have the general formulae $[M(O_2)(SNNS)]$ ($M = Zr^{IV}$ and Th^{IV}) and $[M^1(O)(O_2)(SNNS)]$ ($M^1 = Mo^{VI}$, W^{VI} and U^{VI}). These peroxo complexes were found to be inert towards oxidation. The size of the metals as well as the electronic effect derived from the quadridentate Schiff base influence the mode of coordination of the peroxo moiety. The frequency of the ν_1 mode of the $M(O_2)$ grouping decreases with an increase in the atomic number of the metals in a particular group and in the σ-donor electronic nature of the quadridentate Schiff base used.

Studies on peroxo complexes have received considerable attention in recent years[1–9] because many of these complexes are efficient stiochiometric or catalytic oxidants for organic and inorganic substrates. The reactivity of metal peroxides can be greatly modified by introducing metals of different sizes and ancillary ligands with different donor properties. In particular, peroxo complexes containing lighter metals, for instance, $[Zr(C_5H_5NCOO)_2(O_2)]$ were kinetically stable towards olefinic compounds,[6] whereas the analogous complex of thorium[5] was as an efficient oxidant. The coordination of nucleophilic substrates to zirconium, forming seven-coordinate intermediates prior to oxygen transfer, is not favourable, whereas six-coordinate thorium can adopt an expanded coordination shell very readily. Also, peroxo complexes containing monodentate and bidentate auxiliary ligands were found to undergo oxygen transfer reactions,[1–9] however, those containing tridentate and quadridentate ligands were inert towards oxidation reactions.[5,10,11] We are interested in extending such a study to new peroxo complexes of different elements of groups 4A and 6A containing nitrogen–sulphur donor ligands. We reported earlier a series of peroxo complexes containing a bidentate nitrogen–sulphur donor ligand.[8] No attempt appears to have been made so far to isolate peroxo complexes of transition metals containing quadridentate S,N,N,S ligands. We present here the synthesis of these complexes and their possible attempted oxygen transfer reactions. An attempt has also been made to study the influence of the size of the metal ions and the electronic effect derived from the quadridentate Schiff base on the ν_1(O—O) modes of the complexes in their IR spectra.

EXPERIMENTAL

Reagents

All chemicals used were reagent grade and were used as supplied by Merck.

Physical measurements and elemental analyses

IR spectra (as KBr pellets) were recorded on a Pye–Unicam SP3-300 IR spectrophotometer. Conductivities of 10^{-3} M solutions in dimethyl sulphoxide (DMSO) were measured at 25°C using a WPA CM35 conductivity meter and dip-type cell with platinized electrodes.

Carbon, hydrogen and nitrogen analyses were carried out by Microanalytical Services at the University of St Andrews, Scotland.

* Author to whom correspondence should be addressed.

Preparation of the Schiff base

S-benzyldithiocarbazate, $NH_2NHCSSCH_2C_6H_5$, was prepared by the literature method[12] and its purity checked by elemental analyses, m.p. 125°C.

A solution of S-benzyldithiocarbazate (11.2 g, 0.0564 mol) in absolute ethanol (300 cm^3) was added to a solution of benzil (3.9 g, 0.0188 mol) in the same solvent (100 cm^3). The mixture was refluxed for 6 h, and the yellow crystals which settled on cooling were separated out and washed with ethanol, yield 1.2 g, m.p. 168°C (Found: C, 63.2; H, 4.6; N, 9.8. $C_{30}H_{26}N_4S_4$ requires: C, 63.2; H, 4.6; N, 9.8%).

Preparation of the complexes: general method for the preparation of $[M(O_2)(SNNS)]$ [M = Zr^{IV} (**1**) and Th^{IV} (**2**); SNNS = $(C_{30}H_{24}N_4S_4)^{2-}$]

The Schiff base $C_{30}H_{26}N_4S_4$ (0.0002 mol) was added to a solution of potassium hydroxide (0.0004 mol) in 30% H_2O_2 (20 cm^3). The solution was heated for 5 min, filtered and to the filtrate was added, with stirring, a solution of $M(NO_3)_4 \cdot 4H_2O$ (0.0002 mol) in water (15 cm^3). The resulting precipitate which separated out was filtered, washed several times with water and dried *in vacuo* over P_4O_{10}.

Preparation of $[M(O)(O_2)(SNNS)]$ [M = Mo^{VI} (**3**) and W^{VI} (**4**)]

The Schiff base $C_{30}H_{26}N_4S_4$ (0.005 mol) was added to a solution of potassium hydroxide (0.01 mol) in 30% H_2O_2 (100 cm^3). The solution was heated for 5 min, filtered and to the filtrate was added, with stirring, a solution of MO_3 (M = Mo^{VI} and W^{VI}) (0.005 mol) in 30% H_2O_2 (60 cm^3). The resulting precipitate was filtered, washed successively with water and ether and stored.

Preparation of $[U(O)(O_2)(SNNS)]$ (**5**)

The Schiff base $C_{30}H_{26}N_4S_4$ (0.005 mol) was dissolved in a solution of potassium hydroxide (0.01 mol) in 30% H_2O_2 (100 cm^3). The solution was heated for 5 min, filtered and to the filtrate was added, a solution of $UO_2(NO_3)_2 \cdot 6H_2O$ (0.005 mol) in water (50 cm^3). The solution was boiled and cooled. The resulting precipitate was filtered, washed successively with water and ether and stored.

Attempted reactions of **1** *and* **2** *with allyl alcohol and* **3** *and* **5** *with triphenylphosphine and triphenylarsine, respectively*

Refluxing **1** with allyl alcohol in a 1:1 molar ratio in THF medium for 48 h failed to produce any reaction; **1** was recovered unchanged.

Refluxing **2** with allyl alcohol in the presence of a large excess of 30% H_2O_2 in dioxane medium for 48 h at 90°C also failed to produce any reaction; **2** was recovered unchanged.

Refluxing **3** and **5** with equimolar quantities of triphenylphosphine and triphenylarsine, respectively, in THF for 48 h also failed to produce any reaction; **3** and **5** were recovered unchanged.

RESULTS AND DISCUSSION

Elemental analyses and conductivity data for the complexes are presented in Table 1. The complexes are non-electrolytes in solution suggesting that the anions are covalently bonded in all the cases. The mass spectrum of the Schiff base $C_{30}H_{26}N_4S_4$ does not display the molecular ion peak but shows other diagnostic peaks at *m/z* 285, 211, 149, 105, 77, 51

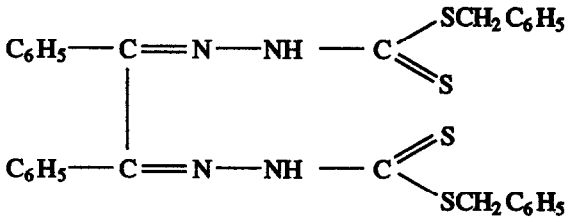

(Ia)

Table 1. Analytical data and other physical properties of the complexes[a]

Compound	Colour	% Carbon Calc.	% Carbon Found	% Hydrogen Calc.	% Hydrogen Found	% Nitrogen Calc.	% Nitrogen Found	Molar conductance ($\Omega^{-1}cm^2\ mol^{-1}$)
$[Zr(O_2)(SNNS)]$ (**1**)	Ash	52.1	52.0	3.5	3.3	8.1	8.1	0
$[Th(O_2)(SNNS)]$ (**2**)	Colourless	43.3	43.1	2.9	2.8	6.7	6.5	2
$[Mo(O)(O_2)(SNNS)]$ (**3**)	Yellow	50.6	50.3	3.4	3.4	7.9	7.7	1
$[W(O)(O_2)(SNNS)]$ (**4**)	Yellow	45.0	45.0	3.0	3.0	7.0	6.8	0
$[U(O)(O_2)(SNNS)]$ (**5**)	Yellow	42.2	42.1	2.8	2.8	6.6	6.5	4

[a] The organic moiety for the compounds indicated is $(C_{30}H_{24}N_4S_4)^{2-}$.

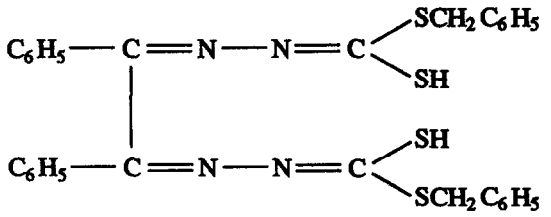

(Ib)

and 28. The Schiff base **I** can exist in the thioketo form (**Ia**) or in enethiol form (**Ib**) or as a mixture of both. The IR spectrum of the Schiff base does not display ν(SH) at *ca* 2570 cm^{-1} but exhibits ν(NH), ν(C=N) and ν(C=S) modes (Table 2), indicating that in the solid state the Schiff base remains in the thioketo form (**Ia**). Its ^1H NMR spectrum in $CDCl_3$ exhibits signals at 4.36, 7.5 and 9.89 ppm corresponding to the methylene, phenyl and —NH— protons, respectively. The ^1H NMR spectrum does not display any peak attributable to a S—H proton. Therefore the Schiff base remains predominantly in the thioketo form (**Ia**) in $CDCl_3$. The Schiff base, however, forms complexes only in basic medium. Attempts to prepare complexes from a neutral medium were unsuccessful. This suggests that the nucleophilicity of the ligand is greatly enhanced in alkaline medium probably due to the creation of an anionic site *in situ*.[12-16] The thione group is relatively unstable in the monomeric form and undergoes a thione (**Ia**)⇌thiol (**Ib**) equilibrium.[17] The deprotonation and consequent formation of an anionic site *in situ* is favoured by the basicity of the medium and the ν(N—H) and ν(C=S) bands of the free ligand disappear in the spectra of the complexes suggesting that the ligand is coordinated in the deprotonated thiol form. This is also evident from the appearance of ν(C—S)[18,19] bands at 710–725 cm^{-1} and ν(M—S) bands[8,14,15,20] at 255–270 cm^{-1} (Table 2) in the IR spectra of the complexes. The ν(C=N) band of the free Schiff base is shifted to lower frequencies in the complexes (Table 2) suggesting that the azomethine nitrogen is coordinated. A molecular model shows that the α-nitrogen (imino nitrogen) is not bonded due to considerable steric strain.[12-16] The far-IR spectra of the complexes exhibit bands in the region 300–325 cm^{-1} (Table 2) which are tentatively attributed to ν(M—N) modes.[4-8,20-22] Complexes **3–5** display bands at 915–925 cm^{-1} assignable to ν(M=O) modes.[4,9,11] The metal peroxo grouping (local C_{2v} symmetry) gives rise to three IR- and Raman-active vibrational modes. These are predominantly O—O stretching (ν_1), the symmetric M—O stretch (ν_2) and the antisymmetric M—O stretch (ν_3). The characteristic ν_1(O—O) modes of **1–5** appear at 800–840 cm^{-1} (Table 2). In particular, the ν_1 mode decreases from the zirconium complex (**1**, 820 cm^{-1}) to the corresponding thorium complex (**2**, 810 cm^{-1}). This is also discernible in the cases of peroxo complexes of the elements of group 6A, there is a decrease in ν_1 upon passing from the molybdenum complex (**3**, 840 cm^{-1}) to the corresponding tungsten complex (**4**, 830 cm^{-1}), which is further decreased in the uranium peroxo complexes (**5**, 800 cm^{-1}). The present data thus clearly reveal that for the $M(O_2)$ grouping, the ν_1(O—O) modes decrease with an increase in the atomic number of the metals in a particular group. In the present examples, ν_3 and ν_2 modes appear at 620–650 and 530–550 cm^{-1}, respectively. It is noteworthy that the ν_1 mode of the present peroxo complexes of zirconium, thorium, molybdenum, tungsten and uranium appear at lower frequencies than the peroxo complexes of these metals containing monodentate, bidentate and tridentate ancillary ligands.[4-11] This is pre-

Table 2. IR spectral data for the Zr^{IV}, Th^{IV}, Mo^{VI}, W^{VI} and U^{VI} complexes[a] [band maxima (cm^{-1})]

Compound	ν(N—H)	ν(C=N)	ν(C=S)	ν(C—S)	ν_1(O—O)	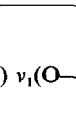	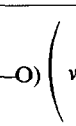	ν(M—N)	ν(M—S)	ν(M=O)
$C_{30}H_{26}N_4S_4$	3285 m	1560 vs	1045 s							
1		1520 s		710 vs	820 s	650 vs	550 s	325 vs	270 vs	
2		1525 s		715 vs	810 s	625 vs	530 vs	315 s	265 s	
3		1515 vs		710 s	840 vs	620 s	535 s	300 vs	255 s	915 vs
4		1525 s		720 s	830 s	630 vs	540 s	315 vs	260 s	920 s
5		1530 s		725 s	800 vs	635 s	545 s	320 m	270 m	925 vs

[a] Relative band intensities are denoted by vs, s and m, representing very strong, strong and medium, respectively.

sumably due to greater charge neutralization of the metal centres by the quadridentate, dinegative σ-donor ligand, causing a weaker coulombic interaction in the M^{n+}—O_2^{2-} moiety ($n = 4$ or 6).

Reactivity

The present peroxo complexes were not found to undergo oxygen transfer reactions. Complexes **1** and **2** failed to oxidize allyl alcohol even when refluxing at 90°C was continued for 48 h. Complexes **3** and **5** were also unreactive towards phosphine and arsine. These negative results outline the enhanced stability of the metal peroxo moiety in the presence of the quadridentate chelating ligand which precludes oxygen transfer reactions. Similar results were also found for the peroxo complexes containing tridentate and quadridentate ligands.[4,6,9,10]

Acknowledgements—Thanks are due to Professor A. D. Westland, Department of Chemistry, University of Ottawa, Canada for the ^{1}H NMR and mass spectra. One of us (M.T.H.T.) gratefully acknowledges the assistance provided by the Microanalytical Services, University of St Andrews, Scotland. We are indebted to the Rajshahi University for the provision of laboratory facilities.

REFERENCES

1. H. Mimoun, *J. Molec. Catal.* 1980, **7**, 1.
2. H. Mimoun, *The Chemistry of Peroxides* (Edited by S. Patai), p. 469, Wiley, New York (1983).
3. A. D. Westland, F. Haque and J. M. Bouchard, *Inorg. Chem.* 1980, **19**, 225.
4. A. D. Westland and M. T. H. Tarafder, *Inorg. Chem.* 1981, **20**, 3992.
5. A. D. Westland and M. T. H. Tarafder, *Inorg. Chem.* 1982, **21**, 3228.
6. M. T. H. Tarafder and M. A. L. Miah, *Inorg. Chem.* 1986, **25**, 2265.
7. M. T. H. Tarafder and A. R. Khan, *Polyhedron* 1987, **6**, 275.
8. M. T. H. Tarafder and A. Ahmed, *Ind. J. Chem.* 1986, **25A**, 729.
9. M. T. H. Tarafder, M. B. H. Howlander, B. Nath, R. Khan and A. A. M. A. Islam, *Polyhedron* 1989, **8**, 977.
10. M. T. H. Tarafder, *Ind. J. Chem.* 1987, **26A**, 874.
11. M. T. H. Tarafder and A. A. M. A. Islam, *Polyhedron* 1989, **8**, 109.
12. M. A. Ali and M. T. H. Tarafder, *J. Inorg. Nucl. Chem.* 1977, **39**, 1785.
13. M. T. H. Tarafder and M. Rahim, *Ind. J. Chem.* 1989, **28A**, 1105.
14. M. T. H. Tarafder, *Ind. J. Chem.* 1989, **28A**, 129.
15. M. T. H. Tarafder and S. Roy, *Ind. J. Chem.* 1988, **27A**, 407.
16. M. T. H. Tarafder, *Ind. J. Chem.* 1989, **28A**, 531.
17. R. Mayer, *Organosulphur Chemistry* (Edited by M. J. Jansen), p. 219. Interscience, New York (1983).
18. F. Basolo, W. H. Baddley and J. L. Burmeister, *Inorg. Chem.* 1964, **3**, 1202.
19. J. Lewis, R. S. Nyholm and P. W. Smith, *J. Chem. Soc.* 1961, 4590.
20. N. M. Karayannis, C. M. Mikulski, M. J. Stroke, L. L. Pytlewski and M. M. Labes, *Inorg. Chim. Acta* 1970, **4**, 455.
21. R. K. Agarwal, M. Srivastava and A. K. Srivastava, *J. Inorg. Nucl. Chem.* 1981, **43**, 204.
22. R. K. Agarwal, A. K. Srivastava, M. Srivastava, N. Bhakru and T. N. Srivastava, *J. Inorg. Nucl. Chem* 1980, **42**, 1778.

Polyhedron Vol. 10, No. 9, pp. 977–991, 1991
Printed in Great Britain

0277–5387/91 $3.00+.00
© 1991 Pergamon Press plc

SYNTHESIS, CHARACTERIZATION AND STEREOCHEMICAL PREFERENCES OF COBALT(III) TERNARY AMINO ACID COMPLEXES CONTAINING *N*-((2-PYRIDYL)METHYL)-2-((2-AMINOETHYL)THIO)ACETAMIDE, A STEREOSPECIFIC LINEAR NSNN TETRADENTATE LIGAND

PAUL J. TOSCANO,* KIMBERLY A. BELSKY, TZE-CHEN HSIEH, TERRENCE NICHOLSON and JON ZUBIETA

Department of Chemistry, State University of New York at Albany, Albany, NY 12222, U.S.A.

(*Received* 11 *October* 1990; *accepted* 14 *January* 1991)

Abstract—The preparation, isolation and characterization of *cis*-β-[Co(pyge)(AA)]PF_6 [pygeH = *N*-((2-pyridyl)methyl)-2-((2-aminoethyl)thio)acetamide; AA = gly, L-ala, L-ile, L-leu, sarcosine (sar), α-aminoisobutyric acid (aiba) and β-ala] are described. ^1H and ^{13}C NMR spectra of the new cobalt complexes strongly suggest that one geometrical isomer is obtained with very high stereoselectivity. β_1-[Co(pyge)(gly)]$PF_6 \cdot 2H_2O$ (**1**) crystallized in the monoclinic space group $P2_1/c$ with $a = 14.518(2)$, $b = 14.583(2)$, $c = 19.783(3)$ Å, $\beta = 98.51(1)°$ and $Z = 8$ and was refined to $R = 0.080$. In both of the two independent cations in the asymmetric unit, the gly chelate had the β_1 configuration with respect to the pyge ligand. The complex β-[Co(pyge)(Cl)(NO_2)]$\cdot H_2O$ was prepared; recrystallization of this complex provided single crystals of β-[Co(pyge)(Cl)(NO_2)]$\cdot$[Co(pyge)$(NO_2)_2$]$\cdot 2H_2O$ (**2**). Complex **2** crystallized in the triclinic space group $P\bar{1}$ with $a = 7.850(1)$, $b = 13.346(2)$, $c = 15.998(2)$ Å, $\alpha = 106.45(1)$, $\beta = 99.07(1)$, $\gamma = 104.78(1)°$ and $Z = 2$, and was refined to $R = 0.052$. The chlorine ligand was found to be *trans* to the amido donor of the pyge ligand, suggesting that the β_1 configuration found for the amino acid complexes stems from kinetically-based substitutions. The complex β-[Co(pyge)Cl_2]$\cdot H_2O$ promotes the hydrolysis of amide and ester bonds of dipeptides and amino acid esters to again give β_1-[Co(pyge)(AA)]PF_6. Finally, evidence is presented for sar and L-ala, that the diastereomeric β_1 complex that predominates at equilibrium is the isomer with the ligand methyl group hydrophobically interacting with the pyridyl moiety of the pyge ligand.

Studies involving the chelation and coordination of amino acids and related ligands to octahedral cobalt (III) centres containing a flexible, linear tetradentate ligand or two bidentate ligands have been an ongoing area of active research.[1–6] Major topics of investigation have included delineation of the factors governing stereoselectivity in the coordination of the optically active amino acids[3,7,8] and activation of the carbonyl or other functionalities of amino acid esters, amides and peptides for hydrolysis,[1,4,9,10] substitution[11] and synthetic reactions.[12]

Recently, we along with others have described the synthesis of *N*-((2-pyridyl)methyl)-2-((2-aminoethyl)thio)acetamide (pygeH).[13–15] Previous studies have demonstrated that complexes of the type

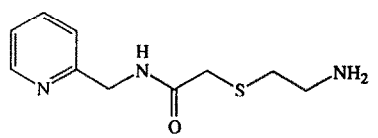

pygeH

$CoL(NO_2)_2$, where L is a flexible, linear NSNN tetradentate ligand that has internal thioether and deprotonated amido nitrogen donor atoms and that coordinates to give three five-membered chelate rings such as pyge, exist in the solid state in the

*Author to whom correspondence should be addressed.

cis-β (unsymmetrical *cis*) geometry.[13,14,16] Further evidence strongly suggests that only the *cis*-β configuration is found for $[Co(pyge)(NO_2)_2]$ in solution.[13,14] More importantly, chemical interconversions of β-$[Co(pyge)(NO_2)_2]$ that yield new complexes of composition $[Co(pyge)X_2]$, where X_2 is two monodentate ligands or one symmetrical bidentate ligand, give only one spectroscopically detectable geometrical isomer.[14] In these cases, the geometry is almost certainly *cis*-β rather than *cis*-α (symmetrical *cis*) or *trans*, since the original *cis*-β dinitrocobalt(III) complex can be recovered via appropriate reaction steps.[14] The apparent stereospecificity for adoption of the *cis*-β geometry by $[Co(pyge)X_2]$ complexes presumably stems from the preference of sulphur for pyramidal coordination when it is at the junction of two five-membered chelate rings flanked by nitrogen (or oxygen) donors at one of the other termini,[17,18] coupled with the planarity enforced about the deprotonated amido donor.[19]

In this contribution we report on our studies involving the synthesis and isolation of complexes of the type β-$[Co(pyge)(AA)]PF_6$, where AA is the anion of an amino acid, from the readily available β-$[Co(pyge)Cl_2]\cdot H_2O$.[14] Since the amino acidato chelates are unsymmetrical, two geometrical configurations are possible for these bidentate ligands which are designated as β_1 and β_2 (see Fig. 1).[20] Thus, for ligands such as gly that contain no asymmetric centres, it is possible to prepare two pairs of enantiomeric complexes that can be designated as Δ,Λ-β_1 and Δ,Λ-β_2.* On the other hand, a chiral amino acid such as L-ala can give rise to four diastereomeric complexes, namely Δ_L-β_1, Λ_L-β_1, Δ_L-β_2 and Λ_L-β_2, due to the additional asymmetric carbon atom.† An *N*-alkylated amino acid such as sarcosine (sar) can also give rise to additional stereoisomers due to the asymmetric coordinated amino group. We will present spectroscopic, as well as crystallographic, evidence that the number of isomeric complexes actually isolated is limited by the kinetic considerations involving the special nature of the tetradentate pyge ligand. We also present results concerning stereochemical preferences within some of the isolated isomeric complexes (AA = sar, L-ala) under equilibrium conditions, as well as evidence that $[Co(pyge)Cl_2]\cdot H_2O$ facilely promotes the cleavage of amide and ester bonds of α-amino carbonyl compounds.

* The cobalt centre itself is asymmetric due to the sense in which the tetradentate ligand is wrapped around the metal (see Fig. 1).

† Here we employ the subscript L to indicate the chirality of the asymmetric carbon atom of the amino acid ligand.

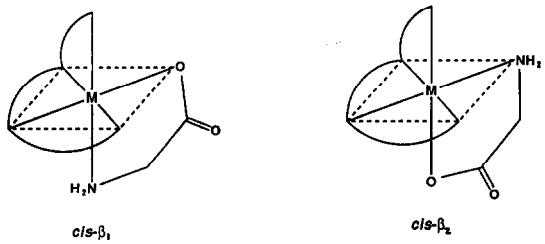

Fig. 1. The two possible geometrical configurations for a chelating gly ligand in a *cis*-β octahedral complex. Only one enantiomer (Δ) is depicted for each configuration. The mirror images would then have the Λ designation.

EXPERIMENTAL

Materials and methods

^1H and ^{13}C NMR spectra were obtained on a Varian XL-300 spectrometer at 299.943 and 75.429 MHz, respectively. Spectra obtained in D_2O solution were referenced to 3-(trimethylsilyl)propionic acid, sodium salt (^1H) or dioxane (^{13}C). Spectra obtained in Me_2SO-d_6 solution were referenced to Me_4Si. The NMR spectra for complex cations having amino acidato ligands with asymmetric centres are complicated, since these compounds are generally isolated as equal mixtures of two diastereomers (see Results and Discussion). If resonances for the same group in the ^1H NMR spectrum of the two diastereomers are sufficiently well separated, then the chemical shift values are presented as pairs next to the assignment. For overlapping or indistinguishable resonances, only one chemical shift value (or range of shift values) is provided. NMR samples for ^1H–^1H NOE experiments were degassed by three freeze–pump–thaw cycles. Visible absorption spectra of dilute aqueous or Me_2SO solutions were recorded on either Varian DMS-80 or Shimadzu UV-160 spectrophotometers at ambient temperature. Molar absorptivity coefficients are given in units of $mol^{-1}\ dm^3\ cm^{-1}$. Elemental analyses were determined by Atlantic Microlab, Inc. (Norcross, GA).

Preparation of compounds

Unless otherwise noted, all starting materials and solvents were obtained from standard sources and used without further purification.

cis-β_1-$[Co(pyge)(AA)]PF_6$ [AA = gly, L-ala, L-val, L-ile, L-leu, β-ala, sarcosine (sar), α-aminoisobutyric acid (aiba)]

A general preparation for the amino acidato complexes will be given. The complex β-$[Co(pyge)Cl_2]\cdot H_2O$[14] (0.75 g, 2.0 mmol) was dissolved in

water (10 cm^3). The free amino acid (2.2 mmol; except for sar, where 5.2 mmol was employed) was added and the pH adjusted to 7.6–7.8 by dropwise addition of NaOH solution (2.5 M). The purple reaction mixture was heated at 50–60°C until a deep red–orange colour was attained (typically 0.5–3.0 h, depending upon the particular AA). After filtration, the filtrate was cooled and NH_4PF_6 (0.49 g, 3.0 mmol) was added. (If a small amount of dull purplish maroon material precipitated at this point, the mixture was refiltered.) Upon slow evaporation, the solution deposited deep red to red–orange, microcrystalline material. Crude yields ranged between 50–70%. Recrystallization from a minimum volume of hot water gave pure compounds. Analytical and spectroscopic data for specific complexes follow.

For AA = gly, the complex was anhydrous. Found: C, 28.6; H, 3.6; N, 11.1. Calc. for $C_{12}H_{18}F_6N_4O_3PSCo$: C, 28.7; H, 3.6; N, 11.2%. Vis (H_2O): λ_{max} 499 nm (ε 420). Vis (Me_2SO): λ_{max} 508 nm (ε 460). ^1H NMR (D_2O): δ 8.36 (d, 1H, H-6 py), 8.14 (t, 1H, H-4 py), 7.70 (m, 2H, H-3 and H-5 py), 4.69 (br s, 2H, $pyCH_2$), 4.08 (d, 1H, SCH_2CO), 3.61 (d, 1H, SCH_2CO), 3.54 (d, 1H, gly—CH_2), 3.24 (d, 1H, gly—CH_2), 2.65–3.15 (complex m, 4H, SCH_2CH_2N). ^{13}C (D_2O): δ 186.47, 178.90, 167.10, 148.95, 141.89, 126.43, 124.45, 53.53, 46.88, 43.59, 39.61, 39.46. Crystals suitable for X-ray diffraction studies were grown by slow evaporation of a saturated aqueous solution of the complex.

For AA = L-ala, the complex was a dihydrate. Found: C, 28.4; H, 4.2; N, 10.0. Calc. for $C_{13}H_{20}F_6N_4O_3PSCo \cdot 2H_2O$: C, 28.3; H, 4.4; N, 10.1%. Vis (H_2O): λ_{max} 500 nm (ε 400). Vis (Me_2SO): λ_{max} 510 nm (ε 530). ^1H NMR (D_2O): δ (8.32, 8.29) (d, 1H, H-6 py), 8.14 (t, 1H, H-4 py), 7.69 (m, 2H, H-3 and H-5 py), (4.72, 4.69) (br s, 2H, $pyCH_2$), 4.08 (d, 1H, SCH_2CO), (3.76, 3.32) (q, 1H, ala—CH), (3.61, 3.59) (d, 1H, SCH_2CO), 2.65–3.15 (complex m, 4H, SCH_2CH_2N), (1.40, 1.24) (d, 3H, ala—CH_3). ^{13}C (D_2O): δ (188.29, 187.63), 179.06, 178.92), (167.23, 167.16), (148.85, 148.61), 141.86, (126.52, 126.44), (124.51, 124.43), (54.92, 53.58), 53.58 (accidental equivalence of $pyCH_2$ with L-ala—CH), (43.49, 43.35), (39.71, 39.54). (39.54, 39.49), (18.76, 18.34).

For AA = L-val, the complex had three and a half water molecules of hydration. Found: C, 29.3; H, 4.7; N, 9.3. Calc. for $C_{15}H_{24}F_6N_4O_3PSCo \cdot 3.5H_2O$: C, 29.7; H, 5.1; N, 9.2%. Vis (H_2O): λ_{max} 500 nm (ε 430). Vis (Me_2SO): λ_{max} 506 nm (ε 530). ^1H NMR (D_2O): δ (8.32, 8.25) (d, 1H, H-6 py), 8.14 (t, 1H, H-4 py), 7.68 (m, 2H, H-3 and H-5 py), (4.74, 4.72) (br s, 2H, $pyCH_2$), (4.17, 4.15) (d, 1H, SCH_2CO), (3.67, 3.17) (d, 1H, val—NCH), (3.59, 3.57) (d, 1H, SCH_2CO), 2.65–3.15 (complex m, 4H, SCH_2CH_2N), 2.23 (m, 1H, val—iPrCH), (0.97, 0.94, 0.92, 0.60) (d, 6H, val—CH_3). ^{13}C (D_2O): δ (187.23, 186.81), (179.15, 179.04), (167.60, 167.45), (148.78, 148.63), (141.93, 141.85), (126.43, 126.27), (124.62, 124.40), (64.47, 62.95), 53.72 (br), (43.44, 43.39), (39.72, 39.49), (39.49, 39.31), (30.98, 30.81), (18.60, 18.50), (16.33, 15.83).

For AA = L-ile, the complex was a dihydrate. Found: C, 32.6; H, 4.7; N, 9.2. Calc. for $C_{16}H_{26}F_6N_4O_3PSCo \cdot 2H_2O$: C, 32.3; H, 5.1; N, 9.4%. Vis (H_2O): λ_{max} 501 nm (ε 430). Vis (Me_2SO): λ_{max} 508 nm (ε 460). ^1H NMR (D_2O): δ (8.34, 8.24) (d, 1H, H-6 py), 8.14 (t, 1H, H-4 py), 7.69 (m, 2H, H-3 and H-5 py), (4.74, 4.72) (br s, 2H, $pyCH_2$), (4.16, 4.14) (d, 1H, SCH_2CO), (3.70, 3.19) (d, 1H, ile—NCH), (3.59, 3.57) (d, 1H, SCH_2CO), 2.65–3.15 (complex m, 4H, SCH_2CH_2N), 1.92 (m, 1H, ile—sBuCH), 1.33 (m, 2H, ile—$sBuCH_2$), 0.75–1.00 (overlapping d and t, 6H, ile—CH_3). ^{13}C (D_2O): δ (187.30, 186.76), (179.11, 179.01), (167.57, 167.45), (148.79, 148.56), (141.89, 141.85), (126.41, 126.24), (124.60, 124.35), (64.58, 62.89), 53.70 (br), 43.55 (br), (39.70, 39.53), (39.43, 39.35), (38.15, 38.06), (24.51, 23.93), (15.50, 15.05), (12.32, 12.06).

For AA = L-leu, the complex was a monohydrate. Found: C, 33.0; H, 4.8; N, 9.7. Calc. for $C_{16}H_{26}F_6N_4O_3PSCo \cdot H_2O$: C, 33.3; H, 4.9; N, 9.7%. Vis (H_2O): λ_{max} 501 nm (ε 500). Vis (Me_2SO): λ_{max} 508 nm (ε 500). ^1H NMR (D_2O): δ (8.31, 8.29) (d, 1H, H-6 py), 8.14 (m, 1H, H-4 py), 7.69 (m, 2H, H-3 and H-5 py), (4.73, 4.71) (br s, 2H, $pyCH_2$), (4.14, 4.13) (d, 1H, SCH_2CO), (3.65, 3.21) (d of d, 1H, leu—NCH), (3.59, 3.57) (d, 1H, SCH_2CO), 2.65–3.15 (complex m, 4H, SCH_2CH_2N), 1.25–1.85 (complex m, 3H, leu—CH_2 and leu—iPrCH), (0.90, 0.87, 0.82, 0.79) (d, 6H, leu—CH_3). ^{13}C (D_2O): δ (188.51, 187.96), (179.13, 179.01), 167.36, (148.70, 148.54), 141.82, (126.44, 126.41), (124.55, 124.46), (57.30, 56.05), 53.62, (43.39, 43.29), (43.14, 42.35), 39.40–39.60 (broadened manifold of four ill-resolved resonances), (24.62, 24.42), (23.19, 23.11), (20.85, 20.79).

For AA = β-ala, the complex was a dihydrate. Found: C, 28.0; H, 3.9; N, 10.3. Calc. for $C_{13}H_{20}F_6N_4O_3PSCo \cdot 2H_2O$: C, 28.3; H, 4.4; N, 10.1%. Vis (H_2O): λ_{max} 502 nm (ε 460). Vis (Me_2SO): λ_{max} 509 nm (ε 460). ^1H NMR (D_2O): δ 8.37 (d, 1H, H-6 py), 8.15 (t, 1H, H-4 py), 7.70 (m, 2H, H-3 and H-5 py), 4.67 (s, 2H, $pyCH_2$), 4.05 (d, 1H, SCH_2CO), 3.59 (d, 1H, SCH_2CO), 2.45–3.15 (complex m, 8H, SCH_2CH_2N and ala—CH_2). ^{13}C (D_2O): δ 182.31, 178.81, 166.93, 149.71, 141.85, 126.32, 124.48, 53.50, 43.80, 39.57, 39.33, 39.26, 34.59.

For AA = sar, the complex was a trihydrate. Found: C, 27.1; H, 4.2; N, 10.1. Calc. for $C_{13}H_{20}F_6N_4O_3PSCo \cdot 3H_2O$: C, 27.4; H, 4.6; N, 9.8%. Vis (H_2O): λ_{max} 503 nm (ε 430). Vis (Me_2SO): λ_{max} 510 nm (ε 500). The isolated complex was a mixture (14 : 86) of two diastereomers due to stereochemistry about the coordinated methylamino group of sar. ^{1}H NMR for the major isomer (D_2O): δ 8.41 (d, 1H, H-6 py), 8.21 (t, 1H, H-4 py), 7.77 (m, 2H, H-3 and H-5 py), 4.84 (br s, 2H, pyCH_2), 4.13 (d, 1H, SCH_2CO), 3.63 (d, 1H, SCH_2CO), 3.63 (d, 1H, gly—CH_2), 3.12 (d, 1H, gly—CH_2), 2.65–3.15 (complex m, 4H, SCH_2CH_2N), 1.66 (s, 3H, NCH_3). Most of the ^{1}H resonances for the minor isomer were either too weak to accurately determine the chemical shifts or overlapping those of the major isomer. However, the NCH_3 resonance was easily observed at 2.73 ppm. ^{13}C NMR of the major isomer (D_2O): δ 183.89, 178.94, 167.02, 149.13, 142.09, 126.63, 124.50, 58.46, 53.43, 43.92, 40.10, 39.22, 37.47. ^{13}C NMR of the minor isomer (D_2O): δ 184.60, 179.03, 167.15, 149.21, 142.09, 126.73, 124.87, 57.46, 53.34, 43.97, 39.50, 39.10, 38.68.

For AA = aiba, the complex was a dihydrate. Found: C, 29.8; H, 4.3; N, 9.9. Calc. for $C_{14}H_{22}F_6N_4O_3PSCo \cdot 2H_2O$: C, 29.7; H, 4.6; N, 9.9%. Vis (H_2O): λ_{max} 504 nm (ε 510). Vis (Me_2SO): λ_{max} 512 nm (ε 540). ^{1}H NMR (D_2O): δ 8.32 (d, 1H, H-6 py), 8.16 (t, 1H, H-4 py), 7.71 (m, 2H, H-3 and H-5 py), 4.72 (br s, 2H, pyCH_2), 4.12 (d, 1H, SCH_2CO), 3.60 (d, 1H, SCH_2CO), 2.65–3.15 (complex m, 4H, SCH_2CH_2N), 1.50 (s, 3H, aiba—CH_3), 1.17 (s, 3H, aiba—CH_3). ^{13}C (D_2O): δ 190.81, 179.05, 167.57, 148.54, 141.92, 126.46, 124.58, 60.62, 53.71, 43.23, 39.68, 39.54, 27.60, 26.84.

β-[Co(pyge)(Cl)(NO_2)] · H_2O

A solution of $NaNO_2$ (0.092 g, 1.33 mmol) was added to a solution of β-[Co(pyge)Cl_2] · H_2O[14] (0.50 g, 1.33 mmol) in water (8 cm^3). After stirring for 10 min, the product began to precipitate. After 1 h, the rose-coloured product (0.093 g, 18% based on the product being a monohydrate) was collected and air-dried. Found: C, 31.5; H, 3.9; N, 14.3. Calc. for $C_{10}H_{14}ClN_4O_3SCo \cdot H_2O$: C, 31.4; H, 4.2; N, 14.6%. ^{1}H NMR (Me_2SO-d_6): δ 9.17 (d, 1H, H-6 py), 8.05 (t, 1H, H-4 py), 7.64 (t, 1H, H-3 py), 7.60 (d, 1H, H-5 py), 4.51 (AB q, 2H, pyCH_2), 4.34 (br s, 1H, NH), 3.85 (br s, 1H, NH), 3.80 (d, 1H, SCH_2CO), 3.44 (d, 1H, SCH_2CO), 2.63 (complex m, 4H, SCH_2CH_2N). ^{13}C NMR (Me_2SO-d_6): δ 176.40, 166.72, 150.19, 138.70, 123.37, 121.79, 52.96, 43.33, 39.48, 36.58.

Crystallization of β-[Co(pyge)(Cl)(NO_2)] · [Co(pyge)(NO_2)$_2$] · $2H_2O$ (**2**)

β-[Co(pyge)(Cl)(NO_2)] · H_2O had limited solubility in water at room temperature; however, dissolution occurred readily in warm (60°C) water. Slow evaporation of a saturated aqueous solution gave dark maroon needles. The ^{1}H NMR spectrum of the crystals in Me_2SO-d_6 was more complex than that of the starting material; the diagnostic H-6 py (*ortho*-hydrogen of the pyridyl group of the pyge ligand) region suggested that the crystals consisted of equal parts β-[Co(pyge)(Cl)(NO_2)] (doublet at δ 9.17) and another cobalt complex, that was likely to be β-[Co(pyge)(NO_2)$_2$] (doublet at δ 8.73).[13] The ^{13}C NMR spectrum (Me_2SO-d_6) of the crystals confirmed this assignment for **2**: in addition to resonances that are attributable to β-[Co(pyge)(Cl)(NO_2)] having the same relative configuration of Cl and NO_2 ligands as in the original starting material before the recrystallization, resonances occurred at δ 175.59, 167.21, 150.38, 138.96, 123.70, 122.17, 52.74, 43.69 and 36.88, in good agreement with literature values for β-[Co(pyge)(NO_2)$_2$].[14]

Promotion of the hydrolysis of amide and ester bonds by β-[Co(pyge)Cl_2] · H_2O

The experiments involving glycine methyl ester, glycylglycine (gly–gly) and L-alanylglycine (L-ala–gly) were conducted in exactly the same fashion as for the preparation of β_1-[Co(pyge)(AA)]PF_6 reported above, except that the above three compounds were substituted for the amino acid. For the first two compounds, the isolated complex had visible, ^{1}H NMR and ^{13}C NMR spectra that were identical to those of independently prepared β_1-[Co(pyge)(gly)]PF_6, while the latter compound gave as the major (> 85%) product a 50 : 50 mixture of the two β_1-[Co(pyge)(L-ala)]PF_6 diastereomers and the minor product (< 15%) β_1-[Co(pyge)(gly)]PF_6. On the other hand, *N*-acetylglycine gave no isolable cobalt(III) amino acid complex, even under forcing conditions of prolonged heating.

Equilibration of diastereomers of β_1-[Co(pyge)(AA)]PF_6 (L = L-ala *and* sar)

The complex β_1-[Co(pyge)(L-ala)]PF_6 was isolated as a 50 : 50 mixture of diastereomers from the preparative procedure employed (*vide supra*). For reasons to be enumerated in the Discussion, we believe that the two isomers have the Δ_L-β_1 and Λ_L-β_1 configurations. If the isolated L-ala cobalt

complex is redissolved in D_2O and the pH adjusted to ~8.0–8.5 (pD ~ 7.6–8.1), the main change in the ^1H NMR spectrum of the solution is the rapid (< 15 min) $^1H/^2H$ exchange of the protons in the $SCH_2C(O)$ moiety of the pyge ligand. If the solution is heated at ~ 50°C, then further spectral changes, involving the coordinated L-ala ligand, occur in the spectrum over a period of time. The L-ala methyl and methine resonances for the two diastereomeric complexes, which are initially equal in intensity, change so that at equilibrium the ratio of major to minor isomer is 63:37. The "major" isomer has resonances at δ 3.76 and 1.24 for the methine and methyl resonances, respectively, while the "minor" isomer displays the analogous peaks at δ 3.32 and 1.40, respectively. The equilibration takes *ca* 1.5–2 days to complete; further monitoring of the solution over an 8-day period revealed no further changes in the ^1H NMR spectrum.

The complex β_1-[Co(pyge)(sar)]PF_6 is also isolated as a mixture of diastereomers due to the formation of an asymmetric centre at the *N*-methyl amino group of sar upon coordination; in this case, each isomeric complex presumably consists of enantiomeric pairs of complexes. The diastereomeric ratio of 14:86 was not affected by added base, implying that the equilibrium ratio of the diastereomers is isolated under the preparative conditions.

X-ray crystallographic studies of **1** *and* **2**

Intensity data for crystals of **1** and **2** were measured on a Nicolet R3mV four-circle diffractometer equipped with a graphite monochromator, using Mo-K_α radiation ($\lambda = 0.71073$ Å). Data were corrected for background, attenuators, Lorentz and polarization effects in the usual fashion, but not for absorption.[21] Heavy atoms were located via Patterson maps and full-matrix least-squares refinement was accomplished with the SHELXTL Plus package of programs. Hydrogen atom positions were calculated geometrically, fixed at a C—H distance of 0.96 Å, and not refined. Crystal data and details of the data collection methods and refinement procedures are given in Table 1 and in supplementary Tables S1 and S10.

The two independent PF_6 anions in **1** were highly disordered and merit some further discussion. From difference Fourier maps, the disorder appeared to be of an axial type, mostly confined to a plane containing four of the six fluorine atoms. The disorder was modelled with some difficulty by inserting six partially occupied fluorine sites for the four atoms and limited the ultimate accuracy of the structure. However, this problem was immaterial to the main purpose of determining the structure of **1**, which was to elucidate the relative configuration

Table 1. Crystallographic data for β_1-[Co(pyge)(gly)]$PF_6 \cdot 2H_2O$ (**1**) and β-[Co(pyge)(Cl)(NO_2)]·[Co(pyge)$(NO_2)_2$]$\cdot 2H_2O$ (**2**)

	1	**2**
Formula	$C_{12}H_{22}F_6N_4O_5PSCo$	$C_{20}H_{32}ClN_9O_{10}S_2Co_2$
M_r	538.29	775.97
Temperature (K)	298	298
Crystal system	Monoclinic	Triclinic
Space group	$P2_1/c$	$P\bar{1}$
a (Å)	14.518(2)	7.850(1)
b (Å)	14.583(2)	13.346(2)
c (Å)	19.783(3)	15.998(2)
α (°)	90	106.45(1)
β (°)	98.51(1)	99.07(1)
γ (°)	90	104.78(1)
V (Å^3)	4142.3(9)	1505.8(8)
$F(000)$	2192	796
Z	8	2
D_c (g cm^{-3})	1.73	1.71
μ (cm^{-1})	10.8	13.9
Number of reflections measured	5916	3247
Number of independent reflections ($\|F_o\| \geq 6\sigma\|F_o\|$)	4053	2495
$R(F_o)$	0.080	0.052
$R_w(F_o)$	0.089	0.058

of the gly ligand with respect to the pyge ligand. Full listings of atomic coordinates, bond lengths and angles, isotropic and anisotropic displacement factors, and hydrogen atom parameters for complexes **1** and **2**, as well as fractional occupancies for the fluorine atoms of the PF_6 anions of **1** have been deposited as supplementary material with the Editor and the Cambridge Crystallographic Data Centre.

RESULTS AND DISCUSSION

The reaction of *cis*-β-[Co(pyge)Cl_2]·H_2O with gly, L-ala, L-val, L-ile, L-leu, β-ala, sar and aiba in aqueous solution at pH 7.7 ± 0.1 and 50–60°C gave good yields of β-[Co(pyge)(AA)]$^+$ (where AA is the corresponding amino acidato ligand). It is likely that intermediates of type β-[Co(pyge)(Cl)(H_2O)]$^+$ or β-[Co(pyge)(H_2O)$_2$]$^{2+}$ are involved in the formation of the amino acid complexes reported herein by analogy to similar known chemistry.[1] Completion of the preparative reaction appeared to be slower in cases where the side group of the amino acid is large (such as in L-val or L-ile) or where a six-membered chelate ring must form (such as for β-ala). The complex ions are readily isolated as their hexafluorophosphate salts in good yields (60–70%).

In general, dilute aqueous solutions of [Co(pyge)(AA)]PF_6 had one broad, relatively symmetrical absorption of modest intensity ($\varepsilon \sim 440 \pm 80$ mol^{-1} dm^3 cm^{-1}) at about 501 ± 3 nm with very little dependence on the identity of the amino acid. A weak shoulder was evident on the higher energy side of this main absorption for some complexes. In dilute Me_2SO solution, the visible band had comparable intensity and line shape to the absorptions in aqueous solution and was bathochromically shifted by 6–10 nm.

In the case of a tertiary *cis*-β octahedral complex with an unsymmetrical bidentate ligand, two geometrical configurations are possible; these isomers are designated as *cis*-β_1 and *cis*-β_2 (see Fig. 1) in accordance with literature convention.[20] Each of these geometrical isomers will exist as a pair of enantiomers (Δ and Λ)[21] for AA = gly, β-ala and aiba and as a pair of diastereomers (Δ_L-β_1, Λ_L-β_1 and Δ_L-β_2, Λ_L-β_2) for AA = L-ala, L-val, L-ile and L-leu due to an intrinsic asymmetric centre in the bidentate ligand. ^{1}H and ^{13}C NMR spectra for [Co(pyge)(AA)]PF_6 strongly indicate that only one of the two possible geometrical configurations (*cis*-β_1 or *cis*-β_2) is found in the isolated complexes for each amino acid ligand, since only one set of NMR resonances is observed for the achiral amino acids and two sets of closely-spaced resonances are observed for the chiral (see Experimental and Fig. 2). The ^{13}C NMR spectra are especially persuasive, since variations in ligating atoms at the two substitutable coordination sites β-[Co(pyge)X_2] result in significant changes in chemical shift for many of the carbon nuclei in the pyge ligand.[13,14,22]

The sar ligand deserves special mention. While sar has no asymmetric centre in the free amino acid, an asymmetric centre at the methylated amino group is generated upon coordination.[8,23] In this case, a mixture of two diastereomeric complexes was isolated in an approximately 14:86 ratio (by integration of the *N*-methyl resonances in the ^{1}H NMR spectrum, which are separated by 1.07 ppm). The presence of two different isomers was most clearly illustrated in the ^{13}C NMR spectrum by the occurrence of pairs of closely spaced resonances. The resonances corresponding to each isomeric complex could be distinguished easily in the ^{13}C NMR spectrum, since there was an approximately 4:1 ratio in intensities for the two resonances in each pair of peaks.

Electronic and NMR spectral results alone were not sufficient to determine the coordination mode (β_1 vs β_2) of the amino acid chelate. Ultimately, the structure of **1** was solved by diffraction methods. Two independent formula units of **1** make up the asymmetric unit of the unit cell. The description of the structure will be limited to that involving the cations, since the PF_6 anions were disordered.

The bonding parameters and ligand conformations within each independent cation are essentially the same. Selected bond distances and angles are provided in Table 2 and an ORTEP representation for "cation A" is depicted in Fig. 3. The pyge ligand adopts the expected *cis*-β configuration.[13,14] Bond lengths and angles within the pyge ligand are very similar to those previously reported for β-[Co(pyge)(NO_2)$_2$]·H_2O.[13]

The geometrical parameters in the cobalt–glycinato moiety are also within expected values.[24–26] The orientation of the gly ligand with respect to the tetradentate ligand is β_1 (with the amino and carboxylato groups of the gly ligand *trans* to the amino and amido groups of the pyge ligand, respectively; see Figs 1 and 3) in each independent cation. The solution visible, ^{1}H NMR and ^{13}C NMR spectra of the crystals of **1** are identical to those of the [Co(pyge)(gly)]PF_6 starting material, strongly suggesting that the β_1 configuration persists in the solution and solid states. Thus, the orientation of the gly ligand in **1** can be reasonably assigned to be β_1; more specifically the Δ,Λ-β_1 pair of enantiomers has been obtained.

As noted above, for [Co(pyge)(AA)]PF_6 (where AA = amino acidato ligands other than gly), NMR

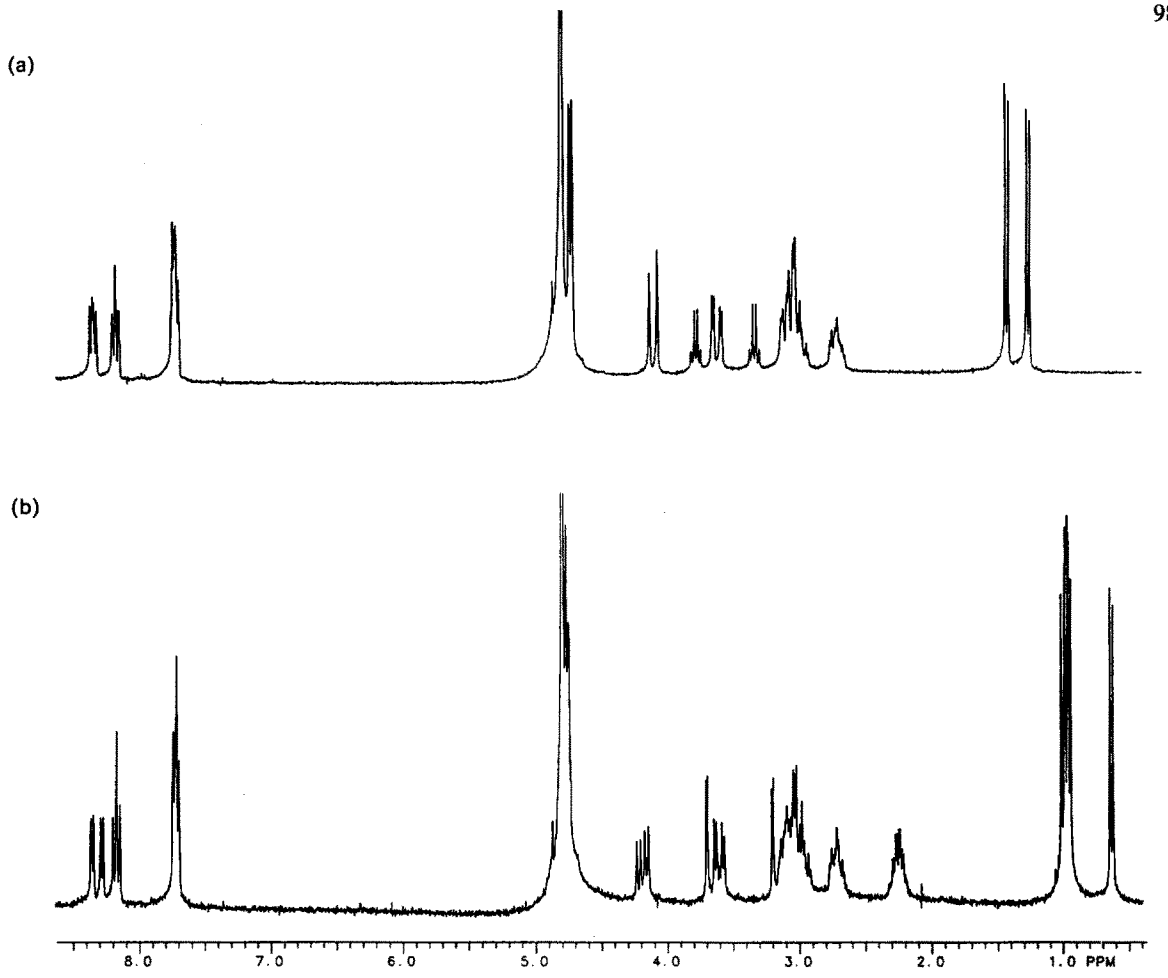

Fig. 2. ^{1}H NMR spectra (D_2O) of (a) β_1-[Co(pyge)(L-ala)]PF_6 and (b) β_1-[Co(pyge)(L-val)]PF_6.

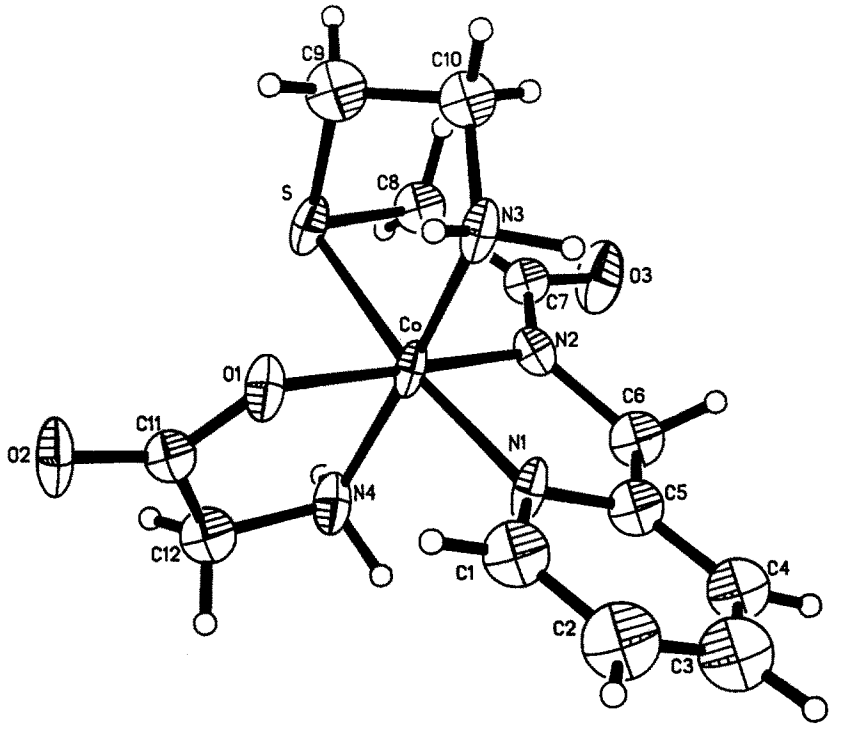

Fig. 3. Molecular structure and atom-numbering scheme for one of the two independent cations of **1**.

Table 2. Selected bond lengths (Å) and angles (°) for the two independent cations of **1**

	Cation A	Cation B
Co—S	2.231(3)	2.222(3)
Co—N(1)	1.920(9)	1.931(8)
Co—N(2)	1.877(8)	1.860(8)
Co—N(3)	1.942(8)	1.958(10)
Co—N(4)	1.983(8)	1.977(10)
Co—O(1)	1.927(7)	1.897(7)
S—Co—O(1)	91.0(2)	89.8(2)
S—Co—N(1)	170.4(2)	171.2(3)
O(1)—Co—N(1)	97.6(3)	98.3(3)
S—Co—N(2)	86.9(3)	87.4(3)
O(1)—Co—N(2)	177.0(3)	176.8(3)
N(1)—Co—N(2)	84.7(4)	84.5(3)
S—Co—N(3)	88.0(3)	89.0(3)
O(1)—Co—N(3)	88.0(3)	89.0(4)
N(1)—Co—N(3)	88.0(3)	87.9(4)
N(2)—Co—N(3)	94.0(3)	92.6(4)
S—Co—N(4)	93.0(3)	93.8(3)
O(1)—Co—N(4)	85.0(3)	85.5(3)
N(1)—Co—N(4)	92.1(4)	90.1(4)
N(2)—Co—N(4)	93.0(3)	93.8(3)
N(3)—Co—N(4)	173.0(4)	173.8(4)

spectral results indicate that the corresponding ^1H and ^{13}C NMR chemical shifts for the pyge backbone ligand are very similar to those in the gly complex and that only one geometrical configuration is isolated. Coupled with the observations that the visible spectra of these complexes are essentially the same in two different solvents as those for AA = gly and that $[Co(pyge)(gly)]^+$ has β_1 geometry, these data imply that the β_1 configuration obtains in general for β-$[Co(pyge)(AA)]^+$.

In order to probe whether the apparent preference for β_1 coordination of the amino acid ligands might be kinetic in origin, β-$[Co(pyge)Cl_2]\cdot H_2O$ was carefully reacted with one equivalent of $NaNO_2$ to give $[Co(pyge)(Cl)(NO_2)]\cdot H_2O$. The ^1H NMR spectrum of the product was typical for a single cobalt complex containing the pyge ligand [see Fig. 4(a) for the portion of the spectrum containing the diagnostic resonance for H-6 of the pyridyl ring of the pyge ligand]. In addition, the ^{13}C NMR spectrum of this material displayed only one set of ligand resonances (see Experimental). Taken together, these pieces of evidence strongly suggest that the isolated material involves the formation of only one new compound. Thus, the occurrence of equal

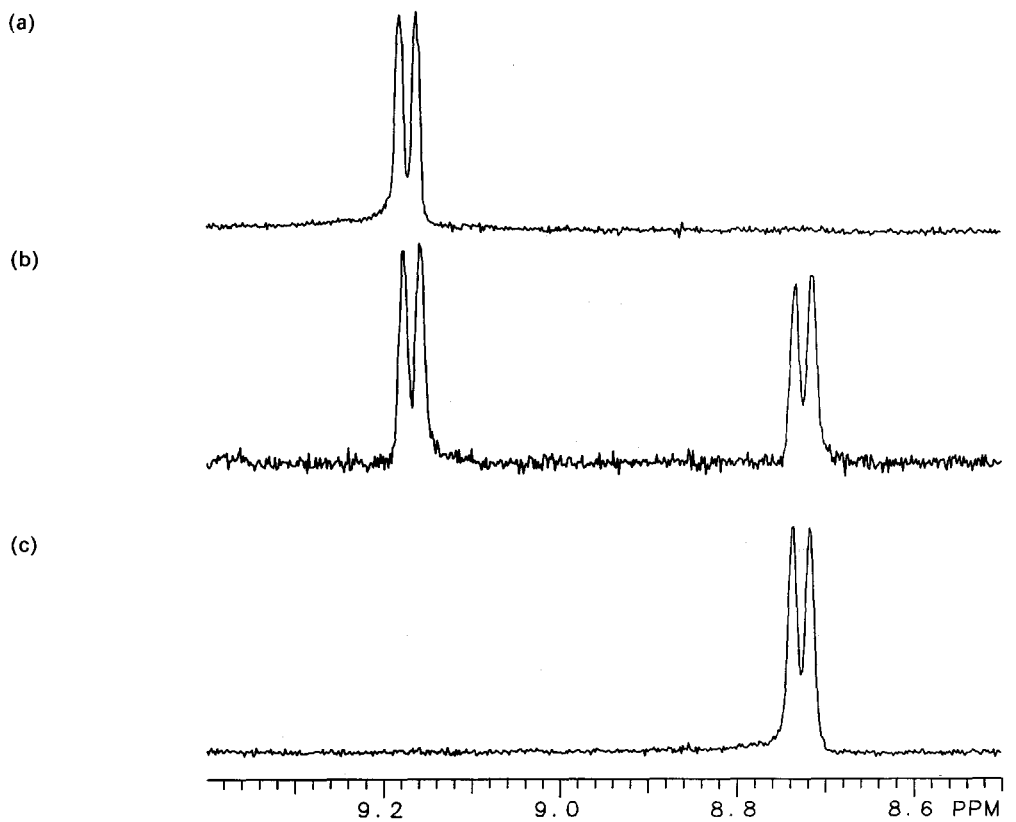

Fig. 4. ^1H NMR spectral expansion (Me_2SO-d_6) of the H-6 pyridyl proton of the pyge ligand for (a) β-$[Co(pyge)(Cl)(NO_2)]\cdot H_2O$, (b) the crystals of **2** and (c) authentic β-$[Co(pyge)(NO_2)_2]$.

mixtures of dinitro and dichloro cobalt(III) complexes was eliminated, as well as the presence of both of the two possible complexes containing one nitro and one chloro ligand. While we could conclude that only one of two possible *cis-β* isomers having one nitrogen and one chloro ligand was present, the relative positions of the two monodentate ligands in the *cis-β* cobalt(III) complex could not be discerned from the NMR spectra.

An attempted recrystallization of *β*-[Co(pyge)(Cl)(NO_2)]·H_2O from hot water led to the isolation of single crystals of the new compound, *β*-[Co(pyge)(Cl)(NO_2)]·[Co(pyge)(NO_2)$_2$]·$2H_2O$ (**2**). Complex **2** possibly arises from the redistribution equilibrium [eq. (1)]:

$$2[\text{Co(pyge)(Cl)}(NO_2)] \rightleftharpoons [\text{Co(pyge)}(NO_2)_2] + [\text{Co(pyge)Cl}_2] \quad (1)$$

The dichloro cobalt(III) complex is very soluble in aqueous solution and could lead to the serendipitous co-crystallization of *β*-[Co(pyge)(Cl)(NO_2)] and *β*-[Co(pyge)(NO_2)$_2$]. The equilibrium mixture of these two complexes could also arise via a series of aquation and anation reactions, as well, without the intervention of *β*-[Co(pyge)Cl_2]. The ^{1}H (see Fig. 4 and the Experimental) and ^{13}C NMR spectra of the crystals consist of a superposition of the resonances for *β*-[Co(pyge)(Cl)(NO_2)] and *β*-[Co(pyge)(NO_2)$_2$]. Most importantly, the NMR spectra confirm that in the crystals of complex **2**, the two monodentate ligands of the *β*-[Co(pyge)(Cl)(NO_2)] moiety have the same relative disposition with respect to one another as in the originally isolated complex, [Co(pyge)(Cl)(NO_2)]·H_2O.

The asymmetric unit of the unit cell for **2** consists of one complex molecule each of [Co(pyge)(Cl)(NO_2)] and [Co(pyge)(NO_2)$_2$] and two water molecules of hydration. Selected bond distances and angles for **2** are collected in Table 3. The pyge ligand in both complexes adopts the *cis-β* geometry that is dictated by the constraints imposed by the tetradentate ligand.[13,14] In general, bond lengths and angles in the two complex molecules are within expected values.[13] The *β*-[Co(pyge)(NO_2)$_2$] molecule is depicted in Fig. 5. The structure is virtually identical to that found for [Co(pyge)(NO_2)$_2$]·H_2O[13] with one minor difference. Although the N(15) nitro ligand is again twisted out of the major coordination plane of ligating atoms and the N(11)—Co(11)—N(15) angle of 99.9(3)° is abnormally large, the twist of this nitro ligand in the present case is in the opposite sense of that found in *β*-[Co(pyge)(NO_2)$_2$]·H_2O.[13] Presumably, the two rotational configurations are comparably stable and allow the nitro ligand to relieve unfavourable steric interactions with the hydrogen atom bonded to C(11) of the pyridyl ring.

The *β*-[Co(pyge)(Cl)(NO_2)] structure is shown in

Table 3. Selected bond lengths (Å) and angles (°) for the two independent molecules of **2**

[Co(pyge)(Cl)(NO_2)]		[Co(pyge)(NO_2)$_2$]	
Co(1)—S(1)	2.230(3)	Co(11)—S(11)	2.241(3)
Co(1)—N(1)	1.953(6)	Co(11)—N(11)	1.952(8)
Co(1)—N(2)	1.895(5)	Co(11)—N(12)	1.901(8)
Co(1)—N(3)	1.992(9)	Co(11)—N(13)	2.008(9)
Co(1)—N(4)	1.932(11)	Co(11)—N(14)	1.925(9)
Co(1)—Cl(1)	2.261(6)	Co(11)—N(15)	1.952(8)
Cl(1)—Co(1)—S(1)	91.5(1)	N(15)—Co(11)—S(11)	90.4(2)
Cl(1)—Co(1)—N(3)	90.9(3)	N(15)—Co(11)—N(13)	91.4(3)
S(1)—Co(1)—N(3)	88.5(2)	S(11)—Co(11)—N(13)	87.9(3)
Cl(1)—Co(1)—N(2)	177.3(2)	N(15)—Co(11)—N(12)	175.7(3)
S(1)—Co(1)—N(2)	86.2(2)	S(11)—Co(11)—N(12)	86.5(2)
N(3)—Co(1)—N(2)	90.6(4)	N(13)—Co(11)—N(12)	91.5(3)
Cl(1)—Co(1)—N(1)	98.5(3)	N(15)—Co(11)—N(11)	99.9(3)
S(1)—Co(1)—N(1)	169.7(3)	S(11)—Co(11)—N(11)	168.9(2)
N(3)—Co(1)—N(1)	89.0(3)	N(13)—Co(11)—N(11)	87.6(3)
N(2)—Co(1)—N(1)	83.8(3)	N(12)—Co(11)—N(11)	83.4(3)
Cl(1)—Co(1)—N(4)	88.5(3)	N(15)—Co(11)—N(14)	89.4(3)
S(1)—Co(1)—N(4)	91.3(3)	S(11)—Co(11)—N(14)	92.9(3)
N(3)—Co(1)—N(4)	179.3(4)	N(13)—Co(11)—N(14)	178.8(3)
N(2)—Co(1)—N(4)	90.0(4)	N(12)—Co(11)—N(14)	87.7(3)
N(1)—Co(1)—N(4)	91.4(3)	N(11)—Co(11)—N(14)	91.4(4)

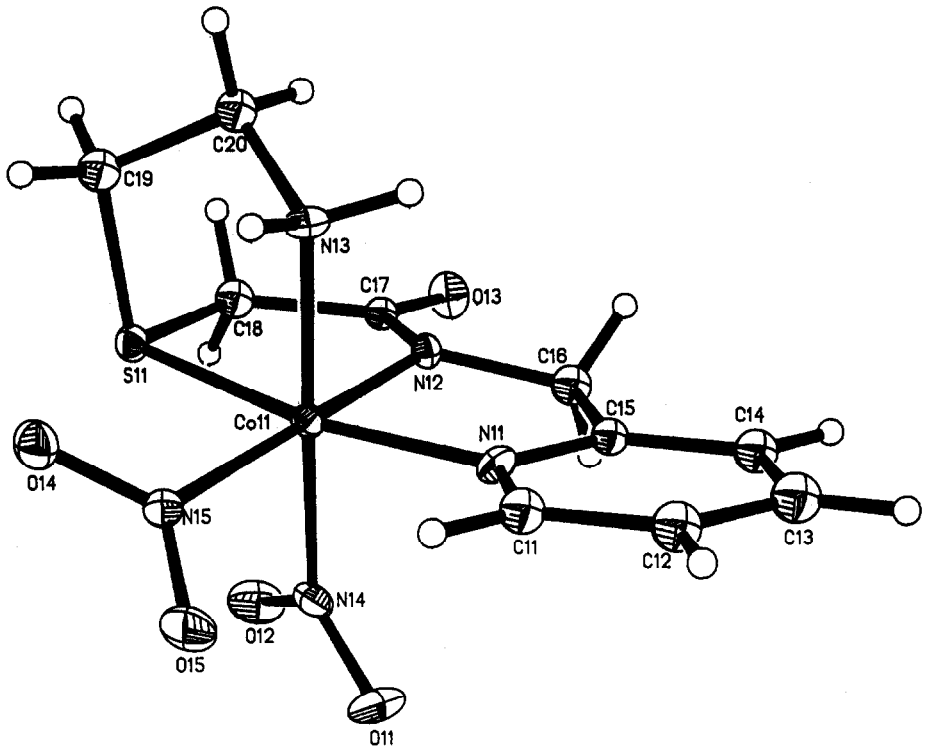

Fig. 5. Molecular structure and atom-numbering scheme for the molecule of β-[Co(pyge)$(NO_2)_2$] of **2**.

Fig. 6. The chloride and NO_2 ligands are *trans* to the amido and amino groups of the pyge ligand, respectively. Thus, coupled with the NMR data reported above, we may conclude that this same configuration of the monodentate ligands also obtains for the original compound from which the crystals of **2** were grown and that the chloride ligand (or possibly aquo ligand) *trans* to the amino donor

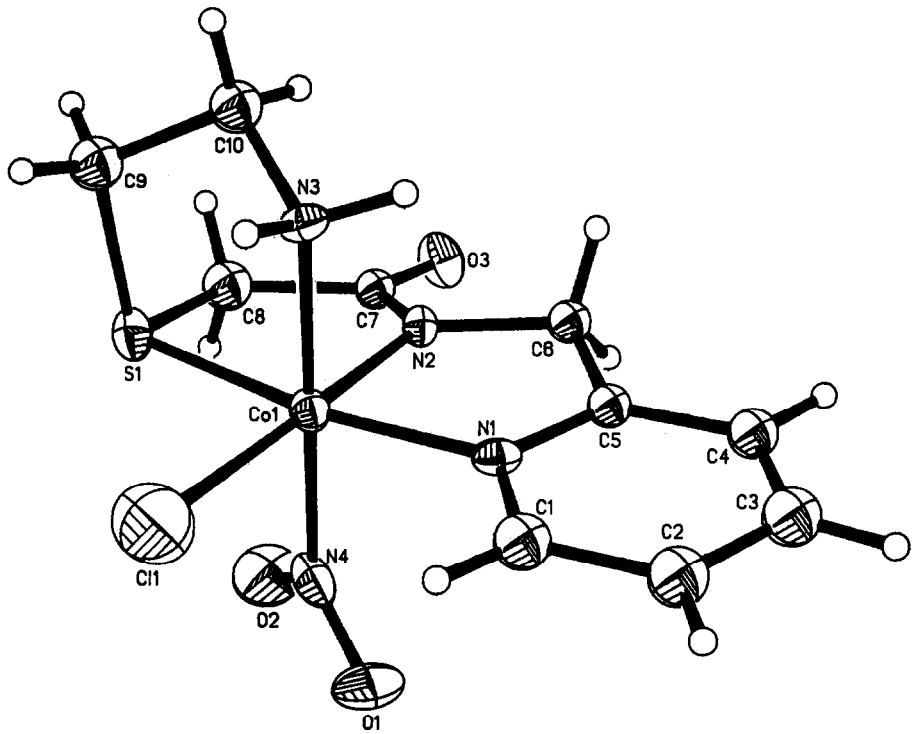

Fig. 6. Molecular structure and atom-numbering scheme for the molecule of β-[Co(pyge)(Cl)(NO_2)] of **2**.

of the pyge ligand is apparently preferentially substituted by the nitro anion in the formation of β-[Co(pyge)(Cl)(NO_2)]. The cobalt(III) centre is known to show a strong affinity for nitrogen donor ligands.[27] We then infer that the β_1 configuration fo the amino acid complexes arises as a result of initial coordination of the amino group of the amino acid ligand to the cobalt ion at the position *trans* to the amino group of the pyge ligand, followed by the chelate ring closure. The isoelectric points (pI) for the amino acids in this study are all near 6.0, so an appreciable fraction of the amino groups of the amino acid ligands should be available for binding under the reaction conditions (pH 7.6–7.8).

The preference for substitution *trans* to the amino donor of the pyge ligand in β-[Co(pyge)Cl_2] could be steric in origin. However, we believe that the steric differences between the two relatively labile coordination sites on cobalt should be too small to account for the extremely high stereoselectivity observed for nitro substitution in the preparation of β-[Co(pyge)(Cl)(NO_2)] and formation of the β_1 amino acid complexes that occurs in the present instance.

We feel that a more likely explanation is that the substitution of the position *trans* to the amino group of the pyge ligand is kinetically favoured; that is, the chloride (or aquo) ligand *trans* to the amino group of pyge is labilized relative to the other chloride (or possibly aquo) ligand *trans* to the amido nitrogen. We would then conclude that the amino group is a better *trans*-labilizer than the deprotonated amido group. Whether this is just intrinsically so, or may be due to the ability of the amino group to readily deprotonate under the slightly basic (pH 7.6–7.8) conditions of the substitution reactions (à la a D-CB type mechanism), is a matter of speculation. We note that in all cases at neutral to basic pH values, the amino protons readily exchange with deuterons from the bulk D_2O solvent by ^1H NMR spectroscopy in support of the above hypothesis. In any event, the geometrical configuration of the amino acid chelate (β_1) would then be established by this kinetically-controlled substitution pattern, combined with the preference of cobalt(III) ions for nitrogen donor ligands.

Examination of the filtrates of preparations of β-[Co(pyge)(AA)]$^+$ revealed little evidence for the formation of significant amounts of complexes with β_2 configuration; essentially only β_1 isomers could be detected within the limits of the NMR techniques. This last result contrasts sharply with elegant studies involving [Co(trien)(gly)]$^{2+}$, where *cis*-α, *cis*-β_1 and *cis*-β_2 isomers could be obtained.[24–26] In the trien case, additional isomerism involving stereochemistry about the coordinated secondary nitrogen donor atoms of the trien ligand must also be considered;[24–26] no such problem occurs in the pyge case of the present investigation. In the case of the chiral AA ligands, we exclude the possibility that Δ_D-β_1 and Λ_D-β_1 isomers might also be present in significant amounts also. In order for these complexes to be formed, either racemization of the asymmetric centre on the amino acid would have to occur before coordination, or epimerization might occur after coordination to the cobalt centre. We feel that the former is unlikely given the mild conditions employed in the synthesis of the amino acid complexes. The latter is more problematic, since epimerization of amino acids chelated to cobalt(III) and other metal ion centres is a well-known phenomenon.[28] However, no evidence for $^1H/^2H$ exchange was found for the methine proton of coordinated L-ala under pH conditions entirely analogous to those employed in the synthesis of the complexes (*vide infra*). Thus, the assignment of the Δ_L-β_1 and Λ_L-β_1 configurations appears to be secure for the asymmetric amino acids.

The equilibration of diastereomeric cobalt(III) amino acid complexes under basic conditions (pH ~ 8.0) was studied for AA = sar and L-ala. For AA = sar, the asymmetry arises as a result of the chiral coordinated *N*—CH_3 group. Two β_1 isomers are isolated (presumably as a mixture of two pairs of enantiomers) in a ratio of 14 : 86, which does not change over a period of time at basic pH values; the only change in the ^1H NMR spectrum involved the $SCH_2C(O)$ protons which were rapidly exchanged for deuterons. The isolation of an equilibrium mixture of isomers is understandable by consideration of the facile $^1H/^2H$ exchange for the protons at coordinated amino groups of the ligands at neutral to basic pH values (*vide supra*).

The *N*—CH_3 resonance for the sar ligand occurs in the ^1H NMR spectrum at δ 1.66 for the major isomer and δ 2.73 for the minor isomer [for free sar, δ(*N*—CH_3) is 2.77 ppm]. The large upfield shift of this resonance for the predominant complex suggests that it is the isomer with the *N*—CH_3 group situated under the pyridyl ring of the pyge ligand and thus, in the shielding region of the aromatic ring. Using tables of computed shieldings due to aromatic ring currents,[29] combined with structural parameters estimated from the molecular structure of **1**,* we can calculate a ring-current shielding of

* The required structural parameters for the sar complex with the *N*—CH_3 moiety under the pyridyl ring are $z = 2.2$ Å and $p = 1.8$ Å, while for the isomer with the opposite configuration at nitrogen, $z = 2.2$ Å and $p = 5.2$ Å. See ref. 29 for definitions of z and p.

−1.07 ppm for the sar complex with the *N*—CH_3 group under the ring and a ring-current contribution of +0.08 ppm for the other isomer with the opposite configuration at nitrogen. The predicted difference in chemical shifts of 1.15 ppm, based solely on ring current effects,[29,*] is very close to the observed difference of 1.07 ppm. Furthermore, irradiation of the *N*—CH_3 ^{1}H NMR resonance at δ 1.66 under NOE conditions resulted in a 10±2% increase in intensity in the H-6 pyridyl proton resonance of the pyge ligand. We estimate that these groups should be *ca* 3.0 Å apart from the structural determination of **1**. Literature results suggest that *ca* 15% enhancement can be expected for ^{1}H–^{1}H NOE for these types of groups separated by this distance.[30]

In terms of the above interpretation, the observed preference in [Co(pyge)(sar)]$^+$ for the β_1 diastereomer with the *N*—CH_3 moiety under the pyridyl group may be explained in terms of electronic, and possibly, steric origins. Stability might be gained via hydrophobic and/or attractive van der Waals' interactions between the methyl and pyridyl groups by having the *N*—CH_3 functionality under the electron-deficient pyridyl ring. In addition, this configuration could allow more favourable solvation of the amino proton of the sar ligand. Such types of interactions are well-documented and depend upon a number of factors, including the nature of the groups involved and solvent polarity.[31–33] We note that unfavourable steric interactions might also come about in the minor diastereomer from van der Waals' interactions between the *N*—CH_3 moiety and one of the hydrogen atoms on C(8), as well as the lone pair of electrons on S(7) of the pyge ligand.

On the other hand, for AA = L-ala, the two β_1 diastereomers (Δ_L-β_1 and Λ_L-β_1) are isolated in essentially equal amounts, but can be equilibrated to a 37 : 63 ratio under basic conditions (pH ~ 8.0) over a period of 2 days (see Fig. 7). If we again presume that the further upfield shift of the L-ala methyl group for the preferred diastereomer arises from its proximity to the shielding region of the pyridyl ring, then similar arguments to that for AA = sar (*vide supra*) obtain in this case in order to explain the observed results. Further support for this hypothesis may be derived from the fact that the L-ala methine resonance for the minor isomer is observed upfield from that of the major isomer (Fig. 7). This reversal in chemical shift order (compared with that of the methyl resonances) is reasonable since the methine proton for the minor isomer should now be the group closest to the shielding region of the pyridyl ring.

However, there is a less marked discrimination of one isomer (Λ_L-β_1) over the other (Δ_L-β_1) at equilibrium in the L-ala vs the sar case. This can be understood from the viewpoint of a less efficient hydrophobic interaction of the methyl group of L-ala with the pyridyl ring of the pyge ligand due to distance constraints, which is in accord with the smaller difference in the chemical shifts for the pertinent methyl group of the two diastereomers in the L-ala case as compared with that for sar. It is also likely that any steric interactions involving C(8) and S(7) (*vide supra*) are lessened with the methyl group attached to the α-carbon atom in L-ala, as opposed to the amino group in sar.

In the case of the base-catalysed equilibration of the β_1-[Co(pyge)(L-ala)]$^+$ diastereomers, another interesting development occurs. Up until this point in the discussion, we have largely presumed that the stereochemistry about the asymmetric centre on the chelated L-ala ligand is preserved during equilibration. The equilibration could occur via carbanionic epimerization of the asymmetric centre at the α-carbon atom of the L-ala ligand as has been previously observed for [Co(en)$_2$(AA)]$^{2+}$ (en = 1,2-diaminoethane).[28] However, essentially *no* deuterium exchange is observed for that methine proton in the ^{1}H NMR spectra during the equilibration of the β_1-[Co(pyge)(L-ala)]$^+$ isomers (see Fig. 7). This consequence means that either the carbanion intermediate is preferentially reprotonated instead of deuterated or that a different mechanism is operational in the instance at hand. Since the equilibration of the β_1-[Co(pyge)(L-ala)]$^+$ complexes was performed at pH ~ 8.0 (at higher pH values, significant decomposition occurs, possibly involving the pyge ligand) vs pH > 11 for the en complexes, and since the reprotonation should be highly unlikely, we favour the latter explanation.

One possible isomerization mechanism to explain the present results is somewhat reminiscent of that proposed for epimerization of *cis*-β-[Co(7,7′-Me_2salen)(AA)] [7,7′-Me_2salen = bis(2′-hydroxyacetophenone)ethylenediimine] and related complexes in which metal–ligand bond-breaking is invoked.[34] In this scenario, the two β_1-[Co(pyge)(L-ala)]$^+$ diastereomers can be equilibrated via exchange of coordination positions by the amino group of the pyge ligand with that of the amino donor of the L-ala ligand under base catalysis, with all other donor atoms remaining in their original coordination sites. One of the amino groups could be deprotonated, thereby labilizing the amino ligand at the *trans* position; the deprotonation of coordinated amino donors in β_1-[Co(pyge)(AA)]$^+$ is

* See footnote on previous page.

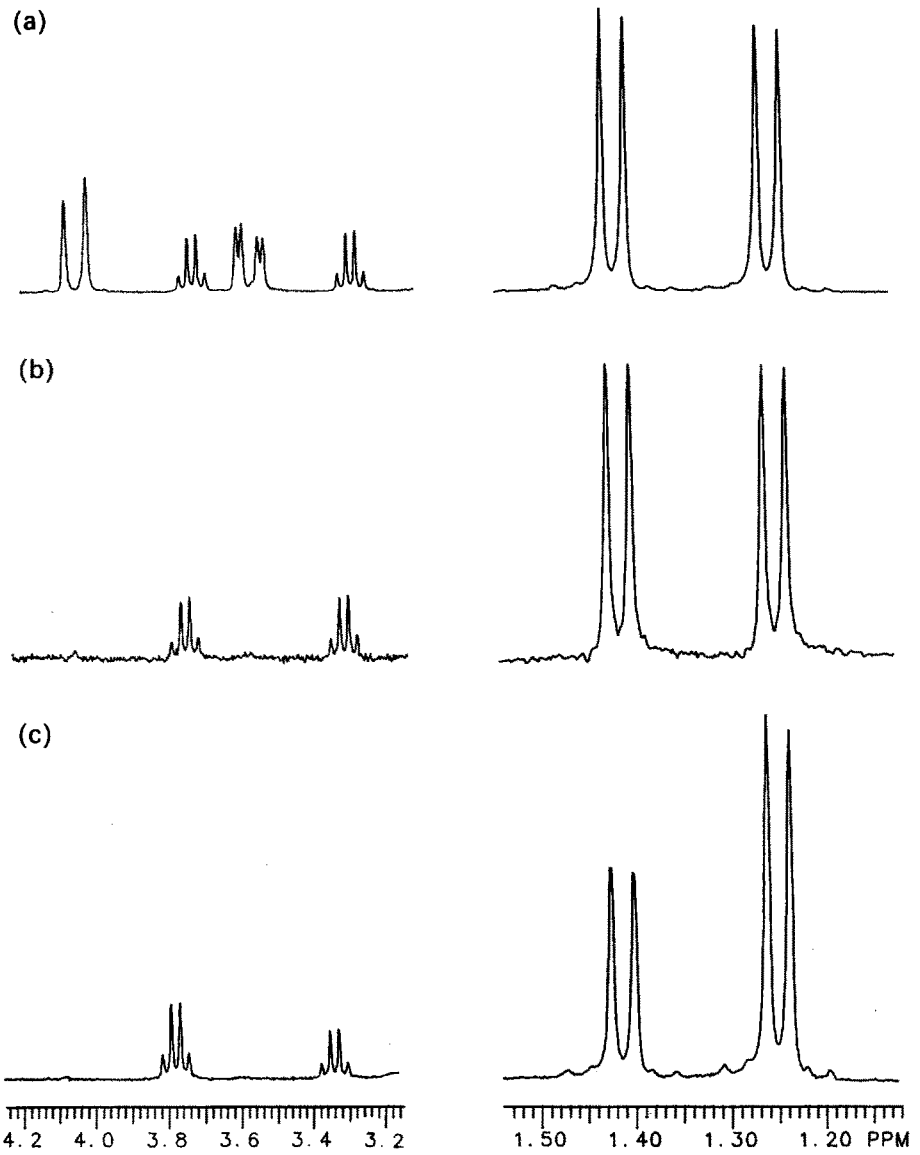

Fig. 7. ^{1}H NMR spectral expansions (D_2O) for the methine and methyl resonances of the L-ala ligand of β_1-[Co(pyge)(L-ala)]PF_6: (a) neutral D_2O, (b) 15 min after addition of NaOD (pH ~ 8.0) and (c) at equilibrium (45 h after addition of NaOD).

feasible as demonstrated above by the facile exchange of amino protons in neutral to basic D_2O solution. We would then require that the dangling amino group swing around to substitute at the position of the other amino ligand, which would then eventually occupy the other, recently vacated site. Considerable reorganization, including an inversion at the sulphur centre, would be required, and may explain the relatively slow approach to equilibrium. Other mechanisms, including intermolecular ones, may be put forth; however, the above speculative mechanism is consistent with the lack of deuterium exchange observed at the α-carbon atom with the L-ala ligand.

The complex β-[Co(pyge)Cl_2]·H_2O (or its corresponding hydrolysis products) is also quite effective in the promotion of the hydrolysis of peptide and amino acid ester bonds under mild conditions (50–60°C, pH 7.6–7.8, 0.5–1.0 h) in much the same manner as $[CoN_4(OH)(H_2O)]^{2+}$ (where N_4 is one tetradentate ligand or two bidentate ligands with four nitrogen donor atoms) and related complexes.[1,4,7,10] Thus, the reaction of the dichloro cobalt complex with either gly–gly or gly methyl ester gives β_1-[Co(pyge)(gly)]$^+$, with no detectable intermediate. The spectroscopic (visible, ^{1}H and ^{13}C NMR) analysis of the isolated complexes indicates that they have the same β_1 configuration as the complex prepared from gly.

With the unsymmetrical dipeptide L-ala–gly, the

major isolated product (> 85–90%) is the mixture of β_1 diastereomers of [Co(pyge)(L-ala)]$^+$. The remainder of the isolated material is mostly β_1-[Co(pyge)(gly)]$^+$. The formation of the gly cobalt complex could occur via a small amount of *O*-terminal cleavage or by competition of gly formed in the N-terminal hydrolysis of L-ala–gly with unreacted L-ala–gly for cobalt reactive sites. In order to determine which of the two possibilities might be operating in this case, the dichloro cobalt complex was treated with *N*-acetylglycine. Essentially no hydrolysis occurred, even after long reaction times. Thus, it appears that the promotion of the cleavage of the dipeptides and amino acid esters proceeds via prior coordination of the *N*-terminal end, followed by chelation with and activation of the carbonyl oxygen of the functionality to be hydrolysed, much as has been elegantly demonstrated for similar cobalt complexes.[1,4,7] The stereoselective control of the configuration (again β_1) of the isolated amino acidato complexes in the hydrolyses would then be the result of the same kinetic factors enumerated above in the direct syntheses of β_1-[Co(pyge)(AA)]$^+$.

Conclusions

The β-[Co(pyge)X_2] complexes have proved to be a versatile system for the study of the stereochemical coordination preferences of amino acid anionic ligands. The tetradentate ligand, pyge, enforces the strict formation of pseudo-octahedral complexes having the *cis*-β geometry. At first glance, this would appear to be a hindrance with regard to unsymmetrical bidentate chelates, since such ligands could potentially coordinate in two different geometrical configurations, β_1 and β_2. However, the unsymmetrical nature of the pyge ligand apparently leads to the kinetically-controlled isolation of only the β_1 isomer. The complex β-[Co(pyge)Cl_2] promotes the hydrolysis of amide and ester bonds of α-amino carbonyl compounds from the *N*-terminal end under mild conditions, again giving only β_1-cobalt(III) amino acid complexes.

In cases where an asymmetric centre is formed upon chelation to the cobalt(III) centre (sar) or is contained in the amino acid ligand (L-ala), diastereomeric β_1-complexes are isolated. In the former case, the diastereomers are isolated in their equilibrium ratio (14 : 86). On the other hand, in the latter case a 50 : 50 mixture of the two diastereomers are isolated, which can be slowly equilibrated under basic conditions to a 37 : 63 proportion, without the involvement of a carbanionic intermediate. In both instances, evidence was presented and arguments put forth that the favoured diastereomer was the β_1-complex with the methyl group of the amino acid chelate in position to interact with the pyridyl moiety of the pyge ligand. Such types of interactions have been proposed to be important with regard to substrate binding to metalloenzymes, including carboxypeptidase A.[31] In view of the peptidase type activity demonstrated by β-[Co(pyge)Cl_2] and the hydrophobic stereochemical preferences shown by sar and L-ala reported herein, work is in progress towards the end of extending these studies to other optically active amino acids and related unsymmetrical bidentate ligands.

Acknowledgements—We thank the State University of New York at Albany Faculty Research Program and the U.S. Army Research Office under Grant DAAL-0388K0198 for their generous financial support. We also thank Professor Shelton Bank for helpful discussions regarding the NMR experiments and Sriram Naganathan for obtaining the NOE NMR spectra.

REFERENCES

1. P. A. Sutton and D. A. Buckingham, *Accts Chem. Res.* 1987, **20**, 357.
2. M. Yashiro, S.Yano, M. Ajioka, S. Yano, K. Toriumi, T. Ito and S. Yoshikawa, *Inorg. Chem.* 1986, **25**, 1709 and refs therein.
3. E. F. Birse, P. A. Williams, F. S. Stephens and R. S. Vagg, *Inorg. Chim. Acta* 1988, **148**, 63 and refs therein.
4. R. W. Hay and P. J. Morris, *Met. Ions Biol. Syst.* 1976, **5**, 173.
5. D. A. Buckingham, in *Biological Aspects of Inorganic Chemistry* (Edited by A. W. Addison, W. R. Cullen, D. Dolphin and B. R. James), p. 141. Wiley, New York (1977).
6. Y. Fujii, Y. Yoshikawa, M. Syoji and H. Shinohara, *Bull. Chem. Soc. Japan* 1990, **63**, 138 and refs therein.
7. D. A. Buckingham, J. Dekkers, A. M. Sargeson and L. G. Marzilli, *Inorg. Chem.* 1973, **12**, 1207.
8. D. A. Buckingham, I. P. Maxwell and A. M. Sargeson, *J. Chem. Soc., Chem. Commun.* 1969, 581.
9. C. J. Boreham, D. A. Buckingham and F. R. Keene, *J. Am. Chem. Soc.* 1979, **101**, 1409 and refs therein.
10. M.-J. Rhee and C. B. Storm, *J. Inorg. Biochem.* 1979, **11**, 17.
11. D. A. Buckingham, J. Dekkers and A. M. Sargeson, *J. Am. Chem. Soc.* 1973, **95**, 4173.
12. A. Hammershoi, R. M. Hartshorn and A. M. Sargeson, *J. Chem. Soc., Chem. Commun.* 1988, 1267.
13. P. J. Toscano, K. A. Belsky, L. M. Engelhardt, K. J. Fordon and A. H. White, *Inorg. Chem.* 1990, **29**, 1357.
14. P. J. Toscano and L. G. Marzilli, *Inorg. Chem.* 1983, **22**, 3342.
15. M. Toprak, E. Gellert and O. Bekaroglu, *Transition Met. Chem. (Weinheim, Ger.)* 1979, **4**, 372.
16. P. J. Toscano, K. J. Fordon, L. M. Engelhardt, B. W.

Skelton, A. H. White and P. A. Marzilli, *Polyhedron* 1990, **9**, 1079.
17. B. Bosnich, W. R. Kneen and A. T. Phillip, *Inorg. Chem.* 1969, **8**, 2567.
18. J. H. Worrell and D. H. Busch, *Inorg. Chem.* 1969, **8**, 1572.
19. H. Sigel and R. B. Martin, *Chem. Rev.* 1982, **82**, 385.
20. D. A. Buckingham and L. G. Marzilli, *Inorg. Chem.* 1967, **6**, 1042.
21. A. Bruce, J. L. Corbin, P. L. Dahlstrom, J. R. Hyde, M. Minelli, E. I. Stiefel, J. T. Spence and J. Zubieta, *Inorg. Chem.* 1982, **21**, 917.
22. P. J. Toscano, unpublished results.
23. Y. Fujii, M. Matsufuru, A. Saito and S. Tsuchiya, *Bull. Chem. Soc. Japan* 1981, **54**, 2029.
24. B. F. Anderson, J. D. Bell, D. A. Buckingham, P. J. Cresswell, G. J. Gainsford, L. G. Marzilli, G. B. Robertson and A. M. Sargeson, *Inorg. Chem.* 1977, **16**, 3233.
25. D. A. Buckingham, R. J. Dellaca, M. Dwyer, G. J. Gainsford, L. G. Marzilli, I. E. Maxwell, W. T. Robinson, A. M. Sargeson and K. R. Turnbull, *J. Am. Chem. Soc.* 1974, **96**, 1713.
26. D. A. Buckingham, M. Dwyer, G. J. Gainsford, V. J. Ho, L. G. Marzilli, W. T. Robinson, A. M. Sargeson and K. R. Turnbull, *Inorg. Chem.* 1975, **14**, 1739.
27. F. A. Cotton and G. Wilkinson, *Advanced Inorganic Chemistry*, 5th edn, p. 732. Wiley, New York (1988).
28. D. A. Buckingham, I. Stewart and P. A. Sutton, *J. Am. Chem. Soc.* 1990, **112**, 845 and refs therein.
29. J. W. Emsley, J. Feeney and L. H. Sutcliffe, *High Resolution Nuclear Magnetic Resonance Spectroscopy*, Vol. 1, pp. 595–604. Pergamon Press, Oxford (1965).
30. T. C. Farrar, *Pulse Nuclear Magnetic Resonance Spectroscopy*, 2nd edn, pp. 136–140. The Farragut Press, Chicago (1989).
31. H. Sigel, *Pure Appl. Chem.* 1989, **61**, 923 and refs therein.
32. H. Sigel, *Chimia* 1990, **44**, 55.
33. O. Yamauchi, A. Odani, T. Kohzuma, H. Masuda, K. Toriumi and K. Saito, *Inorg. Chem.* 1989, **28**, 4066.
34. Y. Fujii, K. Shiono, K. Ezuka and T. Isago, *Bull. Chem. Soc. Japan* 1980, **53**, 3537.

Polyhedron Vol. 10, No. 9, pp. 993–995, 1991
Printed in Great Britain

0277–5387/91 $3.00+.00
Pergamon Press plc

COMMUNICATION

POLYKETONES VIA OXIDATION OF POLYBUTADIENES CATALYSED BY COMPLEXES OF PLATINUM(II)

AHMED IRAQI and DAVID J. COLE-HAMILTON*

Chemistry Department, University of St Andrews, St Andrews, Fife, KY16 9ST, Scotland, U.K.

(*Received* 23 *January* 1991; *accepted* 5 *February* 1991)

Abstract—Polybutadienes containing different ratios of 1,4- and 1,2-polymerized units are converted to polyketones by oxidation with ^{t}BuOOH in the presence of catalytic quantities of $[Pt(diphoe)CF_3(CH_2Cl_2)]^+$ (diphoe = $Ph_2PCH{=}CHPPh_2$); reactivity ratios for the different double bonds are determined as pendant/*trans*/*cis*, 6 : 5 : 3.

Polyketones are known to be good precursors for the synthesis of many other polymers,[1] but they also have considerable potential uses in their own right since they are photodegradable.[2] Polyketones can be synthesized by (i) polymerization of unsaturated ketones using metal alkyl catalysts[3] or free radical initiators;[4] (ii) co-polymerization of unsaturated ketones with other unsaturated monomers such as 2-chloro-1,3-butadiene[5] or vinyl acetate;[6] and (iii) co-polymerization of carbon monoxide with ethene catalysed by palladium(II) complexes.[7]

We have been investigating the synthesis of new polymers via the modification of polybutadiene using homogeneous catalysis. In a previous communication[8] we reported that polybutadiene containing 55% of its double bonds in the backbone of the polymer and 45% pendant from the double bond could be selectively epoxidized only on the backbone double bonds using ^{t}BuOOH as oxidant and a molybdenum-based catalyst that we have developed. In order to attempt to prepare polyketones with different structures using homogeneous catalysis, we have studied reactions of polybutadienes with ^{t}BuOOH in the presence of $[Pt(diphoe)CF_3(CH_2Cl_2)]^+$ (diphoe = $Ph_2PCH{=}CHPPh_2$). This catalyst system has been extensively studied by Strukul *et al.* and has been shown to be selective for the formation of methylketones from terminal alkenes. Very few other catalysts allow oxidation of alkenes to methyl ketones and none is as active and selective as $[Pt(diphoe)CF_3(CH_2Cl_2)]^+$.

Polybutadienes having a variety of different structures were reacted with ^{t}BuOOH in dichloromethane containing the catalyst at 80°C in sealed tubes under nitrogen.† The resulting polymers were isolated and analysed using IR, ^{1}H and ^{13}C NMR spectroscopy. The starting materials were selected so as to have various proportions of *cis* and *trans* backbone or terminal pendant double bonds (see Table 1).

All of the products show strong absorption in their IR spectra at *ca* 1720 cm^{-1} and resonances in the ^{13}C NMR spectra near δ 212 (this is generally a weak resonance and is not observed for the product from *cis*-polybutadiene, where only low conversion is obtained) confirming that ketones are formed. The carbon atoms α to the ketones give resonances at δ 26.5 and 26.6 and resonances from protons on the ketones appear near δ 1.25. From integration of the ^{1}H NMR spectra it is possible to determine the extent of oxidation as well as the pendant/backbone

* Author to whom correspondence should be addressed.

† In the absence of added catalyst, a low conversion (~5%) to alcoholic type products [^{13}C NMR: δ 82 (pendant double bonds) and 86 (backbone double bonds)] is observed. These are not peroxides of the polymer since they are not removed by shaking with acidified ferrous ammonium sulphate, but are obtained as a side product (> 5%) in the catalytic reaction.

Table 1. Composition of polymers (%) formed by oxidation of polybutadienes; figures in parentheses represent per cent conversion of the particular type of double bond

	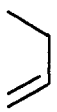		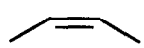	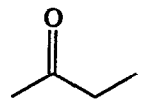	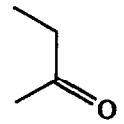	Overall conversion (%)
cis-Polybutadiene, 100% *cis*-1,4	—	—	88 (12)	12	—	12
Polybutadiene, 21% vinyl, 19% *cis*-1,4 and 60% *trans*-1,4	9 (57)	34 (43)	13 (31)	32	12	44
Polybutadiene, 47% vinyl, 17% *cis*-1,4 and 36% *trans*-1,4	18 (61)	17 (52)	12 (29)	24	29	53
Polybutadiene, 83% vinyl, 17% *trans*-1,4	34 (59)	9 (47)	—	8	49	57

selectively, whilst integration of resonances at δ 27.5 and 32.8 gives the relative amounts of *cis* and *trans* backbone double bonds remaining in the polymer.[10] Integration of these resonances relative to the resonances at δ 26.5 and 26.6 gives an internal check on the calculations.

The results of these analyses are shown in Table 1 and indicate that in all cases partial oxidation to ketones occurs. Unlike simple alkenes, in which high selectivities to oxidation of terminal double bonds are observed,[9] both internal and terminal double bonds in the polymers are oxidized and it is therefore possible to calculate reactivity ratios of terminal/internal of *ca* 4:3 for a polymer with approximately equal amounts of pendant and backbone double bonds. The relatively high reactivity of the internal double bonds is somewhat surprising in view of the results obtained with simple alkenes.[9]

The overall conversion of double bonds to ketonic functions increases as the proportion of pendant double bonds in the polymer increases, although not simply as a result of the higher reactivity of the pendant double bonds. Thus, if only *cis* double bonds are present in the polymer, 12% of these are oxidized, whereas in other cases the conversion of backbone double bonds under similar conditions can be as high as 47%.

Analysis of Table 1 shows that this arises because of a higher reactivity of the *trans* than of the *cis* backbone double bonds. From a comparison of the data in Table 1, it appears that a reactivity ratio of 6:5:3 for pendant/*trans*/*cis* double bonds is operating. All *cis*-1,4-polybutadiene appears to be less reactive, however, than expected on this basis.

Since the ratio of the different kinds of double bonds in the polymer can readily be controlled, the oxidation reaction that we report and which is illustrated in Scheme 1 provides a versatile route to polymers containing ketone groups pendant from the main chain and/or in the backbone, with ready

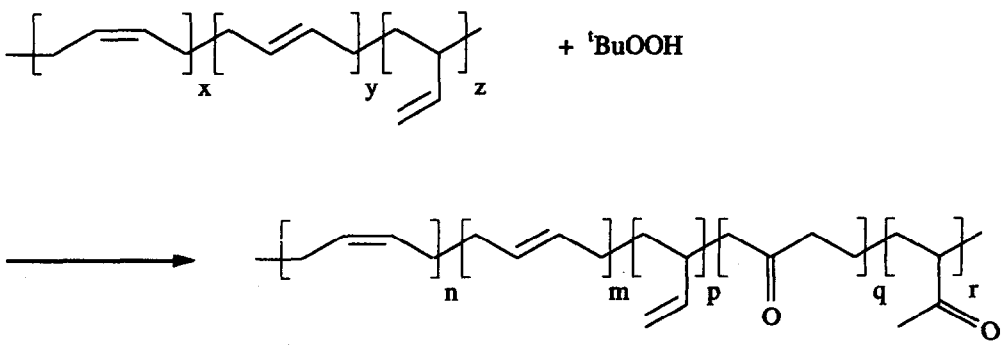

Scheme 1. Oxidation of polybutadiene to polyketones catalysed by $[Pt(diphoe)CF_3(CH_2Cl_2)]^+$.

control of the two types of ketone group. It also provides a simple method for functionalizing at the internal carbon atom of pendant double bonds in polybutadienes. Other reactions that we have studied either functionalize the backbone double bonds (epoxidation)[8] or the terminal atom of the pendant double bonds (hydroformylation, hydrosilation[11]).

Acknowledgements—We thank the SERC for support (A.I.), Johnson Matthey plc for generous loans of platinum metal salts, and the Japanese Soda Company for generous gifts of samples of polybutadienes.

REFERENCES

1. (a) Y. Morishima, T. Takizawa and S. Murahoshi, *Eur. Polym. J.* 1973, **9**, 669; (b) A. Sen, Z. Jiang and J. T. Chen, *Macromolecules* 1989, **22**, 2012.
2. (a) M. Heskins and J. E. Guillet, *Macromolecules* 1970, **3**, 224; (b) Y. Amerik and J. E. Guillet, *Macromolecules* 1971, **4**, 375.
3. (a) T. Tsuruta, R. Fujio and J. Furukawa, *Makromolec. Chem.* 1964, **80**, 172; (b) P. R. Thomas, G. J. Tyler, T. E. Edwards, A. T. Radcliffe and R. C. P. Cubben, *Polymer* 1964, **5**, 525.
4. A. K. Chaudhuri and S. Basu, *Makromolec. Chem.* 1959, **29**, 48.
5. G. S. Wish and N. Brodoway, *J. Polym. Sci. A* 1963, **1**, 2163.
6. H. C. Haas and M. S. Simon, *J. Polym. Sci.* 1952, **9**, 309.
7. T. W. Lai and A. Sen, *Organometallics* 1984, **3**, 866.
8. M. Gahagan, A. Iraqi, D. C. Cupertino, R. K. Mackie and D. J. Cole-Hamilton, *J. Chem. Soc., Chem. Commun.* 1989, 1688.
9. G. Strukul, R. Sinigalia, A. Zanardo, F. Pinna and R. A. Michelin, *Inorg. Chem.* 1989, **28**, 554 and refs therein.
10. A. D. H. Clague, J. A. M. van Broekhouen and L. P. Blaauw, *Macromolecules* 1974, **7**, 348.
11. A. Iraqi, I. D. Utuk and D. J. Cole-Hamilton, unpublished observations.

Polyhedron Vol. 10, No. 10, pp. 997–1005, 1991
Printed in Great Britain

0277-5387/91 $3.00+.00
© 1991 Pergamon Press plc

SYNTHESIS OF ISOTOPOMERIC BINUCLEAR THIO COMPLEXES OF MOLYBDENUM AND TUNGSTEN AND THE STUDY OF THEIR VIBRATIONAL SPECTRA

V. P. FEDIN,* B. A. KOLESOV, Yu. V. MIRONOV, O. A. GERAS'KO and V. YE. FEDOROV

Institute of Inorganic Chemistry, Siberian Branch of Academy of Sciences of the U.S.S.R., Novosibirsk, pr. Lavrentyeva 3, 630090, U.S.S.R.

(*Received* 25 *July* 1990; *accepted* 9 *October* 1990)

Abstract—Alkylammonium salts, $W_2{}^{34}S_4X_4{}^{2-}$ (X = Cl, Br), $M_2{}^{34}S_4Br_8{}^{2-}$ (M = Mo, W) and $Mo_2{}^{34}S_6O_2{}^{2-}$, have been obtained from $^{34}S_8$. IR and Raman spectra of these compounds have been studied and the normal vibrations calculated. A number of vibrations involving sulphur atoms [for example ν(M=S), ν(S—S)] are characteristic, which allows vibrational spectroscopy to be used to study the changes occurring in the metal–sulphur containing fragments. The interaction of $W_2(\mu_2\text{-}S)(\mu_2\text{-}S_2)Br_8{}^{2-}$ with $^{34}S_8$ was shown to produce $W_2(\mu_2\text{-}S_2)_2Br_8{}^{2-}$. The reaction of $Mo_2(\mu_2\text{-}{}^{34}S_2)_2Cl_4Cl_{4/2}$ with $S_x{}^{2-}$ results in the replacement of ^{34}S by ^{32}S to produce the $Mo_2(\mu_2\text{-}S_2)_2(S_2)_4{}^{2-}$ complex.

As a result of studies in the last 10–15 years a large new area of specifically built polynuclear thio complexes of transition metals has been revealed. The greatest number of synthetic results in the study of homometallic complexes have been obtained for molybdenum and tungsten.[1–3] These complexes may undergo complex rearrangements, accompanied by substantial changes in their metal–sulphur containing fragments.[3–5] Important information on the structural changes in these clusters upon their transformations can be obtained by using X-ray structural analysis and vibrational spectroscopy methods.[6–9] In the literature there have been practically no reports on the calculations of normal vibrations, which appears to be due to the difficulty of obtaining isotopomeric thio complexes. Earlier we reported calculations of the vibrational spectra for some triangular thio, thiohalogenide and thioselenohalogenide complexes of molybdenum: $Mo_3S_{13}{}^{2-}$,[7] $Mo_3S_7Cl_6{}^{2-}$[8] and $Mo_3S_4Se_3Cl_6{}^{2-}$.[9] In the present study we discuss the synthesis of thio complexes of molybdenum and tungsten with the ^{34}S isotope and present calculations of the normal vibrations in these complexes. Vibrational spectroscopy has been shown to be the most informative method in the study of the reactions of thio complexes, accompanied by changes in their metal–sulphur containing fragments. Examples are discussed.

EXPERIMENTAL

The syntheses were carried out using standard Schlenk techniques. The compounds with isotopes prepared from elemental sulphur contained 99.95% of the ^{34}S isotope.

The IR spectra were obtained on a IFS-113 (Brüker) Fourier spectrometer, and the Raman spectra on a DFS-24 spectrometer using the 632.8 nm line of a He–Ne laser for excitation.

The synthesis of binuclear complexes of molybdenum and tungsten with the ^{34}S isotopes, proceeding from ^{34}S elemental sulphur, is shown in Scheme 1.

Preparation of $(Bu_4N)_2{}^{34}S_6$

To a solution of $Na_2{}^{34}S_x$ prepared from $NaBH_4$ (1.00 g) and $^{34}S_8$ (0.71 g) in H_2O (20 cm^3),[7] n-Bu_4NBr (3.0 g) was added. The precipitated solid was filtered off, washed with ether and dried *in vacuo*. Obtained: 2.11 g (n-$Bu_4N)_2{}^{34}S_6$. Yield 88%.

* Author to whom correspondence should be addressed.

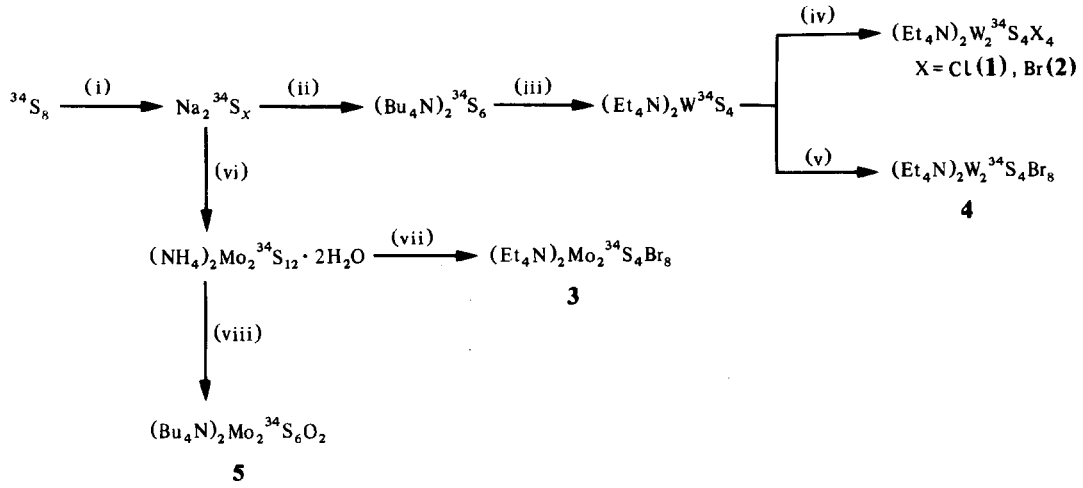

Scheme 1. Preparation of binuclear ^{34}S-thio complexes of molybdenum and tungsten: (i) $NaBH_4$ in H_2O;[7] (ii) Bu_4NBr in H_2O; (iii) $W(CO)_6$ and Et_4NBr in CH_3CN; (iv) HX (X = Cl, Br) in CH_2Cl_2;[10] (v) HBr in CH_2Cl_2;[10] (vi) $K_4Mo_2Cl_8$ and NH_4Br in H_2O;[11] (vii) Br_2 and Et_4NBr in CH_3CN;[13] (viii) NH_4OH and Bu_4NBr.[12]

Preparation of $(Et_4N)_2W^{34}S_4$

$W(CO)_6$ (0.40 g) and $(Bu_4N)_2{}^{34}S_6$ (0.52 g) were boiled in CH_3CN (30 cm^3) for 1 h. The complex, Et_4NBr (1.50 g), was added and the solution cooled to $-5°C$. The precipitated solid was filtered off, washed with alcohol and ether and dried *in vacuo*. Obtained: 0.34 g $(Et_4N)_2W^{34}S_4$. Yield 54%.

RESULTS AND DISCUSSION

Preparation of molybdenum and tungsten binuclear complexes with the ^{34}S *isotope*

Scheme 1 shows the routes by which complexes **1–5** were synthesized, proceeding from $^{34}S_8$. The main difficulty to overcome in the synthesis of these compounds is the preparation of $(Et_4N)_2W^{34}S_4$. The traditional method for the preparation of WS_4^{2-} which consists of passing H_2S through a solution of WO_4^{2-} in ammonia for an extended period of time, turned out to be unsuitable for these purposes. We found that tetrathiotungstate can be obtained in good yield by interacting $W(CO)_6$ with $(Bu_4N)_2{}^{34}S_6$. Upon boiling, the colour of the solution in acetonitrile changes from dark green (S_3^-) to yellow (WS_4^{2-}). After addition of Et_4NBr and cooling, the yellow $(Et_4N)_2W^{34}S_4$ crystallizes in good yield. Again, adding Bu_4NBr to an aqueous solution of $Na_2{}^{34}S_x$ produces $(Bu_4N)_2{}^{34}S_6$ in practically quantitative yield. All other syntheses shown by the reaction schemes were carried out under the conditions described earlier. Thus, the reactions shown in Scheme 1 allow the binuclear thio complexes of molybdenum and tungsten to be synthesized with minimal losses of the ^{34}S isotope.

Vibrational spectra

The structures of $W_2S_4X_4^{2-}$, $M_2S_4Br_8^{2-}$ and $Mo_2S_6O_2^{2-}$ are shown in Fig. 1. The X-ray structures of $W_2S_4Br_8^{2-}$, $Mo_2S_4Br_8^{2-}$ and $Mo_2S_6O_2^{2-}$ are known from the literature.[16–18] The structure of the $W_2S_4X_4^{2-}$ salts has not been determined by X-ray structural analysis and therefore in order to calculate the normal vibrations, use was made of the X-ray structural data for the $W_2S_4Br_2(PPh_3)_2$[19] and $W_2S_2O_2Cl_4^{2-}$[20] complexes. Using probable structural parameters in the absence of experimental ones does not significantly affect the final results within the adopted method of calculation—the approximation of the valence forces[21] (the vibrational frequencies in this method being given by the force constants, quantitites that are independent of interatomic distances). More serious consequences may result from incorrectly chosen bond angles, since in this case there will be considerable changes in the kinematic coefficients. However, deviations within several degrees are quite acceptable. The calculated force constants of the complexes are listed in Table 1.

$W_2S_4X_4^{2-}$ (X = Cl, Br)

The IR and Raman spectra of $W_2S_4Cl_4^{2-}$ and $W_2S_4Br_4^{2-}$ complexes (Fig. 2) are very simple and do not present difficulties in assigning the

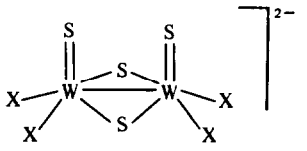

$W_2S_4Cl_4^{2-}$ (1) and $W_2S_4Br_4^{2-}$ (2)

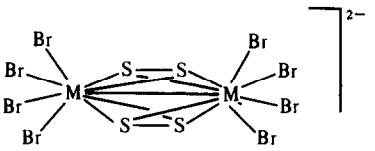

$Mo_2S_4Br_8^{2-}$ (3) and $W_2S_4Br_8^{2-}$ (4)

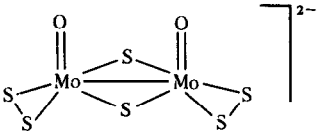

$Mo_2S_6O_2^{2-}$ (5)

Fig. 1. Schematic drawing of the structure of binuclear thio complexes of molybdenum and tungsten.

vibrations, which hardly mix with each other mainly due to substantial differences in force constants between the individual bonds of the molecule. The lines at 530–515 cm^{-1} belong to the W=S vibrations and those at 460–440 cm^{-1}, to the W—S—W fragment.[14,15] This follows both from the isotope shift of these frequencies on going from the ^{32}S to ^{34}S complexes and their almost complete invariance with change of the halogen. A practically zero isotope shift and large variations on going from Cl to Br obviously allow assignment of the 350–280 cm^{-1} vibrations to the valence vibrations of the W—Cl bonds, and those at 280–210 cm^{-1} to W—Br. These conclusions are supported by calculations of the frequencies and shapes of the vibrational modes for the studied complexes. The results are shown in Tables 2 and 3 which list the observed and calculated frequencies, isotope shifts and potential energy distribution among the groups of equivalent vibrational coordinates. The force constants in complexes **1** and **2** (Table 1) practically coincide. It should be noted that the W—W bond constant is the least defined due to the W—W frequency appearing at *ca* 100 cm^{-1}, in the region where both deformational internal and external (translational and librational) vibrations that are strongly mixed with each other appear. Division of the spectrum into a high-frequency region of the internal valence vibrations and a low-frequency region (below 200 cm^{-1}) follows from the differences in the behaviour of these frequencies with the change in the crystal temperature, and holds for all of the complexes. Therefore, the remark concerning the metal–metal bond force constant refers to all of the complexes discussed in the present work.

$M_2S_4Br_8^{2-}$

The spectra of these compounds are also easy to interpret. The most remarkable aspect is the

Table 1. Stretching force constants, f (mdyn $Å^{-1}$)

Compound	Bond					
	M—M	M—μ_2-S	M=Y	S—S	M—X	M—S_t
$W_2S_4Cl_4^{2-}$	1.3	2.7	4.3		1.9	4.3
$W_2S_4Br_4^{2-}$	1.3	2.7	4.4		1.9	4.4
$W_2S_4Br_8^{2-}$	0.9	1.7		3.2	1.5(Br_e) 1.2(Br_a)	
$Mo_2S_4Br_8^{2-}$	0.7	1.5		3.0	1.4(Br_e) 1.1(Br_a)	
$Mo_2S_6O_2^{2-}$	1.2	2.4	7.1	2.3		1.3

M = Mo, W; Y = S, O.

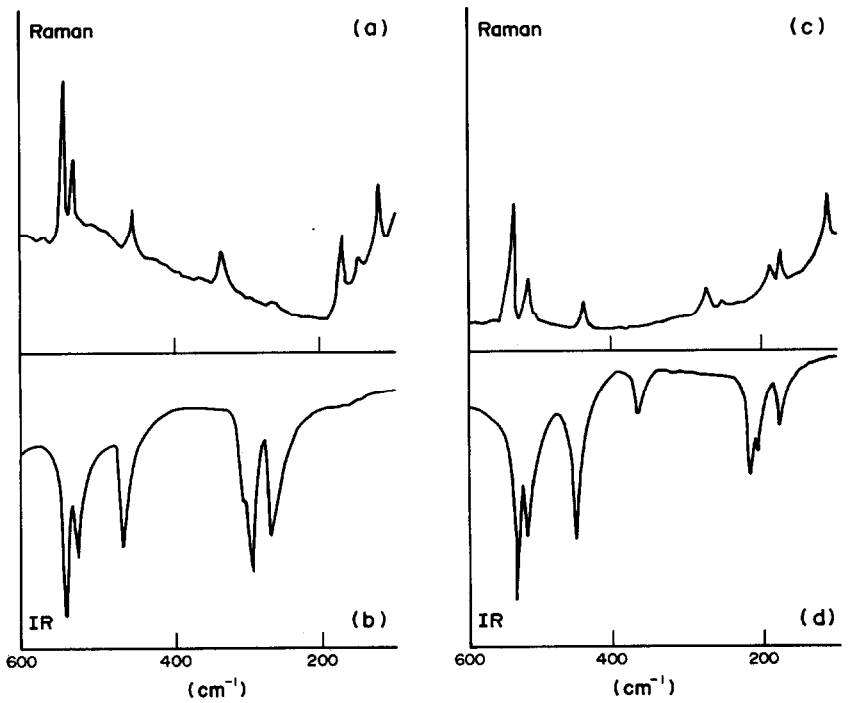

Fig. 2. IR (in polyethylene) and Raman spectra of $(Et_4N)_2W_2S_4Cl_4$ (a) and (b), $(Et_4N)_2W_2S_4Br_4$ (c) and (d).

appearance of an IR- and Raman-active line at $\sim 600\ cm^{-1}$. This vibration is noted for its characteristic nature. It is sufficient to say that upon $^{92}Mo \rightarrow {}^{100}Mo$ substitution its frequency changes within 1 cm^{-1} both in bi- and trinuclear complexes,[6-8] and on going from the ^{32}S to ^{34}S complexes the shift may become as large as 17 cm^{-1} and may serve as a reliable indication of the presence of the S_2^{n-} fragment in the complexes. Although the frequency of the S—S vibration may vary from 610 to 530 cm^{-1},[22] depending on the type of complex, it is not its kinematic relation with other

Table 2. Vibrational frequencies together with the experimental and calculated isotopic shifts and distribution of the potential energy (%) among the groups of equivalent vibrational coordinates for $W_2S_4Cl_4^{2-}$

Bands (cm^{-1})		ν (cm^{-1})		Distribution of the potential energy			
Found	Calc.	Found	Calc.	W—S_{br}	W—S_t	W—Cl	W—W
134, Raman	131, A_1	[a]	0.6	3	4	0	93
269, IR		0					
299, IR	295, A_2	0	0.9	9	0	91	0
311, IR	298, B_2	0	0.3	2	0	98	0
	327, B_1		4.1	38	0	62	0
338, Raman	338, A_1	[a]	0.8	6	2	91	1
	377, B_1		5.8	62	2	36	0
	379, A_2		7.9	92	0	8	0
448, Raman	450, A_1	[a]	11.3	89	6	4	1
459, IR	456, B_2	10	11.3	98	0	2	0
515, Raman, IR	515, B_1	12	13.0	1	99	0	0
527, Raman, IR	523, A_1	12	11.5	6	93	0	1

[a] The Raman spectra of $(Et_4N)_2W_2{}^{34}S_4Cl_4$ are not obtainable.

Table 3. Vibrational frequencies together with experimental and calculated isotopic shifts and distribution of the potential energy (%) among the groups of equivalent vibrational coordinates for $W_2S_4Br_4^{2-}$

Bands (cm^{-1})		ν (cm^{-1})		Distribution of the potential energy			
Found	Calc.	Found	Calc.	W—S_{br}	W—S_t	W—Br	W—W
115, Raman	112, A_1	0	0.4	3	0	23	74
211, IR	209, A_2	1	0.6	8	0	92	0
219, IR	212, B_2	0	0.3	5	0	95	0
260, IR	256, B_1	0	0.4	1	1	98	0
281, Raman	281, A_1	3	0.5	2	1	85	12
362, IR	362, B_1	10	9.1	96	1	2	0
445, Raman	448, A_1	9	6.1	90	1	2	0
455, IR	454, B_2	11	11.1	99	0	1	0
515, IR		13					
520, Raman	524, B_1	13	13.5	1	99	0	0
530, Raman, IR	529, A_1	13	12.8	7	92	0	1

vibrations which is responsible for the variation, but the charge state of the pair itself. The M—S vibrations appear as intense lines at 350–300 cm^{-1} in the Raman spectra and together with the S_2^{n-} vibrations ($\sim$ 600 cm^{-1}) provide spectral proof of the presence of a bridging μ_2-S_2 group in the complex.

It should be noted that upon replacement of the bromine ligands by the chlorine ligands the M—X vibration mixes with the vibrations of the M—S bonds, which results in the shift of the latter to 380–330 cm^{-1}.[6] The M—Br vibrations appear as a series of very intense IR bands at 260–180 cm^{-1}. According to the X-ray structural analysis[16,17] there are two types of bromine in these complexes; the equatorial atoms which lie in the plane defined by the metals

Table 4. Vibrational frequencies together with the experimental and calculated isotopic shifts and distribution of the potential energy (%) among the groups of equivalent vibrational coordinates for $W_2S_4Br_8^{2-}$

Bands (cm^{-1})		ν (cm^{-1})		Distribution of the potential energy				
Found	Calc.	Found	Calc.	W—W	W—Br(1)	W—Br(2)	W—S	S—S
	93, A_g		0.0	88	6	3	3	0
180, Raman	174, A_{1g}	2	1.9	0	0	68	32	0
181, IR	188, B_2	0	0.9	0	0	86	14	0
193, IR	194, B_{1u}	1	1.0	0	91	0	9	0
209, IR	226, B_{3u}	0	1.5	0	76	14	10	0
233, Raman	233, A_g	0	0.7	5	82	13	0	0
	241, A_u		7.2	0	0	0	100	0
	288, A_{1g}		4.8	0	0	23	76	0
299, Raman	307, B_{3u}	6	5.4	0	12	2	86	0
309, Raman	309, B_{2g}	5	4.8	0	14	0	86	0
323, Raman	325, A_g	8	7.7	0	4	1	86	9
331, Raman	334, B_{3g}	7	10.0	0	0	0	100	0
335, Raman	337, B_{1u}	5	6.5	0	7	0	85	8
338, IR		8						
362, IR	362, B_{2u}	7	8.6	0	0	6	94	0
590, IR	592, B_{1u}	17	17.6	0	0	0	13	87
598, Raman	597, A_g	17	17.8	0	0	0	15	85

Table 5. Vibrational frequencies together with the experimental and calculated isotopic shifts and distribution of the potential energy (%) among the groups of equivalent vibrational coordinates for $Mo_2S_4Br_8^{2-}$

Bands (cm^{-1})		ν (cm^{-1})		Distribution of the potential energy				
Found	Calc.	Found	Calc.	Mo—Mo	Mo—Br(1)	Mo—Br(2)	Mo—S	S—S
	100, A_g		0.0	90	8	2	0	0
183, IR	188, A_{1g}	3	3.2	0	0	55	45	0
	191, B_{2g}		1.6	0	86	0	14	0
198, IR	199, B_{1u}	0	1.5	0	91	0	8	0
217, Raman, IR	217, B_{2u}		2.1	0	0	77	23	0
	234, A_u		7.0	0	0	0	100	0
	247, B_{3u}		2.5	0	76	10	14	0
261, Raman	260, A_g	0	1.8	7	80	11	1	1
	326, B_{3u}		3.9	0	19	5	76	0
323, Raman	326, B_{1u}	8	9.7	0	0	0	100	0
	327, A_{1g}		3.2	0	0	42	58	0
333, Raman, IR	338, A_g		6.1	1	10	2	80	7
347, Raman	349, B_{2g}	2	3.9	0	17	0	83	0
	369, B_{1u}		5.5	0	11	0	80	9
381, IR	383, B_{2u}		7.1	0	0	16	84	0
598, IR	597, B_{1u}	13	17.6	0	0	0	14	86
601, Raman	600, A_g	14	17.8	0	0	0	14	86

and the middle points of the S—S bonds, and the axial atoms which are all the other bromines. There is a difference of 0.1 Å between the M—Br bond lengths for the axial and equatorial bromines. Values of the force constants reflect these differences. Thus, the force constant of the M—Br_e bond exceeds that of the M—Br_a bond. Tables 4 and 5 show the experimental and calculated parameters for the thiobromide complexes.

$Mo_2S_6O_2^{2-}$

The IR and Raman spectra of the oxothio complex, $(n\text{-}Bu_4N)_2Mo_2S_6O_2$, are shown in Fig. 4

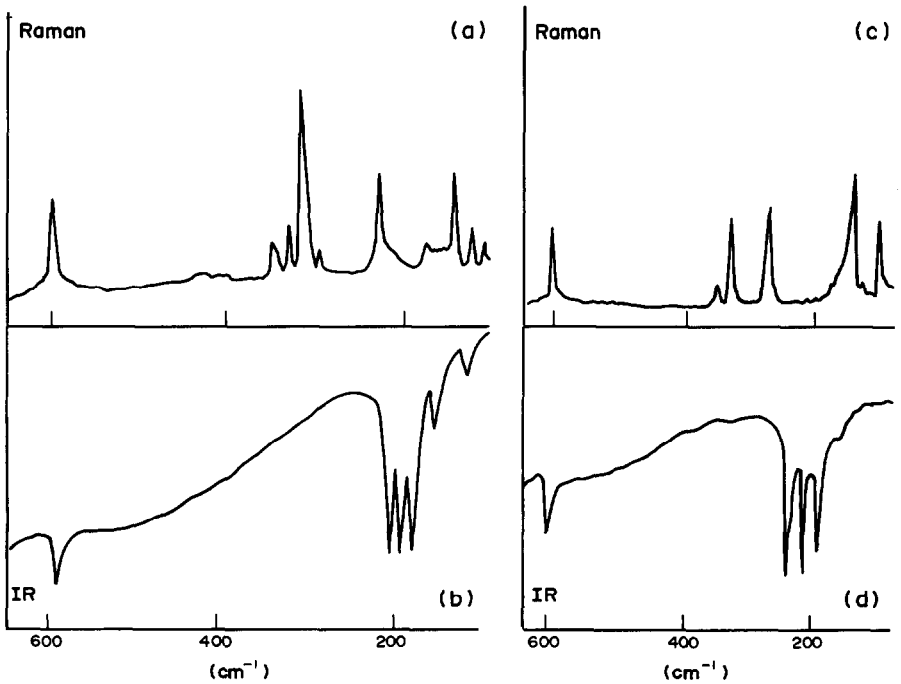

Fig. 3. IR (in polyethylene) and Raman spectra of $(Et_4N)_2W_2S_4Br_8$ (a) and (b), $(Et_4N)_2Mo_2S_4Br_8$ (c) and (d).

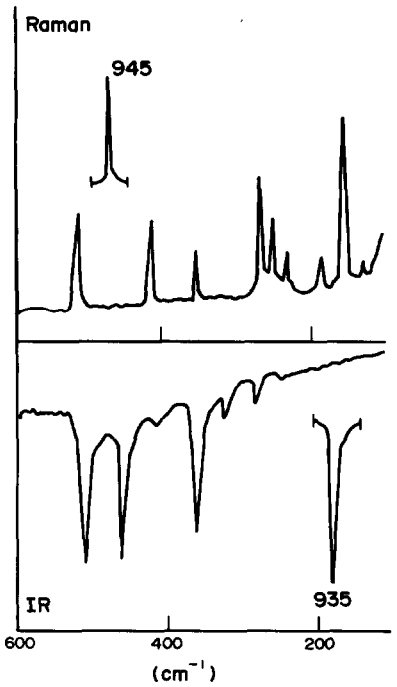

Fig. 4. IR (in polyethylene) and Raman spectra of $(Bu_4N)_2Mo_2S_6O_2$.

and its experimental and calculated characteristics are given in Table 6. The Mo=O vibration is readily recognizable in the spectrum by the high-frequency line at 940 cm^{-1}. Most important from the chemical point of view was the establishment of the vibrational frequencies for the terminal fragment S_2^{n-} and the comparison of its spectral behaviour with that of the bridging ligand S_2^{n-}. The frequency of the terminal S_2^{n-} fragment vibration, 520 cm^{-1} (as follows from the isotope shift values), was found to be below that of its bridging counterpart in each of the studied complexes (bi- and trinuclear complexes).[6-8]

Reactions of binuclear thio complexes of molybdenum and tungsten

The study of the vibrational spectra of binuclear thio complexes of molybdenum and tungsten revealed some characteristic vibrations which are useful in identifying individual fragments of the structure. Thus, in addition to the Mo—O and M—Br (M = Mo, W) vibrations, those of W=S (~ 530 cm^{-1}), S—S of the μ_2-S_2 bridging ligand (~ 600 cm^{-1}) and of S—S of the terminal S_2 ligand (~ 520 cm^{-1}) are also highly characteristic. The high characteristic nature of these bands may help solve chemical problems of establishing the mechanisms or routes by which the reactions of polynuclear thio complexes proceed.

In the present work we present two examples of the use of the vibrational spectroscopy to study the reactions of binuclear thio complexes of molybdenum and tungsten.

Example 1. Earlier we found that the thiobromide

Table 6. Vibrational frequencies together with the experimental and calculated isotopic shifts and distribution of the potential energy (%) among the group of equivalent coordinates for $Mo_2S_6O_2^{2-}$

Bands (cm^{-1})		ν (cm^{-1}) ^{92}Mo—^{100}Mo		ν (cm^{-1}) ^{32}S—^{34}S		Distribution of the potential energy				
Found	Calc.	Found	Calc.	Found	Calc.	Mo—Mo	Mo—S_{br}	Mo—S_t	S—S	Mo—O
	154, A_1		3.8		1.8	92	0	0	1	7
196, Raman		5		3						
232, Raman				2						
253, Raman, IR	253, A_2	0	0.0	5	7.5	0	12	88	0	0
258, Raman	259, B_2		0.4	10	7.5	0	6	94	0	0
280, Raman	279, B_1	2	2.4	7	6.4	0	16	72	12	1
283, IR	280, A_1	0	3.6	8	5.5	4	2	79	13	3
320, Raman, IR		1		7						
359, IR	362, B_1	7	4.7	5	7.0	0	83	12	4	1
368, Raman	397, A_2	6	6.1	5	7.1	0	91	9	0	0
424, IR	428, A_1	4	3.1	9	10.0	1	94	2	1	2
426, Raman		4		9						
466, IR	466, B_2	6	4.9	8	10.0	0	97	3	0	0
518, IR	522, A_1	0	0.0	13	15.2	0	0	12	88	0
525, Raman	523, B_1	0	0.5	15	15.1	0	0	13	87	0
935, IR	937, B_1	6	5.1	0	0.0	0	0	0	0	100
945, Raman	945, A_1	6	5.8	1	0.1	0	0	0	0	100

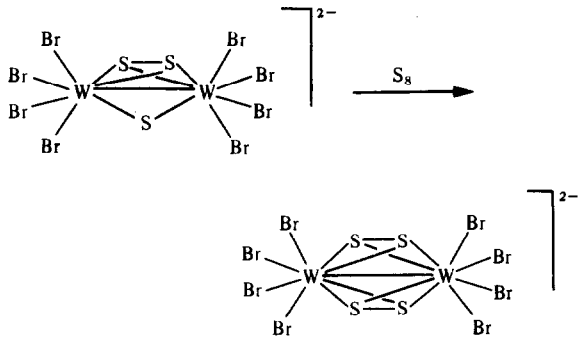

Scheme 2.

complex of tungsten, $W_2S_3Br_8^{2-}$, interacts with S_8 in CH_3CN to form $W_2S_4Br_8^{2-}$.[10]

We have studied the interaction of $W_2S_3Br_8^{2-}$ with ^{34}S under analogous conditions. It is clear that if the reaction proceeds by addition of ^{34}S to the μ_2-S ligand to form μ_2-$^{32}S^{34}S$, in the IR and Raman spectra there must appear an extra band with $\Delta\nu = 8$ cm^{-1} relative to ν(S—S) in $W_2S_4Br_8^{2-}$. According to the vibrational spectroscopy data the interaction of $W_2S_3Br_8^{2-}$ with ^{34}S only produces complex **3** which does not contain ^{34}S. Thus, the interaction of $W_2S_3Br_8^{2-}$ with sulphur in CH_3CN takes a complex route with several directions. This is indicated by the fact that $(Et_4N)_2W_2S_4Br_8$ was obtained in only 20% yield.[10] The other products of this reaction could not be isolated in an analytically pure form.

Example 2. Earlier, the binuclear thiobromide, $Mo_2S_4Cl_6$, was shown to interact with ammonium polysulphide to form $(NH_4)_2Mo_2S_{12}\cdot 2H_2O$.

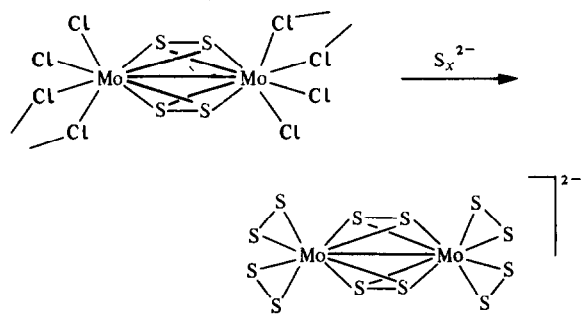

Scheme 3.

We studied this reaction using isotopomeric compounds, and it turned out that the interaction of $Mo_2{}^{34}S_4Cl_6$ with $(NH_4)_2{}^{32}S_x$ produces only $(NH_4)_2Mo_2{}^{32}S_{12}\cdot 2H_2O$.

$$Mo_2{}^{34}S_4Cl_6 \xrightarrow{{}^{32}S_x^{2-}} Mo_2{}^{32}S_{12}{}^{2-}$$

$$\xrightarrow[(2)\,Me_4NCl]{(1)\,NH_4OH} (Me_4N)_2Mo_2{}^{32}S_6O_2$$

In the IR spectra of $Mo_2S_{12}^{2-}$, in the region below 600 cm^{-1} there is only one characteristic band at 520 cm^{-1} resulting from the valence S—S vibrations. The conclusion that substitution of the ^{34}S atoms of the μ_2-S_2 ligands by the ^{32}S atoms took place is made on the basis of the following two observations: (1) there is no shift of the splitting of the 520 cm^{-1} band and (2) the interaction of the reaction product with the aqueous solution of ammonia produces $Mo_2S_6O_2^{2-}$.[12] This complex exhibits very rich IR and Raman spectra which reliably suggest that there are no essential amounts of the ^{34}S isotope.

REFERENCES

1. A. Müller, E. Diemann, R. Jostes and H. Bögge, *Angew. Chem. Int. Ed. Engl.* 1981, **20**, 934.
2. A. Müller, *Polyhedron* 1986, **5**, 323.
3. V. P. Fedin, M. N. Sokolov and V. Ye. Fedorov, *Koord. Khim.* 1990, **16**, 291 (in Russian).
4. A. Hadjikyriacou and D. Coucouvanis, *Inorg. Chem.* 1989, **28**, 2169.
5. D. Coucouvanis, A. Hadjikyriacou, M. Draganjac, M. G. Kanadtzidis and O. Ileperuma, *Polyhedron* 1986, **5**, 349.
6. B. A. Kolesov, V. P. Fedin, O. A. Geras'ko and V. Ye. Fedorov, *Koord. Khim.* 1987, **13**, 771 (in Russian).
7. V. P. Fedin, B. A. Kolesov, Yu. V. Mironov and V. Ye. Fedorov, *Polyhedron* 1989, **8**, 2419.
8. V. P. Fedin, M. N. Sokolov, Yu. V. Mironov, B. A. Kolesov, S. V. Tkachev and V. Ye. Fedorov, *Inorg. Chim. Acta* 1990, **167**, 39.
9. V. P. Fedin, Yu. V. Mironov, M. N. Sokolov, B. A. Kolesov and V. Ye. Fedorov, *Inorg. Chim. Acta* 1990, **174**, 275.
10. V. P. Fedin, Yu. V. Mironov, M. N. Sokolov, Yu. I. Mironov and V. Ye. Fedorov, *Inorg. Chim. Acta* 1989, **163**, 65.
11. V. P. Fedin, O. A. Geras'ko, Yu. V. Mironov and V. Ye. Fedorov, *Zh. Neorg. Khim.* 1988, **33**, 2846 (in Russian).
12. A. Müller, E. Krickemeyer and U. Reinsch, *Z. Anorg. Allg. Chem.* 1980, **B470**, 35.
13. V. P. Fedin, Yu. V. Mironov and V. Ye. Fedorov, *Zh. Neorg. Khim.* 1989, **34**, 2984 (in Russian).
14. J. W. McDonald, G. B. Friesen, L. D. Rosenhein and W. E. Newton, *Inorg. Chim. Acta* 1983, **72**, 205.
15. M. G. B. Drew, R. J. Hobson, P. P. E. M. Mumba, D. A. Rice and N. Turp, *J. Chem. Soc., Dalton Trans.* 1987, 1163.
16. A. V. Virovetz, Yu. L. Slovohotov, Yu. T. Strychkov, V. Ye. Fedorov, Yu. V. Mironov and V. P. Fedin, *Koord. Khim.* 1990, **16**, 198 (in Russian).
17. D. Fenske, B. Czeska, C. Schumacher, R. E. Schmidt and K. Dehnike, *Z. Anorg. Allg. Chem.* 1985, **520**, 7.
18. W. Clegg, N. Mohan, A. Müller, A. Neumann, W.

Rittner and G. M. Sheldrick, *Inorg. Chem.* 1980, **19**, 2066.
19. V. P. Fedin, Yu. V. Mironov, A. V. Virovetz, N. V. Podberezskaya and V. Ye. Fedorov, *Inorg. Chim. Acta* 1990, **171**, 199.
20. M. G. B. Drew, E. M. Page and D. A. Rice, *Inorg. Chim. Acta* 1983, **76**, 33.
21. L. A. Gribov and V. A. Dementjev, *Methods and Algorithms of Calculation in the Theory of Vibrational Spectra of Molecules*. Nauka (1981) (in Russian).
22. A. Müller, W. Jaegerman and J. H. Enemark, *Coord. Chem. Rev.* 1982, **46**, 245.

Polyhedron Vol. 10, No. 10, pp. 1007–1012, 1991
Printed in Great Britain

0277–5387/91 $3.00+.00
© 1991 Pergamon Press plc

RADIATION-CATALYTIC REDUCTION OF MOLECULAR NITROGEN WITH APPLICATION OF THE TUNGSTEN(IV) HYDRIDE COMPLEXES

J. O. DZIĘGIELEWSKI,* J. MAŁECKI and R. GRZYBEK

Institute of Chemistry, Silesian University, 9 Szkolna Street, 40006 Katowice, Poland

(*Received* 1 *June* 1990; *accepted* 13 *December* 1990)

Abstract—A radiation-catalytic experiment of the fixation and reduction of molecular nitrogen has been carried out. The $[WH_4(dtpe)_2]$ complex was applied to fix molecular nitrogen in a γ-radiation field. Plots of the dependence of either the number of molecules of ammonia or hydrazine vs dose are presented. A mechanism for the radiation-catalytic fixation and reduction of molecular nitrogen using the $[WH_4(dtpe)_2]$ complex is suggested. The unusually high radiation yields of ammonia and hydrazine are explained as due to a cyclic process.

In previous work, methanol solutions of the complex $[MoOCl(dppe)_2]Cl$[1,2] and cyclohexane solutions of the complex $[MoH_4(dtpe)_2]$[3] were used in the process of radiation-catalytic reduction of molecular nitrogen [dppe = $(C_6H_5)_2P(CH_2)_2P(C_6H_5)_2$, dtpe = $(o\text{-}CH_3C_6H_4)_2P(CH_2)_2P(o\text{-}CH_3C_6H_4)_2$]. It was determined in these papers[1–3] that in a γ-radiation field the bis-dinitrogen molybdenum(0) complex formed and the coordinated dinitrogen was gradually reduced to $—NNH_2$, then to $—N_2H_4$ and finally to NH_3. The yields obtained were, however, much higher than expected from the amounts of e_s^-, H and R which should be produced in the radiation field (agents reducing central atoms or —NH groups). In another paper[4] it was shown that during the course of irradiation of a methanol solution of $[Mo(NNH_2)(HSO_4)(dppe)_2]HSO_4$ the intermediate $[HMoN_2H_3(dppe)_2]^+$ was formed as a result of the addition of a H^+ ion to the former complex. The hydrido intermediate immediately reacted with H^+ ions and initiated cyclic production of H atoms and H_2 molecules. In order to determine the role of hydrido ligands formed in the course of attaching the H^+ ion to the central atom, the complex $[WH_4(dtpe)_2]$ was used instead of the molybdenum analogue because of its presumed higher stability. It was shown previously[3] that H^- ions participate in the reduction of coordinated dinitrogen, but important problems such as reactions between H^- ions and the negatively-polarized N atom (the terminal one) in the M—N—N group were not considered. In this paper this problem is also explained. Taking into account the higher reducing ability of the tungsten ions than the molybdenum ions and the evident influence of H^+ ions on the yields of ammonia,[1,2] we came to the conclusion that the tungsten(IV) hydrido complex should increase the yields of the reduction of molecular nitrogen.

EXPERIMENTAL

The ligands dppe and dtpe were synthesized as reported elsewhere.[5] The complexes $[WH_4(dtpe)_2]$ and $[W(dtpe)_2]$ were obtained by literature methods.[3,6] Cyclohexane solutions of the $[W(dtpe)_2]$ complex were irradiated in the γ-radiation source "Issledovatel" (stationary ^{60}Co γ-radiation source) with simultaneous saturation with deoxygenated nitrogen. Dose rate in conversion to cyclohexane and methanol was calculated as 2.3×10^{17} eV cm^{-3} min^{-1} on the basis of a Fricke dosimeter. The $[WH_4(dtpe)_2]$ complex was dissolved in cyclohexane, acidified methanol (H_2SO_4) or in a mixture of acidified ethanol and cyclohexane (1 : 1). Acidified solutions of the tungsten(IV) hydride complex were irradiated in the same manner as $[W(dtpe)_2]$ except that in these cases the solutions were saturated either with N_2 or with a mixture of N_2 and H_2 (1 : 3). In order to keep the

* Author to whom correspondence should be addressed.

concentrations of the tungsten complexes constant, the gases were passed through scrubbers filled with the appropriate solvent. The hydrazine and ammonia generated were absorbed in aqueous solutions of H_2SO_4 ($C = 5 \times 10^{-2}$ mol dm^{-3}). Hydrazine[7,8] and ammonia[9,10] were estimated by standard methods. In the case of acidified solutions, products were estimated either in irradiated solutions or in traps filled with aqueous H_2SO_4.

RESULTS AND DISCUSSION

Figure 1 presents typical curves of the dependence of the number of N_2H_4 molecules on dose, generated during the irradiation of cyclohexane solutions of $[W(dtpe)_2]$ and $[WH_4(dtpe)_2]$ complexes saturated with N_2 or with a mixture of N_2 and H_2. These curves have been discussed earlier.[1]

The presence of H^- in the tungsten(IV) complex evidently increases the number of hydrazine molecules (curves 3 and 1) similar to the molybdenum analogues.[3] The maximum on curve 3 is lower than on curve 1 and is shifted towards higher doses. The exponential shape, up to the maximum, of curve 3 suggests that in the course of irradiation of the $[W(dtpe)_2]$ complex solutions the $[WH_4(dtpe)_2]$ complex is formed which accelerates reduction of the generated $[W(N_2)_2(dtpe)_2]$ complex to hydrazine. Generation of the W—H groups in the irradiated cyclohexane solution of $[W(dtpe)_2]$ was determined on observing IR absorptions at 1830, 1796 and 1775 cm^{-1} for the separated substance (after removing solvent). The deeper slope of curve 2 shows that the coordinated dinitrogen is highly reduced, which together with increased hydrazine yield is connected to the constant supply of H_2 into the irradiated solution. This is caused by the high concentration of W—H groups. Table 1 gives yields of hydrazine molecules. These conclusions are generally confirmed by Fig. 2 and Table 2.

The radiation yield of hydrazine is about 10 times greater than in solutions of the tungsten(IV) hydrido complex of lower concentrations. An increase in the $[WH_4(dtpe)_2]$ concentration causes a decrease in the yield of hydrazine and an increase in the ammonia yield in comparison with the $[W(dtpe)_2]$ complex (Tables 1 and 2). Use of the tungsten complexes leads to higher yields of hydrazine and ammonia than in the case of molybdenum complexes (data in Tables 1 and 2 and in Figs 1 and 2, together with the data from a previous paper[3]). Increase in the yield of N_2 reduction is caused by the greater ability of tungsten(IV) complexes and their higher stability. On the basis of the difference

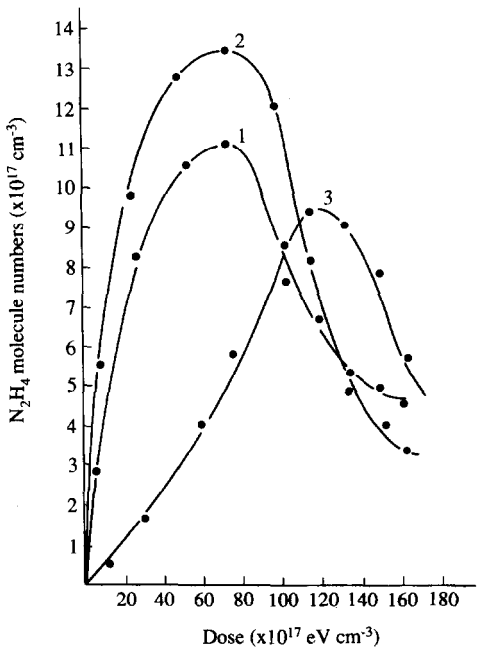

Fig. 1. Plot of the dependence of the number of N_2H_4 molecules on dose: (1) cyclohexane solution of the $[WH_4(dtpe)_2]$ complex, $C = 10^{-2}$ mol dm^{-3} saturated with N_2; (2) cyclohexane solution of the $[WH_4(dtpe)_2]$ complex, $C = 10^{-2}$ mol dm^{-3} saturated with a 1 : 3 mixture of N_2 and H_2; (3) cyclohexane solution of the $[W(dtpe)_2]$ complex, $C = 10^{-2}$ mol dm^{-3} saturated with N_2.

Table 1. Radiation yields (number of molecules per 100 eV) of N_2H_4 for different concentrations of $[W(dtpe)_2]$ and $[WH_4(dtpe)_4]$ dissolved in cyclohexane

Concentration of $[W(dtpe)_2]$ (mol dm^{-3})	Number of hydrazine molecules per 100 eV	Concentration of $[WH_4(dtpe)_2]$ (mol dm^{-3})	Number of hydrazine molecules per 100 eV
10^{-3}	0.5	10^{-3}	5.3
5×10^{-3}	1.3	5×10^{-3}	10.0
10^{-2}	12.8	10^{-2}	36.6
—	—	10^{-2}[a]	52.5

[a] Solution saturated with a mixture of N_2 and H_2 (1 : 3).

Table 2. Radiation yields of NH_3 for different concentrations of $[W(dtpe)_2]$ and $[WH_4(dtpe)_2]$ dissolved in cyclohexane

Concentration of $[W(dtpe)_2]$ (mol dm^{-3})	Number of ammonia molecules per 100 eV	Concentration of $[WH_4(dtpe)_2]$ (mol dm^{-3})	Number of ammonia molecules per 100 eV
10^{-3}	25.0	10^{-3}	48.0
5×10^{-3}	41.7	5×10^{-3}	125.0
10^{-2}	54.5	10^{-2}	238.6
—	—	10^{-2}[a]	395.8

[a] Solution saturated with a mixture of N_2 and H_2 (1 : 3).

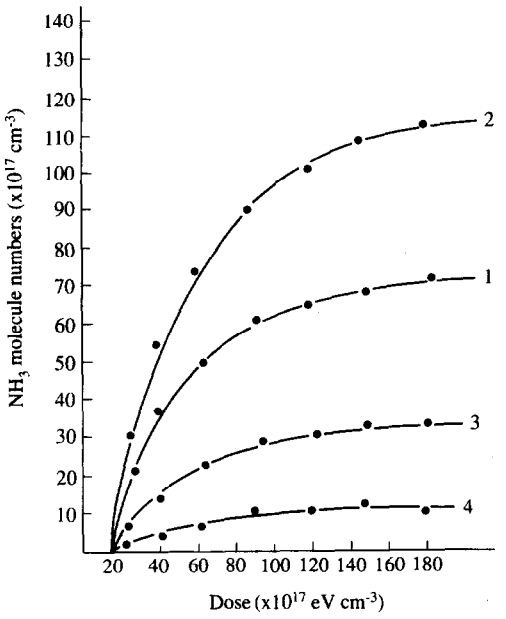

Fig. 2. Plot of the dependence of the number of NH_3 molecules on dose for different concentrations of the $[WH_4(dtpe)_2]$ complex solutions in C_6H_{12}: (1) $C = 10^{-2}$ mol dm^{-3}, saturated with N_2; (2) $C = 10^{-2}$ mol dm^{-3}, saturated with N_2 and H_2 (1 : 3); (3) $C = 5\times10^{-3}$ mol dm^{-3}, saturated with N_2; (4) $C = 10^{-3}$ mol dm^{-3}, saturated with N_2.

between the induction periods in the generation of ammonia (shorter for tungsten complexes), it was stated that the reduction ability in the process of reduction of hydrazine to ammonia is about 25% higher for tungsten complexes than for molybdenum complexes.

Consideration of the differences $G_{NH_3([MH_4(dtpe)_2])} - G_{NH_3([M(dtpe)_2])}$ for tungsten and molybdenum complexes leads to the conclusion that the tungsten(IV) hydrido complex is about 1.75 times more stable than the molybdenum(IV) hydrido complex, under the conditions of the experiment. Such a meaningful difference in the stability of these complexes allows protonation of the tungsten(IV) hydrido complex by the stoichiometric amount of H_2SO_4:

$$[WH_4(dppe)_2] + H_2SO_4 \longrightarrow [WH_5(dtpe)_2]HSO_4.$$

Figures 3 and 4 show the plots of the numbers of $N_2H_6^{2+}$ and NH_4^+ ions as functions of dose, and Table 3 presents yields of these ions.

Acidification of the solutions of the tungsten(IV) hydrido complexes causes effects opposite to those in the case of the $[MoH_4(dtpe)_2]$ complexes.[3] This shows that $[WH_5(dtpe)_2]^+$ ions were present in solution. The stability of these ions depends evidently on the nature of the solvent; they are more stable in a mixture of ethanol and cyclohexane than in pure methanol. It is noticeable (Fig. 3) that the yield of hydrazine is highly dependent on the H^- concentration and independent of the H^+ concentration, as can be seen from the plots. This means that the reduction of W—N_2 groups by W—H groups is the radical process. Therefore, H^- ions are not joined to the negatively polarized terminal N atom in the W—N—N^- group (similar to the molybdenum complexes). So, the H atom is transferred from the W—H group to the W—N_2 group, which changes the charge allocation. Transfer of the H atom from the W—H group onto other ligands was observed earlier.[11] Yields of ammonia are highly dependent on the concentration of H^+ ions, as can be seen in Fig. 4 and was also observed earlier.[1,2] This means that the coordinated hydrazine is reduced by the hydrido complex in an ionic way (e^- from atom centres and H^-). The radical mechanism of reduction of hydrazine seems to be unbelievable because the H—H bond energy is higher than the N—H bond energy (by *ca* 45 kJ mol^{-1}). It also causes the fact that H atoms could not be attached to hydrazine molecules but rather remove H atoms from hydrazine and form H_2 molecules with a constant rate of 2.4×10^4 dm^3 mol s^{-1}.[12] Formation of hydrazine in the reaction of $[Mo(N_2)_2(dtpe)_2]$ with H atoms, together with the lack

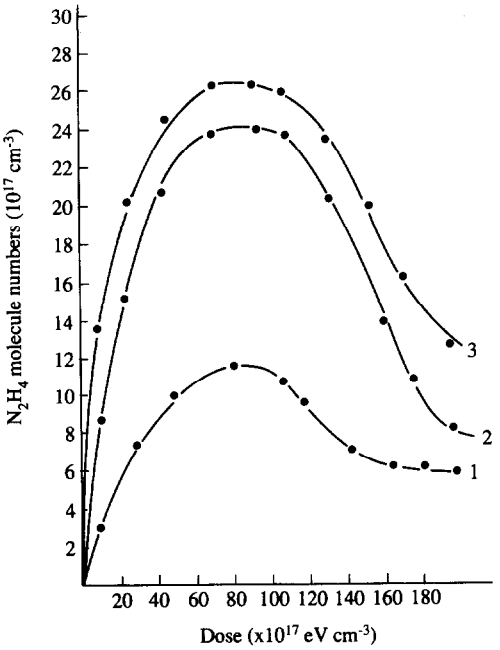

Fig. 3. Plot of the dependence of the number of N_2H_4 molecules on dose: (1) methanol solution of the $[WH_4(dtpe)_2]$ complex acidified with H_2SO_4 ($C = 10^{-2}$ mol dm^{-3}), $C = 10^{-2}$ mol dm^{-3} (the curve is the same for an acid concentration of $C = 10^{-1}$ mol dm^{-3}); (2) $[WH_4(dtpe)_2]$ solution in a mixture of C_2H_5O and C_6H_{12} (1 : 1) acidified with H_2SO_4 ($C = 10^{-2}$ mol dm^{-3}), saturated with N_2; (3) $[WH_4(dtpe)_2]$ solution in a mixture of C_2H_5OH and C_6H_{12} (1 : 1) acidified with H_2SO_4 ($C = 10^{-2}$ mol dm^{-3}), saturated with a 1 : 3 mixture of N_2 and H_2.

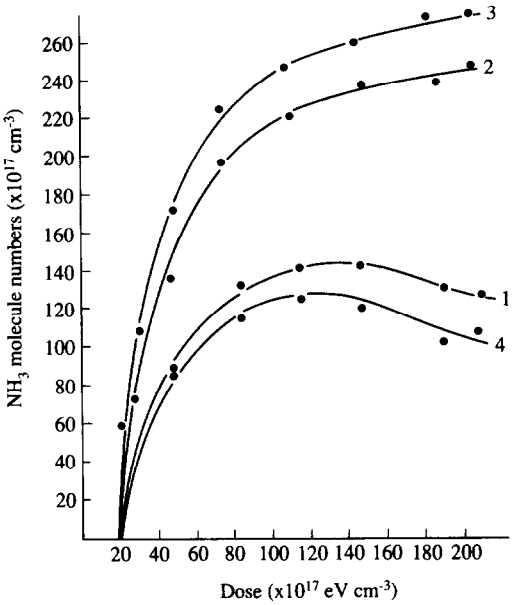

Fig. 4. Plot of the dependence of the number of NH_3 molecules on dose: (1) $[WH_4(dtpe)_2]$ complex in CH_3OH, $C = 10^{-2}$ mol dm^{-3}, acidified with H_2SO_4 ($C = 10^{-1}$ mol dm^{-3}), saturated with N_2; (2) $[WH_4(dtpe)_2]$ complex in a mixture of C_2H_5OH and C_6H_{12} (1 : 1) acidified with H_2SO_4 ($C = 10^{-2}$ mol dm^{-3}), saturated with N_2; (3) $[WH_4(dtpe)_2]$ complex in a mixture of C_2H_5OH and C_6H_{12} (1 : 1) acidified with H_2SO_4 ($C = 10^{-2}$ mol dm^{-3}), saturated with a 1 : 3 mixture of N_2 and H_2; (4) $[WH_4(dtpe)_2]$ complex in CH_3OH, $C = 10^{-2}$ mol dm^{-3}, acidified with H_2SO_4 ($C = 10^{-2}$ mol dm^{-3}), saturated with N_2.

Table 3. Radiation yields of $(N_2H_6)SO_4$ and $(NH_4)_2SO_4$ for different concentrations of the $[WH_4(dtpe)_2]$ complex dissolved in acidified methanol or in mixture of ethanol and cyclohexane (1 : 1)

Irradiated system	Number of molecules per 100 eV	
	$(N_2H_6)SO_4$	$(NH_4)_2SO_4$
CH_3OH solution saturated with N_2 $C_{H_2SO_4} = 10^{-2}$ mol dm^{-3}	46.0	444.4
CH_3OH solution saturated with N_2 $C_{H_2SO_4} = 10^{-1}$ mol dm^{-3}	46.0	500.0
Mixture of C_2H_5OH and C_6H_{12} saturated with N_2 $C_{H_2SO_4} = 10^{-2}$ mol dm^{-3}	95.0	1917.0
Mixture of C_2H_5OH and C_6H_{12} saturated with N_2+H_2 (1 : 3) $C_{H_2SO_4} = 10^{-2}$ mol dm^{-3}	110.0	2182.0

of ammonia in the products was evidenced earlier.[3]

From comparison of Figs 3 and 1 it can be seen that the stationary concentration of hydrazine (at the maximal doses—see figures) is maximal for $[WH_5(dtpe)_2]^+$ solutions saturated with a mixture of N_2 and H_2 and depends on the nature of the solvent. Its value influences the yield of ammonia. Curves 1 and 2 in Fig. 4 are permanently raised and the ammonia concentration (curve 1) at the point corresponding to a dose of 160×10^{17} eV cm^{-3} is 4×10^{-2} mol dm^{-3}. One-third of the $[WH_5(dtpe)_2]^+$ ions could effectively form the bis-dinitrogen tungsten(0) complex which then gives ammonia. The other two-thirds of the tungsten(IV) hydrido complex provide the source of H atoms or H^- ions, which are necessary to reduce coordinated dinitrogen. By considering all these facts it may be stated that the molar ratio of ammonia ($C = 4\times10^{-2}$ mol dm^{-3}) to $[WH_5(dtpe)_2]^+$ ($C = 3.3\times10^{-3}$ mol dm^{-3}) is about 12:1. Thus, the process of fixation and reduction of molecular nitrogen must be cyclic in nature. Also considering that the amount of donor H atoms in W—H groups ($C = 5\times10^{-2}$ mol dm^{-3}) was too low to generate 16×10^{-2} mol dm^{-3} H atoms in N—H groups ($C_{NH_4^+} = 4\times10^{-2}$ mol dm^{-3}), one may predict that the correct amount of $[WH(dtpe)_2(N_2)_2]^+$ converted into $[WH_5(dtpe)_2]^+$ is represented by reaction 1 in the mechanism. The exchange of N_2 for H_2 in the $[W(N_2)_2(dtpe)_2]$ complex proceeds with a lower rate because of the higher energy of the W—N_2 bond.[15] Therefore, the degree of sloping of the part of the curve in Fig. 2 corresponding to higher doses is lower than in Fig. 4. Maxima on curves 3 and 4 in Fig. 4 are connected with the decomposition of NH_4^+ ions by CH_2OH radicals, as was discussed earlier.[2]

On the basis of all the above and on data presented in previous papers[1-4] the following mechanism of the radiation-catalytic process of fixation and reduction of molecular nitrogen could be proposed:

Mechanism (a)

$$\text{solvent} \rightsquigarrow S^+, H, R, e_s^-, S^* \tag{1}$$

$$[WH_4(dtpe)_2] + 2N_2 \overset{e_s^-, S^*, H}{\rightleftharpoons} [W(N_2)_2(dtpe)_2] + 2H_2 \tag{2}$$

$$[W(N_2)_2(dtpe)_2] + [WH_4(dtpe)_2] \longrightarrow \begin{bmatrix} W(dtpe)_2 \\ | \\ N_2H_4 \end{bmatrix} + [W(dtpe)_2] + N_2 \tag{3}$$

$$\begin{bmatrix} N_2H_4 \\ | \\ W(dtpe)_2 \end{bmatrix} \xrightarrow[H^+]{S^+} \begin{bmatrix} N_2H_5^+ \\ | \\ W(dtpe)_2 \end{bmatrix} \tag{4}$$

$$\begin{bmatrix} N_2H_5^+ \\ | \\ W(dtpe)_2 \end{bmatrix} \xrightarrow[e^-, H^-]{H^+, S^+} 2NH_3 + [W(dtpe)_2] \tag{5}$$

$$[W(dtpe)_2] + 2N_2 \longrightarrow [W(N_2)_2(dtpe)_2]. \tag{6}$$

Mechanism (b)
(in acidified solutions)

$$[WH_5(dtpe)_2]^+ + 2N_2 \overset{H, S^*, R}{\rightleftharpoons} [WH(N_2)_2(dtpe)_2]^+ + 2H_2 \tag{1}$$

$$[WH(N_2)_2(dtpe)_2]^+ + [WH_5(dtpe)_2]^+ \longrightarrow \begin{bmatrix} WH(dtpe)_2 \\ | \\ N_2H_4 \end{bmatrix}^+ + [WH(dtpe)_2]^+ + N_2 \tag{2}$$

$$\begin{bmatrix} WH(dtpe)_2 \\ | \\ N_2H_4 \end{bmatrix}^+ + [WH_5(dtpe)_2]^+ \xrightarrow{2H^+} \begin{cases} \xrightarrow{(a)} 2NH_3 + [WH(dtpe)_2]^+ + [WH_3(dtpe)_2]^{3+} + H_2 \\ \xrightarrow{(b)} 2NH_3 + [WH(dtpe)_2]^+ + [WH_3(dtpe)]^+ + H_2 \end{cases} \tag{3}$$

$$[WH_3(dtpe)_2]^{3+} + H_2 \xrightarrow[R]{H} [WH_5(dtpe)_2]^+ \tag{4}$$

$$[WH(dtpe)_2]^+ + 2N_2 \longrightarrow [WH(N_2)_2(dtpe)_2]^+. \tag{5}$$

Complex $[WH(N_2)_2(dtpe)_2]^+$ [reactions (1) and (5)] is well known in the solid phase with dppe,[13–15] whereas hydrogenation reactions of olefins using molybdenum or tungsten hydrido complexes which proceed with reduction of the central atoms [like reactions (2) and (3b)] are also described.[16]

The proposed mechanism of fixation and reduction of molecular nitrogen using $[WH_4(dtpe)_2]$ is in accord with the well known fact that in the course of the reduction of N_2 by nitrogenase together with two ammonia molecules one molecule of H_2 is liberated. This could mean that metal centres in nitrogenase are protonated (H^+ ions from the environment) and then nitrogenase could be reduced as in reaction (3) (in acidified solution) or (4) (in non-acidified solution). Thus, the proposed mechanism could be treated as an alternative one for the simplified explanation of the action of nitrogenase to that proposed earlier.[18]

REFERENCES

1. J. O. Dzięgielewski, *Polyhedron* 1989, **8**, 1463.
2. J. O. Dzięgielewski and R. Grzybek, *J. Radioanalyt. Nucl. Chem. Articles* 1989, **132**, 115.
3. J. O. Dzięgielewski and R. Grzybek, *Polyhedron* 1990, **9**, 645.
4. J. O. Dzięgielewski, R. Gil-Bortnowska and R. Grzybek, *J. Radioanalyt. Nucl. Chem. Articles* 1990, **140**, 415.
5. *Inorganic Syntheses*, Vol. XVI, McGraw-Hill, New York (1976).
6. B. Bell, J. Chatt, G. J. Leigh and T. Ito, *J. Chem. Soc., Chem. Commun.* 1972, 34.
7. M. Pares and A. Retit, *Bull. Soc. Chim. France* 1947, 122.
8. G. V. Watt and J. D. Chisp, *Analyt. Chem.* 1952, **24**, 2006.
9. W. T. Bolleter, C. J. Bushmann and P. W. Tidwell, *Analyt. Chem.* 1961, **33**, 592.
10. C. J. Pickett, K. S. Ryder and J. Talarmin, *J. Chem. Soc., Dalton Trans.* 1986, 1453.
11. S. G. Slater, R. Lusk, B. F. Schumann and M. Darensbourg, *Organometallics* 1982, **1**, 1662.
12. J. DeLaire, P. Cordier and J. Belloni, *J. Phys. Chem.* 1976, **80**, 1687.
13. J. Chatt, G. A. Heath and R. L. Richards, *J. Chem. Soc., Dalton Trans.* 1974, 2074.
14. J. R. Dilworth, S. Donovan-Mtunzi, C. T. Kan and R. L. Richards, *Inorg. Chim. Acta* 1981, **53**, L161.
15. N. J. Lazarowych, R. H. Morris and J. M. Ressner, *Inorg. Chem.* 1986, **25**, 3926.
16. Yu. Kukushkin, *Reakcyonnaya sposobnost koordynacyonnych soedynenyj*, p. 57. Kchimia, Leningrad (1987).
17. J. Chatt (Ed.), *New Trends in the Chemistry of Nitrogen Fixation*, p. 116. Mir, Moscow (1984).
18. R. R. Eady, D. J. Lowe and R. N. F. Thornley, *Nature* 1978, **272**, 557.
19. J. Chatt, R. R. Eady, D. J. Lowe, J. R. Postage, R. L. Richards, B. E. Smith and R. N. F. Thornley, *Proceedings of the Steenbock International Symposium on Nitrogen Fixation, June* 12–16, 1978. University of Wisconsin, Madison, Wisconsin, U.S.A.

Polyhedron Vol. 10, No. 10, pp. 1013–1017, 1991
Printed in Great Britain

0277–5387/91 $3.00+.00
© 1991 Pergamon Press plc

FORMATION OF HETEROBIMETALLIC RUTHENIUM–MERCURY NITROSYL COMPLEXES

LORETO BALLESTER-REVENTOS,* ANGEL GUTIERREZ-ALONSO and MARIA FELISA PERPIÑAN-VIELBA

Departamento de Quimica Inorganica, Facultad de Ciencias Quimicas, Universidad Complutense, 28040-Madrid, Spain

(*Received* 13 *June* 1990; *accepted* 7 *January* 1991)

Abstract—The nitrosyl ruthenium complexes $[RuCl(CO)(NO)(PPh_3)_2]$ and $[Ru(NO)_2(PR_3)_2]$ (R = Ph, CH_2CH_2CN) react with an excess of mercury salts, HgX_2, to give the first nitrosyl ruthenium complexes containing ruthenium–mercury bonds. The reactions take place with substitution of one or more ligands in the parent compound and *cis* addition of the X and HgX groups.

One of the reactions most extensively used in the synthesis of heterobimetallic transition compounds is the addition of a mercury(II) compound to an electron-rich metal complex.[1] The usual reaction implies an adduct type interaction with formation, in some cases, of the oxidative addition product.[2]

There are very few examples of bimetallic ruthenium–mercury compounds, the majority being adduct type complexes, for example $[Ru(C_5H_5)_2 \cdot HgCl_2]$[3] and $[RuCl_2(PPh_3)_3 \cdot HgCl_2]$.[4] Even more scarce are the oxidative addition complexes and only the mononuclear carbonyls $[Ru(CF_3)(HgCF_3)(CO)_2(PPh_3)_2]$[5] and $[Ru(X)(HgX)(CO)_3(PR_3)]$ are known.[6]

The unstable derivative $[RuCl_2(HgCl)(NO)(PPh_3)_2]$ has also been reported as an unisolated intermediate in the reaction between $[RuCl(CO)(NO)(PPh_3)_2]$ and $HgCl_2$.[7] The analogous osmium complex is, however, known.[8]

We report now the isolation and characterization of the first ruthenium–mercury bimetallic nitrosyls, obtained by oxidative addition of mercury salts to ruthenium nitrosyl derivatives.

RESULTS AND DISCUSSION

Reactions of $[RuCl(CO)(NO)(PPh_3)_2]$

The reaction between $[RuCl(CO)(NO)(PPh_3)_2]$ and excess HgI_2 leads to an orange–brown solid of formula $[RuCl(I)(HgI)(CO)(NO)(PPh_3)]$ (**I**). The IR spectrum of which (Table 1) shows increases of 43 and 268 cm^{-1} in the ν(CO) and ν(NO) bands, respectively, relative to the starting material and indicative of oxidation.

This oxidation is not localized over the metal, with a formal oxidation state of +2 in both cases, but over the [RuNO] system which is oxidized from $[RuNO]^8$, with a bent nitrosyl (NO^-) in the starting material,[9] to $[RuNO]^6$, with a linear nitrosyl (NO^+) in the reaction product.

Using $Hg(SCN)_2$ a similar reaction takes place and together with the addition of the mercuric salt, substitution of the halogen by thiocyanate is also observed, with formation of $[Ru(SCN)_2(HgSCN)(CO)(NO)(PPh_3)]$ (**II**). Its IR spectrum shows that the carbonyl and nitrosyl bands shift to higher frequencies due to oxidation. There are also two bands at 2100 and 2130 cm^{-1} due to the ν(CN) stretch of two different thiocyanates, which could be those bonded to mercury and ruthenium.

The ^{31}P NMR spectrum in DMSO for this compound shows one single signal at 25.4 ppm with satellites due to the ^{199}Hg–^{31}P coupling. The coupling constant of 850 Hz is higher than the values reported in the literature,[10] supporting a *trans* arrangement of the Hg(SCN) and PPh_3 groups in the molecule. As the nitrosyl and carbonyl ligands both have a high *trans* influence, it is unlikely that these groups are opposite in the molecule and so the stereochemistry for complex **II** shown in Fig. 1(a) was proposed.

The reaction between $[RuCl(CO)(NO)(PPh_3)_2]$

* Author to whom correspondence should be addressed.

Table 1. IR spectral data for the compounds obtained (cm^{-1})

Compounds	$\nu(CN)_{tcep}$	$\nu(CN)_{cyanide}$	$\nu(CO)$	$\nu(NO)$	$\nu(Ru—Cl)$	
$[RuCl(I)(HgI)(CO)(NO)(PPh_3)]$(**I**)			1968s	1860s	321w	
$[Ru(SCN)_2(HgSCN)(CO)(NO)(PPh_3)]$(**II**)		2100s	2040s	1873s		
		2130sh				
$[RuCl(CN)(HgCN)(CO)(NO)(PPh_3)]$(**III**)		2090s	1993s	1895s	315w	
		2110sh				
$[RuCl(CO)(NO)(PPh_3)_2 \cdot Hg(CN)_2]$(**IV**)		2087m	1935s	1605s	280w	
$[Ru(NO)_2(PPh_3)_2]$(**V**)				1640s		
				1605s		
$[Ru(NO)_2(tcep)_2]$(**VI**)		2240s		1675s		
				1650s		
$[Ru(SCN)(HgSCN)_2(NO)(PPh_3)]$(**VII**)		2110s		1880s		
		2140s				
$[Ru(SCN)_2(HgSCN)(NO)(tcep)]$(**VIII**)	2250s	2130s		1894s		
		2150s				
$[Ru(CN)_2(HgCN)(NO)(PPh_3) \cdot Hg(CN)_2]$(**IX**)		2100s		1867s		
		2140sh				
$[Ru(CN)_2(HgCN)(NO)(tcep)]$(**X**)	2250s	2100s, br		1870s		
$[RuCl_2(HgCl)(NO)(tcep)]$(**XI**)	2240s			1862s	320m	(Ru—Cl)
					270m	(Hg—Cl)
$[RuCl_2(HgPh)(NO)(PPh_3)]$(**XII**)				1844s	325m	
$[RuCl_2(HgPh)(NO)(tcep)]$(**XIII**)	2250s			1869s	320m	

and $Hg(CN)_2$ leads to different compounds depending on the solvent used.

When the reaction takes place in dichloromethane–ethanol the complex $[RuCl(CN)(HgCN)(CO)(NO)(PPh_3)]$ (**III**) is obtained. As is shown in Table 1, the IR spectrum is similar to those of complexes **I** and **II**, suggesting a similar structure. There are also two $\nu(CN)$ stretches corresponding to two different cyanides. The insolubility of this complex and the ready decomposition that occurs in DMSO prevents the attainment of a good NMR spectrum, but as this complex is similar to the thiocyanate complex, a *trans* configuration Hg—Ru—P is expected. By assuming a *cis* disposition of the carbonyl and nitrosyl ligands and according to the proposed mechanism for these reactions (see below), Fig. 1(b) is suggested as the most likely stereochemistry for this complex.

If the reaction occurs in ethanol a different compound of formula $[RuCl(CO)(NO)(PPh_3)_2 \cdot Hg(CN)_2]$ (**IV**) is formed. The IR spectrum shows bands at 1935 cm^{-1}, $\nu(CO)$, and 1605 cm^{-1}, $\nu(NO)$, very close to those of the parent compound (1925 and 1592 cm^{-1}, respectively). This suggests a weak interaction between the metals, probably as an adduct complex where the oxidation state of the ruthenium is not sensibly modified, in contrast to the high shift observed in the oxidative addition complex.

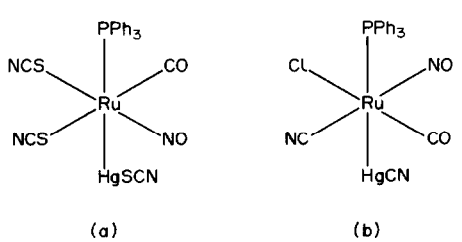

Fig. 1. Proposed structures for complexes (a)**II** and (b)**III**.

Complex **IV** undergoes conversion in solution to the oxidative addition derivative, **III**. This fact suggests that the adduct is an intermediate in the oxidative addition reaction and the proposed mechanism for this reaction is shown in Scheme 1.

The formation of a similar intermediate has been proposed in the reaction of $[RuCl_2(CO)_2(PPh_3)_2]$ with $HgPh_2$ to account for the formation of $[RuCl(Ph)(CO)_2(PPh_3)_2]$ as the final product.[11] The ruthenium–mercury interaction in complex **IV** is assumed to be via pseudohalogen and chlorine bridges due to the low value of the $\nu(Ru—Cl)$ stretch, about 40 cm^{-1} lower than a typical terminal Ru—Cl bond (for example in complex **I**, Table 1), which appears to indicate that the chlorine is acting as a bridge between ruthenium and mercury. Nevertheless, other possible links, like direct bonds between the metals or a single bridge through the cyano group, cannot be excluded, as we have not enough evidence to choose one specific coordination mode.

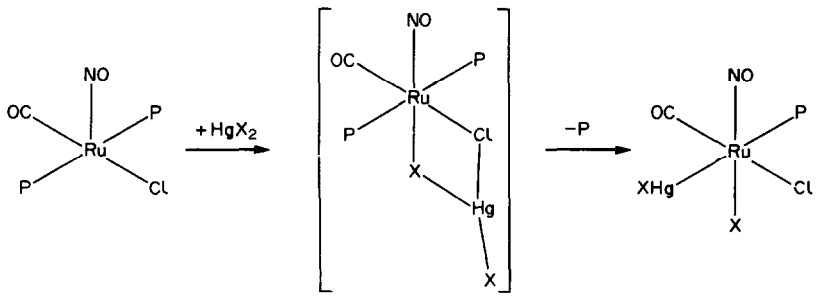

Scheme 1.

The tetrahedral complex $[Ru(NO)_2(PPh_3)_2]$ (**V**) reacts with excess HgX_2 with substitution of one nitrosyl and one phosphine and oxidation to formal ruthenium(II) complexes of formula $[RuX_2(HgX)(NO)(PPh_3)]$. An exception to this behaviour is the reaction with $Hg(SCN)_2$ which gives rise to the formation of $[Ru(SCN)(HgSCN)_2(NO)(PPh_3)]$ (**VII**), although this compound has several similarities with the rest of the complexes of the series.

The complex $[Ru(NO)_2(tcep)_2]$ (**VI**) was obtained from **B** by phosphine substitution. The increase in the ν(NO) band can be explained in terms of the lower basicity of tris-2-cyanoethylphosphine relative to triphenylphosphine.[12]

Complexes **VII–XIII** show an increase of *ca* 250 cm^{-1} in the ν(NO) stretch, indicative of a NO^+ group in ruthenium(II) complexes. Complex **IX** probably contains lattice $Hg(CN)_2$ and the IR spectrum shows, for the three different M—CN bonds of the compound, two bands at 2100 and 2140 $cm.^{-1}$ Since complex **X**, containing only Ru—CN and Hg—CN bonds, has only one broad band at 2100 cm^{-1} which must include both stretches, the extra band in the IR of complex **IX** may be attributable to the lattice mercury cyanide. The high value of this frequency may indicate that the cyanides of these lattice molecules act as bridges, as in free $Hg(CN)_2$ [ν(CN) = 2195 cm^{-1}].

In the reaction of **V** with $HgCl_2$, elimination of mercury and formation of $[RuCl_3(NO)(PPh_3)_2]$ occurs, whereas complex **VI** produces $[RuCl_2(HgCl)(NO)(tcep)]$ (**XI**), with ν(Ru—Cl) and ν(Hg—Cl) at 320 and 270 cm^{-1}, respectively. In a similar manner, complex **V** reacts with ClHgPh to give a mixture of $[RuCl_3(NO)(PPh_3)_2]$ and $[RuCl_2(HgPh)(NO)(PPh_3)]$ (**XII**). Reaction of **VI** and ClHgPh affords the analogous complex **XIII**, whose IR spectrum shows only one ν(Ru—Cl) band, suggesting a Cl—HgPh break in the addition reaction.

The ^{13}C NMR spectrum of **XIII** shows two signals for the cyanide (119.8 and 120.4 ppm) and for the methylene carbons (23.5 and 22.6, and 11.8 and 9.9 ppm) of the tcep, indicating different CH_2CH_2CN groups. This fact can be interpreted in terms of a restricted rotation of the phosphine. The phenyl signals appear slightly shifted to lower fields relative to free ClHgPh,[13] as expected if HgPh acts as a Lewis acid. The *ortho* and *meta* carbons of this phenyl group show coupling to ^{199}Hg of similar magnitude to that in the free ClHgPh, supporting the idea of the Cl—HgPh break and the addition of the Cl and HgPh groups to the ruthenium.

Finally the ^{31}P NMR spectrum of this compound contains a septuplet at 29.6 ppm [^2J(P—H) = 11.5 Hz] with two satellites [^2J(Hg—P) = 486 Hz], indicative of a *trans* Hg—Ru—P arrangement in the molecule. In contrast, the spectrum of **XII** contains the signal at 26.5 ppm with ^2J(Hg—P) = 101.8 Hz. This coupling appears to be smaller than those observed for *trans* dispositions and we cannot determine if mercury and phosphorus are mutually *cis* or *trans* in this compound.

EXPERIMENTAL

All reactions were carried out under oxygen-free nitrogen. $[RuCl(CO)(NO)(PPh_3)_2]$[7] and $[Ru(NO)_2(PPh_3)_2]$[14] were synthesized by the published methods. IR spectra were recorded on KBr pellets using a Perkin–Elmer 1330 spectrophotometer. NMR spectra were recorded with a Bruker WP-80-SY relative to TMS (^{13}C) and 85% $[H_3PO_4(^{31}P)$.

Preparation of $[RuCl(I)(HgI)(CO)(NO)(PPh_3)]$ (**I**)

A suspension of $[RuCl(CO)(NO)(PPh_3)_2]$ (0.36 g, 0.5 mmol) and HgI_2 (0.67 g, 1.5 mmol) in ethanol (30 cm^3) was refluxed for 2 h. The brown solution was filtered and the solvent removed *in vacuo*. The solid was extracted with dicholoromethane. Addition of diethyl ether gave a purple solid in 63% yield. Found: C, 23.9; H, 1.6; N, 1.6. Calc.: C, 25.0; H, 1.7; N, 1.5.

Preparation of [$Ru(SCN)_2(HgSCN)(CO)(NO)(PPh_3)$] (**II**)

A mixture of [$RuCl(CO)(NO)(PPh_3)_2$] (0.36 g, 0.5 mmol) in dichloromethane (20 cm^3) and $Hg(SCN)_2$ (0.47 g, 1.5 mmol) in ethanol (20 cm^3) was refluxed for 2 h. The orange–brown precipitate which formed was collected and washed with dichloromethane, ethanol and diethyl ether. Yield 87%. Found: C, 33.1; H, 1.8; N, 7.2. Calc.: C, 33.2; H, 1.9; N, 7.0.%

Preparation of [$RuCl(CN)(HgCN)(CO)(NO)(PPh_3)$] (**III**)

To a solution of [$RuCl(CO)(NO)(PPh_3)_2$] (0.36 g, 0.5 mmol) in dichloromethane (15 cm^3), a solution of $Hg(CN)_2$ (0.38 g, 1.5 mmol) in ethanol (20 cm^3) was added and the mixture was stirred for 3 h. The solution, which became orange, was concentrated to 5 cm^3 and then 20 cm^3 of diethyl ether were added affording **III** as an orange precipitate. Yield 79%. Found: C, 35.6; H, 2.4; N, 6.0. Calc.: C, 35.5; H, 2.1; N, 5.9%.

Preparation of [$RuCl(CO)(NO)(PPh_3)_2 \cdot Hg(CN)_2$] (**IV**)

A mixture of [$RuCl(CO)(NO)(PPh_3)_2$] (0.36 g, 0.5 mmol) and $Hg(CN)_2$ (0.25 g, 1.0 mmol) in ethanol was refluxed for 3 h. During this time the solid changed from green to orange–brown, then was filtered and washed with ethanol, dichloromethane and diethyl ether. Yield 60%. Found: C, 47.8; H, 3.2; N, 4.4. Calc.: C, 48.2; H, 3.1; N, 4.3%.

Preparation of [$Ru(NO)_2(tcep)_2$] (**VI**)

A solution of [$Ru(NO)_2(PPh_3)_2$] (3.45 g, 5 mmol) and tcep (2.85 g, 15 mmol) in toluene (50 cm^3) was refluxed for 2 h. The solution changed from red to orange and a dark orange precipitate appeared. After cooling to room temperature, the solid was filtered, washed with toluene, ethanol and diethyl ether. Yield 77%. Found: C, 39.6; H. 4.4; N, 20.9. Calc.: C, 39.5; H, 4.4; N, 20.4%.

Preparation of [$Ru(SCN)(HgSCN)_2(NO)(PPh_3)$] (**VII**)

A suspension of [$Ru(NO)_2(PPh_3)_2$] (0.35 g, 0.5 mmol) and $Hg(SCN)_2$ (0.48 g, 1.5 mmol) in ethanol was refluxed for 3 h. The ochre solid was collected, washed with ethanol, toluene and ethanol and dried. Yield 84%. Found: C, 26.2; H, 1.6; N, 5.8. Calc.: C, 26.0; H, 1.6; N, 5.8%.

The following complexes were prepared in a similar way using [$Ru(NO)_2(PPh_3)_2$] or [$Ru(NO)_2(tcep)_2$] and a 1 : 3 excess of the appropriate mercury salt:

[$Ru(SCN)_2(HgSCN)(NO)(tcep)$] (**VIII**): brown solid; yield 71%. Found: C, 20.4; H, 1.8; N, 14.0. Calc.: C, 20.6; H, 1.7; N, 14.0%.

[$Ru(CN)_2(HgCN)(NO)(PPh_3) \cdot Hg(CN)_2$] (**IX**): ochre solid; yield 69%. Found: C, 29.4; H, 1.7; N, 9.1. Calc.: C, 29.9; H, 1.6; N, 9.1%.

[$Ru(CN)_2(HgCN)(NO)(tcep)$] (**X**): brown solid; yield 74%. Found: C, 23.5; H, 2.1; N, 16.4. Calc.: C, 23.9; H, 2.0; N, 16.3%.

[$RuCl_2(HgCl)(NO)(tcep)$] (**XI**): yellow–orange solid; yield 58%. Found: C, 17.0; H, 2.0; N, 8.8. Calc.: C, 17.1; H, 1.9; N, 8.9%.

[$RuCl_2(HgPh)(NO)(PPh_3)$] (**XII**): orange–brown solid; yield 49%. Found: C, 38.9; H, 2.7; N, 2.2. Calc.: C, 40.4; H, 2.8; N, 2.0%.

[$RuCl_2(HgPh)(NO)(tcep)$] (**XIII**): orange–brown solid; yield 76%. Found: C, 26.5; H, 2.5; N, 8.4. Calc.: C, 26.8; H, 2.5; N, 8.4%.

Acknowledgement—We thank the Comision Interministerial de Ciencia y Tecnologia (Project PS87-0028) for financial support.

REFERENCES

1. (a) R. W. Johnson, W. R. Muir and D. A. Sweigart, *J. Chem. Soc., Chem. Commun.* 1970, 643; (b) B. Deubzer and H. D. Kaesz, *J. Am. Chem. Soc.* 1968, **90**, 3276; (c) C. P. Carey, C. R. Cyr, R. L. Anderson and D. F. Marten, *J. Am. Chem. Soc.* 1975, **97**, 3053.
2. (a) D. J. Cook, J. L. Dawes and R. D. W. Kemmitt, *J. Chem. Soc.* 1967, 1547; (b) I. W. Nowell and D. R. Russell, *J. Chem. Soc., Dalton Trans.* 1972, 2393.
3. W. H. Morrison and D. N. Hendrickson, *Inorg. Chem.* 1972, 11, 2912.
4. M. M. Taqui, S. Shareef, S. Vancheeson and R. A. Levenson, *J. Inorg. Nucl. Chem.* 1976, **38**, 1279.
5. G. R. Clark, S. V. Hoskins and W. R. Roper, *J. Organomet. Chem.* 1982, **234**, C9.
6. M. I. Bruce, M. Cooke and M. Green, *J. Organomet. Chem.* 1968, **13**, 227.
7. K. R. Laing and W. R. Roper, *J. Chem. Soc. A* 1970, 2149.
8. G. A. Bentley, K. R. Laing, W. R. Roper and J. M. Waters, *J. Chem. Soc., Chem. Commun.* 1970, 998.
9. J. Mason, D. M. P. Mingos, J. Schaefer, D. Sherman and E. O. Stejskal, *J. Chem. Soc., Chem. Commun.* 1985, 444.
10. (a) M. M. Kubicki, R. Kergoat, J. Y. Le Gall, J. E. Guerchais, J. Douglade and R. Mercier, *Aust. J. Chem.* 1982, **35**, 1543; (b) T. A. George and C. D. Turnipseed, *Inorg. Chem.* 1973, **12**, 394.

11. C. F. J. Barnard, J. A. Daniels and R. J. Mawby, *J. Chem. Soc., Dalton Trans.* 1976, 961.
12. W. A. Henderson and C. A. Streuli, *J. Am. Chem. Soc.* 1960, **82**, 5791.
13. J. Browning, P. L. Goggin, R. J. Goodfellow, N. W. Hurst, L. G. Mallison and M. Murray, *J. Chem. Soc., Dalton Trans.* 1978, 872.
14. J. J. Levison and S. D. Robinson, *Chem. Ind.* 1969, 1514.

Polyhedron Vol. 10, No. 10, pp. 1019–1023, 1991
Printed in Great Britain

0277–5387/91 $3.00+.00
© 1991 Pergamon Press plc

REACTIONS OF CARBONYL AND NITROSYL RUTHENIUM COMPLEXES WITH UNINEGATIVE (X,S)-DONOR LIGANDS (X = S, P)

A. GUTIERREZ-ALONSO and L. BALLESTER-REVENTOS*

Departamento de Quimica Inorganica, Facultad de Ciencias Quimicas,
Universidad Complutense, 28040-Madrid, Spain

(*Received* 13 *June* 1990; *accepted* 7 *January* 1991)

Abstract—Reactions of 1,1-dithiolates ($EtOCS_2^-$ and $Et_2NCS_2^-$) and the related (P,S)-donor ligand ($Ph_2PCSNPh^-$) with halocarbonylphosphine complexes of ruthenium give halide substitution derivatives with chelation of the (S,S)- or (P,S)-donor ligand. The reaction of $[RuCl_2(CO)(CS)(PPh_3)_2]$ with dithiolates gives rise to displacement of the thiocarbonyl ligand, while with $Ph_2PCSNPh^-$ the derivative $[RuCl(Ph_2PCSNPh)(CO)(CS)(PPh_3)]$ is obtained. The carbonyl nitrosyl complex $[RuCl(CO)(NO)(PPh_3)_2]$ reacts with displacement of nitrosyl and formation of $[RuCl(X,S)(CO)(PPh_3)_2]$ complexes.

The halocarbonyl and halophosphine complexes of ruthenium react with 1,1-dithiolates with formation of hexacoordinated $Ru(S,S)_2L_2$ (L = CO, PPh_3),[1] with the (S,S)-donor ligands mutually *cis*. The neutral ligands in these complexes are not easily substituted, unlike the R_2PS_2 analogues[2] which undergo substitution of one neutral ligand, e.g. PPh_3, by carbonyl of other phosphines to give the mixed $Ru(S,S)_2LL'$ complexes. The phosphine carbonyl derivative has also been produced by reaction of $[RuCl(OOCCH_3)(CO)(PPh_3)_2]$ with the alkali dithiocarbamate.[3] To date there are no reports of the reactions of 1,1-dithiolates with thiocarbonyl or nitrosyl ruthenium derivatives.

We report in this paper the study of the reactivity of halocarbonylphosphine ruthenium complexes towards anionic (X,S)-donor ligands: Etxant ($EtOCS_2^-$), Et_2dtc ($Et_2NCS_2^-$) and $Ph_2PCSNPh^-$, the latter usually acting as a (P,S) bidentate ligand.[4,5] The observed reactions take place with substitution of at least one of the chlorine ligands and one or more of the neutral ligands by the (X,S)-donor ligand.

RESULTS AND DISCUSSION

The reaction of $RuCl_2(PPh_3)_2$ and $Ph_2PCSNPh^-$ in ethanol gives the complex $[Ru(Ph_2PCSNPh)_2(PPh_3)_2]$ (**I**), similar to those described for xanthates and dithiocarbamates.[1,3] This complex reacts with phosphines, like tcep {$P(CH_2CH_2CN)_3$} or dppe ($Ph_2PCH_2CH_2PPh_2$) in refluxing acetone to give $[Ru(Ph_2PCSNPh)_2(tcep)_2]$ (**II**) and $[Ru(Ph_2PCSNPh)_2(dppe)]$ (**III**), respectively. The IR spectra of these complexes (Table 1) show a strong band at 1525–1550 cm^{-1} attributed to the ν(C=N) stretch of the exocyclic C=NPh group, which reveals bidentate coordination to the metal[6] via phosphorus and sulphur atoms. A medium intensity band at 940 cm^{-1} is assigned to the ν(C—S) vibration.

The ^{31}P NMR spectrum of complex **I** (Table 2) shows two triplets with a coupling of 20 Hz, indicating two pairs of equivalent phosphorus mutually *cis*. This can be interpreted as being due to *cis* positioning of the PPh_3 ligands, as has been observed in the analogous dithiocarbamate complex[2] and evidenced in their substitution by dppe, and *trans* coordination of the two phosphorus atoms of the phosphinethioformamido ligands, as shown in Fig. 1(a).

The $[RuCl_2(CS)(PPh_3)_2]_2$ complex, obtained from $RuCl_2(PPh_3)_3$ and CS_2,[7] has a dimeric structure with chloro bridges, which can be cleaved by donor ligands like CO and forms $[RuCl_2(CO)(CS)(PPh_3)_2]$. These complexes react in different ways with dithiolate ligands. Thus, $[RuCl_2(CS)(PPh_3)_2]_2$ reacts with the (X,S)-donor ligands to give com-

* Author to whom correspondence should be addressed.

Table 1. IR data for the new complexes (cm^{-1})

Compound	Z—C(S)X⁻ ν(C—Z)	ν(C—S)	ν(C≡S)	ν(C≡O)	ν(Ru—Cl)	Others
$[Ru(Ph_2PCSNPh)_2(PPh_3)_2]$ (I)	1550s	940m				
$[Ru(Ph_2PCSNPh)_2(tcep)_2]$ (II)	1540s	930m				2240s $\nu(CN)_{tcep}$
$[Ru(Ph_2PCSNPh)_2(dppe)]$ (III)	1525s	930m				
$[Ru(Etxant)_2(CS)(PPh_3)]$ (IV)	1240s	1050m	1290s			
$[Ru(Et_2dtc)_2(CS)(PPh_3)]$ (V)	1490s	995m	1275s			
$[Ru(Ph_2PCSNPh)_2(CS)(PPh_3)]$ (VI)	1560s	940m	1270s			
$[Ru(Etxant)_2(CO)(PPh_3)]$ (VII)	1235s	1050m		1940s		
$[Ru(Et_2dtc)_2(CO)(PPh_3)]$ (VIII)	1500s	1005m		1940s		
$[RuCl(Ph_2PCSNPh)(CO)(CS)(PPh_3)]$ (IX)	1550s	935m	1275s	1955s	315w	
$[RuCl(Etxant)(CO)(PPh_3)_2]$ (X)	1215s	1045m		1945w	330w	
$[RuCl(Et_2dtc)(CO)(PPh_3)_2]$ (XI)	1490s	1005m		1935s	330w	
$[RuCl(Ph_2PCSNPh)(CO)(PPh_3)_2]$ (XII)	1555s	935m		1955s		
$[RuH(Ph_2PCSNPh)(CO)(PPh_3)_2]$ (XIII)	1550m	935m		1950s		1970sh $\nu(Ru—H)$
$[RuCl(Etxant)(CO)_2(PPh_3)]$ (XIV)	1240m	1045m		2040s 1970s		
$[RuCl(Et_2dtc)(CO)_2(PPh_3)]$ (XV)	1500s	995m		2030s 1960s	330w	

Table 2. ^{31}P NMR data for some of the new complexes

Complex	δ (ppm)		2J(P—P) (Hz)
I	30.62t	28.51t	20
VI	31.43t	21.90d	22
IX	33.17d	32.36d	81
XI	35.41d	27.07d	48
XII	29.67(A) 28.97(B) 21.33(C)		$J_{AB} = 31$ $J_{AC} = -21$ $J_{BC} = 82$

plexes of formula $[Ru(X,S)_2(CS)(PPh_3)]$ (**IV–VI**), while the carbonyl–thiocarbonyl derivative reacts with Etxant or Et_2dtc to give the previously known $[Ru(S,S)_2(CO)(PPh_3)]$ (**VII–VIII**)[4] and with $Ph_2PCSNPh^-$ forming $[RuCl(Ph_2PCSNPh)(CO)(PPh_3)]$ (**IX**). All these complexes show characteristic IR bands of bidentate (X,S) ligands (Table 1).[1,8,9] Complexes **IV**, **V**, **VI** and **IX** also exhibit a band at 1270–1290 cm^{-1} attributed to ν(CS) of a terminal thiocarbonyl ligand.

The ^{31}P NMR spectrum of **VI** shows a triplet at 31.43 ppm for the triphenylphosphine phosphorous and a doublet at 21.90 ppm for the two equivalent phosphinothioformate ligands. The coupling constant, 22 Hz, suggests a *cis* disposition of the non-equivalent phosphorus [Fig. 1(b)]. The *cis* disposition of PPh_3 and CS is proposed in accordance with that observed in the related carbonyl complexes **VII** and **VIII**.[4]

The substitution of a thiocarbonyl group in the presence of carbonyl ligands is a very unusual reaction and has been interpreted according to the relative strengths of the M—CO and M—CS bonds.[10] Richardson *et al.*[11] suggest that substitution may occur when $\nu(CS) \geqslant 1348$ cm^{-1}, as found in $[Fe(C_5H_5)(CO)_2(CS)]^+$ where both carbonyl and thiocarbonyl can be displaced by other ligands. In our case, the complex $[RuCl_2(CO)(CS)(PPh_3)_2]$ shows ν(CS) at 1295 cm^{-1}, suggesting a stronger M—CS than M—CO bond. The observed behaviour must then be explained on the basis of nucleophilic attack on the thiocarbonyl, as has been reported in reactions with amines or alcohols.[12]

A possible mechanism for this reaction would be the substitution of one chlorine and one phosphine by the dithiolate, followed by nucleophilic attack on CS by a second dithiolate with formation of the metallacycle Ru—C(S)—S—C(X)—S. This ring has been reported in molybdenum(II) chemistry with Et_2dtc and CS ligands.[13] In our complexes the metallacyclic intermediate would not be stable, probably because of the high reaction temperature (reflux of ethanol), and would decompose with loss of CS to isolated $[Ru(S,S)_2(CO)(PPh_3)]$.

The reaction with $Ph_2PCSNPh^-$ stops after the first step and so derivative **IX** is isolated. The most probable chlorine to be substituted in this step is the one situated *trans* to CS, which corresponds to the higher *trans* effect of this ligand relative to CO.

The ^{31}P NMR spectrum of **IX** shows two doub-

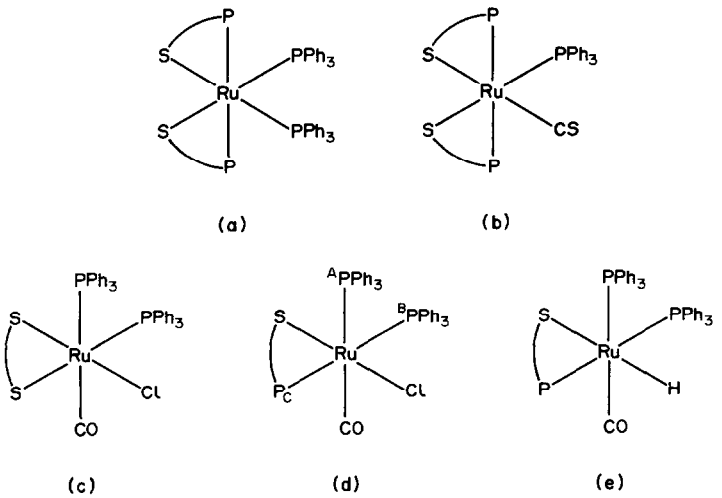

Fig. 1. Proposed structures for complexes: (a) **I**, (b) **VI**, (c) **XI**, (d) **XII** and (e) **XIII**.

lets which can be assigned to two non-equivalent phosphorus atoms. The ^2J(P—P) value of 81 Hz does not distinguish unambiguously between a *cis* or *trans* disposition of both phosphorus atoms. This coupling value is intermediate between the published values found for two *cis* (0–70 Hz) and *trans* (60–800 Hz) phosphorus atoms.[14] However, the coupling constants found in the present work for the ruthenium complexes of *ca* 20 Hz for *cis* coupling and 82 Hz (see below) for *trans* coupling suggest that complex **IX** may have a *trans* arrangement of the two phosphorus atoms.

The reaction of $[RuCl(CO)(NO)(PPh_3)_2]$ with 1,1-dithiolates takes place with substitution of the nitrosyl to give complexes of formula $[RuCl(X,S)(CO)(PPh_3)_2]$ (**X–XII**). The IR spectra show the characteristic bands of chelate (X,S) ligands together with a ν(Ru—Cl) stretch at 330 cm^{-1}, shifted to higher frequencies than the parent compound as a consequence of the loss of nitrosyl.

The ^{31}P NMR spectrum of **XI** shows two doublets for the two *cis* non-equivalent phosphorus atoms and the ^{13}C NMR shows the carbonyl signal as a doublet, $^2J(^{13}C—^{31}P) = 15$ Hz, for a carbonyl *trans* to one phosphine. Although this value is rather small and more typical of a *cis* coupling,[15] the pattern, a doublet, indicates that the carbonyl is coupled only to one phosphorus, e.g. in our case the expected J(C—P) should be nearly zero. On the other hand (see below), the analogous $[RuH(Ph_2PCSNPh)(CO)(PPh_3)_2]$ in which the only variation is the exchange of chlorine by hydride should have the carbonyl *trans* to one phosphine and thus we propose the same stereochemistry for both complexes. The only stereochemistry that fits these conditions for **XI** is shown in Fig. 1(c). The ^{31}P NMR spectrum of **XII** shows an ABC pattern

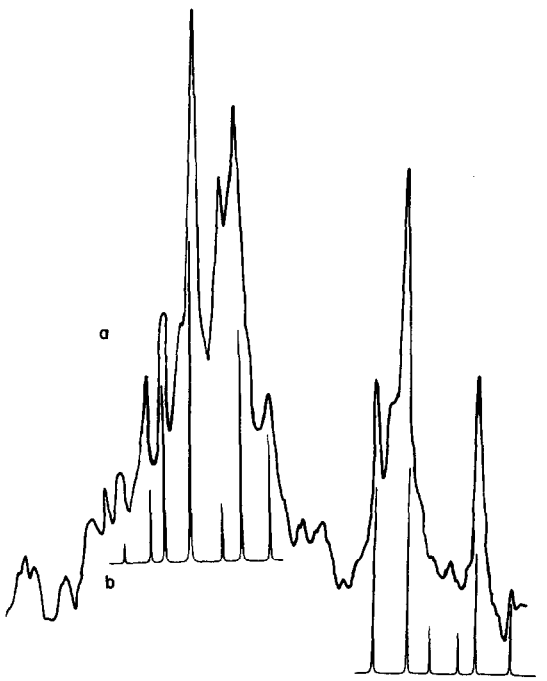

Fig. 2. (a) Observed and (b) simulated ^{31}P NMR spectra of **XII**.

interpreted by a *mer* disposition of the three phosphorus nuclei as shown in Fig. 2, where both the experimental and the simulated spectra are represented. We assign the signal at lower frequencies to the phosphinothioformamido ligand in accordance with that observed in the spectrum of **VI** (Table 2). The most likely structure has been chosen in accordance with the similarities between complexes **XI** and **XII** and is represented in Fig. 1(d).

The reaction of $[RuHCl(CO)(PPh_3)_3]$ with $Ph_2PCSNPh^-$ affords the hydride $[RuH(Ph_2$

$PCSNPh)(CO)(PPh_3)_2]$ (**XIII**), having the same formula as those of Etxant and Et_2dtc previously reported.[3] This derivative shows the ν(Ru—H) stretch as a shoulder at 1970 cm^{-1}, shifted 40 cm^{-1} to lower frequencies relative to the starting chlorohydride and attributed to the substitution of the phosphine *trans* to this hydride. The ^1H NMR spectrum shows a pseudo-quadruplet at -0.64 ppm with ^2J(P—H) = 7.1, 7.4 and 7.5 Hz for similar coupling of the three non-equivalent phosphorus atoms to the hydride. From this result and from comparison with complexes **XI** and **XII** the stereochemistry chosen for complex **XIII** is shown in Fig. 1(e).

The 1,1-dithiolates used react with *cis,cis,trans*-$[RuCl_2(CO)_2(PPh_3)_2]$ with partial substitution of chlorines, and formation of $[RuCl(S,S)(CO)_2(PPh_3)]$ (**XIV–XV**) that show bands for a bidentate dithiolate ligand and for two *cis* carbonyls, which shift to lower frequencies than in the dichloride and are related to the higher donor character of the dithiolates. On the other hand, the reaction with $Ph_2PCSNPh^-$ occurs with substitution of one carbonyl ligand instead of a phosphine. The $[RuCl(Ph_2PCSNPh)(CO)(PPh_3)_2]$ complex thus obtained shows an identical IR spectrum to **XII**, suggesting that the same isomer has been formed. This would imply reorganization of the ligands around the metal had occurred in the reaction.

EXPERIMENTAL

All reactions were carried out under oxygen-free nitrogen. $Ph_2PCSNHPh$,[16] $RuCl_2(PPh_3)_3$,[17] $[RuCl_2(CS)(PPh_3)_2]_2$,[7] $[RuCl_2(CO)(CS)(PPh_3)_2]$,[7] $[RuCl(CO)(NO)(PPh_3)_2]$,[18] $[RuHCl(CO)(PPh_3)_3]$[19] and *cis,cis,trans*-$[RuCl_2(CO)_2(PPh_3)_2]$[20] were prepared as reported. Analyses were carried out by Elemental Microanalysis Ltd (Devon); IR spectra were recorded on KBr discs using a Perkin–Elmer 1330 spectrophotometer; and NMR spectra were recorded on a Bruker WP80SY using TMS and 85% H_3PO_4 as standards.

Preparation of $[Ru(Ph_2PCSNPh)_2(PPh_3)_2]$ (**I**)

An ethanolic solution of $RuCl_2(PPh_3)_3$ (0.96 g) and $Ph_2PCSNHPh$ (0.64 g) with a few drops of NEt_3 was refluxed for 2 h. The orange solution was concentrated *in vacuo* to 10 cm^3 and filtered. Addition of 30 cm^3 of cold Et_2O produces an orange solid, which was filtered and washed with Et_2O. Yield: 86%. Found: C, 70.0; H, 4.8; N, 2.2. Calc.: C, 70.2; H, 4.8; N, 2.2%.

Preparation of $[Ru(Ph_2PCSNPh)_2(tcep)_2]$ (**II**)

A solution of **I** (0.43 g) and tcep (0.55 g) in toluene was refluxed for 3 h. The solvent was then removed *in vacuo* and the solid extracted with CH_2Cl_2 and precipitated as a yellow powder by addition of light petroleum. Yield: 48%. Found: C, 59.8; H, 4.9; N, 10.1. Calc.: C, 59.6; H, 4.8; N, 9.9%.

Preparation of $[Ru(Ph_2PCSNPh_2)(dppe)]$ (**III**)

The compound was obtained as yellow microcrystals from **I** (0.31 g) and dppe (0.15 g) as described for **II**. Yield: 74%. Found: C, 67.3; H, 4.9; N, 2.6. Calc.: C, 67.4; H, 4.8; N, 2.4%.

Preparation of $[Ru(X,S)_2(CS)(PPh_3)]$ (**IV–VI**)

A solution of $[RuCl_2(CS)(PPh_3)_2]_2$ (1 mmol) and the alkali dithiolate (2.1 mmol) (or $Ph_2PCSNHPh$ and excess of NEt_3) in 25 cm^3 of EtOH was refluxed for 2 h. The solvent was removed *in vacuo* and the solid extracted with CH_2Cl_2. Addition of hexane affords the product as an orange solid, which was washed with Et_2O. $[Ru(Etxant)_2(CS)(PPh_3)]$ (**IV**), yield: 83%. Found: C, 46.1; H, 3.8. Calc.: C, 46.2; H, 3.9%. $[Ru(Et_2dtc)_2(CS)(PPh_3)]$ (**V**), yield: 76%. Found: C, 48.7; H, 5.2; N, 4.0. Calc.: C, 49.5; H, 5.0; N, 4.0%. $[Ru(Ph_2PCSNPh)_2(CS)(PPh_3)]$ (**VI**), yield: 74%. Found: C, 65.5; H, 4.0; N, 2.7. Calc.: C, 65.3; H, 4.3; N, 2.6%.

Preparation of $[Ru(S,S)_2(CO)(PPh_3)]$ (**VII–VIII**)

A solution of $[RuCl_2(CO)(CS)(PPh_3)_2]$ (1 mmol) and the alkali dithiolate (2 mmol) in EtOH was refluxed for 2 h. The orange solution was filtered, concentrated to 5 cm^3 and cooled at 0°C for 2 days to give orange microcrystals of the product. $[Ru(Etxant)_2(CO)(PPh_3)]$ (**VII**), yield: 87%. Found: C, 47.1; H, 4.0. Calc.: C, 47.4; H, 4.0%. $[Ru(Et_2dtc)_2(CO)(PPh_3)]$ (**VIII**), yield: 83%. Found: C, 50.5; H, 5.2; N, 4.1. Calc.: C, 50.6; H, 5.1; N, 4.0%.

Preparation of $[RuCl(Ph_2PCSNPh)(CO)(CS)(PPh_3)]$ (**IX**)

A solution of $Ph_2PCSNHPh$ (0.64 g) and NEt_3 (1 cm^3) in 10 cm^3 of EtOH was added to a hot solution of $[RuCl_2(CO)(CS)(PPh_3)_2]$ (0.77 g) in EtOH (15 cm^3) and the mixture was refluxed for 30 min. The solution was then worked-up as above to give **IX** as an orange solid. Yield: 87%. Found: C, 59.0; H, 3.7; N. 2.0. Calc.: C, 59.2; H, 3.8; N, 1.8%.

Preparation of [RuCl(S,S)(CO)(PPh_3)$_2$] (**X–XI**)

A suspension of [RuCl(CO)(NO)(PPh_3)$_2$] (0.72 g) and the alkali dithiolate (2 mmol) in MeOH (25 cm^3) was refluxed for 15 min until the solution turned red–brown. The hot solution was filtered and cooled at 0°C depositing a brown solid. [RuCl(Etxant)(CO)(PPh_3)$_2$] (**X**), yield: 61%. Found: C; 59.6; H, 4.3. Calc.: C, 59.3; H, 4.3%. [RuCl(Et_2dtc)(CO)(PPh_3)$_2$] (**XI**), yield: 74%. Found: C, 61.3; H, 4.6; N, 1.7. Calc.: C, 60.2; H, 4.8; N, 1.7%. ^{13}C NMR (ppm): 201.65 d [*C*O, ^2J(P—C) = 15 Hz], 194.40 s (S_2CNEt_2), 136–126 m (Ph) 43.15 s (NCH_2CH_3), 12.61 s (NCH_2CH_3).

Preparation of [RuCl($Ph_2PCSNPh$)(CO)(PPh_3)$_2$] (**XII**)

Method (a). A solution of $Ph_2PCSNHPh$ (0.48 g) and NEt_3 (1 cm^3) in EtOH (10 cm^3) was added to a refluxing solution of [RuCl(CO)(NO)(PPh_3)$_2$] (0.72 g) in CH_2Cl_2 (20 cm^3). The solution was refluxed for 1 h, concentrated to 10 cm^3 and filtered. Addition of pentane (20 cm^3) and cooling at 0°C overnight afforded orange microcrystals in 76% yield.

Method (b). A solution of [$RuCl_2$(CO)$_2$(PPh_3)$_2$] (0.75 g), $Ph_2PCSNHPh$ (0.64 g) and NEt_3 (1 cm^3) in EtOH (25 cm^3) was refluxed for 5 h. The solution was filtered, the solvent was removed *in vacuo* and the residue extracted with 2 × 10 cm^3 of acetone. Addition of Et_2O (30 cm^3) afforded a yellow solid which was recrystallized from CH_2Cl_2–pentane. Yield: 63%. Found: C, 65.5; H, 4.6; N, 1.4. Calc.: C, 66.6; H, 4.5; N, 1.3%.

Preparation of [RuH($Ph_2PCSNPh$)(CO)(PPh_3)$_2$] (**XIII**)

A solution of [RuHCl(CO)(PPh_3)$_3$] (0.95 g, 1 mmol), $Ph_2PCSNHPh$ (0.35 g, 1.1 mmol) and NEt_3(0.5 cm^3) in acetone (30 cm^3) was refluxed for 2 h and then stirred for 1 h. The green precipitate that appeared was recrystallized from CH_2Cl_2–hexane. Yield: 83%. Found: C, 69.2; H, 4.7; N, 1.4. Calc.: C, 69.0; H, 4.7; N, 1.4%. ^{1}H NMR (ppm): 7.7–7.2 m (40H, *Ph*), 6.2–5.4 m (5H, *Ph*—N), −0.64 q [1H, *H*—Ru, J(P—H) = 7.3 Hz, average].

Preparation of [RuCl(S,S)(CO)$_2$(PPh_3)] (**XIV–XV**)

A suspension of *cis,cis,trans*-[$RuCl_2$(CO)$_2$(PPh_3)$_2$] (0.75 g, 1 mmol) and the alkali dithiolate (2.5 mmol) was refluxed for 3 h in EtOH. The solution was filtered, concentrated to 10 cm^3 and then 15 cm^3 of Et_2O were added. The ochre precipitate that appeared was collected, washed with EtOH and Et_2O, and dried. [RuCl(Etxant)(CO)$_2$(PPh_3)] (**XIV**), yield: 65%. Found: C, 47.8; H, 3.5. Calc.: C, 48.9; H, 3.5%. [RuCl(Et_2dtc)(CO)$_2$(PPh_3)] (**XV**), yield: 58%. Found: C, 49.5; H, 4.2; N, 2.5. Calc.: C, 49.8; H, 4.2; N, 2.3%.

Acknowledgement—We thank the Comision Interministerial de Investigacion Cientifica y Tecnica (Project PS87-0028) for support.

REFERENCES

1. C. O'Connor, J. D. Gilbert and G. Wilkinson, *J. Chem. Soc. A* 1969, 84.
2. D. J. Cole-Hamilton and T. A. Stephenson, *J. Chem. Soc., Dalton Trans.* 1974, 739.
3. P. B. Critchlow and S. D. Robinson, *J. Chem. Soc., Dalton Trans.* 1975, 1367.
4. D. H. M. W. Thewissen, H. P. M. M. Ambrosius, H. L. M. Van Gaal and J. J. Steggerda, *J. Organomet. Chem.* 1980, **192**, 101.
5. A. Gutierrez, L. Ballester, V. Perez-Garcia and C. Ruiz-Valero, *Polyhedron* 1990, **9**, 2163.
6. J. Kopf, R. Lenck, S. N. Olaffson and R. Kramolowsky, *Angew Chem., Int. Edn. Engl.* 1976, **15**, 768.
7. J. D. Gilbert, M. C. Baird and G. Wilkinson, *J. Chem. Soc. A* 1968, 2198.
8. A. N. Bhatt, R. C. Fay, D. F. Lewis, A. F. Lindmark and S. H. Strauss, *Inorg. Chem.* 1974, **13**, 886.
9. A. McAuliffe and B. J. Sayle, *Inorg. Chim. Acta* 1978, **30**, 35.
10. M. A. Andrews, *Inorg. Chem.* 1977, **16**, 496.
11. J. W. Richardson, R. J. Angelici and R. A. Jacobson, *Inorg. Chem.* 1987, **26**, 452.
12. (a) B. D. Dombeck and R. J. Angelici, *Inorg. Chem.* 1976, **15**, 2403; (b) F. Faraone, P. Piraino, W. Marsala and S. Sergi, *J. Chem. Soc., Dalton Trans.* 1977, 859; (c) J. M. Lisy, E. D. Dobrzynski, R. J. Angelici and J. Clardy, *J. Am. Chem. Soc.* 1975, **97**, 656; (d) W. Petz, *J. Organomet. Chem.* 1984, **270**, 81.
13. S. J. N. Gurgmayer and J. L. Templeton, *Inorg. Chem.* 1985, **24**, 3939.
14. E. G. Finer and R. K. Harris, *Prog. NMR Spectrosc.* 1970, **6**, 61.
15. D. W. Krassowski, J. H. Nelson, K. R. Brower, D. Hauenstein and R. A. Jacobson, *Inorg. Chem.* 1988, **27**, 4294.
16. K. Issleib and G. H. Harzfeld, *Chem. Ber.* 1964, **97**, 3430.
17. P. S. Hallman, T. A. Stephenson and G. Wilkinson, *Inorg. Synth.* 1970, **12**, 238.
18. K. R. Laing and W. R. Roper, *J. Chem. Soc. A* 1970, 2149.
19. N. Ahmad, J. J. Levison, S. D. Robinson and M. F. Uttley, *Inorg. Synth.* 1974, **15**, 45.
20. M. I. Bruce and F. G. A. Stone, *J. Chem. Soc. A* 1967, 1238.

Polyhedron Vol. 10, No. 10, pp. 1025–1029, 1991
Printed in Great Britain

0277-5387/91 $3.00+.00
© 1991 Pergamon Press plc

SOLVENT EXTRACTION OF GOLD(III) BY BENZO-15-CROWN-5 AND CHARACTERIZATION OF THE CRYSTALLINE EXTRACTED COMPLEX

YANG HONGWU,* ZHOU ZHIXIAN, ZHANG MINGRUI, ZHANG XIANXIN and RUAN BOYANG

Department of Chemistry, Zhengzhou University, Zhengzhou, Henan 450052, P.R.C.

(*Received* 5 *October* 1990; *accepted* 9 *January* 1991)

Abstract—Gold(III) can be extracted efficiently into 1,2-dichloroethane with benzo-15-crown-5 (B15C5) from an aqueous solution containing hydrochloric acid and potassium ion. It is found that a bulky ion pair is formed by association of a potassium–crown ether complex cation and complex anion $AuCl_4^-$ in the organic phase. The effects of acidity, temperature and other metal ions on the extraction have been studied. The apparent extraction equilibrium constant K_{ex} has been measured to be 2.7×10^7 at 15°C and the enthalpy change ΔH for the extraction process to be -28.4 kJ mol^{-1}. The crystalline extracted complex was characterized by elemental analysis, IR and UV–vis spectra, and its composition is found to be $K(B15C5)_2AuCl_4$.

Although benzo-15-crown-5 (B15C5) has been widely used to extract and separate alkali and alkali-earth metal ions, there are only a few reports on the extraction and separation of anions and complex anions by it. It has been found that B15C5 can be changed into the potassium–crown ether complex in the presence of potassium ion. The complex reaction may be expressed as follows:

$$n\,B15C5 + K^+ \rightleftharpoons K^+(B15C5)_n \quad n = 1\text{–}2.$$

By associating it with a univalent anion, ReO_4^-,[1] or metallic complex anions, $InBr_4^-$ and InI_4^-,[2] these ion-pair species can be easily extracted into the organic phase. In this paper, the extraction of $AuCl_4^-$ by the potassium–crown ether complex was examined and some satisfactory results were obtained.

EXPERIMENTAL

Reagents and apparatus

B15C5, m.p. 79–80.5°C, was obtained from Anyang Oil and Chemical Factory. The purity of gold is 99.99%. Analytical-grade 1,2-dichloroethane and distilled water were saturated with each other prior to use. Other reagents were of analytical grade.

Spectrophotometric measurements were carried out with Hitachi Model UV-220A (Japan) and Shimadzu IR-435 (Japan) spectrophotometers. For elemental and thermal analyses, a Carlo Erba elemental analysis apparatus Model 1106 (Italy) and a Rigaku thermofiex thermal analyser (Japan) were used.

Procedure

(i) *Extraction.* An aqueous solution containing gold(III) (100 μg cm^{-3}) and 1M hydrochloric acid and the same volume of 1,2-dichloroethane containing a certain amount of B15C5 were placed in a stoppered glass tube and shaken for 5 min at 15 ± 1°C, then centrifuged to separate the phases. The aqueous phase was used to measure the absorbance at 314 nm[3] in order to determine the gold concentration (Beer's law is followed in the concentration ranges of 0–35 μg cm^{-3} of gold) and the gold in the organic phase was determined by subtracting the concentration in the aqueous phase from the total concentration added to the tube initially.

* Author to whom correspondence should be addressed.

The distribution ratio of the gold was defined as:

$$D = [Au^{III}]_o/[Au^{III}],$$

where the subscript "o" denotes organic and the lack of a subscript refers to the aqueous phase.

(ii) *Preparation of the crystalline extracted complex.* A saturated organic phase of benzo-15-crown-5–potassium tetrachloroaurate, obtained from successive extractions of the gold(III) in the aqueous solution containing 1 M hydrochloric acid and a certain amount of potassium ion, was evaporated to almost dryness in a water bath. The residue was recrystallized twice with 1,2-dichloroethane and a red–orange, crystalline complex was obtained.

(iii) *Elemental analyses of the crystalline extracted complex.* Carbon and hydrogen were determined using a 1106 elemental analysis apparatus (Italy), and chlorine by silver nitrate titration with a K_2CrO_4 indicator after the complex was decomposed by alkali solution. The amount of gold was measured at 314 nm after the complex was broken down at 700°C and dissolved in the aqua regia.

RESULTS AND DISCUSSION

The study of the extraction mechanism

The effects of diverse metal ions on extraction of gold were tested by mixing an aqueous phase containing 100 $\mu g\ cm^{-3}$ of gold(III), 1 M hydrochloric acid and 1 M of another metal ion with the same volume of organic phase containing 1.0×10^{-3} M B15C5 according to the proposed extraction method. As can be seen in Table 1, by adding the metal ions to the aqueous solution, the extraction efficiency of gold(III) is increased with varying degrees. This is not surprising since the metal ions can coordinate with B15C5 to form complex cations and the gold(III) which should exist as a complex anion $AuCl_4^-$ in the presence of Cl^- can be extracted on forming an ion-pair species.

Although Na^+ fits well into the cavity of the B15C5 molecule, K^+ is the most effective for gold extraction. Because the radius of K^+ is larger than that of the B15C5 cavity (~1.0 Å), it can be sandwiched between two molecules and a 1:2 (K^+:B15C5) hydrophobic complex can be formed.[4,5]

However, with decreasing radii and increasing valency of the metal ions, the interaction between the metal ions and water molecules becomes stronger and the B15C5 molecule mainly forms 1:1 complexes with the metal ions[4,6,7] and for this reason, the most hydrophobic complex of $K^+(B15C5)_2$ displays the highest efficiency for the extraction of $AuCl_4^-$.

In the absence of the metal ion the extraction of $AuCl_4^-$ is very poor, because it is difficult to form the complex cation of B15C5. As can be seen from Fig. 1 and Table 1, if $[H^+]$ in the aqueous phase is $\leqslant 1$ M, the distribution ratio D is $\leqslant 0.03$. However, with increasing acidity in the aqueous phase gold(III) also can be moderately extracted by B15C5, which may be attributed to the formation of an ion-pair species of $H_3O^+(B15C5)\cdot AuCl_4^-$.

The UV–vis spectra of B15C5 and the extracted complex in 1,2-dichloroethane and $KAuCl_4$ in aqueous solution are shown in Fig. 2. The absorption maximum of B15C5 at 278 nm, caused by an electronic transition in the benzene ring, is shifted to 274 nm in the extracted complex $K(B15C5)_2AuCl_4$, indicating the formation of the complex cation $K^+(B15C5)_2$. After the extraction equilibrium, the golden yellow colour of the organic phase is the same as that of the aqueous phase, and the shapes of the UV–vis absorption spectra in the two phases are similar except for a bathochromic shift from 314 nm in the aqueous solution to 325 nm in 1,2-dichloroethane. This originates from the electronic transition from Cl^- to Au^{III} in the complex anion $AuCl_4^-$,[8] whose absorption spectrum will shift to longer wavelengths with decreasing polarity of the solvent. These results indicate that $AuCl_4^-$ has the same configuration in the organic phase as in the aqueous phase.[9]

Table 1. Effect of metal ions

	LiCl	NaCl	KCl	$MgCl_2$	$AlCl_3$	—
D	2.01	6.67	22.04	0.16	0.35	0.03
r'	0.60	0.95	1.33	0.65	0.50	—

[a] Ionic radius of metal (Å).

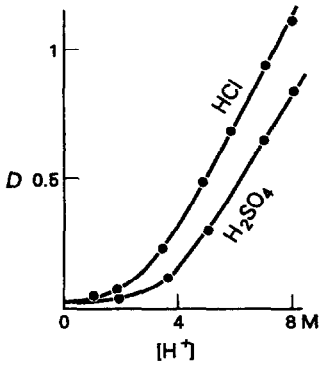

Fig. 1. Effect of acidity on D of gold(III); $[Au^{III}] = 0.50 \times 10^{-3}$ M and $[B15C5] = 1.0 \times 10^{-3}$ M.

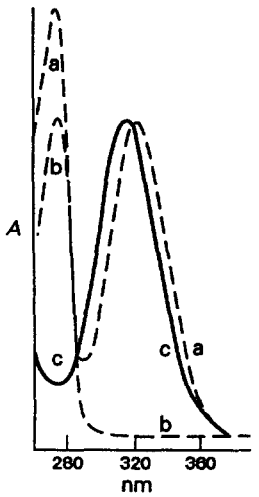

Fig. 2. UV absorption spectra of: (a) $[K(B15C5)_2AuCl_4] = 2.0 \times 10^{-5}$ M, (b) [B15C5] = 2.0×10^{-5} M and (c) $[KAuCl_4] = 2.0 \times 10^{-5}$ M.

On the basis of the above discussion and the electroneutrality principle, the extraction equilibrium may be assumed as:

$$m\,AuCl_4^- + m\,K^+ + n\,B15C5_o \rightleftharpoons [Km(B15C5)_n(AuCl_4)_m]_o \quad (1)$$

and the extraction equilibrium constant can be written as follows:

$$K_{ex} = D/[K^+]^m[B15C5]_o^n \quad (2)$$

$$\log D = m \log [K^+] + n \log [B15C5]_o + \log K_{ex}. \quad (3)$$

According to eq. (1), when two of the concentrations of the three reactants were kept constant and the third reactant concentration was changed, the extractions were carried out and the results are shown in Figs 3 and 4. From slopes

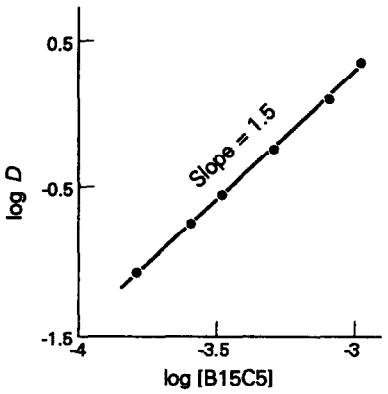

Fig. 4. Effect of log [B15C5] on log D; $[Au^{III}] = 0.50 \times 10^{-3}$ M and $[K^+] = 6.70 \times 10^{-3}$ M.

of the straight lines in the figures and eq. (3), the following conclusions can be obtained: $m = 1$ and $n = 1.5$.

Therefore, the component of the extracted complex in solution was preliminarily determined as $K(B15C5)_{1.5}AuCl_4$, and in accordance with this composition, the extraction equilibrium constant was calculated to be 2.7×10^7 at 15°C.

It should be mentioned that the slope of the straight line in Fig. 4 is 1.5 which may result from two types of extracted complexes of 1 : 1 and 1 : 2 (K^+ : B15C5) species existing simultaneously in the organic phase. A similar result has also been observed in the extraction of $InBr_4^-$ with B15C5 in the presence of K^+.[1]

As shown in Fig. 5 the values of $\ln D$ increase monotonously with a decrease in the temperature. A plot of $\ln D$ against $1/T$ shows a straight line. By using the thermodynamic relation:

$$\ln D = -\Delta H/RT + C, \quad (4)$$

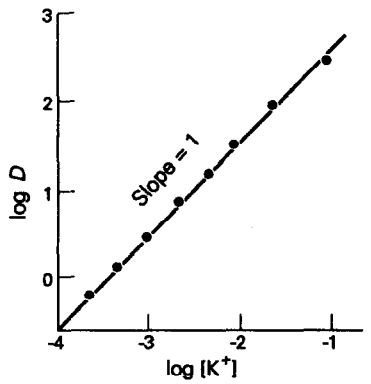

Fig. 3. Effect of $\log[K^+]$ on $\log D$; $[Au^{III}] = 0.50 \times 10^{-3}$ M and [B15C5] = 1.0×10^{-3} M.

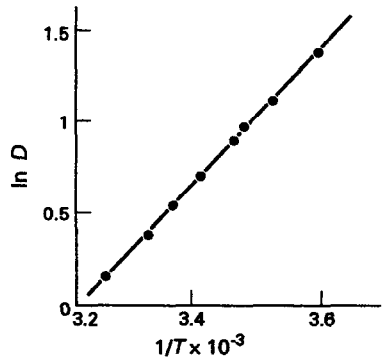

Fig. 5. Effect of T on $\ln D$ of gold(III); $[Au^{III}] = 0.50 \times 10^{-3}$ M and [B15C5] = 1.0×10^{-3} M.

Table 2. Elemental analyses

Complex	Colour		C (%)	H (%)	Cl (%)	Au (%)
$K(B15C5)_2AuCl_4$	Red–orange	Calc.	36.8	4.4	15.5	21.5
		Found	36.8	4.4	15.5	21.6

the value of the enthalpy change, ΔH, was calculated to be -28.4 kJ mol^{-1}. The result indicates that the extraction reaction is exothermic and the extraction efficiency decreases with increasing temperature.

The characterization of the extracted crystalline complex

The extracted crystalline complex is a bright red–orange single crystal, which is stable in air and not deliquescent. It is easily soluble in 1,2-dichloroethane and the solution is also stable, but it is only slightly soluble in methanol and the complex decomposes if left in the air for a long period. The complex is also slightly soluble in water but readily decomposes depositing gold.

The results of elemental analyses are listed in Table 2, which shows that the crystalline complex has the composition $K(C_{14}H_{20}O_5)_2AuCl_4$ ($C_{14}H_{20}O_5$ = B15C5). It is consistent with ref. 2 that the ratio of K^+ : B15C5 is 1 : 2 in the crystalline complex but in the extracted complex in the organic phase it is 1 : 1.5. This may be interpreted as during the process of extraction because of competitive coordination to K^+(B15C5) between free B15C5 and the water molecule the 1 : 1 and 1 : 2 extracted complexes (K^+ : B15C5) are simultaneously present in the organic phase.

Since it is impossible to record real IR spectra of B15C5 and complex $K(B15C5)_2AuCl_4$ using the KBr-pressed-disc technique,[10] their spectra were taken as Nujol mulls and are shown in Fig. 6. In the complex $K(B15C5)_2AuCl_4$, the characteristic frequency of free B15C5 at 978 cm^{-1} almost disappears and a double peak of B15C5 at 1048 and 1040 cm^{-1} becomes a single peak at 1040 cm^{-1}. These results indicate the formation of coordinate bonds in the crystalline complex.[10,11]

The results of thermal analyses of the extracted crystalline complex in nitrogen gas are shown in Fig. 7. The endothermic peak at 198°C on the DTA curve is the melting point of the extracted crystalline complex which is consistent with that measured using a Model X4 micromelting point apparatus. A high and sharp exothermic peak at 225°C on the DTA curve and a corresponding rapid and continuous weight loss in the TG curve indicate the decomposition of the complex. The process continues until the decomposition is complete and the weight is constant.

These results show that in the presence of K^+ in an aqueous solution containing 1 M hydrochloric acid, the complex anion $AuCl_4^-$ can be extracted quantitatively into an organic phase by B15C5 which can coordinate with K^+ extremely well to

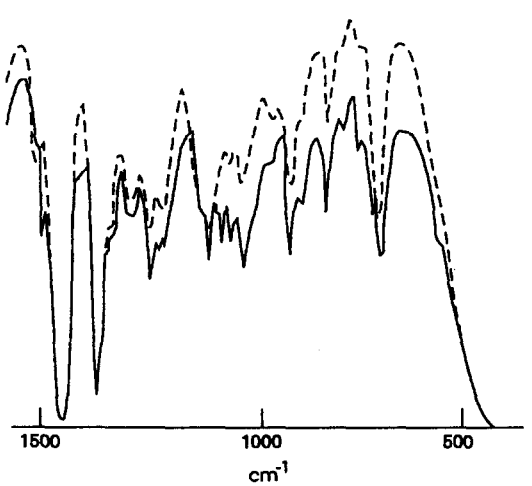

Fig. 6. IR spectra of the crystalline complex and B15C5: – – – B15C5 and —— $K(B15C5)_2AuCl_4$.

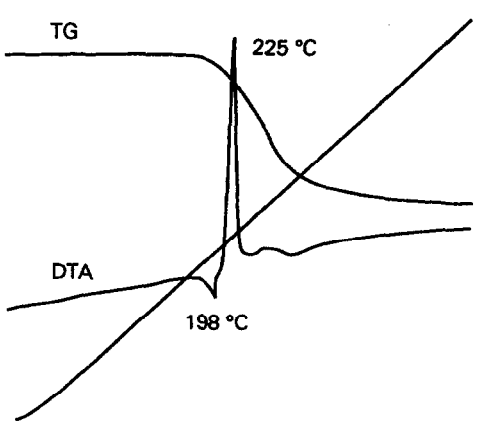

Fig. 7. DTA and TG curves of $K(B15C5)_2AuCl_4$.

form a complex cation of potassium–crown ether. It is certain that the selective coordination of B15C5 with K^+ will restrain other kinds of cations and hydrophilic anions from entering the organic phase, and therefore, it can be predicted that the extraction system proposed in this paper may be applied to the extraction and separation of gold(III) in practical production.

REFERENCES

1. Z. Zhou and J. Yang, *Huaxue Shiji* 1987, **9**, 50; *Chem. Abstr.* 106: 221140e.
2. Z. Zhou and X. Zhang, *Huaxue Xuebao* 1988, **46**, 496; *Chem. Abstr.* 109: 136000b.
3. R. A. Potts, *Inorg. Chem.* 1970, **9**, 1284.
4. V. W. Bhagwat, H. Manohar and N. S. Poonia, *Inorg. Nucl. Chem. Lett.* 1980, **16**, 373; 1981, **17**, 207.
5. Z. Zhou, B. Du, X. Zhang, S. Liu and J. Huang, *Jiegou Huaxue* 1987, **6**, 209; *Chem. Abstr.* 108: 14199g.
6. M. A. Bush and M. R. Truter, *J. Chem. Soc., Perkin II* 1972, 341.
7. N. S. Poonia and A. V. Bajaj, *Chem. Rev.* 1979, **79**, 389.
8. A. K. Gangopadhayay and A. Chakravorty, *J. Chem. Phys.* 1961, **35**, 2206.
9. L. Li, Y. Sun, H. Ren and P. Di, *Gaodeng Xuexiao Huaxue Xuebao* 1985, **6**, 1097; *Chem. Abstr.* 104: 96709c.
10. M. Shi, Z. Wang, S. Chen, Y. Zhao, B. Li, M. Zhou, J. Jin and S. Xu, *He Huaxue Yu Fangshe Huaxue* 1981, **3**, 1; *Chem. Abstr.* 95: 141054u.
11. N. S. Poonia and M. R. Truter, *J. Chem. Soc., Dalton Trans.* 1973, 2062.

Polyhedron Vol. 10, No. 10, pp. 1031–1036, 1991
Printed in Great Britain

0277–5387/91 $3.00+.00
© 1991 Pergamon Press plc

SYNTHESIS, PROPERTIES AND CRYSTAL STRUCTURE OF BIS(METIAMIDE)BIS(ISOTHIOCYANATO)NICKEL(II)

M. A. MARTINEZ* and J. P. LEGROS

Laboratoire de Chimie de Coordination du CNRS, Unité No. 8241 liée par convention à l'Université Paul Sabatier et à l'Institut National Polytechnique, 205 Route de Narbonne, 31077 Toulouse Cédex, France

and

L. SOTO† and A. SANCHO

Departament de Química Inorgánica, Facultat de Farmacia, Universitat de Valencia, Blasco Ibañez No. 13, 46010 Valencia, Spain

(*Received* 5 *October* 1990; *accepted* 9 *January* 1991)

Abstract—The crystal structure of Ni(metiamide)$_2$(NCS)$_2$ was determined by X-ray diffraction methods. Unlike cimetidine, which is a tridentate ligand, metiamide ($C_9H_{16}N_4S_2$): N-Methyl-N-[2-{(5-methylimidazol-4-yl)methylthio}ethyl]thiourea (which also possesses three potential donor sites) is bidentate, coordinated to the nickel atom through N(imidazole) and S(thioether) atoms. The S(thiourea) atom does not take part in the coordination; instead, the isothiocyanate ion is coordinated through nitrogen to the metal atom. The nickel atom lies on a centre of symmetry in an elongated octahedral environment: the nitrogen atoms occupy equatorial positions (Ni—N = 2.04 and 2.06 Å) and S(thioether) atoms occupy apical positions (Ni—S = 2.58 Å). Individual molecules are linked together by a unique S···H—N hydrogen bond involving the uncoordinated S(thiourea) atom. IR, electronic reflectance and magnetic data are consistent with the structural results.

Imidazole is a common component of some important molecules of biological interest. A current field of interest in our group is to study the complexation of such molecules with transition metals. Previous work has been devoted to metal complexes of cimetidine (CM), a histamine H_2-receptor antagonist. Cimetidine contains the imidazole ring linked to a chain containing a thioether function and a cyanoguanidine moiety which provide several potential donor sites. In the complexes $Cu(CM)_2X_2$ [$X_2 = (ClO_4^-)_2$,[1,2] $(NO_3^-)_2$[3] and SO_4^{2-}[4]] the ligand is coordinated through S(thioether), N(imidazole) and N(cyano) atoms; in all these compounds the copper(II) ion has a basically octahedral environment which displays significantly different distortion depending on the nature of the counter-anion, even though no direct interaction exists between the metal atom and the counter-anion.

We have started the study of a series of metal complexes of a new, biologically active ligand, metiamide‡ (Met, Fig. 1), related to cimetidine. Metiamide like CM is a histamine H_2-receptor antagonist[5,6] and the substitution of a thiourea group for the cyanoguanidine moiety is expected to alter the reactivity of this kind of chelate.

In this paper the synthesis, spectroscopic characterization, and X-ray crystal structure of the bis (metiamide)bis(isothiocyanato)nickel(II) complex, $Ni(Met)_2(NCS)_2$, are presented and discussed.

EXPERIMENTAL

Preparation and analyses of the complex

An aqueous solution (30 cm^3) of nickel chloride (2 mmol) was added to an ethanol solution (50 cm^3)

* Permanent address: Departament de Química Inorgánica, Facultat de Farmacia, Universitat de Valencia, Blasco Ibañez No. 13, 46010 Valencia, Spain.

† Author to whom correspondence should be addressed.

‡ Metiamide ($C_9H_{16}N_4S_2$): N-Methyl-N-[2-{(5-methylimidazol-4-yl)methylthio}ethyl]thiourea.

of the ligand (4 mmol) and potassium thiocyanate (4 mmol). The violet crystals obtained from the solution were filtered, washed with ethanol and dried at 100°C. Found: Ni, 9.0; C, 36.3; N, 21.0; S, 28.8; H, 4.8. Calc. for $NiC_{20}H_{32}N_{10}S_6$: Ni, 8.9; C, 36.2; N, 21.1; S, 29.0; H; 4.8%.

Spectroscopic measurements

IR spectra were obtained using a Perkin–Elmer Model 845 spectrophotometer with KBr discs and Nujol mulls (below 400 cm^{-1}). Solid reflectance spectra were recorded with a Perkin–Elmer Lambda 9 spectrophotometer, with a reflectance attachment fitted. Magnetic susceptibility measurements were carried out using the Faraday method with a Brucker Magnet BE-15 balance and $(Ni(en)_3)S_2O_3$ as calibrant. Diamagnetic corrections were estimated from Pascal constants.[7]

Crystal structure determination

General operating procedures have been described previously.[8] Crystal data and relevant parameters of the crystallographic study are given in Table 1. Systematic absences indicate the space group $P2_1/c$. The structure was determined by the Patterson method and refined using standard full-matrix least-squares and Fourier procedures.[9] Structure factors were corrected for anomalous dispersion; no correction was applied for absorption because of the small μ value and small-sized, block-shaped crystal. All hydrogen atoms were located on difference Fourier maps. Their contribution to the structure factors was calculated using idealized, unrefined positions and isotropic temperature factors equal to 1.3 times the B_{eq} of the atoms to which they are bonded. Final atomic positional and thermal parameters and lists of F_o/F_c values have been deposited as supplementary material with the Editor, from whom copies are available on request. Atomic coordinates have also been deposited with the Cambridge Crystallographic Data Centre.

Table 1. Crystallographic data

Formula	$NiC_{20}H_{32}N_{10}S_6$
Mr	663.6
Diffractometer	CAD4 Enraf–Nonius
Radiation	Mo-K_α
Wavelength (Å)	0.71069
Space group	Monoclinic, $P2_1/c$
a (Å)	7.523(1)
b (Å)	12.630(2)
c (Å)	15.341(2)
β (°)	93.08(2)
V (Å^3)	1455.4(6)
Z	2
D_c (g cm^{-3})	1.51
D_m (g cm^{-3})	1.50(2) (flotation)
μ (cm^{-1})	11.1
Temperature (K)	293
Crystal size (mm)	0.3 × 0.2 × 0.2
Maximum Bragg angle (°)	$\theta_{max} = 25$
Number of independent reflections	2547
Number of observed reflections ($I > 2\sigma$)	1802
Number of refined parameters	169
R and R_w	0.031 and 0.035
Weighting scheme	Unit weights

RESULTS AND DISCUSSION

Crystal structure

Bond lengths and angles are listed in Table 2. Atoms are labelled according to Fig. 1. The crystal structure is made up of isolated centro-symmetric $Ni(Met)_2(NCS)_2$ complex molecules (Figs 2 and 3). The nickel atom lies on a crystallographic centre of symmetry and possesses an elongated octahedral NiN_4S_2 environment. Two metiamide molecules are coordinated to the metal atom through the imidazole N(2) and the thioether S(1) atoms. In addition, two NCS^- ions are also coordinated through their N(20) atom. The nitrogen atoms form an almost perfect NiN_4 equatorial square plane [Ni—N(2) = 2.06 Å, Ni—N(20) = 2.04 Å and N(20)—Ni—N(2) = 90.0°]. The axial sulphur atoms are located at a distance [Ni—S(1) = 2.58 Å] indicating a rather weak Ni—S interaction (Ni—S coordination distances are usually close to 2.2 Å for a square-planar geometry). It is worthwhile to compare this coordination with that of copper in

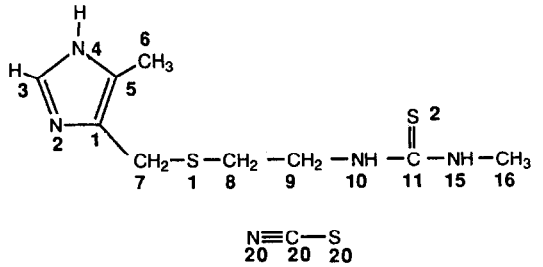

Fig. 1. The metiamide molecule. The numbering of non-hydrogen atoms used throughout the paper is indicated. To facilitate comparisons, the numbering scheme used in previous cimetidine papers[2–4] has been kept as far as possible. The numbering of atoms of the isothiocyanate ligand is also given.

Table 2. Bond lengths (Å) and angles (°) with ESDs in parentheses

Ni—S(1)	2.580(1)	C(7)—S(1)	1.811(3)
Ni—N(2)	2.061(3)	C(8)—S(1)	1.815(3)
Ni—N(20)	2.037(3)	C(9)—C(8)	1.513(5)
N(2)—C(1)	1.381(4)	N(10)—C(9)	1.460(4)
C(5)—C(1)	1.357(5)	C(11)—N(10)	1.342(5)
C(7)—C(1)	1.487(5)	S(2)—C(11)	1.699(4)
C(3)—N(2)	1.329(4)	N(15)—C(11)	1.335(5)
N(4)—C(3)	1.351(5)	C(16)—N(15)	1.456(5)
C(5)—N(4)	1.377(5)	N(20)—C(20)	1.150(4)
C(6)—C(5)	1.491(5)	C(20)—S(20)	1.636(4)

N(2)—Ni—S(1)	83.5(1)	N(4)—C(5)—C(1)	105.1(3)
N(20)—Ni—S(1)	87.8(1)	C(6)—C(5)—C(1)	130.8(3)
N(20)—Ni—N(2)	90.0(1)	C(6)—C(5)—N(4)	124.1(3)
C(7)—S(1)—Ni	91.0(1)	C(1)—C(7)—S(1)	112.2(2)
C(8)—S(1)—Ni	107.2(1)	C(8)—S(1)—C(7)	101.6(2)
C(5)—C(1)—N(2)	109.8(3)	C(9)—C(8)—S(1)	115.4(2)
C(7)—C(1)—N(2)	120.2(3)	N(10)—C(9)—C(8)	113.0(3)
C(7)—C(1)—C(5)	129.9(3)	C(11)—N(10)—C(9)	123.4(3)
C(1)—N(2)—Ni	117.1(2)	S(2)—C(11)—N(10)	120.4(3)
C(3)—N(2)—Ni	132.7(2)	N(15)—C(11)—S(2)	122.4(3)
C(3)—N(2)—C(1)	106.6(3)	C(16)—N(15)—C(11)	124.5(3)
N(4)—C(3)—N(2)	109.3(3)	S(20)—C(20)—N(20)	179.0(3)
C(5)—N(4)—C(3)	109.1(3)	C(20)—N(20)—Ni	172.0(3)

the three previously reported Cu—CM complexes (Table 3). In the three Cu—CM complexes CM acts as a tridentate ligand through the imidazole N(2), the thioether S(1) and the cyano N(14) atoms. In the metiamide molecule a thiourea group replaces the cyanoguanidine moiety of the cimetidine ligand thus providing a third potential coordination site: the S(2) atom of the thiourea group. However, in the Ni—Met complex this atom is not bonded to the metal atom. The C(11)—S(2) distance (1.699 Å) is close to the C—S bond length in the free thiourea (1.707 Å),[10] which is consistent with non-coordination of the S(2) atom. The isothiocyanate group, linear as usual, shows normal bond lengths and coordinates linearly to the nickel atom.

In the metiamide ligand the imidazole ring is

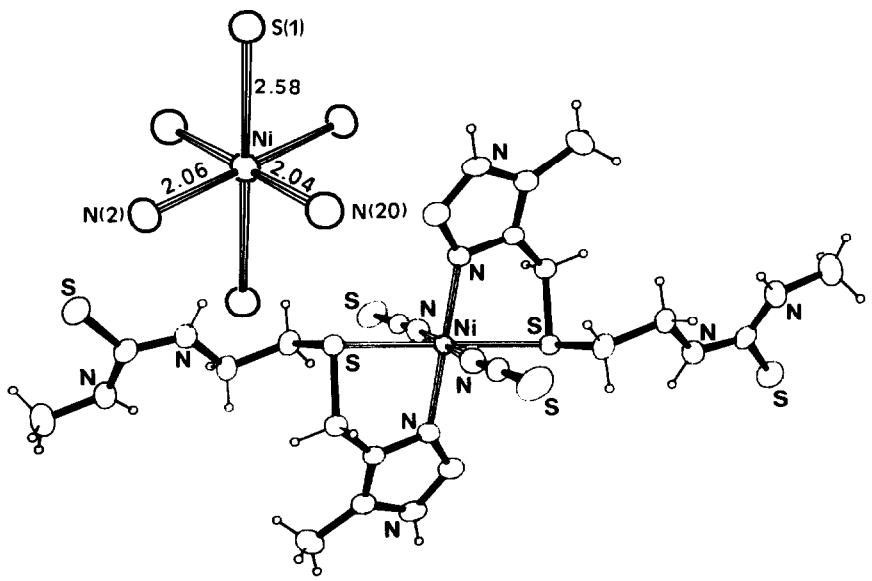

Fig. 2. Perspective view of the $Ni(Met)_2(NCS)_2$ molecule.

Table 3. Geometries around copper(II) in cimetidine complexes and nickel(II) in the metiamide complex

Reference	Cu—N(2) (Å)	Cu—S(1) (Å)	Cu—N(14) (Å)	N(2)—Cu—N(14) (°)	N(2)—Cu—S(1) (°)	S(1)—Cu—N(14) (°)
1, 2	1.980(6)	2.790(2)	2.042(7)	88.6(3)	78.9(2)	86.5(2)
3	1.942(2)	2.419(1)	2.558(2)	88.7(1)	84.9(1)	79.3(1)
4	1.981(3)	2.910(2)	2.001(3)	89.0(1)	77.4(1)	87.3(1)
	Ni—N(2)	Ni—S(1)	Ni—N(20)	N(2)—Ni—N(20)	N(2)—Ni—S(1)	S(1)—Ni—N(20)
This work	2.061(3)	2.580(1)	2.037(3)	90.0(1)	83.5(1)	87.8(1)

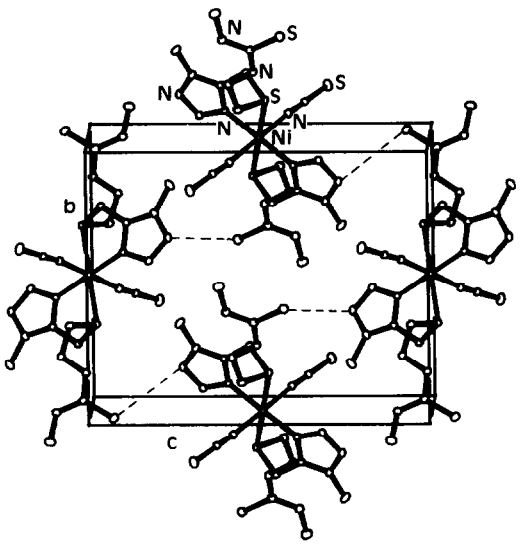

Fig. 3. Crystal packing.

planar with the methyl C(6) atom in the plane of the ring, the thiourea group is also planar although the methyl C(16) atom is located somewhat out-of-plane (Table 4). The dihedral angle between the two planes is 10.8°. The conformation of the coordinated metiamide ligand is described by the torsion angles listed in Table 5. In the absence of other X-ray data on metiamide or its complexes, a comparison could be attempted with related cimetidine and its complexes, however, such a comparison does not show any analogy between the conformation of metiamide in $Ni(Met)_2(NCS)_2$ and the A[11] or Z[12] conformations of cimetidine (or the corresponding chelated forms[4]).

The crystal packing is shown in Fig. 3. The only intermolecular interaction which can be considered as a hydrogen bond, on the basis of the criterion $d(S\cdots N) < 3.6$ Å,[13] involves the non-coordinated S(2) atom. The $S(2)\cdots N(4)^i$ distance is 3.354 Å (the superscript i refers to the transformation $-1+x$, $1/2-y$, $1/2+z$) with $S(2)\cdots H(11)^i = 2.497$ Å and $S(2)\cdots H(11)^i—N(4)^i = 148.8°$. Other intermolecular interactions are van der Waals' contacts.

Table 4. Displacements (Å) from least-squares planes through the imidazole ring and thiourea group. Atoms used to calculate the equations of planes are denoted by asterisks

Imidazole ring		Thiourea group	
C(1)*	−0.022	C(11)*	−0.008
N(2)*	0.023	N(10)*	0.003
C(3)*	0.010	S(2)*	0.002
N(4)*	−0.016	N(15)*	0.003
C(5)*	−0.021	C(16)	−0.115
C(6)*	0.026		

Table 5. Selected torsion angles and dihedral angle (°)

N(10)—C(11)—N(15)—C(16)	−174.8
C(9)—N(10)—C(11)—N(15)	2.9
C(9)—N(10)—C(11)—S(2)	−178.6
C(8)—C(9)—N(10)—C(11)	−179.8
S(1)—C(8)—C(9)—N(10)	−62.0
C(7)—S(1)—C(8)—C(9)	−60.0
C(8)—S(1)—C(7)—C(1)	−70.5
N(2)—C(1)—C(7)—S(1)	−46.4
C(5)—C(1)—C(7)—S(1)	137.2

Dihedral angle between the imidazole ring and the thiourea group: 10.8.

Table 6. Electronic spectrum

Bands (cm^{-1})	Assignments	$10Dq$	B (cm^{-1})
8264	$^3T_{2g} \leftarrow {}^3A_{2g}$	8266	631
11,043	$^1E_g \leftarrow {}^3A_{2g}$		
13,378	$^3T_{1g} \leftarrow {}^3A_{2g}$		
17,542	$^1A_{1g} \leftarrow {}^3A_{2g}$		
22,085	$^3T_{1g}(P) \leftarrow {}^3A_{2g}$		

Spectroscopic and magnetic properties

The IR spectrum of the complex shows two bands at 3330 and 3200 cm^{-1} assigned to the stretching vibrations of the N—H groups.[14] The bands in the 1495–1260 cm^{-1} region correspond to a combination of ν(C=N), ν(C=N—C=C), ν(N—H) and ν(N—C=S) of imidazole and thiourea groups.[15,16] Since the S(thiourea) atom is not included in the coordination sphere, the corresponding stretching frequency, ν(C=S), should be affected mainly by hydrogen bonding. The corresponding absorption band[17] is observed at 740 cm^{-1} for the complex as well as for the free ligand; this result indicates either that the hydrogen bond is rather weak or that the S(thiourea) atom also accepts a hydrogen bond in the solid state structure of the free ligand. Three bands located at 2100, 825 and 475 cm^{-1} are attributed, respectively, to the ν(CN), ν(CS) and δ(NCS) vibration modes of the thiocyanate group. The shifts, relative to the free anion, are in agreement with the presence of a nitrogen-bonded thiocyanate group.[18,19] The ν(CN) vibration appears as a sharp band as expected for a *trans* arrangement of the two thiocyanate groups.[20] The ν(Ni—S) and ν(Ni—N) stretching modes are observed in the 320–290 cm^{-1} region.[21,22]

The electronic reflectance spectrum of $Ni(Met)_2(NCS)_2$ shows bands characteristic of an octahedral geometry.[23] Table 6 lists the assignments of the observed bands. The nature and position of these bands are similar to those observed for Ni—CM complexes[24,25] which also contain a NiN_4S_2 chromophore.

The room temperature magnetic moment μ_{eff} is 3.10 BM, consistent with the octahedral geometry.[26]

CONCLUSIONS

Because of its similarity with the cimetidine molecule, the metiamide molecule is expected to be very flexible. Thus, the non-coordination of the thiourea S(2) atom cannot be attributed to geometrical constraints but rather to the coordination strength of the NCS^- ion. Since it has been shown[4] that the geometry of the coordination polyhedron of the copper atom in the Cu—CM complexes is very sensitive to the nature of the counter-anion (Table 3), it would be interesting to use NCS^- as the counter-anion of a Cu—CM complex. On the one hand, the two N(cyano) atoms of the guanidine moiety and of the thiocyanate ion would compete to enter the coordination sphere and possibly lead to unusual dicoordinated cimetidine. On the other hand, the possibility of the occurrence of sulphur-coordinated thiocyanate cannot be ruled out. In addition, the so-called "plasticity"[27] of copper(II) allows many coordination schemes ranging from severely flattened tetrahedron to strongly elongated octahedron. The $Cu(CM)_2(NCS)_2$ complex was thus prepared, however, no crystal suitable for X-ray analysis could be grown until now.

Acknowledgements—The authors wish to thank the Spanish Ministerio de Educación y Ciencia (DGICYT) and the French Ministère de la Recherche et de la Technologie for financial support (Acción Integrada 182/90F —Action Intégrée 95). M.A.M. also acknowledges the CNRS for the facilities put at her disposal.

REFERENCES

1. F. T. Greenaway, L. M. Brown, J. C. Dabrowiak, M. R. Thompson and V. M. Day, *J. Am. Chem. Soc.* 1980, **102**, 7782.
2. A. Sancho, J. Borras, L. Soto-Tuero, C. Esteban-Calderón, M. Martinez-Ripoll and S. Garcia-Blanco, *Polyhedron* 1985, **4**, 539.
3. L. Soto, J. Borras, A. Sancho, A. Fuertes and C. Miravitlles, *Acta Cryst.* 1985, **C41**, 1431.
4. L. Soto, J. P. Legros and A. Sancho, *Polyhedron* 1988, **7**, 307.
5. R. E. Pounder, J. G. Williams, G. J. Milton-Thompson and J. J. Misiewicz, *Br. Med. J.* 1975, **2**, 307.
6. G. J. Durant, J. C. Emmett, C. R. Ganellin, P. D. Miles, M. E. Parsons, H. D. Prain and G. R. White, *J. Med. Chem.* 1977, **20**, 901.
7. K. Burger, *Coordination Chemistry: Experimental Methods*. Butterworths, London (1973).
8. L. Soto, J. P. Legros, M. C. Molla and J. Garcia, *Acta Cryst.* 1987, **C43**, 834.
9. B. A. Frentz, SDP Structure Determination Package. Enraf–Nonius, Delft (1982).
10. N. R. Kunchur and M. R. Truter, *J. Chem. Soc.* 1958, 3478.
11. E. Hadicke, F. Frickel and A. Franke, *Chem. Ber.* 1978, 3222.
12. L. Parkanyi, A. Kalman, B. Hegedus, K. Harsanyi and J. Kriedl, *Acta Cryst.* 1984, **C40**, 676.
13. E. J. Gabe, M. R. Taylor, J. Pickworth Glusker, J. Minkin and A. L. Patterson, *Acta Cryst.* 1969, **B25**, 1620; A. Wojtczak, M. Jaskolski and Z. Kosturkiewicz, *Acta Cryst.* 1985, **C41**, 1752.
14. L. J. Bellamy, *Infrared Spectra of Complex Molecules*, Vol. 1. Chapman and Hall, London (1975).
15. T. J. Lane, I. Nakagawa, J. L. Walter and A. J. Kandathil, *Inorg. Chem.* 1962, **1**, 267.
16. R. K. Gosavi, U. Agarwala and C. N. Rao, *J. Am. Chem. Soc.* 1967, **89**, 235.
17. B. Beecroft, M. J. M. Campbell and R. Grzeskowiak, *J. Inorg. Nucl. Chem.* 1974, **36**, 55.
18. K. Nakamoto, *Infrared and Raman Spectra of Inor-*

ganic and Coordination Compounds, 4th edn. Wiley, New York (1986).
19. R. J. H. Clark and C. S. Williams, *Spectrochim. Acta* 1966, **22**, 1081.
20. L. F. Larkworthy and B. J. Tucker, *Inorg. Chim. Acta* 1978, **33**, 167.
21. M. Akbar Ali and S. E. Livingstone, *Coord. Chem. Rev.* 1974, **13**, 103.
22. B. C. Cornielsen and K. Nakamoto, *J. Inorg. Nucl. Chem.* 1974, **36**, 2467.
23. A. B. P. Lever, *Inorganic Electronic Spectroscopy*, 2nd edn. Elsevier, Amsterdam (1986).
24. A. Sancho, L. Soto and J. Borras, *Transition Met. Chem.* 1985, **10**, 214.
25. A. Abadia, A. Sancho, L. Soto and J. Borras, *Transition Met. Chem.* 1986, **11**, 8.
26. F. E. Mabbs and D. J. Machin, *Magnetism and Transition Metal Complexes*. Chapman and Hall, London (1973).
27. B. J. Hathaway, *Struct. Bond.* 1984, **57**, 55.

Polyhedron Vol. 10, No. 10, pp. 1037–1048, 1991
Printed in Great Britain

0277–5387/91 $3.00+.00
© 1991 Pergamon Press plc

RAMAN, MASS, AND ^{77}Se NMR SPECTRA OF $SeSCl_2$ AND ITS REACTIONS WITH POTASSIUM IODIDE AND TITANOCENE PENTASULPHIDE TO PRODUCE CYCLIC SELENIUM SULPHIDES*

RALF STEUDEL,† BETTINA PLINKE and DETLEF JENSEN

Institut für Anorganische und Analytische Chemie, Technische Universität Berlin, Sekr. C 2, D-1000 Berlin 12, F.R.G.

and

FRANK BAUMGART

Inwan-N.-Stranski-Institut für Physikalische und Theoretische Chemie, Technische Universität Berlin, D-1000 Berlin 12, F.R.G.

(*Received* 18 *September* 1990; *accepted* 24 *January* 1991)

Abstract—Mixing of S_2Cl_2 and Se_2Cl_2 at 21°C results in the formation of $SeSCl_2$ as shown by ^{77}Se NMR, mass, and Raman spectroscopy. The enthalpy of this reaction has been determined as +13 kJ mol^{-1} (S_2Cl_2), and the equilibrium constant $K_c = 0.066$ at 294 K. In addition, the formation of other Se—S—Cl molecules and of $SeCl_2$ is observed. An Se_2Cl_2–S_2Cl_2–$SeSCl_2$ mixture (Se:S = 1:1) reacts with titanocene pentasulphide to give mainly S_7, SeS_6 and 1,2-Se_2S_5 but small concentrations of six-, eight-, nine- and 12-membered Se—S ring molecules have also been observed. The reaction of Se_2Cl_2–S_2Cl_2 mixtures (Se:S = 1:2) with potassium iodide affords 1,2,5-Se_3S_5 as the major product followed by 1,2-Se_2S_6, 1,4-Se_2S_6 and 1,3-Se_2S_6. HPLC analysis of this reaction shows, however, that selenium sulphide ring molecules of ring sizes 6–8 are formed. Mixing of SCl_2 and Se_2Cl_2 at 21°C results in precipitation of $SeCl_4$ and formation of S_2Cl_2, which reacts with Se_2Cl_2 to give $SeSCl_2$.

The well known similarities between the chemistry of sulphur and selenium can be seen from the ever increasing number of chain- and ring-like compounds with homonuclear SS and SeSe bonds, respectively. More recently compounds with SeS bonds, cyclic selenium sulphides, have been prepared in considerable numbers.[2] From a synthetic point of view the dichlorosulphanes, S_nCl_2 ($n = 1, 2, \ldots$), are of particular importance because of their rôle in the preparation of sulphur rings, sulphanes, organic polysulphanes, etc. Milne *et al.*[3,4] have recently shown that dichloroselenanes, Se_nCl_2 ($n = 1, \ldots, 4$), exist in equilibrium in liquid Se_2Cl_2:

$$2\,Se_2Cl_2 \rightleftharpoons SeCl_2 + Se_3Cl_2, \quad K_c = 6 \times 10^{-4}\,(20°C); \tag{1}$$

$$3\,Se_2Cl_2 \rightleftharpoons 2\,SeCl_2 + Se_4Cl_2, \quad K_c = 3 \times 10^{-6}\,(20°C). \tag{2}$$

Dissolution of elemental selenium in liquid Se_2Cl_2 increases the concentrations of Se_3Cl_2 and Se_4Cl_2, as was shown by ^{77}Se NMR spectroscopy.[3,4] In a similar fashion, pure, freshly distilled S_2Cl_2 is in equilibrium with SCl_2 and S_3Cl_2, but the equilibrium constant is much smaller:[5]

$$2\,S_2Cl_2 \rightleftharpoons SCl_2 + S_3Cl_2. \tag{3}$$

While in liquid Se_2Cl_2 *ca* 5% of the liquid is present as $SeCl_2$ and Se_3Cl_2,[3,4] the self-dissociation of S_2Cl_2 amounts to only *ca* 1% at 20°C.[5] Nevertheless, mixing of Se_2Cl_2 with S_2Cl_2 should result in mixed SeS species:

* Part 137 of the Series *Sulphur Compounds*; for Part 136 see ref. 1.

† Author to whom correspondence should be addressed.

$$S_2Cl_2 + Se_2Cl_2 \rightleftharpoons 2\,SeSCl_2, \quad (4)$$

$$2\,SeSCl_2 \rightleftharpoons SeCl_2 + SeS_2Cl_2, \quad (5)$$

$$SeSCl_2 + Se_2Cl_2 \rightleftharpoons SeCl_2 + Se_2SCl_2. \quad (6)$$

The formation of $SeSCl_2$ has in fact been claimed by Volkov *et al.*[6] who had studied the Raman spectra of Se_2Cl_2–S_2Cl_2 mixtures in molar ratios of 3 : 1, 1 : 1 and 1 : 3 at 20°C, and had compared the spectra with those of the pure components. These authors observed three new lines for the mixtures and assigned them to the molecule $SeSCl_2$ as follows:[6]

410 cm^{-1}: SCl stretching,
396 cm^{-1}: SeS stretching,
164 cm^{-1}: bending (not specified).

Volkov *et al.* suggested the structure $Se{=}SCl_2$ (symmetry C_s) for the new compound which is in contrast to the well established chain-structures of both S_2Cl_2 and Se_2Cl_2 (symmetry C_2).[7] We have therefore repeated this work and studied reaction (4) by mass, ^{77}Se NMR and Raman spectroscopy hoping that we could find additional information to establish both the structure of $SeSCl_2$ and the equilibrium constant of reaction (4).

EXPERIMENTAL

Materials

Carbon disulphide (CS_2; techn. grade) was purified by distillation from phosphorus pentoxide (P_4O_{10}). Disulphur dichloride (S_2Cl_2) was distilled immediately prior to use. Diselenium dichloride (Se_2Cl_2)[8] and titanocene pentasulphide (Cp_2TiS_5; Cp = η^5-C_5H_5)[9] were prepared according to literature methods. Methanol used as an eluent for HPLC was distilled from anhydrous magnesium sulphate (to remove water and nucleophilic impurities) and degassed in a vacuum immediately prior to use. Spectra of Se_2Cl_2–S_2Cl_2 mixtures were measured in sealed glass tubes.

Procedures

^{77}Se NMR spectra were recorded with a Bruker WM 360 spectrometer equipped with Aspect 3000 computer for spectrometer control and data processing (frequency, 68.679 MHz; temperature, 21°C; sample tube diameter, 20 mm). Raman spectra were obtained with an Instruments S.A. spectrometer which is based on a Jobin Yvon U 1000 double monochromator and controlled by a MAC 80 computer. Raman scattering was excited with a Spectra Physics krypton ion laser (647.1 nm) and measured by a Hamamatsu R943-02 GaAs photomultiplier. The wavenumbers were reproducible to within ± 1 cm^{-1}. To prevent the Raman samples from thermal or photolytic decomposition during the measurements they were usually cooled to well below 0°C using a self-made cryostat in which the vapour of liquid nitrogen was used as a coolant. Evaporation of the nitrogen by an electric heater was controlled by a Pt 100 temperature sensor placed next to the sample which was contained in a glass capillary inside a glass Dewar vessel. High-performance liquid chromatography (HPLC) was performed with the following equipment: Perkin–Elmer Liquid Chromatograph (Series 2 with two pumps), Rheodyne Syringe Loading Injector (Model 7125 with a 10-μl sample loop), Millipore-Waters Radial-Pak column cartridges filled with C18 phase for reversed-phase chromatography (column length, 10 cm; inner diameter, 8 mm; particle size, 5 or 10 μm) and contained in a RCM-100 compression module, Perkin–Elmer LC75 UV spectrophotometer with autocontrol (variable wavelength detector with a deuterium lamp), Hewlett–Packard 3390A electronic integrator with an integrated recorder and printer. Mass spectra were recorded using a double-focusing sector-field spectrometer (MAT 311A) controlled by a Kratos DS 90 computer.

Chemical shifts

The NMR spectra of Se_2Cl_2–S_2Cl_2 mixtures were measured with D_2O as an external lock substance and $(CH_3Se)_2$ as an external reference, the shift of which was taken from the literature as 275.0 ppm versus $(CH_3)_2Se$.[10] Shifts therefore refer to $(CH_3)_2Se$. The same holds for the NMR spectra of selenium sulphides dissolved in CS_2 for which C_6D_6 was used as an internal lock and 1,2,3-Se_3S_5 (653.4 and 559.9 ppm[11]) as an internal standard.

Reaction of Se_2Cl_2–S_2Cl_2 *mixtures with* KI

Disulphur dichloride, (1.1 cm^3, 13.3 mmol) and 0.55 cm^3 Se_2Cl_2 (6.7 mmol) dissolved in 100 cm^3 CS_2 were reacted with 19.9 g finely powdered dry potassium iodide (0.12 mol) for 4 h with stirring at 20°C in the dark. After filtration the solution was shaken with powdered $Na_2S_2O_3 \cdot 5H_2O$ (25.3 g, 0.16 mol) to remove elemental iodine followed by filtration and drying with $MgSO_4$. Part of this solution was measured by NMR spectroscopy within 5 h after preparation. Another part was cooled to −60°C for 24 h resulting in orange needle-like crystals of m.p. 110–115°C (360 mg).

Reaction of Se_2Cl_2–S_2Cl_2 *mixtures with titanocene pentasulphide*

To 1.1 g (3.25 mmol) Cp_2TiS_5 dissolved in CS_2 at 20°C in diffuse daylight was added 0.2 cm^3 of an equimolar mixture of Se_2Cl_2 and S_2Cl_2 with stirring. After 5 min (or later) 1 cm^3 of the mixture was diluted to 50 cm^3 with CS_2 and immediately analysed by HPLC.

RESULTS AND DISCUSSION

Mass spectrum of $SeSCl_2$

The electron impact mass spectrum of an equimolar mixture of S_2Cl_2 and Se_2Cl_2 is shown in Table 1. The liquid sample was evaporated into the ion source of the spectrometer. According to the differing volatilities, the ions originating from S_2Cl_2 give rise to the strongest peaks. However, besides the molecular ions $S_2Cl_2^+$ and $Se_2Cl_2^+$ with their characteristic isotopic pattern, we also observed the ion $SeSCl_2^+$ of the mixed species. The isotopic pattern of this signal at m/z 176,..., 192 matched the calculated pattern very well with m/z 182 being the largest peak. Under high-resolution conditions the mass of this ion was determined as 181.8254 (calculated for $^{80}Se^{32}S^{35}Cl_2^+$: 181.8263). According to these results the existence of $SeSCl_2$ in equilibrium with S_2Cl_2 and Se_2Cl_2 is beyond any doubt. The spectrum also shows the presence of $SeCl_2$ since the ion $SeCl_2^+$ can hardly be a fragment ion of the chain-like Se_2Cl_2.

Table 1. Mass spectrum of an equimolar mixture of S_2Cl_2 and Se_2Cl_2 (largest peaks only); electron energy 70 eV

Peak (m/z)	Relative intensity	Assignment
230	0.24	$Se_2Cl_2^+$
195	0.20	Se_2Cl^+
182	0.57	$SeSCl_2^+$
150	4.6	$SeCl_2^+$
134	94.9	$S_2Cl_2^+$
99	100	S_2Cl^+
67	13.8	SCl^+
64	50.7	S_2^+

^{77}Se *NMR spectrum of* $SeSCl_2$

Quantitative data regarding the equilibrium concentrations of $SeSCl_2$ and Se_2Cl_2 can best be obtained using ^{77}Se NMR spectroscopy (^{77}Se: $I = 1/2$, natural abundance, 7.6%). The resonance line of neat Se_2Cl_2 has been observed before: it occurs at 1272 ppm versus dimethylselenide as external standard.[4] We have found that mixtures of S_2Cl_2 and Se_2Cl_2 in molar ratios of 1:1 and 5:1 show up to 10 lines of very different intensity which we assign as shown in Table 2. The chemical shifts slightly depend on the S_2Cl_2 content of the mixture. The assignment of the second most intense line located 13 ppm downfield from the Se_2Cl_2 line is in accord with observations that substitution of one Se by S in an Se_2 unit shifts the signal of the remaining Se atom to lower field.[12,13] The intensity ratio of the $SeSCl_2$ and Se_2Cl_2 lines at various temperatures provides a means to calculate the equilibrium constant (K_c), the reaction enthalpy ($\Delta H°$), the reaction entropy ($\Delta S°$) and the free reaction enthalpy ($\Delta G°$) of reaction (4):

$$K_c = \frac{[SeSCl_2]^2}{[S_2Cl_2][Se_2Cl_2]}. \qquad (a)$$

Table 2. ^{77}Se NMR spectra of two liquid S_2Cl_2–Se_2Cl_2 mixtures at 21°C (molar ratios S:Se = 1:1 and 5:1; b = broad). Chemical shifts relative to $(CH_3)_2Se$

	1:1		5:1		
No.	Shift (ppm)	Peak height	Shift (ppm)	Peak height	Assignment
1	1746.0	3	1753.5	18	$SeCl_2$
2	~1350	>1, b	1352.9	0.5, b	ClSe*SeSCl
3	—		1345.3	1.3	ClSeSSeCl
4	~1340	>1, b	1341.3	0.5, b	ClSeSe*SCl
5	—		1335.4	0.7	ClSeSSSCl
6	—		1327.0	0.5	ClSSeSSCl
7	1314.9	1	1308.9	1	ClSeSSCl
8	1303.0	21	1295.1	42	ClSeSCl
9	1290.2	100	1282.3	100	Se_2Cl_2
10	1284.7	1.5	1278.7	2.5	ClSSeSCl

Neglecting the dissociation of Se_2Cl_2 according to eqs (1) and (2), and of S_2Cl_2 according to eq. (3), we assume $[S_2Cl_2] = [Se_2Cl_2]$. Since the peak area A of Se_2Cl_2 represents two Se atoms it follows:

$$K_c = \frac{[SeSCl_2]^2}{[Se_2Cl_2]^2} = \frac{4A^2(SeSCl_2)}{A^2(Se_2Cl_2)}. \quad \text{(b)}$$

The thermodynamic functions have been calculated from eqs (c) and (d):

$$\frac{d \ln K_c}{dT} = \frac{-\Delta H^\circ}{RT^2}, \quad \text{(c)}$$

$$\ln K_c = -\frac{\Delta G^\circ}{RT} = -\frac{\Delta H^\circ}{RT} + \frac{\Delta S^\circ}{R}, \quad \text{(d)}$$

using the peak areas measured at four different temperatures (see Table 3). The linear regression of the $\ln K_c$ values of Table 3 according to eq. (c) resulted in a correlation coefficient of $r = 0.997$ for the equation $\ln K_c = -(1562/T) + 2.599$, and an enthalpy of $\Delta H^\circ = 13$ kJ mol^{-1} for reaction (4). From the linear regression K_c was obtained as 0.066 for 294 K resulting in $\Delta G^\circ_{293} = 6.6$ kJ mol^{-1} and $\Delta S^\circ_{293} = 22$ J mol^{-1}. The directly measured K_c value for 294 K was 0.065 (Table 3).

The less intense lines in the NMR spectra of S_2Cl_2–Se_2Cl_2 mixtures are assigned as follows. Near 1750 ppm the well known line of $SeCl_2$[3,4] is observed, the relative intensity of which dramatically increases with increasing S_2Cl_2 content. This indicates that S_2Cl_2 oxidizes Se_2Cl_2 partly to $SeCl_2$, which must result in longer-chain sulphur chlorides, e.g. by reactions of types (4)–(8):

$$2\,S_2Cl_2 + Se_2Cl_2 \rightleftharpoons SeCl_2 + S_4Cl_2, \quad (7)$$

$$S_4Cl_2 + Se_2Cl_2 \rightleftharpoons SeSCl_2 + SeS_3Cl_2. \quad (8)$$

All species on the right sides of eqs (4)–(8) have been observed directly or indirectly in this work (see below). The NMR line near 1280 ppm on a first glance may represent Se_3Cl_2,[3,4] which in liquid Se_2Cl_2 has been observed 0.6 ppm upfield from Se_2Cl_2. However, the 1280 ppm line increases in intensity with increasing S_2Cl_2 content. It should also be noted that the relatively high $SeCl_2$ concentration in the 5:1 mixture will result in suppression of Se_3Cl_2 and Se_4Cl_2 in the equilibrium reactions (1) and (2). No Se_4Cl_2 line[3,4] has been observed in S_2Cl_2–Se_2Cl_2 mixtures, although the spectra were recorded in the range 670–1820 ppm. Therefore, the line near 1280 ppm should not be assigned to Se_3Cl_2 but rather to an S—Se—Cl species. The intensity of this line seems to be not related to the intensity of any of the other weak lines. A relationship between the $SeSCl_2$ line near 1300 ppm and the 1280 ppm line can, however, not entirely be excluded and the latter may represent an isomer of $SeSCl_2$, namely S=$SeCl_2$. More likely, however, the chain-like species ClSSeSCl seems to be responsible for this signal. Further evidence for such a molecule in the S_2Cl_2–Se_2Cl_2 mixtures will be presented below.

The other weak signals, located in the range 1305–1355 ppm, have been only tentatively assigned. The most intense lines are probably arising from trichalcogendichlorides and the weakest from the two isomeric SeS_3Cl_2 molecules. Again, evidence for all these species comes also from the HPLC analysis described below.

The two relatively broad signals near 1340 and 1350 ppm are assigned to the two non-equivalent atoms in 1,2-$Se_2S_2Cl_2$, which may undergo an exchange reaction resulting in line broadening.

In the thermodynamic calculations presented above, reactions (1)–(3) and (5)–(8) have been neglected. The data in Table 2 show that in a 1:1 mixture of S_2Cl_2 and Se_2Cl_2 at 21°C only about 4% of the Se atoms are not present in either Se_2Cl_2 or $SeSCl_2$. The approximation therefore seems to be justified.

Table 3. Quantitative analysis of the ^{77}Se NMR spectra of a S_2Cl_2–Se_2Cl_2 mixture (molar ratio 1:1) at various temperatures

Peak areas at T:	294 K	305 K	311 K	325 K
$A_1(Se_2Cl_2)$	1091.0	1447.2	1580.4	1521.3
$A_2(SeSCl_2)$	139.5	207.5	234.7	251.4
$A_2:A_1$	0.128	0.143	0.149	0.165
$(A_2:A_1)^2$	0.0163	0.0206	0.0221	0.0273
$\ln K_c$	−2.727	−2.498	−2.428	−2.214
K_c	0.065	0.082	0.088	0.109

A = peak area; T = temperature in K.

Raman spectrum of $SeSCl_2$

While the mass and NMR spectra allowed the detection and determination of $SeSCl_2$, the Raman spectrum should provide information about its structure. The three alternative structures ClSSeCl, S=$SeCl_2$ and Se=SCl_2 all result in six fundamental vibrations which are all Raman active. The first molecule is of C_1 symmetry and all its Raman lines will be polarized, while the other two are of C_s symmetry resulting in three polarized and three depolarized Raman lines. We have measured the Raman spectra of S_2Cl_2–Se_2Cl_2 mixtures with molar ratios of between 3 : 1 and 1 : 3, and at temperatures between −100 and +20°C. A krypton ion laser operating at 647.1 nm was used to minimize photodecomposition reactions of the deeply coloured reaction mixtures. The spectra obtained were compared with the spectra of the pure components S_2Cl_2 and Se_2Cl_2 which had been reported earlier,[14] and to the spectra of SCl_2–Se_2Cl_2 mixtures. Typical Raman spectra of an S_2Cl_2–Se_2Cl_2 1 : 1 mixture at 20 and −40°C are shown in Fig. 1. They show five weak features at 411, 388, 219, 185 and 164 cm^{-1} which are not present (or much weaker) in the spectra of either S_2Cl_2 or Se_2Cl_2 and which are assigned as follows.

The 411 cm^{-1} line has also been observed for pure Se_2Cl_2,[14,15] although with much lower intensity; in Se_2Cl_2 it disappears completely on cooling to −100°C. Milne *et al.*[15] assigned this signal to ν_1 (a) of $SeCl_2$ originating from reactions (1) and (2). In S_2Cl_2–Se_2Cl_2 mixtures the 411 cm^{-1} line is much stronger than in pure Se_2Cl_2 at the same temperature but it also gradually disappears on cooling and cannot be seen at −75°C anymore, while simultaneously the 388 cm^{-1} line increases in intensity suggesting a conversion of one compound into another. This behaviour is incompatible with the properties of $SeSCl_2$ which, according to its thermodynamic properties (see above), should still be present at −75°C ($K_c = 0.005$) in detectable concentrations, and should not be converted to a compound other than S_2Cl_2 and Se_2Cl_2. We therefore assign the 411 cm^{-1} line to ν_1 of $SeCl_2$ and the 388 cm^{-1} signal to ν_1 of $SeCl_4$, the strongest Raman line of which is located near 390 cm^{-1}.[16–18] Its formation from $SeCl_2$ is shown in eq. (9):[3,4]

$$3\,SeCl_2 \rightleftharpoons SeCl_4 + Se_2Cl_2. \qquad (9)$$

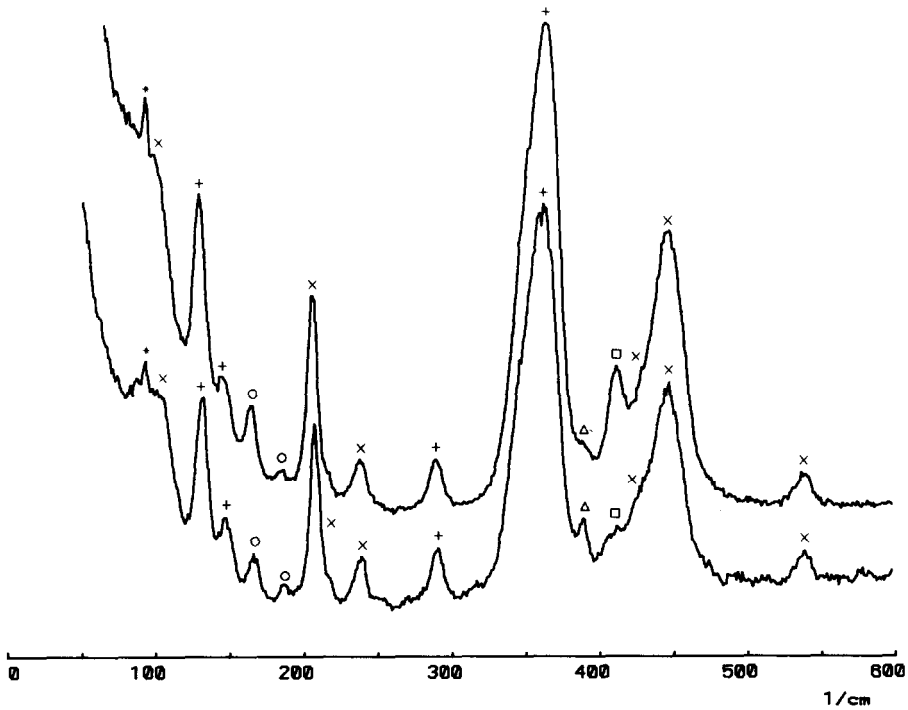

Fig. 1. Raman spectra of a S_2Cl_2–Se_2Cl_2 mixture (molar ratio 1 : 1) at 20°C (top) and −40°C (bottom) showing the lines of S_2Cl_2 (×), Se_2Cl_2 (+), $SeSCl_2$ (○), $SeCl_2$ (□), and $SeCl_4$ (△). The starred line arises from the laser. Wavenumbers (intensities in parentheses): 20°C—537 (m), 446 (s), 428 (sh), 411 (m), 388 (sh), 364 (vs), 352 (sh), 289 (m), 237 (m), 205 (s), 185 (w), 164 (w-m), 145 (w), 129 (m) cm^{-1}; −40°C—539 (w), 446 (s), 424 (sh), 412 (vw), 389 (vw), 362 (vs), 290 (m), 238 (m), 219 (sh), 207 (s), 187 (w), 167 (m), 147 (m), 132 (s) cm^{-1}.

Unfortunately, K_c and ΔH of this reaction are unknown. In addition, redox reactions of type (10),

$$2\,SeCl_2 + S_2Cl_2 \rightleftharpoons SeCl_4 + SeS_2Cl_2, \quad (10)$$

may play a rôle. The higher concentration of $SeCl_2$ in S_2Cl_2–Se_2Cl_2 mixtures has already been discussed above.

Support for the above assignment comes from the observations made with SCl_2–Se_2Cl_2 mixtures. When 3 cm^3 SCl_2 (freshly distilled) were carefully added to 2 cm^3 Se_2Cl_2 at 0°C, with exclusion of light, an exothermic reaction took place resulting in a precipitate and a brownish solution. After filtration the precipitate was washed with pentane and identified as $SeCl_4$ by Raman spectroscopy. The Raman spectrum of the solution measured at −40 and −100°C showed the presence of S_2Cl_2 by the following lines: 542, 445, 240, 209 and 112 cm^{-1}. Obviously, the following reaction had taken place:

$$6\,SCl_2 + Se_2Cl_2 \rightleftharpoons 2\,SeCl_4 + 3\,S_2Cl_2. \quad (11)$$

Since the molar ratio SCl_2–Se_2Cl_2 was only 2:1 some Se_2Cl_2 remained in the mixture, while SCl_2 was consumed completely. The S_2Cl_2 formed may then react according to eq. (4); the molar ratio S_2Cl_2–Se_2Cl_2 must have been 1:0.67. In addition to the Raman lines of S_2Cl_2 and Se_2Cl_2 the following signals were observed (intensities in parentheses):

412 cm^{-1} (sh), not observed at −100°C, probably $SeCl_2$;
392 cm^{-1} (s), probably $SeCl_4$[16–18] (which is soluble in Se_2Cl_2[19]);
303 cm^{-1} (w), observed only at −100°C, probably $SeCl_4$;[16–18]
188 cm^{-1} (vw), 170 cm^{-1} (m) } bending modes of $SeSCl_2$.

The line at 392 cm^{-1} was much stronger than in any of the S_2Cl_2–Se_2Cl_2 mixtures; it is therefore assigned to $SeCl_4$. The two weak features at 170 and 188 cm^{-1} may be identical to the 164 and 185 cm^{-1} lines observed for S_2Cl_2–Se_2Cl_2 mixtures (see above). Since their intensities were not related to the intensity of the line at 390 ± 2 cm^{-1} these lines are not assigned to $SeCl_4$ but to the bending modes of chain-like $SeSCl_2$.

It may be assumed that most of the vibrational wavenumbers of ClSeSCl can be estimated as arithmetic means of the corresponding wavenumbers of the binary chlorides. For example, ν(SS) = 540 cm^{-1} of S_2Cl_2 and ν(SeSe) = 290 cm^{-1} of Se_2Cl_2 result in ν(SSe) = 415 cm^{-1} of ClSeSCl. In a similar fashion the torsional modes of the binary chlorides give, by averaging, δ(ClSeSCl) = 104 cm^{-1}. The arithmetic mean of all bending modes of S_2Cl_2 and Se_2Cl_2 results in δ = 180 cm^{-1}, which indicates the approximate position of δ(ClSeS) and δ(ClSSe) of ClSeSCl. The two stretching modes SCl and SeCl of ClSeSCl will occur at about the same wavenumbers as the corresponding modes of the binary compounds. From the above it is obvious that, at best, four of the six ClSeSCl fundamental modes may be observed since ν(SCl) and ν(SeCl) will be obscured by the strong signals of the simultaneously present binary chlorides.

The SeS stretching mode of ClSeSCl will be of low Raman intensity (cf. S_2Cl_2) and strongly coupled with both ν(SCl) and ν(SeCl) due to the low molecular symmetry. Due to the interference by the broad SCl line of S_2Cl_2 we did not observe ν(SeS), unless one assigns the shoulder of the broad SCl line at *ca* 425 to this mode.

The two bending modes each of S_2Cl_2 and Se_2Cl_2 occur as neighbouring lines with the symmetrical one of somewhat higher intensity and lower wavenumber than the asymmetrical vibration. This pattern fits the two $SeSCl_2$ lines at 166 ± 3 and 186 ± 2 cm^{-1} which are located between the bending modes of the binary chlorides and which therefore are assigned to δ(ClSSe) and δ(ClSeS) of chain-like $SeSCl_2$. For 1:1 mixtures of S_2Cl_2 and Se_2Cl_2 the intensity of these lines decreases with decreasing temperature, as is to be expected. There is no evidence for the presence of any other isomer of $SeSCl_2$ (symmetry C_s) the SeS stretching vibration of which should show up in the range 550–650 cm^{-1}.

There remains to be addressed the question of whether the other strong lines of $SeCl_4$ can be seen in our spectra. Besides the 390 cm^{-1} line, strong to medium signals for dissolved $SeCl_4$ (in CH_3NO_2)[18] are to be expected at:

358 cm^{-1}, hidden under ν(SeCl) of Se_2Cl_2;
264 cm^{-1}, shoulder in Fig. 1;
206 cm^{-1}, shoulder in Fig. 1;
150 cm^{-1}, hidden under $\nu(Se_2Cl_2)$.

As can be seen from Fig. 1, two of the four expected signals are in fact observed (shoulders at 206 and 260 cm^{-1}) in the −40°C spectrum while the other two are obscured by strong Se_2Cl_2 lines.

Reaction of $SeSCl_2$ *with titanocene pentasulphide*

The reaction of sulphur chlorides with $(C_5H_5)_2TiS_5$ can be considered a derivatization reaction since the reaction is quantitative and irreversible and, consequently, the products obtained show what kind of chlorides and in which concentrations have been present before:[20]

$$Cp_2TiS_5 + S_nCl_2 \rightarrow Cp_2TiCl_2 + S_{n+5} \quad (Cp = \eta^5\text{-}C_5H_5). \quad (12)$$

S_2Cl_2 yields S_7 (99%), SCl_2 gives S_6 and S_{12}, and S_3Cl_2 will result in formation of S_8,[20] while with Se_2Cl_2 the analogous 1,2-Se_2S_5 is formed:[21]

$$Cp_2TiS_5 + Se_2Cl_2 \rightarrow Cp_2TiCl_2 + Se_2S_5. \quad (13)$$

If a reaction mixture contained $SeCl_2$, Se_3Cl_2 or $SeSCl_2$ the expected derivatives would be SeS_5, 1,2,3-Se_3S_5 and SeS_6, respectively. HPLC using reversed-phase columns and a UV absorbance detector may be used to separate and identify the above compounds by their retention times.[21–23] It has been shown that the retention of Se_xS_y molecules ($x = 0, 1, \ldots$; $y = 0, 1, \ldots$) of ring sizes 6–12 depends on the ring size, the number of Se atoms, and the number of heteronuclear bonds per molecule only.[23]

Since selenium sulphide molecules are light-sensitive, thermally unstable, and subject to decomposition by nucleophiles, the reactions were carried out under very clean conditions, with exclusion of daylight, and as fast as possible. Cp_2TiS_5 was used in excess to make sure that all chlorides reacted. Between mixing of the components at 20°C in CS_2, followed by dilution to 1 : 50, and injection for HPLC analysis *ca* 9 min passed; deliberately, samples were also analysed 90 min and 24 h after mixing.

Independent of the mixing ratio of S_2Cl_2 and Se_2Cl_2 (3 : 1, 1 : 1 and 1 : 3) the main products from the reaction of the mixture with Cp_2TiS_5 were qualitatively always the same: SeS_5, 1,2-Se_2S_5, SeS_6, S_7 and 1,2,3-Se_3S_5, which may have originated from $SeCl_2$, Se_2Cl_2, $SeSCl_2$, S_2Cl_2 and Se_3Cl_2, respectively. Figure 2 shows a typical chromatogram using a methanol–water mixture (95 : 5, v/v) as eluent; the retention times are listed in Table 4. In addition to the above mentioned compounds, very weak peaks have been observed which can be assigned to other seven-, eight-, nine- and 12-membered Se_xS_y rings on the basis of their retention times and retention indices (RS) as shown in Table 4.

To calculate the RS data the molecules S_6, S_8, S_9 and S_{10} have been measured under identical conditions as reference materials. From their retention data the RS values of the Se_xS_y molecules are obtained.[23] RS values are specific for a certain substance and a certain eluent composition but independent of flow rate and column length.[23] As can be seen from Table 4, most of the peaks can be definitely assigned to certain six-, seven- and eight-membered rings. RS data of nine-membered Se_xS_y molecules are scarce but the two species observed in this work seem to be identical with S_9 and SeS_8 previously observed in the chromatogram of the extract of an Se—S melt.[23] The identity of the two 12-membered rings was checked by comparison with authentic samples;[24] their extremely long retention times result in less accurate RS values and, consequently, the agreement with the literature

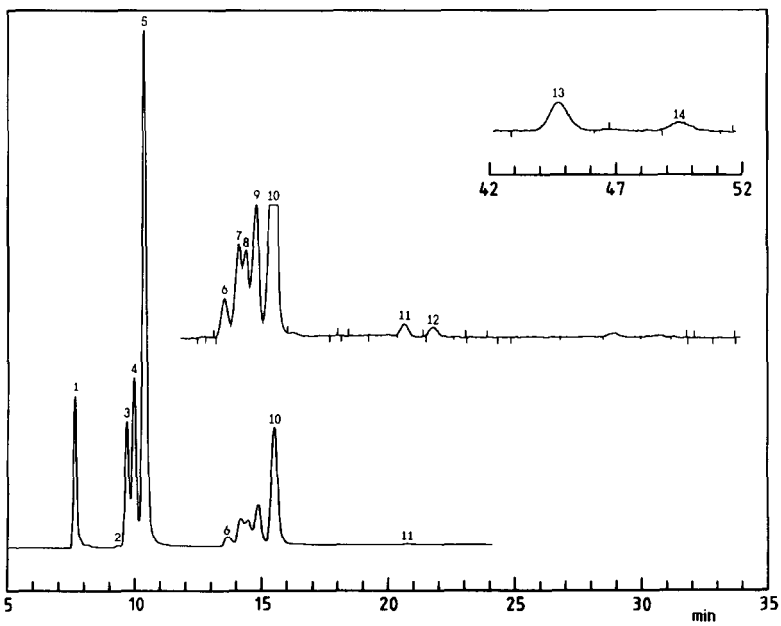

Fig. 2. HPLC analysis of the reaction products from titanocene pentasulphide with a S_2Cl_2–Se_2Cl_2 mixture (1 : 1) showing the presence of 6–12-membered Se_xS_y ring molecules (for details see Table 4).

Table 4. HPLC analysis of the products from the reaction of a S_2Cl_2–Se_2Cl_2 mixture (1 : 1) with titanocene pentasulphide

Peak	Retention time (min)	RS_{exp}	Assignment	RS_{calc}[23]	RS_{exp}[23]
1	7.66	576	SeS_5		575
2	9.30	645	$Se_2S_5{}^4$	643	
3	9.68	659	SeS_6	659	
4	9.96	668	1,2-Se_2S_5		662
5	10.37	682	S_7		681
6	13.61	767	$Se_2S_6{}^4$	761	
7	14.13	778	SeS_7		775
8	14.41	784	$Se_2S_5{}^4$	779	
9	14.80	792	$Se_2S_6{}^2$; S_8	794 ($Se_2S_6{}^2$)	793 (S_8)
10	15.44	804	$Se_3S_5{}^2$		804
11	20.64	886	SeS_8		886
12	21.78	901	S_9		902
13	44.76	1090	1,7-Se_2S_{10}		1059
14	49.46	1116	1,2-Se_2S_{10}		1092

The retention indices RS_{exp} have been calculated as explained in the text and compared with previously published data (columns 5 and 6) for peak assignment. In cases where no experimental RS data (column 6) are known, calculated RS values have been used (column 5). The exponents at some formulae indicate the number of SeS bonds in the molecule (e.g. $Se_2S_6{}^4$ = 1,3-Se_2S_6 or 1,4-Se_2S_6; $Se_2S_6{}^2$ = 1,2-Se_2S_6).

data is less satisfactory. These Se_2S_{10} species originate from a dimerization of SeS_5,[24] and part of SeS_5, and all 1,2,3-Se_3S_5 originate from a dismutation of Se_2S_5:[21]

$$2\ \text{1,2-}Se_2S_5 \rightarrow SeS_5 + \text{1,2,3-}Se_3S_5. \qquad (14)$$

The detection of 1,2,3-Se_3S_5 is therefore no evidence for the presence of Se_3Cl_2.

The other products indicate that the S_2Cl_2–Se_2Cl_2 mixture contains traces of E_nCl_2 compounds (E = S or Se) resulting in $Se_2S_6{}^4$ (from 1,3-Se_2SCl_2), SeS_7 (from SeS_2Cl_2), $Se_2S_6{}^2$ (from 1,2-Se_2SCl_2), S_8 (from S_3Cl_2), SeS_8 (from SeS_3Cl_2) and S_9 (from S_4Cl_2). In this notation the exponents give the number of SeS bonds in the molecule (1,3-Se_2S_6 and 1,4-Se_2S_6 have the same RS value and are therefore collectively denoted as $Se_2S_6{}^4$).

The fact that no S_6 was observed shows that S_2Cl_2–Se_2Cl_2 mixtures do not contain SCl_2. On the other hand, the S_3Cl_2 assumed to explain the formation of S_8 may originate from reaction (15):

$$S_2Cl_2 + S_4Cl_2 \rightleftharpoons 2\,S_3Cl_2. \qquad (15)$$

To determine the rate of reaction (4) the following experiments were carried out. 1 cm^3 each of S_2Cl_2 and Se_2Cl_2 were mixed at 20°C, and after 2, 4 and 5 min, respectively, samples were taken and immediately reacted with titanocene pentasulphide in CS_2. This reaction mixture was then rapidly analysed by HPLC (after sedimentation of Cp_2TiCl_2 and dilution of a sample). The results show that mixing of the two chlorides for 2 min is sufficient to form $SeSCl_2$, which on reaction with Cp_2TiS_5 yields SeS_6. The concentration of SeS_6 neither increased nor decreased when the reaction times were increased.

Reaction of $SeSCl_2$ *with potassium iodide*

The reaction of a S_2Cl_2–Se_2Cl_2 mixture with solid KI results in I_2, KCl and a mixture of cyclic selenium sulphides which have been separated by HPLC and characterized by their retention time, Se content, crystal shape and Raman spectra as six-, seven- and eight-membered rings;[22,25] e.g.:

$$S_2Cl_2 + 2\,KI \rightarrow S_2I_2 + 2\,KCl, \qquad (16)$$

$$Se_2Cl_2 + 2\,KI \rightarrow Se_2I_2 + 2\,KCl, \qquad (17)$$

$$2\,Se_2I_2 + 2\,S_2I_2 \rightarrow Se_4S_4 + 4\,I_2, \qquad (18)$$

$$Se_2I_2 + 3\,S_2I_2 \rightarrow Se_2S_6 + 4\,I_2. \qquad (19)$$

Because of the complex nature of the mixture not all components could initially be identified. We have therefore repeated our previous work and analysed the reaction products simultaneously by HPLC, Raman and ^{77}Se NMR spectroscopy hoping to find compounds directly derived from $SeSCl_2$. Such

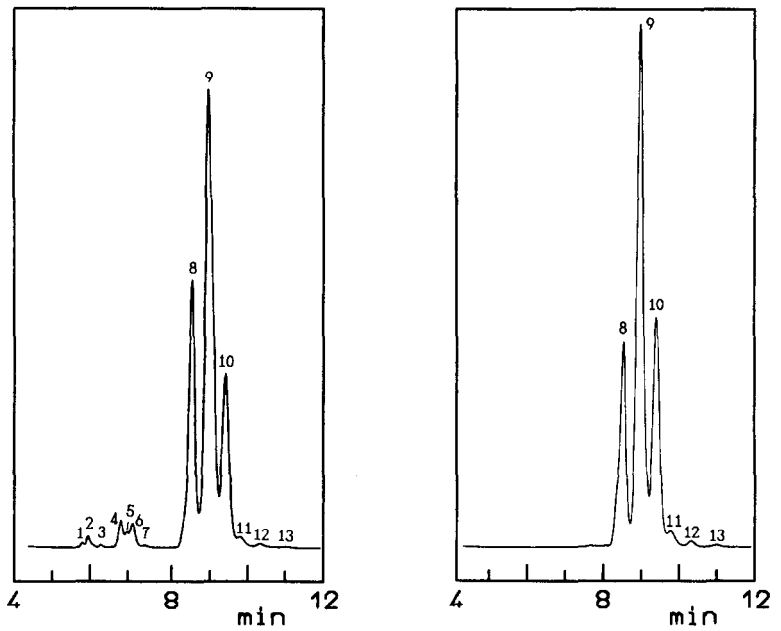

Fig. 3. HPLC analysis of the reaction mixture obtained from treating a S_2Cl_2–Se_2Cl_2 mixture (2 : 1) with potassium iodide at 20°C (left), and of the Se_xS_{8-x} crystals obtained from the reaction mixture at −60°C (right) (for details see Table 5).

molecules should contain single (isolated) Se atoms resulting from reactions of types (20) and (21):

$$ISSI + ISeSI \rightarrow ISSSeSI + I_2, \quad (20)$$

$$2\,ISSSeSI \rightarrow 1,4\text{-}Se_2S_6 \text{ or } 1,5\text{-}Se_2S_6 + 2I_2. \quad (21)$$

In order to increase the $SeSCl_2$–Se_2Cl_2 ratio we have treated a 2 : 1 molar mixture of S_2Cl_2 and Se_2Cl_2 in CS_2 with potassium iodide at 20°C with exclusion of light. After stirring for 4 h and removal of the iodine formed by thiosulphate, the solution was dried with $MgSO_4$ and immediately analysed by HPLC and NMR spectroscopy. Part of the solution was cooled to −60°C for 24 h resulting in orange needle-like crystals of m.p. 110–115°C (360 mg from 1.1 cm^3 S_2Cl_2 and 0.55 cm^3 Se_2Cl_2) which

Table 5. HPLC analysis of the freshly prepared reaction products of a S_2Cl_2–Se_2Cl_2 mixture (2 : 1) with potassium iodide

Peak	Retention time (min)	RS_{exp}	Assignment	RS_{calc} [23]	RS_{exp} [23]
1	5.83	570	SeS_5		575
2	5.98	584	Se_3S_3 [4]	583	
3	6.29	612	Se_4S_2 [2]	601	
4	6.75	649	Se_2S_5 [4]	643	
5	6.96	664	SeS_6 or Se_3S_4 [4]	659/658	
6	7.03	669	Se_2S_5 [2]		662
7	7.30	687	Se_3S_4 [2]	690	
8	8.65	765	Se_2S_6 [4]	761	
9	9.06	785	Se_2S_6 [2] and Se_3S_5 [4]	792/779	
10	9.48	805	Se_3S_5 [2] and Se_4S_4 [4]		804/808
11	9.87	821	Se_4S_4 [2]	831	
12	10.38	842	Se_5S_3 [2]	849	
13	11.00	865	Se_6S_2 [2]		866

The retention indices in column 3 have been calculated from the retention times; the last two columns give the RS values published earlier and used for peak assignment (see also Table 4).

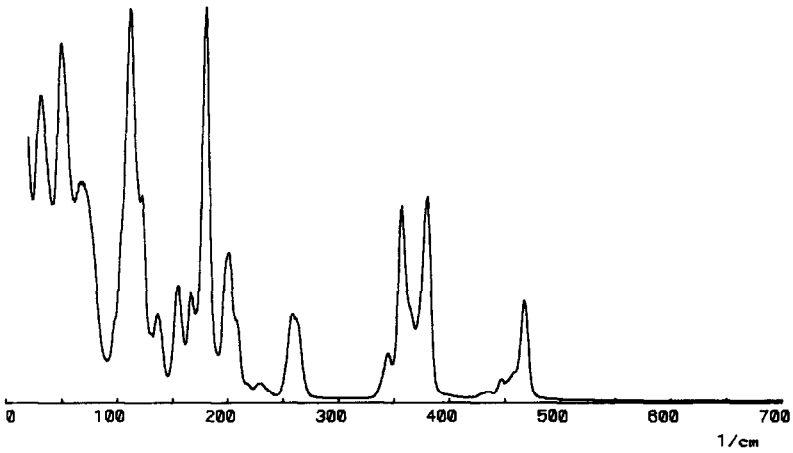

Fig. 4. Raman spectrum of the orange crystals of eight-membered Se_xS_y molecules obtained from the S_2Cl_2–Se_2Cl_2–KI reaction (for wavenumbers and assignment see Table 6).

were analysed by HPLC, ^{77}Se NMR and Raman spectroscopy.

Figure 3 shows the chromatograms of the reaction solution and of the crystals obtained from this solution on cooling; the assignment is given in Table 5. In Fig. 4 the Raman spectrum of the crystals is shown; for wavenumbers and assignment see Table 6. The Raman spectrum shows the typical signals for SS (400–500 cm^{-1}) and SeSe (250–300 cm^{-1}) bonds as well as two types of SeS bonds: those of isolated Se atoms as in S—Se—S units resulting in a strong vibrational coupling between the two neighbouring SeS bonds (340/380 cm^{-1}) and those of cumulated Se atoms as in S—Se—Se—S structural units resulting in weak coupling and lines near 360 cm^{-1} [26] for the SeS stretching vibration. Thus, the Raman spectrum is in agreement with the other analytical findings; the SSeS units are evidence for the presence of $SeSCl_2$ in the initial reaction mixture. To a first approximation, the spectrum indicates a slightly higher con-

Table 6. Raman spectrum of the orange crystals of composition Se_nS_{8-n} obtained from the reaction of S_2Cl_2–Se_2Cl_2 (2:1) with potassium iodide (wavenumbers in cm^{-1}; s = strong, m = medium, w = weak, sh = shoulder)

Wavenumber (intensity)	Assignment
30 (s), 50 (s), 68 (m)	lattice and torsion modes
112 (vs), 123 (sh), 137 (w), 156 (m), 167 (w), 181 (vs), 200 (m), 209 (sh), 229 (vw)	bending modes
259 (m)	ν (SeSe)
344 (w), 357 (s), 380 (s)	ν (SeS)
434 (vw), 446 (vw), 457 (sh), 467 (m)	ν (SS)

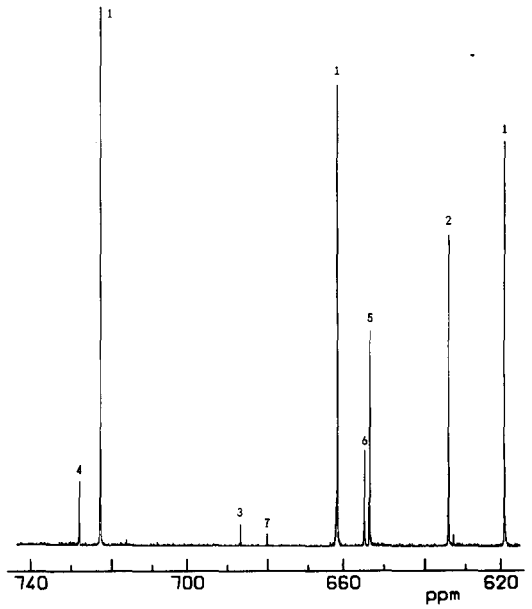

Fig. 5. ^{77}Se NMR spectrum of a freshly prepared carbon disulphide solution of the orange crystals obtained from the S_2Cl_2–Se_2Cl_2–KI reaction (103 mg crystals dissolved in 15 cm^3 CS_2 at 20°C). For peak assignment see Table 7; the region below 600 ppm has been recorded separately.

Table 7. ^{77}Se NMR analysis of the reaction products of S_2Cl_2–Se_2Cl_2 (2:1) mixtures with potassium iodide in CS_2 at 20°C. The relative concentrations have been estimated from peak heights (see Fig. 5). For further details see text; chemical shifts in ppm relative to $(CH_3)_2Se$

Peak	Molecule	Chem. shift	Molar concentration			
			Solution	Crystals		Ref. 28
			a	*b*	*c*	
1	1,2,5-Se_3S_5	723.1/661.9/619.1	31	62	18	7
2	1,2-Se_2S_6	633.2	25	14	24	34
3	1,4-Se_2S_6	686.8	18	1	4	13
4	1,3-Se_2S_6	728.5	15	3	3	7
5	1,2,3-Se_3S_5	653.4/559.9	11	14	25	13
6	1,2,5,6-Se_4S_4	654.7	—	4	2	0
7	1,2,4,5-Se_4S_4	679.8[d]	—	1	0	1
8	1,2,3,4-Se_4S_4	663.6/580.7	—	0	11	4
9	1,2,3-Se_5S_3	657.0/596.9/590.2	—	0	9	2
10	1,5-Se_2S_6	716.3	—	0	4	7
11	SeS_7	699.2	—	0	4	5
12	1,2,4-Se_3S_5		—	—	—	4
13	1,2,3,5-Se_4S_4		—	—	—	1
14	1,2-Se_6S_2		—	—	—	1
15	Se_8		—	—	—	1

[a] Freshly prepared reaction mixture after removal of iodine, recording time 5 h.
[b] Freshly prepared solution of orange crystals (obtained from reaction mixture on cooling) in CS_2.
[c] Same solution as in column *b* but after standing at 20°C for 6 months.
[d] Second line near 654.4 ppm obscured by 1,2,5,6-Se_4S_4.

centration of SSeS over SSe_xS ($x > 1$) units. The spectrum also shows that the sample contains more SeS than SeSe bonds.

In Table 7 the results of the NMR analysis of the freshly prepared reaction solution, of the freshly redissolved orange crystals, and of the same sample after standing at 20°C for 6 months are shown. All peaks could be assigned on the basis of literature data for the chemical shifts of selenium sulphides.[11,13]

All results show that the main products are certain eight-membered Se_xS_y rings, but the HPLC analysis demonstrates the presence of at least four six-membered and three seven-membered Se_xS_y rings in addition. These species are not present in the crystals, the composition of which seems to be less complex since the HPLC trace shows only three strong and three weak peaks, and one shoulder indicating the presence of seven species forming a solid solution. The retention times, RS values and assignment are shown in Table 5. This assignment basically rests on a comparison of RS values with literature data[23] and on the results of the NMR spectra.

The data in Table 7 show 1,2,5-Se_3S_5 as the major reaction product which is also responsible for the largest HPLC peak. This substance is unstable in solution since its concentration decreases on standing, while species with all Se atoms neighbouring increase on ageing; it is known that such species are somewhat more stable[27] which also follows from the positive enthalpy of reaction (4).

We noted that some decomposition of 1,2,5-Se_3S_5 took place already within the first 15 h after preparation of the reaction mixture. At that time 1,2-Se_2S_6 had become the major species in the CS_2 solution followed by 1,2,5-Se_3S_5 with 1,4-Se_2S_6 still being third.

Formally, 1,2,5-Se_3S_5 may be formed by reaction (22):

$$SeSCl_2 + Se_2Cl_2 + 2S_2Cl_2 \xrightarrow[-8KCl,4I_2]{+8KI} \begin{cases} \rightarrow 1,2,5\text{-}Se_3S_5 \\ \rightarrow 1,2,3\text{-}Se_3S_5 \end{cases} \quad (22)$$

When the intermediate ISeSI reacts with ISeSeI via the SeI bond, 1,2,3-Se_3S_5 is formed. In the case that ISeSeI first reacts with two ISSI and then with ISeSI, 1,2,5-Se_3S_5 is to be expected. The other expected isomer, 1,2,4-Se_3S_5, has not been observed in our work. On grounds of the initial mixing ratio of $S_2Cl_2 : Se_2Cl_2 = 2:1$, reaction (22) is more likely

than other reactions and, consequently, Se_3S_5 is the major product. (In Se_3S_5 the S : Se ratio amounts to 1.7 : 1.) Seven eight-membered Se_xS_y molecules can be seen in the NMR spectra of the freshly dissolved orange crystals; the spectrum of the reaction mixture (column 4 of Table 7) showed only five species due to the poor signal-to-noise ratio.

In general, our NMR results are in perfect agreement with the HPLC data which show only traces of selenium-rich rings in the freshly prepared reaction mixture as well as in the freshly prepared solution of the crystals. In contrast, Laitinen *et al.*[28] studying the same reaction have observed reaction products by ^{77}Se NMR spectroscopy which resemble the products in our decomposed (aged) solution. These authors had reacted S_2Cl_2–Se_2Cl_2 mixtures of different molar proportions (1 : 4 through 4 : 1) with potassium iodide in CS_2, obviously following our earlier procedure.[22] Without giving many details the reaction mixtures were analysed quantitatively by ^{77}Se NMR using the natural isotopic composition. For a 2 : 1 (S–Se) mixture the results listed in Table 7, last column, were obtained.[28] These data clearly resemble the composition of our aged solution (column 6 of Table 7) indicating that the samples of Laitinen *et al.* had decomposed prior to NMR spectroscopy. These authors did not state the time elapsed between sample preparation and recording of the NMR spectra. It should be noted that reliable results of unstable selenium sulphides can be obtained only with strict exclusion of light and nucleophilic impurities, which requires special acid treatment of glassware including NMR tubes and solvents. In addition, all solutions should be analysed as rapidly as possible.

Summarizing, we have shown that mixing Se_2Cl_2 with S_2Cl_2 rapidly yields $SeSCl_2$ and other mixed Se—S—Cl molecules together with $SeCl_2$. These species can be detected by NMR and Raman spectroscopy and react with titanocene pentasulphide as well as with potassium iodide to give a variety of cyclic selenium sulphides. SCl_2 and Se_2Cl_2 react quantitatively to give $SeCl_4$ and S_2Cl_2.

Acknowledgements—We are grateful to Dr Maria Papavassiliou for reproducing some experiments, to Ms K. Thiel for typing the manuscript, and to the Deutsche Forschungsgemeinschaft and Verband der Chemischen Industrie for support.

REFERENCES

1. O. Klimmek, A. Kröger, R. Steudel and G. Holdt, *Arch. Microbiol.* 1991, **155**, 177.
2. R. Steudel and R. Laitinen, *Topics Curr. Chem.* 1982, **102**, 177; *Gmelin Handbuch der Anorganischen Chemie* (8th edn) *Selen* [B], pp. 160–176 (1949) and [A 2], p. 179. Springer, Berlin (1980); R. Steudel and E.-M. Strauss, in *The Chemistry of Inorganic Homo-, and Heterocycles* (Edited by I. Haiduc and D. B. Sowerby), Vol. 2, pp. 769–792. Academic Press, London (1987); R. S. Laitinen, *Acta Chem. Scand.* 1987, **A41**, 361.
3. M. Lamoureux and J. Milne, *Can. J. Chem.* 1989, **67**, 1936.
4. M. Lamoureux and J. Milne, *Polyhedron* 1990, **9**, 589.
5. R. Strauss, Dissertation, Techn. Univ. Berlin (1987).
6. S. V. Volkov, Z. A. Fokina, V. F. Lapko, V. E. Pogorelov and G. I. Salivon, *Ukr. Khim. Zh.* 1982, **48**, 899.
7. R. Kniep, L. Korte and D. Mootz, *Z. Naturforsch.* 1983, **38b**, 1.
8. F. Fehér, in *Handbuch der Präparativen Anorganischen Chemie* (Edited by G. Brauer), Vol. I, p. 415. F. Enke, Stuttgart (1975).
9. R. Steudel and R. Strauss, *J. Chem. Soc., Dalton Trans.* 1984, 1775.
10. W. McFarlane and R. J. Wood, *J. Chem. Soc., Dalton Trans.* 1972, 1397.
11. R. Steudel, M. Papavassiliou, D. Jensen and K. Seppelt, *Z. Naturforsch.* 1988, **43b**, 245.
12. R. S. Laitinen and T. A. Pakkanen, *Inorg. Chem.* 1987, **26**, 2598.
13. R. Steudel, M. Papavassiliou and W. Krampe, *Polyhedron* 1988, **7**, 581.
14. R. Steudel, D. Jensen and B. Plinke, *Z. Naturforsch.* 1987, **42b**, 163.
15. J. Milne, *Polyhedron* 1985, **4**, 65.
16. R. Ponsioen and D. J. Stufkens, *Rec. Trav. Chim. Pays-Bas* 1971, **90**, 521.
17. W. Brockner and A. Feza Demiray, *Z. Naturforsch.* 1980, **35a**, 766.
18. J. Milne and P. La Haie, *Inorg. Chem.* 1979, **18**, 3180.
19. M. Lundkvist and M. Lellep, *Acta Chem. Scand.* 1968, **22**, 291.
20. R. Steudel, R. Strauss and D. Jensen, *Chemiker-zeitung* 1985, **109**, 349.
21. R. Steudel and E.-M. Strauss, *Angew. Chem.* 1984, **96**, 356; *Angew. Chem., Int. Ed. Engl.* 1984, **23**, 362.
22. R. Steudel and E.-M. Strauss, *Z. Naturforsch.* 1983, **38b**, 719.
23. R. Steudel, E.-M. Strauss and D. Jensen, *Z. Naturforsch.* 1990, **45b**, 1282.
24. R. Steudel, D. Jensen and F. Baumgart, *Polyhedron* 1990, **9**, 1199.
25. E.-M. Woldt, Diplomarbeit, Techn. Univ. Berlin (1981).
26. R. Laitinen and R. Steudel, *J. Mol. Struct.* 1980, **68**, 19.
27. R. O. Jones and D. Hohl, *J. Am. Chem. Soc.* 1990, **112**, 2590.
28. R. S. Laitinen, P. Pekonen, Y. Hiltunen and T. A. Pakkanen, *Acta Chem. Scand.* 1989, **43**, 436.

Polyhedron Vol. 10, No. 10, pp. 1049–1059, 1991
Printed in Great Britain

0277–5387/91 $3.00+.00
Pergamon Press plc

VOLATILE TRIS-TERTIARY-ALKOXIDES OF YTTRIUM AND LANTHANUM. THE X-RAY CRYSTAL STRUCTURE OF $[La_3(OBu^t)_9(Bu^tOH)_2]$

DONALD C. BRADLEY,* HALINA CHUDZYNSKA, MICHAEL B. HURSTHOUSE* and MAJID MOTEVALLI

Department of Chemistry, Queen Mary and Westfield College, Mile End Road, London E1 4NS, U.K.

(*Received* 19 *December* 1990; *accepted* 30 *January* 1991)

Abstract—Tertiary alkoxides of yttrium and lanthanum have been prepared by addition of excess tertiary alcohol to the metal tris-(bis-trimethylsilylamides), $M\{N(SiMe_3)_2\}_3$ (M = Y, La), and characterized by elemental analyses, NMR, IR and mass spectroscopy. With t-butanol and t-amyl alcohol the alcoholates $[Y_3(OBu^t)_9(Bu^tOH)_2]$ (**1**), $[Y_3(OAm^t)_9(Am^tOH)_2]$ (**2**) and $[La_3(OBu^t)_9(Bu^tOH)_2]$ (**3**) were isolated. With higher tertiary alcohols the tris-t-alkoxides $[M(OR)_3]$ were obtained [M = Y, R = CMe_2Pr^i (**4**), $CMeEtPr^i$ (**5**), CEt_3 (**6**); M = La, R = CMe_2Pr^i (**7**), $CMeEtPr^i$ (**8**)] as dimers. The coordinated Bu^tOH in **1** could be replaced by THF or pyridine but not by trimethylamine. The X-ray crystal structure of **3** showed that the La_3 triangle is capped by two μ_3-OBu^t groups with three μ_2-OBu^t bridges as in $[La_3(\mu_3\text{-}OBu^t)_2(\mu\text{-}OBu^t)_3(OBu^t)_4(Bu^tOH)_2]$. The variable temperature NMR data suggest that compounds **1** and **2** have the same structure in solution as compound **3**.

The alkoxides of yttrium and some of the lanthanides have been known for many years,[1–4] but hitherto have not been fully characterized. In recent years the interest in these compounds has been greatly boosted by their applications in ceramics and electronic materials.[5] The need for volatile or soluble (in organic solvents) metallo-organic compounds containing metal—oxygen bonds, which could serve as precursors for the MOCVD or the sol–gel technique has prompted several workers to reinvestigate the older data[6,7] and to search for new compounds.[8,14] The yttrium and lanthanide alkoxides are known to form polymeric structures which are responsible for their low volatility and solubility.[4] Recently it has been shown[6,7] that yttrium, ytterbium and scandium isopropoxides form pentanuclear complexes $[M_5O(OPr^i)_{13}]$ around a five-coordinated (μ_5) oxygen atom. Evans *et al.*[9] attempted the preparation of yttrium t-butoxide from YCl_3 and $NaOBu^t$ or $LiOBu^t$ in THF and obtained products such as $[Y_3(\mu_3\text{-}OCMe_3)(\mu_3\text{-}Cl)(\mu\text{-}OCMe_3)_3(OCMe_3)_4(THF)_2]$ and $[Y_4(\mu_5\text{-}OCMe_3)_2(\mu\text{-}OCMe_3)_4(OCMe_3)_4(\mu\text{-}O)(\mu\text{-}Cl)_2Li_4(\mu\text{-}OCMe_3)_2]_2$. They succeeded in isolating a chlorine-free compound $[La_3(OBu^t)_9(THF)_2]$, although they were unable to solve the crystal structure due to disorder problems. Further work[10] produced more structures of chloro-t-butoxo complexes of yttrium and demonstrated the general complexity of the system and its dependence on small changes in the preparative conditions.

RESULTS AND DISCUSSION

We have prepared the following tris-t-alkoxides of yttrium and lanthanum: $[M_3(OR)_9(ROH)_2]$ [M = Y, R = Bu^t (**1**), Am^t (**2**); M = La, R = Bu^t (**3**)] and $[M(OR)_3]_n$ [M = Y, R = CMe_2Pr^i (**4**), $CMeEtPr^i$ (**5**), CEt_3 (**6**); M = La, R = CMe_2Pr^i (**7**), $CMeEtPr^i$ (**8**)].

We chose the t-alkoxides because the branched OR groups give greatest shielding of the metal atoms thereby decreasing the degree of oligomerization and enhancing the volatility and solubility.

We were also interested in comparing the t-alkoxides with the isopropoxides which we found previously to form the oxo-complexes $[M_5O$

* Authors to whom correspondence should be addressed.

$(OPr^i)_{13}$]. The mechanism of the formation of the oxo-complexes could be either:

(i) by elimination of propene ($MOPr^i \rightarrow MOH + C_3H_6$), or
(ii) by formation of di-isopropyl ether ($2\ MOPr^i \rightarrow M_2O + Pr^i{}_2O$).

Some t-alkoxides (e.g. $Al_2OBu^t{}_6$) are known to undergo β-elimination with formation of an alkene on thermolysis. However, we have found that all of the yttrium and lanthanum t-alkoxides are tris compounds thermally stable at least up to 150°C. Since t-alkoxide groups should eliminate alkenes much more readily than the isopropoxide group this appears to rule out mechanism (i) for the formation of the $[M_5O(OPr^i)_{13}]$ compounds.

Preparations

To preclude the formation of the chloride alkoxides obtained by Evans *et al.*,[9,10] we chose to prepare the t-alkoxides from a chlorine-free starting material. For this purpose we used the reaction of $M\{N(SiMe_3)_2\}_3$ (M = Y or La)[11] with tertiary alcohols in benzene solution:

$$M\{N(SiMe_3)_2\}_3 + 3\ R^tOH \rightarrow [M(OR^t)_3] + 3\ HN(SiMe_3)_2.$$

This approach was recently used by other workers in synthesizing $[Y(OSiPh_3)_3]$,[12] although they were unsuccessful when applying it to the t-butoxide.

The alcohol in at least 30% excess was added to $M\{M(SiMe_3)_2\}_3$ in benzene solution. The mixture was stirred and refluxed for 1 h and the completion of the reaction checked by NMR. The solvents were evaporated *in vacuo* and the residue either sublimed *in vacuo* or crystallized from toluene or pentane. The compounds were characterized by elemental analysis, NMR, IR and mass spectra. An X-ray crystal structure of $[La_3(\mu_3\text{-}OBu^t)_2(\mu\text{-}OBu^t)_3(OBu^t)_4(Bu^tOH)_2]$ was obtained.

All the compounds were obtained as white solids. Compounds **1** and **3** were moderately soluble in organic solvents, while the higher t-alkoxides were very easily soluble in benzene and pentane. Some data on melting points, volatilities and mass spectra of these compounds are presented in Table 1. It is noteworthy that three of these compounds (**1**–**3**) are formulated as $[M_3(OR)_9(ROH)_2]$ with coordinated alcohol, which was identified by IR and NMR spectroscopy. Such complexes are rare in metal alkoxide chemistry[4] since alkoxide bridging is the preferred mode of metal coordination expansion. The coordinated alcohol could be removed by heating (**1**, 60–70°C; **2**, 40–50°C; **3**, 100°C) *in vacuo* with the lanthanum complex (**3**) being the most stable. Therefore, the volatilities observed for these compounds probably relate to the unsolvated tri-t-alkoxides and their melting points are complicated by decomposition caused by loss of coordinated alcohol. The coordinated t-butanol in **1** was readily replaced by THF giving $[Y_3(OBu^t)_9(THF)_2]$ (**9**) which lost THF when heated to 70°C *in vacuo*. Pyridine also displaced the alcohol from **1** but trimethylamine did not. It is noteworthy that Evans *et al.*[9] obtained $[Y_3(OBu^t)_8Cl(THF)_2]$ and showed that the THF could be replaced by pyridine.

None of the higher t-alkoxides (C_6 or C_7) gave complexes with coordinated alcohol, presumably

Table 1.

Compound	Melting point (°C)	Volatility (°C/torr)	Mass spectra *m/z* Obs.	Calc.	Species
$[Y_3(OBu^t)_9(Bu^tOH)_2]$ (**1**)	171	$235/10^{-2}$	851.2463	851.2403	$[Y_3(OBu^t)_8]^+$
			721.1046	721.1046	$[Y_3(OBu^t)_6O]^+$
$[Y_3(OAm^t)_9(Am^tOH)_2]$ (**2**)	84	$150/10^{-3}$	None observed		
$[La_3(OBu^t)_9(Bu^tOH)_2]$ (**3**)	192	$240/10^{-3}$	610.7948	610.7972	$[La_3O_6C_7H_{14}]^+$
$[Y(OCMe_2Pr^i)_3]$ (**4**)	161	$170/10^{-3}$	742.3499	742.3445	$[Y_2(OCMe_2Pr^i)_6\text{-}2Me]^+$
			683.3007	683.2949	$[Y_2(OCMe_2Pr^i)_5]^+$
$[Y(OCMeEtPr^i)_3]$ (**5**)	196	$170/10^{-3}$	753.3739	753.3731	$[Y_2(OCMeEtPr^i)_5]^+$
$[Y(OCEt_3)_3]$ (**6**)	198	$225/10^{-2}$	753.3713	753.3731	$[Y_2(OCEt_3)_5]^+$
			709.3106	709.3106	$[Y_2(OCEt_3)_5\text{-}Me\text{-}Et]^+$
$[La(OCMe_2Pr^i)_3]$ (**7**)	119	$135/10^{-3}$	783.3023	783.2953	$[La_2(OCMe_2Pr^i)_5]^+$
			597.0961	597.0969	$[La_2(OCMe_2Pr^i)_3O]^+$
$[La(OCMeEtPr^i)_3]$ (**8**)	112	$150/10^{-3}$	853.3729	853.3735	$[La_2(OCMeEtPr^i)_5]^+$

because of steric hindrance which prevents the metals attaining the octahedral coordination required for the trinuclear species $[M_3(OR)_9(ROH)_2]$. Instead it seems that dimeric compounds $[M_2(OR)_6]$ are formed with tetrahedral metal coordination. Although the volatility data in Table 1 are not very precise it does appear that for both $[M(OCMe_2Pr^i)_3]$ and $[M(OCMeEtPr^i)_3]$ the heavier lanthanum compounds are distinctly more volatile than the corresponding yttrium compounds.

Bradley and Swanwick[13] showed several years ago that in the series $[M(OR^t)_4]$ (M = Ti, Zr, Hf; R = Bu or Am) the volatilities were in the unexpected order Hf > Zr > Ti. This was explained in terms of the mass-entropy effect which becomes apparent when the central metal atom is effectively screened by the bulky ligands and prevented from contributing to intermolecular attractive forces. The rather large difference in volatility between the yttrium and lanthanum compounds suggests that other factors must also be involved. For example the dimeric lanthanum compounds may dissociate more readily to monomers than the yttrium dimers. Nevertheless, the mass spectral data show evidence of gaseous dimeric species for both metals.

Mass spectra

None of the compounds gave parent molecular ions but some important fragment ions were identified by accurate masses as shown in Table 1.

Considering first of all the trinuclear species $[M_3(OR)_9(ROH)_2]$, it is clear that loss of coordinated alcohol has occurred but the presence of trinuclear fragment ions $[Y_3(OBu^t)_8]^+$ (*m/z*, 851), $[Y_3O(OBu^t)_6]^+$ (*m/z*, 721) and $[La_3O_6C_7H_{14}]^+$ (*m/z*, 610.8) suggests that the trimer species $[M_3(OR)_9]$ is present in the vapour state. Although $[Y_3(OBu^t)_9(THF)_2]$ gave no identifiable fragment ions, the pyridine complex gave a peak at 856 corresponding to $[Y_3O_9C_{31}H_{45}N_2]^+$.

For all of the higher t-alkoxides a fragment ion corresponding to $[M_2(OR)_5]^+$ was observed, suggesting that these compounds are dimeric in the vapour state. In addition to the agreement between observed and calculated accurate masses, these species were also confirmed by the presence in the correct proportion of the M+1 ion corresponding to the species containing one ^{13}C atom in place of a ^{12}C atom.

NMR spectra

Variable temperature ^1H and ^{13}C NMR studies were carried out in order to derive structural information on these t-alkoxides in solution. All of the compounds were fluxional and required low temperatures to slow down the exchange between distinguishable alkoxide groups.

The limiting low temperature ^1H NMR spectra of the trinuclear species $[M_3(OR)_9(ROH)_2]$ (**1–3**) were very complex and a knowledge of the molecular structure of the lanthanum compound (**3**) obtained by single crystal X-ray analysis was invaluable in their interpretation. The structure (Fig. 1) shows that in $[La_3(OBu^t)_9(Bu^tOH)_2]$ (**3**) there is a triangle of metal atoms bound by two capping μ_3-OBu^t groups (above and below the triangle) and three bridging μ_2-OBu^t groups. Each metal has two terminal ligands of which two out of six are probably the coordinated alcohols.

The t-butoxides (**1**) and (**3**) exhibit very similar spectra which are detailed in Table 2. At around 230 K, each has five major peaks with intensities in the ratio 2:2:2:1:4, reading from left to right lower field to higher field. Assuming that the two coordinated alcohol molecules are bonded to different metals then one μ_2-OBu^t is unique since the other two will be equivalent. If the two μ_3-OBu^t groups are also equivalent then it follows that the six terminal groups are in a 2:4 ratio corresponding to two alcohols and four alkoxides. Closer inspection of the spectra reveals that there are some significant minor peaks adjacent to some of the major peaks and at low temperature the OH peak for the coordinated alcohol splits into two peaks in a 3:1 ratio. This suggests that more than one structure is present and indeed the molecular structure (Fig. 1) depends on whether the coordinated alcohols are both above (or below) the plane of the M_3 triangle (isomer **A**) or one is above and one below (isomer **B**). The X-ray structure unfortunately does not clearly identify the positions of the alcohol ligands, but it is reasonable to suppose that the OH chemical shifts of isomers **A** and **B** will be slightly different. The unique μ_2-OBu^t resonance at *ca* δ 1.50 is also split into an approximately 2:1 ratio, although the two peaks are not sufficiently resolved to give accurate values of integration. The lowest field peak at *ca* δ 1.80, which is believed to be due to the μ_3-OBu^t groups, also has a small satellite as do the other major peaks, but even at 400 MHz it has not been possible to completely resolve the spectra. At higher temperature (300 K) the spectra simplify to three main peaks in the ratio (left to right from lower field to higher field) 2:3:6 corresponding to $2\times\mu_3$, $3\times\mu_2$ and $6\times$terminal groups due, presumably, to rapid exchange involving the coordinated alcohols and the terminal alkoxide groups. The OH peaks also coalesce into a single peak in the correct proportion to the t-butyl peaks of 2:99

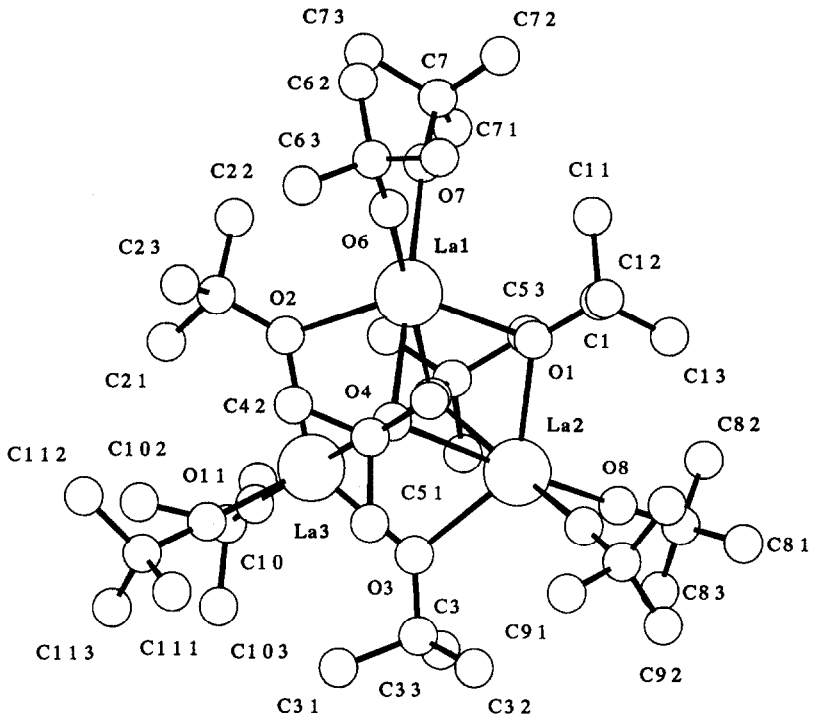

Fig. 1. The molecular structure of $[La_3(\mu_3\text{-}OBu^t)_2(\mu\text{-}OBu^t)_3(OBu^t)_4(Bu^tOH)_2]$ showing the atom numbering scheme: hydrogen atoms omitted for clarity.

required by the formula. On raising the temperature to *ca* 330 K the three t-butyl peaks all coalesced into a single, broad peak due to exchange of terminal, μ_2-bridging and μ_3-bridging alkoxide groups. Addition of t-butanol (δ 1.15 Bu^t, 2.37 OH) to the yttrium compound (**1**) in toluene (d_8) at 300 K had no effect on the lowest field t-butoxide peak (μ_3-OBu^t), or on the peak at intermediate field (μ_2-OBu^t), but caused a substantial shift from δ 1.43 to 1.26 in the highest field peak (terminal OBu^t groups). This behaviour was taken as further confirmation that the highest field peak was due to the terminal alkoxide groups including the coordinated alcohols. The alcohol OH peak was also shifted to higher field (δ 2.52) as expected showing rapid exchange between free and coordinated alcohol molecules.

The t-amyloxide of yttrium (**2**) gave more complex ^{1}H NMR spectra than the t-butoxide because of the presence of singlets (methyl bonded to the quaternary carbon), triplets (methyl of the ethyl) and quartets (methylene of the ethyl). Nevertheless, the overall pattern was similar to that of the t-butoxides with broad singlets, triplets and quartets at 353 K each giving five resonances at low temperatures (253 K). In the case of the singlets, which were best resolved, the ratios of intensities were 2:2:2:1:4 (from low to high field) exactly as found in the t-butoxides. It is therefore reasonable to conclude that the t-amyloxide has the same trinuclear structure as the t-butoxide.

The ^{13}C NMR spectra of compounds **1–3** showed splitting of peaks similar to that found in the ^{1}H spectra, but were less well resolved and not amenable to quantitative evaluation. The ^{89}Y NMR spectra of **1** and **2** at 310 K showed single peaks at δ 166.8 and 199.1 in C_6D_6. No doubt the fluxional nature of these complexes prevented the resolution into two peaks in the 2:1 ratio required by the structure assuming that the yttrium atoms bonded to one terminal alkoxide and one alcohol would have a slightly different chemical shift from the yttrium bonded to two terminal alkoxides.

The ^{1}H NMR spectrum of **9** at 273 K was rather complex corresponding to the presence of a major species having two broad unresolved peaks at δ 1.78 and 1.35 and a minor species with sharp lines at δ 1.92, 1.72, 1.70, 1.53 and 1.49 in the ratios of 1:3:1:2:1:1, respectively. The peaks due to THF were present at δ 1.43 and 3.59. It appears that more than one species is present but one of them could well have the trinuclear structure of **1** with the t-butanol molecules replaced by THF, analogous to the complex $[Y_3Cl(OBu^t)_8(THF)_2]$ obtained by Evans *et al.*[9]

By careful heating *in vacuo* the coordinated

Table 2. ^{1}H NMR spectra

Compound	Temperature (K)	Chemical shifts[a]
$[Y_3(OBu^t)_9(Bu^tOH)_2]$ (1)	323	4.20 (2H), 1.53 (99H)
	297[b]	3.83, 1.83, 1.68, 1.43
	253	1.83, 1.77, 1.76, 1.74, 1.54, 1.52, 1.30
	227	1.83 (18H), 1.81 (18H), 1.77 (18H), [1.56, 1.51, 9H], [1.33, 1.28, 36H].
$[Y_3(OAm^t)_9(Am^tOH)_2]$ (2)	353	1.84 (q, 2H), 1.48 (s, 6H), 0.95 (t, 3H)
	297[b]	2.73 (s, 2H) [1.76, 1.56, 1.38, 0.95br, 122H]
	253	5.53 (s, 2H), 2.40q, 2.22q, 1.98q, 1.78 (s, 22H), 1.74q, 1.69 (s, 22H), 1.66 (s, 22H), 1.51q, 1.49 (s, 11H), 1.31 (s, 44H), 1.21t, 1.08t, 0.96t, 0.92t, 0.88t.
$[La_3(OBu^t)_9(Bu^tOH)_2]$ (3)	338	4.06 (s, 2H), 1.48 (s, 99H)
	297[b]	4.96 (2H), 1.81 (18H), 1.70 (27H), 1.45 (54H)
	273	5.00, 1.74, 1.70, 1.64, 1.50, 1.39
	263	1.75, 1.70, 1.66, 1.49, 1.46, 1.32
	242	5.42, 5.36, 1.77, 1.72, 1.68, 1.49, 1.46, 1.30
	233	[5.42, 5.36, 2H], 1.78 (18H), 1.77 (18H), 1.70 (18H), [1.49, 1.47, 9H], [1.32, 1.28, 36H].
$[Y(OCMe_2Pr^i)_3]$ (4)	297[b]	1.63 (sept. 1H), 1.30 (s, 6H), 1.05 (d, 6H)
	203	[1.92, 1.77, 1H], [1.46, 1.41, 6H], [1.22, 1.16, 1.07, 6H].
$[Y(OCMeEtPr^i)_3]$ (5)	300[b]	1.90 (sept), 1.72 (sept), 1.54q, 1.39s, 1.13 mult.
$[Y(OCEt_3)_3]$ (6)	353	1.54q, 0.97t
	303[b]	1.57 mult, 1.00t
	273	1.61 (q, 2H), 1.54 (q, 4H), [1.04t, 1.00t, 9H].
$[La(OCMe_2Pr^i)_3]$ (7)	297[b]	1.72 (sept, 1H), 1.36 (s, 6H), 1.03 (d, 6H)
	233	[2.52, 2.21, 1.89, sept], [1.69, 1.53, 1.45, 1.40, s], [1.34, 1.15, 1.02, 0.94, d].
$[La(OCMeEtPr^i)_3]$ (8)	298[b]	1.66 (sept, 1H), 1.55 (q, 2H), 1.20 (s, 3H), 1.07 (d, 3H), 1.03 (t, 3H), 0.98 (t, 3H).
$[Y(OBu^t)_3]_n$[c]	297[b]	1.62–1.50 (two broad overlapping peaks)
	217	1.80, 1.77, 1.73, 1.69, 1.58, 1.55, 1.49, 1.44, 1.27.
$[Y(OAm^t)_3]_n$[d]	300[b]	Broad peaks overlapping 1.75, 1.55, 1.43, 0.98
	233	2.20q, 2.05q, 1.95q, 1.70 (s, 2H), 1.63 (s, 2H), 1.52 (s, 2H), 1.52 (s, 2H), 1.45 (s, 2H), 1.35 (s, 2H), 1.28t, 1.22t, 1.0t, 0.97t, 0.84t.

[a] Relative to TMS, in $C_6D_5CD_3$ except when designated [b].
[b] In C_6D_6.
[c] Obtained by removing Bu^tOH from **1** *in vacuo* (see Experimental).
[d] Obtained by removing Am^tOH from **2** *in vacuo*.

t-butanol could be removed from **1** leaving the unsolvated tris-t-butoxide $(Y(OBu^t)_3]_n$, which gave a very broad ^{1}H NMR signal at *ca* δ 1.56 at 297 K. At low temperature (217 K) this was resolved into a complex spectrum of nine peaks (δ 1.80, 1.77, 1.73, 1.69, 1.58, 1.55, 1.49, 1.44 and 1.27) suggesting the presence of polymeric species.

Removal of coordinated t-amyl alcohol from **2** left a solid whose ^{1}H NMR spectrum at 233 K gave five resolved singlets at δ 1.70, 1.63, 1.52, 1.45 and 1.35 in the ratio 2:2:2:1:2, respectively, together with several quartets (δ 2.20, 2.05 and 1.95) and triplets (δ 1.28, 1.22, 1.06, 0.97 and 0.84). Interestingly, the pattern of singlets could be ascribed to trinuclear $[Y_3(\mu_3\text{-}OAm^t)_2(\mu_2\text{-}OAm^t)_3(OAm^t)_4]$, based on the structure in Fig. 1, without the coordinated alcohol molecules. In such a structure the μ_2-ligands would be distinguishable in a 1:2 ratio and the four terminal ligands in a 2:2 ratio. It would seem that the slightly more bulky t-amyloxide groups do not allow the trinuclear cluster to undergo further polymerization resulting in a molecular structure containing one six-coordinate and two five-coordinated yttrium atoms.

The yttrium and lanthanum derivatives of the C_6 t-alcohol dimethylisopropylcarbinol (**4** and **7**)

showed different ^{1}H NMR behaviour compared with the t-butoxides and t-amyloxides. At room temperature, **4** gave a septet (δ 1.63), singlet (δ 1.30) and doublet (δ 1.05) in the correct proportions for the alkyl group. Cooling to 203 K was required to cause splitting to two septets (δ 1.92 and 1.77), two singlets (δ 1.46 and 1.41) and three doublets (δ 1.22, 1.16 and 1.07) which were all broad. The lanthanum analogue (**7**), which also showed only a single alkoxide species at room temperature (δ 1.72 sept., 1.36 sing., 1.03 doub.) gave a more complex spectrum at lower temperatures (233 K) comprising three septets, four singlets and four doublets.

The mass spectra of **4** and **7** gave evidence of dinuclear fragment ions, but the ^{1}H NMR spectra for dimers should give only two alkoxide environments and it may well be that a trinuclear species is present in equilibrium with the dimer. It is noteworthy that for both compounds the signals all moved downfield on cooling. The ^{13}C NMR spectrum of **4** showed no splitting down to 233 K, whereas in **7** splitting into two signals was observed for $C(CH_3)_2$ and $CCH(CH_3)_2$ carbon atoms at 233 K. Interestingly, the ^{89}Y NMR spectrum of **4** gave a single peak at δ 36.8 at very much higher field than the trinuclear compounds **1** and **2**, which contain octahedrally coordinated yttrium. This strongly suggests that in **4** the yttrium is in a lower coordination environment.

The ^{1}H NMR spectrum of **5** gave, at room temperature, two septets, one quartet, two singlets and a multiplet consisting of overlapping triplets and doublets. The ratio of the two septets and two singlets was 2 : 1 in each case, suggesting the presence of a dimer. The spectrum was unchanged on lowering the temperature. The ^{13}C NMR spectrum of **5** showed two unequal signals for the quaternary, CH, CH_2 and CH_3 (ethyl) carbon atoms, but two large (equal) and two small (equal) signals for the CH_3 (isopropyl) carbon atoms. This suggests a dimeric structure in which restricted rotation renders the two methyls of the isopropyl groups non-equivalent. The ^{89}Y NMR signal for **5** was at δ 45.6, which is in the same region as for **4** and also suggests a lower coordination than in **1** and **2**. The ^{1}H NMR spectrum of **8** at room temperature gave a septet, a quartet, a singlet, a triplet and two equal doublets and was unchanged on lowering the temperature. The splitting of the isopropyl methyl doublets suggests non-equivalence as in the yttrium compound (**5**).

The ^{13}C NMR spectrum of **8** also showed one signal for the quaternary, CH, CH_2 and CH_3 (ethyl) carbons, but two (equal) signals for the CH_3 (isopropyl) carbons in agreement with the ^{1}H NMR spectrum.

Finally we mention the ^{1}H NMR spectrum of **6**, which at 353 K gave a quartet (δ 1.54) and a triplet (δ 0.97). At around 303 K the quartet broadens and at 273 K is resolved into two quartets (δ 1.61 and 1.54) in a 2 : 1 ratio. The triplet also broadens and splits into two overlapping triplets (δ 1.04 and 1.00) at 273 K. The ^{13}C NMR spectrum of **6** showed splitting of the quaternary and CH_2 carbon atoms at room temperature, whilst the ^{89}Y spectrum gave one peak at δ 37.5. These data together with the mass spectrum suggest that compound **6** is dimeric with distorted tetrahedral yttrium.

Infrared spectra

Compounds **1–3**, containing coordinated alcohols, have broad bands corresponding to OH-stretching vibrations at 3420, 3439 and 3386 cm^{-1}, respectively. Compound **9** shows one of the characteristic THF bands at 1075 cm^{-1} (cf. 1072 cm^{-1} in free ligand), but the other band at *ca* 913 cm^{-1} is obscured by strong bands due to t-butoxide groups.

X-ray crystal structure of $[La_3(OBu^t)_9(Bu^tOH)_2]$ (**3**)

The molecular structure of **3** was determined by single crystal X-ray diffraction and is shown in Figs 1 and 2. Some bond lengths are listed in Table 3 and bond angles in Table 4. The trinuclear species with the M_3O_{11} metal–oxygen framework has already been described under the NMR section. The presence of two molecules of Bu^tOH in the trinuclear molecule is shown by elemental analysis, IR spectra and ^{1}H NMR spectra, but it was not possible to locate the OH hydrogen atoms in the X-ray structure. It is reasonable to suggest that the coordinated alcohols occupy terminal positions on two of the three lanthanum atoms and their presence might be revealed by longer La—O bond distances compared with the La—OBu^t groups. Looking at the terminal La—O bonds it is noticeable that La(1) has one long (2.604) and one short (2.195 Å) bond suggesting that O(7)C(7)(C71, C72, C73) is one of the alcohol molecules. La(2) is equally bonded to O(8) and O(9) (La—O, 2.304 and 2.308 Å) which must be covalently bonded t-butoxides and therefore La(3) should carry the other alcohol ligand. In fact La(3) is almost equally bonded to O(10) and O(11) (La—O, 2.350 and 2.315 Å) and the difference is barely significant. If the coordinated alcohols are bonded to La(1) and La(3) this would make the μ_2-bridging t-butoxide group O(2)C(2)(C21, 22, 23) slightly different in environment from the other two equivalent μ_2-bridging groups. In fact O(2) forms a symmetrical bridge to La(1) (2.449 Å) and La(3) (2.447 Å), whereas O(3)

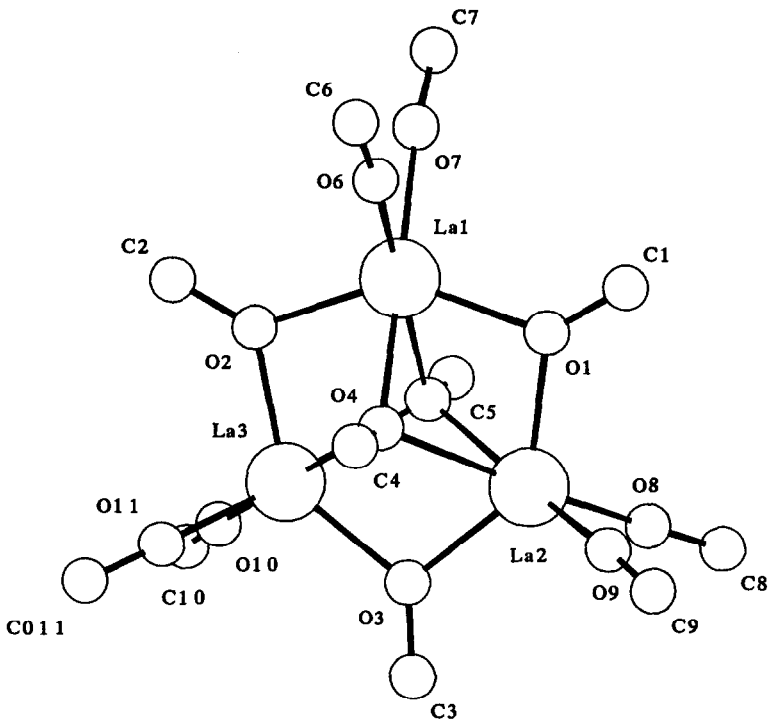

Fig. 2. The structure of the $La_3(OAlk)_{11}$ core. All Bu^t methyls omitted for clarity.

and O(1) form slightly unsymmetrical bridges [La(3)—O(3), 2.417; La(2)—O(3), 2.458; La(1)—O(1), 2.408; and La(2)—O(1), 2.460 Å]. Bearing in mind the uncertainties in these bond distances the data are inconclusive. The presence of coordinated alcohol might be expected to show up in a comparison of La—O—C bond angles. Thus the oxygen atom on a covalently bound alkoxide has two lone pairs of electrons available for π-donation into vacant metal orbitals with a limiting angle of 180° for full π-bonding. The oxygen of a coordinated alcohol has only one lone pair for π-donation leading to an angle nearer to 120°. The data in Table 4 show that three of the terminal groups have LaOC angles very close to 180° (178.9, 178.7 and 177.0), one is 175.1, another is 173.7 and the smallest angle is 167.5°. It is significant that the smallest angle involves La(1)—O(7) which has the longest terminal La—O bond length and was accordingly identified as a coordinated alcohol. The

Table 3. Selected bond lengths (Å) for $[La_3(\mu_3\text{-OBu}^t)_2(\mu\text{-OBu}^t)_3(OBu^t)_4(Bu^tOH)_2]$

O(1)—La(1)	2.408(14)	O(2)—La(1)	2.449(14)
O(4)—La(1)	2.505(13)	O(5)—La(1)	2.548(13)
O(6)—La(1)	2.195(13)	O(7)—La(1)	2.604(15)
O(1)—La(2)	2.460(12)	O(3)—La(2)	2.458(14)
O(4)—La(2)	2.622(14)	O(5)—La(2)	2.573(14)
O(8)—La(2)	2.304(18)	O(9)—La(2)	2.308(18)
O(2)—La(3)	2.447(13)	O(3)—La(3)	2.417(14)
O(4)—La(3)	2.594(14)	O(5)—La(3)	2.586(14)
O(10)—La(3)	2.350(19)	O(11)—La(3)	2.315(16)
C(1)—O(1)	1.442(20)	C(2)—O(2)	1.451(27)
C(3)—O(3)	1.457(22)	C(4)—O(4)	1.461(20)
C(5)—O(5)	1.475(22)	C(6)—O(6)	1.409(23)
C(7)—O(7)	1.500(27)	C(8)—O(8)	1.449(29)
C(9)—O(9)	1.441(29)	C(10)—O(10)	1.423(32)
C(011)—O(11)	1.427(27)		

Table 4. Selected bond angles (°) for $[La_3(\mu_3\text{-}OBu^t)_2(\mu\text{-}OBu^t)_3(OBu^t)_4(Bu^tOH)_2]$

O(2)—La(1)—O(1)	140.9(4)	O(4)—La(1)—O(1)	73.9(5)
O(4)—La(1)—O(2)	74.4(5)	O(5)—La(1)—O(1)	73.3(5)
O(5)—La(1)—O(2)	73.2(5)	O(5)—La(1)—O(4)	65.9(4)
O(6)—La(1)—O(1)	105.1(5)	O(6)—La(1)—O(2)	107.0(5)
O(6)—La(1)—O(4)	110.4(5)	O(6)—La(1)—O(5)	176.2(4)
O(7)—La(1)—O(1)	107.1(5)	O(7)—La(1)—O(2)	102.8(5)
O(7)—La(1)—O(4)	175.3(4)	O(7)—La(1)—O(5)	109.8(5)
O(7)—La(1)—O(6)	73.9(5)	O(3)—La(2)—O(1)	137.0(4)
O(4)—La(2)—O(1)	71.0(4)	O(4)—La(2)—O(3)	72.1(5)
O(5)—La(2)—O(1)	72.0(4)	O(5)—La(2)—O(3)	72.4(5)
O(5)—La(2)—O(4)	63.9(4)	O(8)—La(2)—O(1)	106.6(5)
O(8)—La(2)—O(3)	105.1(5)	O(8)—La(2)—O(4)	168.4(5)
O(8)—La(2)—O(5)	104.5(6)	O(9)—La(2)—O(1)	100.5(5)
O(9)—La(2)—O(3)	110.6(5)	O(9)—La(2)—O(4)	106.5(6)
O(9)—La(2)—O(5)	169.0(4)	O(9)—La(2)—O(8)	85.1(7)
O(3)—La(3)—O(2)	139.3(4)	O(4)—La(3)—O(2)	72.8(5)
O(4)—La(3)—O(3)	73.2(5)	O(5)—La(3)—O(2)	72.6(5)
O(5)—La(3)—O(3)	72.8(5)	O(5)—La(3)—O(4)	64.1(4)
O(10)—La(3)—O(2)	106.6(6)	O(10)—La(3)—O(3)	103.4(6)
O(10)—La(3)—O(4)	170.7(5)	O(10)—La(3)—O(5)	106.7(6)
O(11)—La(3)—O(2)	101.9(5)	O(11)—La(3)—O(3)	108.3(5)
O(11)—La(3)—O(4)	105.6(5)	O(11)—La(3)—O(5)	169.2(4)
O(11)—La(3)—O(10)	83.7(7)	La(2)—O(1)—La(1)	101.0(5)
C(1)—O(1)—La(1)	129.9(11)	C(1)—O(1)—La(2)	129.1(11)
La(3)—O(2)—La(1)	99.7(5)	C(2)—O(2)—La(1)	130.0(11)
C(2)—O(2)—La(3)	130.1(10)	La(3)—O(3)—La(2)	102.1(5)
C(3)—O(3)—La(2)	127.0(13)	C(3)—O(3)—La(3)	130.9(12)
La(2)—O(4)—La(1)	94.2(4)	La(3)—O(4)—La(1)	94.4(4)
La(3)—O(4)—La(2)	93.3(4)	C(4)—O(4)—La(1)	123.8(10)
C(4)—O(4)—La(2)	122.6(11)	C(4)—O(4)—La(3)	120.8(10)
La(2)—O(5)—La(1)	94.4(4)	La(3)—O(5)—La(1)	93.6(4)
La(3)—O(5)—La(2)	94.6(4)	C(5)—O(5)—La(1)	120.3(10)
C(5)—O(5)—La(2)	123.4(12)	C(5)—O(5)—La(3)	123.0(12)
C(6)—O(6)—La(1)	175.1(10)	C(7)—O(7)—La(1)	167.5(12)
C(8)—O(8)—La(2)	178.7(14)	C(9)—O(9)—La(2)	177.0(13)
C(10)—O(10)—La(3)	173.7(15)	C(011)—O(11)—La(3)	178.9(13)

next smallest angle (173.7°) corresponds to La(3)—O(10), which on bond length considerations could be the other alcohol molecule. It is noteworthy that the LaOC angles in the bridging alkoxides are much smaller (μ_2, 127.0–130.1° and μ_3, 120.8–123.8°). In the absence of any clear cut evidence for the position of the second alcohol, we presume it is disordered, together with an alkoxy group, over sites O(10) and O(11).

All of the lanthanum atoms in **3** are in distorted octahedral coordination with each metal bonded to two terminal, two μ_2-bridging and two μ_3-bridging t-butoxide groups. The μ_3-bridging oxygen atoms cannot be involved in π-donation to the metals and it is significant that they are positioned *trans* to the strongly π-donating terminal oxygen atoms. The overall molecular structure of **3** is similar to that reported for $[Y_3Cl(OBu^t)_8(THF)_2]$ by Evans *et al.*[9] who were unable to remove the final chlorine atom in their synthetic procedure. Further work by Evans *et al.*[10] led to the isolation of $[Y_3Cl(OBu^t)_8(THF)_3][BPh_4]$ which contains the interesting trinuclear cation $[Y_3(\mu_3\text{-}Cl)(\mu_3\text{-}OBu^t)(\mu\text{-}OBu^t)_3(OBu^t)_3(THF)_3]^+$ which also has the same framework structure as **3**.

We believe that in solution compound **1** obtained in this research has the same structure as the lanthanum analogue **3**. Although we have grown a single crystal of **1**, the X-ray crystallographic analysis has so far been thwarted by disorder problems. Work is continuing on the X-ray structure determination for compounds **1** and **4**–**6**. It is interesting to note even the very bulky t-alkoxo groups, $OCMe_2Pr^i$, $OCMeEtPr^i$ and $OCEt_3$, result in the formation of dimeric yttrium and lanthanum trialkoxides. By using the bulky substituted phenoxo

ligand, 2,6-$Bu_2^tC_6H_3O$, Lappert *et al.*[8] have obtained the monomeric $[Y(OC_6H_3Bu_2^t)_3]$ compound which sublimed at 250–255°C/10^{-3} torr and is considerably less volatile than compounds **4–6** reported here. Clearly the gain in volatility expected to result from a monomeric species has been more than compensated for by the lowering in volatility caused by the increased number of atoms in the substituted phenoxo group. Work in progress suggests that enhanced volatility of the metal tris-t-alkoxides will be obtained by substituting CF_3 groups for CH_3 due to the anomalously weak intermolecular forces between fluoroalkyl groups.

EXPERIMENTAL

All operations were carried out under an atmosphere of purified N_2 using vacuum line, glove box and Schlenk-style apparatus. Solvents were dried over and distilled from sodium benzophenone and stored over molecular sieves. Bu^tOH was refluxed over sodium butoxide and distilled. Am^tOH, $Pr^i Me_2COH$, $Pr^iEtMeCOH$ and Et_3COH were dried first over molecular sieves, then the amount required for the reaction was put in excess benzene and finally dried azeotropically. The commercial yttrium and lanthanum chlorides were refluxed in $SOCl_2$ (freshly distilled from linseed oil) for 48 h. The $SOCl_2$ was then evaporated off *in vacuo* and the chlorides heated at 50°C for 20 h to remove residual traces of $SOCl_2$. Hexamethyldisilazane was purchased from Aldrich and dried over molecular sieves. Butyl lithium was used as purchased. The compounds $M\{N(SiMe_3)_2\}_3$ (M = Y or La) were prepared as previously described.[11]

NMR spectra were obtained using Bruker WP80FT, WM250FT and WH400FT spectrometers. Calibration was made using solvent signals from incomplete deuteration and made relative to TMS for ^1H and ^{13}C; ^{89}Y was relative to YCl_3. Mass spectra were obtained using a MS-902 EI mass spectrometer, recorded at 70 eV. IR spectra were obtained as Nujol mulls in the range 4000–200 cm^{-1} using a Perkin–Elmer FT 1720× spectrometer.

Microanalytical data on carbon and hydrogen were obtained from University College, London and from B.M.A.C. The metals were analysed gravimetrically as metal oxides.

Crystallography

Crystal data for **3**: $C_{44}H_{101}O_{11}La_3$, $M = 1223.0$, monoclinic space group $P2_1/a$, $a = 28.163(5)$, $b = 10.987(2)$, $c = 19.974(5)$ Å, $\alpha = \beta = 90$, $\gamma = 99.79°$, $V = 6090.49$ Å^3, $Z = 4$, $D_c = 1.33$ g cm^{-3}, $\mu(Mo\text{-}K_\alpha) = 21.2$ cm^{-1}. Data were collected at room temperature with an Enraf–Nonius CAD4 diffractometer and monochromated Mo-K_α radiation. The data were corrected for Lorentz, polarization and absorption effects. Full-matrix least-squares refinement of 514 parameters gave $R = 0.041$, $R_w = 0.037$ for 4170 unique, observed reflections from 7443 measured. The weighting scheme, $w = [\sigma^2(F_0)+]^{-1}$, gave acceptable agreement analyses. Atomic coordinates, full lists of bond lengths and angles, and thermal parameters have been deposited at the Cambridge Crystallographic Data Centre.

Preparation of $[Y_3(OBu^t)_9(Bu^tOH)_2]$ (1)

To $Y\{N(SiMe_3)_2\}_3$ (3.1 g) in benzene (85 cm^3) was added Bu^tOH (15 cm^3) and the solution was refluxed for 2 h. Solvent and $(Me_3Si)_2NH$ were then removed by evaporation *in vacuo* and the residue was crystallized from toluene giving white crystals (1.3 g, 67% yield based on yttrium, m.p. 171°C). Found: 25.0; C, 47.6; H, 9.4. Calc. for $[Y_3(OBu^t)_9(Bu^tOH)_2]$: Y, 24.9; C, 49.2; H, 9.5%. ^{13}C NMR ($C_6D_5CD_3$) at 298 K: δ 74.9, 72.2 ($OCMe_3$); 36.3, 34.3 (CH_3); at 233 K: δ 74.9, 72.5, 72.2, 72.1 ($OCMe_3$); 36.5, 36.3, 35.7, 34.0 (CH_3). ^{89}Y NMR (C_6D_6) at 310 K: δ 166.8. IR: 3420br, 1241m, 1207s, 1165m, 983s, 936s, 901s, 877m, 768m, 741w, 530s, 496s, 478s, 391m, 256s, 230w cm^{-1}.

A sample of **1** was heated *in vacuo* at 60–80°C until no more Bu^tOH remained. Found: Y, 2.85. $Y(OBu^t)_3$ requires: Y, 28.8%. Compound **1** appears to sublime at 235°C/10^{-2} torr with decomposition, yielding a white sublimate (47%, m.p. 240°C). Found: C, 39.6; H, 8.1. $Y(OBu^t)_3$ requires: C, 46.8; H, 8.8%.

Preparation of $[Y_3(OAm^t)_9(Am^tOH)_2]$ (2)

A solution of Am^tOH (6 cm^3) in benzene (40 cm^3) was added to a solution of $Y\{N(SiMe_3)_2\}_3$ (6.2 g) in benzene (160 cm^3) and left overnight. After removing solvent, $(Me_3Si)_2NH$ and excess Am^tOH by evaporation *in vacuo* the residue was recrystallized from Am^tOH (2.8 g, 63% based on yttrium, m.p. 84°C). Found: Y, 21.7. $Y_3(OAm^t)_9(Am^tOH)$ requires: Y, 21.7%. ^{13}C NMR (C_6D_6) at 297 K: δ 75.2 ($OCMe_2Et$); 40.7 (CCH_2Me); 31.3 (CCH_3); 11.2 (CCH_2CH_3); at 253 K ($C_6D_5CD_3$): 77.4, 77.0, 74.4 ($OCMe_2Et$); 41.4, 40.7, 39.5 (CCH_2Me); 31.3, 31.2, 29.6 (CCH_3); 12.1, 11.0, 10.8 (CCH_2CH_3). ^{89}Y NMR (C_6D_6) at 310 K: δ 199.1. IR: 3386br, 1360m, 1331w, 1316w, 1287w, 1227m, 1162s, 1151s, 1059m, 1017m, 981s, 949s,

935m, 890s, 878m, 793w, 735m, 534m, 512s, 480m, 464m, 390w, 305w, 242w, 235w, 228s, 225m cm^{-1}.

A sample of **2** was heated *in vacuo* at 70°C until no more Am^tOH remained. The white solid (m.p. 110°C) was analysed for $Y(OAm^t)_3$. Found: Y, 25.8. $Y(OAm^t)_3$ requires: Y, 25.4%. Compound **2** appeared to distil at 150°C/10^{-3} torr with decomposition, giving a glue-like condensate which could not be crystallized.

Preparation of $[La_3(OBu^t)_9(Bu^tOH)_2]$ **(3)**

To a solution of $La\{N(SiMe_3)_2\}_3$ (4.8 g) in benzene (150 cm^3) was added Bu^tOH (5 cm^3) and the solution was refluxed for 1 h and left overnight. After removing volatiles by evaporation *in vacuo*, the residue was crystallized from toluene (3.2 g, 100% based on lanthanum, m.p. 192°C). Found: La, 34.2; C, 42.3; H, 8.6. $[La_3(OBu^t)_9(Bu^tOH)_2]$ requires: La, 34.1; C, 43.2; H, 8.3%. ^{13}C NMR (C_6D_6) at 297 K: δ 73.7, 73.0, 71.6 ($OCMe_3$); 36.2, 35.5, 34.4 (CCH_3); at 253 K ($C_6D_5CD_3$): 73.4, 72.0, 70.8 ($OCMe_3$); 35.0, 34.6, 32.6 (CCH_3). IR: 3439br, 1378s, 1356s, 1349s, 1202s, 1022w, 972s, 936s, 911s, 889m, 826w, 746m, 513s, 488s, 457m, 379m, 353m, 229s, 226s cm^{-1}.

Preparation of $[Y(OCMe_2Pr^i)_3]$ **(4)**

Me_2Pr^iCOH (8 cm^3) in benzene (50 cm^3) was added to a solution of $Y\{N(SiMe_3)_2\}_3$ (8 g) in benzene (200 cm^3) and refluxed for 2 h and left overnight. After removal of the volatiles *in vacuo* the residue was distilled at 170°/10^{-3} torr (5.0 g, 91% based on yttrium, m.p. 161°C). Found: Y, 22.7; C, 53.4; H, 10.5. $Y(OCMe_2Pr^i)_3$ requires: Y, 22.7; C, 55.1; H, 10.0%. The compound dissolves readily in hydrocarbon solvents. ^{13}C NMR (C_6D_6) at 297 K: δ 76.5 ($OCMe_2Pr_i$); 41.2 ($CCHMe_2$); 30.1 (CCH_3); at 233 K ($C_6D_5CD_3$): 76.7, 41.2, 29.6, 19.4. ^{89}Y NMR ($C_6D_5CD_3$) at 310 K: δ 36.8. IR: 1366s, 1353m, 1321w, 1223m, 1175s, 1149s, 1103s, 1051s, 1010s, 947s, 923m, 911m, 869w, 852w, 795w, 714m, 574s, 558w, 532s, 478m, 429m, 378w, 359w, 300w, 254w, cm^{-1}.

Preparation of $[Y(OCMeEtPr^i)_3]$ **(5)**

Compound **5** was obtained from the reaction of $Y\{N(SiMe_3)_2\}_3$ (7 g) and $MeEtPr^iCOH$ (8 cm^3) in benzene, in the same manner as for **4**, as a white solid by sublimation at 170°C/10^{-3} torr (5.0 g, 94% based on yttrium, m.p. 196°C). Found: Y, 20.7; C, 53.8; H, 10.7. $Y(OCMeEtPr^i)_3$ requires: Y, 20.5; C, 58.0; H, 10.4%. Compound **5** dissolves readily in hydrocarbon solvents. ^{13}C NMR (C_6D_6) at 297 K: δ 80.0, 78.2 ($OCMeEtPr^i$); 38.4, 37.0 ($CCHMe_2$); 36.0, 35.3 (CCH_2Me); 26.9, 25.2 (CCH_3); 19.2, 19.0, 18.8, 18.7 ($CCHCH_3$); 10.2, 9.8 (CCH_2CH_3). ^{89}Y NMR ($C_6D_5CD_3$) at 310 K: δ 45.6. IR: 1362s, 1329m, 1313w, 1281w, 1202m, 1169s, 1147s, 1104s, 1063m, 1023s, 994s, 957m, 941s, 908s, 853m, 792w, 724m, 699m, 580m, 563s, 485m, 442m, 393w, 363w, 328w, 281w, cm^{-1}.

Preparation of $[Y(OCEt_3)_3]$ **(6)**

Compound **6** was prepared in the same manner as **4** and **5** from the reaction of $Y\{N(SiMe_3)_2\}_3$ (7 g) and Et_3COH (8 cm^3) in benzene, and the residual white solid was distilled at 225°C/10^{-2} torr (4.0 g, 75% based on yttrium, m.p. 198°C). Found: Y, 20.4; C, 55.8; H, 10.8. $Y(OCEt_3)_3$ requires: Y, 20.5; C, 58.0; H, 10.4%. Compound **6** dissolves readily in hydrocarbon solvents. ^{13}C NMR (C_6D_6) at 297 K: δ 80.2, 78.0 ($OCEt_3$); 33.7, 33.3 (CCH_2CH_3); 9.7 (CH_2CH_3). ^{89}Y NMR at 310 K: δ 47.8 (C_6D_6), 37.5 ($C_6D_5CD_3$). IR: 1344m, 1324m, 1295w, 1277w, 1259w, 1212m, 1158s, 1050s, 996s, 948s, 923m, 851w, 813w, 795w, 762w, 713m, 669w, 578m, 534s, 479m, 456w, 374m, 314w, 283w, cm^{-1}.

Preparation of $[La(OCMe_2Pr^i)_3]$ **(7)**

Pr^iMe_2COH (4.5 cm^3) in benzene (50 cm^3) was added to a solution of $La\{N(SiMe_3)_2\}_3$ (5.86 g) in benzene (150 cm^3), and after refluxing for 2 h was left overnight. After removal of volatiles *in vacuo* the residue was distilled at 135°C/10^{-3} torr (1.75 g, 42% based on lanthanum, m.p. 119°C). Found: La, 31.9. $La(OCMe_2Pr^i)_3$ requires: La, 31.4%. ^{13}C NMR (C_6D_6) at 297 K: δ 77.2 ($OCMe_2Pr^i$); 40.5 ($CCHMe_2$); 28.6 (CCH_3); 19.4 ($CHCH_3$); at 233 K ($C_6D_5CD_3$): δ 29.7, 29.1 (CCH_3); 19.9, 19.4 ($CHCH_3$). IR: 1308w, 1235vw, 1189m, 1169s, 1146s, 1099s, 1061w, 985s, 974s, 945m, 927m, 905m, 858m, 800w, 706w, 552m, 513m, 492m, 437w, 388w, 312w, cm^{-1}.

Preparation of $[La(OCMeEtPr^i)_3]$ **(8)**

Compound **8** was prepared in the same manner as **7** from the reaction of $La\{N(SiMe_3)_2\}_3$ (4.41 g) and $MeEtPr^iCOH$ (4 cm^3) in benzene and the residual white solid was distilled at 150°C/10^{-3} torr (2.1 g, 61% based on lanthanum, m.p. 112°C). Found, La, 29.5; C, 49.8; H, 9.4. $La(OCMeEtPr^i)_3$ requires: La, 28.7; C, 52.1; H, 9.4%. ^{13}C NMR (C_6D_6) at 297 K: δ 79.7 ($OCMeEtPr^i$); 38.6 ($CHMe_2$); 35.5 (CCH_2Me); 26.0 ($OCCH_3$); 19.1, 19.0 ($CHCH_3$); 10.1 (CH_2CH_3). IR: 1361s, 1327w, 1279w, 1259w, 1181s, 1165s, 1147s, 1102s, 1035m,

1007s, 953m, 932s, 911s, 851w, 787w, 715m, 694w, 574m, 557w, 516s, 437w, 416w, 392w, 330w, 233w, cm^{-1}.

Preparation of $[Y_3(OBu^t)_9(THF)_2]$ (**9**)

A sample of **1** was dissolved in THF, refluxed for 1 h and left overnight. After evaporation of the volatiles *in vacuo* the residue was redissolved in THF and compound **9** crystallized out. Found: Y, 24.5; C, 44.9; H, 8.9. $[Y_3(OBu^t)_9(THF)_2]$ requires: Y, 24.9; C, 49.4; H, 9.1%. On heating *in vacuo* at 70°C the THF was pumped off. Compound **9** begins melting at 142°C with decomposition. ^1H NMR ($C_6D_5CD_3$) at 303 K: δ 3.59, 1.88, 1.68, 1.52, 1.46; at 273 K: 3.59 (THF), 1.92, 1.78, 1.72, 1.70, 1.53, 1.52, 1.49, 1.43 (THF). IR: 1354m, 1239m, 1207s, 1075w, 1002s, 985m, 935m, 903m, 876w, 767w, 528m, 497m, 481m, 391w, 256m, 230m, cm^{-1}.

Reaction of **1** *with pyridine*

A sample of **1** was dissolved in pyridine and left overnight. After evaporating off the volatiles *in vacuo* the residue was crystallized from toluene and recrystallized from pentane to give colourless crystals (m.p. 118°C). Found: Y, 26.2; C, 48.3; H, 8.2; N, 2.5. Calc. for $Y_3(OBu^t)_9(C_5H_5N)_2$: Y, 24.6; C, 51.0; H, 8.5; N, 2.6%. ^1H NMR (C_6D_6) at 297 K: δ 9.25, 7.00, 6.81 (multiplets, 2H, 1H, 2H, C_5H_5N); 1.55 (singlet, 28H, $OCCH_3$).

Addition of NMe_3 *to* **1**

(a) Trimethylamine (3.5 cm^3) was condensed at −90°C onto **1** (1.24 g) and allowed to warm to 0°C. After 1 h at 0°C the volatiles were evaporated off *in vacuo* and **1** was recovered unchanged.

(b) NMe_3 (11 cm^3) was condensed onto **1** in toluene (20 cm^3) and allowed to warm to 0°C. After 2 h at 0°C it was kept at −20°C for a further 60 h and the volatiles then evaporated off *in vacuo*. The residue was unchanged (**1**).

Acknowledgements—We thank SERC for support, Mr G. Coumbarides and Mr P. Haycock for NMR spectra, Mr P. Cook for mass spectra and Mr Ian Harding for mounting the single crystal of **3**. We also acknowledge the use of the University of London Intercollegiate Research Service (ULIRS) 400 MHz NMR spectrometer.

REFERENCES

1. D. C. Bradley and M. M. Faktor, *Chem. Ind.* 1958, 1332.
2. K. S. Mazdiyasni, C. T. Lynch and J. S. Smith, *Inorg. Chem.* 1965, **4**, 342.
3. L. M. Brown and K. S. Mazdiyasni, *Inorg. Chem.* 1970, **9**, 2783.
4. D. C. Bradley, R. C. Mehrotra and D. P. Gaur, *Metal Alkoxides*. Academic Press, London (1978).
5. L. G. Hubert-Pfalzgraf, *New J. Chem.* 1987, 662; D. C. Bradley, *Chem. Rev.* 1989, **89**, 1317.
6. D. C. Bradley, H. Chudzynska, D. M. Frigo, M. B. Hursthouse and M. A. Mazid, *J. Chem. Soc., Chem. Commun.* 1988, 1258; D. C. Bradley, H. Chudzynska, D. M. Frigo, M. E. Hammond, M. B. Hursthouse and M. B. Mazid, *Polyhedron* 1990, **9**, 719.
7. O. Poucelet, W. J. Sartain, L. G. Hubert-Pfalzgraf, K. Foltins and K. G. Caulton, *Inorg. Chem.* 1989, **28**, 263.
8. P. B. Hitchcock, M. F. Lappert and A. Singh, *J. Chem. Soc., Chem. Commun.* 1983, 1499; P. B. Hitchcock, M. F. Lappert and R. G. Smith, *Inorg. Chim. Acta* 1987, **139**, 183; W. J. Evans, J. M. Olofson and J. W. Ziller, *Inorg. Chem.* 1989, **28**, 4309.
9. W. J. Evans, M. S. Sollberger and T. P. Hanusa, *J. Am. Chem. Soc.* 1988, **110**, 1841.
10. W. J. Evans and M. S. Sollberger, *Inorg. Chem.* 1988, **27**, 4417; W. J. Evans, J. M. Olofson and J. W. Ziller, *J. Am. Chem. Soc.* 1990, **112**, 2308.
11. D. C. Bradley, J. S. Ghotra and F. A. Hart, *J. Chem. Soc., Dalton Trans.* 1973, 1021.
12. M. J. McGeary, P. S. Coan, K. Folting, W. E. Streib and K. G. Caulton, *Inorg. Chem.* 1989, **28**, 3284.
13. D. C. Bradley and J. D. Swanwick, *J. Chem. Soc.* 1958, 3207; 1959, 748.
14. O. Poncelet, L. G. Hubert-Pfalzgraf, J. C. Daran and R. Astier, *J. Chem. Soc. Chem. Commun.* 1989, 1846.

Polyhedron Vol. 10, No. 10, pp. 1061–1068, 1991
Printed in Great Britain

0277–5387/91 $3.00+.00
© 1991 Pergamon Press plc

CHIRAL NITROGEN LIGANDS IN LATE TRANSITION METAL-CATALYSED ASYMMETRIC SYNTHESIS—I. ADDRESSING THE PROBLEM OF LIGAND LABILITY IN RHODIUM-CATALYSED HYDROSILATIONS

MICHAEL E. WRIGHT* and STEVEN A. SVEJDA

Department of Chemistry and Biochemistry, Utah State University, Logan, UT 84322-0300, U.S.A.

(*Received* 2 *November* 1990; *accepted* 21 *January* 1991)

Abstract—Treatment of 2,6-dichloropyridine with the potassium salt of ephedrine derivatives afforded the new chiral ligands 2-chloro-6-[(1*R*,2*S*)-2-(R_2N)-1-phenylpropanoxy] pyridine [NR_2 = NH_2 (**1a**), NHMe (**1b**), NMe_2 (**1c**)] in good yield. The isomeric and new ligands 2-(X)-[(1*R*,2*S*)-2-amino-1-phenylpropanoxy]pyridine [X = 3-chloro (**2**); X = 5-chloro (**3**); X = 5-trifluoromethyl (**4**)] were also prepared in the study. Combining ligand **1a** with $[(COD)RhCl]_2$ gave rapid addition and the isolable rhodium(I) complex, (COD)[**1a**]RhCl (**5a**). Complex **5a** provided the highest enantioselectivity to date for the asymmetric hydrosilation of acetophenone (30% enantioselectivity, 78% chemical yield) using a nitrogen-based, chiral, bidentate ligand in a stoichiometric fashion. Ligands **1b–c** and 2-[(1*R*,2*S*)-2-amino-1-phenylpropanoxy]pyridine (**1d**) gave low optical yields for the asymmetric hydrosilation of acetophenone. Ligands **2–4** gave enantioselectivity ranging from 10 to 23% (~1.1 : 1, ligand/rhodium) and similar chemical yields as **1a** for the hydrosilation of acetophenone. Employing a 10-fold excess of ligands **2–4** afforded enantioselectivity of 37–42% for the hydrosilation of acetophenone. The success of ligands **1a** and **2–4** as compared with **1d** (4% optical yield) and other bidentate nitrogen-based ligands is attributed to the increased π-acidity of the pyridine ring as a result of the electron-withdrawing substituents.

The asymmetric catalytic hydrogenation[1] and hydrosilation[2] of the carbonyl group is a valuable synthetic method for the synthesis of chiral alcohols.[3] Asymmetric hydrosilation of ketones can be very chemoselective for the carbonyl functional group and thus complements the hydrogenation reaction which shows preferential reactivity towards alkenes. In the early 1970s the research groups of Kumada,[4a] Kagan[4b] and Ojima[4c] and co-workers pioneered the development of the transition metal-catalysed asymmetric hydrosilation of ketones. Continued efforts in the transition metal-catalysed asymmetric hydrosilation for the 1970s focused on the use of chiral phosphorus-based ligands. In 1982, Brunner and co-workers developed rhodium catalysts employing nitrogen-based ligands which showed a significant increase in optical yield relative to all phosphorus ligands developed at that time (Chart 1).[5] A requisite for high enentioselectivity with nitrogen-based ligands has been a large ligand/metal ratio (~5–13).[6] A recently developed chiral terdentate ligand (Chart 1) by Nishiyama and co-workers[7] gave the first significant optical yield (56%) for a nitrogen-based ligand when employed in a stoichiometric fashion. However, for optimum performance the use of excess ligand (4–8, ligand/rhodium) was still necessary and the "assistance" of a Lewis acid (e.g. AgX, X = OSO_2CF_3 and BF_4) was always required. A very attractive feature of nitrogen-based ligands is that the chirality is usually derived from the inexpensive and readily available pool of optically pure amines.

Even with well over 200 chiral bidentate nitrogen-based ligands[8] synthesized in the last decade, not once has the problem of ligand lability been addressed. Instead the issue has been side-stepped by applying Le Chatelier's principle. In the present

*Author to whom correspondence should be addressed.

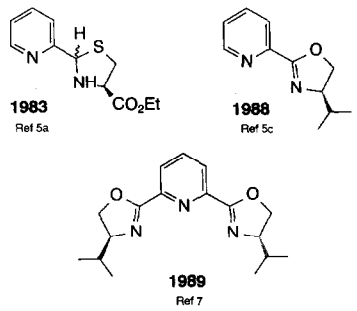

Chart 1.

study we demonstrate that there are options to employing excess ligand. By simply tailoring the π-acceptor character of the nitrogen-based ligand it is possible to overcome the necessity of a high ligand/rhodium ratio.

RESULTS AND DISCUSSION

Ligand preparations

We recently developed the efficient synthesis of chiral 6-alkoxy-2-bromopyridines and utilized these materials to prepare a variety of chiral bis(6-alkoxy-2-pyridyl)silane and -methanol ligands.[9] In an analogous manner, treatment of 2,6-dichloro- or 2-chloropyridine with the potassium salt of three ephedrine derivatives afforded compounds **1a–d** [eq. (1)].[10]

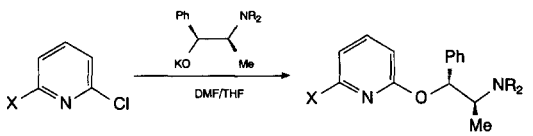

(1)

1a, X = Cl, NR_2 = NH_2
1b, X = Cl, NR_2 = NHMe
1c, X = Cl, NR_2 = NMe_2
1d, X = H, NR_2 = NH_2

Ligands **2–4** were also prepared in reasonable yield from the appropriate chloropyridine derivative and the norephedrine potassium alkoxide. The ligands were obtained as light brown oils after flash chromatography on silica gel. In certain cases the ligands were converted to their monohydrochloride salts to obtain analytically pure samples.

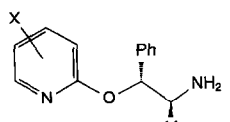

2, X = 3-chloro
3, X = 5-chloro
4, X = 5-trifluoromethyl

Catalytic applications—hydrosilation of acetophenone

Treatment of **1a** with $[(COD)RhCl]_2$[11] produced the addition product **5a** as an air-stable, light yellow solid. Complex **5a** gave analytical and NMR data consistent with a mononuclear rhodium(I) complex. Complex **5a** was found to efficiently catalyse the hydrosilation of acetophenone in 30% enantioselectivity without the addition of free ligand or a co-factor (Scheme 1,[12] Table 1, entry 1). The significance of this result is amplified in light of that *no other bidentate nitrogen-based ligand has ever afforded higher than a 6% optical yield when used in a stoichiometric fashion.* Notably the *in situ* generation of the catalyst is less efficient than using the preformed rhodium(I) complex **5a** (Table 1, entry 3).

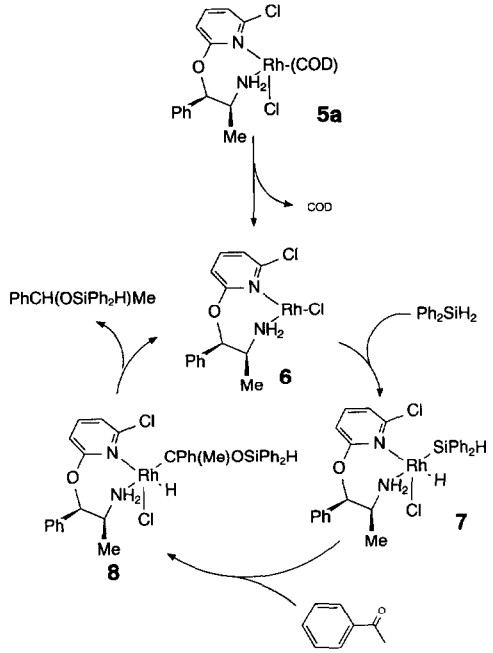

Scheme 1.

Utilization of ligands **1b–c** to generate the catalysts *in situ* afforded much lower optical yields (Table 1, entries 6 and 7). The amine coordination is clearly a requisite to bring the chirality of the ligand in close proximity to the metal centre and also in forming a conformationally rigid ligand environment. The poor results obtained with ligands **1b–c** are likely a consequence of added steric interactions of the N-methyl group(s) in the chelate ring and with substituents on the metal centre.

The integrity of the catalytic system throughout the reaction period is supported by measuring the optical yield of 1-phenylethanol as a function of reaction progress. The relatively constant optical yield ($30 \pm 2\%$) vs reaction progress measured is consistent with the chiral catalytic species remaining intact throughout the entire reaction period. The catalyst stability is limited since at the higher

Table 1. Results for the asymmetric hydrosilation of acetophenone utilizing ligands **1a–d**[a]

Entry	ligand	Substrate/Rh ratio	Ligand/Rh ratio	*ee* (%)	Chemical yield (%)
1	**1a**	100:1[b]	1:1	30 (*S*)	78
2		400:1[b]	1:1	21 (*S*)	75
3		100:1	1.1:1	23 (*S*)	85
4		100:1[c]	1:1	0	65
5		100:1	1.1:1[d]	7 (*S*)	86
6	**1b**	100:1	5:1	0	81
7	**1c**	100:1	5:1	0	87
8	**1d**	100:1	1.2:1	4 (*S*)	77

[a] Catalyst generated *in situ* except where noted, see Experimental for precise experimental conditions.
[b] Precatalyst **5a** was employed.
[c] $[(CO)_2RhCl]_2$ was used as the rhodium(I) source.
[d] Reaction run at 20°C.

substrate/catalyst ratio of 400 we obtain a notably lower optical yield.

The low optical yield for ligand **1d** is an intriguing result. On the basis of steric arguments we would anticipate ligand **1d** to chelate stronger than **1a**. To explore the reasons behind the success of ligand **1a** we synthesized ligands **2–4** and evaluated these ligands in the hydrosilation of acetophenone (Table 2). The results clearly demonstrate that the *electron-withdrawing character of the substituent is a key factor*. Substituents in the 5-position produce a trend in optical yield vs the Hammett σ values which suggests that the electron-withdrawing character of the substituent is controlling the ligand's ability to transfer chirality.

It is well known that for low valent transition metals (i.e. Rh^1) d–π backbonding becomes an important factor in the coordination of bipyridine and related ligands.[13] This may indeed be why all the chiral, nitrogen-based, bidentate and even the terdentate ligands suffer lability problems with the soft and low-valent rhodium(I) metal. The rhodium(I) complex can either lose COD (to generate complex **6**) or the nitrogen ligand to generate the *achiral* species **9** (Scheme 2). The latter catalyst will of course carry out the hydrosilation chemistry producing a racemic product. We have measured the relative rate of hydrosilation for $[(COD)RhCl]_2$ against **5a** and found that the former is considerably faster than **5a** ($k_1 \approx 10 \times k_2$). Additional evidence that such an equilibrium is operative is found by increasing the ligand/rhodium ratio and observing not only that the enantioselectivity increased (37–42%), but more importantly, became nearly the

Table 2. Results for the asymmetric hydrosilation of acetophenone employing ligands **2–4**[a]

Entry	ligand	Substrate/Rh ratio	Ligand/Rh ratio	*ee* (%)	Chemical yield (%)
1	**2**	100:1	1.1:1	14 (*S*)	77
2		100:1	10:1	37 (*S*)	88
3	**3**	100:1	1.1:1	10 (*S*)	87
4		100:1	10:1	42 (*S*)	86
5	**4**	100:1	1.1:1	23 (*S*)	75
6		100:1	10:1	40 (*S*)	88
7	**4(i)**	100:1	1.1:1	1 (*S*)	79
8		100:1	10:1	1 (*R*)	78

[a] All reactions were performed at 0°C in dichloromethane. For specific experimental details see the Experimental under Hydrosilation of acetophenone.

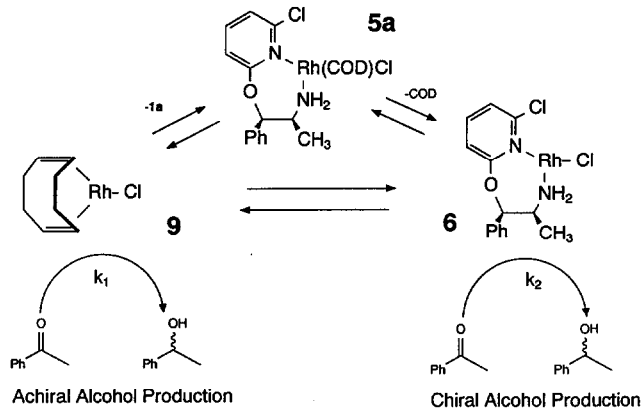

Scheme 2.

same for ligands **2**–**4**. These data would suggest that electronic factors do not affect the optical yield through ligand conformation but rather through controlling the relative concentrations of the active catalysts **6** and **9**.

Molecular modelling of the rhodium catalyst

Molecular mechanics analysis of the proposed catalytic intermediates has been performed using BIOGRAPH (Version 2.0) on an Ardent supercomputing system. We chose to model complex **7** which is the proposed catalytic intermediate responsible for *re* and *si* face selectivity (Fig. 1). Configuration **A** was found to be the lowest energy structure with all other variations being significantly less stable. As suggested by a reviewer we also approached the minimization by supplying a tremendous amount of internal vibrational energy (temperature = 600 K) to the system and then returning to normal (i.e. 273 K). This latter procedure produced conformation **A** as well. On the premise that **A** is responsible for the observed product, then approach of the ketone would be affected by the *axial*-methyl group. The *equatorial*-phenyl group appears to be important for "locking" the ring conformation.

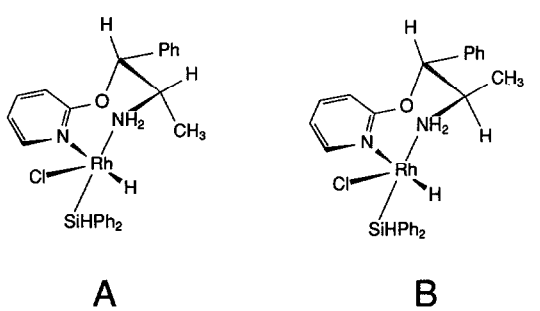

Fig. 1. Drawings illustrating the seven-membered chelate ring for the norephedrine ligands based on molecular mechanics. Structure **A** utilizes the (1*R*,2*S*)-norephedrine ligand and conformation **B** uses the diastereomeric ligand (1*R*,2*R*)-norephedrine.

To test the importance of the *axial*-methyl group in the transmittal of asymmetry we prepared **4(i)**, a diastereoisomer of **4**. As anticipated structure **B** was calculated to be more stable than **A** because both substituents in the chelate ring are equatorial. Utilization of **4(i)** in the hydrosilation of acetophenone gave only a 1% optical yield of 1-phenylethanol even at the high ligand/rhodium ratio of 10 (Table 2). This result confirms the importance of the *axial*-methyl group in the stereochemical outcome of the reaction and suggests a means for modifying and improving ligand performance.

Concluding remarks

Through the synthesis and utilization of a new class of ligands in the rhodium-catalysed hydrosilation of acetophenone we have substantially improved the enantioselectivity for the stoichiometric use of chiral, nitrogen-based, bidentate ligands. The success of our ligands was due to the incorporation of electron-withdrawing groups in the pyridine ring leading to an increase in the π-acidity. This in turn enhanced ligand binding to the soft and low-valent rhodium(I) centre and decreased the concentration of any achiral rhodium catalysts. Modelling of the catalytic systems combined with the synthesis of a diastereomeric analogue provided evidence that the *axial*-methyl group in the chelate ring is crucial for asymmetric induction. Future efforts in our research program will involve the development of chiral nitrogen ligands with a combination of enhanced π-acidity and strong σ-donating capabilities.

EXPERIMENTAL

General

All manipulations of compounds and solvents were carried out by using standard Schlenk techniques. Solvents were degassed and purified by distillation under nitrogen from standard drying agents. Spectroscopic measurements utilized the following instrumentation: ^{1}H NMR, Varian XL 300; ^{13}C NMR, Varian XL 300 (at 75.4 MHz). NMR chemical shifts are reported in δ vs Me_4Si in ^{1}H NMR and assigning the $CDCl_3$ resonance at 77.00 ppm and the DMSO-d_6 resonance at 39.50 ppm in ^{13}C NMR spectra. Optical rotations were measured at ambient temperature (20 ± 1°C) on a Perkin–Elmer 241 polarimeter using the sodium *D*-line. The polarimeter was calibrated using (*R*)-1-phenylethanol (Lancaster Synthesis) by measuring several dichloromethane solutions at concentrations in the range of those prepared from reactions. The (1*R*,2*S*)-(−)-norephedrine, (1*R*,2*R*)-(−)-norpseudoephedrine hydrochloride, (1*R*,2*S*)-(−)-ephedrine, (1*R*,2*S*)-(−)-N-methylephedrine and $[(CO)_2RhCl]_2$ were purchased from Aldrich Chemical Company and used as received. The 2,3-, 2,5- and 2,6-dichloropyridines and 2-chloro-5-trifluoromethylpyridine were purchased from Lancaster Synthesis. The $[(COD)RhCl]_2$ was prepared by the literature method.[11] The acetophenone was distilled from barium oxide and the diphenylsilane was distilled from calcium hydride prior to use and stored under nitrogen. Elemental analyses were performed at Atlantic Microlab Inc., Norcross, Georgia.

Preparation of **1a–d**

Potassium alkoxides were prepared by treatment of the appropriate alcohol with potassium metal in THF for 48 h under reflux. The potassium alkoxide THF solution was transferred by cannulation to a DMF (100 cm^3) solution of 2,6-dichloropyridine (5.92 g, 40 mmol) at 20°C. The mixture was allowed to react for 60 min, then was poured on to water and extracted with ether (2×150 cm^3). The organic layers were combined and washed with brine and then dried over potassium carbonate. Removal of the solvent under reduced pressure afforded compounds **1a–d** in > 82% crude yield. Ligand **1a** was purified by chromatography on silica gel eluting with ethyl acetate/hexanes (1 : 19, v/v) (oil, 50%). Ligand **1b** was purified by chromatography on silica gel eluting with methanol/dichloromethane (1 : 9, v/v) (oil, 46%). Ligand **1c** was flash-columned on alumina (MPLC grade, neutral, non-activated) with ethyl acetate/hexanes (1 : 9, v/v) (oil, 40%).

2-*Chloro*-6-[(1R,2S)-2-*amino*-1-*phenylpropanoxy*] *pyridine* (**1a**)

$[\alpha]^{20}$ −2.84° (c = 0.0193, CH_2Cl_2); ^{1}H NMR ($CDCl_3$): δ 7.45 (dd, J = 8.1, 7.5 Hz, 1H, py H4), 7.43–7.24 (m, 5H, phenyl H's), 6.81 (dd, J = 7.5, 0.6 Hz, 1H, py), 6.67 (dd, J = 8.1, 0.6 Hz, 1H, py), 5.80 (d, J = 5.6 Hz, 1H, C*H*OPh), 3.39 (apparent quintet, J = 6.3 Hz, 1H, C*H*NMe), 1.29 (br s, 2H, N*H*$_2$), 1.15 (d, J = 6.6 Hz, 3H, C*H*$_3$); ^{13}C NMR ($CDCl_3$): δ 162.7 (py C6), 148.2 (py C2), 140.7 (py CH), 138.1 (phenyl C), 128.2, 127.8, 127.5 (phenyl CH's), 116.5, 109.2 (py CH's), 82.1 (*C*HOPh), 51.0 (*C*HNMe), 19.1 (*C*H$_3$). Found: C, 64.0; H, 5.8. Calc. for $C_{14}H_{15}ClN_2O$: C, 64.0; H, 5.7%.

2-*Chloro*-6-[(1R,2S)-2-(*methylamino*)-1-*phenylpropanoxy*]*pyridine* (**1b**)

$[\alpha]^{20}$ −2.35°C (c = 0.0222, CH_2Cl_2); ^{1}H NMR ($CDCl_3$): δ 7.48 (dd, J = 8.2, 7.5 Hz, 1H, py H4), 7.41–7.23 (m, 5H, phenyl H's), 6.83 (dd, J = 7.5, 0.7 Hz, 1H, py), 6.70 (dd, J = 8.2, 0.7 Hz, 1H, py), 6.09 (d, J = 4.9 Hz, 1H, C*H*OPh), 3.03 (dq, J = 6.5, 4.9 Hz, 1H, C*H*NMe), 2.46 (s, 3H, NHC*H*$_3$), 1.57 (br s, 1H, N*H*CH$_3$), 1.13 (d, J = 6.5 Hz, 3H, C*H*$_3$); ^{13}C NMR ($CDCl_3$): δ 162.8 (py C6), 148.2 (py C2), 140.6 (py CH), 138.9 (phenyl C), 128.2, 127.5, 126.9 (phenyl CH's), 116.5, 109.1 (py CH's), 78.8 (*C*HOPh), 59.4 (*C*HNMe), 33.9 (N*C*H$_3$), 15.1 (*C*H$_3$). Found: C, 65.0; H, 6.2. Calc. for $C_{15}H_{17}ClN_2O$: C, 65.1; H, 6.2%.

2-*Chloro*-6-[(1R,2S)-2-(*dimethylamino*)-1-*phenylpropanoxy*]*pyridine* (**1c**)

$[\alpha]^{20}$ −1.95° (c = 0.0206, CH_2Cl_2); ^{1}H NMR ($CDCl_3$) δ 7.47 (apparent t, J = 7.8 Hz, 1H, py H4), 7.36–7.20 (m, 5H, phenyl H's), 6.82 (d, J = 7.6 Hz, 1H, py), 6.69 (d, J = 7.8 Hz, 1H, py), 6.26 d, J = 4.3 Hz, 1H, C*H*OPh), 2.94 (dq, J = 6.8, 4.3 Hz, 1H, C*H*NMe), 2.35 [s, 6H, N(C*H*$_3$)$_2$], 1.13 (d, J = 6.8 Hz, 3H, C*H*$_3$); ^{13}C NMR ($CDCl_3$): δ 162.5 (py C6), 148.3 (py C2), 140.6 (py CH), 128.1, 127.1, 126.5 (phenyl CH's), 116.5, 109.4 (py CH's), 77.0 (*C*HOPh), 64.4 (*C*HNMe), 41.7 (N(*C*H$_3$)$_2$), 9.5 (*C*H$_3$). Found: C, 66.2; H, 6.6. Calc. for $C_{16}H_{19}ClN_2O$: C, 66.1; H, 6.6%.

2-[(1R,2S)-2-*amino*-1-*phenylpropanoxy*]*pyridine* (**1d**)

$[\alpha]^{20}$ −1.00° (c = 0.0258, CH_2Cl_2); ^{1}H NMR ($CDCl_3$): δ 8.07–8.04 (m, 1H, py H6), 7.57–7.51 (m,

1H, py H4), 7.42–7.23 (m, 5H, phenyl H's), 6.82–6.78 (m, 2H, py), 5.89 (d, $J = 5.1$ Hz, 1H, C*H*OPh), 3.44–3.36 (m, 1H, C*H*NMe), 1.54 (br s, 2H, NH_2), 1.14 (d, $J = 6.6$ Hz, 3H, CH_3); ^{13}C NMR ($CDCl_3$): δ 163.1 (py C2), 146.9 (py C6), 138.7 (phenyl C), 138.6 (py CH), 128.1, 127.5, 127.2 (phenyl CH's), 116.9, 111.3 (py CH's), 81.0 (*C*HOPh), 51.4 (*C*HNMe), 18.9 (*C*H_3). Final purification was achieved by chromatography on activated neutral alumina using methanol/dichloromethane (1:4, v/v) as eluant (15% purified yield). The purified compound was dried (63°C, 0.05 torr, 36 h); however, spectroscopic (^{1}H NMR) analysis indicated 1.4 equiv. of methanol remained in the dried sample (white solid, m.p. 56–60°C). Found: C, 72.5; H, 7.1. Calc. for $C_{14}H_{16}N_2O \cdot 1/4CH_3OH$: C, 72.5; H, 7.3%.

Preparation of **2–4**

Ligands **2–4** were prepared by a procedure analogous to **1a–d**. Crude **2–4** were purified by chromatography on silica gel eluting with methanol/dichloromethane (1:9, v/v) (**2**: oil, 48%; **3**: oil, 40%; **4**: oil, 49%).

3-*Chloro*-2-[(1R,2S)-2-*amino*-1-*phenylpropanoxy*] *pyridine* (**2**)

$[\alpha]^{20}$ +0.94° ($c = 0.0216$, CH_2Cl_2); ^{1}H NMR ($CDCl_3$): δ 7.89 (d, $J = 4.9$ Hz, 1H, py H6), 7.60 (d, $J = 7.7$ Hz, 1H, py H4), 7.44–7.24 (m, 5H, phenyl H's), 6.75 (dd, $J = 7.7$, 4.9 Hz, 1H, py H5), 6.03 (d, $J = 2.6$ Hz, 1H, C*H*OPh), 3.49–3.41 (m, 1H, C*H*NMe), 2.06 (br s, 2H, NH_2), 1.16 (d, $J = 6.6$ Hz, 3H, CH_3); ^{13}C NMR ($CDCl_3$): δ 158.3 (py C6), 144.6 (py C4), 138.3, 138.1, 128.1 (2 C's), 127.6, 127.1, 118.7, 117.5, 81.6 (*C*HOPh), 51.4 (*C*HNMe), 18.3 (*C*H_3).

{3-*Chloro*-2-[(1R,2S)-2-*amino*-1-*phenylpropanoxy*] *pyridine*} · HCl

Melting point, 171–174°C; ^{1}H NMR ($CDCl_3$): δ 8.86 (br s, 3H, NH_3), 7.87 (dd, $J = 5.0$, 1.7 Hz, 1H, py H6), 7.61 (dd, $J = 7.7$, 1.7 Hz, 1H, py H4), 7.57–7.53 (m, 2H, phenyl H's), 7.38–7.25 (m, 3H, phenyl H's), 6.75 (dd, $J = 7.7$, 5.0 Hz, 1H, py H5), 6.38 (d, $J = 2.4$ Hz, 1H, C*H*OPh), 3.78 (m, 1H, C*H*NMe), 1.36 (d, $J = 6.8$ Hz, 3H, CH_3). Found: C, 55.6; H, 5.4. Calc. for $C_{14}H_{16}Cl_2N_2O$: C, 56.2; H, 5.4%.

5-*Chloro*-2-[(1R,2S)-2-*amino*-1-*phenylpropanoxy*] *pyridine* (**3**)

$[\alpha]^{20}$ −1.29° ($c = 0.0193$, CH_2Cl_2); ^{1}H NMR ($CDCl_3$): δ 7.97 (d, $J = 2.7$ Hz, 1H, py H6), 7.48 (dd, $J = 8.8$, 2.7 Hz, 1H, py H4), 7.39–7.23 (m, 5H, phenyl H's), 6.75 (d, $J = 8.8$ Hz, 1H, py H3), 5.80 (d, $J = 5.4$ Hz, 1H, C*H*OPh), 3.42–3.34 (m, 1H, C*H*NMe), 1.52 (br s, 2H, NH_2), 1.14 (d, $J = 6.6$ Hz, 3H, CH_3); ^{13}C NMR ($CDCl_3$): δ 161.4 (py C2), 145.2 (py C6), 138.5 (phenyl C), 138.3 (py C4), 128.1, 127.7, 127.2 (phenyl C's), 124.1, 112.2 (py C's), 81.7 (*C*HOPh), 51.2 (*C*HHNMe), 18.9 (*C*H_3).

{5-*Chloro*-2-[(1R,2S)-2-*amino*-1-*phenylpropanoxy*] *pyridine*} · HCl

Melting point, 208–209°C; ^{1}H NMR ($CDCl_3$): δ 8.78 (br s, 3H, NH_3), 7.83 (d, $J = 2.7$ Hz, 1H, py H6), 7.44 (dd, $J = 8.8$, 2.7 Hz, 1H, py H4), 7.40–7.29 (m, 5H, phenyl H's), 7.01 (d, $J = 8.8$ Hz, 1H, py H3), 6.23 (d, $J = 2.6$ Hz, 1H, C*H*OPh), 3.58 (m, 1H, C*H*NMe), 1.23 (d, $J = 6.8$ Hz, 3H, CH_3). Found: C, 56.1; H, 5.4. Calc. for $C_{14}H_{16}Cl_2N_2O$: C, 56.2; H, 5.4%.

5-(*Trifluoromethyl*)-2-[(1R,2S)-2-*amino*-1-*phenylpropanoxy*]*pyridine* (**4**)

$[\alpha]^{20}$ −1.07° ($c = 0.0230$, CH_2Cl_2); ^{1}H NMR ($CDCl_3$): δ 8.33 (d, $J = 2.4$ Hz, 1H, py H6), 7.74 (dd, $J = 8.8$, 2.4 Hz, 1H, py H4), 7.42–7.28 (m, 5H, phenyl H's), 6.88 (d, $J = 8.8$ Hz, 1H, py H3), 5.92 (d, $J = 5.7$ Hz, 1H, C*H*OPh), 3.41 (apparent quintet, $J = 6.6$ Hz, 1H, C*H*NMe), 1.21 (br s, 2H, NH_2), 1.16 (d, $J = 6.6$ Hz, 3H, CH_3); ^{13}C NMR ($CDCl_3$): δ 165.2 (py C2), 144.9 (q, $^3J_{C-F} = 4.5$ Hz, py C6), 138.1 (phenyl C), 135.8 (q, $^3J_{C-F} = 3.1$ Hz, py C4), 128.2, 127.9, 127.3 (phenyl C's), 123.9 (q, $^1J_{C-F} = 271$ Hz, *C*F_3), 120.0 (q, $^2J_{C-F} = 33$ Hz, py C5), 111.4 (py C3), 82.1 (*C*HOPh), 51.1 (*C*HNMe), 19.2 (*C*H_3).

{5-(*Trifluoromethyl*)-2-[(1R,2S)-2-*amino*-1-*phenylpropanoxy*]*pyridine*} · HCl

Melting point, 201–202°C; ^{1}H NMR ($CDCl_3$): δ 8.78 (br s, 3H, NH_3), 8.17 (s, 1H, py H6), 7.69 (dd, $J = 8.7$, 2.3 Hz, 1H, py H4), 7.38–7.27 (m, 5H, phenyl H's), 7.16 (d, $J = 8.7$ Hz, 1H, py H3), 6.33 (d, $J = 2.9$ Hz, 1H, C*H*OPh), 3.58 (m, 1H, C*H*NMe), 1.20 (d, $J = 6.8$ Hz, 3H, CH_3). Found: C, 54.1; H, 4.9. Calc. for $C_{15}H_{16}ClF_3N_2O$: C, 54.1; H, 4.9%.

5-(*Trifluoromethyl*)-2-[(1R,2R)-2-*amino*-1-*phenylpropanoxy*]*pyridine* (**4i**)

$[\alpha]^{20}$ −1.57° (c = 0.0215, CH_2Cl_2); oil, 26% purified yield; ^{1}H NMR ($CDCl_3$): δ 8.33 (s, 1H, py H6), 7.74 (dd, J = 8.8, 2.3 Hz, 1H, py H4), 7.40–7.23 (m, 5H, phenyl H's), 6.89 (d, J = 8.8 Hz, 1H, py H3), 5.82 (d, J = 6.8 Hz, 1H, C*H*OPh), 3.36 (apparent quintet, J = 6.6 Hz, 1H, C*H*NMe), 1.41 (br s, 2H, NH_2), 1.05 (d, J = 6.6 Hz, 3H, CH_3); ^{13}C NMR ($CDCl_3$): δ 165.4 (py C2), 144.9 (q, $^3J_{C-F}$ = 4.5 Hz, py C6), 139.0 (phenyl C), 135.8 (q, $^3J_{C-F}$ = 3.2 Hz, py C4), 128.3, 127.8, 127.1 (phenyl C's), 123.9 (q, $^1J_{C-F}$ = 271 Hz, *C*F$_3$), 120.0 (q, $^2J_{C-F}$ = 33 Hz, py C5), 111.3 (py C3), 83.2 (*C*HOPh), 51.8 (*C*HNMe), 19.4 (*C*H$_3$).

{5-(*Trifluoromethyl*)-2-[(1R,2R)-2-*amino*-1-*phenylpropanoxy*]*pyridine*} · HCl

Melting point, 209–210°C; ^{1}H NMR ($CDCl_3$): δ 8.75 (br s, 3H, NH_3), 8.26 (s, 1H, py H6), 7.70 (dd, J = 8.8, 2.5 Hz, 1H, py H4), 7.36–7.31 (m, 5H, phenyl H's), 7.14 (d, J = 8.8 Hz, 1H, py H3), 6.02 (d, J = 9.2 Hz, 1H, C*H*OPh), 3.55 (m, 1H, C*H*NMe), 0.97 (d, J = 6.8 Hz, 3H, CH_3). Found: C, 54.2; H, 4.9. Calc. for $C_{15}H_{16}ClF_3N_2O$: C, 54.1; H, 4.8%.

{COD}{2-*Chloro*-6-[(1R,2S)-2-*amino*-1-*phenylpropanoxy*]*pyridine*}RhCl (**5a**)

$[\alpha]^{20}$ 9.5° (c = 1, CH_2Cl_2); ^{1}H NMR ($CDCl_3$): δ 7.55 (apparent t, J = 7.8 Hz, 1H, py 4H), 7.35–7.21 (m, 5H, phenyl H's), 6.91 (apparent d, J = 7.3 Hz, 1H, py), 6.74 (apparent d, J = 7.3 Hz, 1H, py), 6.44 (br s, 1H, C*H*OPh), 4.63–4.47 (br m, 2H), 3.66–3.34 (br m, 4H), 2.50–2.26 (br m, 4H), 2.17–1.97 (br m, 2H), 1.84–1.62 (br m, 3H), 1.26 (d, J = 6.3 Hz, 3H, CH_3); ^{13}C NMR (DMSO-d_6): δ 162.7 (py C6), 147.2 (py C2), 142.2 (py C4), 139.2 (phenyl C), 128.3, 127.3, 125.6 (phenyl C's), 116.9, 110.0 (py CH's), 80.9 (*C*HOPh), 80–75 (broad, vinyl COD C's), 52.6 (*C*HNMe), 31.0, 29.4 (allylic COD C's), 15.6 (*C*H$_3$). Found: C, 51.4; H, 5.4; Cl, 13.6; N, 5.3. Calc. for $C_{22}H_{27}Cl_2N_2ORh$: C, 51.9; H, 5.3; Cl, 13.9; N, 5.5%.

Hydrosilation of acetophenone

A Schlenk tube was charged with acetophenone (0.6 g, 5 mmol), [(COD)RhCl]$_2$ (12.3 mg, for 100 : 1, substrate/Rh, mol/mol), the appropriate ligand, and dichloromethane (3 cm^3). The mixture was degassed by three consecutive freeze–pump–thaw cycles. A separate Schlenk tube was charged with diphenylsilane (1.3 cm^3, 7 mmol) and dichloromethane (1 cm^3) and degassed as above. The latter solution was cannulated into the acetophenone mixture and allowed to react at 0°C until the carbonyl band in the IR (1685 cm^{-1}) disappeared (~18 h). The mixture was then diluted with acetone (5 cm^3) and 10% hydrochloric acid (10 cm^3) and then stirred vigorously for 2 h. The mixture was extracted with ether and the organic layer dried over potassium carbonate. The ether was removed and the crude product purified by bulb–bulb distillation (fraction from 60–80°C, 0.7 torr, was collected). Contamination by acetophenone in the samples was taken into account and calculated using the ^{1}H NMR spectra for the distilled product. The product was also analysed by preparing the MPTA ester and analysed by high-field ^{1}H NMR according to the literature procedure,[14] and found to be in excellent agreement with the data from optical measurements.

Monitoring the optical yield vs reaction progress

Complex **5a** was formed by adding [(COD)RhCl]$_2$ (82 mg, 0.33 mmol) and **1a** (97 mg, 0.37 mmol) to 30 cm^3 of dichloromethane. The solution was concentrated to 5 cm^3 and ether (100 cm^3) was added. The precipitate was collected and washed several times with ether to remove excess ligand. The solid was redissolved in dichloromethane and degassed Ph_2SiH_2 (8.7 cm^3, 47 mmol) was added. The mixture was allowed to react at ambient temperature for 30 min and then cooled to 0°C. Acetophenone (4.0 g, 33 mmol) was added to the mixture and aliquots (2.5 cm^3) were removed from the reaction vessel at 1 h intervals. The aliquots were transferred to a flask containing an acetone (10 cm^3) and 10% hydrochloric acid (5 cm^3) mixture which had been chilled to 0°C. The product was isolated after work-up by distillation at reduced pressure. Samples of the distilled product (0.100 g) were diluted to 1.00 cm^3 with dichloromethane and their optical rotations measured and enantiomeric excesses calculated.

Molecular mechanics

The proposed catalytic species were modelled using BIOGRAPH (Version 2.0) on an Ardent super-computing facility. The structures were permitted to minimize without any interatomic restrictions and were approached from several different beginning structures to avoid false minima. The metal centre was modelled with ruthenium since Version 2.0 of BIOGRAPH does not contain rhodium. The energies used in the study represent

the total energy of the molecule which is basically a summation of bond, angle, torsion and van der Waals' energies.

Acknowledgements—We are grateful to the donors of the Petroleum Research Fund, administered by the American Chemical Society, for partial funding of this work. M.E.W. expresses his sincere appreciation for helpful and constructive comments by referees concerning an initial version of this paper.

REFERENCES

1. (a) R. Noyori, T. Ohkuma, M. Kitamura, H. Takaya, N. Sayo, H. Kumobayashi and S. Akutagawa, *J. Am. Chem. Soc.* 1987, **109**, 5856; (b) M. Kitamura, T. Ohkuma, S. Inoue, N. Sayo, H. Kumobayashi, S. Akutagawa, T. Ohta, H. Takaya and N. Noyori, *J. Am. Chem. Soc.* 1988, **110**, 629; (c) E. J. Corey, R. K. Bakshi, S. Shibata, C.-P. Chen and V. K. Singh, *J. Am. Chem. Soc.* 1987, **109**, 7925.
2. For a general review of transition metal-catalysed hydrosilations see: I. Ojima and K. Hirai, in *Asymmetric Synthesis* (Edited by J. D. Morrison), Vol. 5. Academic Press, New York (1985).
3. For general reviews on transition metal-catalysed asymmetric synthesis see: H. B. Kagan, in *Comprehensive Organometallic Chemistry* (Edited by G. Wilkinson, F. G. A. Stone and E. W. Abel), Chap. 53, pp. 463–498. Pergamon Press, Oxford (1982); I. Ojima, *Pure Appl. Chem.* 1984, **56**, 99; I. Ojima, N. Clos and C. Bastos, *Tetrahedron* 1989, **45**, 6901 and refs cited therein.
4. (a) K. Yamamoto, T. Hayashi and M. Kumada, *J. Organomet. Chem.* 1971, **31**, C9; K. Yamamoto, T. Hayashi and M. Kumada, *J. Organomet. Chem.* 1973, **46**, C65; (b) W. Dumont, J.-C. Poulin, T.-P. Dang and H. B. Kagan, *J. Am. Chem. Soc.* 1973, **95**, 8295; (c) I. Ojima, T. Kogure and Y. Nagai, *Chem. Lett.* 1973, 541.
5. (a) H. Brunner, G. Riepl and H. Weitzer, *Angew. Chem., Int. Edn. Engl.* 1983, **22**, 331; (b) H. Brunner, R. Becker and G. Riepl, *Organometallics* 1984, **3**, 1354; (c) H. Brunner and A. Kurzinger, *J. Organomet. Chem.* 1988, **346**, 413.
6. For typical examples where high ligand/rhodium ratios are necessary see: H. Brunner and H. Fisch, *J. Organomet. Chem.* 1987, **335**, 1 (ligand **2** in paper, 10:1, 35% *ee*; 5:1, 4% *ee*). H. Brunner and G. Riepl, *Angew. Chem., Int. Edn Engl.* 1982, **21**, 377 (ligand **1a** in paper, 13:1, 57% *ee*; stoichiometric cation complex, 0% *ee*). Reference 7 of this paper (ligand **1a** in paper, 4:1, 83% *ee*; stoichiometric complex, 56% *ee*).
7. H. Nishiyama, H. Sakaguchi, T. Nakamura, M. Horihata, M. Kondo and K. Itoh, *Organometallics* 1989, **8**, 846.
8. Brunner and co-workers have prepared and tested the majority of chiral, nitrogen-based ligands prepared to date. Other workers include Botteghi and co-workers (*J. Org. Chem.* 1984, **49**, 4290; *Synth. Commun.* 1985, **15**, 807; *J. Organomet. Chem.* 1986, **304**, 217) and Steel *et al.* (*Aust. J. Chem.* 1986, **39**, 1525).
9. M. E. Wright, S. A. Svejda, M.-J. Jin and M. A. Peterson, *Organometallics* 1990, **9**, 136.
10. L. Testaferri, M. Iecco, M. Tingoli, D. Bartoli and A. Massoli, *Tetrahedron* 1985, **41**, 1373.
11. Prepared by literature procedure from $RhCl_3$ (hydrate): G. Giordano and R. H. Crabtree, *Inorg. Synth.* 1979, **19**, 218.
12. Scheme 1 is based upon the presently accepted catalytic sequence for hydrosilation reactions: J. F. Peyronel and H. B. Kagan, *Nouv. J. Chim.* 1978, **2**, 211; I. Ojima, T. Kogure and M. Kumagai, *J. Org. Chem.* 1977, **42**, 1671.
13. F. A. Cotton and G. Wilkinson, in *Advanced Inorganic Chemistry*, p. 119. John Wiley, New York (1980) and refs cited therein.
14. J. A. Dale, D. L. Dull and H. S. Mosher, *J. Org. Chem.* 1969, **34**, 2543.

Polyhedron Vol. 10, No. 10, pp. 1069–1073, 1991
Printed in Great Britain

0277–5387/91 $3.00+.00
© 1991 Pergamon Press plc

ISOLATION OF A SULPHUR-RICH INDIUM POLYSULPHIDE COMPLEX CONTAINING TWO DIFFERENT S_x^{2-} LIGANDS. SYNTHESIS AND STRUCTURE OF $[InS_{10}Br]^{2-}$

SANDEEP DHINGRA and MERCOURI G. KANATZIDIS*

Department of Chemistry, Michigan State University, East Lansing, MI 48824, U.S.A.

(*Received* 15 *November* 1990; *accepted* 21 *January* 1991)

Abstract—The reaction of $InBr_3$ with K_2S_5 (or K_2S_4 and K_2S_6) and Ph_4PBr afforded yellow $(Ph_4P)_2[In(S_4)(S_6)Br]$ (**I**). Complex **I** crystallizes in the monoclinic space group $P2_1/c$ with $a = 14.355(7)$, $b = 17.723(4)$, $c = 20.974(7)$ Å, $\beta = 108.5(1)°$, $V = 5060.6(4)$ Å^3 (at 23°C), $Z = 4$. The $[In(S_4)(S_6)Br]^{2-}$ anion features a trigonal bipyramidal indium centre coordinated by four sulphur atoms and one bromine atom. The latter occupies an axial position. The In^{3+} centre is chelated by two bidentate polysulphide S_4^{2-} and S_6^{2-} ligands. The S_6^{2-} ligand occupies two equatorial positions. The remaining one equatorial and one axial positions are occupied by the S_4^{2-} ligand. The average In—S distance is 2.535(35) Å. The In—Br distance is 2.615(3) Å. Complex **I** shows no absorptions in the UV–vis spectrum. Two strong absorptions at 490 and 457 cm^{-1} in the IR spectrum are attributed to S—S vibrations.

Soluble transition-metal polychalcogenides constitute an important class of compounds with unusual structures and stoichiometries. They are useful as model compounds for sulphided heterogeneous catalysts,[1] metal/sulphur transport agents in geochemistry[2] and precursors to chalcogenide semiconductors.[3] To date, a number of polysulphide, and to a lesser extent, polyselenide and polytelluride complexes with transition metals have been synthesized and structurally characterized.[1–8] In some cases, polysulphides behave differently than their heavier congeners, while in others they behave similarly. It would be important to understand the role of the metal ion in determining similarities and differences in the chemistry of the various polychalcogenide ligands. To date, mostly transition metals have been investigated with respect to coordination to polychalcogenide ligands. On the contrary, the preparation of soluble polychalcogenide compounds containing main-group elements has not been pursued to the same degree. The few existing examples are, $[Bi_2S_{34}]^{4-}$,[9] $[Sn(S_4)_2(S_6)_{0.6}(S_4)_{0.4}]^{2-}$,[10] $[In_2Se_{21}]^{4-}$,[11] $[SnSe_{12}]^{2-}$,[12] $[PbSe_8]^{2-}$[13] and $[M_3Se_{15}]^{3-}$[14] (M = In, Tl). As part of our systematic investigation of polychalcogenide chemistry of the late transition and main group metals[11–14] and in an attempt to prepare the sulphur analogue of the indium–polyselenide $[In_2Se_{21}]^{4-}$ we investigated the corresponding polysulphide chemistry. We have isolated and structurally characterized a new unexpected complex $[InS_{10}Br]^{2-}$, which possesses an unusual structure.

EXPERIMENTAL

All work was carried out in a glove box (Vacuum Atmospheres, Inc.) under a nitrogen atmosphere. Dimethylformamide (DMF) was stored over 4 Å Linde molecular sieves for several days and distilled *in vacuo*. Ether was distilled over sodium (or potassium)/benzophenone under a nitrogen blanket. $InCl_3$ (anhydrous) was purchased from Alpha Products Inc. Satisfactory elemental analyses were obtained. Potassium polysulphides (K_2S_x, $x = 4$–6) were prepared in liquid ammonia from potassium metal and elemental sulphur in the appropriate ratio. The X-ray powder diffraction patterns were recorded either with a standard Debye–Scherrer powder camera mounted on a Phillips Norelco XRG-5000 X-ray generator operating at 40 kV/20

* Author to whom correspondence should be addressed.

mA, or a Phillips XRG-3000 computer controlled powder diffractometer. Ni filtered, Cu radiation was used. Thermal gravimetric analyses were performed on a Cahn TG System 121 under flowing nitrogen. A typical heating rate of 5°C min^{-1} was used. IR spectra were recorded as KBr and CsI pellets on a Nicolet 740 FT–IR spectrometer. Elemental analyses were performed on a JEOL JSM-35C scanning electron microscope equipped with an Energy Dispersive Spectroscopy detector.

Synthesis of **I**

A 20 cm^3 DMF solution of $InBr_3$ (0.200 g, ~0.564 mmol) was added to a 80 cm^3 DMF solution of K_2S_4 (0.117 g, ~0.568 mmol), K_2S_6 (0.153 g, 0.565 mmol) in the presence of Ph_4PBr (0.470 g, 1.121 mmol). The mixture was stirred for ~20 min. Filtration of the pale yellow solution to remove the KBr precipitate, followed by slow addition of *ca* 60 cm^3 of ether, and storage at room temperature for 2 days, afforded 0.41 g of analytically pure, yellow, chunky crystals (61% yield). The synthesis also can be carried out with K_2S_5 (39% yield).

The X-ray diffraction (XRD) powder pattern obtained from this material matches extremely well that calculated from the single crystal coordinates, confirming the purity of the compound. A comparison between the calculated and observed d_{hkl} spacings for this material is shown in Table 1.

X-ray crystallographic studies

The crystallographic data were collected on a Enraf–Nonius diffractometer using an ω–2θ scan

Table 1. Observed and calculated X-ray powder pattern of **I**

h	k	l	D_{calc}	D_{obs}	I_{obs}	h	k	l	D_{calc}	D_{obs}	I_{obs}
1	1	0	10.796			−4	1	5	3.0738	3.0750	18.5
−1	1	1	10.682	10.660	9.09	4	2	1	3.0020	3.0173	27.1
1	1	1	8.622	8.554	16.4	4	0	2	2.9465	2.9410	28.3
−1	1	2	8.4506			2	2	5	2.8756	2.8725	22.3
0	2	1	8.0946	8.0956	36.6	−3	5	2	2.8375	2.8372	27.1
				7.9486	100.0	−3	5	3	2.7755	2.7794	24.4
1	2	0	7.4268	7.4093	4.2	−5	1	4	2.7560	2.7515	18.6
−2	0	2	6.6935	6.6918	21.6	−2	4	6	2.7177	2.7150	28.3
1	1	2	6.5406	6.5368	13.8	−4	4	4	2.6705	2.6699	20.4
1	3	0	5.4194	5.4163	26.1	0	4	6	2.6544	2.6584	22.2
−1	1	4	5.0222	5.0301	49.2	−5	3	3	2.5722	2.5700	22.2
−2	2	3	4.8221	4.8218	60.1	−4	5	3	2.4957	2.4953	19.8
−2	0	4	4.8069			1	7	1	2.4525	2.4588	21.2
2	1	2	4.7539	4.7394	37.1	−5	3	5	2.4386	2.4345	23.4
−3	0	2	4.7345			−4	4	6	2.4110	2.4129	24.4
−1	3	3	4.4826	4.4927	80.1	−3	5	6	2.3771	2.3772	35.9
−2	3	2	4.4293	4.4239	44.6	−3	3	8	2.3393	2.3312	71.3
0	2	4	4.3366	4.3289	31.9	2	2	7	2.2883	2.2854	23.8
−1	4	1	4.2064	4.1905	37.1	−6	2	1	2.2619	2.2582	29.8
3	1	1	4.0390	4.0271	73.1	−3	7	1	2.2357	2.2287	20.4
−3	1	4	3.9508	3.9445	31.7	0	4	8	2.1618	2.1707	22.2
0	3	4	3.8044	3.8022	27.4	−4	6	5	2.1454	2.1478	21.2
3	2	1	3.7569	3.7515	26.7	−4	4	8	2.1126	2.1085	26.1
2	2	3	3.7497			−6	2	7	2.0743	2.0697	36.6
−3	3	2	3.6945	3.6936	25.0	6	0	2	2.0741		
3	3	0	3.5988	3.5979	24.1	6	1	2	2.0599	2.0545	32.4
−4	1	2	3.5163	3.5099	25.9	−6	0	8	2.0264	2.0206	22.7
2	1	4	3.4513	3.4547	27.1	−7	1	1	1.9854	1.9816	45.8
2	3	3	3.3895	3.3875	36.4	−5	3	9	1.9506	1.9573	18.9
−3	3	4	3.3420	3.3438	43.0	−7	3	5	1.9097	1.9028	33.9
−4	2	1	3.2930	3.2940	94.2	2	8	4	1.8748	1.8762	18.2
−2	2	4	3.2076	3.2142	25.0	−6	4	8	1.8428	1.8458	16.1
−4	2	4	3.1309	3.1302	19.5						

mode and Mo–K_α radiation. The crystals were mounted inside glass capillaries and sealed. Crystal data and details for data collection and refinement are shown in Table 2. The intensities of three check reflections were monitored every 100 reflections and did not show any appreciable decay during the data collection period. An empirical absorption correction was applied to all data based on ψ scans for several reflections. The structure was solved with direct methods using SHELXS-86[15] and was refined with the SDP[16] package of crystallographic programs, using a VAXstation 2000 computer. All non-carbon and non-hydrogen atoms were refined anisotropically. The carbon atoms were refined isotropically. The hydrogen atom positions were calculated and included in the structure factor calculation but were not refined. The final coordinates of all atoms, thermal parameters of all non-hydrogen atoms, tables of least-squares planes and a listing of calculated and observed ($10F_o/10F_c$) structure factors (total of 32 pages) have been deposited with the Director, Cambridge Crystallographic Data Centre. There were no significant residual peaks in the final electron density different map. The XRD powder pattern was calculated using the atom coordinates determined from the single crystal data using the program POWD 10.[17]

Table 2. Data for crystal structure analysis[a] of I

Formula	$C_{48}H_{40}P_2InS_{10}Br$
FW	1194.17
a (Å)	14.355(7)
b (Å)	17.723(4)
c (Å)	20.974(7)
α (°)	90.0
β (°)	108.50
γ (°)	90.00
V (Å^3)	5060.6
Z	4
Space group	$P2_1/c$
D_{calc} (g cm^{-3})	1.57
μ(Mo-K_α) (cm^{-1})	17.3
2θ range (°)	4–40
Data collected	5288
Number of data unique	4577
Data used [$F_o^2 > 3\sigma(F_o^2)$]	2989
Min. max. absorbance correction	0.823/0.999
Number of variables	319
Number of atoms per asymmetric unit	102
Final R/R_w (%)	6.6/9.6

[a] At 23°C.

RESULTS AND DISCUSSION

Synthesis

Our original aim was to prepare In^{3+}/S_x^{2-} complexes structurally and compositionally analogous to the selenium analogues, $[In_2Se_{21}]^{4-}$[11] and $[In_3Se_{15}]^{3-}$,[14] by reacting $InCl_3$, K_2S_5 and Ph_4PBr in DMF. As it often happens with polychalcogenide ligands, a different complex than anticipated was obtained. The rational preparation of **I** was subsequently carried out by reacting $InBr_3$ with K_2S_5 (or a mixture of K_2S_4 and K_2S_6) in DMF in the presence of Ph_4P^+ according to eq. (1):[18]

$$InBr_3 + 2K_2S_5 + 2Ph_4PBr \longrightarrow (Ph_4P)_2[InS_{10}Br] + 4KBr. \quad (1)$$
$$\textbf{(I)}$$

The UV–vis spectrum of **I** in DMF solution has no characteristic absorption bands (300–800 nm) and features a rising absorbance at higher energies. The absence of an absorption band around 650 nm suggests that the complex does not dissociate in this solvent to form S_x^- radical anions which are responsible for this absorption.[11] In the IR region of the spectrum we observe strong absorptions at 490 and 457 cm^{-1} and a weak absorption at 470 cm^{-1}. These are most likely due to S—S vibrations. A medium intensity absorption is also observed at 352 cm^{-1} which currently is not assigned with certainty.

Thermal gravimetric analysis examination of the thermolysis of **I** under flowing nitrogen shows that the compound begins to lose weight at −335°C. This onset temperature of initial weight loss is shared by other Ph_4P^+ salts of polyselenide complexes. It represents the thermal stability of the Ph_4Ph^+ ion with respect to nucleophilic attack from the S_x^{2-} ligands.[3] The weight loss curve is complicated lacking any well-defined plateaux. At 1000°C, the highest temperature studied, the material continues to lose weight. The grey–black residue obtained contains In, S and P in the 2:2:1 ratio. Its X-ray powder pattern does not show the presence of known In/S, In/P or In/S/P phases.

Description of the structure of **I**

The monoclinic unit cell contains well separated $[InS_{10}Br]^{2-}$ anions and Ph_4P^+ cations. The latter have the usual tetrahedral structure and will not be discussed further. The structure of the $[InS_{10}Br]^{2-}$ anion is shown in Fig. 1. In view of the structure of $[In_2Se_{21}]^{4-}$, and that described here, it appears that five coordination in indium polychalcogenide chem-

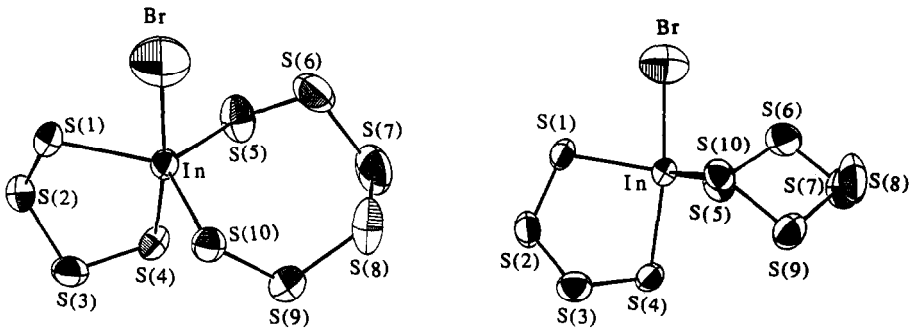

Fig. 1. Two views of the $[In(S_4)(S_6)Br]^{2-}$ anion with labelling scheme, as drawn by ORTEP.

istry is readily accessible. The coordination of indium is best described as a trigonal bipyramid with three equatorial sulphur ligands and two axial (a sulphur and a bromide) ligands. It is somewhat surprising that the bromide ligand occupies an axial site in the molecule since an equatorial position is predicted based on VSEPR arguments. The indium atom is chelated by a S_4^{2-} and a S_6^{2-} ligand. The latter occupies two equatorial positions. The occurrence of S_6^{2-} ligands is rather rare. Another example of a polysulphide complex in which both S_4^{2-} and S_6^{2-} ligands are present is found in $[Sn(S_6)(S_4)_2]^{2-}$.[10] It should be noted, however, that while in the latter complex the S_4^{2-} and S_6^{2-} ligands are disordered about the same crystallographic site, in **I** they are ordered and occupy distinct sites. The average In—S bond distance is 2.535(35) Å. The equatorial In—S bonds are shorter than the axial In—S(4) bond as expected. A listing of selected bond distances and angles for $[InS_{10}Br]^{2-}$ is given in Table 3. The observed S—S bonds are in the normal range of single S—S bond distances reported for other metal polysulphide compounds.[19] It is interesting to note that in the seven-membered InS_6 ring the In, S(5), S(7), S(8) and S(10) atoms lie very close to a plane with S(6) and S(9) positioned, respectively, 1.16 and 1.19 Å above and below it. The same con-

Table 3. Selected distances (Å) and angles (°) in the $[In(S_4)(S_6)Br]^{2-}$ anion. Standard deviations are given in parentheses[a]

In—S(1)	2.526(4)	S(1)—S(2)	2.061(8)
In—S(4)	2.596(5)	S(2)—S(3)	2.045(7)
In—S(5)	2.506(5)	S(3)—S(4)	2.035(6)
In—S(10)	2.514(5)	S(5)—S(6)	2.017(8)
In—S(mean)	2.535(35)	S(6)—S(7)	2.060(8)
		S(7)—S(8)	2.080(10)
In—Br	2.615(3)	S(8)—S(9)	2.029(8)
		S(9)—S(10)	2.048(6)
		S—S(mean)	2.046(19)

S(1)—In—S(4)	91.0(2)	In—S(1)—S(2)	106.3(2)
S(1)—In—S(5)	125.2(2)	In—S(5)—S(6)	107.1(3)
S(4)—In—S(5)	85.4(2)	In—S(4)—S(3)	98.8(2)
S(4)—In—S(10)	97.2(2)	In—S(10)—S(9)	105.0(3)
S(5)—In—S(10)	115.7(2)	S(1)—S(2)—S(3)	103.5(3)
S(1)—In—Br	80.8(1)	S(2)—S(3)—S(4)	103.7(3)
S(4)—In—Br	170.3(1)	S(5)—S(6)—S(7)	107.2(4)
S(5)—In—Br	95.2(2)	S(6)—S(7)—S(8)	107.4(4)
S(10)—In—Br	91.4(2)	S(7)—S(8)—S(9)	107.9(4)
		S(8)—S(9)—S(10)	107.0(3)

[a] The estimated standard deviations in the mean bond lengths and the mean bond angles are calculated by the equations $\sigma_1 = \{\Sigma_n(l_n - l)^2/n(n-1)\}^{1/2}$. Where l_n is the length (or angle) of the nth bond, l is the mean length (or angle) and n is the number of bonds.

formation has also been observed in the seven-membered HgS_6 ring of the $[Hg(S_6)_2]^{2-}$ complex.[20] The equatorial position of the S_6^{2-} ligand in **I** is rationalized by its ability to provide a wide enough "bite" to span the 4.25 Å needed between equatorial ligands. The smaller S_4^{2-} ligand cannot offer such a large bite (3.7 Å max.) and thus is better stabilized in the fashion in which it is found in $[In(S_4)(S_6)Br]^{2-}$. The position of the S(9) atom in the S_6^{2-} ligand affects the S(4)—In—S(10) angle which becomes 12° larger than the S(4)—In—S(5) angle, suggesting that the S(9) atom exerts a significant steric repulsion on S(4). The flexibility of the S_6^{2-} ligand to tune its "bite" size is evident by the fact that it has now been found to participate in chelating fashion in tetrahedral, trigonal bipyramidal and octahedral coordination. The five-membered InS_4 ring adopts an envelope conformation with S(3) lying 1.1 Å above the In(1)S(2) S(4) plane. To the best of our knowledge, $[In(S_4)(S_6)Br]^{2-}$ is the first molecular example of an In^{3+} polysulphide complex.

The In—Br bond length in $[In(S_4)(S_6)Br]^{2-}$ is 2.615(3) Å, in the correct range for axial binding, five-coordinate indium, being 0.055 Å shorter than the In—Br bond in the six-coordinate $[InBr_6]^{3-}$,[21] and longer than the same bond in the tetrahedral $[InBr_4]^-$.[21] When the bromide is equatorially bound to five-coordinate indium such as in $InBr_3(Me_3AsS)_2$, it forms a shorter In—Br distance in the range of 2.53–2.55 Å.[22] Work is continuing to isolate homoleptic indium polysulphide complexes.

Acknowledgements—Financial support from the Donors of the Petroleum Research Fund, administered by the American Chemical Society, is gratefully acknowledged. We thank Drs Grahame Williams, Kay Fair and James Phillips of Enraf–Nonius Corp. for the kind collection of X-ray crystallographic data for **I**.

REFERENCES

1. (a) A. Müller, *Polyhedron* 1986, **5**, 323; (b) M. Draganjac and T. B. Rauchfuss, *Angew. Chem., Int. Edn Engl.* 1985, **24**, 742.
2. K. B. Krauskopf, *Introduction to Geochemistry*, 2nd edn. McGraw-Hill, New York (1979).
3. (a) S. Dhingra and M. G. Kanatzidis, *MRS Symp. Proc.* 1990, **180**, 825; (b) K.-W. Kim, S. Dhingra and M. G. Kanatzidis, 199th American Chemical Society Meeting, Boston MA (1990), INOR 141; (c) S. Dhingra, K.-W. Kim and M. G. Kanatzidis, *MRS Symp. Proc.*, in press.
4. (a) H. Strasdeit, B. Krebs and G. Henkel, *Inorg. Chim. Acta* 1984, **89**, L11; (b) J. Adel, F. Weller and K. Dehnicke, *Z. Naturfor.* 1988, **43B**, 1094.
5. M. G. Kanatzidis and S.-P. Huang, *J. Am. Chem. Soc.* 1989, **111**, 760.
6. (a) W. A. Flomer and J. W. Kolis, *J. Am. Chem. Soc.* 1988, **110**, 3682; (b) W. A. Flomer, S. C. O'Neal, W. T. Pennington, D. Jeter, A. W. Cordes and J. W. Kolis, *Angew. Chem., Int. Edn Engl.* 1988, **27**, 1702; (c) S. C. O'Neal and J. W. Kolis, *J. Am. Chem. Soc.* 1988, **110**, 1971.
7. R. D. Adams, T. A. Wolfe, B. W. Eichhorn and R. C. Haushalter, *Polyhedron* 1989, **8**, 701.
8. (a) M. A. Ansari and J. A. Ibers, *Coord. Chem. Rev.* 1990, **101**, 223; (b) M. G. Kanatzidis, *Comm. Inorg. Chem.* 1990, **10**, 161.
9. A. Müller, M. Zimmermann and H. Bögge, *Angew. Chem., Int. Edn Engl.* 1986, **25**, 273.
10. A. Müller, J. Schimanski, M. Römer, H. Bögge, F.-W. Baumann, W. Eltzner, E. Krickemeyer and U. Billerbeck, *Chimia* 1985, **39**, 25.
11. M. G. Kanatzidis and S. Dhingra, *Inorg. Chem.* 1989, **28**, 2024.
12. S.-P. Huang, S. Dhingra and M. G. Kanatzidis, *Polyhedron* 1990, **9**, 1389.
13. R. M. H. Banda, J. Cusick, M. L. Scudder, D. C. Craig and I. G. Dance, *Polyhedron* 1989, **8**, 1995.
14. M. G. Kanatzidis and S. Dhingra, submitted.
15. G. M. Sheldrick, in *Crystallographic Computing 3* (Edited by G. M. Sheldrick, C. Kruger and R. Goddard), pp. 175–189. Oxford University Press, Oxford (1985).
16. B. A. Frenz, The Enraf–Nonius CAD4 SDP System, in *Computing in Crystallography*, pp. 64–71. Delft University Press, Delft, Holland (1978).
17. D. K. Smith, M. C. Nichols and M. E. Zolensky, POWD 10: A FORTRAN Program for Calculating X-ray Powder Diffraction Patterns, Version 10. Pennsylvania State University (1983).
18. The isostructural $(Ph_4P)_2[InS_{10}Cl]$ has been synthesized in DMF by the reaction of $InCl_3$ and K_2S_5 in the presence of Ph_4PCl. It shows an identical X-ray powder diffraction pattern with that of **I** and its unit cell is $a = 14.314(7)$, $b = 17.623(8)$, $c = 20.861(15)$ Å, $\beta = 108.28(5)°$, $V = 5022$ Å^3.
19. (a) D. Coucouvanis, P. R. Patil, M. G. Kanatzidis, B. Detering and N. C. Baenziger, *Inorg. Chem.* 1985, **24**, 24; (b) A. Müller, E. Krickemeyer and H. Bögge, *Z. Anorg. Allg. Chem.* 1987, **554**, 61.
20. A. Müller, J. Schimanski and U. Schimanski, *Angew. Chem., Int. Edn Engl.* 1984, **23**, 159.
21. M. A. Khan and D. G. Tuck, *Acta. Cryst.* 1981, **B37**, 683.
22. W. T. Robinson, C. J. Wilkins and Z. Zeying, *J. Chem. Soc., Dalton Trans.* 1988, 2187.

Polyhedron Vol. 10, No. 10, pp. 1075–1078, 1991
Printed in Great Britain

0277-5387/91 $3.00+.00
© 1991 Pergamon Press plc

THE MOLECULAR STRUCTURE OF (ALLYL)BIS(METHYLCYCLOPENTADIENYL)NIOBIUM(III)

LINDA K. CHEATHAM, JOHN J. GRAHAM, ALLEN W. APBLETT and ANDREW R. BARRON*

Department of Chemistry and Materials Research Laboratory, Harvard University, Cambridge, MA 02138, U.S.A.

(*Received* 26 *November* 1990; *accepted* 14 *January* 1991)

Abstract—The compound $(\eta^5\text{-}C_5H_4Me)_2Nb(\eta^3\text{-}C_3H_5)$ (**1**) has been prepared and characterized by ^1H, ^{13}C and ^{93}Nb NMR spectroscopy. The molecular structure of **1** has been confirmed by X-ray crystallography and the nature of the bonding between the allyl ligand and the niobium is discussed. Compound **1** crystallizes in the monoclinic space group $P2_1/c$, $a = 6.029(2)$, $b = 7.752(2)$, $c = 26.115(6)$ Å, $\beta = 92.33(2)°$, $V = 1219.5(5)$ Å^3, $Z = 4$, $R = 0.031$, $R_w = 0.050$.

There is a remarkably rich chemistry of bent bis (cyclopentadienyl)transition metal complexes, $(\eta^5\text{-}C_5H_5)_2ML_n$, when $n = 1$–3. Within these complexes the L_n groups are forced, due to the nature of the frontier orbitals, to lie in a common plane perpendicular to the Cp centroid—M—Cp centroid plane. Such an arrangement is indeed observed for $(\eta_5\text{-}C_5H_5)_2NbH_3$.[1] However, derivatives in which the L_n group are constrained from being co-planar such as η^3-allyl pose an interesting question concerning the bonding between the metal and the ligand. Lauher and Hoffman[2] have presented the molecular orbital treatment of $(\eta^5\text{-}C_5H_5)_2M$(allyl) complexes shown in Fig. 1, in which three allyl-to-metal bonding interactions are proposed. Firstly, the lowest filled allyl orbital, *a'*, overlaps with the higher *a'* metal orbital, forming a σ ligand-to-metal bonding interaction. Secondly, the non-bonding *a''* ligand orbital donates into the *a''* metal orbital. In addition, they proposed that significant back-bonding would occur from the lower metal *a'* orbital and the allyl, *a'*, π-antibonding orbital. The two former interactions were also reported from photoelectron spectroscopy studies by Green *et al.*, however, the latter was proposed to be primarily metal lone pair in character.[3]

We have recently reported the preparation of niobium carbide-containing thin films by metal organic chemical vapour deposition, using (allyl) bis(cyclopentadienyl)niobium compounds as single source precursors.[4] As part of this study we have undertaken an X-ray crystallographic structural determination of one of the precursor compounds, $(\eta^5\text{-}C_5H_4Me)_2Nb(\eta^3\text{-}C_3H_5)$ (**1**). The results of which are herein discussed with respect to the theoretical and spectroscopic studies noted above.

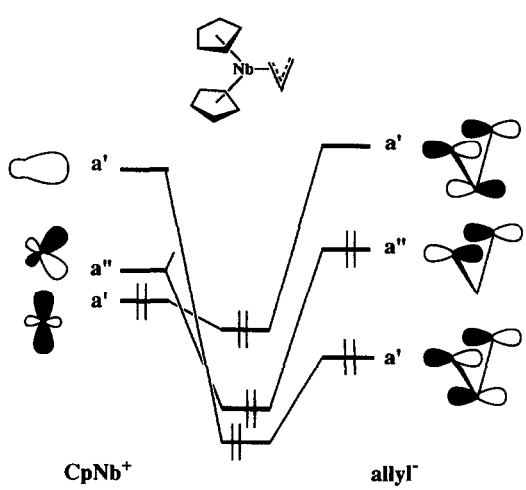

Fig. 1. Orbital interaction diagram for $(\eta^5\text{-}C_5H_5)_2M(\eta^3\text{-}C_3H_5)$.

*Author to whom correspondence should be addressed.

RESULTS AND DISCUSSION

Treatment of $(\eta^5\text{-}C_5H_4Me)_2NbCl_2$ with two molar equivalents of allyl Grignard in diethyl ether affords the dark green compound $(\eta^5\text{-}C_5H_4Me)_2Nb(\eta^3\text{-}C_3H_5)$ (**1**). Compound **1** is air and moisture sensitive but may be stored under an inert atmosphere at −20°C. The ^1H and ^{13}C NMR spectra (see Experimental) of **1** are consistent with a symmetrically-bound allyl ligand. No exchange is observed between either the exo and endo protons of the allyl group, or the inequivalent methylcyclopentadienyl ligands, even at elevated temperatures (90°C). This indicates that the allyl ligand is non-fluxional.

The molecular structure of **1** has been determined by X-ray crystallography. The crystal structure of **1** consists of discrete molecules separated by van der Waals' contacts. A perspective view of an individual molecule of **1** is shown in Fig. 2, together with the atom numbering scheme. Pertinent bond lengths and bond angles are given in Table 1.

The structural features of **1** are typical of bent sandwich transition metal bis(η^5-cyclopentadienyl) complexes, i.e. the two planar C_5H_4Me groups bend back away from the coordinated η^3-allyl ligand. The angle between the centroids of the two methylcyclopentadienyl ligands [X1—Nb(1)—X2] (134.0°) is within experimental error of the narrow range observed for $(\eta^5\text{-}C_5H_5)_2NbX_2$ complexes [129.3(10)–133.2(3)],[5] but lower than that found for $(\eta^5\text{-}C_5H_5)_2NbH_3$ (141.6°).[1] The C—C distances within the aromatic rings are essentially equivalent, within experimental error, averaging 1.417(4) Å for C(12) to C(16), and 1.421(3) Å for C(22) to C(26). The Nb—C(C_5H_4Me) distances are not equivalent, ranging from 2.368(2) to 2.474(2) Å for C(12) to C(16) and from 2.310(2) to 2.491(3) Å for C(22) to C(26). Similar differences in Nb—C distances were noted for the bis(η^5-cyclopentadienyl)niobium complexes, $(C_5H_5)_2Nb(CS_2)(\eta^1\text{-}C_3H_5)$[5c] and $(C_5H_5)_2NbCl_2$,[5a] in which the Nb—C distances range from 2.37(2) to 2.50(2) Å and 2.33(4) to 2.44(3) Å, respectively.

The allyl ligand is nearly planar, with the C—C distances towards the long end of the range commonly observed for transition-metal allyl systems (1.35–1.45 Å),[6] consistent with the presence of σ-donation from the allyl π-orbital to the metal a'.

Since the allyl hydrogens were located and freely refined, the geometries around the allyl carbons may be readily defined. Whereas C(2) is close to trigonal planar, C(1) and C(2) are in distorted tetrahedral geometries. In addition, the plane of the allyl group is not perpendicular to the plane defined by Nb(2), C(1) and C(3), but is at an angle of 117.6°. These structural features are consistent with a strong bonding interaction betwen the allyl nonbonding orbital and the metal a'' orbital, but little or no back-bonding from the metal to allyl. The latter is therefore in accord with the results obtained from photoelectron spectroscopy[3] which indicates the presence of a metal-centred lone pair. The close structural similarity between **1** and $(\eta^5\text{-}C_5H_5)_2Ti(\eta^3\text{-}C_3H_3\text{-}1,2\text{-}Me_2)$[7] which have d^2 and d^1 metal centres, respectively, is also an indication that metal-to-ligand back donation is negligible.

EXPERIMENTAL

NMR (^1H, ^{13}C and ^{93}Nb) spectra, in C_6D_6, were recorded on Bruker AM-500 and WM-300 spectrometers [δ in parts per million relative to $SiMe_4$ (^1H, ^{13}C external) and $KNbCl_6$ in CH_3CN (^{93}Nb, external)]. The ^1H–^1H connectivity was established by a COSY NMR experiment. Spectra were collected using a standard pulse sequence[8] with a 45° mixing pulse, a 1 s relaxation delay, and a resolution of 4 Hz/pt. The FIDs were not weighted before Fourier transformation and the spectral matrix was symmetrized about the diagonal. The assignment of the methylcyclopentadienyl ligands relative to

Table 1. Selected bond lengths (Å) and angles (°) for **1**

Nb(1)—C(1)	2.325(2)	Nb(1)—C(2)	2.345(2)
Nb(1)—C(3)	2.346(2)	Nb(1)—C(12)	2.474(2)
Nb(1)—C(13)	2.419(3)	Nb(1)—C(14)	2.368(2)
Nb(1)—C(15)	2.388(3)	Nb(1)—C(16)	2.424(3)
Nb(1)—C(22)	2.491(3)	Nb(1)—C(23)	2.400(2)
Nb(1)—C(24)	2.310(2)	Nb(1)—C(25)	2.347(2)
Nb(1)—C(26)	2.435(2)	C(1)—C(2)	1.421(3)
C(2)—C(3)	1.412(4)		
C(1)—Nb(1)—C(2)	35.4(1)	C(1)—Nb(1)—C(3)	65.1(1)
C(2)—Nb(1)—C(3)	35.0(1)	C(1)—C(2)—C(3)	125.0(2)

the allyl ligand was determined by the observation of NOE enhancement of the signals of the methylcyclopentadienyl ligand closest to the proton attached to the central carbon of the allyl group. In a similar manner, the irradiation of the methyl resonances of the cyclopentadienyl ligands allowed for the assignment of the ring C—*H* resonances. The individual ^1H–^1H coupling constants were determined by the appropriate selective decoupling experiments. The ^{13}C resonances were assigned using a ^1H–^{13}C correlation experiment. Spectra were collected using a standard pulse sequence[9] with a 45° mixing pulse and a 2 s relaxation delay. The FIDs were weighted with a line broadening of 1 Hz prior to transformation. ^1H and ^{13}C NMR assignments are given relative to the atom numbering scheme in Fig. 2. Mass spectra were obtained using a Kratos MS-50L mass spectrometer and associated data system. EI spectra were recorded with an ionization energy of 70 eV at a scan rate of 3 s decade^{-1}. Samples were introduced into the instrument from a direct insertion probe. All manipulations were carried out under argon. Solvents were dried, distilled and degassed before use. The compound $(\eta^5\text{-}C_5H_4Me)_2NbCl_2$ was prepared by an improved modification of previous procedures[10] by the reduction of an ethereal suspension of $NbCl_5$ with ^{i}PrMgBr to give $NbCl_4$. Subsequent reaction with $Na(C_5H_4Me)$ in diethyl ether allowed the isolation of dark brown $(\eta^5\text{-}C_5H_4Me)_2NbCl_2$ in high yield (70–80%). Allyl Grignard, $(C_3H_5)MgBr$, was prepared by literature methods.[11]

$(\eta^5\text{-}C_5H_4Me)_2Nb(\eta^3\text{-}C_3H_5)$ (1)

$(C_3H_5)MgBr$ (23 cm^3, 1.15 M in diethyl ether, 26 mmol) was added dropwise to a stirred suspension of $(\eta^5\text{-}C_5H_4Me)_2NbCl_2$ (4.3 g, 13 mmol) in 100 cm^3 of diethyl ether. The dark green solution was stirred overnight and then the solvent was removed *in vacuo*. The solid was dissolved in 200 cm^3 of pentane, heated at reflux for 1 h, and filtered warm through a medium porosity frit. A green pentane solution was obtained and stored at −20°C under nitrogen. Dark green crystals precipitated upon cooling. Yield: 60–70%.

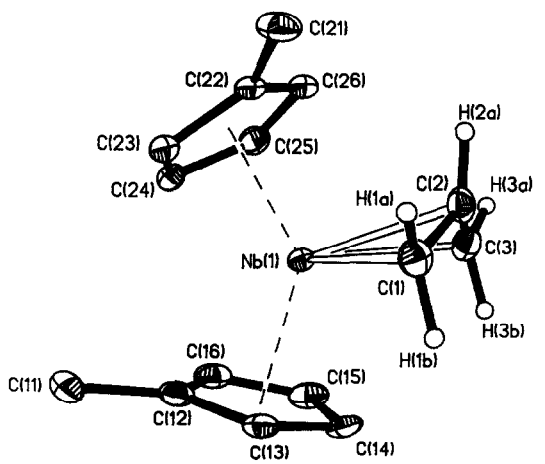

Fig. 2. X-ray crystal structure of **1** showing the numbering scheme. The hydrogen atoms on the methylcyclopentadienyl ligands are omitted for clarity.

Mass spectrum, *m/z*: 292 (M), 250 (M − C_3H_6), 105 (NbC), 79 (C_5H_4Me).

^1H NMR: 4.44 [2H, d, *J*(H—H) = 2.2 Hz, C(14,15)—*H*], 4.23 [2H, d, *J*(H—H) = 2.2 Hz, C(13,16)—*H*], 4.16 [2H, d, *J*(H—H) = 2.2 Hz, C(23,26)—*H*], 3.75 [2H, d, *J*(H—H) = 2.2 Hz, C(24,25)—H], 2.65 {2H, dd, *J*[H(1,3)a—H(1,3)b] = 4.6 Hz, *J*[H(1,3)a—H(2)a] = 9.4 Hz, C(1,3)—Ha}, 2.00 {1H, tt, *J*[H(2)a—H(1,3)a] = 9.4 Hz, *J*[H(2)a—H(1,3)b] = 14.0 Hz, C(2)—H}, 1.84 [3H, s, C(21)—H], 1.29 [3H, s, C(11)—H], 0.71 {2H, dd, *J*[H(1,3)b—H(1,3)a] = 4.6 Hz, *J*[H(1,3)b—H(2)a] = 14.0 Hz, C(1,3)—Hb}.

^{13}C-{^1H} NMR: 107.2, 106.3 [C(12), C(22)], 93.9 [C(13), C(16)], 91.7 [C(24), C(25)], 88.9 [C(14), C(14)], 78.8 [C(23), C(26)], 77.0 [C(2)], 42.6 [C(1), C(3)], 15.6 [C(21)], 14.4 [C(11)].

^{93}Nb-{^1H} NMR: −1738 ($w_{1/2}$ = 14,300 Hz).

X-ray crystallography

Unit-cell parameters and intensity data were obtained by following previously detailed

Table 2. Crystal data, details of intensity measurements and structure refinement for **1**

Formula	$C_{15}H_{19}Nb$
Mr	292.2
Crystal dimensions (mm)	0.10 × 0.20 × 0.15
Crystal system	Monoclinic
a (Å)	6.029(2)
b (Å)	7.752(2)
c (Å)	26.115(6)
β (°)	92.33(2)
V (Å^3)	1219.5(5)
Space group	$P2_1/c$
D_c (g cm^{-3})	1.592
Z	4
μ (mm^{-1})	0.915
Minimum, maximum 2*θ* (°)	4.0, 55.0
T (K)	193
Total data	3962
Total unique data	3413
Total observed data	2894
Weighting scheme parameter	$1/[(\lvert F_o\rvert)^2+0.0099\lvert F_o\rvert^2]$
Final *R*	0.031
Final R_w	0.050

procedures,[12] using a Nicolet R3m/v diffractometer operating in the θ–2θ scan mode with graphite-monochromated Mo-K_α radiation ($\lambda = 0.71069$ Å). Empirical absorption corrections were applied to the data using the program PSICOR. Further experimental data are given in Table 2.

The structure was solved using the direct methods program XS,[13] which revealed the position of the niobium atom. The remainder of the atoms were found using standard difference map techniques. Hydrogen atoms were located and refined with fixed isotropic thermal parameters.

Details of the refinement are given in Table 2. Selected bond lengths and angles are given in Table 1. Atomic scattering factors and anomalous scattering parameters are given in ref. 14.

Acknowledgements—We thank the Office of Naval Research and the National Science Foundation for financial support, and NSERC for a postdoctoral fellowship (A.W.A.).

REFERENCES

1. R. D. Wilson, T. F. Koetzle, D. W. Hart, A. Kvick, D. L. Tipton and R. Bau, *J. Am. Chem. Soc.* 1977, **99**, 1775.
2. J. W. Lauher and R. Hoffman, *J. Am. Chem. Soc.* 1976, **98**, 1729.
3. J. C. Green, S. E. Jackson and B. Higginson, *J. Chem. Soc., Dalton Trans.* 1975, 403.
4. P. D. Stupik, L. K. Cheatham, J. J. Graham and A. R. Barron, *Mater. Res. Soc. Symp. Proc.* 1990, **168**, 363.
5. (a) K. Prout, T. S. Cameron, R. A. Forder, S. R. Critchley, B. Denton and G. V. Rees, *Acta Cryst.* 1974, **B30**, 2990; (b) L. J. Guggenberger, P. Meakin and F. N. Tebbe, *J. Am. Chem. Soc.* 1974, **96**, 5420; (c) M. G. B. Drew and L. S. Pu, *Acta Cryst.* 1977, **B33**, 1207; (d) P. B. Hitchcock, M. F. Lappert and C. R. C. Milne, *J. Chem. Soc., Dalton Trans.* 1981, 180.
6. (a) H. J. Clarke, *J. Organomet. Chem.* 1974, **80**, 155; (b) J. A. Kaduk, A. T. Poulos and J. A. Ibers, *J. Organomet. Chem.* 1977, **127**, 245.
7. R. B. Helmholdt, F. Jellinck, H. A. Martin and A. Vos, *Recueil* 1967, **86**, 1263.
8. (a) W. P. Ave, E. Bartholdi and R. R. Ernst, *J. Chem. Phys.* 1976, **64**, 2229; (b) K. Nagayam, A. Kumar, K. Wüthrich and R. R. Ernst, *J. Magn. Reson.* 1980, **40**, 321.
9. A. Bax and G. Morris, *J. Magn. Reson.* 1981, **42**, 501.
10. (a) R. Broussier, H. Normand and B. Gautheron, *J. Organomet. Chem.* 1978, **155**, 337; (b) M. J. Bunker, A. DeCian, M. L. H. Green, J. J. E. Moreau and N. Siganporia, *J. Chem. Soc., Dalton Trans.* 1980, 2155.
11. R. E. Benson and B. C. McKusick, *Org. Synth.* 1963, **4**, 749.
12. M. D. Healy, D. A. Wierda and A. R. Barron, *Organometallics* 1988, **7**, 2543.
13. G. M. Sheldrick, SHELXTL PLUS. Nicolet Corporation, Madison, Wisconsin, U.S.A. (1986).
14. *International Tables for X-ray Crystallography*, Vol. 4. Kynoch Press, Birmingham (1974).

Polyhedron Vol. 10, No. 10, pp. 1079–1083, 1991
Printed in Great Britain

0277–5387/91 $3.00+.00
Pergamon Press plc

INFLUENCE OF LACTAM RING SIZE ON METALLAMACROCYCLE RING TYPE; SYNTHESIS AND CRYSTAL STRUCTURE OF THE HETEROMETALLIC COMPLEX $[Hg_2Er(C_8H_{14}NO)_4(NO_3)_3]_n$

DAVID M. L. GOODGAME,* ARWA M. KHALED and DAVID J. WILLIAMS

Chemistry Department, Imperial College of Science, Technology and Medicine, London SW7 2AY, U.K.

(*Received* 17 *October* 1990; *accepted* 5 *February* 1991)

Abstract—Reaction of 2-azacyclononanone (= LH) with mercury(II) acetate and erbium(III) nitrate in methanol yields the compound $[Hg_2ErL_4(NO_3)_3]_n$ (**1**), which has been characterized by X-ray diffraction. Each erbium atom is eight-coordinate and has two bidentate nitrates and two chelating HgL_2 units bonded to it. The remaining nitrate ion serves to link molecules of **1** to produce polymeric chains. The formation of the eight-membered mercury/erbium-containing rings results in a structure which is radically different from those previously found for the mercury/lanthanide complexes formed by the smaller ring lactams, 2-azacyclobutanone and 2-azacyclopentanone.

In previous work we have demonstrated the remarkable versatility of lactams of general formula **I** to produce polymeric mercury/metal hetero-

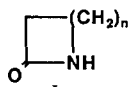

I

a; n = 1
b; n = 2
c; n = 6

metallic compounds containing large ring systems incorporating the metal atoms *within the ring framework*. Even with constant lactam ring size (e.g. 2-azacyclopentanone, 2-pyrrolidone, **Ib**) a wide diversity of metallamacrocycle ring sizes and structural types resulted from changes in the metal, M, employed.[1] Also, equally dramatic changes can be induced by reducing the size of the lactam ring to 2-azacyclobutanone[2](β-propiolactam, **Ia**) whilst keeping the metal unchanged. This has prompted us to explore lactams with larger rings, where the small, but potentially significant, changes in the coordination "bite" of the N—C—O lactam unit, coupled with the increased steric influences of the larger alicyclic rings, are likely to result in appreciable modifications to the polymeric structures adopted.

Although the use of larger ring lactams has not proved as amenable as **Ia** and **Ib** to the formation of heterometallic complexes of good crystalline quality—microcrystalline powders or even oils often result—the use of 2-azacyclononanone (**Ic**) has afforded good crystals of the complex $[Hg_2ErL_4(NO_3)_3]_n$ (**1**). X-ray structural studies on **1** show it to have a totally different structure from any of the heterometallic mercury/metal compounds formed by **Ia** or **Ib**.

EXPERIMENTAL

Preparation

Pale pink crystals of **1** separated over 3 days from a methanolic solution of mercury(II) acetate (0.16 g), hydrated erbium(III) nitrate (0.11 g) and **Ic** (0.14 g). Found: C, 28.9; H, 4.2; N, 7.3. Calc. for $C_{32}H_{56}ErHg_2N_7O_{13}$: C, 29.2; H, 4.3; N, 7.5%.

X-ray study

The crystal data are: $C_{32}H_{56}ErHg_2N_7O_{13}$, M_r = 1315.3, monoclinic, a = 12.385(2), b = 17.481(2), c = 19.853(2) Å, β = 106.10(1)°, V = 4130 Å^3, space group $P2_1/c$, Z = 4, D_c = 2.12 g cm^{-3}, Cu radiation, λ = 1.54178 Å, μ(Cu-K_α) = 183 cm^{-1},

* Author to whom correspondence should be addressed.

$F(000) = 2515$. Data were measured on a Nicolet R3m diffractometer with Cu-K_α radiation (graphite monochromator) using ω-scans.

A crystal of dimensions $0.03 \times 0.17 \times 0.30$ mm was used. 5004 independent reflections ($2\theta \leqslant 116°$) were measured, of which 4152 had $|F_o| > 3\sigma(|F_o|)$ and were considered observed. The data were corrected for Lorentz and polarization factors; a numerical absorption correction (face-indexed crystal) was applied; maximum and minimum transmission factors, 0.617 and 0.115.

The structure was solved by the heavy atom method. The non-hydrogen atoms were refined anisotropically. The positions of the hydrogen atoms were idealized, C—H = 0.96 Å, assigned isotropic thermal parameters, $U(H) = 1.2U_{eq}(C)$, and allowed to ride on their parent carbon atoms. Refinement was by block-cascade full-matrix least-squares to $R = 0.038$, $R_w = 0.034$ [$w^{-1} = \sigma^2(F) + 0.00017F^2$]. The maximum and minimum residual electron densities in the final ΔF map were 1.15 and -0.69 e Å^{-3}, respectively. The mean and maximum shift/error in the final refinement were 0.004 and 0.020, respectively. Computations were carried out on an Eclipse S140 computer using the SHELXTL program system.[3] Selected bond lengths and angles are listed in Table 1.

RESULTS AND DISCUSSION

We observed previously[2,4] that the stoichiometries of the mercury/erbium complexes formed by **Ia** and **Ib** were both of the type $Hg_3Er_2L_6(NO_3)_6$ (where L = the anions of **Ia** and **Ib**), and no compounds of other stoichiometries were obtained on varying the mole ratios of the reactants. In the case of ligand **Ic**, use of the same synthetic method has given a complex of different stoichiometry: $Hg_2ErL_4(NO_3)_3$.

The X-ray analysis shows the erbium atom to be eight-coordinate, adopting a distorted dodecahedral geometry (Fig. 1). The distortion parameters[5] are ϕ_A 26.4°, ϕ_B 101.4° and MA/MB = 1.08. This arrangement may alternatively be visualized as the erbium atom being coordinated axially by two bidentate nitrate groups and equatorially by four oxygen atoms from **Ic** ligands, which, if one regards each nitrate as a single group, produces a distorted octahedral array (Fig.

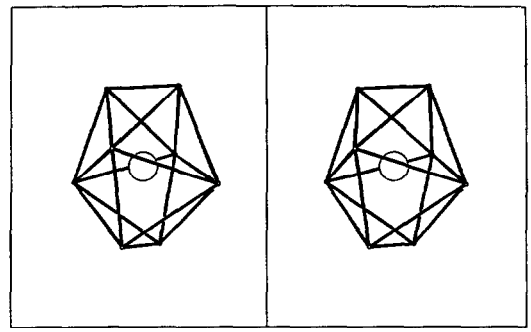

Fig. 1. Stereoscopic view of the dodecahedral arrangement of the oxygen atoms surrounding the erbium atom.

Table 1. Selected bond lengths (Å) and angles (°) for **1**

Hg(1)—N(1)	2.054(8)	Hg(2)—N(1″)	2.048(8)
Hg(1)—N(1′)	2.050(8)	Hg(2)—N(1*)	2.051(7)
Er—O(2)	2.216(7)	Er—O(21)	2.418(7)
Er—O(2′)	2.239(7)	Er—O(22)	2.413(7)
Er—O(2″)	2.242(8)	Er—O(31)	2.423(6)
Er—O(2*)	2.250(6)	Er—O(32)	2.416(7)
N(1)—Hg(1)—N(1′)	171.3(3)	N(1″)—Hg(2)—N(1*)	169.8(3)
O(2)—Er—O(2′)	94.6(3)	O(2)—Er—O(2″)	158.5(2)
O(2′)—Er—O(2″)	93.2(2)	O(2)—Er—O(2*)	88.7(3)
O(2′)—Er—O(2*)	156.0(2)	O(2″)—Er—O(2*)	92.2(2)
O(2)—Er—O(21)	79.8(2)	O(2′)—Er—O(21)	127.7(2)
O(2″)—Er—O(21)	79.6(3)	O(2*)—Er—O(21)	76.3(2)
O(2)—Er—O(22)	78.4(2)	O(2′)—Er—O(22)	75.0(2)
O(2″)—Er—O(22)	84.4(3)	O(2*)—Er—O(22)	128.8(2)
O(21)—Er—O(22)	52.8(2)	O(2)—Er—O(31)	74.0(2)
O(2′)—Er—O(31)	77.4(2)	O(2″)—Er—O(31)	127.3(3)
O(2*)—Er—O(31)	80.8(2)	O(21)—Er—O(31)	145.3(2)
O(22)—Er—O(31)	138.8(2)	O(2)—Er—O(32)	126.6(2)
O(2′)—Er—O(32)	81.3(3)	O(2″)—Er—O(32)	74.4(3)
O(2*)—Er—O(32)	77.7(3)	O(21)—Er—O(32)	142.1(3)
O(22)—Er—O(32)	147.2(3)	O(31)—Er—O(32)	53.0(3)

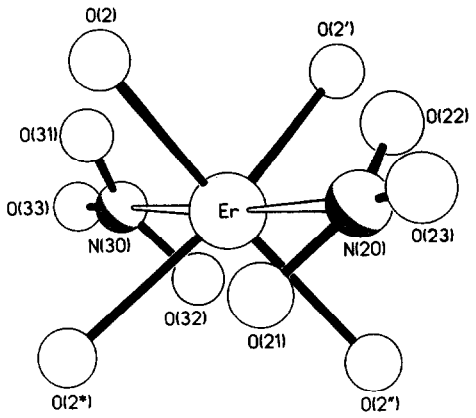

Fig. 2. Coordination geometry about the erbium atom.

2). The overall symmetry approximates to S_4 about the N(20)ErN(30) axis. The nitrate groups are arranged such that O(2), O(31), N(30), O(32) and O(2″) lie in one plane and O(2′), O(22), N(20), O(21) and O(2*) lie in another perpendicular to it. The Er—O bond lengths fall into two groups; those to nitrate oxygen atoms [range 2.413(7)–2.423(6) Å] being *ca* 0.2 Å longer than those to the carbonyl oxygen atoms [range 2.216(7)–2.250(6) Å].

Pairs of **Ic** ligands link via the deprotonated nitrogen atom to crystallographically independent mercury atoms in a nearly linear [Hg(1) 171.3(3)°, Hg(2) 169.8(3)°] arrangement. Each of these HgL_2 units binds to the erbium atom via the exocyclic oxygen atoms forming an eight-membered heterobimetallic ring (Fig. 3) in which only the erbium atom lies significantly out of the ring plane. (There are no significant out-of-plane distortions at any of the four amide nitrogen atoms.) The trans-annular Er...Hg distances are 3.78(1) and 3.83(1) Å to Hg(1) and Hg(2), respectively.

It is noticeable that in this complex the COEr angles are appreciably opened out from an idealized 120° and tend towards linearity (159, 160, 168 and 173°). The largest COM angle we have observed previously in related mercury metal lactam complexes was 156° [for $Hg_2Th(C_4H_6NO)_4(NO_3)_4$],[6] and, in general, the average value lies in the range 135–140°.

Despite the conformational flexibility of the 2-azacyclononanone ring, three of the four have virtually identical conformations (Table 2). Rings B and D (Fig. 3) are the same, C is enantiomeric, but ring A adopts a totally different geometry. A comparison of the conformations of rings A and B, using the amide groups on each ring as a common basis, is shown in Fig. 4.

Compound **1** differs from the related mercury/erbium complexes formed by **Ia** and **Ib** in that only two of the three nitrate anions are bonded to the erbium atom. The remaining nitrate ion does, however, play a key role in the formation of an overall polymeric structure (Fig. 5). It links Hg(1) in one molecular unit to Hg(2) in the next. This is achieved by O(12) binding to both Hg(1) and Hg(2)

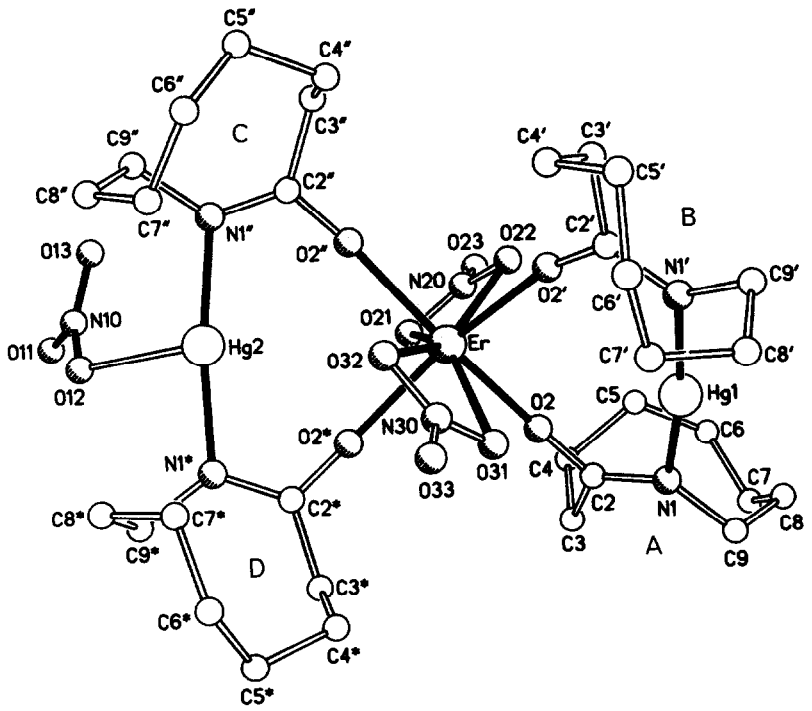

Fig. 3. Perspective view of each $[Hg_2Er(C_8H_{14}NO)_4(NO_3)_3]$ unit, giving the atom numbering.

Table 2. Torsion angles (°)[a] for the 2-azacyclononanone rings in **1**[b]

	A	B	C[c]	D
C(9)—N(1)—C(2)—C(3)	−3	9	5	11
C(2)—N(1)—C(9)—C(8)	84	102	106	103
N(1)—C(2)—C(3)—C(4)	−107	−85	−90	−86
C(2)—C(3)—C(4)—C(5)	48	90	90	85
C(3)—C(4)—C(5)—C(6)	80	−104	−103	−102
C(4)—C(5)—C(6)—C(7)	−61	54	60	58
C(5)—C(6)—C(7)—C(8)	−59	64	57	61
C(6)—C(7)—C(8)—C(9)	98	−76	−70	−79
C(7)—C(8)—C(9)—N(1)	−81	−54	−50	−50

[a] Average ESD *ca* 1°.
[b] Rings A–D are identified in Fig. 3.
[c] Enantiomer of C.

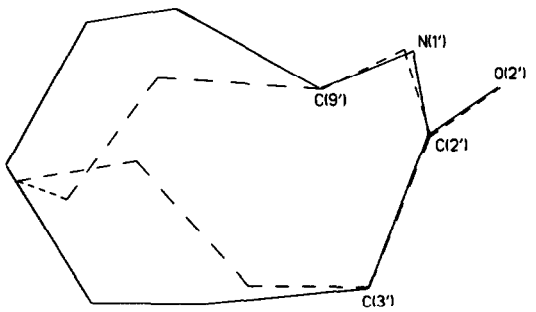

Fig. 4. A comparison of the conformations of rings A and B. Ring A is depicted by broken lines.

[Hg(1)—O(12) 2.75(1) and Hg(2)—O(12) 2.62(1) Å; Hg(1)...Hg(2) 4.5 Å]; O(11) binds to just a single mercury atom, Hg(1) [Hg(1)—O(11) 2.75(1) Å]. In both cases the approach of the nitrate oxygen atoms is virtually orthogonal to the N—Hg—N directions. For Hg(1) the O—Hg—N angles are in the range 91–96° and for Hg(2) they are in the range 84–106°. The direction of the polymer chain is along the crystallographic *b* direction—the chain being made up of screw-related molecules.

Despite the bulk of the alkane rings, the crystal packing is very efficient, with adjacent, centrosymmetrically related polymer chains inter-

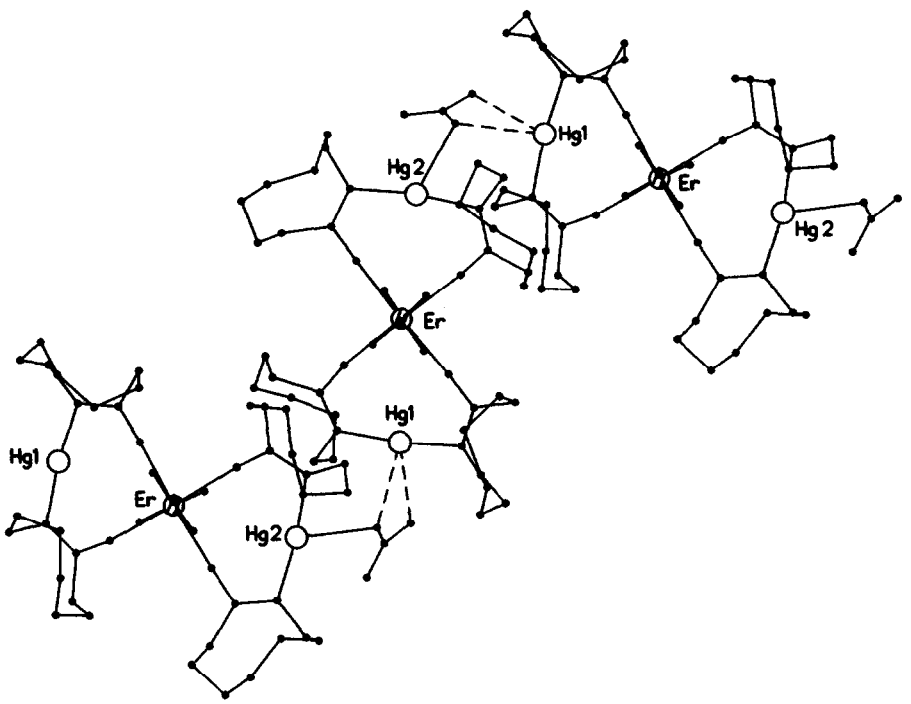

Fig. 5. Part of one of the nitrate-linked polymeric chains of **1**.

leaving with each other. The packing gives rise to short, non-bonded CH...O(NO_3) contacts, e.g. C(3)...O(11) 3.09, C(3″)...O(13) 3.24 Å; in this latter case the H(3A″)...O(13) distance is 2.40 Å and the C—H...O angle, 146°.

It is interesting that the use of the larger ring lactam, **Ic**, produces a structure in which, for the first time for a mercury/lanthanide ion combination, the minimum size (eight-membered) metallamacrocycle is formed. This is in striking contrast to the very large macrocycles (up to 80-membered[1]) previously encountered. The only other eight-membered rings we have found are in the homobimetallic mercury/mercury complex $[Hg_2(C_4H_6NO)_2Cl_2]_n$[1] and the mercury/silver complex $[HgAg(C_4H_6NO)_2(NO_3)]_2$[7] formed by 2-pyrrolidone; in the latter of those two compounds one of the oxygen atoms of the chelating 2-pyrrolidone additionally serves as a bridge between pairs of silver atoms.

Acknowledgement—We thank the SERC for the X-ray diffractometer.

REFERENCES

1. D. M. L. Goodgame, D. J. Williams and R. E. P. Winpenny, *Polyhedron* 1989, **8**, 1913 and refs therein.
2. D. M. L. Goodgame, A. M. Khaled, C. A. O'Mahoney and D. J. Williams, *J. Chem. Soc., Chem. Commun.* 1990, 851.
3. G. M. Sheldrick, SHELXTL, An Integrated System for Solving, Refining, and Displaying Crystal Structures from Diffraction Data, Revision 5.1. University of Göttingen, F.R.G. (1985).
4. D. M. L. Goodgame, D. J. Williams and R. E. P. Winpenny, *J. Chem. Soc., Dalton Trans.* 1989, 1439.
5. D. L. Kepert, *Progr. Inorg. Chem.* 1978, **24**, 179.
6. D. M. L. Goodgame, D. J. Williams and R. E. P. Winpenny, *Polyhedron* 1988, **7**, 1807.
7. D. M. L. Goodgame, D. J. Williams and R. E. P. Winpenny, *Polyhedron* 1988, **7**, 1299.

Polyhedron Vol. 10, No. 10, pp. 1085–1090, 1991
Printed in Great Britain

0277–5387/91 $3.00+.00
Pergamon Press plc

CRYSTAL STRUCTURE AND COORDINATION CHEMISTRY OF (2-CARBOMETHOXYETHYL)IODODIPHENYLSTANNANE, $IPh_2SnCH_2CH_2CO_2Me$

PAUL HARSTON, R. ALAN HOWIE, GEOFFREY P. McQUILLAN, JAMES L. WARDELL* and ENRICO ZANETTI

Department of Chemistry, University of Aberdeen, Meston Walk, Old Aberdeen AB9 2UE, Scotland, U.K.

and

SOLANGE M. S. V. DOIDGE-HARRISON and NEIL S. STEWART

School of Applied Sciences, Robert Gordon's Institute of Technology, St Andrews Street, Aberdeen AB1 1HG, Scotland, U.K.

and

PHILIP J. COX

School of Pharmacy, Robert Gordon's Institute of Technology, Schoolhill, Aberdeen, AB1 1FR, Scotland, U.K.

(*Received* 23 *October* 1990; *accepted* 5 *February* 1991)

Abstract—The crystal structure of $IPh_2SnCH_2CH_2CO_2Me$: $C_{16}H_{17}IO_2Sn$ (**10**; X = I) has been determined; the tin atom adopts a distorted trigonal bipyramidal geometry, with iodine and the internal carbonyl oxygen in axial sites. The chelated structure of **10** (X = I) [ν(CO) 1684 cm^{-1}] persists in such solvents as dichloromethane, chloroform, tetrahydrofuran and acetonitrile. Pyridine is able to compete with the intramolecular ester coordination in CH_2Cl_2 solution with the formation of unchelated $IPh_2Sn(py)CH_2CH_2CO_2Me$ (**11**) [ν(CO) 1734 cm^{-1}]; the formation constant of **11** is 0.07 ± 0.01 1 mol^{-1} at 25°C.

Ester groups are generally weak donors towards organotin acceptors. However, when sited intramolecularly, for example as in $Cl_2Sn(CH_2CH_2CO_2Me)_2$ (**1**),[1] $Cl_3SnCH_2CH_2CO_2R$ (**2**), (R = Me;[1] R = Pr^i [2]) and $Cl_3SnCH_2CH_2CH_2CO_2Et$ (**3**),[3] they are able to complex strongly to tin centres.[4] Crystal structure determinations[1–3] and spectral data[4–6] for **1–3** and related compounds show that $RO_2C(CH_2)_n$ groups do act as chelating ligands in the solid state. Similar conclusions are obtained in non-coordinating solvents.[2,3] However in coordinating solvents such as MeCN[2,3] or in the presence of nitrogen donors, e.g. pyridine or 2,2′-bipyridine, the coordination by the ester groups, e.g. in **2** and **3**, can be broken.[2,3] From comparison of stability constants, the five-membered chelate ring in **2** is found to be stronger than the six-membered ring in **3**.

The chelating abilities of $RO_2CCH_2CH_2$ and other groups (Me_2NCS_2 and 8-quinolinato) have been compared in appropriate compounds, e.g. $[MeO_2CCH_2CH_2SnCl_{3-n}(S_2CNMe_2)_n]$ (**4**; n = 1–3),[7,8] $[(MeO_2CCH_2CH_2)_2Sn(S_2CNMe_2)_2]$ (**5**)[9] and $[(MeO_2CCH_2CH_2)_2SnCl(8\text{-quinolinate})]$ (**6**):[10] structural studies indicate that the $MeO_2CCH_2CH_2$ group has the weakest chelating ability of these three groups. The sulphido compounds, $[(MeO_2CCH_2CH_2)_2SnS]_3$ (**7**)[11] and $[MeO_2CCH_2CH_2Sn(S)(S_2CNMe_2)]_3$ (**8**),[11] in the solid state, both

* Author to whom correspondence should be addressed.

contain monodentate $RO_2CCH_2CH_2$ units as does $[(RO_2CCH_2CH_2)(Me_2NCS_2)Sn(XCH_2CH_2)_2Y]$ (**9** R = Me, X = S, Y = O; R = Et, X = O, Y = NMe).[12]

The Lewis acidity of organotin halides generally decreases in the sequence: $RSnX_3 > R_2SnX_2 > R_3SnX$. Thus it is anticipated that the tin atom in $XPh_2SnCH_2CH_2CO_2Me$ (**10**) would be a poorer acceptor centre than that in $X_3SnCH_2CH_2CO_2Me$ (X = halide) towards both the internal ester group and external donors. In order to investigate the coordination chemistry of **10**, we have determined the crystal structure of **10** (X = I) and have studied its coordination by donor molecules. We now wish to report our results.

EXPERIMENTAL

The compound $Ph_3SnCH_2CH_2CO_2Me$ (**11**) was prepared from Ph_3SnH and $CH_2{=}CHCO_2Me$ by a published procedure.[13] The reaction of **11** (4.37 g 0.01 mol) and I_2 (2.54 g, 0.01 mol) in CCl_4 (50 ml) gave $IPh_2SnCH_2CH_2CO_2Me$. The reaction residue, after removal of all volatiles, was recrystallized from EtOH to give a solid; melting point 77°C (ref. 13, 76°C). Found: C, 39.3; H, 3.5; I, 26.2. Calc. for $C_{16}H_{17}IO_2Sn$: C, 39.5, H, 3.5; I, 26.1%. ^{119}Sn NMR ($CDCl_3$, 33.35 MHz): δ −92.07 ppm (relative to Me_4Sn).

$Cl_3SnCH_2CH_2CO_2Me$ was a recrystallized sample from a previous study.[6]

Solvents and donor molecules

MeCN was purified by a standard procedure;[14] CH_2Cl_2 and THF were dried over CaH_2 and distilled prior to use. Donor molecules were either redistilled or recrystallized prior to use.

The compound $Cl_2Pt(COD)$ (COD = 1,5-cyclooctadiene) was obtained by a literature procedure.[15]

Formation constants

These were determined from IR data, from the carbonyl region, at 25 ± 1°C in CH_2Cl_2 solution as previously described.[6]

Reaction between **11** *and* $Cl_2Pt(COD)$

Solutions of **11** (0.0437 g, 1 mmol) and $Cl_2Pt(COD)$ (0.0374 g, 1 mmol) in CD_2Cl_2 (total volume 1 cm^3) were mixed and the reaction monitored by ^1H NMR spectroscopy (220 MHz) at 30°C. The successive formations of $ClPh_2SnCH_2CH_2CO_2Me$ and $Cl_2PhSnCH_2CH_2CO_2Me$ were indicated (see Table 1 for ^1H NMR details).

The platinum products—ClPhPt(COD) and $Ph_2Pt(COD)$—were also detected by NMR.

ClPhPt(COD). δ ^1H 2.46 (m, 8H, CH_2), 4.55 (t, 2H, $J^{119}Pt$–^1H 75 Hz, CH), 5.70 (t, 2H, 34 Hz, CH), 6.7–7.4 (m, 5H, phenyl).

$Ph_2Pt(COD)$. δ^1H 2.5 (m, 8H, CH_2), 5.02 (t, 4H, $J^{119}Pt$–^1H, 40 Hz, CH), 6.6–7.5 (m, 10H, phenyl).

Crystal structure determination

Crystal data. $C_{16}H_{17}IO_2Sn$, $M = 486.91$, monoclinic, space group $P2_{1/n}$, $a = 10.073(8)$, $b = 17.721(14)$, $c = 10.427(10)$ Å, $\beta = 112.11(7)°$, $V = 1725(2)$ Å^3, $Z = 4$, $D_c = 1.875$ g cm^{-3}, $D_m = 1.88$ g cm^{-3}, $F(000) = 928$, μ(Mo-K_α) = 3.26 mm^{-1}, $\lambda = 0.71069$ Å, T = room temperature.

Table 1. ^1H NMR spectra (220 MHz) for $Ph_nX_{3-n}SnCH_2CH_2CO_2Me$ in CD_2Cl_2 $\delta(J^{119}Sn$–^1H Hz)

Compound	CH_2^a α	CH_2^a β	OMe	Ph[b]	
				m+*p*	*o*
$Ph_3SnCH_2CH_2CO_2Me$	1.61 (55)	2.65 (68)	3.43	7.35	7.53
$IPh_2SnCH_2CH_2CO_2Me$	1.96	2.82	3.73	7.35	7.76
$ClPh_2SnCH_2CH_2CO_2Me$	1.73	2.82	3.78	7.38	7.77
$Cl_2PhSnCH_2CH_2CO_2Me$	1.96	2.92	3.86	7.46	7.90
$Cl_3SnCH_2CH_2CO_2Me$	2.23 (108)	2.96 (191)	3.97	—	—

[a] Triplet $J_{H,H}$ 8 Hz.
[b] Multiplets.

Data collection and processing. Colourless crystal, $0.31 \times 0.14 \times 0.25$ mm. The cell dimensions were obtained from setting angles of 14 independent reflections with $2\theta \approx 20°$ on a Nicolet P3 4-circle diffractometer using monochromatic Mo-K_α radiation. 3059 unique intensities were measured with $\theta \leqslant 25°$ as $\theta/2\theta$ scans; 1958 reflections had $F > 5\sigma(F)$. Range of $h\ k\ l$: $0 \leqslant h \leqslant 11$; $0 \leqslant k \leqslant 21$; $-11 \leqslant l \leqslant 11$.

The data were corrected for Lorentz and polarization effects but absorption was ignored. Two reference reflections, monitored periodically, showed no significant variation in intensity.

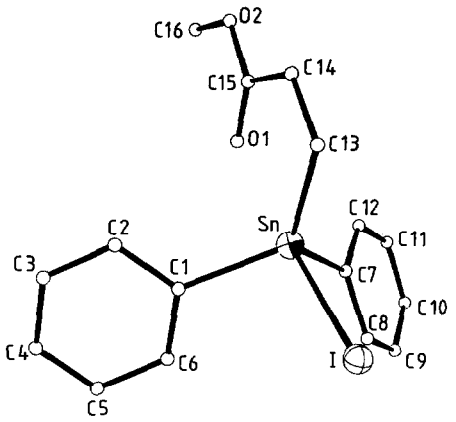

Fig. 1. Molecular structure of **10** (X = I).

Structure analysis and refinement

The structure was determined by the heavy-atom method (Patterson function), which revealed the approximate positions of the tin and iodine atoms. The remaining non-hydrogen atoms were located from successive Fourier difference maps using SHELX 76.[16] The hydrogen atoms were placed in calculated positions and refined relative to their bonded carbons. Full-matrix least squares calculations on F with unit weights and anisotropic thermal parameters for all non-hydrogen atoms and isotropic thermal parameters for hydrogen atoms converged at $R = 0.052$. Atomic scattering factors for carbon, hydrogen, oxygen and tin were taken[16] from SHELX 76. Data for iodine was taken from the *International Tables for X-ray Crystallography*.[17] Final $\Delta\rho_{max} = +0.76$ eÅ^{-3}, $\Delta\rho_{min} = -0.66$ eÅ^{-3}. Molecular geometries were generated by the GX package.[18]

RESULTS AND DISCUSSION

Compound **10** (X = I) was obtained by the reaction of **11** with I_2; this cleavage reaction occurs particularly readily, due to the nucleophilic assistance afforded by the ester group in the rate-determining step. Other reactions of **11** with electrophilic reagents are facile, e.g. even the weakly electrophilic, Me_3SiX, is able to cleave a Ph—Sn bond[19] in **11** to give **10** (X = Cl, Br or I); $Cl_2Pt(COD)$ can cause cleavage of two Ph—Sn bonds to give successively **10** (X = Cl) and $Cl_2PhSnCH_2CH_2CO_2Me$, as shown in this study. ^{1}H NMR spectral data for $Ph_nX_{3-n}SnCH_2CH_2CO_2Me$ compounds are given in Table 1.

Crystal structure of **10** (X = I)

The atomic arrangements are shown in Fig. 1. Bond lengths are given in Table 2 and bond angles in Table 3. Compound **10** (X = I) exists as discrete molecules, containing five-membered chelate rings.

The geometry about tin is that of a distorted trigonal bipyramid, the axial atoms being I [Sn—I 2.811(2) Å] and the carbonyl oxygen [Sn—O 2.55(2) Å] with the valence angle, I—Sn—O, equal to 170.5(3)°. The three carbon units are in equatorial sites [Sn—C = 2.10(2)–2.16(2) Å]: the sum of the C—Sn—C valence angles is 353.8°.

Intramolecular Sn—O distances in other $RO_2(CH_2)_n$—Sn compounds are given in Table 4. It can be seen in Table 3 that the Sn—O distance in **10** (X = I) is comparable with those in **1** (Sn—O 2.52), but is appreciably greater than in **2** [Sn—O 2.337(5)–2.357(5) Å]. The sum of the covalent radii of tin and oxygen is 2.13 Å, while the sum of the van der Waals' radii is 3.70 Å. The Sn—I bond distance is relatively long, cf. the value of 2.764(2) Å in the five-coordinate tin compound,[20] 3-*C*-(IBu_2SnCH_2)-1,2 : 5,6-di-*O*-isopropylidene-α-D-allofuranose, in which the intramolecular Sn—O distance is 2.68(2) Å. Sn—I bond lengths in a number of tetrahedral tin compounds range[21] from 2.69(3) to 2.729(3) Å.

Solution study

Compound **10** (X = I) remains completely chelated in chlorocarbon solvents (CH_2Cl_2 and CCl_4) [ν(CO) 1684 cm^{-1}] as well as in MeCN and THF solutions: the values of ν(CO) for **10** (X = I) in a KBr disc is 1670 cm^{-1}, while ν(CO) for $Ph_3SnCH_2CH_2CO_2Me$ in KBr is 1740 cm^{-1}. Similar findings are obtained for **10** (X = Cl). As can be seen from the ^{1}H NMR spectral data given in Table 1, complexation of the MeO_2C group to tin [in $Ph_nX_{3-n}SnCH_2CH_2CO_2Me$ ($n = 0$, 1 or 2)] results in shifts for δMe and in β-CH_2, from values in $Ph_3SnCH_2CH_2CO_2Me$.

Table 2. Bond lengths (Å) for **10** (X = I) with ESDs in parentheses

Sn—I	2.811(2)	Sn—O(1)	2.55(2)
Sn—C(1)	2.14(2)	Sn—C(7)	2.16(2)
Sn—C(13)	2.10(2)	C(13)—C(14)	1.45(4)
C(14)—C(15)	1.48(3)	C(15)—O(1)	1.20(2)
C(15)—O(2)	1.30(3)	C(16)—O(2)	1.47(3)
C(1)—C(2)	1.38(3)	C(7)—C(12)	1.33(3)
C(2)—C(3)	1.39(3)	C(11)—C(12)	1.37(3)
C(3)—C(4)	1.35(4)	C(10)—C(12)	1.34(4)
C(4)—C(5)	1.35(4)	C(9)—C(10)	1.35(3)
C(5)—C(6)	1.38(3)	C(8)—C(9)	1.40(3)
C(6)—C(1)	1.37(3)	C(7)—C(8)	1.39(3)

In CH_2Cl_2 solution, pyridine is able to compete with the intramolecular ester coordination in **10** (X = I) and equilibrium (1) is set up. The value of the formation constant, K_1, at 25°C was calculated to be 0.07 ± 0.01 dm^3 mol^{-1}. Only one pyridine molecule is able to coordinate to **10**. The value of K_1 indicates the difficulty of opening the chelate ring; even in pyridine as solvent, only *ca* 40% has the open structure. One molar equivalents of such donors as 2,2′-bipyridine, acridine and Ph_3P, had no impact on the spectrum of **10** (X = I) in CH_2Cl_2 solution.

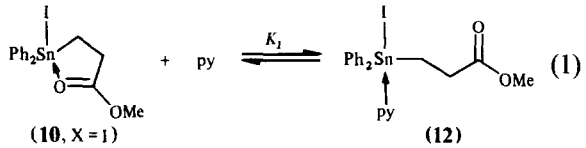

(1)

(10, X = I) **(12)**

ν(CO) 1684 cm^{-1} ν(CO) 1734 cm^{-1}

$K_1 = [(\mathbf{12})] / [(\mathbf{10}, X = I)][py]$

The compound $Cl_3SnCH_2CH_2CO_2Me$ has been previously shown to take part in equilibria with pyridine in CH_2Cl_2 solution (Scheme 1).[6] With $Cl_3SnCH_2CH_2CO_2Me$ **2** (R = Me), both one and two molecules of pyridine could be coordinated; however only on coordination of the second molecule of pyridine is the chelate ring broken.

From comparison of values of K_1 and K_3, it can be seen that the chelate ring in **10** (X = I) is considerably more resistant to opening than in **13**; in other words, the intramolecular ester coordination in **10** (X = I) is surprisingly stronger than that in **13**. The relative strengths of the chelate rings in **10** (X = I) and **2** are also borne out by the effects of MeCN on the opening of the chelates.

Formation constants for 1 : 1 R_3SnCl–py complexes have also been reported:[22,23] values obtained are 1.9 dm^3 mol^{-1} for R = Me in CCl_4 at 27°C (and also in C_6H_6 at 30°C) and 1.1 dm^3 mol^{-1} for R = Ph

Table 3. Bond angles (°) for **10** (X = I) with ESDs in parentheses

I—Sn—C(1)	96.9(5)	O(1)—Sn—C(1)	85.5(6)
I—Sn—C(7)	100.3(5)	O(1)—Sn—C(7)	87.2(5)
I—Sn—C(13)	97.6(6)	O(1)—Sn—C(13)	73.4(6)
I—Sn—O(1)	170.5(3)	C(1)—Sn—C(7)	112.1(7)
C(1)—Sn—C(13)	119.8(7)	C(7)—Sn—C(13)	121.9(7)
Sn—C(13)—C(14)	116.6(14)	C(14)—C(15)—O(2)	115.4(16)
C(13)—C(14)—C(15)	119.4(19)	C(15)—O(2)—C(16)	116.0(15)
C(14)—C(15)—O(1)	120.0(18)	O(1)—C(15)—O(2)	124.6(16)
C(15)—O(1)—Sn	110.7(11)		
Sn—C(7)—C(12)	123.6(14)	Sn—C(1)—C(2)	122.0(13)
C(7)—C(12)—C(11)	123.3(19)	C(1)—C(2)—C(3)	118.9(17)
C(12)—C(11)—C(10)	120.7(19)	C(2)—C(3)—C(4)	122.1(19)
C(11)—C(10)—C(9)	117.7(17)	C(3)—C(4)—C(5)	119.6(20)
C(10)—C(9)—C(8)	122.6(20)	C(4)—C(5)—C(6)	119.2(17)
C(9)—C(8)—C(7)	117.9(17)	C(5)—C(6)—C(1)	122.4(18)
C(8)—C(7)—C(12)	117.5(16)	C(6)—C(1)—Sn	120.2(13)
C(8)—C(7)—Sn	118.8(12)	C(2)—C(1)—C(6)	117.8(16)

Table 4. Crystal structure data for $RO_2C(CH_2)_n$-Sn compounds

Compound	Crystal structure details	ν(CO) solid (cm^{-1})	Reference
$(MeO_2CCH_2CH_2)_2SnCl_2$	Six-coordinate Sn; both =O complexed Sn—O 2.52 Å	1675[a]	1
$(MeO_2CCH_2CH_2)_2SnCl$(8-quinolinate)	Six-coordinate Sn; one =O complexed Sn—O 2.847(4) Å	1732[a] 1712[a]	10
$(MeO_2CCH_2CH_2)_2Sn(S_2CNMe_2)_2$	Seven-coordinate Sn; one =O complexed Sn—O 2.751(5) Å	1730[a] 1693[a]	9
$[(MeO_2CCH_2CH_2)_2SnS]_3$	Four-coordinate Sn; no =O complexed bridging S	1713	11
$MeO_2CCH_2CH_2SnCl_3$	Five-coordinate Sn; =O coordinated Sn—O 2.347(5) Å	1658	1
$Pr^iO_2CCH_2CH_2SnCl_3$	Five-coordinate Sn =O coordinated Sn—O 2.337(5) Å		2
$MeO_2CCH_2CH_2SnCl_2(S_2CNMe_2)$	Six-coordinate Sn; complexed Sn—O 2.436(6) Å	1652	7
$MeO_2CCH_2CH_2SnCl(S_2CNMe_2)_2$	Six-coordinate Sn =O not complexed	1724	8
$[MeO_2CCH_2CH_2Sn(S)(S_2CNMe_2)]_2$	Five-coordinate Sn; =O not complexed [Sn———O 3.19 Å]	1730	11
$MeO_2CCH_2CH_2Sn(S_2CNMe_2)$ $[(SCH_2CH_2)_2O]$	Six-coordinate Sn; =O not complexed		12
$EtO_2CCH_2CH_2Sn(S_2CNMe_2)$ $[(OCH_2CH_2)_2NMe]$	Six-coordinate Sn; =O not complexed		12
$EtO_2CCH_2CH_2CH_2SnCl_3$	Five-coordinate Sn; =O complexed Sn—O 2.405(8) Å	1645	3
$MeO_2CCH_2CH_2SnIPh_2$	Five-coordinate Sn; =O complexed Sn—O 2.55(2) Å	1684	[b]

[a] V. G. Kumar Das, N. S. Wang and P. J. Smith, *Inorg. Chim. Acta.* 1981, **49**, 149.
[b] This study.

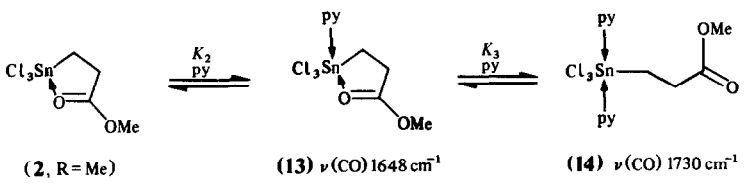

(**2**, R = Me) ν(CO) 1684 cm^{-1} (**13**) ν(CO) 1648 cm^{-1} (**14**) ν(CO) 1730 cm^{-1}

K_2 = [**13**] / [(**2**, R = Me)] > 10^5 at 25 °C
K_3 = [**14**] / [**13**] [py] = $10^{0.85}$ at 25 °C

Scheme 1.

in C_6H_6 at 30°C. Compounds R_3SnCl and R_3SnI have similar Lewis acidities, and so the reduction of the Lewis acidity of **10** (X = I) arising from chelation can be deduced to be a factor of *ca* 20.

1 : 1 Complexes of Me_3SnX–py (**15**) have been isolated; moreover the crystal structure of **15** (X = Cl) has been determined.[24] As predicted by the values of the formation constants of **15**, it is completely dissociated in non-polar solvents.

Acknowledgements—Support under the European Community's Erasmus Training Programme (No. ICP89UK0206) to enable E.Z. (normally of the Dipartimento de Chimica Inorganica, Metallorganica and Analitica, Universita di Padova, Italy) to spend a period at Aberdeen is gratefully acknowledged, as is a SERC CASE award (to P.H.).

REFERENCES

1. P. G. Harrison, T. J. King and M. A. Healy, *J. Organomet. Chem.* 1979, **182**, 17.
2. R. A. Howie, E. S. Paterson, J. L. Wardell and J. W. Burley, *J. Organomet. Chem.* 1983, **259**, 71.
3. R. A. Howie, E. S. Paterson, J. L. Wardell and J. W. Burley, *J. Organomet. Chem.* 1986, **304**, 301.
4. R. E. Hutton and V. Oakes, in Organotin compounds: new chemistry and applications, *Adv. Chem. Soc.* 1976, **157**, 123; R. E. Hutton, J. W. Burley and V. Oakes, *J. Organomet. Chem.* 1978, **156**, 369; R. M. Haigh, A. G. Davies and M.-W. Tse, *J. Organomet. Chem.* 1979, **174**, 163.
5. V. G. Kumar Das, S. W. Ng and P. J. Smith, *J. Organomet. Chem.* 1987, **49**, 149.
6. D. Maughan, J. L. Wardell and J. W. Burley, *J. Organomet. Chem.* 1981, **212**, 59.
7. O.-S. Jung, J. H. Jeong and Y. S. Sohn, *Polyhedron* 1989, **8**, 1413.
8. O.-S. Jung, J. H. Jeong and Y. S. Sohn, *Acta Cryst.* 1990, **C46**, 31.
9. S. W. Ng, C. Wei, V. G. Kumar Das, G. B. Jameson and R. J. Butcher, *J. Organomet. Chem.* 1989, **365**, 75.
10. S. W. Ng, C. Wei, V. G. Kumar Das, J.-P. Charland and F. E. Smith, *J. Organomet. Chem.* 1989, **364**, 343.
11. O.-S. Jung, J. H. Jeong and Y. S. Sohn, *Polyhedron* 1989, **8**, 2557.
12. O.-S. Jung, J. H. Jeong and Y. S. Sohn, unpublished observation.
13. J. G. Noltes and G. J. M. van Der Kerk, Functionally Substituted Organotin Compounds. Tin Research Institute, Greenford, Middlesex; see also L. Verdonck and G. P. van der Kelen, *J. Organomet. Chem.* 1968, **11**, 491.
14. J. F. Coltzee, *Pure and Appl. Chem.* 1966, **13**, 429.
15. D. Drew and J. R. Doyle, *Inorg. Synth.* 1972, **13**, 48.
16. G. M. Sheldrick, SHELX 76, Program for Crystal Structure Determination. University of Cambridge, U.K. (1976).
17. *International Tables for X-Ray Crystallography*, Vol. IV. Kynoch Press, Birmingham, U.K. (1974).
18. P. R. Mallinson and K. W. Muir, *J. Appl. Cryst.* 1985, **18**, 51.
19. J. C. Podesta, A. B. Chopa, A. D. Ayala and L. C. Koll, *J. Organomet. Chem.* 1987, **333**, 25.
20. P. J. Cox, S. M. S. V. Doidge-Harrison, R. A. Howie, I. W. Nowell, O. J. Taylor and J. L. Wardell, *J. Chem. Soc., Perkin Trans.* 1 1989, 2017.
21. F. Meller and I. Fankucken, *Acta Cryst.* 1955, **8**, 343; N. W. Alcock and J. F. Sawyer, *J. Chem. Soc., Dalton Trans.* 1977, 1090; V. Cody and E. R. Corey, *J. Organomet. Chem.* 1969, **19**, 359; L. H. Zakhanov, B. I. Betrov, V. A. Lobedev, E. A. Kuz'min and N. V. Belov, *Kristallografiya* 1978, **23**, 1049; H. A. Skinner and L. E. Sutton, *Trans. Faraday Soc.* 1944, **90**, 164.
22. D. P. Graddon and B. A. Rana, *J. Organomet. Chem.* 1976, **105**, 51; Y. Farhangi and D. P. Graddon, *J. Organomet. Chem.* 1975, **87**, 67.
23. T. F. Bolles and R. S. Drago, *J. Am. Chem. Soc.* 1966, **88**, 3921.
24. E. V. van den Berghe and G. P. van der Kelen, *J. Organomet. Chem.* 1968, **11**, 479; I. R. Beattie and G. P. McQuillan, *J. Chem. Soc.* 1963, 1519; R. Hulme, *J. Chem. Soc.* 1963, 1524.

Polyhedron Vol. 10, No. 10, pp. 1091–1096, 1991
Printed in Great Britain

0277-5387/91 $3.00+.00
© 1991 Pergamon Press plc

SPECTROSCOPIC CHARACTERIZATION, ELECTROCHEMISTRY AND SINGLE-CRYSTAL STRUCTURE OF BIS[CHLOROBIS (DIMETHYLPHOSPHITO-*P*)(HEXAMETHYLBENZENE) RUTHENIUM(II)-μ-(*O,O,Cl*)]COPPER(II) DICHLOROMETHANE (1:2), AN UNUSUAL LINEAR, HETEROTRINUCLEAR COMPLEX

GERARD A. VAN ALBADA, RUDOLF A. G. DE GRAAF, RONALD HAGE and JAN REEDIJK

Department of Chemistry of Leiden University, P.O. Box 2300, RA Leiden, The Netherlands

and

ELKE BUCHHOLZ and WOLFGANG KLÄUI

Institut für Anorganische Chemie, TH Aachen, Templergraben 55, D-5100 Aachen, F.R.G.

(*Received* 10 *September* 1990; *accepted* 12 *February* 1991)

Abstract—The X-ray crystal structure of the heterotrinuclear compound $[Cu\{ClRu[(MeO)_2PO]_2(C_6Me_6)\}_2]\cdot 2CH_2Cl_2$ is described, together with its spectroscopic and electrochemical properties. The copper ion is tetragonally coordinated by four, short copper–oxygen bonds [Cu—O = 1.931(4) and 1.965(4) Å] and two, long Cu—Cl bonds of 2.881(2) Å. The chloride ions bridge directly between the copper and ruthenium, with Ru—Cl = 2.292(2) Å and Ru—Cl—Cu = 93.6(1)°. The other bridging ligands are the $OP(OMe)_2^-$ ligands, which coordinate to copper with oxygen and to ruthenium with phosphorus. The ruthenium coordination is completed by the η^6-C_6Me_6 ligand. The structure of the complex is retained in solutions of CH_2Cl_2 and CH_3CN. Electrochemical studies (CV and DPP) show that both ruthenium(II) ions can be oxidized subsequently at, respectively, 0.69 and 0.87 V. The copper(II) ion is not redox active. The compound has been further characterized by ligand-field spectra and EPR spectra for copper(II). These spectra agree with a tetragonal chromophore CuO_4Cl_2, both for the solid and the (frozen) solution.

Heteronuclear coordination compounds have gained much interest during the last decade,[1] both as synthetic analogues for metalloproteins and as catalytic centres. In the preparation of such heteronuclear species, an asymmetric bridging ligand usually plays a key role.

The coordination chemistry of mono-anionic tridentate ligands is mainly that of the N,N,N-ligands tris(pyrazolyl)borate, $[RB(pz)_3]^-$,[2] and of the O,O,O-ligands $[(C_5H_5)Co\{P(O)R_2\}_3]^-$.[3] Both are 6e-ligands that almost always act as facially coordinating tris-chelating ligands and they are in that respect formally equivalent to the cyclopentadienyl ligands $C_5R_5^-$. The tris(pyrazolyl)borate ligands have a well-developed organometallic chemistry and despite the fact that the O,O,O-ligands $[(C_5H_5)Co\{P(O)R_2\}_3]^-$ are similar to fluoride and oxide[4] (they have electronic properties distinctly different from those of the cyclopentadienyl ligands), they form low-valent transition metal carbonyl complexes as well. Many of them are surprisingly inert. Often they are too unreactive to be valuable catalyst components. In order to control the reactivity of such complexes we designed O,O,X-ligands, where X is a donor centre that coordinates less strongly to metal ions than the P=O oxygen donor centres. Complexes of the type [(ring) metal$\{P(O)R_2\}_2X]^-$ are only useful as the O,O,X-ligands when they themselvers are inert building blocks.

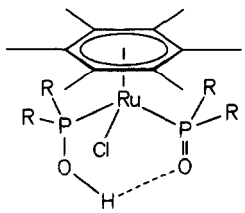

R = OMe

Fig. 1. Schematic drawing of the ligand $L^- = [(C_6Me_6)Ru\{P(O)(OMe)_2\}_2Cl]^-$.

To achieve this we have looked for substitutionally robust d^6 low-spin metal ions protected by a large ring to gain additional inertness. Of the many systems that we have tried, the complexes $[(C_5Me_5)M\{P(O)(OMe)_2\}_2X]^-$ (M = Co, Rh; X = Cl)[5] and $[(C_6Me_6)Ru\{P(O)(OMe)_2\}_2Cl]^-$ (in the following abbreviated as L^-) turned out to be useful as ligands. We have now developed an elegant synthesis of $HL = [(C_6Me_6)Ru\{P(O)(OMe)_2\}\{P(OH)(OMe)_2\}Cl]$, the hydronated form of this O,O,Cl-ligand[6] (see Fig. 1).

In the case of coordination towards copper(II), the ligand has produced a compound[7] analysing as $[Cu\{ClRu[(MeO)_2PO]_2(C_6Me_6)\}_2]$. Preliminary ligand-field spectral data showed a ligand-field maximum at 740 nm, suggesting at least some coordination of the chloride ligand to copper(II) and certainly no CuO_4 chromophore. To find out the details of the structure, a crystal structure determination was performed and solution data were obtained (EPR and electrochemistry).

In this paper we describe the first crystal structure of a compound containing this ligand, thereby forming a heterotrinuclear complex, which proves unequivocally that it can act as a tris-chelating ligand.

EXPERIMENTAL

Starting materials and synthesis

The title compound was synthesized as described before.[6,7] Recrystallization from CH_2Cl_2 provided crystals suitable for diffraction studies.

Physical measurements and analyses

Ligand-field spectra were recorded in the diffuse reflectance mode. Spectra were measured on a Perkin–Elmer 330 instrument equipped with a data station (33,000–5000 cm^{-1}) fitted with a reflectance attachment using MgO as reference material.

IR spectra from 4000 to 200 cm^{-1} were recorded as KBr pellets on a Perkin–Elmer 580 spectrometer. EPR powder spectra were recorded on a Varian E3 instrument (X-band frequencies) using standard conditions. Frozen solution and solution spectra were obtained in CH_2Cl_2 on the same instrument.

Cyclic voltammograms and differential pulse polarograms were obtained in CH_3CN/CH_2Cl_2 solutions, with 0.1 M tetrabutylammonium perchlorate (TBAP) as the electrolyte. The experiments were performed on a EG&G PAR C Model 303 polarograph with an EG&G 384B polarographic analyser. A glassy-carbon electrode was used as working electrode, a platinum wire was used as auxiliary electrode and a saturated calomel electrode (SCE) as reference electrode. The scan rate for the differential pulse polarograms (DPP) was 4 mV s^{-1} and for the cyclic voltammograms (CV) 100 mV s^{-1}.

X-ray structural determination of $[Cu\{ClRu[(MeO)_2PO]_2(C_6Me_6)\}_2]\cdot 2CH_2Cl_2$

A rod-shaped single crystal of $[Cu\{ClRu[(MeO)_2PO]_2(C_6Me_6)\}_2]\cdot 2CH_2Cl_2$ of $0.40\times 0.30\times 0.20$ mm^3 was obtained through slow evaporation of a solution in CH_2Cl_2. Data collection was carried out by an ω–2θ scan on an Enraf–Nonius CAD-4 diffractometer with use of graphite monochromatized MoK_α radiation (λ = 0.71073 Å). Unit-cell parameters and final orientation matrices were determined by least-squares refinement of 25 reflections with $4.93 < \theta < 21.90°$. Details of scan rate and background estimation have been described elsewhere.[8] Standard reflections measured every 5400 s showed no significant changes in intensity. Of the 4717 reflections measured, 4515 were independent of which 3746 were significant [with $I > 2\sigma(I)$]. Intensity data were corrected for Lorentz and polarization effects. No correction for absorption was applied.

Positions of the metal atoms did not follow unequivocally from a three-dimensional Patterson synthesis. The other non-hydrogen positions within the molecule were determined with use of the program MULTAN.[9] Standard refinement revealed the positions of the other non-hydrogen atoms and were refined anisotropically, except for the non-hydrogen atoms of the methylene chloride. Due to the disorder of the methylene chloride the non-hydrogen atoms C(7), Cl(2) and Cl(3) were refined at four positions with 40, 20, 20 and 20% occupancy, and with temperature factors of 5 $Å^2$. Waser constraints were applied for C(7)—Cl(2) [= 1.81(3) Å] and the angle Cl(2)—C(7)—Cl(3) [109(3)°]. Due to the quality of the dataset and the disorder mentioned above, no hydrogen atoms

Table 1. Crystal and diffraction data of [Cu{ClRu [(MeO)$_2$PO]$_2$(C$_6$Me$_6$)}$_2$]·2CH$_2$Cl$_2$

Chemical formula	$CuC_{34}Cl_6H_{64}O_{12}P_4Ru_2$
Molecular weight	1267.18
Crystal system	Monoclonic
a(Å)	19.136(1)
b(Å)	15.157(1)
c(Å)	8.884(1)
β(°)	92.91(3)
V(Å^3)	2573.7
Space group	$P2_1/n$ (No. 14)
Z	2
D_c (g cm^{-3})	2.41
μ (cm^{-1})	24.81
λ	Mo-K_α
h Range	−22 to +22
k Range	0 to +18
l Range	0 to +10
Radiation	Mo-K_α (0.71073 Å)
T(°C)	21
R, R_w	0.0457, 0.0629
θ Range (°)	1.10–25.00
F(000)	1143.74
Number of measured reflections	4717
Significant independent reflections	3746 [$I < 2\sigma(I)$]
R(int)	0.001228

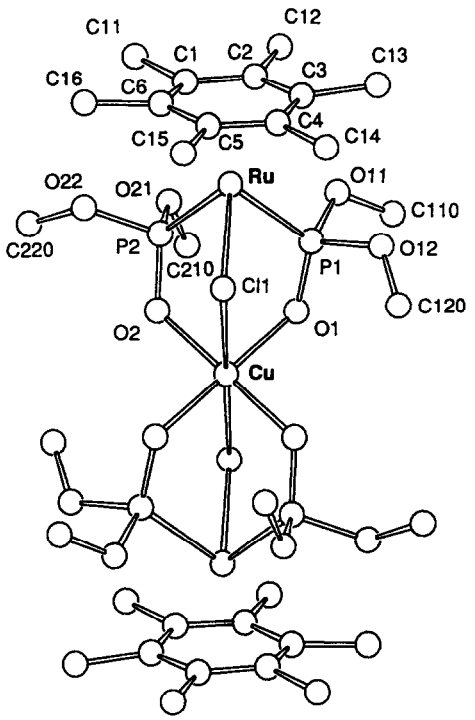

Fig. 2. Projection of the molecular complex [Cu{ClRu [(MeO)$_2$PO]$_2$(C$_6$Me$_6$)}$_2$] and the numbering of the atoms; methylene chloride molecules have been omitted for clarity.

could be located. Further full-matrix least-squares refinements, minimizing the function $\Sigma w(|F_o| - |F_c|)^2$, where $w = [\sigma^2(F)]^{-1}$ was terminated when the maximum shift/error was < 0.3. Atomic scattering factors were taken from literature tabulations.[10] Other details of data collection and structure refinement are given in Table 1. Atomic coordinates, anisotropic thermal parameters, less important geometric information and tables of F_o and F_c are given in the supplementary tables.

RESULTS AND DISCUSSION

Structure description

An ORTEP plot of the trinuclear complex is presented in Fig. 2. The cell contains two molecules of CH_2Cl_2 per Ru_2Cu unit. Unfortunately these are rotationally disordered, but could be refined with a few more positions; these have been omitted for clarity. A list of bonding distances is given in Table 2 and relevant bond angle information is given in Table 3.

The centrosymmetric structure consists of a copper ion which is tetragonally coordinated by four, short oxygen contacts [Cu—O = 1.931(4) and 1.965(4) Å] and two, long Cu—Cl contacts of 2.881(2) Å. The chloride ions bridge directly between the copper and ruthenium, with Ru—Cl = 2.292(2) Å and Ru—Cl—Cu = 93.6(1)°. The other bridging ligands are the $OP(OMe)_2^-$

Table 2. Relevant bond lengths (Å) for [Cu{ClRu [(MeO)$_2$PO]$_2$(C$_6$Me$_6$)}$_2$]·2CH$_2$Cl$_2$

Cu—Cl(1)	2.881(2)	P(2)—O(22)	1.616(5)
Cu—O(2)	1.931(4)	O(21)—C(210)	1.43(1)
Cu—O(1)	1.965(4)	O(22)—C(220)	1.46(1)
Ru—P(1)	2.263(2)	O(11)—C(110)	1.45(1)
Ru—P(2)	2.274(2)	O(12)—C(120)	1.43(1)
Ru—Cl(1)	2.392(2)	C(1)—C(2)	1.42(1)
Ru—C(1)	2.221(6)	C(1)—C(6)	1.43(1)
Ru—C(2)	2.232(6)	C(1)—C(11)	1.52(1)
Ru—C(3)	2.281(7)	C(2)—C(3)	1.42(1)
Ru—C(4)	2.275(7)	C(2)—C(12)	1.533(9)
Ru—C(5)	2.278(7)	C(3)—C(4)	1.43(1)
Ru—C(6)	2.307(7)	C(3)—C(13)	1.52(1)
P(1)—O(1)	1.520(5)	C(4)—C(5)	1.41(1)
P(1)—O(11)	1.603(5)	C(4)—C(14)	1.52(1)
P(1)—O(12)	1.620(6)	C(5)—C(6)	1.41(1)
P(2)—O(2)	1.520(5)	C(5)—C(15)	1.54(1)
P(2)—O(21)	1.607(5)	C(6)—C(16)	1.54(1)

Table 3. Relevant bond angles (°) in $[Cu\{ClRu[(MeO)_2PO]_2(C_6Me_6)\}_2]\cdot 2CH_2Cl_2$

Cl(1)—Cu—O(2)	81.9(1)	P(1)—Ru—P(2)	84.02(7)
Cl(1)—Cu—O(1)	84.9(1)	P(1)—Ru—Cl(1)	84.00(7)
Cl(1)—Cu—O(2)*	98.1(1)	P(1)—Ru—C(1)	130.9(2)
Cl(1)—Cu—O(1)*	95.1(1)	P(1)—Ru—C(4)	109.6(2)
O(2)—Cu—O(1)	90.9(2)	P(2)—Ru—Cl(1)	87.62(6)
O(2)—Cu—O(1)*	89.1(2)	P(2)—Ru—C(1)	91.8(2)
O(1)—Cu—Cl(1)*	95.1(1)	P(2)—Ru—C(4)	166.3(2)
O(1)—Cu—O(2)*	89.1(2)	Cl(1)—Ru—C(1)	144.8(2)
O(1)—Cu—O(1)*	180.0(0)	Cl(1)—Ru—C(4)	94.8(2)
Cl(1)*—Cu—O(2)*	81.9(1)	C(1)—Ru—C(4)	78.4(2)
Cl(1)*—Cu—O(1)*	84.9(1)	O(2)*—Cu—O(1)*	90.9(2)
Ru—P(1)—O(1)	119.7(2)	Ru—C(1)—C(2)	71.8(4)
Ru—P(1)—O(11)	108.5(2)	Ru—C(1)—C(6)	74.8(4)
Ru—P(1)—O(12)	112.0(2)	Ru—C(1)—C(11)	131.1(5)
O(1)—P(1)—O(11)	108.7(3)	C(2)—C(1)—C(6)	120.2(6)
O(1)—P(1)—O(12)	107.2(3)	C(2)—C(1)—C(11)	119.8(7)
O(11)—P(1)—O(12)	98.8(4)	C(6)—C(1)—C(11)	119.7(7)
Ru—P(2)—O(2)	120.3(2)	C(1)—C(2)—C(3)	120.2(6)
Ru—P(2)—O(21)	112.8(2)	C(1)—C(2)—C(12)	119.5(7)
Ru—P(2)—O(22)	107.3(2)	C(3)—C(2)—C(12)	120.1(7)
O(2)—P(2)—O(21)	107.2(3)	C(2)—C(3)—C(4)	119.5(6)
O(2)—P(2)—O(22)	107.3(3)	C(2)—C(3)—C(13)	119.7(7)
O(21)—P(2)—O(22)	100.0(3)	C(4)—C(3)—C(13)	120.8(7)
Cu—Cl(1)—Ru	93.62(6)	Ru—C(4)—C(3)	72.0(4)
Cu—O(2)—P(2)	125.6(3)	Ru—C(4)—C(5)	72.1(4)
P(2)—O(21)—C(210)	120.3(6)	Ru—C(4)—C(14)	128.0(5)
P(2)—O(22)—C(220)	119.1(6)	C(3)—C(4)—C(5)	119.4(6)
P(2)—O(22)—C(11)	89.0(3)	C(3)—C(4)—C(14)	121.2(7)
C(220)—O(22)—C(11)	113.9(6)	C(5)—C(4)—C(14)	119.4(7)
Cu—O(1)—P(1)	125.6(3)	C(4)—C(5)—C(6)	121.9(6)
C(4)—C(5)—C(15)	118.5(7)	C(6)—C(5)—C(15)	119.6(7)
P(1)—O(11)—C(110)	120.7(6)	C(1)—C(6)—C(5)	118.5(6)
P(1)—O(11)—C(12)	108.5(3)	C(1)—C(6)—C(16)	120.2(7)
C(110)—O(11)—C(12)	128.8(6)	C(5)—C(6)—C(16)	121.3(7)
P(1)—O(12)—C(120)	122.2(5)	O(22)—C(11)—C(1)	81.9(4)
P(1)—O(12)—C(13)	89.9(3)	O(11)—C(12)—C(2)	83.8(4)
C(120)—O(12)—C(13)	136.7(6)	O(12)—C(13)—C(3)	85.0(4)

* Related by centre of symmetry.

ligands, which coordinate to copper with oxygen and to ruthenium with phosphorus [Ru—P = 2.263(2) and 2.274(2) Å]. The ruthenium coordination is completed by the η^6-C_6Me_6 ligand, with Ru—C contacts varying from 2.221(6) to 2.307(7) Å. The copper–oxygen distances are significantly shorter than those found in the related $[\{CpCo[P(O)(OEt)_2]_3\}_2Cu]$, where Cu—O contacts of 2.03–2.05 Å (equatorial) and 2.13–2.15 Å (axial) were found.[11] Apparently, the weaker chloride ligands allow the Cu—O contacts to be shorter in the present compound. The molecules $[CuL_2]$ and solvent molecules appear to be packed in the lattice by normal van der Waals' contacts and no unusual phenomena were observed.

Spectral, electrochemical and analytical data

Ligand-field spectral data of the solid compound show a broad doublet with maxima at 13,800 and 10,900 cm^{-1}. According to literature data[12] this band agrees with an elongated, tetragonal chromophore CuO_4Cl_2. In addition, a broad and strong band is observed with a maximum at 26,250 cm^{-1} and a tail into the visible range. This absorption is a MLCT band of the ruthenium centre and causes the light yellow colour of the ligand, L^-, and its metal complexes.

Powder EPR spectra at 300 and 77 K show an axial spectrum, typical for elongated tetragonal symmetry,[12] with parameters $g_\parallel = 2.41(1)$,

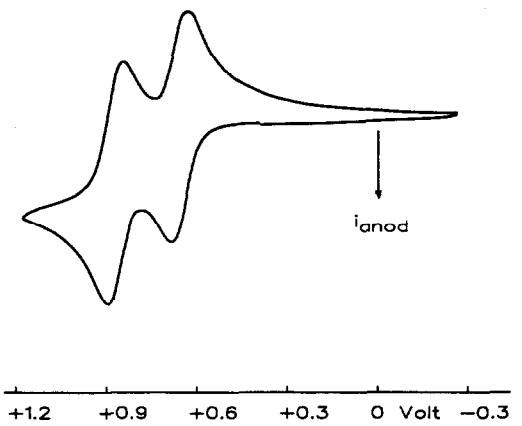

Fig. 3. Cyclic voltammogram of [CuL$_2$] recorded in CH$_2$Cl$_2$; supporting electrolyte NBu$_4$PF$_6$, 50 mV s^{-1}.

$g_\perp = 2.07$ and $A_\parallel = 120(5)$ gauss. The parameters at 77 K have a slightly smaller value for $g_\parallel$ and a slightly larger value for $A_\parallel$, indicative of a somewhat larger degree of tetragonality.[12] A frozen solution in CH$_2$Cl$_2$ shows a spectrum with identical spectral parameters (within experimental error).

Due to the poor solubility of the title complex in CH$_3$CN, electrochemical measurements were performed in a mixture of CH$_3$CN and CH$_2$Cl$_2$ and also in pure CH$_2$Cl$_2$. The cyclic voltammogram exhibits two quasi-reversible oxidation waves at 0.65 V (peak-to-peak separation 70 mV) and 0.86 V (peak-to-peak separation 60 mV) vs SCE, with an approximate intensity ratio of 1:1. Also the differential pulse polarogram reveals the presence of two oxidation processes at 0.69 and 0.90 V, again with an appropriate intensity ratio of 1 : 1 (see Fig. 3). In CH$_3$CN as solvent the ratio deviates from 1 : 1.

The two redox processes of [CuL$_2$] at 0.65 and 0.86 V are tentatively assigned as both being $Ru^{II} \rightarrow Ru^{III}$, with the second oxidation being more difficult as a consequence of the higher charge.[13] To verify the assumption that the copper(II) ion is not redox active in this system, we have measured the cyclic voltammograms of comparable compounds. In [MgL$_2$], two redox processes occur at +0.67 and *ca* 0.83 V (vs SCE). At 0.92 V a further, but only quasi-reversible, oxidation was observed. Furthermore, we have measured the cyclic voltamograms of NaL, [LH$_2$]PF$_6$ and [{(C$_6$Me$_6$)RuCl$_2$}$_2$]. NaL is reversibly oxidized at 0.72 V (peak-to-peak separation 115 mV, 20 mV s^{-1}). [LH$_2$]PF$_6$ is reversibly oxidized at 0.92 V (peak-to-peak separation 80 mV, 100 mV s^{-1}). [{(C$_6$Me$_6$)RuCl$_2$}$_2$] can be oxidized in the presence of extra chloride to give [(C$_6$Me$_6$)RuCl$_3$] at 0.82 V (peak-to-peak separation 80 mV, 200 mV s^{-1}). Thus we can be fairly certain that the redox reactions of [CuL$_2$] are ruthenium centred, without the involvement of copper(II).

The differential pulse polarogram did not reveal the presence of a reversible reduction wave down to −1.5 V. Scanning at more negative potentials leads to decomposition (and deposition) of the compound at the electrodes.

Conclusions

In the present paper the crystal structure and electrochemistry of the copper(II) complex [CuL$_2$] have been described. The results show that L$^-$ (= [(C$_6$Me$_6$)Ru{P(O)(OMe)$_2$}$_2$Cl]$^-$) can indeed act as a tris-chelating agent with an O,O,Cl-donor set; however, the two Cu—Cl bond lengths are quite long. The ligand-field spectrum and the EPR data are in agreement with a very weak ligand field for copper(II). The ruthenium(II) ion in ligand L$^-$ can be oxidized to ruthenium(III). It will be interesting to study how the coordination chemistry and spectroscopic properties of L$^-$ are influenced by the oxidation state of the central metal ion.

Acknowledgements—The authors are indebted to Jouk Janssen (Amsterdam) for collecting the X-ray dataset. We thank T. Schmitz for his help with the preparation of the ligand and its copper complex. We are indebted to Bayer AG (Leverkusen, F.R.G.) and to Degussa AG (Frankfurt, F.R.G.) for valuable chemicals. W.K. thanks the Fonds der Chemischen Industrie and the Minister für Wissenschaft und Forschung des Landes Nordrhein Westfalen for financial support of this work.

Supplementary material available. A listing of atomic fractional coordinates and anisotropic thermal parameters, a table of C—Cl bond information and tables of F_o and F_c for the title compound.

REFERENCES

1. R. J. P. Williams, *J. Molec. Catal.* 1985, **30**, 1.
2. S. Trofimenko, *Prog. Inorg. Chem.* 1986, **34**, 115.
3. W. Kläui, A. Müller, W. Ebersprach, R. Boese and I. Goldberg, *J. Am. Chem. Soc.* 1987, **109**, 164; W. Kläui, *Angew. Chem.* 1990, **102**, 661; *Angew. Chem., Int. Edn Engl.* 1990, **29**, 627 and refs cited therein.
4. W. Kläui, W. Eberspach and P. Gütlich, *Inorg. Chem.* 1987, **26**, 3977.
5. E. Buchholz and W. Kläui, unpublished.
6. W. Kläui and E. Buchholz, *Angew. Chem.* 1988, **100**, 603; *Angew. Chem., Int. Edn Engl.* 1988, **27**, 580.
7. W. Kläui and E. Buchholz, *Inorg. Chem.* 1988, **27**, 3500.

8. G. Germain, P. Main and M. M. Woolfson, *Acta Cryst.* 1970, **B26**, 274.
9. P. Main, in *Crystallographic Computing Techniques* (Edited by F. R. Ahmed), Copenhagen (1976).
10. D. T. Cromer and J. T. Waber, *International Tables for X-ray Crystallography*, Vol. IV. Kynoch Press, Birmingham (1974).
11. E. Dubler, L. Linowsky and W. Kläui, *Transition Met. Chem.* 1979, **4**, 191.
12. B. J. Hathaway and D. E. Billing, *Coord. Chem. Rev.* 1970, **3**, 140.
13. K. A. Goldsby and T. J. Meyer, *Inorg. Chem.* 1984, **23**, 3002.

Polyhedron Vol. 10, No. 10, pp. 1103–1104, 1991
Printed in Great Britain

0277–5387/91 $3.00+.00
Pergamon Press plc

A CONVENIENT ROUTE TO LEAD(II) ALKOXIDES

R. C. MEHROTRA,* A. K. RAI and A. JAIN

Chemical Laboratories, University of Rajasthan, Jaipur 302 004, India

(*Received* 14 *November* 1990; *accepted* 18 *February* 1991)

Abstract—A convenient route for synthesis of lead(II) isopropoxide (**I**) by interaction (1 : 2 molar ratio) of PbF_2 with $KOPr^i$ is described. Other alkoxy derivatives can be synthesized by alcoholysis and trans-esterification of **I**.

Following a few earlier publications on bis-aryloxide[1] and oxide–alkoxides,[2,3] there has been a recent spurt of interest in the chemistry of lead(II) alkoxides in view of their potential applications for lead based superconductors,[4,5] as evinced by the synthesis:[6]

$$Pb[N(SiMe_3)_2]+2ROH \longrightarrow 1/n[Pb(OR)_2]_n+2HN(SiMe_3)_2$$

(with R = $HCMe_2$, CMe_3, CMe_2Et, H_2CCH_2OMe, $HCMeCH_2NMe_2$), and structural studies on $[Pb(OBu^t)_2]_3$[6,7] and $[Pb(OCH_2CH_2OMe)_2]_n$.[6]

In view of the above, we now report our work on the quantitative synthesis of $Pb(OPr^i)_2$ by the reaction between anhydrous PbF_2 (freshly prepared from $Pb(NO_3)_2 \cdot nH_2O$ and Na_2F_2 in aqueous medium) and 2 mol of $KOPr^i$ (prepared *in situ* by the interaction of K with Pr^iOH):

$$PbF_2+2KOPr^i \xrightarrow{\text{Benzene}} Pb(OPr^i)_2+2KF\downarrow. \quad \textbf{(I)}$$

Compound **I** is a pale yellow solid, soluble in benzene in which it shows (ebullioscopically) a degree of association between 3.5–4.7, but it tends to polymerize on standing overnight into a deeper yellow solid which becomes sparingly soluble in organic solvents. It forms a mono-adduct with THF, $Pb(OPr^i)_2 \cdot THF$, but not with C_5H_5N.

The freshly prepared $Pb(OPr^i)_2$ is highly reactive and undergoes alcoholysis with some alcohols to yield the corresponding soluble alkoxides, which do not tend to show a similar ageing phenomenon:

$$Pr(OPr^i)_2+nROH \xrightarrow{\text{Benzene}} Pb(OPr^i)_{n-2}(OR)_n+nPr^iOH\uparrow$$

(R = n-Bu, t-Bu and t-Am; n = 1, 2).

The trans-esterification reactions of **I** appear to be more facile:

$$Pb(OPr^i)_2+2CH_3COOEt \xrightarrow[\text{reflux}]{\text{Cyclohexane}} Pb(OEt)_2+2CH_3COOPr^i. \quad \textbf{(II)}$$

Compound **II** was found to be insoluble in common organic solvents, but it is converted to soluble $Pb(OBu^t)_2$ on refluxing (approx. 20 h) under a fractionating column with excess of Bu^tOH in benzene:

$$Pb(OEt)_2+2Bu^tOH \xrightarrow[\text{reflux}]{\text{Benzene}} Pb(OBu^t)_2+2EtOH\uparrow. \quad \textbf{(III)}$$

Compound **III** can also be prepared by the trans-esterification reaction between $Pb(OPr^i)_2$ and CH_3COOBu^t:

$$Pb(OPr^i)_2+2CH_3COOBu^t \xrightarrow[\text{reflux}]{\text{Cyclohexane}} Pb(OBu^t)_2+2CH_3COOPr^i\uparrow.$$

The analysis of lead and alkoxide group(s) in all the products is within experimental (±0.5%) error; as are the estimations of isopropanol/ethanol liberated in the reactions.

$[Pb(OBu^t)_2]_3$ shows a trimeric unit[6,7] in the crystalline form, whereas $[Pb(OCH_2CH_2OMe)_2]_n$, with which $[Pb(OPr^i)_2]_n$ has been shown[6] to be isostructural, exhibits a chain structure. It appears

*Author to whom correspondence should be addressed.

plausible that freshly prepared $Pb(OPr^i)_2$ has structural features similar to those of $Pb(OBu^t)_2$[6,7] and ages into a polymeric form similar to that of $[Pb(OCH_2CH_2OMe)_2]$.[6]

Acknowledgements—Thanks are due to Professor W. E. Buhro and Dr S. C. Goel of Washington University (St. Louis, U.S.A.) for helpful discussions.

REFERENCES

1. B. Cetinkaya, I. Gümrückü, M. F. Lappert, J. L. Atwood, R. D. Rogers and M. J. Zaworotko, *J. Am. Chem. Soc.* 1980, **102**, 2088.
2. A. I. Yanovskii, N. Ya. Turova and E. P. Turevskaya, *Koord. Khim.* 1982, **8**, 153 (English translation, *Soviet J. Coord. Chem.* 1982, 76), and references therein.
3. R. Papiernik, L. G. Hubert-Pfalzgraf and M. C. Massiani, *Inorg. Chim. Acta* 1989, **169**, 1.
4. S. A. Sunshine, T. Siegrist, L. F. Schneemeyer, D. W. Murphy, R. J. Cava, B. Batlogg, R. B. Dover, R. M. Fleming, S. H. Glarum, S. Nakahara, R. Farrow, I. J. Krajewski, S. M. Zajurak, J. V. Waszczak, J. H. Marshall, P. Marsh, L. W. Rupp and W. F. Peck, *Phys. Rev. B* 1988, **38**, 893.
5. F. Chatput, J. P. Boilot, M. Lejeune, R. Papiernik and L. G. Hubert-Pfalzgraf, *J. Am. Ceram. Soc.* 1989, **72**, 1335.
6. S. C. Goel, M. Y. Chiang and W. E. Buhro, private communication.
7. M. Veith, *Chem. Rev.* 1990, **90**, 3.

APPENDIX

Supplementary data. Analytical data for lead(II) alkoxides

Compound	Analyses Found (%) Pb	Found (%) OPr^i	Calc. (%) Pb	Calc. (%) OPr^i
$Pb(Oi\text{-}C_3H_7)_2$	63.9	36.1	63.7	36.3
$Pb(OC_2H_5)_2$	69.6	30.3[a]	69.7	30.3[a]
$Pb(On\text{-}C_4H_9)_2$	58.9	—	58.7	—
$Pb(Ot\text{-}C_4H_9)_2$	58.8	—	58.7	—
$Pb(Ot\text{-}C_5H_{11})_2$	54.3	—	54.4	—
$Pb(Oi\text{-}C_3H_7)_2 \cdot THF$	52.9	29.2	52.2	29.7
$Pb(Oi\text{-}C_3H_7)(On\text{-}C_4H_9)$	61.1	17.0	61.2	17.4
$Pb(Oi\text{-}C_3H_7)(Ot\text{-}C_4H_9)$	61.9	16.8	61.1	17.4
$Pb(Oi\text{-}C_3H_7)(Ot\text{-}C_5H_{11})$	59.1	16.8	58.7	16.7

[a] For —OEt group.

Polyhedron Vol. 10, No. 10, pp. 1105–1111, 1991
Printed in Great Britain

0277-5387/91 $3.00+.00
© 1991 Pergamon Press plc

CHEMICAL SPECIATION MODELLING AND THERMODYNAMIC DATABASE COMPILATION—I. DATA UNCERTAINTIES

J. R. DUFFIELD,* F. MARSICANO† and D. R. WILLIAMS‡

School of Chemistry and Applied Chemistry, University of Wales College of Cardiff, P.O. Box 912, Cardiff CF1 3TB, U.K.

(*Received* 20 *November* 1990; *accepted* 18 *February* 1991)

Abstract—This article addresses the critical appraisal of thermodynamic data for inclusion in databases for use with computer-based chemical speciation models. The uses of chemical speciation analysis, the need for accurate and applicable thermodynamic data and the uncertainties associated with the modelling of "real-life" processes are considered. Where appropriate, examples are given to illustrate and expand upon individual points.

A comprehensive understanding of the metal–ligand equilibria pertaining to many aqueous environments and fluids including groundwaters, blood plasma, gastro–intestinal juices and food extracts is essential in an ever-increasing number of endeavours. Such equilibria will be of fundamental importance in any area where a knowledge of the chemical form of an element is a prime requirement. Examples of such areas might include research into radioactive waste disposal, assessment of the metal-dependent side-effects of modern pharmaceuticals, the bioavailability of metal ions from foods and the use of metal complexes to suppress bacterial activity.[1–4]

All such studies require detailed analysis of the chemical "speciation" of each metal and ligand present in the system. In this context, speciation is used to denote the chemical form of a given metal ion or ligand with respect to valence state(s), concentrations of complexes and free aquated metal ions in equilibrium with solid precipitates. It is not sufficient only to know the total concentrations.

In most cases, however, due to the very low concentrations coupled with the extremely complicated, and labile, equilibrium processes involved, such systems are inaccessible to direct analytical measurements. One method of overcoming these problems is to model the systems of interest using computer simulation programs and associated databases. These enable the extent of metal–ligand interactions to be quantified as percentages of the total concentrations of any component.

There are a number of computer programs available for the simulation of metal–ligand equilibria in aqueous systems. An abbreviated selection of those used in our laboratories is given in Table 1. Programs such as those listed model the systems in question using the Laws of Mass Action and Mass Balance and thermodynamic formation constants for all of the possible metal–ligand species, in conjunction with defined parameters such as pH, E_h and total metal and total ligand concentrations. Thus, each program solves a series of mass balance relationships expressed in terms of each metal ion and ligand.[1] Clearly, the success of such calculations and their chemical predictions will be critically dependent upon the accuracy of the thermodynamic formation constants of all possible reactions occurring in the system.

The purpose of this series of articles is to review the criteria which should be considered when selecting such thermodynamic data for inclusion in a database from the vast number of sources available (see Part 2), to point out possible deficiencies in existing data and to recommend how these might be remedied.

* Present address: Department of Chemistry, Faculty of Science and Engineering, Manchester Polytechnic, John Dalton Building, Chester Street, Manchester M1 5GD, U.K.

† Department of Chemistry, University of Witwatersrand, P.O. Wits 2050, Johannesburg, South Africa.

‡ Author to whom correspondence should be addressed.

Table 1. Chemical speciation programs at UWCC, Cardiff, U.K.

System	Programs
Chemical speciation analysis: These are static models which calculate the chemical equilibrium distribution of aqueous species in a solution and, in some cases, the saturation indices for solid phases.	COMICS[a] ECCLES[b] HALTAFALL[c] MINEQL[d] MINIQUAD[e] SCOGS[f] SOLMNQ[g] GEOCHEM[h] ESTA[i]
Reaction path analysis: These may perform the same function as the chemical speciation models but, in addition, they may be used as dynamic models capable of predicting the path of a reacting system. For example, mass transfer in and out of a system, or changes in the distribution of an aqueous species, either as a reaction progresses or with time.	PHREEQE[j] EQ3/6[k]

[a] D. D. Perrin and I. G. Sayce, *Talanta* 1967, **14**, 833.
[b] P. M. May, P. W. Linder and D. R. Williams, *J. Chem. Soc., Dalton Trans.* 1977, 588.
[c] N. Ingri, W. Kakolowicz, L. G. Sillen and B. Warnqvist, *Talanta* 1967, **14**, 1261.
[d] J. C. Westall, J. L. Zachary and F. M. M. Morel, Tech. Note No. 18, Dept. Civil Engineering, MIT, Cambridge MA (1976).
[e] A. Sabatini, A. Vacca and P. Gans, *Talanta* 1974, **21**, 53.
[f] I. G. Sayce, *Talanta* 1968, **15**, 1397.
[g] Y. K. Kharaka and I. Barnes, NTIS Tech. Report, PB214–899, Springfield VA (1973).
[h] S. V. Mattigod and G. Sposito, in *Chemical Modeling in Aqueous Systems* (Edited by E. A. Jenne), p. 837. ACS Symposium Series No. 93, Washington (1979).
[i] P. M. May, K. Murray and D. R. Williams, *Talanta* 1985, **32**, 483.
[j] D. L. Parkhurst, D. C. Thorstenson and L. N. Plummer, U.S. Geol. Survey, Water Resources Investigations 80–96, NTIS Tech. Report, PB81-167801 (1980) (Revised 1985).
[k] T. J. Wolery, UCRL-52658, Lawrence Livermore National Laboratory, Livermore CA (1979) (Revised 1983, 1985).

UNCERTAINTIES ASSOCIATED WITH MODELLING

In any assessment of "real-life" processes made using simulation techniques, there are three major sources of uncertainty. These have been referred to as "modelling", "data" and "completeness" uncertainties as described below.[5]

Modelling uncertainties

These stem from an imperfect understanding of the processes being modelled and/or from numerical approximations used in the mathematical representations of processes.

Data uncertainties

These arise as a result of poor quality and/or applicability of data and parameters used as input to a mathematical model.

Completeness uncertainties

These refer to possible omissions from the model because of lack of knowledge. Random events will fall into this category. In the case of chemical speciation modelling, "completeness uncertainties" will constitute a component of "modelling uncertainties".

The contribution of each type of uncertainty to the overall uncertainty which is intrinsic to a given simulation exercise will vary depending upon the process(es) being modelled.

The total of these three uncertainties associated with a model can be quantified by a combination of uncertainty analysis and exercises in verification and validation. Uncertainty analysis is used to make reliable estimates of the probability that a parameter will have a specific value. It is a subjective approach to the problem of data uncertainty assessment in which the assigned probabilities are expressions of "degrees of belief" that a parameter will have a particular value. The belief is derived

from expert judgement and the concepts adumbrated in this paper are aimed at (i) improving the wisdom of those "experts" who compile databases and (ii) making database users more aware of the origins and possible shortcomings of the individual data.

Verification and validation exercises compare the models and their predictions with experimental results, thereby checking both the mathematics and the input data. These procedures, and especially verification, are also used in "inter-code" comparisons to further assess the success, or otherwise, of calculation procedures.[1]

In principal, completeness uncertainties are unquantifiable, although some allowance can generally be made by extending probability ranges in uncertainty analysis.

In simulations of chemical speciation in dilute aqueous media, the main source of uncertainty is normally due to the quality of the input, specifically that of the formation constants and the composition of their associated complexes. In such purely aqueous phase systems, the physical chemistry theory of metal–ligand interactions and the mathematical models derived therefrom are relatively well understood, i.e. in this instance, mathematical models are more advanced than the associated formation constant databases. Thus, this series addresses the problem of data.

DATA UNCERTAINTIES

Determination of reliable formation constants and solubility products involves a great deal of painstaking experimental work as well as judicious use of whatever graphical and/or computerized numerical methods were available for data analysis at the time at which the work was carried out. Inevitably, values published in the literature will be of varying reliability and it is not uncommon for published values of formation constants for particular metal–ligand systems obtained at various dates by different workers to be in disagreement by a few orders of magnitude.

Factors affecting the quality and reliability of formation constants found in the chemical literature have been considered in various recent publications.[6,7] They are brought together and listed below for convenience and completeness. Where a factor is thought to be particularly important in the present context, it is presented in depth with examples.

Factors affecting the accuracy of formation constants

In the current context, accuracy is used to denote not only the closeness of a given formation constant to its true value, but also the capability of the measured set of formation constants to completely describe the metal–ligand experimental data from which they are derived.

Experimental method. Due regard should be taken of the sensitivity and appropriateness of the method adopted to the type of chemical reaction being investigated. Aspects such as kinetics, solubility and redox properties of the system may be crucial in selection of an appropriate method. A technique which at one time was regarded as suitable for use in the study of a particular system may later be shown to be inadequate. For example, the zinc amalgam electrode was at one stage used for the study of complexes formed in the zinc-cyanide system.[8] Later, it was shown that such electrodes react chemically with cyanide-containing solutions[9] and are, therefore, inappropriate as probes for zinc in such solutions unless special precautions are taken.[10] A faulty experimental method can often be the largest source of error.[6]

Purity of reagents. The presence of impurities in the reagents used, and particularly in the background electrolyte which is present in relatively high concentrations, can lead to unsuspected side reactions and errors in formation constants which are difficult to estimate but often lead to erroneously low values for the constants.

Selection of background electrolyte. By far, the majority of studies of metal–ligand complex formation reactions are now carried out in the presence of a relatively high and constant concentration of a supposedly inert background electrolyte. By this means, activity coefficients of ionic species in solution are held constant and subsequent calculations are greatly simplified. Popular electrolytes for this purpose include KNO_3, $NaClO_4$, KCl and NaCl. In instances where the ligand species has an appreciable basicity, part or all of the cationic component of the background electrolyte may be replaced by the protonated form of the ligand. This lowers the pH of the solutions studied and tends to suppress hydrolysis both of the metal aqua ion and of the complex species formed. If, however, the background electrolyte ions interact significantly and in a specific manner with the system under study, this leads to competing side reactions and usually underestimation of formation constants. Such interactions need not necessarily be of a chemical nature, i.e. they need not involve bond formation, but may involve "outer-sphere" complex formation, i.e. formation of loosely associated ion pairs. If the Fuoss equation[11] is used to estimate values for the logarithm of the equilibrium constant for outer-sphere complex formation log K_{os}, it is found that this quantity depends sensitively on the product of the

charge numbers z_+z_- of the interacting ions, and also on the charge separation a of the ions involved. Thus, for values of a_h ranging between 4.0–8.0 Å, one obtains a variation in the value of log K_{os} as shown in Table 2.

Table 2. The variation of log K_{os} with the product of charge numbers (z_+z_-) and charge separation (a) of interacting ions

	Log K_{os}	
z_+z_-	$a = 4.0$ Å	$a = 8.0$ Å
−1	0.02	0.25
−2	0.76	0.77
−3	1.53	1.29
−4	2.30	1.80
−6	3.85	2.83
−8	5.40	3.86

Thus, even in the absence of chemical interactions, ions from a uni-univalent background electrolyte will associate significantly with reagent ions having charge numbers of 2 or larger and of opposite sign. Since different background electrolytes lead to different values of the charge separation, a, it follows that different uni-univalent background electrolytes which may be quite inert in the chemical sense may, at the same ionic strengths, lead to somewhat differing values of formation constants for a given system. The tabulation above indicates that such a situation may be expected to occur when the charge number of a reagent ion is equal to, or greater than, 3.

This may account at least in part for the effect of background electrolyte on the first protonation constant of polyaminopolycarboxylic acids shown in Table 3,*[12] all determined at an ionic strength of 150 mmol dm^{-3}. As the size of the cation in the background electrolyte is increased in the sequence Na^+, K^+, $(CH_3)_4N^+$, so the corresponding concentration formation constant is seen to increase noticeably. The larger the cation, the larger the corresponding a value for the cation–ligand anion interaction, leading to relative destabilization of the ligand anion and, therefore, increased relative affinity for the hydrogen ion.

Ideally, if the metal–ligand system under investigation has a highly charged metal ion, a background electrolyte containing a large anion should be used. Conversely, if the system involves a highly charged ligand, the background electrolyte should contain a large cation. This will minimize the influence of ionic association effects on measured formation constants. Interesting background electrolytes in this connection are the tetraalkylammonium perchlorates (not all of which have the required solubility properties)[7] and tetrabutylammonium tetrafluoroborate.

Reagent concentrations. These will, of necessity, be reflections of the constraints imposed by the sensitivity of the analytical method used and by the ionic strength changes produced. However, in order to identify all possible equilibria, the metal and ligand concentrations, both absolute and relative, should be varied as widely as possible within the range set by these two limiting factors, as well as by metal ion hydrolysis. It is to be hoped that the concentration ranges used will be reported with the subsequently determined formation constant. The same comments hold true for the variation of pH.

When reviewing data for inclusion in a database reagent concentration ranges will be important indicators, amongst other factors, of the completeness of a proposed set of formation constants for the interaction of a metal ion with a ligand. This is particularly true when concentrations have been specifically chosen so as to focus upon only one major species to the exclusion of minor protonated or hydroxy complexes.

Reagent concentrations are relevant not only to identification of equilibria, but also to the precision of the constants finally obtained. Although it is difficult to generalize on this point, experience in our laboratories has indicated that, for the potentiometric technique, particular care is needed in cell calibration and solution standardization when working solution concentrations are below the millimolar level.

Ionic strength. To achieve the best balance

Table 3. First protonation constants of EDTA and DTPA at 37°C in different background electrolytes (I = 150 mmol dm^{-3})

Background electrolyte	Log β	
	EDTA	DTPA
NaCl	9.120	9.673
KCl	9.844	10.047
$(CH_3)_4N^+Cl^-$	10.074	10.645

* The polyaminopolycarboxylic acids are also known to bind alkali metal ions to a slight extent.[13] Thus, in the present example, the situation will be further complicated by competition between the alkali metal ions and protons for the first protonation site.

between the conflicting requirements of keeping ionic strength constant and covering a sufficiently wide range of reagent concentrations, it would seem that, ideally, solution equilibria should be studied at ionic strengths of at least 1 mol dm^{-3}.[7]

Nevertheless, studies that are carried out with a specific chemical modelling application in view are often carried out at the ionic strength appropriate to that application, viz. 150 mmol dm^{-3} for blood plasma, and 0.7 mol dm^{-3} for sea water. Variations of ionic strength that take place as a result of complex formation should not exceed 1% of the concentration of the background electrolyte, although this restriction can be relaxed a little if the calculation procedures used make allowance for small variations in ionic strength, as is the case in some recently reported computer programs.[14,15]

Computational procedures. These have recently been reviewed in depth.[16] The quality, sophistication and type of optimization procedures used in the calculation of formation constants from the experimental data will have a bearing on their accuracy. It is particularly important that the numerical values and sources of any auxiliary data used (e.g. metal hydrolysis constants, ligand pK_a, pK_w, etc.) should be specified. The use of protonation constants determined by other workers can introduce significant errors since systematic errors are often eliminated when both proton and metal complexes are studied under identical conditions.[17] Another major and often overlooked source of error relates to uncertainties in the set of species or complexes assumed to be present, i.e. uncertainties in the model proposed to account for the experimental data.

Two general strategies have been described for use in tackling the problem of model selection: the Baes and Mesmer approach of using the smallest possible number of species and considering more only if no acceptable fit is found, and the approach of the Sillén school where a number of plausible species is considered and those of low stability rejected. These two approaches often lead to models which differ somewhat, particularly with regard to the proposed minor species but, fortunately, seem to lead to similar conclusions about predominant species.[18] A systematic approach to the sequential introduction of species into an equilibrium model has recently been described by Marsicano *et al.*[19] Whatever method is used, it is most desirable that authors give an indication, with reasons, of possible models that have been rejected during fitting procedures. If, as often happens, two or more models can be proposed that fit the data almost equally well, then the uncertainty limits quoted for the formation constants of complexes common to both models (usually the predominant species) must take account of the unavoidable model uncertainties.

Additional factors affecting the accuracy of solubility products

A wide variety of methods are available for the determination of solubility products of sparingly soluble electrolytes. In principle, any solution property whose value depends upon the extent of dissolution of the sparingly soluble electrolyte can be used. In practice, the most commonly used techniques are EMF measurements (yielding activities or concentrations of uncomplexed ions in solution) or solubility measurements (yielding total or analytical concentrations of both complexed and uncomplexed species in solution).

In this context, for the sparingly soluble solid, M_mL_n, it is important to distinguish between the conventional solubility product,

$$K_s^0 = [M]^m[L]^n$$

(at constant ionic strength/activity coefficients)

and an apparent solubility product,

$$K_s^* = T_M^m T_L^n,$$

which is calculated in terms of analytical (total) concentrations of M and L in solution, with no account taken of any complex formation equilibria involving the species M or L.

The quantity, K_s^*, has little thermodynamic significance and can be expected to have a constant value only if $T_M \approx [M]$ and $T_L \approx [L]$ under conditions in which activity coefficients are held constant and negligible complex formation takes place.

It is evident that reliable values of K_s^0 can only be obtained under conditions in which complex formation in the solution phase is negligible or, alternatively, when the state of knowledge about the solution phase equilibria is sufficiently advanced so that the concentrations of free (uncomplexed) components [M] and [L] can be reliably calculated from values of T_M and T_L determined analytically. This point is illustrated in Table 4, where the solubility product of the sparingly soluble solid $Zn(CN)_2$ is calculated on the basis of various assumptions concerning the presence and nature of the species present in the solution phase. The (analytically determined) solubility[20] of $Zn(CN)_2$ in freshly boiled, triple-distilled water at 25.000 ± 0.02°C is such that the total concentration of zinc in solution is 12.8 ± 1.0 ppm, i.e. $T_{Zn} = 1.96 (\pm 0.15) \times 10^{-4}$ mol dm^{-3} and $T_{CN} = 2T_{Zn} = 3.92(\pm 0.30) \times 10^{-4}$ mol dm^{-3}.

It can be seen that, based on the same exper-

Table 4. Values of the solubility product of sparingly soluble $Zn(CN)_2$ calculated on the basis of various models of the speciation of the aqueous phase

Species allowed for in solution	Literature reference and data of study	Calculated solubility product
Assumption: no complex formation in solution	Pre-1903	3.01×10^{-11}
$Zn(CN)_4^{2-}$	ref. 21 (1953)	4.17×10^{-13}
$Zn(OH)^+$, $Zn(OH)_2$, $Zn(OH)_3^-$, $Zn(OH)_4^{2-}$	ref. 21 (1953)	2.35×10^{-13}
$Zn_2(OH)^{3+}$, $Zn(CN)_4^-$,	ref. 22	
$Zn(OH)^+$, $Zn(OH)_2$, $Zn(OH)_3^-$		
$Zn(OH)_4^{2-}$, $Zn_2(OH)^{3+}$, $ZnCN^+$	ref. 23 (1972)	1.82×10^{-15}
$Zn(CN)_2$, $Zn(CN)_3^-$, $Zn(CN)_4^{2-}$		
$Zn(OH)^+$, $Zn(OH)_2$, $Zn(OH)_3^-$, $Zn(OH)_4^{2-}$		
$Zn_2(OH)^{3+}$, $Zn(CN)_2$, $Zn(CN)_3^-$	ref. 19 (1987)	3.41×10^{-16}
$Zn(CN)_4^{2-}$, $Zn(CN)_3(OH)^{2-}$, $Zn(CN)_3(OH)_2^{3-}$		
$Zn(CN)_5^{3-}$		

imental data, the solubility product of $Zn(CN)_2(s)$ changes by some five orders of magnitude, depending upon the level of sophistication to which the composition of the solution phase is described. It follows that reported values of solubility products are of rather little value unless all the equilibria existing in the solution phase are adequately accounted for and clearly specified.

Most of the other factors listed previously as affecting the accuracy of formation constants apply equally well to solubility products, with one additional requirement that the solid phase be unambiguously identified, e.g. by X-ray powder diffraction studies.

It is known, for example, that europium oxalate in the presence of sodium ions exists as two solid phases, $2NaEu(oxalate)_2 \cdot 7H_2O$ and $Eu_2(oxalate)_3 \cdot 10H_2O$, with the latter phase being more stable at higher ligand concentrations.[24] Transition between these two phases is slow. Failure to detect changes of this sort will clearly lead to substantial error.

Finally, since solubility equilibrium is usually attained only slowly, adequate tests for equilibrium should be applied, and separation of solid from solution phase, whether done by filtration or centrifugation, should preferably be carried out at the equilibration temperature.

CONCLUSIONS

There is an expanding need for an accurate analysis of the chemical speciation occurring in a wide range of industrial, pharmaceutical and environmental processes.[25] To be successful, such computer-based speciation analyses require a sound understanding of the potential pitfalls generated by uncertainties inherent in the modelling assumptions and in the thermodynamic data used. It is hoped that the discussion of the possible sources of error and the accompanying examples presented in this article will aid experimentalists in the design of their equilibrium measurements and thus increase their relevance for modelling purposes. In addition, the discussion should also assist modellers in their choice of data from the extensive original literature and secondary compilations now available, as will be discussed in Part 2 of this series.

REFERENCES

1. J. R. Duffield and D. R. Williams, *Chem. Soc. Rev.* 1986, **15**, 291.
2. A. Cole, P. M. May and D. R. Williams, *Agents Actions* 1981, **11**, 296.
3. G. L. Christie, J. R. Duffield and D. R. Williams, *Biofluid Speciation Models and Bioavailabilities of Metals from Milk, Intestinal Fluid and Saliva*, in *Proceedings of 1986 Summer Computer Simulation Conference*, 28–30 *July* 1986, *Reno, Nevada*, p. 405.
4. S. R. Hurford, G. L. Smith, D. R. Williams, D. Cummins and P. I. Riley, *Rev. Port. Quim.* 1985, 423.
5. M. D. Hill and M. J. Crick, NRPB, Chilton, Didcot, personal communication (1986).
6. M. T. Beck, *Pure Appl. Chem.* 1977, **49**, 127.
7. G. Anderegg, *Pure Appl. Chem.* 1982, **54**, 2693.
8. H. T. S. Britton and E. N. Dodd, *J. Chem. Soc.* 1932, 1940.
9. E. Ferrell, J. M. Ridgion and H. L. Riley, *J. Chem. Soc.* 1936, 1121.
10. H. Persson, *Acta Chem. Scand.* 1971, **25**, 543.
11. R. M. Fuoss, *J. Am. Chem. Soc.* 1958, **80**, 5059.
12. J. R. Duffield, Ph.D. Thesis, University of Wales (1982).
13. G. Schwarzenbach and H. Ackermann, *Helv. Chim. Acta.* 1947, **30**, 1798.

14. P. M. May, K. Murray and D. R. Williams, *Talanta* 1985, **32**, 483.
15. K. Murray and P. M. May, *ESTA Users' Manual*, UWCC, P.O. Box 912, Cardiff CF1 3XF (1984).
16. D. J. Leggett (Ed.), *Computational Methods for the Determination of Formation Constants*. Plenum Press, New York (1985).
17. L. D. Pettit, *Pure Appl. Chem.* 1984, **56**, 247.
18. H. Rossotti, *The Study of Ionic Equilibria*, p. 150. Longman, London (1978).
19. F. Marsicano, C. Monberg, B. S. Martincigh, K. Murray, P. M. May and D. R. Williams, *J. Coord. Chem.* 1988, **16**, 321.
20. P. J. Harris, F. Marsicano and N. P. Finkelstein, *A Preliminary Investigation into the Mechanism of Depression in the Flotation of Sulphide Minerals at the Prieska Copper Mine*. Report No. 1721 dd. 10 June 1975. Project 02670. Council for Mineral Technology (MINTEK), Private Bag X3015, Randburg 2125, South Africa.
21. S. Suzuki, *Sci. Report Res. Inst. Tohoku Univ. A* 1953, **5**, 311.
22. R. M. Smith and A. E. Martell, *Critical Stability Constants, Vol. 4. Inorganic Complexes*, Plenum Press, New York (1976). (Constants for zinc hydroxyl species, corrected to the appropriate ionic strength.)
23. M. Collier, L. Donneau, M. Fournier and M. Quintin, *J. Chim. Phys.* 1972, **69**, 945. (Values at $\mu = 0.5$ M corrected to appropriate ionic strength by use of Davies equation.)
24. I. Grenthe and G. Gardhammer, *Acta Chem. Scand.* 1969, **23**, 93.
25. J. R. Duffield and D. R. Williams, *Chem. Brit.* 1989, 375.

Polyhedron Vol. 10, No. 10, pp. 1113–1120, 1991
Printed in Great Britain

0277–5387/91 $3.00 + .00
© 1991 Pergamon Press plc

CHEMICAL SPECIATION MODELLING AND THERMODYNAMIC DATABASE COMPILATION—II. DATABASE COMPILATION AND SENSITIVITY ANALYSES

J. R. DUFFIELD,* F. MARSICANO,† M. WATERS and D. R. WILLIAMS‡

School of Chemistry and Applied Chemistry, University of Wales College of Cardiff, P.O. Box 912, Cardiff CF1 3TB, U.K.

(*Received* 20 *November* 1990; *accepted* 18 *February* 1991)

Abstract—The collation of thermodynamic data describing metal–ligand interactions in solution to produce useful, coherent and internally consistent compilations known as thermodynamic databases is discussed. In addition, procedures to update and manipulate equilibrium data in a meaningful and scientifically rigorous way are discussed using an approach known as MASAD (a Multivariate Approach to the Sensitivity Analysis of Data).

The scientific literature from many disciplines abounds with data, of varying degrees of precision and accuracy, describing metal–ligand interactions. The measurement and use of such equilibrium data and the associated uncertainties have already been discussed[1] and recently a book by Martell and Motekaitis has underlined these points.[2] In this paper, we first describe some of the existing compilations of thermodynamic equilibrium data which are available. This description is not exhaustive, however, because the fields of application of the subject are numerous and because interest in the topic, with respect to both measurement and use, spans many disciplines. Therefore, the compilations detailed in the next section have been limited to represent those most readily accessible within the chemistry-based literature, and omission of a compilation from discussion does not imply untoward criticism of that work.

Even taking into account the vast and expanding library of equilibrium data which already exists in compilations, current knowledge of the majority of such systems of potential interest is either inadequate or uncertain, or still awaits investigation. In such situations, a number of approaches can be tried to overcome the problems posed. These include (a) estimation of data from chemical trends and free energy relationships,[3,4] and (b) assessing the robustness of data and models using sensitivity analyses of the type used in modelling radioactive waste disposal scenarios.[5,6] The latter of these two approaches is discussed at some length in this paper.

EXISTING COMPILATIONS OF DATA AND ONGOING CRITICAL ASSESSMENT ACTIVITIES

Various compilations of data covering formation constants of proton–ligand and metal–ligand complexes, as well as solubility products, are available to researchers working in the field of solution equilibria, as well as to prospective users of solution thermodynamic data. Under the auspices of the Commission on Equilibrium Data of the Analytical Chemistry Division of the International Union of Pure and Applied Chemistry (IUPAC), a series of comprehensive but uncritical tabulations of data have appeared in the literature[7–10] covering all data published up to the end of 1973 for organic ligands, and up to the end of 1974 for inorganic ligands. These compilations provide rapid access to the primary literature but no attempt is made to assess the accuracy of published data. The advent of computerization of Chemical Abstracts and the increasing use of computerized literature search facilities

* Present address: Department of Chemistry, Faculty of Science and Engineering, Manchester Polytechnic, John Dalton Building, Chester Street, Manchester M1 5GD, U.K.

† Department of Chemistry, University of Witwatersrand, P.O. Wits 2050, Johannesburg, South Africa.

‡ Author to whom correspondence should be addressed.

has, to some extent, relieved the pressure for production of updated uncritical data compilations. However, anyone who has used both methods of accessing the primary literature will attest to the continued usefulness, convenience and economy of the uncritical data compilations, and it is hoped that compilers will continue to be willing to devote time and energy to this activity.

The task of producing critical tabulations of protonation and metal–ligand complex formation constants and solubility products is indeed a massive one. The size of the task, and the degree and range of expertise required are such that the task can probably only be adequately tackled on the basis of extended international cooperation.

With regard to protonation/acid dissociation constants, an early critical survey of the literature by Kortüm *et al.*[11] surveyed the literature to the end of 1956. This survey was later extended by Perrin[12,13] and by Sergeant and Dempsey[14] to include literature up to the end of 1970.

For metal–ligand formation constants, an important source of critically selected formation constants available at the present time is a set of volumes published by Martell and Smith between 1974–1977,[15–18] supplemented by further volumes in 1982[19] and 1989.[20] These six volumes cover the literature up to and including 1985. In addition, the IUPAC Commission on Equilibrium Data has, in an editorial capacity, launched an ongoing series of Critical Surveys of Stability Constants of Metal Complexes,[21] which are published initially in the IUPAC official journal, *Pure and Applied Chemistry*, with a view to later binding in a permanent hard-cover form and publication as part of the IUPAC Chemical Data Series.

Some surveys in this series that have appeared to date include formation constants for complexes of EDTA,[22] 1,10-phenanthroline, 2,2′-bipyridyl and related compounds,[23] fluoride,[24] nitrilotriacetate,[25] histidine, phenylalanine, tyrosine, L-DOPA and tryptophan,[26] ethylenediamine,[27] indium[28] and acetylacetonate.[29] In the IUPAC critical surveys, reference is made to all published data, which are then classified into the categories: recommended, tentative, doubtful, or rejected,[21] with full justifications given. Such critical and authoritative surveys, carried out by acknowledged experts in their fields, probably represent the ultimate that can be achieved by way of critical assessment of formation constant data. However, the coverage of each survey is of necessity limited, as is the rate at which such detailed and closely argued surveys can be produced. They, therefore, complement, but in no way supercede or displace, the much wider ranging critical compilations of Martell and Smith. Even the latter ongoing compilation lags behind the primary literature by some 8 years or so. It follows that a user of formation constants, for example, in connection with a chemical modelling application, is likely to construct his initial, or feasibility model (see below) using, say, the Martell and Smith compilations and then, once the really important or critical items of data for the particular application have been identified, the researcher is likely to consult the primary literature to update his information, and to draw his own conclusions about the reliability of that information. At that stage, any IUPAC Critical Survey that may be available and that relates to the systems of interest would be of prime importance.

With regard to solubility products, the uncritical compilations referred to earlier[7–9] are a useful source of data. As pointed out in Part 1 of this series of papers, such values should be read in conjunction with the corresponding formation constants for solution species, and corrected by the prospective user if the situation viz-a-viz the constants for the solution species has changed since the original work was published. Critically selected values can be found in the Martell and Smith compilations.[14–20] In general, the recovery of solubility data from the literature and the selection of the best solubility data for a particular application are held to be frequently so difficult that researchers are often forced to redetermine solubility values for themselves, sometimes rather inexpertly.[30] Since solubility data are required and used by a variety of disciplines, a Solubility Data Project was initiated under the coordination of the Committee on Data for Science and Technology (CODATA) of the International Council on Scientific Unions (ICSU), with contributions envisaged from the various world scientific unions and federations, including IUPAC.

The Solubility Data Project is concerned with preparation of a comprehensive critical compilation involving three board categories of data: solubility of gases in liquids, solubility of liquids in liquids, and solubility of solids in liquids. The entire field was subdivided into 20 series for publication by Pergamon Press.[30] The approach underlying the Solubility Data Project is similar to that of the IUPAC-sponsored Critical Surveys of Stability Constants of Metal Complexes, in that the compilations are prepared by experts in the field, operating according to review procedures established under the direction of topic editors. Surveys that have appeared to data and are of interest in the present context are volumes dealing with the solubility of silver azide, cyanide, cyanamides, cyanate, selenocyanate and thiocyanate,[31] scandium, yttrium, lanthanum and lanthanide nitrates,[32] alka-

line-earth metal halates,[33] copper, silver, gold, zinc, cadmium and mercury oxides and hydroxides,[34] lead sulphates, selenates and tellurates,[35] beryllium, barium, strontium and sodium sulphates,[36] silver chloride,[37] alkali metal and ammonium chlorides,[38] alkali and alkaline-earth oxides and hydroxides,[39] alkali metal and ammonium halates,[40] and copper and silver halates.[41] In addition, various volumes have appeared dealing with the solubility of organic substances and gases in aqueous and other solvents.

It is clear, however, that given the wide range of systems that are potentially of interest to users, and the limited rate at which such surveys can be completed and published, the researcher at the present time is generally still confronted with the need to select critically between values of solubility products appearing in the literature.

Heats or enthalpy changes for ligand protonation and metal–ligand complex formation reactions form an integral part of any thermodynamic database for solution chemical applications because such values (together with partial molar heat capacities if these are available) are used to compute the temperature dependence of the equilibrium constant for the corresponding protonation or complex formation reaction. Critical compilations are available that cover heats of proton ionization reactions reported in the published (refereed) literature through mid-1975,[42] and heats of metal–ligand complex formation reactions through 1973.[43]

CRITERIA FOR SELECTION OF DATA

Many of the criteria that are being applied in the selection of formation constant data for the thermodynamic database used by the authors of this review have been described by Smith and Martell,[14–20] by Beck,[44] and have been applied in practice by authors of Critical Surveys.[22–29] These, together with one or two others, will be summarized briefly below.

Many of the selection criteria stem directly from a consideration of the factors affecting the accuracy of formation constants (dealt with in Part I)[1], and can be summarized as follows:

(a) *The adequacy of the experimental method*

This must be appropriate to the system studied and have survived criticism by later workers.

(b) *The precision of the experimental work*

This can sometimes be gauged by the efforts made at reagent purification, solution standardization and tests for attainment of equilibrium, as well as reproducibility of measurements. Adequate tests for side reactions like oxidation are also desirable.

(c) *The proper choice of medium*

This must be chemically inert towards reactant species.

(d) *Adequate coverage of reagent concentration range, with its implications viz-a-viz ionic strength*

(e) *Adequate level of sophistication of calculation techniques*

This should allow for the effect of all relevant equilibria other than the equilibria studied. Values of all auxiliary data used should be stated and should be reliable.

(f) *Model selection*

Preferably, this should be based on more than simply the prejudices of the authors concerned, and uncertainty limits quoted should in some way reflect uncertainties in the model.

Another class of selection criteria stems from comparisons that can be made between the work of various authors on the same or similar system(s).

First, when several workers are in close agreement on a value for a particular complex, the average of these results is often selected. Values showing considerable scatter could be eliminated.[14–20]

Secondly, a particular difficulty arises when two authors who have studied the same system disagree on the question of what complex species are formed in that system. The disagreement often concerns minor species. The problem of critical selection then becomes a problem, not only of selection of the best value(s), but also one of selection of the best model. It is of paramount importance to ensure that the selected species are not mutually exclusive. It may be that two different sets of species are considered to describe the system equally well and inclusion of complexes and numerical values from both data sets will lead to erroneous results. As a general rule, it is probably safer to accept or reject models (including both species and formation constants) as a whole, rather than to proceed on the assumption that all the complex species reported by both authors have an objective existence. If, however, the two reported studies involved work at very different conditions of reagent concentration, then this rule could be relaxed. It is, for example, well known that polynuclear complexes form to a greater extent at higher metal ion concentrations. In such circumstances, it may be acceptable to "mix models".

Thirdly, when there is poor agreement between published values, and other supporting evidence is lacking, the "track-record" of the authors concerned may influence the selection of values. Other factors being equal, preference may sometimes be given to results of more experienced research groups who have supplied reliable values for other ligands, or who have published other reliable values obtained by the same experimental technique.[14–20]

Fourthly, established trends among similar metal ions and among similar ligands can be useful in deciding between widely differing values.[14–20] The linear free energy relation (LFER) in various forms can be particularly useful here. There are numerous examples in the literature of the use of LFERs to correlate protonation constants of series of structurally related organic acids. Use of the equations of Hammett, Yukawa and Tsuno, Swain and Lumpton, and Pavelich and Taft for this and other purposes have been reviewed recently by Exner and Shorter.[45–47] The use of LFERs for the correlation of formation constants of metal–ligand complexes is less well developed than for ligand protonation but certain quantitative approaches adopted by physical organic chemists in the 1920s only began to be applied to inorganic chemistry in the 1950s.[48] There are various examples in the literature of the use of LFERs to correlate formation constants of pairs of ligands with a series of similar metal ions,[49–52] and also of pairs of metal ions with a series of similar ligands.[49,53–55] The accuracy of these correlations depends, of course, on the degree of similarity of the metal ions or ligands being compared.

Finally, correlation analysis based on two and three term equations of a factor analytic type have had some success in correlating the stabilities of a wide variety of metal ions with certain simple monodentate ligand species.[54,56,57]

Where such correlations are used in deciding between widely differing values, or in assessing whether a single reported value may be worth checking experimentally, they must, as pointed out by Martell and Smith,[15–20] be used cautiously to avoid overlooking real examples of anomalous behaviour.

DATABASE COMPILATION

Once the chemical literature has been accessed and critically reviewed, the resulting thermodynamic data must be collated and then compiled into a database. This latter stage may not be straightforward and probably will involve a number of important scientific and managerial decisions, although these may be constrained by the uses to which the database will be put.

For many uses, in addition to defining a database standard state (e.g. a temperature of 25°C with pure water as the solvent), it may be necessary to define the "master components" whose interactions in solution give rise to the individual complex species. In the majority of cases, this latter consideration will present no real difficulty. Only in the case where different oxidation states of an element can exist is a choice of master component(s) really necessary. Here, two possibilities exist: (a) the individual oxidation states can be the master components for that element, or (b) one oxidation state can be the master component, the other states being defined from that master component using the reduction potentials for the relevant half-cell reactions.

One interesting and potentially very useful approach to the problem of database compilation which endeavours to account for many of the problems posed is currently being researched and put into operation by May and Murray in their Joint Expert Speciation System (JESS) initiative.[58] In this initiative, which is well advanced, it is proposed to provide a computer library of thermodynamic data with utilities allowing update and retrieval of species so that choice of "master component" can be rapidly and easily altered. Furthermore, utilities are provided to enable data to be adjusted to account for changes in temperature (van't Hoff) and in ionic strength (14 ionic strength correction methods have been included). In this way, it is hoped that JESS will provide a user-friendly environment in which databases can be compiled and tailored in a flexible manner as required. It should be noted, however, that the ultimate choice of data used will be the user's responsibility; JESS provides the tools.

As is apparent from much of the above discussion, database compilation is, at present, a time-consuming and often tedious occupation. Whilst the production and use of the best possible thermodynamic database must be the ultimate aim in any chemical speciation modelling exercise, it is often difficult to achieve this task in the short term. In such a situation, database compilation itself may become an iterative process as illustrated in Fig. 1. Here, modelling and compilation combine to help identify and evaluate both the important complex species in a given system and the accuracy and precision of their associated formation constants. Indeed, it is arguable that database compilation should never be divorced from modelling as the two tend to complement each other. This may be particularly important where two data sets exist for a given complex system and where the inclusion of both sets would overestimate the importance of the system. In this case, one possible solution is to use both data sets in a simulation–validation exercise

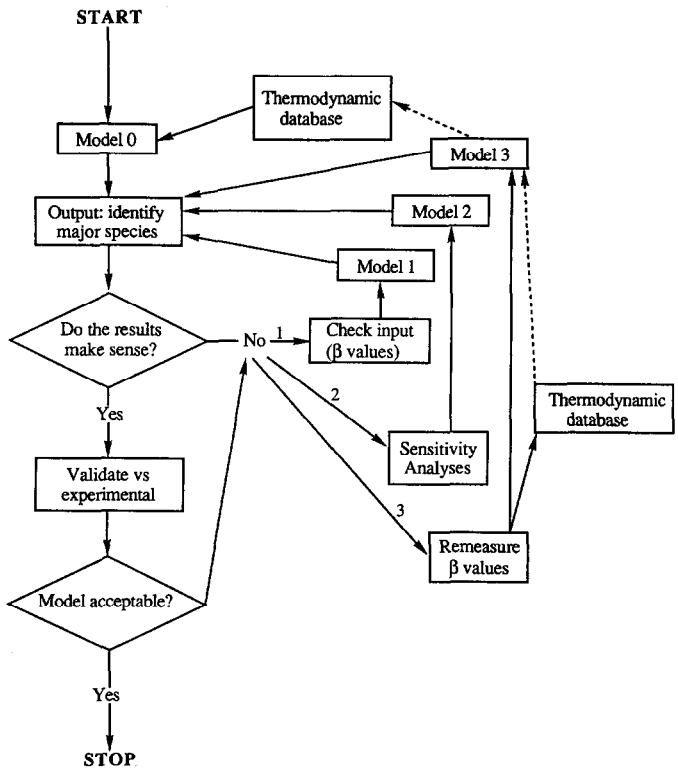

Fig. 1. A flow-diagram showing the interdependence between chemical speciation modelling and the maintenance and improvement of a thermodynamic database. Initially, a feasibility model [model 0] is constructed using the best available input data, i.e. component concentrations, system parameters (pH, E_h) and formation constants. Model 0 is then run and the output examined to identify errors in the input data, particularly with respect to concentrations. From this point on, database maintenance and updating becomes important and is accomplished via an iterative procedure to ensure that predictions made concerning species concentrations are the best possible. This procedure relies to a great extent on the use of sensitivity analyses which allow uncertainties in formation constant data to be identified and so give an indication of metal–ligand systems which may require experimental investigation.

and to choose the data set giving the more accurate predictions. This may be time-consuming and expensive.

Alternatively, the data and model used to simulate the experimental system of interest can be subjected to some form of sensitivity analysis to enable the more important chemical species to be identified and subsequently assessed.

MASAD—A MULTIVARIATE APPROACH TO THE SENSITIVITY ANALYSIS OF DATA

The ultimate aim of the sensitivity analysis of chemical data is to identify the "pivotal" chemical species, changes in whose values lead to significant perturbations in modelling predictions. MASAD has been designed to enable such sensitivity analyses to be automated so that much of the time-intensive analysis of variability of predicted chemical speciation is encompassed within a computer program. The concept is described more fully below.

The concept of sensitivity analysis is familiar in the fields of linear programming[59] and of modelling dynamic systems.[60] However, in the field of chemical speciation modelling, where systems are non-linear and taken to be at equilibrium, neither of the methodologies used in the above disciplines is entirely appropriate.

In the context of chemical speciation modelling, the aim is to determine the sensitivity of the model output to changes in the values of its input parameters, the latter of which are the log β and log K_{sp} values describing the formation of aqueous species and solid phases, respectively. Thus, for any given model some critical output parameter must first be identified, e.g. the solubility of a given element in the system of interest. Overall, MASAD seeks to assess model sensitivity in four main stages:

(i) the input to the chemical model is defined and the critical output parameter identified,
(ii) the model is run and major chemical species determined,
(iii) the model is re-run a number of times with varying log β and log K_{sp} values of important species, and
(iv) the pivotal species identified from a multivariate statistical analysis of the results from (iii).

These stages are described in more detail below.

Once the system of interest has been chosen and the output parameter identified, the system is modelled and the chemical speciation determined. Those complexes considered significant, i.e. which form to $> 0.1\%$ in the initial model, are then selected for inclusion in the sensitivity analysis along with any others which, based upon chemical knowledge, are felt to be questionable.

The next step involves remodelling the system but with simultaneous variation of the significant log β and log K_{sp} values about their base ("accepted") values. If a full factorial design[61,62] was applied to this modelling it would allow the determination of the contributions to the overall sensitivity of the system of all the log β variations and all the interactions between them. This approach would require a great amount of computing time which, for most systems of interest, is unrealistic.

In MASAD, therefore, a probabilistic Monte Carlo approach has been adopted[63] giving a significant saving in resources and time. This reduction in the resource requirement is, of course, at the expense of information describing *all* of the interaction effects.

The method used to obtain the variations in log β values is based upon the random sampling of statistical distributions,[64,65] one per log β value. It is thus necessary to describe which distribution to use and to obtain the relevant parameters for each log β value of interest. As the results obtained from the modelling work will need to be analysed using multivariate analysis to determine both direct and interaction effects, then the statistical tool which would seem to be best able to satisfy the requirements is multiple regression analysis.[66,67] There are non-parametric tools[68,69] available which might be suitable for some of the data analysis but these lack the necessary power to resolve the results into the contributions of each log β and interaction effect.

The use of a parametric tool such as multiple regression requires that the errors associated with the data to be analysed are randomly distributed according to the Gaussian or normal distribution.[70]

Therefore, the Gaussian distribution is employed in the MASAD sampling step. It should be noted, however, that the parameters used by multiple regression do possess a degree of robustness in that they are not affected significantly by slight departures from the Gaussian distribution and the underlying assumption of normality.[71] This latter assumption appears appropriate, especially when the log β values selected for inclusion in a given database are the best unbiased estimates of the true formation constants for the species concerned so that the probability that a formation constant will have a particular value decreases as we move away from the value in the database.

As the Gaussian distribution is employed, each log β value in a database must have a standard deviation assigned to it and this assignment must be based upon some assessment of the quality of the original data. To a certain extent, this is subjective but by employing the ideas promulgated here and in Part I of this series of reviews the authors have developed a five point scale, namely:

(i) very good quality data, vary log $\beta \pm 1.0$ ($\equiv$ SD of 0.5);
(ii) good quality data, vary log $\beta \pm 2.0$ ($\equiv$ SD of 1.0);
(iii) moderate quality data, vary log $\beta \pm 3.0$ ($\equiv$ SD of 1.5);
(iv) poor quality data, vary log $\beta \pm 5.0$ ($\equiv$ SD of 2.5);
(v) species of questionable existence, as for (iv) plus removal from system.

Each log β (describing a chemical species) is assigned a distribution, $N(\log \beta, \text{SD})$, and for each modelling run a random number is obtained from each distribution to represent that log β value in that particular run.

If no quality assessment is possible for a given log β value, a quality class is selected at random from those given above. However, the resource requirement of this approach is significantly higher than is the case when a data quality assessment is available. Furthermore, the resultant output is less reliable. The final stage of MASAD is to analyse the model output to determine the pivotal chemical species, including interactions thereof. As stated above, this is carried out using multiple regression analysis.

CONCLUSIONS

It is apparent that to model aqueous metal–ligand systems and to predict the chemical speciation occurring within such systems, thermodynamic data describing the interactions are

required. The better and the more complete the thermodynamic data used to model the interactions, the greater the certainty with which the predictions can be used and the results believed. Thus, the quality of data (formation constants and solubility products) within the thermodynamic database is crucial and every effort must be made to trace data to source for assessment purposes. Therefore, an "audit trail" for all constants used is a pre-requisite in the management of a thermodynamic database.

Even when such good management techniques are utilized, there will be occasions when uncertainties arise as to the quality and completeness of data concerning metal–ligand interactions. Here, the impact of data uncertainty can be gauged by careful use of sensitivity analyses which will help to indicate whether or not a given species, or set of species, is pivotal in the system of interest. If a species is considered to be pivotal and the associated thermodynamic data is uncertain, the species can then be measured experimentally. In all cases, however, neither the modeller nor the database manager should forget or neglect their chemical knowledge. Individual data points should not be treated in isolation but considered as part of a whole so that chemical trends can be identified and the conformity of relevant data to them assessed. The maxim "garbage in, garbage out" (GIGO) is all too correct in the field of chemical speciation modelling and database users and managers alike must seek to minimize situations where such criticisms can be levelled.

REFERENCES

1. J. R. Duffield, F. Marsicano and D. R. Williams, *Polyhedron* 1991, **10**, 1105.
2. A. E. Martell and R. J. Motekaitis, *Determination and Use of Stability Constants*. VCH Publishers, Weinheim (1988).
3. C. K. Jorgensen and J. Pouradier, *J. Chim. Phys.* 1970, **67**, 124.
4. R. D. Hancock and A. E. Martell, *Chem. Rev.* 1989, **89**, 1875.
5. P. G. Doctor, *Engin. Geol.* 1989, **26**, 411.
6. R. L. Iman and J. C. Helton, *A Comparison of Uncertainty and Sensitivity Analysis Techniques for Computer Models*, Sandia National Laboratories Report NUREG/CR-3904, SAND84-1461 (1985).
7. L. G. Sillén and A. E. Martell, *Stability Constants of Metal-ion Complexes*, 2nd Ed., Special Publication No. 17. The Chemical Society, London (1964).
8. L. G. Sillén and A. E. Martell, *Stability Constants of Metal-ion Complexes*, Special Publication No. 25. The Chemical Society, London (1971).
9. E. Högfeldt, *Stability Constants of Metal-ion Complexes. Part A. Inorganic Ligands. IUPAC Chemical Data Series*, No. 21. Pergamon Press, Oxford (1982).
10. D. D. Perrin *Stability Constants of Metal-ion Complexes. Part B. Organic Ligands. IUPAC Chemical Data Series*, No. 22. Pergamon Press, Oxford (1979).
11. G. Körtum, W. Vogel and K. Andrussow, *Pure Appl. Chem.* 1961, **1**, 190.
12. D. D. Perrin, *Dissociation Constants of Organic Bases in Aqueous Solution. IUPAC Chemical Data Series*, No. 12. Pergamon Press, Oxford (1965).
13. D. D. Perrin, *Dissociation Constants of Inorganic Acids and Bases in Aqueous Solution. IUPAC Chemical Data Series*, No. 19. Pergamon Press, Oxford (1972).
14. E. P. Sergeant and B. Dempsey, *Ionisation Constants of Organic Acids in Aqueous Solution. IUPAC Chemical Data Series*, No. 23. Pergamon Press, Oxford (1979).
15. A. E. Martell and R. M. Smith, *Critical Stability Constants. Volume* 1: *Amino Acids*. Plenum Press, New York (1974).
16. R. M. Smith and A. E. Martell, *Critical Stability Constants. Volume* 2: *Amines*. Plenum Press, New York (1975).
17. A. E. Martell and R. M. Smith, *Critical Stability Constants. Volume* 3: *Other Organic Ligands*. Plenum Press, New York (1977).
18. R. M. Smith and A. E. Martell, *Critical Stability Constants. Volume* 4: *Inorganic Complexes*. Plenum Press, New York (1976).
19. A. E. Martell and R. M. Smith, *Critical Stability Constants. Volume* 5: *First Supplement*. Plenum Press, New York (1982).
20. R. M. Smith and A. E. Martell, *Critical Stability Constants. Volume* 6: *Second Supplement*. Plenum Press, New York (1989).
21. IUPAC Commission on Equilibrium Data, *Coord. Chem. Rev.* 1975, **17**, 358.
22. G. Anderegg, *Critical Survey of Stability Constants of EDTA Complexes*. Pergamon Press, Oxford (1977).
23. W. A. E. McBryde, *A Critical Review of Equilibrium Data for Proton and Metal Complexes of* 1,10-*Phenanthroline*, 2,2′-*Bipyridyl and Related Compounds*. Pergamon Press, Oxford (1978).
24. A. M. Bond and G. T. Hefter, *Critical Survey of Stability Constants and Related Thermodynamic Data of Fluoride Complexes in Aqueous Solution. IUPAC Chemical Data Series*, No. 27. Pergamon Press, Oxford (1980).
25. G. Anderegg, *Pure Appl. Chem.* 1982, **54**, 2693.
26. L. D. Pettit, *Pure Appl. Chem.* 1984, **56**, 247.
27. P. Paoletti, *Pure Appl. Chem.* 1984, **56**, 491.
28. D. G. Tuck, *Pure Appl. Chem.* 1983, **55**, 1477.
29. J. Stary and J. O. Liljenzin, *Pure Appl. Chem.* 1982, **54**, 2557.
30. A. S. Kertes, R. Battino, H. L. Clever, S. S. Davis, W. Gerrard, G. K. Sigworth and C. L. Young, *CODATA Bull.* 1976, **21**, 74.
31. M. Salomon (Ed.), *Silver Azide, Cyanide, Cyanamides, Cyanate, Selenocyanate and Thiocyanate.*

Solubility Data Series, Vol. 3. Pergamon Press, Oxford (1979).
32. S. Siekierski, T. Mioduski and M. Salomon (Eds), *Scandium, Yttrium, Lanthanum and Lanthanide Nitrates. Solubility Data Series*, Vol. 13. Pergamon Press, Oxford (1983).
33. H. Miyamoto and M. Salomon (Eds), *Alkaline-earth Metal Halates. Solubility Data Series*, Vol. 14. Pergamon Press, Oxford (1983).
34. T. P. Dirkse (Ed.), *Copper, Silver and Gold, and Zinc, Cadmium and Mercury Oxides and Hydroxides. Solubility Data Series*, Vol. 23. Pergamon Press, Oxford (1986).
35. K. R. Bullock (Ed.), *Lead Sulphates, Selenates and Tellurates. Solubility Data Series*. Pergamon Press, Oxford (1988).
36. J. W. Lorimer (Ed.), *Beryllium, Barium, Strontium and Radium Sulphates. Solubility Data Series*. Pergamon Press, Oxford (1986).
37. E. M. Woolley (Ed.), *Silver Chloride and Water Systems. Solubility Data Series*. Pergamon Press, Oxford (1986).
38. R. Cohen-Adad (Ed.), *Alkali Metal and Ammonium Chlorides. Solubility Data Series*. Pergamon Press, Oxford (1986).
39. J. E. Bauman (Ed.), *Alkali and Alkaline Earth Metal Oxides and Hydroxides in Water. Solubility Data Series*. Pergamon Press, Oxford (1986).
40. H. Miyamoto and M. Salomon, *Alkali Metal and Ammonium Halates. Solubility Data Series*. Pergamon Press, Oxford (1986).
41. H. Miyamoto and E. M. Woolley, *Copper and Silver Halates. Solubility Data Series*. Pergamon Press, Oxford (1986).
42. J. J. Christensen, L. D. Hansen and R. M. Izatt, *Handbook of Proton Ionization Heats*. Wiley, New York (1976).
43. J. J. Christensen, D. J. Eatough and R. M. Izatt, *Handbook of Metal Ligand Heats and Related Thermodynamic Quantities*, 2nd Ed. Dekker, New York (1975).
44. M. T. Beck, *Pure Appl. Chem.* 1977, **49**, 127.
45. O. Exner, *The Hammett Equation—The Present Position. Advances in Linear Free Energy Relationships* (Edited by N. B. Chapman and J. Shorter). Plenum Press, New York (1972).
46. J. Shorter, *The Separation of Polar, Steric and Resonance Effects by Use of Linear Free Energy Relationships—Advances in Linear Free Energy Relationships* (Edited by N. B. Chapman and J. Shorter). Plenum Press, New York (1972).
47. J. Shorter, *Multiparameter Extensions of the Hammett Equation—Correlation Analysis in Chemistry* (Edited by N. B. Chapman and J. Shorter). Plenum Press, New York (1978).
48. J. R. Chipperfield, *Linear Free Energy Relationships in Inorganic Chemistry—Advances in Linear Free Energy Relationships* (Edited by N. B. Chapman and J. Shorter). Plenum Press, New York (1972).
49. H. Irving and H. Rossotti, *Acta Chem. Scand.* 1956, **10**, 72.
50. R. D. Hancock, G. J. McDougall and F. Marsicano, *Inorg. Chem.* 1979, **18**, 2847–2848 (Fig. 1).
51. F. Mulla, F. Marsicano, B. S. Nakani and R. D. Hancock, *Inorg. Chem.* 1985, **24**, 3076.
52. R. D. Hancock and B. S. S. Nakani, *Afr. J. Chem.* 1982, **35**, 153.
53. R. D. Hancock and F. Marsicano, *J. Chem. Soc., Dalton Trans.* 1976, 1832 (Figs 1 and 2).
54. R. D. Hancock and F. Marsicano, *Inorg. Chem.* 1978, **17**, 560 (Figs 1 and 2).
55. F. Marsicano and R. D. Hancock, *J. Chem. Soc., Dalton Trans.* 1978, 228 (Figs 1–7).
56. R. D. Hancock and F. Marsicano, *Inorg. Chem.* 1980, **19**, 2709 (Fig. 4).
57. R. D. Hancock and F. Marsicano, *South African J. Chem.* 1980, **33**, 77.
58. K. Murray and P. M. May, *Joint Expert Speciation System Users Manual* (Edited by P. M. May) School of Mathematical and Physical Sciences, Murdoch University, Murdoch, Western Australia (1989).
59. H. P. Williams, *Model Building in Mathematical Programming*, 2nd Ed. Wiley, Chichester (1985).
60. R. Tomovic, *Sensitivity Analysis of Dynamic Systems* McGraw-Hill, New York (1963).
61. O. L. Davies, *The Design and Analysis of Industrial Experiments*, 2nd Ed. Longman, London (1956).
62. J. A. John and M. H. Quenouille, *Experiments: Design and Analysis*. Griffin, London (1977).
63. B. Youens, *Statistics for the Social Scientist, Vol. 2. Applied Statistics*. Penguin Books, Harmondsworth (1967).
64. J. H. Pollard, *A Handbook of Numerical and Statistical Techniques*, pp. 236–252. Cambridge University Press, Cambridge (1977).
65. D. Cook, *Basic Statistical Computing*, pp. 98–99. Edward Arnold, London (1982).
66. N. R. Draper and H. Smith, *Applied Regression Analysis*, 2nd Ed. Wiley, New York (1981).
67. G. B. Wetherill, *Intermediate Statistical Methods*. Chapman and Hall, London (1981).
68. S. Henley, *Non-parametric Geostatistics*. Applied Science Publishers, Barking (1981).
69. G. Desmet, Reliability of Radioactive Transfer Models. Elsevier, London (1988).
70. G. W. Snedecor and W. G. Cochran, *Statistical Methods*, 7th Ed. Iowa State University Press, Iowa (1980).
71. G. B. Wetherill, *Intermediate Statistical Methods*, pp. 8–13. Chapman and Hall, London (1981).

Polyhedron Vol. 10, No. 10, pp. 1121–1129, 1991
Printed in Great Britain

0277-5387/91 $3.00+.00
© 1991 Pergamon Press plc

CHEMICAL SPECIATION MODELLING AND THERMODYNAMIC DATABASE COMPILATION—III. MODELLING SOLID FORMATION AND DISSOLUTION

J. R. DUFFIELD,* J. R. JOHNS, F. MARSICANO† and D. R. WILLIAMS‡

School of Chemistry and Applied Chemistry, University of Wales College of Cardiff, P.O. Box 912, Cardiff CF1 3TB, U.K.

(*Received* 20 *November* 1990; *accepted* 18 *February* 1991)

Abstract—Solids may be introduced into speciation using ion activity products and saturation index plots. The compilation of data required for such models is described and the descaling of cooling pipes in an industrial reactor is modelled as an example of how iron oxide dissolution can be maximized with a minimum of corrosion of pipeline and valves.

Previous papers have dealt with the critical appraisal of thermodynamic data for inclusion in databases for use with computer-based chemical speciation models and on-going critical assessment activities.[1,2]

Computer modelling of the precipitation/dissolution of solids in an aqueous medium is usually achieved by the addition of solubility considerations to general aqueous speciation codes since aqueous speciation knowledge is required before dissolution or precipitation can be calculated.

This paper describes the particular problems associated with the selection of formation/dissolution constants for solids, and the interpretation of results from programs using such data.

Factors affecting solubility

The difference between the lattice energy (the energy consumed in separating the ions or molecules of a substance from the crystal lattice) and the hydration energy (the energy released by solvation of ions or molecules), determines the solubility of a solid in water.

Since lattice and hydration energies often vary in a similar manner with change in the chemical variable, for example, increasing with ionic charge and decreasing with ionic size, solubility trends are difficult to predict even qualitatively from a consideration of the difference between these two parameters.

For most ionic solids, the hydration energy is somewhat less than the lattice energy and, thus, the dissolution reaction is generally endothermic, with the result that solubility increases with increase in temperature.

However, for essentially ionic oxides, the oxide ion hydrolyses on dissolution in water and, thus, the dissolution process is exothermic, i.e. solubility decreases with increasing temperature. For some elements (e.g. beryllium and boron), incomplete ionization occurs, and the oxides formed have substantial covalent characters and generally low solubilities.

An equilibrium constant is related to temperature by the expression:

$$K = A \exp(-\Delta H^{\ominus}/RT),$$

where K is the equilibrium constant, T the absolute temperature, and $\Delta H^{\ominus}$ the standard state enthalpy of reaction (assumed constant over small temperature ranges). The constant, A, is also a function of $\Delta H^{\ominus}$ and is assumed to be nearly constant over small temperature ranges.

The effect of temperature on equilibrium constants for the dissolution of solids is much larger than for the formation of aqueous complex species

* Present address: Department of Chemistry, Faculty of Science and Engineering, Manchester Polytechnic, John Dalton Building, Chester Street, Manchester M1 5GD, U.K.

† Department of Chemistry, University of Witwatersrand, P.O. Wits 2050, Johannesburg, South Africa.

‡ Author to whom correspondence should be addressed.

owing to the generally larger enthalpies associated with dissolution processes. Any modelling work involving solids must, therefore, use equilibrium constants appropriate to the particular temperature considered. Usually, constants at standard temperature are corrected using the van't Hoff equation and reaction enthalpies.

Enthalpies of dissolution are themselves temperature dependent, and the dependence is described by Kirchhoff's law:

$$\left[\frac{\partial \Delta H}{\partial T}\right]_p = \Delta C_p,$$

where ΔC_p is the molar heat capacity change at constant pressure. Very few speciation codes use heat capacities for correcting enthalpies since the effect upon equilibrium constants for solid dissolution is smaller than uncertainties in these parameters.

Since dissolution is an ionic dissociation process, any factors that affect the thermodynamic stability of ions in solution, e.g. ionic strength, will also affect solubility. Ionic strength corrections may be applied in the same way as for aqueous equilibria. Reactions involving the ions formed will also indirectly affect the solubility.

Ion activity products and saturation indices

The solubility product is the inverse of the equilibrium constant for the dissolution reaction of a solid to form ions. For any sparingly soluble salt of the metal ion M^{n+} with the anion X^{m-}, i.e. M_mX_n, the dissolution reaction is:

$$M_mX_n(s) \rightleftharpoons mM^{n+}(aq) + nX^{m-}(aq),$$

and the activity solubility product is given by:

$$K_{sp} = (a_m^{n+})^m \cdot (a_x^{m-})^n = [M^{n+}]^m[X^{m-}]^n \cdot (\gamma_m^{n+})^m \cdot (\gamma_x^{m-})^n,$$

where a = thermodynamic activity and γ = concentration activity coefficient.

The activity of a pure solid is set at unity and need not be included in the expression. The right-hand side is thus the product of $m+n$ concentration (or activity) factors. If the solid is sparingly soluble and the ionic strength of the solution low, the activity coefficients will be near unity, and concentrations can be used rather than activities. Alternatively, if the solid is sparingly soluble and the ionic strength of the solution is constant, but not necessarily low, the activity coefficient factors will have more or less constant values which could be incorporated into the constant, K_{sp}. With this modification to the numerical value of K_{sp}, concentrations rather than activities can once again be used.

The ion activity product (IAP) or activity product, is the product of the activities of the ions produced on dissolution of the solid raised to the power of their stoichiometric coefficients in the balanced reaction equation, i.e. the right-hand side of the solubility product expression. Thus, for the reversible reaction:

$$M_xX_n(s) = mM^{n+}(aq) + nX^{m-}(aq),$$

$$IAP = (a_m^{n+})^m \cdot (a_x^{m-})^n.$$

It is important to note that the IAP differs from K_{sp} in as much as the activities, a_m^{n+} and a_x^{m-}, appearing in the expression for IAP do not necessarily correspond to values at equilibrium but they do correspond to the activities prevailing in a given system which may not be at solubility equilibrium. The saturation index (SI) is defined as the logarithm of the quotient of the ion-activity product to the solubility product, i.e. $SI = \log (IAP/K_{sp})$.

If $SI > 0$ then the solution is supersaturated. Given sufficient time, a precipitate will form and any precipitate present will not dissolve.

If $SI < 0$ then the solution is less than saturated. No precipitate forms and any precipitate present will dissolve.

If $SI = 0$ then the solution is just saturated and no net precipitation or dissolution is expected to occur.

Saturation index plots are a convenient method for representing the propensity of a system for precipitation or dissolution with the need to refer to the actual solubility products involved.

Problems associated with the selection of dissolution constants for databases

Most databases contain a single value for the formation or dissolution constant of a solid, in addition to extra data or a code to correct this value for ionic strength, temperature, etc. Selection of this single value can be problematic for several reasons.

(1) Many values tabulated in compilations are derived from thermodynamic data (such as free energies of formation) rather than direct experimental solubility measurement. Whilst these values can be used in the absence of other data, experimentally determined constants are preferable.

(2) The formation constant may be continuously variable between a lower limit for an amorphous phase or highly hydrated form, and an upper limit for a crystalline phase or less hydrated form, there being no clear delineation between the two. The particular form of solid phase which actually occurs

in a system will depend upon the experimental conditions.

(3) Many solids undergo "ageing" with concurrent stability change as reflected in their formation constants. Ageing can be rapid at elevated temperatures.

(4) The formation constant can be dependent upon the particle size of the precipitate. If the particle size is very small, the surface area per mole becomes sufficiently large to require surface energy to be considered.

(5) Coprecipitation of a foreign ion such as an impurity can alter the stability of the solid. This can occur through:

(a) formation of a solid solution whereby the contaminating ion(s) precipitates with the same lattice structure and similar lattice constants to the solid being considered;
(b) ion entrapment or occlusion whereby foreign ions are trapped during the rapid precipitation occurring in the vicinity. Cation, anion or mixed occlusions can occur, resulting in an impure phase;
(c) adsorption of foreign ions on to the surface of a precipitate. Many precipitates exhibit significant ion-exchange properties.

(6) The accuracy with which a solubility product can be determined depends upon the experimental method and the treatment of the experimental data. Many workers in the past have not taken any account of the complex equilibria between the metal and ligand in solution but, rather, have calculated solubility products from total (analytical) concentrations, giving unreliable constants. Literature reports involving separation of the solid and saturated solution, followed by chemical analysis, often given chronologically decreasing solubility products (decreasing solubility) owing to improvement in the separation (e.g. filtration) technique.

Prediction of solid precipitation

Problems also arise with determining which of several thermodynamically feasible phases will actually form under the conditions being modelled. Furthermore, the particular phase that does, in fact, begin to precipitate may be kinetically controlled and depend upon factors such as:

(1) the concentration of the ions involved in the equilibrium;
(2) the temperature of the solution;
(3) other ions present in solution including impurities;
(4) turbulence;
(5) particle size;
(6) nucleation factors.

Thermodynamic speciation codes can go only as far as indicating phases that might precipitate on the basis of thermodynamic stability. A purely thermodynamic model cannot take into account kinetic effects. Rather, these must be assessed by a skilled professional chemist and used in interpreting such modelling results.

To demonstrate these problems, an example using the iron oxyhydroxide system will be reviewed in the context of aqueous speciation and solid precipitation modelling.

There are a number of iron oxyhydroxide forms reported in the literature. Some occur naturally in geology but can also be synthesized, whilst some are synthetic only. Those relevant to general speciation modelling are described below.

Forms of iron oxyhydroxides

$Fe(OH)_3$. Amorphous ferric hydroxide, an amorphous material which comprises a relatively large proportion of most fresh precipitates and which is formed under conditions of substantial supersaturation with respect to the crystalline oxyhydroxides; it is thermodynamically unstable with respect to both haematite and goethite. An amorphous phase develops by rapid hydrolysis of dissolved ferric species or rapid oxidation and hydrolysis of ferrous iron-rich solutions.

α-Fe_2O_3. Haematite is rarely found as a direct precipitate geologically but slowly crystallizes from amorphous material by dehydration or long term ageing at low temperatures or from short intervals close to 100°C.[3] It may also form to some extent by rapid precipitation at room temperature or from gels around 100°C.[4] The colour is brick red.

γ-Fe_2O_3. Maghemite is rarely found as a direct precipitate but is more usually formed by low temperature oxidation of magnetite, or dehydration of lepidocrocite.[3,5,6] When heated to 200–700°C, it transforms to haematite.[5] It may be produced geologically from other iron oxides by the reducing action of organic matter.[5]

α-FeOOH. Goethite, limonite, precipitates by relatively slow oxidation and hydrolysis of aqueous or solid ferrous iron species.[3,5] Under laboratory conditions, goethite forms most rapidly at pH values higher than 3.5 because the oxidation rate of ferrous iron is extremely slow under more acidic conditions.[3] It also forms by long-term ageing of amorphous material precipitated during hydrolysis

of ferric solutions.[3] Upon dehydration, it forms haematite.[5]

β-FeOOH. Akaganeite is the rarest form under natural conditions,[7,8] The synthetic light brown solid polymorph forms at room temperature by slow hydrolysis of 20–80 mmol dm^{-3} $FeCl_3$ solutions, and it is probable that it only forms from chloride solutions.[3–5,9,10] On heating to 280°C, or boiling in water for 6 days, it transforms to α-Fe_2O_3 (haematite).[9]

γ-FeOOH. Lepidocrocite is dimorphous with goethite. It may be synthesized (indirectly via $Fe_3(OH)_6$)[9] by slow oxidation between pH 4–7 of dilute solutions of ferrous salts or by oxidation of $3Fe_2O_3 \cdot 2FeO$. Usually, its occurrence is accompanied by goethite. Thermally, it dehydrates to form maghemite.[5]

δ-FeOOH. δ-FeOOH is solely synthetic and is obtained by very rapid oxidation of $Fe(OH)_2$. This brown and strongly magnetic material transforms to α-Fe_2O_3 (haematite)[9] on heating above 100°C.

Fe_3O_4. Magnetite is synthesized by oxidation of iron at high temperatures in air by heating Fe_2O_3 in reducing atmospheres, or by precipitation by addition of alkali to solutions of mixed ferrous–ferric ions. It is one of the most abundant oxide minerals in igneous and metamorphic rocks. It frequently occurs as heavy detrital material in sedimentary rocks and it may become concentrated by stream and tidal action to form black magnetite sands.[5] Hydrated Fe_3O_4 (magnetite) rather than hydrated Fe_2O_3 (haematite) is obtained from ferrous hydroxide when the supply of oxygen is limited (e.g. in water at 100°C) and under alkaline conditions.

$FeOOH \cdot nH_2O$. Hydrated haematite and brown haematite are terms used to describe poorly characterized crystalline hydrated oxides whose real identities are not known.[5]

$Fe_2O_3 \cdot 4H_2O$. Crystallized ferric hydroxide may be formed by the slow hydrolysis of ferric ethylate.[11]

$Fe_3(OH)_8$. $Fe_3(OH)_8$ is formed by slow oxidation of $Fe(OH)_2$ under neutral conditions. It forms Fe_3O_4 (magnetite) on heating in water to 100°C. Strong oxidation of the solid forms Fe_3O_4 or γ-Fe_2O_3.[6]

$Fe(OH)_2$. "Ferrous hydroxide" is precipitated as a snow white gel when alkali or ammonia is added to a ferrous solution in the absence of oxygen. It has a green colour if even minute traces of oxygen are present due to iron(III) hydroxide impurities. It immediately oxidizes on contact with oxygen.

The details given above, as well as the relationship between the various oxyhydroxide forms of iron, are summarized in Fig. 1.

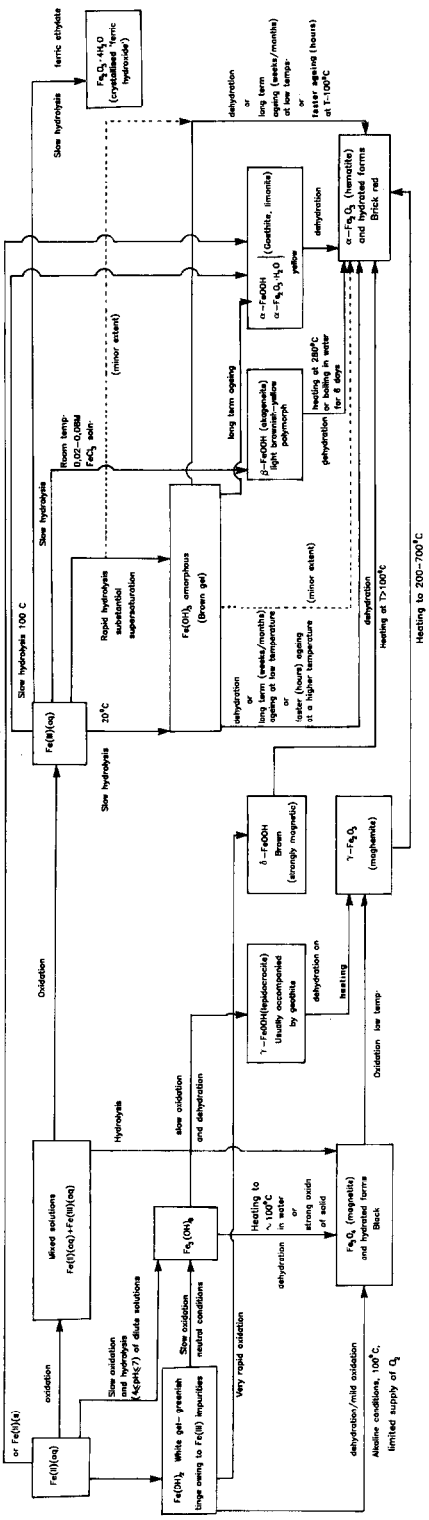

Fig. 1. Relationship between various oxyhydroxide forms of iron that are of interest in the context of aqueous solution modelling.

Redox processes: E_h–*pH relations*

Since iron solids can contain the metal in several oxidation states, the redox potential of the solution needs to be considered carefully when modelling is performed. The interrelationships between all these possible precipitates of iron as a function of redox potential is best shown with an E_h–pH diagram. Figure 2 shows the stability fields for solids and the predominant aqueous species for the Fe–H_2O–O_2 system with 10^{-4} mmol dm^{-3} dissolved iron species (5.6 ppm iron).[3] The procedure for constructing these diagrams can be found in Hem and Cropper[12] and Garrels and Christ.[13]

The boundaries are drawn at equal ion activities. The boundaries between ferric–ferrous aquo iron species and ferric oxyhydroxide solids are drawn for log K_{sp} values of −44 (crystalline solid) and −37.1 (amorphous solid). This difference in log K_{sp} means that at a fixed pH and E_h there can be roughly seven orders of magnitude more dissolved iron in equilibrium with fresh amorphous solid than with well crystallized goethite or haematite. For the E_h and pH values for iron rich aerobic natural waters (pH 5–8, E_h −0.1 to +0.3 V), the system will contain most suspended oxyhydroxides, and lie on the boundary between the regions of stability of the ferrous aquo species and ferric oxyhydroxide solids.

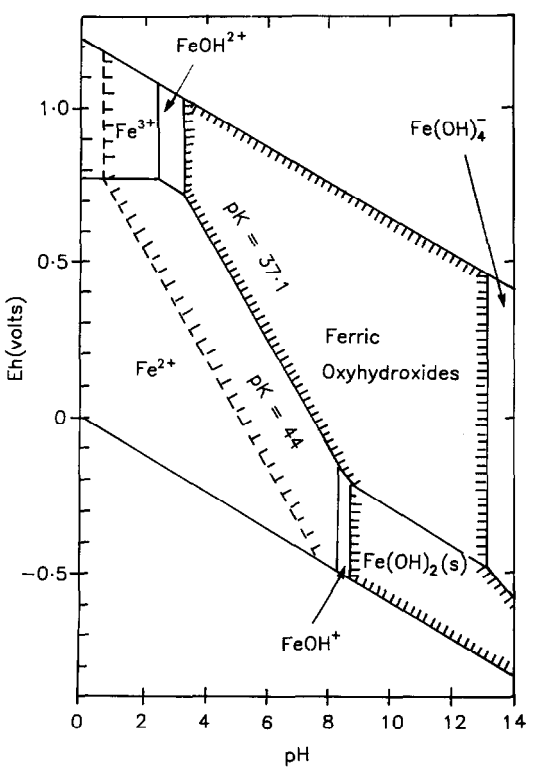

Fig. 2. E_h–pH relations between the predominant aqueous species and iron oxyhydroxides.

General comments

In most cases, the oxyhydroxide first precipitated is amorphous, having been formed under conditions of substantial supersaturation. Early in the precipitation process, poorly crystalline goethite or lepidocrocite may also form. The tendency to form amorphous precipitates increases with the valency of the metal ion.

Many workers refer to this finely divided, disordered precipitate first formed as the "active" form, since it undergoes change with time (ageing) to produce larger and more ordered crystals (the "inactive" form).

The relationship between freshly precipitated amorphous ferric hydroxide and goethite may be written:

$$Fe(OH)_3(\text{amorphous}) = \alpha\text{-FeOOH(crystalline goethite)} + H_2O,$$

and between amorphous ferric hydroxide and haematite is seen to be:

$$2Fe(OH)_3(\text{amorphous}) = \alpha\text{-}Fe_2O_3(\text{crystalline haematite}) + 3H_2O.$$

From free energies of formation,[14,15] the Gibbs free energy for these transformations is found to be −29.18 kJ mol^{-1} (−6.97 kcal mol^{-1}) for goethite and −60.59 kJ mol^{-1} (−14.46 kcal mol^{-1}) for haematite. Thus, with sufficient time, a freshly precipitated ferric hydroxide will transform into the more stable haematite phase.

Oxyhydroxide precipitates are often mixtures of different phases. The apparent thermodynamic stability or the solubility of such mixtures depends mainly on the solubility of the least stable phase present, a phase which is usually amorphous. It must always be remembered, however, that the formation of a particular solid phase may be kinetically controlled owing to slow rates of reaction and may not be observed to occur, even though it is thermodynamically favourable. Another less thermodynamically favourable phase may be observed to form instead. Slow precipitation over long time periods, such as that considered in many geological systems, will favour formation of thermodynamically more stable phases, whereas rapid precipitation, e.g. alkali addition, will favour the kinetic product.

If acid is added to a solution containing precipitated ferric oxyhydroxides, the least stable, more soluble amorphous material may redissolve, leaving behind relatively crystalline particles of lower solubility product.[3]

Oxyhydroxide precipitates usually contain col-

loidal material. Sizes range from molecular $Fe(OH)_3$ to micron sized crystals or crystal aggregates. Both crystalline and amorphous precipitates remain colloidal indefinitely in some solutions. Particle size is probably the major influence on thermodynamic stability of the oxyhydroxides. Other factors include crystallinity, degree of hydration of the precipitate, the presence of impurities, and turbulence.

Thermodynamic relationships

Solution reactions for all the oxyhydroxides can be written in the same form, e.g.

$$Fe(OH)_3(\text{amorphous, s}) \rightleftharpoons Fe^{3+}(aq) + 3OH^-(aq),$$
$$\alpha\text{-}FeOOH(s) + H_2O \rightleftharpoons Fe^{3+}(aq) + 3OH^-(aq),$$
$$1/2\alpha\text{-}Fe_2O_3(s) + 3/2H_2O \rightleftharpoons Fe^{3+}(aq) + 3OH^-(aq).$$

The logarithm of the solubility product expression may be written as:

$$\log K_{sp} = \log[Fe^{3+}][OH^-]^3.$$

Values for log K_{sp} range from -37 for fresh, rapidly precipitated amorphous material to -44 or less for crystalline goethite and haematite.[3]

There is a linear increase in log K_{sp} for oxyhydroxides with decrease in particle size due to surface energy. For equal sized goethite and haematite particles, goethite is more stable when the particle size exceeds 760 Å (0.076 μm) but less stable than haematite at smaller particle sizes. Particle sizes of $\leqslant 100$ Å are common in laboratory solutions and natural waters. Such particles are at least 1.2 and 2.7 log K_{sp} units less stable than well crystallized samples of haematite and goethite, respectively.

Ferric oxyhydroxides precipitated in natural waters are usually mixtures of X-ray amorphous material (does not give an X-ray diffraction pattern) and poorly crystalline goethite (α-FeOOH) and, sometimes, poorly crystalline lepidocrocite. Oxyhydroxides other than these are rarely precipitated from natural waters.

In cases of slight supersaturation of iron solutions with hydroxide ions, nucleation and crystal growth are often slow. The crystalline form may precipitate very slowly and equilibrium is established only very gradually. Under such conditions, short-term measurements of solubility products do not give reliable results.

Solid $Fe(OH)_2$ cannot be formed in air and only forms in solution under reducing conditions. Addition of hydroxide to a ferrous solution in the absence of oxygen yields a fairly crystalline ferrous hydroxide [$Fe(OH)_2$] product. The addition of base to precipitated $Fe(OH)_2$ at high pH gives a material which is easily oxidized at low potential to $Fe(OH)_3$.

The reaction $3Fe(OH)_2(\text{crystalline}) = Fe_3O_4(\text{crystalline}) + H_2(g) + 2H_2O$, has a Gibbs free energy change of -27.3 kJ mol^{-1} (-6.5 kcal mol^{-1}).[14,15] Therefore, $Fe(OH)_2$ is unstable with respect to decomposition into magnetite, water and hydrogen gas. Under a total pressure of 1 atm., a precipitate of ferrous hydroxide should eventually decompose to yield magnetite, and hydrogen would bubble from the system until the conversion was complete.

Solubility can also be represented as a concentration versus pH plot. The solubility of amorphous iron hydroxide as a function of pH is represented in Fig. 3.[16] The hydroxide concentration is determined by the pH, and the plot is of total iron concentration versus pH. The area

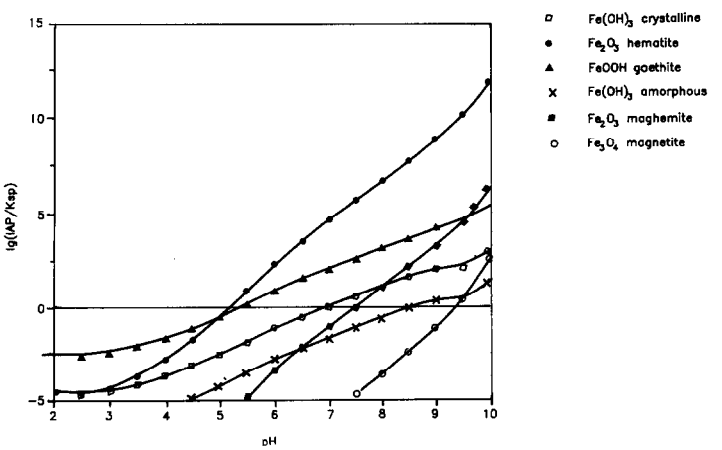

Fig. 3. Solubility of $Fe(OH)_3$(amorphous) depicted on a concentration versus pH plot. A value of -38.7 was used for the solubility product.

above the roughly parabolic hatched envelope represents precipitated amorphous ferric hydroxide (where the ion activity product exceeds the K_{sp} value) while below this the iron is present as a mixture of hydrolysed species. Minimum solubility is observed at a pH of about 8.5. It should be noted that an E_h value was chosen such that all the iron is present as iron(III).

Example of dissolution modelling—descaling a reactor cooling system

The solution used for cleaning the cooling system of a steel reactor was modelled using the PHREEQE code.[17] The oxide corrosion film undergoes dissolution in an acidic aqueous medium (nitric acid added) using EDTA as a chelating agent and with citric acid–ammonium citrate added as a buffer.

Input parameters used for the model were as follows:

Total Fe	20 mmol dm^{-3}
Total EDTA	25 mmol dm^{-3}
Total citric acid	15 mmol dm^{-3}
Total Na^+	50 mmol dm^{-3}
Total NH_4^+	9 mmol dm^{-3}
E_h	0.50 V
Temperature	90°C (363 K).

The system was modelled at pH values between 2–10, fixing the pH by addition of nitric acid or sodium hydroxide as required, in order to maintain the charge balance. The solution was not allowed to equilibrate with solid phases but the saturation indices for solid phases were computed.

Constants

The constants in Table 1 are those from the literature that are believed to be the most reliable at this time. The log K_{sp} values are the logarithms of the solubility products (calculated from the UW* PHREEQE database), in terms of iron(II) or iron(III) as appropriate, and hydroxide ligands. They have been converted into this form so that direct comparison of the numerical values can be made.

The database for PHREEQE, however, uses constants based on water as a master species, and relative to Fe^{2+} as a master species, i.e. the formation constant for hydroxide from water (pK_w) is added to log K_{sp} for each hydroxide ion present in a formula unit of the solid. All Fe^{3+} species include a redox correction of 13.01 for the Fe^{2+}–Fe^{3+} couple for each Fe^{3+} ion present in a formula unit of the solid. Accordingly, they are numerically not directly comparable owing to different oxidation states and numbers of hydroxide ions involved.

* University of Wales College of Cardiff (formerly UWIST, Cardiff).

Table 1. Iron oxyhydroxide constants in the UW database

	PHREEQE		
	Log K_{sp}[a]	Log K[b]	References
$Fe(OH)_3$ amorphous	−37.1	17.90	19, 20
$Fe(OH)_3$ crystalline	−38.8	16.21	21
α-Fe_2O_3 haematite	−41.3	26.72	21
γ–Fe_2O_3 maghemite	−35.6	32.42	19, 22
α-FeOOH geothite	−41.5	13.51	20, 21
Fe_3O_4 magnetite	−45.3	36.71	23
$Fe_3(OH)_8$	−91.8	46.24	20, 24, 25
$Fe(OH)_2$	−14.4	13.61	22, 26
FeO	−0.5	13.53	22

[a] Solubility products (dissolution to give Fe^{2+} or Fe^{3+} and OH^-), calculated from the UW PHREEQE database.

[b] Dissolution constants corrected for formation from water and Fe^{2+} only (PHREEQE[17] format).

Table 2. Formation constants for aqueous iron species

Species	Log β	References
Iron(II)		
$[FeOH]^+$	−9.50	21
$[Fe(OH)_2]^0$	−20.6	21
$[Fe(OH)_3]^-$	−31.0	21
$[Fe(OH)_4]^{2-}$	−46.0	21
$[Fe(EDTA)]^{2-}$	16.00	28
$[FeH(EDTA)]^-$	19.17	28
$[FeH_2(EDTA)]^0$	22.30	28
$[Fe(EDTA)(OH)]^{3-}$	6.301	28
$[Fe(EDTA)(OH)_2]^{4-}$	−4.38	28
Iron(III)		
$[FeOH]^{2+}$	−15.2	21
$[Fe(OH)_2]^+$	−18.68	21
$[Fe(OH)_3]^0$	−25.01	21
$[Fe(OH)_4]^-$	−34.61	21
$[Fe_2(OH)_2]^{4+}$	−28.97	21
$[Fe(OH)_4]^{5+}$	−45.33	21
$[FeNO_3]^{2+}$	−12.01	28
$[Fe(EDTA)]^-$	14.513	28
$[FeH(EDTA)]^0$	16.123	28
$[Fe(EDTA)(OH)]^{2-}$	6.702	28
$[Fe(EDTA)(OH)_2]^{3-}$	−4.81	28
$[Fe_2(EDTA)_2(OH)_2]^{4-}$	12.216	28

Table 3. Iron citrate formation constants corrected for formation from water and Fe^{2+} only (PHREEQE[17] format) at $I = 0$

Iron(II)		Iron(III)	
$[Fe(Cit)]^-$	6.13	$[Fe(Cit)]^0$	−0.17
$[FeH(Cit)]^0$	10.17	$[Fe(Cit)(OH)]^-$	−2.43
$[FeH_2(Cit)]^+$	13.64	$[Fe(Cit)(OH)_2]^{2-}$	−7.69
$[Fe(Cit)(OH)]^{2-}$	−0.86	$[Fe(Cit)_2]^{3-}$	5.88
$[Fe(Cit)_2]^{4-}$	7.80	$[FeH(Cit)_2]^{2-}$	10.37
		$[FeH(Cit)_2(OH)]^{4-}$	−0.21

The justification for the selection of these particular constants for the UW database will not be discussed here, but are consistent with those of the EIR MINEQL database and the CHEMVAL (Mirage 2 project of EEC) database. Selection was done by expert groups in line with the guidelines proposed by IUPAC.[18]

The formation constants given in Table 2 were used for aqueous iron species.

The iron(II) and iron(III) citrate constants (given at $I = 0$) in Table 3, which were measured at UW, have also been included in the model.

The following iron citrate constants, which have been considered by other workers but which were not consistent with the iron citrate model at UW and were, therefore, not used, were:

$[Fe(OH)_2(Cit)_2]^{4-}$	−4.54
$[FeH(Cit)_2]^{3-}$	13.58
$[FeH(Cit)]^+$	1.28
$[Fe_2(Cit)_2(OH)_2]^{2-}$	−1.61

A plot of saturation index versus pH is shown in Fig. 4 for the iron solids that may, from thermodynamic considerations, possibly precipitate.

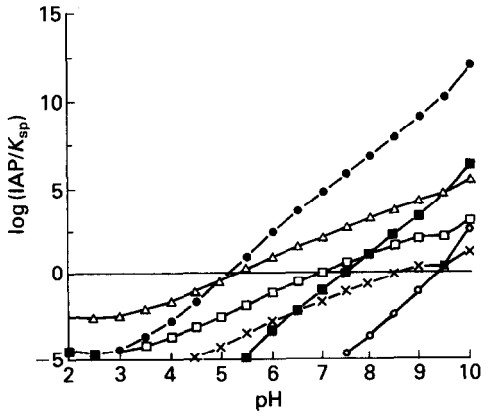

Fig. 4. Saturation index plot for model of reactor cooling system cleaning solution. Key: □, $Fe(OH)_3$ crystalline; ●, Fe_2O_3 haematite; △, FeOOH goethite; ×, $Fe(OH)_3$ amorphous; ■, Fe_2O_3 maghaemite; ○, Fe_3O_4 magnetite.

RESULTS

It may be observed that below a pH value of 5, no solubility products are exceeded, i.e. all saturation indices are less than zero. As the pH increases, the solubility limits for various phases are reached (i.e. the lines cross the horizontal saturation limit line). Of all the solid phases considered, $Fe(OH)_3$ (amorphous) is likely to be the precipitate first formed, on the basis of "real" experimental observations[3] rather than thermodynamic considerations, even though it is not the most thermodynamically stable.

Under the conditions being modelled, maghemite ought not to form since it rarely precipitates directly from aqueous iron solutions but usually forms under reducing conditions from other iron solids.[3,5,6]

Magnetite is unlikely to form since, although the level of oxygen is zero and the temperature high (90°C), the conditions are not sufficiently reducing for any significant concentration of ferrous ions to be present, an experimentally observed requirement for magnetite precipitation.[5]

A small amount of poorly crystalline goethite and/or haematite might be expected to precipitate with the initial amorphous solid formed.[3] Ageing is quite rapid at 90°C, however, so after a period of several hours, transformation to more crystalline $Fe(OH)_3$–haematite–goethite will occur. These phases are more thermodynamically stable and far less soluble than the initially precipitated, more hydrated, amorphous phase. It would be necessary to reduce the pH of the solution to a much lower value than that at which the first precipitate formed in order to redissolve the aged precipitate.

The implications of solid precipitation in a cooling system can be of major importance. Pumps, valves and filters can become blocked and solids can deposit in stagnant areas of low flow, and reduction of the pH to a value sufficient to redissolve the precipitate can cause significant corrosion problems to plant materials. The pH must, therefore, be maintained at a value low enough to allow a good rate of oxide film dissolution, but not low enough for corrosion to become a significant problem, yet not above a pH where solids reprecipitation can occur.

CONCLUSIONS

Solid–solution speciation models which are based upon powerful programs and verified thermodynamic databases permit:

(a) an enhanced understanding of the processes present;

(b) the optimization of desirable effects;
(c) the suppression of undesirable side effects;
(d) the outcome of postulated modifications (e.g. a change of sequestering ligand used) to be assessed.

Acknowledgements—We gratefully acknowledge Rolls Royce & Associates (Derby) for encouraging this work.

REFERENCES

1. J. R. Duffield, F. Marsicano and D. R. Williams, *Polyhedron* 1991, **10**, 1105.
2. J. R. Duffield, F. Marsicano, M. Waters and D. R. Williams, *Polyhedron* 1991, **10**, 1113.
3. D. Langmuir and D. O. Whittemore, *Variations in the Stability of Precipitated Ferric Oxyhydroxides, Adv. Chem. Ser.* Vol. 106, p. 209 (1971).
4. H. B. Weiser and W. O. Milligan, *J. Am. Chem. Soc.* 1935, **57**, 238.
5. W. A. Deer, R. A. Howie and J. Zussman, in *Rock Forming Minerals*. Longmans, London (1963).
6. G. Hägg, *Zeit. Phys. Chem.* 1935, **29B**, 95.
7. R. Van Tassel, *Bull. Soc. Belge Geol.* 1959, **68**, 360.
8. K. C. Chandy, *Indian J. Phys.* 1962, **36**, 484.
9. J. D. Bernal, D. R. Dasgupta and A. L. Mackay, *Clay Min. Bull.* 1959, **4**, 15–30.
10. J. H. L. Watson, W. Heller and L. E. Poplawski, Third European Regional Conf. Electron Microscopy, 1964, p. 315 (1964).
11. P. A. Thiessen and R. Köppen, *Zeit. Anorg. Chem.* 1931, **200**, 18.
12. J. D. Hem and W. H. Cropper, *U.S. Geol. Survey. Water Supply Paper* 1959, **4**, 1459A.
13. R. M. Garrels and C. L. Christ, *Solutions, Minerals and Equilibria*, p. 172. Harper and Row, New York (1965).
14. R. A. Robie, B. S. Hemingway and J. R. Fisher, *Geol. Soc. Bull.* No. 1452 (1978).
15. D. Wagman, D. H. Evans, V. B. Parker, R. H. Schumm, I. Halouw, S. M. Bailey, K. L. Churney and R. L. Nuttall, *J. Phys. Chem. Ref. Data* 1982, **11**, Suppl. 2.
16. W. Stumm and J. Morgan, *Aquatic Chemistry*. Wiley, New York (1981).
17. D. L. Parkhurst, D. C. Thorstenson and L. N. Plummer (Eds), *PHREEQE: A Geochemical Speciation and Mass Transfer Code Suitable for Nuclear Waste Performance Analysis*, USGS-WRI, 80–86 (1980).
18. M. T. Beck, *Pure Appl. Chem.* 1977, **48**, 127.
19. A. H. Truesdell and B. F. Jones, *J. Res. U.S. Geol. Survey* 1974, **2**, 232.
20. J. W. Ball *et al.*, *U.S. Geol. Survey Water Resources Invest*, USGS-WRI (1980).
21. A. E. Smith and R. M. Martell, *Critical Stability Constants*, Vol. 4, p. 78. Plenum Press, New York (1976).
22. B. W. Goodwin and M. Munday, *A Reference Guide to SOLMNQ—An Interactive Solution Mineral Equilibrium Program*, AECL-7800 (1983).
23. B. W. Goodwin, Private communication (1984).
24. L. V. Bensen and L. S. Teague, *A Tabulation of Thermodynamic Data.* Lawrence Berkeley Laboratory, San Francisco (1980).
25. F. N. Ponnamperama, E. M. Tianco and L. Teresita, *Soil Sci.* 1967, **103**, 374.
26. Y. K. Kharaka and I. Barnes, *SOLMNQ: Solution Mineral Equilibrium Computations*, USGS-WRD-73-002 (1973).
27. C. F. Baes and R. E. Mesmer, *The Hydrolysis of Cations*. Wiley, New York (1976).

Polyhedron Vol. 10, No. 10, pp. 1131–1138, 1991
Printed in Great Britain

0277–5387/91 $3.00+.00
© 1991 Pergamon Press plc

SYNTHESIS OF NEW SIX-COORDINATE COMPLEXES OF SILICON(IV)

DENNIS F. EVANS* and CHIH Y. WONG

Inorganic Chemistry Laboratories, Imperial College, London SW7 2AY, U.K.

(*Received* 14 *January* 1991; *accepted* 20 *February* 1991)

Abstract—The synthesis of new six-coordinate tris-bidentate complexes of silicon(IV) is reported. Two methods of synthesis have been used, the normal procedure using $SiCl_4$, and a novel method using $Si(OEt)_4$ in the presence of a strong acid. This new route has shown to be preferential for making such compounds in general. The complexes have been characterized by ^1H and ^{29}Si NMR spectrometry in DMSO, elemental analysis and FAB^+ mass spectrometry. Facial and meridional isomerism was normally slow on the NMR time scale and in some cases the rates of isomerism were recorded. Complexes derived from the 3-hydroxypyridin-4-ones were found to be water stable.

Preliminary work on the understanding of the biochemistry of silicon involves an investigation into its aqueous chemistry. Quantitative data for the formation of tris-catecholato silicon(IV) complexes have been previously reported.[1] Since few complexes of silicon are stable in aqueous solution, this present work involves the synthesis of new six-coordinate silicon(IV) complexes in non-aqueous solvents, which are based on a variety of hard bidentate ligands. Several of these ligands, e.g. 1,2-dimethyl-3-hydroxypyridin-4-one and acetohydroxamic acid, have already been shown to chelate efficiently with other hard metal ions, notably with iron(III)[2] and aluminium(III).[3] A new and simple route to these complexes is illustrated below in eq. (1):

$$Si(OEt)_4 + 3LH + HX \rightarrow [SiL_3]^+[X]^- + 4EtOH, \quad (1)$$

where $X^- = CF_3SO_3^-$, HSO_4^-, $CF_3CO_2^-$, Cl^- or the 10-camphor-sulphonate anion. This is found in most cases to be preferable to the normal method used for acac[4] and tropolonato[5] complexes, as shown in eq. (2):

$$SiCl_4 + 3LH \rightarrow [SiL_3]^+[Cl]^- + 3HCl. \quad (2)$$

The complexes have been characterized by ^1H and ^{29}Si NMR spectroscopy, elemental analysis and FAB^+ mass spectrometry.

EXPERIMENTAL

Materials

Silicon tetraethoxide, trifluoromethanesulphonic acid, trifluoroacetic acid, 10-camphorsulphonic acid (camH), maltol (malH), acetohydroxamic acid (aceH), benzohydroxamic acid (benH), 3-hydroxypyridin-2-one (2,3-dihydroxypyridine, dhpH) and 8-hydroxyquinoline-*N*-oxide (hqoH) were obtained commercially from Aldrich and used without further purification. Chrysin (chrH) was obtained from Sigma.

3-Hydroxy-2-methylpyridin-4-one[6] (hmpH), 1,2-dimethyl-3-hydroxypyridin-4-one[7] (dmpH) and 1-ethyl-3-hydroxy-2-methylpyridin-4-one[7] (empH) were prepared by literature methods.

Physical measurements

^1H NMR spectra were recorded on a Jeol GSX270 (270 MHz) spectrometer. $^{29}Si\{^1H\}$ NMR spectra were recorded on a Bruker WM250 (250 MHz) spectrometer. Chemical shifts are quoted relative to internal tetramethylsilane (TMS) for both ^1H and ^{29}Si nuclei. The relaxation reagent, $Cr(acac)_3$, was added (0.08 M) to overcome the

Correspondence should be addressed to: Dr S. R. Drake, Inorganic Chemistry Laboratories, Imperial College, London SW7 2AY, U.K.

*This paper is dedicated to the memory of the late Professor Dennis Frederick Evans, FRS.

problems associated with the long relaxation times and the negative magnetic moment of the ^{29}Si nucleus. Mass spectra were recorded on a Micromass VG 7070E spectrometer in the FAB^+ mode, with the sample suspended in a *m*-nitrobenzylalcohol matrix.

8-*Hydroxyquinaldine*-N-*oxide* (8-*hydroxy*-2-*methylquinoline*-N-*oxide*, hmqH)

This was prepared by slow addition of *m*-chloroperoxybenzoic acid (27 g, 80–85%, 0.125 mol) in chloroform (150 cm^3) to an ice-cooled and vigorously stirred solution of 8-hydroxyquinaldine (20 g, 0.125 mol) in chloroform (100 cm^3). After 4 h the solution was left to stand at room temperature over a period of 48 h. The *m*-chlorobenzoic acid was subsequently removed by extraction with 0.2 M phosphate buffer (1 : 1 sodium dihydrogen orthophosphate and disodium hydrogen orthophosphate) solution (3×150 cm^3, pH *ca* 7). The chloroform solution was evaporated to dryness and the residue recrystallized from benzene (100 cm^3)/light petroleum (20 cm^3). Yield: 9.9 g, 45%. Found: C, 68.5; H, 5.1; N, 7.5. hmqH requires: C, 68.6; H, 5.2; N, 8.0%. M.p. = 99–101°C.

Preparation of solid hexadentate silicon(IV) complexes

There are two general methods of preparation in accordance with eqs (1) and (2), respectively.

Method 1

$[Si(dmp)_3]^+[CF_3SO_3]^-$. To dmpH (1.00 g, 7.19 mmol) in hot ethanol (10 cm^3), under argon, $Si(OEt)_4$ (0.53 cm^3, 2.40 mmol) was added followed by CF_3SO_3H (0.21 cm^3, 2.40 mmol). The mixture was refluxed for 18 h and precipitated with diethyl ether (5 cm^3). The white solid was filtered under excess argon pressure, and then washed with a little ether (10 cm^3) and dried *in vacuo* at 50°C for 2 days. Yield: 1.26 g, 89%. Found: C, 44.5; H, 4.0; N, 7.1. $[Si(dmp)_3]^+[CF_3SO_3]^-$ requires: C, 44.7; H, 4.1; N, 7.1%. ^1H NMR (270 MHz, DMSO-d_6): δ, 2.35 (3H, m*, CH_3^2), 3.90 (3H, m, CH_3^1), 6.81 (1H, m: d $\{J_{H^5\text{-}H^6} = 6.8$ Hz$\}$, H^5), 8.03 (1H, m: d $\{J_{H^5\text{-}H^6} = 6.8$ Hz$\}$, H^6). H^5 and H^6 were assigned by Nuclear Overhauser Enhancement difference spectroscopy.

Similarly, $[Si(dmp)_3]^+[CF_3CO_2]^-$, $[Si(dmp)_3]^+[HSO_4]^-$ and $[Si(dmp)_3]^+[cam]^-$ were prepared in comparative yields; 80, 65 and 87%, respectively. ^1H NMR showed similar chemical shifts and the bisulphate complex showed the presence of ethanol after drying *in vacuo* at 70°C for several weeks, after which decomposition of the metal complex prevented analytical purity.

$[Si(mal)_3]^+[CF_3SO_3]^-$. This was prepared in 50% yield. Found: C, 40.6; H, 2.4. $[Si(mal)_3]^+[CF_3SO_3]^-$ requires: C, 41.3; H, 2.7%. ^1H NMR (270 MHz, DMSO-d_6): δ, 2.53 (3H, m, CH_3^2), 7.44 (1H, m: d $\{J_{H^5\text{-}H^6} = 4.9$ Hz$\}$, H^5), 8.92 (1H, m: d $\{J_{H^5\text{-}H^6} = 4.9$ Hz$\}$, H^6).

$[Si(dhp)_3]^+[CF_3SO_3]^-$. This was prepared in 75% yield using six-fold the volume of ethanol (60 cm^3) due to the limited solubility of dhpH in hot ethanol. Found: C, 38.1; H, 3.0; N, 8.2. $[Si(dhp)_3]^+[CF_3SO_3]^-$ requires: C, 37.9; H, 2.4; N, 8.3. ^1H NMR (270 MHz, DMSO-d_6): δ, 6.92 (1H, m: t, H^5), 7.25 (1H, m: d, H^4), 7.42 (1H, m: d, H^6).

$[Si(hmp)_3]^+[CF_3SO_3]^-$. This was prepared in 57% yield using four-fold the volume of ethanol (40 cm^3). Found: C, 41.2; H, 3.2; N, 7.5. $[Si(hmp)_3]^+[CF_3SO_3]^-$ requires: C, 41.5; H, 3.3; N, 7.6. ^1H NMR (270 MHz, DMSO-d_6): δ, 2.31 (3H, m, CH_3^2), 6.80 (1H, m: d $\{J_{H^5\text{-}H^6} = 6.3$ Hz$\}$, H^5), 7.86 (1H, m: d $\{J_{H^5\text{-}H^6} = 6.4$ Hz$\}$, H^6).

$[Si(emp)_3]^+[HSO_4]^-$. This was prepared in greater than 90% yield but failed to crystallize with ether, thus the complex was isolated by evaporating the ethanol solution to dryness. ^1H NMR (270 MHz, DMSO-d_6): δ, 1.37 (3H, m: t, CH_3^7), 2.41 (3H, m, CH_3^2), 4.25 (2H, m: quart., CH_2^1), 6.85 (1H, m: d, H^5), 8.08 (1H, m: d, H^6), showed contamination by free ligand.

$[Si(emp)_3]^+[Cl]^-$. This was prepared using a stoichiometric amount of conc. hydrochloric acid (35–38%) as the strong acid. The ethanol solution was evaporated to dryness to leave a pinkish, off-white solid. Yield: 55%. ^1H NMR showed similar chemical shifts as $[Si(emp)_3]^+[HSO_4]^-$, but free ligand resonances were appreciable.

$[Si(ace)_3]^+[CF_3SO_3]^-$. This was prepared by evaporation of solvent to dryness. Yield: 60%. ^1H NMR (270 MHz, DMSO-d_6): δ, 2.05, (3H, s, CH_3), showed contamination by free ligand.

$[Si(hqo)_3]^+[CF_3SO_3]^-$. This was prepared by evaporation of solvent to dryness. Yellow solid, yield: 70%. The ^1H NMR spectrum was too complicated in the aromatic region, however, contamination by free ligand was observed.

$[Si(hmq)_3]^+[CF_3SO_3]^-$. This was prepared by evaporation of solvent to dryness. Yellow–green solid, yield: > 90%. ^1H NMR (270 MHz, DMSO-d_6): δ, 2.20 (3H, s, CH_3^{fac}), 2.35 (3H, m, CH_3^{mer}), showed contamination by free ligand.

* δ shown represent the average values observed; multiplicity caused by facial and meridional isomers. m: d represents multiple doublets.

Method 2

$[Si(dmp)_3]^+[Cl]^-$. To dmpH (1.00 g, 7.19 mmol) in hot chloroform (5 cm^3), under argon, $SiCl_4$ (0.27 cm^3, 2.40 mmol) was added. The mixture was refluxed for 18 h. The solution was evaporated to dryness and the white residue was filtered under excess argon pressure and dried *in vacuo* at 50°C for 2 days. Yield: 1.12 g, 98%. ^1H NMR showed similar chemical shifts to $[Si(dmp)_3]^+[CF_3SO_3]^-$ but the chloroform resonance persisted after drying *in vacuo* at 70°C for several weeks, after which decomposition of metal complex prevented analytical purity.

$[Si(mal)_3]^+[Cl]^-$, $[Si(ben)_3]^+[Cl]^-$, $[Si(hmq)_3]^+[Cl]^-$ and $[Si(chr)_3]^+[Cl]^-$ complexes were prepared as above. The ^1H NMR spectra of $[Si(ben)_3]^+[Cl]^-$ and $[Si(chr)_3]^+[Cl]^-$ were complicated but the formation was confirmed by ^{29}Si NMR and FAB^+ mass spectrometry.

RESULTS AND DISCUSSION

Facial and meridional isomers

For the bidentate ligands studied here, the two oxygen atoms are non-equivalent and thus there is the possibility of meridional and facial isomers, each of which is enantiomeric. In the facial isomer the ligands are equivalent but in the meridional isomer they are all different. The meridional facial (*mer*/*fac*) isomer ratio expected at equilibrium, on a purely statistical basis, is 3 : 1. This is simply the probability expected due to the three possible meridional and one facial isomers. The ratio was observed for complexes derived from a number of the ligands, e.g. malH, hmpH, dmpH and empH.

With the $[Si(dmp)_3]^+$ ion, interconversion of *mer* and *fac* isomers was comparatively slow and partial separation by crystallization could be achieved (Fig. 1). For the $[Si(hmq)_3]^+$ ion, the equilibrium was non-statistical with a *mer*/*fac* ratio of *ca* 1.1 (Fig. 2). Detailed mechanistic studies[8] on similar $M(L—L')_3$ systems reveal the diverse rearrangement mechanisms possible, however, the cause of such large magnetic inequivalence of these isomers was not explained. We attribute the large chemical shift differences to long-range shielding effects, i.e. in the $[Si(hmq)_3]^+$ ion the large magnetic inequivalence is caused by the ring currents produced in the large asymmetric quinaldine ligand. The preference for a particular isomer in solution is rarely observed for $M(L—L')_3$ type complexes. The non-statistical isomer distribution observed may arise from O—Si d_π-p_π interaction. The silicon(IV) cation has empty 3*d* orbitals which are available for d_π donation from the filled p_π orbitals of the oxygen atoms. The higher donor capacity of the oxygen in N → O compared with C—O may be sufficient for the *fac* isomer (with no competing N → O donor orbitals on the same axis) to be stabilized relative to the *mer* isomers (which has one axis with two N → O donor orbitals competing for the same orbitals on the silicon atom).

Rate of meridional and facial isomerism

For the equilibrium: $fac \rightleftharpoons mer$,

$$K = \frac{[mer]}{[fac]} = \frac{k_1}{k_2}.$$

If we can assume first-order kinetics, then it can be deduced that:[9]

$$\log_e \frac{[fac]_0 - [fac]_{eqm}}{[fac]_t - [fac]_{eqm}} = (k_1 + k_2)t.$$

In the $[Si(dmp)_3]^+$ ion where a statistical distribution was observed, we also have $k_1 = 3k_2$. From the 270 MHz ^1H NMR intensity measurements, $k_1 = 2.1 \times 10^{-5}$ s^{-1} ($t_{1/2} = 9.2$ h) and $k_2 = 7.0 \times 10^{-6}\,s^{-1}$ ($t_{1/2} = 27.5$ h) (Fig. 3). Similarly, with the $[Si(hmq)_3]^+$ ion where a non-statistical distribution was observed, we have $k_1 = 1.1\ k_2$, which gives $k_1 = 1.1 \times 10^{-6}$ s^{-1} ($t_{1/2} = 184$ h) and $k_2 = 9.5 \times 10^{-7}\,s^{-1}$ ($t_{1/2} = 202$ h).

It is likely that the large differences in rates are associated with the different chelating ring sizes. This may be deduced from comparisons with the rates observed for tropolonato[10] and acac[11] complexes. The observations can be seen as effects caused by the steric bulk of the larger rings. Within the five-membered chelating rings, there is also the possibility of varying rates according to the stability of the complex. Therefore, the fast rate of isomerism [$k_1 = 1.8 \times 10^{-4}\,s^1$ ($t_{1/2} = 1$ h) and $k_2 = 6 \times 10^{-5}\,s^{-1}$ ($t_{1/2} = 3$ h)] observed for the easily hydrolysed $[Si(hmp)_3]^+$ ion is not unexpected.

^{29}Si NMR

The observed ^{29}Si chemical shifts are given in Table 1. It was shown by Cella *et al.*[12] that six-coordinate complexes of silicon give much more negative values of δ than do complexes in which the silicon is bound to four oxygen atoms only, and this is confirmed in the present work. In addition, for six-coordinate complexes with six-membered chelating rings, the ^{29}Si is much more shielded than in complexes with five-membered chelating rings. Within the five- or six-membered rings there is relatively little change in δ with various ligands. Two

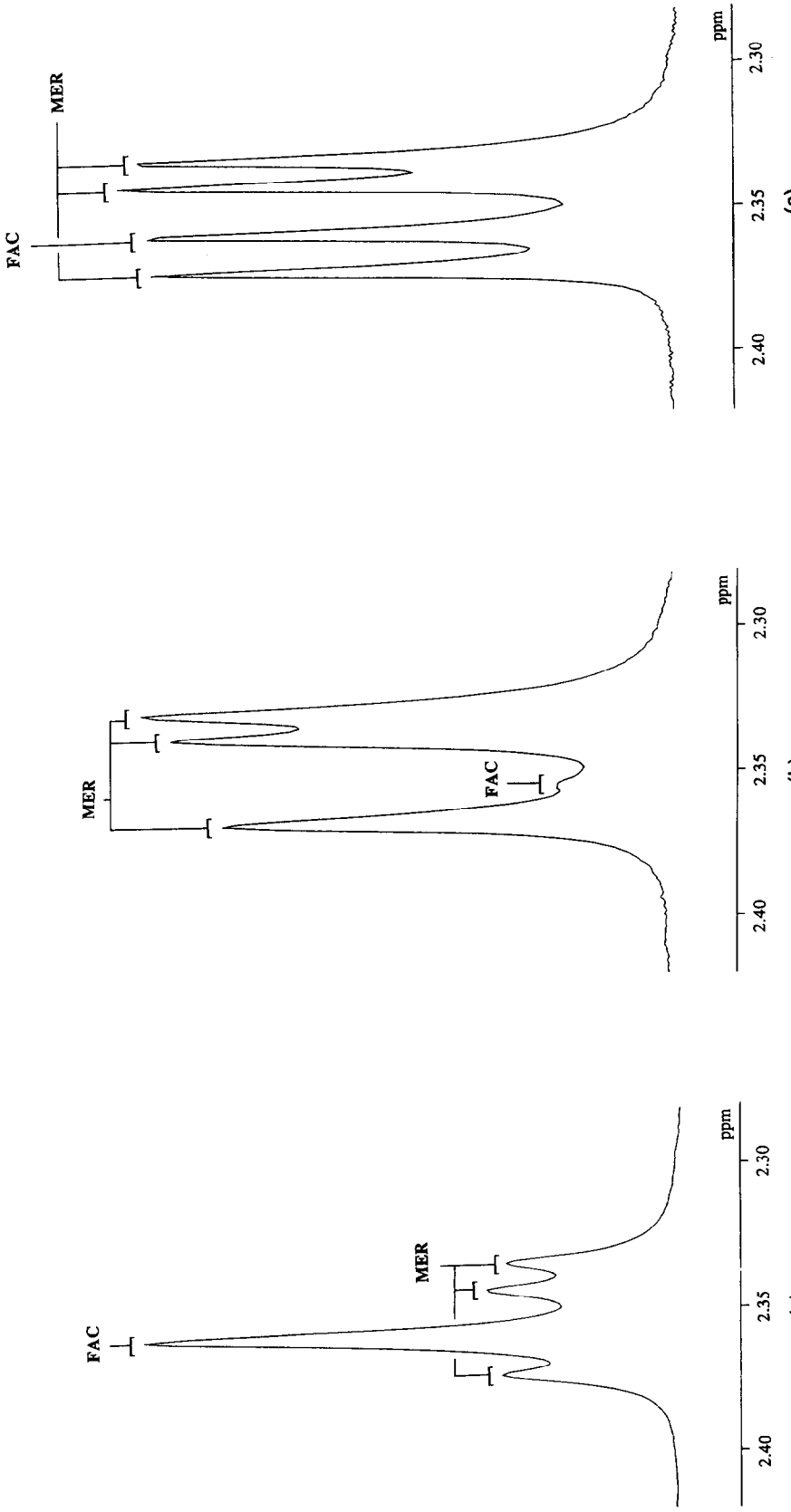

Fig. 1. ^{1}H NMR of 2-Me resonances in $[Si(dmp)_3]^+[Cl]^-$ (270 MHz, DMSO-d_6): (a) recrystallized from chloroform ~ 5 mins after dissolution; (b) recrystallized from ethanol/ether ~ 5 mins after dissolution; (c) solution (a) after 2 days at room temperature.

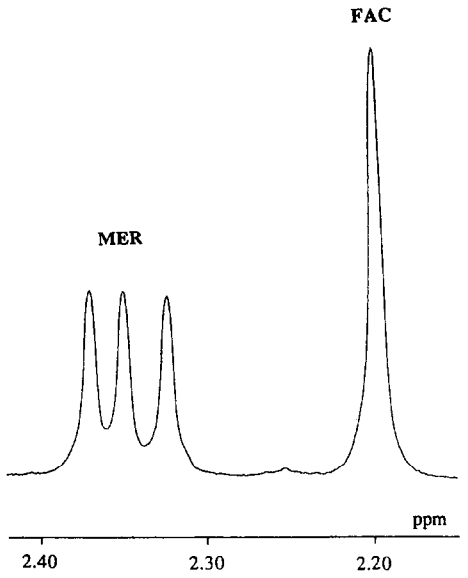

Fig. 2. ^{1}H NMR of 2-Me resonances in $[Si(hmq)_3]^+[CF_3SO_3]^-$ (270 MHz, DMSO-d_6).

^{29}Si resonances are observed for the complexes derived from malH, hqoH and hmqH. One possible explanation for this is the presence of *mer* and *fac* isomers.

Mass spectrometry

Table 2 shows the results of FAB^+ mass spectrometry. In all cases the parent $[SiL_3]^+$ ion is observed. Species corresponding to $[\{SiL_2\}-\{H\}]^+$ and $[SiL_2(OH)]^+$ were observed, the latter species are presumably formed by hydrolysis due to traces of water in the matrix.

CONCLUSIONS

Chelate ring size

The difference in chemical shifts between the five- (^{29}Si, $\delta = -130$ to -150 ppm) and six- (^{29}Si, $\delta = -190$ to -200 ppm) membered chelate rings have been previously reported.[12] Thus, this serves as a method for confirming the formation of six-coordinate silicon(IV) complexes. The important aspects of the ^{29}Si shifts appear to be the *dependence* on chelate ring size and the *independence* of the nature of the coordinating oxygens, overall charge of complex, and the nature of the counter ions. That is, the chemical shifts are dominated by the shielding effects associated with the symmetry around the silicon nucleus. This is in marked contrast to the pentacoordinated and tetracoordinated organosilicon compounds where symmetry is reduced and the nucleus is highly sensitive to the electronic properties of the substituents.[15]

Facial and meridional isomerism

From the above results we also observe a statistical distribution (in DMSO, $t_{1/2} \sim 10^0$–10^1 h) of *fac* and *mer* isomers with the five-membered chelate ring complexes, and non-statistical distribution (in DMSO, $t_{1/2} \sim 10^2$–10^3 h) of *fac* and *mer* isomers with six-membered chelate ring complexes. The difference in rates of isomerization is attributed to steric effects and the difference in isomer dis-

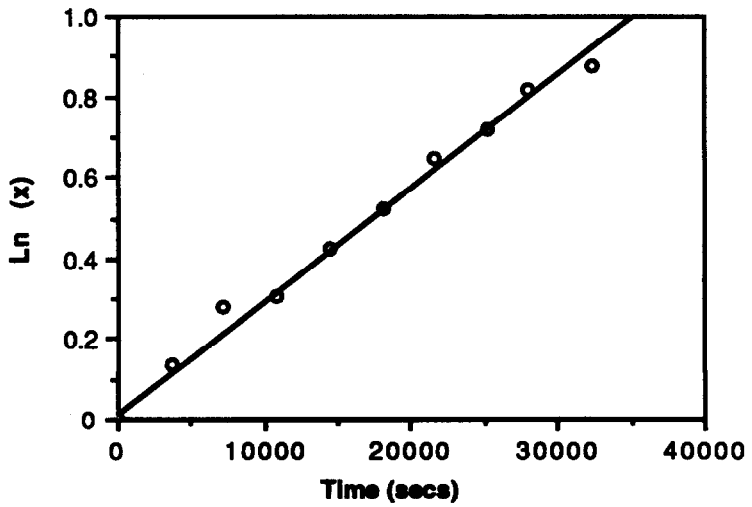

Fig. 3. A plot of $\log_e(x)$ against time, where $x = [Fac]_0 - [Fac]_{eqm}/[Fac]_t - [Fac]_{eqm}$ of $[Si(dmp)_3]^+[Cl]^-$ in DMSO-d_6 at 27°C.

Table 1. ^{29}Si chemical shifts for six-coordinate complexes (the solvent is DMSO unless otherwise stated)

Complex	δ (ppm) relative to TMS
$[Si(mal)_3]^+[Cl]^-$	−134.9, −134.4
$[Si(mal)_3]^+[CF_3SO_3]^-$	−134.9, −134.4
$[Si(dmp)_3]^+[HSO_4]^-$	−135.3 (Fig. 4)
$[Si(dmp)_3]^+[cam]^-$	−135.3
$[Si(dmp)_3]^+[CF_3CO_2]^-$	−135.3
$[Si(dmp)_3]^+[Cl]^-$	−135.5, (−138.3)[a]
$[Si(dmp)_3]^+[CF_3SO_3]^-$	−135.5
$[Si(emp)_3]^+[HSO_4]^-$	−135.4
$[Si(emp)_3]^+[Cl]^-$	−135.5
$[Si(hmp)_3]^+[CF_3SO_3]^-$	−136.4
$[Si(ace)_3]^+[CF_3SO_3]^-$	−137.7
$[Si(ben)_3]^+[CF_3SO_3]^-$	−138.7
$[Si(dhp)_3]^+[CF_3SO_3]^-$	−141.6
$[Si(hmq)_3]^+[CF_3SO_3]^-$	−192.3, −192.7
$[Si(hmq)_3]^+[Cl]^-$	−192.3, −192.7
$[Si(chr)_3]^+[Cl]^-$	−193.1
$[Si(hqo)_3]^+[CF_3SO_3]^-$	−193.4, −193.8
$[Si(cat)_3]^{2-}[(Et_3NH)_2]^{2+}$	−139.3[b]
$[Si(cat)_3]^{2-}[K_2]^{2+}$	−140.3[b]
$[Si(trop)_3]^+[Cl]^-$	−140.7[c]
$[Si(trop)_3]^+[SbF_6]^-$	−139.4[d]
$[Si(acac)_3]^+[ZnCl_3]^-$	−193.7[e]

[a] Tartrate buffer in D_2O, pD = *ca* 4.
[b] Reference 6.
[c] Reference 13.
[d] Reference 14, CD_3OD.
[e] Reference 14.

tribution is attributed to the electronic effects of the ligands.

Synthetic considerations

The new method of synthesis [eq. (1)] has proved to be a more convenient, economical and flexible method of preparing six-coordinate tris complexes of silicon. This was demonstrated using dhpH whose solubility is limited in chloroform, thus the complex could not be easily prepared otherwise. It also allows for the possibility of forming complexes with different anions. ^{29}Si NMR and FAB^+ mass spectroscopy provide an easy criterion to confirm formation of these six-coordinate silicon(IV) complexes.

Stability in aqueous media

Equilibrium studies of tris-catecholato silicon(IV) complexes have shown that for dinegative bidentate ligands, formation is favoured in alkaline conditions and electron-withdrawing groups on the ligand.[1]

For the mononegative bidentate ligands we have

$$Si(OH)_4 + 3LH + H^+ \rightleftharpoons SiL_3^+ + 4H_2O.$$

Hence formation of the complexes is favoured at low pH, and by electron-donating groups on the ligand. The only ligands of this type reported in the literature to form silicon(IV) complexes in aqueous solution are tropolones,[5,13] and even here the complexes are almost completely hydrolysed at pH values above *ca* 2.5. The synthesis of $[Si(emp)_3]^+[Cl]^-$ using conc. hydrochloric acid (35–38%) reflects the stability of the complex in aqueous solution. Equilibrium studies of 3-hydroxypyridin-4-ones are currently under investigation but initial results indicate that the complexes are stable at much greater pH values than those derived from tropolones. All other ligands studied here showed complete hydrolysis in acidic solution.

Table 2. FAB^+ Mass spectra of six-coordinate silicon complexes (using a *m*-nitrobenzyl alcohol matrix unless otherwise stated)

Complex	m/z[a] $[SiL_3]^+$	$[SiL_2(OH)]^+$	$[\{SiL_2\}-\{H\}]^+$
$[Si(mal)_3]^+[CF_3SO_3]^-$	403 (100)	295 (5)	277 (9)
$[Si(ben)_3]^+[CF_3SO_3]^-$	436 (100)	317 (67)	299 (16)
$[Si(dmp)_3]^+[Cl]^-$	442 (100)	321 (19)	303 (24)
$[Si(dmp)_3]^+[CF_3SO_3]^-$	442 (100)	321 (14)	303 (18)
$[Si(dmp)_3]^+[CF_3CO_2]^-$	442 (100)	321 (10)	303 (11)
$[Si(dmp)_3]^+[HSO_4]^-$	442 (100)	321 (10)	303 (17)
$[Si(dmp)_3]^+[cam]^-$	442 (100)	321 (13)	303 (15)
$[Si(hmp)_3]^+[CF_3SO_3]^-$	400 (100)	293 (11)	275 (81)
$[Si(emp)_3]^+[Cl]^-$	484 (100)	349 (6)	331 (8)
$[Si(emp)_3]^+[HSO_4]^-$	484 (100)	349 (8)	331 (9)
$[Si(dhp)_3]^+[CF_3SO_3]^-$	358 (90)	265 (15)	247 (100)
$[Si(ace)_3]^+[CF_3SO_3]^-$	250 (100)	193 (13)	175 (22)
$[Si(hqo)_3]^+[CF_3SO_3]^-$	508 (100)	365 (23)	347 (19)
$[Si(hmq)_3]^+[Cl]^-$	550 (100)	393 (19)	375 (7)
$[Si(chr)_3]^+[Cl]^-$	787 (46)	551 (37)	533 (100)
$[Si(mal)_3]^+[CF_3SO_3]^-$[b]	403		
$[Si(dmp)_3]^+[Cl]^-$[b]	442		
$[Si(ben)_3]^+[CF_3SO_3]^-$[b]	436		

[a] Figures in parentheses represent relative peak intensities.
[b] DMSO matrix.

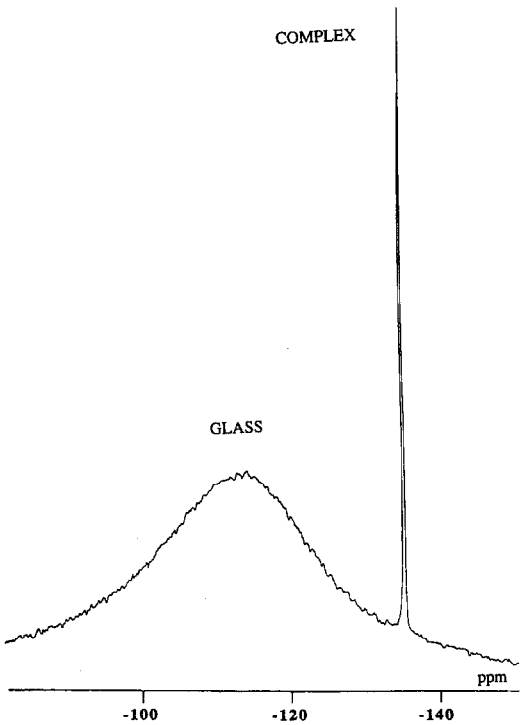

Fig. 4. ^{29}Si NMR of $[Si(dmp)_3]^+[HSO_4]^-$ [49.7 MHz, DMSO, int. TMS, 0.08 M $Cr(acac)_3$ relaxant].

Acknowledgements—We thank Mr P. Hammerton for the ^{29}Si NMR spectra and Mr J. N. Bilton for the mass spectra. One of us (C.Y.W.) thanks the SERC for a grant, and Dr S. R. Drake for his invaluable advice.

REFERENCES

1. D. F. Evans, J. Parr and E. N. Coker, *Polyhedron* 1990, **9**, 813.
2. R. C. Scarrow, P. E. Riley, K. Abu-Dari, D. L. White and K. N. Raymond, *Inorg. Chem.* 1985, **24**, 954; R. C. Scarrow and K. N. Raymond, *Inorg. Chem.* 1988, **27**, 4140.
3. W. O. Nelson, T. B. Karpishin, S. J. Rettig and C. Orvig, *Can. J. Chem.* 1988, **66**, 123; W. O. Nelson, T. B. Karpishin, S. J. Rettig and C. Orvig, *Inorg. Chem.* 1988, **27**, 1045.
4. W. Dilthey, *Berichte* 1903, **36**, 923.
5. E. L. Muetterties and C. M. Wright, *J. Am. Chem. Soc.* 1964, **86**, 5132; S. Sjöberg, N. Ingri, A. M. Nenner and L. O. Öhman, *J. Inorg. Biochem.* 1985, **24**, 267.
6. R. L. N. Harris, *Aust. J. Chem.* 1976, **29**, 1329.
7. G. J. Kontoghiorghes and L. Sheppard, *Inorg. Chim. Acta* 1987, **136**, L11.
8. R. H. Holm, *Dynamic Nuclear Magnetic Spec-*

troscopy (Edited by L. M. Jackman and F. A. Cotton), p. 317. Academic Press, New York (1975).
9. C. H. Bamford and C. F. H. Tipper (Eds), *Comprehensive Chemical Kinetics*, Ch. 2, *The theory of kinetics*. Elsevier, New York (1975).
10. I. Ito, N. Tanka, I. Hanazaki and S. Nakayura, *Inorg. Nucl. Chem. Lett.* 1969, **5**, 781; E. L. Muetterties and C. W. Alegranti, *J. Am. Chem. Soc.* 1969, **91**, 4420.
11. E. Larsen, S. F. Mason and G. H. Searle, *Acta. Chem. Scand.* 1966, **20**, 191.
12. J. A. Cella, J. D. Cargioli and E. A. Williams, *J. Organomet. Chem.* 1980, **186**, 13.
13. J. Parr, PhD thesis, Imperial College, London (1989).
14. Ch. Faure, *Maroc. Med.* 1973, **52**, 572.
15. E. A. Williams, *R. Soc. Chem., An. Rep. NMR Spectrosc.* 1983, **15**, 235.

Polyhedron Vol. 10, No. 10, pp. 1139–1141, 1991
Printed in Great Britain

0277–5387/91 $3.00+.00
© 1991 Pergamon Press plc

COMMUNICATION

THE EFFECT OF SECOND-SPHERE COORDINATION OF 18-CROWN-6 ETHER ON ELECTRONIC SPECTRA AND ELECTROCHEMICAL PROPERTIES OF $[Ru(NH_3)_5L](PF_6)_3$ AND $[Ru(NH_3)_5L](PF_6)_2$

ISAO ANDO,* HIROAKI FUJIMOTO, KAZUTO NAKAYAMA, KIKUJIRO UJIMOTO and HIRONDO KURIHARA

Department of Chemistry, Faculty of Science, Fukuoka University, Nanakuma 8-19-1, Jonan-ku, Fukuoka 814-01, Japan

(*Received* 26 *November* 1990; *accepted* 20 *February* 1991)

Abstract—Ruthenium(III) complexes $[Ru(NH_3)_5L](PF_6)_3$ (L = 4-aminopyridine or 4-dimethylaminopyridine) and ruthenium(II) complexes $[Ru(NH_3)_5L](PF_6)_2$ (L = isonicotinamide or pyrazine) form adducts with 18-crown-6 ether in acetonitrile giving a blue shift of the LMCT band for the ruthenium(III) complex, a red shift of the MLCT band for the ruthenium(II) complex and a negative shift of the ruthenium(III)/ruthenium(II) redox potential for all the complexes.

Macrocyclic polyethers (crown ethers) are known to form stable adducts with a variety of transition metal complexes by virtue of multiple hydrogen bonding between the oxygen atoms of the crown ether and protic ligands such as ammonia or water at the primary coordination sphere of the complexes.[1] Such second-sphere coordination may bring about a change in the microenvironment of the metal complexes to modify their physicochemical properties. Microenvironmental change plays vital roles in biological processes.

So far many crown ether adducts of metal complexes have been obtained for inspection of the effects of second-sphere coordination upon the physicochemical properties of the complexes.[2–4] However, no marked changes in electronic spectra and electrochemical properties have been recognized for the aliphatic crown ether adducts, while an adduct formation of hexacyano complexes with polyammonium macrocycles caused a prominent change in the redox potential associated with the metal centre.[5] In this study we have examined electronic spectra and electrochemical properties of ruthenium(III) complexes $[Ru(NH_3)_5L](PF_6)_3$ [L = 4-aminopyridine (ampy) or 4-dimethylaminopyridine (dmapy)] and ruthenium(II) complexes $[Ru(NH_3)_5L](PF_6)_2$ [L = isonicotinamide (isn) or pyrazine (pz)] in the presence of 18-crown-6 ether (18C6) in acetonitrile and found that the second-sphere coordination of 18C6 caused a prominent effect both on electronic spectra and electrochemical properties of the ruthenium complexes.

EXPERIMENTAL

The ruthenium complexes were prepared by the literature methods.[6] Electronic absorption spectra in acetonitrile were recorded on a Hitachi 228 spectrophotometer at 25°C. Cyclic voltammograms in acetonitrile containing n-tetrabutylammonium hexafluorophosphate as the supporting electrolyte were obtained with a three-electrode cell, equipped with a glassy carbon working electrode, a $Ag/AgNO_3$ reference electrode, and a platinum coil as the auxiliary electrode. All measurements were performed in the dark.

* Author to whom correspondence should be addressed.

RESULTS AND DISCUSSION

Ruthenium(III) complexes $[Ru(NH_3)_5(ampy)](PF_6)_3$ and $[Ru(NH_3)_5(dmapy)](PF_6)_3$ in acetonitrile show the ligand to metal charge-transfer (LMCT) band [transition from the ligand HOMO to the unfilled t_{2g} orbital of ruthenium(III)] at 516 and 598 nm, respectively. On adding 18C6, they shifted to 502 and 576 nm, respectively (see Fig. 1). The intraligand bands found in the region shorter than 300 nm for these ruthenium(III) complexes were practically unaffected by added 18C6, except for only a slight increase in the intensities of the bands.

Ruthenium(II) complexes $[Ru(NH_3)_5(pz)][(PF_6)_2$ and $[Ru(NH_3)_5(isn)](PF_6)_2$ in acetonitrile show the MLCT band [transition from the filled t_{2g} orbital of ruthenium(II) to the ligand LUMO] at 458 and 468 nm, respectively. On adding 18C6 to the solutions the metal to ligand charge-transfer (MLCT) band shifted to 462 and 472 nm, respectively. The intraligand transition bands found in the region shorter than 260 nm for those complexes were little affected by the addition of 18C6.

Such shifts of the LMCT band of the ruthenium(III) complexes and the MLCT band of the ruthenium(II) complexes may be attributed to second-sphere coordination of 18C6 to $[Ru(NH_3)_5L]^{n+}$ ($n = 2, 3$), through ammine-18C6 hydrogen bonding, as demonstrated for other ammine complex/crown ether adducts by the single crystal X-ray method.[2,3,7] It is noteworthy that the LMCT band of the ruthenium(III) complexes shifts toward shorter wavelength, while the MLCT band of the ruthenium(II) complexes shifts toward longer wavelength.

The spectral features observed above can be rationalized as follows. The second-sphere coordination of 18C6 to $[Ru(NH_3)_5L]^{n+}$ ($n = 2, 3$) stabilizes both ruthenium(III) and ruthenium(II) complexes. The ammine–18C6 interaction is expected to be stronger in ruthenium(III) complexes than ruthenium(II) complexes because the ammine proton becomes more acidic when coordinated to higher valent metal ion. Thus, for the ruthenium(III) complexes, the ground state is more stabilized relative to the charge-transfer states and causes a blue shift of the LMCT band, whereas for the ruthenium(II) complexes, the charge-transfer state is more stabilized relative to the ground state and causes a red shift of the MLCT band (Fig. 2).

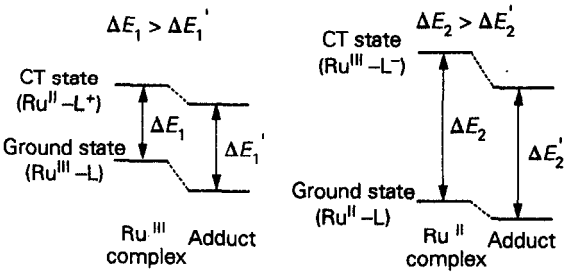

Fig. 2. Schematic energy level diagrams of the ground state and the charge-transfer state for ruthenium(III) and ruthenium(II) complexes and their adducts.

If this is indeed the case, the second-sphere coordination of 18C6 to $[Ru(NH_3)_5L]^{n+}$ ($n = 2, 3$) may also affect the ruthenium(III)/ruthenium(II) redox process. Electrochemical properties of $[Ru(NH_3)_5L]^{n+}$ ($n = 2, 3$) in the absence and presence of 18C6 were investigated by means of cyclic voltammetry. Typical cyclic voltammograms are given in Fig. 3. All the complexes show a

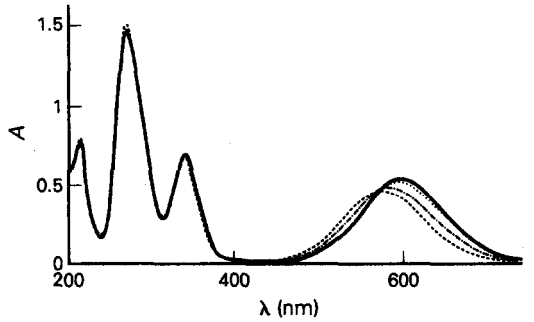

Fig. 1. Absorption spectra of $[Ru(NH_3)_5(dmapy)](PF_6)_3$ in acetonitrile solution. [Complex] = 1.00×10^{-4} mol dm^{-3}; [18C6] = 0 (——), 1.00×10^{-4} (· · ·), 1.00×10^{-3} (—·—) and 1.00×10^{-2} mol dm^{-3} (– – –).

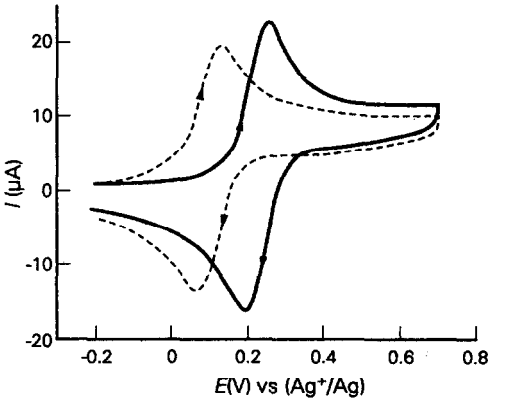

Fig. 3. Cyclic voltammograms of $[Ru(NH_3)_5(pz)](PF_6)_2$ in acetonitrile in the absence (——) and presence (– – –) of 0.10 mol dm^{-3} 18C6. [Complex] = 5.0×10^{-4} mol dm^{-3}; supporting electrolyte: 0.10 mol dm^{-3} n-tetrabutylammonium hexafluorophosphate.

Table 1. Ruthenium(III)/ruthenium(II) redox potnetials of $[Ru(NH_3)_5L](PF_6)_n$ (n = 2, 3) in the absence and presence of 18C6

Complex	$E_{1/2}$ (V) vs Ag^+/Ag		
	[18C6] = 0 mol dm^{-3}	[18C6] = 0.10 mol dm^{-3}	$\Delta E_{1/2}$ (mV)
$[Ru(NH_3)_5(isn)](PF_6)_2$	0.115 (60)	−0.013 (65)	−128
$[Ru(NH_3)_5(pz)](PF_6)_2$	0.225 (60)	0.103 (65)	−122
$[Ru(NH_3)_5(ampy)](PF_6)_3$	−0.125 (60)	−0.255 (60)	−130
$[Ru(NH_3)_5(dmapy)](PF_6)_3$	−0.140 (60)	−0.265 (60)	−125

The $E_{1/2}$ values are taken as the average of the cathodic and anodic peak potentials. The values in parentheses are the peak separations in millivolts.

reversible redox couple attributable to the ruthenium(III)/ruthenium(II) redox process.[8] As seen in Fig. 3, the addition of 18C6 gives rise to a negative shift of the redox couple. The shift was found to be *ca* −130 mV irrespective of the nature of L. The electrochemical results are summarized in Table 1. The electrochemical features observed for the $[Ru(NH_3)_5L]^{n+}$/18C6 system is also compatible with the above discussion; i.e. 18C6 stabilizes the ruthenium(III) complexes more strongly than the ruthenium(II) complexes, so that the half-wave potentials shift cathodically, irrespective of the value of $E_{1/2}$.

The present study demonstrates that the second-sphere coordination of aliphatic crown ethers can significantly affect the spectral and electrochemical properties of ammine complexes. Detailed studies along these lines are in progress.

Acknowledgement—The present work was partially supported by a grant from the Central Research Institute of Fukuoka University.

REFERENCES

1. H. M. Colquhoun, J. F. Stoddart and D. J. Williams, *Angew. Chem., Int. Edn Engl.* 1986, **25**, 487.
2. R. Ballardini, M. T. Gandolfi, L. Prodi, M. Ciano, V. Balzani, F. H. Kohnke, H. S.-Zavareh, N. Spencer and J. F. Stoddart, *J. Am. Chem. Soc.* 1989, **111**, 7072; D. R. Alston, J. F. Stoddart and D. J. Williams, *J. Chem. Soc., Chem. Commun.* 1985, 532.
3. H. M. Colquhoun, S. M. Doughty, J. F. Stoddart and D. J. Williams, *Angew. Chem., Int. Edn Engl.* 1984, **23**, 235.
4. H. M. Colquhoun, D. F. Lewis, J. F. Stoddart and D. J. Williams, *J. Chem. Soc., Dalton Trans.* 1983, 607; P. A. Cusack, B. N. Patel and P. J. Smith, *J. Chem. Soc., Dalton Trans.* 1984, 1239; T. B. Vance Jr, E. M. Holt, C. G. Pierpont and S. L. Holt, *Acta Cryst.* 1980, **36**, 150; T. B. Vance Jr, E. M. Holt, D. L. Varie and S. L. Holt, *Acta Cryst.* 1980, **36**, 153.
5. F. Peter, M. Gross, M. W. Hosseini and J. M. Lehn, *J. Electroanalyt. Chem.* 1983, **144**, 279.
6. R. G. Gaunder and H. Taube, *Inorg. Chem.* 1970, **9**, 2627; C. Creutz and H. Taube, *J. Am. Chem. Soc.* 1973, **95**, 1086; J. E. Sutton and H. Taube, *Inorg. Chem.* 1981, **20**, 3125; R. J. H. Clark and M. J. Stead, *J. Chem. Soc., Dalton Trans.* 1981, 1760.
7. H. M. Colquhoun and J. F. Stoddart, *J. Chem. Soc., Chem. Commun.* 1981, 612.
8. J. R. Winkler, T. L. Netzel, C. Creutz and N. Sutin, *J. Am. Chem. Soc.* 1987, **109**, 2381; C. Cruetz and M. H. Chou, *Inorg. Chem.* 1987, **26**, 2995; R. W. Callahan, G. M. Brown and T. J. Meyer, *Inorg. Chem.* 1975, **14**, 1443; J. C. Curtis, B. P. Sullivan and T. J. Meyer, *Inorg. Chem.* 1983, **22**, 224.

Polyhedron Vol. 10, No. 10, p. 1143, 1991
Pergamon Press plc. Printed in Great Britain

CORRIGENDUM

Synthesis of organotin complexes with ligands of biological significance. F. L. Lee, E. G. Gabe, L. E. Khoo, G. Eng and F. E. Smith (Polyhedron, Vol. 9, No. 5, pp. 653–657, 1990).

In the abstract and the section titled "Intensity data" (p. 655) of the above paper, the number of significant reflections should be 2504 and not 1174.

The authors wish to apologise for any inconvenience caused.

Polyhedron Vol. 10, No. 11, p. 1145, 1991
Pergamon Press plc. Printed in Great Britain

INTRODUCTION

There has been much recent research activity in the area of organo- and transition metal silicon, germanium and tin chemistry. In particular, there have been a number of reports of the synthesis of discrete, molecular homopolyatomic molecules, as well as, new synthetic routes to oligomers and polymers. The isolation and characterization of Group 14 species with new and unexpected geometries are extending our understanding of structure, bonding and reactivity.

It is the purpose of this Polyhedron Symposium-in-Print to bring together contributions on a variety of different, important aspects of recent developments in homopolyatomic and related silicon, germanium and tin chemistry. Areas that have been covered include new synthetic routes to polysilanes, transition metal substituted Group 14 derivatives, the electronic structure and properties of homo-oligomers and -polymers of the Group 14 elements, the chemistry of transition metal substituted silylenes (silanediyls), and the chemistry of carbene analogues.

I am indebted to the authors for their contributions to this issue, the reviewers for their comments and Ms Sheryl Fellows of Pergamon Press.

MARK J. HAMPDEN-SMITH

Polyhedron Vol. 10, No. 11, pp. 1147–1152, 1991
Printed in Great Britain

0277–5387/91 $3.00+.00
© 1991 Pergamon Press plc

SILICON COMPOUNDS WITH STRONG INTRAMOLECULAR STERIC INTERACTIONS—XLIII.* FORMATION AND MOLECULAR STRUCTURES OF TWO ISOMERIC DISILACYCLOBUTANEDIIMINES

MANFRED WEIDENBRUCH,† BRIGITTE BRAND-ROTH, SIEGFRIED POHL and WOLFGANG SAAK

Fachbereich Chemie der Universität Oldenburg, Carl-von-Ossietzky-Strasse 9-11, D-2900 Oldenburg, F.R.G.

Abstract—In the presence of mesityl isocyanide (**7**) or 2,6-diisopropylphenyl isocyanide (**8**), photolysis of hexa-tert-butylcyclotrisilane (**1**) gives dark red crystals of N,N′-dimesityl-2,2,4,4-tetra-tert-butyl-2,4-disilacyclobutane-1,3-diimine (**9**) and violet crystals of N,N′-bis(2,6-diisopropylphenyl)-2,2,4,4-tetra-tert-butyl-2,4-disilacyclobutane-1,3-diimine (**10**), respectively. In the latter case small amounts of the isomeric N,N′-bis(2,6-diisopropylphenyl)-3,3,4,4-tetra-tert-butyl-3,4-disilacyclobutane-1,2-diimine (**11**) are also isolated as green crystals. The X-ray structure analysis of **10** shows that the ring atoms, and the exocyclic nitrogen atoms lie almost exactly in one plane. The two aryl groups are arranged *trans* to each other. The X-ray structure of the ring **11**, however, reveals a folded C_2Si_2 framework with the exocyclic nitrogen atoms being orientated in opposite directions. The aryl groups adopt the *syn*, *anti* conformation.

Despite the great progress made in recent years in the area of unsaturated silicon compounds,[2] stable molecules containing silicon as part of a cumulated double-bond system have not yet been reported.

In 1988, Arrington *et al.*,[3] as well as Pearsell and West,[4] investigated the reactions of silylenes with carbon monoxide in matrices. Reaction of dimethylsilylene was claimed to form a planar silaketene,[3] whereas in the case of the dimesitylsilylene addition product both the electronic spectra and the formation of disilenes on thawing of the matrix indicate that Lewis acid–base adducts of non-planar geometry are formed between the silylene and carbon monoxide.[4] This is corroborated by theoretical calculations[5] which predict an appreciably lower energy of the non-planar form.

Recently, we investigated the photolysis of hexa-tert-butylcyclotrisilane (**1**)[6] in the presence of phenyl isocyanide and isolated ruby-red crystals of N,N′-diphenyl-2,2,4,4-tetra-tert-butylcyclobutane-1,3-diimine (**5**).[7] It is well known that **1**, under photolytic conditions, gives di-tert-butylsilylene (**2**) and tetra-tert-butyldisilene (**3**), both of which can be trapped by various addition reactions.[8] Therefore, we suggested that the reaction is initiated by an addition reaction between **2** and phenyl isocyanide to give a silaketenimine or a Lewis acid–base product of type **4**, which then dimerizes to the isolated **5** (Scheme 1).

To verify that **5** results from dimerization of the suggested silaketenimine and not from a two-fold addition of the phenyl isocyanide to the disilene **3**, we allowed **1** to react with 2,4,6-tri-tert-butylphenyl isocyanide, whose bulky *ortho*-tert-butyl groups should disfavour both cyclodimerization and insertion into the Si—Si bond of a possible disilacyclopropanimine[9] intermediate.

In fact, a monomeric compound consisting of **2** and the aryl isocyanide in a ratio of 1 : 1 was isolated. The spectroscopic data indicated, however, that the expected intermediate of type **4** had rearranged to the trialkylsilyl cyanide **6**.[7]

To determine whether **6** might result from the reaction of **2** with the corresponding isocyanide, or whether it is formed from a precursor of type **5** via a CH activation of the *ortho*-tert-butyl groups, we now have carried out the photolysis of **1** in the presence of mesityl isocyanide (**7**) and of 2,6-diiso-

* For part XLII, see ref. 1.

† Author to whom correspondence should be addressed.

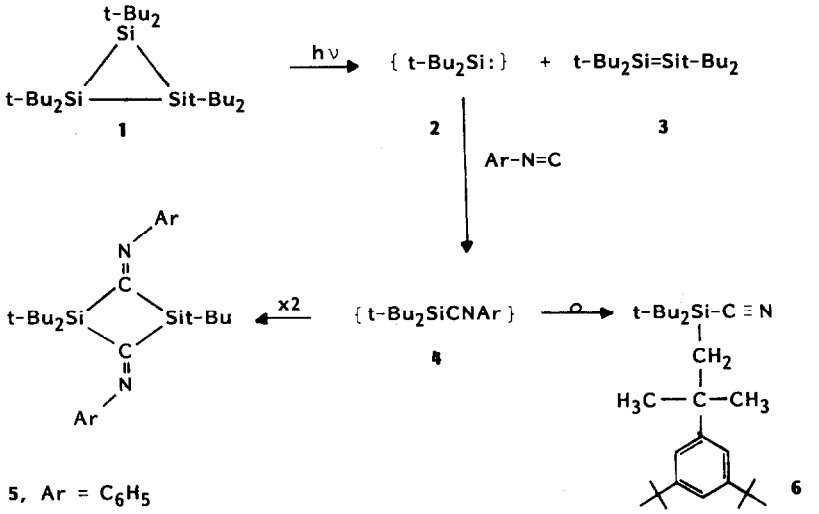

Scheme 1. Suggested mechanism of the addition reactions of aryl isocyanides with photolytically generated di-tert-butylsilylene (**2**).

propylphenyl isocyanide (**8**). These compounds also contain *ortho*-alkyl groups capable of undergoing isomerization reactions (Scheme 2).

Photolysis of **1** in the presence of **7** resulted in a red solution from which red crystals of the 2,4-disilacyclobutane-1,3-diimine (**9**) were isolated. Upon exposure to the ambient atmosphere, **9** decomposes, both in solution and in the solid state. Only a single set of signals is observed in both the ^{1}H and ^{13}C NMR spectra. This suggests that in solution either the barrier to *cis–trans* inversion at silicon is low, or that **9** has exclusively the *trans* geometry at silicon, as was detected for the phenyl analogue **5** in the solid state.[7]

Co-photolysis of **1** and the sterically more crowded isocyanide **8** yielded a dark green solution from which, upon cooling to −30°C, violet crystals of the four-membered cycle N,N′-bis(2,6-diisopropylphenyl)-2,2,4,4-tetra-tert-butyl-2,4-disilacyclobutane-1,3-diimine (**10**) were isolated. The structure of **10** was confirmed by ^{1}H, ^{13}C NMR and mass spectroscopic analyses and also by an X-ray diffraction study (Fig. 1, Table 1). Compound **10** crystallizes with two independent molecules each lying on a crystallographic inversion centre. The molecular geometry and atom numbering scheme for one of the molecules is illustrated in Fig. 1. Since they have the same basic features, the following discussion will refer to only one of the molecules.

The ring atoms and the exocyclic nitrogen atoms lie almost exactly in one plane. The two aryl groups are arranged *trans* to each other in the solid state. The planes of these aryl groups are strictly parallel to each other. The endocyclic as well as the exocyclic Si—C distances are significantly longer than a standard Si—C single bond length. They are com-

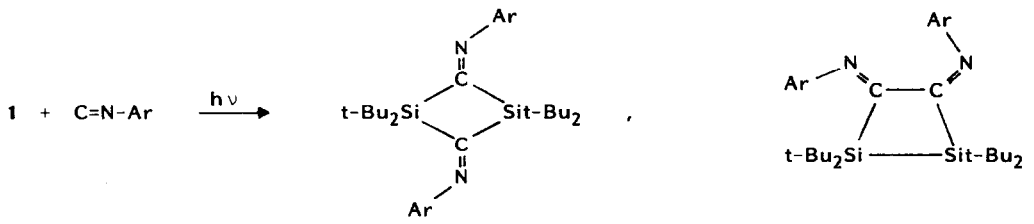

7, Ar = 2,4,6-$(CH_3)_3C_6H_2$ **9**, Ar = 2,4,6-$(CH_3)_3C_6H_2$ **11**, Ar = 2,6-$(i\text{-}C_3H_7)_2C_6H_3$

8, Ar = 2,6-$(i\text{-}C_3H_7)_2C_6H_3$ **10**, Ar = 2,6-$(i\text{-}C_3H_7)_2C_6H_3$

Scheme 2. Photolysis of **1** in the presence of *ortho*-disubstituted aryl isocyanides.

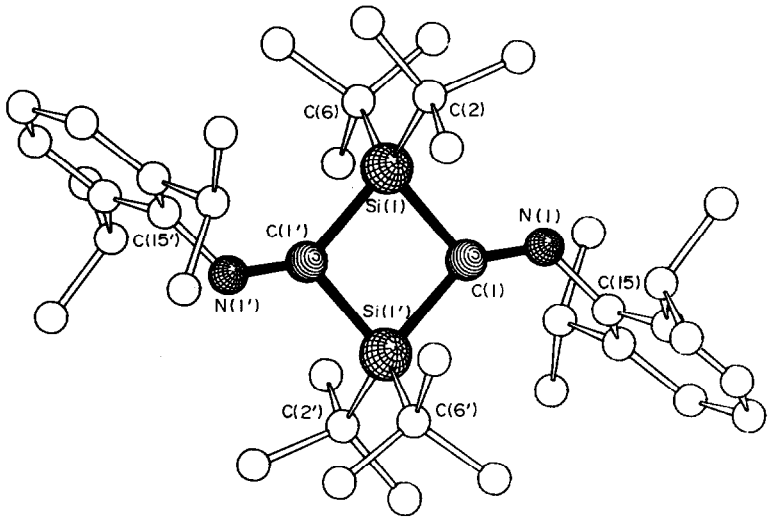

Fig. 1. The molecular structure and atom numbering scheme for crystalline **10** (hydrogen atoms omitted). Only one of the two independent molecules is shown.

parable with the Si—C bond lengths of some sterically crowded 2,4-disilacyclobutanes prepared by Brook and co-workers.[10]

The most striking feature of **10** is its violet colour, which is reflected in the longest wavelength absorption at $\lambda_{max} = 560$ nm. The same absorption lies at 510 nm for a disilacyclopropanimine derivative[9] and at 520 nm for the four-membered ring **5**.[7] The observed red shift of **10** seems to correspond with an increase of ring strain within this series of compounds. This rationalization was recently proposed by West and co-workers[9] in order to explain the bright red colour of the disilacyclopropanimine.[9]

Upon prolonged cooling of the photolysis mixture to −30°C, a minor amount of green crystals was also isolated. The spectroscopic data contribute very little to an elucidation of the structure of these green crystals. The mass spectrum, for example, only shows signals which may be attributed to a disilacyclopropanimine ring system. Therefore, the evidence for the structure of **11** rests ultimately on single-crystal X-ray diffraction data (Fig. 2, Table 2).

The X-ray structure analysis shows that **11** is an isomer of **10** with the imino groups being in the 1,2-position. Contrary to **10**, the Si_2C_2 ring framework is slightly puckered with an interplanar angle of *ca* 26° between the planes formed by the atoms Si(1)—Si(2)—C(1) and Si(2)—C(1)—C(2). The two exocyclic nitrogen atoms are *ca* 0.5 Å above and *ca* −0.65 Å below the mean plane through the ring atoms. The aryl groups adopt a *syn, anti* conformation, with the rings rotated at *ca* 90° against one another. The observed conformation of **11** and the stretching of the Si—Si and Si—C bonds may relieve the sterical strain within this molecule.

These results seem to confirm the mechanism proposed for the formation of **5** and **6** (Scheme 1).

Table 1. Selected intramolecular distances (Å) and angles (°) for molecule 1 [and molecule 2] for **10**, with ESDs in parentheses

C(1)—Si(1)	1.939(3) [1.969(3)]	Si(1)—C(2)	1.935(4) [1.926(4)]
C(1')—Si(1)	1.980(3) [1.940(3)]	Si(1)—C(6)	1.923(4) [1.930(3)]
C(1)—N(1)	1.275(4) [1.276(4)]	N(1)—C(15)	1.432(4) [1.434(4)]
C(1)—Si(1)—C(1')	82.8(2) [82.9(2)]	Si(1)—C(1)—Si(1')	97.1(2) [97.1(2)]
C(1)—N(1)—C(15)	126.9(3) [124.4(3)]	Si(1)—C(1)—N(1)	122.2(2) [122.5(2)]
C(2)—Si(1)—C(6)	111.4(2) [111.4(2)]	Si(1')—C(1)—N(1)	140.5(2) [140.3(2)]

The numbers marked with primes indicate symmetry equivalent atoms.

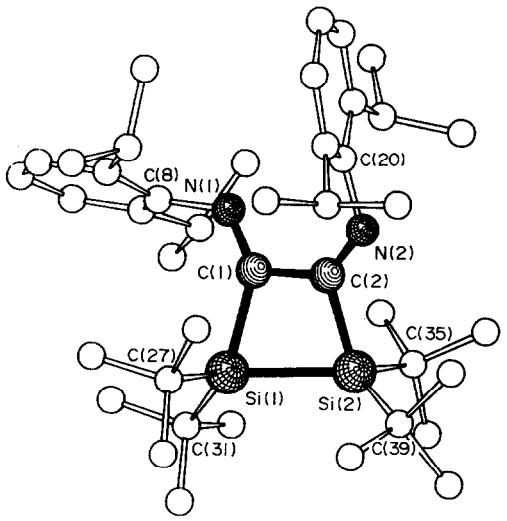

Fig. 2. The molecular structure and atom numbering scheme for crystalline **11** (hydrogen atoms omitted).

Since both **10** and **11** are formed simultaneously in the photolysis reaction, it is possible that they arise from a common intermediate such as a silaketenimine of type **4**. Head-to-tail dimerization then should give the four-membered ring **10**, whereas head-to-head dimerization should yield the isomer **11**. In the absence of trapping reagents some short-lived silaethylenes[13] and silapropadienes[14] bearing bulky substituents also undergo head-to-head dimerizations yielding 3,4-disilacyclobutanes.

Compounds **10** and **11** could also result from reaction of the aryl isocyanide **8** with an intermediate disilacyclopropanimine[9] derivative. However, such insertion reactions of isocyanides into Si—Si single bonds only take place in the presence of a palladium catalyst[15] and should, in this case, be further impaired by the bulky substituents.

EXPERIMENTAL

Materials, measurements and techniques

All reactions were carried out in oven-dried glassware under an atmosphere of dry argon or nitrogen. Photolyses were carried out by using a high pressure mercury lamp (Heraeus TQ 150) which was immersed in the reaction vessel.

The isocyanides **7** and **8** were prepared by the phosgene method[12] from N-(2,4,6-trimethylphenyl)formamide[11] or N-(2,6-diisopropylphenyl) formamide,[11] respectively.

NMR spectra were recorded on a Bruker AM 300 (^{1}H, ^{13}C) or Bruker WP 250 (^{29}Si) spectrometer using deuterated benzene as solvent. IR spectra were recorded on a Beckman 4220 instrument, and mass spectra were recorded by using a Varian-MAT 212 mass spectrometer. UV–vis spectra were recorded on a Shimadzu UV-260 spectrometer. Elemental analyses were performed by Analytische Laboratorien, D-5250 Engelskirchen, F.R.G.

N,N′ - Dimesityl - 2,2,4,4 - tetra - tert - butyl - 2,4 - disilacyclobutane - 1,3 - diimine (**9**)

A solution of **1** (0.436 g, 1.00 mmol) and **7** (0.43 g, 3.00 mmol) in n-hexane (60 cm^3) was photolysed for 5 h. The bright red solution was then cooled to −30°C for several days. After this time red crystals of **9** (0.13 g, 45%), m.p. 224–226°C, had precipitated. ^{1}H NMR : δ 1.19 (s, 36H, t-Bu), 2.13 (s, 6H, *p*-Me), 2.31 (s, 12H, *o*-Me), 6.80 (s, 4H, C_6H_2); ^{13}C NMR : δ 19.75, 20.76, 24.95, 31.42, 124.52, 129.23, 132.61, 156.58, 226.26 (C=N); MS (EI, 70 eV): *m/z* 574 (2, M^+), 429 (36, M^+ − MesNC); IR (KBr): ν(C=N) at 1565(w) and 1550(w) cm^{-1}. Found: C, 75.0; H, 10.1; N, 4.8. Calc. for $C_{36}H_{58}N_2Si_2$: C, 75.2; H, 10.2; N, 4.9%.

Table 2. Selected intramolecular distances (Å) and angles (°) for **11**, with ESDs in parentheses

Si(1)—Si(2)	2.416(3)	C(1)—C(2)	1.527(8)
Si(1)—C(1)	1.990(6)	Si(2)—C(2)	1.935(6)
C(1)—N(1)	1.281(7)	C(2)—N(2)	1.277(7)
N(1)—C(8)	1.423(8)	N(2)—C(20)	1.437(8)
Si(1)—C(27)	1.932(7)	Si(2)—C(35)	1.931(7)
Si(1)—C(31)	1.940(8)	Si(2)—C(39)	1.920(7)
C(1)—Si(1)—Si(2)	75.7(2)	Si(1)—C(1)—C(2)	99.5(4)
C(2)—Si(2)—Si(1)	75.8(2)	Si(2)—C(2)—C(1)	103.2(4)
C(2)—N(2)—C(20)	128.0(6)	C(1)—N(1)—C(8)	123.7(5)
Si(1)—C(1)—N(1)	141.0(5)	Si(2)—C(2)—N(2)	126.0(5)

N,N'-Bis(2,6-diisopropylphenyl)-2,2,4,4-tetra-tert-butyl-2,4-disilacyclobutane-1,3-diimine (**10**) *and N,N'-bis(2,6-diisopropylphenyl)-3,3,4,4-tetra-tert-butyl-3,4-disilacyclobutane-1,2-diimine* (**11**)

A solution of **1** (0.426 g, 1.00 mmol) and **8** (0.56 g, 3.00 mmol) in petroleum ether, 40–60°C (60 cm^3), was co-photolysed for 1.5 h. The solvent was removed and the residue was recrystallized from n-pentane. The dark green solution was cooled to −30°C for several days. After this time violet crystals of **10** (0.25 g, 76%), m.p. 185°C (decomp.), had precipitated. ^{1}H NMR: δ 1.18 (s, 36H, t-Bu), 1.28 (d, 12H, CH_3), 1.35 (d, 12H, CH_3), 3.37 [sept., 4H, $CH(CH_3)_2$, $J = 6.7$ Hz], 7.05 (t, 2H), 7.15 (d, 4H, $J = 7.7$ Hz); ^{13}C NMR: δ 20.27, 24.22, 25.19, 28.88, 31.42, 122.40, 124.42, 134.73, 156.49, 226.97 (C=N); ^{29}Si NMR: δ 1.68; MS (EI, 70 eV): *m/z* 658 (1, M^+), 471 (15, $M^+ - ArNC$); UV–vis: $\lambda(\varepsilon)$ 226 (25,000), 272 (12,000), 480 (350), 560 (230). Found: C, 76.4; H, 10.6; N, 4.2. Calc. for $C_{42}H_{70}N_2Si_2$: (658.29): C, 75.6; H, 10.7; N, 4.2%.

Upon prolonged cooling to −30°C a minor amount of green crystals of **11** was also isolated. ^{1}H NMR: δ 1.27 (s, 36H), 1.44 (not resolved, 24H, CH_3), 3.11 [not resolved, 4H, $CH(CH_3)_2$], 6.97–7.10 (not resolved, 6H); ^{13}C NMR: δ 24.36, 26.82, 28.76, 31.18, 32.37 (broad), 34.70, 122.20, 123.98, 145.15, 149.86, C=N could not be detected; MS (EI, 70 eV): *m/z* 471 (31, $M^+ - ArNC$); UV–vis: $\lambda(\varepsilon)$ 417, 613 (ε values could not be determined).

X-ray structure analyses of **10** *and* **11**

Slow cooling of the photolysis mixture in petroleum ether to −30°C resulted in crystals of **10** and **11** suitable for X-ray diffraction. In each case, the crystal was mounted in a thin-walled glass capillary. Data collection was performed on a Siemens AED 2 diffractometer using graphite-monochromated Mo-K_α radiation. Significant crystal data and data collection parameters are listed in Table 3.

The structures were solved by direct phase determinations using the SHELX 86 program system

Table 3. Summary of crystal data

	10	**11**
Empirical formula	$C_{42}H_{70}N_2Si_2$	$C_{42}H_{70}N_2Si_2$
Molecular weight	658.29	658.29
Colour of crystal	Dark violet	Green
Crystal dimensions (mm)	0.35 × 0.28 × 0.18	0.65 × 0.46 × 0.11
Crystal system	Triclinic	Monoclinic
Space group	$P\bar{1}$	$P2_1/n$
Cell dimensions		
a (Å)	10.750(1)	10.974(1)
b (Å)	12.456(1)	19.114(1)
c (Å)	16.036(1)	20.399(1)
α (°)	89.97(1)	
β (°)	88.95(1)	100.95(1)
γ (°)	79.15(1)	
Z (molecules/cell)	2[a]	4
Volume (Å^3)	2108.4	4200.7
Calculated density (g cm^{-3})	1.038	1.038
Wavelength (Å)	0.71069	0.71069
Linear absorption coefficient (cm^{-1})[b]	0.81	0.81
2θ range (°)	3.0–48.0	3.0–48.0
Number of unique reflections	6611	5471
Number of observed reflections with $I > 2\sigma(I)$	4508	3137
Number of variables	415	412
R	0.060	0.084
R_w	0.058	0.071

[a] Two independent half molecules, each situated on an inversion centre.
[b] No absorption correction was applied.

and refined by full-matrix least-squares techniques. Hydrogen atoms were placed in calculated positions, and all other atoms were refined anisotropically.

Crystallographic data

Further information on the crystal structure investigations are available on request from the Fachinformation Karlsruhe, Gesellschaft für Wissenschaftlich-technische Information mbH, D-7514 Eggenstein-Leopoldshafen 2 (F.R.G.) on quoting the depository number CSD 54831, the names of the authors and the journal citation. Tables of atom coordinates, thermal parameters and remaining bond lengths and angles are also available from the Cambridge Crystallographic Data Centre.

Acknowledgements—Financial support of our work by the Deutsche Forschungsgemeinschaft, the Volkswagen-Stiftung and the Fonds der Chemischen Industrie is gratefully acknowledged.

REFERENCES

1. A. Schäfer, M. Weidenbruch, S. Pohl and W. Saak, *Z. Naturfor.* 1990, **45b**, 1363.
2. Review: G. Raabe and J. Michl, in *The Chemistry of Organic Silicon Compounds* (Edited by S. Patai and Z. Rappoport), Part 2, p. 1015. John Wiley, Chichester (1989).
3. C. A. Arrington, T. J. Petty, S. E. Payne and W. C. K. Haskins, *J. Am. Chem. Soc.* 1988, **110**, 6240.
4. M.-A. Pearsell and R. West, *J. Am. Chem. Soc.* 1988, **110**, 7228.
5. T. P. Hamilton and H. F. Schaefer III, *J. Chem. Phys.* 1989, **90**, 1031.
6. A. Schäfer, M. Weidenbruch, K. Peters and H. G. von Schnering, *Angew. Chem.* 1984, **96**, 311; *Angew. Chem. Int. Edn Engl.* 1984, **23**, 302.
7. M. Weidenbruch, B. Brand-Roth, S. Pohl and W. Saak, *Angew. Chem.* 1990, **102**, 93; *Angew. Chem. Int. Edn Engl.* 1990, **29**, 90.
8. Reviews: M. Weidenbruch, *Comments Inorg. Chem.* 1986, **5**, 247; R. West, *Angew. Chem.* 1987, **99**, 1231; *Angew. Chem. Int. Edn Engl.* 1987, **26**, 1201.
9. H. B. Yokelson, A. J. Millevolte, K. J. Haller and R. West, *J. Chem. Soc., Chem. Commun.* 1987, 1605.
10. K. M. Baines, A. G. Brook, P. D. Lickiss and J. F. Sawyer, *Organometallics* 1989, **8**, 709.
11. J. Burgers, M. A. Hoevnagel, P. E. Verkade, H. Visser and B. M. Webster, *Recl Trav. Chim. Pays-Bas* 1958, **77**, 491.
12. I. Ugi, U. Fetzer, U. Eholzer, H. Knupfer and K. Offermann, *Angew. Chem.* 1965, **77**, 492; *Angew. Chem. Int. Edn Engl.* 1965, **4**, 432.
13. A. G. Brook, S. C. Nyburg, F. Abdesaken, B. Gutekunst, G. Gutekunst, R. K. M. R. Kallury, Y. C. Poon, Y.-M. Chang and W. Wong-Ng, *J. Am. Chem. Soc.* 1982, **104**, 5667.
14. M. Ishikawa, D. Kovar, T. Fuchikami, N. Nishimura, M. Kumada, T. Higuchi and S. Miyamoto, *J. Am. Chem. Soc.* 1981, **103**, 2324.
15. Y. Ito, S. Nishimura and M. Ishikawa, *Tetrahedron Lett.* 1987, **28**, 1293; Y. Ito, T. Matsuura and M. Murakami, *J. Am. Chem. Soc.* 1988, **110**, 3692.

Polyhedron Vol. 10, No. 11, pp. 1153–1161, 1991
Printed in Great Britain

0277–5387/91 $3.00+.00
© 1991 Pergamon Press plc

NEW STABLE GERMENES

M. LAZRAQ, C. COURET,* J. ESCUDIE* and J. SATGE

Laboratoire de Chimie des Organominéraux, URA 477, Université P. Sabatier, 118 route de Narbonne, 31062 Toulouse Cedex, France

and

M. SOUFIAOUI

Laboratoire de Cycloadditions, Département de Chimie, Faculté des Sciences, Université Mohamed V, Av. Ibn Batouta, Rabat, Morocco

Abstract—Two new stable fluorenylidene germenes **5** and **6** substituted on germanium with two bulky bisyls $[(Me_3Si)_2CH]$ or with a bisyl and a mesityl group have been synthesized by dehydrofluorination of the corresponding fluorogermanes by tert-butyllithium. The ditert-butylfluorenylidene germene **7** could not be obtained by this route, but its lithio precursor **8** can be used as its synthetic equivalent.

Alkenes are among the most important compounds in organic synthesis. Their heavier homologues should also be very useful, both as precursors of potentially interesting new kinds of polymers (such polymers including a Group 14 metal could present new and unexpected mechanical or electrical properties) and in organometallic synthesis. So the study of the compounds M=C (M = Si, Ge, Sn) appears very promising.

Some years ago, evidence for the formation of transient germenes (M = Ge) was presented by trapping reactions.[1,2] The first examples of stable germenes **1**[3,4] and **2**[5,6] were reported as recently as 1987. Both compounds are stabilized owing to steric (bulky groups on germanium, and to a small extent on carbon) and electronic effects, involving mesomerism between the germanium–carbon double bond and the fluorenylidene group in the case of **1**,[3,4] or delocalization in the free orbital of boron with an ylide type structure in the case of **2**.[5,6]

Very recently we have been able to stabilize two other compounds with a Ge=C double bond, the fluorenylidene germenes **3** and **4**:[7]

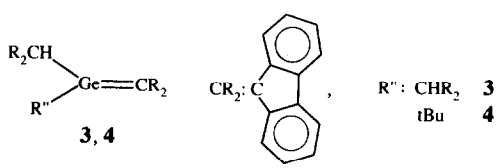

3, 4

The great interest of sterically hindered germenes is the stabilization of cycloadduct derivatives which are normally inaccessible. However,

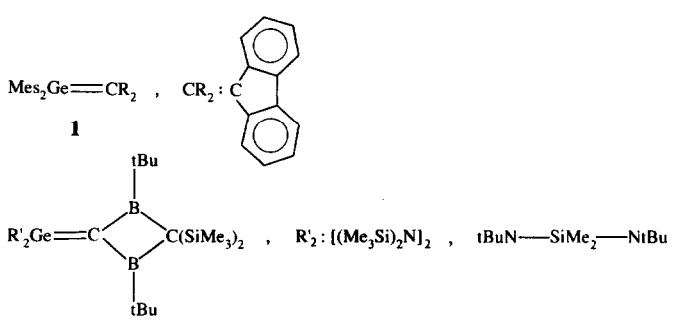

1 **2**

* Authors to whom correspondence should be addressed.

although substituted with two bulky mesityl groups, $Mes_2Ge{=}N{-}N{=}CR'_2$ ($CR'_2 = CR_2$, CPh_2) (obtained by reaction of **1** with diazofluorene or diphenyldiazomethane) could not be stabilized. Very few stable germa-imines have been reported,[9] and their chemical behaviour is not well developed. Also germirane, $Mes_2Ge{-}CH_2{-}CR_2$[10] (obtained from **1** and diazomethane), is unstable but would be of great interest in organometallic synthesis.

So we thought that such interesting but labile species (as well as germanones, Ge=O, and germathiones, Ge=S, which have been invoked in some reactions from **1**) could be rendered kinetically inert by substituting the germanium starting materials with more sterically demanding ligands.

We report here the synthesis of the new fluorenylidene germenes, substituted on germanium by two very large bis(trimethylsilyl)methyl (bisyl) groups **5**, and with one mesityl and one bisyl on germanium, **6**. In **6** steric hindrance should be intermediate between that observed for **1** and **5**. Moreover, owing to the prochiral germanium, **6** could be useful in mechanistic and stereochemical studies. We report also the attempted synthesis of ditert-butylfluorenylidene germene **7** and the use of the lithio compound **8** as its synthetic equivalent.

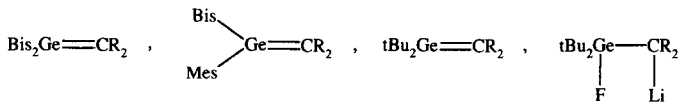

5 **6** **7** **8**

Bis: $(Me_3Si)_2CH$

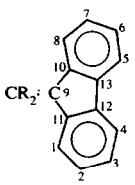

RESULTS AND DISCUSSION

Synthesis of fluorofluorenylgermanes (**15**)–(**17**)

Following our synthesis of germene **1**,[3,4] it appeared that the most convenient route to germenes $R'R''Ge{=}CR_2$ (**5**)–(**7**) would be the dehydrofluorination of fluorogermanes $R'R''Ge(F)CHR_2$ by tert-butyllithium ($R'R'' = tBu_2$, Bis_2, BisMes; CR_2 = fluorenyl). The use of fluorine instead of other halogens eliminates some side reactions, such as direct alkylation of germanium by lithio compounds and lithium–halogen exchange. The first step in the synthesis of **15**–**17** involves the preliminary preparation of dimethoxygermane derivatives **9**–**11**, which are obtained in good yields from tetramethoxygermane[11] and tert-butyllithium or bisyllithium, or from mesityltrimethoxygermane[12] and bisyllithium:

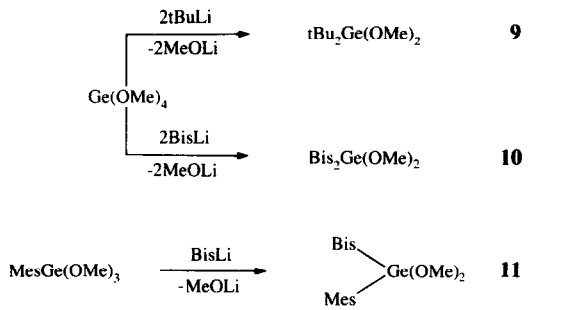

Bis=bisyl: $(Me_3Si)_2CH$

The corresponding difluoro derivatives **12**–**14** are nearly quantitatively obtained by treatment of **9**–**11** with solutions of hydrofluoric acid in water; then addition of fluorenyllithium leads to the fluorofluorenylgermanes **15**–**17**, which are the immediate precursors of germenes **5**–**7**:

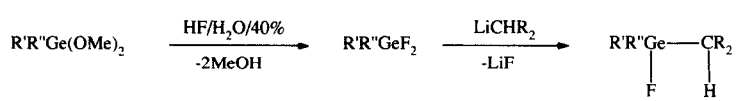

R'R'':			
tBu_2	**9**	**12**	**15**
Bis_2	**10**	**13**	**16**
BisMes	**11**	**14**	**17**

Compounds **9–17** could be easily purified by crystallization and exhibit good air and moisture stability, probably because of the large steric hindrance at germanium.

Dibisyl(fluorenylidene)germene (**5**)

The formation of germene **5** is extremely dependent on the experimental conditions. The best yield of **5** is obtained by using a 50:50 mixture of THF/Et_2O as solvent and an excess of tert-butyllithium (1.7 equivalent), required due to the reaction of tert-butyllithium with THF[13] during the lithiation of fluorogermane **16** to afford the lithio compound **18**. Contrary to the species $Mes_2Ge(F)CHR_2$, which on reaction with tert-butyllithium gives the corresponding lithio compound at low temperature, **18** is obtained only after 1 h at room temperature. This low reactivity of **16** compared with its dimesityl analogue could be explained both by steric hindrance and electronic effects.

Lithio compound **18** is stable to the reaction conditions and when quenched with methyl iodide affords, nearly quantitatively, the corresponding germane **19** after 1 h at room temperature. Elimination of lithium fluoride produces the expected germene, **5**, only after heating for 1 h at 40°C.

The solutions of germene **5** are highly air and moisture sensitive and they immediately turn from orange to green in the presence of traces of oxygen. Compound **5** can be obtained in pure form and physicochemically characterized by ^1H and ^{13}C NMR. However, it has not been possible to assign with certainty the ^{13}C NMR resonance of the carbon doubly-bonded to germanium. This carbon was expected in the chemical shift region of the fluorenyl carbon atoms and might be small, either because of its long relaxation time or due to quadrupolar coupling with germanium.

The presence of the germanium–carbon double bond is chemically unambiguously proven by addition of MeOH to afford the corresponding methoxygermane **20**, as expected from the polarity $Ge^{\delta+}=C^{\delta-}$ of the double bond. Addition of tert-butyllithium to **5**, followed by quenching with MeOH or methyl iodide, respectively, leads to germanes **22** and **23**. The reaction is best explained by a single-electron transfer mechanism involving the intermediates **21** and **21′**, because it seems that the addition of tert-butyllithium across the double bond is unlikely due to the high steric hindrance on germanium.

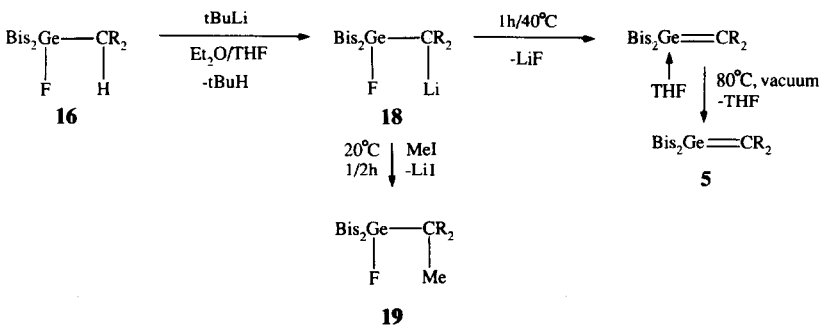

Using Et_2O instead of a mixture of THF/Et_2O in the synthesis of **5** from **16**, gives this germene in poor yield (*ca* 20–25%): addition of tert-butyllithium to **16**, in Et_2O, followed by quenching with MeOH, affords **20**, germane **22** and starting

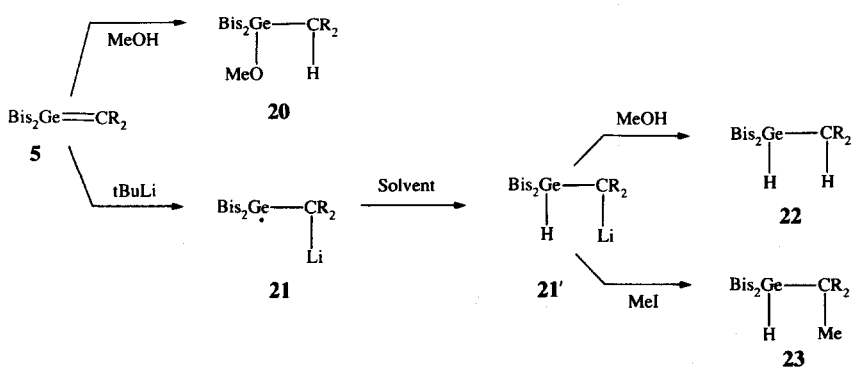

Germene **5** is first obtained complexed with one molecule of THF, but free germene is easily synthesized by heating **5 · THF** at about 80°C *in vacuo*.

material **16**, in about the same ratio. This result can be explained by the slow formation of lithio compound **18**, followed by a rapid elimination of LiF to give germene **5** (in Et_2O, **18** is much less stabilized than in THF). Compound **5** may then react with tert-butyllithium, according to the single-electron transfer mechanism previously described.

Bisyl(mesityl)fluorenylidenegermene (**6**)

Germene **6** is obtained in a good yield by dehydrofluorination of fluorogermane **17** by tert-butyllithium in Et_2O. Addition of tert-butyllithium was performed at low temperature, and the lithio compound **24** was formed rapidly. Contrary to the case of **18**, THF was not necessary.

Methanolysis immediately after the reaction mixture has reached room temperature affords methoxygermane **25** and starting fluorogermane **17** in the ratio 30:70, indicating only partial elimination of lithium fluoride. The complete elimination occurred only after heating the lithio compound **24** for 0.5 h at 35°C. Under these conditions, addition of MeOH to germene **6** leads quantitatively to formation of **25**:

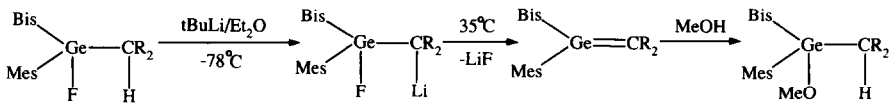

17 **24** **6** **25**

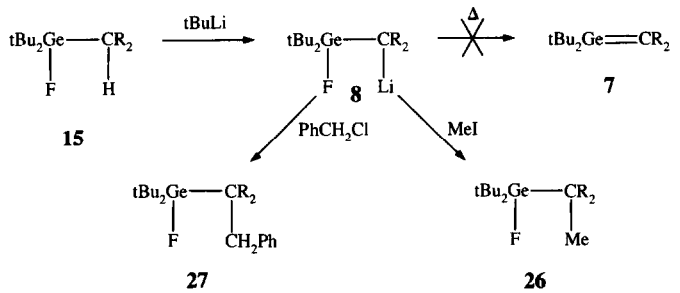

15 **7** **27** **26**

As for germene **5**, orange solutions of **6** are highly air- and moisture-sensitive, but crystals can be handled in air for short periods. In nitrogen or argon atmosphere, **6**, like **5**, is stable and can be stored for long periods.

Germenes **5** and **6** can be isolated as Et_2O or THF adducts, but also free of complexing solvents. The same phenomenon exists in silicon chemistry: silenes $\rangle Si{=}C\langle$,[14] and sila-imines $\rangle Si{=}N{-}$,[15] have already been isolated as ether or amine adducts, and also as free compounds. This complexation is, of course, due to the polarity of Si=C or Si=N double bonds. In contrast, analogous adducts have never been observed in symmetrical doubly-bonded derivatives such as disilenes,[16] digermenes,[2] distannenes,[17] diphosphenes,[18] or in unsymmetrical sila-,[19] germa-[12,20] or stannaphosphenes,[21] in which the double bond is only slightly polarized and the metal has a weaker electrophilic character.

The study of the reactivity of **6** with various unsaturated compounds is now in progress.

Attempted synthesis of ditert-butyl(fluorenylidene) germene (**7**)

Addition of one equivalent of tert-butyllithium to the ditert-butyl(fluoro)fluorenylgermane **15** leads exclusively to the corresponding lithio derivative **8**. Attempts to eliminate lithium fluoride, by using various solvents (Et_2O, THF, pentane) or by thermolysis, were unsuccessful. Formation of **8** is proved by its reaction with methyl iodide or benzyl chloride, leading quantitatively to **26** and **27**:

Therefore, there is a great difference of stability of fluorogermyllithio derivatives, Ge(F)—C(Li), depending on the substituents on germanium: with one or two aryl groups (mesityl,[3] fluorenyl[7]) lithium fluoride is easily eliminated at low temperature, whereas with two alkyl groups such as tert-butyl this elimination did not occur. A rather similar phenomenon has been observed in the synthesis of germaphosphenes, $\rangle Ge{=}P{-}$, in which elimination of lithium fluoride is much easier for Mes_2Ge

(F)P(Li)Ar than for $tBu_2Ge(F)P(Li)Ar$[12] (*ca* −40°C instead of 24 h at room temperature). The easy formation of dibisylgermene **5** from its lithio fluoro precursor **18** could be partly due to the electrophilic assistance of silicon by interaction with fluorine:

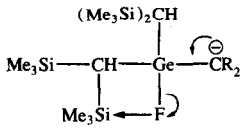

However, lithio compound **8** can be considered to some extent as a synthetic equivalent of germene **7**. For example, addition of benzaldehyde to **8** leads to the three derivatives **28**, **29** and **30** which have been obtained in a pure form by fractional crystallization. Formation of **28** and **29** involves the preliminary formation of the four-membered ring germaoxetane **31**, followed by a [4] → [2+2] cycloreversion, and dimerization of the germanone intermediate **32**. The formation of the six-membered ring derivative **30** can be explained by insertion of the germanone **32** into the germanium–oxygen bond of the germaoxetane intermediate **31**. This reaction is additional proof of the initial formation of this heterocycle.

EXPERIMENTAL

General procedures

All the experiments were carried out under argon or nitrogen with flame-dried apparatus. Solvents must be freshly distilled over sodium/benzophenone. ^1H NMR spectra were recorded on a Bruker AC 80 at 80.13 MHz or on a Bruker AM 300 WB at 300.1 MHz; ^{13}C NMR spectra on a Bruker AC 200 at 50.3 MHz (TMS internal standard); and ^{19}F NMR spectra on a Bruker AM 300 WB at 282.4 MHz (CF_3COOH external standard). IR spectra were recorded on a Perkin–Elmer 457 grating spectrometer. Mass spectra were measured on a Nermag R 10 010 spectrometer (EI). Melting points were determined on a Reichert apparatus. Elemental analyses were performed by the "Service de microanalyse de l'Ecole de Chimie", Toulouse (France). Carbon atoms of fluorenyl groups are numbered C_1 to C_{13} according to the scheme shown in the introduction.

Dibisyl(dimethoxy)germane (**10**)

A solution of bis(trimethylsilyl)methyllithium [prepared from bis(trimethylsilyl)bromomethane[22]

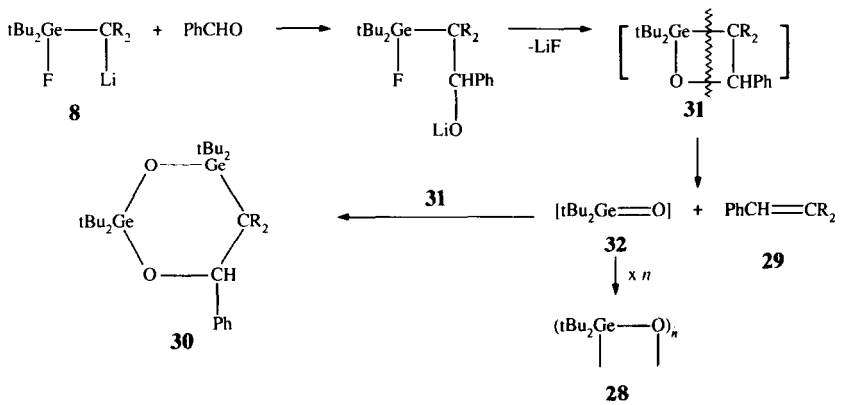

CONCLUSION

The germenes **5** and **6** and the lithio derivative **8** described in this paper present a particular interest for the following reasons. Compound **5**, the most hindered germene isolated to date, may stabilize otherwise unstable adducts or low coordination number species. Studies of its chemistry are now in progress. Compound **6** is the first example of germene with a prochiral germanium atom suitable for stereochemical studies at the Ge=C double bond and **8** can be used as a synthetic equivalent of the ditert-butylfluorenylidene germene **7**.

(16.8 g, 70 mmol) and 44 cm^3 of a solution 1.6 M of butyllithium in hexane] in Et_2O (50 cm^3) was added to a solution of tetramethoxygermane (6.6 g, 33.3 mmol) in Et_2O (20 cm^3). After the end of the addition, the reaction mixture was refluxed for 4 h. MeOLi was eliminated by filtration; **10** can be recrystallized in small amounts of pentane at −20°C: 9.19 g (61%); m.p. 55°C. ^1H NMR (C_6D_6): 0.22 (s, 36H, Me_3Si), 1.82 (s, 6H, OMe). ^{13}C NMR ($CDCl_3$): 3.31 (Me_3Si), 12.03 (CHSi), 52.42 (OMe).

Dibisyl(difluoro)germane (**13**)

To a solution of **10** (8.6 g, 18.9 mmol) in Et_2O (100 cm^3) was added a solution of hydrofluoric acid in water (40%, 5.5 g, 50% excess). The reaction was slightly exothermic. The reaction mixture was heated at reflux of Et_2O for 4 h, then the organic layer was extracted with Et_2O and dried overnight over Na_2SO_4. Removal of solvent *in vacuo* led to crude **13** which can be recrystallized from pentane to afford 6.16 g (76%) of white crystals; m.p. 59°C. ^1H NMR (C_6D_6): 0.18 (s, Me_3Si). ^{19}F NMR (C_6D_6): −58.05 (t, $^3J_{HF}$ 18.6 Hz). ^{13}C NMR ($CDCl_3$): 2.42 (Me_3Si), 14.24 (t, $^2J_{CF}$ 8.12 Hz, CHSi).

Dibisyl(fluoro)fluorenylgermane (**16**)

Fluorenyllithium was prepared by addition of a solution 1.6 M of butyllithium in hexane (11.3 cm^3, 18.0 mmol) to a solution of fluorene (3.0 g, 18.0 mmol) in a 50:50 mixture of THF/Et_2O (100 cm^3). The lithio compound was stirred for 1 h at room temperature, then this red solution was slowly added to a solution of **13** (7.75 g, 18.0 mmol) in Et_2O (50 cm^3) at room temperature. The reaction mixture was heated for 8 h at reflux, then filtered through silica (eluent, THF). The volatile components were removed *in vacuo* and crude **16** was recrystallized in pentane to afford 8.08 g (78%) of white crystals; m.p. 339°C. ^1H NMR (C_6D_6): 0.04 (d, $^5J_{HF}$ 0.3 Hz, 18H, Me_3Si), 0.18 (d, $^5J_{HF}$ 0.7 Hz, 18H, Me_3Si), 4.71 (broad s, 1H, CHR_2), 7.25–7.96 (m, 8H, CR_2). ^{19}F NMR ($CDCl_3$): −87.4. ^{13}C NMR ($CDCl_3$): 3.46 (Me_3Si), 4.04 (Me_3Si), 12.27 (d, $^2J_{CF}$ 12.8 Hz, CHSi), 47.73 (d, $^2J_{CF}$ 10.3 Hz, CHR_2), 120.17 (C_4, C_5), 125.87, 126.44, 126.57 (C_1, C_2, C_3, C_6, C_7, C_8), 141.42 (C_{12}, C_{13}), 143.45 (d, $^3J_{CF}$ 1.0 Hz, C_{10}, C_{11}). MS (EI, 70 eV, ^{74}Ge), *m/z*: 557 (M−F, 7), 411 (Bis_2GeF, 3), 393 (Bis_2Ge+1, 1), 165 (R_2CH, 70), 73 (Me_3Si, 100). Found: C, 56.6; H, 8.3. $C_{27}H_{47}FGeSi_4$ requires C, 56.3; H, 8.2.

Dibisylfluorenylgermane (**22**)

To a solution of **16** (2.00 g, 3.5 mmol) in Et_2O (30 cm^3), cooled in a dry ice–acetone, were added 2.7 molar equivalents of tert-butyllithium, 1.7 M in pentane. The reaction mixture was then warmed to room temperature and became an intense red. Addition of an excess of MeOH immediately decolorized the solution. Solvents were removed *in vacuo* and 20 cm^3 of pentane were added; lithium salts were filtered off, and crude **22** was recrystallized from pentane; 1.65 g (85%) of white crystals of **22** were obtained; m.p. 118–119°C. ^1H NMR ($CDCl_3$): −0.21 (d, $^3J_{HH}$ 3.0 Hz, 2H, CHSi), 0.01 (s, 18H, Me_3Si), 0.22 (s, 18H, Me_3Si), 4.52 (s, 1H, CHR_2), 4.75 (t, $^3J_{HH}$ 3.0 Hz, 1H, GeH), 7.18–7.55 (m, 8H, CR_2). ^{13}C NMR ($CDCl_3$): 1.08 (CHSi), 2.95 (Me_3Si), 3.40 (Me_3Si), 42.58 (CHR_2), 119.68 (C_4, C_5), 125.20, 125.59, 126.36 (C_1, C_2, C_3, C_6, C_7, C_8), 140.60 (C_{12}, C_{13}), 146.63 (C_{10}, C_{11}). IR (KBr): ν(Ge—H) 2068 and 2076 cm^{-1}. MS (EI, 70 eV, ^{74}Ge), *m/z*: 557 (M−1, 2), 543 (M−15, 10), 393 (Bis_2GeH, 100), 165 (CHR_2, 25).

Dibisylfluoro(methylfluorenyl)germane (**19**)

To a solution of **16** (0.50 g, 0.87 mmol) in THF (5 cm^3)–Et_2O (5 cm^3) was slowly added 1.7 equivalents of tert-butyllithium 1.7 M in pentane. The reaction mixture, warmed to 0°C, turned gradually yellow. After 1/2 h stirring at 0°C, MeI (0.12 g, 0.87 mmol) was added. After 1 h at room temperature the reaction mixture was practically colourless; LiI was filtrated and solvents were removed *in vacuo*, and crude **19** was crystallized in pentane; 0.44 g of **19** (86%) were obtained; m.p. 112–113°C. ^1H NMR ($CDCl_3$): −0.16 (d, $^5J_{HF}$ 0.6 Hz, 18H, Me_3Si), 0.18 (d, $^5J_{HF}$ 0.9 Hz, 18H, Me_3Si), 1.77 (d, $^4J_{HF}$ 0.6 Hz, 3H, $MeCR_2$), 7.38–7.88 (m, 8H, CR_2). ^{13}C NMR ($CDCl_3$): 3.95 (Me_3Si), 4.31 (d, $^4J_{CF}$ 1.8 Hz, Me_3Si), 14.10 (d, $^2J_{CF}$ 13.1 Hz, $CHSi_2$), 25.40 (d, $^3J_{CF}$ 27 Hz, $MeCR_2$), 52.17 (d, $^2J_{CF}$ 12.6 Hz, CR_2), 120.25 (C_4, C_5), 125.00, 125.05, 126.93 (C_1, C_2, C_3, C_6, C_7, C_8), 140.61, 149.61 (C_{10}, C_{11}, C_{12}, C_{13}).

Dibisyl(fluorenylidene)germene (**5**)

To a solution of **16** (2.0 g, 3.48 mmol) in Et_2O/THF (50:50) (15 cm^3) cooled to −78°C were slowly added 3.48 cm^3 of a 1.7 M solution of tert-butyllithium in pentane (5.92 mmol). The reaction mixture was warmed to room temperature then heated at reflux for 1 h. A slight precipitate of LiF appeared and the reaction mixture turned orange-red. After elimination of LiF by filtration and of the solvents *in vacuo*, crystallization in pentane afforded orange crystals of germene **5** complexed with one mole of THF; the free germene **5** was obtained by heating **5·THF** *in vacuo* at 80°C; 1.53 g of orange crystals (79%) of **5** were obtained; m.p. 149–150°C. **5·THF**, ^1H NMR (CD_2Cl_2): 0.43 (s, 36H, Me_3Si), 1.87 (m, 4H, CH_2), 3.74 (m, 4H, CH_2O), 7.20–7.46 (m, 4H, CR_2), 7.79–8.00 (m, 4H, CR_2). **5**, ^1H NMR (C_6D_6): 0.46 (s, 36H, Me_3Si), 7.27–8.23 (m, 8H, CR_2).

Dibisyl(methylfluorenyl)germane (**23**)

Two molar equivalents of a solution 1.7 M of tert-butyllithium in pentane were added to a solution of **16** (2.00 g, 3.5 mmol) in Et_2O (30 cm^3) cooled to −78°C. The reaction mixture was then warmed to 20°C and became red; on the addition of a two-fold excess of methyl iodide, it turned gradually colourless. After 1 h stirring, solvents were eliminated *in vacuo* and 20 cm^3 of pentane were added to precipitate LiF and LiI. After filtration, cooling of the solution at −20°C gave white crystals of **23**, 1.20 g (60%); m.p. 160–161°C. ^1H ($CDCl_3$): −0.1 (s, 18H, Me_3Si), 0.14 (s, 18H, Me_3Si), 1.79 (s, 3H, MeC), 4.96 (t, $^3J_{HH}$ 1.5 Hz, 1H, GeH), 7.30–7.84 (m, 8H, CR_2). ^{13}C ($CDCl_3$): 3.51 (Me_3Si), 3.72 (Me_3Si), 4.51 (CHSi), 25.48 (*Me*C), 47.94 (*C*R_2), 120.24 (C_4, C_5), 124.13, 126.26, 126.74 (C_1, C_2, C_3, C_6, C_7, C_8), 139.97, 151.63 (C_{10}, C_{11}, C_{12}, C_{13}). IR (KBr): ν(Ge—H) 2056 cm^{-1}. MS (EI, 70 eV, ^{74}Ge), *m/z*: 557 (M−15, 2), 393 (Bis_2GeH, 35), 179 (R_2CMe, 59), 73 (Me_3Si, 100). Found: C, 59.1; H, 9.0. $C_{28}H_{50}GeSi_4$ requires: C, 58.8; H, 8.8.

Dibisyl(methoxy)fluorenylgermane (**20**)

To a solution of **16** (1.0 g, 1.74 mmol) in Et_2O (20 cm^3) and THF (20 cm^3) at −20°C was slowly added a solution of tert-butyllithium 1.7 M in pentane (1.02 cm^3, 1.74 mmol). The reaction mixture immediately turned light yellow and after 1 h was allowed to gradually warm; it turned orange (probably due to the formation of lithio compound). After 1 h at reflux, a three-fold excess of MeOH (0.15 g, 5.20 mmol) was added, to afford a light yellow solution. Solvents were removed *in vacuo* and 30 cm^3 of pentane were added to precipitate MeOLi. Crystallization from pentane afforded white crystals of **2**, 0.83 g (81%); m.p. 105–106°C. ^1H NMR ($CDCl_3$): −0.10 (s, 1H, CHSi), 0.04 (s, 18H, Me_3Si), 0.07 (s, 18H, Me_3Si), 3.74 (s, 3H, MeO), 4.61 (s, 1H, CHR_2), 7.29–7.91 (m, 8H, CR_2). ^{13}C NMR ($CDCl_3$): 1.10 (CHSi), 4.16 (Me_3Si), 4.34 (Me_3Si), 46.23 (*C*HR_2), 53.77 (MeO), 120.04 (C_4, C_5), 125.69, 126.05, 126.34 (C_1, C_2, C_3, C_6, C_7, C_8), 141.31, 144.48 (C_{10}, C_{11}, C_{12}, C_{13}).

Bisyl(mesityl)dimethoxygermane (**11**)

A solution of BisLi [prepared from BisBr (10 g, 41.7 mmol) and a stoichiometric amount of butyllithium 1.6 M in hexane at −78°C] in Et_2O was added to a solution of $MesGe(OMe)_3$ (11.85 g, 41.7 mmol) in pentane (40 cm^3) cooled to −78°C. After the addition the reaction mixture was allowed to warm to room temperature and then refluxed for 4 h. MeOLi was removed by filtration and the solvents were evaporated *in vacuo* leading to nearly pure waxy **11**, which is very soluble in common organic solvents and can be recrystallized from small amounts of pentane to give 17.17 g (91%) of white waxy crystals; m.p. 39°C. ^1H NMR (C_6D_6): 0.15 (s, 1H, CHSi), 0.33 (s, 18H, Me_3Si), 2.14 (s, 3H, *p*-Me), 2.62 (s, 6H, *o*-Me), 3.55 (s, 6H, OMe), 6.77 (s, 2H, arom. Mes). ^{13}C NMR ($CDCl_3$): 2.61 (Me_3Si), 10.50 (CHSi), 21.05 (*p*-Me), 22.73 (*o*-Me), 51.66 (OMe), 129.40 (*m*-C Mes), 131.33 (*ipso*-C Mes), 139.55 (*p*-C Mes), 143.56 (*o*-C Mes). Found: C, 52.6; H, 8.9. $C_{18}H_{36}GeO_2Si_2$ requires: C, 52.3; H, 8.8.

Bisyl(mesityl)difluorogermane (**14**)

A solution of hydrofluoric acid in water (40%, 4.0 g, 50% excess) was added to **11** (5.28 g, 12.8 mmol) in benzene (30 cm^3). The reaction mixture was heated at reflux for 2 h, then the organic layer was extracted with Et_2O and dried over Na_2SO_4. Solvents were removed *in vacuo* and **14** was recrystallized from pentane to afford 3.78 g (76%) of white crystals; m.p. 62–63°C. ^1H NMR (C_6D_6): 0.23 (s, 18H, Me_3Si), 1.99 (s, 3H, *p*-Me), 2.49 (s, 6H, *o*-Me), 6.62 (s, 2H, arom. Mes). ^{19}F NMR (C_6D_6): −61.9 (d, $^3J_{HF}$ 8.2 Hz). ^{13}C NMR ($CDCl_3$): 2.22 (s, Me_3Si), 13.79 (t, $^2J_{CF}$ 8.2 Hz, CH), 21.17 (s, *p*-Me), 23.30 (s, *o*-Me), 129.50 (s, *m*-C Mes), 141.50 (*p*-C Mes), 142.70 (*o*-C Mes). Found: C, 50.1; H, 7.8. $C_{16}H_{30}F_2GeSi_2$ requires: C, 49.4; H, 7.8.

Bisyl(mesityl)fluorenylgermane (**17**)

A solution of fluorenyllithium [prepared from fluorene (3.0 g, 18.0 mmol) and a solution of butyllithium 1.6 M in hexane (11.3 cm^3, 18.0 mmol) in 100 cm^3 of a 50:50 mixture of THF/Et_2O] was slowly added to a solution of **14** (6.99 g, 18.0 mmol) in Et_2O (80 cm^3) at room temperature. The reaction mixture was heated at reflux for 2 h then filtered on silica (eluent, THF). After removal of solvents *in vacuo*, crude **17** was recrystallized from pentane to afford 6.92 g (72%) of white crystals; m.p. 122–123°C. ^1H NMR ($CDCl_3$): 0.01 (s, 9H, Me_3Si), 0.49 (d, $^5J_{HF}$ 0.5 Hz, 9H, Me_3Si), 0.50 (d, $^3J_{HF}$ 21.0 Hz, 1H, CHSi), 1.74 (s, 3H, *p*-Me), 1.98 (d, $^5J_{HF}$ 2.2 Hz, 6H, *o*-Me), 4.73 (d, $^3J_{HF}$ 1.5 Hz, 1H, CH), 6.32 (s, 2H, arom. Mes), 7.00–8.27 (m, 8H, CR_2). ^{19}F NMR ($CDCl_3$): −95.27. ^{13}C NMR ($CDCl_3$): 2.45 (s, Me_3Si), 3.66 (s, Me_3Si), 9.85 (d, $^2J_{CF}$ 15.2 Hz, CHSi), 20.89 (s, *p*-Me), 23.61 (d, $^4J_{CF}$ 6.0 Hz, *o*-

Me), 48.1 (d, $^2J_{CF}$ 11.3 Hz, *C*HR$_2$), 119.62, 120.22, 124.02, 124.75, 124.79, 125.96, 126.38, 126.41, 128.66, 132.32, 132.49 (C_1, C_2, C_3, C_4, C_5, C_6, C_7, C_8 and *m*-C Mes), 132.3 (d, $^2J_{CF}$ 8.0 Hz, *ipso*-C Mes), 138.94, 140.08, 141.47, 142.40, 143.35 (d, 5.0 Hz), 144.33 (C_{10}, C_{11}, C_{12}, C_{13}, *o*-C Mes, *p*-C Mes). MS(EI, 70 eV, ^{74}Ge), *m/z*: 521 (M−15, 2), 371 [BisGe(F)Mes, 63], 165 (R_2CH, 31), 119 (Mes, 11), 159 (Bis, 2). Found: C, 65.5; H, 7.4. $C_{29}H_{39}FGeSi_2$ requires: C, 65.1; H, 7.3.

Bisyl(mesityl)fluorenylidenegermene (**6**)

An equivalent of tert-butyllithium 1.7 M in pentane (2.8 mmol) was added to a solution of **17** (1.50 g, 2.8 mmol) in Et_2O (20 cm^3) cooled to −78°C. (Note: Et_2O must be very carefully dried and deoxygenated and all the apparatus flame-dried *in vacuo*.) The reaction mixture was then allowed to warm to room temperature: it turned gradually yellow, then orange at room temperature, and orange–red on reflux of Et_2O. Approximately 1/2 h of reflux was necessary for the complete formation of germene. LiF was eliminated by centrifugation. Solvents were removed *in vacuo* giving crude germene **6**. Crystallization in pentane gave 0.88 g (61%) of orange crystals of **6**; m.p. 60–61°C. Solutions of **6** are extremely air-sensitive: they turned green when traces of air were added. ^{1}H NMR (CD_2Cl_2): 0.33 (s, 18H, Me_3Si), 0.37 (s, 1H, CHSi), 2.45 (s, 3H, *p*-Me), 2.61 (s, 6H, *o*-Me), 6.96–8.05 (m, 8H, CR_2), 7.14 (s, 2H, arom. Mes).

Bisyl(mesityl)(methoxy)fluorenylgermane (**25**)

An excess of methanol (carefully dried and deoxygenated) was added to a solution of **6** (1.14 g, 2.2 mmol) in Et_2O (10 cm^3). The orange solution of **6** turned immediately colourless. Et_2O and excess of MeOH were eliminated *in vacuo* and crude **25** was recrystallized in pentane to afford 0.91 g (86%) of white crystals; m.p. 134–135°C. ^{1}H NMR ($CDCl_3$): 0.03 (s, 9H, Me_3Si), 0.47 (s, 9H, Me_3Si), 2.06 (s, 6H, *o*-Me), 2.18 (s, 3H, *p*-Me), 3.83 (s, 3H, OMe), 4.85 (s, 1H, CH), 6.59 (s, 2H, arom. Mes), 7.02–8.01 (m, 8H, CR_2). ^{13}C NMR ($CDCl_3$): 2.92 (Me_3Si), 3.83 (Me_3Si), 7.36 (CHSi), 21.00 (*p*-Me), 23.14 (*o*-Me), 44.69 (*C*HR$_2$), 53.10 (OMe), 119.67, 120.19 (C_4, C_5), 124.64, 124.97, 125.69, 125.99, 126.32, 126.44, (C_1, C_2, C_3, C_6, C_7, C_8), 128.65 (*m*-C Mes), 134.52, 138.40, 140.65, 141.70, 143.02, 145.04, 145.07 (C_{10}, C_{11}, C_{12}, C_{13}, *ipso*-C Mes, *o*-C Mes, *p*-C Mes). MS (EI, 70 eV, ^{74}Ge), *m/z*: 547 (M−1, 11), 383 [Bis(Mes)GeOMe, 100], 351 [Bis(Mes)Ge−1, 10], 193 (MesGe, 11), 165 (R_2CH, 53), 119 (Mes, 10), 73 (Me_3Si, 64). Found: C, 66.3; H, 7.9. $C_{30}H_{42}GeOSi_2$ requires: C, 65.8; H, 7.7.

Ditert-butyl(fluoro)fluorenylgermane (**15**)

A solution of fluorenyllithium [prepared as previously described from fluorene (8.67 g, 52.2 mmol) and butyllithium (52.2 mmol) in 120 cm^3 of THF/Et_2O (50:50)] was added to a solution of **12** (11.73 g, 52.2 mmol) in Et_2O (100 cm^3) at room temperature. The orange reaction mixture was heated at reflux for 2 h, then filtered through silica and the solvents were eliminated *in vacuo*. Recrystallization from pentane afforded 13.34 g (69%) of white crystals of **15**; m.p. 90–91°C. ^{1}H NMR ($CDCl_3$): 1.00 (d, $^4J_{HF}$ 1.0 Hz, 18 H, tBu), 4.52 (broad s, 1H, CH), 7.17–8.00 (m, 8H, CR_2). ^{13}C NMR ($CDCl_3$): 28.41 (s, Me), 31.84 (d, $^2J_{CF}$ 8.6 Hz, *C*Me), 41.40 (d, $^2J_{CF}$ 6.8 Hz, CH), 120.11 (C_4 C_5), 125.35, 126.16, 126.48 (C_1, C_2, C_3, C_6, C_7, C_8), 140.93, 143.91 (C_{10}, C_{11}, C_{12}, C_{13}). MS (EI, ^{74}Ge), *m/z*: 372 (M, 15), 315 (M−tBu, 2), 238 (M−2tBu−HF, 15), 207 (tBu_2GeF, 30), 165 (HCR_2, 100). Found: C, 67.5; H, 7.3. $C_{21}H_{27}FGe$ requires: C, 68.0; H, 7.3.

Ditert-butyl(fluoro)(benzylfluorenyl)germane (**27**)

To a solution of **15** (1.0 g, 2.7 mmol) in Et_2O (15 cm^3) cooled to −78°C was added one equivalent of tert-butyllithium 1.7 M in pentane. After warming to room temperature, the reaction mixture turned red. Benzyl chloride (0.34 g, 2.7 mmol) was added to the lithio compound $tBu_2Ge(F)C(Li)R_2$ at room temperature; the solution immediately became light yellow. After 1 h stirring at room temperature, lithium chloride was removed by filtration and then the solvents were removed *in vacuo*. Crude **27** was recrystallized from pentane, affording 1.06 g (85%) of white crystals of **27**; m.p. 157–158°C. ^{1}H ($CDCl_3$): 1.06 (d, $^4J_{HF}$ 1.3 Hz, 18H, tBu), 4.06 (s, 2H, CH_2), 6.41–8.18 (m, 13H, CR_2Ph). ^{13}C ($CDCl_3$): 29.73 (s, Me), 34.44 (d, $^2J_{CF}$ 8.6 Hz, *C*(Me$_3$), 40.69 (s, CH_2), 57.55 (d, $^2J_{CF}$ 8.6 Hz, *C*R$_2$), 120.00 (C_4, C_5), 125.76–136.05 (C_1, C_2, C_3, C_6, C_7, C_8, Ph) 141.20, 146.62 (C_{10}, C_{11}, C_{12}, C_{13}). MS (EI, ^{74}Ge), *m/z*: 462 (M, 2), 328 [tBuGe(F)CR_2CH_2, 1], 257 [Ge(F)CR_2, 13], 207 (tBu_2GeF, 6), 57 (tBu, 100). Found: C, 72.4; H, 7.2. $C_{28}H_{33}FGe$ requires: C, 72.9; H, 7.2.

Ditert-butyl(fluoro)(methylfluorenyl)germane (**26**)

To the lithio compound **8** [prepared from **17** (0.5 g, 1.35 mmol) and one equivalent of tert-butyllithium in Et_2O] was added methyl iodide (0.19 g,

1.35 mmol) in solution in pentane (5 cm^3). After 15 min at room temperature the orange reaction mixture turned yellow; solvents were removed *in vacuo* and 15 cm^3 of pentane were added; LiI was then eliminated by filtration. Crystallization from pentane afforded 0.31 g (48%) of white crystals of **26**; m.p. 87–88°C. ^1H NMR ($CDCl_3$): 0.96 (s, 18H, tBu), 1.53 (s, 3H, CMe), 7.17–8.11 (m, 8H, CR_2).

Reaction of lithio compound **8** *with benzaldehyde*

To a solution of lithio compound **8** [prepared as previously from **15** (1.0 g, 2.7 mmol), one equivalent of tert-butyllithium and Et_2O (15 cm^3) cooled to −78°C] was added a solution of benzaldehyde (0.29 g, 2.7 mmol) in Et_2O (5 cm^3). The reaction mixture turned brown–black, then was warmed to room temperature. During stirring at 20°C for 10 h, it progressively turned yellow. After filtration to remove lithium fluoride, solvents were evaporated *in vacuo*. Pentane (25 cm^3) was added to the crude resulting mixture; cooling to −20°C allowed the crystallization of alkene **29**,[23] which was separated by filtration (0.38 g, 55%). The filtrate contained **28** and **30**, which were separated by fractional crystallization in Et_2O/pentane (50:50). **28** was the first to crystallize. **28**, ^1H NMR ($CDCl_3$): 0.96, 1.21, 1.24 and 1.46 (4s). ^{13}C NMR ($CDCl_3$): 27.43, 27.99 and 31.91. MS (EI, ^{74}Ge), *m/z*: 437 (M − 3tBu, 0.5), 381 (M − 4tBu + H, 1), 367 (M − 4tBu − Me + 2H, 1), 293 (M − $tBu_2Ge{=}O$ − 2tBu + H, 2), 204 ($tBu_2Ge{=}O$, 2), 57 (tBu, 100). **30**, ^1H NMR ($CDCl_3$): −0.04 (s, 9H, tBu), −0.03 (s, 9H, tBu), 0.11 (s, 9H, tBu), 0.12 (s, 9H, tBu), 4.60 (s, 1H, CH), 7.17–7.93 (m, 13H, CR_2 and Ph). ^{13}C NMR ($CDCl_3$): 20.92, 23.43, 24.14 and 28.10 (Me_3C), 60.86 (CH), 62.59 (CR_2), 119.05 to 145.67 (Ph, CR_2).

REFERENCES

1. T. J. Barton, E. A. Kline and P. M. Garvey, *J. Am. Chem. Soc.* 1973, **95**, 3078; P. Rivière, A. Castel and J. Satgé, *J. Am. Chem Soc.* 1980, **102**, 541; N. Wiberg and Ch. K. Kim, *Chem. Ber.* 1986, **119**, 2966 and 2980; N. Wiberg, P. Karampatses and Ch. K. Kim, *Chem. Ber.* 1987, **120**, 1203.
2. For a recent review on Ge=C compounds, see: J. Barrau, J. Escudié and J. Satgé, *Chem. Rev.* 1990, **90**, 283.
3. C. Couret, J. Escudié, J. Satgé and M. Lazraq, *J. Am. Chem. Soc.* 1987, **109**, 4411.
4. M. Lazraq, J. Escudié, C. Couret, J. Satgé, M. Dräger and R. Dammel, *Angew. Chem.* 1988, **100**, 885; *Angew. Chem. Int. Edn. Engl.* 1988, **27**, 828.
5. H. Meyer, G. Baum, W. Massa and A. Berndt, *Angew. Chem.* 1987, **99**, 790; *Angew. Chem. Int. Edn Engl.* 1987, **26**, 798.
6. A. Berndt, H. Meyer, G. Baum, W. Massa and S. Berger, *Pure Appl. Chem.* 1987, **59**, 1011.
7. G. Anselme, J. Escudié, C. Couret and J. Satgé, *J. Organomet. Chem.* 1991, **403**, 93.
8. M. Lazraq, C. Couret, J. P. Declerq, A. Dubourg, J. Escudié and M. Rivière-Baudet, *Organometallics* 1990, **9**, 845.
9. C. Glidewell, D. Lloyd, K. W. Lumbard and J. S. McKechnie, *Tetrahedron Lett.* 1987, **28**, 343; J. Pfeiffer, W. Maringgele, M. Noltemeyer and A. Meller, *Chem. Ber* 1989, **122**, 245; H. G. Ang and F. K. Lee, *J. Chem. Soc., Chem. Commun.* 1989, 310; H. G. Ang and F. K. Lee, *F. Fluorine Chem.* 1989, **43**, 435.
10. M. Lazraq, J. Escudié, C. Couret, J. Satgé and M. Soufiaoui, *J. Organomet. Chem.* 1990, **397**, 1.
11. D. C. Bradley, L. J. Kay and W. Wardlaw, *J. Chem. Soc.* 1956, 4916.
12. H. Ranaivonjatovo, J. Escudié, C. Couret and J. Satgé, *New J. Chem.* 1989, **13**, 389.
13. R. B. Bates, L. M. Kroposki and D. E. Potter, *J. Org. Chem.* 1972, **37**, 560.
14. N. Wiberg, G. Wagner, G. Muller and J. Riede, *J. Organomet. Chem.* 1984, **271**, 381; N. Wiberg, G. Wagner and G. Muller, *Angew Chem. Int. Edn. Engl.* 1985, **24**, 229.
15. N. Wiberg, K. Schurz and G. Fisher, *Angew. Chem. Int. Edn Engl.* 1985, **24**, 1053; N. Wiberg, K. Schurz, G. Reber and G. Muller, *J. Chem. Soc., Chem. Commun.* 1986, 591; N. Wiberg, G. Preiner, P. Karampatses, Ch. K. Kim and K. Schurz, *Chem. Ber.* 1987, **120**, 1357.
16. R. West, *Angew. Chem. Int. Edn. Engl.* 1987, **26**, 1201.
17. S. Masamune and L. R. Sita, *J. Am. Chem. Soc.* 1985, **107**, 639.
18. S. Lochschmidt and A. Schmidpeter, *Phosphorus and Sulfur* 1986, **29**, 73.
19. C. N. Smit, F. M. Lock and F. Bickelhaupt, *Tetrahedron Lett.* 1984, **25**, 3011; C. N. Smit and F. Bickelhaupt, *Organometallics* 1987, **6**, 1156.
20. J. Escudié, C. Couret, J. Satgé, M. Andrianarison and J. D. Andriamizaka, *J. Am. Chem. Soc.* 1985, **107**, 3378.
21. C. Couret, J. Escudié, A. Raharinirina and J. Satgé, *J. Am. Chem. Soc.* 1985, **107**, 8280.
22. N. Wiberg and G. Wagner, *Chem. Ber.* 1986, **119**, 1455.
23. M. Neuenschwander, R. Vogeli, H. P. Fahrni, H. Lehman and J. P. Ruder, *Helv. Chim. Acta* 1977, **60**, 1073.

Polyhedron Vol. 10, No. 11, pp. 1163–1171, 1991
Printed in Great Britain

0277–5387/91 $3.00+.00
© 1991 Pergamon Press plc

SILYLENE COMPLEXES STABILIZED BY SULPHUR SUBSTITUENTS; A STRUCTURE AND REACTIVITY STUDY

CHRISTIAN LEIS and CHRISTIAN ZYBILL*

Anorganisch-chemisches Institut, Technische Universität München, Lichtenbergstrasse 4, 8046 Garching, F.R.G.

and

JOACHIM LACHMANN and GERHARD MÜLLER

Fakultät für Chemie, Universität Konstanz, 7750 Konstanz, F.R.G.

Abstract—A new base-stabilized silylene (silanediyl) complex (t-BuS)$_2$(HMPA)Si=Fe(CO)$_4$ (**9b**) has been prepared from $Na_2Fe(CO)_4$ and (t-BuS)$_2SiCl_2$ (**2b**) in the presence of HMPA (hexamethylphosphoric triamide). An X-ray structure analysis of **9b** shows the silylene coordinated to the iron atom [Fe—Si = 2.278(1) Å]. The HMPA is bound via its oxygen atom to the unsaturated silicon [O—Si 1.734(2) Å], which adopts a distorted tetrahedral coordination geometry. A comparison of **9b** with the analogous oxo compound (t-BuO)$_2$(HMPA)Si=Fe(CO)$_4$ (**9a**) indicates an almost identical stabilizing effect of the electron-deficient silicon atom in **9b** by π-mesomeric and polarization effects of the t-BuS substituents. The conformation of the substituents found at the silicon atom is reproduced by a force field calculation. A base-free silylene complex (t-BuS)$_2$Si=Fe(CO)$_4$ (**10**) has been observed directly by NMR spectroscopy (^{1}H NMR: δ 1.70, s; ^{29}Si NMR: δ 83.2, s) and was further characterized by a derivatization reaction with HMPA to form **9b**. The HMPA adduct **9b** is a valuable model compound for mechanistic investigations: photolysis of **9b** in the presence of 2,3-dimethylbutadiene as trapping reagent yields 1,4-addition of the silylene to the butadiene. In the absence of any trapping reagents, polysilanes are formed. The experiments provide evidence for a silylene cleavage mechanism.

Interest in organometallic silicon chemistry has considerably increased,[1,2] since the recent discovery of stable coordination compounds with low-valent silicon ligands.[3,4] This refers, in particular, to silylene (silanediyl) complexes (**A**) and their donor adducts (**B**), which are known for the metals iron, ruthenium, chromium and tungsten.[5] Furthermore, cationic silylene complexes (**C**)[4] and cyclic bis-silylene complexes (**D**) have been realized with the compounds Cp*FeSiMe$_2$OMeSi(OMe)Me[6] and CpFeCOSiMe$_2$NH$_2$SiMe$_2$,[7] as well as base adducts of metallasilaallenes (**E**).[8] In a wider sense, the recently isolated complexes of disilaethenes (**F**)[9] and silaethenes (**G**)[10] have also to be considered (Scheme 1).

Base-stabilized silylene complexes are model compounds for extremely reactive, base-free complexes which are proposed as key intermediates in a variety of catalytic reactions. These are, for example, the dehydrogenative coupling of primary silanes to disilanes[11] or the polymerization of silanes by early transition metal catalysts.[12]

A great many research activities have been invested into stable base adducts of silylene (silanediyl) complexes by X-ray structure analysis, NMR and Mössbauer spectroscopy.[1] An X-ray structure study shows important interdependencies between bond lengths, coordination geometry and substituent effects at the silicon atom.[3,5] The bond lengths, as well as the coordination geometry at silicon, are a function of the electronic saturation of silicon, which is given by the respective substituents. Stabilizing substituents induce an elongation of both the metal–silicon and donor–silicon bonds and lead to a stronger distortion of the tetrahedral coor-

* Author to whom correspondence should be addressed.

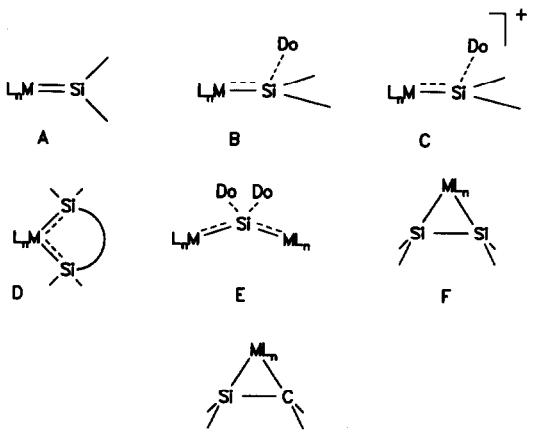

Scheme 1.

dination sphere. Thus, data from X-ray structures are a valuable indicator of the magnitude of the metal–silicon interaction. On the grounds of the extended set of parameters, a fairly good assignment of the effects of particular substituents is possible.[5]

This work describes the effects involved when sulphur is directly bonded to silicon in the coordination compound $(t\text{-BuS})_2(HMPA)Si{=}Fe(CO)_4$ (**9b**). Sulphur, in particular, has been proposed as a stabilizing substituent for low coordinated and low-valent silicon species. Important for the stabilization are π-mesomeric effects, but a strong polarization interaction between sulphur and silicon is also important.[13] Investigations of the stable system $[(i\text{-Pr})_2S]_3Si^+ClO_4^-$ have been reported and are in support of a significant stabilization effect; however, systematic data on sulphur-containing silicon species are still rare.[14] This refers also to the direct observation of silylenes (silanediyls) in a matrix, where exact measurements of the spectroscopic properties of sulphur-substituted silylenes have not been made so far.[14]

A major reason for this lack of information are the great difficulties involved with the synthesis of silicon compounds due to the inherent kinetic lability of the sulphur–silicon bond, which gives rise to an enhanced nucleophilic displacement of the thio substituents by ligand exchange reactions or hydrolysis.

In this article the synthesis of a new silylene coordination compound $(t\text{-BuS})_2(HMPA)Si{=}Fe(CO)_4$ (**9b**) is introduced, together with a crystallographic investigation and a preliminary reactivity study.[15] The given data allow the accurate measurement of the silicon–sulphur interaction and a qualitative assignment of the stabilizing effects which occur.

RESULTS AND DISCUSSION

Synthesis of silylene complexes

A very efficient route to coordination compounds of silylenes is provided via the salt elimination reaction of carbonylate dianions with halosilanes. This reaction is versatile and allows variation of both the metals and the introduced silanes.[3] The required silanes are conveniently synthesized by treatment of the appropriate lithium organyls with $SiCl_4$ at low temperatures.

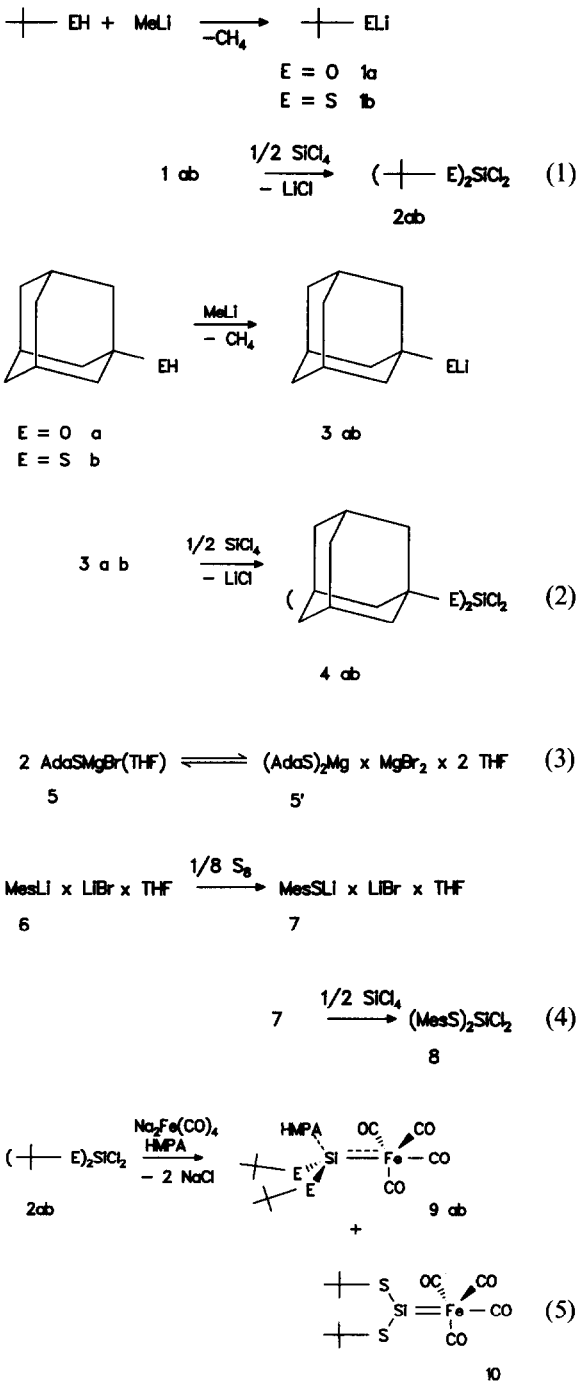

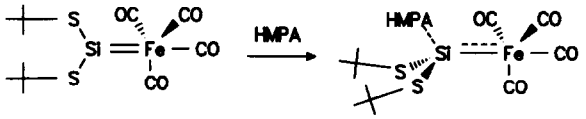

(6)

The observed selectivities for the dichlorosilanes vary and are highest for bis-t-butylthiodichlorosilane (**2b**). $MesS_2SiCl_2$ (**8**) can be obtained in moderate yields from a reaction of lithium mesitylthiolate (**7**) with silicon tetrachloride; the thiolate **7** is prepared from MesLi + LiBr and sulphur. 1-AdaSMgBr (**5**) forms a Schlenk equilibrium, $\mathbf{5} \rightleftharpoons \mathbf{5}'$, according to eq. (3).

The chlorosilanes, R_2SiCl_2, obtained are purified by fractional crystallization. However, for R = MesS, 1-AdaS, a slow exchange reaction, $2R_2SiCl_2 \rightleftharpoons RSiCl_3 + R_3SiCl$, occurs, which renders further reactions of the halosilanes with metalate anions difficult. The t-butylthio compound $(t\text{-BuS})_2SiCl_2$ (**2b**), purified by preparative gas chromatography, is much better suited for further conversion with $Na_2Fe(CO)_4$ in the presence of HMPA to $(t\text{-BuS})_2(HMPA)Si{=}Fe(CO)_4$ (**9b**) in 30% yield. Compound **9b** is a colourless, crystalline compound, sensitive to air and moisture.

The preparation of $(t\text{-BuO})_2SiCl_2$ (**2a**) and its subsequent reaction to $(t\text{-BuO})_2(HMPA)Si{=}Fe(CO)_4$ (**9a**) have already been described,[3b] but **9a** is included for comparison.

Spectroscopic investigations

All compounds have been fully characterized by NMR and IR spectroscopy (see Experimental). In particular, the ^1H NMR spectrum of **9b** shows characteristic shifts [δ 1.63, s, 18H, t-BuS; δ 2.77, d, $^3J(^{31}P^1H) = 29.0$ Hz, 18H, HMPA]. The ^{29}Si NMR spectrum [δ 74.4, $^2J(^{31}P^{29}Si) = 33.1$ Hz] is also of diagnostic value. The observed IR bands for the ν(CO) stretching vibration are typical for an axial coordination of the silylene ligand (C_{3v}). A comparison of the ν(CO)/cm^{-1} A_1 and E vibrational data and the respective force constants $k_0(^{12}CO)$/Nm^{-1} [For **9a**: ν(CO) 2005(w), 1920(s), 1883(s); $k_0(^{12}CO)$ 1623, 1489, 1432. For **9b**: ν(CO) 1995(w), 1910(s), 1870(s); $k_0(^{12}CO)$ 1607, 1473, 1412] indicates a stronger donor capacity of the coordinated silylene in the sulphur compound **9b**.[16]

The spectroscopic analysis of the reaction mixture [eq. (5)] gives, in addition to **9b**, direct evidence for the presence of a donor-free complex **10** [^1H NMR (C_6D_6): δ 1.70, s, 18H, t-BuS; ^{29}Si NMR: δ 83.2, singlet], with no further impurities present. The ^{29}Si resonance clearly excludes a dimeric species.* According to the intensity distribution of both the ^{29}Si and ^1H NMR signals, **10** is formed in a ratio of 1 : 1.6 (**10**/**9b**). Compound **10** decomposes at -30°C into $[(t\text{-BuS})_2Si]_n$ and $Fe_3(CO)_{11}H^-$ with a half-life time of 12 h.† The polysilane has been isolated. By addition of a 10-fold excess of HMPA, **10** is converted to **9b** quantitatively.‡

Molecular structure of **9b**

An X-ray structure analysis of **9b** (Tables 1 and 2) confirms the proposed molecular structure (Fig. 1). The coordination geometry at the iron centre is trigonal bipyramidal with the silicon ligand occupying an apical coordination site. The Fe—Si bond [2.278(1) Å] in **9b** is short compared with the known Fe—Si single bond distances. The Fe—Si bond lengths of donor-stabilized silylene complexes range from 2.289(2) Å in **9a**[3a] to 2.214(1)/2.221(1) Å in $Cl_2(HMPA)Si{=}Fe(CO)_4$[3c] for acyclic complexes, and 2.207(3)/2.222(3) Å in Cp*Fe(CO)SiMe(OMe)-OMe-SiMe$_2$.[6] A rough estimate of the Fe=Si bond lengths of an uncomplexed double bond on the grounds of covalent radii gives 2.18 Å.[3b]

The coordination sphere of the silicon is completed to a distorted tetrahedron by the addition of a HMPA molecule [Si—O 1.734(2) Å]. The HMPA

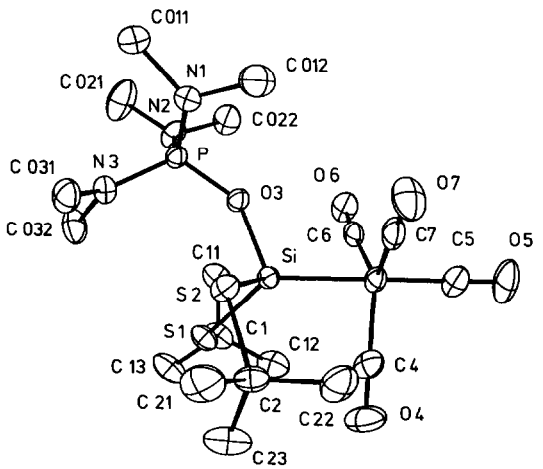

Fig. 1. ORTEP view of **9b**. Displacement ellipsoids at the 50% probability level.

* For $(OC)_4Fe\text{-}SiMe_2\text{-}Fe(CO)_4\text{-}SiMe_2$, ^{29}Si NMR δ 161.0 ppm has been measured, which is typical for metallasilacyclobutanes.

† A dimeric silylene complex would be stable.

‡ This trapping experiment provides further evidence for the presence of a monomeric silylene complex **10**, since the retro-cleavage of a dimeric silylene complex species by a base to a monomeric coordination compound is not known in the literature.

Table 1. Fractional atomic coordinates and equivalent isotropic displacement parameters for **9b** ($U_{eq} = \Sigma_i\Sigma_j U_{ij} a^*_i a^*_j a_i a_j$)

Atom	X/A	Y/B	Z/C	U (eq.)
Fe	0.64056(3)	0.78213(3)	0.70252(2)	0.031
C(4)	0.7209(3)	0.8985(3)	0.6854(2)	0.042
O(4)	0.7713(2)	0.9735(2)	0.6732(1)	0.052
C(5)	0.5776(2)	0.7928(3)	0.6109(2)	0.050
O(5)	0.5363(2)	0.7974(2)	0.5518(1)	0.081
C(6)	0.6773(2)	0.6442(3)	0.6845(1)	0.031
O(6)	0.6966(2)	0.5543(2)	0.6694(1)	0.053
C(7)	0.5261(2)	0.7997(3)	0.7583(2)	0.042
O(7)	0.4515(2)	0.8090(2)	0.7921(1)	0.066
Si	0.72317(5)	0.76789(6)	0.81885(4)	0.025
S(1)	0.88651(5)	0.78771(6)	0.83115(4)	0.036
S(2)	0.67603(5)	0.86429(5)	0.91890(4)	0.031
C(1)	0.9637(2)	0.7083(3)	0.7591(2)	0.045
C(2)	0.6801(2)	1.0159(2)	0.9026(2)	0.037
C(11)	0.9373(2)	0.5860(3)	0.7615(2)	0.054
C(12)	0.9526(3)	0.7548(3)	0.6779(2)	0.053
C(13)	1.0731(2)	0.7253(3)	0.7887(2)	0.064
C(21)	0.6505(3)	1.0632(3)	0.9818(2)	0.053
C(22)	0.6021(3)	1.0519(3)	0.8426(2)	0.061
C(23)	0.7872(2)	1.0525(3)	0.8804(2)	0.058
P	0.70945(5)	0.57608(6)	0.93787(4)	0.027
O(3)	0.6968(1)	0.6419(1)	0.86173(9)	0.029
N(1)	0.5961(2)	0.5751(2)	0.9771(1)	0.035
N(2)	0.7550(2)	0.4576(2)	0.9099(1)	0.043
N(3)	0.7874(2)	0.6200(2)	1.0038(1)	0.034
C(011)	0.5797(2)	0.5112(3)	1.0492(2)	0.040
C(012)	0.5027(2)	0.6008(3)	0.9355(2)	0.064
C(021)	0.7873(4)	0.3747(3)	0.9672(2)	0.087
C(022)	0.7177(3)	0.4072(3)	0.8383(2)	0.053
C(031)	0.7571(2)	0.6942(2)	1.0669(2)	0.042
C(032)	0.8994(2)	0.6058(3)	0.9983(2)	0.055

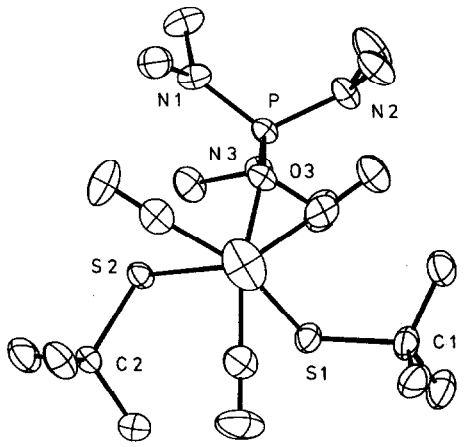

Fig. 2. ORTEP view of **9b** down the Fe—Si axis.

O—Si bond lengths of **9b** and **9a** [Si—O 1.730(3) Å] are identical within the usual three-fold standard deviations. The Si—S distances are relatively short, 2.158(1) and 2.170(1) Å, and indicate a substantial mesomeric π-interaction between the silicon and the sulphur atom, while metal–silicon bond lengths are even shorter due to the more electrophilic silicon atom (π-backbonding).[3c] Thus, a comparison of the Fe—Si bond lengths in **9a** and **9b** allows the conclusion that stabilizing O → Si π-effects are slightly more important in **9a** than S → Si effects are in **9b**. The coordination geometry at the silicon centre shows typical distributions from an ideal tetrahedron, with relatively large bond angles, t-BuS—Si—Fe 123.1(1)/121.3(1)°, and a small angle, t-BuS—Si—S(t-Bu) 98.2(1)°. The sum of the angles between the substituents at silicon, R—Si—R, Fe—Si—R and R—Si—Fe, is virtually the same in **9a** (342.1°) and **9b** (342.6°).

It has been shown that the donor–silicon interaction occurs through the LUMO of the Si=Fe double bond and is strongly influenced by substituent effects.[3c,d] The discussed structural features may be used as a probe for the degree of electronic saturation at silicon and allow a qualitative assignment of the stabilizing effect of sulphur, which is only slightly smaller in **9b** than in the oxo compound **9a**, and substantially greater than in alkyl-substituted silylene complexes.[1]

Table 2. Selected bond distances (Å) and angles (°) in the structure of **9b** (ESDs in units of the last significant digit in parentheses)

Bond distances (Å)			
Fe—Si	2.278(1)	P—O(3)	1.542(2)
Si—S(1)	2.158(1)	S(1)—C(1)	1.866(3)
Si—S(2)	2.170(1)	S(2)—C(2)	1.865(3)
Si—O(3)	1.734(2)		
Bond angles (°)			
Fe—Si—S(1)	123.1(1)	Fe—Si—O(3)	110.2(1)
Fe—Si—S(2)	121.3(1)	S(1)—Si—O(3)	104.7(1)
S(1)—Si—S(2)	98.2(1)	S(2)—Si—O(3)	94.8(1)

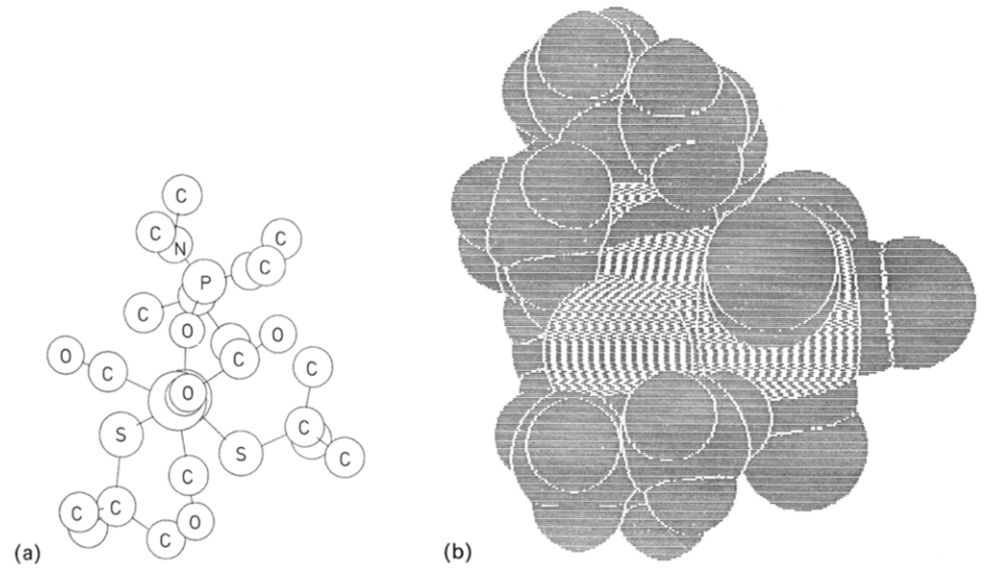

Fig. 3. (a) Projection down the Fe—Si axis of the structure of **9b** obtained by a force field calculation (hydrogen atoms omitted for clarity). (b) View of the van der Waals' surface of **9b** obtained by the force field calculation.

The bond lengths and the coordination geometry at silicon are primarily a result of electronic effects. However, the relative conformation of the organic substituents at the silicon atom represents a minimum of steric interactions. An ORTEP view of the molecule down the Fe—Si bond (Fig. 2) shows that **9b** contains no mirror plane, but the two t-BuS substituents together with HMPA form an asymmetric conformation, which is apparently a minimum of energy. This rotamer is reproduced by a force field calculation.[17] The obtained conformation and van der Waals' surface are depicted in Fig. 3.

Reactions

Previous experiments have shown that coordinated silylenes (with an additional base at silicon) can be activated photochemically or thermally in silylene transfer reactions.[3c]

A reactivity study of **9a,b** provides similar results: photolysis of the complexes $R_2(HMPA)Si{=}Fe(CO)_4$ (R = t-BuO, t-BuS) in the presence of triphenylphosphine leads, after photolytic activation of CO, to the *trans*-phosphine complexes **11a,b**, and subsequently to the displacement of the silylene ligand by a further phosphine to produce the bis-phosphine complex **13**. The liberated silylenes polymerize instantaneously; for **12a**, R = t-BuO, the molecular weight has been determined as 550. $[(t\text{-BuS})_2Si]_n$ (**12b**) is a white, air-sensitive material, soluble in toluene and insoluble in THF. The coordinated HMPA is split off from the silicon during the second step of the photolysis reaction and can be recovered quantitatively.

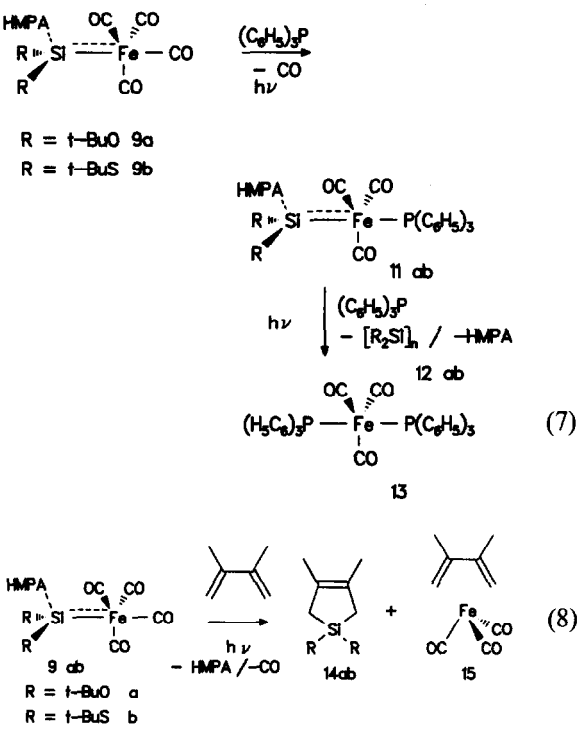

Trapping experiments of the silylenes with 2,3-dimethylbutadiene have been successful for R = t-BuO and R = t-BuS and yield the products **14a,b** and **15**. The photolysis reaction can be monitored by IR spectroscopy [ν(CO) **9a**: 2005, 1920, 1883 cm^{-1}, ν(CO) **15**: 2045, 1971 cm^{-1}], which shows the disappearance of the ν(CO) bands of **9a** or **9b**

together with a simultaneous increase of the bands of **15**. The reaction follows a (pseudo) first-order rate law. The observed reactivity pattern documents the potential of complexes **9a,b** to react as a silylene source and also provides evidence for a silylene polymerization mechanism. Further experiments concerning the reactivity and spectroscopic properties of [(t-BuS)$_2$Si] are underway.

Summary

The obtained results provide a set of data for both a "donor-free" silylene complex, (t-BuS)$_2$Si=Fe(CO)$_4$ (**10**), and its HMPA adduct, (t-BuS)$_2$(HMPA)Si=Fe(CO)$_4$ (**9b**). An X-ray structure analysis of **9b** allows the estimation of the stabilizing effect of the sulphur substituents at silicon. The bond distances Si—S, Si—Fe, Si—O and the overall coordination geometry at silicon show a substantial stabilization of the electron-deficient silicon by sulphur due to mesomeric π-interaction and polarization effects. The observed effects are slightly smaller than in the oxo compound **9a** and allow the assignment of the following gradation of ligand stabilization capacity: O > S ≫ C. This gradation is consistent with results from ^{29}Si NMR and IR spectroscopy.

^{1}H NMR and ^{29}Si NMR data, as well as trapping experiments with HMPA, give evidence for a labile, "base-free" complex (t-BuS)$_2$Si=Fe(CO)$_4$ (**10**). Both **10** and the HMPA adducts **9a,b** undergo silylene cleavage reactions with subsequent polymerization of the silylenes in solution. This mechanism is supported by trapping experiments of the silylenes with 2,3-dimethylbutadiene.

EXPERIMENTAL

All experiments have been performed in an atmosphere of dry nitrogen or argon, respectively. The solvents were dried by conventional techniques (NaK alloy, P_4O_{10}), and residual water contents were in all cases below 3.5 ppm (detected by Karl Fischer titration). Elemental analyses were carried out at Mikroanalytisches Laboratorium der Technischen Universität München. NMR spectra were obtained on Jeol GX 400 and Jeol FX 270 spectrometers, IR spectra on a Nicolet FT-IR-5DX spectrometer and GC–MS analysis was performed on Hewlett–Packard 5890 A and 5970 B instruments with a column CP SIL 5CB (50 m; 0.32 mm).

Bis(t-butylthio)dichlorosilane, (t-BuS)$_2$SiCl$_2$ (**2b**)

To a solution of t-butylthiol (33.8 cm^3, 0.3 mol) in 100 cm^3 of pentane, n-BuLi (190 cm^3, 0.3 mol) (1.71 M solution in hexane) was added at −40°C. The reaction mixture was stirred for a further 2 h at room temperature. After removal of the solvent *in vacuo*, lithium-t-butylthiolate (27.6 g, 0.287 mol) was isolated as a white solid (96%). Further reaction to the chlorosilane was accomplished by the addition of a solution of the thiolate (27.6 g, 0.287 mol) in 100 cm^3 of THF at −60°C to $SiCl_4$ (16.6 cm^3, 0.144 mol) dissolved in 100 cm^3 of THF. After completion of the addition, the reaction mixture was stirred at room temperature for a further 2 h. The LiCl was removed by filtration and the THF stripped off *in vacuo*. The residual colourless oil was contaminated with LiCl and was therefore purified by vacuum distillation or by prep. GC (retention time: 9.7 min; MS analysis: M^+ = 276.3%). Compound **2b** is a colourless liquid. Yield: 10.6 g (27%); b.p. 90°C/1 mbar. ^{1}H NMR ($CDCl_3$): δ 1.2 (s). ^{29}Si NMR (C_6D_6): δ 4.4.

Bis(1-adamantyloxo)dichlorosilane, (AdaO)$_2$SiCl$_2$ (**4a**) *and bis-(1-adamantylthio)dichlorosilane*, (AdaS)$_2$SiCl$_2$ (**4b**)

To magnesium chips (1.69 g, 69.7 mmol) in 50 cm^3 of ether, 1-AdaBr (15.0 g, 69.7 mmol) dissolved in 100 cm^3 of ether was added dropwise. The Grignard reaction was initiated by external local heating of the mixture. After 30 min, the heat formed is self-sufficient for further reaction. After completion of the halide addition, the mixture was refluxed for 3 h and kept at room temperature for 10 h. Then, sulphur (2.23 g, 69.7 mmol) was added portionwise through a special device and the obtained mixture refluxed for a further 5 h. The slightly cloudy, yellow solution was filtrated and the THF removed *in vacuo*. The brown residue obtained was purified by dissolving it repeatedly in 40 cm^3 of THF and precipitating the product by addition of 40 cm^3 of pentane. Compound **4b** formed as a yellow powder (8.96 g; yield: 48%). ^{1}H NMR (C_6D_6): **4b**, δ 1.5 (m, α-methylene-H): 2.3 (m, β-CH); 3.9 (m, γ-methylene-H).

Compound **4a** was prepared by deprotonation of 1-adamantol with methyllithium and subsequent conversion to the chlorosilane by $SiCl_4$ (Yield: 62%).

Synthesis of bis(2,4,6-trimethylphenylthio)dichlorosilane [bis(mesitylthio)dichlorosilane], (MesS)$_2$SiCl$_2$ (**8**)

Mesityllithium·LiBr. The synthetic procedure given in ref. 18 was slightly modified. Mesitylbromide (30.1 cm^3, 0.2 mol) was dissolved in 250

cm^3 of diethyl ether. Then, n-BuLi (250 cm^3, 0.4 mol) (1.71 M solution in hexane) was added under vigorous stirring over a period of 1 h. If necessary, the reaction flask was cooled externally by an ice bath. A white precipitate of **6** formed, which increased during a further hour of refluxing of the reaction mixture. The product was isolated by filtration and dried in high vacuum (10^{-3} torr). Yield: 31.8 g (75%).

Lithium mesitylthiolate, LiSMes·THF (**7**). To a solution of MesLi·LiBr (**6**) (31.8 g, 0.2 mol) in 250 cm^3 of THF, S_8 (4.8 g, 150 mmol) was added portionwise over a period of 30 min at −20°C. The sulphur dissolved completely, and the yellow solution which formed was kept at room temperature for a further 3 h. The obtained crude lithium mesitylthiophenolate was purified by derivatization to the thiophenol. Therefore, the THF was first replaced by ether, and subsequently the thiophenolate was converted to the thiol by addition of 0.1 M sulphuric acid at 0°C. The thiophenol was extracted from the water phase with ether. After removal of ether, the thiol was isolated as a yellow oil with a characteristic odour. Yield: 20.4 g (90%); b.p. 106°C. ^{1}H NMR ($CDCl_3$): δ 2.2 (Br, 6H, 3H; *o*-CH_3, *p*-CH_3); 2.8 (s, 1H, SH); 6.7 (s, 2H, aryl-H).

To a solution of mesitylthiophenol (20.4 g, 134 mmol) dissolved in 200 cm^3 of THF, n-BuLi (74 cm^3, 134 mmol) (1.71 M solution in n-hexane) was added. The colour of the solution changed from yellow to orange during the addition. The mixture obtained was then stirred for a further 3 h at room temperature. After removal of the THF *in vacuo*, **7** was isolated in 70% yield (22.7 g).

Bis(2,4,6-*trimethylphenylthio*)*dichlorosilane*, $(MesS)_2SiCl_2$ (**8**)

To a stirred solution of silicon tetrachloride (5.1 cm^3, 45 mmol) in 100 cm^3 of THF, **7** (22.7 g, 93 mmol) dissolved in 100 cm^3 of THF was added at −25°C (3% access of $SiCl_4$), and the reaction mixture turned slightly yellow. After refluxing for a further 6 h, the lithium halides were removed and the solvent stripped off *in vacuo*. The resulting paste was again dissolved in 100 cm^3 of a 3:1 mixture of pentane–ether. After filtration from the residual lithium halides and removal of the solvent, a yellow oil was obtained, which is sensitive to hydrolysis and oxidation. Yield: 12.2 g (70%). ^{29}Si NMR data show the presence of two reaction products in the ratio 4:1 $(MesS)_2SiCl_2/(MesS)_3SiCl$. Compound **8** could not be further enriched by either fractional crystallization or Kugelrohr distillation due to ligand exchange reactions. ^{1}H NMR ($CDCl_3$): **8** δ 2.3 (m, 9H, *o*-CH_3, *p*-CH_3); 6.9 (s, broad, 2H, aryl H). ^{29}Si NMR (C_6D_6): δ 26.7. MS: *m/z* 400 (M^+; 1.7%)

Reaction of **2b** *with* $Na_2[Fe(CO)_4]$ *to form* (t-BuS)$_2$Si=Fe(CO)$_4$ (**9b**) *and* (t-BuS)$_2$(HMPA)Si=Fe(CO)$_4$ (**10**)

To a solution of $Na_2[Fe(CO)_4]$ (3.3 g, 9.6 mmol) in a mixture of 100 cm^3 of THF and 15 cm^3 of HMPA, **2b** (2.7 g, 9.6 mmol) was added at −50°C. The reaction mixture was stirred for 12 h, filtered, and THF and HMPA were subsequently removed at high vacuum (10^{-4} torr). The crude product contained **9b** and **10** in a 1:1.6 ratio. Compound **10** can be converted to **9b** by addition of 2 cm^3 of HMPA. Alternatively, the mixture could be purified by column chromatography on silica gel (2.5 cm diameter, 40 cm height) with a cooled (−15°C) chromatography column. However, **10** decomposed during chromatography into $HFe_3(CO)_{11}^-$ and polysilane **12b**. Analytical data for **9b**: Found (Calc.): C, 38.98 (39.04); H, 6.59 (6.51); N, 7.62 (7.59). IR for **9b** (KBr): 1995 (w), 1910 (s), 1870 (s) [ν(CO) in cm^{-1}]. MS: *m/z* = 553 (M^+; 1.5%). ^{1}H NMR (C_6D_6): δ 1.63 (s, br, 18H), δ 2.77 [d, $^2J(^{31}P^{29}Si)$ = 29.0, 18H]. ^{29}Si NMR (C_6D_6): δ 74.0, **9b**.

^{1}H NMR (C_6D_6): 1.70; ^{29}Si NMR (C_6D_6): δ 83.2, **10**.

Crystal structure analysis of **9b***

Crystal data and a summary of data pertinent to data collection and refinement are colleced in Table 3. Exact cell dimensions were obtained by least-squares refinement of the Bragg angles of 15 selected reflections centred on the diffractometer. Reduced cell calculations did not reveal symmetry higher than orthorhombic. Three standard reflections, measured after every 50 reflections, showed only random intensity fluctuations. Therefore, a correction for crystal decay was not considered necessary, neither was one for absorption. Refinement was carried out with anisotropic displacement parameters. The methyl groups were treated as rigid groups (H atoms with U_{iso} fixed at 0.05 Å^2). To ensure that the chirality of the single crystal under investigation and that of the coordinate set were identical, the inverse coordinate set was also refined.

*A complete list of fractional atomic coordinates including hydrogen atoms and a list of observed and calculated structure factors ($F_o - F_c$) have been deposited together with the manuscript.

Table 3. Crystal structure data for **9b**

Crystal dimensions (mm^3)	$0.40 \times 0.45 \times 0.50$
Formula	$C_{18}H_{36}FeN_3O_5PS_2Si$
M_r	553.540
Crystal system	Orthorhombic
Space group	$P2_12_12_1$ (No. 19)
a (Å)	13.066(2)
b (Å)	12.155(1)
c (Å)	17.181(3)
V (Å^3)	2728.6
Z	4
d_{calc} (g cm^{-3})	1.347(7)
μ(Mo-K_α) (cm^{-1})	8.3
F(000) (e)	1168
T (°C)	−50
Diffractometer	Syntex-P2$_1$
Radiation	Mo-K_α, $\lambda = 0.71069$ Å
Monochromator	Graphite
Scan	ω
Scan width (in ω)	0.6
Scan speed (° min^{-1})	0.7–29.3
$(\sin/\lambda)_{max}$ (Å^{-1})	0.572
hkl range	+14, +13, ±19
Standard reflections	020, 006, 200
Reflections (measured/unique)	4721/4238
R_{int}	0.021
Reflections observed [$F_o \geqslant 4.0\sigma(F_o)$]	4022
Structure solution	Direct methods (SHELXS-86)
Hydrogen atoms (found/calc)	33/3
Parameters refined	316
r^a	0.026
Rw^b	0.028
$(\text{Shift/error})_{max}$	0.016
$\Delta\rho_{fin}$(max/min) (e/Å^3)	0.57/−0.28

[a] $R = \Sigma(||F_o|-|F_c||)/\Sigma|F_o|$.
[b] $Rw = [\Sigma w(|F_o|-|F_c|)^2/\Sigma w F_o^2]^{1/2}$; $w = 1/\sigma^2(F_o)$. Function minimized: $\Sigma w(|F_o|-|F_c|)^2$.

It yielded substantially higher R values, however ($R/R_w = 0.039/0.044$).

Atomic form factors for neutral, isolated atoms were taken from Cromer and Waber,[19] and those for hydrogen were based on the bonded spherical atom model of Stewart *et al.*[20] Corrections for anomalous scattering were applied for all atoms except hydrogen.[21] The programs used included SHELXS-86[22] (structure solution), SHELXS-76[23] (refinement), ORTEP[24] (molecular drawings), as well as locally written routines. All calculations were performed on a VAX 8200.

Molecular modelling of the structure of **9b**

The molecule was optimized by the ALCHEMY minimizer program with $E_{tot} = E_{str} + E_{ang} + E_{tor} + E_{vdw}$. E_{tot} = total energy, $E_{str} = \Sigma_i^N k^d_i/2(d_i - d^0_i)^2$, $d^0_{FeSi} = 2.300$ Å, $k_{FeSi} = 1500$ kcal mol^{-1} Å^2; $E_{ang} = \Sigma_i^N k^\theta_i/2(\theta_i - \theta^0_i)^2$, $\theta_{0FeSiO} = 115°$, $k^\theta_{FeSiO} = 0.03$ kcal mol^{-1} deg^2; $E_{tor} = \Sigma_i^N k_i/2[1 + \sin(\text{per}_i) \times \cos(|\text{per}_i|\omega_i)]$, $\omega_{SiFe^{**}} = 0.1$ kcal mol^{-1} deg^2; $E_{vdw} = \Sigma_i^n[\Sigma_{j>i} E_{ij}(1.0/a^{12}_{ij} - 2.0/a^6_{ij})]$, $E_{FeSi} = 0.200$ kcal mol^{-1}, $a_{Fe} = 3.000$ Å, $a_{Si} = 2.000$ Å. All other parameters were used from the program without modification. A detailed description is given in ref. 5.

Photolysis of complexes **9a** *and* **9b**

The photolysis reaction of **9b** was carried out as described for **9a**.[3d] A solution of **9b** (1.66 g, 3 mmol) and $(C_6H_5)_3P$ (787 mg, 3 mmol) in 100 cm^3 of THF was photolysed at −40°C for 2 h (Hg high pressure lamp). Complex **11a** was isolated quantitatively.

Further irradiation of **11a** at −40°C in the presence

of $(C_6H_5)_3P$ in a 2 : 1 ratio yielded the bisphosphine complex **13** and polysilane, which were separated as described in ref. 3d. ^1H NMR (C_6D_6): **11b** δ 1.7 (s, 18H, t-BuO), 2.5 [d, $^3J(^{31}P^1H)$ = 10.5 Hz, 18H, HMPA], 7.0–7.3 (m, 15H, C_6H_5); **13** δ 7.1 (m, 18H), 7.5–8.0 (m, 12H). ^{31}P NMR (C_6D_6): **11b** δ 87.8; **13** δ 95.2.

Photolysis of **9a,b** *in the presence of* 2,3-*dimethylbutadiene*

Complex **9a** (1.54 g, 3 mmol) together with 2,3-dimethylbutadiene (5.0 g) in 100 cm^3 of THF were photolysed at −40°C. Every 30 min, an aliquot of the reaction mixture (2 cm^3) was taken and concentrated by a factor of 10 in the vacuum (10^{-2} torr). The GC–MS analysis gave two major peaks at retention time 6.2 min, 70% intensity, M = 256 M^+ **14a**: retention time 5.2 min, 20% intensity, M = 222, M^+ **15**. Furthermore, traces of HMPA, M^+ = 179, were present.

No further by-products were observed. Complexes **14a,b** and **15** can be separated by prep. GC. ^1H NMR (C_6D_6): **14a**, δ 1.74, br, 10H, CH_3, CH_2; 1.70, s, 18H, t-BuO; **14b**, δ 1.75, br, 10H, CH_3, CH_2; 1.70, s, 18H, t-BuS.[25] IR (THF): **15**, 2045 (s), 1971 (s) CO.[26]

Acknowledgements—We wish to acknowledge U. Graf and B. Barth (Mikroanalytisches Laboratorium der Technischen Universität München) for carrying out the elemental analysis.

REFERENCES

1. C. Zybill, *Top. Curr. Chem.* 1991, in press.
2. T. D. Tilley, in *The Chemistry of Organosilicon Compounds* (Edited by S. Patai and Z. Rappoport). John Wiley, New York (1989).
3. (a) C. Zybill and G. Müller, *Angew. Chem.* 1987, **99**, 683; *Angew. Chem. Int. Edn Engl.* 1987, **26**, 669; (b) C. Zybill and G. Müller, *Organometallics* 1988, **7**, 1368; (c) C. Zybill, *Nachr. Chem. Tech. Lab.* 1989, **37**, 248; (d) C. Zybill, D. L. Wilkinson, C. Leis and G. Müller, *Angew. Chem.* 1989, **101**, 206; *Angew. Chem. Int. Edn Engl.* 1989, **28**, 203.
4. (a) D. A. Straus, T. D. Tilley, A. L. Rheingold and S. Geib, *J. Am. Chem. Soc.* 1987, **109**, 5872.
5. C. Leis, D. L. Wilkinson, G. Müller and C. Zybill, *Organometallics* 1991, in press.
6. (a) K. Ueno, H. Tobita, M. Shimoi and H. Ogino, *J. Am. Chem. Soc.* 1988, **110**, 4092; (b) H. Tobita, K. Ueno, M. Shimoi and H. Ogino, *J. Am. Chem. Soc.* 1990, **112**, 3415.
7. W. Malisch, P. Lorz and G. Thum, *Chemiedozententagung Mainz* 1988, 13–16.3, Abs. B36.
8. C. Zybill, D. L. Wilkinson and G. Müller, *Angew. Chem.* 1988, **100**, 574; *Angew. Chem. Int. Edn Engl.* 1988, **27**, 583.
9. (a) E. K. Pham and R. West, *J. Am. Chem. Soc.* 1989, **111**, 7667; (b) D. H. Berry, J. Chey, H. S. Zipin and P. J. Carroll, *J. Am. Chem. Soc.* 1990, **112**, 452; (c) E. K. Pham and R. West, *Organometallics* 1990, **9**, 1517.
10. (a) C. L. Randolph and M. S. Wrighton, *Organometallics* 1987, **6**, 365; (b) B. K. Campion, R. H. Heyn and T. D. Tilley, *J. Am. Chem. Soc.* 1988, **110**, 7558.
11. (a) K. A. Brown-Wensley, *Organometallics* 1987, **6**, 1590; (b) M. Kumada, *J. Organomet. Chem.* 1975, **100**, 127.
12. (a) C. T. Aitken, J. F. Harrod and E. Samuel, *J. Am. Chem. Soc.* 1986, **108**, 4059; (b) L. S. Chang and J. Y. Corey, *Organometallics* 1989, **8**, 1885; (c) H. G. Woo and T. D. Tilley, *J. Am. Chem. Soc.* 1989, **111**, 8043.
13. (a) J. B. Lambert and W. J. Schulz Jr, *J. Am. Chem. Soc.* 1983, **105**, 1671; (b) J. B. Lambert, J. A. McConnell and W. J. Schulz Jr, *J. Am. Chem. Soc.* 1986, **108**, 2482; (c) J. B. Lambert, W. J. Schulz Jr, J. A. McConnell and W. Schilf, in *Silicon Chemistry* (Edited by J. Y. Corey, E. R. Corey and P. P. Gaspar). Ellis Horwood, Chichester (1988).
14. G. Raabe and J. Michl, *Chem. Rev.* 1985, **85**, 419.
15. C. Leis, *Diplomarbeit*, Technische Universität München (1988).
16. P. Bratermann, *Metal Carbonyl Spectra*. Academic Press, New York (1975).
17. N. L. Allinger, *Adv. Phys. Org. Chem.* 1976, **13**, 1.
18. M. J. Fink, M. J. Michalczyk, K. J. Haller, R. West and J. Michl, *Organometallics* 1984, **3**, 793.
19. D. T. Cromer and J. T. Waber, *Acta Cryst.* 1965, **18**, 104.
20. R. F. Stewart, E. R. Davidson and W. T. Simpson, *J. Chem. Phys.* 1965, **42**, 3175.
21. *International Tables for X-ray Crystallography*, Vol. IV. Kynoch Press, Birmingham, U.K. (1974) (Present distributor: Kluwer Academic Publishers, Dordrecht).
22. G. M. Sheldrick, in *Crystallographic Computing 3* (Edited by G. M. Sheldrick, C. Krüger and R. Goddard), p. 175. Oxford University Press, Oxford (1985).
23. G. M. Sheldrick, SHELX-76, Program for Crystal Structure Determination. University of Cambridge, U.K. (1976).
24. C. K. Johnson, ORTEP-II, Report ORNL-5138. Oak Ridge National Laboratory, Oak Ridge, Tennessee (1976).
25. The ^1H NMR data are comparable to literature data of $Me_2Si\text{-}CH_2\text{-}C(CH_3)=C(CH_3)\text{-}CH_2$ and clearly exclude any isomeric structure: M. Ishikawa, F. Ohi and M. Kumada, *J. Organomet. Chem.* 1975, **86**, C23.
26. For comparison see: E. O. Fischer and H. Werner, *Metal π-Complexes 1*. Elsevier, Amsterdam (1966).

Polyhedron Vol. 10, No. 11, pp. 1173–1176, 1991
Printed in Great Britain

0277–5387/91 $3.00+.00
© 1991 Pergamon Press plc

REACTIONS OF THE RUTHENIUM SILYLENE DERIVATIVE $[(\eta^5\text{-}C_5Me_5)(PMe_3)_2RuSiPh_2(NCMe)]BPh_4$ WITH ALCOHOLS, KETONES AND ACETIC ACID

CHENG ZHANG, STEVEN D. GRUMBINE and T. DON TILLEY†

Department of Chemistry, D-006, University of California at San Diego, La Jolla, CA 92093-0506, U.S.A.

Abstract—The cationic ruthenium silylene complex $[Cp^*(PMe_3)_2RuSiPh_2(NCMe)]^+BPh_4^-$ (**1**, $Cp^* = \eta^5\text{-}C_5Me_5$) reacts with alcohols (MeOH, EtOH and ^{t}BuOH) to produce the ruthenium acetonitrile complex $[Cp^*(PMe_3)_2Ru(NCMe)]^+BPh_4^-$ (**2**) and the corresponding alkoxysilanes $HSiPh_2OR$ (R = Me, Et, ^{t}Bu). At low temperature (−60°C), an intermediate (**3**) was observed in the reaction involving ethanol (by ^{1}H NMR spectroscopy). This intermediate gives rise to a RuH hydride signal (δ 11.08), which appears as a triplet ($^2J_{PRuH}$ = 11 Hz). This species may therefore be *cis*-$[Cp^*(PMe_3)_2Ru(H)SiPh_2OEt]BPh_4$, however, the very low $^2J_{PRuH}$ coupling constant suggests a structure involving an η^2-H-$SiPh_2OEt$ ligand. The mechanism of these reactions is suggested to consist of dissociative loss of acetonitrile to produce the base-free silylene complex $[Cp^*(PMe_3)_2Ru{=}SiPh_2]^+$, which adds alcohol across the double bond to form **3**. The observed silane products are then formed via reductive elimination from ruthenium. The enolizable ketones MeCOMe and MeCOPh react with **1** in a similar fashion to give **2** and the silyl enol ethers $HSiPh_2(OCR{=}CH_2)$ (R = Me, Ph). Acetic acid reacts with **1** to afford **2** and $HSiPh_2(OOCMe)$.

Transition metal silylene complexes ($L_nM = SiR_2$) have been implicated in a number of processes involving metal-mediated transfer of silylene groups.[1] In particular, it appears that such species may be key intermediates in metal-catalysed Si—Si bond-forming reactions.[2–6] For example, $(PEt_3)_2PtCl_2$ acts as a catalyst for redistributing the disilanes $RMe_2SiSiMe_2H$ (R = H or Me) to a mixture of oligomers $R(SiMe_2)_nH$ (n = 1–6).[6a] Addition of diphenylacetylene to this reaction mixture resulted in trapping of $SiMe_2$ groups to form $Me_2Si(CPh{=}CPh)_2SiMe_2$. Based on these observations, Yamamoto *et al.* proposed that an intermediate $Pt{=}SiMe_2$ complex was responsible for transfer of silylene groups.[6b] Recently, Zybill *et al.* have shown that the dimethylsilylene derivative $(CO)_4FeSiMe_2$(HMPA) thermally decomposes to $Fe_3(CO)_{12}$ and polysilane of low molecular weight.[7a]

Direct, conclusive evidence for participation of silylene complexes in reaction schemes awaits reactivity studies based on isolated, well-characterized examples. To date only a few transition metal silylene complexes have been reported, and these all display coordination of a Lewis base to the silylene silicon atom.[7–9] Furthermore, very little has been reported regarding reactivity trends for these species. We have described the synthesis and characterization of a cationic ruthenium silylene complex, $[Cp^*(PMe_3)_2Ru{=}SiPh_2(NCMe)]^+BPh_4^- \cdot CH_2Cl_2$ (**1**, $Cp^* = \eta^5\text{-}C_5Me_5$), which is labile in solution and serves as a source of the base-free silylene species $Cp^*(PMe_3)_2Ru{=}SiPh_2^+$.[8b] Here we describe reactivity studies of this complex, which involve transfer of the silylene group to alcohol, ketone and acetic acid substrates.

RESULTS AND DISCUSSION

Complex **1** exhibits very limited reactivity toward the aryl silanes $PhSiH_3$, Ph_2SiH_2 and Ph_3SiH. Whereas Ph_2SiH_2 and Ph_3SiH do not react with **1** in dichloromethane over a 3-day period, $PhSiH_3$ reacts slowly with **1** over 1 week to produce a number of unidentified products.

Addition of excess methanol, ethanol or tert-butanol to a dichloromethane solution of **1** results in immediate, quantitative (by ^{1}H NMR spectroscopy) conversion to the ruthenium acetonitrile

† Author to whom correspondence should be addressed.

complex **2** and the corresponding alkoxysilanes $HSiPh_2OR$ [eq. (1), R = Me, Et, or ^tBu].

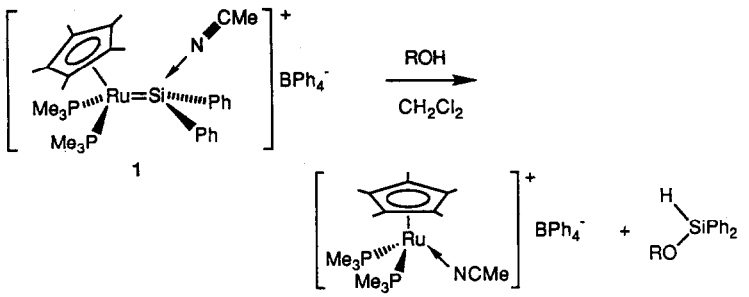

(1)

Ruthenium complex **2** was identified by comparison of ^1H and ^{31}P NMR data with an authentic sample, prepared from $Cp^*(PMe_3)_2RuCl$ and $AgBPh_4$ in acetonitrile.[8b] Spectroscopic characterization of the alkoxysilanes was also facilitated by independent syntheses. These $HSiPh_2OR$ compounds were obtained in high yields by reaction of $HSiPh_2Cl$ with pyridine and the corresponding alcohol in diethyl ether. These reactions are related to the previously reported conversion of **1** and water to **2** and $Ph_2Si(H)OSi(H)Ph_2$.[8b]

Variable temperature ^1H NMR spectroscopy showed that **1** and ethanol react in dichloromethane-d_2 at $-60°C$ to form an intermediate hydride complex **3**. This species exhibits a triplet resonance at δ −11.08 in the ^1H NMR spectrum, characteristic for a ruthenium hydride complex with equivalent coupling to two phosphorous nuclei. However, the $^2J_{PRuH}$ coupling constant appears to be too low (11 Hz) to be due to the silyl-hydrido complex *trans*-$[Cp^*(PMe_3)_2Ru(H)SiPh_2OEt]BPh_4$, since the related alkyl-hydrido complex $[Cp^*(PMe_3)_2Ru(H)Me]BF_4$ has a $^2J_{PRuH}$ coupling constant of 41.8 Hz.[10] The low $^2J_{PRuH}$ coupling constant for **3**, and the equivalence of the phosphine ligands, is consistent with a structure involving an η^2-silane ligand, $[Cp^*(PMe_3)_2Ru(\eta^2\text{-}HSiPh_2OEt)]BPh_4$. Note that the related silyl complexes $Cp^*(PMe_3)Ru(SiR_3)_2H$ [SiR_3 = $Si(OEt)_3$, $SiPh_2Cl$ and $SiMe_2OEt$] also possess low $^2J_{PRuH}$ coupling constants (3 Hz), suggesting the possibility of η^2-$HSiR_3$ ligands.[8b] Other η^2-$HSiR_3$ complexes have been reported,[11] and it has been observed that similar dihydrogen complexes $Cp(L)(L')Ru(\eta^2\text{-}H_2)^+$ are relatively stable species.[12] Unusually small $^2J_{PMH}$ coupling constants for the "hydride" atom(s) of both η^2-H_2 and η^2-$HSiR_3$ complexes have been observed. Note that for $Cp(Me_2PCH_2CH_2PMe_2)RuH_2^+$, $^2J_{PRuH}$ = 31 Hz, whereas for $Cp(Me_2PCH_2CH_2PMe_2)Ru(\eta^2\text{-}H_2)^+$, $^2J_{PRuH}$ = 3.6 Hz.[12c] As the reaction solution is warmed above $-60°C$, intermediate **3** decomposes to **2** and $HSiPh_2OEt$ ($t_{1/2}$ at $-40°C$ = 40 min).

Reactions of **1** with alcohols and ketones (*vide infra*) are severely inhibited by addition of acetonitrile, suggesting that reactions occur via initial loss of acetonitrile from **1**. Indeed we have previously shown that the lability of **1** in solution is due to rapid, dissociative loss of acetonitrile.[8b] The above experimental observations suggest the proposed mechanism shown in Scheme 1. Intermediate **4** was not detected, but it is presumed that coordination of alcohol to the silylene silicon atom precedes Si—H bond formation. Migration of hydrogen may then proceed via transfer to ruthenium, giving the observed $[Cp^*(PMe_3)_2Ru(H)SiPh_2OR]^+$ intermediate complex that decomposes to **2** and $HSiPh_2OR$ by reductive elimination. A kinetic isotope effect, determined by use of a 1 : 1 EtOH/EtOD mixture, was found to be k_H/k_D = 1.0. This negligible isotope effect suggests that a hydrogen migration step is not rate-limiting.

Silylene complex **1** also reacts with enolizable ketones over the course of *ca* 1 h to provide quantitative yields (by ^1H NMR spectroscopy) of **2** and silyl enol ethers [eq. (2), R = Me, Ph].

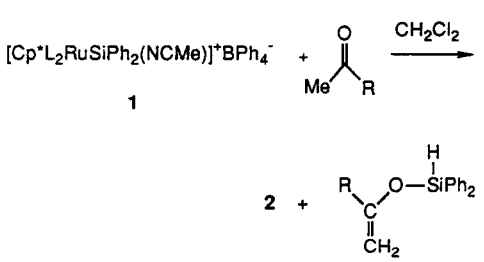

(2)

Under comparable conditions, no reaction of benzophenone occurred over 12 h. The silyl enol ethers were separated from the reaction mixtures by removal of volatiles under vacuum and extraction with pentane. After filtration, removal of the pentane under reduced pressure afforded the pure silyl enol ethers as colourless oils in high yields. For these reactions, no intermediates could be observed

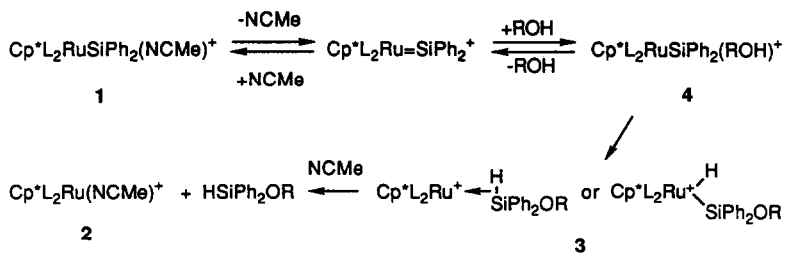

Scheme 1. (L = PMe_3.)

by variable temperature ^{1}H NMR spectroscopy, but we assume that coordination of substrate to the silylene ligand is a crucial step. In a similar process, reaction of **1** with acetic acid gives **2** and $HSiPh_2(OOCMe)$.

The reactions reported here involve transfer of a silylene fragment ($SiPh_2$) from a metal centre to another molecule. In addition, it is interesting to note that the silicon-containing products are those that would be expected from reactions of alcohols, ketones and carboxylic acids with free silylenes.[13] However, reactions involving the ruthenium silylene derivative **1** appear to be mechanistically distinct, in that the metal centre plays an important role. It is clear that there is much to be learned about reactions of transition metal silylene complexes, and future reports will address additional features of this chemistry.

EXPERIMENTAL

Manipulations were carried out under inert atmospheres of nitrogen or argon using standard Schlenk line and glovebox techniques. Dry, oxygen-free solvents were employed throughout. IR spectra were recorded on a Perkin–Elmer 1330 infrared spectrometer. NMR spectra were recorded on a GE QE-300 instrument at 300 MHz (^{1}H) and 121.5 MHz (^{31}P). Mass spectra were obtained with a Hewlett–Packard 5988-A mass spectrophotometer. Complexes **1**,[8b] **2**[8b] and $Cp^*(PMe_3)_2RuCl$[14] were prepared according to literature procedures.

Reactions of **1** *with protic substrates*

A representative procedure is given for the reaction with methanol. Methanol (4.4×10^{-3} cm^3, 0.108 mmol) was added to a dichloromethane solution (2 cm^3) of **1** (0.100 g, 0.108 mmol). After stirring the solution for 0.5 h, the volatiles were removed under vacuum. The sticky solid was extracted with pentane (5 cm^3) and volatiles were removed from this extract to afford an oily liquid. The remaining solid was shown to be **2** by ^{1}H NMR spectroscopy. The oily liquid was identified as $HSiPh_2(OMe)$ (*ca* 96% pure), by comparison of spectroscopic properties with an independently prepared sample.

Independent syntheses of silanes

These syntheses were accomplished using the reaction of $HSiPh_2Cl$ with pyridine and the appropriate protic reagent. A representative procedure is given for $HSiPh_2OMe$. The silane $HSiPh_2Cl$ (2.0 cm^3, 0.010 mol) and methanol (0.44 cm^3, 0.012 mol) were combined with diethyl ether (40 cm^3) in a flask. Pyridine (1.1 cm^3, 0.012 mol) was then added by syringe, and the resulting solution was stirred for 2 h. The reaction mixture was filtered and the volatiles were removed from the solution containing the product. This afforded an oily liquid which was distilled *in vacuo* (98°C, 0.01 torr) to obtain 2.0 cm^3 of product (85% yield).

(i) $HSiPh_2OMe$. ^{1}H NMR (23°C, benzene-d_6): δ 3.37 (s, 3H, OMe), 5.60 (s, 1 H, SiH), 7.15 (m, 6 H, Ph), 7.63 (m, 4 H, Ph). MS (EI): parent ion observed at *m/z* 214. IR (neat, CsI, cm^{-1}): 3065 m, 3046 m, 2995 w, 2932 m, 2830 mn, 2118 s (SiH), 1588 w, 1428 s, 1182 m, 1115 s, 1080 s, 840 s, 815 s, 762 m, 735 s, 698 s, 678 w.

(ii) $HSiPh_2OEt$. ^{1}H NMR (23°C, benzene-d_6): δ 1.09 (t, J = 7 Hz, 3 H, CH_2CH_3), 3.69 (q, J = 7 Hz, 2 H, CH_2CH_3), 5.66 (s, 1 H, SiH), 7.16 (m, 6 H, Ph), 7.66 (m, 4 H, Ph). MS (EI): parent ion observed at *m/z* 228. IR (neat, CsI, cm^{-1}): 3065 w, 3045 w, 2970 m, 2865 w, 2117 s, (SiH), 1587 w, 1427 s, 1388 w, 1160 w, 1112 s, 1024 w, 949 m, 849 s, 815 s, 730 s, 695 s.

(iii) $HSiPh_2O^tBu$. ^{1}H NMR (23°C, benzene-d_6): δ 1.34 (s, 9 H, $OCMe_3$), 5.55 (s, 1 H, SiH), 7.40 (m, 6 H, Ph), 7.61 (m, 4 H, Ph). IR (neat, CsI, cm^{-1}): 2110 s (SiH).

(iv) $HSiPh_2(OCMe{=}CH_2)$. ^{1}H NMR (23°C, benzene-d_6): δ 1.88 (s, 3 H, CH_3), 4.12 (d, J = 1.5 Hz, 1 H, $=CH_2$), 4.18 (d, J = 1.5 Hz, 1 H, $=CH_2$),

5.59 (s, 1 H, SiH), 7.44 (m, 6 H, Ph), 7.67 (m, 4 H, Ph). MS (EI): parent ion observed at *m/z* 240. IR (neat, CsI, cm^{-1}): 2130 s (SiH).

(v) $HSiPh_2(OCPh{=}CH_2)$. ^1H NMR (23°C, benzene-d_6): δ 4.53 (d, $J = 2$ Hz, 1 H, $=CH_2$), 4.96 (d, $J = 2$ Hz, 1 H, $=CH_2$), 5.72 (s, 1 H, SiH), 7.59 (m, 5 H, Ph), 7.70 (m, 6 H, Ph), 7.95 (m, 4 H, Ph). MS (EI): parent ion observed at *m/z* 302. IR (neat, CsI, cm^{-1}): 2131 s (SiH).

(vi) $HSiPh_2OOCMe$. ^1H NMR (23°C, benzene-d_6): δ 2.18 (s, 3 H, CH_3), 5.65 (s, 1 H, SiH), 7.41 (m, 6 H, Ph), 7.63 (m, 4 H, Ph). MS (EI): parent ion observed at *m/z* 242. IR (neat, CsI, cm^{-1}); 2964 w, 2944 w, 2910 w, 2168 m (SiH), 1725 s, 1588 w, 1426 s, 1367 s, 1240 s, 1120 s, 1015 m, 993 m, 820 s, 733 m, 695 m.

NMR data for **3**

^1H NMR (−85°C, dichloromethane-d_2): δ −11.14 (t, $J = 11$ Hz, 1 H, RuH), 1.11 (t, $J = 7$ Hz, 3 H, CH_2CH_3), 1.39 (br, 18 H, PMe_3), 1.51 (s, 15 H, C_5Me_5), 3.56 (q, $J = 7$ Hz, 2 H, CH_2CH_3), 6.86 (t, 8 Hz, 4 H, BPh), 7.02 (t, $J = 8$ Hz, BPh), 7.25 (br, 8 H, BPh), 7.41 (br, 10 H, SiPh). ^{31}P NMR (−85°C, dichloromethane-d_2): δ −0.18.

Acknowledgements—Acknowledgement is made to the National Science Foundation for generous support of this work. T.D.T. thanks the Alfred P. Sloan Foundation for a research fellowship (1988–1990). We also thank Johnson Matthey Inc. for a loan of ruthenium trichloride.

REFERENCES

1. T. D. Tilley, in *The Chemistry of Organic Silicon Compounds* (Edited by S. Patai and Z. Rappoport), Ch. 24, p. 1415. Wiley, New York (1989).
2. T. D. Tilley, *Comm. Inorg. Chem.* 1990, **10**, 37.
3. M. D. Curtis and P. S. Epstein, *Adv. Organomet. Chem.* 1981, **19**, 213.
4. C. Aitken, J. F. Harrod and U. S. Gill, *Can. J. Chem.* 1987, **65**, 1804.
5. I. Ojima, S. I. Inaba, R. Kogure and Y. Nagai, *J. Organomet. Chem.* 1973, **55**, C7.
6. (a) K. Yamamoto, H. Okinoshima and M. Kumada, *J. Organomet. Chem.* 1970, **23**, C7; (b) K. Yamamoto, H. Okinoshima and M. Kumada, *J. Organomet. Chem.* 1971, **27**, C31.
7. (a) C. Zybill, D. L. Wilkinson, C. Leis and G. Müller, *Angew. Chem. Int. Edn Engl.* 1989, **28**, 203; (b) C. Zybill and G. Müller, *Angew. Chem. Int. Edn Engl.* 1987, **26**, 669; (c) C. Zybill, D. L. Wilkinson and G. Müller, *Angew. Chem. Int. Edn Engl.* 1988, **27**, 583; (d) C. Zybill and G. Müller, *Organometallics* 1988, **7**, 1368.
8. (a) D. A. Straus, T. D. Tilley, A. L. Rheingold and S. J. Geib, *J. Am. Chem. Soc.* 1987, **109**, 5872; (b) D. A. Straus, C. Zhang, G. E. Quimbita, S. D. Grumbine, R. H. Heyn, T. D. Tilley, A. L. Rheingold and S. J. Geib, *J. Am. Chem. Soc.* 1990, **112**, 2673.
9. (a) K. Ueno, H. Tobita, M. Shimoi and H. Ogino, *J. Am. Chem. Soc.* 1988, **110**, 4092; (b) H. Tobita, K. Ueno, M. Shimoi and H. Ogino, *J. Am. Chem. Soc.* 1990, **112**, 3415.
10. H. E. Bryndza, L. K. Fong, R. A. Paciello, W. Tam and J. E. Bercaw, *J. Am. Chem. Soc.* 1987, **109**, 1444.
11. (a) A. Colomer, R. J. P. Corriu and A. Vioux, *Inorg. Chem.* 1982, **21**, 368; (b) U. Schubert, J. Müller and H. G. Alt, *Organometallics* 1987, **6**, 469; (c) U. Schubert, G. Scholz, J. Müller, K. Ackermann, B. Wörle and R. F. D. Stansfield, *J. Organomet. Chem.* 1986, **306**, 303; (d) X.-L. Luo and R. H. Crabtree, *J. Am. Chem. Soc.* 1989, **111**, 2527.
12. (a) F. M. Conroy-Lewis and S. J. Simpson, *J. Chem. Soc., Chem. Commun.* 1986, 506; (b) F. M. Conroy-Lewis and S. J. Simpson, *J. Chem. Soc., Chem. Commun.* 1987, 1675; (c) M. S. Chinn and D. M. Heinekey, *J. Am. Chem. Soc.* 1987, **109**, 5865.
13. (a) T.-Y. Y. Gu and W. P. Weber, *J. Organomet. Chem.* 1980, **184**, 7; (b) P. P. Gaspar, in *Reactive Intermediates* (Edited by M. Jones Jr and R. A. Moss), Vol. 2, p. 335. Wiley, New York (1981) and refs therein; (c) P. Jutzi, U. Holtmann, H. Bögge and A. Müller, *J. Chem. Soc., Chem. Commun.* 1988, 305.
14. T. D. Tilley, R. H. Grubbs and J. E. Bercaw, *Organometallics* 1984, **3**, 274.

Polyhedron Vol. 10, No. 11, pp. 1177–1187, 1991
Printed in Great Britain

0277–5387/91 $3.00+.00
Pergamon Press plc

PENTAMETHYLDISILYLMETHYL DERIVATIVES OF THE TRANSITION METALS, $LMCH_2SiMe_2SiMe_3$ [LM = $(\eta^5\text{-}C_5R_5)M(CO)_n^-$, M = Fe, W, R = H, Me, $n = 2, 3$; $(\eta^5\text{-}C_9H_7)Fe(CO)_2^-$; $(\eta^5\text{-}C_5H_5)_2MCl^-$, M = Ti, Zr, Hf]*

SNEH SHARMA, RAMESH N. KAPOOR, FRANCISCO CERVANTES-LEE and KEITH H. PANNELL†

Department of Chemistry, The University of Texas at El Paso, El Paso, TX 79968-0513, U.S.A.

Abstract—Pentamethyldisilylmethyl derivatives of the transition metals have been synthesized, $LMCH_2SiMe_2SiMe_3$ [LM = $(\eta^5\text{-}C_5R_5)M(CO)_n^-$, M = Fe, W, R = H, Me, $n = 2$, 3; $(\eta^5\text{-}C_9H_7)Fe(CO)_2^-$; $(\eta^5\text{-}C_5H_5)_2MCl^-$, M = Ti, Zr, Hf]. The cyclopentadienylcarbonyl complexes are photochemically labile with respect to rearrangement to LM-$SiMe_2CH_2SiMe_3$ and are also subject to base-induced migration to the cyclopentadienyl ring to form $(\eta^5\text{-}Me_3SiCH_2SiMe_2C_5H_4)$ derivatives. The titanium, zirconium and hafnium complexes exhibit neither property; the only compound isolated from the photochemical treatment of these complexes being $Me_3SiSiMe_3$. Structural analyses of $(\eta^5\text{-}C_5H_5)W(CO)_3CH_2SiMe_2SiMe_3$ and its phosphine-substituted rearrangement product, $(\eta^5\text{-}C_5H_5)W(CO)_2(PPh_3)SiMe_2CH_2SiMe_3$, are presented.

In a communication published in 1974 we reported that the complex $(\eta^5\text{-}C_5H_5)Fe(CO)_2CH_2SiMe_2SiMe_3$, containing a Si—Si bond, was photochemically labile with respect to rearrangement to a complex containing a direct Fe—Si bond, $(\eta^5\text{-}C_5H_5)Fe(CO)_2SiMe_2CH_2SiMe_3$.[2] Furthermore we observed that when the complex was subjected to base treatment, followed by addition of MeI, a migration of the disilylmethyl group to the cyclopentadienyl ring occurred, during which the group again rearranged to form $(\eta^5\text{-}Me_3SiCH_2SiMe_2C_5H_4)Fe(CO)_2Me$.[3] These two brief communications are the only reports concerning the chemistry of the ligand $Me_3SiSiMe_2CH_2$-. We are presently reinvestigating this area of chemistry, and now report the synthesis, structural characterization and chemical reactivity, of a series of such disilylmethyl complexes of iron, tungsten, titanium, zirconium and hafnium.

RESULTS AND DISCUSSION

The synthesis of the complexes $LMCH_2SiMe_2SiMe_3$ was accomplished via two distinct chemical pathways, outlined in eq. (1) for the cyclopentadienylcarbonyl complexes, and eq. (2) for the group 4 chlorometallocene complexes:

$$[(\eta^5\text{-}C_5R_5)M(CO)_n]^-Na^+ + ClCH_2SiMe_2SiMe_3 \longrightarrow (\eta^5\text{-}C_5R_5)M(CO)_nCH_2SiMe_2SiMe_3 \quad (1)$$

$[(\eta^5\text{-}C_5H_5)M(CO)_n]^- = (\eta^5\text{-}C_5Me_5)Fe(CO)_2$ (IV), $(\eta^5\text{-}C_5H_5)W(CO)_3$ (V)

$$(\eta^5\text{-}C_5H_5)_2MCl_2 + Mg + ClCH_2SiMe_2SiMe_3 \longrightarrow (\eta^5\text{-}C_5H_5)_2M(CH_2SiMe_2SiMe_3)Cl \quad (2)$$

M = Ti (I), Zr (II), Hf (III).

A reaction similar to those described in eq. (1) was performed using $(\eta^5\text{-}C_9H_7)Fe(CO)_2$, the π-indenyl analogue of the $(\eta^5\text{-}C_5H_5)Fe(CO)_2$ (Fp) anion, to produce $(\eta^5\text{-}C_9H_7)Fe(CO)_2CH_2SiMe_2SiMe_3$ (VI). The yields from such direct salt elimination reactions were in the range 50–70%, while whose for the reactions outlined in eq. (2) were more moderate and variable, 7–40%. The complexes IV, V and VI are thermally stable at room temperature, and may also be handled in the air for brief periods of time. The group 4 complexes are very susceptible to decomposition in the presence

*Organometalloidal derivatives of the transition metals—27. For part 26 see ref. 1.

†Author to whom correspondence should be addressed.

of trace amounts of moisture to form $[(\eta^5\text{-}C_5H_5)_2MCl]_2O$. Such behaviour was also reported by Lappert's group for the related monosilylmethyl analogues, $(\eta^5\text{-}C_5H_5)_2MCl(CH_2SiMe_3)$.[4] We were unable to obtain satisfactory analyses on these complexes.

Spectroscopic analysis of the new complexes was performed via the usual techniques, IR, ^1H, ^{13}C and also ^{29}Si NMR. The various data from such investigations are in total accord with the proposed structures, and are recorded in Table 1.

We have performed a single crystal X-ray analysis on **V**, Fig. 1(a). The various bond lengths and angles for the $(\eta^5\text{-}C_5H_5)W(CO)_3^-$ portion of the complex are as expected, and the W—C σ bond length of 2.28 Å is also well within the expected range. The Si—Si bond length of 2.347(4) Å is also in the middle of the published permethylated disilane Si—Si bond lengths. We have previously reported that direct substitution of a transition metal onto a disilane fragment, $(\eta^5\text{-}C_5H_5)Fe(CO)_2$ substituents, causes a pronounced elongation of the Si—Si bond. In the case of complex **V** the effect of the tungsten substituent is essentially muted by the intervening CH_2 group.

We have investigated the chemical properties of the complexes with respect to two main reaction conditions, photochemistry and base treatment, and the results are discussed below.

Photochemistry

The new π-cyclopentadienyl(π-indenyl)carbonyl complexes are readily rearranged when treated with UV light, for example eq. (3):

$$\mathbf{VI} \xrightarrow{h\nu/hexane} (\eta^5\text{-}C_9H_7)Fe(CO)_2SiMe_2CH_2SiMe_3. \quad (3)$$
(VIII)

The new rearranged materials are isolable as stable complexes for the iron systems, but could not be isolated from the reaction with the tungsten complex **V**. In this latter case it was neccessary to perform the photochemical reaction in the presence of triphenylphosphine in order to isolate the corresponding rearranged dicarbonyl(phosphine) complex (**IX**), eq. (4):

$$\mathbf{V} + PPh_3 \xrightarrow{h\nu/hexane} (\eta^5\text{-}C_5H_5)W(CO)_2(PPh_3)SiMe_2CH_2SiMe_3. \quad (4)$$
(IX)

The photochemical rearrangement reactions may be followed by IR spectroscopy, since the metal–carbon complexes exhibit ν(CO) stretching modes at higher frequencies than their metal–silicon bonded counterparts. ^{29}Si NMR is useful for complete characterization. Cleavage of the Si—Si bond transforms the silicon resonances from typical disilane resonances, modified by the transition metal substituent, into a pair of essentially isolated silane fragments. Thus, whereas the two ^{29}Si resonances in **IV** occur at −8.7 ppm (Fe—CH_2*Si*Si) and −20.6 ppm (FeCH_2Si*Si*), the product **VII** resonances are at 42.0 ppm (Fe—*Si*CH_2Si) and 0.4 ppm (Fe—SiCH_2*Si*). As with other iron complexes, the effect

Table 1. New complexes: analytical data, yields, melting points and spectral data[a]

Complex	Yield (%)	Analysis Found(Calc.) C; H	Melting point
$(\eta^5\text{-}C_5H_5)_2Ti(CH_2SiMe_2SiMe_3)Cl$ **(I)**	8		108
^1H: 0.0 ($SiMe_3$+$SiMe_2$); 2.16 (CH_2); 6.24 ($\eta^5\text{-}C_5H_5$)			
^{13}C: −1.68 ($SiMe_3$); 0.39 ($SiMe_2$); 38.1 (CH_2); 116.0 ($\eta^5\text{-}C_5H_5$)			
^{29}Si: −13.9 ($SiMe_2$); −19.7 ($SiMe_3$)			
$(\eta^5\text{-}C_5H_5)_2Zr(CH_2SiMe_2SiMe_3)Cl$ **(II)**	31		98
^1H: 0.18 ($SiMe_3$); 0.19 ($SiMe_2$); 0.98 (CH_2); 5.91 ($\eta^5\text{-}C_5H_5$)			
^{13}C: −1.67 ($SiMe_3$); 0.75 ($SiMe_2$); 46.0 (CH_2); 112.8 ($\eta^5\text{-}C_5H_5$)			
^{29}Si: −15.9 ($SiMe_2$); −19.6 ($SiMe_3$)			
$(\eta^5\text{-}C_5H_5)_2Hf(CH_2SiMe_2SiMe_3)Cl$ **(III)**	35		95
^1H: 0.19 ($SiMe_3$); 0.20 ($SiMe_2$); 0.48 (CH_2); 5.84 ($\eta^5\text{-}C_5H_5$)			
^{13}C: −1.69 ($SiMe_3$); 0.80 ($SiMe_2$); 42.5 (CH_2); 111.8 ($\eta^5\text{-}C_5H_5$)			
^{29}Si: −15.8 ($SiMe_2$); −18.6 ($SiMe_3$)			
$(\eta^5\text{-}C_5Me_5)Fe(CO)_2CH_2SiMe_2SiMe_3$ **(IV)**	46	54.4; 8.00 (55.1; 8.21)	56

Table 1—*continued*

Complex	Yield (%)	Analysis Found(Calc.) C; H	Melting point
IR: ν(CO): 1991, 1938 ^{1}H: −0.54 (CH_2); 0.14 ($SiMe_3$); 0.24 ($SiMe_2$); 1.41 (Me) ^{13}C: −14.3 (CH_2); −0.56 ($SiMe_3$, $SiMe_3$); 9.22 ($C_5\mathit{Me}_5$); 95.3 (η^5-C_5Me_5) ^{29}Si: −8.72 ($SiMe_2$); −20.6 ($SiMe_3$)			
(η^5-C_5H_5)W(CO)$_3$$CH_2SiMe_2SiMe_3$ (V)	60	35.5; 4.51 (35.2; 4.63)	55
IR: ν(CO): 2016, 1929 ^{1}H: 0.08 (CH_2); 0.18 ($SiMe_3$); 0.28 ($SiMe_2$); 4.62 (η^5-C_5H_5) ^{13}C: −39.2 (CH_2); −1.70 ($SiMe_3$); 0.80 ($SiMe_2$); 91.6 (η^5-C_5H_5); 218.6, 230.2 (CO) ^{29}Si: −7.2 ($SiMe_2$); −19.4 ($SiMe_3$)			
(η^5-C_9H_7)Fe(CO)$_2$$CH_2SiMe_2SiMe_3$ (VI)	40	54.7; 6.60 (54.8; 6.50)	oil
IR: ν(CO): 2008, 1954 ^{1}H: −0.76 (CH_2); 0.19 ($SiMe_2$+$SiMe_3$); 4.34, 4.80, 6.83 (η^5-C_9H_7) ^{13}C: −18.9 (CH_2); −1.70 ($SiMe_3$), −0.55 ($SiMe_2$); 73.6, 92.3, 104.6, 124.6, 126.6 (η^5-C_9H_7); 218.2 (CO) ^{29}Si: −7.79 ($SiMe_2$); −20.6 ($SiMe_3$)			
(η^5-C_5Me_5)Fe(CO)$_2$$SiMe_2CH_2SiMe_3$ (VII)	80	54.6; 8.51 (55.1; 8.21)	oil
IR: ν(CO): 1988, 1929 ^{1}H: 0.19 ($SiMe_3$); 0.50 (CH_2); 0.62 ($SiMe_2$); 1.54 ($C_5\mathit{Me}_5$) ^{13}C: 2.12 ($SiMe_2$); 7.70 (CH_2); 9.98 ($SiMe_3$); 11.05 ($C_5\mathit{Me}_5$); 94.7 (C_5Me_5) 218.4 (CO) ^{29}Si: 42.0 ($SiMe_2$); 0.37 ($SiMe_3$)			
(η^5-C_9H_7)Fe(CO)$_2$$SiMe_2CH_2SiMe_3$ (VIII)	80	53.5; 6.60 (54.8; 6.50)	oil
IR: ν(CO): 1994, 1941 ^{1}H: −0.24 (CH_2); 0.0 ($SiMe_3$); 0.23 ($SiMe_2$); 4.11, 4.35, 4.38, 7.00 (m) (η^5-C_9H_7) ^{13}C: 1.50 ($SiMe_2$); 7.90 (CH_2); 12.31 ($SiMe_3$); 72.0, 74.8, 76.2, 96.3, 111.1, 124.2, 126.6 (η^5-C_9H_7); 215.4 (CO) ^{29}Si: 48.8 ($SiMe_2$); 0.0 ($SiMe_3$)			
(η^5-C_5H_5)W(CO)$_2$(PPh_3)$SiMe_2CH_2SiMe_3$ (IX)	20	51.8; 5.23 (52.3; 5.19)	74
IR: ν(CO): 1936, 1859 ^{1}H: 0.12 ($SiMe_3$); 0.33 (CH_2); 0.63 ($SiMe_2$); 4.85 (η^5-C_5H_5), 7.33 (m, Ph) ^{13}C: 2.30 (CH_2); 6.68 ($SiMe_3$); 10.7 ($SiMe_2$); 90.3 (η^5-C_5H_5), 128.4, 130.3, 133.6, 137.1 (Ph); 227.2 (CO) ^{29}Si: 19.4 [d, J(Si—P) = 11.9 Hz, $SiMe_2$]; 1.51 ($SiMe_3$) ^{31}P: 52.7			
(η^5-$C_5H_4SiMe_2CH_2SiMe_3$)W(CO_3)Me (X)	60	36.4; 4.88 (36.6; 5.11)	35
IR: ν(CO): 2009, 1914 ^{1}H: −0.24 (CH_2); 0.0 ($SiMe_3$); 0.16 ($SiMe_2$); 0.52 (W—CH_3); 4.55 (m), 4.77 (s, C_5H_4) ^{13}C: −34.1 (W—CH_3); 0.76 ($SiMe_3$); 1.41 ($SiMe_2$); 4.54 (CH_2); 95.8 (η^5-C_5H_4); 217.3 (CO) ^{29}Si: −4.24 ($SiMe_2$); 0.11 ($SiMe_3$)			

[a] NMR spectra were recorded in C_6D_6, with the exception of **IX** which was recorded in $CDCl_3$. All IR spectra were recorded in n-hexane. Melting points were recorded in open capilliary tubes and are uncorrected.

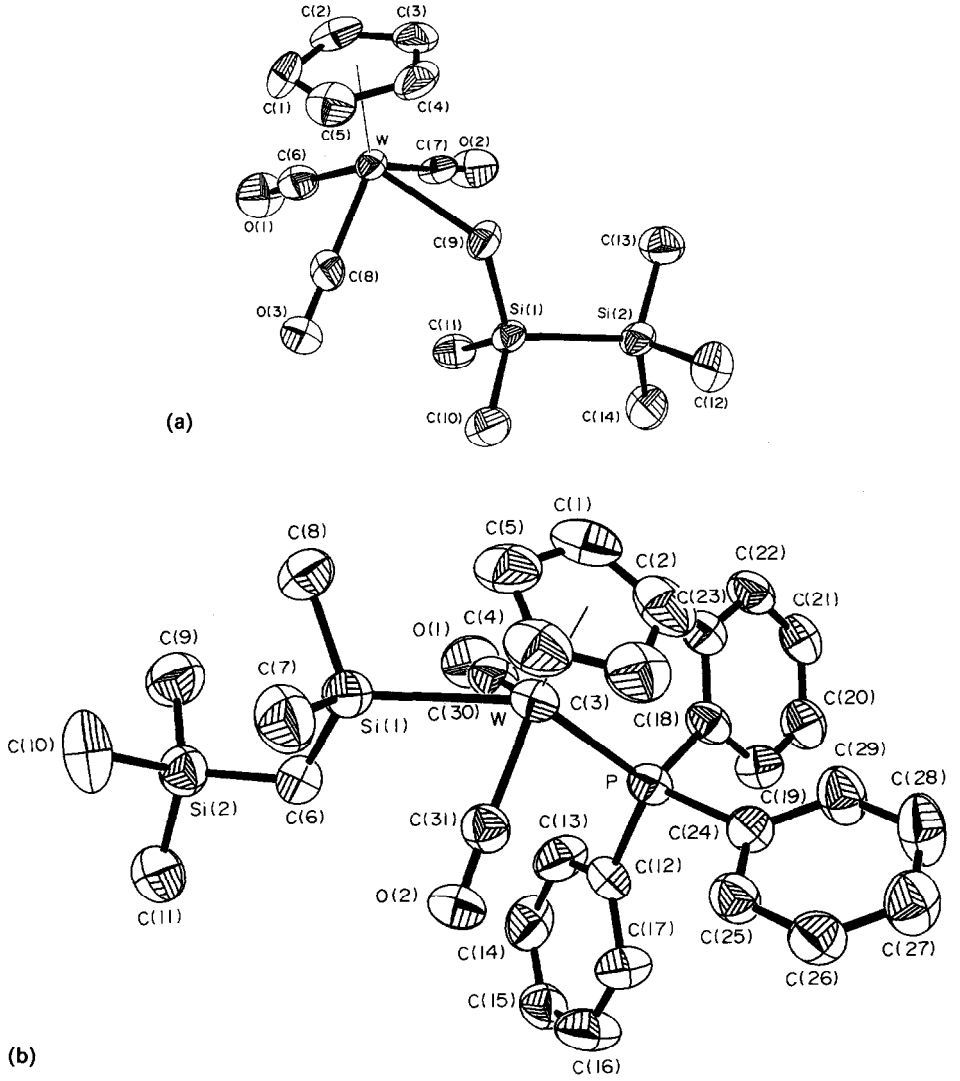

Fig. 1. (a) Structure of $(\eta^5\text{-}C_5H_5)W(CO)_3CH_2SiMe_2SiMe_3$ (V); (b) structure of $(\eta^5\text{-}C_5H_5)W(CO)_2(PPh_3)SiMe_2CH_2SiMe_3$ (IX).

of the transition metal upon the ^{29}Si NMR chemical shift in comparison to the corresponding methyl analogue, i.e. $FeSiR_3$ vs $MeSiR_3$, $\Delta\delta$, is great when the silicon atom is directly attached to the metal, e.g. 49 ppm for $FeSiCH_2SiMe_3$ (VIII) vs $Me_3SiCH_2SiMe_3$, but almost negligible in the case of a silicon atom removed from the iron by three bonds.[5,3] Similar results may be observed for the tungsten complexes, except that the shielding effect created by the tungsten atom upon directly bound silicon atoms is considerably less than that observed in the case of iron complexes.

We have also characterized the rearranged tungsten complex IX by single crystal X-ray structural analysis, Fig. 1(b). The various aspects of the structure are unremarkable, but the structure represents only the third example of the structural characterization of a W—Si bond, and the first in the $(\eta^5\text{-}C_5H_5)W(CO)_n^-$ type system. The W—Si bond length is 2.633(2) Å, significantly longer then those in $(PMe_3)_3IW(H)_2SiMe_3$, 2.389 Å,[6] and $(CO)_4W(\mu\text{-}SiEt_2)_2W(H_2)(CO)_4$, 2.586 Å.[7] The three complexes are very different with respect to the ligands on tungsten, and of course one of the complexes contains a bridging silyl group, thus until a greater series of complexes are available for study the significance of such data is unclear. Selected bond lengths and bond angles are presented in Table 2.

In general the nature of the W—Si bond precludes the ready formation and examination of a large range of complexes of the type $(\eta^5\text{-}C_5H_5W(CO)_3SiR_3$, cf. the large number of complexes of the type $(\eta^5\text{-}C_5H_5)Fe(CO)_2SiR_3$. The rearrangement illustrated here suggests a possible

Table 2. Bond lengths (Å) and bond angles (°) for complexes V and IX

Complex V			
Bond lengths (Å)			
W—C(1)	2.283(10)	W—C(2)	2.302(11)
W—C(3)	2.332(10)	W—C(4)	2.365(12)
W—C(5)	2.330(10)	W—C(6)	1.956(12)
W—C(7)	1.981(9)	W—C(8)	1.948(9)
W—C(9)	2.336(9)	Si(1)—Si(2)	2.347(4)
Si(1)—C(9)	1.870(9)	Si(1)—C(10)	1.882(9)
Si(1)—C(11)	1.873(9)	Si(2)—C(12)	1.842(11)
Si(2)—C(13)	1.867(10)	Si(2)—C(14)	1.856(12)
O(1)—C(6)	1.147(16)	O(2)—C(7)	1.150(12)
O(3)—C(8)	1.179(11)	C(1)—C(2)	1.428(15)
C(1)—C(5)	1.355(16)	C(2)—C(3)	1.401(16)
C(3)—C(4)	1.397(16)	C(4)—C(5)	1.392(15)
Bond angles (°)			
C(6)—W—C(7)	79.6(4)	W—C(9)—Si(1)	126.1(5)
C(6)—W—C(8)	76.0(4)	C(7)—W—C(8)	111.0(4)
C(7)—W—C(9)	73.3(4)	C(8)—W—C(9)	75.9(4)
Si(2)—Si(1)—C(9)	110.7(3)	W—C(6)—O(1)	177.4(8)
W—C(7)—O(2)	176.1(8)	W—C(8)—O(3)	177.2(8)
Complex IX			
Bond lengths (Å)			
W—P	2.431(2)	W—Si(1)	2.633(2)
W—C(1)	2.361(8)	W—C(2)	2.355(9)
W—C(3)	2.337(9)	W—C(4)	2.330(10)
W—C(5)	2.318(9)	W—C(30)	1.948(9)
W—C(31)	1.933(7)	P—C(12)	1.832(7)
P—C(18)	1.847(6)	P—C(24)	1.842(6)
Si(1)—C(6)	1.886(7)	Si(1)—C(7)	1.888(10)
Si(1)—C(8)	1.887(9)	Si(2)—C(6)	1.855(8)
Si(2)—C(9)	1.873(10)	Si(2)—C(10)	1.850(10)
Si(2)—C(11)	1.862(9)	O(1)—C(30)	1.172(10)
O(2)—C(31)	1.173(8)	C(1)—C(2)	1.394(14)
C(1)—C(5)	1.400(13)	C(2)—C(3)	1.397(13)
C(3)—C(4)	1.396(15)	C(4)—C(5)	1.384(13)
C(12)—C(13)	1.386(10)	C(12)—C(17)	1.382(10)
C(13)—C(14)	1.392(11)	C(14)—C(15)	1.372(12)
C(15)—C(16)	1.322(14)	C(16)—C(17)	1.386(11)
C(18)—C(19)	1.380(11)	C(18)—C(23)	1.376(9)
C(19)—C(20)	1.362(10)	C(20)—C(21)	1.365(11)
C(21)—C(22)	1.374(12)	C(22)—C(23)	1.392(9)
C(24)—C(25)	1.385(9)	C(24)—C(29)	1.383(9)
C(25)—C(26)	1.409(10)	C(26)—C(27)	1.348(11)
C(27)—C(28)	1.372(11)	C(28)—C(29)	1.383(11)
Bond angles (°)			
P—W—Si(1)	133.9(1)	P—W—C(30)	80.0(2)
P—W—C(31)	82.1(2)	C(30)—W—C(31)	101.2(3)
W—Si(1)—C(6)	115.3(3)	Si(1)—C(6)—Si(2)	122.7(4)
W—C(30)—O(1)	177.5(6)	W—C(31)—O(2)	175.9(6)

route to stable complexes with a W—Si bond. The rearrangement is related to that initially observed in our laboratories for the complex $(\eta^5\text{-}C_5H_5)Fe(CO)_2CH_2SiMe_2H$,[8] and studied extensively by Wrighton and co-workers for $(\eta^5\text{-}C_5Me_5)Fe(CO)_2CH_2SiMe_2H$ and related tungsten complexes, eq. (5):[9]

$$(\eta^5\text{-}C_5H_5)Fe(CO)_2CH_2SiMe_2H \xrightarrow{h\nu} (\eta^5\text{-}C_5H_5)Fe(CO)_2SiMe_3 \quad (5a)$$

$$(\eta^5\text{-}C_5Me_5)W(CO)_3CH_2SiMe_2H \longrightarrow (\eta^5\text{-}C_5Me_5)W(CO)_3SiMe_3. \quad (5b)$$

Using low temperature matrix isolation spectroscopy, Wrighton and his group confirmed our original suggestion that this reaction proceeded via initial loss of CO, followed by a β-elimination reaction to form a hydrido-metal silene intermediate which rearranged to the observed products upon recombination of CO, or in the presence of other ligands, e.g. PPh_3. We suggest that the mechanism of the disilylmethyl rearrangement reaction is similar to that operating for the $LMCH_2SiMe_2H$ complexes in which an intermediate of type **XII** is formed, eq. (6). This also has the potential for rotation about the metal–silene bond, with recombination to form the observed products upon recoordination of the CO or phosphine ligand.

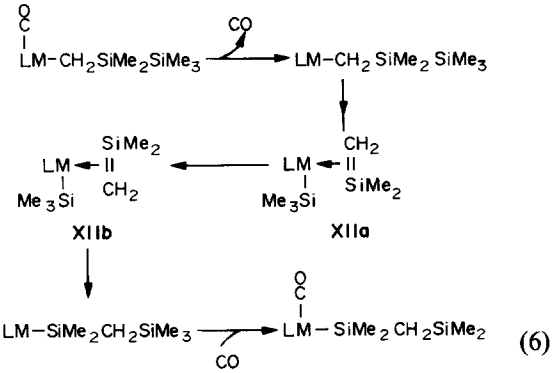

(6)

We are pursuing a program of chemical modification of the $LMCH_2SiR_2SiR_3$ complexes in the hope of isolating silene intermediates of the type **XII**. It is pertinent that both the Berry and Tilley groups have recently discussed and isolated transition metal silene complexes that can be thought of as models for the system discussed here.[10,11]

As in the case of $FpCH_2SiMe_2H$, the rearrangement observed for the iron complexes $(\eta^5\text{-L})Fe(CO)_2CH_2SiMe_2SiMe_3$ (L = C_5Me_5, C_9H_7) may also be effected thermally. The rates of transformation to the corresponding $(\eta^5\text{-L})FeSiMe_2CH_2SiMe_3$ complexes vary considerably. The π-indenyl complex transforms the fastest, 16 h in refluxing hexane, as might be expected if η^5- to η^3-ring slippage is occurring providing a low-energy route to 16e$^-$ coordinatively-unsaturated intermediates. The ability of the π-indenyl group to activate carbonyl insertion reactions via such η^5–η^3 slippages is well established.[12] The $(\eta^5\text{-}C_5Me_5)$ complex rearranged smoothly after 60 h, but the $(\eta^5\text{-}C_5H_5)$ complex does not yield any significant product after 80 h, exhibiting considerable Fe—C bond cleavage such that the only isolated product was $[(\eta^5\text{-}C_5H_5)Fe(CO)_2]_2$. We are currently investigating the nature of the thermal transformation in the case of the π-indenyl system to note if loss of CO is important.

We have subjected the group 4 chlorometallocene complexes **I**, **II** and **III** to similar photochemical treatment. Monitoring the reaction progress via ^{29}Si NMR, it was apparent that no rearrangements of the type illustrated above occur in this system. After prolonged irradiation in inert hydrocarbon solvents the only identifiable silicon-containing product was $Me_3SiSiMe_3$. This is probably formed via homolytic cleavage of the M—C bond, followed by hydrogen abstraction from the solvent.

Base treatment

Treatment of cyclopentadienylcarbonylmetal complexes of the type $(\eta^5\text{-}C_5H_5)M(CO)_n(L)R$, (M = Fe, Mo, W, Ru, Re, n = 2, 3, R = alkyl, acyl, silyl, germyl, stannyl, plumbyl) with bases such as n-BuLi and LDA at −78°C has been shown to result in deprotonation of the cyclopentadienyl ring to produce a ring-centred anion.[13] This anion is stable in the case of R = alkyl and may be trapped by addition of the appropriate quench, e.g. methyliodide. In the other cases a migration of the R group occurs, sometimes not until elevated temperatures, i.e. 25°C, to produce a metal-centred anion $[(\eta^5\text{-}RC_5H_4)M(CO)_n(L)]^-$ which can also be trapped with appropriate reagents. Treatment of **V** with LDA at low temperature, followed by warming to ambient temperature, led to the formation of the corresponding metal-centred anion as illustrated in eq. (7):

$$(\eta^5\text{-}C_5H_5)W(CO)_3CH_2SiMe_2SiMe_3 \xrightarrow{LDA} [(\eta^5\text{-}LiC_5H_4)W(CO)_3CH_2SiMe_2SiMe_3] \downarrow$$
$$(\eta^5\text{-}SiMe_3CH_2SiMe_2C_5H_4)W(CO)_3Me \xleftarrow{MeI} [(\eta^5\text{-}Me_3SiCH_2SiMe_2C_5H_4)W(CO)_3]^-Li^+. \quad (7)$$
(X)

The migration of the disilylmethyl group occurs with a rearrangement that involves the cleavage of the Si—Si bond and it appears that this is a general type of reaction. The spectroscopic data for the migration product is in accord with the structure. In the case of the rearranged complex **X**, the two ^{29}Si resonances are at −4.2 and 0.1 ppm, respectively. The former resonance is due to the silicon atom directly bonded to the cyclopentadienyl ring, and is typical of such atoms being shifted 3–5 ppm to lower field than the related $MeSiR_3$ compound.[3]

Treatment of the group 4 chlorometallocene-disilylmethyl complexes with LDA did not result in straightforward chemistry and we are still investigating this system.

EXPERIMENTAL

All reactions were performed under nitrogen atmosphere using oxygen-free dry solvents. Titanocene dichloride, zirconocene dichloride and hafnocene dichloride were purchased from Aldrich Chemical Co., Milwaukee, Wisconsin. The pentamethylcyclopentadienylirondicarbonyl dimer was obtained from Strem Chemical Co., Newburyport, Massachusetts, and the indenylirondicarbonyl dimer was prepared by literature procedures.[14] Tungsten hexacarbonyl was purchased from Pressure Chemical Co., Pittsburgh, Pennsylvania, and $Me_5Si_2CH_2Cl$ and $Me_5Si_2CH_2I$ were prepared by literature procedures.[15]

IR spectra were recorded on a Perkin–Elmer 1600 series FT–IR spectrophotometer, and NMR spectra were recorded on an IBM NR/200 FT–NMR spectrometer. All analyses were performed by Galbraith Laboratories Inc, Knoxville, Tennessee.

The syntheses of the new compounds are typified by the examples given below. The analytical and spectral data are given in Table 1.

Synthesis of $(\eta^5\text{-}C_5H_5)_2Ti(CH_2SiMe_2SiMe_3)Cl$ **(I)**

Into a 100-cm^3 side-arm flask, magnesium turnings (0.24 g, 0.01 g atom), titanocene dichloride (2.0 g, 8.0 mmol) and $Me_5Si_2CH_2Cl$ (1.8 g, 10 mmol) were placed in 20 cm^3 of THF. A crystal of iodine was introduced into the reaction mixture which was stirred at room temperature for 2 h. After about 10 min the colour of solution changed to dark red. The solvent was removed *in vacuo* and the dark residue was extracted with a 1 : 1 hexane–methylene chloride mixture. The solution was filtered under nitrogen and subsequent to evaporation of the solvents, a dark red solid was obtained, which on sublimation at 80°C *in vacuo*, yielded 0.22 g (0.6 mmol, 7.5%) of the red, crystalline title complex.

$(\eta^5\text{-}C_5H_5)_2Zr(CH_2SiMe_2SiMe_3)Cl$ **(II)** and $(\eta^5\text{-}C_5H_5)_2Hf(CH_2SiMe_2SiMe_3)Cl$ **(III)** were synthesized in a similar manner, 31 and 35% respective yields, and were purified by recrystallization from hexane.

Synthesis of $(\eta^5\text{-}C_5Me_5)Fe(CO)_2CH_2SiMe_2SiMe_3$ **(IV)**

A 250-cm^3 round-bottomed flask fitted with a septum and a magnetic stirring bar was charged with 40 g of 1% Na/Hg amalgam and 60 cm^3 of THF. To this was added $[(\eta^5\text{-}C_5Me_5)Fe(CO)_2]_2$ (1.5 g, 3.0 mmol). The mixture was stirred for 24 h, at which time IR monitoring indicated that the starting material had been transformed into $[(\eta^5\text{-}C_5Me_5)Fe(CO)_2]^-Na^+$, ν(CO), 1993, 1875, 1860, 1791 and 1755 cm^{-1}. Mercury was removed and the solution was cooled to 0°C, and $ClCH_2Si_2Me_5$ (1.0 g, 5.0 mmol) was added. The solution was stirred for 2 h and the solvent removed *in vacuo*. To the resulting residue was added 60 cm^3 of hexane and the solution was stirred for 1 h and then filtered. The filtrate was concentrated to 5 cm^3 and passed through a silica gel column. A yellow band was formed and eluted with hexane to yield **IV** (1.1 g, 2.4 mmol, 46%) as a yellow solid.

Synthesis of $(\eta^5\text{-}C_5H_5)W(CO)_3CH_2SiMe_2SiMe_3$ **(V)**

A 250-cm^3 side-arm flask was charged with sodium metal (0.30 g, 1.3 g atom) and 60 cm^3 of THF. The sodium suspension in THF was treated with cyclopentadiene (1.5 cm^3, 2.4 mmol) (freshly distilled) in order to react with all the sodium to form a light pink sodium cyclopentadienide solution. The resulting solution was treated with tungsten hexacarbonyl (3.6 g, 10.2 mmol) and the solution heated to reflux for 72 h to form a yellow solution of $[(\eta^5\text{-}C_5H_5)W(CO)_3]^-Na^+$. To this solution was added 5.5 g of $Me_5Si_2CH_2I$ and the solution was refluxed for 18 h. THF was removed and a yellowish-brown liquid was extracted with hexane. Upon concentration to 5 cm^3 and chromatography on a 2 × 25 cm silica gel column with hexane, a yellow band was developed which yielded **V** (2.70 g, 6.1 mmol, 60%).

Photolysis of $(\eta^5\text{-}C_5H_5)_2Ti(CH_2SiMe_2SiMe_3)Cl$ **(I)**

Compound **I** (0.10 g) was dissolved in 1 cm^3 of degassed C_6D_6. This was irradiated for 20 h in a sealed Pyrex NMR tube and monitored by ^{29}Si NMR. The only observable new product was $Me_3SiSiMe_3$.

Photolysis of $(\eta^5\text{-}C_5Me_5)Fe(CO)_2CH_2SiMe_2SiMe_3$ **(IV)**

A solution of the title complex (0.150 g dissolved in 1 cm^3 of degassed C_6D_6) was irradiated for 15 h in a sealed Pyrex NMR tube and monitored by ^{29}Si NMR. After 12 h it was evident that no starting material was present and the irradiation was stopped. The solution was placed directly onto a 2.5×10 cm silica gel column and eluted with hexane. A single yellow band formed, that upon removal and recrystallization from the same solvent yielded **IV** (0.12 g, 80%).

Photolysis of $(\eta^5\text{-}C_5H_5)W(CO)_3CH_2SiMe_2SiMe_3$ **(V)** *with* Ph_3P

A mixture of **V** (0.6 g, 1.25 mmol) and Ph_3P (0.6 g, 2.2 mmol) in 40 cm^3 of hexane, in a quartz tube, was irradiated for 15 h and was monitored by IR spectroscopy. Upon complete removal of the starting material, the solvent was removed and the resulting reddish-orange solid was dissolved in a minimum quantity of methylene chloride and passed through a 2×25 cm silica gel column. An initial yellow–red fraction, eluted with hexane, was collected and after removal of the solvent yielded $(\eta^5\text{-}C_5H_5)W(CO)_2(PPh_3)SiMe_2CH_2SiMe_3$ (0.3 g, 40%). This material was further purified by recrystallization from hexane.

LDA *treatment of* $(\eta^5\text{-}C_5H_5)W(CO)_3CH_2SiMe_2SiMe_3$ **(V)**

To **V** (0.65 g, 1.3 mmol) in 20 cm^3 of THF, in a side-arm flask at 0°C, was added dropwise freshly prepared LDA (4 cm^3, 2.2 mmol). The colour of the solution immediately changed to orange. The solution was stirred for 45 min, at which time the ν(CO) bands of the starting material had been replaced by bands at 1898, 1800, 1778(sh) and 1713 cm^{-1} indicative of a cyclopentadienyltungstentricarbonylate. Addition of excess methyl iodide (2 cm^3), followed by stirring for 10 min, gave ν(CO) absorptions at 2010 and 1914 cm^{-1}. The solvent was removed and an orange compound was extracted with a 1:1 hexane–methylene chloride mixture. This was recrystallized from hexane to yield yellow, crystalline $(\eta^5\text{-}C_5H_4SiMe_2CH_2SiMe_3)W(CO)_3Me$ (0.4 g, 60%).

Table 3. Summary of crystal data

	V	**IX**
Empirical formula	$C_{14}H_{22}O_3Si_2W$	$C_{31}H_{37}O_2Si_2PW$
Molecular weight	478.3	712.6
Colour of crystal	Yellow	Yellow
Crystal dimensions (mm)	$0.8 \times 0.4 \times 0.2$	$0.2 \times 0.5 \times 0.5$
Crystal system	Monoclinic	Monoclinic
Space group	$P2_1/n$	$P2_1/n$
Cell dimensions		
a (Å)	6.876(2)	11.567(3)
b (Å)	22.657(8)	19.113(3)
c (Å)	11.992(3)	14.246(4)
β (°)	92.24(2)	103.22(2)
Z (molecules/cell)	4	4
Volume (Å^3)	1866.9(10)	3066.0(15)
Calculated density (g cm^{-3})	1.702	1.544
Wavelength (Å)	0.71073	0.71073
Linear absorption coefficient (cm^{-1})	64.5	40.0
2θ range (°)	3.5–45	3.5–45
Number of unique reflections	2268	3938
Number of observed reflections with $I > 3\sigma(I)$	1980	3507
Number of variables	182	350
R	0.037	0.037
R_w	0.053	0.045

Structural analysis of $(\eta^5\text{-}C_5H_5)W(CO)_2(PPh_3)SiMe_2CH_2SiMe_3$ **(IX)**

An irregularly shaped crystal, $0.22 \times 0.48 \times 0.50$ mm, was mounted on a glass fibre and covered with epoxy glue. Crystal data were collected at room temperature on a R3m/V Nicolet four-circle diffractometer with graphite monochromated Mo-K_α, $\lambda = 0.71073$ Å, radiation. Unit cell parameters and standard deviations were obtained by a least-squares fit to 25 reflections randomly distributed in reciprocal space and lying in the 2θ range 15–30°. Intensity data were collected in the ω scan mode, with scans from 0.75° below $K_{\alpha 1}$ to 0.75° above $K_{\alpha 2}$, with a variable scan speed of 3–20° min^{-1}. Background counts were taken with a stationary crystal and total background time/scan time of 0.5. Three standard reflections were monitored every 100 reflections and showed no significant decay. The data were corrected for Lorentz and polarization effects and a semi-empirical absorption correction was also applied giving a min/max transmission of 0.020/0.044.

The space group $P2_1/n$ was determined from the systematic absences. The structure was solved by the heavy-atom method and refined by full-matrix least-squares using the SHELXTL-PLUS software package on a Microvax II computer. Selected bond lengths and bond angles are provided in Table 2, and the various collection and refinement data are recorded in Table 3.

Structural analysis of $(\eta^5\text{-}C_5H_5)W(CO)_3CH_2SiMe_2SiMe_3$ **(V)**

A yellow plate of **V**, $0.8 \times 0.4 \times 0.18$ mm, was used for the structural characterization. Three standard reflections were monitored every 100 reflections and used in a profile analysis to allow for approximately 5% of intensity decay during the experiment. The data were corrected for Lorentz and polarization effects and a semi-empirical absorption correction factor was applied giving a min/max transmission ratio of 0.72/0.99. Selected bond lengths and angles are recorded in Table 2, and the various collection and refinement data are recorded in Table 3. Atomic coordinates and equivalent isotropic displacement coefficients for both structures are presented in Table 4.

Table 4. Atomic coordinates ($\times 10^4$) and equivalent isotropic displacement coefficients (Å$^2 \times 10^3$) for complexes **V** and **IX**

	x	y	z	U (eq)[a]
		Complex **V**		
W	178(1)	2577(1)	6091(1)	40(1)
Si(1)	−1511(3)	1005(1)	6257(2)	43(1)
Si(2)	−2005(4)	399(1)	7809(2)	54(1)
O(1)	4029(13)	2537(3)	4828(9)	92(4)
O(2)	2743(12)	1803(3)	7732(6)	89(3)
O(3)	−979(11)	1927(3)	3864(5)	72(3)
C(1)	−323(18)	3551(5)	5681(9)	71(4)
C(2)	734(18)	3523(5)	6728(9)	77(4)
C(3)	−543(18)	3263(4)	7466(8)	68(4)
C(4)	−2304(17)	3141(4)	6891(10)	72(4)
C(5)	−2124(15)	3320(5)	5790(8)	65(4)
C(6)	2614(18)	2566(4)	5301(10)	60(4)
C(7)	1793(14)	2070(4)	7104(8)	53(3)
C(8)	−492(14)	2168(4)	4700(7)	51(3)
C(9)	−1811(14)	1800(4)	6629(8)	50(3)
C(10)	−3360(13)	802(4)	5123(7)	65(4)
C(11)	941(13)	815(4)	5733(8)	63(4)
C(12)	−4610(16)	289(5)	8049(8)	87(5)
C(13)	−819(17)	737(5)	9083(7)	80(5)
C(14)	−928(22)	−342(5)	7602(9)	94(6)
		Complex **IX**		
W	1447(1)	2001(1)	80(1)	55(1)
P	2621(2)	2109(1)	−1126(1)	53(1)
Si(1)	1655(2)	1250(1)	1659(1)	66(1)

Table 4—*continued*

	x	*y*	*z*	*U* (eq)[a]
Si(2)	3285(2)	30(1)	2946(2)	73(1)
O(1)	1750(5)	420(3)	−352(4)	87(2)
O(2)	3838(5)	2391(3)	1474(4)	83(2)
C(1)	−613(7)	2127(5)	−564(7)	87(4)
C(2)	−39(8)	2650(5)	−967(7)	92(4)
C(3)	535(8)	3095(5)	−228(7)	87(4)
C(4)	318(7)	2847(5)	638(7)	86(4)
C(5)	−370(7)	2251(5)	430(7)	85(4)
C(6)	3080(6)	738(4)	2032(5)	70(3)
C(7)	1582(9)	1848(5)	2699(6)	101(4)
C(8)	383(7)	615(5)	1561(7)	92(4)
C(9)	2457(8)	−787(5)	2479(7)	105(4)
C(10)	2772(10)	290(5)	4035(6)	116(5)
C(11)	4893(8)	−191(5)	3320(7)	105(4)
C(12)	4152(6)	1786(3)	−800(5)	55(2)
C(13)	4333(7)	1069(4)	−774(6)	81(3)
C(14)	5478(7)	797(5)	−495(7)	89(4)
C(15)	6442(7)	1234(5)	−259(6)	78(3)
C(16)	6267(8)	1917(5)	−270(8)	98(4)
C(17)	5143(7)	2209(4)	−551(6)	75(3)
C(18)	2097(6)	1679(3)	−2309(5)	56(2)
C(19)	2802(6)	1663(4)	−2970(5)	63(3)
C(20)	2388(7)	1401(4)	−3874(5)	73(3)
C(21)	1262(7)	1138(4)	−4135(5)	66(3)
C(22)	551(7)	1128(4)	−3484(5)	71(3)
C(23)	970(6)	1403(3)	−2564(5)	59(2)
C(24)	2720(6)	3028(3)	−1493(5)	56(2)
C(25)	3254(6)	3512(4)	−808(5)	66(3)
C(26)	3319(7)	4222(4)	−1061(6)	72(3)
C(27)	2829(8)	4440(4)	−1964(6)	84(3)
C(28)	2263(9)	3966(4)	−2638(6)	93(4)
C(29)	2216(8)	3265(4)	−2413(5)	77(3)
C(30)	1664(6)	1016(5)	−186(5)	66(3)
C(31)	2953(7)	2219(4)	942(5)	60(3)

[a] Equivalent isotropic *U* defined as one-third of the trace of the orthogonalized U_{ij} tensor.

Acknowledgements—Support of this research by the NSF, grant No. RII-88-02973, is gratefully acknowledged. Preliminary studies on this topic were performed by Dr D. Jones.

REFERENCES

1. K. H. Pannell and H. K. Sharma, *Organometallics*, in press.
2. K. H. Pannell and J. R. Rice, *J. Organomet. Chem.* 1974, **78**, C35.
3. K. H. Pannell, S. P. Vincenti and R. C. Scott III, *Organometallics* 1987, **6**, 1593.
4. J. Jeffery, M. F. Lappert, N. T. Luong-Thi, M. Webb, J. L. Atwood and W. E. Hunter, *J. Chem. Soc., Dalton Trans.* 1981, 1593.
5. K. H. Pannell and A. R. Bassindale, *J. Organomet. Chem.* 1982, **229**, 1.
6. M. J. Bennett and K. A. Simpson, *J. Am. Chem. Soc.* 1971, **93**, 7156.
7. A. R. Barron, G. Wilkinson, M. Motavelli and M. B. Hursthouse, *J. Chem. Soc., Dalton Trans.* 1987, 837.
8. K. H. Pannell, *J. Organomet. Chem.* 1970, **21**, 17.
9. (a) C. L. Randolf and M. S. Wrighton, *Organometallics* 1987, **6**, 365; (b) C. Lewis and M. S. Wrighton, *J. Am. Chem. Soc.* 1983, **105**, 7768.
10. (a) D. H. Berry and L. J. Procopio, *J. Am. Chem. Soc.* 1989, **111**, 4099; (b) D. H. Berry, J. H. Chey, C. H. Zipin and P. J. Carroll, *J. Am. Chem. Soc.* 1990, **112**, 452.
11. B. K. Campion, R. H. Heyn and T. D. Tilley, *J. Am. Chem. Soc.* 1990, **112**, 4079; (b) 1988, **110**, 1558.

12. (a) C. White and R. J. Mawby, *Inorg. Chim. Acta* 1970, **4**, 261; (b) T. C. Forschner and A. R. Cutler, *Organometallics* 1987, **6**, 889.
13. (a) W. K. Dean and W. A. G. Graham, *Inorg. Chem.* 1977, **16**, 1060; (b) S. R. Berryhill and B. J. Sharenow, *J. Organomet. Chem.* 1981, **221**, 143; (c) G. Thum, W. Ries and W. Malisch, *J. Organomet. Chem.* 1983, **252**, C67; (d) S. R. Berryhill, G. L. Clevenger and Y. P. Burdurli, *Organometallics* 1985, **4**, 1509; (e) P. C. Heah and J. A. Gladysz, *J. Am. Chem. Soc.* 1984, **106**, 7636; (f) G. L. Crocco and J. A. Gladysz, *J. Chem. Soc., Chem. Commun.* 1985, 283; (g) S. Abbot, G. J. Baird, S. G. Davies, I. M. Dordor-Hedgecock, T. D. Maberly, J. C. Walker and P. Warner, *J. Organomet. Chem.* 1985, **285**, C17; (h) K. H. Pannell, C. Hernandez, J. Cervantes, J. Cassias and S. P. Vincenti, *Organometallics* 1986, **5**, 1056; (i) J. L. Crocco, C. S. Young, K. E. Lee and J. A. Gladysz, *Organometallics* 1988, **7**, 2158; (j) J. Cervantes, S. P. Vincenti, R. N. Kapoor and K. H. Pannell, *Organometallics* 1989, **8**, 744.
14. T. C. Forschner and A. R. Cutler, *Inorg. Chim. Acta* 1985, **102**, 113.
15. (a) M. Kumada, J. Nakajima, M. Ishikawa and Y. Yamamoto, *J. Org. Chem.* 1958, **23**, 292; (b) M. Kumada and M. Ishikawa, *J. Organomet. Chem.* 1964, **1**, 411.

Polyhedron Vol. 10, No. 11, pp. 1189–1201, 1991
Printed in Great Britain

0277-5387/91 $3.00+.00
© 1991 Pergamon Press plc

REACTIVITY OF MOLYBDENUM AND TUNGSTEN DISILENE COMPLEXES

DONALD H. BERRY,† JEAN CHEY, HOWARD S. ZIPIN and PATRICK J. CARROLL

Department of Chemistry and Laboratory for Research on the Structure of Matter, University of Pennsylvania, Philadelphia, PA 19104-6323, U.S.A.

Abstract—The reactions of the η^2-disilene complexes $Cp_2M(\eta^2\text{-}Me_2Si{=}SiMe_2)$ (M = Mo, **1a**; W, **1b**) with a variety of inorganic and organic substrates are reported. Compound **1a** reacts with methanol to yield $Cp_2Mo(SiMe_2H)(SiMe_2OMe)$ (**2**, >80%) and $Cp_2Mo(H)(SiMe_2SiMe_2OMe)$ (**3**, < 20%), products of Si—Si and Mo—Si bond cleavages. Nucleophilic attack by methylenetrimethylphosphorane leads to opening of the $MoSi_2$ ring and yields the disilyl-substituted ylide $Cp_2Mo(H)(SiMe_2SiMe_2CH{=}PMe_3)$ (**4**). Although oxygen atom sources such as O_2, N_2O, epoxides and Ph_3PO do not react cleanly with **1**, reaction with elemental sulphur yields the symmetrical sulphur-atom insertion product cyclo-$Cp_2Mo(SiMe_2SSiMe_2)$ (**5**). In contrast, reaction with triphenylphosphine sulphide principally yields the unsymmetrical insertion product cyclo-$Cp_2Mo(SiMe_2SiMe_2S)$ (**6**). Compounds **5** and **6** have been characterized by X-ray diffraction studies. Insertion into the Si—Si bond of **1a** and **1b** is also observed in reactions with trimethylsilylazide and carbon dioxide, which yield cyclo-$Cp_2Mo(SiMe_2N(TMS)SiMe_2)$ (**7**) and cyclo-$Cp_2W(SiMe_2C(O)OSiMe_2)$ (**10**), respectively. Benzophenone also appears to insert between the two silicon atoms in **1a** to yield a five-membered ring compound, but the instability of this product has precluded a definitive assignment of the structure. The four-membered ring compound cyclo-$Cp_2Mo(SiMe_2)_3$ (**8**) has been identified in the reaction of **1a** with dimethylsilylene, generated by the thermolysis of hexamethylsilacyclopropane. Dimethylsilylene insertion is relatively unselective in non-coordinating solvents such as benzene, and the secondary insertion product cyclo-$Cp_2Mo(SiMe_2)_4$ (**9**) is also produced. However, only **8** is formed in tetrahydrofuran, an observation which can be attributed to the higher selectivity of the intermediate silylene–base adduct formed in the coordinating solvent.

There has been remarkable progress over the last few years in the preparation of transition metal complexes of unsaturated silicon ligands. Stable complexes of disilenes ($R_2Si{=}SiR_2$),[1–3] silenes ($R_2Si{=}CR_2$)[4,5] and silylenes ($=SiR_2$)[6,7] have been isolated and characterized to varying degrees. Although stable free silaolefins have been known for nearly 10 years,[8–11] their high reactivity requires the use of extremely bulky substituents for the preparation of stable species. In contrast, the stabilization afforded by coordination to transition metals has allowed the isolation of relatively unhindered silaolefin complexes.

The bonding of a silaolefin to a metal centre can be expected to be similar to that of an organic olefin, which is best described by the Dewar–Chatt–Duncanson model.[12] In this model synergistic σ and π interactions between the olefin p–π and π^* orbitals and metal orbitals of appropriate symmetry lead to a continuum of possible structures bounded by species containing formal sp^2 and sp^3 centres ("olefin complexes" and "metallacyclopropanes") as shown below.

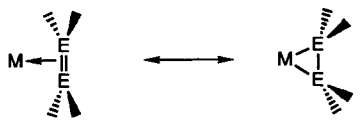

In accord with this model, structural and spectroscopic evidence suggests that partial double bond character is maintained in the ground state structures of silaolefin complexes.[1–3,5] Reactivity is another measure by which the nature of silaolefin complexes can be gauged. This report describes the

† Author to whom correspondence should be addressed.

reactivity of molybdenum and tungsten disilene complexes towards a variety of inorganic and organic reagents. In many cases analogies can be found between the observed transformations and reactions of three-membered ring silicon compounds such as siliranes and disiliranes. In other instances, however, the chemistry parallels that of free disilenes or metal complexes of organic olefins. For the sake of clarity and convenience, the different classes of reactions have been organized and described in terms of transformations of a MSi_2 ring (e.g. ring-opening and insertion reactions).

The molybdenum and tungsten disilene complexes $Cp_2M(\eta^2\text{-}Me_2Si{=}SiMe_2)$ (M = Mo, **1a**; W, **1b**) can be prepared in multi-gram quantities using the procedures described recently by our group.[1,5] The tungsten analogue has been structurally characterized and exhibits a Si—Si bond length intermediate between single and double bond distances and a relatively small degree of pyramidalization at the silicon atoms. These features are analogous to those found in metal complexes of organic olefins.

In considering the reactivity of these Group 6 disilene complexes it is important to note that although the two extreme bonding limits described above differ in formal oxidation states, both formalisms lead to an $18e^-$ configuration at the metal. Thus it is unlikely that the disilene complexes would undergo nucleophilic processes such as associative ligand substitution or oxidative addition reactions at the saturated metal centre.† The transformations described below are consistent with this expectation and can be most easily analysed in terms of initial interactions between the silicon centres and the substrate.

RESULTS AND DISCUSSION

General comments

Disilene complexes **1a** and **1b** are stable for prolonged periods of time at 25°C in the solid state or as hydrocarbon solutions. However, their stability in solution at higher temperatures is limited, and benzene solutions decompose with a half-life of *ca* 1 day at 65°C. Non-polar reagents such as H_2 and $HSiMe_3$ were found to be unreactive towards the disilene complexes at 25 and at 65°C. Compound **1** also does not react with donor ligands such as CO, PMe_3 and C_2H_4. This is in contrast to the analogous tungsten *silene* complexes, $Cp_2W(\eta^2\text{-}Me_2Si{=}CH_2)$, which has been found to react readily at 25°C with H_2, H-$SiMe_3$, PMe_3 and C_2H_4 via a reversible "ring-slip" mechanism.[5] This process is apparently not viable for the disilene complexes.

Although most of the reactions are described for either **1a** or **1b**, the reactions of the other analogues were examined in small-scale NMR tube experiments in several cases (MeOH, Ph_3PS, CO_2) and the chemistry of both disilene complexes appears to be comparable.

Reactions which lead to opening of the MSi_2 *ring*

(a) *Methanolysis of* $Cp_2Mo(\eta^2\text{-}Me_2SiSiMe_2)$ (**1a**). Reaction of **1a** with methanol in benzene yields two products (4 : 1) within 18 h at 25°C. The structures of both can be assigned on the basis of the ^1H NMR spectra. The major product exhibits resonances attributable to equivalent Cp ligands, a —$SiMe_2H$ group and a —$SiMe_2OMe$ group, and can be formulated as $Cp_2Mo(SiMe_2H)(SiMe_2OMe)$ (**2**). In contrast, the minor product exhibits resonances for equivalent Cp ligands, a —$SiMe_2SiMe_2OMe$ group and a molybdenum hydride ($\delta - 7.64$, s, 1H) and is assigned as $Cp_2Mo(H)(SiMe_2SiMe_2OMe)$ (**3**).

Thus methanolysis of **1a** proceeds by two net pathways [eq. (1)]: addition of the methanol O—H bond across the Si—Si bond vector (major) and addition across a M—Si bond vector (minor). In both instances a new Si—O bond is formed. At this point it has not been established whether the mixture represents a kinetic or thermodynamic product distribution.

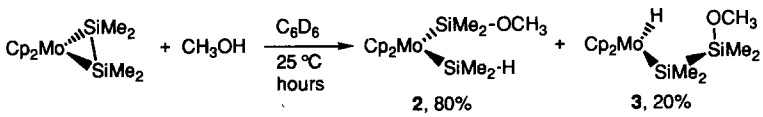

(1)

Methanolysis of **1a** could be initiated by nucleophilic attack of methanol or methoxide at silicon. Approach of the oxygen towards the different sides of the $SiMe_2$ plane could then determine whether M—Si or Si—Si bonds are cleaved. Alternatively, proton transfer from methanol to **1a** could lead to the observed products by an initiating electrophilic interaction.

In contrast to the methanolysis of **1a**, Pham and West have recently reported that reaction of the platinum disilene complex $(Et_3P)_2Pt(\eta^2\text{-}Mes_2SiSiMes_2)$ (Mes = 2,4,6-trimethylphenyl) with ethanol yields only the product of Pt—Si bond cleavage, $(Et_3P)_2Pt(H)(SiMes_2SiMes_2OEt)$.[2b] Interestingly, the methanolysis of platinum complexes of less hindered disilenes is reported to yield an uncharac-

† Note, however, that a degree of unsaturation can be gained by a change in the bonding mode of a Cp ligand. See, for example, ref. 5.

terized mixture containing the products of both Pt—Si and Si—Si bond cleavage.[2b]

Cleavage by alcohols of the Si—Si bond in disilene complexes is reminiscent of the analogous reaction of a disilacyclopropane described by Seyferth and co-workers in 1980.[13] Another interesting parallel can be found in the chemistry of an *organic* olefin complex. In 1974, Wiberg and co-workers described the alcoholysis of the platinum complex of an extremely strained olefin, 2,2,0-bicyclohexene, which yields the product of C—C bond cleavage [eq. (2)].[14] This strained olefin and free disilenes share a common driving force for increased pyramidalization at the olefinic atoms (i.e. greater sp^3-character), which is partially relieved by coordination to a metal centre. Although mechanistic details are not available for either of these Si—Si or C—C bond cleavage reactions, it is clear that Si—Si bond cleavage in **1** is not driven solely by the thermodynamics of Si—O bond formation, or by other factors unique to silicon.

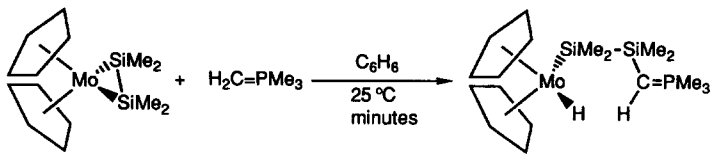

(3)

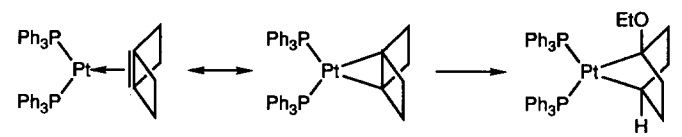

(2)

(b) *Reaction of* **1a** *with methylenetrimethylphosphorane.* Reaction of **1a** with methylenetrimethylphosphorane in benzene at 25°C quantitatively yields a single product within 15 min (55% yield after recrystallization). The product has been identified as the unusual disilyl-substituted ylide $Cp_2Mo(H)(SiMe_2SiMe_2CH{=}PMe_3)$ (**4**) on the basis of spectroscopic and analytical data. In addition to the Cp resonance, the ^1H NMR spectrum of **4** exhibits resonances for a PMe_3 group (δ 0.93, d, $J = 6.09$ Hz, 9H), two $SiMe_2$ groups (δ 0.63 and 0.43, 6H each), the ylide proton (δ 0.55, d, $J_{P-H} = 5.0$ Hz, 1H), and the metal hydride (δ −7.77, 1H). The shift of the single resonance observed in the ^{31}P NMR (δ −1.98) is similar to that seen in other silyl-substituted ylides such as $Me_3SiCH{=}PMe_3$ (δ −1.2).[15] In addition, resonances are observed in the ^{29}Si NMR at δ 1.39 (d, $^3J_{Si-P} = 38.9$ Hz) and −17.1 (d, $^2J_{Si-P} = 14.3$ Hz). The chemical shift and J_{P-C} of the upfield resonance compare well with the silicon in $Me_2HSiCH{=}PMe_3$ (δ −27.9, d, $^2J_{Si-P} = 15.8$ Hz)[16] and suggest the resonance at δ −17.1 in **4** is due to the silicon attached to the ylide carbon. Note that the magnitude of three-bond phosphorus couplings are generally larger than two-bond couplings.[17]

Formation of **4** can be reasonably viewed as occurring by initial attack at silicon by the nucleophilic ylide carbon to yield a zwitterionic intermediate containing both cationic phosphonium and anionic molybdenum centres. Proton transfer from the phosphonium methylene to the metal would then yield **4**. Seyferth and co-workers have reported a similar transformation in the reaction of a silacyclopropane with an ylide, and proposed an analogous zwitterionic intermediate.[18]

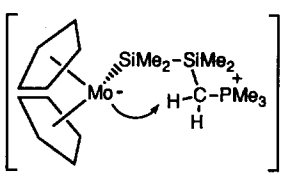

Net one-atom insertion reactions

(a) *Reaction of* **1a** *with elemental sulphur.* Free disilenes have been shown to react with chalcogens to produce the corresponding three-membered ring compounds [e.g. eq. (4)].[19] Analogous reactions of the coordinated disilene in **1a** would yield four-membered ring compounds. Although reaction of **1a** with a variety of oxygen-atom sources (O_2, Ph_3PO, propylene oxide) led to extensive decomposition, sulphur-atom sources were found to yield tractable products.

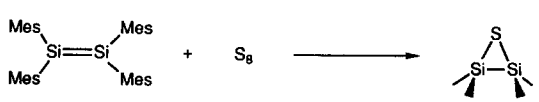

(4)

Treatment of **1a** with elemental sulphur leads to the rapid formation of the symmetrical insertion product, cyclo-$Cp_2Mo(SiMe_2SSiMe_2)$ (**5**), which has been isolated as a red crystalline solid in 54% yield [eq. (5)]. The ^1H NMR spectrum of **2** exhibits

a single resonance due to the Cp ligand and a single resonance due to two $SiMe_2$ groups, consistent with a symmetrical structure. The ^{29}Si NMR spectrum exhibits a single resonance at δ 14.29.

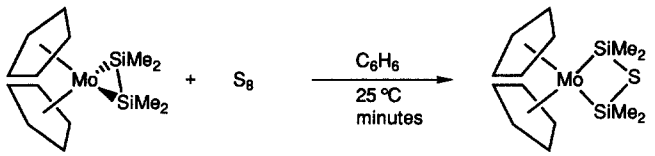

(5)

The structure of **5** was determined by single crystal X-ray diffraction methods. The two unique molecules in the unit cell (**A** and **B**) are shown in Figs 1 and 2. Crystallographic details are summarized in Table 1, and bond distances and angles are listed in Table 2. Structural parameters for the two independent molecules are virtually identical, except for the planarity of the $MoSi_2S$ ring. Each molecule exhibits the pseudo-tetrahedral coordination environment at molybdenum typical for bent metallocenes. The angles subtended at the metals by the Cp ring-centroids in molecules **A** and **B** are 141.2 and 140.9°, and the respective Si—Mo—Si angles are 67.97(6) and 68.83(6)°. The four Mo—Si bond distances measure from 2.550(2) to 2.566(2) Å, in the range expected for typical single bonds.[1] A search of the Cambridge Structural Database found 33 compounds containing a total of 77 Si—S bonds, with a mean distance of 2.134(26) Å. The four Si—S bond lengths in **5** [2.166(3)–2.177(3) Å] are somewhat longer than this mean distance, which can most likely be attributed to the strain of the four-membered ring and the electronic effect of the transition metal on the silicon.

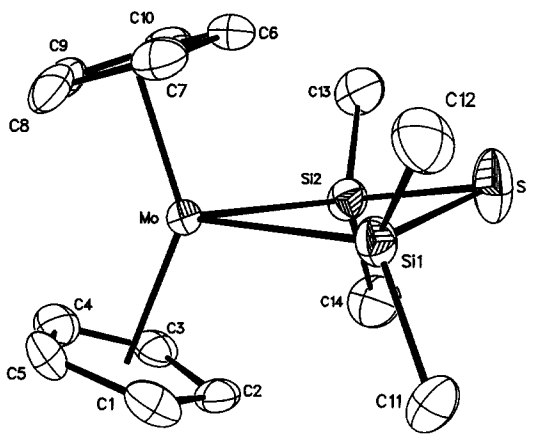

Fig. 1. ORTEP drawing of $Cp_2Mo(SiMe_2SSiMe_2)$ (**5**), molecule **A** showing 30% probability thermal ellipsoids.

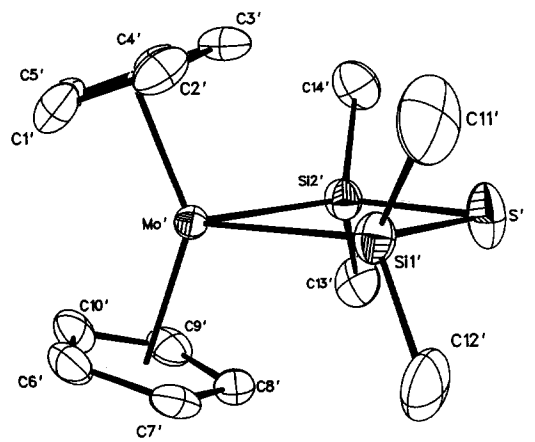

Fig. 2. ORTEP drawing of $Cp_2Mo(SiMe_2SSiMe_2)$ (**5**), molecule **B** showing 30% probability thermal ellipsoids.

The four-membered ring in molecule **B** is essentially planar; the sulphur atom lies only 0.031 Å above the $MoSi_2$ plane and the dihedral angle formed by the $MoSi_2$ and Si_2S planes is only 1.1°. In contrast, the ring in molecule **A** is puckered, with the sulphur atom 0.413 Å above the $MoSi_2$ plane and the corresponding dihedral angle is 14.6°. The conformations of the four-membered rings in molecules **A** and **B** must be very close in energy, and it is likely that crystal packing forces are responsible for the two different geometries. Further evidence for a very soft potential energy surface for distortion of the $MoSi_2S$ ring is found in the thermal ellipsoids of the sulphur atoms, which are elongated perpendicular to the $MoSi_2$ planes in both molecules, and indicate the ease of thermal movement in this direction.

West and Pham have recently reported the structure of a related four-membered ring compound, cyclo-$(Ph_3P)_2Pt(SiMe_2OSiMe_2)$, formed by oxidation of a platinum disilene complex.[2b] This complex exhibits a relatively short trans-annular Si—Si separation of 2.549(2) Å, which has been interpreted in terms of possible cross-ring bonding between the silicon atoms. Typical Si—Si single bond lengths are *ca* 2.34 Å.[20] The trans-annular Si—Si distances in the two molecules of **5** are 2.865 and 2.888 Å, and are long enough to preclude any significant bonding interaction. Short Si—Si contacts are clearly not an inherent feature of MSi_2X rings.

Although the parallel can be made between the

Table 1. Crystallographic data for structure determinations of **5** and **6**

	5	**6**[a]
Formula	$MoSSi_2C_{14}H_{22}$	$MoSSi_2C_{14}H_{22}$
Formula weight	374.51	374.51
Crystal dimensions (mm)	$0.42 \times 0.20 \times 0.12$	$0.45 \times 0.33 \times 0.30$
Crystal class	Orthorhombic	Monoclinic
Space group	*Pbca* (No. 61)	$P2_1/c$ (No. 14)
Z	16	4
Cell constants		
a (Å)	17.101(3)	12.720(3)
b (Å)	17.604(2)	8.136(3)
c (Å)	21.601(3)	16.178(7)
β (°)		97.06(3)
V (Å^3)	6503(3)	1662(2)
μ (cm^{-1})	10.39	10.16
D_{calc} (g cm^{-3})	1.53	1.50
$F(000)$	3072	768
Radiation	Mo-$K_{\bar{\alpha}}$	Mo-$K_{\bar{\alpha}}$ ($\lambda = 0.71073$ Å)
θ Range (°)	2.5–27.5	2.5–27.5
Scan mode	ω–2θ	ω–2θ
h, k, l collected	20, 20, 25	16, 10, ± 20
Number of reflections measured	6304	4266
Number of unique reflections	5712	3819
Number of reflections used in refinement	3281 ($> 3.0\sigma$)	2380 ($> 3.0\sigma$)
Number of parameters	325	163
Data/parameter ratio	10.1	14.6
R_1	0.035	0.099
R_2	0.041	0.139
GOF	1.104	3.983

[a] The structure of compound **6** was determined from a twinned crystal (see Experimental).

Table 2. Selected bond distances (Å) and angles (°) in **5**[a]

Mo—Si(1)	2.559(2)	Mo′—Si(1′)	2.558(2)
Mo—Si(2)	2.566(2)	Mo′—Si(2′)	2.550(2)
Si(1)—S	2.166(3)	Si(1′)—S′	2.168(3)
Si(1)—C(11)	1.884(7)	Si(1′)—C(11′)	1.887(8)
Si(1)—C(12)	1.880(7)	Si(1′)—C(12′)	1.871(8)
Si(2)—S	2.177(3)	Si(2′)—S′	2.176(3)
Si(2)—C(13)	1.873(8)	Si(2′)—C(13′)	1.892(7)
Si(2)—C(14)	1.892(8)	Si(2′)—C(14′)	1.888(7)
Cp(1)[b]—Mo—Cp(2)[b]	141.2	Cp(1′)[b]—Mo′—Cp(2′)[b]	140.9
Si(1)—Mo—Si(2)	67.97(6)	Si(1′)—Mo′—Si(2′)	68.83(6)
Mo—Si(1)—S	103.82(9)	Mo′—Si(1′)—S′	103.91(9)
Mo—Si(1)—C(11)	120.2(2)	Mo′—Si(1′)—C(11′)	120.5(3)
Mo—Si(1)—C(12)	120.5(2)	Mo′—Si(1′)—C(12′)	120.9(3)
S—Si(1)—C(11)	104.9(2)	S′—Si(1′)—C(11′)	104.0(3)
S—Si(1)—C(12)	104.7(2)	S′—Si(1′)—C(12′)	104.1(3)
C(11)—Si(1)—C(12)	101.0(3)	C(11′)—Si(1′)—C(12′)	101.2(4)
Mo—Si(2)—S	103.29(9)	Mo′—Si(2′)—S′	103.94(9)
Mo—Si(2)—C(13)	121.1(2)	Mo′—Si(2′)—C(13′)	120.5(2)
Mo—Si(2)—C(14)	120.1(3)	Mo′—Si(2′)—C(14′)	119.3(2)
S—Si(2)—C(13)	103.3(2)	S′—Si(2′)—C(13′)	105.2(3)
S—Si(2)—C(14)	105.6(3)	S′—Si(2′)—C(14′)	106.5(2)
C(13)—Si(2)—C(14)	101.5(4)	C(13′)—Si(2′)—C(14′)	100.1(4)
Si(1)—S—Si(2)	82.53(9)	Si(1′)—S′—Si(2′)	83.31(9)

[a] Numbers in parentheses are ESDs in the least significant digits.
[b] Cp(1) and Cp(2) refer to the C_5H_5 ring centroids.

Table 3. Selected bond distances (Å) and angles (°) in **6**[a]

Mo—S	2.524(4)	Cp(1)[b]—Mo—Cp(2)[b]	138.9
Mo—Si(1)	2.588(5)	S—Mo—Si(1)	75.1(1)
S—Si(2)	2.125(7)	Mo—S—Si(2)	98.4(2)
Si(1)—Si(2)	2.315(6)	Mo—Si(1)—Si(2)	91.9(2)
Si(1)—C(11)	1.91(2)	Mo—Si(1)—C(11)	121.0(6)
Si(1)—C(12)	1.94(2)	Mo—Si(1)—C(12)	118.0(7)
Si(2)—C(13)	1.93(3)	C(11)—Si(1)—C(12)	101.5(9)
Si(2)—C(14)	1.91(2)	S—Si(2)—Si(1)	89.1(2)
		C(11)—Si(1)—C(12)	101.5(9)
		S—Si(2)—Si(1)	89.2(1)
		C(13)—Si(2)—C(14)	108.0(1)

[a] Numbers in parentheses are ESDs in the least significant digits.
[b] Cp(1) and Cp(2) refer to the C_5H_5 ring centroids.

reactions of sulphur with complexed and free disilenes, there are similar analogies with small-ring silicon compounds. Boudjouk and Samaraweera recently reported formation of a silathietane by treatment of the silirane *cyclo*-(t-Bu)$_2$SiCHMeCHMe with elemental sulphur; i.e. net sulphur-atom insertion into the Si—C bond of a three-membered ring.[21] A similar insertion of a sulphur atom into the Si—Si bond of a disilacyclobutane has been reported by Seyferth and co-workers.[22]

(b) *Reaction of* **1a** *with triphenylphosphine sulphide.* In contrast to the reaction with elemental sulphur, reaction of **1a** with triphenylphosphine sulphide in benzene at 25°C (6 days) yields principally the unsymmetrical sulphur-atom insertion product cyclo-$Cp_2Mo(SiMe_2SiMe_2S)$ (**6**), in addition to the symmetrical isomer **5** (*ca* 3 : 1). Recrystallization of the mixture from toluene affords **6** as a pure material (40% yield). The ^{1}H NMR spectrum of **6** exhibits a singlet due to the Cp and two singlets due to inequivalent $SiMe_2$ groups, consistent with the unsymmetrical structure. In addition, resonances at δ 47.0 and −24.5 are observed in the ^{29}Si NMR spectrum.

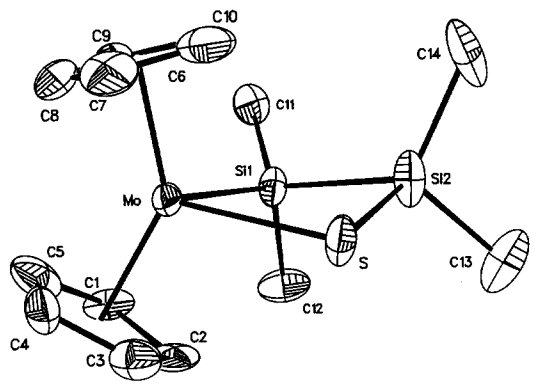

Fig. 3. ORTEP drawing of $Cp_2Mo(SiMe_2SiMe_2S)$ (**6**), showing 30% probability thermal ellipsoids.

Although well-formed crystals of **6** could be readily grown from a variety of organic solvents, preliminary X-ray diffraction studies indicated that all were twinned. The geometrical relationship of the two interpenetrating unit cells was determined and diffraction data were collected for one of the unit cells (see Experimental). Solution by heavy atom methods and refinement of the data yielded the structure shown in Fig. 3. Crystallographic details are summarized in Table 1. Although the basic structural features should be reliable and all bond parameters are within chemically reasonable ranges (Tables 4 and 5), the twinning complication dictates that the values of the bond lengths and angles be interpreted with some caution.

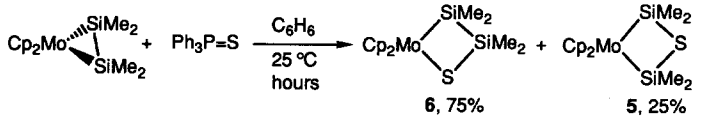

(6)

The structure consists of a puckered four-membered ring and is made up of molybdenum, sulphur and two silicon atoms. As expected on the basis of the spectroscopic data, the sulphur atom is situated between the metal and one of the silicon atoms. The $MoSi_2S$ ring in **6** is non-planar, and Si(2) lies 0.65 Å above the MoSiS plane. The MoSiS and Si_2S planes subtend a dihedral angle of 24.5°.

The formation of **6** may be related to the reaction of **1** with methylenetrimethylphosphorane. Attack at silicon by phosphine sulphide would lead to an analogous zwitterionic intermediate in which proton transfer cannot readily occur. Displacement of triphenylphosphine by the anionic metal centre in the intermediate would then result in ring closure to produce **6**. Consistent with this premise, reaction of **1a** with *triethyl*phosphine sulphide yields a mixture of several products exhibiting upfield resonances characteristic of molybdenum hydrides in the ^{1}H NMR spectrum. These products presumably arise from proton transfer to the metal from the acidic phosphonium alkyl groups in the proposed intermediate, accompanied by decomposition of the resulting sulphur-substituted ylide.

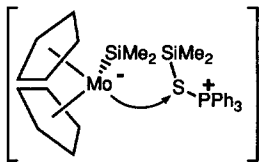

(c) *Reaction of* **1a** *with trimethylsilylazide.* Compound **1a** reacts with trimethylsilylazide in benzene at 25°C to yield the symmetrical nitrogen-atom insertion product, cyclo-$Cp_2Mo(SiMe_2(NSiMe_3)SiMe_2)$ (**7**). Analysis of the reaction mixture by NMR indicates that **7** is produced quantitatively, although the high solubility of the compound resulted in a low isolated yield (29%) following recrystallization. The reaction is complete in less than 1 h, and no intermediates were observed by ^{1}H NMR. The ^{1}H NMR spectrum shows a single resonance due to the Cp ligand and a singlet due to four equivalent silicon methyl groups indicative of a symmetrical structure. In addition, a singlet due to the trimethylsilyl group on the azide is observed. The ^{29}Si NMR spectrum exhibits two singlets at δ 15.63 and −6.21.

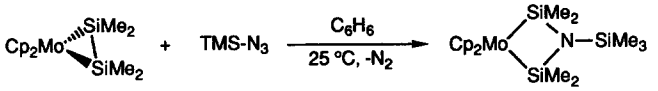

(7)

It should be noted that trimethylsilylazide does not decompose to the nitrene under the extremely mild reaction conditions used to prepare **7**, thus a simple nitrene insertion process can be excluded from consideration. West and co-workers, however, have reported that the stable disilene Mes_4Si_2 undergoes 1,3-dipolar additions with a variety of organic azides.[19a] In two instances the initial five-membered ring product is observed prior to formation of the azadisiliranes by N_2 extrusion [eq. (8)].

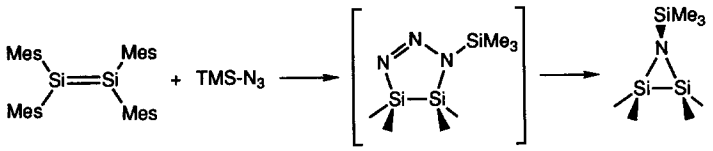

(8)

The facile reaction of **1a** with TMS-N_3 may reflect partial π-character in the coordinated disilene fragment, and could thus involve a formal dipolar addition of the azide.

(d) *Reaction of* **1a** *with hexamethylsilacyclopropane.* Dimethylsilylene has been shown to react readily with a wide variety of substrates. Examples include insertion of dimethylsilylene into silicon and transition metal hydride bonds,[23,24] insertion into Si—C bonds of a silacyclopropane to form a disilacyclobutane,[22] and addition to multiple bonds in organic compounds.[23] However, the harsh thermal or photochemical conditions employed for silylene generation are not suited for studying the reactions of silylenes with most transition metal complexes. However, as reported by Seyferth *et al.*,[25] the thermolysis of hexamethylsilacyclopropane (HMS) generates dimethylsilylene at *ca* 65°C, conditions sufficiently mild to allow examination of the reaction of dimethylsilylene with **1a**.

Reaction of **1a** with hexamethylsilacyclopropane in benzene-d_6 at 65°C initially yields the single insertion product, cyclo-$Cp_2Mo(SiMe_2)_3$ (**8**), as shown in eq. (9). The silylene insertion is not particularly selective in benzene solution, and the secondary insertion product, cyclo-$Cp_2Mo(SiMe_2)_4$ (**9**), is also observed before 50% of **1a** has been consumed. In addition, octamethyl-1,2-disilacyclobutane is also formed as a result of competing insertion of dimethylsilylene into HMS.[22] Compound **8** exhibits resonances in the ^{1}H NMR spectrum due to a single Cp ligand and two unequal sets of silicon methyl groups (δ 0.47, 6H and 0.46, 12H). The double insertion product, **9**, shows a similar spectrum,

of equal intensity (δ 0.42, 12H and 0.33, 12H). It has not been established whether silylene insertion occurs into M—Si or Si—Si bonds.

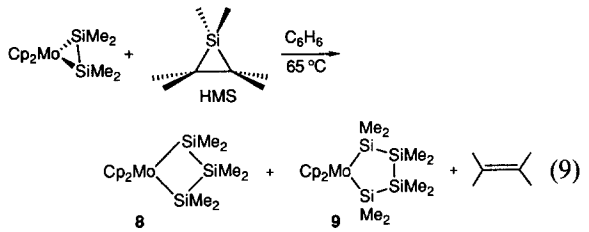

(9)

Previous studies by our group[24] and other workers[26–30] have shown that the selectivity of silylene reactions is greatly enhanced in the presence of Lewis bases. The increased selectivity is attributed to the formation of intermediate base-silylene adducts, which are more discriminating than free dimethylsilylene. Indeed, reaction of **1a** with HMS in the coordinating solvent tetrahydrofuran-d_8 at 65°C yields the single insertion product **8** as the only molybdenum-containing compound.

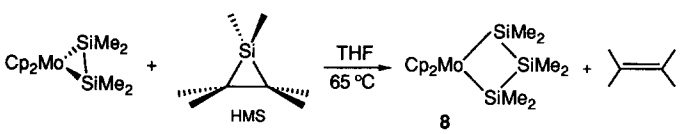

(10)

Net two-atom insertion reactions

(a) *Reaction of* **1a** *with carbon dioxide.* Carbon dioxide generally behaves as a Lewis acid towards transition metal complexes. Typical reactions of carbon dioxide with transition metal complexes involve simple coordination through carbon, or insertion into metal–alkyl or –hydride bonds to produce carboxylates of the general form MO_2CR.[31] Less commonly, metalloesters of the form MCO_2R are produced. Although not as extensively studied, reaction of carbon dioxide with metal silyl complexes yields products derived from initial metalloester (MCO_2SiR_3) formation.[32–35] The latter presumably reflects the favourable thermodynamics of Si—O bond formation, as well as differences in the electronic polarization of M—Si and M—C bonds.

Treatment of **1b** with 1 equiv. of carbon dioxide at 25°C leads to a rapid reaction in which cyclo-$Cp_2W(SiMe_2OC(O)SiMe_2)$ (**10**) is produced in nearly quantitative yield by ^{1}H NMR (72% isolated). Compound **10** is the net result of C=O insertion into the Si—Si bond of the disilene complex. The regiochemistry of the insertion is confirmed by the ^{29}Si NMR spectrum, which exhibits two resonances showing satellites due to the ^{183}W nucleus (δ 50.4, $^1J_{W-Si}$ = 112.7 Hz and δ 15.2, ^1J = 103.9 Hz). The magnitude of these spin–spin couplings clearly indicates both silicon atoms are directly attached to the tungsten centre. The resonance at δ 15.2 can be assigned to the silicon between the metal and the carbonyl carbon by the large ^{13}C coupling observed in a sample prepared with $^{13}CO_2$ ($^1J_{C-Si}$ = 59.6 Hz). In contrast, the silicon resonance at δ 50.4 exhibits a relatively small coupling to the carbonyl ($^2J_{C-Si}$ = 7.2 Hz). The ^{1}H NMR spectrum of the ^{13}C-enriched sample also exhibits spin–spin coupling between the carbonyl carbon and the protons of one $SiMe_2$ group ($^3J_{C-H}$ = 2.0 Hz). The carbonyl is observed in the ^{13}C NMR spectrum as a singlet at δ 197.6, which does not exhibit tungsten satellites. The carbonyl stretching mode is observed as a band at 1675 cm^{-1} in the IR spectrum.

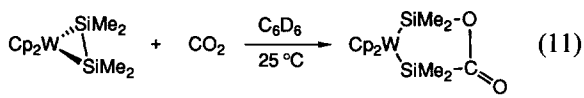

(11)

Although the reaction of carbon dioxide with the disilene complex could be viewed as proceeding by nucleophilic attack at silicon by an oxygen centre, an initial electrophilic interaction would be more consistent with the established reactivity of carbon dioxide.

(b) *Reaction of* **1a** *with benzophenone.* Free disilenes react with aldehydes and ketones to produce disilaoxetanes.[36] Siliranes also react with organic carbonyl compounds, yielding five-membered rings as products.[37] The latter reaction only proceeds readily with α,β-unsaturated ketones and aldehydes.

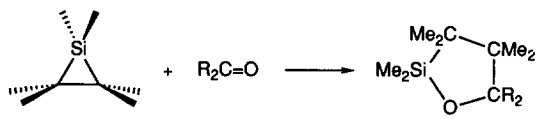

(12)

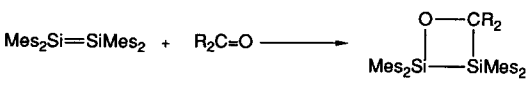

(13)

Disilene complex **1a** cleanly reacts with 1 equiv. of benzophenone within 1 h at 25°C to yield a single product exhibiting resonances in the ^{1}H NMR spectrum for a single Cp, two $SiMe_2$ groups (δ 0.54, 6H

and 0.59, 6H) and the phenyl groups. Unfortunately, the product is unstable and decomposes within hours to a complex mixture, thwarting all attempts to isolate the adduct. Although the 1 : 1 stoichiometry of the reaction is clear from the ^{1}H NMR, the regiochemistry of the addition is less certain. We favour the regiochemistry shown in eq. (14), in which the carbonyl fragment has been inserted between the Si—Si bond of **1a**, analogous to the carbon dioxide reaction described above.

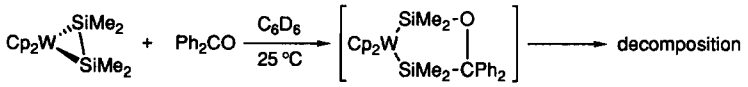

(14)

Acetone reacts only very slowly with **1a** and yields a complex mixture of products. The observation of resonances characteristic of vinylic protons in the ^{1}H NMR of this mixture suggests that acetone may react as a weak acid (cf. methanol), rather than undergoing an insertion reaction. The greater reactivity of benzophenone relative to acetone towards **1a** may reflect the greater electrophilicity of the carbonyl carbon in benzophenone. Alternatively, the benzophenone insertion may involve an initial electron transfer step to form a benzophenone radical anion, which subsequently attacks a silicon centre in the radical cation of **1a**.

CONCLUSIONS

In summary, although η^2-disilene complexes **1a** and **1b** are coordinatively saturated at the transition metals, reaction is observed with a wide variety of both nucleophilic and electrophilic reagents under extremely mild conditions. The reactions are presumably initiated by interactions with the reactive disilicon moiety. Analogies with the reaction chemistry of both disilenes and three-membered ring compounds can be found for most of the observed reactions of the disilene complexes. However, the preponderance of reactions which lead to cleavage of the Si—Si bond suggests that the three-membered ring analogy will be the most helpful for predicting the outcome of new reactions.

EXPERIMENTAL

General considerations

All manipulations were carried out under dry nitrogen using high vacuum-line or Schlenk techniques or in a Vacuum Atmospheres glovebox. Glassware was oven-dried before use. Petroleum ether (boiling range 35–65°C), tetrahydrofuran (THF), benzene and toluene were freshly distilled from sodium/benzophenone ketyl. IR spectra were measured on a Perkin–Elmer 1430 spectrophotometer. ^{1}H NMR spectra were obtained using IBM-Bruker AC 250 or AM 200 spectrometers. ^{13}C NMR and ^{29}Si experiments were measured using the DEPT or INEPT pulse sequences or gated coupled spectra to obtain coupling constants. Elemental analyses were performed by Desert Analytics (Tucson). High resolution mass spectral analyses were performed on a VG Instruments ZAB-E spectrometer.

Reaction of **1a** *with methanol: formation of* **2** *and* **3**

An NMR tube containing 0.05 cm^3 of methanol, 10 mg of **1a** and 0.5 cm^3 of benzene-d_6 was sealed under vacuum. The reaction was monitored by ^{1}H NMR, which indicated that the reaction was complete after 18 h. ^{1}H NMR of $Cp_2Mo(SiMe_2H)(SiMe_2OMe)$ (**2**): δ 4.7 (m, 1H, Si—*H*), 4.03 (s, 10H, *Cp*), 3.40 (s, 3H, OCH_3), 0.54 (s, 6H, $SiMe_2$), 0.47 (d, J = 1.94 Hz, 6H, $SiMe_2$). ^{1}H NMR of $Cp_2Mo(H)(SiMe_2SiMe_2OMe)$ (**3**): δ 4.22 (s, 10H, *Cp*), 3.38 (s, 3H, OCH_3), 0.30 (s, 6H, $SiMe_2$), 0.28 (s, 6H, $SiMe_2$), −7.64 (s, 1H, Mo*H*).

Synthesis of $Cp_2Mo(H)(SiMe_2SiMe_2CHPMe_3)$ (**4**)

A solution of **1a** (100 mg, 0.29 mmol) and methylenetrimethylphosphorane (3.25 cm^3, 0.29 mmol) in 15 cm^3 of benzene was stirred for 1 h under nitrogen at 25°C. Solvent was removed *in vacuo*, yielding 80 mg (63%) of **4**. Recrystallization from toluene/petroleum ether at −30°C yielded 70 mg (55%). ^{1}H NMR: 4.39 (s, 10H, *Cp*), 0.93 (d, 9H, PMe_3), 0.64 (s, 6H, $SiMe_2$), 0.44 (s, 6H, $SiMe_2$), −0.5 (d, 1H, =C*H*), −7.8 (s, 1H, Mo*H*). ^{31}P NMR: δ −1.98. ^{29}Si NMR (DEPT): δ 1.39 (d, J = 38.86 Hz), −17.13 (d, J = 14.25 Hz). Found: C, 49.80; H, 7.26. Calc. for $C_{18}H_{33}MoPSi_2$: C, 49.98; H, 7.69%.

Synthesis of cyclo-$Cp_2Mo(SiMe_2SiMe_2S)$ (**5**)

A solution of **1a** (197 mg, 0.585 mmol) in 40 cm^3 of toluene was slowly added to S_8 (155 mg, 0.60 mmol) and stirred for 1.5 h under nitrogen. Solvent

was removed *in vacuo* and recrystallization from toluene at −78°C yielded 119 mg (54%) of **5**. ^{1}H NMR: δ 4.02 (s, 10H, *Cp*), 0.70 (s, 12H, Si*Me*$_2$). ^{29}Si NMR (DEPT): δ 14.29. Satisfactory analysis for **5** could not be obtained despite multiple recrystallizations and submissions, possibly as a result of residual sulphur. Found: C, 40.32; H; 5.14. Calc. for $C_{14}H_{22}SSi_2Mo$: C, 44.90; H, 5.92%.

Synthesis of cyclo-$Cp_2Mo(SiMe_2SiMe_2S)$ (**6**)

A solution of **1a** (145 mg, 0.424 mmol) and triphenylphosphine sulphide (125 mg, 0.37 mmol) in 100 cm^3 of benzene was stirred for 6 days at 25°C under nitrogen. Solvent was removed *in vacuo*, yielding a 3:1 mixture of **6** and **5** (^{1}H NMR). Triphenylphosphine and residual triphenylphosphine sulphide were extracted with 100 cm^3 of petroleum ether. Recrystallization of the residue from toluene at −30°C yielded 65 mg (41%) of pure **6**. ^{1}H NMR: δ 4.26 (s, 10H, *Cp*), 0.62 (s, 6H, Si*Me*$_2$), 0.51 (s, 6H, Si*Me*$_2$). ^{29}Si NMR (DEPT): δ 46.96, −24.48. Found: C, 44.79; H, 5.78. Calc. for $C_{14}H_{22}SSi_2Mo$: C, 44.90; H, 5.92%.

Synthesis of cyclo-$Cp_2Mo(SiMe_2N(TMS)SiMe_2)$ (**7**)

A solution of **1a** (140 mg, 0.438 mmol) and azidotrimethylsilane (0.120 cm^3, 0.86 mmol) in 20 cm^3 of benzene was stirred at 25°C for 1 h. Examination of the reaction mixture by ^{1}H NMR indicates that **7** was the only product formed. Solvent was removed *in vacuo* and the product was recrystallized from toluene/hexanes at −35°C to yield 50 mg (29%) of pure **7**. ^{1}H NMR: δ 4.0 (s, 10H, *Cp*), 0.49 (s, 9H, Si*Me*$_3$), 0.30 (s, 6H, Si*Me*$_2$). ^{29}Si NMR (DEPT): 15.63, −6.21. Found: C; 47.79; H, 7.31. Calc. for $C_{17}H_{31}MoSi_3N$: C, 47.55; H, 7.23%.

Reaction of **1a** *with* HMS *in benzene-d*$_6$: *formation of* **8** *and* **9**

To an NMR tube containing **1a** (14 mg, 0.41 mmol) and 0.5 cm^3 of benzene-d$_6$ was added hexamethylsilacyclopropane (0.015 cm^3, *ca* 0.80 mmol). After 20 min at 65°C (15% conversion of **1a**), only cyclo-$Cp_2Mo(SiMe_2)_3$ (**8**) was observed. ^{1}H NMR: δ 0.94 (s, 10H, *Cp*), 0.47 (s, 6H, Si*Me*$_2$), 0.46 (s, 12H, Si*Me*$_2$). With further heating (< 50% conversion of **1a**), formation of cyclo-$Cp_2Mo(SiMe_2)_4$ (**9**) was observed. ^{1}H NMR: δ 3.88 (s, 10H, *Cp*), 0.42 (s, 12H, Si*Me*$_2$), 0.33 (s, 12H, Si*Me*$_2$).

Reaction of **1a** *with* HMS *in tetrahydrofuran-d*$_8$: *formation of* **8**

To an NMR tube containing **1a** (14 mg, 0.41 mmol) and 0.5 cm^3 of tetrahydrofuran-d$_8$, was added hexamethylsilacyclopropane (0.015 cm^3, *ca* 0.80 mmol). Thermolysis at 65°C for 18 h resulted in complete conversion of **1a** and formation of **8** as the only molybdenum-containing product observed.

Synthesis of cyclo-$Cp_2W(SiMe_2OC(O)SiMe_2)$ (**10**)

Carbon dioxide (0.18 mmol) was condensed onto a frozen solution containing **1b** (74 mg, 0.17 mmol) in 15 cm^3 of benzene at −196°C and the mixture allowed to warm to room temperature. A rapid colour change from dark orange to yellow was observed and then solvent was removed *in vacuo*. The solid was extracted with benzene and recrystallized from THF, yielding 59 mg (72%) of **10** as yellow crystals. ^{1}H NMR (C_6D_6): δ 3.75 (s, 10H, *Cp*), 0.50 (s, 6H, Si*Me*$_2$), 0.47 (s, 6H, Si*Me*$_2$). ^{29}Si NMR (DEPT, in THF-d$_8$): δ 50.4 ($^1J_{W-S}$ = 112.7 Hz, *Si*OC), 15.2 ($^1J_{W-Si}$ = 103.9 Hz, *Si*CO). ^{29}Si NMR (**10**-$^{13}CO_2$, DEPT, C_6D_6): δ 50.4 ($^2J_{C-Si}$ = 7.2 Hz), 15.5 ($^1J_{C-Si}$ = 59.6 Hz). ^{13}C NMR (**10**-$^{13}CO_2$, C_6D_6): δ 197.61 (Si*C*O$_2$Si), 76.49 (Cp), 8.66 (Si*Me*$_2$), 4.44 (Si*Me*$_2$). IR (C_6D_6 solution): ν(C=O) = 1675 cm^{-1}. Found: C, 38.01; H, 4.72. Calc. for $C_{15}H_{22}O_2Si_2W$: C, 37.98; H, 4.67%.

Reaction of **1a** *with benzophenone*

The reaction of **1a** (6 mg) and benzophenone (3 mg) in benzene-d$_6$ in an NMR tube was followed by ^{1}H NMR. After 1 h the reaction had reached 90% completion with formation of a single product. ^{1}H NMR: δ 7.0 (m, Ph), 3.84 (s, 10H, *Cp*), 0.54 (s, 6H, Si*Me*$_2$), 0.59 (s, 6H, Si*Me*$_2$). The product is not stable and decomposes within hours at 25°C.

Structure determinations of **5** *and* **6**

General crystallographic procedures. Crystals of suitable size were grown from toluene/hexanes at −35°C, sealed in 0.5-mm thin-walled Pyrex capillaries in the glove box and the capillaries mounted on the diffractometer. Refined cell dimensions and their standard deviations were obtained from least-squares refinement of 25 accurately centred reflections with $2\theta > 25°$. Crystal data are summarized in Table 1.

Diffraction data were collected at 295 K on an Enraf–Nonius four-circle CAD-4 diffractometer employing graphite monochromated Mo-K_α radiation. The intensities of three standard reflections

were measured at intervals of *ca* 80 reflections to check for systematic change during data collection. Data collection is summarized in Table 1. The raw intensities were corrected for Lorentz and polarization effects by using the program BEGIN from the SDP+package.[38]

All calculations were performed on a VAX 11/785 computer using the SDP+software package.[38] The full-matrix least-squares refinement was based on F, and the function minimized was $\Sigma w(|F_o|-|F_c|)^2$. The weights (w) were taken as $4F_o^2/[\sigma(F_o^2)]^2$, where $|F_o|$ and $|F_c|$ are the observed and calculated structure factor amplitudes. Atomic scattering factors and complex anomalous dispersion corrections were taken from refs 39–41. Agreement factors are defined as $R_1 = \Sigma||F_o|-|F_c||/\Sigma|F_o|$ and $R_2 = [\Sigma w||F_o|-|F_c||^2/\Sigma w|F_o|^2]^{1/2}$. The goodness-of-fit is defined as GOF $= [\Sigma w(|F_o|-|F_c|)^2/(N_o-N_p)]^{1/2}$, where N_o and N_p are the number of observations and parameters. Final positional and thermal parameters for both structures have been deposited with the Cambridge Crystallographic Data Centre.

Solution and refinement of **5**. A decay correction (18% maximum, 8% average, based on F) was applied to the data. The orthorhombic space group *Pbca* was uniquely determined by the systematic absences. On the basis of the calculated density, 16 molecules (two unique) were expected in the unit cell. The coordinates of two independent molybdenum atoms were obtained by using the program Multan.[38] Analysis of subsequent Fourier maps led to location of the remaining heavy atoms. Refinement using anisotropic Gaussian amplitudes followed by difference Fourier synthesis resulted in the location of most of the Cp hydrogen atoms and at least one hydrogen atom on each methyl group. All remaining hydrogen atoms were placed at idealized locations [D(C—H) = 0.95 Å] using the program HYDRO.[38] Final refinement included anisotropic Gaussian amplitudes for all non-hydrogen atoms and fixed positions and fixed isotropic parameters for the hydrogen atoms. Structure refinement is summarized in Table 1.

Solution and refinement of **6**. A unit cell could not be initially determined from 25 accurately centred reflections. However, approximately half of the reflections fit one monoclinic cell, and the remaining reflections fit a second, related, monoclinic cell, suggestive of a twinned crystal. Approximately 10 well-formed crystals were examined and found to exhibit this twinning, thus data collection was attempted using one of the apparent cells (see Table 1). The molybdenum atom was located from a Patterson map and Fourier methods led to the location of all remaining heavy atoms. Hydrogen atoms were found or placed as described above. Refinement using anisotropic Gaussian amplitudes led to agreement factors of $R_1 = 0.099$, $R_2 = 0.139$ and GOF = 3.983.

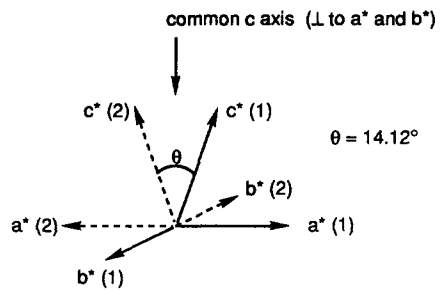

Fig. 4. Relationship of twinned unit cells in crystals of **6**.

The intensities of several reflections were compared in both of the twins and found to be approximately equal, suggesting a *ca* 1 : 1 twin. Analysis of the two twinned unit cells showed the cells were related by a rotation of 180° about a common c axis, resulting in the coincidence of the a^* axis of twin 1 with the $-a^*$ axis of twin 2 and the b^* axis of twin 1 with the $-b^*$ axis of twin 2 (Fig. 4). The c^* axes of the two twins subtend an angle of 14.12°. It was further possible to calculate that reflections for the two cells would be roughly coincident for all reflections in which the l-index is a multiple of *ca* 5 (e.g. $l = 5$, 10, 15, etc). This prediction was confirmed by analysis of the full data set using the program PERFACT, which showed the expected trend of agreement factor as a function of the l-index.† Refinement of the structure excluding reflections with $l = 5$, 10 and 15 led to improved agreement factors $R_1 = 0.077$, $R_2 = 0.118$ and GOF = 3.408. Bond distances and angles did not change significantly in this test refinement (Δ distances < 0.03 Å, Δ angles < 1°). Deconvolution of the coincident data in the full data set was not attempted. As mentioned in the Discussion, it is important to stress that this partial structure determination is included only as a measure of the basic structural features in **6**, and the exact values of the metrical data should be interpreted with caution.

† Maximum overlap of the reciprocal lattices occurs at intervals along c^* corresponding to l-index values which are multiples of slightly greater than 5, hence the intensities of reflections with $l = 6$, 11 and 16 also have contributions from the second twin.

Acknowledgements—This work was supported by the National Science Foundation (Grant No. CHE-88-08161) and the Pew Science Program. D.H.B. also thanks

the Alfred P. Sloan Foundation for a research fellowship (1990–1992) and the University of Pennsylvania Natural Science Association for a Young Faculty Award.

REFERENCES

1. D. H. Berry, J. H. Chey, H. S. Zipin and P. J. Carroll, *J. Am. Chem. Soc.* 1990, **112**, 452.
2. (a) E. K. Pham and R. West, *J. Am. Chem. Soc.* 1989, **111**, 7667; (b) E. K. Pham and R. West, *Organometallics* 1990, **9**, 1517.
3. (a) E. A. Zarate, C. A. Tessier-Youngs and W. J. Youngs, *J. Am. Chem. Soc.* 1988, **110**, 4068; (b) E. A. Zarate, C. A. Tessier-Youngs and W. J. Youngs, *J. Chem. Soc., Chem. Commun.* 1989, 577; (c) A. B. Anderson, P. Shiller, E. A. Zarate, C. A. Tessier-Youngs and W. J. Youngs, *Organometallics* 1989, **8**, 2320.
4. (a) B. K. Campion, R. Heyn and T. D. Tilley, *J. Am. Chem. Soc.* 1988, **110**, 7558; (b) B. K. Campion, R. Heyn and T. D. Tilley, *J. Am. Chem. Soc.* 1990, **112**, 4079.
5. (a) T. S. Koloski, P. J. Carroll and D. H. Berry, *J. Am. Chem. Soc.* 1990, **112**, 6405; (b) T. S. Koloski, P. J. Carroll and D. H. Berry, manuscript in preparation.
6. Most silylene complexes prepared to date are stabilized by the coordination of a Lewis base to the silicon: (a) D. A. Straus, T. D. Tilley, A. L. Rheingold and S. J. Geib, *J. Am. Chem. Soc.* 1987, **109**, 5872; (b) D. A. Straus, C. Zhang, G. E. Quimbita, S. D. Grumbine, R. H. Heyn, T. D. Tilley, A. L. Rheingold and S. J. Geib, *J. Am. Chem. Soc.* 1990, **112**, 2673; (c) C. Zybill and G. Müller, *Angew. Chem., Int. Edn Engl.* 1987, **26**, 669; (d) C. Zybill, D. L. Wilkinson and G. Müller, *Angew. Chem., Int. Edn Engl.* 1988, **27**, 583; (e) C. Zybill and G. Müller, *Organometallics* 1988, **7**, 1368; (f) C. Zybill, D. L. Wilkinson, C. Leis and G. Müller, *Angew. Chem., Int. Edn Engl.* 1989, **28**, 203; (g) K. Ueno, H. Tobita, M. Shimoi and H. Ogino, *J. Am. Chem. Soc.* 1988, **110**, 4092; (h) H. Tobita, K. Ueno, M. Shimoi and H. Ogino, *J. Am. Chem. Soc.* 1990, **112**, 3415.
7. Evidence for stable base-free silylene complexes has also been presented: D. A. Straus, S. D. Grumbine and T. D. Tilley, *J. Am. Chem. Soc.* 1990, **112**, 780.
8. For a general review of multiply-bonded silicon compounds see: G. Raabe and J. Michl, in *The Chemistry of Organic Silicon Compounds* (Edited by S. Patai and Z. Rappoport), Ch. 17. Wiley, New York (1989).
9. R. West, *Angew. Chem., Int. Edn Engl.* 1987, **26**, 1201 and refs therein.
10. A. G. Brook and K. M. Baines, *Adv. Organomet. Chem.* 1986, **25**, 1 and refs therein.
11. (a) N. Wiberg and K. Schurz, *J. Organomet. Chem.* 1988, **341**, 145; (b) C. N. Smit, F. M. Lock and F. Bickelhaupt, *Tetrahedron Lett.* 1984, **25**, 3011.
12. (a) M. J. S. Dewar, *Bull. Soc. Chim. Fr.* 1951, **18**, C71; (b) J. Chatt and L. A. Duncanson, *J. Chem. Soc.* 1953, 2939.
13. D. Seyferth, D. C. Annarelli, S. C. Vick and D. P. Duncan, *J. Organomet. Chem.* 1980, **201**, 179.
14. M. E. Jason, J. A. McGinnety and K. B. Wiberg, *J. Am. Chem. Soc.* 1974, **96**, 6531.
15. H. Schmidbaur, J. Eberlein and W. Richter, *Chem. Ber.* 1977, **110**, 677.
16. T. S. Koloski and D. H. Berry, unpublished results.
17. C. J. Jameson, Methods in stereochemical analysis, in *Phosphorus-31 NMR Spectroscopy in Stereochemical Analysis* (Edited by J. G. Verkade and L. D. Quin), Vol. 8, Ch. 6. VCH, Weinheim (1987).
18. D. Seyferth, D. P. Duncan, H. Schmidbaur and P. Holl, *J. Organomet. Chem.* 1978, **159**, 137.
19. (a) R. West, G. R. Gillette, H. B. Yokelson and A. J. Millevolte, *Phosphorus, Sulfur and Silica* 1989, **41**, 3; (b) R. West, D. J. D. Young and K. J. Haller, *J. Am. Chem. Soc.* 1985, **107**, 4942.
20. S. G. Baxter, K. Mislow and J. F. Blount, *Tetrahedron* 1980, **36**, 605.
21. P. Boudjouk and U. Samaraweera, *Organometallics* 1990, **9**, 2205.
22. D. Seyferth, E. Goldman and W. J. Escudie, *J. Organomet. Chem.* 1984, **271**, 337.
23. Reviews: P. P. Gaspar, in *Reactive Intermediates* (Edited by M. Jones Jr and R. A. Moss), Wiley Interscience, New York (1978), Vol. 1, p. 229; (1981), Vol. 2, p. 335; (1985), Vol. 3, p. 333.
24. D. H. Berry and Q. Jiang, *J. Am. Chem. Soc.* 1987, **109**, 6210.
25. D. Seyferth, D. C. Annarelli and D. P. Duncan, *Organometallics* 1982, **1**, 1288.
26. D. Seyferth and T. F. O. Lim, *J. Am. Chem. Soc.* 1978, **100**, 7074.
27. W. P. Weber and K. P. Steele, *J. Am. Chem. Soc.* 1980, **102**, 6095.
28. K. Raghavachari, J. Chandrasekhar, M. S. Gordon and K. J. Dykema, *J. Am. Chem. Soc.* 1984, **106**, 5853.
29. (a) G. R. Gillette, G. H. Noren and R. West, *Organometallics* 1987, **6**, 2617; (b) G. R. Gillette, G. H. Noren and R. West, *Organometallics* 1989, **8**, 487.
30. (a) W. Ando, K. Hagiwara and A. Sekiguchi, *Organometallics* 1988, **7**, 558; (b) G. Levin, P. K. Das, C. Bilgrien and C. L. Lee, *Organometallics* 1989, **8**, 1206.
31. For a general review, see: D. J. Darensbourg and R. A. Kudaroski, *Adv. Organomet. Chem.* 1983, **22**, 129.
32. T. C. Eisenschmid and R. Eisenberg, *Organometallics* 1989, **8**, 1822.
33. (a) P. Svoboda and J. Hetflejs, *Collect. Czech. Chem. Commun.* 1975, **40**, 1746; (b) P. Svoboda and J. Hetflejs, *J. Organomet. Chem.* 1974, **65**, C37.
34. G. Suss-Fink and J. Reiner, *J. Organomet. Chem.* 1981, **221**, C36.
35. H. Koinuma, F. Kawakami, H. Kato and H. Hirai, *J. Chem. Soc., Chem. Commun.* 1981, 213.
36. (a) M. J. Fink, D. J. De Young, R. West and J. Michl, *J. Am. Chem. Soc.* 1983, **105**, 1070; (b) A. Schäfer, M. Weidenbruch and S. Pohl, *J. Organomet. Chem.* 1985, **282**, 305.
37. D. Seyferth, S. C. Vick, M. L. Shannon, T. F. O.

Lim and D. P. Duncan, *J. Organomet. Chem.* 1977, **135**, C37.
38. B. A. Frenz and Associates, Inc., College Station, TX 77840, and Enraf–Nonius, Delft, Holland.
39. *International Tables for X-ray Crystallography*, Vol. IV, Table 2.2B. Kynoch Press, Birmingham (1974).
40. R. F. Stewart, E. R. Davidson and W. T. Simpson, *J. Chem. Phys.* 1965, **42**, 3175.
41. *International Tables for X-ray Crystallography*, Vol. IV, Table 2.3.1. Kynoch Press, Birmingham (1974).

Polyhedron Vol. 10, No. 11, pp. 1203–1213, 1991
Printed in Great Britain

0277–5387/91 $3.00+.00
Pergamon Press plc

SUBVALENT GROUP 14 METAL COMPOUNDS—XIII.* OXIDATIVE ADDITION REACTIONS OF GERMANIUM AND TIN AMIDES $M(NR_2)_2$ (R = $SiMe_3$, M = Ge OR Sn) WITH SULPHUR, SELENIUM, TELLURIUM OR MeOOCC≡CCOOMe; X-RAY STRUCTURES OF $[Ge(NR_2)_2(\mu\text{-}Te)]_2$ AND $Sn(NR_2)_2CC(OMe)OSn(NR_2)_2CC(OMe)O$†

PETER B. HITCHCOCK, HATAM A. JASIM, MICHAEL F. LAPPERT, WING-POR LEUNG,‡ AUDESH K. RAI and ROSEMARY E. TAYLOR§

School of Chemistry and Molecular Sciences, University of Sussex, Brighton BN1 9QJ, U.K.

Abstract—The germanium and tin divalent amide $M(NR_2)_2$ (R = $SiMe_3$, M = Ge or Sn) readily reacts with a chalcogen (E) or MeOOCC≡CCOOMe to yield the appropriate metal(IV) oxidative addition product $[M(NR_2)_2(\mu\text{-}E)]_n$ (E = S, Se or Te) (**1–6**) or $Sn(NR_2)_2CC(OMe)OSn(NR_2)_2CC(OMe)O$ (**7**), respectively. Each of the compounds **1–7** has been characterized by microanalysis and NMR spectra and two of the compounds $[Ge\{N(SiMe_3)_2\}_2(\mu\text{-}Te)]_2$ (**3**) and **7**, by single crystal X-ray diffraction. Some selected geometric parameters are as follows. **3**: ⟨Ge—N⟩ 1.86(1), ⟨Ge—Te⟩ 2.595(2), ⟨Si—N⟩ 1.76(2) Å; ⟨TeGeTe′⟩ 94.38(6), ⟨GeTeGe′⟩ 85.59(6)°. **7**: (MeO)C—C(OMe) 1.40(2), CC—C(OMe) 1.36(2), MeOCO—Sn 2.125(9), Sn—C 2.07(1), ⟨Sn—N⟩ 2.031(9), ⟨Si—N⟩ 1.75(1) Å. Each of the compounds $Sn(\eta\text{-}C_5H_4R)(NR_2)$ (**8**) and $Sn(\eta\text{-}C_5H_3R_2\text{-}1,3)(NR_2)$ (**9**) was obtained in a mixture with $Sn(NR_2)_2$ and the appropriate bis(cyclopentadienyl)tin(II) compound. ^{119}Sn NMR chemical shifts are reported for compounds **4** and **6–9**.

The majority of papers in this series have dealt with bivalent Group 14 metal molecules $M'X_2$ [M′ = Ge, Sn or Pb; X̄ = a bulky monohapto ligand such as C̄HR_2, N̄R_2, Ō$Ar^{R'}$ or SAr^{Bu^t}: R = $SiMe_3$, $Ar^{R'}$ = $C_6H_2Bu^t_2$-2,6-R′-4 (R′ = H, Me or Bu^t)], which are monomeric in dil. hydrocarbon solution and, except for the dimer $M_2(CHR_2)_4$ (M = Ge or Sn), in the crystal. Such a MX_2 species behaves as a:[1] (i) Lewis base, (ii) Lewis acid or as a substrate for (iii) oxidative addition, (iv) a redox reaction, (v) an insertion reaction, (vi) a metathetical exchange reaction or (vii)[2] a reaction [which may belong to any of classes (i)–(vi)] with a transition metal complex. This paper is principally concerned with some new reactions of type (iii) involving the germanium(II) or tin(II) bis(trimethylsilyl)amide, $M(NR_2)_2$; a minor theme concerns reactions of class (vi) leading to the novel heteroleptic cyclopentadienyltin(II) amides **8** and **9**.

In Part XI, oxidative addition reactions of $M(NR_2)_2$ with various reagents AB to yield the metal(IV) adducts $M(NR_2)_2(A)B$ were described [A—B = R″—Hal (e.g. = Bu^nCl, Bu^tBr or PhI), CH_2Cl—Cl, $CHCl_2$—Cl, CCl_3—Cl, Br—NR_2 or $CF_3C(O)O$—$C(O)CF_3$].[3] Related reactions of $Sn(CHR_2)_2$ have been studied,[3] including those where A—B = H—Cl,[1] H—F or $Bu^tC(O)$—Cl.[3]

Relevant to the present paper are reactions of MX_2 with a chalcogen or those with a conjugated organic compound leading to a cycloadduct.

Treatment of $Sn(CHR_2)_2$ with Me_3NO gave the dimeric tetravalent cyclostannoxane **I**,[4] whereas with a trace of air in the presence of $[Mo\{O(O)CMe\}_2(NCMe)_6][BF_4]$ the stannaozonide **II** was obtained.[5]

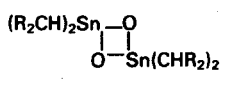

I

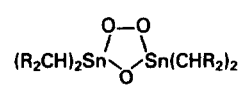

II

* For Part XII, see ref. 16.

† No represents available.

‡ Present address: Chemistry Department, The Chinese University of Hong Kong.

§ née Kelly.

Both these unusual compounds probably owe their stability to the exceptionally sterically demanding bis(trimethylsilyl)methyl substituents at tin; e.g. bulky cyclostannoxanes such as $[SnBu^t_2(\mu\text{-}O)]_3$[4] are generally trimers in contrast to the linear polymer found for the less crowded analogue $[SnPr^i_2(\mu\text{-}S)]_n$.

The carbene-like behaviour of $Sn(CHR_2)_2$ was demonstrated in Part II by its ready transformation into its oxidative cycloadduct **III** with 2,3-

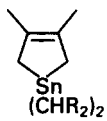

III

dimethylbuta-1,3-diene.[6] Similar reactions of $Sn(CHR_2)_2$ with a wider series of 1,3-dienes have been examined.[7] That study was extended to other conjugated 4-π-systems such as vinyl ketones or aldehydes, which likewise yielded 1,4-cycloadducts, e.g. **IV** from $OCC(CH_2)_4CCR^1R^2$.[8] The transient $GeMe_2$ has been trapped with various non-functionalized alkynes to give cycloadducts, e.g. **V** from PhC≡CH.[9]

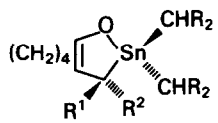

IV

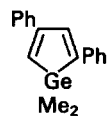

V

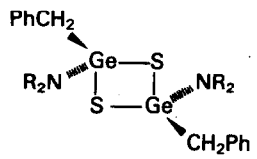

VI

The present study of the oxidative addition of the heavier chalcogens to $Ge(NR_2)_2$ was prompted by our earlier discovery of the unusual reaction between $Ge(NR_2)_2$ and $(Me_3Si)_3CSH$ in toluene at *ca* 20°C to give the X-ray characterized compound **VI** [in solution it was a mixture of *cis* (**VI**) and *trans* isomers].[10] Other four-membered ring compounds of the type $[MR'R''(\mu\text{-}E)]_2$ which have been prepared have invariably been obtained from metal(IV) precursors: e.g. the X-ray-authenticated $[GeBu^t_2(\mu\text{-}S)]_2$[11] and $[SnBu^t_2(\mu\text{-}E)]_2$ (E = S, Se or Te)[12] from the appropriate $MBu^t_2Cl_2$ and Na_2E. A similar procedure was employed for the cyclotrimers $[SnR'_2(\mu\text{-}E)]_3$ (R = Me and E = S, Se or Te; or R = Ph and E = S or Te); the crystalline $[SnMe_2(\mu\text{-}Te)]_3$ was found to have a puckered $(SnTe)_3$ skeleton.[13] A "mixed" four-membered ring compound $[Sn(C_6H_2Pr^i_3\text{-}2,4,6)_2]_2(\mu\text{-}O)(\mu\text{-}S)$ has been reported.[14]

A brief mention of some of the synthetic data relating to compounds **1**–**7** was made in ref. 1.

EXPERIMENTAL

Materials, measurements and techniques

The starting germanium(II) and tin(II) bis(trimethylsilyl)amides were prepared as described in Part V.[15] Manipulative procedures for air-sensitive materials were outlined in Part XII.[16] NMR spectra were run on a Bruker WM360 instrument. Colours, melting points, yields and microanalytical data for compounds **1**–**7** are shown in Table 1, while NMR spectroscopic data are given in Table 2. The complexes containing selenium or tellurium (**2**, **3**, **5** and **6**) were stored in the dark.

Synthesis of bis(bistrimethylsilylamido)germanium(IV) sulphide, $1/n[Ge\{N(SiMe_3)_2\}_2(\mu\text{-}S)]_n$ (**1**)

Powdered sulphur (0.1 g, 3.13 mmol) was added to a stirred solution of $Ge[N(SiMe_3)_2]_2$ (1.23 g, 3.13 mmol) in THF (*ca* 50 cm^3). The resultant mixture was a pale orange suspension, which, after 30 min, had become a clear, pale yellow solution. The solution was stirred for 24 h. All volatiles were removed *in vacuo*, leaving a cream solid, which was extracted into n-hexane (*ca* 40 cm^3); the extract was filtered. Cooling the filtrate to *ca* −30°C afforded the white, crystalline *title product* **1** (1.10 g, 75%), which was washed with cold (*ca* −78°C) n-pentane and dried *in vacuo*.

Synthesis of bis(bistrimethylsilylamido)germanium(IV) selenide, $1/n[Ge\{N(SiMe_3)_2\}_2(\mu\text{-}Se)]_n$ (**2**)

Powdered selenium (0.30 g, 3.81 mmol) was added to a stirred solution of $Ge[N(SiMe_3)_2]_2$ (1.50 g, 3.8 mmol) in THF (*ca* 50 cm^3). The initial cloudy, orange–brown suspension cleared rapidly to give a pale yellow solution which was stirred for 24 h. Volatiles were removed *in vacuo*, leaving a pale yellow solid, which was extracted into n-pentane (*ca* 40 cm^3) and the extract was filtered. Cooling of the filtrate to *ca* −30°C produced the white, crystalline *title product* **2** (1.28 g, 71%), which was washed with cold (*ca* −78°C) n-pentane and dried *in vacuo*.

Synthesis of bis(bistrimethylsilylamido)germanium(IV) telluride, $[Ge\{N(SiMe_3)_2\}_2(\mu\text{-}Te)]_2$ (**3**)

Powdered tellurium (0.55 g, 4.29 mmol) was added to a stirred solution of $Ge[N(SiMe_3)_2]_2$ (1.69

Table 1. Colours, melting points, yields and microanalysis results for the complexes 1–7 (R = $SiMe_3$)

Compound	Colour	Yield (%)	Melting point[a] (Boiling point) (°C)	Analysis (%)[b] C	H	N
$1/n[Ge(NR_2)_2(\mu\text{-}S)]_n$ (1)	White	75	> 300°C	33.8 (33.9)	8.53 (8.53)	6.53 (6.56)
$1/n[Ge(NR_2)_2(\mu\text{-}Se)]_n$ (3)	White	71	264	30.5 (30.5)	7.67 (7.68)	5.90 (5.93)
$[Ge(NR_2)_2(\mu\text{-}Te)]_2$ (5)	Orange	64	159 (dec.)	27.6 (27.7)	6.92 (6.96)	5.32 (5.37)
$1/n[Sn(NR_2)_2(\mu\text{-}S)]_n$ (2)	White	54	281 (dec.)	30.6 (30.6)	7.70 (7.70)	5.93 (5.94)
$1/n[Sn(NR_2)_2(\mu\text{-}Se)]_n$ (4)	Yellow	59	265 (dec.)	27.8 (27.8)	6.94 (6.99)	5.37 (5.40)
$1/n[Sn(NR_2)_2(\mu\text{-}Te)]_n$ (6)	Orange–red	53	128 (dec.)	25.4 (25.4)	6.36 (6.40)	4.95 (4.94)
$Sn(NR_2)_2CC(OMe)OSn(NR_2)_2CC(OMe)O$ (7)	Deep red	48	192–194 (dec.)	34.7 (35.3)	7.74 (7.70)	5.17 (5.49)

[a] In sealed capillary tubes under argon and are uncorrected.
[b] Calculated values in parentheses.

g, 4.29 mmol) in THF (*ca* 50 cm^3). The resultant cloudy, grey suspension was stirred for 24 h. There appeared to be some remaining unreacted tellurium powder; the mixture was filtered. Volatiles were removed from the filtrate *in vacuo* to give a bright orange solid, which was extracted into n-pentane (*ca* 40 cm^3), the extract was filtered and the filtrate concentrated (to *ca* 30 cm^3) and cooled to *ca* 0°C. After 24 h, there was no sign of crystallization and so the solution was cooled to *ca* −30°C to afford red crystals of the *title product* **3** (1.43 g, 64%), which were washed with cold (*ca* −78°C) n-pentane and dried *in vacuo*.

Synthesis of bis(bistrimethylsilylamido)tin(IV) *sulphide*, $1/n[Sn\{N(SiMe_3)_2\}_2(\mu\text{-}S)]_n$ (**4**)

Powdered sulphur (0.095 g, 2.98 mmol) was added to a stirred solution of $Sn[N(SiMe_3)_2]_2$ (1.31 g, 2.98 mmol) in THF (*ca* 50 cm^3). The resultant cloudy, orange suspension was stirred for 24 h. The colour had then faded to a pale yellow. The reaction mixture was refluxed (*ca* 65°C) for 2 h, then cooled to room temperature, set aside for 12 h and filtered. Volatiles were removed from the filtrate *in vacuo* to give a pale yellow solid, which was extracted into n-hexane (*ca* 50 cm^3); the filtered extract was concentrated to (*ca* 35 cm^3) and cooled to *ca* −30°C. After 24 h some flaky white solid had appeared; all volatiles were removed *in vacuo* and the solid was redissolved in toluene (*ca* 40 cm^3). The resulting pale yellow suspension was filtered; the filtrate was concentrated to *ca* 30 cm^3 and then cooled to *ca* −30°C to give, as a white powder, the *title product* **4** (0.76 g, 54%), which was washed with cold (*ca* −78°C) n-pentane and dried *in vacuo*.

Synthesis of bis(bistrimethylsilylamido)tin(IV) *selenide*, $1/n[Sn\{N(SiMe_3)_2\}_2(\mu\text{-}Se)]_n$ (**5**)

Powdered selenium (0.34 g, 4.28 mmol) was added to a stirred solution of $Sn[N(SiMe_3)_2]_2$ (1.88 g, 4.28 mmol) in THF (*ca* 50 cm^3). The resultant cloudy, orange–brown suspension was stirred for 24 h, whereafter the mixture was still slightly cloudy but most of the selenium appeared to have reacted. Filtration and removal of volatiles from the filtrate *in vacuo* gave a yellow solid, which was extracted into n-pentane (*ca* 40 cm^3). The extract was filtered, the filtrate concentrated (to *ca* 30 cm^3) and cooled to *ca* −30°C to afford yellow crystals of the *title product* **5** (1.31 g, 59%), which were washed with cold (*ca* −78°C) n-pentane and dried *in vacuo*.

Table 2. ^{1}H, ^{13}C and ^{119}Sn NMR chemical shifts (δ) for complexes **1**–**7** (R = $SiMe_3$) recorded at ambient temperatures at 360.13 MHz (^{1}H), 90.66 MHz (^{13}C) or 134.29 MHz (^{119}Sn) in C_6D_6

Compound	$\delta(^{1}H)$ $N(SiMe_3)_2$	$\delta(^{13}C)$	$\delta(^{119}Sn\{^{1}H\})^a$
$1/n[Ge(NR_2)_2(\mu\text{-}S)]_n$ (**1**)	0.50	7.03	—
$1/n[Ge(NR_2)_2(\mu\text{-}Se)]_n$ (**2**)	0.505	7.29	—
$[Ge(NR_2)_2(\mu\text{-}Te)]_2$ (**5**)	0.52	7.53	—
$1/n[Sn(NR_2)_2(\mu\text{-}S)]_n$ (**2**)	0.46	6.73	—
$1/n[Sn(NR_2)_2(\mu\text{-}Se)]_n$ (**4**)	0.43	7.02	−382.6[d,e]
$1/n[Sn(NR_2)_2(\mu\text{-}Te)]_n$ (**6**)	0.49	7.29	−988.8[e,f]
$Sn(NR_2)_2CC(OMe)OSn(NR_2)_2CC(OMe)O$ (**7**)	0.47[b]	5.48[c]	−69.2

[a] For data on the cyclopentadienyltin(II) amides **8** and **9**, see Experimental.
[b] OCH_3 at δ 3.62.
[c] OCH_3 at δ 53.31, $C{=}C$ at δ 89.93, and OCO at δ 163.20.
[d] $^{2}J(^{119}Sn\text{–}^{117}Sn)$ 790 Hz, $^{1}J(^{119}Sn\text{–}^{77}Se)$ 1128 Hz.
[e] Data of E. S. Jang.
[f] $^{2}J(^{119}Sn\text{–}^{117}Sn)$ 569 Hz, $^{1}J(^{119}Sn\text{–}^{125}Te)$ 2700 Hz.

Synthesis of bis(bistrimethylsilylamido)tin(IV) *telluride*, $1/n[Sn\{N(SiMe_3)_2\}_2(\mu\text{-}Te)]_n$ (**6**)

Powdered tellurium (0.51 g, 3.98 mmol) was added to a solution of $Sn[N(SiMe_3)_2]_2$ (1.75 g, 3.98 mmol) in THF (*ca* 50 cm^3). The cloudy, orange–brown suspension was stirred for 24 h and filtered. Volatiles were removed from the filtrate *in vacuo* to give an orange–red solid. This solid was extracted into n-pentane (*ca* 50 cm^3); the extract was filtered, the filtrate was concentrated to *ca* 40 cm^3 and cooled to −10°C to afford orange needles of the *title product* **6** (1.20 g, 53%), which were washed with cold (*ca* −78°C) n-pentane and dried *in vacuo*.

Displacement of tellurium from $1/n[Sn\{N(SiMe_3)_2\}_2(\mu\text{-}Te)]_n$ (**6**) *by sulphur*

Powdered sulphur (0.1 g, excess) was added to a stirred solution of **6** (0.17 g, 2.99 mmol) in THF (*ca* 50 cm^3). The cloudy, orange mixture was stirred for 24 h, whereafter the colour of the mixture had lightened to pale orange and a fine, dark grey precipitate had formed. The mixture was filtered; volatiles were removed from the filtrate *in vacuo*, leaving an off-white solid, which was extracted into n-hexane (*ca* 40 cm^3). The filtered extract was cooled to *ca* −30°C to yield after *ca* 24 h the white, microcrystalline $1/n[Sn\{N(SiMe_3)_2\}_2(\mu\text{-}S)]_n$ (**4**) (0.58 g, 41%), identified by comparison with an authentic sample.

Synthesis of $Sn(NR_2)_2CC(OMe)OSn(NR_2)_2CC(OMe)O$ (**7**)

A solution of $Sn[N(SiMe_3)_2]_2$ (2.08 g, 4.75 mmol) in THF at −78°C was added dropwise to a solution of dimethyl acetylenedicarboxylate (0.67 g, 4.75 mmol) in THF. The reaction mixture was allowed to warm to *ca* 25°C. The pale yellow solution gradually changed to deep red over a period of 30 min. After stirring for 2 h, volatiles were removed *in vacuo* and the residue was extracted into n-hexane (*ca* 100 cm^3). The filtered extract was concentrated to *ca* 50 cm^3 and cooled to *ca* −30°C to give deep red crystals of the *title compound* **7** (1.10 g, 48%), which were filtered off and dried *in vacuo*.

Miscellaneous reactions

(i) Attempts were made to make the mixed cyclopentadienyltin(II) amides $Sn(\eta\text{-}C_5H_4R)(NR_2)$ (**8**) and $Sn(\eta\text{-}C_5H_3R_2\text{-}1,3)(NR_2)$ (**9**); each reaction product was a mixture of **8** or **9** and its symmetrical redistribution products the appropriate tin(II) bis(cyclopentadienyl) and $Sn(NR_2)_2$.

Anhydrous tin(II) chloride (5.96 g, 30 mmol) was added to a stirred solution of trimethylsilylcyclopentadienyl-lithium (4.29 g, 30 mmol) in THF (*ca* 70 cm^3). The mixture immediately turned pale brown and a copious precipitate was produced. The mixture was stirred for 24 h to yield a pale yellow supernatant liquid and a brown precipitate. Volatiles were removed *in vacuo*; the residual solid was extracted into n-hexane (*ca* 60 cm^3) and the extract was filtered. [Bis(trimethylsilyl)amido]lithium etherate (7.24 g, 30 mmol) was added to the stirred filtrate. The reaction mixture became orange and more precipitate was produced. The mixture was stirred for 24 h. Volatiles were removed *in vacuo* to leave a sticky, orange solid, which was extracted into n-pentane (*ca* 40 cm^3). Removal of solvent from the filtered extract gave an orange oil, b.p. 112–115°C at 0.01 mbar.

The distillate comprised the *title product* **8** mixed with bis(trimethylsilylcyclopentadienyl)tin(II) and the tin(II) amide. A further distillation under reduced pressure failed to separate these three compounds.

A solution of bis(trimethylsilyl)cyclopentadienyllithium (3.32 g, 15.9 mmol) was added to a stirred solution of anhydrous tin(II) chloride (3.01 g, 15.9 mmol) in THF (*ca* 60 cm^3). Bis(trimethylsilyl) amidolithium etherate (3.83 g, 15.9 mmol) was added in portions to this solution and the mixture was stirred for 24 h. Volatiles were removed *in vacuo*, leaving a sticky, orange–brown solid, which was extracted into n-pentane (*ca* 40 cm^3). Volatiles were removed from the filtered extract *in vacuo* to leave a red oil, b.p. 110–115°C at 0.02 mbar. The distillate comprised the *title product* **9** mixed with bis[bis(trimethylsilyl)cyclopentadienyl]-tin(II) and the tin(II) amide. Despite further distillations, these three compounds were not separated.

Compounds **8** and **9** were identified by their NMR spectra; the ^{119}Sn NMR chemical shifts were particularly decisive; these were measured at ambient temperature at 134.29 MHz in C_6D_6: δ −525.5 for **8** and δ −569.0 for **9**, compared with δ +771.9 for $Sn(NR_2)_2$, δ −2190.3 for $Sn(\eta\text{-}C_5H_4R)_2$ and δ −2203.6 for $Sn(\eta\text{-}C_5H_3R_2\text{-}1,3)_2$.

(ii) Treatment of the orange $Sn(NR_2)_2$ with several MeC≡CCOOMe, PhC≡CCOOEt, EtC≡CEt and PhC≡CH resulted in a colour change (to yellow for PhC≡CH but red for the other alkynes); each mixture proved to be intractable.

X-ray structures of **3** *and* **7**

Crystal and refinement data are summarized in Table 3. X-ray quality crystals of each of compounds **3** and **7** were obtained by recrystallization from n-hexane at −30°C. Intensities for unique reflections with $2 < \theta < 25°$ were measured in the $\theta/2\theta$ mode with a scan width of $\Delta\theta = (0.8 - 0.35 \tan\theta)°$ and a maximum scan time of 1 min. Two standard reflections monitored every hour showed no significant variation. Data were corrected for Lp effects and an empirical correction for absorption based on psi scan measurements was applied to the data for **7**, but not for **3** (the crystal shape was such that a correction would have been small, bearing in mind the reasonably low μ value).

Each structure was solved by location of heavy atoms (Ge, Sn or Te) using the MULTAN program[17] followed by location of remaining non-hydrogen atoms on difference maps; these atoms were refined with anisotropic thermal parameters by full-matrix least-squares. The hydrogen atoms for **3** were held fixed at calculated positions (C—H 1.08 Å) with $B_{iso} = 6.0$ Å^2: those for **7** were omitted

Table 3. Crystallographic data for the structural analyses of **3** and **7**

	3	**7**
Formula	$C_{24}H_{72}Ge_2N_4Si_8Te_2$	$C_{30}H_{78}N_4O_4Si_8Sn_2$
Formula weight	1041.9	1021.5
Crystal dimensions (mm)	0.35 × 0.30 × 0.20	0.25 × 0.15 × 0.50
Crystal system	Triclinic	Monoclinic
a (Å)	8.874(2)	9.985(5)
b (Å)	11.153(1)	18.124(3)
c (Å)	25.698(5)	14.219(3)
α (°)	78.75(1)	
β (°)	81.45(2)	95.17(4)
γ (°)	72.14(2)	
V (Å^3)	2363.7	2562.8
Z	2	2
Space group	$P\bar{1}$	$P2_1/n$
D_{calc} (g cm^{-3})	1.46	1.32
μ (cm^{-1})	26.9	11.9
Number of observed reflections, $(F^2) > \sigma(F^2)$	4966	3472
$\sigma(F^2)$	$[\sigma^2(I)+(0.02I)^2]^{1/2}$Lp	$[\sigma^2(I)-(0.04I)^2]^{1/2}$Lp
R	0.087	0.088
R_w	0.098	0.119
λ(Mo-K_∞) (Å)	0.71069	0.71069

(they were not all located on a difference map). Refinement with a weighting scheme of $w = 1/\sigma^2(F)$ converged at residuals shown in Table 3, when the maximum shift /ESD was less than 0.3. For both **3** and **7**, a final difference map was calculated and showed no solvate molecules or disorder. Programs from the Enraf–Nonius SDP program package were run on a PDP 11/34 computer. Scattering factors for neutral atoms were taken from ref. 18. Tables of atom coordinates and thermal parameters are available from the Cambridge Crystallographic Data Centre. Final structure factors are available from one of the authors (P.B.H.).

RESULTS AND DISCUSSION

The reactions leading to the new compounds $[M(NR_2)_2(\mu\text{-}E)]_n$ (**1–6**) and $Sn(NR_2)_2CC(OMe)OSn(NR_2)_2CC(OMe)O$ (**7**) are summarized in Scheme 1, which also shows that (i) hydrolysis of **7** yields dimethyl succinate and (ii) treatment of $[Sn(NR_2)_2(\mu\text{-}Te)]_n$ (**6**) with sulphur leads via Te^{2-}/S^{2-} exchange to $[Sn(NR_2)_2(\mu\text{-}S)]_n$ (**4**).

Each of the complexes **1–6** was prepared in a similar fashion by adding the powdered chalcogen to a stirred THF solution of $M(NR_2)_2$. These reactions appeared to be slower for the heavier (a) chalcogens and (b) the Group 14 metal; but all six reactions were complete within 24 h. Each of the complexes **1–6** was readily crystallized from n-pentane.

Although the solution molecular weights of compounds **1–6** were not determined, they are probably dimers; i.e. $n = 2$ in $[M(NR_2)(\mu\text{-}E)]_n$. This assertion is based on (i) their high hydrocarbon solubility (i.e. they are not likely to be linear polymers), (ii) analogy with some of the data cited in the introduction and (iii) the X-ray results on crystalline $[Ge(NR_2)_2(\mu\text{-}Te)]_2$ (**3**), *vide infra*.

At ambient temperature each of the complexes $[M(NR_2)_2(\mu\text{-}S)]_n$ [M = Ge (**1**) or Sn (**4**)] is a white solid, less hydrocarbon-soluble than the appropriate starting metal(II) amide,[15] but with a considerably higher melting point (Table 1). The selenium analogues are white [M = Ge (**2**)] or yellow [M = Sn (**5**)] solids, and each of the tellurium compounds is an orange solid. The colour trends upon increasing the atomic number of the chalcogen are consistent with the colours being due to $n \rightarrow \pi^*$ transitions (involving charge transfer from Ė to a vacant metal-centred *d*-orbital). All have high melting points. The decomposition temperatures at their melting point (Table 1) decreased in the sequence (i) S > Se > Te and (ii) Ge > Sn: these trends follow relative M—E bond strengths. This thermal and particularly photochemical instability was most marked in the case of **6**, which gradually deposited a fine black powder (presumably Te) over the orange crystals after *ca* 24 h exposure to daylight at *ca* 25°C. The selenium analogue **5** showed similar, but less marked, photolability. There was a marked difference in air-sensitivity between the sulphur-containing complexes **1** and **4** and the heavier chalcogenide congeners. The sulphides **1** and **4** were almost air-stable, but the others rapidly decomposed, presumably as a consequence of hydrolysis.

The ^1H, ^{13}C and $^{119}Sn\{^1H\}$ chemical shift data of Table 2 for complexes **1–7** are unexceptional.

The thermal lability of **6** led us to the notion that **6** might be a suitable substrate for reductive elimination into its factors $Sn(NR_2)_2 + Te$. This was put to the test by heating **6** with S_8, whence $[Sn(NR_2)_2(\mu\text{-}S)]_n$ was obtained. Reactions of related metal(IV) tellurides might well offer a general route

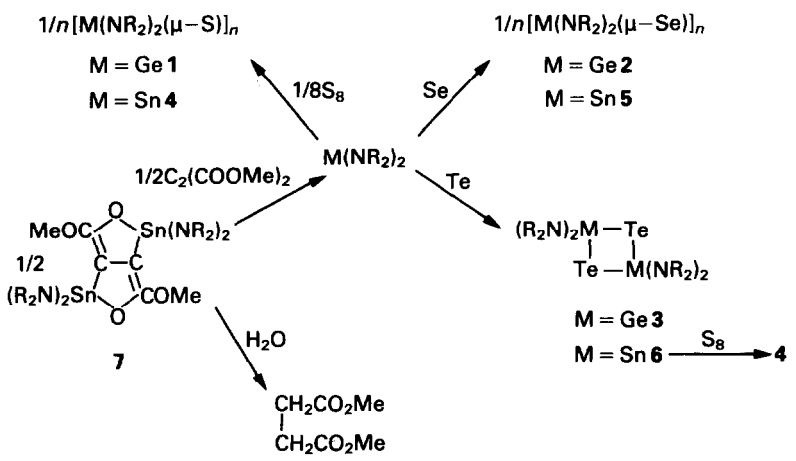

Scheme 1.

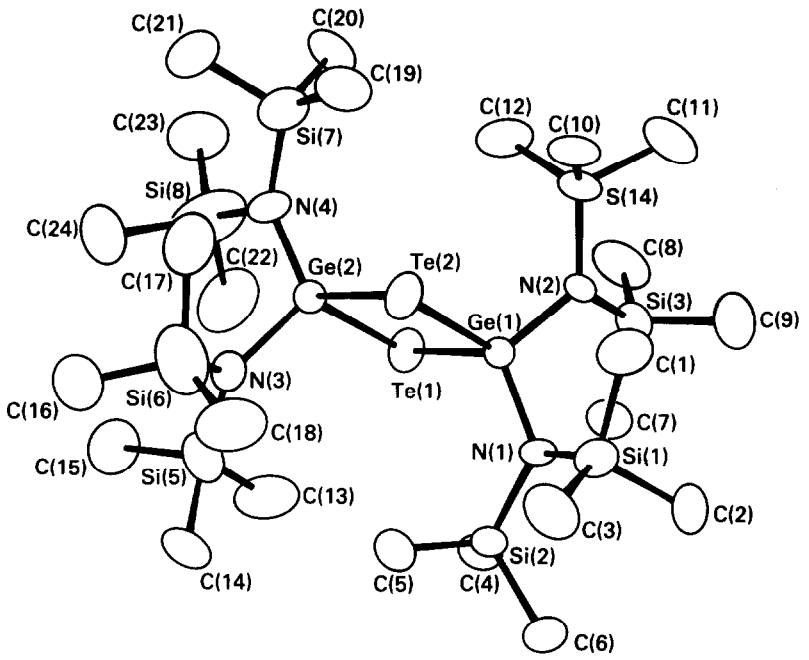

Fig. 1.

to metal(II) products which, if kinetically labile, may be trapped (e.g. with S_8).

The bicyclic di(stanna)-heterocycle **7** is evidently the product of two successive 1,4-cyclo-additions of $Sn(NR_2)_2$ to dimethyl acetylenedicarboxylate, with **VII** as a possible intermediate. The overall reaction

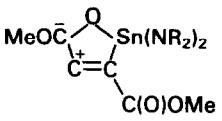

VII

can also be regarded as an unusual redox process, shown most clearly by including the hydrolysis step [**7** → $(CH_2CO_2Me)_2$] in the reaction scheme. Thus, the oxidation $Sn^{II} \rightarrow Sn^{IV}$ is accompanied by the change in oxidation level of the organic moiety from acetylenic into paraffinic.

The synthesis of the mixed metal(II) compounds $Sn(\eta\text{-}C_5H_4R)(NR_2)$ (**8**) and $Sn(\eta\text{-}C_5H_3R_2\text{-}1,3)(NR_2)$ (**9**) was examined with a view to using them as substrates for oxidative additions, e.g. with a chalcogen. In the event, their preparation was explored (by means only of pilot experiments using ^{119}Sn NMR spectroscopy) from $SnCl_2$ and successively the appropriate lithium cyclopentadienyl and $LiNR_2$, but they were not separated from the symmetrical species $Sn(NR_2)_2$ and the appropriate

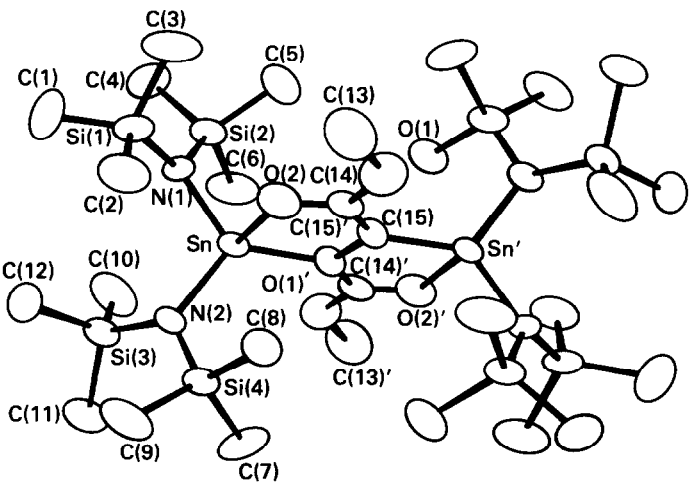

Fig. 2.

Table 4. Intramolecular distances (Å) and angles (°) with ESDs in parentheses for **3** (R = $SiMe_3$)

Bond distances (Å)

Te(1)—Ge(1)	2.595(2)	Te(1)—Ge(2)	2.596(2)
Ge(1)—Te(2)	2.592(2)	Ge(1)—N(1)	1.867(12)
Ge(1)—N(2)	1.869(10)	Te(2)—Ge(2)	2.599(2)
Ge(2)—N(3)	1.873(12)	Ge(2)—N(4)	1.858(13)
Si(1)—N(1)	1.742(14)	Si(1)—C(1)	1.85(2)
Si(1)—C(2)	1.82(2)	Si(1)—C(3)	1.86(2)
Si(2)—N(1)	1.777(11)	Si(2)—C(4)	1.85(2)
Si(2)—C(5)	1.85(2)	Si(2)—C(6)	1.87(2)
Si(3)—N(2)	1.719(13)	Si(3)—C(7)	1.87(2)
Si(3)—C(8)	1.86(2)	Si(3)—C(9)	1.86(2)
Si(4)—N(2)	1.780(11)	Si(4)—C(10)	1.83(2)
Si(4)—C(11)	1.88(2)	Si(4)—C(12)	1.83(2)
Si(5)—N(3)	1.746(13)	Si(5)—C(13)	1.81(2)
Si(5)—C(14)	1.91(2)	Si(5)—C(15)	1.89(2)
Si(6)—N(3)	1.76(2)	Si(6)—C(16)	1.82(2)
Si(6)—C(17)	1.94(2)	Si(6)—C(18)	1.89(3)
Si(7)—N(4)	1.746(13)	Si(7)—C(19)	1.91(3)
Si(7)—C(20)	1.91(2)	Si(7)—C(21)	1.90(2)
Si(8)—N(4)	1.77(2)	Si(8)—C(22)	1.85(2)
Si(8)—C(23)	1.81(3)	Si(8)—C(24)	2.14(4)

Bond angles (°)

Ge(1)—Te(1)—Ge(2)	85.58(6)	Te(1)—Ge(1)—Te(2)	94.47(6)
Te(1)—Ge(1)—N(1)	118.0(4)	Te(1)—Ge(1)—N(2)	109.0(4)
Te(2)—Ge(1)—N(1)	109.3(4)	Te(2)—Ge(1)—N(2)	117.9(4)
N(1)—Ge(1)—N(2)	108.1(5)	Ge(1)—Te(2)—Ge(2)	85.59(6)
Te(1)—Ge(2)—Te(2)	94.28(6)	Te(1)—Ge(2)—N(3)	116.3(4)
Te(1)—Ge(2)—N(4)	110.9(5)	Te(2)—Ge(2)—N(3)	110.0(5)
Te(2)—Ge(2)—N(4)	116.0(4)	N(3)—Ge(2)—N(4)	109.0(6)
N(1)—S(1)—C(1)	112.5(8)	N(1)—Si(1)—C(2)	110.7(9)
N(1)—Si(1)—C(3)	112.3(8)	C(1)—Si(1)—C(2)	106.2(8)
C(1)—Si(1)—C(3)	104(1)	C(2)—Si(1)—C(3)	111(1)
N(1)—Si(2)—C(4)	115.7(7)	N(1)—Si(2)—C(5)	110.7(7)
N(1)—Si(2)—C(6)	110.4(7)	C(4)—Si(2)—C(5)	110.6(9)
C(4)—Si(2)—C(6)	102.0(9)	C(5)—Si(2)—C(6)	106.8(9)
N(2)—Si(3)—C(7)	111.5(7)	N(2)—Si(3)—C(8)	112.3(8)
N(2)—Si(3)—C(9)	110.9(9)	C(7)—Si(3)—C(8)	105(1)
C(7)—Si(3)—C(9)	107.0(9)	C(8)—Si(3)—C(9)	110(1)
N(2)—Si(4)—C(10)	117.2(8)	N(2)—Si(4)—C(11)	110.5(8)
N(2)—Si(4)—C(12)	110.7(8)	C(10)—Si(4)—C(11)	103(1)
C(10)—Si(4)—C(12)	108(1)	C(11)—Si(4)—C(12)	107(1)
N(3)—Si(5)—C(13)	119.6(8)	N(3)—Si(5)—C(14)	110(1)
N(3)—Si(5)—C(15)	112.3(8)	C(13)—Si(5)—C(14)	103(1)
C(13)—Si(5)—C(15)	107(1)	C(14)—Si(5)—C(15)	104(1)
N(3)—Si(6)—C(16)	114(1)	N(3)—Si(6)—C(17)	111(1)
N(3)—Si(6)—C(18)	112(1)	C(16)—Si(6)—C(17)	105(1)
C(16)—Si(6)—C(18)	109(1)	C(17)—Si(6)—C(18)	106(1)
N(4)—Si(7)—C(19)	117.0(9)	N(4)—Si(7)—C(20)	112(1)
N(4)—Si(7)—C(21)	111.2(8)	C(19)—Si(7)—C(20)	106(1)
C(19)—Si(7)—C(21)	101(1)	C(20)—Si(7)—C(21)	109(1)
N(4)—Si(8)—C(22)	113.2(9)	N(4)—Si(8)—C(23)	116.0(9)
N(4)—Si(8)—C(24)	102(1)	C(22)—Si(8)—C(23)	110(1)
C(22)—Si(8)—C(24)	108(1)	C(23)—Si(8)—C(24)	107(1)
Ge(1)—N(1)—Si(1)	118.1(6)	Ge(1)—N(1)—Si(2)	120.0(7)
Si(1)—N(1)—Si(2)	117.8(7)	Ge(1)—N(2)—Si(3)	118.8(6)
Ge(1)—N(2)—Si(4)	119.8(6)	Si(3)—N(2)—Si(4)	118.1(7)
Ge(2)—N(3)—Si(5)	130.2(9)	Ge(2)—N(3)—Si(6)	114.0(7)
Si(5)—N(3)—Si(6)	114.5(8)	Ge(2)—N(4)—Si(7)	131.5(8)
Ge(2)—N(4)—Si(8)	113.9(7)	Si(7)—N(4)—Si(8)	114.6(8)

tin(II) bis(cyclopentadienyl). The reactions of $Sn(NR_2)_2$ with various non-functionalized alkynes was examined, but the results were inconclusive.

The X-ray structures of crystalline $[Ge(NR_2)_2(\mu\text{-}Te)]_2$ (**3**) and **7**, together with the appropriate numbering scheme, are illustrated in Figs 1 and 2, respectively, while geometric parameters are in Tables 4 (**3**) and 5 (**7**).

Some selected geometric parameters for a number of crystalline, four-membered ring compounds $[MXX'(\mu\text{-}E)]_2$, together with those for crystalline $Ge(NR_2)_2$,[19] are listed in Table 6 in order to put the new data on **3** into context. Each of the $(ME)_2$ rings is planar, with the EME′ angle larger than MEM′ and the MEM′ angle smaller for sulphur than tellurium, but for $[SnBu^t_2(\mu\text{-}E)]_2$ this order is reversed (S > Se > Te).[12] The difference in Ge—E bond lengths between the tellurium (**3**) and sulphur (**VI**) compounds is *ca* 0.35 Å, compared with *ca* 0.32 Å between $[SnBu^t_2(\mu\text{-}Te)]_2$ and the sulphur analogue.[12]

The Ge—N bond lengths in the two germanium(IV) compounds **3** and **VI** might have been anticipated to be similar in magnitude, but shorter than in the germanium(II) precursor, $Ge(NR_2)_2$; the difference in *l*(Ge—N) between the latter and **3**

Table 5. Intramolecular distances (Å) and angles (°) with ESDs in parentheses for **7** (R = $SiMe_3$)[a]

Bond distances (Å)			
Sn—O(2)	2.125(9)	Sn—N(1)	2.031(8)
Sn—N(2)	2.031(9)	Sn—C(15)′	2.073(11)
Si(1)—N(1)	1.755(9)	Si(1)—C(1)	1.88(2)
Si(1)—C(2)	1.879(15)	Si(1)—C(3)	1.89(2)
Si(2)—N(1)	1.743(10)	Si(2)—C(4)	1.881(15)
Si(2)—C(5)	1.88(2)	Si(2)—C(6)	1.941(15)
Si(3)—N(2)	1.741(10)	Si(3)—C(10)	1.86(2)
Si(3)—C(11)	1.877(14)	Si(3)—C(12)	1.87(2)
Si(4)—N(2)	1.753(9)	Si(4)—C(7)	1.882(14)
Si(4)—C(8)	1.873(15)	Si(4)—C(9)	1.878(15)
O(1)—C(13)	1.42(2)	O(1)—C(14)	1.337(15)
O(2)—C(14)	1.323(14)	C(14)—C(15)	1.36(2)
C(15)—C(15)′	1.40(2)		
Bond angles (°)			
O(2)—Sn—N(1)	96.9(3)	O(2)—Sn—N(2)	114.6(4)
O(2)—Sn—C(15)′	81.3(4)	N(1)—Sn—N(2)	110.5(3)
N(1)—Sn—C(15)′	124.3(4)	N(2)—Sn—C(15)′	120.7(4)
N(1)—Si(1)—C(1)	111.1(7)	N(1)—Si(1)—C(2)	112.0(5)
N(1)—Si(1)—C(3)	111.1(6)	C(1)—Si(1)—C(2)	107.6(7)
C(1)—Si(1)—C(3)	109.2(9)	C(2)—Si(1)—C(3)	105.5(7)
N(1)—Si(2)—C(4)	111.0(6)	N(1)—Si(2)—C(5)	110.1(6)
N(1)—Si(2)—C(6)	111.6(5)	C(4)—Si(2)—C(5)	109.2(7)
C(4)—Si(2)—C(6)	107.5(7)	C(5)—Si(2)—C(6)	107.3(7)
N(2)—Si(3)—C(10)	111.1(6)	N(2)—Si(3)—C(11)	113.8(6)
N(2)—Si(3)—C(12)	110.7(6)	C(10)—Si(3)—C(11)	105.3(8)
C(10)—Si(3)—C(12)	110.0(8)	C(11)—Si(3)—C(12)	105.8(7)
N(2)—Si(4)—C(7)	110.5(6)	N(2)—Si(4)—C(8)	111.0(5)
N(2)—Si(4)—C(9)	110.4(6)	C(7)—Si(4)—C(8)	109.3(7)
C(7)—Si(4)—C(9)	110.4(8)	C(8)—Si(4)—C(9)	105.2(7)
C(13)—O(1)—C(14)	121(1)	Sn—O(2)—C(14)	109.7(7)
Sn—N(1)—Si(1)	116.7(5)	Sn—N(1)—Si(2)	116.5(4)
Si(1)—N(1)—Si(2)	120.8(5)	Sn—N(2)—Si(3)	120.8(5)
Sn—N(2)—Si(4)	117.3(5)	Si(3)—N(2)—Si(4)	120.5(5)
O(1)—C(14)—O(2)	114.6(9)	O(1)—C(14)—C(15)	125(1)
O(2)—C(14)—C(15)	120(1)	Sn′—C(15)—C(14)	131.3(9)
Sn—C(15)′—C(15)	108.4(8)	C(14)—C(15)—C(15)′	120(1)

[a] Symmetry element ′ is $1-x, 1-y, 1-z$.

Table 6. Some comparative X-ray crystallographic data for the four-membered ring compounds $[MXX'(\mu\text{-}E)]_2$

	⟨M—N⟩ (Å) [⟨M—C⟩ (Å)]	⟨M—E⟩ (Å)	⟨E—M—E⟩ (°)	⟨M—E—M⟩ (°)	N—Ge—N′ (°) [C—Sn—C′ (°)]	Reference
$Ge(NR_2)_2$	1.875(5)	—	—	—	107.1(2)	19
$[Ge(NR_2)(\mu\text{-Te})]_2$ (**3**)	1.86(1)	2.597(2)	94.38(6)	85.59(6)	108.7(6)	This work
cis-$[Ge(CH_2Ph)(NR_2)(\mu\text{-S})]_2$	1.82(2), [1.96(2)]	2.249(6)	95.6(2)	84.3(2)	[111.0(8)][a]	10
$[GeBu^t_2(\mu\text{-S})]$	[2.02(1)]	2.246(3)	94.5(1)	85.5(2)	[113.8(5)]	11
$[SnBu^t_2(\mu\text{-S})]_2$	[2.21(1)]	2.432(4)[b]	93.8(1)	86.2(1)	[117.8(6)[b] 118.0(6)[c]]	12
		2.427(4)[c]				
$[SnBu^t_2(\mu\text{-Se})]_2$	[2.20(2)]	2.549(2)	97.5(1)	82.5(1)	[115.4(8)]	12
$[SnBu^t_2(\mu\text{-Te})]_2$	[2.17(2)]	2.754(1)	100.0(1)	80.0(1)	[117.0(4)]	12

[a] N—Ge—C.
[b] Monoclinic.
[c] Triclinic.

is in practice rather small. The N—Ge—N′ bond angles in $Ge(NR_2)_2$ and **3** are remarkably similar. The Si—N bond lengths [1.76(1) Å in **3** and **VI** and 1.75(1) Å in $Ge(NR_2)_2$] in these three $Ge(NR_2)_2$ derivatives and in **7**, 1.74(1) Å, are closely similar. In **7** the N—Sn—N angle of 110.5(3)° is slightly wider than in the other three compounds but significantly wider than in crystalline $Sn(NR_2)_2$, 104.7(2)°,[20] while the Sn—N bond length in **7** is slightly shorter than in $Sn(NR_2)_2$, 2.09(1) Å.

The molecular structure of crystalline **7** is entirely consistent with its formulation shown in Scheme 1 as a fused, bicyclic compound having an inversion centre at the mid-point of the C(15)—C(15)′ bond and as mirror plane the planar eight-membered bicyclic skeleton. There is no conjugation in the C=C—C=C fragment as evident from the various C—C bond lengths. The Sn—O bond is significantly longer than in $[Sn(CHR_2)_2(\mu\text{-O})]_2$ (**I**), 1.94(2) Å, or in $[SnR_2(OH)]_2(\mu\text{-O})$, 1.956(1) and 2.032(7) Å (the latter being the Sn—OH).[4]

Acknowledgements—We are grateful to SERC and the Leverhulme Trust for support, and to Mr E. S. Jang for some NMR data (see Table 2).

REFERENCES

1. M. F. Lappert, *Silicon, Germanium, Tin and Lead Compounds* 1986, **9**, 129.
2. M. F. Lappert and R. S. Rowe, *Coord. Chem. Revs* 1990, **100**, 267.
3. M. F. Lappert, M. C. Misra, M. Onyszchuk, P. P. Power, R. S. Rowe and M. J. Slade, *J. Organomet. Chem.* 1987, **330**, 31.
4. M. A. Edelman, P. B. Hitchcock and M. F. Lappert, *J. Chem. Soc., Chem. Commun.* 1990, 1116.
5. C. J. Cardin, D. J. Cardin, M. M. Devereux and M. A. Convery, *J. Chem. Soc., Chem. Commun.* 1990.
6. J. D. Cotton, P. J. Davidson and M. F. Lappert, *J. Chem. Soc., Dalton Trans.* 1976, 2275.
7. R. Marx, W. P. Neumann and K. Hillner, *Tetrahedron Lett.* 1984, **25**, 625.
8. K. Hillner and W. P. Neumann, *Tetrahedron Lett.* 1986, **27**, 5347.
9. G. Billeb, W. P. Neumann and G. Steinhoff, *Tetrahedron Lett.* 1988, **29**, 5245.
10. P. B. Hitchcock, H. A. Jasim, R. E. Kelly and M. F. Lappert, *J. Chem. Soc., Chem. Commun.* 1985, 1776.
11. M. Wojnowska, M. Noltemyer, H.-J. Füllgrabe and A. Meller, *J. Organomet. Chem.* 1982, **228**, 229.
12. H. Puff, G. Bertram, B. Ebeling, M. Franken, R. Gattermayer, R. Hundt, W. Schuh and R. Zimmer, *J. Organomet. Chem.* 1989, **379**, 235, and refs therein.
13. A. Blecher and M. Dräger, *Angew. Chem., Int. Edn. Engl.* 1979, **18**, 677.
14. P. Brown, M. F. Mahon and K. C. Molloy, *J. Chem. Soc., Chem. Commun.* 1989, 1621.
15. M. J. S. Gynane, D. H. Harris, M. F. Lappert, P. P.

Power, P. Rivière and M. Rivière-Baudet, *J. Chem. Soc., Dalton Trans.* 1977, 2004.
16. [Titled in error as Part XI (that designation had already been used for ref. 3)], M. F. Lappert, M. J. McGeary and R. V. Parish, *J. Organomet. Chem.* 1989, **373**, 107.
17. G. Germain, P. Main and M. M. Woolfson, *Acta Cryst.* 1971, **A27**, 360.
18. *International Tables for X-Ray Crystallography*, Vol. 4. Kynoch Press, Birmingham (1974).
19. R. A. Bartlett, M. F. Lappert, W.-P. Leung and P. P. Power, unpublished work.
20. T. Fjeldberg, H. Hope, M. F. Lappert, P. P. Power and A. J. Thorne, *J. Chem. Soc., Chem. Commun.* 1983, 639.

Polyhedron Vol. 10, No. 11, pp. 1215–1219, 1991
Printed in Great Britain

0277-5387/91 $3.00 + .00
© 1991 Pergamon Press plc

THE SYNTHESIS, CHARACTERIZATION AND X-RAY STRUCTURE OF *ANTI*-$W_2(GePh_3)_2(NMe_2)_4$

M. H. CHISHOLM,* I. P. PARKIN and J. C. HUFFMAN

Department of Chemistry and Molecular Structure Center, Indiana University, Bloomington, IN 47405, U.S.A.

Abstract—The reaction between $LiGePh_3$ and $W_2Cl_2(NMe_2)_4$ in toluene–THF produces $W_2(GePh_3)_2(NMe_2)_4$ in high yield (69%). The product is air-stable, decomposes at 209°C and is soluble in aromatic hydrocarbon solvents. The ^1H NMR spectrum reveals only an *anti*-isomer with $T_c = 115°C$, $\Delta G^\dagger = 74$ kJ mol^{-1} for amide rotation. The X-ray structure is consistent with the ^1H NMR spectrum and reveals a central *anti*-ethane-like $W_2N_4Ge_2$ core with bond lengths and angles: W≡W = 2.2970(9) Å, W—Ge = 2.625(1) Å, W—N = 1.95(av) Å, W—W—Ge = 95.89(3)°. The compound crystallized in the $P2_1/n$ space group with the cell parameters $a = 19.770(6)$, $b = 11.685(2)$, $c = 9.326(2)$ Å, $\beta = 99.74(1)°$, $Z = 2$, $V = 2123.3$ Å^3, $d_c = 1.802$ g cm^{-3} at −172°C.

There are a number of germanides of the chromium triad, especially for metal centres supported with carbonyl and cyclopentadiene ligands.[1] Despite this very few have been structurally characterized. To our knowledge no dimetallic compounds of this triad containing a metal to germanium bond is known. Previously compounds of the type $M_2(R)_2(NMe_2)_4$ [M = Mo, W; R = Cl, $Si(SiMe_3)_3$, $Sn(SnMe_3)_3$, $SeC_6H_2Me_3$, $SC_6H_2Me_3$, $OCPh_3$] have been synthesized, normally by metathesis reactions involving LiR and the substitutionally labile $M_2Cl_2(NMe_2)_4$ compounds.[2–4] Here we report the reaction of $LiGePh_3$ with $W_2Cl_2(NMe_2)_4$ to produce the first group VI dimetallic germanyl $M_2(GePh_3)_2(NMe_2)_4$. This species could be considered as an example of a heteropolyatomic germanium-containing metal oligomer.

RESULTS AND DISCUSSION

Preparation

Reaction of $W_2Cl_2(NMe_2)_4$ with $LiGePh_3$ proceeds in a toluene–THF solution to produce $W_2(GePh_3)_2(NMe_2)_4$ in high yield (69%), eq. (1):

$$W_2Cl_2(NMe_2)_4 + 2LiGePh_3 \longrightarrow 2LiCl + W_2(GePh_3)_2(NMe_2)_4. \quad (1)$$

The reaction proceeds quite rapidly in that seemingly all the LiCl is immediately precipitated on mixing the reagents. Filtering the solution to remove the LiCl and allowing the filtrate to stand at room temperature yielded orange crystals of $W_2(GePh_3)_2(NMe_2)_4$. These crystals were suitable for an X-ray determination as noted below. The compound is air-stable and soluble in aromatic hydrocarbon solvents (0.2 g/25 cm^3 toluene). It thermally decomposes at 208–209°C but seems relatively inert to hydrolysis either by 6 N HNO_3 or EtOH/KOH (6 N) solutions. These physical properties are probably attributable to the steric shielding provided by the $GePh_3$ ligands, which limits access to the metal centres.

Characterization

$W_2(GePh_3)_2(NMe_2)_4$ had the expected dimethylamide and phenyl ring vibrations in the IR. No assignable M—Ge stretches were seen in the region 4000–200 cm^{-1} [W—Ge = 190 cm^{-1}].[5] The ^1H NMR spectrum of $W_2(GePh_3)_2(NMe_2)_4$ in C_6D_6 is consistent with only the *anti*-rotamer being present in solution. All the dimethylamide ligands are equivalent (related by symmetry elements σ and C_2) but the methyl groups on each dimethylamide ligand are different, being either proximal or distal to the M≡M bond. A difference in chemical shift of 1.55 ppm between these groups is attributable to the diamagnetic anisotropy produced by the M—M triple bond. Variable temperature ^1H NMR spectra in $C_6D_5CD_3$ show extreme broadening at 105°C (Fig. 1) ($\Delta\nu = 465$ Hz) and give an estimated coales-

* Author to whom correspondence should be addressed.

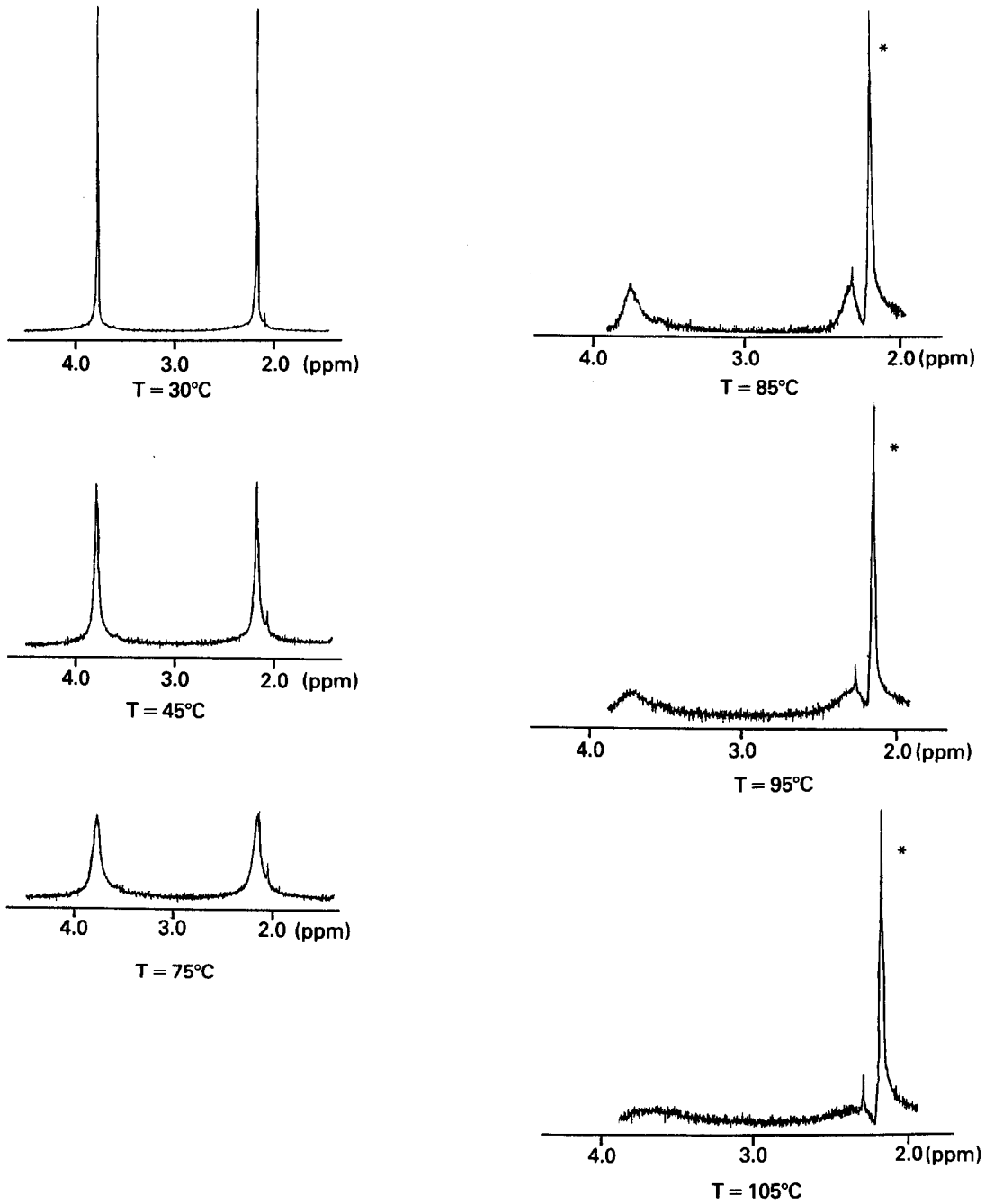

Fig. 1. Variable temperature ^1H NMR spectra recorded in toluene-d_8 at 300 MHz showing the dimethylamide resonances of *anti*-$W_2(GePh_3)_2(NMe_2)_4$. * Residual protio toluene.

cence temperature of 115°C at 300 MHz for free rotation about the M—N bond of a dimethylamide ligand. This is amongst the highest T_c values recorded for M—NMe_2 rotation in $M_2R_2(NMe_2)_4$ complexes[2,3] and is consistent with the large steric pressure of the $GePh_3$ ligands. Cooling a sample of $W_2(GePh_3)_2(NMe_2)_4$ to −40°C does not reveal any other dimethylamide environments.

Solid-state molecular structure

The molecular crystal structure of $W_2(GePh_3)_2(NMe_2)_4$ found in the solid state (X-ray) is shown in Fig. 2, looking perpendicular to the W—W vector, and a parallel view is shown in Fig. 3. The structure reveals an "ethane-like" staggered conformation with the $GePh_3$ ligands disposed in

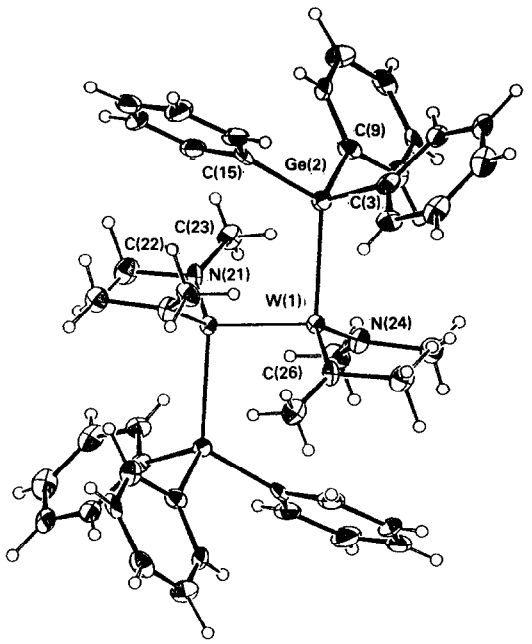

Fig. 2. An ORTEP view of the centrosymmetric $W_2(GePh_3)_2(NMe_2)_4$ giving the atom numbering scheme used in the tables.

an *anti*-configuration. The molecule has a crystallographically imposed centre of inversion.

The W—W distance of 2.2970(9) Å is typical for a W—W triple bond, and considerably shorter than the W—Ge distance of 2.625(1) Å. This later distance is shorter[2] than the corresponding Mo—Sn distance in $Mo_2\{Sn(SnMe_3)_3\}_2(NMe_2)_4$, 2.77 Å, and shorter than the Mo—Si distance in $Mo_2\{Si(SiMe_3)_3\}_2(NMe_2)_4$, 2.67 Å. It is also shorter than the sum of covalent radii of tungsten and germanium. The angles subtended at tungsten reveal the steric pressure of the $GePh_3$ ligand across the M—M bond. Most notable is the enlarged N—W—N angle, 124°, relative to the Ge—W—N angles, 109(av)° (Table 1).

The M—N distance of 1.95(av) Å is consistent with other dimethylamide tungsten distances in $W_2R_2(NMe_2)_4$ complexes, and together with the planarity at nitrogen is indicative of a strong M—N $d\pi$–$p\pi$ interaction.[7]

The observed *anti*-configuration is expected on steric grounds to be more stable than the *gauche* configuration in the presence of the large $GePh_3$ groups. Indeed the large "propeller-like" phenyl rings would seem to preclude the *gauche* conformation even in solution and provide a hydrophobic shield for the NMe_2 ligands. Presumably it is this shielding that makes the compound inert to air, acid and alcoholic alkaline solutions.

EXPERIMENTAL

General procedures and the preparation of $W_2Cl_2(NMe_2)_4$ have been reported.[8]

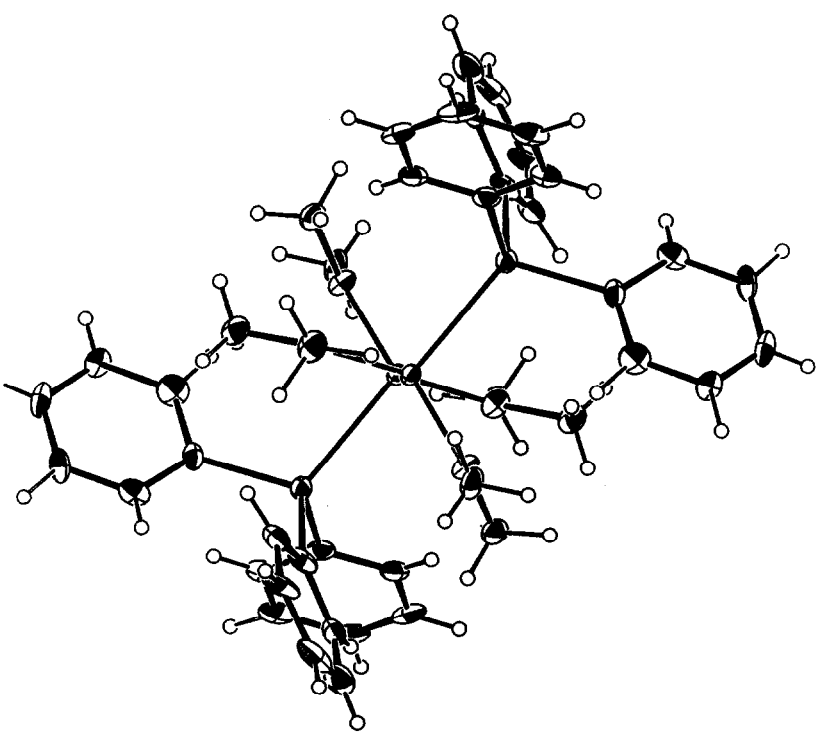

Fig. 3. An ORTEP view of the $W_2(GePh_3)_2(NMe_2)_4$ molecule viewed down the metal–metal bond.

Table 1. Selected bond distances (Å) and angles (°) in $W_2(GePh_3)_2(NMe_2)_4$

W(1)—W(1)	2.2970(9)	Ge(2)—C(15)	1.971(10)
W(1)—Ge(2)	2.625(1)	N(21)—C(22)	1.471(13)
W(1)—N(21)	1.954(8)	N(21)—C(23)	1.447(13)
W(1)—N(24)	1.945(7)	N(24)—C(25)	1.457(12)
Ge(2)—C(3)	1.990(9)	N(24)—C(26)	1.469(13)
Ge(2)—C(9)	1.976(9)		
W(1)′—W(1)—N(21)	106.82(21)	W(1)—N(21)—C(22)	112.3(6)
W(1)′—W(1)—N(24)	106.99(22)	W(1)—N(21)—C(23)	137.9(6)
W(1)′—W(1)—Ge(2)	95.89(6)	C(22)—N(21)—C(23)	109.3(8)
Ge(2)—W(1)—N(21)	110.4(2)	W(1)—N(24)—C(25)	135.4(6)
Ge(2)—W(1)—N(24)	108.3(2)	W(1)—N(24)—C(26)	116.0(6)
N(21)—W(1)—N(24)	124.5(3)	C(25)—N(24)—C(26)	107.9(8)
C(3)—Ge(2)—C(9)	106.1(4)	Ge(2)—C(3)—C(4)	120.7(7)
C(3)—Ge(2)—C(15)	104.3(4)	Ge(2)—C(3)—C(8)	121.5(7)
C(9)—Ge(2)—C(15)	103.9(4)		

Preparation of $W_2(GePh_3)_2(NMe_2)_4$

Triphenylgermanium chloride (0.500 g, 1.47 mmol) was dissolved in THF (5 cm^3) and added over 10 min to a stirred lithium suspension (0.060 g, 8.6 mmol) in THF (5 cm^3). This mixture was stirred for 5 h to generate a yellow solution and a white precipitate. The $LiGePh_3$ solution was filtered through a fine porosity frit and added to a solution of $W_2Cl_2(NMe_2)_4$ (0.405 g, 0.75 mmol) in toluene (15 cm^3) at room temperature to produce an immediate white precipitate. The reaction solution was allowed to stand for 5 min then filtered through a celite/glass frit. The filtrate was allowed to stand at room temperature for 12 h and deposited orange crystals which were collected by decanting the solvent and washing with hexane (10 cm^3), toluene (10 cm^3) and diethyl ether (10 cm^3). These were suitable for X-ray crystallography as described below. Yield: 0.47 g, 0.40 mmol, 53%. Cooling the filtrate to −20°C produced a further small crop, 0.19 g, 0.16 mmol; combined yield: 69%.

Found: C, 46.3; H, 4.6; N, 4.8. Calc: C, 45.8; H, 4.7; N, 4.7%. The crystals were air-stable for over a week at room temperature and had a decomposition point of 208–209°C. ^1H NMR at room temperature in C_6D_6: δ 7.61 (m, 12H), 7.20 (m, 18H), 3.73 (s, 12H), 2.18 (s, 12H). VT: ^1H NMR $T_c = 115$°C (estimated), $\Delta\nu = 465$ Hz, $\Delta G^\dagger = 74$ kJ mol^{-1} in $C_6D_5CD_3$. IR data (KBr pellet, cm^{-1}): 3040m, 2980m, 2940m, 2845s, 2800m, 2750m, 1560m, 1470m, 1450?, 1435s, 1420vs, 1380w, 1290m, 1250m, 1230s, 1173m, 1150w, 1125m, 1085w, 1070s, 1015s, 985w, 955w, 935vs, 920vs, 840m, 805m, 725vs, 685vs, 655w, 600w, 540m, 460s, 360w, 300s, 290s.

Crystallographic determination

A suitable crystal was located and transferred to the goniostat using standard inert atmosphere handling techniques, employed by the Indiana University Molecular Structure Center, and cooled to −172°C for characterization and data collection.

A systematic search of a limited hemisphere of reciprocal space located a set of diffraction maxima with symmetry and systematic absences corresponding to the unique monoclinic space group $P2_1/n$ (alternate setting of $P2_1/c$). Subsequent solution and refinement of the structure confirmed this choice.

Data were collected by using a continuous θ–2θ scan with fixed backgrounds. Data were reduced to a unique set of intensities and associated sigmas in the usual manner. The structure was solved by a combination of direct methods (MULTAN 78) and Fourier techniques. Data were corrected for absorption, based on well-defined crystal faces. All hydrogen atoms were clearly visible in a difference Fourier synthesis phased on the non-hydrogen parameters. All hydrogen atoms were refined (full-matrix least-squares) isotropically and non-hydrogen atoms anisotropically in the final cycles (see Table 2 for crystallographic data).

A final difference Fourier was featureless, with the largest peak being 0.45 e/$Å^3$.

Atomic coordinates have been deposited with the Director, Crystallographic Data Center, Cambridge.

Acknowledgements—We thank the National Science Foundation for support. I.P.P. acknowledges SERC for financial support through a NATO fellowship.

Table 2. Summary of crystallographic data

Empirical formula	$W_2C_{44}H_{54}N_4Ge_2$
Colour of crystal	Orange
Crystal dimensions (mm)	$0.124 \times 0.22 \times 0.22$
Space group	$P2_1/n$
Cell dimensions	
Temperature (°C)	−172
a (Å)	19.770(6)
b (Å)	11.685(2)
c (Å)	9.326(2)
β (°)	99.74(1)
Z (molecules/cell)	2
Volume (Å^3)	2123.30
Calculated density (g cm^{-3})	1.802
Wavelength (Å)	0.71069
Molecular weight	1151.82
Linear absorption coefficient (cm^{-1})	69.349
Detector to sample distance (cm)	22.5
Sample to source distance (cm)	23.5
Average omega scan width at half height	0.25
Scan speed (° min^{-1})	8.0
Scan width (° + dispersion)	2.0
Individual background (s)	4
Aperture size (mm)	3.0×4.0
2θ range (°)	$6 \leqslant \theta \leqslant 45$
Total number of reflections collected	3598
Number of unique intensities	2762
Number with $F > 0.0$	2563
Number with $F > 2.33\sigma(F)$	2380
Number of variables	342
$R(F)$	0.0356
$R_w(F)$	0.0330
Goodness-of-fit for the last cycle	1.030
Maximum delta/sigma for last cycle	0.23

REFERENCES

1. G. Wilkinson, F. G. A. Stone and E. W. Abel (Eds), *Comprehensive Organometallic Chemistry*, Vol. 6, p. 1043. Pergamon Press, Oxford (1982); K. Triplett and M. D. Curtis, *Inorg. Chem.* 1976, **15**, 431.
2. M. H. Chisholm, H. T. Chiu, K. Folting and J. C. Huffman, *Inorg. Chem.* 1984, **23**, 4097.
3. M. H. Chisholm, J. C. Huffman, I. P. Parkin and W. E. Streib, *Polyhedron* 1990, **9**, 2941.
4. M. H. Chisholm, J. F. Corning and J. C. Huffman, *Inorg. Chem.* 1984, **23**, 754.
5. D. J. Cardin, S. A. Keppie, M. F. Lappert, M. R. Litzow and T. R. Spalding, *J. Chem. Soc. A* 1971, 2262.
6. M. H. Chisholm, *Polyhedron* 1983, **2**, 681.
7. M. J. Chetcuti, M. H. Chisholm, K. Folting, D. A. Haitko, J. C. Huffman and J. Janos, *J. Am. Chem. Soc.* 1983, **105**, 1163.
8. M. Akiyama, M. H. Chisholm, F. A. Cotton, M. W. Extine and C. A. Murillo, *Inorg. Chem.* 1983, **22**, 38.

Polyhedron Vol. 10, No. 11, pp. 1221–1225, 1991
Printed in Great Britain

0277–5387/91 $3.00+.00
Pergamon Press plc

SONOCHEMICAL SYNTHESIS OF 1,1-DIMETHYL-1-GERMACYCLOPENT-3-ENES AND THE EXTRUSION OF DIMETHYLGERMYLENE UPON THEIR PYROLYSIS

DEQING LEI and PETER P. GASPAR*

Department of Chemistry, Washington University, St Louis, MO 63130, U.S.A.

Abstract—The ultrasound-promoted reaction of dichlorodimethylgermane with lithium in the presence of substituted 1,3-dienes results in the formation of the corresponding germacyclopent-3-enes in good yields. The gas-phase flow pyrolysis of 1,1,3-trimethyl- and 1,1,3,4-tetramethyl-1-germacyclopent-3-enes leads to the extrusion of dimethylgermylene that has been trapped by addition to 1,3-dienes.

Almost all known silylene reactions are reversible, but carbene reactions usually are not. Extrusion of silylenes from 1-silacyclopent-3-enes is a topic of interest not only because this process is virtually unknown in carbene chemistry, but because study of this process has assisted the elucidation of the mechanisms of silylene–diene addition reactions.[1] While Kolesnikov *et al.* were able to trap dichlorogermylene that was extruded from 1,1-dichloro-1-germacyclopent-3-enes, no dimethylgermylene was captured in the pyrolysis of 1,1-dimethyl-1-germacyclopent-3-ene.[2] We thought it was important to determine whether germylene–diene addition reactions, like those of silylenes, are reversible under flow pyrolysis conditions by preparing 1,1-dialkyl-1-germacyclopent-3-enes and examining their use as a germylene source.[3] Lei and Hampden-Smith have already utilized these findings to generate transition metal substituted germylenes from 1,1-dimetalla-1-germacyclopent-3-enes.[4] Here we report the sonochemical synthesis of a series of 1,1-dimethylgermacyclopenta-3-enes and the extrusion of dimethylgermylene upon their pyrolysis.

RESULTS AND DISCUSSION

Previously, 1,1-dialkyl-1-germacyclopent-3-enes have been synthesized in a two-step sequence by the reaction of alkyl magnesium halides with 1,1-dihalogeno-1-germacyclopent-3-enes, which were obtained from addition of germanium dihalides to suitable 1,3-dienes.[5] We have found that a series of 1,1-dimethyl-1-germacyclopent-3-enes can be prepared by the reaction of dichlorodimethylgermane[6] and lithium metal with the appropriate 1,3-dienes in tetrahydrofuran, promoted by irradiation in an ultrasonic cleaning bath. The reaction was complete within 15–60 min, depending on the diene used. For example, when a solution of 11.5 mmol of dichlorodimethylgermane and excess 2,3-dimethylbutadiene in 30 cm^3 of tetrahydrofuran, together with 0.4 g of lithium metal, was irradiated with ultrasonic waves for 15 min, 1,1,3,4-tetramethyl-1-germacyclopent-3-ene (**1**) was isolated in 54% yield. This series of experiments is summarized below:

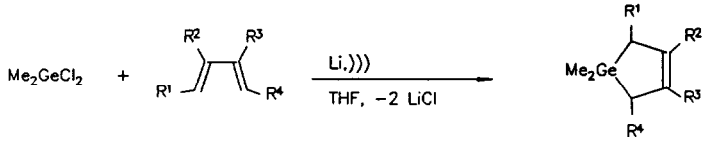

(1)

1: $R^1 = R^4 = H, R^2 = R^3 = Me$, 54%

2: $R^1 = R^2 = R^4 = H, R^3 = Me$, 51%

3: $R^2 = R^4 = H, R^1 = R^3 = Me$, 43%

4,5: $R^2 = R^3 = H, R^1 = R^4 = Me$, 15%.

* Author to whom correspondence should be addressed.

The results shown in eq. (1) suggest that the yields depend on the structure of the 1,3-diene used. The formation of 1,1-dimethyl-1-germacyclopent-3-enes is more facile when there are no substituents on the terminal carbon atoms of 1,3-dienes, i.e. isoprene and 2,3-dimethylbutadiene. The yield of the product decreases dramatically if methyl substituents are present at both termini of the diene π-system. In the reaction of *trans,trans*-2,4-hexadiene (> 99% pure) a mixture of *cis*- and *trans*-1,1,2,5-tetramethyl-1-germacyclopent-3-enes was formed with a *cis*- to *trans*- ratio of 8.5 : 1 [see eq. (2)]. The dominant product stereoisomer retains the geometry of the starting diene.

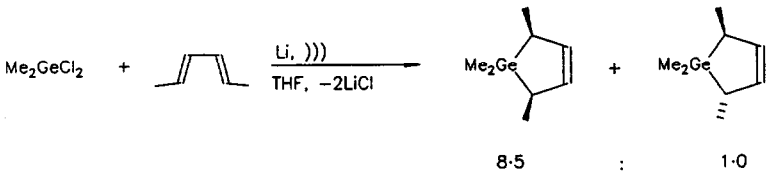

(2)

These reactions provide a convenient and efficient method to synthesize a variety of 1-germacyclopent-3-enes. It is not suggested that a free germylene is produced by lithium-induced dehalogenation of dichlorodimethylgermane. More likely, "germylenoid" species, $Me_2GeClLi$ or Me_2Ge-LiCl, are involved, analogous to the "silylenoid" species encountered by Boudjouk *et al.*[7] and Pae *et al.*[8] in the analogous dehalogenation of sterically crowed dihalodialkylsilanes $(t\text{-but})_2SiX_2$ and Ad_2SiI_2.

We next studied the gas-phase flow pyrolysis reactions of these germacyclopent-3-enes. We found that the extrusion of dimethylgermylene is an efficient process. When 1,1,3-trimethyl-1-germacyclopent-3-ene (**2**) was subjected to vacuum flow pyrolysis at 470°C, *ca* 2 torr, with contact time *ca* 8 ms, in the presence of a 10-fold excess of 2,3-dimethylbutadiene, the dimethylgermylene adduct, 1,1,3,4-tetramethylgermacyclopent-3-ene (**1**), was obtained in 83% yield based on 44% of the starting material consumed. When the reaction temperature was raised to 500°C, conversion increased to 75% but the yield dropped to 61% :

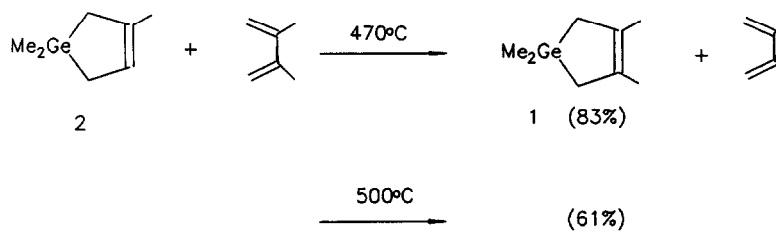

(3)

Under the same conditions pyrolysis of 1,1,3,4-tetramethylgermacyclopent-3-ene (**1**) in the presence of a 10-fold excess of isoprene gave 3-methylgermacyclopent-3-ene (**2**) in 71% yield based on the 47% of the starting material converted :

(4)

These results indicate that dimethylgermylene is efficiently generated by extrusion from the germacyclopent-3-enes under relatively mild conditions.

Flow pyrolysis of 1,1,3-trimethyl-1-germacyclopent-3-ene (**2**) in the presence of a 10-fold excess of *trans,trans*-2,4-hexadiene at 460°C gave a mixture of *cis*- and *trans*-1,1,2,5-tetramethyl-1-

germacyclopent-3-enes (**4**) and (**5**) in a combined 15% yield with a 9:1 ratio of *cis*- to *trans*-isomers (35% decomposition of the starting material):

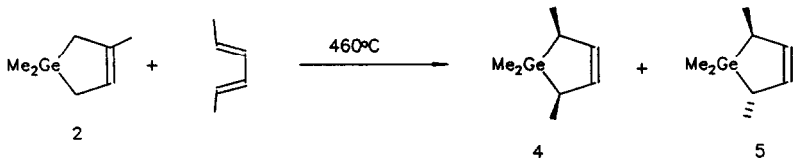

2 4 5 (5)

Under the same conditions, the pyrolysis of neat *trans,trans*-2,4-hexadiene, originally greater than 99% pure, indicated that the recovered diene substrate contained 8% of *cis,trans*-2,4-hexadiene and 2% of a mixture of *E*- and *Z*-1,3-hexadienes. Thus the *trans*-isomer might result from addition of dimethylgermylene to *cis,trans*-2,4-hexadiene produced by isomerization of the starting diene under the reaction conditions. These results are therefore not inconsistent with the previously observed stereospecific addition of dimethylgermylene to the 1,3-dienes.[9,10]

CONCLUSION

A series of 1,1-dimethylgermacyclopent-3-enes has been efficiently synthesized by the ultrasound-promoted, lithium-induced dehalogenation of dichlorodimethylgermane in the presence of 1,3-dienes. It has been demonstrated that the 1,1-dimethyl-1-germacyclopent-3-enes are efficient precursors for the thermal generation of dimethylgermylene.

The high temperature addition of germylenes to 1,3-dienes results only in formation of formal 1,4-adducts. However, a stepwise mechanism for addition of silylene to 1,3-dienes has been well established, whose first step is a concerted 1,2-addition followed by competing processes depending on the structure of the key intermediates, *vinylsiliranes*.[1,3] At room temperature, addition of Me_2Ge to a variety of dienes leads to 1:2-adducts, 3,4-dialkyl-1-germacyclopentanes, products whose formation seems to demand the intermediacy of vinylgermiranes.[11] Kinetic studies on Me_2Ge: suggest that at room temperature, 1,2-addition is more rapid than 1,4-addition.[12]

Therefore, one can ask whether the exclusive formation, often in high yield, of formal 1,4-adducts from Me_2Ge: and dienes at high temperatures also involves a vinylgermirane intermediate. Rearrangement of the vinylgermirane to a germacyclopent-3-ene may be sufficiently rapid to account for the stereospecificity that has been observed.[9] The intramolecular rearrangements may be too rapid at high temperatures for reaction with a second diene molecule to occur.

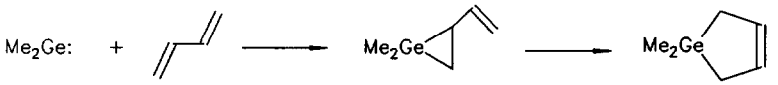

(6)

EXPERIMENTAL

Unless indicated otherwise, all chemicals used were reagent grade and used as supplied. All preparative reactions were carried out under an atmosphere of argon. Tetrahydrofuran solvent was dried over and distilled immediately before use from benzophenone sodium ketyl under a nitrogen atmosphere.

^{1}H NMR spectra were recorded on a Varian XL-300 NMR spectrometer. Combined gas chromatography–mass spectrometry was performed on a Finnigan 3200 instrument operating at an ionization energy of 70 eV. All mass spectra were calibrated internally against perfluoroalkane. Flame ionization detector and thermal conductivity detector instruments were employed for the analytical gas chromatography. A preparative gas chromatograph with dual rhenium tungsten filament TCD detectors was used for separation of the products and for absolute yield determinations on the basis of the amount of the unrecovered precursors, using isomeric compounds as external standards.

Flash vacuum pyrolyses were performed by slowly distilling reactants through a vertical quartz tube (10 mm i.d., 18 cm long) heated by approximately 22 ft of 26 gauge nichrome wire. The nicrome wire was insulated from the quartz tube and the atmosphere with asbestos ribbon. The flow system was evacuated by an oil diffusion pump to *ca* 10^{-5} torr. A gaseous reaction mixture was delivered from a 1-litre reservoir through a ball-type flow meter, and the pressure was measured just upstream from the hot zone by a calibrated thermocouple gauge. The flow system was throttled downstream from the hot zone by a copper plate with a 0.036 in. diameter orifice, and the pyrolysate was condensed in a U-trap immersed in liquid nitrogen. The

temperature was measured at the centre of the hot zone between the outer surface of the tube and the asbestos ribbon by an iron–constantan thermocouple.

1,1,3-*Trimethyl*-1-*germacyclopent*-3-*ene* (**2**)

A mixture of dichlorodimethylgermane (2.0 g, 11.5 mmol), 2-methylbutadiene (1.5 g, 22.1 mmol) and finely cut lithium metal (0.3 g) in 30 cm^3 of THF was sonicated for 30 min under an atmosphere of argon in an ultrasonic cleaning bath (L & R Maxomatic Ultrasonic Generator). The reaction mixture turned light yellowish from what was originally a cloudy suspension, and a white precipitate was formed. The unreacted lithium and precipitate were removed by filtration. The filtrate was distilled at an atmosphere to give 1.4 g of crude product, **2**, which was 72% pure shown by GC (51% yield). The product was further purified by GC (10 ft × 1/4 in. 20% OV-17). ^{1}H NMR (C_6D_6): 0.25 (s, 6H, Ge-Me), 1.34 (bs, 2H, C_5-H), 1.53 (bs, 2H, C_2-H), 1.80 (bs, 3H, C_3-Me), 5.67 (bs, 1H, C_4-H). Mass: 172 (parent), 157 (base). These spectral data are essentially identical to those reported.[3]

1,1,3,4-*Tetramethyl*-1-*germacyclopent*-3-*ene* (**1**)

This was prepared by the procedure described above for germacyclopentene **2**. A mixture of dichlorodimethylgermane (2.0 g, 11.5 mmol), 2,3-dimethylbutadiene (1.9 g, 23.2 mmol) and finely cut lithium metal (0.4 g) in 30 cm^3 of THF was sonicated for 15 min. 1.1 g of germacyclopentene **1** was isolated in 54% yield. ^{1}H NMR (C_6D_6): 0.25 (s, 6H, Ge-Me), 1.56 (bs, 4H, C_2- and C_5-H), 1.76 (bs, 6H, C_3- and C_4-Me). Mass: 186 (parent), 171 (base). These spectral data are consistent with those reported.[3]

1,1,2,4-*Tetramethyl*-1-*germacyclopent*-3-*ene* (**3**)

This was synthesized by the same procedure described for compound **2**. A mixture of dichlorodimethylgermane (1.8 g, 10.3 mmol), 2-methylpentadiene-1,3 (1.7 g, 20.7 mmol) (a mixture of 75% *cis* and 25% *trans*) and lithium (0.3 g) in 20 cm^3 of THF was sonicated for 20 min. 0.8 g of product **3** was isolated in 43% yield. ^{1}H NMR (C_6D_6): 0.19 (s, 3H, Ge-Me), 0.25 (s, 3H, Ge-Me), 1.11 (d, 3H, J = 7.5 Hz, C_2-Me), 1.40 (m, 2H, C_5-H), 1.78 (bs, 3H, C_4-Me), 1.87 (bs, 1H, C_2-H), 5.52 (bs, 1H, C_3-H). Mass: 186 (parent), 171 (base).

1,1,2,5-*Tetramethylgermacyclopent*-3-*enes* (**4**) *and* (**5**)

These were synthesized by the same procedure indicated above for compound **2**. A suspension of *trans,trans*-2,4-hexadiene (1.4 g, 17 mmol), dichlorodimethylgermane (2.9 g) and lithium (0.3 g) was sonicated for 1 h. 0.44 g of products **4** and **5** were isolated in a total of 14% yield. The ratio of *cis*- to *trans*-isomer was 8.5 : 1. ^{1}H NMR (C_6D_6): *cis*-isomer **4**, 0.11 (s, 3H, Ge-Me), 0.22 (s, 3H, Ge-Me), 1.10 (d, 6H, J = 7.8 Hz, C_2- and C_5-Me), 1.78 (q, 2H, J = 7.8 Hz, C_2- and C_5-H), 5.81 (bs, 2H, ole finic H); *trans*-isomer **5**, 0.17 (s, 6H, Ge-Me), the rest of the data are the same as those for its *cis*-isomer **4**. These spectral data are in good agreement with those reported.[9]

Pyrolysis of **1** *in the presence of* 2-*methylbutadiene*

In a typical experiment, a mixture of **1** (47 mg, 0.25 mmol) and a 10-fold excess of 2-methylbutadiene (170 mg, 2.5 mmol) was pyrolysed at 470°C, *ca* 2 torr with residence time *ca* 8 ms. The pyrolysate was separated by GC (10 ft × 1/4 in. 20% OV-17, column temperature at 90°C, He flow rate at 45 cm^3 min^{-1}) to give the starting material in 47% and **2** in 71% yield based on the unrecovered 53% starting material.

Pyrolysis of **2** *in the presence of* 2,3-*dimethylbutadiene*

A gaseous mixture of **2** (69 mg, 0.40 mmol) and a 10-fold excess of 2,3-dimethylbutadiene (328 mg, 4.0 mmol) was passed through the hot zone at 470°C, *ca* 2 torr with residence time *ca* 8 ms. The pyrolysate was separated by gas chromatography (10 ft × 1/4 in. 20% OV-17, column temperature at 90°C and He flow rate at 45 cm^3 min^{-1}). 44% of starting material **2** was recovered. The germylene–diene adduct **1** was isolated in 83% yield based on the unrecovered material **2**. When this reaction was carried out at 500°C, only 25% of starting material **2** was recovered and product **1** was obtained in 61% yield.

Pyrolysis of **2** *in the presence of* trans,trans-2,4-*hexadiene*

A gaseous mixture of **2** (69 mg, 0.40 mmol) and a 10-fold excess of *trans,trans*-2,4-hexadiene (328 mg, 4.0 mmol) was passed through the hot zone at 460°C, *ca* 2 torr with residence time *ca* 8 ms. The pyrolysate was separated by GC (10 ft × 1/4 in. 20%

OV-17, column temperature at 90°C, He flow rate at 50 cm^3 min^{-1}). 65% of **2** was recovered. A mixture of **4** and **5** with a 9:1 ratio of *cis*- to *trans*-isomer was obtained. The ratio of *cis*- to *trans*-isomer was determined by the peak intensity at 0.11 and 0.22 ppm (*cis*-isomer **4**), and 0.17 ppm (*trans*-isomer **5**) in the ^1H NMR spectrum.

Acknowledgement—We thank the United States National Science Foundation for support of this work under Grant No. CHE-88-02677.

REFERENCES

1. D. Lei and P. P. Gaspar, *Organometallics* 1985, **4**, 1471; 1986, **5**, 1276; *Res. Chem. Intermediates* 1989, **2**, 103.
2. S. P. Kolesnikov, I. S. Rogozhin, M. H. Safarov and O. M. Nefedov, *Izv. Akad. Nauk SSSR, Ser. Khim.* 1981, **6**, 1423; *Bull. Acad. Sci. USSR, D.V. Chem. Sci* (*Engl. Transl.*) 1981, 1143.
3. D. Lei, A mechanistic study of the addition of silylenes to 1,3-dienes in both the forward and reverse directions, Doctoral dissertation. Washington University, St Louis (December 1988).
4. D. Lei and M. Hampden-Smith, *J. Chem. Soc., Chem. Commun.* 1989, 1211.
5. P. Mazerolles and G. Manuel, *Bull. Soc. Chim. Fr.* 1966, **1**, 327.
6. M. E. Lee, K. L. Robbitt, D. Lei and P. P. Gaspar, *Synth. React. Inorg. Met.-Org. Chem.* 1990, **20**, 77.
7. P. Boudjouk, U. Samaraweera, R. Sooriyakamaran, J. Chrusciel and K. Anderson, *Angew. Chem. Int. Edn Engl.* 1988, **27**, 1355.
8. D. H. Pae, M. Xiao, M. Chiang and P. P. Gaspar, *J. Am. Chem. Soc.* 1991, **113**, 1281.
9. E. C.-L. Ma, K. Kobayashi, M. W. Barzilai and P. P. Gaspar, *J. Organomet. Chem.* 1982, **224**, C13.
10. M. Schriewer and W. P. Neumann, *J. Am. Chem. Soc.* 1983, **105**, 897.
11. W. P. Neumann, E. Michels and J. Kocher, *Tetrahedron Lett.* 1987, **28**, 3783.
12. K. L. Bobbitt, V. M. Maloney and P. P. Gaspar, *Organometallics*, in press.

Polyhedron Vol. 10, No. 11, pp. 1227–1229, 1991
Printed in Great Britain

0277–5387/91 $3.00+.00
© 1991 Pergamon Press plc

ELECTRICAL CONDUCTIVITY OF SOME PERMETHYLPOLYSILANES DOPED WITH ARSENIC PENTAFLUORIDE

A. LOUIS ALLRED* and DONALD A. VAN BEEK JR

Department of Chemistry, Northwestern University, Evanston, IL 60208, U.S.A.

Abstract—Permethylpolysilanes, $Me(SiMe_2)_nMe$ in which n is approximately 48, and long-chain poly(dimethylsilylenes), with or without extensive branching, exhibit electrical conductivity and electron spin resonance when doped with arsenic pentafluoride.

Diverse polymers become conductors when combined with strong electron acceptors or donors, and numerous related observations have been published.[1] Though nearly all of these polymers contain π systems, electrical conductivity in doped, high molecular weight organosilicon polymers and in polysilane, $(SiH_2)_x$, has also been reported.[2,3] Herein we summarize early observations[4] of conductivity in some other polysilane systems which involved either relatively short chains or polysilane branches.

EXPERIMENTAL

Coupling of a 1:3 molar ratio of $Cl(SiMe_2)_6Cl$ and $Me(SiMe_2)_6Cl$ with potassium metal gives linear chains, $Me(SiMe_2)_nMe$, where $n = \ldots 42, 48, 54\ldots$. This mixture of products, obtained under conditions similar to those previously[5] used to prepare $Me(SiMe_2)_{18}Me$ and $Me(SiMe_2)_{24}Me$, was treated repeatedly with hot ethanol to remove short permethylpolysilane chains and then Soxhlet-extracted by refluxing carbon tetrachloride for 4 days to leave behind the insoluble polymer. The extracted white, powdery product, amounting to a 53% yield based on total $SiMe_2$, was slightly soluble, 7.0 g dm^{-3}, in 1,2,4-trichlorobenzene at 120°C and was shown by analytical HPLC with a 60 Å size exclusion column to consist of $Me(SiMe_2)_nMe$ oligomers starting at $n = 18$ and approximately centred at $n = 48$.

Two-dimensional and three-dimensional polymers were prepared by coupling with sodium/potassium alloy either $Cl(SiMe_2)_6Cl$ or Me_2SiCl_2 as the monomer, either $MeSiCl_3$ or $SiCl_4$ as the crosslinking agent, and either hexane or tetrahydrofuran as the solvent. The one-dimensional polymer, $(SiMe_2)_x$, was obtained from coupling of Me_2SiCl_2 with sodium/potassium alloy in refluxing hexane. The above preparations involved adding the monomers to the stirred alloy under gentle reflux conditions, refluxing the resulting solution for 24 h, adding Me_3SiCl and refluxing for an additional 24 h to replace any chloro groups remaining in the polymer. Then work-up involved careful hydrolysis, extraction with water and hexane, and Soxhlet-extraction of impurities with ethanol for 24 h. A weak absorption at 1045 cm^{-1} in the IR spectra of the amorphous products indicated the presence of some siloxane linkages. The optimum solvents and molar per cents of crosslinking agents are given in Table 1.

Arsenic pentafluoride was purified by trap-to-trap distillation on a vacuum line until it displayed no IR-detectable impurities. This dopant was added in measured amounts by vacuum line techniques to previously pulverized $Me(SiMe_2)_nMe$ where $\bar{n} = 48$ (**I**), to polymers **II–VI** having the formulae indicated in Table 1, and to dodecamethylcyclohexasilane. Samples **I–VI** became light brown when exposed to AsF_5 at room temperature, but exposure at −78°C gave vivid blue–green products that became light brown upon warming. The doped samples were compressed (320 kg cm^{-2}) into 1.3 cm diameter × 0.1–0.2 cm thick pellets and transferred to a four-probe conductivity apparatus[6] in a dry box. Cooling the stainless steel press with liquid nitrogen facilitated the removal of the pasty $Me(SiMe_2)_nMe \cdot (AsF_5)_{0.17n}$, and satisfactory contact of this material with platinum electrodes was ensured using Electrodag.

* Author to whom correspondence should be addressed.

Table 1. Conductivities at 25°C of methylsilicon polymers doped with arsenic pentafluoride

	Polymer	Precursors	Optimum conditions[b]	Y (moles As/Si)	$\sigma(\Omega^{-1}/cm^{-1})$
I	$Me(SiMe_2)_nMe$[a]	6 $Cl(SiMe_2)_6Cl$ 2 $Me(SiMe_2)_6Cl$	—	0.17	1×10^{-5}
II	$(SiMe_2)_x$	Me_2SiCl_2	Hexane	0.17	2×10^{-6}
III	$-(SiMe_2)_x-Si(Me)-$	Me_2SiCl_2 $MeSiCl_3$(0.5–5.0%)	THF; 0.5%	0.17	3×10^{-5}
IV	$-(SiMe_2)_{6x}-Si(Me)-$	$Cl(SiMe_2)_6Cl$ $MeSiCl_3$(25%)	THF	0.17	9×10^{-7}
V	$-(SiMe_2)_x-Si-$	Me_2SiCl_2 $SiCl_4$(1–8%)	Hexane; 3%	0.19	2×10^{-6}
VI	$-(SiMe_2)_{6x}-Si-$	$Cl(SiMe_2)_6Cl$ $SiCl_4$(20%)	THF	0.17	8×10^{-7}

[a] $n = \ldots42, 48, 54\ldots$, prepared with potassium in heptane–benzene and residual chloro groups replaced by reaction with MeMgI.

[b] Solvent and molar per cent of crosslinking reagent leading to polymers with the highest conductivities.

RESULTS AND DISCUSSION

$Me(SiMe_2)_nMe$ and all of the higher polymers were found to be electrical insulators ($\sigma < 10^{-10}$ Ω^{-1} cm^{-1} at room temperature) in their undoped states, as expected. Their conductivities increase many orders of magnitude upon being doped with AsF_5. The conductivity of $Me(SiMe_2)_nMe\cdot(AsF_5)_{0.17n}$ ($\bar{n} = 48$) is 1×10^{-5} Ω^{-1} cm^{-1}. Table 1 presents conductivity data for the various doped polymers. The polymers **IV, V** and **VI**, which have extensive branching as indicated in Table 1, relative to polymers **I–III**, had a higher siloxane content, as indicated by IR spectra, absorbed AsF_5 slower, and generally exhibited lower conductivities upon doping. Polymer **III**, when synthesized from a 5:995 mixture of $MeSiCl_3$ and Me_2SiCl_2 and thus having low crosslinking, exhibited conductivity comparable with that of linear polymers. Polymers **III–VI**, with complete linking of silicon in two- and three-dimensional frameworks, were not obtainable by our method of synthesis, and thus siloxane formation upon work-up is expected. The conductivities of both the doped two-dimensional methylpolysilane (**III**), $\sigma = 3\times10^{-5}$, and the linear poly(dimethylsilylene) (**II**), $\sigma = 2\times10^{-6}$, are much lower than those reported[2] for polysilanes having other side chains which facilitate the synthesis of soluble, high molecular weight polymers. The highest conductivities were obtained for polysilanes with silicon-to-AsF_5 ratios of approximately 6 : 1.

Activation energies of 0.6 ± 0.1 eV were calculated using the equation $\sigma_T = \sigma_o \exp(-E_a/kT)$, for conductivities measured at 5 Hz. The a.c. conductivities increased by a factor of approximately two in the frequency range 5–100 Hz. The conductivity of the doped polymers is electronic in nature: two-probe d.c. measurements taken with blocking platinum electrodes and a steady 10 mV potential showed a constant current for long periods. Observed currents were proportional to applied potentials.

Condensing AsF_5 onto $Me(SiMe_2)_nMe$ at or below -78°C led to an intense blue–green colour which bleached above -73°C. Irradiation of a bleached sample at -100°C with a high-pressure mercury–xenon lamp reproduced the blue–green colour, which again disappeared upon warming. Both blue–green samples gave identical ESR spectra with a slightly asymmetric (non-Dysonian) single line having a g-value of 2.005 ± 0.002 and a width of 19 gauss. The g-value and line width were temperature-independent in the -196 to -78°C range and were independent of doping level. The signal intensity decreased slowly at -100°C and decayed with a 4 min half-life at -75°C. Pure **I** did

not exhibit an ESR signal in the temperature range −196 to 0°C or upon irradiation at either −196 or −78°C. Thus, the species which is responsible for both the colour and the ESR signal is not present during the conductivity measurements. Difficulties in preparing pellets and in making electrical contacts at low temperatures precluded making conductivity measurements on the blue–green samples.

The cyclic $(SiMe_2)_6$ absorbed AsF_5 but no blue–green colour was observed at −78°C, and the sample remained white and an insulator ($\sigma < 10^{-10}\ \Omega^{-1}\ cm^{-1}$) at room temperature.

The mechanism of conduction most likely involves migration of positive holes, as proposed earlier for other systems.[1,2,7] Oxidation of the polysilane chains, with hole formation, is consistent with the IR spectra of doped samples having bands at 500, 695 and 720 cm^{-1} attributable[8] to AsF_3 and AsF_6^- but not to Si—F. Oxidative interactions of polysilanes with electron acceptors have been observed.[9,10] The unpaired spin on fully oxidized $(SiMe_2)_6^+$ is found to delocalize on the ring.[10] These polysilanes, in contrast to intensely studied conducting polymers such as $(SN)_x$, polyacetylene and poly(*p*-phenylene), have no significant p_π unsaturation prior to doping. However, the polysilanes should be easily oxidized since the reported oxidation potentials[11] for short-chain permethylpolysilanes are low: 1.33 V (vs saturated calomel electrode) for $Me(SiMe_2)_4Me$, 1.18 V for $Me(SiMe_2)_5Me$ and 1.08 V for $Me(SiMe_2)_6Me$. For photogenerated holes in poly(phenylmethylsilylene) having a molecular weight corresponding to 3750 silicon atoms in the backbone chain, the mobility is $10^{-4}\ cm^2\ V^{-1}\ s^{-1}$ at room temperature in a field of 2×10^5 V cm^{-1} and is thermally activated with an activation energy of 0.24 eV.[7(a)] The relatively high activation energy of −0.6 eV for conductivity in the above systems probably reflects carrier hopping between polymer chains.

The electrical conductivity of these arsenic pentafluoride-doped polysilanes decreases greatly within a few weeks at room temperature, even in the absence of air and light. The thermal, photolytic and chemical instabilities of these systems are formidable obstacles to their applications in devices.

Acknowledgements—This research was partially supported by the National Science Foundation (Grant No. GP 33530). The authors thank James R. Anderson for assistance with the conductivity measurements.

REFERENCES

1. (a) T. A. Skotheim (Ed.), *Handbook of Conducting Polymers*, Vols 1 and 2. Marcel Dekker, New York (1986) and refs therein; (b) M. Aldissi (Ed.), Proceedings of the International Conference on Science and Technology of Synthetic Metals, *Synth. Met.* 1988–1989, **27–28** and refs therein.
2. (a) R. West, L. D. David, P. I. Djurovich, K. L. Stearley, K. S. V. Srinivasan and H. Yu, *J. Am. Chem. Soc.* 1981, **103**, 7352; (b) R. West, *J. Organomet. Chem.* 1986, **300**, 327; (c) A. Usuki and M. Murase, *Jpn Kokai Tokkyo Koho* JP62 **59**, 632 (87 **59**, 632); *Chem. Abstr.* 1987, **107**, 218592u; (d) Z. Du, X. Wen and J. Lin, *Shandong Daxue Xuebao, Ziran Kexueban* 1987, **22**, 115; *Chem. Abstr.* 1988, **108**, 56695w; (e) H. Naarmann, N. Theophilo, L. Geral, J. Sledz and F. Schue, German Patent DE3634281, 1988, *Chem. Abstr.* 1988, **109**, 120989u.
3. P. John, I. M. Odeh and J. Wood, *J. Chem. Soc., Chem. Commun.* 1983, 1496.
4. D. A. Van Beek Jr, PhD thesis. Northwestern University (1980).
5. W. G. Boberski and A. L. Allred, *Organomet. Chem.* 1974, **71**, C27.
6. D. Cahen, J. R. Hahn and J. R. Anderson, *Rev. Sci. Instrum.* 1973, **44**, 1567.
7. (a) R. G. Kepler, J. M. Zeigler, L. A. Harrah and S. R. Kurtz, *Phys. Rev. B* 1987, **35**, 2818; (b) M. Stolka, H.-J. Yuh, K. McGrane and D. M. Pai, *J. Polym. Sci. A* 1987, **25**, 823; (c) M. Fujino, *Chem. Phys. Lett.* 1987, **136**, 451; (d) M. Abkowitz, F. E. Knier, H.-J. Yuh, R. J. Weagley and M. Stolka, *Solid State Commun.* 1987, **62**, 547; (e) M. J. Rice and S. R. Phillpot, *Phys. Rev. Lett.* 1987, **58**, 937; (f) M. Abkowitz and M. Stoka, *Philos. Mag. Lett.* 1988, **58**, 239; (g) L. M. Samuel, P. N. Sanda and R. D. Miller, *Chem. Phys. Lett.* 1989, **159**, 227; (h) R. D. Miller and J. Michl, *Chem. Rev.* 1989, **89**, 1359.
8. K. O. Christe and A. E. Pavlath, *Z. Anorg. Allg. Chem.* 1965, **335**, 210.
9. V. F. Traven and R. West, *J. Am. Chem. Soc.* 1973, **95**, 6824; H. Sakurai, M. Kira and T. Uchida, *J. Am. Chem. Soc.* 1973, **95**, 6826.
10. H. Bock, W. Kaim, M. Kira and R. West, *J. Am. Chem. Soc.* 1979, **101**, 7667.
11. W. G. Boberski and A. L. Allred, *J. Organomet. Chem.* 1975, **88**, 65.

Polyhedron Vol. 10, No. 11, pp. 1231–1237, 1991
Printed in Great Britain

0277–5387/91 $3.00+.00
© 1991 Pergamon Press plc

NEW DEVELOPMENTS IN THE CHEMISTRY OF SILICON SELENIDES

PHILIP BOUDJOUK

Department of Chemistry, North Dakota State University, Fargo, ND 58105, U.S.A.

Abstract—The development of a convenient route to selenide anions under conditions that permit the use of organosilicon halides opened the way to a variety of organosilicon selenides. Reactivity studies on these selenide anions as well as our efforts to prepare cyclosilselenanes and subsequent photolysis and thermolysis studies are summarized.

The importance of the chemistry of compounds with silicon–oxygen bonds raises questions about the potential of the relatively virgin field of the sulphur, selenium and tellurium analogues. In attempts to explore this area we found a need for developing improved synthetic procedures for making linear, cyclic and cage silathianes and silselenanes. In this review we summarize our efforts leading to convenient syntheses of silicon chalcogenides with an emphasis on selenium derivatives. Some of these compounds are useful precursors to reactive intermediates containing the silicon–selenium double bond. The results of our work in this area are also discussed.

ANIONS OF SULPHUR, SELENIUM AND TELLURIUM

Sulphur, selenium and tellurium anions react with organic halides to form sulphides, disulphides, selenides, diselenides, tellurides and ditellurides,[1] eqs (1) and (2):

$$2RX + E_2^{2-} \longrightarrow R_2E_2 \quad (1)$$

$$2RX + E^{2-} \longrightarrow R_2E. \quad (2)$$

Historically, the syntheses of sulphur, selenium and tellurium salts of the type M_2Se_n (where M is an alkali metal and $n = 1$ or 2) were limited to liquid ammonia and protic solvents, although Sandman *et al.*[2] have recently produced Na_2Se, Na_2Se_2, K_2Se and K_2Se_2 and their tellurium analogues by the direct reaction of selenium or tellurium powder with sodium or potassium in high boiling, polar, aprotic solvents such as N,N-dimethylformamide (DMF), hexamethylphosphoramide (HMPA) or N-methylpyrrolidinone (NMP), eq. (3):

$$2M + nE \xrightarrow{DMF,\ 110°C,\ 1\ h} M_2E \quad (3)$$

$$M = Na, K;\ E = Se, Te;\ n = 1, 2.$$

Gladysz *et al.* found that lithium triethylborohydride reduced elemental selenium to give Li_2Se or Li_2Se_2 depending on the stoichiometry,[3] eq. (4):

$$2Li(C_2H_5)_3BH + nSe \longrightarrow Li_2Se_n + 2(C_2H_5)_3BH + H_2. \quad (4)$$

$$n = 1, 2$$

Our interest in developing new routes to these anions was first aroused by the report of Degrand and co-workers[4] that a combination of electrochemical reduction and ultrasound was required to generate modest yields of Se_2^{2-}, Se^{2-}, Te_2^{2-} and Te^{2-} in THF, acetonitrile and DMF. Our programme for studying the effects of ultrasonic waves on heterogeneous reactions,[5] as well as our need for a more convenient route to these anions as intermediates for group 14 chalcogenides, provided the motivation to investigate.

To our surprise, we found that simply by adding a catalytic quantity of naphthalene to a slurry of THF, sulphur (selenium, tellurium) and an alkali metal, very high yields of the desired anions are obtained.[6] We were able to produce lithium, sodium and potassium salts of sulphur, selenium and tellurium under very mild conditions. Presumably, the naphthalene forms the naphthalene radical anion which acts as a soluble charge-transfer agent and facilitates reduction. The product is controlled by

Table 1. Reductions of selenium by potassium, sodium and lithium

Reaction	Number	Conditions[a]	Time
$2K + 2Se \longrightarrow K_2Se_2$	1	Reflux	40 min
	2	Ultrasound	85 min
	3	Stir	150 min
$2K + Se \longrightarrow K_2Se$	4	Reflux	55 min
	5	Ultrasound	120 min
	6	Stir	130 min
$2Na + 2Se \longrightarrow Na_2Se_2$	7	Reflux	65 min
	8	Ultrasound	65 min
	9	Stir	135 min
$2Na + Se \longrightarrow Na_2Se$	10	Reflux	80 min
	11	Ultrasound	85 min
	12	Stir	180 min
$2Li + 2Se \longrightarrow Li_2Se_2$	13	Reflux	8 h
	14	Ultrasound	9.5 h
	15	Stir	15 h
$2Li + Se \longrightarrow Li_2Se$	16	Reflux	12 h

[a] All ultrasound and stirring reactions were carried out at 20–25°C except numbers 8 and 9 which were at 35–40°C.

the stoichiometry. Our results for selenium are given in Table 1.

Relative reactivity studies

The *in situ* reduction of selenium by potassium, sodium and lithium in THF produces suspensions of selenide or diselenide salts which were treated with organic bromides. Considerable reactivity differences were observed. For example, diselenides are signifiantly more reactive then selenides for all three cations. However, within the diselenide series, Li_2Se_2 is more reactive than the sodium and potassium analogues, while among the selenides the potassium salt is the most active.

Relative reactivities toward organic bromides in THF:

$$Li_2Se_2 \gg Na_2Se \gg K_2Se_2 \gg K_2Se > Na_2Se > Li_2Se.$$

APPLICATIONS IN THE SYNTHESIS OF SILICON CHALCOGENIDES

Linear systems

We applied this methodology to simple silicon halides to prepare disilathianes and disilselenanes.[7] Of these, hexamethyldisilathiane is particularly important because of its utility in organic synthesis.[8] Prior to our work, the best available procedures called for either hydrogen sulphide[9] or lithium triethylborohydride,[10] both of which have inconvenient aspects in handling and/or work-up. Hexamethyldisilathiane and analogous compounds can now be easily prepared in high yields, eq. (5):

$$S + 2Na \xrightarrow[THF]{\text{naphthalene}} Na_2S \xrightarrow[R = H, Me]{2RMe_2SiCl} \underset{90\text{–}95\%}{RMe_2Si—S—SiMe_2R}. \quad (5)$$

This approach also applies to selenium and tellurium, although the latter produces compounds that are very sensitive to water, oxygen and light.

Cyclic and cage systems

When dichlorosilanes are used with sulphur and selenium anions prepared in this fashion, cyclic compounds are obtained, eq. (6):[11,12]

$$M_2E + R_2SiCl_2 \xrightarrow[E = S, Se]{} (R_2SiE)_n. \quad (6)$$

$$n = 2, 3$$

We have been focusing on the cyclosilselananes and found that we could prepare useful quantities of cyclodisilselenanes and cyclotrisilselenanes (Scheme 1). All of these compounds are sensitive to moisture with the exception of the highly hindered $[(Me_3Si)_2SiSe]_2$.

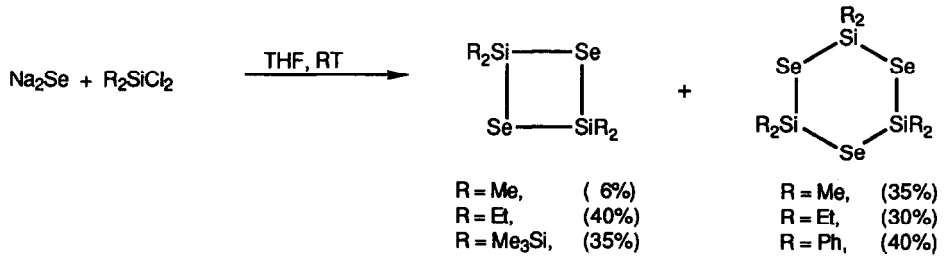

Scheme 1. Synthesis of cyclosilselenanes.

Some physical and spectroscopic properties of cyclosilselenanes
$(Me_2SiSe)_2$: air-sensitive, yellow liquid; decomposes in minutes at 25°C under nitrogen.
$(Me_2SiSe)_3$: air-sensitive, yellow liquid; decomposes in ~ 1 h at 25°C under nitrogen; λ_{254}, $\varepsilon = 1250$.
$(Et_2SiSe)_2$: air-sensitive, yellow liquid; decomposes in ~ 1 h at 25°C under nitrogen.
$(Et_2SiSe)_3$: air-sensitive, yellow liquid; decomposes in ~ 1 h at 25°C under nitrogen; λ_{254}, $\varepsilon = 1100$.
$(Ph_2SiSe)_3$: colourless, crystalline solid; stable for several hours in air.
$[(Me_3Si)_2SiSe)]_2$: light green needles; stable for several days in air.

Tricyclo-[3.3.1.1^{3,7}]tetrasilselenanes

There are only two papers describing the synthesis of adamantane-like structures composed of silicon and selenium, $(RSi)_4Se_6$, both of which report very low yields.[13] Using the methodology that led to cyclosilselenanes, but with organotrichlorosilanes rather than dichlorosilanes, we were able to prepare adamantanes in much improved yields [eq. (7)].[14] All three compounds are white, crystalline solids which decompose over the course of a few hours if left in air.

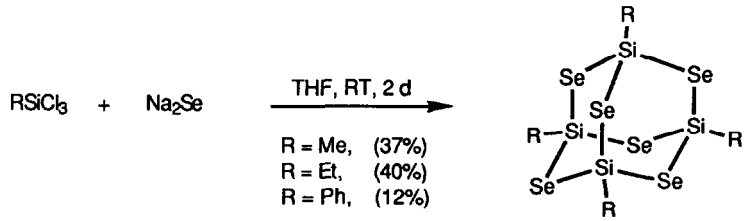

(7)

The structure given in eq. (7) is one of two reasonable isomers from this reaction. The other is the bridged system below:

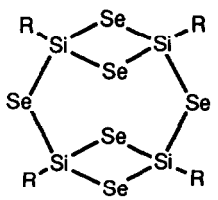

We used ^{77}Se NMR to discriminate between the two possibilities. The adamantane structure gives only one signal since all six selenium atoms are equivalent. The isomer, on the other hand, has two kinds of selenium atom, one set of four in the four-membered rings and one set of two that bridge these rings and should exhibit two absorptions.

Reactive intermediates

We are interested in investigating the chemistry of reactive species containing multiple bonds between elements of groups 14 and 16. In particular, those of the general formula, $R_2E{=}X$, where E = Si, Ge, Sn and X = O, S, Se, Te. Thus it is necessary to develop convenient high yield routes to these intermediates. For spectral studies it is critical that these routes generate innocuous by-products. Thus "clean" sources of these species is an important goal of our work. Here we discuss the results of our efforts with selenium.

Silaneselones via ring contraction of cyclosilselenanes

Pyrolysis of cyclic compounds of the type $(R_2E{-}X)_n$, $n = 2, 3, 4$, is a well-known route to reactive intermediates of the type $R_2E{=}X$ [eq.

Table 2. Ring contractions of $(Me_2SiSe)_3$ and $(Et_2SiSe)_3$

$$(R_2SiSe)_3 \longrightarrow (R_2SiSe)_2$$

Entry	R	Conditions	Time (h)	Yield (%) of $(R_2SiSe)_2$[a]	Per cent conversion[b]
1	Me	254 nm/hexane	23	68	95
2	Me	150°C/decane	48	~ 3	~ 3
3	Me	225°C/decane	70	39	46
4	Me	225°C/decane	94	35	48
5	Et	254 nm/hexane	18	90	100
6	Et	225°C/decane	40	80	100
7	Et	155°C/decane	40	15	16

[a] Yields determined by glc.
[b] Per cent cyclotrisilselenane reacted.

(8)].[15] This approach has been used to generate reactive intermediates for E = C and X = S, Se, such as thiocarbonyl fluoride,[16] thioacetaldehyde and thioacetone,[17] thioformaldehyde[18] and selenoacetaldehyde,[19] as well as for some of the heavier analogues like dimethylsilathione (R = Me, E = Se, X = O)[20,21] and diethylgermathione (R = Et, E = Ge, X = S).[22]

$$(R_2E{-}X)_n \xrightarrow{\Delta} R_2E{=}X \qquad (8)$$

R = alkyl, H, halogen; E = C, Si, Ge; X = O, S, Se.

The first cyclosilselenanes were prepared by Schmidt and Ruf in 1963,[23] but no attempts to generate silaneselones from these compounds, with the exception of our own, have been reported.

$(Me_2SiSe)_3$ and $(Et_2SiSe)_3$ undergo ring contraction, photochemically and thermally, to form $(Me_2SiSe)_2$ and $(Et_2SiSe)_2$, respectively (Table 2). The UV spectra of $(Me_2SiSe)_3$ and $(Et_2SiSe)_3$ show absorbances at 254 nm, while the absorbances of $(Me_2SiSe)_2$ and $(Et_2SiSe)_2$ cut off at 220 nm. Photolysis (Raynonet, 254 nm lamps, hexane) of $(Et_2SiSe)_3$ produces $(Et_2SiSe)_2$ in 90% yield and is the only product observed by gas chromatography (Table 2, entry 5). In a separate experiment, it was shown that $(Et_2SiSe)_2$ is essentially inert to photolysis [254 nm, 48 h, 93% recovery, no evidence of $(Et_2SiSe)_3$]. Photolysis of $(Me_2SiSe)_3$ produces $(Me_2SiSe)_2$ in 68% yield (Table 2, entry 1). Decomposition was observed in the form of discharged elemental selenium in all reactions, photochemical and thermal.

Replacing methyl groups with ethyl groups significantly alters the chemistry of the ring systems. For example, $(Me_2SiSe)_2$ has a $t_{1/2}$ of 60 h at 69°C (refluxing hexane) producing a 22% yield of $(Me_2SiSe)_3$, whereas $(Et_2SiSe)_2$ is stable indefinitely at that temperature and even after 32 h at 250°C, 80% can be recovered [no $(Et_2SiSe)_3$ was detected]. For the six-membered rings, the stabilities are reversed: $(Me_2SiSe)_3$ is stable to 110°C, is only 3% converted to $(Me_2SiSe)_2$ at 150°C, and is less than 50% converted at 225°C even after 94 h (Table 2, entries 1, 6 and 7). The ethyl analogue $(Et_2SiSe)_3$, on the other hand, shows much higher conversion rates to $(Et_2SiSe)_2$, thermally and photochemically (Table 2, entries 2–4). Photolysis of $(Me_2SiSe)_3$ at 254 nm in hexane produces a mixture of $(Me_2SiSe)_2$ and $(Me_2SiSe)_3$ in an 11 : 1 ratio. This mixture was then transferred to a sealed tube and heated to 225°C. After 36 h the ratio changes to about 5.3 : 1, but significant quantities of elemental selenium were also produced.

Thus only for the methyl case does there appear to be an equilibrium between the four- and six-membered rings and then only under thermal conditions. Accurate determination of an equilibrium constant is prevented by the accompanying side reactions. An equilibrium under our photochemical conditions is not possible because $(Me_2SiSe)_2$ and $(Et_2SiSe)_2$ do not absorb at 254 nm.

Ring contraction in the presence of D_3. *Evidence for silaneselones*

Photolysis or thermolysis of $(Me_2SiSe)_3$ [or $(Et_2SiSe)_3$] in the presence of D_3, $(Me_2SiO)_3$, gives $(Me_2SiSe)_2$ and 2,2,4,4,6,6,8,8-octamethyl-1,5,7,3,2,4,6,8-trioxatetrasilselenocane (**3**) [or $(Et_2SiSe)_2$ and 4,4,6,6,8,8-hexamethyl-2,2-diethyl-1,5,7,3,2,4,6,8-trioxatetrasilaselenocane (**4**)], in good yields (Table 3). By analogy to known two atom insertion reactions observed for other $R_2Si{=}X$ species (X = CR_2, NR, O, S),[24] we postulate the inter-

Table 3. Ring contractions in the presence of D_3

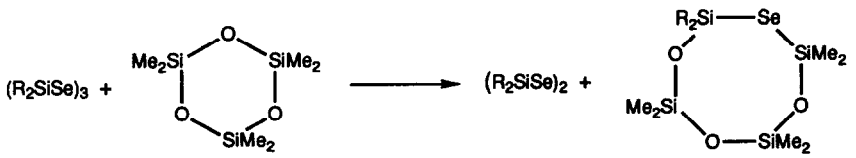

A D3 B C

Experiment[a]	R	D_3/A ratio	Conditions	C/B ratio	Per cent recovered Se as B and C
1	Me	20:1	254 nm/hexane	2.40:1	80
2	Me	100:1	254 nm/hexane	> 100:1	60
3	Me	20:1	225°C/decane	3.00:1	65
4[b]	Me	100:1	225°C	> 100:1	70
5	Et	8:1	254 nm/hexane	0.33:1	81
6	Et	20:1	254 nm/hexane	0.55:1	85
7	Et	100:1	254 nm/hexane	3.00:1	85
8	Et	30:1	225°C/decane	0.65:1	84
9[b]	Et	100:1	225°C	2.70:1	72

[a] All reactions showed complete consumption of starting material.
[b] Experiments run without solvent.

mediacy of silaneselones **1** and **2**, eq. (9):

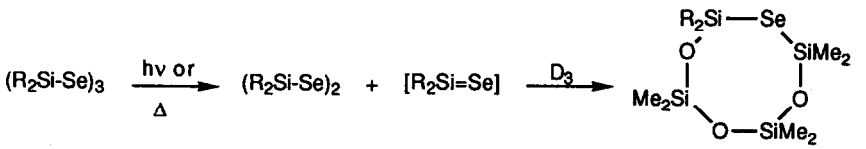

(9)

1, R=Me
2, R=Et

3, R=Me
4, R=Et

The structures of **3** and **4** can be assigned unambiguously on the basis of ^{13}C NMR data. For example, the carbon spectrum of **3** exhibits two singlets at 6.79 and 1.14 ppm, respectively. The alternative structure, **5**, would have at least three absorp-

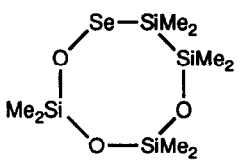

5

tions. The data in Table 3 illustrate important differences in the chemistries of $(Me_2SiSe)_3$ and $(Et_2SiSe)_3$. While $(Me_2SiSe)_3$ is more stable with respect to ring contraction than $(Et_2SiSe)_3$ (Table 1), $(Me_2SiSe)_3$ is a far better source of a silaneselone than is $(Et_2SiSe)_3$.

The experiments with D_3 affect overall silaneselone production. For example, when the ratio of $D_3/(Me_2SiSe)_3$ is 100:1, < 1% of $(Me_2SiSe)_2$ is detected (Experiments 2 and 4). On the other hand, when a $D_3/(Et_2SiSe)_3$ ratio of 100:1 is used, the product mixture contains > 30% $(Et_2SiSe)_2$ (Experiments 7 and 9). While the product distribution may be affected by relative trapping efficiencies, i.e. the smaller dimethylsilaneselone **1** probably reacts faster with D_3 than diethylsilaneselone **2**, the reactivities of the cyclodisilselenanes play a key role because they are sources of silaneselones. When $(Me_2SiSe)_2$ and a 12-fold excess of D_3 is refluxed in hexane for 60 h, no selenocane is observed, but $(Me_2SiSe)_3$ is obtained in 22% yield. This suggests that $(Me_2Si Se)_2$ is a better trap for the silaneselone than D_3, but $(Me_2SiSe)_2$ is approximately 10 times more reactive (Table 4). In these reactions, cyclodisilselenanes are not traps of chemical consequence, since any six-membered ring which is formed should fragment to give silaneselone.

We propose the following pathways for the thermal (> 200°C) reactions of hexaalkylcyclotrisilselanes in the presence of D_3 (Scheme 2). The reaction begins with the extrusion of dialkylsilaneselone

Table 4. Thermolysis of $(R_2SiSe)_2$ with D_3

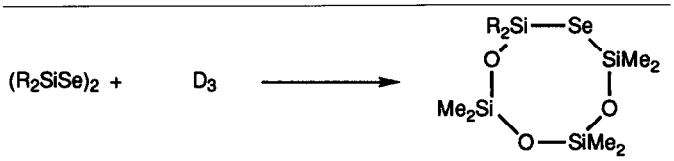

B C

R	D_3/**B** ratio	Conditions	Yield (%) of **C**	Per cent conversion of **B**
Me	12:1	225°C/decane/48 h	70	90
Et	12:1	250°C	5	9

by the cyclotrisilselane. The silaneselone once formed may dimerize, insert into D_3 giving the selenocane or insert into newly formed cyclodisilselenane reforming starting material. We see no evidence of insertion of silaneselone into cyclotrisilselenane to produce cyclotetrasilselenane (in similar experiments with cyclotrisilthianes no cyclotetrasilthianes were observed[20,21]). Cyclodisilselenane formed in the reaction is also capable of extruding silaneselone [e.g. $(Me_2SiSe)_2$ is a more efficient source of silaneselone than $(Me_2SiSe)_3$].

When $(Et_2SiSe)_3$ is photolysed or thermolysed in the presence of triethylsilane, no Si—H insertion is observed. The only observable product is $(Et_2SiSe)_2$ in 90% yield. This indicates that the silaneselone does not readily insert into Si—H bonds under these conditions, and further evidence that silylene formation is not an important pathway in the decomposition of alkylated cyclotrisilselenanes.

No cycloaddition reactions between silaneselones and dienes or alkenes were observed. When $(Et_2SiSe)_3$ is photolysed in a 12-fold excess of cyclohexene, or heated (225°) in a 12-fold excess of anthracene, the only product observed is $(Et_2SiSe)_2$ in approx. 90% yield.

We also investigated the possibility that silaneselones might be intermediates in the synthesis of cyclosilselenanes by treating Et_2SiCl_2 with sodium selenide in the presence of D_3. No selenocanes were detected. This suggests that ring formation occurs primarily through bimolecular reactions involving ionic intermediates (Scheme 3).

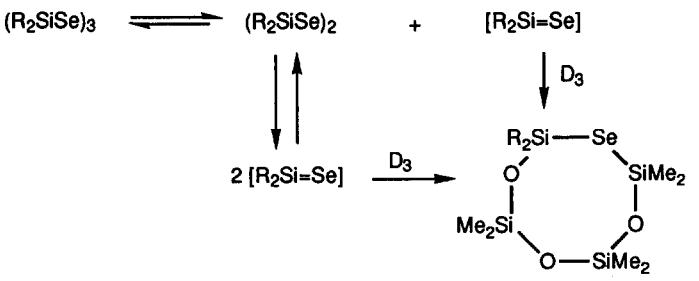

Scheme 2.

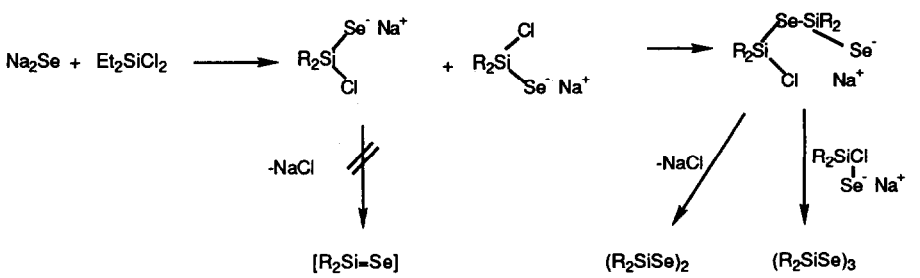

Scheme 3.

Thermolysis and photolysis of $(Ph_2SiSe)_3$ *and* $[(Me_3Si)_2SiSe]_3$

The photolysis of hexaphenylcyclotrisilselenane in D_3 is more complex than $(Me_2SiSe)_3$ and $(Et_2SiSe)_3$, presumably because the initial photoproducts probably absorb at 254 nm. When a 20 : 1 mixture of D_3 and $(Ph_2SiSe)_3$ was photolysed in methylene chloride at 254 nm for 24 h, six products were detected. Only one could be fully characterized: 4,4,6,6,8,8-hexamethyl-2,2-diphenyl-1,5,7,3,2,4,6,8-trioxatetrasilaselenocane (**6**) which was about 20% of the product mixture and is probably the result of insertion of diphenylsilaneselone, $Ph_2Si{=}Se$, into D_3.

When a decane solution of $(Ph_2SiSe)_3$ was heated to 275°C in a sealed tube for 90 h, only starting material was recovered. However, when a mixture of $(Ph_2SiSe)_3$ and a 20-fold excess of D_3 was heated in decane (275°C, 72 h) $(Ph_2SiSe)_3$ and **6** (30%) were isolated. No tetraphenylcyclodisilselenane was observed. This implies that, at 275°C in the absence of a trap, $(Ph_2SiSe)_3$ is fragmenting to produce tetraphenylcyclodisilselenane and diphenylsilaneselone, but the four-membered ring is either converted back to $(Ph_2SiSe)_3$ or decomposed to the silenselone. We pyrolysed $(Ph_2SiSe)_3$ in the presence of Et_3SiH in an effort to trap diphenylsilylene. We were unable to detect the insertion product, $Et_3Si{-}SiPh_2{-}H$, by GC–MS.

A mixture of tetrakis(trimethylsilyl)cyclodisilselenane and a 12-fold excess of D_3 in decane were heated in a sealed tube at 250°C. After 5 days, analysis of the reaction mixture indicated no volatile products and > 95% recovery of starting material. Photolysis produced similar results.

SUMMARY

Convenient routes to dianions of sulphur and selenium have led to useful syntheses of linear, cyclic and cage silathianes and silselenanes. Ready access to these compounds will lead to a more facile exploration of the chemistry of silicon chalcogenides. Our preliminary studies on cyclosilselenanes has opened the way to the generation of new reactive intermediates containing the silicon–selenium double bond.

REFERENCES

1. D. A. Armitage, The chemistry of compounds with silicon–sulfur, silicon–selenium and silicon–tellurium bonds, in *The Chemistry of Organic Silicon Compounds* (Edited by S. Patai and Z. Rappoport), Ch. 23. John Wiley, New York (1989), *The Chemistry of Organic Selenium and Tellurium Compounds* (Edited by S. Patai and Z. Rappoport), Vol. 1. John Wiley, New York (1986).
2. D. J. Sandman, J. C. Stark, L. A. Acampora and P. Gagne, *Organometallics* 1983, **2**, 549.
3. J. A. Gladysz, J. L. Hornby and J. E. Garbe, *J. Org. Chem.* 1978, **43**, 1204.
4. B. Gautheron, G. Rainturier and C. Degrand, *J. Am. Chem. Soc.* 1985, **107**, 5579.
5. For a recent review on the effects of ultrasonic waves on heterogeneous reactions see: (a) P. Boudjouk, Acceleration of synthetically useful heterogeneous reactions using ultrasonic waves, in *High Energy Processes in Organometallic Chemistry* (Edited by K. S. Suslick), ACS Symposium Series 333, Ch. 13. American Chemical Society, Washington, DC (1987); (b) P. Boudjouk, Heterogeneous sonochemistry, in *Ultrasound: Chemical, Physical and Biological Effects* (Edited by K. S. Suslick). Verlag Chemie International, Weinheim, F.R.G. (1988).
6. D. P. Thompson and P. Boudjouk, *J. Org. Chem.* 1988, **53**, 2109.
7. J.-H. So and P. Boudjouk, *Synthesis* 1989, 306.
8. (a) T. Aida, T. H. Chan and D. N. Harpp, *Tetrahedron Lett.* 1981, **22**, 1089; (b) K. Steliou, P. Salama and J. Corriveau, *J. Org. Chem.* 1985, **50**, 4969.
9. D. N. Harpp and K. Steliou, *Synthesis* 1976, 721.
10. M. R. Detty and M. D. Seidler, *J. Org. Chem.* 1982, **47**, 1354.
11. D. P. Thompson and P. Boudjouk, *J. Chem. Soc., Chem. Commun.* 1987, 1466.
12. D. P. Thompson, PhD thesis. North Dakota State University, Fargo, North Dakota.
13. (a) J. A. Forstner and E. L. Muetterties, *Inorg. Chem.* 1966, **5**, 552; (b) A. Hass, R. Hitze, C. Kruger and K. Angermund, *Z. Natur.* 1984, **39B**, 890.
14. P. Boudjouk and S. R. Bahr, unpublished work.
15. For reviews on heavy atom analogues of ketones see: (a) J. C. Guziec, in *Organoselenium Chemistry* (Edited by D. Liotta), p. 237. John Wiley, New York (1987); (b) C. Raabe and J. Michl, *Chem. Rev.* 1985, **85**, 419; (c) J. Satge, *Pure Appl. Chem.* 1984, **56**, 137.
16. H. W. Kroto and R. J. Suffolk, *Chem. Phys. Lett.* 1972, **17**, 213.
17. H. W. Kroto, B. M. Landsberg, R. J. Suffolk and A. Vodden, *Chem. Phys. Lett.* 1972, **29**, 265.
18. H. Block, T. Hirabayashi, S. Mohmand and B. Solouki, *J. Am. Chem. Soc.* 1982, **104**, 3119.
19. M. Hutchinson and H. W. Kroto, *J. Molec. Spect.* 1978, **70**, 347.
20. W. P. Weber and H. S. D. Soysa, *J. Organomet. Chem.* 1979, **165**, C1.
21. K. Moedritzer, *J. Organomet. Chem.* 1970, **21**, 315.
22. H. Lavayssiere, G. Dousse, J. Barrau, J. Satge and M. Bouchart, *J. Organomet. Chem.* 1978, **161**, C59.
23. V. M. Schmidt and H. F. Ruff, *Z. Anorg. Allg. Chem.* 1963, **53**, 2109.
24. (a) C. M. Golino, R. D. Bush, P. On and L. H. Sommer, *J. Am. Chem. Soc.* 1975, **97**, 1957; (b) C. M. Golino, R. D. Bush and L. H. Sommer, *J. Am. Chem. Soc.* 1975, **97**, 7371; (c) H. Okinoshima and W. P. Weber, *J. Organomet. Chem.* 1978, **149**, 279; (d) D. R. Parker and L. H. Sommer, *J. Am. Chem. Soc.* 1976, **98**, 618.

Polyhedron Vol. 10, No. 11, pp. 1239–1245, 1991
Printed in Great Britain

0277–5387/91 $3.00+.00
© 1991 Pergamon Press plc

CATALYTIC DEHYDROCOUPLING: A GENERAL METHOD FOR THE FORMATION OF ELEMENT–ELEMENT BONDS

JOHN F. HARROD* and YING MU

Chemistry Department, McGill University, Montreal, PQ, Canada H3A 2K6

and

E. SAMUEL

Laboratoire de Chimie Organométallique de l'ENSCP (URA 403 CNRS),
11 rue P. et M. Curie, 75005 Paris, France

Abstract—The general status of catalytic dehydrocoupling as a method for the synthesis of element–element bonds is discussed and evaluated in the context of studies carried out in the authors' and other laboratories. Available thermodynamic data show that dehydrocoupling is favourable for the formation of homopolar bonds between a number of the heavier congeners of the *p*-groups, and heteropolar bonds between first members and lower members of the *p*-groups. Metallocene alkyls and hydrides of group 4 show a particularly high catalytic activity in a number of dehydrocoupling reactions, including Si—H/Si—H, Ge—H/Ge—H, Si—H/O—H, Si—H/N—H and B—H/N—H reactions. The role of some novel silyl intermediates in the dimethyltitanocene- and dimethylzirconocene-catalysed silane coupling reactions is discussed. Current views on the mechanism of these reactions are presented, particularly with respect to the intervention of cyclization reactions and their role in molecular weight limitation.

The formation of element–element (E—E or E—E′) bonds is one of the most fundamental of chemical reactions. In organic chemistry, the existence of innumerable metastable unsaturated compounds, whose multiple bonds are easily opened by electrophilic, nucleophilic or free radical attack, provides a wide range of methods for the formation of C—C and C—E bonds. The few unsaturated compounds of the heavier congeners of the *p*-groups depend for their stability and isolation on the use of sterically demanding substituents which suppress the normal addition reactions that render these types of compounds so useful in organic chemistry.[1–4]

A very general route to the formation of E—E′ bonds is the reaction of a hydride of the more electronegative elements (e.g. N, O and the halogens) with a covalent halide to give the hydrogen halide and the E—E′ bond. The thermodynamics and rates of such reactions can be improved, when necessary, by the addition of a base to scavenge the hydrogen halide.

One of the more important general reactions for the formation of E—E bonds is the Wurtz–Fittig type coupling of element halides by reaction with reactive metals, particularly the metals of group 1. Such reactions have an exceptionally wide application for the formation of E—E bonds, but show little or no selectivity for the synthesis of E—E′ bonds. Many cross-coupling reactions can, however, be carried out in two steps: the preformation of an E-group 1 or group 2 compound, followed by reaction with an E′ halide. There is also voluminous literature on specific cross-coupling reactions using transition metal organometallics and element halides, but this goes far beyond the scope of the present article.

In general, reactions of the kind described above

* Author to whom correspondence should be addressed.

present major problems for large scale industrial synthesis. Halide intermediates are relatively expensive and their use generally leads to contaminated salt wastes that are increasingly difficult and costly to dispose of. Batch handling of alkali metals under severe reaction conditions is dangerous and costly. Stoichiometric use of transition metal or main group organometallics is intrinsically costly and always involves difficult by-product recovery and/or disposal problems. Thus, there is considerable incentive to develop alternative syntheses which avoid such problems, while avoiding the introduction of a new set of equally serious problems.

A reaction which is attractive from many points of view is dehydrocoupling, shown in a generalized form in eq. (1):

$$EH + EH \text{ (or } E'H) \longrightarrow E{-}E \text{ (or } E{-}E') + H_2. \quad (1)$$

Such a reaction is appealing since many main group hydrides are in reality, or in principle, easily available at reasonable cost. In addition, the hydrogen by-product is easily recovered. As written, eq. (1) is of little use in the case of the first members of the *p*-groups since the reactions are, for the most part, strongly endothermic under "ambient" conditions. This problem can be, and in some cases has been, overcome by coupling reaction (1) into an exothermic hydrogen-consuming reaction, such as water formation, thus:

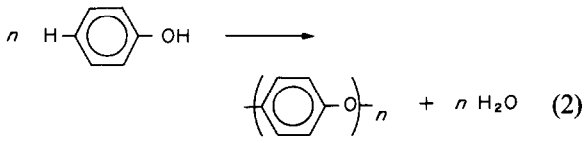

(2)

In the present paper we will review recent developments in the application of coordination catalysis to reactions (1) and attempt to interpret some of the results in mechanistic terms.

THE THERMODYNAMICS OF DEHYDROCOUPLING

Although a thorough analysis of the thermodynamics of reactions (1) is still precluded by the relative paucity of data for the bond dissociation energies of the E—H, E—E and E—E′ bonds, some general trends are obvious. Table 1 presents some data for the binary hydrides. From this table it is obvious that the general trend is for reactions (1) to become more exothermic on descending a group. It is also clear that there are many thermodynamically feasible dehydrocoupling reactions.

Although the data in Table 1 are useful to illustrate some general trends, they should be treated with considerable care when attempting to assess the thermodynamic viability of a particular reaction. The E—H energies are average bond energies for the binary hydrides and the E—E energies are for the pure elements. The numbers can be quite different for molecules carrying organic substituents, but unfortunately there is very little data for such cases. An exception to this is the case of silicon, whose industrial importance has encouraged a number of high quality thermodynamic studies.

Table 1. Thermodynamics of dehydrocoupling for some main group hydrides (energies in kJ mol^{-1})[a]

E	D_{E-H}	$D_{E-E \text{ or } E-E'}$	ΔD_R[b]
C	415	331	+64
Si	320	197	+8
Ge	289	163	−20
N	389	159	+184
P	318	214	−13
As	247	178	−119
O	465	138	+357
S	364	264	+29
Se	314	193	−20
C O	415 465	343	−102
Si O	320 465	368	−18
Si S	320 364	226	+23

[a] Data from ref. 5.

[b] The quantity ΔD_R is the sum of the bond energy changes for the reaction and it is expected to approximate the reaction enthalpy. The values of ΔD_R are based on a value of 435 kJ mol^{-1} for D_{H-H}.

Some data relevant to the dehydrocoupling of silanes is shown in Table 2. From these data two important conclusions may be drawn. In the first place, the dehydrocoupling of silanes is thermodynamically favoured by organic substitution at silicon. Secondly, there is a very large variation in the thermodynamic viability of the reaction, depending on the substitution at silicon. The effect of substitution with silicon is particularly marked, although this must be qualified by the fact that we have no good data on the effect of silicon catenation on the strength of the Si—Si bond. It is also evident that data based on the binary hydrides and the pure elements can be quite misleading.

In conclusion, we draw attention to the fact that the above discussion considers only enthalpic factors. It is not expected that the entropy contributions would be large in a dehydrocoupling reaction, but the high fugacity of hydrogen and its

Table 2. Some bond energies for E—H and E—E bonds (E = C or Si) (energies in kJ mol^{-1})[a]

Molecule	D_{C-H}	D_{Si-H}	D_{C-C}	D_{Si-Si}	$\Delta D_{R(Si)}$ (calc.)
EH_4	437	376	—	—	+9
$MeEH_3$	408	373	~350[b]	—	−9
Me_3EH	383	375	291	335	−20
$PhEH_3$	366	367	~350[b]	~320	−21
E_n (diamond)	—	—	354	225	—
$Me_3SiSiMe_3SiH$	—	355[c]	—	~330[b]	−55
$(Me_3Si)_3SiH$	—	325[c]	—	~300[b]	−85

[a] All data from ref. 6, except those labelled [c].
[b] Estimated by interpolation.
[c] Data from ref. 7.

low solubility could contribute to driving reactions that are thermodynamically marginal. For example, although the data in the tables indicate that the dehydrocoupling of SiH_4 is not thermodynamically favoured, we have in fact observed this reaction in the laboratory.[8]

SOME GENERAL FEATURES OF CATALYTIC DEHYDROCOUPLING OF ORGANOSILANES

A wide range of organometallic complexes has been screened with respect to the catalysis of reaction (1) (E = Si).[9–14] It can be broadly concluded that all compounds so far screened fall into one of two categories. The most common type of activity, and one which seems to occur with virtually any metal complex under approporiate conditions, is a slow stepwise oligomerization which, even in the most promising cases, only leads to low oligomers (n = 2–6). The second category of activity, which up until now is manifest exclusively by some compounds Cp_2MR_2 (M = Ti, Zr, Hf; R = alkyl, H; Cp = η^5-cyclopentadienyl or an alkyl substituted derivative), results in rapid oligomerization to higher oligomers (typically, n = 10–20, but in a few cases to higher values).[15,16] These reactions usually proceed rapidly, even violently, under ambient conditions, while those in the first category normally require the application of heat to achieve reasonable rates. Even some group 4 metallocene complexes exhibit the first rather than the second category of reactivity with primary organosilanes, e.g. bis (indenyl)dimethyltitanium(IV) with phenylsilane, and all group 4 metallocene-catalysed oligomerizations of secondary silanes fall into this category.

The reactivity of organosilanes towards dehydrocoupling is quite sensitive to the nature of the silane. In general, the order of reactivity is 1° > 2° ≫ 3°. Given the thermodynamic values in Table 2, it may be assumed that this order is largely the result of steric constraints. Platinum group complexes are less sensitive to this effect and they commonly couple primary and secondary silanes at comparable rates,[12] but to our knowledge, no effective catalyst for the coupling of tertiary silanes has yet been found.

The group 4 metallocene catalysts are highly sensitive to steric effects. Titanocene derivatives only catalyse the coupling of certain secondary silanes to dimers at an extremely slow rate and even sterically encumbered primary silanes, such as tertbutyl- and cyclohexylsilanes do not oligomerize. Zirconocene-based catalysts are about an order of magnitude more reactive than titanocene analogues[16e] and have been shown to oligomerize some secondary silanes to n = 5 to 6 at higher temperatures and long reaction times.[10]

Catalysts derived from the elements of groups 6–10 also tend to catalyse redistribution of arylsilanes, a serious impediment to the achievement of high polymers.[12,13] Binary carbonyls of manganese, iron and cobalt also catalyse the redistribution of phenylsilane at temperatures where coupling is also catalysed (*ca* 100°C).[17]

A special feature of the group 4 metallocene catalysts is their exceptional ability to couple 1,2-disubstituted disilanes at a more rapid rate than the analogous monosilanes.[18] As a result of this ability, only small amounts of dimer accumulate during the reaction of phenylsilane. We have shown that dimethyltitanocene (DMT) catalyses the coupling of 1,2-diphenyldisilane to the tetramer and higher, even-numbered oligomers at a faster rate than phenylsilane is polymerized by the same catalyst. Only a small amount of redistribution to the monomer occurs and it seems that the reaction is predominantly one of dehydrocoupling. The greater

reactivity of the disilane may not seem surprising in view of the greater weakness of the SiSi—H bond[7] and the more favourable thermodynamics indicated in Table 2. However, the phenomenon is not general and most other catalyst systems are more effective in the oligomerization of monosilane than of disilane. For example, vanadocene catalyses the dehydrocoupling of primary silanes, but requires temperatures in excess of 100°C to give reasonable rates. The reactions proceed in a stepwise fashion to give first the dimer, then the trimer, etc. In this case, the dimer is less reactive than the monomer and can accumulate up to *ca* 50% of the reaction mixture.[9] Similarly, platinum group catalysts also give high yields of dimer.[12]

SOME SILYLMETALLOCENE INTERMEDIATES

A number of silyltitanocene(III) and silylzirconocene(IV) complexes have been isolated from reactions of the dimethylmetallocenes with organosilanes. On the basis of NMR and ESR spectroscopies, the products of DMT reactions with silanes are entirely in the form of titanium(III).[16c,19] The only products isolated so far from dimethylzirconocene (DMZ) reactions are zirconium(IV) complexes.[16d,e] There is, however, ample evidence from NMR and ESR spectra that zirconium(III) species are also produced in solution.[16e]

The first complexes isolated from DMT reactions were the silyl-bridged bimetallic species **1** and **2**.[16c]

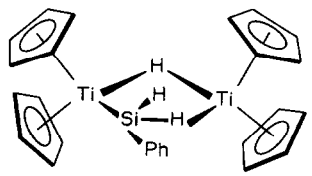

1

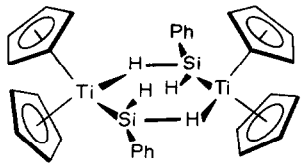

2

These complexes can be observed by virtue of their highly characteristic NMR spectra, and in some cases isolated, with all silanes which undergo polymerization. With sterically hindered primary silanes, or secondary silanes, which do not undergo polymerization, there is no evidence for the bimetallic intermediates by NMR, despite the fact that all the titanium is reduced to titanium(III).

More recently we have reported that silyltitanocene species can be trapped with phosphine ligands to give the monomeric complexes **3**.[19] Such complexes can be produced with secondary silyl ligands, thus proving that the main difference between polymerizable and non-polymerizable silanes is their ability to give the dimetallic species **1** and **2**, and not their ability to transform DMT to silyltitanocene(III) species. This should not be taken as indicating that the bimetallic species are necessary to catalytic activity, but rather that steric repulsion may be responsible for both effects.

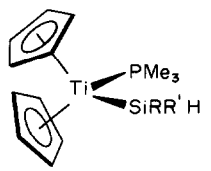

a: R = Ph, R′ = H

b: R = R′ = Ph

3

An examination of the structural details of complexes **3a** and **3b** reveals: (i) the ligands on the silicon adopt a staggered conformation with respect to the ligands on the titanium, with the Ph and PR_3 groups *trans* to each other [see Fig. 1(a)] and (ii) in the diphenyl complex, one of the Ph—Si—Ti angles (that in a *cis* relation to the phosphorus) is opened up to accommodate the steric repulsion between the phenyl group and the phosphine ligand.[19]

The formation of near planar rings via the Si—H—Ti bridges in complexes **1** and **2** forces the ligands on the silicon into a nearly eclipsed configuration with respect to the ligands on the titanium [see Fig. 1(b)]. Excessive steric repulsion between the extraannular ligands on the silicon and titanium atoms is avoided by the assumption of a very large Ph—Si—Ti angle. The angles for the complexes of interest are listed in Table 3. From these data, it is evident that the monometallic diphenylsilyl complex can form by accommodating steric strain via opening up of one of the Ph—Si—Ti angles. The bimetallic complexes cannot form in this case since even the monophenyl species, for both **1** and **2**, has to open up the Ph—Si—Ti angle because of the near-eclipsed configuration. A second substituent on the silicon would be forced

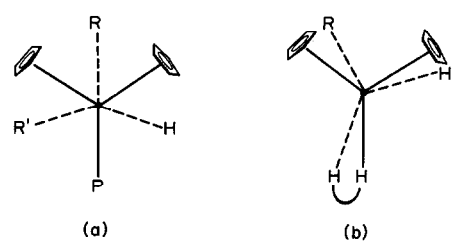

(a) (b)

Fig. 1. Projections showing (a) the staggered conformation of complexes **3** and (b) the near-eclipsed conformation of **1** and **2**.

Table 3. Some bond angles (°) and distances (Å) for silyltitanocene(III) complexes

Complex	Ti—Si—Ph angle	Cp—Ti—Cp angle	Ti—Ti distance
1	130.5(9)	130.6(1)	3.461(2)
2	123.3(1)	130.5(2)	3.866(2)
3a	114.4(5)	135.6(3)	—
3b	116.8(1); 121.3(1)	135.4(1)	—

into unacceptably close interaction with the neighbouring cyclopentadienyl group on the titanium.

OTHER DEHYDROCOUPLING REACTIONS CATALYSED BY GROUP 4 METALLOCENE DERIVATIVES

Dimethyltitanocene is a very active catalyst for the dehydrocoupling of primary and secondary organogermanes.[20] The reactions are quite complicated and in the case of primary germanes lead to cross-linked gels. Secondary germanes react rapidly, but the products are only low molecular weight oligomers ($n = 4$ and 5). Rather surprisingly, DMZ reacts neither stoichiometrically, nor catalytically, with phenyl- or diphenylgermane. We believe that this lack of reactivity may be due to the fact that equilibrium (3) lies too far to the left in the case of zirconium:

$$Cp_2MMe_2 + RGeH_3 \longrightarrow Cp_2MMe(GeH_2R) + MeH. \quad (3)$$

DMT also is a very potent catalyst for the cross-dehydrocoupling of silanes with —OH and —NH functions. These reactions can be used for synthesis of either simple, or polymeric alkoxy- and aryloxy-silanes, or silazanes.[21]

A quite remarkable case of DMT-catalysed dehydrocoupling was recently discovered by Sneddon *et al.*[22] This reaction involves the dehydrocoupling of borazine to a soluble polymer, whose structure is probably that shown in eq. (4).

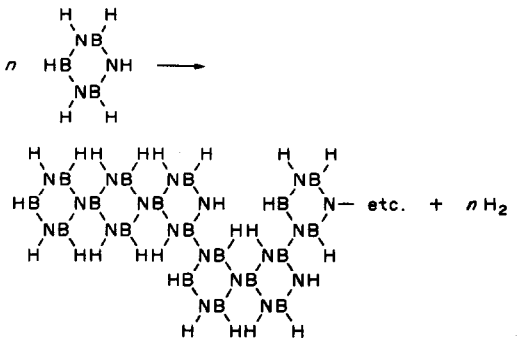

(4)

The fact that the polymer remains soluble, even at high conversions, proves that the three BH and the three NH functions on a given ring do not react with equal reactivity. This is probably another manifestation of the rigorous steric constraints operating at the catalytic metallocene centre during the propagation reactions. In the borazine case, formation of a B—N bond between two rings probably prevents reaction of the vicinal NH and BH bonds due to steric hindrance.

THE MECHANISM OF GROUP 4 METALLOCENE-CATALYSED DEHYDROCOUPLING

Although other mechanisms may be operating with other catalysts,[12,13] it now seems likely that all of the group 4 metallocene-catalysed dehydrocoupling reactions described above involve a series of σ-bond metatheses, as described by Tilley and co-workers.[15] Tilley's conclusions were based on a series of observations of stoichiometric metatheses between silicon hydrides and bis(silyl)- and silyl-hydridometallocenes of zirconium and hafnium. In addition, kinetic studies yielded activation parameters and kinetic isotope effects typical of other σ-bond metatheses.

Our earlier reservations on this matter were largely due to the erroneous conclusion that the titanocene-catalysed reaction did not produce small oligomers. More recent results have shown that the failure to observe these oligomers by NMR spectroscopy is due to their being in rapid equilibrium with the catalyst.[18] Carrying out the NMR analysis at low temperature (−40°C), or using GC to analyse for the low oligomers, shows unequivocally that the reaction proceeds by a stepwise build-up and not by a rapid addition polymerization. It has also been shown that 1,2-diphenyldisilane and 1,2,3-triphenyltrisilane both polymerize by a stepwise mechanism to give oligomers with degrees of polymerization of 4, 6, 8, etc., or 6, 9, 12, etc., respectively.[18]

There are only subtle differences between the

polymerization profiles for titanocene- and zirconocene-based catalyst systems, strongly suggesting that the polymerization mechanism is the same for both.[16e] However, major differences are evident in the manner in which the active catalyst is generated for the two cases. We believe, in agreement with Tilley, that the key catalyst species is $Cp_2M(H)SiH_2R$.[15c,23] The differences in the behaviour of DMT and DMZ are mostly due to the different routes, whereby they are transformed to the active catalyst species. In the case of titanium, there is little doubt that the catalyst cycles through the dimetallic complexes **1** and **2**, possibly by way of titanocene. Complex **1** may dissociate directly to give the hydridosilyltitanocene(IV) and titanocene(II), or it may react with silane as shown in eq. (5):

$$Cp_2Ti(\mu\text{-}H)(\mu\text{-}SiH_2R)TiCp_2 + RSiH_3 \longrightarrow 2\,Cp_2Ti(H)(SiH_2R). \quad (5)$$

Although DMZ also gives zirconocene(III) species, which are detectable in silane–DMZ reaction mixtures by ESR and NMR spectroscopies, there is no evidence that these species are important to the polymerization mechanism.[16d] Most of the zirconium is in the form of zirconium(IV) and in the case of reactions of secondary silanes, the stepwise transformation of DMZ to the silylhydride, according to eqs (6) and (7), can be observed by NMR spectroscopy.[16e]

$$Cp_2ZrMe_2 + RR'SiH_2 \longrightarrow Cp_2Zr(SiRR'H)Me + MeH \quad (6)$$

$$2\,Cp_2Zr(SiRR'H)Me \longrightarrow Cp_2Zr(SiRR'H)H + Cp_2Zr(SiRR'Me)Me. \quad (7)$$

Both of these reactions are readily explained as σ-bond metatheses. In reaction (7), the Si—H bond is probably activated towards metatheses by the geminal zirconium atom.

THE PROBLEM OF CYCLIZATION AND DEPOLYMERIZATION

The dehydrocoupling chemistry described above has already provided a number of useful syntheses of compounds containing Si—Si bonds. Whereas the usefulness of the method has so far proved to be very limited for the synthesis of high polymers. The major problem is the occurrence of competing cyclization reactions. Although the di- and trisilanes are both more reactive than the monosilane, the reactivities of higher oligomers fall off rapidly with increasing chain length because of the dilution of the reactive end groups.[18] Cyclic products always form during the chain propagation step, and in certain experimental situations they may be the only products. This is the case under conditions of high dilution with certain monomers (e.g. benzylsilane) and with certain catalyst/monomer combinations [e.g. phenylsilane with 1,2-bis(indenyl)ethanedimethylzirconium(IV)].[24] With neat phenylsilane and either a DMT or DMZ catalyst, linear oligomers dominate until most of the monomer is consumed (*ca* 1 h under the usual experimental conditions). At this point linear oligomers peaking at about 16 silicon atoms are the most abundant species in the reaction product. However, if the reaction mixture is left for much longer periods (several days) a depolymerization occurs, which results in the conversion of linear chains into cyclics.[16e,18]

The formation of cyclic species during chain propagation is most likely the result of an intramolecular metathesis between the distal SiH_2 end group and the M—Si bond at the growing chain end, as shown in eq. (8).[11] This process obviously has a high probability when the silicon chain is about six atoms long. The different propensities for different silanes to form cyclic species are likely due to the steric constraints operating on the intramolecular metathesis, as opposed to intermolecular metathesis. At the present time, we have no data which allow us to choose between the several possible mechanisms for the depolymerization reaction. These include the random cleavage of Si—Si bonds by some reactive intermediate and an intramolecular, back-biting metathesis, as shown in eq. (9):

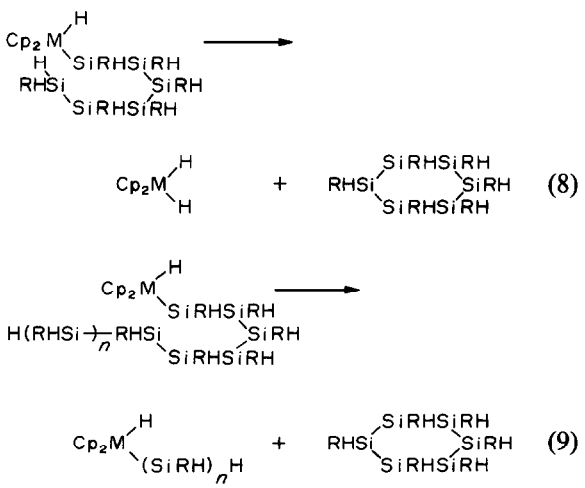

CONCLUSIONS

Studies of dehydrocoupling reactions catalysed by transition complexes have already yielded a fascinating new family of organosilicon complexes

of transition elements. Studies of the structures of these compounds give some indication of the subtle ways in which stereochemistry can influence the outcome of the reaction. Present systems, while highly interesting from the point of view of formation of E—E and E—E′ bonds, have thus far failed to provide a new route to high molecular weight polysilanes. On the basis of our present understanding of the mechanism, there does not seem to be any intrinsic reason why new catalysts with higher propagation/depropagation ratios cannot be developed. The present results are still sufficiently encouraging to justify a continued search for new catalysts.

Acknowledgements—The work described above was funded through grants from the Natural Sciences and Engineering Research Council of Canada and the Fonds FCAR du Quebec. J.F.H. acknowledges the kind hospitality of E.S. and of Professor G. Jaouen on his frequent visits to ENSCP. Y.M. thanks the Faculty of Graduate Studies and Research of McGill University for a scholarship.

REFERENCES

1. R. West, *Angew. Chem. Int. Edn. Engl.* 1987, **26**, 1201.
2. A. H. Cowley, J. Lasch, N. C. Horman and M. Pakulski, *J. Am. Chem. Soc.* 1983, **105**, 5506.
3. M. Regitz and P. Binger, *Angew. Chem. Int. Edn. Engl.* 1988, **27**, 1484.
4. M. Yoshifuji, I. Shima, N. Imamoto, K. Hirotsu and T. Higuchi, *J. Am. Chem. Soc.* 1981, **103**, 4587.
5. R. Steudel, *Chemistry of the Non-metals* (Edited by F. C. Nachod and J. J. Zukerman), p. 130. Walter de Gruyter, Berlin (1977).
6. R. Walsh, *Accts Chem. Res.* 1981, **14**, 246.
7. J. M. Kanabus-Kaminska, J. A. Hawari, D. Griller and C. J. Chatgilialoglu, *J. Am. Chem. Soc.* 1987, **109**, 5267.
8. J. F. Harrod, unpublished results.
9. C. Aitken, J.-P. Barry, F. Gauvin, J. F. Harrod, A. Malek and D. Rousseau, *Organometallics* 1989, **8**, 1732.
10. (a) J. Y. Corey, L. S. Chang and E. R. Corey, *Organometallics* 1987, **6**, 1596; (b) L. S. Chang and J. Y. Corey, *Organometallics* 1989, **8**, 1885; (c) J. Y. Corey, X.-H. Zhu and T. C. Bedard, *XXIII Organosilicon Symposium*. Midland, Michigan (20–21 April 1990); Abstract D1.
11. W. H. Campbell, T. K. Hilty and L. Yurga, *Organometallics* 1989, **8**, 2615.
12. K. A. Brown-Wensley, *Organometallics* 1987, **6**, 1590.
13. I. Ojima, S. Inaba, T. Kogure and Y. Nagai, *J. Organomet. Chem.* 1973, **55**, C7.
14. K. Yamamoto, H. Okinoshima and M. Kumada, *J. Organomet. Chem.* 1970, **23**, C7.
15. (a) H.-G. Woo and T. D. Tilley, *J. Am. Chem. Soc.* 1989, **111**, 8043; (b) H.-G. Woo and T. D. Tilley, *J. Am. Chem. Soc.* 1989, **111**, 3757; (c) T. D. Tilley, *Comments Inorg. Chem.* 1990, **10**, 37.
16. (a) J. F. Harrod, in *Inorganic and Organometallic Polymers* (Edited by H. R. Allcock, K. Wynne and M. Zeldin), ACS Symposium Series No. 360, Ch. 7. American Chemical Society, Washington DC, (1988); (b) J. F. Harrod, in *Transformation of Organometallics into Common and Exotic Materials: Design and Activation* (Edited by R. M. Laine), NATO ASI Series E: Appl. Sci. No. 14, p. 103. Martinus Nijhoff, Amsterdam (1988); (c) C. A. Aitken, J. F. Harrod and E. Samuel, *J. Am. Chem. Soc.* 1986, **108**, 4059; (d) C. A. Aitken, J. F. Harrod and E. Samuel, *Can. J. Chem.* 1987, **64**, 1677; (e) Y. Mu, B. Cote, C. A. Aitken, J. F. Harrod and E. Samuel, *Can. J. Chem.* 1991, in press.
17. A. Malek and J. F. Harrod, unpublished results.
18. Y. Mu and J. F. Harrod, unpublished results.
19. E. Samuel, Y. Mu, J. F. Harrod, Y. Dromzee and Y. Jeannin, *J. Am. Chem. Soc.* 1990, **112**, 3435.
20. C. Aitken, J. F. Harrod, A. Malek and E. Samuel, *J. Organomet. Chem.* 1988, **285**, 349.
21. J. F. Harrod and E. Samuel, unpublished results; R. M. Laine, personal communication.
22. L. G. Sneddon, P. J. Fazen, K. Su, A. T. Lynch, J. S. Bech and E. E. Remsen, *Abstracts of the 33rd IUPAC Symposium on Macromolecules*. Montreal (8–13 July 1990); Session 2.11.3.
23. J. F. Harrod and S. S. Yun, *Organometallics* 1987, **6**, 1381.
24. F. Gauvin and J. F. Harrod, *Can. J. Chem.* 1990, **68**, 1638.

Polyhedron Vol. 10, No. 11, pp. 1247–1264, 1991
Printed in Great Britain

0277–5387/91 $3.00+.00
Pergamon Press plc

THE STRUCTURE AND BONDING IN GROUP IV [1.1.1]PROPELLANES

MARK S. GORDON,* KIET A. NGUYEN and MARSHALL T. CARROLL†

Department of Chemistry, North Dakota State University, Fargo, ND 58105-5516, U.S.A.

Abstract—The structures of Group IV [1.1.1]propellanes are determined using *ab initio* all-electron and effective core potential methods. The bonding in these systems is examined using the theory of atoms in molecules and localized molecular orbital analysis. Singlet–triplet splittings are also calculated. Comparisons with the corresponding bicyclopentanes are made. The bonding interaction between the two bridgehead atoms decreases upon descending the group. Further, the similarities in the internuclear bridgehead region between the propellanes and bicyclopentanes increase upon descending the group.

In a recent series of papers Sita and co-workers[1] have prepared several intriguing polycyclic tin compounds. One of these species, 2,2,4,4,5,5-hexakis(2,6 - diethylphenyl)pentastanna[1.1.1]propellane (**1**) is particularly interesting, in view of the continuing discussion of the nature of bonding, especially between the bridge atoms, in propellanes.[1–11]

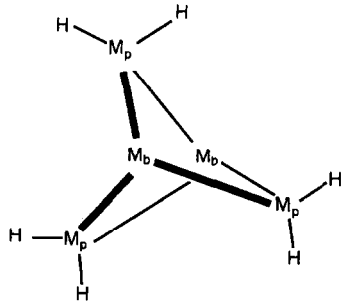

1

According to the X-ray crystal structure of **1** (M = Sn), the distance between the bridgehead (b) atoms, 3.367 Å, is much longer than that between the bridgehead and peripheral (p) atoms, 2.841–2.871 Å. This suggests that the bond connecting the two bridgehead atoms is extremely weak, if it exists at all. Significantly, addition across the b–b bond yields a pentastannabicyclopentane (**2**, M = Sn)

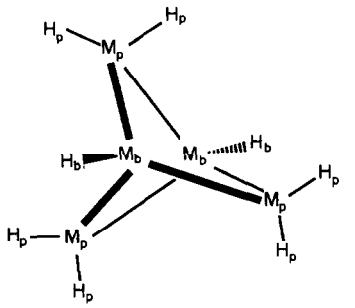

2

whose b–b distance (3.361 Å) differs only slightly from that in the parent [1.1.1]propellane **1** (M = Sn). This reinforces the notion that there is little or no b–b bonding in **1** (M = Sn).

The simplest group IV [1.1.1]propellane, with M = C, has received considerable attention from both experimentalists[12–14] and theoreticians[2,3,7–11,15] in recent years, in an attempt to unravel the nature of the bonding in this compound. In contrast to the case of tin, the b–b bond in the parent [1.1.1]propellane (1.60 Å)[13] is only slightly longer than the b–p bond length in the same compound (1.52 Å) and much shorter than the corresponding b–b distance in **2** with M = C (1.84 Å[16]). These experimental distances suggest that there is much more likely to be a bond connecting the bridgehead atoms in the parent propellane than in its pentastanna analogue.

The numerous theoretical studies of the parent [1.1.1]propellane have recently been reviewed by

* Author to whom correspondence should be addressed.
† Natural Sciences and Engineering Research Council of Canada Postdoctoral Fellow

Wiberg.[12] A detailed analysis of the bonding in this compound has been presented by Wiberg *et al.*,[2] using the density analysis developed by Bader and co-workers.[15,17,18] These authors emphasize the point that it is essential in analysing molecular structure and bonding to consider the *total* electron density and not just the contributions from a subset of orbitals. Indeed, the density analysis based on a self-consistent field (SCF) calculation with the 6–31G(*d*) basis set[19] reveals a *bond critical point*[15] (that is, a saddle point in the total electron density) connecting the bridgehead atoms. Such a point is indicative of the existence of a bond connecting these atoms and is at variance with the conclusions of earlier analyses,[8,9] based on a subset of the occupied molecular orbitals. Further evidence for the b–b bond is the existence of three *ring critical points*, one for each three-membered ring.

The pentasila analogue of [1.1.1]propellane is unknown experimentally, but has been investigated by Schleyer and Janoschek.[3] Using a two-configuration (TCSCF) wave function and an effective core potential, these authors find a rather long (2.735 Å) b–b bond length and "substantial singlet diradical character". If the latter is defined as twice the square of the coefficient for the excited configuration, the per cent diradical character from the TCSCF wavefunction is 12.5%. This plus a very small natural atomic orbital bond order[20] is taken as an indication that there is only very weak b–b bonding in this compound. Schoeller *et al.* have also predicted a long b–b bond length in the pentasila compound.[6] The ring strain in pentasila[1.1.1]propellane has been investigated by Nagase and Kudo[4a] and Allen and co-workers,[10] both of whom find this species to be less strained than the carbon parent. In a related paper, Nagase *et al.* have suggested that placement of electronegative elements in the peripheral positions should stabilize the b–b interaction in the pentasila compound[4b] and also in the pentagerma compound.[5] To our knowledge, no calculations have been reported to date on pentastanna[1.1.1]propellanes.

In the present paper, we present a systematic analysis of the Group IV [1.1.1]propellanes **1**, with M = C, Si, Ge, Sn, in an attempt to develop a broad understanding of the structure and bonding in these compounds. An ancillary objective of this work is to assess the ability of effective core potentials[21,22] to reproduce the structures and (valence) electron densities predicted by full *ab initio* calculations.

COMPUTATIONAL APPROACH

The electronic structure calculations presented here have been carried out at several levels of theory. Species which are formally closed shell singlets have been investigated with restricted Hartree–Fock (RHF) wavefunctions, within the linear combination of atomic orbitals (LCAO) approximation. Because there is a question with regard to the existence of a b–b bond in species **1**, with M = Si, Ge, Sn, and there is the possibility that significant diradical character exists in these compounds,[3] the propellane structures were also investigated with generalized valence bond[23] wavefunctions. The corresponding triplet states, investigated to obtain a *qualitative* handle on the relative singlet–triplet splittings as a function of M, were studied with unrestricted Hartree–Fock (UHF) wavefunctions.

The fully *ab initio* calculations have been performed with the 3–21G(*d*) basis set,[24] with *d* orbital exponents taken from the original papers. Two different sets of effective core potentials, due to Stevens, Basch and Krauss[21] (SBK) and Wadt and Hay[22] (WH) have also been used to analyse the same set of compounds, using the same *d* orbital exponents as in the full *ab initio* calculations. Geometries were determined using the analytical gradients and algorithms contained in GAMESS.[25] Structures were established as minima by verifying that the hessians (matrices of energy second derivatives) are positive definite. These hessians were constructed from second derivatives obtained analytically (RHF *ab initio*) or from finite differences of the analytically determined gradients.

The nature of the bonding in the compounds of interest have been investigated using the density analysis developed by Bader and co-workers.[15,17,18] Because we have found[26] that spurious behaviour can be obtained in this analysis when heavier elements (such as silicon) are involved and standard basic sets are used, two, rather than one, sets of *d* functions have been used for this analysis. The *d* orbital exponents used for this purpose are 1.12, 0.32 (C), 0.79, 0.1975 (Si), 0.492, 0.123 (Ge), 0.366, 0.0915 (Sn) for the all-electron calculations. For the ECP basis sets the same values are used except 1.6, 0.4 is used for carbon. The density analysis has been discussed in detail elsewhere,[15,17,18] and only a few key points will be repeated here. Bond ($\mathbf{r}_b$), ring ($\mathbf{r}_r$) and cage ($\mathbf{r}_c$) critical points will be of interest in the following discussion. A bond critical point exists between two atoms if there is a "saddle point" in the electron density $\rho(\mathbf{r})$ between the two atoms. At such a point the hessian of the electron density has one positive eigenvalue along the bond axis (λ_3) and two negative eigenvalues (λ_1, λ_2) along the axes orthogonal to the bond axis. The existence of a bond critical point implies the existence of a bond path (path of maximum electron density passing

through r_b), and the two atoms are said to be bonded. The hessian at a ring critical point has two positive and one negative eigenvalues, with the density $\rho(\mathbf{r}_r)$ at the ring critical point being smaller than that at all of the surrounding bond critical points. The hessian at a cage critical point has three positive curvatures and $\rho(\mathbf{r})$ is a local minimum at this point. According to this analysis, a [1.1.1]propellane should have a bond critical point between the two bridgehead atoms if a b–b bond exists, as well as three ring critical points, one on the face of each three-membered ring. The lack of such a bond critical point is evidence that there is no "formal bond" connecting these two atoms.[15,17,18] However, such arguments may not reflect the existence of very flat electron density surfaces.

As an additional tool, the localized molecular orbitals (LMOs) obtained using the prescription of Foster and Boys[27] have been calculated. These LMOs will prove to enhance the Bader analysis outlined above.

RESULTS AND DISCUSSION

Structures

The calculated geometries for the [1.1.1]propellanes and the bicyclopentanes are listed in Tables 1 and 2, respectively. All structures have been predicted at all levels of theory using the SBK effective core potentials. The same is true for the WH ECPs, except that these are not available for carbon. The *ab initio* GVB structures for the germanium and tin compounds and the RHF Sn_5H_8 structure have been omitted in the interest of conservation of

Table 1. Geometries of M_5H_6 systems (distances in Å; angles in degrees; M_b denotes bridgehead atom and M_p denotes peripheral atom)

Systems	Wavefunction	Distances			Angles		
		M_b—M_b	M_b—M_p	M_p—H	M_b—M_b—M_p	M_b—M_p—M_b	M_b—M_p—H
C_5H_6	RHF 3–21G(*d*)	1.554	1.508	1.079	59.0	62.0	117.5
	SBK(*d*)	1.573	1.517	1.080	58.8	62.5	117.5
	GVB 3–21G(*d*)	1.611	1.518	1.080	57.9	64.2	117.3
	SBK(*d*)	1.625	1.523	1.081	57.8	64.5	117.4
	UHF 3–21G(*d*)	1.834	1.555	1.084	53.9	72.3	116.8
	SBK(*d*)	1.835	1.556	1.086	53.9	72.3	117.0
Si_5H_6	RHF 3–21G(*d*)	2.694	2.331	1.476	54.7	70.6	117.2
	SBK(*d*)	2.736	2.352	1.480	54.4	71.2	117.4
	WH(*d*)	2.635	2.309	1.462	55.2	69.6	117.4
	GVB 3–21G(*d*)	2.759	2.340	1.479	53.9	72.3	117.2
	SBK(*d*)	2.793	2.358	1.481	53.7	72.6	117.4
	WH(*d*)	2.700	2.316	1.463	54.4	71.3	117.4
	UHF 3–21G(*d*)	2.933	2.364	1.480	51.7	76.7	116.6
	SBK(*d*)	2.952	2.382	1.484	51.7	76.6	116.8
	WH(*d*)	2.895	2.343	1.466	51.8	76.3	116.9
Ge_5H_6	RHF 3–21G(*d*)	2.884	2.449	1.545	53.9	72.1	116.9
	SBK(*d*)	2.980	2.492	1.533	53.3	73.5	117.4
	WH(*d*)	2.974	2.503	1.540	53.6	72.9	117.5
	GVB SBK(*d*)	2.991	2.488	1.533	53.0	73.9	117.5
	WH(*d*)	2.993	2.500	1.540	53.2	73.5	117.5
	UHF 3–21G(*d*)	3.044	2.470	1.548	52.0	76.1	116.3
	SBK(*d*)	3.097	2.504	1.553	51.8	76.4	116.7
	WH(*d*)	3.120	2.517	1.540	51.7	76.6	116.7
Sn_5H_6	RHF 3–21G(*d*)	3.463	2.876	1.748	53.0	74.1	117.7
	SBK(*d*)	3.462	2.863	1.709	52.8	74.4	117.7
	WH(*d*)	3.500	2.881	1.715	52.6	74.8	117.9
	GVB SBK(*d*)	3.469	2.857	1.708	52.6	74.8	117.8
	WH(*d*)	3.497	2.875	1.715	52.5	74.9	117.9
	UHF 3–21G(*d*)	3.627	2.888	1.748	51.1	77.8	117.0
	SBK(*d*)	3.578	2.867	1.707	51.4	77.2	116.8
	WH(*d*)	3.605	2.884	1.715	51.3	77.4	116.9

Table 2. RHF geometries of M_5H_8 systems (distances in Å; angles in degrees; M_b and H_b denote bridgehead atoms and M_p and H_p denote peripheral atoms)

System	Basis set	Distances				Angles			
		M_b—M_b	M_b—M_p	M_b—H_b	M_p—H_p	M_b—M_b—M_p	M_b—M_p—M_b	M_p—M_p—H_b	M_b—M_p—H_p
C_5H_8	3–21G(*d*)	1.879	1.552	1.084	1.087	52.8	74.5	127.2	116.6
	SBK(*d*)	1.883	1.555	1.087	1.089	52.7	74.5	127.3	116.9
Si_5H_8	3–21G(*d*)	2.905	2.353	1.478	1.481	51.9	76.3	128.1	116.7
	SBK(*d*)	2.925	2.368	1.480	1.484	51.9	76.3	128.1	117.0
	WH(*d*)	2.869	2.334	1.465	1.466	52.1	75.8	127.9	117.1
Ge_5H_8	3–21G(*d*)	3.025	2.444	1.534	1.548	51.8	76.5	128.2	116.3
	SBK(*d*)	3.053	2.477	1.527	1.534	52.0	76.1	128.0	116.9
	WH(*d*)	3.076	2.494	1.535	1.540	51.9	76.2	128.1	117.0
Sn_5H_8	SBK(*d*)	3.509	2.840	1.698	1.708	51.8	76.3	128.2	117.0
	WH(*d*)	3.534	2.857	1.707	1.713	51.8	76.4	128.2	117.2

computer time. The ECP structures are generally in quite good agreement with the fully *ab initio* geometries. For carbon, silicon and germanium, the SBK ECP tends to over-estimate bond lengths, the worst case being the Ge_b—Ge_b bond which is over-estimated by 0.1 Å. On the other hand, the WH ECP under-estimates bond lengths to carbon and silicon, but over-estimates those to germanium and tin. In general, the SBK bond lengths are closer to the fully *ab initio* ones. The bond angles predicted by all three methods are quite similar.

Since the GVB wavefunction mixes anti-bonding character into the previously RHF description, it is expected that the GVB bond lengths will be longer than those obtained at the RHF level. This will be particularly true for the M_b—M_b distance, since the highest occupied (HOMO) and lowest unoccupied (LUMO) orbitals correspond to the bonding and antibonding interactions for these atoms. This is indeed seen to be the case in Table 1. For the 3–21G(*d*) structures, the GVB−RHF difference in the M_b—M_b distance is 0.06 and 0.07 Å for carbon and silicon, respectively. The corresponding differences for the SBK ECP are 0.05 and 0.06 Å, respectively, so the trend is well reproduced. In contrast, both ECP methods predict a progressively smaller change in this bond length upon going from RHF to GVB, when M = Si, Ge and Sn. This suggests that as M gets heavier, the bonding interaction between the bridgehead atoms decreases. Further evidence for this conclusion is provided by comparing the predicted b–b distances in M_5H_6 with those in M_5H_8 (Table 2). For M = C, the RHF/3–21G(*d*) b–b distance in bicyclopentane is 0.27 Å longer than the GVB/3–21G(*d*) value for the same distance in [1.1.1]propellane. This considerable difference is expected if one is comparing a bonded to a non-bonded interaction. The SBK ECP comparison is similar. For M = Si, this difference decreases to 0.15 Å [3–21G(*d*)], 0.13 Å (SBK), 0.17 Å (WH). This suggests, as before, that the b–b bonding interaction is smaller for silicon than for carbon. The M_5H_6 vs M_5H_8 b–b distance is even smaller for M = Ge and virtually non-existent for tin. So, the calculated geometries suggest a successively decreasing bonding interaction between the bridgehead atoms as M moves vertically downward in group IV.

As discussed by Schleyer and Janoschek,[3] the loss of bonding interaction between the bridgehead atoms can result in significant diradical character in the propellane species. The calculated GVB coefficients and corresponding natural orbital occupation numbers (NOON) are listed in Table 3. Taking the latter values as a measure of the per cent diradical character, we do find a slight increase

Table 3. GVB–PP coefficients and natural orbital occupation numbers (NOON) for M_5H_6 systems

Systems	Basis set	GVB–PP coefficients HOMO	GVB–PP coefficients LUMO	NOON HOMO	NOON LUMO
C_5H_6	3–21G(*d*)	0.975	−0.223	1.900	0.100
	SBK(*d*)	0.975	−0.223	1.903	0.097
Si_5H_6	3–21G(*d*)	0.964	−0.265	1.860	0.140
	SBK(*d*)	0.964	−0.265	1.860	0.140
	WH(*d*)	0.963	−0.269	1.854	0.146
Ge_5H_6	SBK(*d*)	0.972	−0.233	1.891	0.109
	WH(*d*)	0.968	−0.252	1.873	0.127
Sn_5H_6	SBK(*d*)	0.970	−0.241	1.883	0.117
	WH(*d*)	0.968	−0.250	1.875	0.125

upon going from carbon to silicon. (Note that the calculated value of 14% for silicon is similar to the value of 12.5% found by Schleyer and Janoschek.[3]) However, the per cent diradical character calculated by this measure for M = Ge and Sn is actually lower than that found for Si!

Another approach to this question of diradical character is to investigate the structures and energies of the corresponding triplets, since the triplet states are, by definition, true radicals. The triplet propellane structures are also listed in Table 1. While the difference between the UHF triplet and GVB singlet M_b—M_b distance does decrease as M gets heavier, this difference is still greater than 0.1 Å, even for M = Sn. One would expect the singlet and triplet distances to be the same if the singlet were really a diradical. Similarly, one would expect the triplet to be the ground electronic state in this case. Instead, the triplet is at least 1 eV higher in energy than the singlet, even for M = Sn (Table 4). Further, these splitting values actually are lower limits since the UHF level of theory describes the triplet state better than RHF describes the singlet state. As these observations suggest fairly small diradical character in the ground state [1.1.1]propellanes, it is imperative to examine in detail the characteristics of the electron distributions in these systems.

Analysis of electron density and bonding

While the examination of internuclear distances allows for suggestions as to the strengths of interactions between atoms, shorter internuclear distances do not always imply stronger interactions.[28] A topological analysis of the charge density is a more useful tool to probe the strength and nature of the bonding in these systems.

In general, the electron densities in the valence region generated from ECP wavefunctions (RHF, GVB or UHF) are of the same topological form as the corresponding densities generated from all-electron (AE) wavefunctions (Figs 1–4). Therefore, the two charge distributions have the same number of bond, ring and cage critical points located in approximately the same positions. What is remarkable is that the AE and ECP values of the charge density at these points are very similar (Table 5). For example, differences in the RHF AE and ECP charge densities evaluated at cage critical points do

Table 4. Singlet (RHF)–triplet (UHF) splittings for M_5H_6 systems

System	ΔE (kcal mol^{-1})[a] 3–21G(2*d*)	3–21G(*d*)	SBK(2*d*)	SBK(*d*)	WH(2*d*)	WH(*d*)
C_5H_6	65.3	63.4	63.7	64.4	—	—
Si_5H_6	32.9	29.6	30.2	29.4	28.3	27.5
Ge_5H_6	36.4	38.3	40.1	40.3	33.8	32.9
Sn_5H_6	25.3	26.4	31.9	31.9	29.9	28.9

[a] Energies (triplet minus singlet) are calculated at the SCF optimized geometries where only 1*d* set of functions is placed on each heavy atom.

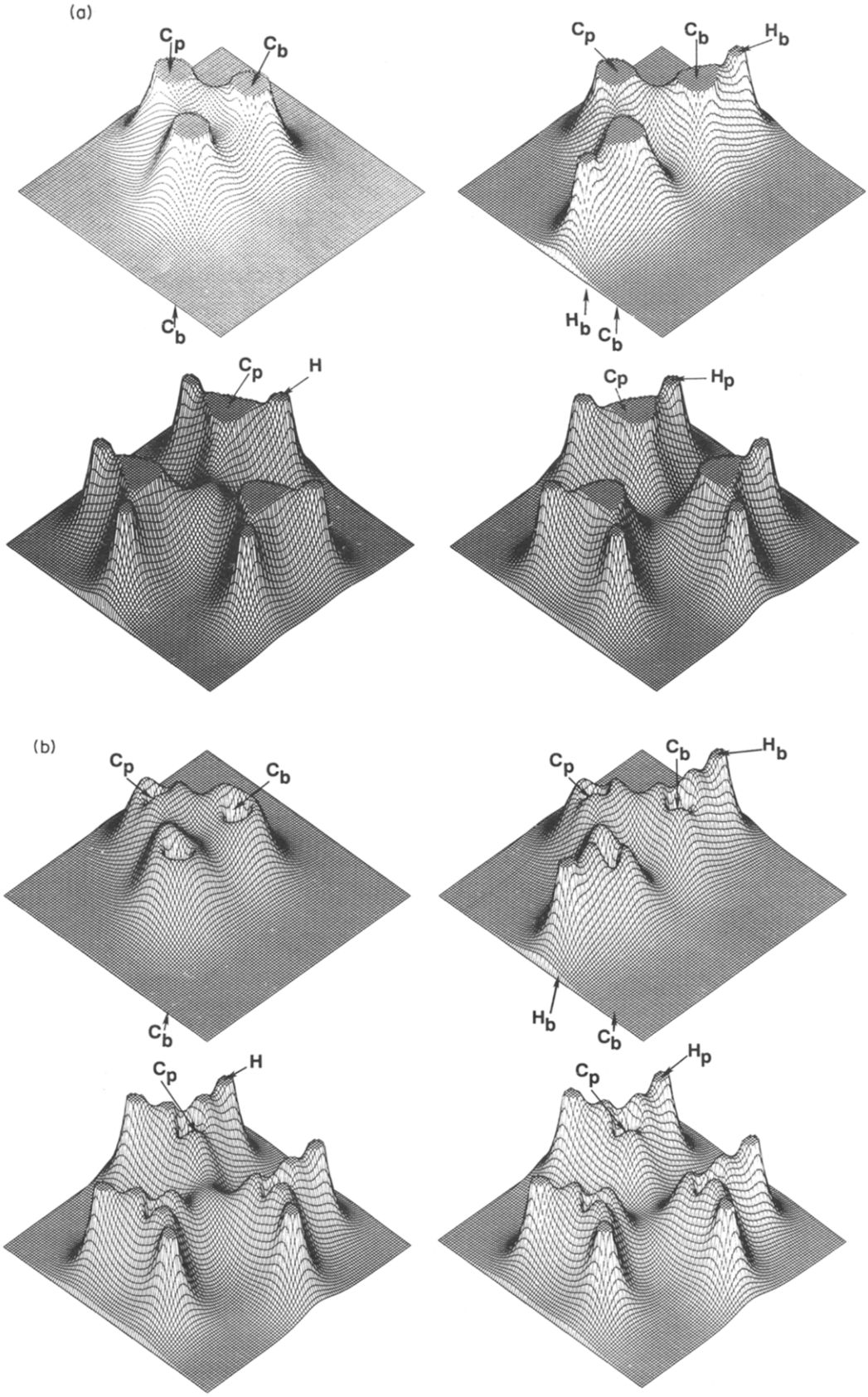

Fig. 1. (a) Relief maps of the charge distributions of C_5H_6 and C_5H_8 systems in the σ_v and σ_h planes. The σ_v maps are displayed in the top half of the figure and the σ_h planes are displayed in the bottom half of the figure. C_5H_6 maps are on the left side of the figure and C_5H_8 maps are on the right side of the figure. The charge distributions are generated from all-electron RHF/3–21G(2*d*)//RHF/3–21G(*d*) wavefunctions. The charge density cutoff is 0.30 au. (b) Corresponding maps to (a) except that here the charge distributions are generated from RHF/SBK(2*d*)//RHF/SBK(*d*) wavefunctions.

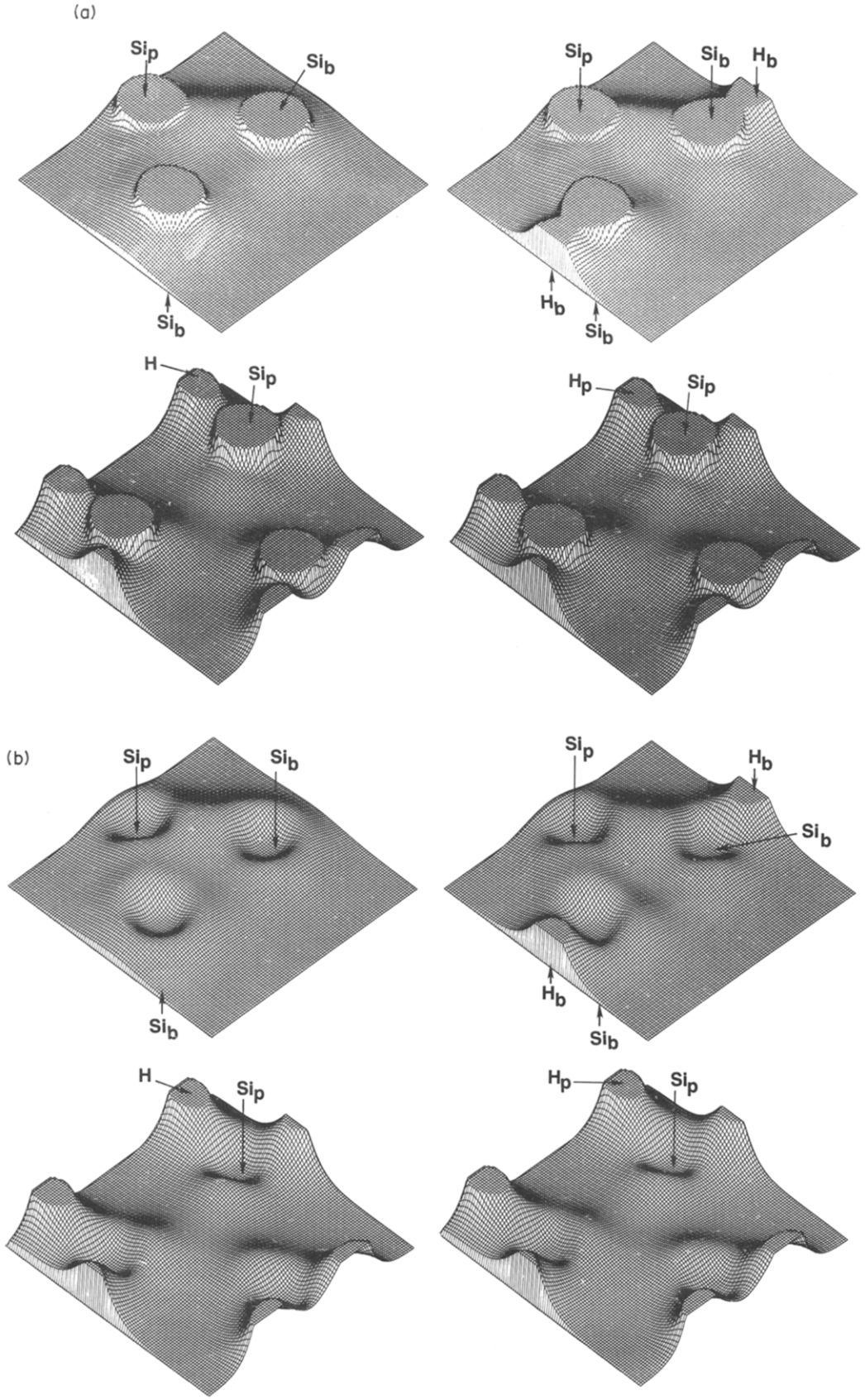

Fig. 2. (a) Relief maps of the charge distributions of Si_5H_6 and Si_5H_8 in the σ_v and σ_h planes. The σ_v maps are displayed in the top half of the figure and the σ_h planes are displayed in the bottom half of the figure. Si_5H_6 maps are on the left side of the figure and Si_5H_8 maps are on the right side of the figure. The charge distributions are generated from all-electron RHF/3–21G(2*d*)//RHF/3–21G(*d*) wavefunctions. The charge density cutoff is 0.10 au in the σ_v plane and 0.13 au in the σ_h plane. (b) Corresponding maps to (a) except that here the charge distributions are generated from RHF/SBK(2*d*)//RHF/SBK(*d*) wavefunctions.

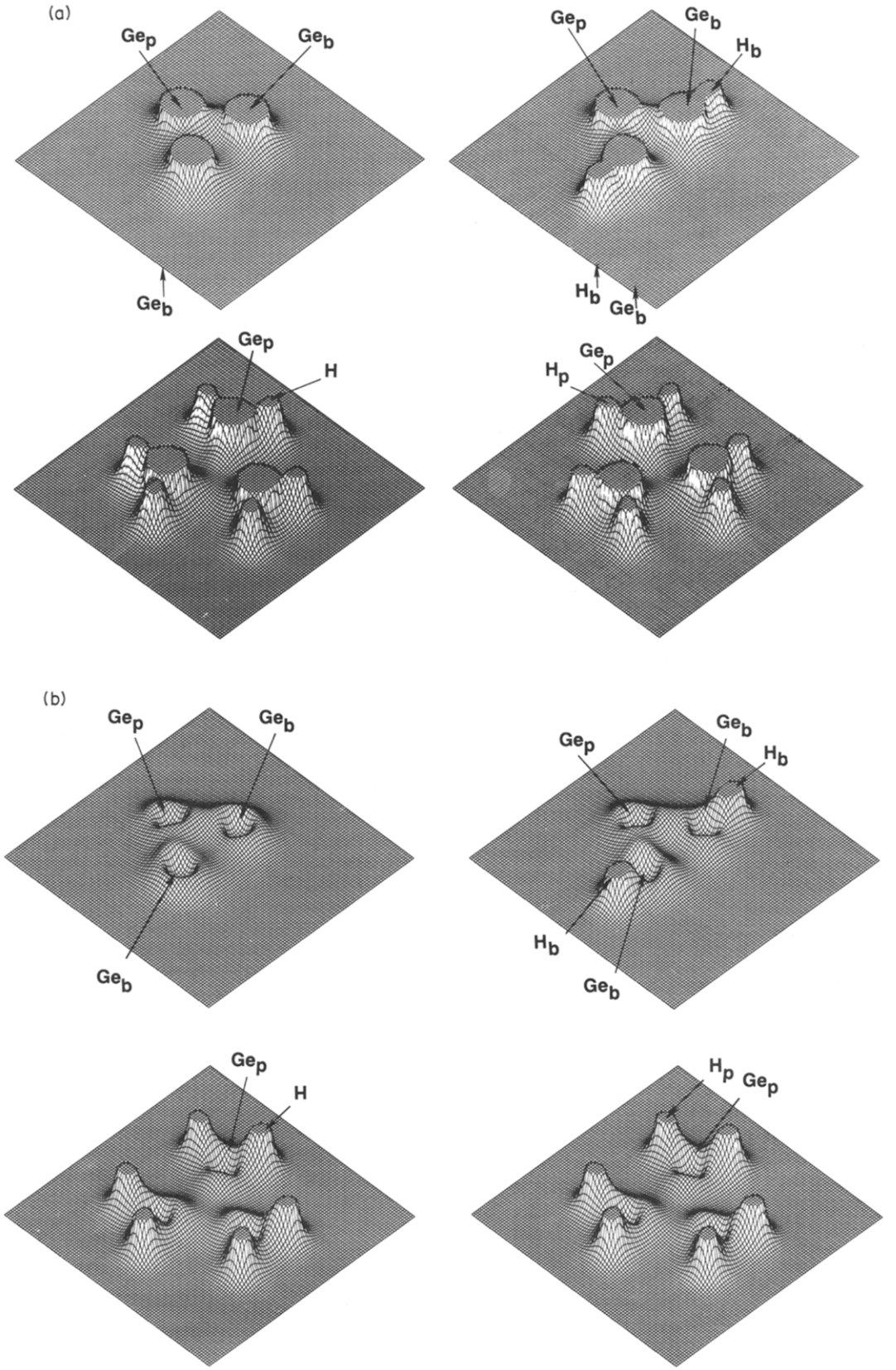

Fig. 3. (a) Relief maps of the charge distributions of Ge_5H_6 and Ge_5H_8 in the σ_v and σ_h planes. The σ_v maps are displayed in the top half of the figure and the σ_h planes are displayed in the bottom half of the figure. Ge_5H_6 maps are on the left side of the figure and Ge_5H_8 maps are on the right side of the figure. The charge distributions are generated from all-electron RHF/3–21G(2*d*)//RHF/3–21G(*d*) wavefunctions. The charge density cutoff is 0.10 au in the σ_v plane and 0.13 au in the σ_h plane. These maps are scaled down by a factor of two compared with the carbon and silicon maps. (b) Corresponding maps to (a) except that here the charge distributions are generated from RHF/SBK(2*d*)//RHF/SBK(*d*) wavefunctions.

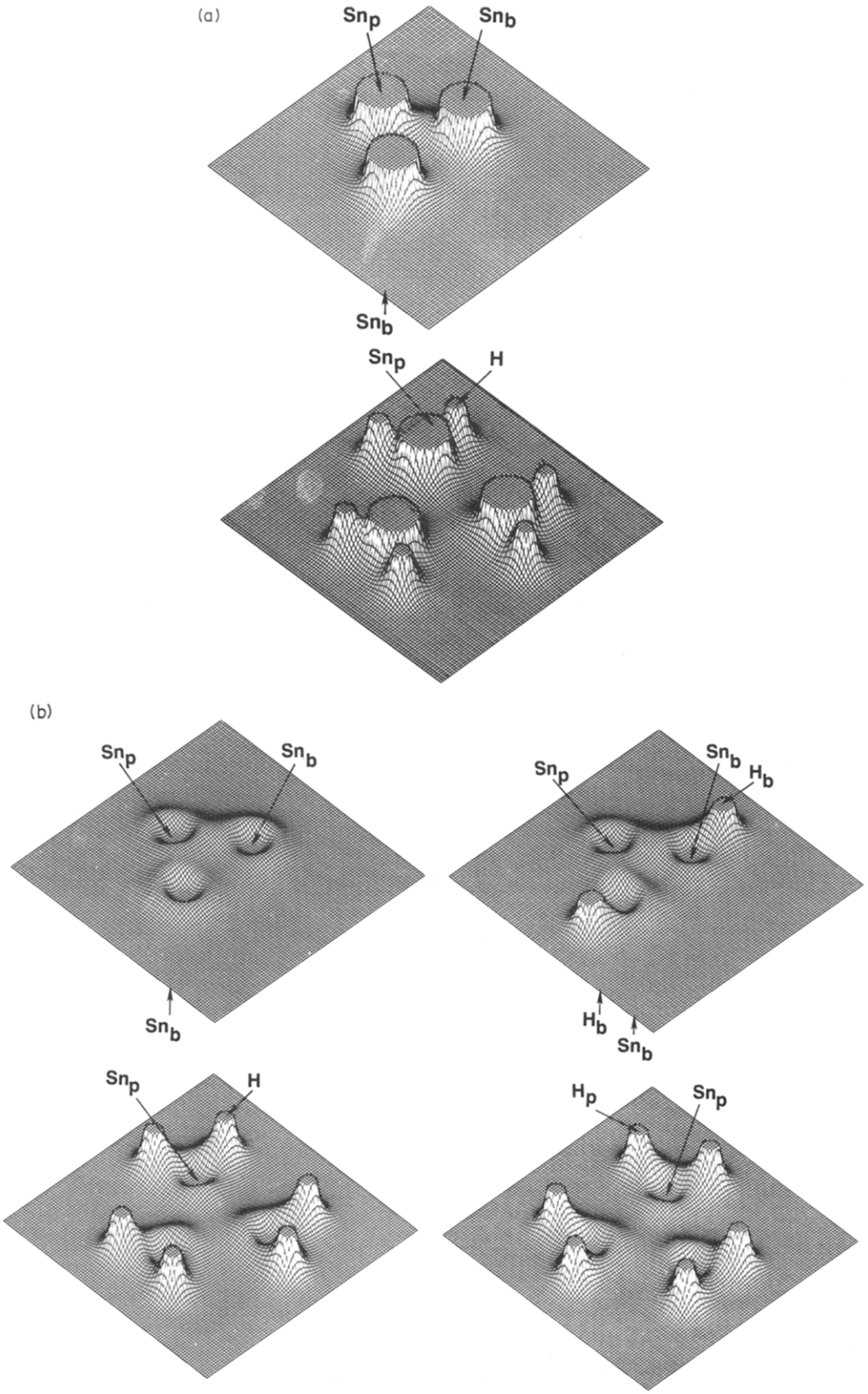

Fig. 4. (a) Relief maps of the charge distributions of Sn_5H_6 in the σ_v and σ_h planes. The σ_v map is displayed in the top half of the figure and the σ_h plane is displayed in the bottom half of the figure. The charge distributions are generated from all-electron RHF/3–21G(2*d*)//RHF/3–21G(*d*) wavefunctions. The charge density cutoff is 0.10 au in the σ_v plane and 0.13 au in the σ_h plane. These maps are scaled down by a factor of two compared with the carbon and silicon maps. (b) Corresponding maps to (a) except that here the charge distributions are generated from RHF/SBK(2*d*)//RHF/SBK(*d*) wavefunctions. In addition, Sn_5H_8 maps are displayed on the right side of this figure.

Table 5. Bond, ring and cage critical point analysis of M_5H_6 and M_5H_8 systems. M_b and H_b denote bridgehead atoms; M_p and H_p denote peripheral atoms. All values are in atomic units

Systems	Bond A—B	Wavefunction	$\rho(\mathbf{r})$	$\nabla^2\rho(\mathbf{r})$
C_5H_6	M_b—M_b	RHF 3-21G(2*d*)	0.2046	−0.1600
		SBK(2*d*)	0.1890	0.0031
		GVB 3-21G(2*d*)	0.1762	0.0424
		SBK(2*d*)	0.1660	0.1491
	M_b—M_p	RHF 3-21G(2*d*)	0.2552	−0.7165
		SBK(2*d*)	0.2403	−0.4972
		GVB 3-21G(2*d*)	0.2542	−0.7346
		SBK(2*d*)	0.2397	−0.5129
		UHF 3-21G(2*d*)	0.2459	−0.7340
		SBK(2*d*)	0.2340	−0.5319
	M_p—H	RHF 3-21G(2*d*)	0.2866	−1.0139
		SBK(2*d*)	0.2831	−1.0835
		GVB 3-21G(2*d*)	0.2855	−1.0066
		SBK(2*d*)	0.2816	−1.0683
		UHF 3-21G(2*d*)	0.2817	−0.9832
		SBK(2*d*)	0.2774	−1.0227
	Ring[a]	RHF 3-21G(2*d*)	0.1977	0.0288
		SBK(2*d*)	0.1840	0.1273
		GVB 3-21G(2*d*)	0.1747	0.1052
		SBK(2*d*)	0.1652	0.1822
		UHF 3-21G(2*d*)	0.1020	0.4812
		SBK(2*d*)	0.1027	0.4371
	Cage[a]	UHF 3-21G(2*d*)	0.1005	0.4870
		SBK(2*d*)	0.1005	0.4738
Si_5H_6	M_b—M_p	RHF 3-21G(2*d*)	0.0850	−0.1142
		SBK(2*d*)	0.0813	−0.1024
		GVB 3-21G(2*d*)	0.0855	−0.1176
		SBK(2*d*)	0.0821	−0.1056
		UHF 3-21G(2*d*)	0.0874	−0.1280
		SBK(2*d*)	0.0841	−0.1144
	M_p—H	RHF 3-21G(2*d*)	0.1165	0.3106
		GVB 3-21G(2*d*)	0.1158	0.3096
		UHF 3-21G(2*d*)	0.1150	0.3128
	Ring[a]	RHF 3-21G(2*d*)	0.0467	0.0348
		SBK(2*d*)	0.0433	0.0393
		WH(2*d*)	0.0494	0.0305
		GVB 3-21G(2*d*)	0.0414	0.0506
		SBK(2*d*)	0.0391	0.0491
		WH(2*d*)	0.0450	0.0419
		UHF 3-21G(2*d*)	0.0307	0.0718
		SBK(2*d*)	0.0299	0.0614
		WH(2*d*)	0.0313	0.0771
	Cage[a]	RHF 3-21G(2*d*)	0.0466	0.0340
		SBK(2*d*)	0.0430	0.0403
		WH(2*d*)	0.0493	0.0297
		GVB 3-21G(2*d*)	0.0409	0.0507
		SBK(2*d*)	0.0382	0.0536
		WH(2*d*)	0.0448	0.0406
		UHF 3-21G(2*d*)	0.0280	0.0849
		SBK(2*d*)	0.0269	0.0793
		WH(2*d*)	0.0285	0.0902
Ge_5H_6	M_b—M_p	RHF 3-21G(2*d*)	0.0751	−0.0762
		SBK(2*d*)	0.0655	−0.0633
		WH(2*d*)	0.0702	−0.0832
		GVB SBK(2*d*)	0.0658	−0.0643
		WH(2*d*)	0.0670	−0.0760
		UHF 3-21G(2*d*)	0.0782	−0.0992
		SBK(2*d*)	0.0692	−0.0777
		WH(2*d*)	0.0701	−0.0870
	M_p—H	RHF 3-21G(2*d*)	0.1226	0.1597
		UHF 3-21G(2*d*)	0.1215	0.1654
	Ring[a]	RHF 3-21G(2*d*)	0.0356	0.0409
		SBK(2*d*)	0.0300	0.0377
		WH(2*d*)	0.0302	0.0429
		GVB SBK(2*d*)	0.0301	0.0381
		WH(2*d*)	0.0309	0.0359
		UHF 3-21G(2*d*)	0.0255	0.0663
		SBK(2*d*)	0.0230	0.0536
		WH(2*d*)	0.0231	0.0548
	Cage[a]	RHF 3-21G(2*d*)	0.0353	0.0398
		SBK(2*d*)	0.0292	0.0388
		WH(2*d*)	0.0302	0.0421
		GVB SBK(2*d*)	0.0292	0.0394
		WH(2*d*)	0.0303	0.0356
		UHF 3-21G(2*d*)	0.0235	0.0738
		SBK(2*d*)	0.0210	0.0633
		WH(2*d*)	0.0210	0.0632
Sn_5H_6	M_b—M_p	RHF 3-21G(2*d*)	0.0505	−0.0095
		SBK(2*d*)	0.0451	−0.0390
		WH(2*d*)	0.0444	−0.0386
		GVB SBK(2*d*)	0.0462	−0.0424
		WH(2*d*)	0.0448	−0.0403
		UHF 3-21G(2*d*)	0.0532	−0.0222
		SBK(2*d*)	0.0484	−0.0468
		WH(2*d*)	0.0478	−0.0467
	M_p—H	RHF 3-21G(2*d*)	0.0974	0.1136
		UHF 3-21G(2*d*)	0.0970	0.1159
	Ring[a]	RHF 3-21G(2*d*)	0.0215	0.0230
		SBK(2*d*)	0.0194	0.0211
		WH(2*d*)	0.0191	0.0196
		GVB SBK(2*d*)	0.0188	0.0239
		WH(2*d*)	0.0188	0.0206
		UHF 3-21G(2*d*)	0.0159	0.0334
		SBK(2*d*)	0.0152	0.0300
		WH(2*d*)	0.0148	0.0301
	Cage[a]	RHF 3-21G(2*d*)	0.0211	0.0237
		SBK(2*d*)	0.0186	0.0220
		WH(2*d*)	0.0184	0.0198
		GVB SBK(2*d*)	0.0180	0.0254
		WH(2*d*)	0.0180	0.0210
		UHF 3-21G(2*d*)	0.0142	0.0396
		SBK(2*d*)	0.0137	0.0356
		WH(2*d*)	0.0132	0.0352

[*continued*

Table 5—*continued*

Systems	Bond A—B	Wavefunction	$\rho(\mathbf{r})$	$\nabla^2\rho(\mathbf{r})$	Systems	Bond A—B	Wavefunction	$\rho(\mathbf{r})$	$\nabla^2\rho(\mathbf{r})$
C_5H_8	M_b—M_p	RHF 3-21G(2*d*)	0.2484	−0.7492	Ge_5H_8	M_b—M_p	3-21G(2*d*)	0.0818	−0.1094
		SBK(2*d*)	0.2353	−0.5367			SBK(2*d*)	0.0726	−0.0876
	M_b—H	3-21G(2*d*)	0.2814	−0.9939			WH(2*d*)	0.0731	−0.0963
		SBK(2*d*)	0.2767	−1.0332		M_b—H	3-21G(2*d*)	0.1241	0.1610
	M_p—H	3-21G(2*d*)	0.2800	−0.9740		M_p—H	SBK(2*d*)	0.1214	0.1684
		SBK(2*d*)	0.2557	−1.0050		Ring[a]	3-21G(2*d*)	0.0270	0.0707
	Ring[a]	3-21G(2*d*)	0.0999	0.4999			SBK(2*d*)	0.0246	0.0246
		SBK(2*d*)	0.1012	0.4435			WH(2*d*)	0.0243	0.0592
	Cage[a]	3-21G(2*d*)	0.0977	0.5126		Cage[a]	3-21G(2*d*)	0.0249	0.0790
		SBK(2*d*)	0.0986	0.4847			SBK(2*d*)	0.0227	0.0684
Si_5H_8	M_b—M_p	RHF 3-21G(2*d*)	0.0895	−0.1352			WH(2*d*)	0.0224	0.0676
		SBK(2*d*)	0.0853	−0.1171	Sn_5H_8	M_b—M_p	WH(2*d*)	0.0500	−0.0519
	M_b—H	3-21G(2*d*)	0.1153	0.2979		Ring[a]	SBK(2*d*)	0.0162	0.0332
	M_p—H	3-21G(2*d*)	0.1146	0.3126			WH(2*d*)	0.0156	0.0332
	Ring[a]	3-21G(2*d*)	0.0313	0.0747		Cage[a]	SBK(2*d*)	0.0148	0.0386
		SBK(2*d*)	0.0310	0.0631			WH(2*d*)	0.0143	0.0382
		WH(2*d*)	0.0319	0.0794					
	Cage[a]	3-21G(2*d*)	0.0285	0.0882					
		SBK(2*d*)	0.0278	0.0837					
		WH(2*d*)	0.0291	0.0920					

[a]See text.

not exceed 0.0061 au. This value is found for Ge_5H_6 in which the geometric differences between AE and ECP are also the largest. In general, valence densities generated from ECP wavefunctions are both qualitatively and quantitatively similar to the corresponding densities generated from AE wavefunctions.

The above observation is encouraging and suggests that a topological analysis of the charge density of large organic, biochemical or transition metal systems determined using ECPs may well yield results which are similar to a corresponding analysis using AE. Since all-electron calculations are often not feasible for these large systems, the usefulness of ECPs becomes readily apparent. Charge distributions calculated from ECP wavefunctions contain the necessary topological features to determine which atoms are bonded to each other, as well as the relative strengths of the interactions.

Though in the vast majority of cases the absence of the core density in the ECP charge distributions does not affect the determination of critical points in the valance region, the bond critical point between M and H (M = Si, Ge, Sn) cannot be located using the ECP wavefunctions. Hydrogen withdraws electrons from M in these cases due to the relative electronegativities of M and H. Since there is no core density on M, there is no maximum at this nuclear position in the charge distribution. Therefore, instead of a saddle point in $\rho(\mathbf{r})$, $\rho(\mathbf{r})$ monotonically increases from the beginning of the valence region of M_p to H (Figs 2–4).

The SBK density has a bond critical point between Si_b and Si_p but WH does not. The WH charge density at the beginning of the valence region is not of sufficient magnitude to cause a saddle to form between Si_b and Si_p. Instead, a non-nuclear local maximum is found and this point is purely an artifact of the WH basis set. For the Sn_bSn_p bond in Sn_5H_8, it is with SBK that this type of critical point is found; WH yields a bond critical point.

We now proceed to analyse bonding in the propellane systems. With the exceptions noted above, the observations made from AE densities are the same as those made from ECP densities. Where possible, we quote AE values; otherwise we use SBK values.

Relief maps of the RHF all-electron total charge distributions in σ_v and σ_h planes for the M_5H_6 and M_5H_8 systems are given in Figs 1–4. Note that the charge density is a maximum only at the nuclear positions. In the σ_v plane, containing the two M_b and one M_p atoms, there are maxima at the two M_b and one M_p nuclei (and also at the H_b nuclei in M_5H_8). In the σ_h plane, containing the three M_p and six H atoms, there are maxima at the three M_p

and six H nuclei. In the σ_v plane there is a saddle point in each charge distribution between each (M_b, M_p) pair. This saddle point has one positive curvature of ρ along the bond axis and two negative curvatures of ρ orthogonal to the bond axis. As noted in the Introduction, such a saddle point is termed a bond critical point. The σ_v plane affords a view of the positive curvature and one of the negative curvatures associated with a (M_b, M_p) pair. The two gradient paths of ρ that originate at the bond critical point and terminate at the M_b and M_p nuclei define the bond path between these atoms. The charge density is a maximum with respect to any lateral displacement along the bond path. For C_5H_6, there is also a bond path between the two bridgehead carbons. The σ_v plane shows the positive and one of the negative curvatures of the C_b—C_b bond, while the σ_h plane shows both negative curvatures. Only for this system is there a bond critical point between the two M_b atoms. In the remaining systems, a cage critical point is found between the two M_b atoms. This kind of critical point is a local minimum and has three positive curvatures: two are displayed in the σ_v plane in M_5H_6 (M = Si, Ge, Sn), and the third curvature (along with one of the positive curvatures also seen in the σ_v plane) is displayed in the σ_h plane.

There are three ring critical points in C_5H_6, one on each three-membered ring face. The σ_v plane shows the two positive curvatures in the ring surface and the σ_h plane shows the negative curvature perpendicular to the ring surface and one of the positive curvatures. There are also three ring critical points in C_5H_8, one associated with each four-membered ring. The arrangement of ring critical points in C_5H_8 is similar to that in the heavier M_5H_6 and M_5H_8 systems (M = Si, Ge, Sn).

Having identified the different types of critical points (points at which the gradient of the charge density, $\nabla\rho$, vanishes), it is now useful to discuss the values of the charge density, ρ, and the Laplacian of the charge density, $\nabla^2\rho$, at these points to gain a better understanding of the bonding and strengths of interaction in the M_5H_6 and M_5H_8 systems.

The M_b and M_p atoms are said to be bonded because a bond critical point, and hence a bond path, exists between them.[15,17,18] For homologous series of molecules, the value of the charge density at this point has been correlated with the bond order and strength of the bond.[2,29–31] These studies have shown that the bond order increases with increasing $\rho(\mathbf{r}_b)$. In the hydrocarbon study, ethane, ethene and ethyne were assigned bond orders of 1, 2 and 3, respectively.[2,29] Since the value of $\rho(\mathbf{r}_b)$ for C_bC_p in C_5H_6 (Table 5) is very close to the analogous value for the CC bond in ethane (Table 6), the C_bC_p bond in propellane may be referred to as a single bond of approximately unit bond order. The $\rho(\mathbf{r}_b)$ value for C_bC_p in C_5H_8 is also close to the ethane value.

The M_bM_p $\rho(\mathbf{r}_b)$ values for M_5H_6 and M_5H_8 (M = Si, Ge, Sn) are slightly smaller than the corresponding M_2H_6 values but never less than 84% of the latter value. These bonds in the propellane and bicyclopentane systems can therefore be referred to as single bonds with bond orders slightly smaller than one.

An analysis of the Laplacian of the charge density, $\nabla^2\rho$, determines the nature of the interaction between bonded atoms.[32,33] If the value of $\nabla^2\rho(\mathbf{r}_b)$ is negative, then a shared or covalent interaction results. If the value is positive, then a closed-shell (e.g. ionic) interaction results. In the M_2H_6 systems, the sign of $\nabla^2\rho(\mathbf{r}_b)$ is negative, implying a covalent interaction. This value becomes less negative as the family is descended, because the charge density to be shared between the heavy atoms is more diffuse

Table 6. bond distances (Å) and bond critical point ($\mathbf{r}_b$) analysis (au) of M_2H_6 systems

System	Wavefunction	M—M Distance	M—M $\rho(\mathbf{r}_b)$	M—M $\nabla^2\rho(\mathbf{r}_b)$	M—H Distance	M—H $\rho(\mathbf{r}_b)$	M—H $\nabla^2\rho(\mathbf{r}_b)$
C_2H_6	RHF/3–21G(2*d*)//RHF/3–21G(*d*)	1.533	0.2562	−0.8481	1.089	0.2766	−0.9545
	RHF/SBK(2*d*)//RHF/SBK(*d*)	1.542	0.2392	−0.5949	1.090	0.2724	−0.9764
Si_2H_6	RHF/3–21G(2*d*)//RHF/3–21G(*d*)	2.350	0.0960	−0.1651	1.482	0.1141	0.3194
	RHF/SBK(2*d*)//RHF/SBK(*d*)	2.367	0.0920	−0.1488	1.486	—	—
Ge_2H_6	RHF/3–21G(2*d*)//RHF/3–21G(*d*)	2.443	0.0862	−0.1327	1.550	0.1201	0.1766
	RHF/SBK(2*d*)//RHF/SBK(*d*)	2.449	0.0784	−0.1446	1.536	—	—
Sn_2H_6	RHF/3–21G(2*d*)//RHF/3–21G(*d*)	2.845	0.0598	−0.0383	1.748	0.0972	0.1203
	RHF/SBK(2*d*)//RHF/SBK(*d*)	2.812	0.0542	−0.0666	1.709	—	—

and because some of this density has been removed by the more electronegative hydrogens. The M_bM_p bonds in the propellanes and bicyclopentanes have negative values for $\nabla^2\rho(\mathbf{r}_b)$ though the magnitudes are slightly smaller than those in the corresponding M_2H_6 systems. The ECP $\nabla^2\rho(\mathbf{r}_b)$ values are not in as good agreement with the corresponding AE values as are the $\rho(\mathbf{r}_b)$ values themselves.

In summary, topological analyses of the M_5H_6 and M_5H_8 charge distributions and comparison with M_2H_6 distributions and distances reveal that the M_bM_p bond is basically a covalent single bond, slightly weaker than the prototype MM bond in M_2H_6.

Using the same analyses as above reveals that the MH bond is a single bond, slightly stronger than the prototype MH bond in M_2H_6. The interaction is a covalent one only for the carbon compounds. In the heavier systems, where the electronegativity of hydrogen substantially exceeds that of silicon, germanium and tin, the interaction is closed-shell (ionic).

A bond path exists between the two bridgehead atoms only in C_5H_6. The ring critical points are in close proximity to the bond critical point (0.096 Å away) and the value of $\rho(\mathbf{r}_r)$ is 97% the value of $\rho(\mathbf{r}_b)$. This means there is a broad bonded maximum in ρ in the interatomic surface (Fig. 1) and a substantial accumulation of charge between the bridgehead nuclei. Wiberg *et al.*[2] have referred to the C_bC_b interaction as a "fat bond" in order to reflect the flat density surface in the bonding region. The value of $\rho(\mathbf{r}_b)$ for the C_bC_b bond in C_5H_6 is 80% of the corresponding value in C_2H_6. The bond order of the C_bC_b bond in C_5H_6 has been calculated to be 0.73.[2]

A similar "fat bond" is not found for C_bC_b in C_5H_8. In fact, a cage critical points exists in the bridgehead region, not a bond critical point. Therefore, a bond path does not connect the M_b nuclei in this (or any of the other) group IV bicyclopentane investigated here. The value of ρ at the cage critical point is only half the value of $\rho(\mathbf{r}_b)$ in C_bC_b of C_5H_6. Figure 1 displays little charge density in the C_bC_b internuclear region of C_5H_8.

As mentioned above, there are three ring critical points in C_5H_8, one associated with each of the three curved four-membered ring surfaces. These ring critical points are in close proximity to the cage critical point (0.054 Å away) and are also very close in ρ values [$\rho(\mathbf{r}_r) = 0.0999$ au; $\rho(\mathbf{r}_c) = 0.0977$ au]. Since the cage critical point is a local minimum in ρ, the ring critical points near it will always be higher in ρ value, even if the difference is very small as it is in this and the other bicyclopentanes.

It is important to recognize that the charge distribution in the bridgehead region of C_5H_8 is different in form from the corresponding region in C_5H_6. In C_5H_8, there is not much charge density in the shallow, flat region between the two bridgehead nuclei, and there is no bond path. In C_5H_6, there is a significant accumulation of charge density and a bond path exists between the two bridgehead nuclei.

The value of $\rho(\mathbf{r}_c)$ in the internuclear bridgehead region in Si_5H_6 is only 48% of the value of $\rho(\mathbf{r}_b)$ in Si_2H_6. This suggests that the interaction between the two silicons is weaker in Si_5H_6 than that in Si_2H_6. The ring critical points in Si_5H_6 are only 0.021 Å from the cage critical point and $\rho(\mathbf{r}_r)$ are only very slightly higher than $\rho(\mathbf{r}_c)$. Thus, a shallow, flat distribution of charge exists between the bridgehead silicons in Si_5H_6 and no bond path is found.

In Si_5H_8, the value of $\rho(\mathbf{r}_c)$ is 61% of the corresponding value in Si_5H_6. The formation of the M_bH_b bonds upon going from M_5H_6 to M_5H_8 removes density from the bridgehead region more than from other regions of the molecule. Though the charge distributions differ quantitatively, qualitatively they have the same topological form. Thus, in the bridgehead region M_5H_6 and M_5H_8 are qualitatively identical in form for M = Si, Ge and Sn (Figs 2–4).

In Ge_5H_6, the value of $\rho(\mathbf{r}_c)$ is 41% the value of $\rho(\mathbf{r}_b)$ in Ge_2H_6. In Ge_5H_8, the value of $\rho(\mathbf{r}_c)$ is 70% of the corresponding value in Ge_5H_6. In Sn_5H_6, the value of $\rho(\mathbf{r}_c)$ is 35% the value of $\rho(\mathbf{r}_b)$ in Sn_2H_6. In Sn_5H_8, the value of $\rho(\mathbf{r}_c)$ is 80% of the corresponding value in Sn_5H_6.

These results lead to the following conclusions: (i) In as much as ρ at the critical point between M_bM_b is a measure of the strength of the M_bM_b interaction (the greater the value of ρ, the stronger the interaction), the M_bM_b interaction in M_5H_6 is weaker than that in M_2H_6, with the interaction becoming progressively weaker as Group IV is descended. (ii) The M_bM_b interaction is weaker in M_5H_8 than in M_5H_6. As the group is descended, the charge distribution in the bridgehead region in M_5H_6 more closely resembles that in M_5H_8, both qualitatively and quantitatively. Thus, the Sn_bSn_b interaction is the weakest of all the interactions.

It has been shown for C_5H_6 that when the C_bC_b distance is increased over the equilibrium distance, the C_bC_b bond critical point eventually coalesces with the three ring critical points and an unstable critical point (possessing one zero curvature) is formed.[2,15] A further infinitesimal increase in the C_bC_b distance yields a cage critical point in the internuclear bridgehead region and three new ring critical points, one associated with each of the newly formed four-membered rings. We have performed this procedure in reverse for the heavier systems. If

we squeeze the two Si_b atoms closer together by 0.20 Å in Si_5H_6 (reducing the M_bM_b distance to 2.494 Å), the three ring critical points coalesce with the cage critical point. Upon a further infinitesimal compression, a bond critical point and three new ring critical points are created, one on the face of each three-membered ring. Thus it takes only 0.20 Å (and a corresponding energy increase of only 1.9 kcal mol^{-1}) to form a bond path between the two Si_b atoms. It should be noted that the remainder of the geometry was not re-optimized upon compression of the bridgehead distance, and so, the energy increase values are upper limits. The value of $\rho(\mathbf{r}_b)$ in the compressed geometry is 0.0590 au and this value is 0.0124 au greater than the cage value in the equilibrium geometry. Still, the value of $\rho(\mathbf{r}_b)$ is 0.0260 au less than the M_bM_p $\rho(\mathbf{r}_b)$ value of 0.0850 au, where the M_bM_p distance = 2.331 Å. Therefore, the shortening of the M_bM_b distance creates a bond path between these atoms although the bond is still weak compared to a normal SiSi bond.

For a similar change in the molecular graph to occur in Ge_5H_6, the bridgehead nuclei must be squeezed together by 0.29 Å. The energy increase is 11.9 kcal mol^{-1}. The value of ρ at the newly created bond critical point is 0.0506 au, 0.0153 au greater than that at the cage critical point in the equilibrium geometry. This newly created bond (of distance 2.593 Å) is weaker than the Ge_bGe_p bond (the Ge_bGe_p distance is 2.449 Å) because $\rho(\mathbf{r}_b)$ in the former is 0.0161 au smaller than the corresponding value in the latter bond.

For a similar change in the molecular graph change to occur in Sn_5H_6, the bridgehead nuclei must be squeezed together by 0.37 Å and the energy increase is 13.2 kcal mol^{-1}. The value of ρ at the newly created bond critical point is 0.0315 au, 0.0104 au greater than the cage critical point in the equilibrium geometry. This newly created bond (of distance 3.092 Å) is weaker than the Sn_bSn_p bond (of distance 2.876 Å) because $\rho(\mathbf{r}_b)$ in the former is smaller than $\rho(\mathbf{r}_b)$ in the latter bond by 0.0190 au.

The ease with which a molecule can change from one structure to another is related to the weakness of the interaction of primary importance in the change.[2,15,34] The equilibrium M_bM_b distances need to decrease by 7, 10 and 11% for the M_bM_b bond path to form (M = Si, Ge, Sn, respectively). The energy needed to bring about this compression increases upon descending Group IV. This supplies further evidence that the Si_bSi_b interaction is stronger than the Ge_bGe_b interaction, which in turn is stronger than the Sn_bSn_b interaction. The two bridgehead silicon atoms are more predisposed to bond path formation than the other heavier systems.

Table 5, in addition to listing the RHF values, also includes the GVB (for singlets) and UHF (for triplets) values. The conclusions made above in the RHF discussion hold for GVB and UHF with one exception. No bond path is found between the C_b atoms in C_5H_6(UHF). The C_bC_b distance is much greater in UHF than RHF (UHF − RHF = 0.28 Å) and the UHF C_bC_b interaction is weaker.

Since the coefficient of the RHF term in the GVB wavefunction is dominant (Table 3), it is useful to inspect localized orbitals.[27] The M_bM_b Boys localized orbital densities are displayed in Fig. 5. The all-electron and effective core potential densities are similar in the valence regions. This observation is further evidence of the success with which ECPs describe valence density. There are two electrons in each of the localized molecular orbitals, and there is a critical point (a maximum) in the orbital density at the M_bM_b midpoint. The values of ρ at this point are 0.1899, 0.0411, 0.0288 and 0.0174 au for M = C, Si, Ge, Sn, respectively. These values are 93, 88, 82 and 82% of the *total* density at the same point for the respective propellanes. Thus, the localization procedure works well to localize the bonding electrons in the bridghead bonding orbital. From the above ρ values and from the contour maps, one sees that there is less density in the M_bM_b bonding region as the family is descended. The amount of density in the localized bridgehead orbital is smallest for Sn_5H_6 owing to the fact that the M_bM_b distance is largest for this system and the effective orbital overlap is smallest.

Though there exists a localized M_bM_b bond orbital in each of the propellane systems, a bond path in the total density exists only in the C_5H_6 case. This is because inclusion of the remaining occupied orbital densities to form the total density creates ring critical points of smaller ρ value than the M_bM_b bond critical point in C_5H_6. However, in the remaining systems, the M_bM_b critical point becomes a cage critical point as the surrounding ring critical points are slightly higher in ρ value. Thus, the existence or lack of a bond critical point and associated bond path as a function of M, especially upon going from carbon to silicon, arises from a subtle difference in the role played by the other LMOs in the M_bM_b region.

Figure 6 displays maps of the singlet RHF minus triplet UHF densities at the RHF geometries for the σ_h plane of the M_5H_6 systems. Going from the triplet to the singlet, the greatest build-up of charge is in the bridgehead bonding region in the vicinity of the M_bM_b critical point. The density differences become increasingly smaller as the group is descended and the M_bM_b bonding interaction descreases. Indeed the difference in the value of $\rho(\mathbf{r}_c)$

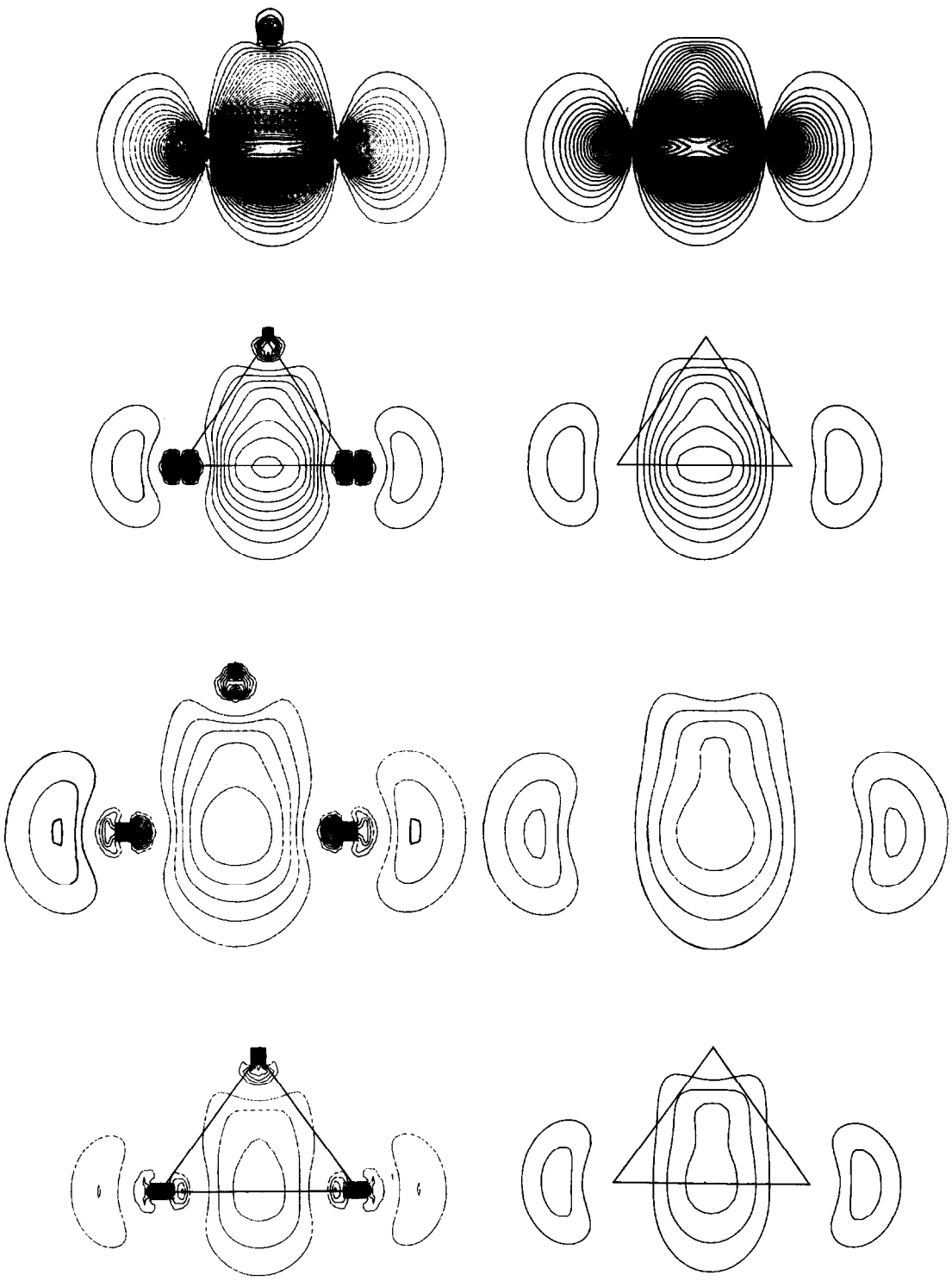

Fig. 5. Contour maps of M_bM_b localized orbital densities in the σ_v plane. The charge distributions for the four maps displayed down the left side of the figure (C_5H_6, Si_5H_6, Ge_5H_6 and Sn_5H_6) are generated from all-electron RHF/3–21G(2*d*)//3–21G(*d*) wavefunctions, while the charge distributions for the corresponding four maps displayed down the right side of the figure are generated from RHF/SBK(2*d*)//RHF/SBK(*d*) wavefunctions.

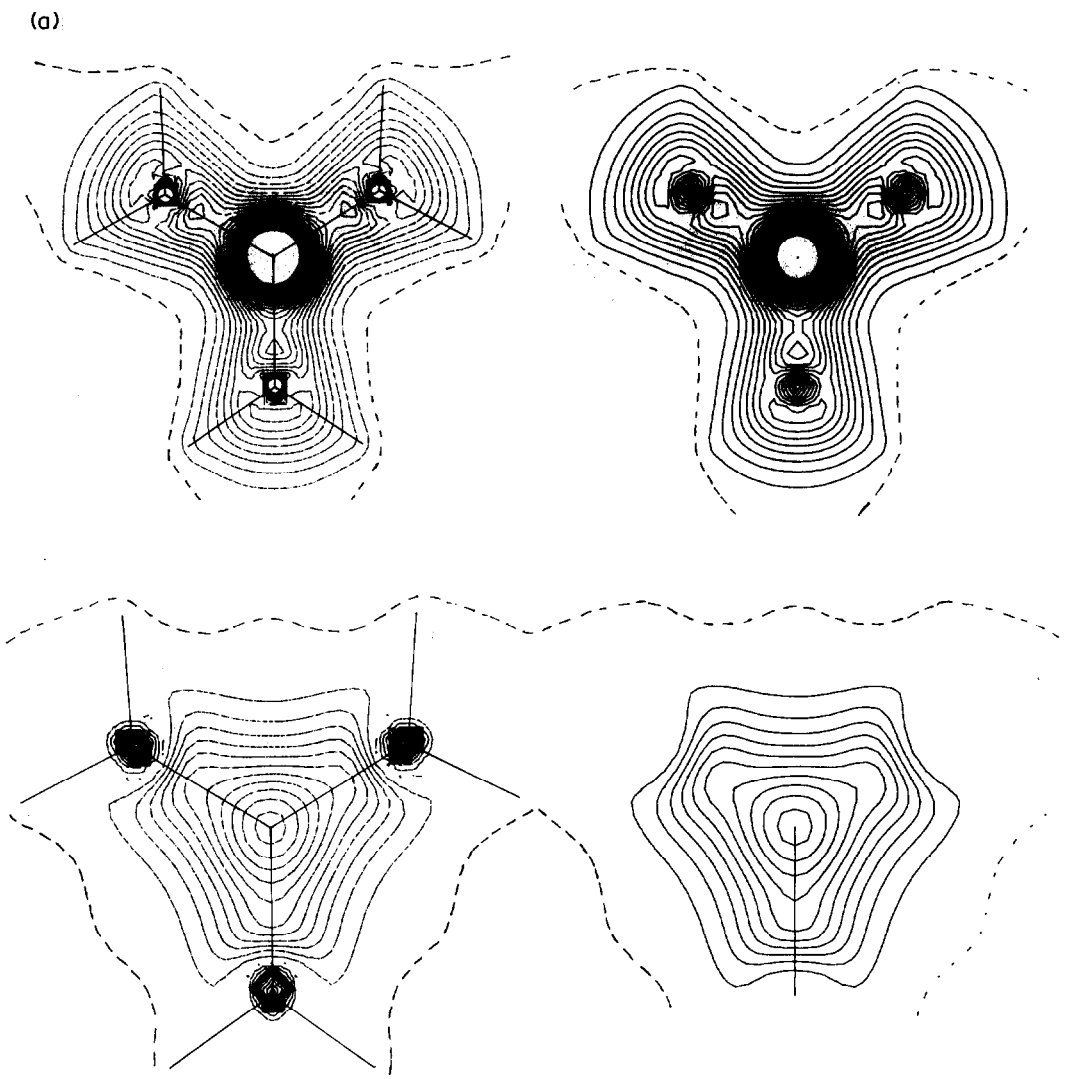

Fig. 6. Contour maps of the RHF minus UHF densities at the RHF geometries for the M_5H_6 σ_h planes. Solid (dashed lines) are positive (negative) values. The largest magnitude contour has a value of ± 0.025 au in all cases. Left-hand side maps are determined by subtracting densities generated using the all-electron 3-21G(2*d*) basic set, while right-hand side maps use the SBK (2*d*) basis set. (a) Top half: C_5H_6; bottom half: Si_5H_6. (b) Top half: Ge_5H_6; bottom half: Sn_5H_6.

between RHF and UHF is smallest in Sn_5H_6, and Sn_5H_6 has the smallest magnitude for the singlet–triplet splitting. In the carbon cases, enough density flows into the singlet system for a bond critical point to form between the bridgehead atoms. In the heavier systems, this is not the case. Note that the same conclusions are reached using either the all-electron or ECP basis set.

CONCLUSIONS

The structures and bonding in [1.1.1]propellanes have been studied in this work. The following points are emphasized:

(i) The bonding interaction between the two bridgehead atoms decreases on descending Group IV so that for tin, there is little difference between Sn_5H_6 and Sn_5H_8 in the M_bM_b region, in agreement with the experimental observations of Sita and co-workers.[1] This statement is supported by geometry comparisons to the corresponding bicyclopentanes and ethanes, by a topological examination of the charge density, by GVB–PP calculations, by singlet–triplet energy and density differences and by localized orbital density analyses.

(ii) Valence electron densities generated from effective core potential basis sets are similar to the corresponding densities generated from all-electron

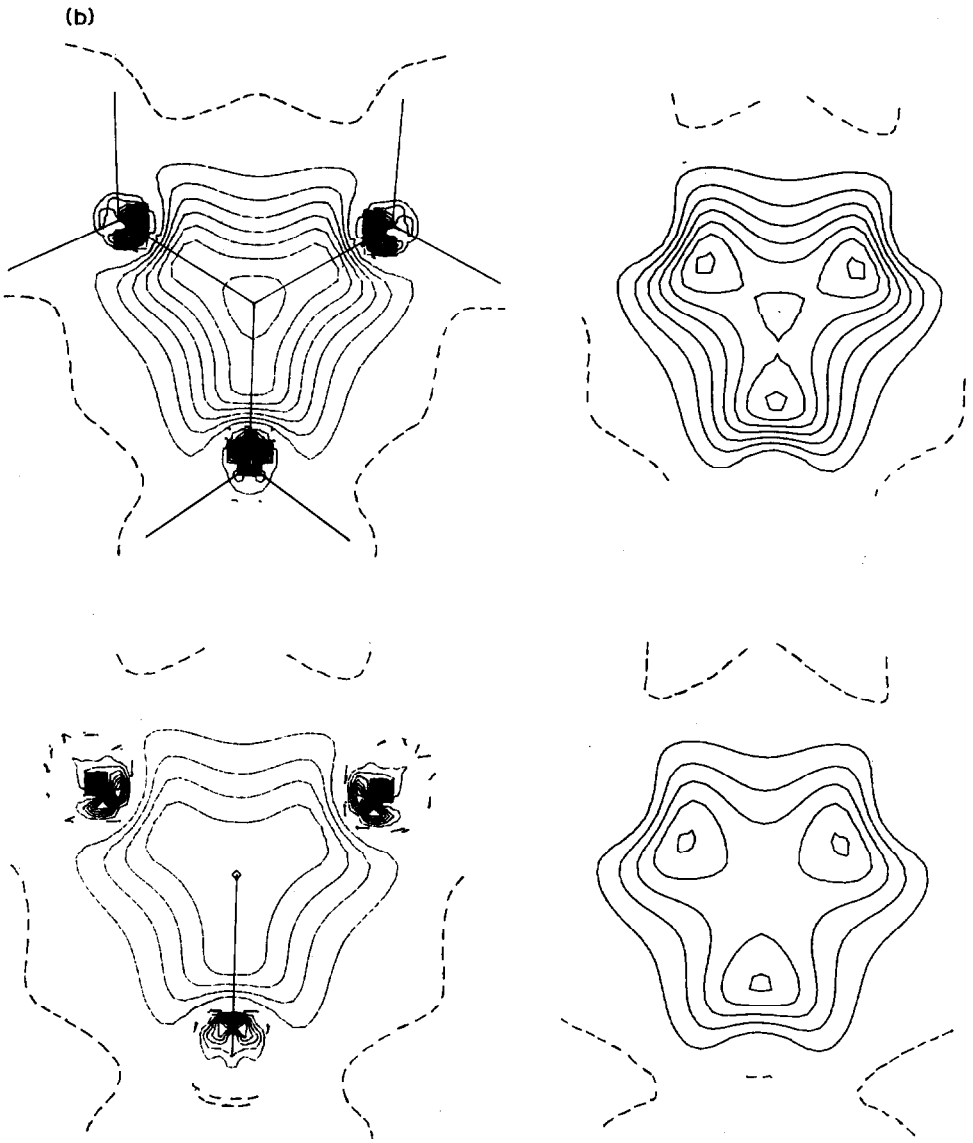

Fig. 6—*continued.*

basis sets. Since these densities are alike, so will be the second derivative density field (the Laplacian). It has been shown that the Laplacian of the charge density field determines the sites of electrophilic and nucleophilic attack and the reactivity of the molecule.[35,36] Therefore, the reactivity of large biochemical and transition metal systems not amenable to all-electron calculations, may well be successfully determined by analysing the Laplacian of the charge density generated from ECP basis sets.

Acknowledgements—The computations described in this work were performed on the North Dakota State University IBM 3090/120E vector computer, obtained, in part, with the aid of a joint study agreement between IBM and NDSU, and on the Cray Y-MP at the San Diego Supercomputer Center. This work was supported in part by a grant from the National Science Foundation (CHE-8911911). We thank Professors Richard Bader, Michael Schmidt, Larry Sita and Keith Laidig for useful discussions, and Dr Walter Stevens for making the SBK ECPs available prior to publication.

REFERENCES

1. L. R. Sita and R. D. Bickerstaff, *J. Am. Chem. Soc.* 1989, **111**, 6454; L. R. Sita and R. D. Bickerstaff, *J. Am. Chem. Soc.* 1989, **111**, 3769; L. R. Sita and I. Kinoshia, private communications (1990).

2. K. B. Wiberg, R. F. W. Bader and C. D. H. Lau, *J. Am. Chem. Soc.* 1987, **109**, 985.
3. P. v. R. Schleyer and R. Janoschek, *Angew. Chem. Int. Edn Engl.* 1987, **26**, 1267; a derivative of bicyclo-[1.1.1]pentasilane has recently been synthesized: Y. Kabe, T. Kawase and K. Okada, *Angew. Chem. Ind. Edn Engl.* 1990, **29**, 794.
4. (a) S. Nagase and T. Kudo, *Organometallics* 1987, **6**, 2456; (b) S. Nagase, T. Kudo and T. Kurakake, *J. Chem. Soc., Chem. Commun.* 1988, 1063.
5. S. Nagase and T. Kudo, *Organometallics* 1988, **7**, 2534.
6. W. W. Schoeller, T. Dabisch and T. Busch, *Inorg. Chem.* 1987, **26**, 4383.
7. W. D. Stohrer and R. Hoffmann, *J. Am. Chem. Soc.* 1972, **94**, 779.
8. M. D. Newton and J. M. Schulman, *J. Am. Chem. Soc.* 1972, **94**, 773.
9. J. E. Jackson and L. C. Allen, *J. Am. Chem. Soc.* 1984, **106**, 591.
10. D. B. Kitchen, J. E. Jackson and L. C. Allen, *J. Am. Chem. Soc.* 1990, **112**, 3408.
11. N. D. Epiotis, *J. Am. Chem. Soc.* 1984, **106**, 3170.
12. K. B. Wiberg, *Chem. Rev.* 1989, **89**, 975.
13. (a) K. B. Wiberg and F. H. Walker, *J. Am. Chem. Soc.* 1982, **104**, 5239; (b) K. B. Wiberg, W. P. Dailey, F. H. Walker, S. T. Waddell, L. S. Crocker and M. D. Newton, *J. Am. Chem. Soc.* 1985, **107**, 7247.
14. K. B. Wiberg and S. T. Waddell, *J. Am. Chem. Soc.* 1990, **112**, 2194.
15. R. F. W. Bader, T. T. Nguyen-Dang and Y. Tal, *Rep. Prog. Phys.* 1981, **44**, 893.
16. K. B. Wiberg and J. J. Wendoloski, *J. Am. Chem. Soc.* 1982, **104**, 5679.
17. R. F. W. Bader and T. T. Nguyen-Dang, *Adv. Quant. Chem.* 1981, **14**, 63.
18. R. F. W. Bader, *Accts Chem. Res.* 1985, **18**, 9.
19. (a) P. C. Hariharan and J. A. Pople, *Theoret. Chim. Acta.* 1973, **28**, 213; (b) M. S. Gordon, *Chem. Phys. Lett.* 1980, **76**, 163.
20. (a) A. E. Reed and F. Weinhold, *J. Chem. Phys.* 1985, **83**, 1736; (b) A. E. Reed, R. B. Weinstock and F. Weinhold, *J. Chem. Phys.* 1985, **83**, 735.
21. W. J. Stevens, H. Basch and M. Krauss, *J. Chem. Phys.* 1984, **81**, 6026.
22. W. R. Wadt and P. J. Hay, *J. Chem. Phys.* 1985, **82**, 284.
23. W. A. Goddard III, T. H. Dunning, W. J. Hunt and P. J. Hay, *Accts Chem. Res.* 1973, **6**, 368.
24. (a) J. S. Binkley, J. A. Pople and W. J. Hehre, *J. Am. Chem. Soc.* 1980, **102**, 1980; (b) M. S. Gordon, J. S. Binkley, J. A. Pople, W. J. Pietro and W. J. Hehre, *J. Chem. Phys.* 1982, **104**, 2997.
25. M. W. Schmidt, K. K. Baldridge, J. A. Boatz, J. H. Jensen, S. Koseki, M. S. Gordon, K. A. Nguyen, T. L. Windus and S. T. Elbert, *QCPE Bulletin, GAMESS, North Dakota State University* 1990, **10**, 52.
26. J. A. Boatz and M. S. Gordon, *J. Phys. Chem.* 1989, **93**, 3025.
27. J. M. Foster and S. F. Boys, *Rev. Mod. Phys.* 1963, **32**, 300.
28. See, for example: (a) M. S. Gordon, T. J. Packwood, M. T. Carroll and J. A. Boatz, *J. Phys. Chem.* 1990 (on 1,3 disilacyclobutanes), in press; (b) M. W. Schmidt, K. A. Nguyen, M. S. Gordon and J. A. Montgomery, *J. Am. Chem. Soc.* 1990 (on Si—O—Si bridges), in press; (c) K. A. Nguyen, M. T. Carroll and M. S. Gordon (on oxygen and sulphur substituted propellanes), submitted.
29. R. F. W. Bader, T. S. Slee, D. Cremer and E. Kraka, *J. Am. Chem. Soc.* 1983, **105**, 5061.
30. E. Kraka, PhD thesis. University of Köln (1984).
31. M. T. Carroll, PhD thesis. McMaster University (1989).
32. R. F. W. Bader and H. Essén, *J. Chem. Phys.* 1984, **80**, 1943.
33. R. F. W. Bader, P. J. MacDougall and C. D. H. Lau, *J. Am. Chem. Soc.* 1984, **106**, 1594.
34. S. M. Bachrach, *J. Molec. Struct. (Theochem.)* 1990, **204**, 131.
35. R. F. W. Bader and P. J. MacDougall, *J. Am. Chem. Soc.* 1985, **107**, 6788.
36. M. T. Carroll, J. R. Cheeseman, R. Osman and H. Weinstein, *J. Phys. Chem.* 1989, **93**, 5120.

Polyhedron Vol. 10, No. 11, pp. 1265–1284, 1991
Printed in Great Britain

0277–5387/91 $3.00+.00
Pergamon Press plc

SINGLET EXCITATION IN POLYSILANES: *AB INITIO* CALCULATIONS ON OLIGOSILANE MODELS

V. BALAJI and JOSEF MICHL†

Center for Structure and Reactivity, Department of Chemistry and Biochemistry, The University of Texas at Austin, Austin, TX 78712-1167, U.S.A.

Abstract—All-electron SCF–CI calculations with several basis sets have been performed for excited singlet states of the linear oligosilanes Si_nH_{2n+2}, $n = 2$–5, in order to establish their nature as a function of chain length. The results suggest that the lowest $\sigma_{SiSi} \rightarrow \pi^*_{SiH}$ excited state lies below the first $\sigma_{SiSi} \rightarrow \sigma^*_{SiSi}$ state in the shortest few oligosilanes, and that the order of the states changes as the number of silicon atoms in the chain increases. An assignment is proposed for the lowest observed two-photon allowed state of polysilanes. In the gas phase, Rydberg states are expected to dominate the low-energy region of the spectra of oligosilanes shorter than Si_6H_{14}. An increase in the SiSiSi valence angle is computed to lower the $\sigma_{SiSi} \rightarrow \sigma^*_{SiSi}$ excitation energy, and torsion around a central SiSi bond from *trans* towards *cis* geometry is computed to increase it. The effect of alkyl substitution was studied using 2,2-dimethyltrisilane as a model compound. It lowers the $\sigma_{SiSi} \rightarrow \sigma^*_{SiSi}$ excitation energy, primarily by destabilizing the highest σ_{SiSi} orbital by hyperconjugative interaction with the substituents. The results for the $\sigma_{SiSi} \rightarrow \sigma^*_{SiSi}$ state are in agreement with simple, qualitative arguments and prior semiempirical calculations.

Polysilanes, $(R_2Si)_n$, high-molecular weight, fully saturated polymers with an all-silicon backbone,[1,2] have remarkable optical properties. These are of considerable importance for the possible use of these materials as photoresists,[3] photoconductors,[4] polymerization initiators,[5] non-linear optical materials,[6] etc., but are as yet poorly understood.

The current theoretical understanding of the spectroscopy of polysilanes relies on a series of semiempirical and *ab initio* calculations on the ground state[7–22] and of semiempirical calculations on electronically excited singlet states[23–31] by a variety of methods. These calculations were performed on model short chains containing no more than 40, and usually only 20 or fewer, silicon atoms. Band theory calculations for infinite chains of perfect translational symmetry have been reported as well.[32–37] We now report results of *ab initio* calculations on vertically excited singlet states of the model systems Si_nH_{2n+2}, $n = 2$–5.

Excited states of polysilanes. Experimental evidence strongly suggests that in room-temperature solutions of poly(di-n-alkylsilane)s the coherence of the lowest-energy electronic excitation extends over no more than two dozen silicon atoms or so.[27,39,40] It has been proposed[25–27,41,42] on the basis of fluorescence depolarization studies and semiempirical calculations that under these conditions the "chromophore length" is conformationally determined. The chromophores were visualized as being approximately planar, all-*trans* chain segments terminated by stronger twists, e.g. *gauche* (*cis*-planar geometry would inhibit delocalization the most), and it was assumed that the polymer backbone contains a fairly wide distribution of segment lengths. If this proposal is correct, the band structure calculations published so far[32–37] are of limited relevance for the interpretation of spectra observed in room-temperature solutions, where these polymers form random coils, and in warm (disordered), neat polymer solids. They would be more pertinent

† Author to whom correspondence should be addressed. Present address: Department of Chemistry and Biochemistry, University of Colorado, Boulder, CO 80309-0215, U.S.A.

to the understanding of the low-temperature solution and ordered solid forms, which have distinctly different conformational structure and optical properties, apparently containing significantly longer chain segments with translational symmetry.

According to this model, the spectra of the disordered polymers, which are of primary interest to us presently, are presumably interpretable as a weighted incoherent sum of contributions from a variety of chromophoric segments differing in length and absorption peak wavelength. On this source of inhomogeneous broadening is superimposed additional broadening due to the fact that each chromophore of a given length can exist in a variety of forms deviating from ideal all-*trans* planarity towards a helical or a more randomly non-planar arrangement, plus the presumably smaller broadening due to a distribution of side-chain geometries and solvent molecule arrangements.

In an alternative view of the high-temperature form of the polymer,[43] the coherence of the excitation is terminated by any of the numerous usual random deviations from perfect symmetry (large number of small twists as in the "worm-like"[44] model, vibrations, zero-point motion, side-chain or backbone conformations, solvent arrangement) without sharp twists in the backbone conformation playing a special role. It has been argued recently[45] that the worm-like model provides a superior description of the low-temperature form of the polymers. It certainly represents a viable possibility for the high-temperature form as well.

There is little doubt of the $\sigma_{SiSi} \rightarrow \sigma^*_{SiSi}$ nature of the transition to the lowest excited singlet state that is strongly allowed in absorption and emission of all of the forms of the polymers, based on the very high intensity and particularly on the long-axis polarization observed in the stretched solid[25,38,46] and in a streaming solution.[27] Transition assignments that can be excluded for the lowest strongly allowed energy band of the polymers are Rydberg, normally broadened beyond recognition in solution spectra, and $\sigma_{SiSi} \rightarrow \pi^*_{SiC}$, expected to be fairly weak and polarized perpendicular to the chain direction. Transitions to states of these types are undoubtedly present at higher energies. For long, chromophoric segments, such as those presumably present at low temperatures in glasses and in the ordered, neat solid, the question of the interband vs excitonic nature of the excited state arises, but this is not an issue for the relatively short model segments which will be of interest here, since in these the hole and the excited electron are necessarily localized in the same small region of space.

According to some[23] CNDO (however, see ref. 24) and all INDO/S[25-27] calculations, the $\sigma_{SiSi} \rightarrow \sigma^*_{SiSi}$ transition is more or less dominated by an electron excitation from the highest σ_{SiSi} to the lowest σ^*_{SiSi} orbital. Note that this does not imply that the σ^*_{SiSi} orbital is the lowest unoccupied molecular orbital (LUMO) and indeed certain calculations,[22,47] as well as the most straightforward interpretation of the very small *s* spin densities observed in the ESR–ENDOR spectra of the radical anions of some cyclic oligosilanes,[48] suggest that the lowest empty orbital of oligosilanes may be of the π^*_{SiC} type, locally antisymmetric to the plane of the silicon backbone. On the other hand, there seems to be general agreement that the highest occupied molecular orbital (HOMO) of polysilanes is of the σ_{SiSi} type, based both on calculations and on photoelectron spectra of model oligosilanes.[8] It is not known to what degree *d* orbitals are needed in the basis set in order to provide an adequate description of the σ and, particularly, the σ^* orbitals. They were not included in the semiempirical calculations reported for excited states.[23-27]

The proposal that excitation coherence length ("chromophore length") in random-coil polysilanes is conformationally determined[25-27,41,42] depends critically on two results of the INDO/S calculations. The first of these is the convergence of the $S_0 \rightarrow S_1$ singlet excitation energy of an all-*trans* or other regular (helical) structures to a finite limit as the silicon chain length increases. There is no doubt that this result is correct in principle and the question is only, at what chain length is the limit reached in practice? The INDO/S method suggests that the excitation energy drops significantly only up to about a dozen silicon atoms in the chain,[25] but it could err in either direction. The simplest way to see that the $\sigma_{SiSi} \rightarrow \sigma^*_{SiSi}$ excitation energy must tend to a finite gap is to note that the vicinal resonance integral from the *n*th silicon atom to the $(n+1)$th silicon atom, $sp^3_{Si(n)} - sp^3_{Si(n+1)}$, is substantially more negative than the geminal one, $sp^3_{Si(n)} - sp^3_{Si(n')}$, so that this linear σ-conjugated system of silicon backbone orbitals exhibits strong resonance integral alternation and is isoelectronic with the π system of a polyene with strong bond length alternation (Fig. 1).

The second critically important INDO/S result on which the proposal depends is the strong increase of the $S_0 \rightarrow S_1$ excitation energy with the twist of one or more bonds away from the *trans* planar geometry towards the *cis* geometry. It is this feature that permits an approximately *gauche* twist to interrupt effective conjugation in the linear chain of interacting σ_{SiSi} bond orbitals. Without this property, there would be no reason to expect a strong twist in the chain, or several such twists, to terminate a chromophore and start another on the other side. The requirement that rotation around

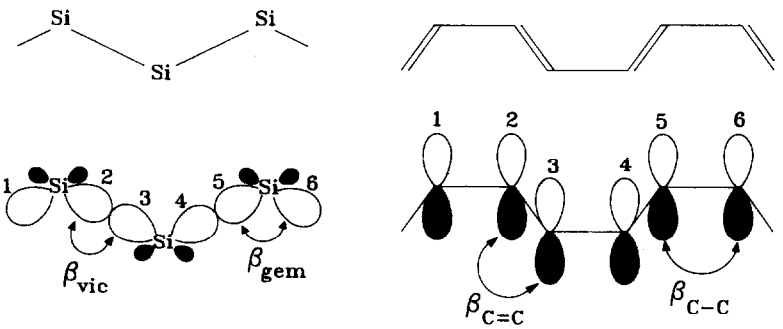

Fig. 1. Basis set orbitals in a σ-conjugated linear chain of interacting silicon sp^3 orbitals in a polysilane (left) and in a π-conjugated linear chain of interacting carbon p orbitals in a polyene with alternating bond lengths (right).

a presumably cylindrically symmetrical σ_{SiSi} bond should affect the degree of σ conjugation may appear counterintuitive at first, but is well grounded in standard theory of *anti*-periplanar through-bond interactions in organic molecules, known to account for numerous experimental observations.[49]

Excited states of oligosilanes. If the segment model for the high-temperature form of polysilanes is correct, an understanding of the electronic states of relatively short oligosilanes will be immediately applicable to the understanding of the optical spectra of the polymers. Even if the worm-like model is correct, one can hope to gain useful insight from an investigation of short oligosilanes, as long as the properties of the shorter oligosilanes can be extrapolated to the long ones.

The present study of a series of simple model segments (Si_nH_{2n+2}) attempts to address at the *ab initio* level several points previously not investigated or examined only at the semiempirical level. It attempts to: (i) verify the nature of the lowest one- and two-photon allowed singlet excitations and the role played by Rydberg and *d* orbitals in their description; (ii) check the sensitivity of the excitation energy to the value of the SiSiSi valence angle; (iii) confirm the proposed effect of chain twisting on the $S_0 \rightarrow S_1$ excitation energy; and (iv) examine the role played by alkyl substitution.

While there is little doubt that the ground state bond lengths in poly(di-n-alkylsilane)s are normal. the valence and particularly the dihedral angles are less sharply defined[2,50] and are sensitive to the nature of the alkyl groups. In this work, we adopt a set of standard model geometries and examine the effect of variation of the angles. We believe this approximation to be adequate for the purpose of examining general trends, but recognize that it contributes to the observed lack of quantitative agreement of the calculated excitation energies with the experimental ones.

It would have been preferable to choose the permethylated oligosilanes [$Si_n(CH_3)_{2n+2}$] and not the parents (Si_nH_{2n+2}) as models for the chromophoric segments in polysilanes, but it was not computationally feasible. As a compromise, we have investigated the unsubstituted parent oligosilanes and explored the effect of methyl substitution in trisilane by performing calculations on 2,2-dimethyltrisilane. *Ab initio* calculations of excitation energies can be presently only carried out for short oligosilane chains if they are to be of credible quality at all, and we have been forced to limit them to disilane (Si_2H_6), trisilane (Si_3H_8), n-tetrasilane (Si_4H_{10}) and n-pentasilane (Si_5H_{12}). Even then, we have only been able to perform them at a level that we consider adequate for the understanding of qualitative features and general trends, but not for quantitative agreement with respect to excitation energies.

METHOD OF CALCULATION

The electronic states of Si_nH_{2n+2}, $n = 2$–5, at standard ground-state geometries were calculated at the level of all-electron SCF followed by configuration interaction (CI). Huzinaga's double-zeta (DZ) basis set[51] was adopted. The effect of silicon *d* orbitals on the nature of the electronic states of silanes was tested by adding *d* functions with an exponent of 0.395 (DZ+d)[52] to the silicon DZ basis. To describe Rydberg orbitals, the silicon DZ basis was augmented with diffuse *s* and *p* functions with exponents of 0.017 and 0.014, respectively (DZ+R).[53]

The configuration list was generated by single and double excitations (CISD) with SCF orbitals as the reference space. The active space in the CISD calculations involved six to 10 highest occupied SCF orbitals and all the virtual SCF orbitals. The

number of configurations thus generated ranged from 20,000 to 50,000.

The following standard bond lengths and bond angles were adopted:[54] SiSi = 2.344 Å, SiH = 1.48 Å, SiC = 1.87 Å, CH = 1.08 Å, ∠SiSiSi = 111.2°, ∠HSiH = 108.0°, ∠CSiC = 109.47° and ∠HCH = 109.0°.

All calculations were performed using a GAMESS[55] program on a Cray X-MP/24 supercomputer at The University of Texas at Austin.

RESULTS AND DISCUSSION

The convention for the axis and orbital labels used in this paper is as follows: (i) The z axis is the long axis of the silicon chain. For structures with all silicon atoms in a single plane, the y axis is the short axis in this plane and the x axis is perpendicular to this plane. (ii) Molecular orbitals that are symmetric with respect to the yz mirror plane containing the silicon atoms are labelled as σ orbitals. Those that are antisymmetric with respect to the yz plane are labelled as π orbitals. Our convention for the σ and π orbitals thus differs from the uncommon convention used in a recent study[22] where even some molecular orbitals that are symmetric with respect to the mirror plane containing the silicon atoms were labelled as π orbitals.

All the electronic states discussed in the following sections are singlet states and the excitation energies correspond to vertical excitations.

*Qualitative molecular orbital bonding model for an all-*trans *polysilane chain*

The extremely simple Sandorfy[56] models C and H provide a natural starting point for a qualitative understanding of the valence and conduction bands in all-*trans* polysilane and of their relation to the delocalized molecular orbitals in all-*trans* oligosilanes (see, for example, ref. 2). In these models, the bonding at each silicon atom centre can be described by using a sp^3 hybrid orbital basis set. Two of the four sp^3 orbitals point towards the in-plane silicon neighbours and the other two point towards the orbitals on the α atoms of the out-of-plane substituents.

In Sandorfy model C, one considers only the silicon backbone orbitals. These can be most easily derived in two steps. First we consider the vicinal interaction between two neighbouring silicon atoms, due primarily to the resonance integral, β_{vic}, between the two strongly overlapping sp^3 orbitals located on these silicon atoms (Fig. 1). It results in the formation of a strongly bonding σ_{SiSi} localized bond orbital and a strongly antibonding σ^*_{SiSi} localized bond orbital. The σ_{SiSi} bond orbital has no interatomic node and the σ^*_{SiSi} bond orbital has one interatomic node across the bond. Second, a weaker geminal resonance integral, β_{gem}, between two sp^3 hybrid orbitals located on the same silicon atom (Fig. 1) couples the σ_{SiSi} localized bond orbitals into delocalized σ_{SiSi} backbone orbitals, and the localized σ^*_{SiSi} bond orbitals into delocalized σ^*_{SiSi} backbone orbitals.

The nodal patterns of the σ_{SiSi} and σ^*_{SiSi} backbone orbitals obtained within this model are shown on the left in Fig. 2. The bonding σ_{SiSi} backbone orbitals have no nodes at SiSi bond midpoints and their relative stability decreases with increasing number of nodes at the silicon atoms. The most stable one has no nodes at the silicon atoms and the least stable one has a node at every silicon atom. The antibonding σ^*_{SiSi} backbone orbitals have nodes at SiSi bond midpoints. Their energy again increases with an increasing number of nodes at the silicon atoms, i.e. the most stable one has no nodes at the silicon atoms and the least stable one has nodes at every silicon atom. In terms of an atomic orbital basis, the least stable σ_{SiSi} backbone orbital contains only $3p_z$ atomic orbitals of silicon and the most stable σ^*_{SiSi} backbone orbital contains only $3s$ and $3p_y$ atomic orbitals of silicon.

In Sandorfy model H, the two sp^3 hybrid orbitals that are not used in the backbone bonding are considered as well. They interact with the orbitals of the substituents (H $1s$ orbitals in the parent polysilane) to form low-energy bonding σ_{SiH} and high-energy antibonding σ^*_{SiH} localized bond orbitals. The former has a larger coefficient on the more electronegative hydrogen, the latter on the less electronegative silicon. Pairwise symmetry adaptation of these bond orbitals with respect to mirror reflection in the silicon backbone yz plane results in the formation of π-symmetry and σ-symmetry bonding and antibonding group orbitals (Figs 2 and 3). The π_{SiH} and π^*_{SiH} group orbitals cannot mix with the previously derived silicon backbone orbitals, which are of σ symmetry. They interact among themselves to yield delocalized bonding π_{SiH} molecular orbitals and antibonding π^*_{SiH} molecular orbitals. Since this interaction occurs primarily through the overlap of $3p_x$ atomic orbitals on silicon, the π^*_{SiH} band is broader than the π_{SiH} band (right-hand side of Fig. 2).

The mixing between the σ_{SiH} group orbitals and the bonding backbone σ_{SiSi} orbitals destabilizes the latter (centre of Fig. 2). The strength of this interaction depends on the energy difference between the interacting orbitals and on the number of nodes. The energy differences between the bonding back-

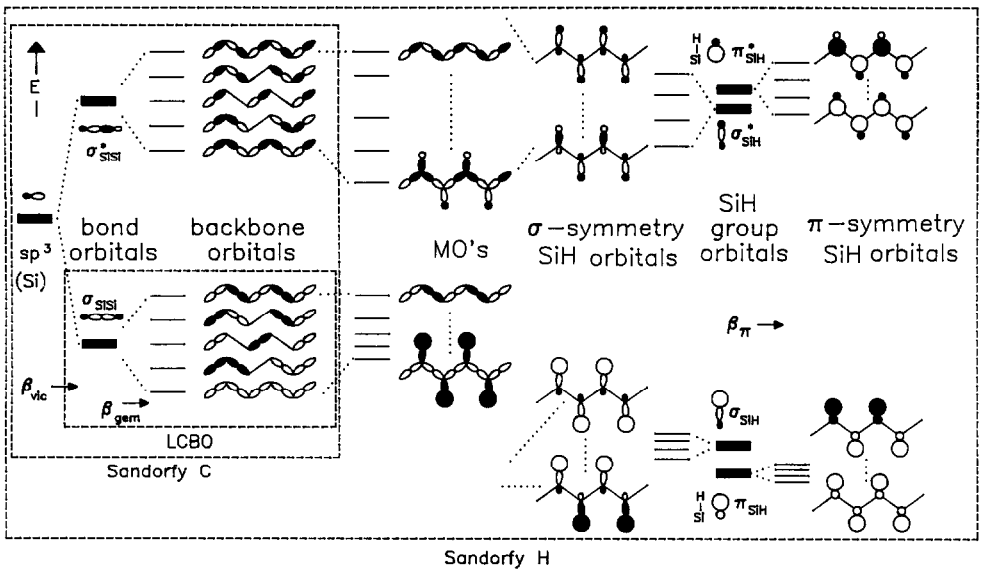

Fig. 2. The construction of σ- and π-symmetry orbitals of a long all-*trans* polysilane chain (schematic).

bone σ_{SiSi} orbitals and the σ_{SiH} group orbitals are large and the coefficients of the latter on the silicon atom small, since silicon is electropositive relative to hydrogen, hence, the interaction is weak. Moreover, at the silicon atom nodal points on the bonding backbone σ_{SiSi} orbitals, the resonance integral between the backbone orbital and the substituent orbital vanishes. For the highest-energy σ_{SiSi} backbone orbitals the interaction is therefore particularly weak and for the HOMO it is absent. Since the most stable σ_{SiSi} backbone orbital is most destabilized and the least stable one is the least affected, the band of σ_{SiSi} backbone orbitals is compressed by the interaction with the σ_{SiH} group orbitals as it forms the final bonding molecular orbitals. We shall continue to refer to these as σ_{SiSi} molecular orbitals for brevity, even though they contain some σ_{SiH} character.

The energy differences between the σ^*_{SiSi} backbone orbitals and the σ^*_{SiH} group orbitals are much smaller (centre of Fig. 2), and the coefficients of the latter on silicon relatively large. Therefore, the σ^*_{SiSi} backbone orbitals are affected more strongly than the σ_{SiSi} backbone orbitals. The most stable σ^*_{SiSi} backbone orbital is stabilized particularly strongly because of the absence of nodal points at the silicon atoms (in the drawing of this orbital in Fig. 4 of ref. 2, analogous to our Fig. 2, the bond-cutting nodes were inadvertently omitted). In general, the σ^*_{SiSi} backbone orbital band is expanded as it forms the final antibonding molecular orbitals. Although the most stable resulting molecular orbitals are mixed heavily with the σ^*_{SiH} orbitals, we shall continue to refer to them as σ^*_{SiSi} molecular orbitals for brevity.

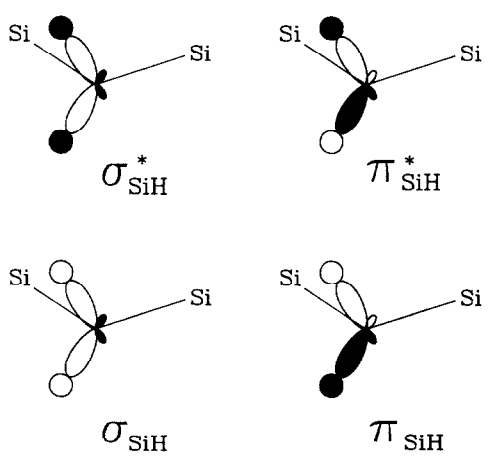

Fig. 3. A schematic drawing of the σ_{SiH}, σ^*_{SiH}, π_{SiH} and π^*_{SiH} group orbitals.

Molecular orbitals and single-reference configuration interaction calculation of excited electronic states (*Table* 1)

The above simple picture for polysilanes of infinite chain length may not be applicable without modification for finite chain oligosilanes because of end effects in the latter. However, we find that the end effects are surprisingly small and that the simple picture provides valuable guidance in the analysis of the results of our *ab initio* calculations. A qualitative picture of the highest few occupied and lowest few

Table 1. Calculated excitation energies in Si_nH_{2n+2} ($n = 2$–5)[a]

Molecule	Excitation energy[b]	Symmetry	Nature of excitation	Leading configuration	Weight[c] (%)
Si_2H_6	275	^1E_u	$\sigma \rightarrow \pi^*$	HOMO → LUMO	51
	297	$^1A_{2u}$	$\sigma \rightarrow \sigma^*$	HOMO → LUMO+3	46
				HOMO → LUMO+2	44
	298	$^1A_{1u}$	$\pi \rightarrow \pi^*$	SHOMO → LUMO	28
				HOMO−2 → SLUMO	28
	302	^1E_u	$\pi \rightarrow \sigma^*$	HOMO−2 → LUMO+2	77
	309	$^1A_{1g}$	$\sigma \rightarrow \sigma^*$	HOMO → LUMO+4	88
Si_3H_8	262	$^1B_2$	$\sigma \rightarrow \sigma^*$	HOMO → LUMO	74
	264	$^1A_2$	$\sigma \rightarrow \pi^*$	HOMO → SLUMO	89
	277	$^1A_1$	$\sigma \rightarrow \sigma^*$	SHOMO → LUMO	75
	282	$^1B_1$	$\sigma \rightarrow \pi^*$	SHOMO → LUMO	40
			$\pi \rightarrow \sigma^*$	HOMO−2 → SLUMO	40
	283	$^1B_2$	$\sigma \rightarrow \sigma^*$	HOMO → LUMO+3	74
Si_4H_{10}	232	^1B_u	$\sigma \rightarrow \sigma^*$	HOMO → LUMO	85
	241	^1A_u	$\sigma \rightarrow \pi^*$	HOMO → SLUMO	89
	258	^1B_u	$\sigma \rightarrow \sigma^*$	SHOMO → LUMO	81
	262	^1A_g	$\sigma \rightarrow \sigma^*$	HOMO−2 → LUMO	59
	262	^1B_g	$\sigma \rightarrow \pi^*$	HOMO → LUMO+4	61
Si_5H_{12}	202	$^1B_2$	$\sigma \rightarrow \sigma^*$	HOMO → LUMO	88
	218	$^1A_2$	$\sigma \rightarrow \pi^*$	HOMO → SLUMO	86
	230	$^1B_1$	$\sigma \rightarrow \pi^*$	HOMO → LUMO+2	77
	232	$^1A_1$	$\sigma \rightarrow \sigma^*$	SHOMO → LUMO	75
	238	$^1A_1$	$\sigma \rightarrow \sigma^*$	HOMO−2 → LUMO	60

[a] DZ basis.
[b] In kcal mol^{-1}.
[c] The per cent contribution to the total CI wavefunction.

unoccupied computed molecular orbitals is shown in Fig. 4 and agrees quite well with the simple expectations.

Disilane. The ground-state properties of disilane, such as equilibrium geometry, rotational barrier and vibrational spectra have been reasonably well studied by electronic structure methods.[57] However, very little is known about the excited states of this molecule. Experiments[58] and calculations[22,47,57] agree that the equilibrium geometry of disilane corresponds to a staggered conformation, similar to that of ethane. We report here the results of SCF–CISD calculations for staggered (D_{3d}) disilane performed using DZ, DZ+d, DZ+R and DZ+d+R basis sets.

At the SCF level, the HOMO is of a_{1g} symmetry and is the σ_{SiSi} bonding orbital (Fig. 4). The second highest occupied molecular orbital (SHOMO) is of e_g symmetry and is of the π_{SiH} type. The difference in the orbital energies of HOMO and SHOMO is 43 kcal mol^{-1} at the DZ level and increases to 46 kcal mol^{-1} at the DZ+d level. The large energy difference of these σ_{SiSi} and π_{SiH} orbitals, and their opposite ordering compared with ethane, have been noted before by others.[22,47] Koopmans' theorem ionization potential (IP) for the removal of an electron from the HOMO is calculated to be 260 kcal mol^{-1} and 259 kcal mol^{-1} at DZ and DZ+d levels, respectively. These results are in agreement with the *ab initio* calculations reported in the literature.[22,47] CNDO calculations predict the first IP to be about 294 kcal mol^{-1}.[8] The measured first IP is 243 kcal mol^{-1}.[8] More detailed calculations of oligosilanes[19,20] have shown that it is possible to predict their IPs more quantitatively than by Koopmans' approximation. However, this is not of particular relevance to this paper and we shall be content with the 15–20 kcal mol^{-1} overestimation of IPs.

The LUMO is a degenerate π^*_{SiH} orbital of e_u symmetry (Fig. 4). The second lowest unoccupied molecular orbital (SLUMO) is the σ^*_{SiSi} orbital of symmetry a_{2u}, located only 1 kcal mol^{-1} higher in energy than the LUMO at the DZ level and 12 kcal mol^{-1} at the DZ+d level. The ordering of these

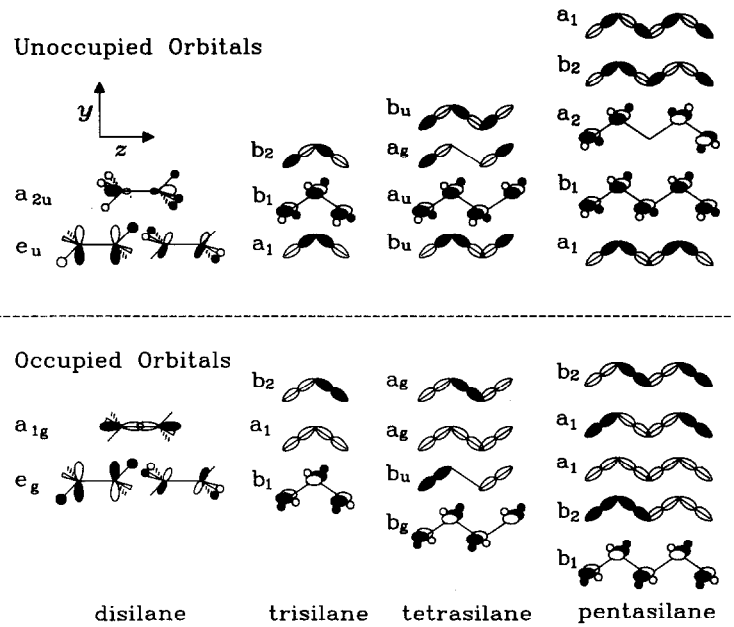

Fig. 4. Schematic representation of the first few highest occupied and lowest unoccupied molecular orbitals in Si_nH_{2n+2} ($n = 2$–5) and their ordering (SCF/DZ).

unoccupied orbitals is consistent with that reported in the literature[22,47] but the energy difference seems to be sensitive to the basis set and/or geometry. The HOMO–LUMO gap is calculated to be 368 and 365 kcal mol^{-1} at DZ and DZ+d levels, respectively. For comparison, an SCF calculation using the 3–21G* basis set predicted 346 kcal mol^{-1} at optimized geometry.[22] The effect of *d* orbitals on the energy of the LUMO σ^*_{SiSi} orbital is more pronounced than their effect on the energies of the σ_{SiSi}, π_{SiH} and π^*_{SiH} orbitals.

At the CISD level, both the DZ and DZ+d basis sets predict the first excited singlet state to be a degenerate $\sigma_{SiSi} \rightarrow \pi^*_{SiH}$ state of ^1E_u symmetry, located at about 275 and 280 kcal mol^{-1}, respectively, above the ground state. The lowest $^1A_{2u}$ $\sigma_{SiSi} \rightarrow \sigma^*_{SiSi}$ state lies 298 kcal mol^{-1} above the ground state with the DZ basis set and 310 kcal mol^{-1} above it with a DZ+d basis. Thus, the $\sigma_{SiSi} \rightarrow \pi^*_{SiH}$ excitation energy increases by only 5 kcal mol^{-1} upon the introduction of *d* orbitals into the basis, while the $\sigma_{SiSi} \rightarrow \sigma^*_{SiSi}$ excitation energy increases by nearly 12 kcal mol^{-1}. This effect is mainly due to the relative destabilization of the σ^*_{SiSi} SCF orbital as discussed above.

The addition of Rydberg functions to the DZ basis produces several low-lying Rydberg transitions at 245–280 kcal mol^{-1}. The lowest Rydberg transition was found to be of the $\sigma_{SiSi} \rightarrow (4s+4p_y)$ type and of $^1A_{1g}$ symmetry. The introduction of *d* orbitals into the basis set (DZ+d+R) again failed to alter the composition of the wavefunctions significantly, but the excitation energy increased by 20 kcal mol^{-1}.

The first five observed excited states have been assigned to Rydberg transitions.[59] The first electronic transition occurs at about 174 kcal mol^{-1} (164 nm). It has been assigned as $\sigma_{SiSi} \rightarrow 4s$ Rydberg, in only qualitative agreement with our results.

The excitation energies calculated for the first few valence excited states at the SCF–CISD level using the DZ basis set are listed in Table 1. A higher-level calculation would certainly be possible for this smallest member of the series, but comparison of the results with those for the longer oligosilanes would then be very unbalanced.

Trisilane. The SCF–CI calculations for trisilane (C_{2v} point group) were carried out using DZ, DZ+d and DZ+R basis sets. In addition, a test calculation where the DZ+d basis set was augmented with a set of *p* polarization functions on all the hydrogen atoms (DZ+dp) was also carried out. Furthermore, a three-configuration MCSCF followed by a three-reference CISD calculation using the MCSCF natural orbitals of the ground state once and those of the first excited state ($\sigma_{SiSi} \rightarrow \sigma^*_{SiSi}$) once were performed at the DZ level in order to check the effect of optimizing the orbitals for the excited state.

The SCF ordering of the high-lying occupied orbitals at the DZ level is as follows (Fig. 4): (i) the HOMO is of b_2 symmetry and corresponds to the

least stable σ_{SiSi} bonding molecular orbital, containing mostly $3p_z$ silicon atomic orbitals, (ii) the SHOMO is of a_1 symmetry and 21 kcal mol^{-1} more stable than the HOMO, corresponding to another σ_{SiSi} bonding MO, and contains mostly $3s+3p_y$ silicon and $1s$ hydrogen atomic orbitals, and (iii) the next highest occupied orbital, 50 kcal mol^{-1} lower in the energy than the HOMO, is of b_1 symmetry and is the least stable of the π_{SiH} orbitals. It is composed mostly of $3p_x$ silicon and $1s$ hydrogen atomic orbitals. The orbital ordering and composition remain the same with no significant changes in the orbital energies at the DZ+d and DZ+dp levels. They are in agreement with the earlier *ab initio*[22,47] and CNDO[8] calculations. The first IP based on Koopmans' theorem is calculated to be 250 kcal mol^{-1} compared with the experimental[8] value of 228 kcal mol^{-1}.

All three basis sets agree in the assignment of LUMO, SLUMO and the next lowest unoccupied molecular orbital to a_1, b_1 and b_2 symmetries, respectively (Fig. 4). The a_1 orbital is the most stable σ^*_{SiSi} orbital (mostly Si $3s+3p_y$ and H $1s$). The b_1 orbital is the most stable π^*_{SiH} orbital (mostly Si $3p_x$ and H $1s$), and the b_2 orbital is the σ^*_{SiSi} molecular orbital (mostly Si $3p_z$). For the three basis sets, less than 1 kcal mol^{-1} change is observed in the orbital energy of the low-lying unoccupied a_1 and b_1 orbitals. The b_2 orbital is destabilized by 4 kcal mol^{-1} upon the addition of silicon d orbitals to the basis set and no further change was observed for the DZ+dp basis set.

The ordering and structure of the bonding and antibonding molecular orbitals thus are as expected for an infinite polysilane from the qualitative Sandorfy models C and H even though in such a short chain the end effects ought to be particularly severe. The HOMO–LUMO gap is calculated to be 337, 335 and 335 kcal mol^{-1} at DZ, DZ+d and DZ+dp levels, respectively. Together with the changes in the orbital energies, these numbers indicate that the addition of silicon d functions and/or hydrogen p functions has an even less significant effect on the properties associated with the frontier orbitals of trisilane than is the case for disilane.

At the DZ level, CISD calculations (Table 1) predict the $\sigma_{SiSi} \rightarrow \sigma^*_{SiSi}$ excitation to be about 2 kcal mol^{-1} lower in energy than the $\sigma_{SiSi} \rightarrow \pi^*_{SiH}$ excitation. The addition of d functions reverses the order. In contrast to the situation in disilane, it lowers the energy of the $\sigma_{SiSi} \rightarrow \sigma^*_{SiSi}$ excitation by 24 kcal mol^{-1} and the energy of the $\sigma_{SiSi} \rightarrow \pi^*_{SiH}$ excitation by about 27 kcal mol^{-1}. The addition of hydrogen p functions to the DZ+d basis lowers the $\sigma_{SiSi} \rightarrow \sigma^*_{SiSi}$ and the $\sigma_{SiSi} \rightarrow \pi^*_{SiH}$ excitation energies by about 8 and 12 kcal mol^{-1}, respectively. The MCSCF–CI calculation described above reduces the $\sigma_{SiSi} \rightarrow \sigma^*_{SiSi}$ excitation energy by about 33 kcal mol^{-1} upon orbital optimization.

The DZ+R basis set predicted a group of Rydberg states located in the range of 210–235 kcal mol^{-1}. The lowest Rydberg transition again is of the $\sigma_{SiSi} \rightarrow (4s+4p_y)$ type and is about 35 kcal mol^{-1} lower than in disilane. The observed energy for the first electronic transition of trisilane is around 153 kcal mol^{-1} (187 nm),[59] 21 kcal mol^{-1} lower in energy than disilane. As in the case of disilane, the three absorption bands that were observed at energies below the first IP of trisilane have been assigned to Rydberg-like transitions,[59] in qualitative agreement with our results.

Trans-*n-tetrasilane*. The SCF–CI calculations were carried out using DZ, DZ+d and DZ+R basis sets, assuming C_{2h} symmetry for the planar *trans* conformation of tetrasilane.

As expected from the qualitative molecular orbital picture, the HOMO of n-tetrasilane is the least stable σ_{SiSi} molecular orbital, with nodes at every silicon atom and no nodes across the bonds (Fig. 4). It is of a_g symmetry. The two other σ_{SiSi} molecular orbitals are a b_u orbital, with one node across the middle SiSi bond, and a totally symmetric a_g orbital with no modes across the SiSi bonds. The qualitative molecular orbital picture based on the Sandorfy C model predicts the a_g orbital with no nodes as the most stable σ_{SiSi} backbone orbital, followed by the b_u orbital with one node and then the a_g HOMO. This indeed is the order of σ_{SiSi} molecular orbitals predicted by CNDO calculations.[8] However, *ab initio* SCF calculations with the DZ, DZ+d or better basis sets[19–22] predict the order of the b_u and the nodeless a_g σ_{SiSi} molecular orbitals to be reversed relative to the σ_{SiSi} backbone orbitals of the Sandorfy C model, so that the resulting SHOMO is of a_g symmetry. This is attributable to the stronger destabilizing interaction of the nodeless a_g backbone orbital with the σ_{SiH} group orbitals (cf. the Sandorfy H model and Fig. 2). The orbital energy differences between the SHOMO a_g and the b_u orbitals are calculated to be only 6 and 2 kcal mol^{-1} at the DZ and DZ+d levels, respectively. The highest bonding π_{SiH} orbital is of b_g symmetry and is much lower in energy, 57 kcal mol^{-1} compared with the HOMO at the DZ level. The first IP (Koopmans' theorem) is calculated to be 241 kcal mol^{-1} at both the DZ and DZ+d levels, compared with the experimental value of 222 kcal mol^{-1}.[8]

The LUMO, calculated at the DZ and DZ+d levels, is a b_u σ^*_{SiSi} molecular orbital. It is a linear combination of the backbone σ^*_{SiSi} orbital and the σ^*_{SiH} orbital, as expected from the Sandorfy H model (Fig. 4). The lowest π^*_{SiH} orbital is of a_u symmetry

and is calculated to be the SLUMO, 19 kcal mol^{-1} above the LUMO at the DZ level. This energy difference is reduced slightly to 17 kcal mol^{-1} at the DZ+d level.

The HOMO–LUMO gap is calculated to be 315 and 314 kcal mol^{-1} at the DZ and DZ+d levels, respectively. The analysis of orbital ordering and the energy differences shows that the silicon *d* functions do not influence the ordering or the orbital energies of the σ_{SiSi} (HOMO), σ^*_{SiSi} (LUMO) and π^*_{SiH} (SLUMO) orbitals. However, for conformational studies the silicon *d* functions may possibly be of some importance.

The DZ basis predicts the first $\sigma_{SiSi} \rightarrow \sigma^*_{SiSi}$ transition to be 9 kcal mol^{-1} lower in energy than the lowest $\sigma_{SiSi} \rightarrow \pi^*_{SiH}$ excitation. However, at the DZ+d level, the $\sigma_{SiSi} \rightarrow \sigma^*_{SiSi}$ excitation energy is decreased by 16 kcal mol^{-1} and the $\sigma_{SiSi} \rightarrow \pi^*_{SiH}$ excitation by 24 kcal mol^{-1}. The net result is that the energy gap between $\sigma_{SiSi} \rightarrow \sigma^*_{SiSi}$ and $\sigma_{SiSi} \rightarrow \pi^*_{SiH}$ excitation is reduced to about 1 kcal mol^{-1}. The lowest Rydberg excitation occurs at around 203 kcal mol^{-1} and is of the $\sigma_{SiSi} \rightarrow (4s+4p_y+4p_z)$ type.

The experimental UV spectrum of n-tetrasilane in cyclohexane has a broad absorption at 140 kcal mol^{-1} (205 nm).[60] Our calculations indicate that the first excited state is more like a Rydberg state than a valence state. However, Rydberg-like transitions are most likely broadened beyond recognition in the solution spectra, and the observed peak is probably attributable to the calculated $\sigma_{SiSi} \rightarrow \sigma^*_{SiSi}$ transition. A weaker $\sigma_{SiSi} \rightarrow \pi^*_{SiH}$ transition is expected to be buried underneath, and our calculations do not permit any reliable statement as to their relative energies.

All-trans-*n-pentasaline*. The SCF–CI calculations were feasible only for the DZ basis set. C_{2v} symmetry was imposed for the all-*trans* conformation.

The highest four occupied orbitals (Fig. 4) are the four σ_{SiSi} orbitals. The energy order of these orbitals predicted by the SCF calculation is b_2, a_1, a_1 (SHOMO) and b_2 (HOMO), in good agreement with earlier calculations.[19,20,22] The occupied π_{SiH} orbitals are below these four orbitals. The highest two are calculated to be 63 (b_1) and 68 (a_2) kcal mol^{-1} lower in energy than the HOMO. The first IP of pentasilane is calculated to be 234 kcal mol^{-1}, compared with the experimental valuc of 216 kcal mol^{-1}.[8]

The σ^*_{SiSi} orbital of a_1 symmetry is predicted by the SCF calculation to be the LUMO. The next higher SLUMO is of π^*_{SiH} character and lies 24 kcal mol^{-1} higher. As expected from the Sandorfy H model, the LUMO shows a considerable silicon 3*s* and σ^*_{SiH} character. The ordering of the unoccupied molecular orbitals at this level of calculation is: a_1 (σ^*_{SiSi} LUMO), b_1 (π^*_{SiH} SLUMO), a_2 (π^*_{SiH}), b_2 (σ^*_{SiSi}), a_1 (σ^*_{SiSi}) and b_2 (σ^*_{SiH}). This ordering is quite different from the ordering obtained from a previous SCF/3-21G* calculation[22] (a_1, a_1, b_1 and b_2). It is possible that the inclusion of silicon *d* functions can alter the ordering of unoccupied molecular orbitals. The HOMO–LUMO gap calculated at the DZ level is 299 kcal mol^{-1}.

The CISD/DZ calculation predicts a $\sigma_{SiSi} \rightarrow \sigma^*_{SiSi}$ $^1B_2$ state described predominantly by the HOMO → LUMO configuration (88%) as the first excited singlet, with an excitation energy of 202 kcal mol^{-1}. Earlier CNDO/2(S+DES CI) calculations[23,24] predict the first excited state to be 124 kcal mol^{-1} above the ground state. However, their HOMO → LUMO configuration contributes only about 50% to the total CI wave function.

A $\sigma_{SiSi} \rightarrow \pi^*_{SiH}$ (HOMO → SLUMO) excited state of $^1A_2$ symmetry lies about 16 kcal mol^{-1} higher. Other nearby excited states include a $^1B_1$ state, represented mostly by the $\sigma_{SiSi} \rightarrow \pi^*_{SiH}$ (HOMO → LUMO+2) configuration, with an excitation energy of 230 kcal mol^{-1}, and a $^1A_1$ state, represented mostly by the $\sigma_{SiSi} \rightarrow \sigma^*_{SiSi}$ (SHOMO → LUMO) configuration, with an excitation energy of 232 kcal mol^{-1}. The measured broad first electronic absorption of n-pentasilane in cyclohexane lies at around 133 kcal mol^{-1} (215 nm).[60] As in the case of tetrasilane, this is most likely due to the calculated $\sigma_{SiSi} \rightarrow \sigma^*_{SiSi}$ transition, with a $\sigma_{SiSi} \rightarrow \pi^*_{SiH}$ absorption band buried underneath.

Summary. Effect of chain length. Our results for molecular orbitals and their energies have brought no surprises, in that they are essentially fully in line with the simple Sandorfy models, with prior semiempirical and *ab initio* work, and with the known trends in experimental ionization potentials.

More noteworthy are the results for the excited states (Fig. 5), and we are now in position to comment on the nature of the lowest excited singlet state as a function of the number of silicon atoms in a linear oligosilane. The distinctions that need to be made are (i) Rydberg vs valence states and (ii) valence $\sigma_{SiSi} \rightarrow \sigma^*_{SiSi}$ vs $\sigma_{SiSi} \rightarrow \pi^*_{SiH}$ states. Another point of interest has been the importance of *d* orbitals for proper description of the valence excited states.

(i) Our results indicate that for disilane, trisilane and tetrasilane, the lowest few Rydberg excitations are of the $4s+4p$ type and are lower in energy than the valence excitations. The trends in the energies of the Rydberg states are expected to parallel the trends in the IPs.[61] Based on the measured first IPs, the Rydberg excitation energy is expected to drop by about 15 kcal mol^{-1} as we go from disilane

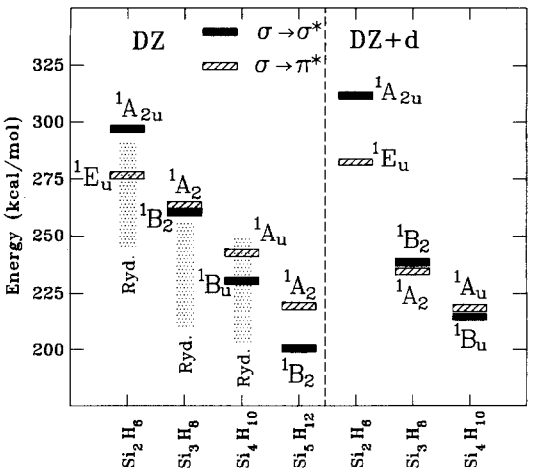

Fig. 5. Energies of the lowest $\sigma_{SiSi} \rightarrow \sigma^*_{SiSi}$ and $\sigma_{SiSi} \rightarrow \pi^*_{SiH}$ singlet excited states in Si_nH_{2n+2} (n = 2–5), obtained from CISD/DZ, CISD/DZ+d, and CISD/DZ+R calculations. See text.

to trisilane and by about 6 kcal mol^{-1} from trisilane to tetrasilane. Our calculated result of 35 kcal mol^{-1} at the SCF–CISD/DZ+R level does not correspond well to the expected value as we go from disilane to trisilane. However, the calculated difference in the lowest Rydberg excitation energy for trisilane and tetrasilane agrees well. The measured first IPs for tetrasilane and pentasilane differ by 6 kcal mol^{-1}.[8] Based on the trends in Rydberg and valence excitation energies, we can estimate that the $\sigma_{SiSi} \rightarrow \sigma^*_{SiSi}$ excitation and not Rydberg excitation will be the lowest excitation in n-hexasilane and higher linear oligosilanes. (ii) Perhaps the most important single outcome of our computations is the realization that two types of valence transitions, $\sigma_{SiSi} \rightarrow \sigma^*_{SiSi}$ and $\sigma_{SiSi} \rightarrow \pi^*_{SiH}$, compete nearly evenly for the position of lowest energy and that the outcome of the competition is a function of chain length. At the DZ and DZ+d basis set levels, the $\sigma_{SiSi} \rightarrow \sigma^*_{SiSi}$ excitation energy decreases more rapidly than the $\sigma_{SiSi} \rightarrow \pi^*_{SiH}$ excitation energy as the number of backbone silicon atoms increases. Except in the case of disilane, each of these valence states is quite well described by a single configuration (Table 1). The configurations correspond to excitation from the HOMO (σ_{SiSi}) into the lowest of the σ^*_{SiSi} molecular orbitals or the lowest of the π^*_{SiH} molecular orbitals. The former agrees with the INDO/S description[25–27] and some,[23] but not all,[24] of the CNDO results.

It is clear from Fig. 5 that the lowest valence excited state in a long enough oligosilane will surely be $\sigma_{SiSi} \rightarrow \sigma^*_{SiSi}$, at least in the all-*trans* conformation. This result is consistent with the previously reported semiempirical and experimental results.[25–27,38,46,62] The trend in the $\sigma_{SiSi} \rightarrow \sigma^*_{SiSi}$ excitation energy as a function of increasing chain length cannot be extrapolated quantitatively to long chains, but is compatible with the convergence limit of about n = 12, suggested by the INDO/S calculations.[25–27] This limit is not known experimentally. The observed excitation energies of polysilane chains $(R_2Si)_n$ continue to decrease up to $n \simeq 100$,[62] but these observations reflect the contributions of a whole distribution of segment lengths, and do not relate to the properties of a single all-*trans* chromophore of a specific length.

At the DZ level, the cross-over point between $\sigma_{SiSi} \rightarrow \pi^*_{SiSi}$ and $\sigma_{SiSi} \rightarrow \sigma^*_{SiSi}$ as the lowest excited singlet appears to be reached at trisilane. Inclusion of polarization *d* orbitals on silicon alters the picture slightly in that it shifts the cross-over point towards tetrasilane. In general, the silicon *d* orbitals play a rather insignificant role. Clearly, we cannot pinpoint the cross-over point, particularly since we have not optimized the geometries. However, it is reasonable to expect that in the shortest oligosilanes, and presumably also in the shortest segments of a disordered polysilane, $\sigma_{SiSi} \rightarrow \pi^*_{SiH}$ will be the lowest excited singlet, so that their photophysical properties will be quite different from those normal in longer oligosilanes and longer polymer chain segments. A $\sigma_{SiSi} \rightarrow \pi^*_{SiH}$ lowest singlet will have a much smaller oscillator strength and much longer radiative lifetime. This will tend to shift the competition between fluorescence on the one hand and intersystem crossing or photochemical decay on the other in favour of the latter two.

Since the equilibrium geometries of the ground and the excited states undoubtedly differ, the vertical absorption energy and the vertical emission energy plots against n may contain different cross-over points. As the equilibrium geometries of the $\sigma_{SiSi} \rightarrow \sigma^*_{SiSi}$ and $\sigma_{SiSi} \rightarrow \pi^*_{SiH}$ excited states undoubtedly also differ, the lowest excited singlet surface of an oligosilane or polysilane segment of a length characteristic of the cross-over region may contain two distinct minima at comparable energies.

Certain otherwise puzzling experimental observations on polysilanes will indeed be accounted for naturally if the shorter chromophoric segments in a poly(di-n-alkylsilane) chain, absorbing primarily below 300 nm, have a lowest excited singlet state of a much longer radiative lifetime than usual for the longer segments, which absorb primarily at longer wavelengths. The chain abridgement reaction, which proceeds with the expulsion of a R_2Si unit, only proceeds upon irradiation at wavelengths

below 300 nm,[63] and many of the photophysical properties of a series of poly(di-n-alkylsilane)s change abruptly at that same wavelength of irradiation in a fashion compatible with the notion that at shorter wavelengths an essentially non-fluorescent segment is being excited.[64] The present results might account for these anomalies in the behaviour of polysilanes, but it is clearly desirable to first investigate experimentally the short model oligosilanes themselves.

The quantitative agreement between the measured electronic excitation energies in simple oligosilanes[59,60] and the results obtained at the SCF–CISD/DZ level is rather poor. Valence-like excitations in disilane and trisilane are probably higher in energy than their first IPs and are difficult to measure. It is highly likely that we overestimate their energies significantly. The first excitation energies for *trans*-n-tetrasilane and all-*trans*-n-pentasilane are higher than the experimental numbers by 93 and 67 kcal mol^{-1}, respectively. The latter presumably refer to a mixture of conformers. The difference between experimental and calculated excitation energies for *trans*-n-tetrasilane is reduced to 77 kcal mol^{-1} at the SCF–CISD/DZ+d level, but this is still rather high.

Multireference CI calculation of excited electronic states. Although we expect that the lack of quantitative agreement does not play a critical role for the qualitative picture that we are primarily interested in presently, we have attempted to improve the quality of the single reference SCF–CISD results by performing multi-reference CI (MRCI) calculations with the DZ basis set for all four oligosilanes. We have generated 490 reference configurations by exciting eight electrons in the orbital space composed of four highest occupied and three lowest unoccupied SCF orbitals, with an excitation level of four. The CI list included all the single excitations from the reference space to the rest of the unoccupied orbital space (multi-reference first-order CI). The results are shown in Fig. 6. They are qualitatively identical to those of the CISD calculations: in disilane the $\sigma_{SiSi} \rightarrow \pi^*_{SiH}$ excitation lies below $\sigma_{SiSi} \rightarrow \sigma^*_{SiSi}$, and the ordering is reversed for the higher oligomers. The vertical excitation energies are lower than those obtained from CISD calculations but still nearly 59 and 51 kcal mol^{-1} above the experimental values for *trans*-n-tetrasilane and all-*trans*-n-pentasilane, respectively. A quantitatively reliable computation of the excitation energies would clearly require the use of optimized geometries, of a larger basis set, optimized excited state orbitals and higher-order CI terms. Some or all of this may be attainable in the near future, particularly with recourse to the pseudopotential approximation.

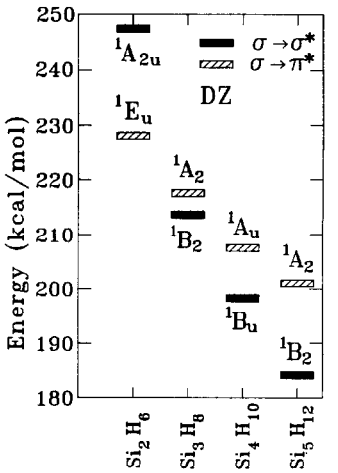

Fig. 6. Energies of the lowest $\sigma_{SiSi} \rightarrow \sigma^*_{SiSi}$ and $\sigma_{SiSi} \rightarrow \pi^*_{SiH}$ singlet excited states in Si_nH_{2n+2} (n = 2–5), obtained from MR–CI/DZ calculations. See text.

A fundamental problem standing in the way of quantitative agreement is the inadequate consistency in the treatment of electron correlation in the oligomers. For a size-consistent quantitative estimation of electron correlation energy in disilane through pentasilane, the minimum number of electrons to be correlated in either a calculation of the $\sigma_{SiSi} \rightarrow \sigma^*_{SiSi}$ state or a calculation of the $\sigma_{SiSi} \rightarrow \pi^*_{SiH}$ state in disilane would be two, in trisilane four, in tetrasilane six and in pentasilane eight. A full CI calculation for the correlation of six and eight electrons over the entire virtual space in tetrasilanes and pentasilanes, respectively, is currently beyond our reach. Further, this type of CI calculation does not include contributions from $\pi_{SiH} \rightarrow \pi^*_{SiH}$ and $\pi_{SiH} \rightarrow \sigma^*_{SiSi}$ excitations, respectively. These will double the electron count for uniform treatment of correlation along the oligosilane series. As a consequence, the current results cannot provide accurate relative energies of the $\sigma_{SiSi} \rightarrow \sigma^*_{SiSi}$ and $\sigma_{SiSi} \rightarrow \pi^*_{SiH}$ excitations as a function of the silicon chain length. However, since the trends remain the same at all levels of calculation that we have performed (Figs 5 and 6), we believe that they are qualitatively correct.

Remarks on two-photon absorption spectroscopy of polysilanes

Recent investigations[43] of simultaneous two-photon absorption of poly(di-n-hexylsilane) in methylcyclohexane glass and in thin films show a

strongly allowed two-photon absorption band at about 23 kcal mol^{-1} above the lowest strong one-photon absorption band. Two-photon polarization measurements have ruled out the possibility of a final state of $\sigma_{SiSi} \rightarrow \pi^*_{SiH}$ character. The absence of any one-photon absorption band at 23 kcal mol^{-1} above the lowest absorption band in the polymer demonstrates that this strongly two-photon allowed state is at best weakly allowed as a one-photon electric dipole excitation. No secure assignment of this two-photon transition has yet been offered.[30,31,43,65]

Our SCF–CISD/DZ calculations for all-*trans* oligosilanes (Table 1) indicate the presence of a higher $\sigma_{SiSi} \rightarrow \sigma^*_{SiSi}$ one-electron excited singlet state of the same symmetry as the ground state (^1A_g for even n, $^1A_1$ for odd n), located 15–30 kcal mol^{-1} above the strongly allowed first excited $\sigma_{SiSi} \rightarrow \sigma^*_{SiSi}$ singlet state (^1B_u when n is even and $^1B_2$ when n is odd). A transition from the ground state to this higher $\sigma_{SiSi} \rightarrow \sigma^*_{SiSi}$ ^1A state is one-photon electric-dipole forbidden for even n and weakly allowed, with short-axis (y) polarization, for odd n, and we propose that this makes this type of state a good candidate for the final state in the observed two-photon transition. In trisilane, tetrasilane and pentasilane, the dominant configuration for this excited state corresponds to the promotion of one electron from the SHOMO (HOMO-2 in tetrasilane) σ_{SiSi} orbital composed of silicon $3s+3p_y$ and hydrogen $1s$ atomic orbitals to the LUMO σ^*_{SiSi} orbital composed mostly of silicon $3s+3p_y$ and hydrogen $1s$ atomic orbitals.

A comparison with linear π-conjugated systems is instructive. In polyenes,[66] the final state for two-photon absorption is a "doubly excited state" with SHOMO → LUMO, HOMO → SLUMO and HOMO^2 → LUMO^2 having roughly equal weights as the dominant configurations. These approximately degenerate configurations are the only three that carry two-photon absorption intensity in the simplest approximation, as they are the only ones obtained from the ground configuration by two successive applications of an "allowed" single-electron promotion (i.e. one that increases the "quantum number", given by the number of nodes in a molecular orbital, by one). The mixing of the three configurations produces three excited ^1A states: 2^1A^-, 1^1A^+ and 3^1A^- in the order of increasing energy (the superscript indicates pseudoparity in the sense of Pariser's[67] alternant pairing). The two $^1A^-$ states are two-photon allowed for a transition from the 1^1A^- ground state, with the two-photon intensity concentrated heavily in the transition to the upper state, 3^1A^-, as a result of balancing contributions from the three contributing configurations. In long polyenes and perhaps already in butadiene, the 2^1A^- state actually lies below the first one-electron excited $^1B^+$ singlet state (HOMO → LUMO). The near degeneracy of the SHOMO → LUMO and HOMO → SLUMO configurations in polyenes is a consequence of their alternant nature (in approximate models, in which alternant symmetry holds exactly, the degeneracy is exact),[67] whereas the closeness of the HOMO^2 → LUMO^2 configuration to the others is "accidental".

At the level of Sandorfy model C, polysilanes are exactly isoconjugate with polyenes and are alternant, too. One might therefore expect that they, too, will have a low-lying doubly excited state of equally mixed "SHOMO" → "LUMO", "HOMO" → "SLUMO" and "HOMO"^{2} → "LUMO"^{2} nature (the orbital labels are placed into quotation marks to indicate that only molecular orbitals of σ^*_{SiSi} nature are counted). Yet, our calculations reveal that the higher $\sigma_{SiSi} \rightarrow \sigma^*_{SiSi}$ state, that we propose as a candidate for the terminal state of strong two-photon absorption, contains only minuscule amounts of "HOMO"^{2} → "LUMO"^{2} and "HOMO" → "SLUMO" configurations and cannot be considered "doubly excited" in the usual sense at all.

Recent CASSCF calculations[28] for trisilane suggest that a vertically doubly excited state with dominant "HOMO"^{2} → "LUMO"^{2} configuration actually exists but lies much higher in energy. It drops rapidly along the chain abridgement reaction coordinate (extrusion of silylene from trisilane), as expected from a Woodward–Hoffmann type correlation diagram.[28,68] Indeed, very recent examination[65] of the successive absorption of two photons by poly(di-n-hexylsilane) revealed not only the two-photon state already discussed above, but also an additional totally symmetrical state at higher energies. This higher state gives rise to an intense $S_1 \rightarrow S_x$ absorption band at energies only a little lower than those of the first intense transition from the ground state, "HOMO" → "LUMO". It is quite plausible that this higher state corresponds to the "HOMO"^{2} → "LUMO"^{2} excitation (^1A_g or $^1A_1$ symmetry). The "HOMO" → "SLUMO" configuration then presumably provides two-photon intensity to one or more yet other transitions at even higher energies. Clearly, judging by our *ab initio* results and the experimental results on simultaneous and successive two-photon absorptions, the oligosilane and polysilane chromophores are not even approximately alternant.

The reason for the loss of alternant symmetry is immediately apparent when one proceeds from the simplest Sandorfy C model to the Sandorfy H model (Figs 2 and 4). Although the energies of the σ_{SiSi} and σ^*_{SiSi} backbone orbitals in themselves still satisfy

the pairing symmetry (identical gaps between "HOMO" and "SHOMO" and between "LUMO" and "SLUMO" and therefore comparable energies for the "HOMO" → "SLUMO" and "SHOMO" → "LUMO" configurations), the interaction of the σ_{SiSi} backbone orbitals with the σ_{SiH} group orbitals has a very different effect than the interaction of the σ^*_{SiSi} backbone orbitals with the σ^*_{Si} group orbitals. As noted above, the resulting band of σ_{SiSi} orbitals is compressed, whereas that of the resulting σ^*_{SiSi} orbitals is expanded. The "HOMO"–"SHOMO" gap is greatly reduced and the "LUMO"–"SLUMO" gap is greatly increased (requiring the introduction of quotation marks, since "SLUMO" is now pushed well above the lowest π^*_{SiH} state or states). As alternant pairing is lost, so is the degeneracy of the "SHOMO" → "LUMO" and "HOMO" → "SLUMO" configurations, and so is their strong mixing. After such uncoupling, the energies of the "SHOMO" → "LUMO", "HOMO"^{2} → "LUMO"^{2} and "HOMO" → "SLUMO" configurations are free to be widely different and their mixing is minimal. One ends up with three two-photon allowed states of comparable intensities at energies not too different from those of the configurations, and all potential for an extremely low-lying "doubly excited" two-photon allowed state is gone.

Inspection of Fig. 2 makes it clear that the root of the problem lies in the lack of mirror-image relation between the σ_{SiH} and σ^*_{SiH} group orbitals and thus is ultimately due to the much higher electronegativity of hydrogen (or carbon), whose 1*s* (or sp^3) orbital dominates the σ_{SiH} (or σ_{SiC}) group orbital, compared with silicon, whose *s*–*p* hybrid orbital dominates the σ^*_{SiH} group orbital. A partial remedy would be to reduce the *s* character of the silicon hybrid orbital used to form the σ_{SiH} and σ^*_{SiH} group orbitals by opening up the SiSiSi valence angle through the use of bulky substituents, but it is unlikely that this effect could be sufficiently large if the lateral substituent remains as electronegative as hydrogen or carbon.

A laterally silylated polysilane of the type $[Si(SiR_3)_2]_n$ ought to have a much better chance at being alternant and exhibiting a more polyene-like, two-photon absorption spectrum. Of course, the stronger resonance integral alternation in the silicon backbone compared with the polyene chain disfavours the "HOMO"^{2} → "LUMO"^{2} configuration energetically relative to "HOMO" → "LUMO", so that even then, the 2^1A state will not be as strikingly low in energy and will not have as much "doubly excited" character. Also, hyperconjugation with the SiR_3 group will introduce additional complications (cf. the following section on alkyl substitution). It would be interesting to see whether lateral substitution with groups less electronegative than silicon, as in $[Si(SnMe_3)_2]_n$, would reverse the situation, making the "HOMO"–"SHOMO" gap larger than the "LUMO"–"SLUMO" gap.

Since the removal of alternant symmetry from the σ_{SiSi} and σ^*_{SiSi} backbone orbitals by interaction with the σ_{SiH} and σ^*_{SiH} group orbitals, respectively, is not at all described by the Sandorfy model C, we believe that the recent attempts to revitalize model C by introduction of electron repulsion at the Pariser–Parr–Pople level[30,31,69] are not likely to provide a correct description of the two-photon states. Although it is possible to manipulate the relative energies of the first one-photon allowed $\sigma_{SiSi} \rightarrow \sigma^*_{SiSi}$ excitation and the first two-photon allowed $\sigma_{SiSi} \rightarrow \sigma^*_{SiSi}$ excitation by adjustment of the β_{gem}/β_{vic} ratio, alternant pairing cannot be removed by this device alone.

Finally, we note that even the Sandorfy H model still neglects some parts of the Hamiltonian that remove alternant pairing, specifically, next-nearest neighbour resonance integrals (β_{13}).

Methyl substitution

Unlike a hydrogen atom, the methyl substituent can interact with the σ_{SiSi} and π_{SiH} orbitals of the silicon backbone of an oligosilane through hyperconjugation. The occupied combined orbitals of the methyl C—H bonds that possess π symmetry with respect to the Si—C bond (not to be confused with π symmetry relative to the plane of the silicon atoms) can act as donors and their unoccupied antibonding counterparts can act as acceptors. The least stable σ_{SiSi} molecular orbital (HOMO) has the right nodal properties (local symmetry) to interact with the methyl donor orbitals (Fig. 7). This interaction should result in a destabilization of the HOMO. The most stable σ^*_{SiSi} molecular orbital, normally the LUMO, has the wrong nodal properties at each silicon to permit interaction with the methyl group orbitals and is not affected. The π^*_{SiH} orbitals of the oligosilane chain can interact both with the occupied and the unoccupied methyl orbitals. The interaction with the donor orbital of the methyl group would destabilize and the interaction with the acceptor orbital of the methyl group would stabilize the antibonding π^*_{SiH} orbital. Semiempirical calculations[33] suggest that the interaction with the unoccupied methyl group orbital is dominant and that the π^*_{SiH} orbital is stabilized.[2] In order to test this simple picture and to examine the influence of methyl orbital interactions on the lowest singlet $\sigma_{SiSi} \rightarrow \sigma^*_{SiSi}$ and $\sigma_{SiSi} \rightarrow \pi^*_{SiH}$ excitation ener-

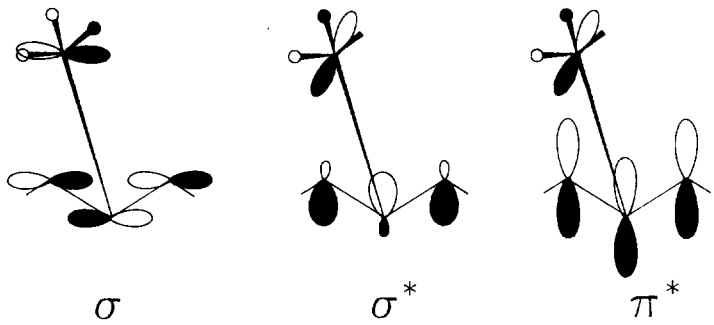

Fig. 7. Schematic representation of the interaction between the local π-symmetry orbitals of a methyl group with the highest σ_{SiSi}, lowest σ^*_{SiSi} and the lowest π^*_{SiC} backbone orbitals of a long all-*trans* polysilane.

gies, we carried out SCF–CI calculations on 2,2-dimethyltrisilane, using the DZ basis set and assuming C_{2v} symmetry.

As in trisilane, the HOMO of 2,2-dimethyltrisilane is the least stable σ_{SiSi} bonding orbital. It has b_2 symmetry and is destabilized relative to the HOMO of trisilane by about 15 kcal mol^{-1}, in accordance with the simple expectations. The experimental IP for 2,2-dimethyltrisilane is not known. However, the measured first IPs for permethylated disilane and tetrasilane are 200 and 184 kcal mol^{-1},[70] respectively. From these numbers, we can guess the IP of permethylated trisilane to be approximately 192 kcal mol^{-1}, which is about 36 kcal mol^{-1} lower than that of parent trisilane. Based on these numbers, it is not unreasonable to expect 15 kcal mol^{-1} reduction of the first IP (destabilization of the HOMO in Koopmans' context) in 2,2-dimethyltrisilane relative to parent trisilane.

The LUMO of 2,2-dimethyltrisilane, which is the most stable of the antibonding σ^*_{SiSi} orbitals, is calculated to be virtually unaffected (destabilized by only 2 kcal mol^{-1} relative to trisilane), again as expected from the simple arguments. The HOMO–LUMO gap in 2,2-dimethyltrisilane is calculated to be 325 kcal mol^{-1}, about 12 kcal mol^{-1} smaller than that of trisilane.

The π^*_{SiH} orbital (SLUMO) of b_1 symmetry is destabilized by 3 kcal mol^{-1} relative to trisilane and shows practically no hyperconjugative interactions. The slight destabilization is most likely due to the larger CSiC angle. Semiempirical calculations[33] suggest that this orbital is stabilized upon methylation, and the reason for the discrepancy is not known.

The $\sigma_{SiSi} \rightarrow \sigma^*_{SiSi}$ (HOMO $\rightarrow$ LUMO) configuration was found to represent well the first excited state of 2,2-dimethyltrisilane, with an excitation energy of about 239 kcal mol^{-1}, reduced by 23 kcal mol^{-1} from that in trisilane. The $\sigma_{SiSi} \rightarrow \sigma^*_{SiSi}$ excitation energy is about 2 kcal mol^{-1} lower and the SHOMO $\rightarrow$ LUMO $\sigma_{SiSi} \rightarrow \sigma^*_{SiSi}$ excitation energy about 12 kcal mol^{-1} higher than the lowest $\sigma_{SiSi} \rightarrow \pi^*_{SiC}$ excitation. The experimental UV spectrum of 2,2-dimethyltrisilane is not available and the valence transitions in parent trisilane are not well known, making a comparison with experiment difficult. However, for comparison, the energy for the first electronic excitation of permethylated tetrasilane in isooctane is about 132 kcal mol^{-1} (216 nm)[71] which is red-shifted by 7 kcal mol^{-1} (11 nm) relative to the first transition in n-tetrasilane.[60]

These results show that methyl substitution on the oligosilane chain lowers the HOMO–LUMO gap by hyperconjugative destabilization of the HOMO, causing the $\sigma_{SiSi} \rightarrow \sigma^*_{SiSi}$ excitation energy in 2,2-dimethyltrisilane to be considerably red-shifted from that in trisilane. The calculated gap between the lowest $\sigma_{SiSi} \rightarrow \sigma^*_{SiSi}$ and $\sigma_{SiSi} \rightarrow \pi^*_{SiC}$ excited states remains almost unchanged.

Variation of the SiSiSi *valence angle*

Previous calculations on the equilibrium geometry of the parent oligosilanes yielded an equilibrium SiSiSi valence bond angle, θ, of 111.2°.[21,22]

In order to evaluate the effect of θ on the excitation energies, we carried out SCF–CISD/DZ calculations on trisilane and the *trans* conformer of n-tetrasilane as model compounds. The angle θ was varied from 100 to 130°. To accommodate for the changes in the hybridization of the atomic orbitals of the central silicon atoms whose valence angle θ is varied, the HSiH angles were also changed, in the opposite direction. For the two extreme values of θ, 100 and 130°, the corresponding HSiH angles were fixed to be 118 and 88°, respectively, as suggested by MNDO calculations.[72]

The SCF orbital energies of the two highest occupied orbitals and the two lowest unoccupied orbitals of trisilane and *trans*-n-tetrasilane are shown in Fig. 8 as a function of θ, which also provides a schematic representation of the orbitals. The behaviour of these orbitals in both trisilane and *trans*-n-tetra-

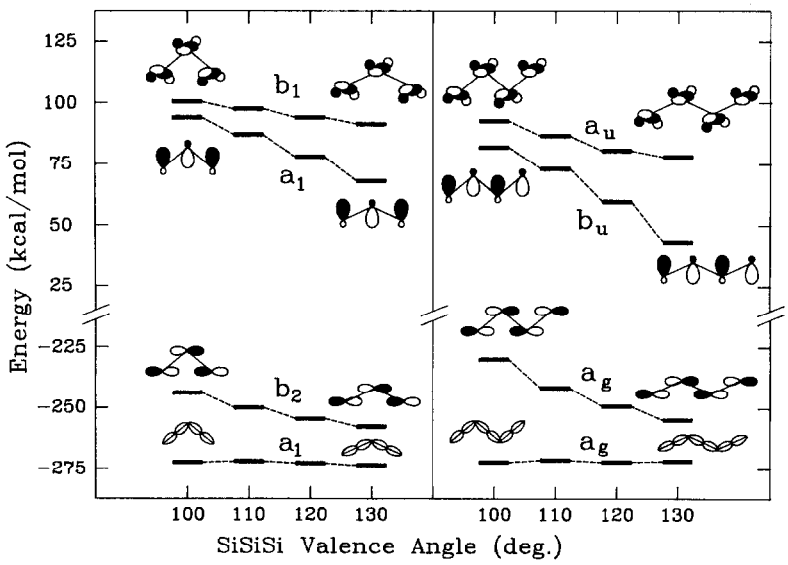

Fig. 8. Changes in the SCF SHOMO, HOMO, LUMO and SLUMO energies of trisilane (left) and n-tetrasilane (right) as a function of the SiSiSi valence angle θ.

silane is similar. In both cases, the ordering of these orbitals does not change as θ is varied from 100 to 130°.

The HOMO σ_{SiSi} orbital (b_2 in trisilane and a_g in *trans*-n-tetrasilane), composed largely of silicon $3p_z$ orbitals, is stabilized as θ is increased, and this is readily understood. At very large values of θ, this orbital is stabilized by the predominantly σ-type positive overlap of the silicon $3p_z$ atomic orbitals at neighbouring silicon atoms. At very small θ, this overlap develops into predominantly π type, its sign changes, and the orbital is destabilized. Significant negative overlap between the $3p_z$ orbitals on the next-nearest neighbour silicon develops as well. The SHOMO σ_{SiSi} orbital (a_1 in trisilane and a_g in *trans*-tetrasilane), composed of the silicon $3s+3p_y$ and hydrogen $1s$ atomic orbitals, is quite insensitive to the changes in the valence angle θ.

The LUMO σ^*_{SiSi} orbital (a_1 in trisilane and b_u in *trans*-n-tetrasilane), composed mostly of silicon $3s+3p_y$ and hydrogen $1s$ atomic orbitals, shows a very strong stabilization as θ is increased. This is mainly due to the decreasing negative overlap of the $3s+3p_y$ atomic orbitals on neighbouring silicon atoms. At the valence angles considered here, the SLUMO is the π^*_{SiH} orbital (b_1 in trisilane and a_u in *trans*-tetrasilane) in both cases. An increase in θ has little effect but the concomitant decrease in the HSiH angle causes a decrease in the overlap between the hydrogen $1s$ and the silicon p_x atomic orbitals and stabilizes the π^*_{SiH} orbital.

The net changes in the HOMO–LUMO and the HOMO–SLUMO gaps as a function of θ are shown in Fig. 9 for the two model compounds. Qualitatively, they suggest that an increase in θ will indeed reduce the first $\sigma_{SiSi} \rightarrow \sigma^*_{SiSi}$ excitation energy and increase the first $\sigma_{SiSi} \rightarrow \pi^*_{SiH}$ excitation energy slightly.

The calculated energies of the lowest $\sigma_{SiSi} \rightarrow \sigma^*_{SiSi}$ and the lowest $\sigma_{SiSi} \rightarrow \pi^*_{SiH}$ excited states of trisilane and *trans*-n-tetrasilane, obtained as a function of θ by performing single-reference CISD/DZ calculations using an active space of first few highest occupied SCF orbitals (seven in trisilane and five in *trans*-n-tetrasilane) and all the unoccupied SCF orbitals, are given in Fig. 10. The ground state energies of both compounds increase by nearly 5 kcal mol^{-1} as θ is increased to 130° or decreased

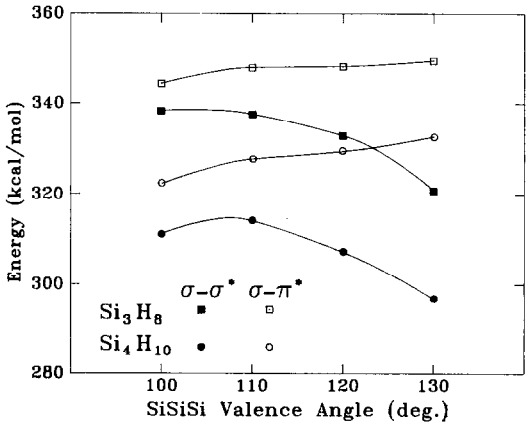

Fig. 9. The variation in the σ_{SiSi}–σ^*_{SiSi} HOMO–LUMO and σ_{SiSi}–π^*_{SiH} HOMO–SLUMO energy gap as a function of θ in trisilane and n-tetrasilane.

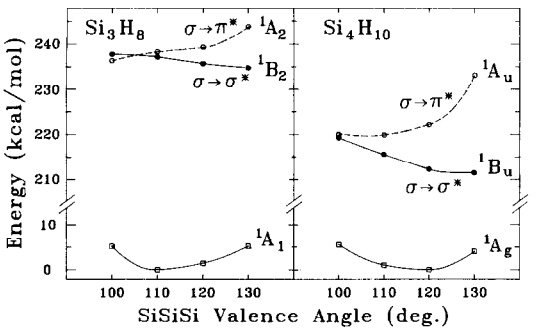

Fig. 10. CISD/DZ energies of the ground state and the lowest $\sigma_{SiSi} \rightarrow \sigma^*_{SiSi}$ and $\sigma_{SiSi} \rightarrow \pi^*_{SiH}$ excited states of trisilane and n-tetrasilane as a function of the SiSiSi valence angle θ, relative to the energy of the ground state at $\theta = 111.2°$.

to 100° from the equilibrium value of 111.2°. As expected from the behaviour of molecular orbital energies just described, as θ is increased, the energy of the lowest $\sigma_{SiSi} \rightarrow \sigma^*_{SiSi}$ excited state of both compounds decreases and that of the $\sigma_{SiSi} \rightarrow \pi^*_{SiH}$ excited state increases.

In trisilane, the CISD/DZ calculation predicts the $\sigma_{SiSi} \rightarrow \pi^*_{SiH}$ excited state to be 2 kcal mol^{-1} lower in energy than the $\sigma_{SiSi} \rightarrow \sigma^*_{SiSi}$ excited state at $\theta = 100°$, and the opposite ordering with $\sigma_{SiSi} \rightarrow \sigma^*_{SiSi}$ excited state lower in energy by 9 kcal mol^{-1} at $\theta = 130°$. In *trans*-n-tetrasilane, the $\sigma_{SiSi} \rightarrow \sigma^*_{SiSi}$ excited state is predicted to be below the $\sigma_{SiSi} \rightarrow \pi^*_{SiH}$ excited state at all valence angles considered here and the separation between the two states increases from 1 to 22 kcal mol^{-1} as θ is increased from 100 to 130°. These results suggest that in the first $\sigma_{SiSi} \rightarrow \sigma^*_{SiSi}$ excited state, oligosilanes and most likely also the chromophoric segments of polysilanes have a tendency to become longer by increasing θ.

Previous INDO/S calculations[26] on parent and permethylated oligosilanes containing up to 20 silicon atoms are at variance with these results in that they predict the first $\sigma_{SiSi} \rightarrow \sigma^*_{SiSi}$ excitation energy to increase as θ increases to 115–120° and then to decrease at larger θ. Previous band gap calculations[37] for infinite chain all-*trans* parent polysilanes, based on a CNDO model Hamiltonian, also disagree. They predict the band gap between the valence and conduction bands to increase as θ is increased from 90 to nearly 120°. While we believe our calculations to be more reliable than the semiempirical ones, more detailed *ab initio* studies using larger basis sets and better model systems are necessary for a definitive understanding of the valence angle effects on excited states.

Experimental evidence available at this time for the $\sigma_{SiSi} \rightarrow \sigma^*_{SiSi}$ transition is certainly compatible with the *ab initio* prediction of a red shift with increasing θ, but is only indirect. Three observations may be relevant. (i) In room-temperature solution, poly(di-n-alkylsilanes) with bulkiest alkyl groups are known[38] to have red-shifted absorption peaks relative to those with smaller alkyl groups, and one may be tempted to ascribe this to increased SiSiSi valence angles θ, whose actual magnitudes are however not known, nor are the CSiC valence angles.

(ii) The distance between the next-nearest neighbouring silicon atoms measured by X-ray diffraction experiments[73,74] of stretch-oriented samples of neat polysilanes in their all-*trans* form increases as one proceeds gradually from poly(dimethylsilane) to poly(di-n-alkylsilane)s, with longer alkyl chains. Assuming the SiSi bond length to be constant in all these polysilanes,[22,54] the SiSiSi valence angles, θ, increase along the same series from 111.7 to about 120°. Simultaneously, the first absorption peak observed in the neat solid polymer shifts from about 340 nm for the shortest alkyls to over 370 nm for the longest. Again, this suggests that there is a correlation between θ and the excitation energy, since the electronic effects of the various alkyl groups must be nearly the same. The correlation does not appear to be linear, however, and changes in the size of the CSiC valence angle along the series may play a role as well.

(iii) Finally, one way to account for the red shift of the first intense transition of certain poly(di-n-alkylsilanes) in the all-*trans* ordered neat solid phase (~ 370 nm)[75] relative to the presumably also all-*trans* low-temperature solution phase (~ 350 nm),[76,77] is to postulate that it is due to a higher value of θ in the neat solid phase enforced by the need to accommodate the side chains.[29,37] Recently, the blue shift of the $\sigma_{SiSi} \rightarrow \sigma^*_{SiSi}$ transition of neat poly(di-n-hexylsilane) with increasing pressure[78,79] has been interpreted in terms of increasing disorder in the silicon backbone. It could also be due to a decrease in the SiSiSi valence angle, θ, with chain compression, since this should be a relatively soft distortion coordinate.

Effects of the SiSiSiSi *twist angle*

As the chain length increases beyond trisilane, conformational effects on the excited states can be explored. As outlined in the introduction, their understanding is critical for the current debate of the nature of the factors responsible for the incomplete delocalization of excitation in polysilane high polymers.

A series of SCF–CISD/DZ calculations were performed on the n-tetrasilane molecule at various

SiSiSiSi twist angles, ϕ, from 0 (planar eclipsed *cis* conformation) to 180° (planar *anti* conformation). For these calculations, the CI active space was restricted to the three highest SCF occupied orbital plus the 13 lowest virtual orbitals, i.e. the minimum basis virtual orbitals. The validity of this restricted CI was checked by performing CI calculations that included the three highest SCF occupied orbitals and all the virtual orbitals at $\phi = 180$, 60 and 0°. The restricted CI calculation was found to reproduce qualitatively the results of the larger CI calculations.

Figure 11 shows the energies of the ground and the first excited states of tetrasilane as a function of ϕ. The *anti* and the *gauche* conformations have nearly identical energy in the ground state and are separated by a 2.2 kcal mol^{-1} barrier for rigid rotation around the central SiSi bond. The top of this conformational barrier is located near a dihedral angle of *ca* 120°. For relaxed rotation, the barrier would be lower still, but its exact value is of limited interest in the present context. The potential energy curve, shown in Fig. 11, is rather flat in the ϕ interval from 60 (*gauche* form) to 0° (eclipsed *cis* form). Previous higher-level *ab initio* calculations for the ground state indicate that the *gauche* form is a local minimum and the eclipsed *cis* form is higher in energy by 1.3 kcal mol^{-1}.[20]

In contrast to the very flat ground state potential energy curve, the first excited singlet state exhibits a strong dependence on ϕ. Its energy minimum corresponds to the planar *anti* conformation ($\phi = 180°$). At this point, the first excited state is of

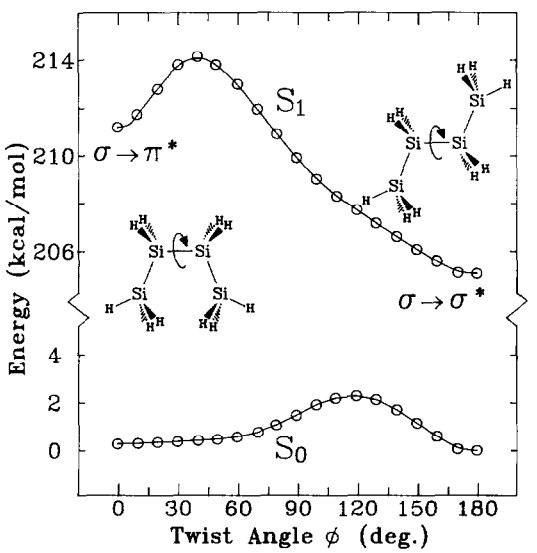

Fig. 11. Energies of the lowest two singlet states, S_0 and S_1, of n-tetrasilane as a function of the SiSiSiSi twist angle ϕ (restricted CISD/DZ, see text), relative to the ground state energy of *trans*-n-tetrasilane.

$\sigma_{SiSi} \rightarrow \sigma^*_{SiSi}$ (HOMO → LUMO) character. Twisting around the central SiSi bond causes a rapid increase in the excitation energy, which reaches a maximum at $\phi = 35°$, near the *gauche* conformation. Further increase in ϕ lowers the excitation energy again and a local minimum in the first excited state occurs at the *cis* conformation ($\phi = 0°$). At this geometry, the excited state is of $\sigma_{SiSi} \rightarrow \pi^*_{SiH}$ character. The presence of two apparent minima in the lowest excited singlet surface as a function of rigid rotation is due to an avoided crossing between the $\sigma_{SiSi} \rightarrow \sigma^*_{SiSi}$ and $\sigma_{SiSi} \rightarrow \pi^*_{SiH}$ excited states, which occurs near the dihedral angle of 35°. The avoidance is related to the loss of symmetry and of strict distinction between the σ and π symmetries during the conformational change. We have made no attempts to actually optimize the geometry of either minimum. In longer chain polysilanes the $\sigma_{SiSi} \rightarrow \pi^*_{SiH}$ excitation is not likely to be below the $\sigma_{SiSi} \rightarrow \sigma^*_{SiSi}$ excitation even at the *cis* conformation and most likely, these would show only one minimum in the first excited singlet state along the rigid rotation path, at the all-*trans* conformation ($\phi = 180°$).

If polysilane chromophoric segments behave in the same fashion as the model oligosilanes, there is a thermodynamic driving force towards the all-*trans* conformation in the lowest $\sigma_{SiSi} \rightarrow \sigma^*_{SiSi}$ singlet excited state and as a consequence, a tendency to convert the approximately *gauche* links terminating the chromophoric segment into *trans* links. Such a process would cause the all-*trans* segment lengths to increase and would appear similar to the process of actual transfer of the excitation energy to a longer segment by the Dexter or Förster mechanism.

The behaviour of the $\sigma_{SiSi} \rightarrow \sigma^*_{SiSi}$ excited state as a function of ϕ is readily rationalized by considering the limits of *anti*-periplanar and *syn*-periplanar orbital interactions.[25-28] The Sandorfy models C and H described earlier provide a qualitative description of the delocalized molecular orbitals of an all-*trans* polysilane chain. In these models, only the effects of vicinal and geminal interactions between the sp^3 hybrid orbitals are considered. Then, a rigid rotation around any Si—Si bond does not affect the σ_{SiSi} bonding and σ^*_{SiSi} antibonding backbone orbitals, because of the cylindrical symmetry of the σ bond. In order to understand qualitatively the effect of conformational changes on the energies of the backbone molecular orbitals one needs to include interactions between more distant non-bonded sp^3 hybrid orbitals, and these can be treated as weak perturbations to the Sandorfy models C and H. Like the vicinal and geminal interactions, a 1–3 interaction is still invariant to a rigid rotation around a Si—Si bond, but a 1–4 interaction is not (Fig. 12).

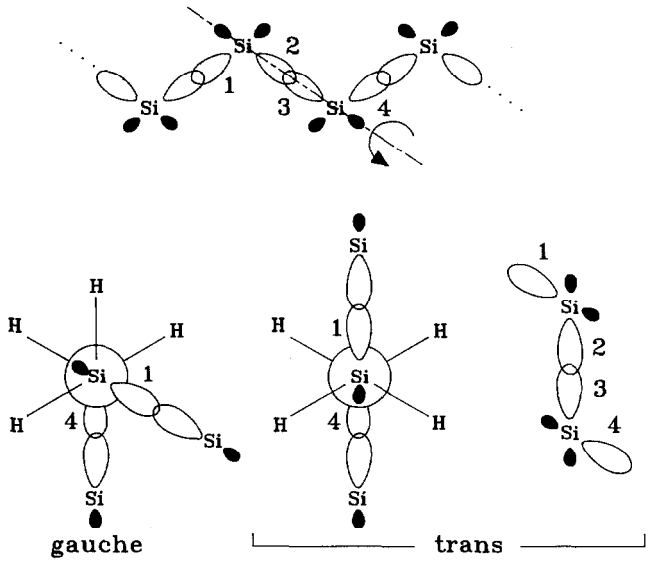

Fig. 12. Relative orientation of silicon sp^3 basis set orbitals 1–4 in *gauche* and *trans* conformations of an oligosilane chain.

In the *trans* planar arrangement of silicon atoms in polysilane, the 1–4 interaction of two sp^3 hybrid orbitals in the silicon chain is *anti*-periplanar in geometry and is dominated by the negative π-type overlap between their p components, which produces a positive resonance integral β_{14}. In the *cis* planar arrangement, π-type overlap between the now *syn*-periplanar orbitals 1 and 4 is positive and the resonance integral β_{14} is negative. It is clear from Fig. 12 that β_{14} must pass through zero partway along the twisting coordinate. When the resonance integrals, β_{14}, are introduced everywhere along the silicon chain, they will perturb the energies of the molecular orbitals in a way dictated by the nodal properties of the latter. Figure 2 shows that the HOMO coefficients have equal signs on every pair of hybrid orbitals that are disposed 1–4 relative to each other, so that a perturbation by a positive β_{14} will cause a destabilization to first-order in perturbation theory. To the contrary, in LUMO the coefficients on hybrid orbitals disposed 1–4 relative to each other differ in sign, so that a perturbation by a positive β_{14} will cause a stabilization.

Upon rotation along the SiSi bond away from the *anti*-periplanar geometry, β_{14} will decrease and go through zero, at which point it will have no destabilizing effect on HOMO nor stabilizing effect on LUMO, and eventually, as the *syn*-periplanar arrangement is reached, β_{14} will attain its most negative value and cause the maximum stabilization of the HOMO and destabilization of the LUMO. The net outcome of this behaviour will be a gradual reduction of the σ_{SiSi}–σ^*_{SiSi} (HOMO–LUMO) gap as one proceeds from the *cis* to the *trans* geometry. The computed reduction of the $\sigma_{SiSi} \rightarrow \sigma^*_{SiSi}$ excitation energy along this coordinate is thus readily accounted for. Since only the p-part of the hybrid orbital overlap is angle-dependent, the effects on HOMO should be larger than those on LUMO, which has considerable silicon 3*s* character, and this is indeed observed in the calculations.

Conclusions

Although only qualitative in nature, the results of the *ab initio* SCF–CISD calculations on simple oligosilanes ($n = 2$–5) lead to useful conclusions: (i) for oligosilanes that have more than about five silicon atoms, all Rydberg excitations will be higher in energy than the lowest valence excitations; (ii) for the planar all-*trans* parent oligosilanes with only a few silicon atoms the first valence excited singlet state is of $\sigma_{SiSi} \rightarrow \pi^*_{SiH}$ nature, and as the silicon chain is extended, a $\sigma_{SiSi} \rightarrow \sigma^*_{SiSi}$ (HOMO → LUMO) state becomes the lowest; (iii) inclusion of silicon *d* orbitals in the basis set has very little influence on the nature of the calculated low-lying excited states; (iv) the lowest excited state with a large two-photon absorption cross-section is well represented by the SHOMO → LUMO $\sigma_{SiSi} \rightarrow \sigma^*_{SiSi}$ configuration and has essentially no doubly excited character, with the HOMO^2 → LUMO^2 $\sigma^2_{SiSi} \rightarrow \sigma^{*2}_{SiSi}$ configuration entering only into much higher energy states; (v) methylation of oligosilanes reduces the HOMO–LUMO gap by hyperconjugative destabilization of the σ_{SiSi} HOMO by the methyl donor orbitals and decreases the $\sigma_{SiSi} \rightarrow \sigma^*_{SiSi}$ excitation energy; (vi) an increase in the SiSiSi valence angle causes a red shift

in the $\sigma_{SiSi} \rightarrow \sigma^*_{SiSi}$ excitation energy; (vii) the *trans* planar conformation leads to lower $\sigma_{SiSi} \rightarrow \sigma^*_{SiSi}$ excitation energies than the *cis* planar conformation; and (viii) conformational changes towards the all-*trans* conformation and an increase in the SiSiSi valence angle are expected upon electronic excitation into the lowest $\sigma_{SiSi} \rightarrow \sigma^*_{SiSi}$ excited state.

Simple rationalization has been provided for several of these results. In particular, the difference between the nature of the wave functions of the states accessible by two-photon absorption in oligosilanes and in polyenes has been attributed to the absence of even only approximate alternant pairing in the former, and the conformational dependence of the excitation energies has been attributed to *anti*-periplanar secondary interactions in the *trans* form and *syn*-periplanar ones in the *cis* form.

The overall agreement between the current *ab initio* calculations and the semiempirical calculations reported in the literature is reasonably good. The absolute excitation energies obtained from the *ab initio* calculations do not agree well with the experimental ones. The agreement can presumably be improved in the future by using optimized geometries, better basis sets, MCSCF methods to optimize the excited state orbitals and by multi-reference CI procedures that include higher order excitations.

Acknowledgements—This work was supported by the Air Force Office of Scientific Research (Grant 87-0001) and by a grant of computer time on a CRAY X-MP/24 by The University of Texas at Austin. We are grateful to Professor Mark S. Gordon and Dr Mike Schmidt for supplying us with the latest versions of the GAMESS program, to Dr John Downing for implementing the program, and to Dr A. J. Lovinger for the communication of unpublished results.

REFERENCES

1. R. West, *J. Organomet. Chem.* 1986, **300**, 327.
2. R. D. Miller and J. Michl, *Chem. Rev.* 1989, **89**, 1359.
3. D. C. Hofer, K. Jain and R. D. Miller, *IBM Tech. Discl. Bull.* 1984, **26**, 5683; R. D. Miller and R. Sooriyakumaran, *J. Polym. Sci., Polym. Lett. Edn* 1987, **25**, 321.
4. R. G. Kepler, J. M. Zeigler, L. A. Harrah and S. R. Kurtz, *Phys. Rev. B* 1987, **35**, 2818; M. Fujino, *Chem. Phys. Lett.* 1987, **136**, 451.
5. R. West, A. R. Wolff and D. J. Peterson, *J. Radiat. Curing* 1986, **13**, 35; A. R. Wolff and R. West, *Appl. Organomet. Chem.* 1987, **1**, 7.
6. F. Kajzar, J. Messier and C. Rosilio, *J. Appl. Phys.* 1986, **60**, 3040; J. C. Baumert, G. C. Bjorklund, D. H. Jundt, M. C. Jurich, H. Looser, R. D. Miller, J. Rabolt, R. Sooriyakumaran, J. D. Swalen and R. J. Twieg, *Appl. Phys. Lett.* 1988, **53**, 1147.
7. H. Bock and W. Ensslin, *Angew. Chem., Int. Edn Engl.* 1971, **10**, 404.
8. H. Bock, W. Ensslin, F. Fehér and R. Freund, *J. Am. Chem. Soc.* 1976, **98**, 668.
9. P. N. Dyachkov, N. V. Ioslovich and A. A. Levin, *Theoret. Chim. Acta* 1975, **40**, 237.
10. P. P. Shorygin, V. A. Petukhov, O. M. Nefedov, S. P. Kolesnikov and V. I. Shiryaev, *Teor. Eksp. Khim., Akad. Nauk Ukr. SSR* 1966, **2**, 190; *Chem. Abstr.* 1966, **65**, 14660f.
11. A. Herman, B. Dreczewski and W. Wojnowski, *Chem. Phys.* 1985, **98**, 475.
12. A. Herman, B. Dreczewski and W. Wojnowski, *J. Organomet. Chem.* 1983, **251**, 7.
13. A. L. Allred, C. A. Ernst and M. A. Ratner, in *Homoatomic Rings, Chains and Macromolecules of Main-Group Elements* (Edited by A. L. Rhingold), p. 307. Elsevier, New York (1977).
14. W. G. Boberski and A. L. Allred, *J. Organomet. Chem.* 1975, **88**, 65.
15. C. G. Pitt, M. M. Bursey and P. F. Rogerson, *J. Am. Chem. Soc.* 1970, **92**, 519.
16. W. S. Verwoerd, *J. Comput. Chem.* 1982, **3**, 445.
17. E. A. Halevi, G. Winkelhofer, M. Meisl and R. Janoschek, *J. Organomet. Chem.* 1985, **294**, 151.
18. R. W. Bigelow and K. M. McGrane, *J. Polym. Sci., Polym. Phys. Ed.* 1986, **24**, 1233.
19. J. W. Mintmire and J. V. Ortiz, *Macromolecules* 1988, **21**, 1189.
20. J. V. Ortiz and J. W. Mintmire, *J. Am. Chem. Soc.* 1988, **110**, 4522.
21. C. Battistoni, A. Lapiccirella, E. Semprini, F. Stefani and N. Tomassini, *Nuovo Cimento Soc. Ital. Fis.* 1984, **3d**, 663 (Engl.).
22. J. T. Nelson and W. J. Pietro, *J. Phys. Chem.* 1988, **92**, 1365.
23. R. W. Bigelow, *Chem. Phys. Lett.* 1986, **126**, 63.
24. R. W. Bigelow, *Organometallics* 1986, **5**, 1502.
25. K. A. Klingensmith, J. W. Downing, R. D. Miller and J. Michl, *J. Am. Chem. Soc.* 1986, **108**, 7438.
26. J. Michl, J. W. Downing, T. Karatsu, A. J. McKinley, G. Poggi, G. M. Wallraff, R. Sooriyakumaran and R. D. Miller, *Pure Appl. Chem.* 1988, **60**, 959.
27. J. Michl, J. W. Downing, T. Karatsu, K. A. Klingensmith, G. M. Wallraff and R. D. Miller, in *Inorganic and Organometallic Polymers*, ACS Symposium Series 360 (Edited by M. Zeldin, K. J. Wynne and H. R. Allcock), Ch. 5. American Chemical Society, Washington, DC (1988).
28. J. Michl and V. Balaji, in *Computational Advances in Organic Chemistry* (Edited by C. Ogretir and I. C. Csizamadia), p. 323. NATO-ASI Series C, Kluwer Academic Publishers, Dordrecht, Holland (1991).
29. P. R. Surjan, R. A. Poirier and H. Kuzmany, *Solid State Sci.* 1987, **76**, 314.
30. Z. G. Soos and G. W. Hayden, *Chem. Phys.* 1990, **143**, 199.
31. Z. G. Soos, G. W. Hayden and P. C. M. McWilliams, *Polym. Prepr.* 1990, **31**, 286.

32. K. Takeda, N. Matsumoto and M. Fukuchi, *Phys. Rev. B* 1984, **30**, 5871.
33. K. Takeda, M. Fujino, K. Seki and H. Inokuchi, *Phys. Rev. B* 1987, **36**, 8129.
34. K. Takeda, H. Teramae and N. Matsumoto, *J. Am. Chem. Soc.* 1986, **108**, 8186.
35. H. Teramae, T. Yamabe and A. Imamura, *Theoret. Chim. Acta (Berl.)* 1983, **64**, 1.
36. J. W. Mintmire, *Phys. Rev. B* 1989, **39**, 13350.
37. K. Takeda and N. Matsumoto, *J. Phys. C.* 1985, **18**, 6121.
38. L. A. Harrah and J. M. Zeigler, *Macromolecules* 1987, **20**, 601.
39. Y. R. Kim, M. Lee, J. R. G. Thorne, R. M. Hochstrasser and J. M. Zeigler, *Chem. Phys. Lett.* 1988, **145**, 75.
40. J. R. G. Thorne, R. M. Hochstrasser and J. M. Zeigler, *J. Phys. Chem.* 1988, **92**, 4275.
41. L. A. Harrah and J. M. Zeigler, in *Photophysics of Polymers*, ACS Symposium Series 358 (Edited by C. E. Hoyle and J. M. Torkelson), Ch. 35. American Chemical Society, Washington, DC (1987).
42. K. S. Schweizer, L. A. Harrah and J. M. Zeigler, in *Silicon-based Polymer Science*, Adv. Chem. Book Ser. 224 (Edited by J. M. Zeigler and F. W. G. Fearon), p. 379. American Chemical Society, Washington, DC (1990).
43. J. R. G. Thorne, Y. Ohsako, J. M. Zeigler and R. M. Hochstrasser, *Chem. Phys. Lett.* 1989, **162**, 455.
44. G. Wenz, M. A. Muller, M. Schmidt and G. Wegner, *Macromolecules* 1984, **17**, 837.
45. A. Tilgner, J. P. Pique, H. P. Trommsdorff, J. M. Zeigler and R. M. Hochstrasser, *Polym. Prepr.* 1990, **31**, 244.
46. V. R. McCrary, F. Sette, C. T. Chen, A. J. Lovinger, M. B. Robin, J. Stohr and J. M. Zeigler, *J. Chem. Phys.* 1988, **88**, 5925.
47. R. S. Grev and H. F. Schaefer III, *J. Am. Chem. Soc.* 1987, **109**, 6569.
48. B. Kirste, R. West and H. Kurreck, *J. Am. Chem. Soc.* 1985, **107**, 3013.
49. E.g., R. Hoffmann, A. Imamura and W. J. Hehre, *J. Am. Chem. Soc.* 1968, **90**, 1499; S. David, O. Eisenstein, W. J. Hehre, L. Salem and R. Hoffmann, *J. Am. Chem. Soc.* 1973, **95**, 3807.
50. W. J. Welsh, J. R. Damewood Jr. and R. West, *Macromolecules* 1989, **22**, 2947.
51. S. Huzinaga, J. Andzelm, M. Klobukowski, E. Radzio-Andzelm, Y. Sakai and H. Tatewaki, *Gaussian Basis Sets for Molecular Calculations*. Elsevier, Amsterdam (1984).
52. M. S. Gordon, *Chem. Phys. Lett.* 1980, **76**, 163.
53. T. H. Dunning and P. J. Hay, in *Methods in Electronic Structure Theory* (Edited by H. F. Schaefer III), Vol. 3, p. 1. Plenum Press, New York (1977).
54. E. Lukevics, O. Pudova and R. Sturkovich, *Molecular Structure of Organosilicon Compounds*. Ellis Horwood, Chichester (1989).
55. M. W. Schmidt, J. A. Boatz, K. K. Baldridge, J. H. Jensen, S. Koseki, M. S. Gordon, K. A. Nguyen, T. L. Windus, S. T. Elbert and B. Lam, *GAMESS: General Atomic and Molecular Electronic Structure System; QCPE Bulletin* 1990, **10**; M. Dupuis, D. Spangler and J. J. Wendoloski, *National Resource for Computations in Chemistry*, Program QG01 (1980).
56. C. Sandorfy, *Can. J. Chem.* 1955, **33**, 1337.
57. Y. Apeloig, in *The Chemistry of Organic Silicon Compounds* (Edited by S. Patai and Z. Rappoport), Ch. 2. John Wiley, New York (1989).
58. J. R. Durig and J. S. Church, *J. Chem. Phys.* 1980, **73**, 4784; B. Beagley, A. R. Conrad, J. M. Freeman, J. J. Mohaghan, B. G. Norton and G. C. Holywell, *J. Molec. Struct.* 1972, **11**, 371.
59. U. Itoh, Y. Toyoshima and H. Onuki, *J. Chem. Phys.* 1986, **85**, 4867.
60. R. Freund, PhD thesis. University of Cologne (1973).
61. M. B. Robin, *Higher Excited States of Polyatomic Molecules*, Vol. 1. Academic Press, New York (1974).
62. P. Trefonas III, R. West, R. D. Miller and D. Hofer, *J. Polym. Sci., Polym. Lett. Ed.* 1983, **21**, 823.
63. T. Karatsu, R. D. Miller, R. Sooriyakumaran and J. Michl, *J. Am. Chem. Soc.* 1989, **111**, 1140.
64. Y.-P. Sun, R. D. Miller, R. Sooriyakumaran and J. Michl, *J. Inorg. Organomet. Polym.* 1991, **1**, 3.
65. J. R. G. Thorne, S. T. Repinex, S. A. Abrash, J. M. Zeigler and R. M. Hochstrasser, *Chem. Phys.* 1990, **146**, 315.
66. B. S. Hudson, B. E. Kohler and K. Schulten, in *Excited States* (Edited by E. C. Lim), Vol. 6, p. 1. Academic Press, New York (1982).
67. R. Pariser, *J. Chem. Phys.* 1956, **24**, 250; A. D. McLachlan, *Molec. Phys.* 1959, **2**, 271; 1961, **4**, 49; J. Koutecký, *J. Chem. Phys.* 1966, **44**, 3702; 1967, **47**, 1501.
68. B. G. Ramsey, *J. Organomet. Chem.* 1974, **67**, C67; E. A. Halevi, G. Winkelhofer, M. Meisl and R. Janoschek, *J. Organomet. Chem.* 1985, **294**, 151.
69. A. Herman, *Chem. Phys.* 1988, **122**, 53.
70. K. Seki, T. Mori, H. Inokuchi and K. Murano, *Bull. Chem. Soc. Japan* 1988, **61**, 351.
71. C. G. Pitt, *J. Am. Chem. Soc.* 1969, **91**, 6613.
72. G. Poggi, J. W. Downing and J. Michl, unpublished results.
73. A. J. Lovinger, D. D. Davis, F. C. Schilling, F. J. Padden Jr., F. A. Bovey and J. M. Zeigler, *Macromolecules* 1991, **24**, 132.
74. J. F. Rabolt, D. Hofer, R. D. Miller and G. N. Fickes, *Macromolecules* 1986, **19**, 611.
75. R. D. Miller, D. Hofer, J. Rabolt and G. N. Fickes, *J. Am. Chem. Soc.* 1985, **107**, 2172.
76. P. Trefonas III, J. R. Damewood Jr., R. West and R. D. Miller, *Organometallics* 1985, **4**, 1318.
77. L. A. Harrah and J. M. Zeigler, *J. Polym. Sci., Polym. Lett. Ed.* 1985, **23**, 209.
78. K. Song, H. Kuzmany, G. M. Wallraff, R. D. Miller and J. F. Rabolt, *Macromolecules* 1990, **23**, 3870.
79. J. F. Rabolt, K. Song, H. Kuzmany, R. Sooriyakumaran, G. Fickes and R. D. Miller, *Polym. Prepr.* 1990, **31**, 262.

Polyhedron Vol. 10, No. 11, pp. 1285–1297, 1991
Printed in Great Britain

0277-5387/91 $3.00+.00
Pergamon Press plc

ELECTRON PROPAGATOR THEORY OF BONDING IN SATURATED SILICON CHAINS

J. V. ORTIZ

Department of Chemistry, University of New Mexico, Albuquerque, NM 87131, U.S.A.

Abstract—*Ab initio* electron propagator calculations produce accurate electron binding energies and Feynman–Dyson amplitudes for oligosilanes as a function of bond angle and dihedral angle distortions. Ground state energies are also calculated for equilibrium and distorted structures. While the ground state energies are fairly insensitive to the distortions, changes in electron binding energies can be much larger. Examination of the Feynman–Dyson amplitudes leads to an electronic structure model that is based on phase relationships between bond orbital and antibond orbitals that are localized in Si—Si bond regions. This model is successful in explaining the calculated shifts in electron binding energies and changes in polymer absorption spectra.

INTRODUCTION

In spite of their lack of multiple bonds, lone pairs or *d*-electrons, polysilanes have large oscillator strengths in the near-UV and a rich chemistry in ground and excited states.[1–4] A variety of new applications, including self-developing photoresists,[5] ceramic precursors[6] and photoconducting polymers,[7] has awakened more widespread interest in these polymers.[8] These potentialities are grounded in the electronic structures[9–14] of saturated silicon-containing backbones and how these are influenced by steric effects that are under the control of substituent and environmental factors. To analyse these disparate causes of various electronic properties, *ab initio* calculations on the simplest species, small oligosilanes, are undertaken. These calculations should include no prejudicial assumptions about the locations or types of bonds that may be present. At the same time, the results of the calculations should be produced in a form that lends itself to deep, yet succinct analysis. Electron propagator theory fulfils both of these requirements admirably, for in addition to generating accurate energetic information, it also rigorously produces a one-electron picture that incorporates the effects of electron correlation. Calculations on the electron binding energies of Si_2H_6 will show the origin of a model of electronic structure built on localized bond and antibond functions. As a result of calculations on Si_3H_8, the influence of bond angle changes will be determined and insights into how the localized functions are combined in larger oligomers will be gained. The large influence that dihedral angles can have on electronic structure will be illustrated in calculations on Si_4H_{10} and will show the importance of non-neighbour interactions. Extrapolations of these results will explain how polymer electronic structure can be related to concepts developed through precise work on small oligomers.

METHODS

Gaussian 88[15] is used in the Hartree–Fock and integral transformation steps, and EPT90[16] is used for the propagator calculations.

Structures optimized at the Hartree–Fock double ζ plus polarization level[17,18] are used in calculations with an effective core potential (which excludes the Si 1*s*, 2*s* and 2*p* electrons), its double ζ basis,[19] and a set of *d* functions ($\alpha_d = 0.45$) on each silicon, as well as a double ζ hydrogen basis.[20] This treatment is adequate for the calculation of ionization energies. Electron affinities of small oligomers require diffuse functions. However, the chief purpose of these calculations is the examination of trends in the limit of an infinitely large polymer, where diffuse functions have negligible importance in the conduction band. Therefore, electron affinity calculations are performed with and without a set of diffuse silicon ($\alpha_s = 0.028$, $\alpha_p = 0.026$) and diffuse hydrogen ($\alpha_s = 0.011$) functions. At the geometries under consideration, cor-

relation corrections to the ground state energy are calculated with second-order many-body perturbation theory.[21]

Electron propagator theory[22] is used to generate electron binding energies and corresponding Feynman–Dyson amplitudes. The former, negatives of ionization energies and electron affinities, are obtained with relaxation and correlation corrections that are absent from Koopmans' theorem[23] predictions, the negatives of canonical orbital energies. For every electron binding energy, there is a Feynman–Dyson amplitude (FDA):

$$\int \Psi^*_{N-1}(2,3,4,\ldots,N)\Psi_N(1,2,3,\ldots,N)\, d(2)d(3)d(4)\ldots d(N) = \phi^{FDA}(1),$$

for ionization energies or

$$\int \Psi^*_N(2,3,4,\ldots,N+1)\Psi_{N+1}(1,2,3,\ldots,N+1)\, d(2)d(3)d(4)\ldots d(N+1) = \phi^{FDA}(1),$$

for electron affinities. Because it is a function of the coordinates of one electron, the FDA is an orbital, or more strictly speaking, a spin-orbital. Phase relationships between localized functions and the extent of delocalization are revealed in FDA plots. Unlike representations of total densities or localized molecular orbitals, plots of the FDA show how the electronic structure of the molecule changes upon removing or adding an electron, for they depend on the initial state, Ψ_N, and on the final states, $\Psi_{N\pm1}$. (Total density and localized molecular orbital plots contain information about Ψ_N only.) FDAs have the advantages generally associated with delocalized, canonical molecular orbitals for describing spectra, but they are more general in that they incorporate the effects of electron correlation. Each electron binding energy corresponds to a Feynman–Dyson amplitude in the same way that an energy corresponds to a canonical molecular orbital in Koopmans' theorem. Hartree–Fock molecular orbital theory constitutes the zeroth-order reference for the electron propagator calculations. The present electron propagator calculations utilize the full second-order approximation.[24]

RESULTS AND DISCUSSION

Reliability of the methods

Previous all-electron calculations with larger basis sets and extensive explorations of correlation effects have shown that the diagonal and second-order approximations yield accurate electron binding energies for Si_2H_6, Si_3H_8 and Si_4H_{10} in their equilibrium, ground state geometries.[17,18] For example, Table 1 shows results of a previous study[17] of the ionization energies of Si_2H_6 with various basis sets and propagator approximations. The methods used in this work are equally accurate. As will be discussed below, for Si_3H_8 there are two cationic final states where an electron has been removed chiefly from Si—Si bonding regions. Comparison of the previous calculations[17] with results of this paper (Table 2) shows close agreement among all propa-

Table 1. Si_2H_6 ionization energies (eV)

Method	$^2A_{1g}$	^2E_g	^2E_u
All-electron, Koopmans' theorem, 6–31*G*(2*d*,*p*)	10.97	12.87	13.61
All-electron, Koopmans' theorem, 6–31*G*(*d*)	10.99	12.88	13.62
All-electron, diagonal second-order, 6–31*G*(2*d*,*p*)	10.36	12.13	12.86
All-electron, diagonal second-order, 6–31*G*(*d*)	10.30	11.99	12.74
All-electron, diagonal third-order, 6–31*G*(2*d*,*p*)	10.46	12.15	12.89
All electron, diagonal third-order, 6–31*G*(*d*)	10.26	11.92	12.68
Photoelectron spectroscopy	10.53	11.9, 12.1	12.73, 13.08
This work	10.59	12.10	12.86

Table 2. Si_3H_8 ionization energies (eV)

Method	$^2B_2$	$^2A_1$
All-electron, Koopmans' theorem, 6–31*G*(*d*)	10.45	11.48
All-electron, diagonal second-order, 6–31*G*(*d*)	9.69	10.57
All-electron, diagonal third-order, 6–31*G*(*d*)	9.70	10.57
Photoelectron spectroscopy	9.87	10.72
This work	9.91	10.71

Table 3. Si_2H_6 electron binding energies (eV)

D_{3d}		C_{2h}	
$Si_2H_6^+ {}^2E_u$	−12.86	$Si_2H_6^+ {}^2A_u$	−12.86
		$Si_2H_6^+ {}^2B_u$	−12.86
$Si_2H_6^+ {}^2E_g$	−12.10	$Si_2H_6^+ {}^2B_g$	−12.10
		$Si_2H_6^+ {}^2A_g$	−12.09
$Si_2H_6^+ {}^2A_{1g}$	−10.59	$Si_2H_6^+ {}^2A_g$	−10.60
$Si_2H_6^- {}^2E_u$	3.32	$Si_2H_6^- {}^2B_u$	3.03
		$Si_2H_6^- {}^2A_u$	3.25
$Si_2H_6^- {}^2A_{2u}$	3.34	$Si_2H_6^- {}^2B_u$	3.31

gator treatments and photoelectron spectra.[25] All of the predicted electron affinities are negative: the extra electron is not bound. When diffuse functions are added to the basis, this finding is not changed. The additional functions contribute chiefly to diffuse FDAs with negative electron affinities. With increasing chain length, the ordinary valence functions will form FDAs that evolve into the conduction band of the polymer.[10,11] The diffuse functions will continue to contribute to unbound levels embedded in the continuum.

Si_2H_6

In addition to the ionization energies obtained for the equilibrium, D_{3d} geometry of Si_2H_6, propagator results for electron binding energies at a distorted, C_{2h} structure are displayed in Table 3. Note that ionization energies and electron affinities are considered. (A bound final state corresponds to a negative electron binding energy, i.e. a positive ionization energy or electron affinity.) In the distorted structure, two Si—H bonds that are *anti* to each other are elongated by 0.1 Å in order to imitate an Si_2H_4 fragment embedded in a polysilane chain. Destruction of the three-fold axis of symmetry implies breaking the degeneracy of the e_g and e_u FDAs. Changes in the ionization energies are small compared with some of the electron affinity shifts.

Examination of the FDAs reveals the importance of symmetry in understanding how fragments evolve into oligomers and polymers. For the higher cationic states, FDAs with e_g and e_u symmetry are concerned with Si—H bonding and display constructive interference of Si p functions perpendicular to the C_3 axis with neighbouring H s functions. In the e_u case, the Si ps have a π bonding relationship and in the e_g case, they have a π antibonding relationship. These final states are substantially altered when hydrogens are removed in favour of organic substituents.

Of greater interest are the FDAs that pertain to the silicon backbone regions. In the D_{3d} structure, the FDA for the lowest cationic final state is easily described as a σ bond orbital between two silicons. In Fig. 1, contours of this FDA are shown, where solid (dotted) lines are positive (negative) contours and dashed lines designate nodes. Contours are drawn in intervals of 0.015. Nuclear positions are indicated by squares. Note the accumulation of oval contours in the centre of the yz plane, between the two silicon nuclei. Nodes intersect the silicon nuclei and suggest the importance of p_z functions. Contributions from hydrogen s functions, although clearly in evidence from the extrema close to the hydrogen nuclei, are relatively minor. When the symmetry of the molecule is reduced to C_{2h}, this FDA remains virtually the same.

Consideration of the electron affinity FDAs with e_u symmetry shows them to be the Si—H antibonding counterparts of the ionization energy FDAs of the

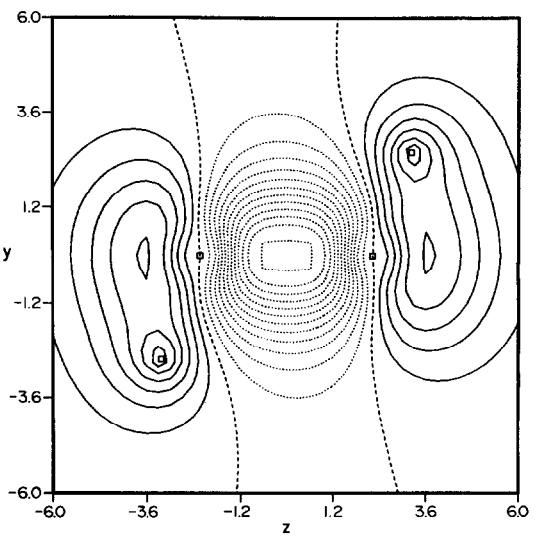

Fig. 1. (D_{3d}) $Si_2H_6^+ {}^2A_{1g}$ Feynman–Dyson amplitude.

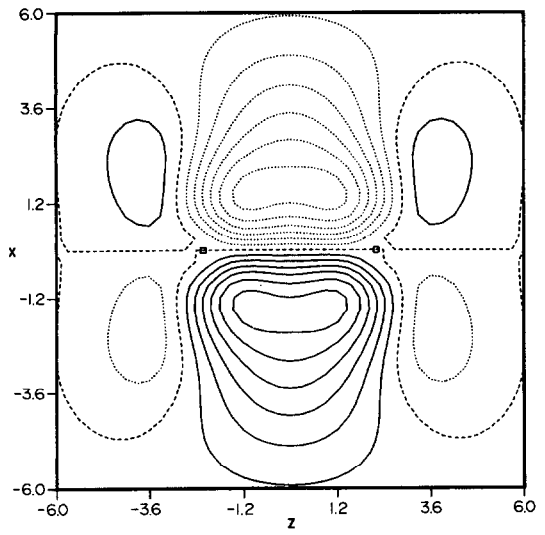

Fig. 2. (D_{3d}) $Si_2H_6^- {}^2E_u$ Feynman–Dyson amplitude.

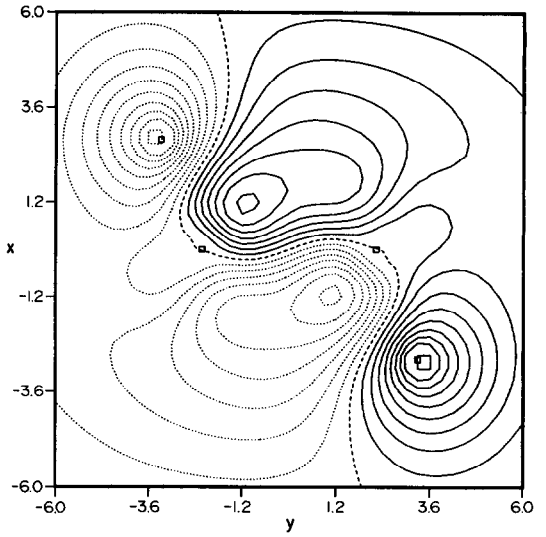

Fig. 4. (C_{2h}) $Si_2H_6^- {}^2B_u$ Feynman–Dyson amplitude.

same symmetry discussed above. Figure 2, a contour plot of an FDA in the xz plane, has nodes along the z axis and extrema in the Si—Si bond region characteristic of a π bonding relationship. Note the presence of four contours surrounded by nodes near values of z corresponding to hydrogen nuclear positions. This suggests an antibonding relationship between the silicons and hydrogens.

Within a trivial amount of energy, 0.02 eV, there is another unbound electron affinity whose FDA has a_{2u} symmetry. Examination of Fig. 3 discloses a wealth of contours in the Si—Si bond region again, but this time with a central node that denotes a σ antibonding relationship. Much of the electron density is therefore pushed to the exterior regions of the molecule. Nodes appear in the vicinity of the hydrogen nuclei.

At this point, it should be re-emphasized that the electron affinity FDAs do not correspond to bound anions. Even when diffuse functions are added to the basis, the largest electron affinity is -1.2 eV. Feynman–Dyson amplitudes for these additional anionic states are non-bonding and are spread over regions remote from the bonds. States such as these are imbedded in the continuum of electron–molecule scattering states.

Breaking the three-fold axis of symmetry in Si_2H_6 allows a_{2u} and e_u FDAs to mix. In the latter degenerate set, one member in C_{2h} symmetry is symmetric with respect to the remaining plane of symmetry and the other is antisymmetric. Group theoretical arguments by themselves cannot tell to what extent mixing takes place between a_{2u} and the symmetric member of the e_u set. From Fig. 4, however, it is evident that the rearrangements are extensive. A lone nodal contour threads its way between the various nuclei in the same plane as that of Fig. 3. (Axis labels have been changed for the lower symmetry calculation, but this is of no consequence.) This FDA, like the FDA in Fig. 2, exhibits much Si—Si π character, but the node connecting the silicons is not straight. It has curves because of contamination from the FDA of Fig. 3. Such interaction produces the local maxima above and to the right of the left-hand silicon nucleus and below and to the left of the right-hand silicon nucleus. Two lobes with opposite sign curl around each other in the Si—Si bond region in resemblance to the Yin–Yang symbol found in the centre of the

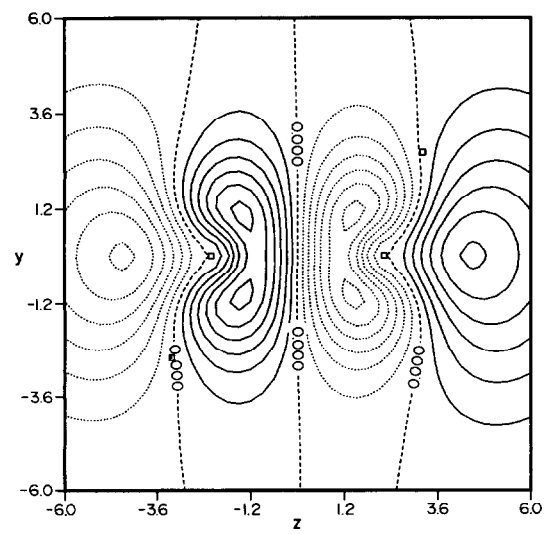

Fig. 3. (D_{3d}) $Si_2H_6^- {}^2A_{2u}$ Feynman–Dyson amplitude.

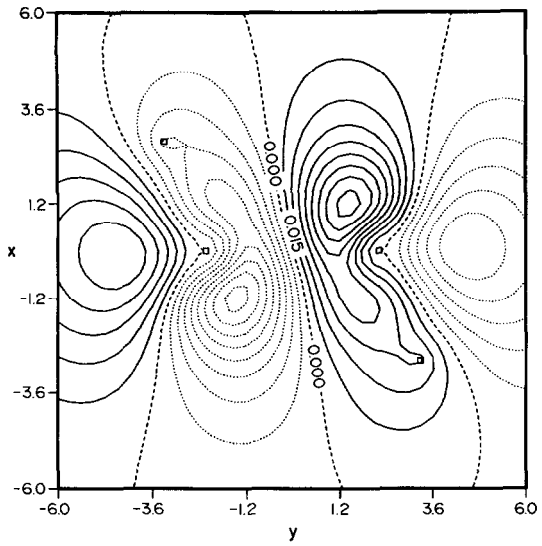

Fig. 5. (C_{2h}) $Si_2H_6^- {}^2B_u$ Feynman–Dyson amplitude.

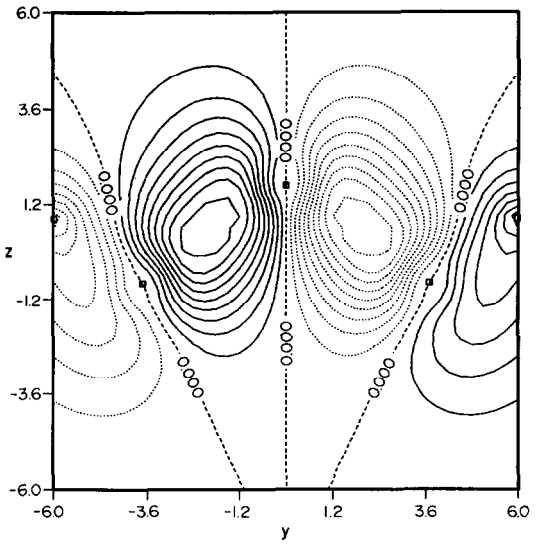

Fig. 7. $Si_3H_8^+ {}^2B_2$ Feynman–Dyson amplitude.

South Korean flag. Such a device has π bonding character and σ antibonding character at once. Because of the presence of the elongated Si—H distances, there is a large deposit of electron density near the two hydrogen nuclei. As shall be seen below, this is an artefact that is obliterated as soon as longer chains are considered.

If two D_{3d} FDAs are mixing, then there must be a remaining combination. This is shown in Fig. 5, where σ antibonding has greater prominence than π bonding. Now the two lobes of Yin–Yang have turned their backs on each other, producing two paisley patterns. Instead of tracing a path perpendicular to this axis, the central node now inclines somewhat because of the π bonding contribution that has been introduced.

These motifs in the broken-symmetry electron affinity FDAs, Yin–Yang and two paisleys, will recur in longer oligomers. These are the antibonding counterparts of the oval bond orbital that occurs in the FDA of the lowest ionization energy.

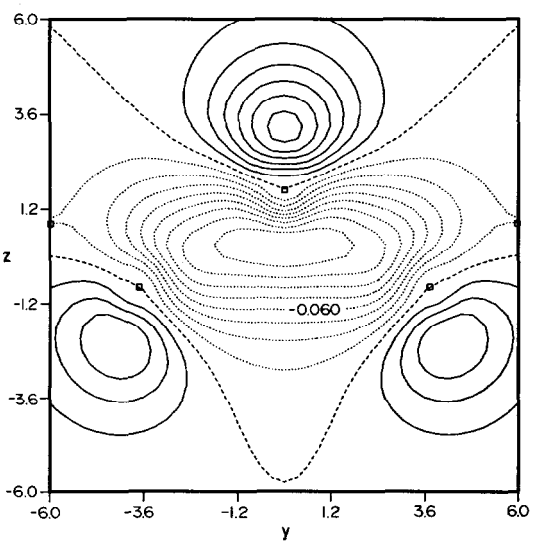

Fig. 6. $Si_3H_8^+ {}^2A_1$ Feynman–Dyson amplitude.

Si_3H_8

If one adopts the bond orbitals as an approximate localized basis for constructing the ionization energy FDAs, then for Si_3H_8 there should be two FDAs of this type. Two bond orbitals in the equilibrium, C_{2v} geometry of Si_3H_8 are related by symmetry and therefore symmetric and antisymmetric combinations are formed. In the former case, constructive interference near the central silicon takes place. Ample confirmation of these suppositions is found in Fig. 6. Negative contours concentrate near the centre of the y axis. An even more obvious success obtains in Fig. 7, where two bond orbitals with opposite signs interfere destructively in the xz plane, as mandated by the b_2 irreducible representation of the FDA.

Because the Si_2H_6 calculations on electron affinity FDAs showed two types of Si—Si antibond orbitals, there is some ambiguity about how the corresponding FDAs of Si_3H_8 should be constructed. Returning to Figs 4 and 5, one notices an important difference between the extrema in the Si—Si bond regions. These extrema are closer to the terminal hydrogens in Fig. 4 than they are in Fig. 5. In the latter FDA, the terminal hydrogen nuclei are within the tails of the paisley lobes. In Si_3H_8, symmetry

projection of these Si—Si antibonding functions produces a total of four combinations. Symmetric combination of two Yin–Yang patterns produces constructive interference in the vicinity of the z axis and three local extrema in the Si—Si bond regions. This combination should be lower in energy than the antisymmetric combination, where destructive interference near the z axis should lead to an antibonding relationship between the Si—Si antibond functions. Two combinations of the paisley patterns can likewise be imagined. A symmetric combination implies constructive interference between the tails of two paisley lobes near the central silicon and along the y axis. For the antisymmetric combination, there is destructive interference between these tails.

Calculations determine the energy ordering and mixings pertaining to these combinations. The qualitative arguments made above are confirmed to a great extent. In the FDA of the largest electron affinity, one sees (Fig. 8) that the most stable combination with a_1 symmetry is built from Yin–Yang lobes instead of paisley patterns. This is reasonable when one considers that in the former case, constructive interference takes place between the Si—Si local extrema near the central silicon, while in the latter case, constructive interference only involves the narrow tails of the paisley lobes. There follows an anionic $^2B_1$ state whose FDA is built from Si—H antibonding combinations of hydrogen s and silicon p_x orbitals; a π bonding relationship prevails among the silicons. In the next FDA, which has b_2 symmetry, interference of paisley patterns is clearly evident (Fig. 9). Note the tails of the paisley lobes that reach over to the terminal hydrogen nuclei.

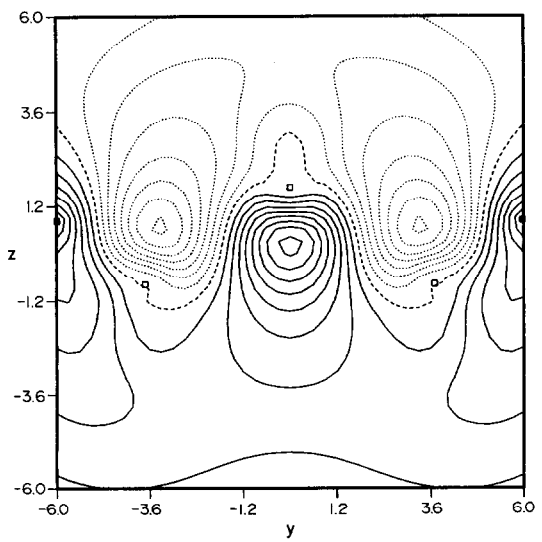

Fig. 8. $Si_3H_8^-$ $^2A_1$ Feynman–Dyson amplitude.

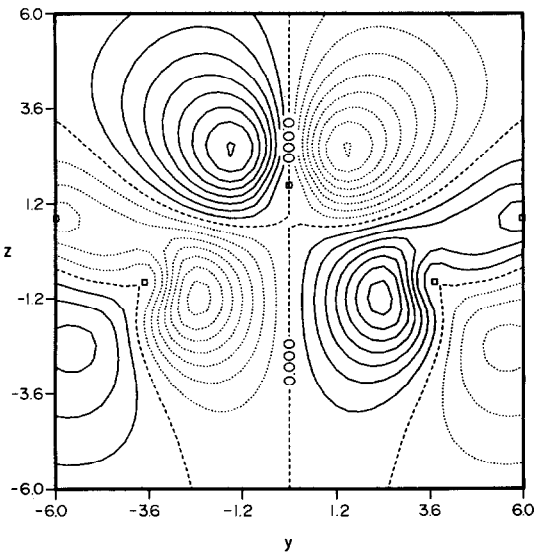

Fig. 9. $Si_3H_8^-$ $^2B_2$ Feynman–Dyson amplitude.

One does not see the tails of the other two paisley lobes because they have destructively interfered with each other near the z axis. Following the same reasoning used for Fig. 8, the lower b_2 combination has less destabilization from destructive interference near the z axis because tails of paisley lobes are involved instead of the thick parts of the Yin–Yang patterns.

Addition of diffuse functions to the basis again produces more anionic states corresponding to negative electron affinities. For the lowest of the new states the electron affinity, -1.1 eV, is nearly the same as its counterpart for the Si_2H_6 case, -1.2 eV. Feynman–Dyson amplitudes for these states are essentially diffuse functions that have been orthogonalized to the valence basis functions.

Si_3H_8 is the simplest possible model for studying the effects of bond angle changes in a silicon backbone. Recent evidence of steric repulsions between bulky side groups producing 120° Si—Si—Si bond angles[26,27] provokes the question as to whether a fundamental change in electronic structure accompanies such distortions. Different hybridization schemes in a valence bond picture may arise from such geometries. To tackle this issue, calculations are repeated for a structure where the central angle is fixed at 120° and where the other geometrical parameters are allowed to relax. The energy difference between the equilibrium and optimized distorted structure is about 0.4 kcal mol^{-1}.[18] (Repeating the same procedure for propane produces an energy difference of 1.3 kcal mol^{-1}.) Electron binding energies shift by about 0.1 eV (Table

Table 4. Si_3H_8 electron binding energies (eV)

	$Si_3H_8^+ {}^2A_1$	$Si_3H_8^+ {}^2B_2$	$Si_3H_8^- {}^2A_1$	$Si_3H_8^- {}^2B_1$	$Si_3H_8^- {}^2B_2$
Equilibrium	−10.71	−9.91	2.46	3.01	3.15
Distorted	−10.62	−10.00	2.34	3.04	3.25

4). These data do not indicate a fundamental change in electronic structure.

There are, nevertheless, interesting trends that emerge from these calculations. From the equilibrium structure to the distorted structure, the lowest electron binding energy is destabilized, but the next electron binding energy declines. These trends appear to follow from phase relationships between the bond orbitals that contribute to the corresponding FDAs. In the first case, this relationship is constructive and the reduced proximity of the bond orbital maxima implied by the increased bond angle causes the destabilization. The opposite trend obtains when the two bond orbitals have opposite phases. The a_1 electron affinity FDA declines and the next higher level ascends as the bond angle increases. Apparently the relationship between the lobes that interfere just below the central silicon is not as important as that between the lobes which interfere above the central silicon in Figs 8 and 9.

Si_4H_{10}

Dihedral angles can be studied when Si_4H_{10} calculations are performed. Rotations about single bonds have often been invoked as causes for red shifts in polysilane absorption spectra accompanying order–disorder transitions.[28] Steric effects and intermolecular forces determine conformations in the silicon backbone and these conformations affect the spectra. Calculations of ground state energies and electron binding energies as a function of the Si–Si–Si–Si dihedral angle are therefore useful as a model of how conformations influence spectra in organopolysilanes.

First, consider the ground state energies in four conformations: *anti* (180° dihedral angle), *gauche* (60°), *eclipsed*$_{120}$ (120°) and *eclipsed*$_0$ (0°). There is essentially no energy difference between the *anti* and *gauche* forms. Preferences for one form over the other found for related compounds are related to the substituents that may take the place of hydrogen. The two eclipsed structures lie 0.7 and 1.1 kcal mol,$^{-1}$ respectively, above the minima. These results are in excellent agreement with all-electron calculations.[17]

While the potential energy surface for dihedral angle variation is quite flat for the ground state of the neutral, electron binding energies exhibit a much more sensitive dependence. These are summarized in Figs 10 and 11, which plot vertical electron binding energies as a function of dihedral angle. Changes from one conformation to another can be several tenths of an electron-volt. The photoelectron spectrum,[25] because it represents a mixture of isomers, has broad maxima at 9.62, 10.3 and 10.85 eV, where the second energy represents overlapping bands. The present *anti* (−9.45, −10.54, −10.86) and *gauche* (−9.64, −10.17, −10.89) electron binding energies are in excellent agreement.

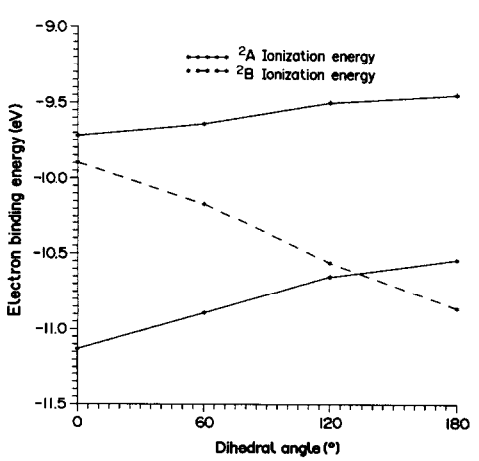

Fig. 10. Si_4H_{10} electron binding energies vs dihedral angle: ionization energies.

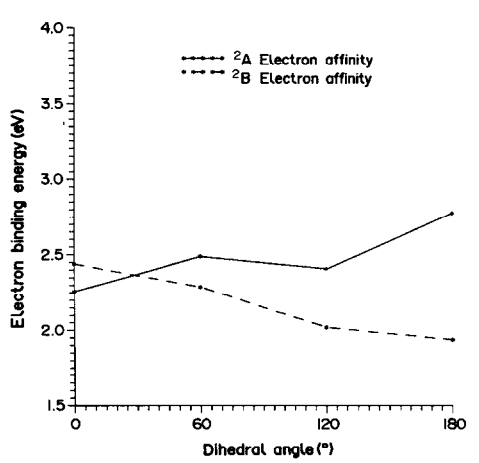

Fig. 11. Si_4H_{10} electron binding energies vs dihedral angle: electron affinities.

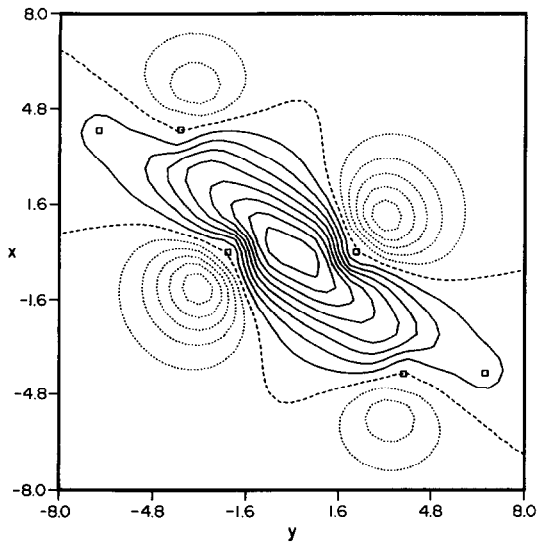

Fig. 12. *Anti* $Si_4H_{10}{}^+ {}^2A_g$ Feynman–Dyson amplitude.

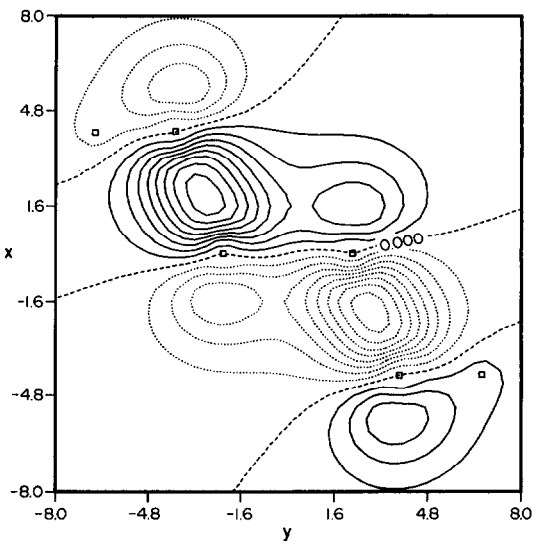

Fig. 13. *Anti* $Si_4H_{10}{}^+ {}^2B_u$ Feynman–Dyson amplitude.

Once again, one can appeal to a qualitative understanding of bond orbitals and antibond orbitals to explain the trends. For the ionization energies, FDAs can be constructed from three bond orbitals. There is always a rotation axis relating the terminal SiH_3 groups to each other, so the FDAs have either *a* or *b* symmetry. (Higher symmetry obtains for the *anti* and *eclipsed*$_0$ cases.) One combination of three bond orbitals has no nodes and *a* symmetry. A *b* symmetry combination has contributions with opposite signs from the terminal bond orbitals. Finally, there should be a combination with alternating signs in the bond functions and *a* symmetry. Another way of classifying these possibilities is to count the number of nodes between bond orbitals: zero, one or two, respectively.

For the *anti* conformation, it is possible to draw contour plots in which all the silicon nuclei are in the same plane. Feynman–Dyson amplitudes for ionization energies are displayed in Figs 12–14. In the first case, constructive interference obtains throughout the silicon backbone region, with a global maximum between the two central silicon nuclei. The long extent of this positive lobe is an excellent indication that all three bond orbitals are contributing to this FDA. In Fig. 13, one sees a node that connects the two central silicons. Two bond orbitals with opposite signs in the terminal Si–Si regions are clearly delineated. In the discussion above of the *b* symmetry combination of bond functions, it was stated that there should be a single node between the two bond orbitals. This node is not perpendicular to the central Si—Si bond axis, but parallel, allowing delocalization of the bond orbitals to occur in such a way as to create a π bonding interaction in the central Si—Si bond region. The curvature of the node in question suggests an alternative formulation where the Yin–Yang antibond orbital contributes in the middle of the molecule. For the FDA corresponding to the lowest ionization energy, one expects three bond orbitals with alternating signs. Figure 14 confirms this conjecture.

To understand the trends in Figs 10 and 11, the opposite extreme in the dihedral angle is considered. Feynman–Dyson amplitudes for the *eclipsed*$_0$ struc-

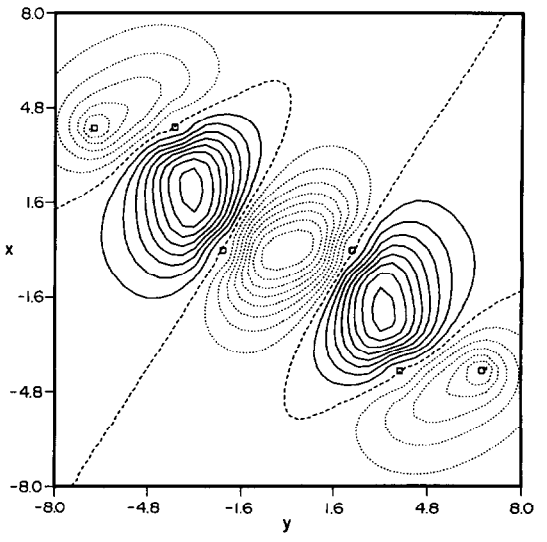

Fig. 14. *Anti* $Si_4H_{10}{}^+ {}^2A_g$ Feynman–Dyson amplitude.

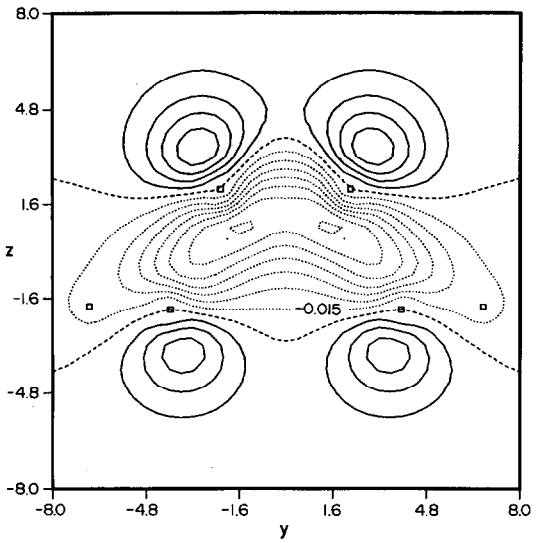

Fig. 15. *Eclipsed*$_0$ $Si_4H_{10}^+$ $^2A_1$ Feynman–Dyson amplitude.

ture also have the representational advantage of coplanar silicon nuclei. In Fig. 15, the analogue of Fig. 12 is displayed. There is still completely constructive interference of bond functions in the silicon backbone region. Note that there are now two extrema instead of just one and that they are displaced away from the central Si—Si bond axis. Of even greater importance is the presence of several negative contours directly connecting the non-neighbour bond orbitals. Such an interaction is not feasible in the *anti* conformation. An in-phase relationship of non-neighbour bond orbitals leads to the stabilization of this level as the dihedral angle decreases. The opposite trend obtains for the next FDA, depicted in Fig. 16. With the closer proximity of the non-neighbour bond orbitals, the FDA is destabilized because the phase relationship is antibonding. In addition, any π bonding that took place between the central silicons in the *anti* geometry has been destroyed. Finally, comparison of Figs 17 and 14 indicates the importance of the non-neighbour interaction. Constructive interference in this case leads to a stabilization of the electron binding energy as the dihedral angle decreases, bringing the non-neighbour bond regions closer to each other.

Based on experience gained in the Si_3H_8 case, the electron affinity FDAs in the *anti* conformation can be constructed from combinations of antibond orbitals. The most stable possibility should retain as many bonding interactions between neighbouring antibond orbitals as possible. Because of the node that is present in the Yin–Yang device in each Si—Si region, the FDA should be antisymmetric with respect to the C_2 axis. Figure 18 confirms these hypotheses and shows three Yin–Yang patterns interfering constructively near the two central silicon nuclei. Consider the patterns near the central silicon nucleus that lies on the positive side of the y axis. Constructive interference takes place between lobes of neighbouring Yin–Yang patterns below and to the left of this nucleus. Tails of the partners of these lobes are also interfering constructively above and to the right of the silicon nucleus. The former type of interference is the reason why one sees four extrema in the silicon backbone region instead of six.

The next issue to arise is the most stable way of arranging three paisley patterns. There is an *a*

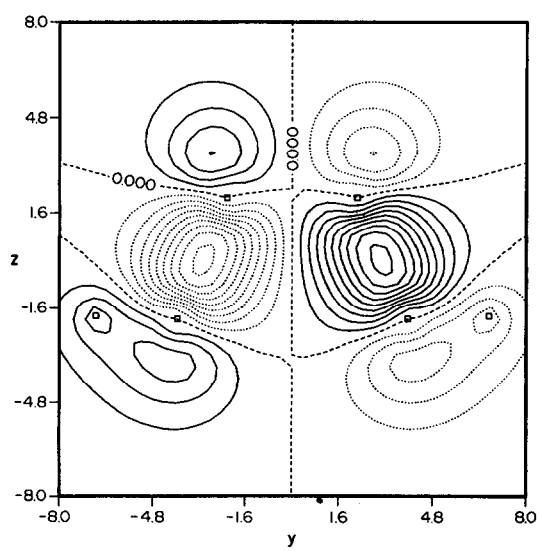

Fig. 16. *Eclipsed*$_0$ $Si_4H_{10}^+$ $^2B_2$ Feynman–Dyson amplitude.

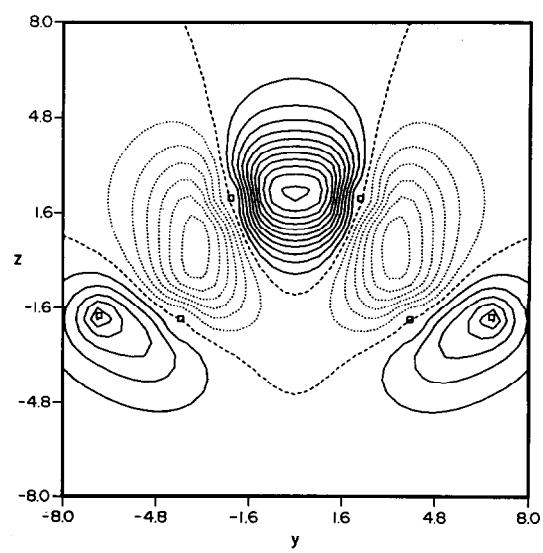

Fig. 17. *Eclipsed*$_0$ $Si_4H_{10}^+$ $^2A_1$ Feynman–Dyson amplitude.

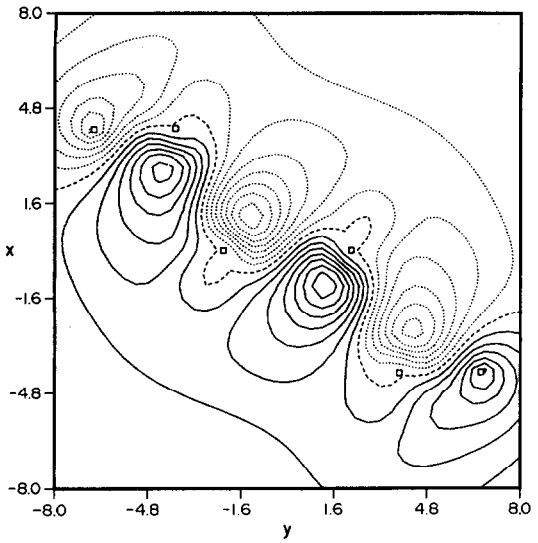

Fig. 18. *Anti* $Si_4H_{10}^-$ ^2B_u Feynman–Dyson amplitude.

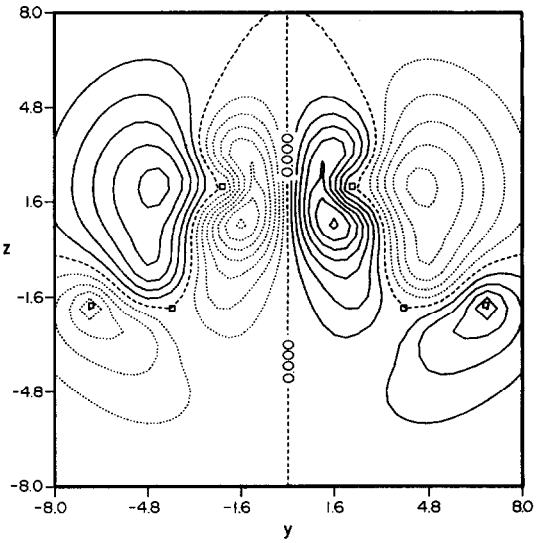

Fig. 20. *Eclipsed*$_0$ $Si_4H_{10}^-$ $^2B_2$ Feynman–Dyson amplitude.

combination formed from paisley patterns on the two terminal Si—Si regions. Two *b* combinations arise from the paisley pattern on the central Si—Si region and the antisymmetric counterpart of the *a* combination. While the *a* combination, through constructive interference of tails, can actually create a bonding interaction in the central Si—Si region, neither of the *b* combinations has anything but antibonding character in this sector of the molecule. The only thing that mixing the two *b* combinations can do is to adjust the nature of the antibonding relationship between the two central silicons. The lowest combination of the three is therefore the one with *a* symmetry. In the FDA shown in Fig. 19, these arguments are verified. Note the somewhat distorted paisley lobes whose tails begin near the terminal hydrogens. The extrema near the terminal silicons of these lobes are more delocalized than their counterparts in previously considered molecules. Near the central silicon nuclei, the wide parts of two paisley lobes are deployed away from the centre of symmetry. Constructive interference between the two tails takes place near the origin.

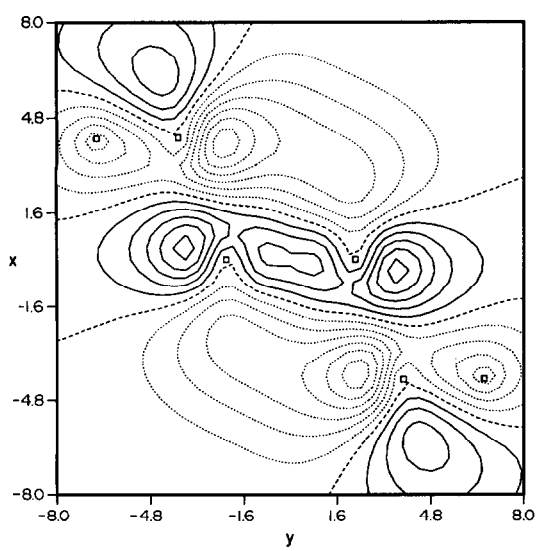

Fig. 19. *Anti* $Si_4H_{10}^-$ ^2A_g Feynman–Dyson amplitude.

Si—H antibonding FDAs that have a_u or b_g symmetry in the *anti* conformation have higher electron binding energies. With only four silicons, the π levels are already above the two lowest electron affinity levels with σ symmetry.

Two reasons underlie the destabilization of the lowest electron binding energy for anionic final states in the *eclipsed*$_0$ form. When the dihedral angle is changed to 0°, the lower of the two anionic FDAs necessarily acquires, because of C_{2v} symmetry, a node that bisects the central Si—Si bond. This is incompatible with the presence of a Yin–Yang form in this region and necessarily introduces more σ antibonding. The other two bond regions are not as drastically affected, but their closer proximity also leads to destabilization, as suggested by their phase relationships. The consequences of these factors for the FDA are shown in Fig. 20, where two Yin–Yang patterns on non-adjacent Si—Si bond regions have opposite signs. Note the distortion of the lobes that lie on the extreme right and left: their local extrema are shifted vertically away from the terminal silicon nuclei. In the central bond region, the pattern is similar to one of the electron affinity FDAs of D_{3d} Si_2H_6. Both of these situations arise from symmetry's enforcement of a central node that is perpendicular to a Si—Si axis.

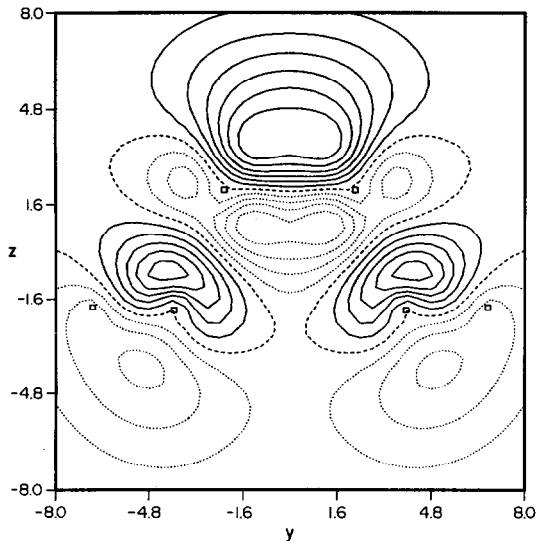

Fig. 21. *Eclipsed*$_0$ $Si_4H_{10}^-$ $^2A_1$ Feynman–Dyson amplitude.

In the remaining FDA, stabilization takes place due to improved constructive interference of paisley lobes from non-adjacent Si—Si bond regions just below the two central silicon nuclei (Fig. 21). One might expect the two remaining paisley lobes to also constructively interfere, but it appears that they have surrounding nodes. The latter pair of lobes is considerably distorted, as evidenced by the locations of their extrema. One might have expected these extrema to lie closer to the z axis. Constructive interference taking place above pushes the extrema to positions just above the terminal silicon nuclei.

Polymers

Based on these findings, one can make some inferences about the valence and conduction bands of a polymer. For the lowest ionization energy, the FDA consists of the most antibonding combination possible of bond orbitals. Alternating phases, one creates the maximum number of nodes. Such an FDA has opposite phases in neighbouring bond orbitals and like phases in first non-neighbour bond orbitals (Fig. 22). As one twists the polymer from an all-*anti* conformation into an all-*gauche* conformation (if the sense of the twist is kept constant, one obtains a helical structure), this FDA is stabilized. For the largest electron affinity, one constructs the corresponding FDA as the most bonding combination possible of antibond, or Yin–Yang orbitals. (Diffuse functions will continue to contribute to unbound anionic states in the polymer.) This FDA exhibits constructive interference about each silicon. An in-phase relationship between neighbouring orbitals and an out-of-phase relationship between first non-neighbour orbitals obtains (Fig. 22). As the dihedral angles decrease, non-neighbour interactions become important, and the electron binding energy is destabilized. In going from a straight chain to a helix, one gets an increase in the ionization energy and a decrease in the electron affinity. Put another way, from helix to straight chain, there is a red shift in the absorption spectrum.

These inferences are confirmed by polymer band calculations.[10,11] In all-*anti* polysilane, the two highest occupied bands exhibit Si—Si σ bonding. The lowest of these states has no nodes along the silicon backbone and the highest has nodes that coincide

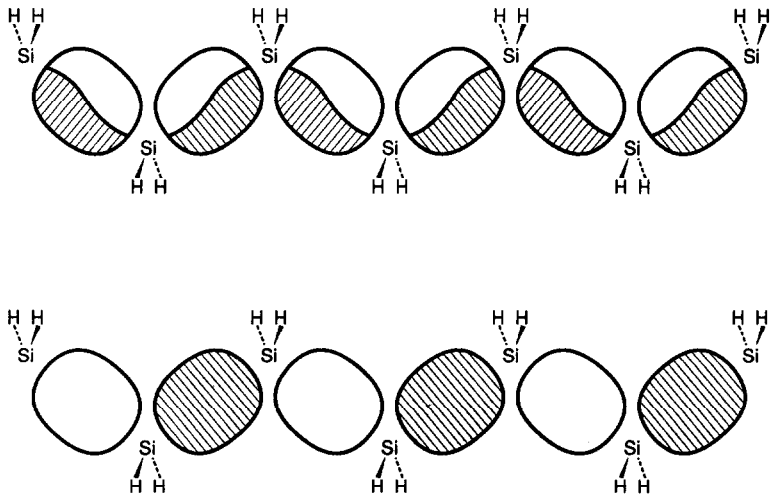

Fig. 22. Feynman–Dyson amplitudes for the lowest ionization energy and highest electron affinity of a polymer.

with each SiH_2 plane. For the lowest state in the conduction band, *sp* hybrids perpendicular to the chain axis have alternating phases on successive silicon nuclei. Phase relationships for the top of the valence band and for the bottom of the conduction band are identical to those in Fig. 22.

CONCLUSIONS

Localized bond orbitals and their antibond counterparts arise in the broken-symmetry FDAs of Si_2H_6. Through application of group theory and criteria of phases and overlap, one can explain how FDAs for larger oligomers are constructed from FDAs of Si_2H_6. A purely localized picture of bonding would be unable to explain how conformations and spectra are related, for there are interactions between neighbouring and non-neighbouring bond and antibond functions that are important. Plots of oligomer FDAs show how localized functions combine to form delocalized states. Phase relationships between the constituent localized orbitals within the FDAs are useful in qualitative predictions of how electron binding energies vary with respect to changes in Si—Si—Si bond angles and Si—Si—Si—Si dihedral angles. Extrapolation to the limit of an infinite polymer shows how shifts in absorption spectra are related to conformational changes.

Acknowledgement—This material is based on work supported by the National Science Foundation under Grant No. CHE-8723185. The Government has certain rights in this material.

REFERENCES

1. C. G. Pitt, in *Homoatomic Rings, Chains and Macromolecules of the Main Group Elements* (Edited by A. L. Rheingold). Elsevier, New York (1977).
2. R. West, *J. Organomet. Chem.* 1986, **300**, 327.
3. P. Trefonas III, R. West and R. D. Miller, *J. Am. Chem. Soc.* 1985, **107**, 2737; A. J. McKinley, T. Karatsu, G. M. Walraff, R. D. Miller, R. Sooriyakumaran and J. Michl, *Organometallics* 1988, **7**, 2567; T. Karatsu, R. D. Miller, R. Sooriyakumaran and J. Michl, *J. Am. Chem. Soc.* 1989, **111**, 1140.
4. R. D. Miller and J. Michl, *Chem. Rev.* 1989, **89**, 1359.
5. D. C. Hofer, R. D. Miller, C. G. Willson and A. Neurather, *Proc. SPIE, Advances in Resist Technology* 1984, **469**, 108; J. M. Zeigler, L. A. Harrah and A. W. Johnson, *Proc. SPIE, Advances in Resist Technology* 1985, **539**, 166.
6. R. West, in *Ultrastructure Processing of Ceramics, Glasses and Composites* (Edited by L. Hench and D. L. Ulrich). John Wiley, New York (1984).
7. R. G. Kepler, J. Zeigler, L. A. Harrah and S. R. Kurtz, *Phys. Rev. B* 1987, **35**, 2818; M. Fujino, *Chem. Phys. Lett.* 1987, **136**, 451.
8. J. Zeigler and F. W. Gordon Fearon (Eds), *Silicon-Based Polymer Science. Adv. Chem. Ser.* 1989, **224**.
9. J. V. Ortiz and J. W. Mintmire, *Adv. Chem. Ser.* 1989, **224**, 551 (Edited by J. Zeigler and F. W. Gordon Fearon); J. W. Mintmire and J. V. Ortiz, *Adv. Chem. Ser.* 1989, **224**, 543 (Edited by J. Zeigler and F. W. Gordon Fearon).
10. J. W. Mintmire, *Phys. Rev. B* 1989, **39**, 13350; J. W. Mintmire, *Mater. Res. Soc.* 1989, **141**, 235.
11. H. Teramae and K. Takeda, *J. Am. Chem. Soc.* 1989, **111**, 1281; H. Teramae, *J. Am. Chem. Soc.* 1987, **109**, 4140; K. Takeda, H. Teramae and N. Matsumoto, *J. Am. Chem. Soc.* 1986, **108**, 8186.
12. J. T. Nelson and W. J. Pietro, *J. Phys. Chem.* 1988, **92**, 1365.
13. R. W. Bigelow and K. M. McGrane, *J. Polym. Sci. B* 1986, **24**, 1233.
14. K. A. Klingensmith, J. W. Downing, R. D. Miller and J. Michl, *J. Am. Chem. Soc.* 1986, **108**, 7438.
15. M. J. Frisch, M. Head-Gordon, H. B. Schlegel, K. Ragavachari, J. S. Binkley, C. Gonzalez, D. J. DeFrees, D. J. Fox, R. A. Whiteside, R. Seeger, C. F. Melius, J. Baker, R. Martin, L. R. Kahn, J. J. P. Stewart, E. M. Fluder, S. Topiol and J. A. Pople, Gaussian 88. Gaussian Inc., Pittsburgh (1988).
16. J. V. Ortiz, EPT90, An Electron Propagator Program. University of New Mexico.
17. J. V. Ortiz and J. W. Mintmire, *J. Am. Chem. Soc.* 1988, **110**, 4522; J. W. Mintmire and J. V. Ortiz, *Macromolecules* 1988, **21**, 1189.
18. J. V. Ortiz and J. W. Mintmire, *J. Phys. Chem.*, accepted.
19. W. R. Wadt and P. J. Hay, *J. Chem. Phys.* 1985, **82**, 284.
20. T. H. Dunning and P. J. Hay, in *Modern Theoretical Chemistry* (Edited by H. F. Schaefer), Vol. 3. Plenum Press, New York (1976).
21. R. Bartlett, *Ann. Rev. Phys. Chem.* 1981, **32**, 359; J. S. Binkley and J. A. Pople, *Int. J. Quant. Chem.* 1975, **9**, 229.
22. J. Linderberg and Y. Öhrn, *Propagators in Quantum Chemistry*. Academic Press, New York (1973); W. von Niessen, J. Schirmer and L. S. Cederbaum, *Comput. Phys. Rep.* 1984, **1**, 57; J. Simons, in *Theor. Chem. Adv. Persp.* 1978, **3** (Edited by H. Eyring); M. F. Herman, K. F. Freed and D. L. Yeager, *Adv. Chem. Phys.* 1981, **48**, 1; Y. Öhrn and G. Born, *Adv. Quant. Chem.* 1981, **13**, 1.
23. T. Koopmans, *Physica* 1933, **1**, 104.
24. J. V. Ortiz, *Int. J. Quant. Chem., Quant. Chem. Symp.* 1988, **22**, 431.
25. H. Bock, W. Ensslin, F. Feher and R. Freund, *J. Am. Chem. Soc.* 1976, **98**, 668.
26. H. Kuzmany, J. F. Rabolt, B. L. Farmer and R. D. Miller, *J. Chem. Phys.* 1986, **85**, 7413.

27. A. J. Lovinger, F. C. Schilling, F. A. Bovey and J. M. Zeigler, *Macromolecules* 1986, **19**, 2657.
28. L. A. Harrah and J. M. Zeigler, *J. Polym. Sci. Polym. Lett.* 1985, **23**, 209; P. Trefonas III, J. R. Damewood and R. West, *Organometallics* 1985, **4**, 1318; R. D. Miller, D. Hofer, J. Rabolt and G. N. Fickes, *J. Am. Chem. Soc.* 1985, **107**, 2172.

Polyhedron Vol. 10, No. 11, pp. 1299–1309, 1991
Printed in Great Britain

0277-5387/91 $3.00+.00
© 1991 Pergamon Press plc

INTERESTING PROPERTIES OF THE HEAVIER GROUP 14 ANALOGUES OF AROMATIC AND POLYCYCLIC CARBON COMPOUNDS. A THEORETICAL STUDY

SHIGERU NAGASE

Department of Chemistry, Faculty of Education, Yokohama National University, Yokohama 240, Japan

Abstract—This summarizes recent theoretical and experimental studies of the compounds whose skeletons are made of the heavier Group 14 elements. Included are the heavier analogues of benzene and strained polycyclic alkanes of current interest. Several interesting and novel properties of silicon, germanium, tin and lead skeletons are demonstrated by means of *ab initio* molecular orbital calculations. To characterize the properties, the applicability of the concepts such as aromaticity, strain and bonding established in carbon chemistry is discussed.

Carbon compounds have played a central role in organic chemistry. In recent years there has been considerable interest in replacing the skeletal carbons by the heavier Group 14 atoms in the expectation of novel physical and chemical properties. We report here our recent theoretical studies of the heavier Group 14 analogues of aromatic and strained polycyclic carbon compounds, together with the recent experimental data on the successful syntheses and isolations. Our primary concern is to test if the well-established concepts such as aromaticity, strain and bonding in carbon chemistry are also valid and to clarify the characteristics of silicon, germanium, tin and lead skeletons compared with carbon skeletons.

All calculations were carried out by using *ab initio* molecular orbital theory. Geometries were fully optimized at the Hartree–Fock (HF) level. For the geometrical optimization of the compounds with diradical character, the two-configuration self-consistent field (TCSCF) theory was used. Carbon and silicon compounds were calculated using the split-valence *d*-polarized 6-31G(*d*) basis set.[1] Calculations were also carried out with *ab initio* effective core potentials (ECP)[2] on silicon, germanium, tin and lead using the double-zeta (DZ) basis set augmented by a set of six *d*-type polarization functions on each heavy atom [*d* exponents 0.262 (Si), 0.246 (Ge), 0.183 (Sn), 0.164 (Pb), 0.75 (C) and 0.85 (O)].[3,4] The ECPs on tin and lead incorporate the mass–velocity and Darwin relativistic effects.[2] The DZ basis sets of the heavier atoms were obtained by contracting the inner two primitive Gaussian functions in the (3*s*3*p*) sets developed by Wadt and Hay,[2] while those of the second-row atoms such as carbon and oxygen were the standard Huzinaga–Dunning contractions specified by (9*s*5*p*)/[3*s*2*p*];[4] the basis set used for hydrogen was of DZ quality.[5] The effect of electron correlation was calculated using Møller–Plesset (MP) perturbation theory up to full fourth order (MP4).[6] Throughout this report, the symbol "//" means "at the geometry of": thus, single point MP calculations using the DZ(*d*) optimized geometries are labelled MP/DZ(*d*)//HF/DZ(*d*).

AROMATIC COMPOUNDS

As well known, benzene (C_6H_6) is unique among conjugated compounds with respect to its stability and reactivity. This has been attributed to "aromaticity" or the cyclic delocalization of π electrons, as the $(4n+2)$ Hückel rule suggests.

Silicon is contiguous to carbon in Group 14. Thus, it is expected that hexasilabenzene (Si_6H_6) also has an aromatic structure of D_{6h} symmetry since it contains six π electrons. To test this, we undertook the first *ab initio* calculations.[7] As expected, the minimum energy structure of hexasilabenzene was calculated to be planar with D_{6h} symmetry. The optimized Si—Si distance of 2.220 Å was 0.077 Å longer than the Si—Si double bond in $H_2Si{=}SiH_2$, but was 0.162 Å shorter than the Si—Si single bond in $H_3Si{-}SiH_3$, reflecting aromaticity. The planar D_{6h} structure has also been calculated by other research groups.[8,9]

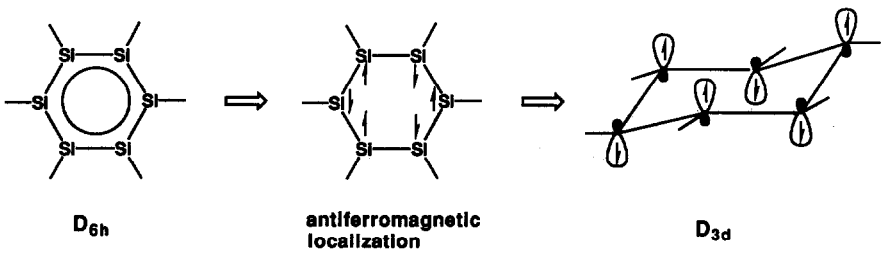

Fig. 1. Deformation of the planar D_{6h} to the non-planar D_{3d} structure in hexasilabenzene.

However, our recent calculations at higher levels revealed that the planar D_{6h} structure is not a minimum on the Si_6H_6 potential energy surface but corresponds to a transition structure with one single imaginary b_{2g} frequency.[10] We have indicated that displacement along the b_{2g} vibrational mode leads to a minimum which is a chair-like puckered structure of D_{3d} symmetry.

As shown in Fig. 1, the skeletal bonding of hexasilabenzene is characterized in terms of a spin density wave (alternative localization of α and β spins); for the HF instability, see ref. 10. A tendency of the antiferromagnetic localization of π electrons onto each silicon atom generates "silyl radical" character at each silicon atom and leads to the preference of the non-planar D_{3d} structure; as well-known, the SiH_3 radical takes a non-planar and pyramidalized structure, unlike the CH_3 radical. The deviation from planarity is however relatively small, as is the gain in energy (*ca* 1 kcal mol^{-1}), probably because π bonding becomes unfavourable upon pyramidalization. The slight preference of the non-planar D_{3d} structure is confirmed also in a subsequent theoretical study at the MCSCF and CI levels.[11]

The non-planar D_{3d} structure is increasingly favoured as the skeletal silicon atoms in hexasilabenzene are replaced by the heavier germanium, tin and lead atoms.[12] Figure 2 shows the optimized D_{6h} and D_{3d} structures of hexagermabenzene (Ge_6H_6), hexastannabenzene (Sn_6H_6) and hexaplumbabenzene (Pb_6H_6) at the

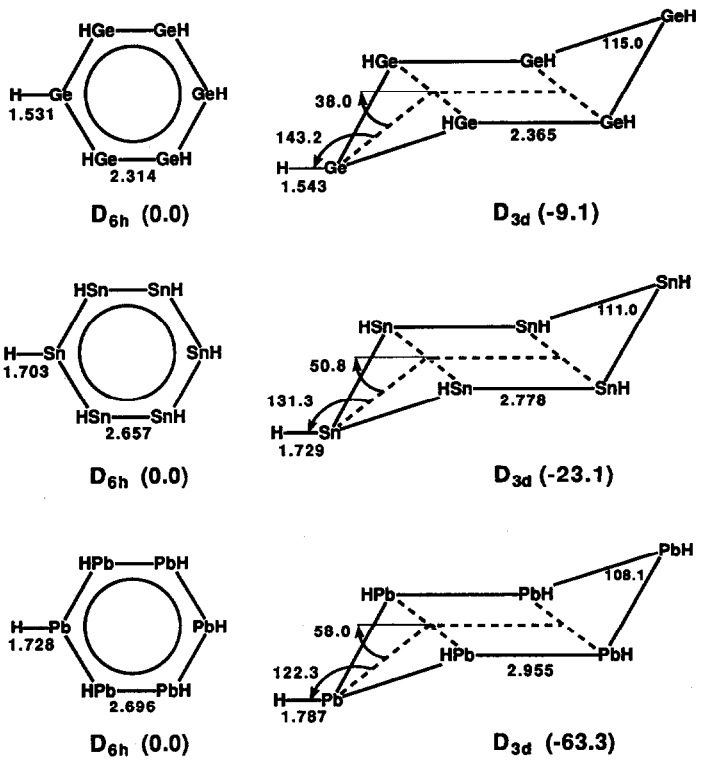

Fig. 2. The optimized D_{6h} and D_{3d} structures (Å and °) of hexagermabenzene, hexastannabenzene and hexaplumbabenzene at the HF/DZ(*d*) level. Values in parentheses are the relative energies (kcal mol^{-1}) at the MP2/DZ(*d*)//HF/DZ(*d*) level.

HF/DZ(*d*) level. The non-planar D_{3d} structures are 9.1 (Ge_6H_6), 23.1 (Sn_6H_6) and 63.3 (Pb_6H_6) kcal mol^{-1} more stable than the planar D_{6h} structures at the MP2/DZ(*d*)//HF/DZ(*d*) level. This suggests that planar hexagonal structures have no special meaning in the heavier analogues, unlike for benzene. The pronounced preference of the non-planar D_{3d} structures in Ge_6H_6, Sn_6H_6 and Pb_6H_6 is due to the increased tendency of the π electrons to localize in an antiferromagnetic way; upon going to GeH_3, SnH_3 and PbH_3 radicals, the pyramidalized structures are progressively favoured. Atomaticity based on electron delocalization is of limited value when it is applied to the heavier analogues of benzene.

It should be noted that the localized nature of π electrons is not characteristic of the heavier analogues. According to spin-coupled valence-bond calculations,[13] the delocalization of π electrons is energetically unfavourable even in benzene. The π electrons are essentially localized in deformed atomic orbitals and the aromatic properties of benzene arise from the symmetric coupling of electron spins. This may suggest that aromaticity is not simply the result of the topological properties of electron count or mode of delocalization. In addition, it has recently been pointed out from the valence-bond correlation diagram and σ–π energy separation that the D_{6h} hexagonal structure of benzene is determined not by the π electrons but by the σ framework, the π electrons themselves preferring a bond-alternated localized D_{3h} structure (a Kekulé structure).[14] We think that the propensity of the π electrons to form singlet pairs alternatively around the ring is analogous in origin to the bond alternation in long polyenes which occurs against the resistance of the σ framework, as known in terms of Peierls distortion in solid physics.

Another interesting point to be noted is the relative stability of the valence isomers.[7] Benzene is 85–130 kcal mol^{-1} more stable than its valence isomers such as Dewar benzene (C_{2v}), benzvalene (C_{2v}) and prismane (D_{3h}). In contrast, the Si_6H_6 valence isomers lie very close in stability to hexasilabenzene and are progressively favoured as the number of double bonds decreases. Thus, hexasilaprismane, being 13.4 kcal mol^{-1} more stable than hexasilabenzene, becomes the most stable Si_6H_6 isomer.[7,10] The preference of prismane structures was also calculated for the heavier Ge_6H_6, Sn_6H_6 and Pb_6H_6 systems.[12] In the heaviest Pb_6H_6 system, even hexaplumbaprismane is not a minimum in D_{3h} symmetry and highly distorted structures were calculated to be more stable. The dramatic differences between the C_6H_6 isomers and their heavier analogues are ascribed to the fact that the heavier atoms have a strong tendency to prefer saturated bonds and are capable of forming less strained compounds.

STRAINED POLYCYCLIC COMPOUNDS

Polycyclic cage compounds $C_{2n}H_{2n}$ such as tetrahedrane ($n = 2$), prismane ($n = 3$) and cubane ($n = 4$) are known as fascinating synthetic targets in carbon chemistry, because of the unusual properties and aesthetic appeal due to high symmetry. As is apparent from the carbon bond angles which deviate greatly from the normal tetrahedral value of 109.5°, they are highly strained. For instance, the strain energies of tetrahedrane and cubane are as large as 140.0 and 154.7 kcal mol^{-1}, respectively, from the experimental evaluation.[15] Summarized in Table 1 are the calculated strained energies of $C_{2n}H_{2n}$ and the silicon analogues $Si_{2n}H_{2n}$ obtained from the homodesmic reactions[16] at the HF/6–31G(*d*) level.[17] The calculated strained energies of tetrahedrane (141.4 kcal mol^{-1}) and cubane (158.6 kcal mol^{-1}) agree well with the experimental values. Thus, comparable accuracy would be expected for the calculated values of the silicon analogues where experimental data are unavailable.

Table 1 reveals an interesting contrast with silicon and carbon compounds.[17] Tetrasilatetrahedrane is as highly strained as tetrahedrane; as the number of four-membered rings increases, however, the strain decreases significantly in silicon compounds while it increases in carbon compounds. Thus, hexasilaprismane is 32 kcal mol^{-1} less strained than prismane, while octasilacubane with only four-membered rings is 65 kcal mol^{-1} less strained than cubane. This suggests that octasilacubane is a reasonable target for synthesis and isolation. In fact, a derivative of octasilacubane (Si_8R_8, R = t-$BuMe_2Si$) has been recently synthesized and its novel properties investigated.[18]

In light of the recent synthesis and structural determination of the bridgehead-coupled cubane, cubylcubane,[19] we have also calculated the silicon-based compound at the HF/6–31G(*d*) level, as shown in Fig. 3.[20] The calculated strained energy of 182.0 kcal mol^{-1}, being somewhat smaller than

Table 1. Strain energies (kcal mol^{-1}) calculated using homodesimic reactions at the HF/6–31G(*d*) level

	X = Si	X = C
Tetrahedrane (X_4H_4; T_d)	140.9	141.4
Prismane (X_6H_6; D_{3h})	113.8	145.3
Cubane (X_8H_8; O_h)	93.5	158.6

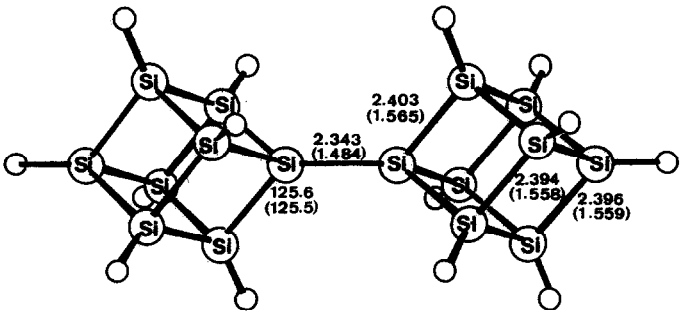

Fig. 3. The HF/6–31G(d) optimized D_{3d} structures of persilacubylcubane and cubylcubane (in Å and °). Values in parentheses are for cubylcubane. The total energies (HOMO and LUMO levels) of persilacubylcubane and cubylcubane are −4630.75593 au (−7.8 and 1.1 eV) and −613.64064 au (−9.6 and 6.0 eV), respectively.

the sum of the strains of two octasilacubanes (2×93.5 kcal mol^{-1}), is 127.8 kcal mol^{-1} smaller than that of 309.8 kcal mol^{-1} for cubylcubane at the HF/6–31G(d) level. This suggests that persilacubylcubane also forms an interesting synthetic target.

Figure 4 shows the optimized structure of larger polycyclic silicon compounds ($Si_{2n}H_{2n}$, n = 5, 6 and 8) at the HF/6–31G(d) level.[20] These were calculated to be minima in D_{nh} symmetry. The calculated strained energies were 82.8 (n = 5), 102.1 (n = 6) and 166.8 (n = 8) kcal mol^{-1}. In the corresponding carbon compounds ($C_{2n}H_{2n}$) known as [n]-prismanes, pentaprismane (n = 5) is the largest that has ever been synthesized.[21] The next largest hexaprismane (n = 6), a formal face-to-face dimer of benzene, is now challenged. However, its synthesis is not yet successful, although the related compound, secohexaprismane, was recently prepared.[22] It is interesting that the strain energies of the silicon-based [n]-prismanes ($Si_{2n}H_{2n}$) are 53.2 (n = 5), 70.1 (n = 6) and 141.0 (n = 8) kcal mol^{-1} smaller than those of 136.0, 172.2 and 307.8 kcal mol^{-1} in [n]-prismanes ($C_{2n}H_{2n}$), respectively;[20] the dimerization of benzene to give hexaprismane was 132 kcal mol^{-1} endothermic, while that of hexasilabenzene to give hexasilaprismane was 153 kcal mol^{-1} exothermic at the HF/6–31G(d) level.

It is also instructive to note that the strain energies of pentasila[1.1.1]propellane (70.2 kcal mol^{-1}) and octasila[2.2.2]propellane (55.7 kcal mol^{-1}) are 34.1 and 40.3 kcal mol^{-1} smaller than those of [1.1.1]propellane (104.3 kcal mol^{-1}) and [2.2.2]propellane (96.0 kcal mol^{-1}) at the HF/6–31G(d) level.[23]

We now discuss the effect of substitution of the skeletal silicon atoms of $Si_{2n}H_{2n}$ (n = 2–4) by heavier atoms such as germanium and tin.[24] As Fig. 5 shows, the substitution has again little effect on the strain energies in the tetrahedrane system.

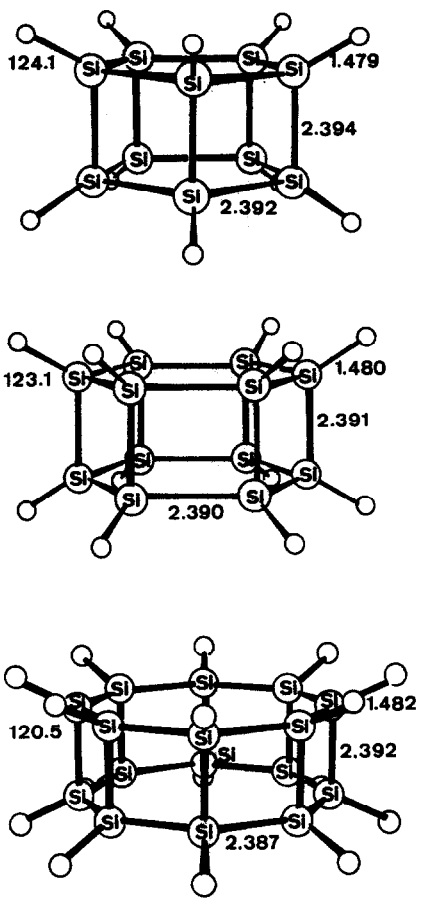

Fig. 4. The HF/6–31G(d) optimized D_{nh} structures of persila[n]prismane ($Si_{2n}H_{2n}$) (in Å and °). The total energies are −2894.98369 (n = 5), −3473.97455 (n = 6) and −4631.91717 (n = 8) au. The HOMO and LUMO levels are −8.6 and 1.3 (n = 5), −8.2 and 1.2 (n = 6), and −8.2 and 1.1 (n = 8) eV, respectively.

This is because three-membered germanium and tin rings are as highly strained as three-membered silicon rings, as is apparent from the fact that the strain energies of cyclotrigermane (39.4 kcal mol^{-1}) and

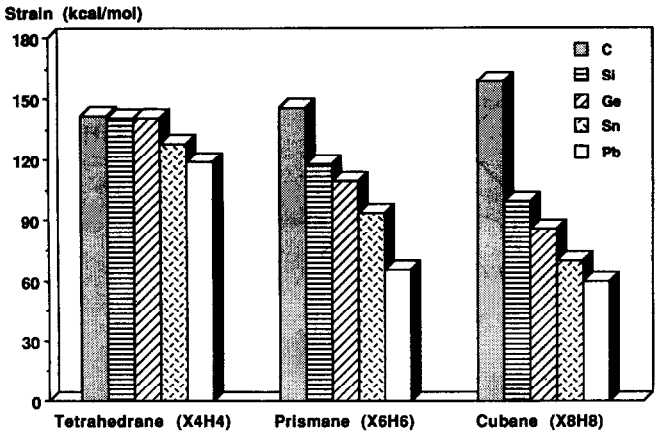

Fig. 5. The strain energies (kcal mol^{-1}) of tetrahedrane, prismane and cubane systems at the HF/DZ(*d*) level.

cyclotristannane (36.6 kcal mol^{-1}) differ little from the strain energy of cyclotrisilane (39.2 kcal mol^{-1}) at the HF/DZ(*d*) level;[24] in addition, these strain energies are all larger than that of cyclopropane (28.7 kcal mol^{-1}).

However, the strain energies of hexasilaprismane and octasilacubane decrease significantly by 9 and 24 kcal mol^{-1} and 13 and 29 kcal mol^{-1}, respectively, upon replacement by the germanium and tin atoms.[24] In this context, it is interesting that a stable hexagermaprismane derivative [Ge_6R_6, R = CH $(SiMe_3)_2$] has recently been synthesized and its X-ray structure determined.[25]

The relief of strain in the prismane and cubane systems is due to the fact that the strain energies of four-membered carbon, silicon, germanium and tin rings decrease successively in the order of cyclobutane (26.7 kcal mol^{-1}), cyclotetrasilane (17.2), cyclotetragermane (15.2), cyclotetrastannane (12.2).[24] These values agree well with the strain energies per four-membered ring in the cubane system: 26.4 (C_8H_8), 16.5 (Si_8H_8), 14.3 (Ge_8H_8) and 11.7 (Sn_8H_8) kcal mol^{-1}. These decreases in strain are due to a stronger reluctance of the heavier atoms to form hybrid orbitals, that is, an increasing tendency to maintain the $(ns)^2(np)^2$ valence electron configurations even in compounds. Apparently, this property of the heavier atoms is favourable for making 90° bond angles with low strain in four-membered rings.[24] However, it becomes unfavourable in forming three-membered rings with bond angles of 60° where hybrid orbitals with sufficiently high *p* character are essential for a description of the bent bond orbitals.[26]

Thus, it is not surprising that a successive decrease in strain due to replacement by the heavier atoms is also seen in the bicyclic compounds consisting of only four-membered rings.[27–29] For instance, the strain energy of bicyclo[2.2.0]hexane decreases by *ca* 20, 25, 30 and 35 kcal mol^{-1}, respectively, upon replacement of the skeletal carbon atoms by the heavier silicon, germanium, tin and lead atoms.[29] In the last 2 years the first synthetic and X-ray structural studies have been made of a derivative of bicyclo[2.2.0]hexasilane.[30] Although the germanium analogues have not as yet been subject to experimental tests, a bicyclo [2.2.0]hexastannane derivative was recently synthesized as the first tin example and its X-ray structure determined.[31] The heaviest analogue, bicyclo[2.2.0]hexaplumbane, is the least strained and prefers a skewed C_2 structure, unlike the lighter analogues of C_{2v} symmetry. However, the energy difference favouring the C_2 over C_{2v} structures is only 0.03 kcal mol^{-1}, despite the considerable geometrical differences between these structures, suggesting that the lead skeleton is remarkably flexible.[29] This structural feature may be ascribable to the fact that lead is most reluctant to form hybrid orbitals with highly directional *p* character because of the inert $(6s)^2$ pair originating from the relativistic effect;[32] lead is most eager to be divalent in compounds.

Reflecting the inert pair, cyclotetraplumbane (c-Pb_4H_8) also tends to take a C_{4h} structure with the hydrogen atoms skewed around the four-membered ring (as shown in Fig. 6) with some divalent character at each lead. The tendency is enhanced in three-membered rings. Thus, cyclotriplumbane (c-Pb_3H_6) adopts a skewed C_{3h} structure, unlike its lighter analogues of D_{3h} symmetry; the energy difference favouring C_{3h} over D_{3h} is as large as 10 kcal mol^{-1} at the MP4/DZ(*d*)//HF/DZ(*d*) level. As suggested in Fig. 7, cyclotriplumbane is best represented as a weak interaction among three singlet plumbylenes (PbH_2). It should be mentioned that skewed-type

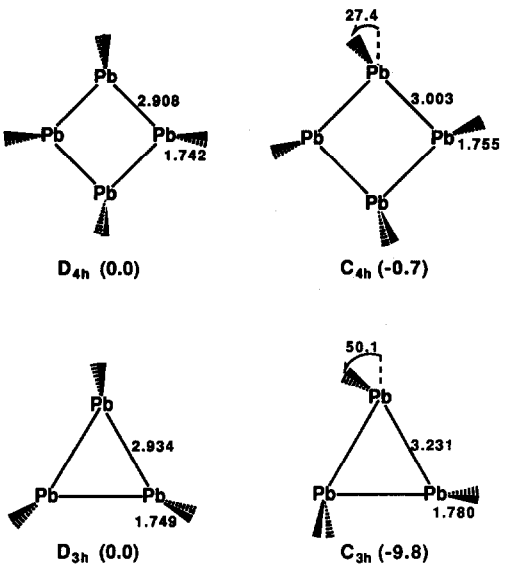

Fig. 6. The HF/DZ(*d*) optimized structures of cyclotetraplumbane (c-Pb_4H_8) and cyclotriplumbane (c-Pb_3H_6) (in Å and °). Values in parentheses are the relative energies (kcal mol^{-1}) at the MP4/DZ(*d*)//HF/DZ(*d*) level.

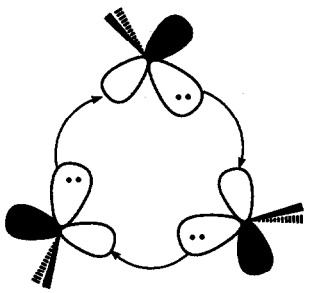

Fig. 7. Interaction of three singlet divalent species (PbH_2).

structures are also favoured in the lighter analogues (c-Si_3H_6, c-Ge_3H_6 and c-Sn_3H_6) when the hydrogens are substituted by the electronegative groups such as fluorine atoms, because the singlet states of the divalent species become much lower in energy than the triplet states.

In an attempt to assess the stability of three-membered and four-membered rings, the energy gain (*E*) due to cyclization from nXH_2 to c-X_nH_{2n} (X = Si, Ge, Sn and Pb) was calculated and compared for $n = 3$ and 4 at the MP4/DZ(*d*)//HF/DZ(*d*) level. As Table 2 shows, the calculated *E* values are larger in forming four-membered rings than in forming three-membered rings, as expected from a lower strain in four-membered rings. The *E* values per "*n*" may measure the strength of the X—X bond in c-X_nH_{2n}. As shown in Table 2, the X—X bonds in the three-membered rings are significantly weaker than those in the four-membered rings.

Table 2. The gain (*E*) in stabilization (kcal mol^{-1}) upon going from nXH_2 to c-X_nH_{2n} at the MP4/DZ(*d*)//HF/DZ(*d*) level

	c-X_4H_8		c-X_3H_6	
X	*E*	*E*/4	*E*	*E*/3
Si	223.4	55.9	142.3	47.4
Ge	164.5	41.1	96.9	32.3
Sn	119.7	29.9	64.1	21.4
Pb[a]	58.9	14.7	20.3	6.8
	59.6	14.9	30.1	10.0

[a] Values in the second entry are for the skewed structures.

As a consequence, heavier polycyclic compounds constructed only from three-membered rings are subject to "bond stretch" isomerism because of the weaker bonds and higher strain. Thus, tetrasilatetrahedrane, containing four three-membered rings, isomerizes, with no significant barrier, by breaking two Si—Si bonds to form an isomer with one four-membered silicon ring.[33] For the silicon[27,34–37] and germanium[28] analogues of bicyclo[1.1.0]butane containing two fused three-membered rings, two distinctly different structures were located as minima, the isomer with the longer central bond being more stable than the normal bond structure. Upon going to the even heavier tin and lead analogues of bicyclo[1.1.0]butane, only bond-stretch isomers were located at the TCSCF/DZ(*d*) level.[38] As shown in Fig. 8, the central Sn—Sn and Pb—Pb bond distances become 0.832 and 0.986 Å longer than the Sn—Sn and Pb—Pb single bond

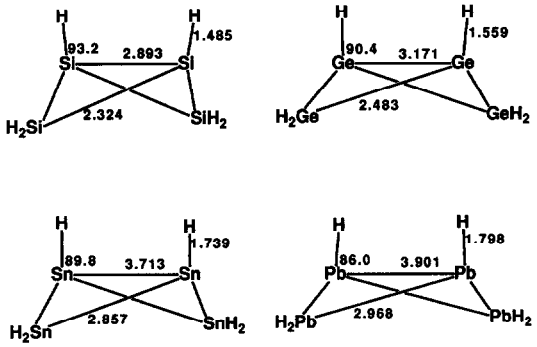

Fig. 8. The TCSCF/DZ(*d*) optimized structures of bond stretch isomers of bicyclic compounds (in Å and °). Interflap angles between the three-membered rings are 138.7 (Si), 140.8 (Ge), 144.0 (Sn) and 151.6° (Pb).

distances in $H_3Sn—SnH_3$ and $H_3Pb—PbH_3$ at the TCSCF/DZ(*d*) level, respectively. The bond-stretch isomers can be viewed as four-membered monocyclic rings with a very weak transannular bond.[28] As is apparent from these results, bond stretching is caused so as to decrease the number of three-membered rings and to create instead less strained four-membered rings.

The silicon analogue of [1.1.1]propellane, containing three fused three-membered rings, undergoes bond-stretching in the central Si—Si bond.[23,39] This was also calculated for the germanium analogue.[40] This theoretical prediction was recently verified by the successful synthesis of 2,2,4,4,5,5-hexakis(2,6-diethylphenyl)pentastanna[1.1.1]propellane.[41] According to its X-ray structure, the central Sn—Sn bond is stretched to 3.367 Å, for which significant singlet diradical character is suggested. Figure 9 shows the optimized structure of the parent compound.[42] The calculated Sn—Sn distances of 3.495 [HF/DZ(*d*)] and 3.502 [TCSCF/DZ(*d*)] Å are *ca* 0.1 Å longer than the value in the X-ray structure of the derivative. This discrepancy may be, in part, ascribed to the presence of the 2,6-diethylphenyl groups on the peripheral tin atoms in the derivative.

The TCSCF wave function (Ψ) of pentastanna[1.1.1]propellane is expressed as

$$\Psi = c_1(\sigma)^2 - c_2(\sigma^*)^2,$$

where σ and σ^* are the bonding and antibonding natural orbitals associated with the central Sn—Sn bond. The closer the square of the c_2 expansion coefficient is to 0.5, the more the wave function corresponds to a singlet diradical. The calculated $(c_2)^2$ value of 0.06 is six times larger than the value of 0.01 in $H_3Sn—SnH_3$: this may support a somewhat diradical character. However, the small value (compared with 0.5) is surprising in light of the stretched central Sn—Sn bond and is comparable with the value of 0.05 calculated for [1.1.1]propellane.[43] In the generalized valence bond approach to the bonding in [1.1.1]propellane, the overlap between the orbitals forming the central C—C bond is calculated to be 0.62.[44] This value is also comparable with the value of 0.59 calculated for pentastanna[1.1.1]propellane.[42] Incidentally, the overlaps were 0.57 and 0.59 in the silicon and germanium analogues, respectively.[42]

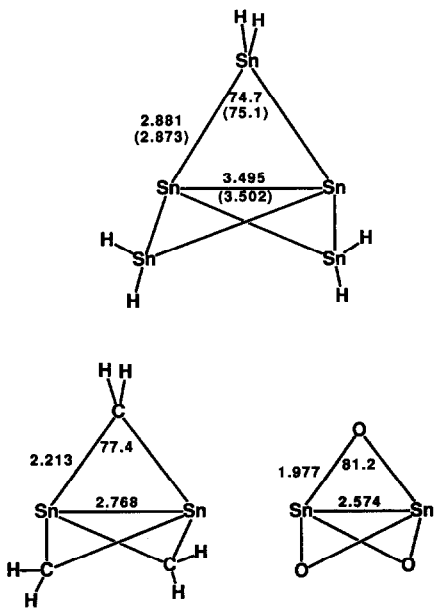

Fig. 9. Pentastanna[1.1.1]propellane and its derivatives at the HF/DZ(*d*) and TCSCF/DZ(*d*) (in parentheses) levels.

It is instructive to view pentastanna[1.1.1]propellane as resulting from a donor–acceptor interaction between SnSn and three SnH_2 units. The SnSn part participates in the interaction as an acceptor, as the negative charge of −0.12e on SnSn suggests. The electron donation into the antibonding π^* vacant orbital of the original SnSn unit may be responsible for the stretching of the central Sn—Sn bond. If this view is correct, electron-accepting substituents at the peripheral positions should significantly suppress the stretching of the central Sn—Sn bond.

As an attempt, the peripheral SnH_2 groups in pentastanna[1.1.1]propellane were all replaced by CH_2 groups because carbon is electronegative to tin. This generated a large amount of positive charge (+0.61e) on each bridgehead tin atom as a result of the increased electron donation from SnSn to three CH_2 units and the decreased back donation into the π^* orbital of SnSn. Thus, the central Sn—Sn bond distance was shortened to 2.768 Å in 1,3-distanna[1.1.1]propellane (Fig. 9). This clearly suggests that the greater the accepting capacity of the peripheral groups, the shorter the central Sn—Sn bond, as emphasized in the silicon and germanium analogues.[23,40]

To confirm this further, we next replaced the CH_2 groups by more electronegative oxygen atoms. The great difference in electronegativity between oxygen and tin leads to the predominance of a π (SnSn) → O forward donation over O → π^*(SnSn) back donation and makes the bridgehead tin atoms more positively charged to 1.37e. The predominance of the forward donation will lead to the formation of a π complex or a three-centre, two-electron bond between SnSn and O. On the other hand, little back donation into the π^* orbital of SnSn and the resultant large charge separation ($Sn^{+1.37}$ and $O^{-0.91}$) and suitable for the proximity of the central bridge-

head tin atoms. Reflecting these, the Sn—Sn bond distance becomes as short as 2.574 Å in 2,4,5-trioxa-1,3-distanna[1.1.1]propellane (Fig. 9).

In contrast to the heavier analogues of [1.1.1]propellane, the heavier analogues of [2.2.2]propellane, consisting of only four-membered rings, have normal central bond distances.[23,42]

For [2.2.2]propellane it was predicted long ago that there are two minima as a result of the crossing in orbital energies of the symmetric (bonding) and asymmetric (antibonding) orbitals of the central C—C bond.[45] The crossing arises from the advantage of through-bond over through-space interactions as the central bond is severely elongated, giving a diradical (see Scheme 1). This was also calculated for the heavier silicon, germanium and tin analogues of [2.2.2]propellane.[42] According to the calculations at the TCSCF/DZ(*d*)//TCSCF/DZ level, normal-bond structures were more stable than diradical structures by 6.0 (Si), 3.0 (Ge) and 2.4 (Sn) kcal mol^{-1}. In addition, the isomerizations of the normal closed-shell structures to diradicals were hindered by significant barriers of 11.5 (Si), 10.2 (Ge) and 9.8 (Sn) kcal mol^{-1}. However, more sophisticated calculations will be essential since these energy values are sensitive to electron correlation.[43]

UNUSUALLY SHORT PHANTOM BONDS

We have recently found that the Si—Si and Ge—Ge distances become unusually short in 2,4,5-trioxa-1,3-disilabicyclo[1.1.1]pentane (**1**)[46] and 2,4,5-trioxa-1,3-digermabicyclo[1.1.1]pentane (**2**),[40] despite the separations between the formally non-bonded atoms. We explained these short distances in terms of a small amount of back donation from the linked oxygen atoms and the resultant large charge separation. In addition, a purely ionic model was also suggested.[47]

Figure 10 shows the optimized structures of the even heavier analogues, 2,4,5-trioxa-1,3-distannabicyclo[1.1.1]pentane (**3**) and 2,4,5-trioxa-1,3-diplumbabicyclo[1.1.1] pentane (**4**), at the HF/DZ(*d*) level. For comparison, **1** and **2** were also calculated at the same level. The optimized Si—Si and Ge—Ge distances of 2.069 and 2.235 Å agree well with our previous values of 2.060 Å [HF/6-31G(*d*)][46] and 2.222 Å [HF/3-21G(*d*)],[40] respectively; the present values are calculated to be only slightly longer.

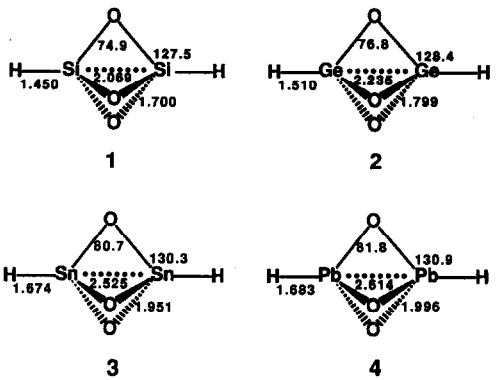

Fig. 10. HF/DZ(*d*) optimized structures of D_{3h} symmetry (in Å and °).

As Fig. 10 shows, **3** and **4** also have very short distances between the formally non-bonded atoms: Sn—Sn = 2.525 Å in **3** and Pb—Pb = 2.614 Å in **4**. These structures of D_{3h} symmetry are indeed energy minima, as shown by all real vibrational frequencies in Table 3. The Sn—Sn and Pb—Pb distances in **3** and **4** are 0.314 (11%) and 0.254 (9%) Å shorter than the Sn—Sn and Pb—Pb single bond distances of 2.839 Å in $H_3Sn—SnH_3$ and 2.868 Å in $H_3Pb—PbH_3$ at the HF/DZ(*d*) level, respectively. These compare favourably with the corresponding Si—Si and Ge—Ge shortenings of 0.275 Å (12%) in **1** from $H_3Si—SiH_3$ and 0.245 Å (10%) in **2** from $H_3Ge—GeH_3$.

Noteworthy is the fact that the Sn—Sn distance of 2.525 Å in **3** is *ca* 0.23 Å shorter than the double bond distances in distannenes ($R_2Sn{=}SnR_2$): 2.768 Å in the X-ray structure of a derivative [R = CH $(SiMe_3)_2$] with a *trans*-bent C_{2h} framework[48] and 2.747 [HF/DZ(*d*)] Å in the parent $H_2Sn{=}SnH_2$ (C_{2h}). The enforced optimization of $H_2Sn{=}SnH_2$ in higher D_{2h} symmetry leads to a shorter Sn—Sn distance of 2.558 Å [HF/DZ(*d*)], but this less stable planar D_{2h} form corresponds to a transition structure for *trans*-bending, as well known for the silicon and germanium analogues.[48,49] The Sn—Sn double bond distances in distannenes exceed the sum of the double bond covalent radii (2.60 Å)[50] and are only slightly shorter than the Sn—Sn single bond distances in distannanes ($R_3Sn—SnR_3$).[48,51] This is because tin is much more reluctant to form distinct double bonds[48,52–54] than silicon and germanium: for a weak dative bond description, see refs 48 and 52; for a σ conjugative interaction, see ref. 53; for a resonating-unshared-pair bond, see ref. 54. In this context, the short Sn—Sn distance in **3** is surprising

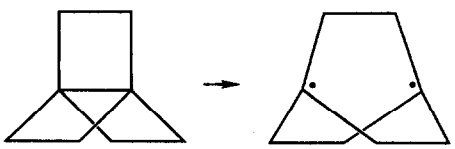

Scheme 1.

Table 3. Harmonic vibrational frequencies (cm^{-1}) and IR intensities (km mol^{-1}) of **1–4** in D_{3h} symmetry at the HF/DZ level[a]

Symmetry	1	2	3	4
e''	536(0)	426(0)	400(0)	316(0)
e'	545(78)	461(91)	400(77)	364(77)
e'	706(2)	649(2)	575(37)	542(20)
e''	736(0)	676(0)	595(0)	557(0)
a_1'[b]	750(0)	467(0)	352(0)	254(0)
a_2''	766(339)	635(240)	598(242)	545(187)
e'	898(393)	765(258)	660(297)	614(234)
a_1'	917(0)	817(0)	731(0)	677(0)
a_2''	2504(58)	2347(55)	2109(117)	2047(205)
a_1'	2510(0)	2350(0)	2113(0)	2056(0)

[a] Values in parentheses are IR intensities.
[b] Stretching between the central heavy atoms.

since its shortening percentage of 11% (0.314 Å) from $H_3Sn—SnH_3$ differs little from that of 13% (0.192 Å) for the C—C bond from $H_3C—CH_3$ to $H_2C{=}CH_2$.[55] In this sense, **3** is the first example with a "true (?)" double bond distance.

Despite recent great developments in the chemistry of the heavy analogues of alkenes,[56] very little is still known about the heaviest lead analogues, diplumbenes ($R_2Pb{=}PbR_2$). According to the calculations of the parent $H_2Pb{=}PbH_2$, the double bond breaks down even in the *trans*-bent C_{2h} form: its optimized Pb—Pb distance is as long as 3.116 [HF/DZ(*d*)] and 3.026 [MCSCF/DZ(*d*)] Å and becomes much longer than the Pb—Pb single bond in $H_3Pb—PbH_3$. This suggests that lead does not form double bonds.[57] In this connection, the non-

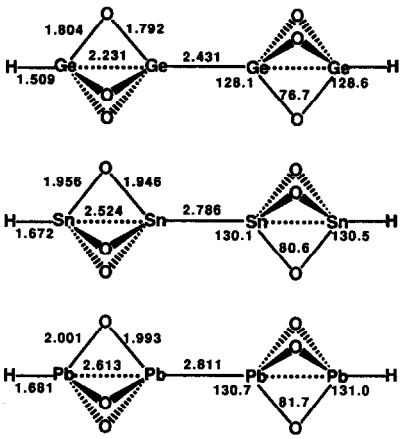

Fig. 11. HF/DZ(*d*) optimized structures of D_{3d} symmetry (in Å and °).

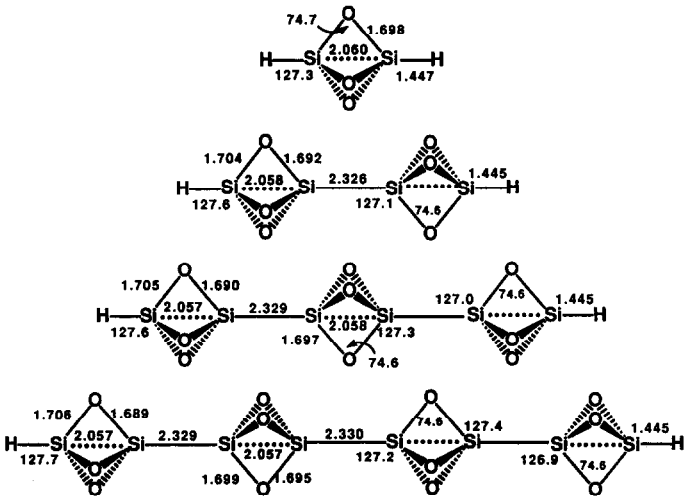

Fig. 12. The HF/6-31(*d*) optimized structure of $H—(Si_2O_3)_n—H$ of D_{3h} (n = 1 and 3) and D_{3d} (n = 2 and 4) symmetry in the staggered forms.

bonded Pb—Pb separation of 2.614 Å in **4** is unprecedentedly short which imitates a double bond distance.

It is interesting that the record distances are kept even in the dimeric forms, as shown in Fig. 11. In addition, it is also interesting to note that the central Ge—Ge (2.431 Å), Sn—Sn (2.786 Å) and Pb—Pb (2.811 Å) single bonds are significantly shorter than the normal single bonds, as in recent topics of the short C—C central single bonds in the cage and bridged ring systems with widened bond angles.[58]

Figure 12 shows the HF/6–31G(*d*) optimized structure of the silicon polymer, H—$(Si_2O_3)_n$—H (n = 1–4).[20] The non-bonded Si—Si separations of *ca* 2.06 Å are considerably shorter than the Si—Si double bond distances of 2.134 Å [HF/6-31G(*d*)] in $H_2Si{=}SiH_2$ and 2.14–2.16 Å in the X-ray structures of the derivatives.[56] No Si—Si triple bond has yet been isolated, although the possible transient existence of *trans*-bent dimethyldisilyne (MeSi≡SiMe) has recently been suggested.[59,60] In this context, it is noteworthy that the non-bonded Si—Si separations in H—$(Si_2O_3)_n$—H compare favourably with the formal Si—Si triple bond distance of 2.083 [HF/6–31G(*d*)] Å in *trans*-bent disilyne (HSi≡SiH). Thus, the silicon skeletons of the polymers having alternatively single and double (or triple) bond distances in the linear chain provide a long-sought polysilene (or polysilyne).

Acknowledgements—This work was undertaken with T. Kudo, M. Nakano and M. Souma in our research group and was, in part, supported by a grant from the Ministry of Education, Science and Culture in Japan. All calculations were carried out at the Computer Room of the Faculty of Education of Yokohama National University and at the Computer Center of the Institute of Molecular Science using the GAUSSIAN 82, 86 and 88 programs.[61–63] Thanks are also due to Dr T. Kudo for the critical reading of the manuscript.

REFERENCES

1. M. N. Francl, W. J. Pietro, W. J. Hehre, J. S. Binkley, M. S. Gordon, D. J. DeFrees and J. A. Pople, *J. Chem. Phys.* 1982, **77**, 3654.
2. W. R. Wadt and P. J. Hay, *J. Chem. Phys.* 1985, **82**, 284.
3. S. Huzinaga, J. Andzelm, M. Klobukowski, E. Radzio-Andzelm, Y. Sakai and H. Tatewaki, *Gaussian Basis Sets for Molecular Calculations*. Elsevier, New York (1984).
4. S. Huzinaga, *J. Chem. Phys.* 1965, **42**, 1293; T. H. Dunning, *J. Chem. Phys.* 1970, **53**, 2823; T. H. Dunning and P. J. Hay, in *Modern Theoretical Chemistry* (Edited by H. F. Schaefer), Vol. 3, p. 1. Plenum Press, New York (1977).
5. J. S. Binkley, J. A. Pople and W. J. Hehre, *J. Am. Chem. Soc.* 1980, **102**, 939.
6. J. S. Binkley and J. A. Pople, *Int. J. Quantum Chem. Symp.* 1975, **9**, 229; J. A. Pople, J. S. Binkley and J. A. Pople, *Int. J. Quantum Chem. Symp.* 1976, **10**, 1; R. Krishnam, M. J. Frisch and J. A. Pople, *J. Chem. Phys.* 1980, **72**, 4244.
7. S. Nagase, T. Kudo and M. Aoki, *J. Chem. Soc., Chem. Commun.* 1985, 1121.
8. D. A. Clabo and H. F. Schaefer, *J. Chem. Phys.* 1986, **84**, 1664.
9. A. F. Sax and R. Janoschek, *Angew. Chem., Int. Edn Engl.* 1986, **25**, 651.
10. S. Nagase, H. Teramae and T. Kudo, *J. Chem. Phys.* 1987, **86**, 4513.
11. A. F. Sax, J. Kalcher and R. Janoschek, *J. Comput. Chem.* 1988, **9**, 564.
12. S. Nagase and T. Kudo, to be published.
13. D. L. Cooper, J. Gerratt and M. Raimondi, *Nature* 1986, **323**, 699.
14. G. Ohanessian, P. C. Hiberty, J.-M. Lefour, J.-P. Flament and S. S. Shaik, *Inorg. Chem.* 1988, **27**, 2219; S. S. Shaik, P. C. Hiberty, G. Ohanessian and J.-M. Lefour, *J. Phys. Chem.* 1988, **92**, 5086; K. Jug and A. M. Koster, *J. Am. Chem. Soc.* 1990, **112**, 6772; refs cited therein.
15. K. B. Wiberg, *Angew. Chem., Int. Edn Engl.* 1986, **25**, 312.
16. P. George, M. Trachtman, C. W. Bock and A. M. Brett, *Tetrahedron* 1976, **32**, 317.
17. S. Nagase, M. Nakano and T. Kudo, *J. Chem. Soc., Chem. Commun.* 1987, 60.
18. H. Matsumoto, K. Higuchi, Y. Hoshino, H. Koike, Y. Naoi and Y. Nagai, *J. Chem. Soc., Chem. Commun.* 1988, 1083; private communication from Professor Matsumoto.
19. R. Gilardi, M. Maggini and P. E. Eaton, *J. Am. Chem. Soc.* 1988, **110**, 7232; K. Hassenruck, J. G. Radziszewski, V. Balaji, G. S. Murthy, A. J. McKinley, D. E. David, V. M. Lynch, H.-D. Martin and J. Michl, *J. Am. Chem. Soc.* 1990, **112**, 873.
20. S. Nagase and M. Souma, to be published.
21. P. E. Eaton, Y. S. Or and S. J. Branca, *J. Am. Chem. Soc.* 1981, **103**, 2134; P. Engel, P. E. Eaton and B. K. Ravi Shankar, *Z. Kristall.* 1982, **159**, 239; E. Honegger, P. E. Eaton, B. K. Ravi Shankar and E. Heilbronner, *Helv. Chim. Acta* 1982, **65**, 1982; P. E. Eaton, Y. S. Or, S. J. Branca and B. K. Ravi Shankar, *Tetrahedron* 1986, **42**, 1621.
22. G. Mehta and S. Padma, *J. Am. Chem. Soc.* 1987, **109**, 2212.
23. S. Nagase and T. Kudo, *Organometallics* 1987, **6**, 2456.
24. S. Nagase, *Angew. Chem., Int. Edn Engl.* 1989, **28**, 329.
25. A. Sekiguchi, C. Kabuto and H. Sakuri, *Angew. Chem., Int. Edn Engl.* 1989, **28**, 55.
26. D. Cremer, J. Gauss and E. Cremer, *J. Molec. Struct. (Theochem)* 1988, **169**, 531.
27. S. Nagase and T. Kudo, *J. Chem. Soc., Chem. Commun.* 1988, 54.

28. S. Nagase and M. Nakano, *J. Chem. Soc., Chem. Commun.* 1988, 1077.
29. S. Nagase and T. Kudo, *J. Chem. Soc., Chem. Commun.* 1990, 630.
30. H. Matsumoto, H. Miyamoto, N. Kojima and Y. Nagai, *J. Chem. Soc., Chem. Commun.* 1987, 1316; H. Matsumoto, H. Miyamoto, N. Kojima, Y. Nagai and M. Goto, *Chem. Lett.* 1988, 629.
31. L. R. Sita and R. D. Bickerstaff, *J. Am. Chem. Soc.* 1989, **111**, 3769.
32. P. Pyykko, *Chem. Rev.* 1988, **88**, 563.
33. S. Nagase and M. Nakano, *Angew. Chem., Int. Edn Engl.* 1988, **27**, 1081.
34. P. v. R. Schleyer, A. F. Sax, J. Kalcher and R. Janoschek, *Angew. Chem., Int. Edn Engl.* 1987, **26**, 364.
35. T. Dabisch and W. W. Schoeller, *J. Chem. Soc., Chem. Commun.* 1986, 896; W. W. Schoeller, T. Dabisch and T. Busch, *Inorg. Chem.* 1987, **26**, 4383.
36. J. A. Boatz and M. S. Gordon, *J. Phys. Chem.* 1989, **93**, 2888.
37. D. B. Kitchen, J. E. Jackson and L. C. Allen, *J. Am. Chem. Soc.* 1990, **112**, 3408.
38. T. Kudo and S. Nagase, to be published.
39. P. v. R. Schleyer and R. Janoschek, *Angew. Chem., Int. Edn Engl.* 1987, **26**, 1267.
40. S. Nagase and T. Kudo, *Organometallics* 1988, **7**, 2534.
41. L. R. Sita and R. D. Bickerstaff, *J. Am. Chem. Soc.* 1989, **111**, 6454.
42. S. Nagase, to be published.
43. D. Feller and E. R. Davidson, *J. Am. Chem. Soc.* 1987, **109**, 4133.
44. R. P. Messmer and P. A. Schultz, *J. Am. Chem. Soc.* 1986, **108**, 7407.
45. W.-D. Stohrer and R. Hoffmann, *J. Am. Chem. Soc.* 1972, **94**, 779.
46. S. Nagase, T. Kudo and T. Kurakake, *J. Chem. Soc., Chem. Commun.* 1988, 1063.
47. A. Streitwieser, *J. Chem. Soc., Chem. Commun.* 1989, 1261.
48. D. E. Goldberg, P. B. Hitchcock, M. F. Lappert, K. M. Thomas, A. J. Thorne, T. Fjeldberg, A. Haaland and B. E. R. Schilling, *J. Chem. Soc., Dalton Trans.* 1986, 2387; D. E. Goldberg, D. H. Harris, M. F. Lappert and K. M. Thomas, *J. Chem. Soc., Chem. Commun.* 1976, 261.
49. G. Trinquier, J.-P. Malrieu and P. Riviere, *J. Am. Chem. Soc.* 1982, **104**, 4529; S. Nagase and T. Kudo, *J. Molec. Struct. (Theochem)* 1983, **103**, 35; S. Nagase, T. Kudo and K. Ito, in *Applied Quantum Chemistry* (Edited by V. H. Smith, H. F. Schaefer and K. Morokuma), p. 249. Reidel, Dordrecht (1986); K. Somasundran, R. D. Amos and N. C. Handy, *Theor. Chim. Acta* 1986, **70**, 393; H. Teramae, *J. Am. Chem. Soc.* 1987, **109**, 4140; J.-P. Malrieu and G. Trinquier, *Theor. Chim. Acta* 1989, **111**, 5916; A. Marquez, G. G. Gonzalez and J. F. Sanz, *Chem. Phys.* 1989, **138**, 99.
50. L. Pauling, *The Nature of the Chemical Bond.* Cornell University Press, Ithaca, New York (1960).
51. H. Puff, B. Breuer, G. Gehrke-Brinkmann, P. Kind, H. Reuter, W. Schuh, W. Wald and G. Weidenbruck, *J. Organomet. Chem.* 1989, **363**, 265.
52. K. W. Zilm, G. A. Lawless, R. M. Merrill, J. M. Miller and G. G. Webb, *J. Am. Chem. Soc.* 1987, **109**, 7236.
53. M. J. S. Dewar, G. L. Grady, D. R. Kuhn and K. M. Merz, *J. Am. Chem. Soc.* 1984, **106**, 6773.
54. L. Pauling, *Proc. Natl. Acad. Sci. USA* 1983, **80**, 3871.
55. W. J. Hehre, L. Radom, P. v. R. Schleyer and J. A. Pople, Ab Initio *Molecular Orbital Theory*, p. 147. John Wiley, New York (1986).
56. G. Raabe and J. Michl, *Chem. Rev.* 1985, **85**, 419; A. H. Cowley and N. C. Norman, *Prog. Inorg. Chem.* 1986, **34**, 1; R. West, *Angew. Chem., Int. Edn Engl.* 1987, **26**, 1201; J. Barrau, J. Escudie and J. Satge, *Chem. Rev.* 1990, **90**, 283.
57. G. Trinquier, *J. Am. Chem. Soc.* 1990, **112**, 2130.
58. O. Ermer, P. Bell, J. Schafer and G. Szeimies, *Angew. Chem., Int. Edn Engl.* 1989, **28**, 473; P. v. R. Schleyer and M. Bremer, *Angew. Chem., Int. Edn Engl.* 1989, **28**, 1226; Y. Xie and H. F. Schaefer, *Chem. Phys. Lett.* 1989, **161**, 516.
59. A. Sekiguchi, S. S. Zigler, R. West and J. Michl, *J. Am. Chem. Soc.* 1986, **108**, 4241.
60. B. S. Thies, R. S. Grev and H. F. Schaefer, *Chem. Phys. Lett.* 1987, **140**, 355.
61. J. S. Binkley, M. J. Frisch, D. J. DeFrees, K. Raghavachari, R. A. Whiteside, H. B. Schlegel, E. M. Fluder and J. A. Pople, Gaussian 82. Department of Chemistry, Carnegie-Mellon University, Pittsburgh.
62. M. J. Frish, J. S. Binkley, H. B. Schlegel, K. Raghavachari, R. Martin, J. J. P. Stewart, F. Bobrowicz, D. J. DeFrees, R. Seeger, R. A. Whiteside, D. Fox, E. M. Fluder and J. A. Pople, Gaussian 86, Release C. Gaussian Inc., Pittsburgh.
63. M. J. Frisch, M. Head-Gordon, H. B. Schlegel, K. Raghavachari, J. S. Binkley, C. Gonzales, D. J. DeFrees, D. J. Fox, R. A. Whiteside, R. Seeger, C. F. Melius, J. Baker, R. Martin, L. R. Kahn, J. J. P. Stewart, E. M. Fluder, S. Topiol and J. A. Pople, Gaussian 88, Release C. Gaussian Inc., Pittsburgh.

Polyhedron Vol. 10, No. 12, pp. 1311–1317, 1991
Printed in Great Britain

0277–5387/91 $3.00+.00
© 1991 Pergamon Press plc

MECHANOCHEMICAL SYNTHESIS OF SOLUBLE COMPLEXES CONTAINING $M_3S_7^{4+}$ AND $M_3Se_7^{4+}$ FRAGMENTS FROM POLYMERIC $M_3Y_7Br_4$ (M = Mo, W; Y = S, Se). THE CRYSTAL STRUCTURE OF $(PPN)_2W_3S_7Cl_6$

V. P. FEDIN,* M. N. SOKOLOV, K. G. MYAKISHEV, O. A. GERAS'KO and V. Ye. FEDOROV

Institute of Inorganic Chemistry, Siberian Branch of the U.S.S.R. Academy of Sciences, 630090 Novosibirsk, Pr. Lavrentyeva 3, U.S.S.R.

and

J. MACIČEK

Institute of Applied Mineralogy, Bulgarian Academy of Sciences, Sophia, Rakowskij str 92, 1000, Bulgaria

(*Received* 7 *September* 1990; *accepted* 7 *January* 1991)

Abstract—The interaction of solid $W_3S_7Br_4$ or $W_3Se_7Br_4$ with Et_4NBr under vibrational mill conditions followed by extraction with acetonitrile resulted in the isolation of $(Et_4N)_2W_3S_7Br_6$ (**1**) and $(Et_4N)_2W_3Se_7Br_6$ (**2**) salts. Treatment of the product of the analogous reaction of $Mo_3Se_7Br_4$ and Et_4NBr with sodium diethyldithiocarbamate (Nadtc) resulted in $[Mo_3Se_7(dtc)_3]dtc$ (**4**). The $M_3Y_7^{4+}$ (Y = S, Se) cluster fragments are retained in all of these reactions. By dissolving **1** in conc. hydrochloric acid and adding PPNCl, the $(PPN)_2W_3S_7Cl_6$ salt (**5**) was obtained, for which an X-ray study has been performed. Selected distances for the cluster anion $W_3(\mu_3\text{-}S)(\mu_2\text{-}S_2)_3Cl_6^{2-}$ are 2.7270(7)–2.7445(6) Å for W—W, 2.360(3)–2.361(3) Å for W—(μ_3-S), 2.032(4)–2.052(4) Å for S—S, 2.429(3)–2.459(2) and 2.493(4)–2.519(3) Å for W—Cl (for *cis* and *trans* positions with respect to μ_3-S, respectively). Rather short distances (3.17–3.21 Å) between the chlorine atoms and sulphur atoms of the μ_2-S_2 ligands of the adjacent anions were noted. The interaction of **2** with 1,2-bisdiphenylphosphine ethane (dppe) is accompanied by elimination of selenium to produce $[W_3Se_4Br_3(dppe)_3]Br$ (**6**).

Although the first cluster chalcogenides of molybdenum of the composition $Mo_3Y_7X_4$ (Y = S, Se; X = Cl, Br) had been synthesized in 1968,[1] the study of their chemical properties was strongly hampered by their low reactivity. X-ray studies of $Mo_3S_7Cl_4$[2] indicated this cluster to have a polymeric structure with the four chlorines being bridging atoms connecting adjacent $Mo_3S_7^{4+}$ units which is described by the crystallochemical formula $[Mo_3S_7Cl_2Cl_{4/2}]_\infty$. The recently obtained thiobromide, $W_3S_7Br_4$,[3] has the same structure also and, apparently, so have all other $M_3Y_7(Hal)_4$ (Y = S, Se; Hal = halogen) compounds.

The known examples of depolymerization of these compounds occurring with breaking of the halogenide bridges to produce molecular complexes take place under rather severe conditions. Thus $Mo_3S_7X_4$ (X = Cl, Br) and $W_3S_7Br_4$ interact with PPh_4X only in melts at 270–300°C to produce the $(PPh_4)_2Mo_3S_7X_6$ (X = Cl, Br) and $(Ph_4P)_2W_3S_7Br_6$ salts in high yields, which have been structurally characterized.[4,5] The interaction of the same chalcohalogenides with Et_4NX in boiling solutions of conc. HX (X = Cl, Br) produces Et_4N^+ salts in very low and poorly reproducible yields.

In the present work we have found that the reactivity of $M_3Y_7(Hal)_4$ considerably increases under the conditions of mechanochemical activation

* Author to whom correspondence should be addressed.

Table 1. Analytical and spectral data for triangular complexes of molybdenum and tungsten

Compound	Colour		Analyses Found (%)	Calc. (%)	Spectral data
$(Et_4N)_2W_3Se_7Br_6$ (**2**)	Brown	W	30.9	29.9	IR: 314, 296, 252, 248, 232, 212, 201, 182, 158, 148, 139, 124 cm^{-1}
		Se	29.3	29.9	
		Br	25.0	26.0	Raman: 313, 282, 252, 231, 200 cm^{-1}
		N	1.4	1.5	
$[Mo_3Se_7(dtc)_3]dtc$ (**4**)	Red	Mo	20.0	20.1	IR (4000–400 cm^{-1}): 2980, 2920, 1510, 1500, 1450, 1430, 1400, 1370, 1350, 1290, 1270, 1250, 1200, 1140, 1120, 1070, 990, 900, 840, 770, 605, 590, 575, 565 cm^{-1}
		Se	37.9	38.6	
		S	17.6	17.9	
		C	16.7	16.7	
		H	2.4	2.8	Raman: 336, 309, 272, 254, 171, 138 cm^{-1}
		N	3.8	3.9	^1H NMR: $\delta(CDCl_3$, from TMS) 4.14 (4H), 3.77 (4H), 3.69 (4H) (m, CH_2), 1.26 (24H) (t, CH_3)
$[W_3Se_4Br_3(dppe)_3]Br$ (**6**)	Green	Se	12.6	13.3	$^{31}P\{^1H\}$ NMR (0.5 M in $CDCl_3$): 36.455 MHz (ppm, from 85% H_3PO_4), +8.6(3P), −1.5(3P)
		Br	14.3	13.4	
		C	39.4	39.2	Electronic spectrum (CH_2Cl_2): $\lambda = 645$ nm ($\varepsilon = 1070$ dm^3 mol^{-1} cm^{-1})
		H	3.2	3.0	

which opens up new possibilities for the synthesis of complexes of $M_3Y_7^{4+}$ and $M_3Y_4^{4+}$.

EXPERIMENTAL

The synthesis of $W_3S_7Br_4$ from the elements followed ref. 5. Bromine was purified over P_4O_{10}, and the molybdenum and tungsten metals were annealed under H_2O before use. The organic solvents were purified by the standard methods.[6] dppe was synthesized according to ref. 7. All other reagents were of reagent-grade purity and used without further purification. $M_3Se_7Br_4$ compounds were obtained by heating stoichiometric amounts of the elements in evacuated quartz ampoules at 300–350°C for 70–90 h.

Experimental equipment

The IR spectra were recorded on a IFS-113 Fourier spectrometer (Bruker) in polyethylene. The Raman spectra were obtained on a Triplimate-2I spectrometer. The ^1H and ^{31}P NMR spectra were taken on a SXP-4-100 (Bruker) instrument at 290 K. The UV–vis spectra were taken on a "Specord" spectrometer. Mo, W, S and Se were determined gravimetrically as $Mo(C_9H_6NO)_2$, WO_3, $BaSO_4$ and Se, respectively. C, H, N and Br were determined at the Laboratory of Microanalysis, Institute of Organic Chemistry (Novosibirsk). The analytical and spectral data for the synthesized complexes are listed in Table 1.

The mechanochemical synthesis was performed using the apparatus described in ref. 8. The conditions were as follows. The grinding packing (3 mm diam. steel balls of total mass 300 g filling 72% of the reactor volume) and starting crystalline materials were charged into a cylindrical steel reactor (100 cm^3 volume and 50 mm height) fitted with a flange cover. The frequency of the vertical reciprocating motion of the reactor was 23 Hz, the amplitude 6 mm. The activation continued for 3–4 h. Under these conditions the reactor warmed up to 80–90°C within the first hour of activation.

Interaction of $M_3Y_7Br_4$ *with* Et_4NBr *(a typical procedure)*

Approximately equal amounts of the two reagents (charges of 3–6 g) were ground in the vibrational mill, after which the mixture was taken out and extracted with hot acetonitrile. Then ether was added to the extract and the precipitated solid was filtered, washed with alcohol, ether and vacuum-dried. For further purification, **1** can be recrystallized from acetonitrile or concentrated HBr. In contrast to this, the compounds of selenium quickly decompose in solutions which make their purification difficult. The typical yields were 50–60% for $(Et_4N)_2W_3S_7Br_6$ (**1**), 20–25% for $(Et_4N)_2W_3Se_7Br_6$ (**2**) and 30% for $(Et_4N)_2Mo_3Se_7Br_6$ (**3**).*

* Not obtained in analytically pure form.

Synthesis of $[Mo_3Se_7(dtc)_3]dtc$ (**4**)

Complex **3** (0.62 g) and $NaS_2CNEt_2 \cdot 3H_2O$ (1.00 g) in acetonitrile were boiled under argon for 2.5 h. After cooling, the red crystalline precipitate was filtered and extracted with dichloromethane on a filter. By adding ether to the extract, 0.44 g of red, crystalline substance were obtained. Yield: 25% (in terms of the starting molybdenum metal).

Synthesis of $(PPN)_2W_3S_7Cl_6$ (**5**)

Complex **2** (0.20 g) was dissolved in 30 cm^3 of conc. hydrochloric acid under heating. After addition of 1 g of PPNCl the solution was heated until a solid coagulated and then placed into a refrigerator (−5°C). After 12 h of standing the solid was filtered off, washed with alcohol and ether. 0.26 g of a pink powder **5** were obtained (quantitative yield).

Crystals suitable for an X-ray study were obtained by diffusion of ether vapours into an acetonitrile solution of the complex.

Synthesis of $[W_3Se_4Br_3(dppe)_3]Br$ (**6**)

Complex **2** (0.30 g, 0.11 mmol) and dppe (0.40 g, 0.49 mmol) in 25 cm^3 of acetonitrile were boiled under argon. After 2 h, the hot, green solution was filtered and allowed to stand at −5°C for crystallization. The precipitated green crystals were filtered to give 0.06 g of complex **6**. By adding ether to the mother solution, a further 0.16 g of **6** were obtained which were recrystallized with hexane from dichloromethane for purification. Combined mass obtained, 0.22 g. Yield: 55%.

Table 2. Crystal data and summary of intensity data collection and structure refinement for $(PPN)_2W_3S_7Cl_6$

Formula	$C_{72}H_{60}P_4N_2W_3S_7Cl_6$
M_r	2065.91
Crystal system	Triclinic
Space group	$P\bar{1}$
a (Å)	13.657(1)
b (Å)	18.148(2)
c (Å)	19.009(2)
α (°)	99.45(1)
β (°)	109.54(1)
γ (°)	109.35(1)
V (Å)	3984(2)
Z	2
D_x (g cm^{-3})	1.722
Crystal size (mm)	$0.25 \times 0.30 \times 0.55$
μ (cm^{-1})	49.14
$F(000)$	2004
T (K)	292
Data collection instrument	CAD-4
Radiation	Mo-K_α
Orientation reflections, range (θ)	22, 20–22
Scan method	−2
Data collection, range	$\sin\theta/\lambda < 0.572$ $-15 < h < 14$ $-20 < k < 20$ $0 < l < 21$
Number of unique data, total with $I > 3\sigma(I)$	10 008 9331
Trans. factor, max., min.	99.876, 85.583
R	0.0398
R_w	0.0673
S	2.0965
Maximum shift/error	0.567
Residual densities (e/Å^3)	
max.	5.59
min.	−4.98

Crystal structure determination of **5**

A well-shaped, dark violet crystal with dimensions $0.25 \times 0.30 \times 0.55$ mm was used. The data were collected on an Enraf–Nonius CAD-4 diffractometer using Mo-K_α radiation (graphite monochromator). The unit cell parameters were determined from a total of 22 reflections ($20.0 < \theta < 22.0$). The details of the X-ray experiment are given in Table 2. Three standard reflections were checked every 3 h during data collection. The intensity variations were less than 1%. The measured intensities were corrected for Lorentz and polarization effects. An empirical correction for absorption was made. The materials decomposition due to the X-rays was not taken into account. The three tungsten atoms were located from a Patterson map and the structure was solved finally by full-matrix least-squares. The positions of the hydrogen atoms were calculated and their contributions added to the structure factors but were not refined. No correction for secondary extinction was made. The atomic scattering factors and the anomalous dispersion coefficients were taken from the SDP/PDP V 3.0 Enraf–Nonius package. All calculations were performed on a PDP 11/44 computer.

RESULTS AND DISCUSSION

The study of the chemistry of molybdenum chalcogenide has shown that the $Mo_3S_7^{4+}$ cluster fragment is stable and shows a distinct tendency to form in systems rich in sulphur. This may be illustrated by the diversity of the synthetic routes to $Mo_3S_7X_4$ thiohalcogenides (X = Cl–I). They may be obtained

from elements, or from MoX_2 or MoX_3 and sulphur, or, vice versa, by heating MoS_3 with bromine[1,9–12] or by thermolysis of MoS_4X_2 (X = Br, I).[1] The cluster thio complex $(NH_4)_2Mo_3S_7(S_2)_3$ was obtained by reduction of $(NH_4)_6Mo_7O_{24}$ with ammonium polysulphide,[13] whereas oxidation of $Mo(CO)_6$ or $K_4Mo_2Cl_8$ with $[R_2P(S)]_2S_2$ (R = Et, Pr, Bu) gives rise to $[Mo_3S_7(R_2PS_2)_3]R_2PS_2$.[14] Maoyu *et al.*[15] obtained $[Mo_3S_7\{(EtO)_2PS_2\}_3]Cl$ by the reaction of K_2MoOCl_5 and P_2S_5 in ethanol. Another molybdenum(V) compound, $MoCl_5$, in the reaction with NaSH forms the $(Et_4N)_3Mo_3S_7Cl_7$ salt in 3% yield.[16]

In the case of $W_3S_7^{4+}$ and $M_3Se_7^{4+}$ clusters the only starting compounds to develop the chemistry are the $M_3Y_7X_4$ chalcogenides and the corresponding selenohalogenides of tungsten have not been described at all. Selenohalogenides of molybdenum, first described in 1968,[9] were obtained by heating di- and trihalogenides of molybdenum with selenium at 300–350°C. We have found that the same samples of $Mo_3Se_7Br_4$ can be obtained from the elements by the ampoule method (heating of stoichiometric amounts of elements in evacuated quartz ampoules at 300–350°C for 70–100 h). In the case of tungsten, heating of stoichiometric amounts of the elements under the above conditions affords a product consisting to a considerable extent of $W_3Se_7Br_4$. Because of the lower reactivity of tungsten and selenium in comparison with molybdenum and sulphur, respectively, the individual product is difficult to obtain; but the selenobromides obtained in this way turned out to be convenient sources of the $M_3Se_7^{4+}$ clusters and presented no problems of separation from the side reaction products.

As a result of the mechanochemical reactions [eq. (1)],

$$M_3Y_7Br_4 + 2Et_4NBr \longrightarrow (Et_4N)_2M_3Y_7Br_6$$

M = W, Y = S (**1**)
M = W, Y = Se (**2**)
M = Mo, Y = Se (**3**) (1)

complexes with molecular structure are produced from the polymeric chalcogalogenides. Vibrational spectra of **1** indicate it to be identical to the product produced in low yield in the reaction Et_4NBr with $W_3S_7Br_4$ in boiling, conc. HBr.[5] In the case of selenohalogenides, comparison of the vibrational spectra of the starting $Mo_3Se_7Br_4$ and the products of reaction (1) indicates that the central, structural fragment $M_3Se_7^{4+}$ is retained. Although, in contrast to the thio complexes, the cluster seleno complexes are not practically studied by the vibrational spectroscopy methods (determination of the types and the symmetry of the vibrations, the force constants), the bands in the region 330–310 cm^{-1} in the IR and Raman spectra of **1** and **3** and of the starting $Mo_3Se_7Br_4$ and $W_3Se_7Br_4$ can be suggested to correspond essentially to the valence vibrations of the μ_2-Se_2 ligand and the lower energy bands 270–280 cm^{-1} to be associated with the μ_3-Se ligand. In the IR spectra of $NbSe_2Cl_2$ and $NbSe_2Br_2$[17] the bands at 352 and 343 cm^{-1}, respectively, were attributed to ν(Se—Se). The lower-lying M—M, M—Br and M—(μ_2-Se) vibrations must strongly mix with each other. The spectra of **2** and **4** (Raman and IR) are shown in Fig. 1.

As pointed out above, selenohalogenide complexes cannot be recrystallized without decomposition. Compound **3** could not be isolated in analytically pure form. Therefore, in this case, the product of reaction (1) was transformed to the more stable diethyldithiocarbamate complex [eq. (2)]:

$$Mo_3Se_7Br_6^{2-} + 4\,dtc^- \xrightarrow{\text{acetonitrile}} [Mo_3Se_7(dtc)_3]dtc + 6Br^- \quad (2)$$
(**4**)

Complex **4** is poorly soluble in CH_3CN and CH_3NO_2 but readily dissolves in chlorinated and aromatic hydrocarbons. The ^1H NMR spectrum of **4** shows the following features due to the structure of **4**:

(1) Non-equivalence of the methylene groups of the coordinated and uncoordinated dithiocarbamates (the ratio of the signals 3:1); (2) Non-equivalence of the methylene groups of the coordinated dithiocarbamate (the intensity ratio 1:1) due to the retarded rotation about the C—N bond.[18] As a result, two methylene groups from each ligand occupy different positions with respect to the Mo_3 plane. The $[Mo_3S_7(Et_2PS_2)_3]^+$ dtc^- complex, containing dithiocarbamate as a counterion, has been described in ref. 14. Thus, the following structure can be proposed for the $Mo_3Se_7(dtc)_3^+$ cation:

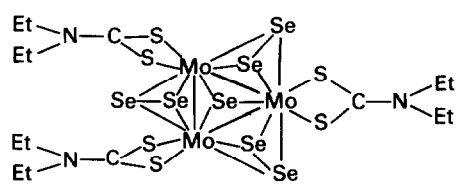

The easy replacement of the halogen atoms in **1**–**3** is also illustrated by the production of the $W_3S_7Cl_6^{2-}$ salt when **1** is recrystallized from conc. hydrochloric acid. Adding PPNCl to this solution results in the isolation of **5** in quantitative yield.

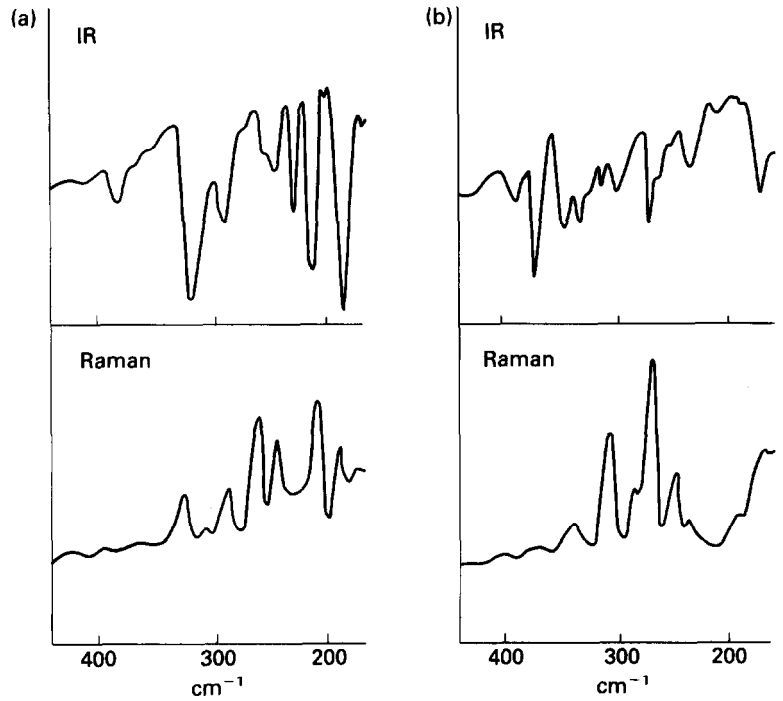

Fig. 1. IR and Raman spectra of (a) $(Et_4N)_2W_3Se_7Br_6$ and (b) $[Mo_3Se_7(dtc)_3]dtc$.

The literature has already described quite a number of examples of transitions from $M_3S_7^{4+}$ to $M_3S_4^{4+}$ derivatives. These reactions consist of the elimination of the equatorial sulphur atoms of the μ_2-S_2 ligand under the action of different nucleophiles.[3,5,19-21] On the whole, the problem of obtaining $Mo_3S_4^{4+}$ and $W_3S_4^{4+}$, both in aqueous and non-aqueous media, can be considered to be solved. In 1985 $Mo_3Se_4^{4+}$(aq) and $Mo_3Te_4^{4+}$(aq) were obtained by Sykes and co-workers[22] by the electrolysis of aqueous solutions of $Mo_2O_4(cys)_2^{2+}$ with a selenium or tellurium cathode. However, no individual solid compounds containing such cluster fragments have been described. Saito *et al.* described[23] the interaction of $Mo_3Se_7Cl_4$ with PEt_3 which probably gives a mixture of several phosphine complexes of $Mo_3Se_4^{4+}$. The $W_3Se_4^{4+}$ derivatives have not been described. We found that **2** readily reacts with dppe upon boiling in acetonitrile to give a bright green solution which crystallizes **6** [eq. (3)]:

$$(Et_4N)_2W_3Se_7Br_6 + 4.5\,dppe \longrightarrow [W_3Se_4(dppe)_3Br_3]Br + 1.5\,dppeSe_2. \quad (3)$$

Complex **6** is soluble in acetonitrile, dichloromethane and chloroform. The electronic spectra of **6** in the visible region contain an absorption band at 645 nm ($\varepsilon = 1070$). Its position and intensity is close to those observed for other $M_3Y_4^{4+}$ chromophores (M = Mo, W; Y = S, Se), indicating, in all appearances, the presence of the $W_3Se_4^{4+}$ chromophore. The ^{31}P NMR spectrum contains two unresolved singlets with an intensity ratio 1 : 1, which indicates the presence of two types of phosphorus atoms coordinated at the tungsten atom in *cis* and *trans* positions with respect to the μ_3-Se ligand. This type of coordination is characteristic of all of the studied complexes $[M_3S_4(\widehat{P\ P})_3X_3]^+$ (M = Mo, W; $\widehat{P\ P}$ = dmpe, dppe; X = Cl, Br, H):[3,18,19,23,24]

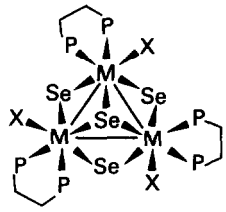

The structure of the $W_3S_7Cl_6^{2-}$ *anion*

The crystal structure of two pairs of polymeric chalcogenides and their anionic complexes have been studied in the chemistry of molybdenum and tungsten: $Mo_3S_7Cl_4$,[2,3] $W_3S_7Br_4$,[3] $(Ph_4P)_2Mo_3S_7Cl_6$[4] and $(Ph_4P)_2W_3S_7Br_6$.[5] The structure has been also determined for $(Et_4N)_3Mo_3S_7Cl_7$[16] in which the anion contains μ_3-Cl weakly coordinated by the axial sulphurs of the μ_2-S_2 ligands (d_{S-Cl} = 2.91–2.95 Å). Here we report the structure of $(PPN)_2W_3S_7Cl_6$.

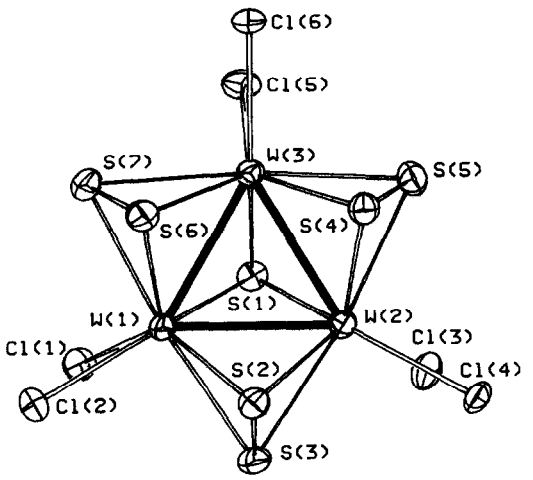

Fig. 2. Structure of $W_3S_7Cl_6^{2-}$ showing the atom labelling scheme.

The structure of the $W_3(\mu_3\text{-}S)(\mu_2\text{-}S_2)_3Cl_6^{2-}$ anion is shown in Fig. 2. There are two independent PPN^+ cations slightly differing in their geometrical parameters but which do not go beyond that typical

Table 3. Bond distances (Å) for the $W_3S_7Cl_6^{2-}$ anion

W(1)—W(2)	2.7451(7)	W(3)—S(1)	2.3698(20)
W(1)—W(3)	2.7270(7)	W(3)—S(4)	2.4015(29)
W(1)—S(1)	2.3595(31)	W(3)—S(5)	2.4909(33)
W(1)—S(2)	2.3966(30)	W(3)—S(6)	2.4000(31)
W(1)—S(3)	2.4885(30)	W(3)—S(7)	2.4915(33)
W(1)—S(6)	2.4021(20)	W(3)—Cl(5)	2.4292(34)
W(1)—S(7)	2.4934(31)	W(3)—Cl(6)	2.5194(20)
W(1)—Cl(1)	2.4498(25)		
W(1)—Cl(2)	2.4977(31)		
W(2)—W(3)	2.7445(6)		
W(2)—S(1)	2.3608(30)		
W(2)—S(2)	2.4006(32)		
W(2)—S(3)	2.4961(32)		
W(2)—S(4)	2.4082(20)		
W(2)—S(5)	2.5071(34)		
W(2)—Cl(3)	2.4587(24)		

Table 5. Deviations of the $W_3S_7Cl_6^{2-}$ atoms from the plane W_3S_3 (Å)

W(1)	0.0344(4)	S(1)	−1.6996(27)
W(2)	0.0928(4)	S(2)	1.7080(27)
W(3)	0.0410(4)	S(4)	1.7209(27)
S(3)	−0.0648(29)	S(6)	1.7125(28)
S(5)	−0.0681(29)	Cl(1)	−1.8796(29)
S(7)	−0.0353(28)	Cl(2)	1.2798(27)
		Cl(3)	−1.6995(29)
		Cl(4)	1.4701(25)
		Cl(5)	−1.8635(29)
		Cl(6)	1.2930(25)

for this cation. In Table 3 are listed the interatomic distances in the $W_3S_7Cl_6^{2-}$ anion. The W—W bond length is, on average, 2.739(1) Å; S—S, 2.039(3) Å; and W—μ_3-S, 2.364(3) Å.

The three tungsten atoms defining an equilateral triangle and the three sulphur atoms of the asymmetrically coordinated μ_2-S_2 ligands practically lie in one plane (deviations from the root-mean-square plane do not exceed 0.1 Å, Table 5). In addition to two μ_2-S_2 and one μ_3-S ligands each tungsten is coordinated by two chlorine atoms at different distances. For the chlorine atoms in the *trans* position to the μ_3-S ligand [Cl(2), Cl(4) and Cl(6)] the average W—Cl distance is 2.524 Å, and in the *cis* position [Cl(1), Cl(3) and Cl(5)] it is 2.446 Å. An analogous situation occurs in the previously studied anions. This appears to be due to the steric effects of the μ_2-S_2 ligands which are strongly tilted towards the M_3 plane and all actually lie on the side of the M_3 triangle which is opposite to μ_3-S (Table 4).

The sulphur atoms of the μ_2-S_2 ligands in such compounds are capable of additionally coordinating halogen atoms, as was shown for $Mo_3S_7Cl_7^{3-}$,[16] $[Mo_3S_7\{(EtO)_2PS_2\}_3Cl]$,[15] with the S—Cl distance (2.9 Å) being intermediate between the covalent (1.9–2.0 Å) and van der Waals' (3.65 Å) interactions. The reason for this behaviour is not clear. We have discovered[4] that the $Mo_3S_7Cl_6^{2-}$

Table 4. Comparison of the $M_3S_7^{4+}$ core dimensions (Å)[a]

Type of bond	$W_3S_7Cl_6^{2-}$[b]	$Mo_3S_7Cl_4^{2}$	$W_3S_7Br_4^{3}$	$Mo_3S_7Cl_6^{2-}$[4]	$W_3S_7Br_6^{2-}$[5]	$Mo_3S_7Cl_7^{3-}$[16]
M—M	2.739(1)	2.745(3)	2.721(3)	2.757(1)	2.739(2)	2.758(1)
S—S	2.039(3)	2.03(1)	1.99(2)	2.023(4)	2.025(9)	2.042(3)
M—μ_3-S	2.364(3)	2.36	2.374(10)	2.348(3)	2.357(6)	2.347(3)
M—μ_2-$S_{eq.}$	2.496(3)	2.50	2.48(2)	2.485(3)	2.490(7)	2.484(3)
M—μ_2-$S_{ax.}$	2.402(3)	2.39	2.39(2)	2.391(3)	2.392(7)	2.392(3)

[a] Middle bond distances are given.
[b] Our data.

anions in the structure of $(Ph_4P)_2Mo_3S_7Cl_6$ are united with centrosymmetric dimers at the expense of the interaction between the chlorine atoms and the sulphur atoms of the μ_2-S_2 ligands (3.12–3.47 Å). Such short S—Cl contacts have also been found by us in the structure of **5** (3.17–3.21 Å).

Acknowledgement—We are grateful to Ms M. P. Primanchuk for halpful discussions.

REFERENCES

1. V. Ye. Fedorov, A. V. Mischenko and V. P. Fedin, *Russ. Chem. Rev.* (*Engl. Transl.*) 1985, **54**, 408.
2. J. Marcoll and A. Rabenau, *Rev. Chim. Minerale* 1974, **11**, 607.
3. F. A. Cotton, P. A. Kibala, M. Matucz, Ch. S. McCaleb and R. B. Sangor, *Inorg. Chem.* 1989, **28**, 2623.
4. A. V. Virovetz, Yu. L. Slovohotov, Yu. T. Struchkov, V. Ye. Fedorov, N. G. Naumov, O. A. Geras'ko and V. P. Fedin, *Koord. Khim.* 1990, **16**, 332.
5. V. P. Fedin, M. N. Sokolov, O. A. Geras'ko, B. A. Kolesov, V. Ye. Fedorov, A. V. Mironov, D. S. Yufit, Yu. L. Slovohotov and Yu. T. Struchkov, *Inorg. Chim. Acta* 1990, **175**, 217.
6. A. J. Gordon and R. A. Ford, *The Chemists Companion*. Wiley, New York (1972),
7. J. Chatt and F. A. Hart, *J. Chem. Soc.* 1960, 1378.
8. V. V. Volkov, K. G. Mjakishev and I. I. Gorbacheva, *Izv. SO AN SSSR, Ser. Khim.* 1983, **12**, 79.
9. A. A. Opalowskii, V. Ye. Fedorov and K. A. Khaldoyanidi, *Dokl. Akad. Nauk SSSR* 1968, **182**, 1095.
10. A. A. Opalowskii, V. Ye. Fedorov, A. P. Mazhara and I. M. Cheremisina, *Zh. Neorg. Khim.* 1972, **17**, 2876.
11. A. P. Mazhara, A. A. Opalowskii, V. Ye. Fedorov and S. D. Kirik, *Zh. Neorg. Khim.* 1977, **22**, 1827.
12. V. Ye. Fedorov, A. P. Mazhara, V. K. Yevstafiev and S. D. Kirik, *Izv. SO AN SSSR, Ser. Khim.* 1978, **14**, 56.
13. A. Müller, R. G. Bhattacharyya and B. Pfeffercorn, *Chem. Ber.* 1979, **112**, 778.
14. H. Keck, W. Kucher and J. Mathow, *Z. Anorg. Allg. Chem.* 1986, **535**, 123.
15. S. Maoyu, H. Jinling and Lu Jiaxi, *Acta Cryst.* 1984, **C40**, 759.
16. P. Klingelhöfer, U. Müller, C. Friebel and J. Pebler, *Z. Anorg. Allg. Chem.* 1986, **543**, 22.
17. J. Rijnsdorp, PhD thesis. University of Reading (1977).
18. F. Duss, in *Comprehensive Organic Chemistry*, Vol. 3. Pergamon Press, New York (1979).
19. V. P. Fedin, M. N. Sokolov and V. Ye. Fedorov, *Koord. Khim.* 1990, **16**, 291.
20. T. Saito, N. Yamamoto, T. Yamagata and H. Imoto, *Chem. Lett.* 1987, 2025.
21. V. P. Fedin, M. N. Sokolov, Yu. V. Mironov, B. A. Kolesov, S. V. Tkachev and V. Ye. Fedorov, *Inorg. Chim. Acta* 1990, **167**, 39.
22. P. Kathirgamanathan, M. Martinez and A. G. Sykes, *Polyhedron* 1986, **5**, 505.
23. T. Saito, N. Yamamoto, T. Nagase, T. Tsuboi, K. Kobayashi, T. Yamagata, H. Imoto and Kei Unoura, *Inorg. Chem.* 1990, **29**, 764.
24. F. A. Cotton, R. Llusar and C. T. Eagle, *J. Am. Chem. Soc.* 1989, **111**, 4332.

Polyhedron Vol. 10, No. 12, pp. 1319–1326, 1991
Printed in Great Britain

0277–5387/91 $3.00+.00
© 1991 Pergamon Press plc

REDOX AND COORDINATIVE PROPERTIES OF N,N′-DITHIOBISAMINES: OXIDATIVE DESULPHURIZATION BY COPPER(II) IONS AND $Cr(CO)_5[S_2(NR_2)_2]$ COMPLEXES

CARLOS DÍAZ

Universidad de Chile, Facultad de Ciencias, Departamento de Química, Casilla 653, Santiago, Chile

(*Received* 20 *November* 1990; *accepted* 9 *January* 1991)

Abstract—N,N′-dithiobisamines, $R_2N—S—S—NR_2$, NR_2=$N(CH_3)_2$, $N(CH_2CH_3)_2$, 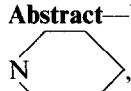 , 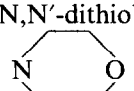 or $N(CH_2—C_6H_5)_2$, are oxidized to SO_2 by copper(II) salts with formation of copper(I) complexes, while from the reaction with pentacarbonyl (tetrahydrofuran)chromium the novel complexes $Cr(CO)_5[S_2(NR_2)_2]$ were isolated. They have been characterized by elemental analysis as well as by spectroscopic methods. The π-acceptor abilities of the sulphur-containing ligands in the $Cr(CO_5)L$ complexes are discussed and compared with those found for their analogous monothio derivatives. Reactivity of the coordinated sulphur compounds towards acids and copper(II) salts is less than that of the free ligands.

Interest in the chemistry of the metal–disulphide interaction has accelerated markedly over the last 50 years, largely because of the importance of this linkage in biological systems.[1,2] Nevertheless, the isolation of metal complexes with organic disulphide is not always facile because certain metal ions cause cleavage of the disulphide bond.[3] The great majority of such studies have been made with disulphide compounds of the type R—S—S—R[3–8] and investigations with disulphides containing bonds other than C—S are scarce.[9–11] As a part of a study of the reactivity and coordination properties of S—N compounds[12–20] we are now investigating the N,N′-dithiobisamines, $R_2N—S—S—NR_2$. These compounds were prepared in 1895[21] but little attention has been paid to their reactivity.[9,22] N,N′-dithiobisamines undergo sulphur–nitrogen fission in reactions with sulphurous acids,[23] thiols[23] and *p*-toluenesulphinic acid,[10] whereas sulphur–sulphur cleavage has been reported in reactions with lithium[24] and chlorine.[9] In spite of the expected coordinative properties arising from the lone electron pairs on the sulphur and nitrogen atoms, to our knowledge the only metal complexes containing N,N′-dithiobisamines as a ligand are the iron(II) and cobalt(II) complexes with N,N′-dithiomorpholine.[25]

Many of the investigations on N,N′-dithiobisamines have been stimulated by their activity as insecticides,[26] fungicides,[26] polymerization catalysts,[27] corrosion inhibitors in lubricating oil[28] and as stabilizers for polyurethane fibres.[29] In addition, much effort has gone into evaluating the usefulness of such disulphides for the vulcanizations of rubber.[30] The extensive use of N,N′-dithiobismorpholine as a catalyst in the vulcanization of natural rubber has prompted a toxicological study on this compound.[31]

Previously we have reported the synthesis and spectroscopic studies of some N,N′-dithiobisamines[32,33] and in this paper we present the results about some of the redox and coordinative behaviour of a series of N,N′-dithiobisamines towards copper(II) salts and the $Cr(CO)_5$ fragment, respectively.

RESULTS AND DISCUSSION

Redox properties of N,N′-*dithiobisamines*

The initial attempt to obtain coordination compounds was made by reaction of copper(II) salts with N,N′-dithiobisamines.

However, we conclude that similar to the behav-

iour of other sulphur–nitrogen compounds,[12,16] N,N′-dithiobisamines reduced copper(II) perchlorate hexahydrate in acetonitrile according to:

$$R_2N—S—S—NR_2 + 6\,Cu(ClO_4)_2 6\,H_2O \xrightarrow{CH_3CN} 6\,[Cu(CH_3CN)_4]ClO_4 + 2\,SO_2 + 32\,H_2O + 4\,HClO_4 + 2\,[R_2NH_2]ClO_4$$

where NR_2 = $N(CH_3)_2$, $N(CH_2CH_3)_2$, 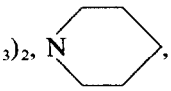 , 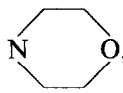 , $N(CH_2—C_6H_5)_2$.

The copper(I) acetonitrile complex[16,34] was identified by IR, ^1H NMR and elemental analysis. The sulphur dioxide evolved from the reaction was detected by the usual method.[16] The corresponding $H_2NR_2^+$ salt was isolated and characterized by IR and ^1H NMR in the case of the reaction with N,N′-dithiobismorpholine and by NMR of the solutions in the case of the other dithiobisamines (see Experimental). Yields of the reactions based on the copper(I) product are similar to those found in the reactions with N,N′-thiobisamines.[16]

On the other hand, from the reaction of N,N′-dithiomorpholine with $CuCl_2 \cdot 2H_2O$ in ethanol, the complex $[Cu_2Cl_3][H_2N$ 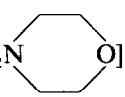 $O]$[12] and sulphur dioxide were identified. Similar products have been found in the reaction of N,N′-thiobisamines with copper(II) chloride dihydrated in ethanol.[17]

The formation of sulphur dioxide and the respective $H_2NR_2^+$ species from these reactions indicate S—N as well as S—S bond cleavage in N,N′-dithiobisamines. This behaviour is readily understood since it is well established that electrophiles such as H^+, Ag^+, Co^{III} and R^+ can assist in the nucleophilic cleavage of the disulphide bond in R—S—S—R compounds.[3] Thus it is known that copper(II) ions destabilize the S—N bond in thiobisamines.[12,15–17]

Although several Cu—RSSR compounds have been reported,[4,6,7] the difficulty in the synthesis of the metal–disulphide complexes has already been noted.[7] The reaction of copper(II) salts with sulphur compounds in a low oxidation state normally results in the reduction of the metal. The copper(I) oxidation state is usually stabilized by the formation of complexes in which the ligand remains intact and (or) by the formation of $(Cu—SR)_n$ complex polymers. In the case of N,N′-thiobisamines and similar to other S—N compounds,[12,16] copper(I) is stabilized by the solvent (acetonitrile) in the reaction with $Cu(ClO_4)_2 \cdot 6H_2O$ or by the anion of the copper(II) salt in the reaction with $CuCl_2 \cdot 2H_2O$.

Coordinative properties

From the above results it can be concluded that metal ions destabilize the S—S as well as the S—N bonds in the N,N-dithiobisamines studied. Hence we attempted their coordination with a metal in a low oxidation state as the fragment $Cr(CO)_5$.[35] Reaction of the labile intermediate $[Cr(CO)_5(THF)]$ with the sulphur–nitrogen ligands in THF affords the complexes $Cr(CO)_5[S_2(NR_2)_2]$:

$$[Cr(CO)_5(THF)] + S_2(NR_2)_2 \xrightarrow{THF} Cr(CO)_5[S_2(NR_2)_2]$$

NR_2

(1) $N(CH_3)_2$

(2) $N(CH_2CH_3)_2$

(3)

(4) 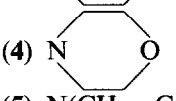

(5) $N(CH_2—C_6H_5)_2$.

The complexes obtained by this procedure are yellow solids, soluble in organic solvents but unstable both in air and particularly in solution. Compounds **2** and **5** were obtained as yellow oils and all crystallization attempts were unsuccessful.

The IR spectra of the complexes in the carbonyl stretching region show the four bands expected for $Cr(CO)_5L$ complexes where L is a bulky sulphur ligand.[36] The splitting of the *E* mode is not observed as found for other sulphur(II)–nitrogen complexes.[14,20] Values of the ν(C—O) frequencies are presented in Table 1. Bands corresponding to the Cr—C stretch and Cr—C—O bending vibrations have also been assigned. Coordination by $Cr(CO)_5$ causes only small changes in the IR bands of N,N′-dithiobisamines.[32] The S—N bands appear to be split and shifted with respect to the free ligand, as is shown in Table 2. The splitting of the S—N bond may be due to the non-equivalent S—N bonds caused by coordination to one of the sulphur atoms:

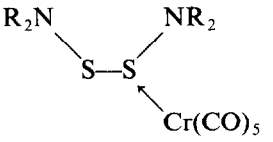

Consistent with this, the coordination of $Cr(CO)_5$ to N,N′-thiobisamines causes only a shift of the ν(S—N) frequency as may be expected, and no splitting is observed.[14]

The NMR spectra of the complexes show, in general, the expected signals corresponding to the

Table 1. IR spectra of $Cr(CO)_5[S_2(NR_2)_2]$[a]

Complex	ν(CO) (cm^{-1})[b] $A_1^{(2)}$	B_1	E	A_1	ν(Cr—C) (cm^{-1})[c] A_1	E	δ(Cr—CO) (cm^{-1})[c] A_1	A_1
$Cr(CO)_5[S_2(N(CH_3)_2)_2]$ (1)	2070w	1990vw	1952vs	1939m	554w	448s	670sh,s	652vs
$Cr(CO)_5[S_2(N(CH_2CH_3)_2)_2]$ (2)	2068w	1990vw	1951vs	1937m	555v[d]	449m[d]	667s[d]	650vs[d]
$Cr(CO)_5[S_2(N$ 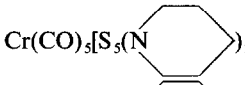 $)_2]$ (3)	2070m	1989w	1950w	1935s	551s	444s	664s	654s
$Cr(CO)_5[S_2(N$ 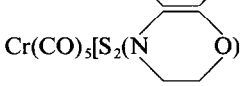 $)_2]$ (4)	2070w	1990w	1953vs	1940s	550vw	446s	655	642
$Cr(CO)_5[S_2(N(CH_2—C_6H_5)_2)_2]$ (5)	2068w	1990w	1950vs	1937m	558w[d]	450s[d]	668vs[d]	650vs[d]

[a] The assignments were made according to refs 14, 20 and 41.
[b] n-Hexane solution.
[c] KBr, solid unless otherwise indicated.
[d] Thin films between NaCl windows.
Abbreviations: s, strong; m, medium; w, weak; v, very; sh, shoulder.

coordinated ligands. Small chemical shift differences in the signals in going from the free to coordinated ligand were observed (see Table 2). The spectra of compounds **1** and **5** could not be recorded at room temperature (35°C) due to the extensive decomposition of the samples. The spectrum of complex **1** at low temperatures (−20°C) consists of two singlets of equal intensity at 2.58 and 2.68 ppm. On standing at room temperature, rapid decomposition of the complex with separation of a green, insoluble solid as well as broadening of the signals by loss of resolution was observed. At the same time a signal corresponding to the free ligand[32] formed in the decomposition appears and increases in intensity on raising the temperature. On the other hand, the ^1H NMR spectrum of **5** at low temperature consists of a slightly broadened (nearly two unresolved signals) signal corresponding to methylene protons, giving rise to a sharp singlet at higher temperatures. Simultaneous appearance of a second singlet, attributable to the free ligand,[32] was observed. On standing at room temperature, decomposition of the complex was also observed. We believe that these changes may be caused by a 1,2 metal-shift between the adjacent pair of sulphur atoms, as observed for pentacarbonylchromium derivatives of dialkyldisulphides.[37] However, for complex **1** and **5** unfortunately the 1,2 shift dynamic

Table 2. Selected spectral data for $Cr(CO)_5[S_2(NR_2)_2]$ complexes

Complex	ν(S—N)$_{as}$ (cm^{-1})[a] Free	Complex	λ_{max} (nm)[b]	^1H NMR[c] Free	Complex
1	942	964,935	403 (1.10)	2.53	2.68, 2.58 (s, CH_3)[d]
2	892	915,890	406 —	1.16 2.71	1.16 (12H, t, CH_3) 2.81 (8H, q, CH_2)
3	919	939,913	403 (0.70)	1.55 2.80	1.60 [12H, m, $(CH_2)_3$] 2.81 (8H, m, CH_2N)
4	938	950,925	401 (1.08)	2.80 3.70	3.00 (8H, m, CH_2N) 3.80 (8H, m, CH_2O)
5	935	945,905	405 —	3.93 7.13	3.95 (8H, s, CH_2)[e] 7.31 (20H, m, C_5H_5)

[a] KBr, solid.
[b] In n-hexane solution.
[c] In $CDCl_3$ and at room temperature unless stated otherwise, δ from TMS.
[d] Spectrum at −20°C.
[e] Spectrum at −35°C.

process could not be observed because of the rapid decomposition of the sample at higher temperatures. For complexes **2–4**, the spectra do not exhibit any significant change at low temperatures.

The differences in the chemical shift values on going from the free to coordinated ligand are comparable with those found in other organic sulphur(II)–nitrogen ligands ligated to chromium(0) which, as has been established, are evidence for coordination via the sulphur atom.[14,20]

The UV–visible spectra of the complexes show a band at about 400 nm, close to those found in pentacarbonylchromium–sulphur complexes[14,20] and assigned to a $^1A_1 \rightarrow {}^1E$ transition.[38]

Attempts to obtain the mass spectra for the complexes were successful only for **3** and **4**. For these compounds the molecular ion peaks in addition to other fragments can be observed, and the ions are listed in Table 3. The fragments arising from decomposition of the molecular ion were identified with the aid of previous fragmentation studies of dithiobisamines[33] and chromium carbonyl complexes.[39] For compound **3** fragmentation occurs principally by loss of three carbon monoxide molecules to give a $Cr(CO)_2[S_2(N\text{-}C_5H_8)_2]^+$ fragment. Subsequently this undergoes successive loss of sulphur to give the species $Cr(CO)_2[S(N\text{-}C_5H_8)_2]^+$ and $Cr[N\text{-}C_5H_8]_2^+$. Fragmentation arising from the Cr—S bond cleavage of the molecular ion is also evident by the presence of the ions $[Cr(CO)_{5-n}]^+$ $(n = 0–5)$ and $[S_2(N\text{-}C_5H_8)_2]^+$. Consistent with this, the

Table 3. The mass spectra of $Cr(CO)_5[S_2(NR_2)_2]$

Fragment	$Cr(CO)_5[S_2(N\text{-}C_5H_8)_2]$ (3) m/z[a]	I (%)	Fragment	$Cr(CO)_5[S_2(N\text{-}C_4H_8O)_2]$ (4) m/z[b]	I (%)
M^+	424	0.73	M^+	428	0.7
M^+-3CO	340	0.18	$M^+-S_2(N\text{-}C_4H_8O)_2$	191.1	3.5
$M^+-3CO-S$	308	5.82	$M^+-S_2(N\text{-}C_4H_8O)_2-CO$	163.9	3.4
$M^+-5CO-S_2$	220	9.88	$M^+-S_2(N\text{-}C_4H_8O)_2-2CO$	135.9	5.8
$M^+-S_2(N\text{-}C_5H_8)_2$	191.9	2.26	$M^+-S_2(N\text{-}C_4H_8O)_2-3CO$	108	13.7
$M^+-S_2(N\text{-}C_5H_8)_2-CO$	163.9	2.11	$M^+-S_2(N\text{-}C_4H_8O)_2-4CO$	80	11.9
$M^+-S_2(N\text{-}C_5H_8)_2-2CO$	136	2.53	$S_2(N\text{-}C_4H_8O)_2^+$	236.1	28
$M^+-S_2(N\text{-}C_5H_8)_2-3CO$	108	8.61	$S{=}S^+{-}N\text{-}C_4H_8O$	150	43
$S_2(N\text{-}C_5H_8)_2^+$	232.1	3.31	$S{=}N\text{-}C_4H_8O$	118	31
$H_2{}^+N\text{-}C_5H_8$	84.1	84.17	$H_2{}^+N\text{-}C_4H_8O$	86.1	100
$C_4H_7{}^{+\cdot}$	55.1	38.77	C_3H_7	57.1	40.7
CO^+	27.9	100			

[a] 20 eV, 350 K.
[b] 20 eV, 335 K.

Table 4. Force constants[a] and Graham parameters[b] in $Cr(CO)_5[S_2(NR_2)_2]$ and other $Cr(CO)_5L$ complexes

Complex	k_1[c]	k_2	δ	π
$Cr(CO)_5[S_2(N(CH_3)_2)_2]$ (**1**)	15.36	15.99	0.09	0.12
$Cr(CO)_5[S_2(N(CH_2CH_3)_2)_2]$ (**2**)	15.33	15.99	0.12	0.09
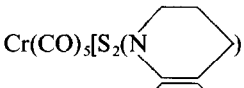 (**3**)	15.30	15.97	0.11	0.08
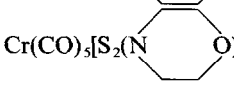 (**4**)	15.37	15.99	0.08	0.13
$Cr(CO)_5[S_2(N(CH_2—C_6H_5)_2)_2]$ (**5**)	15.34	15.99	0.11	0.10
$Cr(CO)_5S[N(CH_3)_2]_2$	15.32	15.95	0.12	0.05
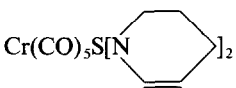	15.29	15.97	0.12	0.07
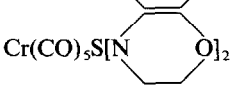	15.37	15.97	0.10	0.09
$Cr(CO)_5S[N(CH_2—C_6H_5)_2]_2$	15.36	15.99	0.13	0.08
$Cr(CO)_5S_2(CH_3)_2$	15.31	15.91	−0.02	0.15
$Cr(CO)_5S(CH_3)_2$	15.36	15.94	−0.01	0.17
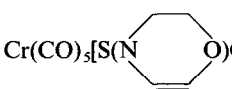	15.54	16.00	−0.07	0.29
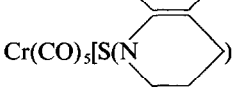	15.38	15.95	−0.01	0.18
$Cr(CO)_5(SCHCH_3)_3$	15.30	15.91	−0.01	0.14
$Cr(CO)_5S(C_2H_5)_2$	15.28	15.81	−0.19	0.22
$Cr(CO)_5S(C_2H_5)CH_2—C_6H_5$	15.29	15.84	−0.14	0.20

[a] Calculated according to the method of Cotton and Kraihanzel.[41]
[b] Calculated according to ref. 40.
[c] In mdyn $Å^{-1}$.
[d] Data from ref. 20.

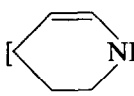 and $[C_4H_7]^+$ fragments observed in the mass spectrum of the free ligand[33] were also observed in the mass spectrum of **3**.

For compound **4** the decomposition of the molecular ion occurs principally with Cr—S cleavage. The 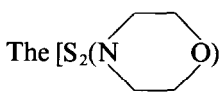 ion and its typical decomposition fragments[33] are observed with high intensity.

Information about the donor–acceptor abilities of the N,N′-dithiobisamines towards $M(CO)_5$ fragments (M = Cr, Mo, W) can be obtained using the σ–π parameters of Graham.[40] For complexes **1–5** these were calculated using the Cotton–Kraihanzel[41] force constants for the C—O bonds obtained from the ν(C—O) values reported in Table 1. For comparison the respective π and σ values for the monothiobisamines analogous compounds,[14] as well as for other ligands,[38] have been included in Table 4. By inspection of the π values, it can be seen that N,N′-dithiobisamines are better π acceptors than their corresponding monothio derivatives but they possess a lower π acceptor ability than alcoxythioamines.[20] From the table it can also be

observed that the π values for complexes **1–5** are close to those found for divalent sulphur compounds. The change in the π acceptor capacity in going from the dithio to the monothio derivatives in the S—N compounds is the reverse of that found in disulphide and thioether ligands.[6]

Stability of the complexes and reaction with $Cu(ClO_4)_2 \cdot 6H_2O$

As mentioned before, solutions in common organic solvents were unstable on exposure to air, but the solids were fairly stable, **1** being the most unstable. The complexes are also unstable to acids, and decomposition with hydrogen sulphide evolution was observed. Decomposition in acid media has also been reported for the free ligands.[23] Towards bases, the complexes are fairly stable. Similar to the free ligands, the complexes reduce the copper(II) perchlorate in acetonitrile to give the copper(I)–acetonitrile complex and sulphur dioxide, but in minor yields.

Consequently, it seems possible to suggest that the reactivity of N,N′-dithiobisamines towards acids decreases in going from the free to the coordinated sulphur–nitrogen compound.

EXPERIMENTAL

N,N′-dithiobisamines were prepared as described previously.[3,2] Commercially available chromium hexacarbonyl (Alfa) was used without further purification. All preparations and manipulations were carried out under purified nitrogen. Spectroscopic measurements were made as described elsewhere.[13–20]

Reactions of N,N′*-dithiobisamines with* $Cu(ClO_4)_2 \cdot 6H_2O$ *in acetonitrile*

Dithiobisamine (1.5–3.5 mmol) in acetonitrile was added to the copper(II) salt solution with stirring and at ambient temperature. The white solid which formed was filtered and dried with a stream of dry nitrogen gas. In some cases a green, basic copper(II) salt was obtained as an impurity which was eliminated by disolution of the solid in hot acetonitrile followed by filtration of the green solid and evaporation of the solvent to afford the white, crystalline product $Cu(CH_3CN)_4ClO_4$.

Found: Cu, 19.2. Calc. for $C_8H_{12}O_4N_4ClCu$: Cu, 19.4%. ^{1}H NMR (acetone-d^6, δ from TMS) 2.15 s (CH_3). IR_{max} (KBr) 2300, 2260 m $\nu(C{\equiv}N)$; 1200–1000s, br $\nu(ClO_4)_{asym}$; 922 s $\nu(ClO_4)_s$; 620 m $\delta(ClO_4)$. Amounts of reactants used, yields of the $Cu(CH_3CN)_4ClO_4$ product and ^{1}H NMR data for the $[H_2NH_2]^+$ salts are as follows: $[(CH_3)_2N]_2S_2$, 0.54 g; $Cu(ClO_4)_2 \cdot 6H_2O$ 2.39 g, yield 82%. $[(CH_3CH_2)_2N]_2S_2$, 0.5 g; $Cu(ClO_4)_2 \cdot 6H_2O$, 2.1 g, yield 70%. ^{1}H NMR $[(CH_3CH_2)_2NH_2]^+$ (filtrate CH_3CN): 3.07 (2H, q, CH_2), 1.25 (3H, t, CH_3).

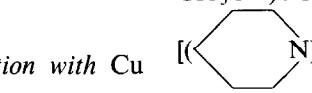

$]_2S_2$ 0.35 g; $Cu(ClO_4)_2 \cdot 6H_2O$ 1.12 g, yield 50%. ^{1}H NMR

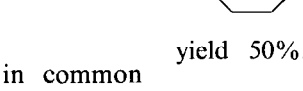

(filtrate CH_3CN): 3.0 (4H, m, NCH_2), 1.66 [6H, m, $(CH_2)_3$].

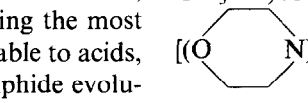

$]_2S_2$ 0.81 g; $Cu(ClO_4)_2 \cdot 6H_2O$ 2.54 g, yield 88%. ^{1}H NMR

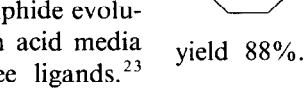

(filtrate CH_3CN): 3.86 (4H, m, OCH_2), 3.26 (4H, m, NCH_2). $[(C_6H_5{-}CH_2)_2N]_2S_2$ 0.7 g; $Cu(ClO_4)_2 \cdot 6H_2O$ 1.15 g, yield 90%. ^{1}H NMR $[(C_6H_5{-}CH_2)_2NH_2]^+$ (filtrate, CH_3CN): 7.3 (10H, m, C_6H_5), 3.9 (4H, s, CH_2).

Isolation of 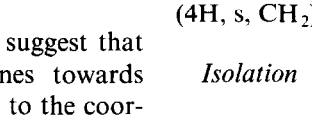 *from reaction with* N,N′*-dithiomorpholine*. After filtration of the white crystals of $Cu(CH_3CN)_4ClO_4$ a second portion of this compound was precipitated by slow evaporation of the solution. Slow evaporation of the solvent of the filtrate at room temperature afforded colourless crystals, soluble in water. ^{1}H NMR (acetone-d_δ δ from TMS): 3.93 (4H, m, OCH_2), 3.53 (4H, m, NCH_2), 3.03 (2H, br, s, NH_2). IR ν_{max} (KBr): 3125 m $\nu(NH_2)_{sym}$; 3060 s $\nu(NH_2)_{asym}$ 2461 m; 1580 s $\delta(NH_2)$.

Reaction of N,N′*-dithiomorpholine with copper*(II) *chloride dihydrate*. To a solution of copper(II) chloride dihydrate (1.73 g, 10.16 mmol) in ethanol (previously deoxygenated with nitrogen) dithiomorpholine (2.5 g, 10.16 mmol) in the same solvent was added dropwise. Evolution of sulphur dioxide and the formation of white crystals was observed. The solid product was filtered, washed with ethanol and dried *in vacuo*, m.p. 110–115°C (dec.) (ref. 12, 110–111°C dec). IR_{max} (KBr) 3185 $\nu(NH_2)_{asym}$; 3060 $\nu(NH_2)_{sym}$; 1580 $\delta(NH_2)$; 1100 s $\nu(COC)_{asym}$; 865 s $\nu(COC)_{sym}$.

Synthesis of $Cr(CO)_5[S_2(NR_2)_2]$ *complexes*

$Cr(CO)_5[S_2(N(CH_3)_2)_2]$ (**1**). A solution of $Cr(CO)_6$ (0.99 g, 4.5 mmol) in *ca* 60 cm^3 of THF was irradiated for 90 min at room temperature. To this a solution of $S_2[N(CH_3)_2]$ (0.6 g, 3.9 mmol) was added and the mixture stirred for 60 min. After removing the solvent *in vacuo* the excess of hexa-

carbonyl was sublimed from the residue *in vacuo* at room temperature. The solid residue was stirred in n-hexane and the solution filtered through Kieselghur. The solution was then concentrated at room temperature *in vacuo* and then placed in the freezer overnight. Filtration of the resulting yellow solid affords **1** (60 % yield), m.p. 53°C. Found: C, 30.2; H, 3.1; N, 7.0. Calc. for $C_9H_{12}O_5N_2S_2Cr$: C, 31.4; H, 3.5; N, 8.0%.

$Cr(CO)_5[S_2(N(CH_2CH_3)_2)_2]$ (**2**). A solution of $[Cr(CO)_5(THF)]$ generated as described for **1** was stirred with the corresponding dithiobisamine (0.82 g, 3.9 mmol) in THF for 1 h. After removing the solvent *in vacuo* the residue was stirred with n-hexane and filtered. Evaporation of the solvent afforded a non-crystallizable, yellow oil which was only spectroscopically characterized (see Tables 1 and 2).

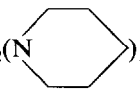

$Cr(CO)_5[S_2(N\quad)_2]$ (**3**). A solution of $[Cr(CO)_5(THF)]$ was stirred with N,N′-dithiobispiperidine (0.8 g, 3.4 mmol) for 1 h. After removing the solvent *in vacuo* the excess of $Cr(CO)_6$ was sublimed under reduced pressure at room temperature. The solid residue was then redissolved in n-hexane, filtered through Kieselghur and the resulting solution was concentrated and placed in a freezer overnight to give **3** as yellow crystals (75% yield), m.p. 92–93°C (dec.). Found: C, 42.1; H, 4.8; N, 6.5. Calc. for $C_{15}H_{20}O_5N_2S_2Cr$: C, 42.4; H, 4.7; N, 6.5%.

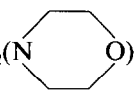

$Cr(CO)_5[S_2(N\quad O)_2]$ (**4**). This compound was obtained using the same procedure as for **3**, as yellow crystals (80% yield), m.p. 86–88°C (dec.). Found: C, 36.1; H, 3.8; N, 6.4. Calc. for $C_{13}H_{16}O_7N_2S_2Cr$: C, 36.8; H, 3.8; N, 6.6%.

$Cr(CO)_5[S_2(N(CH_2—C_6H_5)_2)_2]$ (**5**). To a solution of $[Cr(CO)_5(THF)]$ was added N,N′-dithiobisdibenzylamine (1.52 g, 0.33 mmol) in THF at room temperature. The mixture was stirred for 1 h, then the THF was evaporated *in vacuo* and the resulting oil residue dissolved in n-hexane. The yellow solution was filtered, concentrated and cooled to −20°C overnight. After this no crystals were formed. By evaporation of n-hexane, **5** was obtained as a yellow oil which was spectroscopically characterized (see Tables 1 and 2).

Reaction of **4** *with* $Cu(ClO_4)_2 \cdot 6H_2O$ *in acetonitrile*

To a solution of $Cu(ClO_4)_2 \cdot 6H_2O$ (0.754 g, 0.20 mmol) in acetonitrile, **4** (0.0674 g, 0.157 mmol) was added dropwise with stirring at room temperature. Slow evolution of sulphur dioxide was observed and the solution turned green. A small amount of green, insoluble solid formed which was filtered and the solvent evaporated slowly from the solution. From the residue, 0.0213 g of the complex $[Cu(CH_3CN)_4]ClO_4$ was isolated.

Acknowledgement—Support from the DTI of the University of Chile is gratefully acknowledged.

REFERENCES

1. J. M. Guss, E. A. Merrit, R. F. Phizackerley, B. Hedman, M. Murata, K. O. Hodgman and H. C. Freeman, *Sciences* 1988, **241**, 806.
2. P. M. Colman *et al.*, *Nature* 1978, **272**, 319.
3. J. D. Lydon, R. C. Elder and K. Deutsch, *Inorg. Chem.* 1982, **21**, 3186 and refs therein.
4. M. M. Kadooka, L. Warner and K. Seff, *Inorg. Chem.* 1976, **15**, 812.
5. C. A. Stein and H. Taube, *Inorg. Chem.* 1979, **18**, 2212.
6. H. Siegel, K. H. Scheller, V. M. Rheinberger and B. F. Fisher, *J. Chem. Soc., Dalton Trans.* 1980, 1022.
7. P. M. Boorman, K. A. Kerr, R. A. Kydd, K. J. Moynihan and K. A. Valentine, *J. Chem. Soc., Dalton Trans.* 1982, 1401.
8. H. W. Roesky, T. Gries, P. G. Jones, K. L. Weber and G. M. Sheldrick, *J. Chem. Soc., Dalton Trans.* 1981, 1781.
9. G. Fendler, in *Methoden der Organischen Chemie* (Houben-Weyl), Vol. E11 "Organische Shwefel-Verbindungen", p. 22. G. Thieme Verlag, Stuttgart (1985).
10. T. Okawara, T. Yamasaki, K. Sato, H. Miyazaki and M. Furukawa, *Chem. Pharm Bull.* 1985, **33**, 5225.
11. G. Nickless, *Inorganic Sulfur Chemistry*, pp. 305 and 424. Elsevier, Amsterdam (1969).
12. G. González, C. Díaz and S. Copaja, *Monatsh. Chem.* 1983, **114**, 177.
13. C. Díaz, E. Clavijo and G. González, *Spectrochim. Acta* 1983, **39A**, 537.
14. C. Díaz and G. González, *Inorg. Chim. Acta* 1984, **85**, 61.
15. C. Díaz, S. Copaja and G. González, *Phosphorus and Sulfur* 1985, **22**, 317.
16. C. Díaz V, *Polyhedron* 1985, **4**, 1269.
17. C. Díaz V, *Polyhedron* 1986, **5**, 655.
18. I. Chadwick, C. Díaz, G. González, M. A. Santa Ana and N. Yutronic, *J. Chem. Soc., Dalton Trans.* 1968, 1867.
19. G. González, C. Díaz and H. Binder, *Z. Naturfor.* 1988, **43B**, 513.
20. C. Díaz V, *Sulfur Letts* 1989, **9**, 1.
21. A. Michaelis and K. Luxenbourg, *Chem. Ber.* 1895, **28**, 165.
22. G. E. Thompson, *Quart. Rep. Sulfur Chem.* 1970, **5**, 245.
23. R. W. Saville, *J. Chem. Soc.* 1958, 2880.

24. D. H. R. Barton, S. V. Jey and P. D. Magnus, *J. Chem. Soc., Chem. Commun.* 1975, 855.
25. T. H. Gudimovich, A. Prisyazknyuk, A. I. Vilkova, L. M. Tikhonenko and R. J. Makordei, *Zh. Neorg. Khim.* 1986, **31**, 1309; *Chem. Abstr.* **105**, 90085 v.
26. W. D. Stewart and J. H. Standen, *U.S. Patent 2.501.191* (March 1950); *Chem. Abstr.* 1950, **44**, 6570.
27. K. Machida, H. H. Kegomi and K. Hisamura, *Japanese Patent 6.921.101* (9 September 1969); *Chem. Abstr.* 1970, **72**, 13204 f.
28. D. H. Clement, *U.S. Patent 3.394.185* (23 July 1968); *Chem. Abstr.* 1968, **69**, 95953 z.
29. I. Suzuki, K. Ichikawa, K. Murayama and S. Morimura, *German Patent 1.928.915* (December 1969); *Chem. Abstr.* 1970, **72**, 44845 k.
30. N. R. Datte, P. K. Das and K. D. Basu, *J. Appl. Polym. Sci.* 1986, **32**, 5849.
31. I. I. Datsenko, E. P. Korneichuk, U. S. Petrus and L. Komissanova, *Zh. Ya. Loptneva. Gig. Sanit.* 1988, **3**, 90; *Chem. Abstr.* 1988, **108**, 199752 y.
32. C. Díaz and A. Arancibia, *Phosphorus, Sulfur, Silicon* 1989, **44**, 1.
33. C. Díaz V, *Phosphorus, Sulfur, Silicon* 1990, **48**, 141.
34. P. Hammerich and C. Sigwart, *Experientia* 1965, **19**, 488.
35. T. A. Albright, R. Hoffman, J. C. Thibeault and D. L. Thorn, *J. Am. Chem. Soc.* 1979, **101**, 3801.
36. E. W. Ainscough, A. M. Brodie and A. R. Furness, *J. Chem. Soc., Chem. Commun.* 1971, 1357.
37. E. W. Abel, S. K. Bhargava, P. K. Mittal, K. G. Orrel and U. Sik, *J. Chem. Soc., Dalton Trans.* 1985, 4561.
38. C. Díaz and N. Yutronic, *Polyhedron* 1987, **6**, 503.
39. J. Müller, *Angew Chem. Int. Edn Engl.* 1972, **11**, 653.
40. W. A. G. Graham, *Inorg. Chem.* 1986, **7**, 315.
41. F. A. Cotton and C. S. Kraihanzel, *J. Am. Chem. Soc.* 1962, **83**, 4432.

Polyhedron Vol. 10, No. 12, pp. 1327–1332, 1991
Printed in Great Britain

0277–5387/91 $3.00+.00
© 1991 Pergamon Press plc

THE PREPARATION AND CHARACTERIZATION OF SOME NICKEL(II) AND COPPER(II) COMPLEXES OF ONS LIGANDS

M. NAZIMUDDIN and M. AKBAR ALI*

Department of Chemistry, Chittagong University, Bangladesh

and

F. E. SMITH

Department of Chemistry, Laurentian University, Subdury, Ontario, Canada

(*Received* 9 *July* 1990; *accepted* 24 *January* 1991)

Abstract—New nickel(II) and copper(II) complexes of four Schiff base ligands formed from benzoylacetone and 2-hydroxynaphthaldehyde with S-alkyl esters of dithiocarbazic acid have been prepared and characterized by IR, NMR, ESR and electronic spectroscopic techniques. The Schiff bases yield neutral 1:1 complexes of general formula M(ONS) (ONS^{2-} = dinegatively charged anions of the Schiff base ligands; M = Ni, Cu). Magnetic and spectral evidence support a dimeric structure for these complexes. The complexes, M(ONS)B (B = py, dipy, phen), were also prepared. The complexes, M(ONS)py, are square-planar but electronic and ESR spectroscopic data support a five-coordinate geometry for the Cu(ONS)B (B = dipy, phen) complexes. Based on spectroscopic and magnetic data, a thiolato, sulphur-bridged, octahedral structure is assigned to the Ni(ONS)B (B = dipy, phen) complexes.

Metal complexes of tridentate NNS-bonding ligands have been extensively investigated because of their interesting physicochemical properties and marked biological activities.[1–6] In contrast, comparatively little work has been carried out on metal complexes of chelating agents containing the ONS set of donor atoms. We now report the synthesis and characterization of metal complexes of four new ONS-chelating ligands.

EXPERIMENTAL

Physical measurements and analytical procedures were similar to those described before.[7]

* Author to whom correspondence should be addressed. Present address: Department of Chemistry, University of Brunei Darussalam, Bandar Seri Begawan, Brunei Darussalam.

Preparation of the ligands

The ligands were prepared by heating ethanolic solutions of the appropriate aldehyde or diketone with S-methyl- or S-benzyl-dithiocarbazate. Recrystallization from absolute ethanol afforded pure products.

H_2L^1: $C_{13}H_{12}N_2S_2O$, m.p. 230°C; Found: C, 56.8; H, 4.45; N, 9.8. Calc. for $C_{13}H_{12}N_2S_2O$: C, 56.5; H, 4.4; N, 10.1%.

H_2L^2: $C_{19}H_{16}N_2S_2O$, m.p. 201°C; Found: C, 64.5; H, 4.6; N, 7.9. Calc. for $C_{19}H_{16}N_2S_2O$: C, 64.75; H, 4.6; N, 7.95%.

H_2L^3: $C_{12}H_{14}N_2S_2O$, m.p. 201°C; Found: C, 54.2; H, 5.4; N, 10.5. Calc. for $C_{12}H_{14}N_2S_2O$: C, 54.1; H, 5.3; N, 10.5%.

H_2L^4: $C_{18}H_{18}N_2S_2O$, m.p. 128°C; Found: C, 62.9; H, 5.3; N, 7.9. Calc. for $C_{18}H_{18}N_2S_2O$: C, 63.3; H, 5.3; N, 8.2%.

Preparation of the complexes

The metal complexes were prepared by heating the ligand and metal acetates in a 1 : 1 molar ratio in ethanol. On cooling, the complexes crystallized as microcrystalline powders. Complexes containing the heterocyclic bases were prepared by heating a mixture of the appropriate Schiff base, metal acetate and base in a 10 : 1 mixture of ethanol and 2,2-dimethoxypropane.

RESULTS AND DISCUSSION

The IR spectra of the solid Schiff bases (Table 1) contain no ν(S—H) band at *ca* 2600 cm^{-1} indicating that they remain as the thioketo forms (**IA** and **IIA**), however, in solution there may be an equilibrium mixture of both the thioketo and thioenol (**IB** and **IIB**) forms.

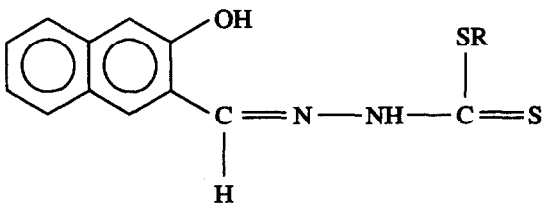

(IA; R = CH_3, H_2L^1; R = $CH_2C_6H_5$, H_2L^2)

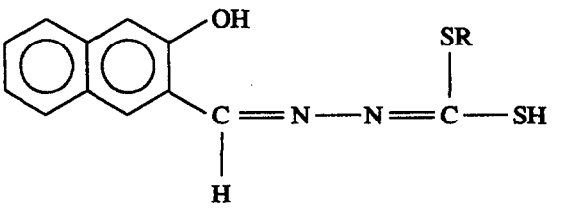

(IB)

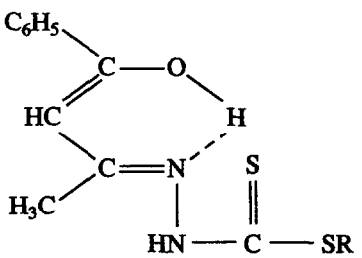

(IIA; R = CH_3, H_2L^3; R = $CH_2C_6H_5$, H_2L^4)

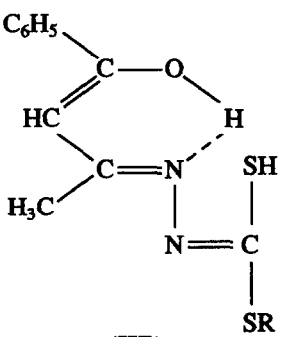

(IIB)

The ^1H and ^{13}C NMR spectral data for the Schiff bases (Table 2) are consistent with structures **IA** and **IIA** but do not support the thioenol tautomeric structures **IB** and **IIB**. The ν(C=N) band[8] of the free ligands shifts to lower wavenumbers (Table 1) in the complexes suggesting coordination via the azomethine nitrogen atoms. This is further supported by ^{13}C NMR. The spectrum of H_2L^1 displays a ^{13}C resonance at 145.73 ppm, whereas as a result of coordination via the CH=N— nitrogen atom this appears at 153.30 ppm in the spectrum of the nickel(II) chelate. The appearance of ν(M—S) bands at *ca* 300 cm^{-1} in the IR spectra of all the metal complexes supports coordination through the mercapto sulphur atoms.

The mono-ligated nickel(II) complexes, Ni(ONS), are diamagnetic and presumably square-planar. Their electronic spectra (Table 1) show *d–d* bands characteristic of square-planar nickel(II).[9] Since the ligands can provide a maximum of three donor atoms, the Ni(ONS) complexes must dimerize in order to attain a square-planar structure. A thiolato sulphur-bridged dimeric structure is proposed for the monoligated nickel(II) complexes. An oxygen-bridged dimeric structure is unlikely since the phenolic ν(C—O) band occurs at 1520 cm^{-1} which is lower than that found for a bridged C—O group.[10] The IR spectra of Ni(ONS)B (B = py, dipy, phen) (Table 1) suggest that the heterocyclic bases are coordinated to the nickel atom. The diamagnetism and electronic spectra of Ni(ONS)py support a monomeric square-planar geometry. The electronic spectra of Ni(ONS)phen and Ni(ONS)dipy (Table 1) do not resemble the spectra of other five-coordinate nickel(II) complexes,[11] but are similar to those of pseudo-octahedral nickel(II) complexes.[12] The lower values of the room-temperature magnetic moments may be due to inter-

Table 1. Selected IR absorption bands and electronic spectral data

Compound	IR assignments					Electronic spectra, λ_{max} (nm)
	ν(NH)/ν(OH)	ν(C=N)	ν(C—O)	ν(M—S)	Bands due to heterocyclic bases	
H_2L^1	3140s 3100sh	1618s	1520w	—	—	
H_2L^2	3111s 2985s	1622s	1518s	—	—	
H_2L^3	3280s,br	1615s	1105s	—	—	
H_2L^4	3361s	1630s	1106s	—	—	
NiL^1	—	1610s	1520w	330w	—	550sh, 455, 400, 334, 295
NiL^2	—	1616s	1523s	300s	—	580, 450, 400, 335, 296
NiL^3	—	1580s	1068s	356w	—	650sh, 429, 300
$NiL^4 \cdot H_2O$	—	1586s	1071s	350sh	—	630sh, 520sh, 435, 338
$NiL^1 \cdot py$	—	1595s	1525s	290s	1240w, 618s, 420s	520sh, 470, 450sh, 400, 341, 318, 297
NiL^2py	—	1615s	1525s	300s	1258sh, 620m, 440m	520sh, 435, 339
NiL^3py	—	1578s	1065s	396w	1210m, 690s, 420s	520, 450sh, 430, 341, 300
NiL^4py	—	1586s	1070s	348s	1213s, 698s, 419w	540, 423, 338, 297
$NiL^2dipy \cdot 2H_2O$	—	1613s	1532s	285s	1440s, 764s, 410s	1111, 833, 455
$NiL^2pheno \cdot 5H_2O$	—	1616s	1533s	295s	1654w, 856m, 60m	1110, 769, 455
$NiL^4dipy \cdot H_2O$	—	1567s	1064s	350w	1472s, 1105m, 762s, 653s	880, 560sh, 433, 339, 297
$CuL^1 \cdot 0.5H_2O$	—	1610s	1530s	315s	—	550, 480sh, 425, 341, 299
CuL^2	—	1616s	1535s	298s	—	600, 520, 450sh, 429, 338
$CuL^3 \cdot H_2O$	—	1580m	1070m	350w	—	647, 340, 298
$CuL^1py \cdot 0.5H_2O$	—	1608s	1528s	290s	1230m, 422s	520sh, 450, 437, 341, 299
$CuL^2py \cdot 0.5H_2O$	—	1616s	1535s	289s	1250w, 640m, 410s	550, 450, 434, 337, 297
$CuL^3py \cdot H_2O$	—	1580s	1065s	350s	1212m, 632m, 410m	625, 570sh, 460sh, 433, 341, 300
CuL^4py	—	1580s	1065s	346w,br	1217s, 639m, 415w	620, 520sh, 420sh, 416, 336, 297
CuL^2dipy	—	1614s	1534s	290s	1440s, 1055m, 763s, 765s	833, 555, 454, 337
CuL^1dipy	—	1610s	1528s	285s	1055s, 770m, 730s, 410s	850sh, 550sh, 410, 341
$CuL^1phen \cdot 0.5H_2O$	—	1602s	1528s	290s	830s, 640s, 408m	770, 520, 450, 436, 358, 299
$CuL^2phen \cdot 0.5H_2O$	—	1614s	1531s	280s	841s, 725s, 638s, 424s	758, 543, 438, 329
CuL^3dipy	—	1593sh	1070m	357w	1498s, 1485s, 1033s, 768s, 700s, 405s	750, 500, 435, 300
CuL^4dipy	—	1594s	1071s	355sh	1485s, 1033s, 763s, 710s, 406w	877, 575, 417, 338, 297
CuL^3phen	—	1586s	1068s	355w	1612m 840m, 725s, 638m	877, 575, 417, 338, 297
$CuL^4phen \cdot H_2O$	—	1578s	1070s	355sh	1619m, 842s, 727s, 639m	880, 540sh, 439, 300

Table 2. ^{1}H and ^{13}C NMR data for the Schiff bases and some of their complexes

Compound	^{1}H NMR assignments (δ, ppm)				^{13}C NMR assignments (δ, ppm)				
	$-SCH_3/SCH_2$	$CH{=}N-/-CCH_3{=}N-$	$-CH=$	Aromatic	$-SCH_3/SCH_2-$	$-C-O$	$-CSS-$	$CH{=}N/CCH_3{=}N$	Aromatic
H_2L^1	2.58s	8.20s	—	7.22, 7.40, 7.58, 7.85, 7.92	16.82	158.07	196.11	145.73	109.13, 118.21, 123.54, 124.09, 127.99, 128.07
H_2L^2	4.52s	8.70s	—	7.20, 7.34, 7.37, 7.51, 7.81, 8.01	38.10	159.52	189.24	142.47	124.35, 127.06, 127.41, 128.35, 128.61, 129.05, 131.41
H_2L^3	2.52s	2.14s	6.49s	7.25, 7.29, 7.31, 7.34, 7.35	17.64	58.85	193.10	158.38	123.97, 128.12, 128.80, 142.60
H_2L^4	4.35d	2.12s	6.48s	7.18, 7.20, 7.30, 7.48	—	54.85	191.73	158.41	123.60, 123.79, 124.09, 128.81, 128.19, 128.55, 129.45, 135.85, 142.67
NiL^1	2.41	8.08d	—	7.09, 7.30, 7.48, 7.58, 7.85	17.40	161.08	169.55	153.30	119.91, 122.63, 124.83, 126.65, 127.44, 128.61, 132.31, 133.98
NiL^2	4.32s	8.02s	—	6.78, 7.10, 7.30, 7.37, 7.49, 7.51, 7.79, 7.81, 8.00, 8.15	38.33	161.35	167.35	139.39	119.95, 122.60, 108.68, 126.50, 126.93, 127.26, 128.72, 131.97, 134.14
NiL^3	2.57s	2.15s	5.90s	7.26, 7.29, 7.39, 7.40, 7.79, 7.81	17.40	58.85	166.40	—	126.33, 128.57, 129.67, 138.52
NiL^4	4.30s	2.20s	5.92	7.20, 7.30, 7.45, 7.66–7.77	39.52	58.45	174.48	152.45	124.07, 128.43, 128.93, 137.69
NiL^1py	2.59s	8.02s	—	7.06, 7.26, 7.28, 7.34, 7.47, 7.64, 7.81, 8.86	17.82	152.48	186.98	162.48	118.74, 118.52, 119.75, 122.68, 124.76, 127.16
NiL^3py	2.59s	2.37s	5.89s	7.25, 7.26, 7.28, 7.30, 7.32, 7.34, 7.63, 7.75, 7.77	17.86	58.44	168.54	152.54	128.21, 129.38, 137.82
NiL^4py	4.30s	2.25s	5.89s	7.18, 7.20, 7.25, 7.28, 7.30, 7.32, 7.34, 7.60, 7.63, 7.75, 7.77	39.42	58.50	—	152.66	124.41, 126.56, 127.17, 128.27, 129.46, 137.85, 138.08, 128.51, 129.02

H_2L^1 = The 2-hydroxy-1-naphthaldehyde Schiff base of S-methyldithiocarbazate; H_2L^2 = the 2-hydroxynaphthaldehyde Schiff base of S-benzyldithiocarbazate; H_2L^3 = the benzoylacetone Schiff base of S-methyldithiocarbazate; H_2L = the benzoylacetone Schiff base of S-benzyldithiocarbazate.

Table 3. Colour, decomposition temperatures, conductivities, magnetic moments and analytical data for the complexes

Compound	Colour	Decomposition temperature (°C)	Λ^a (Ω^{-1} cm^2 mol^{-1})	μ(BM)	Analytical data[b] C	H	N	M
NiL^1	Brown	382	0.5	0.12	47.1	3.2	8.4	18.0
					(46.9)	(3.0)	(8.4)	(17.6)
NiL^2	Yellowish brown	335	0.8	Diam.	55.6	3.5	6.6	14.8
					(55.8)	(3.45)	(6.85)	(4.35)
NiL^3	Dark brown	280	1.5	0.2	44.2	3.9	8.5	18.4
					(44.6)	(3.7)	(8.7)	(18.2)
NiL^4	Dark brown	172	1.4	Diam.	53.9	4.1	6.9	14.6
					(54.3)	(4.1)	(7.0)	(14.7)
NiL^1py	Dark brown	172	1.0	Diam.	52.5	3.7	10.4	14.5
					(52.45)	(3.7)	(10.2)	(14.2)
NiL^2py	Reddish brown	167	0.3	0.15	58.9	3.9	8.3	12.4
					(59.0)	(3.9)	(8.6)	(12.0)
NiL^3py	Brown	140	1.1	Diam.	50.8	4.4	10.6	14.7
					(50.8)	(4.3)	(10.4)	(14.6)
NiL^4py	Dark brown	144	0.5	Diam.	57.4	4.4	8.5	12.7
					(57.8)	(4.4)	(8.8)	(12.3)
$CuL^1 \cdot 0.5H_2O$	Green	225	0.2	2.10	45.2	3.1	8.0	12.7
					(45.0)	(3.2)	(7.5)	(12.3)
CuL^2	Greenish brown	197	0	2.12	54.5	3.3	6.4	15.8
					(54.4)	(3.4)	(6.8)	(15.4)
$CuL^3 \cdot H_2O$	Green	145	1.3	1.93	42.0	3.7	8.4	19.0
					(41.7)	(4.1)	(8.1)	(18.4)
$CuL^1py \cdot 0.5H_2O$	Greenish yellow	223	0.5	1.85	51.1	3.7	10.0	14.8
					(50.7)	(3.8)	(10.1)	(14.9)
$CuL^2py \cdot 0.5H_2O$	Greenish yellow	160	0.7	1.79	57.5	3.9	8.1	12.3
					(58.0)	(4.0)	(8.4)	(11.8)
$CuL^3py \cdot H_2O$	Brown	138	1.1	1.93	48.5	4.7	9.5	15.3
					(48.1)	(4.5)	(9.9	(14.9)
CuL^4py	Chocolate	132	0.4	1.95	56.9	4.3	8.5	13.3
					(57.2)	(4.4)	(8.7)	(13.2)
CuL^1dipy	Pale green	200	0.3	1.93	55.6	3.7	11.0	12.6
					(55.9)	(3.7)	(11.3)	(12.9)
CuL^2dipy	Bottle green	155	0.8	1.3	60.7	4.0	9.5	11.4
					(61.1)	(3.9)	(9.8)	(11.1)
CuL^3dipy	Dark green	193	1.3	2.0	54.2	4.4	11.1	13.2
					(54.6)	(4.2)	(11.6)	(13.1)
CuL^4dipy	Dark green	170	1.1	1.98	60.4	4.3	9.7	11.1
					(60.2)	(4.3)	(9.9)	(11.3)
$CuL^1phen \cdot H_2O$	Greenish yellow	220	1.0	1.84	55.7	4.1	10.8	12.2
					(56.0)	(3.8)	(10.8)	(11.8)
$CuL^2phen \cdot 0.5H_2O$	Dark brown	215	0.7	1.97	61.4	3.7	8.9	10.8
					(61.6)	(4.0)	(9.3)	(10.5)
CuL^3 phen	Dark green	188	0.4	1.96	56.5	4.2	10.5	12.7
					(56.7)	(4.0)	(10.8)	(12.5)
CuL^4 phen	Dark green	172	1.3	1.74	61.9	4.2	9.4	11.1
					(61.6)	(4.1)	(9.6)	(10.9)
NiL^2 dipy $\cdot 2H_2O$	Dark brown	155	0.3	2.57	58.1	3.85	8.2	10.1
					(57.9)	(4.4)	(8.3)	(9.8)
$NiL^2phen \cdot 0.5H_2O$	Dark brown	197	0.7	2.14	54.5	3.3	6.4	15.8
					(54.4)	(3.4)	(6.8)	(15.4)
$NiL^4phen \cdot H_2O$	Brown	130	0.3	1.89	60.6	4.2	9.9	10.0
					(60.3)	(4.4)	(9.4)	(9.8)
$NiL^4dipy \cdot H_2O$	Brown	125	2.5	1.78	58.2	4.3	10.1	10.0
					(58.6)	(4.6)	(9.8)	(10.2)

[a] Molar conductance of *ca* 10^{-3} solutions in dimethylsulphoxide.
[b] Calculated values are given in parentheses.

action between the nickel(II) ions in a mercapto sulphur-bridged dimeric structure or to strong in-plane π-bonding and axial ligation, as has been found in the case of some other nickel(II) complexes.[13]

The copper(II) complexes, $Cu(ONS)\cdot xH_2O$ ($x = 0$, 0.5, 1), are insoluble in most common organic solvents suggesting that they are not monomeric structures. The frozen solution ESR spectrum of CuL^1 in DMSO with two g values ($g_\parallel = 2.16$, $g_\perp = 2.06$) supports a tetragonal geometry. A simple phenolic oxygen- or mercapto sulphur-bridged dimeric structure cannot be assigned to CuL^1 since such a bridging arrangement generally leads to antiferromagnetic interactions.[14] The present copper complexes display room temperature moments of 2.10–1.95 BM which do not support dimeric structures. The colour, magnetic moments and electronic spectra of the present copper(II) complexes (Table 3) resemble those of the copper(II) complex of the 5-nitrosalicylaldehyde Schiff base of S-methyldithiocarbazate, for which a tetrameric structure has been proposed.[15] Unfortunately due to the very low solubilities in suitable non-donor solvents, molecular weights of these compounds in solution could not be measured.

The room temperature moments of Cu(ONS)B (B = py, dipy, phen) fall in the range 1.79–2.0 BM. The electronic spectra of the Cu(ONS)py complexes (Table 1) display *d–d* bands which compare well with those of four-coordinate, square-planar copper(II).[16] The frozen solution ESR spectra of the CuLpy complexes with $g_\perp = 2.07, g_\parallel = 2.17$ and $A_\parallel = 160$ G are typical of square-planar copper(II) complexes.[17]

The electronic spectra of CuLdipy and CuLphen (Table 1) contain *d–d* bands at *ca* 758 and 543 nm which do not resemble either square-planar or tetragonal copper(II) complexes but compare well with those of five-coordinate copper(II) species.[18] The ESR spectral data for these complexes (CuL^2 phen: $g_\perp = 2.07$, $g_\parallel = 2.20$; CuL^4phen: $g_\parallel = 2.16$, $g_\perp = 2.04$; CuL^3phen: $g_\parallel = 2.17$, $g_\perp = 2.05$ with $g_\parallel > g_\perp$) support a square-pyramidal rather than a trigonal-bipyramidal geometry.[18]

Acknowledgements—Some of the spectroscopic measurements were performed at the University of Missouri–Columbia by Dr Michael S. Tempesta, thanks to the support of the IOCD, which is gratefully acknowledged. One of us (M.N.) thanks the UNESCO, New Delhi for financial assistance.

REFERENCES

1. M. Akbar Ali and S. E. Livingstone, *Coord. Chem. Rev.* 1974, **13**, 101.
2. D. H. Petering, in *Metal Ions in Biological Systems* (Edited by H. Sigel), Vol. 2, p. 197. Marcel-Dekker, New York (1980).
3. N. E. Spingram and A. C. Sartorelli, *J. Med. Chem.* 1979, **22**, 1314.
4. L. A. Saryan, K. Mailer, C. Krishnamurti, W. Antholine and D. H. Petering, *Biochem. Pharmacol.* 1981, **30**, 1595.
5. A. G. Bingham, H. Bogge, A. Muller, E. W. Ainscough and A. M. Brodie, *J. Chem. Soc., Dalton Trans.* 1987, 493.
6. S. Padhye and G. B. Kauffman, *Coord. Chem. Rev.* 1985, **63**, 127.
7. S. M. M. H. Majumder, M. Akbar Ali, F. E. Smith and M. A. U. Mridha, *Polyhedron* 1988, **7**, 2183.
8. D. M. Adams, *Metal–Ligand and Related Vibrations.* Arnold, London (1967).
9. G. Maki, *J. Chem. Phys.* 1958, **29**, 1129.
10. C. M. Harris and E. Sinn, *J. Inorg. Nucl. Chem.* 1986, **30**, 2723.
11. M. Akbar Ali, S. E. Livingstone and D. J. Phillips, *Inorg. Chim. Acta* 1972, **6**, 39.
12. A. B. P. Lever, *Inorganic Electronic Spectroscopy.* Elsevier, Amsterdam (1964).
13. S. Balasubramanium and C. N. Krishnan, *Polyhedron* 1986, **5**, 6691.
14. M. Akbar Ali, S. E. Livingstone and D. J. Phillips, *Inorg. Chim. Acta* 1973, **7**, 531.
15. M. Akbar Ali, S. E. Livingstone and D. J. Phillips, *Inorg. Chim. Acta* 1973, 7, 179.
16. L. Sacconi and M. Ciampolini, *J. Chem. Soc.* 1964, 276; J. P. Facklar Jr, F. A. Cotton and D. Branum, *Inorg. Chem.* 1963, **2**, 97.
17. U. Sakaguchi and A. W. Addison, *J. Chem. Soc., Dalton Trans.* 1979, 600.
18. B. R. McGarvey, *Transition Met. Chem.* 1966, **3**, 89.

Polyhedron Vol. 10, No. 12, pp. 1333–1341, 1991
Printed in Great Britain

0277–5387/91 $3.00+.00
Pergamon Press plc

PREPARATION AND CHARACTERIZATION OF NEW TRANSITION METAL COMPLEXES OF NITROIMIDAZOLES. X-RAY CRYSTAL STRUCTURES OF TWO COPPER COMPLEXES: BIS-[(μ-CHLORO)CHLORO-BIS-(1-(2-HYDROXYETHYL)-2-METHYL-5-NITROIMIDAZOLE)COPPER(II)] AND DICHLORO-BIS-(2-METHYL-5-NITROIMIDAZOLE)COPPER(II). FIRST OBSERVATION OF NITRO GROUP COORDINATION TO THE METAL ION IN THESE HETEROCYCLES

NORAH BARBA-BEHRENS*

Departamento de Química Inorgánica, División de Estudios de Posgrado, Facultad de Química, Universidad Nacional Autónoma de México, México, D.F. 04510 Mexico

and

ANA MARÍA MUTIO-RICO

Area de Química Inorgánica, Departamento de Química, Division CBI, Universidad Autónoma Metropolitana Iztapalapa, México, D.F. 09340 Mexico

and

PEDRO JOSEPH-NATHAN and ROSALINDA CONTRERAS

Departamento de Química, Centro de Investigación y de Estudios Avanzados del I.P.N, Apdo. Postal 14-740, México, D.F. 07000 Mexico

(*Received* 24 *July* 1990; *accepted* 24 *January* 1991)

Abstract—2-Methyl-5-nitroimidazole [MNIH, (**1**)] forms the complexes $Cu(MNIH)_2X_2$ [X = Cl (**1a**), Br (**1b**), NO_3 (**1c**), OH (**1d**)] and $Co(MNIH)_2X_2$ [X = Cl (**1e**), OAc (**1f**)]. X-ray crystal structure of **1a** shows a distorted octahedral geometry for the copper(II) ion bonded to two chlorine atoms and two nitroimidazole molecules through N(1) and with a *trans* diaxial coordination to one of the oxygen atoms of the nitro groups. This is the first example of nitroimidazole derivatives in which the nitro group occupies a coordination site. Spectroscopic evidence suggests that for compounds **1b–1f** the preferred coordination site for the metal ion is N(1), with interaction of the nitro group adjacent to it, giving extra stability to the complexes. The copper complexes, **1b** and **1c**, contain six coordinated metal atoms, while **1e** is tetrahedral and **1f** is a carboxylate-bridged dimer. The other ligand, 1-(2-hydroxyethyl)-2-methyl-5-nitroimidazole [metronidazole, HEMNI (**2**)] forms the complexes $Cu(HEMNI)_2X_2$ [X = Cl (**2a**, **2b**), Br (**2c**), OAc (**2d**)] and $Co(HEMNI)_2Cl_2$ (**2e**). An X-ray crystal structure determination on $Cu(HEMNI)_2Cl_2$ (**2a**) shows a centrosymmetric chloro-bridged dimer. The coordination geometry around each copper atom is trigonal bipyramidal with three equatorial chlorine atoms and two axial imidazole molecules. The rest of the metronidazole complexes obtained were shown to be a dimeric compound with bridging

* Author to whom correspondence should be addressed.

acetates, **2d**, two monomeric octahedral (X = Cl, Br) copper compounds, **2b** and **2c**, and a tetrahedral cobalt compound, **2e**.

Metal ions play a vital role in a vast number of widely differing biological processes. The interaction of these ions with drugs administered for therapeutic reasons is a subject of considerable interest.

Continuing our work in this area[1-3] we have been studying the complexing ability of 2-methyl-5-nitroimidazole [MNIH, (**1**)] and 1-(2-hydroxyethyl)-2-methyl-5-nitroimidazole [metronidazole, HEMNI (**2**)], Fig. 1. Nitroimidazoles are used as chemotherapeutic agents particularly in protozoal and anaerobic microbial infections.[4] They have also been proposed as radiosensitizers, this property being related to the presence of the nitro group.[5] Previous work on metal complexes with **2** is limited to two brief reports on copper complexes[6,7] and the research carried out on its platinum compounds has been focused on their radiosensitization properties.[8-12]

EXPERIMENTAL

Reagents

The metal salts, ligands and solvents were obtained from Merck and J. T. Baker as analytical reagents. All reagents were used without further purification.

Physical measurements

IR spectra in the range 4000–600 cm^{-1} were recorded in KBr pellets and as Nujol mulls using CsI plates in the region 600–200 cm^{-1} on a Perkin–Elmer 599B spectrophotometer. Electronic spectra of microcrystalline samples were measured by the diffuse reflectance method on a Cary 17 Varian spectrophotometer over the range 850–350 nm.

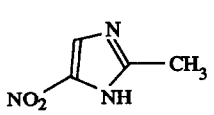

1

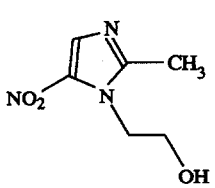

2

Fig. 1. 2-Methyl-5-nitroimidazole (MNIH) **1** and 1-(2-hydroxyethyl)-2-methyl-5-nitroimidazole (metronidazole, HEMNI) **2**.

Magnetic moments were measured using Evans' technique with a Johnson Mathey balance. Elemental analyses were performed by Butterworth Ltd Laboratories in the U.K. and by the Analytical Chemistry Department, DEPg, Facultad de Química UNAM.

Synthesis: general technique

The copper coordination compounds were prepared using ethanol as solvent and 1:1, 1:2 and 2:1 ligand/Cu^{II} molar ratios were employed (mmol scale). The same products were obtained regardless of the variation in ligand/metal ratio, but the ratio 2:1 gave the best yield. The ligand was dissolved in 50 cm^3 of boiling ethanol and added to a solution of the metal salt in 50 cm^3 of hot ethanol. The reaction mixture was refluxed for *ca* 6 h and then allowed to stand at room temperature for 7 days. The resulting precipitates were filtered, washed and dried.

In the case of the cobalt complexes, the molar ratios and the preparation were the same as described above but acetone was used as solvent. When the metal salts were used in excess, only impure compounds were isolated. For the cobalt chloride complexes of both ligands, oleus blue solutions were obtained and the compounds were precipitated by adding 25 cm^3 of a 1:1 ethanol/hexane mixture. The solid products were filtered and washed with ethanol. With cobalt acetate, the metal salt was added to the ligand **1** (2-methyl-5-nitroimidazole, MNIH) and a fine orange powder precipitated immediately; this was centrifuged and washed with hot ethanol. It was not possible to obtain the cobalt acetate complex with the ligand **2** [1-(2-hydroxyethyl)-2-methyl-5-nitroimidazole, HEMNI].

Preparation of $Cu(MNIH)_2Cl_2$ (**1a**)

Copper(II) chloride dihydrate (0.0852 g, 0.5 mmol) was dissolved in hot ethanol (50 cm^3) and a hot solution of **1** (0.1704 g, 1 mmol) in ethanol was added. The green solution was refluxed for 4 h and then allowed to stand for 4 days. The deep blue crystals were filtered off, dried *in vacuo* and sent for X-ray diffraction study. Storage of the mother liquor after filtration resulted in the formation of a few green crystals which changed back to the original blue crystals on attempting to isolate them.

Preparation of $Cu(HEMNI)_2Cl_2$ (**2a**)

Ligand **2** (0.1710 g, 1 mmol) was dissolved in hot ethanol (50 cm^3) and added to a hot solution of $CuCl_2 \cdot 2H_2O$ (0.0852 g, 0.5 mmol) in 50 cm^3 of ethanol. The reaction mixture was refluxed for 6 h. The green solution was allowed to stand at room temperature for 1 week. The bright green crystals (**2a**) which had grown were filtered off, dried *in vacuo* and sent for X-ray diffraction study. Storage of the mother liquor after filtration resulted in the formation of blue crystals with the formula $[Cu(HEMNI)_2Cl_2] \cdot H_2O$ (**2b**). Unfortunately, the crystals were not suitable for X-ray study.

Crystal structure determination of **1a** and **2a**

The single crystal X-ray data collections, structure resolution and refinements were performed on a Nicolet R3m four circle diffractometer using graphite monochromated Cu-K_α radiation (λ = 1.54178 Å) operating in the θ–2θ scanning mode. The unit cell parameters were established by least-squares adjustment on the setting angles of 25 machine centred strong reflections. The crystal data for compounds **1a** and **2a** are summarized in Table 1. During the data collections two standard reflections were monitored after the measurement of groups of 46 reflections and they showed no significant intensity decay. The data measured were corrected for background, Lorentz and polarization effects as well as for absorption, for which the crystal was considered to have a pseudo-ellipsoid shape. The structures were solved by direct methods using the software package provided by the diffractometer manufacturer using data for which $I \geqslant 3\sigma(I)$. All non-hydrogen atoms were refined anisotropically using the full-matrix least-squares procedure. The hydrogen atoms bonded to carbon atoms were placed at fixed positions (C—H, 1.09 Å) and included in the structure factor calculation with their isotropic contribution. After several full-

Table 1. Crystal data, collection and refinement parameters for **1a** and **2a**

(A) Crystal parameters	**1a**	**2a**
Stoichiometry	$C_8H_{10}O_6N_6Cl_2Cu$	$C_{12}H_{18}O_6N_6Cl_2Cu$
Molecular weight	420.652	476.766
Crystal system	Monoclinic	Monoclinic
Space group	$P2_1/a$	P_1/c
Crystal size (mm)	$0.3 \times 0.08 \times 0.02$	$0.4 \times 0.8 \times 0.08$
Crystal colour	Deep blue	Green
a (Å)	7.685(2)	7.075(3)
b (Å)	13.587(4)	19.051(7)
c (Å)	7.796(2)	14.161(7)
β (°)	114.80(2)	90.42(4)
Cell volume (Å^3)	726.53(4)	1896.8(14)
ρ(calc) (g cm^{-3})	1.92	1.67
Z	2	4
$F(000)$, e^-	422	972
(B) Data collection parameters		
μ, cm^{-1}	59.7	46.5
Scan, width, below $K_{\alpha 1}$, above $K_{\alpha 2}$ (°)	1.0–1.2	1.0–1.1
2θ Limits (°)	3–110	3–110
Scan speed (variable) (° min^{-1})	4.0–29.3	3.0–29.3
Exposure time (h)	24.15	75.48
Total reflections collected	1054	2733
Unique reflections	786	2006
(C) Structure refinement		
Reflections for final refinement	725	1998
Parameters refined	105	262
$R(F)$ (%)	5.79	4.56
$R(W)$ (%)	6.41	5.16
Goodness-of-fit for the last cycle	1.128	1.078
Final G	0.00368	0.00228

matrix least-squares cycles of refinement, the two hydroxyl group hydrogen atoms of **1a** became evident from a difference Fourier synthesis and were included in the structure factor calculation. The least-squares weighting scheme used is $w = 1/\sigma^2(F_o)+G(F_o)^2$, where σ is the standard deviation of observed amplitudes based on counting statistics and G is a variable adjusted after each cycle to minimize the function $\Sigma w(\Delta F)^2$. The final G values and other relevant refinement values are given in Table 1.

Table 3. Bond lengths (Å) for **1a**

Cu—Cl	2.307(2)	Cu—N(1)	1.985(5)
Cu—Cl(+)	2.307(2)	Cu—N(1+)	1.985(5)
N(1)—C(2)	1.330(9)	Cu—O(5b+)	2.600(5)
C(2)—N(3)	1.365(8)	N(1)—C(5)	1.370(7)
N(3)—C(4)	1.354(9)	C(2)—C(6)	1.480(10)
C(5)—N(5)	1.429(10)	C(4)—C(5)	1.366(9)
N(5)—O(5b)	1.235(7)	N(5)—O(5a)	1.222(8)

RESULTS AND DISCUSSION

The coordination compounds of copper(II) and cobalt(II) with **1** and **2** obtained in this study, **1a**–**1f** and **2a**–**2e**, are listed in Table 2, together with their analytical data. In the reactions of the metal (II) ions with ligands **1** and **2** in ethanol the same products were obtained regardless of the variation in ligand/metal ratio (1 : 1, 1 : 2 and 2 : 1).

Structure of dichloro-bis-(2-methyl-5-nitroimidazole)copper(II) (**1a**)

The crystal structure of **1a** shows two nitroimidazole and two chlorine atoms bonded to the copper(II) ion, Fig. 2 and Tables 3–5, the structure presents a symmetry centre at the metal ion with an octahedral geometry tetragonally distorted and a *trans* diaxial coordination to one of the oxygen atoms of the nitro groups. The O—Cu distance is 2.6 Å indicating weak coordination, which is also evident from the angle deformation of the ligand which allows the oxygen atom to approach the metal ion. Furthermore, the N—O distance of the nitro groups are longer for the oxygen atoms which are coordinated to the metal ions. The same distance was found in a similar complex between an acetate and a copper(II) atom interacting through a four-membered ring.[13] Compound **1a** is the first example in nitroimidazoles derivatives where the nitro group occupies a coordination site. It is noteworthy that in another nitroimidazole platinum complex[14] the nitro group is not interacting with the metal ion (O—Pt distance 3.28 Å). In compound **1a** the distances Cu—Cl and Cu—N have normal values. The formation of a chelate ring produces a change in the angles of the heterocyclic molecule, the C(5)—N(1)—C(2) angle is decreased (105°) and as a consequence Cu—N(1)—C(2) (132.3°) and Cu—N(1)—C(5) (122°) angles are very large.

Ligand **1** presents a tautomerism, Fig. 3, and the metal has the possibility of coordination to any of these tautomers. A rhodium complex of a methylimidazole has been reported,[15] where coordination takes place through the less hindered nitrogen, Fig. 4. In our case it is noteworthy that the copper ion coordinates to the most hindered nitrogen atom, adjacent to the nitro group. This behaviour is explained by stabilization of the structure through coordination of the nitro group to the metal ion.

Table 2. Elemental analyses for some coordination compounds of MNIH and HEMNI

Compound	Colour	Found (Calc.) (%) C	H	N
$Cu(MNIH)_2Cl_2$ (**1a**)	Deep blue	24.4(24.7)	2.6(2.6)	21.2(21.6)
$Cu(MNIH)_2Br_2$ (**1b**)	Green	19.8(20.1)	2.5(2.1)	17.0(17.6)
$Cu(MNIH)_2(NO_3)_2$ (**1c**)	Blue	22.8(20.1)	2.5(3.0)	22.9(23.4)
$Cu(MNI)_2(OH)_2$ (**1d**)	Deep blue	29.5(27.3)	3.0(3.4)	23.8(23.9)
$Co(MNIH)_2Cl_2$ (**1e**)	Blue	24.7(25.0)	2.7(2.6)	22.9(21.9)
$Co(MNIH)(OAc)_2$ (**1f**)	Orange	29.1(31.5)	3.6(3.6)	14.0(13.8)
$Cu(HEMNI)_2Cl_2$ (**2a**)	Green	30.2(30.2)	3.8(3.8)	17.5(17.6)
$Cu(HEMNI)_2Cl_2$ (**2b**)	Blue	29.7(30.2)	4.2(3.8)	17.7(17.6)
$Cu(HEMNI)_2Br_2$ (**2c**)	Green	27.0(25.5)	3.5(3.2)	14.3(14.9)
$Cu(HEMNI)(OAc)_2$ (**2d**)	Green	33.9(34.0)	4.3(4.3)	11.9(11.9)
$Co(HEMNI)_2Cl_2$ (**2e**)	Deep blue	32.8(31.5)	4.0(4.0)	18.1(17.2)

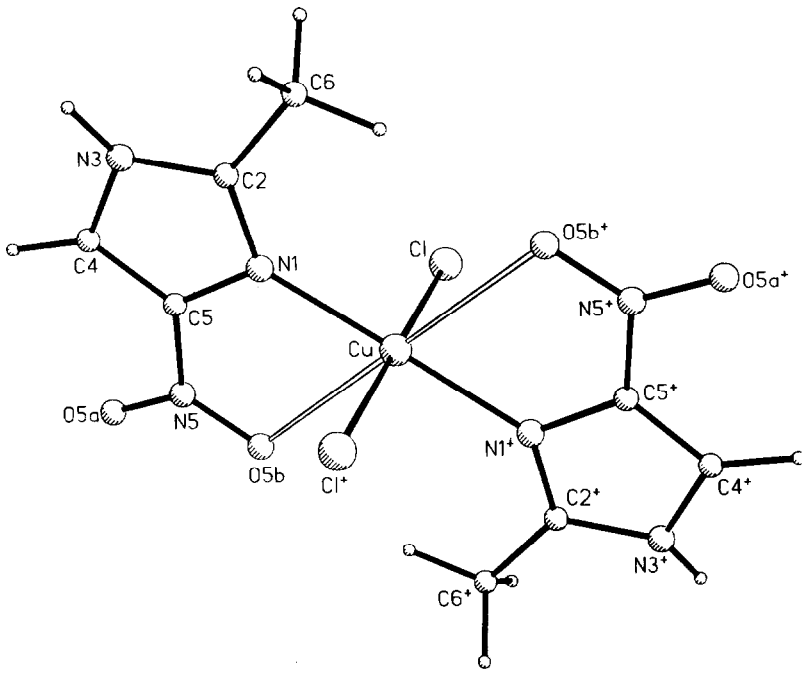

Fig. 2. Crystal structure of **1a**

Structure of bis-[(μ-chloro)chloro-bis-(1-(2-hydroxyethyl)-2-methyl-5-nitroimidazole)copper(II)] (**2a**)

The molecular structure obtained for compound **2a** is a centrosymmetric chloro-bridged dimer, as is shown in Fig. 5. The coordination geometry around each copper atom in the dimer is trigonal bipyramid with three equatorial chlorine atoms and two axial imidazole molecules. Representative bond lengths and angles are given in Tables 6–8. Two different Cu—Cl bond lengths (2.418 and 2.619 Å) in Cu_2Cl_2 appear to be the common feature among the chloro-bridged dimeric complexes of copper(II).[16] The equatorial Cu—Cl bond lengths (2.297 Å) are normal for this type of complex. The angle between the two bridging chlorine atoms and the copper ion is

Table 4. Bond angles (°) for **1a**

Cl—Cu—N(1)	89.6(2)	Cl—Cu—Cl(+)	180.0
N(1)—Cu—Cl(+)	90.4(2)	Cl—Cu—N(+)	90.4(2)
N(1)—Cu—N(1+)	180.0	Cl(+)—Cu—N(1+)	89.6(2)
Cu—N(1)—C(2)	132.3(4)	Cu—N(1)—C(5)	122.1(4)
C(2)—N(1)—C(5)	105.4(5)	N(1)—C(2)—N(3)	109.1(6)
N(1)—C(2)—C(6)	127.0(6)	N(3)—C(2)—C(6)	123.9(6)
C(2)—N(3)—C(4)	110.1(6)	N(3)—C(4)—C(5)	103.7(5)
N(1)—C(5)—C(4)	111.8(6)	N(1)—C(5)—N(5)	121.1(5)
C(4)—C(5)—N(5)	127.1(5)	C(5)—N(5)—O(5a)	117.8(6)
C(5)—N(5)—O(5b)	117.7(5)	O(5a)—N(5)—O(5b)	124.5(7)

Table 5. Selected torsion angles (°) for **1a**

Cl(+)—Cu—N(1)—C(5)	−87.9(0.5)	N(1)—C(5)—N(5)—O(5b)	6.8(1.0)
Cl(+)—Cu—N(1)—C(2)	85.4(0.7)	Cu—N(1)—C(2)—C(6)	9.0(1.2)
N(1)—C(5)—N(5)—O(5a)	−172.1(0.7)	C(4)—C(5)—N(5)—O(5b)	−173.4(0.7)
Cl—Cu—N(1)—C(5)	92.1(0.5)	Cu—N(1)—C(2)—N(3)	−174.8(0.5)
C(2)—N(3)—C(4)—C(5)	−1.3(0.9)		

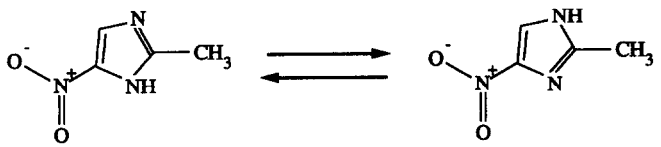

Fig. 3. Tautomerism of **1**.

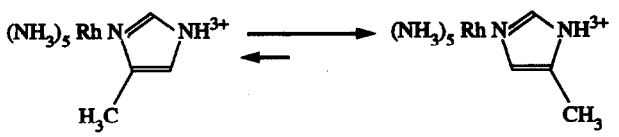

a **b**

Fig. 4. The isomer mixture of $(NH_3)_5Rh(4CH_2imH)^{3+}$ (a) and $(NH_3)_5Rh(5CH_3imH)^{3+}$ (b) slowly converts to 100% of the less hindered isomer (b).

smaller than expected due to the effect of the four-membered ring, nevertheless the sum of the three equatorial angles is 360°, the remainder of the angles around the copper atoms are normal for a bipyramidal structure. Coordination to the metal ion does not produce any deformation of the ligand angles, as can be appreciated from the X-ray data of the free ligand.[17] The two axial imidazole molecules are bonded to copper through the imine nitrogen with a normal Cu—N distance of 1.993 Å.

Infrared and electronic spectroscopy studies

Copper complexes. The electronic spectrum of the crystalline complex **1a** (Table 9) presents a band indicative of a tetragonally distorted octahedral geometry, Fig. 6. The ν(Cu—Cl) stretching band in the far-IR is as expected for terminal Cu—X (290 cm^{-1}) and its magnetic moment is consistent with this structure. A similar structure is proposed for the complexes **1b** and **1c** (Table 9). In the IR spectra (Table 10), the free heterocyclic ligand (MNIH) has

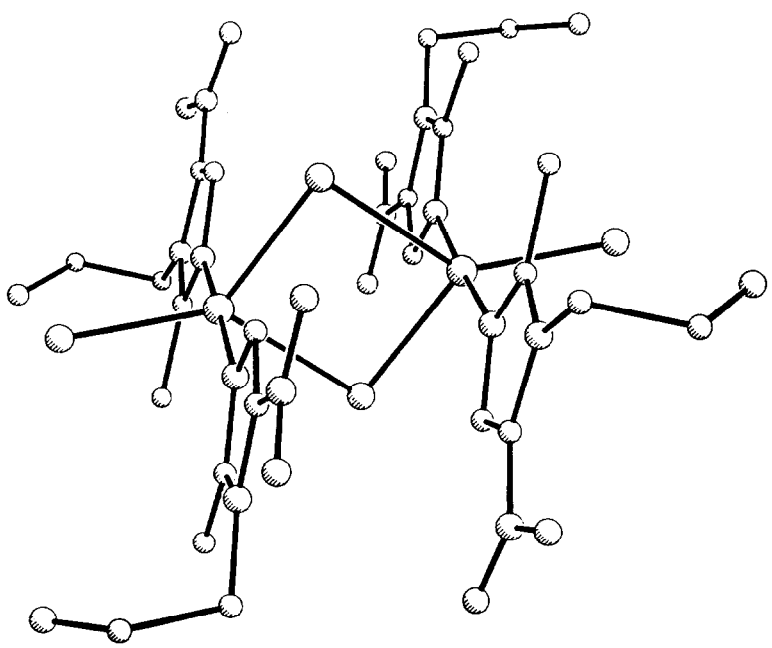

Fig. 5. Crystal structure of **2a**.

Table 6. Bond lengths (Å) for **2a**

Cu—Cl(1)	2.297(2)	Cu—Cl(2)	2.418(1)
Cu—N(1)	1.993(4)	Cu—N(11)	2.002(4)
Cu—Cl(2+)	2.619(1)	Cl(2)—Cu(+)	2.619(1)
N(1)—C(2)	1.339(6)	N(1)—C(5)	1.370(6)
C(2)—N(3)	1.363(6)	C(2)—C(8)	1.489(7)
N(3)—C(4)	1.391(6)	N(3)—C(6)	1.481(6)
C(4)—N(4)	1.415(6)	C(4)—C(5)	1.358(6)
N(4)—O(4a)	1.215(6)	N(4)—O(4b)	1.219(6)
C(6)—C(7)	1.499(8)	C(7)—O(7)	1.417(8)
N(11)—C(12)	1.338(6)	N(11)—C(15)	1.369(7)
C(12)—N(13)	1.348(6)	C(12)—C(18)	1.488(8)
N(13)—C(14)	1.397(7)	N(13)—C(16)	1.485(7)
C(14)—N(14)	1.426(7)	C(14)—C(15)	1.351(7)
N(14)—O(14a)	1.214(8)	N(14)—O(14b)	1.223(7)
C(16)—C(17)	1.529(8)	C(17)—O(17)	1.402(8)

bands assigned to the ν_{as} and ν_s stretching modes of NO_2 at 1510 and 1385 cm^{-1}, which increased in intensity, became broader and shifted a few wave numbers in complexes **1a**, **1b** and **1c**, supporting the interaction of this group with the metal ion *vide infra*; it is also interesting that a set of bands due to the ligand skeletal vibration modes (825, 815, 790 and 750 cm^{-1}) presents exactly the same pattern in these three complexes indicating that they must share the same coordination mode and structure. The difference in the IR spectrum of compound **1d** indicates that copper(II) has another coordination mode. The compound has a strong symmetric band ν(OH) at 3440 cm^{-1} and another broad band, δ(OH), at 1145 cm^{-1} assigned to a bridging OH^- group. The electronic spectrum characteristic of a distorted octahedral geometry (Table 9) and its low magnetic moment ($\mu = 1.58$) allow the proposal of a polymeric structure with hydroxo bridges.

The 1-(2-hydroxyethyl)-2-methyl-5-nitroimidazole copper complexes, **2a**, **2b**, **2c** and **2d**, have similar IR spectra in which the bands assigned to $\nu_{as}(NO_2)$ and $\nu_s(NO_2)$ remain in the same position as observed in the ligand (Table 10), indicating that this group does not participate as a coordination site, *vide infra*; the bands assigned to the ν(OH) group (3220 cm^{-1}) are shifted to higher wave numbers indicating that the original hydrogen bridge

Table 7. Bond angles (°) for **2a**

Cl(1)—Cu—Cl(2)	134.5(1)	Cl(1)—Cu—N(1)	90.1(1)
Cl(2)—Cu—N(1)	91.4(1)	Cl(1)—Cu—N(11)	89.0(1)
Cl(2)—Cu—N(11)	92.4(1)	N(1)—Cu—N(11)	175.4(2)
Cl(1)—Cu—Cl(2+)	135.3(1)	Cl(2)—Cu—Cl(2+)	90.2
N(1)—Cu—Cl(2+)	87.9(1)	N(11)—Cu—Cl(2+)	89.5(1)
Cu—Cl(2)—Cu(+)	89.8	Cu—N(1)—C(2)	125.6(3)
Cu—N(1)—C(5)	127.2(3)	C(2)—N(1)—C(5)	107.2(4)
N(1)—C(2)—N(3)	110.8(4)	N(1)—C(2)—C(8)	125.2(4)
N(3)—C(2)—C(8)	124.0(4)	C(2)—N(3)—C(4)	105.5(4)
C(2)—N(3)—C(6)	125.2(4)	C(4)—N(3)—C(6)	129.3(4)
N(3)—C(4)—N(4)	125.9(4)	N(3)—C(4)—C(5)	108.3(4)
N(4)—C(4)—C(5)	125.7(5)	C(4)—N(4)—O(4a)	118.2(4)
C(4)—N(4)—O(4b)	119.2(5)	O(4a)—N(4)—O(4b)	122.6(5)
N(1)—C(5)—C(4)	108.2(4)	N(3)—C(6)—C(7)	111.2(5)
C(6)—C(7)—O(7)	110.2(5)	Cu—N(11)—C(12)	127.6(3)
Cu—N(11)—C(15)	125.4(3)	C(12)—N(11)—C(15)	106.9(4)
N(11)—C(12)—N(13)	111.1(4)	N(11)—C(12)—C(18)	124.5(4)
N(13)—C(12)—C(18)	124.4(4)	C(12)—N(13)—C(14)	105.6(4)
C(12)—N(13)—C(16)	126.0(4)	C(14)—N(13)—C(16)	128.4(4)
N(13)—C(14)—N(14)	125.4(4)	N(13)—C(14)—C(15)	107.9(4)
N(14)—C(14)—C(15)	126.7(5)	C(14)—N(14)—O(14a)	117.3(5)
C(14)—N(14)—O(14b)	119.5(5)	O(14a)—N(14)—O(14b)	123.2(5)
N(11)—C(15)—C(14)	108.5(4)	N(13)—C(16)—C(17)	111.7(4)
C(16)—C(17)—O(17)	111.7(5)		

Table 8. Selected torsion angles for **2a**

C(8)—C(2)—N(3)—O(6)	1.5(0.8)	Cl(1)—Cu—N(1)—C	−112.6(0.4)
N(3)—C(4)—N(4)—O(4b)	−6.5(0.8)	C(2)—N(1)—C(5)—C	0.5(0.5)

Table 9. Electronic spectra (800–350 nm) and magnetic moments [μ_{eff} (BM)] of some coordination compounds with MNIH and HEMNI

Compound	λ_{max} (nm)		μ
$Cu(MNIH)_2Cl_2$[a] (**1a**)	660	580 sh	1.70
$Cu(MNIH)_2Br_2$ (**1b**)	640		1.69
$Cu(MNIH)_2(NO_3)_2$ (**1c**)	595		1.91
$Cu(MNIH)_2(OH)_2$ (**1d**)	610		1.58
$Co(MNIH)_2Cl_2$ (**1e**)	560		4.32
$Co(MNIH)(OAc)_2$ (**1f**)	490	510	4.75
$Cu(HEMNI)_2Cl_2$[b] (**2a**)	725		2.0
$Cu(HEMNI)_2Cl_2$[c] (**2b**)	595		[d]
$Cu(HEMNI)_2Br_2$ (**2c**)	655		1.8
$Cu(HEMNI)(OAc)_2$ (**2d**)	710		1.49
$Co(HEMNI)Cl_2$ (**2e**)	610	580 sh	4.42

[a] Deep blue.
[b] Green.
[c] Blue.
[d] Not enough sample available.

observed in the ligand[17] is lost in the metal complexes. The blue compound **2b** presents new bands (3120 and 3165 cm^{-1}) in that region, most probably due to a different crystal packing of this compound with respect to the analogous green compound **2a**. There were important changes in the ring vibration region due to N(3) coordination to the metal ion. The electronic spectrum and the magnetic moment of **2a** (Table 9) is characteristic of a pentacoordinated copper(II) ion.[18] The acetate compound, **2d**, has a similar electronic spectrum to **2a**, Fig. 6, and a low magnetic moment (1.49 BM), suggesting the presence of a dimeric structure with a copper–copper interaction.[13] This is supported by the presence of bridging acetates in the IR spectrum, in which vibrations assigned to the COO^- group were at $\nu_{as}(COO^-)$ 1555, $\nu_s(COO^-)$ 1435, $\delta(OCO)$ 650 and $\pi(COO^-)$ 600 cm^{-1}. The structure of this compound is proposed to have a pentacoordinate copper(II) ion with acetate bridges and apical **2**. The electronic spectra of **2b** (blue) Fig. 6, and **2c** are typical of a distorted octahedral geometry (Table 9).

Cobalt complexes. The blue cobalt(II) complexes **1e** and **2e** have magnetic moments and diffuse electronic spectra (Table 9) typical of tetrahedral complexes, Fig. 7, the bands at *ca* 600 nm are assigned to the $^4T_1(P) \leftarrow {}^4A_2(F)$ transition.[19] The low frequency vibrational spectra (Table 10) contain bands assignable to ν(Co—Cl) at 295 and 280 cm^{-1} for **1e** and at 340 and 300 cm^{-1} for **2e**.

The orange compound **1f** has a diffuse electronic spectra, suggesting the presence of a non-centrosymmetric cobalt environment possibly due to a distorted tetragonal arrangement or to a pentacoordinate geometry, with two complex bands at 490 and 510 nm, its magnetic moment ($\mu = 4.75$ BM) is as expected for a cobalt(II) ion. The acetate shows IR bands at *ca* 1545 cm^{-1} [$\nu_a(COO^-)$], 1430 cm^{-1}[$\nu_s(COO^-)$] and 620 cm^{-1} [$\pi(COO^-)$], which are consistent for a carboxylate-bridged cobalt(II) dimer;[20] and most probably has the ligands occupying the terminal positions in the dimer, as has been observed in this type of structure.

Conclusions

Stable complexes with both ligands were obtained. The copper chloride compounds **1a** and

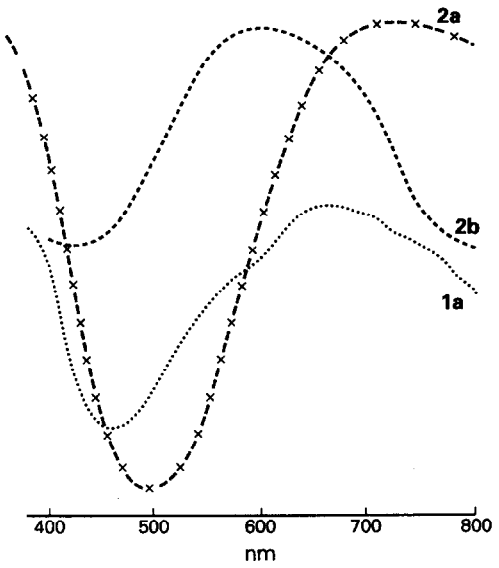

Fig. 6. Electronic spectra of **1a**, **2a** and **2b**.

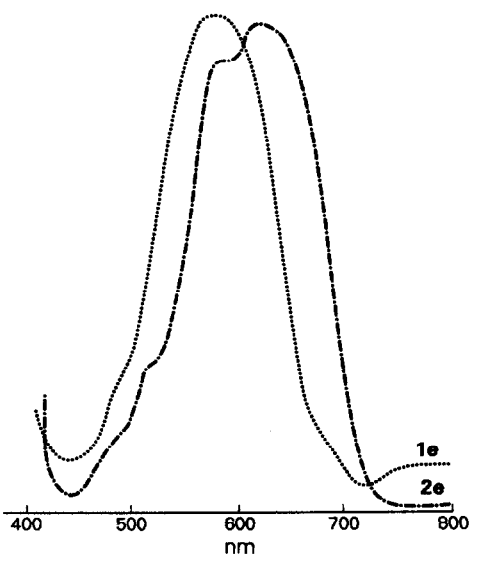

Fig. 7. Electronic spectra of **1e** and **2e**.

Table 10. Selected IR bands (1600–600 cm^{-1}) of coordination compounds with MNIH and HEMNI

Compound	Assignment				Ring vibrations			
	$\nu_{as}(NO_2)$	$\nu_s(NO_2)$	ν(C=C)	ν(C—N)	δ(C—N), δ(C=C), δ(C—H)			
MNIH (**1**)	1510	1385	1405	1290	815,	825,	—	750
$Cu(MNIH)_2Cl_2$ (**1a**)	1520sb	1375sb	1420b	1295s	830,	850,	790m,	750
$Cu(MNIH)_2Br_2$ (**1b**)	1525s	1380s	1420sb	1295s	830,	850,	785m,	750s
$Cu(MNIH)_2(NO_3)_2$ (**1c**)	1520sb	1378sb	1420sb	1292s	828,	848,	785m,	750s
$Cu(MNIH)_2(OH)_2$ (**1d**)	1540sb	[a]	1420sb	1260s	815,	845,	—	730
$Co(MNIH)_2Cl_2$ (**1e**)	1522sb	1378s	1400sb	1280s	810,	825,	—	750
$Co(MNIH)(OAc)_2$ (**1f**)	1500	1390	1405b	1310	835,	845,	—	760
HEMNI (**2**)	1530	1365	1420	1265	985w,	965m,	945m,	905s
$Cu(HEMNI)_2Cl_2$ (**2a**)	1560sb	1370	1425b	1275s	1000b,	950bW,	—	—
$Cu(HEMNI)_2Cl_2$ (**2b**)	1565s	1395b	1425w	1280	1000b,	950bW,	—	—
$Cu(HEMNI)_2Br_2$ (**2c**)	1560b	1370b	1425wsh	1280sb	1000wb,	960b,	—	—
$Cu(HEMNI)(OAc)_2$ (**2d**)	1555b[b]	1435b	[a]	1270	970sb,	—	—	—
$Co(HEMNI)_2Cl_2$ (**2e**)	1560b	1390	1430	1270	995,	—	—	—

[a] Not observable.
[b] Band with $\nu_{as}(COO^-)$ contribution.

2a, were suitable for X-ray diffraction studies. It is noteworthy that the ligand structure modulates the geometry and the coordination sites in these copper complexes.

The results obtained from the electronic spectra for both groups of complexes showed that the ligand **1** is stronger than the ligand **2**, as can be appreciated from the electronic transitions at higher energies for the 2-methyl-5-nitroimidazole complexes, indicating a stronger ligand field. This is most probably due to the presence of a nitro group adjacent to the preferred coordination site, N(1), giving extra stability to the complexes by its interaction with the metals. These complexes are the first examples of the nitroimidazole derivatives in which an interaction of the metal ions with the nitro group is observed. A study of the biological activity of the compounds obtained in this work is in progress.

REFERENCES

1. N. Barba-Behrens, G. Mendoza-Díaz and D. M. L. Goodgame, *Inorg. Chim. Acta* 1986, **125**, 21.
2. N. Barba-Behrens and R. Acevedo-Chávez, *Transition Met. Chem.* 1990, **15**, 434.
3. N. Barba-Behrens, J. L. Bautista, M. E. Ruiz, P. Joseph-Nathan, A. Flores-Parra and R. Contreras, *J. Inorg. Biochem.* 1990, **40**, 201.
4. A. Breccia, B. Cavalleri and G. E. Adam (Eds), *Nitroimidazoles: Chemistry, Pharmacology and Clinical Application*. Plenum Press, New York (1982).
5. D. W. Whillans and G. E. Adams, *Radiat. Res.* 1975, **62**, 407.
6. Y. W. Chien, H. J. Lambert and D. R. Sanvordeker, *J. Pharm. Sci.* 1975, **64**, 957.
7. V. Callaghan, D. M. L. Goodgame and R. P. Tooze, *Inorg. Chim. Acta* 1983, **78**, L1.
8. J. R. Bales, P. J. Sadler, C. J. Coulson, M. Laverick and A. H. W. Nias, *Br. J. Canc.* 1982, **46**, 701.
9. J. R. Bales, C. J. Coulson, D. W. Gilmour, M. A. Mazid, S. Neidle, R. Kuroda, B. J. Peart, C. A. Ramsden and P. J. Sadler, *J. Chem. Soc., Chem. Commun.* 1983, 432.
10. R. Chibber, I. J. Stratford, I. Ahmed, A. B. Robbins, D. Goodgame and B. Lee, *Int. J. Rad. Onc. Biol. Phys.* 1984, **10**, 1213.
11. J. R. Bales, M. S. Mazid, P. J. Sadler, A. Aggarwal, R. Kuroda, S. Neidle, D. W. Gilmour, B. J. Peart and C. A. Ramsden, *J. Chem. Soc., Dalton Trans.* 1985, 795.
12. N. Farrell and K. A. Skov, *J. Chem. Soc., Chem. Commun.* 1987, 1043.
13. L. P. Battaglia, A. B. Corradi, G. M. Trigiano, L. Menabue and G. C. Pellacani, *Inorg. Chem.* 1981, 1075.
14. J. R. Bales, M. A. Mazid, P. J. Sadler, A. Aggarwall, R. Kuroda, S. Neidle, D. W. Gilmour, B. J. Peart and C. A. Ramsden, *J. Chem. Soc., Dalton Trans.* 1985, 795.
15. M. G. Elliot and R. E. Shepherd, *Transition Met. Chem.* 1989, **14**, 251.
16. S. J. Brown, X. Tao, T. A. Wark, D. W. Stephan and P. K. Mascharak, *Inorg. Chem.* 1988, **27**, 1581.
17. N. M. Blaton, O. M. Peeters and C. J. Deranter, *Acta Cryst.* 1979, **B35**, 2465.
18. B. J. Hathaway, *Structure and Bonding*, Vol. 57, p. 56. Springer-Verlag, Berlin (1984).
19. A. B. P. Lever, *Inorganic Electronic Spectroscopy*, 2nd edn. Elsevier, New York (1986).
20. J. Drew, M. B. Hursthouse, P. Thornton and A. J. Welch, *J. Chem. Soc., Chem. Commun.* 1973, 52.

Polyhedron Vol. 10, No. 12, pp. 1343–1352, 1991
Printed in Great Britain

0277–5387/91 $3.00+.00
© 1991 Pergamon Press plc

EFFECTS OF SULPHUR SUBSTITUENTS ON THE GEOMETRIES OF DIPALLADIUM μ-THIOLATO COMPLEXES: CRYSTAL STRUCTURES OF $Pd_2Cl_2(\mu\text{-}Cl)(\mu\text{-}SR)(PMe_3)_2$ (R = Me, t-Bu AND Ph) AND $Pd_2Cl_2(\mu\text{-}SPh)_2(PEt_3)_2$

ESTHER M. PADILLA, JAMES A. GOLEN,* PAUL N. RICHMANN and CRAIG M. JENSEN†

Department of Chemistry, University of Hawaii, Honolulu, HI 96822, U.S.A.

(*Received* 9 *November* 1990; *accepted* 21 *January* 1991)

Abstract—The mono(μ-alkylthiolato) complexes, *cis*-$Pd_2Cl_2(\mu\text{-}Cl)(\mu\text{-}SR)(PMe_3)_2$ (R = Me, **1**; t-Bu, **2**) are obtained as the exclusive products of the reaction of acetone solutions of *trans*-$[PdCl(\mu\text{-}Cl)(PMe_3)]_2$ with the corresponding thiols at 25°C, whereas reaction with stoichiometric amounts of thiophenol gives mixtures of *cis*-$Pd_2Cl_2(\mu\text{-}Cl)(\mu\text{-}SPh)(PMe_3)_2$ (**3**) and *trans*-$Pd_2Cl_2(\mu\text{-}SPh)_2(PMe_3)_2$ (**5**). Reaction of *trans*-$[PdCl(\mu\text{-}Cl)(PR_3)]_2$ with thiophenol in a 1:2 stoichiometry gives exclusively *trans*-$Pd_2Cl_2(\mu\text{-}SPh)_2(PR_3)_2$ (R = Et, **4**; Me, **5**). The molecular structures of **1**, **2**, **3**·CH_2Cl_2 and **4** have been determined by X-ray diffraction. Complexes **1** and **2** have non-planar geometries with dihedral angles of 140 and 146°, respectively, between the coordination planes of the palladium atoms. By contrast, the μ-arylthiolato complexes are planar with dihedral angles of 180° between the coordination planes of the palladium atoms. The Pd—S bond distances 2.262(2)–2.272(2) Å in complexes **1** and **2** are significantly shorter than the Pd—S distances in **3**, 2.288(2) and 2.301(2) Å, indicating enhanced metal–sulphur bonding in the alkylthiolato complexes. The bent geometries of the alkylthiolato complexes as well as the dichotomy of *cis* and *trans* phosphine geometries preferred by $M_2Cl_2(\mu\text{-}SR)_2(PR'_3)_2$ (M = Pd, Pt) alkylthiolato and arylthiolato complexes, respectively, are discussed in view of the enhanced sulphur–metal donor interactions in the alkylthiolato complexes. The isolation of mono(μ-thiolato) complexes from the reaction of *trans*-$[PdCl(\mu\text{-}Cl)(PMe_3)]_2$ with alkylthiols and not arylthiols is also accounted for by the additional stabilization of the metal–sulphur bonds in the alkylthiolato complexes. Crystallographic data: for **1**, orthorhombic, $Pbc2_1$, $Z = 4$, $a = 11.630(6)$, $b = 11.667(3)$, $c = 12.816(4)$ Å, $V = 1739(1)$ Å^3, $\rho_{calc.} = 1.980$ g cm^{-3}; for **2**, orthorhombic, $P2_1cn$, $Z = 4$, $a = 8.158(3)$, $b = 10.345(3)$, $c = 24.106(6)$ Å, $V = 2035(1)$ Å^3, $\rho_{calc.} = 1.830$ g cm^{-3}; for **3**·CH_2Cl_2, monoclinic $C2/2$, $Z = 8$, $a = 27.38(1)$, $b = 11.477(9)$, $c = 16.506(7)$ Å, $\beta = 124.12(3)°$, $V = 4294(4)$ Å^3, $\rho_{calc.} = 1.924$ g cm^{-3}; for **4**, triclinic $P\bar{1}$, $Z = 2$, $a = 8.694(5)$, $b = 9.570(6)$, $c = 10.203(7)$ Å, $\alpha = 68.72(5)$, $\beta = 76.86(5)$, $\gamma = 85.27(5)°$, $V = 770.3(8)$ Å^3, $\rho_{calc.} = 1.592$ g cm^{-3}.

Dimetallic μ-thiolato complexes of palladium and platinum have been known for many years[1] and a wide variety of these complexes have been prepared.[1–11] However, the factors responsible for their thermodynamically preferred conformations remain poorly understood. One enigma has been the preferred geometries of $M_2Cl_2(\mu\text{-}SR)_2(PR'_3)_2$ complexes: the bis(μ-alkylthiolato) complexes are stabilized as *cis* isomers, while the bis(μ-arylthiolato) complexes are stabilized as *trans* isomers. To account for this dichotomy, Chatt and Hart proposed[2] that the metal–sulphur interaction in the alkylthiolato complexes involved an aromatic, inor-

* Present address: Department of Chemistry, University of Southeastern Massachusetts, North Dartmouth, MA 02747, U.S.A.

† Author to whom correspondence should be addressed.

ganic $d\pi$–$d\pi$ ring system into which *p*-electrons from the sulphur atoms were delocalized. They speculated that the aromatic ring was somehow stabilized by the *cis*-phosphine geometry. However, in the case of the arylthiolato complexes dipole measurements indicated non-planar coordination about sulphur. This precludes delocalization of sulphur *p*-electrons into an aromatic $d\pi$–$d\pi$ system and provided a rationale for the arylthiolato complexes adopting the more common *trans*-phosphine geometry.

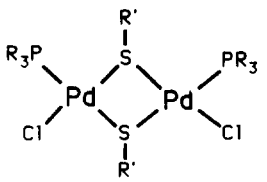

Cis phosphine configuration
when R = alkyl and R' = alkyl.

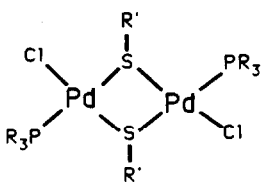

Trans phosphine configuration
when R = alkyl and R' = aryl.

A subsequent X-ray structure determination of *cis*-$Pt_2Cl_2(\mu\text{-}SEt)_2(PPr_3)_2$ by Owston and coworkers[12] showed the Pt—S—Pt—S ring to be non-planar with a dihedral angle of 130° between the two platinum coordination planes and that the thiolato α-carbon atoms were out of the Pt—S—Pt plane. The existence of an aromatic $d\pi$–$d\pi$ ring system in the bis(μ-alkylthiolato) complex was therefore ruled out by these results. Owston instead attributed the stabilization of the *cis* isomer of the bis(μ-alkylthiolato) to a continuous zigzag chain, P—Pt—S—Pt—P, of strong *cis* bonds involving only one sulphur atom.

We have synthesized and determined the crystal structure of several μ-thiolato complexes. From these studies, structural patterns have emerged. We report here the results of our structural studies as well as our insights into the connections between the geometries of the μ-thiolato complexes and the nature of the metal–μ-thiolato bonds.

EXPERIMENTAL

General details

The following were purchased and used without further purification: 2-methyl-2-propanethiol, triethylphosphine (Fluka Chemical Corp.); thiophenol, acetone, chloroform, dichloromethane-d_2 (Aldrich Chemical Co.); trimethylphosphine (Strem Chemicals Inc.) and methyl mercaptan (Matheson). The complexes, *trans*-[PdCl(μ-Cl)$(PR_3)]_2$ (R = Me, Et) were prepared by the method of Chatt and Venanzi.[13]

Caution: Trimethylphosphine and methyl mercaptan are volatile toxins, therefore use of an efficient fume hood is mandatory.

The ^1H and $^{31}P\{^1H\}$ NMR spectra were recorded on a Nicolet NT300 spectrometer at 300 and 122 MHz, respectively. The ^1H NMR data are listed in ppm downfield from TMS at 0.00 ppm. ^{31}P NMR chemical shifts were measured relative to the deuterium resonance of the solvent by using the internal frequency lock of the spectrometer so that the resonance from a capillary of 85% H_3PO_4, centred in a 5 mm NMR tube containing the deuterated solvent, appeared at 0.0 ppm at 20°C. Microanalyses were performed by Oneida Research Services Inc. (Whitesboro, New York).

Preparation of cis-$Pd_2Cl_2(\mu\text{-}Cl)(\mu\text{-}SMe)(PMe_3)_2$ (1)

Synthesis of **1** has been reported previously.[3] However, we find the following preparation more convenient. A slow stream of methyl mercaptan was passed through a solution of *trans*-[PdCl(μ-Cl)$(PMe_3)]_2$ (1.507 g, 2.97 mmol) in acetone (125 cm^3) at room temperature for 5 min. The initially orange solution became green–yellow. The solution was then stirred at room temperature for 24 h. After reduction of the solvent to 30 cm^3, the resulting green, crystalline product (1.443 g, 93.6% yield) was isolated from the reaction mixture by filtration. The ^1H NMR spectrum of the product was identical with that which has previously been reported[3] for **1**. $^{31}P\{^1H\}$ NMR (CD_2Cl_2): δ 6.0 (s). Found: C, 16.1; H, 3.8. Calc.: C, 16.2; H, 4.0%.

Preparation of cis-$Pd_2Cl_2(\mu\text{-}Cl)(\mu\text{-}SCMe_3)(PMe_3)_2$ (2)

A solution of *trans*-[PdCl(μ-Cl)$(PMe_3)]_2$ (0.998 g, 1.97 mmol) in acetone (125 cm^3) was treated at room temperature with 2-methyl-2-propanethiol (0.90 cm^3, 7.90 mmol). The initially orange solution became yellow–green within 5 min and was stirred at room temperature for 24 h. After reduction of the solvent to 40 cm^3, the resulting green, crystalline product (0.924 g, 82.5% yield) was isolated from the reaction mixture by filtration. ^1H NMR (CD_2Cl_2): δ 1.71 (s, $SCCH_3$, 9H), 1.66 [d, J_{P-H} = 12.6 Hz, $P(CH_3)_3$, 18H]. $^{31}P\{^1H\}$

NMR (CD_2Cl_2): δ 5.8 (s). Found: C, 21.3; H, 4.7. Calc.: C, 21.4; H, 4.8%.

Preparation of cis-$Pd_2Cl_2(\mu\text{-}Cl)(\mu\text{-}SPh)(PMe_3)_2$ (**3**)

Method 1. A solution of *trans*-[PdCl(μ-Cl)$(PMe_3)]_2$ (1.011 g, 2.00 mmol) in acetone (100 cm^3) was treated at room temperature with thiophenol (0.205 cm^3, 2.00 mmol). The initially orange solution became yellow within 5 min and was stirred at room temperature for 24 h. After reduction of the solvent to 10 cm^3, the resulting yellow, crystalline solid was isolated by filtration and seen by ^1H NMR to consist of a 85:15 mixture of **3** and **5**. The bis(μ-thiolato) complex was removed by extraction with 150 cm^3 of benzene leaving pure **3** (0.214 g, 18.6% yield). ^1H NMR (CD_2Cl_2): δ 8.13 m, 7.37 m (aromatic, 5H), 1.51 [d, J_{P-H} = 10.2 Hz, $P(CH_3)_3$, 18H]. $^{31}P\{^1H\}$ NMR (CD_2Cl_2): δ 5.8 (s). Found: C, 24.3; H, 3.8. Calc.: C, 24.8; H, 4.0%.

Method 2. A solution of *trans*-[PdCl(μ-Cl$)(PMe_3)]_2$ (1.005 g, 2.00 mmol) in acetone (125 cm^3) was treated at room temperature with thiophenol (0.437 g, 4.00 mmol). The initially orange solution became yellow within 5 min and was stirred at room temperature for 24 h. After reduction of the solvent to 20 cm^3, the resulting yellow, crystalline product, **5**, was isolated from the reaction mixture by filtration (1.204 g, 92.0% yield). ^1H NMR (CD_2Cl_2): δ 8.01 m, 7.21 m (aromatic, 10H), 1.28 (d, J_{P-H} = 11.9 Hz, $P(CH_3)_3$, 18H). $^{13}P\{^1H\}$ NMR (CD_2Cl_2): δ −0.9 (s). Found: C, 32.8; H, 4.2. Calc.: C, 33.0; H, 4.3%. The bis(μ-thiolato) complex (0.418 g, 0.64 mmol) was then refluxed in chloroform with an equimolar amount of *trans*-[PdCl(μ-Cl$)(PMe_3)]_2$ (0.324 g, 0.64 mmol) for 1 h. The resulting yellow, crystalline solid was isolated by filtration, 0.583 g, 78.6% yield.

Preparation of trans-$Pd_2Cl_2(\mu\text{-}SPh)_2(PEt_3)_2$ (**4**)

A solution of *trans*-[PdCl(μ-Cl$)(PEt_3)]_2$ (1.012 g, 1.71 mmol) in acetone (125 cm^3) was treated at room temperature with thiophenol (0.35 cm^3, 3.42 mmol). The initially orange solution became yellow within 5 min and was stirred at room temperature for 24 h. After reduction of the solvent to 10 cm^3, the resulting yellow, crystalline product was isolated from the reaction mixture by filtration (1.069 g, 94.6% yield). ^1H NMR (CD_2Cl_2): δ 8.02 m, 7.21 m (aromatic, 10H), 1.64 [dq, J_{P-H} = 10.2 Hz, $P(CH_2CH_3$, 12H)], 1.06 [dt, J_{P-H} = 9.3 Hz, $P(CH_3)_3$, 18H]. $^{31}P\{^1H\}$ NMR (CD_2Cl_2): δ 30.3 (s). Found: C, 39.0; H, 5.4. Calc.: C, 39.0; H, 5.4%.

Crystallographic studies

Crystals suitable for X-ray diffraction were obtained by slow evaporation of dichloromethane solutions of the respective complexes. The crystals were mounted on glass fibres with epoxy and centred on a Nicolet P3 automated diffractometer. The unit-cell parameters were obtained by least-squares refinement of the setting angles of 20 reflections. Crystal and instrument stability were monitored with a set of three standard reflections measured every 97 reflections; in all cases no significant variations were found. Details of other crystal data and relevant information are summarized in Table 1.

The structures were solved by direct methods using SHELX PLUS computer programs (Nicolet Instrument Corp.) and refined by full-matrix least-squares procedures. All non-hydrogen atoms were refined with anisotropic coefficients. The hydrogen atoms were introduced in fixed, calculated positions and the coordinates and isotropic thermal parameters for hydrogen atoms were allowed to vary in the final cycles of full-matrix least-squares refinement. During the refinement of **3** a group of peaks not associated with the palladium complex became apparent in the difference Fourier maps. The peaks were refined as a methylene chloride solvate. The carbon atom of the solvate lies on a special position about which the symmetry unique chlorine is disordered over two positions which refined with occupancies of 0.765 and 0.235 in the Cl(4) and Cl(4′) sites, respectively.

RESULTS AND DISCUSSION

Syntheses

The mono(μ-thiolato) complexes, *cis*-$Pd_2Cl_2(\mu\text{-}Cl)(\mu\text{-}SR)(PMe_3)_2$ (R = Me, **1**; t-Bu, **2**; Ph, **3**) are obtained by reaction of acetone solutions of *trans*-[PdCl(μ-Cl$)(PMe_3)]_2$ with thiols at 25°C (Scheme 1). In the case of the alkyl thiols, mono(μ-thiolato) complexes were obtained exclusive of bis(μ-thiolato) complexes even when the reaction is carried out in the presence of excess thiol. Analytically pure $Pd_2Cl_2(\mu\text{-}Cl)(\mu\text{-}SR)(PR'_3)_2$ complexes have previously been obtained only through a disproportionation of $[PdCl(\mu\text{-}Cl)(PR_3)]_2$ and purified $Pd_2Cl_2(\mu\text{-}SR)_2(PR'_3)_2$ complexes.[1,3,9,10] The reaction of *trans*-[PdCl(μ-Cl$)(PMe_3)]_2$ with one equivalent of thiophenol produces a mixture of the mono(μ-thiolato) complex, **3**, and the bis(μ-thiolato) complex, **5** (Scheme 1). Analytically pure **3** could be obtained in high yield only from disproportionation of equimolar amounts of **5** and *trans*-[PdCl(μ-Cl$)(PMe_3)]_2$. The bis(μ-thiolato)

Table 1. Summary of crystal data

	1	2	3·CH_2Cl_2	4
Formula	$Pd_2Cl_3P_2SC_7H_{21}$	$Pd_2Cl_3P_2SC_{10}H_{27}$	$Pd_2Cl_5P_2SC_{13}H_{25}$	$Pd_2Cl_2P_2S_2C_{24}H_{40}$
fw	518.6	560.2	665.46	737.7
Crystal dimensions (mm)	0.3 × 0.2 × 0.2	0.3 × 0.3 × 0.7	0.2 × 0.4 × 0.6	0.4 × 0.2 × 0.2
Space group	$Pbc2_1$	$P2_1cn$	$C2/c$	$P\bar{1}$
a (Å)	11.630(6)	8.158(3)	27.38(1)	8.694(5)
b (Å)	11.667(3)	10.345(3)	11.477(9)	9.570(6)
c (Å)	12.816(4)	24.106(6)	16.506(7)	10.203(7)
α (°)	90	90	90	68.72(5)
β (°)	90	90	124.12(3)	76.86(5)
γ (°)	90	90	90	85.27(5)
V (Å^3)	1739(1)	2035(1)	4294(4)	770.3(8)
Z	4	4	8	2
$\rho_{calc.}$ (g cm^{-3})	1.980	1.830	2.06	1.592
λ (Å) (Mo-K_α radiation)	0.71073	0.71073	0.71073	0.71073
T (K)	293	297	295	295
Scan type	2θ–θ	ω	2θ–θ	2θ–θ
Scan rate (° min^{-1})	1.5–15	1.5–15	1.5–15	1.5–15
2θ Range	4.0–60.0	4.0–55.0	4.0–55.0	4.0–60.0
μ (cm^{-1})	27.82	23.85	25.21	15.92
Transmission coefficient	0.492–0.586	0.518–0.600	0.693–0.760	0.588–0.750
Extinction correction	N/A	0.00007(4)	0.00081(7)	0.017(1)
Reflections collected	3070	2703	6248	4893
Unique data with $I > 3\sigma(I)$	2317	2173	4438	4180
R^a (%)	2.29	2.57	3.10	3.01
$R_w{}^b$ (%)	3.81	3.39	7.95	7.01
Goodness of fit^c	0.76	1.00	0.77	1.27

[a] $R = \Sigma||F_o|-|F_c||/\Sigma F_o$.
[b] $R_w = [w\Sigma(|F_o|-|F_c|)^2/\Sigma w(F_o{}^2)]^{1/2}$.
[c] $GOF = [\Sigma w(|F_o|-|F_c|)^2/(N_o-N_v)]^{1/2}$.

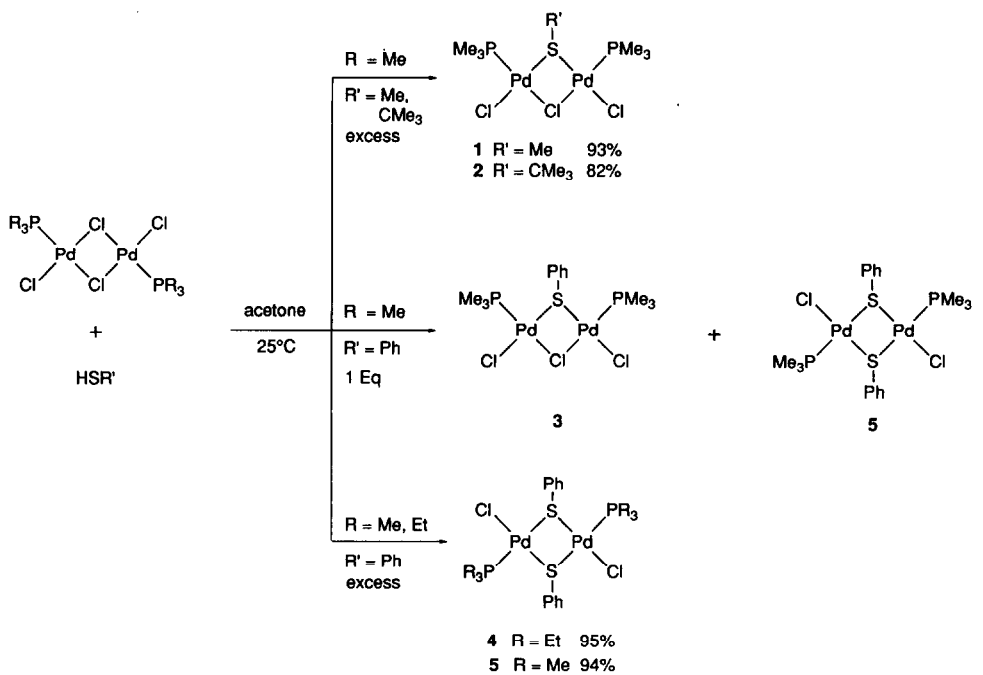

Scheme 1.

complexes, *trans*-$Pd_2Cl_2(\mu\text{-}SPh)_2(PR_3)_2$ (R = Et, **4**; Me, **5**) are obtained as the exclusive product from the reaction of *trans*-$[PdCl(\mu\text{-}Cl)(PR_3)]_2$ with thiophenol in a 1 : 2 stoichiometry (Scheme 1).

Structures of cis-$Pd_2Cl_2(\mu\text{-}Cl)(\mu\text{-}SR)(PMe_3)_2$ (R = Me, **1**; CMe_3, **2**; Ph, **3**) *and* trans-$Pd_2Cl_2(\mu\text{-}SC_6H_5)_2(PEt_3)_2$ (**4**)

ORTEP projections of the molecular structures of **1**, **2**, **3** and **4** are shown in Figs 1–4, respectively. Selected bond angles and distances are given in Tables 2–5. The complexes exhibit nearly square-planar geometry about each of the palladium centres. In the mono(thiolato) complexes **1–3**, the phosphine ligands are arranged in a *cis* configuration as was found[10] in the X-ray structure determination of $Pd_2Cl_2(\mu\text{-}Cl)(\mu\text{-}SEt)(PMe_2Ph)_2$ and has been indicated by electric dipole measurements[1] and spectroscopic[3,7–10] analysis to be the preferred configuration of $M_2Cl_2(\mu\text{-}Cl(\mu\text{-}SR)(PR'_3)_2$ (M = Pd, Pt) complexes. By contrast, the phosphine ligands of **4** are arranged in a *trans* configuration as was found in the X-ray structure determination[4] of $Pd_2(SC_6F_5)_2(\mu\text{-}SC_6F_5)_2(PPh_3)_2$ and has been indicated by electric dipole measurements[2] to be the preferred configuration of $M_2Cl_2(\mu\text{-}SR)_2(PR'_3)_2$ (M = Pd, Pt; R = aryl) complexes. As has been found[4–7,12] for other bis(μ-thiolato) complexes, the μ-thiolato groups of **4** are in an *anti* conformation.

Generality of bent vs planar structures of dipalladium alkylthiolato vs arylthiolato complexes

The μ-alkylthiolato complexes, **1** and **2**, have non-planar geometries with dihedral angles of 140 and 146°, respectively, between the coordination planes of the palladium atoms, while the μ-arylthiolato complexes, **3** and **4**, are planar with corresponding dihedral angles of 180°. The non-planar structures as seen for **1** and **2**, appear to be common to all dipalladium and diplatinum complexes containing μ-alkylthiolato groups as $Pd_2(S_2CSCMe_3)_2(\mu\text{-}SCMe_3)_2$,[5,5] *cis*-$Pd_2Cl_2(\mu\text{-}Cl)(\mu\text{-}SEt)(PMe_2Ph)_2$,[10] *cis*-$PtCl_2(\mu\text{-}SEt)_2(PPr_3)_2$,[12] *cis*-$Pt_2(SCH_2Ph)_2(\mu\text{-}SCH_2Ph)_2(PMePh_2)_2$,[6] and (dppe)Pt(μ-SMe)$_2$-Pt $ClMe_3$[7] all been found to have dihedral angles of 130–154° between the coordination planes of the metals. The planar structures of **3** and **4** match that previously found[4] for *trans*-$Pd_2(SC_6F_5)_2(\mu\text{-}SC_6F_5)_2(PPh_3)_2$, thus suggesting that the planar geometry is preferred by μ-arylthiolato complexes. Both bent[14] and planar[15] structures have also been found for bis(μ-chloro)dipalladium and -diplatinum complexes. In the case of the μ-chloro complexes, the planar and bent structures appear to be energetically very similar[16] and it has been suggested[17] that crystal packing forces are responsible for the variation in the solid-state configuration. However, ^1H and ^{31}P NMR spectroscopic studies of *cis*-$Pt_2(SCH_2Ph)_2(\mu\text{-}SCH_2Ph)_2(PMePh_2)_2$[6] and *cis*-$Pt_2X_2(\mu\text{-}SR)_2(PMe_2Ph)_2$ (X = Cl, I; R = Me)[18] indicate these complexes

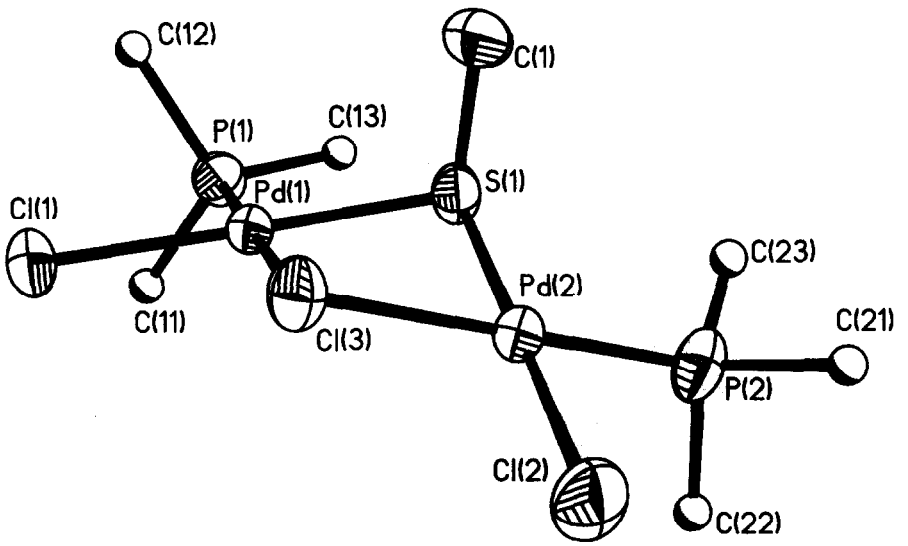

Fig. 1. ORTEP projection of *cis*-$Pd_2Cl_2(\mu\text{-}SMe)(\mu\text{-}Cl)(PMe_3)_2$ (**1**) thermal ellipsoids at 50% probability. The hydrogen atoms have been omitted and PMe_3 carbon atoms given an arbitrary radius for clarity.

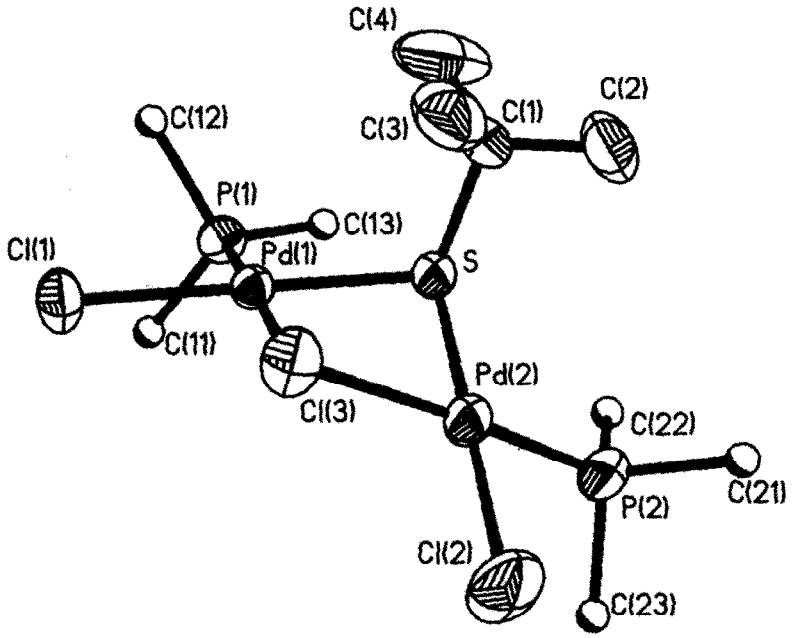

Fig. 2. ORTEP projection of *cis*-$Pd_2Cl_2(\mu\text{-}SCMe_3)(\mu\text{-}Cl)(PMe_3)_2$ (2) thermal ellipsoids at 50% probability. The hydrogen atoms have been omitted and PMe_3 carbon atoms given an arbitrary radius for clarity.

have bent geometries in solution. Therefore, energetic considerations other than solid-state crystal packing forces are responsible for the configurations of these and most likely other bis(μ-thiolato) complexes.

The bending of palladium and platinum μ-alkylthiolato complexes has previously been ascribed to steric interactions.[12] However, comparison of the nearly equal dihedral angles between the coordination planes of **1** and **2** with the planar molecules **3** and **4** demonstrates that electronics rather than sterics are responsible for the geometries of these

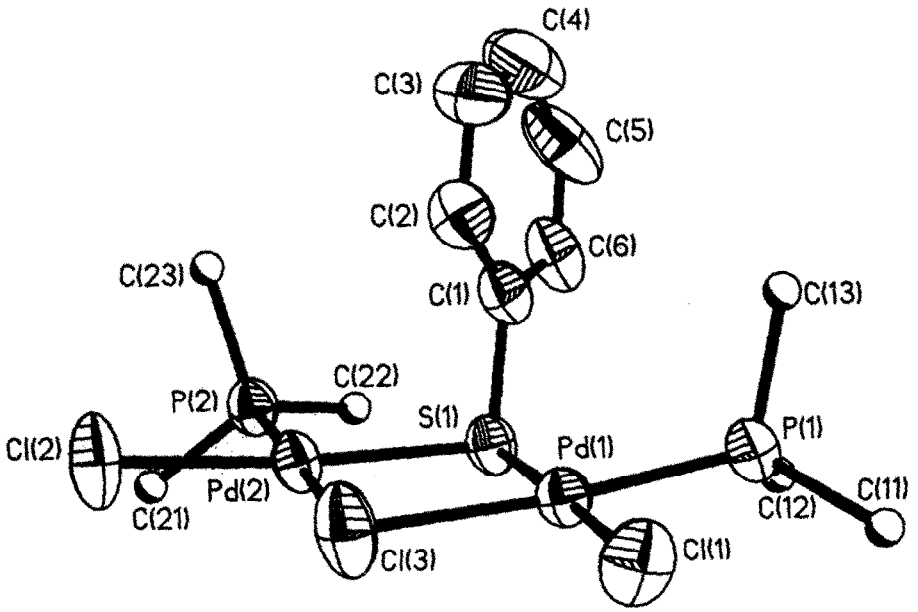

Fig. 3. ORTEP projection of *cis*-$Pd_2Cl_2(\mu\text{-}Cl)(\mu\text{-}SPh)(PMe_3)_2$ (3) thermal ellipsoids at 50% probability. The hydrogen atoms have been omitted and PMe_3 carbon atoms given an arbitrary radius for clarity.

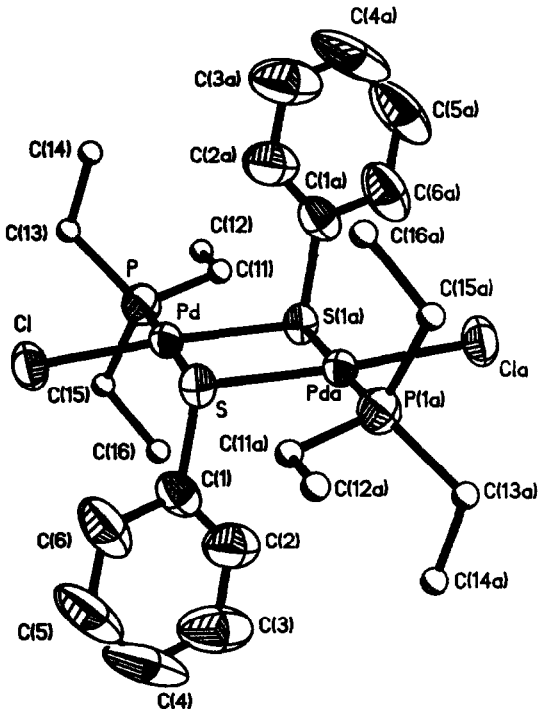

Fig. 4. ORTEP projection of *trans*-$Pd_2Cl_2(\mu\text{-}SPh)_2(PEt_3)_2$ (**4**) thermal ellipsoids at 50% probability. The hydrogen atoms have been omitted and PMe_3 carbon atoms given an arbitrary radius for clarity.

complexes. Finally, the Pd—Pd distances of 3.294(4), 3.208(1), 3.934(3) and 3.463(2) Å in **1**–**4**, respectively, demonstrate the lack of bonding interactions between the palladium atoms and thus metal–metal bonding plays no role in the determination of molecular geometry of these complexes.

The Pd—S bond distances of 2.262(2) and 2.272(2) Å in complexes **1** and **2** are significantly shorter than the Pd—S distances in **3**, 2.288(2) and 2.301(2) Å, indicating enhanced metal–sulphur bonding in the alkylthiolato complexes. One explanation of the consistently bent geometries of the alkylthiolato complexes is that electron-donating alkyl groups, as opposed to electron-withdrawing aryl groups, significantly enhance the donor ability of the thiolato sulphur. As a result, metal–sulphur bonding interactions involving the sulphur p_z orbital and the metal $d_{x^2-y^2}$ orbitals are established thus distorting the complexes from planarity as seen below.

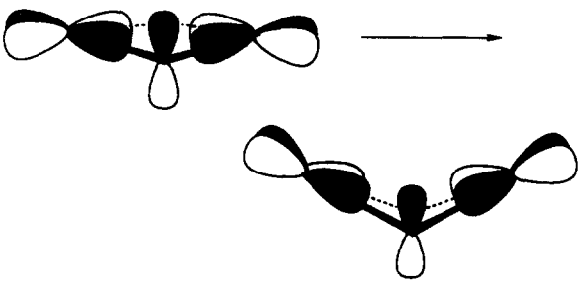

Owston and co-workers proposed[12] that the distortion is favourable to the establishment of a multiple overlap zigzagging P—M—S—M—P chain of π-bonding orbitals. We find no evidence for the involvement of the Pd—P bonds in such a multiple overlap bonding system as the Pd—P bond distances in the mono(μ-arylthiolato) complex **3**, of 2.214(2) and 2.222(2) Å, are within the 2.209(2)–

Table 2. Selected bond distances (Å) and angles (°) for *cis*-$Pd_2Cl_2(\mu\text{-}Cl)(\mu\text{-}SMe)(PMe_3)_2$ (**1**)

		Distances	
Pd(1)—S(1)	2.272(2)	Pd(2)—S(1)	2.272(2)
Pd(1)—P(1)	2.221(2)	Pd(2)—P(2)	2.220(2)
Pd(1)—Cl(1)	2.338(2)	Pd(2)—Cl(2)	2.330(2)
Pd(1)—Cl(3)	2.439(2)	Pd(2)—Cl(3)	2.448(2)
S(1)—C(1)	1.838(9)		
		Angles	
S(1)—Pd(1)—Cl(3)	85.9(1)	S(1)—Pd(2)—Cl(3)	85.7(1)
Cl(3)—Pd(1)—Cl(1)	93.8(1)	Cl(3)—Pd(2)—Cl(2)	81.4(1)
Cl(1)—Pd(1)—P(1)	87.7(1)	P(2)—Pd(2)—Cl(2)	88.9(1)
S(1)—Pd(1)—P(1)	92.6(1)	S(1)—Pd(2)—P(2)	91.7(1)
Cl(3)—Pd(1)—P(1)	178.5(1)	S(1)—Pd(2)—Cl(2)	179.1(1)
S(1)—Pd(1)—Cl(1)	178.7(1)	Cl(3)—Pd(2)—P(2)	177.0(1)
Pd(1)—S—Pd(2)	92.9(1)	Pd(2)—S—C(1)	102.1(3)
Pd(1)—S—C(1)	101.6(3)		

Table 3. Selected bond distances (Å) and angles (°) for *cis*-$Pd_2Cl_2(\mu\text{-}Cl)(\mu\text{-}SCMe_3)(PMe_3)_2$ (**2**)

Distances			
Pd(1)—S	2.265(2)	Pd(2)—S	2.262(2)
Pd(1)—P(1)	2.209(2)	Pd(2)—P(2)	2.214(2)
Pd(1)—Cl(1)	2.339(2)	Pd(2)—Cl(2)	2.339(3)
Pd(1)—Cl(3)	2.441(2)	Pd(2)—Cl(3)	2.450(2)
S—C(1)	1.871(7)		
Angles			
S—Pd(1)—P(1)	93.4(1)	S—Pd(2)—P(2)	92.1(1)
P(1)—Pd(1)—Cl(1)	86.3(1)	P(2)—Pd(2)—Cl(2)	89.0(1)
S—Pd(1)—Cl(3)	86.9(1)	S—Pd(2)—Cl(3)	86.8(1)
Cl(1)—Pd(1)—Cl(3)	93.4(1)	Cl(2)—Pd(2)—Cl(3)	92.2(1)
S—Pd(1)—Cl(1)	179.5(1)	S—Pd(2)—Cl(2)	178.9(1)
P(1)—Pd(1)—Cl(3)	176.3(1)	P(2)—Pd(2)—Cl(3)	174.7(1)
Pd(1)—S—Pd(2)	90.2(1)	Pd(2)—S—C(1)	108.8(2)
Pd(1)—S—C(1)	107.5(2)		

2.221(2) Å range of those in the mono(μ-alkylthiolato) complexes, **1** and **2**.

Effect of metal–sulphur bonding in cis *vs* trans *phosphine geometries*

Dipalladium and diplatinum complexes containing weak σ-donor bridging ligands prefer[14] a *trans*-phosphine geometry. Thus the *trans*-phosphine configuration of **4** and other bis(arylthiolato) complexes is consistent with our model whereby μ-arylthiolato ligands are simple σ-donors. The *cis*-phosphine geometry of $M_2Cl_2(\mu\text{-}SR)_2(PR'_3)_2$ (M = Pd, Pt; R = alkyl) complexes is more problematic. *A priori* it would seem that the alkyl(thiolato) groups should participate in balanced bonding to the metal centres. It would then seem logical for the complex to adopt a *trans*-phosphine geometry whereby the destabilizing *trans* influence of the phosphines would be equally distributed among both thiolato groups. Our model in which the metal–sulphur bonding in the alkylthiolato complexes involves the sulphur p_z and metal $d_{x^2-y^2}$ orbitals provides a new basis for the *cis*-phosphine geometry in the bis(μ-alkylthiolato) complexes. If the additional bonding component involves mainly

Table 4. Selected bond distances (Å) and angles (°) for *cis*-$Pd_2Cl_2(\mu\text{-}Cl)(\mu\text{-}SPh)(PMe_3)_2$ (**3**)

Distances			
Pd(1)—S(1)	2.301(2)	Pd(2)—S(1)	2.288(2)
Pd(1)—P(1)	2.214(2)	Pd(2)—P(2)	2.222(2)
Pd(1)—Cl(1)	2.310(2)	Pd(2)—Cl(2)	2.296(2)
Pd(1)—Cl(3)	2.401(2)	Pd(2)—Cl(3)	2.391(2)
S(1)—C(1)	1.784(5)		
Angles			
S(1)—Pd(1)—P(1)	92.5(1)	S(1)—Pd(2)—P(2)	94.8(1)
P(1)—Pd(1)—Cl(1)	90.8(1)	P(2)—Pd(2)—Cl(2)	87.7(1)
Cl(1)—Pd(1)—Cl(3)	90.3(1)	Cl(2)—Pd(2)—Cl(3)	90.6(1)
S(1)—Pd(1)—Cl(3)	86.4(1)	S(1)—Pd(2)—Cl(3)	87.0(1)
S(1)—Pd(1)—Cl(1)	176.7(1)	S(1)—Pd(2)—Cl(2)	173.4(1)
P(1)—Pd(1)—Cl(3)	174.7(1)	P(2)—Pd(2)—Cl(3)	178.3(1)
Pd(1)—S—Pd(2)	95.9(1)	Pd(2)—S—C(1)	100.3(1)
Pd(1)—S—C(1)	104.3(1)		

Table 5. Selected bond distances (Å) and angles (°) for *trans*-$Pd_2Cl_2(\mu\text{-}SPh)_2(PEt_3)_2$ (**4**)

Distances			
Pd—S	2.382(2)	Pd—Cl	2.323(2)
Pd—S(1a)	2.289(2)	Pd—P	2.266(2)
S—C(1)	1.772(4)		
Angles			
Cl—Pd—S	91.9(1)	S—Pd—S(1a)	84.3(1)
Cl—Pd—P	88.9(1)	Cl—Pd—S(1a)	175.6(1)
P—Pd—S(1a)	94.8(1)	S—Pd—P	178.1(1)
Pd—S—C(1)	101.7(1)	Pd—S—Pd(a)	95.7(1)
Pd(a)—S—C(1)	106.6(1)		

the metal $d_{x^2-y^2}$ orbital, this interaction would be effectively disrupted by the strong *trans* influence of a phosphine ligand. Thus the bis(μ-alkylthiolato) complexes prefer a *cis*-phosphine geometry whereby one thiolato group is *trans* to both chlorides and significantly stabilized by an enhanced metal–sulphur bonding interaction.

CONCLUSION

Our results suggest that the establishment of an enhanced metal–sulphur bonding interaction is responsible for the non-planar geometries of dipalladium and diplatinum μ-alkylthiolato complexes. Furthermore, we believe the dichotomy of *cis* and *trans* geometries preferred by $M_2Cl_2(\mu\text{-}SR)_2(PR'_3)_2$ (M = Pd, Pt) alkylthiolato and arylthiolato complexes, respectively, can be explained by the requirement of weak *trans* donors for the stabilization of this enhanced bonding interaction in the alkylthiolato complexes. Finally, the isolation of mono(μ-thiolato) complexes from the reaction of *trans*-$[PdCl(\mu\text{-}Cl)(PMe_3)]_2$ with alkylthiols and not arylthiols can be accounted for by the additional stabilization of the metal–sulphur bonds in the alkylthiolato complexes.

Acknowledgements—We thank Professor R. E. Cramer for his assistance in the X-ray diffraction studies and Mr J. Chung for helpful discussions. This work was supported by the University of Hawaii Research Council.

REFERENCES

1. J. Chatt and F. A. Hart, *J. Chem. Soc.* 1953, 2363.
2. J. Chatt and F. A. Hart, *J. Chem. Soc.* 1960, 2807.
3. P. L. Goggin, R. J. Goodfellow and F. J. S. Reed, *J. Chem. Soc. A* 1971, 2031.
4. (a) R. H. Fenn and G. R. Segrott, *J. Chem. Soc. A* 1970, 3197; (b) R. H. Fenn and G. R. Segrott, *J. Chem. Soc., Dalton Trans.* 1972, 330.
5. J. C. Fackler and W. J. Zegarski, *J. Am. Chem. Soc.* 1973, **95**, 8566.
6. P. H. Bird, U. Siriwardane, R. Lai and A. Shaver, *Can. J. Chem.* 1982, **60**, 2075.
7. E. W. Abel, N. A. Cooley, K. Kite, K. G. Orrell, V. Sik, M. B. Hursthouse and H. M. Dawes, *Polyhedron* 1987, **6**, 1261.
8. V. K. Jain and G. S. Rao, *Inorg. Chim. Acta* 1987, **127**, 161.
9. V. K. Jain, *Inorg. Chim. Acta* 1987, **133**, 261.
10. V. K. Jain, R. P. Patel, K. V. Muralidharan and R. Bohra, *Polyhedron* 1989, **8**, 2151.
11. (a) R. S. Nyholm, J. F. Skinner and M. B. Stiddard, *J. Chem. Soc. A* 1968, 38; (b) R. O. Gould and M. M. Harding, *J. Chem. Soc. A* 1970, 875; (c) T. Boschi, L. Crociani, L. Toniolo and U. Belluco, *Inorg. Chem.* 1970, **9**, 532; (d) A. R. Dias and M. L. H. Green, *J. Chem. Soc. A* 1971, 1951; (e) K. R. Dixon, K. C. Moss and M. A. R. Smith, *J. Chem. Soc., Dalton Trans.* 1974, 971; (f) C. A. Briant, C. J. Gardner, T. S. A. Hor, N. D. Howell and D. M. P. Mingos, *J. Chem. Soc., Dalton Trans.* 1984, 2645; (g) H. C. Clark, V. K. Jain and G. S. Rao, *J. Organomet. Chem.* 1985, **279**, 181.
12. M. C. Hall, J. A. J. Jarvis, B. T. Kilbourn and P. G. Owston, *J. Chem. Soc., Dalton Trans.* 1972, 1544.
13. J. Chatt and L. M. Venanzi, *J. Chem. Soc.* 1957, 2351.
14. (a) G. R. Davies, R. H. B. Mais, S. O'Brien and P. G. Owston, *J. Chem. Soc., Chem. Commun.* 1967, 1151; (b) J. Lukas, J. E. Ramakers-Blom, T. G. Hewitt and J. J. DeBoer, *J. Organomet. Chem.* 1972, **46**, 167.
15. (a) J. N. Dempsey and N. C. Baenzinger, *J. Am. Chem. Soc.* 1955, **77**, 4984; (b) J. R. Holden and N. C. Baenzinger, *J. Am. Chem. Soc.* 1955, **77**, 4987; (c) W. E. Oberhansli and L. F. Dahl, *J. Organomet. Chem.* 1965, **3**, 43; (d) A. E. Smith, *Acta Cryst.* 1965, **18B**, 331; (e) W. E. Oberhansli and L. F. Dahl, *Inorg. Chem.* 1965, **3**, 629; (f) W. A. Whitla, H. M. Powell

and L. M. Venanzi, *J. Chem. Soc., Chem. Commun.* 1966, 310; (g) R. Mason and A. G. Wheeler, *Nature* 1968, **217**, 1253; (h) M. Black, R. H. B. Mais and P. G. Owston, *Acta Cryst.* 1969, **25B**, 1760; (i) S. F. Watkins, *J. Chem. Soc. A* 1970, 168; (j) F. Dahan, C. Agami, J. Levisalles and F. Rose-Munch, *J. Chem. Soc., Chem. Commun.* 1974, 505.

16. (a) R. H. Summerville and R. Hoffmann, *J. Am. Chem. Soc.* 1976, **98**, 7240; (b) J. K. Burdett, *J. Chem. Soc., Faraday Trans.* 1974, 1599.
17. M. Parra-Hake, M. F. Rettig and R. M. Wing, *Organometallics* 1983, **2**, 1013.
18. M. P. Brown, R. J. Puddephatt and C. E. E. Upton, *J. Chem. Soc., Dalton Trans.* 1976, 2490.

Polyhedron Vol. 10, No. 12, pp. 1353–1361, 1991
Printed in Great Britain

0277–5387/91 $3.00+.00
© 1991 Pergamon Press plc

PREPARATION OF MONO- AND BINUCLEAR COMPLEXES OF COPPER(II), NICKEL(II), COBALT(II), IRON(III) AND VANADYL(V) WITH 2,2′-DIHYDROXY-3,3′-DIACETYL-5,5′-DICHLORODIPHENYLMETHANE

U. RUSSO, B. ZARLI,* P. ZANONATO and M. VIDALI

Dipartimento di Chimica Inorganica, Metallorganica e Analitica, Università di Padova, Via Loredan, 4-35131 Padova, Italy

(*Received* 27 *June* 1990; *accepted* 29 *January* 1991)

Abstract—The synthesis of mononuclear complexes $M(HL)_2 \cdot nS$ [M = copper(II), nickel (II) and cobalt(II), S = solvent] and $M'(HL)_2OH \cdot nS$ [M′ = iron(III) and vanadyl(V)] and of the binuclear complexes $M_2L_2 \cdot nS$ [M = copper(II), nickel(II) and cobalt(II)] and $Fe_2L_2(OH)_2 \cdot H_2O$ and $(VO)_2L_2SO_4 \cdot 4H_2O$ derived from 2,2′-dihydroxy-3,3′-diacetyl-5,5′-dichlorodiphenylmethane (H_2L) is reported. Their coordination geometry is discussed on the basis of physico-chemical data. Magnetic measurements at room temperature suggest that no interactions between metal ions are present in the binuclear chelates. Iron(III) and vanadyl(V) complexes were used as catalysts for the oxidation of 3,5-di-t-butyl-1,2-dihydroxybenzene (3,5-DBTC). From the oxidative cleavage, 3,5-di-t-butyl-*o*-quinone (3,5-DTBQ), 3,5-di-t-butyl-1-oxacyclohepta-3,5-diene-2,7-dione (3,5-DTBODD), 3,5-di-t-butyl-5-carboxymethyl-2-furanone (3,5-DTBCF) and 4,6-di-t-butylpyrone-2-one (4,6-DTBP) were isolated and identified by mass, IR and ^{1}H NMR data. The title compound was reacted to give a hexaketone by application of the Wittig method. A polymeric Schiff base was obtained by reaction of the diacetyl derivative with ethylenediamine, also in the presence of nickel(II) perchlorate or boric acid.

In recent years the increased awareness of the potential importance of molecules containing polymetallic centres has developed. The involvement of compounds containing such centres in catalytic processes has been the primary interest, and this is reflected in the growth and development of metal-cluster chemistry. Further stimulus has come from the discovery that many proteins and enzymes require two or more metal ions for their activity, and from the need to understand the nature of the active site and intermetallic interplay in these metallo-species.

Different approaches have been developed for the design and synthesis of polymetallic centres in order to exploit their mentioned potentials. One strategy has been to design and prepare multidentate ligands capable, through the siting of their donor atoms, of coordinating metal ions into juxtaposition (e.g. compartmental,[1] face-to-face,[2] cylindrical macrotricycles,[3] polypodal ligands,[4] etc.). The development of these so-called binucleating ligands has led to the successful synthesis of homo- and heterobinuclear metal chelates which have found application in the area of biomimic chemistry.[5,6]

As a part of our program on polynuclear chelates, we report the synthesis and the properties of the ligand 2,2′-dihydroxy-3,3′-diacetyl-5,5′-dichlorodiphenylmethane and its interactions with metal salts. In addition, a ligand extension via a modified Wittig reaction is reported.

EXPERIMENTAL

Microanalytical data were obtained by the Microanalytical Service of the University of Padova. Mass spectra were run on a VG Micromass 16 F spectrometer, IR spectra on a Nicolet 5DX FTIR

* Author to whom correspondence should be addressed.

spectrophotometer as KBr disks or Nujol mulls and electronic spectra on a Cary 14 spectrophotometer. Magnetic meausurements were carried out using the Gouy technique at room temperature with $HgCo(NCS)_4$ as calibrant. ^1H NMR spectra were recorded on a Jeol FX 900 in $CDCl_3$ solution. Mössbauer effect spectra were recorded at 78 K in a conventional acceleration spectrometer which utilized a room temperature rhodium matrix ^{57}Co source and was calibrated at room temperature with natural abundance α-iron foil. The spectra were fitted to Lorentzian line shapes by using standard least-squares computer minimization techniques.

Preparation of 2,2′-*dihydroxy*-3,3′-*diacetyl*-5,5′-*dichlorodiphenylmethane* (**V**)

The title compound has been prepared by the following two methods.

Method A

Preparation of acetoxy-4-*chlorophenol* (**I**). *p*-Chlorophenol (50 g) was dissolved in acetic anhydride (120 cm^3) and concentrated sulphuric acid (0.5 cm^3) was added. The solution was refluxed for 2 h and after cooling poured into 500 cm^3 of ice-cooled water. The brown oil was extracted with diethyl ether and the organic phase was washed with water, treated with active charcoal and dried over anhydrous sodium sulphate. The solvent was evaporated and the residue distilled at reduced pressure (78°C/1 mm Hg) to give 64 g of a colourless liquid (yield 96%).

Preparation of 4-*chloro*-2-*hydroxyacetophenone* (**II**). Compound **I** (40 g) was mixed with aluminium trichloride (73 g) and the mixture heated at 120°C for 15 min under vigorous stirring. After cooling, the green solid was poured into 500 cm^3 of ice-cooled 2 N hydrochloric acid. The suspension was filtered and the solid washed with water and crystallized from petroleum ether 40–60°C to give 38 g of colourless needles (yield 95%).

Preparation of 2,2′-*dihydroxy*-3,3′-*diacetyl*-5,5′-*dichlorodiphenylmethane* (**V**). Compound **II** (5 g) was dissolved in a solution of sulphuric acid and methanol (2 : 1 v/v) at −5°C. The resulting solution was further cooled down to −10°C and then formalin (38%; 2 cm^3) was slowly added under stirring. The stirring was continued for 2 h at the same temperature. The solution was left to stand overnight and then poured into 500 cm^3 of cool water. The brown solid was filtered, washed with water and dissolved in 300 cm^3 of NaOH (3%). The solution was treated with active charcoal and the solid was again precipitated with 2 N hydrochloric acid. The brown solid was recrystallized from hot ethanol to give a pale green compound (3.2 g; yield 60%; m.p. 202–203°C).

Method B

Preparation of 2,2′-*dihydroxy*-5,5′-*dichlorodiphenylmethane* (**III**). *p*-Chlorophenol (30 g) was dissolved in methanol (70 cm^3) and water (7 cm^3) was added. The resulting solution was cooled to −10°C and then sulphuric acid (120 cm^3) was added dropwise under stirring. Formalin (38%; 9 cm^3) was added under cooling and the mixture was stirred for 2 h. The white suspension was poured into ice (700 g) and stirred for 30 min. The white powder was filtered, washed with water, dissolved into 120 cm^3 of 2 N sodium hydroxide and treated with active charcoal. The clear solution was acidified with 2 N hydrochloric acid and the precipitate that formed was filtered, washed with water and dried at 50°C *in vacuo*. The white solid was recrystallized from ethanol (21.8 g; yield 70%; m.p. 172–175°C).

Preparation of 2,2′-*diacetoxy*-5,5′-*dichlorodiphenylmethane* (**IV**). Compound **III** (10 g) was dissolved in 100 cm^3 of acetic anhydride and 0.5 cm^3 of concentrated sulphuric acid. The solution was refluxed for 1 h, poured into ice-cooled water and then extracted with diethyl ether; the aqueous phase was discharged while the ethereal phase was washed with aqueous sodium bicarbonate (5%; 2×100 cm^3) and distilled water (100 cm^3), treated with active charcoal and then dried over magnesium sulphate. By evaporation of the solution to dryness the product was obtained as a white solid (12.2 g; yield 92%; m.p. 98–100°C).

Preparation of 2,2′-*dihydroxy*-3,3′-*diacetyl*-5,5′-*dichlorodiphenylmethane* (**V**). Anhydrous aluminium trichloride (20 g) and **IV** (10 g), in a 250 cm^3 flask, were heated in an oil bath at 140–150°C to obtain a homogeneous mixture; the temperature was allowed to rise to 170–180°C and maintained for 30 min. After cooling, the solid was added to 400 cm^3 of 2 N hydrochloric acid. The precipitate was filtered, washed with water and dried. The crude mixture was crystallized from ethanol to give a pale green product (4.0 g; yield 40%; m.p. 200–203°C).

Preparation of mononuclear complexes

The metal perchlorate (1 mmol) dissolved in methanol (50 cm^3) was slowly added to a methanolic solution (100 cm^3) of ligand **V** (2 mmol) and lithium hydroxide (2 mmol). The fine suspension which resulted was heated at 50°C under stirring.

The precipitate was filtered, washed with methanol and dried *in vacuo*.

Preparation of binuclear complexes

Ligand **V** (1 mmol) and lithium hydroxide (2 mmol) were dissolved in hot methanol (100 cm^3) and then added to a methanolic solution (50 cm^3) of the metal salt (1 mmol). The resulting mixture was refluxed for several hours. The precipitate so obtained was filtered, washed with methanol and dried *in vacuo*.

Oxidation of 3,5-*di-t-butyl*-1,2-*dihydroxybenzene*

The oxidation of the 3,5-di-t-butylcatechol (3,5-DTBC) was carried out both in air and under an oxygen atmosphere.

In air. Catechol (2.22 g, 10 mmol) was dissolved in the appropriate solvent (50 cm^3) and poured into a 100 cm^3 flask. The solution was stirred and the iron(III) or vanadyl(V) complex (1×10^{-2} mmol) was added. The solution was stirred for several hours, during which the reaction was monitored by thin layer chromatography. After this, the mixture was evaporated to dryness and the residue was eluted on silica gel using chloroform as eluant. The three main fractions recovered were identified as 3,5-di-t-butyl-*o*-quinone (3,5-DTBQ), 3,5-di-t-butyl-1-oxacyclohepta-3,5-diene-2,7-dione (3,5-DTBODD) and 4,6-di-t-butylpyran-2-one (4,6-DTBP) with vanadyl as catalyst and two 3,5-di-t-butylquinone and 3,5-di-t-butyl-5-carboxymethyl-2-furanone (3,5-DTBCF) with iron(III) as catalyst.

In oxygen. A solution (50 cm^3) of catechol (2.22 g, 10 mmol) and the iron or vanadyl complex (1×10^{-2} mmol) in a 100 cm^3 flask was stirred under oxygen (1 atm) for several hours at room temperature. The reaction mixture was evaporated to dryness and the residue chromatographed on silica gel using chloroform as eluant.

Preparation of the hexaketone 3,3′-*methylene bis*(2-*hydroxy*-1-*acetoacetylbenzene*)

Compound **V** (10 mmol) was dissolved in 200 cm^3 of ethyl acetate heated to 50°C and stirred under a nitrogen atmosphere. Metallic sodium (13 mmol) was slowly added over 30 min. Stirring was continued until the yellow sodium salt was precipitated. The reaction was cooled and the sodium salt filtered, washed with ethyl acetate and dried. The solid was added to dilute aqueous acetic acid solution (10%) and the resulting compound extracted with diethyl ether. The ethereal phase was filtered, washed with aqueous bicarbonate (5%) and distilled water, and finally dried over magnesium sulphate. The product was obtained by evaporation of the solution to dryness as a pale yellow solid (3.3 g; yield 75%; m.p. 172–173°C).

Reaction of **V** *with ethylenediamine*

(A) Nickel(II) perchlorate (1 mmol) and ethylenediamine (2 mmol) were dissolved in ethanol (100 cm^3). The solution was stirred for 30 min at 50°C, heated up to reflux, then **V** (2 mmol) in ethanol (50 cm^3) was added dropwise and the reflux continued for 90 min. During the reaction a yellow–green powder precipitated which was filtered and washed with ethanol and diethyl ether. Elemental analysis agrees with the formula $C_{19}H_{17}Cl_2N_2O_2Ni$ (Found: C, 51.9; H, 4.1; N, 6.5; Cl, 15.8; Ni, 13.0. Calc.: C, 52.5; H, 3.9; N, 6.4; Cl, 16.3; Ni, 13.5%.)

The precipitate was suspended in water and hydrogen sulphide (1 atm) was bubbled through for 30 min. The yellow–black solid was filtered and treated with dimethylsulphoxide to give a black solid and a yellow solution. The solid was filtered and the yellow solution evaporated to dryness to give a solid that was digested in ethanol, filtered, washed with ethanol and diethyl ether and dried *in vacuo*.

(B) Compound **V** (2 mmol) was suspended in methanol and then heated to reflux. Boric acid (1.2 mmol) was added and after 20 min a yellow solution was formed. A methanolic solution of ethylenediamine (2 mmol in 20 cm^3) was added and the reflux was continued for 2 h. During the reaction a yellow solid precipitated, this was filtered, washed with methanol and diethyl ether and dried *in vacuo*.

RESULTS AND DISCUSSION

Compound **V** has been prepared by two different methods according to a modified Erlenmeyer procedure[7] (Scheme 1). The first route seems to be better than the second because it operates at lower temperature; moreover the acetyl derivative (**I**) is liquid and it will mix better with aluminium(III) chloride than the solid diacetyl derivative (**IV**).

Compound **V** has been characterized by elemental analysis (Found: C, 57.6; H, 4.1; Cl, 19.8. Calc. for $C_{17}H_{14}Cl_2O_4$: C, 57.8; H, 4.0; Cl, 20.1%.) and spectral data. The mass spectrum, in addition to the principal fragmentation peaks, shows a strong M^+ peak at 352 *m/z* corresponding to the formula weight of the compound. The ^1H NMR spectrum consists of four signals at 12.43 (phenolic H), 7.58 and 7.37 (aromatic H), 3.95 (CH_2) and 2.60 ppm (CH_3). The hydroxyl IR stretching vibration consists of a broad band centred at *ca* 3050 cm^{-1}. Its

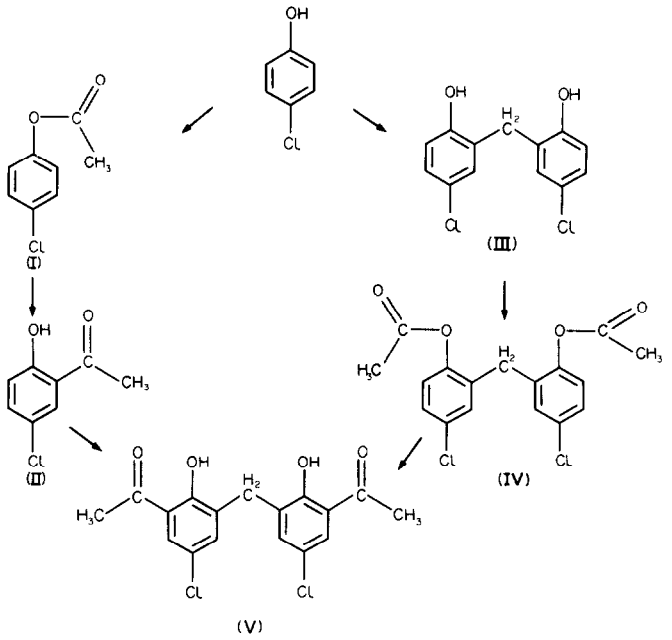

Scheme 1. The two pathways for obtaining V.

position and extreme width (400 cm^{-1}) are compatible with strong intramolecular association. The C=O stretching mode lies at 1638 cm^{-1} and confirms the presence of the intramolecular hydrogen bond.

Interaction with metal ions

Mononuclear complexes. By reacting ligand V with metal perchlorates in a 2:1 molar ratio in methanol, we have obtained mononuclear chelates of the type $M(HL)_2 \cdot nS$ (where S = water or methanol; M = copper(II), nickel(II) and cobalt(II)] and $Fe(HL)_2OH \cdot H_2O$. The synthesis of the vanadyl complex is very sensitive to the reaction conditions; in our case, by reaction of vanadyl(IV) sulphate with the ligand we obtained a compound of vanadyl(V), $VO(HL)_2OH$, even under a nitrogen atmosphere. Almost all the mononuclear compounds are soluble in the common organic solvents and they were crystallized before the analyses (Table 1).

The compounds present similar IR spectra, characterized by a broad band at 3400 cm^{-1} due to the coordinated solvent and a strong band at 1638 cm^{-1} which is also present in the free ligand. The presence of a single absorption for the carbonyl group can be explained assuming that the covalent bond between metal ion and C=O is comparable with a hydrogen bond. This hypothesis is confirmed by the spectra of the mononuclear and dinuclear sodium complexes. In fact, the mononuclear chelate shows two bands due to the C=O groups at 1670 and 1638 cm^{-1}, while the binuclear compound shows only a single band at 1670 cm^{-1}. Since the sodium forms an ionic M—O bond, the first band in the mononuclear chelate can be assigned to a free carbonyl group and the second to the C=O group involved in a hydrogen bond. The C—O phenol stretching frequency at 1323 cm^{-1} in the free ligand is not shifted after the coordination of metal ions, but appears at 1359 cm^{-1} in the sodium compound. A reasonable explanation is connected with an increased electron density on the oxygen atom as a result of increased ionicity of the Na—O bond. The stretching frequencies of the M—O modes, which should occur in the 400–500 cm^{-1} range, cannot be assigned because of the presence of bands due to the free ligand in the same region. The vanadyl complex presents a strong band at 850 cm^{-1} due to the V=O vibration.

The electronic spectra of these complexes show two absorption bands at 255 nm due to the phenyl ring and 350 nm. Since the latter one is present in the free ligand and is insensitive to metal change we assume that it is due to the ligand transition. The copper complex shows a broad band centred at 650 nm comparable with that of copper(II) bis(*o*-hydroxyacetophenonate),[8] suggesting a square-planar geometry. Its magnetic moment (1.80 BM) is that expected for an isolated copper(II) ion. The electronic spectrum of the nickel(II) complex presents a single band (630 nm) in the visible region,

as found for nickel(II) bis(acetylacetonate) and nickel(II) bis(*o*-hydroxyacetophenonate),[9,10] suggesting an octahedral coordination around the nickel(II) ion. This agrees with the room temperature magnetic moment (3.30 BM) typical of octahedral high-spin nickel(II). An octahedral coordination geometry can also be postulated for the cobalt(II) complex on the basis of the magnetic moment (4.90 BM) and electronic spectrum (a band at 600 nm) which are similar to those found for octahedral cobalt(II) bonded to the O_6 chromophore.[10,11] For the $Fe(HL)_2OH \cdot H_2O$ complex obtained by reaction of both iron(II) or iron(III) salts with the ligand under a nitrogen atmosphere, the spectral data suggest the presence of high-spin iron(III). In addition, the magnetic moment (5.90 BM) and the Mössbauer spectra (Fig. 1) are both typical of species containing isolated octahedral high-spin iron(III).[12,13]

Binuclear complexes

The binuclear complexes have been prepared by reaction of the ligand with a slight excess (molar ratio, 1 : 2.2) of the metal salts. The elemental analyses agree with formulae of the type $M_2L_2 \cdot nS$ [where M = nickel(II), copper(II) and cobalt(II)] and $Fe_2L_2(OH)_2 \cdot H_2O$. For the vanadyl ion, the $(VO)_2L_2SO_4 \cdot 4H_2O$ complex has been isolated, as confirmed by elemental analyses (Table 1).

The IR spectra do not differ from the mononuclear complexes as three main bands are present at 3400 (water), 1640 (C=O group) and 1320 cm^{-1} (C—O phenolic). For the vanadyl complex the bands due to ν(V=O) at 868 cm^{-1} and to the coordinated sulphate anion are also present. The electronic spectra of all these complexes are similar to those of the mononuclear chelates and suggest an analogous coordination geometry. The magnetic moments are typical of an isolated metal ion, excluding spin-exchange coupling. The Mössbauer effect spectra of the two iron-containing complexes have been measured at liquid nitrogen temperature and the resulting parameters are reported in Table 2. The spectra (Fig. 1) consist of a single asymmetric quadrupole-split doublet with hyperfine parameters typical of high-spin iron(III) complexes with the metal ion coordinated to six oxygen atoms in a nearly octahedral geometry. No difference can be found between the isomer shift values of the two compounds, and this points to a virtually identical electronic structure. The very small increase of the quadrupole splitting indicates a slightly higher distortion in the coordination of the bis-iron adduct.

Since the X-ray diffraction study[14] of the ligand has shown that the phenyl rings are twisted (Fig. 2), two possible structures for the binuclear complexes can be postulated (Fig. 3): a monomeric (**2a**) or a polymeric one (**2b**). Their low solubilities in coordinating organic solvents and the interactions of the

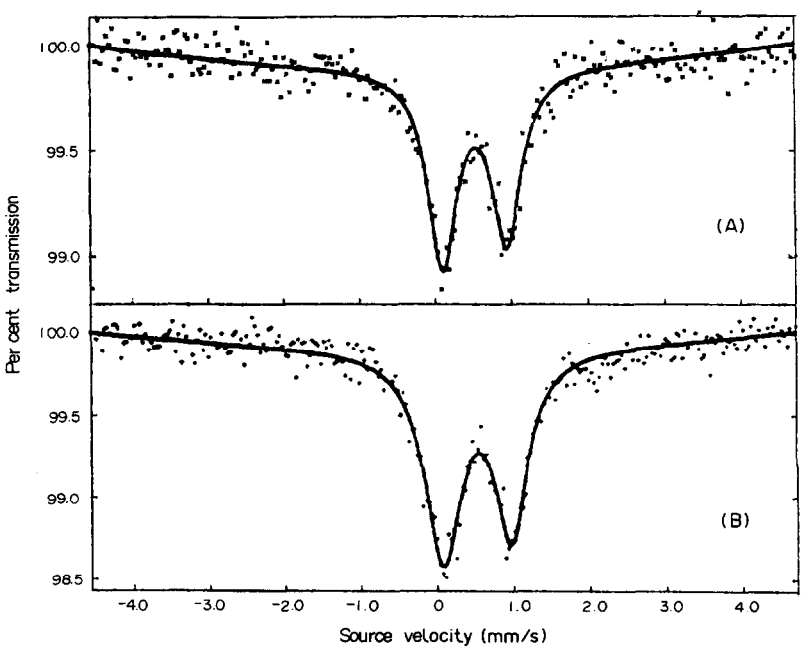

Fig. 1. The Mössbauer spectra of (A) $Fe(HL)_2OH \cdot H_2O$ and (B) $Fe_2L_2(OH)_2 \cdot H_2O$.

Table 1. Elemental analyses[a] and magnetic moments[b] of the complexes

Compound	Colour[c]	Yield (%)	C (%)	H (%)	Metal (%)	μ_{eff} (BM)
$VO(HL)_2OH$	Green	75	51.2 (51.8)	3.6 (3.4)	— —	Diam.
$Fe(HL)_2OH \cdot H_2O$	Brown	50	52.5 (52.5)	3.6 (3.5)	6.3 (7.2)	5.90
$Co(HL)_2 \cdot H_2O$	Yellow	80	52.4 (52.3)	3.5 (3.6)	7.3 (7.5)	4.40
$Cu(HL)_2$	Green	80	53.4 (53.2)	3.3 (3.4)	8.0 (8.3)	1.80
$Ni(HL)_2 \cdot CH_3OH$	Yellow	60	53.0 (52.9)	3.8 (3.8)	6.9 (7.4)	3.30
$(VO)_2L_2SO_4 \cdot 4H_2O$[d]	Deep green	40	40.4 (40.7)	3.1 (3.2)	— —	Diam.
$Fe_2L_2(OH)_2 \cdot H_2O$	Violet	70	46.5 (46.4)	3.3 (3.3)	12.2 (12.9)	5.90
$Fe_2L_2(OH)_2$	Violet	80	48.3 (48.1)	3.2 (3.1)	12.8 (13.2)	5.90
$Co_2L_2 \cdot 4H_2O$	Yellow	60	45.5 (45.8)	3.6 (3.6)	13.0 (13.2)	4.50
Cu_2L_2	Green–yellow	80	49.0 (49.2)	2.8 (2.9)	14.4 (15.3)	1.70
$Ni_2L_2 \cdot CH_3OH$	Yellow	60	49.7 (49.7)	3.4 (3.3)	13.4 (13.8)	3.30

[a] Calculated values are in parentheses.
[b] Given per metal ion.
[c] All the complexes were obtained as powders.
[d] SO_4: Found 8.9, Calc. 9.5%.

binuclear complexes with ethylenediamine to give polymeric Schiff bases suggest a polymeric configuration.

Oxidation reactions in the presence of vanadyl(V) *and iron*(III) *complexes*

The binuclear iron(III) or vanadyl(V) complexes were dissolved in a 0.1 M CH_2Cl_2 solution of 3,5-DTBC and then the reaction mixture was stirred at room temperature under oxygen (1 atm) or in air. At the end of the reaction, the 3,5-DTBC disappeared and the oxidation products (Scheme 2) were separated by a chromatography column on silica gel using chloroform as eluant; they were recrystallized and characterized by IR, ^1H NMR and mass spectroscopy (Table 3). All the investigated complexes were effective catalysts for the oxidation of 3,5-DTBC as shown in Table 4.

In presence of the iron(III) complexes isolation

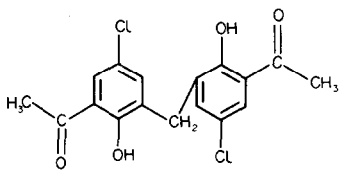

Fig. 2. A schematic view of **V**.

yielded unreacted catechol, a minor amount of lactone 3,5-DTBCF and 3,5-DTBQ as the main product. The results under various conditions are presented in Table 4. While both the mononuclear and binuclear complexes function as catalysts for the formation of 3,5-DTBQ and 3,5-DTBCF, the use of bimetallic complexes decreases the reaction time and increases the percentage of conversion. The same results can be obtained if the reaction is carried out in air even if the reaction time is longer than in an oxygen atmosphere.

In the presence of a catalytic amount of the van-

Table 2. Mössbauer spectral parameters of the iron complexes at 78 K

Compound	δ^a	ΔEq	Γ^b	A_1/A_2^c
$Fe(HL)_2OH \cdot H_2O$	0.53	0.85	0.45–0.45	1.14
$Fe_2L_2(OH)_2 \cdot H_2O$	0.53	0.90	0.59–0.52	1.31

[a] Relative to room temperature α-iron foil.
[b] Full width at half maximum.
[c] Ratio of lower energy to higher energy absorption bands.

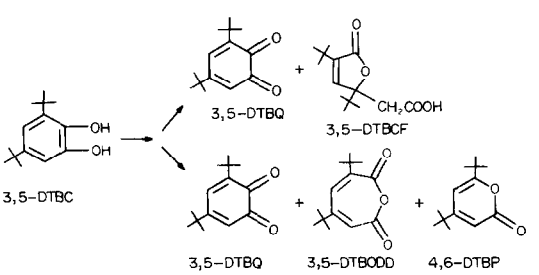

Scheme 2. The oxidation reactions of 3,5-DTBC.

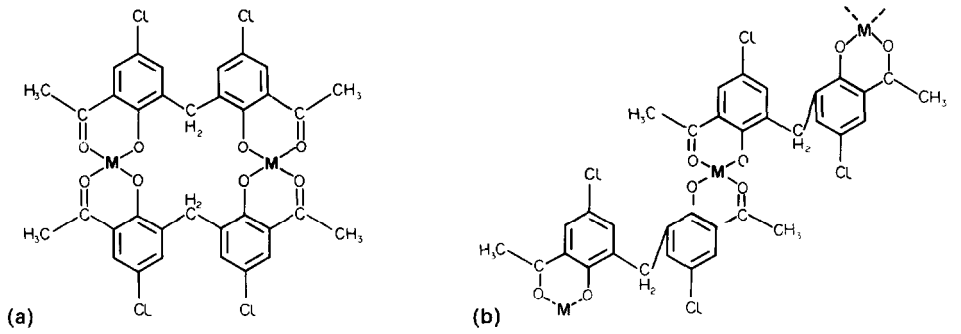

Fig. 3. The proposed structures of the binuclear complexes, (a) monomeric and (b) polymeric.

adyl complex, 5,5-di-t-butylcatechol is oxidized by molecular oxygen to afford three products: 3,5-DTBODD, 4,6-DTBP and 3,5-DTBQ; no catechol has been recovered. 3,5-DTBODD is the main product of this reaction, indicating that vanadium catalyses cleavage of the catechol incorporating an oxygen atom. This reaction compares well with results reported in the literature for other vanadium compounds.[15,16] The most remarkable feature of these oxygenation reactions, in methylene chloride solutions, is the high catalytic activity of the vanadyl complexes as compared with the iron complexes. As the main product, 3,5-DTBODD is analogous to the intermediate found in enzymatic intra-diol cleavage reactions,[17] suggesting that the vanadium catalyst favours an intra-diol rather than an extra-diol oxidative cleavage. The presence of 4,6-DTBP as a minor product can be attributed to an extra-diol cleavage of the catechol ring and subsequent loss of a CO group.[18] Although the 3,5-DTBQ was an intermediate product in several oxidative ring cleavages,[19,20] it cannot be further oxidized in this reaction just as in the enzyme reaction. However, methanol leads to a poor yield of the oxygenated products (3,5-DTBODD, 4,6-DTBP), while pyridine completely inhibits the oxidation. The same results were obtained when the reactions were carried out in air.

Table 3. ^{1}H NMR and IR spectra of the oxidation products of 3,5-DTBC

	^{1}H NMR	IR (cm^{-1})
4,6-DTBP (m.p. 114–115°C; P^+ *m/z* 208)	1.19(9H) 1.26(9H) 6.01(1H)	1710 1630 1550 1255
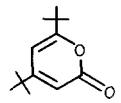		
3,5-DTBODD (m.p. 94–95°C; P^+ *m/z* 236)	1.15(9H) 1.26(9H) 6.13(1H) 7.44(1H)	1780 1740
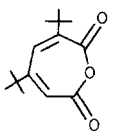		
3,5-DTBCF (m.p. 134–135°C; P^+ *m/z* 245)	0.95(9H) 1.21(9H) 2.76(1H) 2.91(1H) 6.91(1H) 9.47(1H)	1748 1721 1640
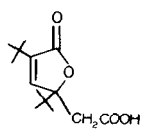		

Table 4. Catalytic oxidation of 3,5-DTBC by iron(III) and vanadyl(V) complexes in methanol and methylene chloride solutions at room temperature

Catalyst	Amount of catalyst[a]	Solvent	Atmosphere	Time	Conversion (%)	Product (%)[b] DTBQ	3,5-DTBODD	4,6-DTBP	Lactone
$Fe(HL)_2OH \cdot H_2O$	1	MeOH	Air	8 h	60	60	—	—	—
		CH_2Cl_2	Air	8 h	60	52	—	—	8
		MeOH	O_2	8 h	85	70	—	—	15
		CH_2Cl_2	O_2	8 h	85	65	—	—	20
$Fe_2L_2(OH)_2 \cdot H_2O$	1	MeOH	Air	5 h	70	60	—	—	10
		CH_2Cl_2	Air	5 h	70	60	—	—	10
		MeOH	O_2	5 h	90	75	—	—	15
		CH_2Cl_2	O_2	5 h	90	72	—	—	18
$VO(HL)_2OH$	1	MeOH	Air	4 h	100	93	Trace	Trace	—
		CH_2Cl_2	Air	4 h	100	23	45	5	—
		MeOH	O_2	3 h	100	92	Trace	Trace	—
		CH_2Cl_2	O_2	3 h	100	24	46	7	—
$(VO)_2L_2SO_4 \cdot 4H_2O$	1	MeOH	Air	3 h	100	94	Trace	Trace	—
		CH_2Cl_2	Air	3 h	100	25	45	8	—
		MeOH	O_2	2 h	100	94	Trace	Trace	—
		CH_2Cl_2	O_2	2 h	100	24	48	10	—

[a] Molar percentage on 3,5-DTBC.
[b] The yield of the isolated products based on 3,5-DTBC.

Interaction of the diacetyl derivative (V) *with ethylenediamine*

We have tried to prepare macrocyclic complexes starting from V, using nickel(II) perchlorate or boric acid as template. The compound was reacted in ethanol solution with a stoichiometric amount of ethylenediamine in the presence of metal perchlorate; a yellow precipitate was formed containing the metal ion. It was treated with H_2S to precipitate NiS, and the black residue was extracted with dimethylsulphoxide. The solution was evap-

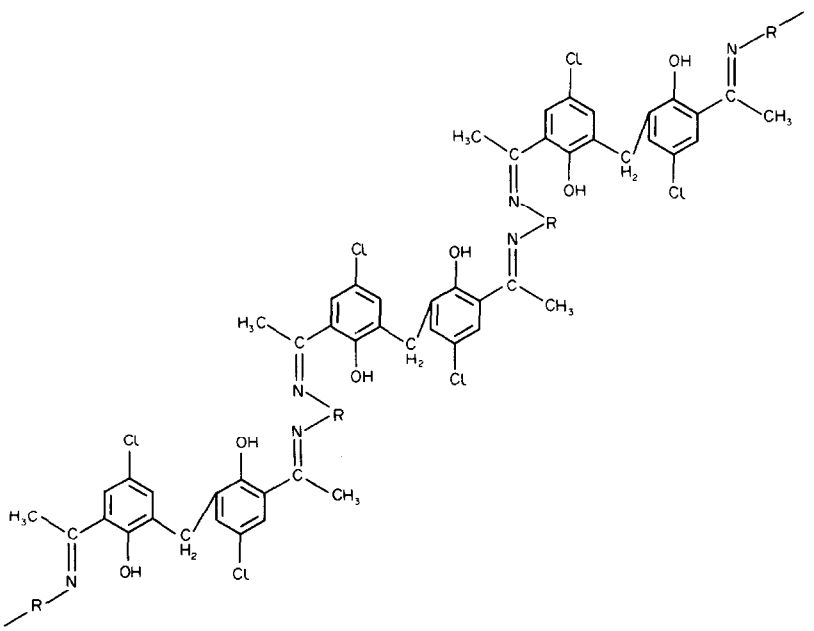

Fig. 4. The polymeric Schiff base obtained from the reaction of V with ethylenediamine.

orated to dryness to give a yellow solid. In the IR spectrum of the compound, the C=O and N—H stretching modes are absent, while a peak at 1605 cm^{-1} is present due to the C=N stretching mode involved in a hydrogen bond. The elemental analysis agrees with this suggestion but the mass spectrum (absence of P^+ at m/z 378 and presence of fragments at higher values m/z) indicates that a polymeric species is present (Fig. 4).

The same result was obtained when **V** was reacted with ethylenediamine in the presence of boric acid.

Interaction of the diacetyl derivative (**V**) *with ethyl acetate*

Compound **V** provides a versatile precursor for polynucleating ligand species or for a hexaketonic array after ligand extension via a modified Wittig condensation. This involves the condensation of the diacetyl derivative with ethyl acetate in the presence of sodium wire. The compound (Fig. 5) was crystallized from hot ethanol to give a pale yellow, microcrystalline powder in good yield. It was characterized by IR, mass (P^+ at $m/z = 437$) and ^1H NMR spectra.

The hydroxyl stretching band of 3,3′-methylene-bis-(2-hydroxyl-1-acetoacetylbenzene) consists of a broad signal, about 400 cm^{-1} wide, centred at 3060 cm^{-1}. This band could result from two overlapping OH absorptions. In the carbonyl region only a band at 1610 cm^{-1} is present, due to a C=O group involved in a hydrogen bond. No bands due to free C=O are present, suggesting that the enol form is predominant in the solid state. The enol tautomer is the major form also in chloroform solution as confirmed by the ^1H NMR spectrum. The principal resonances occur at 2.14, 3.98, 6.20, 12.56 and 14.97 ppm due to CH_3-C, CH_2, phenyl *H*, phenolic O*H* and enolic O*H*, respectively. Other weak signals at 2.30 and 13.65 ppm could be assigned to the keto-methyl and phenolic hydrogen in the keto tautomer. The integrated peak areas are in agreement with these assignments.

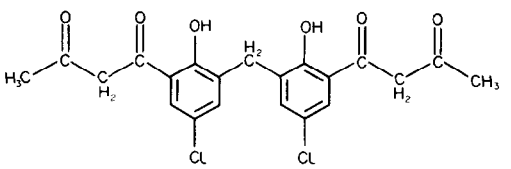

Fig. 5. The hexaketone 3,3′-methylene-bis-(2-hydroxy-1-acetoacetylbenzene).

Work is in progress to prepare complexes with this ligand.

Acknowledgements—We thank Mrs Sandra Boesso, Mr Letterio Turiaco and Mr Sergio Mazzuccato for technical assistance. This work has been supported by the Italian M.P.I.

REFERENCES

1. U. Casellato, P. A. Vigato, D. E. Fenton and M. Vidali, *Chem. Soc. Rev.* 1979, **8**, 199.
2. J. P. Collman, C. M. Elliott, T. R. Halberg and B. S. Tovrog, *Proc. Natn. Acad. Sci. U.S.A.* 1977, **74**, 8.
3. A. H. Alberts, R. Annunziata and J. M. Lehn, *J. Am. Chem. Soc.* 1977, **99**, 8502.
4. Y. Nishida, K. Takahashi, H. Kuramoto and S. Kida, *Inorg. Chim. Acta* 1981, **54**, L103.
5. K. D. Karlin and Y. Gultneh, *Chem. Educ.* 1985, **62**, 983.
6. J. A. Ibers and R. H. Holm, *Science* 1980, **209**, 223.
7. A. Moshfegh, S. Fallab and H. Erlenmeyer, *Helv. Chim. Acta* 1957, **40**, 1157.
8. Y. Taguchi, F. Sagara, H. Kobaiashi and K. Ueno, *Bull. Chem. Soc. Japan* 1970, **42**, 2470.
9. D. P. Graddon and G. M. Mockler, *Aust. J. Chem.* 1967, **20**, 21.
10. S. Yamada, *Coord. Chem. Rev.* 1965, **1**, 145.
11. R. H. Holm, G. W. Everett and A. Chakravorty, *Prog. Inorg. Chem.* 1966, **6**, 83.
12. B. N. Figgis and J. Lewis, *Prog. Inorg. Chem.* 1967, **6**, 37.
13. G. J. Long, T. Wrobleski, R. V. Thundathil, D. M. Sparlin and E. O. Schlaemper, *J. Am. Chem. Soc.* 1980, **102**, 6040.
14. F. Nowshad and M. Ul-Haque, *J. Chem. Soc., Perkin II* 1976, 623.
15. B. Galeffi, M. Postell, A. Grand and P. Rey, *Inorg. Chim. Acta* 1987, **129**, 1.
16. U. Casellato, P. A. Vigato, S. Tamburini, M. Vidali and D. E. Fenton, *Inorg. Chim. Acta* 1984, **84**, 101.
17. G. A. Hamilton, in *Molecular Mechanism of Oxygen Activation* (Edited by O. Hayashi), p. 405. Academic Press, New York (1974).
18. M. Matsumoto and K. Kuroda, *J. Am. Chem. Soc.* 1982, **104**, 1433.
19. A. Nishinaga, T. Itahara and T. Matsuura, *Bull. Chem. Soc. Japan* 1976, **49**, 3353.
20. G. Speier and Z. Tyeklar, *J. Molec. Catal.* 1980, **9**, 233.

Polyhedron Vol. 10, No. 12, pp. 1363–1366, 1991
Printed in Great Britain

0277–5387/91 $3.00+.00
Pergamon Press plc

TRANSITION METAL COMPLEXES OF THE SCHIFF BASES DERIVED FROM S-ALKYLDITHIOCARBAZATE WITH 2-PYRIDINECARBOXALDEHYDE N-OXIDE—II. SYNTHESES, PROPERTIES AND X-RAY CRYSTAL STRUCTURE OF FIVE-COORDINATE COPPER(II) COMPLEXES

SHAOHUA GOU,* XIAOZENG YOU and ZHENG XU

Coordination Chemistry Institute, Nanjing University, Nanjing, P.R.C.

and

ZHONGYUAN ZHOU and KAIBE YU

Chengdu Center of Analysis and Determination, Academia Sinica, Chengdu, P.R.C.

(*Received* 6 *October* 1990; *accepted* 29 *January* 1991)

Abstract—Four five-coordinate copper(II) complexes of deprotonated S-R-β-N-(pyridine N-oxide-2-ylmethylidene)dithiocarbazates (R = methyl, abbreviated SMPDH; R = benzyl, abbreviated SBPDH) with *o*-phenanthroline or 2,2′-bipyridine, were synthesized and characterized by UV, IR spectra and magnetic susceptibilities at room temperature. The X-ray crystal structure of [Cu(SBPD)Phen]ClO_4 was determined. The crystal structure contains a mononuclear unit in which copper(II) displays a distorted square pyramidal geometry.

A large number of transition metal complexes with Schiff bases as ligands containing sulphur and nitrogen atoms have been widely studied, since such complexes of platinum(II), palladium(II), nickel(II), copper(II) and zinc(II) were found to show certain anti-cancer activities.[1–4] Recently, we reported two new tridentate ligands of the above class derived from a Schiff base condensation reaction of S-R-dithiocarbazates (R = methyl and benzyl) with 2-pyridinecarboxaldehyde N-oxide, and their four-coordinate planar copper(II) complexes.[5] As part of our series, four five-coordinate copper(II) complexes of the above two ligands with *o*-phenanthroline or 2,2′-bipyridine are discussed in this paper.

EXPERIMENTAL

Preparation of the copper(II) complexes

The two ligands S-R-β-N-(pyridine N-oxide-2-ylmethylidene)dithiocarbazates (R = methyl, abbreviated SMPDH; R = benzyl, abbreviated SBPDH) have already been reported.[5] A general procedure for preparing copper(II) complexes is as follows. The ligand (1 mmol) was dissolved in ethanol (50 cm^3) with heating and an ethanol solution (10 cm^3) of $Cu(ClO_4)_2 \cdot 6H_2O$ (1 mmol) was added. After refluxing for 10 min, the mixture was added to an equivalent mole of *o*-phenanthroline or 2,2′-bipyridine in ethanol (5 cm^3), and was further refluxed for 5 min, then filtered while hot. Dark green crystals were obtained when the filtrate was cooled to room temperature. Yields and elemental analyses are given in Table 1.

Measurements

UV spectra were obtained using a Shimadzu 240 spectrophotometer. IR absorption spectra from 4000 to 400 cm^{-1} were recorded using a Nicolet 170 SXFT–IR spectrophotometer; samples were prepared as KBr pellets. Magnetic susceptibilities were measured at room temperature by the Gouy method with a CTP-F82 Faraday balance. The corrected magnetic moments and main IR data of the four complexes are listed in Table 2.

* Author to whom correspondence should be addressed.

Table 1. Yields and elemental analyses

Compound[a]	Formula	Yield (%)	Analyses (%)[b] C	H	N
[Cu(SMPD)Phen]ClO_4 (1)	$C_{20}H_{16}N_5ClO_5S_2Cu$	89	41.6 (42.1)	2.9 (2.8)	12.0 (12.3)
[Cu(SMPD)Bipy]ClO_4 (2)	$C_{18}H_{16}N_5ClO_5S_2Cu$	75	39.4 (39.6)	2.6 (2.9)	12.1 (12.8)
[Cu(SBPD)Phen]ClO_4 (3)	$C_{26}H_{20}N_5ClO_5S_2Cu$	91	47.8 (48.4)	2.9 (3.1)	10.7 (10.8)
[Cu(SBPD)Bipy]ClO_4 (4)	$C_{24}H_{20}N_5ClO_5S_2Cu$	67	46.1 (46.4)	3.0 (3.2)	11.1 (11.3)

[a] Phen = *o*-phenanthroline; Bipy = 2,2′-bipyridine.
[b] Calculated values in parentheses.

X-ray structure determination of [Cu(SBPD)Phen] ClO_4 (3)

Single crystals were obtained by slow diffusion of ether into an acetonitrile solution of the complex.

Crystal data: $CuC_{26}H_{20}ClN_5O_5S_2$, Mr = 645.57, monoclinic, space group $C2/c$, $a = 19.227(5)$, $b = 14.506(3)$, $c = 20.487(4)$ Å, $\beta = 106.00(2)°$, $V = 5493(2)$ Å^3, $Z = 8$, $D_c = 1.56$ g cm^{-1}, μ(Mo-K_α) = 10.83 cm^{-1}, $F(000) = 2567$. Crystal size: a tabular crystal, $0.4 \times 0.5 \times 0.05$ mm.

The unit-cell parameters were determined from 25 reflections with the CHDU program, devised by ourselves for searching reflection peaks automatically. Intensity data were collected with a R3M/E four-circle diffractometer operating in the ω–2θ scan mode, using graphite monochromatized Mo-K_α radiation ($\lambda = 0.71069$ Å) and $2\theta_{max} = 42°$. A total of 3307 independent reflections were measured and corrected by Lorentz-polarization factors, but not absorption. Only 2360 [$I > 3\sigma(I)$] reflections were used in structural determination and refinement. The structure was solved by direct methods. The 30 non-hydrogen atoms were revealed from the best E-map, the rest were located from the Fourier syntheses. Hydrogen atoms were obtained from a difference Fourier map. The coordinates of all the atoms, anisotropic thermal parameters for non-hydrogen atoms and isotropic thermal parameters for hydrogen atoms, were refined by block diagonal least-squares with 441 variables. The final $R = 0.046$, $R_w = 0.046$. Maximum peak in final difference synthesis was 0.48 e/Å^{-3} and minimum peak −0.30 e/Å^{-3}; the largest shift/ESD was 0.068 in O_4 atom.

Lists of atomic coordinates, thermal parameters, calculated hydrogen coordinates, least-square planes and torsion angles have been deposited as supplementary material with the Editor, from whom copies are available on request.

RESULTS AND DISCUSSION

The corrected magnetic moments of polycrystalline samples at 283 K are representative of magnetically dilute copper(II) complexes, compatible with the proposed stereochemistry. The reflectance electronic spectra of the compounds studied exhibit one broad unresolved band at *ca* 24.4 kK, unlike other pentacoordinated copper chromophores.[6] The *d–d* bands in these copper(II)

Table 2. Magnetic moments and main IR absorptions

Compound	μ_{eff} (283 KBM)	ν(C=N) (cm^{-1})	ν(C—S) (cm^{-1})	ν(N—O) (cm^{-1})	δ(N—O) (cm^{-1})	ν(Cl—O) (cm^{-1})
1	1.80	1438 vs	1044 w	1201 m	865 w	1101 vs
2	1.68	1416 vs	1043 w	1198 m	877 w	1079 vs
3	1.69	1431 s	1042 w	1198 w	866 w	1086 vs
4	2.10	1410 s	1043 w	1202 m	878 w	1089 vs

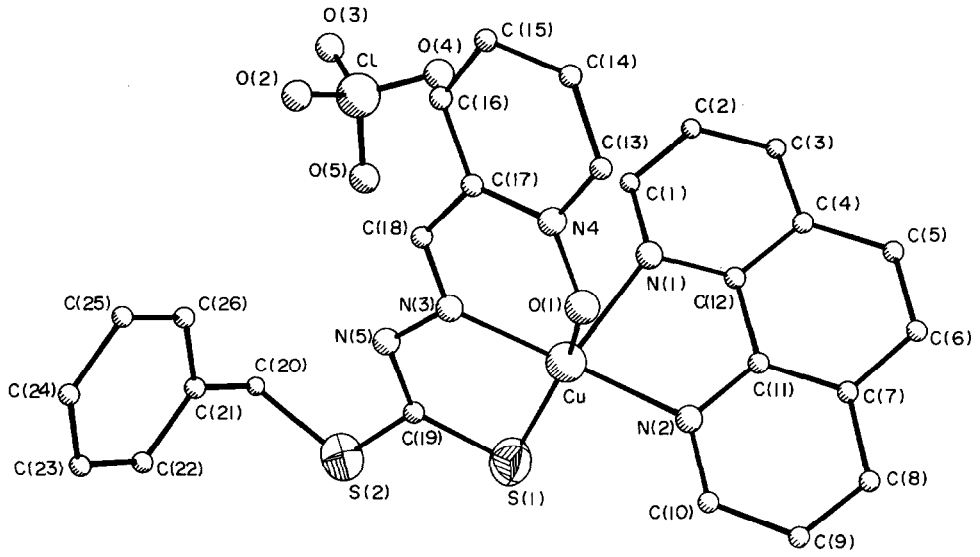

Fig. 1. Molecular structure of **3**.

complexes are not observed, which may result from the charge-transfer absorptions of ligands containing sulphur atoms.

The strong IR bands in the region 1410–1440 cm^{-1} of these complexes are due to the stretching vibrations of C=N bonds. ν(C=N) of complexes **1** and **3** are near 1415 cm^{-1}, whereas those of complexes **2** and **4** are at *ca* 1435 cm^{-1}. Bands appearing at *ca* 1200 cm^{-1} are assigned to ν(N—O) modes, and δ(N—O) modes are found at *ca* 870 cm^{-1}; these

Table 3. Selected bond lengths (Å) and angles (°) for **3**

Cu—S(1)	2.276(2)	Cu—N(1)	2.220(4)
Cu—N(2)	1.985(5)	Cu—N(3)	1.941(5)
Cu—O(1)	2.035(4)	S(1)—C(19)	1.710(7)
S(2)—C(19)	1.756(6)	S(2)—C(20)	1.815(9)
N(1)—C(1)	1.325(8)	N(1)—C(12)	1.341(8)
N(2)—C(10)	1.311(8)	N(2)—C(11)	1.373(7)
N(3)—N(5)	1.403(6)	N(3)—C(18)	1.288(8)
N(4)—C(13)	1.356(8)	N(4)—C(17)	1.368(8)
N(4)—O(1)	1.308(7)	N(5)—C(19)	1.301(8)
C(17)—C(18)	1.451(8)	C(20)—C(21)	1.488(10)
S(1)—Cu—N(1)	121.1(1)	S(1)—Cu—N(2)	96.8(1)
N(1)—Cu—N(2)	79.8(2)	S(1)—Cu—N(3)	85.9(1)
N(1)—Cu—N(3)	101.9(2)	N(2)—Cu—N(3)	175.6(2)
S(1)—Cu—O(1)	150.4(1)	N(1)—Cu—O(1)	88.4(2)
N(2)—Cu—O(1)	88.9(2)	N(3)—Cu—O(1)	87.0(2)
Cu—S(1)—C(19)	93.1(2)	C(19)—S(2)—C(20)	102.6(3)
Cu—N(1)—C(1)	133.3(4)	Cu—N(1)—C(12)	108.3(3)
C(1)—N(1)—C(12)	118.3(4)	Cu—N(2)—C(10)	125.8(4)
Cu—N(2)—C(11)	115.2(4)	C(10)—N(2)—C(11)	118.8(5)
Cu—N(3)—N(5)	120.7(4)	Cu—N(3)—C(18)	25.8(4)
N(5)—N(3)—C(18)	113.5(5)	C(13)—N(4)—C(17)	118.8(6)
C(13)—N(4)—O(1)	118.0(5)	C(17)—N(4)—O(1)	123.2(5)
N(3)—N(5)—C(19)	111.9(5)	N(1)—C(1)—C(2)	122.8(6)
Cu—O(1)—N(4)	122.9(3)	N(4)—C(17)—C(16)	119.4(5)
N(4)—C(17)—C(18)	121.5(5)	C(16)—C(17)—C(18)	119.0(6)
N(3)—C(18)—C(17)	126.3(6)	S(1)—C(19)—S(2)	116.0(4)
S(1)—C(19)—N(5)	128.2(4)	S(2)—C(19)—N(5)	115.8(5)
S(2)—C(20)—C(21)	115.9(5)	C(21)—C(22)—C(23)	120.7(7)

bands are in agreement with literature reports.[7–12] The frequencies of the two ligands decrease by *ca* 22–33 cm^{-1} upon complex formation, indicating N-oxide coordination by two ligands.[13] The ν(C—S) absorption appears near 1043 cm^{-1}, but no stretching vibrations of C=S bonds are observed, which indicates that the two ligands are in the thiolate form in these complexes, similar to those of other metal chelates with S-alkyldithiocarbazates and their derivatives as ligands.[14–16] Very strong bands are found in the range 1079–1101 cm^{-1}, which are assigned to ν(Cl—O) of the ClO_4^- group.

An X-ray study of **3** was carried out. Figure 1 shows the molecular structure with the atomic numbering scheme and selected bond lengths and bond angles are presented in Table 3.

The geometry of the pentacoordinated copper atom is distorted square pyramidal. The basal coordination positions are occupied by the O(1), N(3) and S(1) atoms of the tridentate ligand together with the N(2) atom of *o*-phenanthroline, and the apical position is occupied by the N(1) atom—the other nitrogen atom in the *o*-phenanthroline moiety. The Cu—S(1), Cu—N(2) and Cu—N(3) distances fall within the normal range, corresponding to the bond lengths in [Cu(SMPD)ImH]ClO_4.[5] The axial Cu—N(1) bond, however, is significantly longer (2.220 Å) than the equatorial Cu—N(2) bond (1.985 Å), owing to the coordination of the much larger *o*-phenanthroline group.

The coordination plane composed of Cu N(1) N(2) and N(3), from which the maximum deviation of atoms is −0.0462 Å, has a dihedral angle of 8.8° with the *o*-phenanthroline plane. The pyridine ring of the ligand is planar, and the two connected atoms, C(1) and C(18), are also in the plane with deviations less than 0.0900 Å. The dihedral angle between the pyridine plane and the *o*-phenanthroline plane is 120.5°; it is the spatial resistance of the above two planes that leads to the distorted square pyramidal configuration of the copper atom and the non-coplanarity of the N(2), O(1), N(3) and S(1) atoms. Coordination planes, Cu N(2) N(3) O(1) and Cu S(1) N(1) O(1), with the dihedral angle of 101.1°, are almost perpendicular to that of the Cu N(1) N(2) N(3), the dihedral angles to one another are 91.1 and 89.0°, respectively.

The atoms O(1), N(4), C(17), C(18), N(3), N(5), C(19) and S(1) are all conjugated via the pyridine group, consistent with the case in [Cu (SMPD)ImH]ClO_4.

REFERENCES

1. D. L. Klayman, J. P. Scovill, J. F. Bartosevich and J. Bruce, *J. Med. Chem.* 1983, **26**, 35 and refs therein.
2. J. P. Scovill, D. L. Klayman and C. F. Franchino, *J. Med. Chem.* 1982, **25**, 1261.
3. J. P. Scovill, D. L. Klayman, C. Lambros, G. E. Childs and J. D. Nortsh, *J. Med. Chem.* 1984, **27**, 87.
4. D. X. West and L. K. Pannell, *Transition Met. Chem.* 1989, **14**, 457.
5. S. Gou, X. You, Z. Xu, K. Yu and Z. Zhou, *Polyhedron*, 1990, **9**, 2981.
6. J. Suarez-Varela, L. Soto, J. P. Legros, C. Esteve and J. Gracia, *Polyhedron* 1988, **7**, 229.
7. A. E. Landers and D. J. Phillips, *Inorg. Chim. Acta* 1977, **25**, L39.
8. A. E. Landers and D. J. Phillips, *Inorg. Chim. Acta* 1981, **51**, 109.
9. A. E. Landers and D. J. Phillips, *Inorg. Chim. Acta* 1982, **59**, 41.
10. A. E. Landers and D. J. Phillips, *Inorg. Chim. Acta* 1982, **59**, 125.
11. A. E. Landers and D. J. Phillips, *Inorg. Chim. Acta* 1983, **74**, 43.
12. A. E. Landers and D. J. Phillips, *Inorg. Chim. Acta* 1984, **86**, 77.
13. N. M. Carayannis, L. L. Pylewski and C. M. Mikulski, *Coord. Chem. Rev.* 1973, **11**, 93.
14. M. Das and S. E. Livingstone, *Inorg. Chim. Acta* 1976, **19**, 5.
15. M. A. Ali and M. T. H. Tarafdar, *J. Inorg. Nucl. Chem.* 1977, **39**, 1785.
16. M. A. Ali and S. E. Livingstone, *Coord. Chem. Rev.* 1974, **13**, 101.

Polyhedron Vol. 10, No. 12, pp. 1367–1372, 1991
Printed in Great Britain

0277–5387/91 $3.00+.00
© 1991 Pergamon Press plc

SYNTHESIS AND X-RAY CRYSTAL STRUCTURES OF $[Me_2NH_2]^+[Al(OSiMe_3)_4]^-$ AND $Al_2(OSiMe_3)_6$

MALCOLM H. CHISHOLM,* JOHN C. HUFFMAN and JODI L. WESEMANN

Department of Chemistry and Molecular Structure Center, Indiana University, Bloomington, IN 47405, U.S.A.

(*Received* 16 *October* 1990; *accepted* 29 *January* 1991)

Abstract—The reaction between $Al_2(NMe_2)_6$ and excess Me_3SiOH in hydrocarbon solvents yields $[Me_2NH_2]^+[Al(OSiMe_3)_4]^-$ (**I**), which has been characterized by X-ray crystallography. Hydrogen bonding occurs between oxygen atoms on the siloxides and hydrogen atoms of the dimethylammonium cations. Under a dynamic vacuum **I** sublimes (50°C, 10^{-2} torr) but with some decomposition to $Al_2(OSiMe_3)_6$ (**II**). The latter compound is better prepared by addition of Me_3SiOH to $Al(OPr^i)_3$. The addition of Me_3SiOH and Me_2NH to hydrocarbon solutions of **II** regenerates **I**. These results are compared with previous studies of the reaction between $Al_2(NMe_2)_6$ and Bu^tOH. The X-ray crystal structure of **II** has been determined at −100°C.

In a previous study we observed that the reaction between $Al_2(NMe_2)_6$ and Bu^tOH in hydrocarbon solvents proceeded to give $Al_2(OBu^t)_6$ by way of two kinetic intermediates, $Al_2(\mu\text{-}NMe_2)(\mu\text{-}OBu^t)(OBu^t)_4$ and $(Me_2NH)Al(OBu^t)_3$[1,2] (see Scheme 1). Both of the kinetic products showed remarkable persistence with respect to the formation of $Al_2(OBu^t)_6$ at 0°C and were isolated and fully characterized by single crystal X-ray diffraction. These findings prompted us to investigate the related reaction between $Al_2(NMe_2)_6$[3] and Me_3SiOH. We describe here results of these investigations together with the single crystal X-ray structure of $Al_2(OSiMe_3)_6$, a compound that has previously been reported in the literature from alternative synthetic procedures.[4,5]

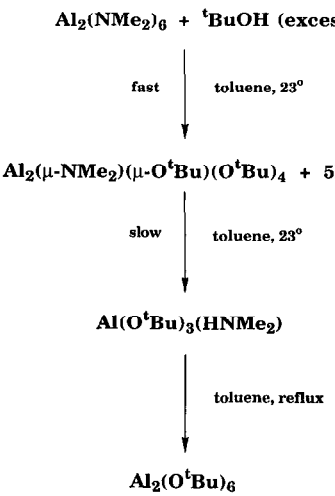

Scheme 1.

RESULTS AND DISCUSSION

Syntheses: $[Me_2NH_2]^+[Al(OSiMe_3)_4]^-$ (**I**) *and* $Al_2(OSiMe_3)_6$ (**II**)

The reaction between $Al_2(NMe_2)_6$ and Me_3SiOH ($\geq$ 6 equiv.) in hydrocarbon solvents proceeds quite differently from the related reaction involving Bu^tOH. The kinetic and thermodynamic product in the reaction is the amine salt, $[Me_2NH_2]^+[Al(OSiMe_3)_2]^-$ (**I**), which is a white, crystalline, hydrocarbon-soluble solid. Although an amine adduct $(Me_2NH)Al(OSiMe_3)_3$ might seem a plausible precursor to **I**, this compound has not been detected. Moreover, addition of Me_2NH to hydrocarbon solutions of $Al_2(OSiMe_3)_6$ does not yield $(Me_2NH)Al(OSiMe_3)_3$ but rather the salt **I** and other unidentified products.

Compound **I** sublimes at 45–50°C, 10^{-2} torr, but with some decomposition. The latter leads to the formation of $Al_2(OSiMe_3)_6$ (**II**), but does not pro-

* Author to whom correspondence should be addressed.

Table 1. Summary of crystal data

Empirical formula	$AlC_{12}H_{36}Si_4O_4{}^-C_2NH_8{}^+$	$Al_2C_{18}H_{54}Si_6O_6$
Colour of crystal	Colourless	Colourless
Crystal dimensions (mm)	$0.25 \times 0.25 \times 0.25$	$0.15 \times 0.35 \times 0.35$
Space group	$P2_1/a$	$P2_1n$
Cell dimensions		
Temperature (°C)	−172	−100
a (Å)	20.003(4)	9.722(3)
b (Å)	14.910(3)	19.944(6)
c (Å)	20.471(4)	11.527(4)
β (°)	118.82(1)	120.69(2)
Z (molecules/cell)	8	8
Volume (Å^3)	5349.22	1921.97
Calculated density (g cm^{-3})	1.067	1.025
Wavelength (Å)	0.71069	0.71069
Molecular weight	429.83	589.10
Linear absorption coefficient (cm^{-1})	2.635	2.816
Detector to sample distance (cm)	22.5	22.5
Sample to source distance (cm)	23.5	23.5
Average omega scan width at half height	0.25	0.25
Scan speed (° min^{-1})	6.0	4.0
Scan width (° + dispersion)	2.0	2.0
Individual background (s)	3	4
Aperture size (mm)	3.0×4.0	3.0×4.0
Two-theta range (°)	6–45	6–45
Total number of reflections collected	8345	2708
Number of unique intensities	6947	2511
Number with $F > 0.0$	5749	2130
Number with $F > 3.0\sigma(F)$	4593	1738
$R(F)$	0.0857	0.0767
$Rw(F)$	0.0764	0.0758
Goodness-of-fit for the last cycle	1.200	1.439
Maximum delta/sigma for last cycle	0.12	0.35

vide a reliable synthesis of **II**. Compound **II** is best prepared by the addition of Me_3SiOH to $Al(OPr^i)_3$.

The addition of Me_3SiOH and Me_2NH to hydrocarbon solutions of **II** regenerates **I** thereby establishing the equilibrium shown in eq. (1). In view of the fact that compound **I** sublimes *in vacuo* with some formation of **II**, the position of equilibrium in eq. (1) must lie well to the right, under ambient conditions.

$$Al_2(OSiMe_3)_6 + Me_2NH + Me_3SiOH \rightleftharpoons [Me_2NH_2]^+[Al(OSiMe_3)_4]^- \quad (1)$$

Compound **I** shows $\tilde{\nu}$(NH) at 2780 and 2470 cm^{-1} in the IR spectrum. Complete IR, ^1H and ^{13}C NMR data are given in the Experimental. The anion $[Al(OSiMe_3)_4]^-$ has been previously reported in both alkali (M = Li, Na, K)[6] and stibonium $[(SbMe_4)^+]$[7] salts. The Si—O—Al stretch in the IR spectrum has been assigned to a band at 966 cm^{-1} for the Na^+ and K^+ salts.[6] We observe a strong band at 948 cm^{-1} for the $Me_2NH_2{}^+$ salt, **I**.

X-ray crystal structures

A summary of pertinent crystal data for **I** and **II** is given in Table 1.

$[Me_2NH_2]^+[Al(OSiMe_3)_4]^-$ (**I**). In the space group $P2_1/a$ there are two independent ion pairs in the asymmetric unit of the unit cell. They differ little with respect to their metric parameters. A view of one of the ion pairs is shown in Fig. 1 and selected

Table 2. Selected bond distances (Å) for $[Me_2NH_2]^+$ $[Al(OSiMe_3)_4]^-$ (**I**)

Al(1)—O(2)	1.733(5)	Al(22)—O(23)	1.771(6)
Al(1)—O(7)	1.780(5)	Al(22)—O(28)	1.729(6)
Al(1)—O(12)	1.750(6)	Al(22)—O(33)	1.765(6)
Al(1)—O(17)	1.747(5)	Al(22)—O(38)	1.765(6)
O(2)—Si(3)	1.620(5)	O(23)—Si(24)	1.634(6)
O(7)—Si(8)	1.633(6)	O(28)—Si(29)	1.618(6)
O(12)—Si(13)	1.621(6)	O(33)—Si(34)	1.618(6)
O(17)—Si(18)	1.622(6)	O(38)—Si(39)	1.637(6)

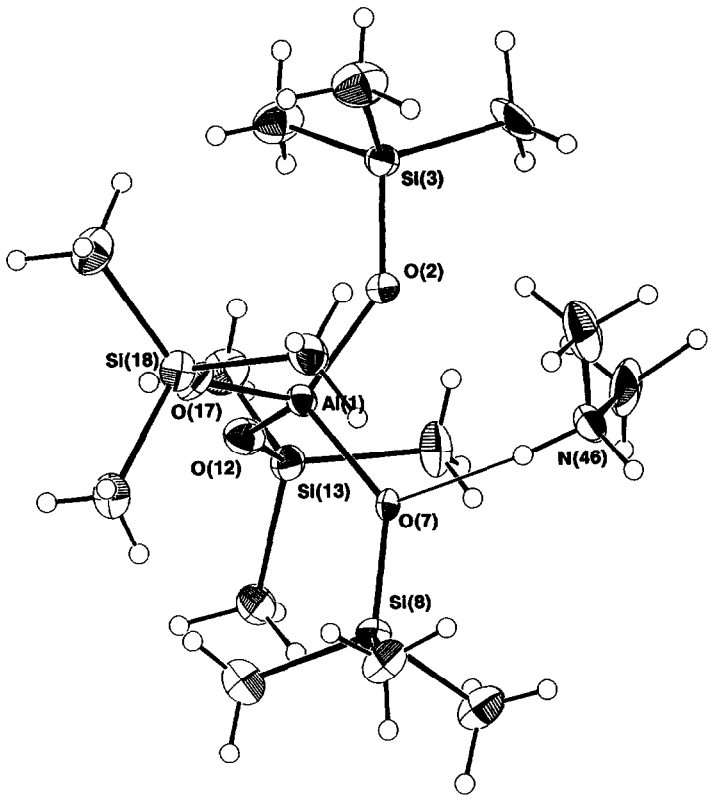

Fig. 1. An ORTEP drawing of $[Me_2NH_2]^+[Al(OSiMe_3)_4]^-$ (I) showing the atom numbering scheme.

bond distances and bond angles are given in Tables 2 and 3.

The aluminium atoms are in a pseudo-tetrahedral environment. The Al—O distances span the range 1.73–1.78 Å with the longer Al—O distances being associated with the oxygen atoms that are nearest and hydrogen bonded to the $[Me_2NH_2]^+$ hydrogen atoms. (H atoms were located in the X-ray determination.) The O—Al—O angles span a range from 104 to 113°. The Si—O distances were all essentially equivalent with an average distance of 1.625 Å. The Al—O—Si angles span the range 130–150° with a greater variation being observed in the ion pair containing Al(22). The smaller Al—O—Si angles are for oxygen atoms that are involved in hydrogen-bonding.

$Al_2(OSiMe_3)_6$ (**II**). Selected bond distances and angles for the centrosymmetric dimer are given in Table 4, wherein a comparison is also made with the previously reported alkoxide dimer, $Al_2(OBu^t)_6$.[2] A ball-and-stick drawing of **II** is shown in Fig. 2.

There is considerable motion associated with the methyl groups and a disorder involving the bridging $OSiMe_3$ ligand. There are two alternate positions for Si(13) (50% occupancy) with each sharing a common position for O(12), C(15) and C(16). There

Table 3. Selected bond angles (°) for $[Me_2NH_2]^+[Al(OSiMe_3)_4]^-$ (I)

O(2)—Al(1)—O(7)	104.07(26)	O(23)—Al(22)—O(28)	110.9(3)
O(2)—Al(1)—O(12)	112.65(21)	O(23)—Al(22)—O(33)	105.3(3)
O(2)—Al(1)—O(17)	112.93(23)	O(23)—Al(22)—O(38)	111.0(3)
O(7)—Al(1)—O(12)	111.44(27)	O(28)—Al(22)—O(33)	112.6(3)
O(7)—Al(1)—O(17)	110.91(26)	O(28)—Al(22)—O(38)	105.8(3)
O(12)—Al(1)—O(17)	105.02(28)	O(33)—Al(22)—O(38)	111.3(3)
Si(3)—O(2)—Al(1)	143.0(4)	Si(24)—O(23)—Al(22)	133.9(4)
Si(8)—O(7)—Al(1)	133.8(4)	Si(29)—O(28)—Al(22)	150.0(4)
Si(13)—O(12)—Al(1)	135.5(4)	Si(34)—O(33)—Al(22)	140.7(4)
Si(18)—O(17)—Al(1)	137.1(4)	Si(39)—O(38)—Al(22)	129.9(4)

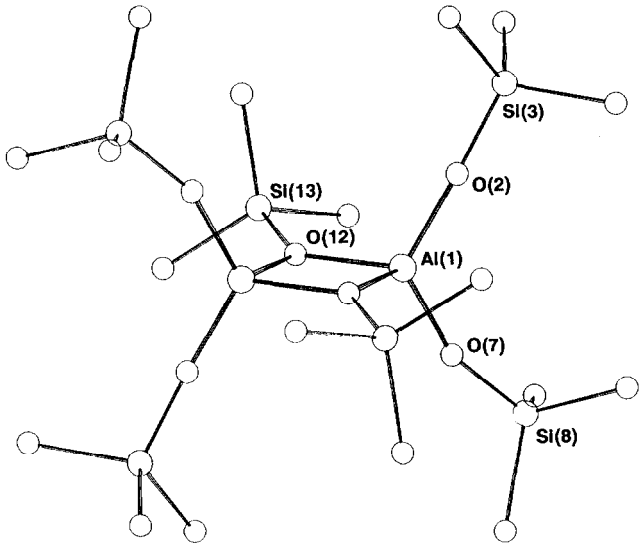

Fig. 2. A ball-and-stick drawing of the $Al_2(OSiMe_3)_6$ (**II**) molecule showing the atom numbering scheme.

are two 50 : 50 occupancies for C(14) and C(14)′ to complement Si(13) and Si(13)′.

Then crystallographic problems notwithstanding, the present structural determination of **II** reveals the remarkable similarity of the Al_2O_6 core with that seen for $Al_2(OBu^t)_6$. In particular, the Al—O distances are equivalent in the two molecules. The Al—O—Si angles of the terminal siloxide ligands are, however, notably larger than their Al—O—C counterparts in the $Al_2(OBu^t)_6$ molecule. The Al(1)—O(2)—Si(3) angle, for example, is 175°, essentially linear. While the Al—O distances differ by *ca* 0.015 Å, the Si—O bond distances differ by *ca* 0.08 Å. In both instances the distances associated with the bridging oxygen atoms are longer which is explainable in terms of either the hybridization at oxygen or the coordination number of oxygen, 2 vs 3. Comparison of Al—O and Si—O distances is also worthy with those seen in $Al_2(OSiMe_3)_4(acac)_2$[8] which adopts the structure depicted by **A**.

Table 4. Selected bond distances (Å) and angles (°) for $Al_2(OSiMe_3)_6$ (**II**) and the equivalent metric parameters for $Al_2(OBu^t)_6$

	II	$Al_2(OBu^t)_6$
Al(1)—Al(1)′	2.692(3)	2.777(2)
Al(1)—O(12)	1.813(4)	1.824(3)
Al(1)—O(2)	1.667(5)	1.698(3)
Al(1)—O(7)	1.678(5)	1.683(3)
O(12)—Si(13)	1.681(2)	1.474(4)
O(7)—Si(8)	1.583(5)	1.421(4)[a]
O(2)—Si(3)	1.601(5)	1.422(4)[a]
Al(1)—O(12)—Al(1)′	95.4(2)	98.9(1)
O(2)—Al(1)—O(7)	118.1(3)	115.1(1)
Al(1)—O(2)—Si(3)	174.3(4)	136.7(2)[b]
Al(1)—O(7)—Si(8)	159.4(4)	148.4(2)[b]

[a] O—C distances.
[b] Al—O—C angles.

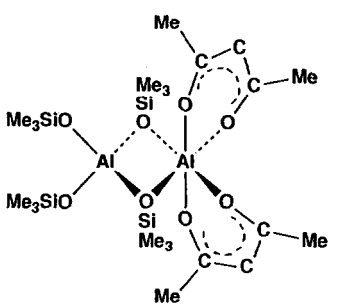

A

Concluding remarks

Bu^tOH and Me_3SiOH differ in two important ways. (1) The pK_a of the silanol is *ca* 4 units lower, indicating greater acidity of the silanol.[9] (2) Although the Me_3Si group is larger in volume than the Bu^t group, the effective steric pressure at a metal centre is greater for Bu^tO than for Me_3SiO as a ligand. Both of these factors are at work in causing the different behaviour of $Al_2(NMe_2)_6$ towards Me_3SiOH and Bu^tOH. The high formation tendency of the $[Al(OSiMe_3)_4]^-$ anion is favoured by both the greater pseudo-halide character and the

lesser steric demand of the $OSiMe_3$ ligand. The greater acidity and lesser steric demand of Me_3SiOH also presumably works to make species such as $Al_2(\mu\text{-}NMe_2)(\mu\text{-}OSiMe_3)(OSiMe_3)_4$ and $(Me_2NH)Al(OSiMe_3)_3$ kinetically more labile than their Bu^tO analogues. The structure of the Al_2X_6 dimers, where X = OBu^t and $OSiMe_3$, are remarkably similar in their Al_2O_6 cores which testifies to the fact that reactivity differences can only be traced in extreme cases to structural origins. The Al—O and Si—O distances in **I** and **II** for the terminal groups are roughly 0.2 Å smaller than the sum of the covalent radii. In view of the fact that the terminal Al—O distances in $Al_2(OBu^t)_6$ and $Al_2(OSiMe_3)_6$ are essentially identical, the short Al—O distances cannot be due to solely oxygen p_π–Al bonding.

EXPERIMENTAL

All procedures were carried out under nitrogen using air-sensitive techniques. Solvents were dried and degassed using standard procedures, and stored over activated molecular sieves. Glassware was presilylated by heating with hexamethyldisilazane. 99.99% $Al(OPr^i)_3$ was purchased from Aldrich and used without further purification in the preparation of $Al_2(OSiMe_3)_6$.[4] Me_3SiOH was synthesized by water hydrolysis of hexamethyldisilazane in diethyl ether, followed by neutralization with 2 M hydrochloric acid, separation of the aqueous layer, removal of ether and vacuum distillation.[2] $Al_2(NMe_2)_6$[3] was made from $AlCl_3$ and $LiNMe_2$ in hexane and purified by sublimation.

^1H and ^{13}C NMR spectra were obtained on a Varian XL-300 spectrometer, ^1H NMR at 300 MHz, referenced to proton impurities of d_6-benzene at δ 7.15; ^{13}C NMR at 75 MHz referenced also to benzene at δ 128.0. Microanalyses were obtained from Oneida Research Services, Whitesburo, New York, and IR spectra were obtained using a Nicolet FT–IR using KBr pellets.

Preparation of $[Me_2NH_2]^+[Al(OSiMe_3)_4]^-$ (I)

$Al_2(NMe_2)_6$ (0.381 g, 1.197 mmol) was dissolved in *ca* 25 cm^3 of toluene. Me_3SiOH (1.8 cm^3, 16.25 mmol) was added and the solution was heated with stirring to 80°C in an oil bath for 6 h. Toluene was removed *in vacuo* to give a white solid, that subsequently was dissolved in hexane. The solution was filtered. The product crystallized at −30°C with a yield of 0.80 g (78%). NMR data showed some concentration dependence. ^1H NMR (C_6D_6): δ 1.35 (br, 6H, NMe_2), 0.32 (s, 36H, $OSiMe_3$); ^{13}C NMR (C_6D_6): δ 33.04 (NMe_2), 3.45 ($OSiMe_3$); ^{29}Si NMR (C_6D_6): δ 0.27; IR (cm^{-1}): 2957s, 2901m, 2780br, 2470br, 1473m, 1257s, 1022s, 947s, 833s, 750s, 650m, 580m, 555m. Found: C, 39.4; H, 10.3; N, 3.1. Calc. for $AlC_{14}H_{44}NO_4Si_4$: C, 39.1; H, 10.3; N, 3.3%.

Addition of $HNMe_2$ *and* Me_3SiOH *to* $Al_2(OSiMe_3)_6$

Four equivalents of Me_3SiOH (0.285 cm^3, 2.63 mmol) were added to $Al_2(OSiMe_3)_6$ (0.387 g, 0.657 mmol) dissolved in *ca* 15 cm^3 of toluene. Me_2NH was bubbled through the solution for 1 min. The volume was reduced *in vacuo* to *ca* 5 cm^3. The solution was cooled to −15°C and within several hours white crystals had formed. They were isolated and dried *in vacuo* yielding 0.07 g, **I** by NMR data.

Sublimation of I

Compound **I** (0.17 g, 0.40 mmol) was placed in a silylated Schlenk and heated to 40°C in an oil bath. After 5 h a white solid had collected on the cold finger. This was collected and examined by ^1HNMR spectroscopy and thereby found to be a mixture of **I** (δ 1.4 and 0.32) and **II** (δ 0.27 and 0.24). From extended sublimations the residue yielded pure **II** as sublimate, δ 0.27 s, 12H (μ-$OSiMe_3$), 0.23 s, 24H (t-$OSiMe_3$). Found: C, 36.5; H, 8.8; N, 0.0. Calc. for **II**: C, 36.7; H, 9.2; N, 0.0%.

X-ray structural determinations

General operating procedures and listings of programs have been previously given.[10] Data collection, solution and refinement parameters are given in Table 1.

$[Me_2NH_2]^+[Al(OSiMe_3)_4]^-$ (**I**). Colourless, rod-like crystals were obtained from a hexane solution. A suitable crystal was located and transferred to the goniostat using standard inert atmosphere handling techniques employed by the IUMSC and cooled to −172°C for characterization and data collection. A systematic search of a limited hemisphere of reciprocal space located a set of diffraction maxima with symmetry and systematic absences corresponding to the unique monoclinic space group $P2_1/a$. Subsequent solution and refinement of the structure confirmed this choice. Data were collected in the usual manner using a continuous θ–2θ scan with fixed backgrounds. Data were reduced to a unique set of intensities and associated sigmas in the usual manner. The structure was solved by a combination of direct methods (MULTAN78) and Fourier techniques. All hydrogen atoms were clearly visible in a difference Fourier synthesis phased on the non-hydrogen atom parameters. All

hydrogen atoms were refined isotropically and non-hydrogen atoms anisotropically in the final cycles. A final difference Fourier was featureless, with the largest peak being 0.45 e/Å^3. Two independent molecules are present in the structure.

$Al_2(OSiMe_3)_6$. Similar crystals were obtained from both toluene and benzene solutions. When the sample was first transferred to the goniostat and cooled using the standard glove-bag techniques developed by the IUMSC, the crystal went through a violent phase transition, completely fracturing at -150°C. A subsequent crystal was transferred at -70°C, and slow cooling indicated the phase transition occurs near -130°C. A third crystal was then transferred and cooled to -100°C, at which temperature all data were collected. A systematic search of a limited hemisphere of reciprocal space located a set of diffraction maxima with symmetry and systematic absences corresponding to the unique monoclinic space group $P2_1/n$. Subsequent solution and refinement of the structure confirmed this choice. Data were collected in the usual manner using a continuous θ–2θ scan with fixed backgrounds. Data were reduced to a unique set of intensities and associated sigmas in the usual manner. The structure was solved by a combination of direct methods (MULTAN78) and Fourier techniques. The thermal motion is best described as severe, and in addition, a disorder is present with the bridging-$OSiMe_3$ group. There are two alternate positions for Si(13) with each sharing C(15) and C(16) as well as O(12). C(14) is also 50% occupancy, and a second position C(14)′ completes the alternate Si(13)′ sphere. In spite of the disorder and large thermal parameters, all atoms behaved properly when refined anisotropically. Hydrogen atoms were placed in fixed idealized positions for the final four cycles of refinement. There are no significant peaks in the final difference Fourier, the largest being 0.40 e/Å^3.

Atomic coordinates for compounds **I** and **II** have been deposited with the Cambridge Crystallographic Data Centre.

Acknowledgement—We thank the National Science Foundation for support.

REFERENCES

1. M. H. Chisholm, V. F. DiStasi and W. E. Streib, *Polyhedron* 1990, **9**, 253.
2. R. H. Cayton, M. H. Chisholm. E. R. Davidson, V. F. DiStasi, P. Du and J. C. Huffman, *Inorg. Chem.* 1991, **30**, 1020.
3. J. Ruff, *J. Am. Chem. Soc.* 1961, **83**, 2835.
4. D. C. Bradley, J. W. Lorimer and C. Prevedorou-Demas, *Can. J. Chem.* 1971, **49**, 2310.
5. H. Schmidbaur, *Chem. Ber.* 1963, **96**, 2696.
6. H. Schmidbaur and M. Schmidt, *Angew. Chem.* 1962, **74**, 589.
7. P. J. Wheatley, *J. Am. Chem. Soc.* 1963, **85**, 3200.
8. M. F. Garbauskas, J. H. Wengrovious, R. C. Going and J. S. Kasper, *Acta. Cryst.* 1984, **C40**, 1536.
9. The pK_a for Et_3SiOH has been determined[a] to be 14 which compares to 19[b] for Bu^tOH: (a) H. Arm, K. Hochstramer and P. W. Schindler, *Chimia* 1974, **28**, 237; (b) W. K. McEwan, *J. Am. Chem. Soc.* 1937, **58**, 1124.
10. M. H. Chisholm, K. Folting, J. C. Huffman and C. C. Kirkpatrick, *Inorg. Chem.* 1984, **23**, 1021.

Polyhedron Vol. 10, No. 12, pp. 1373–1377, 1991
Printed in Great Britain

0277–5387/91 $3.00+.00
© 1991 Pergamon Press plc

PULSE RADIOLYSIS OF MONO- AND BINUCLEAR COPPER(II) MACROCYCLIC COMPLEXES

PAUL V. BERNHARDT and GEOFFREY A. LAWRANCE*

Department of Chemistry, The University of Newcastle, NSW 2308, Australia

and

DAVID F. SANGSTER

Australian Nuclear Science and Technology Organization,
Lucas Heights Research Laboratories, Sutherland 2232, Australia

(*Received* 1 *November* 1990; *accepted* 5 *February* 1991)

Abstract—Pulse radiolytic reduction of a series of nitro-substituted tetraaza copper(II) complexes with the aquated electron (e_{aq}) results in formation of nitro radical anions. By contrast, reaction of pendent nitro dithia-diaza copper(II) analogues with e_{aq} achieves exclusive reduction of the metal centre. Oxidation of all tetraaza copper(II) complexes with the hydroxyl radical (OH) resulted in formation of stable copper(III) complexes, whereas no metal-centred oxidation was observed for the corresponding $Cu^{II}N_2S_2$ complexes. The variation in reactivity, effectively evidence for selectivity in reduction with e_{aq} or oxidation with OH, was attributed to the shift in the $Cu^{II/I}$ half-wave potentials going from a tetraaza to a dithia-diaza donor set.

In a previous paper, we reported the pulse radiolysis and electrochemistry of a series of tetraaza macrocyclic and acyclic nickel(II) complexes.[1] Both nickel(I) and nickel(III) derivatives of the precursor complexes were characterized. The electrochemical behaviour of tetraaminecopper(II) complexes is somewhat similar to that displayed by nickel(II) analogues, in that both the copper(I) and copper(III) oxidation states are also accessible from redox reactions of the precursor complexes. Electrochemical studies of the copper(II) complexes of L^1–L^{12} have been reported with their syntheses,[2–6] and a pulse radiolysis study of the products of both one-electron oxidation (with hydroxyl radicals, OH) and one-electron reduction (with aquated electrons, e_{aq}) of these complexes is contained herein.

* Author to whom correspondence should be addressed.

EXPERIMENTAL

The mononuclear copper(II) complexes of the ligands L^1–L^7 were prepared via metal-directed condensation reactions, as described previously.[2–5] The dicopper(II) complexes of the ligands L^8–L^{12} were also prepared according to literature syntheses.[6]

Pulse radiolysis experiments were performed with a Van de Graaf electron accelerator that delivered electron pulses (3 μs) at *ca* 1 MeV (1 eV = 1.60×10^{-19} J) through the thin wall of a 1 cm optical path cell as previously described.[7] Dosimetry was performed with an aerated aqueous solution of KSCN, employing values of $\varepsilon_{480\ nm} = 7600$ M^{-1} cm^{-1} and $G(OH) = G([(NCS)_2^{-}]) = 2.8$; a dose of *ca* 40 Gy was observed. All reductions were effected by e_{aq}, with OH being scavenged by the addition of 2-methylpropan-2-ol (*ca* 0.01 M) to each solution. Oxidation was achieved with OH, with e_{aq} being quenched by purging each solution

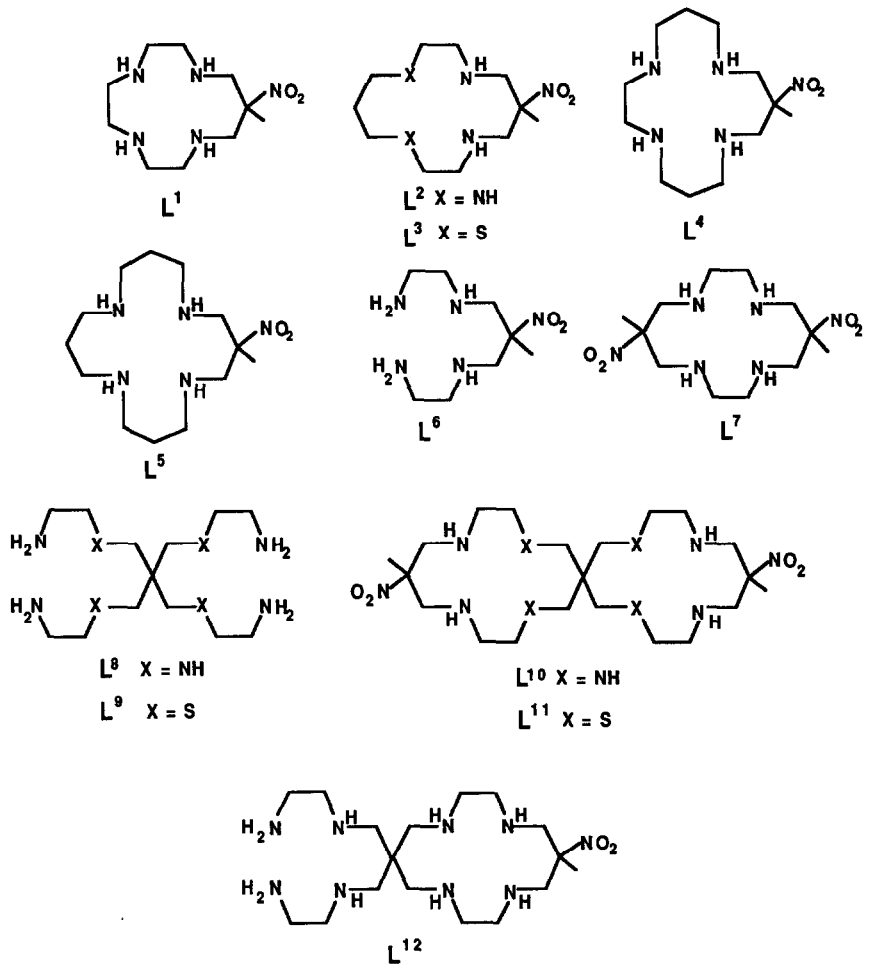

with nitrous oxide, which effectively doubled the yield of OH. Formation rate constants for e_{aq} and OH reactions were determined according to previously described methods.[1]

RESULTS AND DISCUSSION

Reductions

Reactions of all copper(II) complexes with e_{aq} resulted in the formation of species at effectively diffusion controlled rates ($\sim 10^{10}\,M^{-1}\,s^{-1}$). The large excess (100-fold) of precursor complex to reductant (e_{aq}) permitted only single electron redox processes. A summary of the electronic spectra and reactivity of each reduced complex is given in Table 1. In all but four cases, those being the copper(II) complexes of L^3, L^8, L^9 and L^{11}, the electronic spectrum of each reduced species exhibited a single maximum in the range 280–290 nm (ε, 2000–4000 $M^{-1}\,cm^{-1}$). Maxima of comparable energy and intensity have previously been shown to be characteristic of nitro radical anions ($-NO_2^{\bullet -}$),[1,8] and since each of the eight complexes displaying a maximum around 290 nm possess a pendent nitro group, a similar assignment is made for the present set. These nitro radical anion complexes decay via first-order processes (Table 1) to a similar copper(II) complex, or dicopper(II) complex.

The dicopper(II) complexes of the acyclic ligands L^8 and L^9 do not possess pendent nitro groups, and therefore only metal-centred reductions are possible for these complexes. The electronic spectrum of the reduced $[Cu_2L^8]^{4+}$ ion did not differ appreciably from that of its precursor complex, nor were large changes in the spectra anticipated upon reduction to the putative $[Cu_2L^8]^{3+}$ ion, which is a mixed-valence Cu^{II}–Cu^{I} complex. The Cu^{I} moiety (d^{10}) of this reduced species would most likely be transparent in the near UV–vis region of the spectrum, and indeed the Cu_{aq}^{+} ion has been shown to exhibit no electronic maxima in this region.[9] Moreover, bleaching of the relatively weak visible absorption maximum of the copper(II) unit, upon reduction, was not great enough to be precisely determined by the present equipment. By contrast, reduction of the thio-ether analogue $[Cu_2L^9]^{4+}$ with e_{aq} resulted in complete bleaching of the intense near-UV

Table 1. Physical properties of one electron reduced species

Precursor complex	k_d (s^{-1})	λ_{max} (ε) (nm) (M^{-1} cm^{-1})	$E_{1/2}$ ($Cu^{II/I}$)[a] (V *vs* SHE)
$[CuL^1]^{2+}$	5000	280 (4000)	−0.34
$[CuL^2]^{2+}$	5200	280 (2900)	−0.54
$[CuL^3]^{2+}$	<100	—	−0.03
$[CuL^4]^{2+}$	5000	280 (4200)	−0.42
$[CuL^5]^{2+}$	5000	280 (2000)	−0.18
$[CuL^6]^{2+}$	4000	290 (2700)	−0.39
$[CuL^7]^{2+}$	210	290 (3600)	−0.46
$[Cu_2L^8]^{4+}$	<100	No change	−0.36, −0.44
$[Cu_2L^9]^{4+}$	<100	—	+0.41, +0.29
$[Cu_2L^{10}]^{4+}$	3000	290 (3500)	−0.52
$[Cu_2L^{11}]^{4+}$	<100	—	+0.21
$[Cu_2L^{12}]^{4+}$	44,000	290 (4000)	−0.22, −0.39

[a] References 2–6.

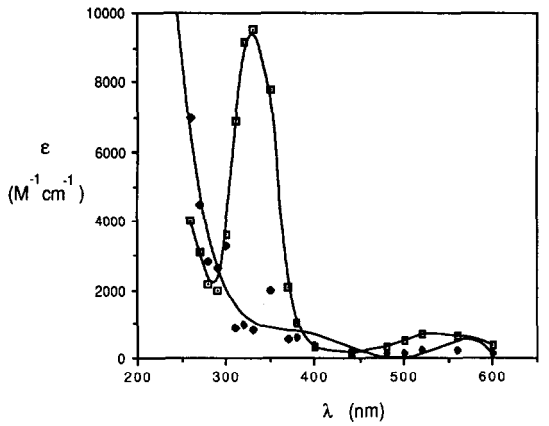

Fig. 1. Electronic spectrum of $[Cu_2L^{11}]^{4+}$ (□) and its one electron reduced product (◆).

maximum (330 nm) characteristic of copper(II) complexes with S-donor ligands.[4] It is apparent that the presence of this maximum is a direct indicator of a copper(II) complex [or dicopper(II) complex], and its disappearance upon reduction or oxidation implies a metal-centred redox reaction. The more intense visible *d–d* maximum exhibited by the N_2S_2 donor complex also allowed the observation of bleaching of this maximum upon reduction. It is notable that the spectrum of the resultant $[Cu_2L^9]^{3+}$ ion displayed no maximum near 330 nm, when one might anticipate a halving of intensity relative to the precursor as a result of a reduction of one of the two metal centres. The origins of this phenomenon are not certain, but it appears that there is definitely a strong intramolecular interaction between the two copper centres upon reduction, despite the absence of π-conjugation in the molecule. Previously we have reported[6] that strong intramolecular dipole–dipole coupling, as defined by EPR spectroscopy, occurs in the dicopper(II) complexes of L^8–L^{12}. The present results indicate a rapid intramolecular exchange of the single "hole" in the saturated mixed-valence d^9/d^{10} $[Cu_2L^9]^{3+}$ ion.

A similar result was obtained when the pendent nitro thio-ether amine complexes $[Cu_2L^{11}]^{4+}$ and $[CuL^3]^{2+}$ were reduced with e_{aq}, where a complete disappearance of the intense maximum at 330 nm (indicative of a metal-centred redox reaction) was found upon reduction of the precursor complex. No evidence of nitro radical formation was found and the resultant spectrum displayed no large maxima in the range 270–600 nm (Fig. 1). Products of the e_{aq} reductions of $[Cu_2L^9]^{4+}$, $[Cu_2L^{11}]^{4+}$ and $[CuL^3]^{2+}$ were stable for the duration of the experiment (*ca* 1 ms). It is generally believed that e_{aq} is an indiscriminant reductant, so the present selectivity in reduction of the pendent nitro groups in the $Cu^{II}N_4$ and $Cu^{II}{}_2N_8$ complexes as opposed to metal-centred reduction of the $[CuL^3]^{2+}$ and $[CuL^{11}]^{4+}$ ions is remarkable. The origins of this selectivity presumably lie in the disparate $Cu^{II/I}$ $E_{1/2}$ values for the $Cu^{II}N_4$ and $Cu^{II}N_2S_2$ systems (Table 1), where reduction of the copper(II) centre in $[Cu_2L^{11}]^{4+}$ and $[CuL^3]^{2+}$ is thermodynamically more viable than nitro group reduction [$E_{1/2}$ (—NO_2) −0.85 V *vs* SHE]. The difference in potential between the $Cu^{II/I}$ couple and the nitro group reduction is not nearly as great in the CuN_4 systems, and the nitro group is apparently reduced in preference to the metal centre, although competition between the metal centre and the nitro group for e_{aq} cannot be discounted, since reduction of the copper(II) centre would not result in a large change in the electronic spectrum (*vide supra*).

Oxidations

Oxidation of all $Cu^{II}N_4$ and $Cu_2{}^{II}N_8$ complexes with OH, like reductions with e_{aq}, occurred at effectively diffusion-controlled rates ($\sim 10^{10}$ M^{-1} s^{-1}), the large excess of precursor complex over oxidant again defining only a primary single electron redox process. Generated species exhibit electronic maxima at 370–400 nm and 280–300 nm (Table 2). These products were stable for at least 1 ms, and the spectrum of the final product retained the features of the initially formed complex. The energies and intensities of these maxima are comparable with those reported for the spectra of complexes

Table 2. Electronic spectra of one electron oxidation products

Precursor complex	λ_{max} (ε) (nm) (M^{-1} cm^{-1})
$[CuL^1]^{2+}$	370 (1400), 300 (3500)
$[CuL^2]^{2+}$	390 (1900), 300 (5200)
$[CuL^3]^{2+}$	No change observed
$[CuL^4]^{2+}$	390 (1600), 280 (6600)
$[CuL^5]^{2+}$	360 (1000), 280 (6000)
$[Cu_2L^8]^{4+}$	380 (500), 300 (2300)
$[Cu_2L^9]^{4+}$	No change observed
$[Cu_2L^{10}]^{4+}$	400 (1900), 290 (6000)
$[Cu_2L^{11}]^{4+}$	No change observed
$[Cu_2L^{12}]^{4+}$	380 (560), 300 (3000)

generated by electrochemical,[10,11] pulse radiolysis[12] and flash photolysis[13] oxidation of copper(II) tetraamines. The stability of the complexes is also consistent with other studies that have found tetraazamacrocyclic copper(III) complexes are stable for several minutes in aqueous solution.[10,11] The origins of these electronic maxima are less certain. It has been suggested,[12] albeit tentatively, that these maxima are both of charge-transfer origin, however one would anticipate at least one *d–d* transition ($^1A_2 \leftarrow {}^1A_1$) by analogy with isoelectronic low-spin d^8 nickel(II) complexes. The situation could not be further resolved, and no definitive assignment is made of the copper(III) spectra.

Metal-centred oxidation of the thio-ether amine complexes $[Cu_2L^9]^{4+}$, $[Cu_2L^{11}]^{4+}$ and $[CuL^3]^{2+}$ was not observed, and the intense maximum at 330 nm present in the precursor complexes did not change significantly upon reaction with OH. It is known that hydrogen abstraction is a competitive reaction to metal-centred oxidation,[14] and evidently such a process is occurring upon reaction of the thio-ether complexes with OH. The absence of metal-centred oxidation of these complexes in contrast to the $Cu^{II}N_4$ species may be explained, again, by reference to the $E_{1/2}$ values for the present complexes. It has already been mentioned that there exists a large difference between the $Cu^{II/I}$ $E_{1/2}$ values for the CuN_4 and CuN_2S_2 systems. Although the $Cu^{III/II}$ couples for the present set of complexes lay outside the potential range within which they could be determined with our equipment, other studies of tetraazamacrocyclic copper(II) complexes have defined $Cu^{III/II}$ $E_{1/2}$ values in the range +1.0–1.2 V *vs* SHE in acidic solution.[10,11,15] Recalling that the $Cu^{II/I}$ couples were some 400 mV more negative for the $Cu^{II}N_4$ complexes relative to their $Cu^{II}N_2S_2$ analogues, a similar shift is anticipated for the $Cu^{III/II}$ couple of the thio-ether complexes, i.e. at least to +1.4 V *vs* SHE. Oxidations with OH are unlikely to occur at such extreme potentials in preference to hydrogen abstraction, where the availability of amine and aliphatic hydrogen atoms offers a ready alternative to metal-centred oxidation.

Conclusions

Selectivity in reduction (e_{aq}) and oxidation (OH) has been shown to occur in redox reactions of copper(II) complexes with different ligand fields. The stronger field tetraazacopper(II) complexes exhibit $Cu^{II/I}$ and $Cu^{III/II}$ couples at significantly more negative potentials than the $Cu^{II}N_2S_2$ analogues. The result of this was found to be a preferential reduction of the copper(II) centre instead of the nitro groups in the $Cu^{II}N_2S_2$ complexes, whereas reduction of the pendent nitro $Cu^{II}N_4$ complexes led to nitro radical anions. Oxidation of the $Cu^{II}N_4$ complexes with OH achieved a metal-centred oxidation in contrast to the $Cu^{II}N_2S_2$ complexes which resulted in hydrogen abstraction.

Acknowledgements—Financial assistance by the Australian Research Council and the Australian Institute for Nuclear Science and Engineering is gratefully acknowledged.

REFERENCES

1. P. V. Bernhardt, G. A. Lawrance and D. F. Sangster, *Inorg. Chem.* 1988, **27**, 405.
2. P. Comba, N. F. Curtis, G. A. Lawrance, M. A. O'Leary, B. W. Skelton and A. H. White, *J. Chem. Soc., Dalton Trans.* 1988, 2145.
3. G. A. Lawrance, M. Rossignoli, B. W. Skelton and A. H. White, *Aust. J. Chem.* 1987, **40**, 1441.
4. P. Comba, G. A. Lawrance, M. Rossignoli, B. W. Skelton and A. H. White, *Aust. J. Chem.* 1988, **41**, 773.
5. P. Comba, N. F. Curtis, G. A. Lawrance, A. M. Sargeson, B. W. Skelton and A. H. White, *Inorg. Chem.* 1986, **25**, 4260.
6. P. V. Bernhardt, P. Comba, L. R. Gahan and G. A. Lawrance, *Aust. J. Chem.* 1990, **43**, 2035.
7. H. A. Boucher, A. M. Sargeson, D. F. Sangster and J. C. Sullivan, *Inorg. Chem.* 1981, **20**, 3719.
8. M. Z. Hoffman, M. Simic and N. V. Brezniak, *J. Am. Chem. Soc.* 1977, **99**, 2166.
9. J. H. Baxendale, E. M. Fielden and J. P. Keene, in *Pulse Radiolysis*, Academic Press, New York (1965).
10. C. Bisi Castellani, L. Fabbrizzi, M. Licchelli, A. Perotti and A. Poggi, *J. Chem. Soc., Chem. Commun.* 1984, 806.

11. D. C. Olson and J. Vasilevskis, *Inorg. Chem.* 1971, **10**, 463.
12. D. Meyerstein, *Inorg. Chem.* 1971, **10**, 2244.
13. K. Kumar, F. P. Rotzinger and J. F. Endicott, *J. Am. Chem. Soc.* 1983, **105**, 7064.
14. S. N. Bhattacharyya and P. Neta, *J. Phys. Chem.* 1981, **85**, 1527.
15. M. Ciampolini, L. Fabbrizzi, M. Licchelli, A. Perotti, F. Pezzini and A. Poggi, *Inorg. Chem.* 1986, **25**, 4131.

Polyhedron Vol. 10, No. 12, pp. 1379–1383, 1991
Printed in Great Britain

0277-5387/91 $3.00+.00
© 1991 Pergamon Press plc

KINETIC STUDY OF THE REACTION OF *MESO*-TETRAKIS (*p*-TRIMETHYLAMMONIUMPHENYL)PORPHINATODIAQUACOBALT(III) WITH THIOCYANATE AND IODIDE IONS IN AQUEOUS SOLUTION

J. G. LEIPOLDT,* W. PURCELL and H. MEYER

Department of Chemistry, University of the Orange Free State, Bloemfontein, Republic of South Africa

(*Received* 2 *November* 1990; *accepted* 5 *February* 1991)

Abstract—The reaction of *meso*-tetrakis(*p*-trimethylammoniumphenyl)porphinatodiaquacobalt(III) with NCS^- and I^- ions has been studied at 15, 25 and 35°C in 0.1 mol dm^{-3} $[H^+]$ (HNO_3) and $\mu = 1.0$ mol dm^{-3} ($NaNO_3$). The values of the acidity constants, K_{a1} and K_{a2}, for the diaqua complex at 25°C are $3.3(5) \times 10^{-7}$ and $2.0(2) \times 10^{-11}$ mol dm^{-3}, respectively. The reactions are first order in ligand concentration up to 0.9 mol dm^{-3}. The values of the second-order rate constants at 25°C are 89.0(5) and 76.0(4) dm^3 mol^{-1} s^{-1} for NCS^- and I^-, respectively. The values of $\Delta S^{\ddagger}$ for the different incoming ligands are positive or nearly positive, which is indicative of dissociative activation. The value of the activation volume [$\Delta V^{\ddagger} = 18.8(8)$ cm^3 mol^{-1}] indeed points to a dissociative mechanism. The porphine ligand greatly labilizes the cobalt(III). There is about a 10^8-fold increase in the rate constant for substitution compared with that of $[Co(NH_3)_5(H_2O)]^{3+}$. It is proposed that the electron-rich porphine not only labilizes the M^{III} ion (M = Co, Rh and Cr) but also promotes a more dissociative activation mode relative to that of the corresponding $[M(NH_3)_5(H_2O)]^{3+}$ complexes. The extent of labilization depends on the electron-donating ability of the porphine as well as the nature of the central metal ion. It is also shown that the overall charge of the complex, whether positive or negative (as determined by the formal charge of the porphine), plays a minor role in the mechanism of the substitution reaction.

It is well known that the porphine ligand labilizes the axial positions in complexes of cobalt(III), rhodium(III) and chromium(III).[1–8] The extent of labilization is dependent upon the metal ion and the other complex to which it is being compared. For example, the anation reactions of *trans*-$[M(TPPS)(H_2O)_2]^{3-}$ [TPPS = *meso*-tetrakis(*p*-sulphonatophenyl)porphine] are about 10^9, 10^3 and 10^2 times faster than those of $[M(NH_3)_5(H_2O)]^{3+}$, where M = Co, Rh and Cr, respectively.[4–6,9] The extent of labilization also depends on the porphine. The relative rate constants for the anation reactions of $[CoP(H_2O)_2]^{n+}$ complexes are 1, 150 and 225 for P = TMPP, TPPS and TCPP, respectively; TMPP = *meso*-tetrakis(4-N-methylpyridyl)porphine and TCPP = *meso*-tetrakis(4-carboxyphenyl)porphine.[2,4,8] The anation reaction of $[Cr(TPPS)(H_2O)_2]^{3-}$ are, however, only about six times faster than those of $[Cr(TMPP)(H_2O)_2]^{5+}$.[6,7]

The large labilization effect of the porphine ligand, especially in the case of the cobalt(III) complexes, has been explained in terms of a dissociative activation. The electron-rich porphine ligand donates electron density to the central metal ion making the cobalt(III) ion (d^6 species) more like a labile d^7 cobalt(II) ion and also stabilizes the five-coordinated intermediate in a dissociative reaction mode.

Strong support for a dissociative activation was recently obtained from high-pressure studies of the reaction between $[Co(TPPS)(H_2O)_2]^{3-}$ and $[Co(TMPP)(H_2O)_2]^{5+}$ and thiocyanate ions as well as thiourea.[10–12] In an attempt to gain more insight into the mechanism of the substitution reactions of porphine complexes of cobalt(III), rhodium(III)

* Author to whom correspondence should be addressed.

and chromium(III), and to compare the labilization effect of different porphines, we have decided to extend this work to the anation reactions of another water-soluble porphine, *meso*-tetrakis(N-trimethyl ammoniumphenyl)porphine (TAPP), complex of cobalt(III).

EXPERIMENTAL

The iodide salt of TAPP was synthesized as described by Krishnamurthy.[13] The cobalt(III) complex of TAPP was synthesized by heating a solution of the iodide salt (150 mg) and $CoCl_2 \cdot 6H_2O$ (600 mg, a large excess) in 50 cm^3 of water for 2 h on a waterbath while oxygen was bubbled through. During this time all the free porphine was converted into the cobalt(III) complex as was indicated by the visible spectrum of the solution. The solution was filtered to remove all the insoluble impurities and allowed to cool. About 10 drops of concentrated perchloric acid were added. The addition of perchloric acid caused the perchlorate salt, $[Co(TAPP)(H_2O)_2](ClO_4)_5$, to precipitate. The product was filtered, washed with ethanol and ether and allowed to dry in the atmosphere at room temperature. The Soret band for this complex is at 426 nm with a molar absorptivity of 2.01×10^5 mol^{-1} dm^3 cm^{-1}.

A plot of absorbance vs pH at 431 nm (Fig. 1) clearly showed that $[Co(TAPP)(H_2O)_2]^{5+}$ is diprotic. It is obvious that the two steps are sufficiently separated to evaluate K_{a1} and K_{a2} (see Scheme 1) independently. From the equilibrium constant expression, the mass balance and Beer's law equation (1) could be derived. A_a is the absorbance of the acid form and A_b of the basic form. The absorbance vs pH data were fitted to eq. (1) using a non-linear least-squares program.

$$A = (K_a A_b + A_a[H^+]/K_a + [H^+]) \quad (1)$$

The values pK_{a1} and pK_{a2} were determined, respectively, as 6.48 ± 0.08 and 10.70 ± 0.09 at 25°C and $\mu = 1.00$ mol dm^{-3} ($NaNO_3$).

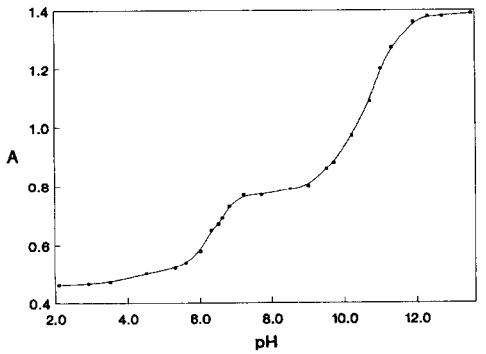

Fig. 1. Change in absorbance as a function of pH at 431 nm.

The values of the stability constants, K_1, for the different incoming ligands at 25°C in 0.1 mol dm^{-3} HNO_3 and $\mu = 1.0$ mol dm^{-3} ($NaNO_3$) were determined spectrophotometrically. The absorbance was measured at different ligand concentrations. From Beer's law, mass balance and the stability constant expression, eq. (2) could be derived:

$$A = (A_r + A_p K_1[L])/(1 + K[L]). \quad (2)$$

A_r is the absorbance of a solution of $[Co(TAPP)(H_2O)_2]^{5+}$, A_p is the absorbance of the product and L is the incoming ligand. The values of K_1 were determined by fitting the absorbance vs [L] data to eq. (2) using a non-linear least-squares program and are listed in Table 1.

The anation reactions between $[Co(TAPP)(H_2O)_2]^{5+}$ and NCS^- and I^- ions were studied at 15, 25 and 35°C in 0.1 mol dm^{-3} HNO_3 and $\mu = 1.0$ mol dm^{-3} ($NaNO_3$). The reaction rates are independent of the $[H^+]$ at $[H^+] > 10^{-3}$ mol dm^{-3}. This clearly indicates that $[Co(TAPP)(H_2O)_2]^{5+}$ is the only reactive species under the experimental conditions. All the kinetic runs were performed under pseudo-first-order conditions, $[L] \gg [Co(TAPP)(H_2O)_2^{5+}]$, where the value of k_{obs} is given by eq. (3), see also Scheme 1:

$$k_{obs} = k_1[L]. \quad (3)$$

Figure 2 is a typical plot of k_{obs} vs [L]. The kinetic results obtained in this way are summarized in Table 1. The activation parameters ($\Delta H^\ddagger$ and $\Delta S^\ddagger$) were calculated by means of a non-linear least-squares fit of the k_1 vs temperature data to the Eyring–Polanyi equation and are also reported in Table 1.

The high-pressure kinetic data for the anation reaction with thiocyanate ions were obtained by means of a thermostatted high-pressure stopped-flow system.[14] The value of $\Delta V^\ddagger$ was calculated from the slope of the linear plot of ln k vs P using eq. (4):

$$\ln k = -\Delta V^\ddagger P/RT. \quad (4)$$

The results are summarized in Tables 1 and 2.

DISCUSSION

The relative high values of pK_{a1} and pK_{a2} {compared with other cobalt(III) complexes like $[Co(en)_2(H_2O)_2]^{3+}$ [15]} indicate that the four nitrogen atoms of TAPP are donating electron density to cobalt(III), since the pK_a values should depend on the electron density on the aqua-oxygen atom and thus also on that on the cobalt ion. The pK_{a1} values

$$[Co(TAPP)(H_2O)_2]^{5+} + L^{n-} \underset{k_{-1}}{\overset{k_1; K_1}{\rightleftharpoons}} [Co(TAPP)(H_2O)L]^{(5-n)+} + H_2O$$

$$K_{a1},\ H^+ \Big\| \Big\downarrow +H^+$$

$$[Co(TAPP)(H_2O)(OH)]^{4+}$$

$$K_{a2},\ -H^+ \Big\| \Big\downarrow +H^+$$

$$[Co(TAPP)(OH)_2]^{3+}$$

Scheme 1. Reaction scheme under the experimental conditions.

of different porphine complexes of cobalt(III) (see Table 3) increase in the order TMPP < TAPP < TPPS < TCPP, which is the expected order since the electron donating ability of the porphines increase in the same order.

The trend in the values of the stability constants (see Table 1; no reaction was observed for Br^- and Cl^- ions as incoming ligands, indicative of very low stability constants for the bromide and chloride complexes) indicates that cobalt(III) behaves as a soft acid. This is also the case for the porphine complexes of rhodium(III) studied so far[5,16] and may be explained in terms of the delocalized electron density in the porphine ligand that is apparently available to the central metal ion. The stability constants for $[Co(TPPS)(H_2O)(NCS)]^{4-}$, 2640 M^{-1} (see ref. 3) and $[Co(TAPP)(H_2O)(NCS)]^{4+}$, 3300 M^{-1} (see Table 1), are about the same, indicating that the overall charge on the complex plays a minor role in determining the stability constants. This may be explained by the fact that the formal charge on the complex is spread over a very large planar surface area, especially since the negatively-charged sulphonato groups (in TPPS) and the positively-charged ammonium groups (in TAPP) are far removed from the positive metal centre. The mode of bonding of the thiocyanate ion is unknown but one would anticipate that the ligand is sulphur bonded because of the apparent softness of cobalt(III).

The reaction of $[Co(TAPP)(H_2O)_2]^{5+}$ with NCS^- and I^- shows no deviation from second-order kinetics up to 0.9 mol dm^{-3} concentration of the incoming ligand. Under our experimental conditions the overall reaction studied can be represented by Scheme 1. The positive values for the entropy of activation is indicative of a dissociative activation. The comparison of the stability and the rate constants also gives an indication of the mode of activation. The stability constants for the NCS^- and I^- complexes differ by a factor of about 35 while the rate constants for these incoming ligands are about the same. This indicates that the rate is not sensitive to the nature of the incoming ligand but sensitive to the nature of the leaving group, which also points to a dissociative activation.

The equilibrium constant, K_1, for the reaction with NCS^- and the $[NCS^-]$ used in the high-pressure study were such that the observed rate constant is given by eq. (3). The pressure dependence of k_1 was therefore calculated from the pressure dependence of k_{obs} at excess NCS^-. The plot of ln k_1 vs pressure was linear and the volume of activation, $\Delta V^{\ddagger}_{expt}$, was calculated from the slope of this line. The large positive value of $\Delta V^{\ddagger}_{expt}$ can also be interpreted as evidence for a dissociative mechanism as

Table 1. Kinetic and equilibrium data for the reaction $[Co(TAPP)(H_2O)_2]^{5+} + L^{n-} \rightleftharpoons [Co(TAPP)(H_2O)(L)]^{(5-n)+} + H_2O$[a]

	NCS^-	I^-
k_1 ($dm^3\ mol^{-1}\ s^{-1}$)	89.0	76.0
K_1 ($dm^3\ mol^{-1}$)	3300	95
$\Delta H^{\ddagger}$ (kJ mol^{-1})	66(1)	63(8)
$\Delta S^{\ddagger}$ (J $mol^{-1}\ K^{-1}$)	14(4)	3(30)
$\Delta V^{\ddagger}$ ($cm^3\ mol^{-1}$)	18.8	—

[a] $[H^+] = 0.1$ mol dm^{-3}, $\mu = 1.0$ mol dm^{-3} ($NaNO_3$). The rate constants are at 25°C.

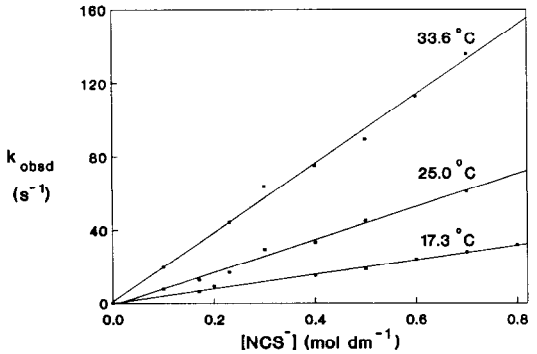

Fig. 2. Plot of k_{obs} vs $[NCS^-]$ at $[H^+] = 0.1$ mol dm^{-3} and $\mu = 1.0$ mol dm^{-3}.

Table 2. k_{obs} as a function of pressure for the anation of [Co(TAPP)$(H_2O)_2]^{5+}$ by NCS^- at 20°C[a]

P (bar)	20	250	500	750	1000
k_1 (dm^{-3} mol s^{-1})	61.2	52.5	42.0	34.5	29.0

[a] $[H^+] = 0.1$ mol dm^{-3} and $[NCS^-] = 0.1$ mol dm^{-3}.

outlined in reactions (5) and (6) :

$$[Co(TAPP)(H_2O)_2]^{5+} \underset{k_{-2}}{\overset{k_2}{\rightleftharpoons}} [Co(TAPP)(H_2O)]^{5+} + H_2O \quad (5)$$

$$[Co(TAPP)(H_2O)]^{5+} + NCS^- \xrightarrow{k_3} [Co(TAPP)(H_2O)(NCS)]^{4+}. \quad (6)$$

For this reaction scheme

$$k_{obs} = \frac{k_2 k_3 [NCS^-]}{k_{-2} + k_3 [NCS^-]}, \quad (7)$$

which can be simplified to

$$k_{obs} = \frac{k_2 k_3}{k_{-2}} [NCS^-], \quad (8)$$

since it was observed that plots of k_{obs} vs $[NCS^-]$ were linear with a zero intercept, indicating that $k_{-2} \gg k_3[NCS^-]$ under our experimental conditions.

From eq. (8) it follows that $\Delta V^{\ddagger}_{expt} = \Delta V^{\ddagger}(k_2) + \Delta V^{\ddagger}(k_3) - \Delta V^{\ddagger}(k_{-2})$. It is expected that both k_3 and k_{-2} would be negative since these steps involve bond formation. It may further be assumed that $|\Delta V^{\ddagger}(k_3)| \geq |\Delta V^{\ddagger}(k_{-2})|$ since the molar volume of NCS^- is larger than that of H_2O. This means that $\Delta V^{\ddagger}(k_2)$ should be at least as large as $\Delta V^{\ddagger}_{expt}$, 18.8 cm^3 mol^{-1}, and clearly points to a dissociative mechanism.

Comparison of the volume of activation for the reaction between $[Co(TPPS)(H_2O)_2]^{3-}$ and NCS^- ($\Delta V^{\ddagger}_{expt} = 15.4$ cm^3 mol^{-1} [10]) and that between $[Co(TMPP)(H_2O)_2]^{5+}$ and thiourea ($\Delta V^{\ddagger}_{expt} = 12.6$ cm^3 mol^{-1} [12]) with the volume of activation for the reaction between $[Co(TAPP)(H_2O)_2]^{5+}$ and NCS^- indicates that the overall charge of the porphine complex, as well as the charge of the incoming ligand, do not play a very significant role in determining the volume of activation.

The order of the rate constants for the reaction of thiocyanate ions with the different porphine complexes (TMPP < TAPP < TPPS < TCPP, see

Table 3. Kinetic and equilibrium parameters for the anation by NCS^- for selected compounds at 25°C and $\mu = 1.0$ mol dm^{-3}

Complex	pK_{a1}	k_1 (M^{-1} s^{-1})	$\Delta V^{\ddagger}$ (cm^3 mol^{-1})	Reference
$[Co(TCPP)(H_2O)_2]^+$	7.40	450	—	2
$[Co(TPPS)(H_2O)_2]^{3-}$	7.02	300	15.5	3, 10
$[Co(TAPP)(H_2O)_2]^{5+}$	6.48	89	18.8	This work
$[Co(TMPP)(H_2O)_2]^{5+}$	5.50	2.0	12.6[a]	12, 17
$[Co(NH_3)_5(H_2O)]^{3+}$	—	1.3×10^{-6}	1.2[b]	9, 18
$[Rh(TPPS)(H_2O)_2]^{3-}$	7.01	2.73×10^{-2}	8.8	5, 10
$[Rh(TAPP)(H_2O)_2]^{5+}$	8.36	2.09×10^{-2}	—	16
$[Rh(NH_3)_5(H_2O)]^{3+}$	—	2.95×10^{-6}[c]	−4.1[b]	19, 20
$[Cr(TPPS)(H_2O)_2]^{3-}$	7.63	4.7×10^{-3}	7.4	6, 10
$[Cr(TAPP)(H_2O)_2]^{5+}$	7.33	4.2×10^{-3}	9.2	21
$[Cr(NH_3)_5(H_2O)]^{3+}$	—	3.0×10^{-5}	−4.9	9

[a] Reaction with thiourea, see ref. 12.

[b] Volume of activation for the water-exchange of the aqua complex, see refs 18 and 20.

[c] Reaction with Cl^- ions, see ref. 19.

Table 3) is the expected trend, since the electron-donating ability of the different porphines increases in the same order. It is, however, noticeable that this effect of the different substituents on the porphine, as well as the amount of labilization (compared with the pentammineaqua complexes), is much less for the rhodium(III) and especially the chromium(III) complexes, see Table 3. The changes in the volumes of activation of the pentammineaqua complexes to that of the porphine complexes point to a change from an Ia to an Id mechanism for the chromium(III) and rhodium(III) complexes and from an Id to a D mechanism for the cobalt(III) complexes, see Table 3. The central metal ion thus seems to control the extent to which the porphine can modify the reactivity as well as the mode of the substitution process.

Finally, the results of this investigation clearly demonstrate how the presence of the porphine ligand promotes a dissociative reaction mode and thus accounts for the large labilizing effect of the porphine ligand. The electron-rich porphine presumably donates electron density to the cobalt(III) ion making it more like a labile cobalt(II) ion and thus also stabilizes the five-coordinated intermediate in a dissociative mechanism.

Acknowledgements—We thank the Foundation of Research Development of the South African C.S.I.R. and the University of the Orange Free State for financial support.

REFERENCES

1. R. F. Pasternack, M. A. Cobb and N. Sutin, *Inorg. Chem.* 1975, **14**, 866.
2. R. F. Pasternack and G. R. Parr, *Inorg. Chem.* 1976, **15**, 3087.
3. K. R. Ashley and S. Au-Young, *Inorg. Chem.* 1976, **15**, 1937.
4. K. R. Ashley and J. G. Leipoldt, *Inorg. Chem.* 1981, **20**, 2326.
5. K. R. Ashley, Shaw-Bey Shyu and J. G. Leipoldt, *Inorg. Chem.* 1980, **19**, 1613.
6. K. R. Ashley, J. G. Leipoldt and V. K. Joshi, *Inorg. Chem.* 1980, **19**, 1608.
7. J. G. Leipoldt, S. S. Basson and D. R. Rabie, *J. Inorg. Nucl. Chem.* 1981, **43**, 3239.
8. J. G. Leipoldt, S. S. Basson, G. J. Lamprecht and D. R. Rabie, *Inorg. Chim. Acta* 1981, **51**, 67.
9. R. van Eldik, D. A. Palmer and H. Kelm, *Inorg. Chem.* 1979, **18**, 1520.
10. J. G. Leipoldt, R. van Eldik and H. Kelm, *Inorg. Chem.* 1983, **22**, 4146.
11. S. Funahashi, M. Inamo, K. Ishihara and M. Tanaka, *Inorg. Chem.* 1982, **21**, 447.
12. G. J. Lamprecht, J. G. Leipoldt and T. W. Swaddle, *Inorg. Chim. Acta* 1987, **129**, 21.
13. M. Krishnamurthy, *Indian J. Chem.* 1977, **15B**, 964.
14. R. van Eldik, D. A. Palmer, R. Schmidt and H. Kelm, *Inorg. Chim. Acta* 1981, **50**, 131.
15. R. G. Pearson, R. E. Meeker and F. Basolo, *J. Am. Chem. Soc.* 1956, **78**, 709.
16. J. G. Leipoldt and H. Meyer, *Polyhedron* 1985, **4**, 1527.
17. K. R. Ashley, M. Berggren and M. Cheng, *J. Am. Chem. Soc.* 1975, **97**, 1422.
18. H. R. Hunt and H. Taube, *J. Am. Chem. Soc.* 1958, **80**, 2642.
19. H. L. Bott, A. J. Poë and K. Shaw, *J. Chem. Soc. A* 1970, 1745.
20. T. W. Swaddle and D. R. Stranks, *J. Am. Chem. Soc.* 1972, **94**, 8357.
21. J. G. Leipoldt and H. Meyer, *Polyhedron* 1987, **6**, 1361.

Polyhedron Vol. 10, No. 12, pp. 1385–1394, 1991
Printed in Great Britain

0277–5387/91 $3.00+.00
© 1991 Pergamon Press plc

NMR, LUMINESCENCE, AND X-RAY CRYSTALLOGRAPHIC STUDIES OF THE INTERACTION OF UNCHARGED N-DONOR LIGANDS WITH EUROPIUM(III) IN THE MACROCYCLIC COMPLEX $[Eu(CH_3COO)_2(C_{22}H_{26}N_6)]Cl\cdot 4(H_2O)$

G. BOMBIERI

Istituto di Chimica Farmaceutica, Università di Milano, Milano, Italy

and

F. BENETOLLO and A. POLO

Istituto di Chimica e Tecnologia dei Radioelementi, Area di Ricerca C.N.R., Corso Stati Uniti 4, Padova, Italy

and

K. K. FONDA and L. M. VALLARINO*

Department of Chemistry, Virginia Commonwealth University, Richmond, VA 23284, U.S.A.

(*Received* 2 *November* 1990; *accepted* 5 *February* 1991)

Abstract—The interaction of uncharged N-donor ligands with the complex $[Eu(CH_3COO)_2L]Cl\cdot 4(H_2O)$, where L is the macrocyclic ligand $C_{22}H_{26}N_6$, was investigated in solution by NMR spectroscopy and luminescence titration. Both experiments indicated little or no interaction of the N-donor ligands with the metal centre of the macrocyclic complex. Attempts to isolate a 1,10-phenanthroline complex of the europium macrocycle produced instead $\{[Eu(CH_3COO)L]_2(\mu\text{-}CO_3)\}(OH)_2\cdot 7H_2O$, which incorporated atmospheric carbon dioxide. The X-ray crystal structure showed a bis-chelating carbonato group linking two europium macrocycles, each of which was folded in a butterfly configuration towards the external bidentate chelating acetates. Ionic hydroxides and clathrated water molecules completed the structure.

The lanthanide(III) complexes of formula $M(CH_3COO)_2LCl\cdot n(H_2O)$,[1] in which L is the macrocyclic ligand $C_{22}H_{26}N_6$ shown in Fig. 1, afford a unique opportunity to investigate the interaction of the metal centre with external ligands due to the kinetic inertness of the metal–macrocycle moiety. These complexes dissolve in water as well as organic solvents, and are inert to metal release even under acidic or basic conditions, and in the presence of competing ligands. The integrity of the ML entity in solution is confirmed, for both diamagnetic and paramagnetic analogues, by ^1H and ^{13}C NMR spectroscopy.[2,3] In contrast, the exocyclic acetate ligands are labile and easily exchanged; in aqueous solution they are partly replaced by water unless an excess of acetate is present.[4] Because the quasi-equatorial macrocyclic ligand remains bound to the

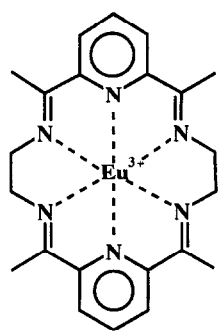

Fig. 1. Schematic formula of the $[Eu(C_{22}H_{26}N_6)]^{3+}$ macrocyclic moiety.

* Author to whom correspondence should be addressed.

metal in solution, the number and geometry of external ligands which may interact with the metal centre are limited. Thus, investigations in solution are greatly simplified by the small number of species which may be present.

The solution behaviour of these complexes is consistent with the solid state structure established for the neodymium,[2] europium,[2] and gadolinium[5] analogues by X-ray crystallography. In these species the metal centre is linked to the six N-donor atoms in a quasi-planar arrangement, while the organic portion of the molecule adopts a folded "butterfly" configuration that minimizes strain. The two bidentate acetates occupy staggered positions on opposite sides of the macrocycle, and an ionic chloride balances the residual charge of the complex.

In the present work, the interaction of the $[M(CH_3COO)_2L]Cl{\cdot}n(H_2O)$ complexes with uncharged nitrogen-donor ligands has been investigated using europium(III) as the metal centre. Europium was chosen because it lends itself to two sensitive and complementary investigative techniques. First, europium(III) retains appreciable Lewis-acidic character in many of its complexes, and can interact with substrates bearing Lewis-basic functionalities to cause paramagnetic shifts and possible broadening of the substrate resonances; certain europium(III) complexes are widely employed as NMR shift reagents.[6] Thus, NMR experiments may serve to determine how the presence of the paramagnetic {EuL} moiety alters the spectral properties of an external ligand. Second, europium(III) exhibits a narrow-band luminescence which arises from electronic transitions within the 4*f* manifold and may be sensitized by the addition of appropriate ligands.[7] Thus, luminescence titration studies can probe the effects of an external ligand on the luminescent behaviour of the europium macrocycle centre. We report here the results of this dual investigation for a series of neutral N-donor ligands including primary amines, as well as monodentate and bidentate chelating heterocycles.

EXPERIMENTAL

Materials and procedures

The complex $[Eu(CH_3COO)_2L]Cl{\cdot}4(H_2O)$ was prepared as previously described.[1] Ligands (1-aminobutane, 2-aminobutane, 2-amino-2-methylbutane, ethylenediamine, aniline, pyridine, 1,10-phenanthroline and 2,2′-bipyridyl) were commercially available and were purified as appropriate before use. Absorption spectra (UV–vis) were obtained with a Beckmann Acta MVIII spectrophotometer. Luminescence measurements were carried out with an SLM-Model 8000 spectrofluorometer. Proton NMR spectra were recorded on a GE QE-300 spectrometer and referenced to TMS.

NMR experiments

Methanol-d_4 (Aldrich) and deuterochloroform (Aldrich) were employed as solvents. In all experiments the ^1H NMR spectrum of a 3.0×10^{-2} M solution of the N-donor ligand was obtained first. An equivalent molar amount of the crystalline europium macrocyclic complex was then added to the NMR tube and the spectrum of the resulting solution was recorded.

Luminescence titrations

All experiments were carried out according to the following general procedure. A set of four solutions was prepared, containing the same concentration (2.0×10^{-4} M) of the $[Eu(CH_3COO)_2L]Cl{\cdot}4(H_2O)$ complex but increasing concentrations of the N-donor ligand (europium–ligand mole ratios = 1 : 1, 1 : 2, 1 : 3 and 1 : 4). Emission and excitation spectra were recorded under identical conditions for each set of solutions and the relative intensities of the $^5D_0 \rightarrow {}^7F_2$ Eu^{III} emission at *ca* 614 nm were compared with the emission of an equimolar solution of the europium complex alone. No appreciable change in either the excitation or emission spectrum was observed for any of the ligands, with the exception of 2,2′-bipyridyl which gave a modest luminescence enhancement for 1 : 1 to 1 : 1.5 mole ratios.

Attempted isolation of solid adducts

Concentration of the stoichiometric 1 : 1 mixtures from NMR experiments, or dilution of the same with diethyl ether, consistently failed to produce any solid (EuL)-(N-donor) adduct. Similarly, no adducts were obtained from bulk solutions (in chloroform or methanol) containing an excess of the N-donor ligands. In each case, only the original complex and the "free" N-donor ligand were recovered. Attempts using a europium–1,10-phenanthroline mole ratio of 1 : 10 in methanol gave, by slow evaporation of the solution in air, minute yields of a yellow crystalline compound of formula $\{[Eu(CH_3COO)L]_2(\mu\text{-}CO_3)\}(OH)_2{\cdot}7H_2O$.

X-ray measurements and structure determination

A transparent pale yellow prismatic single crystal of $\{[Eu(CH_3COO)L]_2(\mu\text{-}CO_3)\}(OH)_2{\cdot}7H_2O$, measuring $0.1 \times 0.22 \times 0.16$ mm, was centred on a four-

circle Philips PW 1100 diffractometer with graphite-monochromated Mo-K_α radiation. The intensity data were corrected for Lorenz-polarization effects and for absorption, following the method of North *et al.*[8] The structure was solved using Patterson and Fourier techniques and refined with full-matrix least squares. Non-hydrogen atoms were allowed to vibrate anisotropically. Carbon-linked hydrogen atoms were introduced at calculated positions and allowed to ride on associated carbon atoms during the least squares refinement ($d_{C-H}=0.98$ Å and $U=0.08$ Å^2). The H atoms of the water molecules, which were disordered among two or three positions, were not introduced. The final difference Fourier map showed a few residuals of the order of 0.6 e/Å^3, close to the water positions and assigned to the disordered hydrogens; two major residuals of about 1 e/Å^3 were present near each europium(III) position. The programs used were SHELX 76[9] for structure solution and refinement, ORTEP[10] and PLUTO[11] for drawings, and PARST[12] for geometrical calculations. Atomic scattering factors were taken from ref. 13.

Crystal data are reported in Table 1, bond lengths and angles in Table 2, and torsion angles in Table 3. Supplementary material (tables of atomic coordinates, atomic vibrations, and calculated structure amplitudes) has been deposited at the Cambridge Data Centre.

RESULTS AND DISCUSSION

Solution studies

The results of the NMR experiments are summarized in Tables 4 and 5. The N-donor ligands investigated in methanol included primary aliphatic and aromatic amines (1-aminobutane, 2-aminobutane, 2-amino-2-methylbutane, ethylenediamine and aniline), as well as nitrogen-containing heteroaromatics (pyridine, 1,10-phenanthroline and 2,2′-bipyridyl). In each case the chemical shifts of the macrocycle protons were sufficiently removed from those of the added ligands so that the two sets of resonances did not interfere. In methanol, a comparison between the spectra of the N-donor ligands alone and the spectra of solutions containing the metal-macrocycle and the

Table 1. Crystal data for $\{[Eu(CH_3COO)L]_2(\mu\text{-}CO_3)\}(OH)_2 \cdot 7H_2O$

Formula	$Eu_2C_{49}H_{74}N_{12}O_{16}$
Molecular weight	1391.11
Crystal system	Orthorhombic
a(Å)	24.929(3)
b(Å)	12.912(2)
c(Å)	19.205(3)
V(Å^3)	6181.77
Space group	*Pccn*
D_c(g cm^{-3})	1.49
Z	4
F(000)	2824
Radiation	Mo-K_α
μ(cm^{-1})	19.52
Reflections measured	6038
Scan method	$\theta/2\theta$
Scan speed (° min^{-1})	1.8
Scan width (°)	1.20
Background counts (s)	20
$2\theta_{max}$ (°)	50
σ limit $[I>n\sigma(I)]$	3
Unique observed data with $[I>3\sigma(I)]$	5451
Number of parameters	348
Weighting scheme w	$[\sigma^2(F_o)+0.003343(F_o)^2]^{-1}$
$R=\Sigma[\|F_o\|-\|F_c\|]/\Sigma\|F_o\|$	0.054
$R_w=[\Sigma w(\|F_o\|-\|F_c\|)^2/\Sigma w\|F_o\|^2]^{1/2}$	0.061
Max Δ/σ on	0.023
Goodness of fit	1.229
Standard reflections	502 504

Table 2. Bond lengths (Å) and angles (°) for $\{[Eu(CH_3COO)L]_2(\mu\text{-}CO_3)\}(OH)_2 \cdot 7H_2O$ with ESDs in parentheses

(a) Europium environment

Eu—O(1)	2.52(1)	Eu—O(2)	2.55(1)
Eu—O(3)	2.493(1)	Eu—O(4)	2.394(8)
Eu—N(1)	2.64(1)	Eu—N(2)	2.56(1)
Eu—N(3)	2.65(1)	Eu—N(4)	2.63(1)
Eu—N(5)	2.56(1)	Eu—N(6)	2.66(1)
O(1)—Eu—O(2)	50.4(3)	O(3)—Eu—O(4)	54.3(3)
N(1)—Eu—N(2)	60.4(4)	N(1)—Eu—N(6)	59.9(4)
N(2)—Eu—N(3)	64.6(4)	N(3)—Eu—N(4)	60.1(3)
N(4)—Eu—N(5)	60.7(4)	N(5)—Eu—N(6)	63.2(4)
O(1)—C(30)	1.25(2)	O(2)—C(30)	1.24(2)
C(30)—C(31)	1.51(2)		
O(3)—C(40)	1.34(2)	O(4)—C(40)	1.27(1)

(b) Ligands

Eu—N(1)—C(1)	122(1)	C(10)—C(12)—C(13)	123(1)
Eu—N(1)—C(5)	119.0(9)	C(13)—C(12)—N(4)	120(1)
N(1)—C(1)—C(2)	122(1)	C(12)—C(13)—C(14)	118(1)
C(2)—C(1)—C(21)	120(1)	C(13)—C(14)—C(15)	122(1)
C(1)—C(2)—C(3)	118(1)	C(14)—C(15)—C(16)	117(1)
C(2)—C(3)—C(4)	118(2)	C(15)—C(16)—C(17)	123(1)
C(3)—C(4)—C(5)	121(1)	C(15)—C(16)—N(4)	124(1)
N(1)—C(5)—C(4)	121(1)	Eu—N(4)—C(12)	120(1)
C(4)—C(5)—C(6)	121(1)	Eu—N(4)—C(16)	121.0(8)
C(5)—C(6)—C(7)	118(1)	C(16)—C(17)—C(18)	116(1)
C(7)—C(6)—N(2)	129(1)	C(18)—C(17)—N(5)	125(1)
Eu—N(2)—C(6)	127(1)	Eu—N(5)—C(17)	123(1)
Eu—N(2)—C(8)	112.7(9)	Eu—N(5)—C(19)	112.7(8)
Eu—N(3)—C(9)	116.0(9)	Eu—N(6)—C(20)	116.7(9)
Eu—N(3)—C(10)	123(1)	Eu—N(6)—C(21)	123(1)
N(3)—C(10)—C(11)	126(1)	N(6)—C(21)—C(22)	125(1)
C(11)—C(10)—C(12)	118(1)	C(1)—C(21)—C(22)	121(1)
N—C(py)	1.34(2)	C—C(aliphatic)	1.50(3)
C—C(py)	1.39(3)		
Eu—N(py)—C	121(1)	Eu—N(aliphatic)—C	119(1)
O(1)—C(30)—O(2)	120(1)	O(1)—C(30)—C(31)	119(1)
O(3)—C(40)—O(4)	117.0(8)	O(2)—C(30)—C(31)	122(1)

ligand in 1 : 1 mole ratio indicated only minimal metal–ligand association. No significant shift was observed for the resonances of any of the N-donors, even though the ability of $[Eu(CH_3COO)_2L]Cl \cdot 4(H_2O)$ to shift ligand resonances has been demonstrated for a series of carboxylate ligands.[14] The heteroaromatic ligands, which are known to form complexes with "free" europium(III), were also investigated in $CDCl_3$ to minimize solvent competition. Even in this non-coordinating solvent, no significant shifts in the proton NMR spectra were observed. It is reasonable to conclude that the association of the acetate groups with the metal must persist in solution, prohibiting significant interaction of the N-donor ligand with the metal centre.

These conclusions are in full agreement with the results of the luminescence titration experiments. Minimal or no change in the intensity of the typical europium(III) emissions was observed upon addition of the N-donor ligands to the $[Eu(CH_3COO)_2L]Cl \cdot 4(H_2O)$ complex, even with 1,10-phenanthroline or 2,2′-bipyridyl, which are known to form highly luminescent complexes with the "free" europium(III) ion.[15,16] Still more significantly, there was no appreciable shift in the excitation spectrum,

Table 3. Macrocycle torsion angles (°) for $\{[Eu(CH_3COO)L]_2(\mu\text{-}CO_3)\}(OH)_2 \cdot 7H_2O$

Atoms	Distances 2–3 (Å)	Angles 1–2–3 (°)	Torsion angles 1–2–3–4 (°)
C(1)—N(1)—C(5)—C(6)	1.30(2)	119(1)	175(1)
N(1)—C(5)—C(6)—N(2)	1.52(2)	118(1)	−5(2)
C(5)—C(6)—N(2)—C(8)	1.23(2)	114(1)	179(1)
C(6)—N(2)—C(8)—C(9)	1.46(2)	118(1)	−107(2)
N(2)—C(8)—C(9)—N(3)	1.49(3)	109(1)	−56(1)
C(8)—C(9)—N(3)—C(10)	1.48(2)	109(1)	−169(1)
C(9)—N(3)—C(10)—C(12)	1.26(2)	118(1)	177(1)
N(3)—C(10)—C(12)—N(4)	1.46(2)	116(1)	12(2)
C(10)—C(12)—N(4)—C(16)	1.36(2)	117(1)	−178(1)
C(12)—N(4)—C(16)—C(17)	1.36(2)	119(1)	−176(1)
N(4)—C(16)—C(17)—N(5)	1.46(2)	113(1)	−10(2)
C(16)—C(17)—N(5)—C(19)	1.27(2)	119(1)	−179(1)
C(17)—N(5)—C(19)—C(20)	1.48(2)	122(1)	−99(2)
N(5)—C(19)—C(20)—N(6)	1.46(2)	108(1)	−58(1)
C(19)—C(20)—N(6)—C(21)	1.50(2)	107(1)	−163(1)
C(20)—N(6)—C(21)—C(1)	1.28(2)	119(1)	175(1)
N(6)—C(21)—C(1)—N(1)	1.50(2)	115(1)	−9(2)
C(21)—C(1)—N(1)—C(5)	1.32(2)	118(1)	177(1)

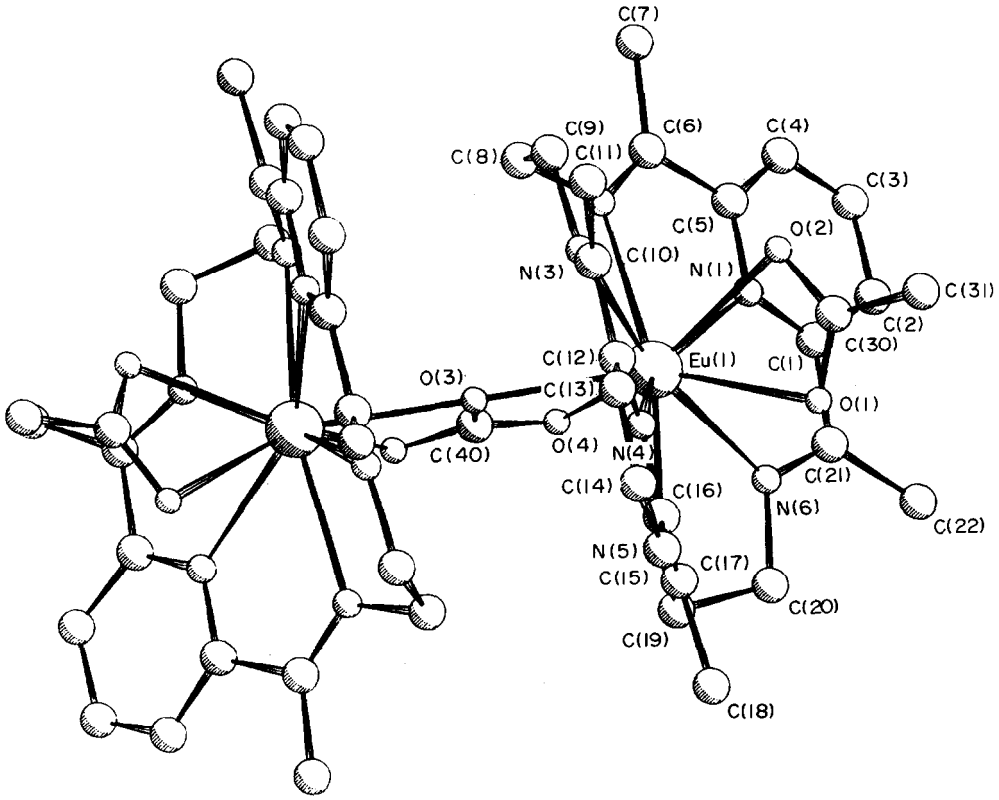

Fig. 2. Structure of the dimeric complex cation $\{[Eu(CH_3COO)L]_2(\mu\text{-}CO_3)\}^{2+}$ (PLUTO view).

Table 4. Proton NMR data for amine substrates with $[Eu(CH_3COO)_2(C_{22}H_{26}N_6)]Cl{\cdot}4(H_2O)$[a]

Substrate	Position	Chemical shift			
		0.03 M Substrate	Substrate–Europium, 3 : 1	Substrate–Europium, 2 : 1	Substrate–Europium, 1 : 1
1-Aminobutane	1	2.62 t (J=7.1 Hz)	2.63 t (J=7.1 Hz)	2.63 t (J=6.9 Hz)	2.64 t (J=7.1 Hz)
	2	1.45 m	1.45 m	1.46 m	1.46 m
	3	1.35 m	1.35 m	1.35 m	1.35 m
	4	0.93 t (J=7.2 Hz)	0.93 t (J=7.2 Hz)	0.93 t (J=7.1 Hz)	0.93 t (J=7.1 Hz)
2-Aminobutane	1	1.05 d (J=6.3 Hz)	1.05 dd (J=6.2, 1.3 Hz)	1.07 d (J=6.6 Hz)	1.07 d (J=6.3 Hz)
	2	2.75 m	2.76 m	2.77 m	2.78 m
	3	1.38 m	1.38 m	1.39 m	1.39 m
	4	0.91 t (J=7.4 Hz)	0.91 td (J=7.5, 1.2 Hz)	0.92 t (J=7.5 Hz)	0.92 t (J=7.5 Hz)
2-Amino-2-methylbutane	1	1.10 s	1.10 s	1.11 s	1.11 s
	3	1.45 q (J=7.5 Hz)	1.44 q (J=7.5 Hz)	1.46 q (J=7.5 Hz)	1.46 q (J=7.6 Hz)
	4	0.91 t (J=7.5 Hz)	0.91 t (J=7.5 Hz)	0.91 t (J=7.5 Hz)	0.91 t (J=7.6 Hz)
Ethylenediamine		2.67 s	2.67 s	2.67 s	2.68 s
Aniline	2	6.71 m	6.69 m	6.69 m	6.69 m
	3	7.07 m	7.06 m	7.06 m	7.06 m
	4	6.67 m	6.65 m	6.65 m	6.65 m

[a] In CD_3OD; chemical shifts in ppm vs TMS. Amino protons unobservable due to deuterium exchange. All integrations as expected.

Table 5. Proton NMR data for nitrogen heteroaromatics with $[Eu(CH_3COO)_2[C_{22}H_{26}N_6)]Cl{\cdot}4(H_2O)$[a]

Substrate–Solvent	Position	Chemical shift			
		0.03 M Substrate	Substrate–Europium 3 : 1	Substrate–Europium 2 : 1	Substrate–Europium 1 : 1
Pyridine–CD_3OD	2	8.53 dd (J=5.9, 1.7 Hz)	8.53 m	8.53 m	8.52 m
	3	7.44 m	7.43 m	7.43 m	7.43 m
	4	7.85 tt (J=7.7, 1.7 Hz)	7.85 tt (J=7.8, 1.7 Hz)	7.85 t (J=7.7 Hz)	7.85 tt (J=7.7, 1.5 Hz)
Pyridine–$CDCl_3$[b]	2	8.63 d (J=5.1 Hz)	8.62 dd (J=5.6, 1.8 Hz)	8.62 dd (J=4.2, 2.1 Hz)	8.62 dd (J=4.2, 1.8 Hz)
	3	7.33 m	7.29 m	7.30 m	7.30 m
	4	7.73 tt (J=7.7, 1.7 Hz)	7.69 tt (J=7.7, 1.8 Hz)	7.69 tt (J=7.7, 1.8 Hz)	7.69 tt (J=7.7, 1.7 Hz)
2,2′-Bipyridyl–CD_3OD	2	8.66 d (J=5.1 Hz)	8.65 d (J=4.5 Hz)	8.65 d (J=4.8 Hz)	8.65 d (J=4.8 Hz)
	3	7.45 ddd (J=7.2, 4.8, 0.9 Hz)	7.44 ddd (J=7.5, 5.1, 0.9 Hz)	7.44 ddd (J=7.2, 4.8, 0.9 Hz)	7.44 m
	4	7.95 td (J=7.7, 1.7 Hz)	7.94 td (J=7.8, 1.7 Hz)	7.94 td (J=7.8, 1.5 Hz)	7.95 td (J=7.8, 1.4 Hz)
	5	8.30 d (J=8.1 Hz)	8.29 d (J=7.8 Hz)	8.29 d (J=7.8 Hz)	8.29 d (J=8.1 Hz)
2,2′-Bipyridyl–$CDCl_3$	2	8.69 dm (J=4.8 Hz)	8.69 d (J=4.5 Hz)	8.69 d (J=4.2 Hz)	8.69 dm (J=4.8 Hz)
	3	7.32 ddd (J=7.5, 4.8, 1.2 Hz)	7.31 dd (J=6.6, 4.8 Hz)	7.32 ddd (J=7.5, 4.8, 0.6 Hz)	7.31 ddd (J=7.5, 4.8, 0.9 Hz)
	4	7.83 td (J=7.8, 1.8 Hz)	7.83 td (J=7.8, 1.5 Hz)	7.82 td (J=7.8, 1.8 Hz)	7.82 td (J=7.8, 1.8 Hz)
	5	8.40 d (J=7.8 Hz)	8.40 d (J=8.1 Hz)	8.40 d (J=8.1 Hz)	8.40 d (J=8.1 Hz)
1,10-Phenanthroline–CD_3OD	2	9.08 dd (J=4.2, 1.5 Hz)	9.06 d (J=4.5 Hz)	9.07 dd (J=4.2, 1.2 Hz)	9.08 br s
	3	7.76 dd (J=8.1, 4.5 Hz)	7.74 dd (J=8.1, 4.5 Hz)	7.74 dd (J=8.1, 4.2 Hz)	7.75 m
	4	8.45 dd (J=8.1, 1.5 Hz)	8.42 dd (J=8.1, 1.5 Hz)	8.43 dd (J=8.1, 1.7 Hz)	8.44 d (J=7.8 Hz)
	5	7.94 s	7.90 s	7.91 s	7.93 s
1,10-Phenanthroline–$CDCl_3$	2	9.20 dd (J=4.2, 1.8 Hz)	9.19 br s	9.19 br s	9.20 dd (J=4.2, 1.2 Hz)
	3	7.65 dd (J=8.0, 4.4 Hz)	7.64 br s	7.65 br m	7.65 dd (J=8.1, 4.5 Hz)
	4	8.26 dd (J=8.1, 1.8 Hz)	8.26 br s	8.27 d (J=7.5 Hz)	8.28 dd (J=8.0, 1.4 Hz)
	5	7.81 s	7.80 br s	7.81 s	7.82 s

[a] Chemical shifts in ppm vs TMS. All integrations as expected.
[b] 0.015 M.

indicating that whatever luminescence was observed arose from the original complex and did not involve energy transfer from the N-donor ligand to the europium(III) centre.

Efforts to isolate solid (EuL)-(N-donor) adducts consistently failed. In one set of experiments with a europium–1,10-phenanthroline ratio of 1 : 10, a novel yellow crystalline complex was obtained as a result of the absorption of atmospheric carbon dioxide by the strongly basic solution. The structure of this unusual complex is described in the following section.

Crystal structure of the carbonato-bridged complex, $\{[Eu(CH_3COO)L]_2(\mu\text{-}CO_3)\}(OH)_2 \cdot 7H_2O$

The compound is ionic, with dimeric complex cations (Fig. 2) consisting of two EuL moieties linked through a bridging as well as chelating carbonate. The two moieties are related by a crystallographic two-fold axis passing through the carbon atom [C(40)] and one of the oxygen atoms [O(3)] of the carbonato bridge. Each europium ion is further linked to a bidentate chelating acetate on the external side of the {Eu—CO_3—Eu} core. Thus the coordination sphere of each europium includes the six nitrogen atoms of the macrocycle in the equatorial plane and two pairs of oxygen atoms, one from the acetate and one from the carbonate, on opposite sides of the macrocycle. An ORTEP view of the asymmetric half-dimer is shown in Fig. 3. Two ionic hydroxides balance the residual charges of the complex cations; clathrated water molecules (seven per dimeric unit) complete the structure. The unit cell is illustrated in Fig. 4.

The two macrocycle moieties of the dimer are folded toward the external acetates and have the "butterfly" configuration found in other lanthanide complexes of this ligand. Each macrocycle consists of two quasi-planar sections containing the pyridine rings and hinged at the —CH_2CH_2— side chains, with an angle of 131.8(2)°. This value is very close to that found in the monomeric $[Eu(CH_3COO)_2L]^+$ moiety of the diacetate chloride complex [132.37(6)°].[2] The torsion angles at the —CH_2CH_2— side chains, −56(1)° [N(2)—C(8)—C(9)—N(3)] and −58(1)° [N(5)—C(19)—C(20)—N(6)], are also nearly identical with the corresponding angles of the diacetate chloride, −55.8(5)° and −58.0(5)°. A ring puckering analysis[17] of the six N-donor atoms showed a minor deviation from planarity, in a twisted boat conformation with puckering constants $Q = 1.00(1)$, $\Theta = 88.3(7)°$, and $\Phi = -138.7(6)°$.

The two acetate ligands of the dimeric complex are staggered with respect to the bridging carbonate and are oriented along the fold line of the respective macrocycle. However, the plane of each acetate is

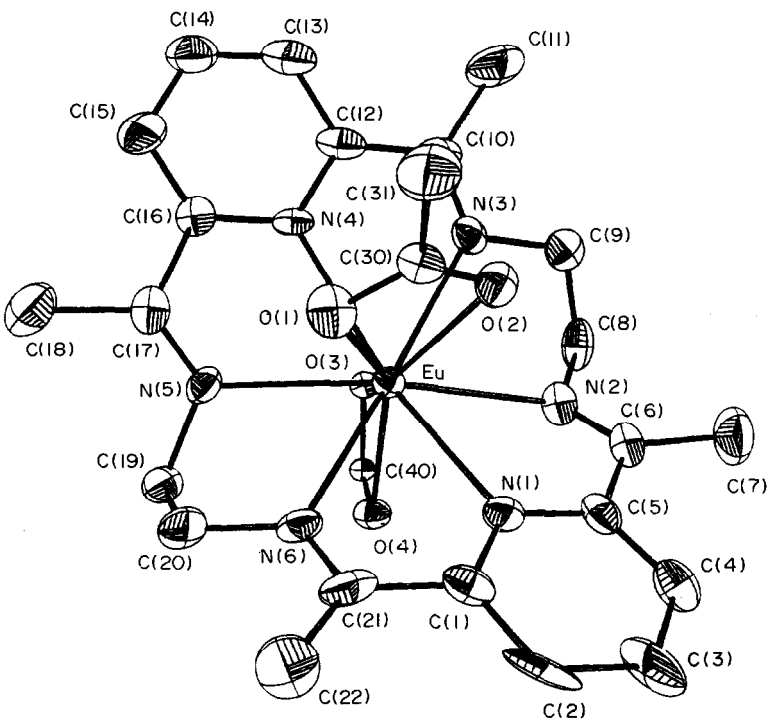

Fig. 3. ORTEP view of the asymmetric half-dimer.

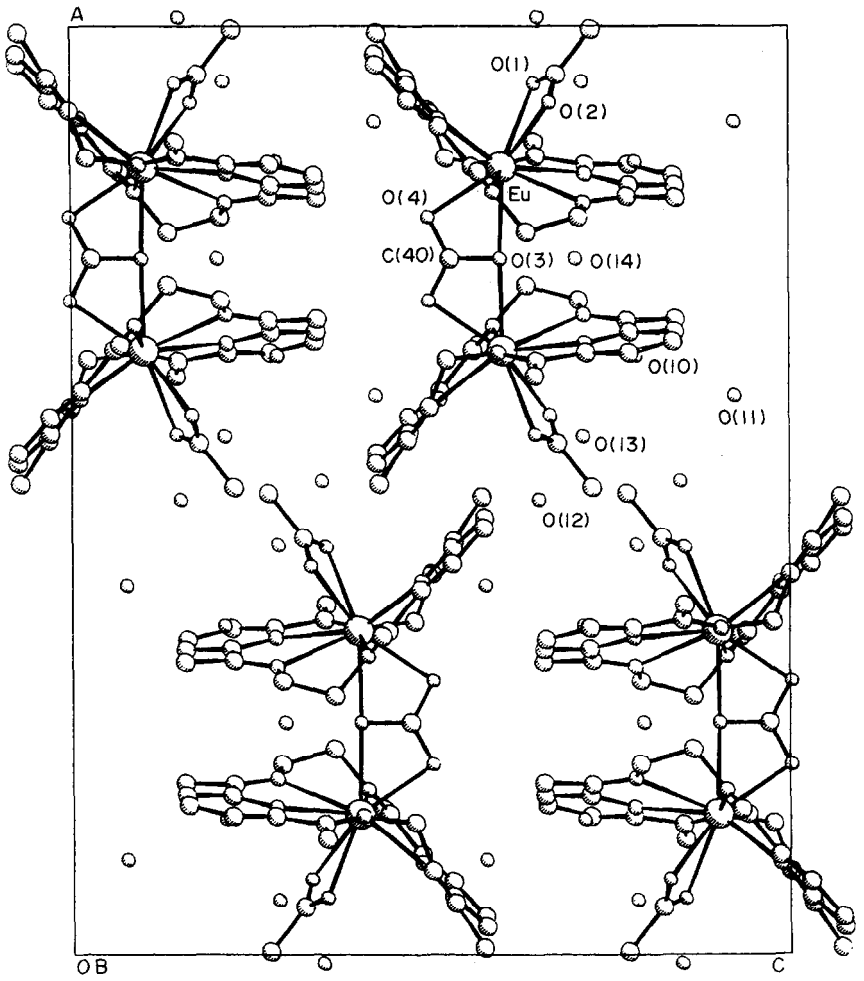

Fig. 4. Unit cell of $\{[Eu(CH_3COO)L]_2(\mu\text{-}CO_3)\}(OH)_2 \cdot 7H_2O$ (PLUTO view down the *b*-axis).

tilted relative to the plane bisecting the macrocycle at the fold. The angle formed by the acetate with the C(9)... N(4)... C(19) section of the macrocycle is 127.0(4)°, whereas the angle formed with the C(8)... N(1)... C(20) section is 78.8(4)°. A similar asymmetry was observed for the acetate ligand on the concave side of the $[Eu(CH_3COO)_2L]^+$ species; the corresponding angles were 102.6(2)° and 55.1(2)°. The dimeric complex Eu—O(acetate) distances are, on average, appreciably longer than the Eu—O(carbonate) distances [2.53(1) versus 2.444(1) Å], and are also somewhat longer than the average Eu—O(acetate) distances [average value 2.48(1) Å] of the $[Eu(CH_3COO)_2L]^+$ complex.[2] This difference between two europium complexes having the same coordination number and containing the same macrocyclic ligand shows that substitution of an acetate by a bridging carbonate influences, either sterically or electronically, the strength of the bonding between the metal and the acetate on the opposite side of the macrocycle. The effect is limited to the anionic axial ligands, since the Eu—N distances are extremely similar in the two complexes.

The features of the bridging carbonate group, although not completely novel, are unusual and deserve comment. A bridging carbonate most commonly exhibits bidentate chelation to one metal centre and monodentate coordination to the other, through the third oxygen atom. In the dimeric complex discussed here the bridging CO_3^{2-} ion acts instead as a chelating ligand to both europium ions and is symmetrically positioned between the two halves of the dimer due to the presence of the crystallographic two-fold axis. Within each half-dimer the Eu—O and C—O distances are rather asymmetric. The Eu—O(3) distance, 2.493(1) Å, is significantly longer than the Eu—O(4) distance, 2.394(8) Å, whereas the C(40)—O(3) distance, 1.34(2) Å, is correspondingly shorter than the C(40)—O(4) distance, 1.27(1) Å. This relationship contrasts with that existing in the carbonato-bridged copper(II) complex $[(CuL)_2(\mu\text{-}CO_3)](ClO_4)_2$

(L = 2,4,4,9-tetramethyl-1,5,9-triazacyclododec-1-ene),[18] in which the shorter C—O distances are those corresponding to the shorter Cu—O distances. Both the europium and the copper dimers, however, show the same decrease of the O—C—O angle from the trigonal planar 120° to 117° upon formation of the strained four-atom chelate ring. The C—O distances in the europium complex indicate that the C=O double bond on the side of the shorter Eu—O bond is stabilized. A similar situation was reported for the asymmetric bridging carbonate in the $Rh_2H_2(O_2CO)(PhC{\equiv}CPh)[P(i\text{-}Pr)_3]_2$ dimer,[19] where electronic factors related to the π-bonding ligands may play an important role in determining the C—O bond lengths.

As illustrated in Fig. 4, the unit cell of $\{[Eu(CH_3COO)L]_2(\mu\text{-}CO_3)\}(OH)_2\cdot 7H_2O$ contains a total of nine non-coordinated oxygen atoms per dimeric complex unit. Two of these oxygen atoms must belong to OH^- ions, as required for ionic charge balance; the others belong to clathrated water molecules. Of the nine oxygen atoms, eight form symmetry-related pairs and one, O(14), occupies a unique position in the plane bisecting the complex perpendicular to the Eu—Eu axis. The H-atoms are disordered; thus their positions cannot be defined unambiguously and it becomes difficult to differentiate between the OH^- ions and the water molecules. A possible distinguishing feature is the presence of six pairs of short contact distances [O(14)...O(10) 3.08(2), O(10)...O(11) 2.92(2), O(10)...O(13) 3.12(2) Å, and the symmetry-related pairs] that most likely arise from hydrogen bonding among the water molecules. The two oxygen atoms [O(12) and its symmetry counterpart], which are not involved in hydrogen bonding, may then be assigned to the OH^- ions.

CONCLUSIONS

It is evident from the results of the NMR and luminescence experiments, and also from the unsuccessful attempts to isolate solid adducts, that uncharged N-donor ligands have no tendency to coordinate to the $[Eu(CH_3COO)_2L]^+$ entity, regardless of their type or denticity. This behaviour contrasts with that of the anionic NCS^- ligand, which replaces the acetates readily to yield a molecular complex of the formula $[Eu(NCS)_3L]$, in which the central europium is bound only to nine nitrogen donor atoms.[20] It may be concluded that the lack of interaction between $[Eu(CH_3COO)_2L]^+$ and uncharged N-donor species results from the inability of the latter to replace the negatively charged acetates, rather than from any intrinsic preference of the europium(III) for O-donor ligands.

Acknowledgements—This work has been supported in part by Coulter Electronics, Hialeah, Florida, by a Virginia Commonwealth University Grant-in-Aid, and by NATO Bilateral Project No. 184–185.

REFERENCES

1. G. Bombieri, F. Benetollo, A. Polo, L. De Cola, D. L. Smailes and L. M. Vallarino, *Inorg. Chem.* 1986, **25**, 1127.
2. F. Benetollo, A. Polo, G. Bombieri, K. K. Fonda and L. M. Vallarino, *Polyhedron* 1990, **9**, 1411.
3. K. K. Fonda and L. M. Vallarino, *Abstr. INOR* 311. 41st Southeast Regional Meeting of the American Chemical Society, Winston-Salem, NC (1989).
4. N. Sabbatini, L. De Cola, L. M. Vallarino and G. Blasse, *J. Phys. Chem.* 1987, **18**, 4681.
5. P. H. Smith, J. R. Brainard, D. E. Morris, G. D. Jarvinen and R. R. Ryan, *J. Am. Chem. Soc.* 1989, **111**, 7437.
6. T. J. Wenzel, *NMR Shift Reagents*. CRC Press, Boca Raton, Florida, (1987).
7. G. A. Crosby, *Molec. Cryst.* 1966, **1**, 37.
8. A. C. T. North, D. C. Philips and F. S. Mathews, *Acta Cryst., Sect. A* 1968, **24**, 351.
9. G. M. Sheldrick, *SHELX*-76. University of Cambridge, Cambridge (1976).
10. C. K. Johnson, *ORTEP II*. Oak Ridge National Laboratory Report ORNL-5138, Oak Ridge, Tennessee (1976).
11. W. D. S. Motherwell and W. Cleeg, *PLUTO*. University of Cambridge, Cambridge (1978).
12. M. Nardelli, *Comput. Chem.* 1983, **22**, 95.
13. *International Tables for X-Ray Crystallography*, Vol. 4. Kynoch Press, Birmingham (1974).
14. G. Bombieri, F. Benetollo, L. De Cola, K. K. Fonda, A. Polo and L. M. Vallarino, *Abstr. INOR* 458. 200th National Meeting of the American Chemical Society, Washington, DC (1990).
15. W. H. Watson, R. J. Williams and N. R. Stemple, *J. Inorg. Nucl. Chem.* 1972, **34**, 501.
16. L. I. Konanenko, S. V. Bel'tyukova, S. B. Meshkova, V. N. Drobyazko and N. S. Polvektov, *Dopov. Akad. Nauk. Ukr. RSR Ser. B* 1975, **9**, 816; *Chem. Abstr.* 1975, **84**, 10577s.
17. D. Cremer and J. A. Pople, *J. Am. Chem. Soc.* 1975, **97**, 1354.
18. A. R. Davis and F. W. B. Einstein, *Inorg. Chem.* 1980, **19**, 1203.
19. T. Yoshida, W. J. Youngs, T. Sakaeda, T. Ueda, S. Otsuka and J. A. Ibers, *J. Am. Chem. Soc.* 1983, **105**, 6273.
20. G. Bombieri, F. Benetollo, A. Polo, L. De Cola, W. T. Hawkins and L. M. Vallarino, *Polyhedron* 1989, **8**, 2157.

Polyhedron Vol. 10, No. 12, pp. 1395–1400, 1991
Printed in Great Britain

0277–5387/91 $3.00+.00
Pergamon Press plc

THE PREPARATION AND STRUCTURAL CHARACTERIZATION OF A DOUBLE-HELICAL BINUCLEAR DICOBALT(II) COMPLEX OF 2,2′:6′,2″:6″,2‴:6‴,2⁗-QUINQUEPYRIDINE; THE X-RAY CRYSTAL STRUCTURE OF ACETATO(*O,O′*)BIS (2,2′:6′,2″:6″,2‴:6‴,2⁗-QUINQUEPYRIDINE)DICOBALT(II) HEXAFLUOROPHOSPHATE TRIS-ACETONITRILE SOLVATE

EDWIN C. CONSTABLE,* SUSAN M. ELDER, PAUL R. RAITHBY and MICHAEL D. WARD†

University Chemical Laboratory, Lensfield Road, Cambridge CB2 1EW, U.K.

(*Received* 13 *November* 1990 ; *accepted* 5 *February* 1991)

Abstract—The reaction of cobalt(II) acetate with 2,2′:6′,2″:6″,2‴:6‴,2⁗-quinquepyridine (**L**) in acetonitrile results in the spontaneous assembly of a binuclear double helical complex. The electrochemical behaviour of this compound is complex. The driving force for the assembly of the complex is probably associated with the close stacking contacts between approximately co-planar pyridine rings; there are no direct metal–metal interactions.

Although the coordination chemistry of 2,2′-bipyridine[1,2] and 2,2′:6′,2″-terpyridine[3] has been intensively investigated over the past century, the interactions of the higher oligopyridines with metals has only recently attracted any interest.[3] We have been particularly interested in the coordination behaviour of 2,2′:6′,2″:6″,2‴:6‴,2⁗-quinquepyridine[4–11] (qpy) and 2,2′:6′,2″:6″,2‴:6‴,2⁗:6⁗,2⁗′-sexipyridine,[12,13] which we have demonstrated to form double- or single-helical binuclear coordination compounds with a range of metals. We have commented elsewhere upon the various factors which control the assembly of a double-helical ligand array.[14,15] In this paper, we wish to describe the formation of a double-helical binuclear complex of qpy with cobalt(II).

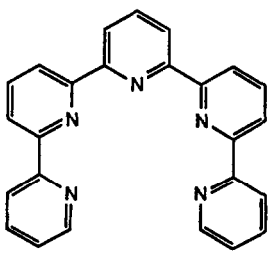

qpy

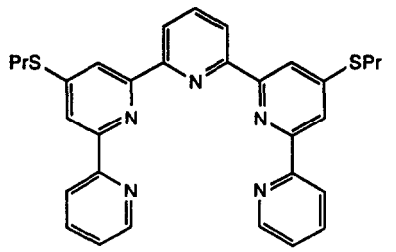

ptqpy

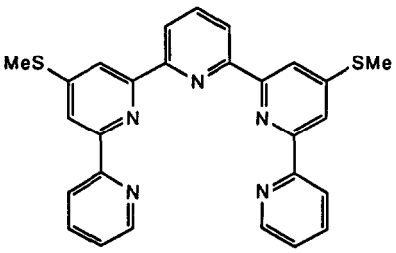

mtqpy

* Author to whom correspondence should be addressed.

† Current address: Department of Inorganic Chemistry, The University, Bristol BS8 1TS, U.K.

EXPERIMENTAL

IR spectra were recorded on a Perkin–Elmer 1710 Fourier transform spectrophotometer, with the samples in compressed KBr discs. Fast atom bombardment (FAB) and electron impact (EI) mass spectra were recorded on a Kratos MS-50 spectrometer, with 3-nitrobenzyl alcohol as matrix for the FAB spectra; ESR spectra were recorded on a Varian E-109 spectrometer as frozen acetonitrile glasses at 90 K. Electrochemical measurements were performed using an AMEL model 553 potentiostat, model 567 function generator and model 721 integrator connected to an *X–Y* recorder via an AMEL model 560/A interface. A conventional three-electrode configuration was used, with platinum bead working and auxiliary electrodes and an Ag/AgCl reference. Ferrocene was added at the end of each experiment as an internal standard. Controlled-potential electrolyses were performed using a cylindrical platinum gauze as working electrode and a smaller, co-axial platinum gauze as auxiliary electrode (separated by a frit). The solvent was acetonitrile in all cases, distilled from CaH_2 and then P_4O_{10} and stored over 4 Å molecular sieve. The base electrolyte was 0.1 M $[Bu^n_4N][BF_4]$, recrystallized twice from methanol/water. Potentials are quoted *vs* ferrocene/ferrocenium couple ($Fc/Fc^+ = 0.0$ V), and all potentials were referenced to internal ferrocene added at the end of each experiment. 2,2′:6′,2″:6″,2‴:6‴,2⁗-Quinquepyridine was prepared by the Krohnke method[16] as we have described earlier,[4–11] cobalt acetate was used as supplied by Aldrich.

Preparation

2,2′:6′,2″:6″,2‴:6‴,2⁗-Quinquepyridine (0.1 g, 0.26 mmol) was added to a solution of $Co(OAc)_2 \cdot 4H_2O$ (0.07 g, 0.28 mmol) in methanol (25 cm^3) and the mixture heated to reflux for 1 h, after which period an orange–brown solution had been obtained. This solution was filtered through Celite and the clear filtrate treated with a methanolic solution of ammonium hexafluorophosphate to yield an orange precipitate. Recrystallization of this solid from acetonitrile by the diffusion of diethyl ether vapour into the solution yielded orange blocks of $[Co_2(qpy)_2(OAc)][PF_6]_3$ (Found: C, 44.7; H, 2.8; N, 9.8. Calc. for $C_{52}H_{37}N_{10}Co_2O_2P_3F_{18}$: C, 45.0; H, 2.7; N, 10.1%) and pink needles of $[Co_2(qpy)_2][PF_6]_4$ (Found: C, 38.9; H, 2.7; N, 9.6. Calc. for $C_{50}H_{34}N_{10}Co_2P_4F_{24}$: C, 39.8; H, 2.5; N, 9.3%).

Crystal structural determination of $[Co_2(qpy)_2(OAc)][PF_6]_3 \cdot 3MeCN$

Orange blocks of the compound were obtained by the diffusion of diethyl ether vapour into an acetonitrile solution of the complex. An orange single crystal was mounted in a glass capillary tube. All geometric and intensity data were taken from this crystal using an automated four-circle diffractometer (Nicolet R3mV) following procedures described previously.[17] Pertinent crystallographic data are given in Table 1. Lattice dimensions were verified by axial photography. Intensity data, gathered by the ω-2θ method were reduced by routine procedures. Calculations were carried out using a Micro-Vax II with the program SHELXTL PLUS.[18] Empirical absorption corrections were applied.

All the non-hydrogen atoms were located by direct methods, and the cobalt, carbon, nitrogen, oxygen and phosphorus atoms refined anisotropically. Pyridine and acetate hydrogen atoms were placed

Table 1. Crystal data for $[Co_2L_2(OAc)][PF_6]_3 \cdot 3MeCN$

Formula	$C_{58}Co_2H_{46}F_{18}N_{13}O_2P_3$
fw	1509.79
Space group	$P\bar{1}$ (No. 2)
a (Å)	11.576(2)
b (Å)	13.965(3)
c (Å)	20.638(4)
α (°)	105.13(1)
β (°)	95.22(1)
γ (°)	104.21(1)
V (Å^3)	3079
Z	2
F(000)	1704
d_{calc} (g cm^{-3})	1.628
Crystal size (mm)	0.65 × 0.38 × 0.38
μ (Mo-K_α) (cm^{-1})	7.30
Data collection instrument	Nicolet R3mV
Radiation	Mo-K_α (λ = 0.71073 Å)
Orientation reflections: number; range (2θ)	35, 20.0° ≤ 2θ ≤ 25.0°
Temperature (°C)	18
Total reflections collected	8776
Number of unique data	8006
Total with $F \geq 4\sigma(F)$	6121
Number of parameters	772
Minimum/Maximum transmission factors	0.7336/0.7958
R	0.082
R'	0.108
Weighting scheme	$w^{-1} = \sigma^2 F + 0.0010\ F^2$
Largest shift/ESD, final cycle	0.49
Largest peak (e/Å^3)	0.95

Table 2. Selected bond lengths (Å) and bond angles (°) for $[Co_2L_2(OAc)][PF_6]_3 \cdot 3MeCN$

Co(1)—N(1)	2.154(7)	Co(1)—N(2)	2.054(8)
Co(1)—N(3)	2.250(7)	Co(1)—N(6)	2.177(6)
Co(1)—N(7)	2.053(7)	Co(1)—N(8)	2.227(6)
Co(2)—N(4)	2.142(7)	Co(2)—N(5)	2.089(8)
Co(2)—N(9)	2.155(6)	Co(2)—N(10)	2.110(8)
Co(2)—O(1)	2.206(6)	Co(2)—O(2)	2.137(6)
N(1)—Co(1)—N(2)	76.8(3)	N(1)—Co(1)—N(3)	151.7(3)
N(2)—Co(1)—N(3)	75.0(3)	N(1)—Co(1)—N(6)	102.0(2)
N(2)—Co(1)—N(6)	95.6(3)	N(3)—Co(1)—N(6)	83.4(2)
N(1)—Co(1)—N(7)	76.0(3)	N(2)—Co(1)—N(7)	167.7(2)
N(3)—Co(1)—N(7)	112.2(3)	N(6)—Co(1)—N(7)	76.0(3)
N(1)—Co(1)—N(8)	86.5(2)	N(2)—Co(1)—N(8)	113.8(3)
N(3)—Co(1)—N(8)	102.4(2)	N(6)—Co(1)—N(8)	150.6(3)
N(7)—Co(1)—N(8)	75.2(3)	N(4)—Co(2)—N(5)	77.2(3)
N(4)—Co(2)—N(9)	107.1(2)	N(5)—Co(2)—N(9)	104.3(3)
N(4)—Co(2)—N(10)	111.8(3)	N(5)—Co(2)—N(10)	170.2(2)
N(9)—Co(2)—N(10)	77.4(3)	N(4)—Co(2)—O(1)	148.7(2)
N(9)—Co(2)—O(1)	103.7(2)	N(5)—Co(2)—O(1)	90.0(2)
N(10)—Co(2)—O(1)	80.2(2)	N(4)—Co(2)—O(2)	90.2(2)
N(5)—Co(2)—O(2)	87.8(3)	N(9)—Co(2)—O(2)	160.6(3)
N(10)—Co(2)—O(2)	88.2(3)	O(1)—Co(2)—O(2)	60.5(3)

in idealized positions with fixed isotropic thermal parameters, $U_{py}=0.07$ Å^2, $U_{acetate}=0.16$ Å^2. The hydrogen atoms of the lattice acetonitrile solvent molecules were not located. The PF_6 anions showed positional disorder and were treated as two interlocking octahedra with a common isotropic temperature factor for F and the two positional sets for each anion were refined with occupancies of k and $1-k$. One of the three lattice MeCN molecules exhibited a two-fold positional disorder. The final difference Fourier map had no peaks larger than 0.95 e/Å^3. Selected bond angles and bond distances are given in Table 2.

RESULTS AND DISCUSSION

Upon heating a suspension of qpy with a methanolic solution containing an equivalent amount of cobalt(II) acetate, an orange–brown solution was obtained. Concentration of this solution, followed by the addition of ammonium hexafluorophosphate resulted in the precipitation of a solid. Recrystallization of this product from acetonitrile by the diffusion of diethyl ether vapour into the solution resulted in the formation of two different types of crystal (orange blocks and pale pink needles) which could be separated by hand. Both of these crystalline products were found to lose solvent and collapse to powders upon standing in air or upon drying *in vacuo*. The FAB mass spectra of these two compounds both exhibited peaks at m/z 1327, 1182, 1037, 892 and 446 which may be assigned to the species $\{[Co_2(qpy)_2][PF_6]_3\}^+$, $\{[Co_2(qpy)_2][PF_6]_2\}^+$, $\{[Co_2(qpy)_2][PF_6]\}^+$, $\{[Co_2(qpy)_2]\}^+$ and $\{[Co_2(qpy)]\}^+$, respectively. Partial elemental analyses of the two compounds were in accord with the formulation $[Co_2(qpy)_2][PF_6]_4$ for the pink compound and $[Co_2(qpy)_2(OAc)][PF_6]_3$ for the orange blocks. The IR spectra of the two complexes in the region 1300–1600 cm^{-1} are different, but there are numerous qpy absorptions in this part of the spectrum and it is not possible to unambiguously assign stretching modes to the acetate groups. The orange complex is paramagnetic with a room temperature magnetic moment of 4.90 BM per cobalt centre, which compares favourably with the value of 4.78 BM reported for the mononuclear complex $[Co(ptqpy)Cl_2]$.[19] The ESR spectrum at −196 K of an acetonitrile glass containing the complex exhibits a broad, featureless, apparently isotropic absorption at g_{av} 3.71 which does not show any hyperfine splitting.

The orange compound is electrochemically active and exhibits an unusually rich and complex redox behaviour, in contrast to that observed for the copper[5,6] and nickel[4,8] analogues. The cyclic voltammogram of an acetonitrile solution is presented in Fig. 1. The behaviour is consistent with the pres-

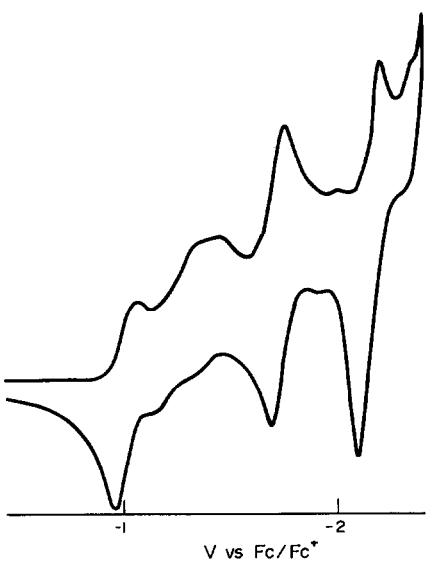

Fig. 1. Reductive cyclic voltammogram of an acetonitrile solution of $[Co_2(qpy)_2(OAc)][PF_6]_3$ (50 mV s^{-1} scan rate, 0.1 M $[^nBu_4N][BF_4]$ supporting electrolyte).

ence of a number of solution species (possibly formed by partial or complete displacement of the acetate by acetonitrile), but it is significant that recrystallization from acetonitrile yields $[Co_2(qpy)_2(OAc)][PF_6]_3$, and so these processes must be reversible or electrochemically initiated. The cyclic voltammogram exhibits reduction processes at -1.10 V (asymmetrical, semi-reversible, $E_a - E_c$ 95 mV), -1.19 V ($E_a - E_c$ 170 mV), -1.37 V ($E_a - E_c$ 130 mV), -1.71 V (reversible, $E_a - E_c$ 90 mV), -1.93 V (very low intensity, but repeatable between various samples, $E_a - E_c$ 90 mV), -2.11 V (return wave amplified by an absorption spike) and -2.30 V (very low intensity) (all potentials quoted *vs* the Fc/Fc^+ couple). The only process that we have been able to unambiguously assign is that associated with the -1.10 V feature; bulk electrolysis at this potential generates a green–brown solution. Coulometry indicates that this wave is associated with the passage of 1.0 ± 0.1 electrons per mole of complex. The assymetry of this peak is scan-rate independent. The ESR spectrum of a frozen acetonitrile glass of this green–brown compound exhibits no absorption close to free-spin, and we can assign the first reduction process to the reduction of the dicobalt(II) complex to a mixed oxidation state (Co^{II}, Co^{I}) species. We have not assigned the remaining processes in the reductive cyclic voltammogram; all of the features are scan-rate dependent and repeatable between different samples of the compound. Perhaps the most surprising feature is the lack of well-defined oxidation processes for the complex. The oxidation of a d^7 cobalt(II) centre to d^6 cobalt(III) should be strongly favoured in a pseudo-octahedral strong ligand field environment. Three small waves are observed at $+0.32$, $+0.53$ and $+0.74$ V, each of which has a small return wave and $E_a - E_c$ values of 80–120 mV (Fig. 2). The reductive feature labelled C in Fig. 2 is only present if the scan includes the oxidative processes (*cf.* Fig. 1) and is a return wave associated with the oxidative processes. Coulometric studies

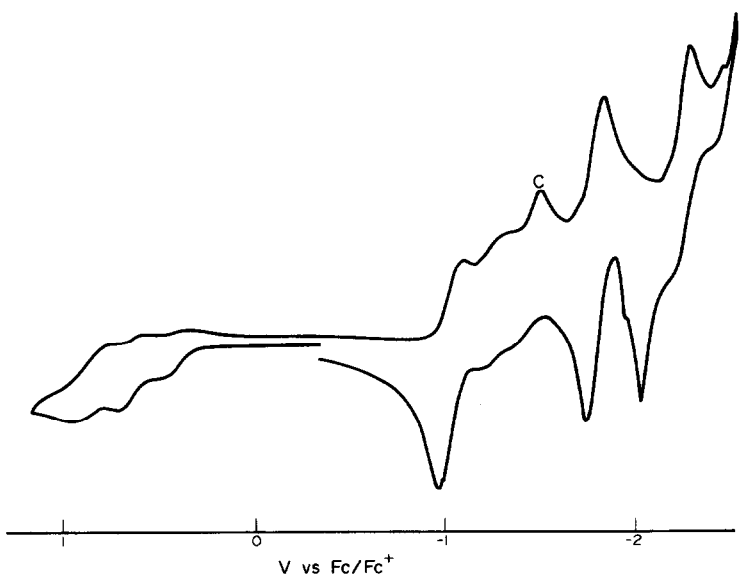

Fig. 2. Full sweep cyclic voltammogram of an acetonitrile solution of $[Co_2(qpy)_2(OAc)][PF_6]_3$ (50 mV s^{-1} scan rate, 0.1 M $[^nBu_4N][BF_4]$ supporting electrolyte).

indicate that the three oxidation processes *combined* are responsible for the transfer of 1.0 ± 0.1 electrons per mole of complex. This observation is in accord with our earlier suggestion of there being a number of solution species. We have been unable to isolate or obtain an ESR spectrum of the oxidized species, which is presumably a mixed oxidation state (Co^{III},Co^{II}) complex.

The X-ray crystal structure of the orange compound has been determined, and the structure of one of the two enantiomers of the cation $[Co_2(qpy)_2(OAc)]^{3+}$ in the complex $[Co_2(qpy)_2(OAc)][PF_6]_3 \cdot 3MeCN$ is shown in Fig. 3. The gross structure of the cation confirms the presence of a binuclear complex with a double helical ligand array about the dicobalt(II) core. The two cobalt centres are both six-coordinate, but are non-equivalent. The structure closely resembles that of $[Ni_2(qpy)_2(OAc)][PF_6]_3 \cdot 3MeCN$ which we recently reported.[8] One of the metal centres [Co(2)] is in a six-coordinate N_6 environment, in which two "2,2′:6′,2″-terpyridyl" portions from the two ligands provide the donor atoms, whilst the second [Co(2)] is in a N_4O_2 environment, provided by the remaining two nitrogen atoms of each qpy ligand presenting a "2,2′-bipyridyl" donor set and the two oxygen donor atoms of a bidentate chelating acetate group. The Co(1)—N bonds show the expected pattern with long contacts to the "terminal" pyridyl rings of the "2,2′:6′,2″-terpyridyl" fragment [2.154(7), 2.177(6), 2.227(6), 2.250(7) Å] and short contacts to the "central" ring [2.054(6), 2.053(7) Å]. In each case, the contact to the central pyridine ring of the ligand is longer than that to the terminal ring. The Co(2)—N and Co(2)—O distances are unremarkable. The N—Co—N bite angles for each "2,2′-bipyridyl" group around Co(1) are unremarkable and are in the range 75.0(3)–76.8(3)°. The corresponding angles about Co(2) are still typical but are slightly larger [77.2(3) and 77.4(3)°] as a consequence of introducing the less sterically demanding acetate ligand, with a bite angle of 60.5(3)°.

There is no significant interaction between the two metal atoms which lie 4.461 Å apart (*cf.* the sum of the *covalent* radii of 2.32 Å). The double helical ligand array is achieved by a series of twists about interannular C—C bonds within each ligand. The major twists occur between the "2,2′-bipyridyl" and "2,2′:6′,2″-terpyridyl" portions of each ligand (59.9° between rings 3 and 4, 58.1° between rings 8 and 9, with the rings numbered according to the

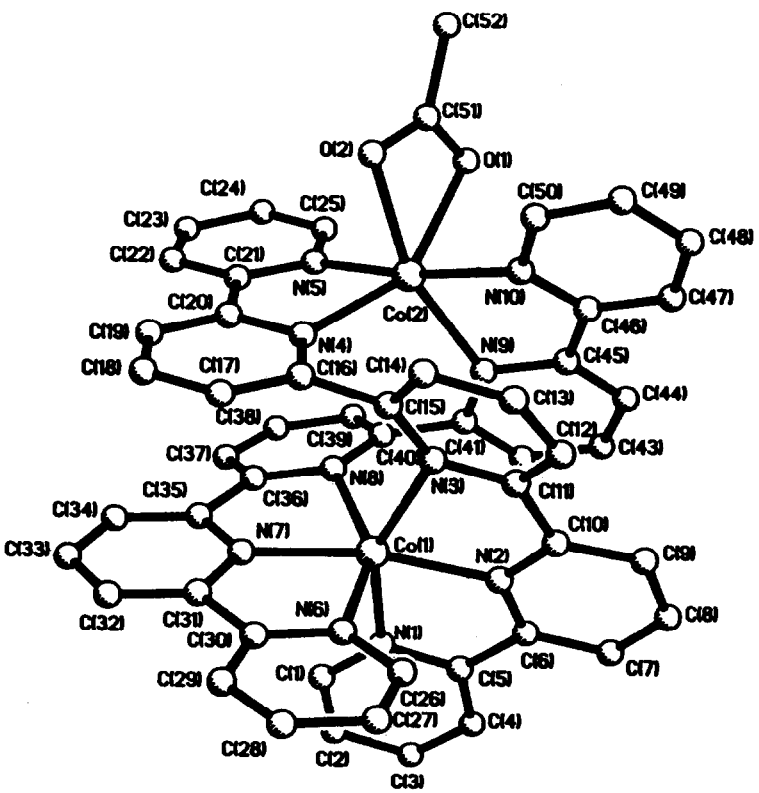

Fig. 3. Structure of one of the two enantiomers of the $[Co_2(qpy)_2(OAc)]^{3+}$ cation in $[Co_2(qpy)_2(OAc)][PF_6]_3 \cdot 3MeCN$ showing the numbering scheme adopted.

numbering of the nitrogen atom). Smaller deviations from planarity are observed between rings 1 and 2 (6.3°), 2 and 3 (17.9°), 4 and 5 (4.9°), 6 and 7 (5.3°), 7 and 8 (14.5°) and 9 and 10 (5.8°). Stacking interactions are observed between approximately parallel rings of the two ligands; rings 4 and 7 make an angle of 2.5° with each other and are separated by an average of 3.307 Å, whilst rings 2 and 9 are twisted by 8.1° and lie 3.389 Å apart. The twisting and the co-planar stacking interactions are emphasised in the projection of the cation presented in Fig. 4.

It is of interest that the reaction of cobalt(II) acetate with qpy results in the high-yield formation of the double-helical binuclear complex, in view of the recent report that the reaction of cobalt(II) chloride with the related ligand 4′,4‴-bis(n-propylthio)-2,2′:6′,2″:6″,2‴:6‴,2⁗-quinquepyridine (ptqpy) yields a green mononuclear complex in high yield.[19] This is in accord with our observations that double-helical complexes may not always be prepared in the presence of competitive halide ligands. We believe that the change in structure is associated with the presence of halide rather than with the substituents on the ligand; support for this comes from the observation that 4′,4‴-bis(methylthio)-2,2′:6′,2″:6″,2‴:6‴,2⁗-quinquepyridine (mtqpy) forms a double-helical binuclear complex with nickel(II).[20]

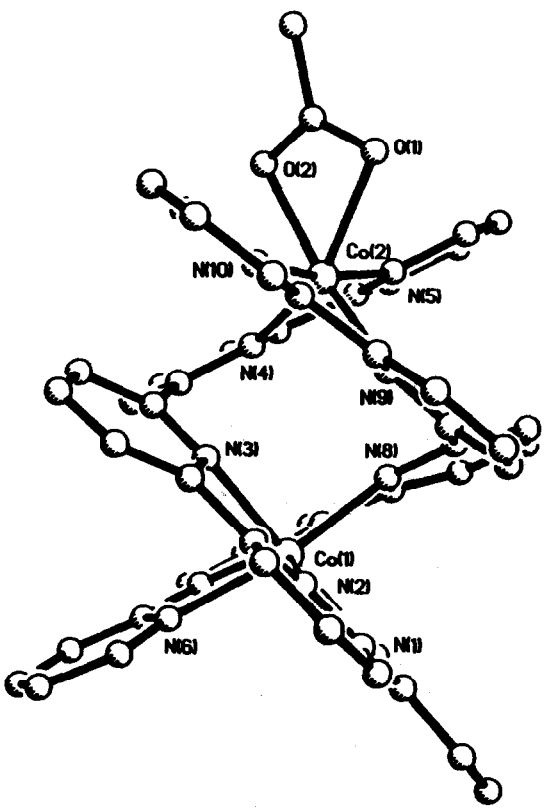

Fig. 4. An alternative view of one of the two enantiomers of the $[Co_2(qpy)_2(OAc)]^{3+}$ cation in $[Co_2(qpy)_2(OAc)][PF_6]_3 \cdot 3MeCN$.

Acknowledgement—We should like to thank the SERC for the award of a research studentship (M.D.W.).

REFERENCES

1. W. R. McWhinnie and J. D. Miller, *Adv. Inorg. Chem. Radiochem.* 1969, **12**, 135.
2. E. C. Constable, *Adv. Inorg. Chem.* 1989, **34**, 1.
3. E. C. Constable, *Adv. Inorg. Chem. Radiochem.* 1986, **30**, 69.
4. E. C. Constable, J. Lewis and M. Schröder, *Polyhedron* 1982, **1**, 311.
5. E. C. Constable, M. G. B. Drew and M. D. Ward, *J. Chem. Soc., Chem. Commun.* 1987, 1600.
6. M. Barley, E. C. Constable, S. A. Corr, R. C. S. McQueen, J. C. Nutkins, M. D. Ward and M. G. B. Drew, *J. Chem. Soc., Dalton Trans.* 1988, 2655.
7. E. C. Constable, M. G. B. Drew, G. Forsyth and M. D. Ward, *J. Chem. Soc., Chem. Commun.* 1988, 1450.
8. E. C. Constable, M. D. Ward, M. G. B. Drew and G. A. Forsyth, *Polyhedron* 1989, **8**, 2551.
9. C. J. Cathey, E. C. Constable, M. J. Hannon, M. D. Ward and D. A. Tocher, *J. Chem. Soc., Chem. Commun.* 1990, 621.
10. E. C. Constable, S. M. Elder, J. A. Healy and D. A. Tocher, *J. Chem. Soc., Dalton Trans.* 1990, 1010.
11. E. C. Constable, S. M. Elder, J. A. Healy, M. D. Ward and D. A. Tocher, *J. Am. Chem. Soc.* 1990, **112**, 4590.
12. E. C. Constable, M. D. Ward and D. A. Tocher, *J. Chem. Soc., Dalton Trans.*, manuscript submitted.
13. E. C. Constable, M. D. Ward and D. A. Tocher, *J. Am. Chem. Soc.* 1990, **112**, 1256.
14. E. C. Constable, *Nature*, 1990, **346**, 314.
15. E. C. Constable, J. M. Holmes and P. R. Raithby, *Polyhedron* 1991, **10**, 127.
16. F. Krohnke, *Synthesis* 1976, 1.
17. E. C. Constable, M. J. Doyle, S. M. Elder and P. R. Raithby, *J. Chem. Soc., Chem. Commun.* 1989, 1377.
18. G. M. Sheldrick, SHELXTIL PLUS, University of Göttingen, F.R.G. (1986).
19. K. A. Gheysen, K. T. Potts, H. C. Hurrell and H. D. Abruna, *Inorg. Chem.* 1990, **29**, 1589.
20. E. C. Constable, M. G. B. Drew and P. D. Wood, unpublished results.

Polyhedron Vol. 10, No. 12, pp. 1401–1403, 1991
Printed in Great Britain

0277-5387/91 $3.00+.00
© 1991 Pergamon Press plc

COMMENTS ON MACROSPECIES AND MACROCONSTANTS VERSUS MICROSPECIES AND MICROCONSTANTS

TAMAS KISS* and IMRE SOVAGO*

Department of Inorganic and Analytical Chemistry, Lajos Kossuth University, H-4010 Debrecen, Hungary

and

R. BRUCE MARTIN*

Chemistry Department, University of Virginia, Charlottesville, VA 22903, U.S.A.

(*Received* 23 *July* 1990; *accepted* 12 *February* 1991)

Abstract—In response to a misunderstanding of our presentation of microconstants and microspecies, some of the relations between them and macrospecies and macroconstants are discussed, with specific reference for metal ion binding to catecholamines. For ligands, such as the catecholamines, of high and unknown basicity, either proton displacement constants or conditional stability constants avoid the need to know the ligand pK_a values. The relation between the two formulations is derived.

In a recent paper in this journal, Martell *et al.*[1] commented on our paper dealing with Al^{3+} binding to catecholamines.[2] Their critical comments indicate misunderstandings of our analysis, so we offer this statement clarifying the principles involved.

At issue is an appreciation of the uses of and differences between the macroscopic and microscopic descriptions of a system. Potentiometric methods yield macroscopic equilibrium constants relating macrospecies each of a single overall composition. They may be used to calculate the free metal ion concentration and the total concentration of all microspecies of a given overall composition. All microspecies of a given composition appear as one species in the macroscopic presentation. In many ligand systems there is only one main complex structure referring to each species composition and ambiguities in interpretation do not arise.

In some systems, however, such as the so-called catecholamines, there is more than one microspecies or structure of importance with a given overall macrospecies composition. For example, in DOPA (3,4-dihydroxyphenylalanine) the species of an overall -1 charge consists of several microspecies, the major one of which bears a negative carboxylate group, a protonated ammonium group and one deprotonated, anionic hydroxy group.[3–5] Hence the molecule is better described as an ammonium catecholate.[4] Which of the two catecholate hydroxy groups is the more extensively ionized is not easily determinable nor of concern as the spectrum of the species is a weighted average over the two microspecies. (Ionization from the hydroxy group occurs with $pK_a = 9.54$ in tyrosine and a comparable 9.45 in *meta*-tyrosine.)[6] Moreover, the remaining catecholate proton hydrogen bonds the catecholate oxygen atoms, contributing to the low pK_a of the first and the high pK_a of the second catechol ionizations.[4] It is possible that there is a single potential well with the proton equidistant between the two oxygen atoms, merging the two microspecies.[6,7] In any case, for practical purposes, the writing of a single microspecies for a catecholate monoanion is fully justified.

Loss of the next DOPA proton from the net -1 charged ammonium catecholate is from the ammonium group leaving a -2 charged species with the lone proton hydrogen bonding the catecholate oxygen pair in the main microspecies. Note

* Authors to whom correspondence should be addressed.

that if we consider the -1 charged species to be a catecholamine, there is no ammonium group proton to lose and the macroconstant for the -1 to -2 deprotonation is wrongfully interpreted as being due to ionization of a catechol proton.

In weakly acid and neutral solutions most metal ions bind the -2 charged DOPA species at the catecholate locus with the bridging proton transferring to the amino group.[2,4,8,9] Thus the macroscopic equilibrium constant for metal ion binding to a -2 charged species includes three microscopic equilibrium constants: ionization of the second catecholate proton, protonation of the amino group and metal ion chelation at the catecholate locus. It is often important to resolve the macroconstant into its three component microconstants, for only the last microconstant value should be used when comparing stability constants to other catechols such as catechol itself and tiron.[2]

Since microconstant values are always made consistent with those of macroconstants, exactly the same information is available from microconstants as from macroconstants. Microconstants, however, probe chemical structure more deeply. If one desires molecular and not just phenomenological information in a system such as DOPA, one needs to estimate the microscopic equilibrium constants and hence the relative populations of microspecies. Only then may comparisons among stability constants be made with other ligand systems. Macroconstants contain a mixture of microconstants relating a mixture of microspecies.

Partly due to the intramolecular hydrogen bonding between the catecholate oxygen atoms, but mainly due to the electrostatic effect, the second ionization in catechols yields a high $pK_a \sim 13$.[4] Owing to the high pH region this ionization constant is not known as well as those with lower pK_a values. We determine these high values in separate measurements without added potassium chloride and titrate with concentrated base giving results uncertain to ± 0.2 log units.[10] Since we choose to conduct most of our work in a region of physiological ionic strength, we prefer to include the necessarily higher ionic strengths in the uncertainty of the results for high pK_a values, rather than perform all measurements at a higher ionic strength. Though highly basic pK_a values are quoted to one decimal place, e.g. 13.4 for DOPA, calculations are carried through as if there are two decimal places, i.e. 13.40 in this case.[2] There is no harm in this procedure because the 13.40 value included in log β values cancels out in subsequent manipulation. Since this dissociation in the free ligand occurs to a negligible extent in the pH range of metal complex formation, the greater uncertainty in high pK_a values does not affect the reliability of metal ion stability constants. All log β values were derived from many data points by modern computer methods.

The basis of potentiometric determination of stability constants is the monitoring of proton displacement on a ligand by a metal ion. We write and define the following reactions and equilibrium constants:

$$HL \rightleftharpoons H^+ + L \qquad K_a = [H^+][L]/[HL]$$

$$M + L \rightleftharpoons ML \qquad K_S = [ML]/([M][L])$$

$$M + HL \rightleftharpoons H^+ + ML \qquad K_{SH} = [H^+][ML]/([M][HL]).$$

Most stability constants are expressed as K_S, but if the pK_a is high enough to be uncertain the proton displacement constant, K_{SH}, may be employed. With the acidity constant of the free ligand, K_a, the equations are related by $K_{SH} = K_a K_S$. Martell recommends the proton displacement formulation (third reaction) for ligands with high pK_a values such as catechols. This formulation has been used for years in reactions of metal ions with highly basic ligands such as peptides, where the amide pK_a of *ca* 15 is even greater than that for catechols.[11] Instead of proton displacement constants, in the catecholamine case we used conditional stability constants, which also avoid the use of uncertain, high pK_a values.[2] The conditional stability constant is defined as $K_C = \alpha K_S$, where $\alpha = K_a/([H^+]+K_a)$ is the fraction of free ligand that is deprotonated. Thus in solutions where $[H^+] \gg K_a$, we have $K_C = K_{SH}/[H^+] = [ML]/([M][HL])$ and when $[H^+] \ll K_a$, we have $K_C = K_S$. Once calculated, the conditional stability constant is usable directly at the pH of interest. Conditional stability constants have a long history,[12] accomplish many of the same purposes as proton displacement reactions and have the advantage of being directly applicable at the chosen pH. More applications of and details concerning conditional constants may be found in refs 2, 5 and 13–15. Almost the entire discussion section of our paper deals with conditional constants and Table 2 lists values for several catechol ligands at pH 7.00.[2] Virtually all the criticisms of our paper are met by our use, indeed emphasis, of conditional stability constants.

Microconstants are not only a valid concept but for systems with several microspecies are also useful in ways that macroconstants are not. Microconstants are routinely determined by a combination of potentiometric and spectral absorption, NMR, etc.) methods. It is incorrect to say of microconstants that they are "only accessible through estimative deduction".[16] When an absorption change is used to measure the extent of depro-

tonation of a group in the pH region where a second group also is deprotonating, the pK_a value is not given directly by the usual equations for a single deprotonating group, because the second deprotonation affects the first. Thus one cannot obtain the "true macroscopic pK" by the normal procedure as suggested.[16] It is necessary to use fuller equations developed more than 30 years ago for this purpose.[3,5,17]

Though claimed to be "of theoretical interest only",[16] microconstants are associated with specific structural changes. In larger systems such as proteins, investigators have gone to considerable trouble to identify individual proton and metal ion binding sites by NMR spectroscopy. The microconstants obtained by this and other techniques are not any more "theoretical" nor any less "true" than macroconstants determined wholly potentiometrically.

REFERENCES

1. A. E. Martell, R. J. Motekaitis and R. M. Smith, *Polyhedron* 1990, **9**, 171.
2. T. Kiss, I. Sovago and R. B. Martin, *J. Am. Chem. Soc.* 1989, **111**, 3611.
3. R. B. Martin, *J. Phys. Chem.* 1971, **75**, 2657.
4. R. K. Boggess and R. B. Martin, *J. Am. Chem. Soc.* 1975, **97**, 3076.
5. R. F. Jameson, G. Hunter and T. Kiss, *J. Chem. Soc. Perkin Trans. II* 1980, 1105.
6. T. Kiss and B. Toth, *Talanta* 1982, **29**, 539.
7. B. Noszal, *J. Phys. Chem.* 1986, **90**, 4104.
8. T. Kiss and A. Gergely, *Inorg. Chim. Acta* 1983, **78**, 247.
9. R. B. Martin, *Metal Ions Biol. Syst.* 1988, **23**, 123.
10. T. Kiss and A. Gergely, *Inorg. Chim. Acta* 1979, **36**, 31.
11. H. Sigel and R. B. Martin, *Chem. Rev.* 1982, **82**, 385.
12. S. Fallab and H. Erlenmeyer, *Arch. Exp. Path. Pharmak.* 1957, **230**, 205.
13. R. B. Martin, *Clin. Chem.* 1986, **32**, 1797.
14. R. B. Martin, *Metal Ions Biol. Syst.* 1988, **24**, 1.
15. H. Sigel and D. B. McCormick, *Accts Chem. Res.* 1970, **3**, 201.
16. A. E. Martell and R. J. Motekaitis, *The Determination and Use of Stability Constants*, Ch. 7. VCH Publishers, New York (1988).
17. J. T. Edsall, R. B. Martin and B. R. Hollingworth, *Proc. Natn. Acad. Sci.* 1958, **44**, 505.

Polyhedron Vol. 10, No. 12, pp. 1405–1409, 1991
Printed in Great Britain

0277–5387/91 $3.00+.00
© 1991 Pergamon Press plc

ASSOCIATION OF TRIS(PENTANE-2,4-DIONATO)COBALT(III) WITH CHLORINATED PHENOLS BY HYDROGEN BONDING

HISANORI IMURA,* SHOICHI KATSUTA and NOBUO SUZUKI†

Department of Chemistry, Faculty of Science, Tohoku University, Sendai 980, Japan

(*Received* 8 *May* 1990; *accepted* 12 *February* 1991)

Abstract—Association of tris(pentane-2,4-dionato)cobalt(III) [$Co(acac)_3$] with chlorophenols, dichlorophenols, trichlorophenols and pentachlorophenol in heptane has been studied by the liquid–liquid partition technique in the heptane–0.10 mol dm^{-3} aqueous perchlorate solution system. From the partition equilibrium, the association complexes with the chlorinated phenols(HA) were found to be $Co(acac)_3 \cdot HA$ and $Co(acac)_3 \cdot 2HA$, and the association constants were determined. Existence of the hydrogen bond between the hydroxyl proton of the phenols and $Co(acac)_3$ was evidenced from the ^1H NMR measurement. The relationship between the association constant and the acid-dissociation constant of the phenols is discussed.

In our recent studies, the specific solute–solvent interaction such as coordination and hydrogen bonding has been demonstrated to be an important factor governing the liquid–liquid partition coefficient of metal complexes.[1–4] In the case of tris-pentane-2,4-dionato complexes of aluminium(III), chromium(III) and cobalt(III), the partition coefficient is remarkably lowered probably due to the hydrogen bond interaction between the metal(III) complexes and water molecules.[4] The specific interaction of such tris-pentane-2,4-dionato complexes with chloroform and methanol has been studied by means of the physicochemical measurements of vapour pressure,[5,6] heat of dissolution,[7] IR absorption spectrum,[8] and NMR relaxation rate.[9–11] In those studies, the hydrogen bond interaction was suggested. However, no systematic study on the hydrogen bonding of metal complexes to a series of proton donors has been carried out.

In this paper, we report studies on the association of tris(pentane-2,4-dionato)cobalt(III) [$Co(acac)_3$] with a series of chlorinated phenols which can be considered to be strong proton donors. The chlorinated phenols used are 2-chlorophenol (2-CP), 3-chlorophenol (3-CP), 2,3-dichlorophenol (2,3-DCP), 3,5-dichlorophenol (3,5-DCP), 2,3,5-trichlorophenol (2,3,5-TCP), 2,3,6-trichlorophenol (2,3,6-TCP), 2,4,5-trichlorophenol (2,4,5-TCP), and pentachlorophenol (PCP). Chloroform was also examined as a proton donating solute. The partition equilibrium of $Co(acac)_3$ between heptane and 0.10 mol dm^{-3} aqueous perchlorate solution in the presence of the chlorinated phenols or chloroform were studied in detail, and the composition as well as the equilibrium constant for the association complex of $Co(acac)_3$ with each chlorinated phenol and chloroform in the organic phase were determined. The effect of acidity and steric effects of the chlorinated phenols on the association is discussed. Additionally, the existence of the hydrogen bond between $Co(acac)_3$ and the phenols is examined by the nuclear magnetic resonance (NMR) spectrometry.

EXPERIMENTAL

Materials

Tris(pentane-2,4-dionato)cobalt(III) was obtained from Dojin Chem. Lab., recrystallized from hexane, and dried *in vacuo*. (Found: C, 50.9; H, 6.1. Calc. for: C, 50.6; H, 5.9%.) Chlorinated phenols were commercially obtained: 3-CP, 2,3-DCP, 3,5-DCP, 2,3,5-TCP, 2,3,6-TCP and 2,4,5-TCP

* Present address: Department of Chemistry, Faculty of Science, Ibaraki University, Mito 310, Japan.
† Author to whom correspondence should be addressed.

were of more than 98% purity and further purified by recrystallization from hexane; 2-CP (guaranteed reagent grade) and PCP (99% purity) were used as obtained. The purity of these phenols was checked by their melting points and UV spectra. Chloroform (spectroscopic grade) was used after washing with water several times. Heptane was purified in the usual manner. Carbon tetrachloride used for the NMR measurements was of spectroscopic grade. Water was doubly distilled. Other reagents were of analytical reagent grade and were used without further purification.

To prevent adsorption of the solute onto the wall of the glassware such as extraction vials and pipettes, they were treated with dimethyldichlorosilane before use.

Procedure

Partition coefficient of tris(pentane-2,4-dionato) cobalt(III). An aqueous solution containing 0.010 M perchloric acid, 0.090 M sodium perchlorate, and 4.0×10^{-5}–2.2×10^{-4} M $Co(acac)_3$ was shaken with heptane for 15 min at 25°C. After centrifugation, the aqueous phase was taken out and the absorbance of $Co(acac)_3$ in the aqueous phase was measured at 255.0 nm. Denoting the absorbance of initially prepared aqueous $Co(acac)_3$ solution by $A_{i,aq}$, and that of the aqueous phase after shaking by A_{aq}, the partition coefficient (P_0) of $Co(acac)_3$ was given as follows:

$$P_0=\frac{(A_{i,aq}-A_{aq})V_{aq}}{A_{aq}V_{org}}, \qquad (1)$$

where V_{aq} and V_{org} were the volume of aqueous and organic phase, respectively. The backward partition was also carried out. A heptane solution of $Co(acac)_3$ was shaken with an aqueous phase (0.010 M perchloric acid–0.090 M sodium perchlorate) for 15 min. The absorbance of the organic phase before ($A_{i,org}$) and after (A_{org}) shaking was measured at 257.0 nm, and the partition coefficient was calculated as follows,

$$P_0=\frac{A_{org}V_{aq}}{(A_{i,org}-A_{org})V_{org}}. \qquad (2)$$

The partition coefficients determined by using eqs (1) and (2) agreed well.

Partition coefficient of tris(pentane-2,4-dionato) cobalt(III) in the presence of chlorinated phenols. An aqueous solution (0.0010 M perchloric acid–0.10 M sodium perchlorate or 0.010 M perchloric acid–0.090 M sodium perchlorate) containing 3.2×10^{-5}–6.3×10^{-4} M $Co(acac)_3$ was shaken with a heptane solution containing 9.0×10^{-5}–3.7×10^{-1} M chlorinated phenols (or chloroform as a solute) for 15–60 min. The absorbance of $Co(acac)_3$ in the aqueous phase before and after shaking was measured at 325.0 nm, where the absorbance of the phenols (or chloroform) in the aqueous phase could be ignored. No change in the absorption spectrum and the molar absorption coefficient of $Co(acac)_3$ in the aqueous phase was observed in the presence of the phenols. The partition coefficient (P') of $Co(acac)_3$ was calculated using eq. (1). When the P' value was so high that the absorbance of $Co(acac)_3$ in the aqueous phase could not be directly measured, the aqueous phase was taken out, mixed with a sodium hydroxide solution (to be 0.05 M sodium hydroxide), and shaken with a small volume of chloroform to concentrate $Co(acac)_3$ into the organic phase. The P' value was obtained knowing the absorbance of the organic phase and the molar absorption coefficient (ε) of $Co(acac)_3$ in chloroform: $\varepsilon=8090\pm70$ M^{-1} cm^{-1} at 325.6 nm.

NMR measurement. ^1H NMR spectra of 0.10 M chlorinated phenol in carbon tetrachloride and the mixture of 0.10 M chlorinated phenol with 0.010–0.050 M $Co(acac)_3$ were measured with a 90 MHz NMR spectrophotometer (Varian EM-390) at 35°C. Tetramethylsilane was used as a reference material.

RESULTS AND DISCUSSION

The partition coefficient of $Co(acac)_3$ between heptane and the aqueous perchlorate solution (ionic strength 0.10 M) was determined to be -1.025 ± 0.023 as the logarithmic values for 15 measurements. This value is in good agreement with the literature values, -0.979[12] and -1.036.[13]

The partition coefficient of $Co(acac)_3$ was measured in the presence of a series of chlorinated phenols and chloroform. Figure 1 shows the plots of the partition coefficient (P') of $Co(acac)_3$ against the equilibrium concentration of the chlorinated phenols and chloroform in the organic phase, where the equilibrium concentration can be readily calculated knowing the partition coefficient and the initial concentration of those solutes. The partition coefficients of the chlorinated phenols[14] and chloroform[15] were quoted: the logarithmic values were: 0.785 for 2-CP, -0.273 for 3-CP, 1.333 for 2,3-DCP, 0.416 for 3,5-DCP, 1.953 for 2,3,5-TCP, 1.985 for 2,3,6-TCP, 1.799 for 2,4,5-TCP, 2.990 for PCP, and 1.844 for chloroform. In all of the systems, the partition coefficient of $Co(acac)_3$ rapidly increased with increase in the chlorinated phenol and chloroform concentration in the organic phase. This enhancement effect was remarkably different

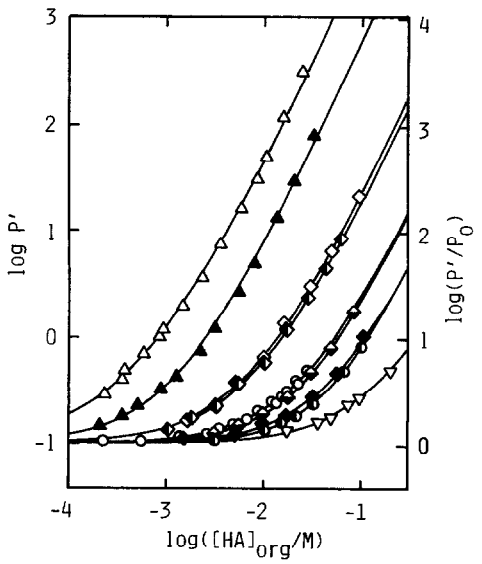

Fig. 1. Effect of chlorinated phenols and chloroform in the organic phase on the partition coefficient of $Co(acac)_3$ between heptane and 0.10 M perchlorate solution. ◆, 2-CP; ▲, 3-CP; ⬙, 2,3-DCP; △, 3,5-DCP; ◐, 2,3,5-TCP; ◑, 2,3,6-TCP; ◇, 2,4,5-TCP; ○, PCP; ▽, $CHCl_3$.

among the chlorinated phenols and increased in the following order: chloroform < 2,3,6-TCP < 2-CP < 2,3-DCP ~ PCP < 2,3,5-TCP ~ 2,4,5-TCP < 3-CP < 3,5-DCP.

Table 1 shows the chemical shift of the hydroxyl proton of each chlorinated phenol in the absence and the presence of $Co(acac)_3$, and the magnitude of the difference in shifts. The data for PCP are not included because its solubility in carbon tetrachloride was so low that the data could not be obtained under the given conditions. In the case of chloroform, the magnitude of the change in chemical shift was as small as 0.04 ppm. The change in chemical shift observed can be explained by hydrogen bonding.[16] In addition, the position of the single peak for the hydroxyl proton indicates the weighted averages of the respective chemical shifts for the free and the hydrogen-bonded phenol molecules. The increasing order of the magnitude of the shift difference is in good agreement with that for the enhancement effect on the partition coefficient of $Co(acac)_3$.

Table 1. NMR chemical shift change for the hydroxyl proton of the chlorinated phenols with $Co(acac)_3$

Chlorinated phenol	δ_0[a] (ppm)	δ[b] (ppm)	$\delta-\delta_0$ (ppm)
2-CP	5.33	5.83	0.50
3-CP	4.77[c]	6.77[c]	2.00[c]
2,3-DCP	5.52	6.22	0.70
2,6-DCP	5.62	5.85	0.23
3,5-DCP	4.77	7.04	2.27
2,3,5-TCP	5.57	6.73	1.16
2,3,6-TCP	5.79	6.16	0.37
2,4,5-TCP	5.37	6.74	1.37

[a] 0.10 M chlorinated phenol in CCl_4.

[b] 0.10 M chlorinated phenol–0.050 M $Co(acac)_3$ in CCl_4.

[c] It was somewhat uncertain because of overlapping of the proton signals.

Association equilibrium

When the association complex of $Co(acac)_3$ with a proton donor (HA) is formed by hydrogen bonding in the organic phase, the apparent partition coefficient (P') of $Co(acac)_3$ in the presence of proton donors can be expressed using the intrinsic partition coefficient (P_0) of $Co(acac)_3$ in the absence of proton donors:

$$P' = \frac{[Co(acac)_3]_{org} + \sum_{n=1}^{m} [Co(acac)_3 \cdot nHA]_{org}}{[Co(acac)_3]_{aq}} \quad (3)$$

$$= P_0\left(1 + \sum_{n=1}^{m} \beta_{ass,n}[HA]_{org}{}^n\right), \quad (4)$$

where the subscripts "org" and "aq" denote the organic and aqueous phase, respectively, and $\beta_{ass,n}$ is the association constant in the organic phase corresponding to the following equilibrium:

$$Co(acac)_{3,org} + nHA_{org} \rightleftharpoons Co(acac)_3 \cdot nHA_{org}. \quad (5)$$

Therefore, the following equation can be derived:

$$\log(P'/P_0) = \log\left(1 + \sum_{n=1}^{m} \beta_{ass,n}[HA]_{org}{}^n\right). \quad (6)$$

Figure 1 also shows the plots of $\log(P'/P_0)$ vs $\log[HA]_{org}$. The plots for 3-CP and 3,5-DCP are almost straight lines with a slope of two in the higher concentration region of the phenols. In other chlorinated phenol systems, such a limiting slope cannot be clearly observed even at the higher concentration region of the phenols (0.1 M), but the slopes of the plots go up to higher than unity. These results mean that the one or two molecules of each chlorinated phenol associate with one molecule of $Co(acac)_3$. From these plots, the association constants, $\beta_{ass,1}$ and $\beta_{ass,2}$ were computed by the least-squares fitting (SALS program, University of Tokyo) based on eq. (6). The association constants obtained are listed in Table 2. In the case of chloro-

Table 2. Association constant of $Co(acac)_3$ with chlorinated phenols and chloroform in heptane at 25°C

Proton donor	log $\beta_{ass,1}$	log $\beta_{ass,2}$	log $K_{ass,2}$[a]
2-CP	1.64 (0.02)	2.57 (0.04)	0.93
3-CP	3.27 (0.03)	5.78 (0.02)	2.51
2,3-DCP	1.87 (0.01)	3.14 (0.01)	1.27
3,5-DCP	3.88 (0.03)	6.58 (0.02)	2.70
2,3,5-TCP	2.55 (0.02)	4.19 (0.02)	1.65
2,3,6-TCP	1.47 (0.02)	2.61 (0.02)	1.14
2,4,5-TCP	2.58 (0.02)	4.29 (0.01)	1.71
PCP	1.98 (0.01)	3.15 (0.04)	1.17
$CHCl_3$	1.18 (0.02)	1.4 (0.1)[b]	0.2[b]

Numerals in parentheses show standard deviations calculated by SALS program.

[a] $K_{ass,2} = \beta_{ass,2}/\beta_{ass,1}$.

[b] See the text.

form, although the slope of the plots is less than unity even in a higher concentration region of chloroform, the association constant was computed by assuming the formation of the 1 : 1 and 1 : 2 association complexes. Hence, the value for the 1 : 2 complex involves somewhat large uncertainty. The solid lines in Fig. 1 indicate the values computed using these association constants. They are in good agreement with the experimental plots.

Figure 2 shows the correlation between the association constant for the $Co(acac)_3$–chlorinated phenol complexes and the magnitude of the shift difference for the hydroxyl proton of the phenols. A good linear correlation between both parameters is clearly seen, so that it is strongly suggested that the association is caused by the hydrogen bonding of the hydroxyl proton of chlorinated phenols to $Co(acac)_3$.

When the association of $Co(acac)_3$ with the chlorinated phenols is due to the hydrogen bonding as described above, the correlation between the association constant and acid-dissociation constant of the phenols should be expected. The latter can be considered to be a measure for the proton donor ability of the phenols, as cited from the literature.[17] Figure 3 shows the association constant of the $Co(acac)_3$–chlorinated phenol complexes as a function of the acid-dissociation constant of the phenols. A good correlation is found for each group of the chlorinated phenols with the same steric conditions around the hydroxyl group: (1) 2,3,6-TCP and PCP, which possess two chlorine substituents at the 2,6-positions; (2) 2-CP, 2,3-DCP, 2,3,5-TCP and 2,4,5-TCP, which possess one chlorine substituent at the 2-position; (3) 3-CP and 3,5-DCP, which do not possess any chlorine atoms at the 2,6-positions but hydrogen atoms instead. The association constants for these three groups lie at the different regions in Fig. 3 and decrease as follows: group (3) > group (2) > group (1). Since the chlorine atom is more bulky than the hydrogen atom, e.g. the van der Waals volume of the chlorine atom is given to be 12.0 $cm^3\ mol^{-1}$ and that of the hydrogen atom only 2.52 $cm^3\ mol^{-1}$,[18] the chlorine atoms adjacent to the hydroxyl group in the chlorinated phenol molecule may bring about the steric hindrance for the association with $Co(acac)_3$. The

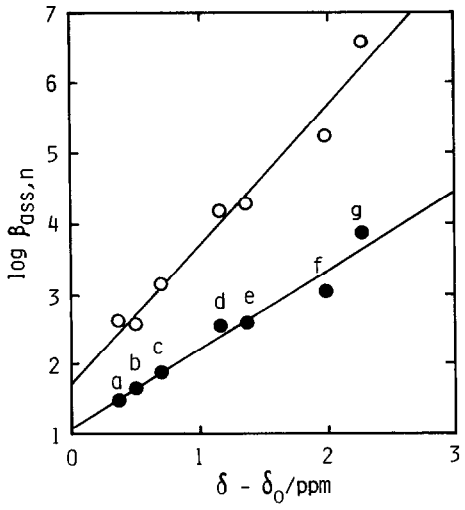

Fig. 2. Correlation between the association constant and the magnitude of the change in NMR chemical shift of the hydroxyl proton of chlorinated phenols. ●, $\beta_{ass,1}$; ○, $\beta_{ass,2}$. a, 2,3,6-TCP; b, 2-CP; c, 2,3-DCP; d, 2,3,5-TCP; e, 2,4,5-TCP; f, 3-CP; g, 3,5-DCP.

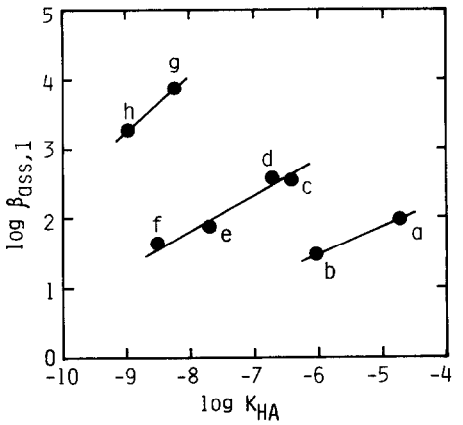

Fig. 3. Correlation between the association constant and the acid-dissociation constant (K_{HA}) of chlorinated phenols. a, PCP; b, 2,3,6-TCP; c, 2,3,5-TCP; d, 2,4,5-TCP; e, 2,3-DCP; f, 2-CP; g, 3,5-DCP; h, 3-CP.

difference in the association constants among the three groups is ascribable to such steric effect.

Consequently, we should discuss the correlation between the association constant and the acid-dissociation constant of chlorinated phenols within each group of the phenols having the same steric structure around the hydroxyl group. In each group, the association constant increases with increase in the acid-dissociation constant of the phenols. This is quite reasonable because the proton donor ability of acids increases with increase in the acid-dissociation constant. Such a linear free energy relationship observed here is also evidence that the association of $Co(acac)_3$ with the chlorinated phenols is attributed to hydrogen bonding.

Tris(pentane-2,4-dionato)cobalt(III) has two open-octahedral faces perpendicular to the C_3 axis of the tris-complex. On each octahedral face, three oxygen atoms from three pentane-2,4-dionato ligands are positioned. The hydrogen bond between $Co(acac)_3$ and the chlorinated phenols can be formed among those oxygen atoms on the octahedral face and the hydroxyl proton of the phenols. Consequently, since two open-octahedral faces of $Co(acac)_3$ can take part in the association, the 1 : 1 and 1 : 2 association complexes should be formed. This model for the association complex is perfectly supported by our experimental results described previously. Such a model has been proposed for the association complex of tris(pentane-2,4-dionato) chromium(III) with chloroform.[5,11]

In conclusion, the existence of the hydrogen bond and the association equilibrium between $Co(acac)_3$ and the chlorinated phenols was clarified. These results revealed that $Co(acac)_3$ acts as a proton acceptor or a base. Such a property of metal complexes is an important factor in their solution chemistry.

REFERENCES

1. H. Imura and N. Suzuki, *Talanta* 1985, **32**, 785.
2. N. Suzuki, S. Matsumora and H. Imura, *Polyhedron* 1987, **6**, 497.
3. N. Suzuki, J. Kodera and H. Imura, *Inorg. Chim. Acta* 1987, **128**, 261.
4. H. Watarai, H. Oshima and N. Suzuki, *Quant. Struct.-Act. Relat.* 1984, **3**, 17.
5. J. F. Steinbach and J. H. Burns, *J. Am. Chem. Soc.* 1958, **80**, 1839.
6. F. R. Clarke, J. F. Steinbach and W. F. Wagner, *J. Inorg. Nucl. Chem.* 1964, **26**, 1311.
7. R. J. Irving and R. A. Schulz, *J. Chem. Soc., Dalton Trans.* 1973, 2414.
8. T. S. Davis and J. P. Fackler Jr, *Inorg. Chem.* 1966, **5**, 242.
9. S. O. Chan and D. R. Eaton, *Can. J. Chem.* 1976, **54**, 1332.
10. G. S. Vigee and C. L. Watkins, *Inorg. Chem.* 1977, **16**, 709.
11. P. L. Wang, J. H. Lee and L. P. Hwang, *J. Phys. Chem.* 1987, **91**, 4856.
12. H. Awano, H. Watarai and N. Suzuki, *J. Inorg. Nucl. Chem.* 1979, **41**, 124.
13. P. D. Hopkins and B. E. Douglas, *Inorg. Chem.* 1964, **3**, 357.
14. S. Katsuta, MSc Thesis, Tohoku University (1989).
15. M. Takahashi, MSc Thesis, Tohoku University (1983).
16. W. G. Schneider, H. J. Bernstein and J. A. Pople, *J. Chem. Phys.* 1958, **28**, 601.
17. J. Drahonovsky and Z. Vacek, *Collect. Czech. Chem. Commun.* 1971, **36**, 3431.
18. A. Bondi, *J. Phys. Chem.* 1964, **68**, 441.

Polyhedron Vol. 10, No. 12, pp. 1411–1421, 1991
Printed in Great Britain

0277–5387/91 $3.00+.00
© 1991 Pergamon Press plc

SYNTHESIS AND SPECTROSCOPIC CHARACTERISTICS OF BIS-[DIMETHYL(PHENYL)SILYLMETHYL]PLATINUM(II) COMPLEXES WITH PHOSPHORUS DONOR LIGANDS

BERNARDETA C. ANKIANIEC and G. BRENT YOUNG*

Inorganic Chemistry Laboratories, Imperial College of Science, Technology and Medicine, London SW7 2AY, U.K.

(*Received* 19 *November* 1990; *accepted* 18 *February* 1991)

Abstract—A series of bis-[dimethyl(phenyl)silylmethyl]platinum(II) complexes *cis*-$Pt(CH_2SiMe_2Ph)_2L_2$ and $Pt(CH_2SiMe_2Ph)_2(BiL)$ with mono- and bidentate tertiary phosphine ligands {L = PMe_3, PEt_3, PMe_2Ph, $PMePh_2$, PPh_3, $P(4\text{-}C_6H_4CH_3)_3$, $P(2\text{-}C_6H_4CH_3)_3$, $PPh_2(2\text{-}C_6H_4CH_3)$, $PPh_2(2\text{-}C_6H_4CF_3)$; BiL = bis(diphenylphosphino)methane [dppm], 1,2-bis(diphenylphosphino)ethane [dppe], 1,3-bis(diphenylphosphino)propane [dppp], 1,4-bis(diphenylphosphino)butane [dppb], 1,1′-bis(diphenylphosphino)ferrocene [dppf]} has been synthesized by metathetical displacement of the dialkene from $Pt(CH_2SiMe_2Ph)_2(cod)$ or $Pt(CH_2SiMe_2Ph)_2(nbd)$ {cod = cycloocta-1,5-diene; nbd = bicyclo[2.2.1]hepta-2,5-diene}. These new complexes have been characterized by IR and NMR [^1H, ^{13}C and ^{31}P] spectroscopy and their notable features are discussed. The sila-neophyl [sila-neophyl = dimethyl(phenyl)silylmethyl] ligand exhibits a weaker NMR *trans*-influence than its carbon analogue.

Recently, we reported that bis-(trimethylsilylmethyl)platinum(II) complexes *cis*-$Pt(CH_2SiMe_3)_2L_2$ with phosphorus donor ligands, L, undergo a novel thermolytic rearrangement involving β-carbon migration from silicon to platinum.[1] This reactivity contrasts with those of the analogous palladium and nickel complexes, which favour thermolytic reductive C—C elimination,[2] and also with those of related, d-block trimethylsilylmethylmetal systems featuring, for example, ruthenium,[3] osmium,[4] rhodium[5] and iridium,[5,6] where γ-hydrogen transfer reactions afford 2,2-dimethyl-2-silametallacyclobutanes. Corresponding neopentylmetal derivatives, including those of platinum,[7] generally undergo similar cyclometallations. Neophylmetal complexes, too, may be susceptible to cyclometallation, this time via aromatic δ-C—H activation; we have elucidated some of the reaction controls in platinum(II) systems *cis*-$Pt(CH_2CMe_2Ph)_2L_2$, with both nitrogen- and phosphorus-donor ligands, L.[8] Preliminary investigations of sila-neophylplatinum† complexes, *cis*-$Pt(CH_2SiMe_2Ph)_2L_2$ with N-donor L, have revealed a thermolytic preference for a cyclometallation path analogous to the neophylplatinum species.[9] In view of the unusual reactivity of *cis*-$Pt(CH_2SiMe_3)_2(PR_3)_2$,[1] however, it was of clear interest to investigate the corresponding sila-neophylplatinum derivatives with P-donor ancillary ligands. Here, we describe their syntheses and some notable spectroscopic characteristics.

EXPERIMENTAL

General and instrumental

Elemental analyses were determined by Imperial College Microanalytical Laboratories. NMR spectra were recorded on Brüker WM250 (^1H, 250.13 MHz; ^{13}C, 62.9 MHz), Jeol GSX270 (^1H, 270.17 MHz; ^{13}C, 67.9 MHz) and Jeol FX90Q (^1H, 89.55 MHz; ^{31}P, 36.21 MHz) spectrometers. IR data were collected on a Perkin–Elmer 683 or a Perkin–Elmer 1720 FT instrument as 4% KBr dispersions.

All reactions were carried out under argon, using standard anaerobic techniques. All apparatus was flame dried before use.[10] Solvents were distilled under nitrogen prior to use: diethyl ether and *n*-

* Author to whom correspondence should be addressed.
† Sila-neophyl = dimethyl(phenyl)silylmethyl.

hexane from sodium–benzophenone; toluene from sodium.

Cycloocta-1,5-diene, bicyclo[2.2.1]hepta-2,5-diene, phosphorus trichloride, diphenylchlorophosphine, triphenylphosphine, bis(1,2-diphenylphosphino)ethane, bis(1,3-diphenylphosphino)propane, and bis(1,1′-diphenylphosphino)ferrocene were all used as supplied by Aldrich Chem. Co. Trimethylphosphine, triethylphosphine, dimethylphenylphosphine and diphenylmethylphosphine, supplied by Strem Chemicals, were stored under argon but used without further purification. Bis(diphenylphosphino)methane and bis(1,4-diphenylphosphino)butane were also used as supplied by Strem Chemicals.

Syntheses

$Pt(CH_2SiMe_2Ph)_2$(cod) and $Pt(CH_2SiMe_2Ph)_2$(nbd) were prepared as described previously.[9]

Preparation of tri-4-tolylphosphine.[11] A solution of $Mg(C_6H_4\text{-}4\text{-}CH_3)Br$ (50 mmol) in diethyl ether (15 cm^3) was added to a stirred solution of PCl_3 (2.00 g, 14.6 mmol) in diethyl ether (40 cm^3). The mixture, which had turned cloudy, was refluxed for 24 h, then cooled to −20°C and quenched with saturated aqueous ammonium chloride (30 cm^3). The organic layer was separated and the aqueous phase washed with diethyl ether (2 × 10 cm^3). The combined ether extracts were dried over anhydrous $MgSO_4$, decolourized with charcoal and filtered. Removal of the ether *in vacuo* yielded a pale yellow solid, which was recrystallized from the minimum amount of hot ethanol (7 cm^3) affording colourless crystals of tri-4-tolylphosphine. (Yield: 2.93 g, 9.6 mmol, 66%.) [^{31}P: $\delta = -6.90$ ppm, s.]

Preparation of diphenyl-2-tolylphosphine.[11] To a stirred solution of PPh_2Cl (2.00 g, 9.1 mmol) in diethyl ether (15 cm^3) cooled to 0°C was added dropwise a solution of $Mg(C_6H_4\text{-}2\text{-}CH_3)Br$ in diethyl ether (50 cm^3). Upon addition, the reaction mixture was stirred vigorously for 24 h then cooled to −25°C and quenched with saturated ammonium chloride solution (30 cm^3). The organic layer was separated and the aqueous phase repeatedly washed with diethyl ether (3 × 15 cm^3) until the washings were colourless. The ether extracts were combined, dried over anhydrous $MgSO_4$, decolourized with activated charcoal, filtered and evaporated to dryness *in vacuo*, yielding a pale yellow crystalline solid. The solid was dissolved in hot ethanol (10 cm^3) and cooled slowly to ambient temperature. The white crystalline solid was filtered, washed with cold ethanol (2 × 4 cm^3) and dried *in vacuo*. (Yield: 2.26 g, 8.2 mmol, 90%.) [^{31}P: $\delta = -14.1$ ppm, s.]

Preparation of diphenyl-2-trifluoromethylphenylphosphine.[12] Diphenyl-2-trifluoromethylphenylphosphine was prepared as a white crystalline solid by the reaction of excess $Li(C_6H_4\text{-}2\text{-}CF_3)$ and PPh_2Cl by a method analogous to that used for diphenyl-2-tolylphosphine. (Yield: 2.12 g, 6.4 mmol, 71%.) [^{31}P: $\delta = -11.4$ ppm, q; $J_{P\text{-}F} = 53.2$ Hz.]

Preparation of cis-*bis-(sila-neophyl)-bis-(trimethylphosphine)platinum*(II). $Pt(CH_2SiMe_2Ph)_2$(cod) (0.20 g, 0.33 mmol) was dissolved in toluene (10 cm^3) and trimethylphosphine (100 μl, 0.76 mmol) added by microsyringe. The reaction mixture was heated to 60°C for 14 days. The toluene was removed *in vacuo* to give a white solid, which was recrystallized from toluene (1 cm^3) and *n*-hexane (0.5 cm^3) and cooled to −20°C to give colourless crystals of $Pt(CH_2SiMe_2Ph)_2(PMe_3)_2$. (Yield: 0.19 g, 0.29 mmol, 89%.) IR: 1421 m, 1283 m, 1258 wm, 1250 m, 1233 s, 1102 s, 967 s, 961 s, 946 vs, 936 s, 809 vs, 763 s, 729 s, 714 s, 539 m.

Preparation of bis-(sila-neophyl)[bis-(diphenylphosphino)methane]platinum(II). $Pt(CH_2SiMe_2Ph)_2$(nbd) (0.20 g, 0.34 mmol) was dissolved in toluene (8 cm^3) and dppm (0.131 g, 0.34 mmol) added. After 10 days at 60°C, the toluene was removed *in vacuo* affording a pale yellow crystalline solid. Recrystallization from dichloromethane (2 cm^3) and methanol (1 cm^3) gave the product as a white crystalline solid. (Yield: 0.27 g, 0.31 mmol, 91%.) IR: 1485 wm, 1438 s, 1426 wm, 1265 m, 1242 m, 1109 s, 1031 m, 831 vs, 819 vs, 729 vs, 702 vs, 694 vs, 585 m, 502 s, 478 m.

Prepared according to the same procedure were:

Bis-(sila-neophyl)[1,4-*bis(diphenylphosphino)butane]platinum*(II). Product: white crystalline solid from dichloromethane and *n*-hexane. (Yield: 0.16 g, 0.17 mmol, 85%.) IR: 1485 wm, 1438 s, 1426 m, 1265 m, 1238 m, 1109 s, 1097 s, 1031 m, 839 s, 811 vs, 745 s, 729 s, 702 vs, 533 m, 506 s.

Bis-(sila-neophyl)[1,3-*bis(diphenylphosphino)propane]platinum*(II). Product: white crystalline solid from dichloromethane and methanol. (Yield: 0.26 g, 0.29 mmol, 85%.) IR: 1489 wm, 1438 s, 1426 m, 1265 m, 1241 m, 1109 s, 839 vs, 815 vs, 718 m, 737 s, 702 vs, 666 m, 518 vs.

Preparation of cis-*bis-(sila-neophyl)-bis-(dimethylphenylphosphine)platinum*(II). $Pt(CH_2SiMe_2Ph)_2$(nbd) (0.20 g, 0.34 mmol) was dissolved in diethyl ether (6 cm^3), dimethylphenylphosphine (120 μl, 0.70 mmol) added and the solution allowed to stand at ambient temperature for 7 days. The solvent was removed *in vacuo*, dissolved in the minimum of benzene (1 cm^3) and *n*-hexane (0.5 cm^3) added. Cooling to −20°C produced colourless crys-

tals of the product. (Yield: 0.25 g, 0.32 mmol, 95%.) IR: 1440 m, 1302 m, 1240 s, 942 s, 917 s, 906 m, 837 vs, 815 vs, 765 s, 753 s, 543 s, 504 s, 489 m, 430 s.

Prepared according to an analogous procedure were:

Cis-*bis*-(*sila-neophyl*)-*bis*-(*diphenylmethylphosphine*) *platinum*(II). Product: colourless crystals from *n*-hexane. (Yield: 0.23 g, 0.26 mmol, 76%.) IR: 1433 m, 1330 m, 1236 s, 939 s, 910 s, 904 s, 839 s, 831 vs, 811 vs, 762 s, 747 s, 726 s, 706 m, 539 s, 494 m, 424 s.

Cis-*bis*-(*sila-neophyl*)-*bis*-(*triethylphosphine*)*platinum*(II). Product: colourless crystals from *n*-hexane. (Yield: 0.23 g, 0.315 mmol, 93%.) IR: 1575 m, 1457 m, 1426 m, 1379 m, 1265 m, 1242 m, 1113 s, 1038 s, 1031 s, 835 s, 819 vs, 772 vs, 741 vs, 721 s, 709 vs, 635 m, 475 m.

Cis-*bis*-(*sila-neophyl*)-*bis*-(*triphenylphosphine*)*platinum*(II). Product: white crystalline solid from benzene and *n*-hexane. (Yield: 0.34 g, 0.33 mmol, 98%.) IR: 1482 m, 1476 m, 1431 s, 1247 m, 1103 m, 1092 s, 828 s, 806 s, 763 m, 737 s, 722 s, 692 vs, 544 m.

Cis-*bis*-(*sila-neophyl*)-*bis*-(*tri*-4-*tolylphosphine*)*platinum*(II). Product: white crystalline solid from benzene and *n*-hexane. (Yield: 0.42 g, 0.38 mmol, 89%.) IR: 1504 s, 1430 m, 1402 wm, 1191 m, 1113 s, 1101 s, 831 s, 806 vs, 726 s, 680 s, 628 s, 524 vs, 514 vs, 499 m, 448 m.

Cis-*bis*-(*sila-neophyl*)-*bis*-(*diphenyl*-2-*tolylphosphine*)*platinum*(II). Product: white crystalline solid from benzene and *n*-hexane. (Yield: 0.28 g, 0.27 mmol, 79%.) IR: 1481 wm, 1438 s, 1246 m, 1113 s, 1101 s, 829 s, 805 vs, 747 s, 728 s, 698 vs, 540 m, 529 s, 499 m, 473 s.

Bis-(*sila-neophyl*)[1,2-*bis*(*diphenylphosphino*)*ethane*] *platinum*(II). Product: white solid from toluene and *n*-hexane. (Yield: 0.31 g, 0.35 mmol, 93%.) IR: 1432 m, 1402 wm, 1259 wm, 1236 m, 1102 s, 828 m, 803 vs, 762 m, 748 s, 741 m, 730 m, 699 vs, 524 s.

Bis-(*sila-neophyl*)[1,1′-*bis*(*diphenylphosphino*)*ferrocene*]*platinum*(II). Product: amber crystalline solid from toluene and *n*-hexane. (Yield: 0.28 g, 0.27 mmol, 78%.) IR: 1485 m, 1438 s, 1430 m, 1265 m, 1109 s, 1101 s, 1042 m, 1031 s, 835 s, 811 vs, 749 m, 733 s, 702 vs, 643 m, 553 m, 498 s, 471 s.

Preparation of cis-*bis*(*sila-neophyl*)-*bis*-[*diphenyl* (2-*trifluoromethylphenyl*)*phosphine*]*platinum*(II). To $Pt(CH_2SiMe_2Ph)_2$(nbd) (0.20 g, 0.34 mmol) dissolved in diethyl ether (7 cm^3) was added excess diphenyl-2-trifluoromethylphenylphosphine (0.45 g, 1.36 mmol). The solution was allowed to remain at ambient temperature for 21 days. After this time, the reaction had reached 75% completion as established by ^{31}P NMR. Unreacted $Pt(CH_2SiMe_2Ph)_2$ (nbd) and excess phosphine were removed by column chromatography at 0°C (neutral alumina, 30 cm) using *n*-hexane as eluent. The product was then obtained using toluene as the eluent. Removal of the solvent *in vacuo* afforded a white solid.

^{31}P NMR showed that the sample was 30% contaminated with the rearranged species. The desired product is very labile and rearranges quickly at ambient temperature in non-polar solvents.

RESULTS AND DISCUSSION

Synthesis

Reaction of the diene complexes with stoichiometric amounts of tertiary phosphines, yielded a series of *cis*-bis-(phosphine)platinum(II) dialkyls in essentially quantitative yields in most cases. With the exception of $Pt(CH_2SiMe_2Ph)_2$(dppf) which is yellow, the remainder are colourless crystalline solids. Where L = PEt_3 and PPh_2Me, some problems were encountered in obtaining crystalline samples. Substitution was generally complete within 14 days at either 60°C or ambient temperature, depending on the diene complex and solvent employed. These air inert solids do not decompose in deoxygenated hydrocarbons. They do react slowly with chlorocarbon solvents, affording *cis*-$PtCl_2(PR_3)_2$; the reaction is accelerated at higher temperatures and in the presence of oxygen. All have satisfactory elemental analyses (Table 1), except *cis*-$Pt(CH_2SiMe_2Ph)_2(PPh_2C_6H_4\text{-}2\text{-}CF_3)_2$ which was not isolated pure.

Spectroscopic studies

Infrared. Selected IR data are listed in the experimental section. These complexes show the same characteristic vibrations in the sila-neophyl skeleton as those previously described.[9] Additionally, the band at 1090 cm^{-1} is a characteristic P—Ph "X-sensitive" band and bands occurring at 545–520 cm^{-1} are out of plane C—H bending modes typical of phosphine bound phenyl groups.

^1H *NMR.* The site designations used in the ensuing discussions appear in Fig. 1. A general feature

Table 1. Analytical data for bis-(sila-neophyl)platinum(II) complexes with P-donor ligands

Complex	Colour	Found (calculated), % C	H
$Pt(CH_2SiMe_2Ph)_2(PMe_3)_2$	White	44.5 (44.6)	6.9 (6.9)
$Pt(CH_2SiMe_2Ph)_2(PEt_3)_2$	White	49.5 (49.4)	7.8 (7.8)
$Pt(CH_2SiMe_2Ph)_2(PMe_2Ph)_2$	White	53.0 (53.0)	6.3 (6.3)
$Pt(CH_2SiMe_2Ph)_2(PPh_2Me)_2$	White	59.3 (59.4)	6.0 (5.8)
$Pt(CH_2SiMe_2Ph)_2(PPh_3)_2$	White	63.8 (63.7)	5.5 (5.5)
$Pt(CH_2SiMe_2Ph)_2(P\text{-}4\text{-}tol_3)_2 \cdot \frac{1}{2}C_6H_6$	White	66.2 (66.3)	6.3 (6.3)
$Pt(CH_2SiMe_2Ph)_2(PPh_2\text{-}2\text{-}tol)_2$	White	64.0 (64.3)	5.7 (5.8)
$Pt(CH_2SiMe_2Ph)_2$(dppm)	White	58.6 (58.8)	5.5 (5.5)
$Pt(CH_2SiMe_2Ph)_2$(dppe)	White	59.0 (59.2)	5.5 (5.6)
$Pt(CH_2SiMe_2Ph)_2$(dppp)$\cdot\frac{1}{2}CH_2Cl_2$	White	57.8 (57.6)	5.8 (5.6)
$Pt(CH_2SiMe_2Ph)_2$(dppb)	White	59.9 (60.0)	5.9 (6.0)
$Pt(CH_2SiMe_2Ph)_2$(dppf)	Amber	59.6 (59.6)	5.0 (5.2)

of all these spectra (Table 2) is the multiplet obtained from the hydrogens of the methylene group bound to platinum, typified by *cis*-$Pt(CH_2SiMe_2Ph)_2(PMe_3)_2$. This second order resonance arises from an $A_2A_2'MRR'X_9X_9'$ system [A = $^1H_{CH_2}$, M = ^{195}Pt, R = ^{31}P and X = $^1H_{P\text{-}CH_3}$]. In practice it generates an apparent quartet with platinum satellites. This multiplet exhibits considerable broadening for several of the complexes in spectra measured at 250 MHz but a well resolved quartet is usually observed at lower field. This phenomenon has been attributed to more efficient relaxation of the ^{195}Pt nucleus by increasing field gradient anisotropy.[13]

Similar general observations have been noted for related *cis*-PtR_2L_2 [R = neophyl, trimethylsilylmethyl, ethenyldimethylsilylmethyl; L = PEt_3, PPh_3 dppe].[8,14-16] Comparisons with bis-(neophyl) analogues show that $^2J_{Pt\text{-}H}$ values are 5–15 Hz larger for sila-neophyl derivatives. Also, the magnitude of $^2J_{Pt\text{-}H}$ coupling constants are consistently *ca* 10 Hz smaller for phosphine complexes than for corresponding nitrogen donor derivatives, implying less *s*-orbital character in the Pt—C—H skeleton and reflecting the generally stronger *trans*-influence of P-donor ligands.[17]

Characteristic patterns-are also observed for the hydrogens on phosphine substituents. These often emerge as doublets of "triplets" due to coupling to both ^{31}P and ^{195}Pt nuclei. An exception is $Pt(CH_2SiMe_2Ph)_2$(dppf), where H_2 and H_6 of the phenyl group generate a very broad singlet at room temperature and the four cyclopentadienyl protons H_Y, $H_{Y'}$, H_Z, $H_{Z'}$ display slightly broadened but unresolved resonances (Fig. 2). Lowering the temperature initially broadens each of these signals, then subsequently they become resolved into doublets. Rate constants (k_c) for the processes responsible for this exchange can be determined from the linewidths at half-height ($\Delta\nu$) at each coalescence point. These rate constants were used to determine the free energies of activation ($\Delta G_c^{\ddagger}$, Table 3) at the coalescence temperature, T_c.[18]

The complex lacks a plane of symmetry unless the phosphine adopts a syn-eclipsed conformation on chelation,[19] resulting in conformers which are enantiomeric. H_Y and $H_{Y'}$ are now magnetically inequivalent, as are H_Z and $H_{Z'}$, and generate distinct resonances. Assuming that there is negligible coupling between hydrogens on different cyclo-

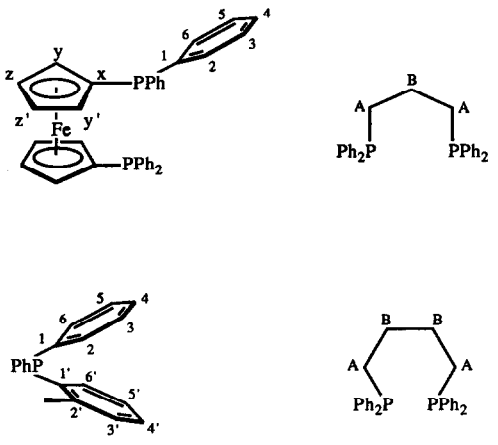

Fig. 1. NMR site designations for P-donor ligands.

Table 2. ^{1}H NMR characteristics of bis-(sila-neophyl)platinum(II) complexes with P-donor ligands

Complex	δ ^{1}H ppm : hydrocarbyl ligand (J_{Pt-H}), Hz [*assignment*]			δ ^{1}H ppm : ancillary ligand (J_{Pt-H}), Hz [*assignment*]
	Pt—CH_2	Si—CH_3	Aromatic ($J_{H_2-H_3}$), Hz	
$Pt(CH_2SiMe_2Ph)_2(PMe_3)_2$[a]	0.50 (**72.3**)	0.19	7.17–7.22m, [H_3, H_4, H_5]; 7.62dd, [H_2, H_6] (**7.6**)	1.14m, (**20.2**) [$P—CH_3$] (J_{P-H} = 7.8 Hz)
$Pt(CH_2SiMe_2Ph)_2(PEt_3)_2$[a]	0.64 (**79.5**)[b]	0.46	7.15–7.19m, [H_3, H_4, H_5]; 7.78dd, [H_2, H_6] (**7.8**)	0.73m, (**14.8**) [$P—CH_2CH_3$] (J_{P-H} = 14.5 Hz); 1.36m, (**15.1**) [$P—CH_2CH_3$] (J_{P-H} = 15.0 Hz)
$Pt(CH_2SiMe_2Ph)_2(PMe_2Ph)_2$[c]	1.15 (**76.3**)	0.66	7.20–7.32m, [H_3, H_4, H_5]; 7.91dd, [H_2, H_6] (**7.7**)	0.91m, (**19.8**) [$P—CH_3$] (J_{P-H} = 7.6 Hz); 6.98–7.03m, [H_3, H_4, H_5]; 7.27[b] [H_2, H_6]
$Pt(CH_2SiMe_2Ph)_2(PMePh_2)_2$[a]	0.75 (**79.8**)	0.13	d[H_3, H_4, H_5]; 7.45dd, [H_2, H_6] (**7.5**)	1.43m, (**20.1**) [$P—CH_3$] (J_{P-H} = 7.2 Hz); 7.16–7.26m, [H_3, H_4, H_5]; 7.29dd, [H_2, H_6]
$Pt(CH_2SiMe_2Ph)_2(PPh_3)_2$[e]	1.18 (**81.7**)[f]	0.37	7.15–7.18m, [H_3, H_4, H_5]; 7.60dd, [H_2, H_6] (**7.8**)	6.80–6.85m, [H_3, H_4, H_5]; 7.37td, [H_2, H_6]
$Pt(CH_2SiMe_2Ph)_2(P\text{-}4\text{-}tol_3)_2$[a]	0.80 (**81.3**)[f]	0.03	7.13–7.19m, [H_3, H_4, H_5]; 7.30dd, [H_2, H_6] (**7.5**)	2.23s, [$Ar—CH_3$]; 6.79d, [H_3, H_5]; 7.12d, [H_2, H_6]
$Pt(CH_2SiMe_2Ph)_2(PPh_2\text{-}2\text{-}tol)_2$[e]	0.89[g]	0.39[g]	7.11–7.18m, [H_3, H_4, H_5]; 7.47dd, [H_2, H_6] (**7.5**)	1.92s, [$Ar—CH_3$]; 6.67–6.89m, [H_3, H_4, H_5]; 6.96–7.05m, [H_2, H_6]; 7.33[g] [$H_{3'}$, $H_{4'}$, $H_{5'}$]; 7.88[g] [$H_{6'}$]
$Pt(CH_2SiMe_2Ph)_2(PPh_2C_6H_4\text{-}2\text{-}CF_3)_2$[e]	0.91[g] (**70.4**)	0.29	7.21–7.28m, [H_3, H_4, H_5]; 7.61dd, [H_2, H_6] (**7.9**)	6.79–6.84m, [H_3, H_4, H_5]; 6.88–7.00m, [$H_{3'}$, $H_{4'}$, $H_{5'}$]; 7.40–7.44m, [H_2, H_6]; 7.65m, [$H_{6'}$]
$Pt(CH_2SiMe_2Ph)_2(dppm)$[c]	1.16 (**86.6**)	0.01	7.12–7.21m, [H_3, H_4, H_5]; 7.45dd, [H_2, H_6] (**7.9**)	4.19m, (**18.8**) [$P—CH_2$] (J_{P-H} = 20.4 Hz); 7.22–7.37m, [H_3, H_4, H_5]; 7.50m, [H_2, H_6]
$Pt(CH_2SiMe_2Ph)_2(dppe)$[c]	1.32 (**81.1**)	0.20	7.17–7.21m, [H_3, H_4, H_5]; 7.52dd, [H_2, H_6] (**6.9**)	1.75m, [$P—CH_2$]; 7.00–7.15m, [H_3, H_4, H_5]; 7.43m, [H_2, H_6]
$Pt(CH_2SiMe_2Ph)_2(dppp)$[a]	0.74 (**80.3**)	0.08	d[H_3, H_4, H_5]; 7.52dd, [H_2, H_6] (**6.3**)	1.85[g]m, [C_BH_2]; 2.42[g]m, [C_AH_2, C_CH_2]; 7.17–7.33m, [H_3, H_4, H_5] 7.42m, [H_2, H_6]
$Pt(CH_2SiMe_2Ph)_2(dppb)$[c]	1.16 (**79.2**)	0.40	7.19–7.26m, [H_3, H_4, H_5]; 7.65dd, [H_2, H_6] (**7.4**)	1.44[g]m, [C_BH_2, C_CH_2]; 2.09[g]m, [C_AH_2, C_DH_2]; 7.04[g] [H_3, H_4, H_5]; 7.45[g] [H_2, H_6]
$Pt(CH_2SiMe_2Ph)_2(dppf)$[c]	1.12[g]	0.33	7.10–7.17m, [H_3, H_4, H_5]; 7.56dd, [H_2, H_6] (**7.9**)	3.71s, [H_Y, $H_{Y'}$]; 3.99s, [H_Z, $H_{Z'}$]; 7.05[g]m, [H_3, H_4, H_5]; 7.70[g]m, [H_2, H_6]

[a] Chloroform-d^1.
[b] Partially obscured by ligand resonances.
[c] Benzene-d^6.
[d] Obscured.
[e] Toluene-d^8.
[f] Obtained at 90 MHz.
[g] Broad resonance.

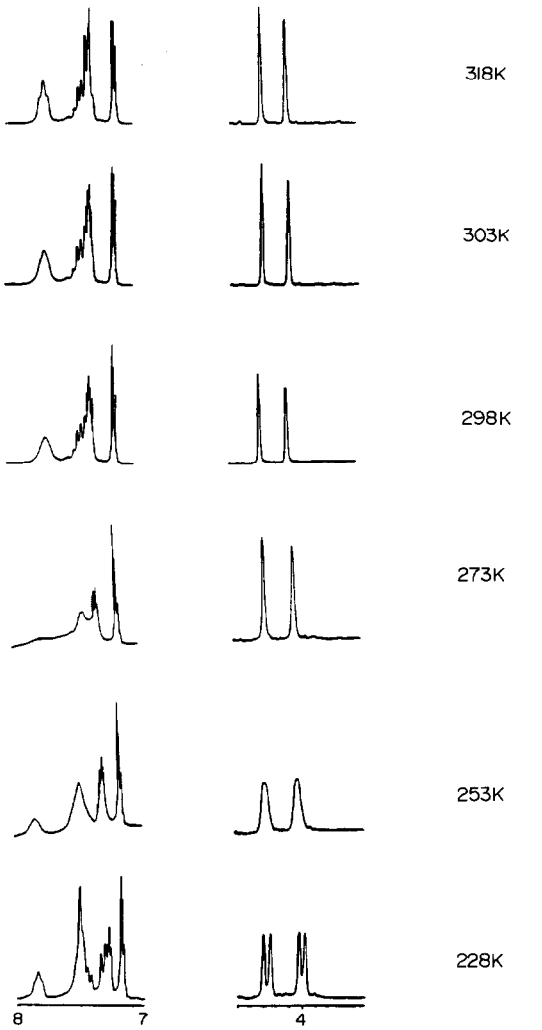

Fig. 2. Temperature-dependence of ^{1}H NMR spectrum of $Pt(CH_2SiMe_2Ph)_2(dppf)$.

pentadienyl rings, the observed low temperature spectrum (representing, ideally, an $A_2B_2C_2D_2$ system) may be explained by slow exchange of these conformers. At high temperatures, rapid exchange gives rise to a time-averaged spectrum ($A_2A_{2'}B_2B_{2'}$) in which H_Y, $H_{Y'}$ and H_Z, $H_{Z'}$ exhibit single resonances. Similarly the two phenyl substituents on each phosphorus are magnetically non-equivalent. Although all the phenyl hydrogens exhibit this type of behaviour, it is most prominent in the resonances due to H_2 and H_6 which collapse forming a broadened triplet at higher temperatures.[20] Assuming that the values of $\Delta G_c^{\ddagger}$ derive from the same process, then $\Delta H_c^{\ddagger}$ is estimated at 43.0 ($\pm$1.0) kJ mol^{-1} and $\Delta S_c^{\ddagger}$ at -43.4 ($\pm$2.0) J K^{-1} mol^{-1}. These values are very similar to those observed previously for related systems[16] indicating that the process is essentially independent of the nature of the alkyl group.

^{31}P NMR. The $^{31}P\{^1H\}$ NMR data for bis-(silaneophyl)bis-(phosphine)platinum(II) complexes appear in Table 4. Spin–spin coupling of ^{31}P to ^{195}Pt results in the expected "triplet" observed for all of these complexes. For L = PPh_2-2-$C_6H_4CF_3$ a "triplet" of quartets due to coupling of three ^{19}F nuclei to ^{31}P was anticipated, instead, a broad "triplet" was observed. The ^{19}F NMR, however, showed the expected doublet with $^4J_{P\text{-}F} = 4.4$ Hz. With the exception of $Pt(CH_2SiMe_2Ph)_2(dppm)$, the $^1J_{Pt\text{-}P}$ coupling constants are in the range 1950–2065 Hz, typical for *cis*-bis-(phosphine)platinum(II) dialkyl compounds.[1,8,16] The especially low value of 1615 Hz for $Pt(CH_2SiMe_2Ph)_2(dppm)$ is a general coordination feature of this ligand and can be ascribed to angular constraints around Pt and P due to the four-membered ring.[21]

Phosphorus nuclei incorporated in chelate rings display a ring contribution, Δ_R, to their chemical shift change upon coordination. The magnitude and direction of Δ_R depend on ring substitution and size.[22] The ring contribution, defined as $\Delta_R = \Delta - \Delta_{R^\circ}$ [where Δ is the difference in the chemical shift upon coordination (δP–δF) and Δ_{R° is a standard ring contribution] has been determined for the series of bidentate phosphine complexes (Table 5). The four-membered ring has a shielding effect

Table 3. Variable temperature ^{1}H NMR data for $Pt(CH_2SiMe_2Ph)_2(dppf)$

Resonance	T_c, K[a]	$\Delta\nu$, Hz[b]	k_c, s^{-1}[c]	$\Delta G_c^{\ddagger}$, kJ mol^{-1}[d]
H_2, H_6	275	102.3	227.2	54.76
H_Y, $H_{Y'}$	253	17.8	39.3	53.88
H_Z, $H_{Z'}$	251	16.2	38.2	53.66

[a] Error $\pm$1 K.
[b] Error $\pm$2%.
[c] Error $\pm$2%.
[d] Error $\pm$1%.

Table 4. ^{31}P NMR characteristics for bis-(sila-neophyl)platinum(II) complexes with P-donor ligands

Complex	δ^a, ppm	$J_{Pt\text{-}P}$, Hz
$Pt(CH_2SiMe_2Ph)_2(PMe_3)_2$[b]	−28.1	1987
$Pt(CH_2SiMe_2Ph)_2(PEt_3)_2$[c]	2.6	2016
$Pt(CH_2SiMe_2Ph)_2(PMe_2Ph)_2$[b]	−16.9	2020
$Pt(CH_2SiMe_2Ph)_2(PMePh_2)_2$[b]	0.9	2029
$Pt(CH_2SiMe_2Ph)_2(PPh_3)_2$[c]	23.3	2034
$Pt(CH_2SiMe_2Ph)_2(P\text{-}4\text{-}tol_3)_2$[d]	21.7	2054
$Pt(CH_2SiMe_2Ph)_2(PPh_2\text{-}2\text{-}tol)_2$[d]	22.3	1976
$Pt(CH_2SiMe_2Ph)_2(PPh_2C_6H_4\text{-}2\text{-}CF_3)_2$[d]	34.0	2029
$Pt(CH_2SiMe_2Ph)_2(dppm)$[b]	−43.5	1615
$Pt(CH_2SiMe_2Ph)_2(dppe)$[c]	40.8	1954
$Pt(CH_2SiMe_2Ph)_2(dppp)$[d]	−1.3	1923
$Pt(CH_2SiMe_2Ph)_2(dppb)$[b]	11.5	1996
$Pt(CH_2SiMe_2Ph)_2(dppf)$[b]	18.1	2060

[a] ppm relative to 85% H_3PO_4–D_2O.
[b] Chloroform-d^1.
[c] Toluene-d^8.
[d] Benzene-d^6.
[e] $J_{P\text{-}F}$ = 4.4 Hz.

relative to *cis*-$Pt(CH_2SiMe_2Ph)_2(PPh_2Me)_2$, whilst the five-membered ring has a deshielding effect. These values are in good agreement with those obtained for other PtR_2L compounds (L = dppm, dppe, dppp, dppb; R = Me, $CH_2SiMe_2CH_2$:CH_2, CH_2SiMe_3)[1,16,22].

Also noteworthy is the magnitude of $^1J_{Pt\text{-}P}$, which is consistently 300–400 Hz greater in sila-neophyl than in neophyl analogues. The same trend has been observed in comparison of analogous neopentyl and trimethylsilylmethyl derivatives (cf. Fig. 3).[14]

^{13}C NMR. $^{13}C\{^1H\}$ NMR characteristics of sila-neophyl complexes are presented in Table 6. Assignments have been made by comparison with the free ligand, by the magnitude of Pt—C coupling constants, on the basis of peak intensities and (in some cases) ADEPT measurements, and are in accord with those noted elsewhere.[8,15,16,23] Typically, carbon atoms on coordinated phosphine show coupling to both ^{31}P and ^{195}Pt producing a doublet of "triplets". $^3J_{Pt\text{-}C}$ coupling is observed to the silicon-bound methyl carbons and to C_1 of the aromatic ring, of magnitude 20–30 Hz. Notably, for unhindered monodentate phosphines, the value of $^3J_{Pt\text{-}C}$ for Si—CH_3 groups is noticeably larger than for Si—C_1. As the steric bulk of the ligand is increased, a decrease in $^3J_{Pt\text{-}C_{methyl}}$ and a corresponding increase in $J_{Pt\text{-}C_1}$ are observed—presumably reflect-

Table 5. ^{31}P NMR ring shift contributions for $Pt(CH_2SiMe_2Ph)_2L_2$ complexes[a]

L	δP, ppm	δF, ppm	Δ, ppm	Δ_R, ppm	Chelate ring size
dppm[b]	−43.5	−22.7	−20.8	−57.9	4
dppe[c]	40.8	−13.2	+54.0	+16.9	5
dppp[d]	−1.3	−17.3	+16.0	−12.1	6
dppb[b]	11.5	−15.0	+26.5	−0.6	7
dppf[b]	18.1	−28.1	+29.0	−8.1	(7)
PPh_2Me[b]	0.9	−28.1	+37.1	0.0	—

[a] Free phosphine chemical shifts obtained from ref. 22.
[b] Chloroform-d^1.
[c] Toluene-d^8.
[d] Benzene-d^6.

Table 6. ^{13}C NMR characteristics of bis-(sila-neophyl)platinum(II) complexes with P-donor ligands

Complex	$\delta^{13}C$ ppm : hydrocarbyl ligands (J_{Pt-C}), Hz [*assignment*]			$\delta^{13}C$ ppm: ancillary ligands (J_{Pt-C}), Hz [*assignment*]
	Pt—CH_2	Si—CH_3	Aromatic	
$Pt(CH_2SiMe_2Ph)_2(PMe_3)_2$[a]	5.97, 8.63 **(524.6)** ($J_{C\text{-}P_{Trans}}$ = 94.3 Hz) ($J_{C\text{-}P_{Cis}}$ = 8.8 Hz)	2.32 **(28.4)**	126.97 [C_3, C_5]; 127.34 [C_4]; 134.29 [C_2, C_6]; 146.37 **(21.8)** [C_1]	17.17 **(29.4)** [*P—CH*$_3$] ($J_{C\text{-}P}$ = 31.4 Hz)
$Pt(CH_2SiMe_2Ph)_2(PEt_3)_2$[a]	3.12, 4.62 **(540.7)** ($J_{C\text{-}P_{Trans}}$ = 94.0 Hz) ($J_{C\text{-}P_{Cis}}$ = 8.0 Hz)	2.80 **(28.6)**	127.13 [C_3, C_5]; 127.31 [C_4]; 133.85 [C_2, C_6]; 146.55 **(23.1)** [C_1]	8.28 [*P—CH*$_2$—*CH*$_3$] ($J_{C\text{-}P}$ = 17.9 Hz); 16.92 **(24.1)** [*P—CH*$_2$*CH*$_3$] ($J_{C\text{-}P}$ = 27.2 Hz)
$Pt(CH_2SiMe_2Ph)_2(PMe_2Ph)_2$[a]	4.22, 5.70 **(536.2)** ($J_{C\text{-}P_{Trans}}$ = 93.6 Hz) ($J_{C\text{-}P_{Cis}}$ = 8.3 Hz)	2.51 **(27.5)**	127.15 [C_3, C_5]; 127.45 [C_4]; 134.20 [C_2, C_6]; 146.19 **(23.6)** [C_1]	14.83 **(28.7)** [*P—CH*$_3$] ($J_{C\text{-}P}$ = 31.5 Hz); 128.02 **(13.8)** [C_3, C_5] ($J_{C\text{-}P}$ = 8.3 Hz); 129.21 [C_4]; 130.87 **(13.9)** [C_2, C_6] ($J_{C\text{-}P}$ = 10.6 Hz); 138.96 **(17.2)** [C_1] ($J_{C\text{-}P}$ = 45.0 Hz)
$Pt(CH_2SiMe_2Ph)_2(PPh_2Me)_2$[a]	5.28, 6.75 **(551.6)** ($J_{C\text{-}P_{Trans}}$ = 92.5 Hz) ($J_{C\text{-}P_{Cis}}$ = 7.4 Hz)	2.44 **(26.8)**	127.02 [C_3, C_5]; 127.31 [C_4]; 134.08 [C_2, C_6]; 146.05 **(25.8)** [C_1]	14.24 **(22.7)** [*P—CH*$_3$] ($J_{C\text{-}P}$ = 31.3 Hz); 127.84 **(12.9)** [C_3, C_5] ($J_{C\text{-}P}$ = 9.4 Hz); 129.26 [C_4]; 132.86 **(13.5)** [C_3, C_5] ($J_{C\text{-}P}$ = 10.1 Hz); 136.08 **(19.6)** [C_1] ($J_{C\text{-}P}$ = 44.6 Hz)
$Pt(CH_2SiMe_2Ph)_2(PPh_3)_2$[a]	6.38, 7.84 **(575.9)** ($J_{C\text{-}P_{Trans}}$ = 92.2 Hz) ($J_{C\text{-}P_{Cis}}$ = 6.1 Hz)	2.66 **(24.4)**	126.87 [C_3, C_5]; 127.17 [C_4]; 134.16 [C_2, C_6]; 145.80 **(28.1)** [C_1]	127.40 **(7.0)** [C_3, C_5] ($J_{C\text{-}P}$ = 8.3 Hz); 129.16 [C_4]; 133.48 **(18.9)** [C_1] ($J_{C\text{-}P}$ = 44.2 Hz); 134.77 **(11.8)** [C_2, C_6] ($J_{C\text{-}P}$ = 10.8 Hz)
$Pt(CH_2SiMe_2Ph)_2(P\text{-}4\text{-}tol_3)_2$[a]	5.53, 7.13 **(573.9)** ($J_{C\text{-}P_{Trans}}$ = 92.7 Hz) ($J_{C\text{-}P_{Cis}}$ = 6.5 Hz)	2.75 **(23.4)**	126.76 [C_3, C_5]; 126.99 [C_4]; 134.08 [C_2, C_6]; 146.26 **(29.6)** [C_1]	21.16 [*Ar—CH*$_3$]; 128.00 **(14.5)** [C_3, C_5] ($J_{C\text{-}P}$ = 8.6 Hz); 130.60 **(18.7)** [C_1] ($J_{C\text{-}P}$ = 46.33 Hz); 134.73 **(12.3)** [C_2, C_6] ($J_{C\text{-}P}$ = 10.9 Hz); 138.91 [C_4]
$Pt(CH_2SiMe_2Ph)_2(PPh_2\text{-}2\text{-}tol)_2$[a]	4.97, 6.44 **(587.3)** ($J_{C\text{-}P_{Trans}}$ = 92.1 Hz) ($J_{C\text{-}P_{Cis}}$ = 5.1 Hz)	2.22 **(22.1)**	126.85 [C_3, C_5]; 127.14 [C_4]; 133.87 [C_2, C_6]; 145.78 **(31.0)** [C_1]	23.15 [*Ar—CH*$_3$]; 125.05 [$C_{5'}$] ($J_{C\text{-}P}$ = 10.8 Hz); 127.38 [$C_{3'}$]; 127.49 [C_3, C_5]; 128.85 [C_4]; 130.08 [$C_{4'}$]; 131.33 [$C_{6'}$] ($J_{C\text{-}P}$ = 4.9 Hz); 134.94 **(12.3)** [C_2, C_6] ($J_{C\text{-}P}$ = 10.9 Hz); 135.24 [$C_{2'}$]; 138.00 [C_1] ($J_{C\text{-}P}$ = 14.0 Hz); 142.75 [$C_{1'}$]
$Pt(CH_2SiMe_2Ph)_2(dppm)$[b]	2.74, 4.34 **(571.2)** ($J_{C\text{-}P_{Trans}}$ = 94.6 Hz) ($J_{C\text{-}P_{Cis}}$ = 7.0 Hz)	2.6 **(27.9)**	127.47 [C_3, C_5]; c[C_4]; 134.32 [C_2, C_6]; 146.33 **(29.1)** [C_1]	48.55 **(10.6)** [*P—CH*$_2$—*P*]; ($J_{C\text{-}P}$ = 50.7 Hz); 128.79 **(10.3)** [C_3, C_5] ($J_{C\text{-}P}$ = 9.9 Hz); 130.35 [C_4]; 132.67 **(26.5)** [C_1] ($J_{C\text{-}P}$ = 19.6 Hz); 133.18 **(13.8)** [C_2, C_6] ($J_{C\text{-}P}$ = 12.1 Hz)

Table 6—*continued*

Complex	δ^{13}C ppm: hydrocarbyl ligands (J_{Pt-C}), Hz [*assignment*]			δ^{13}C ppm: ancillary ligands (J_{Pt-C}), Hz [*assignment*]
	Pt—CH_2	Si—CH_3	Aromatic	
$Pt(CH_2SiMe_2Ph)_2(dppe)$[a]	−0.04, 1.38 (**548.6**) ($J_{C\text{-}P_{Trans}}$ = 89.7 Hz) ($J_{C\text{-}P_{Cis}}$ = 5.1 Hz)	1.76 (**36.5**)	126.89 [C_3, C_5]; 127.04 [C_4]; 133.71 [C_2, C_6]; 146.55 (**34.6**) [C_1]	27.70m, [*P*—CH_2—CH_2—*P*]; 128.28 [C_3, C_5] ($J_{C\text{-}P}$ = 9.7 Hz); 130.13 [C_4]; 132.91 (**26.3**) [C_1] ($J_{C\text{-}P}$ = 45.2 Hz); 133.50 [C_2, C_6] ($J_{C\text{-}P}$ = 11.0 Hz)
$Pt(CH_2SiMe_2Ph)_2(dppp)$[a]	4.47, 5.94 (**551.4**) ($J_{C\text{-}P_{Trans}}$ = 92.5 Hz) ($J_{C\text{-}P_{Cis}}$ = 9.5 Hz)	2.47 (**25.7**)	126.79 [C_3, C_5]; 127.47 [C_4]; 134.17 [C_2, C_6]; 146.26 (**25.4**) [C_1]	20.05 [C_BH_2]; 26.74m, [C_AH_2]; 127.88 (**9.3**) [C_3, C_5] ($J_{C\text{-}P}$ = 8.3 Hz); 128.23 [C_4]; 133.46 (**12.7**) [C_2, C_6] ($J_{C\text{-}P}$ = 14.2 Hz); 135.00 (**19.3**) [C_1] ($J_{C\text{-}P}$ = 30.6 Hz)
$Pt(CH_2SiMe_2Ph)_2(dppb)$[b]	5.84, 7.29 (**552.8**) ($J_{C\text{-}P_{Trans}}$ = 90.9 Hz) ($J_{C\text{-}P_{Cis}}$ = 7.3 Hz)	2.68 (**26.8**)	127.32 [C_3, C_5]; 127.42 [C_4]; 134.61 [C_2, C_6]; 146.38 (**25.5**) [C_1]	27.47 [C_BH_2]; 27.69m, [C_AH_2]; 128.30 [C_3, C_5] ($J_{C\text{-}P}$ = 4.8 Hz); 129.62 [C_4]; 133.97d, [C_2, C_6]; 135.65 (**22.6**) [C_1] ($J_{C\text{-}P}$ = 44.8 Hz)
$Pt(CH_2SiMe_2Ph)_2(dppf)$[a,e]	5.42, 6.91 (**559.4**) ($J_{C\text{-}P_{Trans}}$ = 93.8 Hz) ($J_{C\text{-}P_{Cis}}$ = 6.1 Hz)	2.36 d	126.80 [C_3, C_5]; 127.14 [C_4]; 133.93 [C_2, C_6]; 146.03 (**29.3**) [C_1]	71.93 [C_Z, $C_{Z'}$]; 74.85 [C_Y, $C_{Y'}$] ($J_{C\text{-}P}$ = 3.1 Hz); 77.79 (**51.6**) [C_X]; 127.66 [C_3, C_5]; ($J_{C\text{-}P}$ = 7.0 Hz); 128.31 [C_4]; 134.27d, [C_1]; 134.98d, [C_2, C_6]

[a] Chloroform-d[1].
[b] Benzene-d[6].
[c] Obscured.
[d] Broad resonance.
[e] Measured at −10°C.

ing changes in *s*-orbital contributions to the Pt—CH_2—Si—C skeleton. Relatedly, a corresponding increase in the magnitude of $^1J_{Pt\text{-}C}$ from PMe_3 (524 Hz) to $PPh_2C_6H_4$-2-CF_3 (587 Hz) is also observed.

Just as $^1J_{Pt\text{-}P}$ is larger (*vide supra*), the magnitude of $^1J_{Pt\text{-}C}$ for sila-neophyl derivatives is characteristically 130–160 Hz smaller than that for the analogous neophyl complexes and is very similar to those for corresponding *cis*-$Pt(CH_2SiMe_3)_2L_2$[23] and *cis*-$Pt(CH_2SiMe_2CH_2:CH_2)_2L_2$.[16] Comparing, for instance, $Pt(CH_2SiMe_2Ph)_2(dppe)$ with its carbon equivalent, a reduction of 133 Hz in $^1J_{Pt\text{-}C}$ is matched by an increase in $^1J_{Pt\text{-}P}$ of 370 Hz. The extent of change in the two couplings is—perhaps fortuitiously—similar (*ca* 24%), and typical for analogues for which comparative data are available; notably, the methylplatinum homologue exhibits intermediate values (Fig. 3). These variations may be attributed to a greater carbon 2*s*-orbital contribution to Pt—C bonding in the presence of the more electronegative (and, perhaps, sterically more demanding) β-carbon, which, as has been discussed by us elsewhere,[16,23] affects the disposition of the platinum 6*s*-orbital in the linear C—Pt—P skeleton.

These observations are further substantiation of an apparently weaker *trans*-influence for the β-silaalkyl than for the analogous carbon ligand—and, by conventional wisdom, stronger Pt—C bonds involving the latter. Ancillary ligand dissociation is often a prerequisite for thermolytic rearrangements

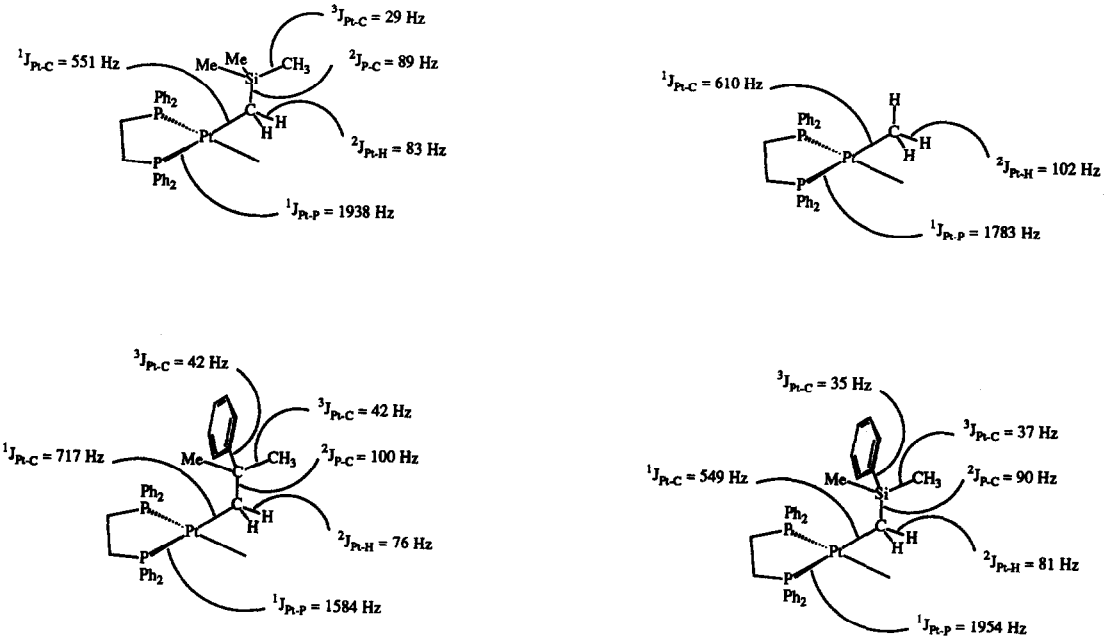

Fig. 3. Selected NMR spin–spin coupling constants for $PtR_2(dppe)$.

of this type of complex (see ref. 8, and references cited therein) and, therefore, such a difference in ground state energies may have a kinetic influence on lability, perhaps contributing to the (usually) readier reactivity of neophyl (and related) complexes compared to silicon-bearing analogues. We are engaged in other studies to evaluate more fully the internal energetics of these systems. As will emerge,[24] however, while Pt—P scission is generally a mechanistic prerequisite in both cases, the preferred modes of reactivity for corresponding silaneophyl- and neophylplatinum(II) complexes may differ completely.

Acknowledgements—We thank Dick Sheppard and Sue Johnson for high field NMR measurements and Ms D. J. Wilkes for an experimental contribution at the outset of this work. The award of a studentship by the SERC (to B.C.A.) is also acknowledged gratefully. As ever, we are greatly indebted to Johnson-Matthey plc for their continuous support via generous loans of platinum.

REFERENCES

1. S. K. Thomson and G. B. Young, *Organometallics* 1989, **8**, 2068.
2. Pan Yi and G. B. Young, manuscript in preparation.
3. R. A. Andersen, R. A. Jones and G. Wilkinson, *J. Chem. Soc., Dalton Trans.* 1978, 446.
4. P. J. Desrosiers, R. S. Shinomoto and T. C. Flood, *J. Am. Chem. Soc.* 1986, **108**, 7964.
5. T. H. Tulip and D. L. Thorn, *J. Am. Chem. Soc.* 1981, **103**, 2448.
6. T. Gregory, P. Harper, P. J. Desrosiers and T. C. Flood, *Organometallics* 1990, **9**, 2523.
7. (a) P. Foley and G. M. Whitesides, *J. Am. Chem. Soc.* 1979, **101**, 2732; (b) P. Foley, R. DiCosimo and G. M. Whitesides, *J. Am. Chem. Soc.* 1980, **102**, 6713.
8. D. C. Griffiths and G. B. Young, *Organometallics* 1989, **8**, 875.
9. B. C. Ankianiec and G. B. Young, *Polyhedron* 1989, **8**, 56.
10. D. F. Shriver, *The Manipulation of Air Sensitive Compounds*. McGraw-Hill, New York (1986).
11. J. E. Leffler and R. D. Temple, *J. Am. Chem. Soc.* 1967, **89**, 5235.
12. H. A. Brune, M. Falck, R. Hemmer, G. Schmidtberg and H. G. Alt, *Chem. Ber.* 1984, **117**, 2791.
13. I. M. Ismail, S. J. S. Kerrison and P. J. Sadler, *Polyhedron* 1982, **1**, 57.
14. S. K. Thomson, Ph.D. Thesis, University of London (1988).
15. R. D. Kelly, Ph.D. Thesis, University of London (1988).
16. R. D. Kelly and G. B. Young, *Polyhedron* 1989, **8**, 433.
17. T. G. Appleton, H. C. Clark and L. E. Manzer, *Coord. Chem. Rev.* 1973, **3**, 62.
18. (a) H. Kessler, *Angew. Chem. Int. Ed. Engl.* 1970, **9**, 219; (b) D. Kost, E. H. Carlson and M. Raban, *J. Chem. Soc., Chem. Commun.* 1971, 656.
19. (a) E. W. Abel, M. Booth and K. G. Orrell, *J. Organ-*

omet. Chem. 1980, **186**, C37; (b) J. J. Bishop and A. Davidson, *Inorg. Chem.* 1971, **10**, 826.
20. (a) I. R. Butler, W. R. Cullen, T. J. Kim, S. J. Rettig and J. Trotter, *Organometallics* 1985, **4**, 972; (b) W. R. Cullen, T. J. Kim, F. W. B. Einstein and T. Jones, *Organometallics* 1983, **2**, 714.
21. (a) T. G. Appleton, M. A. Bennett and I. B. Tompkins, *J. Chem. Soc., Dalton Trans.* 1976, 439; (b) P. S. Braterman, R. J. Cross, L. Manojlović-Muir, K. W. Muir and G. B. Young, *J. Organomet. Chem.* 1975, **84**, C40.
22. P. E. Garrou, *Chem. Rev.* 1981, **81**, 229.
23. S. K. Thomson and G. B. Young, *Polyhedron* 1988, **7**, 1953.
24. B. C. Ankianiec, V. Christou, D. T. Hardy, S. K. Thomson and G. B. Young, manuscript in preparation.

Polyhedron Vol. 10, No. 12, pp. 1423–1425, 1991
Printed in Great Britain

0277–5387/91 $3.00+.00
© 1991 Pergamon Press plc

A NEW RHENIUM–COBALT CARBONYL CLUSTER. X-RAY CRYSTAL STRUCTURE OF $ReCo_3(\mu_3\text{-}NBu^t)_2(\mu\text{-}CO)_2(CO)_8$

VAHE SABOONCHIAN, ANGEL GUTIERREZ and GEOFFREY WILKINSON*

Johnson Matthey Laboratory, Chemistry Department, Imperial College, London SW7 2AY, U.K.

and

BILQUIS HUSSAIN-BATES and MICHAEL B. HURSTHOUSE*

Chemistry Department, Queen Mary and Westfield College, Mile End Road, London E1 4NS, U.K.

(*Received* 10 *December* 1990; *accepted* 20 *February* 1991)

Abstract—The interaction of $Re(NBu^t)_3Cl$ with dicobalt octacarbonyl in hexane gives rise to the cluster $ReCo_3(NBu^t)_2(CO)_{10}$ that has the metal atoms with a "butterfly" type core together with two (μ_3-NBu^t) and two (μ-CO) groups. The rhenium atom has three CO terminal groups, and the two wingtip cobalt atoms have two terminal CO groups.

The interaction of $Re(NBu^t)_3Cl$[1] and $Co_2(CO)_8$ in hexane leads to the isolation of dark red–violet crystals of a compound of stoichiometry $ReCo_3(NBu^t)_2(CO)_{10}$. The compound is moderately air and moisture sensitive and is soluble in common organic solvents. Spectroscopic data are not instructive but the ^1H NMR spectrum has a singlet at 0.88 pm for the NBu^t group, while the IR spectrum has a complicated carbonyl region. The structure of the molecule which has mirror symmetry was determined by X-ray crystallography and is shown in Fig. 1. Bond lengths and angles are given in Table 1.

The geometry is best described in terms of a butterfly[2] structure with the wing fold along the vector Re...Co(1) which lies on the crystallographic mirror plane. In each $ReCo_2$ wing triangle the Re—Co distances are very similar [2.581, 2.602(5) Å] and the Co—Co distance of 2.435(6) Å seems to indicate equivalent strength. The capping imido function bonds slightly asymmetrically, with Co—N distances of 1.98(1) Å[Co(1)] and 1.89(1) Å[Co(2)] and Re—N 2.02(1) Å. On the other hand, the CO bridging across the Co(1)...Co(2) edge is almost symmetrical, with Co—C distances of 1.94(2) and 1.96(2) Å. The Co(2)...Co(2a) distance between wingtips is 3.571(7) Å. If the imido functions act as four electron donors, then the total electron count is 62 e and the structure is then immediately classified as an arachno derivative of an octahedral parent (for electron counting schemes see ref. 2, p. 1068).

There are several precedents for μ_3-NR groups in cluster chemistry, e.g. for tungsten,[3b] where π overlaps in the NPh bridge are discussed and for ruthenium.[3c] Gold compounds[3d] have PhN bridging separate $AuPR_3$ groups. As far as we are aware no μ_3 bridged species of rhenium have previously been reported.

EXPERIMENTAL

To a solution of $Re(NBu^t)_3Cl$ (0.35 g, 0.80 mmol) in hexane (30 cm^3) at −78°C was added a solution of $Co_2(CO)_8$ (0.42 g, 1.2 mmol) in hexane (10 cm_3), and the solution allowed to warm. After 5 h stirring, filtration from black insoluble matter, concentration (to *ca* 7 cm^3) and cooling (−20°C) gave dark red–violet crystals. Yield: 0.2 g (33%). m.p.: 178–180°C. [Found: C, 28.1; H, 2.6; N, 3.7; O, 18.7; $C_{17}H_{18}Co_3N_2O_9Re$ requires C, 27.5; H, 2.3; N, 3.6; O, 20.4%.] MS(EI). The spectrum

* Authors to whom correspondence should be addressed.

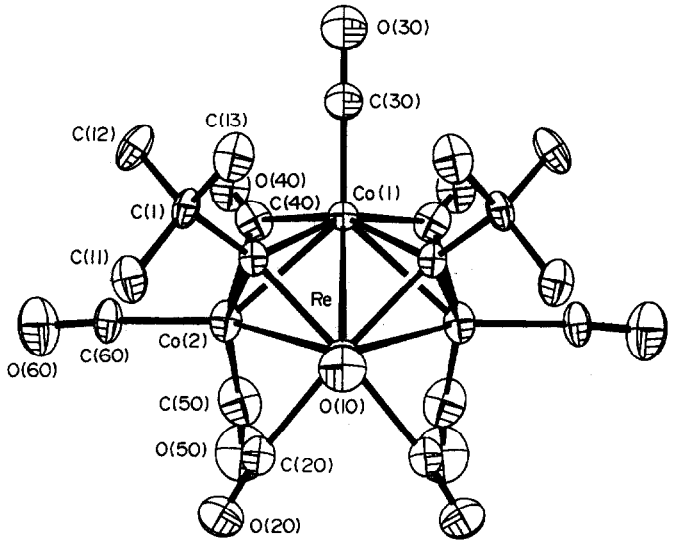

Fig. 1. The X-ray structure of $ReCo_3(NBu^t)_2(CO)_{10}$.

Table 1. Bond lengths (Å) and angles (°) for $ReCo_3(\mu_3\text{-}NBu^t)_2(\mu\text{-}CO)_2(CO)_8$

Bond lengths (Å)

C(10)—Re(1)	1.918(24)	C(20)—Re(1)	2.026(17)
N(1)—Re(1)	2.017(13)	C(30)—Co(1)	1.758(23)
C(40)—Co(1)	1.957(18)	N(1)—Co(1)	1.982(13)
N(1)—Co(2)	1.888(13)	C(40)—Co(2)	1.941(16)
C(50)—Co(2)	1.803(21)	C(60)—Co(2)	1.809(18)
O(10)—C(10)	1.132(27)	O(20)—C(20)	1.088(20)
O(30)—C(30)	1.137(28)	C(1)—N(1)	1.548(19)
C(11)—C(1)	1.537(24)	C(12)—C(1)	1.498(22)
C(13)—C(1)	1.501(24)	O(40)—C(40)	1.168(18)
O(50)—C(50)	1.125(21)	C(60)—O(60)	1.093(22)
Co(1)—Co(1a)	3.571(7)	Co(1)—Re(1)	2.602(5)
Co(2)—Re(1)	2.581(5)		

Bond angles (°)

C(20)—Re(1)—C(10)	92.7(7)	C(20)—Re(1)—C(20a)	78.5(5)
N(1)—Re(1)—Co(1)	48.8(3)	N(1)—Re(1)—Co(2)	46.5(3)
N(1)—Re(1)—C(10)	99.0(6)	N(1)—Re(1)—C(20)	96.8(6)
N(1)—Re(1)—C(20a)	167.6(4)	N(1)—Re(1)—N(1a)	85.5(7)
Co(2)—Co(1)—Co(2a)	94.3(2)	C(40)—Co(1)—C(30)	94.4(9)
N(1)—Co(1)—C(30)	107.5(8)	N(1)—Co(1)—C(40)	157.9(5)
N(1)—Co(1)—N(1a)	87.4(6)	C(40)—Co(1)—C(40a)	88.3(10)
C(50)—Co(2)—N(1)	157.2(7)	C(60)—Co(2)—N(1)	106.1(8)
C(60)—Co(2)—C(50)	94.0(10)	C(40)—Co(2)—N(1)	90.7(6)
C(50)—Co(2)—C(40)	96.1(8)	C(60)—Co(2)—C(40)	101.0(8)
O(10)—C(10)—Re(1)	177.7(18)	O(20)—C(20)—Re(1)	171.2(15)
Co(1)—N(1)—Re(1)	81.2(5)	Co(2)—N(1)—Re(1)	82.7(5)
C(1)—N(1)—Re(1)	138.0(8)	Co(2)—C(40)—Co(1)	77.7(6)
O(30)—C(30)—Co(1)	173.6(24)	O(40)—C(40)—Co(1)	143.4(13)
Co(2)—N(1)—Co(1)	77.9(5)	C(1)—N(1)—Co(1)	131.2(8)
C(1)—N(1)—Co(2)	124.7(10)	O(40)—C(40)—Co(2)	139.0(13)
O(50)—C(50)—Co(2)	174.8(19)	O(60)—C(60)—Co(2)	170.3(19)
C(11)—C(1)—N(1)	105.1(13)	C(12)—C(1)—N(1)	109.0(13)
C(12)—C(1)—C(11)	112.8(15)	C(13)—C(1)—N(1)	109.0(13)
C(13)—C(1)—C(11)	110.8(15)	C(13)—C(1)—C(12)	110.0(15)
C(50)—Co(2)—Co(1)	117.0(7)		

Key to symmetry operations relating designated atoms to reference atoms at (x, y, z): (a) x, 0.5-y, z.

shows the correct rhenium isotope patterns; data only for ^{187}Re; 758(M^+—CO); 730(M^+—2CO); 702(M^+—3CO); 674(M^+—4CO); 646(M^+—5CO); 618(M^+—6CO); 590(M^+—7CO); 562 (M^+—8CO); 534(M^+—9CO); 506(M^+—10CO). IR (Nujol mull): 2077s, 2033s, 1994s, 1923s, 1893s, 1387m, 1362m, 1171m, 1014w, 673w, 641w, 622w, 602m, 563w, 531w, 510w, 493w, 459m, 405w. NMR $^1H(C_6D_6)$: 0.88 (s, NBu^t).

X-ray crystallography

The crystal used for X-ray work was sealed in a thin-walled glass capillary. Following preliminary photography, unit cell dimensions and intensity data were obtained using standard procedures and a CAD4 diffractometer with graphite monochromated Mo-K_α radiation ($\lambda = 0.71069$ Å) operating in the $\omega/2\theta$ scan mode. The structure was solved by direct methods and refined by full matrix least-squares. All atoms were refined with anisotropic displacement factor coefficients; no hydrogens were included. Experimental details are as follows.

Crystal data. $C_{18}H_{18}N_2O_{10}Co_3Re$, $M_r = 785.36$, monoclinic $a = 8.764(2)$, $b = 16.822(3)$, $c = 9.225(2)$ Å, $\beta = 116.71(2)°$, $V = 1214.9$ Å^3, space group $P2_1/m$, $Z = 2$, $D_c = 2.14$ g cm^{-3}, μ(Mo-K_α) = 64.5 cm^{-1}, $F(000) = 752$.

Data collection. $1.5 \leqslant \theta \leqslant 23.0°$, $0 \leqslant h \leqslant g$, $0 \leqslant k \leqslant 18$, $-10 \leqslant l \leqslant 10$, 1886 data collected, 1752 unique, 1371 observed [$F_o > 3\sigma(F_o)$]. *Lp* and empirical absorption corrections based on psi-scans.

Refinement. 163 Parameters, weights = $[\sigma(F)^2 + 0.01F_o]^{-1}$, $R = 0.059$, $R_w = 0.063$. All calculations made using SHELX 80 installed on a T800 transputer hosted by an IBM/AT clone.

Acknowledgements—We thank the SERC (V.S.) for a studentship and X-ray facilities and Universidad Complutense, Madrid, for study leave (A.G.).

REFERENCES

1. A. A. Danopoulos, C. J. Longley, G. Wilkinson, B. Hussain and M. B. Hursthouse, *Polyhedron* 1989, **8**, 2657.
2. F. A. Cotton and G. Wilkinson, *Advanced Inorganic Chemistry*, 5th edn, p. 1059. Wiley, New York (1988).
3. (a) See ref. 2, p. 370; (b) D. C. Bradley, R. J. Errington, M. B. Hursthouse and R. L. Short, *J. Chem. Soc., Dalton Trans.* 1990, 1043; (c) M. Pizzotti, F. Porta, S. Cenini and F. Demartin, *J. Organomet. Chem.* 1988, **356**, 105; M. Pizzotti, S. Cenini, C. Crotti and F. Demartin, *J. Organomet. Chem.* 1989, **375**, 123; S.-H. Han, G. L. Geoffroy and A. L. Rheingold, *Inorg. Chem.* 1987, **26**, 3426; (d) V. Ramamoorthy and P. R. Sharp, *Inorg. Chem.* 1990, **29**, 3336.

Polyhedron Vol. 10, No. 12, pp. 1427–1431, 1991
Printed in Great Britain

0277-5387/91 $3.00+.00
© 1991 Pergamon Press plc

ORGANOCHROMIUM π-COMPLEXES—V.† COMPOUNDS CONTAINING η^4-1,3-DIENE AND η^2-ALKYNE MOLECULES

P. W. JOLLY‡ and U. ZAKRZEWSKI

Max-Planck-Institut für Kohlenforschung, D-4330 Mülheim a.d. Ruhr, F.R.G.

(*Received* 10 *December* 1990; *accepted* 20 *February* 1991)

Abstract—$Cr(PMe_3)_2Cl_2$ reacts with active-Mg and butadiene or Mg(butadiene) in a stepwise manner to give initially $(\eta^4\text{-}1,3\text{-}C_4H_6)Cr(PMe_3)_2Cl$ which reacts further to $(\eta^4\text{-}1,3\text{-}C_4H_6)_2CrPMe_3$. Related compounds are formed in the presence of PMe_2Ph or 2,3-dimethylbutadiene. $Cr(PEt_3)_2Cl_2$ reacts to give the dimeric species $[(\eta^4\text{-}2,3\text{-dimethylbutadiene})Cr(PEt_3)Cl]_2$, whereas in the presence of the bidentate ligand bis(diisopropylphosphino)ethane, $(\eta^4\text{-}1,3\text{-}C_4H_6)Cr(Pr^i_2PC_2H_4PPr^i_2)$ is formed. Related reduction of $CrCl_2$-derivatives in the presence of alkynes leads to the formation of $(\eta^2\text{-}R'C{\equiv}CR')_2Cr(PR_3)_2$ (R′ = Me, Ph) and $(\eta^2\text{-}PhC{\equiv}CPh)_3CrPMe_3$.

Although it is assumed that complexes containing metal-bonded 1,3-diene or alkyne molecules play a role in the chromium-catalysed oligomerization of dienes[2] and cyclotrimerization of alkynes,[3] examples of carbonyl-free compounds are apparently limited in the first case to a few chromium(I)-compounds, e.g. $Cp(\eta^4\text{-}1,3\text{-}C_4H_6)CrPR_3$[4] and $(\eta^4\text{-}1\text{-}EtC_4H_5)(\eta^3\text{-}C_3H_5)Cr(Me_2PC_2H_4PMe_2)$;[5] the zerovalent chromium compounds, $(\eta^4\text{-}1,3\text{-}C_4H_6)Cr(Me_2PC_2H_4PMe_2)_2$[6] and $(\eta^4\text{-}1,3\text{-}C_4H_6)Cr(PF_3)_4$;[7] in the second to $(\eta^2\text{-}PhC_2Ph)Cr(Me_2PC_2H_4PMe_2)$[6] and $Cp_2(\eta^2\text{-}CF_3C_2CF_3)Cr$;[8] and a dinuclear species formulated as $(HC_2H)[Cr(Ph_2PC_2H_4PPh_2)_2]_2$.[9]

Here, we describe the preparation of further examples of both types of compound by reducing $CrCl_2$-derivatives with active-Mg in the presence of a diene or alkyne.

RESULTS AND DISCUSSION

It has been shown that commercially available magnesium is sufficiently reactive to reduce some transition metal halides. For example, $CrCl_3$ in the presence of trimethylphosphine and dinitrogen reacts to give $Cr(PMe_3)_4(N_2)_2$,[10] while $FeCl_2$ in the presence of the same phosphine reacts to give $Fe(PMe_3)_4$.[11] In other cases, activation of the magnesium with anthracene has proved advantageous, and this variation has been used to prepare complexes of a variety of transition metals including iron, cobalt and palladium.[12–15]

Our initial attempts to prepare organochromium compounds by reducing $CrCl_2$ with magnesium failed: for example, $Cr(PMe_3)_2Cl_2$ does not react with butadiene and commercial magnesium activated with methyl iodide at −30°C, while at 0°C uncontrolled reduction takes place to give metallic chromium and a brown oil. Reduction can, however, be successfully carried out at −30°C using a highly active magnesium powder (Mg*) produced by the thermolysis of MgH_2[15] and compounds **1**–**4** have been isolated by reacting the appropriate $Cr(PR_3)_2Cl_2$ species with the active-Mg in the presence of butadiene or 2,3-dimethylbutadiene [eq. (1)]:

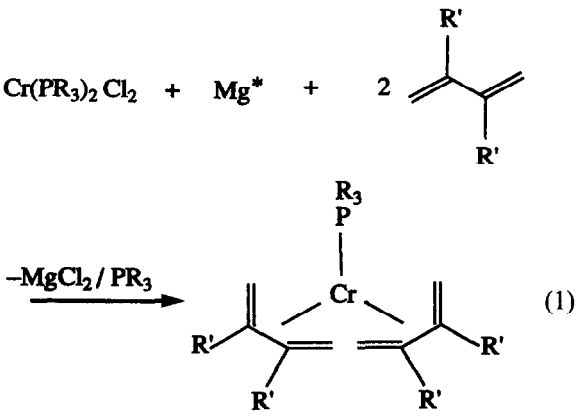

(1)

1 (R=Me, R'=H); **2** (R=Me, R'=Me); **3** (R_3=Me_2Ph, R'=Me)

† For part IV, see ref. 1.

‡ Author to whom correspondence should be addressed.

The green, paramagnetic compounds **1–3** decompose in ether at *ca* 0°C, and their structure follows from the elemental analysis and mass spectra while the protolytic decomposition of **2** is accompanied by the quantitative release of 2,3-dimethylbutadiene.

An analogous reaction carried out in the presence of the bidentate ligand $Pr^i_2PC_2H_4PPr^i_2$ does not lead to a diamagnetic bis(η^4-diene)Cr(L–L)-species but instead the mono(η^4-diene)Cr-species, **4**, is formed [eq. (2)]:

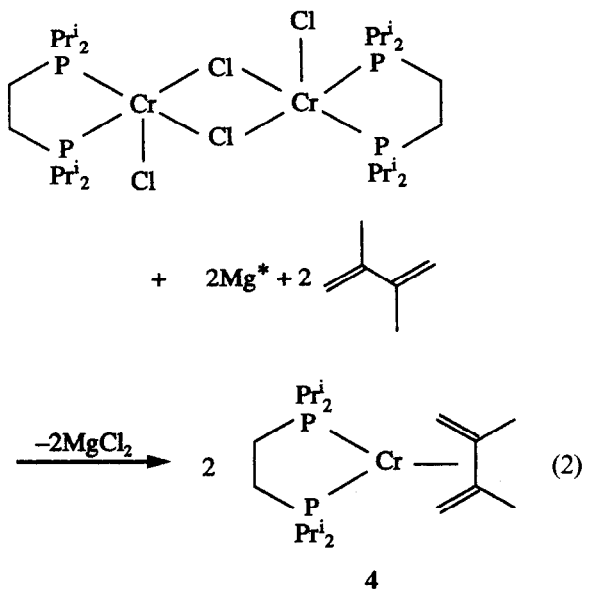

(2)

4

Compound **4** is a violet solid which decomposes above −20°C and inflames in the air.

The attempted extension of the method to $Cr(PEt_3)_2Cl_2$ in the presence of 2,3-dimethylbutadiene produced a brown, crystalline compound whose elemental analysis and molecular weight suggest that a partial reduction has occurred to give the dinuclear (η^4-1,3-diene)Cr^I-species, **5** [eq. (3)]:

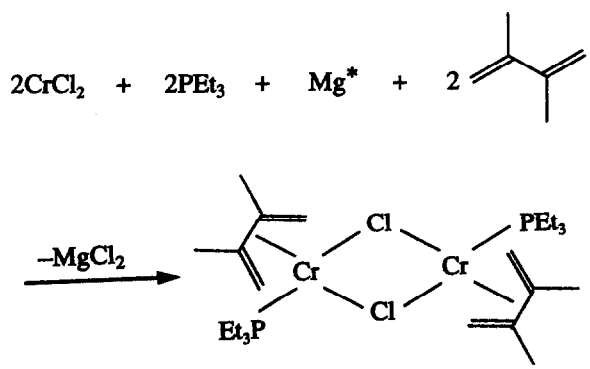

5 (3)

Compound **5** disproportionates in the mass spectrometer to give $CrCl_2$ and fragments assignable to (η^4-2,3-dimethylbutadiene)$_2$CrPEt$_3$. We were, however, unable to make preparative utility of this observation.

A further (η^4-1,3-diene)Cr^I-species, **6**, could be prepared by reacting $Cr(PMe_3)_2Cl_2$ or $Cr(PMe_3)_2Cl_3$ with magnesium–butadiene and it is also formed in low yield upon reacting $Cr(PMe_3)_2Cl_2$ with one equivalent of active-Mg and butadiene [eq. (4)]:

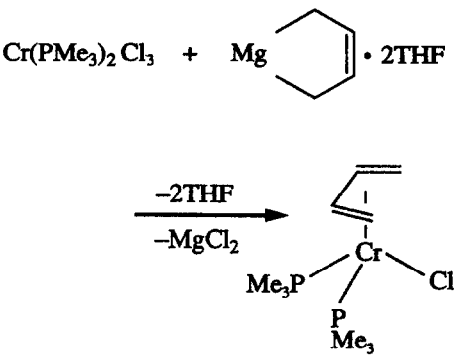

6

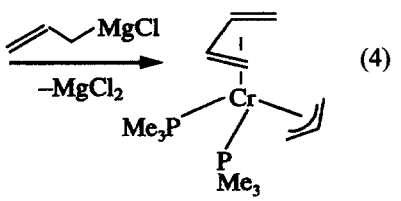

(4)

7

Molecular weight determinations confirm that **6** is monomeric. Compound **6** reacts further at room temperature in a vacuum to give **1** and can be used in the synthesis of further organochromium species. For example, the product of the reaction with allylmagnesium chloride is **7**. Interestingly, the dinuclear-Cr^ICl compound, **5**, does not react with the Grignard reagent.

In contrast to the behaviour of $FeCl_2$, which reacts to give initially an (η^4-1,3-diene)$Fe(PR_3)_3$ species from which P-donor ligands are displaced by a second diene molecule,[13] the results described above suggest that the $CrCl_2$-derivatives are reduced in a stepwise manner in the presence of 1,3-dienes.

The use of active-Mg in the preparation of π-complexes from $CrCl_2$-derivatives is not limited to (η^4-1,3-diene)Cr-species and compounds containing η^2-bonded alkyne molecules can also be synthesized. For example, the reduction of $Cr(PMe_2Ph)_2Cl_2$ in the presence of 2-butyne leads to the formation of the green, crystalline compound, **8** [eq. (5)]:

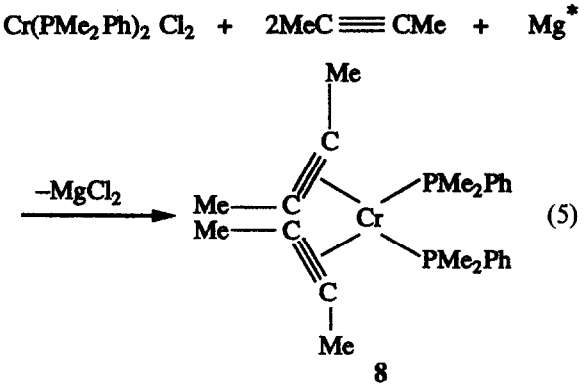

(5)

8

Compound **8** is surprisingly stable and can even be handled briefly at room temperature. The compound is diamagnetic, and the presence of an absorption at 1665 cm^{-1} in the IR spectrum is typical for species in which the alkyne is acting as a 4-electron donor to the metal.[16] The related compounds, **9** and **10**, have been prepared analogously and in the case of **10** the alkyne-C atoms are assigned to a singlet at 212.5 ppm in the ^{13}C NMR spectrum.[17,18]

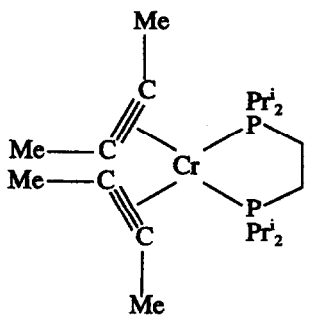

9

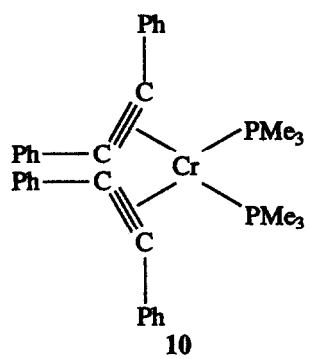

10

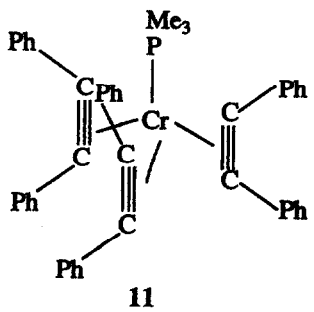

11

Compound **10** reacts further in diethyl ether at 0°C to give the orange–yellow, crystalline compound, **11**. The suggested pseudo-tetrahedral structure (C_{3v}-symmetry) in which the three alkyne groups donate 10 electrons to the metal atom is supported by the observation of an absorption at 1700 cm^{-1} in the IR spectrum and of two singlets at 205.0 and 186.4 ppm in the ^{13}C NMR spectrum measured at −80°C which are assigned to the alkyne C-atoms. Rotation about the chromium–alkyne axis leads to broadening of these signals at −30°C, while at higher temperatures decomposition with the release of hexaphenylbenzene is observed. Mass spectral evidence suggests that a related species (*m/z* 290, M^+) is formed upon reacting $Cr(PMe_3)_2Cl_2$ with active-Mg and 2-butyne, but the compound was contaminated with hexamethylbenzene and could not be isolated pure. A CO-stabilized analogue to **11** has been mentioned,[19] and related compounds are known for molybdenum, tungsten and rhenium.[16,20] An MO-description of the bonding has been developed and need not be reiterated here.[19,21,22]

EXPERIMENTAL

The experimental conditions and the preparation of the $CrCl_2$-derivatives have been described earlier.[23] The active-Mg (Mg*) [composition Mg (96.65%), C (0.98%), H (0.19%), Fe (1.21%) and Cl (0.90%)] was prepared by the thermolysis of MgH_2, and was kindly provided by Professor B. Bogdanović and his co-workers.[15] Mg-butadiene was prepared from magnesium and butadiene.[24]

(η^4-1,3-C_4H_6)$_2$CrPMe$_3$ (1)

A suspension of $Cr(THF)Cl_3$ (1.89 g, 9.7 mmol) and PMe_3 (1.1 cm^3, 10 mmol) in diethyl ether (100 cm^3) was cooled to −30°C and treated with liq. 1,3-butadiene (3.5 cm^3, 30 mmol) and active-Mg (0.5 g, 20.8 mmol). The reaction mixture was stirred at −30°C for 24 h and the resulting brown–green mixture filtered and evaporated to dryness. The residue was extracted with precooled hexane at −30°C, and the green extract cooled to −78°C to give the compound as dark green crystals which were washed with precooled hexane at −78°C and dried at −30°C. Yield: 1.1 g (48% theory). Found: C, 56.0; H, 9.0; Cr, 21.8; P, 13.2. Calc. for $C_{11}H_{21}CrP$: C, 56.9; H, 9.0; Cr, 22.0; P, 13.1%.

MS (70 eV, 70°C): *m/z* 236 (M^+), 182, 128, 76. IR (KBr): *ν* 3040, 1470, 1420, 1280, 960 cm^{-1}.

(η^4-2,3-*Dimethyl*-1,3-*butadiene*)$_2$CrPMe$_3$ (**2**)

Prepared as above as a dark-green crystalline solid (m.p. 85°C dec.) in 48% yield from Cr(THF)Cl$_2$, PMe$_3$, active-Mg and 2,3-dimethyl-1,3-butadiene. Found: C, 61.5; H, 10.3; Cr, 17.7; P, 10.7. Calc. for $C_{15}H_{29}CrP$: C, 61.6; H, 10.0; Cr, 17.8; P, 10.6%.

MS (70 eV, 40°C): *m/z* 292 (M^+), 210, 128, 82. IR (KBr): *v* 3026, 1480, 1420, 1280, 940 cm^{-1}. Treatment of the compound with HCl leads to the release of 2,3-dimethyl-1,3-butadiene (70% theory, GC).

(η^4-2,3-*Dimethyl*-1,3-*butadiene*)$_2$CrPMe$_2$Ph (**3**)

Prepared as above as a dark-green crystalline solid (m.p. 120°C dec.) in 51% yield from Cr(THF)Cl$_2$, PMe$_2$Ph, active-Mg and 2,3-dimethyl-1,3-butadiene. Found: C, 66.6; H, 9.2; Cr, 15.0; P, 9.1. Calc. for $C_{20}H_{31}CrP$: C, 67.8; H, 8.8; Cr, 14.7; P, 8.7%.

MS (70 eV, 70°C): *m/z* 354 (M^+), 272, 216, 190, 138, 134. IR (KBr): *v* 3025, 1485, 1430, 1295, 940 cm^{-1}.

(η^4-2,3-*Dimethyl*-1,3-*butadiene*)Cr(Pr$^i_2$PC$_2$H$_4$PPr$^i_2$) (**4**)

A suspension of [Cr(Pr$^i_2$PC$_2$H$_4$PPr$^i_2$)Cl$_2$]$_2$ was prepared from Cr(THF)Cl$_2$ (1.37 g, 7.03 mmol) and Pr$^i_2$PC$_2$H$_4$PPr$^i_2$ (1.85 g, 7.04 mmol) in diethyl ether (70 cm^3), cooled to −30°C and treated with active-Mg (0.5 g, 20.8 mmol) and 2,3-dimethyl-1,3-butadiene (0.8 ml, 7.1 mmol). The reaction mixture was stirred at −30°C for 24 h, filtered and evaporated to dryness. The residue was extracted with precooled pentane at −30°C and the extract cooled to −78°C to give the compound as violet crystals which were washed with pentane at −78°C and dried at −30°C. Yield: 1.07 g (38% theory). Found: C, 60.6; H, 10.5; Cr, 13.4; P, 15.6. Calc. for $C_{20}H_{42}CrP_2$: C, 60.6; H, 10.7; Cr, 13.1; P, 15.6%.

IR (KBr): *v* 3020, 1460, 1230 cm^{-1}.

[(η^4-2,3-*Dimethyl*-1,3-*butadiene*)Cr(PEt$_3$)Cl]$_2$ (**5**)

A suspension of Cr(THF)Cl$_2$ (1.52 g, 7.8 mmol) and PEt$_3$ (1.2 ml, 8.0 mmol) in diethyl ether (70 cm^3) was cooled to −30°C and treated with active-Mg (0.48 g, 20.0 mmol) and 2,3-dimethyl-1,3-butadiene (1.1 cm^3, 10.0 mmol) and stirred for 24 h at −25°C. The reaction mixture was filtered at −20°C and evaporated to dryness in high vacuum. The residue was extracted with pentane at −10°C and the extract cooled to −78°C to give the compound as red–black crystals which were isolated and washed with precooled pentane (10 cm^3) at −78°C and dried at −30°C. Yield: 1.07 g (48% theory). Found: C, 49.8; H, 9.2; Cl, 12.1; Cr, 18.0; P, 10.9. Calc. for $C_{24}H_{50}Cl_2Cr_2P_2$: C, 50.1; H, 8.8; Cl, 12.3; Cr, 18.1; P. 10.8%.

MW(cryoscopic): 594 g mol^{-1} (calc. 575 g mol^{-1}). IR (KBr): *v* 3016, 1458, 1039 cm^{-1}. Magn. suscept.: μ_B 4.9.

(η^4-1,3-C$_4$H$_6$)Cr(PMe$_3$)$_2$Cl (**6**)

A suspension of Cr(THF)$_3$Cl$_3$ (2.46 g, 6.6 mmol) and PMe$_3$ (1.4 cm^3, 13.5 mmol) in THF (50 cm^3) was cooled to −78°C and treated with (C$_4$H$_6$)Mg(THF)$_2$ (1.56 g, 7.0 mmol). The reaction mixture was stirred for 3 h at −30°C, filtered at −20°C and the solution evaporated to dryness under oil-pump vacuum. The residue was extracted at −10°C with precooled pentane and the extract cooled to −78°C to give the compound as red–black crystals (m.p. 85°C dec.). Yield: 1.6 g (83% theory). The compound can also be prepared by reacting preformed Cr(PMe$_3$)$_2$Cl$_2$ with either (C$_4$H$_6$)Mg(THF)$_2$ (yield 42%) or active-Mg and 1,3-butadiene (yield 19%). Found: C, 40.8; H, 8.3; Cl, 12.2; Cr, 17.6; P, 20.9. Calc. for $C_{10}H_{24}ClCrP_2$: C, 40.9; H, 8.2; Cl, 12.1; Cr, 17.7; P, 21.1%.

MW(cryoscopic): 223 g mol^{-1} (calc. 293.7 g mol^{-1}). IR (KBr): *v* 3030, 1480, 1420, 1280, 950 cm^{-1}.

(η^4-1,3-C$_4$H$_6$)(η^3-C$_3$H$_5$)CrPMe$_3$ (**7**)

(η^4-1,3-C$_4$H$_6$)Cr(PMe$_3$)$_2$Cl (**6**) (1.0 g, 3.4 mmol) was dissolved in diethyl ether (50 cm^3) at −30°C and ethereal allylmagnesium chloride (11 cm^3 of a 0.33 mol soln, 3.6 mmol) was added slowly. The green reaction mixture was stirred for 24 h at −30°C, filtered and evaporated to dryness. The residue was dissolved in hexane (20 cm^3) at −30°C, filtered and the filtrate cooled to −78°C to give the compound as green crystals. Yield: 0.84 g (83% theory). Found: C, 52.8; H, 10.0; Cr, 16.6; P, 19.8. Calc. for $C_{13}H_{29}CrP_2$: C, 52.2; H, 9.8; Cr, 17.4; P, 20.7%.

MS (70 eV, 50°C): *m/z* 299 (M^+), 245, 233, 204, 169. IR (KBr): *v* 3020, 1470, 1420, 1280, 1215, 940 cm^{-1}.

(η^2-MeC≡CMe)$_2$Cr(PMe$_2$Ph)$_2$ (**8**)

A suspension of Cr(PMe$_2$Ph)$_2$Cl$_2$ was prepared from Cr(THF)Cl$_2$ (1.03 g, 5.3 mmol) and PMe$_2$Ph (1.6 cm^3, 11.0 mmol) in diethyl ether (50 cm^3), cooled to −30°C and active-Mg (0.48 g, 20.0 mmol) and 2-butyne (1.2 cm^3, 15 mmol) were added. The

reaction mixture was stirred for 24 h, filtered at −20°C and evaporated to dryness at −30°C under high vacuum. The residue was extracted with pre-cooled pentane at −20°C, the extract concentrated, hexane (10 cm^3) added and the solution cooled to −78°C. The compound was deposited as green crystals which were isolated, washed with pentane at −78°C and dried in high vacuum at −30°C; m.p. 75°C dec. Yield: 1.3 g (56% theory). Found: C, 66.2; H, 7.8; Cr, 11.6; P, 14.3. Calc. for $C_{24}H_{34}CrP_2$: C, 66.0; H, 7.9; Cr, 11.9; P, 14.2%.

MS (70 eV, 73°C): 436 (M^+), 328, 190. IR (KBr): ν 1675, 1665, 1430, 1265, 930 cm^{-1}. ^1H NMR (d_8 THF, −30°C): δ 7.20 (m, Ph), 2.62 (d, MeC≡), 1.40 [d, MeP, J(P,H) 6.8]. ^{31}P NMR (d_8 THF, −30°C): δ 78.83.

(η^2-MeC≡CMe)$_2$Cr($Pr^i_2PC_2H_4PPr^i_2$) (**9**)

Prepared as above as a green crystalline solid (m.p. 85°C dec.) in 57% yield from Cr(THF)Cl_2, $Pr^i_2PC_2H_4PPr^i_2$ active-Mg and 2-butyne in diethyl ether. Found: C, 62.5; H, 10.8; Cr, 12.2; P, 14.6. Calc. for $C_{22}H_{44}CrP_2$: C, 62.5; H, 10.5; Cr, 12.3; P, 14.7%.

IR (KBr): ν 1653, 1460, 1240 cm^{-1}. ^1H NMR (d_8 THF, −30°C): δ 2.77 [d, MeC≡, J(P,H) < 1], 2.03 (m, PCH_2), 1.83 [(m, CH, J(P,H) 7); 0.78/0.61] [dd, Me, J(P,H) 10.8/13.4]. ^{31}P NMR (d_8 THF, −30°C): δ 146.0.

(η^2-PhC≡CPh)$_2$Cr(PMe_3)$_2$ (**10**)

Prepared as above as a red crystalline solid in 55% yield from Cr(THF)Cl_2, PMe_3 active-Mg and diphenylacetylene in diethyl ether. Found: C, 71.9; H, 6.6; Cr, 8.8; P, 10.2. Calc. for $C_{34}H_{38}CrP_2$: C, 72.8; H, 6.8; Cr, 9.3; P, 11.1% (PMe_3-dissociation occurs at 0°C).

IR (KBr): ν 1670, 1650, 1440, 1295, 940 cm^{-1}. ^1H NMR (d_8 THF, −30°C): δ 7.25 (m, Ph), 1.10 [d, PMe, J(P,H) 7.5]. ^{13}C NMR (d_8 THF, −10°C): δ 212.5 (C≡C), 144.7/128.8/127.5/126.1 [Ph, J(C,H) 0/159/159/160], 23.1 [PMe, J(C,H) 128]. ^{31}P NMR (d_8 THF, −30°C): δ 56.34.

(η^2-PhC≡CPh)$_3$CrPMe$_3$ (**11**)

(η^2-PhC≡CPh)$_2$Cr(PMe_3)$_2$ (**10**) (1.5 g, 2.7 mmol) was dissolved in diethyl ether (100 cm^3) and the solution stirred at room temperature for 24 h. The colour changed from red to yellow. The solution was filtered and cooled to −78°C to give the compound as orange crystals which were isolated, washed with pentane at −30°C and dried. Yield: 0.46 g (39% theory). Found: Cr, 7.9; P, 4.5. Calc. for $C_{45}H_{39}CrP$: Cr, 7.9; P, 4.7%.

IR (KBr): ν 1700, 1440, 950 cm^{-1}. ^1H NMR (d_8 THF, −30°C): δ = 7.6–6.5 (m, Ph), 1.45 [d, PMe, J(P,H) 10]. ^{13}C NMR (d_8 THF, −80°C): δ 205.0/186.4 [d, C≡C, J(P,C) 12.5/38.1], 147.9/143.3/129.5/128.5/128.3/126.7/126.0/125.8 (Ph), 18.5 [PMe, J(P,C) 20.9, J(C,H) 128]. ^{31}P NMR (d_8 THF, −30°C): δ 33.34.

REFERENCES

1. P. W. Jolly, C. Krüger and U. Zakrzewski, *J. Organomet. Chem.* In press.
2. G. Wilke, B. Bogdanović, P. Hardt, P. Heimbach, W. Keim, M. Kröner, W. Oberkirch, K. Tanaka, E. Steinrücke, D. Walter and H. Zimmermann, *Angew. Chem.* 1966, **78**, 157.
3. R. P. A. Sneeden and H. H. Zeiss, *J. Organomet. Chem.* 1971, **28**, 259.
4. P. Betz, A. Döhring, R. Emrich, P. W. Jolly, C. Krüger and K. U. Schönfelder, unpublished results.
5. F. Iczek, P. W. Jolly and C. Krüger, *J. Organomet. Chem.* 1990, **382**, C11.
6. J. E. Salt, G. S. Girolami, G. Wilkinson, M. Motevalli, M. Thornton-Pett and M. B. Hursthouse, *J. Chem. Soc., Dalton Trans.* 1985, 685.
7. P. S. Skell, D. L. Williams-Smith and M. J. McGlinchey, *J. Am. Chem. Soc.* 1973, **95**, 3337.
8. M. H. Chisholm, T. D. Gallagher and W. W. Reichert, *Synth. React. Inorg. Metal.-Org. Chem.* 1977, **7**, 279.
9. P. Sobota and B. Jezowska-Trzebiatowska, *J. Organomet. Chem.* 1977, **131**, 341.
10. H. H. Karsch, *Angew. Chem.* 1977, **89**, 57.
11. H. H. Karsch, H. F. Klein and H. Schmidbaur, *Chem. Ber.* 1977, **110**, 2200.
12. H. Bönnemann, B. Bogdanović, R. Brinkmann, D. W. He and R. Spliethoff, *Angew. Chem.* 1983, **95**, 749.
13. H. Hoberg, K. Jenni, E. Raabe, C. Krüger and G. Schroth, *J. Organomet. Chem.* 1987, **320**, 325.
14. R. Benn, P. W. Jolly, R. Mynott, B. Raspel, O. Schenker, K. P. Schick and G. Schroth, *Organometallics* 1985, **4**, 1945.
15. B. Bogdanović, *Acc. Chem. Res.* 1988, **21**, 261.
16. J. L. Templeton, *Adv. Organomet. Chem.* 1989, **29**, 1.
17. D. J. Wink, J. R. Fox and N. J. Cooper, *J. Am. Chem. Soc.* 1985, **107**, 5012.
18. K. H. Dötz and J. Mühlmeier, *Angew. Chem.* 1982, **94**, 936.
19. D. J. Wink and B. T. Creagan, *Organometallics* 1990, **9**, 328.
20. A. B. Manion, T. K. G. Erikson, E. Spaltenstein and J. M. Mayer, *Organometallics* 1989, **8**, 1871.
21. R. B. King, *Inorg. Chem.* 1968, **7**, 1044.
22. D. P. Tate, J. M. Augl, W. M. Ritchey, B. L. Ross and J. G. Grasselli, *J. Am. Chem. Soc.* 1964, **86**, 3261.
23. P. Betz, P. W. Jolly, C. Krüger and U. Zakrzewski, *Organometallics.* In press.
24. K. Fujita, Y. Ohnuma, H. Yasuda and H. Tani, *J. Organomet. Chem.* 1976, **113**, 201.

Polyhedron Vol. 10, No. 12, pp. 1433–1441, 1991
Printed in Great Britain

0277–5387/91 $3.00+.00
© 1991 Pergamon Press plc

ESTIMATION OF STANDARD ENTHALPIES OF FORMATION OF INORGANIC AND ORGANOMETALLIC COMPOUNDS—III. HOMOLEPTIC METAL HALIDES

A. R. DIAS, J. A. MARTINHO SIMÕES* and C. TEIXEIRA

Departamento de Engenharia Química and Centro de Química Estrutural, Instituto Superior Técnico, 1096 Lisboa Codex, Portugal

and

C. AIROLDI and A. P. CHAGAS

Instituto de Química, Universidade Estadual de Campinas, 13081 Campinas, S. Paulo, Brazil

(*Received* 12 *December* 1990; *accepted* 20 *February* 1991)

Abstract—Linear plots of standard enthalpies of formation of homoleptic metal halides, MX_m, against the standard enthalpies of formation of the gaseous hydrogen halides, HX, were used to assess a large number of literature data and to gain a better understanding of the correlations themselves. The method is extremely simple, and enables the estimation of new data.

Enthalpies of formation of organic substances can be estimated through several well known methods.[1–5] These so-called "schemes", which rely on the additivity of bond enthalpies or group contributions and have been refined to account for second order effects such as strain and resonance,[6] yield reliable data for a large number of molecules. A much less favourable situation occurs for inorganic compounds. The wide variety of elements and bonds, together with experimental difficulties in probing the energetics of many inorganic materials, has limited the size of the thermochemical data bank and hindered the development of prediction methods. Efforts in this direction have only become available in recent years, thanks to the work of several groups.[7–14]

In two early papers[7,8] we described a method to estimate enthalpies of formation of inorganic and organometallic molecules, both in their standard reference states (i.e. their stable physical states at 298.15 K and 1 bar) and in the gas phase.[7,8] The method consists of linear correlations between the enthalpies of formation of a given family of compounds, MX_nL_m, and the enthalpies of formation of ligands L or LH [eq. (1)]. As the latter quantities are usually available with good accuracies, the correlations can be used to derive unknown values of $\Delta H_f^\ominus(MX_nL_m,rs/g)$ or even to assess experimental data.

$$\Delta H_f^\ominus(MX_nL_m,rs/g) = a\Delta H_f^\ominus(LH,rs/g)+b. \quad (1)$$

Another good feature of the linear correlations represented by eq. (1) is their apparent physical meaning. Although any empirical method which enables predicting enthalpies of formation of inorganic compounds is itself rather valuable, some understanding of *why* the method works is also desirable. Interesting conclusions, concerning, for example, the trends of metal–ligand and ligand–hydrogen bond disociation enthalpies, were inferred from the above linear relationship.[8] This early discussion revealed, however, some less understood features of the correlation. One of them is related to the slope, a, in eq. (1), which, according to the simple thermochemical model used (see below), should be equal to the number of ligands, L, bonded to the metal atom. Yet, it is observed that a is often different from that number of ligands. In order to gain new insights into this problem we decided to

* Author to whom correspondence should be addressed.

apply the method to analyse the fairly comprehensive thermochemical data of homoleptic metal halides, MX_n. In addition to some general patterns that have emerged from this exercise, the analysis was also used as an assessment of tabulated data and to help in the selection of several controversial values.

DESCRIPTION OF THE METHOD

Consider Scheme 1, which represents an hypothetical reaction involving the metal halide, MX_m. Here, ΔH_1 and ΔH_2 are the enthalpies of reaction with MX_m in the standard reference state (usually solid) and in the gas phase, respectively, and ΔH_V are vaporization (or sublimation) enthalpies.

$$\begin{array}{ccccc} MX_m(rs)+(m/2)H_2(g) & \xrightarrow{\Delta H_1} & M(c)+mHX(g) \\ \downarrow \Delta H_{V1} \quad \downarrow 0 & & \downarrow \Delta H_{V2} \quad \downarrow 0 \\ MX_m(g)+(m/2)H_2(g) & \xrightarrow{\Delta H_2} & M(g)+mHX(g) \end{array}$$

Scheme 1.

As shown in the next section, there is a linear correlation between $\Delta H_f^\ominus(MX_m,g)$ and $\Delta H_f^\ominus(HX,g)$ [eq. (2)]. The implications of this relationship can be derived by expressing ΔH_2 in terms of M—X and H—X bond dissociation enthalpies [eq. (3)].

$$\Delta H_f^\ominus(MX_m,g) = a\Delta H_f^\ominus(HX,g)+b, \quad (2)$$

$$\Delta H_2 = \Delta H_f^\ominus(M,g)+m\Delta H_f^\ominus(HX,g) - \Delta H_f^\ominus(MX_m,g) = m[\bar{D}(M—X) - D(H—X)]+(m/2)D(H—H). \quad (3)$$

It is easily concluded that if eq. (2) is observed and $m = a$, then ΔH_2 is constant for a given metal and so is the difference between the metal–halogen *mean* bond dissociation enthalpy and the halogen–hydrogen bond dissociation enthalpy. This parallel trend of $\bar{D}$(M—X) and D(H—X) had been noted before by ourselves[8] and by Bercaw and co-workers,[15] and its use for predicting new values of metal–ligand bond dissociation enthalpies has been suggested. If the slope a of the empirical correlation [eq. (2)] equals the number of ligands m, then $\bar{D}$(M—X) $-\bar{D}$(M—Y) = D(H—X) $-D$(H—Y) for any pair of halogens X,Y. In the most general case, however, $a \neq m$ and the difference $\bar{D}$(M—X) $-\bar{D}$(M—Y) is related to D(H—X) $-D$(H—Y) through eq. (4). In turn, this implies that in the sequence F → Cl → Br → I [i.e. $\Delta H_f^\ominus(HX,g) < \Delta H_f^\ominus(HY,g)$] the correction term will be positive when $a > m$ and negative when $a < m$. In other words, the parallel trend holds but the differences $\bar{D}$(M—X) $-\bar{D}$(M—Y) may be higher or lower than D(H—X) $-D$(H—Y), depending on the ratio a/m. This obvious conclusion is not restricted to X,Y = halogen: it holds for any ligands L,L′ from a given family (i.e. that belong to the same correlation). It is therefore important to know the value of a whenever the difference D(L—H) $-D$(L′—H) and $\bar{D}$(M—L) [or D(M—L)] are used to estimate M—L′ bond dissociation enthalpy.

$$\bar{D}(M—X)-\bar{D}(M—Y) = D(H—X)-D(H—Y) +[\Delta H_f^\ominus(HX,g)-\Delta H_f^\ominus(HY,g)](1-a/m). \quad (4)$$

Let us go back to Scheme 1 in order to address a final point. As shown below, the linear correlations do not hold just for the enthalpies of formation of MX_m and HX in the *gas phase*, but they are usually observed (and often have better statistical fits) when the enthalpies of formation of MX_m in their *standard reference states* (usually solid) are used. This second empirical relationship can be compared with eq. (5), which was derived with the help of Scheme 1. As ΔH_{V2} is constant for a given metal, the correlation between $\Delta H_f^\ominus(MX_m,rs)$ and $\Delta H_f^\ominus(HX,g)$ implies that the enthalpy of vaporization of MX_m, ΔH_{V1}, which of course varies with X, is itself a linear function of $\Delta H_f^\ominus(HX,g)$.

$$\Delta H_f^\ominus(MX_m,rs) = m\Delta H_f^\ominus(HX,g) - m[\bar{D}(M—X)-D(H—X)] - \Delta H_{V1}+\Delta H_{V2}-(m/2)D(H—H). \quad (5)$$

BRIEF ANALYSIS OF LITERATURE DATA

The method described above will now be applied to review the literature data of homoleptic metal halides of groups 1–12. Included are also the values for thorium and uranium halides. It is stressed that this survey is not comprehensive. One of the points of doing such an exercise was to analyse the values recommended in the two most currently used thermochemical tables for inorganic compounds, JANAF and NBS tables.[16,17] Occasionally, however, data from other sources were included in the discussion. Whenever possible, JANAF tables were preferred over NBS, since they usually provide uncertainty intervals. $\Delta H_f^\ominus(HX,g)$ were taken from the latter compilation, viz. −271.1, −92.307, −36.4 and 26.48 kJ/mol, respectively for X = F, Cl, Br, and I.

Correlations similar to eq. (2) were analysed through a standard least-squares program and the results are shown in Tables 1 and 2. The error bars indicated for the slopes and the intercepts are standard deviations.

Table 1. Parameters for the least-squares fits of $\Delta H_f^{\ominus}(MX_m,c/l)$ vs $\Delta H_f^{\ominus}(HX,g)$

Family	a	b	r	Obs.	Family	a	b	r	Obs.
Group 1					Group 8				
LiX	1.157±0.020	−303.6±2.9	0.9997	J	FeX_3	3.368±0.239	−120.9±39.9	0.9975	M
NaX	0.951±0.034	−320.2±4.9	0.9988	J	RuX_3	1.172±0.014	−96.3±0.8	0.9999	M
KX	0.791±0.043	−357.9±6.2	0.9971	J	FeX_2	2.000±0.049	−163.6±7.1	0.9994	J
RbX	0.737±0.040	−361.6±5.7	0.9971	N	Group 9				
CsX	0.677±0.045	−374.0±6.5	0.9956	N	CoX_2	2.022±0.053	−139.8±7.6	0.9993	N
Group 2					Group 10				
BeX_2	2.829±0.071	−252.7±10.3	0.9994	J	PtX_4	1.338±0.005	−108.1±0.3	1.0000	N
MgX_2	2.533±0.070	−426.7±10.1	0.9992	J	NiX_2	1.911±0.036	−133.4±5.2	0.9997	N
CaX_2	2.315±0.045	−594.4±6.5	0.9996	J	PdX_2	1.131±0.298	−83.5±17.7	0.9669	N
SrX_2	2.183±0.045	−627.5±6.6	0.9996	J	Group 11				
BaX_2	2.001±0.061	−670.5±8.9	0.9991	J	AuX_3	1.335±0.043	−0.2±7.2	0.9995	N
Group 3					CuX_2	1.732±0.078	−70.8±12.9	0.9990	N
ScX_3	3.815±0.131	−590.7±21.9	0.9994	N	CuX	0.724±0.038	−79.9±5.5	0.9972	M
YX_3	3.184±0.169	−730.6±10.0	0.9986	F	AgX	0.470±0.026	−79.6±3.7	0.9971	N
Group 4					AuX	0.291±0.043	−6.3±2.5	0.9894	N
TiX_4	4.313±0.207	−459.3±30.0	0.9977	J	Group 12				
ZrX_4	4.815±0.197	−585.9±28.5	0.9983	J	ZnX_2	1.866±0.045	−254.8±6.5	0.9994	N
TiX_3	3.750±0.119	−407.4±17.2	0.9990	J	CdX_2	1.662±0.040	−247.8±5.9	0.9994	N
ZrX_3	3.346±0.161	−485.1±23.3	0.9977	E	HgX_2	1.002±0.023	−132.7±1.4	0.9997	N
TiX_2	2.102±0.071	−324.0±4.2	0.9994	J	Thorium				
ZrX_2	2.365±0.023	−318.5±3.3	0.9999	E	ThX_4	4.797±0.131	−779.3±19.0	0.9993	N
Group 5					Uranium				
NbX_5	5.240±0.228	−370.0±33.0	0.9981	N	UX_5	5.496±0.248	−585.3±41.3	0.9990	N
TaX_5	5.630±0.226	−370.0±37.7	0.9992	N	UX_4	4.720±0.140	−621.5±20.4	0.9991	N
VX_3	2.609±0.013	−339.4±0.75	1.0000	N	UX_3	3.479±0.063	−557.4±9.2	0.9997	N
VX_2	1.734±0.047	−298.9±2.8	0.9996	L					
Group 6									
WX_6	6.102±0.379	−81.8±63.2	0.9981	J					
WX_5	4.977±0.322	−97.2±53.7	0.9979	B					
MoX_4	2.978±0.060	−199.9±3.6	0.9998	J					
CrX_3	3.219±0.112	−278.7±18.6	0.9994	N					
MoX_3	2.215±0.196	−189.7±11.6	0.9961	M					
CrX_2	2.071±0.052	−214.8±7.5	0.9994	N					
MoX_2	1.501±0.046	−145.1±2.7	0.9995	M					

B, refs 16 and 23; E, ref. 19; F, ref. 18; J, ref. 16; L, ref. 20; M, refs 16 and 17; N, ref. 17.

Group 1

Although the experimental uncertainties of the enthalpies of formation of solid alkaline metal halides are less than 2 kJ/mol, the correlations for these families are not as good as could have been anticipated, a fact that is likely to reflect a limitation of the method itself. Nevertheless, it is observed that in one of the worst cases (KX) the data are fitted within *ca* 6 kJ/mol. Of similar quality are the correlations for the gas phase enthalpies of formation (Table 2) despite their higher experimental uncertainties (up to *ca* 13 kJ/mol). It is worth noting that the fit for NaX in Table 2 relies on three points only, since JANAF tables do not recommend a value for $\Delta H_f^{\ominus}$(NaI,g). An estimate of −106.1±1.7 kJ/mol, obtained by using the correlation together with $\Delta H_f^{\ominus}$(HI,g), disagrees with the value given in NBS tables, −79.5 kJ/mol. Even considering the risk of a long extrapolation, the discrepancy indicates that the value quoted in NBS tables for gaseous sodium iodide is fairly inconsistent with the remaining sodium halide data, which, incidentally, are similar in both tables (within 4 kJ/mol).

An interesting point that is also observed for other groups addressed below, concerns the variation in the slope of the correlations in Table 1: *a*

Table 2. Parameters for the least-squares fits of $\Delta H_f^{\ominus}(MX_m,g)$ vs $\Delta H_f^{\ominus}(HX,g)$

Family	*a*	*b*	*r*	Obs.	Family	*a*	*b*	*r*	Obs.
Group 1					Group 6				
LiX	0.828±0.026	−118.2±3.7	0.9990	J	WX_6	6.438±0.458	38.5±76.3	0.9975	J
NaX	0.619±0.010	−122.5±1.7	0.9999	J	MoX_4	3.522±0.235	−16.0±34.0	0.9956	J
KX	0.662±0.031	−150.1±4.5	0.9978	J	MoX_3	2.626±0.085	101.8±13.5	0.9995	J
RbX	0.654±0.041	−158.3±6.0	0.9960	N	CrX_2	1.655±0.154	26.1±22.4	0.9914	N
CsX	0.680±0.034	−176.6±4.9	0.9976	N	MoX_2	1.411±0.005	219.6±0.8	1.0000	J
Group 2					MoX	0.730±0.015	481.4±2.3	0.9998	J
BeX_2	2.448±0.026	−133.8±3.7	0.9999	J	WX	0.873±0.067	624.9±11.2	0.9970	J
MgX_2	1.878±0.058	−220.2±8.3	0.9991	J	Group 7				
CaX_2	1.753±0.039	−311.4±5.6	0.9995	J	MnX	0.432±0.037	92.1±5.3	0.9929	N
SrX_2	1.617±0.073	−329.3±10.5	0.9980	J	Group 8				
BaX_2	1.667±0.042	−351.6±6.1	0.9994	J	FeX_3	2.991±0.095	−2.6±13.8	0.9990	M
Group 4					FeX_2	1.571±0.106	25.6±15.3	0.9955	J
TiX_4	4.278±0.067	−386.3±9.7	0.9998	J	Group 12				
ZrX_4	4.401±0.050	−477.0±7.3	0.9999	J	ZnX_2	1.504±0.149	−132.7±8.8	0.9951	K
TiX_3	3.484±0.076	−238.1±11.0	0.9995	J	CdX_2	1.342±0.079	−94.6±4.7	0.9983	S
ZrX_3	2.943±0.074	−305.9±10.8	0.9994	E	HgX	0.433±0.008	122.1±1.1	0.9997	H
TiX_2	2.227±0.160	−73.2±23.1	0.9949	J	Thorium				
ZrX_2	1.646±0.062	−117.7±8.9	0.9986	E	ThX_4	4.295±0.090	−583.8±13.1	0.9996	N
TiX	1.159±0.044	251.6±6.4	0.9986	J	Uranium				
ZrX	0.880±0.168	315.8±28.1	0.9821	E	UX_4	4.425±0.053	−429.2±7.7	0.9999	I
Group 5					UX_3	3.033±0.039	−261.3±6.5	0.9999	U
NbX_5	5.605±0.202	−213.6±33.6	0.9994	N	UX_2	2.067±0.030	20.6±5.0	0.9999	U
TaX_5	5.540±0.127	−270.6±21.1	0.9997	W	UX	1.355±0.052	320.4±8.7	0.9993	U
VX_2	2.175±0.143	−66.2±8.5	0.9978	L					

E, ref. 19; H, refs 17 and 31; I, refs 17 and 36–38; J, ref. 16; K, refs 17 and 29; L, ref. 20; M, refs 16 and 17; N, ref. 17; S, refs 17 and 30; U, refs 36–38; W, refs 17, 21 and 22.

decreases with increasing atomic number. The trend is not so smooth for the values in Table 2, but this probably results from experimental errors of the individual values of the enthalpies of formation.

Group 2

Uncertainties of 1–6 kJ/mol are assigned to the enthalpies of formation of most solid alkaline earth metal halides. A noticeable exception is found for BeI_2 (−189±21 kJ/mol). Good linear fittings of these data are seen in Table 1. For the gaseous species, on the other hand, although the error bars are considerably larger, the correlations are even better (Table 2). As noted for Group 1, a decrease of *a* with the atomic number is also observed in this group (Fig. 1).

Group 3

The three enthalpies of formation of solid scandium halides used to derive the correlation in Table 1 were taken from NBS tables. The experimental uncertainties are not available, but the errors in *a* and *b* indicate some inconsistency in the data. A value of −490±22 kJ/mol is predicted for $\Delta H_f^{\ominus}(ScI_3,c)$.

A better correlation is observed for YX_3,

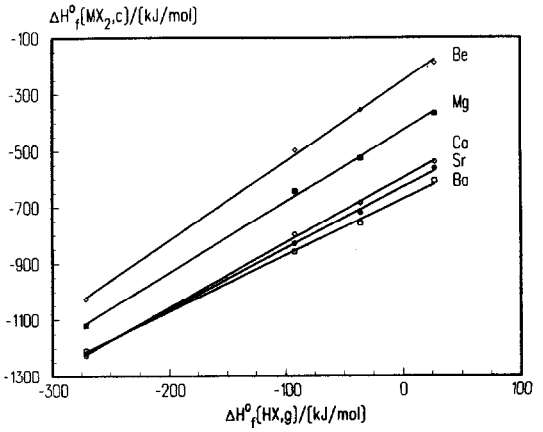

Fig. 1. Enthalpies of formation of solid metal halides from Group 2 against the enthalpies of formation of gaseous hydrogen halides.

obtained from three values (Cl, Br, I) reported by Fuger and co-workers.[18] The NBS values (F, Cl, I) lead to $a = 3.729 \pm 0.217$ and $b = -693.1 \pm 36.0$. Our method is of course unable to assess absolute values (e.g. the discrepancy between the values recommended for $\Delta H_f^\ominus(YI_3,c)$ in the two publications is 24 kJ/mol) but the data fitted in Table 1 look more consistent.

Group 4

The plots of $\Delta H_f^\ominus(MX_m,g)$ vs $\Delta H_f^\ominus(HX,g)$ (M = Ti, Zr; m = 1–4) are illustrated in Figs 2 and 3. They rely on JANAF data, with the exception of $\Delta H_f^\ominus(ZrCl_m,g)$, m = 1–3, which were quoted from a recent work by Efimov *et al.*[19] These values lead to significantly better correlations than the $\Delta H_f^\ominus(ZrCl_m,g)$ data taken from JANAF tables. Despite this improvement, it is observed in Fig. 3 (or in Table 2) that the plot involving ZrX molecules is far from satisfactory, even by excluding from the fit the value recommended by JANAF for $\Delta H_f^\ominus(ZrI,g)$, which looks too high. The worst correlation in the case of the titanium halides is for TiX_2, which is not surprising, given the large uncertainties (13–42 kJ/mol) assigned to the experimental values. The error bars are also large for $\Delta H_f^\ominus(TiX,g)$, *ca* 42 kJ/mol, but the data seem fairly consistent.

The correlations for TiX_m and ZrX_m (m = 3, 4) in their standard reference state are poorer than the gas phase plots. As the uncertainties of both sets of data are similar, this could be related to the trend of ΔH_{VI} with $\Delta H_f^\ominus(HX,g)$ [see the discussion before eq. (5)]. More likely, however, it merely results from inaccuracies of experimental values. Note, for example, that the plots involving solid state enthalies of formation of TiX_2 and ZrX_2 are better than those made with the gas phase values. In addition, the trend in the slopes (a) for TiX_4 and ZrX_4 (Tables 1 and 2) is opposite to what could be expected.

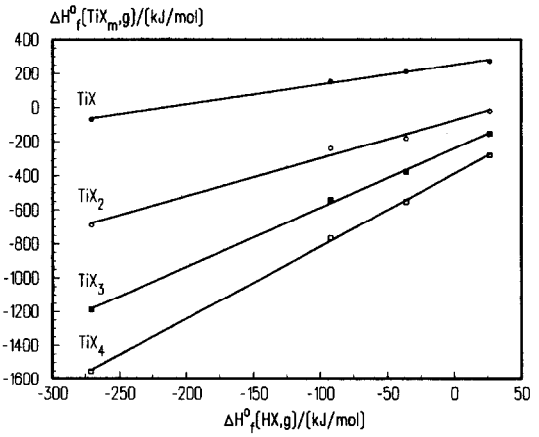

Fig. 2. Enthalpies of formation of gaseous titanium halides against the enthalpies of formation of gaseous hydrogen halides.

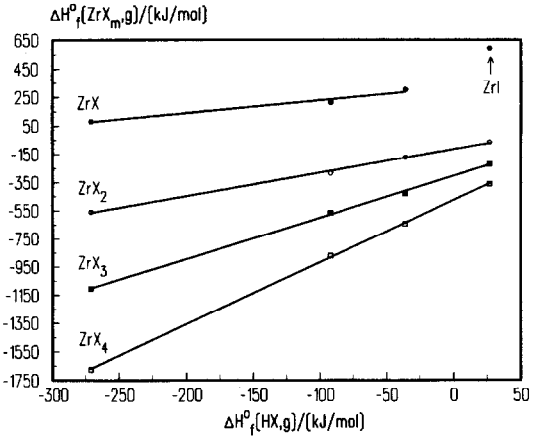

Fig. 3. Enthalpies of formation of gaseous zirconium halides against the enthalpies of formation of gaseous hydrogen halides.

Group 5

The excellent three-point correlation of $\Delta H_f^\ominus(VX_3,c)$ lends some confidence to the estimated value for $\Delta H_f^\ominus(VF_3,c)$, -1047 ± 1 kJ/mol, which is not reported in NBS tables. Probably less reliable is the predicted value for $\Delta H_f^\ominus(VF_2,c)$, -769 ± 13 kJ/mol. This latter three-point plot relies on NBS data for X = Br, I and on a new value for $\Delta H_f^\ominus(VCl_2,c)$, -457.3 ± 1.1.[20]

The correlations for NbX_5 and TaX_5 are less satisfactory, particularly those involving the solid state data. The gas phase plot of the enthalpies of formation of NbX_5 (Table 2) can be used to predict $\Delta H_f^\ominus(NbI_5,g)$, -65 ± 34 kJ/mol. The same exercise for $\Delta H_f^\ominus(TaX_5,g)$ leads to $\Delta H_f^\ominus(TaI_5,g) \approx -124 \pm 21$ kJ/mol. The three points that define this latter correlation were taken from three literature sources.[17,21,22]

Group 6

The correlation for CrX_3 (Table 1) does not include $\Delta H_f^\ominus(CrBr_3,c)$, which is not available but can be estimated as -396 ± 19 kJ/mol. The inconsistency of gas phase enthalpies of formation of CrX_2, on the other hand, is apparent by the error bars in Table 2. Better is the plot involving $\Delta H_f^\ominus(CrX_2,c)$, Table 1. For the analogous MoX_2 molecules, both gas phase and solid three-point plots are very good, allowing estimation of the missing

data: $\Delta H_f^\ominus(MoF_2,c) = -552 \pm 13$ kJ/mol and $\Delta H_f^\ominus(MoCl_2,g) = 89 \pm 1$ kJ/mol. It is worth mentioning that the NBS value for $\Delta H_f^\ominus(MoBr_2,c)$, -261.1 kJ/mol, seems inconsistent with the remaining data. The value recommended in JANAF tables, -202.9 ± 25 kJ/mol, was preferred to define the correlation.

The uncertainties assigned to most of the available enthalpies of formation of solid and gaseous MoX_3 are large, but both three-point plots are reasonable, yielding the following estimates, the first being much less reliable than the second, which is an interpolation: $\Delta H_f^\ominus(MoF_3,c) = -790 \pm 54$ kJ/mol and $\Delta H_f^\ominus(MoCl_3,g) = -141 \pm 16$ kJ/mol.

The inconsistency of JANAF data for the enthalpies of formation of gaseous MoX_4 is reflected by the poor fit seen in Table 2. A better plot is obtained when the three available solid state values are considered (Table 1). This correlation leads to $\Delta H_f^\ominus(MoF_4,c) = -1007 \pm 17$ kJ/mol.

Some of JANAF data for gaseous and standard reference state enthalpies of formation of WX_6 are rather uncertain. This and also the large slope of these plots justify the huge error bars in *a* and *b* seen in Tables 1 and 2. The picture is somewhat similar for the fit involving $\Delta H_f^\ominus(WX_5,c)$, Table 1, which also relies on three experimental values, but here one (WF_5) is an estimate (-1457 kJ/mol) by Burgess *et al.*[23]

Large uncertainties (13–42 kJ/mol) are assigned to the three available $\Delta H_f^\ominus(MoX,g)$ values, but the plot (Table 2) is better than could be anticipated. The missing value, $\Delta H_f^\ominus(MoCl,g)$, is estimated as 414 ± 3 kJ/mol. Not surprisingly, the analogous correlation for WX is worse, reflecting the rather high uncertainties (42–84 kJ/mol) that affect the experimental data. The error bars in *a* and *b* are not as large because the slope is small and because the $\Delta H_f^\ominus(WX,g)$ values are fairly consistent. This three-point correlation leads to an estimate for $\Delta H_f^\ominus(WI,g)$: 648 ± 11 kJ/mol.

Group 7

Only the values of $\Delta H_f^\ominus(MnX,g)$ are available to define a linear correlation (Table 2).

Group 8

JANAF and NBS data had to be used together to yield the parameters displayed in Tables 1 and 2 for FeX_3. The solid state correlation relies on three points only and enables estimation of $\Delta H_f^\ominus(FeI_3,c)$, -32 ± 40 kJ/mol. The high uncertainty is likely to indicate poor quality of experimental data. Recent values reported for $\Delta H_f^\ominus(FeCl_3,c)$, -395.3 ± 0.7 kJ/mol,[24] and $\Delta H_f^\ominus(FeBr_3,c)$, -262.6 ± 0.2 kJ/mol,[25] make small (*ca* 5 kJ/mol) differences from those tabulated in JANAF and NBS tables. This suggests that the value recommended for $\Delta H_f^\ominus(FeF_3,c)$, -1042 ± 13 kJ/mol,[16] may be the source of the inconsistency and is probably too low.

The correlation for gaseous FeX_3 (Table 2) is fairly good and so are those obtained for FeX_2 (Tables 1 and 2). A slight improvement to that involving $\Delta H_f^\ominus(FeX_2,g)$ is achieved if the JANAF values for X = Cl, Br are replaced by the data measured by Efimov and Evdokimova,[24,25] used together with the sublimation enthalpies taken from JANAF.

Values of RuX_3 from the JANAF (Br, I) and NBS (Cl) tables look very consistent and lead to -414 ± 4 kJ/mol for $\Delta H_f^\ominus(RuF_3,rs)$.

Group 9

Data for $\Delta H_f^\ominus(CoX_2,c)$ chosen to define the correlation in Table 1, were taken from JANAF (F, Cl) and NBS (Br, I) tables and seem quite reliable. The values for the chloride and the iodide were remeasured by Lavut *et al.* (-311.1 ± 0.3 kJ/mol),[26] and Efimov and Evdokimova (-215.4 ± 0.3 kJ/mol),[27] respectively, and support that idea. A small improvement of the fit is, however, obtained if the last value is used instead of the NBS result (-220.9 kJ/mol).

Group 10

The three-point fit of $\Delta H_f^\ominus(PtX_4,c)$ data is excellent and leads to an estimate for $\Delta H_f^\ominus(PtF_4,c)$, -471 ± 1 kJ/mol. There is, however, a controversy around this quantity. The above prediction is some 210 kJ/mol higher than a value quoted in a recent paper![28] As stated above, our method is unable to decide for an absolute value. The only valid comment on that discrepancy is that NBS data for PtX_4 are totally inconsistent with the lower number (-681 ± 25 kJ/mol)[28] for the tetrafluoride. One can also speculate on the slope of the PtX_4 correlation in Table 1. Despite the consistency, the slope appears too small, since a higher value could be expected (compare, for example, with the slopes for the correlations involving NiX_2 and PdX_2). Thus, it may well be possible that the observed consistency of NBS data is fortuitous.

Excellent and unsatisfactory correlations are observed for $\Delta H_f^\ominus(NiX_2,c)$ and $\Delta H_f^\ominus(PdX_2,c)$, respectively (Table 1). The latter is a three-point (Cl, Br, I) fit.

Group 11

The parameters derived from the enthalpies of formation of gold halides (Table 1) rely on data for the fluoride, chloride and bromide. On this basis, the value of $\Delta H_f^{\ominus}(AuI_3,c)$ is predicted as 35 ± 7 kJ/mol (it is noted, however, that the slope in Table 1 seems too small, suggesting that this estimate is a lower limit). A similar exercise made for $\Delta H_f^{\ominus}(CuI_2,c)$, by using the three-point fit in Table 1, leads to -25 ± 13 kJ/mol.

The slopes of the correlations for copper, silver and gold mono-halides are in the expected trend, but the consistency of data is not very good, particularly for AuX. In this case, the fit was defined with three points (Cl, Br, I).

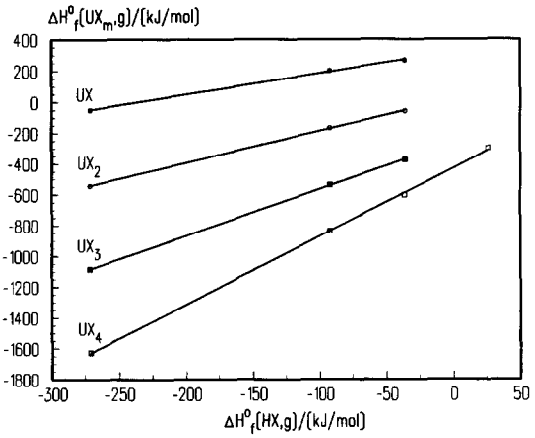

Fig. 4. Enthalpies of formation of gaseous uranium halides against the enthalpies of formation of gaseous hydrogen halides.

Group 12

Data for zinc, cadmium and mercury dihalides in their standard reference states lead to the correlations shown in Table 1. The HgX_2 plot relies on values for the chloride, bromide and iodide, and indicates that $\Delta H_f^{\ominus}(HgF_2,c) = -404 \pm 6$ kJ/mol.

A three-point fit involving $\Delta H_f^{\ominus}(ZnX_2,g)$, Table 2, was obtained from NBS data together with the enthalpies of sublimation of $ZnBr_2$ and ZnI_2 quoted from a different source.[29] In the case of CdX_2, also a three-point correlation, the NBS data were coupled with the enthalpies of sublimation of $CdCl_2$, $CdBr_2$, and CdI_2.[30] Finally, the plot of HgX was obtained with NBS data (F, Cl, I) and a value for $\Delta H_f^{\ominus}(HgBr,g)$ taken from a survey by Hepler and Olofsson.[31]

Thorium

Enthalpies of formation of the solid and gas phase ThX_4 given in NBS compilation must be fairly reliable, as indicated by the correlations in Tables 1 and 2, and by a comparison of some values with more recent literature data. For example, Lau and Hildenbrand determined $\Delta H_f^{\ominus}(ThF_4,g)$ and $\Delta H_f^{\ominus}(ThCl_4,g)$ as -1759 ± 4 kJ/mol and -962 ± 4 kJ/mol, respectively.[32,33] These values differ by 10 and 4 kJ/mol from those recommended by the NBS tables.

Uranium

Values of a and b for UX_5 in Table 1 rely on a three-point correlation (F, Cl, Br) defined with NBS data. The error bars are considerable, probably indicating lack of consistency of those data. A slight improvement of the fit is achieved when the NBS value for $\Delta H_f^{\ominus}(UCl_5,c)$, -1059 kJ/mol, is replaced by a result taken from another source, -1042 ± 2 kJ/mol.[34]

Some controversy surrounds the experimental value of $\Delta H_f^{\ominus}(UF_4,c)$. NBS tables recommend -1914.2 kJ/mol, but O'Hare's estimate is -1897 ± 6 kJ/mol.[35] While the fitting parameters in Table 1, relying on NBS data, cannot judge the discrepancy, a significantly better correlation is obtained when O'Hare's estimate and his experimental value for $\Delta H_f^{\ominus}(UCl_4,c)$, -1022.8 ± 3.8 kJ/mol, are used ($a = 4.657 \pm 0.114$, $b = -623.9 \pm 16.6$, $r = 0.9994$).

The correlation defined for $\Delta H_f^{\ominus}(UX_3,c)$, Table 1, is good, and much better are those shown in Table 2 and in Fig. 4, involving the gaseous halides UX_m ($m = 1$–4). With the exception of UX_4, all rely on data obtained by Lau and Hildenbrand for the fluorides, chlorides, and bromides.[36–38] The NBS value for $\Delta H_f^{\ominus}(UI_4,g)$ was included in the fit of $\Delta H_f^{\ominus}(UX_4,g)$.

FINAL REMARKS

The previous, somewhat tedious, analysis of some literature values of standard enthalpies of formation of metal halides illustrated how an extremely simple method can be used to assess or to estimate new data. As emphasized above, the latter exercise has to be done with caution, since the linear correlations assess the internal consistency of a set of data, rather than absolute magnitudes. In addition, examples were found where good linear fits, indicating consistent values, yield slopes which are perhaps too different from the number of ligands bonded to the metal atom (see, for example, the comments for PtX_4). Incidentally, it is sur-

prising that the correlations hold so well for solid compounds.

The data surveyed are not enough to draw firm conclusions on the variation of the slope throughout the Periodic Table, but, as noted above, a seems to decrease with increasing atomic number for a given group. The most obvious parameter to relate with this change would be the electronegativity of the metal, χ_M, and indeed a qualitative trend is apparent. On the other hand, when Pauling's original equation for his electronegativity scale[39] is introduced in eq. (4), the complex equation obtained indicates also a relationship between a and metal–metal bond dissociation enthalpy, D(M—M).[40] A qualitative trend is observed in this case, for Group 1. Bond order is another parameter that may be related with the slope of the correlations and this possibility is presently being investigated. Further reliable *gas phase* data are, however, probably necessary in order to try a more thorough discussion about the meaning of a.

Acknowledgements—We thank Fundação de Amparo à Pesquisa do Estado de S. Paulo (FAPESP, Brazil) and Junta Nacional de Investigação Científica e Tecnológica (JNICT, Portugal) for providing the funds for collaboration between our groups. Support from Instituto Nacional de Investigação Científica, Portugal, is also acknowledged.

REFERENCES

1. J. D. Cox and G. Pilcher, *Thermochemistry of Organic and Organometallic Compounds*. Academic Press, London (1970).
2. S. W. Benson, *Thermochemical Kinetics*. Wiley, New York (1976).
3. J. B. Pedley, R. D. Naylor and S. P. Kirby, *Thermochemical Data of Organic Compounds*. Chapman and Hall, London (1986).
4. (a) R. T. Sanderson, *Chemical Bonds and Bond Energy*. Academic Press, New York (1976); (b) R. T. Sanderson, *Polar Covalence*. Academic Press, New York (1983); (c) R. T. Sanderson, *J. Am. Chem. Soc.* 1975, **97**, 1367; (d) R. T. Sanderson, *J. Org. Chem.* 1982, **47**, 3835.
5. J. F. Liebman and A. Greenberg (Eds), *Molecular Structure and Energetics*, Vol. 2. VCH, New York (1987).
6. See refs 1–3, 5 and also, for example, N. F. Moiseeva, O. V. Dorofeeva and V. S. Jorish, *Thermochim. Acta* 1989, **153**, 77.
7. A. R. Dias, J. A. Martinho Simões, C. Teixeira, C. Airoldi and A. P. Chagas, *J. Organometal. Chem.* 1987, **335**, 71.
8. A. R. Dias, J. A. Martinho, C. Teixeira, C. Airoldi and A. P. Chagas, *J. Organometal. Chem.* 1989, **361**, 319.
9. M. W. M. Hisham and S. W. Benson, *J. Phys. Chem.* 1987, **91**, 3631.
10. M. W. M Hisham and S. W. Benson, *J. Phys. Chem.* 1989, **93**, 3308. This is part 9 of a series of papers on estimates of thermochemical data of inorganic solids.
11. H. Ohashi, *Thermochim. Acta* 1988, **130**, 115.
12. H. Ohashi, *Thermochim. Acta* 1988, **132**, 187.
13. Yu. M. Kiselev, A. I. Popov, N. S. Kopelov and V. I. Spitsyn, *Dokl. Akad. Nauk S.S.S.R.* 1988, **298**, 1416.
14. K.-Y. Kim and C. E. Johnson, *J. Chem. Thermodyn.* 1981, **13**, 13.
15. H. E. Bryndza, L. K. Fong, R. A. Paciello, W. Tam and J. E. Bercaw, *J. Am. Chem. Soc.* 1987, **109**, 1444.
16. M. W. Chase Jr, C. A. Davies, J. R. Downey Jr, D. J. Frurip, R. A. McDonald and A. N. Syverud, *J. Phys. Chem., Ref. Data* 1985, **14**, Suppl. No. 1.
17. D. D. Wagman, W. H. Evans, V. B. Parker, R. H. Schumm, I. Halow, S. M. Bailey, K. L. Churney and R. L. Nuttall, *J. Phys. Chem., Ref. Data* 1982, **11**, Suppl. No. 2.
18. W. Xiang-Yun, J. T. Zhu, J. Goudiakas and J. Fuger, *J. Chem. Thermodyn.* 1988, **20**, 1195.
19. M. E. Efimov, I. V. Prokopenko, V. A. Medvedev, V. I. Tsirelnikov, G. A. Berezovskii and I. E. Paukov, *J. Chem. Thermodyn.* 1989, **21**, 677.
20. E. G. Lavut, B. I. Timofeyev, V. M. Yuldasheva and N. Raupov, *J. Chem. Thermodyn.* 1989, **21**, 715.
21. A. D. Westland, *Can. J. Chem.* 1979, **57**, 2665.
22. K. H. Lau and D. L. Hildenbrand, *J. Chem. Phys.* 1979, **71**, 1572.
23. J. Burgess, I. Haigh and R. D. Peacock, *J. Chem. Soc., Dalton Trans.* 1974, 1062.
24. V. P. Evdokimova and M. E. Efimov, *Russ. J. Phys. Chem.* 1989, **63**, 1226.
25. M. E. Efimov and V. P. Evdokimova, *Russ. J. Phys. Chem.* 1989, **63**, 1224.
26. E. G. Lavut, B. I. Timofeyev and V. M. Yuldasheva, *J. Chem. Thermodyn.* 1989, **21**, 673.
27. M. E. Efimov and V. P. Evdokimova, *Russ. J. Phys. Chem.* 1987, **61**, 440.
28. A. A. Bondarenko, M. V. Korobov, V. N. Mitkin and L. N. Sidorov, *J. Chem. Thermodyn.* 1988, **20**, 299.
29. O. Kubaschewski, E. L. Evans and C. B. Alcok, *Metallurgical Thermochemistry*. Pergamon Press, Oxford (1967).
30. K. Skudlarski, J. Dudek and J. Kapala, *J. Chem. Thermodyn.* 1987, **19**, 857.
31. L. G. Hepler and G. Olofsson, *Chem. Rev.* 1975, **75**, 585.
32. K. H. Lau and D. L. Hildenbrand, *J. Chem. Phys.* 1989, **90**, 1158.
33. K. H. Lau and D. L. Hildenbrand, *J. Chem. Phys.* 1990, **92**, 6124.
34. E. H. P. Cordfunke, W. Ouweltjes and G. Prins, *J. Chem. Thermodyn.* 1982, **14**, 495.
35. P. A. G. O'Hare, *J. Chem. Thermodyn.* 1985, **17**, 611.

36. K. H. Lau and D. L. Hildenbrand, *J. Chem. Phys.* 1982, **76**, 2646.
37. K. H. Lau and D. L. Hildenbrand, *J. Chem. Phys.* 1984, **80**, 1312.
38. K. H. Lau and D. L. Hildenbrand, *J. Chem. Phys.* 1987, **86**, 2949.
39. L. Pauling, *The Nature of the Chemical Bond*, 3rd edn. Cornell University Press, Ithaca (1973).
40. J. A. Connor and H. A. Skinner, in *Molecular Structure and Energetics* (Edited by J. F. Liebman and A. Greenberg), Vol. 2. VCH, New York (1987).

Polyhedron Vol. 10, No. 12, pp. 1443–1448, 1991
Printed in Great Britain

0277-5387/91 $3.00+.00
© 1991 Pergamon Press plc

STUDIES OF THE *CIS–TRANS* ISOMERISM OF SOME SQUARE-PLANAR PLATINUM(II) NITROIMIDAZOLE COMPLEXES

FIONA M. MACDONALD and PETER J. SADLER*

Department of Chemistry, Birkbeck College, University of London, Gordon House and Christopher Ingold Laboratory, 29, Gordon Square, London WC1H 0PP, U.K.

(*Received* 14 *December* 1990; *accepted* 20 *February* 1991)

Abstract—*Cis–trans* isomerism reactions of *cis*-$Pt(MNZ)_2X_2$ complexes, where MNZ is metronidazole [1-(2′-hydroxyethyl)-2-methyl-5-nitroimidazole] and X = Cl, Br or I, occur in both the solid-state and in solution, and were studied by differential scanning calorimetry and multinuclear NMR spectroscopy. For the solid-state process, enthalpies of isomerization ranged from −21 to −49 kJ mol^{-1}. First order rate constants were determined from ^{195}Pt NMR measurements in solution; consideration of the effects of added halides and free ligand suggests that the reaction mechanism involves associative processes.

The stereochemistry of platinum(II) complexes is often of critical importance to their biological activity. For example, the *cis* isomer of $PtCl_2(NH_3)_2$ is an active antitumour agent, whereas the *trans* isomer is inactive.[1] In contrast, the *cis* isomer of $PdCl_2(NH_3)_2$ is inactive.[2] This can be attributed to the rapid *cis–trans* isomerism of palladium(II) complexes in solution, whereas for platinum(II), although the *trans* isomer is 13 kJ mol^{-1} more stable than the *cis* isomer,[3] the isomerization takes place very slowly.

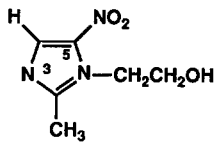

MNZ

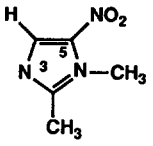

DMZ (4)

The relative stabilities of the isomers are determined largely by the nature of the ligands, but *trans* isomers of platinum(II) complexes are frequently more thermodynamically stable than their *cis* isomers. Thus *trans*-$PtCl_2(py)_2$, where py is pyridine, is *ca* 21 kJ mol^{-1} more stable than the *cis* form.[4] For complexes of the type $Pt(NRZ)_2X_2$ (where X is halide) the *trans* isomer is thermodynamically more stable but the *cis* isomer is the kinetically favoured product. In certain cases a *cis–trans* isomerization process may be observed—this may occur spontaneously or be induced thermally, photochemically or in the presence of a nucleophile.[5] Once formed, the *trans* isomer cannot revert to the *cis* configuration. The reverse situation, where the *cis* isomer is the thermodynamic product and the *trans* is the kinetic product, is rarer but in a few cases *trans–cis* isomerism has been observed. An example is provided by $Pt(dialkylsulphoxide)_2Cl_2$ complexes.[6]

Isomerization reactions may occur in the solid state as well as in solution. We report here studies of the isomerization of platinum(II) nitroimidazole complexes in the solid state and in solution using differential scanning calorimetry (DSC) and NMR spectroscopy. The complexes are of interest because of their potential ability to sensitize tumour cells towards radiation damage and could therefore be useful in cancer treatment.[7–11]

EXPERIMENTAL

Metronidazole (MNZ) and dimetridazole (DMZ) were supplied by Rhône Poulenc (Dagenham), and the platinum(II) complexes were prepared by the routes described previously.[8] NMR

* Author to whom correspondence should be addressed.

Abbreviations: DMZ, Dimetridazole: 1,2-dimethyl-5-nitroimidazole; DSC, Differential scanning calorimetry; MNZ, Metronidazole 1-(2′-hydroxyethyl)-2-methyl-5-nitroimidazole.

solvents were purchased from Aldrich, and glycerine formal from Fluka.

Samples for DSC measurements were ground up using a pestle and mortar, and one sample of *cis*-$Pt(MNZ)_2Cl_2$ was subjected to a commercial milling procedure by Rhône Poulenc (sample B).

DSC

DSC thermograms were obtained on a Perkin–Elmer DSC-2 instrument. Samples were prepared by weighing out milligram quantities of sample into aluminium pans which were then sealed with lids. An empty sealed pan was used as a reference. Unless otherwise stated, samples were run at a heating rate of 10°C min^{-1}, chart speed 10 mm min^{-1} and range setting of 2 mcal (8.368 mJ) s^{-1}. The temperature ranges depended on the complex being studied. A sample with a known heat of fusion (indium; $\Delta H_{fus} = 6.793$ cal g^{-1}) was used for calibration. The areas under the peaks were measured using a planimeter. All runs were carried out in triplicate.

NMR

Information regarding the kinetics of the isomerization reaction in solution was obtained from the rates of disappearance of the ^{195}Pt-$\{^1H\}$ NMR peak for the *cis* isomer and of the appearance of the peak for the *trans* isomer.

^{195}Pt-$\{^1H\}$ NMR spectra at 85.7 MHz were obtained on a Bruker WH 400 spectrometer equipped with a 10 mm broad band probe and a B-VT-1000 variable temperature unit. For each experiment a series of spectra were collected using the same parameters: 500 transients, 0.4 s acquisition time, 0.6 s relaxation delay, 45° flip angle together with broad band decoupling. The chemical shift reference was Na_2PtCl_6 (1 M in D_2O, external).

A means of measuring accurately the temperature inside the probe was required. The temperature dependence of ^{195}Pt chemical shift is well documented (Pregosin, 1982) and so it was decided to calibrate the probe by monitoring the ^{195}Pt chemical shift of the complex under investigation—this, in effect, produced a "platinum thermometer" which provided a rapid means of determining the temperature over the range 300–380 K.

The calibration was achieved by means of a coaxial arrangement involving a 125 mM solution of *cis*-$Pt(MNZ)_2Cl_2$ in glycerine formal in a 5 mm o.d. tube, ethylene glycol plus a trace of HCl in an 8 mm o.d. tube within a 10 mm o.d. tube containing DMSO-d_6 for lock. The temperature was adjusted in steps of 15°C with 45–60 min allowed for equilibration. The probe temperature was measured via the ^1H spectrum of ethylene glycol using the decoupler coils of the broad-band probe. The chemical shift of the ^{195}Pt sample was then recorded, followed by a second check on the probe temperature. This procedure was repeated over the temperature range 300–375 K. Linear relationships between temperature and $\delta(^{195}Pt)$ were obtained (Table 1). The probe temperature was calculated from the separation ($\Delta\nu$ in Hz) between the —OH and CH_2— resonances of ethylene glycol, according to the equation given by van Geet (400 MHz ^1H NMR).[12]

$$T = 466 - 0.254\,\Delta\nu.$$

Table 1. ^{195}Pt NMR chemical shifts of $Pt(MNZ)_2X_2$ at 301 and 373 K in glycerine formal

Complex	$-\delta$ (ppm) 301 K	373 K	$d\delta/dT$
cis-$Pt(MNZ)_2Cl_2$	2070	2031	+0.54
trans-$Pt(MNZ)_2Cl_2$	2069	2021	+0.66
cis-$Pt(MNZ)_2Br_2$	2403	2368	+0.49
trans-$Pt(MNZ)_2Br_2$	2444	2412	+0.44
cis-$Pt(MNZ)_2I_2$	3313	3304	+0.13
trans-$Pt(MNZ)_2I_2$	3371	3352	+0.27

The isomerization reaction was studied in glycerine formal (commercial solvent mixture; 75% 5-hydroxy-1,3-dioxan, 25% 4-hydroxymethyl-1,3-dioxolan) at a temperature of 378 K. Samples were prepared by dissolving the platinum complex in glycerine formal (2 cm^3) to give concentrations of up to 250 mM. The probe was preheated to the specified temperature and the sample inserted. Accumulation was started immediately using a microprogram which enabled a series of spectra to be collected. First order rate constants were obtained from plots of isomer concentration versus time using a computer fitting routine.[13]

RESULTS AND DISCUSSION

Solid state isomerization

Thermograms were obtained for the following complexes: *cis*-$Pt(MNZ)_2Cl_2$, *trans*-$Pt(MNZ)_2Cl_2$, *cis*-$Pt(MNZ)_2Br_2$, *cis*-$Pt(MNZ)_2I_2$ and *cis*-$Pt(DMZ)_2Cl_2$. In the case of *cis*-$Pt(MNZ)_2Cl_2$, two samples were studied: one which had been subjected to a commercial milling procedure (sample A), and one which had been ground in a pestle and mortar (sample B). The two thermograms are shown in Fig. 1. Calculated values for ΔH_f and ΔH_{isom} are listed in Table 2.

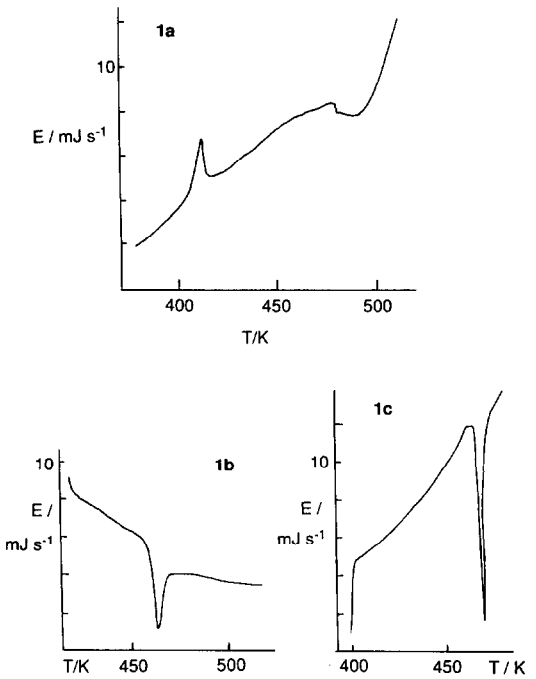

Fig. 1. DSC Thermograms of (a) *cis*-Pt(MNZ)$_2$Cl$_2$ (sample A) (b) *cis*-Pt(MNZ)$_2$Cl$_2$ (sample B) and (c) *cis*-Pt(MNZ)$_2$Br$_2$.

Investigation of *cis*-Pt(MNZ)$_2$Cl$_2$ (sample A) by DSC indicated two endothermic events occurring at 452 and 523 K. The first endotherm correlates with the melting point of the *cis* isomer, and thin layer chromatography of a sample heated to 453 K proved *cis–trans* isomerization to have occurred during this time. This process was found to be irreversible. The second endotherm at 523 K corresponded to the melting of the *trans* isomer, and was followed by a very broad exotherm characteristic of a decomposition process.

Melting transitions are usually endothermic and decompositions exothermic. The observation of an apparently endothermic isomerization is unusual, in that previously such processes have been reported to be exothermic for square-planar platinum(II) complexes. The fact that, in this case, isomerization is accompanied by extensive melting may account for this. A repeat experiment using sample B showed an endo–exotherm [Fig. 1(b)], a trace which is similar to results from previous reports of platinum complexes.[14,15] It is not clear why sample A yielded anomalous results; it can only be inferred that the much smaller particle size has a profound effect on solid state reactions. Endo–exotherms were observed for all the remaining complexes.

Table 2. Values for ΔH_f and ΔH_{isom} obtained from DSC measurements (in kJ mol^{-1})

Complex	ΔH_f	ΔH_{isom}
cis-Pt(MNZ)$_2$Cl$_2$		
Sample A[a]	+26.3	—
Sample B[b]	+7.1	−49.9
cis-Pt(MNZ)$_2$Br$_2$	+12.3	−32.2
cis-Pt(MNZ)$_2$I$_2$	+8.3	−21.3
cis-Pt(DMZ)$_2$Cl$_2$	—	−31.7

[a] Ground with mortar and pestle.
[b] Commercial milling procedure.

In previous studies of the isomerism of platinum(II) complexes using thermal analysis, Nikolaev[16] obtained a sharp exotherm for *cis*-Pt(NH$_3$)$_2$Cl$_2$ prior to the endothermic dissociation peak, a phenomenon not seen for the *trans* isomer. He concluded that this exothermic transition corresponded to an isomerization process. Further proof was provided by a determination of the heats of formation of the two isomers:[17]

$$\textit{cis}\text{-Pt(NH}_3\text{)}_2\text{Cl}_2, \quad \Delta H_f = -483 \text{ kJ mol}^{-1};$$

$$\textit{trans}\text{-Pt(NH}_3\text{)}_2\text{Cl}_2, \quad \Delta H_f = -496 \text{ kJ mol}^{-1}.$$

Similar exothermic effects have been reported for several related square-planar complexes, *cis*-Pt(α-picoline)$_2$Cl$_2$ and *cis*-Pt(β-picoline)$_2$Cl$_2$;[18] *cis*-Pt(pyridine)$_2$X$_2$.

DTA studies on a series of palladium(II) and platinum(II) phosphine complexes have previously given rise to an interesting range of effects.[19] The thermogram of *cis*-Pd(PhPEt$_3$)$_2$Cl$_2$ indicated three thermal events: two endotherms corresponding to the melting points of the *cis* and *trans* isomers, and, shortly after the first endotherm, an exothermic transition. This represented the simultaneous solidification and isomerization of the *cis* isomer. As solidification is an exothermic process, it is difficult to determine whether the isomerization process itself is endo- or exothermic. For the propyl analogue, *cis*-Pd(PhPr$_2$P)$_2$Cl$_2$, only one endotherm was seen and this corresponded to the melting point of the *cis* isomer. On cooling, analysis of this sample revealed that, in fact, the *trans* isomer had been formed—evidently melting and isomerization had occurred simultaneously. The platinum complex, *cis*-Pt(*n*-Bu$_3$P)$_2$Cl$_2$, provided a clearer example: endothermic melting of the *cis* isomer was seen followed by a broader endotherm, subsequently found to correspond to isomerization.

The reverse situation, where the *cis* isomer is the thermodynamic and the *trans* isomer is the kinetic product, has not been so widely studied. Two examples involving *trans*-Pt(pentamethylenesulphide)$_2$

Cl_2[20] and *trans*-$Pt(CO)(NH_2R)Cl_2$[15] have both shown the isomerism process to be exothermic and to be distinct from the melting of the *trans* isomer.

Based on studies of the Pd—N symmetric and antisymmetric stretching bands of *cis*-$PdCl_2(NH_3)_2$ and the bromo analogue, Durig and Mitchell[21] have proposed mechanisms involving intermediates with either trigonal pyramidal geometry (axial Cl^-) or intermolecular association (via Pd---Cl). Some support for the latter comes from the early observation that the following transformation occurs:

$$[PtCl_4]^{2-} [Pt(NH_3)_4]^{2+} \rightarrow 2\ trans\text{-}Pt(NH_3)_2Cl_2.$$

Although intermediates involving tetrahedral geometries have also been proposed,[22] they are unlikely to be favourable for d^8 complexes in their ground states.

Thus for bis(5-nitroimidazole) platinum(II) complexes, the *trans* isomer is likely to be the more thermodynamically stable and the small endotherm can be attributed to melting of the *cis* isomer; it is possible that rapid molecular motion is a requirement for isomerization to occur. The crystal structure of *cis*-$Pt(MNZ)_2Cl_2$[8] shows head-to-tail stacking of the complex in the unit cell, a configuration which could lead to ligand exchange via the associative mechanism.

Isomerizations of $Pt(MNZ)_2X_2$ complexes appear to be less exothermic in the order X = Cl > Br > I (Table 2), which implies that the difference in stability between *cis* and *trans* isomers is smallest for the iodo complex.

Isomerization in solution

A typical series of ^{195}Pt-$\{^1H\}$ NMR spectra, obtained during the isomerization of *cis*-$Pt(MNZ)_2Br_2$ are shown in Fig. 2. Plots of *cis* isomer concentration versus time for the different reaction conditions are given in Figs 3(A), 3(B) and 3(C), and the first order rate constants calculated from these data are listed in Table 3. The temperature coefficients for ^{195}Pt shifts decrease in the order Cl > Br > I (Table 1) and are similar in size to those observed for other platinum(II) complexes, consistent with an increase in the paramagnetic contribution to the chemical shift.

Firstly, the effect of added free ligand, MNZ, on the isomerization rate was studied [Fig. 3(B)]. No species other than the *cis* or *trans* isomers were detected in the ^{195}Pt spectrum. After completion of the reaction, a small sample was withdrawn and checked by ^1H NMR, but only *trans*-$Pt(MNZ)_2Cl_2$ and metronidazole were observed. Addition of metronidazole causes a dramatic increase in reaction rate: by more than a factor of 10 in the presence of 1 mol equiv. (Table 3).

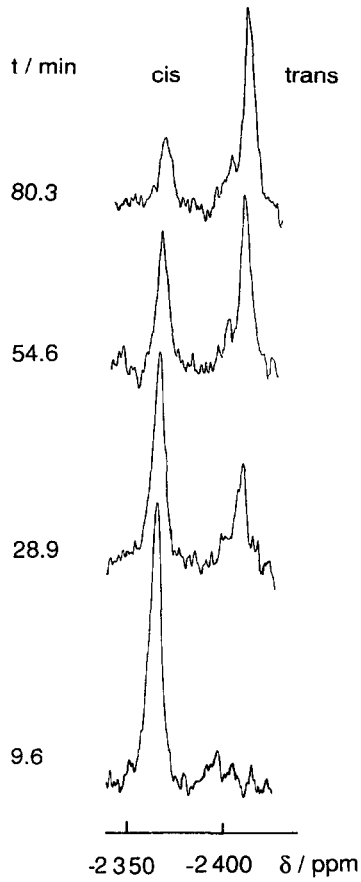

Fig. 2. ^{195}Pt-$\{^1H\}$ NMR spectra of *cis*-$Pt(MNZ)_2Cl_2$ at various times (t) after heating at 378 K in glycerine formal showing the formation of the *trans* isomer.

The effects of added halides on the rate of isomerization were also studied. When LiCl was added to *cis*-$Pt(MNZ)_2Cl_2$ in a mol ratio of 1 : 1 and 2 : 1, again no species other than the *cis* and *trans* isomers were detected during the reaction. The observed increase in isomerization rate may be due to an

Table 3. First order rate constants for the *cis–trans* isomerization reactions of $Pt(MNZ)_2X_2$ at 378 K

Experiment	Rate constant, k (min^{-1})
cis-$Pt(MNZ)_2Cl_2$	4.15×10^{-3}
+0.1 mol equiv. MNZ	6.80×10^{-3}
+0.5 mol equiv. MNZ	4.59×10^{-2}
+1.0 mol equiv. MNZ	5.54×10^{-2}
+1.0 mol equiv. Cl^-	7.00×10^{-3}
cis-$Pt(MNZ)_2Br_2$	1.66×10^{-2}
cis-$Pt(MNZ)_2I_2$	0.29

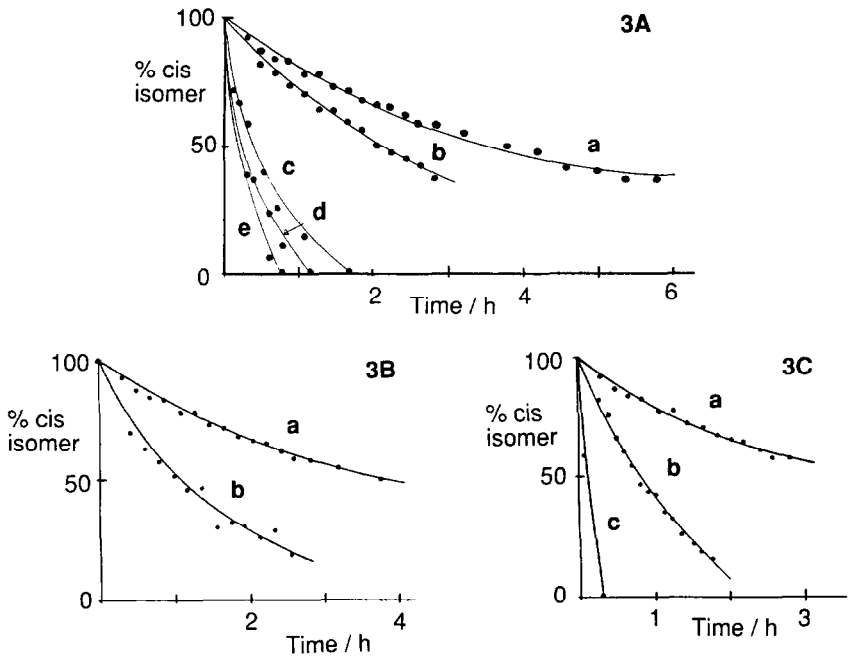

Fig. 3. Plots showing the concentration of the *cis* isomer versus time at 378 K for: (A) *cis*-Pt(MNZ)$_2$ Cl_2 (a), and in the presence of 0.1 (b), 0.5 (c), 1.0 (d) and 2.0 (e) mol equiv. of free ligand MNZ; (B) *cis*-Pt(MNZ)$_2Cl_2$ (a), and in the presence of 1 mol equiv. of LiCl (b); (C) *cis*-Pt(MNZ)$_2Cl_2$ (a), *cis*-Pt(MNZ)$_2Br_2$ (b) and *cis*-Pt(MNZ)$_2I_2$ (c). The initial concentration of each platinum complex was 250 mM.

ionic strength effect since Cl^- should inhibit the reaction if breaking of a Pt—Cl bond is involved in the rate-determining step. An increase in reaction rate with increase in ionic strength is usually observed when an ionic intermediate is involved in the reaction.[23] This was verified by addition of $KAsF_6$, a non-coordinating salt.

A 1 : 1 mixture of *cis*-Pt(MNZ)$_2Cl_2$ with LiBr was prepared in glycerine formal and heated on an oil bath at 420 K for 4 h. After cooling to room temperature, the ^{195}Pt-{^{1}H} NMR spectrum showed three peaks at −2041.4, −2223.7 and −2431.3 ppm with relative intensities of 1 : 1.4 : 0.5. The latter peak is assigned to *trans*-Pt(MNZ)$_2Br_2$ (see Table 1), and that at −2041.4 ppm as *trans*-Pt(MNZ)$_2Cl_2$. The most intense peak is likely to be [Pt(MNZ)$_2$ClBr], probably also a *trans* complex. These results suggest that *cis–trans* isomerism has a step involving halide attack on the *cis* complex.

Isomerization mechanisms have been considered in detail for the case of *cis*-Pt(PEt_3)$_2Cl_2$ in benzene. Although the *cis* complex is indefinitely stable at room temperature, it rapidly isomerizes to the *trans* form on the addition of a trace of free triethylphosphine.[24] Thermodynamic data show that the increased stability is the result of an increase in entropy. This arises from the stronger solvation of the highly polar *cis* isomer, such that isomerization to the *trans* form is accompanied by the release of benzene. Two hypotheses concerning the mechanism have been proposed. The first proposed by Haake and Pfeiffer[25] involves association of the free ligand to give a distorted five-coordinate intermediate [PtL_3X_2] which undergoes a fluxional change, enabling isomerization to occur. Cooper and Powell[26] have suggested an alternative scheme which includes the formation of an ionic intermediate, $[PtL_3X]^+X^-$, in a multistage double displacement mechanism. Experimental evidence lends support to both theories, and it appears that the choice of reaction pathway for such systems depends on the metal, solvent, anion, steric hindrance of the ligands, basicity and catalytic effects.[27]

The uncatalysed isomerization reaction of *cis*-[Pt(PEt_3)$_2$(*o*-MeC_6H_5)Cl] has also been studied[28,29] and a dissociative reaction mechanism proposed. Usually square-planar platinum(II) complexes have been found to favour associative mechanisms, but in this case steric hindrance from the aryl ligand forces a change to a three-coordinate intermediate.

In the present case the evidence points to an associative mechanism involving an ionic intermediate. However, candidate complexes such as $[Pt(MNZ)_3Cl]^+$ are likely to be short-lived and no

species other than the *cis* and *trans* isomers were detected by ^{195}Pt NMR during isomerization reactions. It would have been interesting to examine the effect of solvent polarity on reaction rate, but unfortunately the solubilities of the complexes used here are poor in alternative solvents. Three-coordinate intermediates are unlikely to be favoured in the present case since the isomerization was not retarded by added chloride. However, mechanisms involving pseudorotation of a five-coordinate intermediate to form the *trans* isomer are more difficult to rule out.

Acknowledgements—We thank the SERC, Rhône Poulenc, MRC and Wolfson Foundation for their support for this work. We are very grateful to Drs B. Peart, S. Acott, D. Gilmour and G. Buddle of Rhône Poulenc for their encouragement, advice and assistance. We also thank the University of London Intercollegiate Research Service and MRC for the provision of NMR facilities.

REFERENCES

1. M. J. Cleare and P. C. Hydes, *Metal Ions Biol. Syst.* 1980, **11**, 1.
2. D. S. Gill, in *Platinum Coordination Complexes in Cancer Chemotherapy* (Edited by M. P. Hacker, E. B. Douple and I. H. Krakoff), p. 267. Martinus Nijhoff, Boston (1984).
3. I. I. Chernyaev, V. A. Palkin, R. A. Baranova and N. N. Kuz'mina, *Zh. Neorg. Khim.* 1960, **5**, 693.
4. S. J. Ashcroft and C. J. Mortimer, *Thermochemistry of Transition Metal Complexes.* Academic Press, London (1970).
5. F. R. Hartley, *The Chemistry of Platinum and Palladium.* Applied Sciences Publishers, London (1973).
6. J. H. Price, J. P. Birk and B. B. Wayland, *Inorg. Chem.* 1978, **17**, 2245.
7. J. R. Bales, C. J. Coulson, D. W. Gilmour, M. A. Mazid, S. Neidle, R. Kuroda, B. J. Peart, C. A. Ramsden and P. J. Sadler, *J. Chem. Soc., Chem. Commun.* 1983, 432.
8. J. R. Bates, M. A. Mazid, P. J. Sadler, A. Aggarwal, R. Kuroda, S. Neidle, D. W. Gilmour, B. J. Peart and C. A. Ramsden, *J. Chem. Soc., Dalton Trans.*1985, 795.
9. N. Farrell and K. A. Skov, *J. Chem. Soc., Dalton Trans.* 1987, 1043.
10. N. Farrell, *Transition Metal Complexes as Drugs and Chemotherapeutic Agents*, p. 190. Kluwer Academic, Dordrecht (1989).
11. D. M. L. Goodgame, A. S. Lawrence, A. M. Z. Slawin, D. J. Williams and I. J. Stratford, *Inorg. Chim. Acta.* 1986, **125**, 143.
12. A. L. Van Geet, *Anal. Chem.* **40**, 2227.
13. F. M. Macdonald, PhD Thesis, University of London (1987).
14. N. A. Astakhova, V. S. Bondarenko, S. P. Gabuda, G. D. Mal'chikov and N. A. Shestakhova, *Zh. Strukt. Khim.* 1978, **19**, 427.
15. R. Ellis, T. A. Weil and M. Orchin, *J. Am. Chem. Soc.* 1970, **92**, 1078.
16. A. V. Nicholaev, *Priroda* 1939, **10**, 56.
17. I. I. Chernyaev, V. A. Palkin, R. A. Baranova and N. N. Kuz'mina, *Zh. Neorg. Khim.* 1960, **5**, 693.
18. M. I. Ivanova, *Zh. Neorg. Khim.* 1957, **2**, 1317.
19. G. Beech, G. Marr and S. J. Ashcroft, *J. Chem. Soc.(A)* 1970, 2903.
20. E. A. Allen, N. P. Johnson, D. T. Rosevear and W. Wilkinson, *J. Chem. Soc., Chem. Commun.* 1971, 171.
21. J. R. Durig and B. R. Mitchell, *Appl. Spectrosc.* 1967, **21**, 221.
22. A. Grimson, J. H. Ridd and B. V. Smith, *J. Chem. Soc.* 1960, 1352.
23. G. K. Anderson and R. J. Cross, *Chem. Soc. Rev.* 1980, **9**, 185.
24. J. Chatt and R. G. Wilkins, *J. Chem. Soc.* 1952, 273.
25. P. Haake and R. M. Tfeiffer, *J. Am. Chem. Soc.* 1970, **92**, 4996.
26. D. G. Cooper and J. Powell, *J. Am. Chem. Soc.* 1973, **95**, 1102.
27. R. Romeo, D. Minniti and M. Trozzi, *Inorg. Chem.* 1976, **15**, 1134.
28. R. Romeo, *Inorg. Chem.* 1978, **17**, 2040.
29. G. Farone, V. Ricevuto, R. Romeo and M. Trozzi, *J. Chem. Soc. (A)* 1971, 1877.

Polyhedron Vol. 10, No. 12, pp. 1449–1451, 1991
Printed in Great Britain

0277–5387/91 $3.00+.00
© 1991 Pergamon Press plc

PRESSURE EFFECT ON THE HYDROLYSIS VELOCITY OF α- AND β-CHLOROTETRAETHYLENEPENTAAMINECOBALT(III) CATIONS

YOICHI KITAMURA,* SHINJI MATSUZAKI and TOURU BUTOU

Department of Chemistry, Faculty of Science, Ehime University, Matsuyama 790, Japan

(*Received* 3 *January* 1991; *accepted* 20 *February* 1991)

Abstract—Activation volumes obtained for the title reactions are −3.6 and 42 $cm^3\ mol^{-1}$ for aquation and base hydrolysis of the α-cation, and −1.7 and 35 $cm^3\ mol^{-1}$ for aquation and base hydrolysis of the β-cation. These magnitudes are consistent with the interchange mechanism of aquation or with the S_N1 CB mechanism of base hydrolysis.

We have recently investigated the activation volume for the hydrolysis reaction of a cobalt(III) complex and consider that the magnitude of the activation volume can provide good mechanistic information on the dissociative-associative character of a reaction or the existence of a pre-equilibrium.[1–3] In the present report, we are interested in the effect of the size of a non-labile ligand on the magnitude of the activation volume and study the effect of pressure on the velocity of the title reactions which proceed via two pathways, i.e. aquation [eq. (1)] and base hydrolysis [eq. (2)].[4] Activation volumes for aquation ($\Delta V_{aq}^{\ddagger}$) and base hydrolysis ($\Delta V_b^{\ddagger}$) are calculated therefrom and are discussed in comparison with those of analogous reactions of chloropentaaminecobalt(III).

$$\alpha\text{- or }\beta\text{-[Co(tetren)Cl]}^{2+} + H_2O \xrightarrow{k_{aq}} \alpha\text{-[Co(tetren)OH}_2\text{]}^{3+} + Cl^- \quad (1)$$

$$\alpha\text{- or }\beta\text{-[Co(tetren)Cl]}^{2+} + OH^- \xrightarrow{k_b} \alpha\text{-[Co(tetren)OH]}^{2+} + Cl^-, \quad (2)$$

where tetren = $H_2N(CH_2)_2NH(CH_2)_2NH(CH_2)_2NH(CH_2)_2NH_2$.

The configurations of the α- and β-complexes are shown in Fig. 1.

$$\Delta V_{aq}^{\ddagger} \equiv -RT\frac{d\ln k_{aq}}{dP}$$

$$\Delta V_b^{\ddagger} \equiv -RT\frac{d\ln k_b}{dP}.$$

The activation volume for the aquation of $[Co(NH_3)_5Cl]^{2+}$ at high ionic strength has also been obtained.

EXPERIMENTAL

α- and β-[Co(tetren)Cl]$ZnCl_4$ were obtained according to the literature and identified by elemental analysis and UV–vis absorption spectra.[5] $[Co(NH_3)_5Cl](ClO_4)_2$ was obtained as in previous work.[1] Aliquots of the reaction solution were taken out at certain time intervals and analysed spectrophotometrically.[6]

RESULTS AND DISCUSSION

Experimental first-order rate constants (k_{obs}) are summarized in Table 1. For $[Co(tetren)Cl]^{2+}$, k_{obs} is composed of two contributions:

$$k_{obs} = k_{aq} + k_b[OH^-] = k_{aq} + \frac{k_b K_w}{[H^+]},$$

where K_w is the ionization constant of water. At $[HClO_4] = 1.0$ M, the contribution from base hydrolysis is negligible and $\Delta V_{aq}^{\ddagger}$ can be calculated

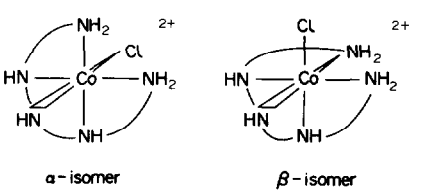

Fig. 1. Configuration of the α- and β-isomers.

* Author to whom correspondence should be addressed.

Table 1. The effect of pressure on the velocity of hydrolysis

Complex	C^a (mM)	$[HClO_4]$ (M)	$[NaClO_4]$ (M)	t (°C)	λ^b (nm)	$10^4 k_{obs}$ (s^{-1})^c at P (MPa) of 5	50	100	150	200
$[Co(NH_3)_5Cl]^{2+}$	1.0	0.10	0.90	66	282	1.40	1.62	1.86	2.16	2.31
α-$[Co(tetren)Cl]^{2+}$	1.0	0.01	0.99	80	290	2.27	2.06	1.40	1.41	1.25
α-$[Co(tetren)Cl]^{2+}$	1.0	1.00	—	80	290	0.760	0.797	0.927	0.898	0.975
β-$[Co(tetren)Cl]^{2+}$	1.0	0.01	—	60	295	1.92	1.42	1.21	1.07	0.90
β-$[Co(tetren)Cl]^{2+}$	1.0	1.00	—	80	295	6.26	6.53	5.85	6.65	7.15

[a] Concentration of the complex.
[b] The reaction was followed at this wavelength.
[c] Mean of duplicate runs.
M = mol dm^{-3}.

using

$$\Delta V_{aq}^{\ddagger} = -RT\frac{d \ln k_{obs}}{dP}.$$

In the hydrolysis of the α-complex at $[HClO_4]$ = 0.01 M, $\Delta V_b^{\ddagger}$ is calculated by

$$\Delta V_b^{\ddagger} = -RT\frac{d \ln (k_{obs}-k_{aq})}{dP} - \Delta V_w + RT\frac{d \ln (\gamma_{2+}/\gamma_{+}^2)}{dP}, \quad (3)$$

where k_{aq} is assumed to be equal to k_{obs} for this complex at $[HClO_4]$ = 1.0 M. The reaction volume (ΔV_w) for the autoprotolysis of water is estimated as -30.5 cm^3 mol^{-1} at 80°C:[7]

$$\Delta V_w = -RT\frac{d \ln K_w}{dP}.$$

γ_{2+} and γ_+ denote the activity coefficients of a 2+ and a 1+ charged ion, respectively. Their pressure dependence is estimated according to the Debye–Hückel approximation and the last term in eq. (3) equals 2.4 cm^3 mol^{-1}.[8] In the hydrolysis of the β-complex at $[HClO_4]$ = 0.01 M, $\Delta V_b^{\ddagger}$ is calculated by

$$\Delta V_b^{\ddagger} = -RT\frac{d \ln k_{obs}}{dP} - \Delta V_w,$$

where the contribution from aquation and the pressure dependence of the activity coefficients are neglected. ΔV_w is estimated as -24.8 cm^3 mol^{-1} at 60°C,[7] and the resultant activation volumes are summarized in Table 2. From the table, the following can be inferred.

(1) $\Delta V_{aq}^{\ddagger}$ for $[Co(NH_3)_5Cl]^{2+}$ does not depend significantly on the ionic strength (μ) or temperature (t). Therefore, we assume generally that $\Delta V_{aq}^{\ddagger}$ for a chloropentaaminecobalt(III) complex, $[Co(N_5)Cl]^{2+}$, is independent of the reaction conditions.

(2) The magnitude of $\Delta V_{aq}^{\ddagger}$ is within the range -8 to ~ -2 cm^3 mol^{-1}. This magnitude may be interpreted by the interchange mechanism, as has been discussed for $[Co(NH_3)_5Cl]^{2+}$ and *trans*-

Table 2. Activation volume for the hydrolysis of the chloropentaaminecobalt(III) complex

Complex	$\Delta V_{aq}^{\ddagger}$ (cm^3 mol^{-1})	t (°C)	μ (M)	Reference	$\Delta V_b^{\ddagger}$ (cm^3 mol^{-1})	t (°C)	μ (M)	Reference
$[Co(NH_3)_5Cl]^{2+}$	−6.0	65	0.1	3	33	25	~0	1
	−7.9	25	0.1	3				
	−7.4±0.6	65	1.0	This work				
trans-$[Co(en)_2(NH_3)Cl]^{2+}$	−5.0	70	0.1	3				
cis-$[Co(en)_2(NH_3)Cl]^{2+}$					32	25	0.06	10
$[Co(NH_2CH_3)_5Cl]^{2+}$	−2.3	39	0.1	9	33	10	0.01	10
$[Co(NH_2CH_2CH_3)_5Cl]^{2+}$					31	12	~0	10
trans-$[Co(NH_3)_4(NH_2CH_3)Cl]^{2+}$	−4.6	49	0.1	9	29	25	0.01	11
α-$[Co(tetren)Cl]^{2+}$	−3.6±0.9	80	1.0	This work	42±1.3	80	1.0	This work
β-$[Co(tetren)Cl]^{2+}$	−1.7±1.0	80	1.0	This work	35±1.0	60	0.01	This work

$[Co(en)_2(NH_3)Cl]^{2+}$.[2,3] It can be noted that the value of $\Delta V_{aq}^{\ddagger}$ is somewhat large for a complex containing a bulky, non-labile N_5 ligand. In the case of the limiting dissociative mechanism, the transition state is long-lived so that the surrounding solvent molecules can equilibrate and the volume effect of a bulky N_5 ligand will cancel out in the transition state and in the initial state.[12] On the other hand, in the case of the interchange mechanism, the transition state is not long-lived enough for the solvent molecules to equilibrate and the effect of a bulky N_5 ligand does not cancel out in both states. Thus, the observed dependence of the magnitude of $\Delta V_{aq}^{\ddagger}$ on the size of a pentaamine ligand is consistent with the interchange mechanism of aquation.

(3) The magnitudes of $\Delta V_b^{\ddagger}$ are large and positive and can be explained by the S_N1 CB mechanism, where the volume change of the pre-equilibrium

$$[Co(N_5)Cl]^{2+} + OH^- = [Co(N_5—H)Cl]^+ + H_2O \quad (4)$$

may amount to *ca* 22 $cm^3\ mol^{-1}$.[13] The N_5—H represents the conjugate base of a N_5 ligand. Except for the β-tetren complex, the magnitude of $\Delta V_b^{\ddagger}$ appears to be independent of the size of the N_5 ligand. This is consistent with the limiting dissociative character of the S_N1 CB mechanism. One explanation for the relatively large $\Delta V_b^{\ddagger}$ value of the β-tetren complex is that the reaction volume of pre-equilibrium (4) is large at a temperature of 80°C. This is surmised from the reaction volume ($-\Delta V_w$) of an analogous neutralization reaction

$$H^+ + OH^- = H_2O$$

which is large at higher temperatures.[7]

REFERENCES

1. Y. Kitamura, R. van Eldik and H. Kelm, *Inorg. Chem.* 1984, **23**, 2038.
2. Y. Kitamura, *Inorg. Chem.* 1985, **24**, 2.
3. Y. Kitamura, S. Taneda and K. Kuroda, *Inorg. Chim. Acta* 1989, **156**, 31.
4. T-L. Ni and C. S. Garner, *Inorg. Chem.* 1967, **6**, 1071.
5. D. A. House and C. S. Garner, *Inorg. Chem.* 1966, **5**, 2097.
6. Y. Kitamura, T. Itoh and M. Takeuchi, *Inorg. Chem.* 1986, **25**, 3887.
7. F. J. Millero, E. V. Hoff and L. Kahn, *J. Solution Chem.* 1972, **1**, 309.
8. S. D. Hamann, *J. Chem. Soc., Faraday Trans. I* 1984, **80**, 2541.
9. G. A. Lawrance, K. Schneider and R. van Eldik, *Inorg. Chem.* 1984, **23**, 3922.
10. Y. Kitamura, G. A. Lawrance and R. van Eldik, *Inorg. Chem.* 1989, **28**, 333.
11. R. van Eldik, Y. Kitamura and C. P. Piriz Mac-Coll, *Inorg. Chem.* 1986, **25**, 4252.
12. M. L. Tobe, *Inorganic Reaction Mechanisms*. Nelson, London (1972).
13. Y. Kitamuta and R. van Eldik, *Ber. Bunsenges. Phys. Chem.* 1984, **88**, 418.

Polyhedron Vol. 10, No. 12, pp. 1453–1455, 1991
Printed in Great Britain

0277–5387/91 $3.00+.00
Pergamon Press plc

COMMUNICATION

THE TRIS((*R*)-CYSTEINESULPHINATO-N,S)COBALTATE(III) ION: A CONVENIENT AND RELIABLE RESOLVING AGENT

R. D. GILLARD

School of Chemistry and Applied Chemistry, University of Wales College of Cardiff, P.O. Box 912, Cardiff CF1 3TB, U.K.

(*Received* 5 *December* 1990; *accepted* 4 *April* 1991)

Abstract—The use of the triply-charged resolving agent tris((*R*)-cysteinesulphinato-N,S) cobaltate(III) for the convenient, reliable and reproducible resolution of triply-charged cations is summarized, following ill-founded criticism.

The utility of potassium tris-fac-Δ-[(*R*)-cysteinesulphinato-N,S)cobaltate(III)] hydrate [synthesized from natural-*R*-cysteine and hexamminecobalt(III) salts in two steps, following simple directions] as a clean resolving agent for triply-charged cations $[M(NN)_3]^{3+}$ has been shown repeatedly.[1] Here, M = Cr, NN = bipy,[1c,d,h] phen,[1c,d] en,[1a] 5,5′-dimethylbipy;[1a] M[1a] = Co, NN = en, pn, bipy, phen; M = Rh,[1a] NN = bipy, phen. Mixed complexes and chelates have also been resolved this way, including, for example, $[Rh(phen)_2(NH_3)_2]^{3+}$ [1a] and the series[1b] from $[Co(phen)_3]^{3+}$ to $[Co(en)_3]^{3+}$. The agent has been sold since 1983 by a Swiss company,[2] quite independently of this laboratory.

Our synthesis[1] starts from hexaamminecobalt(III) salts, and our typical overall reported yield[1c] is 21%.

The characterization of our product as a single, pure compound rests on (i)[1c] the failure of determined efforts via ion-exchange chromatography to separate isomers (the chiroptical properties of leading and trailing parts were identical); (ii)[1c] the constancy during 20 years of the CD of our many samples; and (iii)[1a,b,c] the very clean optical resolutions through its salts. The assignment of linkage isomerism (N,S) stems from that in the green precursor $[Co(cys)_3]^{3-}$ which is, *inter alia*, readily oxidized by hydrogen peroxide (the other known linkage isomer[1d] S,O-bonded, does not undergo this oxidation). Our assignment of the *facial* structure rests essentially on the magnetic resonance spectra. The assignment of handedness [Δ or $R(C_3)$] at the cobalt(III) ion rests on an empirical relation for the lowest energy spin-allowed *d–d* transition.

We have drawn attention[1a,e] to properties which may cause potential difficulties—the photolability of $[Co(R\text{-}cysSO_2)_3]^{3-}$; its thermal lability [particularly via the formation of cobalt(II) species]; the kinetic control of some routes to isomers. However, the route[1a,e] to the versatile and useful resolving agent $[Co(R\text{-}cysSO_2)_3]^{3-}$, arrived at after much experience, is very dependable.

These compounds and their potential isomerism must be described as extremely well known:[3] they have even formed the subject of undergraduate courses.[3b] Nonetheless, a recent paper[4] comments on the earliest work reported from here, but in ignorance of the extensive reported work since 1973,[1b–h] with the strange exception that a single remark in a published lecture[1e] is quoted. (Ironically, that lecture[1e] drew attention again to the possible difficulties[1a] arising from kinetic control: these have been noticed yet again[4] by Arnold and Jackson). In consequence chiefly of that ignorance, the tenor of the short paper[4] by Arnold and Jackson is (in the extensive areas of apparent overlap with our published work[1]) critical. In particular, the final paragraph of their text[4] says: "the inference is that if one intends to use the Δ-tris-(cysteinate) tri-anion (sic) as a resolving agent, the material should be carefully recrystallized to remove the more soluble form . . . *which may well have been present*". The green tris-cysteinate itself is not, of course, yet used as a resolving agent (it is too unstable) but, taking the sense, the quoted extract[4] must refer to the peroxide-oxidized yellow sulphinate compound, so often recommended[1] as a resolving agent. If one

intends to use that as a resolving agent, all that is required is to follow the published directions[1] properly. The comment[4] is otiose. The present note puts the matter straight: the criticism (overt or implied)[4] is incorrect.

Singling out some remarks:[4]

(i) "The ^{13}C NMR spectrum[16] has not been published previously (sic), but Gillard[21] has described it as 'remarkably simple'.[11]" That reference 21 is to a lecture (the present reference 1e) at a summer school, summarizing principles of diastereoisomeric interactions and dissymmetric transformations. Reference 16 in this quotation is to a footnote,[4] giving, for our resolving agent, albeit not made by our method, in D_2O at 25°C (although the experimental section of the paper[4] says 18°C!), values of δ (relative to dioxane): 107.15, −0.46, −13.18. These agree well with the *two* sets of values previously published from here (both recorded with reference to tetramethylsilane). Accepting the value[5] for dioxane relative to TMS, of +67.40, our values were 107.87,[1b] −0.73, −9.46 and 109.1,[1c] 1.3, −8.9.

(ii)[4] "The peroxidized derivative $[Co((R)\text{-cysSO}_2\text{-N,S})_3]^{3-}$ appears[14] to be a useful resolving agent, *and the success of resolutions using this ion could hinge critically on the diastereoisomeric purity*". (My italics.) Reference 14 in this quotation is the present ref. 1a. The methods given[1] remove any such implied problem. Our prescribed synthesis of the solid resolving agent gives[1] a single diastereoisomer which works well as described.[1]

(iii)[4] ". . . the yellow $[Co((R)\text{-cysSO}_2\text{-N,S})_3]^{3-}$ anion, . . . the Δ isomer, the Λ isomer, or a mixture might be obtained . . . accordingly, we have repeated (sic) Dollimore and Gillard's experiments[14] using not only the Δ form but also the Λ and the . . . 1 : 1 mixture . . .". Reference 14 is the present ref. 1a.

The results[4] on the Δ form (the one we always use[1]) fully confirm our own.[1] We have done no experiments on the other forms, so they cannot be repeated.

(iv) The reaction of L-cysteine with cobalt ions, in varied forms, gives[3a] various products. For example, the red isomer $[Co((R)\text{-cis-O,S})_3]^{3-}$ is made[1g] (following Schubert[6]) from cobalt(II) nitrate by air oxidation (typically in 60% yield).

The green isomers (sometimes a diastereo-isomeric mixture) may also be made in a similar way (Schubert's original route[6]) through air oxidation of cobalt(II) reagents. This is the route used[4] (with others) by Arnold and Jackson, who have been able to obtain at least two green isomers *in solution* and who have studied their interconversions. We recommend[1] and use another quite distinct route via $[Co(NH_3)_6]^{3+}$, and our recorded yields (e.g.[1c] 21%) and many other comments[1] make it clear that the word "stereospecific" relates to the final *solid* product $K_3\text{-fac-}\Lambda\text{-}[Co(R\text{-cysSO}_2)_3]nH_2O$. This usage of the word is said[4] to be "erroneously based on . . . the isolated material".

(v) The recent work[4] has confirmed that "the Δ-*RRR*" isomer is much the more abundant under equilibrium conditions". Indeed,[4] "we could detect no Λ-*RRR* isomer by ^{13}C NMR spectroscopy". Rather oddly in view of that (correct) finding, Arnold and Jackson then say in their very last sentence of text[4] "The material should be routinely checked for the presence of the other diastereomer by a technique such as ^{13}C NMR spectroscopy".

In conclusion, the recent paper[4] reports some new facts about the green tris-cysteine compound, intermediate in our synthesis. Otherwise, in covering much of the same ground[1] as that studied by Dollimore and by Cartwright and Sillanpaa with me, Arnold and Jackson have confirmed the following facts:[1] the stereoselectivity of formation of the green compound, in solution and as a crystalline potassium salt; the purity of the single isomer of the peroxide-oxidation product, the spectroscopic properties of this latter, and its structure. They have apparently not attempted to confirm any resolutions: others[1h,2] of course have.

The recent paper[4] implies that its findings show substantial disagreement with our work.[1] It[4] actually confirms all that has been said[1] previously from this laboratory. That confirmation has become concealed, chiefly through ignorance of our extensive work published since 1973.

In much the same way, in his reply to criticisms and misquotation[7] by Jackson of his earlier work (in a field quite distinct from the present one) Brown said[8] "on examination . . . shows that there is no disagreement between our two approaches. Any apparent disagreements have to do with the language employed". The failure by Arnold and Jackson to acknowledge relevant, prior work extends in the present case to the structural work[9] of Okamoto and collaborators. In establishing (by X-ray diffraction) the absolute configuration of $(+)^{CD}_{600}$-bis[tris(L-cysteinato-N,S)cobaltate(III)-μ-S,μ-S′,μ-S″]cobalt(III) nitrate pentahydrate, they too had gone over the question of the stereoselectivity of the formation of green $\Delta_{LLL}\text{-}fac(S)\text{-}[Co(L\text{-cys-N,S})_3]^{3-}$ but were able to agree in full with our earlier work.[1]

REFERENCES

1. (a) L. S. Dollimore and R. D. Gillard, *J. Chem. Soc., Dalton Trans.* 1973, 933; (b) L. S. Dollimore and R. D. Gillard, *J. Chem. Soc., Dalton Trans.* 1975, 369; (c) P. S. Cartwright, R. D. Gillard and E. R. J.

Sillanpää, *Polyhedron* 1987, **6**, 105; (d) P. S. Cartwright and R. D. Gillard, *Polyhedron* 1989, **8**, 1453; (e) R. D. Gillard, in *Optical Activity and Chiral Discrimination* (Edited by S. F. Mason), p. 339. D. Reidel, Dordrecht, The Netherlands (1979); (f) R. D. Gillard, in *F.E.C.S. Internat. Conf. on Circular Dichroism*, Sofia, Bulgaria, p. 52 (1985); (g) R. D. Gillard and P. S. Cartwright, *Polyhedron* 1988, **7**, 1243; (h) N. A. P. Kane-Maguire and J. S. Hallock, *Inorg. Chim. Acta* 1979, **35**, L309.

2. J. P. S. Chimie, *Optically Active Compounds* (Catalogue). CH-2200 Bevaix (Neuchatel), Switzerland (1984).
3. (a) D. A. Buckingham and C. R. Clark, in *Comprehensive Coordination Chemistry* (Edited by G. Wilkinson, R. D. Gillard and J. A. McCleverty), Vol. 4, pp. 837 and 839. Pergamon Press, Oxford and London (1987); (b) University of Wales, BSc Chemistry Final examination papers. University of Wales Press, Cardiff (1984).
4. A. P. Arnold and W. G. Jackson, *Inorg. Chem.* 1990, **29**, 3618.
5. G. C. Levy and J. D. Cargioli, *J. Mag. Res.* 1972, **6**, 143.
6. M. P. Schubert, *J. Am. Chem. Soc.* 1933, **55**, 3336 (this reference is given incorrectly in the present ref. 4).
7. W. G. Jackson, *Inorg. Chem.* 1987, **26**, 3004.
8. T. L. Brown, *Inorg. Chem.* 1989, **28**, 3229.
9. K-I. Okamoto, S-I. Aizawa, T. Konno, H. Einaga and J. Hidaka, *Bull. Chem. Soc. Japan* 1986, **59**, 3859.

Polyhedron Vol. 10, No. 12, pp. 1457–1458, 1991
Printed in Great Britain

0277-5387/91 $3.00+.00
© 1991 Pergamon Press plc

COMMUNICATION

SYNTHESIS AND STRUCTURE OF IRIDIUM TETRAMESITYL

ROBYN S. HAY-MOTHERWELL and GEOFFREY WILKINSON*

Johnson Matthey Laboratory, Chemistry Department, Imperial College, London SW7 2AY, U.K.

and

BILQUIS HUSSAIN-BATES and MICHAEL B. HURSTHOUSE*

Chemistry Department, Queen Mary and Westfield College, Mile End Road, London E1 4NS, U.K.

(*Received* 16 *January* 1991; *accepted* 21 *March* 1991)

Abstract—Interaction of anhydrous iridium trichloride and 2,4,6-trimethylphenyl (mesityl)lithium in diethyl ether forms the tetrahedral iridium(IV) tetramesityl that has been characterized by electron paramagnetic resonance spectroscopy and by X-ray diffraction.

The interaction of $RhCl_3(THT)_3$ (THT = tetrahydrothiophen) with 2,4,6-trimethylphenyllithium in tetrahydrofuran–diethyl ether has been shown[1] to give the rhodium(III) compound, Rh(mesityl)$_3$, whose structure was found to be quasi-*fac*-octahedral (3C,3H) due to agostic interaction of three hydrogen atoms of three *o*-methyl groups on the aryl with the metal atom.[1] By contrast, the interaction of $IrCl_3(THT)_3$ under similar conditions with mesityllithium led to no isolable product. However, anhydrous $IrCl_3$ [made from iridium trichloride trihydrate (Johnson Matthey) by dehydration with thionyl chloride] in diethyl ether on reaction with mesityllithium in ether in four-fold excess at room temperature, led, after evaporation, extraction of the residue with hexane and crystallization at −20°C to Ir(mesityl)$_4$ as brown crystals, m.p. 138–139°C (dec), in about 15% yield. The formation of an iridium(IV) compound from $IrCl_3$ may be due to a disproportionation reaction, but no other product could be isolated and the residue after hexane extraction is black and insoluble in organic solvents. The tetramesityl compound is stable in air as the solid and in hexane solutions, but these decompose on heating in air to give a green, diamagnetic material, characterized analytically and spectroscopically as Ir(mesityl)$_3$(O_2).

The structure of the tetramesityl compound has been determined by X-ray crystallography† and is shown in Fig. 1. The geometry is reasonably described as distorted tetrahedral, with C—Ir—C angles varying from 89.0(4) to 123.9(5)°. The Ir—C bond lengths range from 1.99(1) to 2.02(1) Å. With a low-spin d^5 iridium(IV) system, the origin of the distortion will not be electronic and must therefore be steric, with the ligands distributed and oriented so as to minimize interligand non-bonding interactions. It is therefore not surprising that the

* Authors to whom correspondence should be addressed.

† Crystal data: $C_{36}H_{44}Ir$, M = 668.97, monoclinic, a = 12.192(3), b = 18.876(2), c = 13.223(2) Å, β = 107.09(5)°, V = 2908.7 Å, space group = $P2_1/c$, Z = 4, D_c = 1.53 g cm^{-3}, μ(Mo-K_α) = 44.2 cm^{-1}, F(000) = 1348. Data were collected using an Enraf–Nonius FAST area detector diffractometer and graphite monochromated Mo-K_α radiation. With a diffractometer swing angle of 24.97° and a crystal-to-detector distance of 40.7 mm, data corresponding to slightly more than one hemisphere were scanned. Of the 22,081 data measured, 12,297 were observed and merged (R = 0.06) to give 4001 unique data. The structure was solved via the heavy atom method and refined by least squares to R = 0.052.

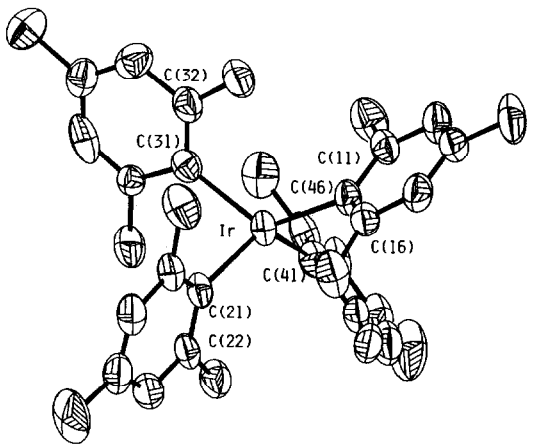

Fig. 1. The structure of Ir(2,4,6-$Me_3C_6H_2)_4$. Selected bond lengths and angles are: Ir—C(11) 2.04(1), Ir—C(21) 1.99(1), Ir—C(31) 2.04(1), Ir—C(41) 2.03(1) Å; C(11)—Ir—C(21) 123.9(5), C(11)—Ir—C(31) 122.0(5), C(11)—Ir—C(41) 92.2(5), C(21)—Ir—C(31) 89.0(4), C(21)—Ir—C(41) 117.0(5), C(31)—Ir—C(41) 115.1(5); Ir—C(11)—C(12) 119(1), Ir—C(11)—C(16) 121(1), Ir—C(21)—C(22) 124(1), Ir—C(21)—C(26) 117(1), Ir—C(31)—C(32) 118(1), Ir—C(31)—C(36) 125(1), Ir—C(41)—C(42) 123(1), Ir—C(41)—C(46) 115(1)°.

geometry of this complex is similar to that found[2] for $[Li(THF)_4][LuAr_4]$ (Ar = 2,6-$Me_2C_6H_3$), in which the Lu—C interaction is likely to be predominantly ionic.

The structure was solved via the heavy-atom method and refined by full-matrix least-squares. The data were corrected for absorption at the isotropic refinement stage using the DIFABS procedure, and the final R, Rw values were 0.052, 0.071, respectively with all carbon atoms and iridium refined anisotropically. No hydrogen atoms were included.

The X-band EPR spectrum in toluene at 77 K agrees with that expected for a tetrahedral molecule with $g_{\parallel} = 2.437$, $g_{\perp} = 2.005$: hyperfine structure due to Ir^{191} and Ir^{193} isotopes (38 and 61% abundance, respectively) is observed.

In cyclic voltammetry in dichloromethane, two reversible, one-electron reduction waves at -0.44 and -1.12 V vs the ferrocene/ferricenium standard were observed.

This mesityl is the first monomeric neutral homoleptic iridium(IV) compound to be synthesized. This now gives hope for the synthesis of compounds with other ligands such as RO, RS, R_2N and R_2P with bulky alkyl or aryl groups.

Acknowledgements—We thank Johnson Matthey plc for loan of iridium and the SERC for X-ray facilities.

REFERENCES

1. R. S. Hay-Motherwell, B. Hussain-Bates, M. B. Hursthouse and G. Wilkinson, *J. Chem. Soc., Chem. Commun.* 1990, 1242.
2. S. A. Cotton, F. A. Hart, M. B. Hursthouse and A. J. Welch, *J. Chem. Soc., Chem. Commun.* 1972, 1225.

Polyhedron Vol. 10, No. 13, pp. 1459–1463, 1991
Printed in Great Britain

0277–5387/91 $3.00+.00
© 1991 Pergamon Press plc

ELECTRONIC STATES OF HOT IONS AND THE REACTIVITY OF [$MoOCl_3$(dppe)] TOWARDS SOLVATED ELECTRONS IN TRI-n-BUTYLPHOSPHATE

J. O. DZIĘGIELEWSKI* and K. FILIPEK

Department of Inorganic and Radiation Chemistry, Institute of Chemistry, Silesian University, 9 Szkolna Street, 40006 Katowice, Poland

(*Received* 19 *July* 1990; *accepted* 13 *December* 1990)

Abstract—The reactivity of molybdenum(V) ions towards solvated electrons (e_s^-) was studied by spectroscopic analysis. The crystal-field parameters, $Dq = 2470\ cm^{-1}$, $Ds = -6710\ cm^{-1}$ and $D\tau = 370\ cm^{-1}$, for the complex [$MoOCl_3$(dppe)] were determined and the energy terms were calculated. The mechanism of the reaction, involving the formation of the hot ion of $[d_{xy}]^1[d_{yz}]^1$ and $[d_{xy}]^1[d_{x^2-y^2}]^1$ configuration was suggested. The rate constant of the reaction of e_s^- with [$MoOCl_3$(dppe)] [dppe = 1,2-bis-diphenylphosphineethane] was calculated as $4.5 \times 10^{10}\ dm^3\ mol^{-1}\ s^{-1}$. The higher reactivity of such a complex of *cis*-symmetry towards e_s^- was explained.

In our recent works[1–4] we examined the reactivity of molybdenum complexes towards solvated electrons (e_s^-). We explained these phenomena as due to higher symmetry complexes having different structural features. We have described the complexes of the general formula $MoAB_3L_2$, and these compounds, according to the Bailar's analysis,[5] could have three isomers. We have also described in detail the reaction of t-$MoOCl_3(PPh_3)_2$ with e_s^-.[4]

The aim of the present work is to determine the reactivity of *cis*-[$MoOCl_3$(dppe)] (i.e. the *mer*-isomer regarding the positions of the Cl ligands) towards e_s^- in TBP (tri-n-butylphosphate) solutions.

The *cis* complexes are known to differ from the *trans* isomers taking into account their thermodynamics and kinetic stabilities. The *cis* isomers are more reactive, for example in reactions with the absorbent media forming hydrogen bonds or in hydrolysis reactions.[6–9] In *cis*-[$M(N_2)_2(PMe_2Ph)_4$] the yields of protonation of dinitrogen groups by the central atoms are much higher than in the *trans* isomers.[10] The biological activity of the *cis*-platinum(II) complexes has been established also.[11,12] However, the rate constants of the reactions of $[Co(en)_2Cl_2]^+$ and $[Cr(C_2O_4)_2(H_2O)]^-$ with e_s^- have been calculated as 7.1×10^{10} and $1.3 \times 10^{10}\ dm^3\ mol^{-1}\ s^{-1}$, respectively, and these values were equal for both *trans* and *cis* isomers.[13] The bidentate ligands such as dppe are known to prefer complexes of lower symmetry.[14] On the other hand, the chelating effect of dppe, abolishing the symmetry requirements, could increase the reactivity of the complex.[15]

EXPERIMENTAL

[$MoOCl_3$(dppe)] (red form, *cis* isomer, *mer*) was prepared according to the literature.[16] TBP (puriss p.a., Fluka) was extracted with 10% KOH, then washed with distilled water and distilled *in vacuo*.

The irradiations were made at 300 K and 77 K. Solutions of [$MoOCl_3$(dppe)] in TBP were saturated with argon or N_2O for 15 min, irradiated in a cobalt source Issledovatel (USSR) using a dose rate of $0.4 \times 10^{16}\ eV\ cm^{-3}\ s^{-1}$ (determined with a Fricke dosimeter and converted into the electron density of TBP). In addition, the solutions saturated with argon were frozen at 77 K then irradiated in a cryostat. In frozen solutions the appearance and decay of the absorption bands as a function of temperature were recorded. In irradiations (at room temperature) of solutions of the molybdenum(V) complex in TBP the changes of the band intensities in the UV–vis region were measured. These spectral measurements were made using a Beckman 5240

* Author to whom correspondence should be addressed.

spectrophotometer. The changes in the magnetic susceptibility due to the irradiation of the solutions examined were determined by the ^1H NMR method described by Evans[17] using a Varian FT-80 A multinuclear spectrometer.

RESULTS AND DISCUSSION

Absorption bands of $[MoOCl_3(dppe)]$ in TBP are shown in Fig. 1 and the band characteristics are presented in Table 1. It is easy to notice that the number of bands attributed to *d–d* transitions is higher than for the *trans* complexes of this type,[18] however, this is in agreement with the spectral characterization of the lower symmetry complexes of the type $[MoOCl_3(LL)]$.[19,20] Assuming C_2 symmetry of the tested complex, the ligand-field parameters, *Dq*, *Ds* and D_τ, were determined and the energies of the terms were calculated as shown in Fig. 2.

Due to the high value of ε and the width of the band at 730 nm one could assume that the *d–d* transition is partially affected by the $Cl^- \rightarrow d_{xy}$ transition (see Fig. 2). The latter transition makes the probability of the $d_{xy} \rightarrow d_{yz}$ transition more likely, therefore the band at 465 nm increased in intensity.

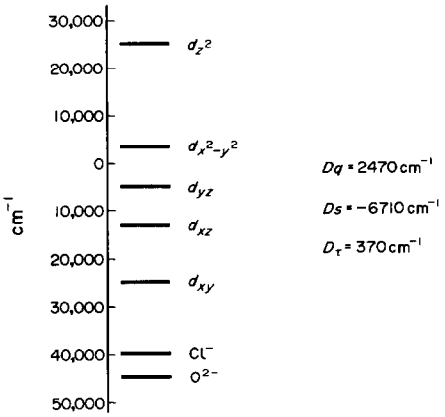

Fig. 2. Ligand-field parameters and the energy level diagram of the central atom orbitals for the complex $[MoOCl_3(dppe)]$.

On the basis of the results presented (see Fig. 2), the absorption bands appearing as a result of irradiation of the frozen solution of $[MoOCl_3(dppe)]$ in TBP were interpreted (Fig. 3). The

Table 1. Band positions, molar extinction coefficients (ε) and assignments for $[MoOCl_3(dppe)]$ (red isomer)

Band (nm)	ε	Assignment
235	16,000	$\pi_0 \longrightarrow d_{yz}$
255	15,000	$\pi_{phen} \longrightarrow 3d_P$
315	3500	$\pi_{Cl} \longrightarrow d_{xz}$
405	400	$d_{xy} \longrightarrow d_{x^2-y^2}$
465	550	$d_{xy} \longrightarrow d_{yz}$
730	80	$d_{xy} \longrightarrow d_{xz}$ ($\pi_{Cl} \longrightarrow d_{xy}$, a small contribution)

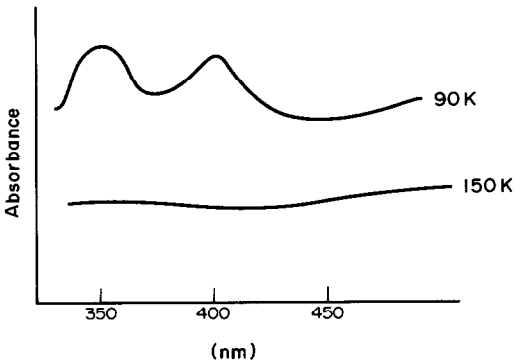

Fig. 3. Absorption bands appearing after the irradiation of the frozen solution of the molybdenum(V) complex in TBP ($C = 5 \times 10^{-3}$ M, dose $= 2 \times 10^{18}$ eV cm^{-3}).

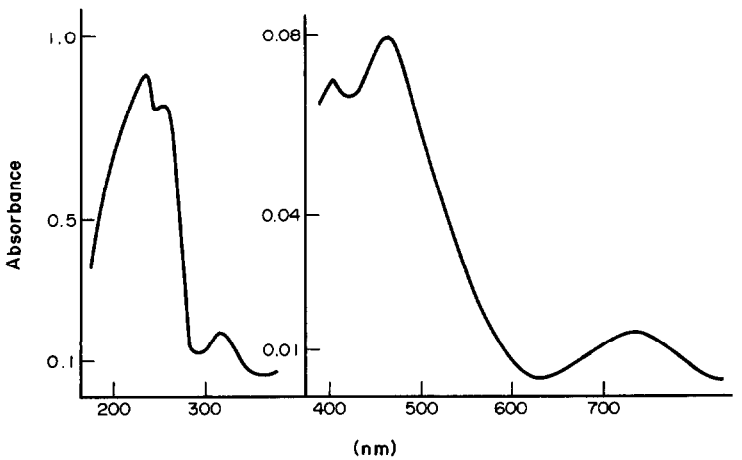

Fig. 1. Absorption bands of $[MoOCl_3(dppe)]$ in TBP.

bands at 350 and 400 nm appearing at 80 K and disappearing at 150 K (the non-irradiated complex solution was used as reference) were assigned as $(d_{xy})^1(d_{yz})^2 \rightarrow (d_{xy})^1(d_{z^2})^1$ and $(d_{xy})^1(d_{x^2-y^2})^1 \rightarrow (d_{xy})^1(d_{z^2})^1$, respectively. Thus, the electronic state of the hot ion, as the immediate product of the molybdenum(V) complex reaction with e_s^-, is $(d_{xy})^1(d_{x^2-y^2})^1$ and $(d_{xy})^1(d_{yz})^1$. The excited state, formed as a result of the direct acceptance of e_t^- and/or the decay of the hot ion could not be observed. The transitions $(d_{xy})^1(d_{xz})^1 \rightarrow (d_{xy})^1(d_{yz}, d_{x^2-y^2})^1$ and $(d_{xy})^1(d_{xz})^1 \rightarrow (d_{xy})^1(d_{xz})^1$ attributed to the excited state are at 300 and 880 nm and are impossible to record due to the significant scattering. The energetic neighbourhood of the $d_{x^2-y^2}$ and d_{yz} levels and their equal electron acceptor abilities are the reason for the similar thermal stability of the bands at 400 and 350 nm in the frozen solutions. According to common views, the higher energy electronic states usually have less thermal stability.

The final, molybdenum(IV), stable product of the molybdenum(V) ion reduction with e_s^- has the configuration $(d_{xy})^2$ and, according to the magnetic susceptibility measurements, is diamagnetic. The effective magnetic moment, after *ca* 40 min of irradiation of the complex solution, was reduced to 0 BM. After irradiation, no changes were found in the intensities of the bands at 235 and 255 nm, while the other bands were decreased. The decrease was proportional to the dose of irradiation and the difference between the intensities of the bands in solutions saturated with Ar and N_2O was significant. Thus, it can be assumed that the molybdenum(V) complex was reduced by e_s^- and, according to the decrease in the band intensity at 315 nm, Cl^- ions were simultaneously liberated from the coordination sphere of the complex. The detailed mechanism of the type of reaction described was presented earlier.[4] The number of reduced molecules of the complex vs dose and concentration were presented in Figs 4 and 5. These were calculated for the band at 730 nm. The number of liberated Cl^- ions vs dose and concentration of the complex solution are presented in Fig. 6. The calculated yields of reduction are presented in Table 2.

The main reactions in the system examined are:

$$TBP \longrightarrow e_s^-, TBP^+, R, \ldots \quad (1)$$

$$[MoOCl_3(dppe)] + e_s^- \longrightarrow [MoOCl_3(dppe)]^- \quad (2)$$

$$TBP + e_s^- \longrightarrow \text{radiolysis products} \quad (3)$$

$$[MoOCl_3(dppe)]^- + TBP \longrightarrow [MoOCl_2(dppe)(TBP)] + Cl^-. \quad (4)$$

By applying the steady-state approximation to reac-

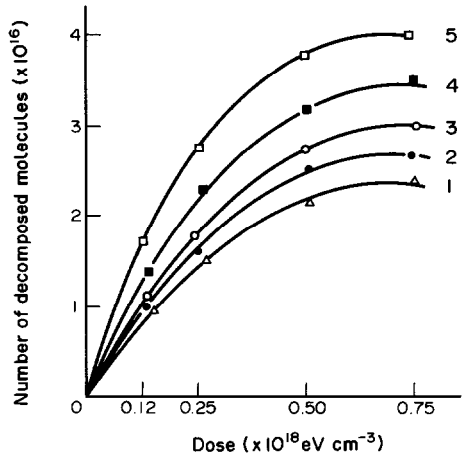

Fig. 4. Number of decomposed molybdenum(V) molecules in TBP solutions saturated with argon vs dose. Concentrations: (1) 1×10^{-3}, (2) 2×10^{-3}, (3) 3.1×10^{-3}, (4) 4.1×10^{-3}, (5) 5×10^{-3} mol dm^{-3}.

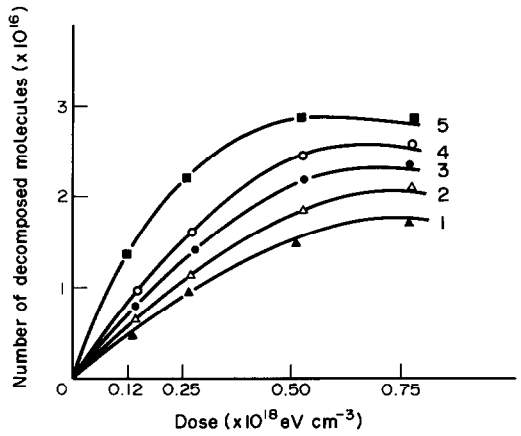

Fig. 5. Number of decomposed molybdenum(V) molecules in TBP solutions saturated with N_2O vs dose. Concentrations: (1) 1×10^{-3}, (2) 2×10^{-3}, (3) 3.1×10^{-3}, (4) 4.1×10^{-3}, (5) 5×10^{-3} mol dm^{-3}.

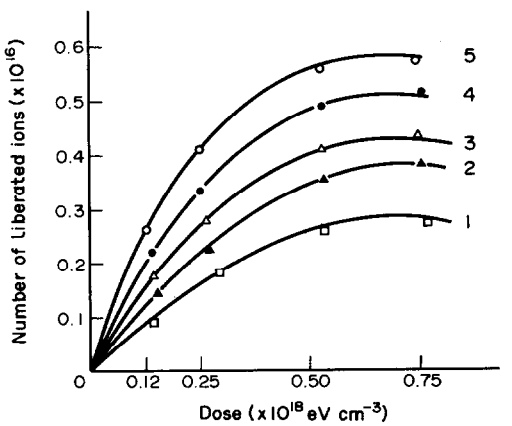

Fig. 6. Number of liberated Cl^- ions in irradiated molybdenum(V) solutions vs dose for the following molybdenum(V) concentrations in TBP: (1) 1.6×10^{-4}, (2) 2.2×10^{-4}, (3) 3×10^{-4}, (4) 3.8×10^{-4}, (5) 5.5×10^{-4} mol dm^{-3}.

Table 2. Radiation yields of reduced molybdenum(IV) molecules and cleaved Mo—Cl bonds as a function of the concentration of the molybdenum(V) complex in TBP

Concentrations $\times 10^{-3}$ (mol dm^{-3})	G (Mo^{IV}) Ar	G (Mo^{IV}) N_2O	ΔG	G (Mo—Cl) Ar
0.16				0.32
0.22				0.36
0.30				0.46
0.38				0.50
0.55				0.60
1.0	5.66	5.06	0.60	
2.0	5.75	5.09	0.66	
3.1	5.84	5.13	0.71	
4.1	5.94	5.17	0.77	
5.0	5.99	5.19	0.80	

G = number of molecules per 100 eV (= radiation yields).

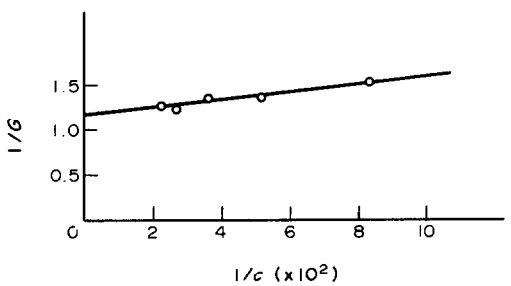

Fig. 7. Dependence of the reciprocal of ΔG on the reciprocal of the concentration of the molybdenum(V) complex.

tions (1)–(3) the following relationship was derived:

$$\frac{1}{\Delta G} = \frac{1}{G_{e_s^-}} + \frac{k_3[\mathrm{TBP}]}{k_2 G_{e_s^-}[\mathrm{Mo^V}]}$$

where $\Delta G = G_{Ar} - G_{N_2O}$, k_2 = rate constant of reaction (2) and k_3 = rate constant of reaction (3). Figure 7 shows G^{-1} as a function of the reciprocal of molybdenum(V) concentration.

From Fig. 7, the values of $G_{e_s^-} = 0.83$ and $K_3[\mathrm{TBP}]/k_2 G_{e_s^-} = 0.5 \times 10^{-3}$ were found. Thus, assuming $k_3 = 5 \times 10^6$ dm^3 mol^{-1} s^{-1} which was determined earlier,[21] we found $k_2 = 4.5 \times 10^{10}$ dm^3 mol^{-1} s^{-1}. On the basis of the results in Table 2, i.e. the yields of the Mo—Cl bond cleavage, the values $G_{e_s^-} = 0.80$ and $k_4 = 4.9 \times 10^{10}$ dm^3 mol^{-1} s^{-1} were calculated in a similar manner. Hence, our expectations concerning the liberation of Cl^- ions from the coordination sphere of the molybdenum complex as a result of molybdenum(V) reduction are confirmed. The calculated rate constant of the reaction of $[MoOCl_3(dppe)]$ with e_s^- is a few times higher than in the case of the reaction of $[MoOC_3(PPh_3)_2]$ with e_s^-.[4] This result and, as a consequence, the greater reactivity of the former complex is due to its lower symmetry and the greater number of orbitals which could accept electrons. Thus, there is no doubt that the symmetry and number of acceptor levels of the central atom in the complex compounds must not be neglected in the reactions with electrons.

REFERENCES

1. J. O. Dzięgielewski, *Polyhedron* 1984, **3**, 1131.
2. J. O. Dzięgielewski, *Polyhedron* 1985, **4**, 1901.
3. J. O. Dzięgielewski, B. Jeżowska-Trzebiatowska, R. Gil-Bortnowska and R. Grzybek, *Polyhedron* 1986, **5**, 833.
4. J. O. Dzięgielewski and K. Filipek, *Polyhedron* 1989, **8**, 447.
5. J. O. Dzięgielewski, *Chemia Nieorganiczna, Cześć III. Chemia Metali Grup Pobocznych./Inorganic Chemistry. Part III. Transition Metals Chemistry./* p. 26. Wydawnictwo Uniwersytetu Sląskiego, Katowice (1987).
6. Y. Mitsuri, J. Susumi and J. Rieko, *Bunseki Kagau* 1983, **32**, 605.
7. B. Wenclawiak and R. E. Sievers, *Z. Analyt. Chem.* 1983, **314**, 682.
8. S. K. Bhowal, M. Fleming and F. Umland, *Z. Analyt. Chem.* 1987, **328**, 235.
9. K. F. Purcell and J. C. Kotz, *Inorganic Chemistry*, p. 725. Holt Saunders, New York (1977).
10. J. Chatt, A. J. Pearman and R. L. Richards, *J. Chem. Soc., Dalton Trans.* 1977, 1853.
11. M. J. Cleare and J. D. Hoeschele, *Platinum Met. Rev.* 1973, **17**, 2.
12. M. J. Cleare, *Coord. Chem. Rev.* 1974, **12**, 349.
13. A. K. Pikaev and S. A. Kabakchi, *Reakcyonnaya*

Sposobnost Pervichnykh Produktov Radyoliza Wody. Energoizdat, Moskva (1982).
14. P. C. H. Mitchell, *J. Inorg. Nucl. Chem.* 1963, **25**, 963.
15. P. C. Braterman, *Top. Curr. Chem.* 1980, **92**, 149.
16. A. V. Butcher and J. Chatt, *J. Chem. Soc. A* 1971, 2356.
17. D. P. Evans, *J. Chem. Soc.* 1959, 2003.
18. D. A. Edwards, *J. Inorg. Nucl. Chem.* 1965, **27**, 303.
19. A. B. P. Lever, *Inorganic Electronic Spectroscopy*, 2nd edn. Elsevier, Amsterdam (1984).
20. H. E. Pence and J. Selbin, *Inorg. Chem.* 1969, **8**, 353.
21. J. O. Dzięgielewski and K. Filipek, *J. Radioanal. Nucl. Chem.* 1988, **128**, 109.

Polyhedron Vol. 10, No. 13, pp. 1465–1472, 1991
Printed in Great Britain

0277–5387/91 $3.00+.00
© 1991 Pergamon Press plc

MONO-ORGANOMERCURY AND DIORGANOTHALLIUM DERIVATIVES OF RHODANINE: CRYSTAL STRUCTURE OF DIMETHYL(RHODANINATO)THALLIUM(III)

NURIA PLAYÁ, ALEJANDRO MACÍAS,* JOSÉ Ma VARELA, AGUSTÍN SÁNCHEZ, JOSÉ S. CASAS* and JOSÉ SORDO

Departamento de Química Inorgánica, Universidade de Santiago de Compostela, 15706 Santiago de Compostela (A Coruña), Spain

(*Received* 28 *September* 1990; *accepted* 24 *January* 1991)

Abstract—The complexes HgR(Rd) and $TlR_2(Rd)$ (R = Me, Ph; HRd = rhodanine) have been prepared from the reaction of the ligand with the appropriate organometallic hydroxide (Tl) or acetate (Hg). The crystal structure of $TlMe_2(Rd)$ was obtained and shows that the thallium atom is coordinated by two oxygen atoms and a sulphur atom from three different ligands, as well as the two carbon atoms of the methyl groups. The compound crystallizes, forming a planar association along the plane defined by the crystallographic axes *ac*. Comparison of this compound with $TlPh_2(Rd)$ and HgR(Rd) was undertaken using mass, IR, and multinuclear (^1H, ^{13}C, ^{199}Hg, ^{205}Tl) NMR spectra.

The reaction of TlR_2^+ in basic media with heterocyclic ligands (HL) that can have the tautomeric equilibrium

$$—NH—C(S)— \rightleftharpoons —N=C(SH)—, \quad (1)$$

gives metallated compounds in which the ligand only partially changes to the thiolic form, the strongest ligand–metal bond forms across the nitrogen atom, although the sulphur atom also takes part in thallium coordination.[1,2]

Furthermore, the tendency of the thallium atom to take coordination numbers of 5 or more produces intermolecular associations in $TlMe_2L$; across bridging sulphur atoms if there are no other donor groups apart from those implicated in the equilibrium [eq. (1)],[1] or, across these groups if they are present in the ligand molecules.[2] The structures are very different from those formed by HgR^+ cations with the same ligands.[1,3]

In the light of these facts, it would be expected that the reaction of dimethylthallium(III) hydroxide with rhodanine (HRd) ought to give a complex showing a coordinative situation for the thallium atom similar to that found in dimethyl(2-thiouracilato)thallium(III),[2] given the similar donor groups and tautomeric possibilities of the two ligands. Nevertheless this work has shown that the compounds are markedly different, indicating the complexity of coordination chemistry of the TlR_2^+ cations.

At the same time, comparing $TlR_2(Rd)$ with HgR(Rd) has revealed unusual spectroscopic differences in solution in DMSO, that distinguish rhodanine from other heterocyclic ligands studied previously.[1–3]

As far as we know, this is the first X-ray diffraction structural study of a complex of the rhodaninate anion Rd^-, although adducts of rhodanine and 3-methylrhodanine have been studied.[4]

EXPERIMENTAL

Rhodanine (Ega-Chemie), and methylmercury and phenylmercury acetates (Merck) were used without prior purification. Dimethylthallium and diphenylthallium hydroxides were obtained from the corresponding iodide and bromide compounds[5] using freshly prepared Ag_2O. Analytical data of the mercury compounds were obtained from Galbraith Lab. Inc. (Knoxville, TN, USA); thallium compounds were analysed in a Perkin–Elmer 240-B

* Authors to whom correspondence should be addressed.

Table 1. Most important bands in the IR spectra of HRd and its complexes

	HRd	HgMe(Rd)	HgPh(Rd)	$TlMe_2$(Rd)	$TlPh_2$(Rd)
ν(N—H)	3160m	—	—	—	—
	3080m	—	—	—	—
ν(C=O)	1705vs,b	1680vs	1695vs	1600vs	1650vs
ν_{as}(C—N—C)	1230vs	1310vs	1315vs	1300vs	1320vs
ν(C=S)	1080vs	—	990vs	1010vs	1030vs
ν(C=S)	820s	820s[a]	780m	810m[a]	—
	780s	785s	770m	790m	780m
ν(C—S_{ring})	680s	680s	690s	680s	680s
ν(Hg—C)	—	545m	—	—	—
ν_{as}(C—Tl—C)	—	—	—	550m	—

[a] $+\rho(CH_3)$.

apparatus. The IR spectra, in nujol suspensions or KBr tablets, were obtained in a Perkin–Elmer 180 spectrometer. ^1H and ^{13}C NMR were recorded on a Bruker WM-250 apparatus except for $TlPh_2$(Rd) for which a Varian CFT-80A apparatus was used. ^{199}Hg (at 44.8 MHz) and ^{205}Tl (at 230.8 MHz) NMR spectra were recorded, in 10 mm o.d. tubes, on a Bruker WM-250 and a Bruker AM-400 spectrometers, respectively. Mass spectra were made on a Kratos MS50TC spectrometer connected to a DS-90 data system, and operating in EI conditions (direct insertion probe, 70 eV, 250°C). All the fragments included in Table 3 were identified using DS-90 software.

Synthesis of $TlMe_2$(Rd)

An aqueous solution containing 2.00 g (7.8 mmol) of $TlMe_2$(OH) was slowly added with stirring to 1.06 g (7.8 mmol) of rhodanine (HRd) dissolved in methanol. After 24 h of stirring a white–violet solid formed that was isolated by filtration and vacuum dried over calcium chloride. A few white–violet crystals, with the same analytical composition as the first solid, were obtained from the mother liquor. They were used in the X-ray diffraction study; m.p. 187-189°C. (Found: C, 16.4; H, 2.1; N, 3.9. $C_5H_8NOS_2Tl$ requires C, 16.3; H, 2.2; N, 3.8%.)

Synthesis of $TlPh_2$(Rd)

An aqueous solution containing 1.28 g (3.4 mmol) of diphenylthallium hydroxide was added to an equimolar amount of rhodanine (0.46 g) dissolved in methanol. After 4 h of stirring, a white solid appeared, which was separated by filtration and vacuum dried over calcium chloride. Dec. pt 170°C. (Found: C, 36.8; H, 2.1; N, 2.9. $C_{15}H_{12}NOS_2Tl$ requires C, 36.7; H, 2.4; N, 2.8%.)

Synthesis of HgMe(Rd)

An aqueous solution of 1.18 g (4.3 mmol) of methylmercury acetate was added to a methanolic solution of rhodanine (0.57 g, 4.3 mmol). The white solid formed was separated by filtration, recrystallized using an ethanol–acetone mixture and vacuum dried over calcium chloride; m.p. 125°C. (Found: C, 13.8; H, 1.5; N, 4.0. $C_4H_5NOS_2Hg$ requires C, 13.8; H, 1.4; N, 4.0%.)

Synthesis of HgPh(Rd)

A solution in ethanol–water (5:2) of 1.22 g (3.7 mmol) of phenylmercury acetate was slowly added with stirring to a solution of rhodanine (0.50 g, 3.7 mmol) in methanol. The white solid that formed was separated by filtration and vacuum dried over calcium chloride; m.p. 130°C. (Found: C, 26.0; H, 1.6; N, 3.3. $C_9H_7NOS_2Hg$ requires C, 26.4; H, 1.7; N, 3.4%.)

Crystal structure determination

Suitable white–violet crystals of $TlMe_2$(Rd) were obtained as described above.

Crystal data. $C_5H_8NOS_2Tl$, M = 366.62, monoclinic, $a = 7.474(2)$, $b = 7.655(1)$, $c = 15.830(4)$ Å, $\beta = 95.45(2)°$, $U = 901.6$ Å^3 (by least-squares refinement on diffractometer angles for 25 automatically centred reflections, $\lambda_{Mo\text{-}K_\alpha} = 0.71073$ Å), space group $I2/m$ (alt. $C2/m$, No. 12), $Z = 4$, $D_c = 2.701$ g cm^{-3}. Crystals of irregular shape. Maximum and minimum dimensions: 0.25 and 0.20 mm, μ(Mo-K_α) = 184.85 cm^{-1}.

Data collection and processing. CAD4 diffractometer, ω–θ mode with scan width and scan speed variables, graphite-monochromated Mo-K_α radiation, 3522 reflections measured ($3 < \theta < 32°$), 1761 unique [merging $R = 0.032$ after empirical absorption correction[6] (max. and min. transmission factors 1.283, 0.612)], giving 849 with $I > 3\sigma(I)$. The standards varied $\pm 3.5\%$ over the course of data collection.

Structure analysis and refinement. Heavy atom method (thallium atom) followed by subsequent Fourier difference syntheses. The hydrogen atoms were not found in the maps and were not included in the model. Full-matrix least-squares refinement with anisotropic thermal parameters for all atoms, and an extinction correction of the form $F_{corr} = F_c(1 + kF_c^2/\sin 2\theta)^{0.25}$, with $k = 3.6803 \times 10^{-8}$, converged for 59 variable parameters to $R = \Sigma(|F_o| - |F_c|)/\Sigma|F_o| = 0.041$ and $R' = [\Sigma w(|F_o| - |F_c|)^2/\Sigma w|F_o|^2]^{1/2} = 0.048$, $w^{-1} = \sigma^2 F_o$). A final difference Fourier map showed some peaks of maximum density 1.265 e Å^{-3} all located at < 1.2 Å from the thallium atom, as previously detected in other dimethylthallium(III) complexes.[2,7,8] Scattering factors and anomalous dispersion corrections were taken from parts (a) and (b) of ref. 9, respectively. Data processing was performed on a DECMicro VAXII computer using the SHELXS-86[10] and VAX-SDP[11] software packages.

RESULTS AND DISCUSSION

Crystal structure

Selected interatomic distances and bond angles for $TlMe_2(Rd)$ are shown in Table 2. The thallium atom is coordinated by two oxygen atoms and a sulphur atom from three different ligands, as well as the two carbon atoms of the methyl groups (Fig. 1). These five atoms form a pseudo-octahedral

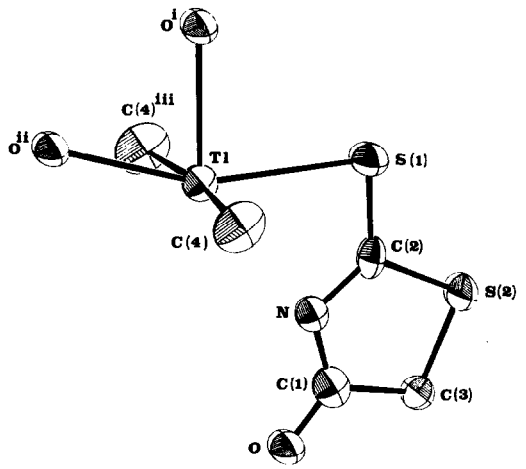

Fig. 1. The environment of the thallium atom in $TlMe_2(Rd)$ and numbering scheme of the compound.

Table 2. Selected interatomic distances (Å) and bond angles (deg) for $TlMe_2(Rd)$

Bond distances			
Tl—S(1)	2.949(3)	S(2)—C(2)	1.743(8)
Tl—O^{i}	2.659(7)	S(2)—C(3)	1.780(9)
Tl—O^{ii}	2.723(7)	O—C(1)	1.22(2)
Tl—N	3.134(7)	N—C(1)	1.32(1)
Tl—C(4)	2.1435(8)	N—C(2)	1.33(2)
S(1)—C(2)	1.67(1)	C(1)—C(3)	1.54(1)
Bond angles			
S(1)—Tl—O^{i}	89.5(1)	C(4)—Tl—C(4)^{iii}	171.4(6)
S(1)—Tl—O^{ii}	160.2(1)	C(2)—S(2)—C(3)	91.3(4)
S(1)—Tl—N	52.2(1)	C(1)—N—C(2)	113.5(7)
S(1)—Tl—C(4)	94.0(3)	O—C(1)—N	124.8(8)
O^{i}—Tl—O^{ii}	70.6(3)	O—C(1)—C(3)	119.8(8)
O^{i}—Tl—N	141.8(2)	N—C(1)—C(3)	115.5(7)
O^{i}—Tl—C(4)	91.6(3)	S(1)—C(2)—S(2)	117.9(5)
O^{ii}—Tl—N	147.6(2)	S(1)—C(2)—N	126.7(6)
O^{ii}—Tl—C(4)	86.7(3)	S(2)—C(2)—N	115.4(7)
N—Tl—C(4)	91.2(3)	S(2)—C(3)—C(1)	104.5(6)

Numbers in parentheses are estimated standard deviations in the least significant digits. Superscipts i, ii, and iii represent the equivalent positions ($x-1$, y, z), ($1-x$, $-y$, $-z$) and (x, $-y$, z), respectively.

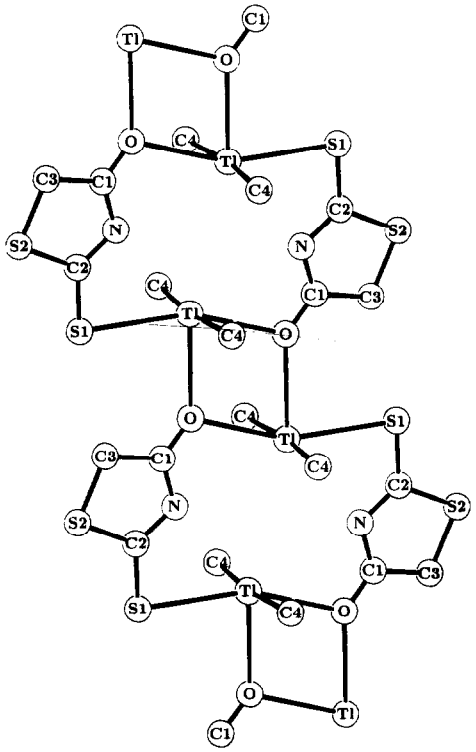

Fig. 2. Polymerization of $TlMe_2(Rd)$ following the crystallographic plane *ac*.

arrangement around the metal atom, with one site of the octahedron vacant. Another thallium atom lies in the approximate direction of the empty site at a distance from the first thallium atom [3.918(1) Å] in the limit of the sum of van der Waals radii (3.92 Å[12]).

The shortest Tl—O distance [2.659(7) Å] is greater than in complexes with the anionic ligands DL-tryptophanate[7] and 1-oxidopyridinium-2-thiolate,[13] which also have asymmetric bridging oxygens, but less than the length of the weak Tl···O bond of dimethyl(2-thiouracilato) thallium(III).[2] The biggest Tl—O distance [2.723(7) Å] is similar to that of the derivative of 2-thiouracil.[2] Similarly, the Tl—S distance [2.949(3) Å] is of the same order as that found in $TlMe_2SCOCH_3$,[14] but greater than those found in other 2-mercapto derivatives[2,8,13] or thiosemicarbazates.[15] The Tl—C distances and the C—Tl—C angle are normal.

That thallium–oxygen and thallium–sulphur distances are greater than those found previously in other compounds of the dimethylthallium(III) cation may come, not so much from the intrinsic donor character of the rhodaninate anion, as from the requirements of the considerably symmetrical laminar configuration of the compound (Fig. 2) (*vide infra*).

The modifications of the rhodanine ring with respect to the free ligand[16] are observed mainly in the C(1)—N and C(2)—N bonds, which shorten in the thallium complex, while the C(2)—S(1) lengthen slightly. These changes suggest that the negative charge of the anion is delocalized along the annular part formed by the atoms O—C(1)—N—C(2)—S(1), strengthening the two nitrogen–carbon bonds and maintaining a high multiplicity in the exocyclic bonds.

The concurrence of two $TlMe_2(Rd)$ units allows the formation of a planar dodecagonal "ring". From this ring protrude the S(2) and C(3) atoms of each rhodanine ring (Fig. 2). It should be noted that the Tl—N distance in these "rings" [3.134(7) Å] is less than the sum of the van der Waals radii (3.51 Å[12]), although the mutual orientation of these two atoms seems ill-suited for a donor interaction to be established by the nitrogen. A pair of weak Tl···O interactions unite each dodecagonal "ring" with its neighbours, forming a planar association along the plane defined by the crystallographic axes *ac*, with the two methyl groups emerging from above and below the plane.

Mass spectra

The spectral behaviour of $TlMe_2(Rd)$ (Table 3) is similar to that observed before in dimethyl(2-thiouracilato)thallium(III),[3] although the molecular ion is less abundant in the present case (0.3% of the base peak). The spectrum shows signals of other fragmentation products with very low intensities ($\leqslant 0.1\%$ of the base peak) and a greater mass than the molecular ion (e.g. *m/z* 450). Although these species could have been generated by an ion–molecule reaction, an origin in the associated character of the compound cannot be excluded.

The spectrum of HgMe(Rd) is clearly different. In the first place, the relative abundance of the molecular ion suggests that the mercury compound is more stable, which agrees with previous thermodynamic studies in solution of the interaction of $HgMe^+$ and $TlMe_2^+$ with sulfhydrilated aminoacids.[17]

Secondly, the HgMe(Rd) spectrum contains minor signals that, judging from their isotopic profile, correspond to the concurrence of two or more ions of related mass. Some of these signals [*m/z* (abundance): 275(14.7) and 260(7.6)] could correspond to the ions [$OCCH_2SHg$]/[OCCHSHg] and [NCSHg]/[MeSHgMe], respectively. The presence of these metallated fragments of the ligand,[18] that are formed in a fragmentation pathway where the

Table 3. Mass spectra (EI) of $TlMe_2(Rd)$[a] and HgMe(Rd)[a]

$TlMe_2(Rd)$			HgMe(Rd)		
Ion	m/z[b]	Relative abundance	Ion	m/z[b]	Relative abundance
[M]	367	0.3	$[S(HgMe)_2]$	464	5.1
[M—Me]	352	32.7	[S(MeHg)Hg]	449	3.2
[M—2Me]	337	5.8	$[SHg_2]$	434	1.0
$[TlMe_2]$	235	59.8	$[MeHg_2]$	417	0.6
[TlMe]	220	13.2	$[Hg_2]$	402	1.6
[Tl]	205	100	[M]	349	18.7
			[M—NCS—H]	290	18.2
			[SHgMe]	249	5.4
			[HgMe]	217	48.0
			[Hg]	202	28.4

[a] Only ions containing thallium or mercury included. [HL] and ligand fragments were also observed.

[b] For the bimetallic species the value of the most intense cluster peak is quoted. In monometallic ions, nominal values are calculated using the most abundant isotope ^{205}Tl or ^{202}Hg.

cleavage of the rhodanine ring precedes the cleavage of the S—Hg bond, demonstrates the high stability of this bond. Finally, the number and intensity of the signals corresponding to binuclear ions in this spectrum (Table 3) are considerable.

The information apported by the spectra of the phenyl derivatives is more restricted. The molecular ion was not detected at all. The ions at higher m/z were [M—Ph] (2.4 referred to $[Ph^+H]$ as base peak) and $[Ph_2Hg]$ (11.5 referred to [Ph] as base peak) for $TlPh_2(Rd)$ and HgPh(Rd), respectively. No Hg—S bond retaining ions have been observed.

IR spectra

Table 1 shows the most significant bands in the IR spectra of the ligand and its complexes. The assignments of the ligand bands are based on previous data.[19,20]

Both ν(N—H) bands of the ligand disappear in the complexes, which corresponds to its deprotonation. In $TlMe_2(Rd)$ the coordination of the C=O and C=S groups to the metal was established on the basis of the X-ray diffraction data (*vide supra*). This coordination strongly shifts the 1705 cm^{-1} band of the ligand, ν(C=O), and the 1080 cm^{-1} band, ν(C=S), to lower wavenumbers. The pattern shown (Table 1) is indicative of similar participation of these groups in the coordination to the metal in the $TlPh_2(Rd)$ complex, whereas in the HgR(Rd) complexes the situation is different. Although ν(C=O) also undergoes slight shifts to lower wavenumbers in this case, these are a consequence of the ligand deprotonation and electron rearrangement due to the C=S group coordination.[19] This coordination is confirmed in HgPh(Rd) from the strong shift of the 1080 cm^{-1} band, which indicates a more pronounced thione---thiol evolution in this complex than in the thallium complexes; in HgMe(Rd) the lack of a strong band in this zone could be indicative of a thiol structure for the ligand in the complex.

On the other hand, the shifts to higher wavenumbers seen for the ν_{as}(C—N—C) band could be based on C—N bond reinforcement or, additionally, on a weak N—M interaction.

A strong band located in the free ligand at 1435 cm^{-1} seems to disappear under complexation. Nevertheless, it might be present as a weak absorption in the complexes as there are several weak bands in the range 1500–1300 cm^{-1}. The lack of intensity of this band on coordination (and also deprotonation) of the ligand can be explained if its assignment previously suggested[21] to ν(C—N—C)+δ(N—H) is considered. The ν(C—S_{ring}) located at 680 cm^{-1} in the free ligand remains in the same position in all the complexes, indicating non-participation of this sulphur atom in the coordination.

With respect to the organometallic fragment, $\rho(CH_3)$ in $TlMe_2(Rd)$ and HgMe(Rd) strengthen the ligand band near 800 cm^{-1}, and the positions of ν(C—Tl—C) and ν(Hg—C) are close to those found in related systems.[13,22]

Table 4. NMR data for the ligand and its organometallic derivatives in DMSO solution

	^{1}H NMR[a]				^{13}C NMR[a]					^{199}Hg, ^{205}Tl NMR
Compound	δ(NH)	δ(CH_2)	δ(MR_n)	$^2J(^1H—M)$	δ[C(2)]	δ[C(4)]	δ[C(5)]	δ(MR_n)	$J(^{13}C—M)$	δM[b]
HRd	10.7	4.3			205.5	176.9	39.5			
HgMe(Rd)		4.2	0.78	201.1	187.0	207.7	43.1	7.0	[c]	−802(39)
HgPh(Rd)		4.3			187.0	207.0	43.7	154.7(C—Hg) 136.9(Co) 128.5(Cm) 128.3(Cp)		−1122(116)
$TlMe_2$(Rd)		3.8	0.93	435.4	213.4	189.8	42.1	25.6	2917	3452(1389)
$TlPh_2$(Rd)		3.9	7.8(Ho) 7.5(Hm) 7.3(Hp)	456(Ho) 140(Hm) 53(Hp)	212.8	188.5	42.6	—(C—Tl)[d] 136.2(Co) 128.8(Cm) 128.4(Cp)	— 302 457 —[e]	2951(2135)

Numbering scheme:

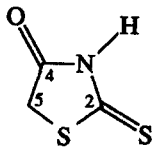

[a] Chemical shift in ppm from TMS. *J* in Hz.

[b] Chemical shift in ppm from Me_2Hg (95% in Et_2O) and infinitely dilute aqueous solution of $TlClO_4$ for M = Hg and Tl, respectively. $W_{1/2}$, in Hz, in parentheses.

[c] Not observed.

[d] One of the peaks of the doublet associated with this carbon is masked by other phenyl carbon signals.

[e] This coupling was not resolved under the experimental conditions used.

NMR spectra

The behaviour of the HgR(Rd) derivatives in solution in DMSO is conventional (Table 4). The C(2) signal is shielded strongly, as expected for the evolution of the ligand to the thiolic form, as a result of the complexation.[23] The carbons C(4,5) are deshielded, possibly due to the combination of the tautomeric change and the inductive effect of the metal. The values of the coupling constant $^2J(^1H–^{199}Hg)$ and the chemical shift of the mercury-bonded carbon of the methyl group, are a little lower and higher, respectively, than values usually observed in thiolated derivatives of methylmercury(II).[24,25] Furthermore, the chemical shift of the metallic nuclide is somewhat less negative than in other neutral compounds with an R—S—HgMe bond.[3,26] These results suggest that there is a dynamic equilibrium in solution between the thiolic S-metallated form and a small fraction of the organomercury N-bonded cation:

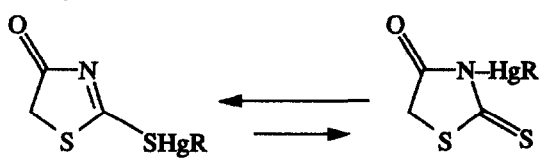

The phenylmercury(II) compound has analogous properties to those of HgMe(Rd).

Surprisingly, the positions of the ligand signals in the ^{13}C NMR spectra of the TlR_2(Rd) compounds (Table 4) are similar to those for HgR(Rd) (see Figs 3 and 4), when, looking at the structure of $TlMe_2$(Rd) in the solid state (*vide supra*), there should be a clearcut difference, at least in the position of the C(2) carbon given the poor thiolic evolution of the ligand in the thallium complex. This apparent anomaly is resolved by considering the proton coupled ^{13}C NMR spectra (insert in Figs 3 and 4). The signal of the C(4) of the carbonyl group is split by the coupling with the hydrogens of the $C(5)H_2$ group, which allows C(4) to be unequivocally identified. Its signal is more shielded than that of the C(2) in HRd (Table 4), and this relative position is maintained in TlR_2(Rd), although both signals are at lower field as a consequence of the coordination to the metal. In HgR(Rd), however, the thiolic evolution of the ligand shields C(2) so much that it changes its relative position with respect to C(4), such that the signal of the latter is placed at lower field in the spectrum. These results suggest that, in DMSO solution, the organothallic derivatives contain the ligand in the keto-thione

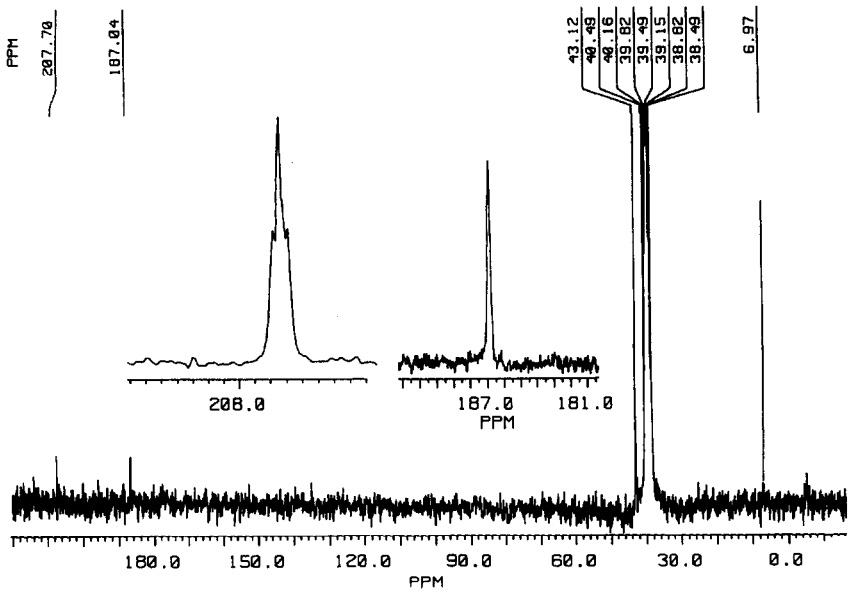

Fig. 3. ^{13}C NMR spectrum of HgMe(Rd) (the insert shows the proton coupled low field signals).

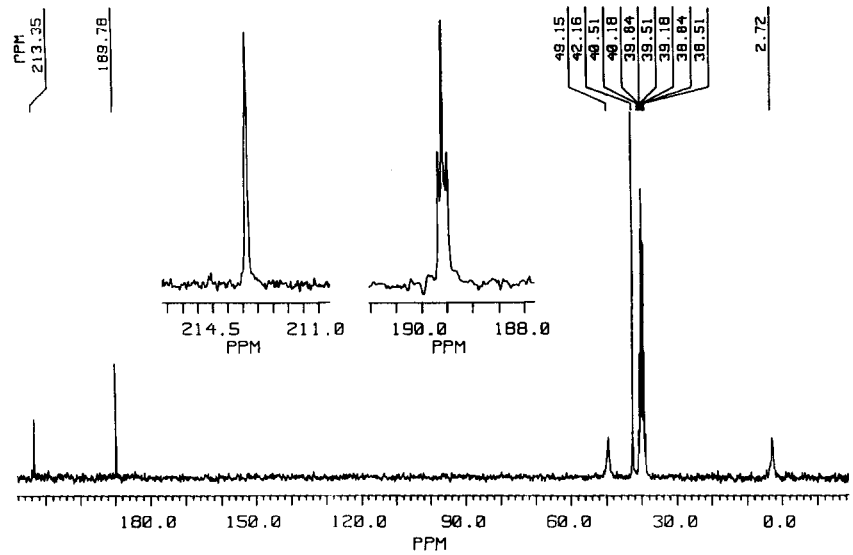

Fig. 4. ^{13}C NMR spectrum of $TlMe_2$(Rd) (the insert shows the proton coupled low field signals).

form as observed in the solid state. Furthermore, the spectral parameters $^2J(^1H-^{205}Tl)$, $^1J(^{13}C-^{205}Tl)$ and the ^{205}Tl chemical shift for $TlMe_2$(Rd) suggest a rather saline behaviour for this compound (i.e. for $TlMe_2ClO_4$ in DMSO, the above mentioned parameters are 438 ± 2.7 Hz, 2918.2 Hz (0.4 M solution) and 3455 ppm (0.4 M solution), respectively).[27]

Acknowledgements—We thank the Comisión Asesora de Investigación Científica y Técnica (PR84-0624), Dirección General de Investigación Científica y Técnica del Ministerio de Educación y Ciencia (PB87-0482), and Xunta de Galicia (A.M.), Spain, for financial support, and Dr Julius Glaser (Inorganic Chemistry Department, The Royal Institute of Technology, Stockholm, Sweden) for the facilities to record the ^{205}Tl spectra.

REFERENCES

1. M. V. Castaño, A. Macías, A. Castiñeiras, A. Sánchez-Gonzalez, E. García-Martinez, J. S. Casas, J.

Sordo, W. Hiller and E. E. Castellano, *J. Chem. Soc., Dalton Trans.* 1990, 1001.
2. M. S. García-Tasende, M. I. Suarez, A. Sánchez, J. S. Casas, J. Sordo, E. E. Castellano and Y. P. Mascarenhas, *Inorg. Chem.* 1987, **26**, 3818.
3. M. S. García-Tasende, M. I. Suarez-Gimeno, A. Sánchez, J. S. Casas, J. Sordo and E. E. Castellano, *J. Organomet. Chem.* 1990, **384**, 19.
4. (a) F. G. Moers, W. P. J. H. Bosman and P. T. Beurskens, *J. Cryst. Mol. Struct.* 1972, **2**, 23; (b) F. G. Moers, J. M. M. Smits and P. T. Beurskens, *J. Cryst. Spectrosc. Res.* 1986, **16**, 101; (c) F. G. Moers, P. T. Beurskens, J. H. Noordik and J. M. M. Smits, *J. Cryst. Spectrosc. Res.* 1986, **16**, 107.
5. H. Gilman and R. G. Jones, *J. Am. Chem. Soc.* 1946, **68**, 517; J. J. Eisch, *Organomet. Synth.* 1981, **2**, 154.
6. DIFABS: N. Walker and D. Stuart, *Acta Cryst.* 1983, **A39**, 159.
7. K. Henrick, R. W. Mattews and P. A. Tasker, *Acta Cryst.* 1978, **B34**, 935.
8. Y. P. Mascarenhas, I. Vencato, M. C. Carrascal, J. M. Varela, J. S. Casas and J. Sordo, *J. Organomet. Chem.* 1988, **344**, 137.
9. Scatt. Fac. (SDP): D. T. Cromer and J. T. Weber, *International Tables for X-Ray Crystallography*, Vol. 4. (a) Table 22B, (b) Table 2.3.1. Kynoch Press, Birmingham (1974).
10. G. M. Sheldrick, *SHELXS-86. Program for Crystal Structure Determination.* University of Cambridge (1986).
11. SDP: B. A. Frenz and Associates, Inc. College Station, Texas and Enraf-Nonius, Delft, The Netherlands, VAXSDP, *Structure Determination Package* (Version 2.2) (1985).
12. A. Bondi, *J. Phys. Chem.* 1964, **68**, 441.
13. M. V. Castaño, A. Sanchez, J. S. Casas, J. Sordo, J. L. Brianso, J. F. Piniella, X. Solans, G. Germain, T. Debaerdemaeker and J. Glaser, *Organometallics* 1988, **7**, 1897.
14. W. Schwarz, G. Mann and J. Weidlein, *J. Organomet. Chem.* 1976, **122**, 303.
15. A. Macías, M. C. Rodriguez-Argüelles, M. I. Suarez, A. Sánchez, J. S. Casas, J. Sordo and U. Englert, *J. Chem. Soc., Dalton Trans.* 1989, 1787.
16. D. Van der Helm, A. E. Lessor Jr and L. L. Merritt Jr, *Acta Cryst.* 1962, **15**, 1227.
17. (a) M. García-Bugarin, M. E. García, G. Berthon, J. S. Casas and J. Sordo, *Polyhedron*, 1988, **24**, 2487; (b) R. S. Reid and D. L. Rabenstein, *Can. J. Chem.* 1981, **61**, 1428.
18. G. Gattow and W. Rach, *Z. Anorg. Allg. Chem.* 1983, **560**, 140.
19. A. C. Fabretti and G. Peyronel, *Trans. Met. Chem.* 1977, **2**, 224.
20. L. Sestili, C. Cauletti and C. Furlani, *Inorg. Chim. Acta* 1985, **102**, 55, and references therein.
21. C. Cogrossi, *Spectrochim. Acta* 1972, **28A**, 855.
22. J. Bravo, J. S. Casas, M. V. Castaño, M. Gayoso, Y. P. Mascarenhas, A. Sánchez, C. O. P. Santos and J. Sordo, *Inorg. Chem.* 1985, **24**, 3435.
23. A. M. Brodie, H. D. Holden, J. Lewis and J. M. Taylor, *J. Chem. Soc., Dalton Trans.* 1986, 633.
24. D. L. Rabenstein, *Acc. Chem. Res.* 1978, **11**, 100.
25. E. Buncel, R. Kumar and A. R. Norris, *Can. J. Chem.* 1986, **64**, 442.
26. A. R. Norris and R. Kumar, *Inorg. Chim. Acta* 1984, **93**, L63.
27. J. F. Hinton, K. R. Metz and R. W. Briggs, *Prog. NMR Spectrosc.* 1988, **20**, 423.

Polyhedron Vol. 10, No. 13, pp. 1473–1477, 1991
Printed in Great Britain

0277-5387/91 $3.00+.00
© 1991 Pergamon Press plc

STRUCTURAL CHARACTERIZATION OF THE PLATINUM(II)–PENICILLIN COMPLEXES

T. GROCHOWSKI* and K. SAMOCHOCKA

Department of Chemistry, Warsaw University, Zwirki i Wigury 101, 02-089 Warsaw, Poland

(*Received* 22 *February* 1990; *accepted* 5 *February* 1991)

Abstract—In the reaction of K_2PtCl_4 with penicillin V and penicillin G, two novel platinum(II) complexes were obtained. The structure of these complexes was determined by using IR and NMR spectroscopy. The structure of natural penicillin was found to be retained in the complex. A new, five-membered ring results from the chelation of the Pt^{2+} ion by the amide and thioether groups of the penicillin moiety. Based on the ^{13}C NMR spectra, the isomerism of the penicillin side chain is established.

Coordination of transition metal ions to the deprotonated nitrogen atom in the amide or peptide bond is a subject of considerable current interest.[1] Relatively few such complexes of platinum(II) have been reported.[2–5] A survey of the literature indicates that the coordination of the amide nitrogen to the Pt^{2+} ion is facilitated if formation of a five-membered ring is involved. However, many platinum complexes with chelating thioether ligands have been investigated[6–14] using spectroscopic techniques and X-ray structural analysis. Among those compounds an important group are complexes with ligands of biological significance. The latter compounds were investigated as models of platinum complexes bonded to proteins.[8–11] An interesting group of bioligands, which feature the amide and thioether functional groups, are penicillins. From a variety of those β-lactam antibiotics, we chose two typical penicillins, penicillin V (PenV) and penicillin G (PenG) (Fig. 1), which are stable in aqueous solution over a wide range of pH. In this study, the complexes of penicillin V and penicillin G with the Pt^{2+} ion were synthesized and isolated. To our knowledge, these are the first platinum complexes of penicillins to be reported. Their structures were determined by NMR and IR spectroscopy.

* Author to whom correspondence should be addressed.

EXPERIMENTAL

Materials

K_2PtCl_4 was obtained[15] from the analytical grade K_2PtCl_6 (POCh Gliwice, Poland). Penicillins V and G (potassium salts) were supplied by Tarchomin Pharmaceutical Works (POLFA), Poland. The purity of the penicillins was checked by HPLC.

NMR measurements

The 500 MHz ^1H and 125 MHz ^{13}C NMR spectra were recorded with a Bruker 500 spectrometer.

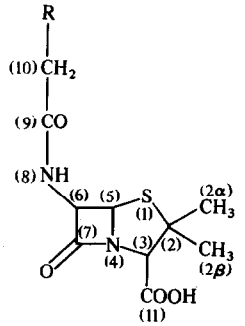

Fig. 1. General structural formula for the penicillin molecule with numbered atoms: R = C_6H_5O for PenV; R = C_6H_5 for PenG.

The 100 MHz ^{1}H NMR spectra were recorded on a Tesla 100 MHz spectrometer. All substances were dissolved in DMSO-d_6. TMS was used as the internal standard for all spectra. An internal lock on deuterium of the solvent was used in ^{1}H and ^{13}C measurements. Spectra of the ^{13}C nucleus were ^{1}H decoupled. The assignments of the ^{13}C signals were confirmed by the DEPT technique.

IR measurements

The IR spectra (3800–400 cm^{-1}) were recorded with an UR-20 IR spectrophotometer (Carl Zeiss Jena) for substances dispersed in KBr disks.

Synthesis of Pt^{2+} *complexes of* PenV *and* PenG

A solution of K_2PtCl_4 (208 mg, 0.5 mmol) in 5 cm^3 of water was added to 5 cm^3 of an aqueous solution of PenV (194 mg, 0.5 mmol) or PenG (186 mg, 0.5 mmol). The change in colour from reddish to yellow was complete within 15 min. The solution was kept at 50°C for 3 h. A yellow precipitate was filtered, rinsed with ethanol and dried over P_4O_{10}. Found: C, 32.8; H, 3.4; S, 5.7; Cl, 4.7; Pt, 32.4. Pt(PenV)(OH)ClPt$C_{16}H_{18}O_6N_2SCl$ requires: C, 32.2; H, 3.0; S, 5.4; Cl, 5.9; Pt, 32.6%. Found: C, 33.4; H, 3.4; S, 5.3; Cl, 5.0; Pt, 32.7. Pt(PenG)(OH)ClPt$C_{16}H_{18}O_5N_2SCl$ requires: C, 33.0; H, 3.1; S, 5.5; Cl, 6.1; Pt, 33.5.

RESULTS AND DISCUSSION

Substitution of chloride by PenV or PenG (Fig. 1) leads in both cases to the formation of a yellow product which precipitates from aqueous solution. The ^{1}H and ^{13}C NMR data for these products are listed in Tables 1 and 2; the IR data are listed in Table 3. The penicillin molecule has three functional groups, i.e. the thioether, amide and carboxylic group, capable of coordinating to the Pt^{2+} ion. It has been shown [2–5] that the formation of a five-membered ring, or a larger chelate containing such a ring, facilitates coordination through the amide group. The formation of a larger, six-membered ring, which involves the amide group, does not occur.[8] Upon coordination, the amide group undergoes deprotonation.[2–5] As shown in Fig. 2, the five-membered ring is formed in the case of the platinum complex with the penicillin molecule. Chelation by the amide group is evident in the IR spectra (Fig. 3): the absence of the amide band II related to the N—H deformational vibrations[16] (1570–1515 cm^{-1}) and the absence of a band related to the N—H stretching vibrations[16] (3300–3100 cm^{-1}). The ^{1}H NMR spectra confirm coordination by the

Table 1. The ^{1}H NMR data for penicillins (V and G) and the Pt^{2+} complexes of penicillins (ppm)

	PenV	Pt—PenV	PenG	Pt—PenG
2α-CH_3	1.46 (s)	1.48 (s)	1.37 (s)	1.47 (s)
2β-CH_3	1.52 (s)	1.59 (s)	1.48 (s)	1.62 (s)
H(3)	3.88 (d)	3.17 (s)	3.78 (s)	3.65 (s)
	$J = 1.1$	4.28[a] (s)		4.23[a] (s)
CH_2-10	4.62	4.56 (m)	3.46	3.53 (m)
	(AB)		(AB)	
H(5)	5.42 (d)	5.51 (d)	5.26 (m)	4.97 (m)
	$J = 3.9$	$J = 4.1$		
		$^3J_{Pt-H} = 20$[b]		
H(6)	5.40 (dd)	5.55 (m)	5.26 (m)	5.46 (m)
	$J_1 = 3.9$			
	$J_2 = 8.1$			
NH	8.41 (d)	8.64[a] (d)	8.64 (d)	8.89[a] (d)
	$J = 8.1$	$J = 7.9$	$J = 7.6$	$J = 8.0$

(s)—singlet, (d)—doublet, (dd)—doublet of doublets, (m)—multiplet and (AB)—AB pattern.
[a] Signal of low intensity.
[b] Measured on a Tesla 100 MHz spectrometer.

Table 2. The ^{13}C NMR data for penicillins (V and G) and the Pt^{2+} complexes of penicillins (ppm)

	PenV	Pt—PenV	PenG	Pt—PenG
C(2)	64.47	63.76	64.35	63.71
C(2α)	27.27	26.46	27.57	26.67
C(2β)	32.22	30.76	31.49	30.30
C(3)	74.02	70.12	74.21	70.31
C(5)	66.78	67.24	66.79	67.29
C(6)	57.24	58.07	57.65	58.48
C(7)	167.50	167.67	169.19	168.86
C(9)	168.60	168.75	170.34	170.34
		168.20		171.09
C(10)	66.22	66.04	41.42	41.84
		66.64		42.10
C(11)	172.22	172.98	173.00	173.55
	Aromatic ring carbons			
	114.49	114.43	126.35	126.27
		114.59		126.35
		114.63		126.40
	121.14	121.10	128.13	128.02
		121.28		128.14
				128.23
	129.41	129.39	129.02	128.62
		129.47		128.80
				128.99
	157.52	157.52	135.81	136.00

Table 3. The IR data for the Pt^{2+}–penicillin complexes (cm^{-1})

PenV	Pt—PenV	PenG	Pt—PenG	
695	700	705	705	Monosubstituted aromatic ring
760	760	765	735	Monosubstituted aromatic ring
1250	1250	1250	1280	
1400	1400	1400	1380	
1505		1500		NH amide band II
1610		1620		
1690	1680	1680	1670	C=O amide band I
1780	1755	1780	1750	COOH, C=O β-lactam
	2600		2600	Broad
2970	3050	2970	3000	CH,CH_2,CH_3 broad
3330		3330		NH
	3400		3400	OH broad

amide group. Since signals related to the amide proton in the spectra of free penicillins were sharp and well integrable, the *ca* 10-fold decrease of these signals in the spectra of the complexes shows the deprotonation of the amide group caused by coordination. The amide proton undergoes rather slow exchange with deuterium from the solvent (DMSO-d_6), because there is no evidence of this process in the spectra of free penicillin ligands. The presence of the prevailing single ^{13}C NMR signals related to the thiazolidine and β-lactam carbon atoms [C+(2), C(2α), C(2β), C(3), C(5), C(6), C(7)] proves that one major isomer is formed in the reactions of K_2PtCl_4 with PenV or PenG.

The substitution reactions were carried out in aqueous solutions of the penicillin salts at an initial pH of about 10 (pK_a of penicillins varies from 4.5 to 5). Under such conditions, in addition to substitution of two chloride ligands by the thioether and amide groups, the hydrolysis of the remaining Pt—Cl bonds may occur.[11,17,18] The presence of hydroxyl hydroxide ligands in these complexes is confirmed by the IR spectra. Broad bands in the range 3600–3300 cm^{-1} are related to the O—H stretching vibrations.[16] The elemental analysis shows that on average one chloride ligand is replaced.

The ^1H NMR spectra of the complexes Pt—PenV and Pt—PenG indicate the presence of some side products. These substances can be identified as chelate complexes coordinated by the thioether and carboxylic groups.[11] The downfield shift of the signals for the methine [H(3)] proton is analogous to the downfield shift of the signals for such protons in Pt—methionine complexes coordinated by thio-

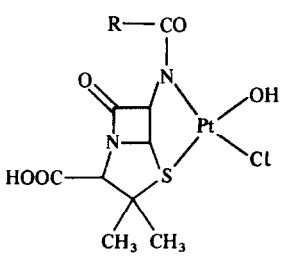

Fig. 2. The structure of the Pt^{2+}–penicillin chelate.

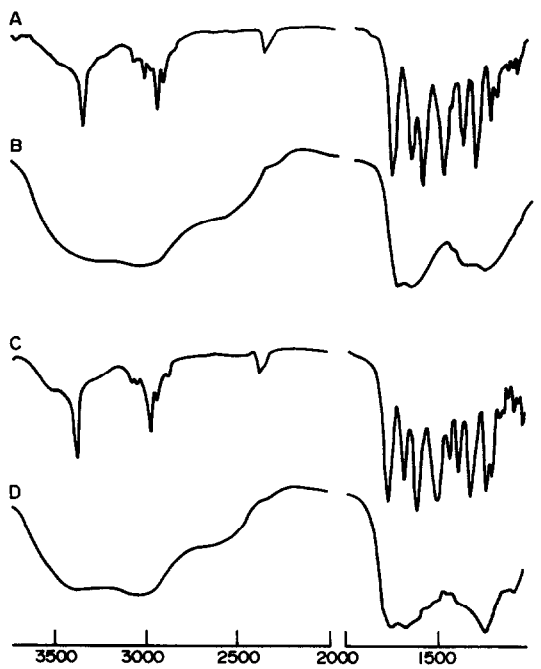

Fig. 3. IR Spectra of free penicillins and their Pt^{2+} complexes: (A) PenG, (B) Pt—PenG complex, (C) PenV and (D) Pt—PenV complex.

ether and carboxylic groups. The presence of signals of low intensity, for the amide N—H proton confirms the existence of such coordinated Pt^{2+} complexes.

Conformation of the penicillin thiazolidine ring and orientation of the Pt—S *bond*

There are two different conformations of the thiazolidine five-membered ring, of which one is typical for natural penicillins [Fig. 4(a)], and the other is found in penicillin sulphoxides [Fig. 4(b)]. Since, the oxidation of the thioether group to the sulphoxide results in a change of ring conformation, the possibility of such an effect during complexation of the Pt^{2+} ion should be considered. The distinction between two conformers can be made on the basis of ^1H NMR data for the two isomers of N-phtalimide–penicillinic acid.[19] For this compound, a transition from structure **4a** to **4b** is evidenced by the downfield shift of the ^1H NMR signal of the 2α-CH_3 protons ($\Delta\delta = -0.16$ ppm) and by the smaller upfield shift of the signal of the 2β-CH_3 protons ($\Delta\delta = +0.02$ ppm). These differences illustrate an interaction between the axial methyl group and β-lactam ring at either the *syn* [Fig. 4(a)] or *anti* [Fig. 4(b)] position.

In the ^1H NMR spectra of Pt—PenG and Pt—PenV complexes dissolved in DMSO, two signals of the 2α-CH_3 and 2β-CH_3 protons are predominant. In both cases, there is no more than a 0.01 ppm downfield shift with respect to the analogous signals of the free ligands. Since both of the penicillins used for synthesis have the thiazolidine ring conformation of type **4a**, the conclusion is drawn that the original **4a**-type conformation of the thiazolidine ring is retained upon complexation of the Pt^{2+} ion.

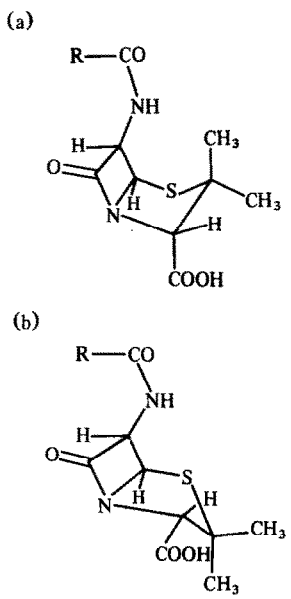

Fig. 4. Conformations of the five-membered thiazolidine ring: (a) typical for prevailing penicillins and (b) typical for penicillin sulphoxides.

Equatorial or axial orientation of the Pt—S bond in the platinum(II)–penicillin complex is possible because of the presence of two lone-pairs of electrons on the thiazolidine sulphur atom. The geometry of the chelate complex **2**, which exhibits the **4a**-type conformation of the thiazolidine ring, determinates the equatorial orientation of the Pt—S bond (Fig. 5). This type of orientation is confirmed by the ^1H and ^{13}C NMR data. Upfield shifts of the C(3) and H(3) NMR signals upon coordination indicate the screening effect along the Pt—S bond.[11]

Conformation of the penicillin side chain

The amide group has a nearly planar structure with restricted rotation around the C—N bond. Two different arrangements are possible when the amide group coordinates the Pt^{2+} ion (Fig. 6). Differences in the arrangements of the substituents at the C(9)—C(10) bond are observed in the ^1H NMR spectra of the free penicillins, in which the signals of the CH_2 protons form the AB pattern. The multiple signals related to the side chain carbon atoms are observed in the ^{13}C NMR spectra of the Pt^{2+} complexes of penicillins. The intensities of these signals are very similar. While β-lactam and thiazolidine carbon atoms produce single NMR signals, the presence of the multiple signals of the side chain atoms proves the existence of the isomeric structures of the penicillin side chain. However, the conformational analysis of the penicillin side chain given above should be considered as preliminary and needs confirmation from further spectroscopic studies of the entire class of similar complexes.

Conclusions

The two novel Pt^{2+} complexes with ligand molecules of biochemical interest were obtained and

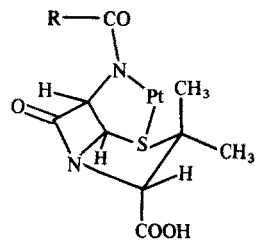

Fig. 5. The conformation of the Pt^{2+}–penicillin complex.

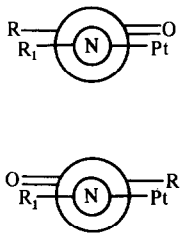

Fig. 6. Two different arrangements of the substituents at the C—N amide bond: R = $C_6H_5OCH_2$ (PenV) or $C_6H_5CH_2$ (PenG); R_1 = penicillin moiety.

their structure was determined by IR and NMR techniques. Coordination of the Pt^{2+} ion in platinum(II)–penicillin complexes involves the amide and thioether groups, and, as a result of the chelation, a new five-membered ring is formed. The structures of the complexes confirm an experimental rule[8] that the formation of five-membered rings involving the amide nitrogen is facile.

The two complexes have *cis* structures and the conformation of the parent penicillin is retained upon complexation. The isomerism of the penicillin side chain was identified in a complex by ^{13}C NMR spectroscopy.

Acknowledgements—Professor Edward Grochowski is thanked for supplying the penicillin samples. This contribution was, in part, supported by grant CPBP 01.17.

REFERENCES

1. H. Sigel and R. B. Martin, *Chem. Rev.* 1982, **82**, 385.
2. G. Kirvan and D. W. Margerum, *Inorg. Chem.* 1985, **24**, 3017.
3. M. F. Mogilevkina, M. V. Sekacheva, I. M. Cheremisina and E. A. Gal'tsova, *Russ. J. Inorg. Chem.* (*Engl. Trans.*) 1976, **21**, 77.
4. M. F. Mogilevkina, V. I. Bessonov and I. M. Cheremisina, *Russ. J. Inorg. Chem.* (*Engl. Trans.*) 1973, **18**, 1396.
5. H. C. Freeman and M. L. Golomb, *J. Chem. Soc., Chem. Commun.* 1970, 1523.
6. D. Dalietos and A. Furst, *Biol. Trace El. Res.* 1982, **4**, 331.
7. L. Olgemöller and W. Beck, *Chem. Ber.* 1984, **117**, 1241.
8. D. D. Gummin, E. M. Ratilla and N. M. Kostič, *Inorg. Chem.* 1986, **25**, 2429.
9. L. M. Peerey and N. M. Kostič, *Inorg. Chem.* 1987, **26**, 2079.
10. J. A. Galbraith, K. A. Menzel, E. M. Ratilla and N. M. Kostič, *Inorg. Chem.* 1987, **26**, 2073.
11. T. G. Appleton, J. W. Connor and J. R. Hall, *Inorg. Chem.* 1988, **27**, 130.
12. E. W. Abel, D. G. Evans, J. R. Koe, M. B. Hursthouse, M. Mazid, M. F. Mahon and K. C. Molloy, *J. Chem. Soc., Dalton Trans.* 1990, **5**, 1697.
13. E. W. Abel, D. G. Evans, J. R. Koe, V. Sik, M. B. Hursthouse and P. A. Bates, *J. Chem. Soc., Dalton Trans.* 1989, **11**, 2315.
14. E. W. Abel, D. G. Evans, J. R. Koe, V. Sik, P. A. Bates and M. B. Hursthouse, *J. Chem. Soc., Dalton Trans.* 1989, **5**, 985.
15. S. E. Livingstone (Ed.), *The Chemistry of Ruthenium, Rhodium, Palladium, Osmium, Iridium and Platinum* (Russian edition), p. 274. Izdat. Mir, Moscow (1978).
16. L. J. Bellamy (Ed.), *The Infra-red Spectra of Complex Molecules* (Russian edition), p. 245. Izdat. Mir, Moscow (1957).
17. D. Banerjea, F. Basolo and R. G. Pearson, *J. Am. Chem. Soc.* 1957, **79**, 4055.
18. R. F. Greene, D. C. Chaterji, P. K. Hiranaka and F. Gallelli, *Am. J. Hosp. Pharm.* 1979, **36**, 38.
19. E. H. Flynn (Ed.), *Cephalosporins and Penicillins. Chemistry and Biology*, p. 331. Academic Press, New York (1972).

Polyhedron Vol. 10, No. 13, pp. 1479–1483, 1991
Printed in Great Britain

0277–5387/91 $3.00+.00
© 1991 Pergamon Press plc

STUDIES ON THE STABILIZATION OF TERBIUM(IV) IN AQUEOUS TETRAMETAPHOSPHATE SOLUTION

XIAOJING LI,* WENJI DONG, YULANG QI, DONGMEI WANG and RUDONG YANG

Department of Chemistry, Lanzhou University, Lanzhou 730000, R.O.C.

(*Received* 16 *October* 1990; *accepted* 12 *February* 1991)

Abstract—Terbium(IV) was obtained by oxidation of trivalent terbium in an alkaline aqueous solution of sodium tetrametaphosphate with ozone. The concentration of terbium(III), the pH and the temperature of the solution all greatly affected the generation and stabilization of terbium(IV). Studies showed that the reduction of terbium(IV) (presumably by water) in alkaline solution was a pseudo first-order reaction. The characteristic absorption spectrum, the molar absorptivity, the rate constants and the activation energy of the reduction reaction of terbium(IV) are reported.

It is well-known that the tetravalent oxidation states of cerium, terbium and praseodymium can exist in the solid state.[1] However, terbium(IV) and praseodymium(IV) are unstable in normal aqueous solutions, since the formal reduction potentials of the Ln^{IV}/Ln^{III} couples (e.g. +3.1 V for terbium[2] in 1 M H^+) are so high that they are reduced by water. As the formal reduction potential of the Ln^{IV}/Ln^{III} couple is a function of the ratio of the stability constants of the lanthanide(IV) and lanthanide(III) compounds, a precipitating or complexing agent should enable the stable compound of lanthanide(IV) to form at a more favourable potential in aqueous solution. The chemical oxidation of terbium(III) in phosphotungstate,[3] tellurate,[4] condensed phosphate[5] and potassium hydroxide solution[6] has been reported. Hobart *et al.*[7] have stabilized terbium(IV) in carbonate solution by means of electrochemical oxidation. A precipitate of terbium(IV) was obtained by photoxidation in pyrophosphate solution.[8]

In the present work, terbium(III) in an aqueous solution of sodium tetrametaphosphate was oxidized by ozonolysis and the colour of the solution changed from colourless to a dark reddish-brown. A study was undertaken to find favourable conditions to produce and stabilize terbium(IV) in the aqueous solution. In addition, further studies of the kinetic properties of terbium(IV) in tetrametaphosphate solution were carried out and it was found that the reduction of terbium(IV) was a pseudo first-order reaction. The rate constants, the half-life and the activation energy of the terbium(IV) reduction have been determined and calculated. As far as we know, these studies have not been previously reported.

EXPERIMENTAL

Apparatus

Spectra were recorded with a Model UV-730 rapid-scan spectrophotometer and a Model 751-G UV spectrophotometer (fitted with constant temperature equipment). The pH of the solution was measured with Model PHS-3 acidometer (precision of 0.01 pH).

Reagents

A $Tb(NO_3)_3$ solution was prepared by dissolving Tb_4O_7 (> 99.9%) in nitric acid and diluting with distilled water. $Na_4P_4O_{12}\cdot 4H_2O$ was prepared according to ref. 9 and the X-ray diffraction, IR spectroscopy, thermal analysis and composition of the product were measured in the same manner as in ref. 9. Ozone (of a content of 20–25 mg dm^{-3}) was generated by passing oxygen at a speed of 0.40

* Author to whom correspondence should be addressed.

$dm^3\ min^{-1}$ through an ozonator. All other reagents were A.R. grade.

Analytical approach

The terbium(IV) concentration was determined by iodimetry.[10] The total concentration of terbium was titrated with EDTA when phosphorus was absent or with DTPA and zinc chloride when phosphorus was present.[11]

Procedure

Solid $Na_4P_4O_{12}\cdot 4H_2O$ was dissolved in an aqueous solution of trivalent terbium nitrate in which the concentration of the terbium ion was 10^{-2}–10^{-1} mol dm^{-3}. When the ratio of the moles of $P_4O_{12}^{4-}$ to the moles of terbium(III) ion was less than 1.5, a white precipitate appeared in the solution. However, the precipitate disappeared gradually and the solution became clear when the ratio was greater than 1.5. The hydroxide ion concentration in the solution was adjusted to *ca* pH = 12 by addition of sodium hydroxide solution. The solution was then cooled with water–ice and oxidized for a few hours to ensure sufficient oxidation of terbium(III) by bubbling ozone through the solution. During the oxidation process, the colour of the terbium solution changed from colourless to yellow to dark reddish-brown.

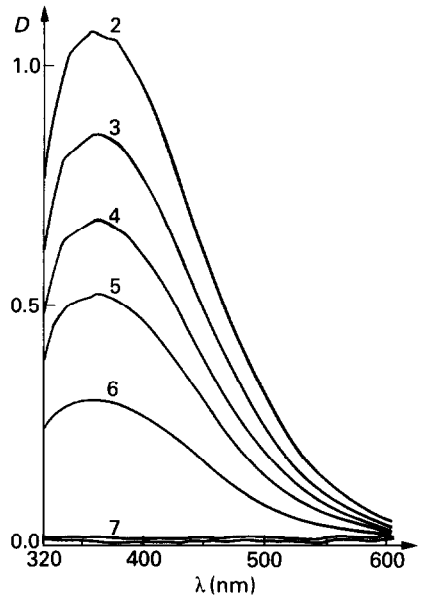

Fig. 1. Absorption spectra of terbium(III) and terbium(III) oxidized by ozone: (1) Tb^{III}–$P_4O_{12}^{4-}$ solution (pH = 12.2); (2) solution 1 was oxidized for 1.5 h (pH = 11.8); (3)–(6) solution 2 was standing for 1, 2.1, 3.3, 5.6 h, respectively; (7) solution 2 was reduced by hydrogen peroxide.

RESULTS AND DISCUSSION

Chemical properties of the terbium(IV) *solution*

The reddish-brown terbium(IV) solution, which is stable for quite a long period (about 2 weeks) in alkaline medium at room temperature, is reduced by water and the colour fades immediately in acid medium. It also oxidizes I^-, Cr^{3+} or Mn^{2+} to I_2, $Cr_2O_7^{2-}$ or Mn^{3+} in acid medium. When an excessively concentrated base (such as sodium hydroxide or potassium hydroxide) is added to the solution, a yellow precipitate of $Tb(OH)_4$ appears.

Spectrum of the terbium(IV) *solution*

The spectrum of the dark reddish-brown terbium(IV) tetrametaphosphate solution is shown in Fig. 1. It is characterized by a broad-band absorption centred at *ca* 365 nm. In comparison, the spectrum of the terbium(III) tetrametaphosphate solution has no absorption peak in the region of *ca* 320–365 nm. When the terbium(IV) solution is left standing for a length of time or some reductants (such as H_2O_2, $NH_2OH\cdot HCl$) are added to the solution, the reddish-brown colour fades and the absorption peak at 365 nm is reduced or disappears (see Fig. 1). Finally, the colour and spectrum of the terbium(IV) solution become the same as that of terbium(III) solution. It is shown that although the formal reduction potential of the Tb^{IV}/Tb^{III} couple is very high in non-complexing, neutral or acidic, aqueous solutions, terbium(IV) can be generated by oxidation by ozone and stabilized by forming a stable complex with a tetrametaphosphate anion in alkaline, aqueous solution. The absorption at 365 nm is the characteristic absorption peak of the terbium(IV) tetrametaphosphate complex solution, and its molar absorptivity is estimated to be $1.7\times 10^3\ dm^3\ mol^{-1}\ cm^{-1}$.

Factors affecting the oxidation of terbium(III)

(a) *The pH of the solution.* In this study it was found that the hydroxide ion concentration of the solution has a great affect on the oxidation of terbium(III). When the pH of the solution is between 11 and 12.7, the oxidation rate of terbium(III) and the stability of terbium(IV) increase with increasing hydroxide ion concentration. If the pH < 11, terbium(III) cannot be oxidized by ozone in the solution, since the formal potential of the Tb^{IV}/Tb^{III} couple is still very high at pH < 11. At pH > 13, the complex of ter-

bium(III) tetrametaphosphate becomes unstable and a great amount of $Tb(OH)_4$ is precipitated from the solution, and the oxidation of terbium(III) becomes difficult (see Fig. 2).

During the reaction, the oxidation of terbium(III) and the reduction of terbium(IV) occur simultaneously in solution. At the beginning of the reaction the rate of oxidation is faster than the rate of reduction; then the reduction rate increases with increasing terbium(IV) concentration and the oxidation rate increases with decreasing terbium(III) concentration in solution. Finally, the oxidation rate and the reduction rate become equal. That is, the oxidation reaction reaches an equilibrium. The lower the initial pH of the solution, the faster the equilibrium. If ozone is bubbled through the solution for too long, the oxidation rate of the reaction will decrease slowly (see Fig. 2).

(b) *The initial concentration of terbium*(III). It is found that when the molar ratio of $[Tb^{III}]/[P_4O_{12}^{4-}]$ in the solution is fixed, the oxidation rate decreases with increase in the initial concentration of terbium(III). The reason is that although the terbium(III) concentration has been increased, the concentration of ozone bubbled through the solution is fixed and therefore the concentration of terbium(IV) produced is not increased.

(c) *The temperature of the solution.* A study was performed to find a correlation between the temperature of the solution and the oxidation of terbium(III). The result shows that the oxidation rate of terbium(III) is decreased with increase in temperature (see Fig. 3). When the temperature is higher than 50°C, the oxidation of terbium(III) is impossible, because at this temperature the $P_4O_{12}^{4-}$ is degraded. The terbium(IV) tetrametaphosphate complex becomes unstable and the reduction rate of terbium(IV) is increased in the solution. It can be seen from Fig. 3 that although the low temperature is beneficial to the oxidation of terbium(III), it reduces the redox rate of reaction and more time is therefore needed to reach the redox equilibrium.

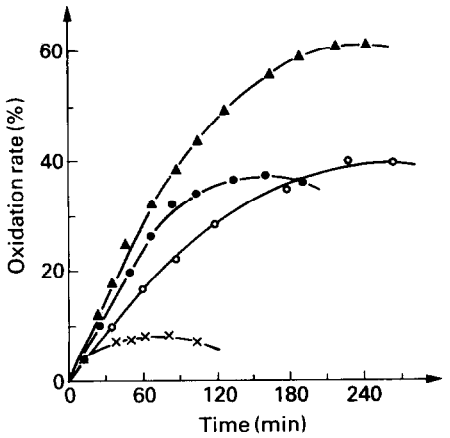

Fig. 2. Correlation of oxidation rate of terbium(III) with pH: $[Tb^{3+}] = 4.91 \times 10^{-3}$ mol dm^{-3}; $[Tb^{3+}]:[P_4O_{12}^{4-}] = 1:4$; $T = 14.0$°C; ▲—pH = 12.56, ●—pH = 12.00, ○—pH = 12.98 (precipitate occurred as ozone was bubbling through the solution), ×—pH = 11.50.

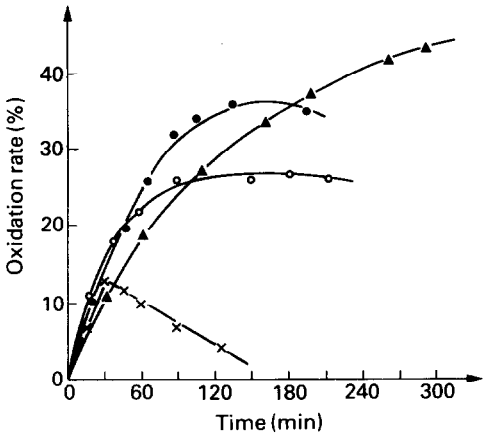

Fig. 3. Correlation of oxidation rate of terbium(III) with temperature: $[Tb^{3+}] = 4.91 \times 10^{-3}$ mol dm^{-3}; $[Tb^{3+}]/[P_4O_{12}^{4-}] = 1:4$; pH = 12.00; ▲—0°C, ●—14.0°C, ○—25.0°C, ×—35.0°C.

(d) *The concentration of tetrametaphosphate.* Our experiments also showed that the concentration of the complexing agent has less influence on the oxidation of terbium(III) than have the initial concentration of terbium(III), the pH and the temperature of the solution.

Study of the reduction kinetics of the terbium(IV) *complex*

The terbium(IV) complex is not very stable and reduces spontaneously at a slow rate in the aqueous solution. A possible equation for the reduction reaction in the alkaline aqueous solution is

$$2Tb^{IV} + 2OH^- \rightarrow 2Tb^{III} + 1/2O_2 + H_2O. \quad (1)$$

Because water is abundant and $[OH^-] \gg [Tb^{IV}]$ in the solution, the concentration of $[OH^-]$ and $[H_2O]$ can be treated as constants. Therefore, reaction (1) is regarded as a pseudo first-order reaction and the kinetics equation is shown below:

$$dC/dt = kC \quad \text{or} \quad \log \frac{C_0}{C} = \frac{k}{2.303} t, \quad (2)$$

where C_0 and C are the concentrations of terbium(IV) at initial time ($t = 0$) and at any time

Table 1. Rate constants of terbium(IV) in solutions of various pH-values[a]

pH of solution	Rate constants 10^6k (s^{-1})
11.20	60.8
11.40	22.8
12.00	5.42
12.56	3.57

[a] $[Tb]/[P_4O_{12}^{4-}] = 1:4$, $t = 15°C$, $[Tb^{IV}] = 2.26 \times 10^{-4}$ mol dm^{-3}.

Table 3. Rate constants of terbium(IV) in solutions of various concentrations of ligand[a]

$[Tb]/[Na_4P_4O_{12}]$	Rate constants 10^6k (s^{-1})
1:2	5.20
1:4	5.42
1:6	5.90

[a] pH = 12.0, $T = 15.0°C$, $[Tb^{IV}] = 2.26 \times 10^{-4}$ mol dm^{-3}.

(t), respectively. As the terbium(IV) complex has a characteristic absorption peak at 365 nm and the terbium(III) complex has no absorption at that wavelength, C_0 and C in eq. (2) can be replaced by the absorbancy, D_0 (at initial time, $t = 0$) and D (at any time, t), of the terbium(IV) complex at 365 nm. Therefore, eq. (2) can be written as

$$\log \frac{D_0}{D} = \frac{k}{2.303}t \quad \text{or} \quad t_{1/2} = 0.693/k, \qquad (3)$$

where $t_{1/2}$ is the half-reduction period of the terbium(IV) complex. The stability of terbium(IV) in the solution can be determined by measuring the change of terbium(IV) absorbancy (D) with change in time (t). The plot of values of log D_0/D against time is linear and it can be shown that the reduction of terbium(IV) in the solution obeys first-order kinetics.

The factors affecting the stability of terbium(IV)

(a) *The* pH *of the solution.* The results given in Table 1 show that the stability of the terbium(IV) complex is greatly increased with increase in the pH of the solution. The main reason is that the coordination of $P_4O_{12}^{4-}$ is influenced by the alkaline nature of the solution. In a certain range of pH, the more basic the solution is, the higher will be the coordination of $P_4O_{12}^{4-}$, the more stable the terbium(IV) complex, and the lower the potential of the Tb^{IV}/Tb^{III} couple. Therefore, the half-reduction period increases with increasing pH.

(b) *The temperature of the solution.* When the pH of the solution is not changed, the stability of the terbium(IV) complex is greatly affected by the temperature. As the temperature increases, the tendency for the terbium(IV) complex to reduce increases (see Table 2), which is similar to the oxidation of terbium(III). The present studies therefore show that a lower temperature is beneficial for the generation and stabilization of the terbium(IV) complex.

In addition, according to the Arrhenius equation:

$$\log k = \frac{E}{2.303RT} + B, \qquad (4)$$

the activation energy (E) of the terbium(IV) tetrametaphosphate complex can be obtained from the slope of log K against $1/T$; $E = 56$ kJ mol^{-1}.

(c) *The concentration of tetrametaphosphate.* It is shown in Table 3 that when the temperature, pH and concentration of the terbium ion are fixed, the influence of the tetrametaphosphate concentration on the stability of terbium(IV) in the solution is not great.

Table 2. Rate constants of terbium(IV) at various temperatures[a]

Temperature (°C)	Rate constants 10^6k (s^{-1})
53.0	85.5
44.0	59.2
36.0	27.7
27.5	10.8
15.0	5.42
6.5	3.33

[a] $[Tb]/[P_4O_{12}^{4-}] = 1:4$, $[Tb^{IV}] = 2.26 \times 10^{-4}$ mol dm^{-3}, pH = 12.00.

Acknowledgement—This research was sponsored by the Chinese Academy of Sciences fund.

REFERENCES

1. F. A. Cotton and G. Wilkinson, *Advanced Inorganic Chemistry* 3rd edn, Ch. 27. Interscience, New York (1972).

2. L. J. Nugent, R. D. Baybarz, J. L. Burnett and J. L. Ryan, *J. Inorg. Nucl. Chem.* 1971, **33**, 2503.
3. A. S. Saprykin, V. I. Spitsyn and N. N. Krot, *Doke. Akad. Nauk SSSR* 1976, **231**, 150.
4. S. M. Hua and R. D. Yang, *Chem. J. Chin. Univ.* 1980, **3**, 573.
5. W. J. Dong and R. D. Yang, *Acta Chim. Sin.* 1986, **44**, 563.
6. R. D. Yang, J. M. Liu and T. R. Ma, *Chem. J. Chin. Univ.* 1982, 153 (A special issue for the 30th anniversary of the founding of the Chinese Chemical Society).
7. D. E. Hobart, K. Samhoum, T. P. Young, V. E. Norvell, G. Mamantov and J. R. Peterson, *Inorg. Nucl. Chem. Lett.* 1980, **16**, 321.
8. X. J. Li and R. D. Yang, *Acta Chim. Sin.* 1987, **45**, 432.
9. R. N. Bell, L. F. Audrieth and O. F. Hill, *Ind. Engng Chem.* 1952, **3**, 568.
10. R. D. Yang, J. M. Liu and T. R. Ma, *J. Lanzhou Univ.* (*Natural Sci.*) 1983, **1**, 72.
11. G. V. Rodichva and N. M. Romanova, *Izv. AN. SSSR Neorg. Mater.* 1979, **6**, 963.

Polyhedron Vol. 10, No. 13, pp. 1485–1490, 1991
Printed in Great Britain

0277–5387/91 $3.00+.00
© 1991 Pergamon Press plc

SUBSTITUENT EFFECT ON LIGAND PROPERTIES AND ^{3}MLCT BEHAVIOUR IN RUTHENIUM(II) DIIMINE COMPLEXES†

ADNAN ATFAH, AHMED H. TUHL and TALAL S. AKASHEH‡

Chemistry Department, Yarmouk University, Irbid, Jordan

(*Received* 16 *October* 1990; *accepted* 12 *February* 1991)

Abstract—New derivatives of 3,6-di(2′-pyridyl)pyridazine (dppn) were used to prepare complexes of the type $[Ru(L)_3]^{2+}$ (where L = dppn or one of its derivatives). The complexes are evaluated as possible solar energy conversion materials.

More effort and interest is concentrated on the study of ruthenium(II) complexes because of their value as photosensitisers for solar energy conversion[1–6] involving the luminescent ^{3}MLCT (metal-to-ligand charge-transfer) excited state that is capable of electron transfer reactions.[7–10] No doubt theoretical methods are needed to predict which ligands would serve our purposes best. In the words of Ernst and Kaim,[11] we are about to "...enter an era in which the first question is not which ligands are available but which ones are desirable". However, the HMO model, thus far utilized,[11–15] needs further refinement and must be combined with experimental data such as basicity of the ligands, cyclic voltammetry data and luminescence properties to make correct predictions regarding photosensitization and photoactivity of the complexes as well as σ and π activities of the ligands. Typically, while ligands with extended π systems (with lower π^* orbitals) are desirable in order to lower MLCT transitions and hopefully ensure the success of photosensitization, 2-(2′-pyridyl)quinoline and 2,2′-biquinoline yield a tris complex that is non-luminescent at room temperature and too photoactive[16] compared with the star of the show, $[Ru(bpy)_3]^{2+}$.[1–10] Recent work shows that the ^{3}MLCT is only reductively quenched by EDTA in the study of the production of hydrogen from water via the methyl viologen cation radical ($MV^{+\cdot}$), provided that the ^{3}MLCT state has a reduction potential, $^*E(2+/1+)$, greater than *ca* 1 V, which applies to the complex $[Ru(bpz)_2(dpq)]^{2+}$ [where bpz = 2,2′-bipyrazine and dpq = 2,3-di(2′-pyridyl)quinoxaline].[16]

The key to the behaviour of ruthenium(II) diimine complexes lies in the properties of the excited ^{3}MLCT state. The redox potentials of this state, largely determined by the relative stability of the metal HOMO t_{2g} orbitals (in octahedral microsymmetry) and the ligand LUMO π^* orbitals, control the probability of the photosensitized electron transfer processes. Electron transfer quenching has to compete with unimolecular processes of the ^{3}MLCT state, such as emission, radiationless decay and photoreactivity via thermal population to a closely lying *d–d* state.[1–10] Needless to say, metal–ligand interactions and, in particular, σ-donor and π-acceptor tendencies of the ligand determine such properties.[7,8,17–20] It is thus not surprising that ligand bonding properties are derivable from ground state and ^{3}MLCT state properties.

Substitution on the ligand is often a good means to finely tune the properties of the excited state.[21,22] Variation of the ligand itself has been attempted[23–25] and even a cage-ligand (ref. 26 and refs therein) has recently been found to protect against photochemistry.

In this work we report the synthesis and properties of new ruthenium tris-diimine complexes where the ligands are derived from 3,6-di(2′-pyridyl)pyridazine (dppn, see Fig. 1).

EXPERIMENTAL

Materials and equipment

The solvents used in this study were Aldrich HPLC grade. Synthesis of the salts (as PF_6^- salts)

† This work is part of the MSc thesis of A. H. Tuhl.
‡ Author to whom correspondence should be addressed.

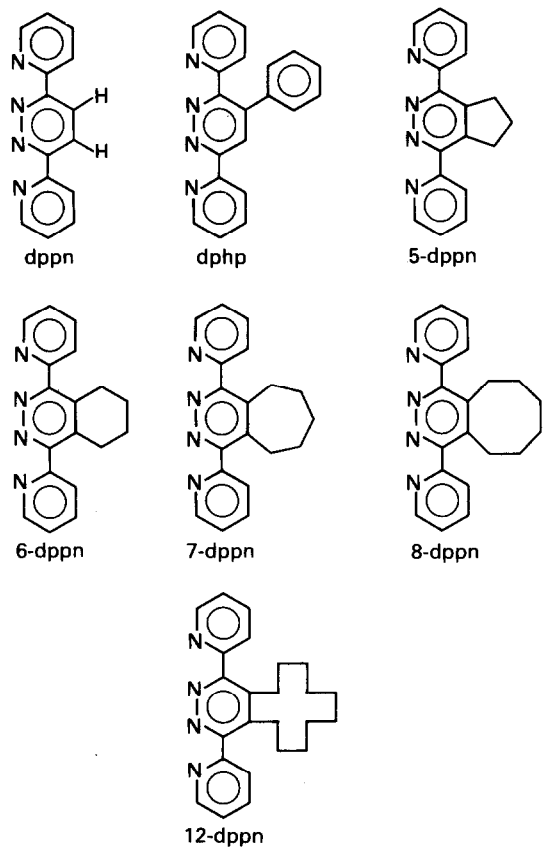

Fig. 1. Structure of the ligand.

was carried out according to standard procedures and is described below. Column chromatography over alumina in acetonitrile was used for purification and characterization was effected by elemental analysis, IR and UV–vis spectroscopy and conductivity measurements. The purity of the samples was checked by the quality of luminescence spectra and lifetime measurements. Cyclic voltammetry, against an SSCE, on a platinum working electrode (and a platinum counter electrode) in DMF (reductions) and acetonitrile (oxidations), with tetra-n-butylammonium hexafluorophosphate (0.1 M) as the supporting electrolyte, was performed on a Hi-Tech potentiostat. A Varian 2300 series UV–vis spectrophotometer and a Perkin–Elmer MPF-44B fluorescence spectrometer were used for recording the spectra in acetonitrile. Lifetimes were measured on an Applied Photophysics K347 laser flash spectrometer in the emission mode, with excitation from a spectron Nd:yAG laser at 355 nm, and/or an Edinburgh Model 199M photon counting system.

Synthesis of ligands and complexes

The dipyridyl pyridazines (dppn and dphp) were prepared according to Butte and Case.[27] The other ligands were prepared according to the procedure described by Atfah.[28]

The tris complexes were prepared by a general procedure. A suspension of $Ru(dmso)_4Cl_2$ (0.27 mmol)[29] or $RuCl_3 \cdot H_2O$ (0.1 g, 0.38 mmol, BDH) in 30% ethanol in water (30 cm^3) was added over an hour to the stoichiometric amount of the ligands in 70 cm^3 of ethanol/water. The mixture was refluxed until the starting ligand disappeared on a TLC plate (3–24 h). The complex was precipitated by adding NH_4PF_6 (2–3 g) in 5 cm^3 of water and cooled in a refrigerator overnight. The vacuum-collected solid was dried after washing in cold water and ether. Dissolution in a small amount of acetonitrile and precipitation by ether (for initial purification) was followed by column chromatography over neutral alumina in dry acetone or acetonitrile. The high quality fractions that were checked by TLC and luminescence spectra were combined, rotatory evaporated to a small volume and precipitated with dry ether. The complexes were characterized by elemental analysis (MHW laboratories P.O. Box 15149, Phoenix, Arizona, USA), in addition to the previously mentioned methods. Data for these are deposited with the Editor and are available from the authors upon request.

RESULTS AND DISCUSSION

Tables 1–3 list the absorbance cyclic voltammetry and excited state characteristics of the complexes as well as some characteristics of the ligands. The excited state redox potentials, $^*E_{1/2}(3+/2+)$ and $^*E_{1/2}(2+/1+)$, were calculated assuming that entropy changes (and thus geometries) upon excitation from the ground state to the ^{3}MLCT are minimal,[8] and the following relations were used:

$$^*E_{1/2}(3+/2+) = E_{1/2}(3+/2+) - E_m$$

and

$$^*E_{1/2}(2+/1+) = E_{1/2}(2+/1+) + E_m.$$

The asterisk labels the excited state, while $E_{1/2}$ is the ground state half-wave potential. While E_m should, in principle, be the 0–0 emission energy, it is usually approximated by the lowest wavelength maxima at 77 K and this gives a lower limit to the energy gap.

Figures 2–4 give typical UV–vis, emission spectra and cyclic voltammograms, respectively.

The UV–vis spectra of the ligands show two features in the range 210–290 nm. The effect of substitution of the electron-releasing phenyl and cyclic alkyl groups leads to a blue shift, resulting from destabilization of the π^* orbitals. This is often accompanied (though not always) by a decrease in

Table 1. UV–vis spectra in acetonitrile (10^{-5}–10^{-6} M as PF_6^- salts)

Compound	Wavelength (nm) [$10^{-4} \times \varepsilon$(dm^3 mol^{-1} cm^{-1})]
dppn	290(1.92); 257(0.90sh)
dphp	281(1.70); 259(1.35sh)
5-dppn	287(1.25); 230(0.85sh)
6-dppn	270(0.55sh); 217(0.87)
7-dppn	267(0.53sh); 223(0.91)
8-dppn	267(0.80sh); 220(1.58)
12-dppn	267(0.80sh); 217(1.04)
$[Ru(dppn)_3]^{2+}$ (I)	477(1.43); 437(sh); 403(sh); 293(7.44); 240(sh)
$[Ru(dphp)_3]^{2+}$ (II)	470(1.55); 440(sh); 400(sh); 287(8.06); 246(sh)
$[Ru(5\text{-}dppn)_3]^{2+}$ (III)	472(1.44); 425(sh); 385(sh); 295(8.12); 250(sh)
$[Ru(6\text{-}dppn)_3]^{2+}$ (IV)	477(1.90); 433(sh); 375(sh); 277(8.90); 217(sh)
$[Ru(7\text{-}dppn)_3]^{2+}$ (V)	470(1.61); 435(sh); 402(sh); 290(5.80); 247(sh)
$[Ru(8\text{-}dppn)_3]^{2+}$ (VI)	473(1.45); 436(sh); 360(sh); 289(4.22); 245(sh)
$[Ru(12\text{-}dppn)_3]^{2+}$ (VII)	473(1.35); 437(sh); 360(sh); 290(3.94); 222(sh)

(sh) = shoulder.

the extinction coefficients. Generally, the effect of complexation leads to red shifts of varying extents of the low energy band due to the general stabilization effect on bonding. The high energy ligand band shows a blue shift for dppn and dphp only.

Complexation largely increases the extinction coefficient of the ligand-centred (LC) bands, which are slightly shifted from those of the ligands. This leads to a definite π,π^* assignment (n,π^* bands should weaken or disappear on complexation). The remaining bands in the complexes are assignable to MLCT bands. In particular, the broad feature around 475 nm is usually considered to be a HOMO metal (d) to LUMO ligand (π^*) transition. Again, electron-releasing effects of the substituents lead to slight blue shifts. The shifts vary between 4 and 7 nm in this band. It has been established that in metal carbonyl complexes of chromium, molybdenum and tungsten containing one diimine ligand[13] and in ruthenium diimine complexes,[11] the extinction coefficient of this band bears a linear relationship with the squared HMO coefficients

Table 2. Cyclic voltammetry results in DMF and acetonitrile vs SSCE[a]

Compound	Reductions, E_{red} (V)			Oxidation, E_{ox} (V)	E	pK_{BH^+}
I	−0.97(60)	−1.15(60)	−1.46(86)	1.47(60)	2.41	3.44
II	−0.95(60)	−1.15(60)	−1.40(80)	1.66(80)	2.61	2.36
III	−1.07(60)	−1.25(60)	−1.50(80)	1.34(80)	2.41	4.17
IV	−1.08(60)	−1.27(100)	−1.53(100)	1.34(60)	2.42	4.17
V	−1.08(100)	−1.25(100)	−1.52(140)	1.34(120)	2.42	4.17
VI	−1.07(80)	−1.25(100)	−1.52(40)	1.32(120)	2.39	4.29
VII	−1.07(70)	−1.25(60)	−1.51(80)	1.29(100)	2.36	4.45
dppn	−1.84(120)					
dphp	−1.85(140)					
5-dppn	−1.96(120)					
6-dppn	−2.07(140)					
7-dppn	−2.09(140)					
8-dppn	−2.11(140)					
12-dppn	−2.10(160)					

[a] Reductions were run in DMF and oxidations is acetonitrile on a platinum working electrode against an SSCE reference electrode and a platinum counter electrode. Supporting electrolyte was 0.1 M tetra-n-butylammonium hexafluorophosphate. Values in parentheses are the differences between anodic and cathodic peaks in millivolts. Scan rates were 0.1 V s^{-1}. pK_{BH^+} values are calculated from $pK_{BH^+} = 11.74\text{–}5.64\ E_{ox}$[11]. $E = E_{ox} - E_{red}$.

Table 3. Characteristics of the ^{3}MLCT excited state

Complex[a]	E_m (RT)[b]	E_m (77 K)[b]	τ (μs)[c]	$^*E_{1/2}(3+/2+)$[d]	$^*E_{1/2}(2+/1+)$[d]
I	642	628,682(sh) 712(sh)	0.614	−0.505	1.01
II	646	632,676(sh)	0.804	−0.266	0.976
III	652	628,684(sh)	0.497	−0.635	0.905
IV	644	634,684(sh)	0.651	−0.626	0.876
V	636	624,676(sh)	0.165	−0.647	0.907
VI	650	628,676(sh)	0.404	−0.655	0.905
VII	650	636,680(sh)	0.418	−0.660	0.885

[a] Emission and lifetime data in acetonitrile.
[b] Wavelength maxima in nanometres.
[c] Degassed with argon.
[d] Excited state redox potentials.
[e] All samples were excited at 476 nm for steady state emission, and 337 nm (N_2 nanosecond flash lamp) or 355 nm (Nd–YAG) for lifetime measurements.

($C_N{}^2$) at the chelating nitrogen centres. The lifetimes of the ^{3}MLCT state follow a similar relationship.[11,13] Thus it is not surprising that ε_{CT} (the extinction coefficients for the lowest energy band) and τ are empirically correlated.[30] In our case, some values of ε_{CT} increase as τ (Table 3) increases. Nevertheless, such a correlation for all the data points could not be established. This could be due to a number of reasons. One reason, apart from their approximate nature, HMO calculations that are restricted to the π-system should be insensitive to cyclic alkyl substitution. Moreover, the MLCT bands in question are broad and may involve transitions to the second LUMO π^* orbital.[31,32] The long tail usually accompanying the MLCT band has been assigned to the luminescent ^{3}MLCT excited state[8] and could add to the poor correlation.

In Table 2 cyclic voltammetry results are presented. Kaim *et al.*[11–15] have found a linear relationship between the basisity of the ligand (pK_{BH^+}: dissociation of the protonated form) and the halfwave potential, $E(3+/2+)$. Since σ-donation largely determines the relative stability of the HOMO metal orbitals,[7,8,17,23,33,34] the pK_b of the ligand (a measure of σ-donation) would naturally affect the redox potential which gauges the metal HOMO orbital stability. The calculated pK_{BH^+} values shown in the table indicate that cycloalkyl substitution leads to more basic ligands with better σ-donation, and this is naturally reflected in the destabilization of the metal orbitals in complexes containing the substituted ligands. 12-dppn exhibits the largest effects, while the other 5, 6, 7 and 8 substituents have very close oxidation potentials. The most stable metal orbital occurs in $Ru(dphp)_3{}^{2+}$.

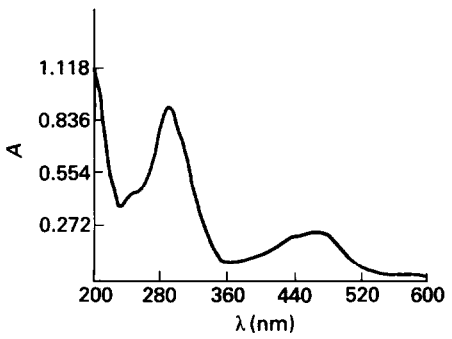

Fig. 2. UV–vis spectrum of $[Ru(12\text{-dppn})_3]^{2+}$ (1×10^{-5} M in acetonitrile).

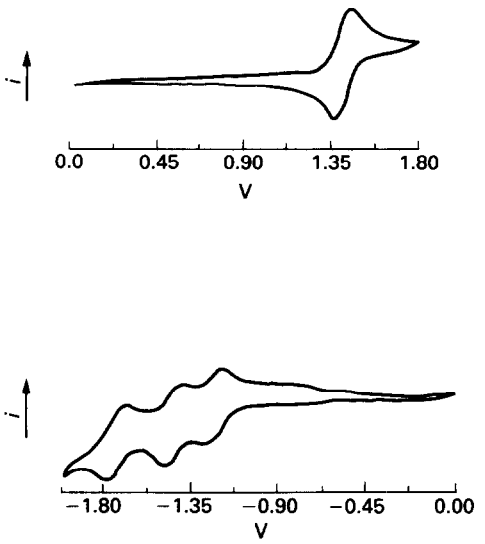

Fig. 3. Cyclic voltammogram of $[Ru(7\text{-dppn})_3]^{2+}$: (a) oxidation in acetonitrile and (b) reduction in DMF.

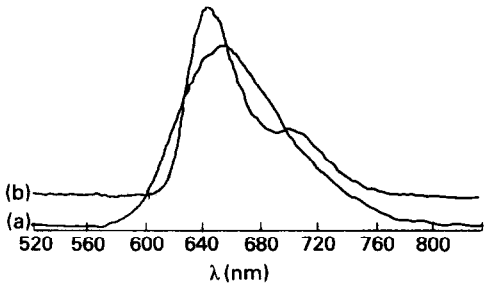

Fig. 4. Emission spectra of $[Ru(5\text{-dppn})_3]^{2+}$ in acetonitrile at (a) room temperature and (b) 77 K.

The cyclic voltammetry results also show three consecutive, reversible or quasi-reversible one-electron peaks which indicate that each reducing electron is localized on one ligand.[8,9,23,25,35] The ligand reduction peaks (Table 2) show mostly irreversible peaks and indicate about a 1 V stabilization of the LUMO π^* orbital upon complexation. We have obtained a linear fit of the complexes' half-wave first reduction potential and that of the ligand (slope = 0.42, correlation coefficient = 0.90), thus substantiating the localized reduction electron picture in the complexes. The first reduction potential largely reflects the stability of the π^* orbitals.[7,8,17,23,33,34] Thus the differences between this reduction peak and the oxidation peak should correlate well with the low energy MLCT absorption band and the ^{3}MLCT emission maximum. The relationship $E_{op} = E_{ox} - E_{red} + A$ (where A is the solvation and reorganization free energies factor) holds well for our complexes, as in other typical complexes.[11-15,23,36] However, in the present study the emission maximum at 77 K correlates much better (correlation coefficient = 0.95) than the lowest energy MLCT absorption maximum (correlation coefficient = 0.83) probably for the same reasons given above for the ε_{cT} and τ values.

The variation of the first reduction potentials of the complexes in the series n-dppn (n = 5–8, 12) show small variations, thus indicating similar π^* stability and thus similar π-accepting properties. The more negative reduction potentials in the series compared with dppn indicate a less stable π^* orbital. Nevertheless, E ($= E_{ox} - E_{red}$) for dppn and n-dppn (n = 5–7) does not vary, thus stressing that π-back-donation is similar for these ligands despite the stronger σ-donation of n-dppn. For n = 8 and 12, slightly stronger σ-donation and weaker π-acceptance are indicated by the redox potentials.

The large metal orbital stability and the slightly larger E for $[Ru(dphp)_3]^{2+}$ give a strong indication that electron-withdrawing phenyl substitution leads to poorer σ-donation but stronger π-acceptor ability than in dppn. In short, σ-donation follows the trend 12-dppn > 8-dppn $\geqslant$ n-dppn > dppn > dphp (n = 5–7), while the π-acceptor trend is dphp > dppn $\approx$ n-dppn $\geqslant$ 8-dppn $\approx$ 12-dppn.

Figure 4 shows the vibrational splitting of the emission spectrum upon cooling to 77 K. Such a result is typical for the ruthenium(II) diimine complexes, in which the rigid medium seems to favour some specific dipole orientations over others. In Table 3, the ^{3}MLCT characteristics are included. The lifetimes are all relatively long and would favour electron-transfer quenching which is necessary for solar energy conversion. The good correlation between the emission maxima and E (mentioned earlier) is indicative of localization of the excited electron on one ligand in the emissive ^{3}MLCT state. The redox potentials for this state can be compared with $[Ru(bpy)_3]^{2+}$ (bpy = 2,2′-bipyridine) which has an $^*E_{1/2}(3+/2+)$ value of -0.83 V and an $^*E_{1/2}(2+/1+)$ value of 0.76 V. All our complexes have better oxidizing excited states than this complex. However, only dppn and dphp have values of $^*E(2+/1+)$ which are close to the minimum (1.03 V) required for quenching by EDTA.[16] Whereas $[Ru(bpy)_3]^{2+}$ is a better reducing agent in the excited state than the complexes reported in this work.

Acknowledgements—T.S.A. gratefully acknowledges the generous support by the Ministry of Planning—Jordan, the Kuwaiti Development Fund and Yarmouk University Research Fund. A.A. wishes to thank Yarmouk University for financial support (Project 18/89).

REFERENCES

1. A. Juris, V. Balzani, F. Barigelletti, S. Campagna, P. Belser and A. von Zelewsky, *Coord. Chem. Rev.* 1988, **84**, 85.
2. D. G. Whitten, *Accts Chem. Res.* 1980, **13**, 83.
3. N. Sutin and C. Creutz, *Pure Appl. Chem.* 1980, **52**, 2717.
4. M. K. De Armond and C. M. Carlin, *Coord. Chem. Rev.* 1981, **36**, 325.
5. K. Kalyanasundaram, *Coord. Chem. Rev.* 1982, **46**, 159.
6. N. Sutin, *J. Photochem.* 1979, **10**, 19.
7. N. Kitamura, Y. Kawanishi and S. Tazuke, *Chem. Phys. Lett.* 1983, **97**, 103.
8. D. P. Rillema, G. Allen, T. J. Meyer and D. Conrad, *Inorg. Chem.* 1983, **22**, 1617.
9. Y. Kawanishi, N. Kitamura, Y. Kim and S. Tazuke, *Sci. Papers Inst. Phys. Chem. Res.* 1984, **78**, 78.
10. C. T. Lin and N. Sutin, *J. Phys. Chem.* 1976, **80**, 97.
11. S. D. Ernst and W. Kaim, *Inorg. Chem.* 1989, **28**, 1520.
12. S. Wolfgang, T. C. Strekas, H. D. Gafney, R. A. Krause and K. Krause, *Inorg. Chem.* 1984, **23**, 2650.
13. S. Ernst and W. Kaim, *J. Am. Chem. Soc.* 1986, **108**, 3578.

14. W. Kaim and S. Kohlmann, *Inorg. Chem.* 1987, **26**, 68.
15. J. Spanget-Larsen, *J. Chem. Soc., Perkin Trans.* 1985, **11**, 417.
16. T. S. Akasheh, unpublished results.
17. R. J. Crutchley and A. B. P. Lever, *Inorg. Chem.* 1982, **21**, 2276.
18. D. P. Rillema, R. W. Callahan and K. B. Mack, *Inorg. Chem.* 1982, **21**, 2589.
19. R. W. Callahan, G. M. Brown and T. J. Meyer, *Inorg. Chem.* 1975, **14**, 1443.
20. R. A. Krause and K. Krause, *Inorg. Chem.* 1982, **21**, 1714.
21. R. P. Thummel and F. Lefoulon, *Inorg. Chem.* 1987, **26**, 675.
22. K. R. Barqawi, A. Llobet and T. J. Meyer, *J. Am. Chem. Soc.* 198, **110**, 7751.
23. T. S. Akasheh and Z. M. Al-Ahmed, *Chem. Phys. Lett.* 1988, **152**, 414.
24. T. S. Akasheh, P. C. Beaumont, B. J. Parsons and G. O. Phillips, *J. Phys. Chem.* 1986, **90**, 5651.
25. D. P. Rillema, D. G. Taghdiri, D. S. Jones, C. D. Keller, L. A. Worl, T. J. Meyer and H. A. Levi, *Inorg. Chem.* 1987, **26**, 578.
26. F. Barigelletti, L. De Cola, V. Balzani, P. Belser, A. von Zelewsky, F. Vogtle, F. Ebmeyer and S. Germmenudi, *J. Am. Chem. Soc.* 1989, **111**, 4662.
27. W. A. Butte and F. H. Case, *J. Org. Chem.* 1961, **26**, 4690.
28. M. A. Atfah, *J. Heterocycl. Chem.* 1989, **26**, 717.
29. I. R. Evans, A. Spencer and G. Wilkinson, *J. Chem. Soc., Dalton Trans.* 1973, 204.
30. R. A. Krause, *Struct. Bond.* 1987, **67**, 1.
31. F. Barigelletti, A. Juris, V. Balzani, P. Belser and A. von Zelewsky, *Inorg. Chem.* 1987, **26**, 4115.
32. A. Juris, P. Belser, F. Barigelletti, A. von Zelewsky and V. Balzani, *Inorg. Chem.* 1986, **25**, 256.
33. A. B. P. Lever, S. Licocia, P. C. Minor, B. S. Ramaswamy, S. R. Pickens and Magnell, *J. Am. Chem. Soc.* 1983, **103**, 6800.
34. R. W. Balk, R. J. Crutchley and A. B. P. Lever, *Inorg. Chim. Acta* 1981, **L49**, 64.
35. C. D. Tait, D. B. McQueen, R. J. Donohoe, M. K. De Armond, K. W. Hanck and D. W. Wertz, *J. Phys. Chem.* 1986, **90**, 1766.
36. E. S. Dodsworth and A. B. P. Lever, *Chem. Phys. Lett.* 1985, **119**, 61.

Polyhedron Vol. 10, No. 13, pp. 1491–1495, 1991
Printed in Great Britain

0277–5387/91 $3.00+.00
© 1991 Pergamon Press plc

MIXED LIGAND COMPLEXES OF LANTHANIDE IONS WITH ACETONE FERROCENECARBONYLHYDRAZONE AND 1,10-PHENANTHROLINE

HAN XIAOJUN* and WANG XINTANG

Department of Chemistry, Xinjiang University, Wulumuqi 830046, P.R.C.

(*Received* 22 *October* 1990; *accepted* 12 *February* 1991)

Abstract—A new ligand, acetone ferrocenecarbonylhydrazone (HL), and 15 mixed ligand complexes of the type $Ln(HL)(Phen)_2Cl_3 \cdot nH_2O$ (Ln = lanthanide and Y; Phen = 1,10-phenanthroline; $n = 4$ and 5) have been prepared by the reaction of hydrated lanthanide chlorides with HL and Phen in ethanol solution. The IR, NMR, UV, molar conductance and thermogravimetry data of the ligands and their complexes are discussed.

Due to their biological activity, especially as potent inhibitors for many enzymes, the coordination chemistry of aroylhydrazines and related compounds has been the subject of extensive investigation.[1,2] Edwards[3] and co-workers have shown that the replacement of the aromatic group by the ferrocenyl moiety in penicillins and cephalosporins improves their antibiotic activity. Therefore, recently a series of hydrazones containing the ferrocenyl moiety and their complexes with anhydrous lanthanide chlorides have been investigated.[4–8] The mixed ligand complexes of hydrazones containing the ferrocenyl moiety with hydrated lanthanide chlorides and other ligands have not, however, been reported as yet. In the present work, acetone ferrocenecarbonylhydrazone (HL) and the mixed ligand lanthanide complexes of it containing 1,10-phenanthroline (Phen) were studied.

EXPERIMENTAL

Ferrocenecarbonylhydrazine was prepared according to the literature.[9] Hexahydrated lanthanide chlorides were prepared from the respective oxides and hydrochloric acid. The other chemicals were analytical reagent grade.

Preparation of acetone ferrocenecarbonylhydrazone

A mixture of ferrocenecarbonylhydrazine and acetone with a molar ratio of 1:1 was reacted in anhydrous ethanol under reflux for 5 h. After filtering, the filtrate was concentrated to dryness, recrystallized from benzene, and the orange crystals were collected on a Buchner funnel, washed twice with cold benzene and dried *in vacuo*; yield, 75% (m.p. 162.5–164°C). Found: C, 59.8; H, 5.8; N, 10.1. Calc. for $C_{14}H_{16}FeN_2O$: C, 59.2; H, 5.6; N, 9.9%.

Preparation of the complexes

Acetone ferrocenecarbonylhydrazone (1.4 mmol) and 1,10-phenanthroline (1.4 mmol) were dissolved in 30 cm^3 of anhydrous ethanol under heating. Hexahydrated lanthanide chlorides (0.7 mmol) in ethanol (8 cm^3) were added dropwise to the above solution. The mixture was maintained under reflux for 8 h. After filtration, the filtrate was concentrated to 10 cm^3 and ether (20 cm^3) was added with stirring. The precipitate which formed was collected, washed four times with 1:4 ethanol/ether and twice with ether and dried *in vacuo*; yield, above 60%. The complexes are listed in Table 1 together with their decomposition temperature and elemental analyses.

Spectral measurements

IR spectra were recorded with a FTS-40 spectrometer using KBr discs in the region 4000–400 cm^{-1}. NMR spectra were obtained on an AC-80 spectrophotometer using deuterodimethyl sulphoxide as solvent and TMS as an internal standard. UV spectra were measured with a Hitachi U-3400 UV–vis spectrophotometer in the region 215–500

* Author to whom correspondence should be addressed.

Table 1. Decomposition temperature and elemental analyses[a] of the complexes

Complex	Formula	Decomposition temperature (°C)	C(%)	H(%)	N(%)
I	$La(HL)(Phen)_2Cl_3 \cdot 5H_2O$	285	46.2(46.6)	3.8(4.3)	9.1(8.6)
II	$Ce(HL)(Phen)_2Cl_3 \cdot 5H_2O$	280	46.5(46.5)	4.0(4.3)	8.6(8.6)
III	$Pr(HL)(Phen)_2Cl_3 \cdot 5H_2O$	278	46.1(46.5)	4.0(4.3)	9.0(8.6)
IV	$Nd(HL)(Phen)_2Cl_3 \cdot 5H_2O$	275	47.0(46.3)	4.2(4.3)	8.8(8.5)
V	$Sm(HL)(Phen)_2Cl_3 \cdot 5H_2O$	272	45.7(46.0)	4.2(4.2)	8.9(8.5)
VI	$Eu(HL)(Phen)_2Cl_3 \cdot 5H_2O$	270	46.0(45.9)	4.0(4.2)	8.9(8.5)
VII	$Gd(HL)(Phen)_2Cl_3 \cdot 4H_2O$	268	46.6(46.5)	4.2(4.1)	8.8(8.6)
VIII	$Tb(HL)(Phen)_2Cl_3 \cdot 5H_2O$	265	44.9(45.6)	4.2(4.2)	8.7(8.4)
IX	$Dy(HL)(Phen)_2Cl_3 \cdot 4H_2O$	260	46.6(46.3)	4.1(4.0)	8.7(8.5)
X	$Ho(HL)(Phen)_2Cl_3 \cdot 5H_2O$	258	45.7(45.4)	4.1(4.2)	8.8(8.4)
XI	$Er(HL)(Phen)_2Cl_3 \cdot 5H_2O$	257	45.3(45.3)	4.1(4.2)	8.6(8.3)
XII	$Tm(HL)(Phen)_2Cl_3 \cdot 5H_2O$	254	45.1(45.2)	3.9(4.2)	8.5(8.3)
XIII	$Yb(HL)(Phen)_2Cl_3 \cdot 5H_2O$	251	44.8(44.9)	4.0(4.1)	8.7(8.3)
XIV	$Lu(HL)(Phen)_2Cl_3 \cdot 5H_2O$	250	45.0(44.9)	4.0(4.1)	8.8(8.3)
XV	$Y(HL)(Phen)_2Cl_3 \cdot 5H_2O$	260	48.6(49.1)	4.4(4.5)	9.5(9.0)

[a] Calculated values are given in parentheses.

nm using a solution in methanol. Electrolytic conductance measurements were made with a DDS-11A molar conductometer and methanol as solvent at 25°C. Thermal characterization studies were carried out with a PE-DTA 1700 thermal analyser in an argon atmosphere.

RESULTS AND DISCUSSION

The lanthanide complexes are amorphous, reddish-orange solids. They are soluble in methanol, ethanol, DMSO and DMF, sparingly soluble in diethyl ether, benzene and water, but insoluble in petroleum ether. Their elemental analyses show that the formula of these complexes is $Ln(HL)(Phen)_2Cl_3 \cdot 4\text{–}5H_2O$.

IR spectra

The important IR frequencies of the ligands and their complexes together with their relative assignments are given in Table 2.

Table 2. Important IR absorption bands (in cm^{-1}) of the ligands and their complexes

Complex	ν(C=O)	δ(N—H)	ν(C=N)	ν(N—N)	ν(Ln—O)	ν(Ln—N)	δ(C—H)	δ(C—H)	ν(C—H)
Ligands	1652vs	1519vs	1633vs	1001m			850vs	737vs	1420vs
I	1634vs	1539vs	1583vs	1004m	416w	546m	845s	729s	1426s
II	1632vs	1538s	1581vs	1003m	417w	544m	845s	731s	1425s
III	1632vs	1539s	1582vs	1002m	417w	543m	846s	728s	1426s
IV	1634vs	1537s	1585vs	1003m	417w	543m	846s	731s	1425s
V	1632vs	1539s	1585vs	1003m	417w	544m	845s	728s	1427s
VI	1636vs	1540s	1586vs	1002m	420w	550m	848s	730s	1424s
VII	1636vs	1540s	1587vs	1003m	419w	549m	847s	730s	1423s
VIII	1634vs	1541s	1580vs	1002m	419w	549m	845s	730s	1426s
IX	1637vs	1542s	1586vs	1003m	421w	550m	849s	730s	1423s
X	1633vs	1545s	1581vs	1002m	418w	550m	849s	729s	1426s
XI	1636vs	1547s	1581vs	1004m	420w	553m	849s	729s	1426s
XII	1636vs	1546s	1581vs	1003m	420w	554m	848s	727s	1426s
XIII	1639vs	1544s	1579vs	1002m	418w	553m	845s	728s	1426s
XIV	1638vs	1540s	1581vs	1004m	417w	555m	843s	726s	1426s
XV	1632vs	1542s	1583vs	1003m	417w	550m	845s	730s	1426s

vs, very strong; s, strong; m, medium; w, weak.

Table 3. NMR spectral data of the ligands and their complexes

Complex	Ferrocenyl moiety C_5H_5	Ferrocenyl moiety C_5H_4 2H(3, 4)	Ferrocenyl moiety C_5H_4 2H(2, 5)	N—H[a]	—CH_3[b]	a	b	c	d
HL	4.17 (5H, s)	4.37 (2H, m)	4.92 (2H, t)	9.70 (1H, s)	2.00 (6H, d)	6.58 (2H, m)	6.70 (2H, s)	7.19 (2H, m)	8.11 (2H, m)
I	4.19 (5H, s)	4.40 (2H, m)	4.96 (2H, t)	9.80 (1H, s)	2.50	7.81 (4H, m)	8.03 (4H, s)	8.54 (4H, m)	9.17 (4H, m)
XIV	4.20 (5H, s)	4.40 (2H, m)	5.00 (2H, t)	9.82 (1H, s)	2.50	7.86 (4H, m)	8.01 (4H, s)	8.55 (4H, m)	9.13 (4H, m)

s, singlet; d, doublet; t, triplet; m, multiplet.
HL = $C_5H_5FeC_5H_4CONHN{=}C(CH_3)_2$
[a] The signal of this proton disappears after adding D_2O.
[b] The signal of these protons is overlapped with that of the protons in deuterodimethyl sulphoxide.

The IR spectra of the complexes are similar. Compared with the IR spectra of ligand HL, ν(C=O)(amide I) and ν(C=N) were shifted to lower frequencies by *ca* 20 and 50 cm^{-1}, respectively, whereas the ν(N—N) and δ(N—H)(amide II) were shifted to higher frequencies by *ca* 2 and 23 cm^{-1}, respectively. These changes show that the HL ligand coordinates with lanthanide ions in the keto form, with the oxygen atom of the carbonyl group and the nitrogen atom of the azomethine.[4-8] Compared with the IR spectra of the Phen ligand, δ(C—H) were shifted to lower frequencies by *ca* 8 and 5 cm^{-1} and ν(C—H) was shifted to higher frequencies by *ca* 6 cm^{-1}. These changes show that Phen participates in coordination.[10] Two new bands observed at *ca* 543–549 cm^{-1} and 415–419 cm^{-1} are attributed to ν(Ln—N) and ν(Ln—O), respectively.[11]

Table 4. Important UV spectral data of the ligands and their complexes

Complex	Ln^{3+}	Absorption bands (log ε) (nm, λ_{max})			
HL		218.9(4.38)		263.5(4.04)	450
Phen			229.6(4.72)	263.7(4.54)	
HL+Phen			228.2	263.5	450
I	La	225.2(5.05)	229.3(5.03)	265.0(4.88)	450
II	Ce	225.0(5.09)	229.0(5.07)	265.6(4.92)	450
III	Pr	225.8(5.06)	229.1(5.06)	264.6(4.90)	450
IV	Nd	224.8(5.07)	229.3(5.06)	264.3(4.90)	450
V	Sm	225.4(5.03)	228.8(5.02)	264.5(4.83)	450
VI	Eu	224.8(5.00)	229.1(5.00)	263.8(4.83)	450
VII	Gd	224.9(5.02)	229.5(5.03)	264.0(4.82)	450
VIII	Tb	224.6(5.04)	229.3(5.03)	264.3(4.84)	450
IX	Dy	224.3(5.01)	229.4(4.99)	265.1(4.83)	450
X	Ho	225.0(5.03)	229.4(5.01)	264.7(4.83)	450
XI	Er	225.5(5.02)	229.8(5.02)	264.0(4.84)	450
XII	Tm	224.5(4.97)	230.4(4.94)	265.1(4.80)	450
XIII	Yb	225.9(5.12)	229.9(5.11)	264.3(4.93)	450
XIV	Lu	225.2(5.05)	229.7(5.01)	264.7(4.82)	450
XV	Y	224.6(4.97)	229.3(4.96)	264.3(4.79)	450

[a] Concentrations: HL = 9.75×10^{-5}M, Phen = 3.96×10^{-5}M, HL+Phen·HL = 2.44×10^{-5}M, Phen = 3.96×10^{-5}M, Complex = approx. 2.00×10^{-5}M.

The IR spectra of the HL ligand show medium, sharp peaks of ν(N—H) at 3240 cm^{-1}, whereas the spectra of the complexes exhibit a strong, broad peak of ν(O—H) at *ca* 3300 cm^{-1}. In addition, the characteristic frequencies of the ferrocenyl moiety appear[12] at *ca* 1452, 1026, 822 and 488 cm^{-1} and the bands at *ca* 1378 cm^{-1} are attributed to $\delta(CH_3)$ in the HL ligand and in all the complexes.

NMR spectra

The NMR spectra of the ligands and their complexes are shown in Table 3.

The protons on the two cyclopentadienyl rings, methyl, the nitrogen atom and all the protons on Phen are shifted downfield. These changes are caused by the deshielding effect which occurs after forming the complexes. This also shows that the HL ligand coordinates with lanthanide ions in the keto form and that the molar ratio HL/Phen in the complexes is 1 : 2.

UV spectra

The UV spectra of the ligands and their complexes in methanol are shown in Table 4 and Fig. 1. It can be seen that the UV spectra of the complexes are similar, but they are somewhat different from those of the ligands. The *K* band (π–π^* transition) of the HL ligand is observed at 219 nm, but in the complexes, a bathochromic shift of *ca* 6 nm occurs resulting from the chelation of the ligand with lanthanide ions, and the band appears at 225 nm.

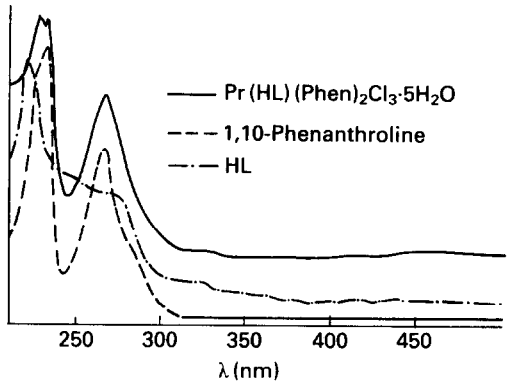

Fig. 1. UV spectra of the ligands and their complexes.

The shoulder peak at 263.5 nm arising from the *B* band of the cyclopentadienyl ring in this ligand changes into a sharp peak at *ca* 265 nm and overlaps with the *B* band of Phen in the complexes. The broad band near 450 nm in the HL ligand and the complexes is attributed to charge-transfer in the ferrocenyl group (transition of the three electrons on iron to either the non-bonding or antibonding orbitals of the cyclopentadienyl ring). The band at 229 nm shows that Phen participates in coordination.

Table 5. Thermal analysis data of the ligands and their complexes

Complex	Ln^{3+}	Decomposition temperature (°C)	Leaving group	Weight loss Found (Calc.)
HL		164–365	Substituent	29.3(34.9)
		365–480	Two cyclopentadienyl rings	46.8(45.4)
		up to 480	Residue (Fe)	23.8(19.7)
Phen		115	H_2O	9.3(9.1)
		160–315	Completely discomposed	
I	La	44.9	$2H_2O$	4.1(3.7)
		150	H_2O	1.8(1.8)
		230	$2H_2O$	3.5(3.7)
		289–695		
		up to 695	Residue (Fe+La+3Cl)	31.4(30.7)
VII	Gd	49.2	$2H_2O$	3.8(3.7)
		200	$2H_2O$	3.9(3.7)
		275–650		
		up to 650	Residue (Fe+Gd+3Cl)	31.0(32.6)
XIV	Lu	45.2	$4H_2O$	6.8(7.1)
		203	H_2O	1.9(1.7)
		262–579		
		up to 579	Residue (Fe+Lu+3Cl)	32.3(33.2)

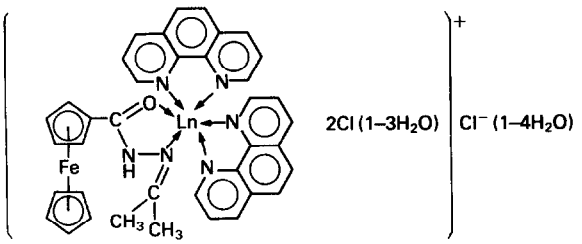

Fig. 2. Structure of these complexes.

Thermal analysis

The thermal analysis data of the ligands and their complexes are listed in Table 5.

It can be seen that the water in these complexes exists in two different forms, crystal and coordinated. The number of coordinated water molecules decreases with a change of lanthanide from light to heavy, i.e. the coordination number of central ions decreases progressively due to the lanthanide contraction. From the start and end temperatures of decomposition, we can see that the thermal stability of the complexes is increased much more than that of the ligands after forming complexes, and that the thermal stability of these complexes is decreased with a change of lanthanide from light to heavy.

Molar conductance

Deep red solutions are obtained by dissolving the complexes in methanol. The molar conductance values of HL, Phen and the complexes are 18.4, 15.0 and 81.7–103.9 $\Omega^{-1}cm^2mol^{-1}$, respectively. These values indicate that in methanol solution HL and Phen are non-electrolytes but the complexes are 1 : 1 electrolytes.[13]

Conclusions

Acetone ferrocenecarbonylhydrazone and 1,10-phenanthroline are bidentate ligands. One molecule of HL (in the keto form), two molecules of Phen, two chloride ions and one to three molecules of water coordinate with one lanthanide ion. The water in these complexes exists in two different forms, crystal and coordinated, and the coordination number is variable (11–9). Therefore, we have established a structure for these complexes shown in Fig. 2.

REFERENCES

1. A. Albert, *Nature (Lond.)* 1953, **9**, 370.
2. R. L. Dutta and M. M. Hossain, *J. Sci. Ind. Res. India* 1985, **44**, 635.
3. E. I. Edwards, R. Epton and G. Marr, *J. Organomet. Chem.* 1975, **85**, C23.
4. Ma Yongxiang and Zhao Gang, *Polyhedron* 1988, **7**, 1101.
5. Ma Yongxiang, Zhang Tongjun and Zhao Gang, *Lanthanide and Actinide Res.* 1988, **2**, 235.
6. Ma Yongxiang and Zhao Gang, *Inorg. Chim. Acta* 1988, **144**, 265.
7. Ma Yongxiang and Li Feng, *Inorg. Chim. Acta* 1988, **149**, 209.
8. Ma Yongxiang and Han Xiaojun, *Lanthanide and Actinide Res.* 1988, **2**, 385.
9. K. Schlogel, *Mh Chem.* 1957, **88**, 601.
10. Yang Luqing and Yang Rudong, *Acta Chim. Sin.* 1989, **47**, 633.
11. Balwan Singh and Harihar Misra, *J. Indian Chem. Soc.* 1986, **63**, 840.
12. Kazuo Nakamoto, *Infrared and Raman Spectra of Inorganic and Coordination Compounds.* John Wiley, New York (1978).
13. W. J. Geary, *Coord. Chem. Rev.* 1971, **7**, 81.

Polyhedron Vol. 10, No. 13, pp. 1497–1506, 1991
Printed in Great Britain

0277–5387/91 $3.00+.00
© 1991 Pergamon Press plc

PERALKYLATED 1,4-DIBORA-2,5-CYCLOHEXADIENES—FORMATION AND REARRANGEMENT INTO PERALKYLATED *NIDO*-2,3,4,5-TETRACARBAHEXABORANES(6)

BERND WRACKMEYER* and GERALD KEHR

Laboratorium für Anorganische Chemie, Universität Bayreuth, Postfach 101251, D-8580 Bayreuth, F.R.G.

(*Received* 3 *January* 1991; *accepted* 20 *February* 1991)

Abstract—Peralkylated 1,4-dibora-2,5-cyclohexadienes (DBCH) (**3a,b**) and a pentaalkylaryl derivative (**3c**) are formed in high yield at low temperature (−78 to −30°C) via the reaction between 1,5,7,11-tetramethyl-2,3,4,8,9,10-hexaisopropyl-3,9-dibora-6-stanna-1,4,7,10-spiro[5.5]undekatetraene (**8**) and organoboron dihalides ($MeBBr_2$, $^iPrBBr_2$, $PhBCl_2$). In contrast with claims in the literature for stable peralkylated DBCH derivatives, compounds **3** rearrange between −30 and +25°C into the *nido*-2,3,4,5-tetracarbahexaboranes(6) (**5**). The specific arrangement of the substituents in the 2,3,4,5-position (Me, ^{i}Pr, Me, ^{i}Pr) is noteworthy. This indicates, together with the formation of carboranes (e.g. **5a** from **3a**) in which substituents at the boron atoms must have been exchanged, that cleavage of the DBCH derivatives (**3**) into borirenes (**1**) is involved at least to some extent. Attempts to prepare a borirene (1-methyl-2,3-ditert-butyl-borirene, **1a**) by the reported reaction between the system $C_8K/MeBBr_2$ and ditert-butylethyne have failed. All reactions were monitored by ^{1}H, ^{11}B, ^{13}C, and ^{119}Sn NMR spectroscopy and the same methods served for the final structural assignment of the DBCH derivatives **3** and the carbaboranes **5**.

The relationship between unsaturated cyclic organoboranes, such as borirenes (**1**), boroles (**2**) and 1,4-dibora-2,5-cyclohexadienes (DBCH, **3**), is of considerable interest, both from a preparative and a theoretical point of view. It has been suggested that the dimerization of **1** leads to **3**[1] and insertion of alkynes into the B—C= bond should give **2**.[1] The reaction of the dianion of **2** (2^{2-}) with boron dihalides does not lead to **3** but to the highly dynamic bicyclic compound **4**[2] which, in the absence of boron ligands with π donor properties, adopts the carborane structure **5**. The carboranes **5** are valence isomers of **3**.

1

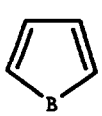

2

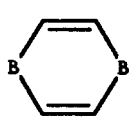

3

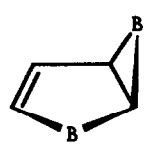

4

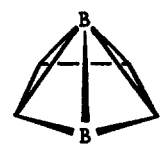

5

Although, derivatives of **4** are potential dimerization products of **1**, the formation of **4** has not been seriously considered[1] since the boron acceptor orbitals are not fully utilized in the dimerization process. On the other hand, the apparently straightforward intramolecular rearrangement of planar **3** into **5** by forming a new C(3)—C(5)— or C(2)—C(6) bond is symmetry forbidden. Inspite of the numerous routes leading to carboranes **5**,[2–7] a direct link between **3** and **5** is still missing. So far, the existence of few derivatives of **3**, mainly species with B—F[8] or B—O[9] bonds, has been proved conclusively. In fact, compound **6**[9] is the only example of a stable DBCH with organyl groups and hydrogen as substituents.

* Author to whom correspondence should be addressed.

6 [Fc = $(\eta^5\text{-}C_5H_5)Fe(\eta^5\text{-}C_5H_4)$-]

The successful synthesis of hexaalkyl-1,4-dibora-2,5-cyclohexadienes was claimed[10] but extensive attempts to reproduce that work failed.[7] Some time ago, as part of a theoretical approach,[1] the claim for stable peralkylated DBCH derivatives has been renewed in the form of a footnote.[11] However, to the best of our knowledge, the experimental details promised have not been published as yet. Based on this unpublished evidence, it has been concluded[1] that "*hexaalkyl derivatives of both* **3** *and* **5** *have been reported and show no evidence of isomerization reactions*". This statement,[1] together with the insufficient experimental evidence,[10] has led to an unsatisfactory situation which prompted us to start a further investigation of this problem.

Firstly, we tried to use the $C_8K/MeBBr_2$ reagent (the "*suitable methylborylene generator*"[10]) and its reaction with ditert-butylacetylene, for preparing and studying the reactivity of the stable[10,12] 1-methyl-2,3-ditert-butyl-borirene (**1a**). Secondly, we reinvestigated the reaction of the peralkylated 1-stanna-4-bora-2,5-cyclohexadiene (**7**) with $MeBBr_2$[6] under very mild reaction conditions, as a potential route to peralkylated DBCH derivatives. The results of the latter study forced us to synthesize and to use the spiro-cyclic compound **8** instead of **7**, in order to prevent side reactions.

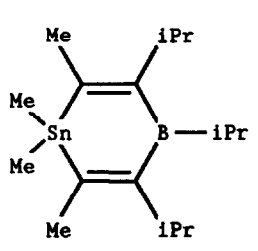

7

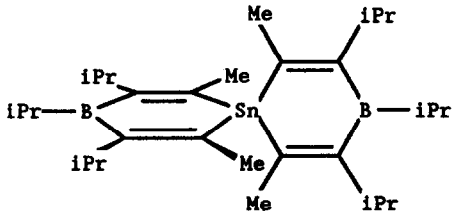

8

RESULTS AND DISCUSSION

Attempted synthesis of 1-*methyl*-2,3-*ditert-butyl-borirene* (**1a**)

As in the previous attempts[7] at reproducing results for the system $C_8K/MeBBr_2$/alkynes, we have used different types of potassium graphite. A well-ordered C_8K-phase (**A**) was prepared and characterized by X-ray diffraction, and a poorly ordered material (**B**) was prepared *in situ*,[13] which apparently has also been used in the original work.[10] All reactions were carried out in hexane (which proved to be inert against both types of "C_8K") and monitored by ^{11}B NMR.

(**A**) After 2 days of stirring the reaction mixture, containing $C_8K/MeBBr_2$/ditert-butylacetylene, at ambient temperature, the ^{11}B NMR spectrum did not show new signals in addition to that of $MeBBr_2$ ($\delta^{11}B$ 63.0). When the mixture was heated to reflux for 24 h, new weak signals at $\delta^{11}B$ 35.4, 41.9, 70.4 and 76.7 had appeared. After heating to reflux for a further 72 h, all $MeBBr_2$ was consumed and major ^{11}B NMR signals appeared at $\delta^{11}B$ 33.3 [presumably $(MeBO)_3$], 42.0, 70.4, 76.8. The signal-to-noise ratio of the ^{11}B NMR spectra was poor in comparison with previous spectra of the same mixture, indicating that most boranes must have been converted into insoluble material.

(**B**) The reaction mixture was treated and monitored as for **A**. Finally, the ^{11}B NMR spectrum showed the same signals in approximately the same ratio as for **A** and, in addition, weak signals at $\delta^{11}B$ 16.6, 13.4, −43.9, −44.0, indicating the presence of some *nido*-2,3,4,5-tetracarbahexaborane(6) derivatives.

Owing to the questionable $\delta^{11}B$ data for **1a**[14a] (**1a** and **9** are reported[10b,12] to be the products of the reaction between $C_8K/MeBBr_2$ and ^{t}Bu—C≡C—^{t}Bu), it is difficult to compare our results with those reported in the literature.[10,12] The $\delta^{11}B$ data for both compounds ($\delta^{11}B$ for **9**: 41.2[14b]) should be in the range $\delta^{11}B$ +35 to +45.[14,15] In

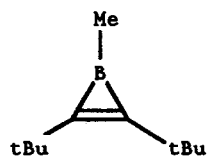

1a

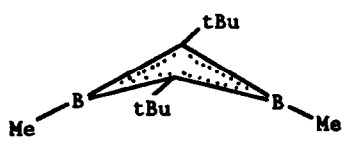

9

any case, the yield of these reactions was very low (no yield has been reported[10b,12]) and we were not able to isolate any definite boron compound from the reaction mixture. Therefore, a study of the reactivity of **1a** towards alkynes (as an interesting route

to borole derivatives **2**) and organoboron halides (ring opening and further reactions) had to be postponed.

Reactions of the peralkylated 1-*stanna*-4-*bora*-2,5-*cyclohexadiene* (**7**) *with alkylboron dibromides*

Compound **7** has been reported[6] to react with $MeBBr_2$ to give Me_2SnBr_2 and a mixture of peralkylated *nido*-2,3,4,5-tetracarbahexaborane(6) derivatives (**3**). We have studied this reaction again with $MeBBr_2$ and $^iPrBBr_2$, using ^1H, ^{11}B, ^{13}C and ^{119}Sn NMR at variable temperature (−78 to +25°C). The reaction starts according to eq. (1), with the Me/Br exchange, leading mainly to **10a** and the dialkylboron bromide, accompanied by a small amount of the DBCH derivative **3a,b** (sub-

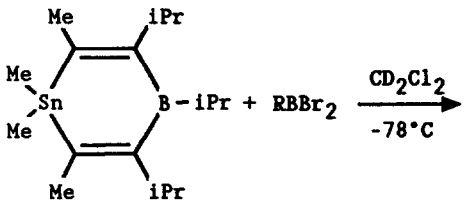

7 R = Me; iPr

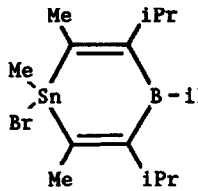

10a

sequently identified, *vide infra*). By warming the samples slowly to room temperature, the amount of **3a,b** did not increase but NMR signals for a mixture of carboranes, as noted previously,[6] appeared and grew rapidly. For both R = Me, ^iPr, a mixture of the carboranes **5a,b** was obtained. Since there can be no doubt as to the distribution of the 2,3,5,6-substituents in **7**, the specific arrangement of the 2,3,4,5-substituents in **5a,b** is remarkable. It is also noteworthy that we did not find an isomer of **5b** with apical ^iPrB— and basal MeB moieties.

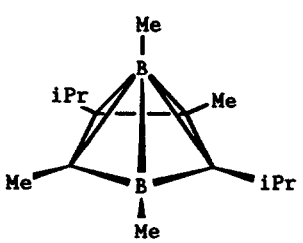

5a

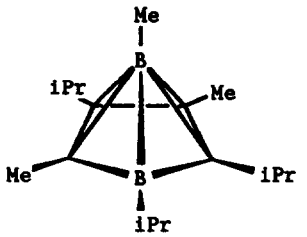

5b

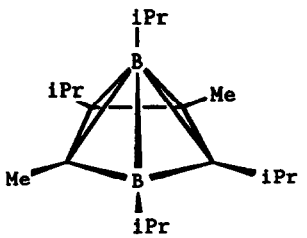

5c

Neither did we observe **5c** (from **7** and $^iPrBBr_2$) in appreciable quantity.

Considering the finding that exocyclic exchange [eq. (1)] is the preferred starting reaction, the whole system becomes exceedingly complex and any discussion of a mechanism leading to **5a,b** as the major, final products would be highly speculative. In order to circumvent the problem of exocyclic exchange [eq. (1)], the spiro-cyclic compound **8** is the better choice for exchange reactions with boron halides.

Synthesis of the spiro-heterocyclic stannane **8** *and its reaction with organoboron dihalides*

The reaction between 2 equivalents of **7** and SnX_4 (X = Cl, Br) does not lead to **8**, but affords only small amounts of **10b,c** [eq. (2)], accompanied by extensive decomposition, including the formation of SnX_2.

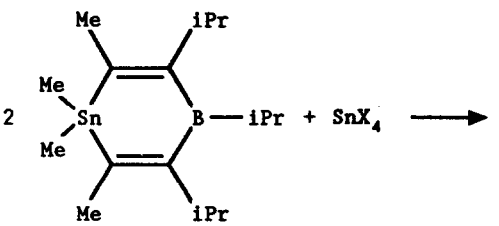

7

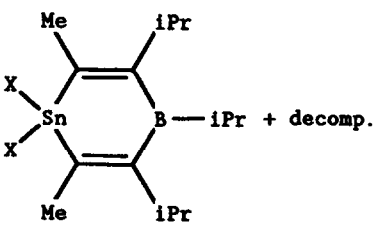

10 b, c

X = Cl, Br

Therefore, we have studied the organoboration[16,17] of tetrakis(alkynyl)stannanes. In the case of the propynide, $Sn(C{\equiv}C{-}Me)_4$, and triisopropylborane [eq. (3)], this has led to the spiro-cyclic compound **8** in high yield.

$$Sn(C{\equiv}C{-}CH_3)_4 + 2\ B(iPr)_3 \longrightarrow$$

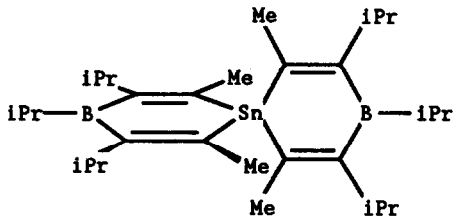

(3)

8

Compound **8** is obtained as a slightly greenish, air-sensitive solid, readily soluble in hexane, benzene, toluene and dichloromethane. It is fully characterized by its NMR data (see Table 1).

The reactions of **8** with $MeBBr_2$, $^iPrBBr_2$ and $PhBCl_2$ in dichloromethane were studied by ^1H, ^{11}B, ^{13}C and ^{119}Sn NMR between -78 and $+25°C$. In all cases, the reaction started [eq. (4)] to give the 1-stanna-4-bora-2,5-cyclohexadienes (**10b,c**) and the corresponding DBCH derivatives (**3a,b,c**). The reactivity towards the boron halides decreased in the order $MeBBr_2 \gg {}^iPrBBr_2 \approx PhBCl_2$.

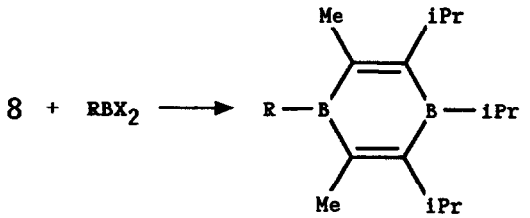

3 a, b, c

R = Me, iPr, Ph

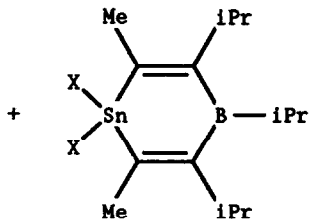

(4)

10 b, c

X = Cl, Br

All NMR data (Table 2), in particular the whole set of ^1H and ^{13}C NMR signals, are consistent with the proposed structures of **3**. An alternative structure of **3b**, with a different arrangement of the 2,3,5,6-substituents, can be ruled out, since there are two

Table 1. ^{119}Sn, ^{11}B and ^{13}C NMR data[a] for the 3,9-dibora-6-stannaspiro[5,5]undecane (**8**) and 1-stanna-4-bora-2,5-cyclohexadienes (**7**, **10a,b,c**)

	$\delta^{13}C$							
Compound	C(2/6)	C(3/5)	Me(2/6)	$^iPr(3/5)$	$^iPr(4)$	R(1)	$\delta^{119}Sn$	$\delta^{11}B$
7	138.1 [464.6]	169.6 (br)[b]	21.3 [53.1]	31.5/23.4 [70.6][7.4]	26.0/21.4 (br)[b]	−9.3 {br}[c]	−121.0	73.1
8	137.3 {br}[c,d]	172.1 (br)[b,d]	21.6 [53.7][d]	31.7/23.1 [69.5][6.8]	25.8/21.5 (br)[b]	—	−201.3	73.0
10a	138.5 {br}[c,f]	170.8 (br)[b,f]	20.4 [54.4]	31.6/22.8; 22.5[e] [93.1][9.2][7.0]	25.8/20.7 (br)	−1.9 {br}[c,f]	−21.6	74.4
10b	139.5 [629.8]	177.8 (br)[b]	19.8 [53.1]	32.4/22.4 [138.5][9.6]	26.4/20.6 (br)[b]	—	−80.3	72.6
10c	139.8 [585.1]	176.6 (br)[b,g]	20.0 [56.7]	32.3/22.5[g] [134.0][10.2]	26.5/20.7 (br)[b]	—	−134.2	73.1

[a] Bruker AC 300; temperature, 300 K; solvent, CD_2Cl_2; external references, $SiMe_4$ [$\delta^{13}C(CD_2Cl_2) = 53.8$; $\delta^1H(CDHCl_2) = 5.33$]; $SnMe_4$ ($\delta^{119}Sn = 0$); BF_3—OEt_2 ($\delta^{11}B = 0$).

[b] $^nJ(^{119}Sn^{13}C)$ values in Hz are given in square brackets and (br) denotes the broad ^{13}C resonances for boron-bonded carbon atoms.

[c] {br} denotes broadened ^{13}C-resonances owing to dynamic effects.

[d] $\delta^{13}C$(233 K): 170.7/170.4; 138.9/134.9; 22.2/21.7.

[e] Diastereotopic groups.

[f] $\delta^{13}C$(233 K): 168.9 [70.0]; 138.8 [499.5]; −1.7 [343.8].

[g] $\delta^{13}C$(233 K): 175.2 [78.6]; 22.0/21.4[e].

Table 2. ^{11}B and ^{13}C NMR data[a] for the 1,4-dibora-2,5-cyclohexadienes (**3a,b,c**)

Compound	C(2/6)	C(3/5)	Me(2/6)	$\delta^{13}C$ $^{i}Pr(3/5)$	$^{i}Pr(4)$	R(1)	$\delta^{11}B$
3a	143.5 (br)[b]	175.1 (br)[b]	16.7[c]	31.5/21.8	22.5/20.8 (br)[b]	8.2[c] (br)[b]	63.6
3b	145.0 (br)[b]	170.1 (br)[b]	16.5	31.2/21.8	22.6/21.0 (br)[b]	n.o./18.8	63.9
3c	143.2 (br)[b]	177.3 (br)[b]	17.6	31.8/21.8	22.5/21.1 (br)[b]	[d]	57.7, 64.0

[a,b] See footnotes [a,b] to Table 1.
[c] δ^1H(233 K): 0.73 s, 3H, BMe; 1.81 s, 6H, =C—Me. δ^1H(300 K): 0.81 s, 3H, BMe; 1.89 s, 6H, =C—Me.
[d] $\delta^{13}C$ (BPh): 127.8 (*m*); 128.7 (*p*); 131.5 (*o*); 145.4 (br, i).

sets of ^1H and ^{13}C NMR signals for the ^{i}PrB groups in **3b**.

Between −78 and −30°C, no carborane was present [see Fig. 1(a)]. A slight excess of compound **8** was used to ensure that all of the boron halide was consumed, in order to suppress its potential influence on the stability of DBCH derivatives (see the complex behaviour of **7** towards boron halides). The rearrangement of **3** into the carboranes **5** starts by warming the reaction solutions from −30°C to room temperature and is almost (> 80%) complete after 48 h for the reactions (**8**+$MeBBr_2$) and (**8**+$PhBCl_2$). In the case of the reaction (**8**+$^{i}PrBBr_2$), a mixture of **3b** and **5c** (*ca* 40:60) is left after 48 h at room temperature, which can be purified by distillation (*ca* 50°C/10^{-4} torr) to give pure **5c**.

The reaction of **8** with $MeBBr_2$ affords pure **3a**

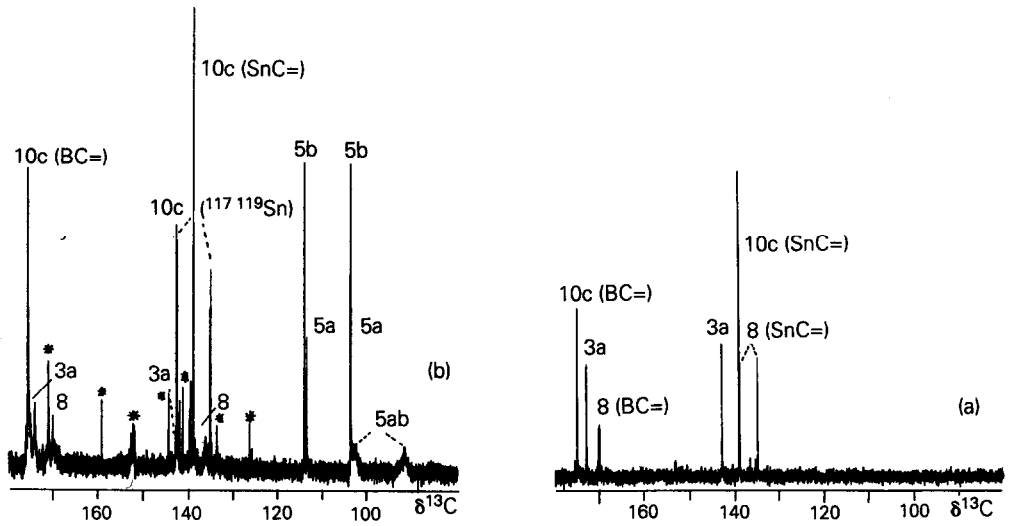

Fig. 1. (a) 75.5 MHz $^{13}C\{^1H\}$ NMR spectrum (233 K, CD_2Cl_2): Reaction between compound **8** (excess) and $MeBBr_2$, showing the region for the olefinic carbons and the carborane cage carbons. Owing to fast quadrupolar relaxation at low temperature, the ^{13}C(B—C=) resonances are fairly sharp[15] and easy to observe. The signals for excess **8**, **10c** and **3a** are readily assigned. The high-field ^{13}C(B—C=) signal of **3a** is on top of the $^{117/119}Sn$ satellites of the ^{13}C(2,6) signals of **10c** [see also Fig. 1(b)]. (b) 75.5 MHz $^{13}C\{^1H\}$ NMR spectrum (300 K, CD_2Cl_2): The same reaction as described in Fig. 1(a), after 2 days at room temperature. In addition to the signals assigned in Fig. 1(a) for **8**, **10c** and **3a**, signals for the cage-carbon atoms of the carboranes **5a** and **5b** are observed. ^{13}C NMR signals for the boron-bonded carbon atoms are broad at room temperature.[15] The ^{13}C(SnC=) resonance signal of **8** is broadened owing to intramolecular dynamic processes. A number of unidentified ^{13}C resonances (marked *) appear in the olefinic region.

at low temperature [see Fig. 1(a)]. However, when the reaction solution is warmed to room temperature a mixture of the carboranes **5a,b** is present [Fig. 1(b)]. Additional ^{13}C NMR signals in the olefinic region indicate that further unknown species have been formed. Selective ^{13}C-{^{11}B} decoupling experiments[6] have shown that there are two different apical BMe groups (**5a,b**) but only one basal BMe (**5a**) and one basal B^{i}Pr group (**5b**). There is no indication of an apical B^{i}Pr group.

Similarly, compound **8** reacts with ^{i}PrBBr$_2$ to give solely **3b** and **10c**. At room temperature, the typical NMR signals for a single carborane **5c** grow.

The NMR spectra for the reaction mixture (**8**+PhBCl$_2$), containing **3c**, **10b** and a small amount of **8**, change slowly at room temperature to a more complex pattern from which the formation of mainly two carboranes, **5d,e**, is evident, accompanied by a small amount of **5c**.

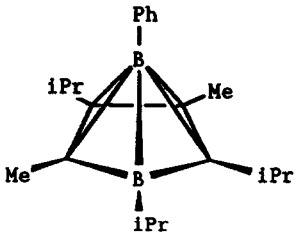

5d

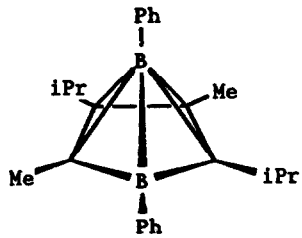

5e

Interconversion between DBCH *derivatives* **3** *and carboranes* **5**

There are mainly two open questions pertinent to the mechanism of the rearrangement of **3** into **5**:

(i) Why does the rearrangement of pure **3a** and pure **3c** lead to mixtures of **5a,b** and **5c,d,e**, respectively?

(ii) How can we explain the specific arrangement of the substituents in the 2,3,4,5-positions of the carboranes **5**?

The experimental evidence relevant to (i) and (ii) rules out the deceptively simple intramolecular process [eq. (5)] which is forbidden by symmetry, anyway. An intermolecular process would either require the rather unlikely reaction between two molecules of DBCH, both loaded with fairly bulky substituents, or the breakage of the six-membered ring into two borirenes [eq. 6(a)]. Recombination of the borirenes could lead back to the starting material (or isomers thereof). However, this would again require the synchronous reaction between sterically crowded centres. Alternatively, derivatives of **4** can be formed from two borirenes [eq. 6(b)] or directly from the DBCH derivatives [eq. 6(c)] via an intramolecular process (*vide infra*) different from that shown in eq. (5). The subscript *n* in eq. (6) denotes that the identity of the substituent is no longer defined.

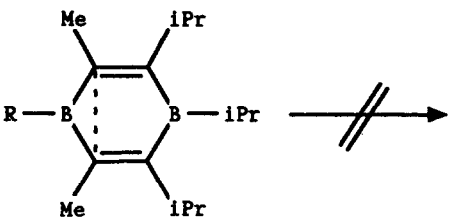

3

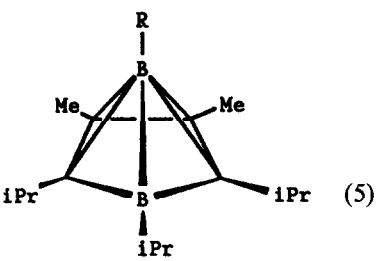

5 (5)

From the derivatives of **4**, there is either a route back to **3** [eq. 6(c)] or the carboranes **5** are formed irreversibly [eq. 6(d)]. The dimerization of the two borirenes to **4** is sterically much less congested if the carbon substituents are alternately ^{i}Pr, Me, ^{i}Pr, Me (in agreement with the experimental data) rather than ^{i}Pr, Me, Me, ^{i}Pr or Me, ^{i}Pr, ^{i}Pr, Me. Since the intermediate **11** has to be considered for the interconversion between **4** and **5**, it is *a priori* unpredictable which RB unit ends up in the apical or basal position. The proposed intramolecular process leading to the intermediate **4**, involving twisted, half-chair or chair conformations of the DBCH derivatives, is symbolized in **12** [dotted lines indicate new B—C bonds and the dashed line indicates a new C—C bond; the B(1)—C(6) and B(4)—C(5) bonds are broken in this process]. Such conformations may be preferred in the presence of bulky substituents such as ^{i}Pr groups on boron as well as on carbon atoms of DBCH. Therefore, both processes [eqs 6(b) and (c)] can be involved in the rearrangement from DBCH derivatives **3** into the carboranes **5**.

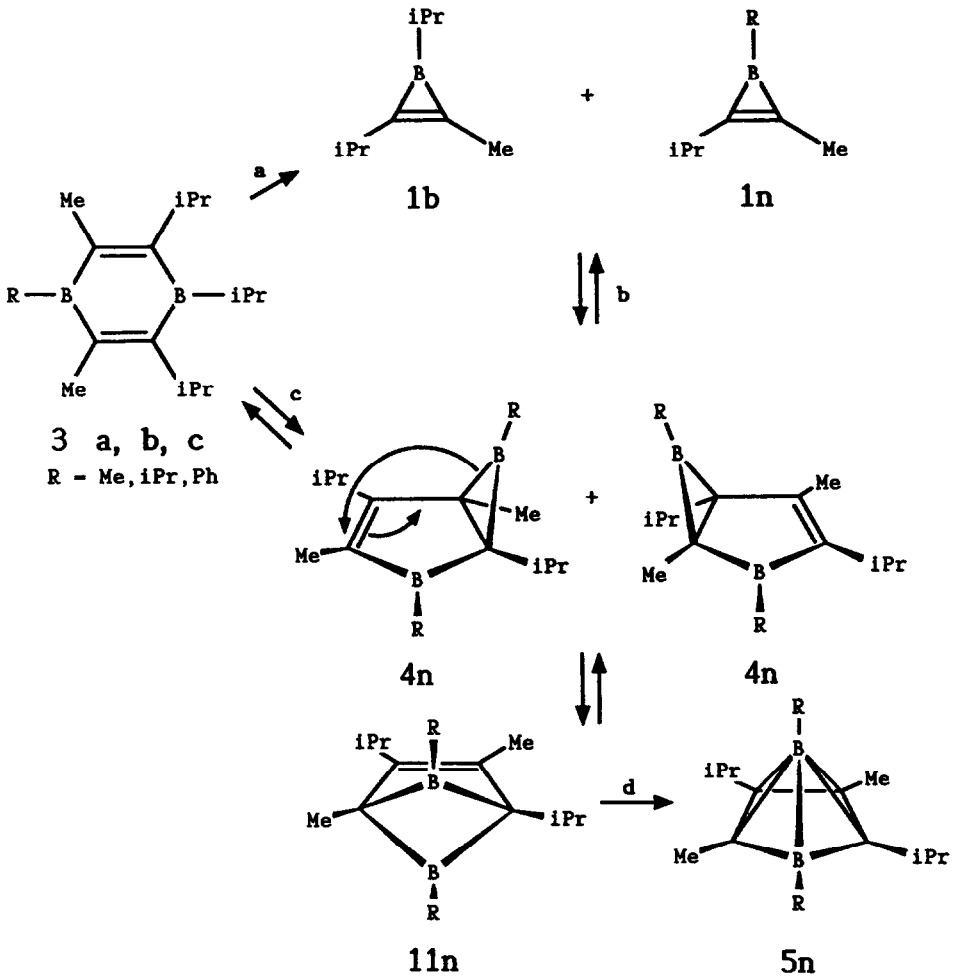

(6)

We have been looking for NMR spectroscopic evidence for the intermediacy of the borirenes **1b,c,d**. There were always weak ^{13}C NMR signals in the olefinic as well as in the aliphatic region which could not be assigned. In the ^{11}B NMR spectra, we find weak signals (see Fig. 2) at $\delta^{11}B+34$ to $+35$, or around $\delta^{11}B+40$ which are in the range expected for borirenes (these signals do not belong to oxidation products, since ^{1}H and ^{13}C resonances for B—O—CH— or $BOCH_3$ groups are missing). However, firm evidence is still missing.

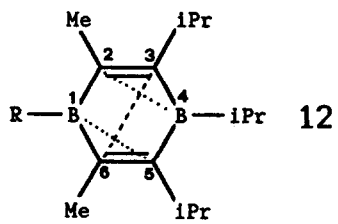

12

EXPERIMENTAL

All compounds were handled in N_2 or Ar atmosphere in carefully dried solvents and dry glassware. The starting materials $BiPr_3$,[18] $MeBBr_2$,[19] $PhBCl_2$[19] and $Sn(C{\equiv}C{-}Me)_4$[20] were prepared according to literature procedures. The reaction between BBr_3 and Sn^iPr_4 (1 : 1) in the absence of solvent gave pure $^iPrBBr_2$ in high yield (89%). [$^iPrBBr_2$: 300 MHz ^1H NMR in C_6D_6 (300 K) δ^1H 0.93 d, 6H, ^{i}Pr; 1.59 sp, 1H, BCH; 96.3 MHz ^{11}B NMR, $\delta^{11}B$ 66.5; 75.5 MHz ^{13}C NMR, $\delta^{13}C$ 19.2 ^{i}Pr; 32.6 (br), BCH.] Potassium graphite has been prepared and characterized as described previously.[7] Mass spectra were recorded with a Varian MAT CH 7 instrument. NMR spectra were obtained with JEOL FX 90Q and Bruker AC 300 spectrometers, both equipped with a multinuclear unit. For further experimental details see the footnotes to Tables 1–3 and Figs 1 and 2.

1,5,7,11-*Tetramethyl*-2,3,4,8,9,10-*hexaisopropyl*-3,9-*dibora*-6-*stanna*-1,4,7,10-*spiro*[5.5]*undecatetraene* (8)

A solution of tetrapropinylstannane (8.2 g, 30 mmol) in 120 cm^3 of toluene was cooled to $-78°C$. After adding triisopropylborane (12.6 cm^3, 90 mmol), the solution was allowed to warm up to room temperature and then heated to 60°C for 12

h. The solvent and the excess of triisopropylborane were removed *in vacuo*, and recrystallization of the residue from hexane at −20°C gave 13.3 g (80%) of **8** as a light green solid (> 180°C decomp.). EI–MS (70 eV): m/z = 556 (M^+, 2%), 531 (56%), 338 (62%), 323 (44%), 295 (44%), 203 (44%), 43 (Me_2CH^+, 100%).

300 MHz ^{1}H NMR in CD_2Cl_2 (300 K): δ^1H [$^nJ(^{119}Sn^1H)$] = 1.104 d, 12H, B^{i}Pr; 1.21 d, 24H, ^{i}Pr; 1.76 sp, 2H, BCH; 1.98 [54.2] s, 12H, =C—Me; 2.94 sp, 4H, =C—CH; (233 K) = 0.94 d, 12H, B^{i}Pr; 1.15 {br}, 24H, ^{i}Pr; 1.73 sp, 2H, BCH; 1.87 [58.0] s, 6H, =C—Me; 1.93 [48.2] 6H, =C—Me; 2.84 br, 4H, =C—CH (see Table 1 for δ^{119}Sn, δ^{13}C and δ^{11}B NMR data).

Reaction of **8** *with organoboron dihalides*

The neat organoboron dihalides were injected into cooled solutions (−78°C) of **8** (0.4 mmol) in

Table 3. ^{11}B and ^{13}C NMR data[a,b] for the *nido*-2,3,4,5-tetracarbahexaboranes(6) (**5a,b,c,d,e**)

Compound	δ^{13}C C(2)	C(3)	C(4)	C(5)	Me(3)	Me(5)	CH(2)	CH(4)	R(1)	R(6)	δ^{11}B(1/6)
5a[d]	103.9 (br)[b]	104.7	114.5	92.8 (br)[b]	10.8	10.5	27.6	27.0	−13.7 (br)[b]	−4.8 (br)[b]	−43.9/17.5
5b[e]	103.9 (br)[b]	104.7	115.8	92.8 (br)[b]	11.8	11.1	27.3	26.6	−13.7 (br)[b]	13.1 (br)[b]	−43.9/19.7
5c[f]	103.1 (br)[b]	106.0	115.4	92.3 (br)[b]	12.0	11.0	27.4	26.6	7.4 (br)[b]	13.3 (br)[b]	−43.3/20.1
5d[g]	104.3 (br)[b]	105.8	117.8	92.5 (br)[b]	12.3	10.8	27.5	26.6	[g]	13.4 (br)[b]	−44.9/20.8
5e[h]	104.3 (br)[b]	106.7	117.5	92.5 (br)[b]	11.3	10.6	27.8	27.1	[h]	[h]	−44.9/18.8

[a,b] See footnotes [a,b] to Table 1.

[c] Diastereotopic groups.

[d] δ^{13}C(^{i}Pr, methyl carbon atoms)[c] = 20.9; 21.0; 21.8; 24.7 (not assigned).
δ^1H(CD_2Cl_2) = −0.36 s (br), 3H, B(1)Me; 0.46 s (br), 3H, B(6)Me; 1.73 s, 3H, C(5)—Me; 1.96 s, 3H, C(3)—Me; 2.71 sp, 1H, C(2)—CH; 3.07 sp, 1H, C(4)—CH;
range for ^{i}Pr methyl protons[c] = 0.80–1.45.
δ^1H(C_6D_6) = −0.39 s (br), 3H, B(1)Me; 0.63 s (br), 3H, B(6)Me; 1.66 s, 3H, C(5)—Me; 1.71 s, 3H, C(3)—Me; 2.34 sp, 1H, C(2)—CH; 2.98 sp, 1H, C(4)—CH;
range for ^{i}Pr methyl protons[c] = 1.00–1.40.

[e] δ^{13}C(^{i}Pr, methyl carbon atoms)[c] = 24.2; 22.5; 21.7; 21.4; 21.1; 20.8 (not assigned);
δ^1H(CD_2Cl_2) = −0.28 s (br), 3H, B(1)Me; n.o. B(6)—CH; 1.82 s, 3H, C(5)—Me; 1.98 s, 3H, C(3)—Me; 2.65 sp, 1H, C(2)—CH; 3.06 sp, 1H, C(4)—CH;
range for ^{i}Pr methyl protons[c] = 0.80–1.45.
δ^1H(C_6D_6) = −0.33 s (br), 3H, B(1)Me; n.o. B(6)—CH; 1.68 s, 3H, C(5)—Me; 1.75 s, 3H, C(3)—Me; 2.52 sp, 1H, C(2)—CH; 2.75 sp, 1H, C(4)—CH;
δ^1H(^{i}Pr, methyl protons)[c] = 1.02 d; 1.05 d; 1.16 d; 1.19 d; 1.26 d; 1.34 d (not assigned).

[f] δ^{13}C(^{i}Pr, methyl carbon atoms)[c] = 21.2; 21.9; 21.9; 22.3; 22.6; 22.6; 23.1; 24.8 (not assigned).
δ^1H(CD_2Cl_2) = 0.85 (br), 2H, BCH; 1.86 s, 3H, C(3)—Me; 2.07 s, 3H, C(5)—Me; 2.63 sp, 1H, C(2)—CH; 3.08 sp, 1H, C(4)—CH; range for ^{i}Pr methyl protons[c] = 0.95–1.40.
δ^1H(C_6D_6) = 1.89 s, 3H, C(5)—Me; 1.92 s, 3H, C(3)—Me; 2.51 sp, 1H, C(2)—CH; 2.82 sp, 1H, C(4)—CH; n.o. B(1)—CH; n.o. B(6)—CH;
δ^1H(^{i}Pr, methyl protons)[c] = 0.99 d; 0.99 d; 1.07 d; 1.07 d; 1.19 d; 1.32 d; 1.37 d; 1.37 d (not assigned).

[g] δ^{13}C(^{i}Pr, methyl carbon atoms)[c] = 21.1; 21.8; 22.0; 22.3; 22.5; 24.6 (not assigned).
δ^{13}C(Ph): 126.2 (*p*); 127.9 (*m*); 134.6 (*o*);
δ^{13}C(i): not observed.
δ^1H(CD_2Cl_2) = 2.82 sp, 1H, C(2)—CH; 3.16 sp, 1H, C(4)—CH;
range for ^{i}Pr methyl protons[c] = 0.5–1.70;
range for C(3/5) methyl protons[c] = 1.85–2.30;
range for the phenyl protons = 7.15–7.60.

[h] δ^{13}C(^{i}Pr, methyl carbon atoms)[c] = 20.9; 21.0; 21.7; 25.1 (not assigned).
δ^{13}C(Ph): 134.5 (*o*); 134.1 (*o*); 127.5; 127.5; 127.7; 128.2 (not assigned); δ^{13}C(i) not observed;
range for ^{1}H NMR: see [g].

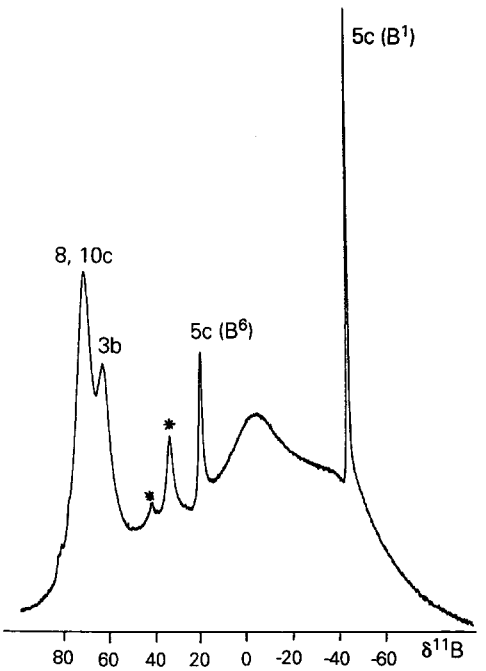

Fig. 2. 96.3 MHz $^{11}B\{^1H\}$ NMR spectrum (300 K, CD_2Cl_2): Reaction between **8** (slight excess) and $^iPrBBr_2$ after 24 h at room temperature. The ^{11}B resonances of **10c**, on top of ^{11}B NMR signal for excess **8**, of the DBCH derivative **3b**, and of the carborane **5c** can be assigned unambiguously. Two signals (marked *) were not assigned (see text).

1.5 cm^3 of CD_2Cl_2. All reactions were monitored by NMR spectroscopy. Depending on the borane, formation of the 1,4-stannabora-2,5-cyclohexadienes (**10b,c**) and DBCH was observed at −40°C (**3a**) or close to room temperature (**3b,c**). In the latter cases the resonances for the DBCH derivatives were always accompanied by resonances for the carboranes (**5**). Except for **3c**/**5de** (decomposition), fractional distillation gave mixtures of the carboranes together with the DBCH derivatives [**3a**/**5ab** (1 : 10) b.p. 50°C/3 × 10^{-4} torr; **3b**/**5c** (1 : 5) b.p. 85°C/3 × 10^{-4} torr]. Chromatography of the mixtures (10 cm SiO_2 column) with hexane gave the pure carborane, whereas the DBCH derivatives decomposed. The reactions between **7** and the organoboron dihalides were carried out by the same method.

300 MHz ^1H NMR in CD_2Cl_2 (300 K): δ^1H [$^nJ(^{119}Sn^1H)$] **10a** = 0.79 [57.2] s, 3H, SnMe; 0.98 d, 6H, B^{i}Pr; 1.22 d, 6H, ^{i}Pr; 1.25 d, 6H, ^{i}Pr; 1.60 sp, 1H, BCH; 2.20 [64.9] s, 6H, =C—Me; 2.93 sp, 2H, =C—CH; **10b** = 1.10 d, 6H, B^{i}Pr; 1.30 d, 12H, ^{i}Pr; 1.98 sp, 1H, BCH; 2.28 [92.0] s, 6H, =C—Me; 2.98 [3.8] sp, 2H, =C—CH; **10c** = 1.06 d, 6H, B^{i}Pr; 1.26 d, 12H, ^{i}Pr; 1.73 sp, 1H, BCH; 2.23 [92.8] s, 6H, =C—Me; 2.94 [4.7] sp, 2H, =C—CH; (see Table 2 for $\delta^{119}Sn$, $\delta^{13}C$ and $\delta^{11}B$ NMR data).

3a = 0.81 s (br), 3H, BMe; 1.00 d, 6H, B^{i}Pr; 1.21 d, 12H, ^{i}Pr; n.o. BCH; 1.89 s, 6H, =C—Me; 2.95 sp, 2H, =C—CH; **3b** = 1.00 d, 6H, B^{i}Pr; 1.10 d, 6H, B^{i}Pr; 1.21 d, 12H, ^{i}Pr, n.o. B(1)CH; n.o. B(6)CH; 1.94 s, 6H, =C—Me; 2.97 sp, 2H, =C—CH; **3c** = 1.16 d, 6H, B^{i}Pr; 1.29 d, 12H, ^{i}Pr; 1.89 s, 6H, =C—Me; 2.10 sp, 1H, BCH; 3.07 sp, 2H, ^{i}Pr; 7.30–7.60 m, 5H, BPh (see Table 3 for relevant ^1H, ^{11}B and ^{13}C NMR data of the carboranes **5**).

Me(^{i}Pr)B—Br in CD_2Cl_2 (300 K): 300 MHz ^1H NMR δ^1H = 1.07 d, 6H, B^{i}Pr; 1.16 s, 3H, BMe; 1.86 sp, 1H, BCH; 96.3 MHz ^{11}B NMR $\delta^{11}B$ = 79.8; 75.5 MHz ^{13}C NMR $\delta^{13}C$ = 16.4 (br), BMe; 18.6, B^{i}Pr; 33.5 (br), BCH.

Acknowledgements—The support of this work by the Deutsche Forschungsgemeinschaft and the Fonds der Chemischen Industrie is gratefully acknowledged. We thank Professor W. Siebert for a sample of ditert-butylethyne.

REFERENCES

1. P. H. M. Budzelaar, S. M. Van der Kerk, K. Krogh-Jespersen and P. v. R. Schleyer, *J. Am. Chem. Soc.* 1986, **108**, 3960.
2. G. E. Herberich, H. Ohst and H. Mayer, *Angew. Chem.* 1984, **96**, 975; *Angew. Chem. Int. Edn Engl.* 1984, **23**, 969.
3. P. Binger, *Tetrahedron Lett.* 1966, 2675.
4. H.-O. Berger, H. Nöth and B. Wrackmeyer, *Chem. Ber.* 1979, **112**, 2884.
5. L. Killian and B. Wrackmeyer, *J. Organomet. Chem.* 1977, **132**, 213.
6. B. Wrackmeyer, *Z. Naturf.* 1982, **37B**, 412.
7. R. Schlögl and B. Wrackmeyer, *Polyhedron* 1985, **4**, 885.
8. P. L. Timms, *Accts Chem. Res.* 1973, **6**, 118 (and refs cited therein).
9. G. E. Herberich and B. Hessner, *J. Organomet. Chem.* 1978, **161**, C36.
10. (a) S. M. Van der Kerk, A. C. M. Van Eekeren and G. J. M. Van der Kerk, *J. Organomet. Chem.* 1980, **190**, C8; (b) S. M. Van der Kerk, P. H. M. Budzelaar, A. C. M. Van Eekeren and G. J. M. Van der Kerk, *Polyhedron* 1984, **3**, 271.
11. S. M. Van der Kerk, P. H. M. Budzelaar, A. Van der Kerk-Van Hoof, unpublished results, cited in ref. 1.
12. S. M. Van der Kerk, P. H. M. Budzelaar, A. Van der Kerk-Van Hoof, G. J. M. Van der Kerk and P. v. R. Schleyer, *Angew. Chem.* 1983, **95**, 61; *Angew. Chem. Int. Edn Engl.* 1983, **22**, 48.
13. H. Podall, W. E. Foster and A. P. Giraitis, *J. Org. Chem.* 1958, **23**, 82.

14. (a) Cited as δ^{11}B 35.9 or 38.5, as a personal communication in C. Pues and A. Berndt, *Angew. Chem.* 1984, **96**, 306; *Angew. Chem. Int. Edn Engl.* 1984, **23**, 313; (b) R. Wehrmann, C. Pues, H. Klusik and A. Berndt, *Angew. Chem.* 1984, **96**, 372; *Angew. Chem. Int. Edn Engl.* 1984, **23**, 372.
15. B. Wrackmeyer, *An. Rep. NMR Spectrosc.* 1988, **20**, 61.
16. (a) B. Wrackmeyer, *Revs Silicon, Germanium, Tin, Lead Compds* 1982, **6**, 75; (b) B. Wrackmeyer, in *Boron Chemistry—Proceedings of the 6th International Meeting on Boron Chemistry–IMEBORON VI* (Edited by S. Hermanek), pp. 387–415. World Scientific, Singapore (1987).
17. L. Killian and B. Wrackmeyer, *J. Organomet. Chem.* 1978, **153**, 153.
18. E. Krause and P. Nobbe, *Chem. Ber.* 1931, **64**, 2112.
19. K. Niedenzu, *Organomet. Chem. Rev. A* 1966, **1**, 305.
20. W. E. Davidsohn and M. C. Henry, *Chem. Rev.* 1967, **67**, 73.

Polyhedron Vol. 10, No. 13, pp. 1507–1512, 1991
Printed in Great Britain

0277–5387/91 $3.00+.00
© 1991 Pergamon Press plc

THE SYNTHESIS AND CHARACTERIZATION OF PYRIMIDINE-2-THIONE COMPLEXES OF PALLADIUM(II)

DIMITRA KOVALA-DEMERTZI* and PARASKEVI KYRKOU

Laboratory of Inorganic Chemistry, Department of Chemistry, University of Ioannina, Ioannina 45110, Greece

and

INESSA ZAKHAROBA

N.S. Kurnakov Institute of General and Inorganic Chemistry, Academy of Sciences, Moscow, U.S.S.R.

(*Received* 25 *April* 1990; *accepted* 22 *February* 1991

Abstract—Complexes of palladium(II) with pyrimidine-2-thione and the thiolate anion were synthesized and characterized. The complexes were prepared in methanolic or aqueous media. The neutral ligand acts as monodentate and exhibits S-coordination in acidic medium or in methanolic solution. In neutral and basic media the thiolate anion of pyrimidine-2-thiol exhibits S,N-ligation through the ring nitrogen and exocyclic sulphur atoms, in the production of an asymmetric, four-membered, chelated ring.

Pyrimidine derivatives containing sulphur in their structure are known to act as potent inhibitors[1] and as antimetabolites.[2] Pyrimidine thiones were found to inhibit the synthesis of t-RNA under certain conditions and thus act as antitumour and antithyroid agents.[3–10] A similar inhibitory behaviour has been found for pyrimidine-2-thione and the compound also shows pronounced *in vitro* bacteriostatic activity.[10,11] The studies on metal complexes of heterocyclic thio derivatives is an area of great interest, as indicated by Raper in a recent review.[12] The thiopyrimidines such as pyrimidine-2-thione have the potential to bind to a single metal through sulphur,[13] nitrogen[14] or one nitrogen and the sulphur atom.[15] Such binding will leave a potential donor free, since it is not feasible for all three donors to bind to the same metal atom. As part of our systematic investigation on the coordination chemistry of pyrimidine derivatives[16–20] and on the study of complexes of platinum group metals,[16–23] we report the preparation and characterization of palladium(II) complexes with pyrimidine-2-thione, abbreviated as LH, and their structural studies by spectral (IR, ^{1}H NMR spectra), thermal and conductivity measurements.

EXPERIMENTAL

$PdCl_2$, K_2PdCl_4 and pyrimidine-2-thione were purchased from Fluka Chemical Company. All the solvents and chemicals used were of high purity. Elemental analysis of the samples was performed at the N.S. Kurnakov Institute, Academy of Sciences, Moscow (U.S.S.R.). The IR spectra were recorded on a Bruker IFS 113 v Fourier transform spectrophotometer using KCl (4000–500 cm^{-1}) and polyethylene (500–40 cm^{-1}) pellets. ^{1}H NMR spectra in d_6-DMSO were recorded at 90 MHz on a Varian EM-390 spectrometer with Me_4Si as internal standard. Thermogravimetric (TG) data have been obtained on a Du Pont R90 instrument equipped with a 951 thermogravimetric analyser. Analyses were carried out using published methods.[16,18,22]

* Author to whom correspondence should be addressed.

Synthesis

$[Pd(LH)X_2]_2$ *and* $[Pd(LH)_2X]_2X_2$ (*where* X = Cl, Br). The complexes were prepared by mixing methanolic solutions of the ligand LH and lithium tetrahalogenopalladate(II) prepared *in situ* from $PdCl_2$ and 2LiX (1.5:3 and 4:2 ligand-to-metal molar ratio). The reaction mixture was stirred for 24 h at room temperature and then left in the refrigerator for 1 day. The powders were filtered off, washed with cold methanol and ether and dried *in vacuo* over silica gel. They were redried at 90°C *in vacuo* over P_4O_{10}.

$PdL_2 \cdot 3H_2O$ *and* $[PdL(OH)]_2 \cdot 2H_2O$. A solution of the ligand LH in 0.2 N KOH was added dropwise, with stirring to a solution of the metal halide, $PdCl_2$, in 0.2 N HCl (4:2 and 1:1.7 ligand-to-metal molar ratio for the complexes $PdL_2 \cdot 3H_2O$ and $[PdL(OH)]_2 \cdot 2H_2O$, respectively). The reaction mixture was stirred for 24 h at room temperature. The powder was then filtered off and washed with cold water, acetone and ether and dried as before.

RESULTS AND DISCUSSION

The analytical data and molar conductivity values are given in Table 1. The complexes are microcrystalline or powders stable in atmospheric conditions. Complexes **1**, **2**, **5** and **6** are insoluble in all common solvents, but complexes **3** and **4** are insoluble in polar solvents and soluble in DMF and DMSO. Because of the insolubility of the prepared complexes in suitable solvents, we could not grow crystals for single crystal X-ray structural analysis. The conductivity values of complexes **3** and **4** are within or near the 110–170 Ω^{-1} cm^2 mol^{-1} range indicated for 1:2 electrolytes in DMF,[24] Table 1.

Complexes **1–4** were formed according to eqs (1)–(4), in methanolic solutions or in aqueous solutions in the pH range 1.0–3.5:

$$Li_2[PdX_4] + LH \xrightarrow{CH_3OH} Pd(LH)X_2 + 2LiX \quad (1)$$

$$Li_2[PdX_4] + 2LH \xrightarrow{CH_3OH} Pd(LH)_2X_2 + 2LiX \quad (2)$$

$$H_2[PdX_4] + LH \xrightarrow{H_2O} Pd(LH)X_2 + 2HX \quad (3)$$

$$H_2[PdX_4] + 2LH \xrightarrow{H_2O} Pd(LH)_2X_2 + 2HX. \quad (4)$$

Complexes **5** and **6** were obtained according to eqs (5) and (6), in basic media in the pH range 4–9:

$$H_2PdCl_4 + LH + 2H_2O \longrightarrow PdL(OH) \cdot H_2O + 4HX \quad (5)$$

$$H_2PdCl_4 + 2LH + 3H_2O \longrightarrow PdL_2 \cdot 3H_2O + 4HX. \quad (6)$$

Table 1. Analytical data, Λ_m values and effects of heat for complexes **5** and **6**

Compound	Colour	Found (%) Calc. (%) C	H	N	S	X	M	Λ_m (S cm^2 mol^{-1})	Removal of water: Temperature weight loss (°C)	% Found (calc.)
$[Pd(LH)Cl_2]_2$ (**1**)	Brown	16.3	2.0	9.0	10.3	23.8	36.7	ins.		
		(16.6)	(1.4)	(9.7)	(11.1)	(24.5)	(36.8)			
$[Pd(LH)Br_2]_2$ (**2**)	Brown	13.0	1.0	7.8	8.8	43.0	27.7	ins.		
		(12.7)	(1.1)	(7.4)	(8.5)	(42.2)	(28.1)			
$[Pd(LH)_2Cl]_2Cl_2$ (**3**)	Brick	24.6	1.9	14.0	15.8	16.8	26.5	98.0[a]		
		(23.9)	(2.0)	(13.9)	(16.0)	(17.6)	(26.5)			
$[Pd(LH)_2Br]_2Br_2$ (**4**)	Brick	19.5	1.7	10.7	12.0	31.2	22.1	132.6[a]		
		(19.6)	(1.6)	(11.4)	(13.0)	(32.6)	(21.7)			
$PdL_2 \cdot 3H_2O$ (**5**)	Brick	25.4	2.6	14.8	16.5		27.4	ins.	70–100	8.9 (9.4)
		(25.0)	(3.2)	(14.6)	(16.7)		(27.3)		100–140	4.5 (4.7)
$[PdL(OH)]_2 \cdot 2H_2O$ (**6**)	Dark brown	19.3	2.3	11.1	12.8		42.0	ins.	70–100	6.8 (7.1)
		(19.0)	(2.4)	(11.1)	(12.7)		(42.1)			

[a] Values of molar conductance for *ca* 10^{-3} M DMF solutions at 25°C. The water percentage was found by TG analysis.

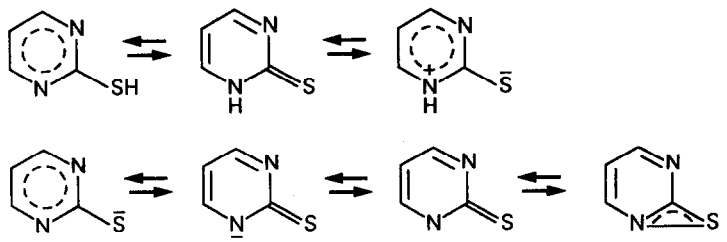

Fig. 1. Tautomeric forms of (a) neutral and (b) anionic forms of pyrimidine-2-thione.

Attempts to isolate complexes in highly acid conditions were unsuccessful.

Tautomeric forms of LH are presented in Fig. 1.

Tautomeric equilibria are modified in solution by changing pH. In highly acid media fully protonated species are likely and may appear to have all available coordination sites blocked. With a pK_a value[25] of 7 deprotonation in the presence of palladium(II) is apparent over a wide pH range, 4–9. Tautomeric equilibria of the thiol–thione type (Fig. 1) are of considerable interest in many areas of chemistry and biochemistry.[26–28]

The principal IR bands of interest are given in Table 2. As a general remark we must emphasize that some stretching modes are coupled, so that the proposed assignments must be regarded as approximate descriptions of the vibrations.[29–31] The assignment for LH is supported by recent normal coordinate treatment.[29] A very broad band at *ca* 2500 cm^{-1} is taken to represent the ν(NH---S) mode due to intermolecular hydrogen bonding. The presence of strong ν(C=S), π(C=S) and δ(C=S) vibrations in LH indicates that the hydrogen atom from the mercapto group migrates to N(1) or N(3) of the ring and the ligand may be better formulated as a pyrimidine-2(1H)-thione rather than as a thiolate,[32]

Table 2. IR spectral data (cm^{-1}) of LH and some representative complexes

Assignments	LH	1	3	5[a]	6[a,b]
$\nu(OH)_{crystal\ water}$				3200–3500vbr	3200–3500vbr
ν(NH)	3040m	3065m	3070m		
ν(CH)	3060w	3050sh	3050sh		
ν(NH---S)	2500vbr				
I Ring str.	1602vvs	1603ms	1601ms	1626ms	1620m
				1602w	1592m
II Ring str.	1560ms	1560vs	1565vvs	1552vvs	1550vvs
III Ring str.	1485ms	1485w	1485br	1480sh	1480sh
Ring str, δ(NH)	1468m	1434m	1422m	1425m	1430m
δ(CH), ν(CN), δ(NH)	1420ms	1385vvs	1381vvs	1372vvs	1368vvs
δ(CH), δ(NH). ν(CN)	1330vvs	1330m	1325s	1320sh	1320sh
δ(CH), δ(NH), ν(C=S)	1222sh	1250m	1250sh	1252m	
ν(C=S), δ(CH)	1207s	1200sh	1200sh		
δ(CH), ν(CN), ν(CC)	1181vs	1182vs	1178vs	1162vs	1165m
π(NH), π(CH)	1050s	1075w	1090mw	1088m	1082br
				1072w	
Ring breathing	1040sh	1045w	1050m	1045sh	1045w
π(NH), π(CH)	980vs	980w	991ms	991ms	992mw
π(CH)	792vs	805s	798br	820mw	790s
ν(C=S), Ring def.	750s	755sh	750sh	772s	775sh
π(CH)	735s	742s	742s	740s	746mw
Ring def.	622vw	650m	650w	650w	650m
π(C=S), Ring tors.	482s		475sh	482ms	470br
ν(C=S), Ring def.	468s	482br	465m	470w	
δ(C=S)	402w				

[a] ν(C—S) band appears at 628(s) cm^{-1}.

[b] $\nu(OH)_b$ band appears at 1260(s) cm^{-1} and $\delta(OH)_b$ at 942(s) cm^{-1}.

but a structure determination would be necessary to decide this. The ν(S—H) band does not appear either in the spectra of the pure ligand or in the spectra of the complexes, indicating that LH and the complexes exist in their thione form. In the free ligand the C=N and C=C bands are observed at 1602 and 1560 cm^{-1} and remain unchanged in the spectra of complexes **1–4** indicating that the cyclic N(1) or N(3) atom is not involved in coordination, while the strong bands at 1207 and 750 cm^{-1} [predominantly the ν(C=S) mode] decrease dramatically and shift to lower frequency upon coordination. All the evidence is consistent with the ligand LH behaving in a monodentate fashion through the sulphur atom of the thione group with no enthiolization process. Since the shifts in complexes **1–4** are in the same direction, the bonding pattern is deduced to be the same for these complexes. The significant change in the ligand bands in complexes **5** and **6** is the absence of the high frequency ν(NH) and δ(NH) bands [great δ(NH) character] at 3090, 1480 and 1320 cm^{-1}, respectively. A new, strong band at 628 cm^{-1} is taken to represent the ν(C—S) vibration. The C—S stretching frequency generally appears in the region 710–570 cm^{-1} [33] and in 4,6-dimethyl-2-mercaptopyrimidine the band at 630 cm^{-1} was attributed to the ν(C—S) vibration.[30] The presence of the bridging hydroxy groups in complex **6** is supported by the appearance of the $\nu(OH)_b$ mode at 1260 cm^{-1} and the bridging OH bending mode at 942 cm^{-1}.[34] In complexes **5** and **6** the band at 1600 cm^{-1} is split and is shifted to higher frequencies, indicating an increase in double bond character of the C=C and C=N links and coordination through the endocyclic nitrogen atom.[12,35]

The far-IR spectra of the complexes (Table 3) give insight into the structure and bonding in the solid state. The far-IR spectra of complexes **1** and **2** are indicative of the presence of both terminal and bridging Pd—$X_{(halogen)}$ bonds, suggesting a dimeric or polymeric structure. The *trans*-planar $M_2L_2X_4$-type compound (C_{2h}) exhibits three IR-active (Bu) ν(MX) modes, one $(MX)_t$ and two $(MX)_b$. For the latter two, the higher frequency band corresponds to $\nu(MX)_b$ *trans* to X, whereas the lower frequency band is assigned to $\nu(MX)_b$ *trans* to L, since it is sensitive to the nature of L.[34] From comparison with the free ligand spectra, a medium and broad absorption in the 320–340 cm^{-1} range could be tentatively attributed to ν(Pd—S)[12,36,37] in the case of the chloro complexes **1** and **3**; this band is masked by ν(Pd—Cl) which has already been assigned. The lower value of ν(Pd—S) obtained for the bromide compounds agrees with the HSAB theory.[18,38,39] The factors affecting the hardness of acids, are size, charge, oxidation state, electronic structure and the nature of attached groups, halogens in this case. The Pd—S bond is stronger when palladium(II) is bonded to chloride since it is more electronegative than bromide and the amount of positive charge on palladium(II) is greater.[18,38,39] The lower value of ν(Pd—S) for the bromide compounds also agrees with the *trans*-influence.[18,34] A slight increase in the position of the ν(M—S) band in complexes **5** and **6**, relative to the corresponding value for the neutral complexes **1–4**, suggests some strengthening of the metal–sulphur bond.[40] The spectra of complexes **5** and **6** differ from those of **1–4** due to the appearance of a band at *ca* 380–390 cm^{-1} attributable to the ν(Pd—N) vibrations.[12,18]

Table 3. Metal–ligand vibrations of the complexes

Compound	$\nu(Pd—X)_t$	$\nu(Pd—X)_b$	ν(Pd—S)	ν(Pd—N)
1	338vsbr	285sh 278m		
2	279ms	212s 202sh	323ms 312sh	
3		280mbr 245m	335mbr 320sh	
4		222ms 215m	322sh 315m	
5			332s 320sh	391s 380sh
6[a]			328m 317sh	379m 369w

[a] $\nu(Pd—O)_b$ appears at 276m (br) cm^{-1}.

The ^{1}H NMR spectrum of LH in d_6-DMSO contains a triplet at 6.87 ppm downfield from TMS assigned to the C(5)H proton, a peak at 8.30 ppm assigned to NH and a peak at 8.38 ppm assigned to the C(4)H and C(6)H protons. The absence of any evidence for the thiol-SH proton (δ 2–5 ppm) confirms the thione tautomer as the dominant species of LH in d_6-DMSO solution, as in the solid state. The ^{1}H NMR spectra of complexes **3** and **4** display peaks at 7.40 ppm assigned to the C(5)H protons, at 8.60 ppm assigned to the NH proton and at 8.75 ppm assigned to the C(4)H and C(6)H protons. The ^{1}H NMR spectra of the complexes **3** and **4** also confirm the participation of the sulphur atom in metal coordination. The spectra of complexes **1**, **2**, **5** and **6** could not be recorded because of their insolubility in d_6-DMSO and other common NMR solvents.

The thermal decomposition of complexes **5** and **6** was studied using TG and DTG techniques. From the data obtained, it can be seen that two

main processes occur—dehydration and pyrolytic decomposition. The thermal decomposition of complex **6** after dehydration is characterized by the complex degradation mechanism without the formation of a stable intermediate. Complex **5** releases water in two steps, as revealed by the appearance of two DTG maxima and an inflection in the TG curve. The presence of a TG plateau after water loss indicates that a stable, anhydrous intermediate is formed. The anhydrous PdL_2 complexes undergo decomposition in two distinct steps, between 250 and 340°C and 350 and 405°C, which corresponds exactly to the release of one L molecule per metal ion. From TG data the following thermal decomposition mechanism has been proposed:

$$PdL_2 \cdot 3H_2O \xrightarrow[endo]{70^\circ C} PdL_2 \cdot H_2O \xrightarrow[endo]{141^\circ C}$$

$$PdL_2 \xrightarrow[exo]{312^\circ C} PdL \xrightarrow[exo]{368^\circ C} PdO.$$

Conclusions

The effect of pH on the coordination properties of the ligand in the presence of the palladium(II) ion has been studied. In methanolic or aqueous acid media (pH = 1–4), complexes of the type $[Pd(LH)X_2]_2$ and $[Pd(LH)_2X]_2X_2$ (where X = Cl, Br) are formed. A sulphur-donating ligand, in the thione form, is proposed. Sulphur donation is also reported for the same ligand in $Pt(LH)_4Cl_2$ and $[Pt(LH)_4] \cdot [PtCl_6]$.[13] In neutral or basic aqueous media $PdL_2 \cdot 3H_2O$ and $[PdL(OH)]_2 \cdot 2H_2O$ complexes are formed. The monoanionic ligand L, in the thiolate form, exhibits bidentate sulphur and nitrogen coordinating behaviour. The involvement of the nitrogen and sulphur atoms in the coordination of L suggests either a bridging or chelated role for the thiolate anion. Some authors described the anion of heterocyclic thiones as S,N-bridging,[40,41] however S,N-chelation has also been proposed for *cis* square palladium and platinum complexes, ML_2 (where L = benzo-1,3-thiazoline-2-thione),[42] and for $[WL_4]$[15] and $[FeL_3]$[32] (where L = the thiolate anion of pyrimidine-2-thiol).

The most plausible structures for the new, isolated complexes based on the above results are dimeric for $[Pd(LH)X_2]_2$ with terminal and bridging halogen atoms and dimeric for $[Pd(LH)_2X]_2X_2$ with bridging halogen atoms. The $[PdL(OH)]_2 \cdot 2H_2O$ complex is described as dimeric with bridging hydroxy groups and chelated S,N-coordinated ligand, while the $PdL_2 \cdot 3H_2O$ complex is described as polymeric with S,N-bridging or monomeric with S,N-chelated thiolate anion (Fig. 2).

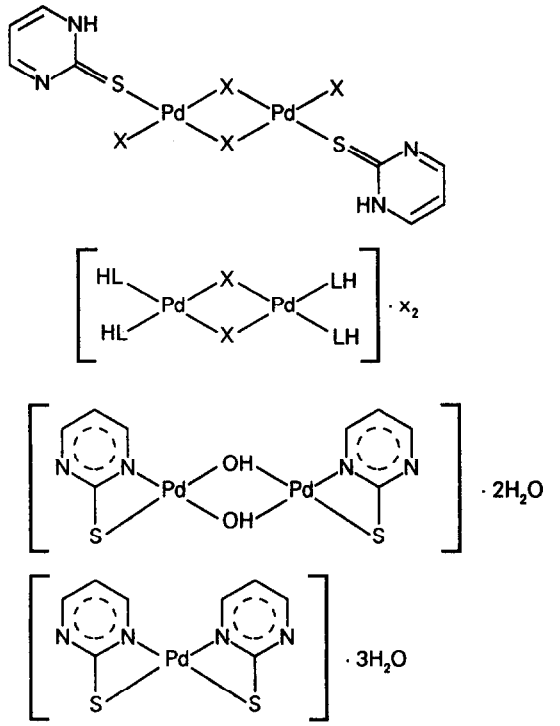

Fig. 2. The proposed geometry for the $[Pd(LH)X_2]_2$, $[Pd(LH)_2X]_2X_2$, $[PdL(OH)]_2 \cdot 2H_2O$ and $PdL_2 \cdot 3H_2O$ complexes

REFERENCES

1. P. K. Robins, *J. Med. Chem.* 1964, **7**, 186.
2. R. Hamers and C. Hamers-Casterman, *J. Med. Biol.* 1972, **3**, 166.
3. J. Abbot, D. M. L. Goodgame and I. Jeeves, *J. Chem. Soc., Dalton Trans.* 1978, 880.
4. J. A. Carbon, L. Hung and D. S. Jones, *Proc. Nat. Acad. Sci. U.S.A.* 1965, **53**, 979.
5. M. L. Lipsett, *Biochem., Biophys. Res. Commun.* 1965, **20**, 224.
6. J. A. Carbon, H. David and M. H. Studier, *Science* 1968, **161**, 1146.
7. J. F. Holland, R. Cuthrie, P. Sheeke and H. Tieckelmann, *Cancer Res.* 1958, **18**, 776.
8. C. B. Lozzio, *Exp. Cell. Res.* 1971, **69**, 377; *J. Cell. Physiol.* 1971, **78**, 25.
9. M. Y. W. Yu, J. Sedlak and R. H. Lindsay, *Arch. Biochem. Biophys.* 1973, **155**, 111.
10. I. Votruba, A. Holly and K. Jost, *FEBS Lett.* 1972, **22**, 287.
11. A. Holly, I. Votruba and K. Jost, *Col. Czech. Chem. Commun.* 1974, **39**, 634.
12. E. S. Raper, *Coord. Chem. Rev.* 1985, **61**, 115.
13. J. M. Bret, P. Castan and J. P. Laurent, *Inorg. Chim. Acta* 1981, **51**, 103.
14. A. C. Skapski and K. A. Woode, *Acta Cryst.* 1979, **356**, 59.
15. F. A. Cotton and W. M. Ilsley, *Inorg. Chem.* 1981, **20**, 614.

16. D. Kovala-Demertzi, J. M. Tsangaris and N. Hadjiliadis, *J. Less. Comm. Met.* 1986, **115**, 1.
17. D. Kovala-Demertzi and J. M. Tsangaris, *Inorg. Chim. Acta* 1986, 125, **3**, L31.
18. D. Kovala-Demertzi, J. M. Tsangaris, H. O. Desseyn and B. J. Van der Veken, *Bull. Soc. Chem. Belg.* 1987, **96**, 7.
19. D. Kovala-Demertzi, J. M. Tsangaris and H. O. Desseyn, *Bull. Soc. Chim. Belg.* 1987, **96**, 335.
20. D. Kovala-Demertzi, *Transition Met. Chem.* 1990, **15**, 23.
21. D. Kovala-Demertzi and D. Nicholls, *J. Coord. Chem. Soc. A* 1988, **17**, 297.
22. D. Kovala-Demertzi, J. M. Tsangaris and N. Hadjiliadis, *Transition Met. Chem.* 1984, **9**, 77.
23. D. Kovala-Demertzi, S. P. Perlepes and G. Lazaras, *Bull. Soc. Chim. Belg.* 1989, **98**, 503.
24. W. J. Geary, *Coord. Chem. Rev.* 1971, **7**, 81.
25. B. Taqui Khan and S. M. Zakeeruddin, *Inorg. Chim. Acta* 1986, **124**, 5.
26. I. C. Paul, *Chemistry of the Thiol Group, Part I* (Edited by S. Pata). John Wiley, New York (1974).
27. M. J. Scanlan, I. H. Hillier and A. A. MacDowell, *J. Am. Chem. Soc.* 1983, **105**, 3568.
28. P. Gund and E. Fluder, *J. Am. Chem. Soc.* 1982, **104**, 5347.
29. D. N. Sathyanarayana and S. V. Kasmir Raya, *Spectrochim. Acta* 1985, **41A**, 809.
30. S. P. Gupta, S. Sharma and R. K. Goel, *Spectrochim. Acta* 1986, **42A**, 1171.
31. S. Aruna and G. Shanmugan, *Spectrochim. Acta* 1985, **41A**, 531,
32. J. A. Latham, G. J. Leigh, J. Pickett, G. Huttner, I. Jibrill and J. Zubieta, *J. Chem. Soc., Dalton Trans.* 1986, 1181.
33. L. J. Bellamy, *Infrared Spectra of Complex Molecules.* Chapman and Hall, London (1975).
34. K. Nakamoto, *Infrared and Raman Spectra of Inorganic and Coordination Compounds.* John Wiley, New York (1986).
35. A. Grigoratos and N. Katsaros, *Inorg. Chim. Acta* 1985, **108**, 41.
36. E. S. Raper and P. H. Crackett, *Inorg. Chim. Acta* 1981, **50**, 159.
37. P. Castan and J. P. Laurent, *Transition Met. Chem.* 1980, **5**, 154.
38. H. Hofmans, H. O. Desseyn and M. A. Herman, *Spectrochim. Acta* 1982, **38A**, 1307.
39. H. Hofmans, H. O. Desseyn, R. Dommisse and M. A. Herman, *Bull. Soc. Chim. Berg.* 1982, **91**, 175.
40. P. O. Knishko, M. I. Michaelenko and K. V. Tsepkasovich, *Zh. Neorg. Khim.* 1969, **91**, 175.
41. W. O. Foye and J. R. Lo, *J. Pharm. Sci.* 1972, **61**, 1209.
42. S. Banerji, R. E. Byrne and S. E. Livingstone, *Transition Met. Chem.* 1982, **7**, 5.

Polyhedron Vol. 10, No. 13, pp. 1513–1519, 1991
Printed in Great Britain

0277–5387/91 $3.00+.00
© 1991 Pergamon Press plc

ORGANODIPALLADIUM(II) CYCLOMETALLATES OF THE SCHIFF BASE N,N′-DIETHYL-2,6-DIALDIMINOBENZENE

SUKLA CHAKLADAR, PARIMAL PAUL and KAMALAKSHA NAG*

Department of Inorganic Chemistry, Indian Association for the Cultivation of Science, Calcutta 700 032, India

(*Received* 18 *September* 1990; *accepted* 22 *February* 1991)

Abstract—Syntheses and reactions of dipalladiobenzene derivatives have been reported. $Li_2[PdCl_4]$ reacts with N,N′-diethyl-2,6-dialdiminobenzene (H_2L) to form the cyclometallated compound, $[Pd_4L_2Cl_4]$, in which metallation occurs at the 3,5-carbon atoms of the aromatic ring. The tetrachloro compound can be converted to a dinuclear precursor complex, $[Pd_2L(MeCN)_2(ClO_4)_2]$, which reacts with pyridine, 4-methylpyridine, pyrazole and imidazole (B) to produce complexes of the type $[Pd_2L(B)_4](ClO_4)_2$, and with 2,2′-bipyridine to produce $[Pd_2L(bpy)_2](ClO_4)_2$. A tetranuclear neutral complex $[Pd_4L_2(pz)_4]$ is formed when the precursor complex interacts with pyrazole and triethylamine. A series of neutral chelate compounds $[Pd_2L(AB)_2]$ has been obtained by reacting the precursor with sodium salts of acetylacetone, ethylacetoacetate, N-methylsalicylaldimine (HAB) and N,N′-dimethyldithiocarbamic acid (HAB). The compounds have been characterized from their ^1H NMR spectra.

Palladium(II), which is classified as a typical electrophile[1–3] for the activation of C—H bonds in hetero-substituted organic molecules, undergoes cyclometallation reactions with remarkable ease and the chemistry of cyclopalladated compounds, especially those derived from N-donor ligands, is very rich.[4–12] In particular, *ortho*-palladated compounds have been extensively studied because of their potential utility in organic synthesis.[13,14] Although the literature abounds with *ortho*-palladated compounds containing one Pd—C linkage per aromatic ring, to our knowledge, there exists only a single report[15] dealing with the formation of *ortho*-metallated dipalladiobenzene derivatives. These compounds have been obtained from N,N,N′,N′-tetraalkyl-*p*-xylene-α,α-diamines and N,N,N′,N′-tetraalkyl-*m*-xylene-α,α-diamines. As part of our interest in exploring the chemistry of 3,5-dipalladiocyclometallates we have recently reported[16] the formation of tetranuclear complexes $[Pd_4L_2(OAc)_4]$ with N,N′-dialkyl-2,6-dialdiminobenzenes (H_2L). These μ-acetato complexes undergo interesting reactions with a variety of nucleophiles. The present study is concerned with the reactions of the dinuclear complex $[Pd_2L(MeCN)_2(ClO_4)_2]$.

* Author to whom correspondence should be addressed.

EXPERIMENTAL

Physical measurements

IR spectra were recorded on a Perkin–Elmer model 783 IR spectrophotometer with KBr pellets or Nujol mulls. ^1H NMR spectra [δ (ppm)] were recorded at 270 MHz on a Bruker WH 270 spectrometer in $CDCl_3$ or Me_2SO-d_6 with Me_4Si as an internal standard. A Philips PR 9500 bridge was used for conductivity measurements. Carbon, hydrogen and nitrogen analyses were performed on a Perkin–Elmer model 240C elemental analyser. Palladium was estimated gravimetrically as the dimethylglyoximate.

Materials

$PdCl_2 \cdot xH_2O$ was obtained from Johnson Matthey, and 1,3-diformylbenzene was prepared by

some minor modifications of the method described in the literature.[17]

The Schiff base N,N′-diethyl-2,6-dialdiminobenzene (H_2L) was prepared by refluxing a benzene solution (50 cm^3) of 2,6-diformylbenzene (2.7 g, 20 mmol) and ethylamine [3.2 cm^3 70% (w/w) aqueous solution, 40 mmol] in a Dean–Stark apparatus for 4 h. The solvent was removed on a rotary evaporator and the oily residue was evacuated to 0.1 torr. The ligand thus obtained was substantially pure and used directly for cyclometallation reactions.

Silver perchlorate was prepared by digesting "silver carbonate" (BDH) with dilute $HClO_4$ to leave some of the carbonate undissolved. The filtrate was evaporated to dryness on a steam bath. The solidified mass after drying over P_4O_{10} *in vacuo* was recrystallized from boiling benzene.

CAUTION! Silver perchlorate and other perchlorate salts described below are potentially explosive. Although $AgClO_4$ was recrystallized in gram quantities without any difficulty, **extreme caution should be exercised in handling this material.**

Preparation of the complexes

$[Pd_4L_2Cl_4]$ (**1**). $Li_2[PdCl_4]$ (2.62 g, 10 mmol) and H_2L (0.94 g, 5 mmol) were stirred in MeOH (100 cm^3) for 5 h. The product deposited was collected by filtration and washed with MeOH and Et_2O; yield 60%.

$[Pd_2L(MeCN)_2(ClO_4)_2]$ (**2**). A stirred suspension of **1** (0.94 g, 1 mmol) in MeCN (30 cm^3) was treated with small portions of $AgClO_4$ (0.83 g, 4 mmol). After 1 h, AgCl was removed by filtration and the filtrate was concentrated to a small volume on a rotary evaporator. The product deposited on cooling at −5°C was collected by filtration and washed with Et_2O; yield quantitative.

$[Pd_4L_2X_4]$ [Z = Br (**3**), N_3 (**4**)]. To a MeCN solution (50 cm^3) of **2** (0.68 g, 1 mmol) was added dropwise, with stirring, an aqueous solution (10 cm^3) of LiBr (0.2 g, 2.4 mmol) or NaN_3 (0.16 g, 2.4 mmol). The product precipitated immediately and after additional stirring for 0.5 h was collected and washed successively with H_2O, MeOH and Me_2CO; yield quantitative.

$[Pd_2L(py)_4](ClO_4)_2$ (**5**). A Me_2CO solution (50 cm^3) of **2** (0.68 g, 1 mmol) was slowly treated with pyridine (0.5 cm^3). The white, crystalline product that deposited on standing was collected by filtration and recrystallized from MeOH; yield 80%.

$[Pd_2L(4\text{-}Mepy)_4](ClO_4)_2 \cdot 0.5CHCl_3$ (**6**). This compound was prepared by the same method as **5** and recrystallized from MeOH–$CHCl_3$; yield 80%.

$[Pd_2L(Hpz)_4](ClO_4)_2$ (**7**). A Me_2CO solution (30 cm^3) of **2** (0.68 g, 1 mmol) and pyrazole (0.27 g, 4 mmol) was stirred for 1 h. The solution was then evaporated to a small volume and stirred with Et_2O to precipitate the product. The compound was recrystallized from MeOH–Et_2O; yield 80%.

$[Pd_2L(Him)_4](ClO_4)_2$ (**8**). The method of preparation of this compound is the same as for **7**.

$[Pd_4L_2(pz)_4]$ (**9**). A solution (30 cm^3) of **2** (0.68 g, 1 mmol) in MeCN was treated dropwise, with stirring, with a solution (10 cm^3) of pyrazole (0.126 g, 2 mmol) and Et_3N (0.2 g, 2 mmol) in MeCN. The product deposited was collected by filtration and washed with MeOH and Me_2CO; yield 80%.

$[Pd_2L(bpy)_2](ClO_4)_2$ (**10**). A MeCN solution (30 cm^3) of **2** (0.68 g, 1 mmol) and an MeOH solution (20 cm^3) of 2,2′-bipyridine (0.31 g, 2 mmol) were mixed together and stirred for 2 h. During this period the colourless solution became intense yellow. The solution was evaporated on a rotary evaporator and the residue triturated with Et_2O. The product was recrystallized from MeOH–Et_2O; yield 90%.

$[Pd_2L(acac)_2]$ (**11**). To a stirred suspension of **2** (0.68 g, 1 mmol) in $CHCl_3$ (40 cm^3) was added an MeOH solution (10 cm^3) of acetylacetone (0.2 g, 2 mmol) and metallic sodium (0.046 g, 2 mmol). The filtrate, on concentration, afforded a yellow, crystalline product which was recrystallized from MeOH–$CHCl_3$; yield 80%.

$[Pd_2L(etacac)_2]$ (**12**). To a stirred suspension of **2** (0.68 g, 1 mmol) in $CHCl_3$ (40 cm^3) was added an EtOH solution (10 cm^3) of ethylacetoacetate (0.26 g, 2 mmol) and KOH (0.11 g, 2 mmol). After 2 h, the solution was filtered and the filtrate was concentrated to *ca* 25 cm^3. The product which deposited on standing was collected by filtration and recrystallized from CH_2Cl_2; yield 80%.

$[Pd_2L(msalmine)_2]$ (**13**). An MeOH solution (10 cm^3) of N-methylsalicylaldimine, obtained by refluxing salicylaldehyde (0.24 g, 2 mmol) and methylamine [0.3 cm^3 40% (w/w) aqueous solution] for 0.5 h, was cooled to room temperature and then added to a stirred suspension of **2** (0.68 g, 1 mmol) in $CHCl_3$ (30 cm^3). After 1 h the filtrate was concentrated to crystallize out the product, which was recrystallized from MeOH–$CHCl_3$; yield 80%.

$[Pd_2L(Me_2dtc)_2]$ (**14**). A freshly prepared MeOH solution (10 cm^3) of sodium dimethyldithiocarbamate[18] (2 mmol) was added in small portions to a solution of **2** (0.68 g, 1 mmol) in Me_2CO (20 cm^3). After 1 h the product was collected by filtration and recrystallized from MeOH–$CHCl_3$; yield 90%.

Analytical data and ^1H NMR spectroscopic data for the complexes are given in Tables 1 and 2, respectively.

Table 1. Analytical data[a] for the complexes

Complex	Colour	Analysis (%) C	H	N	Pd
$[Pd_4L_2Cl_4]$ (1)	Light yellow	31.0(30.6)	3.2(3.0)	5.8(6.0)	45.6(45.3)
$[Pd_2L(MeCN)_2(ClO_4)_2]$ (2)	White	28.5(28.2)	3.0(2.9)	8.0(8.2)	31.0(31.3)
$[Pd_4L_2Br_4]$ (3)	Light yellow	25.3(25.8)	2.7(2.5)	5.1(5.0)	37.8(38.1)
$[Pd_4L_2(N_3)_4]$ (4)	Light yellow	29.5(29.8)	2.9(2.9)	22.8(23.2)	44.5(44.1)
$[Pd_2L(py)_4](ClO_4)_2$ (5)	White	42.2(42.0)	3.6(3.7)	9.0(9.2)	23.6(23.3)
$[Pd_2L(4\text{-}Mepy)_4](ClO_4)_2 \cdot 0.5CHCl_3$ (6)	White	42.9(42.5)	4.0(4.1)	7.9(8.2)	20.5(20.7)
$[Pd_2L(Hpz)_4](ClO_4)_2$ (7)	White	32.7(33.1)	3.6(3.4)	15.8(16.1)	24.8(24.5)
$[Pd_2L(Him)_4](ClO_4)_2$ (8)	White	32.8(33.1)	3.5(3.4)	16.3(16.1)	24.2(24.5)
$[Pd_4L_2(pz)_4]$ (9)	Yellow	41.0(40.5)	3.8(3.7)	15.6(15.8)	40.2(39.9)
$[Pd_2L(bpy)_2](ClO_4)_2$ (10)	Bright yellow	42.0(42.2)	3.5(3.3)	8.9(9.2)	23.2(23.4)
$[Pd_2L(acac)_2]$ (11)	Yellow	44.5(44.2)	4.8(4.7)	4.8(4.7)	36.1(35.7)
$[Pd_2L(etacac)_2]$ (12)	Yellow	44.2(43.8)	4.8(4.9)	4.5(4.3)	32.6(32.4)
$[Pd_2L(msalmine)_2]$ (13)	Greenish-yellow	50.0(50.4)	4.4(4.5)	8.5(8.4)	32.2(31.9)
$[Pd_2L(Me_2dtc)_2]$ (14)	Yellow	34.2(33.8)	4.2(4.1)	9.0(8.8)	33.0(33.3)

[a] Calculated values are given in parentheses.

Table 2. ^1H NMR spectral data[a] for some complexes

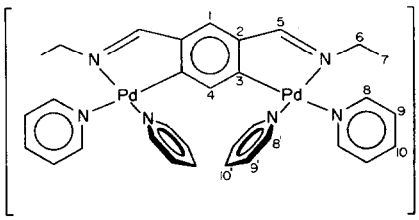

δ^b: 1.08 (t, 6H, 7-CH_3), 3.30 (q, 4H, 6-CH_2), 4.94 (s, 1H, 4-CH), 7.42 (m^d, 4H, 9-CH), 7.50 (s, 1H, 1-CH), 7.53 (m^d, 4H, 9′-CH), 7.96 [t, 4H, (10,10′)-CH], 8.38 (s, 2H, 5-CH), 8.76 (d^d, 4H, 8-CH), 8.88 (d^d, 4H, 8′-CH)

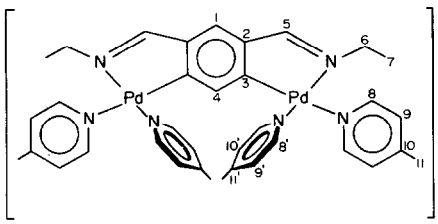

δ^b: 1.04 (t, 6H, 7-CH_3), 2.36 [s, 12H, (11,11′)-CH_3], 3.34 (m, 4H, 6-CH_2), 5.28 (s, 1H, 4-CH), 7.32 [m^d, 8H, (9,9′)-CH], 7.52 (s, 1H, 1-CH), 8.40 (s, 2H, 5-CH), 8.64 [m^d, 8H, (8,8′)-CH]

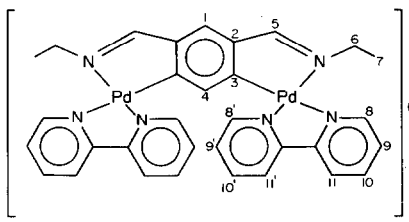

δ^b: 1.44 (t, 6H, 7-CH_3), 4.0 (q, 4H, 6-CH_2), 7.0 (s, 1H, 1-CH), 7.60 (s, 1H, 4-CH), 7.80 [m, 4H, (9,9′)-CH], 8.40 [m, 4H, (11,11′)-CH], 8.62 [m^d, 4H, (10,10′)-CH], 8.74 (s, 2H, 5-CH), 8.88 (d^d, 2H, 8-CH), 8.96 (d^d, 2H, 8′-CH)

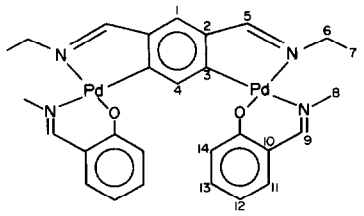

δ^c: 1.43 (t, 6H, 7-CH_3), 3.76 (q, 4H, 6-CH_2), 3.92 (s, 6H, 8-CH_3), 6.52 (t, 2H, 12-CH), 6.89 (d, 2H, 13-CH), 7.10 (s, 1H, 1-CH), 7.16 (d, 2H, 11-CH), 7.25 (d, 2H, 14-CH), 7.63 (s, 1H, 4-CH), 7.83 (s, 2H, 5-CH), 7.88 (s, 2H, 9-CH)

[a] Frequency 270 MHz.
[b] In Me_2SO-d_6.
[c] In $CDCl_3$.
[d] Poorly resolved.

RESULTS AND DISCUSSION

The reaction between N,N′-diethyl-2,6-dialdiminobenzene (H_2L) and $Li_2[PdCl_4]$ in MeOH affords $[Pd_4L_2Cl_4]$ (**1**) in good yield. In this compound metallation occurs simultaneously at the 3- and 5-carbon atoms of the aromatic ring. We have already shown[16] that complex **1** and its analogues can be obtained by the metathetical reaction between the tetra-μ-acetato cyclopalladates, $[Pd_4L_2(OAc)_4]$, and LiCl. The tetranuclear composition of these compounds has been established by determining molecular weights of soluble derivatives.

Although the ability of Schiff bases to form *ortho*-palladated compounds was recognized quite early[18–20] and recent studies[21–25] have covered their important structural aspects, the potential of 2,6-dialdiminobenzenes to form 3,5-dipalladiometallocycles has not been previously investigated. Since *ortho*-palladated compounds derived from Schiff bases have found important applications in organic synthesis,[13,14] we considered that a 3,5-dipalladiometallocyclic derivative of H_2L might widen the scope of synthesis. However, to be useful for reactions such as vinylation or carbonylation, the precursor cyclopalladate should be soluble in organic solvents and contain labile donors. For this purpose **1**, which is practically insoluble in common organic solvents, can be readily converted to a colourless, soluble complex of composition $[Pd_2L(MeCN)_2(ClO_4)_2]$ (**2**) by treating it with four equivalents of $AgClO_4$ in MeCN. The IR spectrum of **2** shows characteristic $\nu(C{\equiv}N)$ due to MeCN at 2250 cm^{-1}. The ν_3 band due to ClO_4^-, which is split into three components with peaks at 1150, 1105 and 1065 cm^{-1}, suggests perchlorate coordination[26] in the solid state. The molar conductivity of **2** in MeCN (250 Ω^{-1} cm^2 mol^{-1}) is in the Λ_M range consistent with a 2:1 electrolyte.[27]

Complex **2** reverts to **1** on treatment with chloride ion. Complexes $[Pd_4L_2Br_4]$ (**3**) and $[Pd_4L_2(N_3)_4]$ (**4**) can be obtained by the same manner. The presence of the 1,3-azido bridge in **4** is indicated by the observation of $\nu_{as}[N_3^-]$ at a higher frequency (2080 cm^{-1}) relative to that of the terminal azide (2050 cm^{-1}).[28,29]

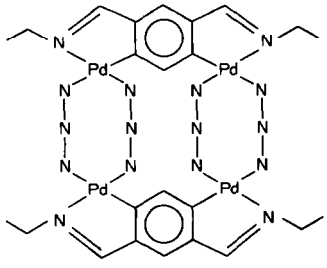

(I)

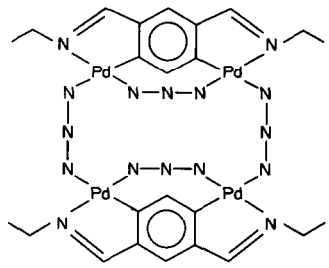

(II)

Complex **4** can be structurally represented either by **I** or **II**, but **I** seems to be more appropriate.

A number of dinuclear cyclopalladates have been derived from **2**. For example, pyridine and 4-methylpyridine afford $[Pd_2L(py)_4](ClO_4)_2$ (**5**) and $[Pd_2L(4\text{-}Mepy)_4](ClO_4)_2$ (**6**), respectively. The ^1H NMR spectrum of **5** (Fig. 1) shows an interesting feature in that the singlet due to 4-CH of the cyclometallated phenyl ring is strongly shielded (δ 4.94) with respect to 1-CH (δ 7.50). Construction of molecular models for **5** revealed that the two pyridine rings which are *trans* with respect to the Pd—N bonds do not lie in the same plane of the cyclometallated aromatic ring. In the sterically favoured configuration the 4-CH proton is exposed to the strong, diamagnetic, anisotropic shielding effect of the adjacent pyridine rings. Inasmuch as the two pyridine rings bound to each palladium are in chemically distinct environments, corresponding hydrogen atoms on each would be expected to resonate at different fields. Indeed Fig. 1 shows that the unresolved multiplets due to 9-CH and 9′-CH appear at δ 7.42 and 7.53, respectively, and also the chemical shifts due to 8-CH (8.76) and 8′-CH (8.88) are different. However, the chemical shifts due to 10-CH and 10′-CH, both being farthest from the metal centre, are least affected by the orientation of the rings and are observed as a triplet at δ 7.96. Complex **6** also shows similar ^1H NMR spectral features (Table 2). In this case the δ values for 4-CH and 1-CH are 5.28 and 7.52, respectively. The relatively stronger shielding of 4-CH in **5** compared with that in **6** can be rationalized in the following way. In **6**, to avoid steric interaction of the methyl substituents the pyridine rings are more tilted which leads to diminution of shielding of 4-CH.

Pyrazole and imidazole also form similar colourless complexes, $[Pd_2L(Hpz)_4](ClO_4)_2$ (**7**) and $[Pd_2L(Him)_4](ClO_4)_2$ (**8**). On the other hand, when **2** is treated with two equivalents of pyrazole and triethylamine, a light yellow complex (**9**) of composition $[Pd_2L(pz)_2]$ is obtained. Complex **9** is not soluble enough for molecular weight determination, nevertheless, the above composition is unlikely in view of the normal stereochemical preferences of

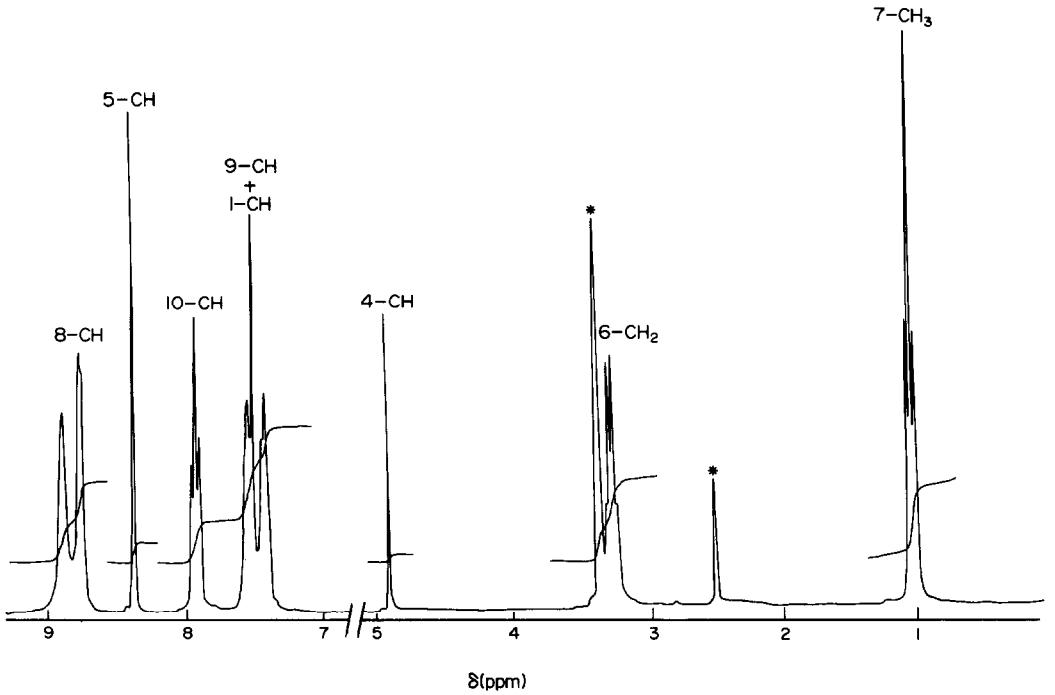

Fig. 1. ^{1}H NMR spectrum of **5** in Me_2SO-d_6. The signal due to the solvent is marked by *.

palladium(II). It is more likely that **9** has the tetranuclear composition $[Pd_4L_2(pz)_4]$ with the structural arrangement shown in **III**.

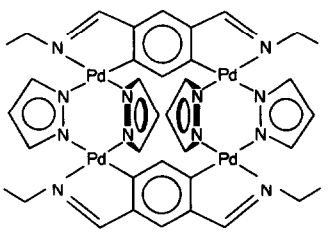

(III)

With 2,2′-bipyridine complex **2** produces $[Pd_2L(bpy)_2](ClO_4)_2$ (**10**). The ^{1}H NMR spectral features of **10** (Table 2) show some interesting changes with respect to those of **5** and **6**. Firstly, the aliphatic protons of **10** are shifted to lower field compared with those of **5** and **6**. Secondly, unlike **5** or **6**, in **10** 4-CH is more deshielded than 1-CH. These changes are plausibly due to more extensive π-electron delocalization in the 2,2′-bipyridine case.

Complex **2** reacts with monoprotic, bidentate ligands (HAB) to form neutral chelate complexes $[Pd_2L(AB)_2]$. $[Pd_2L(acac)_2]$ (**11**) and $[Pd_2L(etacac)_2]$ (**12**), prepared in this way, are identical to those previously obtained by us[16] from the tetranuclear precursor. The ^{1}H NMR spectrum of $[Pd_2L(msalmine)_2]$ (**13**), shown in Fig. 2, is consistent with the structure in which the phenolic oxygen of N-methylsalicylaldimine is *trans* to the Pd—N bond. Similar to **10**, in this case also the aliphatic protons are relatively more deshielded and 4-CH is more deshielded (δ 7.63) compared with 1-CH (δ 7.10). Again this is due to strong electron delocalization in the msalmine chelate ring. A similar observation was also made[16] for **11** and **12**.

Table 3, which summarizes the δ values due to azomethine protons in three ionic and three neutral complexes, discloses an interesting feature. Compared with the ionic complexes for which the chemical shift due to CH=N varies between δ 8.42 and 8.62, in the neutral chelates the chemical shifts remain almost invariant (δ *ca* 7.83) and are appreciably more shielded. The greater shielding of

Table 3. Chemical shifts (δ) due to CH=N

5	8.46
6	8.40
10	8.62
11	7.84[a]
12	7.82[a]
13	7.83

[a] Data taken from ref. 16.

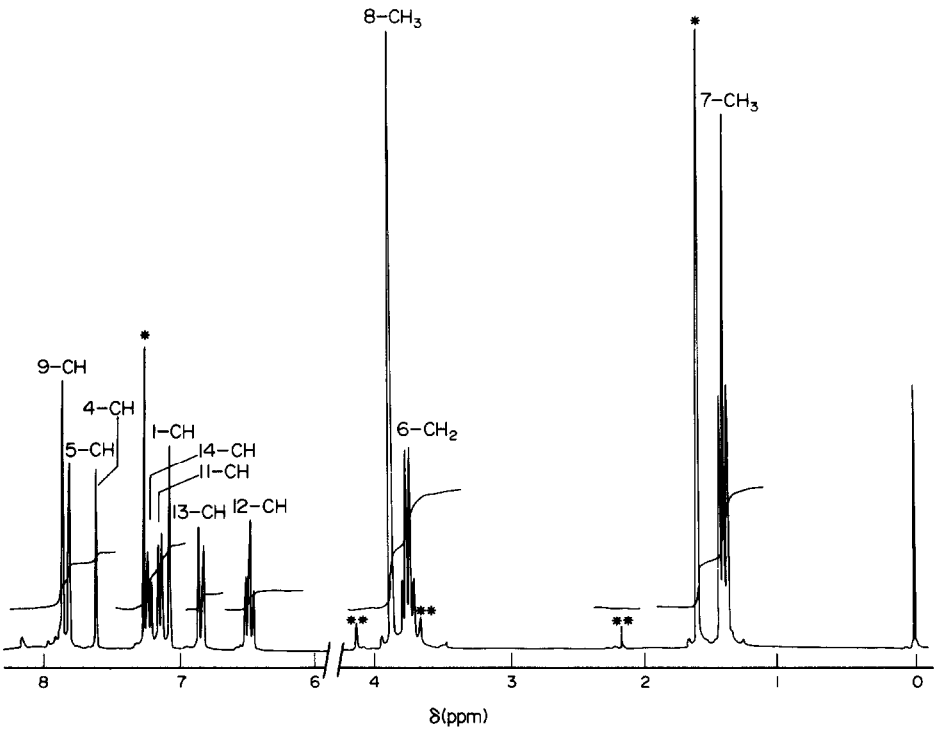

Fig. 2. ^{1}H NMR spectrum of **13** in $CDCl_3$. The signals due to the solvent are marked by * and ** indicates trace impurities.

CH=N in the neutral chelates is a consequence of the quenching of the electrophilicity of palladium.

Finally, complex **2** with N,N′-dimethyldithiocarbamate produces disulphur chelated species, $[Pd_2L(Me_2dtc)_2]$ (**14**). This compound exhibits characteristic IR frequencies due to delocalized

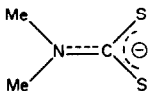

at 1500 [ν(C=N)], 1240 [$\nu_{as}(CS_2^-)$] and 980 cm^{-1} [$\nu_s(CS_2^-)$].

In conclusion, **2** is a useful precursor for the generation of a variety of air-stable, cyclometallated, dipalladiobenzene derivatives. The usefulness of this compound in organic synthesis is currently under investigation.

Acknowledgement—Thanks are due to the Regional Sophisticated Instrumentation Facility, Indian Institute of Science, Bangalore for recording the ^{1}H NMR spectra.

REFERENCES

1. H. Takahashi and J. Tsuji, *J. Organomet. Chem.* 1967, **10**, 511.
2. M. I. Bruce, B. L. Goodall and F. G. A. Stone, *J. Chem. Soc., Dalton Trans.* 1978, 687.
3. K. Hiraki, Y. Fuchita and Y. Kage, *J. Chem. Soc., Dalton Trans.* 1984, 99.
4. J. Dehand and M. Pfeffer, *Coord. Chem. Rev.* 1976, **18**, 327.
5. M. I. Bruce, *Angew. Chem., Int. Edn Engl.* 1977, **16**, 73.
6. I. Omae, *Chem. Rev.* 1979, **79**, 287.
7. E. C. Constable, *Polyhedron* 1984, **3**, 1037.
8. G. R. Newkome, W. E. Puckett, V. K. Gupta and G. E. Kiefer, *Chem. Rev.* 1986, **86**, 451.
9. I. Omae, *Coord. Chem. Rev.* 1988, **83**, 137.
10. V. V. Dunina, O. A. Zalevskaya and V. M. Potatov, *Russ. Chem. Rev.* 1988, **57**, 250.
11. D. W. Evans, G. R. Baker and G. R. Newkome, *Coord. Chem. Rev.* 1989, **93**, 155.
12. A. D. Ryabov, *Chem. Rev.* 1990, **90**, 403.
13. A. D. Ryabov, *Synthesis* 1985, 233.
14. R. F. Heck, *Palladium Reagents in Organic Synthesis.* Academic Press, London (1985).
15. S. Trofimenko, *J. Am. Chem. Soc.* 1971, **93**, 1808; *Inorg. Chem.* 1973, **12**, 1215.
16. S. Chakladar, P. Paul, K. Venkatsubramaniam and K. Nag, *J. Chem. Soc., Dalton Trans.*, in press.
17. H. W. Johnston and J. R. Williams, *J. Am. Chem. Soc.* 1947, **69**, 2065.
18. S. P. Molnar and M. Orchin, *J. Organomet. Chem.* 1969, **16**, 196.
19. H. Onouc and I. Moritani, *J. Organomet. Chem.* 1972, **43**, 431.
20. J. M. Thompson and R. F. Heck, *J. Org. Chem.* 1975, **40**, 2667.
21. J. Albert, J. Granell and J. Sales, *J. Organomet. Chem.* 1984, **273**, 393.

22. J. Granell, D. Sainz, J. Sales, X. Solans and M. Font, *J. Chem. Soc., Dalton Trans.* 1986, 1785.
23. P. W. Clark, S. F. Dykes and G. Smith, *J. Organomet. Chem.* 1987, **330**, 447.
24. J. Albert, J. Granell, J. Sales, X. Solans and M. Font-Altaba, *Organometallics* 1986, **5**, 2567.
25. J. Albert, M. Gomez, J. Granell, J. Sales and X. Solans, *Organometallics* 1990, **9**, 1405.
26. K. Nakamoto, *Infrared and Raman Spectra of Inorganic and Coordination Compounds*, 3rd edn. John Wiley, New York (1978).
27. W. I. Geary, *Coord. Chem. Rev.* 1971, 7, 81.
28. W. Beck, P. Kreutzer and K. W. Werner, *Chem. Ber.* 1971, **104**, 528.
29. Y. Nakao, M. Yamazaki, S. Suzuki, W. Mori, A. Nakahara, K. Matsumoto and S. Ooi, *Inorg. Chim. Acta* 1983, **74**, 159.

Polyhedron Vol. 10, No. 13, pp. 1521–1526, 1991
Printed in Great Britain

0277–5387/91 $3.00+.00
© 1991 Pergamon Press plc

CONVENIENT SYNTHESIS OF NEW BINUCLEATING LIGANDS DERIVED FROM 1,3-DIACETYLBENZENE. POSSIBLE PRECURSORS FOR OLIGOMERIC ORGANOMETALLIC MATERIALS

DOMINIQUE MATT*

Laboratoire de Chimie Inorganique et Analytique, EHICS, URA 405 CNRS, 1 rue Blaise Pascal, F-67008 Strasbourg Cédex, France

and

ALAIN VAN DORSSELAER

Laboratoire de Chimie Organique des Substances Naturelles, Institut de Neurochimie, URA 031 CNRS, 5 rue Blaise Pascal, F-67084 Strasbourg, France

(*Received* 20 *December* 1990; *accepted* 25 *February* 1991)

Abstract—Bis-phosphine 1,3-bis(diphenylphosphinoacetyl)benzene (LH_2) is obtained in high yield by reacting Ph_2PCl with bis(lithium anolate) derived from 1,3-diacetylbenzene in tetrahydrofuran. Its oxidation by air gives quantitatively the corresponding double β-ketophosphine oxide. The ligand LH_2 reacts with $[(o\text{-}C_6H_4CH_2NMe_2)PdCl]_2$ to give the binuclear complex $[\{(o\text{-}C_6H_4CH_2NMe_2)PdCl\}_2(\mu\text{-}LH_2)]$ in which the bis-phosphine behaves as a bridging ligand. The latter complex is conveniently converted by prolonged treatment with sodium hydride in tetrahydrofuran into the bis-enolato complex $[\{(o\text{-}C_6H_4CH_2NMe_2)Pd\}_2(\mu\text{-}L)]$ in which the bridging ligand L contains two chelating subunits. Reaction of LH_2 with $[Pd(acac)_2]$ leads to oligomeric material of formula $(PdL)_n$. Mass spectroscopic measurements suggest the presence of a tetrameric species, $(PdL)_4$, present in the reaction mixture.

There is currently renewed interest in the design and synthesis of binucleating ligands possessing two chelating subunits. Such systems have frequently been used to maintain two metals in close proximity, a situation which, by virtue of reciprocal steric and electronic forces between the metal centres, may induce new physical properties as well as enhanced stoichiometric or catalytic reactivity.[1] More recently, some attention has been focused on ligands with two chelating subunits which are separated by a rigid spacer and therefore cannot bind the same metal centre. This allows the preparation of molecular assemblies built around two distinct metal ions. Such a strategy has been applied, *inter alia*, to the synthesis of dinuclear complexes suitable for the incorporation of bifunctional substrates.[2] Another interesting aspect of binucleating ligands results from the property that the selective chelation of one coordinating subunit may control the orientation of the second one and help to induce predictable organized geometries.[3] In this paper we present a convenient synthesis of 1,3-bis(diphenylphosphinoacetyl)benzene, a ligand with two potentially chelating *P,O* subunits as well as that of the corresponding bis-(phosphine oxide). Some polynuclear palladium complexes obtained from LH_2 are also presented.

EXPERIMENTAL

General procedures

The preparation of the phosphines and the complexes was conducted under an atmosphere of dry

* Author to whom correspondence should be addressed.

dinitrogen by use of standard techniques and equipment (Schlenk flasks, etc.), that of the phosphine oxide LH_2O_2 was performed in air. IR spectra were recorded on a Perkin–Elmer 398 or a IFS 66 Brucker spectrophotometer as KBr pellets. The ^1H and $^{31}P\{^1H\}$ NMR spectra were recorded at 200 and 81 MHz, respectively, on a Bruker WP 200 SY instrument, and the $^{13}C\{^1H\}$ NMR spectra were recorded at 100.6 MHz on a FT Bruker AM 400 spectrometer. ^1H and ^{13}C chemical shifts (in ppm) are given relative to external $SiMe_4$ and those for ^{31}P relative to external H_3PO_4. The mass spectra of the ligands LH_2 and $L^{OMe}H_2$ were recorded on Kratos MS 80 and Finnigan MAT TSQ-70 spectrometers, respectively. The FAB mass spectra of $(PdL)_n$ were recorded on a ZAB HF VG analytical, using *p*-toluenesulphonic acid as protonating agent. The complex $[\{o\text{-}C_6H_4CH_2NMe_2)Pd(\mu\text{-}Cl)\}_2]$[4] and 3,5-diacetylanisole[5] were obtained by literature methods.

Preparation of 1,3-*bis*(*diphenylphosphinoacetyl*) *benzene*

A 1.6 M solution of n-BuLi (12.5 cm^3, 20.0 mmol) was added dropwise to a solution of di-isopropylamine (2.024 g, 20.0 mmol) in tetrahyrofuran (THF) (20 cm^3) at −78°C. The mixture was stirred for 0.5 h and a solution of 1,3-diacetylbenzene (1.622 g, 10.0 mmol) in THF (50 cm^3) was subsequently added with the temperature kept at −78°C. After stirring the viscous purple mixture, a solution of Ph_2PCl (4.413 g, 20.0 mmol) in THF (50 cm^3) was added slowly. The temperature was then raised and the mixture was stirred for 15 h. After removal of the solvent *in vacuo*, the residue was treated with toluene and the resulting suspension was filtered to remove LiCl. The filtered solution was evaporated to dryness and the product was chromatographed on a column containing 450 g of Kieselgel (Kieselgel 60, Merck) using a mixture of CH_2Cl_2/*n*-hexane/AcOEt (450 cm^3 : 550 cm^3 : 50 cm^3) as eluent (yield 4.138 g, 78%). The compound LH_2 eluted first ($R_f = 0.8$ with AcOEt/hexane, 45:55 v/v). Found: C, 76.8; H, 5.5. Calc. for $C_{34}H_{28}O_2P_2$: C, 77.0; H, 5.3%. MS (electron impact) $M_r = 530.54$: 530 (8% M), 386 (8%, $M-2C_6H_5$), 345 (100%, $M-PPh_2$). IR (KBr): 1672 s cm^{-1}. ^1H NMR ($CDCl_3$): δ 3.80 [s, 4H, PCH_2, $^2J(PH) = 0$ Hz], 7.29–7.52 (21H, aromatic H), 8.08 [dd, 2H, H(4) and H(6) of central ring system, $^3J = 8$ Hz, $^4J = 1.5$ Hz], 8.45 [t, 1H, H(2), $^4J = 1.5$ Hz]. $^{31}P\{^1H\}$ NMR (toluene/C_6D_6): δ −16.0 (s). $^{13}C\{^1H\}$ NMR ($CDCl_3$): δ 40.58 [d, PCH_2, $^1J(PC) = 22$ Hz], 128.56–137.11 (aromatic C), 196.30 [d, C=O, $^3J(PC) = 8$ Hz].

Preparation of LH_2O_2

A solution of LH_2 (0.531 g, 1.0 mmol) in CH_2Cl_2 (50 cm^3) was vigorously stirred in a beaker for 72 h. The solvent was removed *in vacuo* and the product was then recrystallized from CH_2Cl_2/pentane (0.435 g, 82%). Found: C, 72.6; H, 5.2. Calc. for $C_{34}H_{28}O_4P_2$: C, 72.6; H, 5.0%. IR (KBr): 1672 vs [ν(C=O)], 1176 vs [ν(P=O)] cm^{-1}. ^1H NMR ($CDCl_3$): δ 4.30 [d, 4H, PCH_2, $^2J(PH) = 15$ Hz], 7.47–9.21 (24 H, aromatic H). $^{31}P\{^1H\}$ NMR ($CDCl_3$): δ 27.2 (s).

Preparation of 3,5-(*diphenylphosphinoacetyl*) *anisole* (L^{OMe})

This compound was prepared using a similar procedure to that described for LH_2 but starting from 3,5-diacetylanisole (0.640 g, 3.33 mmol). The product was chromatographed on Kieselgel (Kieselgel 60, Merck, 100 g) using a mixture of AcOEt/*n*-hexane (25:75 v/v) as eluent ($R_f = 0.45$ with AcOEt/*n*-hexane, 20:80 v/v) (0.300 g, 16%). Found: C, 74.8; H, 5.7. Calc. for $C_{35}H_{30}O_3P_2$: C, 75.0; H, 5.4%. MS (negative ion chemical ionization) $M_r = 560.579$: 592 (6%, M+2O), 576 (34%, M+O), 560 (100%, M). (The peaks due to oxidation of the phosphine could not be avoided.) IR (KBr); 1676 vs [ν(C=O)] cm^{-1}. ^1H NMR ($CDCl_3$): δ 3.77 [s, 4H, PCH_2, $^2J(PH) = 0$ Hz], 3.83 (s, 3H, Me), 7.30–7.49 (20H, aromatic H), 7.61 [d, 2H, H(2) and H(6) of anisole ring, $^4J = 1.5$ Hz], 8.05 [t, 1H, H(4) of anisole ring, $^4J = 1.5$ Hz]. $^{31}P\{^1H\}$ NMR ($CDCl_3$): δ 15.8 (s). $^{13}C\{^1H\}$ NMR ($CDCl_3$): δ 40.77 [d, PCH_2, $^1J(PC) = 22$ Hz], 55.63 (s, Me), 117.88–160.01 (aromatic C), 196.27 [d, C=O, $^3J(PC) = 8$ Hz].

Preparation of $[\{(o\text{-}C_6H_4CH_2NMe_2)Pd(\mu\text{-}Cl)\}_2(\mu\text{-}LH_2)]$ (**1**)

To a solution of $[\{(o\text{-}C_6H_4CH_2NMe_2)Pd(\mu\text{-}Cl)\}_2]$ (0.182 g, 0.33 mmol) in CH_2Cl_2 (10 cm^3) was added a solution of LH_2 (0.175 g, 0.33 mmol) in CH_2Cl_2 (10 mmol). After 5 min stirring, the solution was concentrated to *ca* 10 cm^3 and the product was precipitated with pentane as a white powder, which was recrystallized from CH_2Cl_2/pentane (0.304 g, 85%). Found: C, 57.8; H, 4.9; N, 2.5. Calc. for $C_{52}H_{52}Cl_2N_2O_2P_2Pd_2$: C, 57.7; H, 4.8; N, 2.6%. IR (KBr): 1675 vs [ν(C=O)] cm^{-1}. ^1H NMR ($CDCl_3$): δ 2.75 [d, 12H, NMe_2, $^4J(PH) = 2.5$ Hz], 4.02 [d, 4H, NCH_2, $^4J(PH) < 1$ Hz], 4.55 [d, 4H, PCH_2, $^2J(PH) = 11$ Hz], 6.28–8.29 (32H, aromatic H). $^{31}P\{^1H\}$ NMR ($CDCl_3$): δ 29.9 (s).

Preparation of $[\{(o\text{-}C_6H_4CH_2NMe_2)Pd\}_2(\mu\text{-}L)]$ **(2)**

A solution of complex **1** (0.190 g, 0.18 mmol) in THF (20 cm^3) was stirred with NaH (0.010 g, 0.40 mmol) for 72 h. The solution was evaporated to dryness. Toluene was added and the resulting suspension was filtered through a frit. Addition of pentane to the filtered solution gave **2** as a white powder (0.169 g, 93%). Found: C, 61.6; H, 4.9; N, 2.8. Calc. for $C_{52}H_{50}N_2O_2P_2Pd_2$: C, 61.9; H, 5.0; N, 2.8%. IR (KBr): 1507 vs and 1494 vs [ν(C—O)+ν(C=C)] cm^{-1}. ^1H NMR ($CDCl_3$): δ 2.95 [d, 12H, NMe_2, $^4J(PH) = 2$ Hz], 4.00 [d, NCH_2, $^4J(PH) = 1.5$ Hz], 4.94 [d, 2H, PCH, $^2J(PH) = 2.5$ Hz], 6.69–8.39 (22H, aromatic H). $^{31}P\{^1H\}$ NMR ($CDCl_3$): δ 32.1 (s).

Reaction of LH_2 *with* $Pd(acac)_2$

A solution of LH_2 (0.570 g, 0.93 mmol) in THF (1000 cm^3) was added dropwise to a vigorously stirred solution of $Pd(acac)_2$ (0.283 g, 0.93 mmol) in THF (200 cm^3). The solution instantly turned yellow–green and when *ca* 50% of LH_2 had been added, the solution became turbid. After 1 h stirring, the solution was concentrated to half and filtered through a glass frit. The precipitate was washed several times with Et_2O (0.650 g). The material is only sparingly soluble in THF, CH_2Cl_2 or $CHCl_3$. Found: C, 63.2; H, 4.3. Calc. for $C_{34}H_{26}O_2P_2Pd$: C, 64.3; H, 4.1%. IR (KBr): 1516 vs br and 1509 sh [ν(C—O)+ν(C=C)] cm^{-1}. ^1H NMR ($CDCl_3$): this spectrum was of poor quality because of the low solubility of the compound; a broad signal at δ 4.68 ppm unambiguously reveals the presence of PCH enolate protons. $^{31}P\{^1H\}$ NMR ($CDCl_3$): δ 37.4 (s).

RESULTS AND DISCUSSION

The diphosphine LH_2 was prepared according to the reaction sequence shown in eq. (1), by using THF as solvent. After purification by column chromatography, LH_2 was obtained as a white powder in *ca* 85% yield (see Experimental). Its $^{31}P\{^1H\}$ NMR (toluene/C_6D_6) spectrum displays a single peak at −16.0 pm, a value typical for β-ketophosphines of the type $Ph_2PCH_2C(O)R$.[6] The ketone functions are characterized by (a) a strong absorption band at 1672 cm^{-1} in the IR spectrum and (b) the presence in the $^{13}C\{^1H\}$ NMR spectrum of a doublet at 196.30 ppm [$^2J(PC) = 8$ Hz]. Other characterizing data are given in the Experimental and Table 1. Reaction of air with a dichloromethane solution of LH_2 gave complete conversion into the corresponding bis(phosphine oxide), LH_2O_2 [eq. (2)], after 48 h.

The IR spectrum of LH_2O_2 in KBr shows a typical ν(P=O) absorption band at 1176 cm^{-1}. The ν(C=O) vibration appears at 1672 cm^{-1}, as for the starting compound. We note also that the PCH_2 groups appear as a doublet [$^2J(PH) = 15$ Hz] at 4.30 ppm in the ^1H NMR ($CDCl_3$) spectrum, whereas for LH_2 they appear as a singlet [$^2J(PH) = 0$ Hz] at 3.78 ppm. The spectroscopic data of both ligands clearly indicate that no enol form is present.

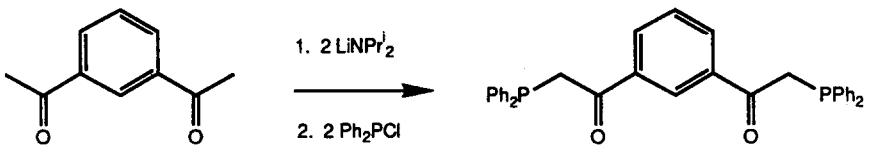

(1)

LH_2

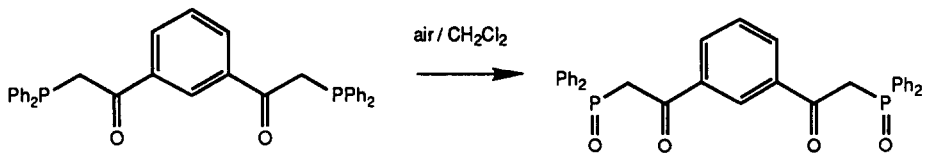

(2)

LH_2 **LH_2O_2**

Another binucleating diphosphine, L_{OMe}, was also prepared according to the procedure used for LH_2 (see Experimental). The spectroscopic data concerning the phosphinoacetyl fragment of this ligand are very similar to those of LH_2 (Table 1 and Experimental) and will not be discussed further.

The ligand LH_2 reacts with the palladium dimer $[(o\text{-}C_6H_4CH_2NMe_2)PdCl]_2$ to yield the binuclear

Table 1. Important spectroscopic data for LH_2, LH_2O_2, $L^{OMe}H_2$, **1** and **2**

Compound	^1H NMR, ppm ($CDCl_3$) δ PCH_2 or PCH [^2J(PH), Hz]	$^{31}P\{^1H\}$ NMR, ppm[a]	ν(C=O), cm^{-1} (KBr)
LH_2	3.80 [0]	−16.0	1672
LH_2O_2	4.30 [15]	27.2	1672
$L^{OMe}H_2$	3.77 [0]	−15.8	1676
1	4.55 [11]	29.9	1675
2	4.94 [2.5]	32.1	1507, 1494

[a] Solvent: $CDCl_3$ except for LH_2, toluene/C_6D_6.

complex **1**, in which the phosphine acts as a bridge between the two palladium atoms [eq. (3)]. Spectroscopic data characteristic of this formulation include the presence of a single ^{31}P NMR signal (29.9 ppm) and a strong ν(C=O) absorption band at 1675 cm^{-1} in the IR spectrum.

When LH_2 was reacted with one equiv. of Pd $(acac)_2$ in THF a sparingly soluble, yellow–green material was obtained (see Experimental). Its IR (KBr) spectrum shows the presence of a strong absorption band at 1516 cm^{-1}, unambiguously showing that the ligand LH_2 has been deprotonated

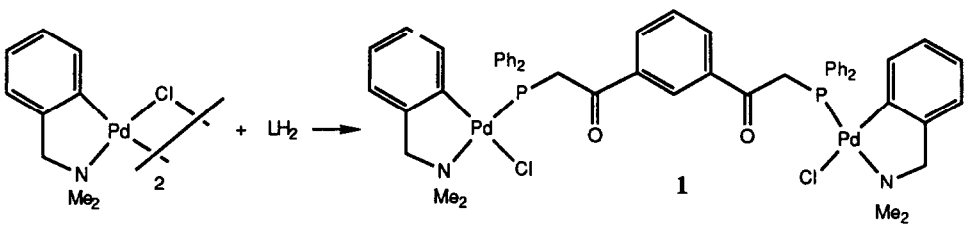

(3)

Treatment of complex **1** with NaH for 72 h quantitatively leads to the bis(enolato) complex **2** [eq. (4)]. The formation of enolato ligands from the two ketone functions is unambiguously demonstrated by the appearance of strong absorption bands at 1507 and 1494 cm^{-1} in the IR spectrum which may be assigned to the ν(C=C)+ν(C—O) vibration.[7] The NMR spectrum of **2** displays a doublet [^2J(PH) = 2.5 Hz] for the PCH protons at 4.94 ppm.

to give the enolato form L. This is also confirmed by the presence of a broad signal at 4.68 ppm (vs 4.94 pm for **2**) in the ^1H NMR spectrum. The $^{31}P\{^1H\}$ NMR ($CDCl_3$) spectrum displays a single peak at 37.4 ppm. This chemical shift, when compared with that found for the complex *cis*-[$\{Ph_2PCH{=}C(O)Ph\}_2Pd$] (37.7 ppm[8]) indicates that each palladium centre is bonded to two phosphorus atoms occupying *cis* positions.

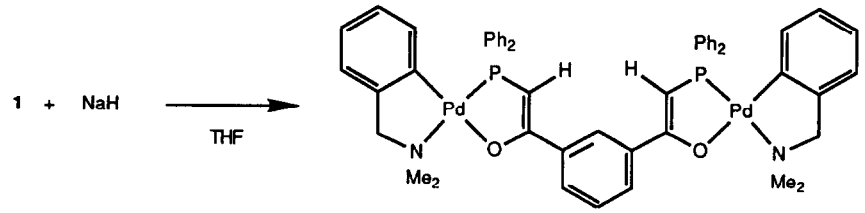

(4)

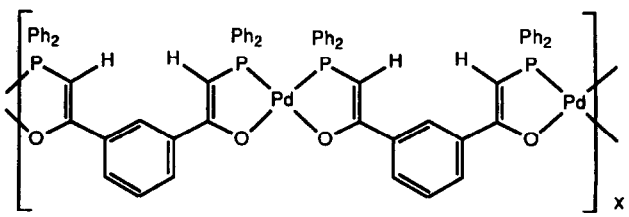

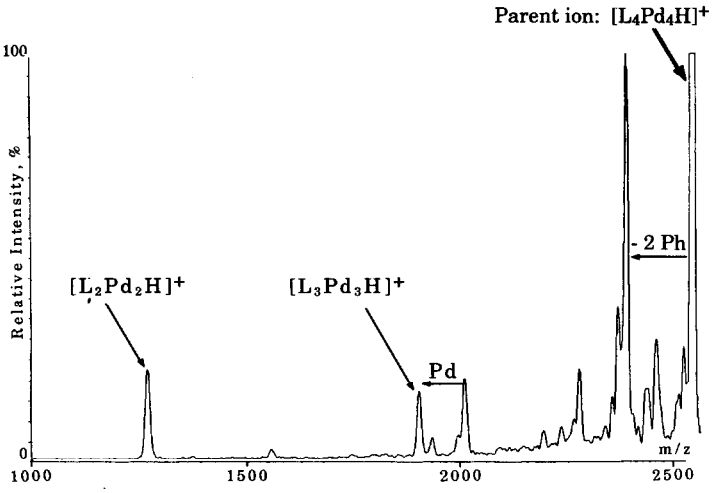

Fig. 1. Mass analysed ion kinetic energy spectrum (MIKES) of the ion at $m/z = 2541 \pm 3$ in the FAB spectrum of the crude reaction mixture. The main fragments observed confirm the tetrameric structure of ion 2541. Dimeric and trimeric species are formed from the parent ion ($[Pd_2L_2H]^+$ at $m/z = 1271$ and $[Pd_3L_3H]^+$ at $m/z = 1905$). The ion at $m/z = 2011$ corresponds to a trimeric species with four palladium atoms and probable loss of a proton to yield a singly-charged ion. The parent ion loses two phenyl groups and yields the ion at $m/z = 2388$.

The FAB–MS spectrum at 1000 resolution of the crude product displays an intense ion at $m/z = 2541.5$ corresponding to a protonated molecular ion $[(PdL)_4H]^+$ (expected value, 2540.8). Two other intense ions appear at $m/z = 1905.9$ and 1270.9 which indicate, respectively, the presence of the fragments $[(PdL)_2H]^+$ (expected value, 1270.9) and $[(PdL)_3H]^+$ (expected value, 1905.7) possibly generated from the ion at $m/z = 2541.5$. The ions at 1905.9 could also partially correspond to a trimeric complex, $(PdL)_3$, present in the crude reaction product. No ion was detected at $m/z = 3175.8$, which would correspond to a pentameric complex, $(PdL)_5$. To confirm that the ion at $m/z = 2541.5$ corresponds to a tetrametallic complex of formula $(PdL)_4$, a MIKES analysis of this ion was performed. In this technique, the molecular isotopical cluster at $m/z = 2541 \pm 3$ was selected using the first sector of the mass spectrometer and its decomposition ions measured with the second sector. This experiment clearly showed (Fig. 1) fragmentation of the selected ion into $(PdL)_3$ ($m/z = 1905$) and $(PdL)_2$ ($m/z = 1271$).

Due to the low solubility product which excludes a detailed NMR study, the question of whether the polymeric material obtained contains only the tetramer $(PdL)_4$ or a mixture of assemblies of formula $(PdL)_n$ cannot be answered at the present time. We are currently investigating this question.

In conclusion, the binucleating ligand LH_2 is conveniently obtained as a P—C coupling product by reacting the bis-enolate, $1,3\text{-}LiCH_2C(O)(C_6H_4)C(O)CH_2Li$, with Ph_2PCl. This ligand allows the synthesis of binuclear complexes containing either a bridging LH_2 moiety or the binucleating L_2 double chelate. The design of this new ligand appears to be of particular interest for the synthesis of new, oligomeric, organometallic materials.

Acknowledgements—We are grateful to Professor M. Leroy, EHICS-Strasbourg, for providing us with facilities to carry out this work and to R. Huber (Service de Spectrométrie de Masse, Université Louis Pasteur) for measuring the mass spectra.

REFERENCES

1. See for example: (a) V. A. Kogan, A. N. Morozov and V. V. Lukov, *Zh. Neorg. Khim.* 1988, **3**, 655; (b) O. Kahn, *Structure and Bonding*, Vol. 68, p. 89. Springer, Berlin (1987); (c) D. Christodoulou, M. G. Kanatzidis and D. D. Coucouvanis, *Inorg. Chem.* 1990, **29**, 191; (d) M. Himmelsbach, R. L. Lintvedt, J. K. Zehetmair, M. Nanny and M. J. Heeg, *J. Am. Chem. Soc.* 1987, **109**, 8003.
2. (a) A. W. Maverick, S. C. Buckingham, Q. Yao, J. R. Bradbury and G. G. Stanley, *J. Am. Chem. Soc.* 1986, **108**, 7430; (b) F. Vögtle, *Supramolekulare Chemie*, pp. 157–158. Teubner, Stuttgart (1989).
3. (a) J. M. Lehn and A. Rigault, *Angew. Chem., Int. Edn Engl.* 1988, **27**, 1095; (b) A. Schepartz and J. P. McDevitt, *J. Am. Chem. Soc.* 1989, **111**, 5976; (c) E. C. Constable and M. D. Ward, *J. Am. Chem. Soc.* 1990, **112**, 1256; (d) R. W. Saalfrank, A. Strark, M. Bremer and H.-V. Hummel, *Angew. Chem., Int. Edn Engl.* 1990, **29**, 311.

4. A. C. Cope and E. C. Friedrich, *J. Am. Chem. Soc.* 1968, **90**, 909.
5. M. J. Jorgensen, *Org. React.* 1970, **18**, 1. The diketone was prepared by reaction of MeLi with the corresponding di-acid in tetrahydrofuran (yield, *ca* 30%). IR (KBr): 1681 vs [ν(C=O)] cm^{-1}. ^1H NMR ($CDCl_3$): δ 2.65 [s, 6H, C(O)Me], 3.92 (s, 3H, OMe), 7.69 (d, 2H, H2 and H5, $^4J \sim 1.5$ Hz), 8.17 (t, H4, $^4J \sim 1.5$ Hz).
6. (a) D. Matt, F. Ingold, F. Balegroune and D. Grandjean, *J. Organomet. Chem.* 1990, **399**, 349; (b) D. Matt and L. Douce, *C. R. Hebd. Séanc. Acad. Sci., Paris* 1990, **t310, Série II**, 721.
7. See for example, (a) C. J. Moulton and B. L. Shaw, *J. Chem. Soc., Dalton Trans.* 1980, 199; (b) J. Dupont, T. M. Gomes Carneiro, M. Luke and D. Matt, *Quim. Nova*, 1988, **11**, 215.
8. P. Braunstein, D. Matt, D. Nobel, F. Balegroune, S.-E. Bouaoud, D. Grandjean and J. Fischer, *J. Chem. Soc., Dalton Trans.* 1988, 353.

Polyhedron Vol. 10, No. 13, pp. 1527–1537, 1991
Printed in Great Britain

0277–5387/91 $3.00+.00
© 1991 Pergamon Press plc

^{31}P AND ^{27}Al NMR STUDY ON THE BINDING ISOMERISM AND ISOMERIZATION EQUILIBRIUM OF ALUMINIUM–CYCLO-POLYPHOSPHATE COMPLEXES IN SOLUTION

QI FENG and HIROHIKO WAKI*

Department of Chemistry, Faculty of Science, Kyushu University, Hakozaki, Higashiku, Fukuoka 812, Japan

and

GENICHIRO KURA

Department of Chemistry, Fukuoka University of Education, Akama, Munakata, Fukuoka 811-41, Japan

(*Received* 23 *April* 1990; *accepted* 28 *February* 1991)

Abstract—The complexes of cyclo-tri-, cyclo-tetra- and cyclo-hexaphosphate with aluminium in solution were studied using ^{31}P and ^{27}Al NMR spectrometry. For the 1 : 1 Al^{3+}–$P_3O_9^{3-}$ complex, only a four-membered bidentate binding complex was found. For the 1 : 1 Al^{3+}–$P_4O_{12}^{4-}$ complex, on the other hand, three kinds of the complex isomers (four-membered, six-membered and eight-membered bidentate binding) were found. For the 1 : 1 Al^{3+}–$P_6P_{18}^{6-}$ complex, four kinds of isomers (four-membered bidentate, six-membered bidentate, 10-membered bidentate and eight-membered tridentate binding) were found. The discovery of new binding isomers is based on the assignment of the ^{31}P or ^{27}Al NMR resonances observed as separate peaks despite the existence of a complexation equilibrium. Furthermore, the stability constants or micro-stability constants and the isomerization constants for the 1 : 1 complexes were evaluated: $K^1_{free} = 1.1 \times 10^3$ for the cyclo-triphosphate complex; $K^1_{free} = 3.3 \times 10^4$, $K^{1-2}_1 = 0.29$ and $K^{1-3}_{1-2} = 6.7$ for cyclo-tetraphosphate complexes; and $K^{1-2}_1 = 8.4$, $K^{1-4}_{1-2} = 0.91$ and $K^{1-3-5}_{1-4} = 0.62$ for cyclo-hexaphosphate complexes, at an ionic strength of 0.1 and 20°C.

Although a large number of papers concerning the equilibrium analysis on metal complexes of cyclo-polyphosphate anions and the hydrolysis of cyclo-polyphosphate has been published,[1–7] an investigation on their binding structure in solution has not so far been reported. Since a cyclo-polyphosphate anion has a large number of donor oxygen atoms, it can coordinate to a metal ion by a variety of binding modes to form various isomers in equilibrium simultaneously. In the conventional equilibrium study only compositional information was given, but the structure of the complexes and the equilibrium distribution of the binding isomers were not given.

Very recently we found the co-existence of two binding modes for chromium–phosphinate complexes and for aluminium–monomeric phosphate complexes in solution by ^{31}P NMR and Raman spectroscopies.[8,9] One of these was a non-chelating mode in which the ligand coordinates to a metal ion with a single oxygen atom and the other was a four-membered chelating mode in which the ligand coordinates with two oxygen atoms.

In this work a distinction between various binding isomers and a quantitative analysis on the equilibrium distribution of these binding isomers in aluminium–cyclo-triphosphate, –cyclo-tetraphosphate and –cyclo-hexaphosphate complex systems were attempted by using ^{31}P and ^{27}Al NMR spectroscopy. The NMR method seemed the most powerful for these purposes, since the aluminium–

* Author to whom correspondence should be addressed.

phosphorus oxoanion complexes are moderately inert and the NMR resonances were observed as separate peaks for each complex in equilibrium.

EXPERIMENTAL

Reagents

The sodium salts of cyclo-triphosphate, $Na_3P_3O_9 \cdot 6H_2O$, cyclo-tetraphosphate, $Na_4P_4O_{12} \cdot 4H_2O$, and cyclo-hexaphosphate, $Na_6P_6O_{18} \cdot 6H_2O$, were prepared by the procedure described in previous papers.[9-11] Aluminium nitrate and other chemicals were of commercially available reagent grade. The acidity of the aluminium nitrate stock solution was maintained at 0.1 M with nitric acid to avoid hydroxo complex formation.

NMR measurement

The sample solutions were adjusted to an ionic strength of 0.1 with $N(CH_3)_4Cl$ and to pH 3 with nitric acid or sodium hydroxide. The NMR spectra were recorded on a FT JEOL spectrometer JNM-GX400 operating at 161.86 MHz for ^{31}P NMR and at 104.4 MHz for ^{27}Al NMR, respectively, at 20°C using a 10 mm i.d. spinning sample tube. The chemical shift was referenced to an external standard of 85% H_3PO_4 for the ^{31}P NMR spectrum and a solution containing 1 M hydrochloric acid for the ^{27}Al NMR spectrum, a positive shift being downfield. The peak area ratio of the complex species and free ligand or free aluminium in the spectrum was determined by measuring the paper weight proportional to each resonance area recorded. When necessary, a Lorentzian curve-fitting computer analysis was employed to resolve the resonance overlapping.

RESULTS AND DISCUSSION

^{31}P *and* ^{27}Al *NMR study of the aluminium–cyclo-triphosphate complex system*

The ^{31}P and ^{27}Al NMR spectra of a series of solutions containing equimolar $Al(NO_3)_3$ and $Na_3P_3O_9$ were measured (Fig. 1). In the ^{31}P NMR spectrum, resonance a_P was due to the free cyclo-triphosphate anion, whereas resonances b_P, c_P, d_P and e_P could be assigned to the aluminium complexes. In the ^{27}Al NMR spectrum, resonance a_{Al} was due to the free Al^{3+} ion and resonances b_{Al} and c_{Al} could be assigned to the complexes. The b_P and c_P resonances in ^{31}P and b_{Al} in ^{27}Al NMR were assigned to a 1 : 1 complex, AlP_3O_9, since they were observed in a sufficiently low concentration range. The presence of two resonances in the ^{31}P NMR spectrum of this complex indicates that the phosphate group exists in two different states in the molecule, one being coordinated and the other uncoordinated. The c_P resonance with a large, upfield coordination shift from the resonance of the free ligand (−10.5 ppm) can be assigned to the aluminium-coordinating phosphate group, while b_P, which has a very small upfield coordination shift (−0.8 ppm), may be assigned to the uncoordinated group in the complex. The b_P resonance is a doublet and its peak area is always twice that of c_P, and b_{Al} is a doublet split by the phosphorus atom of the coordinated phosphate group. Therefore the 1 : 1 aluminium–cyclo-triphosphate complex should exist as structure **I** from the three forms indicated below.

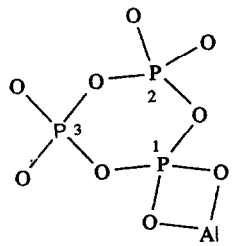

AlP_3O_9 (1)

(I)

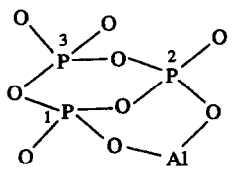

AlP_3O_9 (1–2)

(II)

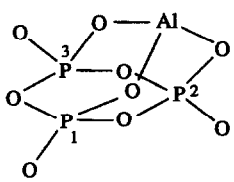

AlP_3O_9 (1–2–3)

(III)

The presence of a single oxygen-binding form in the single phosphate group-binding complex (structure **I**) could also not be denied, as has been previously found in the monomeric phosphate complexes of chromium or aluminium.[8,9] However, the difference in the chemical shifts between the non-chelating and chelating forms may become too small for the polyphosphate complexes to give separate peaks due to perturbation by other uncoordinated phosphate groups in the complex. Therefore, the predominance of the chelate form can be expected, as explained for the monomeric ligand complexes.[9]

The d_P, e_P and c_{Al} resonances can be assigned to a 1 : 2 complex, $Al(P_3O_9)_2^{3-}$, existing as structure **IV** due to the fact that c_{Al} is a triplet and the inten-

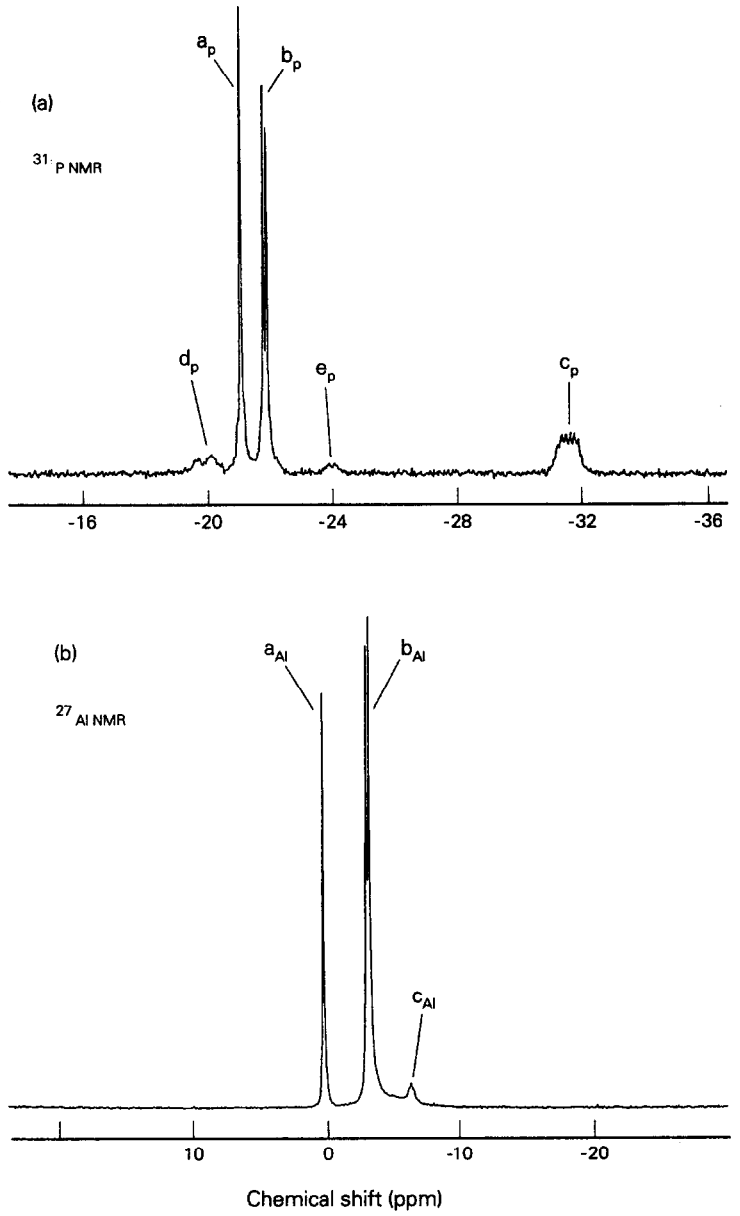

Fig. 1. ^{31}P and ^{27}Al NMR spectra of the solution containing equimolar 2.5×10^{-2} M $Al(NO_3)_3$ and $Na_3P_3O_9$ at pH 3 and 20°C.

sities of these signals increase with increasing ligand concentration, and that the intensity ratio of d_P/e_P remains constant. On the other hand, the 2 : 1 aluminium–cyclo-triphosphate complexes were not detected even in the solution containing excess aluminium ion.

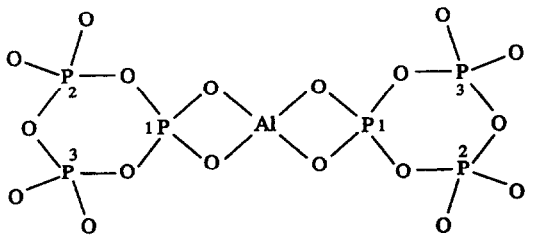

$Al(P_3O_9)_2^{3-}$ (1,1)

(IV)

^{31}P *and* ^{27}Al *NMR study of the aluminium–cyclo-tetraphosphate complex system*

Figure 2 shows examples of ^{31}P and ^{27}Al NMR spectra of the solution containing equimolar $Al(NO_3)_3$ and $Na_4P_4O_{12}$. In the ^{31}P NMR spectrum [Fig. 2(a)], resonance a_P is due to the free cyclo-tetraphosphate ion and the other resonances are

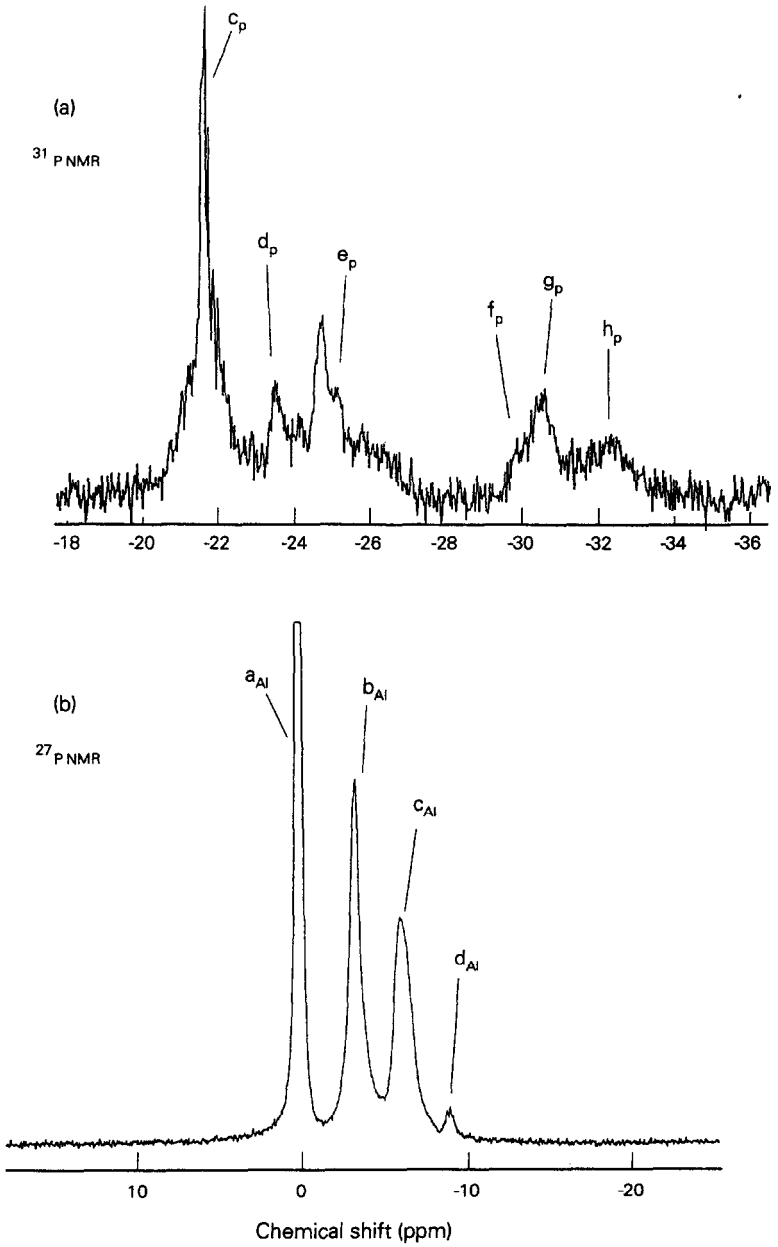

Fig. 2. ^{31}P and ^{27}Al NMR spectra of the solution containing equimolar 4×10^{-3} M $Al(NO_3)_3$ and $Na_4P_4O_{12}$ at pH 3 and 20°C.

due to the aluminium complexes. As the peak area ratio for these complexes did not vary in the lower concentration range, they may be assigned to the 1 : 1 complexes. Resonances g_P, f_P and e_P with large upfield coordination shifts (−6.7, −5.1 and −4.5 ppm) may be assigned to the coordinated phosphate groups, and resonances b_P, c_P and d_P with small coordination shifts (+0.1, −1.3 and −2.0 ppm) may be assigned to the uncoordinated phosphate groups in the complexes, due to the reasons described above. Therefore, there should be at least three types of coordinated phosphate group and three types of uncoordinated phosphate group for the 1 : 1 complexes.

The binding isomers, **V**, **VI** and **VII**, are expected to exist in the Al^{3+}–$P_4O_{12}^{4-}$ complex system, which is different to the Al^{3+}–$P_3O_9^{3-}$ complex system where only the one 1 : 1 complex **I** was formed because of the larger ring size and the presence of more oxygen atoms in the $P_4O_{12}^{4-}$ anion. Cyclotetraphosphate anions coordinate to the aluminium ion by one phosphate group to form four-membered, bidentate binding in complex **V**, and by two phosphate groups to form six-membered

bidentate binding (**VI**) or eight-membered bidentate binding (**VII**).

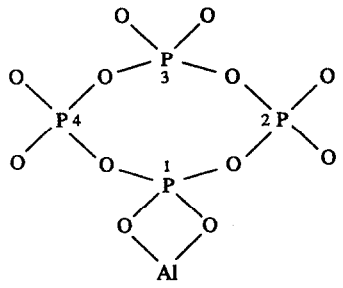

$AlP_4O_{12}^-$ (1)

(V)

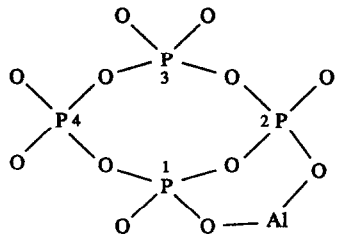

$AlP_4O_{12}^-$ (1–2)

(VI)

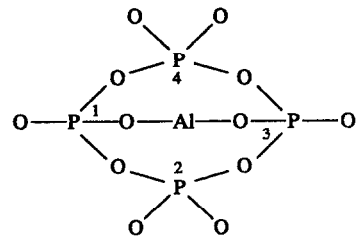

$AlP_4O_{12}^-$ (1–3)

(VII)

It can be considered that a stronger interaction between the phosphate group and aluminium ion should, in general, cause a greater ^{31}P NMR coordination shift. Thus the shift of the coordinated phosphate group may increase with a decrease in the number of phosphate groups coordinating to the aluminium ion, and the shift of the uncoordinated phosphate group decreases with an increase in the distance from the metal ion. The largest upfield shift, g_P, and the smallest shift, b_P, may be assigned to P(1) and P(3) of complex **V**, respectively. Resonance c_P (doublet) may be assigned to P(3) and P(4) of complex **VI**, and resonance e_P, which has the same area as c_P, may be assigned to P(1) and P(2) of complex **VI**. Resonance d_P may be due to overlapping peaks of P(2) and P(4) of complex **VII** with P(2) and P(4) of complex **V**. Therefore, it was concluded that there are three binding isomers for the $AlP_4O_{12}^-$ complex.

In the ^{27}Al NMR spectrum [Fig. 2(b)], resonance a_{Al} is due to the free Al^{3+} ion and resonances b_{Al} and c_{Al} are due to the 1 : 1 complexes. It is expected that the more phosphate groups coordinating to an aluminium ion the larger the shift from the free aluminium ion in the ^{27}Al NMR spectrum. Thus resonance b_{Al} can be assigned to complex **V** and c_{Al} to complexes **VI** and **VII**. Since the chemical shift difference between complexes **V**, **VI** and **VII** is considered to be small, the resonances for the complexes undergo considerable overlapping.

It was observed that the intensities of resonances a_P and b_P decreased and a new resonance with a coordination shift of −11.5 ppm appeared with an increase in the $Al(NO_3)_3$ concentration, when the concentration ratio of $Al(NO_3)_3$ to $Na_4P_4O_{12}$ was larger than unity, reflecting the formation of a 2 : 1 complex. This complex is presumably of structure **VIII** on consideration of the strong repulsion between the two aluminium ions bound to the $P_4O_{12}^{4-}$ anion and the low relative formation of six-membered bidentate binding in the 1 : 1 complex. When cyclo-tetraphosphate is in excess, a new resonance, d_{Al}, with a coordination shift of −6.8 ppm, which is almost the same as that of the $Al(P_3O_9)_2^{3-}$ complex (**IV**), was observed in the ^{27}Al NMR spectrum (Fig. 3). This may be assigned to the 1 : 2 complex (**IX**).

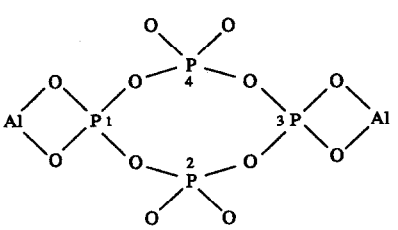

$Al_2P_4O_{12}^{2+}$ (1,3)

(VIII)

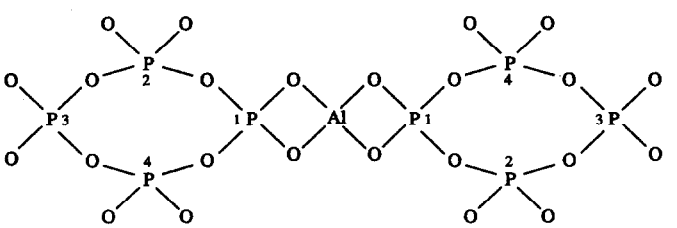

$Al(P_4O_{12})^{5-}$ (1,1)

(IX)

^{31}P *and* ^{27}Al *NMR study of the aluminium–cyclohexaphosphate complex system*

In this system more isomers can be expected. The ^{31}P and ^{27}Al NMR spectra are shown in Fig. 4. Three resonances were observed for the 1 : 1 complexes in the ^{27}Al NMR spectrum [Fig. 4(b)]. On

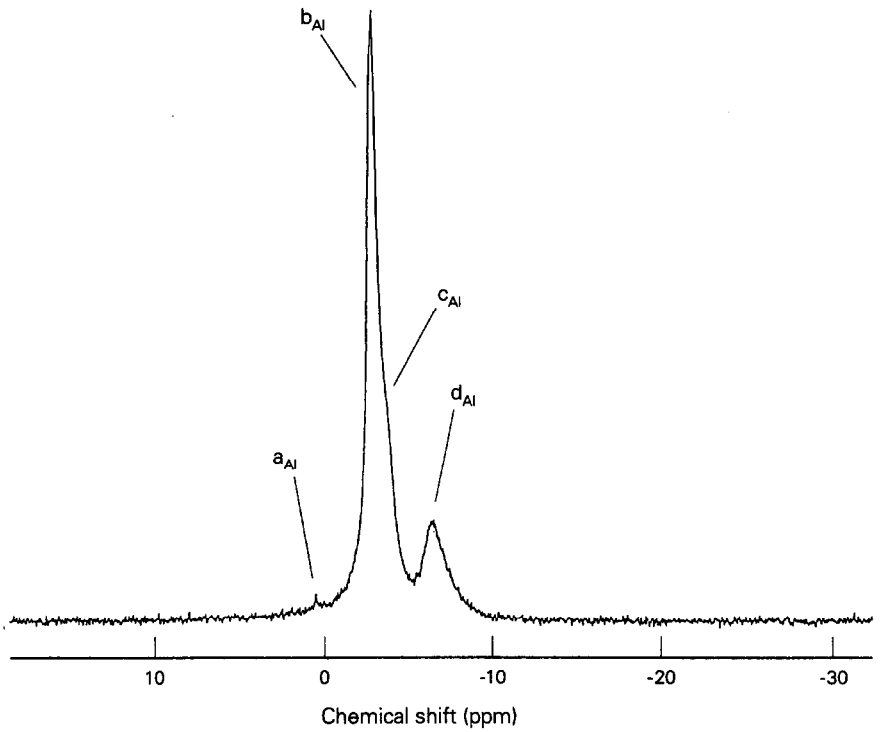

Fig. 3. ^{27}Al NMR spectrum of the solution containing 4×10^{-3} M $Al(NO_3)_3$ and 8×10^{-3} M $Na_4P_4O_{12}$ at pH 3 and 20°C.

the basis of the coordination shift of the resonance and the splitting pattern observed, b_{Al}, c_{Al} and quartet d_{Al} may correspond to a single-phosphate group coordinated isomer, a two-phosphate groups coordinated isomer and a three-phosphate groups coordinated isomer, respectively.

More detailed information can be obtained from the ^{31}P NMR spectrum [Fig. 4(a)]. Resonance a_P is due to the free anion and all the other resonances are due to the 1 : 1 complexes. Similar to the cyclotetraphosphate complex system, e_P, f_P and g_P resonances with large upfield coordination shifts (−4.6, −10.2 and −10.5 ppm from the unprotonated free anion) can be assigned to the coordinated phosphate groups, and b_P, c_P and d_P resonances with smaller upfield coordination shifts (−1.0, −2.0 and −3.5 ppm) can be assigned to non-coordinated phosphate groups. On the basis of the coordination shift and resonance area ratio, d_P and e_P of equal area can be assigned to non-coordinated and coordinated phosphate groups of complex **X**, respectively, in which the $P_6O_{18}^{6-}$ anion coordinates to the aluminium ion via three phosphate groups to form eight-membered tridentate rings. This assignment can be supported by the agreement of concentration of complex **X**, calculated from the areas of ^{31}P NMR resonances d_P or e_P, with that from the area of ^{27}Al NMR resonance d_{Al}. Resonances f_P and g_P can be assigned to the coordinated phosphate groups in the isomers containing 10-membered bidentate binding (**XI**) and six-membered bidentate binding (**XII**), respectively. Since the concentration of the single-phosphate group coordinated isomer (**XIII**) was very low [see ^{27}Al NMR resonance b_{Al} in Fig. 4(b)], the ^{31}P NMR resonance corresponding to this type of binding was not observed under these conditions. Although b_P and c_P can be assigned to the non-coordinated phosphate groups of complexes **XI**, **XII** and **III**, a further detailed assignment is difficult at present.

^{31}P and ^{27}Al NMR spectra of the solution containing $Na_6P_6O_{18}$ and excess $Al(NO_3)_3$ are shown in Fig. 5. The relative intensity of b_{Al} was larger and that of d_{Al} was smaller than those for the equimolar solution. This indicates the formation of 2 : 1 complexes. Using the isomerization constant values of the 1 : 1 complexes (given in Table 3) and the intensity of d_{Al} for the 1 : 1 complex **X**, it was calculated that 17% of c_{Al} is due to the 1 : 1 complexes **XI** and **XII**, and the remaining 83% to the 2 : 1 complexes. The b_{Al} resonance was due mainly to the 2 : 1 complexes.

Two resonances observed for the 2 : 1 complexes in the ^{27}Al NMR spectrum suggest that there are

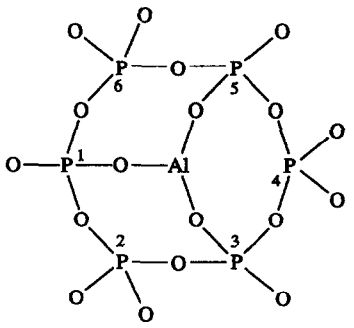

$AlP_6O_{18}^{3-}$ (1–3–5)

(X)

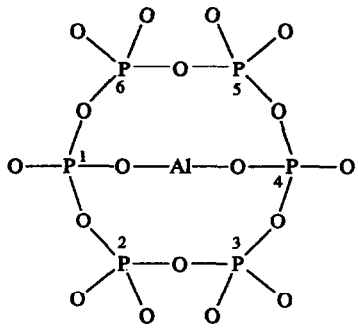

$AlP_6O_{18}^{3-}$ (1–4)

(XI)

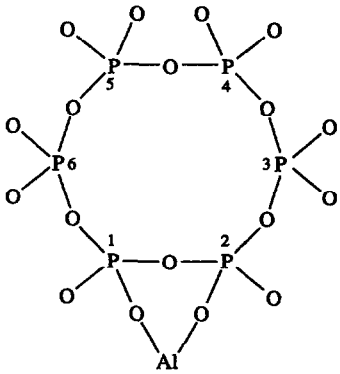

$AlP_6O_{18}^{3-}$ (1–2)

(XII)

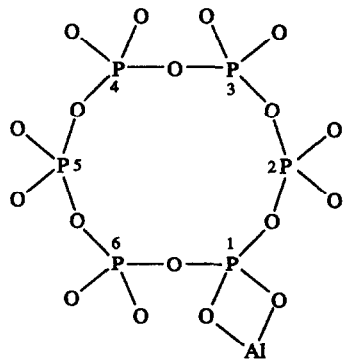

$AlP_6O_{18}^{3-}$ (1)

(XIII)

two binding modes in the complex. In one of the modes, the aluminium ion binds to one phosphate group which has a resonance with a coordination shift of −3.5 ppm (b_{Al}), and in the other mode, the aluminium ion binds to two phosphate groups which has a resonance with a coordination shift of −6.2 ppm (c_{Al}), each value being the same as that for the 1 : 1 complex with the corresponding binding mode. On account of the repulsion between the two positively-charged aluminium ions bound to a $P_6O_{18}^{6-}$ anion, they should be located at the greatest distance from each other. Accordingly, the coordination reactions forming eight- or 10-membered rings may not be predominant. The three isomers are, therefore, possible for the 2 : 1 complexes.

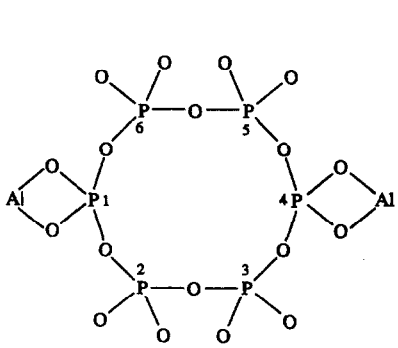

$Al_2P_6O_{18}$ (1,4)

(XIV)

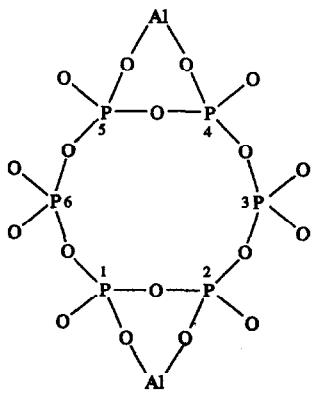

$Al_2P_6O_{18}$ (1–2,4–5)

(XV)

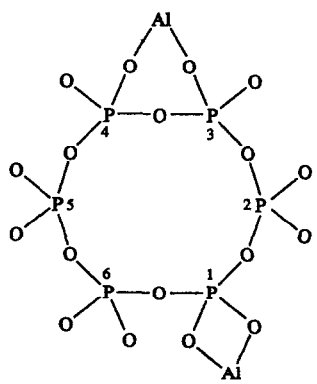

$Al_2P_6O_{18}$ (1,3–4)

(XVI)

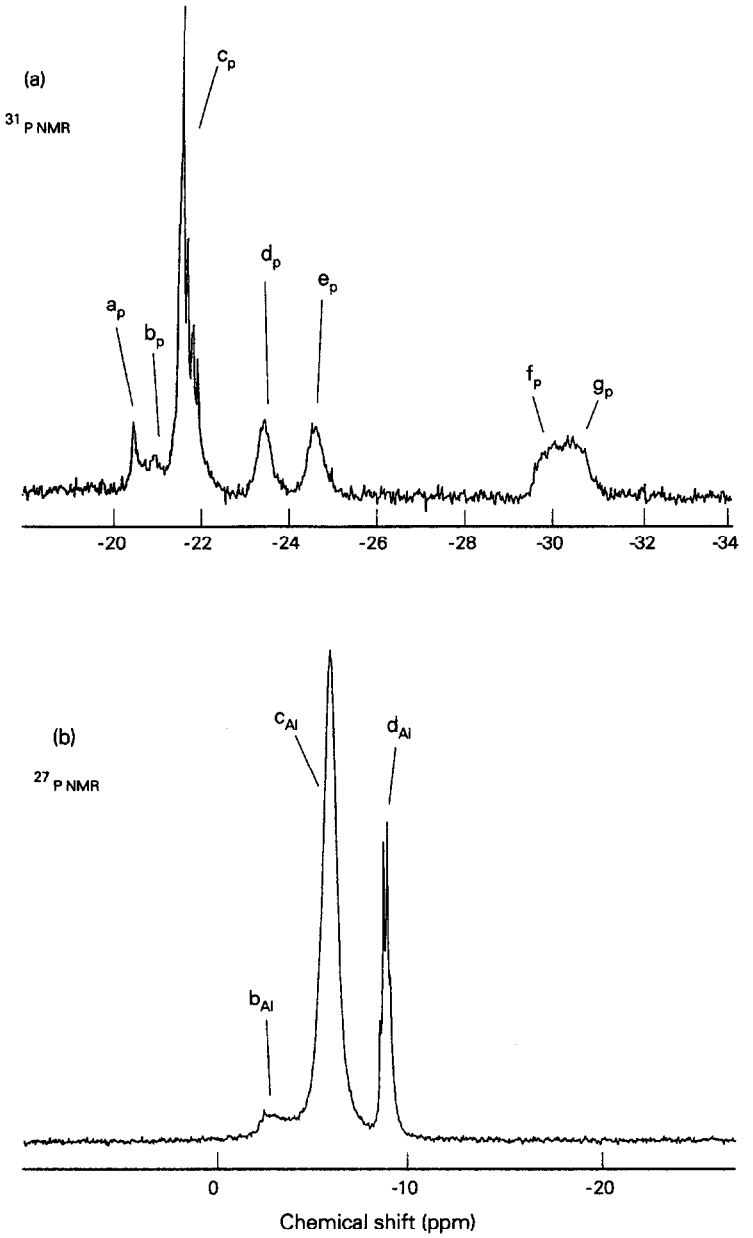

Fig. 4. ^{31}P and ^{27}Al NMR spectra of the solution containing equimolar 4×10^{-3} M $Al(NO_3)_3$ and $Na_6P_6O_{18}$ at pH 3 and 20°C.

Similar conclusions can also be drawn from the ^{31}P NMR investigation. It was observed that resonances a_P, b_P, c_P and f_P decreased, resonance g_P increased and a new resonance h_P appeared with the highest shift in the ^{31}P NMR spectrum of the solution containing excess $Al(NO_3)_3$ (Fig. 5). The h_P resonance can be assigned to P(1) and P(4) of the 2 : 1 complex **XIV** and to P(1) of complex **XVI**; g_P is an overlapping peak consisting of resonances of P(1), P(2), P(4) and P(5) of the 2 : 1 complex **XV** and P(3) and P(4) of complex **XVI** with P(1) and P(2) of the 1 : 1 complex (**XII**). The decrease of f_P due to P(1) and P(4) of complex **XI** indicates that 10-membered bidentate binding does not occur in the 2 : 1 complexes.

Trends in NMR chemical shifts of aluminium–cyclophosphate complexes

The coordination shift data of ^{27}Al and ^{31}P NMR for Al^{3+}–$P_3O_9^{3-}$, –$P_4O_{12}^{4-}$ and –$P_6O_{18}^{6-}$ com-

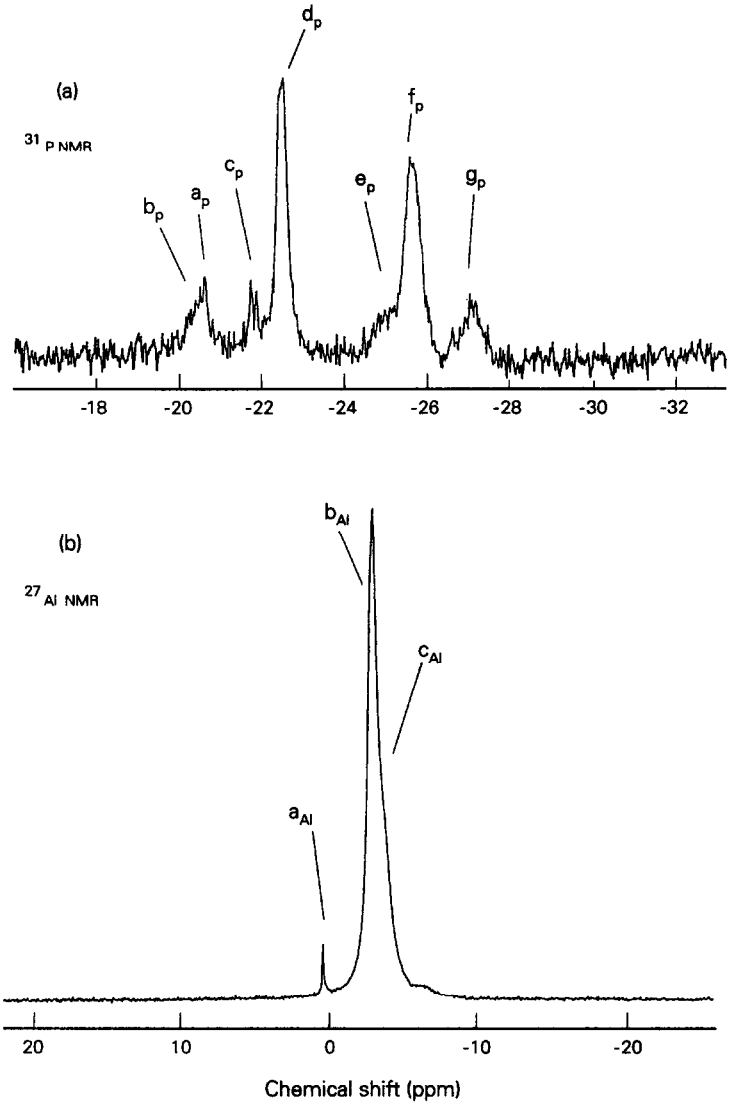

Fig. 5. ^{31}P and ^{27}Al NMR spectra of the solution containing 8×10^{-3} M $Al(NO_3)_3$ and 4×10^{-3} M $Na_6P_6O_{18}$ at pH 3 and 20°C.

plexes are summarized in Tables 1 and 2. It was found that the coordination shift in ^{27}Al NMR depends almost only on the numbers of phosphate groups directly coordinating to an aluminium ion, the shift value increasing with number (Table 1). On the other hand, the coordination shift in ^{31}P NMR for the coordinating phosphate group depends not only on the number of phosphate groups coordinated directly, but also on the binding mode and the ligand structure (Table 2).

Table 1. ^{27}Al NMR coordination shifts (ppm)

	Number of coordinated phosphate groups on the aluminium ion					
	1		2			3
	1 : 1 complex	2 : 1 complex	1 : 1 complex	1 : 2 complex	2 : 1 complex	1 : 1 complex
Al^{3+}–$P_3O_9^{3-}$	−3.4	—	—	−6.7	—	—
Al^{3+}–$P_4O_{12}^{4-}$	−3.4	—	−4.2	−6.8	—	—
Al^{3+}–$P_6O_{18}^{6-}$	−3.5	−3.5	−6.2	—	−6.2	−9.1

Table 2. ^{31}P NMR coordination shifts of the coordinated phosphate groups (ppm)

	Number of coordinated phosphate groups on the aluminium ion							
	1		2					3
	1:1 complex	2:1 complex	1:1 complex			1:2 complex	2:1 complex	1:1 complex
			Six-membered	Eight-membered	10-membered		Six-membered	Eight-membered
Al^{3+}–$P_3O_9^{3-}$	−10.5	—	—	—	—	−3.0	—	—
Al^{3+}–$P_4O_{12}^{4-}$	−6.7	−11.5	−4.5	−5.1	—	—	—	—
Al^{3+}–$P_6O_{18}^{6-}$	—	−12.3	−10.5	—	−10.2	—	−10.5	−4.6

Isomerization constants for the aluminium–cyclophosphate complexes

In order to obtain more quantitative information on the distribution of these new binding isomers, we evaluated the isomerization constants and micro-stability constants for some of these one-to-one complexes, which are defined by the following equations:

$$K^{1}_{free} = \frac{[AlP_3O_9(1)]}{[P_3O_9^{3-}][Al^{3+}]} \quad (1)$$

$$\frac{[AlP_4O_{12}^{-}(1)]}{[P_4O_{12}^{4-}][Al^{3+}]} \quad (2)$$

$$\frac{[AlP_6O_{18}^{3-}(1)]}{[P_6O_{18}^{6-}][Al^{3+}]} \quad (3)$$

$$K^{1-2}_{1} = \frac{[AlP_4O_{12}^{-}(1\text{–}2)]}{[AlP_4O_{12}^{-}(1)]} \quad (4)$$

$$\frac{[AlP_6O_{18}^{3-}(1\text{–}2)]}{[AlP_6O_{18}^{3-}(1)]} \quad (5)$$

$$K^{1-3}_{1-2} = \frac{[AlP_4O_{12}^{-}(1\text{–}3)]}{[AlP_4O_{12}^{-}(1\text{–}2)]} \quad (6)$$

$$K^{1-4}_{1-2} = \frac{[AlP_6O_{18}^{3-}(1\text{–}4)]}{[AlP_6O_{18}^{3-}(1\text{–}2)]} \quad (7)$$

$$K^{1-3-5}_{1-4} = \frac{[AlP_6O_{18}^{3-}(1\text{–}3\text{–}5)]}{[AlP_6O_{18}^{3-}(1\text{–}4)]}. \quad (8)$$

Equations (1)–(3) represent micro-stability constants for the single-phosphate group coordinating complexes, eqs (4) and (5) give intramolecular isomerization constants between the two-phosphate groups coordinating and single-phosphate group coordinating complexes, eqs (6) and (7) give isomerization constants between different two-phosphate groups coordinating complexes, and eq. (8) represents an isomerization constant between the three- and the two-phosphate groups coordinating complexes. If these constants are all determined, the whole distribution of the isomeric complex species may become clear.

The concentrations of the complexes, free ligand and free aluminium ion were estimated from respective peak areas of ^{31}P and ^{27}Al NMR spectra under the given concentrations of each ligand and aluminium atoms. All the constants evaluated for 1 : 1 complexes are summarized in Table 3.

Since the concentration of free aluminium ion in the cyclo-hexaphosphate system was lower than its detection limit in ^{27}Al NMR, the exact K^{1}_{free} value for the cyclo-hexaphosphate complex could not be obtained, but it is predicted to be much larger than that for the cyclo-tetraphosphate complex. The stability constant K^{1}_{free} increased in the order $AlP_6O_{18}^{3-} > AlP_4O_{12}^{-} > AlP_3O_9$, in agreement with an increase in the charge and the number of donor oxygen atoms of the ligand, which is normal behaviour for the complexation reaction.[13–15] The

Table 3. Equilibrium micro-stability constants and isomerization constants of 1 : 1 complexes at $I = 0.1$ and 20°C

	K^{1}_{free}	K^{1-2}_{1}	K^{1-3}_{1-2}	K^{1-4}_{1-2}	K^{1-3-5}_{1-4}
Al^{3+}–$P_3O_9^{3-}$	1.1×10^3	0	—	—	—
Al^{3+}–$P_4O_{12}^{4-}$	3.3×10^4	0.29	6.7	—	—
Al^{3+}–$P_6O_{18}^{6-}$	Very large	8.4	—	0.91	0.62

increase of the isomerization constant K_1^{1-2} following the same order indicates that the larger the size of the ligand, the more convenient is the formation of six-membered bidentate chelate binding. The isomerization constants for the 2 : 1 complexes **XIV**, **XV** and **XVI** were not evaluated because of the difficulty in distinguishing the isomers, but the concentration ratio of total numbers of six-membered bidentate binding form to those of four-membered bidentate form was found to be 0.73. Furthermore, the tendency to form 2 : 1 complexes increased and that of 1 : 2 complexes decreased with an increase in ligand size, though this is a matter of course on considering the increase of charge and numbers of donor oxygen atoms of the ligand.

REFERENCES

1. R. M. Smith and A. E. Martell (Eds), *Critical Stability Constants, Inorganic Complexes*, Vol. 4. Plenum Press, New York (1976).
2. E. Hogfeldt (Ed.), *Stability Constants of Metal-ion Complexes, Part A: Inorganic Ligands*. Pergamon Press, Oxford (1982).
3. L. G. Sillen and A. E. Martell (Eds), *Stability Constants of Metal-ion Complexes*. Special publications No. 17, The Chemical Society, London (1964).
4. L. G. Sillen and A. E. Martell (Eds), *Stability Constants of Metal-ion Complexes*. Special publication No. 25, The Chemical Society, London (1971).
5. G. Kura, *Bull. Chem. Soc. Japan* 1987, **60**, 2857.
6. G. Kura, *Polyhedron* 1987, **6**, 1863.
7. G. Kura, *J. Chromatogr.* 1988, **447**, 91.
8. Q. Feng and H. Waki, *Polyhedron* 1990, **9**, 1555.
9. Q. Feng and H. Waki, *Polyhedron* 1991, **10**.
10. G. Kura and S. Ohashi, *J. Chromatogr.* 1971, **56**, 111.
11. E. J. Griffith and R. L. Buxton, *Inorg. Chem.* 1965, **4**, 549.
12. U. Schulke, *Z. Anorg. Allg. Chem.* 1968, **360**, 231.
13. M. Kohanemaru, H. Waki, S. Ohashi and G. Kura, *J. Inorg. Nucl. Chem.* 1979, **41**, 1457.
14. G. Kura, *Polyhedron* 1986, **5**, 2097.
15. G. Kura and H. Waki, *Polyhedron* 1990, **9**, 511.

Polyhedron Vol. 10, No. 13, pp. 1539–1543, 1991
Printed in Great Britain

0277–5387/91 $3.00+.00
Pergamon Press plc

THE PREPARATION AND CHARACTERIZATION OF SOME IMIDO- AND DIAZENIDO-RHENIUM COMPLEXES OF MALTOL. THE X-RAY CRYSTAL STRUCTURE OF $[Re(maltol)_2(NPh)(PPh_3)][BPh_4]$

COLIN M. ARCHER, JON R. DILWORTH* and PANNA JOBANPUTRA

Department of Chemistry and Biological Chemistry, University of Essex, Colchester CO4 3SQ, U.K.

and

MARY E. HARMAN, MICHAEL B. HURSTHOUSE and ALEXANDER KARAULOV

Department of Chemistry, Queen Mary and Westfield College, Mile End Road, London E1 4NS, U.K.

(*Received* 5 *October* 1990; *accepted* 28 *February* 1991)

Abstract—The imido complex $[ReCl_3(NPh)(PPh_3)_2]$ reacts with excess maltol to give the green complex $[Re(maltol)_2(NPh)(PPh_3)][BPh_4]$ (**1**). Under analogous conditions, $[ReCl_2(N_2COPh)(PPh_3)_2]$ gives $[ReCl(maltol)(N_2COPh)(PPh_3)_2]$ (**2**). An X-ray crystal structure of complex **1** revealed a distorted octahedral structure with *cis*-maltol ligands. Preliminary X-ray data on a poorly diffracting crystal of complex **2** has confirmed the formulation and stereochemistry. The possible structures of products from other precursors are discussed together with their redox and spectroscopic properties.

Although maltol (Fig. 1) has been known since the end of the nineteenth century, its complexes with transition metals were reported comparatively recently. Among the first to be described were the soluble, intensely-coloured species formed with iron(III).[1] Maltol has indeed found some use as a reagent for the spectrophotometric determination of iron in an acidic medium. Currently the neutral, red *tris*-chelate of maltol with iron is showing considerable promise as a clinical reagent for the control of iron *in vivo*.[2] The early studies established that maltol ligates as a chelating ligand via two oxygen atoms. However, there were few complete characterizations of the complexes and many compounds were only studied spectrophotometrically.[3–7] A relatively rare example is $[Fe(maltol)_3]$ which was very recently completely characterized by an X-ray crystal structure.[8]

Recent interest in maltol and its analogues has focused on its use as a reagent for the control of the concentrations of trivalent metals other than iron *in vivo*. Aluminium is linked with Alzheimer's disease but studies of the transport mechanism have been complicated by the facile hydrolysis of Al^{3+} in aqueous solution. However, the complex $[Al(maltol)_3]$ (maltol = monoanion of free ligand) is stable to hydrolysis in aqueous solution at physiological pH and is small enough to cross cell membranes.[9] Studies of the aluminium maltol complex

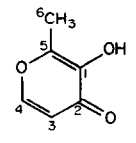

Fig. 1. Structure of maltol.

* Author to whom correspondence should be addressed.

in vivo may well shed light on the mechanism of delivery of aluminium to the brain.[10]

Maltol is established to be non-toxic and to form metal chelates with metal ions that are stable *in vivo*. As a preclude to investigating its suitability as a ligand for technetium, we here report a systematic exploration of its coordination chemistry with rhenium. The chemistry of maltol with technetium will be reported elsewhere.

(1) *Imido complexes*

The rhenium(V) complex $[ReCl_3(NPh)(PPh_3)_2]$ reacts with excess maltol in alcohol in the presence of triethylamine to give a dark green solution. $[Re(maltol)_2(NPh)(PPh_3)]^+$ (**1**) precipitated in good yield by the addition of sodium tetraphenylborate. The complex is isolated as an air-stable, green solid which is diamagnetic both in the solid state and in solution. The Nujol mull IR spectrum shows substantial shifts of *ca* 40 cm^{-1} in the bands at *ca* 1600 cm^{-1} assigned to ν(C=C) and ν(C=O) of maltol, suggesting it is functioning as a bidentate ligand. Due to interfering bands from the PPh_3 and BPh_4 groups no assignment of a band due to ν(Re=N) could be made.

The ^1H NMR spectrum of complex **1** in $CDCl_3$ showed two singlets at 2.00 and 2.60 ppm due to two, magnetically inequivalent methyl groups. There is also a doublet at 6.40 and 6.60 ppm due to one of the vinyl protons of maltol. The other doublet at about 8 ppm is presumably obscured by the phenyl protons. The integrated values are consistent with two coordinated maltol groups and these are magnetically inequivalent. The $^{31}P\{^1H\}$ NMR spectrum shows a singlet at +2.4 ppm, consistent with a single or equivalent phosphine ligands. The HPLC trace for the complex (in dichloromethane with a THF/water gradient in the presence of $[Bu_4N]Br$) showed two peaks with retention times of 4.0 and 4.6 min. This suggests the complex may have two isomers in solution.

X-ray crystal structure of $[Re(maltol)_2(NPh)(PPh_3)][BPh_4]$ (**1**). Crystals suitable for an X-ray crystal structure were grown from dichloromethane–ethanol. A selection of bond lengths and angles is presented in Table 1 and a diagram of the structure (with the atom labelling scheme) is shown in Fig. 2.

The overall geometry for rhenium is best described as distorted octahedral with *cis*-maltol ligands. The Re—O(1) and Re—O(4) bond lengths are almost identical [1.987(7) and 1.996(7) Å] as are Re—O(2) and Re—O(5) [2.122(6) and 2.111(6) Å]. Examination of the bond distances within a maltol ring (Fig. 3) shows that C(1)—C(5) and C(3)—C(4) have significant double bond character, consistent with C(2)—O(5) [1.281(10) Å] being shorter than C(1)—O(4) [1.331(10) Å]. This is also reflected in the asymmetric coordination of maltol to rhenium. The asymmetric coordination of the maltolato anion was also discussed in the structure of $[Fe(maltol)_3]$.[8] The Re=N distance of 1.709(8) Å is within the range found for other imido-rhenium

Table 1. Selected bond lengths (Å) and angles (°) for $[Re(maltol)_2(NPh)(PPh_3)]^+$ (**1**)

Bond lengths			
P—Re	2.407(4)	C(1)—O(4)	1.331(10)
O(1)—Re	1.987(7)	C(2)—O(5)	1.281(10)
O(4)—Re	1.996(7)	C(1)—C(5)	1.377(12)
O(2)—Re	2.122(6)	C(5)—O(6)	1.372(11)
O(5)—Re	2.111(6)	O(6)—C(4)	1.342(13)
N—Re	1.709(8)	C(4)—C(3)	1.330(15)
Bond angles			
N—Re—P	93.3(3)	O(1)—Re—P	97.4(2)
O(1)—Re—N	103.1(3)	O(2)—Re—P	167.8(1)
O(2)—Re—N	99.0(3)	O(2)—Re—O(1)	79.5(3)
O(4)—Re—P	86.7(2)	O(4)—Re—N	170.4(2)
O(4)—Re—O(1)	86.4(3)	O(4)—Re—O(2)	81.3(3)
O(5)—Re—P	90.2(2)	O(5)—Re—N	93.1(3)
O(5)—Re—O(1)	161.6(2)	O(5)—Re—O(2)	89.5(3)
O(5)—Re—O(4)	77.3(3)	C(13)—N—Re	165.5(5)

A complete listing of bond lengths and angles appears in the supplementary data.

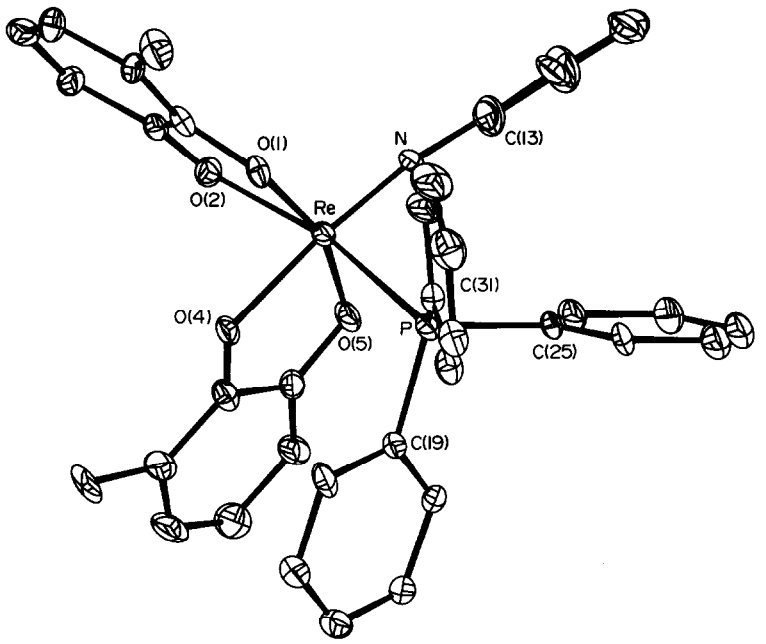

Fig. 2. The molecular structure of $[Re(maltol)_2(NPh)(PPh_3)]^+$ (**1**).

complexes.[11] The Re—N—C(13) angle of 165.5(5)° is consistent with the imido ligand functioning as a linear, four-electron donor ligand.

The O(4)—Re—O(2) angle of 81.3(3)° shows that the *cis*-maltol ligands are forced towards one another as a result of steric pressure from the bulky PPh_3 ligand. The bite angles of the maltol ligands [77.3(3) and 79.5(3)°] are similar to those found for other 1,2-disubstituted aromatic ligands. The bond lengths and angles within the BPh_4 anion are unremarkable.

Electrochemistry of complex **1**. The cyclic voltammetry of complex **1** was studied in acetonitrile solution at a platinum wire working and auxiliary electrodes, silver wire pseudo-reference electrode and 0.2 M $[Bu^n_4N][BF_4]$ as support electrolyte. An irreversible oxidation process at +1.2 V was assigned to the BPh_4 anion. A reversible reduction process is observed at $E_{1/2}$ −0.791 V (relative to SCE). The peak separation of 59.6 mV, at a scan rate of 0.2 V s^{-1}, is consistent with the process being a diffusion-controlled, reversible, one-electron reduction process. This was confirmed by convolution analysis which confirmed that the kinetics of electron transfer are rapid and that there are no accompanying homogeneous chemical processes. The reduction corresponds to the formation of a stable rhenium(IV) d^3 species $[Re(maltol)_2(NPh)(PPh_3)]$. By contrast, the precursor complex $[ReCl_3(NPh)(PPh_3)_2]$ undergoes a reversible, one-electron oxidation process at $E_{1/2}$+0.966 V[12] and two reductions at −1.05 and −1.34 V, relative to SCE, which are irreversible. The irreversibility of the reduction processes for $[ReCl_3(NPh)(PPh_3)_2]$ is almost certainly due to loss of the halide anion.

(2) *Benzoyldiazenido complex*

The chelated benzoyldiazenido(3−) complex $[ReCl_2(N_2COPh)(PPh_3)_2]$ reacts with maltol in alcohol in the presence of base to give the orange complex $[ReCl(maltol)(N_2COPh)(PPh_3)_2]$ (**2**). The IR spectrum of the product shows bands in the 1600 cm^{-1} region which are characteristic of the presence of a linear benzoyldiazenido ligand (see Scheme 1). The shift in the band of the free maltol ligand at *ca*

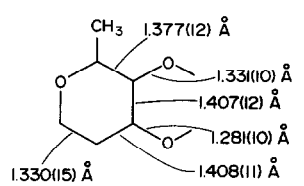

Fig. 3. Bond distances within the maltol ring.

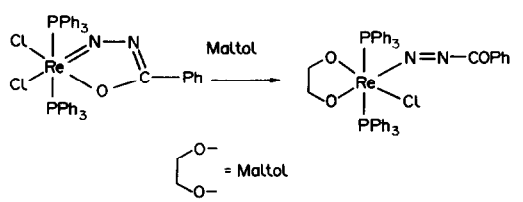

Scheme 1.

1600 cm^{-1} confirms its coordination as a bidentate ligand.

The ^1H NMR spectrum of complex **2** in $CDCl_3$ shows a doublet at 2.40 and 2.10 ppm assigned to the methyl groups of maltol. A complex multiplet at 6.4–6.8 ppm is due to one of the vinylic protons, as above. These observations are consistent with the presence of isomers due to the maltol being present in two possible orientations. The presence of two peaks in the HPLC trace at 11.6 and 13.2 min for this complex might also be in accord with the presence of isomers in solution. The $^{31}P\{^1H\}$ NMR spectrum shows a singlet at +30 ppm due to the two equivalent *trans*-phosphine ligands.

X-ray crystal structure of [ReCl(maltol)(N_2COPh)(PPh_3)$_2$] (**2**). Orange crystals of complex **2** that appeared suitable for an X-ray structure determination were obtained by slow crystallization from dichloromethane–ethanol. However, these crystals did not diffract well and although a data set was collected and the structure solved, the *R* factor remained at 13.8%. This is not appropriate for publication but did suffice to confirm the structure of the complex, a diagram of which is shown in Fig. 4. The structure is in accord with the spectroscopic data with a pseudo-octahedral geometry about rhenium with *trans*-phosphine ligands. There is no sign of disorder in the maltol ligand, so it may be that crystallization has selected single orientation for the maltol ligand shown in Fig. 4.

Electrochemistry of complex **2**. Cyclic voltammetry of **2** under analogous conditions to that above showed a reversible oxidation process at $E_{1/2}$ +0.656 V relative to SCE. The peak separation of 71 mV is suggestive of a one-electron, reversible process and the i_{pa}/i_{pc} ratio is close to unity. This process corresponds to the formation of the rhenium(IV) complex [ReCl(maltol)(N_2COPh)(PPh_3)]$^+$. A second, irreversible process occurs at +1.09 V relative to SCE which remained irreversible at the fastest scan rates. No reduction processes were observed up to potentials of −1.5 V.

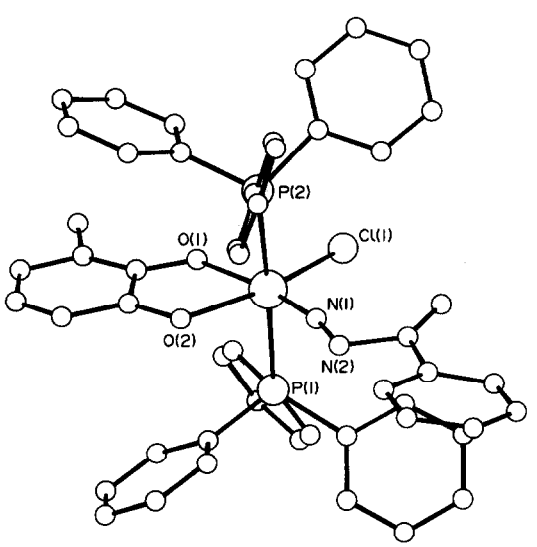

Fig. 4. Molecular structure of [ReCl(maltol)(N_2COPh)(PPh_3)$_2$] (**2**).

(3) *Other rhenium precursors*

Reaction of [$ReOCl_3(PPh_3)_2$] with maltol in ethanol under reflux in the presence of base gave a yellow–brown solution. Subsequent addition of Na[BPh_4] gave a yellow–brown solid which was recrystallized from DMF–diethyl ether. The IR spectrum confirmed the presence of chelated maltol ligands. Elemental analysis suggested the formulation [ReOCl(maltol)(PPh_3)][BPh_4], but the complex was never obtained analytically pure. Similarly, uncharacterizable complexes were obtained from [$ReNCl_2(PPh_3)_2$] and [$ReCl_3$(MeCN)(PPh_3)$_2$].

EXPERIMENTAL

Unless otherwise stated all reactions were carried out in dry solvents in conventional Schlenk glassware under an atmosphere of dinitrogen. IR spectra were recorded on a Perkin–Elmer 1350 spectrophotometer as Nujol mulls and ^1H and ^{31}P NMR spectra were measured on a Bruker WH80 spectrometer. Microanalyses were performed by the Microanalysis service of the University of Manchester. The following complexes were prepared according to the literature methods: [Re$OCl_3(PPh_3)_2$][13] and [$ReCl_2(N_2COPh)(PPh_3)_2$].[14]

Bis (maltolato) phenylimidotriphenylphosphinerhenate (V) *tetraphenylborate* (**1**)

[$ReCl_3$(NPh)(PPh_3)$_2$] (0.40 g, 4.4×10^{-4} mol), maltol (0.28 g, 2.2×10^{-3} mol) and triethylamine (0.62 ml, 4.4×10^{-3} mol) were heated under reflux in absolute ethanol (10 cm^3). Addition of Na[BPh_4] to the resulting deep green solution gave *the complex* as a dark green solid. Found: C, 64.6; H, 4.5; N, 1.2; P, 2.6. Calc. for $C_{60}H_{50}NO_6PBRe$: C, 65.0; H, 4.5; N, 1.3; P, 2.8%. ^1H NMR (ppm): 2.00 s, 2.60 s(6), maltol CH_3; 6.4 d, 6.6 d(2), vinyl protons maltol multiplet 6.8–7.5, multiplet (37), aromatic protons (integrated values in parentheses). ^{31}P NMR (ppm): 2.45.

Chloro (maltolato) benzoyldiazenidobis (triphenylphosphine)rhenium(III) (**2**)

[$ReCl_2(N_2COPh)(PPh_3)_2$] (1.0 g, 1.1×10^{-3} mol), maltol (0.74 g, 5.8×10^{-2} mol) and triethylamine

Table 2. Experimental details for the structure of $[Re(maltol)_2(NPh)(PPh_3)]^+$ (**1**)

Crystal data	
Stoichiometry	$C_{60}H_{50}NO_6PBRe$
a (Å)	13.748(1)
b (Å)	17.382(3)
c (Å)	10.781(2)
α (°)	98.26(2)
β (°)	94.67(1)
γ (°)	77.26(1)
V (Å^3)	2483.96
System	Triclinic
Space group	$P\bar{1}$
Z	2
$F(000)$	1019.9
Radiation	Mo-K_α
Lambda	0.71069
μ (cm^{-1})	25.32
Data collection	
Theta (min./max.)	1.5, 25°
Total data measured	5542
Total data unique	5316
Total data observed	4229
Significance test	$F_o > 3(F_o)$
Refinement	
Number of parameters	834
Absorption correction-psi-scan weighting factor	1.8755
R	0.0399
R_ω	0.0274

(1.6 cm^3, 0.01 mol) were heated under reflux in ethanol (20 cm^3) for 2 h. On cooling, the solution deposited a dark orange solid (0.60 g) which was recrystallized from dichloromethane–diethyl ether. Found: C, 55.0; H, 3.9; N, 2.6. Calc. for $[ReCl(maltol)(N_2COPh)(PPh_3)_2]\cdot CH_2Cl_2$: C, 54.6; H, 3.9; N, 2.6%. Due to apparent decomposition in solution to unidentifiable products, reliable ^1H and ^{31}P NMR spectra could not be obtained.

Determination of the structure of **1**

The experimental data for the structural determination is summarized in Table 2.

Acknowledgements—We are indebted to Amersham International plc for support of P.J. and to Hermann Starck, Berlin for a generous gift of rhenium metal powder.

REFERENCES

1. A. Stefanovic, J. Havel and L. Sommer, *Coll. Czech. Chem. Comm.* 1968, **33**, 4198.
2. R. C. Hider, G. Kontoghiorges, J. Silver and M. A. Stockham, *Chem. Abstr.* 1985, **102**, 694.
3. E. Chiaccierini, J. Havel and L. Sommer, *Coll. Czech. Chem. Comm.* 1968, **33**, 4215.
4. J. Hala, *Coll. Czech. Chem. Comm.* 1967, **32**, 2565.
5. M. Mikesova and M. Bartusck, *Coll. Czech. Chem. Comm.* 1979, **44**, 3256.
6. M. Bartusck and V. Sutacek, *Coll. Czech. Chem. Comm.* 1983, **48**, 2785.
7. R. Petrola, *Finn. Chem. Lett.* 1985, **5**, 219.
8. M. T. Ahmet, C. S. Frampton and J. Silver, *J. Chem. Soc., Dalton Trans.* 1988, 1159.
9. M. W. Finnegan, S. J. G. Lutz, W. O. Nelson, A. Smith and C. Orvig, *Inorg. Chem.* 1987, **26**, 2171.
10. M. W. Finnegan, S. J. Rettig and C. Orvig, *J. Am. Chem. Soc.* 1986, **108**, 5033.
11. D. A. Bright and J. A. Ibers, *Inorg. Chem.* 1969, **8**, 703.
12. J. R. Dilworth and A. Thursfield, unpublished results.
13. J. Chatt and G. A. Rowe, *J. Chem. Soc.* 1964, 2169.
14. J. Chatt, J. R. Dilworth, G. J. Leigh and V. D. Gupta, *J. Chem. Soc. A* 1971, 1012.

Polyhedron Vol. 10, No. 13, pp. 1545–1548, 1991
Printed in Great Britain

0277–5387/91 $3.00+.00
© 1991 Pergamon Press plc

MERCURY THIOETHER CHEMISTRY: THE SYNTHESIS AND X-RAY CRYSTAL STRUCTURE OF $[Hg([15]aneS_5)](PF_6)_2$

ALEXANDER J. BLAKE, ELIZABETH C. PASTEUR, GILLIAN REID and MARTIN SCHRÖDER*

Department of Chemistry, University of Edinburgh, West Mains Road, Edinburgh EH9 3JJ, Scotland, U.K.

(*Received* 9 *November* 1990; *accepted* 28 *February* 1991)

Abstract—Reaction of mercury sulphate with one molar equivalent of $[15]aneS_5$ (1,4,7,10,13-pentathiacyclopentadecane) in refluxing methanol/water for 2 h affords a colourless solution containing the complex cation $[Hg([15]aneS_5)]^{2+}$. Addition of excess NH_4PF_6 gives a white precipitate which can be recrystallized from acetonitrile/diethyl ether to give $[Hg([15]aneS_5)](PF_6)_2$ as a white solid. An X-ray crystal structure determination shows the mercury(II) ion and one thioether sulphur-donor occupying a site of *m* symmetry, with the macrocycle disordered over two equally likely conformations, neither of which possesses *m* symmetry, but which are mirror images of each other. The mercury(II) ion is bound to all five thioether donors of the macrocycle, giving a distorted square-based pyramidal stereochemistry, Hg—S = 2.491(6), 2.717(6), 2.561(8) Å.

We have been investigating the coordination chemistry of a range of thioether and mixed N_2S_4-donor macrocycles such as $[9]aneS_3$, $[15]aneS_5$, $[18]aneS_6$ and $[18]aneN_2S_4$ with transition metal ions.[1] Recently, we reported the synthesis and crystal structure of a highly unusual binuclear silver(I)

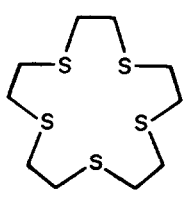

[15] ane S_5

complex $[Ag_2([15]aneS_5)_2](BPh_4)_2$.[2] The structure shows [3+1] thioether coordination to one silver(I) ion and [4+1] thioether coordination to the other, with one sulphur-donor of each macrocycle bridging asymmetrically between the two metal centres, Ag—S = 2.529(3), 2.608(4), 2.537(3), Ag···S′ = 2.907(3), Ag′—S = 2.558(4), 2.623(5), 2.716(5), 2.486(3), Ag′···S′ = 3.131(3) Å. In view of the unexpected geometry exhibited by this complex, we wondered whether similar stereochemical features would be observed upon coordination of $[15]aneS_5$ to other d^{10} metal ions. We report herein the synthesis and single crystal X-ray structure determination of $[Hg([15]aneS_5)](PF_6)_2$. Few examples of macrocyclic mercury thioether complexes have been reported. The dimeric species $[Hg_2([14]aneS_4)Cl_4]$ involves exodentate coordination of two thia-donors, with two chloride ligands completing the tetrahedral environment at each mercury(II) ion.[3] We have previously reported the synthesis and structure of $[Hg([9]aneS_3)_2]^{2+}$: this complex cation involves facial coordination of each trithia macrocycle to give a centrosymmetric, tetragonally compressed stereochemistry, Hg—S_{ap} = 2.638(3), Hg—S_{eq} = 2.728(3), 2.712(3) Å.[4] In contrast, the structure of $[Hg([18]aneN_2S_4)]^{2+}$ shows mercury(II) coordinated through all six macrocyclic donors to give a distorted octahedral geometry with the ligand in a *rac* configuration, Hg—S = 2.655(5), 2.735(4), 2.751(4), 2.639(5), Hg—N = 2.473(11), 2.472(17) Å. The small bite angle of the meridional $SCH_2CH_2NCH_2CH_2S$ linkages in $[Hg([18]aneN_2S_4)]^{2+}$ results in a large tetrahedral distortion of the four

* Author to whom correspondence should be addressed.

thioether donors out of the best S_4 coordination plane.[5]

RESULTS AND DISCUSSION

Treatment of mercury sulphate with one molar equivalent of [15]aneS$_5$ in refluxing methanol/water (1 : 1 v/v) for 2 h affords a colourless solution. Addition of excess NH_4PF_6 gives a white precipitate which was recrystallized from acetonitrile/diethyl ether. The IR spectrum of this product shows peaks consistent with the presence of coordinated [15]aneS$_5$ and of PF_6^- counterion. The FAB mass spectrum exhibits molecular ion peaks at $M^+ = 647$, 521 and 501 assigned to $[^{202}Hg([15]aneS_5)PF_6]^+$, $[^{202}Hg([15]aneS_5)\cdot H_2O+H]^+$ and $[^{202}Hg([15]aneS_5)-H]^+$, respectively. The ^1H NMR spectrum measured in $(CD_3)_2CO$ at 298 K shows a single, broad resonance at δ 3.60 ppm assigned to the methylene protons of coordinated [15]aneS$_5$. Cooling this sample to 218 K results in further broadening of this resonance. The ^{13}C DEPT NMR spectrum [$(CD_3)_2CO$] measured at 298 K shows a single resonance at δ 30.83 ppm indicating that all of the macrocyclic CH_2 groups are equivalent. These data, together with elemental analysis results, indicate the formulation [Hg([15]aneS$_5$)](PF$_6$)$_2$ for the product.

Colourless needles of adequate diffraction quality were obtained by vapour diffusion of diethyl ether into a solution of [Hg([15]aneS$_5$)](PF$_6$)$_2$ in acetone. A single crystal X-ray structure determination showed (Fig. 1) the $[Hg([15]aneS_5)]^{2+}$ cation disordered across a mirror plane. This led to two alternative positions for both C(2) and C(8) and to two independent and equally likely conformations for the macrocyclic ring. Although the mercury ion and S(1) both lie on a crystallographic mirror plane, neither of the conformations determined for the ring possess *m* symmetry, but they are mirror images of each other. This model is chemically sensible since it avoids the eclipsing of macrocyclic CH_2 groups which would occur in a conformer possessing mirror symmetry. By implication, the remaining macrocyclic carbon and sulphur atoms should also have alternative sites, but these conform sufficiently well to the mirror symmetry that different sites are not identifiable. There is a mirror plane through the F—P—F axis of each PF_6^- counteranion. The atoms S(4), S(4D), S(7), S(7D) adopt a slightly distorted square-planar arrangement, S(4)···S(4D) = 3.664(9), S(4)···S(7) = 3.491(10), S(7)···S(7D) = 3.474(12) Å, with the mercury(II) ion displaced by 0.858 Å from this plane, towards the fifth thioether donor, S(1), which occupies an apical site. Thus, the metal ion is bound via all five macrocyclic donor atoms, Hg—S(1) = 2.491(6), Hg—S(4) = 2.717(6), Hg—S(7) = 2.561(8) Å, giving a distorted square-based pyramidal stereochemistry. The plane through S(1), S(4) and S(4D) is inclined at an angle of 79.87° to that through S(4), S(4D), S(7) and S(7D). Clearly, therefore, the structure adopted by [Hg([15]aneS$_5$)](PF$_6$)$_2$ is quite different to that observed for [Ag$_2$([15]aneS$_5$)$_2$](BPh$_4$)$_2$.[2] These results emphasise the coordinative flexibility of [15]aneS$_5$.

Cyclic voltammetry of [Hg([15]aneS$_5$)](PF$_6$)$_2$ measured in acetonitrile at 298 K (0.1 M ^{n}Bu$_4$NPF$_6$

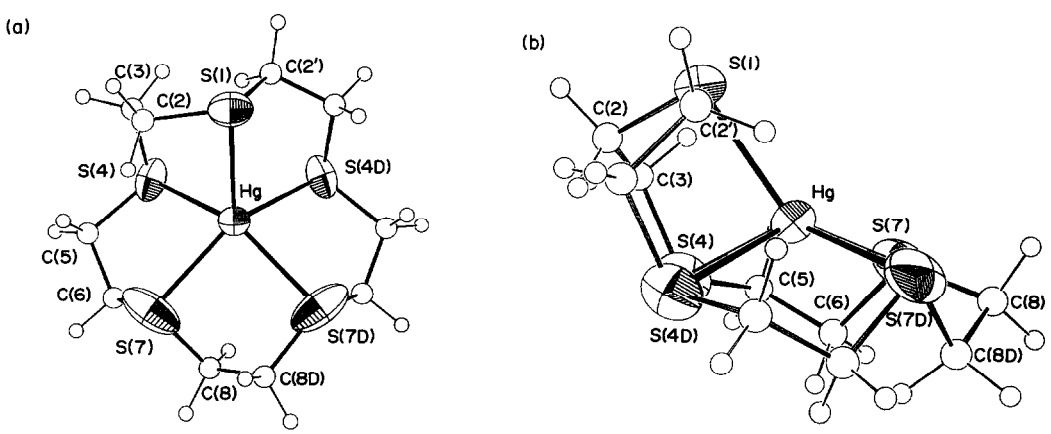

Fig. 1. (a) ORTEP plot of one conformation of $[Hg([15]aneS_5)]^{2+}$ with numbering scheme adopted. A crystallographic mirror plane passes through Hg and S(1) but C(2) and C(8) show significant deviations from this symmetry (see text). (b) Edge view.

supporting electrolyte) at platinum electrodes shows an irreversible reduction at $E_{pc} = +0.17$ V vs Fc/Fc^+ at a scan-rate of 330 mV s^{-1}. The irreversibility may be due to rapid demetallation/decomposition of the reduction product. $[Hg([9]aneS_3)_2]^{2+}$ shows a chemically reversible reduction at $E_{1/2} = -0.15$ V vs Fc/Fc^+,[4] while $[Hg([18]aneN_2S_4)]^{2+}$ shows an irreversible reduction at -1.16 V vs Fc/Fc^+.[5]

EXPERIMENTAL

IR spectra were recorded as KBr and CsI discs using a Perkin–Elmer 598 spectrometer over the range 200–4000 cm^{-1}. UV–vis spectra were measured in quartz cells using Perkin–Elmer Lambda 9 and Pye Unicam SP8-400 spectrophotometers. Microanalyses were performed by the Edinburgh University Chemistry Department Microanalytical service. Electrochemical measurements were performed on a Bruker E310 Universal Modular Polarograph. All readings were taken using a three-electrode potentiostatic system in acetonitrile containing 0.1 M $^nBu_4NPF_6$ or $^nBu_4NBF_4$ as supporting electrolyte. Cyclic voltammetric measurements were carried out using a double platinum electrode and an Ag/AgCl reference electrode. All potentials are quoted vs ferrocene/ferrocenium, Fc/Fc^+. Mass spectra were run by electron impact on a Kratos MS 902 and by fast atom bombardment on a Kratos MS 50TC spectrometer. ^1H and ^{13}C NMR spectra were obtained on Bruker WP80 and WP200 instruments.

Synthesis of $[Hg([15]aneS_5)](PF_6)_2$

Reaction of mercury sulphate (35 mg, 0.118 mmol) and [15]aneS$_5$ (35 mg, 0.116 mmol) in refluxing methanol/water (50 cm^3, 1 : 1 v/v) for 2 h under nitrogen affords a colourless solution. Cooling of the reaction mixture and addition of excess NH_4PF_6 gave a white precipitate which was recrystallized from acetonitrile/diethyl ether (Yield: 52 mg, 57%). Found: C, 15.2; H, 2.55; S, 20.3. Calc. for $[C_{10}H_{20}S_5Hg](PF_6)_2$: C, 15.2; H, 2.5; S, 20.7%. FAB mass spectrum (3-NOBA matrix): Found: $M^+ = 647$, 521 and 501. Calc. for $[^{202}Hg([15]aneS_5)PF_6]^+$: $M^+ = 647$; $[^{202}Hg([15]aneS_5)\cdot H_2O+H]^+$: $M^+ = 521$; $[^{202}Hg([15]aneS_5+H)]^+$: $M^+ = 501$. ^1H NMR spectrum [80.13 MHz, $(CD_3)_2CO$, 298 K]: δ 3.60 ppm (b, CH_2, 20H). ^{13}C DEPT NMR [50.32 MHz, $(CD_3)_2CO$, 298 K]: δ 30.83 ppm (CH_2, 10C). IR spectrum (KBr disc): 3010w, 2910m, 1420m, 1260m, 1205m, 1150w, 1120w, 840vs, 740w, 690w, 680w, 555vs cm^{-1}.

Single crystal X-ray structure determination on $[Hg([15]aneS_5)](PF_6)_2$

A colourless needle ($0.62 \times 0.05 \times 0.04$ mm) was sealed in a Lindemann glass capillary tube and mounted on a Stoë STADI-4 four circle diffractometer.

Crystal data. $[C_{10}H_{20}S_5Hg]^{2+}\cdot 2PF_6^-$, $M = 791.0$, orthorhombic, space group $Cmc2_1$, $a = 11.5487(8)$, $b = 14.4970(8)$, $c = 13.7906(8)$ Å, $V = 2308.8$ Å^3 [from 2θ values for 48 reflections measured at $\pm\omega$ ($26 < 2\theta < 28°$, $\lambda = 0.71073$ Å, $T = 298$ K)], $Z = 4$, $D_c = 2.275$ g cm^{-3}, μ(Mo-K_α) = 7.328 mm^{-1}, $F(000) = 1512$.

Data collection and processing. STADI-4 diffractometer, graphite-monochromated Mo-K_α radiation, ω–2θ scans using the learnt-profile method,[6] 880 reflections measured ($2\theta_{max} = 45°$, h 0 → 12, k 0 → 15, l 0 → 14) giving 759 with $F > 6\sigma(F)$.

Structure analysis and refinement. The mercury position was deduced from a Patterson synthesis. This was then input to DIRDIF[7] which located the positions of one phosphorus and two sulphur atoms. Subsequent iterative cycles of least-squares refinement and difference Fourier syntheses[8] located the positions of all other non-hydrogen atoms. At isotropic convergence, corrections for absorption (min. 0.755, max. 1.204) were made using DIFABS.[9] During refinement, disorder of the macrocyclic carbon atoms was identified and modelled successfully by constraining all C—C and C—S bond lengths to be 1.52 and 1.83 Å, respectively, and the angles around the carbon atoms to be tetrahedral. The two PF_6^- counteranions possess m symmetry, with one phosphorus and two fluorine atoms of each lying on a mirror plane. Anisotropic thermal parameters were refined for mercury, sulphur, phosphorus and fluorine atoms. Hydrogen atoms were included in fixed, calculated positions. The weighting scheme $w^{-1} = \sigma^2(F) + 0.0023F^2$ gave satisfactory agreement analyses. At final convergence, $R = 0.0407$, $R_w = 0.0564$, $S = 1.133$ for 130 independent parameters. At convergence the polarity of the structure was determined. This showed the R values and the uncertainties in the atomic positions to be consistently lower for the hand chosen. Excepting a peak of 1.89 e Å^{-3} close to the metal, the final difference Fourier synthesis showed no feature above 0.88 e Å^{-3}. Illustrations were prepared using ORTEPII,[10] molecular geometry calculations utilized CALC[11] and scattering factor data were inlaid[8] or taken from ref. 12. Bond lengths, angles and torsion angles are given in Table 1. Thermal parameters, fractional atomic coordinates, together with observed and calculated structure factors have been deposited with the

Table 1. Bond lengths, angles and torsion angles for $[Hg([15]aneS_5)]^{2+}$

Bond lengths (Å)			
Hg—S(1)	2.491(6)	Hg—S(7)	2.561(8)
Hg—S(4)	2.717(6)		
Angles (°) with standard deviations			
S(1)—Hg—S(4)	85.87(20)	Hg—S(4)—C(5)	96.8(5)
S(1)—Hg—S(7)	128.55(24)	C(3)—S(4)—C(5)	105.2(8)
S(4)—Hg—S(7)	82.75(22)	Hg—S(7)—C(6)	97.8(6)
S(4)—Hg—S(7D)	142.04(23)	Hg—S(7)—C(8)	91.3(13)
S(7)—Hg—S(7D)	85.4(3)	Hg—S(7)—C(8′)	98.3(14)
Hg—S(1)—C(2)	81.6(7)	C(6)—S(7)—C(8)	94.7(14)
Hg—S(1)—C(2′)	96.4(7)	C(6)—S(7)—C(8′)	122.9(16)
Hg—S(4)—C(3)	92.0(6)		
Torsion angles (°) with standard deviations			
S(1)—C(2)—C(3)—S(4)	83.1(14)	C(5)—C(6)—S(7)—C(8)	−150.6(16)
S(1)—C(2′)—C(3)—S(4)	−82.7(13)	C(5)—C(6)—S(7)—C(8′)	−163.8(19)
C(2)—C(3)—S(4)—C(5)	71.6(14)	C(6)—S(7)—C(8)—C(8D)	164.0(27)
C(2′)—C(3)—S(4)—C(5)	150.4(12)	C(6)—S(7)—C(8′)—C(8B)	64.2(33)
C(3)—S(4)—C(5)—C(6)	−141.2(11)	S(7)—C(8)—C(8D)—S(7D)	−79.3(30)
S(4)—C(5)—C(6)—S(7)	77.9(11)	S(7D)—C(8B)—C(8′)—S(7)	79.3(30)

Editor, from whom copies are available on request. Atomic coordinates have also been deposited with the Cambridge Crystallographic Data Centre.

Acknowledgement—We thank the SERC for support.

REFERENCES

1. A. J. Blake and M. Schröder, *Adv. Inorg. Chem.* 1990, **35**, 1; M. Schröder, *Pure Appl. Chem.* 1988, **60**, 517; G. Reid and M. Schröder, *Chem. Soc. Rev.* 1990, **19**, 43.
2. A. J. Blake, R. O. Gould, G. Reid and M. Schröder, *J. Chem. Soc., Chem. Commun.* 1990, 974.
3. N. W. Alcock, N. Herron and P. Moore, *J. Chem. Soc., Chem. Commun.* 1976, 886.
4. A. J. Blake, A. J. Holder, T. I. Hyde, G. Reid and M. Schröder, *Polyhedron* 1989, **8**, 2041.
5. A. J. Blake, G. Reid and M. Schröder, *Polyhedron* 1990, **9**, 2931.
6. W. Clegg, *Acta Cryst.* 1981, **A37**, 22.
7. P. T. Beurskens, W. P. Bosman, H. M. Doesbury, Th. E. M. van der Hark, P. A. J. Prick, J. H. Noordik, G. Beurskens, R. O. Gould and V. Parthasarathia, DIRDIF. Applications of Direct Methods to Difference Structure Factors, University of Nijmegen, Netherlands (1983).
8. G. M. Sheldrick, SHELX76, Program for crystal structure refinement. University of Cambridge, U.K. (1976).
9. N. Walker and D. Stuart, DIFABS, Program for empirical absorption corrections, *Acta Cryst.* 1983, **A39**, 158.
10. P. D. Mallinson and K. W. Muir, ORTEPII, interactive version, *J. Appl. Cryst.* 1985, **18**, 51.
11. R. O. Gould and P. Taylor, CALC, Fortran77 version, University of Edinburgh, Scotland (1985).
12. D. T. Cromer and J. L. Mann, *Acta Cryst.* 1968, **A24**, 321.

Polyhedron Vol. 10, No. 13, pp. 1549–1557, 1991
Printed in Great Britain

0277–5387/91 $3.00+.00
Pergamon Press plc

CARBONYL COMPLEXES OF MOLYBDENUM AND TUNGSTEN WITH FUNCTIONALIZED DIPHOSPHINES: X-RAY CRYSTAL STRUCTURE OF $[\{W(CO)_3\}_2\{\mu\text{-}P(C_6H_4SMe\text{-}2)_2CH_2CH_2P(C_6H_4SMe\text{-}2)_2\}]$

MOHAMMAD F. M. AL-DULAYMMI, PETER B. HITCHCOCK and RAYMOND L. RICHARDS*

AFRC Institute of Plant Science Research, Nitrogen Fixation Laboratory and School of Chemistry and Molecular Sciences, University of Sussex, Brighton BN1 9RQ, U.K.

(*Received* 14 *November* 1990; *accepted* 28 *February* 1991)

Abstract—The diphosphine-bridged, binuclear complexes $[\{M(CO)_3\}_2(\mu\text{-diphos})]$ (M = Mo or W; diphos = mtppm, mtppe or iptppe) have been prepared. Their binuclear structures are established by the X-ray structure of $[\{W(CO)_3\}_2(\mu\text{-mtppe})]$, in which each tungsten is ligated by three carbonyl groups in a facial arrangement with P,S,S ligation from the bridging mtppe ligand completing the octahedral geometry [average d(W—S) 2.514(9), d (W—P) 2.420(6) Å]. The bridged complexes $[\{M(CO)_4\}_2(\mu\text{-dppmpe})]$ and $[\{MBr_2(CO)_2\}_2(\mu\text{-mtppe})]$ and the mononuclear compounds $[M(CO)_4(dbtpe)]$ and $[MoBr_2(CO)_2(mtppe)]$ are also described.

The chemistry of molybdenum and tungsten with phosphine co-ligands has allowed study of the reactions of a range of small molecules such as N_2, RC≡CR′, CO, RNC, etc., bound at electron-rich centres.[1] Recently there has been great interest in the chemistry of molybdenum and related metals with sulphur-donor ligands because of the involvement of sulphur-ligated molybdenum in catalytic processes such as hydrodesulphurization and dinitrogen reduction.[2,3]

We have prepared a series of functionalized diphosphine ligands[4] which allows us to study the behaviour of metals such as low-valent molybdenum and tungsten in, *inter alia*, a phosphorus–sulphur environment.

We have briefly reported some of our work in this area with molybdenum and tungsten carbonyls[5] and here we describe this work in detail; it involves the preparation of the series of binuclear carbonyl complexes $[\{M(CO)_3\}_2(\mu\text{-diphos})]$, $[\{M(CO)_4\}_2(\mu\text{-diphos})]$ and $[\{MBr_2(CO)_2\}_2(\mu\text{-diphos})]$ and the mononuclear complexes $[M(CO)_4(diphos)]$ and $[MoBr_2(CO)_2(diphos)]$ (M = Mo or W; diphos = diphosphine as described below).

* Author to whom correspondence should be addressed.

RESULTS AND DISCUSSION

We begin by defining our nomenclature for the diphosphines mtppm **(Ia)**, mtppe **(Ib)**, iptppe **(Ic)**, dppmpe **(II)** and dptpe **(III)** as shown in Fig. 1. They were prepared by the methods already described.[4]

Binuclear complexes

The reactions of mtppm, mtppe and iptppe with $[M(CO)_3(MeCN)_3]$ (M = Mo or W) in a 1 : 2 molar ratio in refluxing tetrahydrofuran (THF) produced yellow, crystalline bimetallic complexes of general formula $[\{M(CO)_3\}_2(\mu\text{-diphos})]$ (**1–3** and **6–8** in Table 1) [i.e. eq. (1)]

$$2[M(CO)_3(MeCN)_3] + \begin{matrix}\text{mtppm}\\ \text{mtppe}\\ \text{iptppe}\end{matrix} \xrightarrow[\text{reflux}]{\text{THF}} [\{M(CO)_3\}_2(\mu\text{-diphos})] + 6MeCN. \quad (1)$$

Analytical and spectroscopic data for these complexes are shown in Table 1; all complexes show a singlet in their $^{31}P\{H\}$ NMR spectra and CO bands in their IR spectra characteristic of tricarbonyl complexes.[6,7] They are sparingly soluble in organic solvents but can be recrystallized from hot dimethyl formamide or dimethyl sulphoxide (DMSO). They

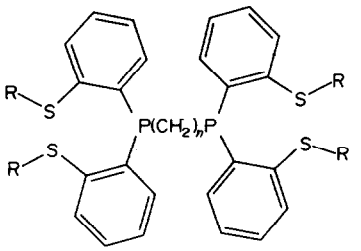

(Ia) $n = 1$, R = methyl
bis{bis(2-methylthiophenyl)phosphino}methane (mtppm)
(Ib) $n = 2$, R = methyl
1,2-bis{bis(2-methylthiophenyl)phosphino}ethane (mtppe)
(Ic) $n = 2$, R = isopropyl
1,2-bis{bis(2-isopropylthiophenyl)phosphino}ethane (iptppe)

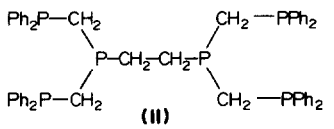

(II)

1,1,4,4-tetrakis(diphenylphosphinomethyl)-1,4-diphosphabutane, or
1,2-bis{(diphenylphosphinomethyl)phosphino}ethane (dppmpe)

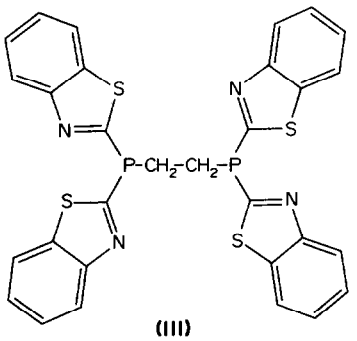

(III)

1,2-bis(dibenzothiazoylphosphino)ethane (dbtpe)

Fig. 1. Functionalized disphosphines.

are stable to air in the solid state but decompose slowly in solution. These complexes and others described later often contain solvent of crystallization, established by analysis and NMR spectroscopy.

The binuclear structure of these compounds has been established by an X-ray structure determination of $[\{W(CO)_3\}_2(\mu\text{-mtppe})]\cdot DMSO$ (7). The molecular structure of **7** is shown in Fig. 2. The unit cell consists of two molecules of the complex, each lying across a crystallographic inversion centre, with two molecules of DMSO in general positions. The single crystal was triclinic, space group $P\bar{1}$.

Each tungsten is coordinated by three facial carbonyl groups, two sulphur atoms and one phosphorus atom, the ethylene bridge of the diphosphine joins the two octahedrally-coordinated metal units. Selected bond distances and angles are given in Table 2. The W—P bond distances, av. 2.420(6) Å are close to the W—S distance [av. 2.514(9) Å]. The metal–carbonyl distances of about 1.97 Å are in the normal range for such compounds.[8] These structures are analogous to that proposed for the tricarbonyl derivative of the hexadentate diphosphine 1,2-bis{bis(diphenylphosphinoethyl)phosphino}ethane (bdpepe), $[\{Mo(CO)_3\}\mu\text{-(bdpepe)}]$.[9]

The hexaphosphine, dppmpe, reacts with two moles of $[M(CO)_3(MeCN)_3]$ to give clear yellow solutions from which complexes (**4** and **9**) have been precipitated as pale yellow solids by addition of hexane. These complexes are more soluble in organic solvents than the thiophenyldiphosphine complexes discussed above. Moreover, their IR spectra show four CO bands (2020, 1937, 1850 and 1830 cm^{-1}, M = Mo; 2017, 1930, 1885 and 1840 cm^{-1}, M = W) which differs considerably from the spectra of complexes **1–3** and **6–8** (Table 1) and of complex $[\{Mo(CO)_3\}_2(\mu\text{-bdpepe})]$, which shows only two characteristic CO bands.[9] The number and frequencies of the CO bands of **4** and **9** are in fact very similar to those observed for tetracarbonyl complexes $[M(CO)_4L_2]$.[9] The $^{31}P\{^1H\}$ NMR spectra for both complexes are more complicated than that of the free ligand,[4] which has an $AA'B_2B_2'$ spectrum,[10] but it can be seen that the chemical shift of the phosphorus giving the B pattern is moved to lower field by about 100 ppm compared with the free ligand (−165 ppm), whereas the A pattern occurs at essentially the same chemical shift as the free ligand (−170 ppm). Thus only the terminal phosphorus atoms (B) are involved in coordination to the metal and the internal phosphorus atoms (A) are uncoordinated. Therefore complexes **4** and **9**

Table 1. Data for carbonyl–polyphosphine complexes

Number[a]	Complex	Analyses[b] C	H	$^{31}P[^1H]$ (δ ppm)[c,d]	^1H (δ ppm)[c,e]	ν(CO) (cm^{-1})[f]
1	$[\{Mo(CO)_3\}_2(\mu\text{-mtppm})]\cdot thf$	46.8(46.8)	3.9(3.8)	−81.5	2.7(s, 12H, CH_3); 4.3(t, 2H, CH_2); 7.4–8.0(m, 16H, Ph)	1935s, 1840sh, 1820sh, 1800b
2	$[\{Mo(CO)_3\}_2(\mu\text{-mtppe})]\cdot thf$	47.2(47.4)	3.7(3.9)	−62.1	2.6(t, 4H, CH_2); 2.9(s, 12H, CH_3); 7.5–8.0(m, 16H, Ph)	1930s, 1835sh, 1800b
3	$[\{Mo(CO)_3\}_2(\mu\text{-iptppe})]\cdot thf$	51.5(51.2)	4.8(5.0)	—	—	1930s, 1836m, 1805m
4	$[\{Mo(CO)_4\}_2(\mu\text{-dppmpe})]$	57.4(57.2)	4.4(4.0)	Multiple bands (−90 to −170)	1.6–3.5(m, 12H, CH_2); 7.2–7.8(m, 40H, Ph)	2020m, 1937s, 1850b, 1830b
5	$[Mo(CO)_4(dbtpe)]\cdot thf$	50.6(50.3)	3.2(3.1)[g]	−80.7	7.3–8.0(m, 16H, Ph)	2038m, 1948s, 1970s, 1859s
6	$[\{W(CO)_3\}_2(\mu\text{-mtppm})]\cdot thf$	35.9(35.7)	2.5(2.6)	−80.9 J_{W-P} = 198 Hz	2.99(s, 12H, CH_3); 5.1(t, 2H, CH_2); 7.4–8.6(m, 16H, Ph)	1932s, 1840sh, 1786b
7	$[\{W(CO)_3\}_2(\mu\text{-mtppe})]\cdot thf$	40.8(40.4)	3.3(3.4)	−65.5 J_{W-P} = 188 Hz	2.6(m, 4H, CH_2); 3.09(s, 12H, CH_3); 7.5–8.0(m, 16H, Ph)	1920s, 1827b, 1790b
8	$[\{W(CO)_3\}_2(\mu\text{-iptppe})]\cdot thf$	44.1(44.3)	4.2(4.3)	−74.2	1.1–1.5(dd, 24H, CH_3); 3.9(t, 4H, CH); 3.6(s, 4H, CH_2); 7.5(m, 16H, Ph)	1920b, 1835b, 1794b
9	$[\{W(CO)_4\}_2(\mu\text{-dppmpe})]$	50.7(50.4)	3.7(3.5)	Multiple bands (−110 to −180)	1.2–2.7(m, 12H, CH_2); 7.2–7.6(m, 40H, Ph)	2017s, 1930s, 1885b, 1840b
10	$[W(CO)_4(dbtpe)]\cdot thf$	45.4(45.9)	2.8(2.8)[h]	—	7.1–8.0(m, 16H, Ph)	2028m, 1960s, 1980s, 1859s
11	$[\{MoBr_2(CO)_2\}_2(\mu\text{-mtppe})]\cdot 2CH_2Cl_2$	31.4(31.4)	2.4(2.6)	−43.7	2.6(t, 4H, CH_2); 3.5(s, 12H, CH_3); 7.7(m, 16H, Ph)	1984ms, 1910ms
12	$[MoBr_2(CO)_2(mtppe)]$	42.7(43.0)	3.7(3.6)	−8.0 AB system $J_{P_A-P_B}$ = 65.9 Hz	2–3 ppm(CH_3 singlets)	1900s
13	$[MoBr_2(CO)_2(dbtpe)]$	41.2(41.0)	2.1(2.1)[i]	—	—	1969s, 1885s
14	$[WBr_2(CO)_2(dbtpe)]$	37.6(37.5)	2.1(2.0)[j]	—	—	1957s, 1871s

[a] See text.
[b] Calculated values in parentheses.
[c] **1** and **10** in $C^2H_2Cl_2$; **2b** and **7** in DMSO-$^2H_6$; **4**, **5** and **9** in C^2HCl_3; **8** in pyridine-$^2H_5$.
[d] Relative to $P(OMe)_3$.
[e] Relative to $SiMe_4$.
[f] Nujol mulls; b = broad, m = medium, s = strong, sh = shoulder.
[g] N; 6.4(6.2).
[h] N; 5.6(5.6).
[i] N; 6.0(6.0).
[j] N; 5.4(5.5).

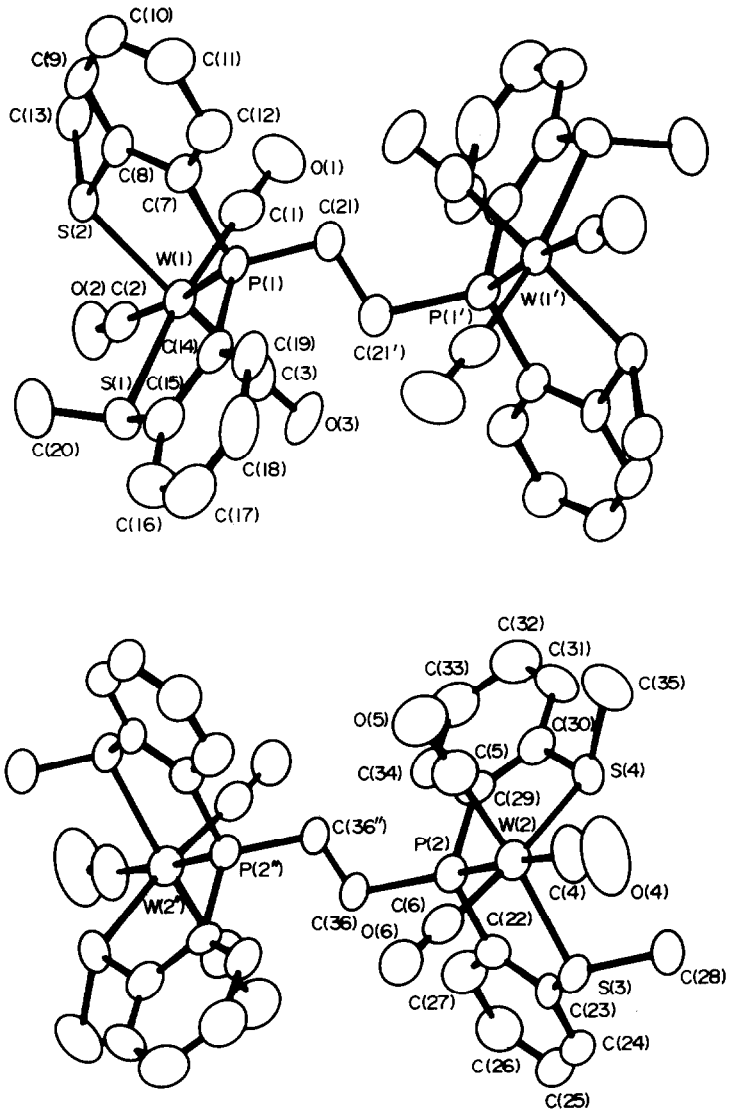

Fig. 2. Structure of $[\{W(CO)_3\}_2(\mu\text{-mtppe})]$ (**7**).

are formulated as binuclear, diphosphine-bridged tetracarbonyl complexes $[\{M(CO)_4\}_2(\mu\text{-dppmpe})]$ as shown in reaction (2):

$$[M(CO)_3(MeCN)_3] + \text{dppmpe} \xrightarrow[\text{reflux}]{\text{THF}} \quad (2)$$

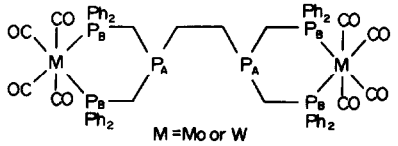

The mechanism of this reaction, which involves disproportionation at some stage to generate extra carbon monoxide, has not been investigated. Presumably the tetracarbonyl species is formed to avoid the highly strained, four-membered ring, which coordination of a third phosphorus atom to each metal would produce.

Mononuclear complexes

When a 1:2 molar ratio of dbtpe and $[M(CO)_3(MeCN)_3]$ was allowed to react in refluxing THF for 20 h, a dark brown pyrophoric mixture was obtained. If, however, a 1:1 molar ratio was used, the mononuclear, olive green complexes $[M(CO)_4(\text{dbtpe})]$ (**5**) and (**10**) were obtained. Their structure [Fig. 3(a)] has been assigned on the basis of the spectroscopic and analytical data shown in Table 1. In particular, for **5**, the $\nu(CO)$ values of 2038, 1948, 1878 and 1839 cm^{-1} are very close to those of $[Mo(CO)_4(Ph_2PCH_2CH_2PPh_2)]$ (2020,

Table 2. Intramolecular distances (Å) and angles (°) with ESDs in parentheses

(a) Bonds

W(1)—S(1)	2.515(3)	W(1)—S(2)	2.509(2)
W(1)—P(1)	2.426(2)	W(1)—C(1)	1.950(11)
W(1)—C(2)	1.974(10)	W(1)—C(3)	1.971(7)
W(2)—S(3)	2.504(2)	W(2)—S(4)	2.529(3)
W(2)—P(2)	2.413(3)	W(2)—C(4)	1.957(12)
W(2)—C(5)	1.959(10)	W(2)—C(6)	1.932(11)
S(1)—C(15)	1.785(10)	S(1)—C(20)	1.765(11)
S(2)—C(8)	1.790(10)	S(2)—C(13)	1.810(11)
S(3)—C(23)	1.771(10)	S(3)—C(28)	1.804(11)
S(4)—C(30)	1.800(11)	S(4)—C(35)	1.809(13)
P(1)—C(7)	1.832(7)	P(1)—C(14)	1.834(10)
P(1)—C(21)	1.827(9)	P(2)—C(22)	1.824(8)
P(2)—C(29)	1.843(10)	P(2)—C(36)	1.825(10)
O(1)—C(1)	1.155(14)	O(2)—C(2)	1.157(12)
O(3)—C(3)	1.152(9)	O(4)—C(4)	1.18(2)
O(5)—C(5)	1.159(13)	O(6)—C(6)	1.160(14)
C(7)—C(8)	1.390(11)	C(7)—C(12)	1.403(14)
C(8)—C(9)	1.382(10)	C(9)—C(10)	1.382(15)
C(10)—C(11)	1.353(15)	C(11)—C(12)	1.374(11)
C(14)—C(15)	1.393(15)	C(14)—C(19)	1.401(14)
C(15)—C(16)	1.38(2)	C(16)—C(17)	1.38(2)
C(17)—C(18)	1.37(2)	C(18)—C(19)	1.375(15)
C(21)—C(21′)	1.506(10)	C(22)—C(23)	1.402(12)
C(22)—C(27)	1.39(2)	C(23)—C(24)	1.382(11)
C(24)—C(25)	1.35(2)	C(25)—C(26)	1.38(2)
C(26)—C(27)	1.394(13)	C(29)—C(30)	1.38(2)
C(29)—C(34)	1.385(14)	C(30)—C(31)	1.37(2)
C(31)—C(32)	1.41(2)	C(32)—C(33)	1.37(2)
C(33)—C(34)	1.39(2)	C(36)—C(36″)	1.524(11)
S(5)—O(7)	1.46(2)	S(5)—C(37)	1.78(2)
S(5)—C(38)	1.75(2)		

(b) Angles

S(1)—W(1)—S(2)	91.03(8)	S(1)—W(1)—P(1)	80.27(9)
S(1)—W(1)—C(1)	169.9(3)	S(1)—W(1)—C(2)	97.0(3)
S(1)—W(1)—C(3)	88.9(3)	S(2)—W(1)—P(1)	80.01(7)
S(2)—W(1)—C(1)	93.5(2)	S(2)—W(1)—C(2)	91.4(2)
S(2)—W(1)—C(3)	179.2(3)	P(1)—W(1)—C(1)	91.7(3)
P(1)—W(1)—C(2)	170.9(2)	P(1)—W(1)—C(3)	99.2(3)
C(1)—W(1)—C(2)	91.9(4)	C(1)—W(1)—C(3)	86.4(4)
C(2)—W(1)—C(3)	89.5(4)	S(3)—W(2)—S(4)	88.42(8)
S(3)—W(2)—P(2)	80.84(8)	S(3)—W(2)—C(4)	92.0(3)
S(3)—W(2)—C(5)	174.8(4)	S(3)—W(2)—C(6)	92.7(3)
S(4)—W(2)—P(2)	78.5(1)	S(4)—W(2)—C(4)	96.1(4)
S(4)—W(2)—C(5)	91.0(4)	S(4)—W(2)—C(6)	174.6(3)
P(2)—W(2)—C(4)	171.0(3)	P(2)—W(2)—C(5)	93.9(4)
P(2)—W(2)—C(6)	96.5(3)	C(4)—W(2)—C(5)	93.3(5)
C(4)—W(2)—C(6)	89.2(5)	C(5)—W(2)—C(6)	87.5(5)
W(1)—S(1)—C(15)	108.6(4)	W(1)—S(1)—C(20)	116.6(4)
C(15)—S(1)—C(20)	99.7(6)	W(1)—S(2)—C(8)	108.3(2)
W(1)—S(2)—C(13)	108.9(3)	C(8)—S(2)—C(13)	101.6(5)
W(2)—S(3)—C(23)	108.7(3)	W(2)—S(3)—C(28)	112.5(3)
C(23)—S(3)—C(28)	100.9(5)	W(2)—S(4)—C(30)	106.2(4)
W(2)—S(4)—C(35)	108.0(5)	C(30)—S(4)—C(35)	103.7(5)
W(1)—P(1)—C(7)	109.7(3)	W(1)—P(1)—C(14)	110.4(3)
W(1)—P(1)—C(21)	122.2(3)	C(7)—P(1)—C(14)	105.8(4)
C(7)—P(1)—C(21)	104.7(4)	C(14)—P(1)—C(21)	102.7(4)
W(2)—P(2)—C(22)	110.5(3)	W(2)—P(2)—C(29)	108.9(3)

Table 2—*continued*

(b) Angles

W(2)—P(2)—C(36)	123.0(3)	C(22)—P(2)—C(29)	103.0(4)
C(22)—P(2)—C(36)	103.2(4)	C(29)—P(2)—C(36)	106.3(4)
W(1)—C(1)—O(1)	176.5(7)	W(1)—C(2)—O(2)	176.4(9)
W(1)—C(3)—O(3)	176.4(9)	W(2)—C(4)—O(4)	174(1)
W(2)—C(5)—O(5)	178(1)	W(2)—C(6)—O(6)	179(1)
P(1)—C(7)—C(8)	119.3(7)	P(1)—C(7)—C(12)	123.2(6)
C(8)—C(7)—C(12)	117.5(7)	S(2)—C(8)—C(7)	119.6(6)
S(2)—C(8)—C(9)	119.2(7)	C(7)—C(8)—C(9)	121.0(9)
C(8)—C(9)—C(10)	119.6(8)	C(9)—C(10)—C(11)	120.4(8)
C(10)—C(11)—C(12)	121(1)	C(7)—C(12)—C(11)	120.8(9)
P(1)—C(14)—C(15)	118.6(7)	P(1)—C(14)—C(19)	123.2(8)
C(15)—C(14)—C(19)	118.0(9)	S(1)—C(15)—C(14)	120.8(8)
S(1)—C(15)—C(16)	118.1(8)	C(14)—C(15)—C(16)	121.0(9)
C(15)—C(16)—C(17)	119(1)	C(16)—C(17)—C(18)	121(1)
C(17)—C(18)—C(19)	120(1)	C(14)—C(19)—C(18)	121(1)
P(1)—C(21)—C(21′)	110.9(6)	P(2)—C(33)—C(23)	118.8(7)
P(2)—C(22)—C(27)	122.1(7)	C(23)—C(22)—C(27)	119.1(7)
S(3)—C(23)—C(22)	120.7(6)	S(3)—C(23)—C(24)	119.3(7)
C(22)—C(23)—C(24)	119.9(9)	C(23)—C(24)—C(25)	120.6(9)
C(24)—C(25)—C(26)	120.9(9)	C(25)—C(26)—C(27)	120(1)
C(22)—C(27)—C(26)	120(1)	P(2)—C(29)—C(30)	117.8(8)
P(2)—C(29)—C(34)	122.5(8)	C(30)—C(29)—C(34)	120(1)
S(4)—C(30)—C(29)	119.6(8)	S(4)—C(30)—C(31)	119.0(9)
C(29)—C(30)—C(31)	121(1)	C(30)—C(31)—C(32)	119(1)
C(31)—C(32)—C(33)	120(1)	C(32)—C(33)—C(34)	120(1)
C(29)—C(34)—C(33)	120(1)	P(2)—C(36)—C(36″)	112.1(7)
O(7)—S(5)—C(37)	115(1)	O(7)—S(5)—C(38)	104(1)
C(37)—S(5)—C(38)	96.3(9)		

Symmetry elements: ′ $1-x, 2-y, -z$; ″ $-x, 1-y, 1-z$.

1919, 1907 and 1881 cm^{-1})[9] and the $^{31}P\{^1H\}$ NMR spectrum has a singlet resonance, i.e. **5** has equivalent phosphorus atoms. Again a disproportionation reaction has taken place to give tetracarbonyls from the tricarbonyl precursor. Compounds **5** and **10** can be prepared by direct reaction of $[M(CO)_6]$ and dbtpe in diglyme, but in low yield.

Treatment of a freshly prepared dichloromethane solution of $[\{MoBr_2(CO)_4\}_2]$ with a dichloromethane solution of mtppe at 20°C gave two products, in the form of red crystals (**11**) and yellow–orange crystals (**12**).

Compound **11** has equivalent phosphorus atoms (singlet ^{31}P NMR spectrum, Table 1) and two CO bands at 1984 and 1910 cm^{-1}, close to the values observed for complex $[\{MoBr_2(CO)_2(dppe)\}_2(\mu\text{-dppe})]$ at 1935 and 1855 cm^{-1}.[11] A likely structure for **11**, consistent with these observations and with analytical data (Table 1), is a bimetallic seven-coordinate structure [as in Fig. 3(b)]. Complex **12** has inequivalent phosphorus atoms (^{31}P NMR spectrum, Table 1) and only one CO band at 1900 cm^{-1} suggesting *trans*-carbonyl groups. A possible structure for **12** is therefore as shown in Fig. 3(c). The reaction of $[WBr_2(CO)_4]$ with tmppe did not give a clean product.

Reaction of $[\{MBr_2(CO)_4\}_2]$ with dbtpe yields salmon pink complexes (**13** and **14**) which are not soluble in common organic solvents. The two CO bands (Table 1) indicate a *cis*-$(CO)_2$ arrangement and a possible structure for **13** and **14** is as shown in Fig. 3(d). Their poor solubility has prevented further characterization.

EXPERIMENTAL

All operations were carried out under pure dinitrogen using standard Schlenk and high vacuum techniques. All solvents were dried and degassed before use. Spectroscopic measurements were made using: NMR, JeoL FX90Q, JeoL GSX270, Brucker WP80 or Brucker WM360 instruments; IR; Perkin–Elmer 598 or 883 instruments; mass spectra, Kratos MS80 RF instrument. Microanalyses were determined by Mr C. J. Macdonald of the Nitrogen

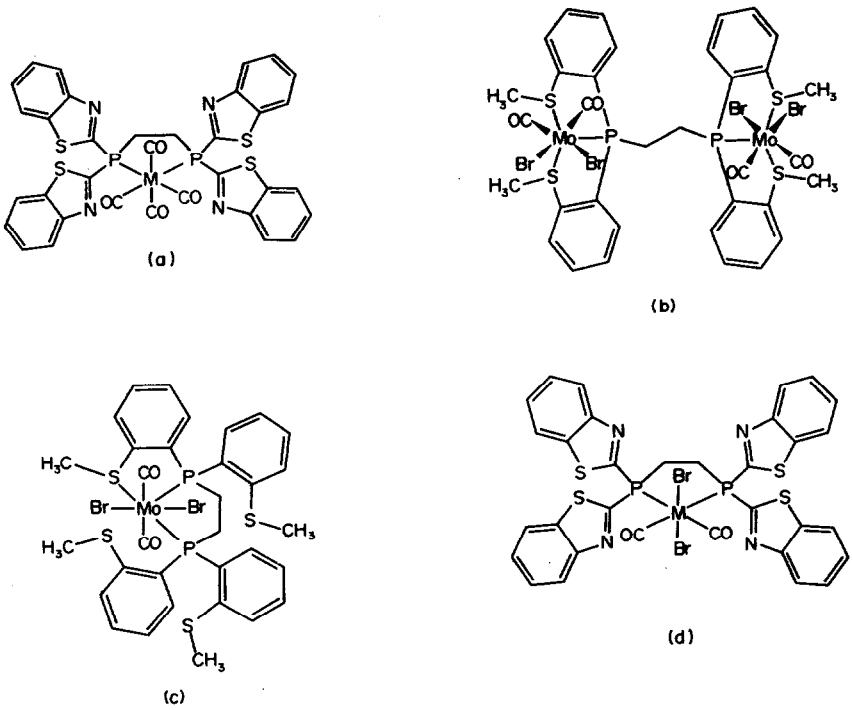

Fig. 3.

Fixation Laboratory or Ms K. Plowman of the University of Sussex. $[M(CO)_3(MeCN)_3]$[12] and $[\{MBr_2(CO)_4\}_2]$[13] were prepared by published methods.

Preparation of $[\{Mo(CO)_3\}_2(\mu\text{-mtppm})]\cdot$thf (**1**)

A mixture of $[Mo(CO)_3(MeCN)_3]$ (0.64 g, 2.1 mmol) and mtppm (0.6 g, 1.1 mmol) in thf (80 cm^3) was refluxed for 40 h, and the resulting yellow solution concentrated to *ca* 40 cm^3. The fine, yellow solid which precipitated was filtered off and dried *in vacuo*. (Yield 0.45 g, 43%.)

Preparation of $[\{Mo(CO)_3\}_2(\mu\text{-mtppe})]\cdot$thf (**2**)

A mixture of $[Mo(CO)_3(MeCN)_3]$ (0.84 g, 2.8 mmol) and mtppe (0.81 g, 1.4 mmol) in thf (100 cm^3) was refluxed under dinitrogen for 20 h, during which time a yellow, crystalline complex formed from the clear solution. This was filtered off and dried *in vacuo*. (Yield 1.0 g, 71%, m.p.: decomposed above 230°C.)

Preparation of $[\{Mo(CO)_3\}_2(\mu\text{-iptppe})]\cdot$thf (**3**)

A mixture of $[Mo(CO)_3(MeCN)_3]$ (0.7 g, 2.3 mmol), iptppe (0.8 g, 1.2 mmol) and thf (100 cm^3) was refluxed for 20 h. The yellow, crystalline solid which precipitated was filtered off, washed with thf and dried *in vacuo*. (Yield 0.85 g, 65.5%:)

Preparation of $[\{Mo(CO)_4\}_2(\mu\text{-dppmpe})]$ (**4**)

A mixture of $[Mo(CO)_3(MeCN_3]$ (1.0 g, 3.3 mmol), dppmpe (1.46 g, 1.65 mmol) and thf (100 cm^3) was refluxed for 48 h. The clear, yellow solution was cooled to room temperature and filtered from the trace of solid, then concentrated to *ca* 40 cm^3. Hexane (50 cm^3) was added to give pale, yellow material which was filtered off and dried *in vacuo*. (Yield 0.9 g, 42%.)

Preparation of $[Mo(CO)_4(dbtpe)]\cdot$thf (**5**)

A mixture of $[Mo(CO)_3(MeCN)_3]$ (0.64 g, 2.1 mmol), dbtpe (1.32 g, 2.1 mmol) and thf (100 cm^3) was refluxed for 24 h. The deep brown solution was filtered and the filtrate concentrated to *ca* 40 cm^3. Hexane (50 cm^3) was added to give an olive green solid, which was filtered off and dried *in vacuo*. (Yield 1.0 g, 52%.)

Preparation of $[\{W(CO)_3\}_2(\mu\text{-mtppm})]\cdot$thf (**6**)

A mixture of $[W(CO)_3(MeCN)_3]$ 0.65 g, 1.66 mmol), mtppm (0.47 g, 0.83 mmol) and thf (80 cm^3) was refluxed for 48 h. The yellow, crystalline solid

was filtered off washed with thf and dried *in vacuo*. (Yield 0.4 g, 41%.)

Preparation of $[\{W(CO)_3\}_2(\mu\text{-mtppe})]\cdot$thf (**7**)

A mixture of $[W(CO)_3(MeCN)_3]$ (0.8 g, 2.0 mmol), mtppe (0.6 g, 1.0 mmol) and thf (100 cm^3) was heated under reflux for 48 h, during which time all the solid material dissolved, then a yellow, crystalline solid precipitated. The mixture was cooled to room temperature and the yellow crystals filtered off, washed with thf and dried *in vacuo*. (Yield 0.6 g, 52%.)

X-ray structure analysis of $[\{W(CO)_3\}_2(\mu\text{-mtppe})]\cdot$DMSO

Crystal data: $[C_{36}H_{32}O_6P_2S_4W_2][C_2H_6OS]$, $M = 1196.7$, triclinic, space group $P\bar{1}$, $a = 11.455(2)$, $b = 11.510(1)$, $c = 17.073(2)$ Å, $\alpha = 105.22(1)$, $\beta = 97.36(1)$, $\gamma = 101.35(1)°$, $U = 2090.6$ Å^2, $Z = 2$, $D = 1.90$ g cm^{-3}, Mo-K_α radiation (graphite monochromator), $\lambda = 0.71069$ Å, $\mu = 59.8$ cm^{-1}.

Data were collected using a crystal, *ca* $0.4\times0.2\times0.1$ mm, on an Enraf–Nonius CAD4 diffractometer in the θ–2θ mode, with $\Delta\theta = (0.8+0.35\tan\theta)°$, and a maximum scan time of 1 min. A total of 5093 unique reflections were measured for $2 < \theta < 22°$ and $+h\pm k\pm l$, and 4112 reflections with $|F^2| > \sigma(F^2)$ were used in the refinement where $\sigma(F^2) = \{\sigma^2(I)+(0.04I)^2\}^{1/2}/\text{Lp}$. There was no crystal decay. An empirical absorption correction was made using DIFABS[14] with maximum and minimum corrections of 1.12 and 0.84.

The structure was solved by routine heavy atom methods and refined by full-matrix least-squares with non-hydrogen atoms anisotropic. Hydrogen atoms, except for those on the molecule of dimethyl sulphoxide solvent, were included at fixed calculated positions and B_{iso} of 6.0 Å. The weighting scheme was $w = 1/\sigma^2(F)$ and the final residuals were $R = 0.032$, $R' = 0.043$. Programs for the Enraf–Nonius SDP-plus package were run on a PDP 11/34 computer. Atomic coordinates, displacement factor coefficients, full lists of bond lengths and angles and F_o/F_c lists have been deposited as supplementary data with the Editor, from whom copies are available on request. Atomic coordinates have also been deposited with the Cambridge Crystallographic Data Centre.

Preparation of $[\{W(CO)_3\}_2(\mu\text{-iptppe})]\cdot$thf (**8**)

A mixture of $[W(CO)_3(MeCN)_3]$ (0.53 g, 1.36 mmol), iptppe (0.47 g, 6.8 mmol) and thf (80 cm^3) was refluxed for 48 h, during which time all the solid initially dissolved and a yellow, crystalline precipitate appeared. This was filtered off, washed with thf and dried *in vacuo*. (Yield 0.45 g, 56%, m.p.: decomposed above 230°C.)

Preparation of $[\{W(CO)_4\}_2(\mu\text{-dppmpe})]$ (**9**)

A mixture of $[W(CO)_3(MeCN)_3]$ (0.71 g, 1.8 mmol), dppmpe (0.8 g, 0.9 mmol) and thf (100 cm^3) was refluxed for 48 h. The clear, yellow solution was cooled to room temperature and filtered. The filtrate was concentrated to *ca* 40 cm^3, then hexane was added to give the product as a pale yellow solid, analytically pure. (Yield 0.9 g, 67.5%.)

Preparation of $[W(CO)_4(\text{dbtpe})]\cdot$thf (**10**)

A mixture of $[W(CO)_3(MeCN)_3]$ (0.81 g, 2.0 mmol), dbtpe (1.3 g, 2.0 mmol) and thf (80 cm^3) was heated under reflux for 20 h, during which time the yellow solution changed to dark green, and most of the solid dissolved. The solution was cooled to room temperature and filtered. The filtrate was concentrated to *ca* 40 cm^3 and hexane was added to give an olive green complex, which was filtered off and dried *in vacuo*. (Yield 1.2 g, 60%.)

Reaction of $[MoBr_2(CO)_4]$ with mtppe

To a suspension of $[Mo(CO)_6]$ (1.0 g, 3.79 mmol) in dichloromethane (30 cm^3), cooled to −78°C, was added bromine (12 drops) and the mixture was left stirring at −78°C for 45 min, then at room temperature for 15 min. The resulting red solution was filtered into another flask containing a suspension of mtppe (1.2 g, 2.1 mmol) in dichloromethane (30 cm^3), and the mixture stirred for a further 4 h. The solution was concentrated *in vacuo* to 30 cm^3 and hexane added until the mixture became turbid. This was then filtered and the filtrate left in the freezer overnight to give red–orange crystals (**11**) which were filtered off and dried *in vacuo*. Hexane was added to the filtrate to give a yellow–orange complex (**12**). Complex **11** was identified as $[\{MoBr_2(CO)_2\}_2(\mu\text{-mtppe})]\cdot 2CH_2Cl_2$ and complex **12** was identified as $[MoBr_2(CO)_2(\text{mtppe})]$.

Preparation of $[MoBr_2(CO)_2(\text{dbtpe})]$ (**13**)

A solution of $[MoBr_2(CO)_2]$ [prepared as described previously from molybdenum hexacarbonyl (1.0 g, 3.78 mmol) in dichloromethane (30 cm^3) and bromine (12 drops)] was added to a suspension of dbtpe (1.8 g, 2.8 mmol) in dichloromethane (30 cm^3). The mixture was stirred at

room temperature for 20 h, then the precipitated salmon pink complex was filtered off, washed with dichloromethane and dried *in vacuo*. (Yield 2.1 g, 80%.)

Preparation of $[WBr_2(CO)_2(dbtpe)]$ (**14**)

In a similar fashion to the above, a solution of $[WBr_2(CO)_4]$ [prepared from tungsten hexacarbonyl (1.0 g, 5.4 mmol) in dichloromethane (30 cm^3) and bromine (15 drops)], was added to a suspension of dbtpe (1.6 g, 2.6 mmol) in dichloromethane (30 cm^3). The resulting mixture was stirred at room temperature for 20 h. The salmon pink complex was filtered off, washed with dichloromethane and dried *in vacuo*. (Yield 2.0 g, 76%.)

REFERENCES

1. A. J. L. Pombeiro and R. L. Richards, *Coord. Chem. Rev.* 1990, **104**, 13 and refs therein.
2. R. Chianelli, *Catal. Rev. Sci. Engng* 1984, **26**, 361.
3. R. L. Richards, *Chem. in Britain* 1988, 29.
4. M. F. M. Al-Dulaymmi, P. B. Hitchcock and R. L. Richards, *J. Organomet. Chem.* 1988, **C31**, 338.
5. M. F. M. Al-Dulaymmi, P. B. Hitchcock and R. L. Richards, *Polyhedron* 1989, **8**, 1976.
6. P. N. Kapoor and P. C. Mercykutty, *J. Organomet. Chem.* 1988, **339**, 97.
7. J. Chatt and H. R. Watson, *J. Chem. Soc.* 1961, 4980.
8. G. Wilkinson, F. G. A. Stone and E. W. Abel (Eds), *Comprehensive Organometallic Chemistry*, Vol. 6, p. 1079. Pergamon Press, Oxford (1982) and refs therein.
9. R. B. King and M. S. Saran, *Inorg. Chem.* 1971, **10**, 1861.
10. M. F. M. Al-Dulaymmi, D. Phil. thesis, Sussex University (1989).
11. R. Colton, *Coord. Chem. Rev.* 1971, **6**, 269.
12. D. P. Tate, W. R. Knipple and J. M. Augl, *Inorg. Chem.* 1962, **1**, 433.
13. J. A. Bowden and R. Colton, *Aust. J. Chem.* 1968, **21**, 2657.
14. N. Walker and D. Stuart, *Acta Cryst.* 1983, **A39**, 159.

Polyhedron Vol. 10, No. 13, pp. 1559–1564, 1991
Printed in Great Britain

0277–5387/91 $3.00+.00
© 1991 Pergamon Press plc

SYNTHESIS AND MOLECULAR STRUCTURE OF $Nd_5(\mu_5\text{-}O)(\mu_3\text{-}OR)_2(\mu_2\text{-}OR)_6(OR)_5(ROH)_2$ (R = Pr^i). THE FIRST EXAMPLE OF A TRIGONAL BIPYRAMIDAL METAL OXOALKOXIDE

G. HELGESSON and S. JAGNER

Department of Chemistry, Chalmers University of Technology, S-41296 Goteberg, Sweden

and

O. PONCELET and L. G. HUBERT-PFALZGRAF*

Laboratoire de Chimie Moléculaire, Université de Nice-Sophia Antipolis, Parc Valrose, 06034 Nice, France

(*Received* 7 *December* 1990; *accepted* 28 *February* 1991)

Abstract—Reaction between neodymium chips and isopropanol (Pr^i) led to the isolation of an oxoisopropoxide solvate $Nd_5(OPr^i)_{13}(Pr^iOH)_2$, which has been characterized by microanalysis and IR spectroscopy, as well as by X-ray diffraction. The molecule corresponds to a trigonal bipyramidal oxoalkoxide $Nd_5(\mu_5\text{-}O)(\mu_3\text{-}OR)_2(\mu_2\text{-}OR)_6(OR)_5(ROH)_2$ (R = Pr^i), in which all metals achieve hexacoordination. The two alcohol molecules are linked to the same neodymium centre, thus leading to distortion of the M_5O_{16} core.

Metal alkoxides are versatile precursors of oxides and are thus widely used in the sol–gel process.[1] High purity neodymium deratives are particularly attractive for their optical properties and thus find application in optical fibers or non-linear optic materials.[2] Various neodymium compounds, including alkoxides $Nd(OR)_3$ (R = Pr^i, Np)[3] associated with ethylaluminum derivatives, have also been found to be interesting for the development of Ziegler–Natta-type catalysts. The bimetallic catalyst, $[Al_3Nd_6(\mu\text{-}Cl)_6(\mu_3\text{-}Cl)_6(\mu\text{-}Et)_9Et_5(OPr^i)]_2$, obtained from the ternary system —$Nd(OPr^i)_3$–Et_3Al–Et_2AlCl—displays high activity and stereospecificity for polymerization of butadiene.[4]

Among the various routes for obtaining lanthanide alkoxides, starting from metal chlorides, nitrates or metal chips, the latter appears to be the most attractive, owing to the available purity of the metal, the absence of alkali metal residues and the high yield reported in the literature.[5] We have previously reported that the compound formulated as "$Y(OPr^i)_3$" actually corresponds to an oxoisopropoxide, $Y_5(\mu_5\text{-}O)(\mu_3\text{-}OR)_4(\mu_2\text{-}OR)_4(OR)_5$ (R = Pr^i), when isolated.[6] The precursor was shown to be a solvate, but its nature remains undetermined, since X-ray diffraction studies have so far failed to solve its structure and ^{1}H NMR data were uninformative as a result of fast exchange processes.

In the case of neodymium, it has, however, proved possible to characterize an isopropanol solvate structurally. We now wish to report the molecular structure of $Nd_5(\mu_5\text{-}O)(\mu_3\text{-}OR)_2(\mu_2\text{-}OR)_6(OR)_5(ROH)_2$ (R = Pr^i), the first example of a trigonal bipyramidal oxoalkoxide.

EXPERIMENTAL

All manipulations were routinely performed under dry argon using vacuum line or Schlenk techniques. Solvents were purified by standard methods. Isopropanol was dried by distillation over $[Al(OPr^i)_3]_4$. ^{1}H NMR and IR spectra were run on Bruker AC-200 and IR-FTS 45 spectrometers, respectively. IR spectra were obtained as Nujol

* Author to whom correspondence should be addressed.

mulls. Analytical data were obtained from the Centre de Microanalyses du CNRS.

Synthesis of the neodymium isopropoxides

The neodymium derivatives were synthesized according to the procedure of Brown and Mazdiyasni.[5] Neodymium chips (Aldrich) (23 g, 0.159 mol) and activated by mercuric salts [$HgCl_2+Hg(OAc)_2$ (1:1, 15 mg) or only $[Hg(OAc)_2]$[6] in 300 cm^3 of toluene/isopropanol (1:1)] were heated under reflux over a period of 48 h. A first crop of pale blue, air-sensitive crystals, analysing as $Nd(OPr^i)_3(Pr^iOH)$[7] (**1**) (yield 46.9 g, 75.6%), was obtained after filtration of the hot reaction medium and cooling at room temperature. These are soluble in toluene, dichloromethane, THF but poorly soluble in isopropanol. Found: C, 37.4; H, 6.9. Calc. for $C_{12}H_{29}O_4Nd$: C, 37.7; H, 7.7%. IR (cm^{-1}): 3348 [ν(OH)]; 1161vs, 1132vs, [ν(C—O)]; 1049s, 993m, 959vs, 872m, 822m, 725w; 544s, 444s, 400m, 334m, 324m, 277m [ν(Nd—O)].

A second crop of crystals (**2**) with comparable solubility properties was obtained by adding isopropanol (100 cm^3) to the filtrate (250 cm_3) (yield 9.3 g, 15%). Found: C, 31.2; H, 6.1. Calc. for $C_{45}H_{107}O_{16}Nd_5$: C, 33.2; H, 6.3%. IR (cm^{-1}): 3337 [ν(O—H)]; 1161vs, 1137, 1120sh [ν(C—O)]; 1049s, 993m, 959vs, 872m, 822m, 727w; 523m, 460sh, 446m, 410, 380sh, 326m, 301m [ν(Nd—O)]. The high lability of the isopropanol molecules in **2** leads to analytical data more in agreement with the $Nd_5O(OPr^i)_{13}$ formulation. Calc. for $C_{39}H_{91}O_{14}Nd_5$: C, 31.1; H, 6.1%. IR (cm^{-1}): 1161vs, 1135vs, 1115sh [ν(C—O)]; 1045m, 995vs, 968vs, 875m, 835w, 720w; 520m, 460sh, 443m, 400sh, 330sh, 300 vs [ν(Nd—O)].

X-ray crystallography of $Nd_5O(OPr^i)_{13}(Pr^iOH)_2$

Crystals of **2** suitable for X-ray were obtained by adding 4 cm^3 of isopropanol to 10 cm^3 of the first filtrate and slow cooling to −20°C. Complex **2** crystallizes as pale blue, irregular-shaped prisms, which decompose within seconds on exposure to air. A crystal was mounted, under nitrogen, in a glass capillary, at approximately −80°C, then cooled to −150°C, and transferred immediately to a Rigaku AFC6R diffractometer. Intensities (h, k, $+l$) were measured at -150 ± 1°C, using graphite-monochromated Mo-K_α radiation from a RU200 rotating anode operating at 9 kW (50 kV, 180 mA). The w–2θ scan mode was employed for $3.5 < 2\theta < 60°$ with a scan rate of 32° min^{-1} and a scan width of $(0.89+0.3\tan\theta)°$. Weak reflections [$F < 10\sigma(F)$] were rescanned up to three times and counts accumulated to improve counting statistics. Stationary background counts were recorded on each side of the reflection. The ratio of peak counting time vs background counting time was 2:1. The fact that the crystal was not subject to decay during the measurement of intensities was checked by monitoring three reflections at regular intervals (after measurement of each 150 reflections). Intensity data were corrected for Lorentz and polarization effects, and an empirical absorption correction, based on azimuthal scans for several reflections, was made (max., min. transmission factors: 1.00, 0.573). Unit-cell parameters were obtained from diffractometer setting angles for 25 reflections in the range $39 < 2\theta < 45°$. Further information on crystal data and intensity data collection is listed in Table 1.

The structure was solved by direct methods (MITHRIL)[8] and subsequent electron density calculations. One of the OPr^i ligands [O(7), C[7); C(71)] was found to be disordered with respect to

Table 1. Summary of crystallographic data for Nd_5 (μ_5-O)(μ_3-OR)$_2$(μ_2-OR)$_6$(OR)$_5$(ROH)$_2$ (R = Pr^i)

Compound	$C_{45}H_{107}Nd_5O_{16}$
Colour	Pale blue
Molecular weight	1625.5
Crystal system	Orthorhombic
Space group	*Aba*2
a (Å)	21.343(6)
b (Å)	21.109(4)
c (Å)	14.338(3)
α (°)	90
β (°)	90
γ (°)	90
V (Å^3)	6460(4)
Z	4
Density (calc.) (g cm^{-3})	1.67
Crystal dimensions (mm)	0.36 × 0.45 × 0.20
F(000) (e^-)	3220
Diffractometer	Rigaku AFC6R
Temperature (°C)	-150 ± 1
Radiation	Mo-K_α
Linear absorption coefficient (cm^{-1})	40.1
Scan type	ω–2θ
Scan width (°)	$(0.89+0.30\tan\theta)$
hkl Limits	0–30, 0–28, −20–0
Data collected	5116
Unique data used [$F_o^2 > 3\sigma(F_o^2)$]	3617
Number of parameters refined	298
$R = \Sigma([F_o]-[F_c])/[F_o]$	0.041
$R_\omega = \Sigma([F_o]-[F_c])^2/(\omega[F_o]^2)^{1/2}$	0.048
Quality-of-fit indicator	1.30
Largest shift/ESD in final cycle	0.12

the two-fold axis through O(4), Nd(3) and O(7), such that C(7) was located and refined as a half-atom. Full-matrix least-squares refinement of positional and anisotropic thermal parameters [isotropic thermal parameter for C(7)] gave a final $R = 0.041$, $R_w = 0.048$. Atomic scattering factors and anomalous dispersion corrections were taken from ref. 9, and the F_o values were weighted according to $w = [\sigma^2(F_o)]^{-1}$ with a p factor of 0.03. A final difference map showed a max., min. residual density of 1.16 and -1.20 e Å^{-3}, respectively. All calculations were carried out with the TEXSAN program system.[10] No hydrogen atoms were included.

Tables of positional and thermal parameters, interatomic distances and angles are given as Supplementary material.

RESULTS AND DISCUSSION

The reaction between neodymium chips, activated by catalytic amounts of mercuric salts (chloride and/or acetate), and isopropanol offered several alkoxide derivatives by crystallization.[7a] The first crop of crystals analysed as a tris-isopropoxide adduct $Nd(OPr^i)_3(Pr^iOH)$ [ν(OH): 3348 cm^{-1}] (75%), and was found by X-ray diffraction to have a tetranuclear structure related to that of $[Ti(OMe)_4]_4$ with hexacoordinated neodymium atoms.[7b] Addition of isopropanol to the filtrate leads to the precipitation of another solvate [ν(OH): 3337 cm^{-1}] in lower yield ($\simeq$ 15%), which was established by X-ray diffraction to correspond to an oxo derivative, $Nd_5O(OPr^i)_{13}(Pr^iOH)_2$. Its molecular structure consists of discrete pentanuclear units, as shown in Fig. 1. Selected distances and bond lengths are reported in Table 2.

The five metals form a distorted trigonal bipyramidal cluster (Fig. 2) with a μ_5-oxo ligand, O(4). Although all metals are hexacoordinated with a distorted octahedral surrounding, they are of three different types, and there are also three types of alkoxide ligands. The trigonal pyramid is elongated along the apex, as evidenced by the Nd(2)—O(4) bond lengths of 2.719(1) Å, compared with those in the equatorial plane, Nd(1)—O(4) 2.468(8) Å and Nd(3)—O(4) 2.355(13) Å, and the non-bonding Nd---Nd distances range from 3.539(1) to 4.409(1) Å. The Nd—O distances vary over a wide range, from 2.121(9) to 2.719(1) Å, with the longest Nd—O distances implying the μ_5-O ligand. The

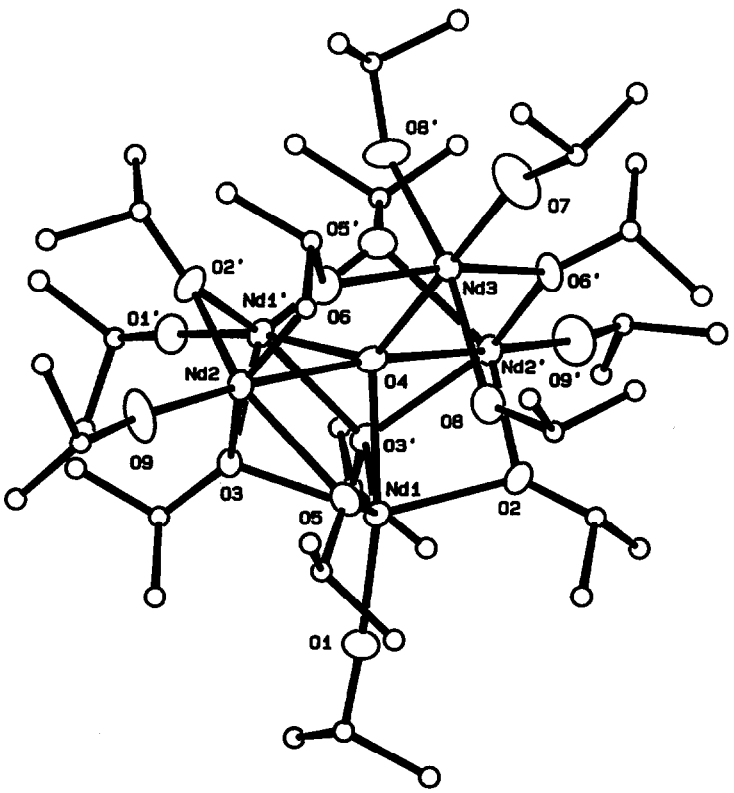

Fig. 1. Molecular structure of $Nd_5(\mu_5\text{-}O)(\mu_3\text{-}OR)_2(\mu_2\text{-}OR)_6(OR)_5(ROH)_2$ (R = Pr^i). Atoms labelled ′ are related by a C_2 axis. Thermal ellipsoids enclose 50% probability. For clarity the carbon atoms have been drawn as spheres of radius 0.12 Å.

Table 2. Selected bond lengths and angles of $Nd_5(\mu_5\text{-}O)(\mu_3\text{-}OR)_2(\mu_2\text{-}OR)_6(OR)_5(ROH)_2$ (R = Pr^i)

Bond lengths (Å)

Nd(1)—O(1)	2.121(9)	Nd(2)—O(5)	2.463(9)
Nd(1)—O(2)	2.358(9)	Nd(2)—O(6)	2.307(10)
Nd(1)—O(3)	2.456(8)	Nd(2)—O(9)	2.140(9)
Nd(1)—O(3′)	2.477(9)	Nd(3)—O(4)	2.355(13)
Nd(1)—O(4)	2.468(8)	Nd(3)—O(6)	2.367(9)
Nd(1)—O(5)	2.407(9)	Nd(3)—O(6′)	2.367(9)
Nd(2)—O(2′)	2.341(9)	Nd(3)—O(7)	2.184(16)
Nd(2)—O(3)	2.450(9)	Nd(3)—O(8)	2.511(10)
Nd(2)—O(4)	2.719(1)	Nd(3)—O(8′)	2.511(10)

Bond angles (°)

O(1)—Nd(1)—O(2)	106.6(3)	O(2′)—Nd(2)—O(3)	76.3(3)
O(1)—Nd(1)—O(3)	101.7(3)	O(2′)—Nd(2)—O(4)	75.5(2)
O(1)—Nd(1)—O(3′)	105.1(3)	O(2′)—Nd(2)—O(5)	143.7(3)
O(1)—Nd(1)—O(4)	169.6(3)	O(2′)—Nd(2)—O(6)	91.7(3)
O(1)—Nd(1)—O(5)	106.9(3)	O(2′)—Nd(2)—O(9)	107.1(4)
O(2)—Nd(1)—O(3′)	143.2(3)	O(3)—Nd(2)—O(4)	65.1(3)
O(2)—Nd(1)—O(3)	75.4(3)	O(3)—Nd(2)—O(5)	77.4(3)
O(2)—Nd(1)—O(4)	80.2(2)	O(3)—Nd(2)—O(6)	141.1(3)
O(2)—Nd(1)—O(5)	114.1(3)	O(3)—Nd(2)—O(9)	112.5(4)
O(3)—Nd(1)—O(3′)	75.0(3)	O(4)—Nd(2)—O(5)	71.0(2)
O(3)—Nd(1)—O(4)	69.0(3)	O(4)—Nd(2)—O(6)	76.2(4)
O(3)—Nd(1)—O(5)	78.4(3)	O(4)—Nd(2)—O(9)	176.1(4)
O(3′)—Nd(1)—O(4)	68.6(3)	O(5)—Nd(2)—O(6)	93.4(3)
O(3′)—Nd(1)—O(5)	141.7(3)	O(5)—Nd(2)—O(9)	105.8(4)
O(4)—Nd(1)—O(5)	76.4(2)	O(6)—Nd(2)—O(9)	106.4(4)

O(4)—Nd(3)—O(6)	82.63(2)
O(4)—Nd(3)—O(7)	180.00
O(4)—Nd(3)—O(8)	82.9(2)
O(6)—Nd(3)—O(6′)	165.3(5)
O(6)—Nd(3)—O(7)	97.4(2)
O(6)—Nd(3)—O(8)	96.8(3)
O(6)—Nd(3)—O(8)	81.4(3)
O(7)—Nd(3)—O(8)	97.1(2)
O(8)—Nd(3)—O(8′)	165.8(5)

Nd(3)—O(4)—Nd(1)	132.1(2)	Nd(1)—O(2)—Nd(2′)	97.7(3)
Nd(3)—O(4)—Nd(2)	94.6(3)	Nd(1)—O(3)—Nd(1′)	95.8(3)
Nd(1)—O(4)—Nd(1′)	95.7(4)	Nd(1)—O(3)—Nd(2)	94.6(3)
Nd(1)—O(4)—Nd(2)	87.9(2)	Nd(1′)—O(3)—Nd(2)	91.8(3)
Nd(1)—O(4)—Nd(2′)	85.9(2)	Nd(1)—O(5)—Nd(2)	95.5(3)
Nd(2)—O(4)—Nd(2′)	170.8(5)	Nd(3)—O(6)—Nd(2)	106.2(4)

Symmetry code for primed atoms: $-x, -y, z$.

only neodymium alkoxide structurally characterized so far corresponds to $Nd_6(\mu_6\text{-}Cl)(\mu_3\text{-}OR)_2(\mu_2\text{-}OR)_9(OR)_6$ (R = Pr^i) and displays metal–oxygen bond lengths varying from 2.05(2) to 2.45(5) Å.[11]

Although the H(OH) of the alcohol molecules could not be located, the position of the alcohol can generally be deduced from the lengthening of the terminal metal–oxygen bonds and/or the bending of terminal ligands in the *cis* position, which allows stabilization of the solvates by hydrogen bonding.[12] By contrast with Nd(1) and Nd(2), Nd(3) bears three terminal ligands; the very different Nd—O distances [2.184(16) and 2.511(10) Å] allow the unambiguous assignment of the latter, Nd(3)—O(8) and Nd(3)—O(8′), to Nd—O(H)R bonds. This is supported by the fact that the Nd(3)—O(8)—C(8) angle is relatively small [136(1)°], while larger M—O—C angles are expected for terminal M—OR bonds. Indeed, the value of the Nd(3)—O(7)—C(7) angle is 158(1)°, and values as large as 174° (av.) are

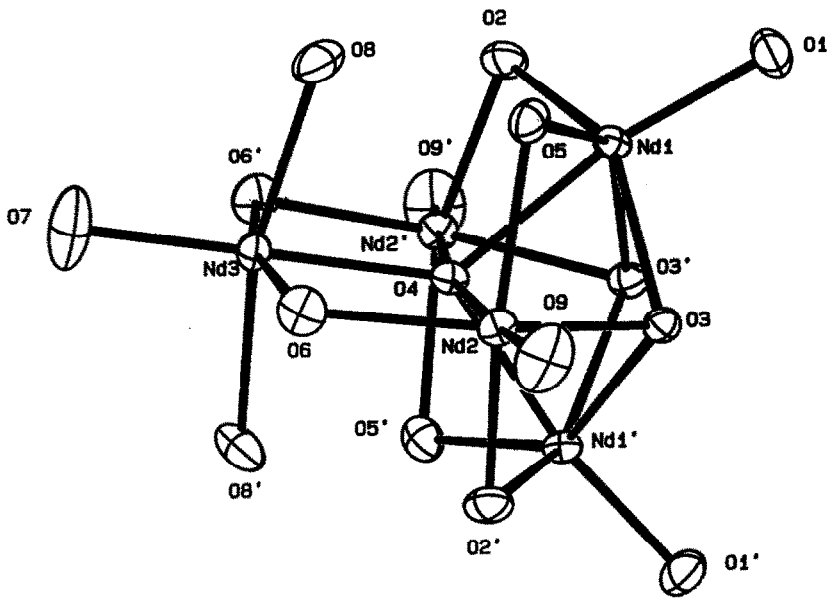

Fig. 2. View of the trigonal bipyramidal Nd_5O_{16} core.

observed for the other terminal Nd—O—C angles. The O(8)···O(5) distance of 2.737(13) Å is consistent with the presence of a hydrogen bond, which is further supported by the broad absorption at 3337 cm^{-1} in the IR spectrum. The Nd—O bond lengths vary in the order Nd—μ_5-O ≈ Nd—O(H)R > Nd—μ_3-OR > Nd—μ_2-OR > Nd—OR, the Nd—μ_5-O bond lengths displaying the largest variations.

Pentanuclear clusters remain relatively scarce, although yttrium and lanthanide oxoalkoxide derivatives such as $(\eta^5\text{-Cp})_5M_5(\mu_5\text{-O})(\mu_3\text{-OR})_4(\mu_2\text{-OR})_4(OR)_5$ (M = Y, R = Pr^i;[13] Gd, R = Bu^t[14]) or $Y_5(\mu_5\text{-O})(\mu_3\text{-OR})_4(\mu_2\text{-OR})_4(OR)_5$ (R = Pr^i[6,15]) have been shown to have a tetragonal pyramidal framework. In fact, the structure of $Nd_5(\mu_5\text{-O})(\mu_3\text{-OR})_2(\mu_2\text{-OR})_6(OR)_5(ROH)_2$ (M_5O_{16} core) can be considered as being derived from that of $Y_5O(OPr^i)_{13}$ (M_5O_{14} core) by the addition of two isopropanol molecules to the same basal metal atom, which results in the conversion of two μ_3-alkoxide groups into μ_2-alkoxide groups in order to preserve hexacoordination for all metal centres. Solvation alters the initial framework, and the resulting coordination polyhedron is a trigonal bipyramid with six doubly-bridging alkoxide groups along the edge connecting the apical and equatorial metal centres. Two μ_3-OR ligands cap the triangular faces formed by Nd(1) and Nd(1′) and one of the apical metals. The overall structure is thus different from the heterometallic lanthanide alkoxide $La_2Na_3(\mu_4\text{-OR})_3(\mu_2\text{-OR})_6(THF)_5$ (R = *p*-tolyl), for which the metal–oxygen core is also a trigonal bipyramid.[16] Distortion of the neodymium cluster is evidenced by the angles around the μ_5-oxo ligand. The presence of three terminal ligands on Nd(3) leads to a reduction of the angle between the two other Nd—O equatorial bonds [Nd(1)—O(4)—Nd(1′) 95.7(4)°] as well as of that of the apical bending [Nd(2)—O(4)—Nd(2′) 170.8(5)°]. In all previously reported examples, the μ_5-O^{2-} ligands have a square pyramidal environment, and thus the geometry observed here appears to correspond to a new coordination mode of the oxo anion, as well as to a metal polyhedron unprecedented for an oxoalkoxide. A change from a square pyramidal polyhedron into a trigonal bipyramidal one by electron donors has also been noted for metal carbonyl clusters,[17] but metal–metal bonding and the nature of the ligands led to an overall metal–carbon core which is different from the metal–oxygen core described here.

These results show that the composition of the solution resulting from reaction between isopropanol and neodymium chips is much more complex than anticipated. Neodymium is less reactive towards isopropanol than yttrium, and no reaction is observed between neodymium, and isopropanol without a catalyst. Mercuric acetate appears to be a better choice than mercuric chloride since it avoids halide contamination of the final material.* Acti-

* Even small amounts of mercuric chloride as catalyst (6.10^{-4} M per Nd) can lead to contamination by the chloroalkoxide $Nd_6Cl(OPr^i)_{17}$, which crystallizes by concentration of the mother liquor and which was identified by the crystal data.[11]

vation of neodymium can also be achieved in neat isopropanol by sonochemistry (600 W over 48 h), but the consumption of the metal and thus the total yield of the neodymium isopropoxide derivatives remains poor ($\approx$ 15%). The IR spectra of the two adducts **1** and **2** mainly contain the absorption bands of the organic ligands and thus they display only small differences in the OH and M—O stretching region. ^{1}H NMR spectra at various temperatures and in different solvents suggest magnetic, non-equivalent isopropoxo groups but the signals are broad and poorly resolved due to the paramagnetism of the compounds and/or exchange phenomena. Thus, the difference in reactivity provide better criteria for the distinction between **1** and **2**. Freshly isolated $[Nd(OPr^i)_3(Pr^iOH)]_4$ reacts with $[Al(OPr^i)_3]_4$ to give the volatile, heterometallic alkoxide $NdAl_3(OPr^i)_{12}$.[18] No reaction is observed in similar conditions between the oxoisopropoxide solvate **2** and the aluminum alkoxide. The oxoalkoxide solvate **2** is much more unstable than **1** with respect to decomplexation reactions.

Oxoisopropoxides, $M_5O(OPr^i)_{13}$, appear to display a special stability, since such compounds are obtained "even with exceptional precaution against hydrolysis"[15] by various synthetic routes and with numerous oxophilic trivalent metals (M = In, Sc, Y, Yb;[15] La[19]). Isolation of an oxoisopropoxide such as **2** directly from the reaction medium without drying provides evidence that oxo derivatives are probably also formed directly in the course of attack of the metal during the electron transfer reactions.

REFERENCES

1. L. G. Hubert-Pfalzgraf, *New J. Chem.* 1987, **11**, 663.
2. S. H. Wang and L. L. Hench, *Science of Ceramic Chemical Processing* (Edited by L. Hench and D. R. Ulrich), p. 20. John Wiley, New York (1986).
3. M. C. Gallazzi, F. Bianchi, A. Giarrusso and L. Parri, *Inorg. Chim. Acta* 1980, **94**, 108.
4. S. Shen, *Inorg. Chim. Acta* 1987, **140**, 7.
5. L. M. Brown and K. S. Mazdiyasni, *Inorg. Chem.* 1970, **9**, 2783.
6. O. Poncelet, W. J. Sartain, L. G. Hubert-Pfalzgraf, K. Folting and K. G. Caulton, *Inorg. Chem.* 1989, **28**, 263.
7. (a) O. Poncelet and L. G. Hubert-Pfalzgraf, *Polyhedron* 1989, **8**, 2183; (b) G. Helgesson and S. Jagner, unpublished results.
8. C. J. Gilmore, *J. Appl. Cryst.* 1984, **117**, 42.
9. *International Tables for X-ray Crystallography*, Vol. IV. Kynoch Press, Birmingham (1974).
10. *TEXSAN Structure Solution Package*. Molecular Structure Corporation, The Woodlands, TX 77381 (1989).
11. R. A. Andersen, D. H. Templeton and A. Zalkin, *Inorg. Chem.* 1978, **17**, 1962.
12. B. A. Vaarstra, J. C. Huffman, P. S. Gradeff, L. G. Hubert-Pfalzgraf, J. C. Daran, S. Parraud, K. Yunlu and K. G. Caulton, *Inorg. Chem.* 1990, **29**, 3126.
13. W. J. Evans and M. S. Sollberger, *J. Am. Chem. Soc.* 1986, **108**, 6095.
14. H. Schumann, G. Koclok and J. Loebel, *Z. Anorg. Allg. Chem.* 1990, **581**, 69.
15. $In_5O(OPr^i)_{13}$ and $Yb_5O(OPr^i)_{13}$ were found to display the same structure: *Polyhedron* 1990, **9**, 719; D. C. Bradley, H. Chudzynska, D. M. Frigo, D. M. Hursthouse and M. B. Mazid, *J. Chem. Soc., Chem. Commun.* 1988, 1258.
16. K. G. Caulton and L. G. Hubert-Pfalzgraf, *Chem. Rev.* 1990, **90**, 969.
17. P. F. Jackson, B. F. G. Johnson, J. Lewis, J. N. Nicholls, M. McPartlin and W. J. H. Nelson, *J. Chem. Soc., Chem. Commun.* 1980, 564.
18. R. C. Mehrotra, M. M. Agrawal and A. Mehrotra, *Synth. Inorg. Met.-Org. Chem.* 1973, **3**, 181.
19. N. El Khokh, Thèse Nouveau Régime, Nice (1990).

Polyhedron Vol. 10, No. 13, pp. 1565–1568, 1991
Printed in Great Britain

0277-5387/91 $3.00+.00
© 1991 Pergamon Press plc

THE CRYSTAL STRUCTURE OF THE MIXED METAL (Ca,Na) COMPLEX WITH BENZENE-1,2-DIOXYDIACETIC ACID, *CATENA*-[PENTAAQUABIS(BENZENE-1,2-DIOXYDIACETATO)CALCIUM(II)–SODIUM(I) DIHYDRATE]

GRAHAM SMITH,* RAYMOND C. BOTT and DALIUS S. SAGATYS

School of Chemistry, Queensland University of Technology, Brisbane 4000, Australia

and

COLIN H. L. KENNARD

Department of Chemistry, The University of Queensland, Brisbane 4072, Australia

(*Received* 12 *December* 1990; *accepted* 20 *March* 1991)

Abstract—The mixed metal (Ca,Na) complex of benzene-1,2-dioxydiacetic acid ($BDDAH_2$), $\{[Na_2Ca(C_{10}H_8O_6)_2(H_2O)_5]\cdot 2H_2O\}_n$ has been prepared and its crystal structure determined by X-ray diffraction from data collected at 178 K. The calcium is bonded to the four "inner" oxygens of two BDDA ligands giving almost square eight-coordination [Ca—O, 2.323–2.513(3) Å]. Sodium ions link the calcium units via the "outer" carboxyl oxygens forming an infinite chain polymer. Water molecules complete four- and five-coordination about each sodium [Na—O, 2.282–2.428(4) Å].

The dicarboxylic acid, benzene-1,2-dioxydiacetic acid ($BDDAH_2$) or *o*-phenylenedioxydiacetic acid, has proved a versatile ligand for complexation of a number of metal ion types.[1] Among these are the univalent metal ions Li,[2] Na,[3] K,[4] Cs,[5] and divalent metal ions Ca, Mn, Zn, Co, Ni[6] and Mg.[3] A univalent–trivalent metal complex (Na,La) is also known.[7] With the exception of the nickel complex $\{[Ni(BDDAH)_2(H_2O)_2]\cdot H_2O\}$, where the BDDAH ligands are unidentate through the carboxylic acid group, the stereochemistry of these complexes is based on a pentagonal plane with four of the donors provided by the "inner" oxygens of the planar ligand. This is the preferred conformation of the free ligand, as seen in the ionic compound $(NH_4)_2(BDDA)$.[3] In a project to investigate the mixed metal complexes of BDDA, using the efflorescent sodium complex $[Na_2(BDDA)_2(H_2O)_8]$[2] as the starting material, small quantities of a stable, colourless crystal were obtained, with cell parameters only slightly different from the parent compound. Crystal structure determination confirmed the presence of calcium in a complex of formula $\{[Na_2Ca(BDDA)_2(H_2O)_5]\cdot 2H_2O\}_n$, reported here.

EXPERIMENTAL

The compound was prepared by the addition of a stoichiometric amount of aqueous $Ca(NO_3)_2$ to an aqueous solution of $[Na_4(BDDA)_2(H_2O)_8]_n$. The latter was prepared by the titration of $BDDAH_2$ with NaOH, as previously described.[3] A small quantity of well-formed, colourless, bipyramidal crystals formed from the solution after partial evaporation at room temperature over several weeks.

Crystal data

$C_{20}H_{30}CaNa_2O_{19}$, $M_r = 660.5$, triclinic, space group $P\bar{1}$, $a = 9.459(6)$, $b = 10.607(7)$, $c = 14.367(8)$ Å, $\alpha = 101.89(4)$, $\beta = 105.33(3)$, $\gamma = 91.55(4)°$, $V = 1355(1)$ Å^3, $Z = 2$, $D_c = 1.618$ g cm^{-3}, $D_m = 1.61$ g cm^{-3}, $T = 178$ K.

* Author to whom correspondence should be addressed.

Table 1. Bond distances (Å) and angles (°) about the metal coordination spheres

Distances			
Ca—O(71)A	2.504(3)	Ca—O(71)B	2.513(3)
Ca—O(72)A	2.463(3)	Ca—O(72)B	2.460(3)
Ca—O(9)A	2.351(3)	Ca—O(9)B	2.357(3)
Ca—O(10)A	2.323(3)	Ca—O(10)B	2.370(3)
Na(1)—Ow(1)	2.358(4)	Na(1)—Ow(4)	2.376(3)
Na(1)—Ow(3)	2.377(3)	Na(2)—Ow(5)	2.302(4)
Na(1)—Ow(7)	2.428(4)	Na(2)—O(12)A	2.282(4)
Na(1)—O(11)A	2.404(4)	Na(2)—O(12)B	2.315(4)
Na(1)—O(11)B	2.347(4)		
Angles			
O(71)A—Ca—O(72)A	61.9(1)	O(71)B—Ca—O(72)B	62.1(1)
O(71)A—Ca—O(9)A	64.7(1)	O(71)B—Ca—O(9)B	64.5(1)
O(71)A—Ca—O(10)A	126.6(1)	O(71)B—Ca—O(10)B	127.5(1)
O(71)A—Ca—O(71)B	136.8(1)	O(72)B—Ca—O(9)B	126.2(1)
O(71)A—Ca—O(72)B	138.3(1)	O(72)B—Ca—O(10)B	66.1(1)
O(71)A—Ca—O(9)B	87.8(1)	O(9)B—Ca—O(10)B	167.7(1)
O(71)A—Ca—O(10)B	80.9(1)	Ow(1)—Na(1)—Ow(3)	88.4(1)
O(72)A—Ca—O(9)A	126.4(1)	Ow(1)—Na(1)—Ow(7)	96.0(1)
O(72)A—Ca—O(10)A	66.2(1)	Ow(1)—Na(1)—O(11)A	107.3(1)
O(72)A—Ca—O(71)B	136.4(1)	Ow(1)—Na(1)—O(11)B	100.4(1)
O(72)A—Ca—O(72)B	137.6(1)	Ow(3)—Na(1)—Ow(7)	89.2(1)
O(72)A—Ca—O(9)B	81.0(1)	Ow(3)—Na(1)—O(11)A	163.1(1)
O(72)A—Ca—O(10)B	89.3(1)	Ow(3)—Na(1)—O(11)B	96.5(1)
O(9)A—Ca—O(10)A	166.0(1)	Ow(7)—Na(1)—O(11)A	83.3(1)
O(9)A—Ca—O(71)B	83.0(1)	Ow(7)—Na(1)—O(11)B	162.7(1)
O(9)A—Ca—O(72)B	88.0(1)	O(11)A—Na(1)—O(11)B	86.8(1)
O(9)A—Ca—O(9)B	92.3(1)	Ow(4)—Na(2)—Ow(5)	83.3(1)
O(9)A—Ca—O(10)B	87.2(1)	Ow(4)—Na(2)—O(12)A	116.8(1)
O(10)A—Ca—O(71)B	90.6(1)	Ow(4)—Na(2)—O(12)B	136.2(1)
O(10)A—Ca—O(72)B	78.0(1)	Ow(5)—Na(2)—O(12)A	112.0(1)
O(10)A—Ca—O(9)B	96.2(1)	Ow(5)—Na(2)—O(12)B	93.9(1)
O(10)A—Ca—O(10)B	86.8(1)	O(12)A—Na(2)—O(12)B	104.8(1)

Data collection, structure solution and refinement

Data were collected from a specimen measuring $0.45 \times 0.27 \times 0.20$ mm^3 on an Enraf–Nonius CAD-4 diffractometer fitted with a low temperature (178 K) accessory. 4552 reflections were collected ($2\theta_{max} = 50°$: *hkl* range: $h = -11$ to 11 $k = -12$ to 12, $l = 0$ to 17), giving 4314 unique of which 3614 with $I > 3\sigma(I)$ were used in structure refinement. Crystal monochromatized Mo-K_α radiation ($\lambda = 0.71073$ Å) was used, with empirical absorption corrections applied to the data. A total loss of *ca* 16% in the intensities of three standards monitored during the 60 h data collection period indicated significant crystal decay, which was allowed for by scaling. The structure was solved using direct methods (SHELXS 86[8]) and refined using SHELX 76.[9] Neutral atom scattering factors and f', f'' terms for anomalous dispersion were taken from ref. 10. Blocked-matrix least-squares refinement with anisotropic thermal parameters on all non-hydrogens gave $R^* = 0.048$. Unit weights were used. Hydrogen atoms were located by difference methods and included in the refinement at fixed positions with their isotropic thermal parameters set invariant at 0.05 Å^2. The maximum peak in the final difference-Fourier analysis was *ca* 0.2 e Å^{-3}.

Bond distances and angles about the coordination polyhedra are given in Table 1. Tables of atomic coordinates, anisotropic thermal parameters, intraligand bond distances and angles, hydrogen atom coordinates and observed and calculated structure factors have been deposited with the Editor as supplementary material: copies are available on request from the Editor or the Authors. Atomic coordinates have also been deposited with the Cambridge Crystallographic Data Centre.

* $R = \Sigma ||F_o| - |F_c|| / \Sigma |F_o|$.

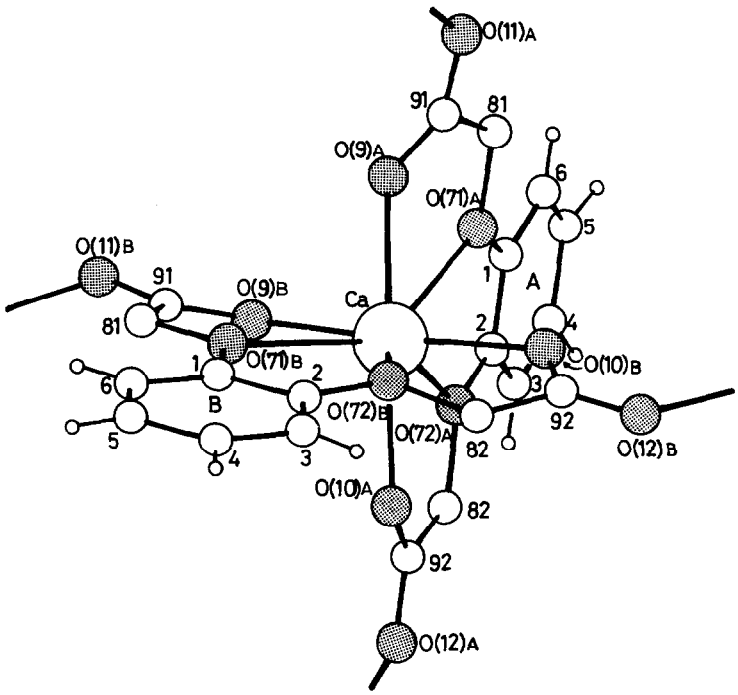

Fig. 1. Molecular configuration for the calcium complex centre. Unless otherwise indicated, atoms are carbons. Methylene hydrogens are omitted for clarity.

DISCUSSION

The structure of the complex comprises eight-coordinate calcium centres involving the four "inner" oxygens of two BDDA ligands (Fig. 1). These units are linked via the "outer" carboxylate oxygens of the ligand through $Na(H_2O)_n$ complex centres to give a cruciform chain motif which extends through the *a* direction of the unit cell (Fig. 2).

The coordination about calcium is best described as distorted square and is quite different from that observed in the 1 : 1 Ca–BDDA complex polymer, $[Ca(BDDA)(H_2O)_2]_n$,[6] in which the stereochemistry is pentagonal bipyramidal, with water molecules occupying the axial sites and an "outer" carboxylate oxygen providing the bridging link in the polymer. This oxygen lies in the fifth site of the pentagonal plane. The links to the four "inner" oxygens of the BDDA ligands are similar in both complexes: Ca—O(ether): Ca—O(carboxyl), 2.460–2.513(3) Å; 2.323–2.357(3) Å, respectively

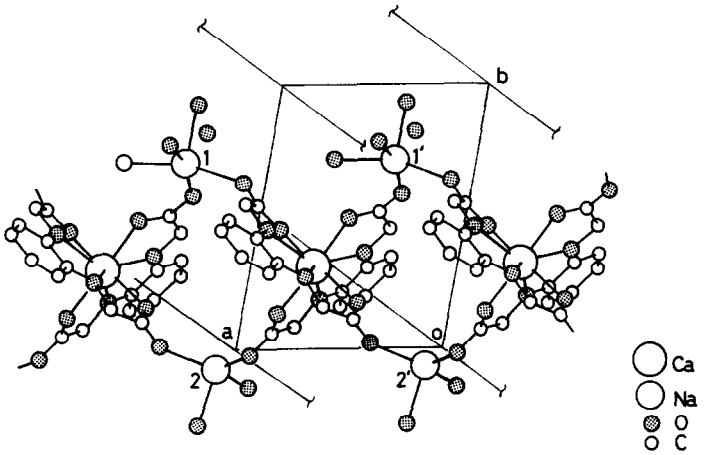

Fig. 2. Packing in the unit cell showing the bis-$Na(H_2O)_n$ bridged chains extending along the *a* cell direction.

(this example), cf. 2.516–2.521(3) Å; 2.308–2.336(3) Å, respectively (the 1 : 1 example).[6] These values are relatively inflexible for most divalent complexes of BDDA where the metal ion lies in the ligand cavity. In the univalent (Group 1A) metal ions, ionic radius is important, with lithium in $[Li_2(BDDA)(H_2O)_3]_2$ giving the best fit and almost equi-dimensional bond distances [Li—O, 2.010–2.097(5) Å].[2] With the polymeric caesium complex $[Cs_2(BDDA)(H_2O)_2]_n$ the caesium ion lies outside the ligand cavity, [Cs—O, 3.070–3.246(6) Å].[5]

Among the other 1 : 2 metal : BDDA complexes, no comparable mode of complexation is found. With $Na[La(BDDA)_2(H_2O_2)]\cdot 4H_2O$,[7] two water molecules as well as the "inner" oxygens of the two BDDA ligands complete an s-bicapped square antiprismatic coordination about La. However, the sodium ions act in a similar manner to the present example in providing $[Na(H_2O)_n]$ bridging systems via BDDA oxygens.

The BDDA ligands in the complex are essentially planar, which is the preferred conformation for this molecule in both coordinated and uncomplexed forms, e.g. $[(NH_4)_2(BDDA)]$.[3] Torsion angles for the two side-chains in the A and B ligands [C(6,3)—C(1,2)—O(7)—C(8), C(1,2)—O(7)—C(8)—C(9), O(7)—C(8)—C(9)—O(9,10)] are −3.1, +3.1, +1.2, −8.6; +170.2, +177.9, +170.1, +178.4; −8.7, +1.9, −6.0, +0.8°, respectively, for the two chains.

The four "outer" carboxylate oxygens of the two BDDA ligands are bonded to sodium atoms [O(11)A—Na(1), 2.404(4) Å; O(11)B—Na(1)′, 2.347(4) Å; O(12)A—Na(2), 2.282(4) Å; O(12)B—Na(2′), 2.315(4) Å] (primed atoms represent translation of one unit along the *a* axis in the cell, forming the chain polymer). The coordination about Na(1) and Na(2) is different, with Na(1) square pyramidal five-coordinate and Na(2) trigonal pyramidal four-coordinate. Apart from the bonds to the bridging carboxyl groups, the coordination about each sodium is completed by water molecules: Na(1)—Ow(1), 2.358(4) Å, 2.377(3) Å; Na(1)—Ow(7), 2.428(4) Å; Na(2)—Ow(4), 2.376(3) Å; Na(2)—Ow(5), 2.302(4) Å. The remaining water molecules in the structure [Ow(2),Ow(6)] are not coordinated and exist as molecules of hydration. Hydrogen bonding interactions between the alternating layers of complex $Ca(BDDA)_2$ and their associated hydrated sodium bridges with the lattice waters are also present.

Acknowledgements—The authors acknowledge the support of the Australian Research Council, the Queensland University of Technology and the University of Queensland.

REFERENCES

1. K. Suzuki, T. Hatori and K. Yamasaki, *J. Inorg. Nucl. Chem.* 1968, **30**, 161.
2. G. Smith, E. J. O'Reilly and C. H. L. Kennard, *Acta Cryst.* 1986, **C42**, 1329.
3. C. H. L. Kennard, G. Smith, E. J. O'Reilly, B. J. Reynolds and T. C. W. Mak, *J. Chem. Soc., Dalton Trans.* 1988, 2357.
4. E. A. Green, W. L. Duax, G. M. Smith and F. Wudl, *J. Am. Chem. Soc.* 1975, **97**, 6689.
5. G. Smith, E. J. O'Reilly, C. H. L. Kennard and T. C. W. Mak, *Acta Cryst.* 1989, **C45**, 1731.
6. G. Smith, E. J. O'Reilly and C. H. L. Kennard, *Polyhedron* 1987, **6**, 871.
7. H. B. Kerfoot, G. R. Choppin and T. J. Kistenmacher, *Inorg. Chem.* 1979, **18**, 787.
8. G. M. Sheldrick, SHELXS 86, Program for Crystal Structure Determination. University of Göttingen, F.R.G. (1986).
9. G. M. Sheldrick, SHELX 76, Program for Crystal Structure Determination. University of Cambridge, U.K. (1976).
10. J. A. Ibers and W. C. Hamilton (Eds), *International Tables for X-ray Crystallography*, Vol. IV. Kynoch Press, Birmingham (1974).

Polyhedron Vol. 10, No. 13, pp. 1569–1572, 1991
Printed in Great Britain

0277–5387/91 $3.00+.00
© 1991 Pergamon Press plc

THE PREPARATION AND CRYSTAL STRUCTURE OF THE CALCIUM COMPLEX WITH THE HERBICIDE ENDOTHALL, *CATENA*-[DIAQUA(7-OXABICYCLO-[2.2.1]-HEPTANE-2,3-DICARBOXYLATO)CALCIUM(II)]

GRAHAM SMITH* and DANIEL E. LYNCH

School of Chemistry, Queensland University of Technology, Brisbane 4000, Australia

and

COLIN H. L. KENNARD

Department of Chemistry, The University of Queensland, Brisbane 4072, Australia

and

THOMAS C. W. MAK

Department of Chemistry, The Chinese University of Hong Kong, Shatin, New Territories, Hong Kong

(*Received* 12 *December* 1990; *accepted* 20 *March* 1991)

Abstract—The calcium complex with the herbicide Endothall (7-oxabicyclo-[2.2.1]-heptane-2,3-dicarboxylic acid) has been synthesized and its structure determined by X-ray methods. The seven-coordination about calcium is irregular comprising four oxygens from two carboxylate groups (two bridging), an ether oxygen [Ca—O, 2.387–2.508(3) Å] and two water molecules [Ca—O, 2.389, 2.398(4) Å]. The carboxylate groups on the Endothall moiety adopt an *exo* rather than an *endo* configuration.

Endothall is the trade name for the herbicide 7-oxabicyclo-[2.2.1]-heptane-2,3-dicarboxylic acid, introduced in 1951 by Pennsalt Chemical Corporation.[1,2]

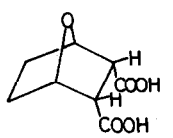

endo-

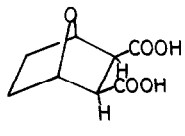

exo-

The carboxylic acid groups in Endothall were assumed to adopt an *endo* configuration relative to the 1,4-oxo-bridged cyclohexane ring.[2] However, a crystal structure determination of Endothall hydrate confirmed the *exo* configurations for the two carboxylic acid groups.[3] In the only known metal complex of this dicarboxylic acid,[4] the acid groups are also *exo* to the ring system. Furthermore, this metal complex is unusual, of the type $[Cu(H_2O)_6]^{2+}[CuL_2]^{2-}$, with each Endothall ligand tridentate (two carboxylate and one ether oxygen). The chemically stable calcium complex reported here is morphologically similar to the copper complex, although it was not expected to be similarly ionic, on the basis of common calcium carboxylate interactions.[5]

EXPERIMENTAL

Preparation

The complex was synthesized by digesting for several hours at 90°C, a 50% aqueous ethanolic solution of Endothall with excess solid calcium carbonate. Unreacted carbonate was removed by

* Author to whom correspondence should be addressed.

vacuum filtration and the solution concentrated by room temperature evaporation over a period of several weeks, giving colourless, pseudo-hexagonal, prismatic crystals suitable for structure determination. Preliminary X-ray studies, density measurement and chemical analysis indicated a formula $[Ca(L)(H_2O)_2]$. (Found: C, 34.7; H, 4.4. Required for $C_8H_{12}CaO_7$: C, 36.9; H, 4.64%.)

Crystal data

$C_8H_{12}CaO_7$, $M_r = 260.3$, triclinic, space group $P\bar{1}$, $a = 6.177(1)$, $b = 8.645(2)$, $c = 10.246(3)$ Å, $\alpha = 70.95(2)$, $\beta = 84.03(2)$, $\gamma = 74.04(2)°$, $V = 497.2(3)$ Å^3, $Z = 2$, $D_c = 1.737$, $D_m = 1.72$ g cm^{-3}, $F(000) = 272$, $\lambda = 0.71073$ Å, μ(Mo-K_α) = 6.3 cm^{-1}, $T = 293$ K.

Data collection

X-ray data were collected on a Nicolet R3m four-circle diffractometer, using graphite crystal monochromatized Mo-K_α X-radiation. A total of 1245 unique reflections were collected up to $2\theta_{max} = 45°$ from a crystal with dimensions 0.08 $\times 0.08 \times 0.14$ mm^3. Of these, 979 with $I > 2.5\sigma(I)$ were considered observed and used in structure refinement. Data were corrected for absorption. The structure was determined using the automatic Patterson procedure of SHELXS 86[6] and refined by full-matrix least-squares (SHELX 76[7]) to residuals $R = (\Sigma \|F_o| - |F_c\|/\Sigma |F_o|)$ of 0.031 and $R_w = [\Sigma w(\|F_o| - |F_c\|^2/\Sigma w \|F_o\|^2)^{1/2}]$ of 0.030. A value of $w = 1.00/(\sigma^2 F_o + 2.7 \times 10^{-4} F_o^2)$ was used. Hydrogen atoms were located in a difference-Fourier analysis and included in the refinement with both positional and thermal parameters refined. Neutral atom scattering factors were used[8] with f', f'' for anomalous dispersion from ref. 8. Bond distances and angles are listed in Table 1, while atomic coordinates, anisotropic thermal parameters, hydrogen atom coordinates and observed and calculated structure factors have been deposited with the Editor as supplementary material; copies are available on request. Atomic coordinates have also been deposited with the Cambridge Crystallographic Data Centre.

DISCUSSION

The structure of the title compound $[Ca(C_8H_8O_5)(H_2O)_2]_n$ involves oxygens of both carboxylate groups and the bridging ether oxygen of the Endothall ligand and two coordinated water molecules, completing an irregular seven-coordination about calcium (Fig. 1). Three of the ligand oxygens [O(111), O(211) (carboxyl) and O(36) (ether)] coordinate symmetrically to calcium [Ca—O, 2.419, 2.445, 2.508(3) Å, respectively]. This is analogous to the tridentate (but bis) mode found for the ligand in the copper(II)–Endothall anion, $[Cu(C_8H_8O_5)_2]^{2-}$.[4] The same carboxylate oxygens form bridges to other calcium ions across inversion centres in the cell [Ca—O(111)′ $(-x, -y, -z)$, 2.452(3) Å: Ca—O(211)′ $(1-x, -y, -z)$, 2.387(2) Å]. The result of this is an infinite zigzag polymer

Table 1. Bond distances (Å) and angles (°) about the coordination sphere

Distances			
Ca—O(111)	2.419(3)	Ca—O(36)	2.508(2)
Ca—O(111)[a]	2.452(3)	Ca—Ow(1)	2.398(3)
Ca—O(211)	2.445(3)	Ca—Ow(2)	2.389(4)
Ca—O(211)[b]	2.387(2)		
Angles			
O(111)—Ca—O(111)[a]	68.3(1)	O(211)—Ca—O(211)[b]	68.5(1)
O(111)—Ca—O(211)	76.5(1)	O(211)—Ca—O(36)	73.8(1)
O(111)—Ca—O(211)[b]	92.8(1)	O(211)—Ca—Ow(1)	147.6(1)
O(111)—Ca—O(36)	73.9(1)	O(211)—Ca—Ow(2)	74.6(1)
O(111)—Ca—Ow(1)	119.1(1)	O(211)[b]—Ca—O(36)	142.0(1)
O(111)—Ca—Ow(2)	146.6(1)	O(211)[b]—Ca—Ow(1)	132.8(1)
O(111)[a]—Ca—O(211)	136.1(1)	O(211)[b]—Ca—Ow(2)	92.8(1)
O(111)[a]—Ca—O(211)[b]	87.6(2)	O(36)—Ca—Ow(1)	83.3(1)
O(111)[a]—Ca—O(36)	118.1(1)	O(36)—Ca—Ow(2)	82.3(1)
O(111)[a]—Ca—Ow(1)	75.1(1)	Ow(1)—Ca—Ow(2)	79.9(1)
O(111)[a]—Ca—Ow(2)	145.0(1)		

[a] Symmetry operation $-x, -y, -z$.
[b] Symmetry operation $1-x, -y, -z$.

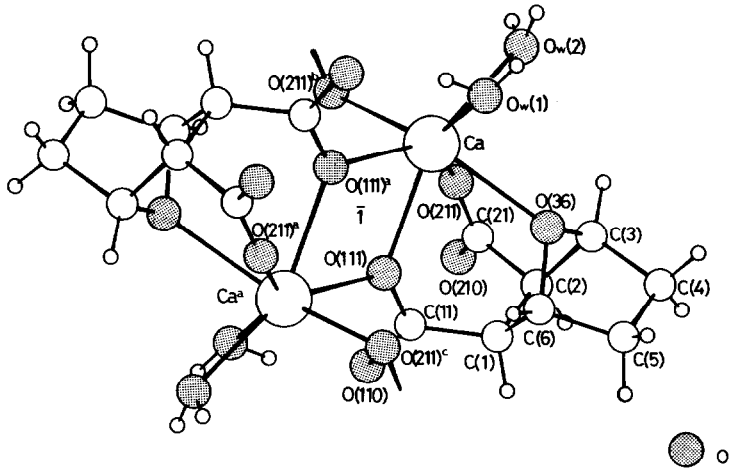

Fig. 1. Molecular conformation and atom naming scheme.

structure which extends through the cell in the *a* direction (Fig. 2). The two water molecules [Ow(1), Ow(2)] complete the coordination sphere about calcium [Ca—O, 2.398, 2.389(4) Å, respectively]. Complex stability is enhanced by the presence of hydrogen bonds involving these water molecules and the uncoordinated carboxyl oxygens [O(110), O(210)] [O(110)···Ow(1)′ $(-x, -y, -z)$, 2.660 Å; O(110)···Ow(2)′ $(x, -1+y, z)$, 2.714 Å; O(210)···Ow(1)′ $(-x, 1-y, -z)$, 2.858 Å], as well as the coordinated oxygen [O(111)···Ow(1)′ $(-x, -y, -z)$, 2.955 Å]. The coordinated oxygens also form intermolecular hydrogen bonds [O(111)···O(111)′ $(-x, -y, -z)$, 2.735 Å; O(211)···O(211)′ $(1-x, -y, -z)$, 2.719 Å]. A polymeric mode is the one expected for calcium carboxylates,[5] although no completely analogous examples are known. The present example is a variation of the Type 3 (malonate) mode of complexation in calcium carboxylates, unique to the dicarboxylates.[9] Furthermore, Ca—O bond distances are considered normal for these compounds.

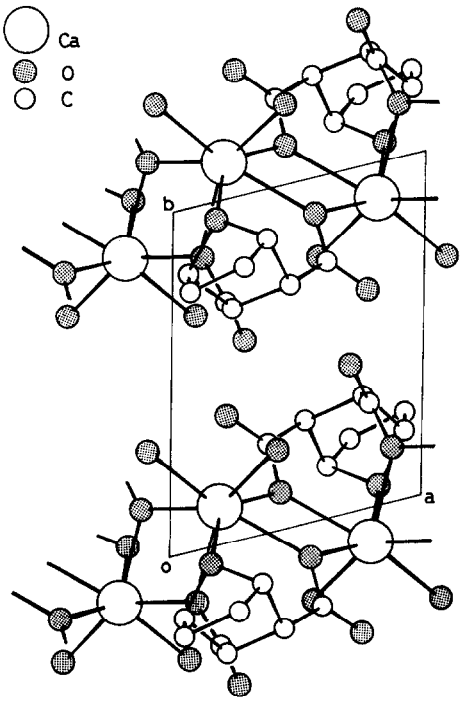

Fig. 2. Packing of the complex in the unit cell viewed down *a*.

Within the Endothall ligand, bond distances and most angles are comparable with those for the parent acid.[3] The configuration of the acid groups is *exo* rather than *endo* relative to the oxo-bridged cyclohexane ring. This is also observed for the copper(II) complex.[4] In both examples, the observed tridentate mode of complexation is possible only with the *exo* configuration. Some conformational differences in the carboxylate groups indicate slight asymmetry in the ligand relative to the metal. The torsion angles about the carboxylate groups [C(6)—C(1)—C(11)—O(111) and C(3)—C(2)—C(21)—O(211)] are −34.1, +24.1° compared with −26.2, +54.9° in the copper complex[4] and −90.5, +0.7° in the parent acid.[3]

Acknowledgements—The authors acknowledge financial assistance from the University of Queensland and the Queensland University of Technology. The Chinese University of Hong Kong is thanked for provision of data collection facilities.

REFERENCES

1. E. Y. Spencer, *Guide to the Chemicals Used in Crop Protection*, 6th edn, p. 248. Agriculture Canada, Ottawa (1973).

2. R. Carlson, R. Whitaker and A. Landskov, in *Analytical Methods for Pesticides and Plant Growth Regulators*, p. 327. Academic Press, New York (1978).
3. H. Yuzhen, X. Xiaogie, Z. Gongdu, T. Youqi, Y. Fuliang and L. Chongxi, *Acta Chim. Sin.* 1983, **41**, 999.
4. G. Smith and C. H. L. Kennard, *Z. Kristallogr.* 1989, **188**, 63.
5. H. Einspar and C. E. Bugg, *Acta Crystallogr.* 1981, **B37**, 1044.
6. G. M. Sheldrick, SHELXS 86, Structure Solution Package. University of Göttingen, F.R.G. (1986).
7. G. M. Sheldrick, SHELX 76, Program for Crystal Structure Determination. University of Cambridge, U.K. (1976).
8. *International Tables for X-ray Crystallography* (Edited by J. A. Ibers and W. C. Hamilton), Vol. 4. Kynoch Press, Birmingham (1974).
9. D. J. Hodgson and R. O. Asplund, *Inorg. Chem.* 1990, **29**, 3612.

Polyhedron Vol. 10, No. 13, pp. 1573–1578, 1991
Printed in Great Britain

0277–5387/91 $3.00+.00
© 1991 Pergamon Press plc

IMINO-ETHER COMPLEXES OF PLATINUM: *cis*-$[PtCl_2(NH{=}C(OR)Me)_2]$ AND $[PtCl_4(NH{=}C(OR)Me)_2]$, WHERE R = Me, Et AND Pr^i. PREPARATION, CHARACTERIZATION AND X-RAY STRUCTURE FOR $[PtCl_2(NH{=}C(OPr^i)Me)_2]_2$

JOSE M. CASAS, MALCOLM H. CHISHOLM,* M. VIOLETA SICILIA and WILLIAM E. STREIB

Department of Chemistry and Molecular Structure Center, Indiana University, Bloomington, IN 47405, U.S.A.

(*Received* 2 *January* 1991; *accepted* 21 *March* 1991)

Abstract—The reaction of *cis*-$PtCl_2(NCMe)_2$ with KOH or KOPh in MeOH, EtOH or Pr^{i}OH produces the imino-ether complexes $[PtCl_2(NH{=}C(OR)Me)_2]$ which have been characterized by IR, NMR and elemental analysis. The crystal structure of $[PtCl_2(NH{=}C(OPr^i)Me)_2]_2$ was determined by X-ray diffraction. Each molecule comprises two units of $[PtCl_2(NH{=}C(OPr^i)Me)_2]$ with a Pt---Pt distance of 3.327(1) Å. The lack of any bridging ligand suggests the presence of hydrogen bonds. The N(4)—Cl(3′) and N(11)—Cl(2′) distances are within the range of van der Waals' interactions. Oxidation reactions of these compounds with $C_6H_5ICl_2$ give the corresponding platinum(IV) complexes $[PtCl_4(NH{=}C(OR)Me)_2]$.

Metal–metal bonding is well known for platinum in stacked platinum(II) complexes[1–3] of type **A**, where the filled d_{z^2}–d_{z^2} interaction is stabilized by mixing with the higher lying p_z–p_z interactions. Also Pt^{III}—Pt^{III} dimers are known,[4–11] wherein two d^7–d^7 ML_5 fragments are united such that the M—M σ bond is formed by Pt $5d_{z^2}$–Pt $5d_{z^2}$ overlap.

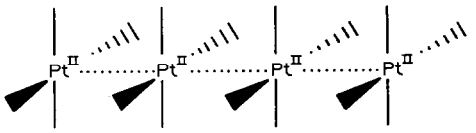

A

In addition, Pt—Pt bonding is often found in Pt^I—Pt^I dimers[12–14] of the type shown in **B**, where the M—M bond is formed from $d_{x^2-y^2}$ interactions. Basically in **B** the M—M bond occupies the fourth coordination site of an otherwise square-planar platinum(II) complex, i.e. the d^3-L_3Pt fragment is isolobal with hydrogen or methyl.

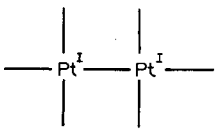

B

The bonding in edge-shared d^8–d^8 square-planar complexes of the general formula shown in **C** below was of interest to us. The principal interactions between the platinum atoms should involve the d_{xy}–d_{xy} orbitals. These are ideally suited to form M—M σ and σ^* interactions.

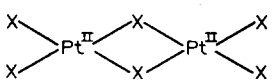

C

Oxidation of an edge-shared Pt^{II}–Pt^{II} dimer of type **C** to give either a mixed valence Pt^{II}—Pt^{III} or Pt^{III}—Pt^{III} dimer could result in the formation of a Pt—Pt bond of order 1/2 and 1, respectively. This has recently been seen where the bridging groups X in **C** are C_6F_5.[15] Here, presumably M—M bonding is assisted by the presence of the μ-C_6F_5 ligand

* Author to whom correspondence should be addressed.

Table 1. Relevant IR data (cm^{-1})

	ν(C=N)	ν(N—H)	ν(Pt—Cl)
$[PtCl_2(NH{=}C(OMe)Me)_2]_2$ (1)	1638(vs)	3230(vs)	320(m), 328(m)
$[PtCl_2(NH{=}C(OEt)Me)_2]_2$ (2)	1636(vs)	3238(vs)	322(m), 328(m)
$[PtCl_2(NH{=}C(OPr^i)Me)_2]_2$ (3)	1630(vs)	3248(vs)	320(s), 328(s)
$[PtCl_4(NH{=}C(OEt)Me)_2]$ (4)	1622(s,b)	3258(m), 3285(m)	335(m), 340(m)
$[PtCl_4(NH{=}C(OPr^i)Me)_2]$ ((5)	1628(s,b)	3224(s,b)	332(m), 340(m)

which provides both an electron-deficient bridge (3c–2e) and a naturally short Pt—Pt distance because of the relatively small Pt—C distances. For X = Cl, the Pt---Pt distance is likely to be too long to allow for significant Pt^{III} to Pt^{III} M—M bonding. We wished, therefore, to prepare alkoxy- or phenoxy-bridged Pt^{II}—Pt^{II} dimers in order to examine their redox properties and their possible ability to support Pt^{III} to Pt^{III} M—M bonds. It is, for example, known that whereas W_2Cl_{10}[16] contains no M—M bond, the compound $W_2(OMe)_{10}$[17] does, cf. W—W = 3.8 Å in W_1Cl_{10} and 2.7 Å in $W_2(OMe)_{10}$. We report here on an investigation intended to yield μ-OR-bridged platinum(II) dimers that proved unsuccessful because of the reactivity of the ancillary ligands. The work described herein provides a general route to imino-ether complexes of platinum(II) chloride.

RESULTS AND DISCUSSION

Syntheses and characterizations

The reaction of the complex *cis*-$PtCl_2(NCMe)_2$ with nucleophiles such as KOPh or KOH in several alcohols as solvents gives the imino-ether complexes $[PtCl_2(NH{=}C(OR)Me)_2]_2$ [R = Me (**1**), Et (**2**) and Pr^i (**3**)] because of the addition of alcohols to the triple C≡N bond. These reactions are base-catalysed, where the bases are not consumed in the process.

When the alcohols are EtOH or Pr^iOH, the corresponding imino-ether complexes are formed in a good yield within a few hours. When the reaction is carried out in MeOH, the solid which precipitated after 2 or 4 h shows strong ν(C=N) and ν(N—H) absorptions in its IR spectra. Its elemental analysis agrees with the stoichiometry $PtCl_2(NH{=}C(OMe)Me)_2$ but its IR spectrum in the region 290–350 cm^{-1} shows several absorptions corresponding to ν(Pt—Cl). This solid is insoluble in all common solvents and only very sparingly soluble in CH_2Cl_2, in contrast to complexes **2** and **3** which are soluble in CH_2Cl_2. If the reaction of *cis*-$PtCl_2(NCMe)_2$ with KOH in MeOH is allowed to proceed for 30 h, the solid precipitated is completely soluble in CH_2Cl_2 and shows similar IR and ^1H NMR spectra to those of complexes **2** and **3**. It is possible that the insoluble form of **1** has a polymeric hydrogen-bonded structure rather than the dimeric type observed for **3** (see later).

All the imino-ether complexes $[PtCl_2(NH{=}C(OR)Me)_2]_2$ [R = Me (**1**), Et (**2**), Pr^i (**3**)] show ν(C=N) and ν(N—H) absorptions in the regions 1630-1640 cm^{-1} and 3230–3250 cm^{-1}, respectively. Two ν(Pt—Cl) absorptions at 320–330 cm^{-1} are observed also, in agreement with their symmetry (C_{2h}) (Table 1).

^1H NMR spectral data for these complexes are collected in Table 2. Characteristic for all samples is the appearance of a N—H signal as a broadened singlet at about 7.9 ppm, a methyl group signal as a singlet at about 2.6 ppm and signals corresponding to the alkoxy group.

X-ray crystal structure of $[PtCl_2(NH{=}C(OPr^i)Me)_2]_2$ (3)

Figure 1 shows the ORTEP drawing of the molecule. In the solid state there are centrosymmetric dimers $[PtCl_2(NH{=}C(OPr^i)Me)_2]_2$ with a distance of only 3.327(1) Å between both metal centres. A summary of crystal data is given in Table 3 and selected bond distances and bond angles are given in Table 4.

Each platinum atom has a local square-planar coordination geometry as expected for platinum(II], with a *cis* disposition of the ligands. Pt—Cl bond lengths [2.309(2) and 2.317(2) Å] and Pt—N bond lengths [2.02(1) Å and 2.01(1) Å] are all longer than those in *cis*-$PtCl_2(NCMe)_2$.[18] These changes reflect the *trans*-influence order of the ligands (imino-ether > nitrile) and the hybridization at nitrogen.

The imino-ether ligands are trigonal with angles Pt(1)—N(11)—C(12), N(1)—C(12)—C(17), N(11)—C(12)—O(13) and C(17)—C(12)—O(13) close to 120° as a consequence of C(sp^2)–N(sp^2) hy-

Table 2. ^{1}H NMR data (ppm)[a]

	N—H	Me	OR
$[PtCl_2(NH{=}C(OMe)Me)_2]_2$ (1)	7.98(s,1)	2.65(s,3)	3.82(s,3)
$[PtCl_2(NH{=}C(OEt)Me)_2]_2$ (2)	7.90(s,1)	2.66(s,3)	4.12(q,2), 1.29(t,3)
$[PtCl_2(NH{=}C(OPr^i)Me)_2]_2$ (3)	7.85(s,1)	2.62(s,3)	4.85(m,1), 1.21(d,6)
$[PtCl_4(NH{=}C(OEt)Me)_2]$ (4)	6.82(s,1)	2.57(s,3)	4.23(q.2), 1.45(t,3)
$[PtCl_4(NH{=}C(OPr^i)Me)_2]$ (5)	6.85(s,1)	2.55(s,3)	4.77(m,1), 1.44(d,6)

[a] $CDCl_3$ solutions, shifts are related to external TMS.

bridization. The C—N bond length is 1.269(11) Å, in agreement with a double C=N bond.[19] The structure of the ligand indicates the *cis* addition of the alcohol to the triple C≡N bond.

The relatively short Pt(1)—Pt(2) distance in the absence of bridging ligands suggests the presence of hydrogen bonds. The observed distances in **3** for N(4)—Cl(3′) = 3.368(7) Å and N(11)—Cl(2′) = 3.322(7) Å, fall within the range expected for NH---Cl bridges, 3.25–3.45 Å.[20] Thus we propose it is hydrogen bonding that is responsible for the observed eclipsed dimer that is reminiscent of d^4–d^4 L_4M—ML_4 complexes.

The weak hydrogen-bonding interactions

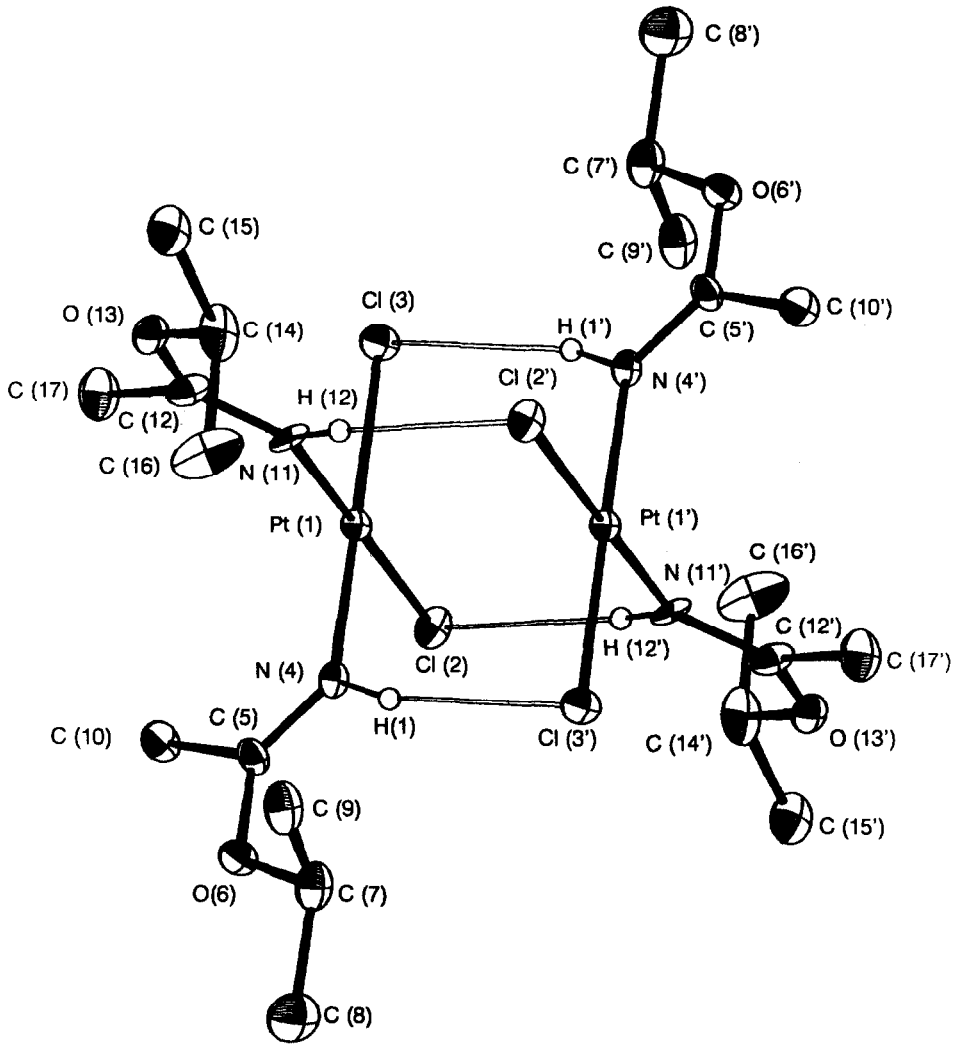

Fig. 1. An ORTEP drawing of the molecular structure of **3** as determined by single-crystal X-ray diffraction. The hydrogen atoms on the nitrogen atom are placed in idealized positions.

Table 3. Summary of crystallographic data

Empirical formula	$C_{20}H_{44}Cl_4N_4O_4Pt_2 \cdot 2CHCl_3$
Colour of crystal	Colourless
Crystal dimensions (mm)	$0.15 \times 0.15 \times 0.15$
Space group	$P2_1/c$
Cell dimensions	
Temperature (°C)	−170
a (Å)	11.115(2)
b (Å)	11.390(2)
c (Å)	15.411(3)
γ (°)	91.88(1)
Z (molecules/cell)	2
Volume (Å^3)	1949.90
Calculated density (g cm^{-3})	2.002
Wavelength (Å)	0.71069
Molecular weight	1175.32
Linear absorption coefficient (cm^{-1})	79.671
Detector-to-sample distance (cm)	22.5
Sample-to-source distance (cm)	23.5
Average omega scan width at half height	2.0
Scan speed (° min^{-1})	8.0
Scan width (° + dispersion)	1.8
Individual background (s)	6
Aperture size (mm)	3.0×4.0
Two-theta range (°)	6–45
Total number of reflections collected	2972
Number of unique intensities	2558
Number with $F\sigma$ 0.0	2426
Number with $F\sigma$ 3.0(F)	2243
$R(F)$	0.0339
$R_w(F)$	0.0348
Goodness-of-fit for the last cycle	0.908
Maximum delta/sigma for last cycle	0.23

responsible for the dimeric structure of these complexes in the solid state probably do not have any effect on the solution chemistry. The reactions of the complexes $[PtCl_2(NH{=}C(OR)Me)_2]_2$ (R = Et, Pr^i) with $C_6H_5ICl_2$ in equimolar amounts, do not lead to Pt^{III}—Pt^{III} dinuclear compounds with M—M bonds, but to mixtures of starting materials and platinum(IV) complexes of stoichiometry $[PtCl_4(NH{=}C(OR)Me)_2]$.

The platinum(IV) complexes can be prepared in

Table 4. Selected bond distances (Å) and bond angles (°) for **3**

Pt(1)—Cl(2)	2.3094(22)	O(6)—C(5)	1.340(11)
Pt(1)—Cl(3)	2.3169(22)	O(6)—C(7)	1.483(10)
Pt(1)—N(4)	2.020(7)	O(13)—C(12)	1.328(11)
Pt(1)—N(11)	2.013(7)	O(13)—C(14)	1.469(11)
Cl(19)—C(18)	1.761(10)	N(4)—C(5)	1.269(11)
Cl(20)—C(18)	1.766(10)	N(11)—C(12)	1.282(12)
Cl(21)—C(18)	1.765(10)		
Cl(2)—Pt(1)—Cl(2)	91.35(8)	Pt(1)—N(11)—C(12)	128.7(6)
Cl(2)—Pt(1)—N(4)	90.20(21)	O(6)—C(5)—N(4)	125.6(8)
Cl(2)—Pt(1)—N(11)	178.31(19)	O(6)—C(5)—C(10)	111.3(7)
Cl(3)—Pt(1)—N(4)	178.44(20)	N(4)—C(5)—C(10)	123.1(8)
Cl(3)—Pt(1)—N(11)	90.15(20)	O(13)—C(12)—N(11)	124.8(8)
N(4)—Pt(1)—N(11)	88.30(28)	O(13)—C(12)—C(17)	112.6(8)
Pt(1)—N(4)—C(5)	127.0(6)	N(11)—C(12)—C(17)	122.5(8)

good yields by the reaction of $[PtCl_2[NH{=}C(OR)Me)_2]_2$ with $C_6H_5ICl_2$ in a 1:2 ratio in $CHCl_3$. Elemental analyses and ^1H NMR data for the platinum(IV) complexes are consistent with the proposed stoichiometry.

Related findings

Certain cationic platinum complexes with imino-ether ligands have been reported. These were prepared by the reactions of [PtClMe(COD)] or *trans*-$PtRXL_2$ (R = Me, X = Cl, L = PMe_2Ph, $AsMe_3$; R = CF_3, X = I, L = PMe_2Ph) with silver salts ($AgPF_6$, $AgBF_4$) and perfluoroaryl nitriles in various alcohols. The final products depend on the alcohol and in some cases on the silver salt used.[21-23]

The authors suggest a mechanism involving the initial formation of a platinum-nitrile π bond, delocalization of the positive charge from platinum onto the C≡N bond leading to activation of the C—N bond towards nucleophilic attack by the alcohol. Refluxing of the coordinated σ-bonded nitrile complexes for several hours did not lead to the imino-ether formation.

In this work, we have found that the synthesis of neutral platinum(II) imino-ether complexes from coordinated σ-bonded nitriles is promoted by a base-catalysed process. The imino-ether ligand is bound more tightly than the nitrile in the *cis*-$PtCl_2L_2$ complexes so that the complexes once formed do not enter into a catalytic cycle.

EXPERIMENTAL

IR spectra were recorded (4000–200 cm^{-1}) on a Perkin–Elmer 283 spectrophotometer, using Nujol mulls between polyethylene sheets. ^1H NMR spectra were recorded on a Varian XL300 instrument. $PtCl_2(NCMe)_2$[24] and $C_6H_5ICl_2$[25] were prepared as already reported. Reactions using KOPh were carried out under N_2.

$[PtCl_2(NH{=}C(OMe)Me)_2]$ (**1**)

To a suspension of *cis*-$PtCl_2(NCMe)_2$ (0.44 g, 1.264 mmol), in 20 cm^3 of anhydrous MeOH, was added KOH (71 mg, 1.264 mmol). The suspension was stirred for 30 h to give a white solid, which was filtered and recrystallized from CH_2Cl_2/OEt_2, 0.2811 g (yield, 54%). Found: C, 17.7; H, 3.3; N, 6.6. Calc. for $[PtCl_2(NH{=}C(OMe)Me)_2]_2$: C, 17.5; H, 3.4; N, 6.8%.

$[PtCl_2(NH{=}C(OEt)Me)_2]_2$ (**2**)

(a) To a solution of KOPh (0.2459 g, 1.86 mmol) in 20 cm^3 of absolute EtOH was added *cis*-$PtCl_2(NCMe)_2$ (0.2163 g, 0.6214 mmol). The suspension was stirred for 2 h to give a white solid, which was filtered and recrystallized from CH_2Cl_2/OEt_2, 0.16 g (yield, 63%).

(b) To a suspension of *cis*-$PtCl_2(NCMe)_2$ (0.5 g, 1.436 mmol) in 30 cm^3 of absolute EtOH was added KOH (80.6 mg, 1.436 mmol). The suspension was stirred for 4 h to give a white solid, which was filtered and recrystallized from CH_2Cl_2/OEt_2, 0.41 g (yield, 70%). Found: C, 21.8; H, 3.9; N, 6.3. Calc. for $[PtCl_2(NH{=}C(OEt)Me)_2]_2 \cdot CH_2Cl_2$: C; 21.3; H, 4.0; N, 6.2%.

$[PtCl_2(NH{=}C(OPr^i)Me)_2]_2$ (**3**)

To a solution of KOPh (0.4476 g, 3.386 mmol) in 20 cm^3 of Pr^iOH was added *cis*-$PtCl_2(NCMe)_2$ (0.3929 g, 1.129 mmol). The suspension was stirred for 2 h to give a white solid, which was filtered and recrystallized from CH_2Cl_2/OEt_2, 0.2955 g (yield, 60%). Found: C, 26.1; H, 4.6; N, 5.6. Calc. for $[PtCl_2(NH{=}C(OPr^i)Me)_2]_2 \cdot CH_2CL_2$: C, 26.3; H, 4.8; N, 5.9%.

$[PtCl_4(NH{=}C(OEt)Me)_2]$ (**4**)

To a solution of **2** (0.25 g, 0.3062 mmol) in 15 cm^3 of $CHCl_3$ was added $C_6H_5ICl_2$ (0.1683 g, 0.6124 mmol). The solution became red immediately, but changed from red to yellow within a few minutes. After 30 min the solvent was removed *in vacuo* and the oily residue was transformed to a yellow solid by adding OEt_2, 0.19 g (yield, 65%). Found: C, 19.5; H, 3.8; N, 5.1. Calc. for $[PtCl_4(NH{=}C(OEt)Me)_2]$: C, 20.1; H, 3.8; N, 5.8%.

$[PtCl_4(NH{=}C(OPr^i)Me)_2]$ (**5**)

To a solution of **3** (0.30 g, 0.34 mmol) in 15 cm^3 of $CHCl_3$ was added $C_6H_5ICl_2$ (0.19 g, 0.69 mmol). The solution became red immediately, but changed to yellow within a few minutes. After 20 min the solvent was removed *in vacuo* and the residue transformed to a yellow solid by adding OEt_2, 0.233 g (yield, 67%). Found: C, 21.8; H, 3.6; N, 5.0. Calc. for $[PtCl_4(NH{=}C(OPr^i)Me)_2] \cdot CHCl_3$: C, 21.1; H, 3.7; N, 4.5%.

X-ray analysis

A crystal of suitable size but with no well-defined faces, was obtained by cleaving a large piece of the sample in a nitrogen atmosphere glove bag. The crystal was mounted using silicone grease and was transferred to a goniostat where it was cooled to −170°C for characterization and data collection.

A systematic search of a limited hemisphere of reciprocal space revealed intensities with Laue symmetry and systematic absences consistent with space group $P2_1/c$, which was later proven correct by the successful solution of the structure. Following complete data collection, data processing gave a residual of 0.042 for the averaging of 193 unique intensities which had been observed more than once. Four standards measured every 300 data showed no significant trends. No correction was made for absorption.

The structure was solved using a combination of direct methods (MULTAN78) and Fourier techniques. The platinum atom position was obtained from an initial E-map. The remaining non-hydrogen atoms were obtained from subsequent iterations of least-squares refinement and difference Fourier calculations. Hydrogen atoms were included in calculated positions to improve the refinement of the non-hydrogen atoms, however the hydrogen atoms were not refined. Hydrogen atom thermal parameters were fixed at one plus the isotropic thermal parameter of the atom to which they were bonded.

In the final cycles of refinement, the non-hydrogen atoms were varied with anisotropic thermal parameters to a final $R(F) = 0.034$. The final difference Fourier had platinum residuals of 0.88–2.2 e/Å^3. All other residual peaks were less than 0.8 e/Å^3.

The centre of the molecule, e.g. the Pt—Pt midpoint, is at a crystallographic centre of symmetry. In addition, the crystal structure contains a molecule of chloroform at a general position.

Atomic coordinates have been deposited with the Director of the Cambridge Crystallographic Centre.

Acknowledgements—We thank the National Science Foundation for financial support. J.M.C. and M.V.S. thank M.E.C. (Spain) for Fulbright postdoctoral fellowships. We also thank Johnson–Mathey for a kind loan of platinum.

REFERENCES

1. D. Washecheck, S. W. Petersou, A. H. Reis and J. H. Williams, *Inorg. Chem.* 1976, **15**, 74.
2. C. Bellito, A. Flamini, O. Piovesana and P. F. Zanazzi, *Inorg. Chem.* 1980, **19**, 3632.
3. (a) H. A. F. Dos Remedios Pinto, P. J. Sadler, S. Neidle, M. R. Sanderson, A. Subiah and R. J. Kuroda, *J. Chem. Soc., Chem. Commun.* 1980, 13; (b) R. E. Marsh and F. H. Herbstein, *Acta Cryst.* 1983, **B39**, 280.
4. J. D. Schagen, A. R. Overbeek and H. Schenk, *Inorg. Chem.* 1978, **17**, 1938.
5. (a) B. R. Steel and K. Vrieze, *Transition Met. Chem.* 1977, **2**, 169; (b) B. R. Steel and K. Vrieze, *Transition Met. Chem.* 1976, **1**, 208.
6. C. Bellitto, A. Flamini, L. Gastaldi and L. Scaramuzza, *Inorg. Chem.* 1983, **22**, 444.
7. D. M. L. Goodgame, R. W. Rollins and A. C. Skapski, *Inorg. Chim. Acta* 1984, **83**, L11.
8. C. M. Che, F. H. Herbstein, W. P. Schaefer, R. E. Marsh and H. G. Gray, *J. Am. Chem. Soc.* 1983, **105**, 4604.
9. G. S. Muraveiskaya, G. A. Kukina, V. S. Orlov, O. N. Evstaf'eva and M. A. Porai-Koshits, *Dokl. Akad. Nauk. SSSR* 1976, **226**, 596.
10. F. A. Cotton, L. R. Falvello and S. Han, *Inorg. Chem.* 1982, **21**, 2889.
11. F. A. Cotton, L. R. Falvello and S. Han, *Inorg. Chem.* 1982, **21**, 1709.
12. M. P. Brown, R. J. Puddephatt, M. Rashidi and K. R. Seddon, *J. Chem. Soc., Dalton Trans.* 1977, 951.
13. R. G. Holloway, B. R. Penfold, R. Colton and M. J. McCormick, *J. Chem. Soc., Chem. Commun.* 1976, 485.
14. M. P. Brown, A. Yavari, L. Manojlovic-Muir and K. W. Muir, *J. Organomet. Chem.* 1983, **256**, C19.
15. J. M. Casas, Thesis Doctoral, Zaragoza (1977).
16. F. A. Cotton and G. Wilkinson, *Advanced Inorganic Chemistry*, 5th edn, p. 820. Wiley Interscience, New York (1988).
17. A. P. Sattelberger, Los Alamos National Laboratories, personal communication.
18. F. D. Rochon, R. Melanson, H. E. Howard-Lock, C. J. L. Lock and G. Turner, *Can. J. Chem.* 1984, **62**, 860.
19. L. Pauling, *The Nature of the Chemical Bond*, 3rd edn, p. 228. Cornell University Press, Ithaca, New York (1960).
20. J. E. Huheey, *Inorganic Chemistry*, 3rd edn, p. 258. Harper & Row, New York (1983).
21. (a) H. C. Clark and L. E. Manzer, *J. Chem. Soc., Chem. Commun.* 1971, **387**; (b) H. C. Clark and L. E. Manzer, *Inorg. Chem.* 1971, **10**, 2699.
22. T. G. Appleton, M. H. Chisholm, H. C. Clark and L. E. Manzer, *Inorg. Chem.* 1972, **11**, 1786.
23. L. E. Manzer, *J. Chem. Soc., Dalton Trans.* 1974, 1535.
24. K. A. Hofmann and G. Bugge, *Chem. Ber.* 1907, **40**, 1772.
25. H. J. Lucas and E. R. Kennedy, *Organic Synthesis Collection*, Vol. 3, p. 482. John Wiley, New York (1988).

Polyhedron Vol. 10, No. 13, pp. 1579–1585, 1991
Printed in Great Britain

0277–5387/91 $3.00+.00
© 1991 Pergamon Press plc

SYNTHESIS AND CHARACTERIZATION OF COPPER(II) COMPLEXES OF 1,5-BIS(QUINOLINE-8′-YL)-1,5-DITHIAPENTANE. CRYSTAL AND MOLECULAR STRUCTURE OF $[Cu(BQDTP)(NO_3)(OH_2)](NO_3)$

E. BERMEJO, R. CARBALLO, A. CASTIÑEIRAS† and A. LOMBAO

Departamento de Química Inorgánica, Universidad de Santiago de Compostela, E-15706 Santiago de Compostela, Spain

and

W. HILLER and J. STRÄHLE

Institut für Anorganische Chemie der Universität Tübingen, Auf der Morgenstelle 18, D-7400 Tübingen 1, F.R.G.

(*Received* 9 *January* 1991; *accepted* 21 *March* 1991)

Abstract—Four new copper(II) complexes of formula $[Cu(BQDTP)Cl_2]\cdot 2H_2O$ (**I**), $[Cu(BQDTP)Br_2]\cdot 2H_2O$ (**II**), $[Cu(BQDTP)(OH_2)_2](ClO_4)_2$ (**III**) and $[Cu(BQDTP)(NO_3)(OH_2)](NO_3)$ (**IV**), where BQDTP is 1,5-bis(quinoline-8′-yl)-1.5-dithiapentane, have been synthesized and characterized by elemental analysis, conductivity measurements, IR and ligand-field spectral studies and magnetic susceptibility measurements. The X-ray crystal structure of **IV** has been solved at 293 K by single-crystal X-ray analysis. It consists of $[Cu(BQDTP)(NO_3)(OH_2)]^+$ cations and nitrate ions, which are connected by hydrogen bonds to a water molecule. The coordination geometry about the copper atom is an elongated octahedron. The measured bond distances are: Cu—S = 2.343(3) and 2.507(3) Å, Cu—N = 1.986(7) and 1.993(7) Å, $Cu—O_{(water)}$ = 2.030(6) Å and $Cu—O_{(nitrate)}$ = 2.677(7) Å. The IR and electronic spectroscopic data, conductivity and magnetic susceptibility are in agreement with the observed structure.

Complete understanding of the mechanisms governing the physiological behaviour of metalloproteins is only possible once their structures, or at least the structure of the active metallic centre, are known. Before crystallography could be employed to determine protein structures, and hence the bonding and the function of the metal in the protein, it was practice to synthesize and analyse low molecular weight metallic complexes whose chemical and physical properties matched those of the corresponding metalloproteins. X-ray crystallography has only served to solve the structure of some proteins, although other techniques such as high-field NMR and EXAFS are proving of great use in this respect. Nonetheless, simple metallic complexes that imitate biological compounds are still very valuable in understanding the structure of the active centre and reaction mechanisms of those proteins with structures too complicated to be resolved by X-ray analysis or which cannot be crystallized.

The response to the discovery in some copper proteins of two nitrogen and two sulphur atoms coordinated to the metal[1] has been the design of several types of chelating ligands containing these atoms.[2] Of these, some of the most interesting are the quadridentate ligands of linear chain NSSN in which the nitrogen atoms belong to heterocyclic compounds such as imidazole,[3] benzimidazole,[4] pirazol[5] or pyridine,[6] and the sulphur atoms belong to thioethers.

Our work over the last few years has been along these lines.[7] This paper presents some recent results obtained using the ligand 1,5-bis(quinoline-8′-yl)-

† Author to whom correspondence should be addressed.

1,5-dithiapentane (BQDTP) in the presence of CuX_2 (X = Cl, Br, NO_3 or ClO_4).

EXPERIMENTAL

Physical measurements

Carbon, hydrogen and nitrogen were determined on a Perkin–Elmer 240B microanalyser.

IR absorption spectra (4000–200 cm^{-1}), as KBr and CsI pellets, were recorded on a Perkin–Elmer 1330 spectrophotometer. Electronic reflectance spectra were recorded on an Hitachi U-3200 spectrophotometer equipped with the standard reflectance accessory. Magnetic susceptibilities were measured in the temperature range 300–70 K by the Faraday method with a DSM-5 susceptometer and $HgCo(SCN)_4$ as the calibration standard. Corrections for the diamagnetism of the ligands were applied.

X-ray crystallographic data were obtained on an Enraf–Nonius CAD4 diffractometer. Data reduction and solution were performed on a Micro VAXII using the SHELXS86[8] and VAX/SDP[9] package of programs.

^1H NMR spectra were determined with a Bruker WM250 instrument in $CDCl_3$ using TMS as the internal standard.

Conductivity measurements were carried out on a WTW LF-3 conductivity bridge. Measurements were made for 10^{-3} M solutions in acetonitrile.

Reagents

The 8-mercaptoquinoline hydrochloride (Lancaster Synthesis Ltd), 1,3-dibromopropane (Merck) and copper(II) salts (Merck) were used without further purification. All solvents used were reagent grade and purified by conventional procedures prior to use.

Ligand synthesis

BQDTP was prepared by the method described in the literature[10] using 8-mercaptoquinoline hydrochloride (2.00 g, 10.1 mmol) in absolute ethanol (15 cm^3) and 1,3-dibromopropane (1.04 g, 5.15 mmol) (70% yield). ^1H NMR ($CDCl_3$): δ 8.95 (c, 2H, H-2q), 8.12 (c, 2H, H-4q), 7.43 (m, 8H, H-3,6,7,8q), 3.33 (t, 4H, S—CH_2—), 2.33 (q, 2H, —CH_2—).

Preparation of the complexes

A solution of BQDTP (0.15 g, 0.40 mmol) in hot ethanol (10 cm^3) was added with stirring to a solution of the copper(II) salt (0.40 mmol) in the same solvent (10 cm^3). After a few minutes the solution became green or garnet in colour. The reaction mixture was stirred at room temperature for 7 days and then filtered. The precipitate obtained was washed well with ethanol and then air-dried.

Determination of the crystal structure of $[Cu(BQDTP)(NO_3)(OH_2)](NO_3)$ (IV)

Green, prismatic crystals were obtained by slow evaporation of an ethanolic solution of the complex. A crystal, dimensions *ca* $0.60 \times 0.10 \times 0.05$ mm, was mounted on a glass fibre. Intensity measurements were performed on a CAD4 Enraf–Nonius four-circle diffractometer in ω–θ scan mode using monochromated Cu-K_α radiation. Of 4599 reflections to $\theta_{max} = 65°$, 3801 were unique ($R_{int} = 0.025$) and 1857 with $I > 3\sigma(I)$ were used in all calculations. An empirical adsorption correction was applied,[11] with correction factors of 0.704–1.600. Cell constants were refined from the θ values of 25 reflections in the range 15–36°.

The structure was solved by the heavy-atom method and subjected to full-matrix, anisotropic, least-squares refinement on *F*. Hydrogen atoms were included at the calculated positions with isotropic temperature factors of 5.0 $Å^2$ and included in the structure factor calculations, but their positional parameters were not refined. A secondary extinction correction was applied,[12] with a final coefficient, refined in the least-squares cycle, of 5.25×10^{-7}. The final *R* value was 0.058, with $R_w = 0.059$ (weighting scheme $w^{-1} = \sigma^2(F)$; 323 parameters; $S = 2.1$; maximum Δ/σ in final cycle 0.01; maximum $\Delta\rho = 0.33$ e $Å^{-3}$ near Cu). For a summary of crystal data, see Table 1.†

RESULTS AND DISCUSSION

Elemental analysis and conductance results are presented in Table 2. In general, the compounds synthesized were sparingly soluble in polar solvents and insoluble in non-polar solvents. Solutions of 10^{-3} M in acetonitrile could only be prepared with compounds **III** and **IV**. Their measured molar conductances were in agreement with values published for similar compounds.[13] The value for compound **III** shows it behaves as a 1 : 2 electrolyte in aceto-

† Further details of the structure determination have been deposited as Supplementary Publication No. CDS-57951. Copies may be obtained through the Fachinformationzentrum Karlruhe, D-7514 Eggenstein-Leopoldshafen 2, F.R.G.

Table 1. Crystallographic data for **IV**

Chemical formula	$C_{21}H_{20}CuN_4O_7S_2$
fw	568.08
Space group	$P2_1/n$
a (Å)	6.480(3)
b (Å)	17.430(5)
c (Å)	21.248(5)
β (°)	97.81(3)
V (Å^3)	2377.8
Z	4
λ(Cu-K_α) (Å)	1.54184
ρ_{cal} (g cm^{-3})	1.587
μ (cm^{-1})	33.29
R	0.058
Rw	0.059
T (K)	293

nitrile, hence the formula $[Cu(BQDTP)(OH_2)_2](ClO_4)_2$. For compound **IV**, the conductance is in keeping with that of 1 : 1 electrolytes, which can be explained by assuming that one of the nitrate groups is coordinated to the copper(II).

IR spectra

Frequencies were assigned to BQDTP and the complexes (Table 3) bearing in mind the assignments for the quinoline molecule and derivatives,[14,15] 8-mercaptoquinoline,[16] pyridine and derivatives,[17] and those proposed for alkyl sulphides.[18]

Structural information was obtained by comparing the spectra of the complexes with that of the ligand. In the 4000–1600 cm^{-1} region a wide band appears between 3600 and 3300 cm^{-1} with a maximum around 3450 cm^{-1}, also two additional peaks appear at 3620 and 3540 cm^{-1} in compound **III**. These have been assigned to the antisymmetric and symmetric ν(OH) stretching modes. The band between 1650 and 1635 cm^{-1} is due to the δ(OH) modes.[19] The positions of these bands show the water molecules are involved in hydrogen bonds.

In the 1600-1350 cm^{-1} region, the ν_{8b} and ν_{8a} vibrations of pyridine are slightly shifted, but those assigned to the ν_{19a} and ν_{19b} modes split and move 15 and 10 cm^{-1}, respectively, to higher frequencies. The cause, as in pyridine complexes, is that the nitrogen of the heteroaromatic ring donates electrons, the C—N bond is strengthened due to an increase in the electron density of the bond, and the corresponding band appears at higher frequencies.

In the 1350–800 cm^{-1} region, the ν_3 band, assigned to the C—H antisymmetric bending modes in the plane, increases in frequency by 6–11 cm^{-1}. This may be explained as the main effect of donation of the free pair on the nitrogen, which is passed around the ring. The ν_1 band, due to the totally symmetric vibrations of the ring, is also shifted to higher frequencies. This has been related to the strength of the donor–acceptor bond,[20] for which the order **I** ≈ **II** < **III** < **IV** can be established in these complexes, even though the magnitude of the displacement is not very large.

Lastly, in the region 800–400 cm^{-1}, the ν_{6a} and ν_{16b} bands, due to deformations of the ring in and out of the plane, undergo shifts of between +20 and +30 cm^{-1} for the first and +17 and +32 cm^{-1} for the second. This is also good indication of coordination of the pyridinic nitrogen to the copper. Also in this region we have assigned the ν(CS) modes. The small shifts of these bands to higher frequencies indicates, though not very rigorously, that the thioether sulphur atoms of BQDTP are coordinated to the metal.

The spectrum of complex **III** contains a wide,

Table 2. Elemental analyses and conductivity measurements for the metal complexes

Compound	Colour	Analysis: calc. (found)(%) C	H	N	Temperature (°C)	Λ_m[a]
BQDTP	White	69.2 (69.6)	5.1 (5.0)	8.1 (7.8)	88	
$[Cu(BQDTP)Cl_2]\cdot 2H_2O$ (**I**)	Green	49.8 (49.0)	4.4 (3.9)	5.4 (5.5)	165	
$[Cu(BQDTP)Br_2]\cdot 2H_2O$ (**II**)	Garnet	41.9 (41.7)	3.6 (3.5)	5.0 (4.4)	150	
$[Cu(BQDTP)(ClO_4)_2]\cdot 2H_2O$ (**III**)	Green	39.1 (39.3)	3.1 (3.3)	4.6 (4.2)	230	287
$[Cu(BQDTP)(NO_3)_2]\cdot H_2O$ (**IV**)	Green	44.1 (43.0)	3.8 (3.8)	10.0 (9.6)	215	128

[a] Molar conductance (Ω^{-1} cm^2 mol^{-1}) for 10^{-3} M solutions at 25°C in acetonitrile.

Table 3. Characteristic IR frequencies (cm^{-1}) of BQDTP and the copper(II) complexes

BQDTP	I	II	III	IV	Assignment
	3440m,a	3460m,a	3620m 3540m	3430m,a	ν(OH)
	1648md	1638md	1635d	1650m	δ(OH)
1601m	1602d	1605d	1610d	1610d	8b, ν(CC)
1590m	1593m	1594m	1591m	1595d	8a, ν(CC)
1483f	1495f	1497f	1495f	1498f	19a, ν(CC)+ν(CN)
	1487f	1487f	1486f,h	1490m,h	
1449f	1460f	1460d,h	1460d	1462m	19b, ν(CC)+ν(CN)
	1452f	1454d	1455d,h	1458m,h	
				1385f	$\nu_a(NO_2)$ (NO_3^-)
1302f	1308m	1309m	1311m	1312m	ν_3
				1290m,h	$\nu_s(NO_2)$ (ONO_2)
			1160- 1020f,a		$\nu_a(ClO_2)$ (ClO_4^-)
				1040d	ν_s(NO) (NO_3^-)
				1015d	ν(NO)* (ONO_2)
982f	988m	987m	991m	997d	ν_1
820f	827f	826f	830f	839m	10a
758m	763m	760m			ν(CS)
658f	680d	679d	685d	691d	6a, α(CCC)
	660m	661m			
626d	625md	628md		630md	ν(CS)
			623mf		$\delta(ClO_2)$ (ClO_4^-)
442d	439d	439d	435d		
433d	452d	452d	450d	465d	16b, ν(CC)
	403d	408d	398d	398d	ν(CuN)
			318d	320d	ν(CuO)
	304m				ν(CuCl)
	280h	375h	285h	275h	ν(CuS)

intense band between 1160 and 1020 cm^{-1} and another strong band at 623 cm^{-1} which have been assigned, respectively, to the $\nu_a(ClO_2)$ antisymmetric stretching mode and to the $\delta(ClO_2)$ bending mode of the perchlorate ion.[21] This is in keeping with the molar conductance value found for this complex.

The spectrum of complex **IV** shows four bands together in the range 1400–1000 cm^{-1}: a strong one at 1385 cm^{-1} and a weak one at 1040 cm^{-1}, which corresponds to the antisymmetrical and symmetrical $\nu(NO_2)$ modes, respectively, of the free nitrate ion,[21] and one of medium intensity at 1290 cm^{-1} and one weak band at 1015 cm^{-1} which represent, respectively, the $\nu_s(NO_2)$ and ν(NO) symmetrical stretching modes of a nitrate group coordinated across an oxygen atom.[22]

In the far-IR region, a medium intensity band at 304 cm^{-1} was found which, since it was not seen in the other complexes, was assigned to the ν(CuCl) modes. The corresponding ν(CuBr) vibration cannot be detected in the spectrum of **II** due to the low resolution of the equipment between 250 and 200 cm^{-1}.

The spectra of compounds **III** and **IV** show weak bands at 318 and 320 cm^{-1}, respectively, which were not seen in the other complexes, and thus suggests they should be assigned to the ν(CuO) modes.[23] In the spectra of all four complexes, a weak band at 400 cm^{-1} and a shoulder at 280 cm^{-1} can be observed, which have been assigned to the ν(CuN) and ν(CuS) modes, respectively.[24]

Electronic spectra

The diffuse reflectance spectra of the complexes (Table 4) contain two classes of bands. One, in the 21,900–22,900 cm^{-1} region, is due to charge-transfer transitions from BQDTP to copper. Additionally, in complexes **I** and **II** there is also a shoulder at 20,390 cm^{-1} and a band at 18,142 cm^{-1}, respectively, which have been attributed to transitions from the halogen to copper.[25]

The solid complexes also exhibit an adsorption

Table 4. Diffuse reflectance spectral data (cm^{-1}) and magnetic moments (BM) for copper(II) complexes[a]

Complex	α	β	θ	μ_{eff}	*d–d*	
I	−48.37	2.66	18.21	1.74	13,558	20,399, 21,949
II	−88.46	3.00	29.45	1.63	13,543	18,142, 22,242
III	−49.50	2.82	17.55	1.68	15,060	22,831
IV	−19.40	2.13	9.10	1.94	14,890	22,742

[a] $1/X = \alpha + \beta T$; θ = Curie–Weiss constant.

band between 13,500–15,500 cm^{-1}. The asymmetric nature of this band is due to an unresolved shoulder at lower frequencies. Although the connection between copper(II) stereochemistry and solid-state electronic spectra is not always straightforward,[26,27] the position of the *d–d* band in all complexes is consistent with a distorted octahedral copper(II) geometry.[28,29]

Magnetic susceptibilities

The solid-state magnetic moments, between 1.60 and 1.95 BM (Table 4) are consistent with an $S = 1/2$ ground state configuration for the d^9 metal ion. Between 70–300 K, all complexes give linear plots of the reciprocal of the molar magnetic susceptibility corrected for temperature; and positive values of 9–30 K for the Curie–Weiss constant (Table 4).

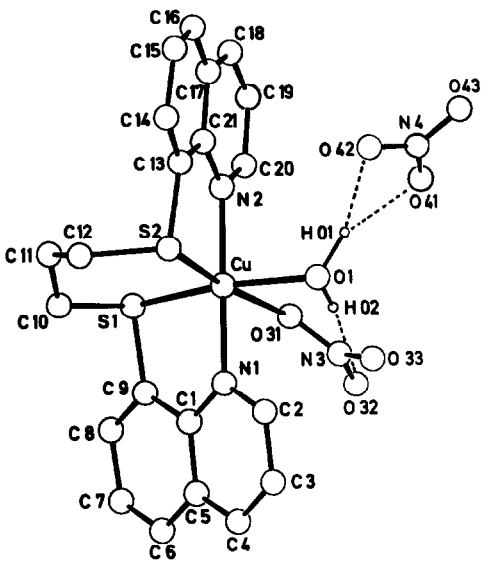

Fig. 1. Perspective view of complex **IV**.

Description of the crystal structure of **IV**

The asymmetric unit of compound **IV** contains a nitrate ion and a monovalent cation formed by a copper atom bound to a molecule of BQDTP, to a nitrate group across one of its oxygen atoms and to the oxygen of a water molecule. The geometry around the copper atom is a tetragonally distorted pseudo-octahedron. The conformation of the complex is shown in Fig. 1. Interatomic bond lengths and angles are shown in Table 5.

In the large number of copper(II) complexes with thioethers that have been characterized structurally,[30] the metal generally sits in a distorted octahedron or is pentacoordinated, with Cu—S bonds lengths in the range 2.297–2.488 Å for equatorial thioether ligands and in the range 2.560–2.919 Å for the axial ligands. The Cu—S bond lengths of 2.343(3) and 2.507(3) Å observed in complex **IV** are typical of thioethers coordinated equatorially and axially, respectively. In keeping with this orientation, the other axial site is filled by an oxygen atom from a nitrate group, with a Cu—O(3) bond length of 2.677(7) Å. This appears to be very large when compared with the bond length of 2.00 Å in copper(II) nitrate in the vapour phase,[31] or with 1.97 Å in other copper(II) complexes where the nitrate group behaves like a monodentate ligand.[32]

In the equatorial plane, two other coordination sites are occupied by the two nitrogen atoms of the quinoline groups, with a mean Cu—N bond length of 1.989(7) Å, in agreement with those observed in copper(II) complexes with a mixture of ligands containing nitrogen heterocycles and oxygen donating ligands.[33] The water molecule occupies the fourth coordination site, the Cu—O(1) bond length being typical of copper(II) complexes with similar coordination.[34] Apart from the excessively large axial bond lengths, departure from octahedral coordination is indicated by the bond angles around the copper atom, in which the greatest differences occur in the angle S(1)—Cu—S(2) [103.5(2)°] and S(1)—Cu—O(1) of [160.3(2)°].

Table 5. Selected bond lengths and angles for the [Cu(BQDTP)(ONO_2)(OH_2)](NO_3) molecule with estimated standard deviations in parentheses

Bond distances (Å)			
Cu—S(1)	2.343(3)	Cu—O(31)	2.677(7)
Cu—S(2)	2.507(3)	Cu—N(1)	1.986(7)
Cu—O(1)	2.030(6)	Cu—N(2)	1.993(7)
Hydrogen bond			
H(01)—O(41)	2.15(8)		
H(01)—O(42)	1.85(8)		
H(02)—O(32)	1.85(8)		
Bond angles (°)			
S(1)—Cu—S(2)	103.5(2)	S(2)—Cu—N(1)	100.2(3)
S(1)—Cu—O(1)	160.3(2)	S(2)—Cu—N(2)	83.5(3)
S(1)—Cu—O(31)	80.9(2)	O(1)—Cu—O(31)	79.4(2)
S(1)—Cu—N(1)	85.3(2)	O(1)—Cu—N(1)	91.4(3)
S(1)—Cu—N(2)	92.9(2)	O(1)—Cu—N(2)	90.0(3)
S(2)—Cu—O(1)	96.3(2)	O(31)—Cu—N(1)	83.3(3)
S(2)—Cu—O(31)	174.6(2)	O(31)—Cu—N(2)	93.2(3)
		N(1)—Cu—N(2)	176.1(3)
Hydrogen bond			
O(1)—H(01)—O(41)	136(6)		
O(1)—H(01)—O(42)	164(7)		
O(1)—H(02)—O(32)	171(8)		

In BQDTP, the bond lengths and angles of the thioether and quinoline groups are in close agreement with those found in similar ligands.[3–7,35]

With regard to the nitrate groups, the N—O bond lengths in the uncoordinated group are somewhat shorter than the usual distances observed in the coordinated group, but this is of no real significance given the high degree of disorder shown. Both groups participate in hydrogen bonds with the water molecule coordinated to copper(II).

Acknowledgements—We thank Professor Alario Franco and Professor Sáez Puche of the Complutense University (Madrid) for their collaboration in the magnetic measurements. We also thank the DGICYT (Spain) for financial support (Project PS88-0051) and DAAD (F.R.G.).

REFERENCES

1. W. H. Armstrong, *Metalloprotein Crystallography: Survey of Recent Results and Relationships to Model Studies in Metal Clusters in Proteins* (Edited by L. Que Jr), p. 1. American Chemical Society, Washington (1988).
2. K. D. Karlin and J. Zubieta (Eds), *Copper Coordination Chemistry: Biochemical and Inorganic Perspectives*. Adenine Press, New York (1983).
3. E. Bouwman, W. L. Driessen and J. Reedijk, *J. Chem. Soc., Dalton Trans.* 1988, 1337; E. Bouwman, J. Ch. Ten Hove, W. L. Driessen and J. Reedijk, *Polyhedron* 1988, **7**, 2591; E. Bouwman, J. S. Wood, R. Day, J. Ch. Ten Hove, W. L. Driessen and J. Reedijk, *Acta Cryst.* 1988, **C44**, 644; A. L. Speek, A. J. M. Duisenberg, E. Bouwman, W. L. Driessen and J. Reedijk, *Acta Cryst.* 1988, **C44**, 1569; E. Bouwman, R. de Gelder, R. A. G. de Graaff, W. L. Driessen and J. Reedijk, *Recl. Trav. Chim. Pays-Bas* 1988, **107**, 163.
4. P. J. M. W. L. Birker, J. Helder, G. Henkel, B. Krebs and J. Reedijk, *Inorg. Chem.* 1982, **21**, 357; M: J. Schilstra, P. J. M. W. L. Birker, G. C. Verschoor and J. Reedijk, *Inorg. Chem.* 1982, **21**, 2637; J. M. M. Smits, R. Janssen, P. T. Beurkens, J. van Rijn and J. Reedijk, *Polyhedron* 1987, **6**, 1843.
5. G. E. Norris, B. F. Anderson and E. N. Baker, *J. Am. Chem. Soc.* 1986, **108**, 2784.
6. E. T. Adman and J. H. Jensen, *Israel J. Chem.* 1981, **21**, 8; J. H. Worrell, J. J. Genova and T. D. Dubois, *J. Inorg. Nucl. Chem.* 1978, **40**, 441; G. R. Brubaker, J. N. Brown, M. K. Yoo, R. A. Kinsey, T. M. Kutchan and E. A. Mottel, *Inorg. Chem.* 1979, **18**, 299; D. E. Nikles, M. J. Powers and F. L. Urbach, *Inorg. Chem.* 1983, **22**, 3210; J. H. Worrell and P. J. Chesky, *Synth. React. Inorg. Met.-Org. Chem.* 1986, **16**, 577.
7. A. Castiñeiras, W. Hiller, J. Strähle, M. V. Paredes and J. Sordo, *Acta Cryst.* 1985, **C41**, 41; A. Castiñeiras, R. Carballo, M. R. Bermejo, M. Gayoso, C. Molleda, W. Hiller and J. Strähle, *Z. Krist.* 1988, **185**, 381; A. Castiñeiras, W. Hiller, J. Strähle, R.

Carballo, M. R. Bermejo and M. Gayoso, *Z. Naturfor.* 1990, **45b**, 1267; A. Castiñeiras, R. Carballo, W. Hiller and J. Strähle, *Z. Krist.* 1990, **193**, 251; W. Hiller, J. Strähle, A. Castiñeiras, R. Carballo, M. R. Bermejo and M. Gayoso, *An. Quim.* 1990, **86**, 506; R. Carballo, A. Castiñeiras, W. Hiller and J. Strähle, *Acta Cryst.*, in press.

8. G. M. Sheldrick, SHELXS86, A Program for the Solution of Crystal Structures from X-ray Diffraction Data. University of Göttingen, F.R.G. (1986).
9. B. A. Frenz, in *Computing in Crystallography* (Edited by H. Schenk, R. Oltof-Hazenkamp, H. van Koningsveld and G. C. Bassi). Delft University Press, Delft (1978).
10. H. A. Goodwin and F. Lions, *J. Am. Chem. Soc.* 1960, **82**, 5013.
11. N. Walker and D. Stuart, *Acta Cryst.* 1983, **A39**, 158.
12. W. H. Zachariasen, *Acta Cryst.* 1963, **16**, 1139.
13. W. J. Geary, *Coord. Chem. Rev.* 1971, **7**, 81.
14. S. S. Singh, *Z. Anorg. Allg. Chem.* 1971, **384**, 81.
15. C. Karr, P. A. Estep and A. J. Papa, *J. Am. Chem. Soc.* 1959, **81**, 152.
16. Y. Mido and E. Sekido, *Bull. Chem. Soc. Japan* 1971, **44**, 2127, 2130.
17. C. H. Klime and J. Turkevich, *J. Chem. Phys.* 1944, **12**, 300; L. Corrsin, B. J. Fax and R. C. Lord, *J. Chem. Phys.* 1953, **21**, 1170; A. R. Kafritaky and M. A. D. Phill, *Quart. Rev.* 1959, **13**, 353; G. C. Kulisingam, W. R. McWhinnie and R. Thomas, *Spectrochim. Acta* 1966, **22**, 1365.
18. M. Ohsaku, Y. Shiro and A. Murata, *Bull. Chem. Soc. Japan* 1972, **45**, 956; M. Ohsaku, *Bull. Chem. Soc. Japan* 1975, **48**, 707.
19. K. Nakamoto, *Infrared and Raman Spectra*, 4th edn. John Wiley, New York (1986).
20. N. N. Greenwood and K. Wade, *J. Chem. Soc. (Lond.)* 1960, 1130.
21. W. Herzberg, *Infrared and Raman Spectra of Polyatomic Molecules*. Van Nostran, New York (1945).
22. J. R. Ferraro and A. Ealker, *J. Chem. Phys.* 1965, **42**, 1278.
23. D. M. Adams and P. J. Lock, *J. Chem. Soc. A* 1971, 2801.
24. J. R. Ferraro, *Low Frequency Vibrations of Inorganic and Coordination Compounds*. Plenum Press, New York (1971).
25. G. Ertem and D. X. West, *Polyhedron* 1985, **4**, 33.
26. E. D. McKenzie, *J. Chem. Soc. A* 1970, 3095.
27. A. Sedov, M. Dunaj-Jurco, M. Kabesova, J. Gazo and J. Garas, *Inorg. Chim. Acta* 1982, **64**, L257.
28. B. J. Hathaway and D. E. Billing, *Coord. Chem. Rev.* 1970, **5**, 143.
29. A. B. P. Lever, *Inorganic Electronic Spectroscopy*, 2nd edn. Elsevier, Amsterdam (1984).
30. J. M. Berg and K. O. Hodgson, *Inorg. Chem.* 1986, **25**, 1800.
31. S. H. Bauer and R. E. La Villa, *J. Am. Chem. Soc.* 1963, **85**, 3597.
32. C. C. Addison, N. Logan, S. C. Wallwork and C. D. Garner, *Quart. Rev.* 1971, **25**, 289.
33. L. Antolini, L. P. Battaglia, A. Bonamartini Corradi, G. Marcotrigiano, L. Menabue, G. C. Pellacini and M. Saladini, *Inorg. Chem.* 1982, **21**, 1391.
34. J. R. Olson, M. Yamauchi and W. M. Butler, *Inorg. Chim. Acta* 1985, **99**, 121.
35. S. Garcia-Granda, C. Jansen, P. T. Beurskens, H. J. J. Behmy and F. Gomez-Beltran, *Acta Cryst.* 1988, **C44**, 176.

Polyhedron Vol. 10, No. 13, pp. 1587–1589, 1991
Printed in Great Britain

0277–5387/91 $3.00+.00
© 1991 Pergamon Press plc

THE PERMUTATIONAL ISOMERISM OF JAHN–TELLER WHEELS

ARNOUT CEULEMANS

Department of Chemistry, Katholieke Universiteit Leuven, Celestijnenlaan 200F, B-3001 Heverlee, Belgium

(*Received* 29 *January* 1991; *accepted* 21 *March* 1991)

Abstract—Molecular rearrangements based on a Jahn–Teller mechanism are characterized by a specific permutational isomerism. This is illustrated for the metallacyclobutane rearrangement, proposed by Wilker and Hoffmann, and for the butterfly isomerisation of $Fe(CO)_4$. It is shown that in both cases a full experimental conformation of the proposed Jahn–Teller mechanisms requires the resolution of enantiomeric reaction cycles.

Platinacyclobutanes undergo highly stereospecific skeletal rearrangements of potential catalytic interest. Puddephatt, Tipper and their co-workers[1] first discovered that a carbon atom in the α position, adjacent to the metal, exchanges with the carbon atom in the β position, opposite to the metal. The simultaneous migration of both phenyl and deuterium substituents in **1** clearly establishes the permutational nature of this rearrangement.

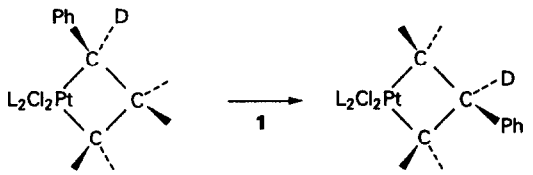

Subsequent experiments by Casey *et al.*[2] demonstrated the high stereospecificity of the Puddephatt reaction. One particularly informative experiment involved the use of platinacyclobutanes with one phenyl and one deuterium on the same side of the metallacycle. There are four such isomers with the phenyl in the α position, as shown in **2**.

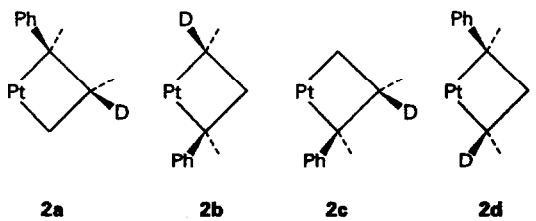

Upon heating a mixture of these isomers the phenyl groups can migrate to the β position, in accordance with reaction **1**. The only two β-phenyl isomers that could be obtained are shown in **3**. In both isomers deuterium and phenyl are still on the same side. This proves that the stereochemistry of the metallacycle is retained.

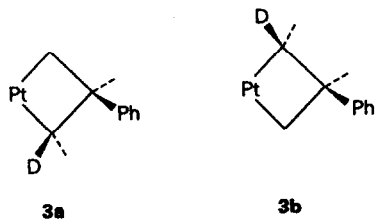

Wilker and Hoffmann[3] have suggested that the Puddephatt rearrangement might be explained by an itinerary around the periphery of a Jahn–Teller wheel. Figure 1 offers a schematic drawing of this mechanism. The structure in the centre has approximate C_{3v} symmetry and is Jahn–Teller unstable. It is surrounded by a Jahn–Teller wheel with three equivalent minima, corresponding to three metallacycle isomers. These isomers have been redrawn below (**4**) in the standard orientation.

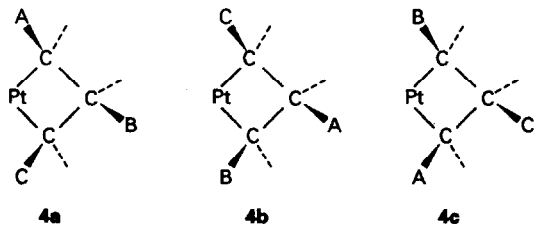

Polytopal rearrangements which interconvert these isomers are characterized by two remarkable geo-

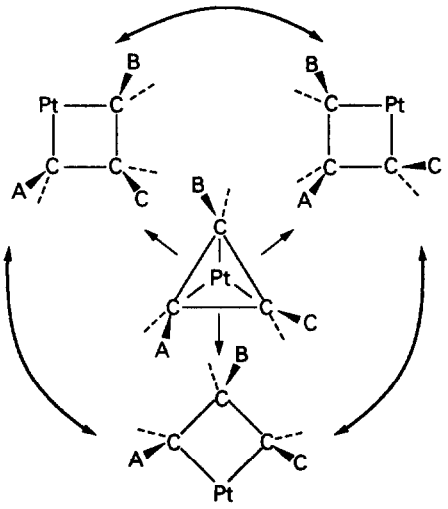

Fig. 1. Metallacyclobutane rearrangement mechanism, according to Wilker and Hoffmann.[3] The structure in the centre is a C_{3v} isomer, which sits atop a Jahn–Teller hill. Distortion of this structure may give rise to three metallacyclobutane isomers. Interconversions of these isomers proceed through a circular potential energy trough, surrounding the Jahn–Teller origin. This trough is the so-called Jahn–Teller wheel.

metric constraints: (i) retention of the orientation of the CH_2 groups with respect to the plane of the three carbon atoms, and (ii) retention of the handedness of the tricarbon structure. The first requirement implies that substituents will retain their relative positions with respect to the plane of the metallacycle. This point is the one that was verified by the labelling experiments of Casey *et al.*[2] The second constraint implies that the permutations associated with the rearrangement must be of an even nature. In fact it is easily verified that the permutations which interconvert the three isomers in **4** are the cyclic permutations of the symmetric group S_3. In combination with the unit element, these permutations form the alternating group A_3 of even permutations on three elements:

$$\mathbf{4a} \xrightarrow{(ABC)} \mathbf{4b}$$

$$\mathbf{4a} \xrightarrow{(ACB)} \mathbf{4c}.$$

Odd permutations, such as the one shown in **5**, are not allowed. This point seems to have been overlooked in the previous treatment.[3] It means that the reaction mixture in the Casey experiment should consist of two enantiomeric cycles, {**2a**,**2b**,**3a**} and {**2c**,**2d**,**3b**}, which are completely separated. Clearly, for an experimental verification of this prediction, we must await experiments with chiral reagents belonging to one of those cycles. Such experiments are certainly within reach, given the current synthetic expertise.[4] If the rearrangement of such a chiral metallacycle is found to induce loss of optical activity, a Jahn–Teller wheel mechanism must be ruled out.

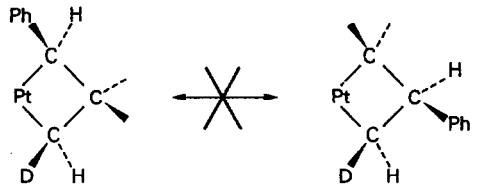

5

The specific permutational isomerism of the Jahn–Teller wheel in Fig. 1 is not an isolated case. An interesting example of a Jahn–Teller "sphere" with the same kind of permutational isomerism as the wheel of Wilker and Hoffmann is offered by the tetrahedral $Tx(e+t_2)$ problem with stable minima of C_{2v} epikernel symmetry.[5] The C_{2v} distortion of a tetrahedron can be viewed as an opening of one of the edges to yield a butterfly-type structure. This type of distortion is encountered in the $Fe(CO)_4$ fragment,[5,6] and in many tetranuclear clusters containing 62 valence electrons.[7] Since a tetrahedron has six edges, six equivalent C_{2v} structures are attainable. These are situated on a Jahn–Teller sphere, as shown in Fig. 2. Rearrangements between these minima correspond to specific permutations of the

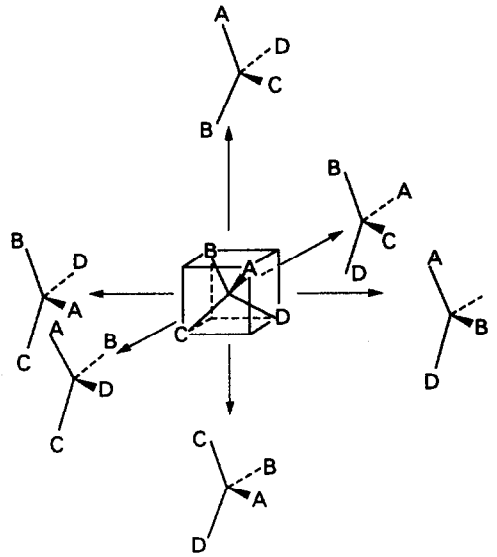

Fig. 2. The rearrangement mechanism for $Fe(CO)_4$, as proposed by Poliakoff and Ceulemans.[6] The structure in the centre has T_d symmetry and is Jahn–Teller unstable. It has six equivalent C_{2v} distortions. All butterfly isomers have been drawn with the same orientation, to make identification easier: the elongated edge between the wingtips of the butterfly is always vertical, while the hinge edge is horizontal.

four ligands (or cluster atoms). The interconversion between two adjacent C_{2v} structures in Fig. 2 is easily identified as a cyclic permutation of one wingtip (w) with the two hinges (h) of the butterfly, while leaving the other wingtip invariant.[8] This permutation can be performed in four different ways, thus connecting a given C_{2v} structure to four adjacent minima, **6**.

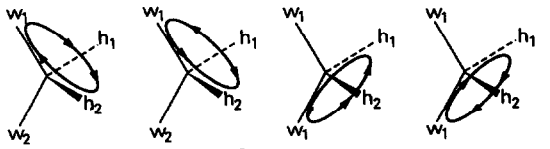

6

Interestingly, the permutational isomerism of this Jahn–Teller process is entirely analogous to a rearrangement mode for a trigonal bipyramid, proposed by Muetterties.[9] The Muetterties mechanism corresponds to a cyclic exchange of one axial (a) with two equatorial (e) ligands, leaving the third equatorial ligand fixed, **7**. The topology of the Jahn–Teller sphere is seen to be a subspace of the rearrangement in **7**, in which one of the ligands is permanently blocked in the equatorial position.

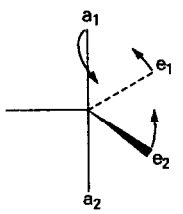

7

This type of permutational isomerism has two important geometrical characteristics: (i) a simultaneous exchange of both axial sites with the equatorial ones, the so-called Berry exchange, requires a minimum number of two elementary processes, and (ii) the mechanism consists of two disjoint enantiomeric cycles.

The first characteristic implies that the open edge of the butterfly cage cannot be transferred to the antipodal site in a single step. For the case of $Fe(CO)_4$, this has indeed been confirmed experimentally in the elegant IR laser study by Poliakoff and co-workers.[10] The second characteristic indicates that the Muetterties mechanism does not invert the stereochemistry. Again experimental verification of this point must await the use of chiral reagents. It seems that butterfly clusters should offer the best chance to reach this goal.

In conclusion, rearrangement[11] mechanisms based on Jahn–Teller wheels[12] are seen to exhibit a specific permutational isomerism. This may explain the remarkable stereochemistries of reactions such as the Puddephatt rearrangement and the Muetterties process. However, for a full experimental confirmation of such proposals, the resolution of enantiomeric reaction cycles seems imperative.

Acknowledgements—Financial support from the Belgian National Science Foundation (NFWO) and the Belgian Government (Ministerie voor Programmatie van het Wetenschapsbeleid) is gratefully acknowledged.

REFERENCES

1. R. J. Al-Essa, R. J. Puddephatt, M. A. Quyser and C. F. H. Tipper, *J. Am. Chem. Soc.* 1979, **101**, 364.
2. C. P. Casey, D. M. Scheck and A. J. Shusterman, *J. Am. Chem. Soc.* 1979, **101**, 4233.
3. C. N. Wilker and R. Hoffmann, *J. Am. Chem. Soc.* 1983, **105**, 5285.
4. See e.g.: W. D. Neilsen, R. D. Larsen and P. W. Jennings, *J. Am. Chem. Soc.* 1988, **110**, 3307.
5. A. Ceulemans, D. Beyens and L. G. Vanquickenborne, *J. Am. Chem. Soc.* 1984, **106**, 5824.
6. M. Poliakoff and A. Ceulemans, *J. Am. Chem. Soc.* 1984, **106**, 50.
7. A. Ceulemans, *J. Chem. Phys.* 1986, **84**, 6442.
8. This permutation corresponds to a three-fold rotation axis in the central tetrahedral frame. Such a rotation interchanges adjacent edges.
9. E. L. Muetterties, *J. Am. Chem. Soc.* 1969, **91**, 4115.
10. B. Davies, A. McNeish, M. Poliakoff and J. J. Turner, *J. Am. Chem. Soc.* 1977, **99**, 7573.
11. See e.g.: J. Brocas, R. Willem and M. Gielen, *The Permutational Approach to Dynamic Stereochemistry*. McGraw-Hill, New York (1983).
12. See e.g.: A. Ceulemans and L. G. Vanquickenborne, *Struct. Bond.* 1989, **71**, 125.

Polyhedron Vol. 10, No. 13, pp. 1591–1592, 1991
Printed in Great Britain

0277–5387/91 $3.00+.00
© 1991 Pergamon Press plc

COMMUNICATION

THE STABILITY OF COMPLEXES OF ALKALI AND ALKALINE EARTH IONS WITH CROWN ETHER CARBOXYLIC ACIDS

HEINZ BUKOWSKY and ERHARD UHLEMANN*

Brandenburgische Landeshochschule, Fachbereich Chemie, O-1571 Potsdam, F.R.G.

and

KARSTEN GLOE and PETER MÜHL

Institut für Festkörperphysik und Werkstofforschung, O-8027 Dresden, F.R.G.

(*Received* 11 *January* 1991; *accepted* 15 *April* 1991)

Abstract—The stability constants of sodium, potassium and calcium complexes with different dibenzo crown ether carboxylic acids were evaluated from the pH dependence of the extraction. There are only small differences between sodium and potassium, but the calcium compound is distinctly more stable.

The extraction of alkali and alkaline earth ions with crown ether carboxylic acids yields a similar curve in the plot of $\log D$/pH as is typical for chelate extraction. In this case, deprotonation of the ligand and complex formation are combined and hence it is possible to determine the stability constant of the extracted complex from the pH dependence of the extraction. Using this model, the stability constants of the sodium, potassium and calcium complexes with 2-(sym-dibenzo-14-crown-4-oxy)hexanoic acid (**1**), 4-(sym-dibenzo-14-crown-4-oxy)butanoic acid (**2**) and 2-(sym-dibenzo-16-crown-5-oxy)hexanoic acid (**3**) were calculated for the chloroform/water system (Table 1).

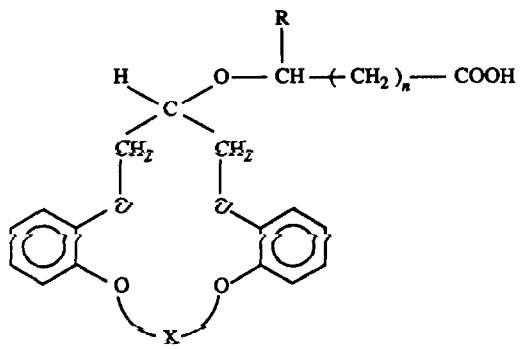

	X	R	n
1	$-CH_2-CH_2-CH_2-$	$-(CH_2)_3-CH_3$	0
2	$-CH_2-CH_2-CH_2-$	H	2
3	$-(CH_2)_2-O-(CH_2)_2-$	$-(CH_2)_3-CH_3$	0

Because of the influence of solvent the evaluated data are distinctly smaller than those which were determined for complexes of (sym-dibenzo-16-crown-5-oxy)acetic acid in methanol/water (Na $\log\beta_1 = 4.02$, 3.27, respectively; K $\log\beta_1 = 3.71$, 3.11, respectively) by potentiometric[1] and calorimetric measurements.[2,3] Furthermore, there is a remarkable difference in stability between the calcium complex and the complexes of alkali ions, which is also reflected in the extraction behaviour.[4,5] Regarding the alkali ions, neither the crown ether cavity nor the length of the carboxylic group have a significant influence on the complex stability. But the potassium complex is somewhat more stable than the sodium compound. For the calcium compound a "sandwich" structure is proposed, but it was not possible to isolate crystals suitable for crystal structure analysis.

* Author to whom correspondence should be addressed.

Table 1. Stability constants of sodium, potassium and calcium complexes with crown ether carboxylic acids

	Ligand 1	2	3
$\log \frac{K_V(HL)}{K_s(HL)}$	7.21	7.33	7.67
$Na^+ \log \beta_1$	1.61	1.58	1.72
$K^+ \log \beta_1$	1.97		2.05
$Ca^{2+} \log \beta_1$	0.79		0.79
$\log \beta_2$	4.23		4.16

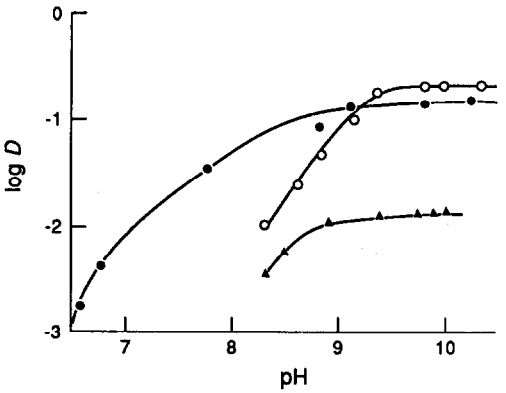

Fig. 1. Plots of log D/pH for the sodium extraction with crown ether carboxylic acids **1** (●), **2** (▲) and **3** (○).

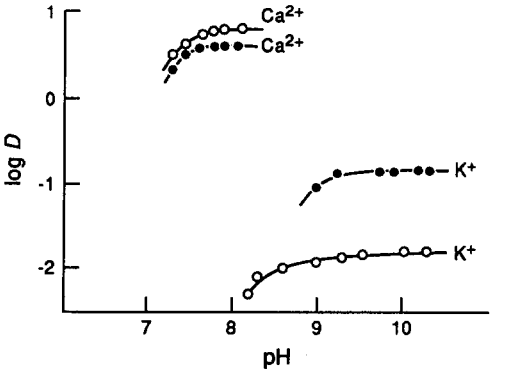

Fig. 2. Plots of log D/pH for the potassium and calcium extraction with crown ether carboxylic acids: **1** (●) and **3** (○).

The syntheses of the crown ether carboxylic acids were reported elsewhere.[4,6,7] The determination of the distribution ratios (Figs 1 and 2) was accomplished radiometrically for sodium and potassium and by flame photometry for calcium. The calculations were made using the program MIQUA[8] following the equations

$$\frac{1}{D} = \frac{1+\beta_1 c_L}{K_V(ML)\beta_1 c_L^-}$$

$$\frac{1}{D} = \frac{1+\beta_1 c_L^- + \beta_2 c_L^{2-}}{K_V(ML_2)\beta_2 c_L^{2-}},$$

respectively, where

$$c_L^- = \frac{c_{HL}(tot)}{c_{H_3O^+}} \frac{K_s(HL)}{K_V(HL)}.$$

The values of $K_s(HL)/K_V(HL)$ were determined from the pH dependence of the two-phase distribution of the crown ether carboxylic acid

$$\log D = \log \frac{K_V}{K_s} - pH$$

$$pH = \log \frac{K_V}{K_s} \quad (\text{for } \log D = 0)$$

using graphical methods.[9]

REFERENCES

1. C. A. Chang, J. Twu and R. A. Bartsch, *Inorg. Chem.* 1986, **25**, 396.
2. R. J. Adamic, E. M. Eyring, S. Petrucci and R. A. Bartsch, *J. Phys. Chem.* 1985, **89**, 3752.
3. R. J. Adamic, B. A. Lloyd, E. M. Eyring, S. Petrucci, R. A. Bartsch, M. J. Pugia, B. E. Knudsen, Y. Liu and D. M. Desai, *J. Phys. Chem.* 1986, **90**, 6571.
4. E. Uhlemann, H. Bukowsky, F. Dietrich, K. Gloe, P. Mühl and H. Mosler, *Anal. Chim. Acta* 1989, **224**, 47.
5. H. Bukowsky, F. Dietrich, E. Uhlemann, K. Gloe, P. Mühl and H. Mosler, *Z. Chem.* 1990, **30**, 33.
6. E. Uhlemann, H. Geyer, K. Gloe and P. Mühl, *Anal. Chim. Acta* 1986, **185**, 279.
7. R. A. Bartsch, G. S. Heo, S. I. Kang, Y. Liu and J. Strzelbicki, *J. Org. Chem.* 1982, **47**, 457.
8. A. Friedrich, H. Bukowsky, E. Uhlemann, K. Gloe and P. Mühl, *Anal. Chim. Acta* 1987, **193**, 373.
9. E. B. Sandell, *J. Am. Chem. Soc.* 1950, **72**, 4660.

Polyhedron Vol. 10, No. 13, p. 1593, 1991
Pergamon Press plc. Printed in Great Britain

BOOK REVIEW

Gmelin Handbook of Inorganic Chemistry (8th edn); Silicon, Supplement Volume B 4, Silicon–Nitrogen Compounds. By P. Eigen, H. Keller-Rudek, W. Kurtz, P. Merlet, H. Schäfer and F. Schröder. Springer, Berlin, 1989, £564.00.

Imagine being presented with a treasure-chest: on opening it, you find it is full of old favourites, half-forgotten pleasures and newly-discovered delights... Such was the imagery that constantly recurred as I dipped into this new volume of Gmelin. For any enthusiast of silicon–nitrogen chemistry, it is guaranteed to produce excitement, coupled with the occasional slight sense of shame on being confronted by references that you should have known about but didn't.

Compared with their silicon–oxygen analogues, silicon–nitrogen molecular compounds generally show a greater variety, but our knowledge of silicon–nitrogen oligomers and polymers is far more sketchy. Much of the polymer work carefully reported in this volume was done in the 1960s, as part of the inorganic polymer initiatives launched at that time, particularly in the U.S., U.S.S.R. and U.K. That particular bubble burst, as bubbles usually do, and we were left with intriguing but perplexing sets of results, often incomplete. Many of these systems need to be re-examined, using modern techniques; this volume may well provide the necessary enthusiasm by pin-pointing systems that could be useful as preceramic polymers. There are also tantalising references to complex thermolysis reactions of some silicon–nitrogen monomers, leading to elimination of amines, H_2, methane and other volatile products, and often catalysed by bases and salts. These have been interpreted as disproportionation, condensation, elimination and rearrangement processes. But are they truly four-centre reactions? Are free radicals involved? Again, answers to such questions could and should be provided by modern investigative methods.

Because of the way in which the Gmelin system operates, this volume contains no compounds with Si—C bonds. This means that only some members of closely-related groups of compounds are included: $HSi(NR_2)_3$ compounds are described, but $R'Si(NR_2)_3$ derivatives are not. On the other hand, exotica such as $\{Si[NCCr(CO)_5]_6\}^{2-}$ are present. The best-studied silicon–nitrogen compound, silicon nitride, Si_3N_4, is excluded, as it will be the subject of another Gmelin volume, soon to be published. A count of pages gives a rough indication of the coverage accorded to various categories of compounds:

	Number of pages
(i) Nitrogen sorbed on silicon	12
(ii) Si_xN_y compounds (except Si_3N_4) and derived gas-phase ions	34
(iii) Anionic $(Si_xN_y)^{n-}$ in solids	17
(iv) Volatile Si/N/H derivatives and derived ions	67
(v) Polymeric Si/N/H species	14
(vi) Other Si/N/X or Si/N/H/X species (X not C, volatile)	5
(vii) Molecular Si/N/C or Si/N/H/C species and their adducts	192
(viii) Si/N/C or Si/N/H/C polymers	10
(ix) Contents	10.

Some surprising entries were encountered: in category (ii), for example, it has been reported that SiN_8, with a spiro structure, is a possible precursor for the deposition of amorphous silicon; an apparently even more unlikely SiN_{12} is in fact the reasonably well-characterized tetraazide, $Si(N_3)_4$. Category (iii) includes compounds such as $LaSi_3N_5$ and Li_5SiN_3, while category (iv) not only details actual compounds such as $(SiH_3)_3N$ but also theoretical studies on unknown monomeric SiN_2H_2 (with nine possible isomers!).

The distinguished group of authors guarantee the scientific authenticity of the volume, while the firm hand of the editor, Dr F. Schröder, ensures an impressive uniformity of style. I have not detected any errors of fact (nor did I expect to). Of course there must always be differences of interpretation, but it was very seldom that I could quarrel with anything other than a nuance of meaning. Despite its very high price, this volume is an essential reference for all those working with silicon–nitrogen compounds. After all, to say that it is worth its weight (0.88 kg) in gold means that it can be bought for only some 3% of its true value.

Department of Chemistry **B. J. AYLETT**
Queen Mary and Westfield College
Mile End Road
London E1 4NS, U.K.

Polyhedron Vol. 10, No. 14, pp. 1595–1598, 1991
Printed in Great Britain

0277–5387/91 $3.00+.00
© 1991 Pergamon Press plc

POLY(1-PYRAZOLYL)BORATOIRIDIUM AND TRIS(1-PYRAZOLYLMETHYL)AMINOIRIDIUM AND -RHODIUM COMPLEXES

MARIA J. FERNANDEZ, MARIA J. RODRIGUEZ and LUIS A. ORO*

Departamento de Química Inorgánica, Instituto de Ciencia de Materiales de Aragón, Universidad de Zaragoza—C.S.I.C., 50009 Zaragoza, Spain

(*Received* 30 *January* 1991; *accepted* 21 *March* 1991)

Abstract—The synthesis of the $Ir(H_nBPz_{4-n})(cod)$ ($n = 2, 0$; Pz = pyrazolyl; cod = cycloocta-1,5-diene) complexes is described. They are prepared by reaction of $[Ir(\mu\text{-Cl})(cod)]_2$ with $Tl(H_nBPz_{4-n})$. The carbonyl compounds $Ir(H_nBPz_{4-n})(CO)_2$ ($n = 2, 0$) are obtained by carbonylation of the cycloocta-1,5-diene derivatives. The preparations of the $[Ir(coe)_2\{N(CH_2Pz)_3\}]BF_4$ (coe = cyclooctene) and $[M(cod)\{N(CH_2Pz)_3\}]BF_4$ (M = Ir, Rh) compounds are also reported. They are prepared by treatment of $[Ir(\mu\text{-Cl})(coe)_2]_2$ or $[M(\mu\text{-Cl})(cod)]_2$ with $N(CH_2Pz)_3$ and $NaBF_4$. The carbonyl compound $[Rh(CO)_2\{N(CH_2Pz)_3\}]BF_4$ is obtained by carbonylation of $[Rh(cod)\{N(CH_2Pz)_3\}]BF_4$.

During the past decade, the interest in the chemistry of transition metal complexes containing poly(1-pyrazolyl)borato (H_nBPz_{4-n}) ligands has grown steadily.[1,2] Part of this interest stems from the proposed structural and electronic similarity between complexes with cyclopentadienyl (C_5H_5) [or pentamethylcyclopentadienyl (C_5Me_5)] and those with H_nBPz_{4-n}.[3,4] Recently we reported[5] the activation of a vinyl carbon–hydrogen bond in a tris(1-pyrazolyl)boratoiridium complex. As part of our studies on the chemistry of iridium complexes with the H_nBPz_{4-n} ligands, we report here the preparation of complexes of the type $Ir(H_nBPz_{4-n})L_2$ ($n = 2, 0$; L_2 = cod; L = CO). This paper also describes the synthesis of a number of new alkenyl and carbonyl iridium and rhodium compounds containing tris(1-pyrazolylmethyl)amine, $N(CH_2Pz)_3$. This ligand has a tripodal shape, similar to H_nBPz_{4-n} ($n = 0$, 1), but differs in that it contains four potential donor sites.[6]

EXPERIMENTAL

All reactions were carried out under a nitrogen atmosphere using Schlenk techniques. $[Ir(\mu\text{-Cl})(coe)_2]_2$,[7] $[Ir(\mu\text{-Cl})(cod)]_2$,[8] $[Rh(\mu\text{-Cl})(cod)]_2$,[9] $Tl(H_nBPz_{4-n})$[10] and $N(CH_2Pz)_3$[6] were prepared as previously reported. IR spectra were recorded on a Perkin–Elmer 783 spectrophotometer. Elemental analyses were carried out on a Perkin–Elmer 240B microanalyser. ^1H NMR spectra were measured in $CDCl_3$ solution at room temperature on a Varian XL 200 spectrometer.

$Ir(H_2BPz_2)(cod)$

$[Ir(\mu\text{-Cl})(cod)]_2$ (300 mg, 0.45 mmol) was added to $Tl(H_2BPz_2)$ (315 mg, 0.90 mmol) in CH_2Cl_2 (20 cm^3). The mixture was stirred for 15 min, then filtered through Kieselguhr. The resulting yellow solution was concentrated under reduced pressure. Addition of pentane (20 cm^3) gave a yellow precipitate which was removed by filtration, washed with pentane and dried *in vacuo*; yield: 132 mg (33%). Found: C, 37.5; H, 4.7; N, 12.6. Calc. for $C_{14}H_{20}BIrN_4$: C, 37.6; H, 4.5; N, 12.5%. ^1H NMR ($CDCl_3$): δ 1.73 [m, 4H, CH_2(cod)]; 2.35 [br, 4H, CH_2(cod)]; 4.00 [br, 4H, =CH(cod)]; 6.20 (t, 2H, Pz); 7.48 (d, 2H, Pz); 7.52 (d, 2H, Pz).

$Ir(BPz_4)(cod)$

The complex was prepared using the procedure described for $Ir(H_2BPz_2)(cod)$, but with $[Ir(\mu\text{-Cl})(cod)]_2$ (253 mg, 0.38 mmol) and $Tl(BPz_4)$ (364 mg, 0.75 mmol). The yellow complex was obtained

* Author to whom correspondence should be addressed.

in 67% yield (292 mg). Found: C, 41.3; H, 4.2; N, 18.7. Calc. for $C_{20}H_{24}BIrN_8$: C, 41.4; H, 4.1; N, 19.3%. ^1H NMR ($CDCl_3$): δ 1.56 [m, 4H, CH_2(cod)]; 2.07 [br, 4H, CH_2(cod)]; 3.71 [br, 4H, =CH(cod)]; 6.32 (br, 4H, Pz); 7.11 (br, 4H, Pz); 7.71 (br, 4H, Pz).

$Ir(H_2BPz_2)(CO)_2$

Carbon monoxide was bubbled through a solution of $Ir(H_2BPz_2)$(cod) (264 mg, 0.59 mmol) in CH_2Cl_2 (20 ml) for 30 min. After concentration of the solution, addition of pentane (15 cm^3) gave an orange precipitate which was filtered off, washed with pentane and dried *in vacuo*; yield: 30 mg (13%). Found: C, 24.7; H, 2.1; N, 13.5. Calc. for $C_8H_8IrN_4O_2$: C, 24.3; H, 2.0; N, 14.2%. ^1H NMR ($CDCl_3$): δ 6.30 (t, 2H, Pz); 7.58 (d, 2H, Pz); 7.69 (d, 2H, Pz). IR ν(C≡O)(CH_2Cl_2): 2070 and 2000 cm^{-1}.

$Ir(BPz_4)(CO)_2$

The complex was prepared using the procedure described for $Ir(H_2BPz_2)(CO)_2$, but with $Ir(BPz_4)$(cod) (180 mg, 0.31 mmol). The yellow compound was obtained in 65% yield (106 mg). Found: C, 31.7; H, 2.1; N, 21.0. Calc. for $C_{14}H_{12}BIrN_8O_2$: C, 31.9; H, 2.3; N, 21.3%. ^1H NMR ($CDCl_3$): δ 6.37 (t, 4H, Pz); 7.07 (d, 4H, Pz); 7.83 (d, 4H, Pz). IR ν(C≡O) (CH_2Cl_2): 2080 and 2010 cm^{-1}.

$[Ir(coe)_2\{N(CH_2Pz)_3\}]BF_4$

$[Ir(\mu\text{-Cl})(coe)_2]_2$ (100 mg, 0.11 mmol) and $NaBF_4$ (26 mg, 0.22 mmol) were added to a solution of $N(CH_2Pz)_3$ (57 mg, 0.22 mmol) in CH_2Cl_2–methanol (1:1, 20 cm^3). The mixture was allowed to react for 30 min. The solution was concentrated to dryness and then CH_2Cl_2 was added. The mixture was filtered through Kieselguhr and the resulting orange solution was concentrated under reduced pressure. Addition of diethyl ether (15 cm^3) led to an orange precipitate, which was filtered off, washed with diethyl ether and dried *in vacuo*; yield: 110 mg (65%). Found: C, 44.8; H, 6.0; N, 13.5. Calc. for $C_{28}H_{43}BF_4IrN_7$: C, 44.4; H, 5.7; N, 13.7%. ^1H NMR ($CDCl_3$): δ 0.8–2.2 [m, 24H, CH_2(coe)]; 2.80 [br, 4H, =CH(coe)]; 5.14 [s, 2H, $CH_2(N(CH_2Pz)_3)$]; 5.69, 6.32 (AB system, 4H, J_{AB} = 14.95 Hz, $CH_2(N(CH_2Pz)_3)$]; 6.30 (br, 3H, Pz); 7.38 (br, 2H, Pz); 7.44 (br, 1H, Pz); 8.01 (br, 1H, Pz); 8.30 (br, 2H, Pz).

$[Ir(cod)\{N(CH_2Pz)_3\}]BF_4$

The complex was prepared using the procedure described for $[Ir(coe)_2\{N(CH_2Pz)_3\}]BF_4$, but with $[Ir(\mu\text{-Cl})(cod)]_2$ (80 mg, 0.12 mmol), $N(CH_2Pz)_3$ (62 mg, 0.24 mmol) and $NaBF_4$ (28 mg, 0.24 mmol). The orange complex was obtained in 78% yield (120 mg). Found: C, 37.6; H, 4.1; N, 15.5. Calc. for $C_{20}H_{27}BF_4IrN_7$: C, 37.3; H, 4.2; N, 15.2%. ^1H NMR ($CDCl_3$): δ 1.80 [br, 4H, CH_2(cod)]; 2.40 [br, 4H, CH_2(cod)]; 3.90 [br, 4H, =CH(cod)]; 5.21 [s, 2H, $CH_2(N(CH_2Pz)_3)$], 5.81, 6.15 [AB system, 4H, J_{AB} = 14.92 Hz, $CH_2(N(CH_2Pz)_3)$]; 6.27 (br, 2H, Pz); 6.34 (br, 1H, Pz); 7.44 (br, 1H, Pz); 7.53 (br, 2H, Pz); 7.94 (br, 1H, Pz); 8.28 (br, 2H, Pz).

$[Rh(cod)\{N(CH_2Pz)_3\}]BF_4$

The complex was prepared using the procedure described for $[Ir(coe)_2\{N(CH_2Pz)_3\}]BF_4$, but with $[Rh(\mu\text{-Cl})(cod)]_2$ (200 mg, 0.41 mmol), $N(CH_2Pz)_3$ (211 mg, 0.82 mmol) and $NaBF_4$ (94 mg, 0.82 mmol). The yellow compound was obtained in 77% yield (350 mg). Found: C, 43.0; H, 4.9; N, 17.9. Calc. for $C_{20}H_{27}BF_4N_7Rh$: C, 43.3; H, 4.9; N, 17.7%. ^1H NMR ($CDCl_3$): δ 2.00 [br, 4H, CH_2(cod)]; 2.60 [br, 4H, CH_2(cod)]; 4.20 [br, 4H, =CH(cod)]; 5.17 [br, 2H, $CH_2(N(CH_2Pz)_3)$], 5.20 [br, 2H, $CH_2(N(CH_2Pz)_3)$]; 6.25 (br, 3H, Pz); 6.30 [br, 2H, $CH_2(N(CH_2Pz)_3)$]; 7.50 (br, 3H, Pz); 7.91 (br, 1H, Pz); 8.10 (br, 2H, Pz).

$[Rh(CO)_2\{N(CH_2Pz)_3\}]BF_4$

Carbon monoxide was bubbled through a solution of $[Rh(cod)\{N(CH_2Pz)_3\}]BF_4$ (60 mg, 0.11 mmol) in CH_2Cl_2 (20 ml) for 30 min. After concentration of the solution, addition of diethyl ether (15 cm^3) gave a yellow precipitate which was filtered off, washed with diethyl ether and dried *in vacuo*; yield: 30 mg (55%). Found: C, 34.2; H, 3.2; N, 18.1. Calc. for $C_{14}H_{15}BF_4N_7O_2Rh$: C, 33.4; H, 3.0; N, 19.5%. ^1H NMR ($CDCl_3$): δ 5.0–6.0 [br, 6H, $CH_2(N(CH_2Pz)_3)$]; 6.3 (br, 3H, Pz); 7.5 (br, 3H, Pz); 8.0 (br, 3H, Pz). IR ν(C≡O) (CH_2Cl_2): 2120, 2105, 2060 and 2040 cm^{-1}.

RESULTS AND DISCUSSION

The synthesis of the $Ir(H_nBPz_{4-n})$(cod) (n = 0, 2) complexes involves a straightforward reaction in dichloromethane between $[Ir(\mu\text{-Cl})(cod)]_2$ and $Tl(H_nBPz_{4-n})$, according to the following equation:

$$1/2[Ir(\mu\text{-Cl})(cod)]_2 + Tl(H_nBPz_{4-n}) \longrightarrow Ir(H_nBPz_{4-n})(cod) + TlCl.$$

The complexes were isolated as yellow, air-stable powders and their purity was ascertained by microanalysis. We have tried to prepare these complexes by reaction in dichloromethane of $[Ir(\mu\text{-Cl})(cod)]_2$ with the sodium salt, $Na(H_nBPz_{4-n})$, but this method also afforded the pyrazolate-bridged complex $Ir_2(\mu\text{-Pz})_2(cod)_2$ as a side product. The yield of $Ir_2(\mu\text{-Pz})_2(cod)_2$ increases if the reaction with $Na(H_nBPz_{4-n})$ carried out in methanol, or by treatment of $[Ir(\mu\text{-OMe})(cod)]_2$ with $Na(H_nBPz_{4-n})$. These results suggest that the presence of a base in solution provides the cleavage of the B—N bond in H_nBPz_{4-n} leading to the formation of the pyrazolate complex.

The ^1H NMR spectrum of $Ir(H_2BPz_2)(cod)$ is compatible with a square-planar structure. It shows a unique resonance, centred at 4.00 ppm, for the vinyl protons of the cod ligand, and only three signals at 6.20, 7.48 and 7.52 ppm attributable to the pyrazolyl protons. The ^1H NMR spectrum of $Ir(BPz_4)(cod)$ at 25°C indicates that the complex is stereochemically non-rigid since the four pyrazolyl rings are equivalent. Thus, the pyrazolyl proton resonances appear as three signals at 6.32, 7.11 and 7.71 ppm. Furthermore, the vinyl protons of the cod ligand are also equivalent, appearing as one broad signal at 3.71 ppm. A similar ^1H NMR spectrum at room temperature has been reported for the stereochemically non-rigid $Rh(BPz_4)(cod)$ complex.[11–13]

Treatment of $Ir(H_nBPz_{4-n})(cod)$ ($n = 0$, 2) with carbon monoxide in dichloromethane gives $Ir(H_nBPz_{4-n})(CO)_2$. Formulation of the compounds was deduced by microanalysis, IR and ^1H NMR. $Ir(H_2BPz_2)(CO)_2$ has been previously prepared by reaction of $Na[Ir_2Cl_{4.8}(CO)_4]$ with $K[H_2BPz_2]$.[14] The IR spectrum of $Ir(BPz_4)(CO)_2$ in dichloromethane exhibits two carbonyl bands at 2080 and 2010 cm^{-1} characteristic of a *cis*-dicarbonyl structure. The ^1H NMR spectrum of $Ir(BPz_{z4})(CO)_2$ at 25°C shows that the compound is again stereochemically non-rigid. Similarly to $Ir(BPz_4)(cod)$, the four pyrazolyl rings are equivalent; the spectrum presents only three signals at 6.37, 7.07 and 7.83 ppm attributable to the pyrazolyl protons.

We have also prepared iridium and rhodium complexes containing the tripodal $N(CH_2Pz)_3$ ligand. The $[Ir(coe)_2\{N(CH_2Pz)_3\}]BF_4$ and $[M(cod)\{N(CH_2Pz)_3\}]BF_4$ (M = Ir, Rh) compounds have been synthesized by reaction of $[Ir(\mu\text{-Cl})(coe)_2]_2$ or $[M(\mu\text{-Cl})(cod)]_2$ with $N(CH_2Pz)_3$ and $NaBF_4$ in dichloromethane. Microanalyses of the compounds are in agreement with the proposed formulation. The ^1H NMR spectra of the complexes at 25°C are consistent with a square-planar structure. Thus, the spectra show the presence of non-equivalent pyrazolylmethylene groups. One of the methylene groups appears as a singlet. The other two methylene units are equivalent, but each of them shows inequivalent protons appearing as an AB spin system. Two of the pyrazolyl groups are equivalent; three signals attributable to these protons are observed. The other pyrazolyl group gives three signals; depending on the complex, some of these signals overlap with those of the other pyrazolyl groups. The vinyl protons of the olefinic ligands appear as a unique, broad signal. In a square-planar structure, two signals would be expected for the "upper" and "lower" protons. The presence of only one signal could be explained in terms of a rapid rotation of the cyclooctene or cycloocta-1,5-diene ligands.[15] An alternative explanation may be that the magnetic environments for the protons are accidentally equivalent.

Carbonylation of $[Rh(cod)\{N(CH_2Pz)_3\}]BF_4$ leads to the formation of $[Rh(CO)_2\{N(CH_2Pz)_3\}]BF_4$. The complex is hygroscopic and this has prevented an accurate microanalysis. The IR and ^1H NMR spectra are in agreement with the proposed formulation. The IR spectrum in dichloromethane at 25°C presents four $\nu(C{\equiv}O)$ frequencies, of similar intensity, at 2120, 2105, 2060 and 2040 cm^{-1}. The presence of four $\nu(C{\equiv}O)$ bands suggests the existence of two species in solution, probably tetra- and pentacoordinate species resulting from the coordination of two or three of the pyrazolyl groups to the rhodium atom. The ^1H NMR spectrum at 25°C suggests that these species undergo rapid exchange on the NMR time scale. Thus, this species shows a broad signal in the 5.0–6.0 ppm range for the six methylene protons and three broad signals at 6.3, 7.5 and 8.0 ppm for the nine pyrazolyl protons.

Carbonylation of $[Ir(cod)\{N(CH_2Pz)_3\}]BF_4$ in dichloromethane leads to a solution containing, most probably, $[Ir(CO)_2\{N(CH_2Pz)_3\}]BF_4$, as is deduced by the IR spectrum. It presents four $\nu(C{\equiv}O)$ bands at 2090, 2070, 2025 and 2000 cm^{-1}, similarly to that of $[Rh(CO)_2\{N(CH_2Pz)_3\}]BF_4$. The low stability of the complex has prevented further characterization.

Acknowledgement—Financial support from the Dirección General de Investigación Científica y Técnica (PB 89-0056) is gratefully acknowledged.

REFERENCES

1. S. Trofimenko, *Prog. Inorg. Chem.* 1986, **34**, 115.
2. S. Trofimenko, J. C. Calabrese and J. S. Thompson, *Inorg. Chem.* 1987, **26**, 1507.

3. P. M. Maitlis, *Chem. Soc. Rev.* 1981, 1.
4. S. May, P. Reinsalu and J. Powell, *Inorg. Chem.* 1980, **19**, 1582.
5. M. J. Fernández, M. J. Rodríguez, L. A. Oro and F. J. Lahoz, *J. Chem. Soc., Dalton Trans.* 1989, 2073.
6. F. Mani and G. Scapacci, *Inorg. Chim. Acta* 1980, **38**, 151.
7. A. van der Ent and A. L. Onderdelinden, *Inorg. Synth.* 1973, **14**, 92.
8. J. L. Herde, J. C. Lambert and C. V. Senoff, *Inorg. Synth.* 1974, **15**, 18.
9. J. Powell and B. L. Shaw, *J. Chem. Soc. A* 1968, 211.
10. S. Trofimenko, J. R. Long, T. Nappier and S. G. Shore, *Inorg. Synth.* 1970, **12**, 99.
11. D. J. O'Sullivan and F. J. Lalor, *J. Organomet. Chem.* 1974, **65**, C47.
12. R. B. King and A. Bond, *J. Organomet. Chem.* 1974, **73**, 115.
13. M. Cocivera, G. Ferguson, F. J. Lalor and P. Szczecinski, *Organometallics* 1982, **1**, 1139.
14. F. Bonati, G. Minghetti and G. Banditelli, *J. Organomet. Chem.* 1975, **87**, 365.
15. G. S. Rodman and K. R. Mann, *J. Organomet. Chem.* 1989, **378**, 255.

Polyhedron Vol. 10, No. 14, pp. 1599–1602, 1991
Printed in Great Britain

0277–5387/91 $3.00+.00
© 1991 Pergamon Press plc

SYNTHESIS AND CHARACTERIZATION OF ORGANOLANTHANIDE COMPLEXES WITH THREE DIFFERENT LIGANDS

YONGFEI YU, SHAOWU WANG, ZHONGWEN YE* and HUAIZHU MA

Institute of Organic Chemistry, Anhui Normal University, Wuhu, Anhui, China

(*Received* 30 *January* 1991; *accepted* 21 *March* 1991)

Abstract—New types of organolanthanide complexes with three different ligands, CpLn(Cl)[$OCOC_6H_4$(*o*-Z)] (Ln = Sm, Yb; Z = H, F, Br, I and OCH_3), were synthesized. These complexes were characterized by elemental analyses, IR, MS and XPS, showing that they are dimers containing carboxylate ions as bridging groups. It was found that the donor atoms (F, Br, I and O) in the complexes only slightly coordinate with lanthanide metal.

Since organolanthanide complexes possess unique and interesting structures and properties, organolanthanide chemistry is currently one of the most rapidly developing areas of organotransition metal chemistry. Up until now, no report on organolanthanide complexes with three different ligands occurs in the literature, though numerous organolanthanide complexes have been synthesized.[1] In view of this, we synthesized 10 new organolanthanide complexes with three different ligands.

RESULTS AND DISCUSSION

By the reaction of the dicyclopentadienyl samarium chloride or dicyclopentadienyl ytterbium chloride with one equivalent of (*o*-Z)C_6H_4COOH at room temperature in THF, 10 new complexes with three different ligands have been synthesized. They are:

CpSm(Cl)[$OCOC_6H_5$]	**(1)**
CpYb(Cl)[$OCOC_6H_5$]	**(2)**
CpSm(Cl)[$OCOC_6H_4$(*o*-F)]	**(3)**
CpYb(Cl)[$OCOC_6H_4$(*o*-F)]	**(4)**
CpSm(Cl)[$OCOC_6H_4$(*o*-Br)]	**(5)**
CpYb(Cl)[$OCOC_6H_4$(*o*-Br)]	**(6)**
CpSm(Cl)[$OCOC_6H_4$(*o*-I)]	**(7)**
CpYb(Cl)[$OCOC_6H_4$(*o*-I)]	**(8)**
CpSm(Cl)[$OCOC_6H_4$(*o*-OCH_3)]	**(9)**
CpYb(Cl)[$OCOC_6H_4$(*o*-OCH_3)]	**(10)**.

All complexes were characterized by elemental analysis, IR and MS spectroscopy. Complexes **3**–**10** were also identified by XPS. All complexes exhibit four characteristic Cp absorption peaks at *ca* 780, 1010, 1440 and 3100 cm^{-1} and an absorption peak at *ca* 250 cm^{-1} due to Ln—C of the π-bonded Cp group.[2] All the complexes are soluble in THF, but they are practically insoluble in benzene. We did not succeed in preparing single crystals for any of them.

Bridged dimeric structure

By studying the relationship between the structure and the IR data of the carboxylato complexes, Deacon[3] and Karraker[4] have pointed out that the value of $\Delta\nu$ [$\nu_{as}(COO^-) - \nu_s(COO^-)$] of the bridged dimeric structure of the complexes is much smaller than that for the corresponding free carboxylate anion. In Table 1, the $\nu_{as}(COO^-)$ and $\nu_s(COO^-)$ frequencies for the complexes of their corresponding free carboxylate anion are listed. It is evident that $\Delta\nu$ of the former is smaller than that of the latter. Thus, the 10 complexes would seem to have bridged dimeric structures. Moreover, the presence of bimolecular species, and fragments thereof in the mass spectra, further support the bridged dimeric structure for all complexes.

Chelate ring

If the substituent atom Z (F, Br, I and O) on the phenyl group in the complexes coordinates with the

* Author to whom correspondence should be addressed.

Table 1. Frequencies of $\nu_{as}(COO^-)$ and $\nu_s(COO^-)$ for complexes **1–10** and their corresponding salts

Complex	$\nu_{as}(COO^-)$ (cm^{-1})	$\nu_s(COO^-)$ (cm^{-1})	$\Delta\nu^a$ (cm^{-1})
1	1531	1415	116
C_6H_5COONa	1552	1413	139
2	1549	1422	127
C_6H_5COONa	1552	1413	139
3	1612	1412	200
(*o*-F)C_6H_4COONa	1612	1403	209
4	1600	1422	178
(*o*-F)C_6H_4COONa	1612	1403	209
5	1573	1409	164
(*o*-Br)C_6H_4COONa	1575	1340	235
6	1590	1413	177
(*o*-Br)C_6H_4COONa	1575	1340	235
7	1571	1404	167
(*o*-I)C_6H_4COONa	1595	1379	216
8	1584	1411	173
(*o*-I)C_6H_4COONa	1595	1379	216
9	1606	1431	175
(*o*-OCH_3)C_6H_4COONa	1590	1380	210
10	1605	1414	191
(*o*-OCH_3)C_6H_4COONa	1590	1380	210

$^a\Delta\nu = \nu_{as}(COO^-) - \nu_s(COO^-)$.

Table 2. IR ν_{C-Z} data for both complexes **3–10** and their reference substances

Complex	ν_{C-Z} (cm^{-1})		
	Found	Reference 5	Reference[a]
3	1162	1400–1000	1271
4	1164	1400–1000	1271
5	448	600–500	553
6	435	600–500	553
7	434	~ 500	490
8	449	~ 500	490
9	1099	1270–1230	1250
10	1181	1270–1230	1250

[a]The data are obtained from measuring the results of the corresponding salts (*o*-Z)C_6H_4COONa, where Z = F, Br, I and OCH_3, respectively.

metal, the electron density at the donor atom will decrease and cause ν(C—Z) to shift to low frequency. The values in complexes **3–10** and those in the corresponding carboxylic salts are listed in Table 2. It is evident that ν(C—Z) in all eight complexes is smaller than that in the free anion, suggesting that the donor atom does indeed coordinate to the lanthanide in these eight complexes. Moreover, the XPS data reveal that the binding energy of the donor atom in the complexes is greater than in the salts. This is further evidence for the coordination of the donor atom to the metal in complexes **3–10** to form chelate rings.

From the above information, we suggest the structures shown in Fig. 1 for the 10 complexes.

EXPERIMENTAL

All reactions and manipulations were conducted under an atmosphere of purified argon using standard Schlenk techniques or a glove box. THF and n-hexane were predried over sodium wire and subsequently refluxed and distilled under argon from sodium benzophenone immediately before use. Benzoic acids with *ortho*-substituted groups were

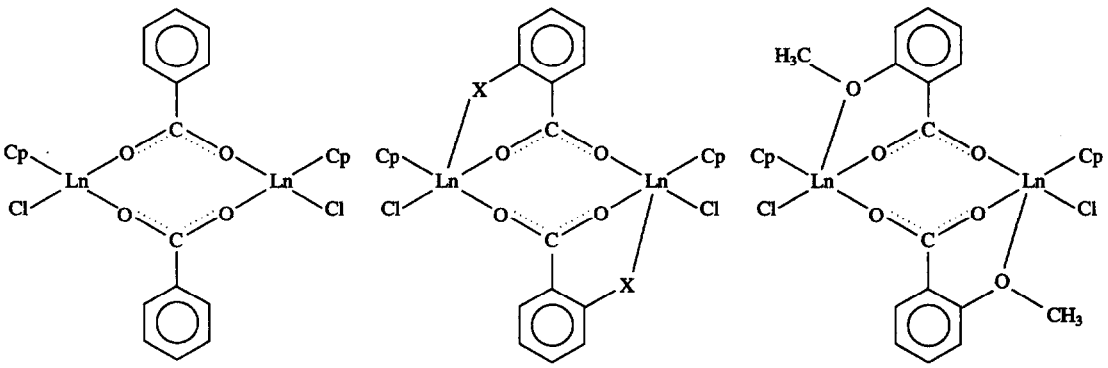

(1) Ln=Sm
(2) Ln=Yb
(3) Ln=Sm X=F (4) Ln=Yb X=F
(5) Ln=Sm X=Br (6) Ln=Yb X=Br
(7) Ln=Sm X=I (8) Ln=Yb X=I
(9) Ln=Sm
(10) Ln=Yb

Fig. 1.

Table 3. Binding energy data of donor atom Z (F, Br, I and O) in complexes **3**–**10** and their corresponding salts

Complex	Binding energy (eV)	ΔE_b[a] (eV)
3	F_{1s} 693.40	+6.57
$(o\text{-F})C_6H_4COONa$	F_{1s} 686.83	
4	F_{1s} 692.35	+5.52
$(o\text{-F})C_6H_4COONa$	F_{1s} 686.83	
5	Br_{3d} 77.20	+7.21
$(o\text{-Br})C_6H_4COONa$	Br_{3d} 69.99	
6	Br_{3d} 75.50	+5.51
$(o\text{-Br})C_6H_4COONa$	Br_{3d} 69.99	
7	$I_{3d5/2}$ 629.00	+8.67
$(o\text{-I})C_6H_4COONa$	$I_{3d5/2}$ 620.33	
8	$I_{3d5/2}$ 626.35	+6.02
$(o\text{-I})C_6H_4COONa$	$I_{3d5/2}$ 620.33	
9	O_{1s}[b] 540.30	+9.40
$(o\text{-OCH}_3)C_6H_4COONa$	O_{1s}[b] 530.90	
10	O_{1s}[b] 536.80	+5.90
$(o\text{-OCH}_3)C_6H_4COONa$	O_{1s}[b] 530.90	

[a] $\Delta E_b = E_{B.E.}(CpLn(Cl)[OCOC_6H_4(o\text{-Z})]) - E_{B.E.}[(o\text{-Z})C_6H_4COONa]$.

[b] The binding energy of O_{1s} in the $-OCH_3$ group and the $-OCOC_6H_4-$ group overlapped, and is not resolved.

dried by heating under vacuum and stored under argon until use. Cp_2LnCl (Ln = Sm, Yb) was prepared following published methods.[6]

IR spectra were obtained as Nujol and Fluorolube mulls on CsI crystal plates. The IR measurements were obtained on a Perkin–Elmer 983(G) spectrometer. The X-ray photoelectron spectra were recorded on a VG ESCALAB MK-II spectrometer. The mass spectra were obtained on a VG ZAB-HS organic mass spectrometer. Mass spectral data are given for isotopes ^{152}Sm, ^{174}Yb, ^{35}Cl and ^{79}Br. The peak patterns correspond to theoretical values based on the natural abundance of the isotopes. Carbon and hydrogen analyses were carried out on a Yanaco MT-2 analyser. Elemental analysis results for Ln (Ln = Sm, Yb) were obtained according to a published method.[2] The elemental analysis data for X (X = F, Br or I) were obtained using a combustion method. Melting points were determined in argon-filled capillaries and were uncorrected.

General method for the preparation of $CpLn(Cl)[OCOC_6H_4(o\text{-Z})]$

To a solution of Cp_2LnCl (Ln = Sm, Yb) (2 mmol) in 50 cm^3 of THF kept under argon in a 100 cm^3 Schlenk flask was added dried $(o\text{-Z})C_6H_4COOH$ (Z = H, F, Br, I and OCH_3) (2 mmol) and the reaction mixture was stirred at room temperature for 24 h. THF was then removed *in vacuo*. THF (5 cm^3) was added, followed by n-hexane (40 cm^3) and the solvent was removed by centrifugation. This procedure was repeated three times. The resulting solid was dried for 2 h *in vacuo* to afford complexes $CpLn(Cl)[OCOC_6H_4(o\text{-Z})]$ (Ln = Sm, Yb; Z = H, F, Br, I and OCH_3).

$CpSm(Cl)[OCOC_6H_5]$ (**1**)

Orange, dec.p., 166°C, yield, 83%. Found (calc.): Ln, 40.4 (40.6), C, 38.7 (38.4), H, 2.7 (2.5), Cl, 9.5 (10.3)%. Main peaks in MS (*m/z*): 746(M_2), 681(M_2-Cp), 373(M), 308(M−Cp), 242($M-C_6H_5COO$), 217($M-Cl-C_6H_5COO$), 152(Sm).

$CpYb(Cl)[OCOC_6H_5]$ (**2**)

Orange, m.p., 46°C, yield, 85%. Found (calc.): Ln, 43.8 (44.0), C, 36.5 (36.0), H, 2.6 (2.7), Cl, 9.0 (9.2)%. Main peaks in MS (*m/z*): 790(M_2), 725(M_2-Cp), 395(M), 330(M−Cp), 264($M-C_6H_5COO$), 239($M-Cl-C_6H_5COO$), 174(Yb).

$CpSm(Cl)[OCOC_6H_4(o\text{-F})]$ (**3**)

Orange, dec.p., 151°C, yield, 86%. Found (calc.): Ln, 38.6 (38.9), C, 37.0 (36.2), H, 2.3 (2.1), F, 4.9 (5.0), Cl. 9.1 (9.6)%. Main peaks in MS (*m/z*): 782(M_2), 717(M_2-Cp), 391(M), 326(M−Cp), 242($M-FC_6H_4COO$), 217($M-Cl-FC_6H_4COO$), 152(Sm).

$CpYb(Cl)[OCOC_6H_4(o\text{-F})]$ (**4**)

Orange, dec.p., 115°C, yield, 83%. Found (calc.): Ln, 41.9 (42.2), C, 34.9 (34.2), H, 2.2 (2.0), F, 4.6 (4.3), Cl, 8.6 (8.9)%. Main peaks in MS (*m/z*): 826(M_2), 761(M_2-Cp), 413(M), 348(M−Cp), 264($M-FC_6H_4COO$), 239($M-Cl-FC_6H_4COO$), 174(Yb).

$CpSm(Cl)[OCOC_6H_4(o\text{-Br})]$ (**5**)

Orange, dec.p., 181°C, yield, 83%. Found (calc.): Ln, 33.3 (33.4), C, 32.0 (31.1), H, 2.0 (2.3), Cl, 7.9 (8.2), Br, 17.7 (18.0)%. Main peaks in MS (*m/z*): 902(M_2), 837(M_2-Cp), 451(M), 386(M−Cp), 242($M-BrC_6H_4COO$), 217($M-Cl-BrC_6H_4COO$), 152(Sm).

$CpYb(Cl)[OCOC_6H_4(o\text{-}Br)]$ (**6**)

Orange, m.p., 82°C, yield, 81%. Found (calc.): Ln, 36.5 (36.8), C, 30.4 (30.0), H, 1.9 (1.8), Cl, 7.5 (8.0), Br, 16.9 (17.0)%. Main peaks in MS (*m/z*): 946(M_2), 881(M_2-Cp), 473(M), 408(M−Cp), 264(M−BrC_6H_4COO), 239(M−Cl−BrC_6H_4COO), 174(Yb).

$CpSm(Cl)[OCOC_6H_4(o\text{-}I)]$ (**7**)

Orange, dec.p., 159°C, yield, 85%. Found (calc.): Ln, 30.2 (30.3), C, 29.0 (28.3), H, 1.8 (2.0), Cl, 7.1 (7.5), I, 25.5 (25.6)%. Main peaks in MS (*m/z*): 998(M_2), 933(M_2-Cp), 499(M), 434(M−Cp), 242(M−IC_6H_4COO), 217(M−Cl−IC_6H_4COO), 152(Sm).

$CpYb(Cl)[OCOC_6H_4(o\text{-}I)]$ (**8**)

Orange, m.p., 57°C, yield, 87%. Found (calc.): Ln, 33.2 (33.3), C, 27.7 (27.1), H, 1.7 (1.8), Cl, 6.8 (7.0), I, 24.4 (24.5)%. Main peaks in MS (*m/z*): 1042(M_2), 977(M_2-Cp), 521(M), 456(M−Cp), 264(M−IC_6H_4COO), 239(M−Cl−IC_6H_4COO), 174(Yb).

$CpSm(Cl)[OCOC_6H_4(o\text{-}OCH_3)]$ (**9**)

Orange, dec.p., 244°C, yield, 81%. Found (calc.): Ln, 37.4 (37.5), C, 38.8 (38.4), H, 3.0 (3.2), Cl, 8.8 (9.2)%. Main peaks in MS (*m/z*): 806(M_2), 741(M_2-Cp), 403(M), 338(M−Cp), 242(M−$CH_3C_6H_4COO$), 217(M−Cl−$CH_3C_6H_4COO$), 152(Sm).

$CpYb(Cl)[OCOC_6H_4(o\text{-}OCH_3)]$ (**10**)

Orange, dec.p., 267°C, yield, 86%. Found (calc.): Ln, 40.7 (40.7), C, 36.8 (36.3), H, 2.9 (2.7), Cl, 8.4 (8.7)%. Main peaks in MS (*m/z*): 850(M_2), 785(M_2-Cp), 425(M), 460(M−Cp), 264(M−$CH_3C_6H_4COO$), 239(M−Cl−$CH_3C_6H_4COO$), 174(Yb).

Acknowledgements—This project was supported by the National Science Foundation of China. The authors gratefully acknowledge Mrs Jiping Hu for carrying out the elemental analysis, Mr Baohui Du for recording the IR spectra and Mr Xianming Liu, who works at the Structure Centre Research Laboratory, University of Science and Technology of China, for measuring the XPS.

REFERENCES

1. H. Schumann and W. Genthe, in *Handbook on the Physics and Chemistry of Rare Earths* (Edited by K. A. Gschneidner Jr and L. Eyring), Vol. 7, p. 445. Elsevier, The Netherlands (1984).
2. Changtao Qian, Changqing Ye, Hanzhang Lu, Yuqin Li, Jialie Zhou, Yuanwen Ge and M. Tsutsui, *J. Organomet. Chem.* 1983, **247**, 161.
3. G. B. Deacon, *Aust. J. Chem.* 1967, **20**, 459.
4. D. G. Karraker, *J. Inorg. Nucl. Chem.* 1969, **31**, 2815.
5. L. T. Bellamy (Ed.), *Infrared Spectra of Complex Molecules*, Chinese Edition (Translated by Mr Weiyuan Huang and Mrs Chongshi Ni), p. 405. Science Press (1975).
6. R. E. Maginn, S. Manastyrskyj and M. Dubeck, *J. Am. Chem. Soc.* 1963, **85**, 672.

Polyhedron Vol. 10, No. 14, pp. 1603–1609, 1991
Printed in Great Britain

0277–5387/91 $3.00+.00
© 1991 Pergamon Press plc

STRUCTURAL DEPENDENCIES OF PYRAMIDAL SULPHUR INVERSION IN HALOGENOTRICARBONYLRHENIUM(I) COMPLEXES OF MONO- AND BIS-(*o*-METHYLTHIO) DERIVATIVES OF TRIPHENYLPHOSPHINE

EDWARD W. ABEL, DAVID ELLIS, KEITH G. ORRELL* and VLADIMIR ŠIK

Department of Chemistry, University of Exeter, Exeter EX4 4QD, U.K.

(*Received* 31 *January* 1991; *accepted* 21 *March* 1991)

Abstract—A series of new halogenotricarbonylrhenium(I) complexes of the hybrid sulphur–phosphine ligands [*o*-(methylthio)phenyl]diphenylphosphine (SP) and bis-[*o*-(methylthio)phenyl]phenylphosphine (DSP) have been prepared and characterized. Both ligands act as sulphur/phosphorus mono-chelates, despite the potential tridenticity of DSP. No evidence of an intramolecular methylthio exchange process involving the uncoordinated and coordinated SMe groups was detected in the $[ReX(CO)_3(DSP)]$ (X = Cl, Br, I) complexes, in contrast to the analogous $[PdX_2(DSP)]$ and $[PtX_2(DSP)]$ complexes. Solution NMR studies revealed pyramidal inversion of the coordinated sulphur atoms in the $[ReX(CO)_3(SP)]$ and $[ReX(CO)_3(DSP)]$ complexes, with energy barriers $[\Delta G^{\ddagger}(298\ K)]$ in the range 51–55 kJ mol^{-1}.

Pyramidal sulphur or selenium inversion in halogenotricarbonylrhenium(I) complexes of dimethyl sulphide,[1] dimethyl selenide[1] and various chelating dichalcogenoethers[2,3] has been the subject of much previous investigation. In these earlier studies all coordinated ligand atoms were stereochemically non-rigid, whereas this present work has been aimed at investigating systems combining rigid and non-rigid coordinated atoms, namely phosphorus and sulphur atoms, respectively.

The ligand [*o*-(methylthio)phenyl]diphenylphosphine(SP) is shown to act as a sulphur/phosphorus chelate ligand towards rhenium(I) pentacarbonyl halides. The ligand bis-[*o*-(methylthio)phenyl]phenylphosphine (DSP) is potentially tridentate towards these reagents, but such a binding mode would require replacement of a carbonyl group *trans* to halogen, and the weak *trans* effect of the latter is unlikely to produce sufficient labilization of the Re—C bond for this to occur. Thus, DSP is more likely to act as a bidentate ligand and form $[ReX(CO)_3(DSP)]$ complexes. Such complexes would contain an uncoordinated methylthio group which might then be involved in an intramolecular sulphur exchange process analogous to those observed in DSP complexes of palladium(II)[4–6] and platinum(II).[5,6]

NMR studies were therefore undertaken to investigate the static and dynamic solution conformations of the two series of complexes $[ReX(CO)_3(SP)]$ (X = Cl, Br, I) and $[ReX(CO)_3(DSP)]$ (X = Cl, Br) in order to clarify their dynamic stereochemistries.

EXPERIMENTAL

Reagents

The ligands[7] and pentacarbonylhalogenorheniums(I)[8,9] were prepared according to literature methods.

Physical methods

IR spectra of the complexes were recorded on a Perkin–Elmer 881 IR spectrophotometer in the region 2200–1800 cm^{-1} as solutions in THF.

^1H NMR and $^{31}P-\{^1H\}$ NMR spectra were recorded on a Bruker AM250 FT spectrometer operating at 250.13 and 101.26 MHz, respectively. ^1H chemical shifts are quoted relative to Me_4Si as the internal standard. $^{31}P-\{^1H\}$ chemical shifts are

* Author to whom correspondence should be addressed.

quoted relative to H_3PO_4 as the external standard. All NMR spectra of the complexes were recorded as solutions in CD_2Cl_2.

Elemental analyses were carried out by Butterworth Laboratories Ltd, Teddington, Middlesex, London.

Melting points were recorded on a digital Gallenkamp melting point apparatus and were uncorrected.

Bandshape analyses were carried out using a modified version of the DNMR3 program of Kleier and Binsch.[10] Computer simulated spectra were fitted visually and energy parameters derived from standard Arrhenius and Eyring plots are based on least-square fittings. The errors quoted for the free energies of activation, $\Delta G^{\ddagger}$, are based on the standard deviation term, $|\sigma(\Delta H^{\ddagger}) - T\sigma(\Delta S^{\ddagger})|$, as described by Binsch and Kessler.[11]

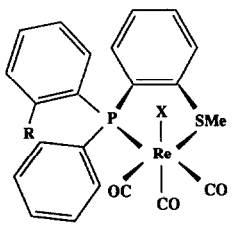

R	X	COMPLEX
H	Cl	I
H	Br	II
H	I	III
SMe	Cl	IV
SMe	Br	V

Fig. 1. Structures of the complexes $[ReX(CO)_3(L—L')]$ (L—L') = (*o*-$MeSC_6H_4)PPh_2$, (SP); X= Cl, Br, I. (L—L') = (*o*-$MeSC_6H_4)_2PPh$, (DSP); X = Cl, Br.

Synthesis of the complexes

Methods for the preparation of all the complexes were analogous, that for the chloride being described below. The reaction time required for the iodide was considerably longer than for the chloro and bromo species.

All manipulations were carried out under nitrogen and freshly dried solvents used in all reactions. Full synthetic and analytical details of these complexes are given in Table 1. Their structures are shown in Fig. 1.

{[o - (methylthio)phenyl]diphenylphosphine}chloro - tricarbonylrhenium(I)

Chloropentacarbonylrhenium(I) (0.25 g, 0.69 mmol) and [*o*-(methylthio)phenyl]diphenylphosphine (0.41 g, 1.3 mmol) were dissolved in THF (10 cm^3) and heated under reflux for 5 h. After this time, the IR spectrum showed three new bands in the carbonyl stretching region, and the bands due to starting material were no longer observed. The solution was concentrated to dryness *in vacuo*, and the white residue washed with hexane. Recrystallization from dichloromethane/hexane gave a white crystalline product which was dried *in vacuo*. Yield: 0.25 g (59%).

RESULTS

The methods outlined above resulted in moderate yields of the complexes, those for the SP complexes being somewhat higher than their DSP analogues (Table 1). IR spectroscopy was a convenient means of monitoring these reactions, the three C—O stretching bands in the product tricarbonyl moiety ($2A' + A''$) being at very different frequencies to those of the reactant pentacarbonyl. Reasoning used elsewhere[3] implies that the three CO groups are in the *fac* configuration.

NMR studies

(i) $[ReX(CO)_3(SP)]$ *complexes*. The ^1H NMR spectra of these complexes in solution at −40°C contained two signals in the SMe region consistent with two invertomeric species. These species are described as *cis* or *trans* according to the relative positions of the ligand SMe group and the halogen with respect to the five-membered metallocycle

Table 1. Synthetic and analytical details of the complexes $[ReX(CO)_3L]$ (L = SP or DSP)

Complex	Reaction time (h)	Yield[a] (%)	Melting temperature (°C)	ν(CO)[b] (cm^{-1})	Elemental analysis [found (calc.) %] C	H
$[ReCl(CO)_3(SP)]$ (I)	5	59	229	2034(vs), 1945(s), 1910(vs)	43.0(43.2)	2.8(2.9)
$[ReBr(CO)_3(SP)]$ (II)	14	59	226	2030(vs), 1939(s), 1904(vs)	40.1(40.0)	2.6(2.5)
$[ReI(CO)_3(SP)]$ (III)	56	40	190	2034(vs), 1943(s), 1912(vs)	38.2(37.4)	2.4(2.4)
$[ReCl(CO)_3(DSP)]$ (IV)	4	44	221	2032(vs), 1914(s), 1906(vs)	41.8(41.7)	2.9(2.9)
$[ReBr(CO)_3(DSP)]$ (V)	19	43	219	2032(vs), 1941(s), 1906(vs)	39.2(40.4)	2.7(2.8)

[a] Based on the $[ReX(CO)_3]$ unit.

[b] (s) = strong, (vs) = very strong.

Table 2. ^{1}H NMR parameters of complexes I–III at low temperature

Complex	Temperature (°C)	Invertomer	Population	Chemical shift: SMe protons (δ)	Chemical shift: aromatic protons[a] (δ)
I	−40	*trans*	0.63	2.63	6.9–8.1 (m)
		cis	0.37	3.11	
II	−40	*trans*	0.74	2.65	6.9–8.1 (m)
		cis	0.26	3.18	
III	−40	*trans*	0.84	2.67	6.9–8.3 (m)
		cis	0.16	3.25	

[a] Aromatic region too complex to distinguish signals due to individual invertomers. (m) = multiplet.

(Fig. 2). Table 2 contains the relevant static NMR parameters of the solution species. It can be seen that the *trans* form is always dominant and is increasingly so as the halogen mass/size increases.

On raising the temperature above −40°C, the two signals in the SMe region broaden and coalesce such that at room temperature a broad singlet is seen which continues to sharpen on further elevation of temperature. Changes were also observed in the aromatic region but these proved too complex for detailed analysis. Addition of free ligand to the samples at temperatures above coalescence produced spectra with separate signals for free and coordinated ligands, confirming the intramolecular nature of the process being monitored.

The changes in the SMe region of the spectrum are consistent with the onset of pyramidal sulphur inversion which exchanges the *cis* and *trans* complexes. Static and dynamic spectra were simulated accurately over the temperature range −40 to 20°C. The "best-fit" rate constants used in the band-shape analysis are given in Table 3.

(ii) $[ReX(CO)_3(DSP)]$ *complexes*. The low temperature ^{1}H NMR spectra of both complexes **IV** and **V** exhibited eight signals in the SMe region. These correspond to the four static invertomers shown in Fig. 3. The additional isomerism of these complexes, compared with the SP complexes, arises from the chiral nature of the tetrahedral phosphorus atom. The four solution species are present

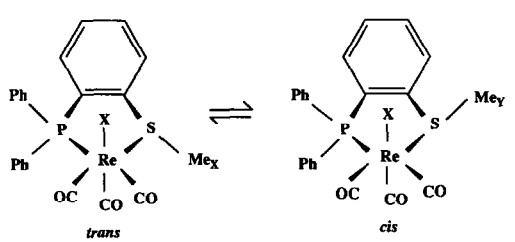

Fig. 2. The static invertomers of complexes I–III.

Table 3. The "best-fit" rate constants obtained from band-shape analyses of complexes I–III

Temperature (°C)	First-order rate constant for sulphur inversion, k (s^{-1}) I	II	III
−20	8.0	5.0	10
−15	22	10	25
−10	40	25	60
−5	68	50	120
0	166	100	220
5	297	180	400
10	513	290	
15	800		
20	1312		

as two diastereomeric pairs, **1** and **2**, resulting from the pendent phenylthioether group being either *trans* or *cis* to the halogen. The two invertomers of each diastereomeric pair arise from the *cis* or *trans* orientation of the coordinated SMe with respect to the halogen. The description of each species refers firstly to the orientation of the pendent SMe group, and secondly to the orientation of the coordinated SMe, both with respect to halogen (Fig. 3). Each of these species exists as a DL pair, but only individual members are shown in Fig. 3 as these cannot normally be distinguished by NMR.

Assignments of signals in the SMe region arise from considerations of steric factors and comparisons with SP complexes. Coordinated SMe protons are expected to be deshielded compared with uncoordinated SMe protons and therefore the methyls A, B, E, F in Fig. 3 will resonate at highest frequencies. In addition, the species **2a** and **2b**, having a pendent phenylthioether moiety *cis* to halogen will be less abundant than the *trans* variety on steric arguments. Thus, the weakest pair of signals in the spectra of the DSP complexes is attributed to the

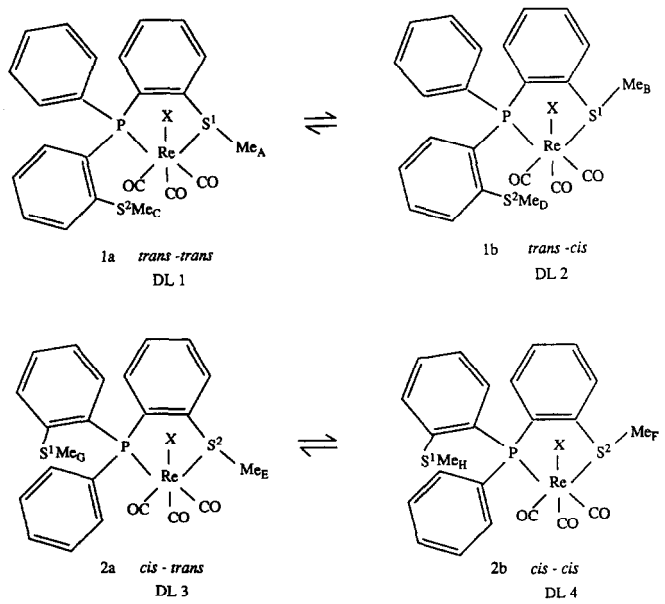

Fig. 3. The static invertomers of complexes **IV** and **V**. The labelling refers to the orientation of the pendent and coordinated SMe groups with respect to halogen, *in that order*. Only single members of the DL pairs are shown.

cis–cis invertomer, **2b**. The non-bonded interactions in this species are only slightly alleviated by placing the coordinated SMe in the *trans* position and thus the *cis–trans* invertomer, **2a**, is only slightly more favoured. The most populous invertomer will contain both SMe groups *trans* to halogen, namely **1a**, and thus the ordering of invertomer populations is expected to be *trans–trans* > *trans–cis* ≫ *cis–trans* > *cis–cis*. Each form should give rise to two SMe signals of identical intensity. However, due to signal overlap this theoretical situation is not realized (Fig. 4).

Before commencing band-shape analyses of the ^{1}H NMR spectra, reliable values of invertomer

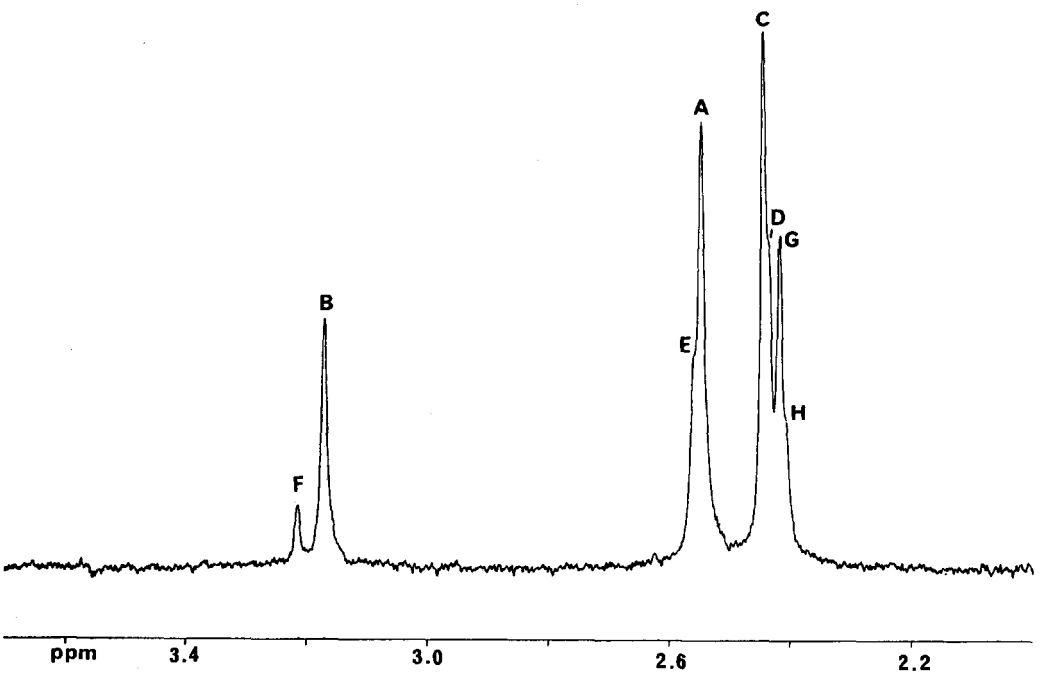

Fig. 4. The ^{1}H NMR spectrum of complex **V** at −40°C in CD_2Cl_2 showing only the SMe region. Labelling refers to Fig. 3.

Table 4. Static ^1H and $^{31}P-\{^1H\}$ NMR parameters of complexes **IV** and **V**

Complex	Temperature (°C)	Invertomer	Population	^1H chemical shift: SMe protons[a] (δ)	^1H chemical shift: aromatic protons[b] (δ)	$^{31}P-\{^1H\}$ chemical shift (δ)
IV	−40	*trans–trans*	0.52	2.54, 2.44	6.8–8.1 (m)	35.9
		trans–cis	0.34	3.16, 2.41		28.4
		cis–trans	0.08	2.55, 2.40		44.6
		cis–cis	0.06	3.21, 2.35		40.8
V	−40	*trans–trans*	0.66	2.54, 244	7.0–8.2 (m)	31.5
		trans–cis	0.32	3.16, 2.44		23.9
		cis–trans	0.01	2.55, 2.41		38.8
		cis–cis	0.005	3.20, 2.40		34.6

[a] Shift of coordinated SMe protons first.
[b] Aromatic region too complex to distinguish signals due to individual invertomers.
(m) = multiplet.

populations were required. These were measured most accurately from low temperature $^{31}P-\{^1H\}$ NMR spectra. Population values and $^{31}P-\{^1H\}$ chemical shifts are given in Table 4. Gross band-shape changes were observed in the ^1H spectra of both the DSP complexes as the temperature was raised. The case of $[ReBr(CO)_3(DSP)]$ (**V**) is illustrated in Fig. 5. The closely spaced set of signals, labelled C, D, G, H (Fig. 4), due to the uncoordinated SMe groups broadened, coalesced around 263 K and then sharpened. The more widely dispersed set of signals, A, B, E, F (Fig. 4), due to the coordinated SMe groups experienced greater exchange broadening and coalesced around ambient temperature. Raising the temperature above ambient led to continued sharpening of all lines until four separated averaged signals, one pair for each diastereomer, were revealed.

The dynamic spin problem was formulated as:

Isomer 1 $A \rightleftharpoons B$ $C \rightleftharpoons D$
Isomer 2 $E \rightleftharpoons F$ $G \rightleftharpoons H$.

Exchanges between isomers **1** and **2** cannot occur without Re—P bond breaking and were therefore discounted from consideration. Interconversions between invertomer pairs were assumed to occur at the same rate and thus theoretical spectra were simulated for a single magnitude of rate constant at each temperature. The best-fit rate constants for **V** at each temperature are given in Fig. 5. These were converted to activation parameters in the usual way and the values are listed in Table 5.

Increasing the temperature of both complexes to *ca* 100°C resulted in further sharpening of the signals and no evidence of the onset of any other exchange process. There is, therefore, no indication of an intramolecular sulphur replacement fluxion involving fission of the Re—S bond and rotation about the Re—P bond to bring the pendent methylthio into the coordination position. Such a process has been detected in the palladium(II) and platinum(II) complexes,[4–6] where the process occurs via a five-coordinate metal transition state.

DISCUSSION

The energy barriers [$\Delta G^{\ddagger}$ (298 K)] to pyramidal sulphur inversion in these hybrid sulphur/

Table 5. Energy parameters for the pyramidal inversion in complexes **I–V**

Complex	E_a (kJ mol^{-1})	$\log_{10}(A/s^{-1})$	$\Delta H^{\ddagger}$ (kJ mol^{-1})	$\Delta S^{\ddagger}$[a] (J K^{-1} mol^{-1})	$\Delta G^{\ddagger}$ (kJ mol^{-1})
I	77.9±2.1	17.1±0.4	75.7±2.1	74.0±7.6	53.6±0.2
II	79.0±2.0	17.5±0.4	76.8±2.0	81.8±7.4	52.4±0.3
III	86.0±3.0	18.8±0.6	83.8±3.0	107.6±11.3	51.7±0.4
IV	72.1±3.5	15.8±0.7	69.9±3.5	50.7±13.0	54.7±0.4
V	84.2±1.9	18.1±0.4	81.9±1.9	93.5±7.1	54.1±0.2

[a] These values are unexpectedly large for purely intramolecular processes, but are considered to be reliable and not artefacts of poor quality band-shape fittings.[14]

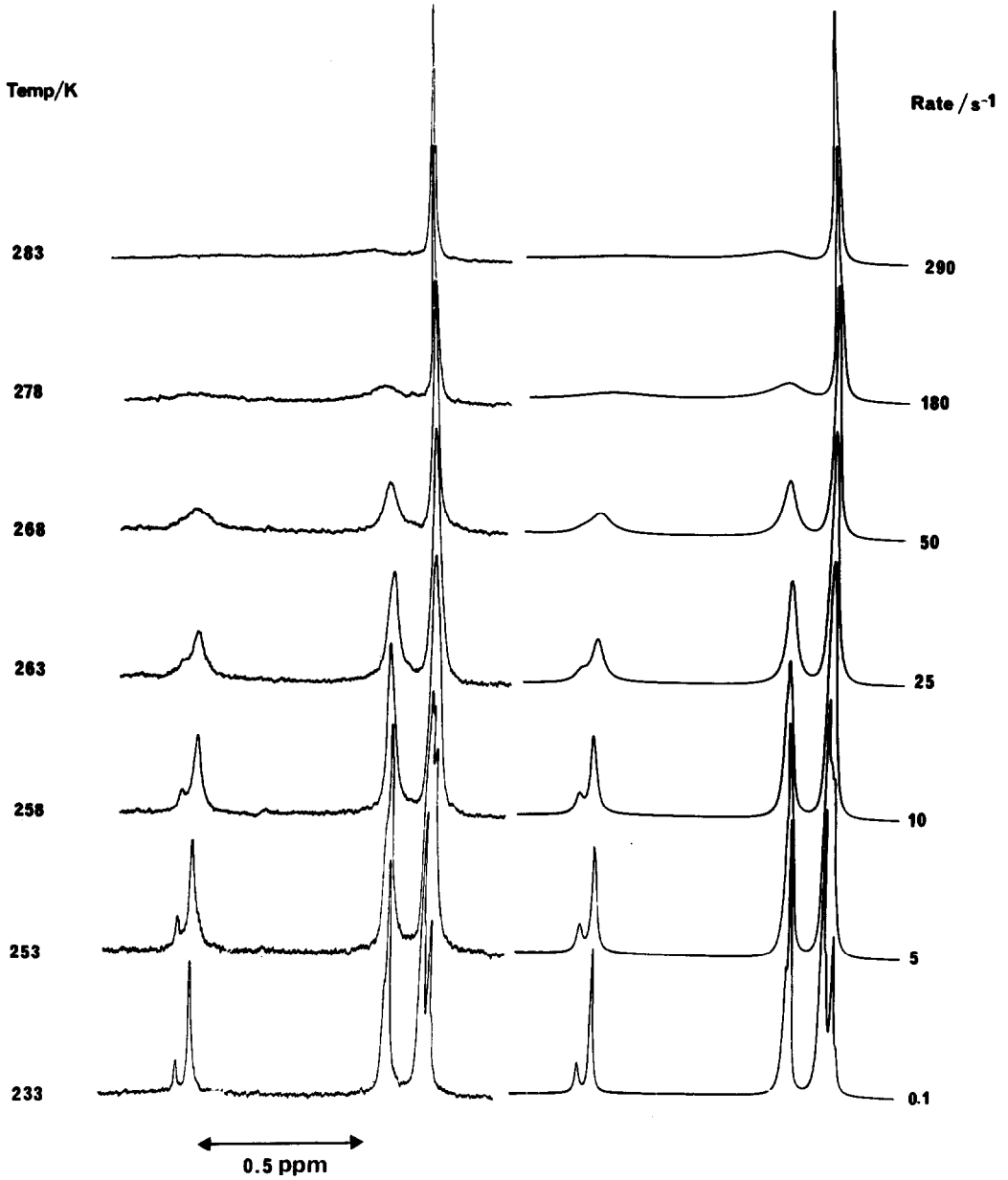

Fig. 5. Experimental and computer synthesized spectra of complex V showing the "best-fit" rate constants.

phosphorus chelate complexes lie in the range 51.7–54.7 kJ mol^{-1}. The values for SP complexes are marginally lower (1.1–1.7 kJ mol) than those for the DSP complexes, possibly the result of a slight steric effect of the uncoordinated SMe group in the latter.

There appears to be a very slight *cis*-halogen influence on the energy barrier, with $\Delta G^{\ddagger}$ values decreasing slightly with increasing halogen size. Previous studies of other $[ReX(CO)_3(L—L)]$ complexes[1–3,12] have revealed no clear halogen dependencies and so the present results should be interpreted with some caution.

The sulphur inversion barriers in these mixed sulphur/phosphorus coordinated ligand chelate complexes are somewhat lower than those in the analogous sulphur/sulphur chelate complexes, viz $[ReX(CO)_3(o\text{-}MeSC_6H_4SMe)]$ (X = Cl, Br, I),[2] where $\Delta G^{\ddagger}$ values are in the range 53.5–56.4 kJ mol^{-1}. Thus, replacement of a pyramidal sulphur atom by a tetrahedral phosphorus atom in the five-membered metallocycle increases slightly the rate

of pyramidal inversion of the coordinated sulphur atom on the other side of the five-membered ring. Whether this is due to an increase in energy of the ground state structure due to steric effects of the phenyl rings or to a stabilization of the planar transition state structure for the inversion process, is uncertain.

An aromatic ligand backbone is known to favour inversion of the heterocyclic sulphur atoms compared with the analogous aliphatic ligand backbone.[13] Thus in the complexes $[ReX(CO)_3\{MeS(CH_2)_2SMe\}]$ (X = Cl, Br, I),[2] $\Delta G^{\ddagger}$ values are *ca* 10 kJ mol^{-1} higher than in the aromatic ligand complexes. This is attributed to the effect of $(p\text{–}p)\pi$ conjugation which is more effective in the planar transition state than in the pyramidal ground-state structure. In the present complexes the conjugation effect is directed towards a single pyramidal sulphur atom rather than towards a pair as in the *o*-$MeSC_6H_4SMe$ complexes, and may be somewhat more effective for that reason. The difference in energies being discussed here, however, is very small and, indeed, the main finding of this paper is that diphenylphosphino and methylthio units appear to have very comparable electronic influences on pyramidal sulphur inversion in five-membered chelate ring complexes of $ReX(CO)_3$.

REFERENCES

1. E. W. Abel, M. M. Bhatti, K. G. Orrell and V. Šik, *J. Organomet. Chem.* 1981, **208**, 195.
2. E. W. Abel, S. K. Bhargava, M. M. Bhatti, K. Kite, M. A. Mazid, K. G. Orrell, V. Šik, B. L. Williams, M. B. Hursthouse and K. M. A. Malik, *J. Chem. Soc., Dalton Trans.* 1982, 2065.
3. E. W. Abel, S. K. Bhargava, K. Kite, K. G. Orrell, V. Šik and B. L. Williams, *J. Chem. Soc., Dalton Trans.* 1984, 365.
4. T. N. Lockyer, *Aust. J. Chem.* 1974, **27**, 259.
5. D. Ellis, PhD thesis. University of Exeter (1991).
6. E. W. Abel, J. C. Dormer, D. Ellis, K. G. Orrell, V. Šik, D. Stephenson, M. B. Hursthouse and M. A. Mazid, manuscript in preparation.
7. D. W. Meek, G. Dyer and M. O. Workman, *Inorg. Synth.* 1976, **16**, 168.
8. W. Hieber, R. Schuh and H. Fuchs, *Z. Anorg. Allg. Chem.* 1941, **248**, 243.
9. M. M. Bhatti, PhD thesis. University of Exeter (1980).
10. D. A. Kleier and G. Binsch, 'DNMR 3', *Quantum Chemistry Program Exchange* 1970, **1**, 165.
11. G. Binsch and H. Kessler, *Angew. Chem., Int. Edn. Engl.* 1980, **19**, 411.
12. E. W. Abel, M. Z. A. Chowdhury, K. G. Orrell and V. Šik, *Polyhedron* 1984, **3**, 331.
13. E. W. Abel, S. K. Bhargava and K. G. Orrell, *Prog. Inorg. Chem.* 1984, **32**, 1.
14. J. Sandström, *Dynamic NMR Spectroscopy*. Academic Press, New York (1982).

Polyhedron Vol. 10, No. 14, pp. 1611–1616, 1991
Printed in Great Britain

0277–5387/91 $3.00+.00
© 1991 Pergamon Press plc

SYNTHESIS OF AN ETHER OXIME LIGAND AND ITS RHODIUM(III) COMPLEX, AND X-RAY STRUCTURE OF THE RHODIUM(III) COMPLEX: UNIQUE RHODIUM(III) BONDING TO A SIMPLE ETHER

G. ERGUN EFE and E. O. SCHLEMPER*

Department of Chemistry, University of Missouri, Columbia, MO 65211, U.S.A.

(*Received* 8 *January* 1991; *accepted* 21 *March* 1991)

Abstract—The ligand 3-methoxy-3-methyl-2-butanone oxime and its rhodium(III) complex have been synthesized, and the complex has been structurally characterized. The octahedron around the rhodium atom involves two *trans*-chlorine atoms [Rh—Cl = 2.3236(8) Å], two *cis*-oxime nitrogen atoms [av. Rh—N = 1.958(3) Å] and two *cis*-ether oxygen atoms [av. Rh—O = 2.117(3) Å]. The oxime oxygen atoms are involved in a short intramolecular hydrogen bond (O---O = 2.391 Å). Synthesis and characterization of the ligand and the rhodium(III) complex are described, and the ^{1}H NMR results are given and discussed. To our knowledge this is the first characterized ether oxime metal complex.

The development of bifunctional chelating ligands and their complexes with Rh-105 as potential radiotherapeutic agents has been under investigation in our laboratory.[1,2] The ligands used in our previous work were all of the nitrogen donor type. In this work, we have uncovered a new approach to the synthesis of 3-methoxy-3-methyl-2-butanone oxime. This compound has been known since 1903 through the work of Schmidt.[3] Additional synthetic approaches were reported in 1964[4] and 1978.[5] Here, we have discovered a rather straightforward approach which should be applicable for the synthesis of other 3-alkoxy-3-methyl-2-butanone oximes.

While many crown ether metal complexes and complexes with macrocyclic ether donors and with bonded tetrahydrofuran or dioxane are known, there are few complexes of bidentate ligands containing a single ether oxygen donor. To our knowledge this is the first reported structure of such a complex with rhodium(III).

EXPERIMENTAL

Preparation of the compounds

3-Methoxy-3-methyl-2-butanone oxime (ether oxime). This compound has been prepared and reported, most recently, by Kisan and Pritzkow,[5] who used the 3-sulphato oxime as the starting oxime. A similar procedure was applied here by using α-chloro-3-methyl-2-butanone (α-chloro oxime). α-Chloro oxime was synthesized as described by Murmann.[6] To prepare the ether oxime, absolute methanol (50 cm^3) and $NaHCO_3$ (5.04 g, 60 mmol) were placed in a round-bottomed flask and warmed up to 50–60°C while stirring. α-Chloro oxime (3.39 g, 25 mmol) was added over a 30 min period and the solution was then refluxed for 4.5 h. The flask was sealed and left at room temperature overnight. The white, inorganic precipitate was filtered out and the solvent was evaporated. The residue was extracted several times into ether and the combined ether extracts were evaporated. The product was recrystallized from hot hexanes to obtain colourless, large crystals. The yield was 30% after recrystallization, m.p. 89–91°C (lit. 92–93°C, ref. 3; 89–90°C, ref. 4). The same compound was also prepared by using triethylamine as base and by refluxing for 24 h, but the yield was lower (14%) in that case.

[Rh(*ether oxime*)$_2$Cl$_2$]. Ether oxime (0.295 g, 2.25 mmol) was dissolved in ethanol (15 cm^3), then $RhCl_3 \cdot 3H_2O$ (0.263 g, 1 mmol) in 5 cm^3 of water was added and the solution was refluxed for 3 h. The pH was adjusted to 7 by the addition of potassium hydroxide, and orange crystals were obtained by

* Author to whom correspondence should be addressed.

slow evaporation of the solvent. Yield: 45%. Found: C, 33.1; H, 5.7; N, 6.1; O, 15.1. Calc. for $RhCl_2O_4N_2C_{12}H_{25}$: C, 33.1; H, 5.8; N, 6.4; O, 14.7%.

^1H *NMR*

Spectra of the compounds were recorded on a JEOL FX90Q Fourier transform NMR spectrometer with TMS as an internal standard in d_6-DMSO. The chemical shifts and the integrated intensities for the designated protons are as follows: ether oxime (a) 1.23s, 6H, (b) 1.71s, 3H, (c) 2.95s, 3H, (f) 10.68s. 1H; [Rh(ether oxime)$_2$Cl$_2$] (a) 1.45s, 12H, (b) 2.21s, 6H, (c) 3.88s, 6H, (f) 18.22s, 1H. The chemical shifts for the complex are at lower fields than those of the ligand, as a result of the deshielding effect of metal and chloride ions. Deshielding due to the double bond results in the protons of the methyl carbon adjacent to the C=N group [(b) protons] resonating at a lower field strength compared with the geminal methyl protons [(a) protons]. The very low-field resonance of the hydrogen-bonded oxime proton in the rhodium complex is characteristic of α-amine oxime complexes which have short, nearly symmetrical hydrogen bonds.[1,7,8] The high symmetry of the complex indicated by the singlet peaks for the methyl protons was confirmed by the X-ray crystal structure.

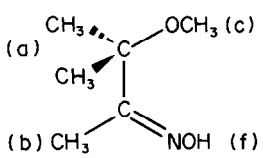

Ether oxime

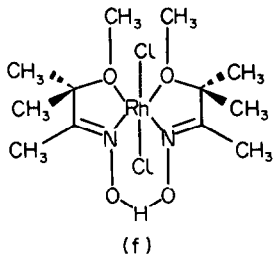

[Rh(ether oxime)$_2$Cl$_2$]

X-ray diffraction

Orange crystals of [Rh(ether oxime)$_2$Cl$_2$] were prepared by the slow evaporation of a solution of ethanol–water (3 : 1 ratio). A crystal of approximate dimensions $0.30 \times 0.10 \times 0.13$ mm was mounted in random orientation on an Enraf–Nonius CAD4 automated diffractometer. The crystal was optically centred. Twenty-five reflections were located by automatic search of reciprocal space and recentred. The setting angles of these reflections were used to obtain the orthorhombic cell constants which are included in Table 1 together with other crystal data and structure solution and refinement parameters.

The intensities were collected with Mo-K_α radiation (0.7107 Å) obtained from a graphite monochromator at a rate to obtain counting statistics of $\pm 3\%$ up to a maximum scan time of 90 s. To check instrument and crystal stability, the intensities of three standard reflections were recorded after every 7200 s of X-ray exposure and showed no significant decay or fluctuation. Orientation was checked after every 200 reflections with the use of the same standards and all 25 original reflections were recentred when the measured position of any scattering vector of any of these standards deviated by more than 0.06° from the calculated position. Systematic absences of $k+l$ odd for $0kl$ and h odd for $h0l$ were consistent with the space groups *Pnam* and $Pna2_1$. Statistical analysis of the intensities did not give a good agreement with the theoretical values for either the non-centrosymmetric or the centrosymmetric structure. Since the agreement in Friedel-pair intensities was good (agreement factor = 0.012), space group *Pnam* was assumed. The choice was confirmed by successful refinement in that space group. The integrated intensities were corrected for background and directly reduced to a set of relative squared structure amplitudes, $|F_o|^2$, by the application of the standard Lorentz-polarization factor (Lp). Individual estimated standard deviations ($\sigma_{counting}$) were derived based on counting statistics. Empirical (Ψ scan) absorption corrections were made with the relative transmission ranging from 0.96 to 1.00.

The structure of the complex was solved by Patterson and Fourier methods, and refinement was by the full-matrix least-squares method. The molecule is very planar, and most of the atoms of the molecule lie on the mirror plane at $z = 1/4$. The only atoms out of this plane are Cl, C(4), C(4′), all C(4) and C(4′) methyl hydrogen atoms and two hydrogen atoms on each of C(3), C(3′), C(5) and C(5′) methyl carbon atoms (see Fig. 1). The symmetry restriction imposed by the mirror plane required

Table 1. Crystallographic data for [Rh(ether oxime)$_2$Cl$_2$]

Formula	$RhCl_2O_4N_2C_{12}H_{25}$
Formula weight	435.2
a (Å)	16.122(4)
b (Å)	11.912(8)
c (Å)	9.355(3)
Z	4
d_{calc} (g cm^{-3})	1.609
μ (cm^{-1})	12.5
Scan method	θ–2θ
Scan range (θ) (°)	$0.6+0.35\tan\theta$
2θ range (°)	4–50
hkl Range	hkl and $-h-k-l$ (2θ = 4–35°) hkl (2θ = 35–50°)
Number of reflections measured	2530
Number of independent reflections measured	1677
Number of reflections above 2α	1327
Function minimized	$\Sigma w(\|F_o\|-\|F_c\|)^2$
w	$4F_o^2/[\sigma^2_{counting}+(0.04F_o^2)]$
R	0.022
wR	0.033
Maximum shift/error on last cycle	0.32
Maximum difference density	0.26 e Å^{-1}

fixed z-coordinates and U_{13} and U_{23} parameters for all the atoms on the mirror plane for subsequent least-squares refinements. The other positional parameters and anisotropic thermal parameters of the non-hydrogen atoms were included in the refinement. The total number of variables was 118.

The final atomic positional parameters and isotropic equivalent thermal parameters have been deposited with the Cambridge Crystallographic Data Centre. The molecular structure is shown in Fig. 1 and important bond distances and angles for non-hydrogen atoms are in Tables 2 and 3, respectively.

RESULTS AND DISCUSSION

The crystal structure consists of discrete, mononuclear, neutral and nearly octahedral rhodium(III)

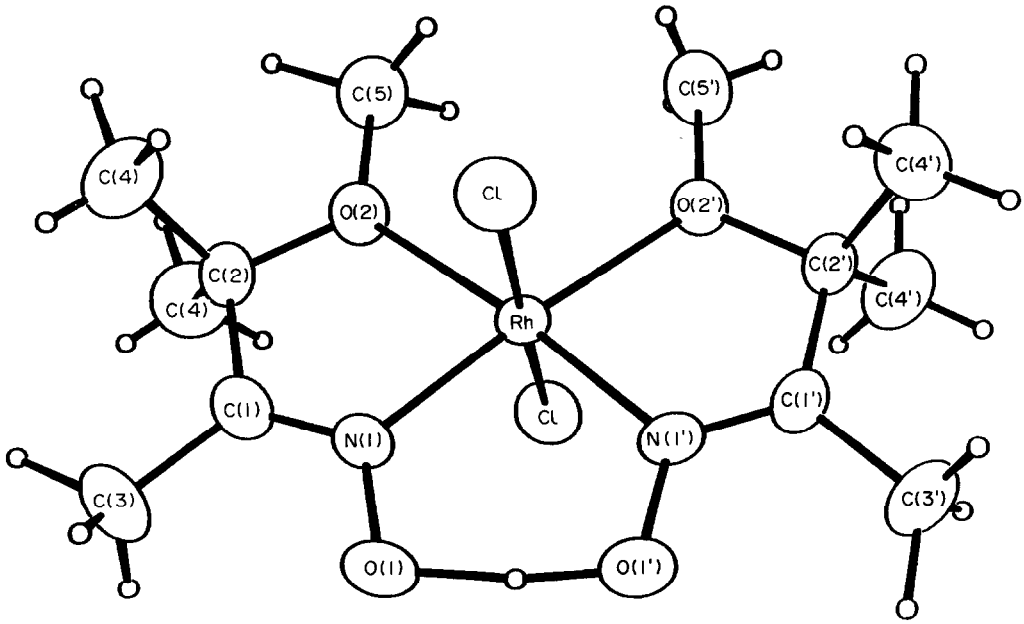

Fig. 1. Perspective view of [Rh(ether oxime)$_2$Cl$_2$].

Table 2. Bond distances (Å) for [Rh(ether oxime)$_2$Cl$_2$]

Rh—Cl	2.3237(8)	O(2′)—C(5′)	1.406(5)
Rh—O(2)	2.119(3)	N(1)—C(1)	1.269(5)
Rh—O(2′)	2.114(2)	N(1′)—C(1′)	1.272(5)
Rh—N(1)	1.952(3)	C(1)—C(2)	1.511(5)
Rh—N(1′)	1.965(3)	C(1)—C(3)	1.503(6)
O(1)—N(1)	1.343(4)	C(1′)—C(2′)	1.505(5)
O(1′)—N(1′)	1.339(4)	C(1′)—C(3′)	1.511(5)
O(2)—C(2)	1.448(4)	C(2)—C(4)	1.516(4)
O(2)—C(5)	1.436(5)	C(2′)—C(4′)	1.519(4)
O(2′)—C(2′)	1.450(4)		

Numbers in parentheses are ESDs in the least significant digits.

molecules. The octahedron around the rhodium atom involves two *trans*-chlorine atoms, two *cis*-ether oxygen atoms and two *cis*-oxime nitrogen atoms. The molecules have very nearly C_{2v} symmetry, but only one mirror is crystallographically fixed, passing through all of the non-hydrogen atoms except Cl, C(4) and C(4′). The mirror plane relates the two chlorine atoms, as well as the two C(4) and two C(4′) methyl carbon atoms. Of special note is the trigonal planar nature of the ether oxygen atoms. Both of these have very nearly 120° angles [range 116.5(2)° for Rh—O(2)—C(2) to 124.9(2)° for Rh—O(2)—C(5)]. This apparent sp^2 hybridization is not observed in the rhodium(I) complex *trans*-[1,5-bis(diphenylphosphino)-3-oxapentane-O,P,P′]carbonylrhodium(I),[9] where the angles around the ether oxygen atom range from 112.5 to 117.5°, or in other metal monoether complexes such as chloro[1-(diphenylphosphino)-2-methoxyethane-O,P][1-(diphenylphosphino)-2-methoxyethane-P]platinum(II),[10] where the angles range from 111.5 to 120.8°.

The least-squares planes of interest are given in Table 4. The two vertical planes, each containing the rhodium, a chlorine, a coordinated ether oxygen and its *trans* oxime nitrogen, are nearly perpendicular to the chelate plane. The dihedral angle between the two vertical planes, internal to the chelate rings, is 76.45(7)°, which is much less than 90° due to chelate ring formation. The two chlorine atoms and the rhodium atom are not strictly linear, with a Cl—Rh—Cl angle of 177.39(4)°. There are no intermolecular contacts between non-hydrogen atoms less than 3.5 Å. The hydrogen bond between the oxime oxygen atoms is quite short, with an O---O distance of 2.391(4) Å. This distance is much shorter than the corresponding hydrogen bond in [Rh(AO)$_2$Cl$_2$][7] which has primary amino groups instead of ether oxygen atoms, with an O---O distance of 2.459(2) Å. Actually, the hydrogen bond distance found in [Rh(ether oxime)$_2$Cl$_2$] is the shortest among the previously studied, mononuclear rhodium(III) amine oxime complexes which have O---O distances ranging from 2.423(3) to 2.626(4) Å.[1,7,8] The dinuclear complex [Rh(BnAO)Cl$_2$]$_2$[8] has an O---O distance of 2.387(5) Å, which is the shortest found in any of the rhodium(III) amine oxime complexes.

Summary

We have prepared a bidentate ligand with an ether oxygen and an oxime nitrogen donor. The

Table 3. Bond angles (°) for [Rh(ether oxime)$_2$Cl$_2$]

Cl—Rh—O(2)	89.54(2)	Rh—N(1)—C(1)	122.0(3)
Cl—Rh—O(2′)	88.99(2)	O(1)—N(1)—C(1)	118.8(3)
Cl—Rh—N(1)	91.09(2)	Rh—N(1′)—O(1′)	118.8(3)
Cl—Rh—N(1′)	90.57(2)	Rh—N(1′)—C(1′)	121.7(3)
O(2)—Rh—O(2′)	108.6(1)	O(1′)—N(1′)—C(1′)	119.5(3)
O(2)—Rh—N(1)	76.8(1)	N(1)—C(1)—C(2)	118.9(4)
O(2)—Rh—N(1′)	174.7(1)	N(1)—C(1)—C(3)	121.0(4)
O(2′)—Rh—N(1)	174.6(1)	C(2)—C(1)—C(3)	120.1(4)
O(2′)—Rh—N(1′)	76.7(1)	N(1′)—C(1′)—C(2′)	119.0(3)
N(1)—Rh—N(1′)	97.9(1)	N(1′)—C(1′)—C(3′)	120.5(4)
Rh—O(2)—C(2)	116.5(2)	C(2′)—C(1′)—C(3′)	120.6(4)
Rh—O(2)—C(5)	124.9(2)	O(2)—C(2)—C(1)	105.8(3)
C(2)—O(2)—C(5)	118.7(3)	O(2)—C(2)—C(4)	108.7(2)
Rh—O(2′)—C(2′)	116.7(2)	C(1)—C(2)—C(4)	110.6(2)
Rh—O(2′)—C(5′)	124.5(3)	O(2′)—C(2′)—C(1′)	105.9(3)
C(2′)—O(2′)—C(5′)	118.8(3)	O(2′)—C(2′)—C(4′)	109.2(2)
Rh—N(1)—O(1)	119.2(2)	C(1′)—C(2′)—C(4′)	109.8(2)

Numbers in parentheses are ESDs in the least significant digits.

Table 4. Least-squares planes for [Rh(ether oxime)$_2$Cl$_2$]

Orthonormal equation of plane 1

$0.0000X+$	$0.0000Y+$	$-1.0000Z-$	$-2.3388=0$
0.0000	0.0000	0.0000	0.0000

Crystallographic equation of plane

$0.0000X+$	$0.0000Y+$	$-9.3552Z-$	$-2.3388=0$
0.0000	0.0000	0.0000	0.0000

Atom	X	Y	Z	Distance ESD
Rh	2.4270	0.9058	2.3388	0.0000±0.0000
N(1)	3.2068	2.6953	2.3388	0.0000±0.0000
N(1′)	4.1041	−0.1179	2.3388	0.0000±0.0000
O(2)	0.7281	2.1723	2.3388	0.0000±0.0000
O(2′)	1.7690	−1.1034	2.3388	0.0000±0.0000

Chi squared = 0.0

Other atoms

Cl	2.3825	0.8774	4.6619	−2.3231±0.0008
O(1)	4.5430	2.8273	2.3388	0.0000±0.0000
O(1′)	5.2657	0.5480	2.3388	0.0000±0.0000
C(1)	2.4892	3.7423	2.3388	0.0000±0.0000
C(1′)	4.1105	−1.3901	2.3388	0.0000±0.0000
C(2)	0.9848	3.5975	2.3388	0.0000±0.0000
C(2′)	2.7971	−2.1254	2.3388	0.0000±0.0000
C(3)	3.1137	5.1088	2.3388	0.0000±0.0000
C(3′)	5.4155	−2.1497	2.3388	0.0000±0.0000
C(4)	0.3918	4.1974	3.5988	−1.2600±0.0038
C(4′)	2.6737	−2.9569	3.6043	−1.2655±0.0034
C(5)	−0.6344	1.7178	2.3388	0.0000±0.0000
C(5′)	0.4205	−1.5005	2.3388	0.0000±0.0000

Orthonormal equation of plane 2

$-0.9347X+$	$0.3531Y+$	$-0.0411Z-$	$-2.1086=0$
0.0003	0.0009	0.0007	0.0029

Crystallographic equation of plane

$-15.0693X+$	$4.2060Y+$	$-0.3847Z-$	$-2.1086=0$
0.0056	0.0109	0.0061	0.0029

Atom	X	Y	Z	Distance ESD
Rh	2.4270	0.9058	2.3388	0.0639±0.0003
C(1)	2.3825	0.8774	4.6619	−0.0001±0.0007
N(1)	3.2068	2.6953	2.3388	−0.0332±0.0030
O(2′)	1.7690	−1.1034	2.3388	−0.0306±0.0026

Chi squared = 0.0

Orthonormal equation of plane 3

$-0.5612X+$	$-0.8263Y+$	$-0.0480Z-$	$-2.2855=0$
0.0008	0.0006	0.0007	0.0029

Crystallographic equation of plane

$-9.0481X+$	$-9.8424Y+$	$-0.4486Z-$	$-2.2855=0$
0.0136	0.0068	0.0063	0.0029

Atom	X	Y	Z	Distance ESD
Rh	2.4270	0.9058	2.3388	0.0628±0.0003
C(1)	2.3825	0.8774	4.6619	−0.0001±0.0007
N(1′)	4.1041	−0.1179	2.3388	−0.0325±0.0032
O(2)	0.7281	2.1723	2.3388	−0.0302±0.0026

Chi squared = 0.0

Table 4.—*continued*

Dihedral angles between planes: Plane number	Plane number	Dihedral angle
1	2	87.64±0.04
1	3	87.25±0.04
2	3	76.42±0.07

rhodium(III) complex of this ligand was synthesized and characterized. To our knowledge this is the first reported metal complex with ligands with donor atoms of this type, and the first rhodium(III) complex with monoether coordination. The formation of this stable complex is unusual since simple ether donors do not generally form good complexes with metals. It also serves as a model for a new series of complexes containing oxygen atoms carrying appropriate functional groups that can be used to couple to protein molecules to form potential radiopharmaceuticals.

Acknowledgement—This work was supported by the U.S. Department of Energy Grant No. DEFG02-86ER60400.

REFERENCES

1. T. Lynde-Kernell and E. O. Schlemper, *J. Coord. Chem.* 1988, **16**, 347.
2. C. S. John, M. R. A. Pillai, J. M. Lo and D. E. Troutner, *Appl. Radiat. Isot.* 1989, **40**, 701.
3. J. Schmidt, *Ber.* 1903, **35**, 3722.
4. C. A. Burkhard and J. F. Brown Jr, *J. Org. Chem.* 1964, **29**, 2235.
5. W. Kisan and W. Pritzkow, *J. Prakt. Chem.* 1978, **320**, 59.
6. R. Kent Murmann, private communication.
7. S. Siripaisarnpipat and E. O. Schlemper, *Inorg. Chem.* 1984, **23**, 330.
8. S. Siripaisarnpipat and E. O. Schlemper, *Inorg. Chem.* 1983, **22**, 282.
9. N. W. Alcock, J. M. Brown and J. C. Jeffrey, *J. Chem. Soc., Dalton Trans.* 1976, 583.
10. G. K. Anderson, E. R. Corey and R. Kumar, *Inorg. Chem.* 1987, **26**, 97.

Polyhedron Vol. 10, No. 14, pp. 1617–1624, 1991
Printed in Great Britain

0277–5387/91 $3.00+.00
© 1991 Pergamon Press plc

RHODIUM COMPLEXES OF TWO BIDENTATE SECONDARY AMINE OXIME LIGANDS AND APPLICATION TO THE LABELLING OF PROTEINS

G. ERGUN EFE, M. R. A. PILLAI,* E. O. SCHLEMPER† and D. E. TROUTNER

Department of Chemistry, University of Missouri, Columbia, MO 65211, U.S.A.

(*Received* 12 *December* 1990; *accepted* 21 *March* 1991)

Abstract—The syntheses of a new, bifunctional ligand, 3-[N-(4-aminobenzyl)]amino-3-methyl-2-butanone oxime, ligand **I**, and a non-bifunctional analogue 3-benzylamino-3-methyl-2-butanone oxime, ligand **II**, the former for labelling proteins with ^{105}Rh complexes for internal radiotherapy applications are reported. The rhodium complex of ligand **II** was isolated and characterized by ^{1}H NMR, IR spectroscopy and X-ray crystallography. The crystal structure consists of discrete mononuclear, neutral and slightly distorted octahedral molecules. The octahedron around rhodium consists of two *trans*-chlorine atoms and four nitrogen atoms from the two bidentate amine oxime ligands. The complex formed *in situ* with the bifunctional ligand **I** gives up to 95% yield with ^{105}Rh in pH 9 bicarbonate buffer. This complex was converted to the isothiocyanate derivative with thiophosgene and extracted into $CHCl_3$ (91%). Conjugation yields of greater than 90% could be obtained with human γ-globulin. The protein conjugation method described is suitable for the preparation of ^{105}Rh labelled antibodies with specific activities of 1.6–9.3 mCi mg^{-1}.

We have been investigating the use of ^{105}Rh as a radionuclide for use in internal radiotherapy. It is a 35.5 h moderate-energy beta-emitter whose usefulness is enhanced by the kinetic inertness and stability of the rhodium(III) complexes. Our goal is to synthesize rhodium(III) complexes of bifunctional chelates which can then be coupled to antibodies or other proteins by standard protein conjugation techniques. Our first approach to this work was to synthesize tetradentate ligands for rhodium with a pendant side arm suitable for coupling to the antibody.[1] Subsequent studies, however, showed that a simple tridentate ligand based on diethylene triamine gave rhodium complexes sufficient stability to permit preforming of the chelate followed by coupling.[2] We also showed that complexes of the simple ligand cysteine could be coupled to proteins through the pendant carboxylate group with chelation through the amine and sulphide groups.[3]

Because of this latter success we report here the design of a bidentate ligand with a pendant coupling group for rhodium. Previous work from this laboratory has shown that bis complexes of rhodium with the ligand 3-amino-3-methyl-2-butanone oxime are readily formed and are very stable.[4] For that reason we chose to modify the ligand to include a functionality for protein conjugation by substitution on the amine nitrogen. The initial modification placed a benzyl group on the amine nitrogen (Fig. 1, ligand **II**), and then we synthesized the 4-aminobenzyl analogue (ligand **I**) which is suitable for conjugation.

Rhodium-105 emits gamma radiation in significant amounts. All operations involving ^{105}Rh were performed in a laboratory approved for the handling of ^{105}Rh up to levels of 8 mCi.

EXPERIMENTAL

Materials and methods

γ-Globulins, human (G-4386) and Sephadex G 75 were purchased from Sigma Chemical Company. 4-Nitrobenzylamine hydrochloride was obtained

* Present address: Isotope Division, Bhabha Atomic Research Center, Trombay, Bombay 400085, India.

† Author to whom correspondence should be addressed.

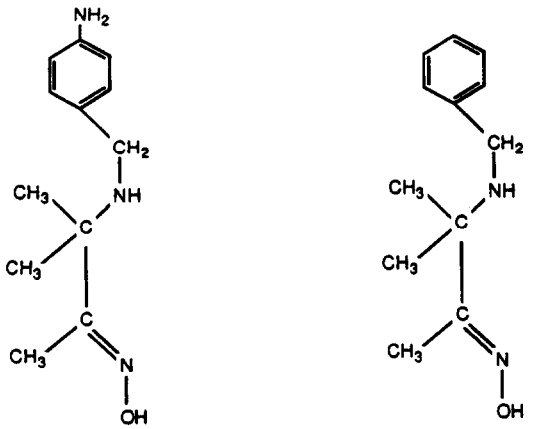

Ligand I Ligand II

Fig. 1. Ligand I, 3-[N-(4-aminobenzyl)]amino-3-methyl-2-butanone oxime and ligand II, 3-benzylamino-3-methyl-2-butanone oxime.

from Aldrich Chemicals. All other reagents or chemicals used were of reagent grade. ^{105}Rh was prepared at the Missouri University Research Reactor and supplied as aqueous $[RhCl_x \cdot (H_2O)_{6-x}]^{(x-3)-}$.

Instrumental methods. ^{1}H NMR spectra were recorded on a JEOL FX-90Q spectrometer. Solid-state IR spectra were recorded on a Nicolet 20 DXB FT–IR spectrometer using fluorolube mulls. Radioactivity was measured on a standard 5 × 5-cm NaI(Tl) well scintillation counter using 319- and 306-keV gamma rays of ^{105}Rh.

Elemental analyses were carried out by Galbraith Laboratories Inc., Knoxville, Tennessee.

Syntheses

3-[N-(4-aminobenzyl)]amino-3-methyl-2-butanone oxime, ligand **I**. 4-Nitrobenzylamine hydrochloride (2.2 g, 11.66 mmol) was dissolved in 70 cm^3 of deionized water and neutralized with 11.66 mmol of sodium hydroxide and extracted with chloroform. The chloroform extracts were combined and evaporated, and the residue was dried. 4-Nitrobenzylamine (1.38 g, 9.07 mmol) was dissolved in 50 cm^3 of absolute methanol and placed in an ice–acetone bath. 3-Chloro-3-methyl-2-butanone oxime (prepared as per ref. 5) (1.41 g, 10.44 mmol) was added to this and the solution warmed to room temperature slowly. It then was refluxed for 24 h. The solvent was evaporated, the residue was suspended in water and 5 M potassium hydroxide was added to change the pH to 8. The white precipitate was collected by filtration and recrystallized from hot ethanol. Yield: 58%.

PtO_2 catalyst (30 mg) in 1 cm^3 of ethanol was first placed in the hydrogenation apparatus and about 45 min later 340 mg of nitrobenzylamine oxime dissolved in 10 cm^3 of ethanol was added. The compound was hydrogenated with 100 cm^3 of hydrogen gas under atmospheric pressure with continuous stirring. The catalyst was removed by filtration, the ethanol was evaporated and the residue was dried. The product weighed 286 mg, yield: 95%. ^{1}H NMR (DMSO-d_6) δ(ppm): 1.17(s) methyl (6H), 1.76(s) methyl(3H), 3.2(s) CH_2 (2H), 4.85(s) NH_2 (2H), 6.46–6.93(m) aromatic (4H), 10.4(s) oxime (1H).

For elemental analysis, the dihydrohexachloroplatinate(IV) salt was prepared as follows. The ligand (0.13 mmol) was dissolved in 2.5 cm^3 of ethanol. 1 cm^3 of water was added, and the solution was acidified to pH 3 by the addition of 1.25 M hydrochloric acid. Then H_2PtCl_6 solution was gradually added and the colour of the solution became darker orange. The solution was filtered and placed in a refrigerator. Orange-coloured crystals formed over 24 h. Found: C, 21.4; H, 3.6; N, 6.1. Calc. $(C_{12}H_{21}N_{30})PtCl_6$: C, 22.8; H, 3.4; N, 6.7%. Lower observed values for carbon and nitrogen suggest that the crystals contain water molecules. For the formula $[C_{12}H_{211}H_{30}]PtCl_6 \cdot 2H_2O$, calculated percentages are as follows: C, 21.6; H, 3.2; N, 6.3%. Ligand **I** was also prepared as the chloride salt and its structure was determined by X-ray diffraction.[6]

3-Benzylamino-3-methyl-2-butanone oxime, ligand **II**. 3-Chloro-3-methyl-2-butanone oxime (2.44 g, 0.018 mol) was added to a solution of benzylamine (0.014 mol) in 25 cm^3 of absolute methanol at 0°C. The solution was stirred in an ice bath for several hours and brought to room temperature slowly. The mixture was then refluxed for 24 h. The solvent was evaporated and the residue was dissolved in water. Upon addition of base, a white precipitate formed which was collected by filtration. Yield: 64%, m.p. 68–69°C. The solid was recrystallized from a methanol–water mixture. ^{1}H NMR (DMSO-d_6) δ(ppm) 1.20(s) methyl (6H), 1.78(s) methyl (3H), 2.2(br) NH (1H), 3.4(s) CH_2 (2H), 7.28(s) aromatic (5H), 10.44(s) oxime (1H).

Rhodium complex of ligand **II**. Rhodium chloride (0.263 g, 1 mmol) was dissolved in 5 cm^3 of deionized water and to this solution, ligand **II** (0.464 g, 2.25 mmol) dissolved in 15 cm^3 of ethanol was added. Potassium hydroxide (1 mmol) was added to change the final pH to ~ 7 and the solution was heated under reflux for 7 h. The initial red colour of the solution turned to light orange, and it was filtered while hot. Orange crystals, suitable for X-ray crystallography, formed by slow evaporation of the

reaction mixture. Yield: 44%. ^{1}H NMR (DMSO-d_6) δ(ppm): 1.03(s) methyl (6H), 1.46(s) methyl (6H), 2.09(s) methyl (6H), 4.34(d) CH_2 (2H), 4.68(d of d) CH_2 (2H), 5.12(d) NH (2H), 7.37–7.44(m) aromatic 10H, 19.51(s) O—H—O (1H). Found: C, 48.9; H, 6.1; N, 9.5. Calc. $RhCl_2O_2N_4C_{24}H_{35}$: C, 49.2; H, 6.0; N, 9.6%.

Rhodium complex of ligand **I**. The procedure above was followed and initially produced an analogous orange solution. Repeated attempts to isolate the corresponding complex of ligand **I** were unsuccessful so that characterization by X-ray diffraction and NMR techniques was not possible. When the ethanol–water solutions were concentrated to attempt isolation, there were obvious additional reactions producing dark-coloured products which could not be redissolved for spectroscopic characterization. We postulate that this might be a result of a polymerization reaction involving the interaction of the dangling aromatic amines with additional rhodium atom(s). We were able to isolate the nickel(II) complex of ligand **I**, and the crystal structure confirms the expected analogous coordination of two ligands in a square plane with the dangling aromatic amines.[6] Because of the square planar preference of nickel(II), the subsequent reactions are not observed.

Collection and reduction of X-ray data

X-ray data were collected at 22(1)°C for the rhodium complex of ligand **II**, on an Enraf–Nonius CAD4 automated diffractometer controlled by a Digital PDP 11/34 computer using Mo-K_α radiation (λ = 0.7107 Å). Lattice constants were obtained by least-squares fit of 25 carefully centred reflections. To check instrument and crystal stability, the intensities of three standard reflections were recorded after every 7200 s of X-ray exposure and showed no significant decay or fluctuation. Orientation was checked after every 200 reflections with the use of the same standards and all 25 original reflections were recentred when the measured deviations of any of the three standards were significant. A summary of crystal data, data collection parameters and refinement results is given in Table 1.

Table 1. Crystal data, data collection parameters and refinement results

Formula	$RhCl_2O_2N_4C_{24}H_{35}$
Formula weight	585.4
Space group	$P2_1/n$
a (Å)	8.802(4)
b (Å)	15.715(6)
c (Å)	19.447(5)
α (°)	90
β (°)	92.87(3)
γ (°)	90
V (Å^3)	2687(1)
T (K)	130(5)
Z	4
λ (Mo-K_α, Å)	0.7107
d_{cal} (g cm^{-3})	1.447
Crystal size (mm)	0.10 × 0.25 × 0.28
μ (cm^{-1})	8.52
Relative transmission factors	91–100% (Ψ scan empirical)
Scan method	θ–2θ
Scan width (°)	$0.90+0.35\tan\theta$
Scan time	to obtain 3% count. stat. to maximum of 90 s
θ Range (°)	2–22.5
Number of reflections measured	3800
Number of independent reflections	3514
Number of independent reflections [$I > 2\sigma(I)$]	2901
Number of variables	403
$R(F)$	0.023
$R_w(F)$	0.031
Maximum shift/error on last cycle	0.03

Solution and refinement of the structures

The X-ray structure was solved by conventional Patterson and difference Fourier methods. The full-matrix least-squares refinements minimized the function $\Sigma w (|F_o|-|F_c|)^2$), where $w = 1/\sigma^2(F_o)$, $\sigma(F_o) = \sigma(F_o^2)/2F_o$ and $\sigma^2(F_o^2) = \sigma^2$ (counting) $+(0.04F_o^2)^2$. Atomic scattering factors were taken from the *International Tables for X-ray Crystallography*[7] and included anomalous scattering contributions. Hydrogen atoms were located by difference Fourier methods or were placed in chemically reasonable positions with B ~ 1.3 × B of atom attached. Positional parameters of hydrogen atoms were also included in the least-squares cycles. The maximum residual electron density was 0.21. The final positional parameters for the non-hydrogen atoms are included in the supplemental material.

Radiochemical studies

^{105}Rh *complexes of ligand* **I**. Bicarbonate buffer (0.5 cm^3 of 0.5 M), saline solution (1 cm^3, 0.9 %), $RhCl_3$ (2×10^{-3} mmol, 0.08 cm^3) and ^{105}Rh (0.1 cm^3, 15 MBq) were refluxed in a 10 cm^3 round-bottomed flask for 2 min. Ligand **I** (1 cm^3, 5×10^{-3} mmol) in ethanol was added to this and refluxing continued for 2 h. The final volume of the solution after refluxing was adjusted to 2 cm^3 and the rhodium concentration was 10^{-3} mmol cm^{-3}.

Estimation complex yield. The complex yield was estimated by the magnesium oxide adsorption technique.[8] Typically, a small aliquot of the complex was diluted to 0.4 cm^3 in saline. Magnesium oxide powder (50 mg) (USP, Light powder) was added to this and mixed over a vortex mixer for about 2 min. The suspension was centrifuged, and the activity associated with the supernatant was compared with the total activity to estimate the complex yield.

Preparation of the isothiocyanate derivative. For conjugation of the complex to protein the amino functional group was converted to the conjugating isothiocyanate group.[9] The complex (0.5 cm^3, 1.25×10^{-3} mmol ligand complexed to 5×10^{-4} mmol of rhodium) was mixed with 0.2 cm^3 of a chloroform solution of thiophosgene (2.7×10^{-2} mmol) for 2 min over a vortex mixer. The organic layer was separated after a 2 min centrifugation, solvent was removed under a stream of nitrogen gas and the residue was redissolved in 0.2 cm^3 of DMF.

Conjugation to γ-globulin. γ-Globulin solution (1 cm^3, 5×10^{-5} mmol) in borate buffer (pH 9) was mixed with 1×10^{-2}–5×10^{-2} cm^3 of activated complex prepared as above (2.3×10^{-5}–11×10^{-5} mmol) and incubated for 5 h at room temperature. Conjugation yields were estimated by gel filtration chromatography over a Sephadex G 75 column (30 × 1.4 cm) using 0.9% saline as eluent. Fractions (2 cm^3) were collected and their activity measured on a NaI(Tl) well scintillation counter.

Challenge studies. Labelled γ-globulin (0.8 cm^3) was mixed with 0.4 cm^3 of diethylenetriamine pentaacetic acid (10^{-2} mmol) and incubated for 24 h. The activity associated with the protein peak was estimated by gel filtration chromatography.

RESULTS

The crystal structure of the rhodium complex of ligand **II** consists of discrete, mononuclear, neutral, slightly distorted octahedral molecules (Fig. 2). The octahedron around rhodium consists of two *trans*-chlorine atoms and four nitrogen atoms from the two bidentate amine oxime ligands. The complex has two five-membered chelate rings and a six-membered ring closed by a strong hydrogen bond between the oxime oxygen atoms formed by the loss of one oxime hydrogen atom. A close examination of Fig. 2 and the torsional angles, e.g. C(2)—N(2)—C(6)—C(7): 108.3(3)°, C(2′)—N(2′)—C(6′)—C(7′): 106.1(3)°, N(2)—C(6)—C(7)—C(12): 115.7(4)°, N(2′)—C(6′)—C(7′)—C(12′): 115.2(4)°, reveals that the molecule nearly has a two-fold axis passing through rhodium and the hydrogen-bonded oxime hydrogen atom (HOO). The intramolecular bond distances and bond angles involving non-hydrogen atoms are given in Tables 2 and 3. The short intra-

Table 2. Bond distances (Å) for the rhodium complex of ligand **I**

Rh—Cl(1)	2.3281(8)	C(2)—C(4)	1.533(5)
Rh—Cl(2)	2.3440(8)	C(2)—C(5)	1.531(5)
Rh—N(1)	1.984(2)	C(2′)—C(4′)	1.539(5)
Rh—N(1′)	1.992(2)	C(2′)—C(5′)	1.529(5)
Rh—N(2)	2.123(2)	C(6)—C(7)	1.518(5)
Rh—N(2′)	2.124(2)	C(6′)—C(7′)	1.501(5)
O—N(1)	1.353(3)	C(7)—C(8)	1.387(5)
O′—N(1′)	1.341(3)	C(7)—C(12)	1.382(5)
N(1)—C(1)	1.275(4)	C(7′)—C(8′)	1.387(5)
N(1′)—C(1′)	1.273(4)	C(7′)—C(12′)	1.385(5)
N(2)—C(2)	1.528(4)	C(8)—C(9)	1.366(6)
N(2)—C(6)	1.510(4)	C(8′)—C(9′)	1.382(6)
N(2′)—C(2′)	1.529(4)	C(9)—C(10)	1.366(6)
N(2′)—C(6′)	1.500(4)	C(9′)—C(10′)	1.354(7)
C(1)—C(2)	1.517(5)	C(10)—C(11)	1.371(6)
C(1)—C(3)	1.503(5)	C(10′)—C(11′)	1.383(6)
C(1′)—C(2′)	1.519(4)	C(11)—C(12)	1.392(6)
C(1′)—C(3′)	1.485(5)	C(11′)—C(12′)	1.377(5)

Numbers in parentheses are ESDs in the least significant digits.

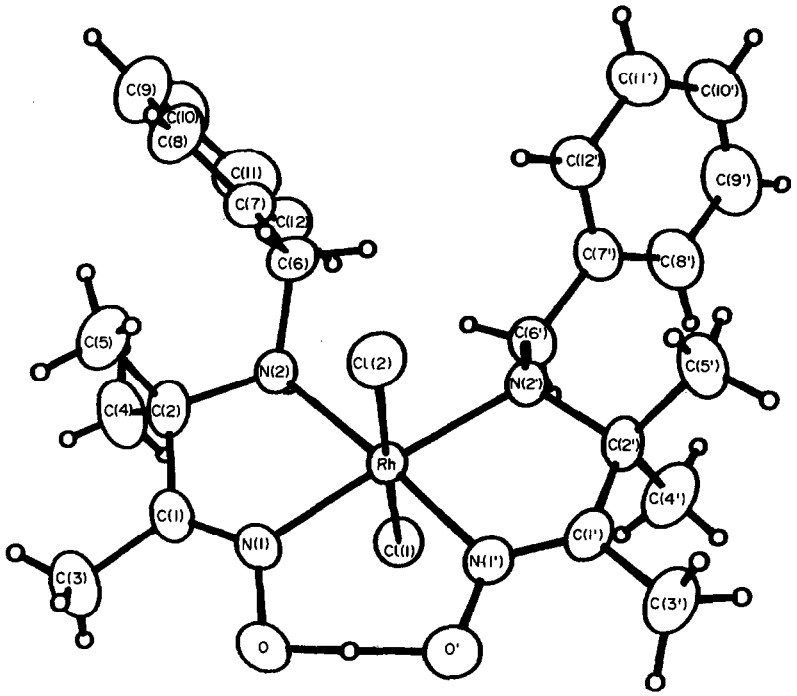

Fig. 2. Perspective view of the rhodium complex of ligand **II**.

molecular O—H—O hydrogen bond length is 2.419(4) Å. The other weaker intramolecular hydrogen bonding interactions in the molecule are between chlorine atoms and the hydrogen atoms on the amine nitrogen atoms; Cl(1)—HN(2) and Cl(2)—HN(2′) distances are 2.65 and 2.67 Å, Cl(1)—HN(2)—N(2) and Cl(2)—HN(2′)—N(2′) angles are 110 and 115°, respectively. The least-squares plane through the four nitrogen atoms and the rhodium atom is the best of the square planes around the rhodium atom and shows only a slight tetrahedral distortion. The *trans* N(1) and N(2′) atoms are slightly out of the plane towards Cl(1) and the *trans* N(1′) and N(2) atoms are slightly towards Cl(2).

The most characteristic peaks of the ^{1}H NMR spectra of the ligands are the low-field oxime proton signal around 10.5 ppm and the high field signals due to the methyl protons. The formation of the complexes is revealed by the movement of the 10.5 ppm oxime peak to *ca* 19 ppm and by splitting of the geminal methyl signal (singlet in the ligand) due to the different environment these methyl groups experience in the complex. The coupling pattern (^{1}H NMR) of the methylene proton in DMSO-d_6 suggests a similar structure in solution to that observed in the crystal structure. Only one of the non-equivalent methylene protons couples with the NH proton as a result of the angular relationship between the methylene protons and NH proton. The IR spectrum of the complex shows the characteristic broad, weak band at 1776 cm^{-1}, due to the intramolecular O—H—O hydrogen bond.

The data in Table 4 include some selected bond distances and angles around the metal atom. The corresponding data for the rhodium complex of the ligand 3-amino-3-methyl-2-butanone oxime are included for comparison.[4] A possible reason for the short distances around the oxime nitrogen atoms is the sp^2 hybridization of these atoms, whereas the amine nitrogens are sp^3 hybridized. The angles around the metal atom show significant deviations from the ideal square planar values because of the bulky phenyl substituent group on the amino nitrogens and the intramolecular O—H—O hydrogen bonding as well as the constraints of the five-membered chelate rings. As a result, the N(amine)—Rh—N(amine) angle opens up as wide as necessary for the most stable configuration. Consequently, N(amine)—Rh—N(oxime) and N(oxime)—Rh—N(oxime) angles are reduced to much smaller values. In the complex, the phenyl rings are oriented away from the rest of the molecule which is important for labelling with proteins, since the functional group on the complex would then be in a position available to react with a protein molecule. The octahedral coordination of the rhodium complexes, with two *trans*-chloride ligands prevents the phenyl rings from twisting above and below the molecular plane. We postulate a similar structure for the rhodium(III) complex of ligand **I** in the solutions discussed below. However, the exact structure

Table 3. Bond angles (°) for the rhodium complex of ligand I

Cl(1)—Rh—Cl(2)	176.84(3)	Rh—N(2′)—C(2′)	111.7(2)
Cl(1)—Rh—N(1)	88.76(7)	Rh—N(2′)—C(6′)	116.8(2)
Cl(1)—Rh—N(1′)	94.38(7)	C(2′)—N(2′)—C(6′)	115.8(2)
Cl(1)—Rh—N(2)	86.79(7)	N(1)—C(1)—C(2)	117.3(3)
Cl(1)—Rh—N(2′)	90.56(7)	N(1)—C(1)—C(3)	120.3(3)
Cl(2)—Rh—N(1)	93.82(8)	C(2)—C(1)—C(3)	122.2(3)
Cl(2)—Rh—N(1′)	87.13(7)	N(1′)—C(1′)—C(2′)	117.6(3)
Cl(2)—Rh—N(2)	91.91(7)	N(1′)—C(1′)—C(3′)	120.7(3)
Cl(2)—Rh—N(2′)	86.99(7)	C(2′)—C(1′)—C(3′)	121.6(3)
N(1)—Rh—N(1′)	96.7(1)	N(2)—C(2)—C(1)	108.1(2)
N(1)—Rh—N(2)	79.0(1)	N(2)—C(2)—C(4)	108.2(3)
N(1)—Rh—N(2′)	176.2(1)	N(2)—C(2)—C(5)	112.1(3)
N(1′)—Rh—N(2)	175.7(1)	C(1)—C(2)—C(4)	110.9(3)
N(1′)—Rh—N(2′)	79.6(1)	C(1)—C(2)—C(5)	106.9(3)
N(2)—Rh—N(2′)	104.69(9)	C(4)—C(2)—C(5)	110.7(3)
Rh—N(1)—O	119.6(2)	N(2′)—C(2′)—C(1′)	108.2(2)
Rh—N(1)—C(1)	121.9(2)	N(2′)—C(2′)—C(4′)	111.7(3)
O—N(1)—C(1)	118.4(2)	N(2′)—C(2′)—C(5′)	108.7(3)
Rh—N(1′)—O′	119.2(2)	C(1′)—C(2′)—C(4′)	106.2(3)
Rh—N(1′)—C(1′)	120.7(2)	C(1′)—C(2′)—C(5′)	110.5(3)
O′—N(1′)—C(1′)	119.4(2)	C(4′)—C(2′)—C(5′)	111.5(3)
Rh—N(2)—C(2)	112.1(2)	N(2)—C(6)—C(7)	115.5(3)
Rh—N(2)—C(6)	115.2(2)	N(2′)—C(6′)—C(7′)	114.8(3)
C(2)—N(2)—C(6)	115.5(2)	C(6)—C(7)—C(8)	120.5(3)
C(6)—C(7)—C(12)	120.9(3)	C(8′)—C(9′)—C(10′)	120.6(4)
C(8)—C(7)—C(12)	118.6(3)	C(9)—C(10)—C(11)	120.5(4)
C(6′)—C(7′)—C(8′)	121.0(6)	C(9′)—C(10′)—C(11′)	120.4(4)
C(6′)—C(7′)—C(12′)	120.7(3)	C(10)—C(11)—C(12)	119.5(4)
C(8′)—C(7′)—C(12′)	118.3(3)	C(10′)—C(11′)—C(12′)	119.1(4)
C(7)—C(8)—C(9)	121.0(4)	C(7)—C(12)—C(11)	120.4(4)
C(7′)—C(8′)—C(9′)	120.2(4)	C(7′)—C(12′)—C(11′)	121.3(4)
C(8)—C(9)—C(10)	120.2(4)		

Numbers in parentheses are ESDs in the least significant digit.

Table 4. Average bond distances and angles involving the rhodium atom

	Rh—ligand II	$Rh(AO)_2Cl_2$
M—N(amine)	2.124(2) Å	2.072(1) Å
M—N(oxime)	1.988(2) Å	1.990(1) Å
N(amine)—Rh—N(amine)	104.7(1)°	101.2(4)°
N(amine)—Rh—N(oxime)	79.3(1)°	80.23(4)°
N(oxime)—Rh—N(oxime)	96.7(1)°	98.2(4)°

of that complex is not critical for the radiochemical results.

Radiochemical studies

Ligand I gave a clear solution after complexation with ^{105}Rh. No appreciable activity was lost as solid when the reaction mixture was centrifuged. The complex yield estimated by the MgO adsorption technique was about 95%. The conversion of the complex into the isothiocyanate derivative was nearly complete. About 91% of the activity was seen in the organic layer, consistent with formation of the expected neutral complex. The remaining 9% of the activity may be the uncomplexed rhodium and a small part of the complex which was not converted to the isothiocyanate derivative (activated complex). The high extractability of the activated

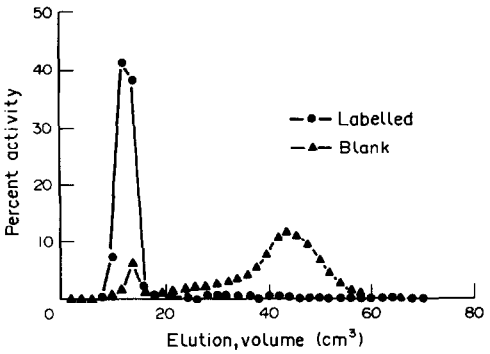

Fig. 3. Gel filtration chromatography pattern of specifically and non-specifically labelled human γ-globulin.

complex suggests a high partition coefficient for the isothiocyanate derivative compared with the original complex. Only 15% of the original complex could be extracted into chloroform under identical conditions. A back extraction of the activated complex from the organic layer was carried out and the distribution ratios of 19 and 69, respectively, were estimated. The change in distribution ratio with subsequent back extraction suggests the presence of more than one complex.

Results of the conjugation experiments are given in Table 5; yields reported are those calculated from gel filtration chromatography, and varied from 76 to 90%. At these values the number of rhodium atoms incorporated per molecule of γ-globulin varied from 0.35 to 2.0 depending on the concentration of the activated complex used for conjugation (average mol. wt of γ-globulins was taken as 15,000 for these calculations). A conjugation experiment with the unactivated complex gave only 10% of the activity in the protein fraction, indicating that the complex is not bound to γ-globulins non-specifically. Figure 3 gives the elution of labelled γ-globulins and non-specifically labelled γ-globulins in the gel filtration column.

No transfer of activity was seen from labelled γ-globulins to DTPA in challenge studies; this is indicative of the high stability of the rhodium complex in the labelled protein. Most of the activity (97%) was found in the protein fraction when the solution was chromatographed on a gel filtration column.

DISCUSSION

Rhodium-105 offers a number of advantages as a radiotherapeutic isotope. It has moderate energy β particles suitable for radioimmunotherapy. Its gamma emissions are less abundant, 306 keV (6%) and 319 keV (19%) and these gamma rays can be used for monitoring the efficacy of treatment. Rhodium forms kinetically inert and stable complexes with many ligands, and hence ^{105}Rh labelled antibodies are expected to be stable *in vivo*. Because ^{105}Rh can be produced in a nuclear reactor it offers the advantage of ready availability and low cost.

This study shows that the bidentate ligands described here form complexes with rhodium in high yields. Crystals of a quality suitable for X-ray diffraction studies were not obtained for the complex of ligand **I**, but there was no difficulty in synthesizing and isolating crystals of the complex of ligand **II**. We believe that the bifunctional ligand **I** probably forms a bis complex with rhodium similar to that with ligand **II**. Rhodium would be chelated to the four nitrogen atoms from the two ligands and the remaining two coordination sites would be satisfied by Cl^- or some other monodentate ligand. The crystal structure of the complex of ligand **II** shows both the phenyl groups to be orientated away from he rhodium atom. The coupling group, $—NH_2$, in the complex with ligand **I** is also expected to be directed away from the rest of the molecule and hence available for activation and conjugation to protein. However, the exact

Table 5. Results of conjugation studies[a]

[γ-Globulins] $\times 10^5$	Rhodium (M) $\times 10^5$	Rhodium/ γ-globulins	Conjugation (%)	Rhodium-labelled/ γ-globulins
5	2.3	0.46	76	0.35
5	4.6	0.92	90	0.83
5	11.4	2.3	87	2.0
5	10.0	2.0	10	0.2[b]

[a] Conjugation reaction was 5 h. Yield calculated by gel permeation chromatography.

[b] The complex used in this experiment was unactivated complex, for estimating the non-specific labelling of the γ-globulins by the complex.

structure of the complex(es) formed at the radiochemical level has not been established and is not critical for the labelling.

Ligand **I** formed complexes with ^{105}Rh at pH 9, HCO_3^- buffer, in yields greater than 95%. No loss of activity as inorganic rhodium during complexation was observed. The complex(es) formed is soluble at the 10^{-3} M concentration studied. Near quantitative conversion of the complex into the isothiocyanate derivative is possible, and hence it is unlikely that the functional group, $—NH_2$, is involved in metal binding. The high extraction ratio of the activated complex into chloroform aids in the isolation of the complex, leaving behind uncomplexed rhodium and most of the unactivated complex.

Depending on the initial complex to γ-globulin ratio, an average of 0.35–2 rhodium atoms could be added to each molecule of γ-globulin. Presently ^{105}Rh is available from the University of Missouri Research Reactor at specific activities greater than 700 Ci $mmol^{-1}$.[10] Using this ^{105}Rh, labelled γ-globulins with specific activities ranging from 1.6 to 9.3 mCi mg^{-1} were prepared by the method described above. It is believed that this work is extendable to label monoclonal antibodies with ^{105}Rh and that the specific activities obtained above are sufficient for radioimmunotherapy.

Acknowledgements—This work was supported by the U.S. Department of Energy, Grant No. DEFG02-86ER60400 and the University of Missouri Research Council.

REFERENCES

1. T. Lynde-Kernall and E. O. Schlemper, *J. Coord. Chem.* 1988, **16**, 347.
2. C. S. John, M. R. A. Pillai, J. M. Lo and D. E. Troutner, *Nucl. Med. Biol.* 1990, **17**, 419.
3. J. M. Lo, M. R. A. Pillai, C. S. John and D. E. Troutner, *Appl. Radiat. Isot.* 1990, **41**, 63.
4. S. Siripaisarnpipat and E. O. Schlemper, *Inorg. Chem.* 1984, **23**, 330.
5. R. K. Murmann, *J. Am. Chem. Soc.* 1957, **79**, 521.
6. G. Ergun Efe, PhD thesis. University of Missouri-Columbia (1989).
7. *International Tables for X-ray Crystallography*, Vol. IV. Kynoch Press, Birmingham (1974) (Present distributor: D. Reidel, Dordrecht).
8. J. M. Lo, M. R. A. Pilai, C. S. John and D. E. Troutner, *Appl. Radiat. Isot.* 1990, **41**, 103.
9. M. W. Brechbeil, O. A. Gansow, R. W. Atcher, J. Schlom, J. Esteban, D. E. Simpson and D. Colcher, *Inorg. Chem.* 1986, **25**, 2772.
10. B. Grazman and D. E. Troutner, *Appl. Radiat. Isot.* 1988, **39**, 257.

Polyhedron Vol. 10, No. 14, pp. 1625–1629, 1991
Printed in Great Britain

0277–5387/91 $3.00+.00
© 1991 Pergamon Press plc

STRUCTURAL CHARACTERIZATION OF THE S-BENZYLDITHIOCARBAZATE DERIVED FROM 2-FORMYLPYRIDINE N-OXIDE AND ITS DIMERIC COPPER(II) NITRATE COMPLEX

ZHENG XU, ELMER C. ALYEA,† GEORGE FERGUSON† and MICHAEL C. JENNINGS

Department of Chemistry and Biochemistry, University of Guelph, Guelph, Ontario, Canada N1G 2W1

(*Received* 12 *December* 1990; *accepted* 21 *March* 1991)

Abstract—The thiobenzyl dithiocarbazate of 2-formylpyridine N-oxide, 2-$C_5H_4N(O)$—CH=N—NH—C(S)—$SCH_2C_6H_5$, crystallizes from ethanol as centrosymmetric dimeric units as a consequence of intermolecular N(O)···H—N bonds [O···N 2.763(4) Å]. In the centrosymmetric copper(II) complex, $\{Cu(ONO_2)[2\text{-}C_5H_4N(O)\text{—}CH\text{=}N\text{—}N\text{=}C(S)\text{—}SCH_2C_6H_5]\}_2$, the anionic ligand is coordinated via the N-oxide oxygen, the azomethine nitrogen and the thiol sulphur atoms. Including the nitrato group, the coordination geometry is primarily distorted square planar [with Cu—O(1) 1.949(1), Cu—N(9) 1.939(2), Cu—S(12) 2.254(1), Cu—O(22) 1.963(2) Å], but weak axial interactions to a second oxygen atom of the nitrato group [2.682(2) Å] and a neighbouring N-oxide oxygen atom [2.674(2) Å] complete an octahedron for the copper atoms in the dimeric units.

Thiosemicarbazones and dithiocarbazates of 2-acetylpyridine have received extensive attention due to their antimalarial, antitumour and antibacterial activity.[1] Their chelating ability with transition metal ions is found to relate to their medicinal activity.[2,3] In investigating the coordinating ability of these ligands with transition metal ions, West and co-workers recently extended their studies to thiosemicarbazones and the related S-methyldithiocarbazate of 2-acetylpyridine N-oxide.[4–6] Our current interest in sulphur–nitrogen donor ligands for copper complexation[7] led us to prepare the new potentially ONS donor ligand derived from 2-formylpyridine N-oxide and thiobenzylthiosemicarbazide, abbreviated as HONS. This paper reports the crystal structure determinations of the ligand and that of a copper(II) nitrato complex of the deprotonated ligand, $Cu(ONO_2)$(ONS); both species occur as dimeric units via bridging N-oxide atoms.

On the basis of IR, electronic and ESR spectral evidence, West and co-workers proposed that thiosemicarbazones of 2-acetylpyridine N-oxide could coordinate to copper(II) in a planar fashion, as depicted in Fig. 1. Since these earlier studies indicated that such ligands could coordinate as neutral, bidentate ligands (R = $NHCH_3$),[5] as well as in the deprotonated form utilizing ONS donor atoms [R = $N(CH_3)_2$,[6] SCH_3[6] and NC_8H_{14}[4]], the present X-ray crystal structure determinations were undertaken in initiating our complexation studies of HONS (R = $SCH_2C_6H_5$, R′ = H in Fig. 1).

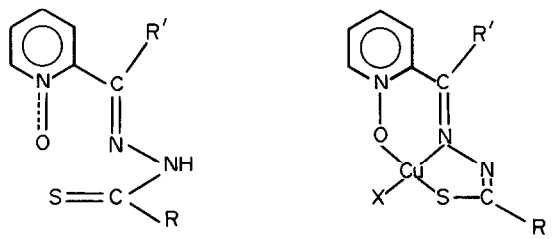

Fig. 1. General structural formula of HONS and its proposed bonding in copper(II) complexes in the deprotonated tridentate form (R′ = H, CH_3).

The structure of the ligand, $C_{14}H_{13}N_3OS_2$, as

† Authors to whom correspondence should be addressed.

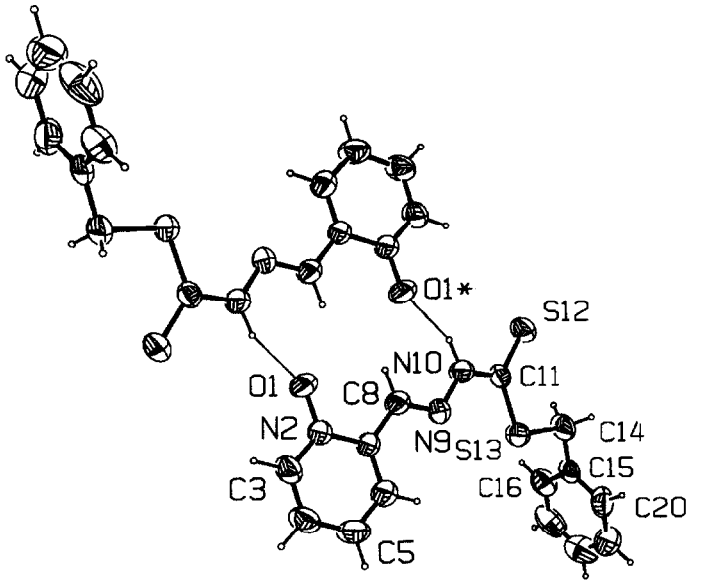

Fig. 2. A view of the HONS ligand with the crystallographic numbering scheme; ellipsoids are at the 50% level.

Table 1. Molecular dimensions for HONS

Bond lengths (Å)			
O(1)—N(2)	1.301(4)	C(11)—S(12)	1.652(4)
N(2)—C(3)	1.353(5)	C(11)—S(13)	1.740(4)
N(2)—C(7)	1.370(4)	S(13)—C(14)	1.822(4)
C(3)—C(4)	1.349(6)	C(14)—C(15)	1.484(5)
C(4)—C(5)	1.376(6)	C(15)—C(16)	1.375(6)
C(5)—C(6)	1.372(6)	C(15)—C(20)	1.377(6)
C(6)—C(7)	1.368(5)	C(16)—C(17)	1.395(7)
C(7)—C(8)	1.452(5)	C(17)—C(18)	1.351(7)
C(8)—N(9)	1.276(5)	C(18)—C(19)	1.342(7)
N(9)—N(10)	1.364(4)	C(19)—C(20)	1.358(7)
N(10)—C(11)	1.347(4)	N(10)···O(1)*	2.763(4)
Bond angles (°)			
O(1)—N(2)—C(3)	119.8(3)	N(10)—C(11)—S(13)	113.3(3)
O(1)—N(2)—C(7)	120.3(3)	S(12)—C(11)—S(13)	126.3(2)
C(3)—N(2)—C(7)	119.9(3)	C(11)—S(13)—C(14)	102.1(2)
N(2)—C(3)—C(4)	121.5(4)	S(13)—C(14)—C(15)	107.6(3)
C(3)—C(4)—C(5)	119.8(4)	C(14)—C(15)—C(16)	121.0(4)
C(4)—C(5)—C(6)	118.9(4)	C(14)—C(15)—C(20)	121.3(4)
C(5)—C(6)—C(7)	120.9(4)	C(16)—C(15)—C(20)	117.6(4)
N(2)—C(7)—C(6)	119.0(3)	C(15)—C(16)—C(17)	120.6(4)
N(2)—C(7)—C(8)	115.9(3)	C(16)—C(17)—C(18)	119.1(4)
C(6)—C(7)—C(8)	125.0(3)	C(17)—C(18)—C(19)	121.0(5)
C(7)—C(8)—N(9)	120.2(3)	C(18)—C(19)—C(20)	120.3(5)
C(8)—N(9)—N(10)	114.9(3)	C(15)—C(20)—C(19)	121.4(4)
N(9)—N(10)—C(11)	121.1(3)	O(1)*···H(10)—N(10)	157.7
N(10)—C(11)—S(12)	120.4(3)		

The * refers to an atom at equivalent position $-x, -y, 1-z$.

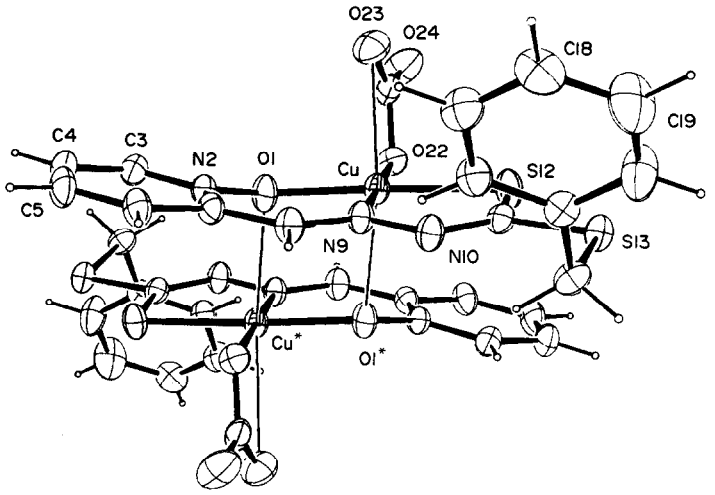

Fig. 3. A view of the dimeric $[Cu(ONO_2)(ONS)]_2$ complex with the crystallographic numbering scheme; ellipsoids are at the 50% level.

shown in Fig. 2,† displays bond lengths consistent with the representation in Fig. 1. The O(1)—N(2) distance of 1.301(4) Å is much shorter than 1.39 Å found in Me_3NO, where there can be no π-bonding,[8] and reflects significant double bond character. Similarly, the azomethine C(8)—N(9) distance [1.276(5) Å] corresponds to a double bond, as does the C(11)—S(12) bond length [1.652(4) Å, cf. 1.740(4) Å for C(11)—S(13)]. The O(1) to S(13) portion of the dithiocarbazate ligand is almost planar, with small dihedral angles between O(1)—C(8) and C(8)—C(11) (8.9°) or N(10)—S(13) (12.8°) moieties. The benzyl group, however, is twisted at right angles relative to the planes containing the potential donor atoms; for example, the dihedral angles between C(14)—C(20) and C(8)—C(11) or N(10)—S(13) planes are 87.1 and 90.8°, respectively (Table 1). An important feature of the crystal structure is the intermolecular hydrogen bond [NO···H—NO···N 2.763(4) Å] between the N-oxide oxygen atom and the amine hydrogen atom of a neighbouring molecule; the HONS ligand thus occurs as centrosymmetric dimeric units in the solid state.

Our crystallographic study of the copper complex establishes it as a centrosymmetric dimer (Fig. 3)‡ with the copper(II) geometry as primarily square planar. The copper atom is bonded to the N-oxide oxygen atom [1.949(1) Å], the azomethine nitrogen atom [1.939(2) Å] and the thiol sulphur atom [2.254(1) Å] of the deprotonated ligand; a copper–nitrato bond [Cu—O(22) = 1.963(2) Å] completes the distorted square plane. Bond length changes [e.g. longer N(2)—O(1), C(8)—N(9), C(11)—S(12) and shorter N(10)—C(11)] as com-

† Crystal data for $C_{14}H_{13}N_3OS_2$, $M_r = 303.4$, monoclinic, space group $P2_1/a$, $a = 8.873(3)$, $b = 11.635(2)$, $c = 14.193(2)$ Å, $\beta = 94.28(2)°$, $V = 1461(1)$ Å^3, $Z = 4$, $D_c = 1.38$ g cm^{-3}, $\mu = 3.5$ cm^{-1}, $F(000) = 632$, Mo-K_α radiation ($\lambda = 0.71073$ Å), $T = 21°C$. 3635 reflections were measured on a CAD4 diffractometer ($2\theta_{max} = 54°$), 3134 were unique and 1435 had $I > 3\sigma(I)$. Lorentz and polarization corrections were applied. The structure was solved using direct methods (SIMPEL). Refinement (with weights derived from the counting statistics) by full-matrix least-squares calculations (with all hydrogen atoms allowed for but not refined) converged with $R = 0.046$ and $wR = 0.057$ for the 1435 observed reflections. An extinction correction was also refined. The final cycle of refinement had 182 variables and maximum shift/error ratio of < 0.005. A final difference map had no chemically significant features. Full details of the analysis are available from the Cambridge Crystallographic Data Centre or from the authors.

‡ Crystal data for $C_{28}H_{24}Cu_2N_8O_8S_4$, $M_r = 855.89$, triclinic, space group $P\bar{1}$, $a = 10.100(2)$, $b = 10.985(2)$, $c = 8.156(2)$ Å, $\alpha = 95.34(2)$, $\beta = 107.98(2)$, $\gamma = 81.98(2)°$, $V = 851.1(6)$ Å^3, $Z = 1$, $D_c = 1.67$ g cm^{-3}, $\mu = 15.5$ cm^{-1}, $F(000) = 434$, Mo-K_α radiation ($\lambda = 0.71073$ Å), $T = 21°C$. 3800 reflections were measured on a CAD4 diffractometer ($2\theta_{max} = 54°$), 3703 were unique and 2950 had $I > 3\sigma(I)$. Lorentz, polarization and Gaussian absorption corrections were applied. The structure was solved using the Patterson heavy-atom method. Refinement (with weights derived from the counting statistics) by full-matrix least-squares calculations (with all hydrogen atoms allowed for but not refined) converged with $R = 0.027$ and $wR = 0.040$ for the 2950 observed reflections. The final cycle of refinement had 226 variables and maximum shift/error ratio of 0.01. A final difference map had no chemically significant features. Full details of the analysis are available from the Cambridge Crystallographic Data Centre or from the authors.

Table 2. Molecular dimensions for $Cu(ONO_2)(ONS)$

Bond lengths (Å)			
Cu—O(1)	1.949(1)	N(9)—N(10)	1.392(2)
Cu—O(1)*	2.674(2)	N(10)—C(11)	1.306(3)
Cu—N(9)	1.939(2)	C(11)—S(12)	1.724(2)
Cu—S(12)	2.254(1)	C(11)—S(13)	1.745(2)
Cu—O(22)	1.963(2)	S(13)—C(14)	1.825(3)
Cu—O(23)	2.682(2)	C(14)—C(15)	1.508(3)
O(1)—N(2)	1.344(2)	C(15)—C(16)	1.381(3)
N(2)—C(3)	1.344(3)	C(15)—C(20)	1.364(3)
N(2)—C(7)	1.368(3)	C(16)—C(17)	1.387(4)
C(3)—C(4)	1.372(4)	C(17)—C(18)	1.340(3)
C(4)—C(5)	1.371(4)	C(18)—C(19)	1.364(5)
C(5)—C(6)	1.364(3)	C(19)—C(20)	1.392(5)
C(6)—C(7)	1.397(3)	N(21)—O(22)	1.292(2)
C(7)—C(8)	1.433(3)	N(21)—O(23)	1.232(3)
C(8)—N(9)	1.291(3)	N(21)—O(24)	1.217(3)
Bond angles (°)			
O(1)—Cu—O(1)*	78.39(6)	N(2)—C(7)—C(8)	123.7(2)
O(1)—Cu—N(9)	91.75(7)	C(6)—C(7)—C(8)	118.6(2)
O(1)—Cu—S(12)	177.36(5)	C(7)—C(8)—N(9)	126.7(2)
O(1)—Cu—O(22)	88.79(6)	Cu—N(9)—C(8)	125.5(2)
O(1)—Cu—O(23)	86.04(6)	Cu—N(9)—N(10)	120.8(1)
O(1)*—Cu—N(9)	104.45(6)	C(8)—N(9)—N(10)	113.7(2)
O(1)*—Cu—S(12)	100.48(3)	N(9)—N(10)—C(11)	112.3(2)
O(1)*—Cu—O(22)	76.14(5)	N(10)—C(11)—S(12)	127.1(2)
O(1)*—Cu—O(23)	126.87(5)	N(10)—C(11)—S(13)	118.9(2)
N(9)—Cu—S(12)	86.21(5)	S(12)—C(11)—S(13)	114.0(1)
N(9)—Cu—O(22)	179.27(6)	Cu—S(12)—C(11)	93.44(7)
N(9)—Cu—O(23)	126.72(7)	C(11)—S(13)—C(14)	103.8(1)
S(12)—Cu—O(22)	93.26(4)	S(13)—C(14)—C(15)	114.6(2)
S(12)—Cu—O(23)	96.52(4)	C(14)—C(15)—C(16)	121.1(2)
O(22)—Cu—O(23)	52.82(6)	C(14)—C(15)—C(20)	121.1(2)
Cu—O(1)—Cu*	101.61(6)	C(16)—C(15)—C(20)	117.9(2)
Cu—O(1)—N(2)	126.2(1)	C(15)—C(16)—C(17)	120.4(2)
Cu—O(1)—N(2)	108.57(9)	C(16)—C(17)—C(18)	121.2(2)
O(1)—N(2)—C(3)	115.7(2)	C(17)—C(18)—C(19)	119.3(2)
O(1)—N(2)—C(7)	122.7(2)	C(18)—C(19)—C(20)	120.2(3)
C(3)—N(2)—C(7)	121.5(2)	C(15)—C(20)—C(19)	121.0(3)
N(2)—C(3)—C(4)	120.7(2)	O(22)—N(21)—O(23)	118.1(2)
C(3)—C(4)—C(5)	119.7(2)	O(22)—N(21)—O(24)	117.8(2)
C(4)—C(5)—C(6)	119.3(2)	O(23)—N(21)—O(24)	124.1(2)
C(5)—C(6)—C(7)	121.2(3)	Cu—O(22)—N(21)	110.9(1)
N(2)—C(7)—C(6)	117.6(2)	Cu—O(23)—N(21)	78.0(1)

The * refers to an atom at equivalent position $-x, 1-y, -z$.

pared with the uncomplexed HONS ligand are consistent with expectations, as represented in Fig. 1. However, the complex crystallizes as a dimer as a consequence of bridging N-oxide oxygen–copper interactions [Cu—O(1)* = 2.674(2) Å]. In the centrosymmetric dimer $[Cu(C_5H_5NO)_2(NO_3)_2]_2$[9] the bridging pyridine N-oxide O—Cu distance to the other copper atom is considerably shorter [2.439(6) Å], whereas the Cu—O bond lengths to the two pyridine N-oxide ligands [1.951(5), 1.968(5) Å] and the pyridine N-oxide N—O distances [1.362(7) Å] are similar to those found in the present complex (Table 2).

Pseudo-octahedral geometry for each copper(II) atom in our complex is completed by virtue of another weak axial bond to a second oxygen atom of the nitrato group [Cu—O(23) = 2.682(2) Å]. The asymmetric bidentate nature of the nitrato group, which is planar, is reflected in the disparate N—O bond distances [N(21)—O(22) 1.292(2),

N(21)—O(23) 1.232(2), N(21)—O(24) 1.217(3) Å]. Whereas the tridentate planar coordinating behaviour of similar thiosemicarbazone and dithiocarbazate ligands and the tetragonal nature of the copper(II) geometry was indicated previously by spectroscopic evidence,[4-6] the specific bonding and unique dimeric interactions are described by this first X-ray analysis of a copper(II) complex with a dithiocarbazate (or thiosemicarbazone) of a pyridine N-oxide. Complexation studies of HONS with a variety of metal ions are underway.

Acknowledgements—We thank NSERC Canada for Operating and Infrastructure Grants (E.C.A. and G.F.) and for a CIDA award (Z.X.). We are grateful to Gou Shaohua of Nanjing University for the synthesis of the compounds.

REFERENCES

1. D. L. Klayman, J. P. Scovill, J. F. Bartosevich and J. Bruce, *J. Med. Chem.* 1983, **26**, 35 and refs therein; M. A. Ali and S. E. Livingstone, *Coord. Chem. Rev.* 1974, **13**, 101; M. Mohan, M. Kumar, A. Kumar, P. H. Madhuranath and N. K. Jha, *J. Inorg. Biochem.* 1988, **33**, 121.
2. J. P. Scovill, D. L. Klayman and C. F. Franchino, *J. Med. Chem.* 1982, **25**, 1261.
3. J. P. Scovill, D. L. Klayman, C. Lambros, G. E. Childs and J. D. Notsch, *J. Med. Chem.* 1984, **27**, 87.
4. D. X. West, R. M. Makeever, J. P. Scovill and D. L. Klagman, *Polyhedron* 1984, **3**, 947.
5. D. X. West, R. M. Makeever, G. Ertem, J. P. Scovill and L. K. Pannell, *Transition Met. Chem.* 1986, **11**, 131.
6. D. X. West and L. K. Pannell, *Transition Met. Chem.* 1989, **14**, 457; D. X. West and D. L. Huffman, *Transition Met. Chem.* 1989, **14**, 190.
7. E. C. Alyea, S. Liu, B. Li, Z. Xu and X. Z. You, *Acta Cryst. C* 1989, **45**, 1566; E. C. Alyea, G. Ferguson, M. C. Jennings, B. Li, Z. Xu and X. Z. You, *Polyhedron* 1990, **9**, 2463.
8. A. Caron, G. J. Palenik, E. Goldish and J. Donohue, *Acta Cryst.* 1964, **17**, 102.
9. S. Šćavničar and B. Matković, *Acta Cryst.* 1969, **B25**, 2046.

Polyhedron Vol. 10, No. 14, pp. 1631–1637, 1991
Printed in Great Britain

0277–5387/91 $3.00+.00
© 1991 Pergamon Press plc

ALCOHOLYSIS OF NITRILES IN GOLD(III) COMPLEXES: THE STRUCTURE OF $[EtC(OEt)NH_2]^+[AuCl_4]^-$

RICHARD A. POTTS,* DEBRA L. GAJ, WILLIAM F. SCHNEIDER and NORMAN S. DEAN

Department of Natural Sciences, University of Michigan, Dearborn, MI 48128, U.S.A.

and

JEFF W. KAMPF and JOHN P. OLIVER*

Department of Chemistry, Wayne State University, Detroit, MI 48202, U.S.A.

(*Received* 7 *January* 1991; *accepted* 21 *March* 1991)

Abstract—The alcoholysis (ROH; R = Me, Et) of nitriles (RCN; R = Me, Et) in the presence of gold(III) chloride and/or hydrogen chloride was investigated. These alcoholysis reactions in the presence of gold(III) chloride occur much more rapidly than the nitrile–alcohol mixture alone. Elemental analyses and IR and NMR spectral data identified two products from the reaction. One product was the imino-ether salt, $[RC(OR')NH_2]^+[AuCl_4]^-$, while the other was the complex of the imino-ether and gold(III) chloride, $RC(OR')NH \cdot AuCl_3$ (R and R′ = Me, Et). The crystal structure of hydrogenethylpropylimidate tetrachloroaurate(III) (**3a**) was determined by X-ray diffraction techniques.

The catalysis of reactions of nitriles by metals has been of major interest for the past 20 years with considerable work focused on the metal-catalysed reactions of nitriles.[1] The coordination of the nitrile nitrogen to the metal or metal complex enhances the electrophilic nature of the nitrile carbon and typically increases the rate of reaction with nucleophiles. These reactions include the alcoholysis of nitriles to form imino-ethers[2–8] which are useful intermediates for the preparation of important acids or esters, but the slow initial reaction of the nitrile with alcohol

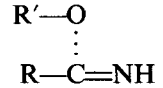

reduces the usefulness of these reactions. Therefore, catalysis of this step by metal complexes or other means is of interest and commercial importance.

Our interest in the alcoholysis arose for these reasons and because of the isolation of a second product in the preparation of nitrile complexes with gold(III) chloride, $RCN \cdot AuCl_3$, in chloroform solvent. The properties of the second product were very different, and analysis indicated the presence of oxygen. This paper describes the characterization and crystal structure of the product which is now known to be the imino-ether salt with the source of the oxygen being the solvent stabilizing ethyl alcohol. The complex between the imino-ether and gold(III) chloride is also described.

EXPERIMENTAL

Materials

Acetonitrile and propionitrile were dried over P_4O_{10} and distilled. All other chemicals were reagent grade. The gold(III) chloride was prepared by dissolving tetrachloroauric acid trihydrate in concentrated perchloric acid and evaporating the solution on a hot plate until crystals began to form. (**CAUTION:** Fumes from perchloric acid must be disposed of properly.) The crystals were collected and dried under vacuum at refluxing toluene temperature.

* Authors to whom correspondence should be addressed.

Preparation of nitrile complexes with gold(III) *chloride*

$EtCN \cdot AuCl_3$ (**1a**) and $MeCN \cdot AuCl_3$ (**1b**) were prepared as described in the literature.[9] The crystals were a very dark red colour and reacted rapidly with water in the air. The analytical results and IR spectral data are collected in Tables 1 and 2.

Preparation of imino-ether and hydrochloride salts

EtC(OEt)NH (**2a**), MeC(OMe)NH (**2b**), EtC(OMe)NH (**2c**), $[EtC(OEt)NH_2]^+[Cl]^-$ (**2d**) and $[MeC(OMe)NH_2]^+[Cl]^-$ (**2e**) were prepared as described in the literature.[10] The salts were also prepared by vacuum-line techniques. The alcohol was added to a 10-fold excess of the nitrile and degassed on a vacuum line. An amount of hydrogen chloride gas, equimolar (0.016 mol) to the alcohol, was transferred to the frozen solution. After slow warming to room temperature, a portion of the excess nitrile was removed by a vacuum until a solid began to form. The solution was placed in a refrigerator to complete crystallization, after which it was filtered, washed with diethyl ether and dried. The colourless crystals reacted slowly with water

Table 1. Analytical data for several $AuCl_3 \cdot$ nitriles, imino-ether salts of the type $[RC(OR')NH_2]^+[AuCl_4]^-$ and adducts of the form $RC(OR')NH \cdot AuCl_3$

Compound	C (%)		H (%)		N (%)		Cl (%)		Au (%)	
	Calc.	Found	Calc.	Found	Calc.	Found	Calc.	Found	Calc.	Found
1a	10.1	9.9	1.4	1.5						
1b	7.0	7.0	0.9	1.1						
3a	13.6	12.4	2.7	2.5	3.2	3.1	32.2	31.6	44.7	44.9
3b	11.3	11.2	2.4	2.3	3.3	3.3	33.2	32.9	46.1	44.3
4a	14.9	14.8	2.8	2.8	3.5	3.4	26.3	26.4	48.7	48.5

Table 2. IR spectral data (cm^{-1}) for several $AuCl_3 \cdot$ nitriles, imino-ether salts of the type $[RC(OR')NH_2]^+[AuCl_4]^-$ and adducts of the form $RC(OR')NH \cdot AuCl_3$

Compound	$\nu_{str.}$(N—H)	$\nu_{bend.}$(N—H)	$\nu_{rock.}$(N—H)	ν(C≡N)	ν(C=N)	ν(Au—Cl)
1a				2342 s		376 m 364 s
1b				2315 s		371 s 356 m 341 w
2a	3330 m				1647 s	
2b	3330 m				1660 s	
2c	3320 m				1655 s	
2d	3300 m,b	1559 m			1656 s	
3a	3360 m 3260 m 3220 m	1562 m	675 m,b		1673 s	361 m 351 s 316 w
3b	3375 m 3305 m 3232 m	1564 m	670 m,b		1681 s	353 s
3c	3404 m 3361 m 3277 m 3225 m	1572 m	662 m,b		1675 s	354 s
4a	3325 m				1637 s	368 m 356 s

from the air. Yields: imino-ethers, 25%; salts, > 95%. **2a**, b.p. 106°C; **2b**, b.p. 72–78°C; **2c**, b.p. 86°C; **2d**, m.p. 95–97°C; **2e**, m.p. 90–91°C. IR and NMR spectral data are collected in Tables 2 and 3.

Preparation of imino-ether tetrachloroaurate(III) *salts*

$[EtC(OEt)NH_2]^+[AuCl_4]^-$ (**3a**), $[EtC(OMe)NH_2]^+[AuCl_4]^-$ (**3b**) and $[MeC(OMe)NH_2]^+[AuCl_4]^-$ (**3c**) were prepared by dissolving gold(III) chloride (0.5 g) in a minimum of purified chloroform (40 cm^3) with equimolar amounts of the alcohol present and adding a 10-fold mole excess of the nitrile. After standing for several days, during which some solvent evaporated and trichloroethane was added, straw yellow crystals were obtained. The same product was obtained by the vacuum-line techniques described above. Equimolar amounts of the alcohol, hydrogen chloride gas, and gold(III) chloride (0.0033 mol) were dissolved in a 10-fold excess of the nitrile and treated as above with the exception that trichloroethane was added to aid precipitation. The crystals were unreactive towards air but did show visual evidence of reduction to gold metal after several weeks. Yield: > 75%. **3a**, m.p. 93–95°C, **3b**, m.p. 88–90°C. Analytical results and IR and NMR spectral data are collected in Tables 1–3.

Preparation of imino-ether complexes with gold(III) *chloride*

$EtC(OEt)NH \cdot AuCl_3$ (**4a**) and $MeC(OMe)NH \cdot AuCl_3$ (**4b**) were prepared by the direct reaction of the imino-ether in alcohol or chloroform solvents with gold(III) chloride in an inert atmosphere. However, the products were of poor quality, and the vacuum-line technique described above was used to prepare products for quantitative purposes. While reaction conditions for the production of the salt and complex were identical, some solutions would produce the salt, another would produce the complex and another would produce a mixture. The two products were identifiable because of differences in colour, melting point and IR spectra. The crystals were orange in colour and unreactive towards air but did show visual evidence of reduction to gold metal after several weeks. **4a**, m.p. 128–130°C; **4b**, m.p. 183–185°C. Analytical results and IR spectral data are collected in Tables 1 and 2.

Instrumentation

IR spectra of Nujol mulls were recorded on a Perkin–Elmer Model 283 spectrophotometer over the range 4000–200 cm^{-1}. ^1H NMR spectra were recorded on a Varian T-60A spectrometer. The spectra were obtained in deuteroacetone and deuteromethanol with TMS as the reference. ^{13}C NMR spectra were recorded on a JEOL JNM-FX60 spectrometer. The spectra were obtained in deuteroacetone with TMS as the reference. Elemental analyses were performed by Spang Microanalytical Laboratory, Eagle Harbor, Michigan and Galbraith Laboratory, Knoxville, Tennessee.

X-ray crystallography

The crystal and molecular structure of the hydrogenethylpropylimidate salt has been determined by

Table 3. NMR spectral data (ppm) for several imino-ether salts of the type $[RC(OR')NH_2]^+[AuCl_4]^-$

Compound	Solvent	δ(MeO)	δ(Me)	δ(EtO)	δ(Et)	δ(C=N)	δ(NH)
			^1H data				
2e	MeOH-d_4	4.2 s	2.5 s				
3a	Acetone-d_6			1.6 t 4.8 q	1.4 t 3.0 q		10.6 br
3b	Acetone-d_6	4.5 s			1.4 t 3.0 q		10.6 br
3c	Acetone-d_6 MeOH-d_4	4.5 s 4.2 s	2.7 s 2.5 s				10.4 br
			^{13}C data				
3a	Acetone-d_6			27.8 70.6	9.3 13.8	183.3	
3c	Acetone-d_6	60.5	19.8			181.6	

single crystal X-ray diffraction. Amber-coloured, rectangular plates of **3a** were grown by slow evaporation of a chloroform solution. The crystals were ground to a tear-shape by use of an air-driven crystal grinder. Crystals were then selected and mounted on glass fibres with epoxy using standard techniques. All data were collected at room temperature on a Nicolet R3 diffractometer. Precession photographs were used to evaluate the crystal quality and confirm the preliminary axial lengths and symmetry information. Corrections were made for decay, background, Lorentz and polarization using the program XTAPE.[11] Complete crystal, experimental and refinement data are given in Table 4. An empirical absorption correction was applied based on a set of appropriate psi-scans using the program XEMP.[11] The structure was solved by the use of the Patterson function to locate the gold atom, followed by successive application of difference Fourier maps and least-squares refinement to locate remaining non-hydrogen atoms.[12] Atoms C(4) and C(5) were refined with isotropic thermal parameters. All other non-hydrogen atoms were refined anisotropically. Hydrogen atoms were placed in calculated positions ($d_{C-H} = 0.96$ Å, riding model) and given an isotropic thermal parameter approximately equal to 1.2 times $U_{(eq)}$ for the atom to which it is bonded. Neutral atomic scattering factors were taken from the usual source[13] and were corrected for anomalous dispersion.

Important interatomic distances and angles are listed in Table 5. Additional data for the structure of **3a** and **3c** are included in the Supplementary Material. See paragraph at the end of the paper for details.

RESULTS AND DISCUSSION

While a mixture of nitrile and alcohol remains unchanged for long periods, the presence of gold(III) chloride and/or hydrogen chloride yields products in reaction times limited only by isolation times. The properties of colour and melting point support the formation of two different compounds and the elemental analyses (Table 1) give strong support to one being the imino-ether tetrachloroaurate(III) salt and the other being the complex between the imino–ether and gold(III) chloride. The IR and NMR spectral data (Tables 2 and 3) further support this conclusion and the crystal structure confirms the formation of the product. These data do indicate that the gold(III) is involved in the alcoholysis reaction. However, whether or not it is catalysing the reaction will have to await results of the kinetic study. The general observation was that it took longer to isolate the product from the gold(III) than from the hydrogen chloride reaction.

IR spectra

The major feature which indicates the formation of the imino-ether from the nitrile is the loss of the C≡N stretching frequency in the 2300 cm^{-1} region[14] and the appearance of the C=N stretching frequency in the 1600–1675 cm^{-1} region.[8] In addition, the appearance of vibrations due to the N—H group is evidence of the formation of the imino-ethers. The presence of the gold(III) and chloride is indicated by the Au—Cl stretching frequency.[15] The frequencies observed for the nitrile complexes, **1a** and **1b**, are indicative of a monosubstituted square planar complex, $AuCl_3 \cdot L$. The observation of similar frequencies for compound **4a** indicates that it is the imino-ether complex. The salts, **3b–3c**, exhibit only a single frequency which is consistent with the tetrachloroaurate(III) anion. While salt **3a** has several Au—Cl frequencies, the crystal structure shows a square planar tetrachloroaurate(III) anion. Further evidence for the formation of the complex is in the N—H frequencies. Only a single stretching frequency appears, and there are no bending or rocking frequencies. This indicates the presence of a single N—H bond.[8] A very similar system has been characterized with the $SbCl_6^-$ anion.[16]

NMR spectra

The NMR spectra (Table 3) are consistent with the presence of the imino-ether cation in solution. In the proton spectra, singlets at the appropriate chemical shift appear when methyl groups are present, and triplets and quartets at appropriate chemical shifts appear when ethyl groups are present. In the ^{13}C NMR spectra, the correct number of peaks appear at the appropriate chemical shifts. Unfortunately, neither the salt nor the complex could be identified due to the instability of the solutions. The cation undergoes further alcoholysis in methanol solution and the gold(III) is reduced in acetone solution. These results are consistent with reports of nickel(II)[1] and platinum(II)[4a] complexes. All of the salts have a broad singlet at 10.5 ppm which can be assigned to the protons on the nitrogen.

Crystal structure

The crystal and molecular structure of the hydrogenethylpropylimidate salt has been determined by single crystal X-ray diffraction. Salt **3a** crystallized

Table 4. Structure determination summary for the X-ray diffraction study of **3a**

Crystal data	
Compound	Hydrogenethylpropylimidate tetrachloroaurate(III)
Empirical formula	$C_5H_{12}NOAuCl_4$
Formula weight	452.94
Crystal colour and habit	Amber-coloured, rectangular plates, ground to tearshape
Crystal dimensions (mm)	$0.29 \times 0.27 \times 0.46$
Crystal system	Triclinic
Space group	$P\bar{1}$ (No. 2)
Z	2
Unit cell dimensions from 25 reflections	$(20.0° \leqslant 2\theta \leqslant 39.0°)$:
a (Å)	7.115(2)
b (Å)	8.152(2)
c (Å)	11.168(2)
α (°)	92.73(1)
β (°)	91.77(1)
γ (°)	106.66(1)
Volume (Å^3)	619.2(2)
Density (calc.) (g cm^{-3})	2.42_9
$F(000)$	420 electrons
Linear absorption coefficient (μ) (cm^{-1})	122.11
Data collection	
Diffractometer	Nicolet R3
Radiation type	Mo-K_α $\lambda = 0.71073$ Å, Lp corrected, graphite monochromator
Temperature	Ambient
Scan type	θ–2θ scan
2θ Scan range (°)	4–55
Octants used	$\pm h$, $\pm k$, $\pm l$ (h: $\bar{10}/10$; k: $\bar{11}/11$; l: $\bar{15}/15$)
Scan rate (° min^{-1})	2.5
Scan width	1.1° below $K_{\alpha 1}$ to 1.1° above $K_{\alpha 2}$
Background/scan ratio	0.5
Standard reflections	3 measured every 100 reflections, linear decay ~ 9%.
Number of data collected	6490
Number of unique reflections	2852, $R_{int.} = 0.0372$
Observed reflections with $(F_o) \geqslant 6.0\sigma(F)$:	2184
Absorption correction	Empirical, psi-scans
R merge before/after correction	0.0739/0.0312
Maximum/minimum transmission	0.204/0.007
Solution and refinement	
System used	SHELX-76, VAX 11/750
Solution	Patterson
Refinement method	Full-matrix least-squares
Function minimized	$\Sigma w(F_o - F_c)^2$
Hydrogen atoms	Riding model, $d_{C-H} = 1.08$ Å, isotropic
U(H) fixed at 1.2 times U(eq) for atom	
Number of parameters refined	99
Observed/parameter ratio	21.9
$R = \Sigma(\lvert F_o \rvert - \lvert F_c \rvert)/\Sigma \lvert F_o \rvert$	0.0459
$R_w = [\Sigma(\lvert F_o \rvert - \lvert F_c \rvert)^2/\Sigma w \lvert F_o \rvert^2]^{1/2}$	0.0604
$w^{-1} = \sigma^2(F_o) + 0.001270(F_o)^2$	
GOF	1.4
Mean shift/error	0.002
Maximum shift/error	0.002
Secondary extinction	15 reflections excluded
Residual electron density	+2.00/−1.20 e/Å^3 near gold

Table 5. Selected interatomic distances (Å) and angles (°) for **3a**

Distances (Å)			
Au(1)—Cl(1)	2.292(2)	C(2)—O(1)	1.46(2)
Au(1)—Cl(2)	2.287(2)	O(1)—C(3)	1.27(1)
Au(1)—Cl(3)	2.287(3)	C(3)—N(1)	1.28(2)
Au(1)—Cl(4)	2.275(3)	C(3)—C(4)	1.48(2)
C(1)—C(2)	1.52(2)	C(4)—C(5)	1.46(3)
Angles (°)			
Cl(1)—Au(1)—Cl(2)	178.6(1)	C(1)—C(2)—O(1)	108(1)
Cl(1)—Au(1)—Cl(3)	89.7(1)	C(2)—O(1)—C(3)	120(1)
Cl(1)—Au(1)—Cl(4)	89.7(1)	O(1)—C(3)—N(1)	123(1)
Cl(2)—Au(1)—Cl(3)	89.5(1)	O(1)—C(3)—C(4)	116(1)
Cl(2)—Au(1)—Cl(4)	91.2(1)	C(3)—C(4)—C(5)	115(2)
Cl(3)—Au(1)—Cl(4)	177.8(1)	N(1)—C(3)—C(4)	121(1)

in the triclinic space group $P\bar{1}$ as discrete ion pairs with a $[EtC(OEt)NH_2]^+$ cation and $[AuCl_4]^-$ anion in the asymmetric unit. The gold atom forms four ionic bonds to chlorine at a mean distance of 2.285(3) Å arranged in a square planar geometry. The maximum deviation is 0.034(4) Å from the plane defined by the four chlorine and the gold atoms. The observed Au—Cl distance is in close agreement with a variety of similar compounds appearing in the Cambridge Structural Database[17] [e.g. 2.271 Å in tetraphenylarsonium tetrachloroaurate(III),[18] 2.273 Å in ammonium tetrachloroaurate(III)[19] and 2.271 Å in hydrogen bis(pyridine-N-oxide) tetrachloroaurate(III)].[20] A search of the database did not reveal an exact match for the cation. Three entries in the database did incorporate the fragment defined by the non-hydrogen atoms of the cation into larger cyclic structures without significant changes from the geometry of the cation observed in **3a**. The N—C(3) bond length of 1.28(2) Å is in the range typical of a formal N—C double bond.[21] N(1), C(2), O(1) and C(3) are co-planar within 0.01(1) Å for the plane defined by the four atoms. The cation and anion do not appear to have any appreciable interaction. The closest contact between non-hydrogen atoms is about 3.35 Å for N(1)—Cl(3). Figure 1 gives an ORTEP view of the ion pair along with the atomic numbering scheme. The structure contains the interesting feature of a near linear chain of gold atoms as illustrated in Fig. 2. The Au···Au distance of 4.264 Å lies well outside the sum of van der Waals' radii for gold of 3.40 Å.[22]

A partial structure for the hydrogenmethylethylimidate tetrachloroaurate(III) compound **3c** also has been determined, giving only the positions for the anion. The probable space group is $P2_1/a$, $Z = 2$, $a = 7.800(2)$, $b = 8.574(2)$, $c = 7.909(4)$ Å, $\beta = 102.15(3)°$, $V = 517.1(3)$ Å^3. The observed mean Au—Cl distance is 2.27(1) Å with the gold atom on an inversion centre. The closest non-bonded distance involving gold is Cl(1)···Au′ of 3.513 Å (primed atom related by $-0.5-x$, $-0.5+y$, $-z$). Experimental data and

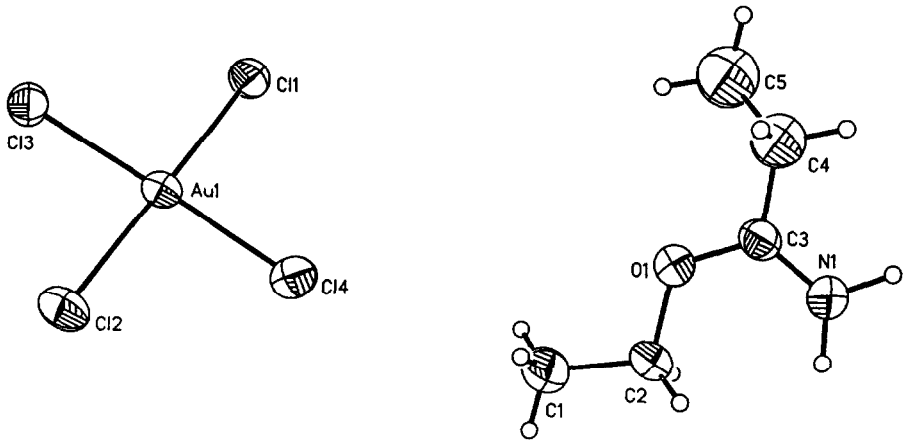

Fig. 1. An ORTEP diagram (50% thermal elipsoids) of **3a**.

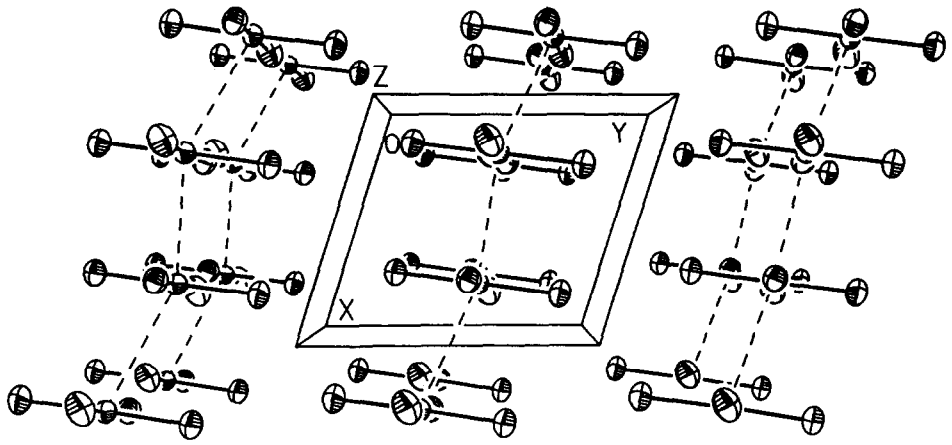

Fig. 2. A packing diagram for **3a** showing the Au—Au stacking arrangement.

positional parameters are available as Supplementary Material. Convergence of the data was achieved at $R = 0.0755$ and $R_w = 0.0921$. Unlike, **3a**, **3c** does not contain the near linear chain of gold atoms.

Supplementary material available. Atomic coordinates and thermal parameters for **3a** have been deposited with the Cambridge Crystallographic Data Centre. A summary of the crystal and data collection parameters, a description of the structure, atomic coordinates and bond lengths for **3c**, as well as observed and calculated structure factors for both compounds, are available from the authors.

REFERENCES

1. (a) B. N. Storhoff and H. C. Lewis Jr, *Coord. Chem. Rev.* 1977, **23**, 1; (b) N. D. Granik, *Russ. Chem. Rev. (Engl. Transl.)* 1983, **52**, 377.
2. G. Rouschias and G. Wilkinson, *J. Chem. Soc. A* 1968, 489.
3. P. F. B. Barnard, *J. Chem. Soc. A* 1969, 2140.
4. (a) H. C. Clark and L. E. Manzer, *Inorg. Chem.* 1971, **10**, 2699; (b) T. G. Appleton, M. H. Chisholm, H. C. Clark and L. E. Manzer, *Inorg. Chem.* 1972, **11**, 1786; (c) H. C. Clark and L. E. Manzer, *Inorg. Chem.* 1972, **11**, 2749; (d) H. C. Clark and L. E. Manzer, *J. Organomet. Chem.* 1973, **47**, C17; (e) L. E. Manzer, *J. Chem. Soc., Dalton Trans.* 1974, 1535.
5. (a) R. Ros, J. Renaud and R. Roulet, *J. Organomet. Chem.* 1975, **87**, 379; (b) R. Ros, J. Renaud and R. Roulet, *J. Organomet. Chem.* 1976, **104**, 271; (c) R. Ros, R. A. Michelin, T. Boschi and R. Roulet, *Inorg. Chim. Acta* 1979, **35**, 43.
6. K. Watanabe and K. Kidokoro, *Chem. Lett.* 1975, 67.
7. M. Wada and T. Shimohigashi, *Inorg. Chem.* 1976, **15**, 954.
8. P. Paul and K. Nag, *Inorg. Chem.* 1987, **26**, 1586.
9. M. S. Kharsch and T. M. Beck, *J. Am. Chem. Soc.* 1934, **56**, 2057.
10. (a) S. M. McElvain and J. W. Nelson, *J. Am. Chem. Soc.* 1942, **64**, 1825; (b) S. A. Glickman and A. C. Cope, *J. Am. Chem. Soc.* 1945, **67**, 1017.
11. XTAPE and XEMP, Programs for Data Reduction and Absorption Correction. Part of Nicolet SHELXTL software, Nicolet Analytical Instruments, Madison, Wisconsin (1984).
12. G. M. Sheldrick, SHELX-76, Program for Crystal Structure Determination. University Chemical Laboratory, Cambridge, U.K. (1976).
13. *International Tables for X-ray Crystallography*, Vol. 4. Kynoch Press, Birmingham, U.K. (1974).
14. R. A. Walton, *Spectrochim. Acta* 1965, **21**, 1795.
15. B. A. Schoenfelner and R. A. Potts, *J. Inorg. Nucl. Chem.* 1981, **43**, 1051.
16. V. E. Allenstein and A. Schmidt, *Z. Anorg. Allg. Chem.* 1966, **344**, 113.
17. F. H. Allen, S. A. Bellard, M. D. Brice, B. A. Cartwright, A. Doubleday, H. Higgs, T. Hummelink, B. G. Hummelink-Peters, O. Kennard, W. D. S. Motherwell, J. R. Rodgers and D. G. Watson, *Acta Cryst.* 1979, **B35**, 2331.
18. P. G. Jones, J. J. Guy and G. M. Sheldrick, *Acta Cryst.* 1975, **B31**, 2687.
19. M. Bonamico, G. Dessy, C. Furlani and F. M. Capece, *Acta Cryst.* 1973, **B29**, 1737.
20. M. S. Hussain and E. O. Schlemper, *J. Chem. Soc., Dalton Trans.* 1982, 751.
21. F. H. Allen, O. Kennard, D. G. Watson, L. Brammer, A. G. Orpen and R. Taylor, *J. Chem. Soc., Perkin Trans. II* 1987, 81.
22. J. Bondi, *J. Phys. Chem.* 1964, **68**, 441.

Polyhedron Vol. 10, No. 14, pp. 1639–1646, 1991
Printed in Great Britain

0277–5387/91 $3.00+.00
© 1991 Pergamon Press plc

CHARACTERIZATION OF ALUMINIUM ISOPROPOXIDE AND ALUMINOSILOXANES

KIRSTEN FOLTING, WILLIAM E. STREIB and KENNETH G. CAULTON*

Department of Chemistry and Molecular Structure Center, Indiana University, Bloomington, IN 47405, U.S.A.

and

OLIVIER PONCELET and LILIANE G. HUBERT-PFALZGRAF*

Laboratoire de Chimie Moléculaire, Unité Associée au CNRS, Université de Nice, Parc Valrose, 06034 Nice, France

(*Received* 5 *October* 1990; *accepted* 21 *March* 1991)

Abstract—Aluminium isopropoxide, in the form of a crystalline solid of melting point 127°C, has been shown by X-ray diffraction to be a tetrameric molecular species of formula $Al[(\mu\text{-}O^iPr)_2Al(O^iPr)_2]_3$, consistent with earlier proposals and spectroscopic data. A central aluminium achieves coordination number six via two bridging alkoxide groups from each of three $Al(O^iPr)_4^-$ groups. The resulting planar $Al(\mu_2\text{-}O)_2Al$ rings have widened ($\sim 132°$) angles at oxygen to increase the non-bonded Al—Al distance. While the terminal O^iPr groups show the shortest (1.70 Å) Al—O distances in the molecule, they are nevertheless strongly bent ($\sim 140°$) at oxygen. The ^1H NMR spectrum of $Al_4(O^iPr)_{12}$ is analysed based on the structure reported here. Characterization of aluminosiloxane derivatives $Al(O^iPr)_{3-x}(OSiMe_3)_x$ ($x = 1$–3) by ^1H and ^{27}Al NMR, mass spectrometry and IR spectroscopy is also reported. For $x = 1$ and 2, these show co-existence of several oligomers. The effect of incorporation of $OSiMe_3$ groups is to favour smaller oligomers.

The materials of empirical formula $Al(OCHMe_2)_3$ have been the focus of a variety of characterization studies and also of applications.[1] Synthetic organic applications include use as a catalyst for the Meerwein–Ponndorf–Verley hydride transfer from the ^iPrO methine carbon to ketones or for the Tishchenko reaction (conversion of aldehydes to esters). More recently, "$Al(O^iPr)_3$" has been a key component in the efforts of the group of Mehrotra to produce aluminium-containing heterometallic alkoxides. Examples include compounds of the type $M[Al(O^iPr)_4]_n$, where M^{n+} is a main group, transition metal, lanthanide or actinide element.[2] Hydrolysis of $Mg[Al(O^iPr)_4]_2$ to spinel $MgAl_2O_4$ is an example of the molecular precursor route to solid oxides.[3] Thermal condensation of $Al(O^iPr)_3$ with metal acetates offers soluble oxoheterometallic alkoxides $\{[(O^iPr)_2AlO]_2M\}_n$ (M = Fe, Co, Cr, . . .) which are catalysts for polymerization of heterocyclic compounds[4] or for oxidation reactions.[5]

The above paragraph began with "the materials . . . $Al(OCHMe_2)_3$ . . ." because this material, when synthesized from aluminium and ^iPrOH and vacuum distilled (100–150°C depending upon the pressure) is obtained as an oil or a viscous ("syrupy")[6] liquid, which is said to "age" over a period of days to give a solid.[7] Such behaviour is unusual and the viscous form has been termed a supercooled melt. Since the degree of aggregation, as measured by cryoscopy, increases with time, the ageing phenomenon is proposed to be due to a reorganization of smaller oligomers into large ones. By heating material at 200°C for 5 min, then cooling rapidly to 25°C for cryoscopy in benzene, a trimeric molecular weight was established.[6,7] The crystalline solid produced after several days (or by recrystallization of the melt from ^iPrOH), with melting

* Authors to whom correspondence should be addressed.

point 118°C, is tetrameric.[6,7] Bradley suggested structure **I** for the tetramer.[8] This represented a

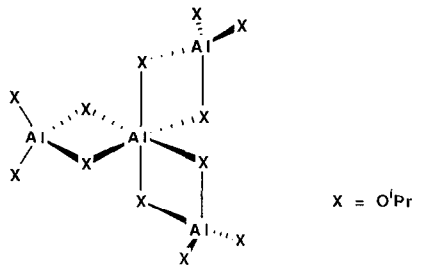

I

dramatic break with the conventional wisdom of that period, which considered both the trimer and the tetramer to have cyclic structures with equivalent aluminium centres. The group of Shiner at Indiana brought ^{1}H NMR spectroscopy to bear on this problem.[6] Particularly noteworthy was their ability to use the *complex* NMR pattern of the tetramer to support the structural proposal (**I**) of Bradley. Kleinschmidt measured[9] the ^{27}Al NMR spectrum of the tetramer in toluene. Two resonances were observed, of relative intensity 3 : 1. The intensity 3 resonance was 30 times broader than the other resonance, and it fell (−59 ppm, using old sign convention) in the chemical shift region diagnostic of four-coordinate aluminium. The unit intensity resonance at −1.5 ppm was very close to the value (0.0 ppm) of six-coordinate aluminium in aluminium(acetylacetonate)$_3$. The cyclic trimer (i.e. a freshly produced melt) exhibited a different ^{27}Al NMR spectrum. These ^{27}Al NMR results have been confirmed recently by Fourier transform instrumentation.[10]

The simplicity of the system described to this point is perturbed by strong assertions[11] that a dimeric form of aluminium isopropoxide also exists.

The single-crystal X-ray determination of the solid-state structure of a sample of $[Al(O^iPr)_3]_m$ was carried out in 1979 and confirmed structure **I**.[12] However, because this determination was not cited in subsequent aluminium alkoxide articles, we remained ignorant of the work. When single crystals of one form (subsequently shown to be the *same* form as that studied earlier[12]) became available to us, we proceeded with a structure determination.

An expanded class of aluminium alkoxides, the siloxides, is also of interest. Materials based on the SiO_2–Al_2O_3 systems are well known for their refractory properties. Aluminosiloxanes $[Al(O^iPr)_{3-x}(OSiMe_3)_x]_m$ can be used as precursors of gels and ceramics. The differential hydrolysis introduced by the siloxo group (less susceptible to hydrolysis than the isopropoxo ones) prevents the precipitation of aluminium hydroxide and thus allows the formation of very homogeneous gels.[13]

We wish now to report further characterization of aluminosiloxanes, as well as our redetermination of the molecular structure of "aged" aluminium triisopropoxide.

EXPERIMENTAL

All operations were carried out under an atmosphere of dry nitrogen gas in solvents that were dried and distilled. ^{1}H and ^{27}Al NMR were registered on Bruker WH-90 and AM-200 spectrometers. ^{27}Al spectra were registered at high temperature and chemical shifts are given with respect to $Al(H_2O)_6^{3+}$ as an external reference. Synthesis of the aluminosiloxanes was achieved according to ref. 14. IR spectra were obtained as Nujol mulls on an FT IRS 45 Bruker spectrometer. Mass spectra were measured on a Ribermag R10-L10 spectrometer. Microanalyses were performed by the Centre de Microanalyses du CNRS.

The aluminium isopropoxide was prepared by a literature method,[15] distilled and allowed to crystallize from toluene at −30°C. Identity and purity of the colourless, crystalline solid (octahedral and truncated octahedral morphology) was established by comparison of the ^{1}H NMR to a literature report, and by comparison of its (sealed tube) melting point (127°C) to that measured on a commercial (Aldrich) sample (128°C), both uncorrected.[16]

X-ray diffraction study of $[Al(O^iPr)_3]_4$

Crystal data at −155°C: $C_{36}H_{84}Al_4O_{12}$, $M = 816.98$, tetragonal, $a = b = 12.317(3)$, $c = 31.724(8)$ Å, $U = 4813.19$ Å^3, $Z = 4$, $D_c = 1.13$ g cm^{-3}, $\lambda = 0.71069$ Å, $\mu = 1.42$ cm^{-1}, space group $P4_12_12$, $R = 0.0491$, $R_w = 0.0457$. This crystal was synthesized and crystallized by a method[15] identical to that used by Turova *et al.*[12] and our space group is identical to theirs.

A crystal was mounted in a nitrogen atmosphere using silicone grease and was transferred to a goniostat where it was cooled to −155°C for characterization and data collection.[17] A systematic search of a limited hemisphere of reciprocal space yielded a set of reflections which exhibited tetragonal symmetry. After intensity data collection using a narrow scan width due to the length of the *c*-axis, a more careful examination revealed systematic absences and Laue symmetry consistent with the non-centrosymmetric space group $P4_12_12$ (No. 92). A total of 4263 reflections (including stan-

dard reflections and space group extinctions) was collected, and 42 reflections which suffered from overlap were rejected. The R for the averaging was 0.066 for 1670 unique data which had been observed more than once. Four standards measured periodically showed no significant trends. No correction was made for absorption.

The structure was solved by a combination of direct methods (MULTAN78) and Fourier techniques. The aluminium positions were obtained from the E-map and the remaining non-hydrogen atoms were located using difference Fourier techniques. Hydrogen atoms were located following the initial refinement. The full-matrix least-squares refinement was completed using anisotropic thermal parameters on the non-hydrogen atoms and isotropic thermal parameters on the hydrogen atoms.

The final difference map was essentially featureless, the largest peak being 0.36 e $Å^{-3}$ in the vicinity of Al(1). No attempt was made at determining the correct absolute configuration. The molecule lies on a crystallographic two-fold axis. Atoms related by the symmetry operation are indicated by ′ in Fig. 1 and Table 1. Tables of atom coordinates and thermal parameters are available from the Cambridge Crystallographic Data Centre. A list of final structure factors is available from one of the authors (K.G.C.).

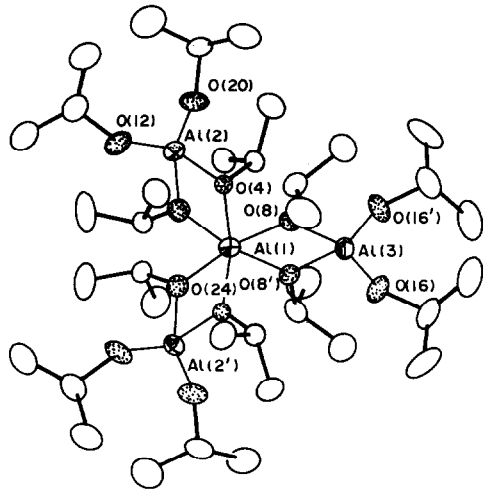

Fig. 1. Stereo ORTEP drawing of the non-hydrogen atoms of $[Al(O^iPr)_3]_4$ viewed down an idealized C_3 axis of symmetry. Selected atoms are labelled, with primed and unprimed atoms being related by a crystallographic C_2 axis passing through Al(1) and Al(3). Stippled atoms are oxygen.

$[Al(O^iPr)_2(OSiMe_3)]_m$

This was synthesized according to the literature procedure[14] from aged $Al(O^iPr)_3$ (9.86 g, 0.048 mol) and $Me_3SiO_2CCH_3$ (6.33 g, 0.048 mol) in 1.30 cm^3 of cyclohexane. Silylacetate was added over a

Table 1. Selected bond distances (Å) and angles (°) for $[Al(CO^iPr)_3]_4$

Al(1)—Al(2)	2.8694(26)	Al(2)—O(12)	1.703(5)
Al(1)—Al(3)	2.866(4)	Al(2)—O(20)	1.692(5)
Al(1)—O(4)	1.918(4)	Al(2)—O(24)	1.804(4)
Al(1)—O(8)	1.923(4)	Al(3)—O(8)	1.798(5)
Al(1)—O(24)	1.933(4)	Al(3)—O(16)	1.704(5)
Al(2)—O(4)	1.803(4)		

O(4)—Al(1)—O(4)′	168.2(3)	O(8)′—Al(3)—O(16)	118.82(21)
O(4)—Al(1)—O(8)′	96.71(19)	O(8)—Al(3)—O(16)	106.08(20)
O(4)—Al(1)—O(8)	92.61(18)	O(16)—Al(3)—O(16)′	119.4(3)
O(4)′—Al(1)—O(24)	76.34(18)	Al(1)—O(4)—Al(2)	100.84(21)
O(4)—Al(1)—O(24)	95.42(19)	Al(1)—O(4)—C(5)	131.2(4)
O(8)—Al(1)—O(8)′	76.11(26)	Al(2)—O(4)—C(5)	126.4(4)
O(8)—Al(1)—O(24)′	95.69(17)	Al(1)—O(8)—Al(3)	100.72(20)
O(8)—Al(1)—O(24)	169.17(19)	Al(1)—O(8)—C(9)	133.8(4)
O(24)—Al(1)—O(24)′	93.26(26)	Al(3)—O(8)—C(9)	125.0(4)
O(4)—Al(2)—O(12)	106.67(23)	Al(2)—O(12)—C(13)	134.5(5)
O(4)—Al(2)—O(20)	118.68(25)	Al(3)—O(16)—C(17)	139.0(5)
O(4)—Al(2)—O(24)	82.57(19)	Al(2)—O(20)—C(21)	146.9(5)
O(12)—Al(2)—O(20)	119.24(25)	Al(1)—O(24)—Al(2)	100.24(20)
O(12)—Al(2)—O(24)′	118.21(24)	Al(1)—O(24)—C(25)	132.9(4)
O(20)—Al(2)—O(24)′	106.28(22)	Al(2)—O(24)—C(25)	126.0(4)
O(8)—Al(3)—O(8)′	82.45(28)		

period of several hours during which azeotropic distillation of cyclohexane/isopropyl acetate was achieved (80°C). The solution was then concentrated and distilled (80°C/0.01 mm Hg) to give 11 g (98% yield). Found: C, 45.4; H, 10.1. Calc. for $C_9H_{23}AlO_3Si$: C, 46.1; H, 10.0%. IR (cm^{-1}): 1250 (Si—C); 1180, 1130 (C—CH_3); 1070; 950 (Si—O); 760; 640 (Al—OR). MS (m/z^+, %); M = [Al(O^{i}Pr)$_2$(OSiMe$_3$)]$_4$; M−OPr (2%); M−OSiMe$_3$ (3%); M−2OPr (6.6%); M−OSiMe$_3$−OPr (4%); $Al_2(O^iPr)_4(OSiMe_3)_2H$ (35%); $Al(OSiMe_3)_2$ (100%); AlO (90%). ^{1}H NMR ($CDCl_3$; 0.1 M, 25°C) (ppm): 4.47–4.08 (m, O*CH*Me$_2$, 2H). 1.42; 1.27; 1.47; 1.36; 1.21, 1.10; 1.06 (d, J = 6 Hz, OCHMe$_2$, 12H); 0.25, 0.22, 0.21 (s, OSiMe$_3$, 9H). We have examined six different crystals at temperatures from −150 to +5°C but found none suitable for an X-ray diffraction study.

$[Al(O^iPr)(OSiMe_3)_2]_p$

Analogous to the previous synthesis, but with a 2:1 ratio of silylacetate to aluminium (0.109 mol). Product was distilled at 105°C/0.01 mm Hg to give 24.2 g (95% yield). Found: C, 39.7; H, 9.7. Calc. for $C_9H_{25}AlO_3Si_2$: C, 40.9; H, 9.5%. IR (cm^{-1}): 1250 (Si—C); 1180, 1130 (C—CH_3); 1070, 950 (Si—O); 640 (Al—OR). MS (m/z^+, CI, NH_3): M = [Al(O^{i}Pr)$_2$(OSiMe$_3$)]$_3$; M−O^{i}Pr (1.4%); M−OSiMe$_3$ (4.6%); M−2O^{i}Pr (3.2%); M−(OSiMe$_3$+O^{i}Pr) (3.9%); M+Al(O^{i}Pr)$_2$(OSiMe$_3$) (19.4%); AlOH(OSiMe$_3$) (100%). ^{1}H NMR ($CDCl_3$; 0.1 M, 25°C) (ppm): 4.18 (m, O*CH*Me$_2$, 1H), 1.22; 1.32 (d, J = 6 Hz, OCH*Me*$_2$, 6H) 0.26; 0.04 (s, OSi*Me*$_3$, 18H).

$[Al(OSiMe_3)_3]_2$

Analogous to the above synthesis, but with a 3:1 ratio of silylacetate to aluminium. The product was purified by sublimation (100°C, 10^{-2} mm Hg). Yield: 70%. Found: C, 35.2; H, 9.3. Calc. for $C_9H_{27}AlO_3Si_3$: C, 36.7; H, 9.2%. IR (cm^{-1}): 1256 (Si—C); 1067; 997, 957 (Si—O), 849, 752, 640, 598, 520, 382, 330. Mass spectrum (m/z^+ %): M (molecular ion, 61%); M−O (100%); M−HSiMe$_3$ (19%); M−OSiMe$_3$−CH$_2$ (10%); M−O(SiMe$_3$)$_2$−CH$_2$ (7%). ^{1}H NMR (d_8-toluene): 0.28, 0.22 (intensity 1:2).

RESULTS

$[Al(O^iPr)_3]_m$

The X-ray diffraction study (Fig. 1) shows the tetragonal crystals to be composed of $Al_4(O^iPr)_{12}$ molecules, each of which has crystallographic C_2 symmetry. The C_2 axis contains Al(1) and Al(3). The formula is best written as Al[(μ_2-O^{i}Pr)$_2$ Al(O^{i}Pr)$_2$]$_3$, in complete confirmation of the conclusions of earlier workers.[6,8,12] One aluminium is six-coordinate and the remaining three are four-coordinate. The overall molecular symmetry approximates D_3, with one Al^{3+} being coordinated by four $Al(O^iPr)_4^-$ units, each of which functions as a bidentate ligand. The material whose structure we report here is identical in composition of matter and space group with that studied by Turova *et al.*[12] Their study, at 25°C, shows high thermal motion and a higher R factor (0.119 for anisotropic refinement of all non-hydrogen atoms), but none of their conclusions is altered by our low-temperature study. The low-temperature study has smaller ESDs and improved agreement between Al—O distances and all bond angles which would be expected to be chemically equivalent.

The Al[(μ-O)$_2$Al]$_3$ core adopts a Mitsubishi motif (**II**). The Al—O bond lengths increase in the order

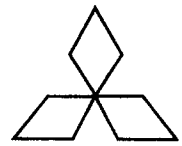

II

^{4}Al—O < ^{4}Al—(μ-O) < ^{6}Al—(μ-O), where the superscript indicates the coordination number. In each step in the above progression, the bond lengthens by 0.10–0.12 Å. In spite of the short Al—O (terminal) bond lengths (average 1.700 Å), bond angles at these oxygen atoms range from 134.5(5) to 136.9(5)°. These are relatively small. Since terminal alkoxides on early transition metals are normally within 15° of being linear at oxygen, oxygen π-donation must be greater for those metals than for aluminium.

The four-membered rings in $Al_4(O^iPr)_{12}$ are all planar. The angle ^{6}Al—O—^{4}Al is large [100.2(2)–100.8(2)°], producing non-bonded ^{6}Al—^{4}Al distances of 2.87 Å. The bridging oxygen atoms are coplanar with their attached groups, and the attached isopropyl groups bend away from the bulkier six-coordinate Al(1) towards the four-coordinate aluminium centres.

Based on the structure determined here, the ^{1}H NMR of $[Al(O^iPr)_3]_4$ warrants some discussion. The molecule has idealized D_3 symmetry, with a C_3 axis making all $Al(O^iPr)_4$ groups equivalent and three C_2 axes, each passing through one four-coordinate aluminium and the six-coordinate

aluminium. This leads to the conclusion that there is only one type of μ_2- and one type of terminal alkoxide, but that the methyl groups on each of these two ^{i}Pr groups are diastereotopic (i.e. inequivalent). One expects four methyl chemical shifts, all of equal intensity.

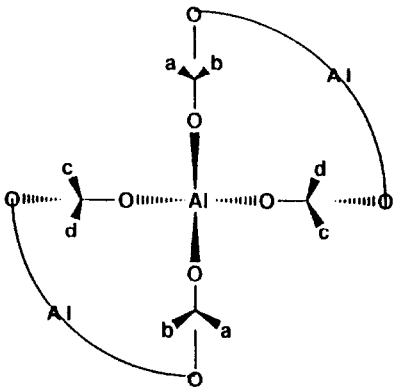

The observed ^{1}H NMR spectrum (300 MHz, 25°C, d_8-toluene) shows the expected two methine chemical shifts, but only *three* methyl resonances (doublets) of intensity 1 : 1 : 2. We assign the intensity 1 peaks to the μ_2-O^{i}Pr groups, so the *absence* of the expected inequivalences of the terminal isopropoxy methyls must be due to either (1) accidental equivalence or (2) some dynamic averaging process. We feel that an intramolecular[18] dynamic process is less likely, since such a process would almost certainly average bridge with terminal alkoxides. A Ray–Dutt twist would maintain the distinction between bridge and terminal groups, but this would cause not only the diastereotopic terminal methyls to coalesce, but also the diastereotopic bridging methyls to coalesce; two doublets are predicted.

Aluminosiloxanes

The various aluminosiloxanes $[Al(O^iPr)_{3-x}(OSiMe_3)_x]_n$ ($x = 1$–3) have been obtained by transesterification reaction in cyclohexane using Me_3SiOAc as a reactant,[14] and characterized by microanalysis, IR, ^{1}H and ^{27}Al NMR (Table 2) as well as by mass spectrometry.

$[Al(O^iPr)_2(OSiMe_3)]_m$

The mass spectrum indicates $[Al(O^iPr)_2(OSiMe_3)]_m$ contains tetrameric units. The ^{27}Al NMR spectrum of this material shows (toluene, 0.1 M, 70°C in order to narrow the signals) a sharp peak at 3.8 ppm ($\Delta_{1/2} = 40$ Hz), as well as broader signals at 40 and 60 ppm which we assign to six-coordinate and two types of four-coordinate metal centres, respectively.[19,20] We proposed structures **III** or **IV** to account for these data. These place

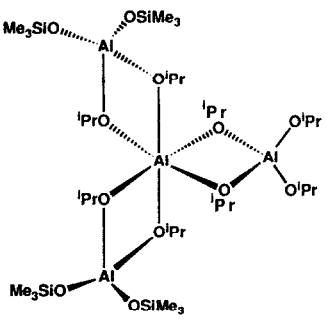

III

Table 2. ^{27}Al NMR data of some aluminosiloxanes

	Chemical shift (ppm) [line width (Hz)]	Solvent	Temperature (°C)	Concentration (mol dm^{-3})
$[Al(OSiMe_3)_3]_2$	59 [1000]	Toluene	80	0.1
$[Al(O^iPr)(OSiMe_3)_2]_p$	10 [1000] 40 [1300] 60 [1250]	Toluene	70	0.1
	13 [750] 50 [1500] 65 [2600]	^{i}PrOH	70	0.5
$[Al(O^iPr)_2(OSiMe_3)]_m$	3.8 [40] 12 [750] 40 [750] 59 [1500]	Toluene	70	0.1
$[Al(O^iPr)_3]_4$	3.5 [50] 61 [1500]	Benzene	70	Saturated

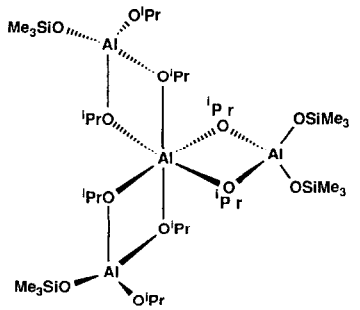

IV

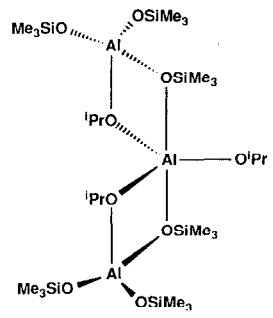

V

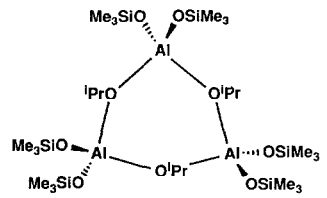

VI

the four more bulky $OSiMe_3$ groups in the least hindered (terminal) positions of the tetramer structure. These incorporate one six-coordinate aluminium and create two distinct types of four-coordinate aluminium centres by means of the $OSiMe_3$ substituent pattern.

The C_2 symmetry of structures **III** and **IV**, interpreted rigorously, requires eight ^{i}Pr methyl chemical shifts and two $OSiMe_3$ chemical shifts. The ^{1}H NMR spectrum (0.1 M, 25°C) shows at least seven ^{i}Pr methyl and two $OSiMe_3$ resonances. This is thus consistent with either structure **III** or **IV**. Since we find the ^{1}H NMR spectrum to be concentration dependent, additional oligomers, or even a mixture of **III** and **IV** may be present under other conditions. In addition, integration of the ^{27}Al NMR spectrum shows that the tetramer comprises only about 25% of the species present at 70°C, and that species with tetracoordinate aluminium predominate. Ligand redistribution in solution [eq. (1)] can be excluded by the absence of any signal due to $[Al(O^iPr)_3]_4$:

$$2[Al(O^iPr)_2(OSiMe_3)]_m \longrightarrow m/4[Al(O^iPr)_3]_4 + [Al(O^iPr)(OSiMe_3)_2]_m. \quad (1)$$

$[Al(O^iPr)(OSiMe_3)_2]_p$

The mass spectrum of $[Al(O^iPr)(OSiMe_3)_2]_p$ shows fragments up to a trinuclear unit. The ^{27}Al NMR spectrum (toluene, 0.1 M) differs mainly from that of $[Al(O^iPr)_2(OSiMe_3)]_m$ by the absence of a sharp signal around 3 ppm, and thus establishes the absence of any six-coordinate aluminium centre. The spectrum shows very broad resonances at 40 ppm (weak) and 60 ppm (strong). We assign the former to five-coordinate and the latter to four-coordinate aluminium, and propose a small amount of structure **V** together with a cyclic trimer (**VI**) or a dimer. Structure **V** has the merit that it is the simplest structure derivable by removal of one aluminium (to give a trimer) from the structure of $[Al(O^iPr)_3]_4$, and in that way it naturally accounts for the absence of six-coordinate aluminium. The central aluminium now has a trigonal bipyramidal geometry, and structural type **V** has been firmly established for $Al_3Cl_5(O^iPr)_4$,[21] $Al_3Br_5(OSiMe_2O SiMe_2O)_2$[22] and $Al_3Cl_5(OBPh_2OBPh_2O)_2$.[23] Five-coordinate aluminium is also established in $Al_{10}(\mu_4\text{-}O)_2(\mu_3\text{-}O)_2(OEt)_{22}$.[24] While structure **V** predicts three $OSiMe_3$ resonances (two are observed) and four ^{i}Pr methyl resonances (two are observed), we feel that the rapid fluxionality common to trigonal bipyramidal structures can account for the simpler observed spectrum.

In contrast to $[Al(O^iPr)_3]_m$ and $[Al(O^iPr)_2(OSi Me_3)]_m$, which transform to solids on "ageing", $[Al(O^iPr)(OSiMe_3)_2]_m$ remains a pasty solid at 25°C. For this reason, crystals suitable for X-ray structure determination could not be obtained. Below −30°C, it is a normal, crystalline solid, but it becomes soft and waxy by 25°C, this suggests plastic phase behaviour.[25] To probe this behaviour further, we have recorded the ^{1}H NMR of neat $[Al(O^iPr)(OSiMe_3)_2]_p$ from −30 to +50°C. A signal is detectable in the solid state at −30°C ($\Delta_{1/2} = 3500$ Hz), which indicates considerable rapid reorientational motion in the solid. The peak width drops rapidly in the range +5–+15°C, and achieves a value of 100 Hz by 20°C. At 20°C, the colourless, crystalline material suddenly converts

into a translucent solid. By 50°C, the spectrum is analogous to that of a solution. This variation in line width reflects a drastic change in molecular freedom, which we assign to a plastic phase transition, above which the molecules begin to rotate or *pseudorotate*, while maintaining their centre of gravity in the solid. This interpretation is supported by differential scanning calorimetry, which shows an endothermic transformation at −27°C; upon cooling, this transition is found at −33°C. Such hysteresis is a common feature of plastic phase transitions.[25] Plastic crystals generally involve highly symmetrical, nearly spherical molecules. The behaviour observed for $[Al(O^iPr)(OSiMe_3)_2]_p$ thus supports a cyclic trimeric structure (**VI**) in the solid state.

$[Al(OSiMe_3)_3]_2$

$[Al(OSiMe_3)_3]_2$ displays a dimeric structure in solution (two types of ^1H NMR signals in a 2:1 ratio), as well as in the vapour phase. Structure **VII**

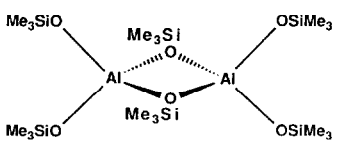

VII

is indicated,[20,26] and has been found for $Al_2Br_4(\mu\text{-}OSiMe_3)_2$.[27] The ^{27}Al NMR chemical shift is in the region characteristic of four-coordinate aluminium.

CONCLUSION

The occurrence of different oligomers of aluminium isopropoxide suggests that they may also have different reactivity. There are already indications that this is true,[18] and this general subject deserves further study.

It appears that substitution of isopropoxo by trimethylsiloxo groups stabilizes smaller oligomers in comparison to $[Al(O^iPr)_3]_4$, apparently because of the larger steric profile of $OSiMe_3$ compared with O^iPr. Higher aggregates entail higher metal coordination numbers and thus larger interligand repulsions.

Since many metal alkoxides and siloxides display *closo* structures, plastic phase behaviour may be responsible for the poor crystallizability, the poor diffraction intensity and the poorly refineable X-ray intensity data for this class of compounds.

Acknowledgements—We thank Professor J. P. Boilot (Paris) for the DSC measurements, B. Septe (Nice) for the NMR spectra, and the CNRS "GRECO 93" and the U.S. Department of Energy for financial support.

REFERENCES

1. D. C. Bradley, *Adv. Inorg. Chem. Radiochem.* 1972, **15**, 259.
2. (a) J. V. Singh and R. C. Mehrotra, *J. Coord. Chem.* 1984, **13**, 273; (b) J. V. Singh and R. C. Mehrotra, *Can. J. Chem.* 1984, **62**, 1003; (c) J. V. Singh and R. C. Mehrotra, *Z. Anorg. Allg. Chem.* 1984, **522**, 211; (d) R. C. Mehrotra, J. M. Batwara and P. N. Kapoor, *Coord. Chem. Rev.* 1980, **31**, 67; (e) J. V. Singh and R. C. Mehrotra, *Inorg. Chem.* 1984, **23**, 1046; (f) N. C. Jain, A. K. Rai and R. C. Mehrotra, *J. Inorg. Nucl. Chem.* 1978, **40**, 349.
3. K. Jones, T. J. Davies, H. G. Emblem and P. Parks, in *Better Ceramics Through Chemistry II* (Edited by C. J. Brinker, D. E. Clark and D. R. Ulrich). Materials Research Society Proceedings, Pittsburgh (1986); H. Dislich, *Angew. Chem., Int. Edn Engl.* 1971, **10**, 363.
4. A. Hamilton, R. Jerome, A. J. Hubert and P. Teyssie, *Macromolecules* 1973, **6**, 651.
5. L. Hocks, P. Durbut and R. Teyssie, *J. Molec. Catal.* 1980, 7, 75.
6. V. J. Shiner, D. Whittaker and V. P. Fernandez, *J. Am. Chem. Soc.* 1963, **85**, 2318.
7. R. C. Mehrotra, *J. Ind. Chem. Soc.* 1953, **30**, 585; 1954, **31**, 85.
8. D. C. Bradley, *Adv. Chem. Ser.* 1959, **23**, 10.
9. D. C. Kleinschmidt, PhD thesis. Indiana University, Bloomington, Indiana (1966).
10. O. Kriz, B. Casensky, A. Lycka, J. Fusek and S. Hermanek, *J. Mag. Reson.* 1984, **60**, 375.
11. D. C. Kelinschmidt, V. J. Shiner and D. Whittaker, *J. Org. Chem.* 1973, **38**, 3334.
12. N. Y. Turova, V. A. Fozunov, A. I. Yanovskii, N. G. Bokii, Y. T. Struchkov and B. L. Tarnopolskii, *J. Inorg. Nucl. Chem.* 1979, **41**, 5.
13. J. C. Plouxviel, J. P. Boilot, O. Poncelet, L. G. Hubert-Pfalzgraf, A. Leconte, A. Dauger and J. C. Beloeil, *J. Non-Cryst. Solids* 1987, **93**, 277.
14. R. C. Mehrotra and B. C. Pant, *Ind. J. Appl. Chem.* 1963, **26**, 109.
15. W. G. Young, W. H. Hartring and F. S. Crossley, *J. Am. Chem. Soc.* 1936, **58**, 100.
16. A. L. Wilds, *Org. Reactions* 1944, **2**, 178.
17. J. C. Huffman, L. N. Lewis and K. G. Caulton, *Inorg. Chem.* 1980, **19**, 2755.
18. It is known that free ^{i}PrOH exchanges slowly with the tetramer: V. J. Shiner and D. Whittaker, *J. Am. Chem. Soc.* 1969, **91**, 394.
19. R. Benn, A. Rufinska, H. Lehmkuhl, E. Janssen and C. Krüger, *Angew. Chem., Int. Edn. Engl.* 1983, **22**, 779.
20. J. H. Wengrovius, M. F. Garbauskas, E. A. Williams,

R. C. Going, P. E. Donahue and J. F. Smith, *J. Am. Chem. Soc.* 1986, **108**, 982.
21. A. I. Yanouskii, V. A. Kozunov and J. Y. Turova, *Dokl. Akad. Nauk. SSSR* 1979, **244**, 119.
22. M. Bonamico and G. Dessy, *J. Chem. Soc. A* 1968, 291.
23. R. Köster, K. Angermund, J. Serwatowski and A. Sporzynski, *Chem. Ber.* 1986, **119**, 1301.
24. A. I. Yanovski, N. I. Kozlova and Y. T. Struchkov, *Koord. Khim.* 1987, **13**, 242.
25. L. A. K. Stabeley, *Tecnica* 1971, **414**, 171; G. W. Smith, *Int. Sci. Technol.* 1967, **61**, 72.
26. H. Schmidbaur and M. Schmidt, *Angew. Chem., Int. Edn Engl.* 1962, **6**, 328.
27. M. Bonamico and G. Dessy, *J. Chem. Soc. A* 1967, 1786.

Polyhedron Vol. 10, No. 14, pp. 1647–1651, 1991
Printed in Great Britain

0277–5387/91 $3.00+.00
© 1991 Pergamon Press plc

EFFECT OF SOLVENT ON THE STABILITY AND ELECTRON-TRANSFER KINETICS OF 1,8-BIS(2-PYRIDYL)-3,6-DITHIAETHER COPPER(II)

K. M. DAVIES,* K. D. WHYTE, J. LIEBERMANN JR† and J. A. MAHR†

Department of Chemistry, George Mason University, Fairfax, VA 22030, U.S.A.

(*Received* 12 *November* 1990; *accepted* 27 *March* 1991)

Abstract—The kinetics of ferrocene reduction of the dithiaether copper(II) complex, $[Cu(pdto)]^{2+}$ [pdto = 1,8-bis(2-pyridyl)-3,6-dithiaoctane], has been studied in the solvents acetone, acetonitrile, methanol and dimethylsulphoxide. Data have been obtained in 0.10 M n-Bu_4NPF_6 and with no added electrolyte. Formal potentials have been measured for the participating couples by cyclic voltammetry, and rate constants have been estimated for $[Cu(pdto)]^{2+}$–$[Cu(pdto)]^{+}$ self-exchange in each solvent. The effect of copper(II)–solvent interactions on the reaction mechanism and on estimated self-exchange rate constants are discussed. Stability constants for $[Cu(pdto)]^{2+}$ have also been determined in a range of dipolar solvents to assess solvent interactions.

The effect of ligand constraints on the electron-transfer self-exchange rates of copper(II)–copper(I) redox couples in coordination environments provided by nitrogen and sulphur donor ligands has been an area of much recent interest.[1] Correlation of self-exchange rate constants obtained with changes in stereochemistry and coordination number that accompany the redox change have been examined and used in some instances to provide insight into factors influencing the kinetic reactivity of blue copper protein active sites.[2–15]

We have previously reported the kinetic behaviour of the $[Cu(pdto)]^{2+}$ complex, with a $Cu^{II}N_2S_2$ coordination environment, on reduction by ruthenium(II) ammine and bipyridyl complexes in aqueous media.[8] Since the geometric change accompanying loss of an inner-sphere water molecule on reduction of the five-coordinate copper(II) reactant, $[Cu(pdto)(H_2O)]^{2+}$, to the four-coordinate copper(I) product is believed to be responsible for the relatively slow copper(I)–copper(II) self-exchange rate constant estimated for the $Cu(pdto)^{2+/+}$ couple, the kinetics of reduction of $Cu(pdto)^{2+}$ have been extended to other donor solvents, using ferrocene as reductant, to explore solvent influences on the reaction and to determine whether different solvent interactions with the copper(II) centre are reflected in the measured reaction rates, and in estimated values of copper(I)–copper(II) self-exchange rate constants. Stability constants, K_f ($Cu^{2+}{}_{(solv)}$ + pdto = $[Cu(pdto)^{2+}]$), for the complexation of Cu^{2+} by the tetradentate ligand pdto, in different solvents, have also been determined to provide information on copper(II)–solvent interactions.

EXPERIMENTAL

Materials

The ligand pdto and the complex $[Cu(pdto)](ClO_4)_2$ were prepared according to the literature method.[16] Ferrocene (Sigma) was purified by sublimation at atmospheric pressure and the electrolytes n-Bu_4NPF_6 (Aldrich) and n-Bu_4NClO_4 (G. F. Smith) were recrystallized from ethanol–water and dried *in vacuo*. Solvents were dried over molecular sieves (3–4 Å) and freshly distilled prior to use. Acetonitrile (Aldrich 99+ spectroscopic grade) was refluxed with P_2O_5 prior to distillation, with only the middle distillate fraction used.

Kinetic measurements

An Aminco stopped-flow spectrophotometer, coupled to a Nicolet 2090 digital oscilloscope and a Hewlett–Packard Vectra ES/12 computer were

* Author to whom correspondence should be addressed.
† Thomas Jefferson High School for Science and Technology, Alexandria, VA 22312, U.S.A.

used for data collection and calculation of rate constants. Reactions were carried out under pseudo-first-order conditions with ferrocene in at least 10-fold excess. First-order plots were linear to at least three half-lives. Reactions were followed at several wavelengths, usually 350 or 520 nm. Three rate determinations were usually carried out for each filling of the stopped flow.

Stability constant measurements

Determinations of $Cu(pdto)^{2+}$ stability constants, K_f, in the solvents acetone, ethylacetate, ethanol, methanol, isopropanol, acetonitrile and N,N-dimethylformamide were made spectrophotometrically using Hewlett–Packard 8452A diode array and Sequoia-Turner 340 spectrophotometers. Equilibrium solutions were thermostatted at 25.0 ± 0.1°C. Values of K_f were obtained by continuous variations and mole ratio methods,[17] with the ionic strength maintained at 0.10 M using sodium perchlorate. In the latter case, determinations were made both with $[Cu^{2+}]$ and [pdto] held constant. Mean values of at least three separate determinations of K_f in each solvent are reported. Data are summarized in Table 3. Apart from differences in intensity, the $[Cu(pdto)]^{2+}$ spectrum was essentially unchanged in all solvents reported except for DMSO. Simple one-to-one complex formation was found in all cases.

Electrochemical measurements

The standard potentials for the $Cu(pdto)^{2+/+}$ and $FeCp_2^{0/+}$ couples in the different solvents were obtained using a BAS CV-1B cyclic voltammetry unit. Potentials were obtained in deoxygenated solvents under argon with a glassy carbon working electrode, a platinum wire auxiliary electrode and a saturated calomel reference electrode (SCE). The BAS electrochemical cell was thermostatted at 25.0 ± 0.1°C. The measurements were uncorrected for liquid junction potentials, since only differences in potential between the $[Cu(pdto)]^{2+/+}$ and $FeCp_2^{0/+}$ couples in a particular solvent were being considered. The reported half-wave potentials were determined at scan rates of 20 mV s^{-1} with 0.10 M n-Bu_4NPF_6 as supporting electrolyte. Values of 0.444, 0.520 and 0.443 V for $[Cu(pdto)]^{2+/+}$, and 0.400, 0.343 and 0.453 V for $[FeCp_2]^{+/0}$, vs SCE, were obtained in acetonitrile, methanol and acetone, respectively. Anodic and cathodic peak separations of close to 0.072 V were found for $[FeCp_2]^{+/0}$, while separations between 0.10 and 0.14 V were observed for the $Cu(pdto)^{2+/+}$ couple in the three solvents. An E_f^0 value of 0.305 V was recorded for a solution of $[Cu(pdto)]^{2+}$ in DMSO, with oxidation and reduction peaks separated by 0.310 V.

RESULTS AND DISCUSSION

In the solvents acetonitrile, acetone and methanol, the reaction was found to follow a second-order rate law, rate $= k_{12}[Cu^{II}][FeCp_2]$ over the concentration ranges employed. Second-order rate constants are shown in Table 1. Similar values were obtained with no added electrolyte and in the presence of 0.10 M n-Bu_4NPF_6, as would be expected for reaction of neutral ferrocene with a dipositive cation in the absence of significant ion-pairing effects. The measured rate constants were also found to be insensitive to variations in excess ligand concentration ($[pdto]/[Cu^{II}] = 2.4$–7.8). The predominant copper(II) species in solution under the experimental conditions is a $Cu(pdto)^{2+}$ complex with a tetradentate pdto ligand and one or two coordinated solvent molecules. Tetradentate coordination by pdto is indicated by the UV–vis spectrum, characterized by an intense *d–d* band at 594 nm and a strong $S(\sigma) \rightarrow d_{x^2-y^2}$ LMCT transition at 360 nm, which appear in each solvent. The $Cu(pdto)^{2+}$ spectrum is essentially the same in acetonitrile, acetone and methanol as in aqueous solution. Similar intense ligand-field and charge-transfer bands at comparable wavelengths also characterize other dithiaether copper(II) complexes.[18,19] $[Cu(pdto)]^{2+}$ stability is expected to result largely from the strong coordinating abilities of the terminal nitrogen atoms, since thiaether coordination to copper(II) in dipolar solvents is believed to be fairly weak. No evidence for pdto complexation was found in DMSO, where the 594 and 360 nm bands characteristic of $Cu(pdto)^{2+}$ were replaced by a single maximum at 206 nm. The much slower second-order rate constant, $k_2 = 3.0 \times 10^{-4}$ M^{-1} s^{-1}, that was obtained from absorbance changes recorded in DMSO, is attributed to the $FeCp_2$ reduction of $[Cu(DMSO)_n]^{2+}$ species formed in that solvent. No anion effects were noted using hexafluorophosphate as medium. The measured rate constants were independant of [n-Bu_4NPF_6], and ion pairing interactions, if present, do not show up kinetically, Similar behaviour was noted with added n-Bu_4NClO_4, in the few experiments carried out with perchlorate salt. This is in contrast to marked anion dependencies, arising from specific anion associations with the copper complex, that were found for $[Cu(pdto)]^{2+}$–$FeCp_2$ electron-transfer rates in acetonitrile, with n-Bu_4NBF_4 and $NaCF_3CO_2$ as electrolytes.[20]

The measured rate constants, k_{12}, and the electron-transfer equilibrium constants, K_{12}, deter-

Table 1. Second-order rate constants at 25°C for $[Cu(pdto)]^{2+}$–$FeCp_2$ electron transfer in acetonitrile, methanol and acetone

	Initial conc. $\times 10^4$ (M)			[n-Bu_4NPF_6] (M)	$10^{-4} \times k_{12}$ (M^{-1} s^{-1})
	$[Cu(pdto)^{2+}]$	[pdto]	$[FeCp_2]$		
Acetonitrile	1.95	10.5	40.4	0	2.28
	1.98	10.1	98.5	0.010	2.06
	1.95	10.5	39.9	0.050	2.18
	1.98	10.1	200.0	0.010	1.74
	1.95	5.4	31.0	0.100	2.14
	1.92	2.5	30.4	0.100	1.98
Methanol	2.02	8.8	30.1	0.102	9.45
	1.98	13.0	30.0	0.100	9.66
	1.96	2.1	15.2	0.100	10.2
	1.80	0.0	30.8	0.100	9.36
	1.98	10.5	30.5	0	8.20
Acetone	1.37	5.6	15.2	0.100	8.95
	1.86	7.1	31.0	0.100	9.42
	1.41	3.1	16.5	0.100	9.36
	1.58	0.0	15.5	0.100	8.87
	1.23	5.0	14.7	0	6.73

Table 2. Summary of kinetic and equilibrium parameters for $FeCp_2$–$[Cu(pdto)]^{2+}$ electron transfer in acetonitrile, methanol and acetone at 25.0°C

	Solvent		
	Acetonitrile	Methanol	Acetone
$k_{12} \times 10^{-4}$, no electrolyte	1.9	8.2	6.7
$k_{12} \times 10^{-4}$, 0.10 M n-Bu_4NPF_6	2.1	9.6	9.1
K_{12}	5.5	980.0	0.68
$k_{12}/K_{12}^{1/2}$	9.0×10^3	3.1×10^3	1.1×10^5
k_{11}[a] $\times 10^{-6}$	5.3	6.0	4.6
k_{22}	15.0	2.2	2.6×10^3

Second order rate constants (M^{-1} s^{-1}).
[a] Reference 21.

mined in each solvent are summarized in Table 2. Also shown are estimated values of the Cu $(pdto)^{2+/+}$ self-exchange rate constant, k_{22}, obtained by the Marcus relations* using known $FeCp_2^{0/+}$ self-exchange rate constants, k_{11},[21] in the different solvents. The values obtained compare to a mean k_{22} value of 0.64 M^{-1} s^{-1} previously estimated for $[Cu(pdto)]^{2+/+}$ self-exchange in 50% aqueous methanol with ruthenium(II) ammine complexes as reductants.[8] Outer-sphere electron-transfer was assumed in the previous study, and a similar mechanism is expected here with ferrocene as reductant. When corrected for driving force ($k_{12}/K_{12}^{1/2}$), the reaction rate in acetone appears more rapid than in the other solvents, which is reflected strongly in the value of the copper(I)–copper(II) self-exchange rate constant obtained (10^2– to 10^3–fold greater in acetone than in the other two solvents). For the $Cu(pdto)^{2+/+}$ system, solvent-dependent rates could arise from solvent influences on both the inner-sphere and outer-sphere components, ΔG_i and ΔG_o, of the activation free energy. Possible outer-sphere solvent influences were explored through the Marcus solvent dielectric continuum expression.[22]

* $k_{12} = (K_{12} k_{11} k_{22} f)^{1/2}$, where $\ln f = \ln (K_{12})^2/4 \ln (k_{11} k_{22}/Z^2)$; Z is the collision frequency, taken to be 10^{11} M^{-1} s^{-1}.

$\Delta G_o = (e^2/4r)[(1/D_{op})-(1/D_s)]$ by plots of $\ln k_{22}$ vs $(1/D_{op})-(1/D_s)$ and $\ln k_{12}/K_{12}^{1/2}$ vs $(1/D_{op})-(1/D_s)$, where ΔG_o, r, D_{op}, and D_s are the outer-sphere solvent reorganization component of the activation energy, the distance between the reactant centres in the transition state and the optical and static dielectric constants. Although a linear dependence was found in both cases, this would appear largely fortuitous, as the value of the slopes obtained in the plots, -169 and -84.7, respectively, correspond to separations, r, in the transition state of 0.83 and 1.7 Å, which are close to an order of magnitude smaller than expected. Failure of the reaction to follow the dielectric continuum theory points to inner-sphere reorganizational changes involving coordinated solvent molecules, rather than outer-sphere solvent effects, being responsible for the solvent-dependent reaction rates that were found. Crystal structures have established five-coordinate copper(II), $[Cu(pdto)ClO_4]ClO_4$, and four-coordinate copper(I), $[Cu(pdto)]PF_6$, structures in the solid state, and the slow self-exchange rate constant estimated for the copper(II)/(I)–pdto couple in aqueous media from k_{12} data involving ruthenium(II)ammine reductants,[6,8] has been previously attributed to the substantial inner coordination sphere reorganizations accompanying electron transfer on reduction of five-coordinate $[Cu(pdto)H_2O]^{2+}$ to the four-coordinate $[Cu(pdto)]^+$ product. With electron transfer coupled to a change in coordination number during the reaction, it is possible for rate control to be tied to either the electron-transfer step or to water loss from the copper centre. Since the reaction in aqueous media was well behaved in the Marcus sense, with $\log k_{12}$ values proportional to G^0 over a fairly wide range of driving force, an electron-transfer controlled reaction rate is indicated. This could result from a concerted one-step process or through a two-step mechanism involving a fast conformational equilibrium prior to a rate-determining electron-transfer step:

$$[Cu(pdto)H_2O]^{2+} \underset{k_{-1}}{\overset{k_1}{\rightleftharpoons}} [Cu(pdto)]^{2+} + H_2O$$

$$[Cu(pdto)]^{2+} + Ru^{II} \xrightarrow[\text{slow}]{k_2} [Cu(pdto)]^{+} + Ru^{III},$$

with $k_{-1} \gg k_2, k_1$. Of interest is the possibility that the more rapid rate constants estimated for $Cu(pdto)^{2+/+}$ self-exchange in acetone indicate a change in mechanism in that solvent, with rate control being tied to a conformational change at the copper centre. Rate controlling structural change at the copper(II) centre, with ferrocene as reductant, could result if $k_2 \gg k_{-1}, k_1$:

$$[Cu(pdto)(acetone)]^{2+} \underset{k_{-1}}{\overset{k_1}{\rightleftharpoons}} [Cu(pdto)]^{2+} + \text{acetone (slow)}$$

$$[Cu(pdto)]^{2+} + FeCp_2 \xrightarrow{k_2} [Cu(pdto)]^{+} + FeCp_2^{+}.$$

Such a change from an electron-transfer controlled reaction rate in aqueous solution ($k_{-1} \gg k_2, k_1$) to one depending on geometric change at the copper(II) centre in acetone ($k_2 \gg k_{-1}, k_1$), would be promoted by a slower rate of association of acetone with the copper(II) centre (k_{-1} step) relative to that of water, and by a more rapid rate of reduction of $[Cu(pdto)]^{2+}$ by $FeCp_2$ (k_2 step) relative to that by ruthenium(II) ammine complexes. A more rapid k_2 step is certainly expected with $FeCp_2$ as reductant on electrostatic grounds, and a *ca* 100-fold rate advantage has previously been demonstrated for the reduction of $Cu(pdto)^{2+}$ by the neutral reductant $Ru(bpy)_2Cl_2$, as compared with dipositive ruthenium(II) ammine complexes.[8] A lower rate constant for the association of acetone with $[Cu(pdto)]^{2+}$ would also be expected on steric grounds. This is also suggested by the stability constant data, where the largest K_f values for $[Cu(pdto)]^{2+}$ formation ($Cu^{2+}{}_{solv} + pdto = [Cu(pdto)(solv)]^{2+}$) have been obtained in acetone (Table 3). If variations amongst the K_f values have their origin largely in copper(II) desolvation changes, which appears likely since entropy changes are expected to be very similar for the complexation process involved, the largest K_f value is found in acetone because this has the weakest Lewis base interaction with copper(II) and is most readily replaced by the pdto ligand. The good electron pair donor solvents, DMSO, DMF and acetonitrile, afford the smallest K_f values.

Brunschwig and Sutin[24] have determined the conditions necessary for a two-step "gated" mechanism involving the intermediate formation of an

* Although rate controlling coordination changes at the copper(I) centre

$$[Cu(pdto)L]^{2+} + Red \underset{k_{-1}}{\overset{k_1}{\rightleftharpoons}} [Cu(pdto)L]^{+} + Ox$$

$$[Cu(pdto)L]^{+} \xrightarrow[\text{slow}]{k_2} [Cu(pdto)]^{+}$$

can result in both electron-transfer ($k_1 \gg k_{-1}, k_2$) and substitution-controlled ($k_{-1} \gg k_1, k_2$) rate constants under certain conditions, provided the spectra of the two copper(I) species are the same, such a mechanism appears unlikely for copper(I), and is not considered.

Table 3. Stability constants, K_f, for $[Cu(pdto)]^{2+}$ formation in dipolar solvents at 25°C

Solvent	K_f (M^{-1})
Acetone	$(1.5\pm0.1)\times10^7$
Ethylacetate	$(2.6\pm0.1)\times10^6$
Isopropanol	$(2.5\pm0.6)\times10^6$
Methanol	$(2.0\pm0.5)\times10^6$
Ethanol	$(1.6\pm0.6)\times10^6$
Acetonitrile	$(2.1\pm0.5)\times10^5$
DMF	$(6.0\pm0.3)\times10^3$
DMSO	<10

unstable reactant to compete with a direct concerted reaction involving only the stable reactant and product. A two-step mechanism is expected to be favourable only at low driving force, and would require that the intermediate, $[Cu(pdto)]^{2+}$, is only slightly less stable than the stable reactant, $[Cu(pdto)(acetone)]^{2+}$. These conditions would appear to be met in acetone, where the solvent coordinates only weakly to the copper(II) centre, and $K_{12} = 0.68$. The data presented, however, do not in themselves confirm a change to a two-step mechanism in acetone, with rate control tied to the coordination change at the copper centre. A concerted one-step reaction involving a smaller inner-shell reorganization energy could also give rise to larger estimated k_{22} values using the Marcus theory.

Amongst other copper(I)–copper(II) self-exchange rate constants (k_{22}, $M^{-1}s^{-1}$) determined for complexes with nitrogen and sulphur donor ligands, fairly large values have been obtained with the multidentate ligands py_2DAP[10] (1.7×10^3), $(imidH)_2DAP$[13] (1.3×10^4), bidhp[12] (4×10^3) and TAAB[7] (5×10^5), where ligand constraints minimize geometric changes between oxidation states. Lower k_{22} values have been estimated with pdto and with tripodal ligands pmas (6–45) and peas[6] (0.7) in CuN_2S_2 environments, where significant structural changes in aqueous solution, particularly changes involving solvent coordination, accompany the redox step. The significantly larger $[Cu(pdto)]^{2+/+}$ self-exchange rate constant obtained in acetone, 2.6×10^3 M^{-1} s^{-1}, is comparable with the self-exchange values obtained for copper(II)–copper(I) systems, where changes in coordination are minimal. This would suggest that the more rapid self-exchange rate in acetone results from a concerted process with a relatively small reorganizational barrier resulting from the weak association of acetone with the copper(II) centre in that solvent.

Acknowledgement—The Authors thank the donors of the Petroleum Research Fund administered by the American Chemical Society for support of this research.

REFERENCES

1. K. D. Karlin and J. Zubieta (Eds), *Copper Coordination Chemistry: Biochemical and Inorganic Perspectives*. Adenine Press, New York (1983).
2. M. A. Augustin and J. R. Yandell, *Inorg. Chem.* 1979, **18**, 577.
3. N. Al-Shatti, A. G. Lappin and A. G. Sykes, *Inorg. Chem.* 1981, **20**, 1466.
4. K. M. Davies, *Inorg. Chem.* 1983, **22**, 615.
5. C.-W. Lee and F. C. Anson, *J. Phys. Chem.* 1983, **87**, 3350.
6. K. D. Karlin and J. K. Yandell, *Inorg. Chem.* 1984, **23**, 1184.
7. E. J. Pulliam and D. R. McMillan, *Inorg. Chem.* 1984, **23**, 1172.
8. K. M. Davies and B. Guilani, *Inorg. Chim. Acta.* 1987, **127**, 223.
9. K. M. Davies and B. Byers, *Inorg. Chem.* 1987, **26**, 3823.
10. J. A. Goodwin, D. M. Stanbury, L. J. Wilson, C. W. Eigenbrot and W. R. Scheidt, *J. Am. Chem. Soc.* 1987, **109**, 2979.
11. M. J. Martin, J. F. Endicott, L. A. Ochrymowycz and D. B. Rorabacher, *Inorg. Chem.* 1987, **26**, 3012.
12. C. M. Groeneveld, J. van Rijn, J. Reedijk and G. W. Canters, *J. Am. Chem. Soc.* 1988, **110**, 4893.
13. J. A. Goodwin, D. M. Stanbury, L. J. Wilson and R. A. Scott, *Inorg. Chem.* 1989, **28**, 42.
14. H. Doine, Y. Yano and T. W. Swaddle, *Inorg. Chem.* 1989, **28**, 2319.
15. S. Knapp, T. P. Keenan, X. Zhang, R. Fikar, J. A. Potenza and H. Schugar, *J. Am. Chem. Soc.* 1990, **112**, 3452.
16. H. A. Goodwin and F. Lions, *J. Am. Chem. Soc.* 1960, **82**, 5013.
17. W. R. Heineman and J. M. Beebe, *Chemistry Experiments for Instrumental Methods by D. T. Sawer.* John Wiley, New York (1984).
18. A. R. Amundsen, J. Whelan and B. Bosnich, *J. Am. Chem. Soc.* 1977, **99**, 6730.
19. D. E. Nikles, M. J. Powers and F. L. Urbach, *Inorg. Chem.* 1983, **22**, 3210.
20. K. M. Davies, K. D. Whyte and A. H. Gilbert, *Inorg. Chim. Acta.* 1990, **177**, 121.
21. E. S. Yang, M.-S. Chan and A. C. Wahl, *J. Phys. Chem.* 1980, **84**, 3094.
22. R. A. Marcus, *J. Chem. Phys.* 1965, **43**, 679.
23. G. R. Brubaker, J. N. Brown, M. K. Yoo, R. A. Kinsey and T. M. Kutchan, *Inorg. Chem.* 1979, **18**, 299.
24. B. S. Brunschwig and N. Sutin, *J. Am. Chem. Soc.* 1989, **111**, 7454.

Polyhedron Vol. 10, No. 14, pp. 1653–1656, 1991
Printed in Great Britain

0277–5387/91 $3.00+.00
© 1991 Pergamon Press plc

MAGNETIC AND ESR STUDIES OF COPPER(II) COMPLEXES WITH N-(AMINOALKYL)SALICYLALDIMINES

M. LELUK and B. JEŻOWSKA-TRZEBIATOWSKA

Institute for Low Temperature and Structure Research, Polish Academy of Sciences, Wrocław, Poland

and

J. JEZIERSKA*

Institute of Chemistry, Wrocław University, 50-383 Wrocław, Poland

(*Received* 16 *July* 1990; *accepted* 5 *April* 1991)

Abstract—The magnetic susceptibility and electron spin resonance (ESR) spectra have been studied for copper(II) complexes with N-(aminoalkyl)salicylaldimines, tridentate Schiff bases containing O(phenol), N(imine) and N(amine) donor atoms. It has been stated that the compounds are anti-ferromagnetically coupled dimers. The ESR spectra show the depolimerization of the dimers by the polar solvents and formation of two types of adducts. On the basis of the ESR hyperfine structural parameters the structure of the adducts has been proposed.

Copper(II) complexes with low magnetic moments are of considerable interest since their magnetic behaviour may usually be attributed to spin–spin coupling within a polynuclear cluster. Often the complexes are dimeric and an exchange interaction occurs between the two copper(II) centres in the dimer. The nature of the interaction is usually interpreted as an isotropic spin–spin interaction, $-2JS_1S_2$. The magnetic properties of these compounds may be studied by electron spin resonance (ESR) and bulk susceptibility methods.

Our previous studies have considered typical binuclear copper(II) complexes with tridentate ONO chelating ligands derived from condensation products of 3-aminopropanol with 2-hydroxyaryl aldehydes (type I complexes) and *o*-aminophenol with *β*-diketones (type II complexes).[1,2]

In the present paper, the six copper(II) complexes with different tridentate ligands which were able to coordinate by the ONN donor set [i.e. O(phenol), N(imine) and N(amine)] were studied by ESR and magnetic susceptibility measurement methods. The synthesis of two of these complexes derived from salicylaldehyde and their room magnetic moments

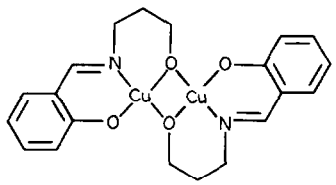

I

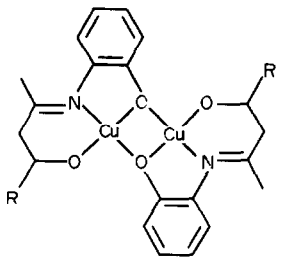

II

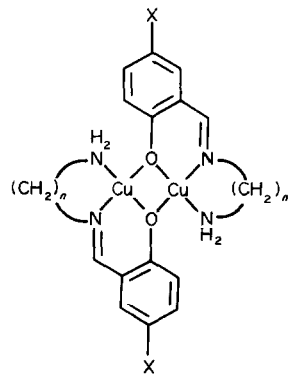

III

$n = 2,3$

$X = H, NO_2$

* Author to whom correspondence should be addressed.

have been reported previously.[3] The results presented here support the dimeric structure of the compounds which are revelant to type III complexes.

In continuation of our studies[2,4] on the adducts of the copper(II) complexes with tridentate Schiff bases, the formation of Cu(ONN)L adducts as the result of dissociation of the dimers in polar solvents, L, has been investigated by the ESR method.

EXPERIMENTAL

The complexes were prepared according to the high dilution reaction described by Mandal and Nag[3] and recrystallized from methanol. The elementary analysis for copper, carbon, nitrogen and hydrogen confirms the formation of copper(II) complexes with N-(aminoalkyl)salicylaldimines showing the following formulae: Cu(sal-enNH$_2$)ClO$_4$, Cu(sal-enNH$_2$)NO$_3$, Cu(sal-pnNH$_2$)ClO$_4$, Cu(sal-pnNH$_2$)NO$_3$, Cu(5-NO$_2$sal-enNH$_2$)NO$_3$·H$_2$O and Cu(5-NO$_2$sal-pnNH$_2$)NO$_3$·H$_2$O. The ligands are the condensation products of salicylaldehyde or 5-nitrosalicylaldehyde with 1,2-diaminoethane (sal-enNH$_2$), (5-NO$_2$sal-enNH$_2$) and salicylaldehyde or 5-nitrosalicylaldehyde with 1,3-diaminopropane, (sal-pnNH$_2$), (5-NO$_2$sal-pnNH$_2$), respectively. The number of water molecules was determined thermogravimetrically. The solvents were purified by the standard methods.

Variable temperature magnetic susceptibility studies between 77 and *ca* 295 K were performed on polycrystalline samples using the Gouy method. Data were corrected for diamagnetism using Pascal constants and TIP, assumed to equal 60×10^{-6} c.g.s.u. The ESR spectra were recorded on a JEOL JES-ME X-band spectrometer using a nuclear magnetometer MJ 11OR and microwave frequency meter JES-SH-30X. The IR spectra were measured on a Perkin–Elmer 180 IR spectrometer.

RESULTS AND DISCUSSION

Properties of the complexes in the solid phase

The significant feature in the IR spectra of the complexes is the presence of the bands associated with N—H (3160–3360 cm^{-1}) as well as C=N bonds (1628–1648 cm^{-1}). Another important characteristic is the appearance of a band associated with the phenolic C—O bond at *ca* 1556 cm^{-1}, which indicates[5] the presence of a bridging phenolic oxygen.

The effective magnetic moments of the compounds derived from the salicylaldehyde decrease with a decrease in temperature; from 1.0 to 1.4 BM at room temperature to near zero at 77 K, indicating antiferromagnetic interactions. The experimental data were interpreted in terms of the isotropic Heisenberg interaction model, based on the exchange Hamiltonian $H = -2JS_1S_2$. The well-known Bleaney–Bowers equation[6] was used to estimate the value of $-2J$ with g fixed at 2.12. A least-squares fitting was carried out and included a term representing a fraction of non-coupled paramagnetic copper centres, p. The results are given in Table 1, and a representative fit for Cu(sal-pnNH$_2$)NO$_3$ is shown in Fig. 1. The experimental susceptibility of the complexes obeys the Bleaney–Bowers equation well, supporting the dimeric structure.

The investigated complexes in the temperature range 77–295 K are ESR silent in the 0–7000 G range; in some cases only very weak signals of the monomeric impurities were observed. The absence of the ESR spectra of the compounds should be related to the pairwise interaction between the copper(II) ions. The complexes derived from 5-nitrosalicylaldehyde exhibit magnetic moments close to the value typical for the non-coupled copper(II) complexes in the temperature range studied. The best fit of their magnetic susceptibilities

Table 1. Magnetic properties of copper(II) complexes with N-(aminoalkyl)-salicylaldimines

Compound	μ_{eff} at 292 K (BM)	$-2J$ (cm^{-1})	p
Cu(sal-enNH$_2$)ClO$_4$	1.12	428	0.0022
Cu(sal-enNH$_2$)NO$_3$	1.40	282	0
Cu(sal-pnNH$_2$)ClO$_4$	1.10	438	0.0168
Cu(sal-pnNH$_2$)NO$_3$	1.01	474	0.0004
Cu(5-NO$_2$sal-enNH$_2$)NO$_3$·H$_2$O	1.80	13	0
Cu(5-NO$_2$sal-pnNH$_2$)NO$_3$·H$_2$O	1.84	$\|2J\| < 4$	—

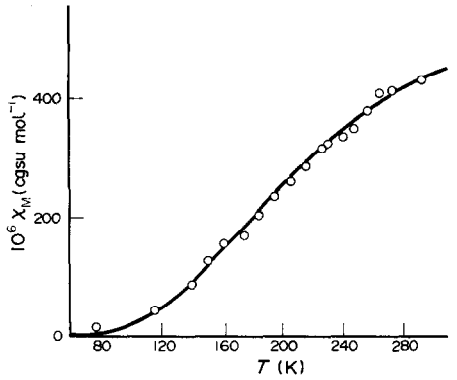

Fig. 1. Temperature dependence of the magnetic susceptibility (per copper atom mole) for $Cu(sal\text{-}pnNH_2)NO_3$.

to the dimer equation yields $-2J = 13$ cm^{-1} and $g = 2.09$ for $Cu(5\text{-}NO_2sal\text{-}enNH_2)NO_3 \cdot H_2O$ and $|2J| < 4$ cm^{-1} and $g = 2.11$ for $Cu(5\text{-}NO_2sal\text{-}pnNH_2)NO_3 \cdot H_2O$, indicating that the strength of the magnetic interactions is generally much smaller than in the corresponding compounds derived from salicylaldehyde. Although only the signals characteristic of the monomeric species are observed in the ESR spectra of these complexes, the appearance of the phenolic C—O band at 1556 cm^{-1} in the IR spectra is important, additional evidence of the binuclear structure. The considerable difference in the strength of antiferromagnetic coupling between the complexes under study may be attributed to the influence of molecular packing on the geometry of the bridging moiety.

Properties of the polymeric complexes in solution

The ESR spectra of the complexes dissolved in methanol, formamide and pyridine are typical for the monomeric species (Figs 2 and 3). They imply

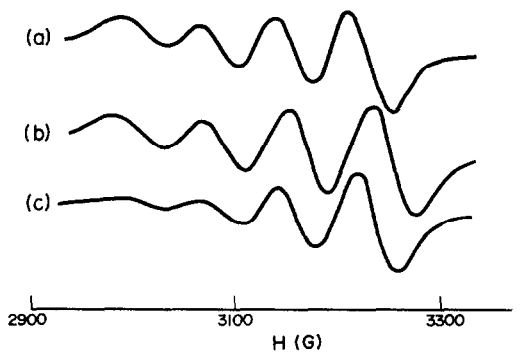

Fig. 2. ESR spectra of $Cu(sal\text{-}enNH_2)NO_3$ at 295 K: (a) in methanol (L), (b) upon addition of L_1 = pyridine to the methanol (L) solution and (c) in pyridine (L).

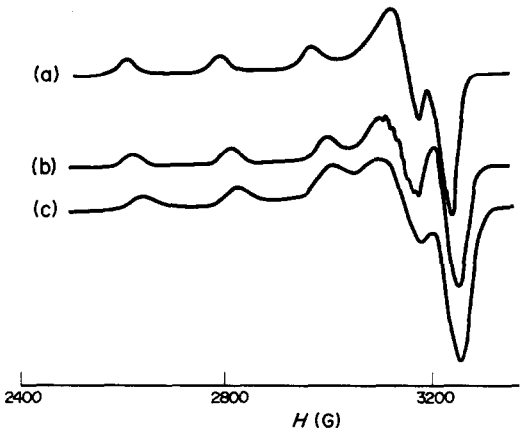

Fig. 3. ESR spectra of $Cu(sal\text{-}enNH_2)NO_3$ at 77 K: (a) in methanol (L), (b) upon addition of L_1 = pyridine to the methanol (L) solution and (c) in pyridine (L).

cleavage of the bridge bonds of dimeric molecules by polar solvents and formation of Cu(ONN)L adducts.

The important features in the interpretation of the ESR parameters (Table 2) are considerably smaller A_{iso} and $A_{\parallel}$ values and greater g_{iso} and $g_{\parallel}$ values for the compound derived from 1,3-diaminopropane compared with the parameters for the compound derived from 1,2-diaminoethane. This trend, which corresponds to the increasing degree of tetrahedral distortion[7] of coordination symmetry, can be associated with the increasing length of the methylene chain joining the nitrogen atoms. Similar chain length–tetrahedral distortion dependence has been observed[8] for tetradentate copper(II) salicylaldimine complexes.

Superhyperfine structure due to the presence of nitrogen nuclei coordinated to the copper(II) ion, which has been observed for ONO Schiff base complexes,[2,4] is not resolved at room temperature for the system under study. The lack of resolution may be explained by the greater number of nitrogen donors and their non-equivalency in our system. Although the perpendicular region of the frozen solution spectra demonstrates superhyperfine splitting due to nitrogen atoms (Fig. 3), it is not possible to determine the number of nitrogen donors on this basis.

Addition of L_1 = pyridine (the molar ratio $L_1/Cu = 6:1$) to a solution of the complexes in oxygen-coordination solvents, L, produced a characteristic change in the ESR parameters [Table 2, Fig. 2(b)]; decrease of the g_{iso} value (about 0.006) and significant increase of A_{iso} (about 10 G) as well as decrease of $g_{\parallel}$ (about 0.02). The observed spectral changes can be interpreted in terms of trans-

Table 2. ESR parameters for copper(II) complexes with N-(aminoalkyl)salicylaldimines in neat solvents (L) and upon addition of pyridine (L_1) to the solution[a]

Compound	Solvent (L)	g_{iso}	A_{iso}	$g_\parallel$	$A_\parallel$	Pyridine (L_1) added g_{iso}	A_{iso}	$g_\parallel$	$A_\parallel$
Cu(sal-enNH$_2$)ClO$_4$	Methanol	2.119	74	2.251	186	2.112	84	2.228	198
	Formamide	2.117	78	2.238	183	2.110	86	2.230	190
	Pyridine	2.114	76	2.226	191				
Cu(sal-enNH$_2$)NO$_3$	Methanol	2.119	75	2.251	188	2.111	83	2.228	198
	Formamide	2.116	77	2.247	185	2.114	85	2.225	189
	Pyridine	2.113	76	2.226	191				
Cu(sal-pnNH$_2$)ClO$_4$	Methanol	2.128	64	2.273	172	2.121	78	2.250	189
	Formamide	2.129	71	2.255	180	2.125	78	2.250	176
	Pyridine	2.121	71	2.246	183				
Cu(sal-pnNH$_2$)NO$_3$	Methanol	2.128	64	2.273	172	2.120	78	2.252	187
	Formamide	2.127	70	2.256	185	2.124	78	2.241	187
	Pyridine	2.122	69	2.243	185				
Cu(5-NO$_2$sal-enNH$_2$)NO$_3$·H$_2$O	Methanol	2.121	73	2.250	189	2.114	83	2.234	194
	Formamide	2.119	79	—	—	2.116	85	—	—
	Pyridine	2.118	79	2.227	192				
Cu(5-NO$_2$sal-pnNH$_2$)NO$_3$·H$_2$O	Methanol	2.133	66	2.276	174	2.122	79	2.254	189
	Formamide	2.126	72	2.251	192	2.125	78	2.249	187
	Pyridine	2.125	72	2.253	185				

[a] Parameters A are in 10^{-4} cm^{-1}; A_{iso} and g_{iso} were measured at 295 K; $A_\parallel$ and $g_\parallel$ were measured at 77 K.

formation of the pseudo-tetrahedral complex of the Cu(ONN)L type into the new adduct containing the pyridine molecule. The stereochemistry of the analogous pyridine adduct has been studied previously for the ONO chelating Schiff base copper(II) complexes.[2,4] On the basis of the changes in the copper hyperfine parameters and, furthermore, analysis of the superhyperfine splitting due to the nitrogen donors, it has been found that the pseudo-tetrahedral Cu(ONO)L complex coordinates one L_1 molecule changing its geometry from pseudo-tetrahedral in Cu(ONO)L to square pyramidal in the Cu(ONO)L_1L complex. L_1 is located in the chelating ring plane, while L adopts an apical position. Although in the present system nitrogen superhyperfine splitting is not informative, the full analogy in the changes of g and A values strongly suggests the same structure in the case of Cu(ONN)pyL (py = pyridine) adducts.

Acknowledgements—This work was financially supported by the Polish Academy of Sciences (Program CPBR 01.12.).

REFERENCES

1. B. Jeżowska-Trzebiatowska, J. Jezierska and J. Baranowski, *Chem. Phys. Lett.* 1977, **52**, 590.
2. J. Jezierska, A. Jezierski, B. Jeżowska-Trzebiatowska and A. Ożarowski, *Inorg. Chim. Acta* 1983, **68**, 7.
3. S. K. Mandal and K. Nag, *J. Chem. Soc., Dalton Trans.* 1984, 2839.
4. J. Jezierska, *Polyhedron* 1987, **6**, 1669.
5. T. Tokki, Y. Muto, M. Kato, K. Imai and H. B. Jonassen, *J. Inorg. Nucl. Chem.* 1972, **34**, 3377.
6. B. Bleaney and K. D. Bowers, *Proc. R. Soc.* 1952, **214A**, 451.
7. H. Yokoi and A. W. Addison, *Inorg. Chem.* 1977, **16**, 1341.
8. S. J. Gruber, C. M. Harris and E. Sinn, *J. Inorg. Nucl. Chem.* 1968, **30**, 1805.

Polyhedron Vol. 10, No. 14, pp. 1657–1662, 1991
Printed in Great Britain

0277–5387/91 $3.00+.00
© 1991 Pergamon Press plc

SYNTHESIS, CHARACTERIZATION AND REACTIVITY OF LEAD(II) ALKOXIDES AND OXOALKOXIDES: CONDENSATION TO OXOALKOXIDES AS A GENERAL STRUCTURAL FEATURE

RENÉE PAPIERNIK, LILIANE G. HUBERT-PFALZGRAF* and MARIE C. MASSIANI

Laboratoire de Chimie Moléculaire, Associé au CNRS, Parc Valrose, 06034 Nice, France

(*Received* 6 *December* 1990; *accepted* 5 *April* 1991)

Abstract—Various routes to lead(II) alkoxides using $PbCl_2$, $Pb(OAc)_2$ and $Pb[N(SiMe_3)_2]_2$ as starting materials have been explored. The formation of homoleptic alkoxides is limited to $[Pb(OBu^t)_2]_m$, while condensation to the oxoalkoxides $Pb_4O(OR)_6$ or $Pb_6O_4(OR)_4$ (R = Et, Pr^i) seems favoured. The various products have been characterized by microanalysis, IR and NMR spectroscopy. $[Pb(OBu^t)_2]_m$ and $Pb_4O(OR)_6$ are soluble precursors of lead oxide, while the tert-butoxide derivates are also volatile. Their reactivity (alcoholysis reactions, formation of complexes) has been examined and ^{207}Pb NMR was used to follow their condensation and/or complexation.

A variety of new materials of technological value—piezoelectric ceramics, superconductors, optico-electronic devices[1]—are multicomponent oxides containing lead. Traditional access to such materials by solid-state reactions at high temperature often results in poor control of the stoichiometry and phase of the final material sought, due, in part, to the volatility of the lead(II) oxide.[2] Sol–gel technology, using molecular precursors of lead oxide, might overcome some of these problems, as lower sintering temperatures are generally required.[3]

However, alkoxides, which often are the most suitable precursors of oxides, have long been practically unknown for lead(II). Poorly characterized, insoluble, polymeric alkoxides of formula $[Pb(OR)_2]_m$ have been reported to form through disproportionation of alkylalkoxides (for R = Me), or substitution reactions from $PbCp_2$ (for R = Me, Bu^t),[4] or from PbX_2[5] (X = I, NO_3 for R = Me). The formation of $Pb(OPr^i)_2$, starting from lead(II) acetate, has been claimed on the basis of its hydrolysis product PbO, but it has not been isolated.[6] Anodic oxidation of lead in absolute isopropanol offered a hexanuclear oxoalkoxide which has been structurally characterized as $Pb_6(\mu_3\text{-}O)_4(\mu_3\text{-}OPr^i)_4$.[7] Monomeric $Pb(OAr)_2$ (Ar = 2,6-ditert-butyl-4-methylphenyl) has been obtained by the metathesis reaction of either $PbCl_2$ or $Pb[N(SiMe_3)_2]_2$.[8]

The work of the group of Buhro[9] concerning the synthesis of $Pb(OR)_2$ (R = Bu^t, Pr^i, CMe_2Et, CEt_3, C_2H_4OMe, $CHMeCH_2NMe_2$) and the crystal structure of $[Pb(\mu,\eta^1\text{-}OC_2H_4OMe)_2]_\infty$ and of $Pb_3(\mu\text{-}OBu^t)_6$ prompts us to report the synthesis of soluble lead(II) alkoxides (R = Bu^t, Pr^i), whose behaviour is dominated by their tendency to undergo condensation reactions to adamantane-like units, $Pb_4O(OR)_6$ and $Pb_6O_4(OR)_4$. ^{207}Pb NMR was used to follow these inorganic polymerization reactions. Part of our work has been published as a preliminary communication.[10]

EXPERIMENTAL

All manipulations were routinely performed under dry argon using Schlenk tubes and vacuum-line techniques. Solvents were purified by standard methods. Anhydrous lead acetate was obtained by allowing the trihydrate to react with acetic anhydride at reflux. $Pb[N(SiMe_3)_2]_2$[11] and $Bu^t{}_3COH$ (tritoxH)[12] were synthesized as reported in the

* Author to whom correspondence should be addressed.

Table 1. Analytical and spectroscopic data of the various lead(II) alkoxides and oxoalkoxides

Compound	Analytical data (%) Found (Calc.) C	H	IR (cm^{-1}) Pb—OR	^1H ($CDCl_3$) (ppm)	$^{207}Pb(C_7D_8)$ (ppm)
$[Pb(OBu^t)_2]_m$ (**1**)	27.1 (27.2)	5.2 (5.1)	534vs, 464w 446m, 374m	1.32	4152
$Pb_4O(OBu^t)_6$ (**2**)	23.1 (22.5)	4.2 (4.2)	532vs, 502sh 446w	1.30	5032
$Pb_4O(OBu^t)_3(OAc)_3$	17.5 (17.4)	2.8 (2.9)	652s, 615m[a] 550w, 485sh, 424sh	2.00 (3H) 1.30 (9H)	
$Pb_4O(OPr^i)_6$ (**3**)	18.2 (18.0)	3.3 (3.5)	530vs, 503vs 394w	1.27d (J = 6.3 Hz) 4.77m	4982[b]
$Pb_6O_4(OPr^i)_4$	9.2 (9.2)	1.7 (1.8)	530vs, 503s	1.11d (J = 6.3 Hz) 4.79m	4985
$Pb_4O(OEt)_6$	12.7 (12.9)	2.5 (2.7)	521vs, 479s	1.39t (J = 7 Hz) 4.35q	4977[c]
$Pb_6O_4(OEt)_4$	5.1 (6.5)	1.1 (1.3)	498vs, 467s	1.19t (J = 7 Hz) 4.13m	5019[c]
$Pb(tritox)_2(tritoxH)$	56.9 (58.2)	10.0 (10.3)	660m, 572w 491w, 450w, 429m	1.29	

[a] ν(Pb—OR) stretching in addition to that of Pb—OAc, $\nu_{as}(CO_2)$ 1533 cm^{-1}, $\nu_s(CO_2)$ 1398 cm^{-1}.
[b] $C_7D_8 + CH_2Cl_2$.
[c] C_7D_8 + THF.

literature. IR spectra were obtained as Nujol or poly(chlorotrifluoroethylene) mulls on a Bruker IFS 45 spectrometer. ^1H and ^{207}Pb NMR spectra were registered, respectively, on Bruker WH-90 and AC-200-E spectrometers, operating in the Fourier transform mode. ^{207}Pb chemical shifts are quoted relative to $Pb(NO_3)_2$ as an external reference, and are negative for high fields. Mass spectra were measured on a Ribermag R-10 spectrometer. Molecular weight data were obtained using the Signer method.[13] Microanalyses were performed at the Centre de Microanalyses du CNRS. Analytical and spectral data are collected in Table 1.

Synthesis of $[Pb(OBu^t)_2]_m$ (**1**)

On addition of Bu^tOH (3 g, 40 mmol) in 15 cm^3 of pentane to a yellow solution of $Pb[N(SiMe_3)_2]_2$ (2.3 g, 4.34 mmol) in 25 cm^3 of pentane at −70°C, the reaction medium immediately became colourless. After 3 h, the volatiles were evaporated and the solid purified by crystallization in pentane at −20°C (2.1 g, 87%). MS (EI, 70 eV) m/z^+, %. M = $[Pb(OBu^t)_2]_2$, M − $C_4H_8O_2$ (15%), M − C_7H_{12} (10%), M/2 (10%), PbO_2 (100%), PbO (20%). Mol. wt: (C_6H_6, 25°C, 0.16 M): 648 ± 65 (calc. 353).

Synthesis of $Pb(tritox)_2(tritoxH)$

A similar procedure applied to $Pb[N(SiMe_3)_2]_2$ (1.18 g, 2.2 mmol) in pentane and tritoxH (0.9 g, 4.4 mmol) at 0°C in the dark gave, after work-up and recrystallization, 0.8 g (45%) of yellow crystals of $Pb(tritox)_2(tritoxH)$. The product is thermally and photochemically unstable, giving colloidal lead.

Synthesis of $Pb_4O(OR)_6$ (R = Bu^t, Pr^i, Et)

R = Bu^t. $Pb_4O(OBu^t)_6$ (**2**) was obtained quantitatively by adding Bu^tOH (32 mmol, 0.3 cm^3) to $Pb[N(SiMe_3)_2]_2$ (0.46 g, 0.85 mmol) in 0.5 cm^3 of hexane.

$Pb_4O(OBu^t)_6$ could also be obtained by reacting $Pb(OAc)_2$ (1.57 g, 4.83 mmol) and $NaOBu^t$ (9.7 mmol) in 100 cm^3 of THF at reflux for 24 h and sublimation of the solid obtained by evaporation to dryness at 200°C (10^{-2} mm Hg); 85%.

R = Pr^i. A suspension of $Pb(OAc)_2$ (10 g, 31.1 mmol) in 50 cm^3 of Pr^iOH was added to 100 cm^3 of 0.6 M $NaOPr^i$ in Pr^iOH. After refluxing for 15 h, the precipitate was eliminated by filtration and washed with Pr^iOH. Recrystallization of the crude product in toluene/pentane gave, as the third crop of crystals, 3 g (32%) of $Pb_4O(OPr^i)_6$ (**3**). MS

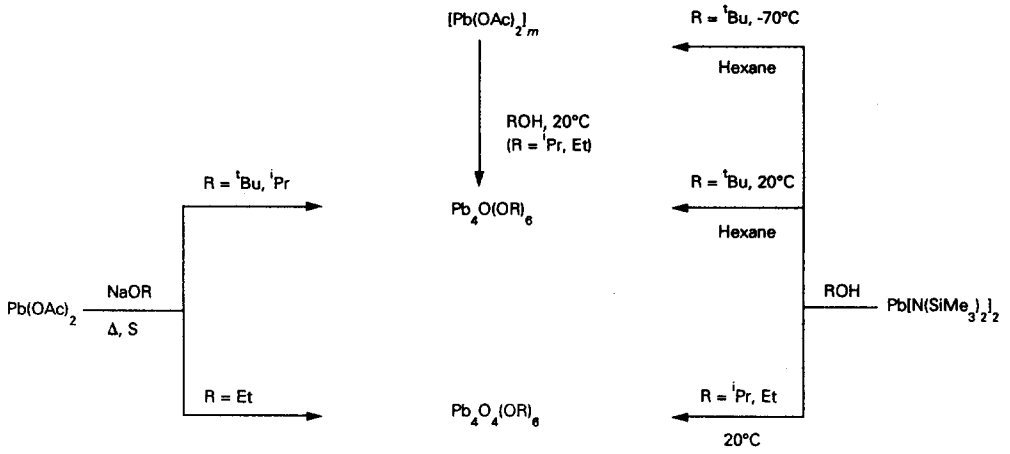

Scheme 1.

[m/z^+, M = $Pb_4O(OPr^i)_6$], M−$PbOC_3H_4$ (10%), M−$Pb(OC_3H_7)_2$ (15%), M−$Pb_2O_2C_3H_7$ (20%), $Pb_2(OC_3H_7)_2$ (30%), $PbO_2C_5H_8$ (20%), Pr_2O (100%).

Alcoholysis of either $[Pb(OBu^t)_2]_m$ or $Pb_4O(OBu^t)_6$ in hexane led to an immediate, quantitative precipitation of $Pb_4O(OR)_6$ (R = Pr^i, Et).

Synthesis of $Pb_6O_4(OR)_4$ (R = Et, Pr^i)

Addition of Pr^iOH (10 cm^3) to neat $Pb[N(SiMe_3)_2]_2$ (0.6 g, 0.96 mmol) at room temperature resulted in a slightly exothermic reaction with immediate precipitation of $Pb_6O_4(OPr^i)_4$.

$Pb_6O_4(OEt)_4$ was also obtained by refluxing $Pb(OAc)_2$ and NaOEt in EtOH for 3 days; the several recrystallizations required for a product without alkali residues led to a poor yield (10%). Cell parameters (−80°C): a = 20.024(5), b = 12.473(3), c = 17.409(3) Å and β = 95.86(4)°, monoclinic.

Synthesis of $Pb_4O(OBu^t)_3(OAc)_3$

Acetic anhydride (0.23 cm^3, 2.3 mmol) in 10 cm^3 of THF was slowly added at 0°C to $Pb(OBu^t)_2$ (0.82 g, 2.3 mmol) in 10 cm^3 of THF. Evaporation to dryness after a 1 h reaction time, left analytically pure $Pb_4O(OBu^t)_3(OAc)_3$ (0.7 g, 97%). The product is unstable in solution; further condensation with elimination of the acetato groups was observed.

The various lead(II) alkoxides are white solids; their solubility decreases with the steric demand of the alkoxo group and increasing nuclearity. The tert-butoxide derivates are highly soluble in the usual solvents, including hexane, while the ethoxides are poorly soluble; the highest solubilities are usually observed in the parent alcohol, CH_2Cl_2 or THF.

RESULTS AND DISCUSSION

(a) *Synthesis and characterization*

Various routes to lead(II) alkoxides using $PbCl_2$, $Pb(OAc)_2$ and $Pb[N(SiMe_3)_2]_2$ as starting materials were estimated (Scheme 1). Lead(II) acetate and lead(II) bis-trimethylsilylamide appear to be the most useful precursors. The novel alkoxides were characterized by microanalysis and the usual spectroscopic techniques including ^{207}Pb NMR (Table 1).

Reaction between $Pb(OAc)_2$ and NaOR (R = Bu^t, Pr^i, Et), in polar solvents (ROH or THF) at reflux for *ca* 24 h, actually led to the isolation of oxoalkoxides, $Pb_4O(OR)_6$ or $Pb_6O_4(OR)_4$. Examples of synthesis of alkoxides starting from acetates remain scarce.[14] In the case of lead, this reaction is highly dependent on the nature of the alkoxo ligand, the reaction is generally incomplete with formation of soluble acetato or oxoacetatoalkoxides [$\nu(CO_2)$ at 1541 and 1456 cm^{-1} in the IR spectra for R = Bu^t for instance].* The volatility of $Pb_4O(OBu^t)_6$ (130°C, 10^{-4} mm Hg) and the poor thermal stability of the various acetatoalkoxides allow its isolation with yields up to 85%. However, the poor selectivity of the reaction results in much lower yields when the work-up requires isolation by crystallization: 35% for R = Pr^i, even less (10%) for the lead ethoxide derivatives whose poor solubility prevented an efficient separation from the starting material. Formation of oxoalkoxides may

*Oxoacetatoalkoxides were also reported as secondary products in the anodic dissolution of lead in ethanol as a result of the reaction of the alkoxide with the supporting electrolyte.[7]

result from acetato groups acting as an oxygen donor or from condensation reactions involving $Pb(OR)_2$ species with elimination of dialkyl ether. Indeed, formation of condensed lead(II) oxoalkoxides appears to be general behaviour in the chemistry of lead(II) alkoxides, and is favoured by a low steric demand of the alkoxo ligand, kinetically fast reactions using $Pb[N(SiMe_3)_2]_2$ as starting material and subsequent recrystallization of the products. Further condensation was also reported to occur by elimination of hexaphenyldisiloxane in the recrystallization of $Pb_4(\mu_4\text{-}O)(OSiPh_3)_6$ giving $Pb_8O_5(OSiPh_3)_6$.[15]

Lead(II) bis-trismethylsilylamide offers a better route to pure lead(II) alkoxides, since the volatile bis-trimethylsilylamine is the only co-product. By contrast with the reactions using the acetate as a starting material which proceed at high temperature, homoleptic alkoxides could be obtained. Highly soluble $Pb(OBu^t)_2$ (**1**) was obtained in 80% yields, by reaction between $Pb[N(SiMe_3)_2]_2$ and the alcohol in dilute medium (pentane), while the formation of $Pb_4O(OBu^t)_6$ (**2**) was quantitative when the reaction was achieved without solvent. Compound **1** was recently established to be a trimer in the solid state, independently by two groups.[9,16] We found this compound to be dimeric in the gas phase (mass spectrometry) as well as in benzene solution at room temperature (M: exp 648 ± 65, calc. 353). Molecular weight data obtained at lower temperature (cryoscopy)[9] account for an equilibrium between dimeric and trimeric species, although we could detect only one type of alkoxo group down to $-60°C$ by ^1H NMR. ^{207}Pb NMR also shows only a single, sharp peak ($A_{1/2} = 16$ Hz).* Dimeric species have also been found for the tin and germanium analogues.[17] An increase in the steric demand of the alkoxo group by using the $OCBu^t_3$ (tritox) moiety (cone angle 125°)[18] prevents the formation of alkoxide bridges, giving a monomeric solvate $Pb(tritox)_2(tritoxH)$. However, this species is unstable and undergoes easy electron-transfer reactions, giving colloidal lead. Synthetic routes using the reactive bis-trimethylsilylamide lead derivative favour the formation of oxoalkoxides of higher nuclearity for alkoxo groups such as R = Et. $Pb_6O_4(OEt)_4$ was obtained, even at low temperature. Reactions between $PbCl_2$ and NaOR (R = Et, Pr^i) were characterized by the poor conversion of the starting material even at high temperature and thus low yields (10%).

The solubility of the various species is mainly governed by the extent of condensation, and therefore, the nature of the alkoxo ligand. $[Pb(OBu^t)_2]_m$ (**1**) is the most volatile species reported here (100°C, 10^{-4} mm Hg) and by contrast with the other lead(II) alkoxides could be sublimed, but with partial conversion to the more stable oxo derivative, $Pb_4O(OBu^t)_6$ (**2**).[10] IR and ^1H NMR spectra generally offer less information, as they mainly display the pattern of the alkoxo ligand.

Characterization was therefore also achieved by using ^{207}Pb NMR. Although it has attractive properties ($I = 1/2$ and adequate natural abundance $\approx 20\%$), ^{207}Pb NMR has been relatively neglected, especially for lead(II) compounds.[19] As a general feature, in the ^{207}Pb spectra of the various lead(II) alkoxides and oxoalkoxides sharp signals were observed in the range 4100–5100 ppm (Table 1). The chemical shifts are nearly independent of the solvent, and for the $Pb_4O(OR)_6$ homologues they move to high field on substituting Bu^t for smaller and more electronegative R groups. ^{207}Pb NMR was especially useful for ascertaining the purity of **1** (4152 ppm), for instance (absence of **2** at 5032 ppm), since IR or ^1H NMR spectra were nearly identical for both compounds and thus uninformative. This method also appears attractive for analysing the composition of the complex reaction media such as $PbCl_2$ or $Pb(OAc)_2$ and $NaOBu^t$ before work-up.

Although $Pb(OAr)_2$,[8] $Pb(OSiMe_3)_2$, $[Pb(OPr^i)_2]_m$[9] and $[Pb(OBu^t)_2]_m$ could be obtained, the stability of homoleptic lead(II) alkoxides appears poor. Condensation to oxoalkoxides of general formula $Pb_4O(OR)_6$ or $Pb_6O_4(OR)_4$ is favoured. The spectroscopic properties of compounds of formula $Pb_4O(OR)_6$ (R = Bu^t, Pr^i, Et) are in agreement with an adamantane-like structure **I**, as previously established for $Pb_4(\mu_4\text{-}O)(\mu\text{-}OSiPh_3)_6$,[15] and in which the lead atoms are in a distorted trigonal bipyramidal environment. The core of the acetatoalkoxide, $Pb_4O(OAc)_3(OBu^t)_3$, can be described accordingly. The small difference (135 cm^{-1}) between the symmetric and antisymmetric COO stretching frequencies in the IR spectra points to bidentate coordination of the acetate groups[20] and a structure of type **II**. This is also in agreement with the structure of $Be_4(\mu_4\text{-}O)(OAc)_6$ and of its derivatives $Be_4(\mu_4\text{-}O)(OAc)_{6-x}(OPr^i)_x$.[21]

Further condensation to oxoalkoxides of general formula $Pb_6O_4(OR)_4$ occurs. Compound **2** appears as the most stable oxoalkoxide towards condensation reactions, but the hexanuclear species is also obtained although in poor yields by reacting $Pb(OAc)_2$ and $NaOBu^t$ and tedious work-up by crystallization. The structure of $Pb_6O_4(OEt)_4$ is

* The line width might be affected by the solvent, the presence of residual alcohol resulted generally in line broadening.

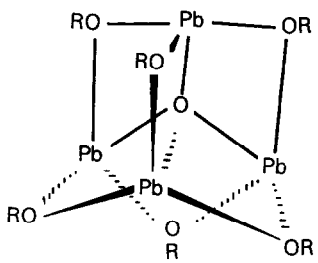

$Pb_4O(OR)_6$ (I)

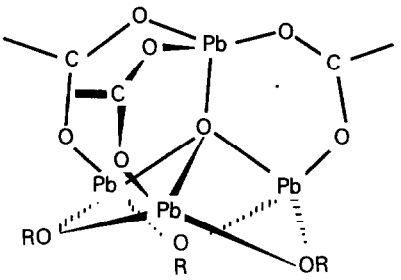

$Pb_4O(OR)_3(OAc)_3$ (II)

probably based on an almost octahedral Pb(6) core (**III**), analogous to that of the isopropoxide derivative,[7] which may be considered as resulting from the condensation of two adamantane units along a common edge. This structural unit also has counterparts in tin(II) chemistry since $Sn_6O_4(OMe)_4$ and $Sn_6O_4(OH)_4$ are known.[22]

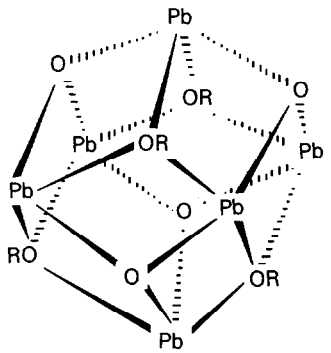

$Pb_6O_4(OR)_4$ (III)

(b) *Reactivity*

The homoleptic alkoxide $[Pb(OBu^t)_2]_m$ (**1**) is more reactive than the oxoalkoxides. Its alcoholysis offers a quantitative route to $Pb_4O(OR)_6$ (R = Et, Pr^i). A selective route to $Pb_4O(OBu)_3(OAc)_3$ can be devised by allowing **1** to react with acetic anhydride. However, the poor stability of all acetatoalkoxides (with respect to further condensation by elimination of the acetato groups, as evidenced by IR) limits the interest of this class of compounds. However, such derivatives might exist as intermediates on the routes to materials when lead acetate is used together with metal alkoxides.[23]

Since the metal atoms should bear some electronic density, complexation was estimated as a way of stabilizing the lead(II) alkoxides and limiting decomposition and/or condensation reactions. Complexes of divalent group 14 elements have been described; however, complexes of lead(II) derivatives remain scarce.[24] Complexation between $W(CO)_5L$ (L = THF or py) and **1** or **2** has been investigated by ligand exchange reactions, since most lead(II) alkoxides display poor photochemical stability. Complexation was evidenced by the rapid appearance of an orange–yellow colour, characteristic of lead–metal carbonyl complexes,[24] while new absorption bands developed in the IR spectra for the carbonyl stretching vibrations [at 1913, 1872, 1809, 1778 cm^{-1} for instance for the reaction between $W(CO)_5(THF)$ and $Pb_4O(OBu^t)_6$]. However, the W(0)—Pb(II) coordination bond is unstable and side reactions involving electron-transfer reactions with formation of colloidal lead are observed. Furthermore, when **1** is a ligand, formation of lead n-butoxide derivatives (^1H and IR evidence) resulting from THF opening[25] was observed when starting from $W(CO)_5 \cdot THF$. These reactions precluded isolation of pure complexes so far and coordination of the lead(II) centre was not further investigated.

The novel alkoxides $[Pb(OBu^t)_2]_m$ and $Pb_4O(OBu^t)_6$ have been used as precursors for the synthesis using sol–gel techniques of $PbMg_{1/3}Nb_{2/3}O_3$ (PNM), a ceramic with interesting dielectric and ferroelectric properties.[26] Since they are both volatile, they might find use in MOCVD techniques, but the higher thermal stability of the oxoalkoxide makes it a more suitable precursor. Even the poorly soluble tetra- or hexanuclear oxoalkoxides can be used as precursors to materials since they were observed to form highly soluble heterometallic alkoxides with niobium, titanium, magnesium or bismuth derivatives. The reaction between $Nb(OEt)_5$ and lead alkoxides in ethanol offered independently of the lead derivative used $[Pb(OBu^t)_2]_m$, $Pb_4O(OEt)_6$ or $Pb_6O_4(OEt)_4$, the compound $Pb_6Nb_4(\mu_4\text{-}O)_4(\mu_3\text{-}OEt)_4(\mu\text{-}OEt)_{12}(OEt)_8$ (**5**) which has been structurally characterized.[27] Compound **5** can be considered as an adduct between $Pb_6O_4(OEt)_4$ and $Nb(OEt)_5$, the lead oxoalkoxide acting as a tetradendate ligand in

which the μ_3-oxo of an electron-rich metal, lead(II), are the donor sites. ^{207}Pb NMR displays a sensitivity to coordination numbers similar to that of ^{119}Sn NMR, although much larger shifts are observed in the case of lead. Indeed, the formation of the heterometallic alkoxide **5** involves an increase in the lead coordination number from 4 to 6, which results in a drastic shift (more than 2000 ppm) to higher fields in the NMR. Large chemical shift variations are also observed for other Pb—O—M (M = Ti, Mg, Bi) systems and thus ^{207}Pb NMR gives an initial indication of the formation or not of heterometallic species and suggests a high coordination number for the lead atoms also. The study of heterometallic alkoxides involving lead and other metals is in progress.

Acknowledgements—We thank the CNRS (GRECO 93) for financial support, and Dr B. Septe for obtaining the ^{207}Pb NMR spectra.

REFERENCES

1. P. Duran and C. Moure, *Mater. Chem. Phys.* 1986, **15**, 193; B. Raveau, C. Michel, M. Hervieu, D. Groult and J. Provost, *Adv. Mater.* 1990, **2**, 290.
2. J. P. Guha and H. U. Anderson, *J. Am. Ceram. Soc.* 1986, C-287.
3. L. G. Hubert-Pfalzgraf, *New J. Chem.* 1987, **11**, 663.
4. R. J. Puddephatt and G. H. Thistlethwaite, *J. Chem. Soc., Dalton Trans.* 1972, 570; A. K. Holliday, P. H. Makin and R. J. Puddephatt, *J. Chem. Soc., Dalton Trans.* 1976, 435.
5. E. Amberger and R. Hönigschmid-Grossich, *Chem. Ber.* 1965, **98**, 3795.
6. O. Yamaguchi, M. Yamadera and K. Shimizu, *Bull. Chem. Soc. Japan* 1977, **50**, 2805; E. Narita, M. Kabayashi, H. Sinjo, H. Tsuchida and H. Naito, *Bull. Chem. Soc. Japan* 1983, **56**, 3129.
7. A. I. Yanovskii, N. Ya. Turova and E. P. Turevskaya, *Koordinatsionnaya Khimiya* 1982, **8**, 153 (Engl. Transl.).
8. B. Cetinskaya, I. Gunrukcu, M. F. Lappert, J. L. Atwood, R. D. Rogers and H. J. Zaworotko, *J. Am. Chem. Soc.* 1980, **102**, 2088.
9. W. E. Buhro, private communication; S. C. Goel, M. Y. Chiang and W. E. Buhro, *Inorg. Chem.* 1990, **29**, 4640.
10. R. Papiernik, L. G. Hubert-Pfalzgraf and M. C. Massiani, *Inorg. Chim. Acta* 1989, **165**, 1.
11. D. H. Harris and M. F. Lappert, *J. Chem. Soc., Chem. Commun.* 1974, 895.
12. T. Syper, *Roczniki Chemii* 1973, **47**, 433.
13. E. P. Clark, *Inorg. Eng. Chem. Anal. Edn* 1941, **13**, 820.
14. D. C. Bradley, R. C. Mehrotra and D. P. Gaur, *Metal Alkoxides*. Academic Press, London (1978); C. E. Sumner and G. R. Steinmetz, *Inorg. Chem.* 1989, **28**, 4290.
15. C. Gaffney, P. G. Harrison and T. J. King, *J. Chem. Soc., Chem. Commun.* 1980, 12.
16. M. Veith, *Chem. Rev.* 1989, **89**, 1.
17. M. Grenz and W. W. du Mont, *J. Organomet. Chem.* 1983, **241**, C5; M. Grenz, Z. Hahn, W. W. du Mont and J. Tickardt, *Angew. Chem., Int. Edn Engl.* 1984, **3**, 977.
18. T. V. Lubben, P. T. Wolczanski and G. D. Van Dyne, *Organometallics* 1984, **3**, 977.
19. J. J. Dechter, NMR of metal nuclides, Part I: Main group elements *Progr. Inorg. Chem.* (Edited by J. S. Lippard), Vol. 29 (1983); K. H. Pannell, J. M. Rozell, S. Cortez and R. Kapoor, *Organometallics* 1990, **9**, 1322; J. D. Kennedy, W. McFarlane and G. S. Pyne, *J. Chem. Soc.* 1977, 2332.
20. G. B. Deacon and R. J. Philipps, *Coord. Chem. Rev.* 1980, **33**, 227.
21. D. E. Fenton, *Comprehensive Coordination Chemistry* (Edited by G. Wilkinson), Vol. 3, p. 1. Pergamon Press, Oxford (1987); A. Tulinsky, C. R. Worthington and E. Pignatora, *Acta Cryst.* 1959, **2**, 623; A. I. Grigor'ev, L. N. Reshetova and A. V. Novoselova, *Dokl. Adad. Nauk. SSSR* 1972, **202**, 85.
22. P. G. Harrison, B. J. Haylett and T. J. King, *J. Chem. Soc., Chem. Commun.* 1978, 112; R. A. Howie and W. Moser, *Nature* 1968, **219**, 372.
23. R. A. Lipeles, N. A. Ives and M. S. Leung, *Science of Chemical Processing* (Edited by L. L. Hench and D. R. Ulrich), p. 320. Wiley, New York (1986).
24. W. Petz, *Chem. Rev.* 1986, **86**, 1019; M. F. Lappert and P. R. Power, *J. Chem. Soc., Dalton Trans.* 1985, 51.
25. A. R. Barron, D. Lyons, G. Wilkinson, M. Motevalli, A. J. Howes and M. B. Hursthouse, *J. Chem. Soc., Dalton Trans.* 1986, 279; C. Tessier-Youngs, W. J. Youngs, S. T. Beachley and W. R. Churchill, *Organometallics* 1983, **2**, 1128.
26. F. Chaput, J. P. Boilot, M. Lejeune, R. Papiernik and L. G. Hubert-Pfalzgraf, *J. Am. Ceram. Soc.* 1989, **72**, 1355.
27. R. Papiernik, L. G. Hubert-Pfalzgraf and J. C. Daran, *J. Chem. Soc., Chem. Commun.* 1990, 695; R. Papiernik and L. G. Hubert-Pfalzgraf *Better Ceramics through Chemistry IV* 1990, **180**, 393.

Polyhedron Vol. 10, No. 14, pp. 1663–1666, 1991
Printed in Great Britain

0277–5387/91 $3.00+.00
© 1991 Pergamon Press plc

REACTIONS OF NONABORANE ANIONS WITH SOME SEVEN-COORDINATE CARBONYL IODIDE COMPLEXES OF MOLYBDENUM(II) AND TUNGSTEN(II)

PAUL K. BAKER, MICHAEL A. BECKETT* and LISA M. SEVERS

Department of Chemistry, University of Wales, Bangor, Gwynedd, LL57 2UW, U.K.

(*Received* 28 *February* 1991; *accepted* 5 *April* 1991)

Abstract—The reactions of $[MI_2(CO)_3L_2]$ (M = Mo, W; L = PPh_3, PPh_2Me, $PPhMe_2$) with $[NMe_4][B_9H_{14}]$ and $[NMe_4][B_9H_{12}]$ in dichloromethane solution have been attempted. The new metalloborane $[6,6,6,6\text{-}(CO)_3(PPh_3)\text{-}6\text{-}W\text{-}B_9H_{13}]$ (**1**) and the previously reported $[6,6,6,6\text{-}(CO)_2(PPh_3)_2\text{-}6\text{-}Mo\text{-}B_9H_{13}]$ were isolable in low yield from the appropriate reaction mixtures. Complex **1** has been characterized by elemental analysis, IR spectroscopy and multielement (^1H, $^{11}B\text{-}\{^1H\}$ and $^{31}P\text{-}\{^1H\}$) NMR spectroscopy. In addition to **1**, moderate yields of $[NMe_4][WI_3(CO)_3(PPh_3)]$ and $[4\text{-}(PPh_3)B_9H_{13}]$ were obtained from the reaction of $[WI_2(CO)_3(PPh_3)_2]$ with $[NMe_4][B_9H_{14}]$.

Considerable interest has been shown in the preparation and reaction chemistry of metal complexes containing polyhedral boron hydride ligands and over 500 metalloboranes have been synthesized.[1] Metalloboranes containing the heavier group 6 metals are surprisingly poorly represented within this wide spectrum of compounds. Hitherto, polyhedral molybdenaborane chemistry and polyhedral wolfraborane chemistry are limited to a dozen or so reported compounds.[2–5] The readily available syntheses of seven-coordinate organophosphine-containing carbonyl iodide complexes of molybdenum(II) and tungsten(II) from $[MI_2(CO)_3(NCCH_3)_2]$ (M = Mo, W)[6] have led us to explore their reactions with the nonaborane anions $[B_9H_{12}]^-$ and $[B_9H_{14}]^-$ in attempts to synthesize new metalloborane complexes of tungsten and molybdenum.

EXPERIMENTAL

General

Reactions were carried out using standard Schlenk techniques under nitrogen, using solvents distilled under nitrogen from an appropriate drying agent. $[NMe_4][B_9H_{12}]$ and $[NMe_4][B_9H_{14}]$ were prepared by reported methods,[7,8] as were the molybdenum(II) and tungsten(II) starting materials.[9] The general procedure for the reaction of the nonaborane anions with the molybdenum(II) or tungsten(II) complexes is outlined below for the preparation of $[6,6,6,6\text{-}(CO)_3(PPh_3)\text{-}6\text{-}W\text{-}B_9H_{13}]$ (**1**).

Elemental analyses (C, H and N) were determined using a Carlo Erba elemental analyser MOD 1106 (using helium as carrier gas). IR spectra were recorded on a Perkin–Elmer F.t IR 1600 spectrophotometer. Multielement NMR spectra were recorded at room temperature in $CDCl_3$ solution on a Bruker AC 250 CP/MAS NMR spectrometer operating at 250 MHz for ^1H, 80.25 MHz for ^{11}B and $^{11}B\text{-}\{^1H\}$ and 101.2 MHz for $^{31}P\text{-}\{^1H\}$. Chemical shifts (δ) are given in ppm to high frequency (low field) of $SiMe_4$ for ^1H, 85% H_3PO_4 for ^{31}P and $BF_3\cdot OEt_2$ for ^{11}B.

Preparation of $[6,6,6,6\text{-}(CO)_3(PPh_3)\text{-}6\text{-}W\text{-}B_9H_{13}]$ (**1**)

To a stirred solution of $[WI_2(CO)_3(PPh_3)_2]$ (2.1 g, 2.00 mmol) in dry dichloromethane (15 cm^3) was added one equivalent of $[NMe_4][B_9H_{14}]$ (0.37 g, 1.98 mmol) under nitrogen. The solution was stirred for a further 24 h, during which time a yellow precipitate formed. A $^{11}B\text{-}\{^1H\}$ NMR spectrum of the reaction solution at this point showed that $[4\text{-}(PPh_3)B_9H_{13}]$ was the major boron-containing species present. The reaction mixture was filtered

* Author to whom correspondence should be addressed.

through a short column of Keiselgel and the filtrate was taken down to *ca* 3 cm^3 in volume under reduced pressure at room temperature and then applied to a series of preparative TLC plates ($20 \times 20 \times 0.1$ cm, silica, Keiselgel GF 254, made in these laboratories as required) and eluted with dichloromethane. Three coloured bands were observed on the preparative TLC plates: two very faint bands at R_f 0.7 (yellow) and R_f 0.65 (orange), and an intense, bright purple band at R_f 0.8. The purple band was removed from the silica and purified by further preparative TLC using (i) dichloromethane and then (ii) 50:50 dichloromethane/hexane as the eluants. The purple component (**1**) was recrystallized from dichloromethane/hexane to yield air-stable, purple crystals of [6,6,6,6-$(CO)_3(PPh_3)$-6-W-B_9H_{13}] (**1**) (0.204 g; 16%). IR: ν(CO) 2014(m), 1948(s), 1892 cm^{-1}; ν(BH) 2549 cm^{-1}. Found: C, 39.6; H, 4.9; N, 0.0. Calc. for $C_{21}H_{28}B_9O_3PW$: C, 39.4; H, 4.4; N, 0.0%.

Identification of the yellow solid

The yellow solid formed from the reaction of reactants as above on a 3.3 mmol scale (3.45 g of $[WI_2(CO)_3(PPh_3)_2]$ and 0.61 g of $[NMe_4][B_9H_{14}]$) was separated from the reaction mixture and washed with 2×10 cm^3 portions of dichloromethane. The mass of this yellow precipatate was 1.85 g. Extraction of this yellow solid with acetone yielded a yellow solution and a white solid (0.31 g). Elemental analysis for this white solid was consistent with it being $[NMe_4]I$; Found: C, 24.0; H, 6.5; N, 5.8. Calc. for $C_4H_{12}IN$: C, 23.9; H, 7.0; N, 6.0%. The yellow solution was evaporated to dryness to yield a yellow solid (1.52 g). Elemental analysis based upon the formula $[NMe_4][WI_3(CO)_3(PPh_3)]$; Found: C, 27.9; H, 3.0; N, 1.5. Calc. for $C_{25}H_{27}I_3NO_3PW$: C, 30.4; H, 2.7; N, 1.5%. IR: ν(CO) at 2004, 1925 and 1901 cm^{-1} comparable to data reported for the related $[N^nBu_4][WI_3(CO)_3(PPh_3)]$ complex.[12] The yellow solid was difficult to isolate free from $[NMe_4]I$.

RESULTS AND DISCUSSION

Synthetic reactions

Organophosphine complexes of the carbonyl iodides of molybdenum(II) and tungsten(II) were prepared as previously described[9] by the reaction of two equivalents of the organophosphine with the labile bis-acetonitrile complexes $[MI_2(CO)_3(NCCH_3)_2]$ (M = Mo, W), eq. (1):

$$[MI_2(CO)_3(NCCH_3)_2] + 2L \longrightarrow [MI_2(CO)_3L_2] + 2CH_3CN$$
$$(M = Mo, W;\ L = PPh_3, PPh_2Me, PPhMe_2). \quad (1)$$

These complexes were reacted separately, in dichloromethane solution, with the $[NMe_4]^+$ salts of the *nido*-$[B_9H_{12}]^-$ and the *arachno*-$[B_9H_{14}]^-$ anions. Only in two cases were metalloborane species identified as reaction products. The new, bright purple *nido*-wolfradecaborane [6,6,6,6-$(CO)_3(PPh_3)$-6-W-B_9H_{13}] (**1**) and the magenta *nido*-molybdenadecaborane [6,6,6,6-$(CO)_2(PPh_3)$-6-Mo-B_9H_{13}] (**2**) were obtained in 16 and 12% yields, respectively, from the reactions of $[MI_2(CO)_3(PPh_3)_2]$ (M = W, Mo) with the *arachno*-$[B_9H_{14}]^-$ anion, eq. (2):

$$[MI_2(CO)_3(PPh_3)_2] + [NMe_4][B_9H_{14}] \longrightarrow \mathbf{1}\ (M = W, 16\%);\ \mathbf{2}\ (M = Mo, 12\%). \quad (2)$$

The cluster geometry of **1** is shown schematically in Fig. 1. Compound **2** has been previously prepared[3] in 4% yield from the reaction of the chloro complex $[MoCl_2(CO)_3(PPh_3)_2]$ with $[N^nBu_4][B_9H_{14}]$. Unexpectedly, the previously reported[3] compound [6,6,6,6-$(CO)_3(PMe_2Ph)$-6-W-B_9H_{13}] (**3**) could not be detected in reactions of $[WI_2(CO)_3(PMe_2Ph)_2]$ with either nonaborane anion. However, the reaction of the *nido*-$[B_9H_{12}]^-$ anion with $[MI_2(CO)_3(PPh_3)_2]$ (M = Mo, W) also resulted in small yields of **1** and **2**, respectively. Compounds **1** and **2** were isolated as air-stable, microcrystalline solids and were characterized by satisfactory elemental

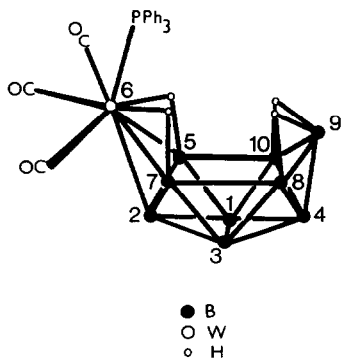

Fig. 1. Schematic representation of the cluster structure of [6,6,6,6-$(CO)_3(PPh_3)$-6-W-B_9H_{13}] (**1**) based upon that proposed for the analogous [6,6,6,6-$(CO)_3(PMe_2Ph)$-6-W-B_9H_{13}] (**3**).[3] The numbering scheme for an open 10-vertex cage is shown. Each unsubstituted boron cluster vertex has an *exo*-terminal hydrogen atom bound to it (not shown).

analysis, and by IR and multielement NMR spectroscopy.

The low yields of the metalloboranes from these reactions mixtures would suggest that they are formed as by-products of a main reaction. Indeed, non-boron-containing, yellow, insoluble materials were observed as the major products from all the reactions attempted. The composition of this yellow material was investigated for the $[WI_2(CO)_3(PPh_3)_2]$/$[NMe_4][B_9H_{14}]$ reaction, where it was found to be a mixture of two compounds which were partially separable by solvent extraction. These two materials were identified by elemental analysis and by IR spectroscopy to be $[NMe_4]I$ and $[NMe_4][WI_3(CO)_3(PPh_3)]$.[10-12] The complex $[WI_2(CO)_3(PPh_3)_2]$ and other seven-coordinate di-iodo tungsten(II) species are well known to decompose in dichloromethane solution to yield seven-coordinate tri-iodo anions.[13-16] The principal boron-containing compound produced in the reaction of $[WI_2(CO)_3(PPh_3)_2]$ with $[NMe_4][B_9H_{14}]$ in dichloromethane solution is the *arachno*-$[4\text{-}(PPh_3)B_9H_{13}]$ borane ligand complex. This was identified by its characteristic $^{11}B\text{-}\{^1H\}$ NMR spectrum.[17] This product presumably results from the reaction of $[B_9H_{14}]^-$ with free PPh_3 produced in the decomposition of the tungsten(II) species outlined above.

Characterization of boron-containing products

The identification of the *nido*-6-metalladecaboranes has been made using primarily $^{11}B\text{-}\{^1H\}$ NMR spectroscopy, augmented by $^{31}P\text{-}\{^1H\}$, ^1H NMR and IR spectroscopy and elemental analysis. The NMR parameters that we have measured for compounds **1** and **2** are given in Table 1, together with comparable NMR data for all other reported non-boron-substituted *nido*-6-metallodecaboranes of molybdenum and tungsten. The $^{11}B\text{-}\{^1H\}$ NMR data in Table 1 for compounds **1**–**4** are similar. Compound **4** is the non-carbonyl-containing species $[6,6,6,6\text{-}(PMe_2Ph)_3H_2\text{-}6\text{-}W\text{-}B_9H_{13}]$.[2] In particular the $^{11}B\text{-}\{^1H\}$ spectrum of **1** shows two high-field resonances (of equal relative intensity 1 : 1) separated from a poorly resolved set of overlapping signals (of relative intensity 7) at lower field in an overall pattern which is entirely characteristic of a *nido*-6-metallodecaborane cluster.[2,18] The $^1J(^{11}B^1H)$ coupling constants that we were able to measure for **1** are in the range 110–140 Hz and are typical for a two-centre/two-electron terminal boron hydrogen bond.[18] The ^1H NMR of compound **1** shows, in addition to a broad hump several ppm wide centred at *ca* δ 2.0 due to terminal hydrogen atoms coupled to ^{11}B, and signals due to the

Table 1. NMR data for unsubstituted *nido*-6-metallodecaboranes of molybdenum and tungsten

Assignment	Compound **1**[a]	**2**[a]	**3**[b]	**4**[c]
$\delta(^{11}B)$ (ppm)				
B(1, 3)	+15.0	+14.9	+13.4	+12.3
B(5, 7)	+11.1	+14.9	+5.2	+7.2
B(9)	+5.1	+4.5	+2.5	+2.5
B(8, 10)	+2.3	+0.5	+2.5	+3.0
B(2)	−23.4	−20.8	−22.9	−23.1
B(4)	−30.1	−30.0	−33.2	−33.0
$\delta(^1H)$ (ppm)				
B—H—B	−4.30	−3.82	−3.71	−3.61
M—H—B	−6.18	−6.45	−6.96	−8.59
$\delta(^{31}P)$ (ppm)	+44.7	+63.5	−1.2	−6.1
$^1J(^{183}W^{31}P)$ (Hz)	207	—	187	227

[a] This work. Literature values for **2** from ref. 3 are $\delta(^{11}B)$ (ppm): B(1, 3) +14.8, B(5, 7) +14.8, B(9) +4.5, B(8, 10) +0.6, B(2) −20.5, B(4) −30.0; $\delta(^1H)$ (ppm): −3.82 (B—H—B), −6.45 (Mo—H—B); $\delta(^{31}P)$ (ppm): +63.4.

[b] Data from ref. 3.

[c] Data from ref. 2.

aromatic protons at low field, two high-field signals of equal intensity at δ −4.30 and −6.18 ppm. These high-field signals are fully consistent with B—H—B and W—H—B bridging hydrogen atoms, respectively. The $^{31}P-\{^{1}H\}$ spectrum of compound **1** appears as a singlet at δ +44.7 ppm flanked by low intensity tungsten satellites with $^{1}J(^{183}W^{31}P)$ of 208 Hz; the magnitude of this $^{183}W-^{31}P$ coupling constant is similar to that found for compounds **3** and **4**.[2,3] Consistent with a tricarbonyl species, the IR spectrum of **1** shows three, strong, carbonyl stretches at 2014, 1948 and 1872 cm^{-1} and a further strong B—H stretch at 2549 cm^{-1}. Elemental analysis and IR data for **1** are given in the Experimental and these are fully in accord with this compound being assigned as a *nido*-6-metallodecaborane with the ligands around the metal centres, as indicated in Fig. 1.

Acknowledgements—We thank the European Social Fund for support for L.M.S. and The Nuffield Foundation for financial aid towards equipment and chemicals.

REFERENCES

1. J. D. Kennedy, *Prog. Inorg. Chem.* 1984, **32**, 211; 1986, **34**, 519.
2. M. A. Beckett, N. N. Greenwood, J. D. Kennedy and M. Thornton-Pett, *J. Chem. Soc., Dalton Trans.* 1986, 795.
3. N. N. Greenwood, J. D. Kennedy, I. Macpherson and M. Thornton-Pett, *Z. Anorg. Allg. Chem.* 1986, **540/541**, 45.
4. P. D. Grebinek, M. L. H. Green, M. A. Kelland, J. B. Leach, P. Mountford, G. Stringer, N. M. Walker and L.-L. Wong, *J. Chem. Soc., Chem. Commun.* 1988, 799.
5. P. D. Grebenik, J. B. Leach, M. L. H. Green and N. M. Walker, *J. Organomet. Chem.* 1988, **345**, C31.
6. P. K. Baker, S. G. Fraser and E. M. Keys, *J. Organomet. Chem.* 1986, **309**, 319.
7. S. K. Boocock, N. N. Greenwood, M. J. Hails, J. D. Kennedy and W. S. McDonald, *J. Chem. Soc., Dalton Trans.* 1981, 1415.
8. B. M. Graybill, J. K. Ruff and M. F. Hawthorne, *J. Am. Chem. Soc.* 1961, **83**, 2669.
9. P. K. Baker, M. A. Beckett and L. M. Severs, *J. Organomet. Chem.* 1991, in press.
10. R. Colton and C. J. Rix, *Aust. J. Chem.* 1969, **22**, 305.
11. W. S. Tsang, D. W. Meek and A. Wojcicki, *Inorg. Chem.* 1968, **7**, 1263.
12. P. K. Baker and S. G. Fraser, *Transition Met. Chem.* 1988, **13**, 284.
13. J. Lewis and R. Whyman, *J. Chem. Soc. A.* 1967, 77.
14. R. Colton and C. J. Rix, *Aust. J. Chem.* 1969, **22**, 305.
15. P. K. Baker and S. G. Fraser, *Inorg. Chim. Acta* 1986, **116**, L1.
16. P. K. Baker, S. G. Fraser and M. G. B. Drew, *J. Chem. Soc., Dalton Trans.* 1988, 2729.
17. B. M. Bodner, F. R. Scholer, L. J. Todd, L. E. Senor and J. C. Carter, *Inorg. Chem.* 1971, **10**, 942.
18. M. A. Beckett, N. N. Greenwood, J. D. Kennedy and M. Thornton-Pett, *J. Chem. Soc., Dalton Trans.* 1985, 1119.

Polyhedron Vol. 10, No. 14, pp. 1667–1674, 1991
Printed in Great Britain

0277–5387/91 $3.00+.00
© 1991 Pergamon Press plc

SYNTHESIS, STRUCTURE AND PROPERTIES OF THE FACE-SHARING BIOCTAHEDRAL $Mo_2X_6(PMe_2Ph)_3$ (X = Br, I) COMPOUNDS

JOHN C. GORDON, HUMBERTO D. MUI and RINALDO POLI†

Department of Chemistry and Biochemistry, University of Maryland, College Park, MD 20742, U.S.A.

and

KAZI J. AHMED

Department of Chemistry, University of Vermont, Burlington, VT 05405, U.S.A.

(*Received* 7 *March* 1991; *accepted* 10 *April* 1991)

Abstract—The title compounds were obtained by reacting the corresponding $MoX_3(THF)_3$ complexes with PMe_2Ph in a 2:3 ratio in refluxing toluene. The compounds assume a face-sharing, bioctahedral structure with three bridging halide ligands, the coordination geometries being completed by one terminal halide and two phosphines for one metal centre, and by two terminal halides and one phosphine for the other one. A comparison with the known chloride analogue shows that the metal–metal separation increases in the order Cl < Br < I and, correspondingly, the paramagnetism of the molecule also increases as shown by solid-state magnetic susceptibility measurements and by the paramagnetic shifts in the solution ^1H NMR spectrum. The NMR spectrum indicates an equilibrium in solution between *anti* and *gauche* isomers. NMR monitoring of the reaction between $Mo_2Br_6(PMe_2Ph)_3$ and PMe_2Ph shows evidence for the formation of the edge-sharing bioctahedral $Mo_2Br_6(PMe_2Ph)_4$ as a short-lived intermediate, the mononuclear $MoBr_3(PMe_2Ph)_3$ being the final product.

We have recently detailed the factors that govern the interconversion between molybdenum(III) complexes of mononuclear, octahedral (MO), $MoCl_3L_3$, edge-sharing, bioctahedral (ESBO), $Mo_2Cl_6L_4$, and face-sharing, bioctahedral (FSBO), $Mo_2Cl_6L_3$ structures, where L = THF[1] or tri-substituted phosphine.[2] In particular, we found that the THF-substituted compounds have the order of relative stability MO < ESBO < FSBO, whereas the phosphine-substituted analogues have an exactly opposite trend. The ESBO compounds are unstable towards disproportionation to a mixture of MO and FSBO systems. However, the ESBO compounds could be prepared by taking advantage of the faster kinetics of the FSBO to ESBO step during the phosphine addition reaction, eq. (1):[2]

$$Mo_2Cl_6L_3 \xrightarrow{+L,\ fast} Mo_2Cl_6L_4 \xrightarrow{+L,\ slow} 2MoCl_3L_3. \quad (1)$$

Since the ESBO chloride complexes show unexpected behaviour in terms of metal–metal bond formation [e.g. the PMe_2Ph complex has a relatively strong metal–metal bond[2] with a Mo—Mo separation of 2.8036(8) Å, whereas the PEt_3 complex[3] has a non-bonded Mo—Mo distance of 3.730(1) Å], we naturally wondered how the metal–metal bonding capability would change on going to the corresponding bromide- and iodide-bridged systems.

We report here the synthesis and structure of the bromide- and iodide-bridged FSBO complexes with

† Author to whom correspondence should be addressed.

PMe_2Ph as the neutral ligand and attempt to convert them into the corresponding ESBO systems by the strategy illustrated in eq. (1).

EXPERIMENTAL

All operations were carried out under an atmosphere of dinitrogen using standard glove-box and Schlenk-line techniques. Solvents were dehydrated by conventional methods and distilled under dinitrogen prior to use. Instruments used were as follows: NMR, Bruker AF200 and WP200; UV–vis, Schimadzu UV-240; magnetic susceptibility, Johnson–Matthey magnetic balance. The elemental analyses were by Midwest Microlab, Indianapolis, Indiana. $MoBr_3(THF)_3$,[4] $MoI_3(THF)_3$[5] and $Mo_2Cl_6(PMe_2Ph)_3$[2] were prepared by literature methods, and PMe_2Ph was purchased from Strem Chemicals and used as received.

Preparation of $Mo_2Br_6(PMe_2Ph)_3$

To a suspension of $MoBr_3(THF)_3$ (1.46 g, 2.64 mmol) in 30 cm^3 of toluene was added PMe_2Ph (0.56 cm^3, 3.9 mmol). The mixture was refluxed for *ca* 7 h, resulting in the formation of a dark, crystalline precipitate and a golden yellow solution. The solid was separated by filtration, washed twice with 5 cm^3 of toluene and dried *in vacuo*. Yield: 523 mg (36.4%). The compound is only sparingly soluble in chloroform and hot toluene. It is somewhat more soluble in dichloromethane to yield intensely coloured forest green solutions. Found: C, 26.5; H, 2.9; P, 8.6. Calc. for $C_{24}H_{33}Br_6Mo_2P_3$: C, 26.5; H, 3.1; P, 8.6%. μ_{eff} (293 ± 2 K) = 0.94 μ_B per molybdenum atom (diamagnetic correction = 403.4×10^{-6} c.g.s.u. per dinuclear unit). UV–vis [CH_2Cl_2, nm (ε, M^{-1} cm^{-1})]: 244 (34,500), 340 (14,200), 418 sh (3000), 612 (2000). A single crystal for the X-ray analysis was obtained by diffusion of n-heptane into a dichloromethane solution.

Preparation of $Mo_2I_6(PMe_2Ph)_3$

This compound was prepared from $MoI_3(THF)_3$ (1.26 g, 1.82 mmol) and PMe_2Ph (0.39 cm^3, 2.7 mmol) in toluene (20 cm^3), following the general procedure described above for the corresponding bromide compound. The mixture was refluxed overnight. Yield: 1.04 g (83%). When the mixture was refluxed only for a short time (*ca* 1/2 h), a comparable amount of dark, crystalline solid was present, but ^1H NMR analysis indicated the presence of impurities. The compound is even less soluble than the bromide analogue, and its dichloromethane solutions are golden yellow. A single crystal for the X-ray analysis was obtained from CH_2Cl_2/n-heptane. Found: C, 20.9; H, 2.3. Calc. for $C_{24}H_{33}I_6Mo_2P_3$: C, 21.1; H, 2.4%. μ_{eff} (293 ± 2 K) = 1.68 μ_B per molybdenum atom (diamagnetic correction = 498.8×10^{-6} c.g.s.u. per dinuclear unit). UV–vis [CH_2Cl_2, nm (ε, M^{-1} cm^{-1})]: 231 (57,000), 318 (20,200), 406 (12,400), 450 sh (10,100), 661 (449).

Magnetism of $Mo_2Cl_6(PMe_2Ph)_3$

μ_{eff} (293 ± 2 K) = 0.23 μ_B per molybdenum atom (diamagnetic correction = 347.6×10^{-6} c.g.s.u. per dinuclear unit).

X-ray crystallography for $Mo_2X_6(PMe_2Ph)_3$ (X = Br, I)

The experimental details are given in Table 1. The cell constants and orientation matrix for data collection for both $Mo_2X_6(PMe_2Ph)_3$ (X = Br, I) compounds were based on 24 carefully centred reflections in the range $20 < 2\theta < 30°$. Acceptable ω scans were obtained. The structures were solved by a combination of direct methods and heavy atom Fourier techniques. Full-matrix least-squares refinement was carried out with anisotropic thermal parameters for all the non-hydrogen atoms. The hydrogen atoms were placed in calculated (d_{C-H} = 0.95 Å) positions. All calculations for the solution and refinement of the structures were performed using the Nicolet SHELXTL PLUS crystallographic package. Selected bond distances and angles for both compounds are listed in Table 2.†

$Mo_2Br_6(PMe_2Ph)_3$

A black, needle-shaped crystal of approximate dimensions $0.25 \times 0.20 \times 0.40$ mm was mounted on the tip of a glass fibre with epoxy resin. θ–2θ scans over the 2θ range 3.5–55.0° produced 7857 unique reflections, of which 3274 [$I > 3\sigma(I)$] were used for structure refinement. The data indicated the centrosymmetric $P\bar{1}$ space group, which was confirmed by the successful solution of the structure. Refinement converged at $R = 0.0485$ and $R_w = 0.0528$.

† Full tables of crystal data, bond lengths, bond angles, anisotropic thermal parameters, calculated hydrogen atom coordinates and F_o/F_c data for the compounds $Mo_2X_6(PMe_2Ph)_6$ (X = Br, I) have been deposited with the Editor as supplementary material. The atomic positional parameters have been deposited with the Cambridge Crystallographic Data Centre.

Table 1. Summary of crystallographic data for $Mo_2X_6(PMe_2Ph)_3$ (X = Br, I)

Compound	$Mo_2Br_6(PMe_2Ph)_3$	$Mo_2I_6(PMe_2Ph)_3$
Formula	$C_{24}H_{33}Br_6Mo_2P_3$	$C_{24}H_{33}I_6Mo_2P_3$
Formula weight	1085.75	1367.75
Space group	$P\bar{1}$	$P\bar{1}$
a (Å)	11.567(4)	11.749(2)
b (Å)	11.711(4)	12.036(2)
c (Å)	13.495(6)	13.741(3)
α (°)	90.27(3)	89.79(2)
β (°)	108.06(3)	72.13(2)
γ (°)	101.33(3)	81.63(2)
V (Å^3)	1699(1)	1828.0(6)
Z	2	2
d_{calc} (g cm^{-3})	2.12	2.48
μ(Mo-K_α) (cm^{-1})	83.44	59.42
Radiation (monochromated in incident beam)	Mo-K_α (λ = 0.71073 Å)	Mo-K_α (λ = 0.71073 Å)
Temperature (°C)	23	23
Transmission factors: max., min.	0.718, 0.657	0.956, 0.799
R^a	0.0485	0.0371
$R_w{}^b$	0.0528	0.0413

[a] $R = \Sigma||F_o|-|F_c||/\Sigma|F_o|$.
[b] $R_w = [\Sigma w(|F_o|-|F_c|)^2/\Sigma w|F_o|^2]^{1/2}$; $w = 1/\sigma^2(|F_o|)+0.002(|F_o|^2)$.

The maximum shift/ESD in the last cycle of refinement was less than 0.02 and the maximum intensity in the final difference Fourier map was < 0.5 e Å^{-3}. An absorption correction based on ψ scans was attempted, without any improvement in the agreement figures.

$Mo_2I_6(PMe_2Ph)_3$

A black, parallelepiped-shaped crystal of approximate dimensions $0.2\times0.2\times0.4$ mm was mounted on the tip of a fibre with epoxy resin. θ–2θ scans over the 2θ range 4.5–50.0° produced 6488 unique reflections, of which 4823 [$I > 3\sigma(I)$] were used for structure refinement. The space group $P\bar{1}$ was chosen and the structure solved and refined to $R = 0.0371$ and $R_w = 0.0413$. The overall geometry of the molecule is very similar to the one observed for $Mo_2Br_6(PMe_2Ph)_3$. The maximum shift/ESD in the last cycle of refinement was less than 0.01. The maximum intensity in the final difference Fourier map was < 0.8 e Å^{-3}. An absorption correction based on ψ scans was applied.

RESULTS AND DISCUSSION

The synthesis of the FSBO $Mo_2X_6(PMe_2Ph)_3$ (X = Br, I) compounds is analogous to that described before[2] for the corresponding chloride compound, eq. (2):

$$2MoX_3(THF)_3+3PMe_2Ph \longrightarrow Mo_2X_6(PMe_2Ph)_3+6THF. \quad (2)$$

Compounds of the $Mo_2X_6L_3$ class (X = halogen, L = neutral donor) are well-known for X = Cl, for instance with L = $PEtPh_2$,[6] PEt_3, PMe_2Ph,[2,7] SMe_2,[8] tetrahydrothiophene,[9] THF,[1,10] or MeCN.[11] Anionic derivatives are known also for the other halides, for instance $Mo_2X_9^{3-}$ (X = Br, I)[12] and $Mo_2X_7L_2^-$ (X = I, L = PMe_3).[13] The two compounds reported in the present paper are the first, uncharged molybdenum(III) systems of the class of FSBO complexes that contain bridging bromide or iodide ligands and, together with the $Mo_2Cl_6(PMe_2Ph)_3$ compound recently described by us, allow a comparison of the properties for the entire series of $Mo_2X_6(PMe_2Ph)_3$ compounds with X = Cl, Br and I to be made.

This comparison is analogous to but presents additional advantages with respect to others done before. It is known that, upon replacement of the chloride bridging ligands with the larger bromide and iodide ions, the metal centres are forced farther from each other and the magnetism in molybdenum(III) FSBO complexes increases. This is the case for $Cs_3Mo_2X_9$ (X = Cl, Br, I)[12a,c] and $[Mo_2X_7(PMe_3)_2]^-$ (X = Cl,[14] I[13]). However, it has recently become apparent that the energy of these systems must have a fairly shallow minimum as a

Table 2. Selected bond distances (Å) and angles (°) for $Mo_2X_6(PMe_2Ph)_3$ (X = Br, I)[a]

	X = Br		X = I	
	(a) Bond distances			
	Mo(1)—Mo(2)	2.749(2)	Mo(1)—Mo(2)	2.909(1)
Mo—(μ-X)	Mo(1)—Br(1)	2.610(2)	Mo(1)—I(1)	2.781(1)
	Mo(1)—Br(2)	2.602(2)	Mo(1)—I(3)	2.788(1)
	Mo(1)—Br(3)	2.558(2)	Mo(1)—I(2)	2.739(1)
	Mo(2)—Br(1)	2.599(3)	Mo(2)—I(1)	2.773(1)
	Mo(2)—Br(2)	2.598(2)	Mo(2)—I(3)	2.782(1)
	Mo(2)—Br(3)	2.632(2)	Mo(2)—I(2)	2.800(1)
Mo—X	Mo(1)—Br(5)	2.547(2)	Mo(1)—I(6)	2.772(1)
	Mo(2)—Br(4)	2.521(2)	Mo(2)—I(4)	2.744(1)
	Mo(2)—Br(6)	2.527(3)	Mo(2)—I(5)	2.753(1)
Mo—P	Mo(1)—P(2)	2.548(4)	Mo(1)—P(2)	2.570(2)
	Mo(1)—P(3)	2.574(4)	Mo(1)—P(1)	2.599(3)
	Mo(2)—P(1)	2.537(4)	Mo(1)—P(3)	2.574(3)
	(b) Bond angles			
Mo—(μ-X)—Mo	Mo(1)—Br(1)—Mo(2)	63.7(1)	Mo(1)—I(1)—Mo(2)	63.2(1)
	Mo(1)—Br(2)—Mo(2)	63.8(1)	Mo(1)—I(3)—Mo(2)	63.0(1)
	Mo(1)—Br(3)—Mo(2)	64.0(1)	Mo(1)—I(2)—Mo(2)	63.3(1)
(μ-X)—Mo—(μ-X)	Br(1)—Mo(1)—Br(2)	88.6(1)	I(1)—Mo(1)—I(3)	88.2(1)
	Br(1)—Mo(1)—Br(3)	95.4(1)	I(2)—Mo(1)—I(3)	96.9(1)
	Br(2)—Mo(1)—Br(3)	100.9(1)	I(1)—Mo(1)—I(2)	100.8(1)
	Br(1)—Mo(2)—Br(2)	89.0(1)	I(1)—Mo(2)—I(3)	88.5(1)
	Br(1)—Mo(2)—Br(3)	93.9(1)	I(2)—Mo(2)—I(3)	95.7(1)
	Br(2)—Mo(2)—Br(3)	99.1(1)	I(1)—Mo(2)—I(2)	99.5(1)
(μ-X)—Mo—L_t	Br(1)—Mo(1)—Br(5)	92.2(1)	I(1)—Mo(1)—I(6)	90.9(1)
	Br(1)—Mo(1)—P(2)	172.0(1)	I(1)—Mo(1)—P(1)	170.7(1)
	Br(1)—Mo(1)—P(3)	86.1(1)	I(1)—Mo(1)—P(2)	82.7(1)
	Br(2)—Mo(1)—Br(5)	89.8(1)	I(3)—Mo(1)—I(6)	91.5(1)
	Br(2)—Mo(1)—P(2)	83.4(1)	I(3)—Mo(1)—P(1)	86.2(1)
	Br(2)—Mo(1)—P(3)	170.0(1)	I(3)—Mo(1)—P(2)	170.7(1)
	Br(3)—Mo(1)—Br(5)	167.0(1)	I(2)—Mo(1)—I(6)	165.7(1)
	Br(3)—Mo(1)—P(2)	85.4(1)	I(2)—Mo(1)—P(1)	87.3(1)
	Br(3)—Mo(1)—P(3)	88.1(1)	I(2)—Mo(1)—P(2)	86.6(1)
	Br(1)—Mo(2)—Br(4)	87.7(1)	I(1)—Mo(2)—I(4)	88.9(1)
	Br(1)—Mo(2)—Br(6)	175.4(1)	I(1)—Mo(2)—I(5)	171.8(1)
	Br(1)—Mo(2)—P(1)	90.9(1)	I(1)—Mo(2)—P(3)	87.6(1)
	Br(2)—Mo(2)—Br(4)	172.7(1)	I(3)—Mo(2)—I(4)	175.9(1)
	Br(2)—Mo(2)—Br(6)	88.1(1)	I(3)—Mo(2)—I(5)	87.5(1)
	Br(2)—Mo(2)—P(1)	86.8(1)	I(3)—Mo(2)—P(3)	92.2(1)
	Br(3)—Mo(2)—Br(4)	87.6(1)	I(2)—Mo(2)—I(4)	87.9(1)
	Br(3)—Mo(2)—Br(6)	90.0(1)	I(2)—Mo(2)—I(5)	88.0(1)
	Br(3)—Mo(2)—P(1)	172.4(1)	I(2)—Mo(2)—P(3)	169.5(1)
L_t—Mo—L_t	Br(5)—Mo(1)—P(2)	88.5(1)	I(6)—Mo(1)—P(2)	86.8(1)
	Br(5)—Mo(1)—P(3)	82.0(1)	I(6)—Mo(1)—P(1)	81.8(1)
	P(2)—Mo(1)—P(3)	101.8(1)	P(1)—Mo(1)—P(2)	102.6(1)
	Br(4)—Mo(2)—Br(6)	94.8(1)	I(4)—Mo(2)—I(5)	94.7(1)
	Br(4)—Mo(2)—P(1)	86.7(1)	I(4)—Mo(1)—P(3)	84.5(1)
	Br(6)—Mo(2)—P(1)	85.4(1)	I(5)—Mo(2)—P(3)	85.5(1)

[a] In each line, geometrically equivalent parameters for the two structures are compared.

function of metal–metal distance. For instance, the metal–metal distance in two different crystalline forms of $Mo_2Cl_6(PEt_3)_3$[2,7] with identical molecular geometry varies by 0.06 Å and the distances in $[Mo_2Cl_9]^{3-}$ and $[Mo_2Br_9]^{3-}$ vary over a 0.25 and 0.54 Å range, respectively, by the mere change of the cation.[13c] Solid-state magnetic measurements may therefore reflect packing and/or counterion effects. The $Mo_2X_6(PMe_2Ph)_3$ molecules reported herein are uncharged (no counterion effects) and the presence of the phosphine protons give the opportunity to at least qualitatively assess the change of magnetic properties *in solution* (no packing effects) through an examination of the paramagnetic shifts in the ^1H NMR. In addition, the two molecules reported here are crystallographically isostructural with each other and with the chloride compound described earlier,[2] thus the packing forces in the solid state should be similar and the correlation between solid-state magnetic susceptibility and solution paramagnetic NMR shifts should be meaningful.

The ^1H NMR spectra of the three complexes show paramagnetic shifts which increase in the order Cl < Br < I, in agreement with the solid-state magnetic data (see Experimental) and with the increase in metal–metal distance on going from the chloride to the iodide derivatives (see crystallographic data below). The methyl proton resonances are shifted upfield, whereas the phenyl proton resonances are shifted downfield with respect to the characteristic regions in diamagnetic complexes. For each molecule, the paramagnetic shifts *increase* upon increasing the temperature. The methyl resonances move from the δ +1 to 0 range at 212 K to the δ −0.8 to −1.5 range at 291 K for the bromide complex, and from the δ 0.5 to −2.5 range at 226 K to the δ −1.2 to −3.4 range at 281 K for the iodide complex. This is consistent with the known electronic structure of these molecules which consists of a diamagnetic ground state ($\sigma^2\pi^4$ metal–metal bond) and low-lying paramagnetic excited states generated by promotion of electrons into the metal–metal π^* orbitals.[12c,15] A reviewer pointed out that the nature of the halogen may in itself cause a change of the phosphine proton chemical shift and thus a strict correlation of paramagnetic shift with magnetic properties is not possible. We note, however, that the position of the PMe_3 proton resonance in the homologous series of *diamagnetic* $Mo_2X_4(PMe_3)_4$ complexes shifts only by 0.29 δ on going from X = Cl to X = I.[16] This shift is very small in comparison with the corresponding shifts observed for the methyl proton resonances in $Mo_2X_6(PMe_2Ph)_3$.

The pattern of ^1H NMR resonances in the methyl region also shows, as already evidenced for the chloride complex,[2] the presence of an equilibrium mixture of *anti* and *gauche* isomers (see Fig. 1). Overlap of some of the peaks occurs in most conditions but examination of the pattern at all temperatures clearly reveals, both for the bromide and for the iodide complex, three absorptions of relative intensity 1 : 1 : 1 (*anti* isomer) and six absorptions of relative intensity 1 : 1 : 1 : 1 : 1 : 1 (*gauche* isomer). The crystalline material that we have obtained for the iodide system after a short (*ca* 1/2 h) reflux time shows more resonances in the methyl region of the ^1H NMR spectrum. These extra resonances have a temperature dependence similar to those of *anti* and *gauche* $Mo_2I_6(PMe_2Ph)$ and are due to an, as yet, unidentified impurity which disappears when the material is refluxed for a longer period.

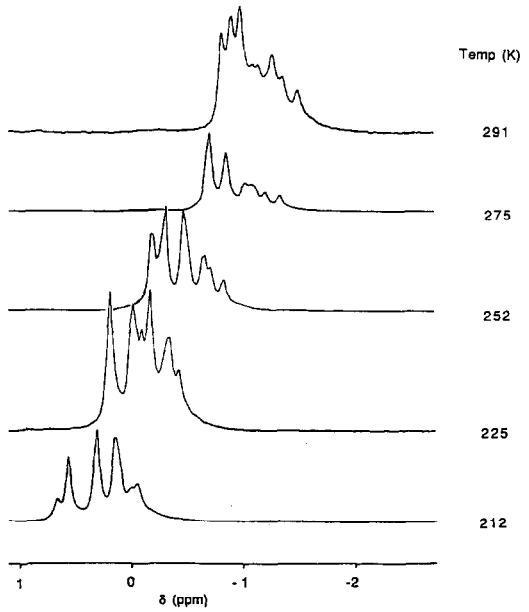

Fig. 1. Representative ^1H NMR spectra of the $Mo_2Br_6(PMe_2Ph)_3$ compound in the methyl region at various temperatures. Solvent = CD_2Cl_2.

The optical properties of the three compounds (X = Cl, Br, I) are also consistent with the known electronic structure. Upon increasing the metal–metal distance and thereby reducing the metal–metal overlap, the HOMO–LUMO gap decreases and the absorption bands experience a red shift.

The $Mo_2X_6(PMe_2Ph)_3$ (X = Br, I) compounds, like their chloride analogue, crystallize in the triclinic space group $P\bar{1}$ with similar cell dimensions. The three molecules show the same face-sharing, bioctahedral geometry with the phosphine ligand system in a relative *anti* configuration. Figure 2 shows a view of the bromide molecule. The octahedral geometry around each metal is slightly distorted, at least in part because of the compression

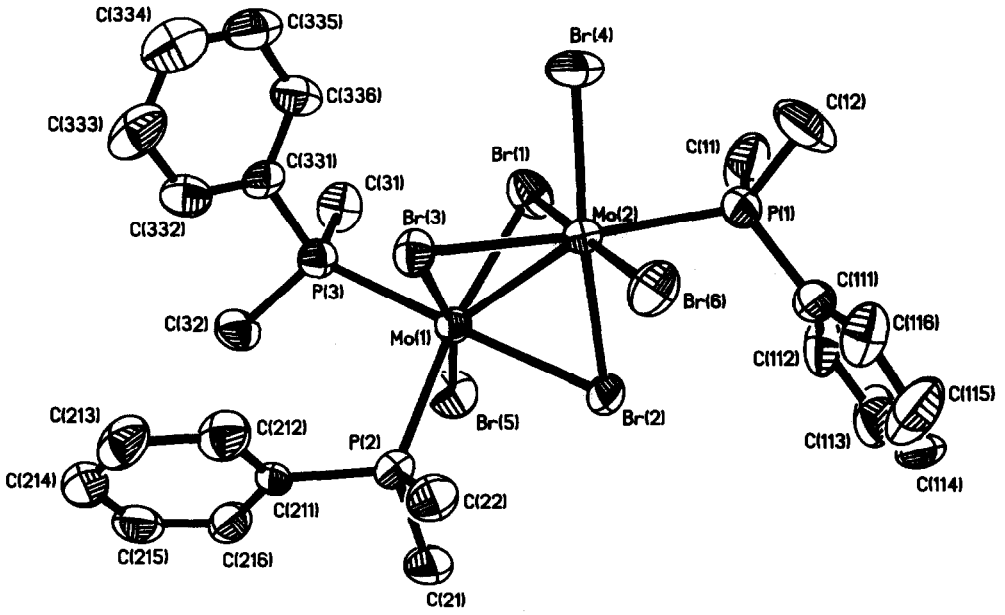

Fig. 2. ORTEP view of the $Mo_2Br_6(PMe_2Ph)_3$ molecule. The iodide analogue has an identical structure.

along the metal–metal axis which is caused by the metal–metal bond. For instance, the average angle between two Mo—(μ-X) vectors is higher than 90°, whereas all the Mo—(μ-X)—Mo angles are less than the value of 70.53° which is the calculated value for an undistorted FSBO structure.[17] Another indication of Mo—Mo bonding is the metal–metal separation, 2.749(2) Å for the bromide complex and 2.909(1) Å for the iodide complex, which compare with 2.6582(5) Å for the corresponding chloride complex.[2] The only other structurally characterized FSBO molybdenum(III) complexes with bridging bromides or iodides are $Cs_3Mo_2Br_9$ [Mo—Mo = 2.816(9) Å],[12] and $[Cat]^+[Mo_2I_7(PMe_3)_2]^-$ [Mo—Mo = 3.021(4) Å, Cat = $PHMe_3$; 3.022(1) Å, Cat = $AsPh_4$].[13]

As one might have anticipated, the Mo—X distances are, on average, shorter for terminal halides, and those involving bridging halide ligands reflect the higher *trans* influence of PMe_2Ph vs X. The Mo—P distances for both compounds are in the range usually found for octahedrally coordinated molybdenum(III) compounds.[4,13,18]

We now come to the original interest of our studies, that is the reaction of the FSBO bromide and iodide complexes with extra phosphine in an attempt to generate the corresponding ESBO complexes and whether the latter would or would not show a direct metal–metal interaction (see Introduction). The reaction of $Mo_2Br_6(PMe_2Ph)_3$ with three equivalents of PMe_2Ph was followed by ^1H NMR at room temperature. Figure 3 shows the salient features of this experiment. Two peaks at *ca* δ −26.5 and −39 in an approximate 1:1 ratio develop initially. These are assigned to the methyl groups of an ESBO $Mo_2Br_6(PMe_2Ph)_4$ molecule containing two phosphine ligands in the axial positions on one molybdenum centre, and the other two in the equatorial positions on the other metal, as shown in structure **I**. This is the geometry that has been found both in the solid state and in solution for the corresponding chloride system.[2,3]

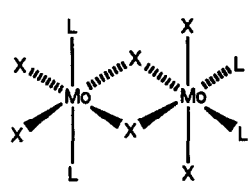

I

The intensity of these resonances, however, never exceeds *ca* 1% of the total amount of the molybdenum complex and two new resonances at δ −26.5 and −40, in a 1:2 ratio, soon start to grow. These correspond to the mononuclear *mer*-$MoBr_3(PMe_2Ph)_3$.[2] Two major conclusions can be drawn from this experiment. The reaction follows the same path as that of the corresponding chloride system,[2] see eq. (2), but the relative rates of the two steps are reversed, the first step (FSBO to ESBO) being slower than the second one (ESBO

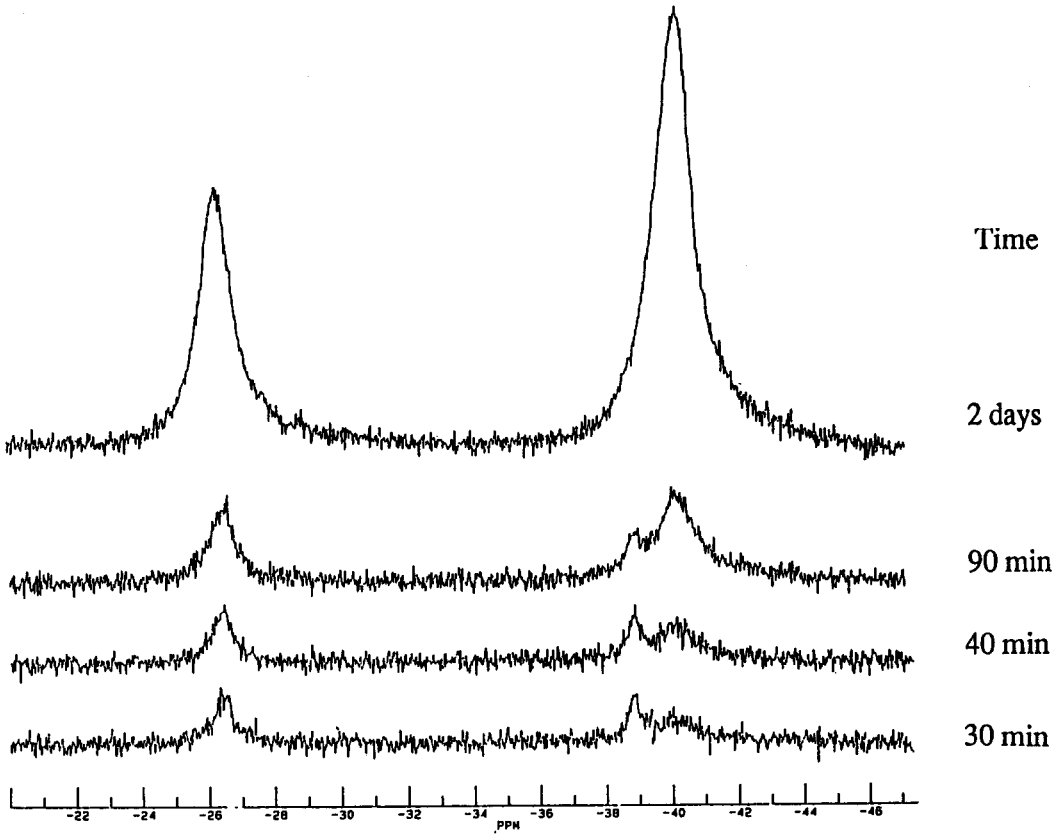

Fig. 3. ^1H NMR spectra in the phosphine methyl region during the reaction of $Mo_2Br_6(PMe_2Ph)_3$ with excess PMe_2Ph.

to MO), see eq. (3):

$$Mo_2Br_6(PMe_2Ph)_3 \xrightarrow[\text{slow}]{+PMe_2Ph} Mo_2Br_6(PMe_2Ph)_4 \xrightarrow[\text{fast}]{+PMe_2Ph} 2MoBr_3(PMe_2Ph)_3. \quad (3)$$

The second conclusion is that the ESBO $Mo_2Br_6(PMe_2Ph)_4$ molecule does not have a direct Mo—Mo bond and its magnetic properties (as indicated by the paramagnetic shifts in the ^1H NMR spectrum) are analogous to those of the mononuclear $MoBr_3(PMe_2Ph)_3$ molecule, i.e. there are three unpaired electrons per metal centre. Therefore, changing the nature of the bridging halide ligands from chloride to bromide is sufficient to change the metal–metal interaction from a situation of strong bonding[2] ($\sigma^2\pi^2\delta^{*2}$) to no bonding at all. This system differs from the corresponding $Mo_2X_6(dppe)_2$ system, in which a Mo—Mo bond exists for both X = Cl[19] and X = Br.[20] The faster second step of eq. (3), as compared with the second step of eq. (1) (L = PMe_2Ph), may be attributed to the increased kinetic barrier in the latter case due to the change of spin state on going from the ESBO to the MO system.

Based on the relative intensities and positions of the peaks in Fig. 3, and comparing the geometrical features of the ESBO $Mo_2Br_6(PMe_2Ph)_4$ with the mononuclear *mer*-$MoBr_3(PMe_2Ph)_3$, it is possible to assign, for the methyl protons of the ESBO molecule, the upfield resonance (δ −39) to the ligands that are *trans* to each other and the downfield resonance (δ −26.5) to the ligands that are *trans* to bridging bromides.

Conclusions

The investigations reported here have shown that, although FSBO systems of the type $Mo_2X_6(PMe_2Ph)_3$ maintain a direct metal–metal bonding on going from X = Cl or X = I, this interaction is lost in the corresponding ESBO $Mo_2X_6(PMe_2Ph)_4$ systems on going from X = Cl to Br. Furthermore, the FSBO to ESBO transformation becomes slower relative to the ESBO to MO transformation on going from X = Cl to X = Br. As a result, although the thermodynamically unstable (toward ligand disproportionation) ESBO chloride system could be kinetically accumulated in solution and isolated by utilizing the strategy illustrated

in eq. (1),[2] the corresponding bromide system can only be generated as a short-lived intermediate. As a corollary, ESBO compounds with monodentate phosphine ligands and bridging *iodide* ligands are not likely to be stable species either.

Acknowledgements—We are grateful to the Petroleum Research Fund, administered by the American Chemical Society, for partial support of this work. Additional support from the Camille and Henry Dreyfus Foundation (New Faculty Award to R.P.) and from the National Science Foundation (Presidential Young Investigator Award to R.P.) is also gratefully acknowledged. H.D.M. thanks the University of Maryland Office of Undergraduate Studies for a Senior Summer Scholarship. The X-ray diffractometer was purchased through a grant provided by the National Science Foundation VT-EPSCoR (Grant No. RII8610679) program.

REFERENCES

1. R. Poli and H. D. Mui, *J. Am. Chem. Soc.* 1990, **112**, 2446.
2. R. Poli and H. D. Mui, *Inorg. Chem.* 1991, **30**, 65.
3. H. D. Mui and R. Poli, *Inorg. Chem.* 1989, **28**, 3609.
4. B. E. Owens, R. Poli and A. L. Rheingold, *Inorg. Chem.* 1989, **28**, 1456.
5. F. A. Cotton and R. Poli, *Inorg. Chem.* 1987, **26**, 1514.
6. M. W. Anker, J. Chatt, G. J. Leigh and A. G. Wedd, *J. Chem. Soc., Dalton Trans.* 1975, 2639.
7. F. A. Cotton, R. L. Luck and K.-A. Son, *Inorg. Chim. Acta* 1990, **173**, 131.
8. P. M. Boorman, K. J. Moynihan and R. T. Oakley, *J. Chem. Soc., Chem. Commun.* 1982, 899.
9. K. J. Moynihan, X. Gao, P. M. Boorman, J. F. Fait, G. K. W. Freeman, P. Thornton and D. J. Ironmonger, *Inorg. Chem.* 1990, **29**, 1648.
10. I. W. Boyd and A. G. Wedd, *Aust. J. Chem.* 1976, **29**, 1829.
11. C. Miniscloux, G. Martino and L. Sajus, *Bull. Soc. Chim. Fr.* 1973, 2179.
12. (a) R. Saillant and R. A. D. Wentworth, *Inorg. Chem.* 1969, **8**, 1226; (b) R. Saillant, R. B. Jackson, W. E. Streib, K. Folting and R. A. D. Wentworth, *Inorg. Chem.* 1971, **10**, 1453; (c) R. Stranger, P. W. Smith and I. E. Grey, *Inorg. Chem.* 1989, **28**, 1271.
13. F. A. Cotton and R. Poli, *Inorg. Chem.* 1987, **26**, 3310.
14. F. A. Cotton and R. L. Luck, *Inorg. Chem.* 1989, **28**, 182.
15. R. H. Summerville and R. Hoffmann, *J. Am. Chem. Soc.* 1979, **101**, 3820.
16. F. A. Cotton and R. Poli, *Inorg. Chem.* 1987, **26**, 3228.
17. F. A. Cotton and D. A. Ucko, *Inorg. Chim. Acta* 1972, **6**, 161.
18. F. A. Cotton and R. Poli, *Inorg. Chem.* 1986, **25**, 3624.
19. P. A. Agaskar, F. A. Cotton, K. R. Dunbar, L. R. Falvello and C. J. O'Connor, *Inorg. Chem.* 1987, **26**, 4051.
20. B. E. Owens and R. Poli, *Polyhedron* 1989, **8**, 545.

Polyhedron Vol. 10, No. 14, pp. 1675–1682, 1991
Printed in Great Britain

0277–5387/91 $3.00+.00
© 1991 Pergamon Press plc

COPPER(II) COMPLEXES OF 1-(PYRIDINE-2-YL)-3-METHYL-3,6-DIAZAHEPTANE (PDAHP). X-RAY CRYSTAL STRUCTURE OF $Cu(PDAHP)Cl_2$

A. CASTIÑEIRAS,* R. CARBALLO and C. VÁZQUEZ

Departamento de Química Inorgánica, Universidad de Santiago de Compostela, E-15706 Santiago de Compostela, Spain

(*Received* 29 *October* 1990; *accepted* 15 *April* 1991)

Abstract—The reactions of the novel tridentate ligand 1-(pyridine-2-yl)-3-methyl-3,6-diazaheptane (PDAHP) with copper(II) salts have been investigated. The ligand and the complexes $Cu(PDAHP)Cl_2$, $Cu(PDAHP)Br_2$, $[Cu(PDAHP)(OH_2)_2](ClO_4)_2$ and $[Cu(PDAHP)(NO_3)](NO_3)$ have been characterized by elemental analyses, conductivity and magnetic susceptibility measurements, mass, IR, electronic absorption and ^1H NMR data. In addition, the X-ray crystal structure of $Cu(PDAHP)Cl_2$ is described. The structure is a distorted trigonal bipyramid in which the copper atom is coordinated by a ligand molecule that spans the two axial and one equatorial sites and by the two chlorine atoms in the remaining equatorial positions.

The preparation and study of inorganic compounds containing biologically important ligands is made easier since certain metal ions are active in many biological processes; species of low molecular weight are hence sought that reproduce, as far as possible, the structural properties and the reactivity of these ions in such processes. The fact that copper, together with magnesium, calcium, iron, zinc, chromium, vanadium and manganese, is one of the essential metallic elements (it is the third most abundant after iron and zinc[1]) and that it has great biological activity when associated with certain metal–protein complexes, participating in the transport of oxygen, electronic transfer reactions or the storage of ions,[2] has brought about enormous interest in the study of systems containing this metallic centre.[3]

Results from spectroscopic and X-ray diffraction studies have established that in many copper-based proteins the metal has either a pseudo-tetrahedral or a square-based pseudo-pyramidal configuration.[4] It may be of use, therefore, to synthesize a series of both tri- and tetradentate ligands that, in the presence of copper(II), give rise to these coordination geometries. As part of our studies of ligands like those referred to above,[5] in this paper we describe the synthesis and characterization of the new tridentate ligand 1-(pyridine-2-yl)-3-methyl-3,6-diazaheptane (PDAHP) and the complexes formed from its reactions with various copper(II) compounds. The structure of one of these complexes has been characterized by X-ray diffraction.

* Author to whom correspondence should be addressed.

EXPERIMENTAL

Materials

The synthesis of the ligand PDAHP was performed using 2-vinylpyridine (Merck) and N,N′-dimethylethylendiamine (EGA). All chemicals were used without further purification.

Physical measurements

Carbon, hydrogen and nitrogen contents were carried out on a Perkin–Elmer 240B microanalyser. Positive ion FAB and electron impact (EI) mass spectra were obtained on a Kratos MS-50 mass spectrometer retrofitted with a Kratos FAB source and interfaced to a Kratos DS-90 data system. Xenon was used as the bombarding gas with atom gun energies of 8 keV. The source was operated

at 250°C. The liquid matrix used was 3-nitrobenzylalcohol.

IR absorption spectra (4000–200 cm^{-1}) using KBr and CsI pellets were recorded on a Perkin–Elmer 1330 spectrophotometer. UV–vis spectra were measured on a Hitachi U-3200 spectrophotometer using the diffuse reflectance technique with MgO as reference.

Magnetic susceptibilities were determined by the Faraday method in the temperature range 70–300 K with a DSM-5 susceptometer, operating at a fixed field strength of 15 kG. $HgCo(NCS)_4$ and $Cd_2(SO_4)_3 \cdot 8H_2O$ were used as calibrants. X-ray crystallographic data were obtained on an Enraf–Nonius CAD4 diffractometer. Data reduction and solution were performed on a MicroVAXII using the SHELXS86[6] and VAX/SDP[7] package of programs.

^1H NMR spectra were recorded on a Bruker WM250 instrument in DMSO-d_6 using TMS as internal standard. Conductivity measurements were carried out on a WTW LF-3 conductivity bridge. Measurements were made for 10^{-3} M solutions in acetonitrile.

Synthesis of the ligand

A solution of concentrated hydrochloride acid (6 cm^3) was carefully added with stirring to a solution of freshly distilled 2-vinylpyridine (8 cm^3, 74.3 mmol) in methanol (30 cm^3) over nitrogen. Stirring was continued for 20 min and an excess of N,N′-dimethylethylendiamine was then added. The mixture was heated under reflux for 1 h. Addition of sodium hydroxide then caused precipitation of sodium chloride. The solvent was removed and the resulting oil was dissolved in ether, dried with calcium sulphate and the solvent removed *in vacuo*. PDAHP was obtained upon removal of the ether solution as a yellow oil (70%).

Synthesis of the complexes

All four complexes were prepared by dissolving CuX_2 crystallized (4 mmol) (X = Cl, Br, ClO_4 or NO_3) in methanol (10 cm^3) and adding the resulting solution to PDAHP (0.77 g, 4 mmol) in methanol (10 cm^3). The mixture was stirred for 7 days after which the volume of the solution was reduced *in vacuo*, and the solids were isolated by filtration. Crystals of $Cu(PDAHP)Cl_2$ suitable for X-ray crystallographic analysis were isolated by slow evaporation of a methanolic solution of the complex.

X-ray data collection and reduction

A light green prismatic crystal of $Cu(PDAHP)Cl_2$ was mounted on a glass fibre and used for data collection. Cell constants and an orientation matrix for data collection were obtained by least-squares refinement of the diffraction data from 25 reflections in the range of $6 < \theta < 12°$. Data were collected at 293 K using Mo-K_α radiation ($\lambda = 0.71073$ Å) and the ω–θ scan technique. The data were corrected for Lorentz and polarization effects and empirical absorption[8] and secondary extinction corrections were applied.[9] The final coefficient, refined in the last least-squares cycle, was 2.13×10^{-7}. A summary of the crystal data, experimental details and refinement results are listed in Table 1.

Structure solution and refinement

The structure was solved by direct methods which revealed the position of all non-hydrogen atoms, and refined on F by a full-matrix least-squares procedure using anisotropic temperature factors. Hydrogen atoms were located from geometrical considerations, added to the structure factors calculations as fixed contributions and their positional parameters were not refined. After all the shift/ESD ratios were less than 0.1, the refinement converged to the agreement factors listed in Table 1. Form factors were taken from ref. 10.*

RESULTS AND DISCUSSION

Our studies show that the reaction of the calculated quantities of copper(II) salts with PDAHP in methanolic solution give the complexes shown in Table 2, which contain a ligand molecule for each metal atom. Elemental analyses, colour and conductivity measurements for the PDAHP ligand and complexes are also listed in Table 2.

Characterization of the ligand

The free ligand was characterized by mass, IR and ^1H NMR spectroscopy.

The molecular ion does not appear in the mass spectrum but fragments are seen that correspond to

* Further details of the structure determination have been deposited as Supplementary Publication No. CDS-54513. Copies may be obtained through the Fachinformationzentrum Karlsruhe, D-7514 Eggenstrin-Leopoldshafen 2, F.R.G.

Table 1. Crystal data, data collection and structure refinement parameters of [Cu(PDAHP)Cl_2]

Formula	$C_{11}H_{19}Cl_2CuN_3$
Molecular weight	327.74
Crystal class	Monoclinic
Space group	$P2_1/c$
Unit cell dimensions	a = 1640.2(2) pm
	b = 788.4(5) pm
	c = 1109.4(5) pm
	β = 104.13(2)°
Volume	1391.2×10^6 pm^3
Z	4
ρ_x	1.565 g cm^{-3}
μ	19.439 cm^{-1}
$F(000)$	676
Crystal shape, dimensions	Prismatic, $0.08 \times 0.08 \times 0.32$ mm
Minimum/maximum absorption correction	0.7561/1.1037
Maximum value of $(\sin\theta)/\lambda$ reached in intensity measurement	0.6162
Range h, k, l	0–13, 0–9, −20–20
Standard reflections	4, 0,1 ; 5,1,3
Interval standard reflections measured	3600 s
Total number of reflections measured, θ range	3095, 3–26°
Number of unique reflections; R_{int}	2793, 0.038
Number of observed reflections	1689
Criterion for observed reflections	$I > 3\sigma(I)$
Weighting scheme	$1/\sigma^2(F)$
Parameters refined	155
Value of R	0.060
Value of wR	0.063
Ratio of max. LS shift to ESD (Δ/σ)	0.069
Max. height in final ΔF map	0.606 e Å^{-3}
Error in an observation of unit weight	2.381
Secondary-extinction coefficient	2.1305×10^{-7}

Table 2. Analytical and physical data for the metal complexes

Compound	Colour	Melting point (°C)	Found (Calc.) % C	H	N	Λ_M[a]
PDAHP·HCl	Yellow		56.2 (57.5)	9.9 (8.7)	18.2 (18.3)	
PDAHP	Yellow		67.8 (68.4)	10.2 (10.2)	21.4 (21.8)	
[Cu(PDAHP)Cl_2]	Blue	223	38.7 (40.4)	5.8 (5.8)	13.0 (12.9)	13.94
[Cu(PDAHP)Br_2]	Green	215	32.8 (31.3)	4.5 (4.5)	9.7 (9.7)	25.96
[Cu(PDAHP)$(H_2O)_2$]$(ClO_4)_2$	Blue	237	27.8 (26.9)	4.6 (4.7)	9.1 (8.5)	236.56
[Cu(PDAHP)(NO_3)](NO_3)	Blue	235	35.1 (34.7)	5.0 (5.0)	18.0 (18.4)	104.89

[a] Ω^{-1} cm^2 mol^{-1}.

the α-splitting of the tertiary amines $[M-CH_2N(H)CH_3]^+$ ($m/z = 149$, relative abundance 90%) and $[M-C_5H_4NCH_2]^+$ ($m/z = 101$, relative abundance 10%) which can be used to deduce the relative molecular mass of the compound. Other abundant ions were $[M—C_5H_4NCH_2CH_2]^+$ ($m/z = 106$, relative abundance 100%) and $[C_5H_4N(H)CH_2]^+$ ($m/z = 93$, relative abundance 26%).

The IR spectrum showed a medium intensity band at 3320 cm^{-1} and a weak one at 1675 cm^{-1} which were assigned to the ν(NH) and δ(NH) modes of the amine group, respectively. Other strong bands at 1588, 1567, 1469 and 1431 cm^{-1} corresponding to the symmetric and asymmetric C=C and C=N vibrations of the pyridine ring. A strong band at 1120 cm^{-1} was assigned to the ν(CN) stretching modes of the amine groups, and the two medium intensity bands at 627 and 406 cm^{-1} were assigned to the deformation modes of the pyridine ring.

The ^{1}H NMR spectrum showed the following signals: 2.18 ppm (s, 3H) and 2.22 ppm (s, 3H), of the methyl groups; 2.42 ppm (m, 4H), of the ethylene group that joins the two amine nitrogen atoms; 2.63 ppm (t, 2H) and 2.82 ppm (t, 2H), of the ethylene group joined to the pyridine; 7.13 ppm (t, 1H), 7.22 ppm (d, 1H), 7.63 ppm (t, 1H) and 8.45 ppm (d, 1H), of the pyridine-1H.

Structure of $Cu(PDAHP)Cl_2$

The most important distances and angles are included in Table 3 and the molecule is represented in Fig. 1 with the atoms shown numbered, and in Fig. 2, a stereoscopic view. The asymmetric unit is formed from a copper atom coordinated by a ligand molecule across its three nitrogen atoms and by the two chlorine atoms that occupy equatorial positions in a polyhedron of distorted trigonal bipyramidal coordination.

The degree of distortion between trigonal bipyramidal and tetragonal pyramidal geometries can be estimated knowing the parameter $\tau = (\beta-\alpha)/60$,[11] where α and β are the maximum basal angles between opposite atoms, such that, ideally, $\tau = 1$ corresponds to the trigonal bipyramid and $\tau = 0$ to the tetragonal pyramid. For the compound under study, Cl(1)—Cu—N(2) = α = 141.8° and N(1)—Cu—N(3) = β = 168.7°, giving $\tau = 0.45$, indicating that there is significant distorsion from the

Table 3. Interatomic distances and bond angles for $[Cu(PDAHP)Cl_2]$[a]

Distances (pm)			
Cu—Cl(1)	233.8(2)	N(3)—C(9)	149.1(6)
Cu—Cl(2)	242.3(1)	N(3)—C(31)	149.6(6)
Cu—N(1)	197.5(4)	C(1)—C(2)	139.6(9)
Cu—N(2)	213.6(4)	C(2)—C(3)	143(1)
Cu—N(3)	199.2(5)	C(3)—C(4)	139(1)
N(1)—C(1)	136.3(8)	C(4)—C(5)	140.3(9)
N(1)—C(5)	136.5(7)	C(5)—C(6)	154.0(9)
N(2)—C(7)	148.3(7)	C(6)—C(7)	149.9(9)
N(2)—C(8)	150.0(7)	C(8)—C(9)	153.6(8)
N(2)—C(21)	151.2(8)		
Angles (°)			
Cl(1)—Cu—Cl(2)	115.89(6)	C(8)—N(2)—C(21)	109.8(5)
Cl(1)—Cu—N(1)	88.3(1)	C(9)—N(3)—C(31)	110.2(4)
Cl(1)—Cu—N(2)	141.8(1)	N(1)—C(1)—C(2)	121.3(7)
Cl(1)—Cu—N(3)	89.2(1)	C(1)—C(2)—C(3)	118.2(8)
Cl(2)—Cu—N(1)	94.9(1)	C(2)—C(3)—C(4)	119.7(8)
Cl(2)—Cu—N(2)	102.3(1)	C(3)—C(4)—C(5)	119.2(8)
Cl(2)—Cu—N(3)	96.1(1)	N(1)—C(5)—C(4)	121.0(7)
N(1)—Cu—N(2)	90.1(2)	N(1)—C(5)—C(6)	116.2(6)
N(1)—Cu—N(3)	168.7(2)	C(4)—C(5)—C(6)	122.9(7)
N(2)—Cu—N(3)	85.0(2)	C(5)—C(6)—C(7)	110.6(7)
C(1)—N(1)—C(5)	120.7(5)	N(2)—C(7)—C(6)	110.2(6)
C(7)—N(2)—C(8)	108.9(4)	N(2)—C(8)—C(9)	108.2(4)
C(7)—N(2)—C(21)	107.5(6)	N(3)—C(9)—C(8)	106.0(4)

[a] ESDs given in parentheses.

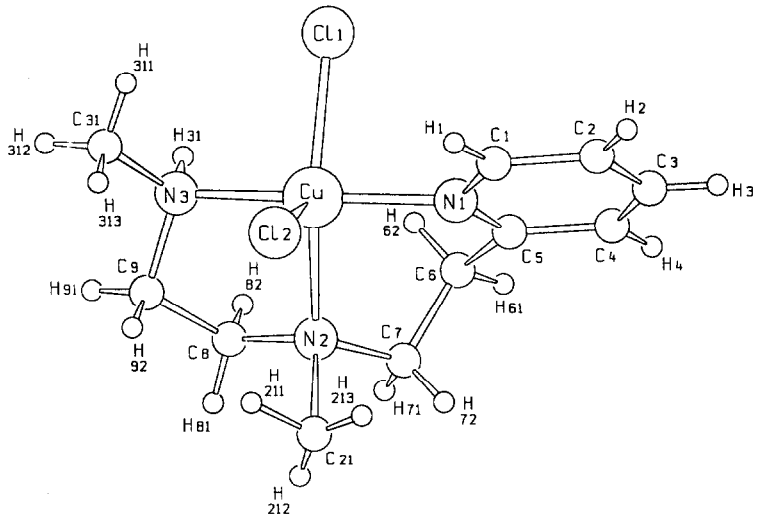

Fig. 1. Structure and numbering scheme for $[Cu(PDAHP)Cl_2]$.

trigonal bipyramid toward a tetragonal pyramidal geometry (Fig. 2). The average deviation of atoms Cl(1), N(1), N(2) and N(3) from the mean basal plane is 26.7 pm. The copper atom is located a distance of 46.16(9) pm above this plane. The distortions can be explained by bearing in mind that PDAHP is a tridentate chelate ligand that coordinates to the metal forming five- and six-membered rings; the resulting tensions cause modifications of the equatorial and axial angles.

The average bond lengths $Cu—N_{(amine)}$, 198.9(5) pm, and $Cu—N_{(pyridine)}$, 213.6(4) pm, are characteristic of copper(II)–nitrogen bonds,[12] and the Cu—Cl distances of 233.8(2) and 242.3(1) pm are slightly greater than those found in other complexes with terminal Cu—Cl bonds in a similar copper coordination.[13]

An "*envelope*" conformation can be deduced for the five-membered ring and a "*boat*" conformation for the six-membered one from the values of the dihedral angles,[14] there being an angle of 32.8(4)° between the mean planes of both rings, comparable to others found in similar systems.[15]

Mass spectra

The mass spectra of all the complexes (Table 4) show two peaks, the one of greater m/z can be assigned to the species $[Cu(PDAHP)X]^+$ and that of lower m/z, coinciding in all cases, to the species $[Cu(PDAHP)]^+$. These species are common in the mass spectra of $[ML_n]X_m$ type coordination compounds of monovalent anions with the metal in oxidation state II or III.[16]

Every spectrum also contained some peaks with higher or lower m/z values than those shown (Table 2), which may be due to oligomeric species, in the

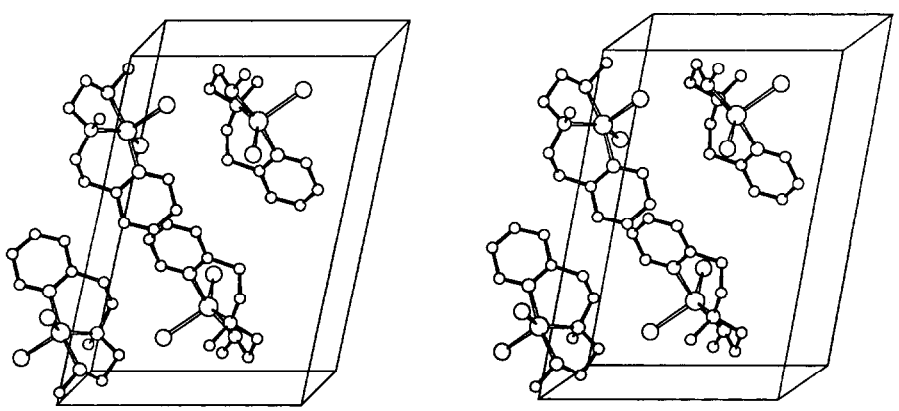

Fig. 2. Stereoscopic view of the unit cell of $[Cu(PDAHP)Cl_2]$.

Table 4. Positive ion FAB spectra of the complexes in *p*-nitrobenzyl alcohol[a]

Compound	[Cu(PDAHP)X]$^+$ *m/z*	RA	[Cu(PDAHP)]$^+$ *m/z*	RA
[Cu(PDAHP)Cl_2]	291	61	256	100
[Cu(PDAHP)Br_2]	337	13	256	55
[Cu(PDAHP)$(H_2O)_2$]$(ClO_4)_2$	355	5	256	71
[Cu(PDAHP)(NO_3)](NO_3)	318	92	256	100

[a] Relative abundances (RA) normalized to a value of 100 units for the most abundant ion, after removal of ions arising from the matrix.

first case, and to the fragmentation of the ligand, in the second.

Conductivity

Values of molar conductivity for 10^{-3} M solutions of the complexes in acetonitrile (Table 4), less than 30 Ω^{-1} cm^2 mol^{-1} in Cu(PDAHP)X_2 (X = Cl or Br), show that they are non-electrolytes with the halide atom coordinated to the metal.[17] The perchlorate derivative has a molar conductivity of 236.56 Ω^{-1} cm^2 mol^{-1}, in agreement with that expected for 1:2 electrolytes in acetonitrile[17] and indicates that the metal is pentacoordinated by the ligand and both water molecules. Cu(PDAHP)$(NO_3)_2$, however, has a molar conductivity of 104.89 Ω^{-1} cm^2 mol^{-1} placing it in the range of 1:1 electrolytes.[17] This is only possible if we suppose that one nitrate group is coordinated to the metal.

IR spectra

A tentative assignment of the most characteristic IR bands has been made (Table 5). The bands due to stretching vibrations in the pyridine ring, between 1590 and 1430 cm^{-1}, and those due to the deformation modes appearing near 625 and 405 cm^{-1}, are displaced to higher frequencies in the complexes. This behaviour is very indicative of the ligand being coordinated to the copper(II) across the nitrogen of the pyridine group.[18] Furthermore, the band corresponding to the ν(NH) mode is displaced between -60 and -140 cm^{-1} in the complexes, and the band assigned to ν(CN), that in the free ligand appears as a strong band at 1120 cm^{-1}, is displaced to higher frequencies by almost 20 cm^{-1} in the complex, to form a weak band. The above indicates that the nitrogen atoms of both amine groups participate in coordination, in agreement with the structural results obtained for Cu(PDAHP)Cl_2.

The spectrum of [Cu(PDAHP)$(OH_2)_2$]$(ClO_4)_2$ contains, in addition to the bands already mentioned, ν(OH) and δ(OH) modes at 3520 and 1665 cm^{-1} indicating the presence of coordinated water molecules,[19] as well as an intense band close to 1100 cm^{-1} and a strong band at *ca* 625 cm^{-1} assignable to the $\nu_3(ClO_4)$ and $\nu_4(ClO_4)$ modes, respectively, of the perchlorate ions.[20]

Table 5. Relevant IR data for the metal complexes

[Cu(PDAHP)Cl_2]	[Cu(PDAHP)Br_2]	[Cu(PDAHP)$(H_2O)_2$]$(ClO_4)_2$	[Cu(PDAHP)(NO_3)](NO_3)	
3165f	3181f	3260m	3220m 3187m	ν(NH)
1609f	1608f	1614f	1609m	8a
1570m	1565m	1550m	1567m	8b
1478f	1475f	1480f	1475f	19a
1441f	1437f	1448f	1445f,a	19b
1140d	1143d		1140d	ν(CN)
653d	650d	652d	650d	6b
490d	470d	485d	477d	ν(CuN)
438d	434d	428d	432d	16a
380d	376d	365d	345d	ν(CuN)
		284d	290d	
		273d	270d	ν(CuO)
240f				ν(CuCl)

Table 6. Magnetic and electronic spectral data for the metal complexes[a]

Compound	α	β	θ	μ	μ(298 K)	d–d (cm^{-1})
$[Cu(PDAHP)Cl_2]$	2.359	2.316	−1.01	1.86	1.79	14,827
$[Cu(PDAHP)Br_2]$	−12.304	2.500	4.92	1.79	1.91	14,285
$[Cu(PDAHP)(H_2O)_2](ClO_4)_2$	51.892	1.080	−48.07	2.72	2.55	17,618–15,479
$[Cu(PDAHP)(NO_3)](NO_3)$	12.966	2.231	−5.81	1.89	1.89	15,271

[a] $1/\chi = \alpha + \beta T$.

In the spectrum of $[Cu(PDAHP)(NO_3)](NO_3)$, the presence of NO_3^- ions is revealed by a strong, narrow band at 1377 cm^{-1} (ν_3) and two weak bands at 815–816 and 726 cm^{-1} (ν_2 and ν_4, respectively),[21] while the bidentate nature of the nitrate ligand is shown by the presence of the bands at 1284 cm^{-1} (ν_3), 1020 cm^{-1} (ν_1) and 832 cm^{-1} (ν_2)[22a] and by the splitting of the combination band $\nu_1+\nu_4$ that appears at 1768 and 1732 cm^{-1}.[22b] The existence of ionic and bidentate nitrates explains the conductivity value found for this complex and the pentacoordination deduced from its electronic spectrum (*vide infra*).

The presence of two low frequency bands at 490–470 cm^{-1} and 380–340 cm^{-1} in the spectra of every complex lead to their assignment as ν(CuN) modes,[23] while a strong absorption at 240 cm^{-1} was identified as ν(CuCl).[24] Lastly, medium intensity bands at 284–273 cm^{-1} and 290–270 cm^{-1} in the spectra of $[Cu(PDAHP)(OH_2)_2](ClO_4)_2$ and $[Cu(PDAHP)(NO_3)](NO_3)$, respectively, which are not seen in the spectra of the other two complexes, can reasonably be assigned to the ν(CuO) modes.[19,25]

Electronic reflectance spectra

The diffuse reflectance spectra of all the complexes (Table 6), except $[Cu(PDAHP)(OH_2)_2](ClO_4)_2$, are very similar and contain a narrow, asymmetric band that is poorly resolved at high energy, with a maxima at 14,827, 14,285 and 15,271 cm^{-1} in the chloro, bromo and nitrate derivatives, respectively, suggesting distorted trigonal bipyramidal geometry,[26] which is consistent with the structural parameters found for $Cu(PDAHP)Cl_2$. The spectrum of $[Cu(PDAHP)(OH_2)_2](ClO_4)_2$, however, presents two peaks of equal intensity at 15,479 and 17.618 cm^{-1} and matches the spectra of other copper(II) complexes with distorted tetragonal pyramidal geometry.[27]

Magnetic susceptibilities

The magnetic moments of the complexes (Table 6) at room temperature have values between 1.79 and 2.55 BM, and lie in the interval expected for pentacoordinated complexes of copper(II).[28,29] Study of the variation in the reciprocal of the molar magnetic susceptibility corrected with the temperature, from 70 to 300 K, indicates that the complexes obey the Curie–Weiss law, and the magnetic moment deduced thereby (Table 6) does not differ greatly from that found at room temperature.

Acknowledgements—We thank Professor Alario Franco and Professor Sáez Puche of Complutense University (Madrid) for their collaboration in the magnetic measurements, and also thank the CICYT of Spain for financial support (Project PS88-0051).

REFERENCES

1. F. A. Cotton and G. Wilkinson, *Advanced Inorganic Chemistry*, 5th edn. John Wiley, New York (1988).
2. G. Albertin, E. Bordignon and A. A. Orio, *Inorg. Chem.* 1975, **14**, 1411.
3. K. D. Karlin and J. Zubieta (Eds), *Copper Coordination Chemistry: Biochemical and Inorganic Perspectives*. Adenine Press, New York (1983).
4. P. H. Berens and D. W. Stephan, *Inorg. Chim. Acta* 1984, **93**, 173.
5. (a) A. Castiñeiras, W. Hiller, J. Strähle, M. V. Paredes and J. Sordo, *Acta Cryst.* 1985, **C41**, 41; (b) A. Castiñeiras, R. Carballo, M. R. Bermejo, M. Gayoso, C. Molleda, W. Hiller and J. Strähle, *Z. Krist.* 1988, **185**, 381.
6. G. M. Sheldrick, SHELXS86, A Program for the Solution of Crystal Structures from X-ray Diffraction Data. University of Göttingen, F.R.G. (1986).
7. B. A. Frenz, in *Computing in Crystallography* (Edited by H. Schrenk, R. Oltof-Hazenkamp, H. van Koningsveld and G. C. Bassi). Delft University Press, Delft (1978).
8. N. Walker and D. Stuart, *Acta Cryst.* 1983, **A39**, 158.
9. W. H. Zachariasen, *Acta Cryst.* 1963, **16**, 1139.
10. *International Tables for X-ray Crystallography*, Vol. IV. Kynoch Press, Birmingham (1974).
11. A. W. Addison, T. N. Rao, J. Reedijk, J. van Rijn and G. C. Verschoor, *J. Chem. Soc., Dalton Trans.* 1984, 1349.
12. (a) G. R. Bribaker, J. N. Brown, M. K. Yoo, R. A. Kiseny, T. M. Kutchan and E. A. Motlel, *Inorg.*

Chem. 1979, **18**, 299; (b) L. P. Battaglia, M. B. Ferrari, A. B. Corradi, G. G. Fava, C. Pelizzi and M. E. V. Tani, *J. Chem. Soc., Dalton Trans.* 1976, 2202; (c) N. Aoi, G. Matsubyashi and T. Tanaka, *Inorg. Chim. Acta* 1984, **85**, 123.
13. W. E. Marsh, W. E. Hatfield and D. J. Hodgson, *Inorg. Chem.* 1982, **21**, 2679.
14. W. L. Duax and D. A. Norton (Eds), *Atlas of Steroid Structure*, Vol. 1. Plenum Press, New York (1975).
15. (a) E. D. Estes, W. E. Estes, W. E. Hatfield and D. J. Hodgson, *Inorg. Chem.* 1975, **14**, 106; (b) P. G. Beckingsdale, A. T. Morcom, C. E. F. Rickard and T. N. Waters, *J. Chem. Soc., Dalton Trans.* 1977, 2135; (c) D. L. Lewis and D. J. Hodgson, *Inorg. Chem.* 1974, **13**, 143; (d) P. C. Jain and E. C. Lingafelter, *J. Am. Chem. Soc.* 1967, **89**, 6131.
16. G. Bojesen, *Org. Mass Spectrom.* 1985, **20**, 413.
17. W. J. Geary, *Coord. Chem. Rev.* 1971, **7**, 81.
18. (a) D. K. Rastoh and K. C. Sharma, *J. Inorg. Nucl. Chem.* 1974, **36**, 2219; (b) G. F. Svatos, C. Curran and J. V. Quagliano, *J. Am. Chem. Soc.* 1955, **77**, 6159.
19. D. M. Adams and P. J. Lock, *J. Chem. Soc. A* 1971, 2801.
20. (a) G. Herzberg, *Infrared and Raman Spectra of Polyatomic Molecules*. Van Nostran, New York (1945); (b) B. J. Hathaway and A. E. Underhill, *J. Chem. Soc.* 1961, 3091.
21. (a) B. M. Gatehouse, S. E. Livingstone and R. S. Nyholm, *J. Inorg. Nucl. Chem.* 1958, **8**, 75; (b) J. R. Ferraro and A. Walker, *J. Chem. Phys.* 1965, **42**, 1278.
22. (a) I. Pavlik, K. H. Thiele, K. Jacob and M. Glanz, *Z. Anorg. Allg. Chem.* 1989, **569**, 106; (b) A. B. P. Lever, E. Mantovani and B. S. Ramaswamy, *Can. J. Chem.* 1957, **49**, 1971.
23. (a) M. L. Niven, G. C. Percy and D. A. Thornton, *J. Molec. Struct.* 1980, **68**, 73; (b) D. X. West and R. J. Hartley, *J. Inorg. Nucl. Chem.* 1980, **42**, 1141.
24. M. Goodgame and K. W. Johns, *Inorg. Chim. Acta* 1980, **46**, 23.
25. G. Ertem and D. X. West, *Transition Met. Chem.* 1985, **10**, 131.
26. (a) M. Duggan, N. Ray, B. Hathaway, G. Tomlinson, P. Brint and K. Pelin, *J. Chem. Soc., Dalton Trans.* 1980, 1342; (b) S. Tyagi and B. J. Hathaway, *J. Chem. Soc., Dalton Trans.* 1983, 199.
27. (a) N. J. Ray, L. Hulett, R. Shahan and B. J. Hathaway, *J. Chem. Soc., Dalton Trans.* 1981, 1461; (b) S. Tyagi and B. J. Hathaway, *J. Chem. Soc., Dalton Trans.* 1981, 2029.
28. A. B. P. Lever, *Inorganic Electronic Spectrocopy*, 2nd edn. Elsevier, Amsterdam (1984).
29. S. K. Jain, B. S. Garg, Y. K. Bhoon, D. L. Klayman and J. P. Scovill, *Spectrochim. Acta* 1985, **41A**, 407.

Polyhedron Vol. 10, No. 14, pp. 1683–1686, 1991
Printed in Great Britain

0277–5387/91 $3.00+.00
© 1991 Pergamon Press plc

TERNARY COMPLEXES OF URANYL BETA-DIKETONES WITH ALIPHATIC AMIDES

P. B. RUIKAR, M. S. NAGAR and M. S. SUBRAMANIAN*

Radiochemistry Division, Bhabha Atomic Research Centre, Trombay, Bombay-400 085, India

(*Received* 9 *November* 1990; *accepted* 15 *April* 1991)

Abstract—Ternary adducts of uranyl beta-diketone chelates [beta-diketones = 1-phenyl-3-methyl-4-benzoyl-pyrazolone-5 (PMBP), 1-phenyl-3-methyl-4-acetyl-pyrazolone-5 (PMAP) and thenoyltrifluoroacetone (TTA)] and dibutyl derivatives of hexanamide (DBHA), octanamide (DBOA) and decanamide (DBDA) have been isolated and characterized as UO_2(beta-diketone)$_2$·amide. The ^{1}H NMR spectra indicate the existence of restricted rotation of the C—N bond in these complexes. Evidence for the existence of the amide adducts of PMBP as an isomeric mixture has been adduced from the presence of four phenyl protons in their ^{1}H NMR spectra. Thermal investigations confirm the existence of two types of PMBP moieties as opposed to the TTA adducts.

Long chain aliphatic amides have potential applications in nuclear fuel processing as they have some specific advantages over the conventional extractant, *viz.* TBP.[1–6] A detailed investigation of several amides for the separation of uranium and plutonium is contained in some excellent review articles.[7,8] Amides can also act as synergistic donors in the extraction of actinides by beta-diketones. Recently, Yi Min and Wang Liya[9] have reported synergistic extraction of uranyl nitrate by a mixture of N,N-diisopropylbutylamide and 1-phenyl-3-methyl-4-benzoyl-pyrazolone-5 (PMBP). Recently we have also investigated the synergistic extraction of uranyl ion with thenoyltrifluroacetone (TTA) and dibutyl derivatives of hexanamide (DBHA), octanamide (DBOA) and decanamide (DBDA).[10] Several binary solid complexes of actinides with amides have also been investigated by Bagnall and co-workers.[11,12] The synthesis, thermal studies, IR and ^{1}H NMR spectra of ternary uranyl complexes with beta-diketones such as TTA, PMBP and 1-phenyl-3-methyl-4-acetyl-pyrazolone-5 (PMAP) with three amides, *viz.* the dibutyl derivatives DBHA, DBOA and DBDA are described in this paper.

* Author to whom correspondence should be addressed.

EXPERIMENTAL

Preparation of the ligands

Pyrazolones and amides were synthesized by the methods of Jensen[13] and Baldwin,[14] respectively, and characterized by elemental analysis, IR and NMR spectra.

Preparation of the complexes

The complexes were prepared by solvent extraction of aqueous uranyl nitrate solution (10 cm^3, 5 mM) at pH = 2 with benzene (10 cm^3) containing 10 mM of the beta-diketone and 5 mM of the amide. The organic layer was dried with anhydrous sodium sulphate, evaporated to dryness and the crude product recrystallized from n-hexane.

Characterization of the complexes

The complexes were characterized by elemental analysis (Table 1) using standard semi-micro analytical methods.[15] Uranium was determined volumetrically, as well as gravimetrically, as reported earlier.[16,17] IR spectra of samples in Nujol mulls between CsI discs were measured using a Pu-9510 spectrophotometer in the range 4000–200 cm^{-1}.

Table 1. Analytical data of uranyl pyrazolone amide complexes[a]

Complex	C (%)	H (%)	N (%)	U (%)[b]	U (%)[c]
$UO_2(PMBP)_2 \cdot DBHA$	48.5	5.6	6.7	26.0	25.5
	(49.1)	(5.5)	(6.7)	(25.7)	
$UO_2(PMBP)_2 \cdot DBOA$	49.6	5.7	6.6	25.0	25.0
	(50.2)	(5.8)	(6.5)	(24.9)	
$UO_2(PMBP)_2 \cdot DBDA$	51.3	5.5	6.3	24.7	24.7
	(51.0)	(5.9)	(6.3)	(24.2)	
$UO_2(PMAP)_2 \cdot DBHA$	54.8	5.3	7.5	23.2	22.6
	(54.7)	(5.4)	(7.6)	(22.6)	
$UO_2(PMAP)_2 \cdot DBOA$	55.6	5.6	7.4	22.4	22.1
	(55.5)	(5.6)	(7.3)	(22.1)	
$UO_2(PMAP)_2 \cdot DBDA$	56.4	5.9	7.0	21.5	21.7
	(56.3)	(5.9)	(7.1)	(21.5)	
$UO_2(TTA)_2 \cdot DBHA$	39.4	3.9	1.5	25.0	24.5
	(38.3)	(4.2)	(1.5)	(25.3)	
$UO_2(TTA)_2 \cdot DBOA$	40.8	4.2	1.5	25.4	24.1
	(39.7)	(4.4)	(1.5)	(24.6)	

[a] Figures in parentheses indicate calculated values.
[b] Volumetric.
[c] Gravimetric.

^{1}H NMR spectra were obtained with a Varian FT-80A spectrophotometer using 0.05 M solutions in d-chloroform. Thermal investigations were carried out using a ULVAC (TGD-7000) differential thermal analyser in air at a heating rate of 10°C min^{-1}.

RESULTS AND DISCUSSION

IR spectra

The empirical assignments of a few typical bands in the IR spectra of the complexes are given in Table 2. The reduction in the stretching frequency of the carbonyl band of the free amide from 1640 to 1600 cm^{-1} indicates its coordination in the molecule.

^{1}H *NMR spectra*

The ^{1}H NMR spectral assignments of a few typical complexes are given in Table 3. In the complexes with TTA as the chelating agent, a broad singlet for the thienyl protons in addition to sharp singlets for the CH protons have been observed. The presence of two clear triplets for the α-CH protons of the butyl group in TTA complexes indicate their non-equivalence caused by restricted rotation of the

Table 2. Typical IR bands of uranyl beta-diketone-amide complexes

X	C=O(v)	Py. ring v	C—H inpl.	O—U—O	C—H *o/p*	M—O(Py)	M—O(X)	O—U—O
			Beta-diketone = PMBP; Amide = X					
DBHA	1610	1510	1065	935	775	430	350	275
DBOA	1610	1505	1065	930	772	420	350	270
DBDA	1695	1495	1060	922	765	420	345	265
			Beta-diketone = PMAP; Amide = X					
DBHA	1600	1495	1060	930	770	420	340	265
DBOA	1600	1495	1060	925	770	415	345	265
DBDA	1705	1508	1070	935	780	432	360	280
			Beta-diketone = TTA; Amide = X					
DBHA	1595		1070	925	795	495	360	260
DBOA	1585		1070	925	790	500	360	250

Table 3. ^{1}H NMR spectra of (a) $UO_2(TTA)_2 \cdot DBHA$ and DBOA, and (b) $UO_2(PMBP)_2 \cdot DBHA$ and DBOA[a] complexes

Nature of proton	Band position (ppm)	Intensity[b]	Multiplicity[c]	Coupling constants (J)
(*a*)				
Thienyl proton(1)	8.16(8.10)	1(1)	Broad singlet	
Thienyl proton(2)	7.70(7.65)	1(1)	Broad singlet	
Thienyl proton(3)	7.20(7.37)	1(1)	Broad singlet	
Proton	6.71(6.65)	1(1)	Singlet	
α-CH_2 of butyl(1)	3.80(3.75)	2(2)	Triplet	8(8)
α-CH_2 of butyl(2)	3.50(3.49)	2(2)	Triplet	8(8)
α-CH_2 of amide	2.80(2.76)	2(2)	Triplet	8(8)
Other CH_2 of butyl	1.70(1.65)	8(8)	Multiplet	
CH_3 and other CH_2 of amide	1.21–1.01 (1.05)	9 (13)	Multiplet	
CH_3 of butyl	0.60(0.55)	6(6)	Triplet	6(4)
(*b*)				
Phenyl and benzoyl	8.25–7.15 (8.25–7.18)	20 20	Broad peak Broad peak	
α-CH_2 of butyl	3.40(3.45)	4	5 (merger of 3 triplets)	
α-CH_2 of amide	2.50(2.53)	2	3	8
CH_3 of pyrazolone	1.93(1.95)	6	Singlet	
Other CH_2 of butyl	1.50(1.53)	8	Multiplet	
CH_3 and other CH_2 of amide	0.98(1.00)	9(13)	Multiplet	
CH_3 of butyl	0.55(0.65)	6	Multiplet	

[a] Results in parentheses indicate values for DBOA complexes.
[b] Number of protons.
[c] Number of peaks.

C—N bond, the triplets arising due to the associated spin coupling by the adjacent methylene protons. Two separate signals for the N-methyl protons have also been observed in the spectra of N,N-dimethylacetamide because of their non-equivalence due to hindered rotation. Methyl protons of the butyl group are observed to be the most shielded, occuring as triplets due to coupling by the adjacent methylene protons. In the PMBP and PMAP complexes with amides, the presence of four and two separate signals, respectively, for the aromatic protons indicate their existence as a mixture of isomers. Four separate signals for the aromatic protons have also been observed in the ^{1}H NMR spectrum of $UO_2(PMBP)_2 \cdot H_2O$ in acetone. The α-methylene protons of the butyl groups in PMBP and PMAP complexes have been observed as a composite peak of six lines (only five peaks observed), involving the merger of two triplets in the PMBP and PMAP complexes, whereas they are observed as two clear triplets in the corresponding TTA complexes. From this, it is clear that the PMBP and PMAP complexes are less sterically hindered to rotation around the C—N bond compared with the TTA complexes.

Thermal investigations

The results of the thermal investigations of $UO_2(PMBP)_2$ complexes with DBHA and DBOA are given in Table 4. The DTA curves of these two complexes show a sharp dip at 125°C, presumably due to a phase change on melting. Three plateaux corresponding to weight loss due to one PMBP, amide and the second PMBP are observed, giving rise to exothermic, endothermic and strong exothermic peaks, respectively. The loss of amide and the second PMBP molecule did not give two clear plateaux and the weight loss has been computed as corresponding to the loss of both. On the other hand, the thermograms of $UO_2(TTA)_2 \cdot DBHA$ and $UO_2(TTA)_2 \cdot DBOA$ show only one plateau due to the loss of both TTA moieties, indicating that they are symmetrically bonded. This agrees with the idea that the amide complexes of pyrazolones exist as a mixture of isomers.

Table 4. Thermal data for $UO_2(PMBP)_2 \cdot X$ complexes[a]

X	H_2O	DBHA	DBOA
Molecular weight	844.6	1052	1080
Water loss at 110°C (%)	3.4		
Total loss of weight (%)	68.9	72.2	72.3
	(68.0)	(73.0)	(74.0)
Loss of one PMBP (%)	30.9	26.2	25.9
	(32.9)	(26.4)	(25.7)
Decomposition temperature (°C)	280	190	210
Peak height temperature (°C)	455	310	305
Nature of peak		Exothermic	Exothermic
Loss of PMBP+X (%)	31.2	47.0	46.4
	(33.0)	(47.9)	(46.7)
(i) Decomposition temperature (°C)		340	340
Peak height temperature (°C)		410	410
Nature of peak		Endothermic	Endothermic
(ii) Decomposition temperature (°C)	380	450	450
Peak height temperature (°C)	510	540	570
Nature of peak	Exothermic	Exothermic	Exothermic
Phase change temperature (°C)		125	125

[a] Figures in parentheses indicate calculated values.

Acknowledgements—The authors wish to express their grateful thanks to Dr P. R. Natarajan for his keen interest in the work.

REFERENCES

1. T. H. Siddall III, *J. Phys. Chem.* 1960, **64**, 1863.
2. G. M. Gasparini and G. Grossi, *Sep. Sci. Tech.* 1980, **15**, 825.
3. T. H. Siddall III, *J. Inorg. Nucl. Chem.* 1963, **25**, 883.
4. T. H. Siddall III, *J. Inorg. Nucl. Chem.* 1967, **29**, 149.
5. K. B. Brown, C. A. Blake and J. M. Schimdt, USAEC Report ORNL-3452 (1963).
6. K. B. Brown, C. A. Blake and J. M. Schmidt, USAEC Report ORNL-3627 (1964).
7. G. M. Gasparini and G. Grossi, *Solv. Ext. Ion Exch.* 1986, **4**, 1233.
8. C. Musikas, *Inorg. Chem. Acta* 1987, **140**, 197.
9. Yi Min and Wang Liya, *Atom. Energy Sci. Tech.* 1987, **21**, 545.
10. R. Veeraraghavan, S. A. Pai and M. S. Subramaninan, *J. Radioanal. Nucl. Chem.* 1990, **141**, 2, 339.
11. A. Ghany, M. Al-Daher and K. W. Bagnall, *J. Less Common Metals* 1985, **108**, 257; 1985, **109**, 381.
12. K. W. Bagnall and G. F. Pyne, *J. Less Common Metals*, 1985, **109**, 31.
13. B. S. Jensen, *Acta Chem. Scand.* 1959, **13**, 1668, 1890.
14. W. H. Baldwin, C. E. Higgins and J. M. Schmitt, USAEC Report ORNL-3679, Chem. Technol. Div. Progr. Report, pp. 56–57. Oak Ridge National Laboratory, Oak Ridge, Tennessee (1965).
15. M. S. Nagar, P. B. Ruikar and M. S. Subramanian, Report BARC-1048 (1980); Report BARC-1299 (1986).
16. M. S. Nagar, P. B. Ruikar and M. S. Subramanian. *Polyhedron* 1987, **6**, 1913.
17. M. S. Nagar, P. B. Ruikar and M. S. Subramanian, *Lanthanide Actinide Res.* 1989, **3**, 21.

Polyhedron Vol. 10, No. 14, pp. 1687–1693, 1991
Printed in Great Britain

0277-5387/91 $3.00+.00
© 1991 Pergamon Press plc

NEW β-DIKETON-(2-PHENYLETHYL)IMINE SCHIFF BASE CHELATES OF COPPER(II), NICKEL(II) AND COBALT(III) AND THEIR ELECTROPHILIC SUBSTITUTION PRODUCTS

S. ABDUL SAMATH, N. RAMAN, K. JEYASUBRAMANIAN and S. K. RAMALINGAM*

Department of Inorganic Chemistry, School of Chemistry, Madurai Kamaraj University, Madurai-625 021, India

(*Received* 13 *November* 1990; *accepted* 15 *April* 1991)

Abstract—New Schiff base chelates of nickel(II), copper(II) and cobalt(III) derived from acac/bzac and 2PEA (acac = 2,4-pentanedionate, bzac = 1-phenyl-1,3-butanedionate anions; 2PEA = 2-phenylethylamine) have been synthesized and characterized. The nickel(II) and copper(II) complexes are non-planar, cobalt(II) does not form any isolable complex and the cobalt(III) complex has an octahedral structure as indicated from UV–vis, IR, ^{1}H and ^{13}C NMR and analytical data. Steric factors arising from the flexible —CH_2—CH_2—Ph substituent on the nitrogen atom of 2PEA force the less hindered, non-planar, tetrahedral geometry for copper(II) and nickel(II) and the meridional octahedral geometry for cobalt(III) to predominate. Electrophilic substitution reactions of these chelates, like γ-halogenation and γ-phenylisocyanation, are also reported.

Transition metal complexes with Schiff bases as ligands have been amongst the most widely studied coordination compounds. An interesting feature of nitrogen-substituted β-ketonimine Schiff base complexes is the stereochemical problems they present.[1] For example, the stereochemistry of N-alkyl β-ketonimine complexes of many transition metals M(II) and (III) are found to be strongly dependent on the nature of the R group bonded to the nitrogen of the >C=N group (Fig. 1).[1,2]

The nickel(II) complexes (where R = CH_3, C_6H_5, *p*-$C_6H_4CH_3$) in the solid state or in solutions of non-polar solvents are planar and diamagnetic. On the other hand, when R is an α-branched alkyl group, like isopropyl or *o*-/*m*-$C_6H_4CH_3$, the complexes are known to be tetrahedral and paramagnetic.[3] In this context, it was of interest to examine the stereochemistry of some four-coordinated metal(II) and six-coordinated cobalt(III) Shiff base ketonimine chelates wherein the chosen ligand system is bulky but flexible due to free rotations around >C—N< and >C—C< bonds

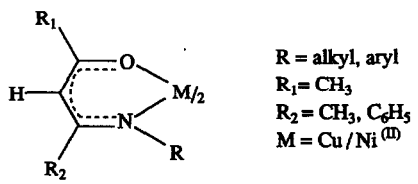

Fig. 1.

of >N—CH_2—CH_2—Ph. This paper reports the isolation and characterization of the title chelates and their γ-substituted electrophilic reaction products.

EXPERIMENTAL

The IR spectra were recorded on a Perkin–Elmer 477 spectrophotometer using KBr discs. The ^{1}H NMR measurements were carried out on a Brucker 270 MHz spectrophotometer in DMSO-d_6 with TMS as an internal standard. ^{13}C NMR spectra of the cobalt(III) Schiff base chelate were recorded on a Brucker instrument (100.62 MHz) in DMSO-d_6. The electronic spectra were recorded in solutions of DMSO and DMF on a Shimadzu UV-160 spectrophotometer.

* Author to whom correspondence should be addressed.

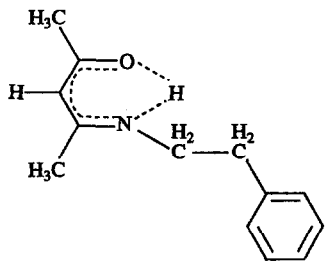

Fig. 2.

Synthesis of Schiff base complexes

The isolation of the title Schiff base ligand (Fig. 2) was not possible by the usual condensation reaction between the β-diketone and 2-phenylethylamine. Therefore, a template-type amine exchange reaction in the presence of metal salt was adopted for the successful synthesis of the title chelates.

(a) *Bis*(4*N* - (2 - *phenylethyl*) - 3 - *penten* - 2 - *ono*) *copper*(II). An ethanolic suspension (150 cm^3) of 1:2:2 stoichiometric quantities of $CuCl_2 \cdot 2H_2O$, β-ketonimine (R = H or CH_3) and 2PEA was left stirring for 2 h at room temperature. The metal salt gradually dissolved to give a clear solution, from which a green solid product separated after a time. This was filtered, washed with water, then with ethanol and dried at 110°C for 2 h.

(b) *Bis*(4*N* - (2 - *phenylethyl*) - 3 - *penten* - 2 - *ono*) *nickel*(II). This nickel(II)(Schiff base complex was prepared by the same method as described for the copper(II) complex.

(c) *Tris*(4*N* - (2 - *phenylethyl*) - 3 - *penten* - 2 - *ono*) *cobalt*(III). The cobalt(II) complex could not be precipitated out by the above method; only a clear solution resulted. But when hydrogen peroxide was added and the solution stirred vigorously, the originally pink-coloured solution turned green and eventually gave a green, solid product. This was filtered, washed with ethanol and dried in a hot air-oven at 110°C for 2 h.

(d) *Bis*/*tris*(3*N*-(2-*phenylethyl*)-1-*phenyl*-2-*buten*-1-*ono*)*metal*(II/III) *chelates*. The benzoylacetoneimine Schiff base chelates of copper(II), nickel(II) and cobalt(III) were prepared by the same methods described above.

Electrophilic substitution reactions

Bromination, chlorination and phenylisocyanation reactions at the γ-carbon of the β-biketonimine chelate ring. The presence of a facile γ-C—H proton in the above chelates offers the possibility to study the electrophilic substitution reactions like bromination, chlorination and phenylisocyanation.

To the chloroform suspension (50 cm^3) of a freshly prepared title chelate was added a stoichiometric quantity of a chloroform solution (100 cm^3) of NBS, NCS or PhNCO. The reaction mixture was heated on a water bath for 2 h with concomittant stirring. The suspension gradually yielded a clear solution, which upon cooling gave a solid, crystalline product. This was filtered, washed with warm chloroform (50 cm^3) and dried *in vacuo* over P_4O_{10}. Stirring or heating of the reaction mixture for a longer period than mentioned led to polymerization, producing dark-coloured products of indefinite composition.

RESULTS AND DISCUSSION

The Schiff base chelates of nickel(II), copper(II) and cobalt(III) and their γ-halo and γ-phenylamido products (Fig. 3) are insoluble in most solvents except DMSO and DMF. The solutions in the later solvents are non-electrolytes as inferred from their low conductivity. The thermal data suggest the presence of two water molecules, coordinated in the case of copper(II) and lattice held in nickel(II) and cobalt(III) complexes. Particulars of the compositions of the β-ketonimine chelates and their reaction products, reaction time, yield and analytical data are presented in Table 1. Important IR vibration data are given in Table 2.

The bands at *ca* 1620, 1200 and 800 cm^{-1} correspond, respectively, to ν(C=N), δ(C=N) and π(C=N) vibrations. By comparison of the IR literature data of the known β-diketonates and their γ-substituted products[4-7] with that of the present chelates the following assignments were made: ν(C=O) (1580 cm^{-1}), ν(C=C) (1550 cm^{-1}), ν(C=O+C—H) (1520 cm^{-1}), in-plane bend δ(C—H) (1190 cm^{-1}) and out-of-plane bend π(C—H) (785 cm^{-1}) vibrations. That an electrophilic substitution has taken place at the γ-carbon by replacement of the C—H proton is indicated by the disappearance of IR bands at 1190 and 785 cm^{-1} and a shift of the band at 1520 cm^{-1} to lower frequency. However, this diagnosis of the reaction product is not straightforward for ketonimines, because the stretching and bending frequencies of >C=N appear in the same diagnostic regions of 1600–1400, 1200–1100 and 750–800 cm^{-1}.

The UV–vis spectral data indicate that for the simplest bidentate Schiff base ligand with limited substituents, the arrangement of bonds in the $[MO_2N_2]$ unit is planar for copper(II) and nickel(II) and tetrahedral for cobalt(II).[1,2] Distortion from planarity of the chelate rings of the Schiff base ligands is known, depending on the nature of the

Table 1. Analytical data, reaction times and yields of metal–β-ketonimine Schiff base complexes and their electrophilic γ-substituted reaction products

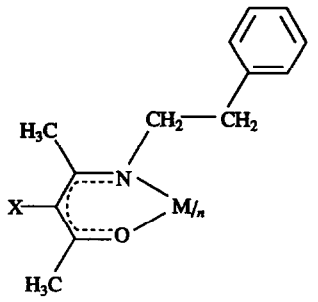

Where X = H, Cl, Br, PhNHCO

Compound	Reaction time (h)	Yield (%)	Colour	Found % (Calculated %) M	C	H	N	Br	Cl
Substrate Schiff base complexes									
$Cu(PEA \cdot AcH)_2 \cdot 2H_2O$	3	70	Green	12.4 (12.6)	62.1 (62.0)	7.1 (7.1)	5.6 (5.6)	—	—
$Ni(PEA \cdot AcH)_2$	5	60	Olive green	12.3 (12.7)	67.2 (67.4)	6.9 (6.9)	6.1 (6.0)	—	—
$Co(PEA \cdot AcH)_3$	10	60	Dark green	8.3 (8.9)	69.6 (70.4)	7.2 (7.2)	6.3 (6.3)	—	—
γ-Brominated products									
$Cu(PEA \cdot AcBr)_2 \cdot 2H_2O$	3	60	Green	9.4 (9.6)	47.2 (47.1)	5.2 (5.1)	4.2 (4.2)	24.0 (24.2)	—
$Ni(PEA \cdot AcBr)_2$	4	50	Yellowish brown	9.5 (9.5)	50.7 (50.3)	4.8 (4.8)	4.4 (4.5)	25.1 (25.8)	—
$Co(PEA \cdot AcBr)_3$	6	55	Green	6.7 (6.5)	52.0 (51.9)	5.0 (5.0)	4.7 (4.7)	26.9 (26.6)	—
γ-Chlorinated products									
$Cu(PEA \cdot AcCl)_2 \cdot 2H_2O$	4	50	Green	11.2 (11.1)	55.0 (54.5)	6.0 (5.9)	4.9 (4.8)	—	12.5 (12.4)
$Ni(PEA \cdot AcCl)_2$	6	50	Yellowish brown	11.5 (11.0)	58.6) (58.7)	5.6 (5.6)	5.8 (5.3)	—	13.7 (13.3)
$Co(PEA \cdot AcCl)_3$	8	50	Dark green	7.6 (7.7)	61.0 (60.9)	5.9 (5.8)	5.5 (5.5)	—	13.1 (13.9)
γ-Phenylisocyanated products									
$Cu(PEA \cdot AcPhNHCO)_2 \cdot 2H_2O$	4	50	Grey–green	8.3 (8.6)	64.7 (64.7)	6.2 (6.2)	7.6 (7.5)	—	—
$Ni(PEA \cdot AcPhNHCO)_2$	8	40	Yellowish brown	8.5 (8.4)	68.6) (68.5)	6.0 (6.0)	8.1 (8.0)	—	—
$Co(PEA \cdot AcPhNHCO)_3$	10	45	Dark green	5.6 (5.8)	70.5 (70.4)	6.2 (6.2)	8.3 (8.2)	—	—

Complexes of nickel(II) and cobalt(III) were obtained in the anhydrous form by dehydration.

substituents present at the imine nitrogen of Fig. 1.[3] When the substituent is large and/or branched as in R = isopropyl, the distortion has been found to be substantial.[1,2] For the copper(II) and nickel(II) complexes, a band at *ca* 10,000 cm^{-1} (Table 3) rules out a square planar geometry.[9–11] The nickel(II) complex in DMSO solution exhibits absorption maxima at *ca* 10,000, 15,000 and 18,000 cm^{-1}, characteristic of a tetrahedral complex. The characteristic absorptions occurring at *ca* 9600 cm^{-1} (ν_1)

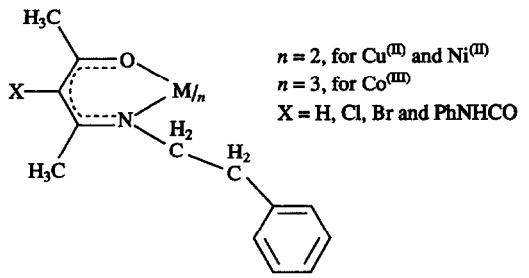

Fig. 3.

for the copper(II) and cobalt(III) ions correspond to an octahedral field around them.

The inability of the cobalt(II) ion to complex with the title Schiff base ligand can be attributed to the hydrolytic instability of cobalt(II) ketonimine complexes, in general, compared with β-diketonates. However, in the attempted preparation of the cobalt (II) complex, when the solution mixture was treated with hydrogen peroxide, the corresponding cobalt(III) complex could be isolated. The UV–vis spectral data (Table 3) coupled with the observed diamagnetism confirm an octahedral spin-paired structure for the cobalt(III) complex.

The ^1H and ^{13}C NMR spectra of the cobalt(III) chelates and their 3-bromo- and 3-phenylamido-substituted products (Tables 4 and 5) display some interesting features.

The observed three-line pattern in the NMR spectra is indicative of a less-strained meridional struc-

Table 2. IR data for the Schiff base chelates[a]

Compound	IR bands (cm^{-1})			
	ν(C=N)	δ(C=N) 1	δ(C=N) 2	ν(C=O) coordinated
$Cu(PEA\text{-}AC)_2 \cdot 2H_2O$	1632	1198	760	1585
$Ni(PEA\text{-}AC)_2$	1635	1201	748	1580
$Co(PEA\text{-}AC)_3$	1641	1220	762	1590

[a] PEA-Ac = 4N-(2-phenylethyl)-3-pentene-2-one.

Table 3. UV–vis data for the Schiff base chelates

Compound	Electronic absorption (cm^{-1})			Geometry
	ν_1	ν_2	ν_3	
$Cu(PEA\text{-}Ac)_2 \cdot 2H_2O$	9765	16,128	21,052	O_h-distorted
$Ni(PEA\text{-}Ac)_2$	10,869	15,385	18,181	Tetrahedral
$Co(PEA\text{-}Ac)_3$	9060	16,400	21,750	O_h-meridional

Table 4. ^1H NMR data for the cobalt(III) Schiff base chelate and its 3-bromo/phenylamido product

Compound	^1H NMR chemical shift (ppm)					
	CH_3 of CH_3CO	CH_3 of CH_3CN	$-CH_2Ph$	$=N-CH_2-Ph$	Ph	γ-C—H
$Co(PEA\text{-}Ac)_3$	1.93	2.25	3.38	3.95	7.59	—
	2.00	2.36	3.40	4.13	7.64	5.39
	2.15	2.48	3.53	4.21	7.84	—
$Co(PEA\text{-}Ac \cdot Br)_3$	1.99	2.29	3.43	4.01	7.69	—
	2.06	2.38	3.56	4.13	7.84	—
	2.21	2.49	3.83	4.27	7.91	—
$Co(PEA\text{-}Ac \cdot PhNHCo)_3$	1.85	2.29	3.29	3.83	7.51	—
	1.93	2.36	3.39	3.99	7.59	—
	2.06	2.46	3.47	4.16	7.73	—

Table 5. ^{13}C NMR chemical shift data for selected resonances (ppm)

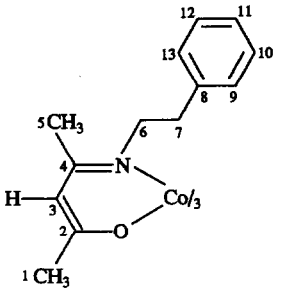

A

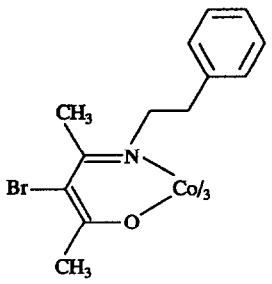

B

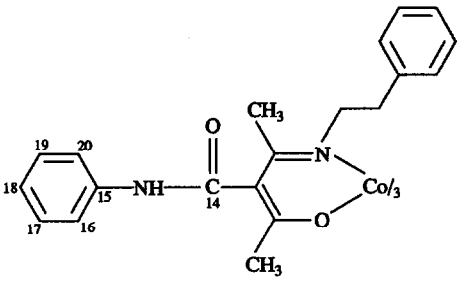

C

NMR Line	Carbon number	Co(PEA-AC·H)$_3$, unsubstituted product—A	Assignment	Co(PEA-AC·Br)$_3$, 3-bromo product—B	Co(PEA-AC·CONHPh)$_3$, 3-phenylamido product—C
1–3	1 (3)	29.52 28.69 27.57	*C*H$_3$—C=O	28.08 27.91 27.02	26.32 25.68 24.90
4–6	2 (3)	183.62 182.21 180.23	CH$_3$—*C*=*O*	184.71 183.54 182.78	183.64 182.48 181.68
7–9	3 (3)	100.92 100.16 (C—H) 90.42	γ-Carbon	188.21 187.81 (C—Br) 186.56	155.32 153.92 152.62
10–12	4 (3)	174.66 172.81 171.69	CH$_3$—*C*=*N*	171.62 170.94 169.76	170.51 169.72 168.82
13–15	5 (3)	18.92 19.53 20.06	*C*H$_3$—C=N	19.64 20.41 21.06	17.81 18.42 19.21
16–18	6 (3)	61.24 60.54 59.18	N—*C*H$_2$	60.54 59.62 58.84	60.92 60.04 59.46
19–21	7 (3)	43.21 42.71 41.04	Ph—*C*H$_2$	42.18 41.72 40.60	42.84 42.00 41.32
22–39	8–13 and 15–20 (m)	148.22 to 120.64 (18) lines	*Ph*—CH$_2$ and *Ph*—NH—Co—	146.21 to 121.46 (18) lines	145.22 to 119.73 (36) lines
59–61	14 (3)	—	—*Co*—NH—Ph	—	176.22 175.64 174.82
62	(m)	37.52	Solvent DMSO-d$_6$	37.56	37.58
Total lines	—	39+1 = 40	—	39+1 = 40	60+1 = 61
Number of carbons	—	13	—	13	20

ture for the tris-chelate. In cobalt(III) chelate, the C—C single bond connecting the azomethine nitrogen and the phenyl group is capable of free rotation, thereby enhancing the steric repulsion between the phenyl groups of the three ligands in the tris-chelate. Furthermore, the methyl groups R_1 and R_2 on the α- and α'-carbon of the β-ketonimine chelate ring could also be expected to contribute to the overall steric influence. It has been found that when $R_1 = CH_3/C_6H_5$ and $R_2 = C_6H_5$, the complex is not formed probably due to the fact that excessive destabilization is brought about by steric crowding between the nine phenyl groups (three in R_1, three in R_2 and three in the chain attached to nitrogen) in a tris-chelated geometry.

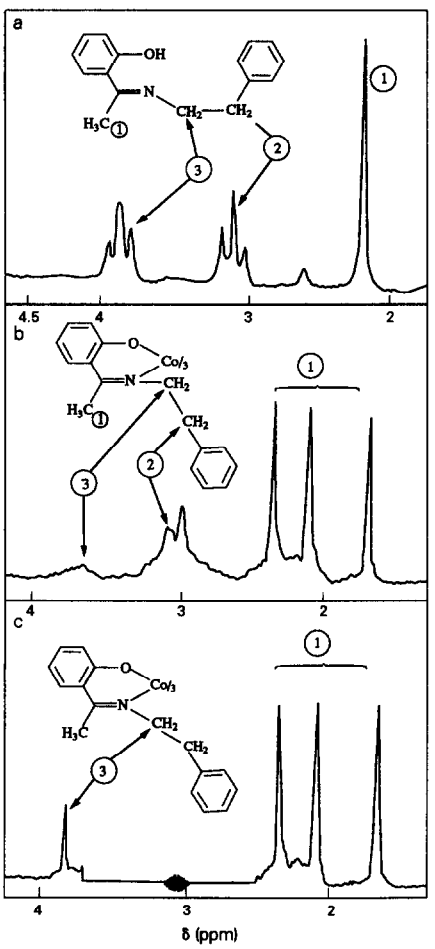

Fig. 4. NMR spectra, (a) the spin–spin splitting of the N—CH_2 and Ph—CH_2 methylene signals with near equal intensities in the isolable analogous ligand PhOH $CH_3C{=}N{-}CH_2{-}CH_2{-}Ph$ (the title ligand not isolable). (b) *Meridional* cobalt(III) complex of the ligand mentioned in (a). The methyl signal consists of 3 lines, Ph—CH_2 methylene multiplets are broad and the N—CH_2 multiplets appear insignificant. (c) Decoupling at signal 2 enhances the intensity of 3.

However, when $R_1 = CH_3$ and $R_2 = CH_3$, the distortion between the chelate rings would be less than that between the $-CH_2-CH_2-Ph$ groups of the three ligands. Still the distortion between the three [O—Co—N] planes of this $M(A—B)_3$ type chelate causes an asymmetric ligand array. Thus, the $(A—B)_3$ ligands, although chemically the same, provide different magnetic environments around the metal ion for adoption of exclusive *meridional* geometry.

Since the Schiff base ligand involved in this work is not isolable, identification of the methylene signals in the spectra of the complexes and the reaction product is carried out as follows. An analogous salicylaldimine Schiff base involving the same amine base (2-phenylethylamine) presents a ^1H NMR spectra [Fig. 4(a)] wherein the two methylene triplets are of equal intensity.[8] Whereas in the ^1H NMR spectra of its cobalt(III) tris-chelated complex [Fig. 4(b)], which exclusively exists in the meridional form, the N—CH_2 of the N—CH_2—CH_2—Ph group signals (triplet) are small in intensity and difficult to distinguish. However, when decoupling is carried out at the Ph—CH_2 resonance (*ca* at δ 3.05) [Fig. 4(c)], a N—CH_2 signal

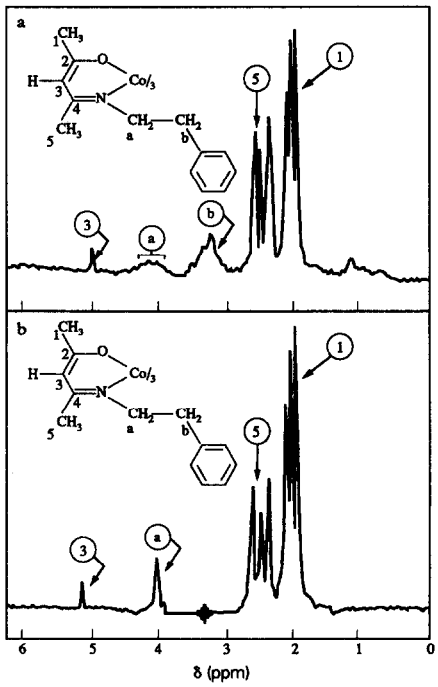

Fig. 5. NMR spectra of the title cobalt(III) Schiff base unsymmetrical tris-chelate (partly unresolved). Multiplet methylene signals appear broad in (a). In (b) decoupling at the Ph—CH_2 resonance raises the intensity of the N—CH_2 proton signal (the multiplets for the methylene signals are not as well resolved as the methyl signals).

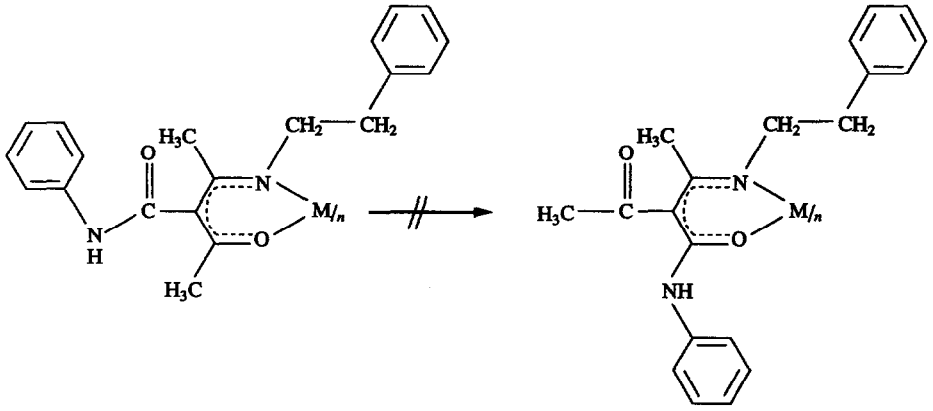

Fig. 6.

conspicuously becomes enhanced in intensity (*ca* at δ 3.90).

Examination of the ^{1}H NMR spectra of the cobalt(III) complex (*mer*) would reveal that a three-line pattern could be observed only for the methyl group resonances [Fig. 5(a)]. Identification of the spin–spin triplet for the N—CH_2 methylene proton of =N—CH_2—CH_2—Ph at *ca* δ 4.00 was difficult since the resonance was weak compared with the triplet observed around δ 3.40 for the methylene protons of Ph—CH_2—CH_2—N=. When decoupling was carried out as indicated above at δ 3.40, a strong, single-line signal appeared at δ 3.95 for the =N—CH_2—CH_2—Ph protons [Fig. 5(b)].

As expected, the ^{1}H–noise decoupled ^{13}C NMR spectra of the pure *mer*-cobalt(III) Schiff base chelate complexes are elegantly simple and most of the signals attributable to the parent Schiff base ligand (though not isolable) are resolved into a three-line pattern. Also, the 3-halo/phenylamido products, exhibit an analogous three-line pattern corresponding to a *meridional* structure without the admixture of the *facial* form. This is reasonable since the already bulky Schiff base ligands would become bulkier still after substitution by halogen or a phenylamido group and would thereby sterically enforce the *meridional* isomeric form. That the γ-substitution reactions have taken place fully is known from the conspicuous disappearance of the signal at δ 5.3 attributable to the γ-C—H proton and the absence of a signal at δ 100.16 in the ^{13}C NMR resonances of the γ-substituted products.

Confirmation by X-ray single crystal analysis was not possible since the substances were only very sparingly soluble in common organic solvents and did not yield single crystals in DMSO solution.

The IR spectra show no additional ν(C=O) (keto) band for any rearranged free acetyl group (expected at *ca* 1700 cm^{-1}), showing that no linkage isomerization has taken place (Fig. 6).

REFERENCES

1. R. H. Holm, G. W. Everett Jr and A. Chakravarthy, *Prog. Inorg. Chem.* 1966, **7**, 83.
2. B. O. West, *New Pathways in Inorganic Chemistry* (Edited by E. A. Ebsworth), p. 303. Cambridge University Press, Cambridge, U.K. (1968).
3. G. W. Everett Jr and R. H. Holm, *J. Am. Chem. Soc.* 1965, **87**, 2117.
4. R. P. Drydon and A. Winston, *J. Phys. Chem.* 1958, **62**, 635.
5. L. J. Bellamy, *The Infra-red Spectra of Complex Molecules*. Methuen, New York (1958).
6. K. Nakamoto, *The Infra-red Spectra and Raman Spectra of Inorganic and Coordination Compounds*. Wiley, New York (1977).
7. L. F. Lindoy, H. C. Lip and W. E. Moody, *J. Chem. Soc., Dalton Trans.* 1974, 44.
8. S. K. Ramalingam, M. Raman and V. Rajaram, *J. Coord. Chem.* 1987, **15**, 329.
9. K. C. Patel and R. R. Patel, *J. Inorg. Nucl. Chem.* 1977, **39**, 1325.
10. M. C. Styka, R. C. Smierciak, E. L. Blinn, R. E. Desimone and J. V. Passariello, *Inorg. Chem.* 1978, **17**, 82.
11. R. S. Nyholm, *Chem. Rev.* 1953, **53**, 263.

Polyhedron Vol. 10, No. 14, pp. 1695–1698, 1991
Printed in Great Britain

0277–5387/91 $3.00+.00
© 1991 Pergamon Press plc

THERMODYNAMICS OF FORMATION, HYDROLYSIS AND IONIZATION OF MONOFLUOROPHOSPHOROUS ACID

JOHN W. LARSON

Department of Chemistry, Marshall University, Huntington, WV 25755-2520, U.S.A.

(*Received* 22 *October* 1990; *accepted* 19 *April* 1991)

Abstract—A NMR study of the equilibrium reaction of HF with aqueous phosphorous acid between 8 and 65°C and various hydrogen ions concentrations gave values of $\Delta G^{\ominus} = 2.2$ kJ, $\Delta H^{\ominus} = -26$ kJ and $\Delta S^{\ominus} = -94$ J K^{-1} for the acid ionization of monofluorophosphorous acid and $\Delta G^{\ominus} = -16.2$ kJ, $\Delta H^{\ominus} = -16.9$ kJ and $\Delta S^{\ominus} = -2.2$ J K^{-1} for the hydrolysis of monofluorophosphorous acid to phosphorous acid and HF.

Monofluorophosphorous acid, $H[FHPO_2]$, was first synthesized in 1968 by Centofanti and Parry[1] from the disproportionation of F_2HPO. Several additional preparative routes have subsequently been discovered.[2–5] Other names used for this acid are phosphinic fluoride, phosphonofluoridous acid and phosphonofluoridic acid.

In this work, aqueous $FHPO_2H$ is shown to be formed by a fast equilibrium reaction between aqueous HF and HPO_3H_2, e.g. (1):

$$HF(aq) + HPO_3H_2(aq) \rightleftharpoons H_2O(l) + FHPO_2H(aq). \quad (1)$$

Thermodynamic properties of monofluorophosphorous acid were obtained from the study of the temperature and hydrogen ion concentration dependence of the equilibrium quotient of this reaction.

The thermochemical properties of $FHPO_2H$ are of interest because: (i) $FHPO_2H$ contains only four heavy atoms and therefore this work may supply useful reference data in relation to theoretical calculations on important phosphorus compounds and reactions, particularly, hydrolysis reactions. (ii) This data may further our understanding of the effects of substituents that are bonded directly to second row atoms. (iii) The thermodynamics of hydrolysis of $FHPO_2H$ [reverse reaction (1)] may be related to and could be helpful in the understanding of biologically important phosphate hydrolysis reactions. No thermochemical properties of this compound are currently available.

EXPERIMENTAL

A concentration solution of phosphorous acid (5.28 mmol of H_3PO_3 per gram of solution) was made from the pure acid obtained from Aldrich. The concentration of this solution and concentrated solutions of hydrofluoric acid (19.85 mmol g^{-1}) and concentrated hydrochloric acid (10.22 mmol g^{-1}), both obtained from Fischer Scientific, were analysed by standard acidimetric titration methods. The HF was stored, dispensed and analysed using plastic labware. The sodium phosphite pentahydrate (BDH Chemicals) was analysed for water by heating *in vacuo* to 200°C. The sample solutions used in this work were prepared by weight with concentrations expressed in terms of molalities and the standard state for the solute taken as the hypothetical one molal solution.

Phosphorus magnetic resonance spectra were obtained using a Varian XL-200 spectrometer. All spectra involving HF solutions were recorded in 10 mm NMR tubes with Teflon sleeves and caps. Temperatures were controlled to within ±0.3°C and calibrated with a mercury thermometer.

The sensitivity of the NMR to low concentration phosphorus species, under the conditions of the equilibrium measurements, was investigated by making up standard solutions containing 0.5 m Na_2HPO_3 and small amounts of NaH_2PO_2. The detection limit of phosphorus as $H_2PO_2^-$ was found to be about 0.0003 m or 0.0006 mole fraction. The equilibrium fractions of phosphorus present as $FHPO_2H$ in the present work covered the range

from 0.013 to 0.007. The intrinsic error in equilibrium quotients is therefore estimated to be between 5 and 10%. This is comparable with the actual scatter in the experimental data.

CALCULATIONS AND RESULTS

When hydrofluoric acid is added to a solution of phosphorous acid, small peaks emerge immediately corresponding to the doublet of doublets of $FHPO_2H$ formed by reaction (1). For the whole temperature range between 5 and 85°C, reaction (1) appears to be fast on the time scale it takes to make the solutions and record the spectrum (20 min) and slow on the NMR time scale that would lead to line broadening (0.01 s). At high HF and H^+ concentrations and at high temperatures, the $FHPO_2H$ peaks broaden appreciably and eventually the PF splitting disappears. This is apparently due to $FHPO_2H$ exchanging F with the HF in solution. At the concentrations of the equilibrium measurements reported here, the broadening is slight and has no effect on the measurements.

Hydrogen decoupling collapses the $FHPO_2H$ spectrum to a doublet. The coupling constants and chemical shifts of the aqueous acid and its conjugate base are reported in Table 1 together with the corresponding value previously determined for liquid monofluorophosphorous acid and aqueous phosphorous acid.

The equilibrium expression for reaction (1) may be written as eq. (2):

$$K_1 = \frac{m_{FHPO_2H}}{m_{HF} m_{HPO_3H_2}}. \quad (2)$$

In this equation and all subsequent equations, the activity coefficients of the neutral species are estimated to be unity and are left out of the equilibrium expressions. The fraction of the phosphorous that is fluorinated as either $FHPO_2H$ or $FHPO_2^-$, X_{PF}, is determined directly from integration of the NMR peaks. Equation (2) may therefore be re-written as eq. (3)

$$K_1 = \frac{X_{FP}}{m_{HF}(1-X_{PF})} \frac{X_2}{X_1} = Q \frac{X_2}{X_1}, \quad (3)$$

where Q is the equilibrium quotient for the reaction and X_1 and X_2 are the respective fractions of phosphite and fluorophosphite in the acid form. Both of these fractions may be obtained via the measured P—H coupling constant of phosphite.

X_1 is calculated directly from the measured coupling constant by the method given in ref. 6, eq. (4):

$$X_1 = (J - 629.5)/56.5. \quad (4)$$

The change in the coupling constants of $FHPO_2$ when it undergoes protonation is too small and the measured values are too uncertain to apply the same procedure in calculating X_2. This fraction is instead obtained by considering the acid equilibrium reaction, eq. (5), and the equilibrium expression, eq. (6), where γ is the mean activity coefficient of H^+ and $FHPO_2^-$:

$$FHPO_2H(aq) \rightleftharpoons H^+(aq) + FHPO_2^-(aq) \quad (5)$$

$$K_5 = m_h m_{FHPO_2} \gamma^2 / m_{FHPO_2H} = H(1-X_2)/X_2. \quad (6)$$

The PH coupling constant of phosphorous acid is used a second time in an empirical method of obtaining the value of $m_H\gamma^2$, defined now as H, from the known acid ionization constant for phosphorous acid and the value of X_1, eq. (7):

$$H = m_H\gamma^2 = \{K_{a,H_3PO_3}\} X_1/(1-X_1). \quad (7)$$

Application of eq. (7) to find the value of $m_H\gamma^2$ appropriate for eq. (6) assumes that the activity coefficient of $FHPO_2^-$ is approximately equal to HPO_3H^-. Considering the similar structures of these species, this assumption is likely to be quite accurate. The fraction of $FHPO_2H$ in the acid form is then given by eq. (8):

$$X_2 = 1/(1 + K_5/H). \quad (8)$$

Table 1. Coupling constants and chemical shifts (relative to 85% phosphoric acid) for monofluorophosphorous and phosphorous acid and their anions

	$FHPO_2H$(aq)	$FHPO_2^-$(aq)	$FHPO_2H$(l)[a]	HPO_3H_2(aq)[b]	HPO_3H^-(aq)[b]
J_{PH} (Hz)	712[c]	698[c]	783	686	629.5
J_{PF} (Hz)	987[c]	973[c]	1028		
δ_P (ppm)	4.0	4.0	−2.74	5.88	3.22

[a] Reference 1.

[b] Reference 6.

[c] Values are apparently effected by hydrogen-bonding to HF and are therefore known to only ±5 Hz.

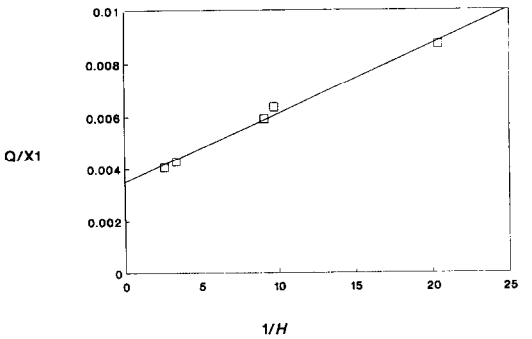

Fig. 1. Determination of K_1 and K_5 by graphing Q/X_1 vs $1/H$, eq. (9), at 65°C.

Substituting eq. (8) for X_2 in eq. (3) and rearranging results in eq. (9):

$$Q/X_1 = K_1 + K_1K_5(1/H). \quad (9)$$

Use of this equation to obtain K_1 and K_5 is demonstrated in Fig. 1. Measurements were made on five different solutions with H ranging between 0.05 and 1.5 m at temperatures of 8, 25, 45 and 65°C to obtain the values given in Table 2. The concentration ranges in these measurements were: 1.75–4.2 m for HF; 0.15–1.3 m for HPO_3H_2; 0–1.3 m for HCl; and 0–2.4 for Na_2HPO_3. None of these concentrations enter directly into the calculations of the equilibrium constants except for the concentration of HF. In the calculation of Q, the initial concentration of HF must be corrected for the amount that reacts to form F^-, $FHPO_2H$, $FHPO_2^-$ and FHF^-. Under the conditions of our measurements, calculations indicate less than 2% of the HF is present in the first three forms. At the highest pH, the concentration of FHF^- becomes appreciable, about 20%. The amount of FHF^- present was easily calculated, eq. (10):

$$m_{FHF^-} = m_{HF}^2 K_a K_d / H, \quad (10)$$

where K_a is the acid dissociation constant of HF,[7] K_d is the equilibrium constant of the reaction of F^- with HF,[7] and function H has been defined previously.

The uncertainties given in Table 2 are the total uncertainties including the uncertainty involved in the estimates of activity coefficients, the uncertainty in the reference values of K_a of phosphorous acid, and the uncertainty involved in the measurement of X_{PF}.

Thermodynamics of ionization of monofluorophosphorous acid

The van't Hoff isochore graph of the equilibrium constants is shown in Fig. 2. Standard thermodynamic analysis leads to values of $\Delta G_5^\ominus = +2.2 \pm 1.1$ kJ, $\Delta H_5^\ominus = -26.0 \pm 4.0$ kJ and $\Delta S_5^\ominus = -94 \pm 13$ J K^{-1} for the acid ionization process.

$FHPO_2H$ is a stronger acid than H_2PO_2H by 0.87 pK_a units and is the strongest known substituted phosphinic acid[8] of formula $XHPO_2H$. This fluoro-substituent effect is somewhat larger than the 0.6 units difference between the pK_{a1} values of FPO_3H_2 and HPO_3H_2 and smaller than the 1.6 units found between their pK_{a2} values. The acidity difference appears to be due entirely to the enthalpy change with the fluoro-substituted acid having a 10 kJ more exothermic heat of ionization.

Thermodynamics of hydrolysis of monofluorophosphorous acid

The value of $\Delta H_1^\ominus = 16.9 \pm 1.3$ kJ obtained from the slope of $\ln K_1$ against $1/T$ is combined with the $\Delta G_1^\ominus = 16.2 \pm 0.6$ kJ at 25°C to obtain $\Delta S_1^\ominus = 2.2 \pm 4.3$ J K^{-1}. The small entropy change is reasonable considering the symmetric nature of reaction (1) and the fact that all of the reactants and products are neutral.

Literature values[9,10] for the thermodynamics of HF(aq), H_3PO_3(aq) and H_2O(l) have been used together with the thermodynamics of reaction (1)

Table 2. Equilibrium constants for reactions (1) and (4) and the pK_a of monofluorophosphorous acid

Temperature (°C)	10^3K_1[a]	K_5	pK_a[b]
8	0.95	0.71	0.15
25	1.4	0.43	0.37
45	2.0	0.27	0.56
65	3.4	0.10	1.0

[a] Uncertainty = ±30%.
[b] Uncertainty = ±0.05+10%.

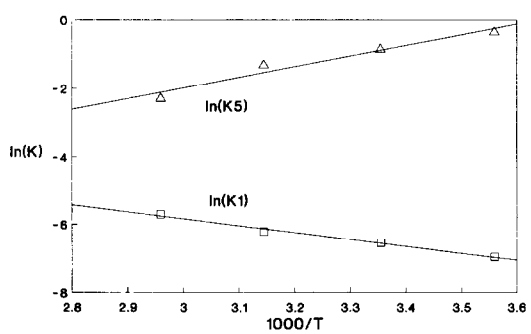

Fig. 2. The van't Hoff isochore graphs for reactions (1) and (5).

Table 3. Thermodynamics of formation[a] of monofluorophosphorous, monofluorophosphite, phosphorous and phosphite at 25°C

	$\Delta G_f^\ominus$ (kJ)	$\Delta H_f^\ominus$ (kJ)	$S^\ominus$
HPO_3H_2(aq)	−836.6	−954.4	(149)[c]
HPO_3H^-(aq)	−829.4	(−969.4)[b]	75
$FHPO_2H$(aq)	−880.1	−971.0	170
$FHPO_2^-$(aq)	−877.9	−997.8	76

[a] Reference values in parentheses.
[b] Reference 9.
[c] Based on $S_{H_3PO_4}$ from ref. 9 and $S_{H_3PO_4} - S_{H_3PO_3} = 8.8$ from ref. 10.

and the thermodynamics of ionization of phosphorous and monofluorophosphorous acid to calculate the thermodynamics of formation reported in Table 3.

Phosphorus appears to be at the borderline between the more electropositive elements which form fluorides that are stable in water and the more electronegative elements which form fluorides that hydrolyse completely in water. Thus SiF_6^{2-} is thermodynamically stable in aqueous solutions, while SO_3F^- is readily hydrolysed. In strong acid solutions, the enthalpy of hydrolysis of these species is calculated to be +24 and −50.1 kJ per mol of HF, respectively. The enthalpy of hydrolysis of $FHPO_2H$(aq), −16.9 kJ, is intermediate between these values.

Related values calculated from literature data[9] are:

$$PF_6^-(aq) + 4H_2O(l) \rightleftharpoons H_2PO_4^-(aq) + 6HF(aq) \quad \Delta H = -19.6\,kJ$$

$$HPO_3F^-(aq) + H_2O(l) \rightleftharpoons H_2PO_4^-(aq) + HF(aq) \quad \Delta G = +8.2\,kJ.$$

The calculated value of ΔG for this second reaction seems peculiar in light of the results of this work on $FHPO_2H$ and the tendency of fluorophosphate to undergo hydrolysis. The thermochemistry of fluorophosphoric acid is therefore currently being re-investigated along with additional substituted phosphonic and phosphinic acids.

REFERENCES

1. L. F. Centofanti and R. W. Parry, *Inorg. Chem.* 1968, **7**, 1005.
2. G. A. Olah and C. W. McFarland, *Inorg. Chem.* 1972, **11**, 845.
3. R. Bender, C. Demay, J. C. Elkaim and J. G. Reiss, *Phosphorus* 1974, **4**, 183.
4. H. Falius, *Angew. Chem., Int. Edn Engl.* 1970, **9**, 733.
5. B. Blazer and K. H. Worms, *Anorg. Allg. Chem.* 1968, **370**, 117.
6. J. W. Larson and M. Pippin, *Polyhedron* 1989, **8**, 527.
7. L. G. Sillen and A. E. Martell, *Stability Constants of Metal Ion Complexes*. The Chemical Society, London (1964).
8. W. P. Jencks and J. Regenstein, *Handbook of Biochemistry and Molecular Biology* (Edited by G. Fasman), Vol. 1, 3rd edn. CRC Press, Cleveland (1976).
9. D. D. Wagman, W. H. Evans, V. B. Parker, R. H. Schumm, I. Halow, S. M. Bailey, K. L. Churney and R. L. Nuttall, *J. Phys. Chem. Ref. Data* 1982, **11**, 1.
10. W. M. Latimer, *Oxidation Potentials*. Prentice–Hall, New York (1952).

Polyhedron Vol. 10, No. 14, pp. 1699–1704, 1991
Printed in Great Britain

0277–5387/91 $3.00+.00
© 1991 Pergamon Press plc

CHROMATOGRAPHIC, SPECTROSCOPIC AND ELECTROCHEMICAL CHARACTERIZATION OF GEOMETRICAL ISOMERS OF THE DICHLOROBIS(2,6-DIMETHYLPYRAZINE)BIS(DIMETHYLSULPHOXIDE)RUTHENIUM(II) COMPLEX

HENRIQUE E. TOMA* and DENISE DE OLIVEIRA

Instituto de Química, Universidade de São Paulo, Caixa Postal 20780, São Paulo, SP, Brazil

(*Received* 7 *December* 1990; *accepted* 22 *April* 1991)

Abstract—The synthesis of the $[RuCl_2(dmso)_2(dmpz)_2]$ complex (dmso = dimethylsulphoxide, dmpz = 2,6-dimethylpyrazine) starting from $[RuCl_2(dmso)_4]$ and dmpz in excess, led to a mixture of two geometrical isomers which were characterized by HPLC, cyclic voltammetry and spectroscopic techniques. The most stable isomer was isolated in pure form, exhibiting a *cis*-Cl_2,*cis*-$(dmso)_2$,*trans*-$(dmpz)_2$ configuration. An all-*cis* configuration was suggested for the second isomer.

Ruthenium(II) sulphoxide complexes, such as $[RuCl_2(dmso)_4]$ and $[RuCl_2(dmso)_2L_2]$ (dmso- = dimethylsulphoxide), have been the subject of renewed interest, with many applications in synthesis,[1–9] oxidation catalysis[10–13] and chemotherapy.[14,17] Because of their mixed nature, the occurrence of geometrical isomers is important, particularly for the understanding of the chemical reactivity of the complexes. Surprisingly, however, this has been little investigated. In this work we studied the $[RuCl_2(dmso)_2(dmpz)_2]$ complex (dmpz = 2,6-dimethylpyrazine) obtained by reacting $[RuCl_2(dmso)_4]$ with dmpz in excess. In contrast to the imidazole analogues reported in the literature,[16,17] this complex exhibits strong charge-transfer bands and is suitable for a detailed investigation of the geometrical isomers using spectroscopic techniques.

EXPERIMENTAL

The starting complex, $[RuCl_2(dmso)_4]$, was obtained in a yellow, crystalline form according to the procedure of Bora and Singh.[18] Found: C, 19.6; H, 4.9. Calc. for $C_8H_{24}O_4S_4Cl_2Ru$: C, 19.8; H, 5.0%.

The $[RuCl_2(dmso)_2(dmpz)_2]$ complex was prepared by reacting $[RuCl_2(dmso)_4]$ with dmpz (Aldrich) in chloroform, under an argon atmosphere, using a molar ratio of 1:8 for these two reactants. The solution was refluxed for 4 h and the volume reduced using a rotary evaporator until it became turbid. At this point, an equivalent volume of diethyl ether was added. The solid was collected on a filter and washed with diethyl ether. The filtrate was kept overnight in the freezer and a second fraction of product was obtained. Found, fraction 1: C, 35.0; H, 5.3; N, 10.4; fraction 2: C, 35.0; N, 5.2; N, 10.3. Calc. for $C_{16}H_{32}N_4S_2O_2Cl_2Ru$: C, 35.3; H, 5.2; N, 10.3%.

The electronic spectra of the complexes were recorded on a Hewlett-Packard model 8451-A diode-array spectrophotometer. High-performance liquid chromatography (HPLC) measurements were carried out using a CG model 480-C instrument attached to the diode-array spectrophotometer. NMR spectra were recorded on a Brucker AC 80 spectrometer; IR spectra of the complexes were recorded on a Perkin–Elmer Model 783 spectrophotometer; and Raman spectra were obtained with a Jarrell–Ash Model 25300 instrument equipped with a krypton ion laser (λ = 647.1 nm). Electrochemical measurements were performed at 25°C, in dry acetonitrile, using a platinum working electrode vs an $Ag/AgNO_3$ (0.010 mol dm^{-3}) reference electrode, as previously reported.[19]

* Author to whom correspondence should be addressed.

RESULTS AND DISCUSSION

Characterization of the geometrical isomers by HPLC

The solids obtained from the synthesis exhibited analytical results consistent with $[RuCl_2(dmso)_2(dmpz)_2]$. In order to evaluate the existence of isomers, HPLC experiments were carried out, starting from 0.3 mmol dm^{-3} solutions of the complexes, freshly prepared in the dark, followed by isocratic elution with a 60:40 methanol–water mixture at a constant flow rate of 0.010 cm^3 s^{-1}, at room temperature. A Zorbax RP C-8 (250 × 4.6 mm) column (Du Pont) was employed, leading to the typical results illustrated in Fig. 1.

According to the HPLC measurements, fraction 1 consists of a single species (**1**), exhibiting a strong absorption band at 294 nm and shoulders at *ca* 330, 380 and 430 nm. Fraction 2 consists of a mixture of species **1** with a second isomer **2**, which exhibits a strong absorption band at 294 nm and a broad composite band at 350 nm.

Attempts at isolating isomer **2** by fractional crystallization of the mixture or by carrying out chromatographic separations were unsuccessful, leading to substantial contamination with isomer **1** or with dissociation products. Photochemical products were also detected after exposing the solutions to daylight for more than 10 min.

Theoretically, the complexes of general formula $[RuCl_2(dmso)_2L_2]$ can exhibit five possible geometrical isomers, with each pair of ligands either in a *cis* or *trans* configuration, as shown in Fig. 2. In this type of complex, it has been shown that the dmso ligand binds to ruthenium(II) preferentially through the sulphur atom.[1,2] Coordination of dmso through the oxygen atom usually leads to labile and less stable complexes with ruthenium(II) ions.

IR, Raman and ^{1}H NMR spectra

Species **1** exhibited the vibrational spectra shown in Fig. 3. The dmso vibrational peaks at 1290 [$\delta_s(CH_3)$], 1095, 1078 [ν(SO)], 1025, 958, 938, 925, 875, 870 [$\rho_r(CH_3)$], 718 [ν_{as}(CSC)], 678 [ν_s(CSC)], 385 and 340 cm^{-1} [δ(CSO)] were assigned based on comparison with the pure ligand (ν, stretching; δ, deformation; ρ, rocking; s, symmetric; as, asymmetric). The ν(SO) vibration of the free dmso ligand is observed at 1040 cm^{-1}. The shift to 1095 and 1078 cm^{-1} in the IR spectra is indicative of sulphur-coordination of dmso, as in the examples reported in the literature.[1-9,20] Coordination through the oxygen atom is expected to decrease the ν(SO) frequencies to values below 1000 cm^{-1}. The dmpz vibrations can also be identified based on the assignment for the free ligand,[21] e.g. 1590, 1525, 1445 [ν(ring)], 1410, 1375 [$\delta(CH_3)$], 1310 [ν(ring)], 1170

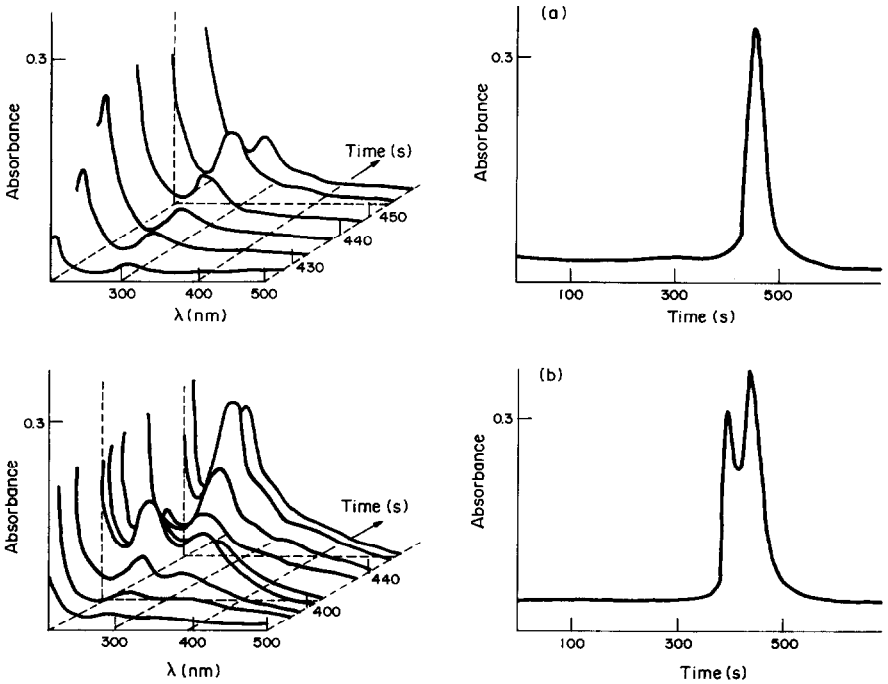

Fig. 1. Three-dimensional plots and chromatograms for the $[RuCl_2(dmso)_2(dmpz)_2]$ complex; (A) fraction **1** and (B) fraction **2**, using a Zorbax RP C-8 column, isocratic elution with 60:40 methanol–water, flow rate = 0.010 cm^3 s^{-1}, temperature = 25°C.

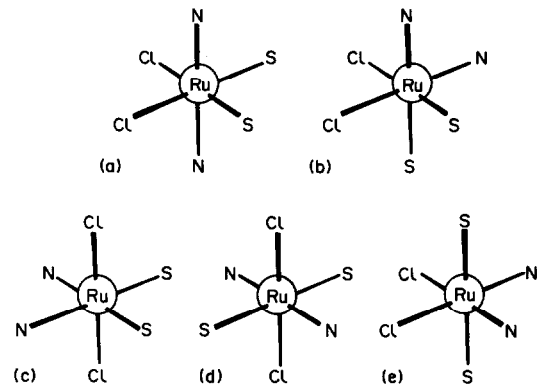

Fig. 2. Geometrical isomers of the $[RuCl_2(dmso)_2(dmpz)_2]$ complex; S = dmso, N = dmpz.

[ν(ring-CH_3)], 1250, 1155, 1150 [β(CH)], 1010 [β(ring)], 975 [ν(ring-CH_3)], 752 [ν(ring)], 732 [γ(CH)], 560, 515 [β(ring)], 450, 435 [γ(ring)], 295 and 268 cm^{-1} (wagging CH_3). The new bands appearing at 325 and 225 cm^{-1} in the IR and Raman spectra are very close to those previously reported[2] for Ru—Cl stretching vibrations in complexes of the type $RuCl_2X_2Y_2$, and are indicative of a *cis*-Cl_2 configuration. Whereas, the coincidence between the IR and Raman spectra, particularly in the case of the metal–ligand vibrations, is consistent with the lack of a symmetry centre in the complex. The additional peak at 420 cm^{-1} in the IR and Raman spectra can be tentatively assigned to Ru—S or Ru—N stretching vibrations.

The ^1H NMR spectra of complex **1** in D_2O solutions exhibited three singlet peaks at 2.42, 3.23 and 8.58 ppm vs TMS, with intensity ratios of 3 : 3 : 1, associated with the methyl protons of dmpz, dmso and the aromatic rings, respectively. The singlet peaks indicate equivalence for each pair of dmpz and dmso ligands.

Based on the information from the Raman, IR and NMR spectral data, complex **1** should exhibit no symmetry centre, with two chloride ligands in the *cis* configuration, and all the ligands in equivalent sites. The only structure compatible with these requirements is for case **A** in Fig. 2. In fact, isomer **A** is expected to be the most stable form, from the viewpoint of cooperative interactions in

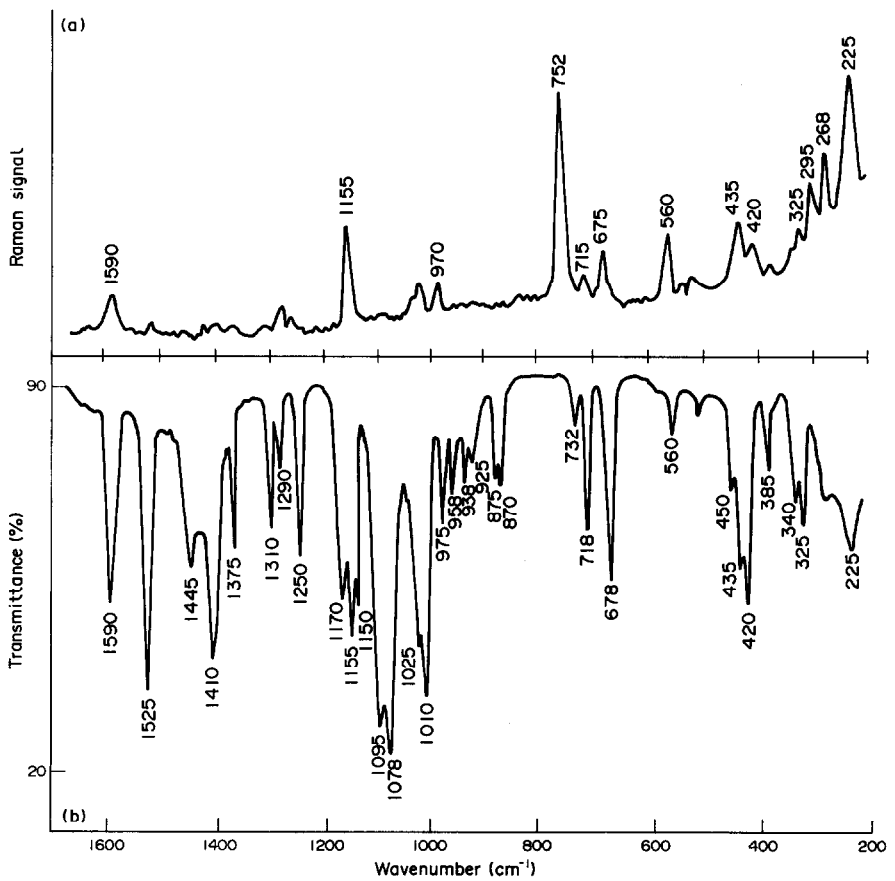

Fig. 3. (A) Raman and (B) IR spectra of the $[RuCl_2(dmso)_2(dmpz)_2]$ complex, corresponding to fraction **1**, obtained, respectively, with the solid sealed in a capillary tube or dispersed in KBr/CsI pellets.

the complex. The chloride ligand is a typical σ,π-electron donor, and dmso is a stronger π-acceptor ligand than dmpz. Therefore, the chloride and dmso ligands in the *trans* configuration can act in a cooperative manner, enhancing the donor–acceptor interactions along the Cl—Ru—S direction.

Based on similar arguments, isomers **C**, **D** and **E** are expected to be much less stable, exhibiting, in contrast to isomer **A**, *trans*-competitive interactions, particularly along the S←Ru→S bonds. It should be noticed, for example, that in the $[RuCl_2(dmso)_4]$ complex the chloride ligands are in *cis*-configuration, interacting in a cooperative manner with the dmso ligands, while the other two dmso ligands adopt a sulphur-bound and oxygen-bound *trans*-cooperative configuration.

Isomer **B**, exhibiting the all-*cis* configuration, is the only isomer which can compete, in terms of stability, with isomer **A**. In fact, this configuration has been proposed for $[RuCl_2(dmso)_2L_2]$ complexes containing substituted 2- and 4-nitroimidazoles, based on XPS, ^1H NMR and IR spectroscopy.[16,17] Therefore, isomer **B** is very likely to occur in fraction 2 from the synthesis. Unfortunately, the vibrational spectra of this material were quite similar to those of isomer **A**, providing little information about the second isomer. NMR measurements were also not conclusive, being complicated by the low solubility of the solid in D_2O and compatible solvents, and by parallel dissociation reactions.

Charge-transfer spectra

The electronic spectrum of species **1**, shown in Fig. 1(A), can be discussed in terms of the geometrical configuration **A** (Fig. 2) which has C_{2v} symmetry. By means of the Gaussian analysis, the UV–vis spectra can be deconvoluted into four bands at 294, 326, 370 and 420 nm. The absorption band around 294 nm is analogous to that observed in N-heterocyclic species, arising from internal $\pi \rightarrow \pi^*$ transitions. The remaining bands are relatively strong and consistent with ruthenium(II)-to-pyrazine, $d_\pi \rightarrow p_\pi^*$ charge-transfer transitions, as in related systems reported in the literature.[22] Analogous to the model proposed by Day and Sanders,[23] the occupied metal d_π orbitals in the C_{2v} group transform according to the symmetry representations a_1, a_2 and b_1. The lowest unoccupied π^* orbitals of the aromatic ligands in the *trans* configuration transform as $a_1(\chi)$ and $b_1(\psi)$. Based on symmetry and orbital overlap considerations,[23] the strongest bands at 326 and 370 nm can be ascribed to the $a_1(d_\pi) \rightarrow a_1(\chi)$ and $b_1(d_\pi) \rightarrow b_1(\psi)$ electronic transitions. The third band at 420 nm is less intense and may be ascribed to the $a_2(d_\pi) \rightarrow b_1(\psi)$ transition, which is symmetry allowed but involves weakly interacting orbitals decreasing the magnitude of the dipole transition moment.[23]

Isomer **B** has global C_1 symmetry. The electronic spectrum can be deconvoluted in terms of one absorption band at 294 nm, ascribed to $\pi \rightarrow \pi^*$ transitions in the aromatic ligand, and three bands at 342, 375 and 425 nm, consistent with metal-to-dmpz charge-transfer transitions. Assuming, for comparison purposes local C_{2v} symmetry for the $Ru(dmpz)_2$ chromophore with two dmpz ligands in the *cis* configuration, the intense charge-transfer bands at 342 and 375 nm could be ascribed to the $a_2(d_\pi) \rightarrow a_2(\psi)$ and $b_1(d_\pi) \rightarrow b_1(\chi)$ transitions, involving strongly interacting metal–ligand orbitals.[23] The less intense band at 425 nm could be ascribed to the $a_1(d_\pi) \rightarrow b_1(\chi)$ transition, which is symmetry allowed, but involves weakly interacting orbitals.

Kinetic aspects

In this work, dissociation reactions were always observed for the complexes in aqueous and non-aqueous solutions. For this reason, all the measurements were carried out using freshly prepared solutions.

The dissociation reactions of species **1** in aqueous solution proceeded according to first-order kinetics, leading to a decay of the charge-transfer bands with a parallel rise of the absorption band at 274 nm of the free dmpz ligand ($k_{obs} = 8.0 \times 10^{-4}$ s^{-1} at 43.8°C). Similar kinetic experiments were also monitored by HPLC, by taking aliquots and analysing their composition as a function of time. These experiments confirmed the preferential aquation of the dmpz ligand ($k_{obs} = 6.3 \times 10^{-4}$ s^{-1} at 43.7°C), in agreement with the spectrophotometrical results.

Electrochemical behaviour

Cyclic voltammograms for species **1** in acetonitrile, at several potential scan rates, are shown in Fig. 4(A). The electrochemical behaviour is consistent with a reversible monoelectronic process, involving the $Ru^{II/III}$ redox couple, with $E_{1/2} = 1.25$ V vs SHE. The pair of shoulders at *ca* 1.0 V is associated with a parallel photochemical process which proceeds to a small extent under normal conditions, leading to preferential labilization of the dmso ligand. This process is accelerated by light. Thermal dissociation can also be observed, however, it proceeds very slowly, with preferential labilization of the dmpz ligand and substitution by

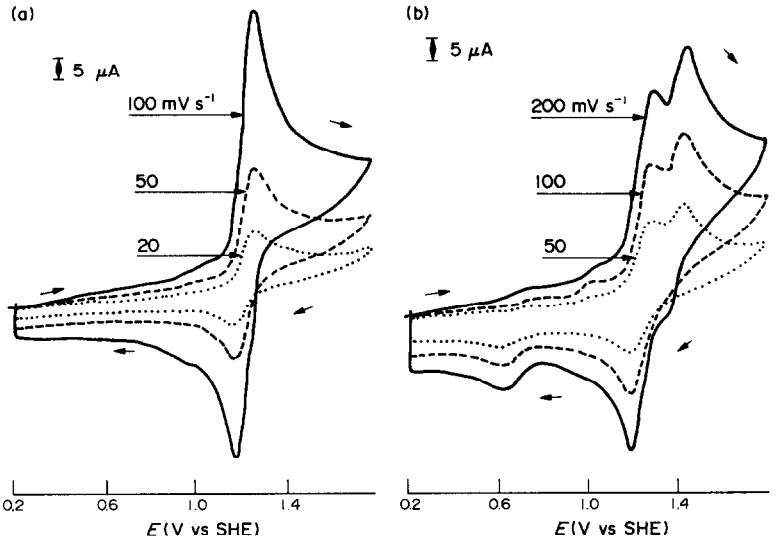

Fig. 4. Cyclic voltammograms of the $[RuCl_2(dmso)_2(dmpz)_2]$ complex (3 mmol dm^{-3}) in acetonitrile; [TEAP] = 0.10 mol dm^{-3}, 25°C; (A) fraction **1** and (B) fraction **2**.

acetonitrile yielding a new species with $E_{1/2}$ of *ca* 1.4 V.

The electrochemical behaviour shown in Fig. 4(B) for fraction 2 is consistent with a mixture of complexes, corresponding to species **1** and **2**, with $E_{1/2} = 1.25$ and 1.43 V vs SHE, respectively. The electrochemical waves of isomer **2** exhibit anodic/cathodic peak ratios smaller than unity. The oxidation of this isomer is followed by a chemical reaction, which is responsible for the rapid decay of the corresponding cathodic peak and for the increase in the cathodic peak at 0.65 V in Fig. 4(B). This species can also be detected in the starting solution after exposure to daylight. We presume that in the oxidized complex, the sulphur-bound dmso ligand is labilized as a consequence of the poor backbonding capability of the ruthenium(III) ions.

Conclusions

The occurrence of geometrical isomers in mixed ruthenium(II)–sulphoxide complexes may be a general phenomenon not readily observed using conventional spectroscopic techniques. This problem requires further investigation because of the many structural and kinetic aspects involved in the synthesis, as recently reported by Jaswal *et al.*[24] in the case of the $[RuCl_2(dmso)_4]$ complex.

Acknowledgements—We thank Professor D. L. A. Faria for obtaining the Raman spectra; and CNPq, FAPESP and FINEP for financial support.

REFERENCES

1. I. P. Evans, A. Spencer and G. Wilkinson, *J. Chem. Soc., Dalton Trans.* 1973, 204.
2. M. M. Taqui Khan and R. Mohuiddin, *Polyhedron* 1983, **2**, 1247.
3. M. M. Taqui Khan and V. V. S. Reddy, *Inorg. Chem.* 1986, **25**, 208.
4. M. M. Taqui Khan and E. Rama Rao, *Polyhedron* 1988, **7**, 29.
5. V. Ravindar, P. Lingaiah and K. L. Reddy, *Inorg. Chim. Acta* 1984, **87**, 35.
6. T. Satyarayama and K. V. Reddy, *Proc. Ind. Acad. Sci., Chem. Sci.* 1987, **99**, 237.
7. K. L. Reddy, P. Lingaiah and K. V. Reddy, *Polyhedron* 1986, **5**, 1519.
8. C. Marzin, G. Tarrago, M. Gal, I. Zidame, T. Hours, D. Lerner, C. Andrieux, H. Gampp and J. M. Savéant, *Inorg. Chem.* 1986, **25**, 1775.
9. T. S. Akasheh, D. Marji and Z. M. Al-ahmed, *Inorg. Chim. Acta* 1988, **141**, 125.
10. D. P. Riley and R. E. Shumate, *J. Am. Chem. Soc.* 1984, **106**, 3179.
11. D. P. Riley and J. D. Oliver, *Inorg. Chem.* 1986, **25**, 1814.
12. D. P. Riley and J. D. Oliver, *Inorg. Chem.* 1986, **25**, 1821.
13. D. P. Riley and J. D. Oliver, *Inorg. Chem.* 1986, **25**, 1825.
14. C. Monti-Bragadin, L. Ramani, L. Sawer, G. Mestroni and G. Zasinovich, *Antimicrob. Agents and Chemotherapy* 1975, **7**, 825.
15. N. Farrell and G. de Oliveira, *Inorg. Chim. Acta* 1982, **66**, L-61.
16. P. K. L. Chan, P. K. H. Chan, D. C. Frost, B. R. James and K. A. Skov, *Can. J. Chem.* 1988, **66**, 117.
17. P. K. L. Chan, B. R. James, D. C. Frost, P. K. H.

Chan, H. L. Hu and K. A. Skov, *Can. J. Chem.* 1989, **67**, 508.
18. T. Bora and M. M. Singh, *J. Inorg. Nucl. Chem.* 1976, **38**, 1815.
19. H. E. Toma and C. Cipriano, *J. Electroanal. Chem.* 1989, **263**, 313.
20. J. A. Davies, *Adv. Inorg. Chem. Radiochem.* 1981, **24**, 115.
21. Y. Ishiabashi, F. Arakawa and R. Shimada, *Bull. Chem. Soc. Japan* 1983, **56**, 1327.
22. H. E. Toma, P. S. Santos and A. Bolanos, *J. Chem. Res. S* 1988, 124.
23. P. Day and N. Sanders, *J. Chem. Soc. A* 1967, 1536.
24. J. S. Jaswal, S. J. Rettig and B. R. James, *Can. J. Chem.* 1990, **68**, 1808.

Polyhedron Vol. 10, No. 14, pp. 1705–1712, 1991
Printed in Great Britain

0277–5387/91 $3.00+.00
© 1991 Pergamon Press plc

THE PHOTOCHEMICAL METHYL MIGRATION IN $(\eta^5\text{-}C_5H_5)Mo(CO)_2LC(O)Me$ [L = $P(OEt)_3$, PPh_3, PBu_3]

R. H. HILL* and JEFF D. DEBAD

The Department of Chemistry, Simon Fraser University, Burnaby, British Columbia, Canada, V5A 1S6

(*Received* 2 *January* 1991; *accepted* 3 *May* 1991)

Abstract—The photolysis of *cis*- and *trans*-$(\eta^5\text{-}C_5H_5)Mo(CO)_2LMe$ [L = $P(OEt)_3$, PPh_3, PBu_3] has been studied at 12 K in 1,2-epoxyethylbenzene glass. All the *trans* species undergo CO loss upon photolysis to generate unsaturated fragments which thermally react with CO to regenerate *trans*-$(\eta^5\text{-}C_5H_5)Mo(CO)_2LMe$. The *cis* species undergo different photochemistry depending on the ligand. For L = $P(OEt)_3$, CO loss is observed to generate a separate isomer of the unsaturated species, which upon thermal reaction with CO produces *cis*-$(\eta^5\text{-}C_5H_5)Mo(CO)_2P(OEt)_3Me$. The photoreaction of *cis*-$(\eta^5\text{-}C_5H_5)Mo(CO)_2LMe$, (L = PPh_3, PBu_3) is not CO loss but loss of L from the coordination sphere. FTIR-monitored photolysis of the acetyl derivatives, *trans*-$(\eta^5\text{-}C_5H_5)Mo(CO)_2LC(O)Me$ [L = $P(OEt)_3$, PPh_3, PBu_3], leads to the stereospecific production of solely *trans*-$(\eta^5\text{-}C_5H_5)Mo(CO)_2LMe$. These products arise from formal CO migration.

Herein we report an example of the migratory insertion reaction which apparently occurs via CO dis-insertion rather than methyl migration. The overall reaction studied is shown in eq. (1):

$$\textit{trans}\text{-}(\eta^5\text{-}C_5H_5)Mo(CO)_2LC(O)Me \xrightarrow{h\nu} \textit{trans}\text{-}(\eta^5\text{-}C_5H_5)Mo(CO)_2LMe + CO \quad (1)$$

[L = $P(OEt_3$, PPh_3, $PBu_3)$]

By FTIR monitoring of the photolytic reaction, we demonstrate that when this reaction is carried out under conditions where both *cis*- and *trans*-$(\eta^5\text{-}C_5H_5)Mo(CO)_2PR_3Me$ are configurationally stable the reaction occurs by CO movement.

Generally, reactions such as this have been found to occur by methyl group migration rather than CO insertion.[1] This was found to be the case in the methyl migration in $(\eta^5\text{-}C_5H_5)Fe(CO)PR_3C(O)Me$[2,3] and $Mn(CO)_5C(O)Me$.[4] There have been reports in the literature concerning formal CO insertion, as opposed to methyl migration.[5–8] In the case of *cis*-$FeMeX(CO)_2(PMe_3)_2$, this result was later shown to be due to a more complicated mechanism in which only alkyl group migration occurred in any one step.[9–11] We are aware of no case in which photochemical decarbonylation leads to formal CO migration.

Previously, we have investigated the low temperature photochemistry of the complexes $(\eta^5\text{-}C_5H_5)Mo(CO)_2LX$ (L = PPh_3, PBu_3; X = Cl, Br, I).[12] In this series we found that photo-induced loss of CO from *cis*-$(\eta^5\text{-}C_5H_5)Mo(CO)_2LX$ (L = PPh_3, PBu_3) led to the production of an unsaturated fragment in which the site of unsaturation was *cis* to the remaining CO ligand. Similarly, loss of CO from the *trans* isomer led to the formation of a molecule in which the remaining CO was *trans* to the site of unsaturation.

The above results suggested that the unsaturated $(\eta^5\text{-}C_5H_5)Mo(CO)LX$ fragments retained the relative geometric position which was present in the precursor molecule. This result has important implications concerning the study of the reaction of $(\eta^5\text{-}C_5H_5)Mo(CO)_2LC(O)Me$ to produce $(\eta^5\text{-}C_5H_5)Mo(CO)_2LMe$ plus CO. If the fragments are indeed rigid we would expect that photo-induced CO loss from *trans*-$(\eta^5\text{-}C_5H_5)Mo(CO)_2LC(O)Me$ (L = phosphine) would lead to different products dependent on whether the reaction is a result of methyl migration or the dis-insertion of CO.

The mechanism of alkyl group migration in

* Author to whom correspondence should be addressed.

molybdenum complexes has been studied previously[13–15] by kinetic methods. In addition, phosphine-substituted complexes have also been examined.[16] It should also be noted that the insertion reaction has been shown to involve intermediates with initial formation of *cis*-acetyl PR_3 relationships.[17]

RESULTS

FTIR studies

Near UV photolysis ($320 < \lambda < 400$ nm) of a 1,2-epoxyethylbenzene glass containing $(\eta^5\text{-}C_5H_5)Mo(CO)_3Me$ at 12 K results in the spectral changes depicted in Fig. 1. Loss of intensity of the IR absorption associated with the starting complex (relevant IR spectral data are tabulated in Table 1) is observed with concomitant growth of absorptions at 2130, 1947 and 1852 cm^{-1}. The band at 2130 cm^{-1} is associated with the production of free CO in the glass.[18] The two remaining bands are logically assigned as due to $(\eta^5\text{-}C_5H_5)Mo(CO)_2Me$.

This fragment has been observed previously in paraffin,[19] CH_4, Ar, N_2 and CO[20] matrices. The absorption bands in a paraffin matrix at 75 K are at 1967 and 1882 cm^{-1} higher energy than those found here. This shift of absorptions is due to the matrix used and not a result of coordination. For example, the FTIR absorption band associated with the coordinatively saturated species, $(\eta^5\text{-}C_5H_5)Mo(CO)_3Me$, are also at lower energy in 1,2-epoxyethylbenzene than those found in a paraffin matrix, where the absorption bands are at 2025 and 1940 cm^{-1}. From the relative intensity of the two CO stretching modes the angle between the CO oscillators (2θ) may be calculated according to the formula $\tan^2\theta = Ias/Is$.[21] The angle found in this manner for $(\eta^5\text{-}C_5H_5)Mo(CO)_2Me$ is 90°.

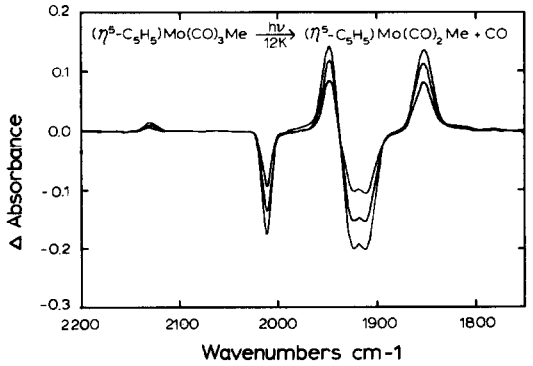

Fig. 1. The changes in the FTIR spectrum of $(\eta^5\text{-}C_5H_5)Mo(CO)_3Me$ associated with photolysis at 12 K for 5, 15 and 60 s.

Photolysis of the $P(OEt)_3$ substituted derivative, $(\eta^5\text{-}C_5H_5)Mo(CO)_2P(OEt)_3Me$, has also been conducted. In Fig. 2(a) we show the result of near-UV irradiation of a glass containing *trans*-$(\eta^5\text{-}C_5H_5)Mo(CO)_2P(OEt)_3Me$. Loss of absorption due to starting material at 1937 and 1832 cm^{-1} and the production of free CO in the glass, together with a new absorption at 1813 cm^{-1}, are observed upon photolysis. The new absorption at 1813 cm^{-1} is assigned as due to the CO loss product $(\eta^5\text{-}$

Table 1. FTIR spectra of relevant complexes at 12 K in 1,2-epoxyethylbenzene

Complex	ν(CO) (cm^{-1}) (Relative intensity)
$(\eta^5\text{-}C_5H_5)Mo(CO)_3Me$	2012(0.9), 1926(1), 1912(1)
$(\eta^5\text{-}C_5H_5)Mo(CO)_2Me$	1947(1), 1852(1)
trans-$(\eta^5\text{-}C_5H_5)Mo(CO)_2P(OEt)_3C(O)Me$	1942(1), 1859(0.5)
trans-$(\eta^5\text{-}C_5H_5)Mo(CO)_2P(OEt)_3Me$	1937(0.4), 1853(1)
cis-$(\eta^5\text{-}C_5H_5)Mo(CO)_2P(OEt)_3Me$	1967(1), 1883(0.7)
Isomer **1** $(\eta^5\text{-}C_5H_5)Mo(CO)P(OEt)_3Me$	1813
Isomer **2** $(\eta^5\text{-}C_5H_5)Mo(CO)P(OEt)_3Me$	1830
trans-$(\eta^5\text{-}C_5H_5)Mo(CO)_2PPh_3C(O)Me$	1933(0.3), 1847(1)
trans-$(\eta^5\text{-}C_5H_5)Mo(CO)_2PPh_3Me$	1930(1), 1843(1)
cis-$(\eta^5\text{-}C_5H_5)Mo(CO)_2PPh_3Me$	1918(1), 1816(0.6)
Isomer **1** $(\eta^5\text{-}C_5H_5)Mo(CO)PPh_3Me$	1800
trans-$(\eta^5\text{-}C_5H_5)Mo(CO)_2PBu_3C(O)Me$	1926(0.5), 1836(1)
trans-$(\eta^5\text{-}C_5H_5)Mo(CO)_2PBu_3Me$	1920(0.7), 1831(1)
cis-$(\eta^5\text{-}C_5H_5)Mo(CO)_2PBu_3Me$	1921(1), 1816(0.8)
Isomer **1** $(\eta^5\text{-}C_5H_5)Mo(CO)PBu_3Me$	1785

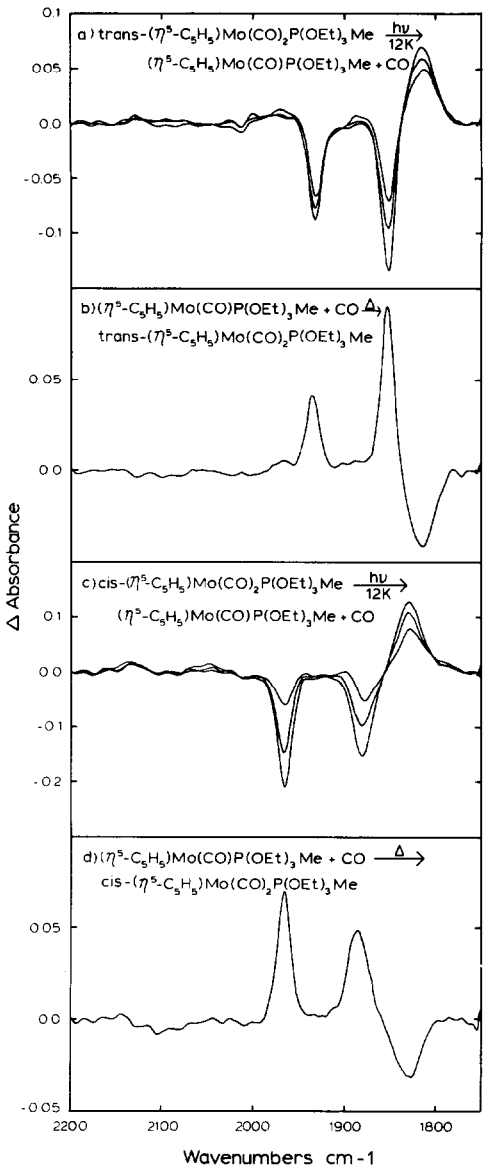

Fig. 2. The FTIR spectral changes associated with photolysis of *trans*-$(\eta^5\text{-}C_5H_5)Mo(CO)_2P(OEt)_3Me$ for 4, 9 and 14 min at 12 K (a). The spectral change associated with warming this sample to 100 K and recooling to 12 K (b). The spectral changes upon photolysis of *cis*-$(\eta^5\text{-}C_5H_5)Mo(CO)_2P(OEt)_3Me$ for 3, 7 and 13 min at 12 K (c). The spectral change associated with warming this sample to 30 K and recooling to 12 K (d).

$C_5H_5)Mo(CO)P(OEt)_3Me$, isomer **1**. Upon warming the glass to 100 K and recooling to 12 K the reaction is reversed [Fig. 2(b)]. It is notable that this thermal reaction is stereospecific, producing only *trans*-$(\eta^5\text{-}C_5H_5)Mo(CO)_2P(OEt)_3Me$.

A similar experiment was conducted with *cis*-$(\eta^5\text{-}C_5H_5)Mo(CO)_2P(OEt)_3Me$. The spectral changes are shown in Fig. 2(c). Once again CO loss occurs upon photolysis, as evidenced by the loss of absorbance due to the dicarbonyl and the production of free CO in the glass. In addition, a monocarbonyl fragment is observed, as evidenced by a single absorption band at 1830 cm^{-1}. This new fragment we assign, again, as the simple CO loss product, $(\eta^5\text{-}C_5H_5)Mo(CO)P(OEt)_3Me$, isomer **2**. The different position of the IR absorption must be due to a different stereochemistry in the unsaturated species. Further evidence for this difference is obtained from its reaction on warming.

The difference in absorption spectra found upon warming the above glass to 30 K and recooling to 12 K is shown in Fig. 2(d). Once again the photochemical reaction is reversed thermally: recombination with CO is observed. The product is solely *cis*-$(\eta^5\text{-}C_5H_5)Mo(CO)_2P(OEt)_3Me$. This is easily distinguished from the *trans* isomer both by the energy and relative intensity of the two absorption bands. The reactions are given by eq. (2):

$$cis\text{-}(\eta^5\text{-}C_5H_5)Mo(CO)_2P(OEt)_3Me \underset{\Delta}{\overset{h\nu}{\rightleftharpoons}} (\eta^5\text{-}C_5H_5)Mo(CO)P(OEt)_3Me + CO. \quad (2)$$

Isomer **2**

Experiments similar to those above have been conducted on *trans*-$(\eta^5\text{-}C_5H_5)Mo(CO)_2PR_3Me$ (R = Ph, Bu) and the results are summarized in eq. (3). The FTIR spectra are given in Table 1. In each case the result was the same as found for the $P(OEt)_3$ derivative. Photo-induced CO loss led to the production of the monocarbonyl fragments, $(\eta^5\text{-}C_5H_5)Mo(CO)PR_3Me$. In both cases, thermal back reaction with CO led to the stereospecific production of *trans*-$(\eta^5\text{-}C_5H_5)Mo(CO)_2PR_3Me$.

$$trans\text{-}(\eta^5\text{-}C_5H_5)Mo(CO)_2PR_3Me \underset{\Delta}{\overset{h\nu}{\rightleftharpoons}} (\eta^5\text{-}C_5H_5)Mo(CO)PR_3Me + CO. \quad (3)$$

Isomer **1**

Unfortunately, the photochemistry of *cis*-$(\eta^5\text{-}C_5H_5)Mo(CO)_2PR_3Me$ (R = Bu, Ph) was not so easily monitored. These isomers are not configurationally stable at room temperature, undergoing isomerism to the *trans* species.[22] In order to prepare these complexes we used our knowledge of the photochemistry of $(\eta^5\text{-}C_5H_5)Mo(CO)_3Me$. As shown earlier this species, upon photolysis, loses CO to generate the 16-electron fragment $(\eta^5\text{-}C_5H_5)Mo(CO)_2Me$. By conducting this photolysis in either PBu_3 or PPh_3 containing 1,2-epoxyethylbenzene solutions at 100 K, we were able to generate small quantities of *cis*-$(\eta^5\text{-}C_5H_5)Mo(CO)_2PR_3Me$. The relevant FTIR absorptions are given in Table 1.

Photolysis of *cis*-(η^5-C_5H_5)Mo(CO)$_2$PBu$_3$Me led rapidly to loss of its absorption bands and the concomitant production of (η^5-C_5H_5)Mo(CO)$_2$Me. This product was identified by comparison of the FTIR spectrum with that observed above in the photolysis of (η^5-C_5H_5)Mo(CO)$_3$Me. Upon warming to 100 K, back reaction to yield the *cis*-phosphine-substituted complex was observed. Unfortunately, the study of *cis*-(η^5-C_5H_5)Mo(CO)$_2$PPh$_3$Me was less satisfactory. We were able to produce only small amounts of *cis*-(η^5-C_5H_5)Mo(CO)$_2$PPh$_3$Me. Photolysis of this led to the production of some (η^5-C_5H_5)Mo(CO)$_2$Me giving evidence that PPh$_3$ loss is the major primary photoprocess for this molecule. The optical density of these products was, however, very low and we cannot rule out the possibility that CO loss occurs competitively. The photochemical and following thermal reactions of the PPh$_3$ and PBu$_3$ derivatives are given in eq. (4):

$$\textit{cis}\text{-}(\eta^5\text{-}C_5H_5)Mo(CO)_2LMe \underset{\Delta}{\overset{h\nu}{\rightleftharpoons}} (\eta^5\text{-}C_5H_5)Mo(CO)_2Me + L. \quad (4)$$

(L = PPh$_3$, PBu$_3$)

The FTIR-monitored photolysis of *trans*-(η^5-C_5H_5)Mo(CO)$_2$P(OEt)$_3$C(O)Me was also conducted at 12 K. The result of photolysis is shown in Fig. 3(a). Loss of absorbance due to the starting material and concomitant production of free CO in the glass is observed. In addition, a new absorption due to a monocarbonyl species is observed at 1813 cm^{-1} and the appearance of new absorption bands at 1937 and 1853 cm^{-1} indicates that *trans*-(η^5-C_5H_5)Mo(CO)$_2$P(OEt)$_3$Me is also formed. The 1813 cm^{-1} absorption is associated with isomer **1** of (η^5-C_5H_5)Mo(CO)P(OEt)$_3$Me. Warming the mixture upon photolysis, to 100 K, results in some reaction with CO. The product of this reaction, as identified by its FTIR, is *trans*-(η^5-C_5H_5)Mo(CO)$_2$P(OEt)$_3$Me [Fig. 3(b)]. Photolysis of this mixture, now containing *trans*-(η^5-C_5H_5)Mo(CO)$_2$P(OEt)$_3$C(O)Me and *trans*-(η^5-C_5H_5)Mo(CO)$_2$P(OEt)$_3$Me, at 12 K, results in the formation of isomer **1** of (η^5-C_5H_5)Mo(CO)P(OEt)$_3$Me. Warming this solution again results in back reaction to form *trans*-(η^5-C_5H_5)Mo(CO)$_2$P(OEt)$_3$Me.

Solutions of *trans*-(η^5-C_5H_5)Mo(CO)$_2$PR$_3$C(O)Me (R = Bu, Ph) in 1,2-epoxyethylbenzene were also cooled to 12 K and photolysed. The FTIR spectral changes were indicative of the loss of (η^5-C_5H_5)Mo(CO)$_2$PR$_3$(CO)$_2$C(O)Me. In each case the production of free CO, *trans*-(η^5-C_5H_5)Mo(CO)$_2$PR$_3$Me and isomer **1** of (η^5-C_5H_5)Mo(CO)PR$_3$Me were observed. These were identified by comparison of the FTIR spectra with those obtained from the corresponding authentic compounds. Warming of the samples led to back reaction with CO to produce only *trans*-(η^5-C_5H_5)Mo(CO)$_2$PR$_3$Me.

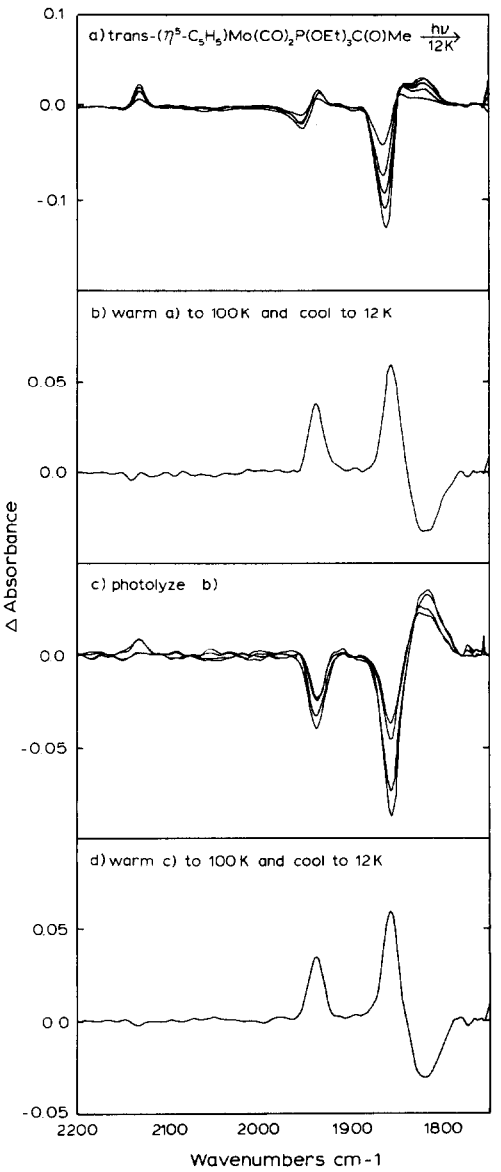

Fig. 3. The FTIR spectral changes associated with the photolysis of *trans*-(η^5-C_5H_5)Mo(CO)$_2$P(OEt)$_3$C(O)Me at 12 K for 2, 6, 9, 12 and 14 min (a). The spectral changes due to warming this solution to 100 K and recooling to 12 K (b). The FTIR changes due to further photolysis of this sample at 12 K for 4, 8, 14 and 20 min (c). The spectral change due to warming this sample to 100 K and cooling to 12 K (d).

NMR studies

In order to confirm the assignment of the molecules formed upon photolysis of the *trans*-acetyl species the following reactions were carried out. A solution containing *trans*-$(\eta^5\text{-}C_5H_5)Mo(CO)_2P(OEt)_3C(O)Me$ was photolysed at 77 K and the reaction monitored by ^1H NMR at room temperature. Upon photolysis, loss of intensity associated with the resonances due to *trans*-$(\eta^5C_5H_5)Mo(CO)_2P(OEt)_3C(O)Me$ was observed. The only photoproduct apparent, as monitored by ^1H NMR, was *trans*-$(\eta^5\text{-}C_5H_5)Mo(CO)_2P(OEt)_3Me$.

The above experiment hence confirms our assignment of the low temperature FTIR spectra. This indicates that not only have we shown that no *cis* isomer is formed but that the sole detectable product, by either FTIR or NMR, is indeed *trans*-$(\eta^5\text{-}C_5H_5)Mo(CO)_2P(OEt)_3Me$.

Similar experiments were conducted for the other phosphine complexes, *trans*-$(\eta^5\text{-}C_5H_5)Mo(CO)_2PR_3C(O)Me$ ($PR_3 = PPh_3$, PBu_3). In each case the sole observable photoproduct, *trans*-$(\eta^5\text{-}C_5H_5)Mo(CO)_2PR_3Me$, confirmed the assignment of the FTIR experiments. In these latter cases, if *cis*-$(\eta^5\text{-}C_5H_5)Mo(CO)_2PR_3Me$ had been formed, isomerism in the room temperature solutions would have led to only the *trans* isomer at room temperature. Their formation would be detectable through the production of $(\eta^5\text{-}C_5H_5)Mo(CO)_3Me$ as a result of the photolysis of the *cis* isomer at low temperature.

DISCUSSION

Previously we have shown that photolysis of $(\eta^5\text{-}C_5H_5)Mo(CO)_2LX$ ($L = PPh_3$, PBu_3; $X = Cl$, Br, I) leads to CO expulsion from the coordination sphere.[12] The product, $(\eta^5\text{-}C_5H_5)Mo(CO)LX$, was shown to be rigid since photolysis of *cis*- and *trans*-$(\eta^5\text{-}C_5H_5)Mo(CO)_2LX$ led to the production of different unsaturated species. These species upon reaction with CO generated only the isomer corresponding to the precursor molecule. Here we have shown that this is also true for photolysis of either *cis*- or *trans*-$(\eta^5\text{-}C_5H_5)Mo(CO)_2P(OEt)_3Me$ and *trans*-$(\eta^5\text{-}C_5H_5)Mo(CO)_2PR_3Me$ (R = Ph, Bu), which all produce CO loss products which depend upon the stereochemistry of the precursor. Each of these CO loss products upon thermal reaction with CO generates the precursor complex in its original geometry. In each case the geometry is consistent with simple CO loss and retention of the stereochemistry associated with the the precursor molecules. The nature of these intermediates, and the possible role of solvation, has been discussed previously with regard to the halide systems and will not be repeated here. Photolysis of *cis*-$(\eta^5\text{-}C_5H_5)Mo(CO)_2PR_3Me$ (R = Ph, Bu) leads to an unsaturated species but through PR_3 loss. In contrast, low temperature photolysis of *cis*- and *trans*-$(\eta^5\text{-}C_5Me_5)Re(CO)_2X_2$ (X = Me, Cl, Br, I) led to the production of a single CO loss product independent of the stereochemistry of the precursor.[18] In this paper we use the retention of stereochemistry in the molybdenum compounds to investigate the decarbonylation of *trans*-$(\eta^5\text{-}C_5H_5)Mo(CO)_2LC(O)Me$ [$L = P(OEt)_3$, PPh_3, PBu_3].

The photolysis of the related acetyl complexes, $(\eta^5\text{-}C_5H_5)Fe(CO)_2C(O)Me$, at temperatures of $\sim$ 12 K was reported to produce the simple CO loss adduct.[23,24] The possibility of η^2-acetyl bonding in this intermediate has also been investigated.[25] We find that under our conditions we do not observe the simple CO loss adduct. We find that following the initial CO loss, rearrangement occurs to generate the saturated molecule, *trans*-$(\eta^5\text{-}C_5H_5)Mo(CO)_2PR_3Me$, which is itself photolysed. Other workers have used both inert gas matrices and PVC films which are apparently considerably harder than 1,2-epoxyethylbenzene used here. It is due to this much softer environment that the migration occurs even at 12 K. In order to test this we repeated experiments with $(\eta^5\text{-}C_5H_5)Fe(CO)_2C(O)Me$ which was observed to give a simple CO loss product, $(\eta^5\text{-}C_5H_5)Fe(Co)C(O)Me$, in Ar and CH_4 matrices and in PVC films.[24] Under our conditions we are unable to stop the migration from occurring and the only product we observe is either the decarbonylated molecule or its CO loss product.

Further evidence that the environment at 12 K in 1,2-epoxyethylbenzene is less restrictive than a gas matrix comes from the observed photochemistry of *cis*-$(\eta^5\text{-}C_5H_5)Mo(CO)_2PR_3Me$ (R = Bu, Ph). For these complexes we find light induced loss of the PR_3 in preference to CO loss. This process is only rarely observed at low temperatures.[26]

Of primary interest in this paper is the stereochemistry at the metal. In all three cases studied the result of photolysis has been an observed formal CO dis-insertion to the coordination site *cis* to the position originally occupied by the acetyl ligand. In addition, we have determined that under our conditions, temperatures of less than 100 K, the coordinatively unsaturated methyl complexes, $(\eta^5\text{-}C_5H_5)Mo(CO)PR_3Me$, are configurationally stable towards isomerism. This result indicates that the formal CO migration is not a result of the isomerism of the product complexes. In addition, due to the extremely low temperatures used in this study, whatever the mechanism is, the reaction is extremely facile at 12 K.

The most likely result of initial photolysis is the generation of an unsaturated species due to CO loss from *trans*-(η^5-C_5H_5)Mo(CO)$_2$PR$_3$C(O)Me to generate (η^5-C_5H_5)Mo(CO)PR$_3$C(O)Me in which the acetyl is *trans* to the phosphine ligand. This step is then followed by simple CO migration, out of the Mo—C bond, to the vacant coordination site producing the observed product, *trans*-(η^5-C_5H_5)Mo(CO)$_2$PR$_3$Me. This sequence of events is illustrated for the P(OEt)$_3$ derivative in Scheme 1. The finding of importance here concerns the stereochemistry of the thermal reaction following photochemical decarbonylation. This formally is a CO dis-insertion rather than a methyl migration. Under the reaction conditions the photoproduced *trans*-(η^5-C_5H_5)Mo(CO)$_2$PR$_3$Me is irradiated, however, we have shown that the result of this secondary photochemistry is reversible [eq. (3)]. Since this secondary photolysis does not result in any observable isomerism it does not affect our conclusion.

The main assumption of this mechanism is that photoproduced (η^5-C_5H_5)Mo(CO)PR$_3$C(O)Me is configurationally stable. In order to test this hypothesis rigorously we would need to study both the *cis*- and *trans*-acetyl complexes. Unfortunately we have been unable, as of yet, to find a synthetic route to these complexes. We have, however, shown that the monocarbonyl fragments, (η^5-C_5H_5)Mo(CO)PR$_3$X, for both the methyl and halides are indeed configurationally stable.[12] It is unlikely that such a small change from methyl to acetyl would result in lowering the barrier to isomerism so significantly as to make the rearrangement facile at 12 K. It should be noted that even at 298 K the barrier for the isomerism via CO loss is significant for the halides.[12,27] In addition, the effect of temperature is not to be underestimated. The isomerism of *cis*- or *trans*-CpMo(CO)$_2$PR$_3$Me (R = Ph, Bu), which is rapid at room temperature,[22] is not observed at all at 100 K. It should be remembered that the isomerism which is observed at room temperature both via thermal[22] and photochemical[12,27] initiation is not a result of a CO loss mechanism but is a direct non-dissociative rearrangement.

An alternative explanation is that the reaction occurs through, not initial CO loss but via radical cleavage. In our case we have some compelling evidence to suggest that this is not occurring. It has been shown[28] that radicals are prone to attack the cyclopentadienyl ring. We see no evidence for products derived from reactions of a radical nature either in NMR or FTIR experiments.

EXPERIMENTAL

The complexes (η^5-C_5H_5)Mo(CO)$_3$Me, *cis*- and *trans*-(η^5-C_5H_5)Mo(CO)$_2$PR$_3$Me (R = Bu, Ph)

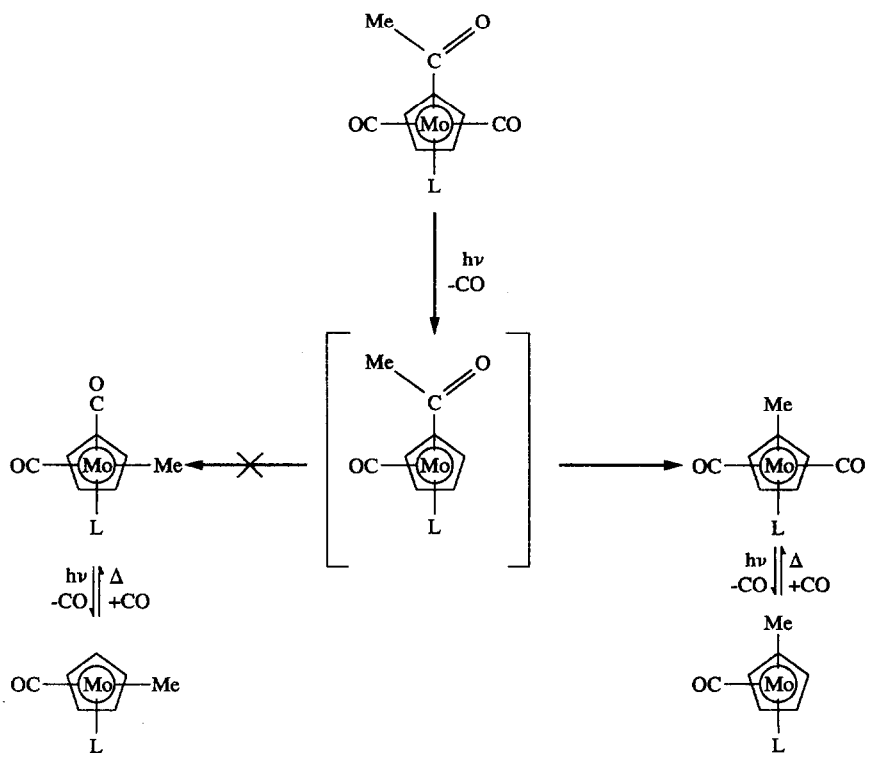

Scheme 1.

were prepared and purified by published methods.[16,29]

FTIR spectra were obtained with a Bruker IFS 85 spectrophotometer. Samples were cooled with a CTI-Cryogenics Model 22 cryocooler attached to a 350R compressor system. Temperatures were controlled and monitored using a Lake Shore Cryotronics silicon diode sensor (DT500 DRC) in conjunction with a Model DRC 80C temperature controller.

The solvent used in the spectroscopic studies, 1,2-epoxyethylbenzene, was obtained from Kodak and used without further purification.

Preparation of $(\eta^5\text{-}C_5H_5)Mo(CO)_2P(OEt)_3X$

The compounds, *cis*- and *trans*-$(\eta^5\text{-}C_5H_5)Mo(CO)_2P(OEt)_3Me$ were prepared by analogy with the methyl complexes above[16] and separated by chromatography on Brockman neutral grade alumina, eluting initially with dichloromethane/hexane (6:1) to separate starting material, then rechromatographed eluting with benzene/hexane (1:1) to separate the isomers. The pure isomers undergo no observable isomerism if stored at 270 K. NMR ($CHCl_3$): *trans*, Cp = 5.02 ppm (d) $^3J(PH) = 1.5$ Hz; Me = 0.28 ppm (d), $^3J(PH) = 3.3$ Hz; *cis*, Cp = 5.31 ppm, Me = 0.38 ppm (d).

FTIR-monitored photolysis of $(\eta^5\text{-}C_5H_5)Mo(CO)_2PR_3X$

Several experiments were conducted in the same manner; here we describe a typical experiment. The complex, *trans*-$(\eta^5\text{-}C_5H_5)Mo(CO)_2P(OEt)_3Me$, was dissolved in 1,2-epoxyethylbenzene to produce a solution of optical density 1.2 for its most intense IR absorption band in the carbonyl region at 1853 cm^{-1}. The sample was then transferred to a CaF_2 faced FTIR cell and loaded into the cold head of the cryostat. The sample chamber was evacuated and then cooled to 12 K. During the cool down FTIR spectra were obtained at different temperatures. At 12 K the sample was photolysed with the water filtered output of a 75 W high pressure mercury lamp for 4 min. The FTIR was then recorded. The above procedure was repeated until no further reaction occurred upon photolysis. At this time the sample was warmed to 100 K then cooled to 12 K. The FTIR spectrum was again recorded.

The sample was then warmed to room temperature and its FTIR spectrum recorded. In other experiments the use of both water and a Corning 7-51 filter isolated the wavelength range 320–400 nm for photolysis.

NMR-monitored photolysis of trans-$(\eta^5\text{-}C_5H_5)Mo(CO)_2LC(O)Me$

A solution containing *trans*-$(\eta^5\text{-}C_5H_5)Mo(CO)_2P(OEt)_3C(O)Me$ (0.005 g) in d^8-toluene (1.0 cm^3) was prepared. From this solution 0.5 cm^3 was taken and degassed with three freeze–pump–thaw cycles in a 5 mm NMR tube and flame-sealed. After obtaining the ^{1}NMR spectrum the sample was photolysed (using the same lamp and filters as above) at 77 K. The changes in the ^{1}H NMR spectra were monitored as a function of photolysis times. Absorptions due to *trans*-$(\eta^5\text{-}C_5H_5)Mo(CO)_2P(OEt)_3C(O)Me$ [Cp = 5.02 ppm, $^3J(PH) = 1.1$ Hz; Me = 2.79 ppm] decreased in intensity with increasing photolysis times. Concomitant production of ^{1}H NMR absorptions due to *trans*-$(\eta^5\text{-}C_5H_5)Mo(CO)_2P(OEt)_3Me$ [Cp = 4.75 ppm, $^3J(PH) = 1.5$ Hz; Me = 0.627 ppm, $^3J(PH) = 3.3$ Hz] was observed.

Similar experiments were conducted with *trans*-$(\eta^5\text{-}C_5H_5)Mo(CO)_2LC(O)Me$ (L = PPh_3, PBu_3). For each of these signals due to the acetyl derivative [L = PPh_3, Cp = 4.83 ppm (d), $^3J(PH) = 1.1$ Hz; Me = 2.90 ppm; L = PBu_3, Cp = 4.91 ppm (d), $^3J(PH) = 0.9$ Hz; Me = 2.86 ppm] were found to decrease with concomitant increase of absorption due to signals associated with *trans*-$(\eta^5\text{-}C_5H_5)Mo(CO)_2LMe$ [L = PPh_3, Cp = 4.50 ppm (d), $^3J(PH) = 1.5$ Hz; Me = 0.78 ppm (d), $^3J(PH) = 2.4$ Hz; L = PBu_3, Cp = 4.63 ppm (d), $^3J(PH) = 1.3$ Hz; Me = 0.66 ppm (d), $^3J(PH) = 2.4$ Hz].

Acknowledgement—We wish to thank the Natural Sciences and Engineering Research Council of Canada for support of this work through an operating grant.

REFERENCES

1. T. C. Flood, *Topics in Stereochemistry* 1981, **2**, 37.
2. A. Davison and N. Martinez, *J. Organomet. Chem.* 1974, **74**, C17.
3. T. G. Attig, R. G. Teller, S.-M. Wu, R. Bau and A. Wojcicki, *J. Am. Chem. Soc.* 1979, **101**, 619.
4. K. Noack and F. Calderazzo, *J. Organomet. Chem.* 1967, **10**, 101.
5. M. Pankowski and M. Bigorne, *J. Organomet. Chem.* 1983, **251**, 333.
6. T. C. Flood, D. C. Cambell, H. H. Downs and S. Nakanishi, *Organometallics* 1983, **2**, 1590.
7. T. C. Flood and D. C. Cambell, *J. Am. Chem. Soc.* 1984, **106**, 2853.
8. H. Brunner, B. Hammer, I. Bernal and M. Draux, *Organometallics* 1983, **2**, 1595.
9. G. Cardaci, G. Reichenbach and G. Bellachioma, *Inorg. Chem.* 1984, **23**, 2936.
10. S. C. Wright and M. C. Baird, *J. Am. Chem. Soc.* 1985, **107**, 6899.

11. G. Cardaci, G. Reichenbach, G. Bellachioma, B. Wassink and M. C. Baird, *Organometallics* 1988, **7**, 2475.
12. J. D. Debad and R. H. Hill, *Can. J. Chem.* 1990, **68**, 2216.
13. I. S. Butler, F. Basolo and R. G. Pearson, *Inorg. Chem.* 1967, **6**, 2074.
14. M. J. Wax and R. G. Bergman, *J. Am. Chem. Soc.* 1981, **103**, 7028.
15. S. L. Webb, C. M. Giandomenico and J. Halpern, *J. Am. Chem. Soc.* 1986, **108**, 345.
16. K. W. Barnett and T. G. Pollman, *J. Organomet. Chem.* 1974, **69**, 413.
17. F. A. Cotton and C. M. Lukehart, *J. Am. Chem. Soc.* 1973, **95**, 3552.
18. R. H. Hill and B. J. Palmer, *Organometallics* 1989, **8**, 1651.
19. R. J. Kazlauskas and M. S. Wrighton, *J. Am. Chem. Soc.* 1982, **104**, 6005.
20. K. A. Mahmoud, R. Narayanaswamy and A. J. Rest, *J. Chem. Soc., Dalton Trans.* 1981, 2199.
21. R. B. King and R. H. Reimann, *Inorg. Chem.* 1976, **15**, 179.
22. J. W. Faller and A. S. Anderson, *J. Am. Chem. Soc.* 1970, **92**, 5852.
23. T. M. McHugh and A. J. Rest, *J. Chem. Soc., Dalton Trans.* 1980, 2323.
24. D. J. Fettes, R. Narayanaswamy and A. J. Rest, *J. Chem. Soc., Dalton Trans.* 1981, 2311; R. H. Hooker, A. J. Rest and I. Whitwell, *J. Organomet. Chem.* 1984, **266**, C27.
25. R. B. Hitam, R. Narayanaswamy and A. J. Rest, *J. Chem. Soc., Dalton Trans.* 1983, 615; R. L. Sweany, *Organometallics* 1989, **8**, 175.
26. J. A. Timney, *Inorg. Chem.* 1979, **18**, 2502.
27. D. G. Alway and K. W. Barnett, *Inorg. Chem.* 1980, **19**, 1533.
28. J. P. Blaha and M. S. Wrighton, *J. Am. Chem. Soc.* 1985, **107**, 2694.
29. P. J. Craig and M. Green, *J. Chem. Soc. A.* 1968, 1978.

Polyhedron Vol. 10, No. 14, pp. 1713–1715, 1991
Printed in Great Britain

0277–5387/91 $3.00+.00
© 1991 Pergamon Press plc

COMMUNICATION

CYCLOPENTADIENYL RUTHENIUM(II) AND (III) COMPLEXES WITH A CHELATING 1,2-BIS(DICYCLOHEXYLPHOSPHINO)METHANE LIGAND

FREDERICK L. JOSLIN, JOEL T. MAGUE and D. MAX ROUNDHILL*

Department of Chemistry, Tulane University, New Orleans, LA 70118, U.S.A.

(*Received* 19 *March* 1991; *accepted* 17 *May* 1991)

Abstract—The reaction between η^5-cpRuCl$(PPh_3)_2$ and 1,2-bis(dicyclohexylphosphino) methane (dcpm) gives η^5-cpRuCl(dcpm). The complex is readily oxidized to η^5-cpRuCl $(dcpm)^+$. Treating η^5-cpRuCl(dcpm) with silver triflate, followed by ammonia or carbon monoxide, gives $[\eta^5$-cpRu(NH_3)(dcpm)$]CF_3SO_3$ or $[\eta^5$-cpRu(CO)(dcpm)$]CF_3SO_3$, respectively. Metathetical replacement of chloride with $LiAlH_4$ gives η^5-cpRuH(dcpm).

There has been much recent interest in the synthesis of low-valent transition metal complexes stabilized by chelating bis-phosphine ligands. In particular, chelating phosphines with electron-donating substituents have been shown to afford transition metal complexes which exhibit unusual reactivity.[1] Recently we have shown that the chelating ligand 1,2-bis(dicylohexylphosphino)ethane (dcpe) can be used to prepare η^5-cpRuCl(dcpe), which can then be converted into a series of novel neutral and cationic complexes.[2] We now report the synthesis of 1,2-bis(dicyclohexylphosphino)methane (dcpm), along with its reactivity as a chelating ligand to the η^5-cyclopentadienyl ruthenium moiety.

Reacting $CH_2(PCl_2)_2$ with 4 equivalents of cyclohexylmagnesium bromide gives the compound $CH_2(PCy_2)_2$ (dcpm) as a colourless, air-sensitive solid.† Treating η^5-cpRuCl$(PPh_3)_2$ with dcpm gives the orange chelate complex η^5-cpRuCl(dcpm) in 45–50% yield, eq. (1):

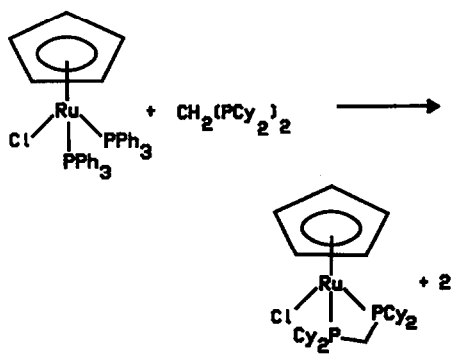

(1)

This complex shows a single $^{31}P\{^1H\}$ NMR resonance at δ 24.6, a triplet $^{13}C\{^1C\}$ NMR signal at δ 36.6 [^1J(PC) = 15.6 Hz] for the methylene carbon and multiplets in the ^1H NMR spectrum at δ 3.45 and 2.95 due to the axial and equatorial hydrogens of the methylene group. The reaction between η^5-cpRuCl(dcpm) and lithium aluminum hydride yields η^5-cpRuH(dcpm) in 90% yield, eq. (2):

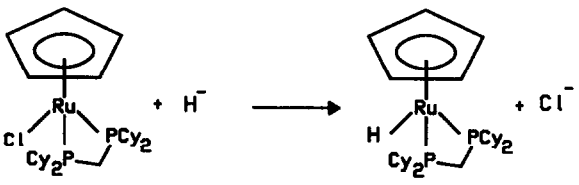

(2)

* Author to whom correspondence should be addressed.

† The compound was purified by vacuum distillation and isolated in 80% yield. Exact *m/z* 408.30790. Calc. for $C_{25}H_{46}P_2$: 408.30748. $^{31}P\{^1H\}$ NMR: δ −10.1. $^{13}C\{^1H\}$ NMR: δ 13.5 t [PCH_2P, ^1J(PC) = 28 Hz], δ 34.7 t [PCH, $|^1J(PC)+{}^3J(PC)| = 5$ Hz], δ 30.6 t [$PC(2)H_2$, $|^2J(PC)+{}^4J(PC)| = 8$ Hz], δ 29.8 t [$PC(6)H_2$, $|^2J(PC)+{}^4J(PC)| = 6$ Hz], δ 26.5–28 t [$PC(3)H_2$, $PC(4)H_2$, $PC(5)H_2$]. The only other mention of $CH_2(PCy_2)_2$ appears to be in a footnote in ref. 3.

The FAB mass spectrum exhibits an envelope of peaks with m/z 572–577, having the maximum relative ion intensity at m/z 575 characteristic of cpRu(dcpm). The complex shows a band in the IR spectrum at 1930 cm^{-1} due to ν(Ru—H). The hydride resonance in the ^1H NMR spectrum is centred at δ −12.2. The double triplet pattern results from coupling to phosphorus [$^2J(PH) = 30.5$ Hz] and one methylene hydrogen [$^4J(HH) = 2.9$ Hz], as confirmed by selective decoupling.[4]

Treating η^5-cpRuCl(dcpm) in THF solution with silver triflate, followed by ammonia or carbon monoxide, gives [η^5-cpRu(NH_3)(dcpm)]CF_3SO_3 or [η^5-cpRu(CO)(dcpm)]CF_3SO_3, respectively, eq. (3):

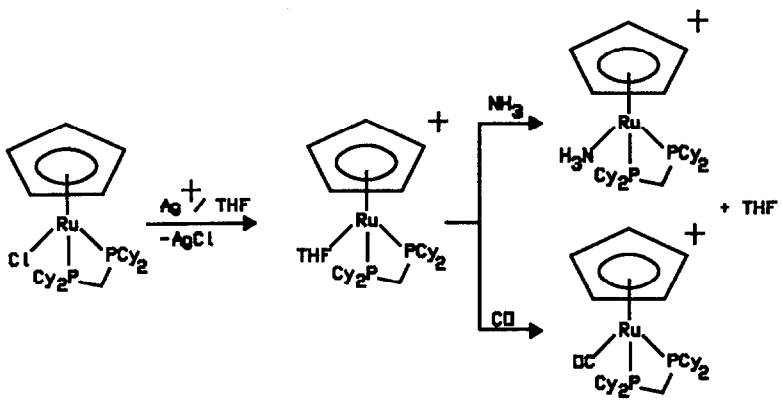

(3)

This unstable carbonyl complex contains ν(CO) at 1933 cm^{-1}, which is lowered by 7 cm^{-1} compared with ν(CO) in the stable complex [η^5-cpRu(CO)(dcpe)]$^+$.[5] Apparently, the electron donation to the carbonyl ligand is greater for the dcpm complex compared with the dcpe analogue.

We find that η^5-cpRuCl(dcpm) undergoes one-electron oxidation to give the red chelate complex η^5-cpRuCl(dcpm)$^+$.* The molecular structure of [η^5-cpRuCl(dcpm)]CF_3SO_3 has been determined by single crystal X-ray diffraction (Fig. 1), which confirms both the monomeric nature of the complex and the chelate bonding of dcpm.† Selected bond distances and angles are collected in Table 1. The P(1)—Ru—P(2) angle within the four-membered ring is 69.57(8)°, and the Cl—Ru—P(1) and Cl—Ru—P(2) angles are slightly different at 91.09(9) and 92.01(8)°, respectively. This finding that the ruthenium(III) complex,

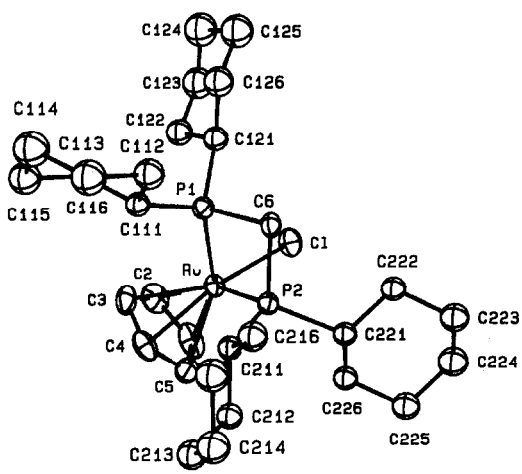

Fig. 1. A perspective view of the [η^5-cpRuCl($Cy_2PCH_2PCy_2$)]$^+$ cation. Thermal ellipsoids are drawn at the 30% probability level and hydrogen atoms are omitted for clarity.

* Possible oxidants are oxygen or silver ion. The crystals were grown from a mixed solution containing acetone and diethyl ether.

† Crystal data for [η^5-cpRuCl(dcpm)]$CF_3SO_3 \cdot 2C_6H_6$; $C_{43}H_{63}P_2O_3F_3SClRu$, mol. wt = 915.58, monoclinic, space group $P2_1/c$ (No. 14), $a = 12.720(3)$, $b = 18.337(4)$, $c = 19.446(3)$ Å, $\beta = 95.58(2)°$, $V = 4485(2)$ Å^3, $Z = 4$, ρ(calc.) = 1.36 g cm^{-3}, μ(Mo-K_α) = 5.6 cm^{-1}, $T = 296$ K, crystal dimensions $0.16 \times 0.16 \times 0.38$ mm. Intensity data were collected on an Enraf–Nonius CAD-4 diffractometer using monochromated Mo-K_α radiation (λ = 0.71073 Å) and were corrected for Lorentz and polarization effects. A total of 4755 unique reflections were collected in the range $3.0 \leqslant 2\theta \leqslant 42$, of which 2804 with $I \geqslant 3.0\sigma(I)$ were used in the structure determination. The structure was solved by Patterson methods and refined using standard difference map techniques. Many hydrogen atoms were located on the difference map. All hydrogen atoms were included as fixed contributions to the scattering with C—H = 0.95 Å, and the isotropic thermal parameters fixed as 1.2 times those of the attached carbon atom. Refinement converged to $R = 0.045$ ($R_w = 0.057$) with the largest shift/ESD in the final cycle being 0.05. The final difference map showed no significant features remaining. Atomic coordinates, bond lengths and angles and thermal parameters, along with Tables of F_o and F_c, have been deposited as supplementary material with the Editor.

Table 1. Bond distance (Å) and interbond angles (°) for [η^5-cpRuCl($Cy_2PCH_2PCy_2$)]$CF_3SO_3 \cdot 2C_6H_6$

Bond distances			
Ru—Cl	2.338(2)	Ru—C′[a]	1.890(9)
Ru—P(1)	2.341(2)	P(1)—C(6)	1.840(8)
Ru—P(2)	2.327(2)	P(2)—C(6)	1.820(8)
Interbond angles			
Cl—Ru—P(1)	91.09(9)	P(1)—Ru—C′[a]	130.1(4)
Cl—Ru—P(2)	92.01(8)	P(2)—Ru—C′[a]	127.9(5)
Cl—Ru—C′[a]	128.1(3)	P(1)—C(6)—P(2)	93.4(4)
P(1)—Ru—P(2)	69.57(8)		

[a] C′ is the centroid of the cyclopentadienyl ring.

η^5-cpRuCl(dcpm)$^+$, is readily isolable further suggests the dcpm confers a higher electron density at the cyclopentadienyl ruthenium(II) centre than does dcpe.

Acknowledgements—We thank the Louisiana Educational Quality Support Fund, administered by the Louisiana Board of Regents, for support of this research. We thank Johnson Matthey Inc. for a loan of ruthenium trichloride. FAB spectra were provided by Dr G. Goodloe at Auburn University.

REFERENCES

1. M. Hackett and G. M. Whitesides, *J. Am. Chem. Soc.* 1988, **110**, 1449; A. Del Zotto, A. Mezzetti, N. B. Pahor and P. Rigo, *J. Chem. Soc., Dalton Trans.* 1989, 1045; A. Del Zotto, A. Mezzetti and P. Rigo, *J. Chem. Soc., Dalton Trans.* 1990, 2515; C. Landis and D. R. Schaad, *J. Am. Chem. Soc.* 1990, **1121**, 1628.
2. F. L. Joslin, M. P. Johnson, J. T. Mague and D. M. Roundhill, *Organometallics* 1991, **10**, 41.
3. H. Heiss, P. Hofmann and P. Neiteler, *Angew. Chem., Int. Edn. Engl.* 1990, **29**, 880.
4. A similar doublet coupling to the hydride resonance in RuH(Ph)$(dcpm)_2$ has not been definitivity assigned; see: P. Palma-Ramircz, D. J. Cole-Hamilton, P. Pogorzelec and J. Campora, *Polyhedron* 1990, **9**, 1107.
5. F. L. Joslin, M. P. Johnson, J. T. Mague and D. M. Roundhill, *Organometallics*, in press.

Polyhedron Vol. 10, No. 14, pp. 1717–1720, 1991
Printed in Great Britain

0277–5387/91 $3.00+.00
© 1991 Pergamon Press plc

COMMUNICATION

SUBSTITUTED SEVEN-COORDINATE MOLYBDENUM–TIN AND TUNGSTEN–TIN COMPLEXES FROM $M(CO)_6$, $BuSnCl_3$ AND PHOSPHITES. X-RAY STRUCTURE OF $[Mo(CO)_2\{P(OMe)_3\}_3(SnBuCl_2)Cl]$

DANIEL MIGUEL, JULIO A. PÉREZ-MARTÍNEZ and VÍCTOR RIERA*

Departamento de Química Organometálica, Universidad de Oviedo, E-33071 Oviedo, Spain

and

SANTIAGO GARCÍA-GRANDA

Departamento de Química Física y Analítica, Universidad de Oviedo, E-33071 Oviedo, Spain

(*Received* 27 *February* 1991; *accepted* 17 *May* 1991)

Abstract—$BuSnCl_3$ reacts with $[M(CO)_3(NCR)_3]$ (M = Mo, R = Me; M = W, R = Et) to produce $[M(CO)_3(NCR)_2(SnCl_2Bu)Cl]$. These complexes react further with three molar-equivalents of $P(OR')_3$ (R' = Me, Et) at room temperature giving dicarbonyl tris-phosphite complexes $[M(CO)_2\{P(OR')_3\}_3(SnCl_2Bu)Cl]$ through displacement of the two nitrile ligands and one CO group. The molybdenum compounds can be prepared in high yields by a one-pot, two-step synthesis by heating $[M(CO)_6]$ with $BuSnCl_3$ in acetonitrile, and then adding the phosphite to the resulting solution. Similar reactions with $SnCl_2Bu_2$ and $SnCl_2Ph_2$ have been explored.

There has been a resurging interest in recent times in the chemistry of seven-coordinate complexes of molybdenum and tungsten, due mainly to their involvement in catalytic processes such as the ring-opening polymerization of norbornene[1] or the hydrostannation of alkynes.[2]

Very recently, Baker *et al.* have reported the oxidation of $[M(CO)_3(NCMe)_3]$ with $SnCl_4$ to give seven-coordinate bis-nitrile complexes $[M(CO)_3(NCMe)_2(SnCl_3)Cl]$, in which the labile acetonitrile groups can be easily replaced by other ligands.[3–5] We are now exploring the reactions of $[M(CO)_3(NCR)_3]$ with haloalkyltin derivatives, $SnCl_{4-n}R_n$, as a general route to seven-coordinate complexes of molybdenum and tungsten containing haloalkylstannate, $SnCl_{3-n}R_n$, ligands. Some preliminary results from this work suggest that the presence of at least one alkyl group bonded to the tin atom substantially modifies the substitution behaviour of the bis-nitrile complexes $[M(CO)_3(NCR)_2(SnCl_{3-n}R_n)Cl]$ when compared with that known for their analogues containing $SnCl_3$. As an example, we wish to report here a facile synthesis for seven-coordinate tris-phosphite complexes of molybdenum and tungsten containing the $SnCl_2Bu$ ligand, and the X-ray crystal structure of one of these derivatives.

$[M(CO)_3(NCR)_3]$ reacts with $BuSnCl_3$ (see Scheme 1) to give $[M(CO)_3(NCR)_2(SnCl_2Bu)Cl]$ [M = Mo, R = Me (**1a**); M = W, R = Et (**1b**)], which can be obtained in virtually quantitative yields as yellow, air-sensitive solids upon evaporation of the solvent. IR specta of **1a** and **1b** show ν(CO) and ν(CN) frequencies very close to those reported for their analogues with $SnCl_3$. Treatment

* Author to whom correspondence should be addressed.

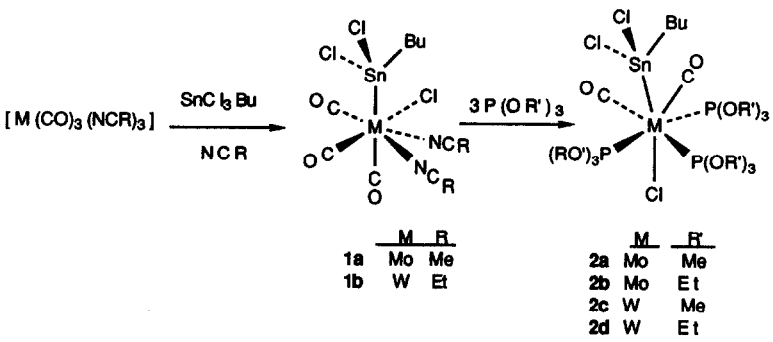

Scheme 1.

of **1a** and **1b** with three equivalents of phosphite leads to the formation, in high yield, of $[M(CO)_2\{P(OR)_3\}_3(SnCl_2Bu)Cl]$ [M = Mo, R = Me (**2a**, 92%), Et (**2b**, 90%); M = W; R = Me (**2c**, 74%), Et (**2d**, 70%)] which have been fully characterized by analytical and spectroscopic methods (see below). Since heating $[Mo(CO)_6]$ and $BuSnCl_3$ in acetonitrile gives the bis-nitrile **1a**, and the presence of excess acetonitrile does not affect the formation of the dicarbonyls **2a** and **2b**, these can be prepared in a one-pot two-step manner, without isolating the intermediate bis-nitrile complexes. In contrast, when $[W(CO)_6]$ was heated with $BuSnCl_3$ in refluxing propionitrile for a long period, IR spectra of the reaction mixture showed only the bands of tungsten carbonyl, without any significant amount of the expected bis-nitrile **1b**, or the intermediate $[W(CO)_3(NCEt)_3]$.[6]

Addition of only one or two molar-equivalents of phosphite to compounds **1a** and **1b** produces the same dicarbonyl tris-phosphite complexes **2a–d**, together with unreacted **1a** and **1b**. This suggests that the change of one chlorine for an alkyl group at the tin atom increases the lability of one of the carbonyl ligands on the molybdenum atom. This behaviour of **1a** and **1b** in substitution reactions contrasts with that reported for their $SnCl_3$ analogues which, when treated with phosphorus ligands, replace only the labile nitrile groups giving tricarbonyl complexes. Thus, it has been reported that the reaction of $[Mo(CO)_3(NCMe)_2(SnCl_3)Cl]$ with two equivalents of $Ph_2P(CH_2)_2PPh_2$ in acetone at room temperature for 24 h gave $[Mo(CO)_3(dppe)(SnCl_3)Cl]$ and unchanged $Ph_2P(CH_2)_2PPh_2$.[3]

Some attempts have been made to explore the oxidative addition of $SnCl_2R_2$ (R = Bu, Ph) to $[Mo(CO)_3(NCMe)_3]$. As expected, the reactions become more difficult as the electron density on the tin atom increases. Thus, $[Mo(CO)_3(NCMe)_3]$ does not react with SnR_2Cl_2 in acetonitrile solution, as shown by the IR monitoring of the mixture. However, when the acetonitrile is evaporated to dryness, and the mixture dissolved in dichloromethane, the oxidative addition takes place readily, and the compounds $[Mo(CO)_3(NCMe)_2(SnR_2Cl)Cl]$ [R = Bu (**1c**), Ph (**1d**)] can be identified by their IR spectra in solution. When three molar-equivalents of phosphite are added to these dichloromethane solutions of **1c** and **1d**, IR spectra of the mixtues show the formation of the dicarbonyl tris-phosphite which is analogous to **2a–d**. Unfortunately, all attempts to isolate and characterize these new compounds have been fruitless to far.

An X-ray study was carried out on a crystal of **2a** (see Fig. 1) to confirm the formulation given in Scheme 1. The molybdenum atom lies in a seven-coordinate environment which can be described as an intermediate between a distorted capped trigonal prism, CTP [with Cl(3) in the capping position], and a distorted capped octahedron, CO [with either C(1) or Sn in the capping position]. Due to the different spatial requirements of the ligands, the angles around Mo(1) deviate from the values expected for the ideal CTP and CO geometries.[7,8] A common feature of the structures reported for related complexes such as $[Mo(CO)_3(bipy)(SnCH_3Cl_2)Cl]$,[9] $[W(CO)_3\{CH_3S(CH_2)_2SCH_3\}(SnCH_3Cl_2)Cl]$[10] and $[Mo(CO)_3\{CH_3S(CH_2)_2SCH_3\}(SnCl_3)Cl]$,[11] is the presence of a chlorine atom bridging the Mo—Sn (or W—Sn) bond. In contrast, in the structure of **2a**, the chlorine atom bonded to molybdenum is at a great distance from the tin atom; Sn, Mo and Cl(3) form a nearly *trans* arrangement [angle 142.0(1)°]. Whereas, the carbon atom of one carbonyl ligand, C(1), is placed near the tin. The distance C(1)···Sn of 2.646(13) Å is too long for any significant bonding, but is short enough to be considered as a contact. Accordingly, although the linear geometry of the carbonyl ligand is not altered [angle Mo—C(1)—O(1) of

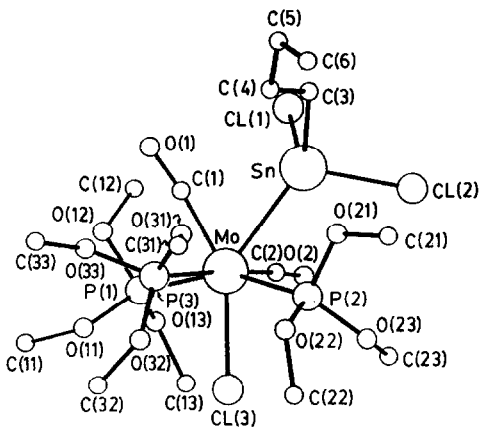

Fig. 1. Perspective view of $[Mo(CO)_2\{P(OMe)_3\}_3(SnCl_2Bu)Cl]$ (**2a**) showing the atom numbering. Selected bond distances (Å) and angles (°): Sn—Mo = 2.774(1), Sn—Cl(1) = 2.410(4), Sn—Cl(2) = 2.387(4), Sn—C(3) = 2.136(14), Mo—Cl(3) = 2.525(4), Mo—C(1) = 1.957(14), Mo—C(2) = 2.024(16), Mo—P(1) = 2.476(4), Mo—P(2) = 2.503(4), Mo—P(3) = 2.536(4); Sn—Mo—Cl(3) = 142.0(1), Sn—Mo—C(1) = 65.4(4), Cl(3)—Mo—C(2) = 90.7(4), C(1)—Mo—C(2) = 105.2(6), Sn—Mo—P(1) = 125.4(1), Cl(3)—Mo—P(1) = 82.7(1), C(1)—Mo—P(1) = 78.4(4), C(2)—Mo—P(1) = 79.7(4), Sn—Mo—P(2) = 74.9(1), Cl(3)—Mo—P(2) = 75.7(1), C(1)—Mo—P(2) = 121.0(4), C(2)—Mo—P(2) = 102.2(4), P(1)—Mo—P(2) = 158.2(1), Sn—Mo—P(3) = 112.2(1), Cl(3)—Mo—P(3) = 86.3(1), C(1)—Mo—P(3) = 75.9(4), C(2)—Mo—P(3) = 174.7(4), P(1)—Mo—P(3) = 95.5(1), P(2)—Mo—P(3) = 81.3(1), Cl(1)—Sn—Cl(2) = 93.9(2), Cl(1)—Sn—C(3) = 98.6(5), Cl(2)—Sn—C(3) = 102.0(5), Cl(1)—Sn—Mo = 109.4(1), Cl(2)—Sn—Mo = 115.6(1), C(3)—Sn—Mo = 130.3(4), Mo—C(1)—O(1) = 173.7(12), Mo—C(2)—O(2) = 176.9(13).

173.7(12)°], the tetrahedral coordination around the tin atom is somewhat distorted to accommodate the C(1) atom.

The $^{31}P\{^1H\}$ NMR spectra of **2a–d** (see below) show only one signal for the three phosphites, revealing the existence of fluxional processes in solution at room temperature. The spectra of the molybdenum compounds **2a** and **2b** exhibit one set of tin satellites (approximate relative intensities 1:10:1), the different ^{31}P–^{117}Sn and ^{31}P–^{119}Sn couplings being unresolved. For the tungsten compounds **2c** and **2d** only one set of broad satellites was observed, instead of the two sets expected (one for ^{31}P–$^{117-119}Sn$ and the other for ^{31}P–^{183}W). This suggests that the coupling constants have about the same value, the observed satellites therefore being the envelope of the two expected sets. The relative intensities measured are in agreement with this assignment. $^{31}P\{^1H\}$ NMR spectra recorded for **2a** and **2c** at −98°C in CD_2Cl_2 exhibit very complex patterns of lines (δ 140–150 ppm for **2a** and δ 120–130 ppm for **2c**), suggesting that the freezing of the dynamic process leads to the formation of more than one isomer at low temperature.

Some additional work is currently in progress to extend the study of the substitution reactions of the bis-nitrile complexes **1a–d** with other phosphorus, nitrogen and sulphur donor ligands.

Selected spectroscopic data

IR spectra (CH_2Cl_2 solution) were recorded on a Perkin–Elmer FT 1720-X spectrometer. ^1H NMR [300.1 MHz, δ(ppm) from internal $Si(Me)_4$] and $^{31}P\{^1H\}$ NMR spectra [121.5 MHz, δ(ppm) to higher frequencies from external 85% H_3PO_4] were recorded in $CDCl_3$ solutions on a Bruker AC-300. Elemental analyses were carried out on a Perkin–Elmer 240B analyser.

$[Mo(CO)_3(NCMe)_2(SnCl_2Bu)Cl]$ (**1a**). IR (cm^{-1}): ν(CO) 2014s, 1935(sh), 1916s; ν(CN) 2317w, 2290w. Satisfactory analysis could not be obtained for bis-nitrile complexes **1a–d** due to their instability.

$[W(CO)_3(NCEt)_2(SnCl_2Bu)Cl]$ (**1b**). IR (cm^{-1}): ν(CO) 2006s, 1915(sh), 1904s; ν(CN) 2320w, 2292w.

$[Mo(CO)_3(NCMe)_2(SnClBu_2)Cl]$ (**1c**). IR (cm^{-1}): ν(CO) 1990s, 1893s(br); ν(CN) 2317 w, 2288 w.

$[Mo(CO)_3(NCMe)_2(SnClPh_2)Cl]$ (**1d**). IR (cm^{-1}): ν(CO) 2001s, 1904s(br); ν(CN) 2317w, 2289w.

$[Mo(CO)_2\{P(OMe)_3\}_3(SnCl_2Bu)Cl]$ (**2a**). (Found: C, 22.1; H, 4.5. Calc. for $C_{15}H_{36}Cl_3MoO_{11}P_3Sn$: C, 22.3; H, 4.5%.) IR (cm^{-1}): ν(CO) 1967m, 1885s. ^1H NMR: δ 3.81 [m, 27H, $3P(OCH_3)_3$], 1.84 [m, 4H, C^1H_2 and C^2H_2 of Bu^n], 1.43 [m, 2H, C^3H_2 of Bu^n], 0.94 [t, J(HH) 7 Hz, 3H, C^4H_3 of Bu^n]. $^{31}P\{^1H\}$ NMR: δ 144.08 [s, J(PSn) 373 Hz].

$[Mo(CO)_2\{P(OEt)_3\}_3(SnCl_2Bu)Cl]$ (**2b**). (Found: C, 30.5; H, 5.8. Calc. for $C_{24}H_{54}Cl_3MoO_{11}P_3Sn$: C, 30.9; H, 5.8%.) IR (cm^{-1}): ν(CO) 1961m, 1883s. ^1H NMR: δ 4.18 [m, 18H, $3P(OCH_2CH_3)_3$], 1.90 [m, 4H, C^1H_2 and C^2H_2 of Bu^n], 1.41 [m, 2H, C^3H_2 of Bu^n], 1.31 [t, J(HH) 7 Hz, 27H, $3P(OCH_2CH_3)_3$], 0.93 [t, J(HH) 7 Hz, 3H, C^4H_3 of Bu^n]. $^{31}P\{^1H\}$ NMR: δ 139.64 [s, J(PSn) 409 Hz].

$[W(CO)_2\{P(OMe)_3\}_3(SnCl_2Bu)Cl]$ (**2c**). (Found: C, 20.3; H, 3.9. Calc. for $C_{15}H_{36}Cl_3O_{11}P_3SnW$: C, 20.1; H, 4.1%.) IR (cm^{-1}): ν(CO) 1954m, 1878s. ^1H NMR: δ 3.82 [s br, 27H, $3P(OCH_3)_3$], 1.81 [m, 4H, C^1H_2 and C^2H_2 of Bu^n], 1.42 [m, 2H, C^3H_2 of Bu^n], 0.93 [t, J(HH) 7 Hz, 3H, C^4H_3 of Bu^n]. $^{31}P\{^1H\}$ NMR ($CDCl_3$): δ 122.99 [s, J(PSn) 330 Hz].

$[W(CO)_2\{P(OEt)_3\}_3(SnCl_2Bu)Cl]$ (**2d**). (Found: C, 27.9; H, 5.3. Calc. for $C_{24}H_{54}Cl_3O_{11}P_3SnW$: C, 28.2; H, 5.3%.) IR (cm^{-1}): ν(CO) 1950m, 1873s. ^1H NMR: δ 4.17 [s br, 18H, $3P(OCH_3)_3$], 1.81 [m, 4H, C^1H_2 and C^2H_2 of Bu^n], 1.42 [m, 2H, C^3H_2 of Bu^n], 1.31 [t, J(HH) 7 Hz, 27H, $3P(OCH_2CH_3)_3$], 0.93 [t, J(HH) 7 Hz, 3H, C^4H_3 of Bu^n]. $^{31}P\{^1H\}$ NMR: δ 119.37 [s, J(PSn) 327 Hz].

Crystal and refinement data for compound **2a**

$C_{15}H_{36}Cl_3MoO_{11}P_3Sn$, $M_r = 806.35$, monoclinic, space group $P2_1/c$, $a = 14.714(5)$, $b = 9.931(6)$, $c = 21.646(7)$ Å, $\beta = 91.12(5)°$, $V = 3162(3)$ Å^3, $D_c = 1.69$ g cm^{-3}, $Z = 4$, $F(000)$ 1608, λ(Mo-K_α) = 0.71073 Å, $\mu = 16.28$ cm^{-1}, room temperature. Pale yellow, prismatic crystal ($0.3 \times 0.1 \times 0.1$ mm) grown by slow diffusion of hexane into a concentrated solution of the compound in dichloromethane. Intensities were collected on an Enraf–Nonius CAD4 diffractometer, using the ω–2θ scan technique. 5520 reflections were measured in the range $0 \leqslant \theta \leqslant 25°$; 1951 with $I \geqslant 3\sigma(I)$ were used in the refinement. An empirical (ψ-scan based) absorption correction was applied. Molybdenum and tin atoms were located from a Patterson synthesis, and the remaining non-hydrogen atoms by DIRDIF.[12] An absorption correction was applied with DIFABS.[13] Full-matrix least-squares refinement was made with SHELX76.[14] All non-hydrogen atoms were refined anisotropically. Hydrogen atoms were geometrically positioned with a given overall isotropic temperature factor of 0.08 Å^2. Number of parameters refined, 308. Final R was 0.043 (R_w 0.038).

Acknowledgement—We thank the Spanish Dirección General de Investigación Científica y Técnica (DGICYT, Project PB88-0467) and Metalúrgica del Nalón S.A. for financial support.

REFERENCES

1. L. Bencze and A. Kraut-Vass, *J. Molec. Catal.* 1984, **28**, 369; L. Bencze, A. Kraut-Vass and L. Prókai, *J. Chem. Soc., Chem. Commun.* 1985, 911.
2. H. X. Zhang, F. Guibé and G. Balavoine, *J. Org. Chem.* 1990, **55**, 1857.
3. P. K. Baker and A. Bury, *J. Organomet. Chem.* 1989, **359**, 189.
4. P. K. Baker and A. Bury, *Polyhedron* 1989, **8**, 7.
5. P. K. Baker and A. J. Quinlan, *Inorg. Chem. Acta* 1989, **162**, 179.
6. G. J. Kubas, *Inorg. Chem.* 1983, **22**, 692.
7. M. G. B. Drew, *Prog. Inorg. Chem.* 1977, **23**, 67.
8. D. L. Keppert, *Prog. Inorg. Chem.* 1979, **25**, 41.
9. M. Elder and D. Hall, *Inorg. Chem.* 1969, **8**, 1268.
10. M. Elder and D. Hall, *Inorg. Chem.* 1969, **8**, 1273.
11. R. A. Anderson and F. W. B. Einstein, *Acta Cryst.* 1976, **B32**, 966.
12. P. T. Beurskens, W. P. Bosman, H. M. Doesburg, Th. E. M. van der Hark, P. A. Prick, J. H. Noordik, G. Beurskens, R. O. Gould and V. Parthasarathi, *Conformation in Biology* (Edited by R. Srinivasan and R. H. Sarma), pp. 389–406. Adenine Press, New York (1982).
13. N. Walker and D. Stuart, *Acta Cryst.* 1983, **A39**, 158.
14. G. M. Sheldrick, SHELX76, Program for Crystal Structure Determinations. University of Cambridge, U.K. (1976).

Polyhedron Vol. 10, No. 14, pp. 1721–1722, 1991
Printed in Great Britain

0277–5387/91 $3.00+.00
© 1991 Pergamon Press plc

COMMUNICATION

ON THE FORMATION OF THE $[RhH(SnCl_3)_5]^{3-}$ COMPLEX ANION: DIRECT ^{119}Sn NMR EVIDENCE FOR THE FACILE PROTONATION OF THE $[Rh(SnCl_3)_5]^{4-}$ SPECIES EXTRACTED INTO CHLOROFORM

IRIS HALL and KLAUS R. KOCH*

Department of Chemistry, University of Cape Town, Private Bag, Rondebosch 7700, Cape Town, South Africa

(*Received* 19 *April* 1991; *accepted* 17 *May* 1991)

Abstract—The $[Rh(SnCl_3)_5]^{4-}$ complex anion, extracted into chloroform containing a quaternary ammonium type liquid anion exchanger, is readily and reversibly protonated in the chloroform phase to yield the stereochemically rigid, $[RhH(SnCl_3)_5]^{3-}$ complex.

The considerable current interest in transition metal–tin chemistry may be ascribed in part to the catalytic utility of these systems, the subject having been recently reviewed.[1] In particular, Saito and co-workers[2,3] have reported the photo-enhanced catalytic dehydrogenation of propan-2-ol using a rhodium–tin chloride system. Furthermore, the yellow solutions obtained when mixing $RhCl_3 \cdot 3H_2O$, $SnCl_2 \cdot 2H_2O$, propan-2-ol and 3 M hydrochloric acid, have been shown by means of ^{119}Sn NMR to contain the $[RhH(SnCl_3)_5]^{3-}$ anion, **1**.[4] In these studies the formation of **1** has been assumed to proceed via the catalytic dehydrogenation of propan-2-ol to yield acetone. While the photo-enhanced dehydrogenation of propan-2-ol (in the *absence* of the hydrochloric acid) doubtlessly involves a hydride complex,[3] the nature and mechanism of formation of such complexes has not been clearly elucidated.

As part of our interest in the selective extraction of the complex anions of the type $[Rh(SnCl_3)_n Cl_{6-n}]^{3-}$ (n = 1–5) by solid polyurethane foams,[5] we have used ^{119}Sn NMR to examine the distribution of these complexes between dilute hydrochloric acid and the quaternary ammonium liquid anion exchanger, tricaprylylmethylammonium chloride (AQ-336, Aldrich) in chloroform. We here report convincing ^{119}Sn NMR evidence that the yellow complex anion **1** is formed by direct protonation of the red–purple (λ_{max} = 470 nm) complex anion $Rh(SnCl_3)_5^{4-}$ (**2**).

When a suitably aged (35°C, 4 h) 0.5 M hydrochloric acid solution containing $RhCl_3 \cdot 3H_2O$ (7 mmol) and sufficient $SnCl_2 \cdot 2H_2O$ (Sn/Rh mole ratio of 10:1) is extracted with an equal volume of 10% (v/v) AQ-336 in $CDCl_3$, the red–purple rhodium–tin complex anions are quantitatively transferred into the organic phase. ^{119}Sn NMR spectroscopy at 25°C (Fig. 1) shows that the predominant species found to be extracted is **2**; this complex is also known to predominate in the aqueous phase under certain conditions.[6] Addition of a small quantity of CF_3COOH directly to the chloroform extract results in a rapid colour change from red to yellow, while the ^{119}Sn NMR spectrum that obtains, is clearly ascribable to the $[RhH(SnCl_3)_5]^{3-}$ complex [$\delta(^{119}Sn) = -14.1$ ppm(eq), +78.7 ppm(ax), $^1J(^{103}Rh–^{119}Sn) = 594$ Hz(eq), 528 Hz(ax), $^2J(^{117}Sn–^{119}Sn) = 1973$ Hz (*cis*, eq–eq), 25,334 Hz (*trans*, eq–eq), 1759 Hz (*cis*, ax–eq), $^2J(^{119}Sn–^{119}Sn) = 1844$ Hz (*cis*, ax–eq), $^2J(^1H–^{119}Sn) = 58$ (*cis*, eq), 1115 Hz (*trans*, ax)]. An identical spectrum may be obtained simply by increasing the hydrochloric acid concentration of the aqueous source phase to greater than 3 M, when the extraction is accompanied by a gradual colour change from red to yellow. The ^{119}Sn NMR spectra of extracts obtained from 5 M hydrochloric acid

* Author to whom correspondence should be addressed.

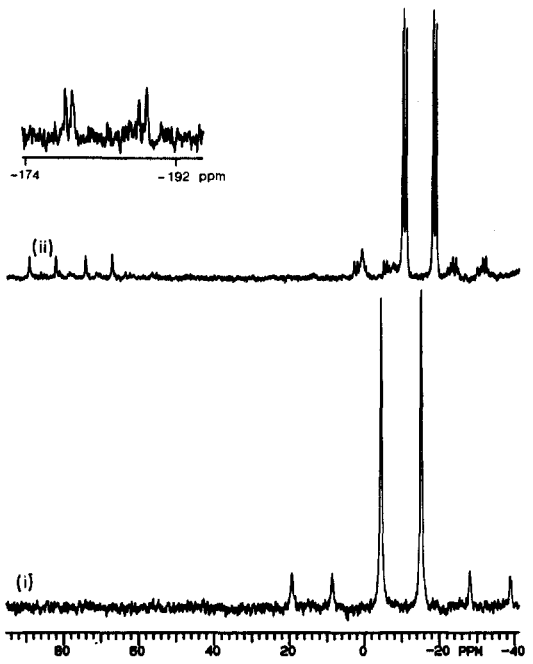

Fig. 1. ^{119}Sn NMR spectra at 74.5 MHz of: (i) a $CDCl_3$/AQ-336 extract obtained from 0.5 M hydrochloric acid containing $RhCl_3$ and $SnCl_2$ (Sn/Rh = 10) and (ii) spectrum after addition to 1 drop of CF_3COOH. [Also shown is the high-field satellite due to *trans* $^2J(^{117}Sn–^{119}Sn)$ coupling.]

solution containing tin chloride in an Sn/Rh mole ratio of 4, reveal the presence of a small amount of a second hydride complex anion assigned to be *trans*-$[RhHCl(SnCl_3)_4]^{3-}$ [$\delta(^{119}Sn) = -92.5$ ppm, $^1J(^{103}Rh–^{119}Sn) = 666$ Hz, $^2J(^{117}Sn–^{119}Sn) = 2398$ Hz, $^2J(^1H–^{119}Sn) = 105$ Hz], in addition to substantial amounts of **1**.

The partial reversibility of the proposed protonation

$$[Rh(SnCl_3)_5]^{4-} + H(org)^+ \rightleftharpoons [RhH(SnCl_3)_5]^{3-}$$

in the AQ-336/$CDCl_3$ phase may be conveniently ascertained by means of a photometric titration. Addition of an appropriate amount of strong acid, e.g. CF_3COOH, to a chloroform extract containing **2**, results in a progressive decrease of the absorbance at 470 nm with a concomitant increase in the absorbance below 350 nm. This trend may be reversed by the subsequent addition of the relatively basic N,N-dimethylformamide.

It is thus clear that the formation of **1** in solutions of propan-2-ol containing dilute hydrochloric acid results from the simple protonation of the pentacoordinate species **2** in the organic phase, and need not involve the deprotonation of propan-2-ol as has been tacitly assumed.[3,4] Further support for this contention is obtained from the observation that the yellow complex anion **1** predominates in 4-methylpentan-2-one (MIBK) extracts obtained from aqueous source phases under a variety of acid concentrations and Sn/Rh ratios. All attempts to detect **2** in the MIBK phase proved fruitless. This observation can now be understood in view of the well established tendency for solvents such as MIBK to co-extract substantial amounts of hydrochloric acid,[7] which results in the rapid protonation of **2** on transfer into the MIBK phase. While the catalytic photo-enhanced dehydrogenation of propan-2-ol most probably involves complex rhodium–chlorotin hydrido species, it is clear that the coordinatively saturated anion **1** is easily formed by facile protonation of **2** in organic solvents, even in the absence of alcohols such as propan-2-ol.

REFERENCES

1. M. S. Holt, W. L. Wilson and J. H. Nelson, *Chem. Rev.* 1989, **89**, 11.
2. S. Shinoda, H. Moriyama, Y. Kise and Y. Saito, *J. Chem. Soc., Chem. Commun.* 1978, 348.
3. H. Moriyama, T. Aoki, S. Shinoda and Y. Saito, *J. Chem. Soc., Perkin II* 1982, 369.
4. T. Yamakawa, S. Shinoda, Y. Saito, H. Moriyama and P. S. Pregosin, *Mag. Res. Chem.* 1985, **23**, 202.
5. L. Jones, I. Nel and K. R. Koch, *Anal. Chim. Acta* 1986, **182**, 61.
6. H. Moriyama, T. Aoki, S. Shinoda and Y. Saito, *J. Chem. Soc., Dalton Trans.* 1981, 639.
7. H. M. Widmer, *J. Phys. Chem.* 1970, **74**, 3251.

Polyhedron Vol. 10, No. 14, pp. 1723–1726, 1991
Printed in Great Britain

0277–5387/91 $3.00+.00
© 1991 Pergamon Press plc

COMMUNICATION

METAL–BETAINE INTERACTIONS—VIII. CRYSTAL STRUCTURE OF *CATENA*-(PYRIDINE BETAINE)(NITRATO)SILVER(I), $[Ag(C_5H_5NCH_2COO)(NO_3)]_n$

XIAO-MING CHEN and THOMAS C. W. MAK*

Department of Chemistry, The Chinese University of Hong Kong, Shatin, New Territories, Hong Kong

(*Received* 17 *January* 1991; *accepted* 23 *May* 1991)

Abstract—The crystal structure of $[Ag(pyBET)(NO_3)]_n$ (pyBET = $C_5H_5N^+CH_2COO^-$) has been characterized by X-ray crystallography. The complex comprises (carboxylato-*O*,*O*′)-bridged one-dimensional polymeric chains with the Ag(I) atom forming two Ag—O(carboxylato) bonds [2.289(1) and 2.334(1) Å to different pyBET ligands] and one Ag—O(nitrato) bond [2.434(2) Å] in a distorted trigonal-planar configuration.

Among the characterized crystal structures of silver(I) carboxylates, most are composed of either discrete dimers or polymeric system constructed by the linkage of dimeric subunits, which have been classified into four principal types [Fig. 1(a)–(d)].[1] Exceptions are extremely rare. The only example to our knowledge is a one-dimensional polymeric arrangement of linear O—Ag—O bonds found in silver(I)(4-chloro-2-methylphenoxy)acetate,[2] where the bridging carboxylato group acts in the *syn–anti* mode [Fig. 1(f)].

Betaines are structurally analogous to the corresponding carboxylate anions, and advantage can be taken of their overall charge neutrality to provide synthetic access to new varieties of metal complexes related to the well-known carboxylates.[3] Recent studies include the preparation and crystal structures of two silver(I) complexes,[4] $[Ag_2(BET)_2(H_2O)_2(NO_3)_2]_n$ (**1**) and $[Ag_2(pyBET)_2(ClO_4)_2]_n$ (**2**) (BET = betaine, $Me_3N^+CH_2COO^-$; pyBET = pyridine betaine, $C_5H_5N^+CH_2COO^-$).† We now report the preparation and single-crystal X-ray analysis of a new betaine silver(I) complex, *catena*-(pyridine betaine)(nitrato)silver(I), $[Ag(pyBET)(NO_3)]_n$ (**3**), which has been found to be the first example of a *syn–syn* (carboxylato-*O*,*O*′)-bridged one-dimensional polymeric structure that is not based on dimeric subunits.

EXPERIMENTAL

Preparation and IR spectra

Pyridine betaine was prepared as described previously.[5] Complex (**3**) was prepared by dissolving $AgNO_3$ (0.250 g, 1.5 mmol) and pyridine betaine (0.411 g, 3.0 mmol) in hot water (3 cm^3, 60°C). After filtration, the solution was evaporated at room temperature in the dark for a week to obtain colourless plate-like crystals.

IR spectra (KBr pellets) were recorded on a Nicolet 20SXC FT-IR spectrometer in the range of 4000–400 cm^{-1}. The complex exhibits the following IR carboxy absorption bands (v = very, s = strong, m = medium; cm^{-1}): ν(COO) at 1633vs, 1384s and δ at 694m. The separation (Δ) between ν_{asym}(COO) and ν_{sym}(COO), 249 cm^{-1}, is smaller than that in uncomplexed pyridine betaine [ν(COO) = 1635, 1377, δ(COO) = 706 cm^{-1}; Δ = 258 cm^{-1}][5] and hence indicative of the bridging mode of carboxylato coordination in the present complex.[6]

* Author to whom correspondence should be addressed.

† The IUPAC names for BET and pyBET are trimethylammonioacetate and pyridinioacetate.

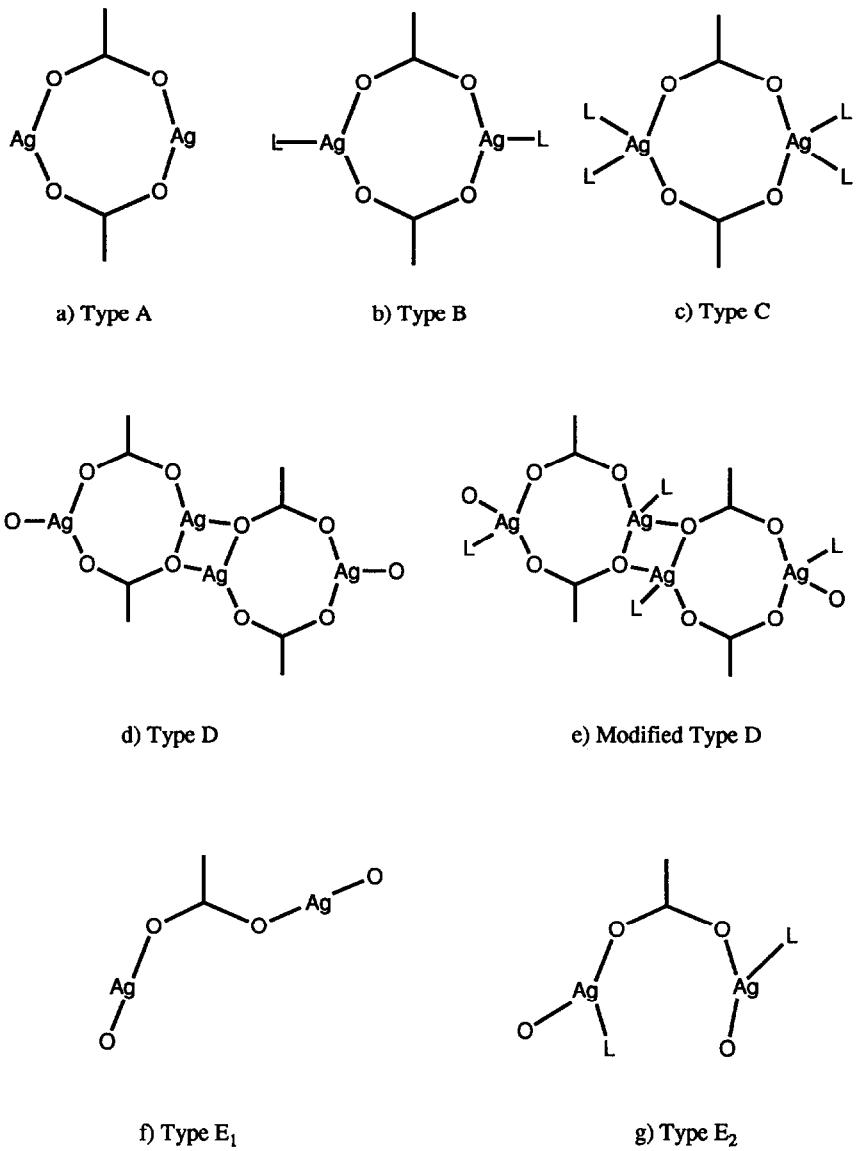

Fig. 1. Principal structural types of silver(I) carboxylates and related betaine complexes. Structures (d)–(g) are polymeric.

X-ray crystallography

$Ag(C_5H_5NCH_2COO)(NO_3)$ (**3**), Mol. wt 307.01, monoclinic, space group $P2_1/c$ (no. 14), $Z = 4$, $a = 12.849(2)$, $b = 4.9992(3)$, $c = 15.047(3)$ Å, $\beta = 113.91(1)°$, $U = 883.6(3)$ Å^3, $D_{calc} = 2.308$ g cm^{-3}, $F(000) = 600$, Mo-K_α radiation ($\lambda = 0.71073$ Å), $\mu = 2.26$ mm^{-1}.

Diffraction intensities (crystal size $0.12 \times 0.28 \times 0.30$ mm; $2\theta_{max} = 55°$, 2024 unique data) were collected at 21°C on a Nicolet R3m/V diffractometer using the ω-scan (2.91–14.63° min^{-1}) mode.[7] Data processing, absorption corrections ($\mu r = 0.27$, transmission factors 0.577–0.795), structure solution, and full-matrix least-squares refinement were performed with the SHELXTL-PLUS program package[8,9] on a DEC MicroVAX-II computer. The non-hydrogen atoms were refined anisotropically. All the hydrogen atoms were generated geometrically (C—H = 0.96 Å), assigned isotropic temperature factors, and included in the structure–factor calculations. Analytic expressions of neutral-atom scattering factors were employed, and anomalous dispersion corrections were incorporated.[10] The final residuals were $R_F = 0.026$ and $R_{wF^2} = 0.028$ for 1706 observed data with $I \geqslant 3\sigma(I)$.

Supplementary materials including non-hydrogen and hydrogen atomic coordinates, bond lengths and angles, and thermal parameters have been

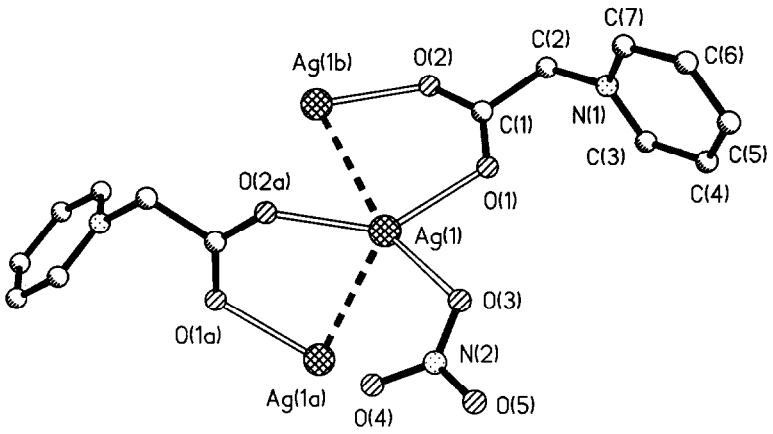

Fig. 2. Perspective view showing the coordination environment of the metal atom in $[Ag(pyBET)(NO_3)]_n$ (**3**) and the atom numbering scheme. Symmetry codes are given in Table 1.

deposited at the Cambridge Crystallographic Data Centre, and observed and calculated structure factors are available upon request from the corresponding author.

RESULTS AND DISCUSSION

As illustrated in Fig. 2, the silver(I) atom in complex (**3**) is coordinated by three oxygen atoms in a nearly planar and distorted trigonal environment. The two metal–ligand bonds involving different carboxylato groups of pyBET ligands [Ag(1)—O(1) = 2.334(3), Ag(1)—O(2a) = 2.289(3) Å] are slightly longer than those [Ag—O(carboxy) = 2.211(6), 2.220(6) Å] found in $[Ag_2(pyBET)_2(ClO_4)_2]_n$ (**2**),[4] and the third linked to a nitrate group [Ag(1)—O(3) = 2.434(3) Å] is shorter than those of axially bonded nitrate groups in the dimeric structure of alanine silver(I) nitrate [2.58(3) Å].[11] There is no other Ag—O contact less than 2.75 Å in the crystal structure. Each pair of adjacent silver(I) atoms are bridged in the *syn–syn* mode by the carboxylato group of a *single* pyBET ligand, resulting in a zigzag polymeric chain running parallel to the 2_1 axis. The metal–metal separation of 3.011(1) Å is significantly larger than the average value (*ca* 2.9 Å) found in dimeric silver(I) carboxylates.[4]

It is worthy of note that the present structure (**3**) is distinct from those of two related silver(I) betaine complexes, $[Ag_2(BET)_2(H_2O)_2(NO_3)_2]_n$ (**1**) and $[Ag_2(pyBET)_2(ClO_4)_2]_n$ (**2**), both of which adopt the modified Type D structure[4] [Fig. 1(e)]. Furthermore, complex (**3**) is different from all the other known silver(I) complexes containing related ligands such as the zwitterionic amino acids; for example, alanine silver(I) nitrate[11] and glycine silver(I) nitrate[12] both have dimeric structures of Type B and D, respectively.

The coordination motif in complex (**3**) is also different from that in the zigzag chain occurring in silver(I) (4-chloro-2-methylphenoxy)acetate,[2] where the silver(I) atom is linearly coordinated by

Table 1. Selected bond distances (Å) and bond angles (°)

Ag(1)—O(1)	2.334(3)	Ag(1)—O(2a)	2.289(3)
Ag(1)—O(3)	2.434(3)		
O(3)—Ag(1)—O(1)	86.0(1)	O(3)—Ag(1)—O(2a)	118.3(1)
O(1)—Ag(1)—O(2a)	139.8(1)	Ag(1)—O(3)—N(2)	119.1(2)
Ag(1)—O(1)—C(1)	120.0(2)	C(1)—O(2)—Ag(1b)	127.0(2)
O(1)—C(1)	1.243(4)	O(2)—C(1)	1.263(4)
C(1)—C(2)	1.527(5)	C(2)—N(1)	1.477(4)
O(1)—C(1)—O(2)	128.3(3)	O(1)—C(1)—C(2)	118.6(3)
O(2)—C(1)—C(2)	113.1(3)	C(1)—C(2)—N(1)	112.9(2)

Symmetry codes: *a* $1-x, -\frac{1}{2}+y, \frac{1}{2}-z$; *b* $1-x, \frac{1}{2}+y, \frac{1}{2}-z$.

two oxygen atoms from different carboxylato groups and extended into a one-dimensional polymeric structure through *syn–anti* bridges [Fig. 1(f)]. Thus complex (**3**) is a new structural variety among silver(I) carboxylates and related complexes [Fig. 1(g)].

REFERENCES

1. T. C. W. Mak, W. H. Yip, C. H. L. Kennard, G. Smith and E. J. O'Reilly, *Aust. J. Chem.* 1986, **39**, 541.
2. G. Smith, C. H. L. Kennard and T. C. W. Mak, *Z. Kristallogr.* 1988, **184**, 275.
3. Part VII. X.-M. Chen and T. C. W. Mak, *Inorg. Chim. Acta.* 1991, in press.
4. X.-M. Chen and T. C. W. Mak, *J. Chem. Soc., Dalton Trans.* 1991, 1219.
5. X.-M. Chen and T. C. W. Mak, *J. Cryst. Spectrosc. Res.* 1991, **21**, 27.
6. G. B. Deacon and R. J. Philips, *Coord. Chem. Rev.* 1980, **33**, 227.
7. R. A. Sparks, *Crystallographic Computing Techniques* (Edited by F. R. Ahmed), p. 452. Munksgaard, Copenhagen (1976).
8. G. M. Sheldrick, *Computational Crystallography* (Edited by D. Sayre), p. 506. Oxford University Press, New York (1982).
9. G. M. Sheldrick, *Crystallographic Computing 3: Data Collection, Structure Determination, Proteins, and Databases* (Edited by G. M. Sheldrick, C. Krüger and R. Goddard), p. 175. Oxford University Press, New York (1982).
10. *International Tables for X-ray Crystallography*, Vol. IV, pp. 55, 99, 149. Kynoch Press, Birmingham (now distributed by Kluwer Academic Publishers, Dordrecht, The Netherlands) (1974).
11. M. E. Kamwaya, R. Papavinasam, S. G. Teoh and R. K. Rajaram, *Acta Cryst.* 1985, **40C**, 1318.
12. J. K. M. Rao and M. A. Viswamitra, *Acta Cryst.* 1972, **28B**, 1484.

Polyhedron Vol. 10, No. 15, pp. 1727–1732, 1991
Printed in Great Britain

0277–5387/91 $3.00+.00
© 1991 Pergamon Press plc

THE REACTIONS OF $[Ru(\eta^6\text{-arene})Cl_2]_2$ COMPOUNDS WITH A SERIES OF AMINOPYRIDINE LIGANDS: X-RAY CRYSTAL STRUCTURES OF $[Ru(\eta^6\text{-}1,4\text{-}MeC_6H_4CHMe_2)Cl_2(NC_5H_4NH_2)]$ AND $[Ru(\eta^6\text{-}C_{16}H_{16})Cl_2(NC_5H_4NH_2)]$

REES ARONSON, MARK R. J. ELSEGOOD, JONATHAN W. STEED and DEREK A. TOCHER*

Department of Chemistry, University College London, 20 Gordon Street, London WC1H 0AJ, U.K.

(*Received* 3 *January* 1991; *accepted* 21 *March* 1991)

Abstract—The reactions of the dimers $[Ru(\eta^6\text{-arene})Cl_2]_2$ (arene = C_6H_6, 1,4-$MeC_6H_4CHMe_2$, [2.2](1,4)$C_{16}H_{16}$) with a range of aminopyridine ligands have been investigated. These ligands can potentially coordinate to a single metal centre in a monodentate fashion through either pyridyl or amino nitrogen atoms, can chelate a single metal centre, or can bridge across two metal ions. Spectroscopic data collected on 12 compounds is exclusively consistent with monodentate coordination via the pyridyl nitrogen atoms. This mode of coordination has been conclusively established by X-ray structure determinations of the compounds $[Ru(\eta^6\text{-}1,4\text{-}MeC_6H_4CHMe_2)Cl_2(NC_5H_4NH_2)]$ and $Ru(\eta^6\text{-}C_{16}H_{16})Cl_2(NC_5H_4NH_2)]$.

Recently we reported the results of our investigations into the reactions of $[Ru(\eta^6\text{-}C_6H_6)Cl_2]_2$ and $[Ru(\eta^6\text{-}C_6H_6)Cl(O_2CCF_3)]$ with α-pyridone and related ligands.[1] Coordination of this series of ligands was almost exclusively of the bidentate type to a single metal centre. In only one instance was monodentate coordination, via the pyridone oxygen atom, observed. Other workers[2] have observed bidentate coordination of the hydroxypyridinate anion in the compound $[Ru(\eta^6\text{-}MeC_6H_4CHMe_2)Cl(NC_5H_4O)]$. In an extension to that earlier work we have examined the reactions of 2-aminopyridine and several variously substituted derivatives with several $[Ru(\eta^6\text{-arene})Cl_2]_2$ compounds, including the paracyclophane compound $[Ru(\eta^6\text{-}[2_2](1,4)C_{16}H_{16})Cl_2]_2$, whose chemistry we are currently studying intensively.[3–5]

EXPERIMENTAL

Microanalyses were carried out by the Chemistry Department of University College London. NMR spectra were obtained on Varian XL-200 and VXR-400 spectrometers (chemical shifts quoted in ppm with positive values to high frequency of $SiMe_4$). IR spectra were recorded in the range 4000–200 cm^{-1} on a Perkin–Elmer 983 spectrophotometer using Nujol mulls on CsI plates.

Materials

The compounds $[Ru(\eta^6\text{-arene})Cl_2]_2$ (arene = C_6H_6, 1,4-$MeC_6H_4CHMe_2$, [2.2](1,4)$C_{16}H_{16}$) were prepared by published literature methods.[6–8] All other reagents were obtained from normal commercial suppliers. All reactions were carried out in degassed solvents under a nitrogen atmosphere.

$[Ru(\eta^6\text{-}C_6H_6)Cl_2(NC_5H_4NH_2)]$

A solution of 2-aminopyridine (0.11 g, 2.2 mmol) in toluene (5 cm^3) was added to a suspension of $[Ru(\eta^6\text{-}C_6H_6)Cl_2]_2$ (0.1 g, 0.2 mmol) in toluene (15 cm^3) and the mixture stirred for 12 h at room temperature. The red–orange product was filtered off, washed with diethyl ether and methanol, and then dried *in vacuo* for 4 h. Yield 36%. IR spectrum ν(N—H) 3287, 3179 cm^{-1}, ν(Ru—Cl) 278 cm^{-1}.

* Author to whom correspondence should be addressed.

Each of the following compounds were prepared in an analogous manner.

$[Ru(\eta^6\text{-}C_6H_6)Cl_2(NC_5H_3CH_3NH_2)]$

Yield 50%. IR spectrum ν(N—H) 3295, 3183 cm^{-1}, ν(Ru—Cl) 291 cm^{-1}.

$[Ru(\eta^6\text{-}C_6H_6)Cl_2(NC_5H_4NHC_6H_5)]$

Yield 26%. IR spectrum ν(N—H) 3234 cm^{-1}, ν(Ru—Cl) 282 cm^{-1}.

$[Ru(\eta^6\text{-}C_6H_6)Cl_2(NC_5H_4NHCH_2C_6H_5)]$

Yield 66%. IR spectrum ν(N—H) 3298 cm^{-1}, ν(Ru—Cl) 278 cm^{-1}.

$[Ru(\eta^6\text{-}MeC_6H_4CHMe_2)Cl_2(NC_5H_4NH_2)]$

Yield 46%. IR spectrum ν(N—H) 3278, 3174 cm^{-1}, ν(Ru—Cl) 282 cm^{-1}.

$[Ru(\eta^6\text{-}MeC_6H_4CHMe_2)Cl_2(NC_5H_3CH_3NH_2)]$

Yield 47%. IR spectrum ν(N—H) 3302, 3235 cm^{-1}, ν(Ru—Cl) 287 cm^{-1}.

$[Ru(\eta^6\text{-}MeC_6H_4CHMe_2)Cl_2(NC_5H_4NHC_6H_5)]$

Yield 69%. IR spectrum ν(N—H) 3229 cm^{-1}, ν(Ru—Cl) 281 cm^{-1}.

$[Ru(\eta^6\text{-}MeC_6H_4CHMe_2)Cl_2(NC_5H_4NHCH_2C_6H_5)]$

Yield 76%. IR spectrum ν(N—H) 3243 cm^{-1}, ν(Ru—Cl) 283 cm^{-1}.

$[Ru(\eta^6\text{-}C_{16}H_{16})Cl_2(NC_5H_4NH_2)]$

Yield 70%. IR spectrum ν(N—H) 3281, 3160 cm^{-1}, ν(Ru—Cl) 297 cm^{-1}.

$[Ru(\eta^6\text{-}C_{16}H_{16})Cl_2(NC_5H_3CH_3NH_2)]$

Yield 94%. IR spectrum ν(N—H) 3306, 3192 cm^{-1}, ν(Ru—Cl) 300 cm^{-1}.

$[Ru(\eta^6\text{-}C_{16}H_{16})Cl_2(NC_5H_4NHC_6H_5)]$

Yield 65%. IR spectrum ν(N—H) 3195 cm^{-1}, ν(Ru—Cl) 297 cm^{-1}.

$[Ru(\eta^6\text{-}C_{16}H_{16})Cl_2(NC_5H_4NHCH_2C_6H_5)]$

Yield 44%. IR spectrum ν(N—H) 3290 cm^{-1}, ν(Ru—Cl) 288 cm^{-1}.

Tables 1 and 2 contain microanalytical and ^1H NMR data for the 12 new compounds.

X-ray studies

The structures of $[Ru(\eta^6\text{-}MeC_6H_4CHMe_2)Cl_2(NC_5H_4NH_2)]$ and $[Ru(\eta^6\text{-}C_{16}H_{16})Cl_2(NC_5H_4NH_2)]$ were determined using general procedures which have been described previously.[9,10] The structures were solved routinely by direct methods and refined, with all non-hydrogen atoms anisotropic, by full-matrix least-squares. Hydrogen atoms were not included in the refinement. In the latter cycles of the refinement of the structure of $[Ru(\eta^6\text{-}C_{16}H_{16})Cl_2(NC_5H_4NH_2)]$, a methanol of crystallization was located on the four-fold axis at $\frac{1}{4}, \frac{1}{4}, y$ and subsequently included in the refinement. Pertinent crystallographic data are

Table 1. Microanalytical data for some ruthenium(II) compounds

Compound	Analyses [Found(calc.)(%)] C	H	N	Cl
$[Ru(\eta^6\text{-}C_6H_6)Cl_2(NC_5H_4NH_2)]$	37.4(38.4)	3.4(3.5)	7.9(8.1)	20.9(20.6)
$[Ru(\eta^6\text{-}C_6H_6)Cl_2(NC_5H_3CH_3NH_2)]$	40.1(40.2)	3.6(3.9)	7.4(7.8)	19.6(19.8)
$[Ru(\eta^6\text{-}C_6H_6)Cl_2(NC_5H_4NHC_6H_5)]$	47.8(48.3)	3.4(3.8)	6.7(7.0)	17.3(16.8)
$[Ru(\eta^6\text{-}C_6H_6)Cl_2(NC_5H_4NHCH_2C_6H_5)]$	49.6(49.8)	3.9(4.1)	5.9(6.4)	16.7(16.3)
$[Ru(\eta^6\text{-}MeC_6H_4CHMe_2)Cl_2(NC_5H_4NH_2)]$	44.7(45.0)	4.7(5.0)	7.4(7.0)	17.1(17.6)
$[Ru(\eta^6\text{-}MeC_6H_4CHMe_2)Cl_2(NC_5H_3CH_3NH_2)]$	46.3(46.2)	5.1(5.3)	6.9(6.9)	16.8(17.1)
$[Ru(\eta^6\text{-}MeC_6H_4CHMe_2)Cl_2(NC_5H_4NHC_6H_5)]$	53.3(53.8)	5.2(5.6)	5.6(5.7)	15.2(14.9)
$[Ru(\eta^6\text{-}MeC_6H_4CHMe_2)Cl_2(NC_5H_4NHCH_2C_6H_5)]$	53.0(53.7)	5.2(5.6)	5.5(5.7)	14.7(14.4)
$[Ru(\eta^6\text{-}C_{16}H_{16})Cl_2(NC_5H_4NH_2)]$	52.3(53.1)	4.5(4.7)	5.4(5.9)	
$[Ru(\eta^6\text{-}C_{16}H_{16})Cl_2(NC_5H_3CH_3NH_2)]$	53.6(54.1)	4.9(4.9)	5.7(5.7)	
$[Ru(\eta^6\text{-}C_{16}H_{16})Cl_2(NC_5H_4NHC_6H_5)]$	58.1(58.9)	4.6(4.7)	4.6(5.1)	
$[Ru(\eta^6\text{-}C_{16}H_{16})Cl_2(NC_5H_4NHCH_2C_6H_5)]$	58.8(59.6)	4.9(5.0)	4.4(5.0)	

Table 2. ^1H NMR data for some ruthenium(II) compounds at 298 K in $CDCl_3$

Compound	δ (ppm) η-Arene	Aminopyridine
$[Ru(\eta^6\text{-}C_6H_6)Cl_2(NC_5H_4NH_2)]$	5.68(s)	8.55(d), 7.34(t), 6.65(t), 6.50(d), 6.06(s, NH_2)
$[Ru(\eta^6\text{-}C_6H_6)Cl_2(NC_5H_3CH_3NH_2)]$	5.67(s)	8.68(d), 7.23(d), 6.78(t), 6.08(s, NH_2), 2.15(s)
$[Ru(\eta^6\text{-}C_6H_6)Cl_2(NC_5H_4NHC_6H_5)]$	5.75(s)	8.84(d), 7.22(m, br), 6.75(t), 9.78(s, NH)
$[Ru(\eta^6\text{-}C_6H_6)Cl_2(NC_5H_4NHCH_2C_6H_5)]$	5.65(s)	8.74(d), 8.11(t, NH), 7.43(t), 7.36(m), 6.59(t), 6.43(d), 4.41(d)
$[Ru(\eta^6\text{-}MeC_6H_4CHMe_2)Cl_2(NC_5H_4NH_2)]$	5.48, 5.33(AB), 2.94(sp), 1.26(d), 1.61(s)	8.57(d), 7.36(t), 6.58(t), 6.50(d), 6.06(s, NH_2)
$[Ru(\eta^6\text{-}MeC_6H_4CHMe_2)Cl_2(NC_5H_3CH_3NH_2)]$	5.43, 5.30(AB), 2.96(sp), 1.62(s), 1.26(d)	8.86(d), 7.23(t), 6.78(d), 6.08(s, NH_2), 2.19(s)
$[Ru(\eta^6\text{-}MeC_6H_4CHMe_2)Cl_2(NC_5H_4NHC_6H_5)]$	5.42, 5.30(AB), 2.96(sp), 1.63(s), 1.28(d)	9.78(s, NH), 8.81(d), 7.21(m), 6.73(t)
$[Ru(\eta^6\text{-}MeC_6H_4CHMe_2)Cl_2(NC_5H_4NHCH_2C_6H_5)]$	5.40, 5.28(AB), 2.96(sp), 1.61(s), 1.26(d)	8.73(d), 8.10(t, NH), 7.35(m), 6.57(t), 6.41(d), 1.50(d)
$[Ru(\eta^6\text{-}C_{16}H_{16})Cl_2(NC_5H_4NH_2)]$	6.85(s), 4.97(s), 3.19, 2.74(AA'XX')	8.32(d), 7.45(t), 6.61(d), 6.51(t), 6.13(s, NH_2)
$[Ru(\eta^6\text{-}C_{16}H_{16})Cl_2(NC_5H_3CH_3NH_2)]$	6.85(s), 4.96(s), 3.19, 2.72(AA'XX')	8.23(d), 7.33(t), 6.46(d), 6.12(s, NH_2)
$[Ru(\eta^6\text{-}C_{16}H_{16})Cl_2(NC_5H_4NHC_6H_5)]$	6.83(s), 5.44(s), 3.16, 2.70(AA'XX')	8.54(d), 7.58(t), 7.35(m), 7.05(d), 6.70(t), 9.51(s, NH)
$[Ru(\eta^6\text{-}C_{16}H_{16})Cl_2(NC_5H_4NHCH_2C_6H_5)]$	6.70(s), 4.84(s), 3.07, 2.64(AA'XX')	8.52(d), 7.30(m), 6.45(t), 6.29(d), 7.76(t, NH)

included in Table 3. Tables 4 and 5 contain selected bond lengths and bond angles for $[Ru(\eta^6\text{-}MeC_6H_4CHMe_2)Cl_2(NC_5H_4NH_2)]$ and $[Ru(\eta^6\text{-}C_{16}H_{16})Cl_2(NC_5H_4NH_2)]$, respectively. Crystallographic calculations used the SHELXTL PLUS program package.[11]

Final atomic coordinates, full listings of bond lengths and angles, thermal parameters and structure factor tables have been deposited with the Editor, and with the Cambridge Crystallographic Data Centre, as supplementary material.

RESULTS AND DISCUSSION

Orange or red, microcrystalline compounds of general formula $[Ru(\eta^6\text{-arene})Cl_2(Hap)]$ (arene = C_6H_6, 1,4-$MeC_6H_4CHMe_2$, $C_{16}H_{16}$; Hap = 2-aminopyridine, 2-amino-3-picoline, 2-benzylaminopyridine, 2-anilinopyridine) have been prepared by the reaction of the dinuclear compounds $[Ru(\eta^6\text{-arene})Cl_2]_2$ with an excess of the appropriate ligand in toluene. Non-polar solvents have frequently been employed in the past to give a wide range of $[Ru(\eta^6\text{-arene})Cl_2L]$ (L = pyridine, tertiary phosphines, etc.) compounds.[12,13] However, when polar solvents have been employed, cationic products, $[Ru(\eta^6\text{-arene})ClL_2]^+$, have usually been formed. Alternatively, if the incoming ligand can be deprotonated, e.g. a carboxylic acid, then a neutral compound such as $[Ru(\eta^6\text{-}C_6H_6)Cl(O_2CCF_3)]$[14] is often formed. Surprisingly the products which were isolated when we reacted $[Ru(\eta^6\text{-arene})Cl_2]_2$ compounds with this series of Hap ligands in methanol were almost invariably identical to those obtained from the non-polar solvent, although admittedly the isolated yield was often smaller. This was particularly surprising given that previously we have been able to prepare a range of neutral compounds of the type $[Ru(\eta^6\text{-arene})Cl(hp)]$[1,15] (Hhp = 2-hydroxypyridine, 6-methyl-2-hydroxypidine, 6-chloro-2-hydroxypyridine) by using precisely these reaction conditions. The differences in reactivity can most likely be explained by invoking the appreciably lower acidity of the amino protons in these ligands, when compared with the hydroxyl protons on the

Table 3. Crystallographic data for $[Ru(\eta^6\text{-}1,4\text{-}MeC_6H_4CHMe_2)Cl_2(NC_5H_4NH_2)]$ (**1**) and $[Ru(\eta^6\text{-}C_{16}H_{16})Cl_2(NC_5H_4NH_2)]CH_3OH$ (**2**)

	1	**2**
Formula	$C_{15}H_{20}N_2Cl_2Ru$	$C_{22}H_{26}N_2OCl_2Ru$
Formula weight	400.34	506.47
Space-group	$P2_12_12_1$	$P4/n$
a (Å)	9.527(2)	21.116(3)
b (Å)	12.265(2)	21.116(3)
c (Å)	14.210(2)	9.128(1)
α (°)	90	90
β (°)	90	90
γ (°)	90	90
V (Å^3)	1660	4069
Z	4	8
$F(000)$	808	2064
d_{calc} (g cm^{-3})	1.60	1.65
Crystal size (mm)	$0.20\times0.26\times0.45$	$0.06\times0.15\times0.55$
μ(Mo-K_α) (cm^{-1})	12.4	10.4
Data collection instrument	Nicolet R3mV	
Radiation	Mo-K_α (λ = 0.71073 Å)	
Orientation reflections: number, range (2θ)	30, $16 \leqslant 2\theta \leqslant 29°$	30, $16 \leqslant 2\theta \leqslant 26°$
Temperature (K)	292	
Unique data measured	1613	3524
Number of unique with $I \geqslant 3.0\sigma(I)$	1534	1949
Number of parameters	181	241
R^a	0.0303	0.0506
$R_w{}^b$	0.0329	0.0620
Weighting scheme	$w^{-1} = \sigma^2(F)+0.00039F^2$	$w^{-1} = \sigma^2(F)+0.00611F^2$
Largest shift/ESD, final cycle	0.01	0.01
Largest peak (e/Å^3)	0.42	0.90

[a] $R = \Sigma[|F_o| - |F_c|]/\Sigma|F_o|$.
[b] $R_w = \Sigma w^{1/2}[|F_o| - |F_c|]/\Sigma w^{1/2}|F_o|$.

various hydroxypyridine ligands used in our earlier study. Given that each of the aminopyridine ligands employed in this study only coordinates unidentately to a ruthenium(II) centre, then there are two potential ligand donor atoms, namely the amino and pyridyl nitrogen atoms. Although it is known[16,17] that ammonia will bind to a "Ru(η^6-arene)" fragment, there are few examples of other coordinated amines in this area of chemistry. In contrast, there are numerous examples of co-ordinated pyridines or pyridyl ligands. Comparison of the H NMR signals from free and coordinated Hap ligands strongly suggested that coordination to the metal was via the pyridyl nitrogen atoms.

Table 4. Selected bond lengths (Å) and bond angles (°) for $[Ru(\eta^6\text{-}1,4\text{-}MeC_6H_4CHMe_2)Cl_2(NC_5H_4NH_2)]$

Bond lengths			
Ru(1)—Cl(1)	2.409(2)	Ru(1)—Cl(2)	2.421(2)
Ru(1)—N(1)	2.160(6)	Ru(1)—C(1)	2.198(7)
Ru(1)—C(2)	2.177(7)	Ru(1)—C(3)	2.160(6)
Ru(1)—C(4)	2.220(7)	Ru(1)—C(5)	2.181(6)
Ru(1)—C(6)	2.178(6)	N(1)—C(11)	1.391(9)
N(1)—C(15)	1.357(9)	N(2)—C(15)	1.377(10)
Bond angles			
Cl(1)—Ru(1)—Cl(2)	85.6(1)	Cl(1)—Ru(1)—N(1)	87.3(1)
Cl(2)—Ru(1)—N(1)	88.6(1)	Ru(1)—N(1)—C(15)	125.4(5)
N(1)—C(15)—N(2)	117.9(6)		

Table 5. Selected bond lengths (Å) and bond angles (°) for $[Ru(\eta^6\text{-}C_{16}H_{16})Cl_2(NC_5H_4NH_2)]$

	Bond lengths		
Ru(1)—Cl(1)	2.405(3)	Ru(1)—Cl(2)	2.402(3)
Ru(1)—C(1)	2.337(9)	Ru(1)—C(2)	2.226(9)
Ru(1)—C(3)	2.146(9)	Ru(1)—C(4)	2.260(8)
Ru(1)—C(5)	2.131(9)	Ru(1)—C(6)	2.159(10)
Ru(1)—N(1)	2.121(7)	N(1)—C(17)	1.374(13)
N(1)—C(21)	1.344(13)	N(2)—C(21)	1.377(17)
	Bond angles		
Cl(1)—Ru(1)—Cl(2)	85.7(1)	Cl(1)—Ru(1)—N(1)	85.7(2)
Cl(2)—Ru(1)—N(1)	92.5(2)	Ru(1)—N(1)—C(21)	125.5(7)
N(1)—C(21)—N(2)	117.3(10)		

This was conclusively established by single crystal X-ray diffraction experiments on $[Ru(\eta^6\text{-}1,4\text{-}MeC_6H_4CHMe_2)Cl_2(NC_5H_4NH_2)]$ and $[Ru(\eta^6\text{-}C_{16}H_{16})Cl_2(NC_5H_4NH_2)]$.

X-ray crystal structures of $[Ru(\eta^6\text{-}1,4\text{-}MeC_6H_4CHMe_2)Cl_2(NC_5H_4NH_2)]$ *and* $[Ru(\eta^6\text{-}C_{16}H_{16})Cl_2(NC_5H_4NH_2)]$

The molecular structures of $[Ru(\eta^6\text{-}1,4\text{-}MeC_6H_4CHMe_2)Cl_2(NC_5H_4NH_2)]$ and $[Ru(\eta^6\text{-}C_{16}H_{16})Cl_2(NC_5H_4NH_2)]$ are shown in Figs 1 and 2, respectively. Important bond lengths and bond angles are presented in Tables 4 and 5. The geometry about each ruthenium ion is that of a distorted octahedron with the η-arene ring and the other ligands adopting a "piano stool" configuration. Both the complexes have an overall geometry similar to that of several $[Ru(\eta^6\text{-arene})Cl_2L]$ and $[Ru(\eta^6\text{-arene})ClL_2]^+$ species[1-3,17,18] described previously. The two Ru—N distances are closely similar, however there are significant variations in the Ru—Cl distances. In particular, the two Ru—Cl distances, 2.409(2) and 2.421(2) Å, in the compound $[Ru(\eta^6\text{-}1,4\text{-}MeC_6H_4CHMe_2)Cl_2(NC_5H_4NH_2)]$ are statistically different. Both chloride ligands are involved in hydrogen bonding to amino nitrogen atoms. The ligand Cl(1) is involved in an intermolecular hydrogen bond of 3.23 Å, while Cl(2) forms an intramolecular hydrogen bond, of 3.24 Å, to N(2). In contrast, only Cl(2) is involved in intramolecular hydrogen bonding, to N(2), 3.16 Å, in $[Ru(\eta^6\text{-}C_{16}H_{16})Cl_2(NC_5H_4NH_2)]$, and the two Ru—Cl bond distances in this molecule are indistinguishable.

In $[Ru(\eta^6\text{-}1,4\text{-}MeC_6H_4CHMe_2)Cl_2(NC_5H_4NH_2)]$ the Ru—C distances lie in the range 2.16–2.22 Å, and the ring centroid is 1.67 Å from the ruthenium ion. Similar distances are observed in the ruthenium(II) *p*-cymene complexes $[Ru(\eta^6\text{-}1,4\text{-}MeC_6H_4CHMe_2)Cl(hp)]^2$, $[Ru(\eta^6\text{-}1,4\text{-}MeC_6H_4CHMe_2)Cl(pyz)_2][PF_6]$[14] and $[Ru_2(\eta^6\text{-}1,4\text{-}MeC_6H_4CHMe_2)_2(\mu\text{-}Cl)_3][BPh_4]$.[19] The C—C bond length alternation which has been observed in several other studies on η^6-arenes coordinated to transition metal ions[18,20] is not readily apparent in this

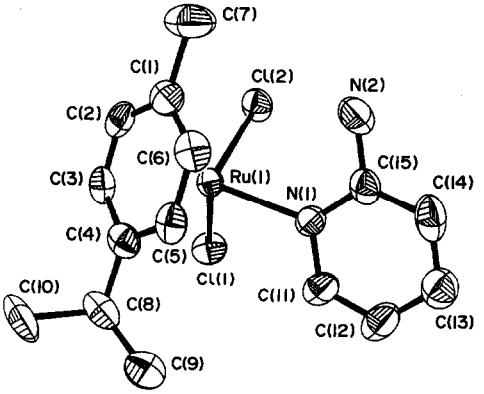

Fig. 1. Thermal ellipsoid plot of the $[Ru(\eta^6\text{-}1,4\text{-}MeC_6H_4CHMe_2)Cl_2(NC_5H_4NH_2)]$ molecule. Atoms are represented by thermal vibration ellipsoids at the 50% confidence level, and the atom-labelling scheme is defined.

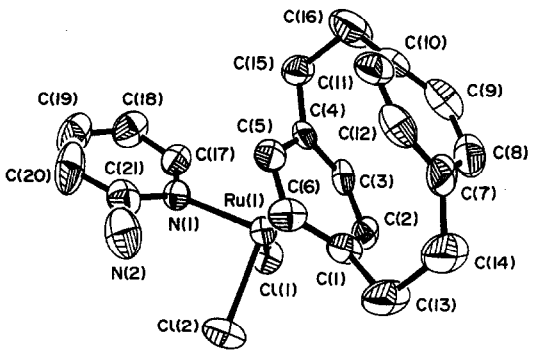

Fig. 2. Thermal ellipsoid plot of the $[Ru(\eta^6\text{-}C_{16}H_{16})Cl_2(NC_5H_4NH_2)]$ molecule. Atoms are represented by thermal vibration ellipsoids at the 50% confidence level, and the atom-labelling scheme is defined.

study. The methyl and isopropyl groups are bent towards the ruthenium ion by 2.3 and 3.4°, respectively. The isopropyl group is not symmetrically placed with respect to the C_6 ring but forms a torsion angle, C(5)—C(4)—C(8)—C(9) = 14.7°, with the mean plane.

In [Ru(η^6-$C_{16}H_{16}$)Cl_2($NC_5H_4NH_2$)] the Ru—C distances fall into two sets; there are four short bonds, to C(2), C(3), C(5) and C(6), 2.13–2.22 Å, and two long bonds to the bridgehead carbons C(1) and C(4), 2.337(9) and 2.260(8) Å, respectively. This variation in metal–carbon bond length is attributed to the presence of the two ethylenic bridges between the aromatic decks of the cyclophane and has been commented on in several previous reports.[3–5,21,22] Indeed, it is a feature of the free ligand, as well as its metal complexes, that the aromatic rings are non-planar. The two bridgehead carbon atoms of the coordinated deck lie, on average, 0.18 Å above the mean plane of the other four coordinated carbon atoms, while the two bridgehead carbons of the non-coordinated deck lie *ca* 0.15 Å below the plane defined by the remaining four carbon atoms of the second deck. It is also noteworthy that the two Ru—C bonds *trans* to the pyridyl nitrogen atom are significantly lengthened with respect to the remaining four Ru—C bonds. Similar observations have been made on the Ru—C bonds *trans* to the tertiary phosphine ligands in the compounds [Ru(η^6-arene)Cl_2(PMe_2Ph)].[18] The two decks are not precisely eclipsed with respect to each other. There is an average torsion angle in the ethylenic bridges of 4.4°. This compares with an estimated value of *ca* 3.2° in the disordered structure of the free ligand.[23] The shallow boat conformation of the free ligand has been ascribed to electronic interactions between the stacked decks. On coordination to a metal ion these unfavourable interactions are reduced and the separation between decks is decreased from 3.09 Å, in the non-coordinated ligand, to 2.99 Å for this compound.

The molecular parameters of the coordinated 2-aminopyridine ligands in the two structures are not significantly different from each other.

Acknowledgements—We thank Johnson–Matthey plc for generous loans of ruthenium trichloride and the SERC for financial support (M.R.J.E.) and for provision of the X-ray diffractometer.

REFERENCES

1. E. C. Morrison, C. A. Palmer and D. A. Tocher, *J. Organomet. Chem.* 1988, **349**, 405.
2. P. Laheurta, J. Latorre, M. Sanau, F. A. Cotton and W. Schwotzer, *Polyhedron* 1988, 7, 1311.
3. M. R. J. Elsegood and D. A. Tocher, *J. Organomet. Chem.* 1988, **356**, C29.
4. M. R. J. Elsegood and D. A. Tocher, *Inorg. Chim. Acta* 1989, **161**, 147.
5. M. R. J. Elsegood and D. A. Tocher, *J. Organomet. Chem.* 1990, **391**, 239.
6. M. A. Bennett and T. W. Matheson, *J. Organomet. Chem.* 1979, **175**, 87.
7. R. T. Swann, A. W. Hanson and V. Beokelheide, *J. Am. Chem. Soc.* 1986, **108**, 3324.
8. T. Arthur and T. A. Stephenson, *J. Organomet. Chem.* 1981, **208**, 369.
9. E. C. Constable, R. P. G. Henney, T. A. Leese and D. A. Tocher, *J. Chem. Soc., Dalton Trans.* 1990, 443.
10. E. C. Constable, S. M. Elder, J. Healy and D. A. Tocher, *J. Chem. Soc., Dalton Trans.* 1990, 1669.
11. G. M. Sheldrick, SHELXTL PLUS, An Integrated System for Refining and Displaying Crystal Structures from Diffraction Data. University of Göttingen, F.R.G. (1986).
12. P. M. Maitlis, *Chem. Soc. Rev.* 1981, **10**, 1.
13. M. A. Bennett, *Comprehensive Organometallic Chemistry*, Vol. IV, Ch. 32. Pergamon Press, Oxford (1982).
14. D. A. Tocher, R. O. Gould, T. A. Stephenson, M. A. Bennett, J. P. Ennett, T. W. Matheson, L. Sawyer and V. K. Shah, *J. Chem. Soc., Dalton Trans.* 1983, 1571.
15. C. A. Palmer, Final Year Project Report. University College London (1987).
16. D. R. Robertson, T. A. Stephenson and T. A. Arthur, *J. Organomet. Chem.* 1978, **162**, 121.
17. R. O. Gould, C. L. Jones, D. R. Robertson and T. A. Stephenson, *Cryst. Struct. Commun.* 1978, **7**, 27.
18. M. A. Bennett, J. P. Ennett and K. I. Gell, *J. Organomet. Chem.* 1972, **43**, C41.
19. D. A. Tocher and M. D. Walkinshaw, *Acta Cryst.* 1982, **B38**, 3083.
20. S. F. Watkins and F. R. Fronczek, *Acta Cryst.* 1982, **B38**, 270.
21. R. T. Swann, A. W. Hanson and V. Boekelheide, *J. Am. Chem. Soc.* 1986, **108**, 3324.
22. Y. Kai, N. Yasuoka and N. Kasai, *Acta Cryst.* 1978, **B34**, 2840.
23. H. Hope, J. Bernstein and K. N. Trueblood, *Acta Cryst.* 1972, **B28**, 1733.

Polyhedron Vol. 10, No. 15, pp. 1733–1739, 1991
Printed in Great Britain

0277–5387/91 $3.00+.00
© 1991 Pergamon Press plc

SYNTHETIC, SPECTROSCOPIC AND MAGNETIC STUDIES OF HETEROMETAL ALKOXIDES OF COBALT(II), NICKEL(II) AND COPPER(II) CONTAINING THE STERICALLY CROWDED TETRAALKOXOALUMINATE LIGAND

G. GARG, R. K. DUBEY, A. SINGH and R. C. MEHROTRA*

Department of Chemistry, University of Rajasthan, Jaipur 302004, India

(*Received* 15 *October* 1990; *accepted* 5 *April* 1991)

Abstract—Heterobimetallic alkoxides of the types $[ClM\{Al(OBu^t)_4\}]$ **(I)** and $[M\{Al(OBu^t)_4\}_2]$ **(II)** ($M = Co^{II}$, Ni^{II} and Cu^{II}) have been prepared by the interactions of MCl_2 with $K\{Al(OBu^t)_4\}$ in 1:1 and 1:2 molar ratios, respectively. These chloro(tetra-t-butoxoaluminato) complexes proved to be useful precursors for the synthesis of a variety of bimetallic alkoxo derivatives such as: $[(OBu^t)M\{Al(OBu^t)_4\}]$, $[\{Al(OEt)_4\}M\{Al(OBu^t)_4\}]$ and $[\{Al(OPr^i)_4\}M\{Al(OBu^t)_4\}]$. All these derivatives are highly moisture-sensitive, coloured solids or viscous liquids. Most of these are volatile except the mixed derivatives like $[ClM\{Al(OBu^t)_4\}]$ and $[(OBu^t)M\{Al(OBu^t)_4\}]$ which tend to disproportionate on heating. These heterometal alkoxides have been characterized by elemental analyses, spectroscopic (IR and visible) and magnetic studies, as well as molecular weight determinations.

Examples of heterometal alkoxides containing the isopropoxoaluminate ligand now include many of the possible combinations of metals[1–4] from group 3 to group 13. Earlier attempts to prepare bis(tetra-t-butoxoaluminato)cobalt,[5] -nickel[6] and -copper[7] by alcoholysis of analogous tetraisopropoxo derivatives $[M\{Al(OPr^i)_4\}_2]$ resulted in the replacement of only three of the four isopropoxide groups in the $\{Al(OPr^i)_4\}^-$ ligands with the formation of $[M\{Al(OPr^i)(OBu^t)_3\}_2]$. Additionally, our earlier findings have also shown that the corresponding alkoxoaluminate derivatives tend to show variation in their coordination state with the nature of the alkyl group. For example, the coordination number in $[Ni\{Al(OR)_4\}_2]$ tends to change from six to four as the R group is changed from methyl in $[\{Ni(\mu\text{-}OMe)_3Al(OMe)\}_2]$ to comparatively more sterically demanding isopropyl groups[6] in $[Ni\{(\mu\text{-}OPr^i)_2Al(OPr^i)_2\}_2]$.

We are, therefore, currently involved in the exploration of the possibility of synthesizing heterobimetallic alkoxides of the types $MCl_{n-x}\{Al(OBu^t)_4\}_x$ and $M\{Al(OBu^t)_4\}_n$ and in examining the effect of the $\{Al(OBu^t)_4\}^-$ group(s) on the stereochemistry of the metal in complexes formed by varied possible combinations with other alkoxo or alkoxometallate group(s). This paper, therefore, is concerned with the synthesis and characterization of heterometal alkoxides of cobalt(II), nickel(II) and copper(II) containing $\{Al(OBu^t)_4\}^-$ group(s).

EXPERIMENTAL

Stringent precautions were taken to exclude moisture throughout all the experimental procedures. Oven-dried (130–140°C) glass apparatus was used throughout all the experimental manipulations. Anhydrous metal chlorides were prepared in a current of dry HCl gas and analysed as reported earlier.[8,9]

Aluminium t-butoxide was prepared by the literature procedure.[10] The metal contents in the derivatives have been analysed as mixed oxides. Copper(II) in the complex was analysed volumetrically. Chloride was estimated by Volhard's method[11] and alcohols (ethanol and isopropanol) were estimated by an oxidimetric method.[12]

* Author to whom correspondence should be addressed.

Table 1. Spectral (IR and UV–vis) and magnetic moment data of heterobimetallic alkoxide derivatives

Compounds	IR (Nujol) (cm^{-1})	UV–vis (cm^{-1}) (solvent)	μ_{eff}
$[ClCo\{Al(OBu^t)_4\}]$ (**Ia**)	1020(m), 1050(m), 1090(m), 1180(m), 1210(m), 1230(m), ν(C—O)M; 530(s), 580(s), 670(m), ν(Al—O); 397(m); 395(m), 480(m), 490(s), 530(s), ν(Co—O); 264(m), 268(m), 272(m), 276(w), 282(m), 376(w), 384(w), ν(Co—Cl)	16,020; 16,890; 18,500; 20,000 (Benzene)	4.82
$[Co\{Al(OBu^t)_4\}_2]$ (**IIa**)	1080(s), 1205(s), ν(C—O)M; 580(s), 660(s), ν(Al—O); 460(s), ν(Co—O)	16,450; 17,300; 19,920 (Benzene)	4.85
$[ClNi\{Al(OBu^t)_4\}]$ (**Ib**)	940(m), 1020(m), 1130(m), 1205(m), 1220(m), 1250(w), ν(C—O)M; 660(m), 690(m), ν(Al—O); 390(m), 420(m), 470(s), 510(s), 540(s), 560(s), ν(Ni—O); 248(m), 260(m), 280(m), 300(m), 320(m), 360(m), 370(m), ν(Ni—Cl)	13,020; 17,120; 18,520; 23,150 (Benzene) 17,980; 18,939; 21,930 (Tetrahydrofuran) 16,440; 17,600; 22,730 (Pyridine) 16,500; 17,790; 22,935 (2,6-Dimethylpyridine)	3.88
$[Ni\{Al(OBu^t)_4\}_2]$ (**IIb**)	1050(m), 1205(s), 905(m), ν(C—O)M; 660(m), ν(Al—O); 490(s), ν(Ni—O)	17,480; 18,940; 24,750 (Benzene) 17,730; 19,080; 24,700 (Tetrahydrofuran) 17,120; 18,380; 23,360 (Pyridine) 17,120; 18,510; 23,150 (2,6-Dimethylpyridine)	3.91

$[(OBu^t)Co\{Al(OBu^t)_4\}]$ (**IIIa**)	920(m), 1080(s), 1205(s), ν(C—O)M; 660(m), ν(Al—O); 450(s), ν(Co—O)	14,530; 16,000; 17,800; 20,300	4.88
$[(OBu^t)Ni\{Al(OBu^t)_4\}]$ (**IIIb**)	940(m), 1020(m), 1130(m), 1220(m), 1250(w), ν(C—O)M; 660(m), ν(Al—O); 390(m), 420(m), 470(s), 510(s), 540(s), 560(s), ν(Ni—O)	14,285; 17,000; 18,315 (Benzene)	3.91
$[\{Al(OEt)_4\}Co\{Al(OBu^t)_4\}]$ (**IVa**)	1029(m), 1050(m), 1090(m), 1180(m), ν(C—O)M; 690(m), ν(Al—O); 395(m), 480(m), 490(s), ν(Co—O)	17,420; 18,940 (Benzene)	4.81
$[\{Al(OPr^i)_4\}Co\{Al(OBu^t)_4\}]$ (**Va**)	950(m), 1080(s), 1205(s), ν(C—O)M; 660(s), 680(m), ν(Al—O); 450(s), ν(Co—O)	14,970; 17,480; 19,085 (Benzene)	4.90
$[\{Al(OEt)_4\}Ni\{Al(OBu^t)_4\}]$ (**IVb**)	1020(s), 1250(s), ν(C—O)M; 665(s), ν(Al—O); 450(s), ν(Ni—O)	—	—
$[\{Al(OPr^i)_4\}Ni\{Al(OBu^t)_4\}$ (**Vb**)	1060(m), 1200(m), ν(C—O)M; 660(m), ν(Al—O); 470(s), ν(Ni—O)	17,120; 18,940; 25,000 (Benzene)	3.95
$[Cu\{Al(OBu^t)_4\}_2]$ (**IIc**)	920(s), 940(s), 1030(s), 1100(s), 1220(s), 1170(s), ν(C—O)M; 620(s), 650(m), ν(Al—O); 470(m), ν(Co—O)	14,045 (Benzene) 14,165 (Tetrahydrofuran) 14,370 (Pyridine) 14,665 (2,6-Dimethylpyridine)	1.96

IR (4000–200 cm^{-1}) spectra were recorded on Perkin–Elmer and Carl Zeiss Specord M80 spectrophotometers. Electronic spectra were recorded on a Pye–Unicam Model 557/SP 8-100 spectrometer. Magnetic susceptibility measurements were made at room temperature (23.5°C) by the Gouy method. The magnetic moments, μ_{eff}, listed in Table 1 have been corrected for the diamagnetic susceptibilities of the ligands and the central metal ion using standard values.[13] Molecular weights were measured ebullioscopically (Gallenkamp apparatus) in benzene.

Synthetic procedure

As preparative procedures are similar in most cases, only details of typical examples of each type are given below, for the sake of brevity.

Preparation of $[ClCo\{Al(OBu^t)_4\}]$ **(Ia)**

A benzene (*ca* 25 cm^3) suspension of $K\{Al(OBu^t)_4\}$ [prepared by dissolving potassium (0.34 g, 8.69 mmol) and $Al(OBu^t)_3$ (2.16 g, 8.76 mmol) in Bu^tOH (*ca* 20 cm^3) and benzene (*ca* 15 cm^3)] was added to a suspension of $CoCl_2$ (1.13 g, 8.71 mmol) in Bu^tOH (*ca* 40 cm^3) and the reaction mixture was stirred for ~12 h at room temperature, during which the colour of the solution changed from light blue to dark blue. The precipitated KCl (1.14 g, 15.31 mmol) was removed by filtration. Removal of volatiles from the filtrate under reduced pressure afforded a dark blue solid (3.10 g, 85%) which was further recrystallized from a benzene/n-hexane mixture.

A similar procedure was used to obtain $[ClNi\{Al(OBu^t)_4\}]$ **(Ib)**.

Preparation of $[Co\{Al(OBu^t)_4\}_2]$ **(IIa)**

To a suspension of $CoCl_2$ (0.82 g, 6.32 mmol) in Bu^tOH (*ca* 30 cm^3) was added a solution of $K\{Al(OBu^t)_4\}$ [prepared by dissolving potassium (0.49 g, 12.5 mmol) and $Al(OBu^t)_3$ (3.16 g, 12.8 mmol) in Bu^tOH (*ca* 20 cm^3) and benzene (*ca* 15 cm^3)]. The reaction mixture was allowed to reflux for about 15 h, during which the colour of the solution changed from blue to purple–red. The precipitated KCl (0.94 g, 12.62 mmol) was removed by filtration. The solvent was removed from the filtrate under reduced pressure to afford a purple solid (4.0 g, 90%).

A similar procedure was used to isolate the coloured solid and viscous liquid products, respectively, $[Ni\{Al(OBu^t)_4\}_2]$ **(IIb)** and $[Cu\{Al(OBu^t)_4\}_2]$ **(IIc)**. Details are given in Table 2.

Reactions of $[ClM\{Al(OBu^t)_4\}]$ $(M = Co^{II})$ *and* Ni^{II}

Reaction of **Ia** *with* $K(OBu^t)$. A benzene suspension of $K(OBu^t)$ [prepared from potassium (0.12 g, 3.00 mmol) and Bu^tOH (*ca* 20 cm^3)] was added to a solution of $[ClCo\{Al(OBu^t)_4\}]$ (1.30 g, 3.00 mmol) in benzene (*ca* 20 cm^3). The resulting reaction mixture was stirred for about 6 h, followed by refluxing for 2 h. Precipitated KCl (0.21 g, 2.82 mmol) was filtered and volatiles were removed under reduced pressure from the filtrate to afford a dirty brown–violet solid $[(OBu^t)Co\{Al(OBu^t)_4\}]$ **(IIIa)** (1.33 g, 94%). The product was purified by recrystallization from a benzene/n-hexane mixture.

A similar procedure was used for the preparation of $[(OBu^t)Ni\{Al(OBu^t)_4\}]$ **(IIIb)**.

Reaction of **Ia** *with* $K\{Al(OR)_4\}$ (R = Et, Pr^i). A benzene (*ca* 20 cm^3) suspension of $K\{Al(OPr^i)_4\}$ [freshly prepared by the interaction of potassium (0.10 g, 2.55 mmol) and $Al(OPr^i)_3$ (0.53 g, 2.59 mmol) in Pr^iOH (*ca* 10 cm^3), followed by removal of the volatiles] was added to a benzene (*ca* 20 cm^3) solution of $[ClCo\{Al(OBu^t)_4\}]$ (1.07 g, 2.58 mmol). The reaction mixture was allowed to reflux for about 6 h, during which the colour changed from blue to violet. Precipitated KCl (0.50 g, 6.71 mmol) was removed by filtration and volatiles were removed under reduced pressure to yield a violet, solid product $[\{Al(OPr^i)_4\}Co\{Al(OBu^t)_4\}]$ **(Va)** (1.30 g, 80%). The product was purified either by distillation under reduced pressure or by recrystallization from n-hexane.

A similar procedure was used for the preparation of $[\{Al(OEt)_4\}M\{Al(OBu^t)_4\}]$ **(IVa** and **IVb)** (M = Co, Ni). Details are given in Table 2.

RESULTS AND DISCUSSION

The new heterobimetallic derivatives of cobalt(II), nickel(II) and copper(II) have been synthesized by the reaction of MCl_2 (anhydrous) with $K\{Al(OBu^t)_4\}$ in 1:1 and 1:2 molar ratios, respectively, in a mixture of benzene and Bu^tOH:

$$MCl_2 + K\{Al(OBu^t)_4\} \xrightarrow[C_6H_6,\ stir]{Bu^tOH} \tfrac{1}{2}[ClM\{Al(OBu^t)_4\}]_2 + KCl\downarrow \quad \textbf{(I)}$$

Ia; $M = Co^{II}$

Ib; $M = Ni^{II}$

Table 2. Preparative, analytical and some physical data of heterobimetallic alkoxide derivatives of Co^{II}, Ni^{II} and Cu^{II}

Reactants (in g)	Product; Nature; Percent yield	Sublimation/ distillation; Percent yield	Analysis: Found (Calc.) (%)				
			Co/Ni/Cu	Mixed oxide	Al	Cl	OR
$CoCl_2 + K\{Al(OBu^t)_4\}$ (1.13) (3.14)	$[ClCo\{Al(OBu^t)_4\}]$ **(Ia)**; blue solid; 80%	Decomposed at 150°C/0.05 mmHg	14.2 (14.2)	—	6.4 (6.5)	8.4 (8.5)	—
$NiCl_2 \cdot x Pr^iOH + K\{Al(OBu^t)_4\}$ (1.38) (2.88)	$[ClNi\{Al(OBu^t)_4\}]$ **(Ib)**; blue–red solid; 85%	Decomposed at 140°C/0.05 mmHg	14.0 (14.2)	—	6.4 (6.5)	8.5 (8.5)	—
$CoCl_2 + 2K\{Al(OBu^t)_4\}$ (0.82) (4.49)	$[Co\{Al(OBu^t)_4\}_2]$ **(IIa)**; purple, crystalline solid; 75%	Sublimed at 160°C/0.05 mmHg; 80	8.4 (8.4)	—	7.6 (7.7)	—	—
$NiCl_2 \cdot x Pr^iOH + 2K\{Al(OBu^t)_4\}$ (0.83) (6.94)	$[Ni\{Al(OBu^t)_4\}_2]$ **(IIb)**; purple, crystalline solid; 75%	Sublimed at 140°C/0.05 mmHg; 80	8.2 (8.4)	—	7.6 (7.7)	—	—
$[ClCo\{Al(OBu^t)_4\}] + K(OBu^t)$ (1.30) (0.12)	$[(OBu^t)Co\{Al(OBu^t)_4\}]$ **(IIIa)**; dirty brown–violet solid; 94%	Decomposed at 175°C/0.07 mmHg	12.7 (13.0)	—	6.0 (5.98)	—	—
$[ClNi\{Al(OBu^t)_4\}] + K(OBu^t)$ (1.27) (0.34)	$[(OBu^t)Ni\{Al(OBu^t)_4\}]$ **(IIIb)**; light purple solid; 80%	Decomposed at 170°C/0.06 mmHg	12.5 (13.0)	—	6.0 (5.98)	—	—
$[ClCo\{Al(OBu^t)_4\}] + K\{Al(OEt)_4\}$ (1.68) (1.00)	$[\{Al(OEt)_4\}Co\{Al(OBu^t)_4\}]$ **(IVa)**; purple, sticky solid; 88%	Distilled at 155°C/0.05 mmHg; 60	10.1 (10.0)	30.6 (30.1)	9.3 (9.2)	—	—
$[ClNi\{Al(OBu^t)_4\}] + K\{Al(OEt)_4\}$ (1.12) (0.67)	$[\{Al(OEt)_4\}Ni\{Al(OBu^t)_4\}]$ **(IVb)**; yellow–green solid; 75%	—	10.2 (10.0)	30.8 (30.1)	9.1 (9.2)	—	—
$[ClCo\{Al(OBu^t)_4\}] + K\{Al(OPr^i)_4\}$ (1.07) (0.77)	$[\{Al(OPr^i)_4\}Co\{Al(OBu^t)_4\}]$ **(Va)**; violet, sticky solid; 70%	Distilled at 150°C/0.05 mm Hg; 80	8.7 (9.1)	—	8.7 (8.4)	—	36.7 (36.8)
$[ClNi\{Al(OBu^t)_4\}] + K\{Al(OPr^i)_4\}$ (1.25) (0.92)	$[\{(Al(OPr^i)_4\}Ni\{Al(OBu^t)_4\}]$ **(Vb)**; purple, sticky solid; 75%	Distilled at 144°C/0.05 mm Hg; 60	8.9 (9.1)	—	8.6 (8.4)	—	36.5 (36.8)
$CuCl_2 + 2K\{Al(OBu^t)_4\}$ (0.51) (2.48)	$[Cu\{Al(OBu^t)_4\}_2]$ **(IIc)**; green, sticky solid; 80%	Distilled at 162°C/0.05 mm Hg; 80	8.9 (9.0)	—	7.6 (7.7)	—	—

$$MCl_2 + 2K\{Al(OBu^t)_4\} \xrightarrow[\text{Reflux}]{C_6H_6,\ Bu^tOH} [M\{Al(OBu^t)_4\}_2] + 2KCl\downarrow$$

(II)

IIa; M = Co^{II}

IIb; M = Ni^{II}

IIc; M = Cu^{II}.

Complexes **IIa**–**IIc** could also be prepared by the equimolar interaction of **Ia**, **Ib** or $[ClCu\{Al(OBu^t)_4\}]$, respectively, with $K\{Al(OBu^t)_4\}$ in benzene.

All these derivatives are moisture-sensitive, coloured [cobalt (purple), nickel (purple) and copper (green)] solids or viscous liquids, soluble in organic solvents (e.g. n-hexane, benzene, toluene). Derivatives **Ia** and **Ib** are dimeric in boiling benzene, whereas complexes **IIa** and **IIb** are monomeric. Derivatives **IIa**–**IIc** are thermally stable and could be sublimed/distilled unchanged under reduced pressure. By contrast, derivatives **Ia** and **Ib** decomposed on heating even under reduced pressure at 150°C/0.05 mmHg.

Derivatives **Ia** and **Ib** proved to be of great synthetic utility for the synthesis of interesting varieties of new heterometal alkoxide derivatives by the reactions shown below:

$$[ClM\{Al(OBu^t)_4\}] + K(OBu^t) \xrightarrow{C_6H_6} [(OBu^t)M\{Al(OBu^t)_4\}] + KCl\downarrow$$

(III)

IIIa; M = Co

IIIb; M = Ni

$$[ClM\{Al(OBu^t)_4\}] + K\{Al(OR)_4\} \xrightarrow{C_6H_6} [\{Al(OR)_4\}M\{Al(OBu^t)_4\}] + KCl\downarrow$$

(IV and V)

IVa; R = Et, M = Co

IVb; R = Et, M = Ni

Va; R = Pr^i, M = Co

Vb; R = Pr^i, M = Ni.

Derivatives **IIIa** and **IIIb**, **IVa** and **IVb** and **Va** and **Vb** are coloured solids, soluble in common organic solvents. Most of these are monomeric (ebullioscopically) in benzene, whereas **IIIa** and **IIIb** depict a dimeric nature.

The reaction of $K\{Al(OBu^t)_4\}$ with $NiCl_2$ was extremely slow, but it could be facilitated by the use of the adduct $NiCl_2 \cdot x Pr^iOH$, in the presence of a few drops of pyridine.

IR spectral studies

Complexes $[ClM\{Al(OBu^t)_4\}]$, $[(OBu^t)M\{Al(OBu^t)_4\}]$ and $[M\{Al(OBu^t)_4\}_2]$ showed structurally useful IR absorptions[14,15] in the regions 1250–1205, 910–905, 800–720 (OBu^t skeleton vibrations); 1080, 1050 ν(C—O), 760–600 ν(Al—O) and 499–400 cm^{-1} ν(M—O) (M = Co, Ni and Cu).

The metal chloride stretching frequency in **Ia** and **Ib** is observed in the range 384–248 cm^{-1}, as expected for bridged chloride[16–18] systems with a coordination environment lower than six.

In the derivatives $[\{Al(OEt)_4\}M\{Al(OBu^t)_4\}]$ and $[\{Al(OPr^i)_4\}M\{Al(OBu^t)_4\}]$, bands were observed in the range 1080, 1060 ν(C—O); 910–905 (due to OBu^t skeleton vibrations); 690, 660, 665 ν(Al—O) and 395–470 cm^{-1} ν(M—O). In the former derivatives, characteristic bands due to OEt skeleton vibrations are observed at 1180 (M = Co), 1160 (M = Ni) cm^{-1}, while in latter complex, bands observed at 1130 (M = Co), 1150 (M = Ni) cm^{-1} are characteristic of OPr^i skeleton vibrations.

Electronic spectral and magnetic studies

The electronic spectrum of $[Ni\{Al(OBu^t)_4\}_2]$ (**IIb**) is characteristic of a tetrahedral environment[19–21] around nickel and the same is corroborated by its magnetic moment (3.91 BM). The electronic spectra of other nickel derivatives show a small equilibrium contribution of octahedral species, increasing from **IIIb** to **Ib** to **Vb**, which is corroborated from their magnetic moments[22,23] (3.88–3.95 BM). These conclusions receive additional support from the spectra (Table 1) observed in different solvents, showing the relative concentration of the octahedral species increasing with the donor capability of the ligand in general: benzene < tetrahydrofuran < pyridine (2,6-dimethylpyridine); in spite of a higher donating capacity expected for 2,6-dimethylpyridine compared with pyridine, the steric effects appear to reduce the donor property of the former ligand.

The spectra of cobalt derivatives[19] **Ia**–**Va** (Table 1) indicate qualitatively an octahedral environment with an increasing component in equilibrium of the tetrahedral form in the sequence **IVa** < **Va** < **IIa** < **Ia** < **IIIa**; however, an alternative possibility of a pentacoordinated species can also not be ruled out. Magnetic moments[22,23] (4.81–4.90 BM) for **Ia**–**Va** are consistent with the above conclusions.

The spectrum of $[Cu\{Al(OBu^t)_4\}_2]$ (Table 1) in benzene shows a medium to weak intensity, very broad absorption band around 14,040 cm^{-1} arising from either a highly distorted tetragonal or a trigonal field. When the spectra were recorded in

different solvents (e.g. tetrahydrofuran, pyridine, lutidine), there was a noticeable blue shift in the position of the band in the following order: tetrahydrofuran < pyridine < lutidine. These observations do indicate, as expected, that as the basicity (or donor strength) of the solvent increases, copper(II) tends to attain an octahedral geometry. The observed magnetic moment, 1.96 BM, for the derivative $[Cu\{Al(OBu^t)_4\}_2]$ also corresponds to the d^9 configuration of copper(II).[22,23]

Although the above limited data do indicate the possibilities of several structural patterns involving fluxional bi- or tridentate bonding of the alkoxometallate ligands in solution, with variations consistent in general with their steric requirements, definite conclusions regarding the structures of these fascinating heterometal alkoxides in the solid state would be possible only after X-ray crystallographic studies, which have not been successful so far.

Acknowledgement—We thank the Department of Science and Technology, Government of India, New Delhi, for support of this research and for research fellowships to two of us (G.G. and R.K.D.).

REFERENCES

1. D. C. Bradley, R. C. Mehrotra and D. P. Gaur, *Metal Alkoxides*. Academic Press, London (1978).
2. R. C. Mehrotra, *Adv. Inorg. Radiochem.* 1983, **26**, 269 and refs therein.
3. R. C. Mehrotra, *J. Ind. Chem. Soc.* 1982, **LIX**, 715.
4. A. Shah, A. Singh and R. C. Mehrotra, *Inorg. Chim. Acta* 1988, **141**, 289.
5. R. C. Mehrotra and J. V. Singh, *J. Coord. Chem.* 1984, **13**, 273.
6. R. C. Mehrotra and J. V. Singh, *Can. J. Chem.* 1984, **62**, 1003.
7. R. C. Mehrotra and J. V. Singh, *Z. Anorg. Allg. Chem.* 1984, **512**, 221.
8. R. K. Dubey, A. Singh and R. C. Mehrotra, *Polyhedron* 1987, **6**, 427.
9. R. K. Dubey, A. Shah, A. Singh and R. C. Mehrotra, *Recl. Trav. Chim.* 1988, **107**, 273.
10. W. Wayne and H. Adkins, *Org. Synth.* 1941, **21**, 8.
11. A. I. Vogel, *A Text Book of Quantitative Inorganic Analysis*. Longman, London (1978).
12. R. C. Mehrotra, *J. Ind. Chem. Soc.* 1953, **30**, 585; D. C. Bradley, F. M. A. Halim and W. Wardlaw, *J. Chem. Soc.* 1950, 3450.
13. A. Earnshaw, *An Introduction to Magnetochemistry*, pp. 4–8. Academic Press, New York (1968).
14. L. J. Bellamy, *The Infrared Spectra of Complex Molecules*. Chapman and Hall, London (1975).
15. K. Nakamoto, *Infrared Spectra of Inorganic and Coordination Compounds*. Wiley Interscience, London (1970).
16. D. M. Adams, *Metal–Ligand and Related Vibrations*. Edward Arnold, London (1967).
17. R. J. H. Clark, *Halogen Chemistry*, Vol. 3. Academic Press, New York (1968).
18. J. R. Ferraro, *Low Frequency Vibrations of Inorganic and Coordination Compounds*. Plenum Press, New York (1971).
19. A. B. P. Lever, *Inorganic Electronic Spectroscopy*, 2nd edn. Elsevier, Amsterdam (1984).
20. C. Furlani and G. Morpurgo, *Z. Phys. Chem. (Frankfurt)* 1961, **28**, 93.
21. H. A. Weakliem and D. S. McClure, *J. Appl. Phys. Suppl.* 1962, **33**, 347.
22. L. Sacconi, M. Cianpolini and N. Narli, *J. Am. Chem. Soc.* 1964, **86**, 819.
23. B. N. Figgis and J. Lewis, *Prog. Inorg. Chem.* 1964, **6**, 37.

Polyhedron Vol. 10, No. 15, pp. 1741–1748, 1991
Printed in Great Britain

0277–5387/91 $3.00+.00
© 1991 Pergamon Press plc

SUBSTITUENT EFFECTS IN MULTIPLY TRIMETHYLSILYL-SUBSTITUTED FERROCENES. MOLECULAR STRUCTURE OF 1,1′,2,2′,4,4′-HEXAKIS(TRIMETHYLSILYL)FERROCENIUM TETRAFLUOROBORATE

JUN OKUDA,† ROLF W. ALBACH and EBERHARDT HERDTWECK

Anorganisch-chemisches Institut der Technischen Universität München, Lichtenbergstrasse 4, D-8046 Garching, F.R.G.

and

FRIEDRICH E. WAGNER

Institut für Kernphysik und Nukleare Festkörperphysik der Technischen Universität München, Frank-James-Strasse, D-8046 Garching, F.R.G.

(*Received* 21 *January* 1991; *accepted* 8 *April* 1991)

Abstract—Cyclic voltammograms, electronic and Mössbauer spectra were recorded for a series of sterically hindered ferrocenes bearing trimethylsilyl and tert-butyl groups Fe[η^5-$C_5H_3(EMe_3)_2$-1,3]$_2$, Fe[η^5-$C_5H_2(EMe_3)$-4-$(SiMe_3)_2$-1,2]$_2$ (E = C, Si), and Fe[η^5-$C_5H_2(SiMe_3)_3$-1,2,4](η^5-C_5R_5) (R = H, CH_3). The redox potential of Fe[η^5-$C_5H_2(SiMe_3)_3$-1,2,4]$_2$ is more negative than is expected for the trimethylsilyl group's electron-withdrawing property, which is confirmed by the value of the lowest wavenumber electronic absorption and of the quadrupole splitting. Oxidation of Fe[η^5-$C_5H_2(SiMe_3)_3$-1,2,4]$_2$ with $AgBF_4$ gives [Fe{η^5-$C_5H_2(SiMe_3)_3$-1,2,4}$_2$]BF_4. A single crystal X-ray structural analysis shows that the cation adopts a conformation with a pair of trimethylsilyl groups eclipsed. The compound crystallizes in the monoclinic space group $P2_1/n$, with $a = 10.597(1)$, $b = 20.739(4)$, $c = 18.450(3)$ Å, $\beta = 105.49(1)°$ and $V = 3907$ Å^3.

1,1′,3,3′-Tetra(tert-butyl)ferrocene[1] represents the first metallocene which has a rotational barrier of the cyclopentadienyl ligand which is high enough to be determined by conventional solution NMR spectroscopy.[2] Recently, we have shown that in addition to the 1,3-di(tert-butyl)cyclopentadienyl (Bu_2Cp) ligand, multiply trimethylsilyl-substituted ligands such as 1,3-bis(trimethylsilyl)cyclopentadienyl (Si_2Cp),[3] 1,2,4-tris(trimethylsilyl)cyclopentadienyl (Si_3Cp)[4] and 4-tert-butyl-1,2-bis(trimethylsilyl)cyclopentadienyl ($BuSi_2Cp$)[5] also form ferrocenes that show similar values of barriers to ring rotation about the metal–ligand axis.[6] The conformational rigidity of these metallocenes has been ascribed to consequences of purely steric effects, viz. to pronounced interligand repulsions.[3,4,6] In order to detect further manifestation of steric influences on the iron centre, we have studied a series of ferrocenes bearing the above mentioned ligands by cyclic voltammetry as well as by electronic and Mössbauer spectroscopy. In this context, we have also performed the preparative oxidation of multiply trimethylsilyl-substituted ferrocenes $Fe(Si_nCp)_2$ ($n = 2$, 3) and an X-ray structural determination of $[Fe(Si_3Cp)_2]BF_4$.

RESULTS AND DISCUSSION

Cyclic voltammograms of the previously synthesized ferrocenes $Fe(Bu_2Cp)_2$,[1] $Fe(Si_2Cp)_2$,[3,7] $Fe(Si_3Cp)_2$,[4,8] $Fe(BuSi_2Cp)_2$,[5] $Fe(Si_3Cp)Cp$[4] and $Fe(Si_3Cp)Cp^*$[4] ($Cp = \eta^5$-C_5H_5; $Cp^* = \eta^5$-C_5Me_5) were obtained at room temperature in dichloro-

† Author to whom correspondence should be addressed.

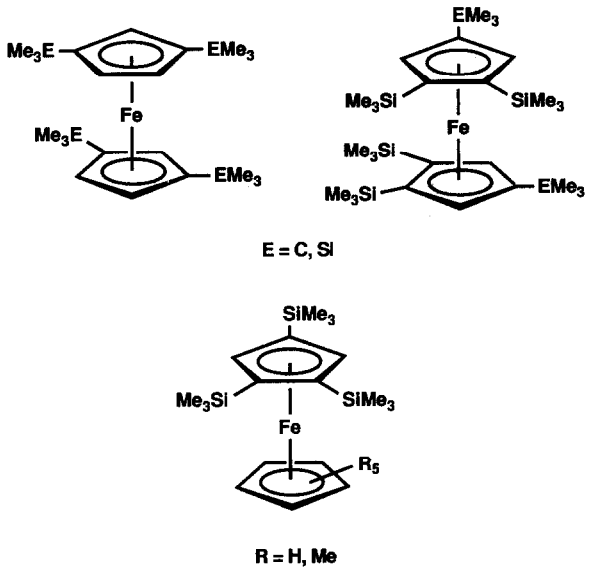

methane solution. All compounds exhibit reversible one-electron oxidations. The redox potentials, $\Delta E_{1/2}$, compiled in Table 1 were internally referenced to ferrocene. For the sake of comparison we have also added $\Delta E_{1/2}$ values of FeCp* Cp[9] and FeCp*$_2$.[10] In Fig. 1 the redox potentials are plotted against the sum of resonance parameters $\Sigma\sigma_R$ (σ_R for Me, 0.11; CMe_3, 0.16; and $SiMe_3$, 0.12[11]). In accordance with literature reports,[10,12] each alkyl group such as methyl or tert-butyl at the ring periphery cathodically shifts the oxidation potential of the substituted ferrocene by *ca* 50 mV relative to the parent compound. Thus, a fairly good linear correlation of $\Delta E_{1/2}$ values with substituent constants is obtained for the alkylated ferrocenes FeCp*$_2$, FeCp*Cp and Fe(Bu$_2$Cp)$_2$. This reflects the steady increase of electron density at the iron centre by successive ring substitution

Table 1. Redox potential, electron and Mössbauer spectroscopic data for substituted ferrocene derivatives

Compound	$\Delta E_{1/2}$ (mV)	UV–vis λ_{max} (nm) [ε]	Mössbauer δ (mm s^{-1})	QS (mm s^{-1})
Fe(Bu$_2$Cp)$_2$	−250	228[11,700] 333[100] 462[165]	0.49[a]	2.48[a]
Fe(Si$_2$Cp)$_2$	+33	228[12,100] 332[115] 477[170]	0.469	2.22
Fe(Si$_3$Cp)$_2$	−104	235[10,500] 361[210] 515[180]	0.519	2.20
Fe(BuSi$_2$Cp)$_2$	−144	233[30,000] 364[162] 496[170]	0.536	2.33
Fe(Si$_3$Cp)Cp	+17	229[8300] 335[110] 454[120]	0.463	2.30
Fe(Si$_3$Cp)Cp*	−359	232[32,700] 345[230] 453[150]	0.478	2.36
FeCp$_2$	0	200[50,000] 325[49] 441[54][c]	0.49[b]	2.39[b]
FeCp*$_2$	−550[d]	222[35,000] 328[180] 426[120][d]	0.53[e]	2.50[e]
FeCpCp*	−270[f]	—	—	—

[a] R. A. Stukan, S. P. Gubin, A. N. Nesmeyanov, V. I. Goldanskii and E. F. Makarov, *Teor. Eksp. Khim.* 1966, **2**, 805.
[b] A. V. Lesikar, *J. Chem. Phys.* 1964, **40**, 2746.
[c] Reference 19.
[d] Reference 10.
[e] S. Iijima, I. Motoyama and H. Sano, *Bull. Chem. Soc. Japan* 1980, **53**, 3180.
[f] Reference 9.

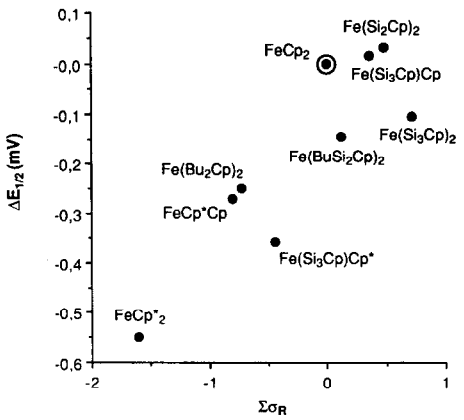

Fig. 1. Plot of redox potentials, $\Delta E_{1/2}$ (V vs internal ferrocene), against the sum of resonance parameters, $\Sigma\sigma_R$, for substituted ferrocenes.

with electron-donating alkyl groups, facilitating the removal of one electron from the bonding orbital ($1e_{2g}$). On the other hand, ferrocenes with trimethylsilyl groups should be more difficult to oxidize, since the electronic effect of this silicon substituent can be summarized as the π-accepting or $-M$ effect prevailing over the weak σ-donating or $+I$ effect.[13] There is indeed an increase of the redox potential within the series $FeCp_2$, $Fe(Si_3Cp)Cp$, $Fe(Si_2Cp)_2$ in keeping with what is expected of the overall electron-withdrawing nature of the trimethylsilyl group. However, the $E_{1/2}$ value of the hexakis-substituted derivative $Fe(Si_3Cp)_2$ is unexpectedly low and is almost comparable with that of 1,1′-dimethylferrocene ($\Delta E_{1/2} = 0.12$ V).[12] The same trend is observed for $Fe(BuSi_2Cp)_2$ and $Fe(Si_3Cp)Cp^*$ when compared with $Fe(BuCp)_2$ and FeCp*Cp, respectively. We believe that this cathodic shift of the redox potential with successive substitution by trimethylsilyl groups is caused by some steric factors. Presumably there is some relief from steric constraint upon oxidation of a sterically-hindered ferrocene to give the corresponding ferrocenium ion which is less hindered due to a longer metal–ligand bond distance. A related sterically-induced shift of redox potential in distorted ferrocenes such as bridged derivatives was reported in the literature,[14] whereas in a number of studies, linear free energy relationships for redox potentials of substituted ferrocenes have been determined.[12,15]

In order to verify that oxidation is also chemically feasible we treated $Fe(Si_2Cp)_2$ and $Fe(Si_3Cp)_2$ with $AgBF_4$ in dichloromethane and isolated the corresponding ferrocenium ion, $[Fe(Si_2Cp)_2]BF_4$ and $[Fe(Si_3Cp)_2]BF_4$, as thermally stable, dark blue crystals in virtually quantitative yield according to eq. (1):

$$Fe(Si_nCp)_2 + AgBF_4 \longrightarrow [Fe(Si_nCp)_2]BF_4 + Ag. \quad n = 2, 3 \qquad (1)$$

Analytical, IR, UV–vis and Mössbauer spectroscopic data clearly indicate the structure of a cationic sandwich complex. Furthermore, we carried out an X-ray structure determination of the hexakis-substituted derivative $[Fe(Si_3Cp)_2]BF_4$. Analogous to the neutral $Fe(Si_3Cp)_2$, for which we performed a detailed conformational analysis,[4] the conformation adopted by $[Fe(Si_3Cp)_2]^+$ is derived from a nearly ideally eclipsed arrangement of the five-membered rings with one pair of trimethylsilyl groups eclipsed (conformation "e_1" of C_2 symmetry[4]). The mean ring carbon–iron distance of 2.137 Å and the ring centroid–iron distance of 1.751

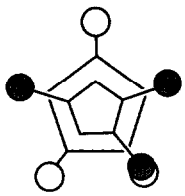

Å are increased by 0.055 and 0.065 Å, respectively, compared with the ferrocene precursor $Fe(Si_3Cp)_2$. This finding clearly indicates a less sterically constrained coordination sphere in the cation. Consequently, the deviation of the two ring ligands from parallel is small, the tilt angle observed is only 4.5°. Also reduced is the degree of the substituents' bending away from the metal centre. Other structural features are comparable with those in analogous sandwich complexes of the type $E(Si_3Cp)_2$ (E = Fe,[4] Mg,[16] Ge,[17] Sn[18]). Figure 2 depicts the molecular structure of the cation, and Table 2 contains selected bond lengths and angles.

The electronic spectra of ferrocene was thoroughly analysed by Gray and co-workers[19] and complete assignment of both charge-transfer and ligand-field absorption bands was undertaken. For the substituted ferrocenes under consideration here the same pattern of one intense metal–ligand charge-transfer band and two d–d absorption bands is observed. The ligand-field absorption at the lowest wavenumber ($^1A_{1g} - {}^1E_{1g}$) is bathochromically shifted as the number of trimethylsilyl substituents at the ring periphery increases. This can qualitatively be ascribed to the electron-withdrawing effect of the trimethylsilyl substituents. However, only poor correlation ($r^2 = 0.52$) between λ_{max} values and substituent parameters such as σ_R (Fig. 3) or redox potentials, $E_{1/2}$, is observed. A good

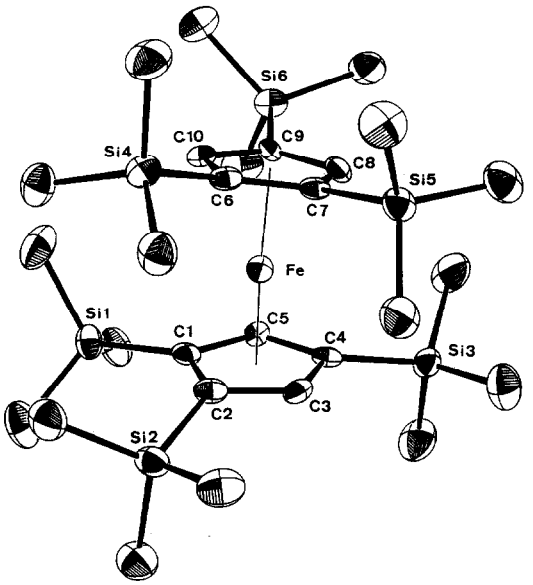

Fig. 2. ORTEP diagram of the cation in $[Fe(Si_3Cp)_2]BF_4$. Atoms are drawn with 50% thermal ellipsoids.

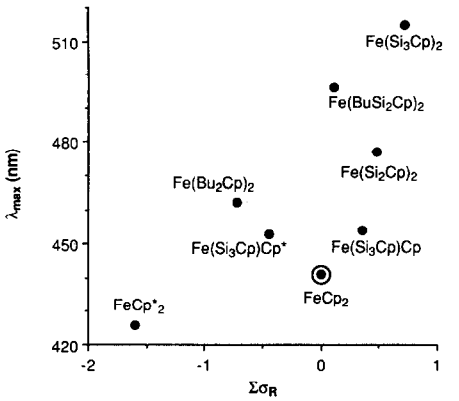

Fig. 3. Plot of lowest wavenumber electronic absorptions, λ_{max} (nm), against the sum of resonance parameters, $\Sigma\sigma_R$, for substituted ferrocenes.

correlation between $E_{1/2}$ and the frequencies of the *d–d* transition bands was found for a series of ferrocenes with electron-withdrawing substituents and this was rationalized in terms of the molecular

Table 2. Selected bond distances (Å) and angles (°) and their standard deviations for the cation in $[Fe(Si_3Cp)_2]BF_4$

Bond lengths			
Fe—C(1)	2.167(3)	Si(1)—C(1)	1.916(3)
Fe—C(2)	2.191(2)	Si(2)—C(2)	1.910(3)
Fe—C(3)	2.128(2)	Si(3)—C(4)	1.883(3)
Fe—C(4)	2.127(2)	Si(4)—C(6)	1.893(2)
Fe—C(5)	2.070(3)	Si(5)—C(7)	1.902(3)
Fe—C(6)	2.181(2)	Si(6)—C(9)	1.913(3)
Fe—C(7)	2.167(2)	C(1)—C(2)	1.464(3)
Fe—C(8)	2.107(2)	C(1)—C(5)	1.425(3)
Fe—C(9)	2.123(2)	C(2)—C(3)	1.437(4)
Fe—C(10)	2.109(2)	C(3)—C(4)	1.438(3)
Fe—Cp(1)	1.751	C(4)—C(5)	1.439(4)
Fe—Cp(2)	1.751	C(6)—C(7)	1.438(3)
		C(7)—C(8)	1.457(3)
		C(8)—C(9)	1.430(4)
		C(9)—C(10)	1.427(3)
Bond angles			
Si(1)—C(1)—C(2)	134.0(2)	Si(4)—C(6)—C(7)	133.0(2)
Si(1)—C(1)—C(5)	119.7(3)	Si(4)—C(6)—C(10)	119.1(2)
Si(2)—C(2)—C(1)	132.0(3)	Si(5)—C(7)—C(6)	131.8(2)
Si(2)—C(2)—C(3)	119.1(2)	Si(5)—C(7)—C(8)	120.8(3)
Si(3)—C(4)—C(3)	128.2(3)	Si(6)—C(9)—C(8)	127.1(2)
Si(3)—C(4)—C(5)	127.0(2)	Si(6)—C(9)—C(10)	125.7(3)
C(2)—C(1)—C(5)	105.8(2)	C(7)—C(6)—C(10)	106.8(3)
C(1)—C(2)—C(3)	106.4(3)	C(6)—C(7)—C(8)	106.6(2)
C(2)—C(3)—C(4)	111.8(2)	C(7)—C(8)—C(9)	110.4(2)
C(3)—C(4)—C(5)	103.3(2)	C(8)—C(9)—C(10)	105.6(2)
C(1)—C(5)—C(4)	112.7(2)	C(6)—C(10)—C(9)	110.5(2)

Cp(1) and Cp(2) denote the centre of the tris(trimethylsilyl)cyclopentadienyl ligands.

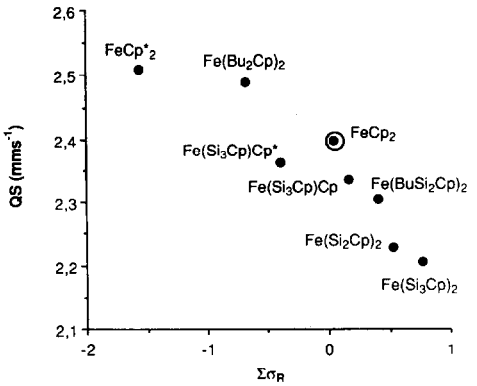

Fig. 4. Plot of quadrupole splittings, QS (mm s^{-1}), against the sum of resonance parameters, $\Sigma\sigma_R$, for substituted ferrocenes.

orbital description for ferrocene.[20] The strong charge-transfer band ($1e_{1u}-2e_{1g}$) was also used to estimate the electron-donating property of a ring ligand,[21] but this relation was not applicable here.

As was noted previously, the isomer shift, δ, in the Mössbauer spectrum of substituted ferrocenes does not significantly reflect the electronic influence of the ring substituents.[22] This is also the case for the sterically-hindered ferrocenes. However, the value of quadrupole splitting, QS, shows a dependence on the groups attached to the five-membered ring and this parameter was also successfully used to probe distortions from the parallel arrangement of the ligands in substituted ferrocenes.[23] When the QS values are plotted against the resonance parameters, $\Sigma\sigma_R$, a fair correlation ($r^2 = 0.84$) results (Fig. 4). In keeping with a reduced electric field gradient caused by introducing electron-withdrawing ring substituents,[24] the QS values for the trimethylsilyl-substituted ferrocenes are significantly decreased. Likewise, electron-donating groups tend to increase the quadrupole splitting, as has been reported recently for a series of dinuclear complexes of the type $[Fe(Bu_nCp)(CO)_2]_2$ ($n = 0$–2).[25] Thus, the QS data for the trimethylsilyl-substituted ferrocenes seem to reflect mainly the electronic effects of the substituents on the iron centre. At this point it remains questionable whether this dependence of the QS values also originates from some steric influence.

Conclusion

On examining the redox potential by cyclic voltammetry, a cathodically-shifted $E_{1/2}$ value for the hexakis-substituted ferrocene, $Fe(Si_3Cp)_2$, has been detected and interpreted as evidence for a sterically-hindered coordination sphere caused by the trimethylsilyl groups. As the solid-state structure of the $[Fe(Si_3Cp)_2]^+$ cation suggests, oxidation of $Fe(Si_3Cp)_2$ clearly leads to a less congested situation around the iron centre. Both UV–vis and Mössbauer spectroscopic data are consistent with the slightly electron-withdrawing property of the trimethylsilyl substituent. This effect, however, is less pronounced than an alkyl group such as methyl or tert-butyl which is electron-donating. Accordingly, a trimethylsilyl group represents a ring substituent that allows the study of the steric effects on ring-substituted cyclopentadienyl metal complexes without inducing a strong electronic perturbation of the metal–ligand bonding.

EXPERIMENTAL

General consideration

All experiments were carried out under nitrogen using standard Schlenk techniques. Solvents were purified, dried and distilled under nitrogen. 1,1′,3,3′-tetra(tert-butyl)ferrocene $[Fe(Bu_2Cp)_2]$,[1] 1,1′,3,3′-tetrakis(trimethylsilyl)ferrocene $[Fe(Si_2Cp)_2]$,[3,7] 1,2,4-tris(trimethylsilyl)ferrocene $[Fe(Si_3Cp)Cp]$,[4] (1,2,3,4,5-pentamethyl)[1′,2′,4′-tris(trimethylsilyl)]ferrocene $[Fe(Si_3Cp)Cp^*]$,[4] 1,1′,2,2′,4,4′-hexakis(trimethylsilyl)ferrocene $[Fe(Si_3Cp)_2]$[4,8] and 4,4′-di(tert-butyl)-1,1′,2,2′-tetrakis(trimethylsilyl)ferrocene $[Fe(BuSi_2Cp)_2]$[5] were prepared as described in the literature.

IR spectra were recorded as KBr pellets with a Nicolet FT–5DX instrument. UV–vis spectra were obtained using dichloromethane solutions with a Perkin–Elmer Lambda 2 spectrophotometer. ^{57}Fe Mössbauer spectroscopic measurements were obtained with a $^{57}Co(Rh)$ source moving in a sinusoidal velocity mode at room temperature. Isomer shifts, δ, and quadrupole splittings, QS, were recorded relative to metallic iron foil. Cyclic voltammograms were recorded with a computer-controlled PAR Model 173 potentiostat. A conventional three-electrode configuration (platinum auxiliary electrode, an Ag/AgCl reference electrode and a glassy carbon working electrode) was employed. Tetra-n-butylammonium hexafluorophosphate was used as supporting electrolyte. Redox potentials were calculated by using the formula $E_{1/2} = 1/2(E_p^{ox} + E_p^{red})$, where E_p^{ox} and E_p^{red} are peak potentials. Elemental analyses were performed by the Microanalytical Laboratory of the Anorganisch-chemisches Institut.

$[Fe(Si_2Cp)_2]BF_4$

To a mixture of $Fe(Si_2Cp)_2$ (0.35 g, 0.74 mmol) and $AgBF_4$ (0.14 g, 0.74 mmol) was added 15 cm^3 of dichloromethane. Immediately, the colour of the

mixture darkened and the mixture was left stirring for 2 h to give a dark green solution. The silver metal was filtered off and the filtrate concentrated to a few cm^3. Ether was layered on top of the solution and after standing overnight at room temperature, dark blue, lustrous platelets were isolated: yield 0.32 g (78%); m.p. 195°C. IR (cm^{-1}): 3098 w, 2954 mw, 2898 w, 1410 m, 1254 s, 1191 m, 1054 s, 891 s, 841 br vs, 754 s, 691 m, 629 m. UV–vis (CH_2Cl_2, ε): λ_{max} 645.5 nm (560), 506 (280), 398 (560), 306.5 (11,740), 269 (14,360), 227 (91.50). Mössbauer: δ 0.441(7) mm s^{-1}. Found: C, 47.0; H, 7.5; Fe, 10.0. Calc. for $C_{22}H_{42}BF_4FeSi_4$: C, 47.0; H, 7.5; Fe, 9.9%.

Table 3. Crystallographic data for $[Fe(Si_3Cp)_2]BF_4$

(a)	*Crystal parameters*	
	Empirical formula	$C_{28}H_{58}BF_4FeSi_6$
	Formula weight	705.9
	Crystal colour	Black prism
	Crystal dimensions (mm)	$0.50 \times 0.45 \times 0.60$
	Radiation	Mo-K_α ($\lambda = 0.70930$ Å)
	Temperature (°C)	-95 ± 5
	Space group	$P2_1/n$ (No. 14)
	a (Å)	10.597(1)
	b (Å)	20.739(4)
	c (Å)	18.450(3)
	β (°)	105.49(1)
	V (Å^3)	3907
	Z	4
	d_{calc} (g cm^{-3})	1.200
	μ(Mo-K_α) (cm^{-1})	102.76
(b)	*Data collection*	
	Diffractometer	CAD4 Enraf–Nonius
	Monochromator	Graphite, incident beam
	Scan type	ω scan
	Scan time (s)	60 (max)
	Scan width (°)	$(1.75 + 0.30 \tan\theta) \pm 25\%$ for background corrections
	Maximum 2θ (°)	50
	Number of reflections measured	5233 ($h01: h+1 = 2n+1$; $0k0: k = 2n+1$)
	Number of independent reflections	4301
	Corrections	Lorentz polarization, numerical absorption (0.0206–0.0854), extinction [ε refined to $\varepsilon = 0.9468 \times 10^{-8}$ in $F_c(\text{corr}) = F_c(1 + \varepsilon \times F_c^2 \times \text{LP})$]
	Standard reflections	3 every 3600 s, intensity check; 3 every 100 reflections, orientation check
(c)	*Refinement*	
	Solution	Patterson method
	Hydrogen atoms	Not found, calculated, included but not refined
	Refinement	Full-matrix least-squares
	Minimization function	$\Sigma w(\lvert F_o\rvert - \lvert F_c\rvert)^2$
	Weighting scheme	$1/\sigma(F_o)^2$
	Anomalous dispersion	All non-hydrogen atoms
	Number of reflections included	3987 $I \geqslant 1.0\sigma(I)$
	Number of parameters refined	349
	R	0.058[a]
	R_w	0.047[b]
	Goodness-of-fit	4.308[c]
	Shift/err	0.001

[a] $R = \Sigma \lvert\lvert F_o\rvert - \lvert F_c\rvert\rvert / \Sigma \lvert F_o\rvert$.
[b] $R_w = [\Sigma w(\lvert F_o\rvert - \lvert F_c\rvert)^2 / \Sigma w F_o^2]^{1/2}$.
[c] $\text{GOF} = [\Sigma w(\lvert F_o\rvert - \lvert F_c\rvert)^2 / (\text{NO} - \text{NV})]^{1/2}$.

$[Fe(Si_3Cp)_2]BF_4$

The compound was prepared in a manner analogous to that used to prepare $[Fe(Si_2Cp)_2BF_4$ and was isolated as lustrous, black cubes in 88% yield; dec. > 250°C. IR (cm^{-1}): 2959 m, 2902 w, 1414 w, 1248 s, 1095 ms, 1060 s, 1048 s, 924 mw, 902 w, 842 br s, 757 ms, 694 mw, 633 mw. UV–vis (CH_2Cl_2, ε): λ_{max} 662 nm (460), 548 (370), 420.5 (840), 323 (10,320), 288 (9910), 227 (11,450). Mössbauer: δ 0.518(1) mm s^{-1}. Found: C, 47.5; H, 8.1; Fe, 8.0. Calc. for $C_{28}H_{58}BF_4FeSi_6$: C, 47.6; H, 8.3; Fe, 7.9%.

Crystal structure determination

Crystal data and details of the X-ray diffraction experiments were reported in Table 3. The compound, obtained as black cubes by layering ether on top of a dichloromethane solution, crystallizes in the monoclinic space group $P2_1/n$ (No. 14). Cell constants were obtained from least-squares refinement by using a set of 44 reflections in the range $34.2° \leqslant 2\theta \leqslant 44.7°$. The iron atom was determined from the Patterson function. All remaining non-hydrogen atoms were located by successive structure factor calculations and difference Fourier maps. Not all hydrogen atoms were found; their ideal positions were added to the calculations but not refined. The tetrafluoroborate ion is partially disordered. A second orientation is obtained from the first by a C_3 rotation about the B(1)—F(1) axis. Occupancies refined to 50% for each of the orientations. Maximum residual electron density of +0.88 e $Å^{-3}$ near the fluorine atoms indicates that the disorder model is imperfect. The refinements converged with unweighted and weighted agreement factors, $R = 0.058$ and $R_w = 0.047$, respectively. All crystallographic calculations were performed on VAX11/730 and VAX8200 computers using SDP[26] and STRUX II[27] systems. Atomic coordinates and thermal parameters have been deposited with the Cambridge Crystallographic Data Centre.

Acknowledgements—Generous financial support by the Volkswagen-Stiftung, the Fonds der Chemische Industrie and the Bund der Freunde der TU München is gratefully acknowledged. We thank Professor W. A. Herrmann for his continued support and interest.

REFERENCES

1. T. Leigh, *J. Chem. Soc.* 1964, 3294; A. N. Nesmeyanov and N. S. Kochetkova, *Dokl. Akad. Nauk SSSR* 1957, **117**, 92; A. N. Nesmeyanov, N. S. Kochetkova, S. V. Vitt, V. B. Bondarev and E. I. J. Kovshov, *Dokl. Akad. Nauk SSSR* 1964, **156**, 99; Z. L. Kaluski, A. I. Gusev, A. E. Kalinin and Y. T. Strukhov, *Zh. Strukt. Khim.* 1972, **13**, 950.
2. W. D. Luke and A. Streitwieser Jr, *J. Am. Chem. Soc.* 1981, **103**, 3241; see also: T. E. Bitterwolf and A. C. Ling, *J. Organomet. Chem.* 1977, **141**, 355.
3. J. Okuda and E. Herdtweck, *J. Organomet. Chem.* 1989, **373**, 99.
4. J. Okuda and E. Herdtweck, *Chem. Ber.* 1988, **121**, 1899.
5. J. Okuda, *Chem. Ber.* 1989, **122**, 1075.
6. Isoelectronic cobaltocenium ions show the same feature: J. Okuda, *J. Organomet. Chem.* 1989, **367**, C1; J. Okuda, *J. Organomet. Chem.* 1990, **385**, C39.
7. G. A. Tolstikov, M. S. Miftakhov and Y. B. Monakov, *Zh. Obshch. Khim.* 1976, **46**, 1778.
8. M. S. Miftakhov and G. A. Tolstikov, *Zh. Obshch. Khim.* 1976, **46**, 930.
9. P. G. Gassman, D. W. Macomber and D. W. Hershberger, *Organometallics* 1983, **2**, 1471.
10. U. Koelle and F. Khouzami, *Angew. Chem., Int. Edn. Engl.* 1980, **19**, 640; J. L. Robbins, N. Edelstein, B. Spencer and J. C. Smart, *J. Am. Chem. Soc.* 1982, **104**, 1882.
11. M. Charton, *Prog. Phys. Org. Chem.* 1981, **13**, 119.
12. D. W. Slocum and C. R. Ernst, *Adv. Organomet. Chem.* 1972, **10**, 79; M. M. Sabbatini and E. Cesarotti, *Inorg. Chim. Acta* 1977, **24**, L9.
13. A. R. Bassindale and P. G. Taylor, in *The Chemistry of Organic Silicon Compounds* (Edited by S. Patai and Z. Rappoport), p. 893. John Wiley, New York (1989).
14. J. E. Gorton, H. L. Lentzner and W. E. Watts, *Tetrahedron* 1971, **27**, 4353.
15. For recent references see: D. W. Slocum, A. L. Edgecomb, J. S. Fowler, H. F. Gibbard and J. Phillips, *Organometallics* 1990, **9**, 307; G. Cerveau, C. Chuit, E. Colomer, J. P. Corriu and C. Reyé, *Organometallics* 1990, **9**, 2415.
16. C. P. Morley, P. Jutzi, C. Krüger and J. M. Wallis, *Organometallics* 1987, **6**, 1084.
17. P. Jutzi, E. Schlüter, M. B. Hursthouse, A. M. Arif and R. L. Short, *J. Organomet. Chem.* 1986, **299**, 285.
18. A. H. Cowley, P. Jutzi, F. X. Kohl, J. G. Lasch, N. C. Norman and E. Schlüter, *Angew. Chem., Int. Edn Engl.* 1984, **23**, 616.
19. Y. S. Sohn, D. N. Hendrickson and H. B. Gray, *J. Am. Chem. Soc.* 1971, **93**, 3603.
20. H. Henning and O. Gürtler, *J. Organomet. Chem.* 1968, **11**, 307.
21. T. P. Hanusa, *Polyhedron* 1982, **1**, 663.
22. M. L. Good, J. Buttone and D. Foyt, *Ann. N.Y. Acad. Sci.* 1974, **239**, 193; R. V. Parish, in *Organic Chemistry of Iron* (Edited by E. A. Koerner von Gustorf, F.-W. Grevels and I. Fischler), p. 194. Academic Press, New York (1978).
23. R. M. G. Roberts, J. Silver, R. J. Ranson and I. E. G. Morrison, *J. Organomet. Chem.* 1981, **219**, 233 and refs therein.
24. R. L. Collins, *J. Chem. Phys.* 1965, **42**, 1072.

25. M. A. El-Hinnawi and M. A. Kobeissi, *Inorg. Chim. Acta* 1989, **166**, 99.
26. R. E. Schmidt, M. Birkhahn, W. Massa, P. Kiprof and E. Herdtweck, STRUX II, Program System for Crystallographic Data Analysis. Universität Marburg (1980) and Technische Universität München, F.R.G. (1985–1987).
27. B. A. Frenz, The Enraf–Nonius CAD 4 SDP system, in *Computing Crystallography*, pp. 64–71. Delft University Press, Delft, Holland (1978).

Polyhedron Vol. 10, No. 15, pp. 1749–1758, 1991
Printed in Great Britain

0277–5387/91 $3.00+.00
© 1991 Pergamon Press plc

QUALITATIVE MODELS FOR THE NMR CHEMICAL SHIFTS OF INTERSTITIAL ATOMS IN CLUSTERS

MELINDA J. DUER and DAVID J. WALES*

University Chemical Laboratories, Lensfield Road, Cambridge CB2 1EW, U.K.

(*Received* 27 *November* 1990; *accepted* 15 *April* 1991)

Abstract—Qualitative models for the NMR chemical shifts of interstitial atoms in clusters are presented which draw heavily upon our present understanding of cluster bonding. The deshielding of interstitial hydrogen atoms can be understood in terms of secondary paramagnetic fields arising on the transition metal centres, whilst that of interstitial carbon and nitrogen atoms is thought to arise from more local sources. In these models, Stone's Tensor Surface Harmonic theory is used to describe the interaction between the interstitial atoms and the metal cluster framework. Model calculations of the susceptibility tensor for $[Ru_6H(CO)_{18}]^-$ and the electronic structures of $[Rh_6C(CO)_{15}]^{2-}$ and $[Rh_6N(CO)_{15}]^-$ support the proposals.

The NMR shielding in a molecule, and hence the chemical shift, depends upon the induced current in the presence of an external magnetic field. To predict the effect of such a field upon the molecular electron density is generally not a simple matter, but much progress has been made, for example, in organic molecules where the bonding is well understood.[1] Successful models have also been developed for the chemical shifts of the central metal atom in octahedral transition metal complexes[2] and for hydride ligands in mononuclear transition metal complexes.[3] However, the bonding in all these systems is relatively simple compared with that in a transition metal cluster. Drawing from the great advances made in understanding the bonding in the latter molecules in recent years, and Stone's Tensor Surface Harmonic (TSH) theory in particular,[4,5] we propose a simple, qualitative model for the chemical shifts of interstitial atoms in a cluster. Estimates of the susceptibility tensor for $[Ru_6H(CO)_{18}]^-$ and electronic structure calculations for $[Rh_6C(CO)_{15}]^{2-}$ and $[Rh_6N(CO)_{15}]^-$ using the Fenske–Hall approximate molecular orbital treatment support this model.

TSH theory has proved to be a highly versatile tool for the discussion of the bonding in cluster compounds.[6] In particular, the method has been used to provide a firmer theoretical foundation for empirical rules of cluster electron counting such as the *Debor Principle*[7] and the *Polyhedral Skeletal Electron Pair Theory*.[8] TSH theory is based upon an approximate descent in symmetry from the full rotation group. Basis functions are classified as σ, π and δ according to the number of nodal planes they possess which contain the radius vector from the centre of the cluster to the atom. Cluster orbitals are formed from σ-type basis functions (with no nodal planes containing the radius vector) using the values of spherical harmonics evaluated at the cluster vertices as expansion coefficients. A helpful comparison may be made with the Hückel wavefunctions for cyclic and linear polyenes: the appropriate linear combinations can be obtained from the wavefunctions for a free electron on-a-ring or in-a-box, respectively. For an approximately spherical cluster we use the eigenfunctions for a free electron on-a-sphere in a similar manner to construct and classify cluster wavefunctions. For example, a σ cluster orbital, $\psi^{\sigma}_{L,M}$ is given by

$$\psi^{\sigma}_{L,M} = \sum_i Y_{L,M}(\theta_i, \phi_i)\sigma(i), \qquad (1)$$

where θ_i and ϕ_i are the angular spherical polar coordinates of vertex i.

To treat π- and δ-type basis functions (which have one and two nodal planes containing the radius vector, respectively) we proceed in a similar manner but use the values of tensor spherical harmonics as expansion coefficients. For further details

* Author to whom correspondence should be addressed.

the reader is referred elsewhere.[5] Recently the method has been extended to consider detailed cluster structure,[9] cluster rearrangements[10] and the relationship between shape and electronic structure.[11]

For $\psi^{\lambda}_{L,M}$ ($\lambda = \sigma, \pi, \delta$) the L and M subscripts reflect the parentage of the orbital under spherical symmetry, where they are good quantum numbers. In a finite point group we find that functions with different L or M do not mix with each other strongly, and hence that L and M are very useful symmetry labels. Furthermore, the cluster orbitals transform under rotations of the point group in the same way as the parent spherical harmonic upon which the expansion coefficients are based. Under reflections, inversions and other "improper" symmetry operations they may transform in the same way or with a change of sign.[9]

NMR SHIELDING—THE RAMSEY THEORY

In this section we summarize the theory of the NMR chemical shift and so introduce the problem to be addressed, bearing in mind that this material may be relatively unfamiliar to cluster chemists. The shielding tensor, σ_{ij}, is defined by

$$\mathbf{B}' = \mathbf{B} - \sigma\mathbf{B}, \tag{2}$$

where $\mathbf{B}$ is the applied field and $\mathbf{B}'$ is the resulting field at the nucleus. Using perturbation theory to express the ground state wavefunction correct to first order in the applied magnetic field and taking the expectation value for the classical expression for $\mathbf{B}'$ gives[12]

$$\sigma_{zz} = \frac{e^2\mu_0}{8\pi m_e}\langle 0|(x^2+y^2)/r^3|0\rangle - \frac{e^2\mu_0}{4\pi m_e^2}\sum_{n>0}\frac{\langle 0|L_z|n\rangle\langle n|L_z/r^3|0\rangle + c.c.}{E_n^0 - E_0^0}, \tag{3}$$

where E_n^0 is the unperturbed energy of state $\psi_n \equiv |n\rangle$, L_z is the z component of the angular momentum operator, $\mathbf{L}$, and *c.c.* denotes the complex conjugate of the previous term in the numerator. This expression, and the analogous terms for the other components of σ, was first given by Ramsey.[13]

The first term depends only upon the ground-state wavefunction and corresponds to the precession of the molecular electron density about the direction of the magnetic field. It is known as the diamagnetic contribution. The second term involves the induced mixing of the ground state with excited states, and is known as the paramagnetic term. It is by reference to the matrix elements of this term that we later rationalize the chemical shift trends in transition metal cluster molecules.

The large, negative values of δ for hydrogen bound to a transition metal complex have been explained by Buckingham and Stephens[3] in terms of a large (anisotropic) paramagnetic shielding contribution (i.e. positive σ) from the metal atom. Essentially, a paramagnetic current centred on the transition metal atom/ion creates a magnetic field which supports the applied field at the transition metal nucleus, but may oppose the applied field at a hydride ligand bound to the transition metal ion. This is illustrated in Fig. 1.

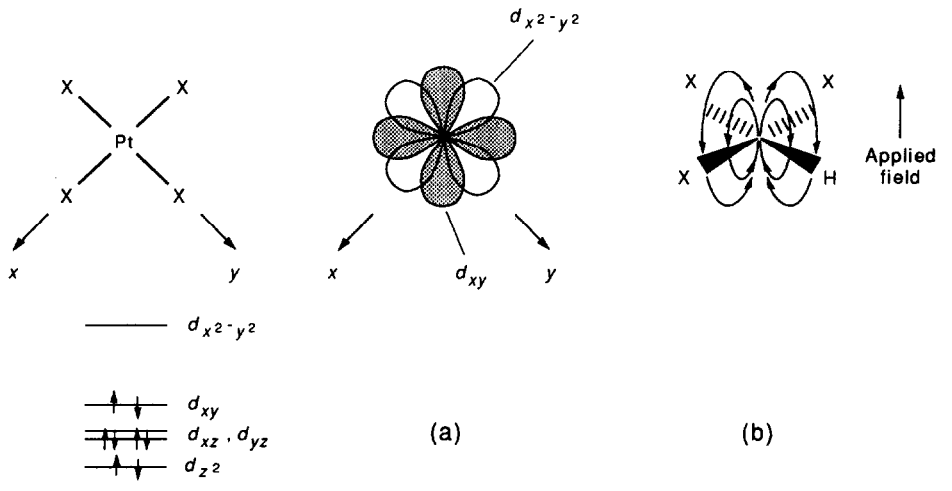

Fig. 1. An induced paramagnetic field arises when a d^8 transition metal ion with square planar coordination is placed in a magnetic field. (a) Electrons from the d_{xy} orbital, for instance, are "rotated" about the z axis into the higher energy $d_{x^2-y^2}$ orbital. This creates the field shown in (b) which supports the applied field at the transition metal centre.

The paramagnetic current arises from the admixture of excited "paramagnetic" mostly *d* electron states into the ground state, through the perturbation provided by the magnetic field. This admixture of excited states may be thought of in one-electron terms as the "rotation" of *d* electrons from a filled or partially filled *d* orbital into higher energy, vacant (or half-filled) *d* orbitals. This "rotation" of charge then gives rise to the magnetic field supporting the applied field at the transition metal nucleus. The precise location of the hydride ligand then determines whether the induced magnetic field has a shielding or a deshielding effect at this nucleus.

In contrast to terminally bound hydride ligands, interstitial hydrogen atoms in clusters are generally only weakly shielded or are deshielded relative to atomic hydrogen. Clearly, the much more complicated electronic structures of cluster molecules do not lend themselves to an analysis as simple as that for single-centre, transition metal complexes. Nevertheless, it is one of the aims of this paper to show how paramagnetic currents on the transition metal atoms, which induce secondary magnetic fields centred on the transition metal atom, may cause the very large chemical shifts of interstitial hydride ligands. Our other aim is to explain the range of chemical shifts observed for clusters with interstitial carbon and nitrogen atoms. A consistent framework must account for the following features:

(i) The chemical shifts of interstitial protons in both symmetrical and unsymmetrical cluster environments.
(ii) Differences between the chemical shifts of interstitial carbon and nitrogen atoms relative to hydrogen.
(iii) Differences between the chemical shifts observed for interstitial carbon and nitrogen atoms in geometrically similar clusters.
(iv) The variation of chemical shifts between octahedral and trigonal prismatic clusters for carbon and nitrogen interstitial atoms.
(v) Variations of chemical shift in analogous clusters with different metal atoms.

We draw heavily upon the TSH description of cluster bonding in the course of rationalizing these trends, even for interstitial hydrogen atoms where a neighbouring group approximation is employed.

CHEMICAL SHIFTS OF INTERSTITIAL PROTONS

We first consider a proton in a symmetrical environment at the centre of a cluster. It is well known that the chemical shifts of protons in the vicinity of aromatic rings can be explained by considering the "ring current" induced by an applied field. In the case of an octahedral cluster, such as $[Ru_6H(CO)_{18}]^-$ or $[Co_6H(CO)_{15}]^-$, the skeletal bonding is essentially delocalized in three dimensions. Hence, on the application of a magnetic field we might expect to observe effects due to a "cylindrical current" arising from a set of current loops. The induced precession of the molecular electron density can be discussed in terms of Larmor Precession or Lenz's Law: the magnetic field of the induced current opposes the change of flux through the electronic orbits (assumed globally delocalized over the cluster skeleton). This term is clearly shielding at the centre of the cluster (Fig. 2).

The above argument considers the diamagnetic contribution to the shielding which correspond to the first term in eq. (3). For a cluster compound with many electrons, the picture of circulating, delocalized currents implies that σ^d is much larger than for the free hydrogen atom; an estimate could be obtained from the Flygare–Goodisman formula.[14] However, there is still the paramagnetic term to consider and this is expected to cancel out much of the diamagnetic effect. In fact, the interstitial protons in both $[Ru_6H(CO)_{18}]^-$ and $[Co_6H(CO)_{15}]^-$ are deshielded with respect to the hydrogen atom and shielded with respect to the bare nucleus. Theoretically we know that the hydrogen 1*s* orbital mixes weakly with an in-pointing S^σ cluster orbital to give bonding and antibonding combinations, leaving the interstitial atom formally associated with two electrons and the energy level pattern of the parent octahedron relatively unperturbed. To calculate the approximate shielding of the hydride nucleus we employ the neighbouring group approximation,[15] where the cluster metal atoms are represented as point magnetic dipoles. The limitations of this approach have been discussed before;[3] however, we feel justified in employ-

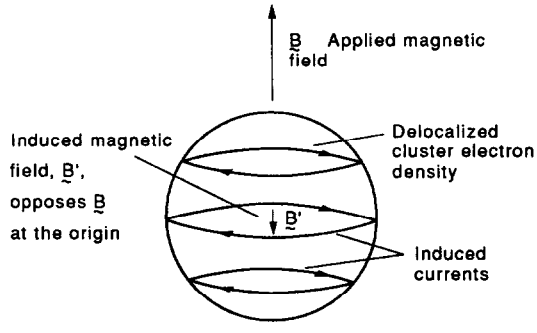

Fig. 2. The induced magnetic field will act to oppose the applied field and lead to shielding of a nucleus at the centre of a spherical cluster with delocalized skeletal bonding.

ing the method in the context of the modest aims of these calculations. The induced field arising on each transition metal atom is then calculated from the magnetic susceptibility tensor, $\chi_{\alpha\beta}$, of the atom using

$$M_\alpha = \chi_{\alpha\beta} H_\beta, \tag{4}$$

where **M** is the associated magnetization. The susceptibility tensor for a transition metal cluster may be written as a sum over the atoms in the cluster. The contribution from a given atom n, is

$$\chi_{zz} = -\frac{e^2\mu_0 N_A \rho}{8\pi m_e M_m} \sum_{i=1}^{Z_n} \langle 0|x_i^2 + y_i^2|0\rangle + \frac{e^2\mu_0 N_A \rho}{4\pi m_e^2 M_m} \sum_{k>0} \frac{\left\langle 0\left|\sum_{i=1}^{Z_n} L_z^i\right|k\right\rangle\left\langle k\left|\sum_{i=1}^{Z_n} L_z^i\right|0\right\rangle + c.c.}{E_k^0 - E_0^0}, \tag{5}$$

where N_A is Avogadro's number, ρ is the density of the sample, M_m is the molar mass, Z_n is the atomic number of nucleus n. All the coordinates are referred to an origin at the local nucleus in question. This form may be derived by explicit transformation of origins[16] or by noting that all the components of the total susceptibility tensor must be gauge-independent. At each atom the local z axis points away from the global origin, which we chose at the centre of the cluster. The shielding at the hydrogen nucleus is then calculated from the total field it experiences due to the induced fields from all the transition metal atoms n:

$$\sigma \approx \frac{M_m}{12\pi\rho N_A} \sum_n (\chi_\parallel^n - \chi_\perp^n) \frac{(1 - 3\cos^2\theta_n)}{R_n^3}, \tag{6}$$

where θ_n is the angle between the radius vector of atom n and the internuclear vector from the interstitial atom to that nucleus, R_n is the distance between the latter atoms and we have assumed local axial symmetry. The expression includes a sum of contributions from all metal atoms in the cluster. It gives an estimate of the shift relative to a hydrogen atom because the diamagnetic contribution local to the interstitial atom has been omitted.

Now we can employ the TSH theory description of the cluster bonding to study the above expressions. The skeletal bonding in an octahedral cluster is essentially delocalized, so we must consider the matrix elements of delocalized cluster orbitals and the true cluster energy levels. The lowest energy virtual excitations in an electron delocalized deltahedral cluster are from L^π to $\overline{L^\pi}$ cluster orbitals, which are linear combinations of p^π and d^π atomic orbitals that have one nodal plane containing the atomic radius vector.[5] In local axes these orbitals are characterized by an m quantum number of ± 1. Now the local angular momentum operators have the following selection rules: for L_z, $\Delta m = 0$ and for L_x and L_y, $\Delta m = \pm 1$ (recall that the latter are linear combinations of the raising and lowering operators). Hence for all the cluster vertices we will have $\chi_\parallel > \chi_\perp$, because all the ψ in question consist mainly of local p^π and d^π functions for which $|m| = 1$. This result should be independent of the precise position of the interstitial atom in the octahedral cavity. When the proton is at the centre of the cluster, $\theta_n = 0$ for all the cluster vertices and σ is negative, i.e. deshielding relative to the hydrogen atom, in agreement with the shifts of $\delta = 23.2$ and 16.4 ppm for the cobalt and ruthenium clusters mentioned above. When the proton moves away from the centre of the cluster some of the θ_n increase from zero and the deshielding due to these terms decreases. Hence we expect the deshielding to be greatest at the centre of a symmetrical cluster. The neighbouring group terms can actually be shielding for larger θ values which may arise for protons in unsymmetrical environments, such as the tetrahedral cavities associated with capping atoms on an octahedron. Furthermore, the TSH bonding description is most appropriate for roughly spherical clusters.[5]

Experimental values of interstitial hydride shifts measured to date are summarized in Table 1; most are qualitatively in accord with the foregoing theory, with positive chemical shifts. The nickel clusters, however, have negative shifts. In these clusters, the hydride ligands effectively cap an interior face of the nickel polyhedron, and are not at all near the centre of an approximately spherical cavity within the cluster. We would expect the hydride ligands in these compounds to behave more like those which cap an exterior face of a cluster. We will not attempt to explain here the precise differences in chemical shift between the deshielded hydrides, since small details of geometry and electronic structure could be significant in determining the magnitude of the deshielding.

To further investigate the validity of our approach some model calculations were performed for $[Ru_6H(CO)_{18}]^-$ as a typical cluster molecule with a deshielded interstitial hydride. All molecular orbital calculations were carried out using the Fenske–Hall method,[17] using tabulated exponential factors for the metal atom.[18] Input molecular geometry was the published structure determined by neutron diffraction[19] and is illustrated in Fig. 3(a). Calculations were also performed for a $[Ru_6H(CO)_{18}]^-$ anion, where the hydrogen atom was placed on the exterior of the metal cluster as

Table 1. Experimental chemical shifts of hydrides for which interstitial geometries have been proposed

Structure	δ (ppm)	Hydride environment
$[Co_6H(CO)_{15}]^-$	+23.2	Octahedral[24]
$[Ru_6H(CO)_{18}]^-$	+16.4	Octahedral[19]
$[Ru_8H_2(CO)_{21}]^{2-}$	+6.88[a]	Octahedral[25]
$[Ru_{10}HC(CO)_{24}]^-$	+0.2	Tetrahedral[26]
$[Ni_{12}H(CO)_{21}]^{3-}$	−24.0	Distorted octahedral,
$[Ni_{12}H_2(CO)_{21}]^{2-}$	−18.0	(3 long, 3 short Ni—H)[28]
$[Rh_{13}H_{5-n}(CO)_{24}]^{n-}$	−16.7 ($n = 3$[b])	Unknown[28]
	−14.3 ($n = 2$[b])	

[a] Note that the proton nucleus giving rise to this signal was not located in the X-ray structure, but was postulated to be interstitial.[26]

[b] The hydrides were postulated to be interstitial from the results of a solution NMR study. However, their precise environment is clearly very important in determining the chemical shift, as discussed in the text; we will not consider these compounds any further here.

shown in Fig. 3(b). These calculations are intended only to demonstrate the qualitative trends in the ^1H chemical shift with changes of the hydride position, and are not expected to give quantitative answers.

We concentrate initially on the $[Ru_6H(CO)_{18}]^-$ anion with an interstitial hydride. The molecular orbital calculation places a charge of −0.4 on the interstitial hydride ligand, confirming that it is not a partial positive charge on the hydride that causes the deshielding of the proton nucleus. In the corresponding metal cluster with an interstitial carbide ligand, the deshielding of the ^{13}C nuclear resonance is ascribed to the carbonium ion nature of the carbon atom.[20]

The paramagnetic part of χ is given in general by Van Vleck's formula:

$$\chi_{\alpha\beta} = \frac{e^2\mu_0 N_A \rho}{4m_e^2 M_m} \sum_{n>0}' \left\{ \frac{\langle 0|l_\alpha|n\rangle\langle n|l_\beta|0\rangle + c.c.}{E_n - E_0} \right\}. \quad (7)$$

Clearly, there is little we can do with this expression without a knowledge of the excited states, $|n\rangle$. Therefore, we approximate the variable energy denominator $(E_n - E_0)$ with a constant Δ, and use the closure approximation to obtain:

$$\chi_{\alpha\beta} = \frac{e^2\mu_0 N_A \rho}{2m_e^2 M_m \Delta} \langle 0|l_\alpha l_\beta|0\rangle. \quad (8)$$

If the ground state is written in terms of molecular orbitals which are themselves linear combinations

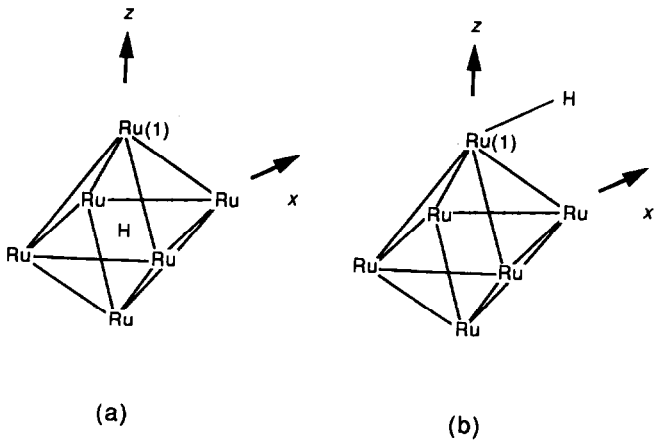

Fig. 3. (a) The structure of the $[Ru_6H(CO)_{18}]^-$ anion in the PPN salt. (b) The structure of the hypothetical $[Ru_6H(CO)_{18}]^-$ anion with an external hydride. The Ru(1)—H distance is 2.03 Å in both cases. In (b) the Ru—H vector is parallel to the x axis.

of atomic orbitals, ϕ, then the above equation becomes

$$\chi_{\alpha\beta} = \frac{e^2\mu_0 N_A \rho}{2m_e^2 M_m \Delta} \sum_j \left\{ \sum_{\nu,\mu} a^*_{\nu j} a_{\mu j} \langle \phi_\nu | l_\alpha l_\beta | \phi_\mu \rangle - \sum_{j'} \sum_{\nu,\mu} \sum_{\lambda,\rho} a^*_{\nu j} a_{\mu j} a^*_{\lambda j'} a_{\rho j'} \langle \phi_\nu | l_\alpha | \phi_\rho \rangle \langle \phi_\lambda | l_\beta | \phi_\mu \rangle \right\}. \quad (9)$$

The subscripts j and j' denote filled molecular orbitals. Equation (9) can also be written in terms of the atomic charges and bond order matrix elements. It can be used to calculate the contribution of a single transition metal atom to the total susceptibility of the molecule if we assume that all the integrals $\langle \phi_\nu | l_\alpha l_\beta | \phi_\mu \rangle$ and $\langle \phi_\nu | l_\alpha | \phi_\mu \rangle$ are negligible if ϕ_ν and ϕ_μ are atomic orbitals on different centres. The sum over atomic orbitals is then restricted to those valence d and p orbitals on the transition metal atom of interest. The resulting susceptibility tensor allows us to calculate the magnetic field arising from paramagnetic currents on that atom. Because the local site symmetry of a ruthenium atom in the octahedral cluster closely approximates C_{3v}, the susceptibility tensor should be approximately diagonal in the local axis frame where the z axis points radially outwards, as above. We estimate the diagonal components to be $\chi_{xx} = 5.71K/\Delta$, $\chi_{yy} = 5.72K/\Delta$ and $\chi_{zz} = 5.79K/\Delta$, where $K = e^2\mu_0 N_A \rho / m_m^2 M_m$ and χ is indeed approximately axial. Then using eq. (6) with $R = 3.86$ bohr, we obtain $\sigma = -0.046/\Delta$ ppm (with Δ measured in hartrees), i.e. deshielded. The HOMO–LUMO gap found in our molecular orbital calculation is 0.07 hartrees (1.7 eV), so that $\sigma = -0.8$ ppm is the contribution to the shielding from each ruthenium centre. This gives the total contribution to σ^p from all six ruthenium atoms around the ^{1}H nucleus as about -5 ppm, i.e. deshielding, which is certainly of the correct order of magnitude.

Using the molecular orbitals calculated for the $[Ru_6H(CO)_{18}]^-$ molecule shown in Fig. 3(b), with an external hydride, we find that the contribution from Ru(1) is $\sigma = 0.026/\Delta$ ppm, i.e. shielded. This is equivalent to $\sigma = 0.7$ ppm for $\Delta = 1$ eV.

The valence d and p orbital populations arising from the Fenske–Hall molecular orbital calculations for both the above molecules are given in Table 2. We note that the d orbital splittings (and indeed populations) change little with the position of the hydrogen atom, as expected.

Table 2. Valence d and p orbital populations of Ru(1) calculated for the structures shown in Fig. 3(a) and (b)

Orbital	(a)	(b)
$4d_{xz}$	0.85	0.84
$4d_{yz}$	0.90	0.95
$4d_{xy}$	1.05	1.03
$4d_{x^2-y^2}$	1.08	1.15
$4d_{z^2}$	1.36	1.33
$5p_z$	0.07	0.06
$5p_y$	0.08	0.09
$5p_x$	0.10	0.12

INTERSTITIAL CARBON AND NITROGEN ATOMS

Above we found that protons in symmetrical, interstitial positions in a cluster are deshielded relative to a hydrogen atom, due to the local field arising from the surrounding transition metal atomic centres. When carbon and nitrogen atoms occupy the centre of an octahedral cluster the deshielding is still more dramatic, even relative to the bare nucleus. A range of values for clusters of interest is given in Fig. 4.†

The presence of valence shell $2s/2p$ orbitals for carbon and nitrogen, which interact with the skeletal cluster orbitals, causes a large, paramagnetic term at the interstitial atom itself. In an octahedral cluster the $2s$ and $2p$ orbitals of these interstitial atoms interact with the inwardly hybridized S^σ and P^σ/P^π cluster orbitals which transform as A_{1g} and T_{1u}, respectively.[5] Bonding and antibonding combinations are formed, of which only the bonding sets are occupied, and the interaction is too large for the neighbouring group approximation applied above to be realistic.

If we denote the bonding and antibonding t_{1u} orbitals by t_{1u} and t^*_{1u}, respectively, then the ground electronic configuration may be denoted by $|t^6_{1u}(^1A_{1g})\rangle$, where we omit the other filled orbitals. The configuration $|t^5_{1u}t^*_{1u}(^1T_{1g})\rangle$ generates a term of symmetry $^1T_{1g}$, and since $\mathbf{L}$ transforms as T_{1g}, the integral

$$\langle t^6_{1u}(^1A_{1g})|\mathbf{L}|t^5_{1u}t^*_{1u}(^1T_{1g})\rangle \quad (10)$$

may be non-zero. Such terms produce a paramagnetic contribution to σ which is deshielding for a central interstitial atom, as *local* paramagnetic effects always are, and larger than the non-local deshielding experienced by interstitial protons. The $|t^5_{1u}t^*_{1u}(^1T_{1g})\rangle$ state is the only excited state which needs to be considered. The $2s/S^\sigma$ bonding and antibonding orbitals, a_{1g} and a^*_{1g}, cannot contribute to

† This tabulation was kindly prepared for us by Dr Joan Mason.

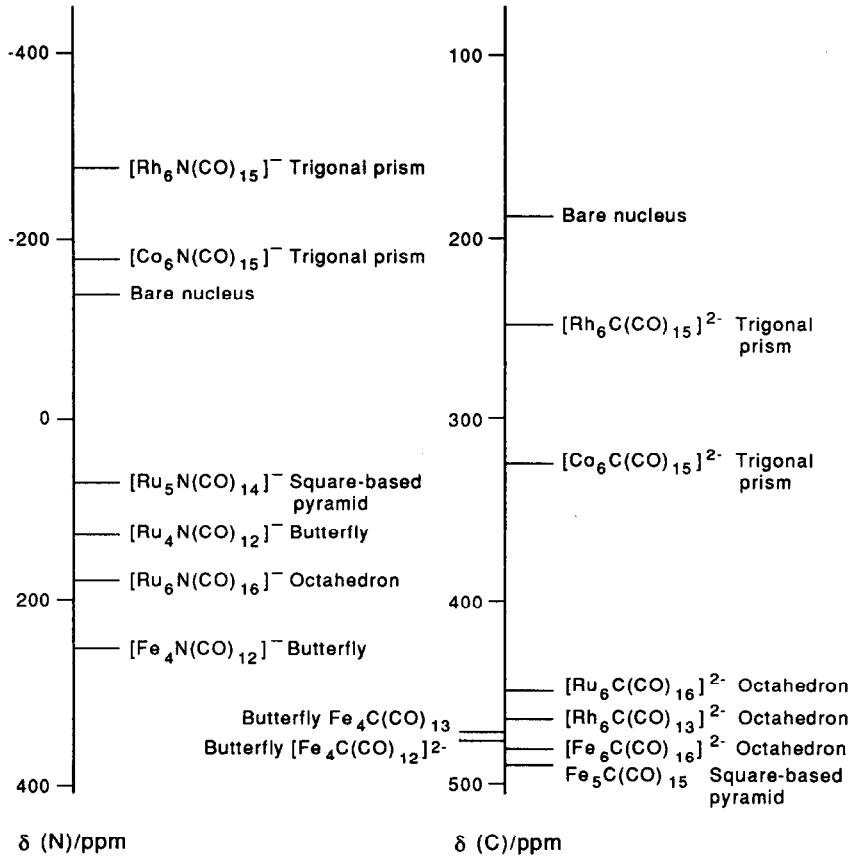

Fig. 4. NMR chemical shifts for interstitial carbon (right) and nitrogen (left) atoms. The origins are for TMS ($SiMe_4$) for carbon and nitromethane ($MeNO_2$) for nitrogen.

the paramagnetic term in this way; the same is true for the $1s/S^{\sigma}$ combinations present for interstitial hydrides. Furthermore, a $^1T_{1g}$ term formed by exciting an electron from the a_{1g} orbital (which is mostly interstitial s in character) to a t_{1g} orbital (with no interstitial s character) is likely to lie rather high in energy. Such contributions are therefore expected to be small.

Hence the shielding of an interstitial carbon or nitrogen atom is rather different from that of a proton. If the critical electronic state is relatively low-lying and the non-vanishing matrix elements have appreciable magnitude, then we expect deshielding relative to the bare nucleus. Furthermore, since the mechanism is now essentially local, the deshielding is greater than for interstitial hydrides. The Extended Hückel calculations for the idealized $[Ru_6C(CO)_{18}]^{2-}$, performed by Wijeyesekera and Hoffmann, support the above model.[21] They show that the bonding and antibonding combinations of $2p$ and P^{σ} orbitals are split by *ca* 4–5 eV in this cluster, so that the energy difference in the denominator of the expression for σ^p would not be excessive.

From Fig. 4 we note that, relative to the bare nuclei, interstitial carbon atoms in cobalt and rhodium trigonal prisms are more deshielded than interstitial nitrogen atoms. However, for the octahedra $[Ru_6C(CO)_{16}]^{2-}$ and $[Ru_6N(CO)_{16}]^{-}$ the deshielding of the interstitial atoms is quite similar, and is greater for the nitrogen atom. Equation (5) suggests that two factors will influence the magnitude of the deshielding: the matrix elements of **L** and the energy difference which appears in the denominator. The valence orbitals of the main group atoms are low-lying compared with those of the metal atoms, and if they did not mix at all then the main group atom would be formally associated with filled $2s$ and $2p$ shells. The matrix elements of the angular momentum operator between such a ground configuration and one involving promotion of a "$2p$" electron to a vacant P^{σ} orbital would be small. Hence, the stronger the metal–interstitial interaction, the greater we expect the deshielding to be. This agrees with both the larger deshielding (relative to the bare nucleus) experienced by the less electronegative interstitial carbon atom in the trigonal prismatic clusters, and with the results of

model calculations described in the next section. However, experience suggests[5] that the energy difference in the denominator will be larger for the octahedral clusters than the trigonal prisms, while the overlap of interstitial and metal valence orbitals should be more favourable, as discussed below. Clearly more data is needed to discern any patterns that may be present, as the identity of the metal must also be important.

CHEMICAL SHIFT AND CLUSTER GEOMETRY

From the data in Fig. 4, we see that interstitial carbon and nitrogen atoms are more deshielded in octahedral clusters than in trigonal prisms. In these metal clusters (with a relatively large density of electronic states) it is likely that the strength of the metal–interstitial interaction is the most variable factor, rather than the energy difference in the denominator. The skeletal bonding orbitals of the trigonal prism can be presented as edge-localized two-centre, two-electron bonds, but for the octahedron the skeletal bonding is delocalized.[6] This, and the fact that the inwardly hybridized p^{σ} orbitals of the octahedron are ideally oriented for overlap with the $2p$ orbitals of the interstitial atom, means that the critical matrix elements of $\mathbf{L}$ are larger for the octahedra. Hence σ^{p} is larger in magnitude (i.e. more negative) and there is a greater deshielding effect in the octahedron.

We would also expect the deshielding to be smaller for an interstitial proton in a trigonal prism than at the centre of an octahedron. In this case we refer back to the neighbouring group model and consider the change in the composition of the frontier orbitals and the effect this has on the local susceptibilities. From the edge-localized bonding pattern of the trigonal prism we know that the frontier orbitals may be written as linear combinations of localized σ-type edge-bonds and antibonds. We expect to find around 33% σ character in the frontier orbitals of a trigonal prism, in contrast to the electron delocalized octahedral clusters, where the frontier orbitals are well described as linear combinations of local π orbitals. To calculate the susceptibility tensors for the metal atoms of the trigonal prism, we define local axes frames (x, y, z) on each atom, rather than $\parallel$ and $\perp$, since the site symmetries are now lower than C_{3v}. The z axis points from the interstitial atom towards the metal atom in each case. Whereas a frontier orbital composed of local π orbitals gives rise to zero matrix elements with L_x and L_y, and to non-zero ones only with L_z, the frontier orbitals in the trigonal prism admit non-zero L_x, L_y matrix elements. This is simply because of the mixing between σ and π cluster orbitals. Hence, we may expect a smaller difference between χ_{xx} (or χ_{yy}) and χ_{zz} in the trigonal prism and, consequently, less deshielding.

To investigate further we performed calculations on the trigonal prismatic clusters $[Rh_6C(CO)_{15}]^{2-}$ and $[Rh_6N(CO)_{15}]$ and octahedral $Ru_6C(CO)_{17}$ using the Fenske–Hall method[17] and tabulated exponential factors for the metal atoms.[18] The geometries of the two trigonal prisms are available from X-ray crystallography, while the octahedral geometry was constructed from idealized parameters.[21]

For the two trigonal prisms (Fig. 5) the cage–

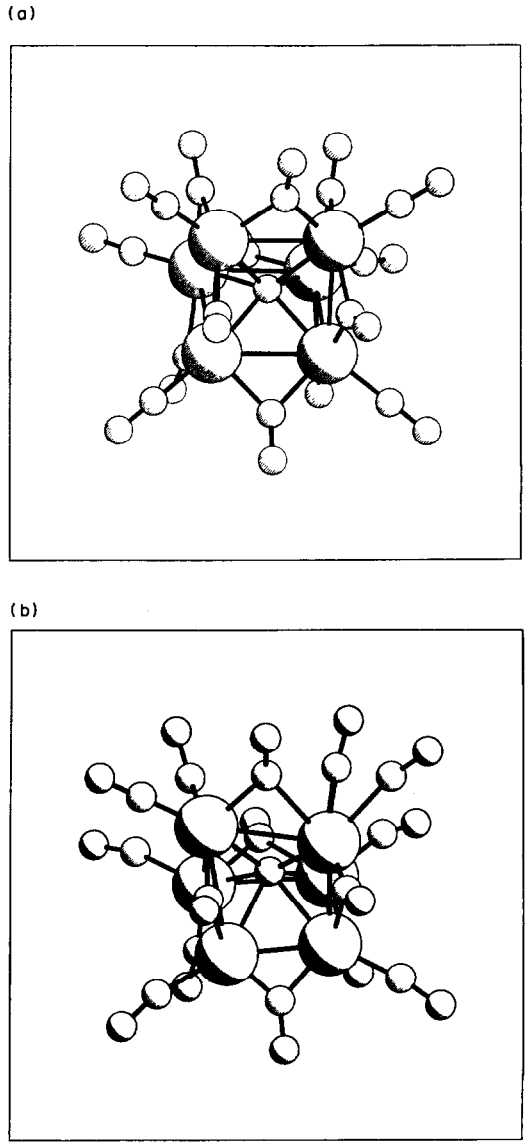

Fig. 5. The structures of (a) $[Rh_6C(CO)_{15}]^{2-}$ and (b) $[Rh_6N(CO)_{15}]^{-}$.

interstitial overlap integrals were found to be around 20% smaller for the nitrogen atom, as expected, and the most significant mixing in both cases was between 2*s* and $S^{\sigma}_{d_{z^2}}$ and 2*p* and $P^{\sigma}_{d_{z^2}}$. The corresponding overlap integrals for the trigonal prisms were found to be only about half the magnitude of those in the octahedral cluster. Both these observations are in accord with the ideas discussed above and with the bonding descriptions of the two types of cluster.

The Mulliken 2*p* atomic orbital populations[22] are also in agreement with the model, lying between 1.4 and 1.8 for the nitrogen and 1.2 and 1.3 for the carbon in the trigonal prismatic cluster, compared with 1.05–1.1 for the carbon atom in the octahedral cluster. The calculated Mulliken atomic charges were −1.7, −1.8 and −0.8 in the same order. These are around 10 times larger than those found using the Extended Hückel method for interstitial carbon atoms in hypothetical cobalt compounds with the same cluster geometries but with hydride ligands instead of carbonyls and large positive charges.[23] The large difference in overall charge between the two sets of clusters probably explains much of the discrepancy. Furthermore, although the Mulliken atomic charges on the interstitial atom vary, it seems unlikely that this would cause σ^d to change sufficiently to explain the wide range of chemical shifts observed.

The other trends in the data of Fig. 4 are also consisent with our qualitative analysis. For example, we know that the energy level patterns in series of *closo*, *nido* and *arachno* clusters are very similar.[5] Hence the interstitial atom chemical shifts in the octahedron, square-based pyramid, butterfly series should be similar, so long as the delocalized bonding pattern is maintained. Considering how large the structural perturbation of losing one or more vertices is, the agreement of the experimental values is quite remarkable.

We can also provide rationalizations and predictions for the changes in chemical shift of a given interstitial atom in cluster cavities of differing size, or for a given polyhedron with different metal atoms. Consider first a change from an octahedron to a tetrahedron. For an interstitial hydride the decrease in the number of neighbouring groups will probably outweigh the somewhat smaller cavity size, and the deshielding should decrease. As for variations in metal atom for otherwise isostructural systems, we predict that the deshielding will be greater for metals with smaller metallic radii. For interstitial hydrogen atoms this effect is largely due to the shorter metal–interstitial distance: for carbon and nitrogen the shorter distance is expected to increase the mixing between the metal and interstitial orbitals. Hence the greatest deshielding is predicted to occur in clusters of late first-row transition metals (smallest metallic radii) and the smallest deshielding for early second- and third-row metals. This is in agreement with the observed shifts of $[Ru_6H(CO)_{18}]^-$ and $[Co_6H(CO)_{15}]^-$, since cobalt has the smaller metallic radius.

CONCLUSIONS

We have proposed qualitative models for rationalizing the chemical shifts of interstitial atoms in clusters. For interstitial hydrogen, it seems reasonable to represent the shielding using the neighbouring group approximation for the skeletal metal atoms. By exploiting our current understanding of cluster bonding in terms of approximate forms for the cluster orbitals, we can explain the chemical shifts of interstitial protons in both symmetrical and unsymmetrical environments.

Interstitial carbon and nitrogen atoms are different from hydrogen, because the interaction of the 2*p* valence orbitals and the $P^{\sigma}_{d_{z^2}}$ cluster orbitals admits significant and large *local* deshielding paramagnetic terms. The magnitude of the deshielding term depends upon the strength of the metal framework–interstitial interaction—greater mixing means more deshielding. The trends observed for the variation of the chemical shift with the electronegativity of the intersitial atom and the geometry (and bonding) in the cluster cage can be rationalized on this basis, and are in accord with our present understanding of the bonding in these clusters.

Current bonding models also suggest that the energy level patterns are largely retained in a *closo*, *nido*, *arachno* series, in agreement with the similar shifts observed for related octahedra, square-based pyramids and butterfly clusters. Finally, we have tried to rationalize and predict the qualitative variation of the chemical shifts of interstitial atoms in isostructural clusters as the identity of the metal atom changes.

Acknowledgements—D.J.W. thanks Lloyd's of London for a Tercentenary Fellowship. M.J.D. is grateful to Dr N. C. Pyper for many helpful discussions. Both authors thank Dr Joan Mason for helpful discussions and providing the data for Fig. 4.

REFERENCES

1. J. Mason, *Adv. Inorg. Chem. Radiochem.* 1976, **18**, 197; J. Mason, *Adv. Inorg. Chem. Radiochem.* 1979, **22**, 199.
2. J. S. Griffith and L. E. Orgel, *Trans. Faraday Soc.* 1957, **53**, 601.

3. A. D. Buckingham and P. J. Stephens, *Chem. Soc. Lond.* 1964, 2747, 4583.
4. A. J. Stone, *Molec. Phys.* 1980, **41**, 1339; A. J. Stone, *Inorg. Chem.* 1981, **20**, 563.
5. D. M. P. Mingos and D. J. Wales, *Introduction to Cluster Chemistry*. Prentice–Hall, Englewood Cliffs (1990).
6. D. M. P. Mingos and R. L. Johnston, *Struct. Bond.* 1987, **68**, 29.
7. R. E. Williams, *Prog. Boron Chem.* 1970, **2**, 51; R. E. Williams, *Inorg. Chem.* 1971, **10**, 210; R. E. Williams, *Adv. Inorg. Chem. Radiochem.* 1976, **18**, 67; K. Wade, *J. Chem. Soc., Chem. Commun.* 1971, 792; R. W. Rudolph and W. R. Pretzer, *Inorg. Chem.* 1972, **11**, 1974; R. W. Rudolph, *Accts Chem. Res.* 1976, **9**, 446.
8. R. Mason, K. M. Thomas and D. M. P. Mingos, *J. Am. Chem. Soc.* 1973, **95**, 3802; D. M. P. Mingos, *Nature Phys. Sci.* 1972, **236**, 99.
9. A. J. Stone and D. J. Wales, *Molec. Phys.* 1987, **61**, 747.
10. D. J. Wales and A. J. Stone, *Inorg. Chem.* 1987, **26**, 3845; D. J. Wales, D. M. P. Mingos and Z. Lin, *Inorg. Chem.* 1989, **28**, 2754; D. J. Wales and D. M. P. Mingos, *Polyhedron* 1989, **8**, 1933.
11. D. J. Wales and D. M. P. Mingos, *Inorg. Chem.* 1989, **28**, 2748.
12. See for example A. Carrington and A. D. McLachlan, *Introduction to Magnetic Resonance*. Chapman and Hall, London (1979).
13. N. F. Ramsey, *Phys. Rev.* 1950, **78**, 699; N. F. Ramsey, *Phys. Rev.* 1952, **86**, 243.
14. W. H. Flygare and J. Goodisman, *J. Chem. Phys.* 1968, **49**, 3122.
15. H. M. McConnell, *J. Chem. Phys.* 1957, **27**, 226.
16. W. H. Flygare, *Chem. Rev.* 1974, **74**, 653.
17. M. B. Hall and F. F. Fenske, *Inorg. Chem.* 1972, **11**, 768,
18. E. Clementi, D. L. Raimondi and W. P. Reinhardt, *J. Chem. Phys.* 1967, **47**, 1300.
19. P. F. Jackson, B. F. G. Johnson, J. Lewis, P. R. Raithby, M. McPartlin, W. J. H. Nelson, K. D. Rouse, J. Allibon and S. A. Mason, *J. Chem. Soc., Chem. Commun.* 1980, 294.
20. V. G. Albano, P. Chini, S. Martinengo, D. J. A. McCaffrey, D. Strumolo and B. T. Heaton, *J. Am. Chem. Soc.* 1974, **96**, 8106.
21. S. D. Wijeyesekera and R. Hoffmann, *Organometallics* 1984, **3** 949.
22. R. S. Mulliken, *J. Chem. Phys.* 1955, **23**, 1833.
23. J.-F. Halet, D. G. Evans and D. M. P. Mingos, *J. Am. Chem. Soc.* 1988, **110**, 87.
24. D. W. Hart, R. G. Teller, C.-Y. Wei, R. Bau, G. Longoni, S. Campanella, P. Chini and T. F. Koetzle, *Angew. Chem., Int. Edn Engl.* 1979, **18**, 779.
25. T. Chihara, Y. Matsuura and H. Yamazaki, *J. Chem. Soc., Chem. Commun.* 1988, 886.
26. P. J. Bailey and M. J. Duer, *J. Chem. Soc., Chem. Commun.* 1989, 1139.
27. R. W. Broach, L. F. Dahl, G. Longoni, P. Chini, A. J. Schulz and J. M. Williams, *Adv. Chem.* 1978, **167**, 93.
28. S. Martinengo, B. T. Heaton, R. J. Goodfellow and P. Chini, *J. Chem. Soc., Chem. Commun.* 1977, 39.

Polyhedron Vol. 10, No. 15, pp. 1759–1765, 1991
Printed in Great Britain

0277-5387/91 $3.00+.00
© 1991 Pergamon Press plc

THE SPECTROCHEMICAL PROPERTIES OF NON-CUBIC TRANSITION METAL COMPLEXES IN SOLUTIONS—II. MIXED TETRAGONAL DISTORTED NICKEL(II) PYRIDINE COMPLEXES IN METHANOL

K. KURZAK* and A. KOŁKOWICZ

Institute of Chemistry, Pedagogical University, 08-110 Siedlce, Poland

and

A. BARTECKI

Institute of Inorganic Chemistry and Metallurgy of Rare Elements, Technical University, 50-370 Wrocław, Poland

(*Received* 2 *July* 1990; *accepted* 22 *April* 1991)

Abstract—The electronic spectra of tetragonal nickel(II) complexes of the type $Ni(Py)_4L_2$ (where Py = pyridine and L = NCS, Cl, Br or I), have been measured in methanol solutions at room temperature. The experimental curves were resolved by Gaussian analysis. The various ligand-field parameters are discussed in terms of their chemical utility and their relation to ligand-field strengths. The ligand-field parameters were examined by two minimization algorithms: the Davidon–Fletcher–Powell method (gradient estimation) and the Powell method (non-gradient). The standard deviations of the parameters were obtained from the former. It was found that the stereochemistry of the complexes in methanol solution differed from that in chloroform solution or in the solid state.

The previous paper[1] presented the theoretical interpretation of the electronic spectra of tetragonal *trans*-$[Ni(Py)_4L_2]$ type complexes in a 10% solution of pyridine in chloroform. The values of the parameters presented for the solutions were comparable with those published before for the solid state.[2–6] These studies are intended to show the effect of methanol on the tetragonal distortion compared to chloroform (as well as the solid state).

EXPERIMENTAL

All the complexes were prepared according to the method of Nelson and Shepherd.[7] Carbon, hydrogen, nitrogen and nickel analyses were performed as before.[1] The measurement conditions for the electronic absorption spectra were the same as reported earlier.[1] The solutions were prepared by dissolving a weighed amount of the complex in methanol. All of the complexes are easily soluble in methanol and are electrolytes in these solutions.

The composition of the complex species in methanol solution has been confirmed by conductance measurements. The molar conductances were measured using the conductivity meter OK-102/1 and electrode OK-902 (Radelkis). The $Ni(Py)_4L_2$ (L = NCS, Cl, Br, I) complexes in methanol solution have the molar conductivity values 20, 72, 102 and 120 Ω^{-1} mol^{-1} cm^2, respectively. The value observed for the dithiocyanatotetrakis(pyridine) nickel(II) is well below the typical range of 1:1 electrolytes, indicating that the coordinated thiocyanate ion is not appreciably removed by the solvent. The molar conductivity of $Ni(Py)_4I_2$ corresponds to that of 1:2 electrolytes.[8] The molar conductivity values of dichloro and dibromo complexes are as expected[8] for 1:1 electrolytes.† More-

* Author to whom correspondence should be addressed.

† For 5×10^{-2} M solutions of $Ni(Py)_4X_2$ (X = Cl, Br, I) and 2.5×10^{-2} M solutions of $Ni(Py)_4(NCS)_2$ at 25°C, i.e. conditions for spectroscopy measurements. The molar conductivity values, measured under the same conditions are: NaCl, 87; NaBr, 101; NaSCN, 76; and KI 112 Ω^{-1} mol^{-1} cm^2, for 1:1 electrolytes.

over, the concentration of chloride ions in the methanol solution of $Ni(Py)_4Cl_2$, measured using the chloride ion sensitive electrode, confirms that the complex studied is a 1 : 1 electrolyte in methanol.

Methods

Spectra were resolved using the procedures described in detail in other work[1,9,10] (and references therein). There is also a description of the procedure used to make band assignments and calculate ligand-field parameters. For CFM calculations the full energy matrices reported by Perumareddi[11] were used. For AOM calculations the matrix elements of the excited states given by Hitchman[4] were used and the one-electron orbital energies given by Hitchman[12] were adopted. In order to apply them to the interpretation presented here (which does allow anisotropy of nitrogen atoms), the elements were zeroed with the $e_{\pi\parallel}$ parameter for a pyridine ligand. Because of the cylindrical symmetry of metal ligand interactions in the axial donor ligands, only one parameter $e_\pi(L)$ (L = NCS, Cl, Br, I) for the complexes was taken into account. The orbital energies for the complexes with different axial ligands are given elsewhere.[4,10,12] Since the orbital energies for the complexes are rather expressed as a function of the sum of the corresponding axial parameters, the AOM parameters were calculated fixing e_σ and e_π of one of the axial ligands.[10]

RESULTS AND DISCUSSION

General

The molar conductivity values of the $Ni(Py)_2Cl_2$ and $Ni(Py)_2Br_2$ complexes in methanol are as expected for 1 : 1 electrolytes, suggesting the formation of $[Ni(Py)_4L]L$ or $[Ni(Py)_4L(solv.)]L$ species (where L = Cl, Br, and solv. refers to solvent). On account of the strong preference of the high-spin nickel(II) ion for the octahedral surrounding, the creation of the first complex is not possible under the conditions of the experiment. Moreover, the calculations show that the parameters of σ-antibonding ability of the halogen ligands ($\sim$7 kK) are much greater than that for pyridine ($\sim$4 kK) for the supposed five-coordinate systems. The relation between these parameters is not in agreement with the data obtained before[1] for the bipyramidal site. Therefore, the formation of the six-coordinate mixed ion seems to be more probable and this one (i.e. $[Ni(Py)_4L(solv.)]L$ structure) was assumed. For the $[Ni(Py)_4(NCS)_2]$ complex in methanol solution we assumed the tetragonal symmetry with *trans*-thiocyanate ions. On account of the conductivity measurements for $Ni(Py)_4I_2$ which corresponded to 1 : 2 electrolytes, we treated that complex as $[Ni(Py)_4(solv.)_2]I_2$ species. The observed solution spectra (see Fig. 1) for all these compounds display only three absorption bands and they do not exhibit any spin-forbidden bands, except for $[Ni(Py)_4(NCS)_2]$. This last compound contains a shoulder related to a triplet–singlet transition at 13350 cm^{-1}.

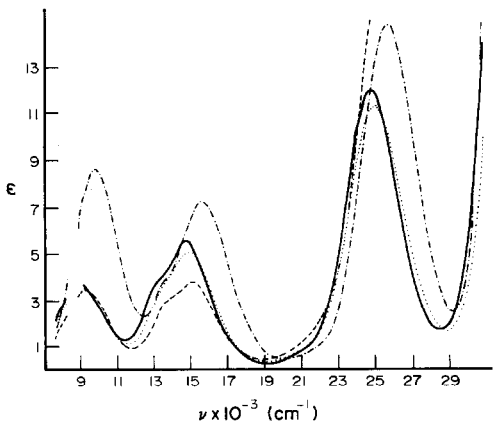

Fig. 1. Electronic absorption spectra of methanol solutions at room temperature of complexes: $[Ni(Py)_4Cl(MeOH)]Cl$, solid line; $[Ni(Py)_4Br(MeOH)]Br$, dot; $[Ni(Py)_4(MeOH)_2]I_2$, dash; $[Ni(Py)_4NCS_2]$, dash–dot.

The theoretical energy level diagram for nickel(II) ions indicates that as many as six triplet–triplet transitions may be observed in the electronic spectra of complexes with C_{4v} and D_{4h} symmetry. This results from tetragonal splittings that are small compared to their band-widths. The *d–d* spectrum may also be further complicated by the overlap of more intense charge-transfer or intramolecular (ligand) spectral bands [for instance in $Ni(Py)_4I_2$]. In general, the solution spectra at room temperature do not provide sufficient resolution to require consideration of the lower symmetry. The presented method assumes that spin–orbital coupling has an effect on the band-widths only in solution at room temperature. The site symmetry was assumed to be $D_{4h}(C_{4v})$ and the electronic spectra fitted this model. The spectra in methanol solution presented in this study differ significantly from those previously reported.[1] From the spectra in chloroform it was immediately evident that except for $[Ni(Py)_4(NCS)_2]$, tetragonal splittings Δ^1_{tetr} and Δ^2_{tetr} of $^3T_{2g}(t_{2g}^5e_g^3)$ and $^3T_{1g}(t_{2g}^5e_g^3)$, respectively, were observed.

The absorption spectrum of $Ni(Py)_4I_2$ in methanol solution consists of two spin-allowed bands at 9260 cm^{-1} and 15120 cm^{-1} (Fig. 2). The observed triplet tetragonal components are related to parent

Table 1. Assignments, observed and calculated transition energies of $Ni(py)_4X_2$ in methanol, in cm^{-1}

Excited state	$[Ni(py)_4(NCS)_2]^a$ Observed	Calculated CFM	Calculated AOM	$[Ni(py)_4(Cl)(MeOH)]Cl$ Observed	Calculated CFM	Calculated AOM	$[Ni(py)_4(Br)(MeOH)]Br$ Observed	Calculated CFM	Calculated AOM	$[Ni(py)_4(MeOH)_2]I_2^a$ Observed	Calculated CFM	Calculated AOM
$^3E(1)$	9507	8985	8985	8618	8403	8403	8686	8525	8522	8897	8363	8362
$^3B_2$	10,381	10,652	10,654	10,015	10,280	10,282	10,049	10,284	10,287	10,062	10,484	10,485
$^1A_1(1)$	13,306	13,465	13,464	12,876	13,212	13,210	13,147	13,314	13,310	13,412	13,259	13,262
$^1B_1(1)$	13,427	13,793	13,793	13,038	13,623	13,623	13,203	13,613	13,611	13,545	13,916	13,918
$^3A_2(1)$	15,264	15,067	15,066	14,604	14,286	14,285	14,810	14,489	14,488	14,806	14,356	14,356
$^3E(2)$	15,976	15,929	15,931	14,978	15,231	15,233	15,107	15,263	15,264	15,287	15,595	15,594
$^1E(1)$	21,597	22,409	22,410	21,278	21,651	21,651	21,257	21,780	21,774	21,284	21,831	21,831
$^1A_1(2)$	23,208	23,056	23,057	22,925	22,762	22,762	22,598	22,669	22,670	24,433	23,688	23,689
$^1B_2(1)$	23,984	23,999	24,002	23,482	23,433	23,435	23,450	23,430	23,429	24,504	23,866	23,868
$^3A_2(2)$	25,651	25,780	25,778	24,732	24,820	24,818	24,831	24,968	24,971	26,298	25,832	25,831
$^3E(3)$	25,957	26,408	26,407	25,148	25,547	25,546	25,280	25,609	25,615	26,369	26,798	26,796
$^1A_2$	26,945	26,473	26,468	26,085	25,690	25,688	26,368	25,993	25,989	25,597	25,932	25,936
$^1E(2)$	28,523	27,826	27,829	27,869	27,205	27,205	27,881	27,102	27,103	27,875	28,277	28,277
$^1B_1(2)$		34,608	34,612		33,440	33,440		33,469	33,466		34,300	34,299
$^1A_1(3)$		34,840	34,841		33,707	33,707		33,911	33,908		34,209	34,212
$^1B_2(2)$		35,054	35,058		33,911	33,911		33,937	33,934		34,835	34,834
$^1E(3)$		35,114	35,114		33,973	33,973		34,134	34,131		34,608	34,610
$^1A_1(4)$		58,783	58,788		57,480	57,480		57,554	57,544		58,416	58,420
r.m.s.		407	407		358	358		346	346		469	469

[a] For D_{4h} term assignments (first column) the "g" subscript is needed.

octahedral transitions $^3T_{2g}$ and $^3T_{1g}(F)$. The other components related to the parent octahedral transition $^3T_{1g}(P)$ are overlapped by a strong band in the near UV region, but allowed a weak shoulder at about 25,000–27,000 cm^{-1}. Figures 2–5 show the experimental spectra of all the studied complexes along with Gaussian components.

Table 1 shows a comparison of the experimental (Gaussian analysis) and theoretical energy levels together with their assignments for all the investigated complexes. The band assignment is based on fitting the resolved band maxima (Gaussian analysis) with the calculated transition energies (eigenvectors) using d^8 quadrate energy levels with full configuration interactions and without spin–orbit coupling. The extension of our calculations to include spin–orbit coupling would be desirable, but since no fine structure was detected the results would have little meaning.

The values of the crystal field, angular overlap and electron correlation parameters for all the investigated complexes are shown in Tables 2 and 3. The transition energies corresponding to these parameters are shown in Table 1.

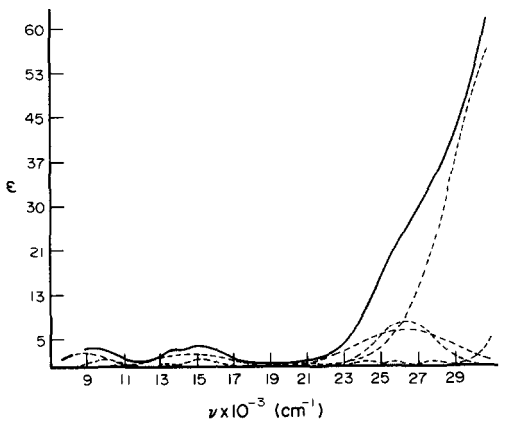

Fig. 2. Absorption spectrum of $Ni(Py)_4I_2$ in methanol solution: experimental spectrum, solid line; component bands, dash.

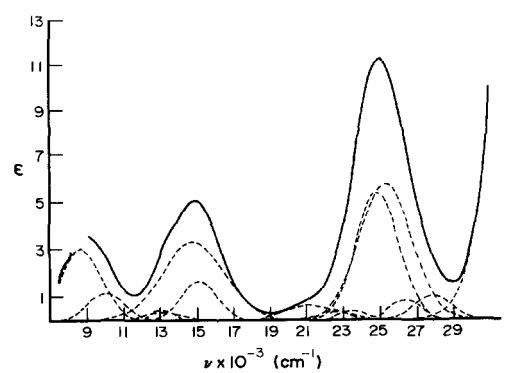

Fig. 3. Absorption spectrum of $Ni(Py)_4Br_2$ in methanol solution: experimental spectrum, solid line; component bands, dash.

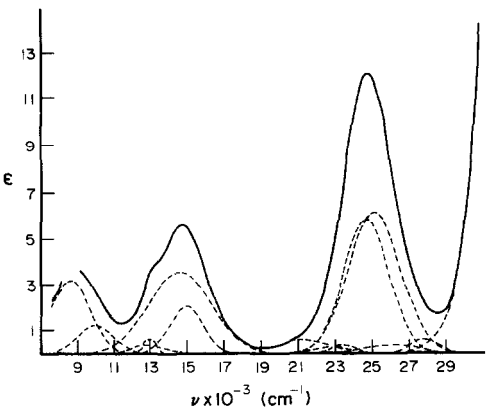

Fig. 4. Absorption spectrum of $Ni(Py)_4Cl_2$ in methanol solution: experimental spectrum, solid line; component bands, dash.

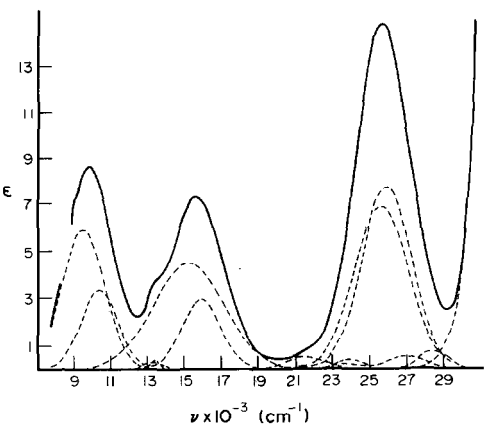

Fig. 5. Absorption spectrum of $Ni(Py)_4NCS_2$ in methanol solution: experimental spectrum, solid line; component bands, dash.

Analysis of the parameters

In the previous paper, the AOM parameters without anisotropy of pyridine were presented [i.e. averaging e_π(Py) values]. If the anisotropy of pyridine is taken into account, the AOM parameters are as given in Table 4. The e_σ and $e_{\pi\perp}$(Py) parameters for all these complexes in chloroform solution are slightly smaller (e_σ about 200 cm^{-1}) than those without anisotropy but e_π(L) is somewhat greater. This gives rise to a change in the ordering of the π-bonding series. Somewhat less π-antibonding ability of pyridine than of chloride is in agreement with Perumareddi's data.[13]

The bonding parameter values of the studied complexes in methanol solution suggest that, as

Table 2. Ligand field parameters (CFM) of $Ni(py)_4L_2$ complexes in methanol solution, in cm^{-1}

Parameter	L NCS	Cl	Br	I
Dq_N	1065(25)	1028(22)	1028(21)	1048(28)
Dq_L	746	671	690	651
Ds	−245(37)	−272(63)	−208(35)	−405(50)
Dt	−182(37)	−204(35)	−193(32)	−227(41)
B	868(28)	860(22)	859(21)	939(26)
C	3645(113)	3602(99)	3598(85)	3470(91)
C/B	4.20	4.19	4.19	3.69
No of bands	13	13	13	13

Table 3. Ligand field parameters (AOM) of $Ni(py)_4L_2$ complexes in methanol solution, in cm^{-1}

Parameter	L NCS	Cl	Br	I
e_σ(Py)	4399(58)	4049(33)	4003(42)	4522(52)
e_σ(L)	3451(63)	2840(41)	3057(53)	—
e_σ(MeOH)	—	3145[a]	3145[a]	3145(79)
$e_{\pi\parallel}$(Py)[b]	0	0	0	0
$e_{\pi\perp}$(Py)	635(49)	466(43)	431(51)	770(66)
e_π(L)	1358(55)	570(56)	568(70)	—
e_π(MeOH)	—	1500[a]	1500[a]	1500(43)
B	868(23)	859(17)	860(15)	939(21)
C	3646(74)	3602(81)	3595(65)	3471(72)
C/B	4.20	4.19	4.19	3.70
No of bands	13	13	13	13

[a] Fixed from $[Ni(Py)_4(MeOH)_2]I_2$.
[b] Assumed.

Table 4. Ligand field parameters (AOM) for *trans*-$[Ni(py)_4L_2]$ complexes in $CHCl_3$ solution with anisotropy of pyridine, in cm^{-1}

Parameter	L NCS This work	Cl Kurzak and Kołkowicz[b]	Br Kurzak and Kołkowicz[b]	I This work
e_σ(Py)	4378(72)	4243(58)	4298(36)	4396(31)
e_σ(L)	4018(86)	2506(71)	2329(94)	1435(66)
$e_{\pi\parallel}$(Py)[a]	0	0	0	0
$e_{\pi\perp}$(Py)	490(54)	438(48)	514(39)	528(33)
e_π(L)	1069(58)	663(88)	832(78)	320(40)
B	815(16)	887(15)	877(17)	1026(27)
C	3466(59)	3325(54)	3342(70)	3860(66)
C/B	4.26	3.75	3.81	3.75
No of bands	13	12	12	7

[a] Assumed.
[b] Reference 10.

expected, the σ-antibonding effects of the halide ions are considerably less than those of pyridine. The estimation of the e_σ parameters seems to be reasonable and quite similar to those reported for two mixed ligand complexes.[1] Both the dichloro and dibromo complexes in methanol are [Ni(Py)$_4$L (solv.)]L species (three mixed ligand complexes). As mentioned above for the complexes with different axial ligands, the AOM parameters were calculated by fixing the parameters for one ligand. These fixed values for the oxygen-donor of methanol (e_σ(O) = 3145, e_π(O) = 1500 cm^{-1}) were taken from the results obtained for [Ni(Py)$_4$(MeOH)$_2$]I$_2$ (see the last column in Table 3). The series for σ-bonding ability of the studied complexes is similar to that for the solid state and in chloroform solution. The σ-antibonding parameter for pyridine is dependent on the axial ligands. The e_σ(Py) in [Ni(Py)$_4$Cl(MeOH)]Cl is approximate to that of [Ni(Py)$_4$Br(MeOH)]Br, but is sightly different for [Ni(Py)$_4$(NCS)$_2$] and [Ni(Py)$_4$(MeOH)$_2$]I$_2$. Values of $e_{\pi\perp}$(Py) for the chloro and bromo complexes are very close (within the error limits), whilst they are somewhat greater for the other complex. It was deduced that the ligand-field strengths of the coordinated solvent are greater than those of the chloro and bromo ligands. That the σ-antibonding parameter is greater for the thiocyanate ion than for the oxygen-donor ligator (methanol) is in agreement with the low molar conductivity value which suggests that the thiocyanate ion is not appreciably substituted by the solvent molecules. Comparison of the results for both of the solutions (i.e. chloroform and methanol) shows a similar relation for the σ- and π-antibonding parameters.

The crystal field parameters of these complexes suggest that, in agreement with the crystal structures, the perturbation of the octahedral environment of the nickel(II) is an elongation along the z-axis. The reduction of the symmetry from O_h to C_{4v} corresponds to a weaker ligand field along the z-axis, i.e. $Dq_z < Dq_{xy}$. The splitting of all the parent cubic levels by the additional ligand field (in-plane) for all the complexes is shown in Fig. 6. This energy term diagram corresponds to tetragonally elongated octahedral systems.

The values of parameters calculated in this work are different from those presented by Kurzak and Bartecki.[1] The Racah B parameters (Tables 2 and 3) of halogen–pyridine systems are slightly less than those obtained from chloroform solution spectra and the C parameters are considerably greater. However, the B and C parameters are due to the free-ion values which are 1042 and 4060 cm^{-1}, respectively for nickel(II). An interesting fact is that the B and C parameters for the dithiocyanato complex are the same as for the chloro and bromo complexes ($C/B = 4.2$), although in chloroform these values were considerably different ($C/B = 4.2$ and 3.8, respectively). The Dq_N values are almost constant at about 1050 cm^{-1}, and they are somewhat less than those given by Kurzak and Bartecki[1] for chloroform solution spectra. No other definite trends for these parameters could be inferred for these tetragonal complexes.

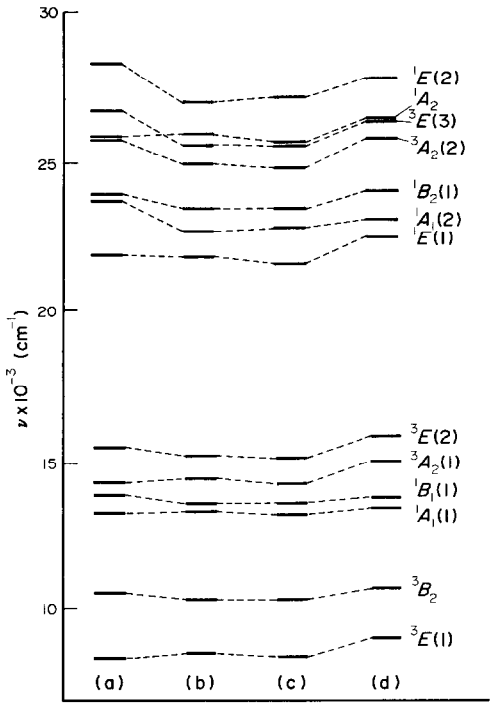

Fig. 6. Term energy diagrams of the complexes: (a) [Ni(Py)$_4$(MeOH)$_2$]I$_2$; (b) [Ni(Py)$_4$Br(MeOH)]Br; (c) [Ni(Py)$_4$Cl(MeOH)]Cl; (d) [Ni(Py)$_4$(NCS)$_2$].

REFERENCES

1. K. Kurzak and A. Bartecki, *Trans. Metal Chem.* 1988, **13**, 224.
2. D. A. Rowley and R. S. Drago, *Inorg. Chem.* 1967, **6**, 1092.
3. D. A. Rowley and R. S. Drago, *Inorg. Chem.* 1968, **7**, 795.
4. M. A. Hitchman, *Inorg. Chem.* 1972, **11**, 2387.
5. A. F. Schreiner and D. J. Hamm, *Inorg. Chem.* 1973, **12**, 2037.
6. J. S. Merriam and J. R. Perumareddi, *J. Phys. Chem.* 1975, **79**, 142.
7. S. M. Nelson and T. M. Shepherd, *J. Chem. Soc.* 1965, 3276.

8. W. J. Geary, *Coord. Chem. Rev.* 1971, **7**, 81.
9. K. Kurzak, A. Kołowicz and A. Bartecki, *Bull. Pol. Acad. Sci., Ser. Sci. Chim.* 1989, **37**, 423.
10. K. Kurzak and A. Kołowicz, *Spectrochim. Acta* 1990, **46A**, 1231.
11. J. R. Perumareddi, *J. Phys. Chem.* 1972, **76**, 3401.
12. M. A. Hitchman, *Inorg. Chem.* 1974, **13**, 2218.
13. J. R. Perumareddi, *Polyhedron* 1988, **8**, 2283.

Polyhedron Vol. 10, No. 15, pp. 1767–1771, 1991
Printed in Great Britain

0277–5387/91 $3.00+.00
© 1991 Pergamon Press plc

COMPLEX FORMATION OF MONOMERIC AND DIMERIC COPPER(II) COMPLEXES WITH CREATININE IN ORGANIC MEDIA

M. MITEWA,* G. GENCHEVA and I. IVANOVA

Department of Chemistry, University of Sofia, 1126 Sofia, Bulgaria

and

E. ZHECHEVA and D. MECHANDJIEV

Institute of General and Inorganic Chemistry, Bulgarian Academy of Sciences, 1113 Sofia, Bulgaria

(*Received* 16 *January* 1991; *accepted* 22 *April* 1991)

Abstract—New monomeric and dimeric copper(II) complexes with creatinine were synthesized in organic media. Formation of different complex species depending on the reaction medium was proved. Using spectroscopic (EPR and IR) and magnetochemical methods, the structure of the complexes obtained was studied.

In our earlier study on the complexation between copper(II) and creatinine (**I**) in aqueous solution, the formation of a monomeric copper(II) complex with a 1 : 2 metal-to-ligand ratio was proved.[1]

By studying the complex formation of creatinine with different metal ions, however, we have found that different complex species are formed depending on the reaction conditions.[2–11] In some cases oligomeric species were obtained,[2,6,8,11] thus proving the ability of creatinine to serve as a bridging ligand, similar to the nucleobases.[12] On the other hand, it has already been shown that in organic solvents dimeric copper(II) complexes with bridging ligands are formed in some cases.[13,14] For that reason the aim of the present study was to obtain dimeric complexes of copper(II) from the copper(II)–creatinine reaction in organic media (methanol and acetonitrile).

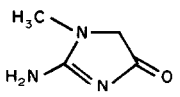

(I)

*Author to whom correspondence should be addressed.

EXPERIMENTAL

Synthetic and analytical procedures

$Cu(creat)_4(OCH_3)_2$ (**1**) (creat = *creatinine*, *bright green*, $\lambda_{Max} = 430$, 670 nm). $Cu(NO_3)_2 \cdot 3H_2O$ (0.1208 g, 0.5 mmol) and creatinine (0.3394, 3.0 mmol) in a 1 : 6 molar ratio were dissolved in 20 cm^3 of methanol. The mixture was refluxed (50–60°C) under constant stirring for 15 min, resulting in the formation of a bright green residue. The latter was filtered off, washed repeatedly with acetone and dried over P_4O_{10} for 2–3 days. Found: C, 37.0; H, 6.0; N, 29.5; Cu, 10.6. Calc.: C, 37.4; H, 5.9; N, 29.1; Cu, 11.0%.

$Cu_2(creat)_6$ (**2**) (*blue–green*, $\lambda_{max} = 438$, 680 nm). $Cu(NO_3)_2 \cdot H_2O$ (0.1208 g, 0.5 mmol) and creatinine (0.4525 g, 4.0 mmol) were dissolved in 20 cm^3 of acetonitrile. The mixture was refluxed (50–60°C) under constant stirring for 1 h, resulting in the formation of a blue–green residue. The latter was filtered off, washed repeatedly with acetone and dried over P_4O_{10} for 2–3 days. Found: C, 35.5; H, 5.0; N, 31.5; Cu, 16.0. Calc. C, 35.8; H, 4.7; N, 31.5; Cu, 15.8%.

$Cu_2(creat)_4$ (**3**) (*reddish-brown*, $\lambda_{max} = 450$ nm). $Cu(NO_3)_2 \cdot 3H_2O$ (0.1208 g, 0.5 mmol) and creatinine (0.4525 g, 4.0 mmol) was dissolved in ace-

tonitrile and refluxed (50–60°C) under constant stirring for 6–7 h, resulting in the formation of a reddish-brown precipitate. The latter was filtered off, washed repeatedly with acetone and dried over P_4O_{10} for 2–3 days. Found: C, 33.3; H, 4.7; N, 29.8; Cu, 21.4. Calc.: C, 33.4; H, 4.2; N, 29.2; Cu, 22.1%.

The compositions of the complexes were determined by elemental analysis, the copper content being determined complexometrically.

Materials and apparatus

The electronic, IR and EPR spectra were recorded on a Specord UV–vis (Carl–Zeiss, Jena), a Perkin–Elmer 983 spectrometer (CsI discs, spectral range 4000–200 cm^{-1}) and an X-band EPR Bruker B-ER 420 spectrometer (g-marker DPPH, temperature range 130–300 K), respectively. The magnetic susceptibility was determined in argon atmosphere by the Faraday method in the range 150–350 K. TG and DTA measurements were carried out with Panton Red Croft 781, appart STA.

All reagents used were of AR grade and the solvents (methanol, deuteriated methanol and acetonitrile) were of spectroscopic grade (Uvasol, Merck).

RESULTS AND DISCUSSION

The first reaction products obtained in different solvents (**1** and **2**) differ significantly in content and structure. Products **2** and **3** were obtained consequently in the course of the copper(II)–creatinine interaction in acetonitrile.

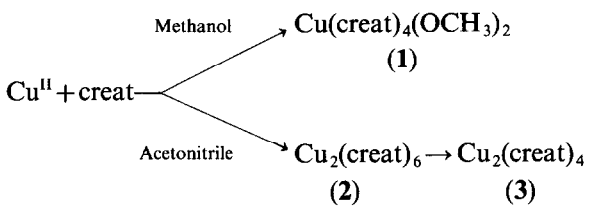

In the protic solvent methanol, the copper(II)–creatinine interaction resulted in the formation of monomeric species and their inner coordination sphere deprotonated solvent molecules were also included. [The autoprotolytic constant of methanol is rather high ($pK_a = 16.9$)[15] and creatinine itself contains the $—NH_2$ group.] The coordination of deprotonated solvent molecules was proved by means of the kinetic isotopic effect. For this purpose the copper(II)–creatinine reaction was carried out in deuterated methanol (CD_3OD) under the same conditions as described for compound **1** in the Experimental. It was found that over 2 h no precipitate was formed thus indicating the coordination of deprotonated methanol.

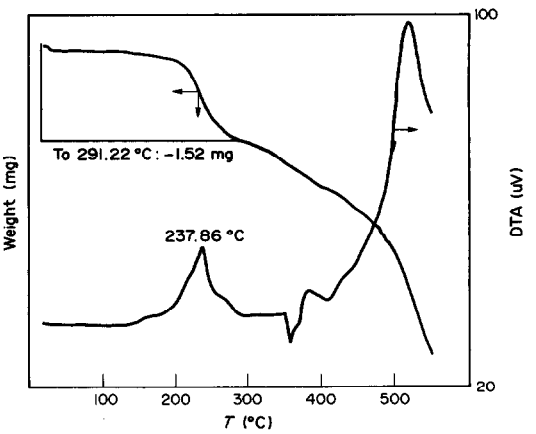

Fig. 1. TG and DTA curves for $Cu(creat)_4(OCH_3)_2$ (**1**).

In order to check this supposition, TG and DTA measurements on **1** were also performed; the data obtained are shown in Fig. 1. It is evident that above 200°C a small mass of the compound was abstracted. This is most likely due to abstraction of two CH_3O^- groups, as the metal alkoxides proved to be rather stable.[16]

In contrast to methanol, in the aprotic solvent acetonitrile, the first reaction product (**2**) was found to be a dimeric copper(II) species. This fact should most probably be connected with the poorer coordination properties of acetonitrile, thus allowing creatinine to act as a bridging ligand.

The reaction in acetonitrile resulted in the formation of another dimeric copper(II) complex (**3**), thus proving the formation of dimeric complexes of copper(II) with the bridging ligand creatinine in organic solvents.

Structure of the complexes

In order to obtain information concerning the structure and coordination mode of the ligand, magnetochemical and spectroscopic (IR and EPR) studies were performed.

The magnetochemical data obtained are represented in Fig. 2. The μ_{eff} values obtained confirm the supposition of the monomeric structure for **1** and the dimeric structure for **2** and **3** (2.0, 1.5 and 1.6 BM, respectively). On the other hand, the temperature dependence of the corresponding μ_{eff} values show a significant difference in the copper(II) stereochemistry.

It is evident that μ_{eff} of **1** is temperature independent, indicating an octahedral structure for the

Table 1. EPR data for the complexes (polycrystalline samples)

Temperature (K)	$Cu(creat)_4(OCH_3)_2$ (1) $g_\perp$ ±0.002	$g_\parallel$ ±0.002	$A_\parallel$(Oe) ±2	$Cu_2(creat)_6$ (2) $g_\perp$ ±0.002	$g_\parallel$ ±0.002	$Cu_2(creat)_4$ (3) g' ±0.02	$g_\perp$ ±0.002	$g_\parallel$ ±0.002
130	2.064	2.400	162	2.044	2.306	2.94	2.066	2.398
300	2.064	2.038	—	2.052	2.294	—	2.066	2.398

Table 2. IR data for the ligand and the complexes[a]

Compound	$\nu_{as}(NH_2)$	$\nu_s(NH_2)$	ν(NH)	ν(C=O)	ν(C=N)	δ(NH)	ν(C—O)
Creatinine	3254 br	3040 br	—	1685	1595	1660	—
$Cu(creat)_4(OCH_3)_2$	3250 br	3150 br	—	1695	1640	1660 sh	1050
$Cu_2(creat)_6$	~ 3260 br	3150 br	~ 3220 br	1705 1690	1640 1650	1665	—
$Cu_2(creat)_4$	—	—	~ 3220 br	1685	1640	—	—

[a]br = broad; sh = shoulder.

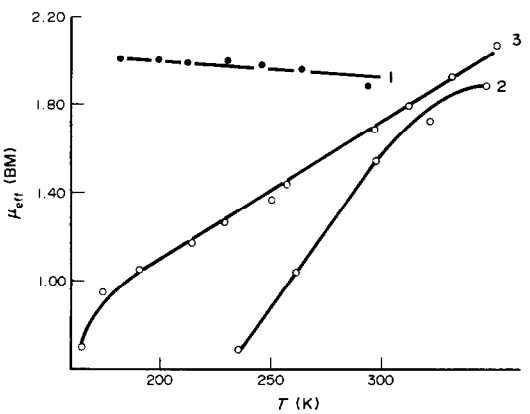

Fig. 2. Temperature dependence of the magnetic moments (μ_{eff}) of the complexes: (1) $Cu(creat)_4(OCH_3)_2$ (1), (2) $Cu_2(creat)_6$ (2) and (3) $Cu_2(creat)_4$ (3).

complex.[17] The EPR data obtained (Table 1) are in agreement with these results. The anisotropic g values obtained ($g_\parallel \gg g_\perp > 2.0$) for **1** correspond to an elongated octahedral structure with a $d_{x^2-y^2}$ ground state.[18] The polycrystalline EPR parameters were found to be temperature independent. A four-component $^{63,65}Cu$ ($I = 3/2$) hyperfine splitting is readily observed in the $g_\parallel$ component allowing evaluation of $A_\parallel$. It should be mentioned that in frozen DMF solution, a poorly resolved nine-component shfs due to four ^{15}N ($I = 1$) atoms ($A_n \sim 13$ G) is also observed, thus indicating coordination via the nitrogen atom of the ligand.

Additional information concerning the coordination mode of the ligand was obtained by studying the IR spectra of the ligand and the complexes (Table 2). It is evident that >C=O and the NH_2-stretching vibrations of complex **1** are observed at higher frequencies than those of the free ligand.* These data indicate coordination via the endocyclic nitrogen atom, as already proved by X-ray diffraction, for platinum(III)–creatinine complexes.[3,4,10]

A band at 1050 cm^{-1} is also observed (absent in the spectra of complexes **2** and **3** and the free ligand) which might be ascribed to the C—O vibration.

On summarizing all the data obtained for the complex, it might be suggested that as a result of a copper(II)–creatinine interaction in methanol, a monomeric copper(II) complex is formed with an elongated octahedral structure (**II**), four creatinine molecules being present in the xy plane and two CH_3O groups occupying the fifth and sixth coordination sites.

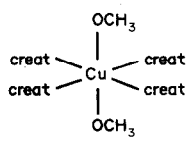

(II)

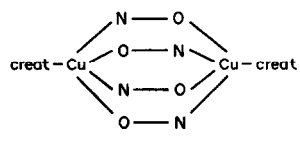

(III)

In contrast to methanol, when acetonitrile was used as solvent the first step of the copper(II)–creatinine interaction resulted in the formation of the

*Most probably due to hydrogen bond interactions between the creatinine molecules.

Table 3. EPR data for the solutions of the complexes in different solvents (T = 130 K)

Solvent	$Cu(creat)_4(OCH_3)_2$ (1)				$Cu_2(creat)_6$ (2)				$Cu_2(creat)_4$ (3)		
	$g_\perp$ ±0.002	$g_\parallel$ ±0.002	$A_\parallel$(Oe) ±2	A_N(Oe) ±0.5	$g_\perp$ ±0.002	$g_\parallel$ ±0.002	$A_\parallel$(Oe) ±2	A_N(Oe) ±0.5	$g_\perp$ ±0.002	$g_\parallel$ ±0.002	$A_\parallel$(Oe) ±2
Formamide	—	—	—	—	2.054	2.277	162	—	2.051	2.260	171
Water	2.053	2.310	144	—	2.053	2.311	144	—	2.056	2.290	157
DMSO	2.053	2.316	144	—	2.054	2.306	144	—	—	—	—
DMF	2.053	2.203	160	12.7	2.054	2.313	140	12.7	—	—	—

DMSO = dimethylsulphoxide; DMF = dimethylformamide.

dimeric copper(II) creatinine complex (**2**) ($\mu_{eff} \sim 1.5$ BM (Fig. 2). In its EPR spectrum a signal with very low intensity and $g = 2.94$ is observed (Table 1), typical for a half-field transition in a copper(II) dimeric species.[14] It may be suggested that in acetonitrile (solvent with weaker coordination properties) the creatinine molecules act as bridging ligands resulting in the formation of the dimeric complex (**III**).

The IR data obtained are in agreement with this supposition. In contrast to the monomeric complex, in the IR spectrum of **2**, two pairs of bands ascribed to ν(C=O) and ν(C=N) are observed (Table 2) due to two types of coordination modes existing. Evidently the ν(C=O) band at 1690 cm^{-1} should be ascribed to the vibration of the bridging ligands and the other band present at higher frequency (1705 cm^{-1}) to the creatinine molecules coordinated as monodentate ligands via the endocyclic nitrogen atom.

As no counterions were found in complex molecules, it may be expected that the positive charge of both copper(II) ions is balanced by four deprotonated creatinine molecules, e.g. four amido anions. In accordance with this supposition, in the IR spectrum of complex **2**, in addition to the two bands ascribed to ν_{as} and ν_s, a new band at $\sim$ 3220 cm^{-1} is also observed. The latter is due most probably to a NH-stretching vibration.

Summarizing the experimental data obtained, a dimeric structure (**III**) is proposed, the latter being consistent with the analytical, magnetochemical and EPR data. As is well documented,[17] the strong temperature dependence of μ_{eff} and the coordination number of five indicate a structure differing significantly from octahedral or square-planar, and most likely a square-pyramidal structure should be expected.

As was mentioned above, in the last step of the reaction in acetonitrile a brown-coloured, almost insoluble,* dimeric copper(II) complex (coordination number four) is obtained. [In this case no signal due to the half-field transition of dimeric copper(II) species was observed, most probably because of the significant broadness of the main EPR signal.] The spectroscopic data (anisotropic EPR signal and the presence of only one band at 450 nm in the visible spectrum) and the strong temperature dependence of μ_{eff} (Fig. 2) again indicate a different stereochemistry. In agreement with a coordination number of four and the IR data obtained (Table 2), structure **IV** may be proposed. In this case the four ligands (as amido anions) act as bridging ligands and therefore only one ν(C=O) (with rather low frequency) and one ν(C=N) band are present in the IR spectrum. As is indicated in Table 2, in this case no bands due to $\nu_{as}(NH_2)$ and $\nu_s(NH_2)$ are observed and only the band at $\sim$ 3220 cm^{-1}, ascribed to the ν(NH) of the amide anion, is present.

In order to obtain some information concerning the structure of the complexes in solution their EPR spectra in different solvents were recorded (Table 3).

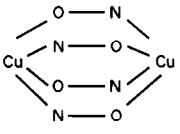

(IV)

It is evident that the EPR parameters obtained for the monomeric complex **1** are different from the corresponding values of the polycrystalline sample, and the $g_\parallel$ and $A_\parallel$ are solvent dependent. This fact may be explained by the $Cu(creat)_4(OCH_3)_2$–solvent interaction.

Rather surprisingly, the EPR parameters obtained for the frozen solutions of the dimeric complex **2** are the same as those for the monomeric complex **1** (Table 3). These data indicate that the

* Showing only low solubility in high-polar solvents (formamide, water).

dissolution of both **1** and **2** results in the formation of one and the same copper(II) complex in the corresponding solvent. Taking into account that in all cases $g_{\parallel} > g_{\perp} > 2.0$, it may be supposed that the monomeric complex $Cu(creat)_4S_2$ (S = solvent molecule) with an elongated octahedral structure is formed, that is to say for **1**, the dissolution is connected with substitution of $^{-}OCH_3$ by solvent molecules and for **2**, with destruction of the dimeric structure. The fact that in a frozen solution of DMF a partially resolved signal due to four ^{15}N ($I = 1$) is observed supports the supposition for the presence of four creatinine molecules in the xy plane (coordination via nitrogen atom).

The dimeric complex **3** proved to be only partially soluble in formamide and water. The EPR data obtained are different from those observed for solutions of **1** and **2** and are also solvent dependent. It might be supposed, therefore, that solvent interaction of the dimeric $Cu_2(creat)_4$ complex also occurs.

REFERENCES

1. M. Mitewa, K. Kabassanov and P. R. Bontchev, *Polyhedron* 1985, **4**, 1159.
2. P. R. Bontchev, M. Mitewa, G. Gencheva, J. Macicek, O. Angelova and V. I. Nefedov, *Proc. 11th Conf. Coord. Chem.*, p. 37. Smolenice, CSSR (1987).
3. M. Mitewa, G. Gencheva, P. R. Bontchev, O. Angelova and J. Macicek, *Polyhedron* 1988, **7**, 1273.
4. M. Macicek, O. Angelova, G. Gencheva, M. Mitewa and P. R. Bontchev, *J. Cryst. Spectr. Res.* 1988, **18**, 651.
5. M. Mitewa, G. Gencheva and P. R. Bontchev, *Proc. 12th Conf. Coord. Chem.*, p. 253. Smolenice, CSSR (1989).
6. P. R. Bontchev, M. Mitewa and G. Gencheva, *Pure Appl. Chem.* 1989, **61**, 897.
7. M. Mitewa, G. Gencheva, P. R. Bontchev, E. Zhecheva and V. I. Nefedov, *Inorg. Chim. Acta* 1989, **164**, 201.
8. G. Gochev, N. D. Yordanov, G. Gencheva, M. Mitewa and P. R. Bontchev, *Electron Magnetic Resonance of Disordered Systems* (Edited by N. D. Yordanov), p. 377. World Scientific, Singapore (1989).
9. M. Mitewa, G. Gencheva, S. Simova and V. I. Nefedov, *C. R. Acad. Bulg. Sci.*, in press.
10. G. Gencheva, M. Mitewa, P. R. Bontchev, G. Gochev, J. Macicek, E. Zhecheva and N. D. Yordanov, *Polyhedron*, in press.
11. G. Gencheva, I. Ivanova and M. Mitewa, *J. Prakt. Chem.*, in press.
12. B. Lippert, *Prog. Inorg. Chem.* 1989, **37**, 1.
13. Y. Nishida and S. Kida, *Bull. Chem. Soc. Japan* 1985, **58**, 383.
14. D. M. L. Goodgame, Y. Nishida and R. E. P. Winpenny, *Bull. Chem. Soc. Japan* 1986, **59**, 344.
15. O. Budevsky, *Osnovi na Analytichnata Khimia*, p. 141. Nauka i Izkustvo, Sofia (1969).
16. D. C. Bradley, *Prog. Inorg. Chem.* 1960, **2**, 303.
17. B. N. Figgis and J. Lewis, 1964, **6**, 37.
18. B. Hathaway, *Struct. Bond.* 1984, **57**, 55.

Polyhedron Vol. 10, No. 15, pp. 1773–1778, 1991
Printed in Great Britain

0277–5387/91 $3.00+.00
© 1991 Pergamon Press plc

TEMPLATE REACTIONS BETWEEN BIS(3-NITRO-2,4-PENTANEDIONATO)COPPER(II) AND α,ω-DIAMINOALKANES IN N,N-DIMETHYLFORMAMIDE SOLUTION

MANABU FUJIWARA* and HISANOBU WAKITA

Department of Chemistry, Faculty of Science, Fukuoka University, Nanakuma, Jonan-ku, Fukuoka 814-01, Japan

and

TAKAYUKI MATSUSHITA

Department of Material Chemistry, Faculty of Science and Technology, Ryukoku University, Seta, Ohtsu 520-21, Japan

(*Received* 22 *January* 1991; *accepted* 22 *April* 1991)

Abstract—The 1:2 adducts of bis(3-nitro-2,4-pentanedionato)copper(II) with ethylenediamine, 1,3-diaminopropane and 1,4-diaminobutane have been isolated and characterized. These adducts have been considered to be intermediates in the formation of the corresponding tetraaza macrocyclic complexes and a template reaction mechanism is proposed.

Reactions of coordinated ligands of metal complexes have been shown to be potentially very useful for their applications to organic syntheses and clarification of the reaction mechanisms involved in living processes. For example, metal chelates of acetylacetonates have been extensively investigated in the reaction with nucleophiles such as nitro[1] and halogen[2] groups. Recently, the metal chelates with acetylacetones having electron-withdrawing substituents on their γ-positions have been reported to exhibit much higher reactivities for amines, and thus these can be applied to the synthesis of tetraaza macrocycles by the so-called template synthesis.[3a–d] The role of metal ions in template reactions has been discussed based on their functions as Lewis acids, as reagents controlling free amine concentration or as genuine templates.[4]

Previously, we have reported that nickel(II) ions are superior to copper(II) ions as template metal ions in the reaction between [dibenzoyl-bis(β-ketoiminato)]metal(II) and ethylenediamine.[5] However, we have also shown that a copper(II) ion can function as a template ion when it is coordinated with acetylacetones having strong electron-withdrawing substituents such as nitro groups.[6]

In this paper we describe the template reactions between a copper(II) complex, bis(3-nitro-2,4-pentanedionato)copper(II), and α,ω-diaminoalkanes such as ethylenediamine, 1,3-diaminopropane and 1,4-diaminobutane in N,N-dimethylformamide (DMF). In addition, the reaction mechanism for the template reaction will be discussed.

EXPERIMENTAL

Materials

All reagents were of reagent grade. DMF was distilled over CaH_2 under reduced pressure before use. Other solvents were purified by the usual manner.

Measurements

UV and visible absorption spectra were recorded on a Hitachi 340 recording spectrophotometer. IR

* Author to whom correspondence should be addressed.

spectra of dimethyl sulphoxide solutions were recorded on a Hitachi 215 grating spectrophotometer by the use of TlI cells with a lead spacer (0.3 mm).

Preparation of bis(3-nitro-2,4-pentanedionato)-copper(II), $Cu(3\text{-}NO_2acac)_2$

This complex was prepared according to the literature.[1]

Preparation of ethylenediamine adduct of $Cu(3\text{-}NO_2acac)_2$, $Cu(3\text{-}NO_2acac)_2 \cdot en_2$

To a suspension of $Cu(3\text{-}NO_2acac)_2$ (5.0 g, 1.4×10^{-2} mol) in ethanol (200 cm^3) was added a slight excess of ethylenediamine (2.0 g, 3.3×10^{-2} mol). The green colour of the complex turned grey immediately. The mixture was stirred at room temperature for 3 h and cooled in an ice–water bath. The resulting grey precipitates were collected on a glass filter, washed with cold ethanol, and dried *in vacuo*. Found: C, 35.7; H, 6.0; N, 17.7. Calc. for $CuC_{14}H_{28}N_6O_8$: C, 35.6; H, 6.0; N, 17.8%.

Other diamine adducts, $Cu(3\text{-}NO_2acac)_2 \cdot pn_2$ and $Cu(3\text{-}NO_2acac)_2 \cdot bn_2$, were obtained by a similar method to that described above, where pn and bn denote 1,3-diaminopropane and 1,4-diaminobutane. In the case of the latter 1:2 adduct, the diamine (4.5 g, 5.6×10^{-2} mol) was required in order to isolate it.

RESULTS AND DISCUSSION

The 1:2 diamine adducts of $Cu(3\text{-}NO_2acac)_2$ and $Cu(3\text{-}NO_2acac)_2 \cdot L_2$, could be isolated by the reaction of $Cu(3\text{-}NO_2acac)_2$ with a diamine (L) in absolute ethanol, where L is ethylenediamine, 1,3-diaminopropane or 1,4-diaminobutane. These adducts were characterized by IR spectra, visible absorption spectra and elemental analyses. The absorption spectral changes of the adducts in hot DMF solution indicate that they may be considered as intermediates in the formation of tetraaza macrocyclic complexes.

IR spectra

The diamine adducts of $Cu(3\text{-}NO_2acac)_2$ were examined by measuring their IR spectra in both solid and solution states. Since these adducts are almost insoluble in non-coordinating solvents such as dichloromethane and chloroform, dimethyl sulphoxide (DMSO) was employed. The DMSO solution spectra are almost the same as those observed in the solid state.[7] The DMSO solution IR spectral data for the diamine, the parent complex and the diamine adducts are shown in Table 1. The IR spectra of the three diamine adducts in the 4000 to 650 cm^{-1} region are quite similar to each other and exhibit characteristic absorption bands around 3400, 3250, 1640, 1580 and 765 cm^{-1}. The bands

Table 1. IR spectral data of diamines, $Cu(3\text{-}NO_2acac)_2$ and its diamine adducts in DMSO

Compound	IR peak (cm^{-1}) ν(N—H)	ν(C—H)	ν(C=O) $+\delta$(HNH)	$\rho(NH_2)$ $+\rho(CH_2)$
en	3360	2850	1600[a]	820
	3290		1600	
pn	3360	2860	1600[a]	870
	3290		1610	765
bn	3280	2860	1660[a]	860
	3210		1600	
$Cu(3\text{-}NO_2acac)_2$			1655	830
			1590	
$Cu(3\text{-}NO_2acac)_2 \cdot en_2$	3420		1640[a]	765
	3230		1580	
	3130			
$Cu(3\text{-}NO_2acac)_2 \cdot pn_2$	3440		1640[a]	830
	3250		1585	765
	3130			
$Cu(3\text{-}NO_2acac)_2 \cdot bn_2$	3450		1640[a]	765
	3250		1580	

[a] Weak absorption band.

at 3400 and 3250 cm^{-1} can be assigned to N—H stretching vibrations due to coordinating diamines; those at 1640, 1580, and 765 cm^{-1} to N—H bending, C=O stretching and a combination of N—H and C—H deformation vibrations, respectively.

It should be noticed that no absorption band around 1700 cm^{-1} is observed due to uncoordinated, free carbonyl moieties of 3-nitro-2,4-pentanedionato groups. These results indicate that the configurations of the diamine adducts in DMSO are maintained in the solid state: the 3-nitro-2,4-pentanedionato groups act as bidentate ligands and the diamine groups coordinate with copper(II) as unidentate ligands. That is, the central copper(II) ions in the diamine adducts are surrounded by donor sets of N_2O_4.

Electronic spectra of copper(II) complexes

Figure 1 shows the electronic spectra of the DMF solutions of the parent complex, $Cu(3\text{-}NO_2acac)_2$, its ethylenediamine adduct, $Cu(3\text{-}NO_2acac)_2 \cdot en_2$, and the macrocyclic compound, $Cu(NO_2\text{-}N_4[14])$, which was obtained in the template reaction of $Cu(3\text{-}NO_2acac)_2$ with ethylenediamine.

The electronic spectrum of $Cu(3\text{-}NO_2acac)_2$ exhibits an absorption band at 14,900 cm^{-1} (672 nm) in the visible region, which can be assigned to ligand field transitions. In the spectrum of its ethylenediamine adduct, the absorption peak is observed at 18,200 cm^{-1} (548 nm). This higher energy shift by 3300 cm^{-1} may be caused by the additional coordination of two molecules of ethylenediamine to the parent complex. On the other hand, in the absorption spectrum of $Cu(NO_2\text{-}N_4[14])$, the absorption band is observed at 17,200 cm^{-1} (580 nm), which can also be assigned to ligand field transitions. The lower energy shift by 1000 cm^{-1} compared to that of the adduct may be due to the transformation from the distorted octahedral $Cu(3\text{-}NO_2acac)_2 \cdot en_2$ to the square planar $Cu(NO_2\text{-}N_4[14])$.

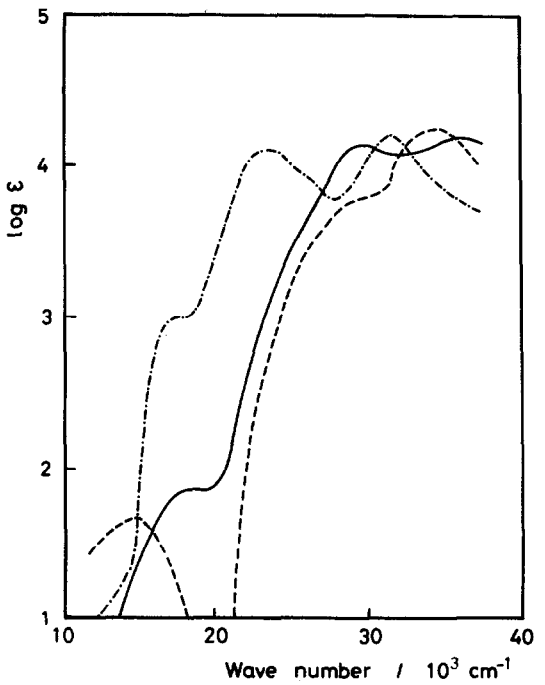

Fig. 1. Electronic spectra of copper(II) complexes in DMF. (·····): $Cu(3\text{-}NO_2acac)_2$; (———): $Cu(3\text{-}NO_2acac)_2 \cdot en_2$; and (–·–·–·–): $Cu(NO_2\text{-}N_4[14])$.

Absorption spectra of the parent complex and its diamine adducts in DMF and DMSO solutions

The absorption spectroscopic data for the parent complex and its diamine adducts in DMF and DMSO are summarized in Table 2. The spectrum of the parent complex in DMF solution has three absorption bands at 676, 337 and 285 nm. That of the ethylenediamine adduct has absorption bands at 549, 336 and 278 nm. Although the band positions in the UV region are almost the same as each other, those in the visible region are different; the absorption peak of the adduct is shifted to shorter wavelengths by approximately 130 nm compared to that of the parent complex. The absorption bands of the 1,3-diaminopropane and 1,4-diaminobutane adducts in the visible region are also shifted to shorter wavelengths by approximately 95 and 85 nm, respectively, compared to that of the parent complex. These shifts are smaller than that observed in the case of ethylenediamine and may

Table 2. Absorption spectral data of $Cu(3\text{-}NO_2acac)_2$ and its diamine adducts in DMF and DMSO solutions

Complex	λ/nm (log ε) in DMF	in DMSO
$Cu(3\text{-}NO_2acac)_2$	676(1.75)	730(1.64)
	337(3.80)	332(3.98)
	285(4.07)	290(4.28)
$Cu(3\text{-}NO_2acac)_2 \cdot en_2$	549(1.88)	550(1.92)
	336(4.17)	339(4.16)
	278(4.21)	279(4.19)
$Cu(3\text{-}NO_2acac)_2 \cdot pn_2$	581(2.06)	578(2.08)
	338(4.16)	341(4.15)
	279(4.26)	280(4.27)
$Cu(3\text{-}NO_2acac)_2 \cdot bn_2$	591(1.94)	594(2.03)
	337(4.13)	340(4.12)
	281(4.23)	280(4.20)

arise from the coordination of diamine molecules to the parent complex. Therefore, it can concluded that coordination bonds between the diamines and the copper(II) ions are stronger in the order ethylenediamine ≫ 1,3-diaminopropane > 1,4-diaminobutane.

All the absorption spectra of these copper(II) complexes in DMSO have three absorption peaks in the UV and visible regions as well as those in DMF. Moreover, the peak positions of the diamine adducts are quite similar to those in DMF. However, the spectrum of the parent complex in DMSO is significantly different from that in DMF, particularly in the visible region. The absorption peak in DMF is observed at 676 nm, which is shifted to shorter wavelengths by about 50 nm compared to that in DMSO. These results suggest that DMF molecules weakly coordinate to the copper(II) ion of $Cu(3\text{-}NO_2acac)_2$.

On the other hand, the fact that the absorption peaks of each diamine adduct are observed at the same positions in DMF and DMSO indicates that these solvent molecules cannot coordinate to the central copper(II) ion of the adducts because the coordination sites of the copper(II) ion in the adducts are already occupied with two nitrogen atoms of the diamines and four oxygen atoms of the 3-nitro-2,4-pentanedianato groups.

It has been reported that in the ethylenediamine adduct of bis(2,4-pentanedionato)copper(II), the central copper(II) ion is surrounded by a donor set of N_4O_2: two molecules of the diamine act as bidentate ligands and two 2,4-pentanedionato groups act as unidentate ligands.[8] This adduct has been found to be very labile and decomposes with elimination of the ethylenediamine. On the contrary, in the present diamine adducts of $Cu(3\text{-}NO_2acac)_2$, β-diketonato ligands act as bidentate ligands and two molecules of the diamines act as unidentate ligands. Moreover, these diamines do not dissociate even in coordinating solvents such as DMF and DMSO, as mentioned above. This is due to the strong electron-withdrawing nitro groups, which can stabilize the coordination bonds between the nitrogen atoms of the diamines and the central copper(II) ion.

Absorption spectral changes caused by the template reaction

In order to clarify a mechanism for the template reaction between $Cu(3\text{-}NO_2acac)_2$ and diamines, absorption spectral changes of their mixed DMF solutions were measured. A DMF solution of the complex $Cu(3\text{-}NO_2acac)_2$ (0.05 mol dm^{-3}) and each diamine (0.10 mol dm^{-3}) was heated to 90°C, and its absorption spectra were measured at regular time intervals. In Fig. 2, the result obtained for the reaction of $Cu(3\text{-}NO_2acac)_2$ with ethylenediamine is given as an example.

In the case of ethylenediamine, addition of the diamine caused an immediate shift of the absorption maximum from 676 nm, due to the parent complex, to 550 nm. This spectrum is almost the same as that of the isolated ethylenediamine adduct, $Cu(3\text{-}NO_2acac)_2 \cdot en_2$. Initially, the absorption maximum of the solution was gradually shifted to longer wavelengths and reached 588 nm after ca. 180 min, and then shifted in the opposite direction to shorter wavelengths with a big increase in intensity. After 360 min, it reached 580 nm with a slight increase in its intensity and shifted no further. This final absorption spectrum is quite similar to that of $Cu(NO_2\text{-}N_4$[14]).

Similar spectral changes were observed for the cases of 1,3-diaminopropane and 1,4-diaminobutane. With 1,3-diaminopropane, its addition to a DMF solution of $Cu(3\text{-}NO_2acac)_2$ caused an immediate shift of the absorption maximum by about 100 nm (from 676 to 576 nm). Initially, this absorption maximum was gradually shifted to longer wavelengths (to 588 nm after 90 min) and then oppositely to shorter wavelengths with an elapse of time. The shift value was smaller than that observed value for the ethylenediamine case but the

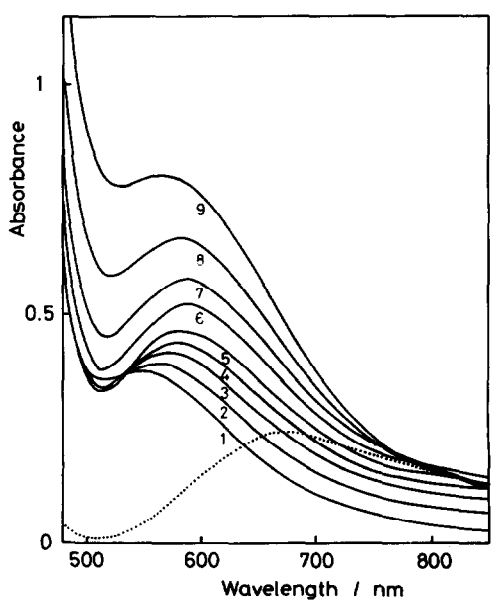

Fig. 2. Absorption spectral changes caused by reacting $Cu(3\text{-}NO_2acac)_2$ with ethylenediamine in DMF at 90°C. (·····): $Cu(3\text{-}NO_2acac)_2$; and (———): 1, 2, 3, 4, 5, 6, 7, 8 and 9, after 5, 30, 60, 90, 120, 180, 300 and 360 min, respectively.

reaction time was shorter than that for the above case; after 180 min the absorption maximum was observed at 580 nm with a high intensity. On the other hand, with 1,4-diaminobutane, the addition of the diamine to the copper(II) complex solution immediately caused a shorter wavelength shift by 60 nm with an increase in intensity. After 30 min, the absorption maximum was observed at 574 nm and its intensity was very high. These absorption spectral changes suggest that the reactivity of the diamines toward the parent complex was in the order en < pn ≪ bn.

Mechanism for the template reaction of Cu(3-NO_2acac)$_2$ *with diamines*

From the results described above, the following mechanism is proposed for the template reaction of Cu(3-NO_2acac)$_2$ with the diamines en, pn and bn. The scheme for the template reaction is shown in Fig. 3. Initially, two diamine molecules coordinate to the central copper(II) ion of Cu(3-NO_2acac)$_2$ as unidentate ligands. In the second stage, the uncoordinated, free amine groups may attack the carbonyl carbons of coordinated β-diketone groups and subsequently can afford two Schiff base bonds, being accompanied with the elimination of two water molecules. In the third stage, the Cu—N bond-fission between the copper(II) ion and the coordinated diamines may take place to leave the free amine groups. At the final stage, these free amine groups react further with the residual and coordinating carbonyl groups of the β-diketones to form the tetraaza macrocyclic Schiff base copper(III) complex, with elimination of two water molecules.

It has been reported that in the reaction of bis(2,4-pentanedionato)copper(II) with ethylenediamine, the desired tetraaza macrocyclic Schiff base copper(II) complex could not be obtained.[8] This significant difference in reactivity between Cu(acac)$_2$ and Cu(3-NO_2acac)$_2$ may be ascribed to the strong electron-withdrawing nitro groups. The electron-withdrawing groups lower the electron density on the carbon atoms of the carbonyl groups, making nucleophilic attack onto the carbon atoms by the amine groups much easier. An important role of the electron-withdrawing groups can be seen in the formation of the tetraaza macrocyclic compound by the template reaction. For example, in the case of the reactions of diamines with bis(3-benzoyl-2,4-pentanedionato)metal(II), where metal(II) is nickel(II) or copper(II), the former complex can form the corresponding tetraaza macrocyclic compound, but the latter gives only an acyclic compound.[5] The reason why the nickel(II) ion is superior to the copper(II) ion as a template ion may be considered to be due to the difference in the stabilizing effect of the metal–nitrogen bond between the metal ion and additional diamines; in the bis(β-diketonato)nickel(II) complex, diamines can coordinate to the central nickel(II) ion to form a six-coordinate complex, whereas in the corresponding copper(II) complex, coordination of two molecules of diamines to the central copper(II) ion is restricted and weakened because of the Jahn–Teller effect. The above-mentioned template reaction is a case of the following. In the reaction of the present Cu(3-NO_2acac)$_2$ with the diamines, the copper(II) ion can act efficiently as a template ion to form the corresponding tetraaza macrocyclic complexes. This is due to the strong electron-with-

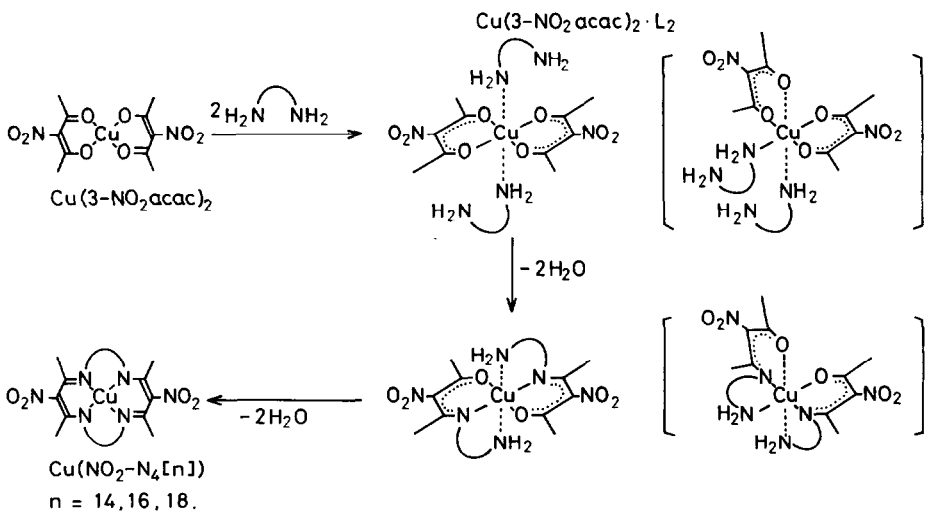

Fig. 3. Mechanistic scheme of the template reaction of Cu(3-NO_2acac)$_2$ with diamine.

drawing effect of the nitro groups on the γ-carbon atoms of acetylacetones. In fact, electrochemical study on the copper(II) complexes indicates that the reduction of $Cu(3\text{-}NO_2acac)_2$ is observed at a much more negative potential, ca. 1.0 V, than that for $Cu(acac)_2$. Both these are effects of the electron-withdrawing nitro groups; that is, to form adequately strong coordination bonds between the copper(II) ion and additional diamines and to coordinate easily by attack on the carbonyl carbon atoms of the coordinated diketones by the free amine moieties of the diamines, to form the desired tetraaza macrocyclic Schiff base complexes by the reaction of $Cu(3\text{-}NO_2acac)_2$ with the diamines.

On the other hand, it has been found that the reactivity of the diamines towards $Cu(3\text{-}NO_2acac)_2$ is very different: reaction rates forming the tetraaza macrocyclic complexes increase in the order $Cu(3\text{-}NO_2acac)_2 \cdot en_2 < Cu(3\text{-}NO_2acac)_2 \cdot pn_2 \ll Cu(3\text{-}NO_2acac)_2 \cdot bn_2$. This agrees with the order of increasing the methylene chain lengths linking the two amine groups of the diamines. These results can be explained as follows: it is necessary for the formation of the Schiff base bonds in the diamine adducts for an adequate distance between the free amine moieties of the coordinated diamines and the coordinated carbonyl groups to exist. Green *et al.* have reported that in the template reaction between 4,7-diaza-2,3:8,9-dibenzodecane-1,10-dione and diamines, a rotation around the C—C bond of ethylenediamine which superimposes the lone pair electrons on the nitrogen atom is less favorable for nucleophilic attack on the carbon atom; whereas this is sterically easy for 1,3-diaminopropane and 1,4-diaminobutane.[9]

However, when the diamines are linked with long methylene chain lengths, it might be inevitable for the formation of Schiff base bonds to take place intermolecularly and intramolecularly. In fact, in the case of the template reaction of $Cu(3\text{-}NO_2acac)_2$ with 1,3-diaminopropane or 1,4-diaminobutane, considerable amounts of by-products which were insoluble in ordinary organic solvents were obtained. These were considered to be polymeric compounds formed by intermolecular reactions, which were not further investigated.

REFERENCES

1. J. P. Collman, R. L. Marshall, W. L. Young and S. D. Goldby, *Inorg. Chem.* 1962, **1**, 704.
2. C. L. Honeybourne, *Inorg. Nucl. Chem. Lett.* 1975, **11**, 191.
3. (a) V. L. Wolf and E. G. Jäger, *Z. Anorg. Allg. Chem.* 1966, **346**, 76; (b) E. G. Jäger, *Z. Chem.* 1968, **8**, 30; (c) D. St. C. Black and P. W. Kortt, *Aust. J. Chem.* 1972, **25**, 281; (d) C. M. Kerwin and G. A. Melson, *Inorg. Chem.* 1973, **12**, 2410.
4. L. F. Lindoy and D. H. Busch, *Preparative Inorganic Reactions* (Edited by W. Jolly), Vol. 6, p. 1. Interscience, New York (1971).
5. M. Fujiwara, K. Yokota, H. Wakita, T. Matsushita and T. Shono, *Fukuoka Univ. Sci. Rep.* 1988, **18**, 141.
6. M. Fujiwara, T. Matsushita and T. Shono, *Polyhedron* 1984, **3**, 1357.
7. M. Fujiwara, H. Wakita and T. Matsushita, *Thermochim. Acta*, in press.
8. T. Kurauchi, M. Matsui, Y. Nakamura, S. Ooi, S. Kawaguchi and H. Kuroya, *Bull. Chem. Soc. Japan* 1974, **47**, 3049.
9. M. Green, J. Smith and P. A. Tasker, *Inorg. Chim. Acta* 1971, **5**, 17.

Polyhedron Vol. 10, No. 15, pp. 1779–1785, 1991
Printed in Great Britain

0277–5387/91 $3.00+.00
© 1991 Pergamon Press plc

SYNTHESIS AND CHARACTERIZATION OF COBALT(II) AND COBALT(III) COMPLEXES OF SUBSTITUTED DIBENZOTETRAAZA[14]ANNULENES

JULITA EILMES

Faculty of Chemistry, Jagiellonian University, Karasia 3, 30-060 Cracow, Poland

(*Received* 12 *February* 1990; *accepted* 25 *April* 1991)

Abstract—The macrocyclic complexes $Co^{II}L_1 \cdot 2H_2O$ and $Co^{II}L_2$ (L_1H_2 = $Bz_2Bzo_2Me_4$[14]hexaeneN$_4$, L_2H_2 = $Bz_2Bzo_2Me_2Ph_2$[14]hexaeneN$_4$) have been synthesized from free ligands and cobalt(II) acetate tetrahydrate. They reacted with dioxygen in pyridine solution to give the corresponding $[Co^{III}L(py)_2]X$ complex (where X = BF_4^-, I^-). The new compounds were characterized by elemental analysis, magnetic moments, IR, ^{1}H NMR and MS data. The steric non-equivalence of the axial sites of the coordinated macrocyclic ligands is discussed on the basis of the ^{1}H NMR spectra of the cobalt(III) complexes. The new cobalt complexes were found to be efficient catalysts for auto-oxidation of benzenethiol to diphenyl disulphide.

The development of synthetic models for naturally occuring metalloenzymes continues to be an important goal.

Synthetic biomimetic systems are of both fundamental and practical interest. They help the understanding of biochemical processes and being capable of imitating some enzymatic functions, can be employed practically as efficient and selective catalysts. Thus, biomimetic oxygenation is considered to be one of the most promising areas of catalysis.[1,2]

Among the macrocyclic systems used for the construction of model complexes, those containing the dibenzotetraaza[14]annulene framework are particularly attractive due to their synthetic accessibility and structural similarity to porphyrins (four donor atoms with substantial unsaturation and delocalization). Moreover, these macrocyclic ligands are able to accommodate a variety of substituents on the phenylene and diimine carbon atoms.

In our previous papers we showed that introduction of the peripheral substituents into the dibenzotetraaza[14]annulene system may be accomplished through a direct synthesis[3] or via substitution/addition reactions at the reactive β-methine carbon centre.[4–6] Further chemical transformations within these pendant groups were also found to be advantageous for the modification of the ligand periphery.[7,8]

Recently, we began studies on the chemistry of the cobalt complexes of previously synthesized, substituted dibenzotetraaza[14]annulenes. This paper reports the synthesis and characterization of the cobalt(II) and cobalt(III) complexes of $Bz_2Bzo_2Me_4$[14]hexaeneN$_4$ (L_1H_2) and $Bz_2Bzo_2Me_2Ph_2$[14]hexaeneN$_4$ (L_2H_2). Use of the new cobalt complexes as efficient catalysts for auto-oxidation of benzenethiol to diphenyl disulphide is also described.

RESULTS

Insertion of the cobalt into the macrocyclic ligand L_1H_2 was accomplished by the reaction with cobalt(II) acetate tetrahydrate (1 equivalent) performed under argon in refluxing acetonitrile–methanol (2:1). In the case of the ligand L_2H_2, the use of ethanol as a solvent was found to be more convenient for the precipitation of the crystalline product in a satisfactory yield. As a result of these reactions the low-spin four-coordinate complexes $Co^{II}L_1 \cdot 2H_2O$ (μ_{eff} = 2.85 BM) and $Co^{II}L_2$ (μ_{eff} = 2.65 BM) were obtained in 90 and 70% yields, respectively.

Diamagnetic cobalt(III) complexes of the L_1H_2 and L_2H_2 ligands were synthesized by the aerial oxidation of cobalt(II) complexes in excess pyridine in the presence of aqueous solutions of the appropriate inorganic salts. On the basis of analytical

and spectral data they have been formulated as six-coordinate $[Co^{III}L(py)_2]X$ complexes.

Scheme 1 outlines the reactions performed. Physical properties and magnetic and spectral data of the complexes are collected in Tables 1 and 2.

The tests of catalytic activity of the cobalt complexes for the auto-oxidation of organic compounds were performed with benzenethiol as a substrate. It was found that in an atmosphere of air, under mild conditions (temperature 20°C), the addition of 1.5 mol% of cobalt(II) and cobalt(III) complexes efficiently catalyse the oxidation of benzenethiol to diphenyl disulphide (yield 58–93%). The results are summarized in Table 3. The general procedure for the catalytic auto-oxidation is given in the Experimental.

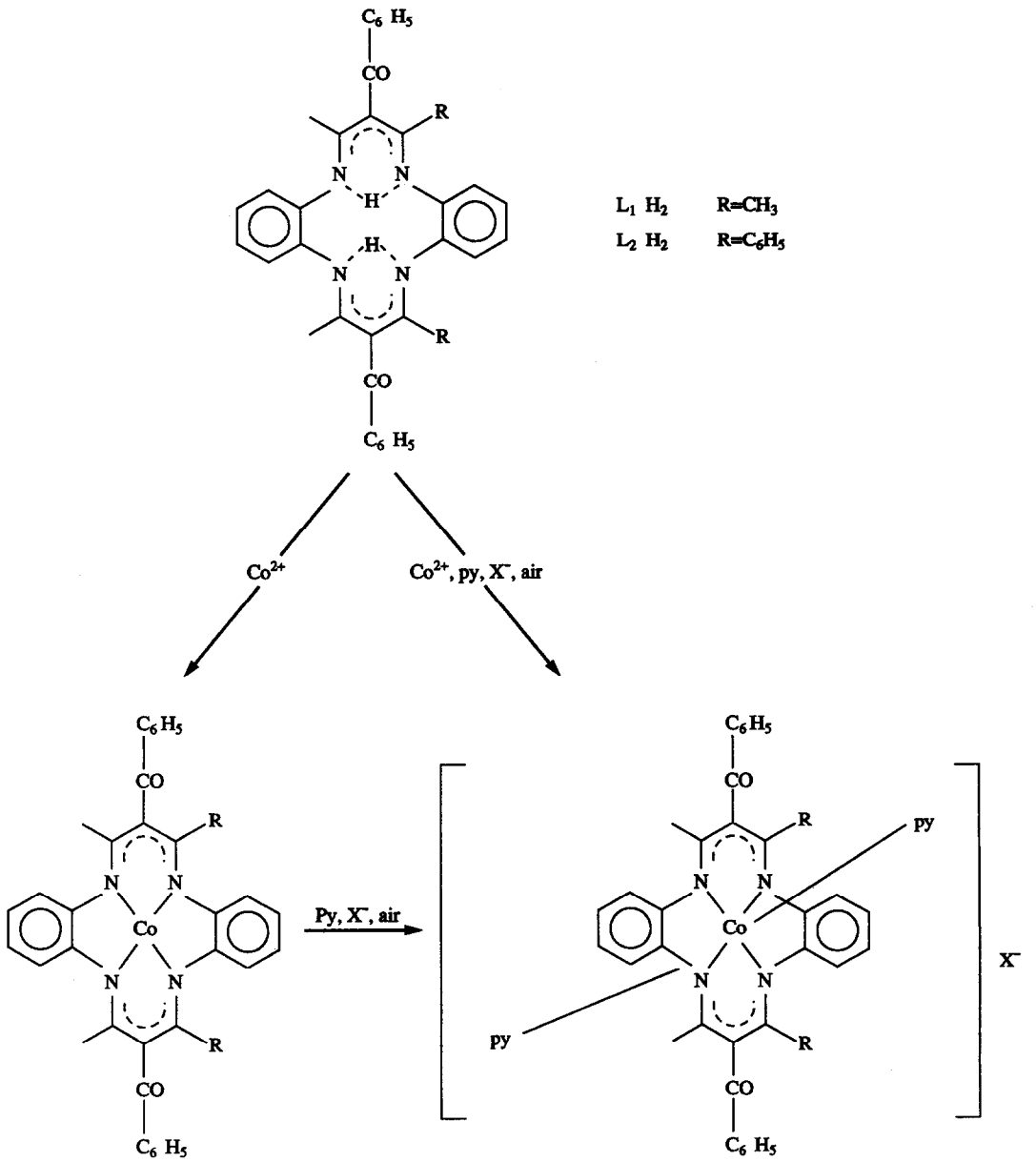

(1) $Co^{II}L_1 \cdot 2H_2O$

(2) $Co^{II}L_2$

(3) $[Co^{III}L_1(py)_2]BF_4$

(4) $[Co^{III}L_1(py)_2]I$

(5) $[Co^{III}L_2(py)_2]BF_4$

(6) $[Co^{III}L_2(py)_2]I$

Scheme 1.

Table 1. Physical properties, magnetic and MS data for complexes **1–6**

Complex	Colour	Yield (%)	Melting point (°C)	$p^+(m/z)$	μ_{eff} (BM)
1	Deep brown	90	255	609	2.85
2	Brown–green	70	170	733	2.65
3	Deep brown	92	276	609	dia.
4	Deep brown	71	210	609	dia.
5	Deep brown	88	280	733	dia.
6	Brown	67	255	733	dia.

Table 2. ^{1}H NMR and IR data for complexes **1–6**

Complex	IR (cm^{-1})	L	py
1	1660s ν(C=O) 1640s $\delta(H_2O)$ 3280s $\nu(H_2O)$ (lattice)		
2	1645 ν(C=O)		
3	1660s ν(C=O) 1060s BF_4	2.05(s, 12H) $-CH_3$ 6.55(m, 4H) } o-C_6H_4 6.74(m, 4H) } AA'BB' 7.37(m, 10H) $-C_6H_5$	9.44(d, 2H) 8.78(b, 1H) 8.01(b, t, 2H) 9.08(d, 2H) 8.75(b, 1H) 7.56(t, 2H)
4	1660s ν(C=O)	2.06(s, 12H) $-CH_3$ 6.57(m, 4H) } o-C_6H_4 6.75(m, 4H) } AA'BB' 7.40(b, m, 10H) $-C_6H_5$	9.5(d, 2H) 8.96(b, 1H) 8.12(b, t, 2H) 9.09(d, 2H) 8.66(b, 1H) 7.58(t, 2H)
5	1630s ν(C=O) 1060s BF_4	2.33(s, 6H) $-CH_3$ 5.43(m, 2H) } o-C_6H_4 5.76(m, 2H) } AA'BB' 6.38(m, 4H) o-C_6H_4 7.07(m, 10H) $-C_6H_5$ 7.31(m, 10H) $-C_6H_5$	10.21(d, 1H) 9.51(d, 1H) 8.68(t, 1H) 8.38(t, 1H) 7.89(t, 1H) 9.15(d, 2H) 7.77(t, 1H) 7.16(t, 2H)
6	1630s ν(C=O)	2.35(s, 6H) $-CH_3$ 5.45(m, 2H) } o-C_6H_4 5.78(m, 2H) } AA'BB' 6.42(m, 4H) o-C_6H_4 7.30(m, 20H) $-C_6H_5$	10.22(d, 1H) 9.45(d, 1H) 9.11(t, 1H) 8.94(t, 1H) 8.05(t, 1H) 9.12(d, 2H) 7.79(t, 1H) 7.37(t, 2H)

Table 3. Auto-oxidation of benzenethiol to diphenyl disulphide under various conditions

Experiment	Catalyst	Gas used	Yield of diphenyl disulphide (%)
(a)	**1**	Air	69
(b)	**2**	Air	93
(c)	**3**	Air	58
(d)	**4**	Air	62
(e)	**5**	Air	79
(f)	**6**	Air	76
(g)	None	Air	1.5
(h)	$Ni^{II}L_1$	Air	1.8
(i)	**1**	Argon	0.5
(j)	**2**	Argon	0.8
(k)	**3**	Argon	0.9
(l)	**5**	Argon	0.9
(m)	**1**, DBMP	Air	1.0
(n)	**2**, DBMP	Air	0.8
(o)	**3**, DBMP	Air	0.5
(p)	**5**, DBMP	Air	0.5

General procedure given in the Experimental; (g) no catalyst added; (h) 1.5 mol% of $Ni^{II}L_1$; (i)–(j) slow stream of argon supplied instead of air; and (m–p) 5 mmol of 2,6-di-tert-butyl-4-methylphenol (DBMP) added.

DISCUSSION

Proof of the proposed structure of the cobalt complexes is supported by analytical and spectral data.

The IR spectra reveal the presence of the coordinated macrocyclic ligands and are fully consistent with their structure. The most diagnostic IR frequencies and their assignments are collected in Table 2.

The EI mass spectra exhibit the expected molecular peaks for all complexes synthesized (Table 1). The cobalt(III) complexes showed additional peaks of remarkable intensity at *m/z* 79, providing evidence for the presence of coordinated pyridine.

The structure of the coordinated macrocycle is confirmed by the ^{1}H NMR spectra of diamagnetic cobalt(III) complexes, showing signals for methyl, phenylene and phenyl groups (Table 2).

Two molecules of pyridine that are present in the complexes $[Co^{III}L(py)_2]X$ and supposed to be axially coordinated, give rise to separate sets of signals (Table 2). This can be explained in terms of the non-equivalence of the axial sites of the coordinated macrocycle and corresponds well with the recent findings on the non-planar conformation of the substituted dibenzotetraaza[14]annulene macrocycle.

Goedken *et al.*[9] first found crystallographically that the tetramethyl-dibenzotetraaza[14]annulene macrocycle adopts the saddle-shaped conformation in which *o*-phenylene rings and the diiminate chelate framework are tilted to opposite sides of the plane defined by four nitrogen atoms. The distortion from planarity is mainly due to steric interactions of β-substituents with the phenylene rings.

Similar pronounced saddle shapes are observed in the free ligands L_1H_2[10] and L_2H_2.[11] In these molecules one side of the non-planar macrocycle is sterically more crowded, due to the benzoyl substituents attached at the *meso* positions of the diiminate framework.

In the ^{1}H NMR spectra of the $[Co^{III}L_2(py)_2]X$ complexes, one of the two non-equivalently coordinated molecules of pyridine is represented by five distinct interpretable resonances [α(d, 1H), α'(d, 1H), γ(t, 1H), β(t, 1H), β'(t, 1H)], whereas the other molecule exhibits only three signals [α(d, 2H), γ(t, 1H), β(t, 2H] (Table 2).

The spectral set of five resonances indicates that one molecule of pyridine does not rotate freely on the NMR time scale and adopts the orientation in which α and α' protons are directed towards the non-equivalent part of the macrocycle. It seems reasonable to assume that the pyridine in question is the one coordinated in the more crowded axial site, i.e. on the non-planar macrocycle face which is equipped with the benzoyl substituents (Fig. 1,* pyridine A). Restrictions in the free rotation is presumed to be mainly due to the steric interactions with pendant benzoyl groups.

For the second molecule of coordinated pyridine, a distinction in the ^{1}H NMR spectra can only be made among the α, β and γ protons (three signals). The question then arises whether the pyridine does rotate freely on the NMR time scale or whether, due to interaction with phenylene rings, it adopts an orientation in which α and α' protons are directed towards the equivalent part of the macrocycle (Fig. 1, pyridine B). Standard ^{1}H NMR spectra cannot provide a conclusive answer to these questions and thus, the problem remains to be solved in further studies.

In the ^{1}H NMR spectra of the complexes $[Co^{III}L_1(py)_2]X$, each of the two non-equivalently coordinated molecules of pyridine gives rise to three signals attributed to the α, β and γ protons (Table 2). Here again, the point in question is whether the

* The figures used for the discussion show only essential features of the structure of free ligands. Complete crystallographic data for the free ligands will be published elsewhere.[10,11]

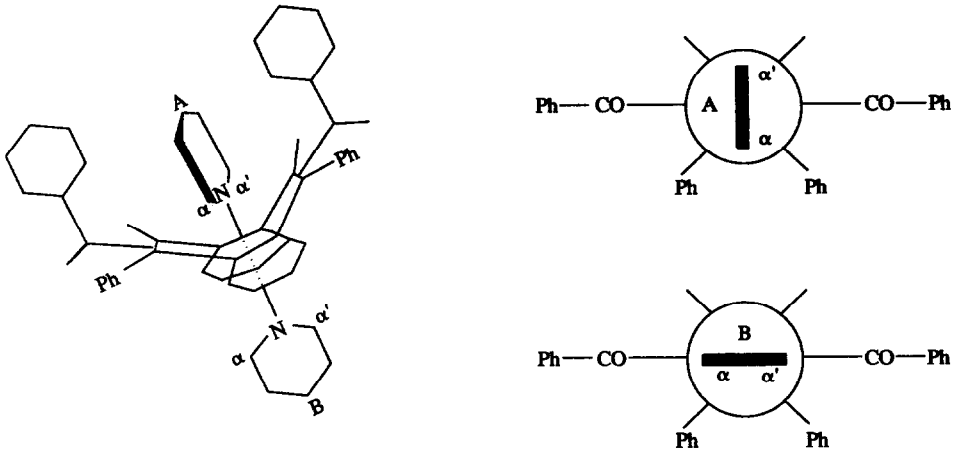

Fig. 1. Schematic representation of the orientation of axial base planes in $[Co^{III}L_2(py)_2]X$.

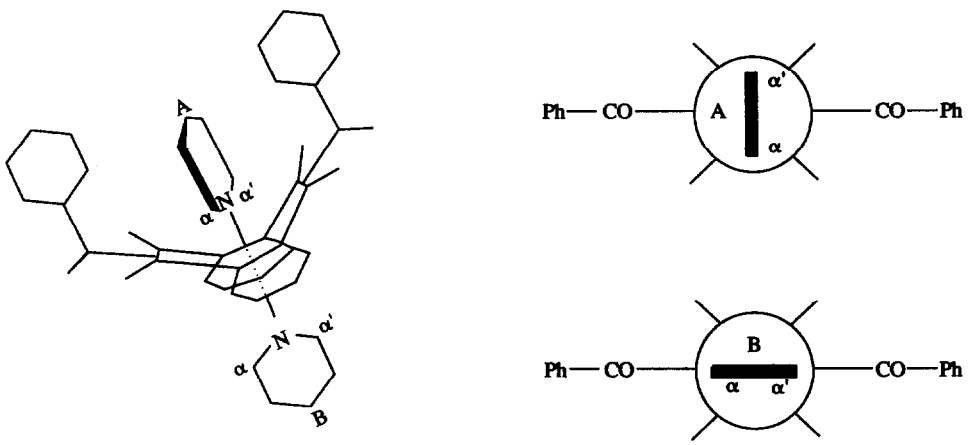

Fig. 2. Schematic representation of the orientation of axial base planes in $[Co^{III}L_1(py)_2]X$.

three resonances represent an average spectrum of freely rotating molecules of pyridine, or whether they correspond to the molecule whose freedom to rotate is restricted on the NMR time scale.

The structural similarity of ligands L_1H_2 and L_2H_2, both non-planar and equipped with pendant benzoyl substituents, strongly suggests similar structures for their complexes. It seems possible that the pyridine coordinated in the more crowded axial position of the complexes $[Co^{III}L_1(py)_2]X$ is also sterically hindered and assumes the orientation shown in Fig. 2* (pyridine A). However, the ^1H NMR spectra mentioned above, although consistent with such an orientation of pyridine A, do not provide straightforward evidence for the restriction of free rotation. It is easily noticed that due to the symmetry of the ligands L_1H_2 (see Fig. 2), ^1H NMR resonances assigned to the sterically hindered pyridine A consist of three signals and in this respect the spectrum does not differ from that which would correspond to the freely rotating molecule.

In conclusion, the ^1H NMR spectra reveal that axial coordination in the cobalt(III) complexes of substituted dibenzotetraaza[14]annulenes is remarkably influenced by the peripheral substituents and the macrocyclic ligand conformation. Two axial coordination sites appear to be sterically non-equivalent in all cobalt(III) complexes synthesized. ^1H NMR spectra of the cobalt(III) complexes derived from non-symmetrically substituted ligands, L_2H_2, allow the detection of hindered rotation of the axial pyridine.

The results show that introducing pendant substituents at the γ,γ' positions of the dibenzotetraaza[14]annulenes may control the rotational orientation of axial ligands in their complexes.

It is worth mentioning at this point that the rotational orientation of the axial base plane remarkably affects various physicochemical prop-

* See footnote on p. 1782.

erties of the complexes[12–14] and is considered to be essential for the activity of the natural haemoproteins.[15–17]

Further experiments are being undertaken in order to investigate the dynamic processes such as axial lability and internal rotation of the pyridine.

The cobalt complexes reported in this paper seem to be suitable for the study of oxygen transport. The structural similairty to the porphyrins and access to various oxidation states of the central metal atom makes them also attractive as potential catalysts.

In this paper we would like only to communicate the results of our preliminary tests of their catalytic activity in the oxidation of organic compounds with molecular oxygen.

As concluded from the results of all the experiments performed (see Table 3), the cobalt complexes **1–6** appeared to be efficient catalysts for the auto-oxidation of benzenethiol to diphenyl disulphide under mild conditions, eq. (1):

$$C_6H_5—SH \xrightarrow[CHCl_3,\ 20°C,\ 30\ min]{O_2,\ complexes\ 1–6} C_6H_5—S—S—C_6H_5. \quad (1)$$

Thus, experiments (a)–(f) showed that the reaction of benzenethiol with molecular oxygen, performed in the presence of 1.5 mol % of complexes **1–6**, led to diphenyl disulphide within 30 min, in fair yield (58–93%). Experiments (g) and (h) provided evidence that the oxidation with air practically did not occur in the absence of the cobalt complexes. Similarly, the presence of molecular oxygen was confirmed to be necessary for the reaction to occur [experiments (i)–(l)]. Furthermore, the yield of diphenyl disulphide was found to be very poor when the reaction was carried out in the presence of the free-radical reaction inhibitor 2,6-di-tert-butyl-4-methylphenol (DBMP) [experiments (m)–(p)].

Although no detailed mechanism can be proposed at this stage, the presumption that the reaction proceeds via a free-radical mechanistic pathway, involving binding and activation of dioxygen by the cobalt complexes, seems to be reasonable. It can be suggested further, that in this respect, the catalytic reaction may be considered as analogous to the auto-oxidation of organic products with the use of the cobalt porphyrins.[18–20]

Investigations of the scope and mechanisms of catalytic activity of the cobalt complexes in the oxidation of organic substrates are presently being carried out.

EXPERIMENTAL

Melting points are uncorrected. IR spectra were recorded in Nujol and hexachlorobutadiene on a Zeiss UR-10 spectrometer. ^{1}H NMR spectra were measured at 500 MHz on a Bruker AM instrument in $CDCl_3$. The spectra were referenced to δ $Me_4Si = 0$. EI mass spectra were run on a Perkin–Elmer 1000 mass spectrometer at 70 eV. The magnetic moments were measured by Evans' method[21] in $CDCl_3$ with Me_4Si at 295 K. Diamagnetic corrections for the ligands were made using Pascal's constants.[22]

All the solvents were distilled before use and degassed where indicated. Inorganic salts were reagent grade and were used without further purification. The ligands L_1H_2 and L_2H_2 were prepared by the procedure described earlier.[4]

[2,3:9,10 - *Dibenzo* - 6,13 - *dibenzoyl* - 5,7,12,14 - *tetra methyl* - 1,4,8,11 - *tetraazacyclotetradeca* - 2,4,6,9,11, 13-*hexaenato*(2−)]*cobalt*(II) *dihydrate* (**1**)

A solution of the cobalt(II) acetate tetrahydrate (0.5 g, 2 mmol) in degassed methanol (10 cm^3) was added to the warm solution prepared by dissolving the ligand L_1H_2 (0.29 g, 0.5 mmol) in degassed acetonitrile (30 cm^3). The reaction mixture was allowed to reflux for 10 min under argon, then left aside for 1 h. The deep brown crystalline product was filtered off, washed with cold water and dried *in vacuo*. Found: C, 67.3; H. 5.0; N, 8.6. Calc. for $C_{36}H_{34}N_4O_4Co$: C, 67.0; H, 5.3; N, 8.7%.

[2,3:9,10 - *Dibenzo* - 6,13 - *dibenzoyl* - 7,12 - *dimethyl* - 5,14 - *diphenyl* - 1,4,8,11 - *tetraazacyclotetradeca* - 2, 5,7,11,13-*hexaenato*(2−)]*cobalt*(II) (**2**)

A solution of the cobalt acetate tetrahydrate (0.53 g, 2 mmol) in degassed water (5 cm^3) was added to a slurry prepared by refluxing the ligand L_2H_2 (0.35 g, 0.5 mmol) in degassed ethanol (100 cm^3). The reaction mixture was refluxed with stirring for 1 h under argon. During this time the colour of the reaction mixture changed from orange to a brown–green, and the whole amount of the ligand dissolved. Upon cooling, the brown–green precipitate was isolated by filtration, then washed with water and dried *in vacuo*. Found: 75.8; H, 4.5; N, 7.3. Calc. for $C_{46}H_{34}N_4O_2Co$: C, 75.3; H, 4.7; N, 7.6%.

Synthesis of the cobalt(III) *complexes* (*general procedure*)

Method (a). A sample of the appropriate complex $Co^{II}L$ was dissolved in warm pyridine to give a deep red solution. Upon cooling, a saturated aqueous solution of the appropriate inorganic salt NaX was added dropwise with stirring to the pyridine

solution, until abundant precipitate appeared. Stirring was continued for a further 2 h and then the reaction mixture was left overnight at room temperature. A crystalline product was filtered off, washed with water and dried *in vacuo*.

Method (b). A violet solution of the cobalt acetate tetrahydrate (0.5 mmol) in warm pyridine (5 cm^3) was added to a slurry of the appropriate ligand (0.5 mmol) in refluxing acetonitrile (10 cm^3). The reaction mixture which became intensively red was gently heated for 5 min and then cooled. A saturated aqueous solution of the appropriate salt (NaX) was added dropwise to the intensively stirred solution until the precipitation of the crystalline product was complete. The mixture was stirred for 2 h and then left overnight at room temperature. The crystalline solid was collected by filtration, washed carefully with water and dried *in vacuo*.

Purification of the cobalt(III) complexes was accomplished by dissolving in a small amount of pyridine and reprecipitating with a saturated aqueous solution of the appropriate inorganic salt NaX. Complex **3**, Found: C, 64.3; H, 4.3; N, 9.4. Calc. for $C_{46}H_{40}N_6O_2CoBF_4$: C, 64.7; H, 4.7; N, 9.8%. Complex **4**, Found: C, 61.4; H, 4.7; N, 9.8. Calc. for $C_{46}H_{40}N_6O_2CoI$: C, 61.8; H, 4.5; N, 9.4%. Complex **5**, Found: C, 68.2; H, 4.6; N, 8.8. Calc. for $C_{56}H_{44}N_6O_2CoBF_4$: C, 68.7; H, 4.5; N, 8.6%. Complex **6**, Found: C, 65.6; H, 4.5; N, 8.6. Calc. for $C_{56}H_{44}N_6O_2CoI$: C, 66.0; H, 4.4; N, 8.3%.

Yields and physical properties of cobalt(II) and cobalt(III) complexes are collected in Table 1.

Catalytic auto-oxidation of benzenethiol to diphenyl disulphide (general procedure)

A stream of air was bubbled through a solution of the catalyst (0.074 mmol) and benzenethiol (0.5 cm^3, 4.9 mmol) in chloroform (15 cm^3). After 30 min, the solvent and unchanged substrate were removed under reduced pressure at room temperature. The residue was chromatographed on neutral alumina. The first fraction eluted with benzene contained pure diphenyl disulphide.

Acknowledgement—This research was financially supported by the Committee of Chemical Sciences of the Polish Academy of Sciences.

REFERENCES

1. R. A. Sheldon and J. K. Kochi, *Metal-Catalyzed Oxidations of Organic Compounds*, Ch. 8, p. 253. Academic Press, New York (1981).
2. T. Matsuura, *Tetrahedron* 1977, **33**, 2869.
3. J. Eilmes, D. Pelan and E. Śledziewska, *Bull. Acad. Pol. Sci.* 1980, **28**, 371.
4. J. Eilmes, *Polyhedron* 1985, **4**, 943.
5. J. Eilmes, *Polyhedron* 1987, **6**, 423.
6. M. Basato, B. Corain, G. Favero, G. Valle and J. Eilmes, *Inorg. Chim. Acta* 1989, **159**, 59.
7. J. Eilmes, *Polyhedron* 1988, **7**, 2197.
8. J. Eilmes, *Polyhedron* 1989, **8**, 1243.
9. V. L. Goedken, J. J. Pluth, S. M. Peng and B. Bursten, *J. Am. Chem. Soc.* 1976, **98**, 8014.
10. J. Śliwiński, J. Eilmes, B. Oleksyn and G. Zanotti, Collected Abstracts of Xth European Crystallography Meeting, Wrocław, Poland, 1986, Abst. No. 2B-75, pp. 224–225.
11. J. Śliwiński, J. Eilmes and B. Oleksyn, *Acta Cryst.*, in preparation.
12. D. K. Geiger, Y. J. Lee and W. R. Scheidt, *J. Am. Chem. Soc.* 1984, **106**, 6339.
13. F. A. Walker, J. Buehler, J. T. West and J. L. Hinds, *J. Am. Chem. Soc.* 1983, **105**, 6923.
14. Y. Uemori, H. Mijakawa and E. Kyuno, *Inorg. Chem.* 1988, **27**, 377.
15. E. J. Heidner, R. C. Ladner and M. F. Perutz, *J. Molec. Biol.* 1976, **104**, 707.
16. J. E. Baldwin and C. Chothia, *J. Molec. Biol.* 1979, **129**, 175.
17. Z. R. Korszun, K. Moffat, K. Frank and M. A. Cusanowich, *Biochemistry* 1982, **21**, 2253.
18. M. Baccouche, J. Ernst, J. H. Fuhrhop, R. Schlözer and H. Arzoumanian, *J. Chem. Soc., Chem. Commun.* 1977, 827.
19. J. H. Fuhrhop, M. Baccouche, H. Graboy and H. Arzoumanian, *J. Molec. Catal.* 1980, **7**, 245.
20. X. Y. Wang, J. Ramunas, J. Motekaitis and A. E. Martell, *Inorg. Chem.* 1984, **23**, 271.
21. D. F. Evans, *J. Chem. Soc.* 1959, 2003.
22. A. Earnshaw, *Introduction to Magnetochemistry*, p. 4. Academic Press, London (1968).

Polyhedron Vol. 10, No. 15, pp. 1787–1790, 1991
Printed in Great Britain

0277–5387/91 $3.00+.00
© 1991 Pergamon Press plc

SYNTHESIS AND MAGNETIC PROPERTIES OF BINUCLEAR COPPER(II)–COBALT(II) COMPLEXES WITH N,N′-BIS (2-AMINOPROPYL)OXAMIDOCOPPER(II)

DAI-ZHENG LIAO,* LI-CUN LI and GEN-LINE WANG

Department of Chemistry, Nankai University, Tianjin, P.R.C.

(*Received* 28 *September* 1990; *accepted* 25 *April* 1991)

Abstract—Three heterobinuclear complexes have been synthesized, namely [Cu(oxap) $Co(L)_2](ClO_4)_2$ [where L = 2,2′-bipyridyl (bpy), 1,10-phenanthroline (phen) and 5-nitro-1,10-phenanthroline (NO_2-phen)], where oxap is N,N′-bis(2-aminopropyl)oxamido. Based on IR, elemental analyses, conductivity measurements and electronic spectra, these complexes are proposed to have extended oxamido-bridged structures and to consist of copper(II) in a planar environment and cobalt(II) in an octahedral environment. The complexes have been characterized by variable temperature magnetic susceptibility (4.2–300 K) and the data were fit by least-squares to a susceptibility equation derived from the spin Hamiltonian, $\hat{H} = -2J\hat{S}\cdot\hat{S}_2 - D\hat{S}_{z1}^2$. The exchange integral, J, was found to be -15 cm^{-1} (for bpy), -24 cm^{-1} (for phen) and -26 cm^{-1} (for NO_2-phen), indicating that a weak antiferromagnetic spin-exchange interaction operates between the metal ions.

Binuclear metal complexes with extended bridged structures are of current interest due to spin-exchange and charge transfer between metal ions and in the domain of metalloenzymes and homogeneous catalysis.[1]

In view of the effective bridging function of the oxamido group, Ojima and Nonoyama[2] first utilized N,N′-bis(2-aminopropyl)oxamidocopper(II), Cu(oxap), as a bidentate mononuclear fragment to prepare the binuclear complex [Cu(oxap)Cu(bpy)] $(NO_3)_2$, but its detailed physicochemical properties have not been reported. Recently, complexes of this kind with various terminal ligands and other metal ions, such as [Cu(oxap)Zn(phen)$_2$] $(ClO_4)_2$ and [Cu(oxap)Ni(phen)$_2$]$(ClO_4)_2$, were synthesized in our laboratory and their magnetic properties and crystal structures were studied.[3] As an extension of the above investigation, this paper deals with the synthesis and the magnetic and EPR properties of three new complexes, [Cu(oxap)$Co(L)_2](ClO_4)_2$ [where L = 2,2′-bipyridyl (bpy), 1,10-phenanthroline (phen) and 5-nitro-1,10-phenanthroline (NO_2-phen)].

* Author to whom correspondence should be addressed.

EXPERIMENTAL

Preparation of [Cu(oxap)$Co(bpy)_2](ClO_4)_2\cdot 1.5H_2O$

N,N′ - bis(2 - aminopropyl)oxamidocopper(II) [Cu(oxap)] was prepared by a literature method.[4] Bpy, phen and NO_2-phen were purchased from Peking Chemical Company.

To an absolute methanol solution (20 cm^3) of Cu(oxpn) (264 mg, 10^{-3} mol) were successively added an absolute methanol solution (10 cm^3) containing $Co(ClO_4)_2\cdot 6H_2O$ (366 mg, 10^{-3} mol) and bpy (312 mg, 2×10^{-3} mol) to give dark purple microcrystals which were separated, washed several times with absolute methanol and diethyl ether and dried *in vacuo*. Found: C, 39.4; H, 3.8; N, 12.6; Cu, 7.0; Co, 6.9. Calc. for $C_{28}H_{32}N_8O_{10}Cl_2CuCo\cdot 1.5H_2O$: C, 39.1; H, 4.1; N, 13.0; Cu, 7.4; Co, 6.8%.

Preparation of [Cu(oxap)$Co(phen)_2](ClO_4)_2\cdot 1.5H_2O$

This complex was obtained as purple microcrystals by the same procedure but by using phen instead of bpy. Found: C, 42.1; H, 3.5; N, 12.3; Cu, 6.9; Co, 6.7. Calc. for $C_{32}H_{32}N_8O_{10}Cl_2CuCo\cdot$

$1.5H_2O$: C, 42.3; H, 3.9; N, 12.3; Cu, 7.0; Co, 6.5%.

Preparation of $[Cu(oxap)Co(NO_2\text{-phen})_2](ClO_4)_2 \cdot 1.5H_2O$

This complex was obtained as light purple microcrystals by the same procedure but by using NO_2-phen instead of bpy. Found: C, 38.1; H, 3.0; N, 14.0; Cu, 6.2; Co, 5.9. Calc. for $C_{32}H_{30}N_{10}O_{14}Cl_2CuCo \cdot 1.5H_2O$: C, 38.5; H, 3.3; N, 14.0; Cu, 6.4; Co, 5.9%.

Measurements

Elemental analyses of carbon, hydrogen and nitrogen were carried out with a Perkin–Elmer analyser, Model 240. Metal contents were determined by EDTA titration, IR spectra were measured on a Shimadzu IR spectrophotometer, Model 408, using KBr pellets, and the electronic spectra (methanol solution) were measured on a Hitachi-240 spectrophotometer. The molar conductance was measured with a DDS-11A conductometer. Variable temperature magnetic susceptibilities were measured on a vibrating sample magnetometer, Model CF. Diamagnetic corrections were made with Pascal's constants for all the constituent atoms, and the magnetic moments were calculated using the equation $\mu_{eff} = 2.828(XT)^{1/2}$. ESR spectra were measured with a JES-FEIXG ESR-apparatus using the X-band.

RESULTS AND DISCUSSION

General characterization

Elemental analyses indicated that the reaction of Cu(oxap) with $Co(ClO_4)_2 \cdot 6H_2O$ and bpy, phen or NO_2-phen yielded the binuclear complexes. For the three $[Cu(oxpn)Co(L)_2](ClO_4)_2$ complexes, the molar conductance values (see Table 1) fall in the expected range for 1 : 2 electrolytes,[5] indicating that the two perchlorate anions are situated outside the metal coordination sphere. The significant bands in the IR spectra of the complexes are given in Table 1. The $\rangle C{=}O$ (carbonyl) stretching vibration at 1588 cm^{-1} for Cu(oxap) and the —C=N— stretching vibration at 1450–1500 cm^{-1} for the terminal ligands (bpy, phen and NO_2-phen) were shifted to higher frequencies in their binuclear complexes. It is likely that the bond order of C=O in the binuclear complexes is higher than that in the mononuclear complexes. These shifts have often been used as definite proof for the existence of the oxamido bridge.[2] In addition, the $-NH_2$ vibration at 3175 cm^{-1} for Cu(oxap) was present for all complexes and a broad, intense band is observed at 1100 cm^{-1}, which is typical for a non-coordinated perchlorate ion. The electronic absorption spectral data for these complexes (methanol solutions) are given in Table 1. A strong absorption in the UV range and only a weak absorption in the visible range can be observed. The former may be attributed to the charge-transfer absorption bands and the latter to the *d–d* transition.[6] Based on the discussion above, these complexes are proposed to have extended oxamido-bridged structures and to contain copper(II) in a planar environment and cobalt(II) in an octahedral environment, as shown in Fig. 1.

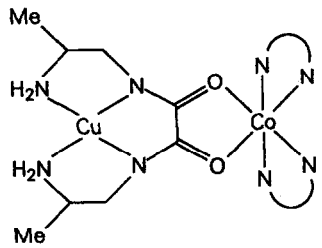

Fig. 1. Structure of $[Cu(oxap)Co(L)_2](ClO_4)_2$ (L = bpy, phen and NO_2-phen).

Table 1. Physical data for the complexes

Complexes	Λ_m (Ω^{-1} cm^2 mol^{-1})	IR (cm^{-1}) C=O	—NH_2	$\rangle C{=}N-$	ClO_4^-	UV (10^3 cm^{-1}) *d–d*	CT
Cu(oxap)		1588	3263				
$[Cu(oxap)Co(bpy)_2](ClO_4)_2$	154	1647	3263	1600	1100	19.49	31.94
$[Cu(oxap)Co(phen)_2](ClO_4)_2$	123	1640	3263	1580	1100	19.52	29.57
$[Cu(oxap)Co(NO_2\text{-phen})_2](ClO_4)_2$	156	1640	3263	1580	1100	19.61	30.21

Magnetic properties

The temperature dependence of the susceptibilities and magnetic moments for the three binuclear complexes are shown in Figs 2–4. The magnetic moments decrease steadily with decreasing temperature, implying the existence of an antiferromagnetic spin-exchange interaction within each molecule. Furthermore, the drastic decrease of magnetic moments around 70 K suggests a zero-field interaction and an intermolecular antiferromagnetic interaction.

The magnetic analyses for the complexes (d^9–d^7) were carried out using the susceptibility equation based on the Heisenberg spin operator ($\hat{H} = -2J\hat{S}_1 \cdot \hat{S}_2$). However, the data at low temperature do not satisfactorily fit this equation, because they neglect the single ion zero-field interaction of the cobalt(II) ion and the intermolecular interaction. We therefore adopted a susceptibility equation based on the modified Heisenberg operator, $\hat{H} = -J\hat{S}_1 \cdot \hat{S}_2 + D\hat{S}_{z1}^2$, where D is the axial zero-field splitting parameter for the cobalt(II) ion. The expression for the susceptibility, χ_m, is given by eq. (1):[7]

$$\chi_m = (2Ng^2\beta^2/K(T-\theta))[\exp(A) + 4\exp(C) + \exp(E)]/[2\exp(A) + \exp(B) + 2\exp(C) + \exp(D) + 2\exp(E)],$$

$$A = [4J + 5D/4 - (4J^2 - 2DJ + D^2)^{1/2}]/KT$$

$$B = (2J + D/4)/KT$$

$$C = (6J + 9D/4)/KT$$

$$D = (6J + D/4)/KT$$

$$E = [4J + 5D/4 + (4J^2 - 2DJ + D^2)^{1/2}]/KT, \quad (1)$$

where N, g, β, K and T have their usual meanings, J is the exchange integral and θ is the Curie–Weiss parameter. As shown in Figs 2–4, good least-squares fits to the experimental data were attained with eq. (1). The agreement factor F defined here as $\Sigma_i (X_i^{obs})^{-1}(X_i^{obs} - X_i^{calc})^2$ is equal to approx. 1×10^{-5} in all cases. Compared with the simple model ($H = 2J\hat{S}_1 \cdot \hat{S}_2$, $F \simeq 10^{-3}$), a much better fit was obtained with the modified Heisenberg operator. The magnetic parameters thus determined are: $J = -15$ cm^{-1}, $g = 2.31$, $D = -1.18$ cm^{-1}, $\theta = -34.9$ K (bpy); $J = -24$ cm^{-1}, $g = 2.47$, $D = -0.04$ cm^{-1}, $\theta = -37.4$ K (phen); and $J = -26$ cm^{-1}, $g = 2.33$, $D = -1.61$ cm^{-1}, $\theta = -6.5$ (NO_2-phen). These results (negative, small J values) indicate that the complexes undergo a weak antiferromagnetic spin-exchange interaction between the metal ions.

To describe the mechanism of the exchange interaction, several models have been proposed.[8–10] According to these models, strict orbital orthogonality results in ferromagnetism, otherwise an antiferromagnetic coupling should be expected. For the present complexes, if the whole molecular symmetry is considered to be C_{2v} and the reference used is shown by Fig. 1, the 3d metallic orbitals of copper(II) and cobalt(II) ions transform as $a_1(d_{z^2}$,

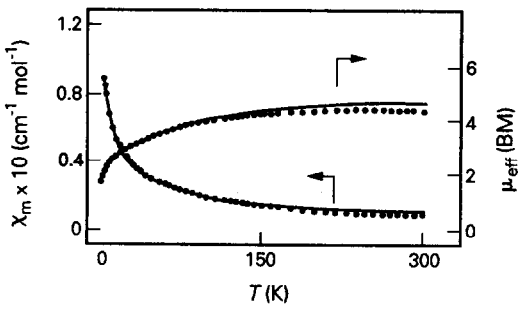

Fig. 4. Temperature variation of the magnetic susceptibility and magnetic moment of [Cu(oxap)Co(NO_2-phen)$_2$](ClO_4)$_2$ · 1.5H_2O.

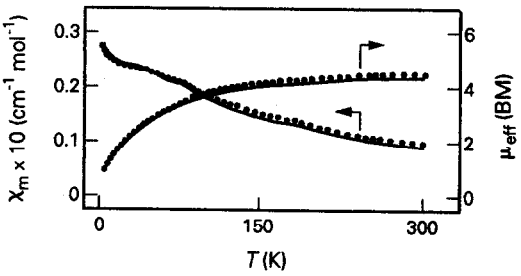

Fig. 2. Temperature variation of the magnetic susceptibility and magnetic moment for [Cu(oxap)Co(bpy)$_2$](ClO_4)$_2$ · 1.5H_2O. The curve is drawn based on eq. (1) using the magnetic parameters given in the text.

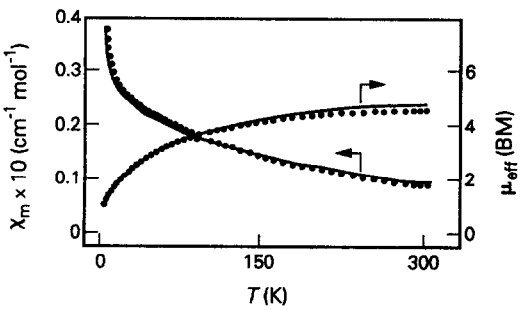

Fig. 3. Temperature variation of the magnetic susceptibility and magnetic moment of [Cu(oxap)Co(phen)$_2$](ClO_4)$_2$ · 1.5H_2O.

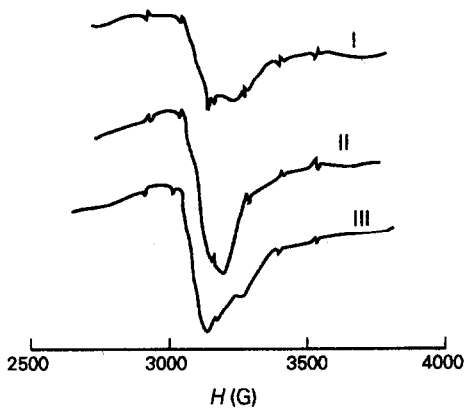

Fig. 5. X-band powder ESR spectra of the complexes at room temperature: **I**, bpy; **II**, phen; and **III**, NO_2-phen.

$d_{x^2-y^2}$), $a_2(d_{yz})$, $b_1(d_{xy})$ and $b_2(d_{zx})$. Around the copper(II) ion there is just one unpaired electron which occupies the b_1(Cu) orbital. Around the cobalt(II) ion the unpaired electron has some distribution in b_1(Co).[11] Because there is no orthogonality between the b_1 magnetic orbitals centred on the copper(II) and cobalt(II) ions, the antiferromagnetic interaction should be observed. We also investigated the magnetic behaviour of Cu^{II}–Cu^{II} and Cu^{II}–Ni^{II} binuclear complexes containing the same oxamido bridge and terminal ligands (e.g. phen) and obtained the following sequence for the magnetic interaction: [CuCu] ($J = -235\ cm^{-1}$) > [CuNi] ($J = -92\ cm^{-1}$) > [CuCo] ($J = -24\ cm-1$).[3] This result is in accordance with Kahn *et al.*'s expectation.[11]

ESR spectra

The powder ESR spectra of the three complexes at room temperature are shown in Fig. 5. They are obviously different from the mononuclear fragments; each exhibits a dissymmetric broad band of upper and lower peaks probably due to coupling of copper(II) ($S_1 = 1/2$) and cobalt(II) ($S_2 = 3/2$), although their assignments have not been made.

Acknowledgement—This project was supported by the National Natural Science Foundation of China.

REFERENCES

1. R. D. Willett, D. Gatteschi and O. Kahn (Eds), *Magneto-structural Correlation in Exchange-coupled Systems*, pp. 523–554. NATO ASI Series, Reidel, Dordrecht, Holland (1985).
2. H. Ojima and K. Nonoyama, *Coord. Chem. Rev.* 1988, **92**, 85.
3. L. C. Li, Thesis, Nankai University, Tianjin (1990).
4. H Ojima and K. Yamada, *J. Chem. Soc. Japan* 1968, **89**, 490.
5. W. J. Geary, *Coord. Chem. Rev.* 1971, **7**, 81.
6. Z. Y. Zhang, D. Z. Liao, Z. H. Jiang, S. Q. hang, X. K. Yao, H. G. Wang and G. L. Wang, *Inorg. Chim. Acta* 1990, **173**, 201.
7. S. L. Lambert, C. L. Spiro, R. R. Gagne and D. N. Hendrickson, *Inorg. Chem.* 1982, **21**, 68.
8. I. G. Dance, *Inorg. Chim. Acta* 1974, **9**, 77.
9. P. J. Hay, J. C. Thibeault and R. Hoffman, *J. Am. Chem. Soc.* 1975, **97**, 4884.
10. O. Kahn and M. F. Charlot, *Nouv. J. Chem.* 1980, **4**, 567.
11. O. Kahn, P. Tola and H. Coudanne, *Chem. Phys.* 1979, **42**, 355.

Polyhedron Vol. 10, No. 15, pp. 1791–1798, 1991
Printed in Great Britain

0277–5387/91 $3.00+.00
© 1991 Pergamon Press plc

COPPER(II) COMPLEXATION BY MICELLE-SOLUBILIZED LONG-CHAIN COMPLEXING AGENTS: UNUSUALLY SLOW REACTION RATES

C. TONDRE,* B. CLAUDE-MONTIGNY and M. ISMAEL

Laboratoire d'Etude des Solutions Organiques et Colloïdales (L.E.S.O.C.), U.A. CNRS No. 406, Université de Nancy I, B.P. 239, 54506 Vandoeuvre-lès-Nancy Cedex, France

and

P. SCRIMIN and P. TECILLA

Dipartimento di Chimica Organica and Centro CNR Meccanismi di Reazioni Organiche, Università di Padova, Via Marzolo 1, 35131 Padova, Italy

(*Received* 3 *January* 1991; *accepted* 25 *April* 1991)

Abstract—We consider in this work the complexation of copper(II) by two different complexing agents [7-4(ethyl-1-methyloctyl)-8-hydroxyquinoline (C_{11}-HQ) and 6-(hexadecylamino)methyl-2-hydroxymethylpyridine (C_{16}NHMePyr)] in different kinds of micellar surfactant solutions (SDS, $C_{12}EO_6$, CTAB and mixed CTAB/butanol). Stopped-flow kinetic experiments at controlled pH have provided values of the apparent rate constants for complex formation, which are discussed with reference to literature data in homogeneous solutions. They show considerable rate decreases, especially in CTAB micellar systems.

Since the pioneering work of Eigen and coworkers, it is well known that the rate of complexation of metal ions with complexing agents correlates with the characteristic rate constant for substitution of water molecules from the inner coordination sphere of metal ions.[1,2] The order of magnitude of this characteristic rate can be assigned to a given metal ion irrespective of the incoming ligand.[2] Apart from very special cases involving unusual mechanisms, this appears to be generally true in homogeneous solutions where the complexation process is always fast. The characteristic rate constants are for instance of the order 10^4, 10^5 and 10^8 s^{-1} for Ni^{2+}, Co^{2+} and Cu^{2+}, respectively. The much larger rate observed for the Cu^{2+} ion compared to the other mentioned ions has been ascribed to the operation of the Jahn–Teller effect, consisting of a distortion in the cation geometry which results in two relatively distant and weakly bonded water molecules in the primary hydration sphere.[3–5] As a consequence, kinetic investigations concerning copper(II) have been particularly difficult, requiring the use of relaxation techniques such as the temperature-jump technique. In some instances the reaction rate could be brought into the lower limit of reaction times attainable by the more classical stopped-flow technique, either by decreasing the concentration of reagents or by using a less reactive protonated form of the ligand.[4]

A class of complexing agents deserving special interest is that of lipophilic extractants which have applications for metal recovery in solvent extraction processes[6] and for functional micellar catalysis.[7,8] These extractant molecules are insoluble or extremely poorly soluble in water but they can be solubilized in an aqueous environment using micellar solutions or micro-emulsions. Such micro-heterogeneous media have been shown to mimic in some way the conditions of an extraction process taking place at an oil/water interface,[9,10] when a "kinetic regime" is established.

In this paper we report results concerning copper(II) complexation by micelle-solubilized long-chain complexing agents, which show very

* Author to whom correspondence should be addressed.

slow complexation rates in comparison to most of the available data in the literature. Such slowing down of the rate of complex formation may prove useful for separation purposes.[11] Compounds **1** and **2** were used as complexing agents:

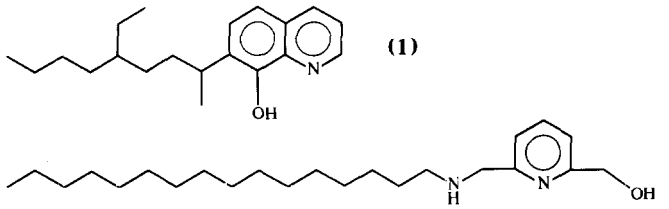

Compound **1**, which will be abbreviated to C_{11}-HQ, had an industrial origin,[9,12] whereas compound **2** (C_{16}NHMePyr in the following) was synthesized in one of our laboratories.[13]

RESULTS AND DISCUSSION

Complexation of Cu^{2+} *with* C_{11}-HQ

Most of the preceding stopped-flow kinetic studies involving this extractant were carried out in conditions where the metal ions (up to now only Ni^{2+} and Co^{2+}) were in a large excess compared to the complexing agent.[9,10,14] The reverse situation, which is closer to that encountered in solvent extraction, is examined here: the final concentration of copper chloride was 3×10^{-4} mol dm^{-3}, whereas the concentration of C_{11}-HQ varied between 3.34×10^{-3} and 1.67×10^{-2} mol dm^{-3} (i.e. 0.1–0.5 in weight by weight per cent). The source solution of C_{11}-HQ had the following composition (values in weight per cent): CTAB (4.5)/butanol (4.5)/C_{11}-HQ (1.0)/water 0.1 mol dm^{-3} TEA/HCl buffer (90.0). Different dilution methods were investigated (see schematic drawing in Fig. 1) leading to different results. In each case, the same diluent (either a micellar solution of the same composition or an aqueous solution) was also used to solubilize the metal ions. Three different kinds of aqueous solutions were tested: (1) solution of 0.1 mol dm^{-3} TEA, pH 6.5; (2) solution of ionic strength 0.25 mol dm^{-3} KBr; and (3) solution with no buffer or salt (pH of the metal ion solution was adjusted with drops of sodium hydroxyde or hydrochloric acid).

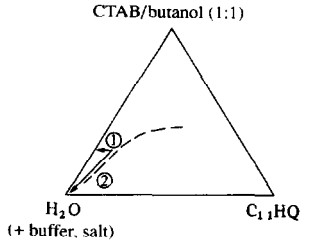

Fig. 1. Schematic phase diagram showing the two possible dilution paths: path (1): dilution with a micellar solution; path (2): dilution with water.

The kinetic curves recorded at 432 nm were generally bi-exponential, with the fastest relaxation process accounting for approximately 90% of the total absorption change. The slow relaxation process whose origin was previously discussed[9] will not be considered here. It was in fact almost undetectable when the aqueous diluent did not contain TEA [cases (2) and (3) above], but this may be due to a slight acidic shift in the final pH.

The variations of the reciprocal relaxation time of the exponential versus concentration of C_{11}-HQ have been plotted in Fig. 2 for the different ways of mixing the solutions described above. Fairly good linear plots were obtained in all cases. The slopes of the straight lines provide the values of the apparent rate constants k_f^{app} for complex formation. This is 3.2×10^3 mol^{-1} dm^3 s^{-1} when the composition of the micellar solution is kept constant during the mixing and from 2 to 2.3 times lower when diluted by an aqueous solution (1.4×10^3 with 0.25 mol dm^{-3} KBr, 1.7×10^3 with no buffer or salt and 2.1×10^3 with 0.1 mol dm^{-3} TEA).

In the case of dilution by an aqueous solution,

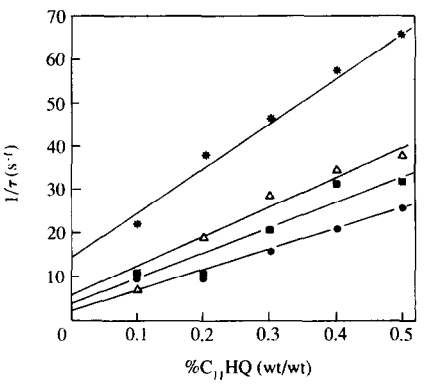

Fig. 2. Reciprocal relaxation time (or observed rate constant) versus concentration of C_{11}HQ in % (wt/wt). Copper concentration: 3×10^{-4} mol dm^{-3}, pH 6.5. Dilution by: (*) micellar solution; (△) water 0.1 mol dm^{-3} TEA; (■) water; (●) water 0.25 mol dm^{-3} KBr.

the final concentration of micelles is half that in the former case and thus the *local* concentration of micelle-solubilized extractants should be larger. Considering this local concentration instead of the overall one does not allow one to rationalize the data. The results would thus indicate that (due to electrostatic repulsions) the probability of a successful collision between Cu^{2+} and an extractant molecule is increased when these molecules are distributed over a larger number of micelles.

We have also examined the complexation of copper ions in the presence of an equivalent concentration of cobalt ions, which are expected to react much more slowly. Two well-separated relaxation processes were obtained in that case: the fastest one, due to copper complexation, remained unaffected by the presence of the second metal ion species. From the variation of the slowest one with concentration of C_{11}-HQ, an apparent rate constant of 8.6 mol^{-1} dm^3 s^{-1} was determined for cobalt complexation. The ratio between the rate constants for copper and cobalt respectively amounts to 372. This value, which is in the order of magnitude expected for the ratio of the water exchange rates in the inner coordination spheres of these metal ions,[1,2] can be taken as proof that the kinetics observed are truly related to metal ion complexation.

The time scale involved in copper complexation by C_{11}-HQ is much longer than what is generally found in homogeneous solutions, as far as neutral ligands are concerned (see Table 1). The values found for k_f^{app} are even smaller than those measured for a number of protonated species, which have been qualified as "abnormal" slow-reacting species.[4] In the present case, as the local pH at the micellar surface is expected to be more basic than the measured one (due to Br^-/OH^- ion exchange[15]), we assume that the extractant exists mainly in its neutral form. Indeed the first pK of the non-alkylated analogue of C_{11}-HQ (8-hydroxyquinoline) was around 5,[16,17] and measurements performed in methanol gave a lower pK value (decrease of about 0.8 units) for C_{11}-HQ than for 8-hydroxyquinoline.[12]

The low rate of complexation can be attributed to several effects whose contributions will have to be investigated more closely: (1) electrostatic repulsions between the metal ions and the micelles in which the extractant is solubilized; (2) hydrophobic interactions between the extractant molecules and the micelles, implying a strong partition of the extractant in favour of the micellar pseudo-phase; (3) a possible effect of reduction of dimensionality if the reaction takes place on the micellar surface;[18] and (4) steric hindrance preventing the approach to the complexing site.

Complexation of Cu^{2+} *with* C_{16}NHMePyr

The kinetics of complex formation were investigated in micellar solutions made respectively of anionic, cationic and non-ionic surfactants. The appearance of the complex in the presence of a large excess of Cu^{2+} ions (1 : 1 complex) was detected at 285 nm (SDS solutions) or at 300 nm (CTAB and $C_{12}EO_6$ solutions). Figure 3 shows that the behaviour of the curves giving the variation of absorbance versus time may be very sensitive to pH changes. In the cases of CTAB and $C_{12}EO_6$, if the solutions of metal and extractant respectively are mixed, with no special pH adjustments, a bimodal curve is obtained which can be nicely fitted with a bi-exponential

Table 1. Comparison of rate constants for Cu^{2+} complexation in homogeneous media (k_f) and in micro-heterogeneous media (k_f^{app})

Ligand	Solvent or particular system	k_f (or k_f^{app}) mol^{-1} dm^3 s^{-1}	Reference
	Homegeneous media		
Miscellaneous neutral ligands	Water, ionic strength 0.3 M	10^7–10^9	4, 30, 31
Miscellaneous protonated ligands	Water, ionic strength 0.3 M	10^3–10^7	4, 30, 31
	Microheterogeneous media		
C_{11}-HQ	CTAB/butanol pH 6.5	1.4–3.2×10^3	This work
$C_{16}\overset{+}{N}H_2$MePyr	SDS 0.2 M pH 3.5	7.1×10^3	This work
$C_{16}\overset{+}{N}H_2$MePyr	$C_{12}EO_6$ 0.02 M pH 3.5	2.4×10^2	This work
$C_{16}\overset{+}{N}H_2$MePyr	CTAB 0.025 M pH 3.5	1.3×10^2	This work

(See text for the abbreviations used.)

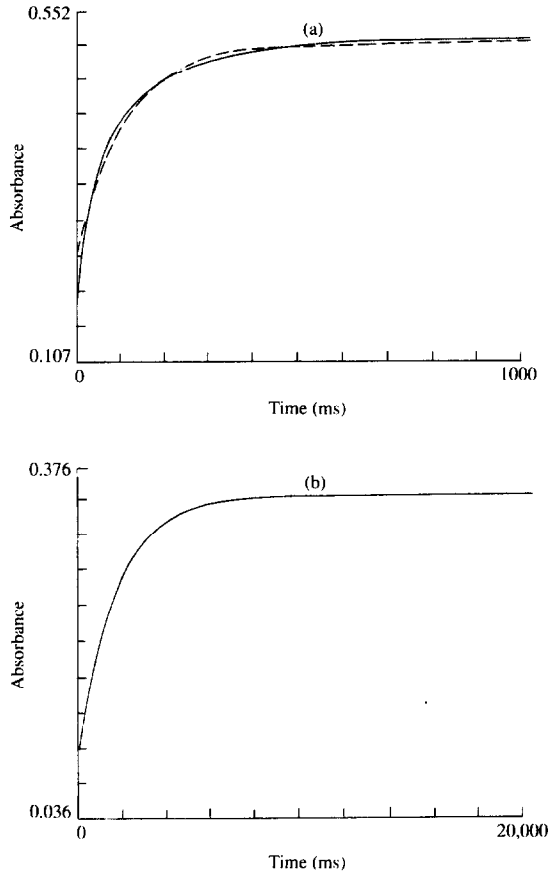

Fig. 3. Typical change of absorbance versus time during $C_{16}NHMePyr/Cu^{2+}$ complexation in CTAB at 300 nm. (a) No HCl added; --- theoretical fit with mono-exponential function; —— experimental curve and fit with biexponential function (undistinguishable). (b) HCl added; experimental curve and monoexponential fit undistinguishable.

function. On the other hand, one always obtains a strictly mono-exponential behaviour if one of the solutions is slightly acidified, so that the final pH is below 4.0. In the case of SDS, the second relaxation time was not observed.

Figures 4–6 indicate the conditions in which one or two relaxation times were obtained (the observed rate constants k_{obs} are equivalent to the reciprocal relaxation times). The pH was adjusted with a few drops of hydrochloric acid or sodium hydroxyde, avoiding the use of any buffer. An aliquot of the mixed solutions was taken out of the stopped-flow apparatus in order to measure the final equilibrium pH values which are plotted in Figs 4–6. The general shape of these curves is as expected when several protonation steps are involved in the mechanism considered.[19,20]

Taking advantage of the preceding observations we fixed the pH at 3.5 ($\pm$0.2) in order to investigate

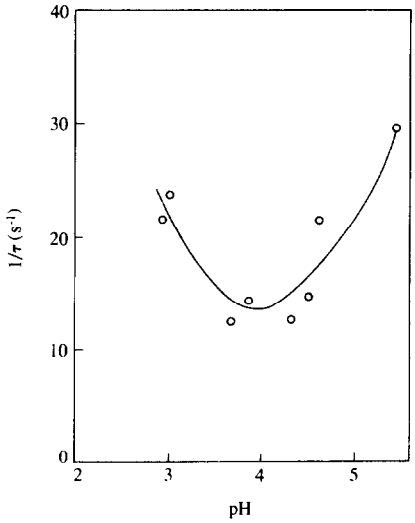

Fig. 4. Reciprocal relaxation times versus pH for $C_{16}NHMePyr/Cu^{2+}$ complexation in SDS 0.2 mol dm^{-3}; $[Cu^{2+}] = 10^{-3}$ mol dm^{-3}.

the effect of the concentration of Cu^{2+} ions on k_{obs}. The results are represented in Fig. 7 for the three micellar systems used as reaction media. A linear variation was always found, the slope of which gives the value of the apparent rate constant for complex formation: 128 mol^{-1} dm^3 s^{-1}, 237 mol^{-1} dm^3 s^{-1} and 7100 mol^{-1} dm^3 s^{-1} for CTAB, $C_{12}EO_6$ and SDS, respectively. These values are likely to be assigned to the reaction between the protonated form of the ligand $C_{16}\overset{+}{N}H_2MePyr$ and the metal ion (see below).

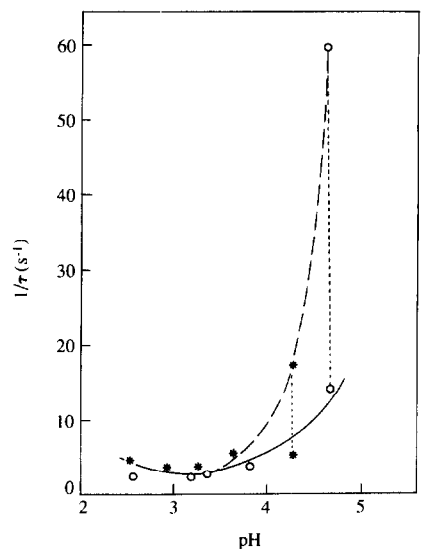

Fig. 5. Reciprocal relaxation times versus pH for $C_{16}NHMePyr/Cu^{2+}$ complexation in $C_{12}EO_6$ 0.02 mol dm^{-3} (○) and 0.2 mol dm^{-3} (*), $[Cu^{2+}] = 5 \times 10^{-3}$ mol dm^{-3}. The dashed lines refer to the second relaxation times.

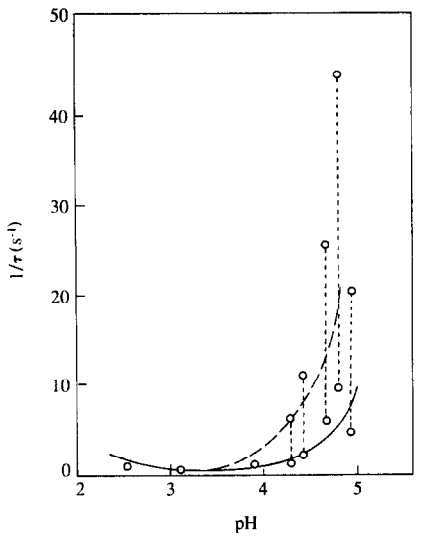

Fig. 6. Reciprocal relaxation times versus pH for $C_{16}NHMePyr/Cu^{2+}$ complexation in CTAB 2.5×10^{-2} mol dm^{-3}; $[Cu^{2+}] = 5 \times 10^{-3}$ mol dm^{-3}. The dashed lines refer to the second relaxation times.

As expected, a much larger value was obtained in SDS solutions than in solutions of the other surfactants. This is due to the high local concentration of Cu^{2+} ions in the Stern layer of the SDS micelles in which the complexing agent is solubilized. It can thus be viewed as a classical micellar "catalysis" effect. Note, however, that the measured rate constant has a value in the same order as that obtained for the protonated form of the non-alkylated ligand aminomethylpyridine ($AmpH^+$) in purely aqueous solution.[4]

The situation is completely different for the case

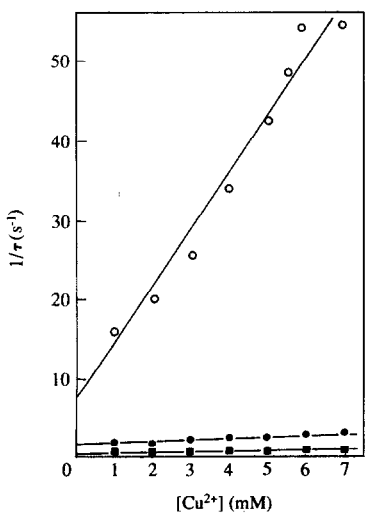

Fig. 7. Reciprocal relaxation times versus concentration of Cu^{2+} at pH 3.5 (±0.2); (○) SDS 0.2 mol dm^{-3}; (●) $C_{12}EO_6$ 0.02 mol dm^{-3}; (■) CTAB 0.025 mol dm^{-3}.

of cationic micelles in which the apparent rate constant has an unusually low value when compared to the literature data (see Table 1). The value obtained with $C_{12}EO_6$ is less than twice as large, which can be taken as an indication that the hydrophobic interactions between the ligand and the micelles play a larger part than the electrostatic repulsions between the metal ions and the surface of the micelles.

The intercepts of the lines shown in Fig. 7 are expected to give the values of the dissociation rate constants. They indicate that the release of Cu^{2+} from its complex is much easier in SDS micelles than in CTAB micelles, with an intermediary situation for $C_{12}EO_6$.

This may be attributed to the fact that in the case of SDS the surfactant ions in the vicinity of the complex can attract the metal ion and thus can destabilize the complex more easily than in the case of cationic or non-ionic micelles.

In the present paper, the micellar systems have been considered as simple reaction media and we will not attempt to define more precisely the site of the reaction of complexation. This will be done in a next step.

Concerning the origin of the two relaxation processes which depend on the pH, additional information regarding the ionization state of the ligand is required. For this reason we have performed potentiometric measurements on a C_4-analogue of $C_{16}NHMePyr$, which is sufficiently water soluble. These measurements indicate a pK of 9.05 for the free ligand [a pK of 8.61 was reported for 2-aminomethylpyridine (Amp) which has a close structure[21]], whereas it is only of 6.1 for the complex with copper(II). The concentration of ligand was 10^{-2} M and a 20% excess of Cu^{2+} ions was used in the second case. If one refers to the case of alkylamines, the pK should be almost independent of the alkyl chain length (pKs are respectively 10.7, 10.63 and 10.61 for ethylamine, $C_{12}NH_2$ and $C_{16}NH_2$).[22] However, the pKs measured in water may be different from the effective pKs in the micellar pseudo-phases.[23,24] The pK shifts are expected to go in opposite directions in SDS and CTAB micellar solutions, respectively. This may explain why the second relaxation time was not observed with SDS.

Neglecting the effect of the micro-environment, the following assumptions can be made from the preceding pK values: (1) essentially the ligand protonated on the amine function should be considered as the reacting species at the pH values used; and (2) the protonation equilibrium of the complex may be responsible for the existence of a second relaxation process.

In fact, according to Roche and Wilkins,[4] the deprotonation of the complex can be quite slow, since proton loss may even be rate-limiting in the reaction of $AmpH^+$ with Cu^{2+}. In this last case the pK shift between the free amine and its complex was estimated to be about 2 units from the comparison with literature data concerning comparable situations. It is close to 3 units in the present case.

From the preceding considerations the simplest mechanism that can be proposed to qualitatively account for our results is the following:

$$Cu^{2+} + LH_2^+ \underset{k_{-1}^{app}}{\overset{k_1^{app}}{\rightleftharpoons}} Cu-LH_2^{3+} \qquad (1)$$

$$Cu-LH_2^{3+} \underset{k_{-2}^{app}}{\overset{k_2^{app}}{\rightleftharpoons}} CuLH^{2+} + H^+. \qquad (2)$$

Protonation of the pyridinium ring has been omitted, but it would have to be taken into consideration in the very low pH range.

The preceding mechanism is characterized by two relaxation times except when the pH is sufficiently acidic that the complex remains entirely protonated. There is no longer a contribution of reaction (2) in that case, and the system is reduced to reaction (1) whose time constant is given by:[25,26]

$$k_{obs} = \frac{1}{\tau} = k_1^{app}[Cu^{2+} + LH_2^+] + k_{-1}^{app}$$

$$\sim k_1^{app}[Cu^{2+}]_0 + k_{-1}^{app}$$

in agreement with the linear behaviours reported in Fig. 7.

Following classical methods of calculations,[26] a complete treatment of the above mechanism was attempted in order to verify how the two relaxation times vary when the pH is changed. Assuming that the equilibrium constants for reaction (1) and (2) are known ($K_1 = k_1^{app}/k_{-1}^{app}$ and K_2 was given the value obtained from pK measurements in water), all the equilibrium concentrations can be calculated. The only unknown quantities for the calculation of the relaxation times are k_2^{app} and k_{-2}^{app}, which are related through K_2. Varying the value of k_2^{app} has not permitted a quantitative agreement with the data, although the same kind of variations could be obtained for the two relaxation times. From these variations the shortest relaxation time could be tentatively assigned to reaction (2) and the longest relaxation time, which was found almost independent of pH, to reaction (1).

This treatment, which considered the micellar solution as an ordinary solvent, provides an explanation for the existence of a second relaxation time but it is inadequate to interpret the data on quantitative grounds because it ignores the actual micro-heterogeneous nature of the solution. One related question is that of the possible existence of free and micellar-bound ligands and the rate controlling their exchange reaction. At pH 3.5, $C_{16}\overset{+}{N}H_2MePyr$ is assumed to behave like a surfactant due to its amphiphilic nature. The mean rate constant for the dissociation of a C_{16}-surfactant monomer from a micelle was shown to be around 10^5 s^{-1}.[27,28] This quantity has to be divided by the micellar number if one particular monomer in the micelle is considered. This would also apply for one single complexing molecule solubilized in a classical micelle made of surfactant ions bearing the same electric charge. In this case, the rate constant for dissociation can thus reasonably be estimated to be in the ms range, which is quite fast in comparison with the time scale of the present experiments. Due to this fast ligand exchange we assumed that we measured an average complexation rate, in which the micelle-solubilized long-chain complexing agent is expected to contribute in an overwhelming manner.

To prove this view to be correct we would need to vary the hydrophobic character of the complexing agent to see if this has an influence on the existence of one or two relaxation times. This should be investigated before a complete treatment, taking into account the micro-heterogeneous nature of the solution, could be attempted as for instance in the work of Miyake *et al.*[29]

Conclusion

We report in this paper unusually slow reaction rates for the complexation of copper(II) with two different complexing agents. However, unlike the case of nickel(II) for which the overall complexation time could be brought down to a time of the order 1 h,[11] the time scale involved always remained shorter than 1 min. This demonstrates that, although considerably decreased, the rate of complexation by micelle-solubilized long-chain complexing agents is still correlated with the rate of substitution of water molecules in the inner coordination sphere of the metal ion.

A direct comparison between ligands **1** and **2** is made difficult due to the existence of different chemical functions, especially the protonatable amine function in compound **2**. In addition, the signal amplitudes had a tendency to vanish when the pH was decreased with compound **1** and increased with compound **2**, preventing us from performing a comparison at the same pH.

The difference by one order of magnitude for the apparent rate constants measured in the presence of CTAB (see Table 1) can hardly be rationalized for this reason. Although a longer alkyl chain may

be responsible for a decrease in k_1^{app}, it is likely that the low value obtained with compound **2** is mainly due to the positive charge on the complexing site. Experiments with ligands having varying alkyl chain lengths appear necessary to go further in the understanding of these complex systems.

EXPERIMENTAL

Chemicals

Recrystallized 99% sodium dodecylsulphate (SDS) was obtained from Roth (Germany), hexaethyleneglycol dodecylether ($C_{12}EO_6$) from Nikko Chemicals (Japan) and cetyltrimethylammonium bromide (CTAB) from Fluka. All these products were used as received with the exception of CTAB, which was twice recrystallized in methanol/diethylether.

$CuCl_2 \cdot 2H_2O$ (normapur) was obtained from Prolabo (France). Compound **1** was obtained by purification of the industrial extractant Kelex 100 (Shering, Germany), according to a previously published procedure.[12] Compound **2** was synthesized by the Padova group.[13] The C_4 analogue was synthesized following the same procedure reported[13] for C_{16}NHMePyr, but using butylamine. The compound is a pale yellow oil. ^{1}H NMR δ ($CDCl_3$, TMS) 0.9 (t, 3H, CH_3), 1.2–1.7 (m, 4H, $2CH_2$), 2.7 (t, 2H, CH_2N), 3.2 (brs, 2H, OH and NH), 3.95 (s, 2H, NCH_2Py), 4.7 (s, 2H, OCH_2), 7.1 and 7.2 (2d, 2H, PyH_3 and H_5), 7.65 (t, 1H, PyH_4). Found: C, 67.9; H, 9.4; N, 14.3. Calc. for $C_{11}H_{18}N_2O$: C, 68.0; H, 9.3; N, 14.4%.

Triethanolamine (TEA) from Merck (pro-analysis) was used in some instances with hydrochloric acid to buffer the solutions (0.1 M concentration).

Techniques

The stopped-flow technique with optical detection was used to investigate the kinetics of complex formation at 25°C. Either a Durrum D-110 apparatus with a 2 cm optical path or a Hi-Tech (SF-3L, England) with a 2 mm optical path was used depending on the extent of light absorption by the metal complex. Both apparatus were on-line with a data acquisition system. The observed rate constants were computed from a least-squares fitting of the experimental curves with mono- or bi-exponential functions.

The stopped-flow experiments involved the rapid mixing of a micellar solution containing the lipophilic extractant with a solution containing the metal ions. This second solution was either a micellar solution having the same composition as the first one or simply an aqueous solution. pH measurements were performed with a combined glass electrode (Metrohm).

All the concentrations refer to the state of the system after rapid mixing. It is not clear whether the terms "micelle" or "micro-emulsion" should be used for the solutions with CTAB/butanol and large concentrations of C_{11}-HQ. The second one is preferable because the extractant was previously shown to play the same part as the oil in a classical microemulsion system.[11]

REFERENCES

1. M. Eigen, *Pure Appl. Chem.* 1963, **6**, 97.
2. M. Eigen and R. G. Wilkins, *Adv. Chem. Series (Am. Chem. Soc.)* 1965, **49**, 55.
3. M. Eigen, *Ber. Bunsenges Phys. Chem.* 1963, **67**, 753.
4. T. S. Roche and R. G. Wilkins, *J. Am. Chem. Soc.* 1974, **96**, 5082.
5. J. Burgess (Ed.), in *Metal Ions in Solution*, p. 361. Ellis Horwood Ltd, John Wiley and Sons (1978)
6. G. M. Ritcey and A. W. Ashbrook, *Solvent Extraction, Principles and Applications to Process Metallurgy*, Part I. Elsevier (1984).
7. R. Fornasier, D. Milani, P. Scrimin and U. Tonellato, *J. Chem. Soc., Perkin Trans II*, 1986, 233.
8. R. Fornasier, P. Scrimin, P. Tecilla and U. Tonellato, *J. Am. Chem. Soc.* 1989, **111**, 224.
9. C. Tondre and M. Boumezioud, *J. Phys. Chem.* 1989, **93**, 846.
10. M. Boumezioud, H. S. Kim and C. Tondre, *Colloids Surf.* 1989, **41**, 255.
11. H. S. Kim and C. Tondre, *Sep. Sci. Technol.* 1989, **24**, 485.
12. M. Boumezioud, P. Lagrange and C. Tondre, *Polyhedron* 1988, **7**, 513.
13. P. Scrimin, P. Tecilla and U. Tonellato, *J. Org. Chem.* 1991, **56**, 161.
14. H. S. Kim and C. Tondre, *Langmuir* 1989, **5**, 395.
15. L. S. Romsted, *Surfactants in Solution* (Edited by K. L. Mittal and B. Lindman), Vol. 2, p. 1015. Plenum Press, New York (1984).
16. W. A. Johnson and R. G. Wilkins, *Inorg. Chem.* 1970, **9**, 1917.
17. M. Boumezioud and C. Tondre, *J. Chim. Phys.* 1988, **85**, 719.
18. R. D. Astumian and Z. A. Schelly, *J. Am. Chem. Soc.* 1984, **106**, 304.
19. D. N. Hague and M. Eigen, *Trans. Faraday Soc.* 1966, **62**, 1236.
20. B. Perlmutter-Hayman, F. Secco and M. Venturini, *J. Chem. Soc. Dalton Trans.* 1982, 1945.
21. K. V. Damu, M. S. Shaikjee, J. P. Michael, A. S. Howard and R. D. Hancock, *Inorg. Chem.* 1986, **25**, 3879.
22. D. D. Perrin, *Dissociation Constants of Organic Bases in Aqueous Solution*. IUPAC, Butterworths, London (1965).

23. A. Berthod and J. Georges, *Nouv. J. Chim.* 1985, **9**, 101.
24. R. A. Mackay, K., Jacobson and J. Tourian, *J. Colloid Interface Sci.* 1980, **76**, 515.
25. M. Eigen and L. De Maeyer, in *Investigation of Rates and Mechanisms of Reactions, Technique of Organic Chemistry* (Edited by S. L. Friess, E. S. Lewis and A. Weissberger), Vol. III, Part II. John Wiley & Sons, New York (1963).
26. C. F. Bernasconi, *Relaxation Kinetics*, pp. 25–27. Academic Press, New York (1976).
27. S. K. Chan, U. Herrmann, W. Ostner and P. Kahlweit, *Ber. Bunsenges Phys. Chem.* 1978, **82**, 380.
28. E. A. G. Aniansson, S. N. Wall, M. Almgren, H. Hoffmann, I. Kielmann, W. Ulbricht, R. Zana, J. Lang and C. Tondre, *J. Phys. Chem.* 1976, **80**, 905.
29. Y. Miyake, M. Shigeto and M. Teramoto, *J. Chem. Soc. Faraday Trans.* 1986, **82**, 1515.
30. D. N. Hague, in *Molecular Biology, Biochemistry and Biophysics* (Edited by I. Pecht and R. Rigler), Vol. 24. Springer-Verlag, Berlin (1977).
31. J. W. Brubaker, A. F. Pearlmutter, J. E. Stuehr and T. V. Vu, *Inorg. Chem.* 1974, **13**, 559.

Polyhedron Vol. 10, No. 15, pp. 1799–1801, 1991
Printed in Great Britain

0277-5387/91 $3.00+.00
© 1991 Pergamon Press plc

REACTIONS OF PRIMARY AROMATIC AMINES WITH STRONGLY ELECTROPHILIC NO COORDINATED TO A RUTHENIUM COMPLEX OF 2-(PHENYLAZO)PYRIDINE

ALOK KUMAR DEB and SREEBRATA GOSWAMI*

Department of Chemistry, North-Eastern Hill University, Shillong 793003, India

(*Received* 18 *March* 1991; *accepted* 3 *May* 1991)

Abstract—The diazotization of primary aromatic amines with a strongly electrophilic mononitrosyl complex, $[Ru(NO)(NO_2)L_2](ClO_4)_2$ [L = 2-(phenylazo)pyridine], in acetonitrile and dichloromethane, is described. The reactions were studied by following the reaction sequence through the isolation of products at various stages of each reaction.

There has been considerable interest in the reactivities of the transition metal nitrosyls,[1,2] in general, and those of Group VIII metal ions,[3–6] in particular. Very recently, we have reported[7] the synthesis of a mononitrosyl complex of the type $[Ru(NO)(NO_2)L_2](ClO_4)_2$ (**1**) [L = 2-(phenylazo) pyridine], and it has been shown from its physicochemical data that the nitrosonium ion (NO^+) character of the coordinated nitric oxide in **1** is very high. Given the presence of a strongly electrophilic NO^+ centre in **1**, we initiated research to study the reactivities of **1** with various nucleophiles. Herein we report the diazotization reaction of aromatic primary amines using **1** as the source material of the nitrosonium cation. This reaction is one of the rare examples of its type and is important in connection with the synthesis of aryldiazonium[8–10] complexes which may be considered as a model[11,12] for dinitrogen complexes.

RESULTS AND DISCUSSION

The amines are abbreviated as $Ar\text{-}NH_2$. Reactions of the nitrosyl complex **1** with $Ar\text{-}NH_2$ were studied by following the reaction sequence through the isolation of products at various stages of the reactions. The reactions which have been studied are shown in Scheme 1. Strategically, the reactions were conducted in two solvents, viz. acetonitrile and dichloromethane, to provide a better insight into the mechanisms of the reactions.

The orange solution of **1** in acetonitrile readily reacted with $Ar\text{-}NH_2$ to produce a mixture of $[Ru(S)(NO_2)L_2]^+$ (**2**) (S = CH_3CN) and $Ar\text{-}N_2^+$. The cationic complex, **2**, has been isolated as a crystalline perchlorate salt. The aryldiazonium cation has been identified by spectral data and also by performing a chemical test with alkaline β-naphthol. Red crystals of the known[13] 1-arylazo-2-naphthol have been isolated from the reaction mixture. The metal part has been characterized by

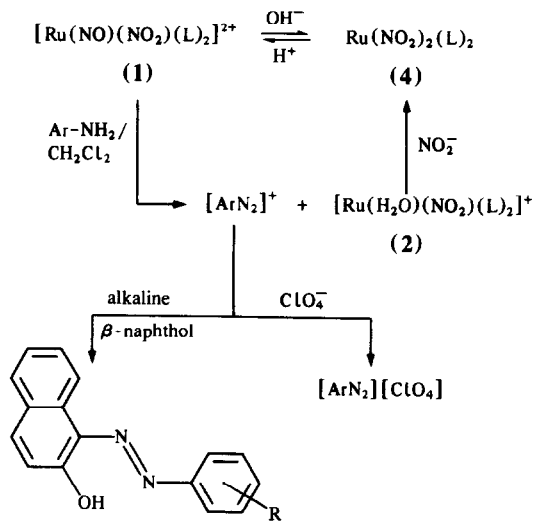

R	Yield (%)
H	45
p-Me	60
p-OMe	55
p-Cl	45

Scheme 1.

* Author to whom correspondence should be addressed.

elemental analysis as well as by examining the spectral data (see Experimental). A strong band at 1370 cm^{-1} assignable to $\nu(NO_2)$ and a weak band at 2300 cm^{-1} assignable to $\nu(C{\equiv}N)$ are observed in the IR spectrum and an intense MLCT absorption band at 515 nm in the visible spectrum. The same reaction, when performed in the presence of very dilute aqueous perchloric acid, yielded the aryldiazonium cation in slightly improved yield together with a diacetonitrile complex of the type $[Ru(CH_3CN)_2L_2]^{2+}$ (**3**), which was isolated as a perchlorate salt. This has been formulated by elemental analysis. This compound showed two $\nu(C{\equiv}N)$ modes in the IR spectrum indicating a *cis* geometry[14] with respect to the solvent. The formation of the diacetonitrile compound **3** from the acidic medium was not unexpected since it has already been shown[7] that the dinitro complex, $Ru(NO_2)_2L_2$, is unstable in acidic media and yields disolvento species of the type $[Ru(S)_2L_2]^{2+}$ (S = solvent). The cationic complex **3** was further characterized by comparison of its spectral data with authentic $[Ru(CH_3CN)_2L_2]^{2+}$, which has been synthesized following the procedure described by Chakravorty and co-workers.[14]

The transformation of **1** to **2** requires firstly diazotization, followed by substitution of coordinated $Ar\text{-}N_2^+$ by acetonitrile. Keeping the high affinity[14] of acetonitrile for ruthenium(II) in mind, we examined the same diazotization reaction in a non-coordinating solvent, dichloromethane, hoping to isolate the coordinated aryldiazonium complex. Unfortunately, the crude reaction product obtained from the red dichloromethane solution showed a strong band at *ca* 2260 cm^{-1}, indicating the presence[9] of free $Ar\text{-}N_2^+$. It is quite significant to note that the IR spectrum of the crude product shows all the characteristic bands for both coordinated NO_2[7] and for coordinated L.[15] Analytically, the crude product was always inconsistent. Therefore, we conclude that the isolated product is a mixture of a salt of $Ar\text{-}N_2^+$ and some ruthenium complex of L. However, extraction of the crude product with water separated $[Ar\text{-}N_2]^+$ from the metal complex. The residue was soluble in dichloromethane which, on slow addition of hexane, yielded crystalline $[Ru(S)(NO_2)L_2]ClO_4 \cdot H_2O$ (**2**) (S = H_2O). Complex **2** (S = H_2O) was characterized by elemental analysis and by spectral data (see Experimental). A strong MLCT absorption band occurred at 530 nm (ε, 8500 $dm^3\ mol^{-1}\ cm^{-1}$). The cationic monoaquo complex **2** (S = H_2O) produced the monoacetonitrile complex **2** (S = CH_3CN) on treatment with acetonitrile, showing its instability in this solvent. This observation also in turn justifies the formation of the monoacetonitrile complex in the reaction when it is carried out in acetonitrile.

Free aryldiazonium ions as well as **2** and **3** are obtained in high yields. The regeneration of **1** can be performed first by treating **2** or **3** with an aqueous solution of sodium nitrite to obtain the known[7] dinitro complex $[Ru(NO_2)_2L_2]$ (**4**), which on treatment with acid produces **1** (Scheme 1). In contrast to the lone example[11,12] of a similar type of reaction, reported previously, free diazonium cations are directly obtained from the reaction of **1** and $Ar\text{-}NH_2$. The results could be interpreted by considering the high π-acidity of L. It is well documented in the literature that aryldiazonium complexes are generally stabilized[12] by π-back donation. In the present complex, L being a very strong π-acceptor[14-17] reduces the back donation to $Ar\text{-}N_2^+$ in the intermediate and thus makes it labile towards solvolysis reactions.

The results of the reactions described above are convincing, and one real advantage of such reactions is the possibility of developing a catalytic route for synthetic nitrosation reactions of organic substrates using **1** as the source of NO^+ under mildly acidic or even neutral conditions.

EXPERIMENTAL

IR spectra were recorded on a Perkin–Elmer IR-983 spectrophotometer in KBr pellets. Electronic spectra were obtained using a Hitachi 330 spectrophotometer. Solution electrical conductivity was measured using a Elico CM 82T conductivity bridge with a solution concentration of 10^{-3} mol dm^{-3}. Spectrograde acetonitrile and dichloromethane were used as the solvents in the diazotization reactions. The substituted anilines used were of reagent grade and used without further purification, aniline was distilled over potassium hydroxide before use. Elemental analyses were obtained using a Haraous CHN-O-RAPID elemental analyser.

Reaction of $[Ru(NO)(NO_2)L_2](ClO_4)_2$ *with* $Ar\text{-}NH_2$ ($Ar\text{-}NH_2$ = *aniline*, p-*anisidine*, p-*chloroaniline*, p-*toluidine*)

The reactions were performed by using a general procedure. Specific details are given for aniline.

Reaction in acetonitrile. The salt $[Ru(NO)(NO_2)L_2](ClO_4)_2$ (0.125 g, 0.17 mmol) was dissolved in acetonitrile (10 cm^3) and aniline (0.016 g, 0.17 mmol) was added. The mixture was stirred for 30 min at room temperature (295 K) and then evaporated to dryness using a vacuum pump. The crude product was then extracted with 30 cm^3 (3 × 10 cm^3) of ice-cold water and the aqueous solution was collected by filtration. To the aqueous solution, an aqueous solution of alkaline β-naphthol was added

with continuous stirring over a period of 15 min. Red crystals of 1-phenylazo-2-naphthol were separated and recrystallized from methanol (m.p. 130°C).

The dark tan residue obtained after water extraction was dried and dissolved in dichloromethane. On slow addition of hexane, light brown crystals of $[Ru(S)(NO_2)L_2]ClO_4 \cdot H_2O$ (S = CH_3CN) were obtained, which were filtered and dried *in vacuo* over P_4O_{10}; yield 60%. Found: C, 42.9; H, 3.3; N, 16.5. Calc. for $C_{24}H_{23}N_8O_7ClRu$: C, 42.9; H, 3.4; N, 16.7%. Λ_M(MeCN): 140 Ω^{-1} cm^2 mol^{-1}; ν_{max} (KBr): 1370 (NO_2), 2300 (C≡N) and 1360 cm^{-1} (N=N); λ_{max} (CH_3CN): 515, 350 and 310 (sh) nm (ε, 6475, 12,050 and 11,920 dm^3 mol^{-1} cm^{-1}).

Reaction in acetonitrile in presence of aqueous perchloric acid. This was carried out similarly except 0.1 cm^3 of 1 M aqueous perchloric acid was added together with Ar-NH_2. The metal part was crystallized from a 1 : 1 acetonitrile/water mixture and left to evaporate at room temperature overnight. The dark crystalline compound was collected by filtration and dried *in vacuo* over P_4O_{10} (compound $[Ru(CH_3CN)_2L_2](ClO_4)_2 \cdot H_2O$; yield 62%. Found: C, 41.0; H, 3.1; N, 14.3. Calc.: C, 40.7; H, 3.4; N, 14.6%. Λ_M(MeCN): 300 Ω^{-1} cm^2 mol^{-1}; ν_{max} (KBr): 2295, 2320 (C≡N) and 1365 cm^{-1} (N=N); λ_{max} (CH_3CN): 500, 470(sh), 365, 310(sh) and 280 nm (ε, 9670, 6400, 7910, 17,200 and 17,500 dm^3 mol^{-1} cm^{-1}).

Reaction in dichloromethane. $[Ru(NO)(NO_2)L_2](ClO_4)_2$ (0.125 g, 0.17 mmol) was suspended in dichloromethane (10 cm^3) and aniline (0.016 g, 0.17 mmol) was added. The mixture was then stirred for 30 min at room temperature (295 K) and the red–brown solution was then filtered. Brownish-white needles of $[C_6H_5N_2](ClO_4)$ were collected, washed with 5 cm^3 of dichloromethane and finally dried *in vacuo* over P_4O_{10}; yield 50%.

The cation $[C_6H_5N_2]^+$ could also be extracted with ice-cold water, and on addition of an aqueous alkaline solution of β-naphthol yielded red crystals of 1-phenylazo-2-naphthol, which were recrystallized from methanol (m.p. 130°C).

The red–brown dichloromethane filtrate was concentrated to 10 cm^3 under reduced pressure and slow addition of hexane yielded dark crystals of $[Ru(S)(NO_2)L_2]ClO_4 \cdot H_2O$ (S = H_2O). These were collected by filtration and dried *in vacuo* over P_4O_{10}, yield 55%. Found: C, 41.0; H, 3.5; N, 15.1. Calc. for $C_{22}H_{22}N_7O_8ClRu$: C, 40.7; H, 3.4; N, 15.1%. Λ_M(MeCN): 140 Ω^{-1} cm^2 mol^{-1}; ν_{max}(KBr): 1370 (NO_2) and 1360 cm^{-1} (N=N); λ_{max}(CH_2Cl_2): 530, 470(sh), 360(sh), 325(sh) and 312 nm (ε, 8500, 4750, 36,950, 58,550 and 67,015 dm^3 mol^{-1} cm^{-1}).

Conversion of $[Ru(S)(NO_2)L_2]ClO_4 \cdot H_2O$ (S = H_2O) *to* $[Ru(S)(NO_2)L_2]ClO_4 \cdot H_2O$ (S = CH_3CN). $[Ru(S)(NO_2)L_2]ClO_4 \cdot H_2O$ (S = H_2O) (0.100 g, 0.15 mmol) was dissolved in acetonitrile (15 cm^3) and stirred at room temperature for 30 min. To the brown solution, an equal volume of water was added and left to evaporate at room temperature overnight. Dark brown crystals of $[Ru(S)(NO_2)L_2]ClO_4 \cdot H_2O$ (S = CH_3CN) were obtained. The analytical and spectral data correspond exactly to those of the previously isolated compound **2** (S = CH_3CN).

Acknowledgements—We are thankful to Professor S. N. Bhat and RSIC for the spectral data.

REFERENCES

1. J. A. McCleverty, *Chem. Rev.* 1979, **79**, 53.
2. F. Bottomley, *Accts Chem. Res.* 1978, **11**, 158.
3. (a) J. B. Godwin and T. J. Meyer, *Inorg. Chem.* 1971, **10**, 2150; (b) W. L. Bowden, W. F. Little and T. J. Meyer, *Inorg. Chem.* 1976, **98**, 444; (c) J. L. Walsh, R. M. Bullock and T. J. Meyer, *Inorg. Chem.* 1980, **19**, 865 and refs therein.
4. P. G. Douglas and R. D. Feltham, *J. Am. Chem. Soc.* 1972, **94**, 5254.
5. F. Bottomley, J. Ekkehardt, J. Pickardt, H. Schumann, M. Mukiada and M. Kakihana, *J. Chem. Soc., Dalton Trans.* 1985, 2427.
6. A. R. Chakravarty and A. Chakravorty, *J. Chem. Soc., Dalton Trans.* 1983, 961.
7. A. K. Deb, P. C. Paul and S. Goswami, *J. Chem. Soc., Dalton Trans.* 1988, 2051.
8. G. Wilkinson, *Comprehensive Coordination Chemistry*, Vol. 2, p. 131. Pergamon Press, Oxford (1987).
9. W. L. Bowden, W. F. Little and T. J. Meyer, *J. Am. Chem. Soc.* 1973, **95**, 5084.
10. W. L. Bowden, W. F. Little and T. J. Meyer, *J. Am. Chem. Soc.* 1977, **99**, 4340.
11. G. Albertin, S. Antoniutti, G. Pelizzi, F. Vital and E. Bordignon, *Inorg. Chem.* 1988, **27**, 829.
12. F. W. B. Einstein, A. B. Gilchrist, G. W. Rayer-Canham and D. Sutton, *J. Am. Chem. Soc.* 1972, **94**, 645.
13. A. I. Vogel, *A Text-Book of Practical Organic Chemistry*, 3rd edn, p. 622. English Language Book Society and Longman Group Limited, London (1956).
14. S. Goswami, A. R. Chakravarty and A. Chakravorty, *Inorg. Chem.* 1983, **22**, 602.
15. R. A. Krause and K. Krause, *Inorg. Chem.* 1980, **19**, 2600.
16. R. A. Krause and K. Krause, *Inorg. Chem.* 1982, **21**, 1714.
17. (a) S. Goswami, A. R. Chakravarty and A. Chakravorty, *Inorg. Chem.* 1982, **21**, 2737; (b) S. Goswami, R. N. Mukherjee and A. Chakravorty, *Inorg. Chem.* 1983, **22**, 2825; (c) G. K. Lahiri, S. Bhattacharya, S. Goswami and A. Chakravorty, *J. Chem. Soc., Dalton Trans.* 1990, 561.

Polyhedron Vol. 10, No. 15, pp. 1803–1808, 1991
Printed in Great Britain

0277–5387/91 $3.00+.00
© 1991 Pergamon Press plc

FORMATION AND SPECTROSCOPIC CHARACTERIZATION OF HETEROBIMETALLIC COMPLEXES CONTAINING SIX-COORDINATE IRON(IV) OR MANGANESE(IV) COMPLEX ANION OF 1,1-DICARBOETHOXY-2,2-ETHYLENE DITHIOLATE AND OCTAHEDRALLY COORDINATED COMPLEX CATIONS OF IRON(II), COBALT(II), NICKEL(II) OR ZINC(II) WITH 1,10-PHENANTHROLINE

NANHAI SINGH,* RAGINI VERMA and N. K. SINGH

Department of Chemistry, Banaras Hindu University, Varanasi 221 005, India

(*Received* 23 *November* 1990; *accepted* 14 *May* 1991)

Abstract—Novel heterobinuclear complexes ($[M(o\text{-phen})_3][M'(DED)_3]$ [M = Fe^{II}, Co^{II}, Ni^{II} or Zn^{II}; M′ = Mn^{IV} or Fe^{IV}; *o*-phen = 1,10-phenanthroline; DED = 1,1-dicarboethoxy-2,2-ethylene dithiolate) have been prepared and characterized. The precursor complex anion $[Fe(DED)_3]^{2-}$ has been isolated as $[Bu_4N)_2[Fe(DED)_3]$. Molar conductivities of these complexes in acetonitrile indicate their 1 : 1 electrolytic behaviour. Bonding modes of the ligands, *o*-phen and DED have been inferred from characteristic IR absorptions suggesting their chelating nature. Room temperature magnetic moments have been measured. Electronic spectral bands suggest octahedral geometry around cobalt(II), nickel(II), iron(II), manganese(IV) and iron(IV) in these complexes. Features of ESR spectra and their *g* values are suggestive of manganese(IV).

The use of the ligand DED is of interest because of its strong tendency to stabilize the high formal oxidation states of certain metals, viz. manganese(IV), iron(IV) or copper(III) in their simple complexes.[1–4] The ligand DED has been characterized by a conjugated π-system.[4] The accessibility of several oxidation states of iron and manganese has evoked a great deal of interest, especially since iron(IV) complexes are important in some biological processes.[5] One of the most interesting characteristics of coordination compounds involving dithioligands is the diversity of their redox properties. The combination of a complex cation and complex anion of different metal ions has been effectively used in the synthesis of polynuclear complexes.[6–8] Our interest in these systems is because heterobimetallic complexes containing a complex cation and a complex anion are important in optical outer sphere ligand-to-metal charge-transfer,[9] and are of great importance in photochemistry[10] as well as electrically conducting materials.[8]

Polypyridine complexes of metal ions such as $Ru(bipy)_3^{2+}$ and related complexes have attracted much attention[11,12] in recent years due to the suitable combination of redox potentials, chemical inertness and excited state life-times which makes them useful as sensitizers. This direction synthesis of heterobimetallic complexes containing $[M(o\text{-phen})_3]^{2+}$ as the cation and $[M'(DED)_3]^{2-}$ as the anion may be interesting. With these points in mind and our continuing effort to explore the tendency of the dithioligands to function as binucleating/bridging ligands in the synthesis of heteronuclear complexes,[13] heterobimetallic complexes of the type $[M(o\text{-phen})_3][M'(DED)_3]$ have been synthesized and characterized. The results of these investigations are described in this paper.

EXPERIMENTAL

Materials and methods

The chemicals used for the synthesis of the complexes were BDH (AR) or equivalent grades. K_2DED was prepared as described earlier.[14] The

* Author to whom correspondence should be addressed.

solvents were freshly distilled and dried before use where necessary.

Preparation of the complexes

$(Bu_4N)_2[Fe(DED)_3]$. $K_2[Fe(DED)_3]$ was prepared[4] *in situ* by slow addition of an aqueous solution (50 cm^3) of anhydrous $FeCl_3$ (0.27 g) to an aqueous solution (200 cm^3) of K_2DED (1.8 g) in a 1 : 3 molar ratio with vigorous stirring. The complex formed immediatedly dissolved to give a dark brownish-black colour. The product was stirred for approx. 15 min and then filtered to an aqueous solution (50 cm^3) containing tetrabutyl ammonium chloride (3.0 g). A shiny black crystalline compound was immediately formed, which was filtered and washed thoroughly with water and dried in air.

Heterobimetallic complexes

$[M(o\text{-phen})_3][Fe(DED)_3]$ [M = Fe^{II}, Co^{II}, Ni^{II} *or* Zn^{II}]

To a solution of $K_2[Fe(DED)_3]$, prepared *in situ* as described above, a solution/suspension of $[Fe(o\text{-phen})_3]^{2+}$, $[Co(o\text{-phen})_3]^{2+}$, $[Ni(o\text{-phen})_3]^{2+}$ and $[Zn(o\text{-phen})_3]^{2+}$ complex ions prepared by mixing an ethanol/methanol–water [80 : 20 (v/v)] mixture solution (30 cm^3) containing $FeSO_4(NH_4)_2SO_4 \cdot 6H_2O$ (0.65 g), $CoCl_2 \cdot 6H_2O$ (0.40 g), $NiCl_2 \cdot 6H_2O$ (0.40 g) and $Zn(CH_3COO)_2 \cdot 2H_2O$ (0.36 g) to an ethanolic solution (20 cm^3) of *o*-phen (1.0 g) in a 1 : 3 molar ratio, were added gradually in a 1 : 1 molar ratio with constant stirring for approx. 30 min. The dark brownish-black microcrystalline complexes formed immediately and were suction filtered, washed thrice with a 50 : 50 ethanol–water (v/v) mixture followed by ethanol, and dried in air.

$[M(o\text{-phen})_3][Mn(DED)_3]$ (M = Fe^{II}, Ni^{II}, Co^{II} *or* Zn^{II})

$K_2[Mn(DED)_3]$ was prepared *in situ* by gradual addition of an ethanolic suspension (30 cm^3) of $Mn(CH_3COO)_3 \cdot 2H_2O$ (0.45 g) to an ethanolic suspension (50 cm^3) of K_2DED (2.0 g) in a 1 : 3 molar ratio (method described elsewhere[1]). The reaction mixture was stirred for 15 min and a dark purple coloured solution was formed. This was filtered, and a solution/suspension (30 cm^3) of $[Fe(o\text{-phen})_3]^{2+}$, $[Co(o\text{-phen})_3]^{2+}$, $[Ni(o\text{-phen})_3]^{2+}$ and $[Zn(o\text{-phen})_3]^{2+}$ complex ions, prepared in ethanol as above, was added in a 1 : 1 molar ratio. Within a short while the dark purple coloured crystalline heterobimetallic complexes were precipitated. The reaction mixture was stirred for approx. 30 min to ensure the completion of the reaction and then suction filtered and washed with dry ethanol. The complexes obtained in this way were suspended in a 90 : 10 (v/v) ethanol–water mixture (50 cm^3) and stirred thoroughly with a glass rod to dissolve the potassium acetate formed by the metathetic reactions. This was filtered and washed with the above solvent mixture and dried in air.

Analysis and physical measurements

The complexes were decomposed with hot concentrated aquaregia and then the metals were gravimetrically determined following standard literature procedures.[15] The molar conductances of the complexes were determined in acetonitrile solution (10^{-3} M). Electronic spectra in the visible and UV region were recorded on a Simadzu UV-160A, UV-vis. spectrophotometer. The experimental details for the elemental analyses, molar conductance and room temperature magnetic susceptibility measurements, and recording of IR and electronic spectra were the same as described earlier.[13] ESR spectra were recorded on a Varian E-117 X-band spectrometer using TCNE radical $g = 2.00277$ as a $\langle g \rangle$ marker. The relevant analytical results and physicochemical data are given in Table 1.

RESULTS AND DISCUSSION

The stoichiometry of the heterobimetallic complexes $[M(o\text{-phen})_3][M'(DED)_3]$ was suggested on the basis of their analytical results. These complexes are formed by the following metathetic reactions:

$$K_2[M'(DED)_3] + [M(o\text{–phen})_3]X_2 \longrightarrow [M(o\text{-phen})_3][M'(DED)_3] + 2KX;$$

where $M' = Fe^{IV}$ or Mn^{IV}; M = Fe^{II}, Co^{II}, Ni^{II} or Zn^{II}; and X = CH_3COO^-, Cl^-, $\frac{1}{2}SO_4^{2-}$.

All the complexes are stable at room temperature, fairly soluble in acetonitrile and DMF but are insoluble in water and ethanol. Their ionic conductivities (S = 80–118 $cm^2\,\Omega^{-1}\,mol^{-1}$) in acetonitrile suggest 1 : 1 electrolytic behaviour.[16] Slightly lower values of conductivities may be regarded due to the presence of two heavier complex ions.

IR spectra

The prominent IR bands of the complexes have been recorded over the range 4000–200 cm^{-1}. There is much evidence that the canonical form of the type shown in **1** plays a key role in the description of the bonding mode of the ligand DED in its

Table 1. Analysis, physicochemical properties and magnetic moments of the complexes

Complex	Colour	m.p. (°C)	M (%)	Fe/Mn (%)	C (%)	H (%)	N (%)	S (%)	μ_{eff} (BM)	δ($cm^2\,\Omega^{-1}\,mol^{-1}$)
$(Bu_4N)_2[Fe(DED)_3]$	Black	172–177	—	4.4	53.9	8.3	2.2	15.3	3.1	138
				(4.5)	(54.2)	(8.2)	(2.2)	(15.4)		
[Fe(*o*-phen)$_3$][Fe(DED)$_3$]	Brownish-black	210–214	—	8.1	53.2	4.1	6.0	13.8	3.0	91
				(8.3)	(53.2)	(4.0)	(6.2)	(14.2)		
[Co(*o*-phen)$_3$][Fe(DED)$_3$]	Black	202–207	4.2	4.0	53.1	4.2	5.9	13.8	5.2	118
			(4.3)	(4.1)	(53.0)	(4.0)	(5.9)	(14.1)		
[Ni(*o*-phen)$_3$][Fe(DED)$_3$]	Black	180–184	4.3	3.9	52.8	3.9	5.9	13.9	4.8	102
			(4.3)	(4.1)	(53.0)	(4.0)	(6.2)	(14.1)		
[Zn(*o*-phen)$_3$][Fe(DED)$_3$]	Black	228–232	4.6	3.9	51.9	4.1	5.9	12.9	2.9	110
			(4.8)	(4.1)	(52.8)	(4.0)	(6.2)	(14.1)		
[Fe(*o*-phen)$_3$][Mn(DED)$_3$]	Purple	190–196	4.2	4.0	51.9	4.2	6.3	12.8	4.3	107
			(4.1)	(4.1)	(53.2)	(4.0)	(6.2)	(14.2)		
[Co(*o*-phen)$_3$][Mn(DED)$_3$]	Dark purple	248–252	4.4	3.9	52.2	3.9	6.1	12.9	5.5	80
			(4.3)	(4.0)	(53.1)	(4.0)	(6.2)	(14.2)		
[Ni(*o*-phen)$_3$][Mn(DED)$_3$]	Dark purple	235–240	4.3	4.1	52.5	4.0	6.0	13.0	4.7	97
			(4.3)	(4.0)	(53.1)	(4.0)	(6.2)	(14.2)		
[Zn(*o*-phen)$_3$][Mn(DED)$_3$]	Purple	210–215	—	8.5[a]	52.6	4.1	6.2	12.9	3.7	112
				(8.8)	(52.9)	(4.0)	(6.2)	(14.1)		

[a] Zinc and manganese have been estimated collectively.
Calculated values appear in parentheses.

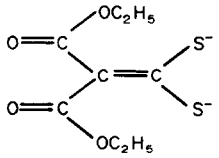

complexes.[1,6,14] The four most important features of the spectra are (a) the occurrence of two absorptions in the 1680–1715 cm^{-1} region in all the complexes due to C=O stretching vibrations indicating twisting of one of the ester groups out of the plane of the ethylene carbons and the non-involvement of the carbonyl group in bonding. (b) The appearance of a sharp band at 1450–1465 cm^{-1}, invariably indicating the presence of a $\nu(C{=}CS_2)$ vibration in all the complexes. (c) The occurrence of bands at 925–1030 cm^{-1}, due to $\nu(CS_2)$ modes. (d) The occurrence of bands at *ca* 630 and 425 cm^{-1}, indicating the coordinated nature[17] of *o*-phen in these complexes. The number and position of the IR spectral bands are suggestive of dinegative bidentate behaviour of DED and bidentate behaviour of *o*-phen in these complexes.

The bands occurring below 400 cm^{-1} in all the complexes may be considered to be associated with metal–sulphur and metal–nitrogen stretching vibrations. The lower frequency bands may be related to metal–sulphur while the higher ones to the metal–nitrogen stretching modes.

Magnetic moments and electronic spectra

The metal ions in higher oxidation states have vacant *d*-orbitals and therefore their visible region spectrum is dominated by charge-transfer bands. With dithioligands this tendency seems to be more pronounced. The $[Zn(o\text{-phen})_3][Mn(DED)_3]$ complex exhibits a broad structured band giving peaks at 400, 511 and 545 nm which are close to the charge-transfer bands of the octahedral $[M(Et_2dtc)_3]BF_4$.[18,19] The magnetic moment, 3.75 BM, for this complex is slightly less than the spin only value (3.88 BM) for a high spin manganese(IV). In the case of $[Fe(o\text{-phen})_3][Mn(DED)_3]$, a broad shaped band comprising peaks at 453, 537, 588 and 800 nm is observed. These are attributed to the charge-transfer bands as well as *d–d* transition bands indicating the presence of octahedral $[Fe(o\text{-phen})_3]^{2+}$ and $[Mn^{IV}(DED)_3]^{2-}$. The tail of this band at 537–588 nm is assigned to MLCT Fe^{II} (t_{2g}^6), to the ligand (π) orbital, and the head at 800 nm to the *d–d* spin triplet.[20–22] The magnetic moment (4.29 BM) for this complex may be related to the presence of high spin manganese(IV) and low spin iron(II).[1,23] The heterobimetallic complexes $[Co(o\text{-phen})_3][Mn(DED)_3]$ and $[Ni(o\text{-phen})_3][Mn(DED)_3]$ exhibit magnetic moments of 5.48 and 4.66 BM, respectively, in which the contributions from both cationic and anionic species are included. Although magnetic data obtained at room temperature are insufficient for evaluating magnetic moments for stereochemical purposes in systems where both cationic and anionic species are paramagnetic, nevertheless, the data obtained at room temperature are comparatively lower than the average values of magnetic moments expected for both paramagnetic centres but higher than those expected for either the cation or anion. This shows the presence of some paramagnetic interactions in the solid state. The former complex shows bands at 454, 473, 520, 545 and 800 nm and the latter at 450, 512 and 545 nm. These bands show the presence of octahedral $[Co(o\text{-phen})_3]^{2+}$ and $[Ni(o\text{-phen})_3]^{2+}$ associated with octahedrally coordinated $[Mn(DED)_3]^{2-}$. The bands at 450–473 nm are mainly due to $[Mn(DED)_3]^{2-}$, while those at 512–800 nm are attributed to octahedral $[Co(o\text{-phen})_3]^{2+}$ and $[Ni(o\text{-phen})_3]^{2+}$ moieties.[22,24]

Magnetic moments (2.88–3.10 BM) for $(Bu_4N)_2[Fe(DED)_3]$, $[Zn(o\text{-phen})_3][Fe(DED)_3]$ and $[Fe(o\text{-phen})_3][Fe(DED)_3]$ are consistent with low spin iron(IV) (d^4 configuration).[1,5,25] $(Bu_4N)_2[Fe(DED)_3]$ shows absorptions at 390, 450, 480 and 530 nm, which are charge-transfer bands.[5] $[Co(o\text{-phen})_3][Fe(DED)_3]$ and $[Ni(o\text{-phen})_3][Fe(DED)_3]$[5] exhibit characteristic electronic spectral bands showing octahedrally coordinated $[M(o\text{-phen})_3]^{2+}$ ($M = Co^{II}$ or Ni^{II}) and $[Fe(DED)_3]^{2-}$ moieties. The magnetic moments 4.81 and 5.15 BM for these complexes may be related to the presence of cationic and anionic species. In all the heterometallic complexes, the bands occurring between 200–300 nm are attributed to the charge-transfer bands.

ESR spectra

The ESR spectra of the heterobimetallic complexes $[M(o\text{-phen})_3][Mn(DED)_3]$ have been recorded in DMF and as polycrystalline samples at room temperature as well as LNT. The spectra of the polycrystalline samples show a single broad, first derivative[23] band at about $g = 2.0$, which is expected for an odd, unpaired electron system showing only the central $Ms = 1/2 \leftrightarrow -\frac{1}{2}$ transition which, in first order, is independent of orientation of the crystallites. The powder ESR spectra with $g = 2.0$ do not unambiguously support the Mn^{IV}, d^3 system since the observed pattern could arise from d^5, Mn^{II} also. Except $[Fe(o\text{-phen})_3][Mn(DED)_3]$, all other heterobimetallic complexes also exhibit a typical solid state spectrum giving $g_{\|} = 4.83$–5.3, which is well in the range

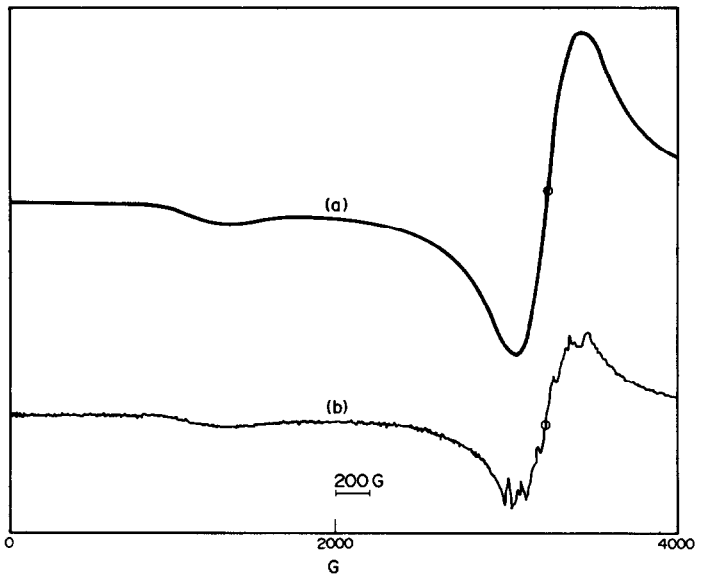

Fig. 1. ESR spectra of (a) [Co(*o*-phen)$_3$][Mn(DED)$_3$] (solid); (b) [Co(*o*-phen)$_3$][Mn(DED)$_3$] (DMF) solution at LNT.

reported[1] for [Mn^{IV}(DED)$_3$](BzPh$_3$P)$_2$. Since our starting material is manganese(III) and the ligand DED has a strong tendency to stabilize manganese(IV), we expect that this pattern arises from manganese(IV).[1]

The ESR spectrum of [Co(*o*-phen)$_3$][Mn(DED)$_3$] in DMF at LNT (Fig. 1) is characterized by isotropic g value = 2.00 and hyperfine interaction constant $\langle A \rangle$ = 92 G, which is quite comparable to the frozen $CHCl_3$ solution spectrum of Mn^{IV} ($R_2Dtc)_3ClO_4$[23] at (113 K). However, other complexes show weak, resolved hyperfine features with g values = 1.99–2.0, but the hyperfine interaction constant $\langle A \rangle$ could not be derived. All the complexes exhibit a weak broad band with g values (4.9–5.00) similar to the solid state spectra. The features of the solid and solution spectra suggest the presence of manganese(IV) in the heterobimetallic complexes. There is no remarkable change in the g values of the complexes recorded as polycrystalline samples or in DMF solution at LNT, which suggests that the structure of the heterobimetallic complexes remains unchanged and rules out the possibility of ligand-exchange reactions in solution.

On the basis of the various physicochemical studies and their close similarity to [M′(DED)$_3$](BzPh$_3$P)$_2$ (M′ = Mn^{IV} or Fe^{IV}), a plausible structure for the heterobimetallic complexes may be suggested where iron(IV) and manganese(IV) have a six coordinate M′S_6 chromophore and iron(II), cobalt(II), nickel(II) or zinc(II) are octahedrally coordinated with three *o*-phen molecules.

Acknowledgement—We are grateful to CSIR for financial support in the form of a research project.

REFERENCES

1. D. Coucouvanis and S. J. Lippard (Eds), *Prog. Inorg. Chem.* 1979, **26**, 301; 1970, **11**, 233.
2. F. J. Hollander, M. L. Caffery and D. Coucouvanis, *J. Am. Chem. Soc.* 1974, **96**, 4682.
3. F. J. Hollander, R. Pedelty and D. Coucouvanis, *J. Am. Chem. Soc.* 1974, **96**, 4032.
4. D. Coucouvanis, F. J. Hollander and R. Pedelty, *Inorg. Chem.* 1977, **16**, 2691.
5. E. A. Pasek and D. K. Straub, *Inorg. Chem.* 1972, **11**, 259.
6. M. L. Caffery and D. Coucouvanis, *J. Inorg. Nucl. Chem.* 1975, **37**, 2081.
7. D. Coucouvanis, N. C. Baenziger and S. M. Johnson, *Inorg. Chem.* 1974, **13**, 1191.
8. Z. J. Zhong, H. Okawa, R. Aoki and S. Kida, *Inorg. Chem. Acta* 1988, **144**, 233.
9. A. Vogler and H. Kunkely, *Inorg. Chim. Acta* 1988, **144**, 149.
10. A. W. Adamson and P. D. Fleischauer (Eds), *Concepts of Inorganic Photochemistry*. Wiley, New York (1975).
11. C. A. Bignozzi and F. Scandola, *Inorg. Chem.* 1984, **23**, 1540.
12. K. Kalyanasundaram, *Coord. Chem. Rev.* 1982, **46**, 159.
13. N. Singh, R. Verma and N. K. Singh, *Polyhedron* 1990, **9**, 1441.
14. K. A. Jensen and L. Henriksen, *Acta Chem. Scand.* 1968, **22**, 1107.
15. A. I. Vogel, *A Textbook of Quantitative Inorganic Analysis*, 3rd edn. Longmans, London (1961).

16. W. J. Geary, *Coord. Chem. Rev.* 1971, **7**, 81.
17. K. Nakamoto, *Infrared and Raman Spectra of Inorganic and Coordination Compounds*, 4th edn, p. 206. John Wiley & Sons, New York (1986).
18. R. Y. Saleh and D. K. Straub, *Inorg. Chem.* 1974, **13**, 3017.
19. R. M. Golding, C. M. Harris, K. J. Jessop and W. C. Tennant, *Aust. J. Chem.* 1972, **25**, 2567.
20. K. Madeja and E. Konig, *J. Inorg. Nucl. Chem.* 1963, **25**, 377.
21. P. Krumholz, O. A. Serra and M. A. De Paoli, *Inorg. Chim. Acta* 1975, **15**, 25.
22. R. A. Palmer and T. S. Piper, *Inorg. Chem.* 1966, **5**, 864.
23. K. L. Brown, R. M. Golding, P. C. Healy, K. J. Jessop and W. C. Tennant, *Aust. J. Chem.* 1974, **27**, 2075.
24. C. K. Jorgenson, *Adv. Chem. Phys.* 1963, **5**, 33.
25. F. J. Hollander and D. Coucouvanis, *J. Am. Chem. Soc.* 1974, **96**, 5646; 1977, **99**, 6268.

Polynedron Vol. 10, No. 15, pp. 1809–1815, 1991
Printed in Great Britain

0277–5387/91 $3.00+.00
© 1991 Pergamon Press plc

IRON(III) AND COPPER(II) COMPLEXES OF POLYDENTATE LIGANDS INCORPORATING BENZIMIDAZOLE AND PHENOLIC RESIDUES

JONATHAN D. CRANE and DAVID E. FENTON*

Department of Chemistry, The University, Sheffield S3 7HF, U.K.

(*Received* 23 *April* 1991; *accepted* 14 *May* 1991)

Abstract—The preparation and complexing properties towards iron(III) and copper(II) of the unsymmetric polydentate ligands 1-(2-hydroxy-phenyl)-2-aza-3,5-bis(benzimidazol-2-yl)pentane, H(**2**), and 1-(2-hydroxy-5-bromo-phenyl)-2-aza-3,5-bis(benzimidazol-2-yl) pentane, H(**3**), are discussed.

The preparation of small molecule complexes as models for dinuclear transition metal biosites may be viewed as essential in helping to gain an understanding of the structure and function of the natural systems.[1] A logical strategy for the synthesis of potential model compounds is to mimic as closely as possible the suspected coordination environment of the metals in these proteins; this can be achieved by designing and preparing synthetically accessible polydentate ligands, and investigating their coordination chemistry with the appropriate transition metal.

Ideally these ligands should contain the correct number of donor groups and these should be as chemically similar as possible to the protein-based donor atoms. Only a few amino acid residues, histidine (imidazole), tyrosine (phenolate), aspartic and glutamic acids (carboxylate) are commonly found coordinated to transition metals in metalloproteins; other residues (e.g. cysteine and methionine) are known to be involved in some cases.[2] The structure and degree of flexibility of the ligands can be used to ensure that the metals are coordinated in an appropriate geometry. Such structural constraints may also be effective in controlling inter-metal distances, therefore favouring the binding of bridging groups that are found (or are believed to be present) in the biosite, but which were not incorporable in the ligand. Finally, for the preparation of a functioning model, consideration must be given to the number, accessibility, and location of any vacant coordination sites on the metal.

To date, two major strategies for ligand based control have been developed for the preparation of dinuclear metal complexes. The first strategy is based on ligands that are large enough and contain sufficient donor atoms to coordinate both metals and any required exogenous bridging groups.[1] At the simplest level these dinucleating ligands comprise two donor sets joined by a non-coordinating linking group. In more complex ligands the linking group may also act as the source of an endogenous bridge. The second strategy is the use of facially coordinating, tridentate ligands such as 1,4,7-triazacyclononane and its tris-N-methylated derivative,[3] and the hydrotris-(1-pyrazolyl)borate anion.[4] Additional coordination of potential bridging groups (three for octahedral and two for trigonal bipyramidal or square based pyramidal geometries) can give dinuclear complexes by spontaneous self assembly. This approach has also been used successfully with the dinucleating ligand 2,2′-dipyridyl.[5–7]

Ligands incorporating benzimidazole groups are of importance for the preparation of model compounds as they contain the biologically relevant imidazole moiety found in histidine. It must be noted however, that benzimidazoles differ from imidazoles in size and chemical properties due to the fused benzene ring. Imidazoles are significantly more basic than their benzimidazole equivalents and the benzimidazole hydrogen is more acidic.[8] The main reason for preparing ligands containing benzimidazoles rather than imidazoles is the

* Author to whom correspondence should be addressed.

relative ease of synthesis. Condensation of 1,2-diaminobenzene with a carboxylic acid under the appropriate reaction conditions gives the corresponding benzimidazole.[9] Similarly, the reaction of polycarboxylic acids yields polybenzimidazole ligands in fair to good yields.

In dinuclear transition metal biosites the metal ions are usually found in chemically or geometrically distinct environments. Such distinctions range from a relatively insignificant difference in coordination geometries (as in haemocyanin), to major differences in donor set and/or coordination number (purple acid phosphatases and haemerythrin). Symmetric dinucleating ligands can only promote minor differences in metal environment upon complexation, and this is always due to steric constraints imposed by other ligands or the metals themselves. Therefore a necessary step towards the synthesis of better models for these metalloproteins is the preparation of unsymmetric dinucleating ligands that provide chemically distinct donor environments.

In this paper we present the synthesis and complexation properties towards copper(II) and iron(III) of unsymmetric polydentate ligands incorporating a phenolic residue and derived from the functionalization of 1,3-bis-(benzimidazol-2-yl)-1-aminopropane (**1**). The ligands contain both imidazole and phenolic functions and therefore may be viewed as appropriate for biosite modelling studies.

RESULTS AND DISCUSSION

Ligands containing phenolic residues are potentially useful for preparing model compounds for transition metal biosites which have tyrosine residues involved in the metal coordination. The primary amine function of (**1**) is readily condensed with salicylaldehyde or its derivatives to give Schiff bases, which were not isolated. The imines were reduced *in situ* to give the corresponding hydrolytically stable secondary amines H(**2**) and H(**3**) (Scheme 1).

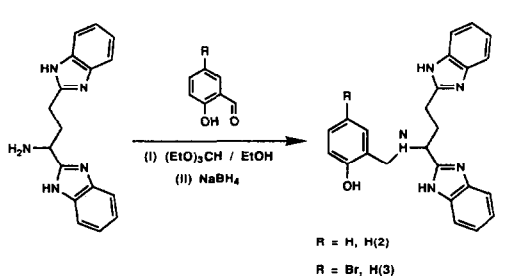

Scheme 1.

Recrystallization from acetone/water gives H(**2**) and H(**3**) as stable 1 : 1 adducts with acetone. In the IR spectra (KBr disc) the characteristic acetone carbonyl stretch occurs at 1705 cm^{-1}. The stoichiometry of the adducts were confirmed by ^1H NMR and elemental analysis. Attempts to grow crystals of these inclusion complexes for X-ray diffraction structure determinations failed, yielding white powders only.

As expected the ^1H NMR spectra (Table 1) show the benzimidazoles to be non-equivalent, with two distinct pairs of A_2B_2 multiplets. Assignments of the benzimidazoles were made by comparison with the spectra of (**1**) and the phenolic groups were assigned by comparison with predicted chemical shifts and coupling for substituted benzenes. The hydrogens of the methylene group formed upon reduction of the Schiff base are non-equivalent and give rise to an AB system. Along with the increased complexity of the propane chain backbone signals, this implies a significant degree of intramolecular hydrogen bonding in solution, preventing rotation of the phenolic group relative to the rest of the molecule on the NMR timescale.

The—CH_2—NH— linkage formed by reduction

Table 1. ^1H NMR assignments of H(**2**) and H(**3**)

H(**2**), δ_H (1 : 1 CD_3OD : $CDCl_3$)

H_d	7.56 (2H, m)
H_j	7.45 (2H, m)
H_e	7.22 (2H, m)
H_k	7.15 (2H, m)
H_p	7.06 (1H, t)
H_n	6.93 (1H, d)
H_q	6.76 (1H, d)
H_o	6.69 (1H, t)
H_a	4.10 (1H, t)
H_l	3.79 (2H, AB)
H_g	2.90 (2H, m)
H_f	2.41 (2H, m)
$(CH_3)_2CO$	2.15 (6H, s)

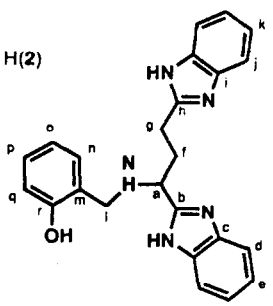

H(**3**), δ_H (CD_3OD)

H_b	7.55 (2H, m)
H_f	7.43 (2H, m)
H_c	7.20 (2H, m)
H_g,H_i,H_l	7.12 (4H, m)
H_k	6.62 (1H, d)
H_a	4.08 (1H, t)
H_h	3.70 (2H, AB)
H_e	2.89 (2H, m)
H_d	2.41 (2H, m)
$(CH_3)_2CO$	2.12 (6H, s)

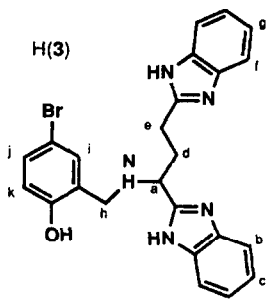

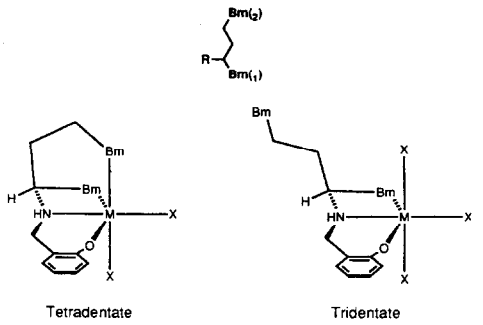

Fig. 1. Possible coordination geometries of (2).

of the Schiff base is benzilic in nature. The ease of fragmentation at this bond is reflected in the c.i. mass spectra of H(2) and H(3). A MH^+ ion is only observed for H(2), at m/z 398 (2%). The dominant peak in both spectra is due to $[H(1)]^+$.

Both (2) and (3) are potentially tetradentate but will possess steric problems similar to (1). Comparison with a similar phenol-containing ligand suggests that the phenol, amine, and Bm(1) will coordinate in a meridional manner.[10] Bm(2) may possibly coordinate as a distant axial ligand (Fig. 1).

Preparation of (2)$FeCl_2(H_2O)$(MeOH) (4) *and* (2)$Fe(NCS)_2(H_2O)_5$ (5)

The phenol group deprotonates in methanolic solutions of iron(III) to give intense purple complexes of the anionic ligand (2). Reaction with iron(III) chloride hexahydrate gave a characterizable product as thin purple needles of (2) $FeCl_2(H_2O)$(MeOH) (4) (Scheme 2). The positive ion FAB mass spectrum confirms that both the ligand and at least one of the chlorides are coordinated to the metal with peaks at m/z 487 (24%), $[(2)Fe(Cl]^+$, and 452 (100%), $[(2)Fe]^+$. By analogy

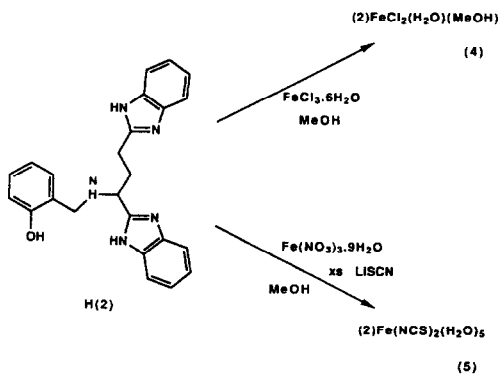

Scheme 2.

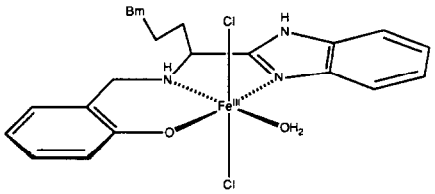

Fig. 2. Proposed structure of (4).

with the closely related benzimidazole complexes $LFeCl_3$ it is probable that both chlorides are bound to the iron in the solid state.[11]

The overall molecular geometry of (4) is hard to predict, but it is likely that one of the benzimidazoles is non-coordinating and the remaining tridentate ligand fragment is bound meridionally. If the complex is octahedral the water molecule is probably the sixth ligand but it is impossible to say which of the three possible sites it occupies (Fig. 2).

The analogous reaction in the presence of excess thiocyanate instead of chloride ions gave the diisothiocyanate complex (2)$Fe(NCS)_2(H_2O)_5$ (5) (Scheme 2), presumably with only one of the water molecules coordinated to the iron to give a similar structure to (4). In the IR spectrum a single band at 2045 cm^{-1} is assignable to the ν_{CN} stretch of the isothiocyanate groups, proving that both SCN— ligands are bound to the iron and that as expected both are coordinated through nitrogen. Compound (4) was too insoluble to record a solution electronic absorption spectrum but (5) was slightly soluble in acetonitrile. Two intense charge-transfer bands are apparent: λ_{max} = 420 (5120) and 590 nm (ε = 1870 $dm^3\ cm^{-1}\ mol^{-1}$). Theoretically the reaction of (2) with iron(III) in the presence of carboxylate should give new multinuclear complexes. Unfortunately no such products could be isolated from such mixtures.

Preparation of dinuclear copper(II) *complexes of the phenol-containing ligands* H(2) *and* H(3)

Reaction of hydrated copper(II) salts with the phenol containing ligands H(2) and H(3) in alcoholic solution and in the presence of base gave complexes in which the phenols are deprotonated and coordinated to the metal. Such complexes were prepared with a range of counterions: Cl^-, $MeCO_2^-$, NO_2^- and ClO_2^- (Scheme 3).

The IR spectra of all six complexes are similar. The spectrum of (6) (chloride counterion) is well resolved and free of anion bands, thus allowing the assignment of these bands in the other compounds. For the acetate complex (7) a single carboxylate symmetric stretch occurs at 1420 cm^{-1}. However there are two antisymmetric stretching bands of

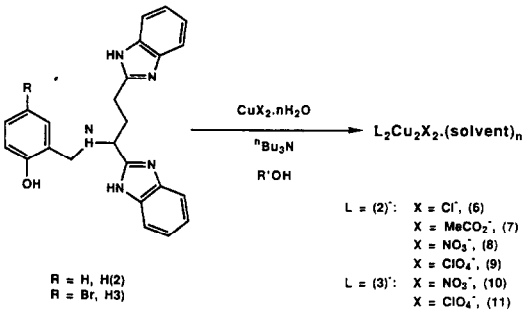

Scheme 3.

approximately equal intensity at 1540 and 1560 cm^{-1}, which implies the presence of two types of acetate. The $\Delta\nu$ values of *ca* 130 cm^{-1} are less than generally found for ionic or monodentate acetates,[12] but nevertheless similar to the values found for the formally monodentate acetates in the mononuclear manganese(II) complex, [N,N-bis(benzimidazol-2-ylmethyl)-amine]bis(acetato) manganese(II) (**12**).[11] Therefore although both acetates are coordinated, it is difficult to say whether they are monodentate, bidentate, or bridging. For the complexes with nitrate [(**8**) and (**10**)] and perchlorate [(**9**) and (**11**)] counterions there is no evidence of coordination, only bands corresponding to the free anions are apparent at 1395 cm^{-1} (NO_3^-), and 1100 and 625 cm^{-1} (ClO_4^-), respectively. In addition, for (**6**) and (**8**) a single sharp band is clearly visible at 3600 cm^{-1}, assignable as the O—H stretch of coordinated water.

As discussed earlier for the coordination of (**2**) and (**3**) with iron(III) it is probable that they act only as tridentate ligands with one of the benzimidazoles, Bm(2), not being coordinated. A copper complex of the structurally similar, tridentate ligand H(**13**), prepared by reduction of the Schiff base formed by condensation of 2-aminomethylpyridine with salicylaldehyde, has been characterized as the neutral mononuclear species (**13**)Cu(NO_3).[10] In this complex the nitrate anion acts as a monodentate ligand but it has already been shown that in (**8**) and (**10**) the nitrates are not coordinated. Hence (**2**) and (**3**) give copper complexes with different metal environments to that found in (**13**)Cu(NO_3). The positive ion FAB mass spectrum of (**13**)Cu(NO_3) has not been reported so it is not known whether high mass aggregation peaks are apparent for this proven mononuclear complex. In all six complexes of (**2**) and (**3**) however, peaks corresponding to dinuclear as well as the expected mononuclear moieties are observed. The high mass peaks are assignable as $[L_2Cu_2(\text{counterion})]^+$ and $[L_2Cu_2—H]^+$ (Table 2). For the complexes of (**3**) the presence of the additional bromine atom means that the observed peak maxima occur at +2 mass units. If the mass spectra are a true reflection of the structure of these complexes in the solid state, it is likely that the phenolate groups are acting as the bridging ligands. Similar dimerizations are known to occur for other phenol containing ligands.[13] For (**8**) and (**10**) this formulation is in agreement with the observed non-coordination of the nitrates, but the reason for the preferred mononuclear nature of the related complex (**13**)Cu(NO_3) is unclear. The presence of the

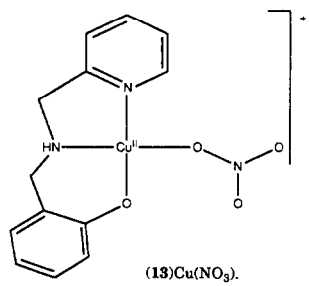

(**13**)Cu(NO_3).

$[L_2Cu_2(\text{counterion})]^+$ peaks does not necessarily mean that the counterion is bound to the dinuclear

Table 2. Positive ion FAB mass spectra assignments of the copper(II) complexes of (**2**) and (**3**)

Compound	Anion (X^-)	*m/z* (% intensity) $[L_2Cu_2(X)]^+$	$[L_2Cu_2—H]^+$	$[LCu]^+$
(a) L = (**2**):				
(**6**)	Cl^-	955 (9)	919 (16)	460 (43)
(7)	$MeCO_2^-$	979 (3)	919 (8)	460 (24)
(**8**)	NO_3^-	982 (3)	919 (18)	460 (29)
(**9**)	ClO_4^-	1019 (20)	919 (15)	460 (63)
(b) L = (**3**):				
(**10**)	NO_3^-	1140 (5)	1077 (22)	540 (71)
(**11**)	ClO_4^-	1175 (10)	1077 (5)	540 (41)

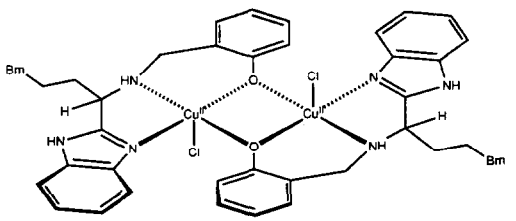

Fig. 3. Proposed structure of (**6**).

metal core, but may be due to ion pairing. However, it has been shown that in (**7**) the acetates are coordinated. There are literature precedents for both terminal and asymmetric bidentate coordination of carboxylates in such dinuclear, phenolate bridged copper complexes.[13] Similarly by comparison with known systems it is likely that the chlorides in (**6**) are coordinated as terminal ligands (Fig. 3).[14]

The room temperature magnetic moment of (**10**) is 1.03 μ_{BM}, significantly less than the theoretical spin only value for copper(II) (1.73 μ_{BM}). This indicates appreciable antiferromagnetic coupling[15] and is consistent with the proposed dinuclear, bis-phenolate bridged nature of these complexes.

EXPERIMENTAL

Elemental analyses were carried out by the Sheffield University microanalytical service. IR spectra were recorded as KBr discs using a Perkin–Elmer 297 IR spectrophotometer (4000–600 cm^{-1}) or a Perkin–Elmer 1710 IR Fourier Transform spectrophotometer (4000–400 cm^{-1}). Electronic absorption spectra were recorded using a Philips PU8720 UV–vis scanning spectrophotometer operating in the range (280–900 nm). ^1H NMR spectra were recorded at 220 MHz on a Perkin–Elmer R34 spectrometer. ^{13}C NMR spectra (62.9 MHz) were recorded using a Bruker AM-250 spectrometer. Electron impact (e.i.) and chemical impact (c.i., ammonia) spectra were recorded on a Kratos MS25 operating at low resolution and positive ion fast atom bombardment (FAB) mass spectra were recorded on a Kratos MS80 spectrometer. The matrix solvent used was 3-nitrobenzylalcohol (NOBA) unless otherwise stated.

1,3-*bis*(*benzimidazol*-2-*yl*)*propylamine* (**1**)

DL-glutamic acid (11.0 g, 75 mmol) and 1,2-diaminobenzene (18.50 g, 170 mmol) were refluxed in aqueous hydrochloric acid (120 cm^3, 5.5 M) for 15 days. The solution changed from an initial deep red colour to intense blue over the first 3 days. The reaction mixture was cooled to room temperature and vigorously stirred while carefully neutralized with excess aqueous ammonia (specific gravity 0.880). The crude product (purple solid) was filtered off and washed with water. Two recrystallizations from methanol/water gave white needles of H(**1**)·1.25(H_2O) (8.70 g, 37%). M.p. 120°C. To confirm the hydration number, a sample was recrystallized a third time for a second analysis. Found: C, 65.1, 64.9; H, 6.1, 6.1; N, 22.3, 22.1. Calc. for $C_{17}H_{19.5}N_5O_{1.25}$: C, 65.0; H, 6.3; N, 22.3%. *m/z* e.i. 291 (M^+, 12%), c.i. 292 (MH^+, 100%). δ_H (CD_3OD) 7.53 (2H, m), 7.48 (2H, m), 7.20 (2H, m), 7.17 (2H, m), 4.24 (1H, t), 2.95 (2H, t), and 2.40 (2H, m). δ_C (CD_3OD) 159.0, 155.8, 139.4, 123.5, 123.2, 115.7, 115.3, 51.1, 36.5 and 26.3.

L-glutamic acid gave white needles with identical spectroscopic properties to H(**1**). Solutions of this product at different concentrations gave no measurable rotation of polarized light, indicating that complete racemization had occurred under the reaction conditions.

1-(2-*hydroxyphenyl*)-2-*aza*-3,5-*bis*(*benzimidazol*-2-*yl*)*pentane* H(**2**)

1,3-bis(benzimidazol-2-yl)propylamine (10.0 g, 30 mmol), salicylaldehyde (3.70 g, 30 mmol), and triethylorthoformate (1 cm^3) was refluxed in ethanol (150 cm^3) for 2 h. The golden yellow solution was cooled to room temperature and sodium borohydride (2 g, 54 mmol) added carefully in small portions. The resulting pale yellow solution was refluxed for 1 h. After cooling, water (50 cm^3) was added and the solution rendered acidic by dropwise addition of concentrated hydrochloric acid. After refluxing for 15 min to hydrolyse any borate esters present, the solution was cooled and the ethanol removed under reduced pressure. The sticky residue was extracted with CH_2Cl_2 (2 × 80 cm^3), dried over $MgSO_4$, filtered, and the solvent removed. The resulting pasty yellow solid was taken up in acetone (100 cm^3) and after *ca* 5 min a thick white precipitate was deposited. This was recrystallized from acetone/water to give H(**2**)(Me_2CO) as a white powder (12.3 g, 90%). M.p. 250°C (decomp.). Found: C, 71.0; H, 6.6; N, 15.2. Calc. for $C_{27}H_{29}N_5O_2$: C, 71.2; H, 6.4; N, 15.4%. *m/z* c.i. 398 (MH^+, 2%). ν_{max} 1705 cm^{-1} (C=O).

The acetone was removed by dissolving a sample in methanol, then evaporating to dryness. This was repeated with CH_2Cl_2 to give a white powder with significantly higher solubilities in organic solvents. δ_C (CD_3OD) 157.6 (s), 156.8 (s), 155.5 (s), 139.3 (s), 130.6 (d), 129.5 (d), 125.1 (s), 123.5 (d), 123.1 (d), 120.3 (d), 116.5 (d), 115.8 (d), 115.3 (d), 57.0 (d), 49.6 (t), 34.4 (t), and 26.4 (t).

1 - (2 - hydroxy - 5 - bromophenyl) - 2 - aza - 3,5 - bis (benzimidazol-2-yl)pentane H(**3**)

This was prepared by the same method as for H(**2**) but using 5-bromosalicylaldehyde. H(**3**) (Me_2CO), white powder (85%). M.p. 240°C (decomp.). Found: C, 60.4; H, 5.3; N, 13.0; Br, 14.9. Calc. for $C_{27}H_{28}BrN_5O_2$: C, 60.7; H, 5.3; N, 13.1; Br, 14.9%. No molecular ion observed in the mass spectrum, highest observed peak: *m/z* c.i. 292 (M—C_7H_5OBr+H, 53%). ν_{max} 1705 cm^{-1} (C=O).

Preparation of (**2**)$FeCl_2(H_2O)(MeOH)$ (**4**)

Iron(III) chloride hexahydrate (0.27 g, 1 mmol) was added to a solution of H(**2**)(Me_2CO) (0.46 g, 1 mmol) and tri-*n*-butylamine (0.19 g, 1 mmol) in methanol (80 cm^3) with stirring. The intense purple solution was filtered as soon as all the iron salt had dissolved. Upon standing overnight (**4**) was deposited as very fine, purple needles (0.51 g, 89%). Found: C, 52.4; H, 4.9; N, 12.2; Cl, 12.3. Calc. for $C_{25}H_{28}Cl_2FeN_5O_3$: C, 52.4; H, 4.9; N, 12.2; Cl, 12.4%.

Preparation of (**2**)$Fe(NCS)_2(H_2O)_5$ (**5**)

Iron(III) nitrate nonahydrate (0.41 g, 1 mmol), H(**2**)(Me_2CO) (0.46 g, 1 mmol), and tri-*n*-butylamine (0.19 g, 1 mmol) were dissolved in methanol (40 cm^3) to give an intense purple solution. Lithium thiocyanate (0.2 g, 3 mmol) in methanol (40 cm^3) was added with stirring. A brown precipitate formed immediately. After 1 h this was filtered off and the filtrate allowed to stand overnight. Purple microcrystals (0.22 g, 33%). Found: C, 47.7; H, 4.7; N, 15.1; S, 9.3. Calc. for $C_{26}H_{32}FeN_7O_6S_2$: C, 47.4; H, 4.9; N, 14.9; S, 9.7%.

Preparation of $(2)_2Cu_2Cl_2(H_2O)_4$ (**6**)

Tri-n-butylamine (0.19 g, 1 mmol) and H(**2**) (Me_2CO) (0.46 g, 1 mmol) were dissolved in methanol (40 cm^3). A solution of copper(II) chloride dihydrate (0.17 g, 1 mmol) in methanol (5 cm^3) was added in one portion with stirring, and the resulting dark green solution was filtered. Thin yellow–green needles began forming almost immediately (*ca* 1 min). After standing overnight the product was filtered off, washed with methanol, and air dried (0.41 g, 77%). Found: C, 54.1; H, 4.5; N, 13.3; Cl, 7.0. Calc. for $C_{48}H_{52}Cl_2Cu_2N_{10}O_6$: C, 54.2; H, 4.9; N, 13.2; Cl, 6.7%.

Preparation of $(2)_2Cu_2(MeCO_2)_2(H_2O)_2(MeOH)_2$ (**7**)

This was prepared as for (**6**) but using hydrated copper(II) acetate (0.20 g, 1 mmol) and more dilute conditions (100+20 cm^3). Yellow–green powder (0.47 g, 83%). Found: C, 56.8; H, 5.5; N, 12.2. Calc. for $C_{54}H_{62}Cu_2N_{10}O_{10}$: C, 57.0; H, 5.5; N, 12.3%.

Preparation of $(2)_2Cu_2(NO_3)_2(H_2O)_2$ (**8**)

This was prepared as for (**6**) but using copper(II) nitrate trihydrate (0.25 g, 1 mmol) in ethanol as solvent. Yellow–green needles (0.38 g, 70%). Found: C, 53.5; H, 4.4; N, 15.4. Calc. for $C_{48}H_{48}Cu_2N_{12}O_{10}$: C, 53.4; H, 4.5; N, 15.6%.

Preparation of $(2)_2Cu_2(ClO_4)_2(H_2O)$ (**9**)

This was prepared as for (**6**) but using copper(II) perchlorate hexahydrate (0.37 g, 1 mmol) in ethanol as solvent. Pale green needles (0.42 g, 69%). Found: C, 50.6; H, 4.4; N, 11.9; Cl, 6.1. Calc. for $C_{48}H_{46}Cl_2Cu_2N_{10}O_{11}$: C, 50.7; H, 4.1; N, 12.3; Cl, 6.2%.

Preparation of $(3)_2Cu_2(NO_3)_2(MeOH)_4$ (**10**)

This was prepared as for (**6**) but using H(**3**)·(Me_2CO) (0.54 g, 1 mmol) and copper(II) nitrate trihydrate (0.25 g, 1 mmol). Green microcrystals (0.56 g, 88%). Found: C, 46.8; H, 4.2; N, 12.8; Br, 11.9. Calc. for $C_{52}H_{58}Br_2Cu_2N_{12}O_{12}$: C, 47.0; H, 4.4; N, 12.6; Br, 12.0%.

Preparation of $(3)_2Cu_2(ClO_4)_2(MeOH)_5$ (**11**)

This was prepared as for (**10**) but using copper(II) perchlorate (0.37 g, 1 mmol). The initial green needles formed redissolved and after standing (*ca* 5 days) dark green intergrown blocks were deposited (0.62 g, 86%). Found: C, 44.3; H, 4.2; N, 9.4; Br, 11.2; Cl, 4.9. Calc. for $C_{53}H_{62}Br_2Cl_2Cu_2N_{10}O_{15}$: C, 44.3; H, 4.3; N, 9.7; Br, 11.1; Cl, 4.9%.

Acknowledgement—We thank the SERC for a studentship.

REFERENCES

1. D. E. Fenton, *Advances in Inorganic and Bio-inorganic Mechanisms* (Edited by A. G. Sykes), Vol. 2, p. 187. Academic Press, London (1983).
2. M. N. Hughes, *The Inorganic Chemistry of Biological Processes*, 2nd edn. Wiley, Chichester (1981).

3. P. Chaudhuri and K. Wieghardt, *Prog. Inorg. Chem.* 1987, **35**, 329.
4. A. Shaver, *Comprehensive Coordination Chemistry* (Edited by G. Wilkinson, R. D. Gillard and J. A. McCleverty), Vol. 2, p. 245. Pergamon Press, Oxford (1987).
5. J. B. Vincent, J. C. Huffman, G. Christou, Q. Li, M. A. Nanny, D. N. Hendrickson, R. H. Fong and R. H. Fish, *J. Am. Chem. Soc.* 1988, **110**, 6898.
6. S. Menage, J-J. Girerd and A. Gleizes, *J. Chem. Soc., Chem. Commun.* 1988, 431.
7. J. S. Bashkin, A. R. Schake, J. B. Vincent, H.-R. Chang, Q. Li, J. C. Huffman, G. Christou and D. N. Hendrickson, *J. Chem. Soc., Chem. Commun.* 1988, 700.
8. M. R. Grimmett, *Comprehensive Heterocyclic Chemistry* (Edited by K. T. Potts), Vol. 5, p. 373. Pergamon Press, Oxford (1984).
9. P. N. Preston, *The Chemistry of Heterocyclic Compounds*, Vol. 40, Benzimidazoles and Congeneric Tricyclic Compounds, Part 1. Wiley-Interscience, New York (1981).
10. J. M. Latour, G. A. Leonard, D. Limosin, D. C. Povey and S. S. Tandon, *Biological and Inorganic Copper Chemistry* (Edited by K. D. Karlin and J. Zubieta), Vol. 2, p. 221. Adenine Press, New York (1985).
11. H. Adams, N. A. Bailey, J. D. Crane, D. E. Fenton, J. M. Latour and J. M. Williams, *J. Chem. Soc., Dalton Trans.* 1990, 1727.
12. G. B. Deacon and R. J. Phillips, *Coord. Chem. Rev.* 1980, **33**, 227.
13. Y.-L. Lee, W. J. Burke and R. B. von Dreele, *Acta Cryst.* C, 1987, **43**, 209.
14. B. F. Hoskins, N. J. McLeod and H. A. Schaap, *Aust. J. Chem.* 1976, **29**, 515.
15. T. N. Sorrell, D. L. Jameson and C. J. O'Connor, *Inorg. Chem.* 1984, **23**, 190.

Polyhedron Vol. 10, No. 15, pp. 1817–1825, 1991
Printed in Great Britain

0277–5387/91 $3.00+.00
Pergamon Press plc

DEOXYGENATION OF OXOVANADIUM(IV) COMPLEXES UNDER MILD CONDITIONS: SYNTHESIS AND STRUCTURAL CHARACTERIZATION OF *CIS*-DIHALOBIS(DIALKYLDITHIOCARBAMATO)VANADIUM(IV)

EDWARD L. JONES and JOHN G. REYNOLDS*

Lawrence Livermore National Laboratory, University of California, Livermore, CA 94550, U.S.A.

and

JOHN C. HUFFMAN and GEORGE CHRISTOU*

Department of Chemistry and Molecular Structure Center, Indiana University, Bloomington, IN 47405, U.S.A.

(*Received* 12 *March* 1991; *accepted* 16 *May* 1991)

Abstract—A new procedure for the deoxygenation of VO^{+2} complexes is described. The synthesis and properties of mononuclear vanadium complexes $VCl_2(S_2CNR_2)_2$ [R = Me, Et, and Py/2 (Me = CH_3, Et = C_2H_5, and Py = C_4H_4) (pyrrolidyl)] and $VBr_2(S_2CNEt_2)_2$ are reported. The compounds were synthesized in high yield by the general reaction of $VO(S_2CNR_2)_2$ with the appropriate acetyl halide in methylene chloride. Single crystal X-ray analysis was performed on both $VCl_2(S_2CN(C_2H_5)_2)_2$ and $VBr_2(S_2CN(C_2H_5)_2)_2$. The analogous structures consist of a mononuclear unit with distorted C_{2v} symmetry, where the halogen atoms are on the same side of the distorted plane formed by the sulphur atoms. The V—Cl distances are inequivalent at 2.260(1) and 2.247(1) Å, as are the V—Br distances at 2.414(1) and 2.401(1) Å. Two sets of V—S bond lengths are also observed for both complexes. The complexes were examined by IR, and the spectra are similar to the spectra of the vanadyl starting material except for the absence of the V=O band at approximately 1000 cm^{-1}. The ligand C—S and C—N bands are slightly higher in energy in the dihalide complexes than in the vanadyl counterpart, contrary to the effects expected from replacing the oxygen with the electron withdrawing halogen atoms. This behaviour, however is indicative of distortions out of the $d_{x^2-y^2}$ orbital bonding plane causing less π bonding and reducing delocalization of charge among the ligands and the metal centre. This is also seen structurally with the two sets of inequivalent V—S and C—S bond lengths. The UV–vis spectra show a weak maximum at around 570 nm with ε_m of approximately 2000 L mol cm^{-1}, typical of dihalogenated V^{IV} complexes.

It is becoming increasingly apparent that the chemistry of vanadium is of great importance to a wide variety of biological and industrial systems. Recent work in the field of inorganic biochemistry indicates there is a class of nitrogenase metallo-enzymes which have vanadium at the active site.[1,2] In these enzymes, vanadium appears to shuttle between V^{II} and V^{IV}, and is possibly bound to an iron–sulphur cluster. However, few models have been made of this active site. One synthetic difficulty is the problem of directly linking iron–sulphur clusters and V^{IV} compounds. This requires functionality on the vanadium atom which can be synthetically manipulated. Thus, having new V^{IV} compounds with functionality is highly desirable.

Vanadium is commercially important in the conversion of crude oils to transportation fuels.[3] Vanadium occurs naturally and can be of high con-

* Authors to whom correspondence should be addressed.

centration in heavier crude oils.[4] It impacts the industry because its necessary removal during upgrading[5] poisons heterogenous catalysts used in processing.[6] The intermediate species in this transformation of the naturally occurring VO^{2+} complexes to the vanadium sulphide on the upgrading catalyst surface are not well characterized. Some evidence suggests VO^{2+} is deoxygenated to V^{IV}.[7-10] Characterizing this transformation is critical to the understanding of catalytic poisoning due to metals.

Vanadium compounds have also been used to generate slurry-type catalysts to upgrade heavy oils and assist in coal liquefaction. These catalysts increase the conversion of petroleum and coal to lower boiling materials,[11] and desulphurize the resulting liquids.[12,13] The exact species responsible could be finely dispersed vanadium sulphides. These are often formed by *in situ* preparation from vanadyl model compounds such as $VO(acac)_2$.[14] The transformation chemistry and the active VS_x species have not been well characterized. Clearly, activation of the V=O bond is a critical part of this mechanism.

The strong V=O bond is extremely stable and generally dominates the coordination chemistry of vanadium.[15] The reactivity of this bond has not been widely studied because access to other types of vanadium compounds has been through easier synthetic routes which do not employ vanadyl reagents. This is unfortunate because many vanadyl compounds are easy to prepare as starting materials (many can be purchased commercially).

Of the limited V^{IV} non-oxo species reported in the literature, many are dihalide complexes. These have been characterized by spectroscopic methods which indicate six coordinate V and both *trans* and *cis* configurations to be possible. However, only one of these complexes, VCl_2(salen-N-Bu^t)$_2$ [salen-N-Bu^t = N-n-butyl(salicylideniminato)] has been characterized by single crystal X-ray analysis.[16] The structure shows an octahedral V centre with *trans* chlorine atoms. We have also recently synthesized and characterized by single crystal X-ray analysis, $VCl_2(acac)_2$ (acac = acetylacetonato),[17] which has a very similar *trans* structure to VCl_2(salen-N-Bu^t)$_2$.

Many methods have been employed to make these types of compounds: (1) by direct halogenation of the corresponding vanadyl complex;[16,19-23] (2) by reactions of VCl_4 and the appropriate free ligand;[18] and (3) by reaction of thiuram disulphides with V^{II} compounds.[24] Although these methods are all adequate, there are some drawbacks. Many of the reagents are difficult to handle, some react with the ligand as well as the vanadium, and some require involved ligand synthesis.

In this report, we describe a useful new method for the mild deoxygenation of VO^{2+} complexes. We present the synthesis and characterization of $VCl_2(S_2CNEt_2)_2$, $VCl_2(S_2CNMe_2)_2$, $VCl_2(S_2CNPy)_2$ and $VBr_2(S_2CNEt_2)_2$ from the reaction of the corresponding vanadyl dithiocarbamates with acetyl halides. In addition, we present the structural characterization by single crystal X-ray analysis of $VCl_2(S_2CNEt_2)_2$ and $VBr_2(S_2CNEt_2)_2$. The described procedure is a new, more facile and direct synthetic method which gives clean products. The crystal structures are the first reported for vanadium dihalodithiocarbamates, and the structures are surprising in as much as the halogen atoms are unexpectedly *cis*.

EXPERIMENTAL

All syntheses were carried out in a dry/inert atmosphere of purified dinitrogen employing standard Schlenk glassware. Air-sensitive samples for spectroscopic study were prepared in a dinitrogen glovebag or Vacuum Atmospheres glove box. IR spectra were recorded as KBr pellets with the Mattson Polaris Model 10410 spectrophotometer. Electronic spectra were recorded on CH_2Cl_2 solutions using a Varian Model 503 spectrophotometer and Spectrochem quartz anaerobic cells. Because the dihalide complexes readily convert back to the corresponding vanadyl complex upon exposure to even trace quantities of water, excess AcCl or AcBr were added to the solutions. Elemental analyses were perfomed by the Lawrence Livermore National Laboratory analytical department and Galbraith Laboratories, Inc., Knoxville, TN.

Reagents

Spectroanalytical grade methylene chloride (0.006% water) and hexanes were obtained from Burdick and Jackson Laboratories, and were dried over CaH_2 and $LiAlH_4$, respectively, under a dinotrogen atmosphere and degassed before use. Ethanol was obtained from Gold Shield Chemical company. Dimethyldithiocarbamic acid, sodium salt dihydrate; diethyldithiocarbamic acid, sodium salt trihydrate; acetyl chloride; and acetyl bromide were purchased from Aldrich. The pyrrolidinedithiocarbamate derivative was purchased from Matheson Coleman and Bell Manufacturing Chemists. The acetyl bromide was distilled before use and the acetyl chloride used as purchased.

Synthesis of complexes

The vanadyl complexes $VO(S_2CNMe_2)_2$, $VO(S_2CNEt_2)_2$ and $VO(S_2CNPy)_2$ were prepared

by the method of McCormick[25] and recrystallized from methylene chloride.

Dichlorobis(dimethyldithiocarbamato)vanadium(IV) $[VCl_2(S_2CNMe_2)_2]$ (**1**). $VO(S_2CNMe_2)_2$ (0.971 g, 0.00358 mol) was dissolved in methylene chloride (125 cm^3) to give a green–brown solution. This was degassed, and acetyl chloride (0.762 cm^3, 0.0107 mol) was added with stirring. The $VO(S_2CNMe_2)_2$ solution slowly turned black. The reaction solution was stirred at room temperature overnight, and then layered with hexanes (125 cm^3) and placed in a freezer. Storage at −10°C for 3 days led to the formation of black crystals. The crystals were filtered and dried *in vacuo*. The yield of crude product was 45% based on vanadium. Recrystallization from a CH_2Cl_2/hexanes mixture (layered) led to pure material as determined by IR, UV–vis and elemental analysis. Found: C, 19.3; H, 4.2; N, 7.4. Calc. for $C_6H_{12}N_2S_4Cl_2V$: C, 19.9; H, 3.3; N, 7.7%. Electronic absorption maxima = λ, nm (ε_m, L mol cm^{-1}); 578.1(1814), 485.9(1575), 379.9^{sh}(6060).

Dichlorobis(diethyldithiocarbamato)vanadium(IV) $[VCl_2(S_2CNEt_2)_2]$ (**2**). This black complex was prepared and purified from $VO(S_2CNEt_2)_2$ (2.06 g, 0.00567 mol) and acetyl chloride (1.21 cm^3, 0.0170 mol) by a similar procedure as above. The yield of the crude product was 56% based on vanadium. Found: C, 28.7; H, 5.6; N, 6.9. Calc. for $C_{10}H_{20}N_2S_4Cl_2V$: C, 28.7; H, 4.8; N, 6.7%. Electronic absorption maxima = λ, nm (ε_m, L mol cm^{-1}); 570.1(1258), 455.2(1459).

Dibromobis(diethyldithiocarbamato)vanadium(IV) $[VBr_2(S_2CNEt_2)_2]$ (**3**). This black complex was prepared and purified from $VO(S_2CNEt_2)_2$ (0.502 g, 0.00138 mol) and acetyl bromide (0.295 cm^3, 0.00415 mol) by similar procedures as above. The yield of the crude product was 58% based on vanadium. Found: C, 23.0; H, 4.1; N, 5.2. Calc. for $C_{10}H_{20}N_2S_4Br_2V$: C, 23.7; H, 4.0; N, 5.5%. Electronic absorption maxima = λ, nm (ε_m, L mol cm^{-1}); 571.4(2023), 484.6(2064), 357.6^{sh}(4314).

Dichlorobis(pyrrolidyldithiocarbamato)vanadium(IV) $[VCl_2(S_2CNPy)_2]$ (**4**). This black complex was prepared and purified from $VO(S_2CNPy)_2$ (1.16 g, 0.00324 mol) and acetyl chloride (0.690 cm^3, 0.00971 mol) by similar procedures as above. The yield of the crude product was 46% based on vanadium. Found: C, 26.5; H, 3.5; N, 5.6. Calc. for $C_{10}H_8N_2S_4Cl_2V(CH_2Cl_2)$: C, 26.9; H, 2.0; N, 5.7%. Electronic absorption maxima = λ, nm (ε_m, L mol cm^{-1}); 578.1(1106), 489.9(959), 417.0^{slsh} (1288).

X-ray crystallography and structure solution

Data were collected on a Picker four-circle diffractometer by using standard low-temperature facilities. Details of the diffractometry, low-temperature facilities, and computational procedures

Table 1. Crystallographic data for *cis*-$VCl_2(S_2CNEt_2)_2$ and *cis*-$VBr_2(S_2CNEt_2)_2$

Property	*cis*-$VCl_2(S_2CNEt_2)_2$	*cis*-$VBr_2(S_2CNEt_2)_2$
Space group	$P\bar{1}$	$P\bar{1}$
a (Å)	9.136(2)	9.233(1)
b (Å)	14.620(4)	14.829(2)
c (Å)	7.186(2)	7.222(1)
α (°)	98.57(1)	98.72(1)
β (°)	110.49(1)	110.12(1)
γ (°)	95.82(2)	95.90(1)
Z	2	2
V (Å^3)	876.77	904.78
Formula	$VC_{10}H_{20}N_2S_4Cl_2$	$VC_{10}H_{20}N_2S_4Br_2$
M_r (g mol^{-1})	418.37	507.27
ρ_{calc} (g cm^{-3})	1.585	1.865
μ (l cm^{-1})	13.028	53.492
T (°C)	−131	−172
λ (Å)	0.71069	0.71069
Range	$6° \leqslant 2\theta \leqslant 55°$	$6° \leqslant 2\theta \leqslant 45°$
Observed data	3424	2161
$R(R_w)$ (%)	3.56(3.70)	4.23(4.31)
Crystal dimensions	0.25 × 0.25 × 0.25 mm	0.28 × 0.32 × 0.30 mm
Colour of crystal	Black–green	Black

employed by the Molecular Structure Center are available elsewhere.[26] Data collection parameters are summarized in Table 1 for $VCl_2(S_2CNEt_2)_2$ and $VBr_2(S_2CNEt_2)_2$. The structures were solved by a combination of MULTAN and Fourier techniques, and refined by full-matrix least-squares.

For both complexes, **2** and **3**, a systematic search of a limited hemisphere of reciprocal space located a set of diffraction maxima with no symmetry or systematic absences indicating a triclinic space group. Subsequent solution and refinement of the structure confirmed the centrosymmetric choice $P\bar{1}$. For **2**, a total of 4825 reflections were collected. Following the usual data processing 4033 unique reflections remained. Of the 4033 reflections, 3424 were considered observed [$F > 2.33\sigma(F)$]. For **3**, a total of 2390 reflections were collected. Following the usual data processing 2366 unique reflections remained. Of the 2366 reflections, 2161 were considered observed [$F > 3\sigma(F)$]. All non-hydrogen atoms were readily located and refined anisotropically for both complexes. All hydrogen atoms were clearly visible in subsequent difference Fourier maps, and were included in the final refinement cycles with isotropic thermal parameters. The final difference maps were essentially featureless, with the largest peak being 0.45 e $Å^{-3}$ near the vanadium atom for complex **2** and 1.02 e $Å^{-3}$ in the immediate vicinity of a bromine atom for complex **3**.

RESULTS AND DISCUSSION

Synthesis

Vanadyl complexes can be deoxygenated by a variety of reagents ($SOCl_2$, $SOBr_2$, PCl_5, $SeOCl_2$, and $COCl_2$)[19,21,23,27] to yield the corresponding dihalide derivative. These reagents, however, are caustic and often react with the ligands. In addition, some dihalide complexes can be made by the direct reaction of VCl_4 (which is difficult to handle) with the ligand,[18] and by less direct methods including going through thiuram disulphide intermediates.[24] We have now discovered acetyl halides can also be used to synthesize V^{IV} dihalide complexes. The cheap and relatively easy to handle AcX reagents (X = Cl, Br) directly afford the dihalide complexes, overcoming the potential side reactions of the other reagents. As a result, we have successfully synthesized, directly from the corresponding vanadyl complexes, $VCl_2(S_2CNMe_2)_2$ (**1**), $VCl_2(S_2CNEt_2)_2$ (**2**), $VBr_2(S_2CNEt_2)_2$ (**3**), and $VCl_2(S_2CNPy)_2$ (**4**) by eq. (1). Previous attempts in the literature to synthesize such compounds using the other halogenating agents mentioned above often led to poorly characterized, impure products, probably due to the halogenating agent reacting with the ligand. The present procedure yields very clean products, and this has also made single crystal growth easy. As a result, single crystal X-ray analyses on **2** and **3** have been performed.

$$VO(S_2CNR_2)_2 + 2AcX \longrightarrow VX_2(S_2CNR_2)_2 + Ac_2O \quad (1)$$

(X = Cl, Br; R = Me, Et, Py/2).

An excess (50%) of AcX was routinely employed after observing incomplete conversion with stoichiometric amounts of reagents (probably due to hydrolysis by adventitious water). Isolation of **4** was difficult because crystals turned to powder upon vacuum drying due to loss of solvent. This was overcome by drying under N_2 purge. However, even under these conditions, the crystals would gradually turn to a powder, making analysis difficult. The inclusion of solvent was verified by elemental analyses which indicated one CH_2Cl_2 in the molecular formula.

Although we have not experimentally studied the mechanism of the reaction, it probably involves electrophilic attack at the VO^{2+}. Reaction Scheme 1 shows a possible pathway.

Description of structures

Figure 1 shows the structure of **2** with the atom numbering scheme. Selected structural parameters are collected in Table 2. The crystal is composed of discrete molecules of $VCl_2(S_2CNEt_2)_2$ with the expected six coodination at vanadium. The geometry around the metal can be described as highly distorted octahedral, with the chlorine atoms

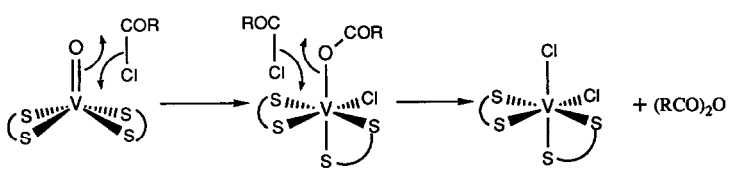

Scheme 1.

Table 2. Selected bond distances (Å) and angles (°) for *cis*-$VCl_2(S_2CNEt_2)_2$

V(1)—Cl(2)	2.2595(10)	N(7)—C(5)	1.309(3)
V(1)—Cl(3)	2.2467(10)	N(7)—C(8)	1.474(3)
V(1)—S(4)	2.4517(11)	N(7)—C(10)	1.481(3)
V(1)—S(6)	2.3777(11)	N(15)—C(13)	1.319(4)
V(1)—S(12)	2.4506(10)	N(15)—C(16)	1.473(4)
V(1)—S(14)	2.3860(11)	N(15)—C(18)	1.477(4)
S(4)—C(5)	1.7126(28)	C(10)—C(11)	1.515(4)
S(6)—C(5)	1.7338(28)	C(16)—C(17)	1.515(5)
S(12)—C(13)	1.709(3)	C(18)—C(19)	1.506(5)
S(14)—C(13)	1.7328(28)		

Cl(2)—V(1)—Cl(3)	98.26(4)	S(4)—V(1)—S(12)	86.11(3)
Cl(2)—V(1)—S(4)	155.63(3)	S(4)—V(1)—S(14)	88.75(4)
Cl(2)—V(1)—S(6)	83.77(4)	S(6)—V(1)—S(12)	86.14(4)
Cl(2)—V(1)—S(12)	92.30(4)	S(6)—V(1)—S(14)	151.63(3)
Cl(2)—V(1)—S(14)	113.86(4)	S(12)—V(1)—S(14)	71.71(4)
Cl(3)—V(1)—S(4)	93.01(4)	V(1)—S(4)—C(5)	87.63(10)
Cl(3)—V(1)—S(6)	116.99(4)	V(1)—S(6)—C(5)	89.56(9)
Cl(3)—V(1)—S(12)	155.37(3)	V(1)—S(12)—C(13)	87.92(10)
Cl(3)—V(1)—S(14)	83.66(4)	V(1)—S(14)—C(13)	89.48(10)
S(4)—V(1)—S(6)	71.86(3)		

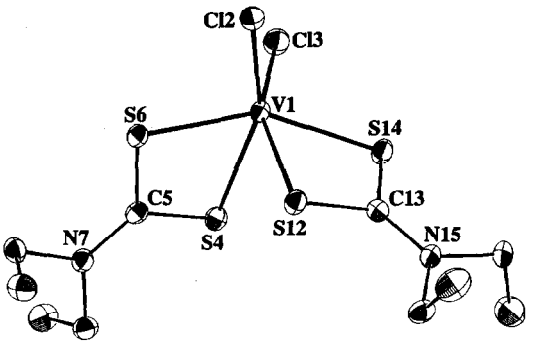

Fig. 1. ORTEP representation of *cis*-$VCl_2(S_2CNEt_2)_2$ showing the atom labelling scheme.

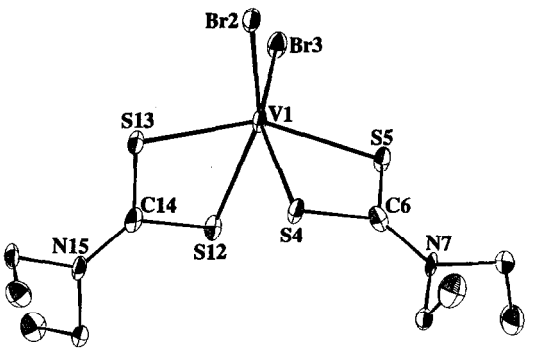

Fig. 2. ORTEP representation of *cis*-$VBr_2(S_2CNEt_2)_2$ showing the atom labelling scheme.

cis to each other on the same side of the distorted plane formed by the four sulphurs of the dithiocarbamate ligands. This is contrary to the structure of VCl_2(salen-N-Bu^t)$_2$, the only reported[19] single crystal determination of a V^{IV} dihalide, which has octahedral coordination with *trans* chlorine atoms. In addition, our crystallographic determination of the structure of $VCl_2(acac)_2$ shows that the latter also exhibits a *trans* geometry.[17] Figure 2 shows the structure of **3** with the atom numbering scheme. Table 3 lists selected structural parameters. The structure is very similar to $VCl_2(S_2CNEt_2)_2$, being composed of discrete molecules of $VBr_2(S_2CNEt_2)_2$, with distorted octahedral coordination at the vanadium. As in the dichloro complex, the bromine atoms are *cis* to each other and on the same side of the plane formed by the four sulphurs of the dithiocarbamate ligands. The structures of **2** and **3** are the first reported single crystal determinations of a V^{IV} *cis* dihalide complex. This geometry was not expected and is contrary to that predicted by several EPR and IR studies.[21,24]

Table 2 shows that the V—Cl bond lengths of **2** are slightly inequivalent. Table 4 compares these bond lengths with other V—Cl bond lengths in the literature. The V—Cl lengths of **2** are slightly shorter than those for two other V^{IV} dichloro complexes. This is probably due to the differences between the *cis* and *trans* structures. The sulphur atoms of the ligands in the *cis* structure are considerably out of the equatorial bonding plane of the metal. As a result, the σ-bonding d_{xy} and π-bonding $d_{x^2-y^2}$ orbital interactions between the vanadium and the dithiocarbamate ligands in the equatorial

Table 3. Selected bond distances (Å) and angles (°) for *cis*-$VBr_2(S_2CNEt_2)_2$

V(1)—Br(2)	2.4137(14)	N(7)—C(6)	1.312(9)
V(1)—Br(3)	2.4007(14)	N(7)—C(8)	1.466(9)
V(1)—S(4)	2.4528(21)	N(7)—C(10)	1.494(9)
V(1)—S(5)	2.3818(21)	N(15)—C(14)	1.316(9)
V(1)—S(12)	2.4586(22)	N(15)—C(16)	1.488(9)
V(1)—S(13)	2.3786(21)	N(15)—C(18)	1.466(9)
S(4)—C(6)	1.713(7)	C(8)—C(9)	1.497(12)
S(5)—C(6)	1.733(7)	C(10)—C(11)	1.504(12)
S(12)—C(14)	1.721(7)	C(16)—C(17)	1.523(11)
S(13)—C(14)	1.725(7)	C(18)—C(19)	1.531(10)
Br(2)—V(1)—Br(3)	97.97(5)	S(4)—V(1)—S(12)	86.74(7)
Br(2)—V(1)—S(4)	92.00(6)	S(4)—V(1)—S(13)	87.10(7)
Br(2)—V(1)—S(5)	113.34(7)	S(5)—V(1)—S(12)	90.09(7)
Br(2)—V(1)—S(12)	154.90(7)	S(5)—V(1)—S(13)	153.20(8)
Br(2)—V(1)—S(13)	83.04(6)	S(12)—V(1)—S(13)	71.86(7)
Br(3)—V(1)—S(4)	155.13(7)	V(1)—S(4)—C(6)	87.65(25)
Br(3)—V(1)—S(5)	83.26(6)	V(1)—S(5)—C(6)	89.54(25)
Br(3)—V(1)—S(12)	93.46(6)	V(1)—S(12)—C(14)	87.13(24)
Br(3)—V(1)—S(13)	116.61(6)	V(1)—S(13)—C(14)	89.65(23)
S(4)—V(1)—S(5)	71.88(7)		

Table 4. Vanadium–chloride bond lengths of selected vanadyl and V^{IV} complexes

Complex	V—Cl (Å)	Vanadium coordination
$VCl_2(S_2CNEt_2)_2$	2.25–2.26	6
$VCl_2(acac)_2$[17]	2.31–2.33	6
$VCl_2(salen\text{-}N\text{-}Bu^t)_2$[16]	2.35	6
$VOCl_2(NMe_3)_2$[41]	2.25	5
$VOCl_2(C_5H_{12}N_2O)_2$[42]	2.34	5
$VOCl_2(C_2H_5O)_2(H_2O)$[43]	2.39	5

plane are not as extensive as in *trans* structures. Consequently, there is less delocalization of charge onto the ligands, resulting in a stronger V—Cl bond. This change in bonding interaction has been substantiated in EPR[21] and far IR[18] examination of *cis* and *trans* dihalide V^{IV} complexes.

The effect of the ligand type on the length of the V—Cl bond cannot be ruled out, however. V=O bond lengths in the corresponding vanadyl complexes are subject to variations due to both the first coordination sphere[28–30] and substituents on the ligands.[31]

For complex **2**, the four V—S bonds are divided into two short (average 2.382 Å) and two long (average 2.451 Å). This is reflected in the corresponding C—S bond lengths, where the two sulphur atoms with the longer V—S bond lengths have the shorter C—S bond lengths (average 1.711 Å), and the two sulphur atoms with the shorter V—S bond lengths have the longer C—S bond lengths (average 1.733 Å). This can be reasoned by considering the structural deviation from the equatorial plane of the molecule. Starting with the *trans* structure, the two dithiocarbamate ligands in a planar configuration distort to the *cis* structure by bending below this plane and also twisting in opposite directions around the C—N axis of each ligand. This removes one sulphur of each ligand from the plane of the π-bonding orbitals more than the other, therefore yielding two sets of V—S bond lengths, as well as two sets of S—V—S bond angles. Indeed, Fig. 1 shows S(6) and S(14) closer to the perpendicular to the plane formed by Cl(2), V, and Cl(3), and shows the planes formed by the S_2CNC_2 atoms in each of the ligands are also twisted with respect to each other. This behaviour is also seen in **3** (Fig. 2), where the longer V—S bond lengths average to 2.4587 Å and the shorter to 2.3804 Å. The corresponding C—S bond lengths average to 1.717 and 1.729 Å, respectively.

Several investigators have shown canonical form I to be particularly important and predominant in binding many dialkyldithiocarbamates to metals.[24,32,33] The C—N stretching frequencies in the IR support this (see below). However, canonical forms II and III cannot be ignored, particularly in light of the two sets of V—S and C—S bond lengths. When the ligands distort out of the equatorial plane, canonical form I is likely to be less important, and either II or III contribute proportionately more to the bonding. If the contribution of II or III is large enough, this would be reflected in each ligand hav-

ing one long and short C—S bond, as observed in the structures.

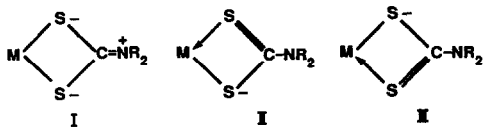

I II III

The single crystal X-ray structure of the vanadyl starting material, $VO(S_2CNEt_2)_2$ is available.[29] Since only the oxygen has been substituted, this allows an interesting comparison of the effects of the chlorine and bromine atom substitution on the $[V(S_2CNEt_2)_2]^{2+}$ subunit structure. The V—S distances reflect more distortion from the equatorial plane in the dihalide complexes than in the vanadyl complex (2.387–2.410 Å). In the vanadyl complex, only one of the four V—S bonds is short, which is considered to be due to crystal packing forces. However, the *average* V—S bond distance for the dichloro complex (2.41 Å), and vanadyl complex (2.40 Å) are similar. These values are slightly shorter than values seen for other vanadium complexes with the $V(S_2C)$ moiety. In these cases, inequivalences in the V—S bond lengths were also seen. $V(S_2CCH_3)_4$,[34] $V(S_2CC_6H_5)_4$,[35] $V(S_2CCH_2C_6H_5)_4$,[35] and $VO(S_2CNEt_2)_3$[36] exhibited the following V—S_{long} distances (Å), V—S_{short} distances (Å), V—S bond ratio (long to short): 2.50, 2.46, 1.02; 2.56, 2.45, 1.05; 2.53, 2.46, 1.03; 2.75, 2.55, 1.08; respectively. These compare to $VO(S_2CNEt_2)_2$, $VCl_2(S_2CNEt_2)_2$ and $VBr_2(S_2CN(Et_2)_2$ with C—S bond ratios of 1.00, 1.03 and 1.03, respectively. The π bonding in $V(S_2CC_6H_5)_4$ and $V(S_2CCH_2C_6H_5)_4$ was also considered weak. Although it is unlikely crystal packing forces would be completely responsible for the V—S bond behaviour described above, it certainly cannot be ruled out and probably accounts for at least some of the distortions in the structures cited.

$VO(S_2CNEt_2)_2$ also exhibits two sets of C—S bond lengths (1.715, 1.727; 1.721, 1.732 Å). Even though the average C—S bond lengths are approximately the same for all three complexes (1.722 Å $\pm$ 0.001 Å), the inequivalences seen in the dihalide complexes are greater than the vanadyl complex. This suggests that the canonical form II or III can have significance even when there is less equatorial distortion, as in the vanadyl complex (the vanadium is 0.7 Å above the basal plane formed by the four sulphur atoms of the dithiocarbamate ligands).

IR spectra

Table 5 lists the most important and characteristic bands of the IR spectra of **1** through **4** and compares them with the corresponding vanadyl starting material. The dihalide derivatives have spectra very similar to the corresponding VO starting material. Both have C—N and C—S bands around 1500 and 950 cm^{-1}, respectively, and a weak C—S stretching band around 850 cm^{-1}. The C—N band is at slightly higher energy than the free ligand (1490 cm^{-1}) for all the complexes.[32] The C—S band is higher for the dihalodialkyldithiocarbamates, and lower or the same for the other complexes compared to the free ligand band (970 cm^{-1}).[32] The most obvious feature of Table 5, however, is the absence of the very intense V=O band in the dihalide complexes. This diagnostic band has been our best indicator of purity during synthesis. The weak C—S absorption which does appear in this region of the dihalide spectra also appears in the vanadyl IR but is partially masked by the very strong V=O stretch.

Table 5. IR data for selected vanadyl and V^{IV} dithiocarbamate complexes (cm^{-1})

Complex	ν(C—N)	ν(C—S)	ν(V=O)
$VO(S_2CNEt_2)_2$	1514	955	988
$VCl_2(S_2CNEt_2)_2$	1521	994	
$VBr_2(S_2CNEt_2)_2$	1520	996	
$VO(S_2CNMe_2)_2$	1539	970	983
$VCl_2(S_2CNMe_2)_2$	1545	981	
$VO(S_2CNPy)_2$	1494	947	994
$VCl_2(S_2CNPy)_2$	1496	947	

In the dihalobisdialkyldithiocarbamate complexes the C—N and C—S stretches are shifted to higher frequencies or, in the case of the pyrrolidine derivative, stay relatively the same upon deoxygenation of the vanadium and addition of the halides [C—N and C—S bands for $VCl_2(S_2CNMe_2)_2$: 6 and 11 cm^{-1} higher, respectively; $VCl_2(S_2CNEt_2)_2$: 7 and 39 cm^{-1} higher, respectively, than the corresponding bands for the vanadyl complexes]. This is in contrast to the other dihalide complexes reported in the literature. Behzadi and Thompson[27] report, for V^{IV} β-diketonate complexes of the form $VX_2(dik)_2$ (X = Cl, Br; dik = acac, bzac), the dichloro derivatives have C—C and C—O bands which are lower frequencies than the same bands in the corresponding vanadyl complexes. From supporting far IR, EPR, and X-ray powder pattern data, these structures appear to have *trans* halogens. Seangprasertkij and Riechel[37] likewise report that for complexes of the type *trans*-VX_2(salen) (X = Phenyl, Cl), the C—N stretch shifts to a lower frequency on going from the vanadyl to the disubstituted derivative. Cuadrado and

Moran[24] report for $VCl_2(S_2CNMe_2)_2$, C—N and C—S bands to be 28 and 15 cm^{-1} lower, respectively, than the corresponding values for $VO(S_2CNMe_2)_2$. However, for $VCl_2(S_2CNEt_2)_2$, they report the C—N and C—S bands to be the same and 21 cm^{-1} higher than the corresponding values for $VO(S_2CNEt_2)_2$. They also conclude, based on the metal–halogen stretch in the far IR (370 cm^{-1}) that these structures have *trans* halogens.

These differences in IR behaviour with respect to the vanadyl precursor can be rationalized by considering the metal complex symmetry and electronic effects of the substituents on the ligands. Jezierski and Raynor[21] in their EPR study of several V^{IV} dihalide complexes deduce that going from the vanadyl structure (where the metal is somewhat out of the plane of the equatorial ligands) to the *trans*-type structure (where the metal is in the plane of the ligands) stabilizes the σ-bonding d_{xy} orbital slightly and stabilizes the π-bonding $d_{x^2-y^2}$ orbital greatly due to increased orbital overlap. This orbital overlap increases delocalization, effectively reducing the charge on the ligand and therefore decreasing the frequencies of the diagnostic ligand bands.

In the *cis*-type structures, the orbital overlap is reduced because the deviation from the ligand plane is increased. This localizes the charge on the ligand, therefore increasing the frequencies of the diagnostic ligand bands, as observed in complexes **1–3**. This is also consistent with the observations of Chatt *et al.*[32] who concluded from examining a large series of metal dithiocarbamate complexes, that the symmetry arrangement in order of decreasing C—N frequencies is planar > tetrahedral > octahedral > distorted octahedral and pyramidal. This is further appreciated if the binding vector of the dithiocarbamates ligand is drawn from the C (on the CS_2) to the metal centre (as opposed to bidentate through the sulphurs), then the coordination around the vanadium in the structures **2** and **3** can be viewed as distorted tetrahedral. The arguments are the same for **4**, except the localized electron density which caused an increase in the C—N and C—S frequencies for **1–3** is offset by delocalization onto the pyrrole ring in **4**. The net effect is the frequencies are almost identical in $VCl_2(S_2CNPy)_2$ and $VO(S_2CNPy)_2$.

CONCLUSIONS

A new and convenient synthesis of vanadium dihalodithiocarbamates from vanadyl starting materials has been developed. The dihalodithiocarbamates, $VCl_2(S_2CNMe_2)_2$, $VCl_2(S_2CNEt_2)_2$, $VCl_2(S_2CNPy)_2$ and $VBr_2(S_2CNEt_2)_2$ show definite physical property deviations from previously characterized dihalide derivatives of V^{IV} coordination complexes. The single crystal structures and IR properties definitely indicate a *cis* configuration of the halides which is contrary to all other structurally characterized V^{IV} dihalide complexes. This *cis* configuration can be considered to be a distortion from octahedral coordination to a tetrahedral-type complex with the dithiocarbamate ligand being smaller than acac, acting like a monodentate ligand instead of a bidentate ligand.

Acknowledgements—The work at the Lawrence Livermore National Laboratory was performed under the auspices of the U.S. Department of Energy under contract number W-7405-ENG-48. Work at Indiana University was supported by the Office of Basic Energy Sciences, Division of Chemical Sciences, U.S. Department of Energy under Grant DE-FG02-87ER13702. We especially thank the Affirmative Action Equal Employment Opportunity Program at Lawrence Livermore National Laboratory for additional support.

Complete listings of atomic coordinates, isotropic and anisotropic thermal parameters, bond distances and angles (20 pages each structure); listing of observed and calculated structure factors for $VCl_2(S_2CNEt_2)_2$ and $VBr_2(S_2CNEt_2)_2$ are available on request. Ordering information is given on any current masthead page. The complex MSC structure reports (No. 90019 and 90056) are available on request from the Indiana Chemistry Library.

REFERENCES

1. R. L. Robson, R. R. Eady, T. H. Richardson, R. W. Miller, M. Hawkins and J. R. Postgate, *Nature* 1986, **322**, 388.
2. J. M. Arber, B. R. Dobson, R. R. Eady, P. Stephens, S. S. Hasnain, C. D. Garner and B. E. Smith, *Nature* 1987, **325**, 372.
3. J. F. Branthaver, *ACS Symp. Ser.* 1987, **344**, 188.
4. J. G. Reynolds and W. R. Biggs, *Acc. Chem. Res.* 1988, **21**, 319.
5. J. G. Speight, *The Chemistry and Technology of Petroleum: Chemical Industries*, Vol. 3. Marcel Dekker, New York (1983).
6. P. W. Tamm, H. F. Harnsberger and A. G. Bridge, *Ind. Eng. Chem. Proc. Res. Dev.* 1981, **20**, 262.
7. B. G. Silbernagel, R. R. Mohan and G. H. Singhal, *ACS Symp. Ser.* 1984, **248**, 91.
8. B. G. Silbernagel, *J. Catal.* 1979, **56**, 315.
9. P. C. H. Mitchell and J. A. Valero, *Inorg. Chem. Acta* 1983, **71**, 179.
10. P. C. H. Mitchell and J. A. Valero, *React. Kinet. Catal. Lett.* 1982, **20**, 219.

11. B. Schuetze and H. Hofmann, *Hydro. Proc.* 1984, **63(2)**, 75.
12. J. G. Reynolds, S. G. Yu and R. T. Lewis, 1985, U.S. Patent 4,559,129.
13. P. A. Montano and B. Granoff, *Fuel* 1980, **59**, 214.
14. W. K. T. Gleim and J. G. Gatis, 1971, U.S. Patent 3,558,474.
15. F. A. Cotton and G. Wilkinson, *Advanced Inorganic Chemistry*, 5th edn. John Wiley and Sons, New York (1988).
16. M. Pasquali, F. Marchetti and C. Floriani, *Inorg. Chem.* 1979, **18**, 2401.
17. E. L. Jones, J. G. Reynolds, J. C. Huffman and G. Christou, manuscript in preparation.
18. R. B. VonDreele and R. C. Fay, *J. Am. Chem. Soc.* 1972, **94**, 7935.
19. M. Pasquali, A. Torres-Filho and C. Floriani, *J. Chem. Soc., Chem. Commun.* 1975, 534.
20. A. Jczicrski and J. B. Raynor, *Inorg. Chim. Acta* 1980, **44**, L153.
21. A. Jezierski and J. B. Raynor, *J. Chem. Soc., Dalton Trans.* 1981, 1.
22. A. Jezierski, *Inorg. Chim. Acta* 1985, **98**, L1.
23. P. Richard, J. L. Poncet, J. M. Barbe, R.Guilard, J. Goulon, D. Rinaldi, A. Cartier and P. J. Tola, *J. Chem. Soc., Dalton Trans.* 1982, 1451.
24. I. Cuadrado and M. Moran, *Trans. Met. Chem.* 1986, **11**, 375.
25. B. J. McCormick, *Inorg. Chem.* 1968, **7**, 1965.
26. M. H. Chisholm, K. Folting, J. C. Huffman and C. C. Kirkpatrick, *Inorg. Chem.* 1984, **23**, 1021.
27. K. Behzadi and A. J. Thompson, *J. Less-Common Met.* 1987, **128**, 281.
28. R. P. Dodge, D. H. Templeton and A. Zalkin, *J. Chem. Phys.* 1961, **35**, 55.
29. K. Henrick, C. Raston and A. White, *J. Chem. Soc., Dalton Trans.* 1976, 26.
30. D. Bruins and D. L. Weaver, *Inorg. Chem.* 1970, **9**, 130.
31. M. Pasquali, F. Marchetti, C. Floriani and S. Merlino, *J. Chem. Soc., Dalton Trans.* 1977, 139.
32. J. Chatt, L. A. Duncanson and L. M. Venanzi, *Suomen Kemistilehti* 1956, **B29**, 75.
33. J. Chatt, L. A. Duncanson and L. M. Venanzi, *Nature* 1956, **177**, 1042.
34. A. L. Fanfani, P. F. Nunzi and A. R. Zanazzi, *Acta Cryst.* 1972, **B28**, 1298.
35. M. Bonamico, G. Dessy, V. Fares and L. Scaramuzza, *J. Chem. Soc., Dalton Trans.* 1974, 1258.
36. J. C. Dewan, D. L. Kepert, C. L. Raston, D. Taylor, A. H. White and E. N. Maslen, *J. Chem. Soc., Dalton Trans.* 1973, 2082.
37. R. Seangprasertkij and T. L. Riechel, *Inorg. Chem.* 1986, **25**, 3121.
38. G. J. M. van der Kerk and H. L. Klopping, *Rec. Trav. Chim.* 1952, **71**, 1179.
39. G. J. M. van der Kerk, M. H. van Raalte, A. K. Sijpesteijn and R. van der Veen, *Nature* 1955, **176**, 308.
40. K. Nakamoto, J. Fujita, R. A. Condrate and Y. Morimoto, *J. Chem. Phys.* 1963, **39**, 423.
41. J. E. Drake, J. Vekris and J. S. Woods, *J. Chem. Soc.* (A), 1968, 1000.
42. J. Coetzer, *Acta Cryst.* 1970, **B26**, 872.
43. J. G. Reynolds, J. C. Huffman and G. Christou. Unpublished data.

Polyhedron Vol. 10, No. 15, pp. 1827–1829, 1991
Printed in Great Britain

0277–5387/91 $3.00+.00
© 1991 Pergamon Press plc

COMMUNICATION

SYNTHESIS AND STRUCTURAL CHARACTERIZATION OF [α,α′-BIS{BIS(2-(DIPHENYLPHOSPHINO)ETHYL)AMINO}ETHANE] BIS(TETRAHYDROBORATO)DICOPPER(I). HYDROGEN BRIDGE ATTACHMENT OF THE TETRAHYDROBORATE GROUP

M. M. TAQUI KHAN,* PARIMAL PAUL and K. VENKATASUBRAMANIAN

Discipline of Coordination Chemistry and Homogeneous Catalysis,
Central Salt and Marine Chemicals Research Institute, Bhavnagar 364 002, India

(*Received* 18 *March* 1991; *accepted* 20 *May* 1991)

Abstract—The synthesis and structural characterization of [α,α′-bis{bis(2-(diphenylphosphino)ethyl)amino}ethane]bis(tetrahydroborato)dicopper(I) complex is reported. Crystal structure analysis shows that each copper atom possesses a distorted tetrahedral geometry with ligation to two phosphorus atoms of the ligand and two hydrogen atoms of BH_4^-. ^1H, ^{13}C, ^{31}P and ^{11}B NMR and IR data are also presented.

Synthesis of metal complexes containing the tetrahydroborate group has gained considerable interest in research due to their catalytic activity in hydrogenation, isomerization, polymerization and oligomerization reactions.[1] A number of such complexes containing copper(I) and tertiary phosphine ligands with different bonding modes of BH_4^- have been reported.[1–4] Recently, photocatalytic behaviour of some of these complexes, viz. $Cu(PPh_3)_2(BH_4)$, Cu(diphos)(BH_4) and Cu(prophos)(BH_4), has also been reported.[5] With a view to investigating the BH_4^- bonding mode and its catalytic activity we have synthesized the title compound with a new hexadentate ligand, viz. α,α′-bis{bis(2-(diphenylphosphino) ethyl)amino}ethane.

EXPERIMENTAL

The compound was synthesized by the reaction of $[Cu(NCCH_3)_4](ClO_4)$[6] and the ligand[7] in a 2:1 mole ratio under refluxing conditions in acetone, followed by the addition of a slight excess of an ethanolic solution of $NaBH_4$ at room temperature. The white compound thus obtained was washed with water and ethanol and on recrystallization from hot DMF gave crystals suitable for single crystal X-ray study.†

* Author to whom correspondence should be addressed.

† *X-ray study.* Intensity data were collected on an Enraf–Nonius CAD4/PDP-11/73 system with graphite-monochromatized Mo-K_α ($\lambda = 0.71069$ Å) radiation in the θ range of 4–47°. After correcting for Lorentz and polarization factors, the intensities were collected for absorption using the empirical absorption correction method with three reflections near $\chi = 90°$. The structure was solved by Multan 82 (P. Main, S. E. Hull, L. Lessinger, G. Germain, J. P. Declercq and M. M. Woolfrom, Universities of York, U.K. and Louvain, Belgium), which gave the positions of the metal and phosphorus atoms unambiguously and the structure was developed by alternated least-squares refinement and difference Fourier maps. Anisotropic refinement of non-hydrogen atoms was by block diagonal matrix and hydrogen atoms were held fixed by stereochemical constraints in the positions in the difference maps with a unit weighting scheme, and the Dunitz–Seiler factor converges to $R = 0.038$ ($R_w = 0.045$).

Crystallographic data. $C_{58}H_{68}Cu_2N_2P_4B_2$, $M_r = 1064.72$, monoclinic, space group $C2/c$, $a = 30.915(3)$, $b = 15.298(2)$, $c = 11.996(1)$ Å, $\beta = 97.33(1)°$, $V = 5627(2)$ Å^3, $Z = 4$, $\mu = 9.07$ cm^{-1}, crystal size $= 0.28 \times 0.24 \times 0.26$ mm, reflections collected = 4142, reflections observed = 3058. Atomic coordinates, bond lengths and angles, and thermal parameters have been deposited with the Cambridge Crystallographic Data Centre.

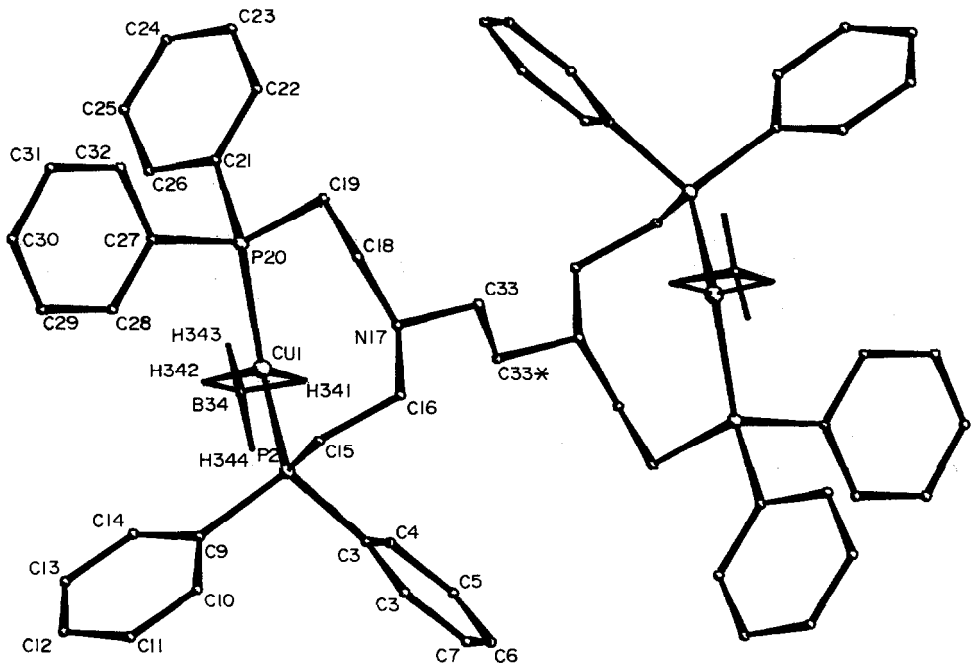

Fig. 1. Molecular structure of the title compound, showing the atom numbering scheme.

RESULTS AND DISCUSSION

The ^{1}H NMR* spectrum of the complex exhibits phenyl protons at 7.25 ppm and methylene protons at 2.16(m), 2.34(m) and 2.40(s) ppm. The first two multiplets are due to the P—CH_2—CH_2—N moiety, their multiplicity is due to coupling between two non-equivalent methylene groups followed by the ^{31}P nucleus. The singlet at 2.40 ppm is assigned to methylene protons of the N—CH_2—CH_2—N bridge. The B—H proton appeared as a broad resonance at 0.9 ppm, consistent with other reported values.[1] The ^{13}C{^{1}H} NMR spectrum contains aromatic carbons in the range 129.30–138.54 ppm, methylene carbons of the P—CH_2—CH_2—N moiety at 28.04 and 50.92 ppm, and the methylene group of the N—CH_2—CH_2—N bridge at 52.14 ppm as a singlet. ^{31}P{^{1}H} NMR exhibits a singlet at -15.68 ppm (in the free ligand this appeared at -19.01 ppm) which indicates the equivalence of phosphorus atoms coordinated to copper(I). The ^{11}B NMR spectrum shows a singlet at -52.48 ppm [relative to $B(OCH_3)_3$], significantly deshielded compared with $NaBH_4$ (-61.00 ppm).

The IR spectrum of the complex exhibits bands at 2365 (broad and strong), 2010 (strong with shoulder) and 1120 (strong and sharp) cm^{-1}, which can be assigned to ν(B—H_t), ν(B—H_b) and BH_2 deformations, respectively, for double hydrogen-bridged BH_4^-.[1,8]

The molecular structure of the complex is shown in Fig. 1. For the sake of clarity, the ORTEP view of the coordination site of one copper atom is displayed in Fig. 2. The crystal structure analysis shows that the complex contains a crystallographic centre of symmetry, which is located at the middle point of the C(33)—C(33′) bond, thus dividing the molecule into identical halves. The copper atom

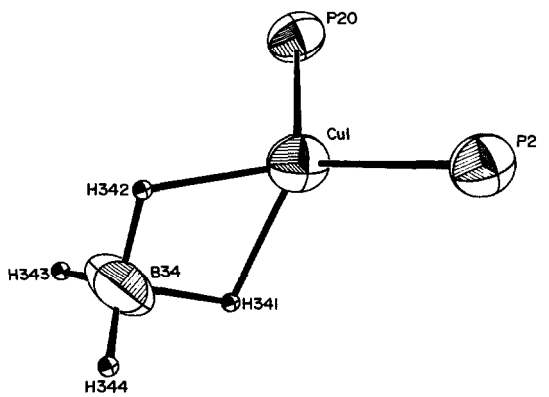

Fig. 2. ORTEP view of the surroundings of the copper(I) polyhedron.

* NMR spectra were recorded on a Jeol FX-100 FT-NMR in $CDCl_3$ (^{1}H) or $CHCl_3$, references used were tetramethylsilane for ^{1}H and ^{13}C, 85% H_3PO_4 for ^{31}P and $B(OCH_3)_3$ for ^{11}B.

Table 1. Selected bond distances (Å) and angles (°) of the title compound

Bond distances		Bond angles	
Cu(1)—P(2)	2.261(1)	P(2)—Cu(1)—P(20)	119.72(6)
Cu(1)—P(20)	2.258(1)	P(2)—Cu(1)—H(341)	113.9
Cu(1)—H(341)	1.683	P(2)—Cu(1)—H(342)	121.4
Cu(1)—H(342)	1.681	P(20)—Cu(1)—H(341)	119.3
Cu(1)—B(34)	2.247(6)	P(20)—Cu(1)—H(342)	108.8
		H(341)—Cu(1)—H(342)	59.8

shows distorted tetrahedral geometry with ligation to two phosphorus atoms of the ligand and the two hydrogen atoms of the tetrahydroborate group. Some selected bond distances and angles are shown in Table 1. The Cu—P distances are slightly shorter compared with those found in $Cu(PPh_3)_2(BH_4)$[2] which has the same coordination site. This can be attributed to the chelating effect of the ligand which results in strong Cu—P bond formation. The Cu—H distances (1.682 ± 1 Å) are also significantly shorter compared with the value of 2.02(5) Å found in $Cu(PPh_3)_2(BH_4)$,[2] which indicates strong bond formation between the copper and the hydrogen atom of BH_4^-. The bond angles found in the coordination sphere (shown in Table 1) indicate a significant distortion in the tetrahedral geometry of copper and is due to different surroundings. The smallest bond angle (59.8°), as expected, is found between two hydrogen atoms [H(341)—Cu(1)—H(342)] due to their small size.

The Cu---B distance of 2.247(6) Å is in the range found for double hydrogen-bridged tetrahydroborato complexes of the first transition metals[1,9,10] but slightly longer compared with the value of 2.184 Å found in $Cu(PPh_3)_2(BH_4)$. Such a short distance between Cu^+ and B^- (even shorter than the sum of the covalent radii of Cu^+ and B^-) indicates a significant interaction between the two atoms, as supported by the significant downfield shift of 8.5 ppm in the ^{11}B NMR spectrum of the complex.

REFERENCES

1. T. J. Marks and J. R. Kolb, *Chem. Rev.* 1977, **77**, 263.
2. S. J. Lippard and K. M. Melmed, *Inorg. Chem.* 1967, **6**, 2223.
3. F. Takusagawa, A. Fumagalli, T. F. Koetzle, S. G. Shore, T. Schmitkons, A. V. Fratini, K. W. Morse, C. Wei and R. Bau, *J. Am. Chem. Soc.* 1981, **103**, 5165.
4. L. M. Engelhardt, C. Pakawatchai and A. H. White, *J. Chem. Soc., Dalton Trans.* 1985, 125.
5. B. Liaw, S. W. Orchard and C. Kutal, *Inorg. Chem.* 1988, **27**, 1311.
6. P. Hemmerich and C. Sigwart, *Experientia* 1963, **19**, 488.
7. M. M. Taqui Khan, P. Paul, K. Venketasubramanian and S. Purohit, *J. Chem. Soc., Dalton Trans.*, submitted.
8. C. Kutal, P. Grutsch, J. L. Atwood and R. D. Rogers, *Inorg. Chem.* 1978, **17**, 3558.
9. M. Y. Darensbourg, R. Bau, M. W. Marks, R. R. Burch Jr, J. C. Deaton and S. Slater, *J. Am. Chem. Soc.* 1982, **104**, 6961.
10. P. Dapporto, S. Midollini, A. Orlandini and L. Sacconi, *Inorg. Chem.* 1976, **15**, 2768.

Polyhedron Vol. 10, No. 15, pp. 1831–1833, 1991
Printed in Great Britain

0277–5387/91 $3.00+.00
© 1991 Pergamon Press plc

COMMUNICATION

SOLID STATE ^{31}P NUCLEAR MAGNETIC RESONANCE OF TRICYANOPHOSPHINE

M. A. H. A. AL-JUBOORI, A. FINCH, P. J. GARDNER* and C. J. GROOMBRIDGE†

Department of Chemistry, Royal Holloway and Bedford New College, Egham Hill, Egham TW20 0EX, Surrey, U.K.

(*Received* 17 *May* 1991; *accepted* 3 *June* 1991)

Abstract—The high resolution ^{31}P NMR spectrum of solid tricyanophosphine is reported. The use of magic angle sample spinning gives the chemical shift much more accurately than the earlier wideline measurement, and spinning sideband analysis gives an improved estimate of the ^{31}P chemical shift anisotropy: -96 ± 5 ppm.

The structure-determining ability of nuclear magnetic resonance spectroscopy is well known, and often depends on interpretation of the chemical shift parameter, most commonly through accumulated empirical knowledge. Considerable progress has been made in recent years in improving the theoretical computation of light element chemical shifts, especially ^{13}C and $^{14/15}$N, and this is gradually being extended to heavier species, of which ^{31}P is of most widespread interest. Chemical shifts (the term "shielding" tends to be used in the context of theoretical work, and has opposite sign) are actually second rank tensors, i.e. functions of orientation relative to the external influence, and it has been pointed out[1] that a full determination (principal components and directions) can lead to a much more complete understanding of the relationship between chemical shifts and structure.

It is clearly important to have experimental values for a range of small molecules and it has become increasingly common for high resolution solid state NMR to be used to provide this, particularly by analysis of spinning sideband patterns given by slow magic-angle sample spinning (MAS). Here we report an investigation of $P(CN)_3$, improving upon an earlier wideline ^{31}P NMR study.[2]

$P(CN)_3$ is pyramidal and crystallizes with tetragonal $I\bar{4}2d$ unit cells in which all molecules are symmetry-equivalent.[3] The bond distances and angles give almost C_{3v} symmetry, but each P—C≡N is slightly bent and weak intermolecular N···P interactions have been implicated.[3]

EXPERIMENTAL

Sample preparation

Tricyanophosphine was prepared from PCl_3 and AgCN by the method of Staats and Morgan[4] and was purified by vacuum sublimation. It was a white crystalline material subsequently handled in a dry nitrogen atmosphere.

NMR spectroscopy

All spectra were obtained on a Bruker MSL-300 spectrometer using a standard double air bearing magic-angle spinning probe. The $P(CN)_3$ sample was packed into a 7 mm zirconia rotor in a nitrogen-filled glove box. A reasonable air seal was made by the use of a small amount of vacuum grease on the rotor endcap. The sample was spun using dry compressed nitrogen gas boiled from a liquid N_2 dewar.

The ^{31}P frequency was 121.481 MHz and the sample was spun at 4433 Hz. The spectrum was recorded using single 90° pulses with a 64 s recycle. An attempt to acquire a ^{13}C spectrum gave no

* Author to whom correspondence should be addressed.
† Present address: BP Research Centre, Chertsey Road, Sunbury-on-Thames TW16 7LN, Middlesex, U.K.

signal. The ^{31}P chemical shift scale was referenced by replacement with 85% orthophosphoric acid in a sealed glass ampoule; positive shifts are to high frequency and are precise to ± 0.2 ppm. The centreband occurs at the intensity-weighted centre of the spectrum, and this was confirmed by spinning speed adjustment; its position gives the isotropic (i.e. "normal") chemical shift. An estimate of the ^{31}P relaxation time, T_1, was made using a saturation-recovery pulse sequence, and it was verified that the relative sideband intensities were not affected by incomplete relaxation.

Spinning sideband analysis was carried out using the least-squares computer program developed by Sales and co-workers,[5] which uses Herzfeld and Berger sideband ratio data.[6] Principal components were determined in the chemical shift sense, and error estimates (95% confidence intervals) were obtained from sum-of-squares derivatives.

RESULTS AND DISCUSSION

The ^{31}P MAS spectrum of $P(CN)_3$ is shown in Fig. 1. The bands were close to Gaussian shape with 164 Hz full width. The isotropic chemical shift was -140.0 ppm, close to the reported MeCN solution value,[7] -137.83 ppm, rather than -129.72 ppm found in iodopropane.[7] Self-coordination in the crystal[3] would thus appear to resemble the MeCN solvent effect. Signal recovery from saturation was found still to be incomplete at 64 s but the ^{31}P T_1 was of the order of 100 s.

Chemical shift principal components were found to be $\delta_{33} = -100(\pm 4)$, $\delta_{22} = -116(\pm 8)$, and $\delta_{11} = -204(\pm 5)$. Different definitions exist for the anisotropy, but if $\delta_\perp = 1/2(\delta_{22}+\delta_{33}) = -108$ ppm, the anisotropy can be taken as $\Delta = \delta_\parallel - \delta_\perp = -96$ ppm. Using the definition for asymmetry $\eta = (\delta_{33}-\delta_{22})/(\delta_{iso}-\delta_{11})$, this is found to differ significantly (0.24) from axial symmetry. These values are not corrected for bulk magnetic susceptibility since this is likely to be less than experimental error. Jameson *et al.*[8] have recently given the shielding on the absolute scale of the phosphoric acid reference, and this can be used to give $P(CN)_3$ *shieldings* as: $\sigma_{iso} = 468.3$ ppm, $\sigma_{11} = 428$, $\sigma_{22} = 444$, $\sigma_{33} = 532$.

Recent *ab initio* molecular calculations of substituted phosphines have suggested[9] a significant participation of phosphorus 3*d* orbitals in the bonding of $P(CN)_3$, due to partial $p\pi$–$d\pi$ overlap (3*p* and 3*d* contributions to P—CN bonding were calculated as 0.57 and 0.14). The simple semi-empirical treatment given by Lucken and Williams[2] yielded a chemical shift anisotropy of -115 ppm, but ignored 3*d* involvement and left considerable flexibility in average excitation energy and electron $\langle r^{-3} \rangle$. An attempt to improve on this would also have to incorporate the intermolecular interaction, since the solvent effect on $P(CN)_3$ shift[7] indicates that this may be of the order of 10 ppm.

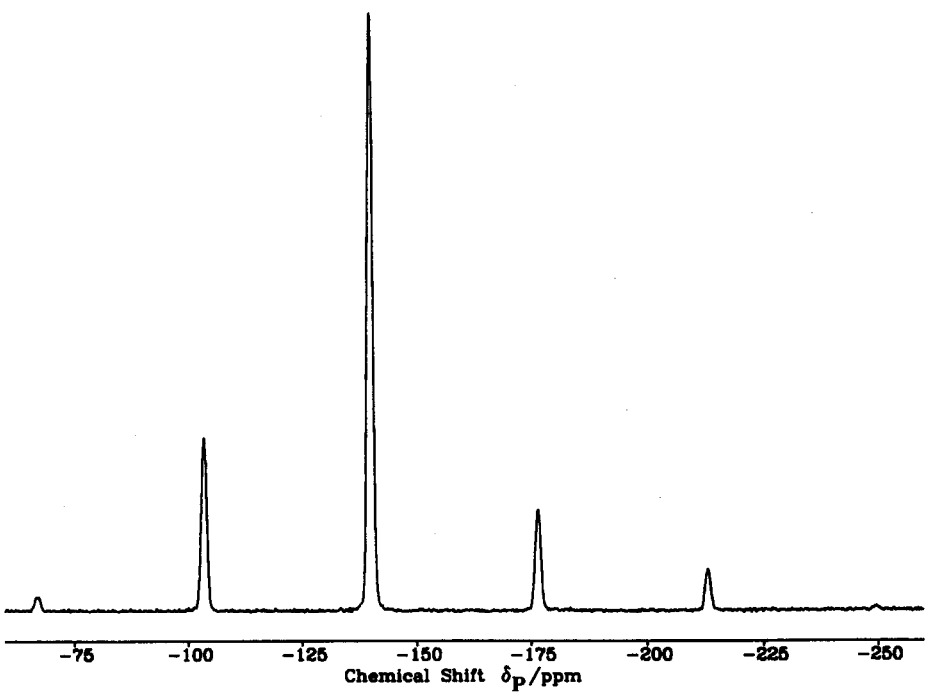

Fig. 1. ^{31}P Magic angle spinning NMR spectrum $P(CN)_3$. Spinning speed 4433 Hz, 400 scans, 64 s recycle.

Acknowledgements—All NMR spectra were obtained using the University of London Intercollegiate Research Service (ULIRS) solid state NMR facility at RHBNC, with assistance from R. T. Mathavan. Our thanks to Dr K. Sales (Queen Mary and Westfield College, London) for use of the SRCH sideband program.

REFERENCES

1. C. J. Jameson, *Nucl. Magn. Reson., Spec. Per. Rep.* 1985, **14**, 11.
2. E. A. C. Lucken and D. F. Williams, *Mol. Phys.* 1969, **16**, 17. [There is an ambiguity in the chemical shift anisotropies given in this paper: different values appear in the abstract (-100 ± 20 ppm) and Table 1 (-128 ± 20 ppm).]
3. K. Emerson and D. Britton, *Acta Cryst.* 1964, **17**, 1134.
4. P. A. Staats and H. W. Morgan, *Inorg. Chem.* 1960, **6**, 84.
5. G. E. Hawkes, K. D. Sales, L. Y. Lian and R. Gobetto, *Proc. R. Soc. Lond. A* 1989, **424**, 93.
6. J. Herzfeld and A. E. Berger, *J. Chem. Phys.* 1980, **73**, 6021.
7. B. W. Tattersall, *Polyhedron* 1990, **9**, 553.
8. C. J. Jameson, A. De Dios and A. K. Jameson, *Chem. Phys. Lett.* 1990, **167**, 575.
9. E. Magnusson, *Phosphorus Sulfur* 1986, **28**, 379.

Polyhedron Vol. 10, No. 15, pp. 1835–1838, 1991
Printed in Great Britain

0277–5387/91 $3.00+.00
© 1991 Pergamon Press plc

COMMUNICATION

AUTOREDUCTION OF COPPER(II) BY A NON-CHELATING AMINE LIGAND: SYNTHESIS AND X-RAY STRUCTURE OF TRIS(2,3-DIMETHYLPYRAZINE)DICOPPER(I) PERCHLORATE

MARK M. TURNBULL*

Department of Chemistry, Clark University, 950 Main St., Worcester, MA 01610, U.S.A.

and

GEORGE PON and ROGER D. WILLETT*

Department of Chemistry, Washington State University, Pullman, WA 99164, U.S.A.

(*Received* 25 *March* 1991; *accepted* 5 *June* 1991)

Abstract—Reaction of $Cu(ClO_4)_2$ with 2,3-dimethylpyrazine (2,3-dmpz) in aqueous solution yields the bright yellow, air-stable, crystalline complex $Cu_2(2,3\text{-dmpz})_3(ClO_4)_2$ (**1**) in 40% yield. The single-crystal X-ray structure reveals a two-dimensional polymeric lattice of tricoordinate copper(I) atoms bridged by 2,3-dimethylpyrazine ligands.

Motivated by our interest in magnetic interactions between metals in two-dimensional lattices, we have begun a series of studies based upon the $Cu(pz)_2(ClO_4)_2$ (pz = pyrazine) 2D-Heisenberg antiferromagnetic system.[1] In the crystalline state, this complex exists as a two-dimensional array of Cu^{2+} ions with bridging pyrazine ligands. Each copper atom is bonded to four pyrazine molecules in a pseudo-square planar array (the perchlorate ions are loosely coordinated in the axial sites). The dihedral angle, δ, between the CuN_4 plane and the plane of the pyrazine molecule is 66°. This canting of the pyrazine ligands, presumably to relieve steric crowding, provides poor overlap between the metal *d*-orbitals and the pyrazine π-system, and reduces the ligands ability to provide an exchange network between Cu^{2+} ions. We are interested in modifying that dihedral angle, either into or perpendicular to the Cu—N plane, to improve the Cu—Cu exchange. Since increasing the steric interactions between the rings would potentially increase the dihedral angle, we attempted the synthesis of $Cu(2,3\text{-dmpz})_2(ClO_4)_2$ [2,3-dmpz = 2,3-dimethylpyrazine].

RESULTS AND DISCUSSION

A deep blue–green solution of $Cu(ClO_4)_2$ and 2,3-dmpz (2:1) was allowed to stand at room temperature for several days.[2] After that time, we noted a distinct change in the colour of the solution to dark green and small yellow crystals appeared at the bottom of the beaker. After another 1–2 days the crystal formation appeared complete and the solid (**1**) was isolated. IR spectroscopy confirmed the presence of the ligand and implied the presence of the metal (via the ClO_4^- absorption at 1100 cm^{-1}). To our surprise, the complex was diamagnetic. The magnetic susceptibility exhibited no temperature dependance over the range 100–300 K. The reduction of Cu^{2+} to Cu^{1+} was confirmed by ^{63}Cu NMR in CH_3CN solution.[3] A single peak was observed at 8.7 ppm ($\nu_{1/2}$ = 40 Hz).

The product proved insoluble in most solvents, but readily dissolved in DMSO and CH_3CN. Unlike the solid material, these solutions proved unstable to air, their bright yellow colour quickly

* Authors to whom correspondence should be addressed.

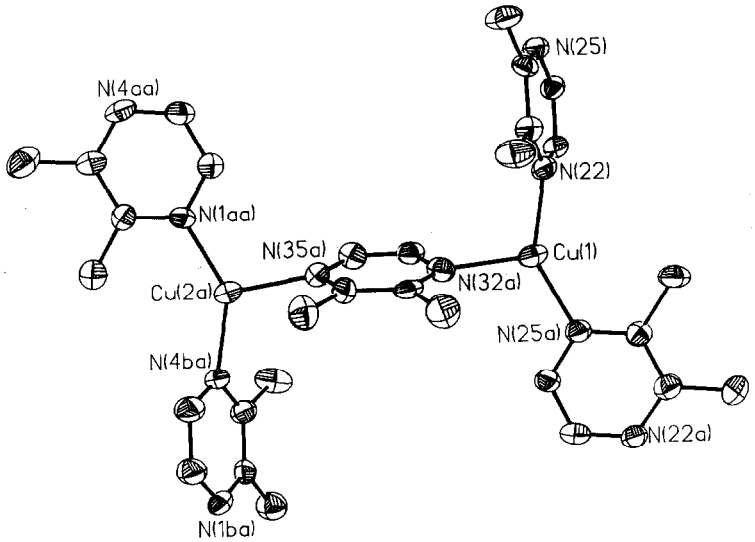

Fig. 1. Illustration of the Cu^{I}–dimethylpyrazine framework showing the planar, three-coordinate geometry of the copper(I) ions. Selected bond lengths (Å) and angles (°) for Cu_2(2,3-dimethylpyrazine)$_3(ClO_4)_2$ (1): Cu(1)—N(22), 1.974(6); Cu(1)—N(25a), 1.967(5); Cu(1)—N(25a), 1.967(5); Cu(1)—N(32a), 2.083(6); Cu(2a)—N(35a), 2.080(6); Cu(2a)—N(1aa), 1.984(5); Cu(2a)—N(4ba), 1.996(6); N(22)—Cu(1)—N(25a), 141.7(2); N(22)—Cu(1)—N(32a), 105.7(2); N(25a)—Cu(1)—N(32a), 112.4(2); N(35a)—Cu(2a)—N(1aa), 110.4(2); N(35a)—Cu(2a)—N(4ba), 107.5(2); N(1aa)—Cu(2a)—N(4ba), 141.0(3).

turning to green. Recrystallization of **1** from CH_3CN under argon gave pale yellow, transparent crystals which appeared to be the solvent adduct (by IR, $\nu(C{\equiv}N) = 2290\ cm^{-1}$) and thus unsuitable for elucidating the structure of complex **1**.

Careful examination of the initial precipitate yielded a small number of crystals suitable for single crystal X-ray diffraction study.[4] An ORTEP drawing showing the coordination spheres about the copper(I) atoms is shown in Fig. 1. A stereodrawing showing the nature of the polymeric sheets is shown in Fig. 2. The structure is described as a pleated sheet. Zigzag chains of alternating copper(I) ions and coordinated 2,3-dmpz molecules run roughly parallel to the *x*-axis. The chains are cross-linked by additional 2,3-dmpz molecules to form the sheets. Adjacent chains are displaced by different amounts along the *z*-axis, providing the pleats (see Fig. 2). The methyl substituents on the pyrazine rings within a given chain are all directed in the same sense relative to the *z*-axis. The methyl substituents on the cross-linking pyrazines are all oriented in the same direction with respect to the *z*-axis.

The coordination spheres of the copper(I) ions are nearly trigonal planar. The sums of N—Cu—N bond angles about copper(1) and (2) are 359.8° and 358.9°, respectively. The coordination geometry about the copper atoms in $KCu_2(CN)_3 \cdot H_2O$ is similar.[5] The pyrazine rings themselves exhibit a

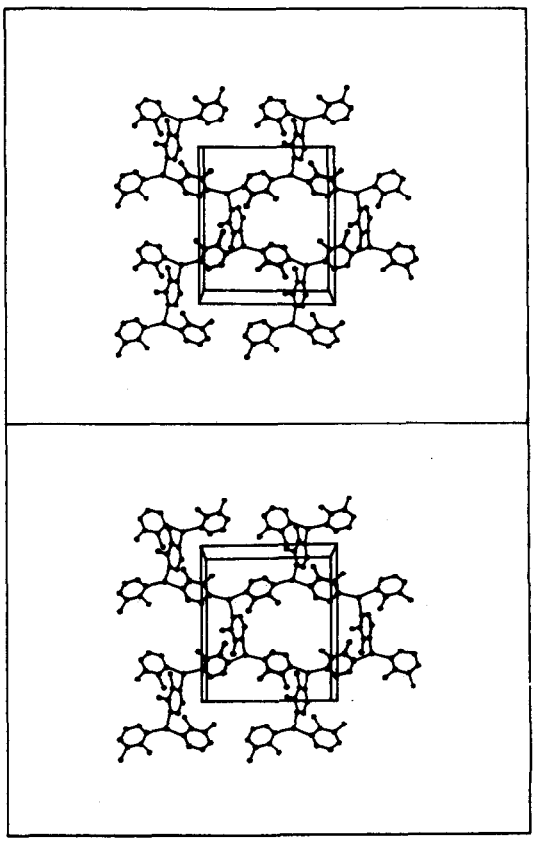

Fig. 2. Stereoview of the Cu_2(2,3-dimethylpyrazine)$_3$ pleated sheets.

wide variety of orientations with respect to the planes defined by the copper ions and their coordinated nitrogen atoms. About copper(1) the δ angles are 72° and 11° along the chain and 111° for the linking pyrazine. For copper(2), the intra-chain δ angles are 68° and 10°, and 110° to the linking pyrazine ring. The δ angles between the chains and one δ angle for each copper within the chains are all within 6° of the 66° angle found in the parent complex $[Cu(pz)_2^{2+}]_n$, but the remaining angles within the chains are substantially reduced. It is difficult to determine how much of the changes in these dihedral angles are due to the methyl substituents, because of the change from four-coordinate to three-coordinate copper centres.

Reduction of copper(II) complexes with chelating amine ligands is well established. Copper(I) complexes with 2,9-dialkylphenanthroline or 6,6′-dialkyl-2,2′-bipyridine have been prepared via chemical[6] or photochemical[7] reduction of the corresponding copper(II) compounds. Autoreduction of bis-chelated copper(II) complexes of 6,6′-dialkyl-2,2′-bipyridines[8] and 8-dimethylarsinoquinoline[9] has also been reported. In these cases, the steric bulk of the ligands is believed to force a tetrahedral geometry about the copper atom which induces a positive shift in the reduction potential. We find no examples in the literature of such a reduction with non-chelating amine ligands in the presence of non-coordinating anions. However, in the presence of halide counter-ions, reduction processes are frequently observed. This includes formation of mixed valence compounds[10] and halogenation of the organic species,[11] as well as isolation of simple copper(I) complexes.[12] The preparation of Cu^I–imidazole complexes via disproportionation of the copper(II) complexes with copper metal has also been described.[13]

We believe the most plausible course for the reaction begins with the initial formation of some Cu^{2+} species with four coordinated 2,3-dimethylpyrazines, perhaps in the manner observed in the $Cu(pz)_2(ClO_4)_2$ lattice. Crowding around the metal ion caused by the methyl groups forces a distortion of geometry to some form of distorted tetrahedron which is then reduced, perhaps by one of the ligands. The non-chelating nature of the pyrazines and the relatively electron-rich nature of the copper(I) ion then make the loss of one ligand, to relieve crowding, a facile process.

Preliminary results indicate that the conditions for reduction of copper(II) to copper(I) in this system are quite specific. Heating the initial solution causes almost immediate formation of **1**, while a solution kept at 5°C showed no evidence of reduction after 10 weeks. Cu(2-methylpyrazine)$_2(ClO_4)_2(H_2O)_2$ and Cu(2-methylpyrazine)$_4(ClO_4)_2(H_2O)$ complexes have been isolated as well and show no evidence of autoreduction.[14] In addition, reaction with 2,5-dimethylpyrazine yielded a copper(II) complex as the major isolated product. Tiny amounts of a yellow crystalline solid were also observed and are believed to be a copper(I) complex analogous to **1**. Further study of this system is in progress.

Acknowledgements—This work was supported by a grant from the National Science Foundation (DMR-9006470). The Bruker MSL-300 NMR spectrometer was purchased with the aid of NSF Grant No. CHE8720106. The X-ray diffractometer facility was established through funds provided by NSF Grant No. CHE8408407 and the Boeing Company. We also thank Professor Christopher P. Landee and Dr Fontaine C. Bradley for helpful discussions and Mr Changan Zhang for obtaining the ^{63}Cu NMR spectrum.

REFERENCES

1. (a) J. Darriet, M. S. Haddad, E. N. Duesler and D. N. Hendrickson, *Inorg. Chem.* 1979, **18**, 2679; (b) M. S. Haddad, D. N. Hendrickson, J. P. Cannady, R. S. Drago and D. S. Bieksza, *J. Am. Chem. Soc.* 1979, **101**, 898.
2. Synthesis of (**1**)—$Cu(ClO_4)_2 \cdot 6H_2O$ (3.70 g, 10 mmol) was dissolved in 5.0 cm^3 of H_2O and added to a stirred solution of 2,3-dimethylpyrazine (2.16 g, 20 mmol) in 5.0 cm^3 of H_2O. The resulting deep blue–green solution was allowed to sit at room temperature in the air for several days (7–10). Initially, a very small amount of blue–green crystalline solid was deposited in the bottom of the beaker (not yet characterized). This was followed by a change in the colour of the solution to dark green and the appearance of a yellow crystalline solid over the course of 24–48 h. The solid was collected by vacuum filtration, washed with H_2O and acetone, and then air-dried to give 2.62 g (40%). Found: C, 32.9; H, 3.5; N, 12.9. Calc. for $C_{18}H_{24}Cl_2Cu_2N_6O_8$: C, 33.2; H, 3.7; N, 13.0%. The formation of **1** can be hastened by heating the initial solution to 60°C, whereupon the previously observed colour change occurs and a bright yellow powder precipitated, 2.80 g (43%). This powder was identical to the crystalline complex according to IR and microanalysis.
3. We do not believe this spectrum represents the actual complex **1**, but rather the acetonitrile adduct. The spectrum was obtained at 79.618 MHz using a 2 μs pulse, on a Bruker MSL-300 spectrometer and referenced to $Cu(CH_3CN)_4Cl$. Attempts to obtain a solid state ^{63}Cu CPMAS spectrum were unsuccessful.
4. X-ray structure determination: Crystal dimensions 0.5 mm × 0.16 mm × 0.08 mm. Data collection was carried out on an upgraded Syntex $P2_1$ diffractometer employing Mo-K_α radiation (λ = 0.71069 Å)

and a graphite monochromator. The orientation matrix and lattice parameters were optimized from a least squares calculation on 25 centred reflections with high Bragg angles (27–30°). Two standard reflections (026, 122) were monitored every 96 reflections and showed no systematic variation. The intensities of 4623 reflections were measured by using an ω-scan (0.9° range) with speeds varying from 3 to 30° min^{-1}. Following the data reduction, 4225 unique reflections remained, with 2642 having $|F_o| \geqslant 3\sigma$. The positions of the copper and chloride atoms were found via direct methods, with the remaining molecules being found from subsequent electron difference maps. All non-hydrogen atoms were refined to final values of $R = 0.0699$ and $R_w = 0.0616$. The final refinement included 325 least squares parameters with a mean value of $|\Delta/\sigma| = 0.007$ and $g = 0.00033$. The goodness of fit was 1.552 and the final difference map showed a residual of 0.64 e $Å^{-3}$ near copper. The hydrogen atoms included were at idealized locations with the C—H distances fixed at 0.96 Å, and isotropic thermal parameters fixed at 0.08. Empirical absorption corrections were applied, resulting in a transmission range of 0.699–0.897. All data reduction, structure solution and refinement and graphics were performed by using SHELXTL 5.1 software. Full data collection information, final atomic coordinates, thermal parameters, all bond lengths and angles and observed and calculated structure factors have been deposited with the Editor. **Crystal data:** Formula: $C_{18}H_{24}Cl_2Cu_2N_6O_8$. Space group: $P2_1/a$, $fw = 650.46$, $T = 22°C$, $a = 12.800(4)$, $b = 14.737(2)$, $c = 12.833(2)$ Å, $\beta = 97.56(2)°$, $V = 2399.6(9)$ $Å^3$, $Z = 4$, $\lambda = 0.71069$ Å, $D_{calc} = 1.80$ g cm^{-3}, $\mu = 20.6$ cm^{-1}, trans. coeff. = 0.699–0.897, $R(F_o) = 0.0699$, $R_w(F_o) = 0.0616$.

5. D. T. Cromer and A. C. Larson, *Acta Cryst.* 1962, **15**, 397.
6. G. Davies and D. J. Loose, *Inorg. Chem.* 1976, **15**, 694, 700.
7. (a) S. Sundararajan and E. L. Wehry, *J. Inorg. Nucl. Chem.* 1972, **34**, 3699; (b) S. Sundararajan and E. L. Wehry, *J. Phys. Chem.* 1972, **76**, 1528.
8. S. Kitagawa, M. Munakata and A. Higashie, *Inorg. Chim. Acta* 1984, **84**, 79.
9. F. H. Jardine, *Adv. Inorg. Chem. Radiochem.* 1975, **17**, 115.
10. B. Scott and R. D. Willett, *Inorg. Chem.* 1991, **30**, 110 and refs therein.
11. R. D. Willett, *Acta Cryst.* 1988, **C44**, 450 and refs therein.
12. (a) F. A. Divillanova, A. Diaz, F. Isaia, G. Verani, L. P. Battaglia and A. Bonamartini-Corrodi, *J. Coord. Chem.* 1986, **15**, 161; (b) J. R. Boehm, A. L. Barch, K. F. Bizot and J. H. Enemark, *J. Am. Chem. Soc.* 1975, **97**, 501; (c) F. A. Cotton, B. A. Frenz, D. L. Hunter and Z. C. Mester, *Inorg. Chim. Acta* 1974, **11**, 111.
13. H. M. J. Hendriks and J. Reedijk, *Recl. J. R. Natl. Chem. Soc.* 1979, **98**, 95.
14. M. M. Turnbull and R. D. Willett, unpublished results.

Polyhedron Vol. 10, No. 15, pp. 1839–1841, 1991
Printed in Great Britain

0277–5387/91 $3.00+.00
© 1991 Pergamon Press plc

COMMUNICATION

ISOSTRUCTURAL POTASSIUM AND SODIUM DI-NITROGEN FUNCTIONALIZED AMIDES: SYNTHESES AND CRYSTAL STRUCTURES OF [Ph(2-Pyr)NK·TMEDA]$_2$ AND [Me(2-Pyr)NNa·TMEDA]$_2$

PHILIP C. ANDREWS, DANIEL R. BAKER and ROBERT E. MULVEY*

Department of Pure and Applied Chemistry, University of Strathclyde, Glasgow G1 1XL, U.K.

and

WILLIAM CLEGG and PAUL A. O'NEIL

Department of Chemistry, The University, Newcastle upon Tyne NE1 7RU, U.K.

(*Received* 12 *March* 1991; *accepted* 17 *June* 1991)

Abstract—Two alkali metal amide complexes, [Ph(2-Pyr)NK·TMEDA]$_2$ and [Me(2-Pyr)NNa·TMEDA]$_2$, synthesized from 1:1:1 mixtures of PhM (M = K or Na), the appropriate secondary amine and the Lewis base TMEDA, have been structurally identified by X-ray diffraction and shown to adopt analogous dimeric structures based on planar (N—M)$_2$ rings with additional "internal"- and "external"-donor N·M links that render the metal cations six-coordinate.

Structural information on potassium amides is particularly scarce.[1] Those which have been identified hitherto exhibit marked differences from their sodium congeners. Two sets of crystal structures illustrate this point. Unsolvated $[(Me_3Si)_2NM]_n$ is dimeric for M = K[2] and polymeric for M = Na.[3] While $\{[Bu^t_2(F)Si]N(Bu^t)M\cdot(THF)_x\}_n$ is dimeric ($n = 2$) for both metals, the larger K^{m+} cation displays additional interactions to F and to THF ($x = 2$) to attain six-coordination, in contrast to the four-coordinate Na^{m+} cations ($x = 1$).[4] Here, however, we report a K/Na pair, [Ph(2-Pyr)NK·TMEDA]$_2$ (**1**) and [Me(2-Pyr)NNa·TMEDA]$_2$ (**2**), which adopt essentially identical solid-state structures as revealed by X-ray diffraction studies (TMEDA = $Me_2NCH_2CH_2NMe_2$).

EXPERIMENTAL

Metal amides **1** and **2** were prepared by the method outlined in Scheme 1. Typically for alkali metal organic compounds, moisture and oxygen must be rigorously excluded during the preparation and subsequent storage of these pale yellow crystalline solids. Yields of first crops were 70 and 72%, m.p. is 253–254 and 95–96°C, respectively. Satisfactory analyses (C, H, N, M) were obtained. Excess tetrahydrofuran co-solvent is necessary to dissolve **1** prior to its recrystallization.

PhM + R(2-Pyr)NH ⟶ PhH + R(2-Pyr)NM
↓ L
½[R(2-Pyr)NM·L]$_2$

Conditions: argon atmosphere, solvent n-hexane, L=TMEDA.
For **1**, R=Ph, M=K : For **2**, R=Me, M=Na

Scheme 1.

Crystallography

1: $C_{34}H_{50}N_8K_2$, $M = 649.0$, triclinic, $P\bar{1}$, $a = 9.203(7)$, $b = 10.891(8)$, $c = 11.072(8)$ Å,

* Author to whom correspondence should be addressed.

$\alpha = 108.25(3)°$, $\beta = 109.90(3)°$, $\gamma = 104.53(3)°$, $V = 908.14$ Å^3, $Z = 1$, $D_{calc} = 1.187$ g cm^{-3}, $F(000) = 348$, $\mu = 0.29$ mm^{-1} for Mo-K_α radiation ($\lambda = 0.71073$ Å). Of 6404 reflections, measured[5] with a Stoe-Siemens diffractometer at 150 K ($2\theta_{max} = 50°$), 3202 were unique ($R_{int} = 0.026$), and 2882 with $F > 4\sigma_c(F)$ were used for structure determination[6] by direct methods and difference syntheses. Blocked-cascade refinement to minimize $\Sigma w\Delta^2$ ($\Delta = |F_o| - |F_c|$; $w^{-1} = \sigma^2(F) = \sigma_c^2(F) + 5 - 9G + 29G^2 - 11H + 6H^2 + 6GH$; $G = F_o/F_{max}$, $H = \sin\theta/\sin\theta_{max}$, $\sigma_c(F)$ (from counting statistics only),[7] anisotropic thermal parameters for all non-hydrogen atoms, constrained hydrogen atoms [C—H = 0.96 Å, H—C—H = 109.5°, aromatic hydrogen on ring external bisectors, $U(H) = 1.2U_{eq}(C)$], gave $R = 0.062$, $R' = (\Sigma w\Delta^2/\Sigma wF_o^2)^{1/2} = 0.068$, a satisfactory analysis of variance and no significant features in the final difference map.

2: $C_{24}H_{46}N_8Na_2$, $M = 492.7$, monoclinic, C2, $a = 14.404(2)$, $b = 13.931(2)$, $c = 8.343(1)$ Å, $\beta = 112.41(1)°$, $V = 1547.8$ Å^3, $Z = 2$, $D_c = 1.057$ g cm^{-3}, $T = 240$ K, $F(000) = 536$, $\mu = 0.085$ mm^{-1}. Data collection and structure determination as for **1** with 4028 measured reflections, 1427 unique ($R_{int} = 0.018$), 1167 with $F > 4\sigma_c(F)$, $w^{-1} = \sigma_c^2(F) + 10 - 19G + 29G^2 - 25H + 16H^2 + 20GH$, extinction correction $F_c' = F_c/(1 + xF_c^2/\sin 2\theta)^{1/4}$ [$x = 1.4(3) \times 10^{-7}$]. $R = 0.044$, $R' = 0.037$.

Tables of atomic coordinates and other crystallographic data for both compounds have been deposited with the Editor and the Cambridge Crystallographic Data Centre.

RESULTS AND DISCUSSION

The structure common to **1** and **2** is built around a planar (amido N—M)$_2$ dimeric ring (Figs 1 and 2,

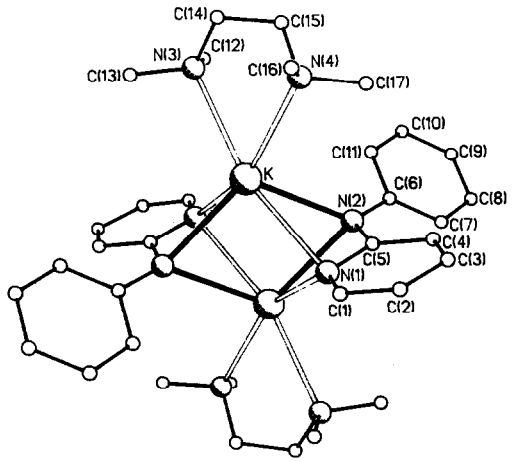

Fig. 1. Molecular structure of **1**, with labelling of important atoms. Amido N—K bonds filled, other N—K bonds open.

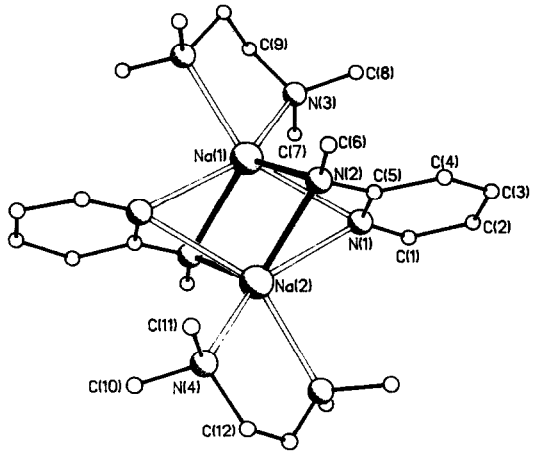

Fig. 2. Molecular structure of **2**, with labelling of important atoms. Amido N—Na bonds filled, other N—Na bonds open.

Table 1. Key dimensions in planar (N—Na)$_2$ and (N—K)$_2$ dimeric ring systems (X-ray diffraction data)

Amide	Amido N—M bond lengths (Å)	Bond angles (°) at N	Bond angles (°) at M	Reference
[Me(2-Pyr)NNa·TMEDA]$_2$ (**2**)	2.446(4), 2.454(4)	70.3(1)	110.0(3) 109.5(3)	This work
[Ph(2-Pyr)NNa·PMDETA]$_2$[a]	2.499(2), 2.552(2)	71.3(1)	108.7(1)	8
(N-sodioindole·TMEDA)$_2$	2.356(5), 2.478(5)	87.1(2)	92.9(2)	9
(N-sodioindole·PMDETA)$_2$	2.474(3), 2.481(5)	89.9(1)	90.1(2)	9
{[Bu$^t_2$(F)Si]N(Bu^t)Na·(THF)}$_2$	2.483(2), 2.497(2)	Not given		4
[Ph(2-Pyr)NK·TMEDA]$_2$ (**1**)	2.805(2), 2.805(3)	73.9(1)	106.0(1)	This work
[(Me$_3$Si)$_2$NK]$_2$	2.770(3), 2.803(3)	85.83(9)	94.47(9)	2
{[Bu$^t_2$(F)Si]N(Bu^t)K·(THF)$_2$}$_2$	2.958(5), 2.961(5)	Not given		4

[a] This structure belongs to the same family as **1** and **2**.

respectively). This feature is beginning to dominate K/Na amide structural chemistry. Table 1 compares the key dimensions of eight four-membered rings of this type. Rings with M = K are inherently larger than those with M = Na, in keeping with periodic M^{m+} radius considerations. The R(2-Pyr) substituents in **1** and **2** occupy *transoid* positions, above and below the ring plane, enabling each pyridyl N to bridge to each pair of M^{m+} cations. Distances involved in these "internal"-donor metal linkages measure 2.841(2)/2.877(3) Å and 2.677(4)/2.709(4) Å, respectively. More unsymmetrical K-(pyridyl)N-K bridging [N—K distances, 2.779(7)/2.956(8) Å] was earlier noted in the binuclear ylide derivative $[(Ph)_2PC(H)P(Ph)_2C(H)(C_5H_4N) \cdot K \cdot (THF)_2]_2$.[10] The dihedral angles between the (amido N—M)$_2$ ring planes and the (pyridyl N—M)$_2$ ones are 120.0° for **1** and 116.9° for **2**. "External"-donor molecules (bidentate TMEDA ligands) complete the hexa-coordination of the M^{m+} cations [N—M distances: 2.825(2)/2.906(3) Å for **1**; 2.510(6)/2.511(2) Å for **2**]. The combined effect of the above structural features is the M^{m+} cations are enclosed within a distorted octahedron of nitrogen atoms. Both M^{m+} cations in each structure carry a high positive charge (greater for K, although *m* approaches one in each case), while an equal negative charge (approaching two in total) is dispersed over the eight nitrogen centres.

Acknowledgement—Financial support from the S.E.R.C. (P.C.A., W.C., R.E.M., P.A.O.) and the Royal Society (R.E.M.) is much appreciated.

REFERENCES

1. M. F. Lappert, P. P. Power, A. R. Sanger and R. C. Srivastava, *Metal and Metalloid Amides*. Ellis Horwood–Wiley, Chichester (1980).
2. K. F. Tesh, T. P. Hanusa and J. C. Huffman, *Inorg. Chem.* 1990, **29**, 1584.
3. R. Grüning and J. L. Atwood, *J. Organomet. Chem.* 1977, **137**, 101.
4. U. Pieper, D. Stalke, S. Vollbrecht and U. Klingebiel, *Chem. Ber.* 1990, **123**, 1039.
5. W. Clegg, *Acta Cryst. Sect. A*. 1981, **A37**, 22.
6. G. M. Sheldrick, SHELXS-86, Program for Crystal Structure Determination. University of Göttingen (1986). SHELXTL, An Integrated System for Solving, Refining and Displaying Crystal Structures from Diffraction Data, Revision 5 (1985).
7. H. Wang and B. E. Robertson, *Structure and Statistics in Crystallography* (Edited by A. J. C. Wilson), p. 125. Adenine Press, New York (1985).
8. P. C. Andrews, W. Clegg and R. E. Mulvey, *Angew. Chem.* 1990, **102**, 1480; *Angew. Chem. Int. Ed. Engl.* 1990, **29**, 1440.
9. K. Gregory, M. Bremer, W. Bauer, P. v. R. Schleyer, N. P. Lorenzen, J. Kopf and E. Weiss, *Organometallics* 1990, **9**, 1485.
10. H. Schmidbaur, U. Deschler and B. Milewski-Mahrla, *Chem. Ber.* 1982, **115**, 3290.

Polyhedron Vol. 10, No. 15, pp. 1843–1846, 1991
Pergamon Press plc. Printed in Great Britain

BOOK REVIEWS

Nomenclature of Inorganic Chemistry: Recommendations 1990. International Union of Pure and Applied Chemistry. Edited by G. J. Leigh. Blackwell Scientific Publications, Oxford, London, Cambridge, MA, 1990, xxiv+289 pp., $70.00 hardback, $27.50 paperback.

Nomenclature has been an integral part of modern chemistry since its very inception. In fact, the publication of Guyton de Morveau, Lavoisier, Berthollet and de Fourcroy's *Méthode de Nomenclature Chimique* (1787), which replaced the ambiguities of alchemical and phlogistic names with those incorporating the reforms of the "new chemistry", preceded by 2 years the publication of Lavoisier's *Traité Élémentaire de Chimie* (1789), were universally regarded as marking the birth of modern chemistry. In accord with the crucial importance of nomenclature, in 1913 the Council of the International Association of Chemical Societies appointed a commission on inorganic and organic nomenclature, but its activities were abruptly ended by World War I. In 1921, the recently formed International Union of Pure and Applied Chemistry (IUPAC) appointed commissions on inorganic, organic and biological chemistry.

The first report of the IUPAC's Commission on the Nomenclature of Inorganic Chemistry (CNIC), known as the "1940 Rules", was published in the leading journals of different countries, e.g. *Ber.* 1941, **A73**, 53; *J. Chem. Soc.* 1940, 1404; and *J. Am. Chem. Soc.* 1941, **63**, 889. These rules, revised and rewritten, were published as a small book, *Nomenclature of Inorganic Chemistry 1957*; Butterworths, London, 1959; ix+93 pp., known as the "1957 Rules" or the "Red Book" from the colour of its cover. A second revision, *Nomenclature of Inorganic Chemistry: Definitive Rules 1970*; Pergamon, Oxford, 1971; xi+110 pp., was more than twice as long as the 1957 rules because, unlike the latter, it no longer included a French version on each right-hand page. The 1970 rules were supplemented by a 36-page IUPAC booklet, *How to Name an Inorganic Substance* and by articles in various publications such as the *Journal of Chemical Education*'s bimonthly series *Notes on Nomenclature* beginning in July 1971 (W. C. Fernelius, K. Loening and R. M. Adams, *J. Chem. Educ.* 1971, **48**, 433).

Since the appearance of the 1970 rules, many new compounds have been prepared, some of which are difficult to name with these rules because they contain new types of bonding or structures. Therefore, trivial and local systems sprouted, especially for coordination and boron compounds, a situation that emphasized the need for a systematic, widely comprehensible nomenclature. Consequently, in 1978 the IUPAC CNIC decided to replace the 1970 red book. The result is "not a revision ... but a completely new version presented in a new way which it is hoped will be much more useful to the general reader". Many of the new fields of chemistry are very highly specialized and need complex types of names. Therefore, the new edition is scheduled to appear in several parts.

Part I, under review here, required a decade to produce and is almost three times as long as its predecessor. It is concerned with the basic principles of nomenclature for the fundamental areas of inorganic chemistry, and the principal authors, 13 eminent chemists from the United States, the United Kingdom, France, the Netherlands and Hungary hope that "its general principles will not be undermined, and that it should retain its currency for many years". Part II will deal with more specialized areas such as quasi-single strand inorganic polymers, organometallic and labelled compounds, and polyoxoanions; some of its contents have already been published in *Pure and Applied Chemistry*. Scheduled for publication in the near future, it will probably require more frequent revision because of its more specialized nature. Subsequent volumes are also planned.

The 1990 edition is presented in an instructional format with numerous examples, rather than as a series of numbered rules as in previous editions. After two entirely new concise chapters on the history and usages of inorganic nomenclature, the remaining nine chapters of Part I deal with elements, atoms, groups of atoms, formulae, names based on stoichiometry, solids, neutral molecular compounds, ions, substituent groups, radicals, salts, oxoacids and derived anions, coordination compounds and boron hydrides and related compounds. Each chapter was written by nominated individuals, assisted by working parties, and was repeatedly reviewed and edited by approx. 15 CNIC members. British spelling is used consistently.

Because of the conflicting use of A and B notation for groups of elements in the periodic table, the unpopular (at least among my acquaintances) 1–18 designation is presented as the preferred one, but the related controversy and other systems are discussed in an appendix, which concludes that "any ultimate recommendation ... must be responsive to the broadest possible constituency" (p. 280). Another recommendation likely to be disputed or ignored by chemists is the use of "lanthanoid" and "actinoid", although "owing to wide current use, 'lanthanide' and 'actinide' are still allowed" (p. 43), even though "the ending -ide normally indicates a negative ion". Similarly, the system recommended for naming elements of atomic numbers greater than 103 which have not yet been discovered and named by their discoverers (p. 37), resulting in such awkward names as ununquadrium (element 114), will probably not find favour with most chemists, who are likely to continue referring

to these species by atomic numbers. Other recommended changes include the avoidance of the term "radical" in anything other than the context of free radicals, the replacement of the terms "Stock number" (G. B. Kauffman and C. K. Jørgensen, *J. Chem. Educ.* 1985, **62**, 243) and "Ewens–Bassett number" (G. B. Kauffman and C. K. Jørgensen, *J. Chem. Educ.* 1985, **62**, 474) by the more readily comprehensible terms "oxidation number" and "charge number", the use of oxide names for anhydrides of fully dehydrated inorganic acids and the use of configuration indexes for *fac* and *mer* isomers "for precise nomenclature purposes".

As expected for such a thoroughly reviewed and edited volume, the errors are few and minor, e.g. Gebieten for Gebiete (p. 2), Jorisson for Jorissen, Damens for Damiens (p. 8) and entitled for titled (p. 9). A useful companion volume dealing with further types of species and providing additional examples has recently been published (B. P. Block, W. H. Powell and W. C. Fernelius, *Inorganic Chemical Nomenclature: Principles and Practice*. American Chemical Society, Washington, DC, 1990; for a review see G. B. Kauffman, *J. Chem. Educ.* 1991, **68**, A158). CNIC Chairmen Joseph Chatt, Yves Jeannin and Daryle H. Busch and their dedicated band of collaborators, including editor G. J. Leigh, deserve our profound thanks for melding "established and traditional practices and systems of nomenclature" into a reference book that should be definitive for many years to come.

GEORGE B. KAUFFMAN
California State University
Fresno
CA 93740
U.S.A.

Advances in Metal Carbene Chemistry. (NATO Advanced Science Institutes Series C, Vol. 269). Edited by U. Schubert. Kluwer Academic Publishers, Dortrecht, 1989, ISBN 0-7923-0156-0, xxiv+407 pp., Dfl 200; $114; £64.

Carbenes, compounds containing a $=CR_1R_2$ moiety bound to a metal, have come of age. Over the last 25 years, they have moved from being unknowns to an organometallic fact of life.

This volume is a collection of papers presented at a NATO Advanced Research Workshop in 1988 (will these workshops fall victim to the end of the Cold War?) and contains 43 contributions from many leading practitioners, including a personal history of metal carbene complexes by E. O. Fischer.

One's response to a compilation like this is essentially a personal one; this reviewer found particular interest in contributions on methylene complexes of ruthenium, osmium and iridium (W. R. Roper), carbene analogues of Wilkinson's catalyst (M. F. Lappert *et al.*) and carbenes of molybdenum(VI) (R. Lai, R. R. Schrock, J. A. Osborn and their co-workers). Carbenes are beginning to be used more widely in organic synthesis (K. H. Dötz, R. Aumann, L. S. Hegedus amongst others) and factors influencing the stability of metal–carbene complexes are better understood.

With a view to rapid publication, this volume has been compiled from camera-ready manuscripts, though this is certainly not obtrusive; it is very thoroughly indexed.

Scientists often have mixed views about the value of this type of publication. I certainly found it very worthwhile for getting an overview of the state of the art in metal–carbene complexes in a way that would not have been possible from scattered publications in the normal literature, and commend it to others similarly placed.

Gmelin Handbook of Inorganic Chemistry. Fe—Organoiron compounds, Part A9—Ferrocene 9. By M. Drössmar-Wolf, 8th edn. Springer-Verlag, Berlin, 1989, ISBN 3-540-93590-8, xiv+384 pp., DM 1742.

The previous volume (A8) of this series completed coverage of the disubstituted ferrocenes with oxygen-containing substituents; this one continues the treatment of the $(C_5H_5)Fe(C_5H_3RR')$ and $(C_5H_4R)Fe(C_5H_4R')$ systems where the substituents R and R′ contain nitrogen, sulphur, selenium, boron and silicon, allotted 197, 71, 4, 15 and 48 pages, respectively. To give an idea of the range of compounds considered, those with nitrogen-containing substituents include amines, amides, isocyanates, nitro-compounds, oximes, and those with N—N and N=N linkages.

As usual, the coverage is extremely comprehensive, with clearly set-out tabulations of data, with all relevant material for any one compound kept together with additional textual discussion. Moreover, all pages of tabulated data have the reminder as a footnote of which page contains the references to that section, an invaluable feature for rapid and accurate locating of references that could well be followed by other book-length review volumes. Another strong point of the Gmelin treatment is the ability to compare alternative synthetic routes and properties. Taking $Fe(C_5H_4CN)_2$ as an example, the relevant table contains references to nine different syntheses (with yields), six reported melting points, two NMR spectra, five IR spectra, two UV spectra and mass spectral information. These are discussed further in another section of the text, along with Mossbauer parameters, ring reactions, and oxidation to the corresponding ferrocenium cation.

Visual representations of many compounds are provided, sometimes a little compressed and distorted, presumably for reasons of spatial economy. There is a 43-page index which provides molecular and line formulae side-by-side.

Like the previous volume, published 3 years ago, this volume is the work of Marianne Drössmar-Wolf, who is to be commended for the thoroughness of her compilation (this must seem rather like the chemical equi-

to these species by atomic numbers. Other recommended changes include the avoidance of the term "radical" in anything other than the context of free radicals, the replacement of the terms "Stock number" (G. B. Kauffman and C. K. Jørgensen, *J. Chem. Educ.* 1985, **62**, 243) and "Ewens–Bassett number" (G. B. Kauffman and C. K. Jørgensen, *J. Chem. Educ.* 1985, **62**, 474) by the more readily comprehensible terms "oxidation number" and "charge number", the use of oxide names for anhydrides of fully dehydrated inorganic acids and the use of configuration indexes for *fac* and *mer* isomers "for precise nomenclature purposes".

As expected for such a thoroughly reviewed and edited volume, the errors are few and minor, e.g. Gebieten for Gebiete (p. 2), Jorisson for Jorissen, Damens for Damiens (p. 8) and entitled for titled (p. 9). A useful companion volume dealing with further types of species and providing additional examples has recently been published (B. P. Block, W. H. Powell and W. C. Fernelius, *Inorganic Chemical Nomenclature: Principles and Practice*. American Chemical Society, Washington, DC, 1990; for a review see G. B. Kauffman, *J. Chem. Educ.* 1991, **68**, A158). CNIC Chairmen Joseph Chatt, Yves Jeannin and Daryle H. Busch and their dedicated band of collaborators, including editor G. J. Leigh, deserve our profound thanks for melding "established and traditional practices and systems of nomenclature" into a reference book that should be definitive for many years to come.

GEORGE B. KAUFFMAN
California State University
Fresno
CA 93740
U.S.A.

Advances in Metal Carbene Chemistry. (NATO Advanced Science Institutes Series C, Vol. 269). Edited by U. Schubert. Kluwer Academic Publishers, Dortrecht, 1989, ISBN 0-7923-0156-0, xxiv+407 pp., Dfl 200; $114; £64.

Carbenes, compounds containing a $=CR_1R_2$ moiety bound to a metal, have come of age. Over the last 25 years, they have moved from being unknowns to an organometallic fact of life.

This volume is a collection of papers presented at a NATO Advanced Research Workshop in 1988 (will these workshops fall victim to the end of the Cold War?) and contains 43 contributions from many leading practitioners, including a personal history of metal carbene complexes by E. O. Fischer.

One's response to a compilation like this is essentially a personal one; this reviewer found particular interest in contributions on methylene complexes of ruthenium, osmium and iridium (W. R. Roper), carbene analogues of Wilkinson's catalyst (M. F. Lappert *et al.*) and carbenes of molybdenum(VI) (R. Lai, R. R. Schrock, J. A. Osborn and their co-workers). Carbenes are beginning to be used more widely in organic synthesis (K. H. Dötz, R. Aumann, L. S. Hegedus amongst others) and factors influencing the stability of metal–carbene complexes are better understood.

With a view to rapid publication, this volume has been compiled from camera-ready manuscripts, though this is certainly not obtrusive; it is very thoroughly indexed.

Scientists often have mixed views about the value of this type of publication. I certainly found it very worthwhile for getting an overview of the state of the art in metal–carbene complexes in a way that would not have been possible from scattered publications in the normal literature, and commend it to others similarly placed.

Gmelin Handbook of Inorganic Chemistry. Fe—Organoiron compounds, Part A9—Ferrocene 9. By M. Drössmar-Wolf, 8th edn. Springer-Verlag, Berlin, 1989, ISBN 3-540-93590-8, xiv+384 pp., DM 1742.

The previous volume (A8) of this series completed coverage of the disubstituted ferrocenes with oxygen-containing substituents; this one continues the treatment of the $(C_5H_5)Fe(C_5H_3RR')$ and $(C_5H_4R)Fe(C_5H_4R')$ systems where the substituents R and R′ contain nitrogen, sulphur, selenium, boron and silicon, allotted 197, 71, 4, 15 and 48 pages, respectively. To give an idea of the range of compounds considered, those with nitrogen-containing substituents include amines, amides, isocyanates, nitro-compounds, oximes, and those with N—N and N=N linkages.

As usual, the coverage is extremely comprehensive, with clearly set-out tabulations of data, with all relevant material for any one compound kept together with additional textual discussion. Moreover, all pages of tabulated data have the reminder as a footnote of which page contains the references to that section, an invaluable feature for rapid and accurate locating of references that could well be followed by other book-length review volumes. Another strong point of the Gmelin treatment is the ability to compare alternative synthetic routes and properties. Taking $Fe(C_5H_4CN)_2$ as an example, the relevant table contains references to nine different syntheses (with yields), six reported melting points, two NMR spectra, five IR spectra, two UV spectra and mass spectral information. These are discussed further in another section of the text, along with Mossbauer parameters, ring reactions, and oxidation to the corresponding ferrocenium cation.

Visual representations of many compounds are provided, sometimes a little compressed and distorted, presumably for reasons of spatial economy. There is a 43-page index which provides molecular and line formulae side-by-side.

Like the previous volume, published 3 years ago, this volume is the work of Marianne Drössmar-Wolf, who is to be commended for the thoroughness of her compilation (this must seem rather like the chemical equi-

to these species by atomic numbers. Other recommended changes include the avoidance of the term "radical" in anything other than the context of free radicals, the replacement of the terms "Stock number" (G. B. Kauffman and C. K. Jørgensen, *J. Chem. Educ.* 1985, **62**, 243) and "Ewens–Bassett number" (G. B. Kauffman and C. K. Jørgensen, *J. Chem. Educ.* 1985, **62**, 474) by the more readily comprehensible terms "oxidation number" and "charge number", the use of oxide names for anhydrides of fully dehydrated inorganic acids and the use of configuration indexes for *fac* and *mer* isomers "for precise nomenclature purposes".

As expected for such a thoroughly reviewed and edited volume, the errors are few and minor, e.g. Gebieten for Gebiete (p. 2), Jorisson for Jorissen, Damens for Damiens (p. 8) and entitled for titled (p. 9). A useful companion volume dealing with further types of species and providing additional examples has recently been published (B. P. Block, W. H. Powell and W. C. Fernelius, *Inorganic Chemical Nomenclature: Principles and Practice*. American Chemical Society, Washington, DC, 1990; for a review see G. B. Kauffman, *J. Chem. Educ.* 1991, **68**, A158). CNIC Chairmen Joseph Chatt, Yves Jeannin and Daryle H. Busch and their dedicated band of collaborators, including editor G. J. Leigh, deserve our profound thanks for melding "established and traditional practices and systems of nomenclature" into a reference book that should be definitive for many years to come.

GEORGE B. KAUFFMAN
California State University
Fresno
CA 93740
U.S.A.

Advances in Metal Carbene Chemistry. (NATO Advanced Science Institutes Series C, Vol. 269). Edited by U. Schubert. Kluwer Academic Publishers, Dortrecht, 1989, ISBN 0-7923-0156-0, xxiv+407 pp., Dfl 200; $114; £64.

Carbenes, compounds containing a $=CR_1R_2$ moiety bound to a metal, have come of age. Over the last 25 years, they have moved from being unknowns to an organometallic fact of life.

This volume is a collection of papers presented at a NATO Advanced Research Workshop in 1988 (will these workshops fall victim to the end of the Cold War?) and contains 43 contributions from many leading practitioners, including a personal history of metal carbene complexes by E. O. Fischer.

One's response to a compilation like this is essentially a personal one; this reviewer found particular interest in contributions on methylene complexes of ruthenium, osmium and iridium (W. R. Roper), carbene analogues of Wilkinson's catalyst (M. F. Lappert *et al.*) and carbenes of molybdenum(VI) (R. Lai, R. R. Schrock, J. A. Osborn and their co-workers). Carbenes are beginning to be used more widely in organic synthesis (K. H. Dötz, R. Aumann, L. S. Hegedus amongst others) and factors influencing the stability of metal–carbene complexes are better understood.

With a view to rapid publication, this volume has been compiled from camera-ready manuscripts, though this is certainly not obtrusive; it is very thoroughly indexed.

Scientists often have mixed views about the value of this type of publication. I certainly found it very worthwhile for getting an overview of the state of the art in metal–carbene complexes in a way that would not have been possible from scattered publications in the normal literature, and commend it to others similarly placed.

Gmelin Handbook of Inorganic Chemistry. Fe—Organoiron compounds, Part A9—Ferrocene 9. By M. Drössmar-Wolf, 8th edn. Springer-Verlag, Berlin, 1989, ISBN 3-540-93590-8, xiv+384 pp., DM 1742.

The previous volume (A8) of this series completed coverage of the disubstituted ferrocenes with oxygen-containing substituents; this one continues the treatment of the $(C_5H_5)Fe(C_5H_3RR')$ and $(C_5H_4R)Fe(C_5H_4R')$ systems where the substituents R and R′ contain nitrogen, sulphur, selenium, boron and silicon, allotted 197, 71, 4, 15 and 48 pages, respectively. To give an idea of the range of compounds considered, those with nitrogen-containing substituents include amines, amides, isocyanates, nitro-compounds, oximes, and those with N—N and N=N linkages.

As usual, the coverage is extremely comprehensive, with clearly set-out tabulations of data, with all relevant material for any one compound kept together with additional textual discussion. Moreover, all pages of tabulated data have the reminder as a footnote of which page contains the references to that section, an invaluable feature for rapid and accurate locating of references that could well be followed by other book-length review volumes. Another strong point of the Gmelin treatment is the ability to compare alternative synthetic routes and properties. Taking $Fe(C_5H_4CN)_2$ as an example, the relevant table contains references to nine different syntheses (with yields), six reported melting points, two NMR spectra, five IR spectra, two UV spectra and mass spectral information. These are discussed further in another section of the text, along with Mossbauer parameters, ring reactions, and oxidation to the corresponding ferrocenium cation.

Visual representations of many compounds are provided, sometimes a little compressed and distorted, presumably for reasons of spatial economy. There is a 43-page index which provides molecular and line formulae side-by-side.

Like the previous volume, published 3 years ago, this volume is the work of Marianne Drössmar-Wolf, who is to be commended for the thoroughness of her compilation (this must seem rather like the chemical equi-

valent of painting the Forth Bridge at times) which makes this book a tremendous timesaver—like the rest of the series—to organometallic chemists.

Gmelin Handbook of Inorganic Chemistry. Tungsten. Supplement Volume A5a, Electrochemistry. By G. Bär, D. Gras, V. Haase and G. Hönes. Springer-Verlag, Berlin, 1990, ISBN 3-540-93605-X, DM 972.

This is the sixth volume of the tungsten supplement dealing with the synthesis, properties and reactions of the metal (in addition, a separate series, of which parts B1–6 have been published, deals with tungsten compounds). It is multi-disciplinary in that much of the content will be of interest to non-inorganic chemists. A wide range of data has been assimilated, mostly from Soviet sources.

The volume opens with a résumé of the standard potentials for tungsten electrodes in a variety of equilibria. There follows an account of the behaviour of tungsten as a cathode and an anode in both aqueous and non-aqueous media. Detailed consideration of hydrogen over-voltages shows the need for scrupulous cleanliness of apparatus to achieve reproducible and consistent results. The effects of various experimental factors—pH, temperature, solvent, anions and cations—on over-voltage are clearly set out. Unfortunately for synthetic chemists, it appears that attempts to use electrochemical oxidation of tungsten in halogen-saturated solvents have been unsuccessful as a route to solutions of tungsten halides (suitable synthetic starting materials), in contrast to uranium and molybdenum. The latter part of the book details polarographic characteristics and electrode position.

The clarity of the layout assists its intelligibility to the non-specialist. The literature is surveyed to the end of 1987, but as usual more recent data are considered.

Organometallic Radical Processes (Journal of Organometallic Chemistry Library 22). Edited by William C. Trogler. Elsevier, Amsterdam and New York (Published in conjunction with Akademie-Verlag, Berlin), 1990, vii+380 pp., ISBM 0-444-98827-0, vii+380 pp., $130.75, Dfl 255.

The 18-electron rule is one of the cornerstones of organometallic chemistry; this book celebrates many of the exceptions in discussing 17- and 19-electron systems. Increasingly sophisticated techniques have revealed them often acting as intermediates in the reactions of even-electron systems, so that this book is of particular interest to the spectroscopist, kineticist and the organometallic chemist.

This latest volume in a well-established series contains 10 self-contained chapters, of which the first (by C. Amatore) details electrochemical methods for generating these radicals. The complementary techniques of chronoamperometry and cyclic voltammetry are contrasted and the power of their combined use propounded. Particular examples studied include oxidative addition to Ni(O) and Pd(O) complexes and the mechanism of formation of Collman's reagent $Fe(CO)_4^{2-}$. Chapter 2 (M. C. Baird) looks at 17-electron metal-centred radicals, beginning with the classic example of the uniquely stable paramagnetic carbonyl, $V(CO)_6$. This chapter contains a considerable amount of comparative IR and ESR data for a very wide range of paramagnetic substituted carbonyl species of vanadium, chromium, molybdenum, tungsten, manganese and iron. In Chapter 3, T. L. Brown starts by examining the formation and reactions of organometallic radicals before getting down to the rich variety of processes involving atom transfer. This very thorough treatment includes several extensive tabulations of data and numerous correlations.

N. J. Coville focuses on ligand substitution reactions from the aspect of synthesis, pointing out the increasing number of techniques (e.g. electrochemical, phase transfer catalysts) now available in addition to the classical methods of thermal and photochemical routes. The very handy listings of catalysts could well serve as springboards for a number of research projects. The prototype 17-electron metallocene system, the ferrocenium ion, is the starting point of W. E. Geiger's chapter on redox reactions of sandwich systems. This brings together a valuable collection of redox potentials, both for cyclopentadienyls and arenes. Chapter 6 (W. Kaim and B. Olbrich-Deussner) reviews paramagnetic main-group and transition-metal complexes with unsaturated nitrogen ligands. As they point out, these are particularly amenable to study by ESR as ^{14}N h.f.s. is easily recognised. There is a comprehensive listing of systems implicated in radical formation; careful study of this chapter could lead to developing ligands calculated to stabilize unusual oxidation states in isolable compounds. J. K. Kochi reviews activation of metal carbonyls in Chapter 7, considering electrochemical, thermal and photochemical electron transfer. The non-thermal routes have been found to proceed at considerably faster rates in certain cases, raising possibilities of alternative synthetic routes and catalytic pathways. The potential of cyclic voltammetry at extremely high scan rates is considered, mainly applied here to manganese. The coupling reactions of carbonyl-containing cations and anions are examined, linked with studies of the charge-transfer salts.

P. H. Rieger's chapter on ESR studies on organometallic radicals gives a number of recorded spectra together with computer simulations. He points out that it is frequently necessary to include second-order corrections in the analysis (does anyone ever use Q-band?); and also the problems that can arise if the g- and hyperfine tensor axes are not coincident. This is an excellent chapter for the ESR spectroscopist, but probably not user-friendly enough for the average organometallic chemist. Chapter 9 (W. C. Trogler) is a review of the mechanisms for ligand substitution, insertion and disproportionation in 17-electron radicals; these mechanisms are in common with 18-electron systems, but faster by a factor of a million to a billion in the case of

valent of painting the Forth Bridge at times) which makes this book a tremendous timesaver—like the rest of the series—to organometallic chemists.

Gmelin Handbook of Inorganic Chemistry. Tungsten. Supplement Volume A5a, Electrochemistry. By G. Bär, D. Gras, V. Haase and G. Hönes. Springer-Verlag, Berlin, 1990, ISBN 3-540-93605-X, DM 972.

This is the sixth volume of the tungsten supplement dealing with the synthesis, properties and reactions of the metal (in addition, a separate series, of which parts B1–6 have been published, deals with tungsten compounds). It is multi-disciplinary in that much of the content will be of interest to non-inorganic chemists. A wide range of data has been assimilated, mostly from Soviet sources.

The volume opens with a résumé of the standard potentials for tungsten electrodes in a variety of equilibria. There follows an account of the behaviour of tungsten as a cathode and an anode in both aqueous and non-aqueous media. Detailed consideration of hydrogen over-voltages shows the need for scrupulous cleanliness of apparatus to achieve reproducible and consistent results. The effects of various experimental factors—pH, temperature, solvent, anions and cations—on over-voltage are clearly set out. Unfortunately for synthetic chemists, it appears that attempts to use electrochemical oxidation of tungsten in halogen-saturated solvents have been unsuccessful as a route to solutions of tungsten halides (suitable synthetic starting materials), in contrast to uranium and molybdenum. The latter part of the book details polarographic characteristics and electrode position.

The clarity of the layout assists its intelligibility to the non-specialist. The literature is surveyed to the end of 1987, but as usual more recent data are considered.

Organometallic Radical Processes (Journal of Organometallic Chemistry Library 22). Edited by William C. Trogler. Elsevier, Amsterdam and New York (Published in conjunction with Akademie-Verlag, Berlin), 1990, vii+380 pp., ISBM 0-444-98827-0, vii+380 pp., $130.75, Dfl 255.

The 18-electron rule is one of the cornerstones of organometallic chemistry; this book celebrates many of the exceptions in discussing 17- and 19-electron systems. Increasingly sophisticated techniques have revealed them often acting as intermediates in the reactions of even-electron systems, so that this book is of particular interest to the spectroscopist, kineticist and the organometallic chemist.

This latest volume in a well-established series contains 10 self-contained chapters, of which the first (by C. Amatore) details electrochemical methods for generating these radicals. The complementary techniques of chronoamperometry and cyclic voltammetry are contrasted and the power of their combined use propounded. Particular examples studied include oxidative addition to Ni(O) and Pd(O) complexes and the mechanism of formation of Collman's reagent $Fe(CO)_4^{2-}$. Chapter 2 (M. C. Baird) looks at 17-electron metal-centred radicals, beginning with the classic example of the uniquely stable paramagnetic carbonyl, $V(CO)_6$. This chapter contains a considerable amount of comparative IR and ESR data for a very wide range of paramagnetic substituted carbonyl species of vanadium, chromium, molybdenum, tungsten, manganese and iron. In Chapter 3, T. L. Brown starts by examining the formation and reactions of organometallic radicals before getting down to the rich variety of processes involving atom transfer. This very thorough treatment includes several extensive tabulations of data and numerous correlations.

N. J. Coville focuses on ligand substitution reactions from the aspect of synthesis, pointing out the increasing number of techniques (e.g. electrochemical, phase transfer catalysts) now available in addition to the classical methods of thermal and photochemical routes. The very handy listings of catalysts could well serve as springboards for a number of research projects. The prototype 17-electron metallocene system, the ferrocenium ion, is the starting point of W. E. Geiger's chapter on redox reactions of sandwich systems. This brings together a valuable collection of redox potentials, both for cyclopentadienyls and arenes. Chapter 6 (W. Kaim and B. Olbrich-Deussner) reviews paramagnetic main-group and transition-metal complexes with unsaturated nitrogen ligands. As they point out, these are particularly amenable to study by ESR as ^{14}N h.f.s. is easily recognised. There is a comprehensive listing of systems implicated in radical formation; careful study of this chapter could lead to developing ligands calculated to stabilize unusual oxidation states in isolable compounds. J. K. Kochi reviews activation of metal carbonyls in Chapter 7, considering electrochemical, thermal and photochemical electron transfer. The non-thermal routes have been found to proceed at considerably faster rates in certain cases, raising possibilities of alternative synthetic routes and catalytic pathways. The potential of cyclic voltammetry at extremely high scan rates is considered, mainly applied here to manganese. The coupling reactions of carbonyl-containing cations and anions are examined, linked with studies of the charge-transfer salts.

P. H. Rieger's chapter on ESR studies on organometallic radicals gives a number of recorded spectra together with computer simulations. He points out that it is frequently necessary to include second-order corrections in the analysis (does anyone ever use Q-band?); and also the problems that can arise if the g- and hyperfine tensor axes are not coincident. This is an excellent chapter for the ESR spectroscopist, but probably not user-friendly enough for the average organometallic chemist. Chapter 9 (W. C. Trogler) is a review of the mechanisms for ligand substitution, insertion and disproportionation in 17-electron radicals; these mechanisms are in common with 18-electron systems, but faster by a factor of a million to a billion in the case of

valent of painting the Forth Bridge at times) which makes this book a tremendous timesaver—like the rest of the series—to organometallic chemists.

Gmelin Handbook of Inorganic Chemistry. Tungsten. Supplement Volume A5a, Electrochemistry. By G. Bär, D. Gras, V. Haase and G. Hönes. Springer-Verlag, Berlin, 1990, ISBN 3-540-93605-X, DM 972.

This is the sixth volume of the tungsten supplement dealing with the synthesis, properties and reactions of the metal (in addition, a separate series, of which parts B1–6 have been published, deals with tungsten compounds). It is multi-disciplinary in that much of the content will be of interest to non-inorganic chemists. A wide range of data has been assimilated, mostly from Soviet sources.

The volume opens with a résumé of the standard potentials for tungsten electrodes in a variety of equilibria. There follows an account of the behaviour of tungsten as a cathode and an anode in both aqueous and non-aqueous media. Detailed consideration of hydrogen over-voltages shows the need for scrupulous cleanliness of apparatus to achieve reproducible and consistent results. The effects of various experimental factors—pH, temperature, solvent, anions and cations—on over-voltage are clearly set out. Unfortunately for synthetic chemists, it appears that attempts to use electrochemical oxidation of tungsten in halogen-saturated solvents have been unsuccessful as a route to solutions of tungsten halides (suitable synthetic starting materials), in contrast to uranium and molybdenum. The latter part of the book details polarographic characteristics and electrode position.

The clarity of the layout assists its intelligibility to the non-specialist. The literature is surveyed to the end of 1987, but as usual more recent data are considered.

Organometallic Radical Processes (Journal of Organometallic Chemistry Library 22). Edited by William C. Trogler. Elsevier, Amsterdam and New York (Published in conjunction with Akademie-Verlag, Berlin), 1990, vii+380 pp., ISBM 0-444-98827-0, vii+380 pp., $130.75, Dfl 255.

The 18-electron rule is one of the cornerstones of organometallic chemistry; this book celebrates many of the exceptions in discussing 17- and 19-electron systems. Increasingly sophisticated techniques have revealed them often acting as intermediates in the reactions of even-electron systems, so that this book is of particular interest to the spectroscopist, kineticist and the organometallic chemist.

This latest volume in a well-established series contains 10 self-contained chapters, of which the first (by C. Amatore) details electrochemical methods for generating these radicals. The complementary techniques of chronoamperometry and cyclic voltammetry are contrasted and the power of their combined use propounded. Particular examples studied include oxidative addition to Ni(O) and Pd(O) complexes and the mechanism of formation of Collman's reagent $Fe(CO)_4^{2-}$. Chapter 2 (M. C. Baird) looks at 17-electron metal-centred radicals, beginning with the classic example of the uniquely stable paramagnetic carbonyl, $V(CO)_6$. This chapter contains a considerable amount of comparative IR and ESR data for a very wide range of paramagnetic substituted carbonyl species of vanadium, chromium, molybdenum, tungsten, manganese and iron. In Chapter 3, T. L. Brown starts by examining the formation and reactions of organometallic radicals before getting down to the rich variety of processes involving atom transfer. This very thorough treatment includes several extensive tabulations of data and numerous correlations.

N. J. Coville focuses on ligand substitution reactions from the aspect of synthesis, pointing out the increasing number of techniques (e.g. electrochemical, phase transfer catalysts) now available in addition to the classical methods of thermal and photochemical routes. The very handy listings of catalysts could well serve as springboards for a number of research projects. The prototype 17-electron metallocene system, the ferrocenium ion, is the starting point of W. E. Geiger's chapter on redox reactions of sandwich systems. This brings together a valuable collection of redox potentials, both for cyclopentadienyls and arenes. Chapter 6 (W. Kaim and B. Olbrich-Deussner) reviews paramagnetic main-group and transition-metal complexes with unsaturated nitrogen ligands. As they point out, these are particularly amenable to study by ESR as ^{14}N h.f.s. is easily recognised. There is a comprehensive listing of systems implicated in radical formation; careful study of this chapter could lead to developing ligands calculated to stabilize unusual oxidation states in isolable compounds. J. K. Kochi reviews activation of metal carbonyls in Chapter 7, considering electrochemical, thermal and photochemical electron transfer. The non-thermal routes have been found to proceed at considerably faster rates in certain cases, raising possibilities of alternative synthetic routes and catalytic pathways. The potential of cyclic voltammetry at extremely high scan rates is considered, mainly applied here to manganese. The coupling reactions of carbonyl-containing cations and anions are examined, linked with studies of the charge-transfer salts.

P. H. Rieger's chapter on ESR studies on organometallic radicals gives a number of recorded spectra together with computer simulations. He points out that it is frequently necessary to include second-order corrections in the analysis (does anyone ever use Q-band?); and also the problems that can arise if the g- and hyperfine tensor axes are not coincident. This is an excellent chapter for the ESR spectroscopist, but probably not user-friendly enough for the average organometallic chemist. Chapter 9 (W. C. Trogler) is a review of the mechanisms for ligand substitution, insertion and disproportionation in 17-electron radicals; these mechanisms are in common with 18-electron systems, but faster by a factor of a million to a billion in the case of

the paramagnetic systems. Organometallic chemists have long been familiar with the cycles involving 16–18-electron systems; similar 17–19-electron changes seem to apply here. Reasons are advanced for the frequently observed stability of the 19-electron systems. Nineteen-electron systems themselves are the subject of D. R. Tyler's final chapter, with an emphasis on photochemically generated radicals, which have grown in importance over the last decade.

The book is well produced, with few obvious errors (e.g. pp. 175 and 202). Apart from a subject index, it very sensibly has a radical formula index.

Felixstowe College **SIMON COTTON**
Felixstowe, IP11 7NQ
U.K.

Polyhedron Vol. 10, No. 16, pp. 1847–1856, 1991
Printed in Great Britain

0277–5387/91 $3.00+.00
© 1991 Pergamon Press plc

SOME SUBSTITUTION REACTIONS OF LIGANDS COORDINATED TO THE BIS(CYCLOPENTADIENYL)TITANIUM MOIETY, THE X-RAY CRYSTAL STRUCTURE OF $Ti(\eta^5\text{-}C_5H_5)_2(OPh)_2$ AND AN ASSESSMENT OF THE ANTI-TUMOUR ACTIVITY OF SOME CYCLOPENTADIENYL TITANIUM COMPOUNDS

BALRAJ S. KALIRAI, JEAN-DOMINIQUE FOULON, THOMAS A. HAMOR,* CHRISTOPHER J. JONES* and PAUL D. BEER†

School of Chemistry, University of Birmingham, Edgbaston, Birmingham B15 2TT, U.K.

and

SIMON P. FRICKER

Johnson Matthey Technology Centre, Blount's Court, Sonning Common, Reading RG4 9NH, U.K.

(*Received* 4 *February* 1991; *accepted* 18 *June* 1991)

Abstract—The new complexes $Ti(\eta^5\text{-}C_5H_5)Cl(OC_6H_4NH_2\text{-}3)_2$, $Ti(\eta^5\text{-}C_5H_5)Cl(O_2CPh)_2$, $Ti(\eta^5\text{-}C_5H_5)_2(O_2C(S)C_6H_4\text{-}1,2)$, $Ti(\eta^5\text{-}C_5H_5)_2Cl(SC_6H_4OH\text{-}4)$, $Ti(\eta^5\text{-}C_5H_5)_2(OC_6H_4NH_2\text{-}3)_2$ and $Ti(\eta^5\text{-}C_5H_5)_2Cl(OC_6H_4Z)$ (Z = NO_2-2, NO_2-3, NO_2-4, NH_2-3) have been synthesized. The free amine group in $Ti(\eta^5\text{-}C_5H_5)_2Cl(OC_6H_4NH_2\text{-}3)$ reacts with RCl [R = MeCO, PhCO, $(OCCO)_{1/2}$, $Br(CH_2)_3CO$] in the presence of base to give $Ti(\eta^5\text{-}C_5H_5)_2Cl(R)$ but, in the absence of base, PhCOCl reacts to give $PhCONHC_6H_4OH$-3 and $Ti(\eta^5\text{-}C_5H_5)_2Cl_2$. The X-ray crystal structure of $Ti(\eta^5\text{-}C_5H_5)_2(OPh)_2$ has been determined and reveals a *pseudo*-tetrahedral arrangement of the two η^5-cyclopentadienyl and two phenoxide ligands around titanium. The Ti—O(Ph) distances are 1.907(3) Å and O—Ti—O is 98.1(2)°. The anti-tumour activities of $Ti(\eta^5\text{-}C_5H_5)Cl(OC_6H_4NH_2\text{-}3)_2$, $Ti(\eta^5\text{-}C_5H_5)Cl(O_2CPh)_2$ and $Ti(\eta^5\text{-}C_5H_5)_2(O_2C(S)C_6H_4\text{-}1,2)$ have been assessed *in vitro* using a panel of seven human tumour cell lines.

The anti-tumour properties of the metallocene dihalides, and in particular $TiCp_2Cl_2$ (Cp = C_5H_5), have aroused considerable interest in recent years.[1,2] A number of derivatives of this titanium compound have been synthesized in the search for a material which might be sufficiently effective for clinical use. So far work in this area has largely concentrated on bis-cyclopentadienyl complexes containing monodentate co-ligands.[1] In the work described here we report the syntheses and anti-tumour activities of two monocyclopentadienyl titanium complexes and of a bis-cyclopentadienyl complex which contains a chelating co-ligand.

In a further development of this work we are interested in incorporating, in the titanium complexes, functional groups which might exhibit interactions with DNA. This approach is based on the proposal that the titanium complexes act through interactions with intracellular DNA[1] and follows precedents set with work on derivatives of the anti-tumour drug cisplatin.[3] As an initial stage in this synthetic programme we have been examining the substitution of the halide ligands in $TiCp_2Cl_2$ with ligands containing functionalized aryl groups. Earlier reports[4] indicate that phenoxide derivatives of

* Authors to whom correspondence should be addressed.
† Present address: Inorganic Chemistry Laboratory, University of Oxford, South Parks Road, Oxford, U.K.

$TiCp_2Cl_2$ may be obtained through the substitution of either cyclopentadienyl[5] or halide[6] ligands. Aryl carboxylate derivatives containing the $\{TiCp_2\}^{2+}$ moiety have also been reported.[4,7-9] Here we describe alternative syntheses which afford mono- or bis-phenoxide derivatives and a reaction in which a Cp^- ligand is displaced by $PhCO_2^-$. The further derivatization of the amine group in $TiCp_2Cl(O\text{-}C_6H_4NH_2\text{-}3)$ to produce amides has been investigated and the molecular structure of $TiCp_2(OPh)_2$ has been determined.

In order to overcome the limitations of murine tumour models, a panel of seven human tumour cell lines has been used to assess the anti-tumour activity of three new compounds *in vitro*. The results obtained are compared with those obtained with $TiCp_2Cl_2$ and with cisplatin.

RESULTS AND DISCUSSION

Synthetic studies

The reaction between $TiCp_2Cl_2$ and $HOC_6H_4NH_2\text{-}3$ in the presence of NEt_3 proceeds in toluene at 90°C over a period of 2 h to give the mono-phenoxide complex $TiCp_2Cl(OC_6H_4NH_2\text{-}3)$ and triethylammonium chloride. Attempts to produce the bis-phenoxide derivative by using more forcing conditions resulted in the displacement of cyclopentadienyl to give $TiCpCl(OC_6H_4NH_2\text{-}3)_2$. However, by using NaH to produce phenoxide ions during the reaction it was possible to obtain $TiCp_2(OC_6H_4NH_2\text{-}3)_2$. When present in two-fold stoichiometric excess, the *meta* and *para* mono-nitrophenols, $HOC_6H_4NO_2$, reacted with $TiCp_2Cl_2$ in the presence of NaH to give only monophenoxide derivatives. In contrast $HOC_6H_4NO_2\text{-}2$ proved more reactive and, under these conditions, afforded the known[6] bis-phenoxide complex $TiCp_2(OC_6H_4NO_2\text{-}2)_2$. The mono-phenoxide derivative $TiCp_2Cl(OC_6H_4NO_2\text{-}2)$ could also be obtained in the presence of NaH if the reactants were present in a 1:1 molar ratio. The known[6] compound $TiCp_2(OPh)_2$ could also be prepared using NaH. The reactivities of the chloride ligands in $TiCp_2Cl_2$ towards substitution by phenoxide contrast markedly with those observed[10,11] for the zirconium halides $ZrCp\{HBpz_3\}Cl_2$ and $Zr\{HB\{3,5\text{-}Me_2C_3N_2H\}_3\}Cl_3$. In the case of the titanium complex, substitution of the second halide generally requires more forcing conditions than substitution of the first and mixed chlorophenoxide complexes have been readily obtained. In the zirconium complexes, substitution of the first chloride appears to facilitate subsequent chloride substitutions so that the reaction between $Zr\{HB(3,5\text{-}Me_2C_3N_2H)_3\}Cl_3$ and $HOC_6N_4NO_2\text{-}4$ in 1:1 molar ratio, for example, affords only $Zr\{HB(3,5\text{-}Me_2C_3N_2H)_3\}(OC_6H_4NO_2\text{-}4)_3$ and unreacted $Zr\{HB(3,5\text{-}Me_2C_3N_2H)_3\}Cl_3$. Mixed chloride–aryloxide or chloride–alkoxide derivatives of the zirconium complexes have only been obtained by the use of highly sterically demanding ligands.[11,12]

In a search for means of further derivatizing the titanium complexes the reactions of the free amine group in $TiCp_2Cl(OC_6H_4NH_2\text{-}3)$ were investigated. Diazotization reactions are not possible since the phenoxide ligand is displaced in the presence of acid. The formation of Schiff base derivatives in reactions with ketones or aldehydes also fails since, even under otherwise anhydrous conditions, the H_2O liberated in the condensation reaction causes hydrolysis of the titanium complex. However, in the presence of a reagent such as NaH or NEt_3 which can absorb the acid liberated, reactions with acyl chlorides can be successfully executed. Thus the complexes $TiCp_2Cl(OC_6H_4NHCOR)$ [R = Me, Ph, $(CH_2)_3Br$] can be obtained from the reactions of the aminophenoxide complexes with RCOCl. The bimetallic complex $TiCp_2Cl(OC_6H_4NHCOR)]_2$ can also be obtained from a reaction with oxalyl chloride. A particularly interesting finding was that, in the absence of base, the reaction with PhCOCl affords $PhCONHC_6H_4OH\text{-}3$ and $TiCp_2Cl_2$ through cleavage of the Ti—O bond by the HCl released during the reaction. Thus, under these conditions $TiCp_2Cl_2$ may be used as a protecting group to prevent reaction with the hydroxy function of 3-aminophenol while producing the amide by reaction with the acyl chloride. The protecting agent is then recovered after the reaction so that the overall process may be described as follows:

$$TiCp_2Cl_2 + HOC_6H_4NH_2\text{-}3 + NEt_3 \longrightarrow TiCp_2Cl(OC_6H_4NH_2\text{-}3) + Et_3NHCl$$

$$TiCp_2Cl(OC_6H_4NH_2\text{-}3) + PhCOCl \longrightarrow TiCp_2Cl(OC_6H_4NHCOPh) + HCl$$

$$TiCp_2Cl(OC_6H_4NHCOPh) + HCl \longrightarrow TiCp_2Cl_2 + HOC_6H_4NHCOPh\text{-}3$$

$$HO\text{-}C_6H_4\text{-}NH_2\text{-}3 + PhCOCl + NEt_3 \longrightarrow HO\text{-}C_6H_4\text{-}NHCOPh\text{-}3 + Et_3NHCl$$

Normally in preparing $HOC_6H_4NHCOPh$ from $HOC_6H_4NH_2$ by reaction with PhCOCl it would be necessary to protect the hydroxy group, form the amide then de-protect the hydroxy function. In this reaction the $TiCp_2Cl_2$ serves as a novel protecting group which is removed in the same reaction step as the amide formation.

The use of the $\{TiCp_2Cl\}^+$ moiety as a protecting group for the —SH functionality in HOC_6H_4SH-4 was also investigated. $TiCp_2Cl_2$ reacts with the thiolate group in HOC_6H_4SH-4, in preference to the hydroxyl group, to give $TiCp_2Cl(SC_6H_4OH$-4). However, the reactions of the free hydroxy group with RCOCl afforded complex product mixtures which we were unable to purify, suggesting that the $\{TiCp_2Cl\}^+$ may not be so useful in this role. An ether synthesis was also attempted by reacting $Me(CH_2)_5Br$ with $TiCp_2Cl(SC_6H_4OH$-4) in dichloromethane in the presence of NaH. This reaction was also unsuccessful.

The reaction of benzoic acid with $TiCp_2Cl_2$ has also been studied using refluxing toluene as the reaction medium and NaH to remove the HCl liberated. The reaction between $PhCO_2H$ and $TiCp_2Cl_2$ in 1:1 molar ratio affords the known complex $TiCp_2Cl(O_2CPh)$. However, when a 2:1 molar ratio was used to obtain the bis-carboxylate, displacement of η^5-C_5H_5 occurred to give $TiCpCl(O_2CPh)_2$. This finding contrasts with the recently reported syntheses[8] of $Ti(\eta^5$-$C_5H_4Me)_2(O_2CC_6H_4X$-2)$_2$ (X = F, Br, NO_2, Me) from $Ti(\eta^5$-$C_5H_4Me)_2Cl_2$ and NaO_2CPh in benzene at 30°C where both chloride ligands are displaced. The reaction of thiosalicylic acid with $TiCp_2Cl_2$ proceeds rapidly in refluxing toluene in the presence of NEt_3 to give the chelate complex $TiCp_2(O_2C(S)C_6H_4$-1,2). Unlike the other phenoxide or carboxylate complexes studied this compound proved to be sufficiently stable to allow purification by column chromatography on silica gel.

The new complexes have been characterized by elemental analyses and IR, ^{1}H NMR and mass spectroscopy. The IR spectra of the new phenoxide complexes contain ν_{C-O} at *ca* 1260 cm^{-1} along with bands attributable to the cyclopentadienyl ligands at 810, 1020 and 3100 cm^{-1}. The spectra of the nitrophenoxide derivatives also contain ν_{NO_2} at 1560 cm^{-1} whilst those of the aminophenoxide derivatives contain ν_{NH} at 3350 cm^{-1}. The 270 MHz ^{1}H NMR spectra of these compounds contain singlets attributable to the cyclopentadienyl ligands in the region 6.2–6.5 ppm in addition to signals in the aromatic region which are of the expected relative intensity for the formulation of mono- or bis-phenoxide complexes as appropriate. In the case of the *meta*-substituted complexes a singlet, two doublets and a triplet ($^3J_{H-H}$ *ca* 8 Hz) are observed for the aromatic protons. The chelate complex $TiCp_2\{O_2C(S)C_6H_4$-1,2} exhibits two doublets and two triplets while the *para*-substituted derivatives exhibit two doublets from the aryl protons. The IR spectra of the amide derivatives obtained from $TiCp_2Cl\{OC_6H_4NH_2$-3} and RCOCl (R = Me, Ph) exhibit $\nu_{C=O}$ at 1680 and 1650 cm^{-1} respectively and the ^{1}H NMR spectra contain additional signals attributable to the acyl substituents.

The mass spectra of the new compounds contain only weak molecular ions, the most abundant ions in the spectra of the monophenoxide complexes are those which retain the chloride substituents and involve loss of the cyclopentadienyl ligands. The electronic spectra of the new complexes generally contain two maxima with high extinction coefficients typical of charge transfer bands.

*Structural studies**

The complex $TiCp_2(OPh)_2$ afforded crystals of sufficient quality to allow an X-ray crystal structure to be determined. Bond lengths and angles are presented in Table 1 using the numbering scheme shown in Fig. 1.[13] The molecule possesses cry-

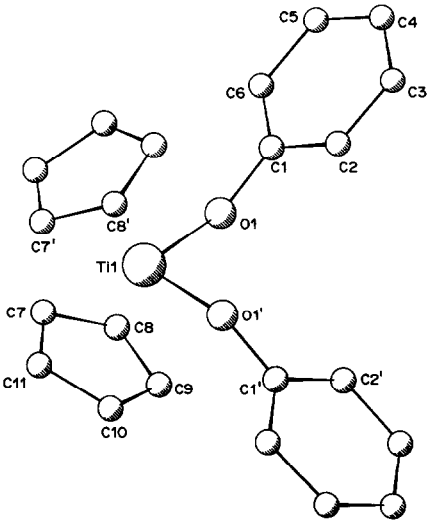

Fig. 1. A view of the molecule in a direction perpendicular to the two-fold axis through the titanium atom. Hydrogen atoms have been omitted for clarity. Primed atoms are related to the corresponding unprimed ones by the two-fold axis.

* Supplementary data available, fractional atomic coordinates and thermal parameters have been deposited with the Cambridge Crystallographic Data Centre.

Table 1. Bond lengths (Å) and bond angles (°) with e.s.d.'s in parentheses.

Ti(1)—O(1)	1.907(3)	C(2)—C(3)	1.367(6)
Ti(1)—C(7)	2.384(5)	C(3)—C(4)	1.377(7)
Ti(1)—C(8)	2.401(5)	C(4)—C(5)	1.369(7)
Ti(1)—C(9)	2.391(5)	C(5)—C(6)	1.391(6)
Ti(1)—C(10)	2.388(5)	C(7)—C(8)	1.355(8)
Ti(1)—C(11)	2.386(5)	C(7)—C(11)	1.392(8)
O(1)—C(1)	1.339(4)	C(8)—C(9)	1.352(8)
C(1)—C(2)	1.388(4)	C(9)—C(10)	1.368(9)
C(1)—C(6)	1.380(5)	C(10)—C(11)	1.357(8)
O(1)—Ti(1)—O(1)′[a]	98.1(2)	C(4)—C(5)—C(6)	121.0(5)
Ti(1)—O(1)—C(1)	139.2(2)	C(1)—C(6)—C(5)	120.1(4)
O(1)—C(1)—C(2)	121.5(4)	C(8)—C(7)—C(11)	107.1(5)
O(1)—C(1)—C(6)	119.9(4)	C(7)—C(8)—C(9)	109.2(6)
C(2)—C(1)—C(6)	118.4(4)	C(8)—C(9)—C(10)	107.9(6)
C(1)—C(2)—C(3)	120.7(4)	C(9)—C(10)—C(11)	108.3(6)
C(2)—C(3)—C(4)	121.2(4)	C(7)—C(11)—C(10)	107.5(6)
C(3)—C(4)—C(5)	118.5(5)		

[a] O(1)′ is related to O(1) by the crystallographic two-fold axis.

stallographic two-fold symmetry, the two-fold axis passing through the titanium atom. The two symmetry related oxygen atoms, together with the centroids (Ct) of the symmetry related cyclopentadienyl rings form a considerably distorted tetrahedral coordination geometry around titanium with angles ranging from 98.1(2) to 131.4(2)° for the O—Ti—O′ and Ct—Ti—Ct′ angles, respectively (see Table 2). The four Ct—Ti—O angles fall into two categories, two angles at 103.3(2)° and two angles at 108.1(2)°. The O—Ti—O angle is just over the upper limit of the 94–97° range for the ligand–metal–ligand angle considered[14] characteristic of MCp_2L_2 compounds, where M is a d^0 metal. A very similar geometry has been found[15] in the crystal structure of $TiCp_2(OC_6H_2Cl_3)_2$ and, apart from the longer Ti—S bond, also in the crystal structure[16] of $TiCp_2(SPh)_2$. Selected parameters are compared in Table 2.

Noteworthy is the large Ti—O—C(aromatic) angle. This appears to indicate some electron $p\pi$–$d\pi$ donation from oxygen to titanium, also indicated by the slight shortening of the Ti—O bond length relative to the single bond value of *ca* 2.0 Å. This is in accord with the observations of others and with EHMO calculations.[17] However, in the sulphur analogue,[16] the angles at sulphur adopt near tetrahedral values of 112.9 and 115.4°. The Ti—S—C (aliphatic) angle in the crystal structure[18] of $TiCp_2(SMe)_2$ is slightly smaller at 109.9(1)° and that in $TiCp_2(SEt)_2$ is 110.7(6)°.[19]

Similar geometries have also been found[20] in a

Table 2. Titanium coordination distances (Å) and angles (°)

	$TiCp_2(OPh)_2$[a]	$TiCp_2(OC_6H_2Cl_3)_2$[b]	$TiCp_2(SPh)_2$[c]
Ti—O(S)	1.907	1.946	2.395, 2.424
Ti—Ct[d]	2.089	2.07	2.072, 2.067
Ct—Ti—Ct′	131.4	130.0	132.4
Ct—Ti—O(S)	103.3	105.5	101.8, 101.9
Ct′—Ti—O(S)	108.1	107.2	108.3, 108.7
O(S)—Ti—O(S)′	98.1	97.0	99.3
Ti—O(S)—C	139.2	141.1	112.9, 115.4

[a] Present work; molecule has C_2 symmetry.
[b] Ref. 15; molecule has C_2 symmetry.
[c] Ref. 16; molecule has approximate C_2 symmetry.
[d] Ct denotes the centroid of the cyclopentadienyl ring.

number of chloroaryloxo and diaryloxo titanocenes. In these compounds, the ligand–Ti–ligand and (cyclopentadienyl)centroid–Ti–(cyclopentadienyl)centroid angles are in the ranges 126–131 and 94–98° respectively, and the Ti–centroid and Ti—O distances are 2.09–2.13 and 1.86–1.93 Å. There is, however, some indication that the Ti—O length is greater in the diaryloxo compounds than in the chloroaryloxo derivatives; 1.91–1.95 Å in the former, compared with 1.86–1.88 Å in the latter.[15,20,21] This effect may be related to the competitive $p\pi$–$d\pi$ donation of the Ti—O bonds. The Ti—O—C(aromatic) angles are in the range 140–150°, in good agreement with the present work. This angle appears to be quite flexible as demonstrated by its relatively small value of 123° in the crystal structure[21] of ethylene bis(4,5,6,7-tetrahydro-(*S*)-1-indenyl)titanium-(*S*)-1′,1″-bi-2-naphtholate. Here it is apparently constrained to a small value by formation of a seven-membered chelate ring. In $TiCp_2(O_2CPh)_2$ a Ti—O—C(carboxyl) angle of 148.3(8)° is observed.[19]

The cyclopentadienyl rings in $TiCp_2(OPh)_2$ are planar to within ±0.01 Å and are inclined at an angle of 130.5(2)° to one another, in good agreement with the Ct—Ti—Ct′ angle. When viewed in a direction perpendicular to the plane bisecting the interplanar angle the cyclopentadienyl rings are close to an eclipsed orientation.

Anti-tumour testing

Primary screening for new anti-neoplatic agents has been predominantly based on transplantable murine tumours such as the P388 and L1210 leukaemias. These screening models have had limited success in identifying drugs capable of acting against solid tumours.[22] In order to overcome the limitations of murine tumour models, a panel of human tumour derived cell lines has been used as a primary *in vitro* screen for metal-containing anti-tumour drugs.[23] The cell lines (SW403, SW620, SW1116 colon carcinoma; HT1376 bladder carcinoma; HT29/219 rectal carcinoma, ZR-75-1 breast carcinoma and SK-OV-3 ovarian carcinoma) are representative of tumours of different tissue origin and clinical responsiveness. All have been shown to exhibit a differential cytotoxic response to known anti-tumour agents, an indicator of anti-tumour activity as opposed to non-selective cytotoxicity.[24]

Four titanium complexes were tested against the cell line panel. The IC_{50} values (the concentration of test compound causing 50% cell death) are shown in Table 3 and are compared with the clinically used metal-containing anti-tumour drug, cisplatin. Cisplatin is particularly active against four of the cell lines (ZR-75-1, HT 1376, HT29/219 and SK-OV-3) and has limited activity against the colon carcinomas. Titanocene dichloride, $TiCp_2Cl_2$, a candidate for phase 1 clinical trials, exhibited limited activity against the tumour panel with some indication of differential activity. This was not as marked as with cisplatin, with the lowest IC_{50} values being against the cisplatin sensitive lines.

Three other titanium cyclopentadienyl complexes were tested against the tumour panel. $TiCp_2(O_2C(S)C_6H_4)$ exhibited marginal activity against the colon carcinoma lines and the ovarian carcinoma line; the monocyclopentadienyl complexes $TiCpCl(OC_6H_4NH_2\text{-}3)_2$ and $TiCpCl(O_2CC_6H_4)_2$ exhibited little or no cytotoxicity against the cell line panel. The titanium cyclopentadienyl complexes tested do not show selective anti-tumour activity *in vitro* against the cell line panel used. The anti-tumour activity of titanocene complexes has been demonstrated in a variety of *in vivo* murine models, and it has been proposed that the limited activity observed *in vitro* may be due to rapid hydrolysis of the complex.[25] This may account for the high IC_{50} values obtained with the titanium complexes tested against the cell line panel. It would appear that the strategy of replacing the chloride ligands in $TiCp_2Cl_2$ with the chelating ligand 1,2-

Table 3. *In vitro* anti-tumour activity of titanium complexes and cisplatin

Formula	IC_{50} (μg/ml) vs cell line						
	SW620	SW1116	SW403	ZR-75-1	HT29/219	HT1376	SKOV-3
$TiCp_2Cl_2$	130	145	> 200	120	130	80	155
$TiCp_2[O_2C(S)C_6H_4\text{-}1,2]$	130	190	138	Inactive	Inactive	> 200	127
$TiCpCl(OC_6H_4NH_2\text{-}3)_2$	> 200	> 200	> 200	180	Inactive	> 200	Inactive
$TiCpCl(O_2CPh)_2$	> 200	> 200	> 200	160	> 200	151	> 200
$PtCl_2(NH_3)_2$	115	140	163	5	9	5	11

$O_2C(S)C_6H_4$ in an attempt to suppress any hydrolysis reactions is ineffective in improving the antitumour activity of this class of compound.

EXPERIMENTAL

Synthetic studies

All reactions were performed under an atmosphere of dry nitrogen, but products were treated as air-stable. Solvents used for these reactions were purified by distillation from standard drying agents under dry nitrogen. Reagents were used as supplied, $TiCp_2Cl_2$ was obtained from Lancaster Synthesis Ltd. Elemental analyses were performed by the Microanalytical Laboratory of the University of Birmingham.

IR and mass spectra were recorded on PE 297 and Kratos MS 80 instruments respectively and ^1H NMR spectra were recorded using PE R12B 60 MHz and JEOL GX270 270 MHz instruments.

Preparations

$TiCp_2(OPh)_2$. In a 25 cm^3 round bottom flask $TiCp_2Cl_2$ (126 mg, 0.5 mmol) was mixed with sodium hyride (excess, 300 mg) and a solution of phenol (93 mg, 1 mmol) in toluene (10 cm^3) added. The mixture was heated under reflux for 3 h, cooled, filtered through kieselguhr and the yellow filtrate was then evaporated to dryness to give a yellow oil. This was redissolved in CH_2Cl_2 (20 cm^3) and pentane added (10 cm^3). Bright yellow crystals of the product were obtained on standing and were dried *in vacuo* (129 mg, 70%). M.p. 142°C. Found: C, 72.2; H, 5.6; M^+, 364. $C_{22}H_{20}O_2Ti$ requires C, 72.5; H, 5.5; M, 365.9. $\delta_H(CDCl_3)$ 6.28 [10H, S, η^5-C_5H_5]; 7.23, 6.80, 6.66 [4H, t; 2H, t; 4H, d, C_6H_5]; *m/z* 364 (M^+), 299 (M—Cp) and 271 (M—OC_6H_5).

$TiCp_2(OC_6H_4NO_2$-3)Cl. An excess of sodium hydride (150 mg) was added to a solution of 3-nitrophenol (420 mg, 3.0 mmol) in toluene (60 cm^3) and $TiCp_2Cl_2$ (380 mg, 1.5 mmol) added. The mixture was then stirred at 100°C for 24 h, allowed to cool, filtered and the red/orange filtrate evaporated to dryness to give a red/orange oil. The crude product was triturated with diethyl ether (30 cm^3) to remove residual $TiCp_2Cl_2$ and 3-nitrophenol. Recrystallization from CH_2Cl_2/*n*-pentane (1 : 1, 20 cm^3) afforded the product as bright orange crystals (273 mg, 51%). M.p. 140°C. Found: C, 54.6; H, 4.2; N, 3.7%; M^+, 351.5. $C_{16}H_{14}NClO_3Ti$ requires C, 54.6; H, 4.0; N, 4.0%; M, 351.4. $\delta_H(CDCl_3)$ 6.43 [10H, s, η^5-C_5H_5]; 7.65, 7.37, 7.35, 7.04 [1H, d; 1H, t; 1H, s; 1H, d, C_6H_4]; *m/z* 351 (M^+); 316 (M—Cl); 286 (M—Cp); 213 (M—$OC_6H_4NO_2$).

$TiCp_2(OC_6H_4NO_2$-2)Cl. An excess of sodium hydride (150 mg) was added to a solution of 2-nitrophenol (197 mg, 1.2 mmol) in toluene (30 cm^3). The mixture was heated under reflux for 3 h and $TiCp_2Cl_2$ (305 mg, 1.2 mmol) was then added. After heating under reflux for a further 2 h, the brown mixture that formed was cooled, filtered and the filtrate evaporated to dryness. The crude product (237 mg, 55%) was recrystallized from dichloromethane/*n*-pentane (1 : 1, 30 cm^3) to give a brownish orange solid. M.p. 131–133°C. Found: C, 54.3; H, 4.3; N, 3.9%; M^+, 352. $C_{16}H_{14}NClO_3Ti$ requires C, 54.6; H, 4.0; N, 4.0%; M, 351.5. ν_{max}: 1600, C_6H_5; 1560, N=O; 1260, Ph—O; 3100, 1020, 810, η^5-C_5H_5; 750, C_6H_4-*o* cm^{-1} (KBr); λ_{max}: 370, 350 nm; ε: 0.74, 3.0 mol^{-1} dm^3 cm; $\delta_H(CDCl_3)$ 6.46 [10H, s, η^5-C_5H_5]; 7.87, 7.45, 7.1, 6.86 [1H, d, J = 8.2 Hz; 1H, t, J = 8.4 Hz; 1H, d, J = 8.4 Hz; 1H, d, J = 8.4 Hz, C_6H_4]; *m/z* 351 (M^+); 316 (M—Cl); 286 (M—Cp); 213 (M—$OC_6H_4NO_2$).

$TiCp_2(OC_6H_4NO_2$-4)Cl. An excess of sodium hydride (150 mg) was added to a solution of 4-nitrophenol (421 mg, 3 mmol) in toluene (60 cm^3). The mixture was stirred for 0.5 h at 100°C and then $TiCp_2Cl_2$ (377 mg, 1.5 mmol) was added. After stirring the mixture at 100°C for a further 24 h, the mixture was cooled, filtered through kieselguhr and the filtrate evaporated to dryness to give a red/orange oil (254 mg, 59%). The crude product was recrystallized from dichloromethane/*n*-pentane (1 : 1, 20 cm^3) to give dark red needles. M.p. 173–175°C. Found: C, 54.6; H, 4.2; N, 3.9%; M^+, 352. $C_{16}H_{14}NClO_3Ti$ requires C, 54.6; H, 4.0; N, 4.0%; M, 352. ν_{max}: 1600, C_6H_5; 1560, N=O; 1260, Ph—O; 3100, 1020, 810, η^5-C_5H_5; 780, C_6H_4-*p* cm^{-1} (KBr); λ_{max}: 250, 355 nm; ε: 1.3, 1.7 mol^{-1} dm^3 cm; $\delta_H(CDCl_3)$ 6.44 [10H, s, η^5-C_5H_5]; 6.65, 8.14 [2H, d, J = 9.4 Hz; 2H, d, J = 9.2 Hz, C_6H_4]; *m/z* 351 (M^+); 316 (M—Cl); 286 (M—Cp); 213 (M—$C_6H_4NO_2$).

$TiCp_2(OC_6H_4NO_2$-2)$_2$. An excess of sodium hydride (300 mg) was added to a solution of 2-nitrophenol (421 mg, 3 mmol) in toluene (30 cm^3). The mixture was heated under reflux for 2 h and then $TiCp_2Cl_2$ (377 mg, 1.5 mmol) was added. After heating under reflux for a further 3 h, the mixture was cooled, filtered and the brownish filtrate evaporated to dryness to give a brownish oil (426, 62%). The crude product was recrystallized from dichloromethane/*n*-pentane (1 : 1, 10 cm^3) to give a brownish/yellow solid. M.p. 195°C. Found: C, 57.8; H, 4.2; N, 6.0%; M^+, 454. $C_{22}H_{18}N_2O_6Ti$ requires C, 58.2; H, 4.0; N, 6.2%; M, 454. ν_{max}: 1600, 1480, C_6H_4; 1560, N=O; 1260, Ph—O;

3100, 1010, 810, η^5-C_5H_5; 750, C_6H_4-*o* cm^{-1} (KBr); λ_{max}; 375, 254 nm; ε: 0.66, 3.7 mol^{-1} dm^3 cm; $\delta_H(CDCl_3)$ 6.38 [10H, s, η^5-C_5H_5]; 7.87, 7.42, 6.89, 6.85 [2H, d, $J = 8.1$ Hz; 2H, t, $J = 7.8$ Hz; 2H, t, $J = 7.9$ Hz; 2H, d, $J = 8.2$ Hz, C_6H_4]; *m/z* 454 (M^+); 389 (M—Cp); 316 (M—$OC_6H_4NO_2$).

$TiCp_2(OC_6H_4NH_2$-3)Cl. In a 100 cm^3 round bottom Schlenk flask, a solution of finely ground 3-aminophenol (56 mg, 0.5 mmol) in toluene (15 cm^3) was stirred at 90°C. Triethylamine (0.3 cm^3) and $TiCp_2Cl_2$ (127 mg, 0.5 mmol) were added and the reddish/brown mixture was stirred for 2 h at this temperature. The mixture was cooled, filtered and the filtrate evaporated to dryness, to give an orange oil. The crude product was then recrystallized from dichloromethane/*n*-pentane (1 : 2, 30 cm^3) to give a shiny orange/brown solid (104 mg, 62%). M.p. 56–58°C. Found: C, 60.0; H, 5.5; N, 4.8%; M^+, 321. $C_{16}H_{16}NClOTi$ requires C, 59.8; H; 5.0; N, 4.4%; M, 322. ν_{max}: 1600, 1480, C_6H_4; 1280, Ph—O; 1200, C—N; 3100, 1020, 810, η^5-C_5H_5 cm^{-1} (KBr); λ_{max}: 350, 248 nm; ε: 0.6, 1.9 mol^{-1} dm^3 cm; $\delta_H(CDCl_3)$ 6.37 [10H, s, η^5-C_5H_5]; 6.99, 6.0–7.0, 6.04 [1H, t, $J = 7.8$ Hz; 2H, d; 1H, s, C_6H_4]; 3.65 [2H, s, NH_2]; *m/z* 321 (M^+); 285 (M—Cl), 256 (M—Cp), 213 (M—$OC_6H_4NH_2$).

$[TiCp_2(OC_6H_4NH_2$-3)$_2$. A solution of 3-aminophenol (330 mg, 3 mmol) in toluene (60 cm^3) was stirred at 100°C with an excess of sodium hydride (400 mg). $TiCp_2Cl_2$ (377 mg, 1.5 mmol) was added and the mixture stirred for 2 days 20 h at this temperature. The mixture was cooled, filtered over kieselguhr and the filtrate evaporated to dryness to give a dark brown oil (364 mg, 61%). The crude product was recrystallized from dichloromethane/*n*-pentane (1 : 1, 30 cm^3) to give a dark brown solid. M.p. 62–64°C(d). Found: C, 67.2; H, 5.6; N, 6.8%; M^+, 394. $C_{22}H_{22}N_2O_2Ti$ requires C, 67.0; H, 5.6; N, 7.1%; M, 394. ν_{max}: 3350, NH_2; 1590, 1480, C_6H_4; 1280, Ph—O; 1190, C—N; 3100, 1010, 810, η^5-C_5H_5; 680, C_6H_4-*m* cm^{-1} (KBr); λ_{max}: 350, 240 nm; ε: 0.86, 2.7 mol^{-1} dm^3 cm; $\delta_H(CDCl_3)$ 6.27 [10H, s, η^5-C_5H_5]; 7.0, 6.2–6.6, 6.1 [2H, t, $J = 7.9$ Hz; 4H, d; 2H, s, C_6H_4]; 3.7 [4H, s, NH_2]; *m/z* 394(M^+); 329 (M—Cp).

$TiCp(OC_6H_4NH_2$-3)$_2$Cl. A solution of 3-aminophenol (131 mg, 1 mmol) and $TiCp_2Cl_2$ (300 mg, 1 mmol) in toluene (80 cm^3) was stirred at 100°C with triethylamine (0.6 cm^3) for 24 h. The mixture was cooled, filtered through kieselguhr and the red/orange filtrate evaporated to dryness (215 mg, 49%). The crude product was recrystallized from dichloromethane/*n*-pentane (1 : 1, 20 cm^3) to give a bright orange solid. M.p. 100°C(d). Found: C, 55.7; H, 4.4; N, 8.0%; M^+, 365. $C_{17}H_{17}N_2ClO_2Ti$ requires C, 56.0; H, 4.7; N, 7.7%; M, 364.5. ν_{max}: 3350, NH_2; 1600, 1460, C_6H_4; 1180, C—N; 3100, 1020, 810, η^5-C_5H_5; 690, C_6H_4-*m*, cm^{-1} (KBr); λ_{max}: 380, 320 nm; ε: 0.24, 0.52 mol^{-1} dm^3 cm; $\delta_H(CDCl_3)$ 6.29 [5H, s, η^5-C_5H_5]; 6.99; 6.94, 6.2, 6.18 [2H, t, $J = 7.9$ Hz; 2H, d, $J = 7.7$ Hz; 2H, $J = 7.9$ Hz; 2H, s, C_6H_4]; 3.7 [4H, s, NH_2]; *m/z* 364 (M^+); 329 (M—Cl); 299 (M—Cp); 256 (M—$OC_6H_4NH_2$).

$TiCp_2(O_2CPh)Cl$. An excess of sodium hydride (150 mg) was added to a solution of benzoic acid (294 mg, 2 mmol) in toluene (60 cm^3) and the mixture was heated under reflux for 3 h. $TiCp_2Cl_2$ (600 mg, 2 mmol) was added and the resulting mixture heated under reflux for a further 2 h. The mixture was then cooled, filtered and the filtrate evaporated to dryness to give a reddish/orange oil (410 mg, 51%). The crude product was recrystallized from dichloromethane/pentane (1 : 1, 20 cm^3) to give a yellow solid. M.p. 105°C(d). Found: C, 60.9; H, 4.2%; M^+, 334. $C_{17}H_{15}ClO_2Ti$ requires C, 61.0; H, 4.5%; M, 334.5. ν_{max}: 1700, C=O; 1600, 1440, C_6H_5; 3100, 1020, 800, η^5-C_5H_5, cm^{-1} (KBr); $\delta_H(CDCl_3)$ 6.43 [10H, s, η^5-C_5H_6]; 7.51, 7.9, 8.04 [1H, t, $J = 6.9$ Hz; 2H, d, $J = 7.0$ Hz; 2H, d, $J = 7.0$ Hz, C_6H_5]; *m/z* 334 (M^+); 298 (M—Cl); 269 (M—Cp); 213 (M—O_2CPh).

$TiCp(O_2CPh)_2Cl$. An excess of sodium hydride (300 mg) was added to a solution of benzoic acid (294 mg, 2 mmol) in toluene (30 cm^3) and the mixture was heated under reflux for 3 h. $TiCp_2Cl_2$ (300 mg, 1 mmol) was added and the mixture heated under reflux for a further 2 h. The mixture was cooled, filtered and the filtrate evaporated to dryness to give a bright yellow oil (334 mg, 71%). The crude product was recrystallized from dichloromethane/pentane (1 : 1; 30 cm^3) to give a yellow solid. M.p. > 300°C. Found: C, 58.5; H, 3.8%; M^+, 390. $C_{19}H_{15}ClO_4Ti$ requires C, 58.4; H, 3.8%; M, 390. ν_{max}: 1690, C=O; 1600, 1440, C_6H_5; 3100, 810, η^5-C_5H_5, cm^{-1} (KBr); λ_{max}: 360, 247 nm; ε: 0.64, 2.8 mol^{-1} dm^3 cm; $\delta_H(CDCl_3)$ 6.62 [5H, s, η^5-C_5H_5]; 8.04, 7.52, 7.43 [4H, d, $J = 7$ Hz; 4H, t, $J = 7.3$ Hz; 2H, t, $J = 7.7$ Hz, C_6H_5]; *m/z* 355 (M—Cl); 234 (M—Cl—O_2CPh).

$TiCp_2\{O_2C(S)C_6H_4$-1,2$\}$. A solution of $TiCp_2Cl_2$ (500 mg, 2 mmol), thiosalicylic acid (309 mg, 2 mmol) and triethylamine (410 mg, 3 mmol) in toluene (40 cm^3) was heated under reflux for 0.5 h. An intense green precipitate formed and the mixture was allowed to cool, then filtered and the filtrate evaporated to dryness to give a green oil. The crude product was purified using a silica gel column (14 cm × 3.5 cm) with methanol as the eluant. The major green band was collected and afforded the product as a dark green solid (440 mg, 82%). M.p. 144–146°C. Found: C, 62.0; H, 4.7%; M^+, 331.

$C_{17}H_{15}SO_2Ti$ requires C, 61.6; H, 4.5%; M, 331. ν_{max}: 1600, 1440, C_6H_4; 1620, C=O; 3100, 1020, 820, η^5-C_5H_5, cm^{-1} (KBr); λ_{max}: 320, 239 nm; ε: 1.1, 3.0 mol^{-1} dm^3 cm; $\delta_H(CDCl_3)$ 6.31 [10H, s, η^5-C_5H_5]; 8.38, 7.52, 7.38 [1H, d, $J = 7.9$ Hz; 1H, d, $J = 7.9$ Hz; 1H, t, $J = 7.9$ Hz, C_6H_4]; *m/z* 330 (M^+): 221 (M—SC_6H_4); 178 (M—$O_2C(S)C_6H_4$).

$TiCp_2(OC_6H_4NHCOCH_3$-3)Cl. A solution of 3-aminophenol (180 mg, 1.7 mmol) in toluene (40 cm^3) was stirred at 95–100°C with triethylamine (0.9 cm^3) and $TiCp_2Cl_2$ (412 mg, 1.7 mmol) for 2 h. The mixture was cooled, filtered through kieselguhr and toluene (20 cm^3), triethylamine (0.3 cm^3) and acetyl chloride (0.12 cm^3, 1.7 mmol) were then added to the filtrate and the mixture stirred at room temperature for 2.5 h. The resulting orange suspension was filtered through kieselguhr and the filtrate evaporated to dryness to give a red/orange oil (248 mg, 41%). The crude product was recrystallized from dichloromethane/*n*-pentane (1 : 1, 20 cm^3) to give a bright orange solid which was dried *in vacuo* at 50°C overnight. M.p. 80°C(d). Found: C, 59.4; H, 4.9; N, 4.3%; M^+, 363.5. $C_{18}H_{18}NClO_2Ti$ requires C, 59.4; H, 5.0; N, 3.9%; M, 364. ν_{max}: 3250, 1540, NH; 1680, C=O; 1600, 1480, C_6H_4; 1280, Ph—O; 3100, 1020, 810, η^5-C_5H_5, cm^{-1} (KBr); λ_{max}: 360, 247 nm; ε: 0.64, 2.8 mol^{-1} dm^3 cm; $\delta_H(CDCl_3)$ 6.38 [10H, s, η^5-C_5H_5]; 6.29–7.15 [4H, C_6H_4]; 7.21 [1H, s, NH]; 2.2 [3H, s, CH_3]; *m/z* 363 (M^+); 298 (M—Cp); 262 (M—Cp—Cl); 213 (M—$OC_6H_4NHCOCH_3$).

$TiCp_2(OC_6H_4NHCOPh)Cl$. A solution of $TiCp_2Cl_2$ (157 mg, 0.6 mmol) in toluene (40 cm^3) was stirred at 95–100°C with triethylamine (0.9 cm^3), finely ground 3-aminophenol (157 mg, 1.4 mmol) for 20 h. The mixture was cooled, filtered and the filtrate stirred with a mixture of toluene (20 cm^3), triethylamine (0.3 cm^3) and benzoyl chloride (0.15 cm^3, 1.5 mmol) at room temperature for $2\frac{1}{2}$ h. The mixture was cooled, filtered through kieselguhr and the filtrate evaporated to dryness, to give a shiny orange solid (48 mg, 56%). The crude product was recrystallized from dicholoromethane/*n*-pentane (1 : 1, 20 cm^3) to give an orange solid. M.p. 125°C. Found: C, 65.0; H, 5.2; N, 3.8%; M^+, 425. $C_{23}H_{20}NO_2ClTi$ requires C, 64.9; H, 4.70; N, 3.3%; M, 425.5. ν_{max}: 3300, 1540, NH; 1650, C=O; 1600, 1440, C_6H_4; 1280, Ph—O; 3100, 1020, 810, η^5-C_5H_5, cm^{-1} (KBr); λ_{max}: 350, 250 nm; ε: 0.59, 4.0 mol^{-1} dm^3 cm; $\delta_H(CDCl_3)$ 6.40 [10H, s, η^5-C_5H_5]; 6.44–7.86 [9H, C_6H_4/C_6H_5]; 7.96 [1H, s, NH]; *m/z* 426 (M^+); 360 (M—Cp); 213 (M—OP $C_6H_4NHCOPh$).

$PhCONHC_6H_4OH$-3. A solution of $TiCp_2(OPC_6H_4NH_2$-3)Cl (276 mg, 0.9 mmol) in dichloromethane (25 cm^3) was stirred at room temperature with benzoyl chloride (0.1 cm^3, 0.9 mmol). The orange precipitate that formed was stirred at this temperature for 0.5 h and at 40°C for 2 h. The mixture was then cooled, filtered through kieselguhr and the filtrate evaporated to dryness forming a pale orange solid. The crude product was recrystallized from dichloromethane/*n*-pentane (1 : 1, 20 cm^3) affording white needles. Crystals of $TiCp_2Cl_2$ were also obtained during purification (356 mg, 77%). Found: C, 73.3; H, 5.0; N, 6.6%; M^+, 213. $C_{13}H_{11}NO_2$ requires C, 73.2; H, 5.2; N, 6.6%; M, 213. ν_{max}: 3300, OH; 3200, 1580, NH; 1640, C=O; 1600, 1440, C_6H_4; *m/z* 213 (M^+); 137 (M—Ph); 105 (M—HOC_6H_4NH).

$\{TiCp_2Cl(OC_6H_4NHCO$-$)\}_2$. A solution of 3-aminophenol (255 mg, 2.3 mmol) in toluene (35 cm^3) was stirred at 95–100°C with triethylamine (0.9 cm^3) and $TiCp_2Cl_2$ (584 mg, 2.3 mmol) for 2 h. The mixture was cooled, filtered and the filtrate was then stirred with a mixture of toluene (25 cm^3), triethylamine (0.3 cm^3) and oxalyl chloride (0.1 cm^3, 1.2 mmol) at room temperature for 1 h and at 45°C for 2 h. The orange precipitate was cooled, filtered through kieselguhr and the orange filtrate evaporated to dryness to give an orange oil (490 mg, 31%). The crude product was recrystallized from dichloromethane/*n*-pentane (1 : 1, 30 cm^3) to give an orange solid. M.p. 105°C(d). Found: C, 57.3; H, 4.6; N, 3.5%; M^+, 697. $C_{34}H_{30}N_2Cl_2O_4Ti_2 \cdot 0.3CH_2Cl_2$ requires C, 57.0; H, 4.2; N, 3.9%; M, 697. ν_{max}: 3250, 1590, NH; 1680, C=O; 1595, 1480, C_6H_4; 1290, Ph—O; 3100, 1100, 810, η^5-C_5H_5, cm^{-1} (KBr); $\delta_H(CDCl_3)$ 6.41 [20H, s, η^5-C_5H_5]; 7.23; 7.1, 6.5, 6.36 [2H, t, $J = 8.2$ Hz; 2H, d; 2H, d, $J = 6.7$ Hz; 2H, d, $J = 8.44$ Hz, C_6H_4].

$TiCp_2Cl(OC_6H_4NHCOCH_2CH_2Br)$. A solution of $TiCp_2Cl(OC_6H_4NH_2$-3) (277 mg, 0.9 mmol), triethylamine (0.3 cm^3) and 4-bromobutyric chloride (0.1 ml, 0.9 mmol) was stirred at 60°C in toluene (30 cm^3) for 3 h. The mixture was cooled, filtered through kieselguhr and the red filtrate evaporated to dryness (163 mg, 41%). The crude product was recrystallized from dichloromethane/*n*-hexane (1 : 1, 20 cm^3) to give a bright orange crystalline solid. M.p. 95°C(d). Found: C, 51.4; H, 4.2; N, 3.2; M^+, 470. $C_{20}H_{21}NBrClO_2Ti$ requires C, 51.1; H, 4.5; N, 3.0; M, 470.5. ν_{max}: 3150, 1530, NH; 2900, CH_2; 1660, C=O; 1590, 1440, C_6H_4; 1280, Ph—O; 3100, 1020, 800, η_5-C_5H_5, cm^{-1} (KBr); $\delta_H(CDCl_3)$ 6.39 [10H, s, η^5-C_5H_5]; 6.4–7.2 [4H, C_6H_4]; 1.44, 2.54, 3.54 [2H, t, $J = 7.2$ Hz; 2H, m, $J = 7.2$ Hz; 2H, T, $J = 6.4$ Hz, $(CH_2)_3Br$]; *m/z* 470 (M^+), 405 (M—Cp), 213 (M—$OC_6H_4NHCO(CH_2)_3Br$).

$TiCpCl(SC_6H_4OH$-4). A solution of $TiCp_2Cl_2$ (223 mg, 0.9 mmol), 4-hydroxythiophenol (0.1 cm^3,

0.9 mmol) and triethylamine (0.12 cm^3, 0.9 mmol) was heated under reflux in toluene (30 cm^3) for 23 h. The reddish precipitate was cooled, filtered and the filtrate evaporated to dryness giving a reddish oil (242 mg, 80%). The crude product was purified using a silica gel column (12 cm × 1.5 cm) with dichloromethane as the eluent, affording a purple brown solid. Found: C, 56.3; H, 4.5%; M^+, 338. $C_{16}H_{15}SClOTi$ requires C, 56.7; H, 4.5%; M, 338.5. ν_{max}: 3400, OH; 1590, 1480, C_6H_4; 1260, Ph—O; 3100, 1020, 820, η^5-C_5H_5, cm^{-1} (KBr); $\delta_H(CDCl_3)$ 6.48 [10H, s, η^5-C_5H_5]; 7.28, 6.96 [2H, d, J = 8.7 Hz; 2H, d, J = 8.7 Hz, C_6H_4]; m/z 300 (M—C_3H_3).

Structural studies

A crystal of $TiCp_2(OPh)_2$ (0.4 × 0.4 × 0.8 mm) was mounted on an Enraf-Nonius CAD-4 diffractometer; cell dimensions and intensities were measured by ω–2θ scans with graphite-monochromated Mo-K_α radiation and scan range $(\omega) = (1.1 + 0.35 \tan\theta)°$. Scan speed varied from 1.7 to 5.0° min^{-1} depending on the intensity. 2244 reflections were scanned within $2 < \theta < 27°$. Of these 2007 were unique (merging $R_{int} = 0.038$).

Three standard reflections measured every 2 h showed no significant variation in intensity. 1069 structure amplitudes with $F > 4\sigma(F)$ were considered observed and used in the analysis. No absorption corrections were applied.

Crystal data. $C_{22}H_{20}O_2Ti$, M_r = 364.3, orthorhombic, space group *Pbcn*, a = 9.801(2), b = 10.861(4), c = 17.297(23) Å, V = 1841 $Å^3$, Z = 4, molecular symmetry 2 (C_2), D_c = 1.314 g cm^{-3}, $F(000)$ = 760, μ(Mo-K_α) = 0.469 mm^{-1}, λ = 0.71069 Å, T = 293 K.

The structure was solved by Patterson and Fourier methods[26,27] and refined by least-squares using anisotropic thermal parameters for the heavier atoms. Hydrogen atoms were placed in calculated positions riding on their respective bonded atoms. Isotropic temperature factors were refined for the hydrogen atoms. Weights $w = [\sigma^2(F) + 0.001F^2]^{-1}$ which resulted in a satisfactory weighting analysis, were used in the least-squares refinement. The refinement converged to R = 0.047, Rw = 0.060, with a maximum shift/error ratio of 0.02. The residual electron density in the final difference map was in the range ±0.35 e $Å^{-3}$.

Complex neutral-atom scattering factors were employed. Computations were carried out on the University of Birmingham IBM 3090 with the SHELXS86[26] and SHELX76[27] programs. Lists of atomic fractional coordinates and anisotropic thermal parameters have been deposited at the Cambridge Crystallographic Data Centre.

Anti-tumour testing

Maintenance of cell lines. Anti-tumour activity was assessed on an *in vitro* panel of seven human tumour cell lines. The colon carcinoma lines (SW403, SW620, SW1116) were maintained in Leibovitz L15 medium; the colorectal carcinoma line (HT29/219), the ovarian carcinoma line (SK-OV-3) and the bladder carcinoma line (HT1376) were maintained in Eagles minimal essential medium with Earles salts; the breast carcinoma line (ZR-75-1) was maintained in RPMI 1640 supplemented with 1 mM sodium pyruvate. All media were supplemented with 10% foetal bovine serum, 2 mM L-glutamine, 100 IU penicillin cm^{-3} and 100 μg streptomycin cm^{-3}. Cell cultures were grown as monolayers at 37°C in a 5% CO_2 atmosphere.

Dosing regimen. On day 1, 96-well microtitre plates were seeded with 200 μl cell suspension at 5×10^4 cells cm^{-3} (HT29/219, HT29/219, HT1376, ZR-75-1, SK-OV-3) and 10^5 cells cm^{-3} (SW403, SW620, SW1116). On day 2, the cells were treated with test compound over a concentration range of 1–200 μg cm^{-3} for 2 h. Compounds were formulated in 0.2 cm^3 1% dimethylacetamide medium, untreated control cells were exposed to 1% dimethylacetamide for 2 h. The compounds were removed after the 2 h incubation period and replaced with fresh medium. The cells were cultured for a further 72 h and total cell protein determined using sulphorhodamine B.[28]

Sulphorhodamine B assay. The medium was removed and the cells fixed in 0.1 cm^3 10% trichloroacetic acid for 30 min at 4°C. The cells were washed five times with tap water followed by staining with 100% 0.1% sulphorhodamine B in 1% acetic acid for 15 min. The cells were washed four times with 1% acetic acid and air dried. The stain was dissolved in 0.2 cm^3 10 mM unbuffered Tris. Absorbance at 540 nm, reference 690 nm, was measured using a microtitre plate reader. Results were normalized with respect to control cells and expressed as per cent survival. Dose/response curves were constructed from the normalized data. The IC_{50}, the concentration of test compound giving 50% survival with respect to controls, was calculated from the dose/response curves.

Acknowledgement—We are grateful to the SERC for support (to B.S.K.).

REFERENCES

1. P. Köpf-Maier and H. Köpf, *Chem. Rev.* 1987, **87**, 1137.

2. P. Köpf-Maier, W. Wagner and H. Köpf, *Cancer Chemother. Pharmacol.* 1981, **5**, 237.
3. W. I. Sundquist and S. J. Lippard, *Coord. Chem. Rev.* 1990, **100**, 293.
4. K. Andra, *J. Organometal. Chem.* 1968, **11**, 567.
5. P. C. Wailes, R. S. P. Coutts and H. Weingold, *Organometallic Chemistry of Titanium, Zirconium, and Hafnium.* Academic Press, New York (1974).
6. A. N. Nesmeyanov, O. V. Nogina, A. M. Berlin, A. S. Girshovich and G. V. Shatalov, *Izv. Akad. Nauk SSSR, Otd. Khim. Nauk* 1961, 2146.
7. G. A. Razuvaev, V. N. Latyaeva and L. I. Vyshinkaya, *Dokl. Akad. Nauk SSSR* 1961, **138**, 1126.
8. Z. Yaokun, W. Zhinqiang, W. Xin and Z. Ying, *Polyhedron* 1990, **9**, 783.
9. D. N. Sen and U. N. Kantak, *Indian J. Chem.* 1971, **9**, 254.
10. R. A. Kresinski, Ph.D. theses. University of Birmingham, U.K. (1990).
11. R. A. Kresinski, T. A. Hamor, C. J. Jones and J. A. McCleverty, *J. Chem. Soc., Dalton Trans.* 1991, **603**, 1835.
12. D. L. Reger and M. E. Tarquini, *Inorg. Chem.* 1983, **22**, 1064.
13. W. D. S. Motherwell and W. Clegg, PLUTO88, Program for plotting molecular and crystal structures, Report "Cambridge Structural Database System", Cambridge Crystallographic Data Centre (1998).
14. K. Prout, T. S. Cameron, R. A. Forder, S. R. Critchley, B. Denton and G. V. Rees, *Acta Cryst.* 1974, **B30**, 2290.
15. Y. Qingchuan, J. Xianglin, X. Xiaojie, L. Genpei, T. Yougi and C. Shoushan, *Scientia Sinica (Series B)* 1982, **25**, 356.
16. E. G. Muller, S. F. Watkins and L. F. Dahl, *J. Organomet. Chem.* 1976, **111**, 73.
17. D. M. Hoffman, N. D. Chester and R. C. Fay, *Organometallics* 1983, **2**, 48.
18. M. A. A. F. de C. T. Carrondo and G. A. Jeffrey, *Acta Cryst.* 1983, **C39**, 42.
19. M. J. Calhorda, M. A. A. F. de C. T. Carrondo, A. R. Dias, C. F. Frazão, M. B. Hursthouse, J. A. Martinho Simões and C. Teixeira, *Inorg. Chem.* 1988, **27**, 2513.
20. J. Besancon, S. Top, J. Tirouflet, Y. Dusausoy, C. Lecomte and J. Protas, *J. Organomet. Chem.* 1977, **127**, 153, and references cited therein.
21. F. R. W. P. Wild, L. Zsolnai, G. Huttner and H. H. Brintzinger, *J. Organomet. Chem.* 1982, **232**, 233.
22. T. H. Corbett, F. A. Valeriote and L. H. Baker, *Invest. New Drugs* 1987, **5**, 3–20.
23. S. P. Fricker, *Metal Ions in Biology and Medicine* (Edited by P. Collery, L. A. Poirier, M. Mangait, J-C. Etienne), pp. 452–456. John Libby Eurotest, Paris (1990).
24. S. P. Fricker and R. G. Buckley, *Biochem. Soc. Trans.* 1984, **17**, 1049.
25. G. P. Breitbach, H. Braun, M. Tesseraux, P. Kopf-Maier, G. Sass, S. Kaul and W. Schmidt, *Trace Elements in Medicine*, 1990, **7**, 88.
26. G. M. Sheldrick, SHELXS-86, Program for the solution of crystal structures. University of Gottingen (1987).
27. G. M. Sheldrick, SHELXS-76, Program for crystal structure determination. University of Cambridge (1976).
28. P. Skehan, R. Storeng, D. Scudiero, A. Monks, J. McMahon, D. Vistica, J. Warren, H. Bokesch, S. Kenney and M. R. Boyd, *Proc. Am. Assoc. Cancer Res.* 1989, **30**, 612.

Polyhedron Vol. 10, No. 16, pp. 1857–1864, 1991
Printed in Great Britain

0277–5387/91 $3.00+.00
© 1991 Pergamon Press plc

ROTATIONAL ISOMERISM IN OCTAHEDRAL d^6-IRIDIUM(III) COMPLEXES *TRANS,MER*-$[IrCl_2(PMe_3)_3L]^+$ WHERE L = PMe_3, PMe_2Ph OR $PMePh_2$; X-RAY CRYSTAL STRUCTURE OF $[IrCl_2(PMe_3)_3(PMe_2Ph)]ClO_4 \cdot CH_2Cl_2$

ANTHONY J. DEEMING,* SIMON DOHERTY and JANE E. MARSHALL

Department of Chemistry, University College London, 20 Gordon Street, London WC1H 0AJ, U.K.

(*Received* 30 *January* 1991; *accepted* 18 *June* 1991)

Abstract—The cationic d^6-complexes $[IrCl_2(PMe_3)_3L]^+$ where L = PMe_3, PMe_2Ph or $PMePh_2$ have been synthesized and the single-crystal X-ray structure of *trans,mer*-$[IrCl_2(PMe_3)_3(PMe_2Ph)]ClO_4 \cdot CH_2Cl_2$ determined; the cation is chiral because of the conformation adopted about the Ir—PMe_2Ph bond. The low-temperature $^{31}P\{^1H\}$ NMR spectrum (−75°C, CD_3COCD_3) of this salt shows a major ABCD component (95%), consistent with the chiral conformer found in the crystal, and a minor AB_2C component (5%) corresponding to a symmetrical achiral isomer. These isomers interconvert by rotation about the Ir—PMe_2Ph bond and at 45°C a sharp coalesced AB_2C spectrum is obtained. In the low-temperature ^1H NMR spectrum, the major chiral isomer shows non-equivalent *ortho*-protons, whereas the minor achiral isomer gives a single resonance for these protons. Related rotamers are observed for the $PMePh_2$ complex but we could not obtain frozen-out spectra for $[IrCl_2(PMe_3)_4]^+$. We conclude that, even for these small tertiary phosphines, it is possible to have rotamers that interconvert slowly enough for line-shape effects to be observed in NMR spectra at ambient temperatures provided that there are four phosphines in each complex. Chiral rotamers may be dominant in rotameric equilibria.

We have described the internal rotational behaviour of the tetrakis-phosphine complex *trans*-$[IrCl_2(PMe_2Ph)_4]ClO_4$, which exists in three clearly identifiable rotameric forms which interconvert slowly at −50°C whereas rotation about the Ir—P bonds is rapid above room temperature. The interpretation of the low-temperature $^{31}P\{^1H\}$ NMR spectrum in terms of overlapping ABCD, AA′BB′ and A_4 spectra was moderately straightforward but a complete analysis of the very rich ^1H NMR spectrum was not possible.[1] In this paper we have examined related complexes containing three PMe_3 ligands and only one tertiary phosphine carrying aryl substituents (PMe_2Ph or $PMePh_2$) to see if there was still restricted rotation about Ir—P bonds in these rather less-crowded systems. Furthermore, we hoped that the analysis of the NMR spectra, especially the ^1H NMR spectra in the aryl region, would be much simpler than for $[IrCl_2(PMe_2Ph)_4]ClO_4$, partly because there would be fewer accessible isomers.

RESULTS AND DISCUSSION

Syntheses

Reaction of chloroiridic acid with an excess of PMe_3 under argon in 2-methoxyethanol gave brick-red crystals of the salt $[IrCl_2(PMe_3)_4][IrCl_4(PMe_3)_2]$, which was characterized by elemental analysis, its conductivity in nitrobenzene and its ^1H NMR spectrum which contained methyl multiplets in the ratio 1:2. Extended thermolysis in the same solvent gave a redistribution of the PMe_3 ligands to give *mer*-$[IrCl_3(PMe_3)_3]$.

The chlorine ligand *trans* to PMe_3 is labile and treatment with silver perchlorate in wet acetone gave a precipitate of AgCl and a yellow solution of the aqua complex *trans,mer*-$[IrCl_2(H_2O)(PMe_3)_3]$

* Author to whom correspondence should be addressed.

ClO_4. This complex gives a ^1H NMR spectrum which is consistent with the static structure unlike that of *trans,mer*-$[IrCl_2(H_2O)(PMe_2Ph)_3]^+$ which shows coalescence behaviour involving rapid and reversible H_2O dissociation and stereochemical non-rigidity of the intermediate, $[IrCl_2(PMe_2Ph)_3]^+$, leading to phosphine exchange.[2] Presumably, the bulkier PMe_2Ph ligands lead to higher rates of H_2O dissociation and we expect that higher temperatures would be required for the PMe_3 species to show comparable behaviour, although we did not test this. Even so, the H_2O ligand in *trans,mer*-$[IrCl_2(H_2O)(PMe_3)_3]^+$ can be easily replaced in dichloromethane at room temperature by tertiary phosphines, L, to give the desired products of the type *trans,mer*-$[IrCl_2(PMe_3)_3L]ClO_4$. The compounds with L = PMe_2Ph (**1**) or $PMePh_2$ (**2**) were isolated as air-stable yellow crystalline solids. The cation with L = PMe_3 (**3**) had already been identified in the salt prepared directly from chloroiridic acid and the room-temperature ^1H and ^{31}P NMR spectra of the nitrate salt have been described.[3] The perchlorate salt with L = PPh_3 was not formed even on treatment of the aqua complex with an excess of this ligand; we believe that the equilibrium leading to the displacement of the aqua-ligand is unfavourable. This gives some indication of the extent of crowding since, in the absence of crowding, one would expect a tertiary phosphine to be more favourably coordinated than H_2O in such complexes.

Crystal structure of $[IrCl_2(PMe_3)_3(PMe_2Ph)]ClO_4 \cdot CH_2Cl_2$ (**1**)

The complexes *trans,mer*-$[IrCl_2(PMe_3)_2L]ClO_4$ (L = PMe_2Ph or $PMePh_2$) exhibit interconverting isomers in solution (see below) so, to establish a basis for understanding this behaviour, we determined the single-crystal X-ray structure of the dimethylphenylphosphine complex (**1**) (Fig. 1). Selected bond lengths and angles are shown in Table 1. The *trans,mer*-configuration is confirmed and, although the geometry is clearly octahedral, the four phosphorus atoms are somewhat distorted from a planar towards a tetrahedral arrangement. The P(1)IrP(2) and P(3)IrP(4) angles are 167.3(1)° and 168.9(1)°, respectively. As in other compounds of this type, such as $[IrCl_2(PMe_2Ph)_4]^+$, two substituents at each phosphorus atom are above the approximate P_4 plane and one is below with this arrangement alternating around the phosphine plane.[1] The Ph group of the PMe_2Ph shares one side of this plane with a Me group so that the molecule is asymmetric and all four phosphorus atoms are different. As an alternative, the Ph ligand might have occupied a central position with the two Me groups on the opposite side of the approximate P_4 plane and in this case there would have been a molecular plane of symmetry and the molecule would have been achiral.

Rotational isomers of $[IrCl_2(PMe_3)_3(PMe_2Ph)]ClO_4$ (**1**) *in solution*

Restricted rotation is normally only associated with bulky tertiary phosphine ligands such as tertiary butyl substituted ligands.[4] However, we have found that there are two rotamers of this cation in solution which give separate signals in low-temperature NMR spectra. Figure 2 shows the $^{31}P\{^1H\}$ NMR spectrum of the complex $[IrCl_2(PMe_3)_3(PMe_2Ph)]ClO_4$ (**1**) in CD_3COCD_3 at −75°C together with a computer simulation. This simulated spectrum requires the presence of an ABCD

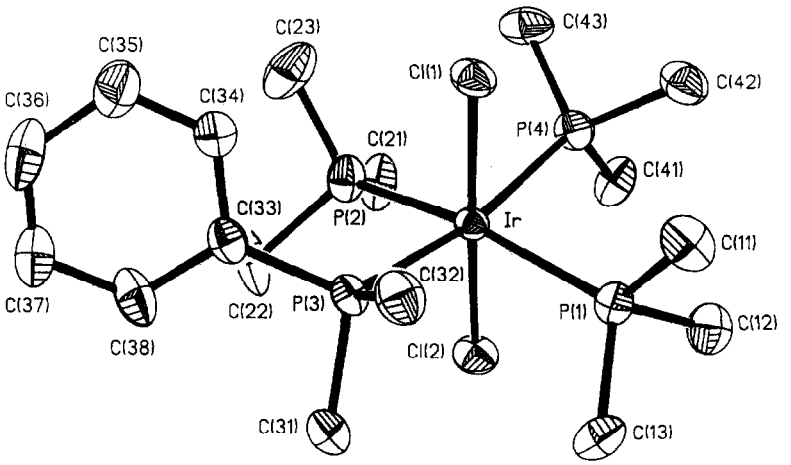

Fig. 1. Molecular structure of the complex cation of the salt $[IrCl_2(PMe_3)_3(PMe_2Ph)]ClO_4 \cdot CH_2Cl_2$ (**1**).

Table 1. Selected bond lengths (Å) and angles (°) for the complex $[IrCl_2(PMe_3)_3(PMe_2Ph)]ClO_4 \cdot CH_2Cl_2$ (**1**)

Ir—Cl(1)	2.375(4)	Ir—Cl(2)	2.366(4)
Ir—P(1)	2.375(4)	Ir—P(2)	2.357(5)
Ir—P(3)	2.381(4)	Ir—P(4)	2.375(4)
Cl(1)—Ir—P(1)	95.1(2)	Cl(1)—Ir—P(2)	97.5(2)
Cl(1)—Ir—P(3)	86.5(1)	Cl(1)—Ir—P(4)	82.4(1)
Cl(2)—Ir—P(1)	83.6(2)	Cl(2)—Ir—P(2)	83.8(2)
Cl(2)—Ir—P(3)	94.7(1)	Cl(2)—Ir—P(4)	96.3(1)
Cl(1)—Ir—Cl(2)	178.2(2)	P(1)—Ir—P(2)	167.3(2)
P(1)—Ir—P(3)	90.7(2)	P(1)—Ir—P(4)	89.9(2)
P(2)—Ir—P(3)	91.6(2)	P(2)—Ir—P(4)	90.2(2)
P(3)—Ir—P(4)	168.9(1)		

pattern (δ 28.3, 26.2, 30.0, 25.5) for the major isomer (**1a**) (95%) and an AB_2C pattern (δ 21.2, 29.4, 33.4) for the minor isomer (**1b**) (5%) (labelled as $A'B_2'C'$ in Fig. 2). Good simulated spectra were obtained by fixing the *cis* coupling constants at −27 Hz and the *trans* coupling constants at 366Hz for **1a** and −30 Hz (*cis*) and 366 Hz (*trans*) for **1b**. This situation may be compared with that of *trans*-$[IrCl_2(PMe_2Ph)_4]ClO_4$ for which *cis* (−23 Hz) and *trans* (363 Hz) couplings between the ^{31}P nuclei were also of opposite sign. We believe that the predominant isomer at low temperature is that observed in the crystal, since the ABCD spectrum is as expected for this particular chiral rotamer (**1a**). The minor isomer (**1b**) with higher symmetry (AB_2C spectrum) would then correspond to a rotamer with a mirror plane and the phenyl group in the central position. The $^{31}P\{^1H\}$ NMR spectra of (**1**) start to broaden above −75°C and at 45°C, rotamers **1a** and **1b** are in fast exchange and a single coalesced AB_2C spectrum (δ 25.98, 23.56, 28.65) is observed (Fig. 3).

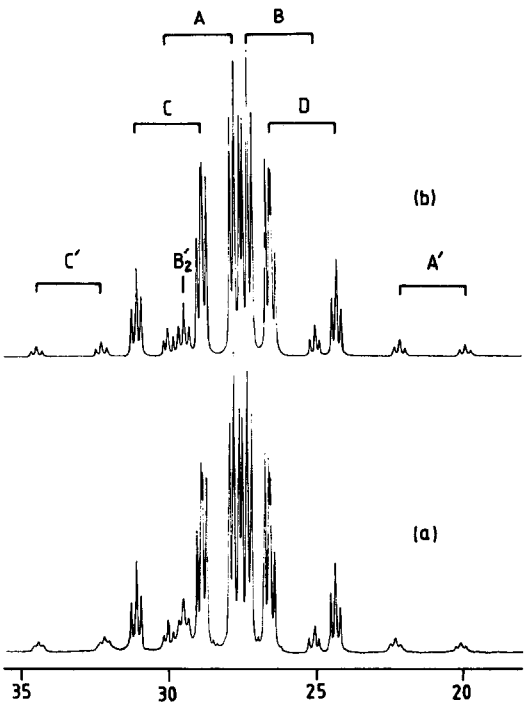

Fig. 2. (a) The $^{31}P\{^1H\}$ NMR spectrum of $[IrCl_2(PMe_3)_3(PMe_2Ph)]ClO_4$ (**1**) in CD_3COCD_3 at −75°C and (b) its computer simulation as the sum of an ABCD spectrum (isomer **1a**) and an AB_2C spectrum (isomer **1b**) with signals labelled A′, B_2' and C′).

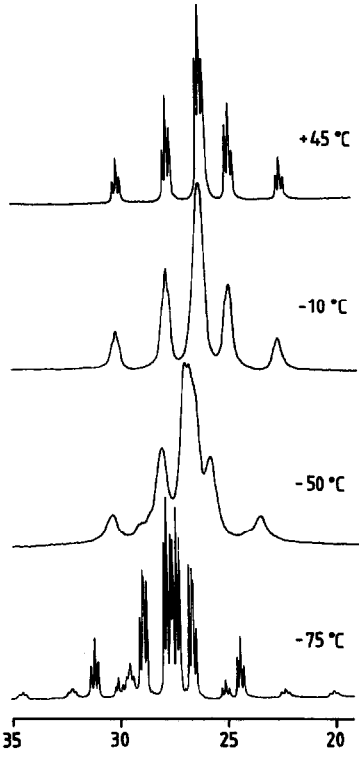

Fig. 3. $^{31}P\{^1H\}$ NMR spectra of $[IrCl_2(PMe_3)_3(PMe_2Ph)]ClO_4$ (**1**) in CD_3COCD_3 at the temperatures given, showing the broadening and collapse of the spectrum (ABCD + AB_2C) at −75°C to give a simple AB_2C spectrum at +45°C.

The ^{1}H NMR spectra are also consistent with this interpretation. Figures 4 and 5 contain the variable-temperature spectra in the phenyl and methyl regions, respectively. The major isomer (**1a**) has non-equivalent *ortho* protons giving separate triplet signals at δ 8.44 and 7.42 at -75°C (the latter resonance is partly obscured by the *meta* and *para* signals), whereas the minor isomer shows a single *ortho* triplet at δ 8.08. This is consistent with the different symmetries of **1a** and **1b** as shown in Scheme 1. As the temperature is raised the spectrum broadens and the three *ortho* resonances finally coalesce to the broad resonance at δ 8.04 at room temperature. At the same time the other resonances simplify (*para*, δ 7.55t and *meta*, δ 7.48t). We presume that the *ortho* resonance would resolve into a sharp triplet at higher temperatures but these spectra were not recorded.

The methyl region of the ^{1}H NMR spectrum (Fig. 5) is too complex to be analysed totally and signals for the minor isomer (**1b**) are largely obscured by those of the major isomer (**1a**). The diastereotopic Me groups of the PMe_2Ph ligand give two overlapping doublets at low tempratures which coalsesce to a single doublet at room temperature as expected. Two doublets (δ 1.04 and 1.12) are at significantly higher field than any others and are assigned to the two Me groups that lie over the face of the Ph group (see Fig. 1). This confirms that the major isomer in solution is that found in the crystal. The complexity of the Me region at low temperatures is only consistent with the restricted rotation about the Ir—PMe_3 bonds as well as about the Ir—PMe_2Ph bond. Fast rotation about Ir—PMe_3 bonds with restricted roation about the Ir—PMe_2Ph bond would give a spectrum much simpler than that in Fig. 5 at low temperature. We believe that the mechanism shown in Scheme 1 hides the fact that, as the PMe_2Ph ligand rotates, there is rotation about the other Ir—P bonds. Presumably this is a cog-wheel type process which maintains the overall arrangement of substitutents at the phosphines with two up and one down, alternately around the molecule. Thus, the PMe_2Ph ligand and the PMe_3 ligand *trans* to it are expected to maintain an eclipsed conformation as in the crystal structure. We can see in Scheme 1 that the interconversion of the enantiomeric forms of **1a**, with its associated exchange of P^1 with P^2, H^1 with H^2, and of Me^1 with Me^2, occurs via the minor isomer (**1b**). Our NMR results are in qualitative agreement with this.

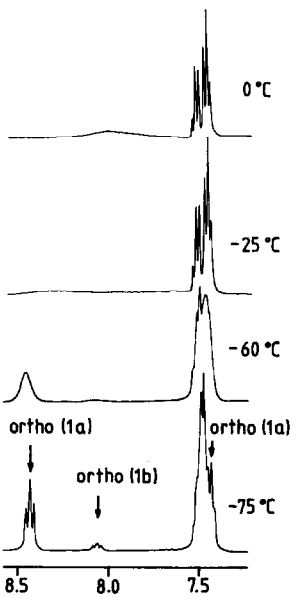

Fig. 4. ^{1}H NMR spectra of $[IrCl_2(PMe_3)_3(PMe_3Ph)]ClO_4$ (**1**) in the phenyl region at different temperatures.

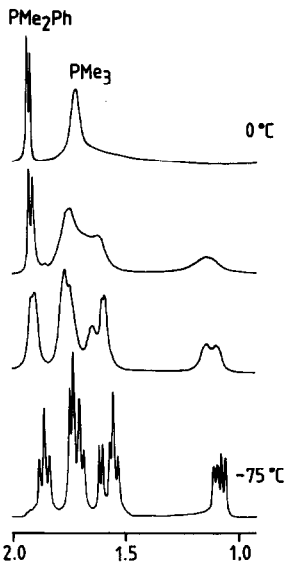

Fig. 5. ^{1}H NMR spectra of $[IrCl_2(PMe_3)_3(PMe_2Ph)]ClO_4$ (**1**) in the methyl region at different temperatures.

Rotational isomers of $[IrCl_2(PMe_3)_3(PMePh_2)]ClO_4$ (**2**) *in solution*

Similarly, the low-temperature $^{31}P\{^1H\}$ NMR spectrum (-75°C, CD_3COCD_3) demonstrates that there are two isomers in unequal abundance which are only slowly interconverting at this temperature. However, in contrast to the PMe_2Ph species, the spectra of both the major and the minor species can both be interpreted in terms of AB_2C patterns (see Fig. 6 for the observed and the simulated spectra); major isomer (**2a**) (δ 26.0, 16.9, 30.8) and minor isomer (**2b**) (δ 32.8, 26.0, 26.0) with *cis* and *trans*

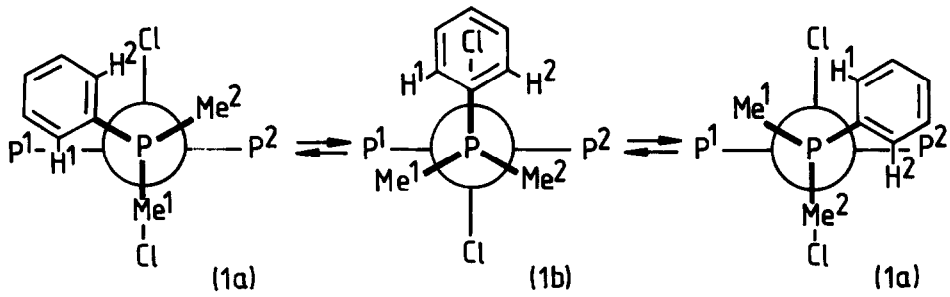

Scheme 1.

coupling of −27 and 366 Hz for both. Above −75°C the effects of exchange are observed and at room temperature exchange is rapid enough to give a coalesced AB_2C spectrum (δ 20.50, 24.20, 29.80).

In spite of the above observations, we propose that the isomers (**2a**) and (**2b**) are unsymmetrical and symmetrical, respectively, as shown in Scheme 2. There are various possible explanations for the AB_2C spectrum for **2a**. There could be a process which is rapid even at −75°C which exchanges P^1 with P^2 of the major isomer (**2a**), without the involvement of the minor isomer (**2b**). For this to be true, the most rapid equilibria in Scheme 2 would need to be one or more of the processes across the middle rather than those on the outer circuit. We believe that this would only be possible if the $PMePh_2$ ligand rotated about the Ir—P bond while the PMe_3 ligand *trans* to it was stationary. This would allow the forms of **2a** to interconvert with each other but not with **2b**. This seems to be unlikely and we propose that the outer circuit is the favoured pathway. We can only explain the observed spectra by an accidental coincidence of chemical shifts leading to the AB_2C spectrum for **2a**.

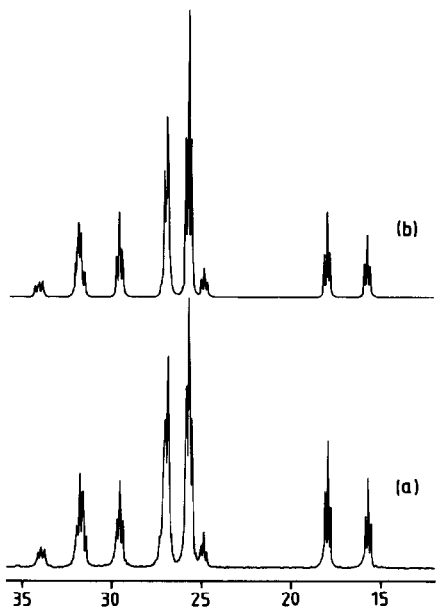

Fig. 6. (a) The $^{31}P\{^1H\}$ NMR spectrum of $[IrCl_2(PMe_3)_3(PMePh_2)]ClO_4$ (**2**) in CD_3COCD_3 at −75°C and (b) its computer simulation as the sum of two ABCD spectra for isomers **2a** and **2b**, respectively.

In principle, the low-temperature ^1H NMR spectrum of the cation $[IrCl_2(PMe_3)_4]^+$ should show separate signals for the Me groups that are up and those that are down in the ratio 1:2 if rotation about the Ir—P bonds was slowed sufficiently. At −90°C the methyl multiplet has broadened but we could not obtain spectra at temperatures lower than this that are necessary to obtain separate resonances.

We believe that the relatively high rotation barriers in the systems described in this paper are the result of having four tertiary phosphines in a plane in an octahedral complex. We have not observed rotational effects in tris-phosphine complexes, but envisage that the introduction of any relatively bulky ligand in complexes of the type *mer*-$[MCl_2L(PR_3)_3]$ should give such effects. We believe that chirality in simple complexes of the kind in this paper has not previously been stressed or even recognized as leading to distinct effects in solution.

EXPERIMENTAL

^1H and $^{31}P\{^1H\}$ NMR data are presented in Tables 2 and 3, respectively.

Synthesis of $[IrCl_2(PMe_3)_4][IrCl_4(PMe_3)_2]$

A solution of chloroiridic acid (1.55 g, 3.6 mmol) in a mixture of 2-methoxyethanol (20 cm^3) and concentrated aqueous HCl (*ca* 0.5 cm^3) was refluxed for 15 min in a Schlenk tube under argon. Trimethylphosphine (1.40 g, 18 mmol) was added and the tube was sealed and the mixture heated under reflux for 8 h, during which time the green solution

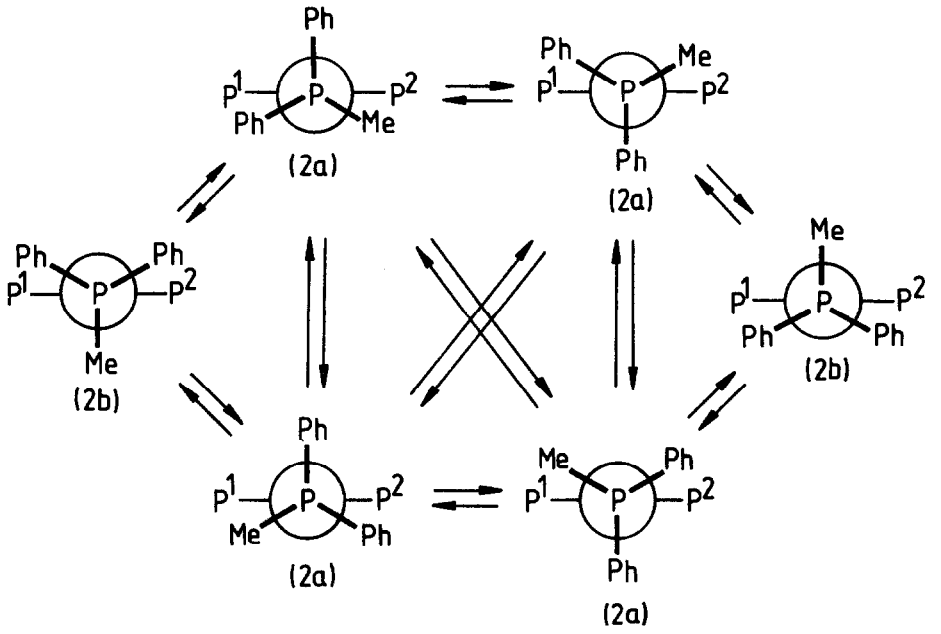

Scheme 2.

Table 2. ^{1}H NMR data for tertiary phosphine complexes of iridium(III)

Compound	δ	Assign.	J(PH)[a] (Hz)
$[IrCl_2(PMe_3)_4][IrCl_4(PMe_3)_2]$[b]	1.45(t)	Me (9H)	8.4
	1.68(t,br)	Me (18H)	6.8
mer-$[IrCl_3(PMe_3)_3]$[b]	1.64(t)	Me (18H)	7.8
	1.67(d)	Me (9H)	10.6
mer-$[IrCl_2(PMe_3)_3(H_2O)]ClO_4$[b]	1.63(t)	Me (18H)	7.8
	1.72(d)	Me (9H)	11.5
	6.80(br)	H_2O (2H)	
mer-$[IrCl_2(PMe_3)_3(PMe_2Ph)]ClO_4$[c]	1.08(d)	PMe_3 (3H)	8.0
	1.10(d)	PMe_3 (3H)	7.0
	1.56(m)	PMe_3 (6H)	
	1.60(d)	PMe_3 (3H)	7.2
	1.71(m)	PMe_3 (12H)	
	1.84(d)	PMe_2Ph (3H)	9.0
	1.87(d)	PMe_2Ph (3H)	9.0
	7.44(m)	Ph (4H)	
	8.40(t)	Ph (1H)	9.1
	8.08(t)	Ph (2H)	9.0
mer-$[IrCl_2(PMe_3)_3(PMePh_2)]ClO_4$[d]	1.55(s,br)	PMe_3 (18H)	
	1.86(d,br)	PMe_3 (9H)	7.5
	2.48(d,br)	$PMePh_2$ (3H)	7.7
	8.02(m)	Ph (4H)	
	7.54(s,br)	Ph (6H)	

[a] For virtually coupled triplets the value given is $|^2J(PH)+{}^4J(PH)|$.
[b] In $CDCl_3$ at 20°C at 200 MHz.
[c] In CD_2Cl_2 at −75°C at 400 MHz.
[d] In $CDCl_3$ at 45°C at 400 MHz.

Table 3. $^{31}P\{^1H\}$ NMR data for tertiary phosphine complexes of iridium(III)

Compound	δ^a	$J(PP)^{trans}$	$J(PP)^{cis}$
mer-$[IrCl_2(PMe_3)_3(PMe_2Ph)]ClO_4$[b]	28.30, 26.20, 30.00, 25.50 (ABCD, major, 95%),	366	−27
	21.20, 33.40, 29.40 (A_2BC, minor, 5%)	366	−30
mer-$[IrCl_2(PMe_3)_3(PMe_2Ph)]ClO_4$[c]	25.98, 23.56, 28.65 (A_2BC)	366	−25
mer-$[IrCl_2(PMe_3)_3(PMePh_2)]ClO_4$[b]	26.00, 16.90, 30.80 (ABCD, major),	366	−27
	32.80, 26.00, 26.80 (A_2BC, minor)	366	−27
mer-$[IrCl_2(PMe_3)_3(PMePh_2)]ClO_4$[c]	29.80, 24.20, 20.50 (A_2BC)	366	−27

[a] In CD_3COCD_3 at 162 MHz with chemical shifts relative to 85% H_3PO_4.
[b] At −75°C.
[c] At 45°C.

became orange–red. The solution stood at room temperature overnight and the brick-red crystals (1.21 g, 67%) were filtered off, washed with diethyl-ether, and dried *in vacuo*. Found: C, 20.7; H, 5.0; P, 17.7. $C_{18}H_{54}Cl_6Ir_2P_6$ requires: C, 20.5; H, 5.1; P, 17.6%. MS (EI): $m/z = 526$ for the parent ion corresponding to $[IrCl_3(PMe_3)_3]^+$, rearrangement apparently occurring in the mass spectrometer probe.

Synthesis of mer-$[IrCl_3(PMe_3)_3]$

An orange–red solution of some of the above salt (0.45 g, 0.43 mmol) in 2-methoxyethanol (50 cm^3) was heated under reflux for 60 min until it became deep yellow. The volume of the solution was reduced under reduced pressure to about 5 cm^3 and the solution stored at −20°C overnight. The yellow precipitate was collected and combined with more precipitate formed on concentrating and cooling the filtrate further. After washing and drying, the combined yield of yellow crystals of the product was 0.411 g (91%). Found: C, 20.4; H, 5.0; P, 16.1. $C_9H_{27}Cl_3IrP_3$ requires: C, 20.5; H, 5.1; P, 17.6%. MS (EI): $m/z = 526$ (parent molecular ion).

Synthesis of trans,mer-$[IrCl_2(H_2O)(PMe_3)_3]ClO_4$

Silver perchlorate (0.027 g, 0.13 mmol) was added to a suspension of *mer*-$[IrCl_3(PMe_3)_3]$ (0.0682 g, 0.13 mmol) in acetone (10 cm^3) and the mixture was shaken for 30 min. The filtered yellow solution was evaporated to dryness under reduced pressure to give a yellow oil which was crystallized from a dichloromethane/diethyl-ether mixture to give the title compound as yellow needles (0.056 g, 71%). Found: C, 17.7; H, 4.8; P, 17.4. $C_9H_{29}Cl_3IrO_5P_4$ requires: C, 17.7; H, 4.7; P, 17.2%.

Synthesis of trans,mer-$[IrCl_2(PMe_3)_3(PMe_2Ph)]ClO_4$

Dimethylphenylphosphine (0.024 cm^3, 0.17 mmol) was added to a solution of the cationic aqua-complex above (0.060 g, 0.10 mmol) in dichloromethane (5 cm^3) and the mixture stirred for 60 min at room temperature. The solvent was removed to give an oil. Careful addition of diethyl-ether to a solution of the oil in dichloromethane gave the product $[IrCl_2(PMe_3)_3(PMe_2Ph)]ClO_4 \cdot CH_2Cl_2$ as pale yellow crystals (0.053 g, 73%) of a quality suitable for X-ray structure determination. Found: C, 26.5; H, 4.8; P, 15.7. $C_{15}H_{40}Cl_5IrO_4P_4$ requires: C, 26.6; H, 4.9; P, 15.2%.

Synthesis of $[IrCl_2(PMe_3)_3(PMePh_2)]ClO_4$

A procedure similar to that above using the aqua-complex (0.0281, 0.053 mmol) and methyl-diphenylphosphine (0.019 cm^3, 0.053 mmol) and

crystallization as above gave the title compound in good yield (0.031 g, 86%). Found: C, 33.4; H, 5.3; P, 13.5. $C_{22}H_{40}Cl_3IrO_4P_4$ requires: C, 33.4; H, 5.1; P, 13.4%.

X-ray crystal structure determination for trans,mer-$[IrCl_2(PMe_3)_3(PMe_2Ph)]ClO_4 \cdot CH_2Cl_2$

A yellow crystal of $C_{18}H_{40}Cl_5IrO_4P_4$ with dimensions $0.22 \times 0.12 \times 0.06$ mm^3 suitable for an X-ray structure determination was obtained by layering diethyl-ether on to a dichloromethane solution of the salt and allowing slow diffusion to occur. Measurements were made at 293 K on a Nicolet R3m/v diffractometer operating with graphite monochromated Mo-K_α radiation ($\lambda = 0.71073$ Å) in the ω–2θ mode. An orthorhombic cell, $a = 13.730(3)$, $b = 20.715(5)$, $c = 21.720(3)$ Å, $U = 6178(2)$ Å^3, was obtained by auto-indexing and least-squares fitting of 30 orientation reflections in the 2θ range 12–26°. A total of 5986 intensity data (5412 unique) in the 2θ range 5–50° were corrected for Lorentz and polarization effects and for absorption by the azimuthal scan method; μ(Mo-K_α) = 49.7 cm^{-1}. No significant decay was found by monitoring three check reflections periodically throughout the data collection.

The structure was solved by direct methods in the space group *Pcab*, $Z = 8$, $F(000) = 3216$, $D_c = 1.75$ g cm^{-3}. The model with 268 parameters was refined to $R = 0.0514$ and $R_w = 0.0549$ using 2859 data with $I_0 > 1.5\sigma(I_o)$, where $R_w = [\Sigma w(|F_o| - |F_c|)^2/\Sigma w|F_o|^2]^{1/2}$ and $w = 1/[\sigma^2(F_o) + 0.000436(F_o)^2]$. All non-hydrogen atoms of the iridium complex cation were refined anisotropically. The disordered perchlorate anions were refined with constrained tetrahedral geometry and with Cl—O distances of 1.417 Å. The chloride atom and one oxygen atom were refined with an occupancy of 1.0 but the other six oxygen sites were given an occupancy of 0.5. Hydrogen atoms on the Me and Ph groups were included in idealized positions and allowed to ride on the carbon atoms with fixed C—H distances (0.96 Å) and thermal parameters ($U = 0.080$ Å^2). The maximum shift/ESD in the final least-squares cycle was 0.024 and the maximum peak in the final difference Fourier map was 1.86 e Å^{-3}. All calculations were carried out using a MicroVax II computer running SHELXTL-PLUS.[5] Atomic coordinates, thermal parameters, full tables of bond lengths and angles, and listings of the observed and calculated structure factors have been deposited with the Editor as supplementary material.

Acknowledgements—We thank the S.E.R.C. for research studentships (for S.D. and J.E.M.) and for funds for the purchase of a diffractometer and Johnson-Matthey for a loan of iridium.

REFERENCES

1. A. J. Deeming, S. Doherty and J. E. Marshall, *J. Chem. Soc., Chem. Commun.* 1989, 1351.
2. A. J. Deeming, G. P. Proud, H. M. Dawes and M. B. Hursthouse, *J. Chem. Soc., Dalton Trans.* 1986, 2545.
3. P. L. Goggin, R. J. Goodfellow, J. R. Knight, M. G. Norton and B. F. Taylor, *J. Chem. Soc., Dalton Trans.* 1973, 2220.
4. B. E. Mann, C. Masters, B. L. Shaw and R. E. Stainbank, *J. Chem. Soc., Chem. Commun.* 1971, 1103.
5. G. M. Sheldrick, SHELXTL-PLUS, Package for crystal structure determination. University of Göttingen, F.R.G. (1986).

Polyhedron Vol. 10, No. 16, pp. 1865–1872, 1991
Printed in Great Britain

0277-5387/91 $3.00+.00
Pergamon Press plc

EARLY STAGES OF THE HYDROLYSIS OF CHROMIUM(III) IN AQUEOUS SOLUTION—7. KINETICS OF CLEAVAGE OF THE HYDROLYTIC DIMER IN ACIDIC SOLUTION†

LEONE SPICCIA

Department of Chemistry, Monash University, Clayton, Victoria 3168, Australia

(*Received* 26 *February* 1991; *accepted* 4 *June* 1991)

Abstract—The kinetics of cleavage of the hydrolytic dimer of chromium(III) have been studied in acidic solution and at elevated temperatures using spectrophotometric methods. The slightly curved dependence of k_{obs} on $[H^+]$ has been attributed to equilibration between a doubly-bridged dimer (DBD) and two singly-bridged dimer forms (fully protonated, SBD and monodeprotonated SBD-H), which are related by a protonation equilibrium that gives rise to the acid dependence of k_{obs}. Two pathways for cleavage of SBD forms into Cr^{3+} are proposed involving SBD and SBD-H and the actual bridge cleavage reactions are concluded to be acid independent. The calculated rate constants and activation parameters at 25°C were as follows: $k_{SBD\text{-}H} = 3.9(\pm 0.4) \times 10^{-7}$ s^{-1} [$\Delta H^* = 98(\pm 3)$ kJ mol^{-1} and $\Delta S^* = 20(\pm 11)$ JK^{-1} mol^{-1}]; $k_{SBD} = 2.7(\pm 0.2) \times 10^{-6}$ s^{-1} [$\Delta H^* = 112(\pm 2)$ kJ mol^{-1} and $\Delta S^* = 83(\pm 5)$ JK^{-1} mol^{-1}]. The significance of these results is discussed and a comparison with existing information on the oxo-bridged hydrolytic dimer of chromium(III) is made. The rate of the dimerization reaction between Cr^{3+} and $CrOH^{2+}$ has been estimated and found to be about 1000 times slower than the dimerization of two $CrOH^{2+}$ ions.

Hydroxy- (or oxo-) bridged binuclear complexes, dimers, are the first products of the hydrolytic polymerization of many metal ions in aqueous solution. Consequently, there is continuing interest in the properties of these complexes.[2,3] However, most work has focussed on complexes in which the metal centre is bound to several N-donor ligands[3] and in comparison very few hydrolytic dimers, in which the ligands are derived entirely from the solvent (H_2O), have been studied in detail.[2–7] Thus, comparisons of the behaviour and properties of binuclear complexes containing, for example, N-donor ligands, with those of purely hydrolytic dimers are generally lacking and there is some uncertainty as to whether the information obtained for the former is directly relevant to the hydrolytic behaviour of aqueous metal ions. The hydrolytic dimer of chromium(III) is one oligomer which has been the subject of extensive characterization studies[3,6–9] as well as comprehensive kinetic and thermodynamic investigations[1,6,9–13] and is particularly well-suited for making such an assessment.

Thompson and Connick[6] have demonstrated that the hydrolytic dimer can exist in both singly-bridged (SBD) and doubly-bridged (DBD) forms. Subsequently, the structure of DBD has been determined,[7] and its magnetic and spectroscopic properties investigated.[14] Thompson[6,9] further showed that the acid cleavage of DBD into Cr^{3+} involves two consecutive, clearly separable processes [eq. (1)]. The order of these processes is believed to be reversed in the dimerization of Cr^{3+}.[11] The overall rate of acid cleavage is much slower for SBD than for DBD which means that each of these processes can be studied with little interference from the other. As a result, measurements of the rate of interconversion[1,9] and equilibrium[13] between SBD and DBD have been possible. In addition, estimates of the overall rate of acid cleavage to give Cr^{3+} are also available but were obtained at variable ionic strength.[9]

$$DBD \rightleftharpoons SBD \rightleftharpoons Cr^{3+} \qquad (1)$$

† Part VI: Ref. 1.

We report here the result of a variable temperature and $[H^+]$ ($I = 1.0$ M) study of the cleavage of the dimer into Cr^{3+}, from which two reaction pathways have been established.

EXPERIMENTAL

Materials

Solutions of the hydrolytic dimer $[Cr_2(\mu\text{-}OH)_2(OH_2)_8](ClO_4)_4$, were prepared using a recently published method,[15] the only modification being that $HClO_4$ rather than aromatic sulphonic acids was used to oxidize chromium metal to Cr^{2+}. The resulting crude dimer solutions were purified and standardized as described previously.[10] When stored at -18°C stock dimer solutions showed no change in composition after several months.

Analytical grade reagents were used throughout. Water was deionized and doubly distilled prior to use. $NaClO_4$ and $LiClO_4$ solutions of known concentration were prepared by neutralization of standardized solutions of either NaOH or LiOH with $HClO_4$. All solutions were filtered through 0.22 μm Sartorius SM11307 cellulose nitrate membrane filters prior to use in kinetic experiments.

Instruments

The instruments and techniques used to measure the pH of the solutions and to carry out kinetic measurements have been described previously.[1]

Kinetic experiments

Reaction mixtures were prepared at the desired temperature (62.3–91.5°C) by mixing equal volumes of a dimer solution ($[Cr_2(\mu\text{-}OH)_2(OH_2)_8]^{4+} = 4.28 \times 10^{-3}$ M, $[HClO_4] = 9.3 \times 10^{-3}$ M and $[NaClO_4] = 0.122$ M, determined at room temperature, *ca* 22°C, according to published methods) with a series of solutions containing varying proportions of $HClO_4$ and $NaClO_4$ (or $LiClO_4$ in some cases) but whose ionic strength was constant (1.83 M at room temperature). The final reaction conditions were [Dimer] $= 2.14 \times 10^{-3}$ M, $[HClO_4] = 0.0271$–0.919 M and $I = 1.0$ M ($NaClO_4$ or $LiClO_4$). In the analysis of the kinetic data these acid concentrations were corrected for the temperature-dependent expansion of the solvent.

The reaction was monitored in the UV region ($\lambda < 300$ nm) where the absorbance was found to decrease as the dimer is converted into Cr^{3+}. The data were analysed at 250 nm where this decrease was between 0.5 and 0.7 units. Pseudo-first order rate constants, k_{obs}, were calculated at this wavelength from the change in absorbance, A_t, with time, t, by means of linear least-squares fitting of the data to the expression $A_t = (A_0 - A_\infty)e^{-k_{obs}t} + A_\infty$. In most cases A_0, A_∞ and k_{obs} were determined from the A_t vs t data. However, as a check on the suitability of the procedure A_∞ was measured experimentally for several runs and used in the calculation of k_{obs}. The values of k_{obs} obtained from the two treatments were within experimental error. Furthermore, experimental and fitted A_∞ values were in excellent agreement.

RESULTS

The overall rate of cleavage of the hydrolytic dimer of chromium(III) was measured in the temperature range 62.3–91.5°C and $[H^+]$ range 0.026–0.90 M, but at constant ionic strength (1.0 M). High temperatures were chosen because this gave reaction rates which could be measured using conventional spectrophotometric methods. Chromatographic analysis was used to show that Cr^{3+} is the only species present at the completion of the reaction. That is, the reaction is irreversible under the conditions used. The spectrophotometric data could be fitted accurately with a single exponential function ($0.002k_{obs} < \sigma_{k_{obs}} < 0.01k_{obs}$), which indicates that the process being followed is first order with respect to the dimer. Table 1 summarizes the $[H^+]$ and temperature dependence of the observed rate constants (k_{obs}).

The dependence of k_{obs} on $[H^+]$ is almost linear (slight curvature becomes apparent at high $[H^+]$) with a non-zero intercept at all temperatures (see Fig. 1). Thus, the cleavage of the dimer involves at

Table 1. Observed rate constants (k_{obs}) for the cleavage of the hydrolytic dimer into Cr^{3+} in acidic solution at various temperatures and $I = 1.0$[a,b]

T (°C)	$[H^+]^c$ (M)	$10^5 k_{obs}$ (s^{-1})
62.3	0.905	5.33
	0.905	5.23
	0.725	4.39
	0.725	4.42
	0.545	3.45
	0.545	3.34
	0.545	3.37
	0.365	2.47
	0.185	1.55
	0.0945	0.984
	0.0495	0.786
	0.0270	0.650

Table 1.—*continued*

T (°C)	$[H^+]^c$ (M)	$10^5 k_{obs}$ (s^{-1})
67.6	0.902	8.68
	0.902	8.56[d]
	0.722	7.08
	0.722	7.24[d]
	0.543	5.71
	0.543	5.56[d]
	0.363	4.08
	0.184	2.37
	0.0942	1.75
	0.0494	1.38
	0.0269	1.18
76.9	0.897	20.0[d]
	0.897	20.1
	0.716	16.7[d]
	0.716	16.6
	0.540	13.4
	0.540	13.4[d]
	0.361	9.75
	0.183	6.28
	0.183	5.92
	0.0937	4.29[d]
	0.0937	4.23
	0.0491	3.50
	0.0491	3.39
83.5	0.894	36.2
	0.716	30.7
	0.538	24.6
	0.360	18.5
	0.182	11.6
	0.0933	8.62
	0.0489	7.28
	0.0266	6.52
91.5	0.712	53.8[d]
	0.535	43.7
	0.535	44.1[d]
	0.358	34.7[d]
	0.358	33.6
	0.181	23.9
	0.0928	16.9
	0.0928	17.2[d]
	0.0486	15.2
	0.0486	14.5
	0.0486	15.0[d]
	0.0265	13.2
	0.0265	13.6

[a] Except where otherwise indicated $NaClO_4$ was used as supporting electrolyte.

[b] A comprehensive table listing $\sigma_{k_{obs}}$ values and the weighting factors used in fitting the data to eq. (4) can be obtained from the author on request.

[c] $[H^+]$ corrected for the temperature dependent expansion of the solvent.

[d] $LiClO_4$ used as supporting electrolyte.

least two pathways, one of which is dependent on $[H^+]$. In contrast, Thompson[9] observed no systematic variation of k_{obs} with $[H^+]$ in the concentration range 1–8 M but in this case no attempt was made to maintain constant ionic strength.

The simplest reaction mechanism which will accommodate the almost linear dependence of k_{obs} on $[H^+]$, and existing information on the interconversion between SBD and DBD forms[1,9] is that given in Scheme I. The overall process involves several pathways which can be subdivided into two types: cleavage of DBD to give SBD forms (top half of Scheme I) followed by cleavage of SBD forms into Cr^{3+}. Thompson[9] has shown that there are substantial differences in the rates at which these processes occur, interconversion between SBD and DBD being *ca* 200 times faster than cleavage to Cr^{3+}. In fact, measurements of the equilibrium between SBD forms and DBD have been possible without interference from the cleavage of SBD forms to Cr^{3+}.[13] This suggests that the overall cleavage of the dimer is rate-determined by the cleavage of SBD forms. In Scheme I, the rate constants of importance are k_{SBD} and $k_{SBD\text{-}H}$, which represent the rate of bridge cleavage within SBD and SBD-H, respectively. Note that the actual bridge cleavage processes are proposed to be acid independent and that the acid dependence of k_{obs} arises from the protonation equilibrium between SBD-H and SBD. If the actual bridge cleavage processes were acid catalysed, a dependence of k_{obs} on $[H^+]^2$ might be expected. The rate law for the

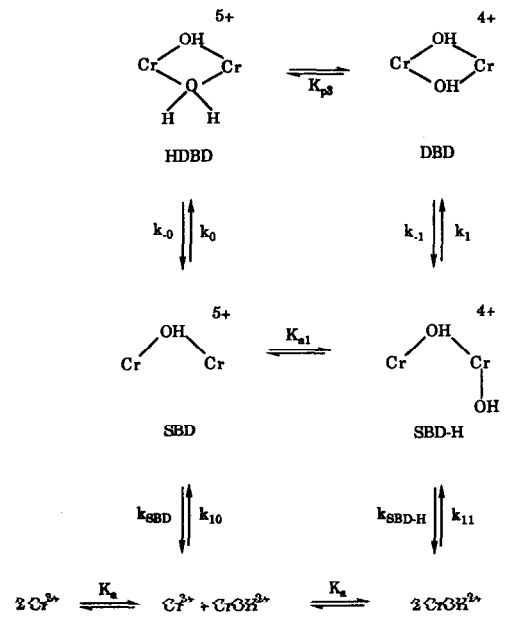

Scheme I.

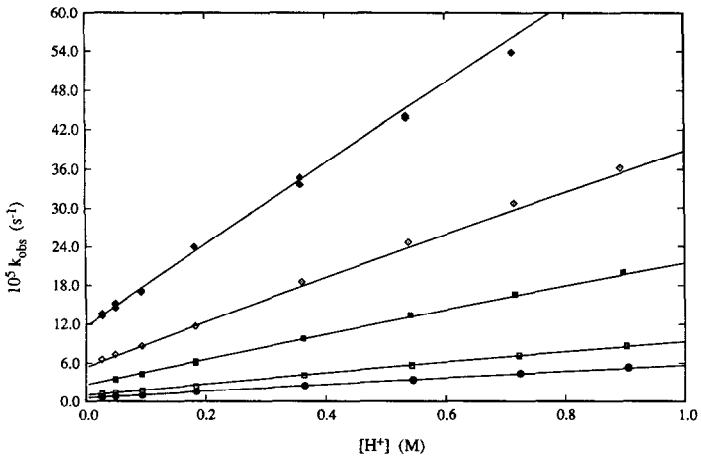

Fig. 1. Acid concentration and temperature dependence of the observed rate constant for cleavage of the hydrolytic dimer of chromium(III) at $I = 1.0$ M. Full lines represent the calculated values of k_{obs} determined from eq. (4). (●) 62.3°C; (□) 67.6°C; (■) 76.9°C; (◇) 83.5°C; (◆) 91.5°C.

cleavage of the dimer may be written as:

$$\frac{d[Cr^{3+}]}{dt} = k_{SBD\text{-}H}[SBD\text{-}H] + k_{SBD}[SBD], \quad (2)$$

where $k_{SBD\text{-}H}$ and k_{SBD} are the rate constants for cleavage of SBD-H and SBD, respectively. Use of the expressions $K_1 = [SBD\text{-}H]/[DBD]$, $K_{a1} = [SBD\text{-}H][H^+]/[SBD]$ and $[DIM]_T = \{[DBD] + [SBD\text{-}H] + [SBD]\} = \{1 + 1/K_1 + [H^+]/K_1K_{a1}\}[DBD]$ followed by simplification gives eq. (3).

$$\frac{d[Cr^{3+}]}{dt} = \left\{\frac{[k_{uc} + k_c[H^+]]}{[1 + 1/K_1 + [H^+]/K_1K_{a1}]}\right\}[DIM]_T = k_{obs}[DIM]_T \quad (3)$$

[In eq. (3), $k_{uc} = k_{SBD\text{-}H}/K_1$ and $k_c = k_{SBD}/K_1K_{a1}$.] In the case where both K_1 and K_1K_{a1} are large and the denominator in eq. (3) is *ca* 1, a linear dependence of k_{obs} on $[H^+]$ would result. Taking into account the temperature dependence of each parameter gives the following expression for k_{obs}:

$$k_{obs} = \frac{\left[\frac{kT}{h}\left\{\exp\left(\frac{\Delta H^*_{k_{uc}} - T\Delta S^*_{k_{uc}}}{RT}\right) + [H^+]\exp\left(\frac{\Delta H^*_{k_c} - T\Delta S^*_{k_c}}{RT}\right)\right\}\right]}{\left[1 + \left\{\exp\left(\frac{-\Delta H^\circ_{K_1} + T\Delta S^\circ_{K_1}}{RT}\right) + [H^+]\exp\left(\frac{-\Delta H^\circ_{K_1K_{a1}} + T\Delta S^\circ_{K_1K_{a1}}}{RT}\right)\right\}\right]}. \quad (4)$$

In analysing the data, previously determined[13] thermodynamic constants for K_1 ($\Delta H^\circ = -10.4$ (± 2.7) kJ mol^{-1} and $\Delta S^\circ = -15.0(\pm 8.9)$ JK^{-1} mol^{-1}) and K_1K_{a1} ($\Delta H^\circ = 29.5(\pm 1.1)$ kJ mol^{-1} and $\Delta S^\circ = 104.4(\pm 3.7)$ JK^{-1} mol^{-1}) were used to reduce the number of parameters in eq. (4). The activation parameters for k_{uc} and k_c (Table 2) were determined from weighted non-linear least squares fitting of the temperature and $[H^+]$ dependence of k_{obs} to eq. (4). The procedure involved minimization of $\Sigma_i W_i(k_{obs,i} - k_{calc,i})^2$ where $W_i = 1/\sigma^2_{k_{obs,i}}$ and $k_{obs,i}$, $k_{calc,i}$, W_i and $\sigma_{k_{obs,i}}$ are the observed rate constants, calculated rate constants, weighting factors and standard error in each k_{obs} value, respectively. An excellent fit of the data is indicated by the small standard errors associated with each parameter (Table 2).

The activation parameters for each cleavage process have been used to calculate k_c and k_{uc} at 25°C, which is outside the range of temperature used in this study. From these values, published values of K_1 and K_1K_{a1}, (respectively, 10.1 and 1.83 at 25°C)[13] and using the expressions $k_{SBD\text{-}H} = K_1k_{uc}$ and $k_{SBD} = k_cK_1K_{a1}$, $k_{SBD\text{-}H}$ and k_{SBD} have been estimated. Activation parameters for $k_{SBD\text{-}H}$ and k_{SBD} were determined from those of k_{uc} and k_c and the thermodynamic constants of K_1 and K_1K_{a1} given above. All of this information is listed in Table 2 and will be used in the discussion to follow.

DISCUSSION

The kinetic data for cleavage of the hydrolytic dimer of chromium(III) can be interpreted in terms of two bridge-cleavage processes (Scheme I), cleav-

Table 2. Activation parameters and calculated rate constants for cleavage of the hydrolytic dimer of chromium(III)

Parameter	$10^6 k$ (s^{-1})	ΔH^* (kJ mol^{-1})	ΔS^* (JK^{-1} mol^{-1})
k_{uc}	0.038(±0.002)[a]	108.7(±0.8)[b]	35(±2)[b]
k_c	1.46(±0.05)[a,c]	82.7(±0.6)[b]	−22(±2)[b]
$k_{SBD\text{-}H}$[d]	0.39(±0.04)	98(±3)	20(±11)
$k_{SBD\text{-}H}$[e]	2.7(±0.2)	112(±2)	83(±5)
k_{-1}[f]	22(±1)	110(±5)	35(±16)
$k_{-0}K_{p3}$[f]	52(±1)[c]	59(±2)	−130(±8)
k_{-0}	520 (est)[g]	104 (est)[h]	0 (est)[h]

[a] Rate constants at 25°C calculated from the activation parameters.

[b] Determined by fitting the data to eq. (4).

[c] Units are M^{-1} s^{-1}.

[d] Activation parameters for $k_{SBD\text{-}H}$ determined assuming $k_{SBD\text{-}H} = K_1 k_{uc}$ and using data for k_{uc} given above and published values of K_1, $\Delta H°(K_1)$ and $\Delta S°(K_1)$ (ref. 13).

[e] Activation parameters for k_{SBD} determined assuming $k_{SBD} = k_c K_1 K_{a1}$ using data for k_c given above and published values of $K_1 K_{a1}$, $\Delta H°(K_1 K_{a1})$ and $\Delta S°(K_1 K_{a1})$ (ref. 13).

[f] Data from ref. 1.

[g] Estimated from $k_{-0}K_{p3}$ assuming $K_{p3} \simeq 0.1$ M^{-1}.

[h] Activation parameters for k_{-0} estimated from parameters for $k_{-0}K_{p3}$ and assuming $\Delta H°$ $(K_{p3}) \simeq -45$ kJ mol^{-1} and $\Delta S°$ $(K_{p3}) = -130$ JK^{-1} mol^{-1}.

age of SBD-H ($k_{SBD\text{-}H}$) and SBD (k_{SBD}). The actual bridge-cleavage reactions are proposed to be acid independent and the acid dependence of k_{obs} attributed to equilibration between DBD and SBD forms. This is much faster than cleavage of SBD forms and involves a protonation equilibrium for SBD-H, which accounts for the acid dependence. Existing data on the cleavage of DBD into SBD suggests that this is not unreasonable (Table 2). In this case, acid-catalysed cleavage becomes apparent at the highest $[H^+]$,[1,9] but the rate for this pathway ($k_{-0}K_{p3}$) in 1 M H^+ at 25°C is only twice as fast as the corresponding uncatalysed process (k_{-1}). The value of K_{p3} has been estimated[3] as < 0.1 M^{-1}. Protonation of the bridging OH^- in SBD is expected to be more difficult than for DBD because of the higher overall charge while for SBD-H protonation is more likely at the terminal OH^-, giving SBD (at 298.15 K, pKa_1(SBD) determined from equilibrium studies[13] and kinetic measurements[1] were 0.74 and 1.00, respectively). It is important to note that decreases in protonation constants of 100 fold (or even higher) per unit charge increase are not uncommon for terminal OH^- groups coordinated to Cr^{3+} or chromium(III) oligomers.[10] Assuming similar variations in the case of bridging OH^- groups the protonation constant for the bridging OH^- group in SBD is likely to be $\ll 0.001$ M^{-1}. Thus, under the conditions of the current study ($[H^+] \sim 0.02$–1 M) acid-catalysed bridge cleavage of SBD forms would become apparent if the rate of cleavage of the protonated form, i.e. Cr—OH_2—Cr, is faster than the uncatalysed pathway by at least 1000 fold. To the author's knowledge there are no examples of singly-bridged binuclear complexes of chromium(III) for which such accelerations in bridge cleavage rate are found (see ref. 3 for a recent review). In the case of rhodium(III), however, acid-catalysed cleavage processes are not uncommon for both singly- and doubly-bridged complexes.[3] An excellent example highlighting this behaviour is the Δ,Λ-$[(en)_2 Rh(OH)_2 Rh(en)_2]^{4+}$ complex.[16]

Holwerda and co-workers[17] claim to have isolated an oxo-bridged aquo dimer $(H_2O)_5CrO Cr(OH_2)_5^{4+}$, as a product of the oxidation of Cr^{2+} with 1,4-benzoquinone. This species cannot be obtained by deprotonation of SBD because this occurs at the more acidic terminal H_2O groups. Indeed the kinetics of conversion of SBD into DBD have been followed over several deprotonations of SBD but no evidence for bridge deprotonation was

obtained.[1] This would be apparent in the UV-vis spectrum where the appearance of intense absorptions characteristic of oxo-bridges would occur, as is the case for $(NH_3)_5CrOHCr(NH_3)_5^{5+}$.[3,18] Furthermore, deprotonation of DBD results in the formation of the "active" dimer hydroxide $Cr_2(\mu\text{-}OH)_2(OH)_4(OH_2)_4 \cdot 2H_2O$ and not an oxo-bridged binuclear species. Cleavage of Holwerda's oxo dimer[17b] in acidic solution (1 M $HClO_4$) is much faster than cleavage of SBD forms, found in this study (difference in rate *ca* 1300 fold) and previously by Thompson.[9] This is a surprising observation given that the oxo-bridged dimer would be expected to be protonated in acidic solution [note that pKa for $(NH_3)_5CrOHCr(NH_3)_5^{5+}$ is 7.6][19] and there are no obvious steric factors which would hinder this protonation process. Thus, it would be expected that an oxo-bridged hydrolytic dimer of this type would be protonated in acidic solution and its cleavage behaviour should parallel that observed for SBD forms.

The rate of bridge cleavage in acidic solution is generally faster for DBD than for SBD forms (Table 2), i.e. k_{-1} and k_0 are larger than $k_{SBD\text{-}H}$ and k_{SBD}. This cannot be attributed to a change in nucleophile because an important feature of these bridge-cleavage reactions is that they involve attack by a common nucleophile, H_2O from the solvent. Note that this is not the case for bridge-formation reactions where coordinated OH^-, H_2O and O^{2-} (in some cases) can all act as nucleophiles. Although the commonality of nucleophiles reduces the complexity of bridge-cleavage processes, cf. bridge formation, there are nevertheless several other factors that could influence the rate of these processes. These include: (i) electrostatic attraction between the differently charged dimer forms and the incoming nucleophile; (ii) the relative lability of the chromium(III) coordination spheres which is known to be influenced by the degree of deprotonation on each chromium(III) centre;[1,11] (iii) geometrical differences between dimer forms which may influence the ease of nuclephilic attack; (iv) hydrogen-bond stabilization of deprotonated forms.[3] In the case of SBD-H, intramolecular hydrogen-bond stabilization is believed to be important[1,3,13] and is likely to influence the rate of both bridge formation and cleavage reactions. This means that $k_{SBD\text{-}H}$ is probably not a true measure of the rate of cleavage of SBD-H and furthermore, the form undergoing bridge cleavage is uncertain. From the well-established accelerations in substitution rates with degree of deprotonation of reactants[11,20] it would seem that cleavage of SBD-H should be faster than cleavage of SBD, but the opposite is true in practice (Table 2). The most likely explanation is that the hydrogen-bonded form does not participate in bridge cleavage and retards the process. Alternatively, the higher charge on SBD (5+), cf. SBD-H (4+), suggests a greater attraction of SBD for H_2O and this might be responsible for the observed faster rate of cleavage of SBD. However, previous work on the rate of H_2O exchange on Cr^{3+} and $CrOH^{2+}$ [20] and intramolecular ring closure within SBD forms[1] has shown that labilization of the coordination sphere of chromium(III), induced by deprotonation, has a much greater effect on reactivity than these electrostatic effects.

The faster rate of bridge cleavage for DBD ($k_{-1} = 2.7 \times 10^{-5}$ s^{-1}) when compared with SBD ($k_{SBD} = 2 \times 10^{-6}$ s^{-1}) is probably reflecting a higher lability of DBD (OH/Cr = 1.0) which overall has a higher degree of deprotonation than SBD (OH/Cr = 0.5). In addition, the double-bridging moiety in DBD (bridging O—Cr—O angle of 78°) introduces constraints which effectively enlarge some adjacent angles in the chromium(III) sphere and expand some of the faces of the chromium octahedron. For an associative substitution this might facilitate nucleophilic attack. The actual rate of bridge cleavage within protonated DBD, $Cr(\mu\text{—}OH)(\mu\text{—}OH_2)Cr^{5+}$ (Scheme I) has been estimated as 5×10^{-4} s^{-1} (assuming $K_{p3} = 0.1$ M^{-1}). A somewhat faster rate of cleavage of protonated DBD, cf. DBD and SBD, would not be unexpected since bridging H_2O would be held less tightly than bridging OH^-, but this difference may not be that large.

The activation enthalpies for bridge cleavage are concentrated in the range 98–112 kJ mol^{-1} while the activation entropies cover a wider range, 0–80 JK^{-1} mol^{-1} (Table 2). In the case of SBD-H, hydrogen-bond stabilization would affect ΔH^* and furthermore, it is not known whether the form undergoing cleavage is the hydrogen-bonded form or not. Apart from this, the remarkably constant values of ΔH^* for dimer bridge cleavage correspond closely with those determined for $(NH_3)_5Cr(OH)Cr(NH_3)_5^{5+}$ and *cis*- and *trans*-$[(NH_3)_5Cr(OH)Cr(NH_3)_4(OH_2)]^{5+}$ which range between 105–113 kJ mol^{-1} [13,21] and more importantly with ΔH^* for H_2O exchange on Cr^{3+} and $CrOH^{2+}$ (respectively, 109 and 111 kJ mol^{-1}).[20] On the basis of these comparisons it could be argued that these reactions all involve a similar mechanism (possibly I_a) and that there are no dramatic differences in the lability of the chromium(III) coordination sphere for each form of the hydrolytic dimer. However, the data for H_2O exchange on Cr^{3+} and $CrOH^{2+}$ has firmly established that changes in mechanism, from I_a to I_d, and lability derived solely from ΔS^* are possible.[20] Indeed, sub-

stantial variations in ΔS^* are found for the bridge-cleavage reactions but their interpretation is not straightforward.

The results of this study together with measurements of the SBD–DBD equilibrium[13] and of the equilibrium distribution of polynuclear species in partially neutralized solutions of Cr^{3+} [12] allow prediction of dimerization rates for mononuclear chromium(III) species. For example, from the reaction sequence for the formation of DBD from Cr^{3+} (Scheme I) it can be shown that k_{11}, the rate of dimerization of $CrOH^{2+}$, is given by eq. (6)

$$k_{11} = \beta_{22}k_{-1}k_{SBD\text{-}H}/k_1K_a^2 = \beta_{22}k_{uc}/K_a^2; \quad (6)$$

where β_{22} is the stability constant for the dimer [$5.6(\pm0.5)\times10^{-6}$ M^{-1} at 25°C],[12] K_a is the first acid dissociation constant of Cr^{3+} [$5.13(\pm0.4)\times10^{-5}$ M at 25°C],[10] $K_1 = (k_1/k_{-1})$ is the equilibrium constant for interconversion between SBD-H and DBD, $k_{SBD\text{-}H}$ is the rate of cleavage of SBD-H and k_{uc} is the overall rate for the uncatalysed cleavage of the dimer (Table 2). This calculation gave $k_{11} = 8(\pm2)\times10^{-5}$ M^{-1} s^{-1} which is in reasonable agreement with the directly determined value of $2.0(\pm0.4)\times10^{-4}$ M^{-1} s^{-1}.[11] Similarly for the reaction of Cr^{3+} with $CrOH^{2+}$, the rate of dimerization k_{10} is given by eq. (7)

$$k_{10} = \beta_{22}k_{-1}k_{SBD}/k_1K_{a1}K_a = \beta_{22}k_c/K_a; \quad (7)$$

where K_{a1} is the first acid dissociation constant of SBD,[13] k_{SBD} is the rate of cleavage of SBD and k_c is the overall rate of acid-catalysed cleavage of dimer (Table 2). The value of k_{10} [$1.6(\pm0.3)\times10^{-7}$ M^{-1} s^{-1}] obtained in this way is much lower than that given previously in ref. 11 where a calculation error was made. The reaction of Cr^{3+} with $CrOH^{2+}$ is *ca* 1000 times slower than dimerization of $CrOH^{2+}$, further demonstrating the dramatic effect of deprotonation on reactivity. The predicted rate of the reaction between $CrOH^{2+}$ and Cr^{3+} is only slightly faster than the rate of H_2O substitution on Cr^{3+} (4.3×10^{-8} M^{-1} s^{-1} when corrected for $[H_2O]$). This indicates that the difference in nucleophilic character between coordinated OH^- and H_2O from the solvent is small, assuming of course, that the coordinated OH^- is the attacking nucleophile in the dimerization reaction. Indirect evidence exists suggesting that this is the case.[3,22]

The constant for the $2CrOH^{2+} \rightleftarrows$ SBD-H equilibrium is $K_{11} = k_{11}/k_{SBD\text{-}H} \simeq 500$ M^{-1} and is much greater than that for the $Cr^{3+} + CrOH^{2+} \rightleftarrows$ SBD equilibrium, where $K_{10} = k_{10}/k_{SBD} \simeq 0.6$ M^{-1}. This comparison suggests that SBD forms become strongly favoured over mononuclear chromium(III) species as the overall degree of deprotonation increases.

CONCLUSION

Bridge formation and cleavage processes play important roles in the formation, cleavage and interconversion reactions of hydrolytic oligomers but the information available on these processes is limited. The current and previous[1,9–13] kinetic investigations of the hydrolytic dimer of chromium(III) have focussed attention on the factors that determine the rate of these substitution processes. The important factors, some of which also determine the behaviour of $A_4M(\mu\text{-}OH)_2MA_4^{4+}$ systems[3] include the degree of deprotonation, lability and overall charge on the dimer species undergoing reaction, the nature of the attacking nucleophile,[3] the mechanism of substitution and in the case of SBD-H, intramolecular hydrogen-bond stabilization.[3] However, it has been difficult to disentangle the relative importance of each of these factors.

In comparing the information for the hydrolytic dimer with the numerous studies on related systems of the type $A_4M(\mu\text{-}OH)_2MA_4^{4+}$, it is found that the behaviour of the hydrolytic dimer parallels closely that of these tetraammine systems at low pH ($\leqslant 2$).[1,3,9] This is true of both bridge-cleavage and formation processes. At higher pH values, such as those found in natural systems, the behaviour of the hydrolytic dimer becomes vastly different from that of the tetraammines.[1,3] In the case of the hydrolytic dimer, many coordinated H_2O ligands are present which when deprotonated allow bridge formation processes, in particular, to occur at greatly enhanced rates. For example, double deprotonation of SBD ($pK_{a2} = 4.30$)[1] has a much greater effect on the rate of ring closure than monodeprotonation ($pK_{a1} = 1.00$).[1] In addition, the dimerization of DBD to give the tetramer occurs at measurable rates at pH > 3 [pK_{a1}(DBD) = 3.68] and is followed by further polymerization.[23] This is in complete contrast to the tetraammine complexes, where once diol formation (DBD forms) is complete further reaction (except for bridge deprotonation) is prevented by the presence of four nitrogen-donor ligands.[3]

Acknowledgements—Part of this work was carried out at the Institut de Chimie, Université de Neuchâtel, Neuchâtel, Switzerland under support from the Swiss National Foundation. Financial support was also received from the Australian Research Council.

REFERENCES

1. L. Spiccia and W. Marty, *Polyhedron* 1991, **10**, 619.
2. C. F. Baes and R. E. Mesmer, *The Hydrolysis of Cations*. Wiley, New York (1976).
3. J. Springborg, *Adv. Inorg. Chem.* 1988, **32**, 55.
4. G. Johansson, *Acta Chem. Scand.* 1962, **16**, 403.
5. (a) S. E. Castillo-Blum, D. T. Richens and A. G. Sykes, *J. Chem. Soc., Chem. Commun.* 1986, 1120; (b) S. E. Castillo-Blum, D. T. Richens and A. G. Sykes, *Inorg. Chem.* 1989, **28**, 954.
6. M. Thompson and R. E. Connick, *Inorg. Chem.* 1981, **20**, 2279.
7. L. Spiccia, H. Stoeckli-Evans, W. Marty and R. Giovanoli, *Inorg. Chem.* 1987, **26**, 474.
8. (a) M. Ardon and G. Stein, *J. Chem. Soc.* 1956, 2095; (b) M. Ardon and R. A. Plane, *J. Am. Chem. Soc.* 1959, **81**, 3197; (c) M. Ardon and A. Linenberg, *J. Phys. Chem.* 1961, **65**, 1443; (d) R. W. Kolaczkowski and R. A. Plane, *Inorg. Chem.* 1964, **3**, 322.
9. G. Thompson, PhD Thesis, Lawrence Radiation Laboratory Report UCRL-11410. University of California, Berkeley (1964).
10. H. Stünzi and W. Marty, *Inorg. Chem.* 1983, **22**, 2145.
11. F. P. Rotzinger, H. Stünzi and W. Marty, *Inorg. Chem.* 1986, **25**, 489.
12. H. Stünzi, L. Spiccia, F. P. Rotzinger and W. Marty, *Inorg. Chem.* 1989, **28**, 66.
13. T. Merakis and L. Spiccia, *Aust. J. Chem.* 1989, **42**, 1579.
14. C. Reber, H. U. Güdel, L. Spiccia and W. Marty, *Inorg. Chem.* 1987, **26**, 3186.
15. T. Merakis, A. Murphy, L. Spiccia, A. Beguin and W. Marty, *Helv. Chim. Acta* 1989, **72**, 993.
16. (a) M. Hancock, B. Nielsen and J. Springborg, *Acta Chem. Scand.* 1982, **A36**, 313; (b) K. Kaas and J. Springborg, *Inorg. Chem.* 1987, **26**, 387.
17. (a) R. A. Holwerda and J. S. Petersen, *Inorg. Chem.* 1980, **19**, 1775; (b) R. F. Johnston and R. A. Holwerda, *Inorg. Chem.* 1982, **22**, 2942; (c) R. F. Johnston and R. A. Holwerda, *Inorg. Chem.* 1985, **24**, 3176, 3181.
18. J. Glerup, *Acta Chem. Scand.* 1972, **26**, 3775.
19. G. Schwarzenbach and B. Maygar, *Helv. Chim. Acta* 1962, **45**, 1425.
20. F.-C. Xu, R. Krouse and T. W. Swaddle, *Inorg. Chem.* 1985, **24**, 267.
21. (a) D. W. Hoppenjans and J. B. Hunt, *Inorg. Chem.* 1969, **8**, 505; (b) H. N. Po, V.-H. Chung and S. R. Davis, *J. Inorg. Nucl. Chem.* 1973, **35**, 2849; (c) H. N. Po and H. Enomoto, *J. Inorg. Nucl. Chem.* 1973, **35**, 2581.
22. F. Christensson and J. Springborg, *Inorg. Chem.* 1985, **24**, 2129.
23. C. Besso, Travail de Diplome. Université de Neuchâtel, Switzerland (1984).

Polyhedron Vol. 10, No. 16, pp. 1873–1876, 1991
Printed in Great Britain

0277–5387/91 $3.00+.00
© 1991 Pergamon Press plc

NEUTRAL PHOSPHINE AND PHOSPHITE DERIVATIVES OF THE FRAGMENT $(\eta^5\text{-}C_5Me_5)Re(CO)_2$ AND THE CATIONIC *cis*-$[(\eta^5\text{-}C_5Me_5)Re(CO)_2\{P(OPh)_3\}I]^+$ COMPLEX

A. HUGO KLAHN,† CARMEN LEIVA and KATHERINE MOSSERT

Instituto de Química, Universidad Católica de Valparaíso, Casilla 4059, Valparaíso, Chile

and

XIAOHENG ZHANG

Department of Chemistry, Simon Fraser University, Burnaby, B.C., Canada V5A 1S6

(*Received* 17 *February* 1991; *accepted* 4 *June* 1991)

Abstract—The phosphine complexes, $(\eta^5\text{-}C_5Me_5)Re(CO)_2PR_2R'$ [R = R′ = Ph (**1**); R = Me, R′ = Ph (**2**)] and the phosphite complexes, $(\eta^5\text{-}C_5Me_5)Re(CO)_2[P(OR)_3]$ [R = Et (**3**); R = Ph (**4**)] have been prepared in 38–70% yield by reaction of the THF complex $(\eta^5\text{-}C_5Me_5)Re(CO)_2(THF)$ with the corresponding phosphine or by direct irradiation of $(\eta^5\text{-}C_5Me_5)Re(CO)_3$ in the presence of the phosphite ligand. From the reaction of the neutral triphenylphosphite complex (**4**) with I_2 in hexane the cationic complex *cis*-$[(\eta^5\text{-}C_5Me_5)Re(CO)_2\{P(OPh)_3\}I]^+$ (**5**) could be isolated in almost quantitative yield. The *cis* orientation of the CO groups for the latter complex has been assigned on the basis of $^2J(CP)$ coupling constants and by the intensity ratio of the symmetric and antisymmetric stretching frequencies of the CO ligands.

Traditionally, cyclopentadienyl complexes of the type $CpM(CO)_2L$, Cp = $\eta^5\text{-}C_5H_5$, with M = Mn or Re and L = neutral two electron donor ligand, have been produced by photosubstitution of a CO ligand from the corresponding tricarbonyl complex.[1] Two experimental procedures have been used to incorporate the ligand L to a metal center. These are direct irradiation of $CpM(CO)_3$, dissolved in a non-coordinating solvent, in the presence of the entering ligand[2] or photochemical generation of an intermediate, usually with a solvent molecule as ligand, followed by thermal reaction in the presence of L. The latter method is currently the most widely used for the preparation of the $CpM(CO)_2L$ complexes. In rhenium complexes, for example, Nesmeyanov *et al.* have used the THF derivatives $CpRe(CO)_2(THF)$ for the preparation of a series of compounds with phosphorus containing ligands $CpRe(CO)_2(PR_3)$ (R = Ph, OEt and OPh).[3] It is worth noting that thermal CO substitution by PMe_3, generating the $CpRe(CO)_2(PMe_3)$ complex, has also been reported.[4] To our knowledge, of analogous pentamethylcyclopentadienyl complexes with phosphorus ligands only the PMe_3 complex, $Cp^*Re(CO)_2(PMe_3)$ ($Cp^* = \eta^5\text{-}C_5Me_5$), is known. This complex has been synthesized in a straightforward photosubstitution reaction involving $Cp^*Re(CO)_3$ and PMe_3,[5] and via the THF complex, $Cp^*Re(CO)_2(THF)$, followed by the addition of PMe_3.[6] The triphenylphosphine analog $Cp^*Re(CO)_2(PPh_3)$ was briefly mentioned with no details of either its synthesis or characterization.[7]

In the present work, we wish to report the synthesis and spectroscopic characterization of a series of pentamethylcyclopentadienylrhenium complexes containing phosphine, namely $Cp^*Re(CO)_2(PR_2R')$ [R = R′ = Ph (**1**); R = Me, R′ = Ph (**2**)], or phosphite ligands, $Cp^*Re(CO)_2[P(OR)_3]$ [R = Et (**3**); R = Ph (**4**)]. In addition, this paper also describes the reaction of the neutral triphenylphosphite complex (**4**) with I_2 leading to the first example of a cationic phosphite complex possessing a four-legged piano stool type of structure *cis*-$[Cp^*Re(CO)_2\{P(OPh)_3\}I]^+$ (**5**).

† Author to whom correspondence should be addressed.

EXPERIMENTAL

All reactions were carried out under nitrogen using Schlenk apparatus connected to a double manifold providing a low vacuum or nitrogen atmosphere. Photochemical reactions were conducted in quartz tubes irradiated with a Hanovia Model 679 A36, 450 W high-pressure mercury vapor lamp. Solvents were dried by conventional methods, distilled under N_2 and used immediately. IR spectra were measured with a Bomen MB-120 FTIR. ^1H and ^{13}C NMR spectra were measured at 400 and 100 MHz respectively, on a Bruker WM-400 instrument. Coupling constants are reported in Hertz. Mass spectra were obtained on a Hewlett-Packard 5985 mass spectrometer with electron impact source. Reported masses are based on ^{187}Re. Microanalyses were performed by M. K. Yang of the SFU Microanalytical Laboratory. Rhenium was purchased as $Re_2(CO)_{10}$ (Strem Chemical Co.) and converted to $Cp^*Re(CO)_3$ according to the literature procedure.[8] The ligands, PPh_3, PMe_2Ph, $P(OEt)_3$ and $P(OPh)_3$ (Strem) were used as received.

Preparation of $Cp^*Re(CO)_2(PPh_3)$ (**1**)

This complex was prepared using a method similar to that reported[6] for $Cp^*Re(CO)_2(PMe_3)$: a solution of $Cp^*Re(CO)_3$ (200 mg, 0.49 mmol) in THF (50 cm_3) was irradiated at 20°C for 40 min. It gradually turned yellow and the IR spectrum indicated a ratio $Cp^*Re(CO)_3$: $Cp^*Re(CO)_2(THF)$ of approximately 1 : 1.5. Upon reduction of the volume of solvent under vacuum to about 10 cm^3, an excess (300 mg, 1.14 mmol) of solid PPh_3 was added. The mixture was heated for 1 h at 50°C. After cooling the IR showed the complete conversion of $Cp^*Re(CO)_2(THF)$ into (**1**), some unreacted $Cp^*Re(CO)_3$ was also present. The solvent was removed under vacuum and the brown oily solid remaining was dissolved in CH_2Cl_2 and chromatographed on a neutral alumina column. Hexane moved first the $Cp^*Re(CO)_3$ and then the product was eluted with a mixture of hexane–diethylether 1 : 1. Removal of the solvents, under vacuum, resulted in a pale yellow solid. Recrystallization from hexane at −10°C gave complex (**1**) (125 mg) as pale yellow crystals in 38% yield [based on $Cp^*Re(CO)_3$]. M.p.: 205–207°C. Elemental analysis for $C_{30}H_{30}O_2PRe$: Found: C, 56.4; H, 4.7. Calc.: C, 56.2; H, 4.7%. IR (CH_2Cl_2, cm^{-1}): ν(CO) 1912 (vs), 1842 (vs). ^1H NMR ($CDCl_3$): δ 1.80 (s, 15H, Cp*), 7.46 (m, 15H, Ph). $^{13}C\{^1H\}$ NMR ($CDCl_3$): δ 10.36 (s, $C_5\mathit{Me}_5$), 96.90 (s, C_5Me_5), 127.85 (d, $J = 9.9$), 129.30 (s), 133.35 (d, $J = 11.5$) and 137.80 (d, $J = 49.5$, Ph), 206.50 (d, $J = 7.8$, CO). MS: m/z 640 (M^+), 612 ($M^+ - CO$), 584 ($M^+ - 2CO$), 563 ($M^+ - Ph$).

Preparation of $Cp^*Re(CO)_2(PMe_2Ph)$ (**2**)

A procedure similar to that used in the synthesis of (**1**) gave the product in 45% yield as pale yellow crystals. M.p. 106–108°C. Elemental analysis for $C_{20}H_{26}PO_2Re$: Found: C, 46.2; H, 4.9. Calc.: C, 46.5; H, 5.0%. IR (CH_2Cl_2, cm^{-1}): ν(CO) 1906 (vs), 1833 (vs). ^1H NMR ($CDCl_3$): δ 1.87 (s, 15H, Cp*), 1.88 (d, $J = 8.8$, 6H, Me), 7.52 (m, 5H, Ph). $^{13}C\{^1H\}$ NMR ($CDCl_3$): δ 10.59 (s, $C_5\mathit{Me}_5$), 22.48 (d, $J = 37.2$, $P\mathit{Me}_2Ph$), 95.82 (s, C_5Me_5), 128.11 (d, $J = 9.1$), 129.18 (s), 130.12 (d, $J = 11.1$) and 139.50 (d, $J = 48.5$, PMe_2Ph), 206.63 (d, $J = 7.0$, CO). MS: m/z 516 (M^+), 501 ($M^+ - Me$), 488 ($M^+ - CO$), 460 ($M^+ - 2CO$), 445 ($M^+ - 2CO - Me$).

Preparation of $Cp^*Re(CO)_2[P(OEt)_3]$ (**3**)

This complex was prepared by following the same procedure used to prepare complex (**4**) (see below) but the photolysis was carried out in THF. It was obtained in 70% yield as slightly yellow crystals. M.p. 50–52°C. Elemental analysis for $C_{18}H_{30}PO_5Re$: Found: C, 40.0; H, 5.8. Calc.: C, 39.8; H, 5.5%. IR (CH_2Cl_2, cm^{-1}): ν(CO) 1923 (vs), 1852 (vs). ^1H NMR ($CDCl_3$): δ 1.28 (t, $J = 7.1$, 9H, $P(OCH_2CH_3)_3$) 2.07 (s, 15H, Cp*), 3.86 (q, $J = 7.1$, 6H, $P(OCH_2CH_3)_3$): $^{13}C\{^1H\}$ NMR ($CDCl_3$): δ 10.61 (s, $C_5\mathit{Me}_5$), 16.03 (s, $P(OCH_2\mathit{CH}_3)$, 60.04 (d, $J = 2.0$, $P(OCH_2Me)_3$), 96.36 (s, C_5Me_5), 204.42 (d, $J = 12.07$, CO). MS: m/z 544 (M^+), 516 ($M^+ - CO$), ($M^+ - OEt$), 471 ($M^+ - CO - OEt$).

Preparation of $Cp^*Re(CO)_2[P(OPh)_3]$ (**4**)

$Cp^*Re(CO)_3$ (300 mg, 0.74 mmol) was dissolved in 100 cm^3 of toluene. To this solution 0.5 cm^3 (1.9 mmol) of $P(OPh)_3$ was added, under stirring, and the mixture was irradiated for 45 min. Evaporation of toluene under vacuum yielded a brown oil which was dissolved in CH_2Cl_2 and chromatographed on a silica gel column. The unreacted $Cp^*Re(CO)_3$ and excess of $P(OPh)_3$ was washed from the column using hexane and compound (**4**) was eluted with diethylether. The solvent was removed with a rotary evaporator yielding a slightly yellow solid. This was crystallized from hexane to give pale yellow crystals. Yield 305 mg (60% based on starting *tricarbonyl* complex). M.p. 130–132°C. Elemental analysis for $C_{30}H_{30}O_5PRe$: Found: C, 52.5; H, 4.3. Calc.: C, 52.4; H, 4.4%. IR (CH_2Cl_2, cm^{-1}): ν(CO) 1944 (vs), 1873 (vs). ^1H NMR ($CDCl_3$): δ 1.87 (s, 15H,

Cp*), 7.35 (m, 15H, Ph). $^{13}C\{^1H\}$ NMR ($CDCl_3$): δ 10.34 (s, C_5Me_5), 96.90 (s, C_5Me_5), 121.46 (d, $J = 4.5$), 124.07 (s), 129.47(s), 153.00 (broad singlet, J not resolved, Ph), 202.55 (d, $J = 11.4$, CO). MS: m/z 688 (M^+), 660 ($M^+ - CO$), 595 ($M^+ - OPh$).

Preparation of cis-$[Cp^*Re(CO)_2[P(OPh)_3]I][I_3]$ (5-(I_3))

This complex was prepared using a method similar to that reported[6] for the PMe_3 analog, *cis*-$[Cp^*Re(CO)_2(PMe_3)I]^+$: a solution of complex (**4**) (100 mg, 0.14 mmol) in hexane (10 cm^3) was treated with a saturated solution of I_2 in hexane with stirring until all the rhenium complex had reacted (by IR). The dark red precipitate formed was separated, washed with diethyl ether, and dried *in vacuo*. Recrystallization from CH_2Cl_2–ether yielded 164 mg (95%) of dark red crystals. M.p. 79–81°C with decomposition. Elemental analysis for $C_{30}H_{30}O_5I_4PRe$: Found: C, 30.1; H, 2.5. Calc.: C, 30.2; H, 2.5%. IR (CH_2Cl_2, cm^{-1}): ν(CO) 2052 (vs), 2002 (s), (intensity ratio 1.3 : 1.0). ^1H NMR ($CDCl_3$): δ 2.52 (s, 15H, Cp*), 7.28 (m, 15H, Ph). $^{13}C\{^1H\}$ NMR ($CDCl_3$): δ 12.02 (s, C_5Me_5), 108.24 (s, C_5Me_5), 120.81 (d, $J = 4.0$), 126.76 (s), 130.31 (s), 151.27 (d, $J = 13.1$, Ph), 182.50 (d, $J = 18.3$, CO), 196.80 (d, $J = 32.0$, CO).

RESULTS AND DISCUSSION

(a) *Neutral phosphine and phosphite complexes*

The phosphine complexes $Cp^*Re(CO)_2(PR_2R')$, [R = R′ = Ph (**1**); R = Me, R′ = Ph (**2**)] were easily prepared following the method described for the synthesis of $Cp^*Re(CO)_2(PMe_3)$,[6] that is a thermal reaction of the THF complex $Cp^*Re(CO)_2(THF)$ [prepared *in situ* by irradiation of $Cp^*Re(CO)_3$ in THF] with the corresponding phosphine. A different method was used to prepare the phosphite derivatives $Cp^*Re(CO)_2[P(OR)_3]$ [R = Et (**3**); R = Ph (**4**)], which involved direct photochemical reaction of the tricarbonyl complex, dissolved in THF (**3**) or toluene (**4**), with the phosphite ligand. A possible disubstituted product $Cp^*Re(CO)[P(OR)_3]_2$ was not observed in the latter reaction even though the bisphosphine complex $Cp^*Re(CO)(PMe_3)_2$ was produced by photolysis of $Cp^*Re(CO)_3$ in the presence of PMe_3 using a 100 W medium-pressure mercury lamp and much prolonged irradiation times.[5]

Since better yields were obtained in the preparation of the phosphite compounds, the same method was also attempted to produce complexes (**1**) and (**2**). However, irradiation of $Cp^*Re(CO)_3$ in THF or toluene with an excess of phosphine produced dark yellow solutions plus some unidentified solid, which showed no ν(CO) absorptions in the IR spectra. From the solutions, only small amount of products could be isolated (10% yield).

Phosphine and phosphite complexes (**1–4**) were isolated as pale or slightly yellow crystals analytically and spectroscopically pure. They are indefinitely stable under N_2 and appear not to deteriorate when exposed to air and light over a period of days. They are soluble in most common organic solvents.

The carbonyl stretching region of the IR spectra of compounds **1–4** consists of two very strong absorption bands near 1930 and 1850 cm^{-1}. As expected these bands are shifted by about 20 cm^{-1} to lower frequencies than those reported for the corresponding Cp analogs.[3] Frequencies decrease in the order $P(OPh)_3 > P(OEt)_3 > PPh_3 > PMe_3Ph$. This is the same order found in the compounds $CpMn(CO)_2(PR_3)$[9,10] and indicates an increase of electron density on the metal as a result of the phosphorus ligands. The observed trend is consistent with that expected from relative basicity and acceptor ability of phosphorus ligands.[11,12]

The electron impact mass spectra of **1–4** clearly established the molecular ion and showed fragments corresponding to loss of CO. In none of the cases is the loss of the intact phosphorus ligand observed.

The ^1H NMR spectra of these complexes showed no unusual features, a singlet for Cp* (between δ 1.80–2.07) and the resonances attributed to the phosphorus ligand. The $^{13}C\{^1H\}$ NMR spectra, in addition to the single resonances for the Cp* and the corresponding carbons of PR_3, showed a doublet in the low field region (δ 204) for the carbonyl carbon resonance. The resonances for the phosphite complexes (**3**) and (**4**) are more shielded and have the greater $^2J_{CP}$, in agreement with the well-established better π-acceptor properties of these ligands compared with the phosphines.[11–14]

(b) *The cationic phosphite complex*, cis-$[Cp^*Re(CO)_2\{P(OPh)_3\}I]^+$ (**5**)

The reaction of the dicarbonyltriphenylphosphite complex (**4**) with I_2 in hexane resulted in an oxidative addition of the iodo ligand with almost quantitative formation of cationic complex **5**. Similar reactions have been observed for $Cp^*Re(CO)_3$[14] and $Cp^*Re(CO)_2(PMe_3)$[6] with I_2. In the IR spectrum of this dark-red, air stable crystalline compound, two ν(CO) absorptions are observed. As expected, they are shifted by more than 100 cm^{-1} to higher frequencies when compared with **4**. The

higher wavenumber band, ν_s(CO) is stronger than ν_{as}(CO), which we interpret to indicate a *cis* orientation of the CO groups by comparison with other dicarbonyl complexes possessing a four-legged piano stool type of structure.[6,14] The *cis* stereochemistry was also confirmed by ^{13}C NMR. In fact, the ^{13}C NMR spectrum of **5** in the CO region showed two doublets at δ 182.50, $J = 18.3$ and 196.80, $J = 32.0$ indicating the non-equivalence of the COs as expected for a *cis* configuration of these groups. We tentatively assign the resonance at higher δ value having the greater ^2J(CP) value to the CO group *cis* to the $P(OPh)_3$ ligand, in an analogous manner to the assignment made in the *cis*-$[Cp^*Re(CO)_2(PMe_3)I]^+$ complex.[6]

Attempts to isomerize **5** to the less hindered *trans* isomer were unsuccessful. The complex was recovered unchanged when boiled in THF for 6 h. After 2 h in refluxing toluene total decomposition was observed.

The formation of only one isomer for this iodo complex is not surprising since it has been tentatively established that the *cis* configuration is preferred to *trans* for the complexes $[Cp^*Re(CO)_2(PMe_3)X]^+$ when the halogen is changed from Cl through Br to I.[6] However, it is important to mention at this point that only the *trans* configuration has been found in the manganese cationic complexes resulting from the reaction of $(C_5H_4Me)Mn(CO)_2L$ ($L = PEt_3$, PPh_3, PMe_2Ph and $P(OPh)_3$) or $Cp^*Mn(CO)_2(PPh_3)$ with I_2.[15] Accordingly, more work has to be done to establish the factors influencing the stereochemistry in these types of complexes.

Acknowledgements—The authors acknowledge Professor D. Sutton for allowing us to obtain the NMR, MS, IR and EA at the Chemistry Department of Simon Fraser University. This work was supported by FONDECYT Chile through an operating grant to A.H.K. (155-89), and Universidad Católica de Valparaíso project 125.761/90.

REFERENCES

1. M. S. Wrighton, *Chem. Rev.* 1974, **74**, 401.
2. P. J. Giordano and M. S. Wrighton, *Inorg. Chem.* 1977, **16**, 160.
3. A. N. Nesmeyanov, N. E. Kolobova, Ye. V. Makarov, B. L. Lokshin and E. B. Rusach, *Isv. Akad. Nauk SSSR, Ser. Khim.* 1976, **3**, 629.
4. C. P. Casey, J. M. O'Connor, W. D. Jones and K. J. Haller, *Organometallics* 1983, **2**, 535.
5. R. G. Bergman, P. F. Seidler and T. T. Wenzel, *J. Am. Chem. Soc.* 1985, **107**, 4358.
6. A. H. Klahn-Oliva, R. D. Singer, J. M. Aramini and D. Sutton, *Inorg. Chem.* 1989, **28**, 4217.
7. J. K. Hoyano and W. A. G. Graham, *J. Chem. Soc., Chem. Commun.* 1982, 27.
8. A. T. Patton, C. E. Strouse, C. B. Knobler and J. A. Gladysz, *J. Am. Chem. Soc.* 1983, **105**, 5804.
9. W. Strohmeier and F. J. Muller, *Chem. Ber.* 1967, **100**, 2812; *Z. Naturforsch. B* 1967, **22**, 451.
10. G. M. Bodner, *Inorg. Chem.* 1974, **13**, 2563.
11. W. A. G. Graham, *Inorg. Chem.* 1968, **7**, 315.
12. Md. M. Rahman, H.-Y. Liu, K. Eriks, A. Prock and W. P. Giering, *Organometallics* 1989, **8**, 1.
13. G. M. Bodner and L. J. Todd, *Inorg. Chem.* 1974, **13**, 1335.
14. F. W. B. Einstein, A. H. Klahn-Oliva, D. Sutton and K. G. Tyers, *Organometallics* 1986, **5**, 53.
15. N. G. Connelly and M. D. Kitchen, *J. Chem. Soc., Dalton Trans.* 1977, 931.

Polyhedron Vol. 10, No. 16, pp. 1877–1882, 1991
Printed in Great Britain

0277–5387/91 $3.00+.00
© 1991 Pergamon Press plc

THE EFFECT OF SODIUM CATIONS ON THE MOLECULAR DYNAMICS OF N-ACETYLAZA-15-CROWN-5†

GRAHAM C. SAUNDERS

Inorganic Chemistry Laboratory, South Parks Road, Oxford OX1 3QR, U.K.

(*Received* 19 *April* 1991; *accepted* 20 *May* 1991)

Abstract—N-acetylaza-15-crown-5 exhibits restricted rotation about the amide N—C bond, with a value of the free energy of activation, ΔG^*, of 73 ± 1 kJ mol^{-1}, as determined by dynamic ^{13}C-{^1H} NMR spectroscopy. Addition of sodium cations leads to a reduction in ΔG^* which is dependent upon the amount of sodium cations added. ΔG^* falls to 54 ± 1 kJ mol^{-1} with three equivalents of Na^+. A simple mathematical model is used to explain the variation of ΔG^* with sodium cations.

Alkali metal cation binding by non-cyclic and cyclic polyethers has been investigated by a number of NMR spectroscopic techniques. Most studies have concentrated on shifts of δ in the ^{13}C and ^1H NMR spectra,[1,2] changes in the value of the spin-lattice relaxation time, T_1,[1,3] and alkali metal NMR spectroscopy.[4] Conformational changes of complexed and uncomplexed crown ethers upon cooling have also been investigated by variable temperature ^{13}C and ^1H NMR spectroscopy.[5] The study of restricted rotation about amide N—C bonds by variable temperature ^{13}C and ^1H NMR spectroscopy in some ferrocene derivatives containing crown ether groups has been reported,[6] but the effect of adding alkali metal cations on the dynamic NMR of these compounds has not. Prior to our study of the effects of alkali metal cations upon the molecular dynamics of bis(aza-15-crown-5)thiuram disulphide‡ (**1**),[7] the only reported investigation into the effects of alkali metal cations upon restricted rotation was that into the molecular dynamics of non-cyclic amides by Jagur-Grodzinski and co-workers.[8] They report an increase in the activation energy for rotation about the amide N—C bond, E_A, of 16 ± 5 kJ mol^{-1} for amide **2** upon the addition of two equivalents of lithium perchlorate in [^2H]$_3$-nitromethane. This can be attributed to an interaction between the lithium cation and the amide oxygen atoms, which through inductive and resonance effects increases the π-electron donation into the N—C bonds from the nitrogen atoms.

Herein is reported the effect of sodium cations upon the molecular dynamics of N-acetylaza-15-crown-5 (**3**) and a mathematical model to explain the effects of cations on the molecular dynamics of compounds **1** and **3**.

RESULTS AND DISCUSSION

Reaction of aza-15-crown-5 with excess acetyl chloride gave N-acetylaza-15-crown-5 (**3**) in *ca* 35% yield as a pale brown oil (Scheme 1), which was characterized by IR, ^1H and ^{13}C NMR spectroscopy and mass spectrometry. The 1 : 1 $NaBPh_4$ complex of **3** and **4**, was prepared by slow evaporation of a dichloromethane solution of a mixture of **3** and $NaBPh_4$. Complex **4** was obtained as a cream-coloured microcrystalline solid, which was characterized by elemental analysis, and IR and ^1H NMR spectroscopy. Both **3** and **4** showed strong bands in their IR spectra at *ca* 1630 cm^{-1}, assigned to the amide C=O stretch. The ^1H NMR spectrum of **3** recorded in [^2H]$_3$-acetonitrile showed a triplet, two multiplets and a singlet, with relative intensities 2 : 14 : 4 : 3. The first three sets of resonances are assigned to the crown-ether ring hydrogen atoms and the singlet to the methyl hydrogen atoms. The ^{13}C-{^1H} NMR spectrum recorded in [^2H]$_3$-acetonitrile at 300 K includes two singlets at 51.8 and 49.3 ppm, assigned to the α-carbon atoms, and six peaks between 69 and 72 ppm, assigned to the other crown-ether ring carbon atoms. These data indicate that, as expected, there is restricted rotation about

† 13-acetyl-1,4,7,10-tetraoxo-13-azacyclopentadecane.

‡ 13,13′ - (1,4 - dithioxo - 2,3 - dithiabutane - 1,4 - diyl) di(1,4,7,10-tetraoxo-13-azacyclopentadecane).

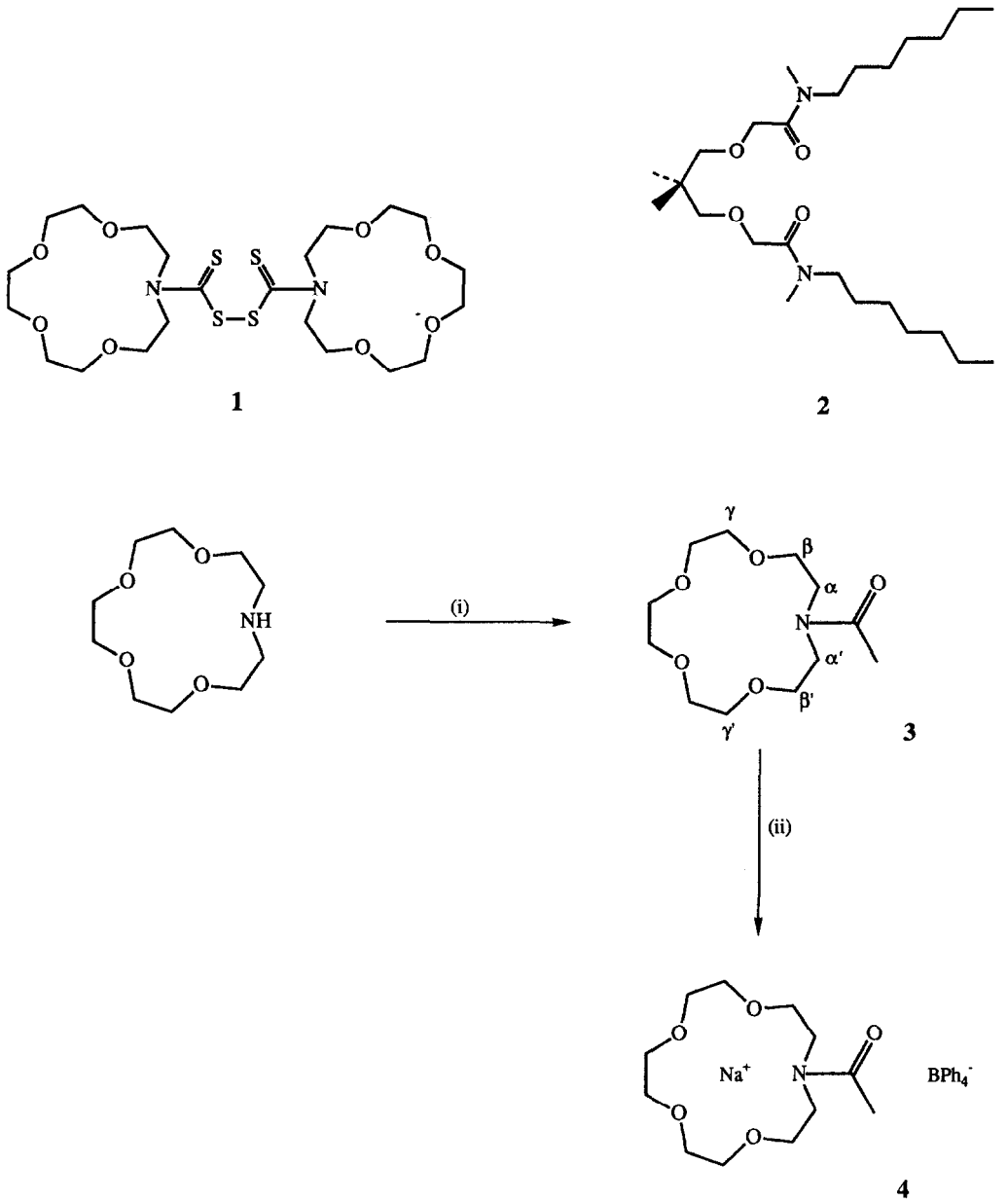

Scheme 1. (i) CH_3COCl, 34%; (ii) $NaBPh_4$, CH_2Cl_2.

the amide N—C bond, which at 300 K causes the inequivalence of the α, β and γ pairs of carbon atoms. At 342 K no coalescence of any of the pairs of peaks was observed.

From eq. (1)[9] the rate constant may be obtained, then from the Eyring equation [eq. (2)],[10] a value for the free energy of activation, ΔG^*, may be calculated. (Contrary to the results reported in the original Holm-Gutowsky papers the overall rate constant is twice the observed rate constant, i.e. $k = 2k_c'$.[11]) The lack of any coalescence at 342 K indicates that ΔG^* is greater than 72.5 kJ mol^{-1}.

$$k_c' = \pi \cdot \delta\nu/(2)^{1/2} \quad (1)$$

$$k = (\kappa k_B T/h)e^{-(\Delta G^*/RT)} \quad (2)$$

Variable temperature ^{13}C-{^1H} NMR spectra of (3) in $[^2H]_8$-toluene gave a value of ΔG^* of 73 ± 1 kJ mol^{-1}.

The ^1H NMR spectrum of **4** in $[^2H]_3$-acetonitrile includes a multiplet, a triplet and a singlet with relative intensities 16:4:3, which are assigned to the 16 OCH_2 crown-ether hydrogen atoms, the four NCH_2 hydrogen atoms and the methyl hydrogen atoms, respectively. Thus, the complexation of a sodium cation by **3** has a significant effect upon the ^1H NMR spectrum. In particular, the NCH_2 hydrogen atoms which are inequivalent in **3** are

equivalent in **4**, suggesting that complexation of a sodium cation has a dramatic effect upon the rotation about the N—CO bond. The IR spectra and the lack of any significant shift of δ for the methyl hydrogen resonance shows that the sodium cation has little effect upon the C=O bond.

The effect of sodium cations upon the value of ΔG^* for **3** at a concentration of 0.1 M in $[^2H]_3$-acetonitrile was investigated by variable temperature $^{13}C-\{^1H\}$ NMR spectroscopy. The spectra indicated that, as expected, intermolecular exchange of the sodium cations is fast on the NMR timescale, and thus the methylene carbon atoms of uncomplexed and complexed **3** gave rise to averaged signals. The results are shown in Fig. 1. Addition of *ca* 0.02 equivalents of $NaBPh_4$ caused a decrease in ΔG^* of *ca* 6 kJ mol^{-1}, and addition of 0.9 equivalents of $NaBPh_4$ led to a decrease in ΔG^* of *ca* 16 kJ mol^{-1}. This decrease in ΔG^* implies that sodium cations interact with the nitrogen atom so as to withdraw electron density available for π-bonding in the N—C bond, and not with the amide oxygen atom, which would have caused an increase in the value of ΔG^*, as observed for **2**. The interaction with the nitrogen atom is due to the preferential binding of the cation to the crown-ether heteroatoms over that to the amide oxygen atom. The ^{23}Na NMR spectrum of $NaBPh_4$ in the presence of excess **3** in $[^2H]_3$-acetonitrile gave a value of the width at half-height, $\Delta\nu(1/2)$, of the single peak observed of 130 Hz, compared to the value of 16 Hz for $NaBPh_4$ alone. Further, the $^{13}C-\{^1H\}$ NMR spectrum of **3** with $NaBPh_4$ added showed shifts of the resonances of the crown ether and amide NCO carbon atoms from those of **3** alone. These data together with the ^1H NMR and IR spectra of **4** confirm that the sodium cations are bound by the crown-ether rings.

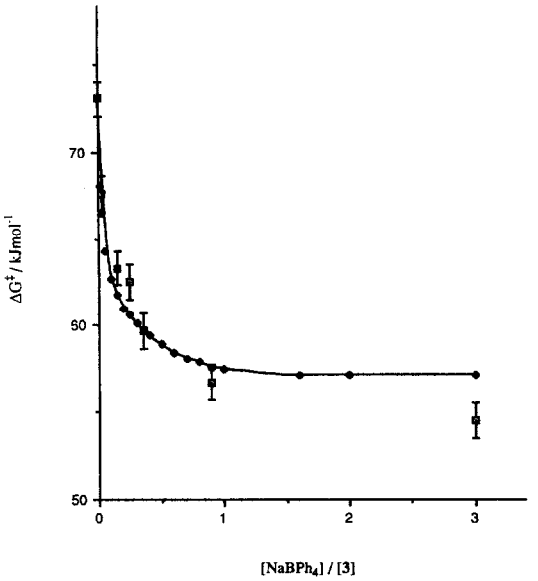

Fig. 1. Plot of ΔG^* for rotation about the amide N—C bond of **3** against equivalents of $NaBPh_4$ (experimental values are shown with error bars, the line represents the theoretical values derived from $K = 250$ mol^{-1} dm^3, $\Delta G^*_{uncomp} = 73$ kJ mol^{-1}, $\Delta G^*_{comp} = 57$ kJ mol^{-1}, at a concentration of **3** of 0.1 M).

Addition of excess $NaBPh_4$ to **3** might be expected to lead to an increase in ΔG^* from a minimum value due to the sodium cation–amide oxygen atom interaction becoming significant as the amount of uncomplexed cations available to interact with the amide oxygen atom increases. However the variable temperature $^{13}C-\{^1H\}$ NMR spectra of **3** with three equivalents of $NaBPh_4$ gave a value of ΔG^* of 54 ± 1 kJ mol^{-1}, which is significantly lower than with 0.9 equivalents of $NaBPh_4$. This indicates that the sodium cation–amide oxygen atom interaction is weak, especially in comparison to the lithium cation–amide oxygen atom interaction in amide **2**.

The shape of the plots of ΔG^* against equivalents of $NaBPh_4$ for thiuram disulphide **1** and amide **3** are similar, and a suitable model can be applied to provide an explanation. For a simple crown-ether amide such as **3**, where intermolecular cation exchange is fast on the NMR timescale, the rate constant for rotation about the amide N—C bond at temperature T, k_T, can be assumed to be the weighted average of the rate constants for the uncomplexed and complexed molecules, k_T^1 and k_T^2, respectively; given by eq. (3).

$$k_T = (1-X)k_T^1 + Xk_T^2; \quad (3)$$

where X is the proportion of complexed crown ether at any instant. An expression for X may be derived from eqs (4)–(6) [eq. (7)], which is similar to one quoted by Popov and co-workers.[12]

$$[M^+ \cdot C] = K_T[C][M^+] \quad (4)$$

$$[C]_0 = [C] + [M^+ \cdot C] \quad (5)$$

$$[M^+]_0 = [M^+] + [M^+ \cdot C]; \quad (6)$$

where $[C]_0$ and $[M^+]_0$ are the total concentrations of crown ether and cation, respectively; [C] and $[M^+]$ are the concentrations of uncomplexed crown ether and cation, respectively; and $[M^+ \cdot C]$ is the concentration of the complex.

$$X = (1/2K')\{(1 + K' + \varepsilon K') - [1 + 2K' + K'^2 + 2K'(1-K')\varepsilon + K'^2\varepsilon^2]^{1/2}\}; \quad (7)$$

where ε is the number of equivalents of cation per crown ether, $[M^+]_0/[C]_0$, and K' is related to the

binding constant of the crown ether at temperature T, K_T, by eq. (8).

$$K' = K_T[C]_0. \quad (8)$$

Thus, values of k and therefore ΔG^* may be calculated from the binding constant, K_T, the concentration of the crown ether, and the number of equivalents of $NaBPh_4$. A theoretical plot of ΔG^* against equivalents of sodium cations was calculated from eqs (2), (3), (7) and (8) using values of k^1_{293} of 0.625 s^{-1} (corresponding to a value of ΔG^* of 73 kJ mol^{-1}), k^2_{293} of 446.0 s^{-1} ($\Delta G^* = 57$ kJ mol^{-1}), and K_{293} of 250 mol^{-1} dm^3, which is a reasonable value to expect for a functionalized 15-crown-5[13] (Fig. 1). The similarity of the experimental and theoretical plots strongly suggests that the original assumption is appropriate for the system. The differences between the theoretical and experimental values of ΔG^* may be attributed to the temperature dependence of both the free energy of activation and the binding constant. The entropy for rotation about a bond is usually considered to be small, and thus the direct effect of temperature upon ΔG^* is also likely to be small. The effect upon K is likely to be large due to the large entropic change accompanying complexation by a crown ether. However, it is noted from eqs (2), (3), (7) and (8) that relatively large changes in the value of K have a small influence on ΔG^* at low equivalents ($< ca$ 0.8) of cation, and thus this technique could not be used for determining K.

This model can also be applied to explain the effects of adding sodium cations to thiuram disulphide **1**, the molecular dynamics of which has been reported previously,[7] but here the values of ΔG^* are corrected to account for the difference between the observed and overall rate constants. Making the assumption that binding of a cation by one of the crown-ether rings of **1** affects neither the binding ability nor the rotation about the N—CS_2 bond of the other crown ether ring of **1**, then eqs (4)–(7) are appropriate. K' must be multiplied by two to account for **1** possessing two crown-ether rings and ε is the number of equivalents per crown ether ring ($\varepsilon = [M^+]_0/2[\mathbf{1}]$). Values of ΔG^* calculated from eqs (2), (3), (7) and (8) for a concentration of **1** of 0.07 M (that used in the experimental study) and values of k^1_{293} of 30.9 s^{-1} ($\Delta G^* = 63.5$ kJ mol^{-1}), k^2_{293} of 320.2 s^{-1} ($\Delta G^* = 52.2$ kJ mol^{-1}), and K_{293} of 250 mol^{-1} dm^3 are shown in Fig. 2. Again the theoretical and experimental results are similar. The differences between the experimentally determined results and the theoretical values may be attributed to the temperature dependence of ΔG^* and K, and also that the assumption that binding of a cation by one crown-ether ring does not affect the other ring is not strictly true.

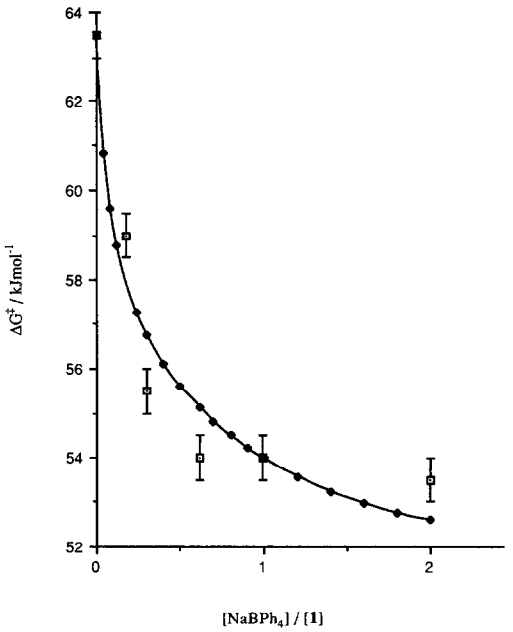

Fig. 2. Plot of ΔG^* for rotation about the N—CS_2 bonds of **1** against equivalents of $NaBPh_4$ (experimental values are shown with error bars, the line represents the theoretical values derived from $K = 250$ mol^{-1} dm^3, $\Delta G^*_{uncomp} = 63.5$ kJ mol^{-1}, $\Delta G^*_{comp} = 52.2$ kJ mol^{-1}, at a concentration of **1** of 0.07 M).

In conclusion, sodium cations cause a dramatic reduction in the free energy of activation for rotation about the amide N—C bond in N-acetyl-aza-15-crown-5, which is explained by the interaction between the cation and the nitrogen atom reducing the amount of π-electron density available for bonding in the N—C bond. A simple mathematical model relating the value of ΔG^* to the binding constant of the crown ether and the amount of cation added is shown to be applicable and theoretical values of ΔG^* for thiuram disulphide **1** and amide **3** agree well with those determined experimentally.

EXPERIMENTAL

^1H, ^{13}C and ^{23}Na NMR spectra were recorded on a Brüker AM300 spectrometer. ^1H NMR spectra were recorded at 300 MHz and referenced internally using the residual protio solvent resonance relative to tetramethylsilane ($\delta = 0$ ppm). ^{13}C NMR spectra were recorded at 75.47 MHz and referenced internally using the solvent resonance relative to tetramethysilane ($\delta = 0$ ppm). ^{23}Na NMR spectra were recorded at 79.35 MHz and

referenced externally to 3 M NaCl in $[^2H]_2$-water ($\delta = 0$ ppm). All chemical shifts are quoted in δ (ppm) and coupling constants in Hz. Abbreviations used in multiplicities are s = singlet, t = triplet and m = multiplet. The variable temperature unit of the NMR spectrometer was calibrated by use of a thermocouple immersed in toluene within an NMR tube. Temperatures were accurate to within ± 1 K.

IR spectra were recorded neat between CsI plates or as a CsI pellet on a Perkin–Elmer IR Fourier transform spectrometer. The mass spectrum was recorded on an AEI m.s. 902 mass spectrometer updated by a data handling system supplied by Mass Spectroscopy Services Ltd.

Where necessary solvents were dried over activated molecular sieves and distilled under nitrogen from over phosphorus pentoxide (dichloromethane). $[^2H]_3$-acetonitrile was dried by storage over activated molecular sieves. Chromatography was performed on columns of neutral alumina (Fluka) deactivated with 6% w/w water.

Aza-15-crown-5 was prepared as described in the literature.[14] Sodium tetraphenylborate (Aldrich) was dried by heating at 80°C *in vacuo* for several hours and stored under nitrogen.

N-Acetylaza-15-crown-5 (**3**)

Acetyl chloride (*ca* 7 cm^3, 0.1 mol) was added slowly to aza-15-crown-5 (1.22 g, 5.6 mmol) in diethyl ether (50 cm^3) and stirred for 10 min. A white precipitate was formed. Sodium hydroxide (2 g) in water (10 cm^3) was added and the diethyl ether allowed to evaporate. The pale yellow aqueous solution was extracted with dichloromethane (5×20 cm^3). The combined extracts were dried over magnesium sulphate, filtered and the solvent removed by rotary evaporation affording a brown oil. Chromatography with 1:1 petroleum ether/dichloromethane as eluant separated the product as a pale brown oil, which was dried *in vacuo*. Yield 0.50 g (34%). Mass spectrum, *m/z* (%): 261 (22), 262 (71), 263 (37) [$(M+H)^+$], 219 (100), 220 (44) [$(M—CH_3CO)^+$]. ^1H (300 MHz, $[^2H]_3$-acetonitrile): 3.69 [t, $^3J(H_\alpha H_\beta$ or $H_{\alpha'}H_{\beta'})$ 6.2 Hz, 2H, H_α or $H_{\alpha'}$], 3.57 (m, 14H, OCH_2), 3.45 (m, 4H, OCH_2), 2.02 (s, 3H, CH_3). ^{13}C-{^1H} (75.47 MHz, $[^2H]_3$-acetonitrile): 171.4 (NCO), 71.6, 71.4, 71.0, 70.8, 70.6, 69.8 (OCH_2), 51.8 and 49.3 (C_α and $C_{\alpha'}$), 22.0 (CH_3). ν (neat) 1629 cm^{-1} (NC=O).

N-Acetylaza-15-crown-5 sodium tetraphenylborate (**4**)

3 (*ca* 0.2 g, 0.8 mmol) and $NaBPh_4$ (excess) were dissolved in acetonitrile (20 cm^3). The solvent was removed under reduced pressure and the solid stirred in dichloromethane for 2 h. The solution was filtered and the solvent removed under reduced pressure to give small cream-coloured crystals of **4**. Found: C, 69.4; H, 7.05; N, 2.2. Calc. for $C_{36}H_{43}NO_5NaB(CH_2Cl_2)_{0.25}$: C, 69.7; H, 7.0; N, 2.2%. ^1H (300 MHz, $[^2H]_3$-acetonitrile): 7.29 (m, 8H, BPh_4), 7.03 [t, ^3J(HH) 7.3 Hz, 8H, BPh_4], 6.85 [t, ^3J(HH) 7.3 Hz, 4H, BPh_4], 5.46 (s, 0.5H, CH_2Cl_2), 3.58 (m, 16H, OCH_2), 3.46 [t, $^3J(H_\alpha H_\beta)$ 5.8 Hz, 4H, NCH_2], 2.03 (s, 3H, CH_3). ν (CsI) 1632 cm^{-1} (NC=O).

Acknowledgements—The author thanks MediSense (U.K.) Ltd and the S.E.R.C. for support. He is also grateful to Professor M. L. H. Green for his support and Dr A. Sella for helpful discussion.

REFERENCES

1. R. Büchi and E. Pretsch, *Helv. Chim. Acta* 1977, **60**, 1141.
2. E. Amble and E. Amble, *Polyhedron* 1983, **2**, 1063; T. W. Robinson and R. A. Bartsch, *J. Chem. Soc., Chem. Commun.* 1985, 990; P. D. Beer, *J. Chem. Soc., Chem. Commun.* 1985, 1115; 1986, 1678.
3. P. D. J. Grootenhuis, E. J. R. Sudholter, C. J. Van Staveren and D. N. Reinhoudt, *J. Chem. Soc., Chem. Commun.* 1985, 1426.
4. Y. M. Cahen, J. L. Dye and A. I. Popov, *J. Phys. Chem.* 1975, **79**, 1289; A. J. Smetana and A. I. Popov, *J. Solution Chem.* 1980, **9**, 183; E. Kauffman, J. L. Dye, J.-M. Lehn and A. I. Popov, *J. Am. Chem. Soc.* 1980, **102**, 2274; J. D. Lin and A. I. Popov, *J. Am. Chem. Soc.* 1981, **103**, 3773; J. Bouquant, A. Delville, J. Grandjean and P. Laszlo, *J. Am. Chem. Soc.* 1982, **104**, 686; A. S. Galiano-Roth and D. B. Collum, *J. Am. Chem. Soc.* 1988, **110**, 3546; R. T. Streeper and S. Khazaeli, *Polyhedron* 1991, **10**, 221.
5. J.-M. Lehn, J.-P. Sauvage and B. Dietrich, *J. Am. Chem. Soc.* 1970, **92**, 2916; F. A. L. Annet, J. Krane, J. Dale and K. Daasvatn, *Acta Chem. Scand.* 1973, **27**, 3395; G. Borgen, J. Dale, K. Daasvatn and J. Krane, *Acta Chem. Scand., Sect. B* 1980, **34**, 249; J. Krane, E. Amble, J. Dale and K. Daasvatn, *Acta Chem. Scand., Sect. B* 1980, **34**, 255.
6. P. J. Hammond, A. P. Bell and C. D. Hall, *J. Chem. Soc., Perkin Trans. I* 1983, 707; P. D. Beer, *J. Organomet. Chem.* 1985, **297**, 313; P. D. Beer and A. D. Keefe, *J. Organomet. Chem.* 1986, **306**, C10; P. J. Hamond, P. D. Beer, C. Dudman, I. P. Danks, C. D. Hall, J. Knychala and M. C. Grossel, *J. Organomet. Chem.* 1986, **306**, 367.
7. M. L. H. Green, S. R. Marder, G. C. Saunders and N. M. Walker, *J. Chem. Soc., Dalton Trans.* 1988, 1697; J. Granell, M. L. H. Green, V. J. Lowe, S. R. Marder, P. Mountford, G. C. Saunders and N. M. Walker, *J. Chem. Soc., Dalton Trans.* 1990, 605.

8. U. Olsher, G. A. Elgavish and J. Jagur-Grodzinski, *J. Am. Chem. Soc.* 1980, **102**, 3338.
9. D. Kost, E. H. Carlson and M. Raban, *J. Chem. Soc., Chem. Commun.* 1971, 656.
10. H. Eyring, *Chem. Rev.* 1935, **17**, 65; J. Sandström, *Dynamic N.M.R. Spectroscopy*. Academic Press, London (1982).
11. J. W. Faller, *Adv. Organomet. Chem.* 1977, **16**, 205.
12. R. L. Bodner, M. S. Greenberg and A. I. Popov, *Spectrosc. Lett.* 1972, **5**, 489.
13. F. De Jong and D. N. Reinhoudt, *Adv. Phys. Org. Chem.* 1980, **17**, 279; A. Masuyama, Y. Nakatsuji, I. Ikeda and M. Okahara, *Tetrahedron Lett.* 1981, **22**, 4665.
14. H. Maeda, S. Furuyoshi, Y. Nakatsuji and M. Okahara, *Bull. Chem. Soc. Japan* 1983, **56**, 212.

Polyhedron Vol. 10, No. 16, pp. 1883–1887, 1991
Printed in Great Britain

0277–5387/91 $3.00+.00
© 1991 Pergamon Press plc

THE CRYSTAL AND MOLECULAR STRUCTURE OF BIS(2,2′:6′,2″-TERPYRIDINE)MAGNESIUM PERCHLORATE MONOHYDRATE

EDWIN C. CONSTABLE* and JOHN HEALY

University Chemical Laboratory, Lensfield Road, Cambridge CB2 1EW, U.K.

and

MICHAEL G. B. DREW*

Department of Chemistry, The University, Whiteknights, Reading RG6 2AD, U.K.

(*Received* 26 *November* 1990; *accepted* 20 *May* 1991)

Abstract—The complex $[Mg(terpy)_2][ClO_4]_2 \cdot H_2O$ (terpy = 2,2′:6′,2″-terpyridine) may be prepared by the direct reaction of magnesium perchlorate with 2,2′:6′,2″-terpyridine. The magnesium is in a pseudo-octahedral environment very similar to that observed in transition metal *bis*-(2,2′:6′,2″-terpyridine) complexes. Crystallographic data: space group $I4_1/a$, $a = 12.531(13)$, $c = 40.52(4)$ Å, $V = 2912$ Å^3, $Z = 8$.

2,2′:6′,2″-Terpyridine (terpy) is a ligand which has found very widespread application in coordination chemistry.[1] The ligand shows all of the versatility of its bidentate analogue 2,2′-bipyridine (bipy)[2,3] and forms complexes with representatives from most of the groups of the periodic table, although those with the transition elements have attracted by far the greatest attention. In general, 2,2′:6′,2″-terpyridine acts as a terdentate chelating ligand, although isolated examples of a bidentate bonding mode have been described.[4–7a] Although the coordination chemistry of the alkali metals and the alkaline earths is dominated by interactions with anionic or oxygen donor ligands, we and others have recently demonstrated that these metal ions form remarkably stable complexes with macrocyclic ligands[8–15] containing only sp^2-hybridized nitrogen donor atoms. Although there have been isolated reports over the years regarding the interactions of the group 1 and group 2 metal ions with open-chain oligopyridine and 1,10-phenanthroline ligands,[16–22] few such complexes have been reported for the terdentate ligand 2,2′:6′,2″-terpyridine (terpy).[22] We have been particularly interested in the interactions of magnesium ions with 2,2′:6′,2″-terpyridine in view of the previous reports of the formation of a relatively stable 1:1 complex ($K = 5.858 \pm 0.023$) in water.[23,24] The solid state species $Mg(NO_3)_2 \cdot terpy \cdot 2H_2O$ has been described, but nothing is known about the coordination environment about the metal atom.[22] This report is concerned with the preparation and structural characterization of the complex $[Mg(terpy)_2][ClO_4]_2 \cdot H_2O$.

EXPERIMENTAL

IR spectra were recorded in compressed KBr pellets on a Perkin–Elmer FT 910 spectrometer; ^{1}H NMR spectra were recorded on Brüker WM 250 or AM 400 spectrometers. Fast atom bombardment (FAB) mass spectra were recorded on a Kratos MS50 mass spectrometer. 2,2′:6′,2″-Terpyridine was prepared as described previously.[25]

Preparation

A solution of $[Mg(H_2O)_6][ClO_4]_2$ (0.165 g, 0.50 mol) in boiling MeCN (25 cm^3) was added to a solution of 2,2′:6′,2″-terpyridine (0.23 g, 0.100 mol) in warm $CHCl_3$ (10 cm^3) to yield a voluminous off-white precipitate. The resulting suspension was heated to reflux for 1 h, cooled, and the solid collected by filtration. The solid was washed with water

* Authors to whom correspondence should be addressed.

(3×1 cm^3) and diethyl ether (3×1 cm^3) and dried *in vacuo* to yield $[Mg(terpy)_2][ClO_4]_2$ as a pale yellow solid. Yield: 0.2 g; 58%. Found: C, 52.3; H, 3.2; N, 12.4. Calc. for $C_{30}H_{22}Cl_2MgN_6O_8$: C, 52.2; H, 3.2; N, 12.4%.

Crystal structural determination of $[Mg(terpy)_2][ClO_4]_2 \cdot H_2O$

Crystals of the monohydrated complex were obtained by the diffusion of diethyl ether vapour into a solution of $[Mg(terpy)_2][ClO_4]_2$ in reagent grade acetonitrile. A very pale pink single crystal of approximate size $0.25 \times 0.3 \times 0.3$ mm was mounted in a capillary and set up to rotate about the {*110*} direction on a Stoe Stadi2 diffractometer and data collected via variable width ω scan. Background counts were for 20 s, and a scan rate of 0.0333° s^{-1} was applied to a width of $(1.5+\sin\mu/\tan\theta)$. A total of 3149 independent reflections were measured with a 2θ(max) of 50°, of which 1260 with $I > 2\sigma(I)$ were used in subsequent refinement.

Starting coordinates for the cation were taken from those of isomorphous structures.[26-30] The perchlorate anion and one water molecule with half occupancy were located in a difference Fourier map. Unlike the anions in the other isostructural compounds, the perchlorate anion showed no sign of disorder. Hydrogen atoms of the 2,2′:6′,2″-terpyridine ligands were placed in trigonal positions with a common refineable thermal parameter (one for each ligand). The structure was given a weighting scheme in the form $\omega = 1/[\sigma_2(F)+0.003F^2]$. The final R value was 0.081 ($R_w = 0.085$). In the final cycle of refinement all shift/error ratios were $< 0.3\sigma$. The final difference Fourier map had no peaks larger than 0.3 e Å^{-3}. Calculations were carried out using SHELX 76[31] and some of our own programs on the Amdahl 5870 at the University of Reading. Pertinent crystallographic data are given in Table 1 and bond distances and bond angles within the metal coordination sphere are given in Table 2.

Table 1. Crystal data for $[Mg(terpy)_2][ClO_4]_2 \cdot H_2O$

Formula	$C_{30}Cl_2H_{24}MgN_6O_9$
f_w	707.4
Space group	$I4_1/a$
a (Å)	12.531(13)
c (Å)	40.52(4)
V (Å^3)	6362
Z	8
$F(000)$	2912
d_{meas} (g cm^{-3})	1.47
d_{calc} (g cm^{-3})	1.48
Crystal size (mm)	$0.25 \times 0.3 \times 0.3$
μ(Mo-K_α) (cm^{-1})	2.94
Data collection instrument	Stoe Stadi2
Radiation	Mo-K_α ($\lambda = 0.7107$ Å)
Number of unique data	3149
Total with $I \geqslant 2\sigma(I)$	1260
R^a	0.081
R'^b	0.085
Weighting scheme	$w = 1/[\sigma^2F+0.003F^2]$

[a] $R = \Sigma[|F_o|-|F_c|]/\Sigma|F_o|$.
[b] $R' = \Sigma w^{1/2}[|F_o|-|F_c|]/\Sigma w^{1/2}|F_o|$.

RESULTS AND DISCUSSION

Very little is known concerning the coordination chemistry of 2,2′:6′,2″-terpyridine with group 2 metal ions. The complexes $Mg(NO_3)_2 \cdot 2H_2O$, $Ca(SCN)_2 \cdot 2terpy \cdot H_2O$ and $Ba(SCN)_2 \cdot terpy \cdot H_2O$ have been reported, but are of unknown structure.[20] The radical anions generated by the reaction of 2,2′:6′,2″-terpyridine with group 2 metals in inert solvents have been studied, and there is ESR evidence for the formation of contact ion-pairs or coordination compounds of significant lifetime, although no further characterization has been made.[4] The only other species which has been described is a 1:1 complex with magnesium sul-

Table 2. Important bond distances (Å) and bond angles (°) within the coordination sphere for $[Mg(terpy)_2][ClO_4]_2 \cdot H_2O$

Distances			
Mg—N(10)	2.109(8)	Mg—N(19)	2.247(6)
Mg—N(20)	2.050(10)	Mg—N(29)	2.244(7)
Angles			
N(10)—Mg—N(19)	74.42(20)	N(10)—Mg—N(20)	180.0
N(19)—Mg—N(20)	105.58(20)	N(10)—Mg—N(29)	105.59(20)
N(19)—Mg—N(29)	96.05(22)	N(20)—Mg—N(29)	74.41(20)
N(19)—Mg—N(19)	149.82(23)	N(19)—Mg—N(29)	92.20(20)

phate which has been characterized as a solution species in aqueous solutions containing the two components.[23,24]

The reaction of magnesium perchlorate with 2,2′ : 6′,2″-terpyridine in a mixed acetonitrile–chloroform solvent yields a white solid. The same product may be obtained from reaction in methanolic solution, and is not decomposed upon treatment with water. X-ray quality crystals may be obtained by the slow diffusion of ether vapour into an acetonitrile solution. The ^{1}H NMR spectrum of a solution of the crystalline compound dissolved in CD_3CN is shown in Fig. 1. This clearly demonstrates that a single 2,2′ : 6′,2″-terpyridine containing product is obtained. The ^{1}H NMR spectrum differs significantly from those of 2,2′ : 6′,2″-terpyridine or 2,2′ : 6′,2″-terpyridinium salts in CD_3CN. This is an important observation, as 2,2′ : 6′,2″-terpyridinium salts are a possible (indeed, in view of the ancitipated low stability of the magnesium salts, a likely) product from the reaction. The ^{1}H NMR spectrum of the compound exhibits a doublet of doublets (δ 7.40, 2H, H_5), a doublet (δ 7.84, 2H, H_6), a triplet of doublets (δ 8.17, 2H, H_4), a doublet (δ 8.53, 2H, H_3) and an AB_2 apparent triplet (δ 8.69, 3H, $H_{3',4',5'}$). The most notable feature is the upfield shift of H_6 with respect to 2,2′ : 6′,2″-terpyridine (δ 8.7) and the downfield shift of $H_{4'}$ (δ 8.1). The upfield shift of H_6 is a feature which is commonly observed in *pseudo*-octahedral *trias*(2,2′-bipyridine) and *bis*(2,2′ : 6′,2″-terpyridine) complexes,[1,32,33] and is usually ascribed to the shielding experienced by these protons lying above another pyridine ring. The FAB mass spectrum of the complex exhibits peaks at *m/z* 490 ({[Mg(terpy)$_2$]}$^{2+}$) and *m/z* 257 ({[Mg(terpy)]}$^+$). These results strongly suggest that a salt containing the six-coordinate $[Mg(terpy)_2]^{2+}$ cation has been formed.

The crystal and molecular structure of the cation in the complex $[Mg(terpy)_2][ClO_4]_2 \cdot H_2O$ is presented in Fig. 2. The structure consists of discrete $[Mg(terpy)_2]^{2+}$ cations with crystallographically imposed C_2 symmetry, together with perchlorate anions in general positions and a water molecule with half occupancy. This structure is startlingly reminiscent of a transition metal *bis*(2,2′ : 6′,2″-terpyridine) complex, and indeed is isomorphous with the compounds $[Co(terpy)_2][ClO_4]_2 \cdot 0.5H_2O$,[26] $[Co(terpy)_2][ClO_4]_2 \cdot 1.3H_2O$,[27] $(Co(terpy)_2][NO_3]_2 \cdot 2H_2O$,[28] and $[Cu(terpy)_2][NO_3]_2$.[29,30] In these structures the anions and water molecules lie in channels created by staggered layers of the $[Co(terpy)_2]^{2+}$ cations. In the present structure no disorder was noted in the perchlorate counter ions, although in all of the previously reported complexes the anions were disordered in some way. The dimensions and anisotropic thermal parameters of the

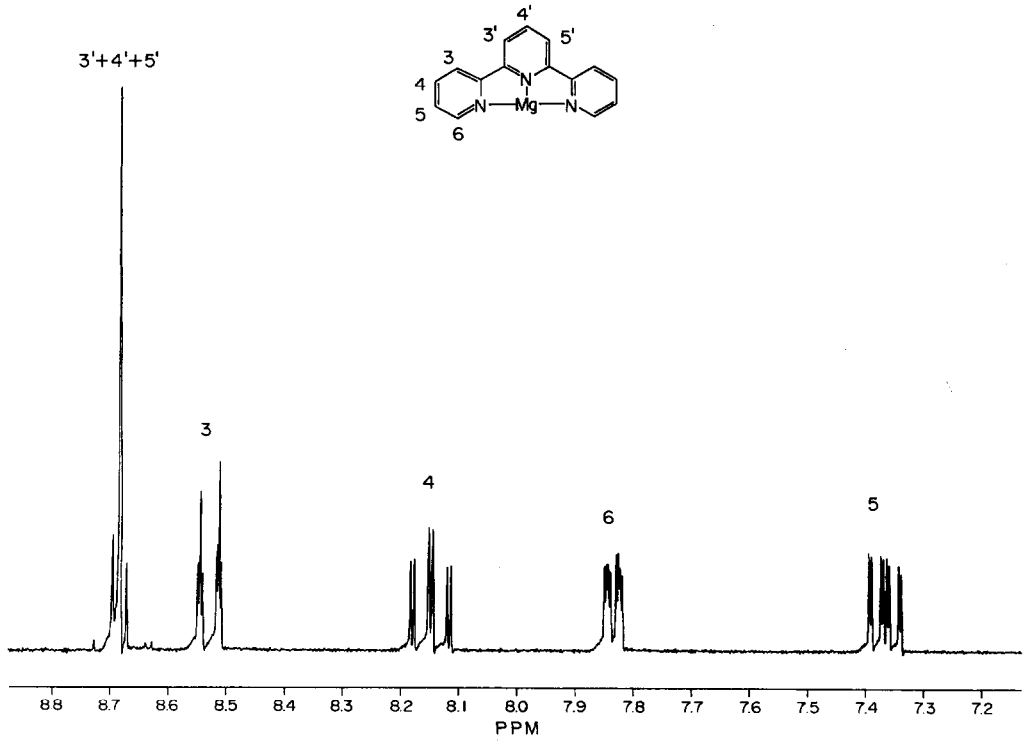

Fig. 1. 250 MHz ^{1}H NMR spectrum of a CD_3CN solution of $[Mg(terpy)_2][ClO_4]_2$.

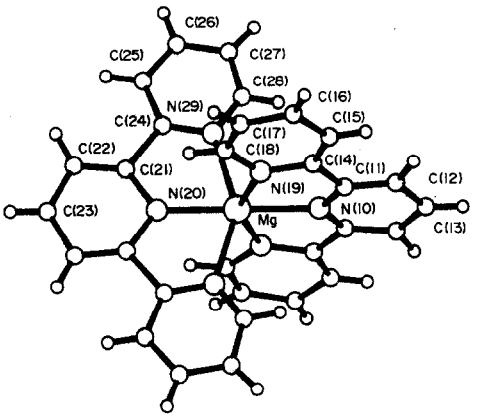

Fig. 2. Crystal and molecular structure of the cation in $[Mg(terpy)_2][ClO_4]_2 \cdot H_2O$ showing the numbering scheme adopted.

perchlorate anion are reasonable and the final difference Fourier map showed no significant areas of electron density in its vicinity. Only one position was found for the water molecule, which was refined with half-occupancy.

Considerable variations in the dimensions within $[M(terpy)_2]^{n+}$ cations have been observed, and these are commonly ascribed to crystal packing effects within the lattice.[1,27] Within a series of $[Co(terpy)_2]^{2+}$ complexes, the angle of intersection between the two terpy ligands was found to range between 84.5 and 90.0° and the N(central)—Co—N(central) angles varied from 175–180° with inter-annular twists of up to 10° between adjacent pyridyl rings of each terpy ligand.[27] It is also a feature common to all $[M(terpy)_2]^{n+}$ structures that the M—N(central) bond distance is significantly shorter than the M—N(terminal) distances.[1] The dimensions within this present structure fall within these trends with Mg—N(central) distances of 2.050(10) and 2.109(8) Å and Mg—N(terminal) distances of 2.247(6) and 2.244(7) Å. The twist angles between the central and terminal pyridine rings are only 2.6 and 3.3°, and the two ligands make an angle of 88.1(1)°.

There are very few structurally characterized compounds containing magnesium ions coordinated to six nitrogen donor ligands. The majority of these complexes are porphyrin complexes in which the two axial sites are occupied by *N*-donor ligands[34,35] but two structures containing the $[Mg(NCMe)_6]^{2+}$ cation are known.[36,37] Of these latter, one is disordered,[36] while in the other[37] the Mg—N bond lengths are in the range 2.134–2.178 Å. In the porphyrin adducts[34,35] the Mg—N(porphyrin) distances are in the range 2.04–2.09 Å, and the Mg—N(axial) distances in the range 2.29–2.42 Å. These values indicate that the dimensions found in the $[Mg(terpy)_2]^{2+}$ cation are reasonable, and the the Mg^{2+} cation is of the right size to form such a complex. The formation of such a cation with six Mg—N bonds is unusual and there are no precedents for such complexes with terpy or similar ligands.

Acknowledgements—We should like to thank the SERC for the award of a Post-Doctoral Fellowship (JH) and for funds for the diffractometer. We thank A. W. Johans for his assistance with the crystallographic investigation.

REFERENCES

1. E. C. Constable, *Adv. Inorg. Chem. Radiochem.* 1987, **30**, 69.
2. W. R. McWhinnie and J. D. Miller, *Adv. Inorg. Chem. Radiochem.* 1969, **12**, 135.
3. E. C. Constable, *Adv. Inorg. Chem.* 1989, **34**, 1.
4. I. M. Brown, S. I. Weissman and L. C. Snyder, *J. Chem. Phys.* 1965, **42**, 1105.
5. K. Nakamura, *Bull. Chem. Soc. Japan* 1971, **45**, 1943.
6. R. D. Chapman, R. T. Loda, J. P. Riehl and R. W. Schwartz, *Inorg. Chem.* 1984, **23**, 1652.
7. G. B. Deacon, J. M. Patrick, B. W. Skelton, N. C. Thomas and A. H. White, *Aust. J. Chem.* 1984, **37**, 929.

7a. N. C. Thomas and J. Fischer, *J. Coord. Chem.* 1990, **21**, 119.

8. L.-Y. Chung, E. C. Constable, J. Lewis and P. R. Raithby, *J. Chem. Soc., Chem. Commun.* 1986, 1719.
9. E. C. Constable, M. J. Doyle, J. Healy and P. R. Raithby, *J. Chem. Soc., Chem. Commun.* 1988, 1262.
10. E. C. Constable, J. A. Healy and M. J. Hynes. In preparation.
11. T. W. Bell, A. Firestone, F. Guzzo and L. Y. Hu, *J. Incl. Phenom.* 1987, **5**, 149.
12. T. W. Bell and F. Guzzo, *J. Am. Chem. Soc.* 1984, **106**, 6111.
13. T. W. Bell and A. Firestone, *J. Am. Chem. Soc.* 1986, **108**, 8109.
14. T. W. Bell and A. Firestone, *J. Chem. Soc., Chem. Commun.* 1986, 769.
15. T. W. Bell and A. Firestone, *Ann. N.Y. Acad. Sci.* 1986, **471**, 291.
16. P. Pfeiffer and W. Christeleit, *Z. Anorg. Allg. Chem.* 1938, **239**, 133.
17. S. Herzog, *Naturwissenschaften* 1956, **43**, 105.
18. G. Oerpen and F. Vögtle, *Liebigs Annln Chem.* 1979, 2114.
19. J. L. Toner, *Tetrahedron Lett.* 1983, **24**, 2707.
20. F. Vögtle, W. M. Muller and W. Raßhoffer, *Isr. J. Chem.* 1979, **18**, 246.
21. M. D. Grillone and M. A. Nocilla, *Inorg. Nucl. Chem. Lett.* 1978, **14**, 49.
22. E. Schmidt, A. Hourdakis and A. I. Popov, *Inorg. Chim. Acta* 1981, **52**, 91.
23. M. M. Emara and C.-T. Lin, *J. Indian Chem. Soc.* 1980, **57**, 876.

24. M. M. Emara, C.-T. Lin and G. Atkinson, *Bull. Soc. Chim. Fr.* Pt. 1, 1980, 173.
25. E. C. Constable, S. Corr and M. D. Ward, *Inorg. Chim. Acta* 1988, **141**, 201.
26. W. Henke and S. Kremer, *Inorg. Chim. Acta* 1982, **65**, L115.
27. B. N. Figgis, E. S. Kucharski and A. H. White, *Aust. J. Chem.* 1983, **36**, 1537.
28. F. Takusaqawa, P. G. Yohannes and K. B. Mertes, *Inorg. Chim. Acta* 1986, **114**, 165.
29. M. Mathew and G. J. Palenik, *J. Coord. Chem.* 1973, **1**, 243.
30. R. Allman, W. Henke and D. Reinen, *Inorg. Chem.* 1978, **17**, 378.
31. G. M. Sheldrick, SHELX 76, Package for Crystal Structure Determination. University of Cambridge (1976).
32. E. C. Constable and J. Lewis, *Inorg. Chim. Acta* 1983, **70**, 251.
33. E. C. Constable, *J. Chem. Soc., Dalton Trans.* 1985, 2687.
34. V. McKee, C. C. Ong and G. A. Rodley, *Inorg. Chem.* 1984, **23**, 4242.
35. R. Bonnett, M. B. Hursthouse, K. M. A. Malik and B. Mateen, *J. Chem. Soc., Perkin II*, 1977, 2072.
36. B. A. Stork-Blaisse, G. C. Verschoor and C. Romers, *Acta Cryst. B* 1972, **28**, 2445.
37. M. G. B. Drew, P. P. K. Claire and G. R. Willey, *J. Chem. Soc., Dalton Trans.* 1988, 215.

Polyhedron Vol. 10, No. 16, pp. 1889–1891, 1991
Printed in Great Britain

0277–5387/91 $3.00+.00
© 1991 Pergamon Press plc

CRYSTAL STRUCTURE OF THE COMPLEX OF DIBENZO-30-CROWN-10 WITH GADOLINIUM ISOTHIOCYANATE

YAN SHIPING and WANG GENGLIN*

Department of Chemistry, Nankai University, Tianjin, China

and

WANG HONGGEN and YAO XINKAN

Central Laboratory, Nankai University, Tianjin, China

(*Received* 17 *October* 1990; *accepted* 20 *May* 1991)

Abstract—The crystal and molecular structures of $Gd(NCS)_3(H_2O)_2L$ (L = dibenzo-30-crown-10) have been determined by single crystal X-ray diffraction. In this compound the gadolinium centre is eight-coordinate (three oxygen atoms of the crown ether, three isothiocyanate anions and two water molecules).

The coordination chemistry of the alkali, alkaline earth metals, lanthanide and transition metals has been extensively studied since the initial discovery[1,2] of the crown ethers. Complexes formed were found to depend not only on the size of the cation and crown ether cavity but also the choice of anion and solvent. Dibenzo-30-crown-10 (hereafter named L) is a larger ether. Very few solid complexes of this ligand with metal ions have been reported.[3–5] Bush and Troter[3] determined the crystal structure of the complex of potassium with dibenzo-30-crown-10 and found the ligand was wrapped round the potassium ion. Ciampolini and Nardi[5] synthesized the compounds of lanthanide perchlorates with L by using anhydrous salts and anhydrous acetonitrile. So far, to our knowledge, no report on the crystal structure of complexes between lanthanide metal ions and L has appeared. Recently, we were successful in the synthesis and structural characterization of the title complex. This complex is very different from the complex of potassium and is the subject of this report.

EXPERIMENTAL

Synthesis and crystallization of $Gd(NCS)_3(H_2O)_2L$

L (1 mmol) in acetonitrile (10 cm^3) was added to a stirred solution of $Gd(NCS)_3 \cdot 6H_2O$ (1 mmol) in the same solvent (10 cm^3). The reaction mixture was heated to 80°C for 2 h, cooled to room temperature, and stored in a desiccator containing P_4O_{10}. Crystals formed over a period of several weeks at room temperature. Found: C, 41.1; H, 4.8; N, 4.3. Calc. for $Gd(NCS)_3(H_2O)_2L$: C, 41.1; H, 4.9; N, 4.6%.

X-ray data collection, structure determination, and refinement for title compound

A transparent colourless crystal of the title compound having approximate dimensions of $0.2 \times 0.2 \times 0.3$ mm was mounted on a glass fibre in a random orientation. The determination of the unit cell and the data collection were performed with Mo-K_α radiation ($\lambda = 0.71073$ Å) on an Enraf–Nonius CAD4 diffractometer equipped with a graphite crystal monochromator. A total of 5200 independent reflections were collected in the range of $2° \leqslant \theta \leqslant 25°$ by the ω–2θ scan technique at room temperature, in which 2667 reflections with ($I \geqslant 3\sigma I$) were considered to be observed and used in the succeeding refinement. A correction for Lp effects was applied to the data.

Crystals are triclinic, space group $P\bar{1}$, with $a = 12.874(2)$, $b = 12.952(3)$, $c = 14.691(5)$ Å, $\alpha = 64.77(2)$, $\beta = 64.43(2)$, $\gamma = 77.17(2)°$; $V = 1996.77$ Å^3, $M_w = 904.07$, $Z = 2$, $D_x = 1.497$ g cm^{-3}, $\mu = 18.7$ cm^{-1}, $F(000) = 910$.

The structure was solved by the Patterson

* Author to whom correspondence should be addressed.

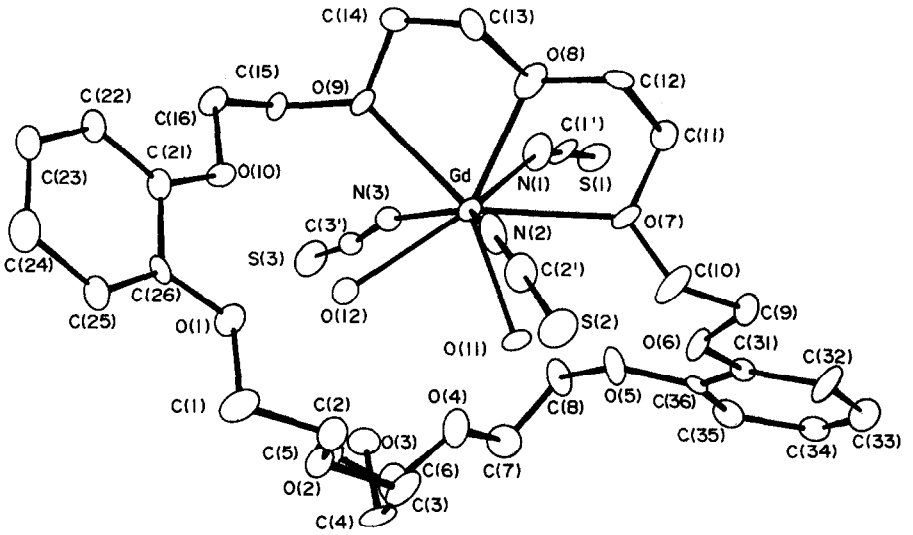

Fig. 1. Perspective view of the $Gd(NCS)_3(H_2O)_2L$ showing the atom numbering.

method. All the other non-hydrogen atoms were determined from successive difference Fourier syntheses.

The final refinement by full-matrix least-squares with anisotropic thermal parameters for non-hydrogen atoms converged with agreement factors of $R = \Sigma|\Delta F|/\Sigma|F_o| = 0.070$ and $R_w = [\Sigma_w|\Delta F|^2/\Sigma_w|F_o|^2]^{1/2} = 0.085$ (unit weights for all observed

Table 1. Bond distances (Å)

Gd—O(7)	2.516(7)	O(8)—C(12)	1.48(1)
Gd—O(8)	2.47(1)	O(8)—C(13)	1.47(1)
Gd—O(9)	2.460(6)	O(9)—C(14)	1.43(1)
Gd—N(1)	2.437(9)	O(9)—C(15)	1.42(1)
Gd—N(2)	2.468(9)	O(10)—C(16)	1.41(1)
Gd—N(3)	2.25(1)	O(10)—C(21)	1.34(2)
Gd—O(11)	2.409(6)	N(1)—C(1')	1.11(1)
Gd—O(12)	2.447(7)	N(2)—C(2')	1.17(1)
S(1)—C(1')	1.63(2)	N(3)—C(3')	1.25(1)
S(2)—C(2')	1.58(1)	C(1)—C(2)	1.50(1)
S(3)—C(3')	1.74(2)	C(3)—C(4)	1.55(2)
O(1)—C(1)	1.49(1)	C(5)—C(6)	1.54(2)
O(1)—C(26)	1.35(2)	C(7)—C(8)	1.44(2)
O(2)—C(2)	1.43(1)	C(9)—C(10)	1.57(1)
O(2)—C(3)	1.43(1)	C(11)—C(12)	1.59(2)
O(3)—C(4)	1.46(1)	C(13)—C(14)	1.52(2)
O(3)—C(5)	1.47(1)	C(15)—C(16)	1.55(1)
O(4)—C(6)	1.41(2)	C(21)—C(22)	1.37(1)
O(4)—C(7)	1.45(1)	C(21)—C(26)	1.46(1)
O(5)—C(8)	1.48(1)	C(22)—C(23)	1.45(1)
O(5)—C(36)	1.39(1)	C(23)—C(24)	1.43(2)
O(6)—C(9)	1.47(1)	C(24)—C(25)	1.42(2)
O(6)—C(31)	1.37(2)	C(25)—C(26)	1.40(1)
O(7)—C(10)	1.47(2)	C(31)—C(32)	1.40(1)
O(7)—C(11)	1.44(1)	C(31)—C(36)	1.36(1)
C(32)—C(33)	1.41(1)	C(34)—C(35)	1.46(2)
C(33)—C(34)	1.40(2)	C(35)—C(36)	1.39(1)

Numbers in parentheses are estimated standard deviations in the least significant digits.

Table 2. Bond angles (°)

O(7)—Gd—O(8)	66.1(2)
O(7)—Gd—O(9)	132.0(3)
O(7)—Gd—N(1)	72.4(3)
O(7)—Gd—N(2)	71.6(3)
O(7)—Gd—N(3)	135.0(3)
O(7)—Gd—O(11)	72.6(3)
O(7)—Gd—O(12)	134.2(3)
O(8)—Gd—O(9)	66.2(3)
O(8)—Gd—N(1)	76.8(4)
O(8)—Gd—N(2)	73.8(4)
O(8)—Gd—N(3)	125.5(3)
O(8)—Gd—O(11)	138.5(2)
O(8)—Gd—O(12)	131.1(2)
O(9)—Gd—N(1)	101.3(2)
O(9)—Gd—N(2)	90.8(2)
O(9)—Gd—N(3)	79.5(3)
O(9)—Gd—O(11)	155.3(3)
O(9)—Gd—O(12)	77.8(2)
N(1)—Gd—N(2)	140.1(3)
N(1)—Gd—N(3)	70.0(3)
N(1)—Gd—O(11)	87.4(3)
N(1)—Gd—O(12)	144.7(4)
N(2)—Gd—N(3)	149.9(3)
N(2)—Gd—O(11)	97.2(3)
N(2)—Gd—O(12)	74.9(3)
N(3)—Gd—O(11)	82.1(3)
N(3)—Gd—O(12)	75.3(3)
O(11)—Gd—O(12)	81.9(2)

Table 3. Hydrogen bonding contact geometries (Å, °)

O(11)—O(4)	2.802		
O(11)—O(6)	2.904	O(4)—O(11)—O(6)	107.1
O(12)—O(1)	3.048		
O(12)—O(3)	2.839	O(1)—O(12)—O(3)	108.3

reflections). The highest peak on the final difference Fourier map had a height of 0.99 e $Å^{-3}$.

All calculations were performed on a PDP11/44 computer using SDP-PLUS program system.

Tables of final atomic positional and thermal parameters, full lists of bond lengths and angles, equations of least-squares planes have been deposited as supplementary material with the Editor.

RESULTS AND DISCUSSION

The crystal structure of the complex is shown with the crystallographic numbering of the atoms in Fig. 1. Some bond lengths, and bond angles are given in Tables 1 and 2.

In the complex, only three oxygen atoms O(7), O(8), O(9) of the cyclic ether interact with the gadolinium(III) ion with the Gd—O distances ranging from 2.460(6) to 2.516(7) Å (mean, 2.482 Å). The nitrogen atoms of the three isothiocyanate anions and two oxygen atoms of coordinated water molecules are also bonded to the gadolinium(III) ion. Two coordinated water molecules contact the cyclic ether oxygen atoms O(1), O(3), O(4) and O(6) with hydrogen bonds (Table 3). The coordination number of the gadolinium(III) ion is eight. The O(7), O(8), O(9), O(11) and gadolinium atoms lie approximately in a plane (Fig. 2). The maximum deviation from the plane is 0.0088 Å (gadolinium). The gadolinium atom simultaneously lies in the plane which consists of N(1), N(2), N(3) and O(12). The maximum deviation from the plane is 0.0246 Å (gadolinium). The dihedral angle between the two planes is 86.94°. All the eight donor atoms around gadolinium(III) ion make up a coordination dodecahedron with D_{2d} symmetry (Fig. 3). The structures of the potassium iodide complex with dibenzo-30-crown-10 and of our complex are very different. In the potassium complex, the cyclic ether is wrapped round the potassium, and all 10 oxygen atoms of the cyclic ether interact with the cation. The difference in crystal structures may be caused by: (i) the K ion has a larger radius than the gadolinium ion (1.33 and 0.93 Å for K^+ and Gd^{3+}, respectively); (ii) the water molecule and isothiocyanate anion have stronger coordination ability than cyclic ether oxygen atoms for gadolinium. The coordinated water molecules and isothiocyanate anions inhibit other oxygen atoms of the cyclic ether from coordinating to Gd.

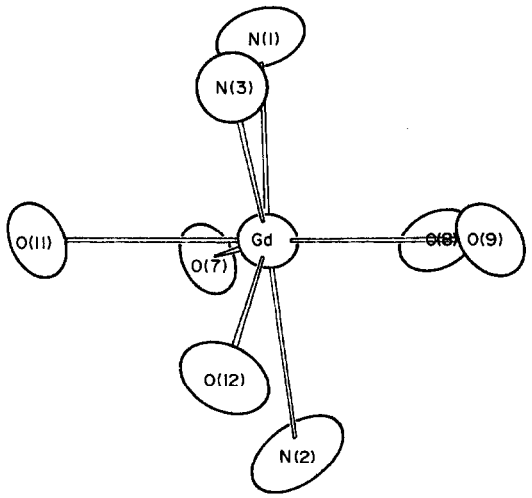

Fig. 2. Gadolinium(III) ion environment.

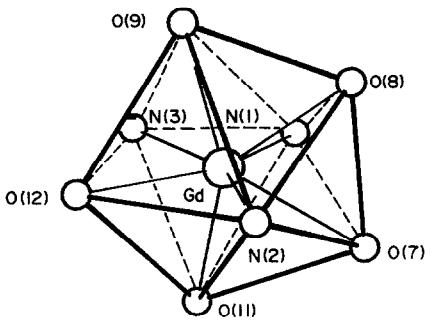

Fig. 3. The coordination polyhedron of gadolinium(III) ion.

Acknowledgement—This research was supported by grants from the National Natural Science Foundation of China.

REFERENCES

1. Michio Hiraoka, *Crown Compounds*. Kodansha, Tokyo (1982).
2. J. C. G. Bunzli and D. Wessner, *Coord. Chem. Rev.* 1984, **60**, 191.
3. M. A. Bush and M. R. Truter, *J. Chem. Soc. Perkin II* 1972, 345.
4. D. G. Parsons and J. N. Wingfield, *Inorg. Chim. Acta* 1976, **18**, 263.
5. M. Ciampolini and N. Nardi, *Inorg. Chim. Acta* 1979, **32**, L9.

Polyhedron Vol. 10, No. 16, pp. 1893–1895, 1991
Printed in Great Britain

0277–5387/91 $3.00+.00
© 1991 Pergamon Press plc

CRYSTAL STRUCTURE OF BIS(α-METHACRYLATO)-2,2′-BIPYRIDINE-MONOHYDRATE COPPER(II)

GAO YICI,* WANG YAOYU, ZHU YING and SHI QIZHEN

Department of Chemistry, Lanzhou University, Lanzhou, Gansu, P.R.C.

(*Received* 27 *July* 1990; *accepted* 20 *May* 1991)

Abstract—The X-ray crystal structure of the title copper(II) complex has been determined and shows that the complex is mononuclear with distorted square pyramidal coordination from two monodentate carboxylates, a bidentate bipyridiyl and one aquo ligands.

There have been many studies[1,2] directed towards extending our understanding of the particularity and diversity of structures of copper(II) complexes. Numerous papers dealing with copper carboxylates have been published,[3–11] but compounds with unsaturated carboxylic acids, especially their structural information, are still very little known. Edmondson and Lever[12] and Morzinski and Heyduk[13–15] synthesized the copper(II) complexes of unsaturated acids with monodentate hetrocyclic amines in 1965 and 1983, respectively, and reported these compounds to have binuclear bridge structures, indicated by spectroscopic (UV–vis, IR, EPR) and magnetic investigations.

In an attempt to obtain more information on these complexes we recently prepared single crystals of copper(II) complexes of α-methacrylic acid and its derivatives with bidentate heterocyclic amines from the mixed solvent system methyl alcohol and ethylene glycol dimethyl ether (2:1, v/v) at room temperature. This, our first study, reports crystal data and important features of the copper(II) complex of α-methacrylate with 2,2′-bipyridine. Further studies will report the syntheses and structures for other copper unsaturated carboxylates.

EXPERIMENTAL

Synthesis

The parent complex [Cu(α-methacrylato)$_2$·H_2O] was first prepared in methyl alcohol by an improvement of the method of Edmondson and Lever.[12] The product was recrystallized from the mixed solvent described above. Found: C, 38.4; H, 4.8; Cu, 25.4. Calc. for $C_8H_{12}CuO_5$: C, 38.2; H, 4.8; Cu, 25.3%.

Methyl alcohol (15 cm^3), the parent complex (1.00 g) and 2,.2′-bipyridine (0.65 g) were mixed and the deep green–blue crystals which formed after refluxing and evaporating for several hours were filtered and dried. The crude product was recrystallized from methyl alcohol and ethylene glycol dimethyl ether (2:1 v/v) at room temperature. Found: C, 53.0; H, 4.9; N, 6.9; Cu, 15.7. Calc. for $C_{18}H_{18}CuN_2O_5$: C, 53.0; H, 4.9; N, 6.9; Cu, 15.7%.

Structure solution

Preliminary photographic examination and data collection were performed with Mo-K_α radiation ($\lambda = 0.7107$ Å) on an Enraf–Nonius CAD-4 computer-controlled K-axis diffractometer with a graphite crystal-incident beam monochromator. The sample selected for investigation, had dimensions of $0.26 \times 0.26 \times 0.19$ mm^3. Accurate unit cell parameters were obtained by least-squares refinement. 4393 independent reflections ($1° \leqslant \theta \leqslant 27°$) were collected by using the ω–2θ scan technique but only 2611 with $I \geqslant 3\sigma(I)$ were used in the refinement. All data were corrected for Lorentz and polarization effects and also for absorption. Crystal data are listed in Table 1.

The crystal structure was solved by direct methods (MULTAN-82). The copper and most non-hydrogen atoms were located from an E map. The remaining non-hydrogen atoms were located by difference Fourier synthesis. The structure was refined by full-matrix least-squares with anisotropic

* Author to whom correspondence should be addressed.

Table 1. Crystal data for the complex

$Cu(CH_2{=}C(CH_3){-}COO)_2(bipy)H_2O$	$C_{18}H_{18}N_2O_5Cu$
M (g mol^{-1})	406.90
D_c (g cm^{-3})	1.445
μ(Mo-K_α (cm^{-1})	12.002
F(000)	836
Crystal system	Monoclinic
Space group	$P2_1/n$
a (Å)	6.851(1)
b (Å)	17.626(2)
c (A°)	15.553(1)
β (°)	96.52(1)
V (Å^3)	1865.9
Z	4

Table 2. Bond distances (Å) for the complex

Cu—O(1)	1.969(2)	C(2)—C(3)	1.363(6)
Cu—O(3)	1.926(2)	C(3)—C(4)	1.372(5)
Cu—O(5)	2.292(2)	C(4)—C(5)	1.382(4)
Cu—N(1)	2.023(3)	C(5)—C(6)	1.467(4)
Cu—N(2)	2.005(3)	C(6)—C(7)	1.384(4)
O(1)—C(11)	1.266(4)	C(7)—C(8)	1.360(5)
O(2)—C(11)	1.248(4)	C(8)—C(9)	1.369(5)
O(3)—C(15)	1.261(4)	C(9)—C(10)	1.385(5)
O(4)—C(15)	1.228(4)	C(11)—C(12)	1.495(5)
N(1)—C(1)	1.344(4)	C(12)—C(13)	1.335(5)
N(1)—C(5)	1.347(4)	C(12)—C(14)	1.435(6)
N(2)—C(6)	1.350(4)	C(15)—C(16)	1.516(5)
N(2)—C(10)	1.334(4)	C(16)—C(17)	1.387(6)
C(1)—C(2)	1.362(5)	C(16)—C(18)	1.398(5)

thermal parameters for the copper atom and isotropic thermal parameters for other atoms. The final discrepancy factor of R is 0.031, R_w was 0.030.

RESULTS AND DISCUSSION

Bond distances and angles for the complex are listed in Tables 2 and 3. The least-squares planes and their dihedral angle are listed in Table 4. Figures 1 and 2 show the molecular structure and crystal packing.

The structure in this five-coordinated complex has the central copper atom in a distorted square pyramidal configuration with two α-methacrylate ligands, a 2,2′-bipyridine ligand and an aquo ligand.

Table 3. Bond angles (°) for the complex

O(1)—Cu—O(3)	91.1(1)	N(2)—C(6)—C(7)	114.7(3)
O(1)—Cu—O(5)	100.26(9)	N(2)—C(6)—C(5)	120.8(3)
O(1)—Cu—N(1)	162.4(1)	C(5)—C(6)—C(7)	124.5(3)
O(1)—Cu—N(2)	93.4(1)	C(6)—C(7)—C(8)	119.9(3)
O(3)—Cu—O(5)	95.44(9)	C(7)—C(8)—C(9)	119.5(3)
O(3)—Cu—N(1)	92.4(1)	C(8)—C(9)—C(10)	118.7(3)
O(3)—Cu—N(2)	170.1(1)	N(2)—C(10)—C(9)	122.2(3)
O(5)—Cu—N(1)	96.3(1)	O(1)—C(11)—O(2)	123.1(3)
O(5)—Cu—N(2)	91.81(9)	O(1)—C(11)—C(12)	118.1(3)
N(1)—Cu—N(2)	80.2(1)	O(2)—C(11)—C(12)	118.8(3)
C(1)—N(1)—C(5)	118.5(3)	C(11)—C(12)—C(13)	119.6(3)
C(6)—N(2)—C(10)	118.9(3)	C(11)—C(12)—C(14)	118.0(3)
N(1)—C(1)—C(2)	122.5(3)	C(13)—C(12)—C(14)	122.4(4)
C(1)—C(2)—C(3)	118.9(3)	O(3)—C(15)—O(4)	125.6(3)
C(2)—C(3)—C(4)	119.9(3)	O(3)—C(15)—C(16)	114.6(3)
C(3)—C(4)—C(5)	118.9(3)	O(4)—C(15)—C(16)	119.8(3)
N(1)—C(5)—C(4)	121.3(3)	C(15)—C(16)—C(17)	118.4(3)
N(1)—C(5)—C(6)	114.7(3)	C(15)—C(16)—C(18)	117.3(4)
C(4)—C(5)—C(6)	124.1(3)	C(17)—C(16)—C(18)	124.2(4)

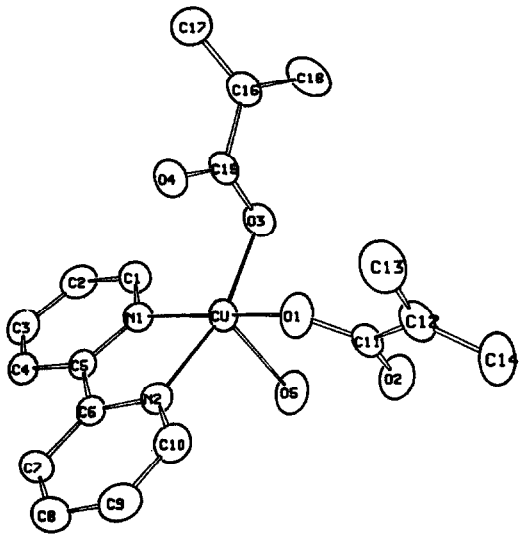

Fig. 1. Perspective view of the molecule of complex.

The heterocyclic amine is bidentate to the copper atom to form a rather stable chelate ring. It is quite interesting that each unsaturated carboxylate contributes only one carboxyl oxygen atom for coordination to copper (Fig. 1). This is the first such example for copper complexes with unsaturated carboxylates. The weakly basic and π accepting character of 2,2′-bipyridine render the copper atom fairly positive and thus increases the interaction between the copper and the negative oxygen atoms.

The observed bond lengths and angles (Tables 2 and 3) are within accepted limits for compounds of this type.[3] In the molecule the distances of Cu—O(1), Cu—O(3), Cu—O(5), Cu—N(1) and Cu—N(2) are 1.969(2), 1.926(2), 2.292(2), 2.023(3) and 2.005(3) Å. The angles of O(1)—Cu—O(5), O(3)—Cu—O(5), N(1)—Cu—O(5) and N(2)—Cu—O(5) are 100.26(9), 95.44(9), 96.3(1) and 91.81(9)°, respectively. Obviously, the distance of Cu—O(5) is much longer than others and this is one of the geometrical features for a square pyramid.

The four atoms N(1), N(2), O(1) and O(3) are nearly in a plane, and the copper atom is 0.297 Å above the pyramid base. The reason for the apparent equivalence of the two C—C bonds (C=C and C—C) is disorder [Table 2; C(16)—C(17) and C(16)—C(18)].

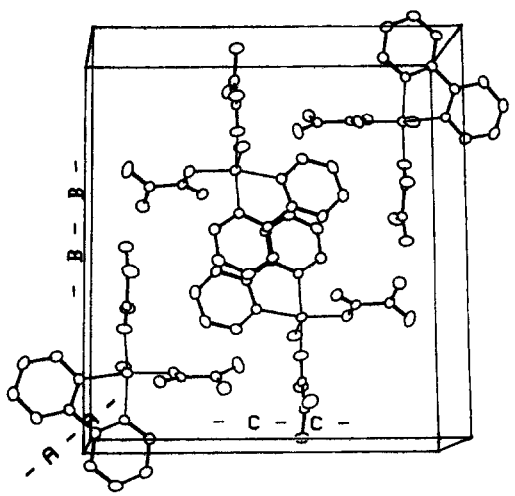

Fig. 2. Model of the packing of the structure of the complex in the unit cell.

REFERENCES

1. F. A. Cotton and G. Wilkinson, *Advanced Inorganic Chemistry*, 3rd edn, p. 492. Wiley, New York (1972).
2. K. Sone, S. Utsuno and T. Ogura, *J. Inorg. Nucl. Chem.* 1969, **31**, 117.
3. W. Fitzgerald, J. Foley, D. M. Sweeney, N. Ray, D. Sheahan, S. Tyagi and B. Hethaway, *J. Chem. Soc., Dalton Trans.* 1982, 1117.
4. V. P. Thomas, D. Rehorek and H. Spindler, *Z. Anorg. Allg. Chem.* 1973, **399**, 175.
5. P. R. Shukla, R. Kamal and S. T. Spees, *J. Indian Chem. Soc.* 1978, 871.
6. S. Gurrieri, S. Musumeci, E. Rizzarelli and A. Seminara, *J. Inorg. Nucl. Chem.* 1976, **38**, 1215.
7. S. Musumeci, E. Rizzarelli, S. Sammartano and A. Seminara, *Z. Anorg. Allg. Chem.* 1977, **433**, 297.
8. R. P. Bonomo, S. Musumeci, E. Rizzarelli and S. Sammartano, *Inorg. Chim. Acta* 1975, **14**, 251.
9. I. M. Procter, B. J. Hathaway and P. G. Hodgson, *J. Inorg. Nucl. Chem.* 1972, **34**, 3689.
10. P. O'Brien, *J. Chem. Soc., Dalton Trans.* 1981, 1540.
11. B. J. Hathaway, *Coord. Chem. Rev.* 1981, **35**, 211.
12. B. J. Edmondson and A. B. P. Lever, *Inorg. Chem.* 1965, **4**, 1608.
13. J. Mrozinski and E. Heyduk, *Pol. J. Chem.* 1983, **57**, 375.
14. J. Mrozinski and E. Heyduk, *Pol. J. Chem.* 1982, **56**, 683.
15. J. Mrozinski and E. Heyduk, *J. Coord. Chem.* 1984, **13(4)**, 291.

Polyhedron Vol. 10, No. 16, pp. 1897–1902, 1991
Printed in Great Britain

0277–5387/91 $3.00+.00
© 1991 Pergamon Press plc

PRIMARY AMIDO AND AMINE ADDUCT COMPLEXES OF GALLIUM: SYNTHESIS AND STRUCTURES OF $[t\text{-}Bu_2Ga(\mu\text{-}NHPh)]_2$ AND $t\text{-}Bu_3Ga \cdot NH_2Ph$

DAVID A. ATWOOD, RICHARD A. JONES* and ALAN H. COWLEY*

Department of Chemistry, The University of Texas at Austin, Austin, TX 78712, U.S.A.

and

SIMON G. BOTT and JERRY L. ATWOOD*

Department of Chemistry, The University of Alabama, Tuscaloosa, AL 35487, U.S.A.

(*Received* 21 *February* 1991; *accepted* 16 *May* 1991)

Abstract—Reaction of $t\text{-}Bu_2GaCl$ with LiNHPh in toluene/diethylether (4:1) at −78°C gives the dimeric primary amido complex $[t\text{-}Bu_2Ga(\mu\text{-}NHPh)]_2$ (**1**) in 60% yield. The reaction of $t\text{-}Bu_3Ga$ with NH_2Ph at −78°C in toluene gives the adduct $t\text{-}Bu_3Ga \cdot NH_2Ph$ (**2**) in 75% yield. The structures of both compounds have been determined by X-ray crystallography. The molecular geometry of **1** consists of a dinuclear unit with two bridging —NHPh groups and two terminal t-Bu groups bound to each gallium atom. The coordination geometry of both the gallium and nitrogen atoms is distorted tetrahedral. The molecular geometry of **2** involves a fairly long dative N→Ga donor bond [2.246(9) Å] and the configuration of the amine is distorted from an idealized tetrahedral geometry due to steric repulsions. Crystallographic data for both **1** and **2** suggest the presence of close interactions between the N—H hydrogen atoms and the gallium atoms (N—H···Ga).

There is currently considerable interest in complexes which feature bonding between the group 13 and 15 elements since such compounds offer potential as precursors to III/V compound semiconductors.[1] In previous studies we have reported details of our work on phosphido (R_2P^-) and arsenido (R_2As^-) derivatives of the group 13 elements.[2] We were therefore interested in the analogous amido (R_2N^-) complexes of the heavier group 13 metals for which several examples have been reported.[3] We have now prepared and characterized a number of new amido and amine adduct complexes of gallium and report here details of the synthesis and structures of $[t\text{-}Bu_2Ga(\mu\text{-}NHPh)]_2$ (**1**) and $t\text{-}Bu_3Ga \cdot NH_2Ph$ (**2**) which are among the first structurally characterized primary amido complexes of gallium and the first X-ray structure featuring the $t\text{-}Bu_3Ga$ group.[4] The X-ray structure of **1** suggests the presence of a close N—H···Ga interaction and we were curious to see if such an interaction might exist in the adduct (**2**). The X-ray structure of **2** again indicates the presence of a close N—H···Ga interaction. However the structural data for both compounds were not of sufficient quality to enable the N—H hydrogens to be fully refined isotropically.

* Authors to whom correspondence should be addressed.

RESULTS AND DISCUSSION

Synthesis of the primary amido complex $[t\text{-}Bu_2Ga(\mu\text{-}NHPh)]_2$ (**1**)

Reaction of $t\text{-}Bu_2GaCl$ with one equivalent of LiNHPh in toluene and diethylether (4:1) at −78°C gives high yields of the primary amido complex (**1**). ^1H NMR data for **1** are in accord with the structure determined crystallographically. Thus the t-*Bu*—Ga units appear as a singlet at δ 0.90 and the N—C_6H_5 group as a broad signal located at δ 6.80. The N—H protons were not observed, possibly due to the large quadrupole of nitrogen. The IR spec-

Table 1. Crystal data, details of intensity measurement and structure refinement for [t-$Bu_2Ga(\mu NHPh)]_2$ (**1**) and t-$Bu_3Ga \cdot NH_2Ph$ (**2**)

Formula	$C_{28}H_{48}N_2Ga_2$	$C_{18}H_{34}NGa$
Crystal dimensions (mm)	$0.06 \times 0.06 \times 0.10$	$0.05 \times 0.08 \times 0.11$
Crystal system	Monoclinic	Monoclinic
Space group	$P2_1/c$	$P2_1/n$
a (Å)	9.757(3)	9.050(1)
b (Å)	9.852(2)	14.325(1)
c (Å)	15.429(2)	15.045(1)
β	101.90(4)	91.959(8)
U (Å^3)	1498.3(6)	1949.4(6)
Mass	552.141	334.193
D_c (g cm^{-3})	1.228	1.143
μ(Mo-K_α) calc. (cm^{-1})	17.45	14.04
Z	2	4
Scan width (°)	$0.8+0.35(\tan\theta)$	$0.8+0.35(\tan\theta)$
Range of indices h, k, l	$+10, +11, \pm 17$	$+10, +15, \pm 15$
2θ range (°)	2–40	2–40
Total reflections	2110	1260
Total observed reflections	1845	841
Significance test	$F_o > 6\sigma(F_o)$	$F_o > 6\sigma(F_o)$
Number of parameters	120	136
Weighting scheme	$[(\sigma F)^2+0.000625F^2]^{-1}$	$[(\sigma F)^2+0.000625F^2]^{-1}$
Final R	0.0932	0.0481
Final R_w	0.0898	0.0570

trum contains peaks assigned to the phenyl groups, however, only a very weak peak at 3260.5 cm^{-1} was observed which could be assigned to a ν(N—H) stretch.

X-ray structure of **1**. Molecules of **1** crystallize in the monoclinic space group $P2_1/c$ with two molecules per unit cell. Figure 1 shows the molecular geometry and atom numbering scheme while Fig. 2 illustrates the location of the nitrogen hydrogen atoms. Selected bond lengths and angles are given in Table 2. The structure of **1** consists of dimeric units with a center of inversion and a crystallographically imposed C_2 axis along the Ga···Ga axis. There is a slight distortion in the bonding of the bridging —NHPh groups. The two Ga—N distances are 2.103(9) and 2.018(9) Å. These lengths are somewhat longer than other bridging Ga—N bonds such as those found in $[H_2GaN(CH_2)_2]_3$,[5] [1.97(2) Å]. This difference may be due to the steric influence of the bulky tert-butyl groups. The Ga—C bond lengths are also somewhat lengthened; Ga—C(1), [2.006(9) Å] and Ga—C(5), [2.18(2) Å]. These lengths may be compared to similar values found in the dimeric compound $[Me_2Ga(\mu$-MeN=C(Me)NMe)$]_2$ [Ga—C, 1.991(5) and 2.005(4) Å].[6]

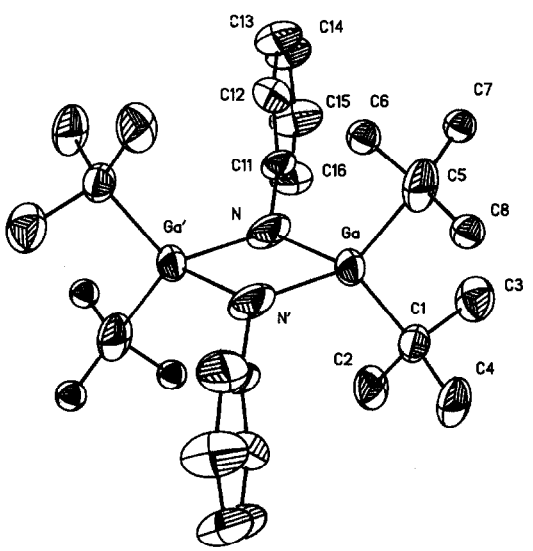

Fig. 1. ORTEP view of (**1**) showing the atom numbering scheme. Hydrogen atoms omitted for clarity.

The nitrogen hydrogen atom was located from difference Fourier maps, but in view of the difficulty of finding one electron between two gallium atoms it was refined with fixed isotropic parameters and allowed to "ride" upon the nitrogen.[7] The location of the hydrogen atom was checked by removal and subsequent location as the largest peak on the final difference map. The hydrogen is symmetrically located 2.037 Å from both gallium atoms. The C(11)—N—H bond angle is acute, 74.5°, demonstrating a close association with the Ga—N plane. The N—H bond length is slightly longer

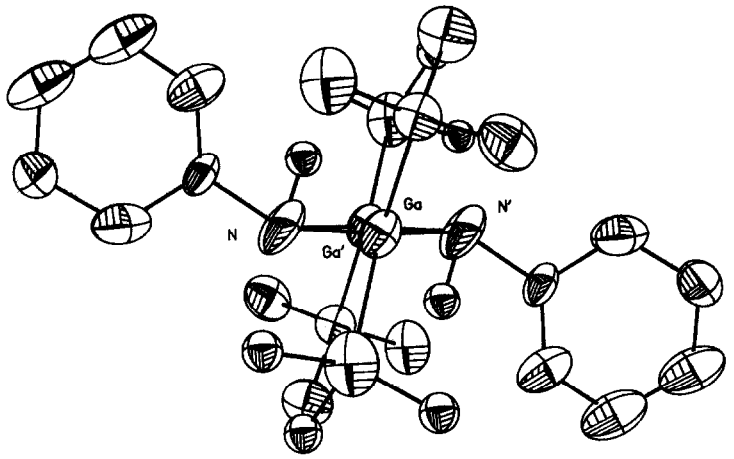

Fig. 2. ORTEP view of (1) showing the location of the nitrogen–hydrogen atoms.

(N—H, 1.105 Å) than the standard length (1.00 Å). Rather than describe this hydrogen as an "agostic" hydride, bonding to empty orbitals on an electron deficient metal atom, it may be more appropriate to describe the interaction as a δ^+–δ^- dipole. In this case the amide proton is attracted to the electron density of the Ga_2N_2 ring; not specifically towards any atom.

Synthesis of the primary amine complex t-Bu_3 Ga · NH_2Ph (2)

Reaction of t-Bu_3Ga with one equivalent of NH_2Ph in toluene at −78°C gives high yields of the primary amine adduct (2). The ^{1}H NMR spectrum of 2 shows a singlet at δ 1.17 (Ga—t-*Bu*) and well resolved peaks at δ 6.5(d), δ 6.8(t), and δ 6.9(t) assigned to N—*Ph*. A broad weak resonance occurs at δ 3.45 for N—*H*. The IR spectrum shows strong peaks at 3347 and 3285 cm^{-1} assigned to ν(N—H).

X-ray structure of (2). Molecules of 2 crystallize in the monoclinic space group, $P2_1/n$ with four molecules per unit cell. The molecular structure of 2 is shown in Fig. 3. Selected bond lengths and angles are given in Table 3. Note that the atoms C(21), Ga, N, and NH(1) are all coplanar with the maximum deviation from the least-squares plane being 0.07 Å for C(21). The Ga—N bond distance of 2.246(9) Å is longer than the corresponding dis-

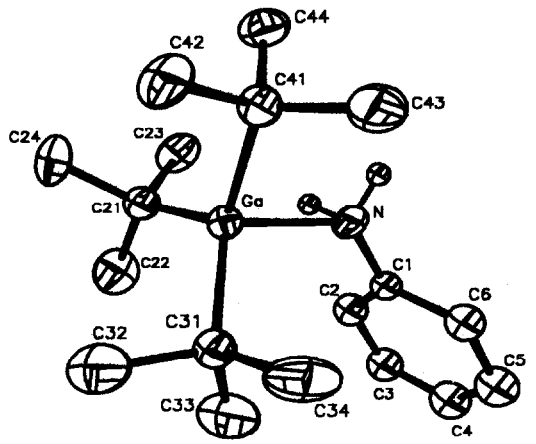

Fig. 3. ORTEP view of (2) showing the atom numbering scheme. Hydrogen atoms omitted for clarity.

Table 2. Selected bond lengths (Å) and angles (°) for (1)

Ga—N	2.103(9)	N—C(11)	1.43(1)
Ga—N′	2.018(9)	Ga—N(H)	2.037
Ga—C(1)	2.006(9)	N—H	1.105
Ga—C(5)	2.18(2)		
N′—Ga—N	83.5(3)	N—Ga—C(1)	105.4(4)
Ga′—N—Ga	96.5(2)	N—Ga—C(5)	124.0(6)
Ga—N—C(11)	122.4(7)	H(N)—N—Ga	71.2
C(1)—Ga—C(5)	114.2(5)	C(11)—N—H	74.5

Numbers in parentheses are the estimated standard deviations in the least significant digits.

Table 3. Selected bond lengths (Å) and angles (°) for (**2**)

Ga—N	2.246(9)	Ga—C(41)	2.04(1)
N—H(1)	1.043	N—C(1)	1.39(1)
N—H(2)	0.918	Ga—H(1)	2.42
Ga—C(21)	2.00(1)	Ga—H(2)	2.63
Ga—C(31)	2.00(1)		
N—Ga—C(31)	106.4(5)	Ga—N—H(2)	104.0
N—Ga—C(41)	95.9(5)	N—Ga—C(21)	101.3(5)
C(21)—Ga—C(31)	116.3(6)	C(21)—Ga—C(41)	115.8(6)
Ga—N—C(1)	125.8(8)	C(31)—Ga—(41)	116.8(6)
Ga—N—H(1)	87.0		

Numbers in parentheses are the estimated standard deviations in the least significant digits.

tance for the adduct of trimethyl gallium with tert-butyl amine which has a value of 2.12(1) Å.[4] This increased length can be partially attributed to steric repulsion between the t-Bu—Ga groups and the phenyl ring. The closest interatomic distance, C(1)—C(3), between these two groups is 3.54(2) Å.

As expected, the configuration of the amine is distorted from the ideal tetrahedral geometry. The C(1)—N—Ga angle of 125.8(8) Å is clearly indicative of steric repulsion between the amine phenyl ring and the t-Bu—Ga groups. Both amine hydrogen atoms were located from difference Fourier maps. However, attempts to refine the hydrogen atoms isotropically led to unrealistic values for the fractional coordinates. Thus, the nitrogen–hydrogen atoms were included in the refinement with fixed isotropic thermal parameters and allowed to "ride" upon the nitrogen. Confirmation of the hydrogen atom locations was achieved by removing these atoms from the refinement and then locating them as the largest two peaks in the final difference map. One of the hydrogen atoms [H(1)] forms an acute angle with the Ga—N bond, H(1)—N—Ga, 87°, while the corresponding H(2)—N—Ga angle is 104°. The N—H(1) distance is correspondingly larger than N—H(2); 1.04 vs 0.92 Å. The Ga···H(1) distance is 2.42 Å which is considerably shorter than the sum of the van der Waals radii for gallium and hydrogen (*ca* 3.1 Å).[8] The other Ga···H(2) distance is 2.63 Å, while the corresponding distances found in the adduct $Me_3Ga \cdot NH_2Bu^t$ are both 2.52 Å.[4]

The IR spectrum of (**2**) displays two strong ν(N—H) stretches at 3347 and 3286 cm^{-1}. There appears to be no particularly low IR active ν(N—H) vibration which may be assigned to a close Ga···H interaction.

Our observation suggests that other derivatives of the heavier group 13 elements may also contain close M···H interactions and further studies are in progress.

EXPERIMENTAL

All reactions were performed under oxygen free nitrogen or under vacuum. Toluene and diethylether were distilled from sodium/benzophenone under nitrogen before use. Aniline was dried over molecular sieves and then distilled from calcium hydride before use. Instruments: IR, Perkin–Elmer, 1330, Digilab FTS-40; NMR, GE QE-300, (^{1}H, 300 MHz). IR spectra were run as Nujol mulls using KBr plates. NMR spectra were recorded in C_6D_6 solution at ambient temperature unless otherwise stated and are in ppm referenced to Me_4Si (δ 0.0, ^{1}H). Melting points were obtained in sealed capillaries under nitrogen (1 atm.) and are uncorrected. t-Bu_3Ga, and t-Bu_2GaCl were prepared as previously described.[9] LiNHPh was prepared *in situ* by the addition of one equivalent of MeLi to NH_2Ph in diethylether at −78°C. The reaction mixture was then allowed to warm to 25°C over the course of 4 h.

Synthesis of (**1**). A solution of LiNHPh (1.33 g, 13.39 mmol) was added dropwise to a solution (−78°C) of t-Bu_2GaCl (2.93 g, 13.35 mmol), prepared *in situ* from the reaction of t-BuLi with $GaCl_3$ in toluene/diethylether (4:1) (50 cm^3) at −78°C. The reaction mixture was stirred (12 h) and allowed to come to room temperature. Volatile materials were removed under vacuum and the residue was extracted with hexane (150 cm^3) and the resulting solution filtered. Reduction in volume of the solution by evaporation under vacuum (10^{-3} Torr) resulted in the immediate formation of **1** as a white micro-crystalline solid. Crystals suitable for X-ray crystallography were grown from a diethylether solution (20 cm^3) cooled to −25°C. For **1**: m.p.

120–123°C, dec. Yield: 2.21 g, 60% based on t-Bu_2GaCl. IR: 3261 w, 1607 m, 1268 m, 1214 m, 1170 m, 1143 m, 991 w, 946 w, 875 m, 857 w, 825 s, 784 m (cm^{-1}). ^1H NMR: δ 6.8 (b, 5H, N—*Ph*), 0.90 (s, 18H, Ga—t-*Bu*).

Synthesis of (**2**). Aniline (NH_2Ph) (0.72 cm^3, 8.30 mmol) was added dropwise to a toluene solution of t-Bu_3Ga (1.00 cm^3, 4.15 mmol) at −78°C. The reaction mixture was stirred (6 h) and allowed to warm to room temperature. The solution was concentrated under vacuum (30 cm^3) and colourless crystals suitable for X-ray crystallography were obtained after several weeks of storage at −30°C. For **2**: m.p. 111–113°C, dec. Yield, 1.04 g based on t-Bu_3Ga. IR: (Nujol mull), 3339 m, 3268 m, 1620 m, 1321 m, 1071 w, 1054 w, 979 w, 929 w, 832 s, 821 m, 755 m, 714 m (cm^{-1}). The N—H stretches do not change significantly in the solid state (KBr disc). ^1H NMR: δ 6.9(t), 6.8(t), 6.5(d) (5H, N—*Ph*), 3.45 (br. s, 2H, N—*H*), 1.17 (s, 27H, Ga—t-*Bu*).

X-RAY EXPERIMENTAL

Details of crystal data and a summary of intensity data collection parameters for **1** and **2** are given in Table 1. Data were collected on an Enraf–Nonius CAD-4 diffractometer at 23±2° using graphite monochromated Mo–K_α radiation. Intensity data were recorded in a manner as described previously.[10] All calculations were performed on a Microvax 3100 computer using the SHELX software package.[11] For each structure the data were corrected for Lorenz and polarization effects.

Compound **1**. Crystals suitable for X-ray diffraction were grown by cooling a diethylether solution to −25°C. Crystals were mounted in thin-walled glass capillaries and sealed under argon. Unit cell parameters were obtained by centering 25 reflections having 2θ values between 20 and 26°. The monoclinic space group $P2_1/c$ was uniquely determined by the systematic absences $h0l$, $l = 2n+1$, $0k0$, $k = 2n+1$. Data were collected in the $+h+k\pm l$ quadrant between 2θ values of 2 and 50°. The reflection intensity standards indicated < 2% decrease in intensity over the course of data collection, and hence no correction was applied. A Ψ scan of four reflections having χ values between 80 and 90° showed a minimum transmission of 80.2% and a maximum transmission of 99.8%. No absorption correction was applied. The structure of **1** was solved by direct methods and successive cycles of difference Fourier maps followed by least-squares refinement. All non-hydrogen atoms were refined anisotropically. The nitrogen–hydrogen atom was located from the final difference map as the largest peak. Attempts to refine the hydrogen separately were unsuccessful and it was included in the refinement with fixed isotropic thermal parameters and allowed to ride upon the nitrogen. All other hydrogen atoms were placed at calculated positions (d_{C-H} = 1.00 Å, H—C—H = 109.5°) and were not refined, rather being constrained to ride upon the appropriate carbon.

Compound **2**. Crystals suitable for X-ray diffraction were grown by cooling a toluene solution to −25°C. The crystals were mounted in thin-walled glass capillaries and sealed under argon. Unit cell parameters were obtained by centering 25 reflections having 2θ values between 22 and 26°. The monoclinic space group $P2_1/n$ was uniquely determined by the systematic absences $h0l$, $h+l = 2n$, $0k0$, $k = 2n+1$. Data were collected in the $+h$, $+k$, $\pm l$ quadrant between 2θ values of 2 and 50°. The intensity standards indicated a < 2% decrease in intensity over the course of data collection, and hence no correction was applied. A Ψ scan of four reflections having χ values between 80 and 90° showed a minimum transmission of 70.0% and a maximum transmission of 98.8%. An empirical absorption correction was applied. The observed structure factors of equivalent reflections were averaged. The gallium atom was found using a Patterson search, and subsequent location of the other non-hydrogen atoms was achieved using difference Fourier maps. The nitrogen hydrogen atoms were located from difference Fourier maps. Attempts to refine these hydrogens led to unrealistic values for the fractional coordinates. Thus these atoms were assigned fixed thermal parameters and then allowed to "ride" upon the nitrogen atom. All other hydrogen atoms were placed at calculated positions (d_{C-H} = 1.00 Å, H—C—H = 109.5°) and were not refined, rather being constrained to ride upon the appropriate carbon.

Acknowledgements—We thank the Robert A. Welch Foundation, the National Science Foundation and the Army Research Office (DAAL 03-89-K-0164) for support.

REFERENCES

1. For a review, see: A. H. Cowley and R. A. Jones, *Angew. Chem., Int. Edn Engl.* 1989, **28**, 1208.
2. A. H. Cowley, P. R. Harris, R. A. Jones and C. M. Nunn, *Organometallics* 1991, **10**, 652; A. H. Cowley, B. L. Benac, J. G. Ekerdt, R. A. Jones, K. B. Kidd, J. Y. Lee and J. E. Miller, *J. Am. Chem. Soc.* 1988, **110**, 6248.
3. G. E. Coates, *J. Chem. Soc.* 1951, 2003; O. T.

Beachley, G. E. Coates and G. Kohnstam, *J. Chem. Soc.* 1965, 3248; A. Storr and A. D. Penland, *J. Chem. Soc. (A)* 1971, 1237.
4. We have also recently structurally characterized $Me_3Ga \cdot NH_2(t\text{-}Bu)$ and $Me_3In \cdot NH_2(t\text{-}Bu)$. D. A. Atwood, A. H. Cowley and R. A. Jones, *J. Organomet. Chem.* To be submitted.
5. W. Harris, A. Storr and J. Trotter, *J. Chem. Soc., Chem. Commun.* 1971, 1101.
6. H. D. Hausen, F. Gerstner and W. Schwarz, *J. Organomet. Chem.* 1978, **145**, 277.
7. For a discussion of problems associated with locating hydrogen atoms from X-ray data, see: F. A. Cotton and R. L. Luck, *Inorg. Chem.* 1989, **28**, 3210.
8. A. Bondi, *J. Phys. Chem.* 1964, **68**, 441.
9. R. A. Kovar, H. Deir, D. Brandau and J. O. Callaway, *Inorg. Chem.* 1975, **14**, 2809; H. M. Schwering, *J. Organomet. Chem.* 1977, **91**, C4.
10. J. Holton, M. F. Lappert, D. G. H. Ballard, R. Pearce, J. L. Atwood and W. E. Hunter, *J. Chem. Soc., Dalton Trans.* 1979, 45.
11. G. W. Sheldrick, SHELX—A System of Computer Programs for X-ray Structure Determination. Cambridge, England (1976).

Polyhedron Vol. 10, No. 16, pp. 1903–1909, 1991
Printed in Great Britain

0277–5387/91 $3.00+.00
© 1991 Pergamon Press plc

SYNTHESIS AND CHEMISTRY OF SECONDARY ALKYL IODIDE COMPLEXES OF THE FORMULA $[(\eta^5\text{-}C_5H_5)Re(NO)(PPh_3)(ICHRR')]^+BF_4^-$

ALAIN IGAU and J. A. GLADYSZ*

Department of Chemistry, University of Utah, Salt Lake City, UT 84112, U.S.A.

(*Received* 4 *April* 1991; *accepted* 16 *May* 1991)

Abstract—Reactions of deuterodichloromethane complex $[(\eta^5\text{-}C_5H_5)Re(NO)(PPh_3)(ClCD_2Cl)]^+BF_4^-$ with (**a**) isopropyl iodide, (**b**) *sec*-butyl iodide, (**c**) cyclopentyl iodide, and (**d**) cyclohexyl iodide give secondary alkyl iodide complexes $[(\eta^5\text{-}C_5H_5)Re(NO)(PPh_3)(ICHRR')]^+BF_4^-$ (**3a–d**) in good to high NMR yields, depending upon the quantity of alkyl iodide employed. These compounds are much less stable than analogous primary alkyl iodide complexes, but analytically pure **3d** can be isolated from the reaction of $(\eta^5\text{-}C_5H_5)Re(NO)(PPh_3)(CH_3)$ and $HBF_4\cdot OEt_2$ in neat cyclohexyl iodide (73%). Complex **3d** decomposes in CD_2Cl_2 to give cyclohexyl fluoride, cyclohexene (74% total) and bridging halide complexes $[(\eta^5\text{-}C_5H_5)Re(NO)(PPh_3)]_2X^+BF_4^-$ (X = I, 33%; Cl, 36%). The formation of cyclohexyl fluoride suggests BF_4^- participation in carbon–iodine bond cleavage. Reaction of **3d** and PPh_3 gives the substitution product $[Ph_3PC_6H_{11}]^+BF_4^-$ (24%), cyclohexyl fluoride (24%), cyclohexene (30%) and $(\eta^5\text{-}C_5H_5)Re(NO)(PPh_3)(I)$ (**7**, 95%). An analogous reaction of **3d** and PPN^+Br^- gives cyclohexene (57%) and **7** (99%).

Stable complexes of alkyl halides and transition metals are scarce.[1–5] Since Crabtree prepared the iridium methyl iodide complexes $[(H)_2Ir(PPh_3)_2(ICH_3)_2]^+X^-$ in pure form a decade ago, the vast majority of adducts isolated have been *primary* alkyl halides. Coordinated alkyl halides have been shown to be dramatically activated towards nucleophilic attack.[1,2,4] Thus, useful applications of secondary and tertiary alkyl halide complexes are readily envisioned. Further, when the metal fragment and alkyl halide are both chiral, there is the possibility that one alkyl halide enantiomer might selectively bind ("chiral recognition").

We have previously studied the synthesis, structure and reactivity of the chiral rhenium primary alkyl iodide complexes $[(\eta^5\text{-}C_5H_5)Re(NO)(PPh_3)(ICH_2R)]^+BF_4^-$ in detail.[4] With few exceptions, these compounds are easily isolated in pure form and in good to high yields from reactions of the substitution-labile dichloromethane complex $[(\eta^5\text{-}C_5H_5)Re(NO)(PPh_3)(ClCH_2Cl)]^+BF_4^-$ (**1**) and alkyl iodides (3–5 equiv.). We therefore sought to systematically define the scope of analogous secondary and tertiary alkyl iodide complexes that can be generated and/or isolated, and to compare their physical and chemical properties with those of the primary alkyl iodide complexes.

* Author to whom correspondence should be addressed.

RESULTS

(1) *Synthesis of secondary alkyl iodide complexes*

The methyl complex $(\eta^5\text{-}C_5H_5)Re(NO)(PPh_3)(CH_3)$ (**2**)[6] and an internal standard were dissolved in CD_2Cl_2 in an NMR tube and treated with $HBF_4\cdot OEt_2$ at −80°C. The generation of the previously reported deuterodichloromethane complex $[(\eta^5\text{-}C_5H_5)Re(NO)(PPh_3)(ClCD_2Cl)]^+BF_4^-$ (**1**-d_2)[5a] was verified by ^1H and ^{31}P NMR (−60°C). The sample was then frozen in liquid nitrogen and treated with 2 equiv. of (**a**) isopropyl iodide, (**b**) *sec*-butyl iodide, (**c**) cyclopentyl iodide and (**d**) cyclohexyl iodide, as shown in Scheme 1. These mixtures were warmed to −40°C in the NMR probe. Secondary alkyl iodide complexes $[(\eta^5\text{-}C_5H_5)Re(NO)(PPh_3)(ICHRR')]^+BF_4^-$ (**3a–d**) formed in 65–75% yields relative to a ^1H NMR resonance of the standard.

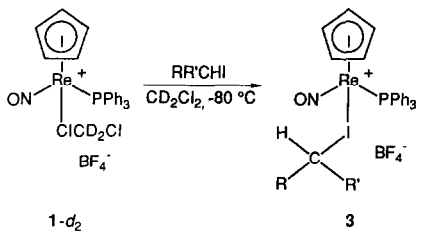

Scheme 1. Synthesis of secondary alkyl iodide complexes **3**.

When larger excesses of secondary alkyl iodides were employed, yields of **3a–d** were somewhat greater. However, extensive efforts to isolate pure complexes by this route were unsuccessful. Therefore, **3a–d** were characterized *in situ* by ^{1}H, ^{13}C and ^{31}P NMR spectroscopy, as summarized in Table 1. Properties were similar to those found earlier for primary alkyl iodide complexes $[(\eta^5\text{-}C_5H_5)Re(NO)(PPh_3)(ICH_2R)]^+BF_4^-$.[4] The ICH ^{13}C NMR resonances (47.9–58.3 ppm) showed diagnostic downfield shifts (22–29 ppm)[7] from those of the free alkyl iodides. The *sec*-butyl complex **3b**, which contains two stereocentres, gave two sets of resonances of equal intensity. Thus, the two possible rhenium/carbon configurational diastereomers formed in equal amounts.

Alternative routes to pure samples of **3** were sought. Thus, the methyl complex **2** was dissolved in *neat* cyclohexyl iodide and treated with $HBF_4 \cdot OEt_2$ at −40°C. Workup gave the cyclo-

Table 1. NMR characterization of secondary alkyl iodide complexes $[(\eta^5\text{-}C_5H_5)Re(NO)(PPh_3)(ICHRR')]^+BF_4^-$ (**3**)

Complex	^{1}H NMR (δ)[a]	$^{13}C\{^{1}H\}$ NMR (ppm)[b]	$^{31}P\{^{1}H\}$ NMR (ppm)[c]
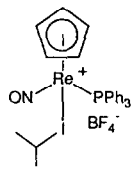 **3a**	7.50–7.22 (m, $3C_6H_5$), 5.59 (s, C_5H_5), 4.44 (sept, J = 6.6, CHI), 1.74 (d, J = 6.6, CH_3), 1.72 (d, J = 6.6, $C'H_3$).	PPh_3 at: 133.2 (d, J = 11.4, *o*), 132.5 (d, J = 57.6, *i*), 131.6 (d, J = 2.5, *p*), 129.0 (d, J = 13.0, *m*); 91.6 (s, C_5H_5), 47.9 (d, J = 2.8, CH), 28.0 (s, CH_3), 27.7 (s, $C'H_3$).	12.20 (s)
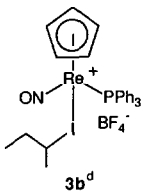 **3b**[d]	7.51–7.22 (m, $3C_6H_5$), 5.57 (s, C_5H_5), 4.41/4.33 (m, CHI), 1.74/1.71 (d, J = 7.1, CH_3CH), 1.68 (m, CHH'), 1.01/1.00 (t, J = 7.0, CH_3CH_2).	PPh_3 at: 133.2 (d, J = 10.9, *o*), 132.6 (d, J = 57.0, *i*), 131.6 (d, J = 2.7, *p*), 129.1 (d, J = 10.9, *m*); 91.6/91.5 (d, C_5H_5), 58.3/58.2 (d, J = 2.6, CH), 33.9/32.9 (s, CH_2), 25.4/25.0 (s, CH_3CH), 13.6/12.4 (s, CH_3CH_2).	13.03/12.98 (s)
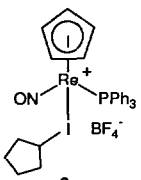 **3c**	7.52–7.24 (m, $3C_6H_5$), 5.58 (s, C_5H_5), 4.64 (m, CHI), 2.00 (m, 4H), 1.78 (m, 2H), 1.59 (m, 2H).	PPh_3 at: 133.6 (d, J = 9.4, *o*), 132.2 (d, J = 58.7, *i*), 131.3 (d, J = 2.5, *p*), 128.8 (d, J = 10.8, *m*); 91.4 (s, C_5H_5), 57.1 (s, CH), CH_2 (s) at 37.1, 36.7, 27.2, 22.8.	12.09 (s)
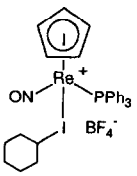 **3d**	7.49–7.18 (m, $3C_6H_5$), 5.57 (s, C_5H_5), 4.45 (m, CHI), 2.30 (m, 2H), 1.87 (m, 2H), 1.50 (m, 3H), 1.20 (m, 3H).	PPh_3 at: 133.2 (d, J = 11.0, *o*), 132.6 (d, J = 57.4, *i*), 131.7 (s, J = 2.0, *p*), 129.3 (d, J = 10.8, *m*); 91.6 (s, C_5H_5), 54.5 (s, CH), CH_2 (s) at 38.8, 37.1, 27.1, 27.0, 25.5.	12.15 (s)

[a] Recorded at 300 MHz in CD_2Cl_2 at −40°C and referenced to internal $CHDCl_2$ (5.32 ppm). All coupling constants are to ^{1}H and are in Hz.

[b] Recorded at 75 MHz in CD_2Cl_2 at −40°C and referenced to CD_2Cl_2 (53.8 ppm). All couplings are to ^{31}P and are in Hz. Assignments of phenyl carbon resonances were made as described in footnote c of Table 1 in ref. 8.

[c] Recorded at 121 MHz (unlocked) in CD_2Cl_2 at −40°C and referenced to external 85% H_3PO_4.

[d] Two diastereoisomers in a 50 : 50 ratio.

hexyl iodide complex **3d** in a 73% yield as an analytically pure, tan powder. An IR spectrum (CH_2Cl_2, −42°C) showed a ν(NO) at 1707 cm^{-1} (vs). This sample was used for all reactions described below.

The chlorobenzene complex $[(\eta^5\text{-}C_5H_5)Re(NO)(PPh_3)(ClC_6H_5)]^+BF_4^-$ is sometimes superior to **1** as a precursor to complexes of the formula $[(\eta^5\text{-}C_5H_5)Re(NO)(PPh_3)(L)]^+BF_4^-$.[5b] Analogous NMR-monitored reactions could not be conducted due to the precipitation of secondary alkyl iodide complexes (**3**) from the chlorobenzene solvent. However, a sample of isopropyl iodide complex **3a** was isolated from a preparative experiment. It was quite pure by ^1H and ^{31}P NMR, but not by microanalysis.

(2) *Thermal and substitution chemistry of cyclohexyl iodide complex* **3d**

A CD_2Cl_2 solution of **3d** and an internal standard was kept at room temperature in an NMR tube. Over the course of 2 days, conversion to two cyclopentadienyl-containing products was observed, as shown in Scheme 2. These were identified, on the basis of ^1H, ^{13}C and ^{31}P NMR spectra, as the previously characterized bridging iodide complex (*RR,SS*)-$[(\eta^5\text{-}C_5H_5)Re(NO)(PPh_3)]_2I^+BF_4^-$ (**4**)[9] and bridging chloride complex (*SS,RR*)-$[(\eta^5\text{-}C_5H_5)Re(NO)(PPh_3)]_2Cl^+BF_4^-$ (**5**).[5a] Yields were 33% and 36%, respectively, relative to an ^1H NMR resonance of the standard. In separate experiments, **4** and **5** were isolated.

The organic products derived from **3d** were assayed by ^1H NMR and gas chromatography (GLC). A mixture of cyclohexyl fluoride (δ 4.65, CHF) and cyclohexene (δ 5.87, =CH) was formed. No cyclohexyl iodide was detected. With time, the cyclohexyl fluoride diminished as the amount of cyclohexene increased until, at the end of 2 days, only cyclohexene (74%) remained.

An authentic sample of cyclohexyl fluoride was treated with $BF_3 \cdot OEt_2$ in CD_2Cl_2 at room temperature. Clean conversion to cyclohexene occurred over the course of 8 h, as assayed by ^1H NMR and GLC [eq. (1)]. However, cyclohexyl iodide and $BF_3 \cdot OEt_2$ did not react after 24 h under analogous conditions.

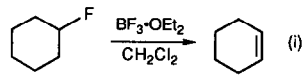

Next, a CD_2Cl_2 solution of **3d** and an internal standard was treated with CH_3CN (1.5 equiv.) at −80°C. The sample was warmed to room temperature. Over the course of 12 h, the acetonitrile complex $[(\eta^5\text{-}C_5H_5)Re(NO)(PPh_3)(NCCH_3)]^+BF_4^-$ (**6**)[5a] formed as the only cyclopentadienyl and PPh_3-containing product, as assayed by ^1H and ^{31}P NMR. The yield was 80% relative to a ^1H NMR resonance of the standard. However, no cyclohexyl iodide was detected by ^1H NMR or GLC, rather, cyclohexene (87%) was the exclusive organic product. Some cyclohexyl fluoride was detected by GLC during the early stages of the reaction, but it subsequently converted to cyclohexene.

(3) *Reactions of cyclohexyl iodide complex* **3d** *and nucleophiles*

A CD_2Cl_2 solution of **3d** and an internal standard was frozen in liquid nitrogen. PPh_3 (1.4 equiv.) was then added, and the sample was gradually warmed to 0°C. After 8 h, the iodide complex $(\eta^5\text{-}C_5H_5)Re(NO)(PPh_3)(I)$ (**7**)[10] had formed in a 95% yield, as assayed by ^1H and ^{31}P NMR and shown in Scheme 3. However, three major cyclohexyl-derived products were present: the phosphonium salt $[Ph_3PC_6H_{11}]^+BF_4^-$ (**8**, 24%), cyclohexyl fluoride (24%) and cyclohexene (30%). The ratio of cyclohexyl fluoride and cyclohexene did not change significantly with time.

An authentic sample of **8** was prepared from the previously characterized bromide salt $[Ph_3PC_6H_{11}]^+Br^-$,[11] as described in the Experimental. Also, cyclohexyl iodide and PPh_3 (2 equiv.) did not independently react in CH_2Cl_2 at room temperature (24 h). This shows that the cyclohexyl iodide ligand in **3d** is activated towards attack by PPh_3.

Two additional phosphorus-containing products were evident in the ^{31}P NMR spectrum of the **3d**/PPh_3 reaction mixture. These were not quanti-

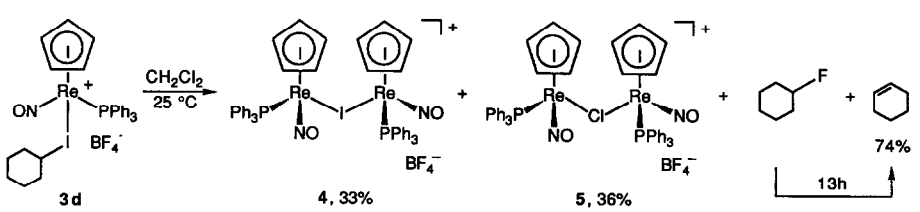

Scheme 2. Thermal decomposition of cyclohexyl iodide complex **3d**.

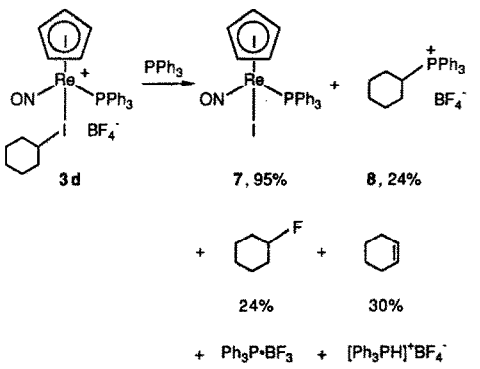

Scheme 3. Reaction of cyclohexyl iodide complex **3d** and PPh_3.

fied, but were assigned as $[Ph_3PH]^+BF_4^-$ (4.45 ppm, d, J(PH) 527.0 Hz) and $Ph_3P \cdot BF_3$ (−5.01 ppm, br, s). The large coupling in the former is diagnostic of a phosphonium salt phosphorus–hydrogen bond.[12] Also, the fluorosulphate analogue $[Ph_3PH]^+FSO_3^-$ has been previously shown to give a similar ^{31}P NMR resonance (CCl_4: 5.4 ppm, d, J(PH) 510 Hz).[13] Accordingly, when a CD_2Cl_2 solution of PPh_3 was treated with $HBF_4 \cdot OEt_2$ (0.7 equiv.), a 4.5 ppm doublet was cleanly generated. The Lewis acid/base adduct $Ph_3P \cdot BF_3$ has also been previously characterized.[14] When a CD_2Cl_2 solution of PPh_3 was analogously treated with $BF_3 \cdot OEt_2$, a broad resonance appeared at −5.0 ppm.

Next, a similar reaction was conducted with **3d** and PPN^+Br^-.[15] The mixture was kept at −40°C for 12 h, and then assayed by ^1H and ^{31}P NMR at room temperature. The iodide complex **7** formed in a 99% yield. However, cyclohexene (57%) was the only organic product detected. An aliquot of the mixture was taken when the sample was at −40°C and analysed by GLC. Some cyclohexyl flouride was present.

(4) *Reactions with tertiary alkyl iodides*

A "less bulky", bridgehead tertiary alkyl iodide was sought for scout experiments. Thus, 1-adamantyl iodide (3 equiv.)[16] was reacted with **1**-d_2 in the presence of an internal standard, as described for the secondary alkyl iodides above. Over the course of several hours at −40°C, a multitude of products formed. The major species (*ca* 20%) exhibited plausible NMR resonances for a 1-adamantyl iodide complex (−20°C: ^1H NMR, δ 5.57, s; ^{31}P NMR 12.1 ppm, s). When the sample was warmed to room temperature, bridging halide complexes **4** (δ 5.42, 49%) and **5** (δ 5.41, 40%) formed. The significant yield of bridging iodide complex **4** also suggests that an appreciable amount of the target complex was generated.

DISCUSSION

We previously reported that isopropyl iodide is about 50% as reactive as methyl iodide, and 67% as reactive as ethyl iodide towards the dichloromethane complex **1** at −41°C.[4a] Thus, secondary alkyl iodides are less nucleophilic than primary alkyl iodides, or poorer Lewis bases in a kinetic sense. This follows logically from their increased bulk. Secondary alkyl iodides are likely poorer Lewis bases in the conventional thermodynamic sense as well. We attempted to demonstrate this by treating cyclohexyl iodide complex **3d** with ethyl iodide (3 equiv.) in CD_2Cl_2 at 0°C. However, the previously characterized[4a] ethyl iodide complex $[(\eta^5\text{-}C_5H_5)Re(NO)(PPh_3)(ICH_2CH_3)]^+BF_4^-$ was not detected by ^1H or ^{31}P NMR. Rather, the independent decomposition of **3d** occurred.

The isolation of secondary alkyl iodide complexes **3** from preparations involving dichloromethane solvent is in all cases complicated by the formation of the bridging halide complexes $[(\eta^5\text{-}C_5H_5)Re(NO)(PPh_3)]_2X^+BF_4^-$. The probable key features of these competing decomposition pathways are sketched in Scheme 4. First, solvolytic displacement of the alkyl iodide ligands in **3** can occur to give dichloromethane complex **1** [step (a)], which rapidly decomposes to the bridging chloride complex **5** above −20°C.[5a] This substitution is likely faster and less endothermic than for the corresponding primary alkyl iodide complexes, accounting for the observed stability trend.

Secondly, carbon–iodine bond cleavage can occur to give the iodide complex **7** [step (b)]. Complex **7** can in turn react with **3** or **1** to give bridging iodide complex **4**.[9] The formation of cyclohexyl fluoride in Scheme 2 suggests that the weakly coordinating[17] BF_4^- anion can participate in the carbon–iodine bond cleavage step, as sketched in **I** (Scheme 4). Alternatively, the carbon–iodine bond might undergo heterolysis, and the carbocation of the resulting intimate "ion pair" could react with BF_4^-. Since some cyclohexene seems to form directly from **3d**, it is also possible that BF_4^- serves as the base in an E2 elimination step, as shown in **II**.

The attack of BF_4^- upon coordinated dichloromethane has been proposed as a key step in the decomposition of **1** to bridging chloride complex **5**.[5a] However, the expected primary product FCH_2Cl could not be conclusively identified in the reaction mixture. Thus, the formation of cyclohexyl

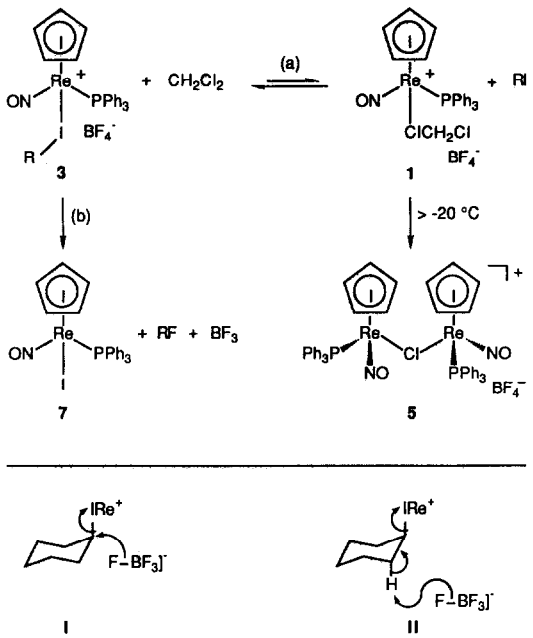

Scheme 4. Some possible decomposition pathways for alkyl iodide complexes **3**.

fluoride from **3d** provides welcome precedent for this step. The anion PF_6^- has been shown to be a poorer fluoride ion donor than BF_4^-.[17] Thus, PF_6^- salts of **3** would likely be somewhat more stable. However, $HPF_6 \cdot OEt_2$, which is required for the formation of the precursor dichloromethane complex, no longer appears to be commercially available in adequate purity.

The mass balance for the organic and inorganic decomposition products of **3d** is only fair. Note that steps **I** and **II** (Scheme 4) give the strong acids BF_3 and HF. These in turn can likely react with many of the primary products. Also, the iodide complex **7** has been shown to undergo a "transalkylation" reaction with dichloromethane complex **1** to give the iodochloromethane complex $[(\eta^5\text{-}C_5H_5)Re(NO)(PPh_3)(ICH_2Cl)]^+BF_4^-$.[9]

In the reaction of **3d** and PPh_3 (Scheme 3), PPh_3 serves both as a nucleophile (to give phosphonium salt **8**) or a base (to give cyclohexene). Pathways analogous to **I** and **II** (Scheme 4) are likely involved. The formation of comparable amounts of cyclohexyl fluoride and **8** suggests that BF_4^- and PPh_3 attack upon the cyclohexyl iodide ligand is competitive. The BF_3 by-product from the former process subsequently binds to PPh_3, therefore, cyclohexyl fluoride does not convert to cyclohexene as in Scheme 2 and eq. (1). Interestingly, cyclohexyl bromide and PPh_3 react to give the phosphonium salt $[Ph_3PC_6H_{11}]^+Br^-$, without any significant amount of competing elimination.[11]

In contrast to PPh_3, PPN^+Br^- appears to function chiefly as a base towards **3d**. However, the formation of cyclohexene (87%) in the reaction of **3d** and acetonitrile is more surprising. Analogous primary iodide complexes and acetonitrile react to give mainly simple substitution products—acetonitrile complex **6** (82–87%) and free alkyl halides (72–82%).[4a] This suggests a more complex mechanistic sequence, possibly involving the BF_4^- anion, with **3d**.

Crabtree has previously reported the isolation of chiral ruthenium isopropyl iodide and cyclohexyl iodide complexes $[(\eta^5\text{-}C_5H_5)Ru(CO)(PPh_3)(ICHRR)]^+PF_6^-$.[2c] He finds that the former undergoes clean reactions with chloride ions to give isopropyl chloride, and pyridine to give the corresponding pyridinium salt. However, the latter gives only cyclohexene upon reactions with nucleophiles. Cyclohexyl halides are well-known to be more susceptible to elimination reactions than acyclic analogues.

We have previously shown that the methyl iodide complex $[(\eta^5\text{-}C_5H_5)Re(NO)(PPh_3)(ICH_3)]^+BF_4^-$ exchanges only slowly with CD_3I (15 equiv.) in CD_2Cl_2 at room temperature.[4a] Also, the diastereotopic methyl groups of isopropyl iodide complex **3a** give distinct ^1H and ^{13}C NMR resonances (Table 1). These would be equivalenced by any rapid dissociative process. Thus, the reactions in Scheme 1 are probably under kinetic control.

This is likely relevant to the lack of diastereoselectivity in the formation of *sec*-butyl iodide complex **3b**. Based upon crystal structures of a primary alkyl iodide complex and bridging iodide complex **4**,[4a,9] the diastereomers of **3b** likely adopt the structures **III** and **IV**. In each, the large *C*—I

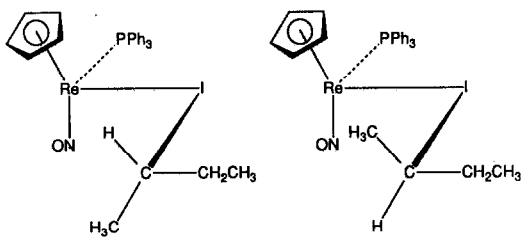

III (*RS,SR*)
(favored, CH_3 and C_5H_5 *anti*)

IV (*RR,SS*)
(disfavored, CH_3 and C_5H_5 *syn*)

substituent, ethyl, is oriented *anti* to the I—Re bond. We had expected **III** to be more stable due to reduced steric interactions between the cyclopentadienyl ligand and the remaining *C*—I substituents. An analogous consideration accounts for the very high diastereoselectivity in the formation of bridging halide complexes **4** and **5**.[9] Thus, we speculate that significant diastereoselection might be realized under thermodynamically controlled conditions.

In summary, this study has established that secondary alkyl iodide complexes (**3**) can be synthesized and in some cases isolated in pure form. However, they are considerably more labile than analogous primary alkyl iodide complexes. Although the cyclohexyl iodide ligand in **3d** is activated towards nucleophilic attack, competing reactions involving the BF_4^- anion are observed and elimination products usually dominate.

EXPERIMENTAL

General

All reactions were conducted under a dry nitrogen atmosphere. IR spectra were recorded on a Mattson Polaris FT-IR spectrometer. NMR spectra were recorded on Varian XL-300 spectrometers. The following chemical shift standards were used: ^{1}H, residual $CHDCl_2$ (δ 5.32); ^{13}C, CD_2Cl_2 (53.8 ppm); ^{31}P, external 85% H_3PO_4 (0.00 ppm). Mass spectra were obtained on a VG 770 spectrometer. Analytical gas–liquid chromatography (GLC) was conducted on a Hewlett Packard 5890 chromatograph utilizing a capillary column (cross-linked 5% phenyl methyl silicone, 25 m × 0.2 mm × 0.33 mm film) and a 0.6 cm^3 min^{-1} helium flow. Microanalyses were conducted by Atlantic Microlab. Melting points were determined in evacuated capillaries.[18]

Solvents, reagents and standards were utilized as follows: CH_2Cl_2 and CH_3CN, distilled from P_2O_5; hexane, distilled from sodium; methanol, distilled from magnesium; CD_2Cl_2, distilled from CaH_2; $HBF_4 \cdot OEt_2$ (Aldrich), standardized as described previously;[5a] alkyl iodides (Aldrich), filtered through a 3.5 cm alumina column, distilled, and stored at −10°C over copper in the dark; PPh_3 (Aldrich), recrystallized from benzene; Ph_3SiCH_3 (Pfaltz & Bauer), $BF_3 \cdot OEt_2$, and $AgBF_4$ (Aldrich), used as received; cyclohexyl flouride (Pfaltz & Bauer) was assayed by GLC and returned to the vendor unless pure. The salt[15,19] PPN^+Br^- and 1-adamantyl iodide[16] were prepared by literature procedures.

Isolation of $[(\eta^5\text{-}C_5H_5)Re(NO)(PPh_3)(IC_6H_{11})]^+ BF_4^-$ (**3d**). A Schlenk flask was charged with $(\eta^5\text{-}C_5H_5)Re(NO)(PPh_3)(CH_3)$ (**2**;[6] 0.339 g, 0.612 mmol), cyclohexyl iodide (3 cm^3), and a stir bar. The mixture was gently warmed to solubilize **2**, and then cooled to −40°C (CH_3CN/dry ice). Then $HBF_4 \cdot OEt_2$ (0.085 cm^3, 0.67 mmol) was added with stirring. The mixture was kept at −40°C for 50 min and then hexane was added. A precipitate formed, which washed with hexane (2 × 3 cm^3) and dried *in vacuo* to give **3d** as a tan powder (0.374 g, 0.447 mmol, 73%), m.p. 100–105°C, dec. Mass spectrum [(+)-FAB (7 kV, Ar, 3-nitrobenzyl alcohol/$CHCl_3$), *m/z* (relative intensity), ^{187}Re]: 754 (M^+, 24%), 671 (M^+-C_6H_{11}, 41%), 544 (M^+-IC_6H_{11}, 57%). Found: C, 41.6; H, 3.8. Calc. for $C_{29}H_{21}BF_4INOPRe$: C, 41.4; H, 3.7%.

Solutions of $[(\eta^5\text{-}C_5H_5)Re(NO)(PPh_3)(ICHRR')]^+ BF_4^-$ (**3**). The following procedure is representative. A 5 mm NMR tube was charged with **2** (0.0453 g, 0.0811 mmol), Ph_3SiCH_3 as a standard (0.0176 g, 0.0641 mmol) and CD_2Cl_2 (0.8 cm^3), and was capped with a septum. The tube was cooled to −80°C, and $HBF_4 \cdot OEt_2$ (0.008 cm^3, 0.073 mmol; 0.85–0.90 equiv.) was added. Next, ^{1}H and ^{31}P NMR spectra were acquired at −60°C, and showed the formation of $[(\eta^5\text{-}C_5H_5)Re(NO)(PPh_3)(ClCD_2Cl)]^+$ (**1**-d_2) in an 85% yield, based upon limiting $HBF_4 \cdot OEt_2$. The sample was frozen in liquid nitrogen, and isopropyl iodide (0.0124 cm^3, 0.124 mmol, 2 equiv.) was added. The tube was slowly warmed to −60°C. Then ^{1}H, ^{13}C and ^{31}P NMR spectra were recorded (negligible reaction). The sample was kept for 8–10 h at −40°C. Subsequent NMR spectra showed the formation of $[(\eta^5\text{-}C_5H_5)Re(NO)(PPh_3)(ICH(CH_3)_2)]^+BF_4^-$ (**3a**, 0.047 mmol relative to the Ph_3SiCH_3 ^{1}H NMR resonance) in a 75% yield based upon **1**-d_2. Table 1 shows the data obtained.

Decomposition of **3d**. A 5 mm NMR tube was charged with **3d** (0.0183 g, 0.0218 mmol), Ph_3SiCH_3 as a standard (0.0123 g, 0.0448 mmol) and CD_2Cl_2 (0.80 cm^3), and was capped with a septum. The tube was kept at room temperature and ^{1}H and ^{31}P NMR spectra were periodically recorded. After 48 h, no **3d** remained. The yields of (*RR,SS*)-$[(\eta^5\text{-}C_5H_5)Re(NO)(PPh_3)]_2I^+BF_4^-$ (**4**, 0.0072 mmol, 33%),[9] (*SS,RR*)-$[(\eta^5\text{-}C_5H_5)Re(NO)(PPh_3)]_2Cl^+BF_4^-$ (**5**, 0.0078 mmol, 36%)[5a] and cyclohexene (0.0083 mmol, 74%) were determined by integration of ^{1}H NMR resonances (C_5H_5, =CH vs Ph_3SiCH_3). The cyclohexene yield was confirmed by GLC. See text for other data.

Reaction of **3d** *and acetonitrile*. A 5 mm NMR tube was charged with **3d** (0.0438 g, 0.0521 mmol), Ph_3SiCH_3 standard (0.0157 g, 0.0599 mmol), and was capped with a septum. The sample was cooled to −80°C, and CD_2Cl_2 (0.8 cm^3) and CH_3CN (0.0040 cm^3, 0.078 mmol) were added via a syringe. The sample was warmed to room temperature, and ^{1}H and ^{31}P NMR spectra were periodically recorded. After 12 h, no **3d** remained. The yields of $[(\eta^5\text{-}C_5H_5)Re(NO)(PPh_3)(NCCH_3)]^+BF_4^-$ (**6**, 0.0417 mmol, 80%)[5a] and cyclohexene (0.0453 mmol, 87%) were determined by integration of ^{1}H NMR resonances (C_5H_5, =CH vs Ph_3SiCH_3).

Reaction of **3d** *and* PPh_3. A 5 mm NMR tube was charged with **3d** (0.0366 g, 0.0435 mmol),

Ph_3SiCH_3 as a standard (0.0143 g, 0.0521 mmol), and was capped with a septum. The sample was frozen in liquid nitrogen, CD_2Cl_2 (0.8 cm^3) was added, followed by solid PPh_3 (0.0160 g, 0.0610 mmol). The sample was slowly warmed to 0°C, and ^1H and ^{31}P NMR spectra were periodically recorded. After 8 h, no **3d** remained. The yields of $(\eta^5\text{-}C_5H_5)Re(NO)(PPh_3)(I)$ (**7**, 0.0413 mmol, 95%),[10] $[Ph_3PC_6H_{11}]^+BF_4^-$ (**8**, 0.0104 mmol, 24%), cyclohexyl fluoride (0.0104 mmol, 24%) and cyclohexene (0.0131 mmol, 30%) were determined by integration of ^1H NMR resonances (C_5H_5, CHX, =CH vs Ph_3SiCH_3). The cyclohexyl fluoride and cyclohexene yields were confirmed by GLC. See text for other data.

Reaction of **3d** *and* PPN^+Br^-. A 5 mm NMR tube was charged with **3d** (0.0244 g, 0.0290 mmol), Ph_3SiCH_3 standard (0.0127 g, 0.0463 mmol), and was capped with a septum. The sample was frozen in liquid nitrogen, CD_2Cl_2 (0.8 cm^3) was added, followed by solid PPN^+Br^- (0.0210 g, 0.0340 mmol). The sample was kept at −40°C for 12 h and then ^1H and ^{31}P NMR spectra were recorded at room temperature. The yields of **7** (0.0287 mmol, 99%) and cyclohexene (0.0281 mmol, 57%) were determined by integration of ^1H NMR resonances (C_5H_5, =CH vs Ph_3SiCH_3). See text for other data.

Preparation of $[Ph_3PC_6H_{11}]^+BF_4^-$ (**8**). A flask was charged with $[Ph_3PC_6H_{11}]^+Br^-$ (0.654 g, 1.54 mmol),[11] $AgBF_4$ (0.352 g, 1.81 mmol), methanol (25 cm^3), and a stir bar. The mixture was stirred for 15 min and was then poured through a 3 cm pad of Celite on a coarse glass frit. The solvent was removed from the filtrate by rotary evaporation. A white microcrystalline powder formed, which was recrystallized from CH_2Cl_2/ether and dried under an oil pump vacuum to give **8** (0.646 g, 1.49 mmol, 94%), m.p. 241°C. IR (cm^{-1}, KBr) ν(BF) 1121 vs, 1054 vs, 996 vs; ^1H NMR (δ, CD_2Cl_2, 25°C) 7.84–7.87 (m, $3C_6H_5$), 3.67 (m, PCH), 2.11 (m, CH_2), 1.83 (m, CH_2), 1.71 (m, CH_2), 1.16 (m, CH_2); $^{13}C\{^1H\}$ NMR (ppm, CD_2Cl_2) 135.2 (d, J(CP) 2.9 Hz, *p*-Ph), 133.8 (d, J(CP) 9.4 Hz, *m*-Ph), 130.7 (d, J(CP) 12.6 Hz, *o*-Ph), 117.3 (d, J(CP) 83.5 Hz, *i*-Ph), 31.0 (d, J(CP) 46.9 Hz, PCH), 26.8 (d, J(CP) 3.0 Hz, $PCCH_2$),[20] 26.0 (d, J(CP) 13.8 Hz, $PCCCH_2$),[20] 25.6 (s, CH_2); $^{31}P\{^1H\}$ (ppm, CD_2Cl_2) 26.7 (s). Found: C, 66.2; H, 6.0. Calc. for $C_{24}H_{28}NF_4P$: C, 66.7; H, 6.1%.

Acknowledgement—We thank the NSF for support of this research.

REFERENCES

1. R. J. Kulawiec and R. H. Crabtree, *Coord. Chem. Rev.* 1990, **99**, 89.
2. (a) R. H. Crabtree, J. W. Faller, M. F. Mellea and J. M. Quirk, *Organometallics* 1982, **1**, 1361; (b) M. J. Burk, B. Segmuller and R. H. Crabtree, 1987, **6**, 2241; (c) R. J. Kulawiec, J. W. Faller and R. H. Crabtree, 1990, **9**, 745 and references therein.
3. (a) M. R. Colsman, T. D. Newbound, L. J. Marshall, M. D. Noirot, M. M. Miller, G. P. Wulfsberg, J. S. Frye, O. P. Anderson and S. H. Strauss, *J. Am. Chem. Soc.* 1990, **112**, 2349 and references therein; (b) M. Bown and J. M. Water, 1990, **112**, 2442; (c) F. M. Conroy-Lewis, A. D. Redhouse and S. J. Simpson, *J. Organomet. Chem.* 1989, **366**, 357.
4. (a) C. H. Winter, W. R. Veal, C. M. Garner, A. M. Arif and J. A. Gladysz, *J. Am. Chem. Soc.* 1989, **111**, 4766; (b) P. T. Czech, J. A. Gladysz and R. F. Fenske, *Organometallics* 1989, **8**, 1810; (c) A. Igau and J. A. Gladysz, *Organometallics* 1991, **10**, 2327.
5. (a) J. M. Fernández and J. A. Gladysz, *Organometallics* 1989, **8**, 207; (b) J. J. Kowalczyk, S. K. Agbossou and J. A. Gladysz, *J. Organomet. Chem.* 1990, **397**, 333.
6. W. Tam, G.-Y. Lin, W.-K. Wong, W. A. Kiel, V. K. Wong and J. A. Gladysz, *J. Am. Chem. Soc.* 1982, **104**, 141.
7. The following chemical shifts were found for the ICH resonances of free alkyl iodides (ppm, CD_2Cl_2, −40°C): (**a**) 21.4; (**b**) 32.4; (**c**) 28.7; (**d**) 32.5.
8. W. E. Buhro, S. Georgiou, J. M. Fernández, A. T. Patton, C. E. Strouse and J. A. Gladysz, *Organometallics* 1986, **5**, 956.
9. C. H. Winter, A. M. Arif and J. A. Gladysz, *Organometallics* 1989, **8**, 219.
10. J. H. Merrifield, J. M. Fernández, W. E. Buhro and J. A. Gladysz, *Inorg. Chem.* 1984, **23**, 4022.
11. H. J. Bestmann and O. Kratzer, *Chem. Ber.* 1963, **96**, 1899.
12. D. G. Gorenstein, *Phosphorus-31 NMR* (Edited by D. G. Gorenstein), Ch. 2 and 18. Academic Press, Orlando (1984).
13. G. A. Olah and C. W. McFarland, *J. Org. Chem.* 1969, **34**, 1832.
14. (a) E. Muylle, G. P. Van der Kelen and Z. Eeckaut, *Spectrochim. Acta* 1975, **31A**, 1039; (b) E. Muylle and G. P. Van der Kelen, *Spectrochim. Acta* 1975, **31A**, 1045; (c) E. Muylle and G. P. Van der Kelen, *Spectrochim. Acta* 1976, **32A**, 599; (d) E. Muylle, G. P. Van der Kelen and E. G. Claeys, *Spectrochim. Acta* 1976, **32A**, 1149; (e) J. M. Van Paasschen and R. A. Geanangel, *Inorg. Chem.* 1978, **17**, 3302.
15. $PPN^+ = [Ph_3P{\cdots}N{\cdots}PPh_3]^+$.
16. G. Molle, P. Bauer and J. E. Dubois, *J. Org. Chem.* 1982, **47**, 4120.
17. (a) W. Beck and K. Sünkel, *Chem. Rev.* 1988, **88**, 1405; (b) R. V. Honeychuck and W. H. Hersh, *J. Am. Chem. Soc.* 1989, **111**, 6056.
18. G. V. D. Tiers, *J. Chem. Educ.* 1990, **67**, 258.
19. A. Martinsen and J. Songstad, *Acta Chem. Scand.* 1977, **A31**, 645.
20. These assignments follow from the trend $^1J(PC) > {}^3J(PC) > {}^2J(PC)$ commonly observed in alkyl phosphonium salts:[4a,12] G. A. Gray, *J. Am. Chem. Soc.* 1973, **95**, 7736; see Table IV, footnotes d–e.

Polyhedron Vol. 10, No. 16, pp. 1911–1919, 1991
Printed in Great Britain

0277–5387/91 $3.00+.00
© 1991 Pergamon Press plc

[COPPER(II)-ARYLTETRAAZANNULENE]I_x COMPLEXES AS CONDUCTIVE MATERIALS. SOLID STATE SYNTHESIS AND CHARACTERIZATION

FRANCESCO LELJ,* GIANCARLO MORELLI, GIAMPAOLO RICCIARDI, MAURIZIO ROMANELLI and ANGELA ROSA

Dipartimento di Chimica, Universita' della Basilicata, Via N. Sauro 85, 85100 Potenza, Italy

and

MARIA F. OTTAVIANI

Dipartimento di Chimica, Universita' di Firenze, Via G. Capponi 9, 50121 Firenze, Italy

(*Received* 12 *December* 1990; *accepted* 14 *May* 1991)

Abstract—Cu(dibenzo[b,i][1,4,8,11]tetraaza[14]annulene), Cu(dbTAA), Cu(dinaphtho-[b,i][1,4,8,11]tetraaza[14]annulene), Cu(dnTAA), Cu(diphenanthro[b,i][1,4,8,11]tetraaza [14]annulene) and Cu(dpTAA) complexes have been used for synthesizing new conductive materials. Chemical oxidation of the three compounds in acetone slurries by variable amounts of iodine yielded microcrystalline conductive powders with a wide range of stoichiometries. Thermal stability of the oxidized materials was investigated by TGA and DTGA techniques showing a relationship between solid phase stability and iodine content and, together with IR data, suggests the presence of a single phase. Raman spectra show strong scatterings attributable to I_3^- (107 cm^{-1}) and (160 cm^{-1}) I_5^- polyiodides, the latter occurs only in highly iodinated complexes (I/Cu ratio larger than three) and the I_2 presence can be excluded. Electrical conductivity measurements of powder samples of the oxidized compounds exhibit some dependence on the iodine content in the I/Cu ratio range 0–0.9. The temperature response of the conductivity of the oxidized compounds, in the range 70–220 K, is interpretable in terms of an activated formation of carriers. ESR spectra, static magnetic susceptibility and IR data as a function of the I/Cu ratio suggest that the oxidative process involves not only the copper unpaired electron, but also electrons associated with delocalized ligand orbitals on the macrocycle. Large enhancement of the conductivity is shown by Cu(dpTAA)$I_{0.2}$ (1.5 S cm^{-1}) and the temperature dependance of conductivity shows metallic behaviour starting from 200 K.

Partially oxidized metalloorganic complexes with aromatic ligands have provided[1–3] an interesting class of molecular conductors. Partial iodine oxidation of tetraazaannulene complexes of various transition metals promises an interesting class of molecular conductors. As a matter of fact, the role played by the nature of the ligand and the degree of oxidation on their properties has not been systematically investigated. However some studies on metal(II) (M = Ni, Cu, Co, Pd) complexes of the dianionic ligands dibenzo[b,i][1,4,8,11]tetraaza [14]annulene^{2-}, (dbTAA),[1,3–6] 5,7,12,14tetramethyldibenzo [b,i] [1,4,8,11] tetraaza [14] annulene^{2-}, (dbTMTAA)[1,7] and of others, variously substituted dibenzo [b,i] [1,4,8,11] tetraaza [14] annulenes^{2-} [1,3] have been undertaken. Among these, the unsubstituted dbTAA complexes give rise to the most conductive materials and show very promising transport parameters slightly smaller than those of "Molecular metals", like (NiPc)I (Pc = Phthalocyanine).[10,11]

In this paper, as part of a systematic study on

* Author to whom correspondence should be addressed.

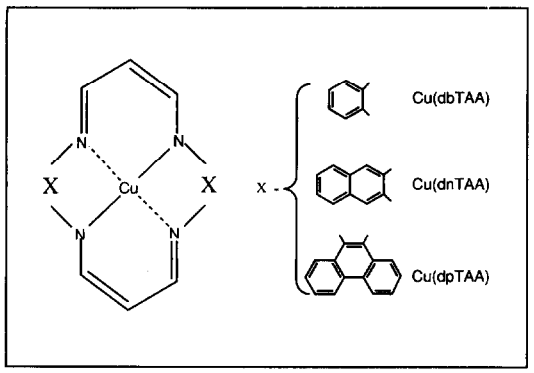

Fig. 1. Scheme of the three complexes.

the properties of these compounds, we present the preparation of the I_2 oxidized compounds of copper(II) with new tetraaza[14]annulene macrocyclic dianionic ligands[12] with larger aromatic moieties, i.e. dinaphtho[b,i][1,4,8,11]tetraaza[14]annulene^{2-} and diphenanthro[b,i][1,4,8,11]tetraaza[14]annulene^{2-} [hereafter $(dnTAA)^{2-}$ and $(dpTAA)^{2-}$, respectively (Fig. 1)]. Our purpose is to gain insight into the influence of the degree of oxidation and the "dimension" of the macrocycle on the solid state conductivity of the material. The results concerning the materials obtained by iodine oxidation of these complexes are discussed in comparison with new data for the analogous copper(II)dibenzo[b,i][1,4,8,11]tetraaza[14]annulene complex, Cu(dbTAA).[12]

EXPERIMENTAL

Reagents

Cu(dnTAA) and Cu(dpTAA) were synthesized following the procedures set up in our laboratory,[12] whereas Cu(dbTAA) was synthesized according to the experimental procedure of Hunziker *et al.* and Wuu *et al.*[3]

Iodination of the copper complexes: procedure. In order to prepare polycrystalline samples of various stoichiometries, finely powdered Cu(dbTAA), Cu(dnTAA) and Cu(dpTAA) in acetone were treated with increasing amounts of iodine dissolved in acetone, in the dark. The reactions were performed by stirring for 18 h at room temperature in a flask stopped with a septum. In a typical experiment Cu(dbTAA) (0.174 g, 0.500 mmol) in 20 cm^3 of acetone was treated with I_2 (0.635 g, 2.500 mmol) dissolved in 15 cm^3 of acetone. The black microcrystalline compound obtained was purified by removing the solvent and the unreacted iodine under a stream of nitrogen. The compound, washed with 5–10 cm^3 of acetone and dried at 40°C and 25 mmHg, was characterized as $Cu(dbTAA)I_{3.3}$.

Physical methods characterization

Spectroscopy. IR spectra were recorded as Nujol mulls with a Perkin–Elmer Model 883 spectrophotometer. Raman spectra were obtained with a Ramanor HG2S spectrometer employing 514.5 nm excitation (250 mW argon ion laser power filtered at 30%). The samples, in glass capillaries, were spun at 3000 rpm. The ESR spectra were recorded with a Bruker 200D spectrometer operating at the X band and equipped with an Aspect 2000 computer for spectra accumulation and magnetic parameter calculation. Susceptibility measurements were carried out by a susceptometer AZTEC-DSM5 operating at 13,500 G equipped with an electromagnet Bruker BE15.

Thermogravimetric analysis. TGA data were obtained by using a B85 Setaram thermal analyser equipped with TGC 85 controller module and a BBC(Goerz Metrawatt) Servogor 120 recorder. Measurements were carried out using a platinum sample boat under a nitrogen atmosphere. A nitrogen flow rate of 50 cm^3 min^{-1} and programmed heating rates of 20°C min^{-1} were employed. Scans were made from room temperature to 600°C. Initial sample mass was nominally 8.0 mg. Iodine contents were directly determined from the thermograms. All the obtained data were in good agreement with the elemental analyses.

Conductivity measurements. Electrical conductivity data by both the linear two-probe and the four-probe van der Pauw[13] methods were obtained. With the linear two-probe technique only room temperature data were acquired. Micropellets, 1 mm in diameter and *ca* 1 mm thick, were introduced in a glass capillary. In the case of van der Pauw measurements sample disks (13-mm diameter, about 0.5-mm thick) were used. The disks were formed using an evacuable die and a Carver press at 12 tons cm^{-2}. Thickness and diameter of samples and probe spacing were determined with the aid of a microscope. Electrical current to the sample was supplied by a Hewlett Packard precision DC current source 6186C. Output DC voltages were detected by Hewlett Packard 3478 A Multimeter. The disks were mounted over zapphire monocrystal, electrical contacts to the samples were made with a palladium paste. The investigated temperature range was between 77 K and room temperature. For measurements at temperatures below room temperature a refrigerator system (Air Product-USA, model LT-3-110) supplied with APD-E

digital indicating temperature controller and equipped with a shroud for conductivity measurements was used. The measurement procedure included: (i) verification of electrical isolation between the sample and mount; (ii) resistance measurements between all four electrodes as a function of current to check for nonohmic behaviour, contact resistance, and sample integrity; and (iii) measurements at zero current to the sample to check for stray voltages. Conductivity data have been collected at least five times on each sample and at least three micropellets with the same I/Cu ratio have been used giving rise to an error of ± 0.05 on $\log \sigma$ (see Table 1).

RESULTS

Iodination chemistry and characterization of the materials

Table 1 reports the most relevant characterization data of iodinated complexes of Cu(dbTAA), Cu(dnTAA) and Cu(dpTAA) prepared according to the outlined procedure. The oxidation afforded black coloured microcrystalline powders for Cu(dbTAA) and Cu(dnTAA), and from red to dark purple powders, depending on iodine content, for Cu(dpTAA). The response of the three complexes to oxidation has been found strongly dependent on the iodine concentration for Cu(dbTAA) and Cu(dnTAA); the iodine uptake reached maximum values for Cu(dbTAA) and Cu(dnTAA) in about 2 h, and in 24 h for Cu(dpTAA); the same general behaviour was also found with iodinating slurries in n-pentane, CH_2Cl_2 or $CHCl_3$; the oxidized compounds were air stable for months, without an appreciable iodine loss. The percentage of iodine reacted is always within 10–50% of the amount used. However, the iodine uptake is not easily predictable and shows large sensitivity to the experimental conditions. Owing to this sensitivity we determined the I/Cu ratio for each sample used by thermogravimetric measurements and elemental analysis (see Table 1) before characterization and physical measurements.

Table 1. Iodination conditions, analytical data and room temperature conductivities for Cu(dbTAA)I_x, Cu(dnTAA)I_x and Cu(dpTAA)I_x

Complex	x	Copper complex (mmol) (weight, g)[a]	I_2 (mmol) (weight, g)[b]	Iodine uptake (%)	Elemental analysis, calc. (found) C	H	N	$-\log \sigma$[c]
	0.00	—	—	—	61.8(62.1)	4.0(3.9)	16.0(15.7)	10.00
	0.11	0.500(0.174)	0.250(0.063)	11	59.4(59.9)	3.8(3.9)	15.4(15.2)	1.69
	0.90	0.500(0.174)	0.500(0.127)	45	46.6(47.1)	3.0(3.2)	12.1(12.3)	2.52
Cu(dbTAA)I_x	1.92	0.500(0.174)	1.000(0.254)	48	36.4(36.9)	2.4(2.7)	9.4(9.7)	2.40
	3.30	0.500(0.174)	2.500(0.635)	33	28.1(28.4)	1.8(1.9)	7.3(7.7)	3.05
	4.80	0.500(0.174)	5.000(1.270)	24	22.5(22.6)	1.5(1.6)	5.8(5.6)	3.20
	6.65	0.500(0.174)	7.500(1.905)	22	18.1(18.3)	1.2(1.1)	4.7(4.9)	3.15
	0.00	—	—	—	69.4(69.8)	4.0(4.3)	12.4(12.6)	5.70
	0.10	0.500(0.225)	0.250(0.063)	10	67.5(67.7)	3.9(4.1)	12.1(12.0)	1.30
	0.26	0.500(0.225)	0.500(0.126)	13	64.7(65.0)	3.7(3.8)	11.6(11.3)	1.33
Cu(dnTAA)I_x	1.26	0.500(0.225)	1.000(0.252)	31	51.2(51.4)	2.9(3.0)	9.2(9.5)	3.00
	2.10	0.500(0.225)	2.500(0.630)	21	43.6(43.9)	2.5(2.7)	7.8(7.6)	3.10
	4.80	0.500(0.225)	5.000(1.260)	24	29.5(29.9)	1.7(1.6)	5.3(5.2)	3.70
	6.20	0.500(0.225)	7.500(1.890)	21	25.2(25.5)	1.4(1.3)	4.5(4.3)	4.05
	0.00	—	—	—	74.2(74.4)	4.0(4.1)	10.2(10.5)	5.10
	0.10	0.500(0.275)	0.250(0.063)	10	72.6(72.8)	3.9(3.7)	10.0(10.3)	−0.18
	0.22	0.500(0.275)	0.350(0.089)	16	70.7(71.0)	3.8(3.6)	9.7(9.9)	0.00
	0.85	0.500(0.275)	0.500(0.126)	42	62.1(62.5)	3.3(3.2)	8.5(8.2)	2.00
Cu(dpTAA)I_x	1.60	0.500(0.275)	0.750(0.190)	52	54.2(54.4)	2.9(2.9)	7.4(7.1)	3.90
	1.75	0.500(0.275)	1.000(0.252)	43	52.8(53.1)	2.8(2.7)	7.3(7.4)	3.95
	1.83	0.500(0.275)	2.500(0.630)	18	52.2(52.5)	2.8(2.7)	7.2(7.3)	4.00
	3.09	0.500(0.275)	5.000(1.260)	15	43.3(43.4)	2.3(2.2)	5.9(5.4)	4.50
	6.72	0.500(0.275)	7.500(1.890)	22	29.1(29.4)	1.6(1.9)	4.0(4.1)	5.30

[a] In 20 cm^3 of acetone.
[b] Dissolved in 15 cm^3 of acetone.
[c] Values reported with estimated errors of ± 0.05.

Thermogravimetric measurements

TGA curves of the three unoxidized complexes are featureless up to 370, 410 and 470°C, respectively. A large weight loss is starting at these temperatures as confirmed by DTGA curves, the shape of which is attributable to sublimation with partial decomposition. The maxima of the differential weight loss lie at 420, 460 and 520°C, respectively. After iodination, the position and the shape of the DTGA curves do not change appreciably at these temperatures. Furthermore the de-iodinated compounds showed the same composition and the same spectroscopic (IR and UV–vis) behaviour as the unoxidized ones. This shows that the iodination process is fully reversible and, likely, does not modify the chemical structure of the complexes.

The iodinated complexes with an iodination degree up to $x = 3$ showed a single step weight loss with sharp and symmetrical DTGA curves centred at 270°C (Cu(dbTAA)I_x and Cu(dnTAA)I_x) and at 180°C (Cu(dpTAA)I_x). Furthermore, Raman spectra show in the range 50–650 cm^{-1} only a strong absorption at 107 cm^{-1} and the superior harmonics at 214, 322 and 438 cm^{-1}, attributable[14,15] to the symmetric stretching mode of I_3^-. These evidences lead to the conclusion that the main iodine species present in the solid phase is I_3^-. Compounds with a higher iodination degree ($x > 3$) showed one more weight loss at 240°C [Cu(dbTAA)I_x and Cu(dnTAA)I_x] and at 150°C [Cu(dpTAA)I_x] attributable to the I_5^- dissociation in I_3^- and I_2, as confirmed by Raman spectroscopy that showed an additional signal at 167 cm^{-1}. This behaviour is similar to that found for some silicon and germanium O-bridged phthalocyanines[14] and Ni(opd)$_2I_x$ [opd = o-phenylendimine][16] complexes although higher thermal stability is displayed by the presently investigated compounds. We exclude the presence of I_2, on the basis of the lack of any Raman band around 207 cm^{-1}, and of I^-, by analogy with previous works[15,17] on iodinated molecular crystals, although this species is undetectable by any of the spectroscopic techniques utilized in this study.

Two trends can be summarized by DTGA: (a) the lower the iodine content the higher the thermal stability of the materials; (b) at comparable x values the DTGA maxima are similar for Cu(dbTAA)I_x and Cu(dnTAA)I_x, both are higher than those found for Cu(dpTAA)I_x by about 100°C.

Electrical conductivity

Conductivity data at room temperature by both the linear two-probe technique on micropellets and van der Pauw's[13] method on pressed discs are in excellent agreement for all the samples. Electrical conductivity data for Cu(dbTAA)I_x, Cu(dnTAA)I_x and Cu(dpTAA)I_x at room temperature are reported in Table 1 and in Fig. 2(b), as a function of the I/Cu ratio determined by DTG. Within the range 0–1 of x, the absolute values of the electrical conductivity at the same x value follow the order Cu(dpTAA)I_x > Cu(dnTAA)I_x > Cu(dbTAA)I_x. The conductivity reaches a pronounced maximum for all the three complexes at a very low x value (0.2). Furthermore Cu(dnTAA) and Cu(dpTAA), also in the unoxidized form, exhibit a not negligible conductive ability. The electrical conductivity, with respect to the unoxidized compounds increases by a factor of 10^8 [Cu(dbTAA)], 10^4 [Cu(dnTAA)] and 10^5 [Cu(dpTAA)]. For x values larger than 0.2 the conductivity drops to nearly constant values for the three oxidized complexes.

This last observation matches with data reported

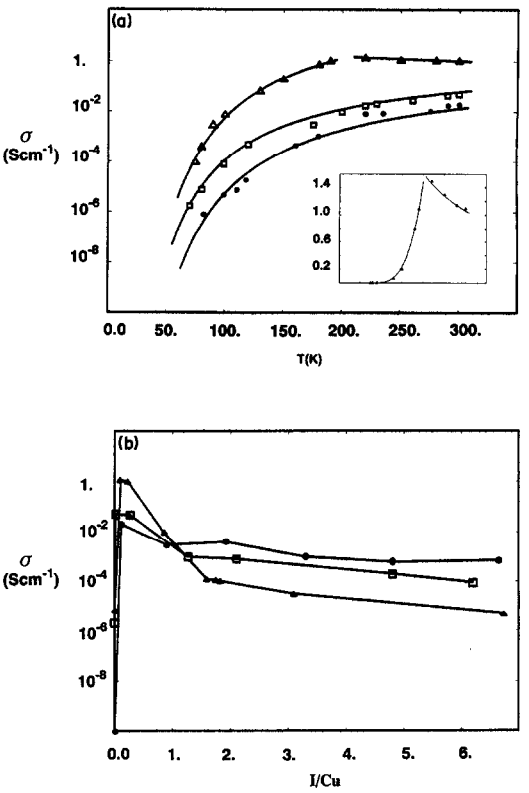

Fig. 2. (a) Temperature dependence of the conductivity. [Plot of log(σ) versus T for Cu(dbTTA)$I_{0.11}$ (●); Cu(dnTAA)$I_{0.10}$ (□), Cu(dpTTA)$I_{0.22}$ (△).] Plot of (σ, T) is reported in the insert for the dpTAA complex in order to point out the different behaviour of the data above and below 200 K. (b) Variation of the conductivity as a function of iodine content. Cu(dbTAA)I_x; Cu(dnTAA)I_x; Cu(dpTAA)I_x. The lines meeting the experimental points are drawn only for eye guide.

for M(dbTAA)I_x powders (M = Cu, Ni, Co, Fe) at x values greater than 0.7, where the conductivity is almost independent of iodination degree. Some authors[3a] have incorrectly concluded that the iodination content does not affect significantly the conductivity of M(dbTAA) oxidized powders, whereas our data point out a strong correlation between iodination extent and electrical conductivity within the range 0–0.9 of x. This correlation parallels that found for $NiPcI_x$ powders,[18] where high conductivity is reached at x values in the range 0.5–1.44.

Although the nature of the correlation between conductivity and degree of iodination might suggest an interpretation based on a percolation model, DTGA results exclude this hypothesis. Moreover IR spectra for all the compounds show a single absorption for the C=N stretching which strongly support the exclusion of the presence of a multiple phase in the iodinated compounds.

The electrical conductivity of $Cu(dbTAA)I_{0.11}$, $Cu(dnTAA)I_{0.10}$ and $Cu(dpTAA)I_{0.22}$ as functions of the temperature is reported in Fig. 2(a). $Cu(dpTAA)I_{0.22}$ shows a "metal like" behaviour ($d\sigma/dt < 0$) between 300 and 220 K, besides near 200 K a semiconducting transition is observed. This trend is clearly shown in the insert of Fig. 2(a). Data between 80 and 200 K are fitted by the following relation valid for activated carrier formation:[19,20]

$$\sigma = AT^{-\alpha}e^{-E_a/2RT} \text{(with } \alpha = 1.02 \text{ and } E_a = 0.21 \text{ eV)}.$$

Moreover the same relation does not fit the data in the whole temperature range, but the data are fitted in the temperature range (200, 300) K by the simple relation $\sigma = AT^{-\alpha}$, where $A = 2.6$ and $\alpha = 1.02$. In the range (80, 220) K both Cu(dbTAA) and Cu(dnTAA) show semiconductive behaviour. The experimental data, in this range, are fitted by the relation $\sigma = A'e^{-E_a/RT}$, where the parameter A' and E_a are 1.08, 0.21 and 1.09, 0.16 for dbTAA and dpTAA complexes, respectively.

A semiconductive behaviour, described by this last equation, is observed in the series $Cu(dbTAA)I_x$, $Cu(dnTAA)I_x$ and $Cu(dpTAA)I_x$, at a higher I/Cu ratio ($x > 5$).

Magnetic susceptibility

The static paramagnetic susceptibility ($\chi^S M$) of $Cu(dbTAA)I_x$, $Cu(dnTAA)_x$ and $Cu(dpTAA)_x$ oxidized complexes have been measured with variable iodine content up to $x = 3$. The results show an analogous trend for the three species and we will discuss here the data obtained for $Cu(dnTAA)I_x$ at x values, 0.26, 1.26 and 2.10. In this species the dominant form of iodine is I_3^- and it is possible to indicate the compounds in the mixed valence form: $[Cu(dnTAA)]^+_{0.09}(I_3^-)_{0.09}$; $[Cu(dnTAA)]^+_{0.42}(I_3^-)_{0.42}$; and $[Cu(dnTAA)]^+_{0.70}(I_3^-)_{0.70}$. The magnetic susceptibility, taking into account the correction for the diamagnetism of the tetraazaannulene ring, of the metal and of the I_3^- polyiodide, are $9.69 \cdot 10^{-4}$, $9.29 \cdot 10^{-4}$ and $9.40 \cdot 10^{-4}$ emu mol^{-1}, respectively. Assuming the same approximation we used[12] for the unoxidized complexes ($1.32 \cdot 10^{-3}$, $1.33 \cdot 10^{-3}$ and $1.28 \cdot 10^{-3}$ emu mol^{-1}, respectively), these values indicate 0.95, 0.46 and 0.46 unpaired electrons for the metallomacrocycle, respectively.

ESR results

The ESR spectra of the oxidized species $Cu(dbTAA)I_x$, increasing the iodine amount, show first a broadening and then a partial resolution of the line; at $x = 0.9$ the spectrum is typical of a copper(II) electron with anisotropic g tensor ($g \approx 2.03$). At higher values of x($x \approx 4$) the spectrum shows another signal centred at $g \approx 2.003$.

This behaviour can be interpreted as due to a progressive decrease of the spin–spin exchange interaction.

Spectra were recorded in the case of $Cu(dnTAA)I_x$ and $Cu(dpTAA)I_x$ at the same oxidation extent where $Cu(dbTAA)I_x$ showed a partially resolved g structure. $Cu(dnTAA)I_x$ exhibited only a slight line broadening ($H \approx 165$ G), but the line shape remained unaltered when compared to the unoxidized sample;[12] at higher oxidation ($x > 6$) the spectrum shows the same behaviour as in $Cu(dbTAA)I_x$.

In the case of $Cu(dpTAA)I_x$ the spectrum shows also the very sharp signal at $g \approx 2.003$ and the copper signal as well; the main difference with respect to the unoxidized sample is the increased linewidth ($H \approx 220$ G) of the signal due to the species in a concentrated environment.

To further check this behaviour and in order to reduce the broadening of the lines we carried out ESR measurements on all three copper complexes, both in the unoxidized and oxidized cases, when diluted (1 : 100 weight ratio) by the corresponding unoxidized nickel complexes.[21]

In all the three unoxidized species, at variance with the case of pure unoxidized samples[12] at low x values, the spectra show two absorptions due to unpaired electrons with different character: one very broad characteristic of copper and a second one at $g \approx 2.003$ whose intensity with respect to

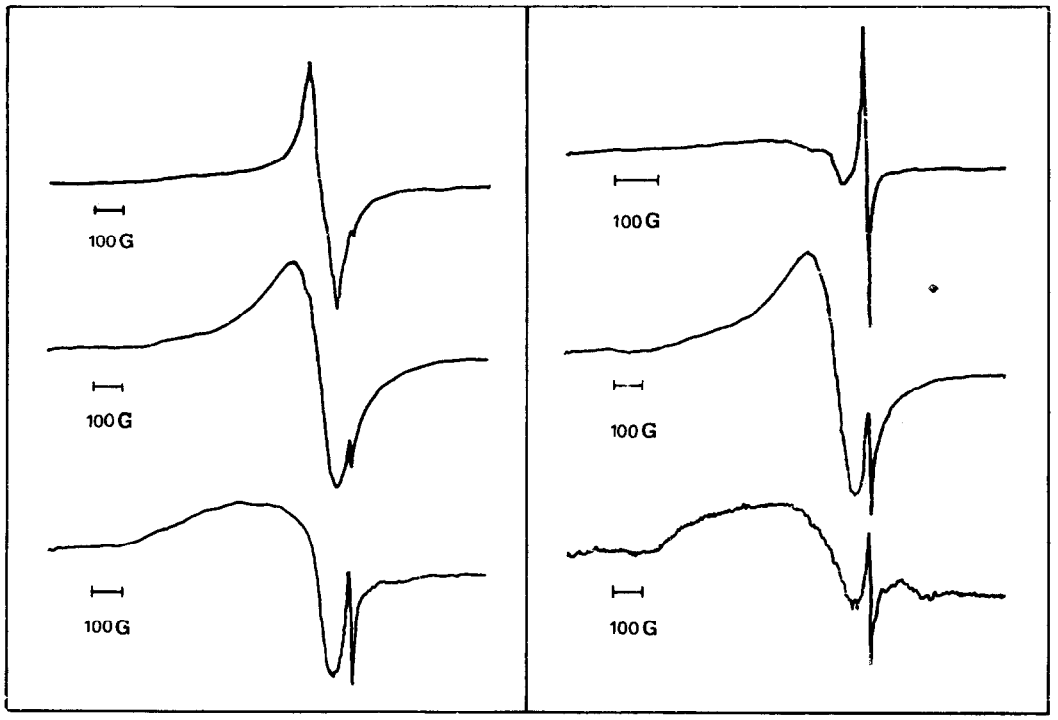

Fig. 3. (a) Room temperature ESR spectra of copper complexes diluted (1 : 100 mg) in the corresponding nickel complexes. Top : Cu(dbTAA) ; field modulation intensity : 2.5 Gpp ; gain : $2.5 \cdot 10^4$; middle : Cu(dnTAA) ; field modulation intensity : 1.25 Gpp ; gain : $8 \cdot 10^4$; bottom : Cu(dpTAA) ; field modulation intensity : 3.2 Gpp ; gain : $1 \cdot 10^5$; central field and scan range as in Fig. 3(b). (b) Room temperature ESR spectra of iodinated copper complexes diluted (1 : 100 mg) in the corresponding unoxidized nickel complexes. Top : $Cu(dbTAA)I_{0.90}$; central field : 3300 G ; scan range : 1000 G ; field modulation intensity : 3.2 Gpp ; gain : $1 \cdot 10^5$; middle : $Cu(dnTAA)I_{0.26}$; field modulation intensity : 3.2 Gpp ; gain : $1 \cdot 10^5$; bottom : $Cu(dpTAA)I_{0.22}$; field modulation intensity : 3.2 Gpp ; gain : $3.2 \cdot 10^5$; the last two spectra were registered at a central field $H = 3200$ G and scan range 1500 G.

the broad band increases from dbTAA to dpTAA complexes.

On oxidation the effects shown in Fig. 3(b) can be summarized : (i) the exchange narrowed signal in Cu(dbTAA) has changed to a broad band with partial resolution in $Cu(dbTAA)I_x$, whereas the line at $g \approx 2.003$ has gained a strong amplitude ; (ii) the central line in Cu(dnTAA) does not undergo significant changes in the shape nor in the width ($H \approx 165$ G) in $Cu(dnTAA)I_x$, whereas the "free-electron" line is slightly increased in amplitude ; and (iii) in the spectrum of $Cu(dpTAA)I_x$ the central absorption is slightly broadened and the line at $g \approx 2.003$ has almost the same amplitude when compared with unoxidized powder.

As a general trend in the diluted Cu(dnTAA) and Cu(dpTAA) systems, oxidation determines only a slight weakening of exchange interaction, whereas in the case of Cu(dbTAA) oxidation is by far more effective. The intensity of the signal at $g \approx 2.003$ increases going from the unoxidized to the oxidized situation ; the change is more evident in the Cu(dbTAA) where also a greater weakening of the exchange interaction is observed.

DISCUSSION

In order to gain a coherent picture of the ESR, magnetic susceptibility, electrical conductivity and IR data, we will follow in the discussion as a guideline two main informations, i.e. the solid state packing of the molecules and the electronic structure of the isolated molecules. Concerning $[Cu(dbTAA)]I_x$ it has been found[22] that the compound with $x = 2.01$ has a structure with planar molecules whose rings stack metal-over-metal with the plane of the rings normal to the stacking axis. Successive rings in the unit cell are staggered by 54°. Chains of I_3^+ lie in the channels between the Cu(dbTAA) stacks as has been found in the case of other dbTAA complexes.[3] It is reasonable to assume that also in the case of Cu(dnTAA) the main packing features are not modified as also indicated by the ESR behaviour of the two systems on oxidation. The

solid state packing suggests that the intermolecular interactions are essentially one-dimensional and limited to the stacking axis. This allows us to give a simple picture of the solid state electronic structure starting from the molecular orbitals of the isolated molecule. The electronic structure[12] of the Cu(dbTAA) complex suggests that the two higher energy bands are those which arise from the b_{1_u} and b_{1_g} orbitals of the isolated molecules; therefore the modifications of the molecular properties following the oxidative processes can be interpreted in terms of symmetry properties and composition of these orbitals. Cu(dnTAA) complex, whose electronic structure was computed following the same theoretical approach of Lelj *et al.*,[12] shows the same ordering of the higher energy occupied levels. In this last case the molecular geometry of the complex was derived from that of Cu(dbTAA)[12] and of naphthalene molecules. Comparison of the susceptivity data with conductivity shows interesting trends. Figure 4 shows the plot of the fraction of electron spin and conductivity data as a function of the I/Cu ratio in the case of Cu(dnTAA); analogous results are found in the case of dbTAA and dpTAA complexes. The correlation between the two properties, although only few points are reported, is fairly clear. Moreover starting from x values near 1.26, both the conductivity and the fraction of free spins remains constant. The trend of the fraction of free spins, which decreases less than expected on the basis of the ionic stoichiometry of the charge-transfer complexes, suggests that a partial removal of electrons from the ligand system is not negligible.

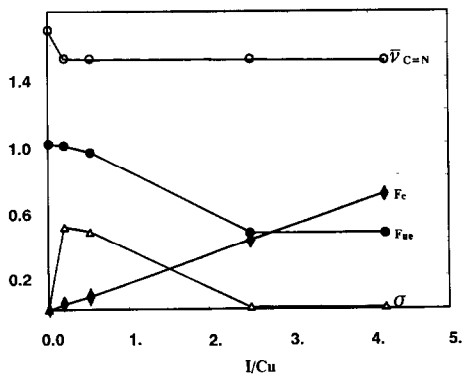

Fig. 4. Plot of the conductivity (σ), fraction of unpaired spin (F_{ue}), wave number of the C=N stretching frequency [$\bar{\nu}$(C=N)] and fraction of positive charge (F_c) in the case of [Cu(dnTAA)]I_x as a function of the I/Cu ratio.

Such a suggestion is further supported by the analysis of the behaviour of the ν(C=N) on increasing the oxidation degree of the system. In fact the oxidation determines a rapid drop of the ν(C=N) which, at x values higher than 1.26, remains constant. This behaviour can be interpreted on the basis of electron density depletion from the C_{aryl}—N bond. At a low I/Cu ratio the electrons are pulled out from the band which arises from the HOMO b_{1_g} level [Fig. 5(b)] with large copper d_{xy}

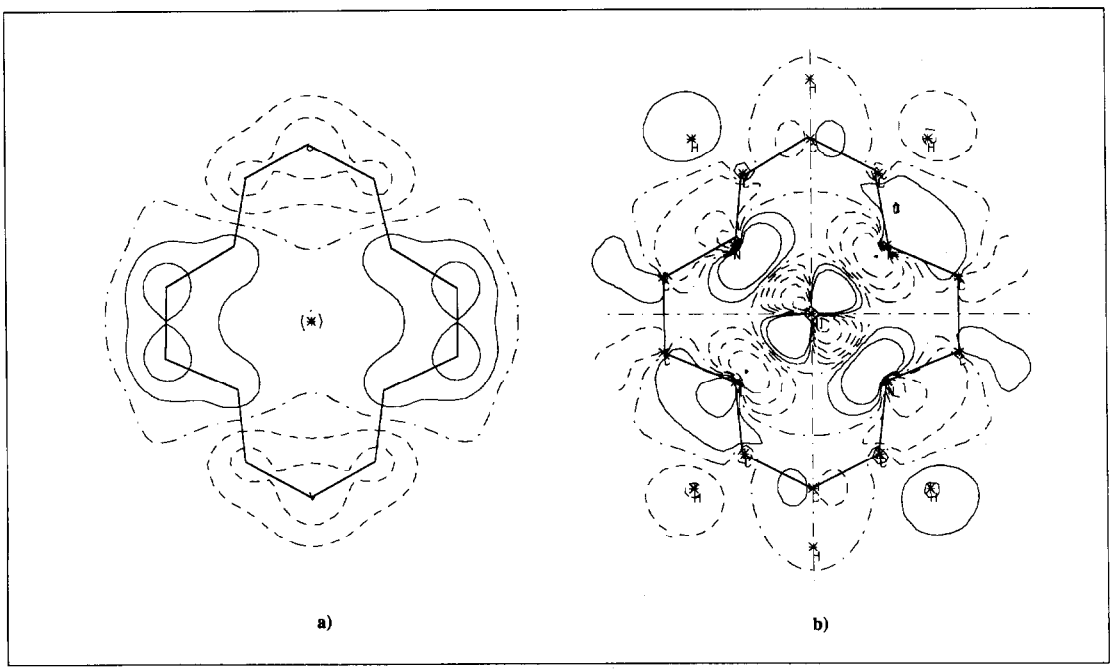

Fig. 5. Contour plot of the b_{1_u} (1.0 a.u. above the molecular plane) (a) and b_{1_g} (in the molecular plane). (b) MOs for Cu(dnTAA) (only the tetraazaannulenic framework is reported). Contour levels: 0, ±0.01, ±0.05, ±0.1, ±0.2, ±0.5 (electron a.u.^{3})$^{1/2}$ (negative: dashed lines; zero: dot-dashed).

character and with a clear metal–nitrogen anti-bonding character.

On the other hand this orbital shows a bonding character between the two mentioned carbon and nitrogen atoms. Ionization from the band which is formed by this orbital induces the reduction of the spin density on the copper atom (then the observed reduction of the static susceptivity) and the reduction of the ν(C=N) as well.

A further increase in the charge (i.e. increasing the I/Cu ratio), obtained at the expense of the b_{1_g} orbital leads to an increased stability of the band formed by HOMO b_{1_g} and to a degeneration with the band formed by SHOMO b_{1_g}. As soon as this last orbital ionizes the π unpaired spin density generated increases the total unpaired spin density on the molecule and then the static magnetic susceptibility is less than expected on the basis of the ionic stoichiometry of the charge-transfer complexes. Moreover the b_{1_u} orbital has π symmetry (with respect to the σ_h plane) mainly localized on the ligand (in the case of the dbTAA and even more in the case of dnTAA) but with a very clear anti-bonding character between the $\text{carbon}_{\text{aryl}}$ and nitrogen atoms [Fig. 5(a)]. Then electron removal from this band increases the strength of the C=N bond against the decrease generated by the ionization of b_{1_g}. This leads to a substantial stabilization of the ν(C=N) value with respect to the modification of the I/Cu ratio.

The above reported ESR spectra, in diluted samples, further suggest that there is a large tendency of the system to be oxidized both on the metal and on the ligand. In fact in all cases, although at different x values, depending on the ligand nature, it is possible to observe a signal at $g \approx 2.003$, characteristic of a "free electron", i.e. an electron mainly localized on the ligand moiety.

The origin of this line might be, in principle, an organic radical (e.g. oxidized free ligand) in the mixture. In the case of the free ligand and phthalocyanine (Pc) metal diamagnetic complexes, this line has been attributed to a radical formed by reversible adsorption of oxygen by Pc.[23] On the other hand, in our case the appearance of this line at very high x values both in the case of Cu(dnTAA) (Fig. 6) and Cu(dbTAA) and its increase, whereas the copper band decreases in the spectra of diluted samples of all the species on increasing the oxidation degree, suggests that the observed phenomenon is indeed dependent on the contemporary oxidation of the metal and ligand in the complex. The interpretation of the nature of the oxidative process can be further strengthened by comparison with the extreme behaviours shown by two already investigated molecular conductors, i.e. CoPcI[24]

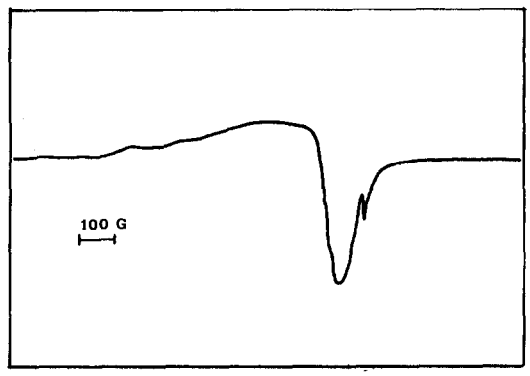

Fig. 6. Room temperature ESR spectra of $\text{Cu(dnTAA)I}_{6.45}$ powder; middle field: 3200 G; scan range 1500 G; field modulation intensity: 1.5 Gpp; gain: $1.6 \cdot 10^{-5}$.

(Pc = phthalocyanine) and CuPcI.[25] In fact, it has been found in CoPcI that oxidation involves only the Co^{2+} paramagnetic centre leading to a totally dz^2 metallic band. The conductivity values are interpreted in terms of relatively short Co—Co distances. The formation of a metallic band is supported by strong coupling phenomena among unpaired electrons, as shown by the calculated number of unpaired electrons for metallomacrocycle which is lower (0.4) than expected for a completely free spin (0.77). On the other hand, recently, the same authors have shown[25] that in CuPcI and in Cu(TATBP)[26] (TATBP = triazatetrabenzoporphyrinato) the oxidative process produces an increase of the number of unpaired electrons for the molecular unit (1.1 against 1.0 of CuPc); this behaviour has been attributed to a fully ring-centred oxidation which leaves intact the Cu^{2+} centres, giving rise to a total susceptibility greater than one spin for the molecular unit. In our complexes the situation seems to be different from the reported cases. In fact a fully metal centred oxidation could not account for the observed trend of conductivity, ν(C=N) and ESR data. Moreover a fully ligand centred oxidation does not match with the decrease of the susceptibility of the oxidized complexes with respect to the unoxidized ones. It is then reasonable to suppose that in our systems the oxidation leads to a removal of electrons from orbitals with large metallic character and from orbitals ligand centred as well.

We can conclude that, as concerns the nature of the carriers, the investigated systems do not differ significantly from NiTAAI_x, CuPcI or NiPcI, which on the other hand exhibit a ligand centred conduction band.

However, unlike CuPcI, the oxidative process in our compounds also strongly affects the metallic

centre, inducing novel magnetic behaviour. This is inferred by the presence of two distinguishable ESR signals that suggest there is no magnetic interaction between carriers and the unpaired electrons of copper centres, at least in the case of dbTAA and dnTAA complexes.

Acknowledgements—We are indebted to Dr C. Caneschi (University of Firenze) for magnetic susceptibility measurements, Dr M. Latronico (University of Basilicata) for elemental analyses and C. Barlaba' for technical support in thermogravimetric and conductivity measurements. We would like to thank C.I.S.I.T. of Universita' della Basilicata for a generous gift of computer time and graphical facilities. This work was partially supported by Italian National Research Council (CNR) and by "Progetto Finalizzato: Materiali Speciali per Tecnologie Avanzate".

REFERENCES

1. T. J. Marks and D. W. Kalina, *Extended Linear Chain Compounds* (Edited by J. S. Miller), Vol. 1, pp. 271–278. Plenum Press, New York (1982); and refs therein.
2. T. J. Marks, *Science* 1985, **227**, 881.
3. (a) M. Hunziker, B. Hilti and G. Rihs, *Helv. Chim. Acta* 1981, **64**, 82; (b) Y. M. Wuu, S. M. Peng and H. Chang, *J. Inorg. Nucl. Chem.* 1980, **42**, 839.
4. K. Sakata, M. Hashimoto, N. Tagami and Y. Murakami, *Bull. Chem. Soc. Japan* 1980, **53**, 2262.
5. M. C. Weiss, G. Gordon and V. L. Goedken, *Inorg. Chem.* 1977, **16**, 305.
6. L. S. Lin, T. J. Marks, C. R. Kannewurf, J. W. Lyding, M. S. McClure, M. T. Ratajack and T. C. Whang, *J. Chem. Soc., Chem. Commun.* 1980, 954.
7. M. Tsutsui, R. L. Bobsein and R. Pettersen, *Inorg. Chem.* 1979, **18**, 758.
8. M. Hunziker, H. Loeliger, G. Rihs and B. Hilti, *Helv. Chim. Acta* 1981, **64**, 2544.
9. F. Adams, R. Gompper and E. Kujath, *Angew. Chem. Int., Edn Engl.* 1989, **28**, 1060.
10. C. J. Schramm, D. R. Stojakovik, B. M. Hoffman and T. J. Marks, *Science* 1978, **200**, 47.
11. J. Martinsen, S. M. Palmer, J. Tanaka, R. C. Green and B. M. Hoffman, *Physical Review* B 1984, **30**, 6269.
12. F. Lelj, G. Morelli, G. Ricciardi and A. Rosa, *Polyhedron*, in press.
13. L. J. van der Pauw, *Philips Res. Rep.* 1958, **13**, 1.
14. R. S. Nohr, P. M. Kuznesof, K. J. Wynne, M. E. Kenney and P. G. Siebenman, *J. Am. Chem. Soc.* 1981, **103**, 4371; and refs therein.
15. S. L. Hsu, A. J. Signorelli, G. P. Pez and R. H. Baughman, *J. Chem. Phys.* 1978, **69**, 106.
16. (a) F. Lelj, G. Morelli, G. Ricciardi, M. F. Brigatti and A. Rosa, *Polyhedron* 1989, **8**, 2603; (b) F. Lelj, A. Rosa, G. P. Ricciardi, M. Casarin, P. L. Cristinziano and G. Morelli, *Chem. Phys. Lett.* 1989, **160**, 1, 39.
17. K. F. Schoch Jr, B. R. Kundalkar and T. J. Marks, *J. Am. Chem. Soc.* 1979, **101**, 7071.
18. C. J. Schramm, R. P. Scaringe, D. R. Stajakovic, B. M. Hoffman, J. A. Ibers and T. J. Marks, *J. Am. Chem. Soc.* 1980, **102**, 6702.
19. A. J. Epstein, E. M. Conwell, D. J. Sandman and J. S. Miller, *Solid State Commun.* 1977, **23**, 355.
20. A. J. Epstein and E. M. Conwell, *Solid State Commun.* 1977, **27**, 627.
21. P. M. Hoffman, J. Martinsen, L. J. Pace and J. A. Ibers, *Extended Linear Chain Compounds* (Edited by J. S. MIller), Vol. 3, pp. 410–490. Plenum Press, New York (1982).
22. M. Hunziger and G. Rihis, *Inorg. Chim. Acta* 1985, **102**, 39.
23. (a) J. M. Assour and W. K. Khan, *J. Am. Chem. Soc.* 1965, **87**, 207; (b) C. M. Guzy, J. B. Raynor and M. C. R. Symons, *J. Chem. Soc.* (A), 1969, 2299; (c) J. M. Assour and S. E. Harrison, *J. Chem. Phys.* 1964, **68**, 872.
24. J. Martinsen, J. L. Stanton, J. Tanaka, R. L. Greene, B. M. Hoffman and J. A. Ibers, *J. Am. Chem. Soc.* 1985, **107**, 6915.
25. M. Y. Ogawa, J. Martinsen, S. M. Palmer, J. L. Stanton, J. Tanaka, R. L. Greene, B. M. Hoffman and J. A. Ibers, *J. Am. Chem. Soc.* 1987, **109**, 1115.
26. K. Liou, M. Y. Ogawa, T. P. Newcomb, G. Quirion, M. Lee, M. Poirier, W. P. Halperin, B. M. Hoffman and J. A. Ibers, *Inorg. Chem.* 1989, **28**, 3889.

Polyhedron Vol. 10, No. 16, pp. 1921–1928, 1991
Printed in Great Britain

0277–5387/91 $3.00+.00
© 1991 Pergamon Press plc

SPECTROSCOPY STUDIES OF LANTHANIDE TRICHLOROACETATE SINGLE CRYSTALS

J. LEGENDZIEWICZ* and G. OCZKO

Institute of Chemistry, University of Wrocław, 50-383 Wrocław, 14 Joliot-Curie, Poland

and

G. MEYER

Institute of Inorganic Chemistry, University of Hannover, Hannover, F.R.G.

(*Received* 4 *April* 1991; *accepted* 14 *May* 1991)

Abstract—The single crystals of some lanthanide carboxylates are characterized by a lack of inversion symmetry, so they could be used for generation of the second harmonic.[1–5] Single crystals of neodymium and erbium trichloroacetate were synthesized and shown to form the polymeric chain linking dimeric subunits, where the lanthanide ions can occupy different site symmetry positions.

The absorption and luminescence spectra of single crystals of the title compounds were measured at room and liquid helium temperatures; Stark components were determined and analysed in terms of interacting ions. Spectroscopic properties were related to the X-ray crystal data.

Probabilities of *f–f* transitions depending on the orientation of biaxial single crystals were considered.

Two aspects of the spectroscopic studies of lanthanide trichloroacetates seem to be very interesting. First, variation in the atoms (Cl, F, Br) which substitute the H atom of the acetate anion must influence the Ln–O distance, so studies of hypersensitive transition intensity can elucidate the covalent effect in the spectra. Second, broad studies were undertaken to obtain monocrystals of lanthanide carboxylates and their spectroscopic characteristics as part of the search for new materials for nonlinear optics.

Recently we have published the spectroscopic results for dysprosium trichloroacetate single crystals as the first part of the series studies.[7] However the full interpretation of spectroscopic effects was not completed since the crystal structure data were unavailable. The crystal structure data for isomorphic erbium and dysprosium trichloroacetate were reported by Takashi Imai[6] and by Poraj-Koshits.[8] Our data indicate that neodymium single crystals are isomorphous with the above ones, but praseodymium probably deviates from that relation. Moreover the X-ray data show that polymeric chains are formed, linking dimeric subunits with two different site symmetry positions for the Ln^{3+} ions. Lanthanide ions in trichloroacetates are characterized by a lack of inversion symmetry.

In this paper, the results of optical absorption and fluorescence measurements are reported, and the spectroscopic effects are discussed and related to the X-ray data. The existence of short range interactions between ions associated as dimeric pairs is also discussed.

EXPERIMENTAL

Crystals of neodymium and erbium trichloroacetate $Ln(CCl_3COO)_3 \cdot 2H_2O$ were grown from water solutions. The lanthanide trichloroacetates were synthesized by slow reaction between lanthanide oxides and trichloroacetic acid, at controlled pH ($\sim$ 5.4). The crystals obtained in this way were then recrystallized from water solu-

* Author to whom correspondence should be addressed.

tions and grown to the dimensions suitable for spectroscopic measurement. The measured crystal densities are: $\rho_1 = 2.22$ g cm^{-3}, $\rho_2 = 2.34$ g cm^{-3}. Concentration of Ln^{3+} ions in crystals are: $C_1 = 3.33$ M, $C_2 = 3.39$ M, respectively. The dimensions of the crystals ($5 \times 5 \times y$ mm^3, $y_1 = 1.98$, 0.825, 0.578, 0.378 mm $\rightarrow Nd^{3+}$ for different spectral regions, $y_2 = 0.71$ mm $\rightarrow Er^{3+}$) allowed the absorption spectra measurement along the *a*-axis only. Absorption spectra in the region 320–920 nm for Nd^{3+} and 350–1600 nm for Er^{3+} were recorded at 293, 118 and 5 K. Stark components were determined at 5 K. The experimental oscillator strength values were used to calculate the Ω_λ parameters from the Judd relation.[9]

Fluorescence spectra of the neodymium trichloroacetate single crystals were recorded at 4.2 K with a spectrophotometer designed in the laboratory of the Institute of Physics, Polish Academy of Sciences (Warsaw, Poland). The instrument has a GDM 1000 grating monochromator (Carl Zeiss, Jena) with a cooled M 10FD29 photomultiplier tube (Carl Zeiss, Jena). An ILA 120 argon laser (Carl Zeiss, Jena) was used as the excitation source. Fluorescence of Nd^{3+} ions was excited with the 488 and 514 nm lines.

RESULTS AND DISCUSSION

The perspective drawings of the complex around the erbium(1) and erbium(2) atoms, respectively, are shown in Fig. 1;[6] a schematic presentation shows the coordination geometries around the metal atoms as well as the bridging modes in accord with the data of Takashi Imai.[6] In the case of Nd^{3+} single crystals, similar to the Er^{3+} ion[6] (because of the isomorphism of both crystals), two different dimeric subunits exist in the polymeric chain with two different Nd^{3+} ion site symmetry positions. Those two different dimeric subunits are bridged by oxygen atoms of water molecules and two carboxylic bridges of the Ln—O—C—O—Ln type. According to the data of Takashi Imai, in this way three different Ln—Ln distances are observed in the structure. On the other hand the Poraj-Koshits X-ray data indicated the coordination number eight for erbium(1) and seven–nine for erbium(2). Unfortunately in both papers the fitting procedure of coordination polyhedra was not made. Even if we consider the distances, Ln—O, and angles in all possible distorted coordination figures we are not able to find the symmetry centre for metal ions. Such a property of single crystals must be reflected in their spectroscopic properties.

The oscillator strengths for all electronic transitions observed in the absorption spectra at 293, 118 and 5 K are given in Tables 1 and 2. Although the intensity measurement was performed for one crystal orientation (along the *a*-axis in Fig. 2) the mean intensity for two other orientations should not change much. Crystals of trichloroacetate are biaxial, so for that type of single crystal (as was

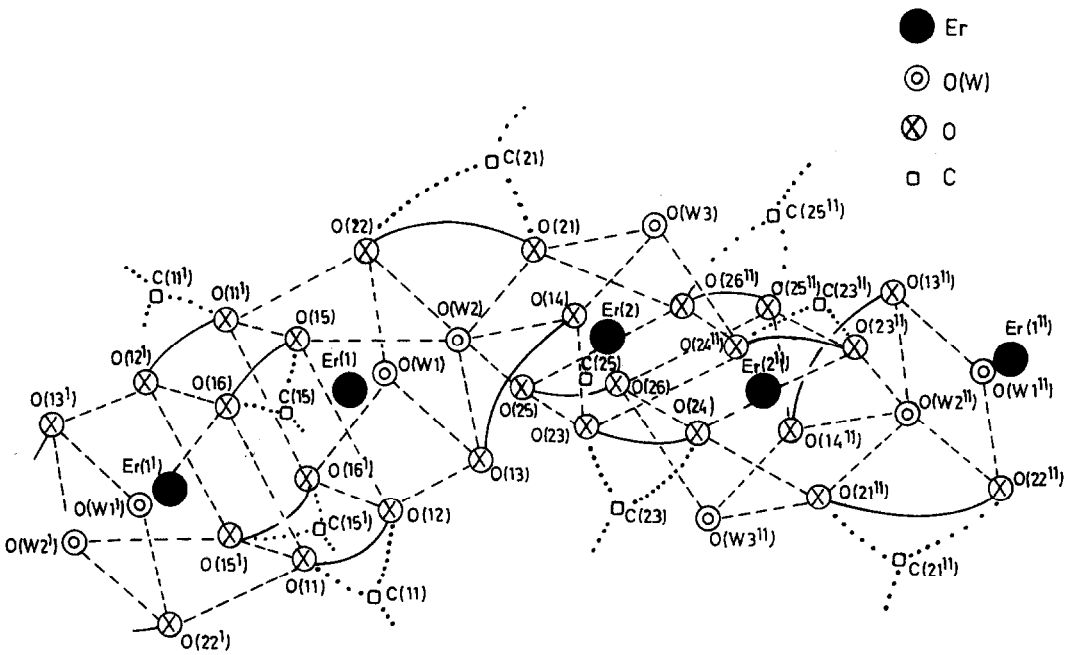

Fig. 1. Schematic presentation to show the coordination geometries around the metal atoms, as well as the bridgings between them.

Table 1. The oscillator strength values of f–f transitions $P\times10^8$ and $\Omega_\lambda\times10^{20}$ parameter values for $Nd(CCl_3COO)_3\cdot2H_2O$ crystals at different temperatures

Term	293 K	5 K
$^4F_{3/2}$	148.46	146.54
$^4F_{5/2}{}^2H_{9/2}$	677.98	407.25
$^4S_{3/2}{}^4F_{7/2}$	906.09	420.88
$^4F_{9/2}$	58.78	34.95
$^2H_{11/2}$	17.31	15.23
$^4G_{5/2}{}^2G_{7/2}$	1345.50	706.77
$^2K_{13/2}{}^4G_{7/2}{}^4G_{9/2}$	694.77	512.80
$^2K_{15/2}{}^2G_{9/2}(^2D,{}^2F)_{3/2}{}^4G_{11/2}$	207.37	250.17
$^2P_{1/2}{}^2D_{5/2}$	40.04	27.44
$^4D_{3/2}{}^4D_{5/2}{}^2I_{11/2}$		
$^4D_{1/2}{}^2L_{15/2}$	858.95	
$^2I_{13/2}{}^4D_{7/2}{}^2L_{17.2}$	246.21	
$^2H_{9/2}$	18.48	
$^2D_{3/2}{}^2H_{11/2}$	58.03	
$^2D_{5/2}$	41.25	
$\Omega_2\times10^{20}$	1.99 ± 0.30	
$\Omega_4\times10^{20}$	1.99 ± 0.27	
$\Omega_6\times10^{20}$	4.20 ± 0.39	

$c = 3.327$ M.
$\rho = 2.2189$ g cm^{-3}.

Table 2. The oscillator strength values of f–f transitions $P\times10^8$ and $\Omega_\lambda\times10^{20}$ parameter values for $Er(CCl_3COO)_3\cdot2H_2O$ crystals at different temperatures

Term	293 K	118 K
$^4I_{13/2}$	239.38	289.41
$^4I_{11/2}$	78.56	75.73
$^4I_{9/2}$	25.57	22.94
$^4F_{9/2}$	216.86	192.60
$^4S_{3/2}$	52.75	42.73
$^2H_{11/2}$	816.21	633.39
$^4F_{7/2}$	234.17	205.75
$^4F_{5/2}{}^4F_{3/2}$	90.98	76.39
$(^2G,{}^4F,{}^2H)_{9/2}$	96.91	97.89
$^4G_{11/2}$	1444.99	974.16
$^4G_{9/2}$	203.82	126.57
$^2K_{15/2}{}^2G_{7/2}$	122.78	85.06
$\Omega_2\times10^{20}$	3.31 ± 0.15	
$\Omega_4\times10^{20}$	1.12×0.23	
$\Omega_6\times10^{20}$	1.10×0.12	

$c = 3.388$ M.
$\rho = 2.3359$ g cm^{-3}.

observed earlier by Lomhein and De Shazer[10–11] and by us[12]) the difference in intensities can vary within the limits of 10%. As regards such a change to the intensity calculations, we can discuss and compare them with those published for other lanthanide carboxylates,[3] especially for single crystals with the same bonding mode of carboxylic group, and with that for the simple acetate $Ln(CH_3COO)_3\cdot3H_2O$.

According to the X-ray data, the substitution of

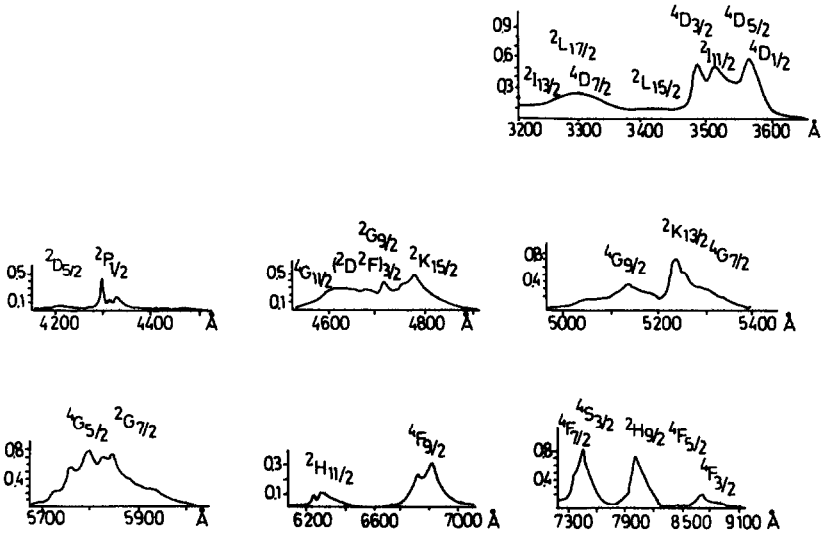

Fig. 2. Absorption spectra of $Nd(CCl_3COO)_3\cdot2H_2O$ crystals at room temperature.

the H atom in the CH_3COO^- anion by one to three F^- ions, as well as by a Cl^- anion leads to the change of structures.[1]

It is also well known that the bonding mode of the carboxylic group in lanthanide acetates changes when the ionic radius is decreased and the Ln—O distance changed (from 2.56 for Ce^{3+} to 2.41 for Er^{3+}). But when we consider the change of ionic radius (from Ce^{3+} to Er^{3+}) we obtain mean values of Ln—O only slightly shorter for erbium. The crystal structure converted from monoclinic $P2_1/b$ to triclinic $P\bar{1}$.[13-14] Aslanov implicated that for the series of acetates the covalency varied, which resulted in coordination of

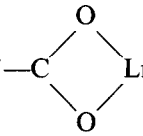

type for the end of the series. As a matter of fact the bonding lengths of such coordination are usually longer than Ln—O—C—O—Ln type.[15]

On the other hand, the stability constants of lanthanide acetate decrease from cerium to erbium.[16-17]

Gubanov and Riskov, on the basis of the theoretical calculation, consider the covalent effect in the series of lanthanide oxides and fluoro-oxides.[18] They have found that the density of overlapping of $2p$ oxygen orbitals and f orbitals of the Ln^{3+} ion decreases from neodymium to ytterbium.

The substitution of H atoms in the CH_3COO^- anion by one–three F^- ions, as well as by a Cl^- anion leads to the change of charge distribution on the $XCOO^-$ anion and, consequently, to the structural change. The substitution of H atoms in acetate by three Cl^- anions leads to the change of structure from dimeric for $Er_2(CH_3COO)_6 \cdot 4H_2O$ ($P\bar{1}$ c.n. = 9) to polymeric for $Er_2(CCl_3COO)_6 \cdot 4H_2O$ ($P\bar{1}$ c.n. = 8) and to a drastic change of coordination mode of the carboxyl group (from chelating bridges of

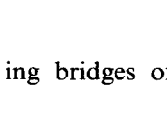

type and chelating

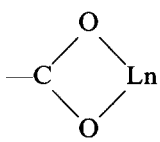

Ln type for the former to simple bridging —Ln—O—C—O—Ln— type for the latter). Coordination number decreased from nine to eight. In consequence the mean bond length decreases (from 2.41 to 2.34 Å) and although the charge distribution and pK_a can suggest the smaller contribution of covalency in trichloroacetates, still the lower coordination number (given by steric effect) leads to a decrease of Ln—O bond lengths. So in consequence we should expect the intensity of hypersensitive transitions to increase as was actually observed

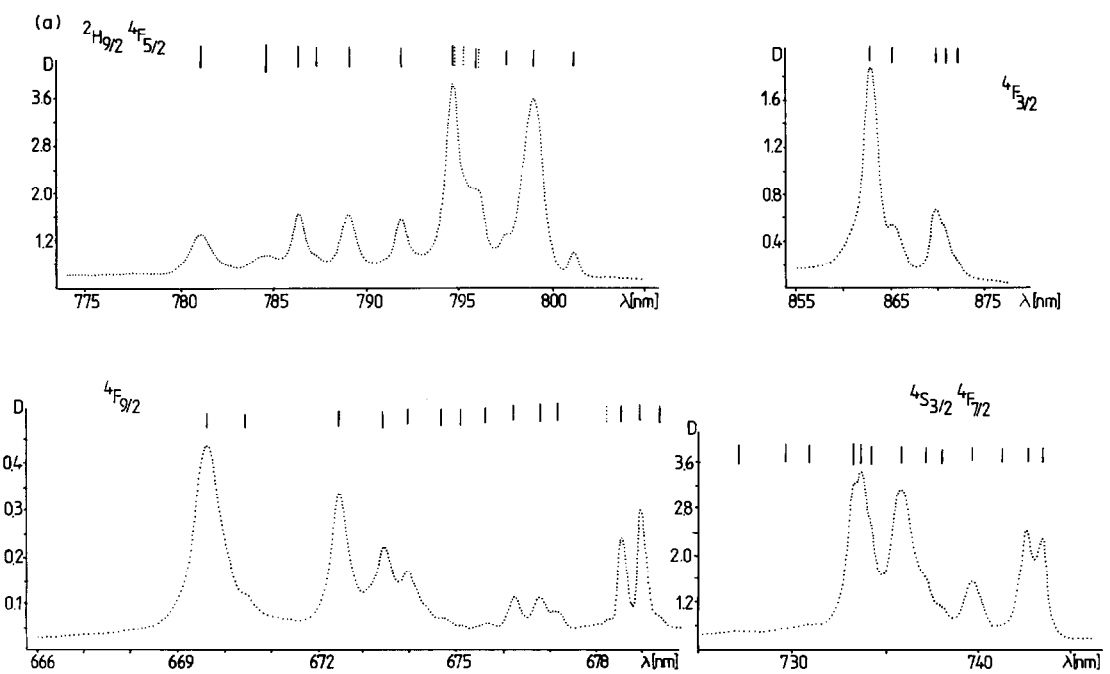

Fig. 3(a).

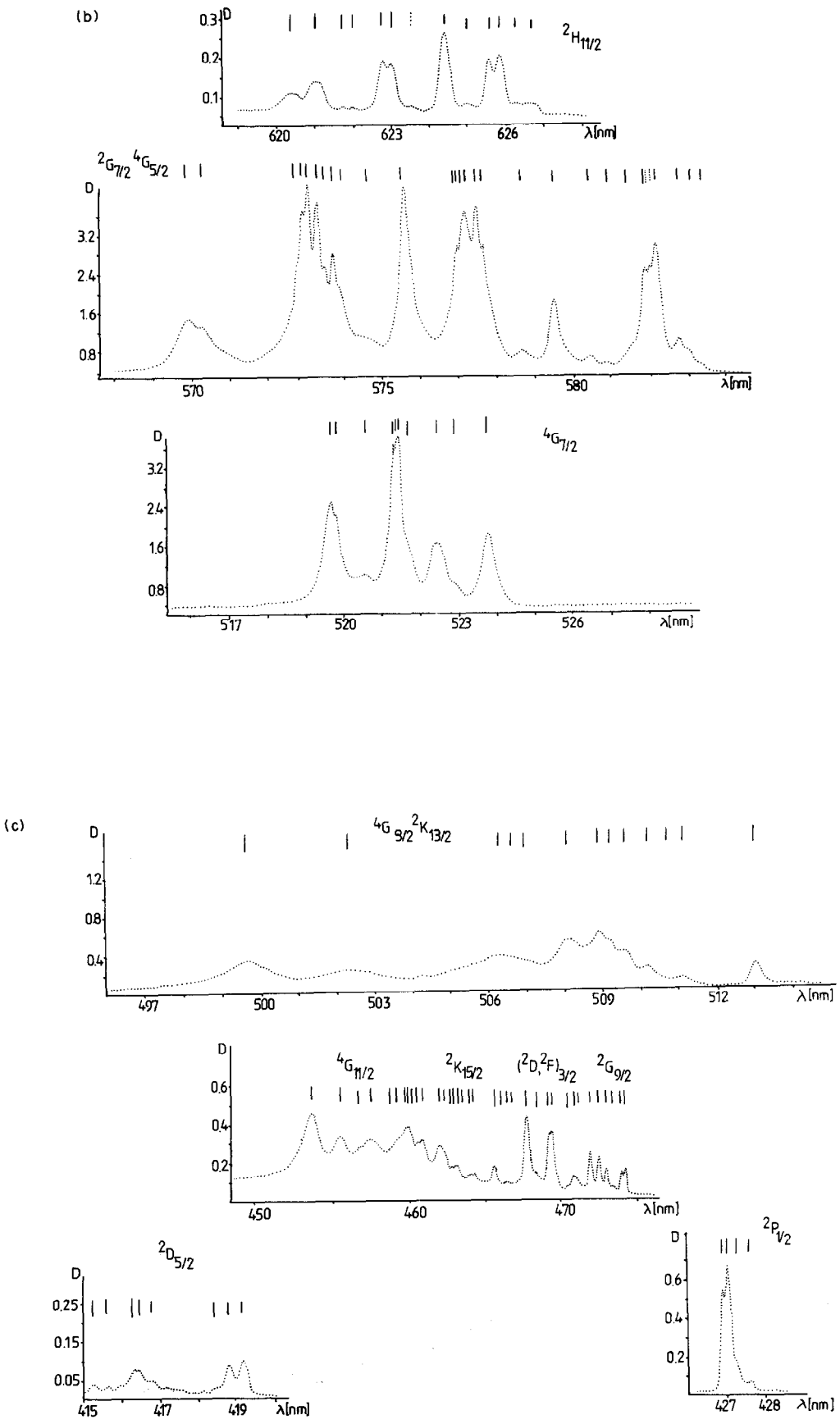

Fig. 3. Absorption spectra of $Nd(CCl_3(COO)_3 \cdot 2H_2O$ crystal at 5 K.

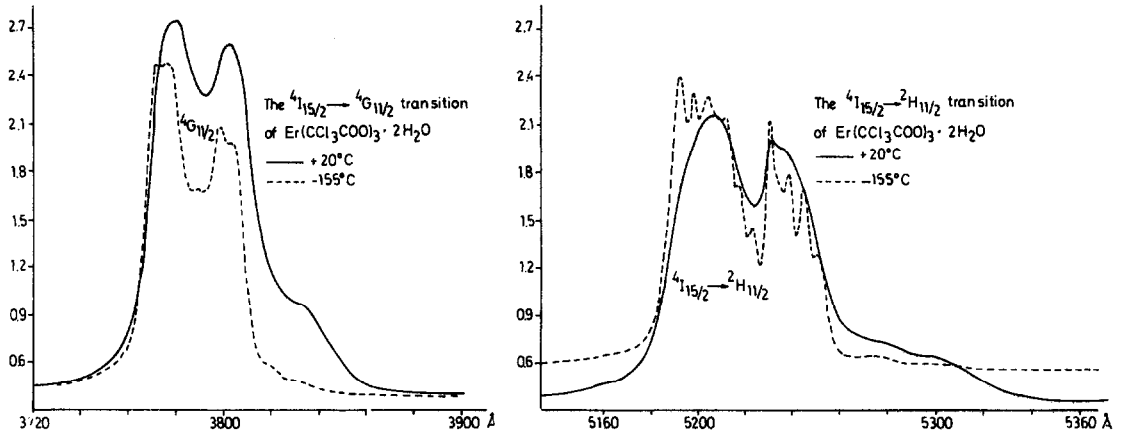

Fig. 4. The hypersensitive transitions of $Er(CCl_3COO)_3 \cdot 2H_2O$ crystals at different temperatures.

(946.84×10^{-8} for erbium acetate to 1444.99×10^{-8} for erbium trichloroacetate) (Figs 2 and 4).[19]

Covalent effect was reported by Henrie *et al.*[20] They consider an increasing basic character of the coordinating ligand (ΣpK_a) resulting in increasing absorption intensity.

If we confront the results of intensity analysis for erbium trichloroacetates and formates (for which the same bonding mode of the carboxyl group appears) and relate them to Ln—O distances, a good direction of intensity change is apparent.[3]

The oscillator strength values at various temperatures are shown in Tables 1 and 2. The drastic decrease of intensity for almost all transitions is obvious. Intensity decays with temperature decrease. It can be given either by change of ground state sublevel population or by vibronic mechanism contribution. If the first effect is involved, the variation of intensity could be almost the same for all transitions. In fact we have observed a different quantity of intensity change, so probably the second mechanism could have taken part also. This last conclusion advocates the shape of absorption bands at 5 K. If we return to the structure data, two Er^{3+} or Nd^{3+} ions occupy two different site symmetry positions, that can implicate the additional Stark components of the second site for a given transition. In fact, however, we have not observed an agree-

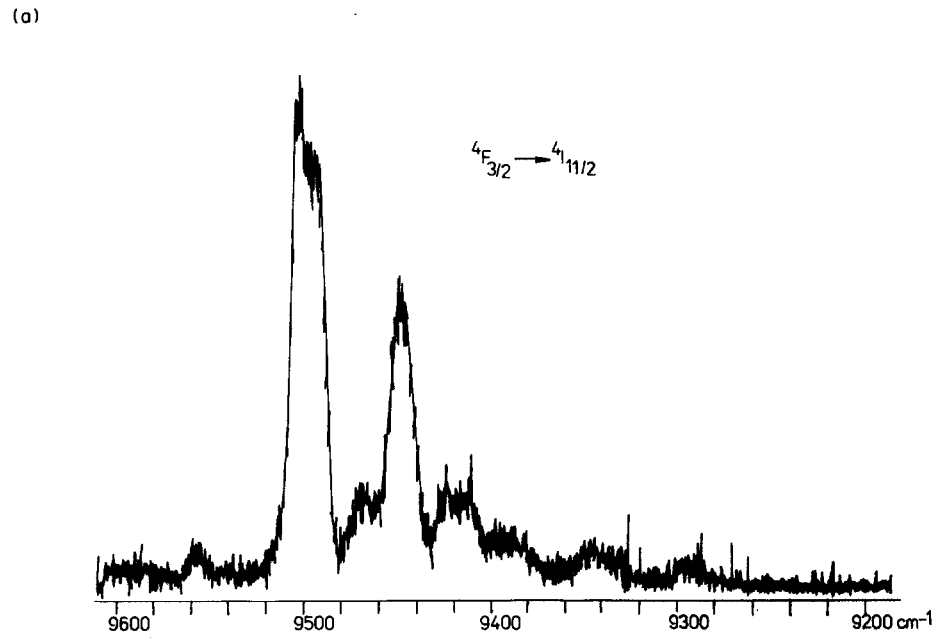

Fig. 5(a).

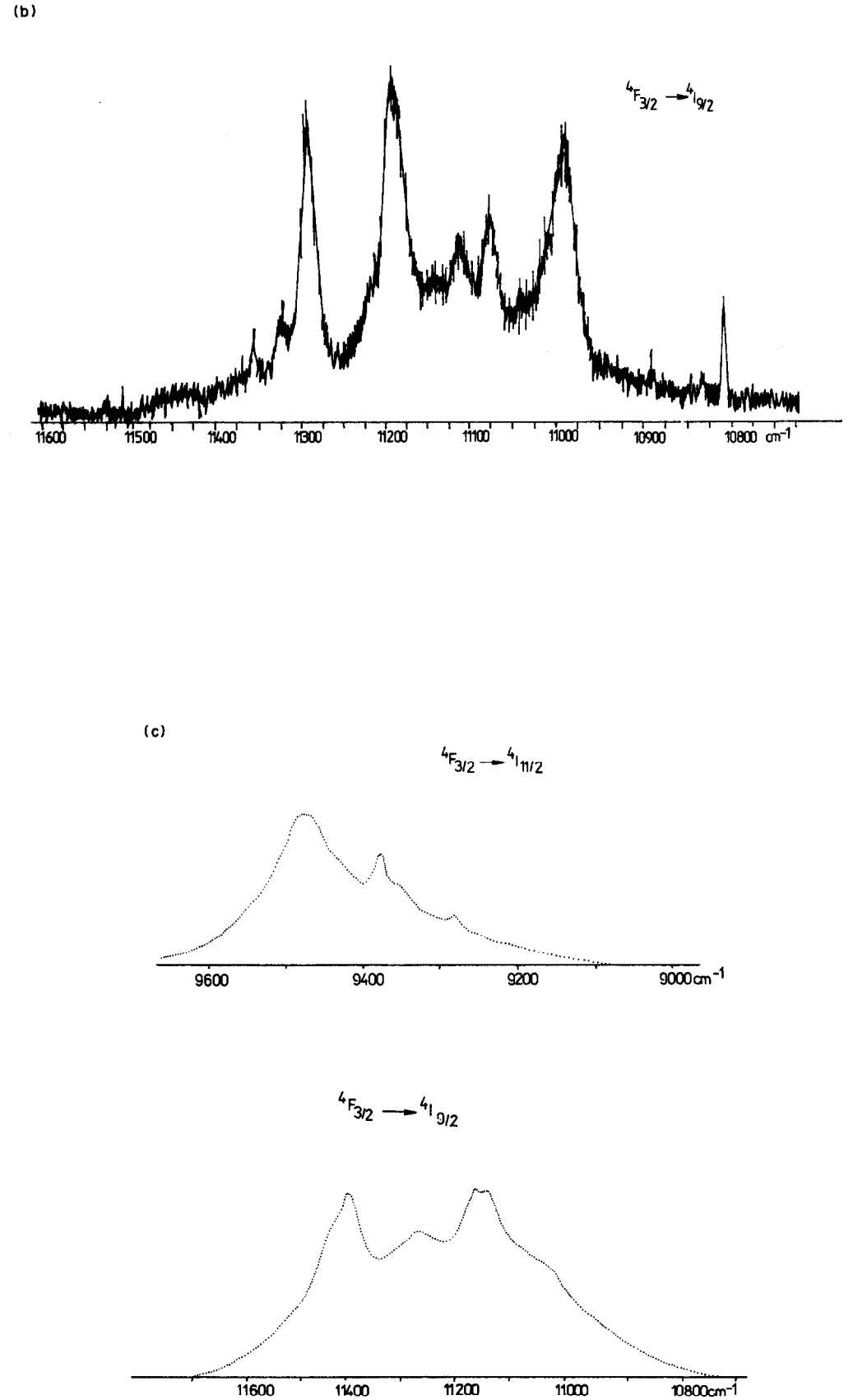

Fig. 5. Luminescence spectra of $Nd(CCl_3COO)_3 \cdot 2H_2O$ crystals. (a) 4.2 K, $\lambda_{exc} = 488$ nm, (b) 4.2 K, $\lambda_{exc} = 488$ nm and (c) 300 K, $\lambda_{exc} = 514$ nm.

ment between the expected and the observed numbers of components. The stronger components are accompanied by the many weak ones. Additional components appeared in almost all transitions which can be given both by vibration and/or by ion-pair interactions. Splitting of $^4I_{9/2} \rightarrow {}^2P_{1/2}$ at 5 K seems to confirm this conclusion. It has been possible due to the mutual perturbation that each ion induces at the site of its neighbour which shifts the energy levels and thus produces satellites of the optical lines (Fig. 3).

Figures 5(a) and (b) show the neodymium trichloroacetate single crystal luminescence spectra at 4.2 K. It was found: 12 Stark components for $^4F_{3/2} \rightarrow {}^4I_{11/2}$; 13 well observed lines and some additional detected as bendings for $^4F_{3/2} \rightarrow {}^4I_{9/2}$ transition. The nature of the additional lines needs further consideration as an effect of vibronic and ion-pair interactions.

REFERENCES

1. L. A. Aslanov, W. M. Ionov and P. D. Keikbaev, *Koord. Khimia* 1976, **2**, 1674.
2. L. M. Belyaev, L. M. Dorozhkin, L. V. Soboleva, B. A. Chayanov, V. D. Shigorin and G. P. Shipulo, *Kristallografiya* 1979, **24**, 842.
3. J. Legendziewicz, T. Głowiak, G. Oczko and C. N. Dao, *J. Less-Common Met.* 1986, **125**, 45.
4. A. A. Kaminskii, *Laser Crystal.* Springer, Berlin (1981).
5. W. Zolin, W. Cariuk and W. Markuszev, *Koord. Khimia* 1986, **12**, 1498.
6. Takashi Imai and Akira Ouchi, *Bull. Chem. Soc. Japan* 1987, **60**, 408.
7. J. Legendziewicz, C. Szafrański, G. Oczko, W. Stręk and B. Jeżowska-Trzebiatowska, *Bull. Acad. Polon. Sci.* 1988, **36**, 189.
8. A. S. Antsyshkina, M. A. Porai-Koshits and V. N. Ostrikova, *Zhur. Neorg. Khimii* 1988, **33**, 1950.
9. B. R. Judd, *Phys. Rev.* 1962, **127**, 750.
10. T. S. Lomheim and L. G. De Shazer, *J. Appl. Phys.* 1978, **49**, 5517.
11. T. S. Lomheim and L. G. De Shazer, *Phys. Rev. B.* 1979, **20**, 4343.
12. J. Legendziewicz, E. Huskowska, A. Waśkowska and Gy. Argay, *Inorg. Chim. Acta* 1984, **92**, 151.
13. G. Sadikov, G. Kukina and M. A. Porai-Koshits, *Zhur. Struc. Khimii* 1967, **8**, 551.
14. L. A. Aslanov, I. Abdulminev and M. A. Porai-Koshits, *Dokl. Akad. Nauk USSR* 1972, **205**, 343.
15. L. A. Aslanov, *Zhur. Struc. Khimii* 1972, **13**, 468.
16. A. Sonesson, *Acta Chem. Scand.* 1958, **12**, 165.
17. A. Sonesson, *Acta Chem. Scand.* 1958, **12**, 1937.
18. W. A. Gubanov and M. W. Riskov, *Zhur. Struc. Khimii* 1986, **27**, 124.
19. K. Bukietyńska and A. Mondry, unpublished.
20. D. E. Henrie, R. L. Fellows and G. R. Choppin, *Coord. Chem. Rev.* 1976, **18**, 199.

Polyhedron Vol. 10, No. 16, pp. 1929–1937, 1991
Printed in Great Britain

0277–5387/91 $3.00+.00
© 1991 Pergamon Press plc

REDOX CHEMISTRY OF 1,4-DIHYDROXY-9,10-ANTHRAQUINONE (QUINIZARINE) AND ITS MANGANESE(II) COMPLEXES IN DIMETHYLSULPHOXIDE

MARIO E. BODINI* and VERÓNICA ARANCIBIA

Laboratorio de Electroquímica, Facultad de Química,
Pontificia Universidad Católica de Chile, Casilla 6177, Santiago, Chile

(*Received* 1 *August* 1990; *accepted* 8 *May* 1991)

Abstract—The redox behaviour of the ligand 1,4-dihydroxy-9,10-anthraquinone (Quinizarine) and its oxidation–reduction products (semiquinones and dianion) has been studied in dimethylsulphoxide, $(CH_3)_2SO$. The combination of Quinizarine in the presence of two equivalents of tetraethylammonium hydroxide (TEAOH) with manganese(II) in a 1 : 2 and 1 : 1 mole ratio forms two complexes. The first one has a stability constant of 9.0×10^{12} M^{-2}, whereas the second one precipitates. On the other hand further oxidation by electrolysis of the solution of Quinizarine in the presence of the two equivalents of TEAOH yields a green solution of the corresponding semiquinone. The combination of this semiquinone with manganese(II) in a 1 : 1 mole ratio forms a violet complex. These complexes and their oxidation reduction products have been characterized by cyclic voltammetry, controlled-potential electrolysis and optical spectroscopy in dimethylsulphoxide solvent. The formation constant for the complex has been evaluated spectrophotometrically and turns out to be 8.9×10^5 M^{-1}. These results may be relevant to the mechanism of the role of manganese in biological systems.

INTRODUCTION

Many manganese complexes have been studied to serve as models for the centre that catalyses the oxidation of water to molecular oxygen in Photosystem II of green-plant photosynthesis.[1–10] A mixed ligand complex in which the manganese atom is bound both to a protein and to another ligand (i.e. a quinone) to facilitate the oxidation of the whole unit has been proposed.[11] Under these conditions the oxidation equivalents would accumulate in this unit to permit the subsequent oxidation of two water molecules to yield hydrogen peroxide and finally molecular oxygen.

The most abundant naturally occuring quinones are paraquinones[12] and among those Quinizarine has the particular feature of having two hydroxy groups in the 1 and 4 positions. Therefore, it can be oxidized to the corresponding *para*-semiquinone which could form a stable complex with manganese, assisted by the 9,10 quinonic system as a second coordinating group. This oxidation process could take place at a more positive potential which would make it more appropriate to develop a model for the active centre of Photosystem II.

In this paper we report the study of the redox chemistry of Quinizarine and the interaction of its different forms with manganese(II).

EXPERIMENTAL

Equipment

A three-electrode potentiostat (Tacussel Model PRT 20-2X potentiostat/galvanostat with Model GSPT wave generator) was used for the cyclic voltammetric and controlled-potential electrolysis experiments.

A current integrator based on operational amplifiers was used as a coulometer in the controlled-potential electrolyses.

Cyclic voltammograms were recorded on a Hewlett–Packard Model 7004 A X-Y recorder.

The electrochemical cell was equipped with a Beckman platinum-inlay working electrode (area 0.23 cm^2), a platinum coil auxiliary electrode, and

* Author to whom correspondence should be addressed.

an Ag/AgCl reference electrode filled with an aqueous tetramethylammonium chloride solution and adjusted to 0.00 V vs SCE.[13] The latter was contained in a Pyrex tube with a soft-glass cracked tip; this electrode was placed inside a Luggin capillary. For controlled potential electrolysis, a platinum-mesh working electrode was employed.

A Beckman Model Acta CV spectrophotometer was used for UV–vis spectrophotometric measurements.

Air-sensitive compounds were handled in a glove bag (Aldrich) under a nitrogen atmosphere and the oxygen content was monitored with a Beckman Model Monitor II Oxygen Analyser.

Reagents

The reagents for the investigation and syntheses included $Mn(ClO_4)_2 \cdot 6H_2O$ (G. Frederick Smith), tetraethylammonium hydroxide (TEAOH) (25% in methanol, Eastman), tetramethylammonium chloride (Aldrich), and tetraethylammonium perchlorate (TEAP) (G. Frederick Smith). The ligand Quinizarine was obtained from Aldrich.

Burdick and Jackson Laboratories "distilled-in-glass" grade solvents were used without further purification for all of the experiments. High purity argon was used to de-aerate solutions.

Because the solvation water of the $Mn(ClO_4)_2 \cdot 6H_2O$ salt interfered with the stoichiometric formation of the complexes under study, $[Mn^{II}(DMU)_6][ClO_4]_2$ (DMU = dimethylurea)[14] was used in all the experiments in which the manganese(II) complexes were formed *in situ*. As a source of manganese(III), $[Mn^{III}(Urea)_6][ClO_4]_3$[15] was used in all the experiments.

RESULTS AND DISCUSSION

The cyclic voltammograms of solutions of Quinizarine in dimethylsulphoxide (DMSO) are illustrated in Fig. 1(a). This ligand presents two reversible couples with reduction peak potentials of -0.58 V vs SCE and -1.14 V vs SCE, and oxidation peak potentials of -0.50 V vs SCE and -1.06 V vs SCE, respectively. Controlled-potential electrolysis after the reduction peaks indicate that one electron has been transferred in each process. Therefore, we can conclude that they correspond to the formation of the semiquinone (species **II**) and the dianion (species **III**) of the ligand as a consequence of the reduction of the quinonic system in the 9 and 10 positions, according to the following half-reactions, eq. (1):

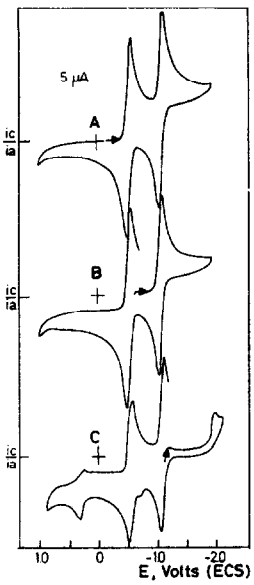

Fig. 1. Cyclic voltammograms in DMSO (TEAP 0.1 M, $v = 0.1$ V s^{-1}) of solutions that are 0.1 mM in Quinizarine [1,4-di(OH)AQ, species **I**] (a); 1.0 mM in semiquinone [1,4-di(OH)SQ$^-$, species **II**] (b); 1.0 mM in dianion [1,4-di(OH)DA^{2-}, species **III**] (c).

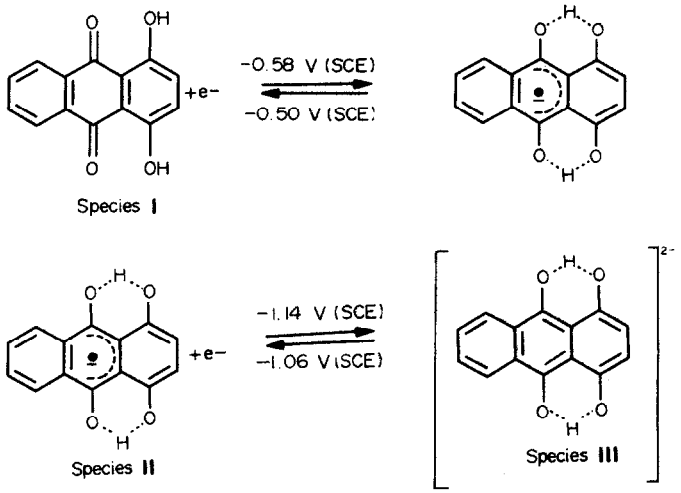

(1)

Quinizarine is yellow–orange in DMSO, whereas the semiquinone **II** is dark brown and the dianion **III** is light brown. Both species **II** and **III** react with molecular oxygen very readily. Figure 1(b) shows the cyclic voltammogram of a solution of the semiquinone **II** generated by controlled-potential electrolysis at −0.78 V vs SCE of a solution of Quinizarine. Figure 1(c) shows the cyclic voltammogram of a solution of the dianion **III** generated by controlled-potential electrolysis at −1.34 V vs SCE of a solution of the semiquinone.

The UV–vis spectrum of Quinizarine [Fig. 2(a)] shows a quinoid electron transfer band at 275 nm (ε = 10,700 M^{-1} cm^{-1}), another quinoid electron transfer band at 325 nm (ε = 3500 M^{-1} cm^{-1}), and an electron transfer band at 470 nm (ε = 8600 M^{-1} cm^{-1}). The last band may involve excitation of the non-bonding electrons of the hydroxy group to the carbonyl anti-bonding orbitals of the quinone.[16] The spectrum of semiquinone [Fig. 2(b)] shows an absorption maximum at 500 nm (ε = 21,100 M^{-1} cm^{-1}) which indicates that in this case the visible peak has shifted bathochromically and its intensity has increased. This effect may be due to the delocalized electrons that produce an aromatic system. Also, it shows a well defined maximum at 390 nm (ε = 6400 M^{-1} cm^{-1}). On the other hand, the dianion **III** shows a very intense absorption maximum at 470 nm (ε = 21,000 M^{-1} cm^{-1}) but it does not show the maximum at 390 nm due to the radical nature of the semiquinone **II** [Fig. 2(c)].

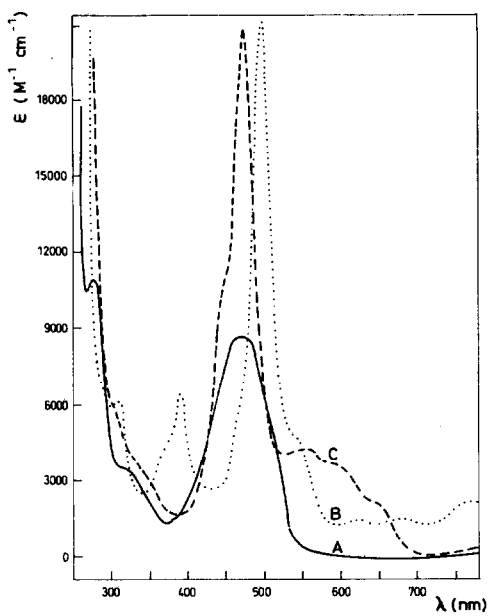

Fig. 2. Absorption spectra, UV–vis, in DMSO of solutions that are 1.0 mM in Quinizarine [1,4-di(OH)AQ, species **I**] (a); 1.0 mM in semiquinone [1,4-di(OH)SQ^{-}, species **II**] (b); 1.0 mM in dianion [1,4-di(OH)DA^{2-}, species **III**] (c).

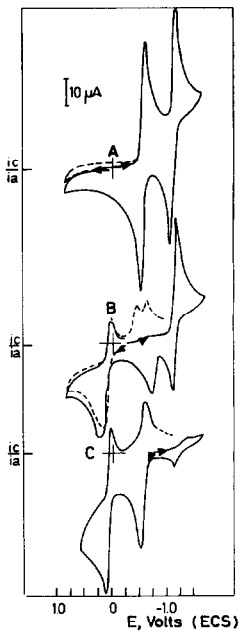

Fig. 3. Cyclic voltammograms in DMSO (TEAP 0.1 M, $v = 0.1$ V s^{-1}) of solutions that are 1.0 mM in Quinizarine [1,4-di(OH)AQ, species **I**] (a); 1.0 mM in Quinizarine and 1.0 mM in TEAOH [1,4-(O^{-},OH)AQ, species **IV**] (b); 1.0 mM in Quinizarine and 2.0 mM in TEAOH [1,4-di(O^{-})AQ, species **V**] (c).

In the presence of one and two equivalents of base the hydroxy protons are neutralized (species **IV** and **V**) and the solutions turn blue. Figures 3 and 4 show the cyclic voltammograms and UV–vis spectra of these compounds.

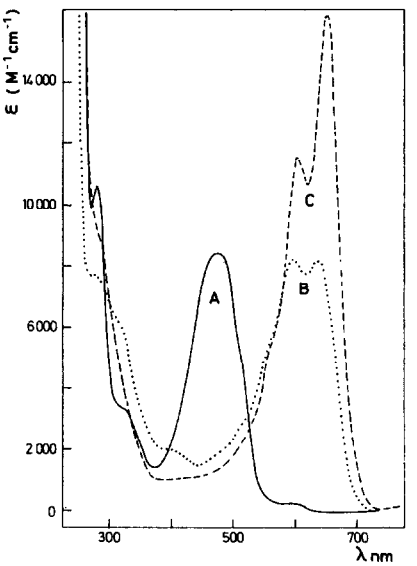

Fig. 4. Absorption spectra, UV–vis, in DMSO of solutions that are 1.0 mM in Quinizarine [1,4-di(OH)AQ, species **I**] (a); 1.0 mM in Quinizarine and 1.0 mM in TEAOH [1,4-(O^{-},OH)AQ, species **IV**] (b); 1.0 mM in Quinizarine and 2.0 mM in TEAOH [1,4-di(O^{-})AQ, species **V**] (c).

After the addition of one equivalent of base the absorption maxima are: 275 nm ($\varepsilon = 7800\ M^{-1}\ cm^{-1}$), 325 nm ($\varepsilon = 6000\ M^{-1}\ cm^{-1}$), 395 nm ($\varepsilon = 2000\ M^{-1}\ cm^{-1}$), 535 nm ($\varepsilon = 3800\ M^{-1}\ cm^{-1}$), 600 nm ($\varepsilon = 8300\ M^{-1}\ cm^{-1}$) and 640 nm ($\varepsilon = 8300\ M^{-1}\ cm^{-1}$) [Fig. 4(b)]. Upon addition of a second equivalent of base only the absorption maxima at 600 nm ($\varepsilon = 11{,}600\ M^{-1}\ cm^{-1}$) and at 650 nm ($\varepsilon = 16{,}300\ M^{-1}\ cm^{-1}$) show up.

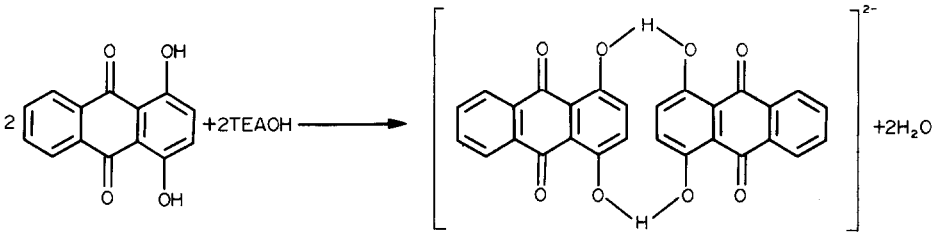

On the basis of our experimental results we have proposed the structure of compound **IV**, because the solution of this species presents absorption maxima at 275 and 325 nm which are characteristic of the protonated quinone (species **I**), and at 600 and 640 nm which are characteristic of the totally deprotonated quinone (species **V**). The cyclic voltammogram of this solution (Fig. 3(b)] presents a reduction peak at −1.14 V vs SCE which involves the transfer of one equivalent of charge, whereas upon reversal of the scan direction two oxidation peaks show up at −0.67 V vs SCE and −1.06 V vs SCE, respectively. Controlled potential electrolysis after these peaks indicate that 0.5 equivalents of charge have been transferred in each case, and the spectra of the solutions obtained after the electrolyses are shown in Fig. 5. Notice that after the reduction of compound **IV** a mixture of protonated dianion (species **III**) and deprotonated dianion (species **V**) is obtained. Species III is characterized by the presence of the maxima at 470 and 560 nm, whereas species **V** can be identified by the maxima at 600 and 650 nm. The oxidation of these two species occur at different potentials: at −1.06 V vs SCE the formation of the protonated semiquinone (species II) is observed whereas at −0.67 V vs SCE the deprotonated semiquinone (species **VI**) corresponding to the oxidation of the 1,4 dihydroxy system, is obtained (the absorption maxima at 390 and 560 nm are not observed). Finally, species **II** and **VI** react to regenerate species **IV**.

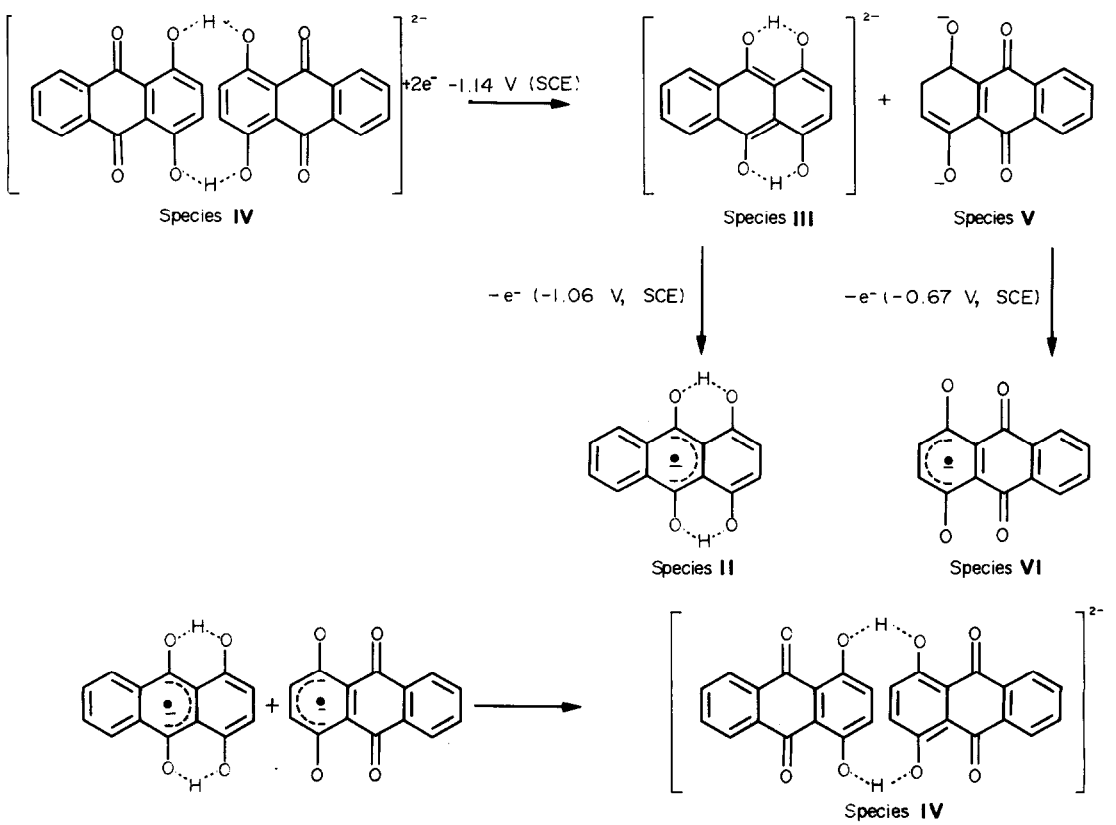

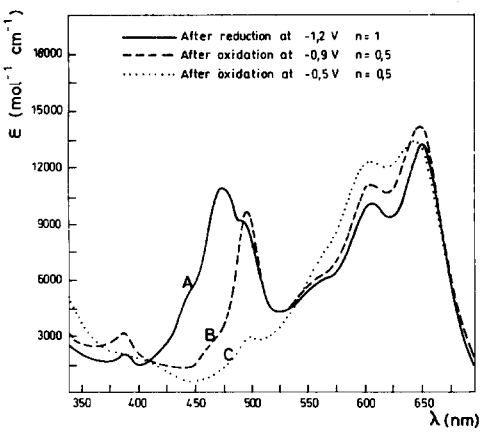

Fig. 5. Absorption spectra, UV–vis, in DMSO of (a) a 1.0 mM solution of Quinizarine and 1.0 mM in TEAOH (species **IV**) after complete electrolysis at −1.34 V vs SCE ($n = 1$), species **III** and **V**; (b) solution A after complete electrolysis at −0.9 V vs SCE ($n = 0.5$), species **II**; (c) solution **B** after complete electrolysis at −0.5 V vs SCE ($n = 0.5$), species **IV**.

Conductometric titration of a 1 mM solution of Quinizarine in DMSO with a 0.095 M solution of NaOH in methanol gave a first break after the addition of one equivalent of base and then the conductance remained constant until the second equivalent of base was added. From then on an increase of conductance was observed upon addition of an excess of base. This is indicative of the formation of an ion aggregate like species **IV**, which is more conductive than Quinizarine (species **I**).[17-18]

The neutralization of the second proton does not change the conductivity of the solution because the effects of the dissociation of the aggregate and the formation of the dianion compensate. The high conductivity of the aggregate of two monoanions is due to the formation of an ion pair with the titrant cation.

If the titration is done using a solution of tetraethylammonium hydroxide in methanol the conductivity curve breaks are not observed clearly and the conductance values are approximately 20% lower than those obtained when sodium hydroxide is used as the titrant.

If the initial scan is made in the positive direction one oxidation peak is observed at +0.20 V vs SCE and three reduction peaks at +0.07 V vs SCE, 0.4 V vs SCE, and −0.58 V vs SCE show up. These processes can be represented by the following set of equations:

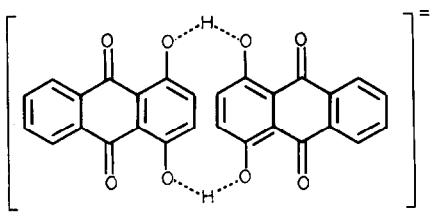

Species **IV**

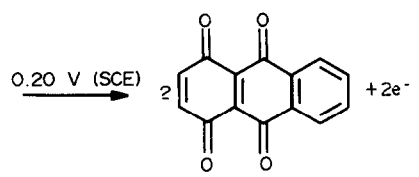

Species **VII**

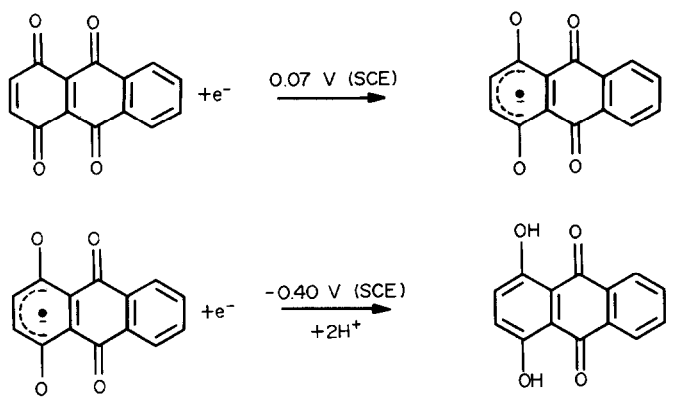

The formation of the diquinonic species **VII** has been verified by controlled-potential electrolysis which indicates that two equivalents of charge are being transferred in this process.

In the presence of two equivalents of base the solution turns blue (species **V**). In this case [Fig. 1(c)] an anodic peak shows up at −0.46 V vs SCE and a second anodic peak at +0.20 V vs SCE is observed. Controlled-potential electrolysis at −0.3 V vs SCE indicates that the first peak corresponds

to a one-electron process that generates a green radical species (species **VI**) produced by the oxidation of the 1,4 dihydroxy system which is then oxidized via another one-electron process to the diquinone **VII**.

The UV–vis spectra of these solutions show absorption maxima at 531 nm ($\varepsilon = 8200\ M^{-1}\ cm^{-1}$), 553 nm ($\varepsilon = 9700\ M^{-1}\ cm^{-1}$) and 606 nm ($\varepsilon = 7850\ M^{-1}\ cm^{-1}$) [Fig. 7(c)].

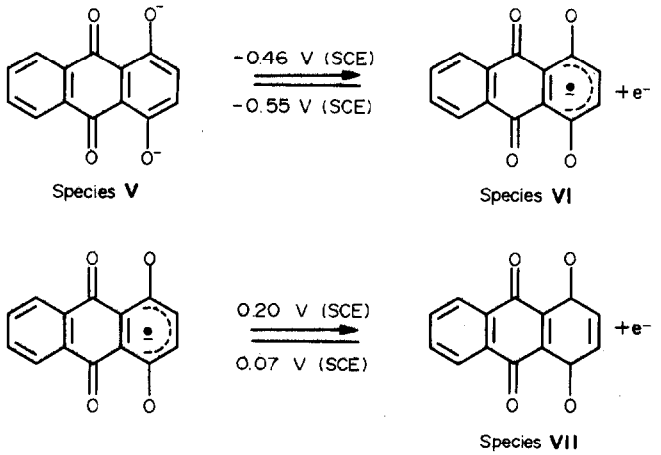

The direct reaction of the semiquinone **II** generated by controlled potential electrolysis at −0.78 V vs SCE with molecular oxygen generates a blue solution which presents the same spectrum as a solution of deprotonated Quinizarine. The blue species is also generated by a strong base such as superoxide ion (produced by chemical reaction of dioxygen with the semiquinone) which is known to be a powerful Bronsted base in aprotic solvents.[9-20]

$$\text{1,4-di(OH)SQ} + O_2 \longrightarrow \underset{\text{blue}}{\text{1,4-(O}^-\text{,OH)AQ}} + HO_2\cdot$$

In the presence of manganese(II) the protonated Quinizarine or its reduced form (semiquinone) does not form complexes as the cyclic voltammograms and the UV–vis spectra do not change in the presence of the metal ion.

On the other hand in the presence of two equivalents of base the cyclic voltammograms and UV–vis spectra of solutions with different concentrations of manganese(II) (Figs 6 and 7) show that with a 1 : 2 metal-to-ligand mole ratio the presence of free ligand is not observed. The solution is blue–violet. An anodic peak shows up at +0.17 V vs SCE which corresponds to the oxidation of the complex formed to $MnSQ^+$ and SQ^-. These species are finally oxidized to the corresponding diquinonic species at 0.42 V vs SCE, and 0.55 V vs SCE, respectively.

$$\underset{\text{blue–violet}}{MnQ_2^{2-}} \xrightarrow{+0.17\,V} MnSQ^+ + SQ^- + 2e^-$$
$$\downarrow 0.55\,V \qquad \downarrow 0.42\,V$$
$$Mn^{II} + DQ + e^- \qquad DQ + e^-$$

Addition of more Mn^{2+} causes the bis blue–violet complex to react, forming another violet complex with a 1 : 1 stoichiometry [Fig. 7(c)] which precipitates if the concentration is higher than 1 mM. This complex oxidizes at +0.26 vs SCE and +0.55 V vs SCE, whereas the oxidized ligand is reduced at +0.09 V vs SCE. The UV–vis spectra [Fig. 7(d)]

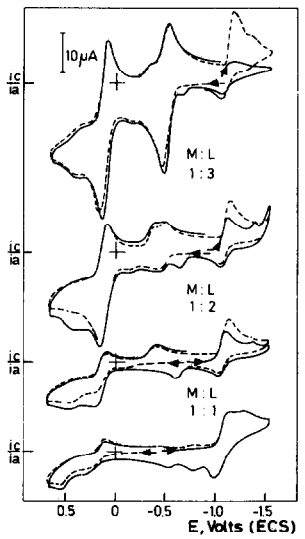

Fig. 6. Cyclic voltammograms in DMSO (TEAP 0.1 M, v = 0.1 V s^{-1}) of (a): a 1.0 mM in Quinizarine and 2.0 mM in TEAOH [1,4-(O⁻,OH)AQ, species **V**]; (b): solution A in the presence of 0.3 mM $Mn^{II}(DMU)_6(ClO_4)_2$; (c): solution A in the presence of 0.5 mM $Mn^{II}(DMU)_6(ClO_4)_2$; (d): solution A in the presence of 1.0 mM $Mn^{II}(DMU)_6(ClO_4)_2$.

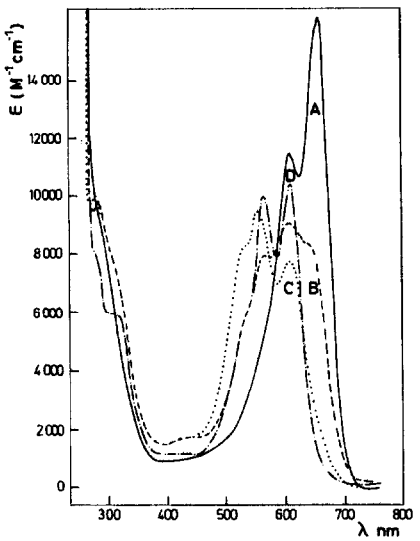

Fig. 7. Absorption spectra UV–vis in DMSO of (a): a 1.0 mM in Quinizarine and 2.0 mM in TEAOH [1,4-(O^-, OH)AQ, species V]; (b): solution A in the presence of 0.3 mM $Mn^{II}(DMU)_6(ClO_4)_2$; (c): solution A in the presence of 0.5 mM $Mn^{II}(DMU)_6(ClO_4)_2$; (d): solution A in the presence of 1.0 mM $Mn^{II}(DMU)_6(ClO_4)_2$.

shows absorption maxima at 569 nm ($\varepsilon = 10{,}000$ M^{-1} cm^{-1}) and 613 nm ($\varepsilon = 10{,}200$ M^{-1} cm^{-1}).

When Quinizarine in the presence of two equivalents of base is oxidized electrochemically at -0.30 V vs SCE it is found that one equivalent of charge is being transferred. Therefore, the semiquinone corresponding to the oxidation of the 1,4 dihydroxy system is obtained. Upon addition of manganese(II) to this green semiquinone a soluble violet complex is formed with a 1.1 stoichiometry. This complex is oxidized at $+0.55$ V vs SCE [Fig. 8(d)] and as a consequence of that it decomposes because after this process the reduction of the diquinone (DQ) is observed at $+0.09$ V vs SCE. This complex presents absorption maxima [Fig. 9(c)] at 520 nm ($\varepsilon = 5000$ M^{-1} cm^{-1}), 555 nm ($\varepsilon = 8200$ M^{-1} cm^{-1}), and 650 nm ($\varepsilon = 9800$ M^{-1} cm^{-1}).

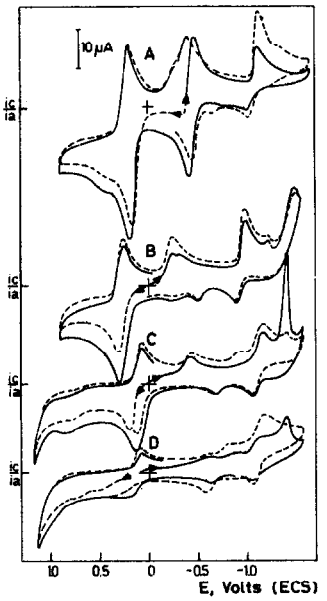

Fig. 8. Cyclic voltammograms in DMSO (TEAP 0.1 M, $v = 0.1$ V s^{-1}) of (a): a 1.0 mM in Quinizarine and 2.0 mM in TEAOH after electrolysis at -0.30 V vs SCE (species VI); (b): solution A in the presence of 0.3 mM $Mn^{II}(DMU)_6(ClO_4)_2$; (c): solution A in the presence of 0.5 mM $Mn^{II}(DMU)_6(ClO_4)_2$; (d): solution A in the presence of 1.0 mM $Mn^{II}(DMU)_6(ClO_4)_2$.

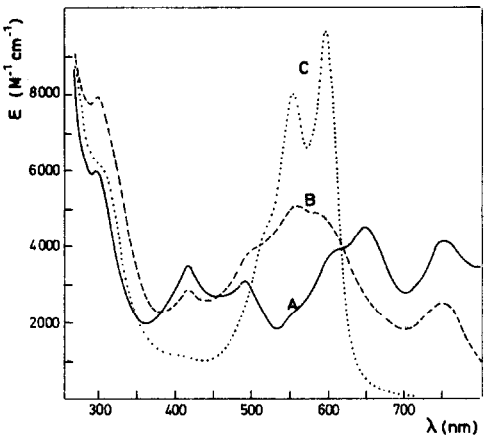

Fig. 9. Absorption spectra UV–vis in DMSO of (a): a 1.0 mM in Quinizarine and 2.0 mM in TEAOH after electrolysis at -0.30 V vs SCE (species VI); (b): solution A in the presence of 0.3 mM $Mn^{II}(DMU)_6(ClO_4)_2$; (c): solution A in the presence of 0.5 mM $Mn^{II}(DMU)_6(ClO_4)_2$; (d): solution A in the presence of 1.0 mM $Mn^{II}(DMU)_6(ClO_4)_2$.

The stability constants of the complexes formed have been evaluated spectrophotometrically. The one corresponding to the $MnSQ^+$ complex has been determined by measuring the absorbance at 750 nm of a solution of the semiquinone produced by controlled-potential electrolysis as the concentration of manganese is increased. This constant turns out to be 8.9×10^5 M^{-1}. In a similar manner the stability constant of the bis complex with quinizarine MnQ_2^{2-} has been evaluated by measuring the absorbance at 660 nm of a solution of the metal as the concentration of ligand is increased. In this case the stability constant is 9.0×10^{12} M^{-2}.

$$Mn^{II} + SQ^{\cdot-} \longleftrightarrow MnSQ^+ \quad Kf = 8.9 \times 10^5\, M^{-1}$$

$$Mn^{II} + 2Q^{2-} \longleftrightarrow MnQ_2^{2-} \quad Kf = 9.0 \times 10^{12}\, M^{-2}$$

In the presence of an excess of manganese(II) a 1:1 complex of manganese with the dianion of

Quinizarine is formed. This complex, being neutral is insoluble in this medium and precipitates, therefore we were not able to determine its stability constant.

Therefore, we can conclude that several complexes are formed between manganese and the different forms of Quinizarine in this medium. The unprotonated ligand, Q^{2-}, forms a 1:1 and a 1:2 complex. The first one is insoluble and probably corresponds to a polymeric structure analogous to those found with copper.[21]

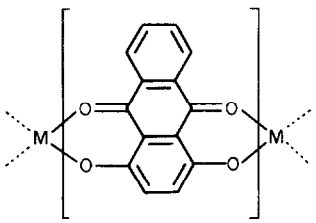

The 1:2 complex is soluble with a stability constant of 9.0×10^{12} M^{-2}. The oxidation of the 1,4 dihydroxy system forms a semiquinone at fairly positive potentials, and this species in the presence of manganese(II) generates a stable complex with a stability constant of 8.9×10^{5} M^{-1}. Probably an intramolecular charge-transfer takes place in this complex, with the metal ion having a manganese(III) character and the semiquinone being reduced to the corresponding dianion. The spectroscopic evidence [Fig. 9(c) compared to Fig. 10(c)] indicates the presence of bound dianion in this complex, which presents the same spectrum as a solution of manganese(III)–dianion (Fig. 10). Consequently, we assume that the manganese atom has a manganese(III) character in this case. This behaviour is analogous to that observed with other ligands such as 3,5-ditertbutyl catechol,[22] Lawsone[23] and Lapachol.[24]

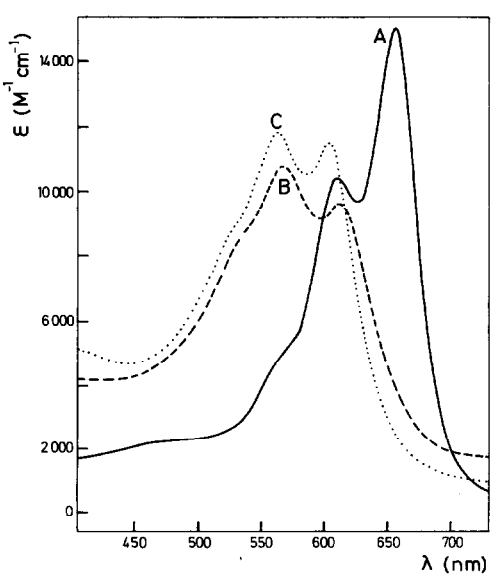

Fig. 10. Absorption spectra UV–vis in DMSO of (a): a 1.0 mM in Quinizarine and 2.0 mM in TEAOH [1,4-(O^-,OH)AQ, species V]; (b): solution A in the presence of 0.5 mM $Mn^{III}(UREA)_6(ClO_4)_3$; (c): solution A in the presence of 1.0 mM $Mn^{III}(UREA)_6(ClO_4)_3$.

Therefore, these results may be relevant for the development of a model system for the active centre of Photosystem II of green-plant photosynthesis. Mixed-ligand complexes of manganese with oxidized Quinizarine and some other ligands that stabilize higher oxidation states of this metal can act as centres that accumulate oxidizing equivalents at a potential positive enough to produce the oxidation of water to molecular oxygen. The study of these mixed ligand complexes is currently in progress in our group.

Acknowledgement—This work was supported by CONICYT-Chile through the FONDECYT No. 309/88 research grant.

REFERENCES

1. H. K. Lichtenthater, *Prog. Photosynth. Res., Proc. Int. Congr.* 1969, **1**, 304.
2. H. H. Stichl and H. T. Witt, *Z. Natur.* 1969, **24B**, 1588.
3. R. L. Heath, *Int. Cytol.* 1973, **34**, 49.
4. H. J. van Gorkom, *Biochem. Biophys. Acta* 1974, **347**, 439.
5. A. J. Bearden and R. Q. Makin, *Rev. Biophys.* 1975, 7, 131.
6. R. Radmer and G. M. Cheniae, *Primary Processes*, Vol. 2. Elsevier–North Holland, New York (1977).
7. D. B. Knaff, R. Malkin, J. C. Myron and M. Stoller, *Biochem. Biophys. Acta* 1977, **459**, 402.
8. J. Livorness and T. D. Smith, *Struct. Bond.* 1982, **48**, 1.
9. K. Sauer, *Accts Chem. Res.* 1980, **13**, 249.
10. D. T. Sawyer, M. E. Bodini, L. A. Willis, T. L. Riechel and K. D. Magers, *Adv. Chem. Ser.* 1977, **162**, 330.
11. G. L. Lawrence and D. T. Sawyer, *Coord. Chem. Rev.* 1978, **27**, 173.
12. S. Patai, *The Chemistry of the Quinoinoid Compounds*, Part 2. John Wiley, London (1974).
13. D. T. Sawyer and J. L. Roberts, *Experimental Electrochemistry for Chemists*, pp. 144–145. Wiley Interscience, New York (1974).
14. P. W. van Loenwen and W. L. Groenwald, *J. Inorg. Nucl. Chem. Lett.* 1967, **3**, 145.
15. H. Oghakozorg and J. Summers, *Inorg. Chem.* 1982, **21**, 3903.
16. I. Singh, R. T. Ogata, R. E. Moore, C. W. J. Chang and P. J. Scheuer, *Tetrahedron* 1968, **24**, 6053.

17. D. B. Bruss and G. A. Harlow, *Analyt. Chem.* 1958, **30**, 1836.
18. G. Franchini, C. Preti, L. Tassi and G. Tosi, *Analyt. Chem.* 1988, **60**, 2358.
19. D. T. Sawyer and J. S. Valentine, *Accts Chem. Res.* 1961, **14**, 393.
20. V. Arancibia and M. Bodini, *An. Quim.* 1988, **84**, 26.
21. H. Dwain Coble and H. F. Holtzclaw Jr, *J. Inorg. Nucl. Chem.* 1974, **36**, 1049.
22. K. D. Magers, C. G. Smith and D. Sawyer, *Inorg. Chem.* 1980, **19**, 492.
23. V. Arancibia and M. Bodini, *An. Quim.* 1986, **82B**, 309.
24. M. Bodini and V. Arancibia, *Polyhedron* 1989, **8**, 1407.

Polyhedron Vol. 10, No. 16, pp. 1939–1949, 1991
Printed in Great Britain

0277-5387/91 $3.00+.00
Pergamon Press plc

PHOSPHOLE COMPLEXES OF GOLD(III) HALIDES: SYNTHESIS, STRUCTURE, ELECTROCHEMISTRY AND LIGAND REDISTRIBUTION REACTIONS

SAEED ATTAR and JOHN H. NELSON*

Department of Chemistry, University of Nevada, Reno, NV 89557, U.S.A.

and

WILLIAM H. BEARDEN

JEOL NMR Application Laboratory, Peabody, MA 91960, U.S.A.

and

NATHANIEL W. ALCOCK

Department of Chemistry, University of Warwick, Coventry CV4 7AL, U.K.

and

LJILJANA SOLUJIC' and EMIL B. MILOSAVLJEVIC'

Institute of Chemistry, Faculty of Sciences, University of Belgrade, 11001 Belgrade, Yugoslavia

(*Received* 26 *October* 1990; *accepted* 3 *May* 1991)

Abstract—The complexes $LAuCl_3$ [L = 1-phenyl-3,4-dimethylphosphole(DMPP), 1-phenyldibenzophosphole(DBP) and triphenylphosphine], $LAuBr_3$ (L = DBP, Ph_3P) and $LAuClBr_2$ (L = DBP, Ph_3P) were prepared and characterized by physical properties, cyclic voltammetry, far IR, $^{31}P\{^1H\}$ and CP/MAS $^{31}P\{^1H\}$ NMR spectroscopy. Ligand redistribution reactions of the types: $LAuCl + L'AuBr \rightleftharpoons L'AuCl + LAuBr$; $LAuCl_3 + LAuBr_3 \rightleftharpoons LAuCl_nBr_{3-n}$; $LAuCl_3 + L'AuBr_3 \rightleftharpoons LAuCl_nBr_{3-n} + L'AuCl_nBr_{3-n}$; and $LAuCl + L'AuBr_3 \rightleftharpoons LAuBr + L'AuCl + L'AuBr + LAuCl_nBr_{3-n} + L'AuCl_nBr_{3-n}$ all occur rapidly and have been studied by $^{31}P\{^1H\}$ NMR spectroscopy. These reactions all appear to proceed by way of halide-bridged intermediates. The solid state identities of $LAuClBr_2$ were established by a combination of far IR and CP/MAS $^{31}P\{^1H\}$ NMR spectroscopies and single crystal X-ray crystallography for Ph_3PAuBr_2Cl. The R_3PAuBr_2Cl complexes are substitutionally disordered, probably with two-thirds bromine and one-third chlorine in each site. Ph_3PAuBr_2Cl crystallized in the monoclinic space group $P2_1/c$ with $a = 9.086(2)$, $b = 11.410(2)$, $c = 18.734(4)$ Å, $\beta = 95.01°(2)$, and $Z = 4$. The structure was solved by least-squares methods with $R_F = 0.074$ for 1919 unique reflections with $I/\sigma(I) \geqslant 3.0$. The gold atom has nearly regular square-planar coordination with Au—P = 2.314(6) A° and Au—X = 2.399(3), 2.413(3) and 2.415(4) A°.

Solid-state nuclear magnetic resonance spectroscopy is attracting increasing interest in inorganic chemistry.[1] We and others have investigated the utility of CP/MAS $^{31}P\{^1H\}$ NMR spectroscopy for the solid-state characterization of phosphines,[2] phosphine-oxides, -sulphides and -selenides;[3] manganese, molybdenum and tungsten;[4] iron, ruthenium and osmium;[5] rhodium,[6,7] nickel,[8] palla-

* Author to whom correspondence should be addressed.

dium,[9-11] platinum,[9,10,12,13] copper,[14-25] silver,[26,27] gold,[28,29] cadmium[30] and mercury[31] phosphine complexes. These studies have shown that the ^{31}P chemical shift is very environmentally dependent and provides information concerning the phosphorus and metal site symmetries and the overall geometries of the complexes. The magnitudes of ^{1}J(CuP) and ^{1}J(AgP) allow determination of metal coordination numbers and metal–phosphorus bond distances. For the palladium, platinum, cadmium and mercury complexes, the magnitude of ^{2}J(PP) is a function of the PMP bond angles. Thus, for some complexes their $^{31}P\{^{1}H\}$ CP/MAS spectra can provide details of solid-state structures similar to those available from the more difficult to obtain EXAFS[32,33] measurements.

Gold(III) phosphine complexes of the type R_3PAuX_3 are prepared by oxidative addition of the appropriate halogen, X_2, to the gold(I) complexes R_3PAuX. Previous workers[34-37] have found that when the oxidative additions (reactions 1 and 2) were studied, highly crystalline homogeneous samples were obtained. In each case elemental analyses were consistent with the $R_3PAuXX'_2$ stoichiometries. NMR studies of these substances in solution[36,38] showed that halide redistribution[10] reactions occurred rapidly to produce all six of the possible compounds: R_3PAuCl_3, *cis*- and *trans*-R_3PAuCl_2Br, *cis*- and *trans*-$R_3PAuClBr_2$ and R_3PAuBr_3. These authors discussed the probable solid state identities suggesting that a mixture of R_3PAuCl_3 and R_3PAuBr_3,[37] pure R_3PAuXX_2[34,35] or a mixture of all six species[36] was present in the solid state. They also discussed the mechanism[36,38] of the halide redistribution. We have conducted a thorough study of the complexes of DMPP, DBP (see Struct. 1) and Ph_3P by solution $^{31}P\{^{1}H\}$ and CP/MAS $^{31}P\{^{1}H\}$ NMR, electrochemistry, far IR spectroscopy and X-ray crystallography to obtain a further insight into the solid state identities and ligand redistribution reactions.

$$R_3PAuCl + Br_2 \longrightarrow R_3PAuBr_2Cl \quad (1)$$

$$R_3PAuBr + Cl_2 \longrightarrow R_3PAuBrCl_2 \quad (2)$$

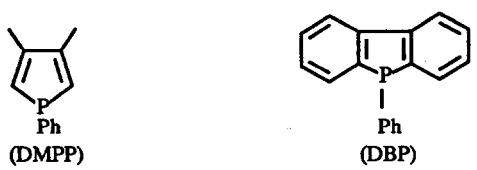

(DMPP) (DBP) 3

EXPERIMENTAL

(a) *Reagents and physical measurements*

All chemicals were reagent grade and were used as received or synthesized as described below. All solvents, when necessary, were dried by standard procedures and stored over Linde 4 Å molecular sieves. All reactions involving phosphines or phospholes were conducted under a nitrogen atmosphere. R_3PAuX,[29,34] 1-phenyl-3,4-dimethylphosphole[40](DMPP) and 1-phenyldibenzophosphole[41] (DBP) were prepared by literature methods.

Elemental analyses were performed by Galbraith Laboratories, Knoxville, TN. Melting points were determined on a Meltemp apparatus and are uncorrected. IR spectra were recorded on a Perkin–Elmer 1800 FT-IR instrument as polyethylene pellets. The solution $^{31}P\{^{1}H\}$ NMR spectra were recorded at 40.26 MHz on a JEOL FX-100 spectrometer in the FT mode. Typical acquisition conditions were 1 and 5 kHz spectral windows, acquisition times of 4 and 0.8 s, recycle time of 5 s; typically 5 to 10 k transients were collected with proton noise decoupling and 2 Hz line broadening was applied. A JEOL NM 5471 controller was used for temperature control and temperatures were measured with a calibrated platinum resistance thermometer. Chemical shifts were referenced to an external sample of PPh_3 in $CDCl_3$ ($\delta = -6$ ppm) and converted to an 85% H_3PO_4 reference with a positive value being downfield of the respective reference. Cross-polarization magic-angle-spinning (CP/MAS) $^{31}P\{^{1}H\}$ NMR spectra were obtained on a JEOL GX-270 wide bore spectrometer operating at 6.43 T (^{31}P at 109.25 MHz) using a 40 kHz sweep width, recycle delay time of 6 s, and a proton-decoupling field of 10 G. No line broadening was applied. Between 200 and 300 mg of the compound was spun at 4 kHz in Delrin or Kel-F rotors. All the CP/MAS chemical shifts were referenced to an external sample of Ph_3P ($\delta = -6.0$ ppm). The uncertainties in chemical shifts are estimated to be ± 0.5 ppm. Cyclic voltammetry was performed as previously described.[42]

(b) *Syntheses* $LAuCl_3$

The three $LAuCl_3$ (L = DBP, Ph_3P and DMPP) complexes were prepared by the same procedure. The following is exemplary. Chlorine gas was slowly bubbled through a $CHCl_3$ (20 cm^3) solution containing 0.25 g (0.51 mmol) DBPAuCl while the solution was magnetically stirred. The originally colourless solution turned bright yellow within a few seconds. This yellow solution was filtered, the solution volume was reduced to a few cm^3 by rotary evaporation, n-hexane was slowly added and the mixture was cooled to 0°C. The precipitate was isolated by filtration, washed with anhydrous diethyl ether, and vacuum dried to yield 0.24 g (82.8%) of orange crystals, m.p. 119–121°C.

Found: C, 38.5; H, 2.5. Calc. for $C_{18}H_{13}AuCl_3P$: C, 38.4; H, 2.3. Ph_3PAuCl_3,[37] yellow plates (58%), m.p. 179–181°C. DMPP $AuCl_3$, yellow powder (98%), m.p. 121–122°C. All three $LAuCl_3$ (L = DBP, Ph_3P, DMPP) complexes are photochemically and thermally unstable, decomposing even in the absence of light to black solids. The DMPP complex decomposes in 2 weeks and the Ph_3P complex decomposes in approx. 5 weeks.

$LAuBr_3$. The $LAuBr_3$ (L = DBP, Ph_3P) complexes were prepared in the same manner. The following is exemplary. To a solution containing 0.17 g (0.31 mmol) DBPAuBr in 20 cm^3 $CHCl_3$ was added 1.0 cm^3 of 0.34 M Br_2 in $CHCl_3$. The resulting dark red solution was magnetically stirred at ambient temperature for 3 h. The solution was then filtered, the filtrate reduced in volume to a few cm^3 by rotary evaporation, anhydrous diethyl ether was slowly added and the mixture was cooled to 0°C. The precipitate was isolated by filtration, washed with anhydrous diethyl ether, and vacuum dried to yield 0.15 g (68.2%) of burgundy-red crystals, m.p. 121–123°C. Found: C, 30.95; H, 2.17. Calc. for $C_{18}H_{13}AuBr_3P$: C, 31.0; H, 1.9. Ph_3PAuBr_3,[37] brick-red plates (92%) m.p. 149–150°C. Attempted preparation of (DMPP)$AuBr_3$ by the same procedure resulted in the formation of a black oil. The $^{31}P\{^1H\}$ NMR spectrum of this oil suggested the addition of Br_2 to the diene system of DMPP.[40,43]

$LAuClBr_2$. The $LAuClBr_2$ (L = DBP, Ph_3P) complexes were prepared in the same manner as for the $LAuBr_3$ complexes except that the starting material was LAuCl. DBPAuClBr$_2$ (84.2%), burgundy-red crystals, m.p. 128–130°C. Found: C, 32.8; H, 2.1. Calc. for $C_{18}H_{13}AuBr_2ClP$: C, 33.1; H, 2.0%. $Ph_3PAuClBr_2$ (52.1%) burgundy-red crystals, m.p. 162–164°C. Found: C, 32.7; H, 2.5. Calc. for $C_{18}H_{15}AuBr_2Cl$: C, 33.0, H, 2.3%.

(c) *Crystal structure analyses*

A 0.04 × 0.10 × 0.40 mm burgundy-red lath of Ph_3PAuBr_2Cl was selected from among the crystals formed by the reaction of Ph_3PAuCl with Br_2 in $CHCl_2/Et_2O$ in stoichiometric quantities. They were found to be only weakly diffracting. Intensity data were taken with a Nicolet $P2_1$ diffractometer in the θ–2θ mode and were corrected for Lorentz, polarization and absorption effects, the last by the Gaussian method. Systematic absences ($h01$, $1 \neq 2n$; $0k0$, $k \neq 2n$) indicated the $P2_1/c$ space group. The heavy atoms were located by Patterson techniques, and the light atoms were then found on successive Fourier syntheses. The three heavy Au ligand atoms were of equal height in Fourier syntheses, and were treated as Br, which gave satisfactory refinement. Substitution of Br by Cl cannot be excluded, and the relatively high thermal parameters of the Br atoms could be consistent with this [Ueq of Br (*trans* to Br) 0.0727 (10) (mean), of Br (*trans* to P) 0.0846 (15)]. This possibility is not testable by direct refinement because of the correlation of thermal parameters and occupancy; random substitution would be equivalent to 0.83 Br at each site. Anisotropic temperature factors were used for all non-hydrogen atoms. Hydrogen atoms were given fixed isotropic temperature factors, $u = 0.07$ Å^2 and were inserted at calculated positions and not refined. Final refinement was by cascaded least-squares methods [minimizing $\Sigma\omega(Fo-Fc)^2$]. The largest positive and negative peaks on final difference Fourier syntheses were of height (e Å^{-3}) +2 and −4 in the vicinity of the Au atom. A weighting scheme of the form $1/(\sigma^2(F)+gF^2)$ with $g = 0.0026$ was used and shown to be satisfactory by a weight analysis. Three standard reflections monitored every 200 reflections showed no regular changes during data collection. Final $R_F = 0.074$ and $R_{WF} = 0.078$. This rather high final figure is likely to result principally from approximations in measurement of the platy crystal, leading to an imprecise absorption correction, and the weakly diffracting crystals. Computing was with the SHEXTL system[44] on a Data General DG30 computer. Scattering factors were taken from ref. 45. $C_{18}H_{15}AuBr_2Cl$, M = 654.33, monoclinic, $a = 9.086(2)$, $b = 11.410(2)$, $c = 18.734(4)$ Å, $\beta = 95.01(2)°$, $U = 1934.8$ Å^3, space group $P2_1/c$, $Z = 4$, $D_c = 2.25$ g cm^{-3}, burgundy-red plates, μ(Mo–K_α) = 138.1 cm^{-1}, $\lambda = 0.71069$ Å, $F(000) = 1288$.

RESULTS AND DISCUSSION

(1) *Oxidative additions to* R_3PAuX *complexes*

Two-coordinate 14-electron d^{10} LAuX complexes may be expected to readily undergo oxidative addition reactions[46] to form four-coordinate 16-electron d^8 $LAuX_3$ complexes. Neither DBPAuCl nor Ph_3PAuCl react with CH_3I, BrCN, ICN or $ClCH_2CN$. In each case the R_3PAuCl complex was quantitatively recovered. However, the colourless DBPAuCl, Ph_3PAuCl and DMPPAuCl complexes each reacted with Cl_2 in $CHCl_3$ at ambient temperature to give the corresponding yellow LAuCl_3 complexes. All three complexes are photochemically and thermally unstable, eventually decomposing into black solids. The relative rates of decomposition are: $DMPPAuCl_3 > DBPAuCl_3 >$

Ph_3PAuCl_3, which is the order of decreasing ease of oxidation of the respective phosphorus donors. The colourless DBPAuBr and Ph_3PAuBr complexes reacted with Br_2 in $CHCl_3$ at ambient temperature to give the photochemically and thermally stable burgundy-red $DBPAuBr_3$ and Ph_3PAuBr_3 complexes. For DMPPAuBr, Br_2 in $CHCl_3$ not only oxidized gold(I) to gold(III) but also brominated the carbon–carbon double bonds[43] of DMPP leading to a complex mixture of 20 phosphorus containing species as a black oil. The colourless DBPAuI and Ph_3AuI when reacted with I_2 in $CHCl_3$ at ambient temperature formed black oils that gave single $^{31}P\{^1H\}$ NMR chemical shifts in $CDCl_3$ at $\delta = 31.8$ ppm (DBP) and 38.4 ppm (Ph_3P), which are identical[29] to those of DBPAuI and Ph_3PAuI, respectively. This is consistent with the observations that gold(III) complexes are reduced to gold(I) complexes by iodide.[47]

Both DBPAuCl and Ph_3PAuCl reacted with Br_2 in $CHCl_3$ at ambient temperature to form burgundy-red homogeneous appearing crystals of the corresponding $LAuClBr_2$ complexes, whose stoichiometry was evidenced by elemental analyses and these substances have narrow melting point ranges. However, DBPAuI and Ph_3PAuI reacted with Br_2 to form $DBPAuBr_3$ and Ph_3PAuBr_3, respectively, and DBPAuBr and Ph_3PAuBr reacted with Cl_2 to form $DBPAuCl_3$ and Ph_3PAuCl_3, respectively.

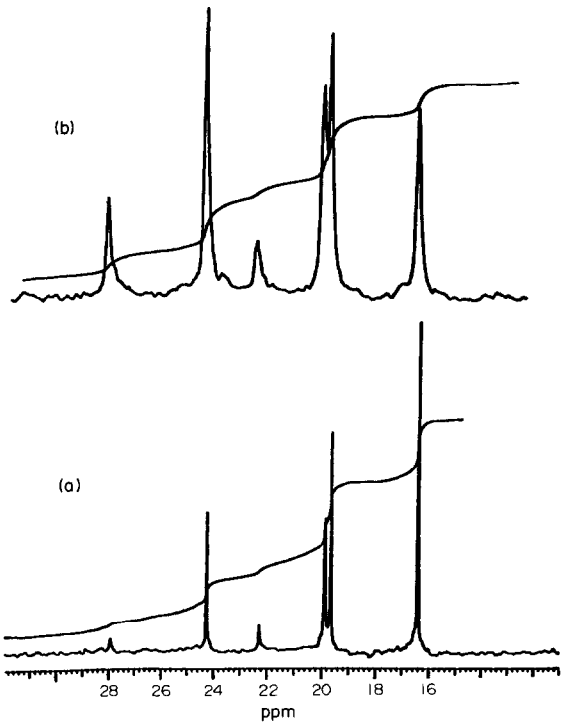

Fig. 1. 40.26 MHz $^{31}P\{^1H\}$ NMR spectra in $CDCl_3$ at 30°C for (a) $DBPAuClBr_2$ and (b) an equimolar mixture of $DBPAuCl_3$ and $DBPAuBr_3$. Assignments as follows: $DBPAuCl_3$ (27.9 ppm), *cis*-$DBPAuCl_2Br$ (24.2 ppm), *trans*-$DBPAuCl_2Br$ (22.3 ppm), *trans*-$DBPAuBr_2Cl$ (19.9 ppm), *cis*-$DBPAuBr_2Cl$ (19.6 ppm), $DBPAuBr_3$ (16.4 ppm).

(2) *Halide redistribution reactions*

Although the elemental analyses and melting point data for the $LAuClBr_2$ complexes would indicate that their solid state identity is as formulated, their $^{31}P\{^1H\}$ NMR spectra in $CDCl_3$ solution at 30°C [Fig. 1(a)] show the presence of more than one species in solution. For both complexes six phosphorus-containing species are present in solution. These species result from halide redistribution[39] reactions of the $LAuClBr_2$ complexes. The $^{31}P\{^1H\}$ NMR resonances are assigned as follows: $DBPAuCl_3$ (27.9 ppm), *cis*-$DBPAuCl_2Br$ (24.2 ppm), *trans*-$DBPAuCl_2Br$ (22.3 ppm), *trans*-$DBPAuBr_2Cl$ (19.9 ppm), *cis*-$DBPAuBr_2Cl$ (19.6 ppm) and $DBPAuBr_3$ (16.4 ppm). These assignments are based upon the chemical shifts of solutions of pure $DBPAuCl_3$ (28.3 ppm) and $DBPAuBr_3$ (16.8 ppm) in $CDCl_3$ at 30°C. We reason that the greater the *trans* influence[47–50] of the halide, the weaker the *trans* Au—P bond and the more upfield the ^{31}P chemical shift. Thus, we expect the ^{31}P chemical shift of *cis*-$DBPAuCl_2Br$ to be upfield of that of $DBPAuCl_3$ but downfield of that of *trans*-$DBPAuCl_2Br$. Also, if the halide redistribution reaction is nearly statistical as is often found for such reactions,[39] then the $DBPAuBr_2Cl$ complexes should be more abundant than the $DBPAuBrCl_2$ complexes and their corresponding ^{31}P resonances should be more intense. The $^{31}P\{^1H\}$ resonances for a $CDCl_3$ solution of Ph_3PAuBr_2Cl at 30°C were similarly assigned: Ph_3PAuCl_3 (42.9 ppm), *cis*-Ph_3PAuCl_2Br (38.3 ppm), *trans*-Ph_3PAuCl_2Br (38.1 ppm), *trans*-Ph_3PAuBr_2Cl (34.8 ppm), *cis*-Ph_3PAuBr_2Cl (33.0 ppm) and Ph_3PAuBr_3 (30.5 ppm).

Heaton and Kelsey[38] similarly observed by ^{31}P NMR spectroscopy that reaction of Cl_2 with Et_3PAuBr in $CHCl_3$ at 25°C resulted in the rapid formation of all six $Et_3PAuCl_nBr_{3-n}$ species but their assignments as to the relative chemical shifts of Et_3PAuCl_2Br and $Et_3PAuClBr_2$ differ from ours. They based their assignments on the systematic trends observed upon *cis*-substitution of chloride by bromide in mixed chloride/bromide platinum(IV) complexes. We believe that our assignments of the relative chemical shifts are more internally consistent than theirs and they are also consistent with the following observation. Figure 1(b) shows the

$^{31}P\{^{1}H\}$ NMR spectrum of a solution prepared from equimolar amounts of $DBPAuCl_3$ and $DBPAuBr_3$ in $CDCl_3$ immediately after mixing at 30°C. The same six species are present in this solution indicating that the halide redistribution reaction is rapid. For a solution of $DBPAuClBr_2$ the Br/Cl ratio is 2 : 1 but in a solution containing equimolar amounts of $DBPAuCl_3$ and $DBPAuBr_3$ the Br/Cl ratio is 1 : 1. Hence, the relative amounts of $DBPAuCl_2Br$ to $DBPAuClBr_2$ species in the latter solution should increase relative to those in the former. The ratio of the integrated intensities of the resonances ascribed to $DBPAuCl_2Br$ complexes to those ascribed to the DBPAu $ClBr_4$ complexes is 0.5 in Fig. 1(a) and 1.0 in Fig. 1(b), consistent with the relative molar ratio of the halides in the two solutions.

(3) *The mechanisms of halide redistribution*

The halide redistributions of $LAuBr_2Cl$ complexes could proceed by two alternative mechanisms: (1) catalysis by LAuCl[36] (reactions 3–6); or (2) simple halide redistribution (reaction 7).

$$LAuCl + Br_2 \longrightarrow LAuClBr_2 \quad (3)$$

$$LAuClBr_2 + LAuCl \longrightarrow LAuCl_2Br + LAuBr \quad (4)$$

$$LAuBr + Br_2 \longrightarrow LAuBr_3 \quad (5)$$

$$LAuCl + LAuCl_2Br \longrightarrow LAuCl_3 + LAuBr \quad (6)$$

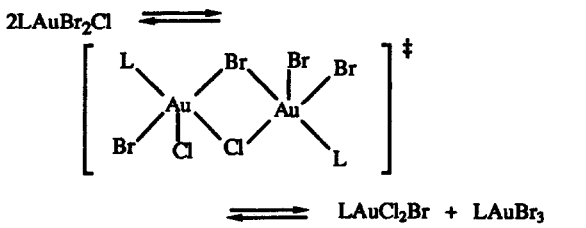

(7)

Reactions (3–6), were first suggested by Puddephatt and Thompson[36] on the basis of similarities with platinum(II) catalysed halide redistributions of platinum(IV) complexes. These reactions imply that the $LAuCl_2Br$ and $LAuClBr_2$ complexes are better oxidants than Br_2 or that they react with the gold(I) complexes faster than Br_2. We have therefore examined the electrochemical behaviour of the R_3PAuX and R_3PAuX_3 complexes most of which have not previously been reported.[51]

The redox potentials, determined by cyclic voltammetry in CH_2Cl_2 solution are given in Tables 1 and 2. All cyclic voltammograms were quasi-reversible.[52] As can be seen, the phosphine generally has a smaller effect on the reduction potential of $LAuX_3$ than on the oxidation potential of LAuX. But none of the effects on the redox potentials are very large.

Table 1. Electrochemical properties of some gold(I) complexes

Complex	E_p (V vs Fc^+/Fc)[a] $Au^I \rightarrow Au^{III}$	$Au^I \rightarrow Au^0$	Others
(DBP)AuCl	1.07	[b]	1.27[c]
(DBP)AuBr	1.03	[b]	1.20[c]
$(Ph_3P)AuCl$	1.13	−2.46	
$(Ph_3P)AuBr$	1.14	−2.52	

[a] Measured by cyclic voltammetry ($v = 200$ mV s^{-1}) in CH_2Cl_2 solution at a platinum working electrode, with 0.1 M tetrabutylammonium perchlorate as supporting electrolyte.

[b] Very near the cathodic limit of the solvent/electrolyte/electrode system used.

[c] Oxidation. The current for this process is less than that for the $Au^I \rightarrow Au^{III}$ oxidation. The two values (1.27 and 1.20 V) are close enough so that ligand (DBP) oxidation may be suggested. DPP (Differential Pulse Polarography) results agree very well with CVs.

For the sequence of reactions (3–6) to occur as redox reactions, the potentials for reactions (4) and (6) must be greater than zero. Although the reduction potentials of $LAuClBr_2$ and $LAuCl_2Br$ are not available, we may approximate them by the appropriate weighted averages of the potentials for the $LAuCl_3$ and $LAuB_3$ complexes.[53] Thus, the redox potential for $Ph_3PAuClBr_2 + 2e^- \rightarrow Ph_3P$

Table 2. Electrochemical properties of some gold(III) complexes

Complex	E_p (V vs Fc^+/Fc)[a] $Au^{III} \rightarrow Au^I$	$Au^I \rightarrow Au^0$	Others
$(DBP)AuCl_3$	−0.49	[b]	1.29[c,d]
$(DBP)AuBr_3$	−0.37	[b]	1.17[c,d]
$(Ph_3P)AuCl_3$	−0.49	−2.55	[e]
$(Ph_3P)AuBr_3$	−0.31	−2.54	1.34[c]

[a] Measured by cyclic voltammetry ($v = 200$ mV s^{-1}) in CH_2Cl_2 solution at a platinum working electrode, with 0.1 M tetrabutylammonium perchlorate as supporting electrolyte.

[b] Very near the cathodic limit of the solvent/electrolyte/electrode system used.

[c] Oxidation. The current for this process is less than that for other processes; see ref. 51.

[d] The closeness of these values may indicate DBP oxidation.

[e] Near the anodic limit.

$AuBr + Br^- + Cl^-$ is estimated to be -0.37 V vs Fc/Fc^+ or -0.03 V vs NHE as Fc/Fc^+ is 0.40 vs NHE. The redox potential[54] for $Br_2 + 2e^- \rightleftharpoons 2Br^-$ is 1.087 V. Thus, $Ph_3PAuClBr_2$ is a much poorer oxidant than Br_2. While this argument suggests that the gold(I) catalysed mechanism for halide scrambling is not likely to compete with oxidation by Br_2 it does not necessarily establish that a redox reaction between a gold(I) and a gold (III) species cannot take place. To test the latter possibility, a series of $^{31}P\{^1H\}$ NMR experiments were performed on $CDCl_3$ solutions containing equimolar mixtures of LAuX and $L'AuX_3$. Since the halides on both complexes are the same, no halide redistribution takes place. The $^{31}P\{^1H\}$ NMR spectrum of one such mixture (DBPAuCl plus Ph_3PAuCl_3) is shown in Fig. 2. All four possible species viz Ph_3PAuCl (32.4 ppm), DBPAuCl (24.0 ppm), Ph_3PAuCl_3 (42.8 ppm) and $DBPAuCl_3$ (27.9 ppm) are present in this solution. The same four species were found in the same relative amounts in a solution prepared from equimolar amounts of $DBPAuCl_3$ and Ph_3PAuCl. Similarly, $CDCl_3$ solutions of DBPAuBr plus Ph_3PAuBr_3 and $DBPAuBr_3$ plus Ph_3PAuBr each showed the presence of Ph_3PAuBr (34.5 ppm), Ph_3PAuBr_3 (30.5 ppm), DBPAuBr (26.6 ppm) and $DBPAuBr_3$ (16.3 ppm) in the same relative amounts. These reactions could be the result of phosphine redistribution[39] or of redox reactions. To ascertain if redox reactions are possible, we can crudely estimate[55] the electrochemical potential for one of these reactions. Consider the following half reactions (8 and 9):

$$Ph_3PAuCl_3 + 2e^- \longrightarrow Ph_3PAuCl + 2Cl^- \qquad E^0 = -0.49\,V \quad (8)$$

$$DBPAuCl + 2Cl^- \longrightarrow DBPAuCl_3 + 2e^- \qquad E^0 = +0.49\,V. \quad (9)$$

Thus, for reaction (10) $E^0 \cong 0.0$ V and from

$$Ph_3PAuCl_3 + DBPAuCl \rightleftharpoons DBPAuCl_3 + Ph_3AuCl, \quad (10)$$

$E^0 = -0.0295 \log K_{eq}$, we predict $K_{eq} \cong 1$ and the redox reaction (10) is thermodynamically feasible. Reaction (10) was found to occur rapidly and $K_{eq} = 0.76$, as measured by $^{31}P\{^1H\}$ NMR spectroscopy at 30°C in $CDCl_3$.

This result poses the interesting question as to what would be the products of reactions (11) and (12)?

$$Ph_3PAuCl + Ph_3PAuBr_3 \xrightarrow{?} \quad (11)$$

$$DBPAuBr + Ph_3PAuCl_3 \xrightarrow{?}. \quad (12)$$

In both these cases, halide redistribution as well as a redox reaction are conceptually possible. The results of $^{31}P\{^1H\}$ NMR assessments of these reactions are shown in Figs 3 and 4. As can be seen, complete ligand scrambling occurs in both cases. The assignments given in these figures are based upon comparisons with the ^{31}P chemical shifts of the pure LAuX and $LAuX_3$ complexes and the previous arguments for the $LAuBrCl_2$ and $LAuBr_2Cl$ complexes. The same equilibria were observed to occur for $CDCl_3$ solutions containing equimolar amounts of Ph_3PAuBr plus Ph_3PAuCl_3 and DBP AuCl plus $DBPAuBr_3$.

Since the two possible pathways of halide redistribution (reactions 3–6 or 7) would lead to the same products, both pathways might be operating in the absence of added halogen. This postulation is supported by the results of an additional series of $^{31}P\{^1H\}$ NMR experiments on equimolar mixtures of LAuX and $L'AuX_3'$. One such example was shown in Fig. 4 where complete ligand redis-

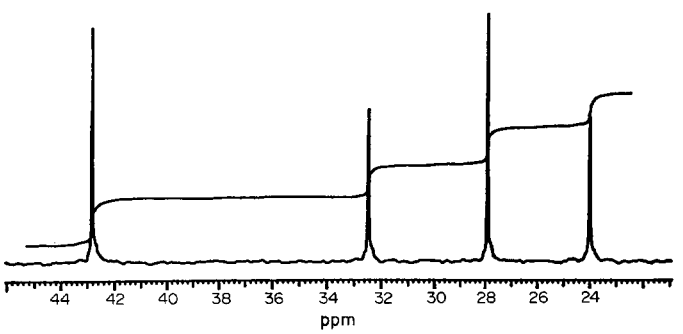

Fig. 2. 40.26 MHz $^{31}P\{^1H\}$ NMR spectrum of an equimolar mixture of DBPAuCl and Ph_3PAuCl_3 in $CDCl_3$ at 30°C. Assignments as follows: Ph_3PAuCl_3 (42.8 ppm), Ph_3PAuCl (32.4 ppm), $DBPAuCl_3$ (27.9 ppm), DBPAuCl (24.0 ppm).

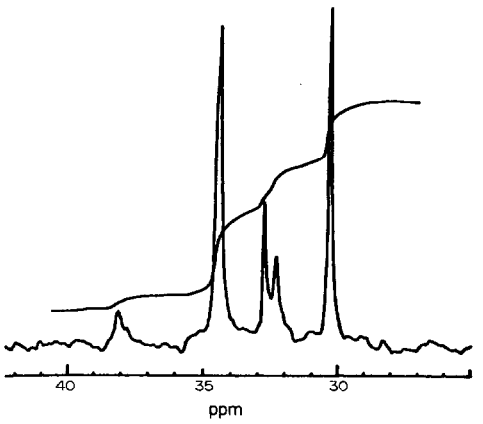

Fig. 3. 40.26 MHz $^{31}P\{^1H\}$ NMR spectrum of an equimolar mixture of Ph_3PAuCl and Ph_3PAuBr_3 in $CDCl_3$ at 30°C. Assignments as follows: *cis*-Ph_3PAuCl_2Br (38.3 ppm), *trans*-Ph_3PAuCl_2Br (37.9 ppm), Ph_3PAuBr (34.5 ppm), *cis*-$Ph_3PAuClBr_2$ (32.9 ppm), Ph_3PAuCl (32.4 ppm), Ph_3PAuBr_3 (30.4 ppm).

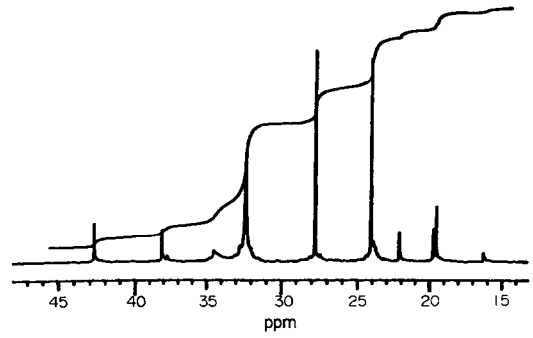

Fig. 4. 40.26 MHz $^{31}P\{^1H\}$ NMR spectrum of an equimolar mixture of DBPAuBr and Ph_3PAuCl_3 in $CDCl_3$ at 30°C. Assignments as follows: Ph_3PAuCl_3 (42.7 ppm), *cis*-Ph_3PAuCl_2Br (38.1 ppm), *trans*-Ph_3PAuCl_2Br (37.8 ppm), Ph_3PAuBr (34.5 ppm), *cis*-$Ph_3PAuClBr_2$ (32.8 ppm), Ph_3PAuCl (32.4 ppm), DBPAuCl$_3$ (27.8 ppm), *cis*-DBPAuCl$_2$Br (24.1 ppm), DBPAuCl (23.9 ppm), *trans*-DBPAuCl$_2$Br (22.1 ppm), *trans*-DBPAuClBr$_2$ (19.5 ppm), *cis*-DBPAuClBr$_2$ (19.5 ppm), DBPAuBr$_3$ (16.2 ppm).

tribution is evident. Ph_3PAuBr plus DBPAuCl$_3$, Ph_3PAuCl plus DBPAuBr$_3$, and DBPAuCl plus Ph_3PAuBr_3 mixtures gave similar results. In each case 12–14 species with the same chemical shifts as given in Fig. 5 and with intensities varying in direct proportion to the varying ligand ratios were observed. In no case were the anticipated 16 resonances observed because of coincidentally equal chemical shifts for some of the species.

Furthermore, complete ligand redistribution was observed for a solution containing an equimolar ratio of Ph_3PAuCl_3 and DBPAuBr$_3$ (Fig. 5). The same species were also found in the same relative amounts for an equimolar mixture of Ph_3PAuBr_3 and DBPAuCl$_3$.

Ligand redistribution also occurs among gold(I) complexes [reaction (13), Fig. 6]. As is evident by the line widths and temperature dependence of this spectrum, the redistributions among gold(I) species are more rapid than those among gold(III) species. Note also that the rate of halide redis-

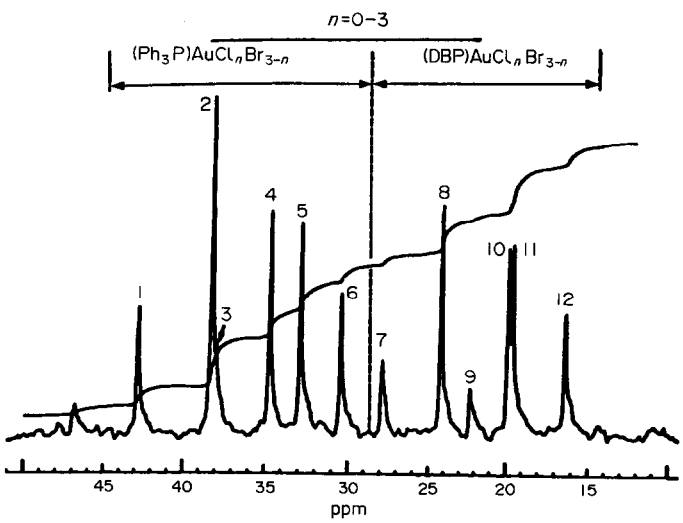

Fig. 5. 40.26 MHz $^{31}P\{^1H\}$ NMR spectrum of an equimolar mixture of Ph_3PAuCl_3 and DBPAuBr$_3$ in $CDCl_3$ at 30°C. Assignments as follows: Ph_3PAuCl_3 (42.9 ppm), *cis*-Ph_3PAuCl_2Br (38.3 ppm), *trans*-Ph_3PAuCl_2Br (38.0 ppm), *trans*-$Ph_3PAuClBr_2$ (34.7 ppm), *cis*-$Ph_3PAuClBr_2$ (32.9 ppm), Ph_3PAuBr_3 (30.5 ppm), DBPAuCl$_3$ (27.9 ppm), *cis*-DBPAuCl$_2$Br (24.3 ppm), *trans*-DBPAuCl$_2$Br (22.3 ppm), *trans*-DBPAuClBr$_2$ (19.9 ppm), *cis*-DBPAuClBr$_2$ (19.6 ppm), DBPAuBr$_3$ (16.5 ppm).

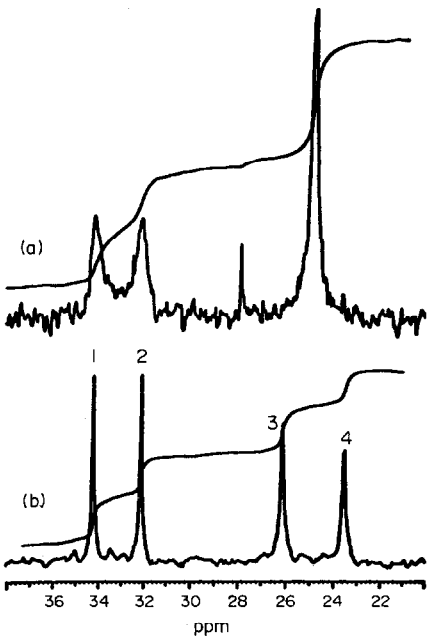

Fig. 6. 40.26 MHz $^{31}P\{^1H\}$ NMR spectra of an equimolar mixture of Ph_3PAuCl and DBPAuBr in $CDCl_3$ at (a) 30°C and (b) −13°C. Assignments as follows: Ph_3P AuBr (34.3 ppm), Ph_3PAuCl (32.2 ppm), DBPAuBr (26.2 ppm), DBPAuCl (23.6 ppm).

tribution is faster for DBPAuX than for Ph_3PAuX species, suggesting that DBP has a greater *trans*-effect than Ph_3P. The same result was observed for an equimolar mixture of Ph_3PAuBr and DBP AuCl.

$$Ph_3PAuCl + DBPAuBr \rightleftharpoons Ph_3PAuBr + DBPAuCl \quad (13)$$

We believe that all of these equilibrium redistribution reactions involve halide-bridged intermediates,[39] similar to that shown in reaction (7). No ionic species such as $[(Ph_3P)(DBP)Au]^+$ or $[(Ph_3P)(DBP)AuX_2]^+$ were ever observed in any of these solutions. Addition of Ph_3P or DBP to solutions containing $LAuX_3$ (L = Ph_3P, DBP; X = Cl, Br) resulted in immediate redox reactions [see eq. (14)]. These results suggest that very little, if any, free Ph_3P or DBP is present during the course of the ligand redistribution reactions. The kinetics and mechanism[56] of the redistribution reactions of pentacoordinate complexes of the type [Au(N ~ N)$(CN)_2$X](N ~ N is a 1,10-phenanthroline; X = Cl, Br) have been described. Anion redistribution of $Ph_3PAuC{\equiv}CPh$ complexes have also been described.[57]

$$Ph_3P + DBPAuCl_3 \longrightarrow Ph_3PCl_2 + DBPAuCl \quad (14)$$

(4) *The solid state identity of* $LAuClBr_2$

The isolated products of the reactions of Ph_3PAuCl and DBPAuCl with Br_2 appear to be homogeneous crystalline substances with narrow melting point ranges and elemental analyses agreeing with the $LAuClBr_2$ composition. However, their $^{31}P\{^1H\}$ NMR spectra in $CDCl_3$ at 30°C show the presence of all six $LAuCl_nBr_{3-n}$ species. Mann and Purdie[34] suggested that only *trans*-$Et_3PAuXX'_2$ is present in the solid state. Williamson and Baird[35] suggested that a mixture of *cis*- and *trans*-LAu $ClBr_2$(L = Ph_3P, Et_3P) is present in the solid state. Puddephatt and Thompson[36] suggested that all six $LAuCl_nBr_{3-n}$ species are present and McAuliffe *et al.*[37] suggested that the solid state products are mixtures of $LAuCl_3$ and $LAuBr_3$ in appropriate proportions. The simplest interpretation of the far IR spectroscopic data (Table 3) is that $LAuBr_3$ and $LAuCl_3$ are present in a 2:1 ratio. This interpretation rests on the fact that the two $LAuClBr_2$ (L = DBP, Ph_3P) complexes show ν(AuCl) and ν(AuBr) vibrations at essentially the same frequencies as those of $LAuCl_3$ and $LAuBr_3$. If the mixed halide species were present in the solid state the ν(AuCl) and ν(AuBr) vibrations for them would be expected to occur at different frequencies, as has been found for HgX_2, HgXX', HgX_2' systems.[58] The CP/MAS $^{31}P\{^1H\}$ NMR spectra (Fig. 7) of the two $LAuClBr_2$ complexes each show two major resonances in a 2:1 intensity ratio (L = Ph_3P, 41.0

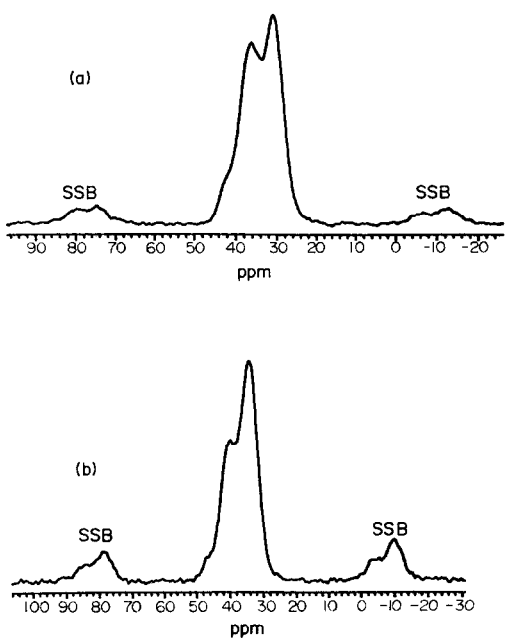

Fig. 7. 109.25 MHz CP/MAS $^{31}P\{^1H\}$ NMR spectra of (a) $DBPAuClBr_2$ and (b) $Ph_3PAuClBr_2$. SSB are spinning sidebands.

Table 3. Gold(III)–halogen stretching frequencies[a] for the $LAuX_3$ and $LAuXX'_2$ complexes[b]

Complex		ν(X—Au—X) (asymm.)[c]	ν(Au—X) (*trans* to L)
(DBP)$AuCl_3$		366	318
(DBP)$AuBr_3$		260	219
(BBP)$AuClBr_2$	Cl:	365	322
	Br:	261	224
$(Ph_3P)AuCl_3$		366, (371)[d] (361)[e]	307, (311)[d] (300)[e]
$(Ph_3P)AuBr_3$		261, (264)[d] (258)[e]	225, (222)[d] (215)[e]
$(Ph_3P)AuClBr_2$	Cl:	366, (347)[d]	310, (313)[d] (301)[e]
	Br:	259, (261)[d] (255)[e]	220, (216)[d]

[a] ν(Au—X) in cm^{-1}.

[b] Recorded as polyethylene pellets.

[c] Refers to the asymmetric (higher energy) as opposed to symmetric (lower energy) stretch of the X—Au—X unit.

[d] From ref. 35, recorded as Nujol mulls mounted between polyethylene discs.

[e] From ref. 37, as Nujol mulls.

and 34.4 ppm; L = DBP, 36.9 and 31.1 ppm). These compare with the CP/MAS $^{31}P\{^1H\}$ NMR spectra of pure Ph_3PAuCl_3 (46.9 ppm), Ph_3PAuBr_3 (36.2 ppm), $DBPAuCl_3$ (42.2 ppm) and $DBPAuBr_3$ (30.5 ppm). Each of these resonances have line widths ($\Delta\nu(1/2)$ ~480 Hz or ~4.4 ppm). We have previously shown that the CP/MAS ^{31}P chemical shift is very environmentally dependent.[9,10,12,29] If $Ph_3PAuCl_nBr_{3-n}$ existed in the solid state with randomly disordered halides, we might expect to see three ^{31}P chemical shifts spanning a range of about 8 ppm. These three resonances would represent Ph_3PAuBr_3 (29.6%), *cis*-Ph_3PAuBr_2Cl (29.6%) plus *trans*-Ph_3PAuBr_2Cl (14.8%) and *cis*-Ph_3AuCl_2Br (14.8%). Given the large CP/MAS line widths together with their lower relative abundances resonances for *trans*-Ph_3PAuCl_2Br (7.4%) and Ph_3PAuCl_3 (3.7%) would probably not be observed (see Fig. 1 for comparison). If only *trans*-Ph_3PAuBr_2Cl was present, only one ^{31}P chemical shift would be observed. Finally, if the solid were a mixture of *cis*- and *trans*-Ph_3PAuBr_2Cl or a mixture of Ph_3PAuCl_3 and Ph_3PAuBr_3, then two resonances should be observed. In the latter case their relative intensities would be 2:1. The observation of three resonances (two major and a minor shoulder) in the CP/MAS ^{31}P NMR spectra (Fig. 7) suggests that these solids probably contain randomly disordered halides.

As further evidence, the X-ray crystal structure of Ph_3PAuBr_2Cl (Fig. 8) was obtained. No inhomogeneity was observable in the crystalline sample. Microscopic observation shows that crystals of Ph_3PAuBr_2Cl are medium-red and those of Ph_3PAuBr_3 are deeper red and that they have different morphologies; they show similar platy morphologies, though the first species gives almost rectangular plates, while crystals of the tribromide are generally diamond-shaped. For Ph_3PAuBr_2Cl the three halides were almost identical in electron density, implying approximately equal substitution of Br by Cl at each site. Bond distances and angles are given in Table 4. Ph_3PAuBr_2Cl is a nearly regular square-planar complex. The two Au—X bonds *trans* to each other [2.399(3) and 2.413(3) Å] are essentially the same length as the Au—X bond *trans* to Ph_3P [2.415(4) Å]. The corresponding distances

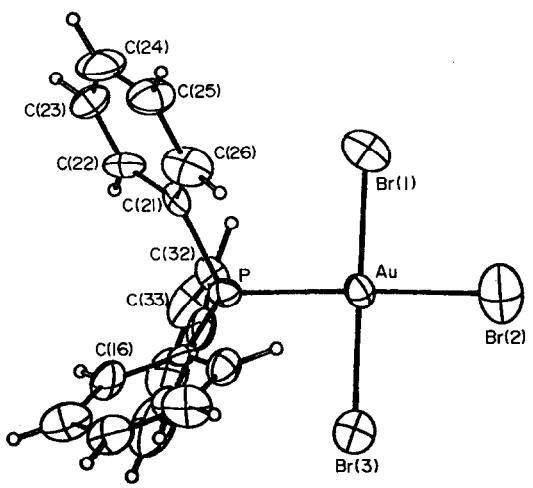

Fig. 8. View of Ph_3PAuBr_2Cl showing the atom labelling scheme; 50% probability ellipsoids. Atoms labelled Br are considered to be substitutionally disordered with approximately 2/3 Br and 1/3 at each site.

Table 4. Selected structural parameters for [$(Ph_3P)AuBr_2Cl$]

Bond lengths (Å)[a]			
Au—Br(1)	2.399(3)	Au—Br(2)	2.415(4)
Au—Br(3)	2.413(3)	Au—P(1)	2.314(6)
P(1)—C(1)	1.794(22)	P(1)—C(21)	1.825(22)
P(1)—C(31)	1.823(26)	Ph: C—C(ave)	1.391(46)
Bond angles (°)			
Br(1)—Au—Br(2)	88.9(1)	Br(1)—Au—Br(3)	177.3(1)
Br(2)—Au—Br(3)	91.1(1)	Br(1)—Au—P(1)	92.6(2)
Br(2)—Au—P(1)	177.2(2)	Br(3)—Au—P(1)	87.3(2)
Au—P(1)—C(11)	112.7(7)	Au—P(1)—C(21)	116.0(7)
C(11)—P(1)—C(21)	102.0(9)	Au—P(1)—C(31)	104.1(8)
C(11)—P(1)—C(31)	111.1(11)	C(21)—P(1)—C(31)	111.1(11)
Ph: C—C—C(ave)	120.0(30)		

[a] Note: the atoms labelled Br are considered to be substitutionally disordered with approximately 2/3 Br and 1/3 Cl at each site.

in Ph_3PAuCl_3[59] [2.273(4), 2.282(4) and 2.347(4) Å] and Et_3PAuBr_3[60] [2.407(1), 2.416(1) and 2.468(1) Å] show that in these complexes the bond *trans* to the phosphine is lengthened because of the high *trans* influence[48–50] of the phosphine. The fact that the Au—X bond *trans* to Ph_3P in Ph_3PAuBr_2Cl is not lengthened to a similar extent suggests greater substitution of Cl for Br in this site, which is consistent with its rather higher apparent thermal parameter.

Acknowledgements—The financial support of the UNR Research Advisory Board and the donors of the Petroleum Research Fund, administered by the American Chemical Socity is gratefully acknowledged.

NOTES AND REFERENCES

1. N. J. Clayden, *Chem. Scr.* 1988, **28**, 211.
2. G. H. Penner and R. E. Wasylishen, *Can. J. Chem.* 1989, **67**, 1909.
3. J. B. Robert and L. Wiesenfeld, *Molec. Phys.* 1981, **44**, 319.
4. E. Lindner, R. Fawzi, H. A. Mayer, K. Eichle and K. Pohmer, *Inorg. Chem.* 1991, **30**, 1102.
5. A. J. Carty, C. A. Fyfe, M. Lettinga, S. Johnson and L. H. Randall, *Inorg. Chem.* 1989, **28**, 4120.
6. J. W. Diesveld, E. M. Menger, H. T. Edzes and W. S. Veeman, *J. Am. Chem. Soc.* 1980, **102**, 7935.
7. A. Naito, D. L. Sastry and C. A. McDowell, *Chem. Phys. Lett.* 1985, **115**, 19.
8. R. Benn, R. Mynott, I. Topalovic and F. Scott, *Organometallics* 1989, **8**, 2299.
9. J. H. Nelson, J. A. Rahn and W. H. Bearden, *Inorg. Chem.* 1987, **26**, 2192.
10. J. A. Rahn, D. J. O'Donnell, A. R. Palmer and J. H. Nelson, *Inorg. Chem.* 1989, **28**, 2631.
11. G. Bodenhausen, J. A. Deli, A. Clements and P. S. Pregosin, *Inorg. Chim. Acta* 1983, **77**, L17.
12. J. A. Rahn, L. Baltusis and J. H. Nelson, *Inorg. Chem.* 1990, **29**, 750.
13. L. Bemi, H. C. Clark, J. A. Davies, C. A. Fyfe and R. E. Wasylishen, *J. Am. Chem. Soc.* 1982, **104**, 438.
14. G. A. Bowmaker, J. D. Cotton, P. C. Healy, J. D. Kildea, S. D. Silong, B. W. Skelton and A. H. White, *Inorg. Chem.* 1989, **28**, 1462.
15. D. A. Edwards and R. Richards, *Spectrochim. Acta* 1978, **34A**, 167.
16. G. A. Bowmaker and D. A. Rogers, *J. Chem. Soc., Dalton Trans.* 1984, 1249.
17. G. A. Bowmaker, J. C. Dyason, P. C. Healy, L. M. Engelhardt, C. Pakawatchai and A. H. White, *J. Chem. Soc., Dalton Trans.* 1987, 1089.
18. G. A. Bowmaker, L. M. Englehardt, P. C. Healy, J. D. Kildea, R. I. Papasergio and A. H. White, *Inorg. Chem.* 1987, **26**, 3533.
19. E. M. Menger and W. S. Veeman, *J. Magn. Reson.* 1982, **46**, 257.
20. P. F. Barron, J. C. Dyason, L. M. Engelhardt, P. C. Healy and A. H. White, *Inorg. Chem.* 1984, **23**, 3766.
21. J. C. Dyason, P. C. Healy, L. M. Engelhardt, C. Pakawatchai, V. A. Patrick and A. H. White, *J. Chem. Soc., Dalton Trans.* 1985, 831.
22. P. E. Barron, J. C. Dyason, P. C. Healy, L. M. Engelhardt, C. Pakawatchai, V. A. Patrick and A. H. White, *J. Chem. Soc., Dalton Trans.* 1987, 1099.
23. P. F. Barron, J. C. Dyason, L. M. Engelhardt, P. C. Healy and A. H. White, *Aust. J. Chem.* 1985, **38**, 261.
24. S. Attar, G. A. Bowmaker, N. W. Alcock, J. S. Frye, W. H. Bearden and J. H. Nelson, *Inorg. Chem.* 1991, **30**.

25. G. A. Bowmaker, A. Camus, P. C. Healy, B. W. Skelton and A. H. White, *Inorg. Chem.* 1989, **28**, 3883.
26. P. F. Barron, J. C. Dyason, P. C. Healy, L. M. Engelhardt, B. W. Skelton and A. H. White, *J. Chem. Soc., Dalton Trans.* 1986, 1965.
27. S. Attar, N. W. Alcock, G. A. Bowmaker, J. S. Frye, W. H. Bearden and J. H. Nelson, *Inorg. Chem.* 1991, **30**.
28. P. F. Barron, L. M. Engelhardt, P. C. Healy, J. Oddy and A. H. White, *Aust. J. Chem.* 1987, **40**, 1545.
29. S. Attar, W. H. Bearden, N. W. Alcock, E. C. Alyea and J. H. Nelson, *Inorg. Chem.* 1990, **29**, 425.
30. J. M. Kessler, J. H. Reeder, R. Vac, C. Yeung, J. H. Nelson, J. S. Frye and N. W. Alcock, *Mag. Reson. Chem.* 1991, **29**.
31. T. Allman and R. E. Lenkinski, *Inorg. Chem.* 1986, **25**, 3202.
32. E. A. V. Ebsworth, D. W. H. Rankin and S. Cradock, *Structural Methods in Inorganic Chemistry*, Ch. 1 and 8. Blackwell Scientific Publications, Oxford (1987).
33. B. K. Teo and D. C. Joy, *EXAFS Spectroscopy, Techniques and Applications.* Plenum, New York (1981).
34. F. G. Mann and D. Purdie, *J. Chem. Soc.* 1940, 1235.
35. D. R. Williamson and M. C. Baird, *J. Inorg. Nucl. Chem.* 1972, **34**, 3393.
36. R. J. Puddephatt and P. J. Thompson, *J. Chem. Soc., Dalton Trans.* 1975, 1810.
37. C. A. McAuliffe, R. V. Parish and P. D. Randall, *J. Chem. Soc., Dalton Trans.* 1979, 1730.
38. B. T. Heaton and R. J. Kelsey, *Inorg. Nucl. Chem. Lett.* 1975, **11**, 363.
39. J. A. Rahn, M. S. Holt and J. H. Nelson, *Polyhedron* 1989, **8**, 897.
40. A. Breque, F. Mathey and P. Savignac, *Synthesis* 1981, 983.
41. S. Affandi, R. L. Green, B. T. Hsieh, M. S. Holt, J. H. Nelson and E. C. Alyea, *Synth. React. Inorg. Met.-Org. Chem.* 1987, **17**, 307.
42. E. B. Milosavljevic', Lj. Solujic', D. W. Krassowski and J. H. Nelson, *J. Organomet. Chem.* 1988, **352**, 177.
43. F. Mercier, S. Holland and F. Mathey, *J. Organomet. Chem.* 1986, **316**, 271.
44. G. M. Sheldrick, *SHEXTL User Manual.* Nicolet, Madison, Wisconsin (1983).
45. *International Tables for X-ray Crystallography*, Vol. IV. Kynoch, Birmingham (1974).
46. For oxidative additions of alkyl halides to gold(I) complexes see: R. G. Pearson and P. E. Figdore, *J. Am. Chem. Soc.* 1980, **102**, 1541; A. Tanaki and J. K. Kochi, *J. Chem. Soc., Dalton Trans.* 1973, 2620; A. Johnson and R. J. Puddephatt, *J. Organomet. Chem.* 1975, **85**, 115.
47. L. I. Elding and L. H. Skibsted, *Inorg. Chem.* 1986, **25**, 4084.
48. T. G. Appleton, H. C. Clark and L. E. Manzer, *Coord. Chem. Rev.* 1973, **10**, 335.
49. M. M. Gofman and V. I. Nefedov, *Inorg. Chim. Acta* 1978, **28**, 1.
50. J. K. Burdett and T. A. Albright, *Inorg. Chem.* 1979, **18**, 2112.
51. J. E. Anderson, S. M. Sawtelle and C. E. McAndrews, *Inorg. Chem.* 1990, **29**, 2627. [Have just shown that electrochemical oxidation of Ph_3PAuCl in CH_2Cl_2 under similar conditions is quasi-reversible ($E_{pa} = 1.22$ V vs Fc/Fc^+) and proceeds by an ECE(C) process, see *Electrochemical Methods* (Edited by A. J. Bard and L. R. Faulkner). John Wiley & Sons, New York, 1980, pages vii–xvi for a list of abbreviations.]
52. P. H. Rieger, *Electrochemistry*, p. 322 ff. Prentice-Hall, Englewood Cliffs, New Jersey (1987).
53. Ligand additivity effects on the redox potentials of transition metal coordination and organometallic compounds have been widely observed. See for example: P. Lemoine, M. Gross, P. Braunstein, F. Mathey, D. Deschamps and J. H. Nelson, *Organometallics* 1984, **3**, 1303; D. Riley and J. Lyon III, *J. Chem. Soc., Dalton Trans.* 1991, 157; A. B. P. Lever, *Inorg. Chem.* 1990, **29**, 1271. The subject has also been treated theoretically: B. E. Bursten, *J. Am. Chem. Soc.* 1982, **104**, 1299.
54. J. E. Huheey, *Inorganic Chemistry, Principles of Structure and Reactivity* 3rd edn, p. A50. Harper and Row, New York (1983).
55. See reference 43, page 334.
56. L. Catalini, M. Giampaolo, G. Paolucci, B. Pitteri and M. L. Tobe, *Inorg. Chem.* 1987, **26**, 2450.
57. R. J. Cross and M. F. Davidson, *J. Chem. Soc., Dalton Trans.* 1986, 411.
58. R. L. Ammlung and T. B. Brill, *Inorg. Chim. Acta* 1974, **11**, 201.
59. G. Bandoli, D. A. Clemente, G. Marangoni and L. Cattalini, *J. Chem. Soc., Dalton Trans.* 1973, 886.
60. D. S. Eggleston, D. F. Chodosh, D. T. Hill and G. R. Girard, *Acta Cryst.* 1984, **C40**, 1357.

Polyhedron Vol. 10, No. 16, pp. 1951–1953, 1991
Printed in Great Britain

0277–5387/91 $3.00+.00
© 1991 Pergamon Press plc

COMMUNICATION

SYNTHESIS AND STRUCTURE OF STABLE INDIUM AND GALLIUM COMPLEXES OF (*R*)-1,4,7-TRIS(2′-METHYLCARBOXYMETHYL)-TRIAZACYCLONONANE

ROBERT C. MATTHEWS and DAVID PARKER*

Department of Chemistry, University of Durham, South Road, Durham DH1 3LE, U.K.

and

GEORGE FERGUSON and BRANKO KAITNER†

Department of Chemistry, University of Guelph, Guelph, Canada N1G 2W1

and

ALICE HARRISON and LOUISE ROYLE

MRC Radiobiology Unit, Chilton, Didcot OX11 0RD, U.K.

(*Received* 12 *June* 1991; *accepted* 28 *June* 1991)

Abstract—The title ligand forms stable neutral complexes with gallium and indium and the structure of the latter has been studied by X-ray crystallography.

Kinetically stable complexes of indium and gallium are being examined for use as imaging agents in diagnostic nuclear medicine (^{67}Ga,γ,$t_{1/2}$ = 3.25 days; ^{68}Ga,β^+,$t_{1/2}$ = 68 min; ^{111}In,γ,$t_{1/2}$ = 2.83 days).[1] In order for these complexes to be used *in vivo* they should resist acid (or cation) mediated decomplexation in the pH range 2–8. The synthesis of a set of C- and N-functionalized macrocyclic ligands based on 1,4,7-triazacyclononane triacetic acid that may be attached to tumour-localizing antibodies and rapidly radiolabelled with indium or gallium isotopes has been reported.[2,3] The structures of a hexacoordinate gallium complex of the parent ligand 1,4,7-triazacyclononane triacetate and of its heptacoordinate chloroindium complex have been defined recently.[4,5] A good model for the N-functionalized ligands **2** and **3** is the chiral triacid **1**. The synthesis and preliminary complexation behaviour of this ligand is reported together with the first structural analysis of a hexacoordinate neutral indium complex which has non-crystallographic C_3 symmetry.

Reaction of 1,4,7-triazacyclononane with (*S*)-2-

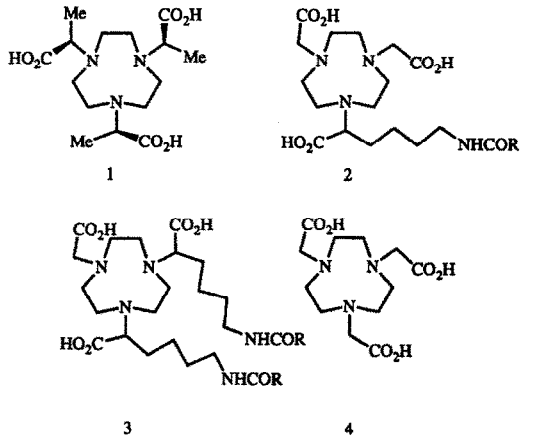

* Author to whom correspondence should be addressed.

† Visiting Professor from Laboratory for General and Inorganic Chemistry, Faculty of Science, University of Zagreb, 41000 Zagreb, Yugoslavia.

Table 1. Protonation constants for **1** and **4** and binding constants (298 K, H_2O, I = 0.1 Me_4NNO_3)[a]

Ligand	pK_1	pK_2	pK_3	$\log K_{CaL}$	$\log K_{CaLH}$	$\log K_{CuLH}$[b]
1	11.2	6.10	3.48	10.8	5.75	2.9
4[c]	11.7	5.74	3.16	8.92	5.06	2.77

[a] Determined by pH-metric analysis with SCOGS2.
[b] From spectrophotometric analysis of the 750 nm $(CuL)^-$ and 660 nm (HCuL) bands.
[c] Data from ref. 7.

chloropropanoic acid in the presence of lithium hydroxide yielded the triacid (*R*)-**1** which was purified by chromatography on alumina as its trimethyl ester ($MeOH/H_2SO_4$ followed by HCl/6 M, 18 h, 120°C). The ligand exhibits similar protonation and complexation behaviour to **4** (Table 1).[6]

The ^{67}Ga complex of **1** was prepared (pH 5, 37°C, 15 min) by admixture of **1** and gallium-67 trichloride (as a solution in 150 mM HCl). Analysis by anion exchange HPLC with radiometric detection revealed that 99.2% of the activity was associated with the neutral gallium complex (**1** · Ga) following addition of an excess of DTPA (Hichrom AX300, elutant 0.2 M NH_4OAc/10% MeCN; $t_R = 4.1$ min). The biodistribution of the (**1** · ^{67}Ga) complex in mice was examined and revealed that > 99% of the activity had been excreted after 24 h, consistent with the high *in vivo* stability of the complex. The (**1** · ^{71}Ga) complex may also be observed in 6 M HNO_3 by ^{71}Ga NMR ($\delta_{Ga} = +149$ ppm).

The neutral indium complex [(*R*)-**1** · In], prepared at pH 1 following admixture of equimolar quantities of **1** and aqueous indium trinitrate solution crystallized slowly from solution. The microanalysis suggested that crystallization occurred with one molecule of water. The crystal structure* revealed that the indium was tightly bound by the nitrogen and oxygen donors, with shorter In—O and In—N bond lengths than any reported previously in analyses of indium complexes with tribasic ligands.[5,7-9] The coordination geometry of the indium atom is a distorted trigonal prism in which the angle of distortion from a regular trigonal prism is 20.8°(2) (*cf.* 60° for an octahedral complex). This value is similar to that found for the ferric complex of **4** (25.2°).[10] The indium complex is apparently much less soluble in water (pH 1–8) than (In · **4**) or (Ga · **4**) perhaps due to the less effective solvation of the more lipophilic complex.

*Crystal data for [(*R*)-In · **1**] $C_{15}H_{42}InN_3O_6$, 0.9 (H_2O): $M = 473.4$, cell dimensions $a = 6.679(2)$, $b = 15.551(3)$, $c = 17.361(3)$ Å, $U = 1803.1(7)$ Å^3, $D_c = 1.744$ g cm^{-3}, $Z = 4$, $F(000) = 964$, Mo-K_α radiation ($\lambda = 0.70903$ Å), $\mu = 13.3$ cm^{-1}. Orthorhombic space group $P22_12_1$ uniquely from the systematic absences. Data collected to a maximum 2θ of 54° and corrected for Lorentz, polarization and absorption effects. 2267 independent reflections measured of which the 1973 with $I > 2.5\sigma(I)$ were labelled observed and used in the analysis. The structure was solved by the heavy-atom method and refined by full-matrix least-squares calculations using the NRCVAX[11] programs. All hydrogen atoms were visible in difference maps and were allowed for as riding atoms. The absolute configuration was established unequivocally by the refinement. At convergence, $R = 0.029$, $R_w = 0.025$. Atomic coordinates, full details of molecular dimensions and thermal parameters have been deposited at the Cambridge Crystallographic Data Centre.

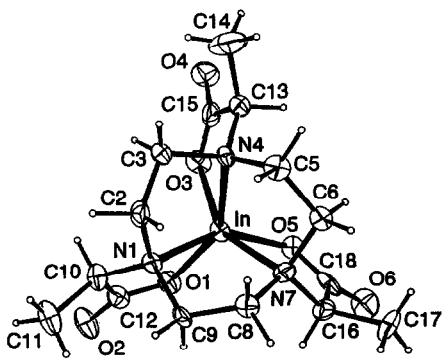

Fig. 1. Perspective (ORTEP) view of the molecule. Selected bond lengths and bond angles: In—N(1) 2.258(4), In—N(4) 2.270(5), In—N(7) 2.254(5), In—O(1) 2.101(4), In—O(3) 2.094(4), In—O(5) 2.094(4) Å; N(1)—In—N(4) 79.7(2), N(1)—In—N(7) 79.7(2), N(4)—In—N(7) 79.3(2), O(1)—In—O(3) 93.6(2), O(1)—In—O(5) 93.9(2), O(3)—In—O(5) 94.1(2), N(4)—In—O(3) 77.0(2), N(7)—In—O(5) 77.0(2), N(1)—In—O(1) 77.7(1).

Acknowledgements—We thank SERC, Celltech Ltd and NSERC for continued support.

REFERENCES

1. D. Parker, *Chem. Soc. Rev.* 1990, **19**, 271; A. E. Martell, R. J. Motekaitis and M. J. Welch, *J. Chem. Soc., Chem. Commun.* 1990, 1748.
2. J. P. L. Cox, A. S. Craig, I. M. Helps, K. J. Jankowski, D. Parker, M. A. W. Eaton, A. T. Millican, K. Millar, N. R. A. Beeley and B. A. Boyce, *J. Chem. Soc., Perkin Trans. I* 1990, 2567.
3. C. J. Broan, K. J. Jankowski, R. Kataky, D. Parker, G. Ferguson, A. Harrison and A. M. Randall, *J. Chem. Soc., Perkin Trans. II* 1991, 87.
4. A. S. Craig, D. Parker, H. Adams and N. A. Bailey, *J. Chem. Soc., Chem. Commun.* 1989, 1793.
5. A. S. Craig, I. M. Helps, D. Parker, H. Adams, N. A. Bailey, M. G. Williams and G. Ferguson, *Polyhedron* 1989, **8**, 2481.
6. A. Bevilacqua, R. I. Gelb, W. B. Hebard and L. J. Zompa, *Inorg. Chem.* **26**, 2699.
7. A. Riesen, T. A. Kaden, W. Ritter and H. R. Macke, *J. Chem. Soc., Chem. Commun.* 1989, 460.
8. H. Prent and F. Haber, *Z. Anorg. Allg. Chem.* 1979, **450**, 120.
9. A. N. Christensen, N. C. Broch, O. Heidenstamm and H. Nilsson, *Acta Chem. Scand.* 1967, **21**, 1046.
10. K. Weighardt, U. Bossek, P. Chaudhuri, W. Herrmann, B. C. Menke and J. Weiss, *Inorg. Chem.* 1982, **21**, 4308.
11. E. J. Gabe, Y. Le Page, J.-P. Charland, F. L. Lee and P. S. White, *J. Appl. Cryst.* 1989, **22**, 384.

Polyhedron Vol. 10, No. 16, pp. 1955–1957, 1991
Printed in Great Britain

0277–5387/91 $3.00+.00
Pergamon Press plc

COMMUNICATION

A NEW ROUTE TO THE PHOSPHINE-SUBSTITUTED CLUSTERS $[Os_3(CO)_{11}(PH_3)]$ AND $[HM_3(CO)_{10}(\mu_2\text{-}PH_2)]$ (M = Ru OR Os)

BRIAN F. G. JOHNSON*

Department of Chemistry, University of Edinburgh, West Mains Road, Edinburgh EH9 3JJ, Scotland, U.K.

and

LUTZ HEUER and JACK LEWIS

University Chemical Laboratory, Lensfield Road, Cambridge CB2 1EW, U.K.

and

C. NIGEL KENNEY

Department of Chemical Engineering, Downing Street, Cambridge CB2 1EW, U.K.

(*Received* 10 *May* 1991; *accepted* 28 *May* 1991)

Abstract—The reaction of $[Ph_4]I$, phosphonium iodide, with the appropriate cluster precursor, e.g. $[Os_3(CO)_{11}(MeCN)]$ or $[M_3(CO)_{10}(MeCN_2)]$ (M = Ru or Os), in the presence of base, BaO, has been shown to be a highly efficient route to the phosphine-substituted clusters $[Os_3(CO)_{11}(PH_3)]$ and the phosphido-bridged cluster $[HM_3(CO)_{10}(\mu_2\text{-}PH_2)]$ (M = Ru or Os).

We have previously reported[1] the synthesis of the phosphine-substituted clusters $[Os_3(CO)_{11}(PH_3)]$ (**2**) and $[Os_3(CO)_{10}(PH_3)_2]$ (**5**) from the direct reaction of $[Os_3(CO)_{11}(MeCN)]$[2] (**1**) or $[Os_3(CO)_{10}(MeCN)_2]$ (**3**) with $[PH_3]$. In a related reaction, the hydrido-cluster $[HRu_3(CO)_{10}(\mu_2\text{-}PH_2)]$ (**7**) has been prepared from $[Ru_3(CO)_{12}]$ and $[PH_3]$. These compounds have been used in the synthesis of higher nuclearity clusters and, in the case of osmium, found to be highly suitable precursors for the formation of the monoanionic hexa-osmium cluster $[Os_6P(CO)_{18}]^-$ containing an interstitial P-atom.[1] Nevertheless, their use has been limited by the potential hazards of $[PH_3]$. In this communication we wish to report a new, highly efficient and safe route to these important precursor materials in which the phosphonium salt $[PH_4]I$ is used as the source of $[PH_3]$.

RESULTS AND DISCUSSION

In a typical reaction the appropriate cluster, e.g. $[Os_3(CO)_{11}(MeCN)]$ (**1**) (120 mg; 0.13 mmol), was treated with $[PH_4]I$ (20 mg; 0.13 mmol) and BaO (140 mg; 0.91 mmol) in CH_2Cl_2 at room temperature for 40 min and then at 40°C for 20 min. After separation by column chromatography on silica, the product, $[Os_3(CO)_{11}(PH_3)]$ (**2**) was isolated in 83% yield and characterized by the usual spectroscopic methods. In addition, a small amount of the iodo-cluster, $[HOs_3(CO)_{10}(\mu_2I)]$, was also obtained. This and other related reactions are illustrated in Scheme 1. In the reaction with $[Os_3(CO)_{10}(MeCN)_2]$ (**3**) the bis-substituted derivative $[Os_3(CO)_{10}(PH_3)_2]$ was the major product. On

* Author to whom correspondence should be addressed.

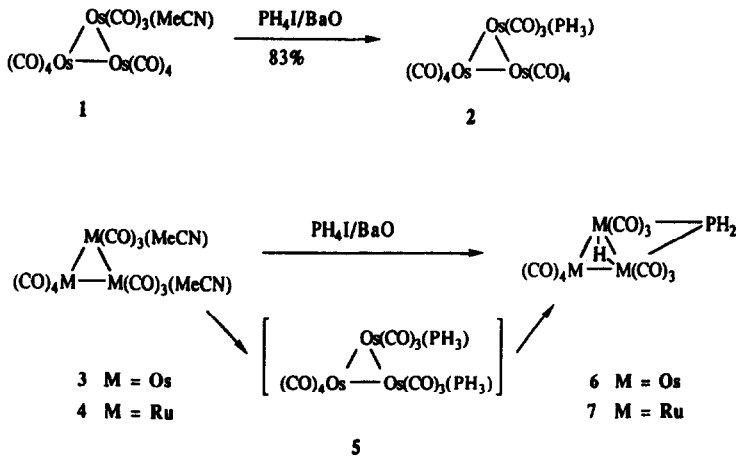

1 2 5

Scheme 1.

warming, further reaction occurred and the hydrido-cluster $[HOs_3(CO)_{10}(\mu_2\text{-}PH_2)]$ (**6**) was obtained. However, with the ruthenium analogue $[Ru_3(CO)_{10}(MeCN)_2]$ (**4**) these reactions are rapid and the only identifiable product was the hydrido-cluster $[HRu_3(CO)_{10}(\mu_2\text{-}PH_2)]$ (**7**). Compounds (**3**), (**5**), (**6**) and (**7**) were characterized by elemental analysis, IR and ^1H NMR spectra. These data were fully in accord with those reported earlier.[1]

This relatively easy route to the compounds (**2**), (**6**) and (**7**) has allowed us to carry out a more extensive examination of their chemistry. We find, for example, that compound (**6**) readily undergoes reaction with electrophilic reagents (RX) to produce the phosphorus-substituted products $[HOs_3(CO)_{10}(PHR)]$ [R = Me (**8**); R = CH_2—$CH{=}CH_2$ (**9**)] which are obtained in both the exo- and endo- isomeric forms. The structures of these isomers was initially derived from a comparison of their IR and NMR spectroscopic data with those of the clusters $[HOs_3(CO)_{10}(PHPh)]$ or $[HRu_3(CO)_{10}(PHPh)]$ (**4**), both of which are known to

Table 1. Selected ^1H NMR spectroscopic data

Compound	Chemical shift values (**8**)		
(**6**) ($CDCl_3$)	5.25 (ddd)	4.98 (dd)	−19.90 (dd)
(**7**) ($CDCl_3$)	5.09 (ddd)	4.43 (dd)	−17.45 (dd)
(C_6D_6)	4.47 (ddd)	3.68 (dd)	−17.62 (dd)
(**8a**) ($CDCl_3$) endo	6.16 (ddqd)	1.80 (dd)	−19.48 (dd)
(C_6D_6) endo	5.62 (ddqd)	1.82 (dd)	−19.14 (dd)
(**8b**) ($CDCl_3$) exo	6.43 (ddq)	1.81 (dd)	−19.00 (dd)
(C_6D_6) exo	5.72 (ddq)	1.81 (dd)	−19.20 (dd)
(**9a**) ($CDCl_3$) endo	2.58 (dddd) (CH_2)	5.19–5.29 (m) (=CH_2) 5.89 (dddt) (=CH) 6.05 (ddt) (C_6H_5)	−19.57 (dd)
(**9b**) ($CDCl_3$) exo	3.36 (ddd)	5.20–5.33 (m) 5.85–6.11 (m) 6.25 (ddt)	−19.04 (dd)

possess exo-geometries on the basis of single crystal X-ray structure analysis.[3] From the ^{1}H NMR spectrum the ratio of exo- to endo- products has been found to be *ca* 4 : 1 in the case of compound (**8**) and 7 : 1 in the case of compound (**9**). Cluster (**9**) readily undergoes isomerization and, on starting with a 7 : 1 mixture of exo- and endo-products, conversion to the pure endo-product occurred readily on warming to *ca* 70°C.

The ^{1}H NMR spectra of these products are given in Table 1. Initially they were assigned on the basis of the arguments given above. Further confirmation that our assignment of the exo- and endo-protons was probably correct came from the spectra obtained for samples in benzene-d_6 as a solvent. In this case, as expected, the exo-proton undergoes the more substantial solvent-shift. Furthermore, the endo-proton shows the unexpected larger coupling to the hydrido-ligand [^1J(HP) and ^3J(HH)].

Acknowledgement—We wish to thank British Gas for their financial support.

REFERENCES

1. (a) S. B. Colbran, F. J. Lahoz, P. R. Raithby, J. Lewis, B. F. G. Johnson and C. J. Cardin, *J. Chem. Soc., Dalton Trans.* 1988, 173; (b) C. J. Cardin, S. B. Colbran, B. F. G. Johnson, J. Lewis and P. R. Raithby, *J. Chem. Soc., Chem. Comm.* 1986, 1288; (c) S. B. Colbran, B. F. G. Johnson, J. Lewis and R. M. Sorrell, *J. Organomet. Chem.* 1985, **C1**, 296.
2. S. R. Drake and R. Khattar, in *Organometallic Synthesis*, Vol. 4, p. 234. Elsevier, Amsterdam (1988).
3. P. L. Taylor, PhD thesis, Cambridge (1982).

Polyhedron Vol. 10, No. 16, pp. 1959–1961, 1991
Printed in Great Britain

0277–5387/91 $3.00+.00
© 1991 Pergamon Press plc

COMMUNICATION

A MONONUCLEAR TERT-BUTYLIMIDO COMPLEX OF NIOBIUM(V). X-RAY CRYSTAL STRUCTURE OF $[Ph_3PCH_2Ph][Nb(NBu^t)Cl_4(py)] \cdot CH_2Cl_2$

WILLIAM CLEGG, R. JOHN ERRINGTON,* DAVID C. R. HOCKLESS and CARL REDSHAW

Department of Chemistry, The University of Newcastle upon Tyne, Newcastle upon Tyne NE1 7RU, U.K.

(*Received* 24 *May* 1991; *accepted* 25 *June* 1991)

Abstract—$NbOCl_3$ reacts with Bu^tNH_2 in the presence of $[Ph_3PCH_2Ph]Cl$ and pyridine in refluxing toluene to give the mononuclear anion $[Nb(NBu^t)Cl_4(py)]^-$, which has been structurally characterized by X-ray crystallography.

Recent interest in organoimido groups as auxiliary ligands for higher oxidation state organometallic chemistry of the early transition metals[1] has stimulated the search for simple synthetic routes to suitable starting materials. The development of molybdenum and tungsten organoimido chemistry has been facilitated by the convenience of the reactions shown in (1) and (2).[2] For the heavier Group 5 elements, the reactions between MX_5 (M = Nb, Ta) and amines, $Me_3SiNHBu^t$ or RNH_2 (R = Et, Pr^i, Bu^t), have been shown to give $[\{M(NBu^t)Cl_3(NH_2Bu^t)\}_2]$ (**1**) or $[\{M(NR)(NHR)Cl_2(NH_2R)\}_2]$ (**2**), respectively, and these can be converted to mononuclear complexes $[M(NR)Cl_3L_2]$ (**3**) or $[M(NR)(NHR)Cl_2L_2]$ (**4**) by treatment with the appropriate ligands.[3] The crystal structure of **2** (M = Ta) has been determined[4] but none of the mononuclear adducts (**3** or **4**) has been characterized crystallographically.

$$WOCl_4 + RNCO \longrightarrow W(NR)Cl_4 + CO_2 \quad (1)$$

$$MoCl_4(thf)_2 + RN_3 \longrightarrow Mo(NR)Cl_4(thf) + N_2 \quad (2)$$

We have been studying the oligomerization of transition metal species $M(X)(Y)Cl_2$ (M = Mo, W; X, Y = O or NR), and have structurally characterized the anions $[W_6O_{14}Cl_{10}]^{2-}$ (**5**), $[W_4(NBu^t)_4O_4Cl_{10}]^{2-}$ (**6**),[5] $[W_3(NBu^t)_3(NPh)_3Cl_7]^-$ (**7**)[6] and $[Mo_2(NBu^t)_4Cl_5]^-$ (**8**).[7] Compound **6** was obtained from the reaction between $WOCl_4$ and Bu^tNH_2 in the presence of Cl^-. In an effort to extend these studies to Group 5 we treated $NbOCl_3$ with Bu^tNH_2 in the presence of $[Ph_3PCH_2Ph]Cl$. The yellow crystalline product obtained has not yet been fully characterized and we have been unable to grow crystals for an X-ray structure analysis, but NMR and IR spectra indicate that it contains terminal NBu^t, μ-O, and coordinated Bu^tNH_2 with diastereotopic hydrogens, which, together with the ^1H NMR inte-

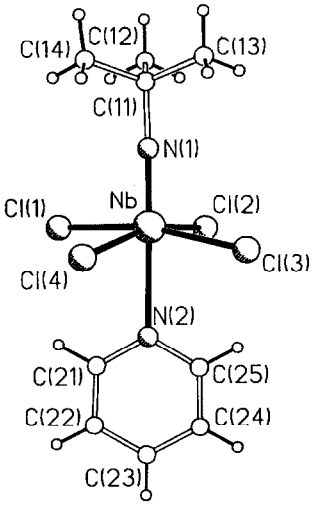

Fig. 1. A view of the molecular structure of $[Nb(NBu^t)Cl_4(py)]^-$, showing the atom numbering scheme.

* Author to whom correspondence should be addressed.

Table 1. Selected bond lengths (Å) and angles (°) for $[Nb(NBu^t)Cl_4(py)]^-$

Nb—Cl(1)	2.446(2)	C(11)—C(13)	1.509(9)
Nb—Cl(2)	2.429(2)	C(11)—C(14)	1.522(9)
Nb—Cl(3)	2.425(2)	N(2)—C(21)	1.329(7)
Nb—Cl(4)	2.434(2)	N(2)—C(25)	1.329(7)
Nb—N(1)	1.731(3)	C(21)—C(22)	1.384(7)
Nb—N(2)	2.479(4)	C(22)—C(23)	1.344(11)
N(1)—C(11)	1.450(5)	C(23)—C(24)	1.358(12)
C(11)—C(12)	1.511(8)	C(24)—C(25)	1.388(8)
Cl(1)—Nb—Cl(2)	88.3(1)	Cl(3)—Nb—N(1)	97.1(1)
Cl(1)—Nb—Cl(3)	168.0(1)	Cl(4)—Nb—N(1)	97.9(1)
Cl(1)—Nb—Cl(4)	88.2(1)	Cl(1)—Nb—N(2)	83.0(1)
Cl(2)—Nb—Cl(3)	89.9(1)	Cl(2)—Nb—N(2)	81.3(1)
Cl(2)—Nb—Cl(4)	163.9(1)	Cl(3)—Nb—N(2)	85.0(1)
Cl(3)—Nb—Cl(4)	90.2(1)	Cl(4)—Nb—N(2)	82.7(1)
Cl(1)—Nb—N(1)	94.9(1)	N(1)—Nb—N(2)	177.8(2)
Cl(2)—Nb—N(1)	98.1(1)	Nb—N(1)—C(11)	176.4(4)

gration, suggest a formula such as $[Ph_3PCH_2Ph][Nb_2(NBu^t)_2(\mu\text{-}O)_2Cl_3(NH_2Bu^t)_2]$.

We repeated the reaction in the presence of pyridine in an attempt to obtain an analogous compound containing pyridine in place of Bu^tNH_2, which we hoped would provide crystals for an X-ray study. Long yellow needles were obtained when the product was recrystallized from CH_2Cl_2/hexane* and the X-ray diffraction study† showed this compound to be the $[Ph_3PCH_2Ph]^+$ salt of a mononuclear tert-butylimido species $[Nb(NBu^t)Cl_4(py)]^-$, an anionic analogue of the adducts (**3**) described by Nielson. The structure of the anion is shown in Fig. 1 and selected bond lengths and angles are given in Table 1.

The anion contains the characteristic features of d^0 transition metal mono-organoimido complexes,[8] although few examples are known for niobium. The distorted octahedral structure with equatorial chlorines displaced away from the multiply-bonded tert-butylimido nitrogen [average Cl—Nb—N(1) = 97°] has a Nb—N_{imido} bond length of 1.731(3) Å, which is similar to that in $[\{Nb(NPh)Cl_2(SMe_2)\}_2(\mu\text{-}Cl)_2]$ [1.733(7) Å][9] but shorter than in other examples of niobium organoimido complexes.[8] The Nb—N_{imido}—C linkage is almost linear, with an angle at N(1) of 176.4(4)°.

Although we have not yet established a mechanism for this transformation of a niobium oxo compound into a tert-butylimido complex, it seems likely that an oxoimido species is formed initially (as in the reaction without pyridine discussed above) which then rearranges to give an insoluble oxo compound and a soluble tert-butylimido complex. We have observed similar redistribution reactions with tungsten oxoimido complexes, where solubility properties seem to determine which products are formed.[10] Further work on this niobium system is in progress.

* Bu^tNH_2 (3.30 cm^3, 31.4 mmol) and pyridine (0.85 cm^3, 10.5 mmol) were added to $NbOCl_3$ (2.25 g, 10.5 mmol) and $[Ph_3PCH_2Ph]Cl$ (4.06 g, 10.4 mmol) in toluene (35 cm^3) and the mixture was heated under reflux for 17 h. After removal of the solvent under reduced pressure, the resulting solid was extracted into CH_2Cl_2 (20 cm^3) and filtered from a white residue. Diffusion of hexane into this solution over several days produced long, yellow needles of $[Ph_3PCH_2Ph][Nb(NBu^t)Cl_4(py)]\cdot CH_2Cl_2$. Satisfactory microanalytical data have been obtained. δ_H (200 MHz, CD_2Cl_2): 1.33 (s, 9H, NC_4H_9), 4.66 [d, 2H, ^2J(PH) 14.2 Hz, PCH_2Ph], 6.8–7.8 (multiplets, 23H, $[Ph_3PCH_2Ph]^+$ and *m*-, *p*-C_5H_5N), 9.29, [d, 2H, ^4J(HH) 4.8 Hz, *o*-C_5H_5N]. $\delta C\{^1H\}$ (50.3 MHz, CD_2Cl_2): 29.5 [s, $NC(Me_3)$], 69.28 (s, $NCMe_3$), 117.37 [d, ^1J(PC) 85.7 Hz, PCH_2Ph], 123.01, 136.79, 151.73, (C_5H_5N), 126.73 [d, J(PC) 8.9 Hz], 128.73 [d, J(PC) 3.7 Hz], 129.04 [d, J(PC) 3.3 Hz], 130.41 [d, J(PC) 12.6 Hz], 131.27 [d, J(PC) 5.5 Hz], 134.15 [d, J(PC) 9.8 Hz], 135.52 [d, J(PC] 2.8 Hz], (Ph_3PCH_2Ph). ν(Nb—Cl) 308, 314 cm^{-1}, s.

† Crystal data for $[Ph_3PCH_2Ph][Nb(NBu^t)Cl_4(py)]\cdot CH_2Cl_2$: $C_{35}H_{38}N_2PCl_6Nb$, Mol. wt = 823.3, monoclinic, a = 11.5933(8), b = 12.0082(8), c = 28.5389(21) Å, β = 100.139(7)°, V = 3911.0 $Å^3$, Z = 4, space group $P2_1/c$; R = 0.0390, R_w = 0.0396 from 3485 unique observed reflections with $3 < 2\theta < 45°$ measured with Mo-K_α radiation (λ = 0.71073 Å) and corrected for absorption. Atomic coordinates, bond lengths and angles, and thermal parameters have been deposited as supplementary material with the editor from whom copies are available on request. Atomic coordinates have also been deposited with the Cambridge Crystallographic Data Centre.

Acknowledgement—We thank the SERC for financial support.

REFERENCES

1. For example, see J. Feldman, W. M. Davis, J. K. Thomas and R. R. Schrock, *Organometallics* 1990, **9**, 2535.
2. D. C. Bradley, M. B. Hursthouse, K. M. A. Malik, A. J. Nielson and R. L. Short, *J. Chem. Soc., Dalton Trans.* 1983, 2651; C. Y. Chou, J. C. Huffman and E. A. Maatta, *J. Chem. Soc., Chem. Commun.* 1984, 1184.
3. P. A. Bates, A. J. Nielson and J. M. Waters, *Polyhedron* 1985, **4**, 1391; A. J. Nielson, *Polyhedron* 1988, **7**, 67.
4. T. C. Jones, A. J. Nielson and C. F. Rickard, *J. Chem. Soc., Chem. Commun.* 1984, 205.
5. W. Clegg, R. J. Errington, D. C. R. Hockless and C. Redshaw, *Polyhedron* 1989, **8**, 1788.
6. D. C. Bradley, R. J. Errington, M. B. Hursthouse and R. L. Short, *J. Chem. Soc., Dalton Trans.* 1990, 1043.
7. W. Clegg, R. J. Errington, D. C. R. Hockless and M. J. Dunn, unpublished results.
8. W. A. Nugent and J. M. Mayer, *Metal–Ligand Multiple Bonds*. Wiley, New York (1988).
9. F. A. Cotton, S. A. Duraj and W. J. Roth, *J. Am. Chem. Soc.* 1984, **106**, 4749.
10. R. J. Errington and C. Redshaw, unpublished results.

Polyhedron Vol. 10, No. 16, p. 1963, 1991
Pergamon Press plc. Printed in Great Britain

BOOK REVIEW

Gmelin Handbook of Inorganic Chemistry. Pb–Organolead Compounds, Part 2. Published by Gmelin Institute for Inorganic Chemistry of the Max Planck Society for the Advancement of Science. Springer, Berlin, 1990, ISBN 3-540-93606-8, 5 ills, xi+273 pp., 830 g, hard cover DM 1203.

System number 47 of the renowned *Gmelin Handbook of Inorganic Chemistry* comprises the chemistry of lead. In the Organolead series two volumes have appeared, dealing with tetramethyllead and tetraethyllead (TEL), respectively. Both compounds are well known to be effective anti-knock agents in the combustion of gasoline in engines.

In the present book the huge body of literature on TEL has been collected, although not all patent data have been included. The literature has been covered through 1988, but *Chemical Abstracts* has been evaluated through No. 110 of 1989.

The book is divided into clear sections describing the various features of TEL. The first section is a comprehensive enumeration of the many routes that are available for the preparation of TEL, including listings of these in well-organized tables. In the same chapter the analytical techniques for TEL which have been used are described. These deal mainly with the detection of TEL in gasolines, air, natural waters, waste waters, marine sediments and biological samples.

The following chapters list the physical properties of TEL, and a wealth of data is presented, again often in the familiar Gmelin tabular format. The majority of the book is dedicated to a thorough description of the chemical reactions of TEL, starting with its thermally or radiation-induced decomposition. On the whole, the data are very well presented, although the part on the decomposition reactions is somewhat disorderly arranged.

Chapters on the physiological properties, toxicity and environmental impact of TEL are included, which is important in view of the extreme toxicity of TEL. The section on the uses of TEL is largely dedicated to its anti-knock properties, although further applications, such as chemical vapour deposition and vapour phase epitaxy, are also listed.

In conclusion, the book is an excellent summary of the profusion of literature on tetraethyllead. The book clearly reflects the German *Gründlichkeit* and subjects of interest are easily accessible for the reader.

Billiton Research B.V., **GUIDO P. M. VAN MIER**
P.O. Box 40,
6800 AA Arnhem,
The Netherlands

Polyhedron Vol. 10, No. 16, p. 1965, 1991
Pergamon Press plc. Printed in Great Britain

ERRATA

A theoretical study of the linear vs bent geometry for several MX_2 molecules: MgF_2, CaH_2, CaF_2, CeO_2 and $YbCl_2$. R. L. DeKock, M. A. Peterson, L. K. Timmer, E. J. Baerends and P. Vernooijs (*Polyhedron*, Vol. 9, No. 15/16, pp. 1919–1934, 1990).

The equation on p. 1930 for the variation of energy as a function of angle has an error. The third line of this equation represents the dipole–dipole term, and here reference is made to the term in parentheses in that third line. As published, this term reads

$$2+\cos^2\theta-1/(2\cos\theta).$$

This term should read

$$(8/3)-1/(2\cos\theta).$$

For the range of angles considered, the correct equation differs little from the equation used. Hence, there is no change in any of the discussion or Figs 1 and 2.

The authors wish to thank Professor H. Stoll of the Universität Stuttgart for pointing out the correction.

The synthesis and reactivity of some μ-phthaloyl and μ-phenylene complexes. S. F. Mapolie and J. R. Moss (*Polyhedron*, Vol. 10, No. 7, pp. 717–723, 1991).

Page 719, right hand column: lines 8, 20 and 40 should refer to compound **3** whereas line 14 should refer to compound **4**.

Page 720, left hand column: line 31 should refer to compound **4**, whereas in the right hand column, line 43 should refer to compound **8**.

Equation (2) on p. 721 should read:

(2)

7 M = $Re(CO)_5$
8 M = $Mn(CO)_5$
9 M = $CpFe(CO)_2$

Polyhedron Vol. 10, No. 17, pp. 1967–1994, 1991
Printed in Great Britain

0277–5387/91 $3.00+.00
Pergamon Press plc

POLYHEDRON REPORT NUMBER 38

ALUMINIUM ALKOXIDES, β-DIKETONATES AND CARBOXYLATES

R. C. MEHROTRA* and A. K. RAI

Department of Chemistry, University of Rajasthan, Jaipur 302 004, India

CONTENTS

1. INTRODUCTION 1967

2. ALKOXIDES OF ALUMINIUM 1968
   2.1. Synthesis 1968
   2.2. Physico-chemical and spectroscopic properties of aluminium alkoxides 1970
      2.2.1. Ageing phenomenon 1971
      2.2.2. Thermal stability 1971
      2.2.3. Hydrolysis 1972
      2.2.4. Reactions of aluminium alkoxides 1972
      2.2.5. Structural features 1973
      2.2.6. Hindered phenoxide derivatives of aluminium 1975

3. BI- AND POLY-METALLIC ALKOXIDES CONTAINING ALUMINIUM 1977

4. ALUMINIUM ALKOXIDES IN SYNTHESES 1980

5. DERIVATIVES OF ALUMINIUM WITH β-DIKETONES AND ALLIED DERIVATIVES 1980
   5.1. Introduction 1980
   5.2. Synthesis 1981
   5.3. Physico-chemical and structural properties 1982

6. ALUMINIUM CARBOXYLATES 1985
   6.1. Introduction and historical background 1985
   6.2. Synthesis 1985
   6.3. Physico-chemical and structural properties 1986

7. ALKANOLAMINE DERIVATIVES OF ALUMINIUM 1988

8. CONCLUSION 1990

1. INTRODUCTION

The chemistry of aluminium, one of the most abundant elements in nature, is well-established. However, a study of the alkoxides, β-diketonates and carboxylates reveals interesting and novel features which are briefly presented in this review.

The three classes of compounds included in this review are obviously correlated, as shown by their general formulae.

* Author to whom correspondence should be addressed.

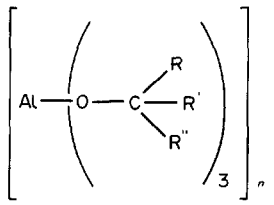

;

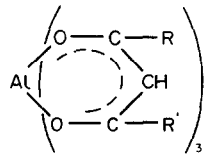

and

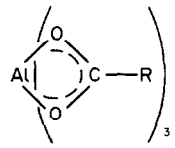

The polarization of the $Al^{\delta+}$—$O^{\delta-}$—C bond is considerably reduced by the +I inductive effect of the alkyl group in alkoxide derivatives. The donation of lone pair(s) of electrons from the alkoxy group(s) of other alkoxide molecule(s) resulting in the formation of associated/polymeric alkoxide species or from a suitably placed oxygen atom in the chelating β-diketonate ligand would further reduce the polarizability of Al—O bonds. On the other hand, the carbonyl group of the carboxylate ligand(s) would enhance significantly the polarity of the Al—O bond although this would tend to be attenuated by the carboxylate group behaving as a bidentate ligand. This article deals mainly with the attempts made during the past 3–4 decades to utilize the above correlationships in the development of new facets in the chemistry of the latter two classes of compounds of alkoxides.

The electron deficient nature of aluminium is clearly depicted by the formation of not only dimeric aluminium chloride, but also dimeric trialkyls, $[AlR_3]_2$. The extraordinary stability of the first homologue, $[Al(CH_3)_3]_2$, of the latter series illustrates clearly the effect of size (steric factor) of aluminium in addition to its electron deficient character. The alkoxides, β-diketonates and carboxylates of aluminium provide some of the most apt examples, depicting the interplay and delicate balance of electronic and steric effects which are generally the key factors affecting the chemistry of any species. In this direction, the possibility of interaction between vacant *p* orbitals on oxygen in some hindered phenoxide derivatives (Section 2.2.5) with π-acceptor *p* orbitals of monomeric aluminium complexes deserves special mention in addition to alkoxy-bridging associated derivatives referred to above.

2. ALKOXIDES OF ALUMINIUM

In spite of aluminium alkoxides being amongst the most widely studied alkoxides of any element and their extensive applications as catalysts in Meerwein–Ponderoff and Openauer reactions, their chemistry (e.g. even the observed degree of association) was highly confused up to the early 1950s. The extension of the concept of the simple "ageing" phenomenon,[1] well known in the case of aluminium hydroxide (or hydrous oxides) to the alkoxides, and the explanation of the same on the basis of a change from coordination state four to six of aluminium, has opened a new phase in the understanding of aluminium alkoxide chemistry.[2]

2.1. *Synthesis*

Aluminium alkoxides can be synthesized by one of the following methods.

(i) *Reaction of aluminium metal with an alcohol.* In spite of its weakly electropositive character, the reaction of aluminium turnings with alcohols in the presence of catalysts like iodine and/or mercuric chloride[3,4] yields the corresponding aluminium alkoxides.

$$Al + 3ROH \xrightarrow[\text{reflux}]{I_2/HgCl_2} Al(OR)_3 + 3/2H_2\uparrow$$

[R = Et, Pr^i, Bu^t).

The nature of alkyl group affects the reaction considerably, significantly reducing the reactivity of long chain and sterically demanding alcohols. In view of their volatility, the products can be conveniently purified by distillation or sublimation under reduced pressure from the reaction mixture.

In contrast to alcohols, phenols are more reactive, yielding aluminium phenoxides without requiring any catalyst.[5,6]

$$\underset{\text{(excess)}}{Al + 3PhOH} \xrightarrow[\text{reflux}]{} Al(OPh)_3 + 3/2H_2\uparrow.$$

The reactions of metallic aluminium with substituted and higher molecular weight phenols has not been studied in detail and their comparatively slow nature is mentioned in a patent[7] only.

(ii) *Reaction of aluminium chloride with an alcohol in the presence of ammonia.* In view of the facile synthetic route of aluminium alkoxides from metallic aluminium itself, the conventional procedure of preparing metal alkoxides[2] from anhydrous metal chlorides has not been pursued actively, except for a report by Teischner.[8]

$$AlCl_3 + 3ROH + 3NH_3 \longrightarrow Al(OR)_3 + 3NH_4Cl\downarrow.$$

The reactions of aluminium chloride with alcohols do not appear to proceed to completion in the absence of a base. For example, Funk *et al.*[9] reported the formation of a product $AlCl_2(OC_2H_5)\cdot 2AlCl_3\cdot 10(EtOH)$ by the reaction of $AlCl_3$ with ethanol. Mehrotra and Mehrotra[10] on repeating the same reaction in benzene solution, isolated a product having the composition $Al_3Cl_7(OEt)_2\cdot 7EtOH$, which on being heated under reduced pressure is converted to $Al_3Cl_5(OEt)_4\cdot 3EtOH$ (the structure of the corresponding isopropoxide analogue, $Al_3Cl_5(OPr^i)_9$ has been elucidated by Turova and co-workers).[11,12]

As in the case of reaction with the metal, phenols are also more reactive[5] with aluminium chloride.

$$AlCl_3 + 3PhOH \xrightarrow{\text{molten}} Al(OPh)_3 + 3HCl\uparrow$$

$$AlCl_3 + 3PhOMe \xrightarrow{70\text{–}80^\circ C} Al(OPh)_3 + 3MeCl\uparrow.$$

(iii) *Alcoholysis reactions of aluminium alkoxides.* In accord with the common characteristic of almost all main group and early transition metal alkoxides,[2,13] aluminium alkoxides undergo facile alcoholysis reactions.

$$Al(OR)_3 + nR'OH \rightleftharpoons Al(OR')_n(OR)_{3-n} + nROH\uparrow.$$

These alcoholysis reactions can be utilized for the preparation of higher alkoxides from the lower analogues like ethoxide or isopropoxide. The reactions can be driven to completion by fractionating out the lower boiling alcohol azeotropically with benzene (used as solvent). Under these conditions, the reactions can be carried out in any desired stoichiometric ratio, yielding mixed alkoxides of the type $Al(OR')_x(OR)_{3-x}$.[1,14]

Alcoholysis reactions are quite facile, but these are subject to steric factors leading to the formation of mixed products only, e.g. $Al_2(OEt)(OBu^t)_5$, with sterically demanding alcohols.

Aluminium phenoxide can also be prepared by this interchange technique.[15] The reactions of aluminium alkoxides with hindered phenols have not received much attention and a preliminary investigation[16] indicates the formation of $Al(OBu^t)(OC_6H_3Bu^t_2\text{-}2,6)_2$ with aluminium in the three-coordination state.

(iv) *Transesterification reactions of aluminium alkoxides.* Baker[17] observed that the reaction between aluminium isopropoxide and higher alkyl acetates could be driven in the forward direction by fractionating off the lower boiling isopropyl acetate.

$$Al(OPr^i)_3 + 3CH_3COOR \longrightarrow Al(OR)_3 + 3CH_3COOPr^i\uparrow.$$

Mehrotra and Kapoor[18,19] while extending the above method to the synthesis of alkoxides of other metal (gallium, iron, niobium, tantalium, etc.) reported that with the use of cyclohexane (which forms a lower boiling azeotrope with ethyl or isopropyl acetate) as solvent, the reactions can also be conveniently accomplished in a desired stoichiometric ratio.

$$Al(OR)_3 + xCH_3COOR' \longrightarrow Al(OR)_{3-x}(OR')_x + xCH_3COOR$$

(R = Et or OPr^i; x = 1, 2, 3).

(v) *Reactions of trialkylaluminium with alcohols and phenols.* Trialkylaluminiums, AlR_3, undergo facile substitution reactions with alcohols[20] and phenols[21] yielding products which can be represented as $Al(R)_{3-n}(OR')_n$ and $Al(R)_{3-n}(OAr)_n$ (where R = Me, Et, Bu etc.; R′ = Me, Et, etc.; Ar = C_6H_5 or C_6H_4X etc.; n = 1–3).

Most of the above products are associated in nature.[20,21] Monomeric alkyl phenoxides with hindered phenols have been studied in considerable detail in recent years and their structural and other interesting features are described in Section 2.2.5.

(vi) *Direct electrochemical synthetic techniques.* Notable success has been claimed[22] in the synthesis (including industrial production) of titanium, zirconium, germanium, niobium, tantalum, yttrium, scandium and gallium by electrolysis in conducting admixtures of alcohols with supporting electrolytes such as Bu_4NBr, $Bu_4N \cdot BF_4$ and NaBr using the relevant metal as anode. It may not be out of place to emphasize that the technique has not yet been successful in the case of aluminium, indicating the need for further investigations.

2.2. *Physico-chemical and spectroscopic properties of aluminium alkoxides*

Taking the electronegativity values of aluminium and oxygen as 1.5 and 3.5, respectively, the Al—O bond could be expected, simply on Pauling's formula, to have ~ 50% ionic character. However, most of the aluminium alkoxides show marked covalent behaviour in their solubility in organic solvents and volatility under reduced pressure. The polarization of the $Al^{\delta+}$—$O^{\delta-}$ bond is reduced by the +I inductive effect (Al⇐O—C) of the alkyl group which should increase from primary to secondary to tertiary. The formation of alkoxy bridges of the type: RO(Al)OR(Al); would also tend to operate in the same direction. The action of reducing the electrophilicity of the central aluminium atom by the increased +I as well as steric demands of the more ramified alkyl group would tend to reduce the degree of association and increase the volatility of the isomeric alkoxides of ramified alcohols (cf. Table 1).

It is difficult to sort out the comparative influence of steric and electronic effects but an effort has been made[14] to assess these by synthesizing all the eight isomeric amyloxides of aluminium

Table 1. Boiling points and molecular association of some aluminium alkoxides

Alkoxides	Boiling point °C mm^{-1}	Molecular association in boiling benzene
$Al(OCH_2CH_3)_3$	184.0/0.5	4.1
$Al(OCH_2CH_2CH_3)_3$	232.5/5.0	4.0
$Al(OCHMe_2)_3$	124.0/5.0	4.0
$Al(OCH_2CH_2CH_2CH_3)_3$	270.0/5.0	3.9
Al(OCHMeEt)	172.0/5.0	2.4
$Al(OCMe_3)_3$	160.0/1.0[a]	2.0
$Al(OCH_2CH_2CH_2CH_2CH_3)_3$	255.0/1.0	4.0
$Al(OCH_2CH_2CHMe_2)_3$	195.0/1.0	4.0
$Al(OCH_2CHMeEt_2)_3$	200.0/0.6	4.1
$Al(OCH_2CMe_3)_3$	180.0/8.0	2.07
$Al(OCHEt_2)_3$	165.0/1.0	2.08
$Al(OCHMeCH_2CH_2CH_3)_3$	162.0/0.5	2.06
$Al(OCHMeCHMe_2)_3$	162.0/0.6	1.98
$Al(OCHMe_2)(OMe_2CH_2Me)_2$	154.0/0.5	1.97

[a] Sublimed.

(Table 1). Out of these, the neopentyloxide is of special interest. It is well known that the neopentyl group exhibits the inductive effect of a primary amyl group, but steric factors are similar to the secondary amyl groups due to the close proximity of a tert. butyl group to the primary CH_2 carbon atom. The properties (volatility as well as molecular association of aluminium neopentyloxide) are almost identical to those of three secondary amyloxides (all dimeric) and sharply different from the other three primary amyloxides (all tetrameric) (Table 1).

It may be noted that efforts to synthesize simple tris-tert.-amyloxides, $Al(OAm^t)_3$, were not successful both from the reaction of aluminium metal with the tertiary amyl alcohol as well as from the alcoholysis of aluminium ethoxide or isopropoxide, in which dimeric mixed alkoxides,[14] $[Al(OR)(OAm^t)_2]_2$ (with R = Et, Pr^i), were the end products. It is suggested that it may be possible to synthesize the tris-tert.-amyloxide of aluminium, $Al(OAm^t)_3$, from the reaction of tert. amyl alcohol on trialkylaluminiums, in which case the intermediate bis-amyloxide products should more easily interact with a third molecule of the tertiary alcohol.

2.2.1. *Ageing phenomenon.* With widely conflicting reports from reliable groups of scientists[23–25] on the molecular association of aluminium isopropoxide ranging from two up to 10, the prevailing confusion was resolved by the observation by Mehrotra[1] of the ageing phenomenon of aluminium isopropoxide. It was shown that the vapour density of aluminium isopropoxide shows dimerization up to a high temperature whereas the freshly distilled supercooled liquid aluminium isopropoxide is essentially trimeric. This trimeric form crystallizes in a few days to a tetrameric species $[Al(OPr^i)_3]_4$, which is fairly stable and tends to show further polymerization only on standing for a long time (some months).

Turova *et al.*[26] confirmed the above observation and showed that the molecular complexity, as well as the melting point of aluminium isopropoxide, depends on ageing of the sample (Fig. 1). The phenomenon of the ageing process has also been discussed by other workers.[27–29]

According to these studies, the degree of association in supercooled melts increases over a period of several minutes from 2 to 2.7/2.8 and then gradually, during several weeks, to 4.

The mass spectrometric studies[30,31] also indicate the existence of penta-, hexa- and even hepta-associates in a very low proportion along with trimeric and tetrameric molecules.

2.2.2. *Thermal stability.* Aluminium alkoxides are in general thermally stable under reduced pressure and can be distilled or sublimed in quantitative yields. However, on heating under atmospheric pressure to ~ 350°C, they tend to undergo decomposition with the formation of a mixture of basic oxides, e.g. the decomposition of aluminium ethoxide[32,33] proceeds as follows.

$$2Al(OC_2H_5)_3 \longrightarrow Al_2(OC_2H_5)_4O + (C_2H_5)_2O$$

$$Al_2(OC_2H_5)_4O \longrightarrow 2Al(OC_2H_5)O + (C_2H_5)_2O$$

$$2Al(OC_2H_5)O \longrightarrow Al_2O_3 + (C_2H_5)_2O.$$

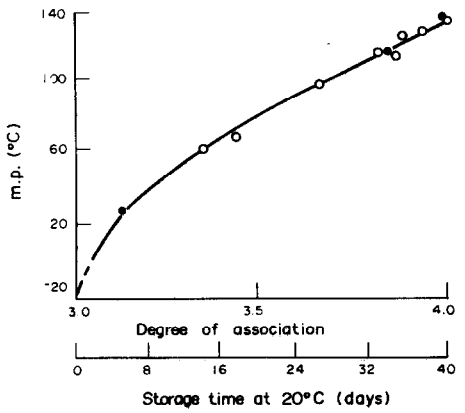

Fig. 1. The dependence of melting point on the degree of association of $Al(OPr^i)_3$: ● data cited by Fieggen and Gerding;[27] ○ data cited by Turova *et al.*[26]

The derivatogram of aluminium isopropoxide showed a three stage decomposition corresponding to the following mechanism.[34]

$$2Al(OPr^i)_3 \xrightarrow{\sim 200^\circ C} Al_2(OPr^i)_2(OH)_4 + 4CH_3CH{=}CH_2$$
$$\downarrow \sim 250^\circ C$$
$$Al_2O_2(OH)_2 + 2Pr^iOH$$
$$\downarrow \sim 330^\circ C$$
$$Al_2O_3 + H_2O.$$

In comparison to alkoxides, the corresponding phenoxides are non-volatile and undergo decomposition with the formation of intermediates like $Ph[OAl(OH)]_4OPh$.[35,36] The D.T.A. studies of aluminium phenoxide show the beginning of decomposition[6] around 100°C with the formation of a residue corresponding in analysis to $Al_6O_7(OPh)_4$ which is later converted to Al_2O_3 at higher temperatures (Scheme 1).

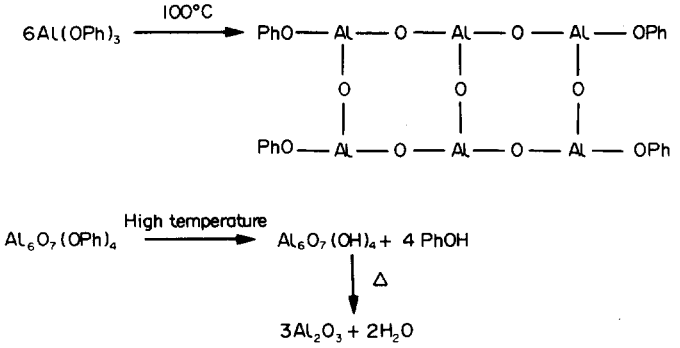

Scheme 1.

2.2.3. *Hydrolysis.* Although aluminium alkoxides like other metal alkoxides are extremely susceptible to hydrolysis, very little work has been carried out in this direction.[37] Alkoxides as well as phenoxides of both metals and metalloids undergo rapid hydrolysis to form basic alkoxides or phenoxides. The nature of the products is dependent on the conditions of hydrolysis. Pfeifer and Flora[35] reported the following order of hydrolytic stability in the mixed butoxy phenoxides of aluminium.

$$Al(OBu)_3 > Al(OPh)(OBu)_2 > Al(OPh)_2(OBu) > Al(OPh)_3.$$

An active interest has arisen in the hydrolysis of aluminium alkoxides used for the preparation of ceramic materials through the solution–sol–gel process, in which alkoxides (either alone or in mixtures) dissolved in organic solvents (generally alcohols) are hydrolysed to give sols. Polycondensation in these sols leads to gel formation which can be sintered into oxide ceramics.[38,39] The hydrolysis of aluminium secondary butoxide in isopropanol has been studied in detail by Chane-Ching and Klein[40] using rheological behaviour and IR spectroscopy.

2.2.4. *Reactions of aluminium alkoxides.* Aluminium alkoxides follow the general characteristics of metal alkoxides in trying to enhance the coordination of the aluminium atom by formation of species with bridging alkoxy groups, rather than by acceptance of lone pairs from donor ligands. In other words, the donor ligands are not generally able to compete thermodynamically with the polymerization process, except in some cases, e.g. formation of species of the type $Al_2(OR)_6(en)$ (where en = ethylenediamine), reported by Bains and Bradley.[41] The recently synthesized monomeric hindered phenoxides of aluminium, $AlMe_x(2,6\text{-}Bu^t, 4\text{-}MeC_6H_2O)_{3-x}$ (where $x = 1$ or 2), form 1 : 1 tetrahedral adducts[42] with PMe_3.

The facile interaction of metal alkoxides with protic reagents in organic solvents in desired stoichiometric ratios has proved to be of great importance in the synthesis of a large number of organic derivatives of aluminium, some of which cannot be prepared by alternative routes. Aluminium isopropoxide which is commercially available has been extensively used for such syntheses. Aluminium isopropoxide reacts with ligands having labile hydrogens in benzene solution, liberating isopropanol, during the course of the reaction, which can be fractionated off azeotropically with

benzene. The fractionation of isopropanol tends to drive the reaction in the forward direction and its estimation by simple chromate oxidation method[43] helps in monitoring the progress of the reaction.

$$Al(OPr^i)_3 + nLOH \xrightarrow{\text{benzene}} Al(OL)_n(OPr^i)_{3-n} + nPr^iOH\uparrow$$

(n = 1, 2 or 3 and LOH = organic ligand).

The versatility of the above synthetic procedure has been demonstrated by the synthesis and characterization of tris- or mixed isopropoxide ligand derivatives of a variety of organic hydroxy ligands, e.g. glycols,[44] catechol,[44] β-diketone,[45,46] β-ketoesters,[45,46] carboxylic acids,[47] fatty acids,[48–50] hydroxy acids,[51] oximes,[52] amidoximes and N-substituted arylbenzimidoximes,[53] unsaturated alkanols,[54] mercapto-carboxylic acids,[55] alkanol amines,[56–58] β-ketoamines,[59] aldamines,[60–62] Schiff bases.[63–74]

Halide alkoxides of aluminium[75–78] have also been synthesized by the reactions of aluminium primary and secondary alkoxides with acyl halides and hydrogen chlorides.

$$Al(OR)_3 + xCH_3COCl \longrightarrow AlCl_x(OR)_{3-x} + xCH_3COOR\uparrow$$

$$Al(OR)_3 + xHCl \longrightarrow AlCl_x(OR)_{3-x} + xROH\uparrow$$

(where R = Et, Pr^i etc.).

The reaction of $Al(OBu^t)_3$ with CH_3COCl has been shown to follow a different route which is represented below in a simplified form.

$$Al(OBu^t)_3 + CH_3COCl \longrightarrow Al(OBu^t)_2Cl + CH_3COOBu^t$$

$$Al(OBu^t)_3 + 2CH_3COCl \longrightarrow Al(OBu^t)Cl(OOCCH_3) + CH_3COOBu^t + Bu^tCl$$

$$Al(OBu^t)_3 + 3CH_3COCl \xrightarrow[\text{reflux}]{} Al(OOCCH_3)_3 + 3Bu^tCl.$$

2.2.5. *Structural features.* The IR spectra of aluminium alkoxides $Al(OR)_3$, where R = Et, Pr^n, Pr^i, Bu^n, Bu^{sec} and Am^{sec}, show a number of absorption bands, amongst which those at 1059, 1015, 1033, 1048, 1058, 1070 cm^{-1} were earlier assigned to Al—O—C vibrations.[79,80] On hydrolysis, the intensity of almost all the above bands decreases,[81] but those at ~ 935 cm^{-1} (νAl—O—Al) and ~ 3340 cm^{-1} (νOH), become broader.

On comparing the IR spectrum of aluminium isopropoxide with a number of those of group IV and V metal isopropoxides, Barraclough *et al.*[82] assigned the absorption frequency in the range of 1000 cm^{-1} to νC—O instead of νAl—O—C, as assumed by earlier workers[79,80] and assigned five new absorptions at 699, 678, 610, 566 and 535 cm^{-1} for νAl—O. The presence of such a large number of bands for νAl—O has been ascribed to the polymeric nature of aluminium isopropoxide.

Robinson and Peak[24] in 1935 proposed the following ring structure for tetrameric aluminium alkoxide, $[Al(OR)_3]_4$, formed by sharing two corners each of four AlO_4 tetrahedra.

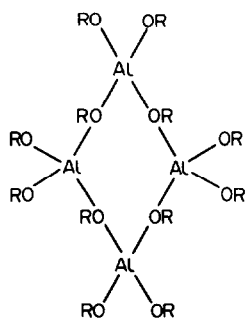

Aluminium tertiary butoxide which was found to be dimeric in a number of solvents, was assigned[1] the following structure.

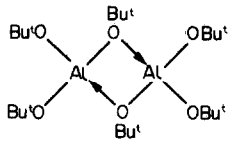

The above structure has been confirmed by Bains[83] and Shiner *et al.*[84] from its ^{1}H NMR spectrum, which depicts two distinct signals for terminal and bridging butyl groups in the ratio 2:1, these have been shown to remain unchanged in the temperature range of −14–74°C.

In the reaction of aluminium ethoxide or isopropoxide with tertiary butanol, two moles of ethoxy (isopropoxy) per aluminium atom can be easily replaced. However, under forcing conditions, the ultimate product was found to be $Al_2(OR)(OBu^t)_5$, where R = Et or Pr^i.

The slow nature of the final stage of the above reactions could be explained by assuming[1] an unsymmetrical structure for $Al_2(OR)_2(OBu^t)_4$ products in which the coordination and subsequent reaction could occur on the less sterically hindered aluminium atom on the left being surrounded by two OR and two OBu^t groups only yielding finally the product $Al_2(OR)(OBu^t)_5$, which does not appear to undergo further alcoholysis due to steric factors (Scheme 2).

Scheme 2.

The unsymmetric structure of $Al_2(OPr^i)_2(OBu^t)_4$ has also been confirmed by Bains[83] and Oliver and Worrall[85] from ^{1}H NMR spectral evidence.

The following structure for trimeric $Al(OPr^i)_3$ was supported by the splitting of the methyl signals of the OPr^i groups in the ratio of 1:1:2:2 in its proton NMR spectrum at low temperature, due to terminal and bridging OPr^i groups.[84]

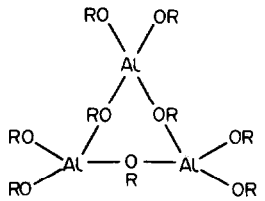

This splitting disappears in the spectrum at room temperature and only a single doublet of the methyl proton is observed.[84] This coalescence of signals may be attributed to a fast exchange of the two types of isopropoxide groups.

Explaining the change in trimeric to tetrameric aluminium isopropoxide on ageing, on the basis of change in coordination number of one of the aluminium atoms from four to six, Bradley[86,87] suggested the following novel structure for $[Al(OPr^i)_3]_4$.

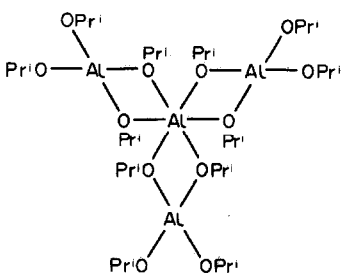

Confirmatory spectral evidence for the above was obtained by PMR spectra, in which three sets of doublets of the methyl proton peaks were observed at 1.70, 1.60, 1.42, 1.33 and 1.33, 1.23 ppm in

the ratio of 1 : 1 : 1 : 1 : 2 : 2.[84,85,88] Shiner *et al.*[84] could observe signals only due to methyl protons but Bradley,[87] Mehrotra and Mehrotra[88] in a 100 MHz PMR spectrum observed two sets of signal for methine protons, having equal intensity, and assigned them to bridging and terminal isopropoxy groups. The splitting in the signal of methyl protons of the isopropoxy group has been attributed to magnetic non-equivalence of two methyls on the same isopropoxy groups.[89] A similar observation had been made earlier by Oliver and co-workers.[90,91]

The appearance of two signals in the ratio 3 : 1 in the ^{27}Al NMR spectrum[92] of aluminium isopropoxide further supports the tetrameric structure proposed earlier and confirms that the molecule contains one central octahedral aluminium surrounded by three isopropoxyaluminate groups.

Earlier X-ray diffraction studies[93] of aluminium alkoxides (methoxide, ethoxide and isopropoxide) supported the tetrameric structure instead of a chain type polymer. The single crystal X-ray structure of aluminium isopropoxide alone appears to have been carried out by Turova *et al.*[26] Aluminium isopropoxide crystallizes out at −30°C in pentane solution with a tetragonal lattice with unit cell dimensions $a = b = 12.595(1)$, $c = 31.823(4)$ Å, $V = 5049(1)$ Å^3, $\rho_{exp} = 1.06$, $\rho_{calcd} = 1.08$, $Z = 16$ and the space group $P4_12_12_1$. These unit cell dimensions are close to those cited by Amma[93] earlier. The crystal structure shown in Fig. 2 has been reported by $[Al(OPr^i)_3]_4$.

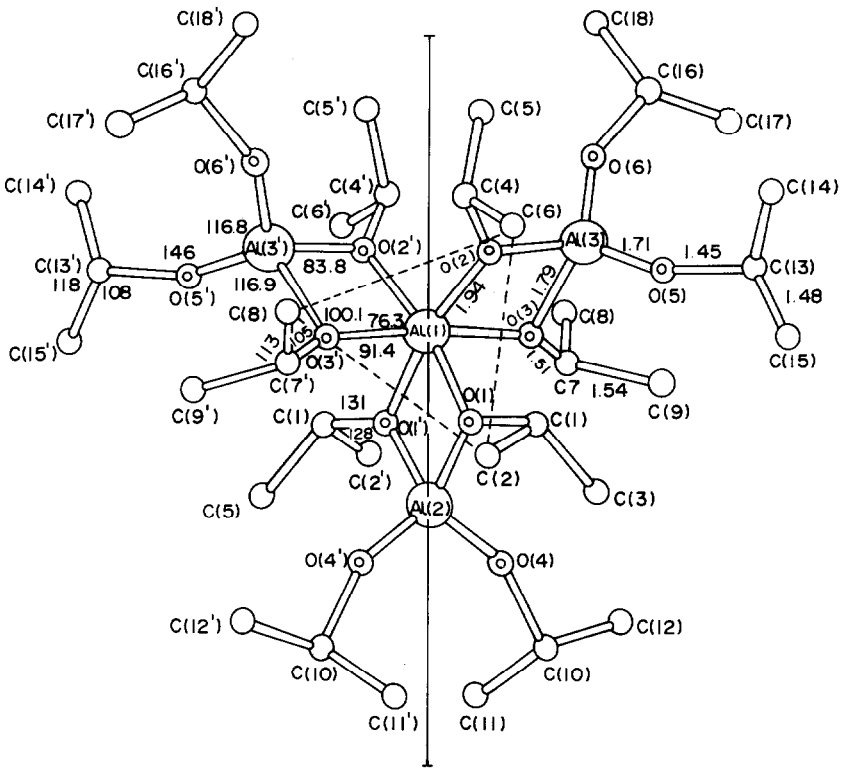

Fig. 2.

2.2.6. *Hindered phenoxide derivatives of aluminium.* Recently (1988), structures of $AlMe(BHT)_2$,[94] $AlMe_2(BHT)PMe_3$[42] and $Me_3NH^+[AlMeCl_2(BHT)]^-$[42] (where BHT = 2,6-di-tert.-butyl-4-methyl phenoxide) have been determined by X-ray crystallography (see Figs 3–5).

The structure of $[AlMe(BHT)_2]$ is planar[94] (bond lengths: Al—O, 1.686 and Al—C, 1.927 Å; bond angles: O—Al—O, 111.9, O—Al—C, 123.6–123.9, Al—O—C, 140.5; 146.8°). As expected, the latter two four-coordinate aluminium derivatives have a distorted tetrahedral geometry[42] with Al—C bond distances of 1.970 and 1.995 Å, respectively; compared to 1.957 Å observed in $Al(CH_3)_3$.[95] This lengthening in Al—C bonds in structures of $[AlMe_2(BHT)PMe_3]$ and $[AlMeCl_2BHT]^-$ is understandable in view of the increase in *p*-character of Al—C bonds on changing from planar to tetrahedral geometry.

Another notable feature of the structures of the latter species is the considerably larger Al—O—C bond angles (164.5–164.0°) than those commonly observed in aluminium alkoxides[26] {cf. Al—O—C

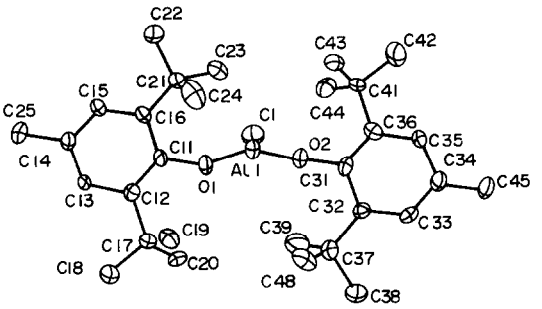

Fig. 3. Crystal structure of $[AlMe(BHT)_2]$.[94]

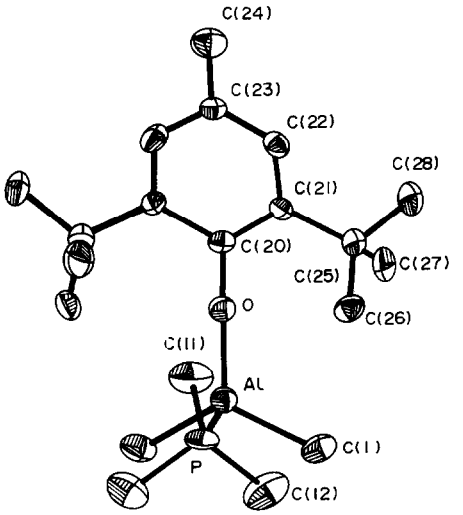

Fig. 4. Crystal structure of $[AlMe_2(BHT)(PMe_3)]$.[42]

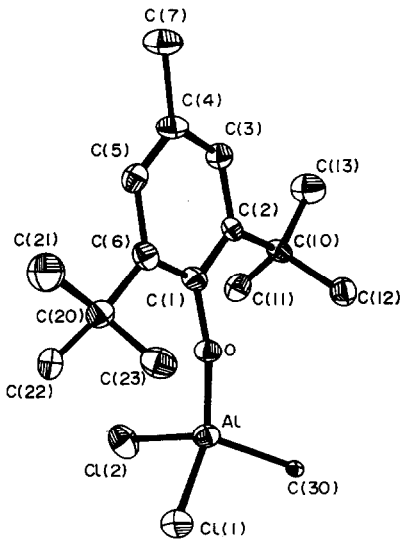

Fig. 5. Crystal structure of the anion $[AlMeCl_2(BHT)]^-$.[42]

for $[Al(OPr^i)_3]_4$, 128.0–135.0°}. In fact this points strongly towards a π interaction between the oxygen *p*-orbitals and the σ anti-bonding orbitals of aluminium derivatives; this conclusion appears to be confirmed by the short Al—O distances of 1.736 and 1.713 Å in the latter two structures, respectively, compared to 1.686 Å in $AlMe(BHT)_2$. However, there appears to be inadequate lengthening in the other Al–ligand bond lengths, a point which deserves further investigation (cf. transition metal derivatives in which *p–d* interaction is quite common).[96]

It is of interest to note that alkylaluminium phenoxides react with Lewis bases[94] (e.g. ethyl toluate) to form four-coordinate derivatives displaying both high activity and stereospecificity in Ziegler–Natta catalytic systems. The reactions of $AlMe_2(BHT)$ and $AlMe(BHT)_2$ with PMe_3 yield mono-phosphine adducts,[42] $AlMe_2(BHT)\cdot PMe_3$ and $AlMe(BHT)_2\cdot PMe_3$. The addition of one equivalent of Me_3NHCl to $AlMe(BHT)_2$ and $AlMe_2(BHT)$ results in the formation of $AlCl(BHT)_2\cdot NMe_3$ and $AlClMe(BHT)\cdot NMe_3$, respectively, whereas addition of two equivalents of Me_3NHCl to $AlMe_2(BHT)$ yields an ionic complex $[Me_3NH][AlCl_2Me(BHT)]$. The molecular structure of methyl toluate adduct, $[AlEt_2(BHT)(MeC_6H_4COOMe)]$, is determined by X-ray crystallography and it is also depicted in Fig. 6.

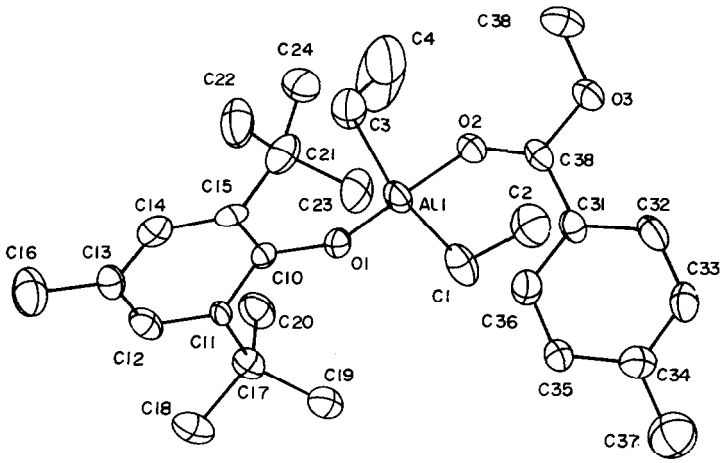

Fig. 6. Crystal structure of $AlEt_2(BHT)(MeO_2CC_6H_4CH_3)$.[94]

3. BI- AND POLY-METALLIC ALKOXIDES CONTAINING ALUMINIUM

Meerwein and Bersin[97] in 1929, using the concept of an acid and base neutralization reaction showed the formation of a species like $K[Al(OPr^i)_4]$ in the titration of potassium isopropoxide and aluminium isopropoxide. In 1952, Albers *et al.*[98] reported the synthesis of $U[Al(OPr^i)_4]_4$ by the following reaction.

$$UCl_4 + 4NaAl(OPr^i)_4 \longrightarrow U[Al(OPr^i)_4]_4 + 4NaCl.$$

Later on another volatile bimetallic compound of uranium, $Al[U(OEt)_6]_3$ was synthesized[99] by the reaction between $Al(OEt)_3$ and $U(OEt)_5$ in the molar ratio 1 : 3.

The existence of ionic species like $[Al(OMe)_4]^-$ was reported by Gut[100] in the titration of aluminium chloride with lithium methoxide in methanol. The formation of similar species has been shown by Mehrotra and co-workers[101] in the titration of aluminium isopropoxide with alkali metal isopropoxides in isopropanol solution. Out of all alkali aluminium isopropoxides, $M[Al(OPr^i)_4]$ (where M = Li, Na and K), only $K[Al(OPr^i)_4]$ was found to be sufficiently soluble in common organic solvents and volatile (with some decomposition). Taking advantage of the solubility of $K[Al(OPr^i)_4]$ species, Mehrotra *et al.*[102–116] have successfully synthesized a number of aluminium containing bimetallic alkoxides by reactions with anhydrous metal chlorides as illustrated by the following equations.

$$MCl_n + nKAl(OPr^i)_4 \xrightarrow[C_6H_6]{Pr^iOH} M[Al(OPr^i)_4]_n + nKCl\downarrow$$

(where M = indium,[102,103] lanthanons,[104-106] tin(IV),[107] tin(II),[108], beryllium,[109] zinc, cadmium, mercury,[110] chromium,[111] iron,[112] manganese,[113] cobalt,[114] nickel[115] and copper[116] etc.).

With pentavalent metals and smaller tetravalent metal atoms like zirconium, all the chlorine atoms are not replaced leading to the formation of heteroleptic products,[117,118] e.g.

$$ZrCl_4 + 2KAl(OPr^i)_4 \longrightarrow ZrCl_2[Al(OPr^i)_4]_2 + 2KCl$$

$$ZrCl_2[Al(OPr^i)_4]_2 + 2KOPr^i \longrightarrow (Pr^iO)_2Zr[Al(OPr^i)_4]_2 + 2KCl.$$

The identity of these products in some cases was established by a fractional distillation of a mixture of alkoxides when the final products indicated in the following equations were distilled out in almost quantitative yields, e.g.

$$Ln(OPr^i)_3 + \underset{\text{(excess)}}{3Al(OPr^i)_3} \longrightarrow Ln[Al(OPr^i)_4]_3 \qquad \text{(Ref. 106, 117)}$$

$$Zr(OPr^i)_4 \cdot Pr^iOH + 2Al(OPr^i)_3 \xrightarrow{Pr^iOH} (Pr^iO)_2Zr[Al(OPr^i)_4]_2 + Pr^iOH \qquad \text{(Ref. 102, 103)}$$

$$Nb(OPr^i)_5 + 2Al(OPr^i)_3 \longrightarrow (Pr^iO)_3Nb[Al(OPr^i)_4]_2$$

$$Nb(OPr^i)_5 + Al(OPr^i)_3 \longrightarrow Nb[Al(OPr^i)_8]$$

$$Ta(OPr^i)_5 + Al(OPr^i)_3 \longrightarrow Ta[Al(OPr^i)_8] \qquad \text{(Ref. 119).}$$

The preparation of similar derivatives, $M[Al(OPr^i)_4]_2$ where M is an alkaline earth metal, e.g. magnesium, calcium, strontium and barium, could finally be effected by the following reaction in which dissolution of the alkaline earth metal appears to be much more facile[120] (may be due to the non-formation of surface layers of insoluble isopropoxides of alkaline earth metals).

$$M + 2Pr^iOH + 2Al(OPr^i)_3 \xrightarrow[Pr^iOH]{HgCl_2} M[Al(OPr^i)_4]_2 + H_2\uparrow$$

(where M = Mg, Ca, Sr, Ba).

Most of these bimetallic alkoxides are volatile under reduced pressure and can be distilled or sublimed. They are soluble in common organic solvents (in which they show generally monomeric behaviour) and thermally stable, but they are hydrolytically unstable.

The bimetallic alkoxides also undergo facile alcoholysis reactions exemplified by the following general equation.

$$M[Al(OPr^i)_4]_n + 4nBuOH \longrightarrow M[Al(OBu)_4]_n + 4nPr^iOH\uparrow.$$

In fact in a number of cases of later "3*d*" metals like nickel, simple alkoxides, $Ni(OR)_2$ do not appear to undergo alcoholysis reaction[117,121] but, even in their cases, the bimetallic alkoxides interchange their alkoxy groups quite readily, following the characteristic feature of alkoxy derivatives of main group and early transition metals. However, this interchange also is subject to steric factors similar to those reported for aluminium isopropoxide, e.g.

$$Ni[Al(OPr^i)_4]_2 + 6Bu^tOH \xrightarrow{\text{facile}} Ni[(\mu\text{-}OPr^i)_2Al(OBu^t)_2]_2 + 4Pr^iOH\uparrow$$

$$Ni[(\mu\text{-}OPr^i)_2Al(OBu^t)_2]_2 + 2Bu^tOH \xrightarrow{\text{slow}} Ni[(\mu\text{-}OPr^i)(\mu\text{-}OBu^t)Al(OBu^t)_2]_2 + 2Pr^iOH\uparrow.$$

Preliminary studies on methanolysis reactions of lanthanon tris-tetraisopropoxyaluminates have shown that initially a transient white insoluble product is formed, but it goes into solution readily from which stable volatile products can be isolated.

$$Ln[(\mu\text{-}OPr^i)_2Al(OPr^i)_2]_3 + 6MeOH \longrightarrow \underset{\text{insoluble}\downarrow}{Ln[(\mu\text{-}OPr^i)_2Al(OMe)_2]_3} + 6Pr^iOH$$

$$Ln[(\mu\text{-}OMe)_2Al(OPr^i)_2]_3$$

soluble, volatile.

The potential of these bimetallic tetraalkoxyaluminates as precursors for ceramics by the solvent–sol–gel process has been emphasized[31] and has already been exploited for the preparation of spinel[122] from magnesium bis-tetraisopropoxyaluminate. Methanolysis and hydrolysis studies of some bimetallic alkoxides like $Mg[Al(OPr^i)_4]_2$, $Ba[Ti(OPr^i)_5]_2$ and $Ca[Al(OPr^i)_4]_2$ etc., are yielding interesting results[16] showing differences in the reactivity of terminal and bridging isopropoxy groups, followed by mutual interchange of the same.

The structures of these bimetallic tetraisopropoxyaluminates can be easily represented in general as the following.

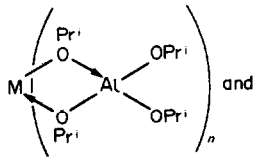

and

(where M = Mg, Ca, Ba, Zn etc.; Fe, Cr, Ga, In, Ln etc.; Th, Sn, Ti etc.; Nb, Ta etc.)

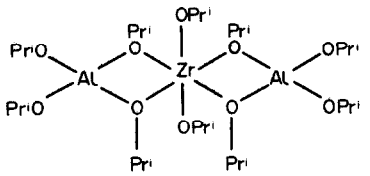

Confirmatory evidence for the plausible structures above has been obtained by IR, ^1H NMR and molecular weight studies and by mass spectroscopic studies of $Ln[Al(OPr^i)_4]_3$,[123] $[Pr^iOBeAl(OPr^i)_4]$,[124] the former show a fragmentation pattern similar to that reported for $[Al(OPr^i)_3]_4$[27] and $La[Al(OPr^i)_4]_3$.[85]

A detailed magnetic and spectroscopic study of tetraisopropoxide aluminates of some 3*d* metals[113–116,125] like iron^{II}, cobalt^{II}, nickel^{II} and copper^{II} showed that for the first two metals, the ligand $[Al(OPr^i)_4]^-$ is bidentate and with copper, it behaves as a tridentate.

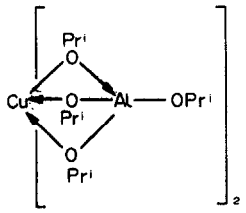

In the case of nickel, the ligand appears to be tridentate when R = Et and bidentate when R = Bu^t, for R = OPr^i, there is an equilibrium between the two forms.

The possibility of the synthesis of trimetallic alkoxides arose out of the behaviour of 1 : 1 beryllium tetraisopropoxyaluminate. When the reaction between MCl_2 (where M = Mg, Ba, Zn, Cd, Hg etc.) and $KAl(OPr^i)_4$ was carried out in a 1 : 1 molar ratio, the bis-product $M[Al(OPr^i)_4]_2$ was obtained in all cases except that of $BeCl_2$. This gave $ClBe[Al(OPr^i)_4]$, which could be easily converted into $(Pr^iO)Be[Al(OPr^i)_4]$[109] by reacting with $KOPr^i$ (1 : 1 molar ratio). This product is monomeric when freshly distilled, but dimerizes on standing[126] for a few days into $(Pr^iO)_2Al(\mu\text{-}OPr^i)_2Be(\mu\text{-}OPr^i)_2Be(\mu\text{-}OPr^i)_2Al(OPr^i)_2$.

The species $Pr^iOBeAl(OPr^i)_4$ also reacts with titanium, zirconium, hafnium, niobium and tantalum isopropoxides and yields termetallic isopropoxides.[127]

$$Pr^iOBe[Al(OPr^i)_4] + M(OPr^i)_4 \longrightarrow (Pr^iO)_3M(\mu\text{-}OPr^i)_2Be(\mu\text{-}OPr^i)_2Al(OPr^i)_2$$

$$2Pr^iOBe[Al(OPr^i)_4] + M(OPr^i)_4 \longrightarrow (Pr^iO)_2M[(\mu\text{-}OPr^i)_2Be(\mu\text{-}OPr^i)_2Al(OPr^i)_2]_2$$

(where M = Ti, Zr and Hf)

$$Pr^iOBe[Al(OPr^i)_4] + M(OPr^i)_5 \longrightarrow (Pr^iO)_4M(\mu\text{-}OPr^i)_2Be(\mu\text{-}OPr^i)_2Al(OPr^i)_2$$

(where M = Nb or Ta).

A number of termetallic isopropoxides containing 3*d* metals have been synthesized by using some stable mixed chloride bimetallic isopropoxides.[128,129]

$$ClM[Al(OPr^i)_4] + K[Ga(OPr^i)_4] \longrightarrow (Pr^iO)_4GaM[Al(OPr^i)_4] + KCl\downarrow$$

$$ClM[Zr_2(OPr^i)_9] + K[Al(OPr^i)_4] \longrightarrow [(Pr^iO)_4Al]M[Zr_2(OPr^i)_9] + KCl\downarrow$$

(where M = Fe^{II}, Co^{II}, Ni^{II} or Cu^{II}).

All these trimetallic alkoxides have been characterized by elemental analyses, molecular weight measurements, spectroscopic and magnetic studies. Almost all are volatile under reduced pressure.

In addition to termetallic alkoxides,[130] tetrametallic alkoxides of trivalent metals like iron have also been isolated.

$$FeCl_3 + K[Zr_2(OPr^i)_9] \longrightarrow Cl_2Fe[Zr_2(OPr^i)_9] + KCl\downarrow$$

$$Cl_2Fe[Zr_2(OPr^i)_9] + K[Al(OPr^i)_4] \longrightarrow ClFe[Al(OPr^i)_4][Zr_2(OPr^i)_9] + KCl\downarrow$$

$$ClFe[Al(OPr^i)_4][Zr_2(OPr^i)_9] + KTa(OPr^i)_6 \longrightarrow (Pr^iO)_6TaFe[Al(OPr^i)_4]Zr_2(OPr^i)_9 + KCl.$$

The synthesis of volatile bi-, ter- and tetra-metallic alkoxides may play an important role in the development of electronic and ceramic materials, particularly in the form of thin films.

The controlled hydrolysis coupled with heat treatment of these polymetallic alkoxides may lead to the formation of mixed metal oxides or oxide hydroxides having potential industrial application.[131–135]

4. ALUMINIUM ALKOXIDES IN SYNTHESES

As early as 1925, the catalytic activity[136,137] of aluminium alkoxides in the reduction of an aldehyde to an alcohol by ethanol was shown.

$$RCHO + CH_3CH_2OH \longrightarrow RCH_2OH + CH_3CHO.$$

Ponndorf[138] in 1926, successfully reduced both aldehydes as well as ketones to the corresponding alcohol by ethanol using aluminium isopropoxide as a catalyst. Aluminium ethoxide was found to be comparatively an inferior catalyst. This reaction is known as the Meerwein–Ponndorf–Verley reaction.

The mechanism for this reaction was developed by Jackman and Macbeth[139] by postulating a cyclic transition state in which hydrogen transfer takes place from the β-C—H bond of an alkoxide to a coordinated aldehyde or ketone.

Nasipuri *et al.*[140,141] used sec.-alkoxy aluminium dichloride, $ROAlCl_2$, prepared *in situ* by the reaction of $LiAl(OR)_4$ with anhydrous aluminium chloride, as a reducing agent for the synthesis of some optically active alcohols from carbonyl compounds, in good yields for the first time. Isobornyloxyaluminium dichloride has been used as catalyst[142] in the reduction of alkyl-methylketones to optically active alcohols.

5. DERIVATIVES OF ALUMINIUM WITH β-DIKETONES AND ALLIED DERIVATIVES

5.1. *Introduction*

The chemistry of β-diketonate derivatives of almost all the transition and main group elements is dominated by the formation of stable chelated derivatives[143,144] with 1,3-diketonate (β-dik) anions.

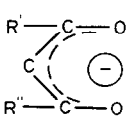

In spite of a number of other bonding modes, e.g. carbon bonded (with elements like sulphur, selenium, mercury, gold etc.) and both carbon as well as oxygen bonded (with metals like platinum or palladium) derivatives of β-diketones,[143,144] the chemistry of aluminium β-diketonate upto 1960's was limited to oxygen bonded simple chelated tris-derivatives[144–149] only. The reactions of

aluminium alkoxides with β-diketones and β-ketoesters[45] leading to the formation of mono-, bis- and tris-derivatives, $Al(OR)_{3-n}(\beta\text{-dik})_n$ (where $n = 1$–3), have not only provided for the first time facile routes for their synthesis but more recently their characterization by physico-chemical techniques has revealed interesting features of the coordination chemistry of aluminium.[43] It may, however, be pointed out that even in oxygen derivatives, no examples are yet known in which the β-diketonate moiety is bonded to aluminium as a monodentate,[150–151] or a neutral coordinating,[143,150] or bridging[143,152] ligand.

Aluminium tris-β-diketonates were synthesized[153–156] for the first time in 1901–1902 and the first X-ray crystallographic study of aluminium tris-acetylacetonate was carried out by Sirkar[157] in 1926.

5.2. *Synthesis*

The following methods of synthesis have been applied for β-diketonate derivatives of aluminium.

(i) $AlCl_3 + 3\beta\text{-dik-H} \xrightarrow{\text{benzene}} Al(\beta\text{-dik})_3 + 3HCl\uparrow$ (Ref. 158).

(ii) $Al_2(SO_4)_3 + 6\beta\text{-dik-NH}_4 \longrightarrow 2Al(\beta\text{-dik})_3 + 3(NH_4)_2SO_4$ (Ref. 156).

(iii) $\underset{\text{(freshly precipitated)}}{Al(OH)_3} + 3\beta\text{-dik-H} \xrightarrow[\text{reflux}]{\text{benzene+ethanol}} Al(\beta\text{-dik})_3 + 3H_2O$ (Ref. 16).

(iv) Mixed alkoxy β-diketonates have been prepared by the reactions of aluminium ethoxide or isopropoxide with various β-diketones and β-ketoesters in different stoichiometric ratios.[45,46,159–162]

$$Al(OR)_3 + nR'COCH_2COR'' \xrightarrow{\text{benzene}} (RO)_{3-n}Al[OC(R')CHCOR'']_n + nROH\uparrow$$

(where R = Et or Pr^i; R′ = R″ = CH_3; R′ = CH_3, R″ = C_6H_5; R′ = CH_3, R″ = OC_2H_5 etc., and $n = 1$–3).

$$Al(OPr^i)_3 + nRCOCH_2COCO_2Me \xrightarrow{\text{benzene}} (Pr^iO)_{3-n}Al[OC(R)CHCOCOOMe]_n + nPr^iOH\uparrow$$

(where $n = 1$–3; R = C_6H_5, *p*-ClC_6H_4, *p*-FC_6H_4 etc.).

(v) The corresponding tertiary butoxide derivatives have also been prepared by alcohol interchange[45,161,162] reactions of the type.

$$Al(OPr^i)_{3-n}(\beta\text{-dik})_n + (3-n)Bu^tOH \xrightarrow{\text{benzene}} Al(OBu^t)_{3-n}(\beta\text{-dik})_n + (3-n)Pr^iOH\uparrow.$$

(vi) Some mixed chloride β-diketone or β-ketoester derivatives[161,162] of aluminium have also been synthesized by the reactions of anhydrous aluminium chloride with corresponding ligands in molar ratio one or two, in dry ether.

$$AlCl_3 + nRCOCH_2COCO_2Me \xrightarrow{\text{ether}} Cl_{3-n}Al[OC(R)CHCOCO_2Me]_n + nHCl\uparrow$$

(where R = *p*-Cl·C_6H_4, *p*-Br-C_6H_4 etc., $n = 1$ or 2)

$$AlCl_3 + n\beta\text{-dik-H} \xrightarrow{\text{ether}} AlCl_{3-n}(\beta\text{-dik})_n + nHCl\uparrow$$

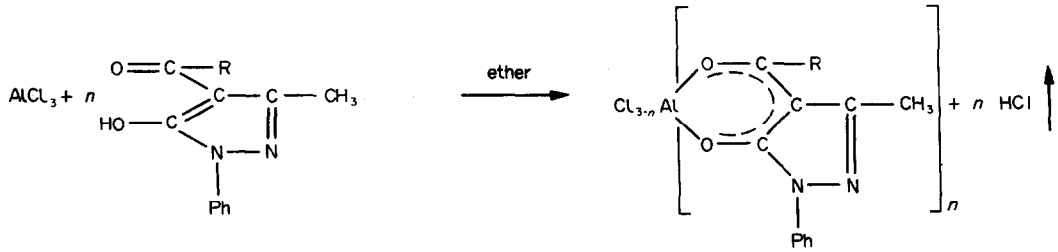

(where $n = 1$ or 2; R = CH_3, C_2H_5, C_6H_5 or *p*-ClC_6H_4 etc.)

(vii) Mixed ligand chelates of the type, $Al(\beta\text{-dik})_n(\beta\text{-dik}')_{3-n}$ (where β-dik and β-dik′ are β-diketonate ligands like acetylacetone, benzoylacetone, hexafluoroacetylacetone etc.) have been synthesized by the following methods.[16,143,163,164]

$$2Al(\beta\text{-dik})_3 + Al(\beta\text{-dik}')_3 \xrightarrow[\text{vacuum}]{\text{heat}} 3Al(\beta\text{-dik})_2(\beta\text{-dik}')$$

$$Al(\beta\text{-dik})_3 + 2Al(\beta\text{-dik}')_3 \xrightarrow[\text{vacuum}]{\text{heat}} 3Al(\beta\text{-dik})(\beta\text{-dik}')_2.$$

The above derivatives can also be synthesized by the following method under much milder conditions.

$$Al(OPr^i)_{3-n}(\beta\text{-dik})_n + 3-n\beta\text{-dik}'\text{-H} \xrightarrow{\text{benzene}} Al(\beta\text{-dik}')_{3-n}(\beta\text{-dik})_n + (3-n)Pr^iOH\uparrow$$

(Ref. 16, 143).

(viii) Mixed ligand complexes of aluminium like $Al(acac)_{3-n}(L)_n$ (where LH is a ligand like 8-hydroxyquinoline) are being synthesized by the following route.[165]

$$Al(OPr^i)_{3-n}(acac)_n + (3-n)LH \longrightarrow Al(acac)_n(L)_{3-n} + (3-n)Pr^iOH\uparrow$$

(where $n = 1$ or 2 and LH = 8-hydroxyquinoline).

(ix) Mixed siloxide β-diketonates of aluminium have been synthesized[46] by the following reactions.

$$Al(OPr^i)_{3-n}(\beta\text{-dik})_n + (3-n)R_3SiOH/R_3SiOOCCH_3 \longrightarrow Al(OSiR_3)_{3-n}(\beta\text{-dik})_n + (3-n)Pr^iOH/CH_3COOPr^i\uparrow$$

(where $n = 1$ or 2; R = CH_3 or C_6H_5)

$$Al(OSiMe_3)_3 + n\beta\text{-dik-H} \longrightarrow Al(OSiMe_3)_{3-n}(\beta\text{-dik})_n + n\text{MeSiOH}$$

(where $n = 1, 2$ or 3).

(x) β-Diketonate and β-ketoester derivatives of a number of aluminium containing bimetallic alkoxides have also been synthesized by the following route.

$$M[(\mu\text{-}OPr^i)_2Al(OPr^i)_2]_n + n\beta\text{-dik-H} \xrightarrow{\text{benzene}} M[(\mu\text{-}OPr^i)_2Al(\beta\text{-dik})(OPr^i)]_n + nPr^iOH\uparrow$$

$$M[(\mu\text{-}OPr^i)_2Al(OPr^i)_2]_n + 2n\beta\text{-dik-H} \xrightarrow{\text{benzene}} M[(\mu\text{-}OPr^i)_2Al(\beta\text{-dik})_2]_n + 2nPr^iOH\uparrow$$

(where $n = 2$, M = Be, Zn, Cd,[109,110] Mg, Ca, Sr, Ba,[2] Mn^{II}, Fe^{II},[149,166] Co^{II},[114] Ni,[115] Cu,[116] Sn^{II}[108] etc.; when $n = 3$, M = Al, Ga, In,[2,149] Cr^{III}[111] etc.).

The occurrence of the initial substitution of terminal isopropoxy groups only has been confirmed by the PMR studies and by the volatilization of the substituted products unchanged.

If the above reactions are extended to the substitution of three isopropoxy groups on aluminium by β-diketonate groups, aluminium tris-β-diketonates are separated out.[106,167]

$$M[(\mu\text{-}OPr^i)_2Al(OPr^i)_2]_n + 3n\beta\text{-dik-H} \longrightarrow M(OPr^i)_n + nAl(\beta\text{-dik})_3 + 3nPr^iOH\uparrow.$$

5.3. *Physico-chemical and structural properties*

Tris-β-diketonate as well as β-ketoester derivatives of aluminium are generally solids, hydrolytically stable and non-volatile. It is now well established that the volatility of metal 1,3-diketonates increases with the substitution of fluorine for hydrogen in the ligand shell.[168–170] Springer *et al.*[171] observed that aluminium tris-fod (1,1,1,2,2,3,3-heptafluoro 7,7-dimethyl-4,6-octanedione) has higher volatility than those of the analogous tris-acetylacetonate or tris-thd(2,2,6,6-tetramethyl-3,5-heptanedione) and only slightly less than that of tris-trifluoroacetylacetone.[169,171] Mixed alkoxy β-diketonates are comparatively more volatile than the corresponding tris-analogues.[45] A comparative thermogravimetric study of β-diketonates of aluminium, gallium and indium revealed that alu-

minium β-diketonates are most volatile.[172] The introduction of an aryl group like phenyl, furyl or thienyl etc. decreases the volatility of the metal chelates.[173]

Aluminium tris-β-diketonates are found to be monomeric[45,161,162] in nature and have an octahedral geometry. The mixed β-diketonate complexes like $Al(\beta\text{-dik})_n(\beta\text{-dik}')_{3-n}$ are optically active. The influence of temperature on optical activity has been studied by NMR. The coalescence temperatures and rate constants for optical inversions for a number of mixed β-diketonate complexes of aluminium have been evaluated.[143,163] Detailed studies have been carried out on the mechanism of such inversion reactions and a number of interesting conclusions involving novel models have been suggested for the same.

The unsymmetrical tris-β-diketone chelates of aluminium are reported to depict *cis*- and *trans*-geometrical isomerism as has been observed in case of a number of other trivalent metal chelates[174–177] also. The NMR (^1H as well as ^{19}F) techniques have been used successfully in differentiating this *cis*- and *trans*-isomerism.

An X-ray study of aluminium tris-(acetylacetonate) derivative[157] was made as early as 1926. This derivative exists in two allotropic modifications,[178] α- and β-forms, having monoclinic and orthorhombic crystal lattice,[179,180] respectively.

Crystal structures for some mixed alkoxide β-diketonate derivatives of aluminium have been reported by Wengrovius *et al.*[46] The crystal structure for $[Al(OPr^i)(Et_2acac)_2]_2$ (Fig. 7) crystallized at −30°C from pentane solution supports our earlier findings[124,161,162] in which we had proposed bonding of two aluminium atoms through isopropoxy bridging.

Aluminium bis-(isopropoxy) acetylacetonate, $Al(OPr^i)_2(acac)$, crystallizes out as a trimer, single crystal X-ray analysis[181] (Fig. 8) of which shows an interesting symmetrical distribution of ligand moieties on the three aluminium atoms, i.e.: (i) two acetylacetonates and two bridging isopropoxides on aluminium (Al2); (ii) one acetylacetonate and four bridging isopropoxide groups on aluminium (Al1); and (iii) four (two bridging and two terminal) isopropoxide groups on aluminium (Al3).

It has been shown that the analogous bis-trimethylsiloxy aluminium acetylacetone is dimeric, $[Al(OSiMe_3)_2(acac)]_2$, and depicts another novel type of unsymmetrical structure[181] (Fig. 9).

In conformity with earlier conclusions on the effect of steric factors on the molecular association of analogous derivatives, it has been further shown that with the substitution of (Me_3SiO-) by (Ph_3SiO-) group, the derivative $[Al(O\text{-}SiPh_3)_2(acac)]$ becomes monomeric tetrahedral structure (Fig. 10).[181]

The above X-ray crystallographic studies of aluminium alkoxide (silyloxide) β-diketonate derivatives reveal that the chemistry and structures of these derivatives are comparatively more complex and the conclusions drawn on the basis of only physico-chemical and spectral data may be misleading

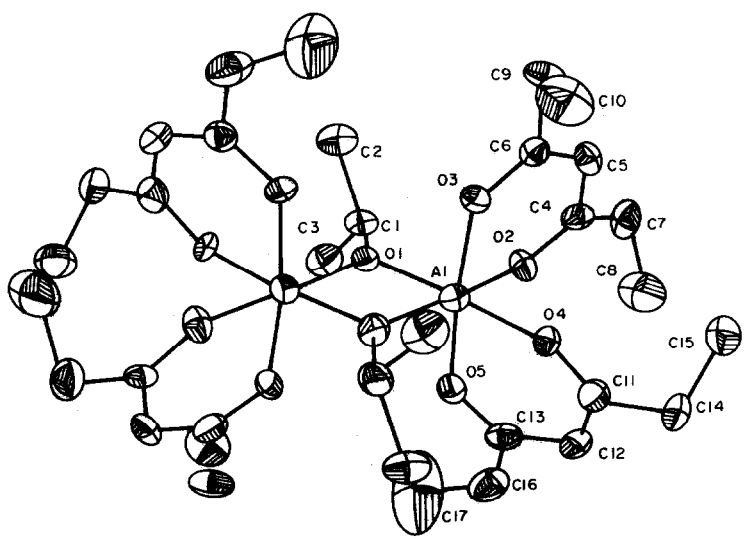

Fig. 7. Crystal structure of $[Al(OPr^i)(Et_2acac)_2]_2$.[46]

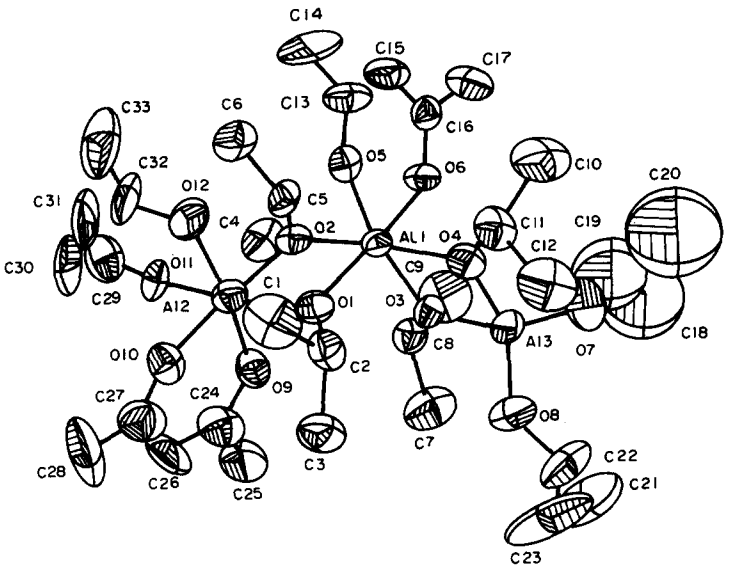

Fig. 8. Crystal structure of $[Al(OPr^i)_2(acac)]_3$.[46]

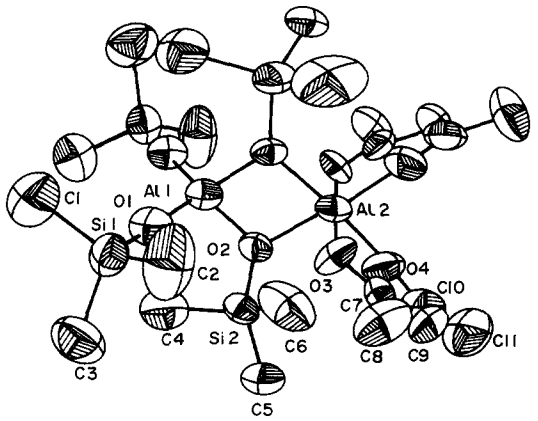

Fig. 9. Crystal structure of $[Al(OSeMe_3)_2(acac)]_2$.[18f]

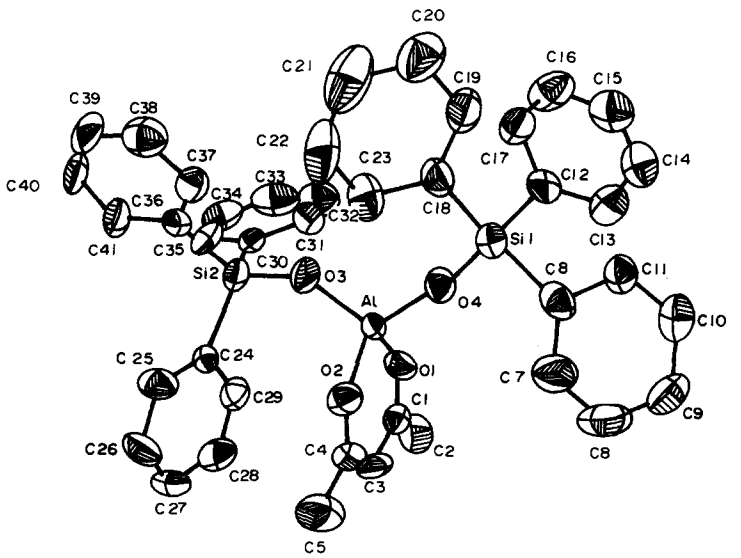

Fig. 10. Crystal structure of $[Al(OSiPh_3)_2(acac)]$.[46]

as the effects of subtle electronic and steric factors on the comparative thermodynamic stability of different possible structures require much more detailed investigations.

6. ALUMINIUM CARBOXYLATES

6.1. *Introduction and historical background*

Aluminium salts of higher fatty acids find commercial applications in several industries[182-185] and are also frequently employed in scientific investigations.[185] In addition to the above and a wide use of aluminium carboxylates in lubrication technology,[182-184] interest in the higher carboxylates (soaps) of aluminium was revived in the 1940s following their use in incendiary Napalm bombs[185(a)] during the Second World War. However, the chemistry, including even the identity of actual derivatives, remained surprisingly obscure.

A review by Gray and Alexander[186] in 1949 cast serious doubts on the very existence of aluminium tri-soaps, arising from numerous failures reported in publications[187-193] from established groups of workers during the decades 1928–1949. Besides reactions in aqueous systems under a variety of conditions, attempts were also made to use aluminium secondary butoxide[186] as a starting material but in all cases, products with the carboxylate : aluminium ratio of only $\leqslant 2$ could be actually isolated.

In fact, the only success claimed in the above direction was that of Glazer *et al.*[194] employing the following route.

$$Al(CH_3)_3 + 3RCOOH \xrightarrow{heat} Al(OOCR)_3 + 3CH_4\uparrow.$$

The main evidence for the formation of aluminium tri-carboxylates in the above reaction was the liberation of 3 moles of methane, but the aluminium analysis of the final tri-carboxylate was far from satisfactory.

Other evidence for the existence of aluminium tri-carboxylates was provided by Lawrence[195] with the observation that 3 moles of alcohol were liberated on heating together aluminium alkoxides with excess fatty acid. Confirming these observations, Gray and Alexander[186] had pointed out that the full amount (3 moles) of alcohol was liberated only at higher temperatures when side-reactions could not be ruled out; they further showed that the analysis of the product(s) obtained after extraction with dioxan in no case showed a carboxylate to aluminium ratio of more than two.

Following his observation[1] that in the alcoholysis reactions of aluminium isopropoxide, two alkoxy groups are replaced with much more facility,[1] Mehrotra[48] carried out the following reaction and confirmed the liberation of 3 moles of isopropanol from a reaction mixture of $Al(OPr^i)_3$ with fatty acids in a 1 : 3 molar ratio, under much milder conditions of azeotropic distillation with benzene.

$$Al(OPr^i)_3 + 3RCOOH \xrightarrow{benzene} Al(OOCR)_3 + 3Pr^iOH\uparrow.$$

Initially received with considerable scepticism the preparation of aluminium tri-soaps by the above route was confirmed by X-ray analysis[196] and IR studies.[197]

The method has since been improved by showing that refluxing of aluminium tert. butoxide with excess fatty acids in benzene solution yielded the tri-soaps[198] without the necessity of any fractionation.

6.2. *Synthesis*

In view of the extreme susceptibility of aluminium derivatives to hydrolysis, non-aqueous media appear to be essential for the preparation of tri-carboxylates, although, hydroxy carboxylates, $Al(OH)_{3-n}(OOCR)_n$ with $n \leqslant 2$ can also be obtained[189-193,199-201] from aqueous solutions. The following methods are therefore available for the preparation of well defined carboxylates of aluminium.

(i) *Reactions of aluminium isopropoxide or ethoxide with carboxylic acids.* Mehrotra[48] in 1953 reported the synthesis of some tri-carboxylates of aluminium viz. laurate, palmitate and stearate, with the corresponding fatty acids.

$$Al(OPr^i)_3 + 3RCOOH \xrightarrow{\text{benzene}} Al(OOCR)_3 + 3Pr^iOH\uparrow$$

(where R = $C_{11}H_{23}$; $C_{15}H_{31}$; $C_{17}H_{35}$).

Later on, a number of aluminium tri-soaps[49] were prepared by interacting aluminium isopropoxide with excess fatty acids in benzene solution and fractionating off the liberated isopropanol azeotropically with benzene.

$$Al(OPr^i)_3 + \underset{\text{(excess)}}{3RCOOH} \xrightarrow{\text{benzene}} Al(OOCR)_3 + 3Pr^iOH\uparrow.$$

The excess fatty acids were removed by repeated crystallization from dry dioxane solution.

Mixed alkoxy carboxylates of aluminium[49] have been synthesized by performing the reactions in molar ratio, 1 : 1 and 1 : 2.

$$Al(OPr^i)_3 + nRCOOH \xrightarrow{\text{benzene}} Al(OPr^i)_{3-n}(OOCR)_n + nPr^iOH\uparrow$$

(where n = 1 or 2).

The lower carboxylates (acetate, propionate and butyrate) of aluminium[47] also were prepared by the following route.

$$Al(OR)_3 + 3\begin{matrix} R'CO \\ \diagdown \\ O \\ \diagup \\ R'CO \end{matrix} \xrightarrow{\text{benzene}} Al(OOCR')_3 + 3R'COOR$$

(where R = Et or Pr^i; R′ = CH_3, C_2H_5 and C_3H_7).

(ii) *Reaction of anhydrous aluminium chloride with acid anhydrides and carboxylic acids.* Anhydrous aluminium trichloride has been reported to react with a mixture of acid anhydride and the corresponding acid yielding the corresponding tri-carboxylates.[202]

$$AlCl_3 + \begin{matrix} RCO \\ \diagdown \\ O \\ \diagup \\ RCO \\ \text{[excess]} \end{matrix} + \underset{\text{[excess]}}{RCOOH} \longrightarrow Al(OOCR)_3 + 3HCl\uparrow$$

(where R = CH_3 and C_2H_5).

These carboxylates are crystallized out from the reaction mixture in quantitative yields. The higher carboxylates of aluminium could not be synthesized from this method.

Aluminium tri-carboxylates as well as chloride carboxylates[203] have been synthesized by refluxing a mixture of anhydrous aluminium chloride and carboxylic acid in benzene solution till the evolution of hydrogen chloride ceased.

$$AlCl_3 + nRCOOH \xrightarrow{\text{benzene}} AlCl_{3-x}(OOCR)_n + nHCl\uparrow$$

(where n = 1, 2, 3 or > 3; R = $C_{11}H_{23}$, $C_{15}H_{31}$, $C_{17}H_{35}$ etc.).

Aluminium chloride carboxylates can also be synthesized by the following alternative route.[49]

$$Al(OPr^i)_{3-n}(OOCR)_n + (3-n)CH_3COCl \xrightarrow{\text{benzene}} Al(Cl)_{3-n}(OOCR)_n + (3-n)CH_3COOPr^i$$

(where n = 1 or 2).

6.3. *Physico-chemical and structural properties*

The lower carboxylates of aluminium like acetates, propionates etc. are sparingly soluble in common organic solvents and the solubility increases with increasing hydrocarbon chain length.

The molecular complexity of aluminium tri-carboxylates in non-aqueous solvents has been studied by many workers[197,204,205] and it has been reported that these derivatives are highly associated in solution. However, molecular weight measurement by Rai and Mehrotra[206] have shown that these derivatives do not depict any tendency of association in refluxing solution, i.e. these are monomeric in nature, but even traces of moisture increase the molecular complexity to such an extent as to exceed the limit of its measurement.[198] The reported increase in viscosity[204,205] with increasing hydrolysis also supports the above observation.

On the basis of IR studies of aluminium tri-laurate in dilute and concentrated solutions, Leger *et al.*[197] suggested the presence of both intra- and intermolecularly-coordinated carboxylate groups.

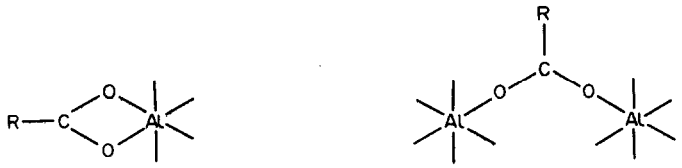

However, Rai and Mehrotra[206] have reported that on refluxing in benzene, the monomeric form is attained by aluminium tri-carboxylates, which may be represented by the following structure.

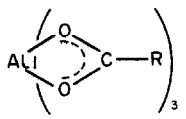

In contrast to aluminium tri-carboxylates, the corresponding alkoxide and chloride carboxylates are reported to be dimeric[206] and trimeric,[203] respectively.

Aluminium carboxylates are highly susceptible to hydrolysis, which explains the repeated failures of earlier workers[183,186,188,192,205,207] to isolate them in the pure state. Aluminium carboxylates including alkoxide carboxylates are non-volatile in nature. The mixed monoisopropoxide bis-carboxylates of aluminium on heating under reduced pressure yield oxide carboxylates and esters.[208]

$$Al(OPr^i)(OOCR)_2 \xrightarrow[\text{under reduced pressure}]{\text{heat}} AlO(OOCR) + RCOOPr^i\uparrow.$$

These oxide carboxylates exhibit association of the order of 9–10 in benzene solution[208] and may have either a ring or chain structure. These oxide carboxylates have also been prepared by the following alternative route.

$$Al(OPr^i)_2(OOCR) + HOH \xrightarrow[\text{heat}]{\text{benzene}} Al(OPr^i)(OH)(OOCR) + Pr^iOH\uparrow$$

$$Al(OPr^i)(OH)(OOCR) \xrightarrow{\sim 170^\circ C} AlO(OOCR) + Pr^iOH\uparrow.$$

These oxide carboxylates are highly soluble in organic solvents and are hydrolytically more stable.

Aluminium triacetate with a heat of formation of -451.8 Kcal mol^{-1}, gives a basic salt $[Al_3(OH)_2(OOCCH_3)_6]^+$ when subjected to hydrolysis.[209] With liquid ammonia, it forms an adduct at lower temperature and undergoes decomposition at room temperature with evolution of ammonia.[210,211]

Aluminium triacetate undergoes decomposition with the loss of acetic anhydride at about 120–140°C and gets converted to oxyacetate at about 200°C.[211]

$$2Al(OOCCH_3)_3 \xrightarrow{120\text{–}140^\circ} Al_2(OOCCH_3)_4O + \begin{matrix} CH_3CO \\ \diagdown \\ \quad O \\ \diagup \\ CH_3CO \end{matrix}$$

$$Al_2(OOCCH_3)_4O \xrightarrow{\sim 200^\circ C} 2AlO(OOCCH_3) + \begin{matrix} H_3C\text{—}CO \\ \diagdown \\ \quad O. \\ \diagup \\ H_3C\text{—}CO \end{matrix}$$

Themogravimetric studies have shown that higher carboxylates like laurate, palmitate, stearate etc. of aluminium undergo decomposition[212,213] with the formation of ketones at about 200°C. Initially, the decomposition proceeds with the evolution of carbon dioxide, the ketone formed during the course of reaction decomposes above 300°C. The DTG curves for these tri-carboxylates have the same nature but different decomposition temperatures.

$$2Al(OOCR)_3 \xrightarrow{\sim 200^\circ C} Al_2O_3 + 3CO_2 + 3\ \begin{matrix} R \\ \diagdown \\ C{=}O \\ \diagup \\ R \end{matrix}$$

$$\begin{matrix} R \\ \diagdown \\ C{=}O \\ \diagup \\ R \end{matrix} \xrightarrow{> 300^\circ C} CO_2 + H_2O.$$

The alkoxide or chloride soaps undergo two step decomposition. The initial decomposition is due to the hydrolysis from the atmospheric moisture.

$$Al(OPr^i)_2(OOCR) + HOH \xrightarrow{120\text{–}250^\circ} Al(OH)(OPr^i)(OOCR) + Pr^iOH\uparrow$$

$$\downarrow \sim 200^\circ C$$

$$Al_2O_3 + \begin{matrix} R \\ \diagdown \\ C{=}O \\ \diagup \\ R \end{matrix} + CO_2 \xleftarrow{> 300^\circ C} AlO(OOCR) + Pr^iOH\uparrow.$$

$$\downarrow > 300^\circ C$$

$$CO_2 + H_2O$$

The two step decomposition has been observed in the derivatogram of both alkoxide and chloride carboxylates of aluminium.[212,213] The oxide carboxylates, synthesized by the hydrolysis of alkoxide carboxylates also follow a similar pattern as has been observed in the decomposition of alkoxide carboxylates.

7. ALKANOLAMINE DERIVATIVES OF ALUMINIUM

A reference has already been made to the reactions of aluminium alkoxides with alkanolamines.[56,57] Hein and Albert[214] reported the synthesis of alumatrane by heating a mixture of aluminium isopropoxide and triethanolamine.

$$Al(OPr^i)_3 + N(CH_2CH_2OH)_3 \xrightarrow{\text{heat above m.p.}} Al[(OCH_2CH_2)_3N] + 3Pr^iOH\uparrow.$$

Mehrotra and Mehrotra[56] studied these reactions in detail. These reactions can be represented by the following equations.

$$Al(OPr^i)_3 + nNH_2CH_2CH_2OH \xrightarrow{\text{benzene}} Al(OPr^i)_{3-n}(OCH_2CH_2NH_2)_n + nPr^iOH\uparrow$$

(where n = 1, 2 and 3)

$$Al(OPr^i)_3 + HN(CH_2CH_2OH)_2 \xrightarrow{\text{benzene}} Al(OPr^i)[(OCH_2CH_2)_2NH] + 2Pr^iOH\uparrow$$

$$2Al(OPr^i)_3 + 3HN(CH_2CH_2OH)_2 \xrightarrow{\text{benzene}} [HN(CH_2CH_2O)_2]Al$$

$$[O\text{-}CH_2CH_2NHCH_2CH_2O\text{-}]Al[(OCH_2CH_2)_2NH] + 6Pr^iOH\uparrow$$

$$Al(OPr^i)_3 + N(CH_2CH_2OH)_3 \xrightarrow{\text{benzene}} Al[(OCH_2CH_2)_3N] + 3Pr^iOH\uparrow.$$

The progress of all these reactions was followed by estimating the isopropanol liberated and collected in the azeotrope with benzene. It may be interesting to record that only the hydroxy groups of mono- and dialkanolamines appear to be reactive in these replacement reactions, which is in contrast to the observations made in the reactions of germanium[215] and tin[216] alkoxides in which both the amino and hydroxy groups are reactive, leading to a ring compound.

The molecular weight measurements of the derivatives $Al(OPr^i)(OCH_2CH_2)_2NH$, $Al_2[(OCH_2CH_2)_2NH]_3$ and $Al(OCH_2CH_2)_3N$ in refluxing benzene showed that the former two are essentially tetrameric whereas the last one is hexameric (cf. its octameric nature reported[214]).

Recently, the reactions of aluminium isopropoxide with substituted mono-alkanolamines[57] in different molar ratios have been shown to yield compounds of the type $Al(OPr^i)_{3-n}(OXNR_1R_2)_n$ (where R_1 = H, CH_3, C_2H_5; R_2 = H, CH_3, C_2H_5 and X = CH_2—CH_2—, —CH_2—CH_2—CH_2—, —CH_2CHCH_3—, —$C_6H_4CH_2 \cdot CH_2$—; n = 1–3). Most of these derivatives are distillable liquids, which are tetrameric in boiling benzene solution. Structures[57] similar to that of tetrameric aluminium isopropoxide have been suggested for these derivatives.

Triethanolamine has been shown to cleave Al—C bonds in triethylaluminium in toluene or hexane solution to form alumatrane.[217]

$$Al(C_2H_5)_3 + (HOCH_2CH_2)_3N \longrightarrow Al(OCH_2CH_2)_3N + 3C_2H_6\uparrow$$

which was shown by mass spectroscopy[218] to be a dimer in the gaseous phase; the following structure has, therefore, been suggested by Voronkov and Baryshok[219] for this derivative.

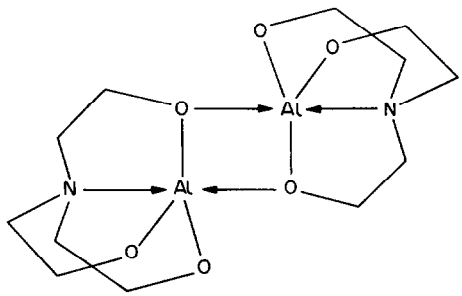

An interesting compound $[N(CH_2CH_2O)_3Al_2(CH_3)_3]_2$[220] has been synthesized by the reaction of $AlMe_3$ with triethanolamine, the structure of which is represented below (Fig. 11).

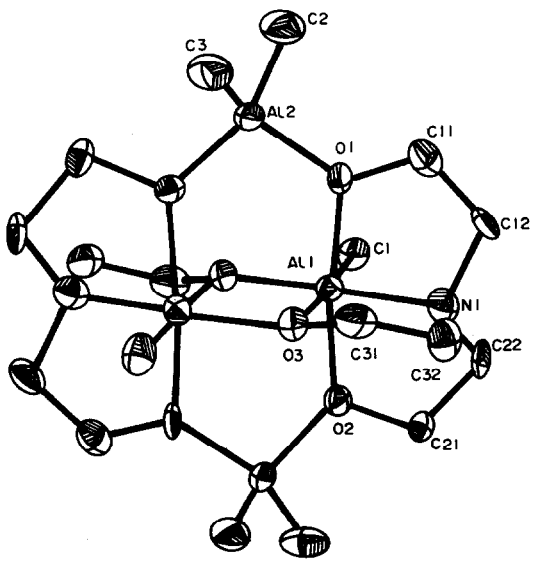

Fig. 11. Crystal structure of $[N(CH_2CH_2O)_3Al_2(CH_3)_3]_2$.[220]

The Al_4O_6 core in the above structure consists of two six-coordinate and two four-coordinate aluminiums and is unlike the one reported previously[221] containing one central octahedral aluminium surrounded by three tetrahedral aluminium isopropoxides. Thus $[N(CH_2CH_2O)_3Al_2(CH_3)_3]_2$ appears to be the first example of a six-coordinate organometallic aluminium derivative.

8. CONCLUSION

The above brief review of the interrelated chemistry of alkoxides, β-diketonates and carboxylates of aluminium indicates that although these derivatives have been known for a long time, they still continue to reveal interesting features. In view of the rapidly growing importance of aluminium oxides in the ceramics industry, the hydrolysis of aluminium alkoxides has been actively pursued[40] during the last few years but further intensive studies on the hydrolytic reactions of aluminium alkoxides including polymetallic derivatives, carboxylates and isomerization studies of β-diketonates are expected to reveal novel features of both academic as well as industrial significance.

The Al—O π-interactions indicated from structural features of recently synthesized hindered phenoxide derivatives of aluminium alkyls are very interesting and should lead to a better understanding of the nature of bonds in such derivatives.

REFERENCES

1. R. C. Mehrotra, *J. Indian Chem. Soc.* 1953, **30**, 585.
2. D. C. Bradley, R. C. Mehrotra and D. P. Gaur, *Metal Alkoxides*. Academic Press, London (1978).
3. W. E. Tistschenko, *J. Russ. Phys. Chem. Soc.* 1899, **31**, 694.
4. J. H. Gladstone and A. Tribe, *J. Chem. Soc.* 1881, 394.
5. R. Muller and O. Sussenguth, German Patent No. 2278550 (1940), *Chem. Abst.* 1942, **35**, 29065.
6. J. Lukasiak, L. A. May, I. Ya. Strauss and R. Piekos, *Rocz. Chem.* 1970, **44**, 1675.
7. G. H. Densin Jr and A. C. Ettling, U.S. Patent No. 2292205 (1942), *Chem. Abstr.* 1943, **37**, 655.
8. S. Teischner, *Comptl Rendul.*, 1953, **237**, 810.
9. H. Funk, J. Schormuller and W. Hensinger, *Z. Anorg. Allg. Chem.* 1932, **205**, 361.
10. R. K. Mehrotra and R. C. Mehrotra, *Z. Anorg. Allg. Chem.* 1961, **311**, 198.
11. V. A. Kozunov, N. I. Koglova and N. Ya. Turova, *Zh. Neorg. Khim.* 1979, **24(6)**, 1526.
12. A. I. Yanovskii, V. A. Kozunov, N. Ya. Turova, M. G. Fumanova and Yu. T. Struchkov, *Dokl. Akad. Nauk. SSSR* 1979, **244**, 119.
13. R. C. Mehrotra, Transition metal alkoxides. In *Recent Advances in Inorganic Radiochemistry* (Edited by H. G. Emeleus and A. G. Sharpe), Vol. 26, p. 269. Academic Press, London (1983).
14. R. C. Mehrotra, *J. Indian Chem. Soc.* 1954, **31**, 85.
15. P. G. David, F. David and V. J. Schiner, *Cienc. Cult.* 1975, **27**, 50.
16. R. C. Mehrotra, unpublished work.
17. R. H. Baker, *J. Am. Chem. Soc.* 1938, **60**, 2673.
18. R. C. Mehrotra, *Inorg. Chim. Acta (Reviews)* 1967, **1**, 99.
19. R. C. Mehrotra and P. N. Kapoor, *J. Less-Common Met.* 1964, **7**, 98; 1966, **10**, 66.
20. T. Mole and E. A. Jeffery, *Organoaluminium Compounds*. Elsevier, Amsterdam (1972).
21. J. J. Esich, *Comprehensive Organometallic Chemistry* (Edited by G. Wilkinson, F. G. A. Stone and E. W. Abel), Vol. 1, Ch. 6. Pergamon, Oxford (1982).
22. V. A. Shreider, E. P. Turevskaya, N. I. Koslova and N. Ya. Turova, *Inorg. Chim. Acta* 1981, **53**, 173.
23. H. Ulich and W. Nespital, *Z. Phys. Chem.* 1933, **165**, 294.
24. R. A. Robinson and D. A. Peak, *J. Phys. Chem.* 1935, **39**, 1125.
25. S. M. McElvain and W. R. Davie, *J. Am. Chem. Soc.* 1951, **73**, 1400.
26. N. Ya. Turova, V. A. Kozunov, A. I. Yanovskii, N. G. Bokii, Yu. T. Struchkov and B. L. Tarnopolskii, *J. Inorg. Nucl. Chem.* 1979, **41**, 5.
27. W. Fieggen and H. Gerding, *Rec. Trav. Chim.* 1968, **87**, 377; 1970, **89**, 175; 1971, **90**, 410; 1972, **91**, 477.
28. V. J. Shiner and D. Whittaker, *J. Am. Chem. Soc.* 1963, **85**, 2318; 1969, **91**, 394.
29. D. C. Kleinschmidt, V. J. Shiner and W. Whittaker, *J. Org. Chem.* 1973, **38**, 3334.
30. L. W. Daasch and H. M. Fales, *Org. Mass-Spec.* 1969, **2**, 1043.
31. L. M. Brown and K. S. Mazdiyasni, *Analyt. Chem.* 1969, **41**, 1243.
32. W. C. Child and H. Adkins, *J. Am. Chem. Soc.* 1923, **45**, 3013.
33. G. P. Shulman, M. Trusty and J. H. Vickers, *J. Org. Chem.* 1963, **28**, 907.
34. M. K. Dongare and A. P. B. Sinha, *Thermochim. Acta* 1982, **57**, 37.
35. G. Pfeifer and T. Flora, *Magy. Kém. Foly.* 1964, **70**, 375.

36. R. S. Macomber, J. C. Ford and W. H. Wenzel, *Synth. React. Inorg. Metal-Org. Chem.* 1977, **7**, 111.
37. D. C. Bradley, Polymetallic Metal Alkoxides, Organosiloxanes and Organometalloxanosiloxanes. In *Inorganic Polymers* (Edited by F. G. A. Stone and W. G. A. Grahm). Academic Press, New York (1962).
38. S. Sakka, in *Treatise on Material Science and Technology*, (Edited by M. Tomozawa and R. Dormeus), Vol. 22, Glass III. Academic Press, New York (1982).
39. R. C. Mehrotra, *J. Non-Cryst. Solids* 1988, **100**, 1.
40. J. Y. Chane-Ching' and L. C. Klein, *J. Am. Ceram. Soc.* 1988, **71**, 83, 86; and refs therein.
41. M. S. Bains and D. C. Bradley, *Can. J. Chem.* 1962, **40**, 2218.
42. M. D. Healy, D. A. Wierda and A. R. Barron, *Organometallics* 1988, **7**, 2543.
43. D. C. Bradley, F. M. Abdel Halim and W. Wardlaw, *J. Chem. Soc.* 1950, 3450.
44. R. C. Mehrotra and R. K. Mehrotra, *J. Indian Chem. Soc.* 1962, **39**, 635.
45. R. K. Mehrotra and R. C. Mehrotra, *Can. J. Chem.* 1961, **39**, 795.
46. J. H. Wengrovius, M. F. Garbauskas, E. A. Williams, R. C. Going, P. E. Donahue and J. F. Smith, *J. Am. Chem. Soc.* 1986, **108**, 982.
47. R. C. Mehrotra and K. C. Pande, *Z. Anorg. Allg. Chem.* 1956, **286**, 291.
48. R. C. Mehrotra, *Nature* 1953, **172**, 74.
49. R. C. Mehrotra and K. C. Pande, *J. Inorg. Nucl. Chem.* 1956, **2**, 60; 1957, **4**, 128.
50. R. C. Mehrotra, *J. Indian Chem. Soc.* 1961, **38**, 509.
51. A. K. Rai, R. K. Mehrotra and R. C. Mehrotra, *J. Pract. Chem.* 1963, **20**, 65.
52. A. Singh, A. K. Rai and R. C. Mehrotra, *Indian J. Chem.* 1973, **11**, 478.
53. L. Nigam, V. D. Gupta and R. C. Mehrotra, *Indian J. Chem.* 1981, **20A**, 65.
54. R. C. Mehrotra and S. C. Goel, *Indian J. Chem.* 1981, **20A**, 1054.
55. R. Ahmad, G. Srivastava and R. C. Mehrotra, *Indian J. Chem.* 1983, **22A**, 32.
56. R. K. Mehrotra and R. C. Mehrotra, *J. Indian Chem. Soc.* 1962, **39**, 677.
57. R. C. Mehrotra and R. Duggal, *Inorg. Chim. Acta* 1985, **98**, 159.
58. W. Tianyong, Iu Kaijuan and Wu. Guanil, *Huaxue Tongbao* 1986, **5**, 33.
59. J. Dayal and R. C. Mehrotra, *Synth. React. Inorg. Metal-Org. Chem.* 1971, **1**, 287.
60. J. Dayal and R. C. Mehrotra, *Indian J. Chem.* 1972, **10**, 435.
61. M. Agarwal, J. P. Tandon and R. C. Mehrotra, *Indian J. Chem.* 1979, **18A**, 151.
62. M. Agarwal, J. P. Tandon and R. C. Mehrotra, *J. Inorg. Nucl. Chem.* 1979, **41**, 1405.
63. J. Dayal and R. C. Mehrotra, *Z. Naturf.* 1972, **27**, 25.
64. K. L. Chawla, P. Parashar and J. P. Tandon, *J. Indian Chem. Soc.* 1972, **49**, 533.
65. R. G. Vijay and J. P. Tandon, *Mh. Chem.* 1976, **107**, 95.
66. J. P. Tandon, S. R. Gupta and R. N. Prasad, *Mh. Chem.* 1976, **107**, 1329.
67. M. Agarwal, J. P. Tandon and R. C. Mehrotra, *J. Indian Chem. Soc.* 1979, **56**, 758.
68. M. Agarwal, J. P. Tandon and R. C. Mehrotra, *Synth. React. Inorg. Metal-Org. Chem.* 1980, **10**, 9.
69. M. Agarwal, J. P. Tandon and R. C. Mehrotra, *Curr. Sci.* 1981, **50**, 174.
70. D. Seidel, E. G. Jaeger and W. Schade, *Z. Chem.* 1984, **24**, 334.
71. K. K. Chaturvedi, R. V. Singh and J. P. Tandon, *Synth. React. Inorg. Metal-Org. Chem.* 1985, **15**, 309.
72. J. Uttamchandani and R. N. Kapoor, *Indian J. Chem.* 1985, **24A**, 242.
73. V. Chaturvedi and J. P. Tandon, *Indian J. Chem.* 1985, **24A**, 422.
74. K. K. Chaturvedi, R. V. Singh and J. P. Tandon, *J. Prakt. Chem.* 1985, **327**, 144.
75. R. K. Mehrotra and R. C. Mehrotra, *J. Indian Chem. Soc.* 1962, **39**, 23.
76. R. K. Mehrotra and R. C. Mehrotra, *J. Prakt. Chem.* 1962, **16**, 251.
77. R. A. Misra and R. C. Mehrotra, *Can. J. Chem.* 1964, **42**, 717.
78. R. A. Misra and R. C. Mehrotra, *J. Indian Chem. Soc.* 1967, **44**, 37.
79. D. L. Guertin, S. E. Wiberley, W. H. Bauer and J. Goldenson, *J. Phys. Chem.* 1936, **60**, 1018.
80. J. V. Bell, J. Heisler, H. Tannennbaum and J. Goldenson, *Analyt. Chem.* 1953, **25**, 1720.
81. R. C. Wilhoit, J. R. Burton, Fu-Tienkuo, Sue-Rong Huang and A. Viquesnel, *J. Inorg. Nucl. Chem.* 1962, **24**, 851.
82. C. G. Barraclough, D. C. Bradley, J. Lewis and I. M. Thomas, *J. Chem. Soc.* 1961, 2601.
83. M. S. Bains, *Can. J. Chem.* 1962, **40**, 381.
84. V. J. Shiner Jr, D. Whittaker and V. P. Fernandez, *J. Am. Chem. Soc.* 1963, **85**, 2318.
85. J. G. Oliver and I. J. Worrall, *J. Chem. Soc.* 1970, 845.
86. D. C. Bradley, *Nature* 1958, **182**, 1211.
87. D. C. Bradley, *Metal Alkoxides, Progress in Inorganic Chemistry*, Vol. II, p. 303. Interscience, New York (1960).
88. R. C. Mehrotra and A. Mehrotra, *J. Chem. Soc., Chem. Commun.* 1972, 189.
89. R. C. Mehrotra and A. Mehrotra, *Proc. Indian Nat. Sci. Acad.* 1974, **40**, 215.
90. J. N. Huckerby, J. G. Oliver and I. J. Worrall, *J. Chem. Soc., Chem. Commun.* 1968, 918.
91. J. G. Oliver, P. K. Philips and I. J. Worrall, *J. Inorg. Nucl. Chem.* 1969, **31**, 1609.

92. J. W. Akitt and R. H. Duncan, *J. Magn. Reson.* 1974, **15**, 162.
93. E. L. Amma, *J. Inorg. Nucl. Chem.* 1963, **25**, 779.
94. A. P. Shreve, R. Mulhaupt, W. Fultz, J. Calabrese, W. Robbins and S. D. Ittel, *Organometallics* 1988, **7**, 409.
95. G. A. Anderson, F. R. Forgaard and A. Haaland, *Acta Chem. Scand.* 1972, **26**, 1947.
96. M. H. Chisholm and I. P. Rothwell, *Alkoxides and Aryloxides, Comprehensive Coordination Chemistry* (Edited by G. Wilkinson, R. D. Gillard and J. A. McCleverty), Vol. 2, p. 235. Pergamon Press, Oxford (1987).
97. H. Meerwein and T. Bersin, *Ann.* 1929, **476**, 113.
98. H. Albers, H. Deutsch, W. Krastinak and H. Von Osten, *Chem. Ber.* 1952, **85**, 267.
99. H. Gilman, G. A. Martin and R. G. Jones, *J. Am. Chem. Soc.* 1956, **78**, 6027.
100. R. Gut, *Helv. Chem. Acta* 1964, **47**, 2262.
101. N. C. Jain, A. K. Rai and R. C. Mehrotra, *Indian J. Chem.* 1976, **14A**, 256.
102. A. Mehrotra and R. C. Mehrotra, *Inorg. Chem.* 1972, **11**, 2170.
103. A. Mehrotra and R. C. Mehrotra, *J. Chem. Soc. A* 1972, 1203.
104. R. C. Mehrotra and M. M. Agarwal, *J. Chem. Soc., Chem. Commun.* 1968, 459.
105. R. C. Mehrotra, M. M. Agarwal and A. Mehrotra, *Synth. React. Inorg. Metal-Org. Chem.* 1973, **3**, 181.
106. R. C. Mehrotra, J. M. Batwara and P. N. Kapoor, *Coord. Chem. Rev.* 1980, **31**, 67.
107. N. C. Jain, A. K. Rai and R. C. Mehrotra, *J. Inorg. Nucl. Chem.* 1978, **40**, 349.
108. R. R. Goel, N. C. Jain and R. C. Mehrotra, *Synth. React. Inorg. Metal-Org. Chem.* 1981, **11**, 345.
109. M. C. Aggrawal and R. C. Mehrotra, *Synth. React. Inorg. Metal-Org. Chem.* 1984, **14**, 139.
110. M. Aggrawal, C. K. Sharma and R. C. Mehrotra, *Synth. React. Inorg. Metal-Org. Chem.* 1983, **13**, 571.
111. J. V. Singh and R. C. Mehrotra, *Inorg. Chem.* 1984, **23**, 1046.
112. J. V. Singh, Ph.D. thesis, Delhi University, Delhi, India (1980).
113. J. V. Singh, N. C. Jain and R. C. Mehrotra, *Synth. React. Inorg. Metal-Org. Chem.* 1979, **9**, 79.
114. J. V. Singh and R. C. Mehrotra, *J. Coord. Chem.* 1984, **13**, 273.
115. J. V. Singh and R. C. Mehrotra, *Can. J. Chem.* 1984, **62**, 1003.
116. J. V. Singh and R. C. Mehrotra, *Z. Anorg. Allg. Chem.* 1984, **522**, 211.
117. R. C. Mehrotra, *Coord. Chem. (IUPAC)* 1981, **21**, 113.
118. R. Jain, A. K. Rai and R. C. Mehrotra, *Synth. React. Inorg. Metal-Org. Chem.* 1985, **15**, 789.
119. S. Govil, P. N. Kapoor and R. C. Mehrotra, *Inorg. Chim. Acta* 1975, **15**, 43.
120. S. Govil and R. C. Mehrotra, *Synth. React. Inorg. Metal-Org. Chem.* 1975, **5**, 267.
121. B. P. Baranwal and R. C. Mehrotra, *Aust. J. Chem.* 1980, **33**, 37.
122. K. Jones, T. J. Davies, H. G. Emblem and P. Parkes, *Mat. Res. Soc. Sym. Proc.* 1986, **73**, 111; and refs therein.
123. A. Mehrotra, Ph.D. thesis, University of Rajasthan, Jaipur, India (1971).
124. M. C. Aggrawal, Ph.D. thesis, University of Rajasthan, Jaipur, India (1984).
125. R. C. Mehrotra and J. V. Singh, *Trans. Met. Chem.* 1984, **9**, 148.
126. R. C. Mehrotra and M. Aggrawal, *Polyhedron* 1985, **4**, 1141.
127. M. Aggrawal and R. C. Mehrotra, *Polyhedron* 1985, **4**, 845.
128. R. K. Dubey, A. Singh and R. C. Mehrotra, *Inorg. Chim. Acta* 1988, **143**, 169.
129. R. K. Dubey, Ph.D. thesis, University of Rajasthan, Jaipur, India (1987).
130. R. K. Dubey, A. Shah, A. Singh and R. C. Mehrotra, *Recl. Trans. Chim. Pays-bas* 1988, **107**, 237.
131. H. Okamura and H. K. Brown, *Ceram. Int.* 1986, **12**, 161.
132. R. J. Ayen and J. H. Burk, *Mat. Res. Soc. Symp. Proc.* 1986, **73**, 80.
133. B. E. Yoldas, *J. Mater. Sci.* 1986, **21**, 1080.
134. S. H. Kwon and S. J. Chung, *Phys. Chem. Glasses* 1987, **28**, 28.
135. S. Hirano, T. Hayashi and T. Kogcyama, *J. Am. Ceram. Soc.* 1987, **70**, 171.
136. A. Verley, *Bull. Soc. Chem. Fr.* 1925, **37**, 537.
137. H. Meerwein and R. Schmidt, *Justus Liebigs Annln Chem.* 1925, **444**, 221.
138. W. Ponndorf, *Z. Angew. Chem.* 1926, **39**, 138.
139. L. M. Jackman and A. K. J. Macbeth, *J. Chem. Soc.* 1952, 3252.
140. D. Nasipuri, M. D. Gupta and S. Banerjee, *Tetrahedron Lett.* 1984, **25**, 5551.
141. D. Nasipuri, A. K. Samadar and M. D. Gupta, *Proc. Indian Acad. Sci. (Chem. Sci.)* 1984, **93**, 601; and refs therein.
142. E. L. Eliel and D. Nasipuri, *J. Org. Chem.* 1965, **30**, 3809.
143. R. C. Mehrotra, R. Bohra and D. P. Gaur, *Metal β-Diketonates and Allied Derivatives.* Academic Press, London (1978).
144. A. R. Siedle, *Comprehensive Coordination Chemistry* (Edited by G. Wilkinson, R. D. Gillard and J. A. McCleverty), Vol. 2, p. 365. Pergamon, Oxford (1987).
145. J. P. Fackler Jr., *Prog. Inorg. Chem.* 1966, **7**, 361.

146. D. P. Graddon, *Coord. Chem. Rev.* 1969, **4**, 1.
147. H. Bock, K. Flatau, H. Junge, M. Kuhr and H. Musso, *Angew. Chem. Int. Ed. Engl.* 1971, **10**, 225.
148. D. W. Thomson, *Struct. and Bonding (Berlin)* 1971, **9**, 27.
149. R. C. Mehrotra, *Pure Appl. Chem.* 1988, **60**, 1349.
150. A. L. Allred and D. W. Thompson, *Inorg. Chem.* 1968, **7**, 1196.
151. A. R. Siedle and L. H. Pignolet, *Inorg. Chem.* 1982, **21**, 135.
152. G. H. Bullen, R. Mason and P. Pauling, *Inorg. Chem.* 1965, **4**, 456.
153. L. Bouveault and A. Bongert, *Compt. Rend.* 1901, **132**, 703.
154. L. Bouveault and A. Bongert, *Bull. Soc. Chim.* 1902, **27**, 1084.
155. A. Hantzsch and C. H. Desch, *Annln* 1902, **323**, 1.
156. V. Kohler, *Am. Chem. J.* 1902, **24**, 355.
157. A. N. Sarkar, *Phil Mag.* 1926, **2**, 1153.
158. G. T. Morgan and H. D. K. Drew, *J. Chem. Soc.* 1921, **119**, 1058.
159. A. G. Charles, N. C. Paterson and G. H. Franke, *Inorg. Synth.* 1967, **9**, 25.
160. L. Maijs and I. Vevere, *Latv. PSR Zinat. Akad. Vestis., Khim. Ser.* 1969, 497; *Chem. Abstr.* 1970, **72**, 18009.
161. Y. P. Singh and A. K. Rai, *Synth. React. Inorg. Metal-Org. Chem.* 1982, **12**, 85.
162. Y. P. Singh, S. Saxena and A. K. Rai, *Synth. React. Inorg. Metal-Org. Chem.* 1984, **14**, 237.
163. J. J. Fortman and R. E. Sievers, *Inorg. Chem.* 1967, **6**, 2022.
164. R. G. Link and R. E. Sievers, *Inorg. Chem.* 1966, **5**, 806.
165. I. Vevere, L. Maijs and D. Reikstina, *Latv. PSR Zinat. Akad. Vestis., Khim. Ser.* 1970, 405; 1971, **74**, 27067.
166. R. C. Mehrotra, *J. Indian Chem. Soc.* 1982, **59**, 715.
167. R. Jain, A. K. Rai and R. C. Mehrotra, *Polyhedron* 1986, **5**, 1017.
168. R. W. Moshier and R. E. Sievers, *Gas Chromatography of Metal Chelates.* Pergamon Press, Oxford (1965).
169. R. E. Sievers, J. W. Conolly and W. D. Ross, *J. Gas Chromat.* 1967, **5**, 241.
170. R. E. Sievers, K. J. Eisentraut, C. S. Springer Jr and D. W. Meek, *Adv. Chem. Ser.* 1967, **NO71**, 141.
171. C. S. Springer Jr, D. W. Meek and R. E. Sievers, *Inorg. Chem.* 1967, **6**, 1105.
172. K. Utsunomiya, *Bull. Chem. Soc. Japan* 1971, **44**, 2688.
173. R. Belcher, C. R. Carnley, J. R. Majer, W. I. Stephen and P. C. Uden, *Analyt. Chim. Acta* 1970, **50**, 423.
174. R. C. Fay and T. S. Piper, *J. Am. Chem. Soc.* 1962, **84**, 2303.
175. R. C. Fay and T. S. Piper, *J. Am. Chem. Soc.* 1963, **85**, 500.
176. R. C. Fay and T. S. Piper, *Inorg. Chem.* 1964, **3**, 348.
177. F. Basolo and R. G. Pearson, *Mechanism of Inorganic Reactions*, 1st edn. Wiley Eastern Reprint, New Delhi (1973).
178. W. T. Astbury, *Proc. Roy. Soc.* 1926, **A112**, 449.
179. E. A. Shugam and L. M. Shkol'nikova, *Kristallografia* 1959, **4**, 419.
180. E. A. Shugam and L. M. Shkol'nikova, *Dokl. Akad. Nauk SSSR* 1960, **133**, 386, 811.
181. M. F. Garbauskas, J. H. Wengrovius, R. C. Going and J. S. Kasper, *Acta Cryst. Sect. C, Cryst. Struct. Commun.* 1984, **C40**, 1536.
182. F. J. Licata, *Metallic Soaps.* Metasap Chemical Company, New Jersey (1940).
183. S. B. Elliot, *Alkaline Earth and Heavy Metal Soaps.* Reinhold Publishing Corporation, New York (1946).
184. R. C. Mehrotra, Wissenschaftliche Zeitschrift Der Friedrich-Schiller-Universitat Jena, Mathematisch-Naturwissenschaft-liche Reihe. Heft 2, 1965, **14**, 171.
185. R. C. Mehrotra and R. Bohra, *Metal Carboxylates.* Academic Press, London (1983).
185(a). W. H. C. Ruegeberg, *J. Phys. Colloid Chem.* 1948, **52**, 1444.
186. V. R. Gray and A. E. Alexander, *J. Phys. Chem.* 1949, **53**, 23.
187. E. Markowicz, *Farben Ztg.* 1928, **34**, 326, 414, 503.
188. J. W. McBain and W. L. McLatchie, *J. Am. Chem. Soc.* 1932, **54**, 3266.
189. Wo. Ostwald and R. Riedel, *Kolloid Z.* 1934, **69**, 185.
190. E. Eigenberger, *Fette U. Seifen* 1940, **49**, 505.
191. E. Eigenberger and A. Eigenberger-Bittner, *Kolloid Z.* 1940, **91**, 287.
192. G. H. Smith, H. H. Pomeroy, C. G. McGee and K. J. Mysels, *J. Am. Chem. Soc.* 1948, **70**, 1053.
193. C. G. McGee, *J. Am. Chem. Soc.* 1949, **71**, 278.
194. J. S. Glazer, T. S. McRoberts and J. H. Schulman, *J. Chem. Soc.* 1950, 2082.
195. A. S. C. Lawrence, *J. Inst. Petrol.* 1945, **31**, 303.
196. A. Gilmour, A. Jobling and S. M. Nelson, *J. Chem. Soc.* 1956, 1972.
197. A. E. Legar, R. L. Hains, C. E. Hubley, Z. C. Hyde and H. Sheffer, *Can. J. Chem.* 1957, **35**, 799.
198. A. K. Rai, Ph.D. thesis, University of Gorakhpur, Gorakhpur, India (1962).
199. R. H. Coe, K. J. Mysels and G. H. Smith, *J. Colloid Sci.* 1943, **3**, 293.

200. G. Spacu and E. Popper, *Kolloid Z.* 1943, **103**, 19.
201. S. S. Marsden Jr, K. J. Mysels, G. H. Smith and S. Ross, *J. Am. Oil. Chem. Soc.* 1948, **25**, 454.
202. G. C. Hood and A. J. Ihde, *J. Am. Chem. Soc.* 1950, **72**, 2094.
203. A. K. Rai and R. C. Mehrotra, *J. Indian Chem. Soc.* 1962, **39**, 1.
204. H. Sheffer, *Can. J. Res.* 1948, **26B**, 481.
205. T. S. McRoberts and J. H. Schulman, *Proc. Roy. Soc.* 1950, **A200**, 136.
206. A. K. Rai and R. C. Mehrotra, *J. Inorg. Nucl. Chem.* 1962, **24**, 961.
207. W. W. Harple, S. E. Wiberly and W. H. Bauer, *Analyt. Chem.* 1952, **24**, 635.
208. A. K. Rai and R. C. Mehrotra, *Indian J. Chem.* 1966, **4**, 295.
209. C. T. Mortimer and P. W. Sellers, *J. Chem. Soc.* 1963, 1978.
210. V. N. Maksimov, K. N. Semenenko, T. N. Naumova and A. V. Novoselova, *Zh. Neorg. Khim.* 1960, **5**, 558.
211. A. I. Grigorev, E. G. Pogodilova and A. V. Novoselova, *Zh. Neorg. Khim.* 1960, **10**, 772.
212. A. K. Rai and R. C. Mehrotra, *J. Indian Chem. Soc.* 1963, **40**, 359.
213. R. C. Mehrotra and A. K. Rai, *Therm. Analyt. Proc. Int. Conf. 4th (1974)* (Edited by I. Buzas), Vol. 2, p. 505. London, England (1975); 1977, **87**, 84470.
214. Fr. Hein and P. W. Albert, *Z. Anorg. Allg. Chem.* 1952, **269**, 67.
215. R. C. Mehrotra and G. Chandra, *Indian J. Chem.* 1965, **3**, 497.
216. R. C. Mehrotra and V. D. Gupta, *Indian J. Chem.* 1967, **5**, 643.
217. H. Higashi and S. Namikawa, *Kogyo Kogaku Zasshi* 1967, **70**, 93, 97.
218. M. J. Lacey and C. G. McDonald, *Aust. J. Chem.* 1976, **29**, 1118.
219. M. G. Voronkov and V. P. Baryshok, *J. Organomet. Chem.* 1982, **239**, 199.
220. M. D. Healy and A. R. Barron, *J. Am. Chem. Soc.* 1989, **111**, 398.
221. V. E. Shklover, Y. T. Struchkov, M. G. Voronkov, A. Z. Obvchinnikova and V. P. Baryshok, *Dokl. Akad. Nauk USSR* 1984, **277**, 1185.

Polyhedron Vol. 10, No. 17, pp. 1995–2023, 1991
Printed in Great Britain

0277–5387/91 $3.00+.00
© 1991 Pergamon Press plc

POLYHEDRON REPORT NUMBER 39

ALKYNE ROTATION ON A Rh—Rh BOND: AN ENTRY TO DIVERSE CHEMISTRY

RON S. DICKSON

Department of Chemistry, Monash University, Clayton, Victoria 3168, Australia

CONTENTS

1. INTRODUCTION 1995

2. RHODIUM AND HEXAFLUOROBUT-2-YNE 1997
   2.1. Reaction of $CpM(CO)_2$ with alkynes 1997
   2.2. Synthesis and physical properties of $Cp_2Rh_2(CO)_2(\mu\text{-}\eta^1\eta^1\text{-}CF_3C_2CF_3)$ (**5**) and $Cp_2Rh_2(\mu\text{-}CO)(\mu\text{-}\eta^2\text{-}CF_3C_2CF_3)$ (**9**) 1999
   2.3. Related dinuclear complexes 2000

3. REACTIVITY OF THE ALKYNE-DIRHODIUM COMPLEXES 2002
   3.1. Some reactions of $Cp_2Rh_2(CO)_2(\mu\text{-}\eta^1\eta^1\text{-}CF_3C_2CF_3)$ (**5**) 2002
   3.2. Some coordinative additions to $Cp_2Rh_2(\mu\text{-}CO)(\mu\text{-}\eta^2\text{-}CF_3C_2CF_3)$ (**9**) 2002
   3.3. C—H bond activation in reactions with unsaturated hydrocarbons 2004
   3.4. Cyclic condensation reactions with alkynes 2007
   3.5. Reactions with diazoalkanes 2011
   3.6. The addition of isocyanide and related ligands 2013

4. THE SYNTHESIS OF CLUSTERS 2015
   4.1. The strategy 2015
   4.2. Clusters of the type $Cp_2LRh_2M(CO)_{1\text{ or }3}(CF_3C_2CF_3)$ 2015
   4.3. The clusters $Cp_2(chel)Rh_3(\mu\text{-}CO)(\mu\text{-}CF_3C_2CF_3)$ 2017
   4.4. Cationic clusters $[Cp_2Rh_3(\mu\text{-}CO)(\mu\text{-}CF_3C_2CF_3)(CNR)_3]^+$ 2018
   4.5. The addition of $[Rh(CO)_2Cl]_2$ to (**9**) 2018
   4.6. Heteronuclear clusters 2019
   4.7. Ligand transfer; a limitation in cluster synthesis 2020
   4.8. The bridge-assisted formation of clusters 2021

5. CONCLUSIONS 2021

1. INTRODUCTION

Alkynes are versatile building blocks in organic synthesis. They can be used to produce products as diverse as atropic acid [eq. (1)][1] and cyclooctatetraene [eq. (2)].[2] The conversion of alkynes to different organic species is generally assisted by the presence of an appropriate metal or metal

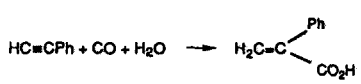

(1)

complex,[3,4] and this is a prime reason for the continuing high level of interest in interactions between alkynes and metal complexes.

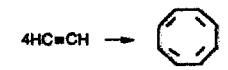

(2)

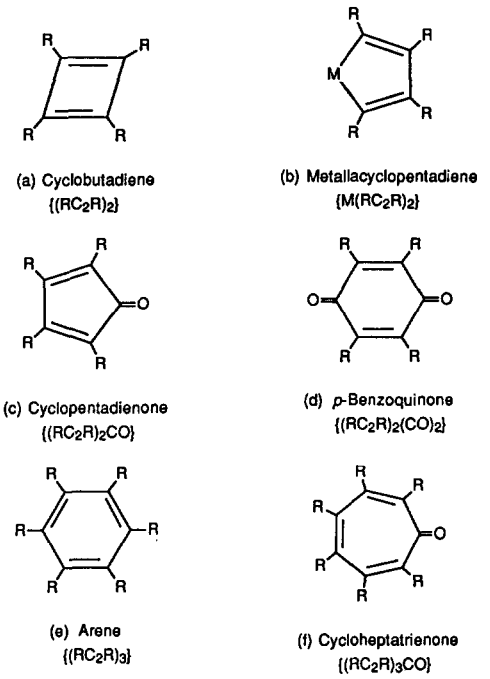

Fig. 1. Examples of cyclic ligands formed by the condensation of alkynes.

Complexes of almost all the transition metals interact in some way with alkynes. With the early transition metals, individual alkyne ligands often remain intact, even when two or more alkynes are coordinated to the same metal centre.[5] In contrast, reactions between complexes of later transition metals and alkynes frequently result in condensation of the alkyne units to form cyclic and other organic ligands.[6] Some of the many cyclic ligands that have been formed through the cyclic condensation of alkynes are given in Fig. 1, and examples of the formation of most of these ligand types are given in later sections of this report. From the perspective of organic synthesis, it is helpful if the cyclic ligand dissociates from the metal under the prevailing reaction conditions. A particular advantage that alkynes offer in metal catalysed alkyne condensation reactions is the potential to control the substituent positions in the organic product. For example, the cyclotrimerization of a terminal alkyne, HC≡CR, can conceivably yield two trisubstituted arenes, (**1**) and (**2**). However,

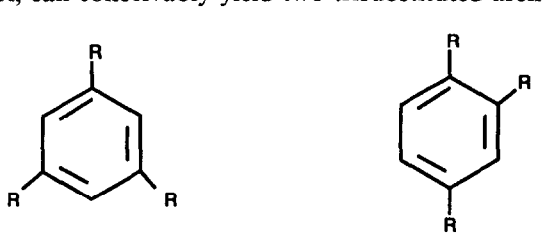

(**1**) (**2**)

such reactions catalysed by $Ni(CO)_2(PPh_3)_2$[7] or $Co_2(CO)_8$[7,8] frequently lead to preferential formation of one isomer, the 1,2,4-trisubstituted product (**2**). With the cobalt system this preference has been rationalized by identifying the substituent pattern in the key intermediate, a trisalkynedicobalt complex of formula $Co_2(CO)_4(HC_2R)_3$.[8] Similar intermediates are presumably implicated in the nickel reactions.

Coordinated alkynes are also able to add to other substrates, **X**, with formation of new C–**X** bonds. A representative example of the many reactions of this type is given in eq. (3).[9,10]

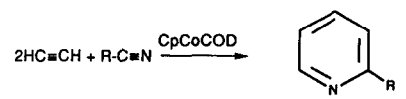

(3)

In extending our knowledge of alkyne transition metal chemistry, considerable attention is currently being directed at the use of di- and poly-nuclear complexes to achieve the chemical modification of alkynes. The well documented studies by Knox[11] and Green *et al.*[12] involving diruthenium and dimolybdenum centres, respectively, and Chisholm *et al.*'s extensive investigations[13] of alkyne complexes of dinuclear tungsten alkoxides, provide just a few examples. Another extremely versatile dinuclear alkyne system is based on the complex $Cp_2Rh_2(\mu\text{-}CO)(\mu\text{-}\eta^2\text{-}CF_3C_2CF_3)$ which was discovered in our laboratories in the late 1970s. Over the past decade or so, we have investigated the addition of a wide range of substrates to this complex, and we continue to be surprised and stimulated by the results obtained. This report presents an overview of our investigations involving this and related complexes.

2. RHODIUM AND HEXAFLUOROBUT-2-YNE

2.1. *Reaction of* $CpM(CO)_2$ *with alkynes*

During a post-doctoral year with Geoffrey Wilkinson in the early 1960s, I prepared[14] the complexes (**3**) and (**4**) by the thermally initiated reaction of $CpRh(CO)_2$ with hexafluorobut-2-yne, $CF_3C{\equiv}CCF_3$. About 10 years later, some discussion of possible pathways for the cyclic trimerization of alkynes on a single metal site was generated in a departmental seminar at Monash. I persuaded a graduate student to repeat my earlier work, and we designed some further experiments that might throw light on the reaction pathway for formation of (**4**). When the experiment to produce (**3**) plus (**4**) was performed, these compounds were isolated in low yields only. However, a significant amount of a new dinuclear product (**5**) was obtained.[15,16] Further study[16,17] established that a range of products (see Scheme 1) was formed in the reaction system, with the yield of each product being critically dependent on the reaction conditions, particularly the temperature. The dinuclear complex (**5**) was the major product obtained when the reaction was carried out between 100–110°C, but the amounts of (**3**) and (**4**) were substantially greater when the temperature was elevated to 120–125°C.

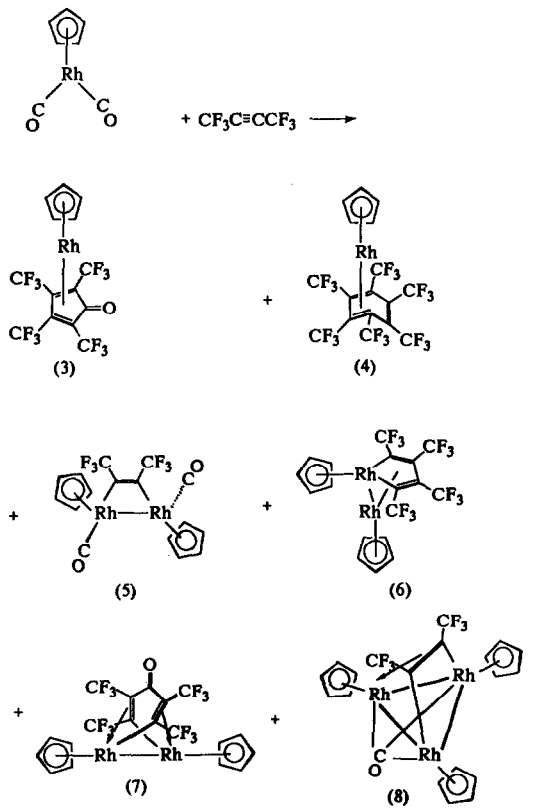

Scheme 1. Products obtained from the reaction of $CpRh(CO)_2$ with $CF_3C{\equiv}CCF_3$.

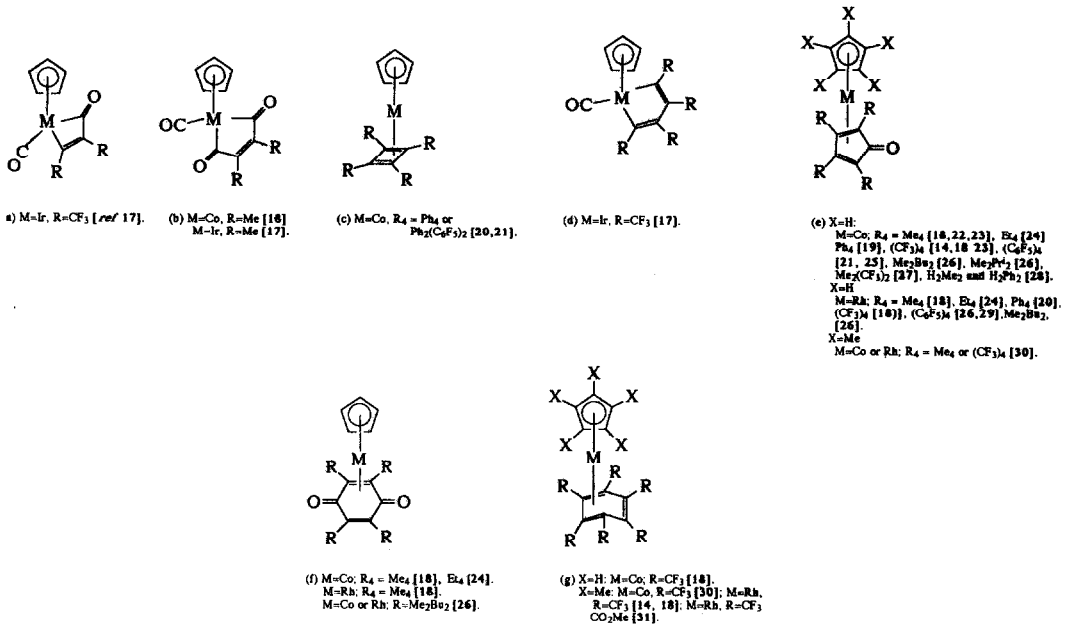

Fig. 2. Examples of mononuclear complexes formed from reactions between $CpM(CO)_2$ or $Cp^*M(CO)_2$ complexes and alkynes. (Reference numbers are given in square brackets.)

Numerous related reactions between $CpM(CO)_2$ complexes and alkynes have been investigated but generally they give mononuclear complexes such as those displayed in Fig. 2. The formation of dinuclear complexes of the type $Cp_2M_2(CO)_n(\mu\text{-}\eta^1\eta^1\text{-}RC_2R)$ is restricted to just a few systems. At about the same time as our report on $Cp_2Rh_2(CO)_2(\mu\text{-}\eta^1\eta^1\text{-}CF_3C_2CF_3)$, Sakurai and Hayashi showed[32] that the dinuclear monocarbonyl complex $Cp_2Co_2(\mu\text{-}CO)(\mu\text{-}\eta^2\text{-}Me_3SiC_2SiMe_3)$ is formed in the thermally initiated reaction of $CpCo(CO)_2$ with $Me_3SiC{\equiv}CSiMe_3$. Later, we established[33] that the related complex $Cp_2Rh_2(\mu\text{-}CO)(\mu\text{-}\eta^2\text{-}Bu^tC_2Bu^t)$ is produced when $Cp_2Rh_2(CO)_3$ and $Bu^tC{\equiv}CBu^t$ are heated together. However, the corresponding reaction with $Me_3SiC{\equiv}CSiMe_3$ gives mainly a trinuclear complex $Cp_3Rh_3(\mu\text{-}CO)(\mu\text{-}\eta^1\eta^1\eta^2\text{-}Me_3SiC_2SiMe_3)$. The iridium complex $Cp_2Ir_2(CO)_2(\mu\text{-}\eta^1\eta^1\text{-}CF_3C_2CF_3)$ is one of the products obtained from the reaction between $CpIr(CO)_2$ and $CF_3C{\equiv}CCF_3$.[17] (See also Section 2.3.)

When the complex $Cp_2Co_2(\mu\text{-}CO)(\mu\text{-}\eta^2\text{-}Me_3SiC_2SiMe_3)$ was treated with other alkynes,[32] several new complexes were formed. However, the rhodium complex $Cp_2Rh_2(\mu\text{-}CO)(\mu\text{-}\eta^2\text{-}Bu^tC_2Bu^t)$ did not display the same reactivity and seemed completely inert to addition reactions. However, the green colour of the dirhodium complex aroused the interest of Geoff Pain, one of my graduate

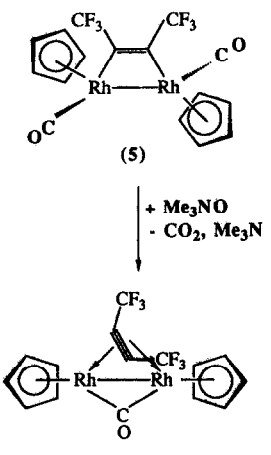

Scheme 2. The conversion of $Cp_2Rh_2(CO)_2(\mu\text{-}\eta^1\eta^1\text{-}CF_3C_2CF_3)$ to $Cp_2Rh_2(\mu\text{-}CO)(\mu\text{-}\eta^2\text{-}CF_3C_2CF_3)$.

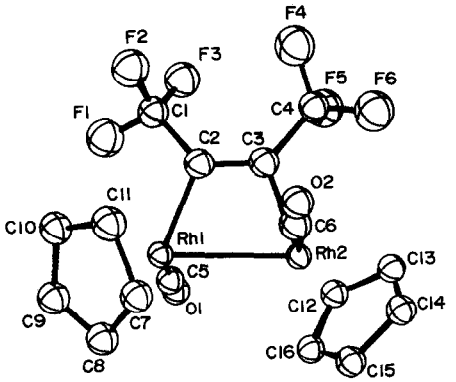

Fig. 3. Molecular structure of $Cp_2Rh_2(CO)_2(\mu\text{-}\eta^1\eta^1\text{-}CF_3C_2CF_3)$.[37] Selected bond distances (Å) and angles (°): Rh(1)—Rh(2), 2.682(1); Rh(1)—C(2), 2.054(10); Rh(2)—C(3), 2.031(10); C(2)—C(3), 1.269(14); C(5)—Rh(1)—Rh(2), 86.6(0.3); C(6)—Rh(2)—Rh(1), 87.2(0.4).

students, and he decided to attempt the conversion of $Cp_2Rh_2(CO)_2(\mu\text{-}\eta^1\eta^1\text{-}CF_3C_2CF_3)$ to the corresponding monocarbonyl complex. The reaction worked well when anhydrous Me_3NO was used as a decarbonylation agent (see Scheme 2),[34] with the formation of $Cp_2Rh_2(\mu\text{-}CO)(\mu\text{-}\eta^2\text{-}CF_3C_2CF_3)$ being signalled by a colour change of the reaction solution from red to green.

2.2. *Synthesis and physical properties of* $Cp_2Rh_2(CO)_2(\mu\text{-}\eta^1\eta^1\text{-}CF_3C_2CF_3)$ (5) *and* $Cp_2Rh_2(\mu\text{-}CO)(\mu\text{-}\eta^2\text{-}CF_3C_2CF_3)$ (9)

Preparation. Subsequent to the above work, we developed a much better route to (**5**) and hence to (**9**). This was based on the initial treatment of $[Rh(CO)_2Cl]_2$ with $CF_3C{\equiv}CCF_3$ which gives an incompletely characterized intermediate of probable formula $[Rh(CO)_2Cl(CF_3C_2CF_3)]_n$, and subsequent reaction of this with TlCp. All stages of the reaction sequence[35,36] are achieved at room temperature, and the overall yield of (**5**) is high. The decarbonylation of (**5**) to (**9**) can then be achieved with Me_3NO as indicated earlier.

Structures. The molecular structures of the two complexes (**5**)[37] and (**9**)[38] were determined from X-ray diffraction data, and these are shown in Figs 3 and 4. This confirmed a very interesting feature of the decarbonylation reaction that had been predicted[34] from spectroscopic data, namely that the bridging alkyne undergoes a 90° rotation when CO is removed. The rotation restores an 18-electron count on each rhodium atom. A rationalization of the electronic requirements for the perpendicular and parallel orientations of the alkyne in these and related complexes has been developed from molecular orbital calculations.[39]

Two further structural features of (**5**) are revealed by spectroscopic studies. Although the two carbonyls are mutually *trans* in the solid state structure, solution IR data indicate that a *cis* isomer also exists. The two isomers can be separated by TLC and are readily distinguished by IR

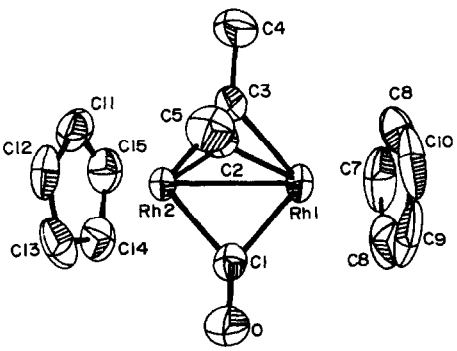

Fig. 4. Molecular structure of $Cp_2Rh_2(\mu\text{-}CO)(\mu\text{-}\eta^2\text{-}CF_3C_2CF_3)$ (**9**).[38] Selected bond distances (Å): Rh(1)—Rh(2), 2.651(1); Rh(1)—C(2), 2.082(5); Rh(1)—C(3), 2.023(5); Rh(2)—C(2), 2.075(5); Rh(2)—C(3), 2.036(5); C(2)—C(3), 1.363(8).

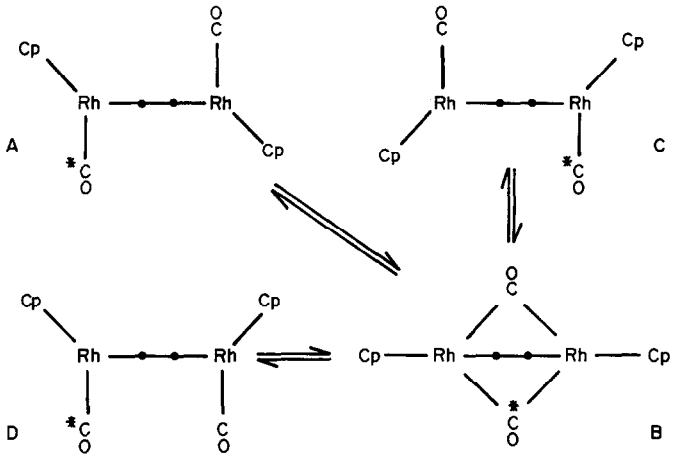

Fig. 5. Proposed pathway for carbonyl site exchange and for *cis* → *trans* isomerization in the complex $(\eta\text{-}C_5H_5)_2Rh_2(CO)_2(CF_3C_2CF_3)$.[40] The molecule is viewed along the 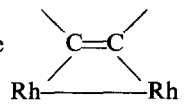 plane, and the CF_3 groups are removed for clarity.

spectroscopy.[40,41] In solution, there is a *cis* to *trans* isomerization, with 50% conversion in 12 h at room temperature. Variable temperature ^{13}C NMR spectroscopy indicates that CO scrambling occurs for the *trans* but it was not detected for the *cis* isomer; a pairwise bridge opening and closing mechanism is invoked[40] (see Fig. 5).

Electrochemistry. A comparison of the electrochemical oxidation and reduction of the two monocarbonyl complexes (**9**) and $Cp_2Rh_2(\mu\text{-}CO)(\mu\text{-}\eta^2\text{-}Bu^tC_2Bu^t)$ has shown[42] that the $CF_3C_2CF_3$ complex is harder to oxidize and easier to reduce than the $Bu^tC_2Bu^t$ complex. However, all of the anionic, cationic and neutral species are kinetically more stable when R = Bu^t rather than CF_3. The stability of the ions is also affected by the solvent used. For example, a very stable cation $[Cp_2Rh_2(\mu\text{-}CO)(\mu\text{-}Bu^tC_2Bu^t)]^+$ is produced in dichloromethane, but when oxidation is achieved in acetonitrile, inherently unstable solvated cations are produced. This behaviour indicates that electron transfer catalysis might prove a useful means of generating some chemistry of the normally inert complex $Cp_2Rh_2(\mu\text{-}CO)(\mu\text{-}Bu^tC_2Bu^t)$. The electrochemical behaviour of (**5**) and (**9**) has also been compared.[43] It is more difficult to reduce and to oxidize the dicarbonyl complex (**5**) than the monocarbonyl species (**9**), and most of the redox products of (**5**) are unstable. The reduction and oxidation pathways are also markedly affected by the orientation of the carbonyls in $Cp_2Rh_2(CO)_2(\mu\text{-}\eta^1\eta^1\text{-}CF_3C_2CF_3)$.

2.3. *Related dinuclear complexes*

We have made numerous attempts to prepare complexes analogous to (**5**) and (**9**), but with metals other than rhodium or alkynes other than hexafluorobut-2-yne. Dinuclear products are rare in reactions of $CpCo(CO)_2$ with alkynes, and we have been unable to form any complexes of the type $Cp_2Co_2(CO)_n(RC_2R')$ except for the previously discussed[32] compound $Cp_2Co_2(\mu\text{-}CO)(\mu\text{-}\eta^2\text{-}Me_3SiC_2SiMe_3)$. Reactions between $CpRh(CO)_2$ and alkynes give a variety of products like those in Scheme 1, but the analogue of (**5**) has been obtained[29] only with $C_6F_5C{\equiv}CC_6F_5$. From the reaction between $CpIr(CO)_2$ and $CF_3C{\equiv}CCF_3$ at 120–160°C, the complex $Cp_2Ir_2(CO)_2(\mu\text{-}\eta^1\eta^1\text{-}CF_3C_2CF_3)$ was obtained,[17] both *cis*- and *trans*- isomers being identified. The complex reacts with Me_3NO, but it is a messy reaction system and $Cp_2Ir_2(\mu\text{-}CO)(\mu\text{-}\eta^2\text{-}CF_3C_2CF_3)$ has not been identified in the reaction products. The related complex $Cp_2Ir_2(CO)_2(\mu\text{-}\eta^1\eta^1\text{-}C_6F_5C_2C_6F_5)$ is formed[20] when $CpIr(CO)_2$ and $C_6F_5C{\equiv}CC_6F_5$ are heated together, and the μ-phenylene complex (**10**) is obtained from the reaction between $CpIr(CO)_2$ and photo-α-pyrone.[44,45]

An alternative synthetic approach used in attempts to increase the variety of complexes analogous to (**5**) involved modifying the Cp groups. In reactions between $Cp^*_2Rh_2(CO)_2$ and various alkynes $RC{\equiv}CR'$ (R = R' = Et, MeO_2C, CF_3, C_6F_5; R = Ph, R' = Me, MeO_2C or C_6F_5) a range of complexes of formula $Cp^*_2Rh_2(CO)_2(\mu\text{-}RC_2R')$ was formed as the major reaction products.[31,46] The

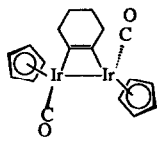

(10)

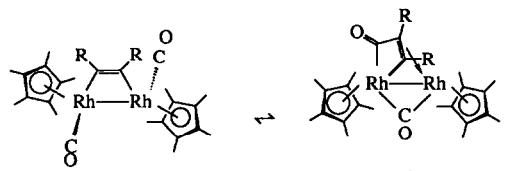

(11) (12)

structures of these complexes vary in an interesting way as the alkyne substituents are changed. The $C_6F_5C_2C_6F_5$ complex exists exclusively in the form (**11**), some others (e.g. PhC_2Ph) adopt only the structure (**12**), and for several of the complexes (e.g. $PhC_2C_6F_5$) (**11**) and (**12**) co-exist. None of these complexes could be decarbonylated with Me_3NO.

The well established "indenyl effect"[47,48] prompted us to extend these investigations to reactions of $indRh(CO)_2$ with $CF_3C{\equiv}CCF_3$ and other alkynes. A rapid reaction did occur under mild conditions[49] with $CF_3C{\equiv}CCF_3$, and the major product was $ind_2Rh_2(CO)_2(\mu\text{-}\eta^1\eta^1\text{-}CF_3C_2CF_3)$ (**13**) with a *trans*-orientation of the carbonyls. Other products formed in this reaction are displayed in Scheme 3. The species (**14**), (**15**) and (**16**) represent new classes of compounds. Treatment of (**13**) with Me_3NO does result in decarbonylation to form $ind_2Rh_2(\mu\text{-}CO)(\mu\text{-}\eta^2\text{-}CF_3C_2CF_3)$. The corresponding reactions of $indRh(CO)_2$ with other alkynes occurred only at elevated temperatures and did not yield complexes analogous to (**13**).

An alternative route to (**5**), which involves a preliminary reaction of the alkyne with $[Rh(CO)_2Cl]_2$ and subsequent treatment of the product with thallium cyclopentadienide, was discussed earlier. Regrettably, attempts[50] to extend this approach to other alkynes led to quite different products. It is interesting, however, that the $\{[Rh(CO)_2Cl]_2 + CF_3C{\equiv}CCF_3 + TlCp\}$ reaction system gives a product of formula $Cp_2Rh_2(CO)_3(\mu\text{-}CF_3C_2CF_3)$ in addition to the *cis*- and *trans*- isomers of $Cp_2Rh_2(CO)_2(\mu\text{-}\eta^2\text{-}CF_3C_2CF_3)$. An X-ray diffraction study[51] on crystals of the tricarbonyl complex revealed the structure shown in (**20**). Spectroscopic results indicate that an isomer with two bridging carbonyls exists in solution, and variable temperature ^{13}C NMR data reveal that the carbonyls are

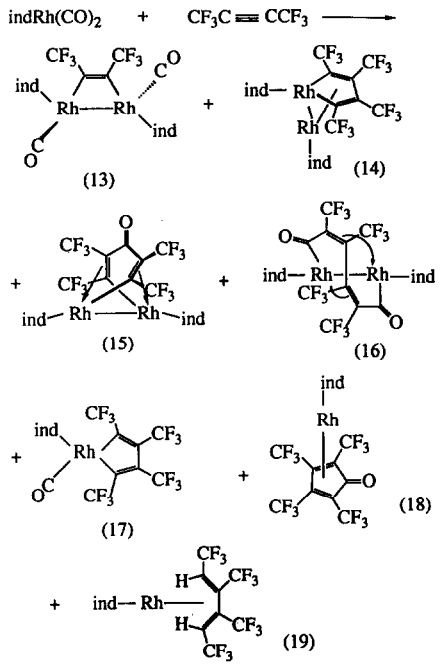

(13) (14) (15) (16) (17) (18) (19)

Scheme 3. Products obtained from the reaction between $indRh(CO)_2$ and $CF_3C{\equiv}CCF_3$ at room temperature. (ind represents η^5-indenyl.)

scrambling rapidly, even at $-100°C$. This complex is readily decarbonylated by treatment with Me_3NO, and both *cis*- and *trans*-isomers of $Cp_2Rh_2(CO)_2(\mu\text{-}\eta^1\eta^1\text{-}CF_3C_2CF_3)$ plus the monocarbonyl complex (**9**) are produced.

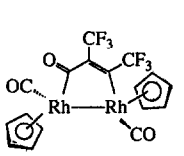

(20)

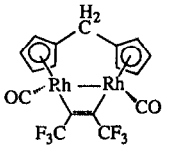

(21)

The bis-cyclopentadienylmethane complex $(CpCH_2Cp)Rh_2(CO)_2(\mu\text{-}\eta^1\eta^1\text{-}CF_3C_2CF_3)$ is formed[52] in the related reaction of $[Rh(CO)_2Cl(CF_3C_2CF_3)]_n$ with $TlCpCH_2CpTl$. This complex necessarily has a *cis*-orientation of the two carbonyls (**21**). There is decarbonylation upon treatment with Me_3NO, but the resultant monocarbonyl complex is unstable presumably due to the need for all ligands to be in bridging positions. Although the decarbonylation product cannot be isolated, ligand additions to the *in situ* product have been investigated.

3. REACTIVITY OF THE ALKYNE-DIRHODIUM COMPLEXES

3.1. *Some reactions of* $Cp_2Rh_2(CO)_2(\mu\text{-}\eta^1\eta^1\text{-}CF_3C_2CF_3)$ (5)

The complex (**5**) is relatively inert, and temperatures exceeding 100°C are needed to initiate substitution reactions. The products formed in these reactions are generally obtained more readily from corresponding reactions with $Cp_2Rh_2(\mu\text{-}CO)(\mu\text{-}\eta^2\text{-}CF_3C_2CF_3)$ (**9**); these are discussed in the following sections of this report. However, an exceptionally facile reaction does occur when protonic acids are added to (**5**). For example, the cation $[Cp_2Rh_2(CO)_2\{CF_3C_2CF_3\cdot H\}]^+$ is formed when (**9**) is dissolved in concentrated sulphuric acid, and the BF_4^- or PF_6^- salts of the protonated species can be isolated.[40] The spectroscopic properties of the salts indicate that protonation of one of the alkyne carbons has occurred to give (**22**).

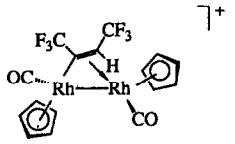

(22)

3.2. *Some coordinative additions to* $Cp_2Rh_2(\mu\text{-}CO)(\mu\text{-}\eta^2\text{-}CF_3C_2CF_3)$ (9)

Although the complex (**9**) is formally coordinatively saturated, it readily adds a variety of substrates under mild conditions. For example, if CO is bubbled through a solution of (**9**), the dicarbonyl complex (**5**) is reformed. This behaviour can be rationalized in terms of an extremely facile interconversion between the perpendicular and parallel bonding modes of the alkyne (see Scheme 4). The addition of numerous other substrates, including $L = PPh_3$, $PMePh_2$, $P(OMe)_3$,

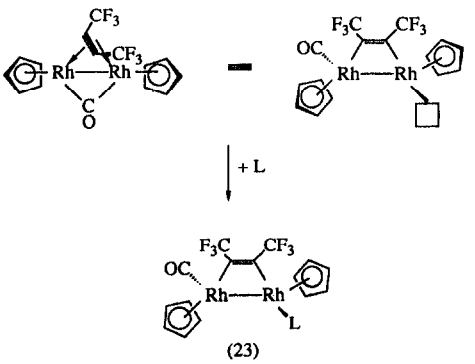

(23)

Scheme 4. A conceptually useful way of rationalizing the high chemical reactivity of (**9**).

PF_3, $PF_2(NEt_2)$, $AsPh_3$ and CNR (R = Bu^t or 2,6-$Me_2C_6H_3$) can be achieved[53] in a similar manner. It is assumed that CO and L are mutually *trans* in all of these complexes, and this has been confirmed[43] by X-ray crystallography for the complex with L = 2,6-$Me_2C_6H_3NC$. Variable temperature ^{13}C NMR spectroscopy establishes that CO and L exchange rapidly in the complexes (**23**, L = CNR), but this is not possible with the other complexes because the group 15 donor ligands cannot assume a bridging position. The electrochemistry of the complexes (**23**, L = PPh_3 or $CNBu^t$) has been investigated,[43] and the redox behaviour is strongly dependent on the electrode and solvent used. Numerous pathways for rearrangement are indicated after oxidative electron transfer.

The complex $Cp_2Rh_2(CO)\{P(p\text{-tolyl})_3\}(\mu\text{-}\eta^1\eta^1\text{-}CF_3C_2CF_3)$ has been prepared[50] from (**9**) and tri-*p*-tolylphosphine. The ^1H NMR spectrum of this complex reveals three distinct *para*-tolyl methyl resonances, and this is consistent with restricted rotation about the Rh—P bond. At elevated temperatures, the methyl resonances begin to merge before there is thermal decomposition of the complex. A similar restricted rotation about the Rh—P bond in $Cp^*Rh\{P(p\text{-tolyl})_3\}(C_6F_5)Br$ has been thoroughly studied[54] by variable temperature ^1H NMR spectroscopy.

Treatment of (**9**) with the secondary phosphine PPh_2H gives the addition product $Cp_2Rh_2(CO)(PPh_2H)(\mu\text{-}\eta^1\eta^1\text{-}CF_3C_2CF_3)$ (**24**).[50] If this complex is left in solution, it undergoes a facile intramolecular H-transfer reaction to yield the bridging alkenyl-phosphido complex (**25**).

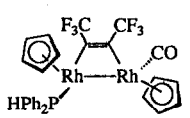

(24)

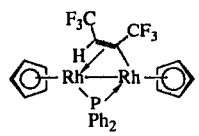

(25)

Several bidentate phosphines have been added to (**9**). Dependent upon the mole ratio of reactants, 1 : 1 (**26**) or 1 : 2 (**27**) adducts are obtained.[55] During chromatography, or when left in solution for extended periods, the complex (**26**, P—P = dppm) decarbonylates to form (**28**).

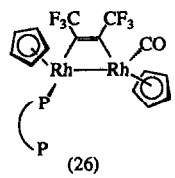

(26)

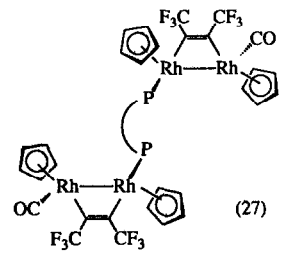

(27)

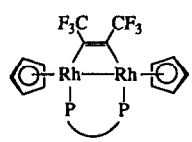

(28)

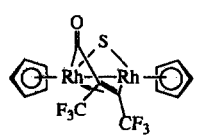

(29)

Related complexes have been formed[56] with the phosphinoalkenes $Ph_2P(CH_2)_nCH{=}CH_2$ (n = 1, 2 or 3) and $F_2POCH_2CH{=}CH_2$, and with the phosphinoalkynes $Ph_2P(CH_2)_nC{\equiv}CR$ (R = Me and n = 0, 1, 2; R = H, n = 1). In every case, coordination was from the phosphorus and there was a dangling alkene or alkyne function.

Some group 16 donors have also been coordinated to (**9**), but the adducts are generally less stable than their group 15 counterparts. At −30°C, CS_2 adds to form $Cp_2Rh_2(CO)(CS_2)(\mu\text{-}\eta^1\eta^1\text{-}CF_3C_2CF_3)$ which decomposes when left in solution to give $Cp_2Rh_2(CO)_2(\mu\text{-}\eta^1\eta^1\text{-}CF_3C_2CF_3)$ and the μ-sulphido complex $Cp_2Rh_2(\mu\text{-}S)(\mu\text{-}CO\cdot CF_3C_2CF_3)$ (**29**). Addition of PPh_3 to the initially

formed adduct results in displacement of the CS_2 and formation of $Cp_2Rh_2(CO)(PPh_3)(\mu\text{-}\eta^1\eta^1\text{-}CF_3C_2CF_3)$.

No reaction was observed when (**9**) was treated with CO_2 under a variety of conditions.[57] However, a similar reaction between (**9**) and carbon oxysulphide gave approximately equimolar amounts of the dicarbonyl complex (**5**) and (**29**). The sulphido complex (**29**) is formed more directly from (**9**) and elemental sulphur in solution at room temperature.[57]

When SO_2 is bubbled into a solution of (**9**), the adduct $Cp_2Rh_2(CO)(SO_2)(CF_3C_2CF_3)$ is obtained.[57] Spectroscopic data on freshly prepared solutions which have been saturated with SO_2 indicate *S*-attachment of the ligand (**30**), but the spectra rapidly become more complex indicating some form of isomerization. In the absence of SO_2, there is reversible dissociation of SO_2 in solution.

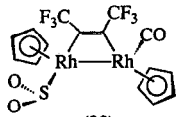

(30)

Weak coordination of dimethylsulphoxide is indicated by a colour change from green to orange–red when (**9**) is dissolved in this solvent. The unsolvated complex is recovered when solvent is removed from the solution. There is no solvation by oxygen-donating solvents such as tetrahydrofuran and acetone, but (**9**) is solvated in solution by acetonitrile.

Not unexpectedly, the indenyl complex $ind_2Rh_2(\mu\text{-CO})(\mu\text{-}\eta^2\text{-}CF_3C_2CF_3)$ displays similar reactivity.[49] The reaction with dppm, for example, occurs rapidly and yields $ind_2Rh_2(\mu\text{-}\eta^1\eta^1\text{-dppm})(\mu\text{-}\eta^1\eta^1\text{-}CF_3C_2CF_3)$. There is no evidence for the intermediate formation of $ind_2Rh_2(CO)(\eta^1\text{-dppm})(\mu\text{-}\eta^1\eta^1\text{-}CF_3C_2CF_3)$. Knowledge of the indenyl effect prompted us to examine corresponding reactions involving the dicarbonyl complex $ind_2Rh_2(CO)_2(\mu\text{-}\eta^1\eta^1\text{-}CF_3C_2CF_3)$. With dppm, $ind_2Rh_2(\mu\text{-}\eta^1\eta^1\text{-dppm})(\mu\text{-}\eta^1\eta^1\text{-}CF_3C_2CF_3)$ was again formed, but addition of the unidentate phosphines PPh_3 or $PMePh_2$ gave unexpected products of formula $(\eta^3\text{-ind})_2Rh_2(PR_3)_2(\mu\text{-CO})(CF_3C_2CF_3)_2$. Possible structures for these complexes are shown in (**31**) and (**32**).

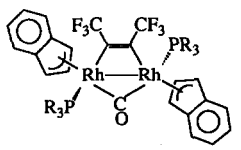

(31)

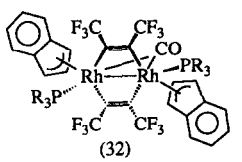

(32)

3.3. C—H *bond activation in reactions with unsaturated hydrocarbons*

Our earliest work on the addition of alkenes to (**9**) was somewhat discouraging. The reactions were slow and not particularly clean. However, a chance discovery that the reactions are greatly accelerated when the reaction solutions are exposed to sunlight opened up an important new area of investigation. In these systems, there is breaking and making of $C(sp^2)$—H bonds with formation of bis-alkenyl complexes. The reaction with ethylene is typical, and gives (**33**) as shown in eq. (4). The ^1H NMR spectrum of (**33**) is given in Fig. 6.

$$Cp_2Rh_2(\mu\text{-CO})(\mu\text{-}\eta^2\text{-}CF_3C_2CF_3) + H_2C{=}CH_2 \xrightarrow[15\text{-}30\ \text{min.}]{\text{sunlight}} Cp_2Rh_2(CO)_2(\mu\text{-}\eta^1\eta^1\text{-}CF_3C_2CF_3) + \quad (4)$$

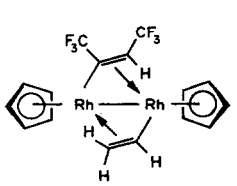

(33)

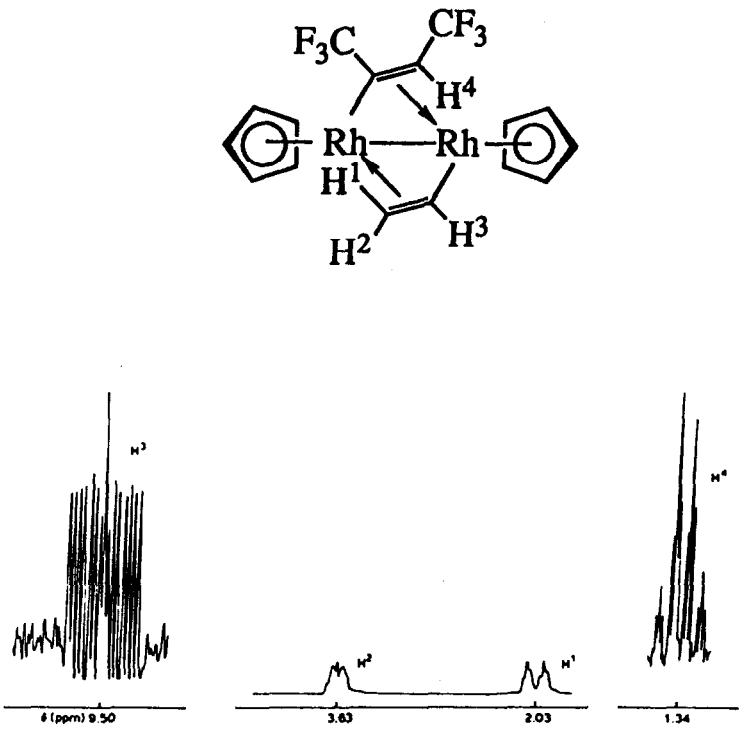

Fig. 6. ^{1}H NMR spectrum of complex (**33**); the resonances for H^3 and H^4 are magnified for clarity.[58]

The spectacular downfield multiplet for H^3 is readily analysed in terms of an ABCXY spin system, and the observed deshielding is diagnostic of a proton in this environment. Related bis-alkenyl complexes are obtained with the acyclic alkenes $H_2C{=}CHR$ (R = Me, Bu^t, Ph, CN), $H_2C{=}CF_2$ and $RHC{=}CHR'$ (R = R′ = Me, Ph, Cl; R = Me, R′ = Et), and the molecular geometries of $Cp_2Rh_2(CH{=}CHCN)\{C(CF_3)C(CF_3)H\}$ (Fig. 7) and $Cp_2Rh_2(CH{=}CF_2)\{C(CF_3)$

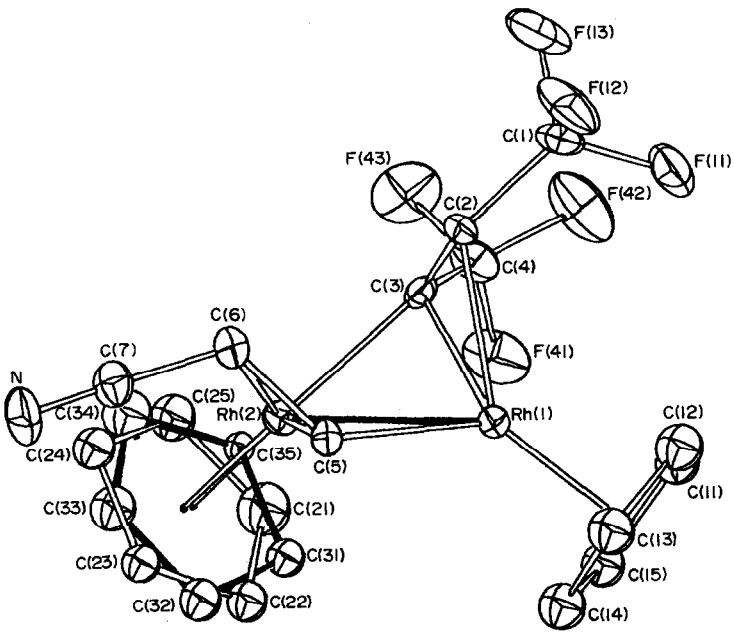

Fig. 7. Molecular structure of the complex $Cp_2Rh_2(CH{=}CHCN)\{C(CF_3){=}C(CF_3)H\}$.[58] Selected bond distances (Å): Rh(1)—Rh(2), 2.627(1); Rh(1)—C(2), 2.15(1); Rh(1)—C(3), 2.09(1); Rh(1)—C(5), 2.00(1); Rh(2)—C(3), 2.04(1); Rh(2)—C(5), 2.10(1); Rh(2)—C(6), 2.19(1); C(2)—C(3), 1.43(2); C(5)—C(6), 1.45(2).

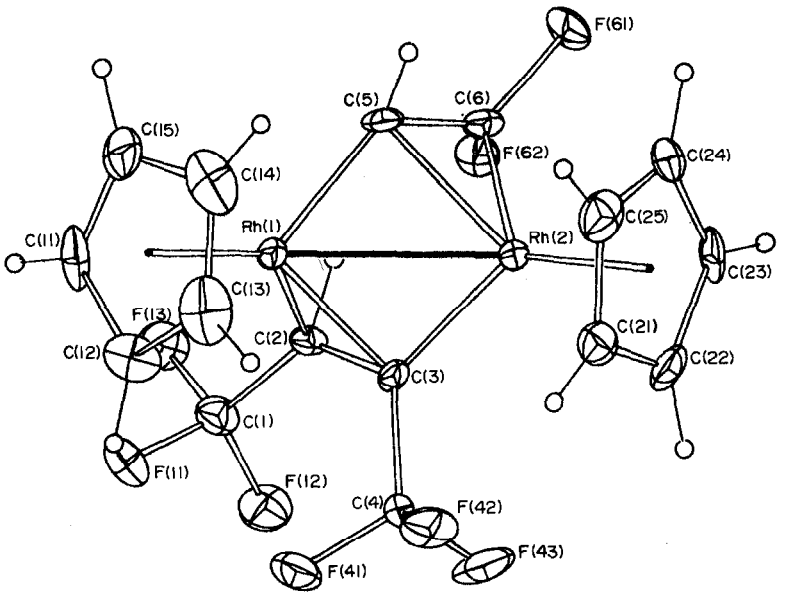

Fig. 8. Molecular structure of the complex $Cp_2Rh_2(CH{=}CF_2)\{C(CF_3){=}C(CF_3)H\}$.[58] Selected bond distances (Å): Rh(1)—Rh(2), 2.628(2); Rh(1)—C(2), 2.14(2); Rh(1)—C(3), 2.07(1); Rh(1)—C(5), 1.95(2); Rh(2)—C(3), 2.03(2); Rh(2)—C(5), 2.14(1); Rh(2)—C(6), 2.06(1); C(2)—C(3), 1.41(2); C(5)—C(6), 1.41(2).

$C(CF_3)H\}$ (Fig. 8) have been determined[58] from X-ray diffraction data. This establishes that the dihedral angle between the two Rh—Rh—C=C planes is close to 90°.

In the reactions with $H_2C{=}CHR$ and $MeHC{=}CHEt$, some regio-selectivity is evident with a preference for C—H bond cleavage at the least crowded alkene-carbon atom. However, this preference is reversed when the substituent incorporates a Lewis base site. Thus, in the reactions with vinyl acetate and allyl cyanide, all three vinylic C—H bonds can be broken, but there is preference for cleavage of the substituted C—H bonds.[59]

Related reactions occur with cyclic alkenes (cyclooctene, norbornene), acyclic dienes (1,3-butadiene, allene and 1-methyl-1,2-butadiene), cyclic polyenes (1,5-cyclooctadiene, norbornadiene, 1,4- and 1,3-cyclohexadiene, cyclopentadiene, methylcyclopentadiene, cycloheptatriene and cyclooctatetraene) and arenes (benzene, chlorobenzene, toluene, dichlorobenzenes). Figure 9 shows the products obtained[60] for butadiene and illustrates the diversity of C—H bond activations achieved in such systems.

Without exception, the reactions with arenes yielded products in which not one but two C—H bonds were activated. Products of the type $Cp_2Rh_2(\text{arene-H})\{C(CF_3)C(CF_3)H\}$ were never observed; instead all products had the formula $[Cp_2Rh_2\{C(CF_3)C(CF_3)H\}]_2(\text{arene-2H})$. An ORTEP view of the molecular structure of the benzene derivative is presented in Fig. 10. Other interesting twists in the patterns of behaviour were experienced when these investigations were extended to heterocyclic compounds.[61] Furan, thiophene and pyrrole behaved as typical aromatic systems and gave complexes of the type (**39**) and (**40**). When X = O, (**39**) is the major product, but (**40**) predominates when X = S. The reaction with pyridine proceeds differently and gives $Cp_2Rh_2\{C(CF_3)C(CF_3)H\}(\text{py-H})$ of probable structure (**41**). This, and related reactions with substituted pyridines such as the 2-fluoro- and 4-methyl-derivatives are fast, even in the dark. However, the reaction with 2-vinylpyridine requires sunlight and proceeds by activation of a vinylic rather than an aromatic proton to give (**42**). The reaction of (**9**) with 2-aminopyridine was slow in the dark but occurred rapidly in sunlight and gave the three products (**43**), (**44**) and (**45**). The latter two products are formed by activation of N—H rather than C—H bonds. There is N—H bond cleavage in the reactions between (**9**) and allylamine, other primary amines, and $NHMe_2$.[59] These reactions occur in the dark and yield the complexes (**46**) which incorporate a bridging carboxamide group.

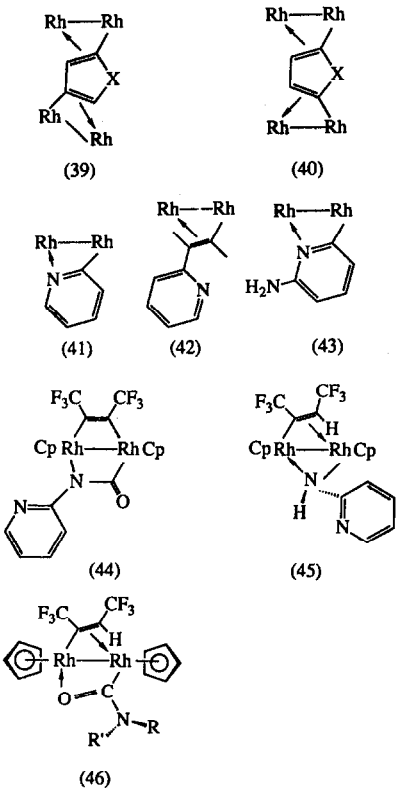

3.4. *Cyclic condensation reactions with alkynes*

Dinuclear complexes with bridging metallacyclopentadiene (**6**) or pentadienone (**7**) groups are formed in reactions of $CpRh(CO)_2$ with $CF_3C{\equiv}CCF_3$.[16] The same complexes are obtained when (**5**) is treated with $CF_3C{\equiv}CCF_3$ at elevated temperatures, or under milder conditions from (**9**) and

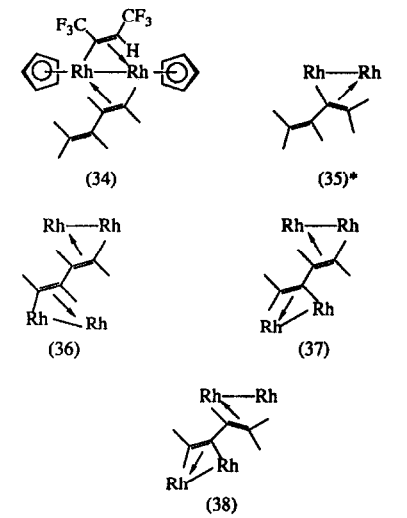

Fig. 9. Products obtained from the sunlight assisted reaction of (**9**) and butadiene. In structural diagrams (**35**) to (**43**), Rh—Rh represents the unit (a):

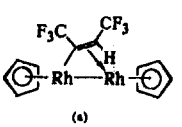

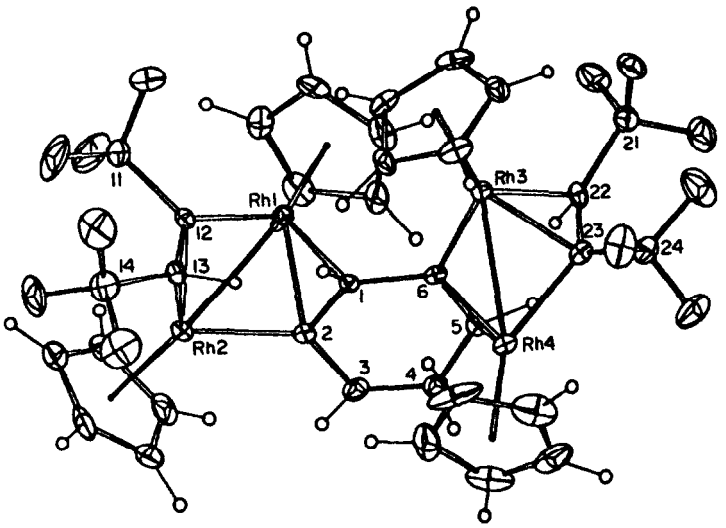

Fig. 10. Molecular structure of the complex $[Cp_2Rh_2\{C(CF_3)C(CF_3)H\}]_2(C_6H_4)$.[60] Selected bond distances (Å): Rh(1)—Rh(2), 2.627(1); Rh(3)—Rh(4), 2.603(1); Rh(1)—C(1), 2.200(7); Rh(1)—C(2), 2.164(7); Rh(1)—C(12), 2.028(8); Rh(2)—C(2), 2.059(10); Rh(2)—C(12), 2.087(8); Rh(2)—C(13), 2.127(8); C(1)—C(2), 1.41(1); C(12)—C(13), 1.415(9).

$CF_3C{\equiv}CCF_3$.[33] The metallacyclopentadiene complex $Cp_2Rh_2\{\mu\text{-}\eta^2\eta^4\text{-}C_4(CF_3)_4\}$ exhibits fluxional behaviour (see Scheme 5) when heated in solution.[18] Similar behaviour has been reported for related complexes including $Cp_2Co_2\{\mu\text{-}\eta^2\eta^4\text{-}C_4H_4\}$[62] and $Cp_2Rh_2\{\mu\text{-}\eta^2\eta^4\text{-}C_4Ph_4\}$.[63]

Other alkynes can be added to (**9**) to form related metallacyclopentadiene and pentadienone complexes. The reactions with $PhC{\equiv}CPh$, $MeC{\equiv}CPh$, $Bu^tC{\equiv}CBu^t$, $MeO_2CC{\equiv}CCO_2Me$, $MeC{\equiv}CCO_2Me$ and $MeC{\equiv}CCF_3$ are highly specific and give equal amounts of the metallacyclopentadiene complexes $Cp_2Rh_2\{\mu\text{-}\eta^2\eta^4\text{-}C_4(CF_3)_2RR'\}$ plus the dicarbonyl complex (**5**).[64]

There is high regio-selectivity when the reactions involve unsymmetrical alkynes $MeC{\equiv}CR$, with the regio-isomer (**47**) being formed exclusively. Related reactions with the terminal alkynes $HC{\equiv}CR$ (R = H, CF_3 or Ph) are extremely fast, and lead initially to precipitation of the cyclobutenyl complexes (**48**).[65] In polar organic solvents, these complexes lose CO and convert to the metallacyclopentadiene complexes (**49**).

The cyclobutenyl intermediate (**48**) is formed with other terminal alkynes $HC{\equiv}CR$ (R = Pr, CH_2CO_2Me, $CMe{=}CH_2$, and $CH_2CH_2CH_2C{\equiv}CH$), but pure samples of the complexes could not be isolated due to their high solubility in hydrocarbon solvents and their rapid conversion in solution to (**49**). The conversion to (**49**) always occurs with high regio-selectivity, with the R and H groups located in the 2- and 3-positions, respectively, of the 1-metallacyclopentadiene ring.

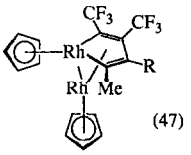

(47)

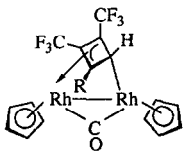

(48)

-CO

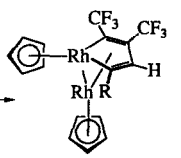

(49)

Some other alkynes lead preferentially to formation of the bridging pentadienone complexes (**50**). This occurs for example with $MeC{\equiv}CMe$, $BuC{\equiv}CBu$ and $MeC{\equiv}CR$ (R = Et, Pr^i, Bu^t). The crystal and molecular structure of the complex $Cp_2Rh_2\{\mu\text{-}1,2,5\text{-}\eta : 1,4,5\text{-}\eta\text{-}C_4(CF_3)_2Me_2CO\}$ has

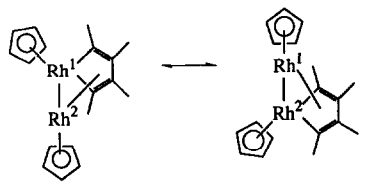

Scheme 5. Ring slippage indicated by the variable temperature NMR spectra of $Cp_2Rh_2\{\mu\text{-}\eta^2,\eta^4\text{-}C_4(CF_3)_4\}$.

been determined,[66] and this establishes that the bridging ligand is attached symmetrically as shown in Fig. 11.

An analogous structure has been determined[67] for the iron complex $Fe_2(CO)_6\{C_4Me_4CO\}$. Both stereoisomers of (**50**) are isolated from reactions with the unsymmetrical alkynes MeC≡CR.

In the reaction of (**9**) with the alkyne $Me_3SiC{\equiv}CSiMe_3$, a complex was intercepted which has two independent alkyne ligands plus a terminal carbonyl.[33] The proposed structure is shown in (**51**). In refluxing hexane, (**51**) converts to the pentadienone complex (**50**, R = R′ = $SiMe_3$).

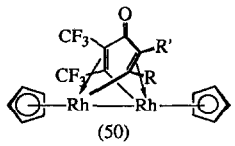

(50)

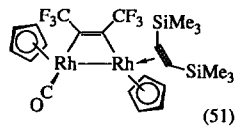

(51)

Some related pentadienone complexes $Cp_2Rh_2\{\mu\text{-}1,2,5\text{-}\eta:1,4,5\text{-}\eta\text{-}C_4R_2R'_2CO\}$ have been obtained by heating $CpRh(CO)_2$ directly with the alkynes MeC≡CR (R = Bu, Pr^i). Three stereoisomers were isolated in each instance.[68] Treatment of $Cp^*Rh(CO)_2$ with MeC≡CMe also gave[30] a small amount of a bridging pentadienone complex $Cp^*_2Rh_2\{\mu\text{-}1,2,5\text{-}\eta:1,4,5\text{-}\eta\text{-}C_4Me_4CO\}$. Some of the complexes $Cp_2Rh_2\{\mu\text{-}1,2,5\text{-}\eta:1,4,5\text{-}\eta\text{-}C_4R_2R'_2CO\}$ have been converted by heating in solution into the mononuclear cyclopentadienone complexes $CpRh\{\eta^4\text{-}C_4R_2R'_2CO\}$.

Since each of the steps depicted in Scheme 6 has been individually verified with certain combinations of M and R, the scheme represents a possible pathway for the formation of mononuclear

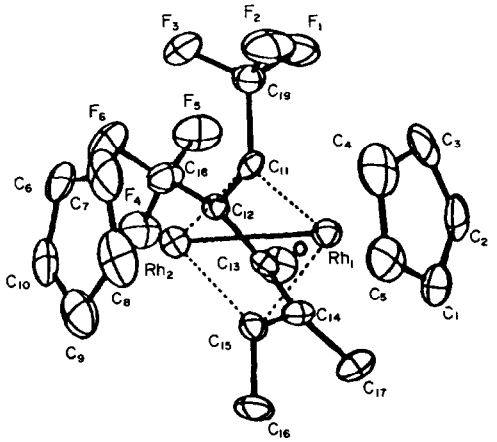

Fig. 11. A drawing of the molecular structure of $Cp_2Rh_2\{C_4(CF_3)_2Me_2CO\}$ viewed down the ketonic carbonyl bond.[66] Selected bond distances (Å): Rh(1)—Rh(2), 2.614(2); Rh(1)—C(11), 2.02(1); Rh(1)—C(14), 2.20(2); Rh(1)—C(15), 2.10(2); Rh(2)—C(11), 2.05(1); Rh(2)—C(12), 2.14(2); Rh(2)—C(15), 2.03(2).

$2CpM(CO)_2$

$\downarrow + RC_2R'$

$Cp_2M_2(CO)_2(\mu\text{-}\eta^1\eta^1\text{-}RC_2R)$

$\downarrow + RC_2R'$

$Cp_2M_2(CO)(\mu\text{-}\eta^1\eta^1\text{-}RC_2R')(RC_2R')$

$\downarrow \Delta$

$Cp_2M_2\{\mu\text{-}1,2,5\text{-}\eta\text{:}1,4,5\text{-}\eta\text{-}C_4R_2R'_2CO\}$

$\downarrow + CO/RC_2R'$

$CpM\{\eta^4\text{-}C_4R_2R'_2CO\}$

Scheme 6. A possible pathway for the formation of cyclopentadienone complexes $CpM\{\eta^4\text{-}C_4R_2R'_2CO\}$ which involves dinuclear intermediates.

cyclopentadienone complexes from $CpM(CO)_2$ and alkynes. However, alternative possible pathways involving mononuclear intermediates such as $CpM(CO)\{CORC_2R'\}$ and $CpM(RC_2R')\{CORC_2R'\}$ cannot be discounted.

Overall, formation of the pentadienone complexes (**50**) from reactions between (**9**) and $RC{\equiv}CR'$ is favoured only when the substituents R and R′ are alkyl groups. With electron-withdrawing substituents and particularly with polar alkynes, the reaction pathway is directed towards formation of the metallacyclopentadiene complexes $Cp_2Rh_2\{\mu\text{-}\eta^2\eta^4\text{-}C_4(CF_3)_2RR'\}$.

Additional unexpected products were isolated from a number of the above reactions. With $MeC{\equiv}CPr^i$, the complex $Cp_2Rh_2\{C_4(CF_3)_2Me(CMe_2OH)CO\}$ was obtained, and the structure (**52**) was confirmed[64] by X-ray crystallography. The source of this complex was an impurity, $MeC{\equiv}CC(OH)Me_2$, in the commercial sample of $MeC{\equiv}CPr^i$. A dinuclear metallacyclopentadiene complex $Cp_2Rh_2\{\mu\text{-}\eta^2\eta^4\text{-}C_4(CF_3)_2Me(COMe)\}$ was isolated from the reaction with a (as supplied) sample of $MeC{\equiv}CEt$, and again final characterization was achieved only by X-ray crystallography.[64]

Another product isolated from the reaction of (**9**) and $HC{\equiv}CSiMe_3$ was identified spectroscopically as (**53**). It could be isolated in significant yield only when TLC of the reaction solution was performed within a short time ($\leqslant$ 10 min) of mixing the reactants.[65]

Some of the most extraordinary products were obtained by treatment of (**9**) with $HC{\equiv}CBu^t$.[69] This reaction does give two isomers of the bridging pentadienone complex $Cp_2Rh_2\{\mu\text{-}1,2,5\text{-}\eta\text{:}1,4,5\text{-}\eta\text{-}C_4(CF_3)_2HBu^tCO\}$ and a single isomer of the metalladiene complex $Cp_2Rh_2\{\mu\text{-}\eta^2\eta^4\text{-}C_4(CF_3)_2HBu^t\}$ (**54**). However, the latter product is isolated only when the product mixture is chromatographed on "non-activated" silica supports. With oven-dried supports, two oxygen atoms are transferred to (**54**) to form (**55**) which incorporates an unsaturated keto-ether ligand.

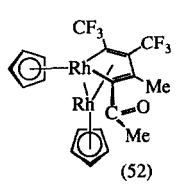

(52)

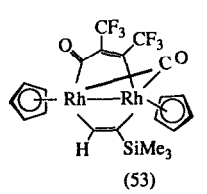

(53)

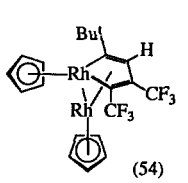

(54)

[SiO2]

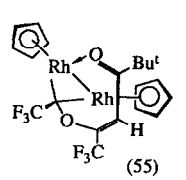

(55)

The molecular structure was established by X-ray crystallography. Two other products isolated from this reaction system could be fully characterized only from X-ray diffraction data. Representations of the molecular structures are given in (**56**) and (**57**).

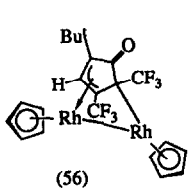
(56)

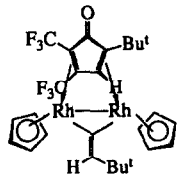
(57)

When the indenyl complex $ind_2Rh_2(\mu\text{-}CO)(\mu\text{-}\eta^2\text{-}CF_3C_2CF_3)$ is treated with $PhC{\equiv}CH$,[49] the complex $ind_2Rh_2\{(CF_3C_2CF_3)_2(PhC_2H)\}$ is formed in addition to $ind_2Rh_2(CO)_2(CF_3C_2CF_3)$. A possible structure for the tris-alkyne complex is shown in (**58**). The analogous reaction with MeC_2Pr^i gives $ind_2Rh_2\{\mu\text{-}1,2,5\text{-}\eta : 1,4,5\text{-}\eta\text{-}C_4(CF_3)_2MePr^iCO\}$ plus the unusual product $ind_2Rh_2\{C_4(CF_3)_2MePr^i(CO_2)\}$. The latter complex has not been structurally characterized. With $Me_3SiC{\equiv}CH$, a pentadienone complex $ind_2Rh_2\{\mu\text{-}1,2,5\text{-}\eta : 1,4,5\text{-}\eta\text{-}C_4(CF_3)_2H(SiMe_3)CO\}$ [**59** ≡ **50** with RR^1 = $(SiMe_3)H$] is the major product.

Another unusual dinuclear product of formula $Cp^*_2Ir_2(CO)_2(CF_3C_2CF_3)_3H$ is formed from $Cp^*Ir(CO)_2$ and $CF_3C{\equiv}CCF_3$ at elevated temperature. It has been characterized crystallographically,[30] and the molecular structure is depicted in (**60**).

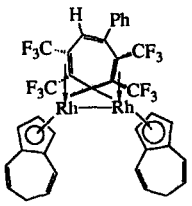
(58)

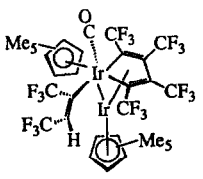
(60)

3.5. *Reactions with diazoalkanes*

The products obtained from reactions of (**9**) with diazoalkanes are influenced markedly by the substituents on $N_2CR^1R^2$. With N_2CH_2,[70] there is a facile elimination of N_2 (Et_2O solution, 0°C) and formation of the μ-alkylidene complex $Cp_2Rh_2(\mu\text{-}CO)(\mu\text{-}CH_2)(\mu\text{-}\eta^1\eta^1\text{-}CF_3C_2CF_3)$ (**61**; $R^1 = R^2 = H$). When left in solution, (**61**) converts to $Cp_2Rh_2(CO)\{\mu\text{-}\eta^1\eta^3\text{-}C(CF_3)C(CF_3)CH_2\}$ (**62**; $R^1 = R^2 = H$) by insertion of the methylene group into an alkyne–rhodium bond.

The same reaction sequence occurs with $N_2CH(CO_2Et)$, and NMR monitoring[71] of the conversion of (**61**; $R^1 = H$, $R^2 = CO_2Et$) to (**62**; $R^1 = H$, $R^2 = CO_2Et$) indicates that the alkylidene migration is accompanied by the isomerization (i.e. a twist that interchanges R^1 and R^2) of both (**61**) and (**62**). All four species can co-exist in solution, but the species that finally crystallizes from aged solutions has the configuration with the ester group in the R^1 position. This was determined unequivocally by determination of the crystal and molecular structure.

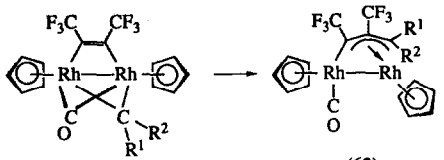
(61) (62)

There are analogous alkylidene addition and migration reactions when (**9**) is treated with $N_2CH(SiMe_3)$ or $N_2CH(CH{=}CH_2)$. With these systems, however, the migration reaction is so rapid in solution at 0°C that spectroscopically pure samples of (**61**) could not be obtained. Only one isomer of the η^1,η^3-allyl complexes (**62**) was detected, and this has the substituent *cis* to the CF_3.[71]

Although a μ-alkylidene complex $Cp_2Rh_2(\mu\text{-}CO)(\mu\text{-}CHCF_3)(\mu\text{-}\eta^1\eta^1\text{-}CF_3C_2CF_3)$ is formed rapidly in the reaction between N_2CHCF_3 and (**9**), there is no subsequent migration of the alkylidene group, even in refluxing solvents. Further investigation of this system establishes that the migration reaction can be achieved indirectly. The reaction path is shown in Scheme 7.

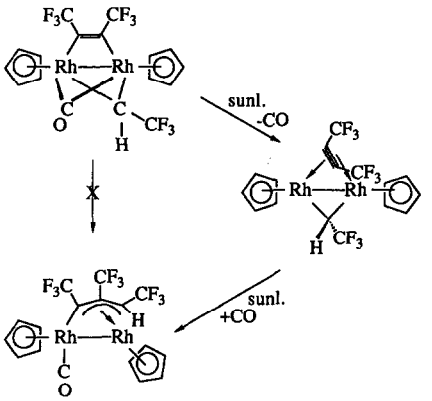

Scheme 7. Indirect pathway for the conversion of $Cp_2Rh_2(\mu\text{-}CO)\{\mu\text{-}CH(CF_3)\}\{\mu\text{-}\eta^1\eta^1\text{-}CF_3C_2CF_3\}$ to $Cp_2Rh_2(CO)\{\mu\text{-}\eta^1\eta^3\text{-}C(CF_3)C(CF_3)CH(CF_3)\}$.

A large variety of addition reactions occur with disubstituted diazoalkanes. The diesters $N_2C(CO_2R)_2$ (R = Me, Et, Bu^t) add with loss of N_2 to form the complexes $Cp_2Rh_2(\mu\text{-}CO)\{\mu\text{-}C(CO_2R)_2\}(\mu\text{-}\eta^1\eta^1\text{-}CF_3C_2CF_3)$ analogous to (**61**). When R = Me or Et, a subsequent migration occurs to give the complexes (**63**; R = Me or Et) in which a new C—O bond has been created. Determination of the crystal and molecular structure[70] of the ethyl ester derivative establishes that the bridging divinyl ether spans the Rh—Rh bond in "flyover" fashion. A migration reaction occurs also when R = Bu^t, but two products have been isolated. One is analogous to (**63**; R = Bu^t), and the other has been spectroscopically characterized[49] as (**64**). Formation of this product has involved hydrolysis of the ester plus migration of $C(CO_2H)_2$ coupled with [H] migration from a carboxylate group to an alkyne carbon.

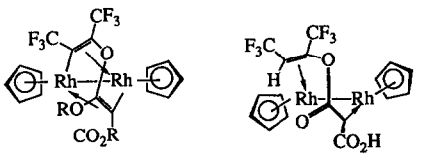

(63) (64)

In the additions of N_2CRR' (R = R' = Me or Ph; R = Ph, R' = Me or CF_3; R = Me, R' = CF_3) to (**9**), there was retention of N_2 and formation of $Cp_2Rh_2\{\mu\text{-}\eta^1:\eta^2:\eta^2\text{-}C(CF_3)C(CF_3)C(O)NNCRR'\}$. Determination of the crystal and molecular structure[49] of the N_2CMePh derivative established that these complexes incorporate a substituted acetophenone hydrazone ligand (**65**). The reactions with N_2CMe_2 and N_2CMePh gave additional products which were formed by loss of N_2. Spectroscopic data for the complex $Cp_2Rh_2(CO)\{CF_3C_2CF_3\cdot CMe_2\}$ are consistent with the structure (**66**), but the X-ray structure of crystals grown from a solution of this complex revealed a different structure (**67**). The latter complex is formed from (**66**) by a 1,4-

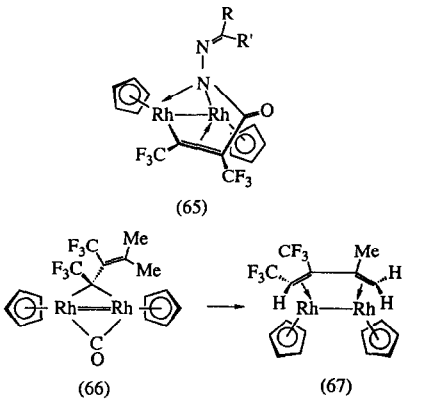

(65)

(66) (67)

hydrogen shift which converts the η^1-propenyl ligand to an $\eta^2\eta^2$-butadiene ligand. A CMePh analogue of (66) was obtained from N_2CMePh,[49] but this compound decarbonylated readily, even in the solid state. A possible structure for the decarbonylation product is given in (68).

Reaction of (9) with diazocyclopentadiene, $N_2C_5H_4$, gave the novel complex $Cp_2Rh_2\{\mu$-$C(O)C(CF_3)C(CF_3)\}\{\mu$-$\eta^1\eta^1$-$C_5H_4\}$ (69).[49] Formation of this complex involves a 1,2-hydrogen shift within the C_5H_4 unit.

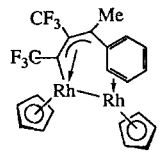

(68)

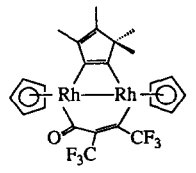

(69)

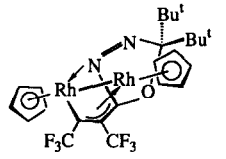

(70)

A very unusual [3 + 2] cyclo-addition[72] of the diazoalkane $N_2CBu^t_2$ to the bridging carbonyl in (9) gives the oxadiazoline complex $Cp_2Rh_2\{N{=}N{-}C(Bu^t)_2\text{-}O\text{-}C\text{-}C(CF_3)C(CF_3)\}$ (70). The molecular structure was confirmed by X-ray diffraction and is shown in Fig. 12. The complex (70) undergoes reversible carbonylation to form $Cp_2Rh_2(CO)\{N{=}N{-}C(Bu^t)_2\text{-}O\text{-}C\text{-}C(CF_3)C(CF_3)\}$.

It is not easy to rationalize the diversity of products obtained from the reactions of (9) and diazoalkanes. When there is loss of N_2, it occurs under very mild conditions, and so an intramolecular elimination seems likely. Subtle stereoelectronic effects seem to influence which of the pathways shown in Scheme 8 is followed. Given that the reaction pathway followed with monosubstituted diazoalkanes N_2CHR is invariably to form (d) whereas disubstituted diazoalkanes frequently give (f), it follows that steric effects will often inhibit the formation of a Rh—C bond in the conversion of (c) to (d). When this pathway is blocked, a complex interplay between steric, electronic and thermodynamic effects dictates the nature of the final product.

3.6. *The addition of isocyanide and related ligands*

It was mentioned in Section 3.2 that the isocyanides CNR (R = *t*-Bu or 2,6-$Me_2C_6H_3$) add coordinatively to (9) to form $Cp_2Rh_2(CO)(CNR)(\mu$-$\eta^1\eta^1$-$CF_3C_2CF_3)$. Similar reactions occur with

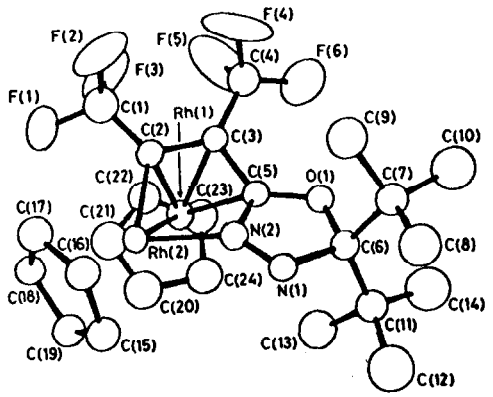

Fig. 12. Molecular structure of complex (70).[72] Selected bond distances (Å): Rh(1)—Rh(2), 2.679(1); Rh(1)—C(2), 2.08(1); Rh(1)—C(3), 2.09(1); Rh(1)—C(5), 2.19(1); Rh(2)—C(2), 2.22(1); Rh(2)—N(2), 2.00(1); C(2)—C(3), 1.43(10); C(3)—C(5), 1.47(1); C(5)—N(2), 1.41(1).

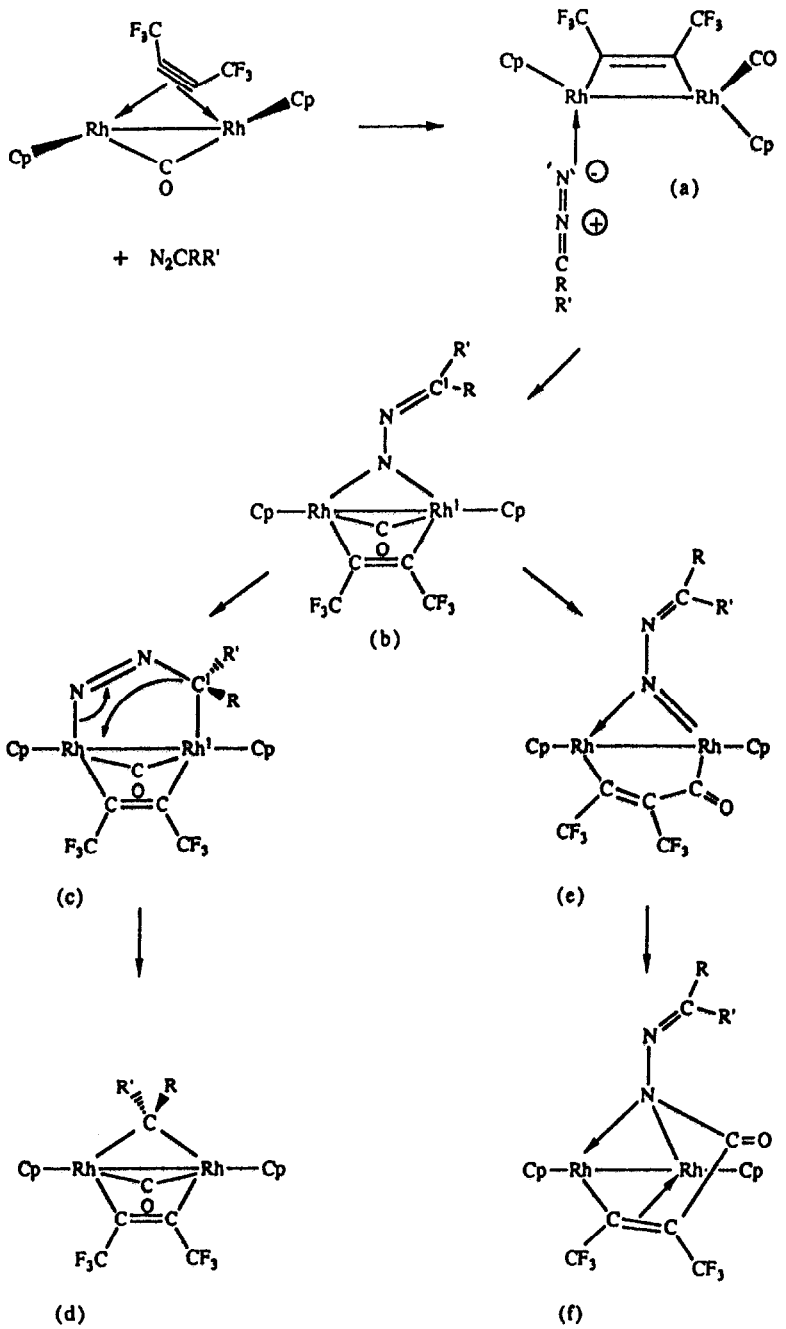

Scheme 8. Alternative pathways in the reactions of diazoalkanes with (**9**).

other isocyanides RNC (R = Et, i-Pr, Cy, Ph, *p*-$MeOC_6H_4$, *p*-$NO_2C_6H_4$) but the products rearrange when left in solution.[73] The rate of rearrangement depends markedly on R and follows the sequence R = Cy, ($t_{1/2}$ = 1740) < i-Pr < Ph < *p*-$MeOC_6H_4$ < *p*-$NO_2C_6H_4$ ($t_{1/2}$ = 1.4 min); it would seem that electronic factors affect the conversion rates. The molecular structure of one of the rearrangement products (R = Et) has been determined by X-ray crystallography. This indicates a terminal carbonyl and a bridging allylimine ligand as shown in (**71**). However, spectroscopic data indicate that when (**71**) is left in solution, it co-exists with two other isomers (**72**) and (**73**). Variable temperature NMR spectroscopy has been used to investigate the rate of interconversion between the three isomers; it is found to be greatest for the aryl systems.

Chemical oxidation of the complexes $Cp_2Rh_2(CO)(CNR)(\mu\text{-}\eta^1\eta^1\text{-}CF_3C_2CF_3)$ can be achieved with the mild oxidant Me_3NO, and the bridging acrylamide complexes $Cp_2Rh_2\{\mu\text{-}\eta^3\text{-}N(R)C(O)$

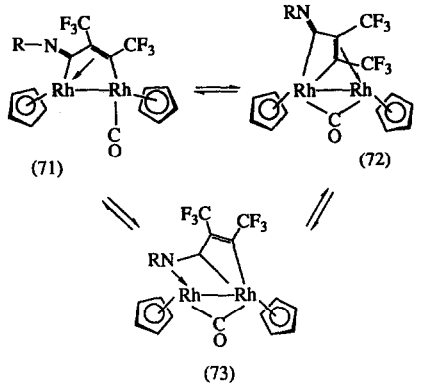

$C(CF_3)C(CF_3)$} are formed. The same complexes are obtained upon treatment of (**9**) or (**5**) with isocyanates RNCO (R = Me, t-Bu, *p*-MeC_6H_4). The best preparative method, however, involves addition of nitrene sources N_3R [R = Ph, PhCO, *p*-$MeC_6H_4SO_2$, $(MeO_2C)CH{=}C(CO_2Me)$] to (**9**); these reactions are instantaneous at 0°C.[74,75] In a variation of this method, (**9**) is treated with a carbodiimide RNCNR (R = Pr^i, Cy). This latter reaction yields the isocyanide complexes $Cp_2Rh_2(CO)(CNR)(\mu\text{-}\eta^1\eta^1\text{-}CF_3C_2CF_3)$ in addition to the appropriate acrylamide complex. The crystal and molecular structure of the complex $Cp_2Rh_2\{CF_3C_2CF_3 \cdot PhNCO\}$ has been determined from single crystal X-ray diffraction data,[74,75] and this reveals the substituted acrylamide ligand as shown in (**74**).

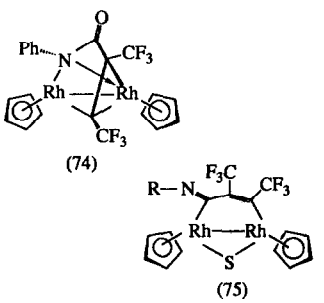

Preliminary investigations of reactions with other heterocumulenes,[76] including isothiocyanates (SCNR), ketenes ($R_2C{=}C{=}O$), thioketenes ($R_2C{=}C{=}S$), ketene–imines ($R_2C{=}C{=}NR'$) and sulphines ($R_2C{=}S{=}O$) have been undertaken. In a number of these reactions, there is evidence for facile ligand fragmentation. For example, the major products obtained from SCNR (R = Me, Et, CH_2Ph, Ph) are formulated as $Cp_2Rh_2(\mu\text{-}S)(CF_3C_2CF_3 \cdot CO)$ and $Cp_2Rh_2(\mu\text{-}S)(CF_3C_2CF_3 \cdot CNR)$ (**75**).

4. THE SYNTHESIS OF CLUSTERS

4.1. *The strategy*

The ease of addition of numerous organic substrates to (**9**) extends readily to the addition of metal nucleophiles and other metal complexes. Such reactions occur under mild conditions and thus provide a useful approach to the controlled synthesis of alkyne metal clusters.

4.2. *Clusters of the type* $Cp_2LRh_2M(CO)_{1\text{ or }3}(CF_3C_2CF_3)$

Our first indication that complexes of this type might be formed readily came from the observation that $Cp_3Rh_3(\mu\text{-}CO)(\mu\text{-}CF_3C_2CF_3)$ is a common by-product in reactions of (**9**) with organic substrates. The same complex is formed in 80% yield when (**5**) is treated with $CpRh(CO)_2$. A more direct approach to this and analogous alkyne complexes $Cp_3Rh_3(\mu\text{-}CO)(\mu\text{-}RC_2R)$ involves reaction of the appropriate alkyne with $CpRh(CO)_2$ or better with $Cp_3Rh_3(CO)_3$.[40] The molecular structures

of two of these complexes prepared in another laboratory were determined[77] from X-ray diffraction data, and two different carbonyl attachments are revealed. When the alkyne is PhC_2Ph, the carbonyl is face-bridging (**76**), but it is edge-bridging (**77**) when $C_6F_5C_2C_6F_5$ is the alkyne. The structures adopted by the $CF_3C_2CF_3$ complex and some related compounds are discussed later.

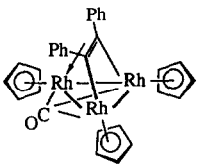

(76)

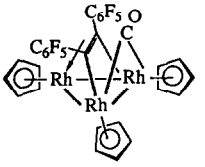

(77)

In an attempt to gain further insight into the conversion of the binuclear complex (**9**) to the trinuclear complex $Cp_3Rh_3(\mu\text{-}CO)(\mu\text{-}CF_3C_2CF_3)$, the former complex was treated with $CpRh(CO)_2$. This gave some $Cp_3Rh_3(\mu\text{-}CO)(\mu\text{-}CF_3C_2CF_3)$ but the tricarbonyl complex $Cp_3Rh_3(CO)_3(\mu\text{-}CF_3C_2CF_3)$ was the major product of this reaction.

Related complexes $Cp_2(\eta\text{-}C_5R_5)Rh_2M(CO)_3(CF_3C_2CF_3)$ are obtained by addition of $(\eta\text{-}C_5R_5)M(CO)_2$ (R = H or Me, M = Co or Rh) to (**9**). The molecular geometry of one of these complexes, $Cp_2Cp^*Rh_3(CO)_3(CF_3C_2CF_3)$, has been established[78] by X-ray diffraction, and there is a V-shaped arrangement of the metal atoms and three different types of carbonyl (**78**). For some of the complexes a second isomer exists but this has not been structurally characterized.

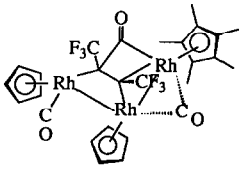

(78)

Although $CpIr(CO)_2$ is expected to be more basic than the corresponding Co and Rh compounds, it reacts exceedingly slowly with (**9**) and the yield of $Cp_3Rh_2Ir(CO)_3(\mu\text{-}CF_3C_2CF_3)$ is < 10% after several weeks.[79] When $Cp^*Ir(CO)_2$ was added to (**9**), an interesting contrast in reaction behaviour was observed[79] in that the only heteropolynuclear product obtained was the monocarbonyl complex $Cp_2Cp^*Rh_2Ir(CO)(CF_3C_2CF_3)$. There is a similar anomalous reaction between $indRh(CO)_2$ and (**9**) which gives $Cp_2indRh_3(\mu\text{-}CO)(\mu\text{-}CF_3C_2CF_3)$.

The tricarbonyl complexes undergo reversible dissociation in solution at room temperature according to eq. (5):

$$Cp_2(C_5R_5)Rh_2M(CO)_3(CF_3C_2CF_3) \rightleftharpoons Cp_2Rh_2(\mu\text{-}CO)(CF_3C_2CF_3) + (C_5R_5)M(CO)_2. \quad (5)$$

The following orders of stability are indicated—R = Me > H; M = Rh > Co (> Ir?). When heated in solution, some of the tricarbonyl complexes undergo partial decarbonylation to give the trinuclear monocarbonyl analogues $Cp_2(C_5R_5)Rh_2M(\mu\text{-}CO)(\mu\text{-}CF_3C_2CF_3)$. However, treatment with Me_3NO provides a better way of converting the tricarbonyl to the monocarbonyl analogues. Thus, either directly or by decarbonylation reactions, an extensive range (Table 1) of trinuclear monocarbonyl complexes has been obtained. It was of interest to determine which of the several possible structures was adopted by these complexes.

Spectroscopic data[40] indicate that the two different structural forms co-exist in solution for the complex $Cp_3Rh_3(\mu\text{-}CO)(\mu\text{-}CF_3C_2CF_3)$. The polarity of the solvent affects the proportions of the isomers present, with greater amounts of the edge bridging form being present in more polar solvents. Similar observations apply to $Cp_3Rh_2Co(\mu\text{-}CO)(\mu\text{-}CF_3C_2CF_3)$ but all three $Cp_2Cp^*Rh_2M(\mu\text{-}CO)(\mu\text{-}CF_3C_2CF_3)$ complexes adopt the μ_3-CO structure. In all of the Rh_2M-complexes, the alkyne is attached symmetrically (i.e. **79**, not **80**).

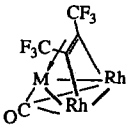

(79)

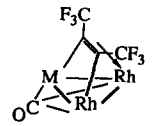

(80)

Table 1. The range of complexes of the type $Cp_2(C_5R_5)Rh_2M(\mu\text{-}CO)(\mu\text{-}CF_3C_2CF_5)$

Complex $Cp_2(C_5R_5)Rh_2M(\mu\text{-}CO)(\mu\text{-}CF_3C_2CF_3)$ R	M	Colour	Carbonyl bonding Mode[a]	Ref.
H	Rh	Purple	face ⇌ edge	40
Me	Rh	Purple–black	face	78
H	Co[b]	Dark green	face ⇌ edge	78
Me	Co	Emerald green	face	78
H	Ir[c]	—		—
Me	Ir	Crimson	face	79
ind	Rh	Green	face ⇌ edge	79

[a] Where isomers exist, the proportions in solution often depend on the polarity of the solvent.
[b] Not fully characterized.
[c] Not prepared.

Relatively few reactions of the complexes $Cp_2(C_5R_5)_6Rh_2M(\mu\text{-}CO)(\mu\text{-}CF_3C_2CF_3)$ have been investigated. Reversible protonation of $Cp_3Rh_3(\mu\text{-}CO)(\mu\text{-}CF_3C_2CF_3)$ occurs in protonic acids, and the tetrafluoroborate salt of $[Cp_3Rh_3(\mu\text{-}CO)(\mu\text{-}CF_3C_2CF_3)H]^+$ has been isolated.[40] The cationic complex incorporates an edge-bridging carbonyl and probably an edge-bridging hydride ligand. A slow reaction occurs between $Cp_3Rh_3(\mu\text{-}CO)(\mu\text{-}CF_3C_2CF_3)$ and $CNBu^t$, and there is cluster fragmentation to produce the new binuclear product $Cp_2Rh_2(CNBu^t)_2(\mu\text{-}\eta^1\eta^1\text{-}CF_3C_2CF_3)$.

4.3. *The clusters* $Cp_2(chel)Rh_3(\mu\text{-}CO)(\mu\text{-}CF_3C_2CF_3)$

A related class of trinuclear clusters has been formed by the addition of $(chel)Rh(CO)_2$ complexes to (**9**). Clusters have been prepared[80] with chel = acetylacetonato and other substituted β-diketonates, 8-hydroxyquinolate, N-*para*-tolylsalicyladimine and other Schiff bases. These are 46-electron clusters in contrast to $Cp_3Rh_3(\mu\text{-}CO)(\mu\text{-}CF_3C_2CF_3)$ which has a 48-electron count. Although 46-electron alkyne-M_3 complexes normally have a perpendicular attachment of the alkyne (**81**), determination of the molecular structure of the 2,2,6,6-tetramethyl-3,5-heptanedionate (thd) complex $Cp_2(thd)Rh_3(CO)(CF_3C_2CF_3)$ establishes that the hexafluorobut-2-yne adopts a parallel bonding mode (**82**).

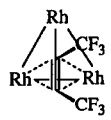

(81)

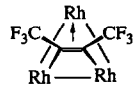

(82)

Spectroscopic results show that two isomers of the $Cp_2(chel)Rh_3(\mu\text{-}CO)(\mu\text{-}CF_3C_2CF_3)$ complexes co-exist in acetone solution, with the major isomer (**83**) exhibiting fluxional behaviour. The major and minor isomers are shown in (**83**) and (**84**), respectively; (**83**) corresponds to the solid state structure of the thd complex.

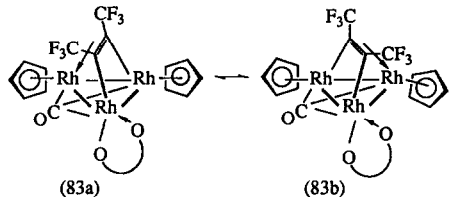

(83a) (83b)

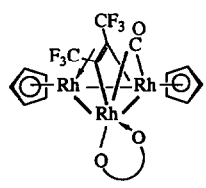

(84)

The clusters $Cp_2(chel)Rh_3(\mu\text{-}CO)(\mu\text{-}CF_3C_2CF_3)$ have been subjected to a range of reactions. In the reactions with CO, $CNBu^t$, PhC≡CPh and $PHPh_2$, cluster fragmentation occurs. Examples of the products obtained are $Cp_2Rh_2(CNBu^t)_2(\mu\text{-}\eta^1\eta^1\text{-}CF_3C_2CF_3)$ and $Cp_2Rh_2(\mu\text{-}PPh_2)\{\mu\text{-}\eta^1\eta^2\text{-}CF_3C_2CF_3\cdot H\}$. There is cluster retention in the reactions with SO_2 and tri-*para*-tolylphosphine which give $Cp_2(acac)Rh_3(\mu\text{-}CO)(\mu\text{-}SO_2)(\mu\text{-}CF_3C_2CF_3)$ and $Cp_2(acac)Rh_3(\mu\text{-}CO)\{P(p\text{-tolyl})_3\}(\mu\text{-}CF_3C_2CF_3)$. The reaction with 1,10-phenanthroline gives the cationic cluster $[Cp_2(phen)Rh_3(CO)(CF_3C_2CF_3)]^+$ resulting from chelate ligand exchange. Treatment of $Cp_2(acac)Rh_3(\mu\text{-}CO)(\mu\text{-}CF_3C_2CF_3)$ with Me_3SiCl results in removal of the acac ligand, and when this is performed in the presence of other ligands new clusters are formed. Examples include $Cp_2Rh_3(CO)(\mu\text{-}CF_3C_2CF_3)(\mu\text{-dppm-H})$ and $Cp_2Rh_3(\mu\text{-}CO)(\mu\text{-}CF_3C_2CF_3)\{P(p\text{-tolyl})_3\}Cl$. Proposed structures for these complexes are shown in (**85**) and (**86**).

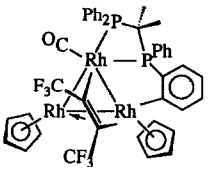

(85)

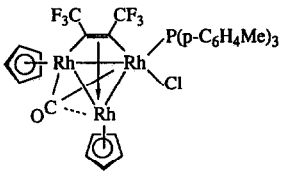

(86)

4.4. *Cationic clusters* $[Cp_2Rh_3(\mu\text{-}CO)(\mu\text{-}CF_3C_2CF_3)(CNR)_3]^+$

The cationic species $[Rh(CNR)_4]^+PF_6^-$ add to (**9**) with loss of one CNR to form the cationic clusters $[Cp_2Rh_3(\mu\text{-}CO)(\mu\text{-}CF_3C_2CF_3)(CNR)_3]^+PF_6^-$ (R = Pr^i, Bu^t). The symmetrical structure shown in (**87**) has been determined[81] from X-ray diffraction data. This is the minor of the two isomers that co-exist in solution. Although the NMR spectra of (**87**) are not temperature dependent, variable temperature NMR results indicate that the major isomer is fluxional at room temperature. The fluxionality is viewed in terms of a "wind-shield wiper" motion of the alkyne as shown in Scheme 9.

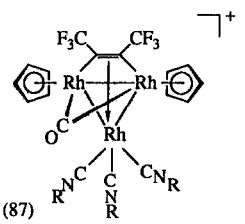

(87)

4.5. *The addition of* $[Rh(CO)_2Cl]_2$ *to* (**9**)

The condensation product $Cp_2Rh_4(CO)_4Cl_2(CF_3C_2CF_3)$ is formed from solutions containing (**9**) and $[Rh(CO)_2Cl]_2$. Crystal structure determination[82] shows that one rhodium of $[Rh(CO)_2Cl]_2$ has added to the Rh—Rh bond of $Cp_2Rh_2(\mu\text{-}CO)(\mu\text{-}CF_3C_2CF_3)$ to give (**88**). In solution, two isomers co-exist and they rapidly interconvert at room temperature.

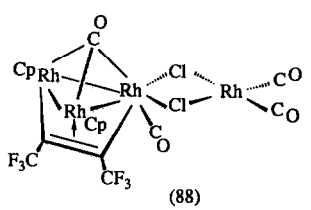

(88)

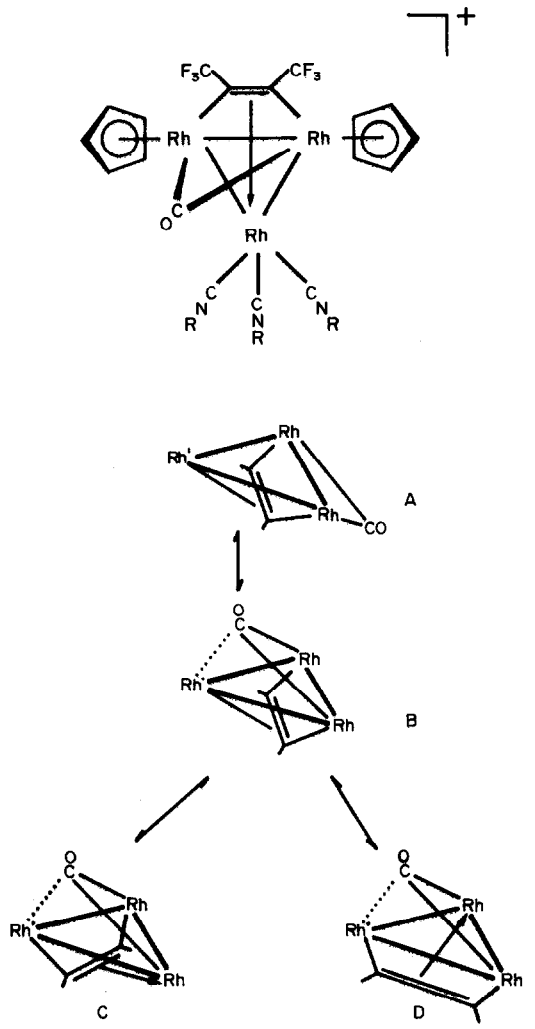

Scheme 9. Interconversion between isomers of the cationic clusters (**87**).[81]

4.6. *Heteronuclear clusters*

Rh_2Pt, Rh_4Pt. Two heteronuclear clusters are obtained[82,83] from the reaction of (**9**) with $Pt(COD)_2$, each being formed by the loss of cyclooctadiene from the Pt^0 complex. With a 1 : 1 ratio of the reactants, the formation of $Cp_2Rh_2Pt(\mu\text{-}CO)(\mu\text{-}CF_3C_2CF_3)(COD)$ is preferred, but substantial amounts of $Cp_4Rh_4Pt(\mu\text{-}CO)(\mu\text{-}CF_3C_2CF_3)$ are obtained when there is an excess of the dirhodium compound in the reaction mixture. The solid state structure of each complex has been established from X-ray diffraction data. In the Rh_4Pt cluster, the Pt is a common apex for two linked Ph_2Pt triangles (**89**).

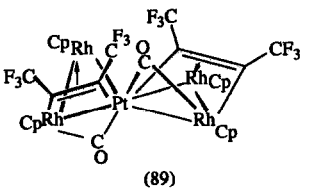

(89)

There is a V-shaped arrangement of the metals in the Rh_2Pt cluster, with one COD remaining on the Pt (**90**). In solution, there is spectroscopic evidence that a second isomer is present, and that it has the structure (**91**). Thus there is facile Rh—Pt bond making and breaking in this system. Variable temperature NMR data indicate fluxional behaviour of the closed cluster.

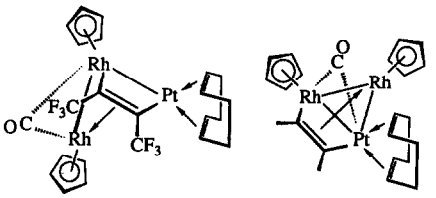

(90) (91)

Rh_2Mn. Numerous products are formed when a solution of $(MeCp)Mn(CO)_3$ and (**9**) is irradiated, or when pre-formed $(MeCp)Mn(CO)_2THF$ is added to (**9**) but only two of the products have been characterized. A ligand transfer reaction gives $(MeCp\text{-}2H)[Cp_2Rh_2(CF_3C_2CF_3 \cdot H)]_2$ (**92**). Interestingly, the isomer obtained in this reaction differs from the four isomers isolated when (**9**) is treated directly with MeCpH (see Section 3.3). The second product is the heteronuclear cluster $Cp_2(MeCp)Rh_2Mn(CO)_3(CF_3C_2CF_3)$ (**93**). Determination of the X-ray crystal structure of this cluster is incomplete because of the apparent need to interchange some of the Mn and Rh atom positions without shifting the MeCp and Cp groups. This problem has not yet been resolved.[84]

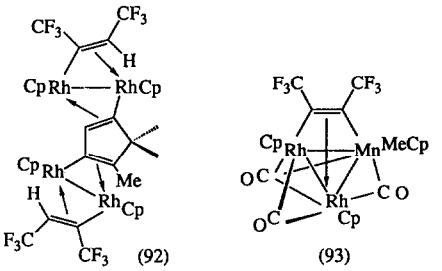

(92) (93)

Rh_2Mo, Rh_2W, Rh_3Mo. The 46-electron clusters $Cp_2Rh_2M(CO)_3(\mu\text{-}CO)(CF_3C_2CF_3)$ (M = Mo or W) are formed[85] in the reactions between (**9**) and $Mo(CO)_3(NCMe)_3$ or the W-analogue. Possible structures for these clusters include (**94**) and (**95**), with the latter favoured because it has the perpendicular orientation of the alkyne normally associated with 46-electron alkyne clusters. The molybdenum but not the tungsten system also gives a tetranuclear cluster which is formulated as $Cp_3Rh_3Mo(CO)_4(CF_3C_2CF_3)$. Several structures are possible, but the most likely is (**96**).

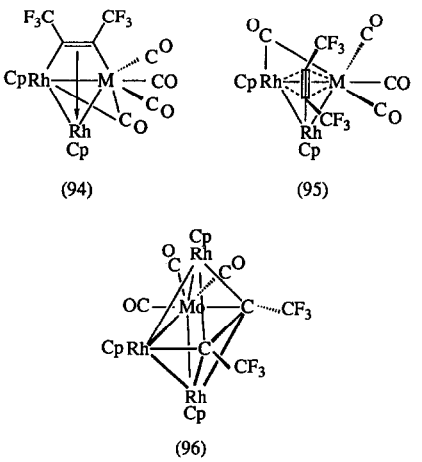

(94) (95) (96)

4.7. *Ligand transfer; a limitation in cluster synthesis*

There is scope for preparing various other heteronuclear clusters through extension of this reaction method. We have noted, however, that one limitation in the approach is that ligand transfer sometimes occurs[84,85] in preference to Rh_2—M bond formation. Some examples that illustrates this tendency include the formation of $Cp_2Rh_2(CO)_2(CF_3C_2CF_3)$ by CO transfer from $Mo(CO)_5(NCMe)$, the isolation of both $Cp_2Rh_2(CO)(CNBu^t)(CF_3C_2CF_3)$ and $Cp_2Rh_2(CNBu^t)_2(CF_3C_2CF_3)$

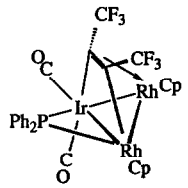

(97)

in the reaction with $Ni(PhC_2Ph)(CNBu^t)_2$, and the transfer of dppm from (dppm-P)$Fe(CO)_4$ to give $Cp_2Rh_2(CO)(dppm)(CF_3C_2CF_3)$.

4.8. *The bridge-assisted formation of clusters*

Two alternative approaches to cluster synthesis based on (**9**) involve prior coordination of a phosphine to the dirhodium complex. One involves complexes of the type $Cp_2Rh_2(CO)(CF_3C_2CF_3)\{Ph_2P(CH_2)_nX\}$ where X = PPh_2, $CH{=}CH_2$, C≡CR etc. The formation of these complexes was discussed in Section 3.2. The dangling functional group is able to coordinate another metal complex. In this way, we have formed several new trimetallic complexes[86] including $Cp_2Rh_2(CO)(CF_3C_2CF_3)(dppe)Cr(CO)_5$, $Cp_2Rh_2(CO)(CF_3C_2CF_3)(Ph_2PCH_2CH_2CH{=}CH_2)\{(MeCp)Mn(CO)_2\}$ and $Cp_2Rh_2(CO)(CF_3C_2CF_3)(Ph_2PCH_2C{\equiv}CMe)\{Co_2(CO)_6\}$. We are currently investigating ways of encouraging Rh_2—M bond formation within the complexes.

There was previous mention of the complex $Cp_2Rh_2(CO)(PPh_2H)(CF_3C_2CF_3)$ (see Section 3.2). The new cluster $Cp_2Rh_2Ir(CO)_2(\mu\text{-}PPh_2)(CF_3C_2CF_3)$ is obtained[85] by treatment of the secondary phosphine complex with n-BuLi and subsequently with $[Ir(COD)Cl]_2$ under a CO atmosphere. The initial reaction presumably gives $Cp_2Rh_2(CO)(PPh_2^-Li^+)(CF_3C_2CF_3)$, and there is elimination of LiCl and replacement of COD by two carbonyls in the subsequent reaction. The structure (**97**) has been established for the Rh_2Ir cluster from X-ray diffraction data. Corresponding reactions with other halo-metal complexes should lead to interesting new phosphido bridged heteronuclear clusters.

5. CONCLUSIONS

The complex (**9**) is a versatile model compound for studying addition reactions, particularly coordinative additions. Reactions generally occur rapidly at or below room temperature. The range of substrates added to (**9**) is considerable and includes phosphines, amines, alkenes, arenes, heterocycles, alkynes, isocyanides, diazoalkanes, azides, heterocumulenes and metal complexes. In many instances, initial coordination of the substrate is followed by further intramolecular reactions to yield new organic ligands. The course of these reactions is very dependent on stereoelectronic influences, and some extremely novel reaction pathways have emerged. In the addition reactions with metal complexes, a range of alkyne metal clusters has been formed and many of these exhibit interesting fluxional effects in solution. Overall, this investigation has revealed a host of novel ligand–metal interactions and many new types of reactions involving the making and/or breaking of C—H, C—C, C—N, C—O, N—H and Rh—M bonds.

Acknowledgements—Many research associates have contributed ideas and their technical skills to various parts of this investigation. Their names appear in the references and I thank all of them for their efforts. I thank the Australian Research Council for financial support and Johnson Matthey Technology Centre for the loan of rhodium trichloride.

REFERENCES

1. I. Amer and H. Alper, *J. Organomet. Chem.* 1990, **383**, 573.
2. G. Wilke, *Angew. Chem., Int. Edn Engl.* 1988, **27**, 185.
3. *Comprehensive Organometallic Chemistry* (Edited by G. Wilkinson, F. G. A. Stone and E. W. Abel), Vol. 8. Pergamon Press, Oxford (1982).
4. N. E. Schore, *Chem. Rev.* 1988, **88**, 1081.
5. D. J. Wink and B. T. Creagen, *Organometallics* 1990, **9**, 328; and refs therein.

6. See, for example: S. Otsuka and A. Nakamura, *Adv. Organomet. Chem.* 1976, **14**, 245.
7. C. Hoogzand and W. Hubel, in *Organic Syntheses via Metal Carbonyls* (Edited by I. Wender and P. Pino), Vol. 1, pp. 343–372. Interscience, New York (1968).
8. R. S. Dickson and P. J. Fraser, *Adv. Organomet. Chem.* 1974, **12**, 323.
9. H. Bönnemann, *Angew. Chem., Int. Edn Engl.* 1985, **24**, 248.
10. P. Diversi, G. Ingrosso, A. Lucherni and D. Vanacore, *J. Molec. Catal.* 1987, **41**, 261.
11. S. A. R. Knox, *Pure Appl. Chem.* 1984, **56**, 81.
12. See, for example: M. Green, P. A. Kale and R. J. Mercer, *J. Chem. Soc., Chem. Commun.* 1987, 375.
13. (a) M. H. Chisholm, B. K. Conroy, D. L. Clarke and J. C. Huffman, *Polyhedron* 1988, **7**, 903; (b) M. H. Chisholm, B. F. Eichorn, K. Folting and J. C. Huffman, *Organometallics* 1989, **8**, 49.
14. R. S. Dickson and G. Wilkinson, *J. Chem. Soc.* 1964, 2699.
15. R. S. Dickson and H. P. Kirsch, *J. Organomet. Chem.* 1971, **32**, C13.
16. R. S. Dickson and H. P. Kirsch, *Aust. J. Chem.* 1972, **25**, 2535.
17. P. A. Corrigan and R. S. Dickson, *Aust. J. Chem.* 1979, **32**, 2147.
18. R. S. Dickson and H. P. Kirsch, *Aust. J. Chem.* 1974, **27**, 61.
19. (a) M. D. Rausch and R. A. Genetti, *J. Am. Chem. Soc.* 1967, **89**, 5502; (b) *J. Org. Chem.* 1970, **35**, 3888.
20. S. A. Gardner, P. S. Andrews and M. D. Rausch, *Inorg. Chem.* 1973, **12**, 2396.
21. S. A. Gardner, E. F. Tokas and M. D. Rausch, *J. Organomet. Chem.* 1975, **92**, 69.
22. R. Markby, H. W. Sternberg and I. Wender, *Chem. Ind. (London)* 1959, 1381.
23. J. L. Boston, D. W. A. Sharpe and G. Wilkinson, *J. Chem. Soc.* 1962, 3488.
24. R. S. Dickson and S. H. Johnson, *Aust. J. Chem.* 1976, **29**, 2189.
25. R. S. Dickson and G. R. Tailby, *Aust. J. Chem.* 1970, **23**, 1531.
26. P. A. Corrigan and R. S. Dickson, *Aust. J. Chem.* 1981, **34**, 1401.
27. R. S. Dickson and P. J. Fraser, *Aust. J. Chem.* 1970, **23**, 2403.
28. R. S. Dickson and H. P. Kirsch, *Aust. J. Chem.* 1973, **26**, 1911.
29. M. D. Rausch, P. D. Andrews, S. A. Gardner and A. Siegel, *Organomet. Chem. Synth.* 1971, **1**, 289.
30. P. A. Corrigan, R. S. Dickson, G. D. Fallon, L. J. Michel and C. Mok, *Aust. J. Chem.* 1978, **31**, 1937.
31. R. S. Dickson, G. S. Evans and G. D. Fallon, *Aust. J. Chem.* 1985, **38**, 273.
32. H. Sakurai and J. Hayashi, *J. Organomet. Chem.* 1972, **39**, 365.
33. P. A. Corrigan, R. S. Dickson, S. H. Johnson, G. N. Pain and M. Yeoh, *Aust. J. Chem.* 1982, **35**, 2203.
34. R. S. Dickson and G. N. Pain, *J. Chem. Soc., Chem. Commun.* 1979, 277.
35. R. S. Dickson and S. H. Johnson, *Aust. J. Chem.* 1978, **31**, 661.
36. R. S. Dickson, S. H. Johnson and G. N. Pain, *Organomet. Synth.* 1988, **4**, 283.
37. R. S. Dickson, H. P. Kirsch and D. J. Lloyd, *J. Organomet. Chem.* 1975, **101**, C48; R. S. Dickson, S. H. Johnson, H. P. Kirsch and D. J. Lloyd, *Acta Cryst.* 1977, **B33**, 2057.
38. R. S. Dickson, G. N. Pain and M. F. MacKay, *Acta Cryst.* 1979, **B35**, 2321.
39. D. M. Hoffman, R. Hoffmann and C. R. Fisel, *J. Am. Chem. Soc.* 1982, **104**, 3858.
40. R. S. Dickson, C. Mok and G. N. Pain, *J. Organomet. Chem.* 1979, **66**, 385.
41. R. S. Dickson, B. M. Gatehouse, M. C. Nesbit and G. N. Pain, *J. Organomet. Chem.* 1981, **215**, 97.
42. J. W. Bixler, A. M. Bond and R. S. Dickson, *Organometallics* 1986, **5**, 1435.
43. J. W. Bixler, A. M. Bond, R. S. Dickson, G. D. Fallon, R. J. Nesbit and H. Pateras, *Organometallics* 1987, **6**, 2508.
44. M. D. Rausch, S. A. Gardner, E. F. Tokas, I. Bernal, G. M. Reisner and A. Clearfield, *J. Chem. Soc., Chem. Commun.* 1978, 187.
45. M. D. Rausch, R. G. Gastinger, S. A. Gardner, B. K. Brown and J. S. Wood, *J. Am. Chem. Soc.* 1977, **99**, 7870.
46. R. S. Dickson, G. S. Evans and G. D. Fallon, *J. Organomet. Chem.* 1982, **236**, C49.
47. F. Basolo, *Inorg. Chim. Acta* 1985, **100**, 33.
48. I. A. Lobanova and V. I. Zdanovich, *Russ. Chem. Rev.* 1988, **57**, 967.
49. B. C. Greaves and R. S. Dickson, unpublished results.
50. O. M. Paravagna and R. S. Dickson, unpublished results.
51. R. S. Dickson, B. M. Gatehouse, M. C. Nesbit and G. N. Pain, *J. Organomet. Chem.* 1981, **215**, 97.
52. G. County and R. S. Dickson, unpublished results.
53. R. S. Dickson, A. P. Oppenheim and G. N. Pain, *J. Organomet. Chem.* 1982, **224**, 377.
54. W. D. Jones and F. J. Feher, *Inorg. Chem.* 1984, **23**, 2376.
55. S. M. Jenkins, J. A. Johnson and R. S. Dickson, unpublished results.
56. M. Wakelam, T. De Simone and R. S. Dickson, unpublished results.
57. W. Baimbridge, A. P. Oppenheim, F. I. McLure and R. S. Dickson, unpublished results.
58. R. S. Dickson, G. D. Fallon, S. M. Jenkins, B. W. Skelton and A. H. White, *J. Organomet. Chem.* 1986, **314**, 333.
59. R. S. Dickson and S. M. Jenkins, *Appl. Organomet. Chem.* 1990, **4**, 493.

60. R. S. Dickson, S. M. Jenkins, B. W. Skelton and A. H. White, *Polyhedron* 1988, **7**, 855.
61. S. M. Jenkins and R. S. Dickson, unpublished results.
62. M. Rosenblum, B. North, D. Wells and W. P. Giering, *J. Am. Chem. Soc.* 1972, **94**, 1239.
63. L. J. Todd, J. R. Wilkinson, M. D. Rausch, S. A. Gardner and R. S. Dickson, *J. Organomet. Chem.* 1975, **101**, 133.
64. W. C. Baimbridge, R. S. Dickson, G. D. Fallon, I. Grayson, R. J. Nesbit and J. Weigold, *Aust. J. Chem.* 1986, **39**, 1187.
65. R. S. Dickson, F. I. McLure and R. J. Nesbit, *J. Organomet. Chem.* 1988, **349**, 413.
66. R. S. Dickson, B. M. Gatehouse and S. H. Johnson, *Acta Cryst.* 1977, **B33**, 319.
67. J. Piron, P. Piret, J. Meunier-Piret and M. Van Meerssche, *Bull. Soc. Chim. Belges* 1968, **78**, 121.
68. P. A. Corrigan and R. S. Dickson, *Aust. J. Chem.* 1978, **31**, 1937.
69. R. S. Dickson, G. D. Fallon, F. I. McLure and R. J. Nesbit, *Organometallics* 1987, **6**, 215.
70. R. S. Dickson, G. D. Fallon, R. J. Nesbit and G. N. Pain, *J. Organomet. Chem.* 1982, **236**, C61; *Organometallics* 1985, **4**, 355.
71. R. S. Dickson, G. D. Fallon, S. M. Jenkins and R. J. Nesbit, *Organometallics* 1987, **6**, 1240.
72. R. S. Dickson, G. D. Fallon and B. C. Greaves, *J. Chem. Soc., Chem. Commun.* 1989, 446.
73. R. S. Dickson, G. D. Fallon, R. J. Nesbit and H. Pateras, *Organometallics* 1987, **6**, 2517.
74. R. S. Dickson, R. J. Nesbit, H. Pateras, J. M. Patrick and A. H. White, *J. Organomet. Chem.* 1984, **265**, C25.
75. R. S. Dickson, R. J. Nesbit, H. Pateras and W. Baimbridge, *Organometallics* 1985, **4**, 2128.
76. W. Baimbridge, F. I. McLure and R. S. Dickson, unpublished results.
77. Trin-Toan, R. W. Broach, S. A. Gardner, M. D. Rausch and L. F. Dahl, *Inorg. Chem.* 1977, **16**, 279.
78. R. S. Dickson, G. S. Evans, G. D. Fallon and G. N. Pain, *J. Organomet. Chem.* 1985, **295**, 109.
79. H. Pateras, M. B. Millikan and R. S. Dickson, unpublished results.
80. R. S. Dickson and O. M. Paravagna, *Organometallics* 1991, **10**, 721.
81. R. S. Dickson, O. M. Paravagna and H. Pateras, *Organometallics* 1990, **9**, 2780.
82. R. S. Dickson, M. J. Liddell, B. W. Skelton and A. H. White, *J. Organomet. Chem.* 1987, **327**, C51.
83. K. Heazle and R. S. Dickson, unpublished results.
84. M. J. Liddell and R. S. Dickson, unpublished results.
85. O. M. Paravagna and R. S. Dickson, unpublished results.
86. T. De Simone, S. M. Jenkins, J. A. Johnson, M. Wakelam and R. S. Dickson, unpublished results.

Polyhedron Vol. 10, No. 17, pp. 2025–2029, 1991
Printed in Great Britain

0277–5387/91 $3.00+.00
© 1991 Pergamon Press plc

PENTACOORDINATE NICKEL(II) COMPLEXES WITH ONE 1,1-DITHIO AND ONE MACROCYCLIC LIGAND. ELECTRO-OXIDATION TO NICKEL(III) IN SOLUTION

ALBERT ESCUER, JOAN RIBAS and RAMON VICENTE*

Departament de Química Inorgánica, Universitat de Barcelona, Diagonal 647, 08028 Barcelona, Spain

and

CHRISTOPHE FAULMANN, DOMINIQUE DE MONTAUZON and PATRICK CASSOUX

Laboratoire de Chimie de Coordination du CNRS, UPR 8241 liée par conventions à l'Université Paul Sabatier et l'Institut national Polytechenique de Toulouse, 205 route de Narbonne, 31077 Toulouse Cedex, France

(*Received* 3 *May* 1991; *accepted* 4 *June* 1991)

Abstract—The synthesis and electrochemical behaviour of the nickel(II) macrocyclic derivatives [Ni(MC1)L](ClO_4) and [Ni(MC2)L](ClO_4) where MC1 is 2,4,4-trimethyl-1,5,9-triazacyclododec-1-ene and MC2 is 2,4,4,9-tetramethyl-1,5,9-triazacyclododec-1-ene, and L^- stands for the 1,1-dithio monoanions, dimethyldithiocarbamate (Me_2Dtc^-), diethyldithiocarbamate (Et_2Dtc^-) or pyrrolidindithiocarbamate ($PyDtc^-$), are described. The analytical and spectroscopic data are consistent with a pentacoordinate geometry. Electrochemical studies of these complexes indicate a reversible oxidation process yielding nickel(III) species unstable at room temperature. EPR studies indicate that these short-lived low-spin d^7 nickel(III) species have their unpaired electron in the d_{z^2} orbital.

In previous work,[1] we have reported the first octahedral macrocyclic nickel(II) compounds containing only one 1,1-dithio ligand. These compounds were prepared from $[Ni(DL\text{-}CTH)]^{2+}$ and $[Ni(Cyclam)]^{2+}$ and a 1,1-dithio anionic ligand L^- to yield the corresponding [Ni(N4-macrocycle)L]$^+$ complexes. DL-CTH and Cyclam, are the tetradentate ligands 5,5,7,12,12,14-hexamethyl-1,4,8,11-tetraazacyclotetradecane and 1,4,8,11-tetraazacyclotetradecane, respectively, while L^- represents dimethyldithiocarbamate, diethyldithiocarbamate or pyrrolidindithiocarbamate. Similarly, starting with a tridentate macrocyclic ligand together with the same 1,1-dithio ligand L^-, the preparation of the corresponding pentacoordinate [Ni(N3-macrocycle)L]$^+$ derivatives may be envisioned. We report here the synthesis and characterization of two series of such derivatives, [Ni(MC1)L](ClO_4) and [Ni(MC2)L](ClO_4), where MC1 is 2,4,4-trimethyl-1,5,9-triazacyclododec-1-ene, MC2 is 2,4,4,9-tetramethyl-1,5,9-triazacyclododec-1-ene, and L^- is dimethyldithiocarbamate (Me_2Dtc^-), diethyldithiocarbamate (Et_2Dtc^-) or pyrrolidindithiocarbamate ($PyDtc^-$). EPR data on the electrogenerated corresponding nickel(III) species are also reported.

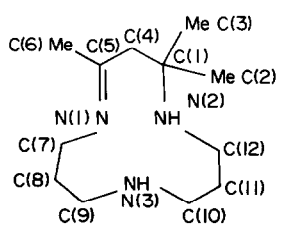

2, 4, 4-Trimethyl-1, 5, 9-Triazacyclododec-1-Ene

* Author to whom correspondence should be addressed.

EXPERIMENTAL

Synthesis

Bis-(3-aminopropyl)amine, N,N-bis(3-aminopropyl)methylamine, sodium dimethyl dithiocarbamate ($NaMe_2Dtc \cdot 2H_2O$), sodium diethyl dithiocarbamate ($NaEt_2Dtc \cdot 3H_2O$), ammonium pyrrolidindithiocarbamate (NH_4Pydtc) and Ni $(ClO_4)_2 \cdot 6H_2O$ were commercially available and used without further purification. $[Ni(MC1)(OH)]_2(ClO_4)_2$ and $[Ni(MC2)(OH)]_2(ClO_4)_2$ were prepared following the general method of Curtis *et al.*[2]

$HClO_4$ (10%) was added to a continuously stirred water suspension of $[Ni(MC1)(OH)]_2(ClO_4)_2$ or $[Ni(MC2)(OH)]_2(ClO_4)_2$ (1 mmol in 75 cm^3 H_2O) until a neutral solution was obtained. To this solution, an aqueous solution of the appropriate L^- ligand (2 mmol in 50 cm^3 H_2O) was added. A blue–green precipitate was immediately formed and, after 30 min of continuous stirring, the complexes were filtered off, washed with water and air-dried. The average yields were 75%. Elemental analysis data are summarized in Table 1 and are consistent with a $[Ni(MCi)L](ClO_4)$ ($i = 1, 2$) formula.

Physical measurements

IR spectra (4000–200 cm^{-1}) were recorded as KBr pellets with a Perkin–Elmer 1130 IR spectrophotometer. UV–vis spectra (acetonitrile solutions) were recorded with a Shimadzu UV-160 A spectrophotometer (Table 2).

Voltammetric measurements and controlled potential electrolysis were carried out using a DACFAMOV 05-03 computer-controlled instrument with ohmic resistance compensation.[3] Rigorously de-aerated acetonitrile was used as a solvent and $(n\text{-}Bu_4N)PF_6$ (0.1 M) as supporting electrolyte. Solutions were de-aerated again by means of a stream of nitrogen and a nitrogen blanket was maintained above the solutions during the electrochemical experiments. Potentials were referenced using an Ag/AgCl (0.1 M KCl) electrode separated from the bulk of the solutions by a medium porosity fritted disc. The potential for the one-electron oxidation of ferrocene is 420 mV versus the Ag/AgCl (0.1 M KCl) electrode. For the voltammetric measurements, a platinum wire auxiliary electrode was used in conjunction with a platinum disc working electrode (TACUSSEL EDI rotating electrode, area 3.14 mm^2). The voltammetric data are summarized in Table 3. Coulometry was performed at 230 K on a large area platinum electrode at 800 mV. Due to experimental requirements (temperature and atmosphere control), a previously described[4] electrolysis cell allowing combined coulometry–EPR studies was used.

The EPR spectra of the electro-oxidized species in CH_3CN glass were recorded at 100 K on a Bruker ER 200 TT spectrometer, equipped with a Bruker B-NM20 gaussmeter and a EIP 548 microwave frequency counter, operating at X-band frequencies.

Table 1. Elemental analysis [Calc.(Found)]

Compound	C	N	H
$[Ni(MC1)(Me_2Dtc)](ClO_4)$	36.8(36.6)	11.4(11.8)	6.4(6.4)
$[Ni(MC1)(Et_2Dtc)](ClO_4)$	39.4(39.3)	10.8(10.5)	6.8(6.7)
$[Ni(MC1)(PyDtc)](ClO_4)$	39.6(39.4)	10.9(10.5)	6.4(6.6)
$[Ni(MC2)(Me_2Dtc)](ClO_4)$	38.2(37.1)	11.1(10.8)	6.6(6.7)
$[Ni(MC2)(Et_2Dtc)](ClO_4)$	40.7(39.6)	10.5(10.0)	7.0(6.8)
$[Ni(MC2)(PyDtc)](ClO_4)$	40.8(40.5)	10.6(10.2)	6.7(6.7)

Table 2. Electronic spectra (in CH_3CN solutions) (λ in nm)

$[Ni(MC1)(Me_2Dtc)](ClO_4)$	604	378	312(sh)	270	238
$[Ni(MC1)(Et_2Dtc)](ClO_4)$	604	376	—	266	232
$[Ni(MC1)(PyDtc)](ClO_4)$	606	382	—	266	240
$[Ni(MC2)(Me_2Dtc)](ClO_4)$	625	387	317	269	244
$[Ni(MC2)(Et_2Dtc)](ClO_4)$	624	389	319	270	243
$[Ni(MC2)(PyDtc)](ClO_4)$	636	389	314	267	242

Table 3. Cyclic voltammetry (in CH_3CN)

Compound	$E_{1/2}$ (mV)	$\Delta E_p = E_p^a - E_p^c$	I_p^a/I_p^c
[Ni(MC1)Me_2Dtc](ClO_4)	511	0.068	1.03
[Ni(MC1)Et_2Dtc](ClO_4)	480	0.058	0.99
[Ni(MC1)PyDtc](ClO_4)	520	0.072	0.99
[Ni(MC2)Me_2Dtc](ClO_4)	569	0.076	0.84
[Ni(MC2)Et_2Dtc](ClO_4)	565	0.067	0.85
[Ni(MC2)PyDtc](ClO_4)	558	0.072	0.94

RESULTS AND DISCUSSION

The IR spectra of all prepared complexes show a doublet in the 3150–3300 cm^{-1} region assignable to ν(N—H) and a strong sharp band at 1650 cm^{-1} assignable to ν(C—N).[2] Additional bands centred at 1100 (s, broad) and 620 (s) cm^{-1} confirm the presence of the ClO_4^- anion. The dithiocarbamate ν(C—N) stretching band is observed in the range 1510–1530 cm^{-1}, as previously observed in [Ni(N3-macrocycle)L](ClO_4);[1] these values indicate a certain amount of double bond character [ν(C=N) = 1690–1640 cm^{-1}, ν(C—N) = 1350–1250 cm^{-1}].[5] In any case, no bands attributable to water molecules are observed. The electronic spectra of all studied complexes (Table 2) show the first maxima at slightly lower energy than that previously reported[1] for octahedral nickel(II) complexes obtained with similar, but tetradentate, macrocyclic ligands and the same 1,1-dithio ligand, L^-. The other intense bands in the UV region are similar to those observed in the octahedral complexes and can be attributed to charge-transfer bands. We can therefore infer from IR and the elemental analysis data that the [Ni(MC*i*)L](ClO_4) (*i* = 1, 2) complexes studied in this work are pentacoordinate systems.

The cyclic voltammogram of all studied complexes (Fig. 1) shows one oxidation couple in the range studied (0–+2 V). The oxidation potential, $E_{1/2}$, the E_p values and the peak intensity ratio are shown in the Table 3. It is interesting to note that these redox potential values are in the same range (500–600 mV) as those previously reported[1] for the [Ni(N4-macrocycle)L](ClO_4) octahedral complexes. By contrast, in the case of complexes with only one N4-macrocyclic ligand, the Ni^{II}/Ni^{III} redox potential values are significantly higher [$\simeq$ 1 V vs $Ag/AgNO_3$ (0.1 M), i.e. $\simeq$ 1.4 V vs Ag/AgCl (0.1 M KCl)].[6] The values of the peak intensity ratio indicate that the Ni^{II}/Ni^{III} couple is reversible in the case of the [Ni(MC1)L](ClO_4) complexes (I_p^a/I_p^c close to one), but only quasi-reversible in the case of the [Ni(MC2)L](ClO_4) complexes (I_p^a/I_p^c lower than one). This indicates that the complexes with the MC2 ligand are less stable at room temperature than the complexes with the MC1 ligand. Cyclic voltammograms were recorded for various voltage-sweep rates: indeed, the lower the sweep rate, the lower the I_p^a/I_p^c ratio. Using these data, the half-life times of nickel(III) oxidized species have been estimated using the method of Nicholson *et al.*[7] to a few minutes in the case of the [Ni(MC1)L](ClO_4) complexes and to a few seconds in the case of the [Ni(MC2)L](ClO_4) complexes.

Controlled potential electrolysis of acetonitrile solutions of the [Ni(MC*i*)L](ClO_4) complexes were carried out at 800 mV and 230 K. The starting nickel(II) complex solutions are blue–green and turn brown–yellow when oxidized. When these solutions are warmed back to room temperature, decomposition occurs and no EPR signal is observed. Consistent with the sweep-rate dependent cyclic voltammetric data discussed above, the vanishing of the signal is faster in the case of the [Ni(MC2)L](ClO_4) complexes compared to the [Ni(MC1)L](ClO_4) complexes.

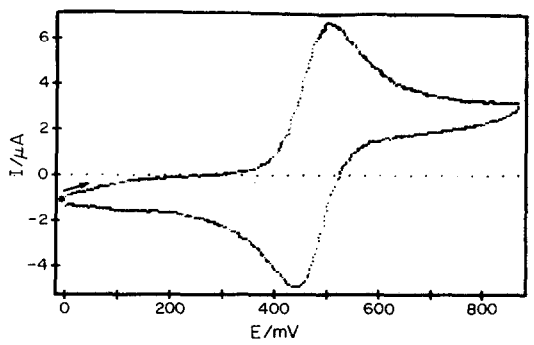

Fig. 1. Cyclic voltammogram of [Ni(MC1)Et_2Dtc](ClO_4). *: starting potential; sweep-rate: 0.1 V s^{-1}; 10^{-3} solution in CH_3CN/(n-Bu_4N)PF_6 (0.1 M); working electrode: platinum rotating disk (area 3.14 mm^2).

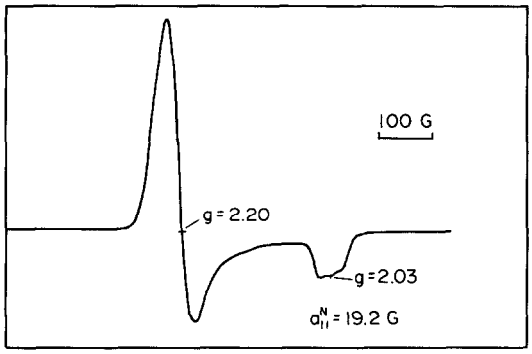

Fig. 2. X-band EPR spectrum (100 K) of [Ni(MC1)$Et_2Dtc]^{2+}$ electrogenerated in CH_3CN at 230 K. (See text for measurement conditions and Table 4 for g and $a_{\parallel}^{N}$ values of the other complexes.)

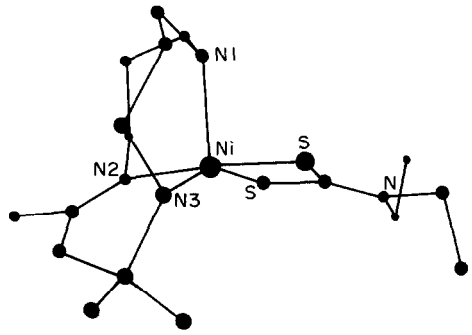

Fig. 3. Proposed penta-coordinate structure for the $[Ni(MC1)Et_2Dtc]^{2+}$ complex cation.

The frozen CH_3CN solution EPR spectra of the product of the electrolysis of the studied nickel(II) complexes confirm that the oxidation process is metal-centred. One typical spectrum, that of [Ni(MC1)Et_2Dtc](ClO_4), is shown in Fig. 2. The spectra consist of axial signals with $g_{\perp}$ and $g_{\parallel}$ values presented in Table 4. Hyperfine splitting (*ca* 20 G) is well-resolved only for $g_{\parallel}$. According to the literature,[6,8,9] such EPR spectra patterns are characteristic of a d^7 system in which the unpaired electron occupies principally the d_{z^2} orbital. The observed hyperfine splitting of the $g_{\parallel}$ feature is due to the interaction with only one nitrogen atom of the N3-macrocyclic ligand ($a_{\parallel}^{N}$ values are given in Table 4). If we assume that the electrogenerated nickel(III) species are also pentacoordinated, this coupling with only one nitrogen atom indicates a square pyramidal geometry with one nitrogen atom in the apical position; in that case, the d_{z^2} orbital is predicted to be lower in energy than the $d_{x^2-y^2}$ orbital.[10] It would be interesting to confirm this structural hypothesis by means of single crystal X-ray diffraction, and work is currently in progress in this direction. Besides, in the present lack of available experimental X-ray structural data of the nickel(II) precursor complexes, the hypothesis of a trigonal bipyramidal geometry with the other position corresponding to the d_{z^2} orbital occupied by one of the sulphur atoms of the 1,1-dithio ligand cannot be ruled out. However, in that case, the d_{z^2} orbital is predicted to be higher in energy than the $d_{x^2-y^2}$ orbital.[10] In the absence of structural data on these complexes, we propose a possible structure for [Ni(MC1)Et_2Dtc](ClO_4) (Fig. 3); this structure was derived and generated from the fractional atomic coordinates of the Et_2Dtc from [Ni(DL-CTH)Et_2Dtc](ClO_4), which structure has been reported,[1] and Ni(MC1) from [Cu(Me_2oxpn)Ni(MC1)](ClO_4), a dinuclear Cu^{II}–Ni^{II} complex we recently structurally characterized[11] (Me_2oxpn is N,N′-bis(2,2′-dimethyl-3-aminopropyl)oxamido).

Table 4. EPR data from frozen (100 K) CH_3CN solutions

Compound	$g_{\perp}$	$g_{\parallel}$	$a_{\parallel}^{N}$
[Ni(MC1)Me_2Dtc](ClO_4)	2.21	2.03	20.5 G
[Ni(MC1)Et_2Dtc](ClO_4)	2.20	2.03	19.2 G
[Ni(MC1)PyDtc](ClO_4)	2.21	2.03	20.5 G
[Ni(MC2)Me_2Dtc](ClO_4)	2.25	2.03	20.5 G
[Ni(MC2)Et_2Dtc](ClO_4)	2.25	2.03	19.2 G
[Ni(MC2)PyDtc](ClO_4)	2.24	2.03	20.5 G

CONCLUSIONS

The first pentacoordinate 1,1-dithio nickel(II) complexes with one N3-tridentate macrocyclic ligand and one dithiocarbamate ligand have been prepared and characterized by elemental analysis and spectroscopic measurements. These complexes undergo one reversible oxidation process in the 475–575 mV range. Controlled electrochemical oxidation of these complexes give oxidized species, unstable at room temperature, which have been characterized by frozen solution EPR spectroscopy as low-spin d^7 nickel(III) species.

Acknowledgements—Financial assistance from the CICYT (Grant No. PB88/0197) is acknowledged. We thank A. Dei, Ph. de Loth and A. Mari for helpful suggestions and stimulating discussions.

REFERENCES

1. R. Vicente, A. Escuer, J. Ribas, A. Dei, X. Solans and J. Calvet, *Polyhedron* 1990, **9**, 1729.
2. J. W. L. Martin, J. H. Johnston and N. F. Curtis, *J. Chem. Soc., Dalton Trans.* 1978, 68.

3. P. Cassoux, R. Dartiguepeyron, P. L. Fabre and D. de Montauzon, *L'Actualité Chimique* 1975, 79; *Electrochim. Acta* 1985, **30**, 1485.
4. P. Cassoux, R. Dartiguepeyron, C. Cross, P. Costes and D. de Montauzon, *Polyhedron* 1984, **3**, 585.
5. A. C. Fabetti, F. Forghieri, A. Giusti, C. Petri and G. Tosi, *Spectrochim. Acta* 1984, **40A**, 343.
6. J. Haines and A. McAuley, *Coord. Chem. Rev.* 1981, **39**, 94.
7. R. S. Nicholson and I. Shain, *Anal. Chem.* 1964, **36**, 706.
8. A. H. Maki, N. Edelstein, A. Davison and R. H. Holm, *J. Am. Chem. Soc.* 1964, **86**, 4580.
9. H. J. Krüger and R. H. Holm, *J. Am. Chem. Soc.* 1990, **112**, 2955.
10. A. Earnshaw, in *Introduction to Magnetochemistry*, p. 44. Academic Press, London (1968) and references 3, 6 and 13, therein.
11. A. Escuer, J. Ribas, R. Vicente, R. Costa and X. Solans, unpublished results. This complex crystallizes in the monoclinic $P2_1/n$ space group, with $a = 13.794$, $b = 27.459$, $c = 9.783$ Å, $\beta = 95.80°$. The five main distances are Ni—O(1) = 2.005, Ni—O(2) = 2.021, Ni—N(1) = 2.050, Ni—N(2) = 2.051 and Ni—N(3) = 2.054 Å. The angles O—Ni—O, O—Ni—N and N—Ni—N are between 80.6 and 103.6°. Consequently, the coordination around nickel(II) ion is slightly distorted square pyramidal.

Polyhedron Vol. 10, No. 17, pp. 2031–2036, 1991
Printed in Great Britain

0277–5387/91 $3.00+.00
© 1991 Pergamon Press plc

REACTIONS OF NIOBIUM AND TANTALUM CLUSTERS WITH ALIPHATIC ALCOHOLS. SYNTHESIS AND PROPERTIES OF $[M_6X_{12}(ROH)_6]X_2$, M = Nb OR Ta, X = Cl OR Br, R = Me, Et, i-Pr OR i-Bu

A. KASHTA, N. BRNIČEVIĆ* and R. E. McCARLEY

Rudjer Bošković Institute, 41000 Zagreb, Croatia, Yugoslavia and Ames Laboratory-USDOE and Department of Chemistry, Iowa State University, Ames, Iowa 50011, U.S.A.

(*Received* 10 *May* 1991; *accepted* 28 *May* 1991)

Abstract—The dissolution and subsequent evaporation of the aliphatic alcohol solutions of $[(M_6X^b_{12})(H_2O)_4X^t_2]\cdot 4H_2O$ (M = Nb or Ta, X = Cl or Br; b, bridging; t, terminal) in a vacuum have resulted in complete exchange of the four coordinated water molecules and two terminal halide atoms by aliphatic alcohols forming insoluble, crystalline, diamagnetic clusters of the composition $[M_6X_{12}(ROH)_6]X_2$ (R = CH_3, C_2H_5, i-C_3H_7 and i-C_4H_9). Spectral evidence indicates occupation of all octahedral coordination sites by aliphatic alcohol molecules.

The solubility of the hexanuclear cluster hydrates $[(M_6X_{12})(H_2O)_4X_2]\cdot 4H_2O$ (M = Nb or Ta, X = Cl or Br) in aliphatic alcohols was observed at the time of their discoveries. Chapin[1] measured the molecular weight of $Ta_6Br_{14}\cdot 7H_2O$ (correct $8H_2O$) using the boiling point method in propyl alcohol solution, and showed that the molecules present in this solvent contain Ta_6 units. Forty years later, X-ray diffraction[2] of an ethanolic solution of $M_6Cl_{14}\cdot 7H_2O$ and $Ta_6Br_{14}\cdot 7H_2O$ confirmed this result and revealed the complex cation $[M_6X_{12}]^{2+}$ with the octahedral arrangement of six metal atoms. The position of the absorption bands in the electronic spectra of these systems was found to be solvent dependent.[3,4] Similar results were obtained from potentiometric titrations.[5] More recently it was demonstrated that the solubility of these $[M_6X_{12}]^{2+}$ cluster units in aliphatic alcohols could be the consequence of reactions with solvents.[6] The specific conductivity and pH measurements at 25°C indicated distinct differences in behaviour between $[M_6Cl_{12}]^{2+}$ and $[M_6Br_{12}]^{2+}$ derivatives in alcohol solutions. For the former the specific conductivity was time dependent, whilst for the latter the equilibrium was reached within a few hours. Support for this proposal was also found in the high resolution ^1H NMR spectra of alcoholic solutions.[7] A complex multiplet consisting of 10 resonances was found in the region δ 3.7–3.8 ppm, arising from the CH_3 groups from coordinated CH_3OH molecules present in the mixed-ligand species $[(M_6X_{12})(H_2O)_{6-x}(CH_3OH)_6]^{2+}$, for X = Br, $0 \leqslant x \leqslant 6$, that are formed in methanolic solutions. The complexity of the ^1H NMR spectra for X = Cl is the consequence of competition between Cl^-, H_2O and CH_3OH for the six octahedral coordination sites. Data on the preparation of $[Nb_6Cl_{12}]Cl_4\cdot 3C_2H_5OH$,[8] $[(C_2H_5)_4N]_2[Nb_6Cl_{12}]X_4\cdot 2C_2H_5OH$[9] or $[M_6Cl_{12}](OH)_2\cdot 6H_2O\cdot 2CH_3OH$[10] also exist. Here we describe the synthetic procedure for the preparation of the completely anhydrous, insoluble cluster alcoholates, $[M_6X_{12}(ROH)_6]X_2$, that are formed in aliphatic alcohol solutions after complete displacement of the four coordinated water molecules and two halide atoms from the first coordination sphere of the parent cluster unit.

EXPERIMENTAL

Materials

Methanol, absolute ethanol, i-butanol (all Merck) and i-propanol (BDH) were dried over activated molecular sieves (3 Å). The clusters $[M_6X_{12}]X_2\cdot 8H_2O$, M = Nb or Ta, X = Cl or Br, were prepared using a published procedure.[11] Their

* Author to whom correspondence should be addressed at: Rudjer Bošković Institute, 41000 Zagreb, Croatia, Yugoslavia.

magnetic susceptibility measurements and electronic spectra agreed with those reported previously[12] for $[M_6X_{12}]^{2+}$ units.

Note. Aliphatic alcohol solutions of chloro and to a lesser extent bromo clusters are oxygen sensitive and slowly oxidize first to $[M_6X_{12}]^{3+}$ and then to $[M_6X_{12}]^{4+}$, and all experiments reported here were carried out on the vacuum line and in a dry-box under an oxygen-free nitrogen atmosphere.

Preparation of the clusters

$[M_6Cl_{12}(ROH)_6]Cl_2$, M = Nb *or* Ta, R = Me *or* Et. The clusters $[Nb_6Cl_{12}]Cl_2 \cdot 8H_2O$ (0.6 g, 0.50 mmol) or $[Ta_6Cl_{12}]Cl_2 \cdot 8H_2O$ (0.7 g, 0.405 mmol) in a round bottom flask and methanol (30 cm^3) or ethanol (50 cm^3) were distilled on the vacuum line. The clusters were dissolved in aliphatic alcohols by mixing and stirring the suspensions at room temperature overnight. The solutions were filtered off and evaporated on the vacuum line until dryness by heating the contents of the flask in a water bath at 35°C. Without heating, the clusters were dried on the vacuum line for a further 2 h. The process of distillation of methanol or ethanol on the vacuum line over the substances and its evaporation was repeated two or three more times for methanol or ethanol, respectively. Complete exchange of water molecules by methanol was recognized by the beginning of crystallization of the insoluble clusters $[M_6Cl_{12}(MeOH)_6]Cl_2$. At this point the suspensions were left for a few days to crystallize. Finally, the flasks and their content were transferred to a dry-box and the dark-green precipitates were separated out, washed with methanol and dried over P_4O_{10} under a nitrogen atmosphere.

After repeating the process of evaporation of ethanol cluster solutions in vacuum four times, the complete exchange of water molecules by ethanol was achieved, but the $[M_6Cl_{12}(EtOH)_6]Cl_2$ clusters were still soluble in ethanol. After the last evaporation to dryness the substances were left on the vacuum line to be evaporated overnight. Found: Nb, 45.9; Cl, 40.0; C, 5.9; H, 2.0. Calc. for $[Nb_6Cl_{12}(MeOH)_6]Cl_2$ (**I**): Nb, 44.7; Cl, 39.8; C, 5.8; H, 1.9%. IR data: 3360 m, 3160 m, 1630 w, 1140 w, 1000 vs, 380 w, 344 vs, 282 m, 245 w. Found: Nb, 42.3; Cl, 37.6; C, 10.6; H, 2.6. Calc. for $[Nb_6Cl_{12}(EtOH)_6]Cl_2$ (**II**): Nb, 41.9; Cl, 37.3; C, 10.8; H, 2.7%. IR data: 3400 w, 3160 w, 1610 w, 1087 w, 1024 vs, 980 sh, 945 sh, 870 s, 808 w, 344 vs, 282 m, 245 w. Found: Ta, 61.5; Cl, 28.1; C, 3.9; H, 1.5. Calc. for $[Ta_6Cl_{12}(MeOH)_6]Cl_2$ (**III**): Ta, 61.2; Cl, 28.0; C, 4.1; H, 1.4. IR data: 3100 m, 1736 w, 1610 w, 1121 m, 1000 vs, 619 w,b, 320 vs, 215 m,b. Found: Ta, 59.0; Cl, 26.9; C, 7.9; H, 2.2. Calc. for $[Ta_6Cl_{12}(EtOH)_6]Cl_2$ (**IV**): Ta, 58.4; Cl, 26.7; C, 7.7; H, 1.9%. IR data: 3400 w, 3150 w, 1618 w, 1089 m, 1024 vs, 1005 sh, 970 sh, 870 m, 808 m, 325 vs, 230 sh.

$[M_6Br_{12}(MeOH)_6]Br_2$, M = Nb *or* Ta. Clusters $[Nb_6Br_{12}]Br_2 \cdot 8H_2O$ (0.5 g, 0.274 mmol) and $[Ta_6Br_{12}]Br_2 \cdot 8H_2O$ (0.5 g, 0.212 mmol) were dissolved in methanol (20 cm^3) by mixing and warming the suspensions at 30°C. The clear, emerald-green solutions were filtered off (G-4 frit) to the ampoules previously filled with nitrogen, sealed off under nitrogen and left at room temperature for about a week. The dark-green clusters started crystallizing on the walls of the ampoules, were collected on a G-4 frit, washed with methanol in which they were not soluble and dried in evacuated tubes overnight.

Compounds of the same composition were precipitated by the addition of an equal volume of concentrated HBr (free of bromine) to the methanolic solution of $[M_6Br_{12}]Br_2 \cdot 8H_2O$. Found: Nb, 29.8; Br, 59.5; C, 3.8; H, 1.3. Calc. for $[Nb_6Br_{12}(MeOH)_6]Br_2$ (**V**): Nb, 29.8; Br, 59.9; C, 3.8; H, 1.3%. IR data: 3050 m, 1610 w, 1120 m, 998 vs, 578 w, 368 m, 267 s, 242 s. Found: Ta, 45.5; Br, 46.4; C, 3.1; H, 1.1. Calc. for $[Ta_6Br_{12}(MeOH)_6]Br_2$ (**VI**): Ta, 45.3; Br, 46.6; C, 3.0; H, 1.0%. IR data: 3160 w, 1600 w, 1120 m, 998 vs, 225 vs.

$[M_6Br_{12}(EtOH)_6]Br_2$, M = Nb *or* Ta. To clusters $[Nb_6Br_{12}]Br_2 \cdot 8H_2O$ (0.6 g, 0.329 mmol) or $[Ta_6Br_{12}]Br_2 \cdot 8H_2O$ (0.7 g, 0.298 mmol) in a round bottom flask the ethanol (50 cm^3) was distilled on the vacuum line. In order to dissolve the clusters completely the suspensions were left overnight, then filtered off, evaporated on the vacuum line until dryness and further dried under vacuum for 2 h. The process of distillation of ethanol over the substances and its evaporation on the vacuum line was repeated three more times. Exchange of water molecules by ethanol was complete when the insoluble $[M_6Br_{12}(EtOH)_6]Br_2$ clusters started to crystallize. The suspensions were left at room temperature for 2 days to crystallize. In a dry-box the precipitates were separated out, washed with ethanol and dried over P_4O_{10} in a nitrogen atmosphere. Found: Nb, 28.8; Br, 57.1; C, 6.9; H, 2.0. Calc. for $[Nb_6Br_{12}(EtOH)_6]Br_2$ (**VII**): Nb, 28.5; Br, 57.3; C, 7.4; H, 1.8%. IR data: 3050 w, 1620 w, 1085 m, 1024 s, 870 m, 808 m, 266 m. Found: Ta, 44.1; Br, 46.9; C, 5.6; H, 1.4. Calc. for $[Ta_6Br_{12}(EtOH)_6]Br_2$ (**VIII**): Ta, 43.8; Br, 46.8; C, 5.8; H, 1.5%. IR data: 1150 vw, 1610 w, 1087 w, 1024 s, 875 m, 804 m, 226 vs.

$[M_6X_{12}(i\text{-}ROH)_6]X_2$, M = Nb *or* Ta, X = Cl *or* Br, R = i-Pr *or* i-Bu. Since the starting substances $[M_6X_{12}]X_2 \cdot 8H_2O$ were poorly soluble in i-PrOH

and i-BuOH, the clusters $[M_6X_{12}(i\text{-}ROH)_6]X_2$ were prepared via the intermediate compounds $[M_6X_{12}]X_2 \cdot n\text{EtOH} \cdot (8-n)H_2O$. To the substances $[M_6X_{12}]X_2 \cdot 8H_2O$ (0.6 g) the ethanol (50 cm^3) in a round bottom flask was distilled on a vacuum line as described for $[M_6X_{12}(EtOH)_6]X_2$. After repeated dissolution of the cluster in ethanol and evaporation of the solution to dryness under vacuum to the solid, dried substances $[M_6X_{12}]X_2 \cdot n\text{EtOH} \cdot (8-n)H_2O$ were obtained. The i-PrOH or i-BuOH (50 cm^3) was distilled over the substances on the vacuum line and after dissolution the clear solutions were also evaporated under vacuum. The dissolution of the cluster in i-ROH and its evaporation on the vacuum line was repeated. During this process the slow crystallization of the insoluble $[M_6X_{12}(i\text{-}ROH)_6]X_2$ occurs as a result of the complete exchange of water and ethanol molecules by i-ROH. The suspensions were left to crystallize for 2 more days. Further methods are as described for $[M_6Cl_{12}(EtOH)_6]Cl_2$. Found: Nb, 39.3; Cl, 35.3; C, 15.0; H, 3.4. Calc. for $[Nb_6Cl_{12}(i\text{-}PrOH)_6]Cl_2$ (**IX**): Nb, 39.4; Cl, 36.1; C, 15.3; H, 3.4%. IR data: 3350 w, 3140 w, 1620 w, 1162 m, 1125 w, 1110 m, 1092 vs, 1030 w, 988 w, 950 w, 924 s, 818 s, 345 s, 280 w, 240 w. Found: Nb, 27.7; Br, 55.1; C, 10.0; H, 2.2. Calc. for $[Nb_6Br_{12}(i\text{-}PrOH)_6]Br_2$ (**X**): Nb, 27.4; Br, 54.9; C, 10.6; H, 2.4%. IR data: 3480 w, 3300 w, 1630 vw, 1165 m, 1128 w, 1112 w, 1095 vs, 1030 vw, 975 w, 950 w, 924 s, 819 s, 263 s. Found: Ta, 56.1; Cl, 25.2; C, 10.9; H, 2.3. Calc. for $[Ta_6Cl_{12}(i\text{-}PrOH)_6]Cl_2$ (**XI**): Ta, 55.9; Cl, 25.5; C, 11.1; H, 2.5%. IR data: 3480 w, 3200 w, 1620 w, 1162 m, 1125 m, 1110 m, 1092 vs, 1030 w, 978 w, 948 sh, 922 vs, 818 vs, 535 w, 395 w, 323 vs, 230 m. Found: Ta, 43.0; Cl, 43.8; C, 8.0; H, 1.9. Calc. for $[Ta_6Br_{12}(i\text{-}PrOH)_6]Br_2$ (**XII**): Ta, 42.3; Cl, 43.6; C, 8.4; H, 1.9%. IR data: 3486 w, 3300 w, 1640 vw, 1165 m, 1128 w, 1112 w, 1095 vs, 950 w, 923 s, 818 s, 230 vs. Found: Nb, 37.2; Cl, 33.4; C, 19.5; H, 3.8. Calc. for $[Nb_6Cl_{12}(i\text{-}BuOH)_6]Cl_2$ (**XIII**): Nb, 37.2; Cl, 33.2; C, 19.2; H, 4.0%. IR data: 3394 m, 3050 w, 1620 w, 1263 m, 1175 sh, 1149 w, 1100 m, 1027 vs, 999 vs, 962 w, 943 m, 901 w, 815 sh, 805 m, 530 m, 505 m, 385 m, 345 vs, 282 m, 241 m. Found: Ta, 53.9; Cl, 24.5; C, 13.8; H, 2.9. Calc. for $[Ta_6Cl_{12}(i\text{-}BuOH)_6]Cl_2$ (**XIV**): Ta, 53.6; Cl, 24.5; C, 14.2; H, 3.0%. IR data: 3400 m, 3060 w, 1615 w, 1265 m, 1175 sh, 1152 w, 1125 w, 1105 w, 1029 vs, 999 vs, 963 w, 945 w, 902 w, 822 w, 805 w, 538 w, 508 w, 388 w, 324 vs, 230 w. Found: Nb, 26.4; Br, 52.6; C, 14.3; H, 3.0. Calc. for $[Nb_6Br_{12}(i\text{-}BuOH)_6]_2$ (**XV**): Nb, 26.3; Br, 52.7; C, 13.6; H, 2.8%. IR data: 3400 m, 3100 w, 1615 w, 1263 w, 1245 sh, 1175 w, 1150 w, 1122 w, 1029 vs, 999 vs, 961 w, 942 w, 899 w, 821 w, 528 w, 504 w, 267 w, 223 vs. Found: Ta, 41.1; Br, 42.3; C, 10.7; H, 2.1. Calc. for $[Ta_6Br_{12}(i\text{-}BuOH)_6]_2$ (**XVI**): Ta, 41.0; Br, 42.2; C, 10.9; H, 2.3%. IR data: 3400 m, 3100 w, 1615 w, 1263 w, 1170 sh, 1135 sh, 1110 w, 1027 vs, 990 s, 962 w, 940 w, 895 w, 868 w, 819 w, 495 w, 230 vs.

Analysis. Niobium or tantalum were determined by the "H-tube" method.[13] The percentage of these metals was also calculated from the amount of M_2O_5 obtained at the end of thermogravimetric decomposition of the alcoholate clusters on the thermobalance. Halogens were determined by potentiometric titrations with standard silver nitrate solution after decomposition of the clusters with KOH and H_2O_2. Carbon and hydrogen were determined by the Rudjer Bošković Institute Microanalytical Service.

Physical measurements. The pH measurements and potentiometric titrations were performed at 25°C with Methrom potentiograph Model E 436. Solid-state IR spectra (4000–180 cm^{-1}) were recorded as Nujol mulls with a Perkin–Elmer Model 580B spectrometer and in methanol solutions with a Perkin–Elmer FTIR 1710 in 0.1 mm KBr cells. Magnetic susceptibility measurements were performed according to Gouy at 22°C for the starting materials and all complexes. Thermogravimetric measurements were carried out on a Cahn RG microanalytical balance in air with a heating rate of 2°C min^{-1}. The X-ray powder diffraction patterns were recorded on a Philips X-ray diffractometer using monochromatized Cu-K_α radiation on powdered samples containing an internal standard[14] of $CaCO_3$, ($R\bar{3}c$, $a = 4.989$, $c = 17.062$.)

RESULTS AND DISCUSSION

$[M_6X_{12}(ROH)_6]X_2$, M = Nb *or* Ta, X = Cl *or* Br, R = Me *or* Et

Crystalline, especially $[M_6Br_{12}(MeOH)_6]Br_2$, diamagnetic substances are the products of the complete exchange of coodinated and lattice water molecules in the starting clusters $[(M_6X_{12})(H_2O)_4X_2] \cdot 4H_2O$ by aliphatic alcohols, methanol or ethanol. Only the bromo clusters $[M_6Br_{12}(MeOH)_6]Br_2$ in this series were simply prepared in two different ways: (1) by leaving the methanolic solution of $[(M_6Br_{12})(H_2O)_4Br_2] \cdot 4H_2O$ in a sealed ampoule under a nitrogen atmosphere for about a week; (2) by acidifying the concentrated solutions of the same clusters by concentrated HBr, the insoluble clusters $[M_6Br_{12}(MeOH)_6]Br_2$ were precipitated out immediately. For the former the beginning of crystallization is concentration- and time-dependent. The synthesis of all of the other alco-

holate clusters was more complicated and was achieved through a long process of subsequent dissolution of the starting eight hydrates in methanol or ethanol, and the evaporation of these solutions *in vacuo* until the insoluble products $[M_6Cl_{12}(MeOH)_6]Cl_2$ and $[M_6Br_{12}(EtOH)_6]Br_2$ were obtained. Only $[M_6Cl_{12}(EtOH)_6]Cl_2$ clusters were found to be soluble in ethanol after complete exchange of water molecules by ethanol.

It was interesting to follow the changes in structure and thermal behaviour of the chloro cluster units upon dissolution in aliphatic alcohols after first and second evaporation *in vacuo* to dryness. For chloro clusters in methanol after the first evaporation *in vacuo* the analytical data were consistent with the substances of the average composition: $Nb_6Cl_{13.98}C_{4.08}H_{22.8}O_{7.86}$ and $Ta_6Cl_{13.98}C_{4.07}H_{23.4}O_{8.01}$, indicating partial exchange of water molecules by methanol. Based on the X-ray powder diffraction patterns new structural arrangements of the cluster units and lower thermal stability (TG measurements) were observed for the mixed ligand alcohol–water clusters as compared to the starting eight hydrates. Also, the solubility in alcohols was considerably higher after the first evaporation than before. After the second evaporation of methanol solutions *in vacuo* only a slight difference in chemical composition was found, yet the insoluble substances $[M_6Cl_{12}(MeOH)_6]Cl_2$ could not be prepared applying one or two evaporations in methanol only, even if the solutions before the first evaporation *in vacuo* were refluxed for several hours. The formation of the insoluble cluster alcoholates was a function of water concentration in alcohol solutions, but also of the process of dissociation of the two halide atoms from the terminal positions. Thus, the conductivity data[6] in methanol or ethanol solution indicated complete dissociation of the two Br^t's from $[(M_6Br^b_{12})(H_2O)_4Br^t_2]\cdot 4H_2O$ within a few hours, while the affinity of the two Cl^t's to be partially coordinated to the cluster units in these solvents was preserved. If ROH solutions were left to be evaporated spontaneously at room temperature without applying vacuum the coordination of ROH molecules to the cluster units failed.

Neither chloro nor bromo derivatives were soluble in polar organic solvents or water, but were soluble in strong oxygen donors like dimethylsulphoxide or N,N′-dimethylformamide. They were sensitive to oxygen and in this respect the bromo derivatives $[M_6Br_{12}(MeOH)_6]Br_2$ were more stable than the chloro derivatives. The process of oxidation to $[M_6X_{12}]^{3+}$ and then to $[M_6X_{12}]^{4+}$ was followed by partial decomposition of some cluster units to hydrated niobium(V) or tantalum(V) oxide. Nicely crystalline (according to the X-ray powder diffraction patterns) derivatives are only obtained with methanol. The analogous $[M_6Cl_{12}(MeOH)_6]Cl_2$ clusters are isostructural, as are $[M_6Br_{12}(MeOH)_6]Br_2$. Neither chloro nor bromo derivatives can be classified in any of the five structural groups[15] previously found within $[M_6X_{12}]^{2+}$ clusters. So far single crystals suitable for the crystal structure determination have not been prepared. The corresponding "*d*" values for $[M_6Br_{12}(MeOH)_6]Br_2$ are measured and listed in Table 1.

IR spectra of all these clusters are very simple and indicate the presence of coordinated alcohol molecules and bridging halides only. The exact position of all absorption bands is given in the Experimental. The strong and unsplit absorption band originating from CO stretchings of coordinated methanol observed at 1000 for **I** and **III** and at 988 cm^{-1} for **V** and **VI** indicates the chemical and structural equivalency among all of the six methanol molecules present. The shift of this absorption band to lower wave numbers in comparison to the position of the same absorption band in liquid[16] methanol (1029 cm^{-1}) indicates strong coordination of the alcohol molecules to the cluster units, reflecting the strong preference of the metal atoms for oxygen-donors in the terminal positions. The position of this band is comparable to that found previously for coordinated methanol molecules.[17] The absence of a strong absorption band in the solid state as well as in the solution IR spectra of these clusters in the 500–350 cm^{-1} region where the MO (oxygen from coordinated methoxo or ethoxo groups) stretching vibrations[18] are expected, suggests that methanol or ethanol are not present as alkoxides. It is interesting that the position of MX_b (b, bridging) vibrations are practically unaffected by the presence of coordinated alcohol molecules in all compounds discussed here as compared to the position of this absorption band in the starting clusters.[19]

$[M_6X_{12}(ROH)_6]X_2$, M = Nb *or* Ta, X = Cl *or* Br, R = i-PrOH *or* i-BuOH

Due to the low solubility of $[(M_6X_{12})(H_2O)_4X_2]\cdot 4H_2O$ in i-PrOH and i-BuOH the synthesis of these alcoholate clusters was only possible via the intermediates $[M_6X_{12}]X_2\cdot n\text{EtOH}\cdot(8-n)H_2O$. The mixed ethanol–water clusters were completely soluble in i-PrOH or i-BuOH and after repeated dissolution and evaporation processes *in vacuo* the isolation of the insoluble $[M_6X_{12}(ROH)_6]X_2$ alcoholate clusters was possible. The i-PrOH deriva-

Table 1. X-ray powder diffraction data

$[Nb_6Br_{12}(MeOH)_6]Br_2$		$[Ta_6Br_{12}(MeOH)_6]Br_2$	
d (Å)	I/I_1	d (Å)	I/I_1
9.41	85	9.39	55
8.81	100	8.78	100
6.54	28	6.42	33
4.47	8	5.06	3
4.41	17	4.46	4
4.16	18	4.39	7
3.986	11	4.15	5
3.461	15	3.976	4
3.34	17	3.450	9
3.218	17	3.319	8
3.143	51	3.211	6
3.087	6	3.132	8
3.030	10	3.030	4
2.963	9	2.959	8
2.940	8	2.929	5
2.805	16	2.797	9
2.722	86	2.714	42
2.564	11	2.557	5
2.495	6	2.536	5
2.446	13	2.488	5
2.365	10	2.447	6
2.288	23	2.438	9
2.281	24	2.358	9
2.239	29	2.280	15
2.170	23	2.276	16
2.142	11	2.233	18
2.021	10	2.164	15
1.978	17	2.136	6
1.926	34	2.016	7
1.886	8	1.972	13
1.859	10	1.921	14
1.848	12	1.879	5
1.783	5	1.854	7
1.762	12	1.843	6
1.729	9	1.776	4
1.698	6	1.758	6
1.668	4	1.727	6
1.641	15	1.697	4
1.585	8	1.639	6
1.574	6	1.579	4
1.537	4	1.557	3
1.518	6	1.514	4
1.495	5	1.491	3
1.471	4	1.466	4
1.434	4	1.381	5
1.385	7		

tives are not isostructural with those of i-BuOH, but the isostructurality was observed within chloro and bromo derivatives of the two series of clusters. Spectral and magnetic properties are relevant to those described for methanol and ethanol derivatives. With the exception of $[M_6Br_{12}(CH_3OH)_6]Br_2$, all of the alcoholate clusters discussed here are slightly moisture-sensitive and if exposed to air a slow transformation to the octahydrates occurs.

CONCLUSION

The large series of alcoholate clusters $[M_6X_{12}(ROH)_6]X_2$ represent a new class of completely

anhydrous cluster species containing the $[M_6X_{12}]^{2+}$ unit. The aliphatic alcohol molecules occupy all available octahedral coordination sites. The crystal structures of these compounds are a function of the particular cluster unit (chloro or bromo) and aliphatic alcohol. In addition to the previously known[10,15] structural groups eight new ones were found within the $[M_6X_{12}]^{2+}$ units. The absence of water molecules makes these clusters suitable as precursors for further reactions with organic and inorganic ligands in non-aqueous solvents. Also, easier oxidation–reduction processes for $[M_6X_{12}]^{n+}$ in solutions are expected in the absence of water molecules.

Acknowledgements—Financial support by the Research Council of the Republic of Croatia and the U.S. Department of Energy, Office of Basic Energy Sciences, Chemical Sciences Division, under Contract JF-891 is gratefully acknowledged.

REFERENCES

1. W. H. Chapin, *J. Am. Chem. Soc.* 1910, **32**, 323.
2. P. A. Vaughan, J. H. Sturdivant and L. Pauling, *J. Am. Chem. Soc.* 1950, **72**, 5477.
3. B. Spreckelmeyer, *Z. Anorg. Allg. Chem.* 1969, **365**, 225.
4. P. B. Fleming and R. E. McCarley, *Inorg. Chem.* 1970, **9**, 1347.
5. N. Brničević and H. Schäfer, *Z. Anorg. Allg. Chem.* 1978, **441**, 219.
6. N. Brničević and D. Plavšić, *Proc. ICCC*, p. 161. Toulouse, France (1980).
7. N. Brničević, R. E. McCarley and V. Rutar, in preparation.
8. B. Spreckelmeyer and H. Schäfer, *J. Less-Common Metals* 1966, **11**, 74.
9. R. A. Mackay and R. F. Schneider, *Inorg. Chem.* 1968, **7**, 455.
10. N. Brničević and B. Kojić-Prodić, *Z. Anorg. Allg. Chem.* 1982, **489**, 235.
11. F. W. Koknat, J. A. Parsons and A. Vongvusharintra, *Inorg. Chem.* 1974, **13**, 1699.
12. J. G. Converse and R. E. McCarley, *Inorg. Chem.* 1970, **9**, 1361.
13. H. Schäfer and K. D. Dohmann, *Z. Anorg. Allg. Chem.* 1959, **300**, 1.
14. Powder Diffraction File, Card No. 5-586, Swarthmore, PA: JCPDS.
15. N. Brničević, B. Kojić-Projić and D. Plavšić, *Z. Anorg. Allg. Chem.* 1981, **472**, 200.
16. M. Falk and E. Whalley, *J. Chem. Phys.* 1961, **34**, 1554.
17. A. Casey and R. J. H. Clark, *Inorg. Chem.* 1969, **8**, 1216.
18. N. Brničević, F. Muštović and R. E. McCarley, *Inorg. Chem.* 1988, **27**, 4532.
19. R. Mates, *Z. Anorg. Allg. Chem.* 1969, **364**, 279.

Polyhedron Vol. 10, No. 17, pp. 2037–2044, 1991
Printed in Great Britain

0277–5387/91 $3.00+.00
© 1991 Pergamon Press plc

ACTIVATION OF AROMATIC CARBON–HYDROGEN BONDS OF METHYL-SUBSTITUTED BENZENES BY THE PALLADIUM(II)ACETATE-DIISOBUTYL SULPHIDE SYSTEM

YOSHIO FUCHITA,* MINA KAWAKAMI and KOHJI SHIMOKE

Laboratory of Chemistry, College of General Education, Kyushu University, Ropponmatsu, Chuo-ku, Fukuoka 810, Japan

(*Received* 8 *April* 1991; *accepted* 28 *May* 1991)

Abstract—Aromatic C—H bond activation of various methyl-substituted benzenes by the $Pd(MeCO_2)_2$-SBu^i_2 system have been studied. In the case of *p*-xylene the new and unusual compound $[(SBu^i_2)(2,5\text{-}Me_2C_6H_3)Pd(\mu\text{-}MeCO_2)_2Pd(\mu\text{-}MeCO_2)_2Pd(2,5\text{-}Me_2C_6H_3)(SBu^i_2)]$ (**1**) has been isolated. Complex **1** reacts with styrene and carbon monoxide to afford (*E*)-1-(2,5-dimethylphenyl)-2-phenylethene and 2,5-dimethylbenzene carboxylic acid, respectively. It has also been found that coupling products, biaryls, are formed in the reaction between $Pd(MeCO_2)_2$-SBu^i_2 and methyl-substituted benzenes. The isolated arylpalladium(II) complexes and the coupling products have been characterized and identified by means of ^1H NMR, GC-MS, and elemental analysis. On the basis of the isomer distribution of both isolated arylpalladium(II) complexes and the coupling products, the effect of the methyl groups on the benzene nucleus towards aromatic C—H bond activation is discussed.

The activation of arene C—H bonds by transition metals is a subject undergoing current research in organometallic chemistry. There are two main ways to prepare σ-aryl complexes directly from arenes: (1) oxidative addition of arene C—H bonds to coordinatively unsaturated metal complexes which are photochemically[1] or thermally[2] generated, and (2) electrophillic substitution of arenes by metal complexes.[3]

We have recently reported the direct activation of benzene C—H bonds by palladium(II) acetate-dialkyl sulphide systems, whose reactions afforded diphenyltripalladium(II) complexes $[(SR_2)PhPd(\mu\text{-}MeCO_2)_2Pd(\mu\text{-}MeCO_2)_2PdPh(SR_2)]$.[4] As an extension of this work, activation of aromatic C—H bonds of methyl-substituted benzenes (toluene, xylenes, trimethylbenzenes and 1,2,3,4-tetramethylbenzene) by the palladium(II) acetate-diisobutyl sulphide system has been investigated. This paper gives a detailed description of the above reactions including isolation and detection of the resulting arylpalladium(II) complexes and the coupling products, biaryls.

* Author to whom correspondence should be addressed.

RESULTS AND DISCUSSION

Synthesis of arylpalladium(II) *complexes*

(a) Activation of *p*-xylene and the resulting arylpalladium(II) complex, $[(SBu^i_2)(2,5\text{-}Me_2C_6H_3)Pd(\mu\text{-}MeCO_2)_2Pd(\mu\text{-}MeCO_2)_2Pd(2,5\text{-}Me_2C_6H_3)(SBu^i_2)]$ (**1**), and its derivative $[PdCl(2,5\text{-}Me_2C_6H_3)(bipy)]$ (**5**). Using the $Pd(MeCO_2)_2$-SBu^i_2 system, *p*-xylene was directly activated to produce **1**. The ^1H and ^{13}C NMR spectra (see Experimental) closely resembled those of $[(SBu^i_2)PhPd(\mu\text{-}MeCO_2)_2Pd(\mu\text{-}MeCO_2)_2PdPh(SBu^i_2)]$ which were similarly obtained from heating palladium(II) acetate in benzene in the presence of diisobutyl sulphide.[4] On the basis of these results, elemental analysis, and its reactions (see below), **1** was formulated as the bis(2,5-dimethylphenyl)tripalladium(II) complex $[(SBu^i_2)(2,5\text{-}Me_2C_6H_3)Pd(\mu\text{-}MeCO_2)_2Pd(\mu\text{-}MeCO_2)_2Pd(2,5\text{-}Me_2C_6H_3)(SBu^i_2)]$, composed of two geometrical isomers, al and ak (Scheme 1). The structure of **1** proposed here tentatively is shown in Scheme 1. X-ray structural analysis of **1** is in progress but difficulties have been encountered owing to the presence of al and ak isomers.

Complex **1** was treated with bipy and then with

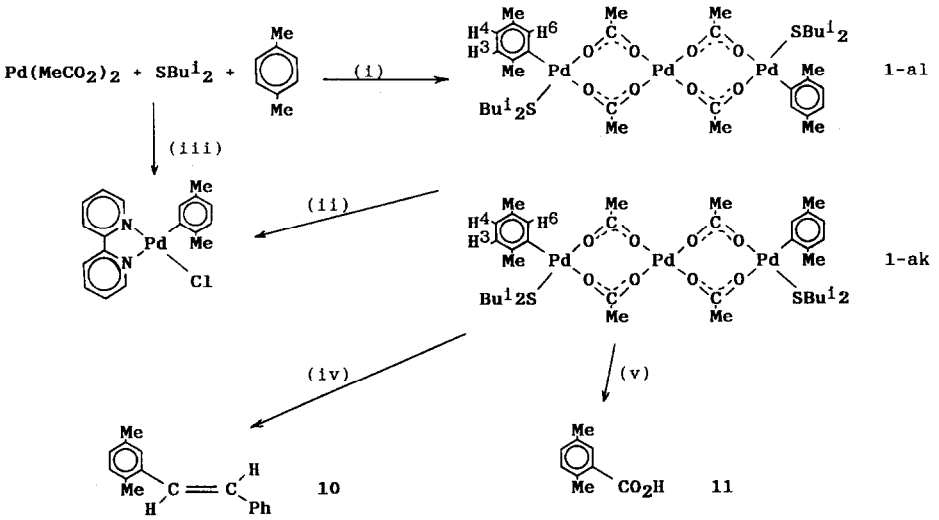

Scheme 1. Reactions of $Pd(MeCO_2)_2$ with *p*-xylene in the presence of SBu^i_2. (i) 90–95°C for 45 min; (ii) bipy, followed by NaCl; (iii) 90–95°C for 45 min, followed by the treatment with bipy and then NaCl; (iv) styrene; and (v) carbon monoxide.

NaCl to afford $[PdCl(2,5\text{-}Me_2C_6H_3)(bipy)]$ (**5**) in 64% yield. This complex was also obtained in 56% yield without isolation of **1**, just by treating the preparative reaction mixture of **1** with bipy and NaCl (Scheme 1). In the ^1H NMR spectrum of **5**, the 5-methyl protons appeared at δ 2.26, while the 2-methyl protons resonated at a comparatively lower field at δ 2.65. Such a deshielding of the methyl resonance *ortho* to the metal atom was found in *trans*-$[Ni(2\text{-}MeC_6H_4)(CCl{=}CCl_2)(PEt_3)_2]$[5] and was ascribed to paramagnetic anisotropy of the metal ion.[5,6]

(b) Activation of other methyl-substituted benzenes and their resulting complexes, [PdCl(aryl)(bipy)] (**2–9**). Diaryltripalladium(II) complexes such as complex **1** could not be isolated by the reactions of the $Pd(MeCO_2)_2$-SBu^i_2 system with corresponding methyl-substituted benzenes except for *p*-xylene, owing mainly to their lower yields. However, by successive treatments with bipy and NaCl after the reactions between the $Pd(MeCO_2)_2$-SBu^i_2 system and the corresponding methyl-substituted benzene, mononuclear aryl-palladium(II) complexes, [PdCl(aryl)(bipy)] (**2–9**), were isolated. Two methods were performed to obtain **2–9** (see Scheme 2), after the activation of the appropriate methyl-substituted benzene by the $Pd(MeCO_2)_2$-SBu^i_2 system: Method A, treatment with bipy followed by NaCl; method B, treatment with NaCl and then with bipy (for further details see Experimental). The results are listed in Table 1 and possible isomers of **2–9** are shown in Fig. 1. It was found that method A afforded a mixture of isomers, while method B yielded only one isomer in which the methyl group is bonded *ortho* to the palladium atom. Previously we have observed that $[(Bu^tSCH_2Bu^t)PhPd(\mu\text{-}MeCO_2)_2Pd(\mu\text{-}MeCO_2)_2PdPh(Bu^tSCH_2Bu^t)]$, whose aryl moiety has no methyl group *ortho* to the palladium atom, decomposed during the reaction with LiCl to afford $[PdCl_2(Bu^tSCH_2Bu^t)_2]$ and biphenyl.[4] Enhanced stability of the aryl complexes involving a methyl group in the *ortho* position relative to those containing methyl substituents on *m*- or *p*-positions is mainly due to an increase in metal—carbon bond strength, caused by the d_π–p_π bonding and to an increase in kinetic stability due to the increase in energy difference between the highest occupied and

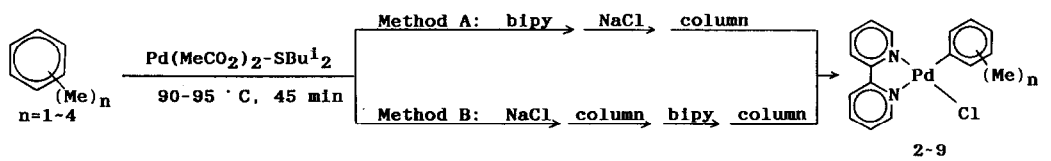

Scheme 2. Two preparative methods for **2–9**.

Table 1. Analytical and physical data for arylpalladium(II) complexes **1–9**

Complex	Method[a]	Yield (%)	M.p.[b] (°C)	Analysis[c] (%) C	H	N
1	—	60	181	45.3(45.4)	6.3(6.3)	—
2a[d]	B	3	191	58.4(59.1)	4.6(4.5)	6.1(6.0)
3a[e]	B	11	197	56.8(57.0)	4.7(4.6)	6.2(6.3)
4a,b,c	A	13[f]	—[g]	54.0(53.6)	4.6(4.3)	6.6(7.0)
4a	B	6	209	53.4(53.6)	4.2(4.3)	6.9(7.0)
5	A	56	144	53.5(53.6)	4.3(4.3)	6.9(7.0)
	C	64	144	—	—	—
6a	B	2	219	55.2(54.7)	4.7(4.6)	6.6(6.7)
7a,b,c	A	16[h]	—[g]	54.6(54.7)	4.6(4.6)	6.5(6.7)
9	A	11	232	55.4(55.7)	4.9(4.9)	6.4(6.5)

[a] See text as for A and B. C: Reaction of **1** with bipy, followed by the treatment of NaCl.
[b] With decomposition, except for **5**.
[c] Calculated values in parentheses.
[d] Obtained as 1 mol of benzene adduct.
[e] Obtained as 0.5 mol of benzene adduct.
[f] Isomer ratio of **4a** : **4b** : **4c** = 45 : 55 : 0.
[g] Not measured since it is a mixture.
[h] Isomer ratio of **7a** : **7b** : **7c** = 25 : 75 : 0.

the lowest unoccupied molecular orbitals.[7] However, in the case of toluene, *o*-xylene and 1,2,3-trimethylbenzene, method A did not produce **2**, **3** or **6** in a pure state.

In the case of the reactions with *m*-xylene, 1,2,4-trimethylbenzene and 1,3,5-trimethylbenzene, there are possibilities to form the arylpalladium(II) complexes, **4c**, **7c** and **8**, respectively, whose aryl moieties contain two methyl groups *ortho* to the central palladium atom. However, they were not obtained;

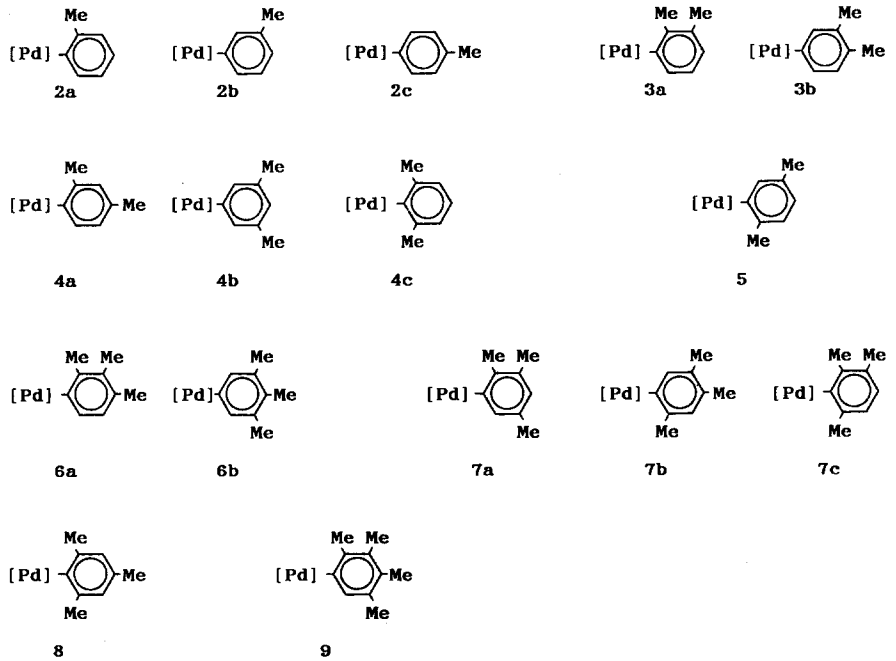

Fig. 1. Possible isomers of [PdCl(aryl)(bipy)] (**2–9**). [Pd] denotes the PdCl(bipy) moiety.

Table 2. ^{1}H NMR spectra of arylpalladium(II) complexes **2–9**[a]

Complex	Arylpalladium moiety	bipy[b]
2a	2.71[s, 2-Me]; 6.9–7.0[c, 3- ~ 6-H]	9.32[d, ^3J(HH) = 5.9 Hz]
3a	2.74[s, 2-Me], 2.25[s, 3-Me]; 6.75–6.9[4- ~ 6-H]	9.32[d, ^3J(HH) = 5.4 Hz]
4a	2.66[s, 2-Me]; 2.27[s, 4-Me]; 6.77[dd, ^3J(HH) = 7.3 Hz, ^4J(HH) = 1.5 Hz, 5-H]; 6.18[d, ^4J(HH) = 7.3 Hz, 3-H]; 7.29[d, ^3J(HH) = 1.5 Hz, 6-H]	9.28[d, ^3J(HH) = 5.4 Hz]
4b	2.26[s, 3-, 5-Me]; 7.06[br s, 2-, 6-H]; 6.62[br s, 4-H]	9.29[d, ^3J(HH) = 5.4 Hz]
5	2.65[s, 2-Me]; 2.26[s, 5-Me]; 6.73[dd, ^3J(HH) = 7.6 Hz, ^4J(HH) = 1.5 Hz, 4-H]; 6.86[d, ^3J(HH) = 7.6 Hz, 3-H]; 7.29 [d, ^4J(HH) = 1.5 Hz, 6-H]	9.31[d, ^3J(HH) = 5.9 Hz]
6	2.79[s, 2-Me]; 2.17, 2.25[s, 3-, 4-Me]; 6.74[d, ^3J(HH) = 7.6 Hz, 5-H]; 7.13[d, ^3J(HH) = 7.6 Hz, 6-H]	9.32[d, ^3J(HH) = 5.4 Hz]
7a	2.69[s, 2-Me]; 2.22, 2.23[s, 3-, 5-Me]; 6.63[br s, 4-H]; 7.11[br s, 6-H]	9.32[d, ^3J(HH) = 5.4 Hz]
7b	2.62[s, 2-Me]; 2.18, 2.19[s, 4-, 5-Me]; 6.77[s, 3-H]; 7.19[s, 6-H]	9.31[d, ^3J(HH) = 5.4 Hz]
8	2.71[s, 2-, 6-Me]; 2.26[s, 4-Me]; 6.66[s, 3-, 5-H]	9.32[d, ^3J(HH) = 5.1 Hz]
9	2.75[s, 2-Me]; 2.15, 2.17, 2.20[s, 3-, 4-, 5-Me]; 7.07 [s, 6-H]	9.30[d, ^3J(HH) = 5.4 Hz]

[a] Key: s = singlet, br s = broad singlet, d = doublet, and dd = doublet of doublets. For the numbering of the methyl group and aromatic protons see Fig. 1.

[b] Assigned to 6-H of one pyridyl moiety *trans* to the aryl group. Other protons of the 2,2′-bipyridyl ligand resonated near δ 7.3, 7.6 and 7.9–8.1 as a complex pattern.

only complex **8** was formed in a yield less than 1% and only its ^{1}H NMR spectrum was measured (Table 2).

The ^{1}H NMR spectrum of the arylpalladium(II) complexes derived from *m*-xylene by method A showed three methyl resonances at δ 2.26 (s, 3.3H), 2.27 (s, 1.35H) and 2.66 (s, 1.35H). Considering that the integral values and the lower field shift characteristic of the methyl signal attached *ortho* to the palladium atom (see above), the methyl signals at δ 2.27 and 2.66 were assigned to the non-equivalent methyl groups of isomer **4a**, while the resonance at δ 2.26 was ascribed to the equivalent methyl groups of isomer **4b**. Assignment of the ^{1}H NMR signals of **4a** was confirmed upon measuring the ^{1}H NMR spectrum of the product from method B, which contained isomer **4a** only. The isomer ratio of **4a** : **4b** was calculated as 45 : 55.

In the ^{1}H NMR spectrum of the reaction products of 1,2,4-trimethylbenzene by method A, a pair of signals (ratio 75 : 25) was observed in the arylpalladium moiety (Table 2), judging from the integral values. The ^{1}H-^{1}H COSY spectrum showed correlation between the resonances at δ 6.63 and 7.11, attributable to a weak ^4J(HH) coupling. On the basis of the above results, the minor and major products of the pair were assigned to **7a** and **7b**, respectively.

(c) Reaction of **1** with styrene or carbon monoxide. Complex **1** reacted with styrene in a THF-CH_2Cl_2 mixed solvent to give (*E*)-1-(2,5-dimethylphenyl)-2-phenylethene (**10**) in 90% yield. When carbon monoxide was bubbled through a CH_2Cl_2 solution of **1** and the reaction mixture was treated with sodium hydrogen carbonate, 2,5-dimethylbenzene carboxylic acid (**11**) was obtained in 26% yield. The formation of both **10** and **11** strongly confirmed that **1** contained the 2,5-dimethylphenylpalladium moiety and was formed by direct C—H bond activation of *p*-xylene by the $Pd(MeCO_2)_2$-SBu^i_2 system.

Coupling reaction of methyl-substituted benzenes promoted by the $Pd(MeCO_2)_2$-SBu^i_2 *system**

The fact that palladium(II) acetate promotes or catalyses the coupling reaction of aromatic compounds via the formation of arylpalladium(II) complexes to give biaryls is well-established.[8,9] It has been found that the reaction mixture of the $Pd(MeCO_2)_2$-SBu^i_2 system and methyl-substituted benzenes contained corresponding biaryls. Yields of the coupling products and their isomer distribution are summarized in Table 3.

In the case of 1,3,5-trimethylbenzene, the $Pd(MeCO_2)_2$-SBu^i_2 system gave practically no coupling product. This is consistent with the result reported previously by Itatani and Yoshimoto[9] in the palladium-catalysed coupling of 1,3,5-trimethyl-

* See ref. 4 for the coupling of toluene.

Table 3. Coupling products promoted by the $Pd(MeCO_2)_2$-SBu^i_2 system[a]

Methyl-substituted benzenes	Yield (%)[b]	Isomers and distribution[c]		
	61	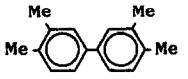 12a(84%)	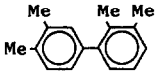 12b(16%)	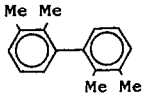 12c(~0%)
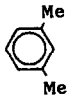	25	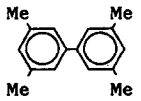 13a(60%)	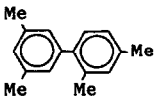 13b(40%)	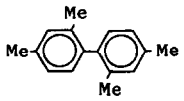 13c(~0%)
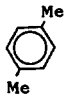	6	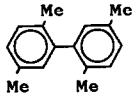 14(100%)		
	56	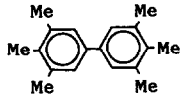 15a(75%)	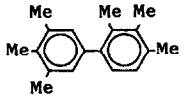 15b(25%)	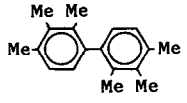 15c(~0%)
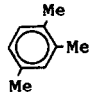	$\ll 1$[d]	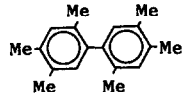 16a	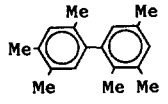 16b	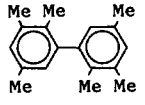 16c
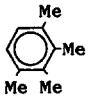	5	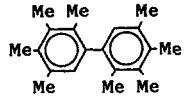 17(100%)		

[a] Conditions: $Pd(MeCO_2)_2$ (0.050 g, 0.223 mmol), SBu^i_2 (0.022 g, 0.148 mmol) and the corresponding methyl-substituted benzene (12 cm^3).

[b] Yields based on $Pd(MeCO_2)_2$.

[c] Determined by GLC.

[d] Isomer distribution could not be determined owing to its low yield.

benzene. This fact indicated that no C—H bond activation occurred and accordingly, the resulting palladation did not proceed on the benzene carbon between two methyl groups. This seemed to be applicable to the 2-carbon of 1,3-dimethylbenzene (*m*-xylene) and the 3-carbon of 1,2,4-trimethylbenzene; formation of the corresponding coupling products derived from such species were excluded.

In the cases of *o*-xylene, *m*-xylene and 1,2,3-trimethylbenzene, the ^1H NMR spectra of the corresponding isolated coupling products showed the absence of **12c**, **13c** and **15c**. These three compounds would be produced by homocoupling of the corresponding arylpalladium(II) species containing one methyl group *ortho* to the central palladium atom. However, the above arylpalladium(II) species coupled with other species involving no methyl groups around the palladium atom produced **12b**, **13b** and **15b** in moderate yields. On the

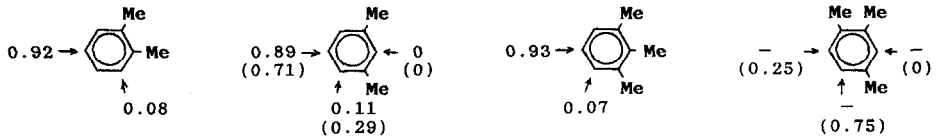

Fig. 2. Relative positional reactivities of methyl-substituted benzenes calculated from the coupling products or from the isolated arylpalladium(II) complexes (shown in parentheses).

contrary, when there is no position to be activated except for the *ortho* position to one methyl group, i.e. *p*-xylene, 1,2,4-trimethylbenzene and 1,2,3,4-tetramethylbenzene, the coupling reaction did occur on these positions to afford **14**, **16** and **17**. However, their yields were generally very low. These results indicated that a C—H bond surrounded by both hydrogen and methyl groups is resistant to activation, owing to steric problems caused by the methyl group.

Relative positional reactivities in each methyl-substituted benzene for C—H bond activation were calculated from the composition of the coupling products formed (Fig. 2). These data suggested that the ease of the C—H bond activation depends considerably on the number of methyl groups around the C—H bond to be activated. Relative positional reactivities were also calculated from the isomer distribution of **4** and **7** (see parentheses in Fig. 2). The value of the 4- or 6-position of *m*-xylene was slightly greater than that of the 5-position, in comparison with the calculated values from the coupling products. This difference might be ascribed to a higher stability of **4a** having an *ortho* methyl group in its aryl moiety (see above). However, in 1,2,4-trimethylbenzene, the 5- and 6-positions are equal in the number of methyl groups around them; reactivity of the 5-position is about three times greater than that of the 6-position. This could be associated with a higher electron density at the 5-position compared with the 6-position: both 5- and 6-positions have one *ortho* methyl group, but in addition the former has another methyl group in the *para* position. On the basis of the arguments presented above, we conclude that the $Pd(MeCO_2)_2$-SBu^i_2 system activates aromatic C—H bonds of methyl-substituted benzenes predominantly at less hindered and more electron-rich positions.

EXPERIMENTAL

All the experiments were performed under nitrogen. Solvents were dried by the usual methods and distilled. Other reagents were used without purification. The NMR spectra were measured on a JEOL JNM GX-270 instrument with $CDCl_3$ as a solvent and reported in δ (ppm) relative to tetramethylsilane. Yields and distribution of the coupling products, biaryls, were analysed with a Shimadzu GC-14A gas chromatograph on a BP-1 (50 m long) capillary column. Coupling products were identified by GC-MS on a Shimadzu GC-MS 9020DF instrument. Melting points were determined on a Yanaco melting point apparatus MP-500D.

Preparation of $[(SBu^i_2)(2,5\text{-}Me_2C_6H_3)Pd(\mu\text{-}MeCO_2)_2Pd(\mu\text{-}MeCO_2)_2Pd(2,5\text{-}Me_2C_6H_3)(SBu^i_2)]$ (**1**)

A suspension of palladium(II) acetate (0.400 g, 1.78 mmol) and SBu^t_2 (0.174 g, 1.19 mmol) was heated in *p*-xylene (20 cm^3) at 90°C for 1 h. Upon cooling, some crystals appeared. After the resulting mixture was concentrated to about 5 cm^3, the precipitated crystals were filtered and washed with hexane to give 0.38 g of **1**. ^1H NMR: δ 0.89 [24H, br, sulphide-CH_3], 1.77 [3H, s, CH_3CO_2], 1.83 [3H, s, CH_3CO_2], 1.86 [3H, s, CH_3CO_2], 1.94 [3H, s, CH_3CO_2], 1.95 [4H, br, sulphide-CH], 2.13 [3H, s, 5-CH_3 of 2,5-xylyl], 2.17 [3H, 5-CH_3 of 2,5-xylyl], 2.83 [8H, br, sulphide-CH_2], 3.02 [6H, s, 2-CH_3 of 2,5-xylyl], 6.64 [2H, d, ^3J(HH) = 7.3 Hz, 3- or 4-H of 2,5-xylyl], 6.75 [2H, d, ^3J(HH) = 7.3 Hz, 3- or 4-H of 2,5-xylyl], 7.51 [1H, s, 6-H of 2,5-xylyl], 7.54 [1H, s, 6-H of 2,5-xylyl]. $^{13}C\{^1H\}$ NMR: δ 20.86 and 20.92 (5-CH_3); 21.61, 21.64, 22.03 and 22.07 (sulphide-CH_3); 23.08, 23.33, 23.47 and 23.57 (acetato-CH_3); 23.89 and 23.92 (2-CH_3), 27.49 and 27.52 (sulphide-CH); 46.29 and 46.32 (sulphide-CH_2); 124.56 (4-C of 2,5-xylyl); 127.34 (3-C of 2,5-xylyl); 132.91 and 133.10 (5-C of 2,5-xylyl); 135.27 and 135.42 (6-C of 2,5-xylyl); 138.51 and 138.67 (2-C of 2,5-xylyl); 140.14 and 140.20 (1-C of 2,5-xylyl); 181.63, 182.07, 183.09 and 183.46 (acetato-CO_2).

Preparation of $[PdCl(2,5\text{-}Me_2C_6H_3)(bipy)]$ (**5**)

(a) Method A: A mixture containing palladium(II) acetate (0.200 g, 0.891 mmol) and SBu^t_2 (0.087 g, 0.594 mmol) was heated in *p*-xylene (20 cm^3) for 1 h. After cooling to room temperature, solid bipy (0.139 g, 0.891 mmol) was added and the mixture was stirred for 3 h. A precipitate appeared which was collected and extracted with $CHCl_3$ (30

cm^3). The $CHCl_3$ extracts were evaporated to dryness and then acetone (10 cm^3) was introduced. After addition of a solution of NaCl (0.260 g, 4.46 mmol) in acetone/water (5 cm^3/2.5 cm^3), the mixture was stirred at room temperature for 1 day and evaporated to dryness. The residue was extracted with $CHCl_3$ to remove the by-product [$PdCl_2$(bipy)] and was chromatographed on a silica gel column (200 mesh, 13 × 1.2 cm) with $CHCl_3$. Complex **5** (0.133 g) was obtained upon the addition of hexane to a yellow fraction. (b) Method C: Solid bipy (0.045 g, 0.286 mmol) was added to a suspension of **1** (0.100 g, 0.0945 mmol) in *p*-xylene (5 cm^3). The resulting mixture was stirred at room temperature for 4 h, and the volatile materials were removed *in vacuo*. The residue in acetone (5 cm^3) was treated with NaCl (0.095 g, 1.63 mmol) in acetone/water (2 cm^3/2 cm^3), and the mixture was stirred at room temperature for 1 day. After evaporating to dryness, the residue was extracted with $CHCl_3$ to remove the by-product [$PdCl_2$(bipy)], and chromatographed on a silica gel column (200 mesh, 11 × 1.2 cm). The yellow fraction which was eluted by $CHCl_3$ was collected and recrystallized from CH_2Cl_2 and hexane to give **5** (0.049 g).

Preparation of the arylpalladium(II) *complexes of the type* [PdCl(aryl)(bipy)] (**2–9**)

Complexes **2–9** were synthesized by two methods A and B. Typical examples are described below:

(a) Method A: A suspension containing $Pd(MeCO_2)_2$ (0.400 g, 1.78 mmol) and SBu^i_2 (0.174 g, 1.19 mmol) in *m*-xylene (20 cm^3) was heated at 90–95°C for 1 h. After the reaction mixture was cooled to ambient temperature, solid bipy (0.278 g, 1.78 mmol) was added and the resulting mixture was stirred for 3 h. Hexane (25 cm^3) was added to the mixture, and the precipitate which appeared was collected. The precipitate was treated with NaCl (0.521 g, 8.91 mmol) in an acetone/water (20/5 cm^3) mixed solvent, and the mixture was stirred for 1 day at room temperature. After the volatile materials were removed *in vacuo*, the residue was extracted with $CHCl_3$ to remove the by-product [$PdCl_2$(bipy)], and was chromatographed on a silica gel column (200 mesh, 22 × 1.2 cm). The yellow fraction which was eluted by $CHCl_3$ was collected and recrystallized from $CHCl_3$–hexane to give a mixture of **4a** and **4b** (0.067 g).

(b) Method B: A suspension containing $Pd(MeCO_2)_2$ (0.400 g, 1.78 mmol) and SBu^i_2 (0.174 g, 1.19 mmol) in *m*-xylene (20 cm^3) was heated at 90–95°C for 1 h. After the volatile materials were removed *in vacuo*, the residue was extracted with acetone (40 cm^3). The extract was treated with NaCl (0.521 g, 8.91 mmol) in water (5 cm^3), and stirred at room temperature for 1 day. The resulting mixture was evaporated to dryness, and extracted with $CHCl_3$ (30 cm^3) to remove the by-product [$PdCl_2$(bipy)]. The $CHCl_3$ extract was then passed through a silica gel column (200 mesh, 27 × 1.2 cm) with $CHCl_3$. The yellow/yellow-orange fraction was treated in benzene (15 cm^3) with bipy (0.278 g, 1.78 mmol) at room temperature for 1 day. The reaction mixture was chromatographed on a silica gel column (200 mesh, 22 × 1.2 cm) with $CHCl_3$ as an eluant. A yellow fraction was obtained and recrystallized from $CHCl_3$–hexane to give **4a** (0.029 g).

Reactions of **1** *with styrene and carbon monoxide*

(a) With styrene: A CH_2Cl_2 solution (15 cm^3) of styrene (0.043 g, 0.416 mmol) was added to a THF solution (10 cm^3) of **1** (0.200 g, 0.189 mmol), and the resulting mixture was stirred for 3 h, whereupon palladium black was precipitated. After the volatile materials were removed *in vacuo*, the residue was chromatographed on a silica gel column (200 mesh, 15 × 1.2 cm). The fraction was eluted with hexane, collected and recrystallized with hexane to give (*E*)-1-(2,5-dimethylphenyl)-2-phenylethene (**10**) (0.071 g, 90%), m.p. 41°C. MS: *m*/*z* 150(M^+). ^{1}H NMR: δ 2.34 and 2.37 [s, Me], 6.9–7.1, 7.2–7.4 and 7.45–7.55 (m, aromatic and olefinic protons). Found: C, 92.3; H, 7.7. Calc. for $C_{16}H_{16}$: C, 92.3; H, 7.7%. (b) With carbon monoxide: At room temperature carbon monoxide was bubbled through a CH_2Cl_2 solution (15 cm^3) of **1** (0.200 g, 0.189 mmol) for 30 min. The reaction mixture containing palladium black was evaporated to dryness and the residue was extracted with ether (20 cm^3). To the ethereal extract saturated sodium hydrogen carbonate in water (15 cm^3) was added, and the aqueous layer was separated and acidified with concentrated HCl. The organic product was extracted with ether (15 cm^3) and the extract was dried over Na_2SO_4. After evaporation of the solvent, the product was recrystallized with hexane to give 2,5-dimethylbenzene carboxylic acid (**11**) (0.015 g, 26%), m.p. 131°C (lit[10] 132°C). MS: *m*/*z* 150(M^+). ^{1}H NMR: δ 2.22 [s, 5-Me], 2.47 [s, 2-Me], 7.02 [s, 3-H], 7.12 [dd, ^3J(HH) = 7.8 Hz, ^4J(HH) = 1.5 Hz, 4-H], 7.74 [d, ^4J(HH) = 1.5 Hz, 6-H]. Found: C, 71.5; H, 6.6. Calc. for $C_9H_{10}O_2$: C, 72.0; H, 6.7%.

Coupling reactions of methyl-substituted benzenes promoted by the $Pd(MeCO_2)_2$-SBu^i_2 *system*

The coupling reactions were performed by the reaction of the $Pd(MeCO_2)_2$ (0.050 g, 0.223 mmol) and SBu^i_2 (0.022 g, 0.148 mmol) system in appro-

priate methyl-substituted benzenes (12 cm^3) at 90°C for 1 h. After cooling, the mixture was analysed by GLC or GC-MS. Yields of corresponding coupling products were determined on GLC using the following calibration curves: bi(*o*-xylyl) for the coupling products of *o*-, *m*-, and *p*-xylene; bi(1,2,3-trimethylphenyl) for 1,2,3- and 1,2,4-trimethylbenzene and 1,2,3,4-tetramethylbenzene. Isomer distributions were determined by comparing the retention times on GLC with corresponding isolated coupling products (see below). Identification of the coupling products **14** and **17** was performed only by GC-MS.

Separation of the coupling products from the reaction mixture

A typical example is shown below. A suspension containing $Pd(MeCO_2)_2$ (1.00 g, 4.45 mmol) and SBu^i_2 (0.434 g, 2.97 mmol) in *o*-xylene (20 cm^3) was heated at 90°C for 1 h. After cooling, the filtered mixture was evaporated to dryness. The residue was chromatographed on a silica gel column (200 mesh, 27 × 1.2 cm), and the fraction was eluted by hexane, collected and evaporated to dryness to give crude bi(*o*-xylyl). This crude product was further purified by preparative TLC (Kieselgel 60 HF) to give 0.20 g [21%, based on the used $Pd(MeCO_2)_2$] of a mixture of **12a** and **12b** (**12a**:**12b** = 12:88, by GLC). GC-MS: *m/z* 210(M^+). Found: C, 91.4; H, 8.6. Calc. for $C_{16}H_{18}$: C, 91.4; H, 8.6%. ^{1}H NMR: **12a**: δ 2.29 and 2.32 [s, 3- and 4-Me], 7.18 [d, ^3J(HH) = 7.8 Hz, 5-H], 7.31 [dd, ^3J(HH) = 7.8 Hz, ^4J(HH) = 1.7 Hz, 6-H], 7.35 [br s, 2-H]; **12b**: only three methyl signals were observed distinctly at δ 2.16, 2.30, and 2.33, and other resonances were obscured due to overlapping.

13: yield 13% [based on $Pd(MeCO_2)_2$] (**13a**:**13b** = 70:30). GC-MS: *m/z* 210(M^+). Found: C, 91.3; H, 8.5. Calc. for $C_{16}H_{18}$: C, 91.4; H, 8.6%. ^{1}H NMR: **13a**: δ 2.37 [s, 3- and 5-Me], 6.97 [br s, 4-H], 7.19 [br s, 2- and 6-H]. **13b**: δ 2.24 [s, 2-Me], 2.35 [s, 4-, 3′- and 5′-Me], 6.92 [br s, 4′-H], 7.02 [br s, 3-H], 7.06 [br d, ^3J(HH) = 7.8 Hz, 5-H], 7.11 [d, ^3J(HH) = 7.8 Hz]; 7.19 [br s, 2′- and 6′-H].

15: yield 23% [based on $Pd(MeCO_2)_2$] (**15a**:**15b** = 95:5). GC-MS: *m/z* 238(M^+). Found: C, 90.7; H, 9.3. Calc. for $C_{18}H_{22}$: C, 90.8; H, 9.2%. ^{1}H NMR: **15a**: δ 2.20 [s, 4-Me], 2.34 [s, 3- and 5-Me], 7.22 [s, 2- and 6-H]. **15b**: only five methyl signals were observed at δ 2.17, 2.22, 2.24, 2.32 and 2.33; other resonances were obscured due to low yield.

Coupling product **16** could not be isolated under the conditions used, and was only detected by GC-MS, *m/z* 238(M^+).

Acknowledgement—The authors are grateful to Professor Mitsuya Shimoda, Department of Food Science and Technology, Faculty of Agriculture, Kyushu University, for GC-MS.

REFERENCES

1. See for example, M. Berry, K. Elmitt and M. L. H. Green, *J. Chem. Soc., Dalton Trans.* 1979, 1950; A. H. Janowicz and R. G. Bergman, *J. Am. Chem. Soc.* 1983, **105**, 3929; W. D. Jones and F. J. Feher, *J. Am. Chem. Soc.* 1984, **106**, 1650.
2. See for example, C. A. Tolman, S. D. Ittel, A. D. English and J. P. Jesson, *J. Am. Chem. Soc.* 1979, **101**, 1742; P. J. Desrosiers, R. S. Shinomoto and T. C. Flood, *J. Am. Chem. Soc.* 1986, **108**, 7964.
3. M. S. Kharasch and T. M. Beck, *J. Am. Chem. Soc.* 1934, **56**, 2057; G. B. Shul'pin, A. E. Shilov, A. N. Kitagorodskii and J. V. Z. Krevor, *J. Organomet. Chem.* 1980, **201**, 319; Y. Aoyama, T. Yoshida, K. Sakurai and H. Ogoshi, *Organometallics* 1986, **5**, 168.
4. Y. Fuchita, K. Hiraki, Y. Kamogawa and M. Suenaga, *J. Chem. Soc., Chem. Commun.* 1987, 941; Y. Fuchita, K. Hiraki, Y. Kamogawa, M. Suenaga and K. Tohgoh, *Bull. Chem. Soc. Japan* 1989, **62**, 1081.
5. R. G. Miller, R. D. Stauffer, D. R. Fahey and D. R. Parnell, *J. Am. Chem. Soc.* 1976, **92**, 1511.
6. A. D. Buckingham and P. J. Stephens, *J. Chem. Soc.* 1964, 4583.
7. M. L. H. Green, *Organometallic Compounds*, Vol. 2, pp. 224–226. Methuen & Co. Ltd, London (1968).
8. See for example, J. M. Davidson and C. Triggs, *Chem. Ind.* 1966, 457; H. Yoshimoto and H. Itatani, *Bull. Chem. Soc. Japan* 1973, **46**, 2490; F. R. S. Clark, R. O. C. Norman, C. B. Thomas and J. S. Willson, *J. Chem. Soc., Perkin Trans.* 1974, **1**, 1289.
9. H. Itatani and H. Yoshimoto, *J. Org. Chem.* 1973, **38**, 76.
10. R. C. Weast and M. J. Astle, *Handbook of Data on Organic Compounds*, Vol. 1. CRC Press, Boca Raton (1985).

Polyhedron Vol. 10, No. 17, pp. 2045–2050, 1991
Printed in Great Britain

0277–5387/91 $3.00+.00
© 1991 Pergamon Press plc

MOLECULAR PRECURSORS OF ALKALINE EARTHS: SYNTHESIS AND STRUCTURE OF $[N(C_2H_4O)(C_2H_4OH)_2]_2Ba \cdot 2EtOH$. THE FIRST STRUCTURALLY CHARACTERIZED BARIUM ALKOXIDE

OLIVIER PONCELET and LILIANE G. HUBERT-PFALZGRAF*

Laboratoire de Chimie Moléculaire, Associé au CNRS,
Université de Nice—Sophia Antipolis, Parc Valrose, 06034 Nice, France

and

LOIC TOUPET

Laboratoire de Physique Cristalline, Associé au CNRS, Campus de Beaulieu, 35042 Rennes, France

and

JEAN CLAUDE DARAN

Laboratoire de Chimie des Métaux de Transition, Associé au CNRS, 75230 Paris, France

(*Received* 31 *January* 1991; *accepted* 23 *May* 1991)

Abstract—The reaction between barium and triethanolamine in toluene/THF affords, after recrystallization in ethanol, the barium alkoxide $[N(C_2H_4O)(C_2H_4OH)_2]_2Ba \cdot 2EtOH$, which has been characterized by X-ray crystallography. The tetradentate character of the triethanolamine molecule allows the barium atom to be octacoordinated in a monomeric $Ba[(OC_2H_4)(OHC_2H_4)_2N]_2$ unit. However, these units are associated by intermolecular hydrogen-bonding due to the ethanol lattice molecules, thus forming an extensive two-dimensional network. The hydrogen-bonding reduces the volatility of the precursor, but is favourable to the formation of gels by hydrolysis.

Low temperature routes to materials using molecular precursors via sol–gel[1] or MOCVD techniques[2] form an area of considerable interest and technological significance. Barium is involved in many useful dielectric materials based on oxides such as barium titanate or $BaMg_{1/3}Ta_{2/3}O_3$, as well as in the high T_c superconductors.[3] However, while barium alkoxides can be easily obtained via direct attack by alcohols due to the electropositive character of the metal, they remain poorly characterized, and various derivatives, sometimes called "barium extract", have so far been used in the sol–gel process.[4] MOCVD techniques require isolation as well as a better knowledge of the properties of the precursor. Although homoleptic barium alkoxides with classical alkoxo groups have been reported, they appear, once isolated, to display a poor stability with respect to the formation of oxoalkoxides and/or photochemical decomposition.[5] Indeed, the only structurally characterized barium alkoxides —$HBa_5O(OPh)_9(THF)_8$ and $H_3Ba_6O(OBu^t)_{11}(OCEt_2CH_2O)(THF)_3$—are actually penta- or hexanuclear oxo aggregates.[6] Functional alcohols such as triethanolamine are commonly used in the sol–gel process, especially for mixed oxide

* Author to whom correspondence should be addressed.

materials. This aminoalcohol has, for instance, been used as a means of obtaining superconducting coatings.[7] A $Ti(OR)_4$-triethanolamine product was used as the precursor for the preparation of titanium nitride by pyrolysis.[8] Such potentially polydentate alcohols may also be useful for the stabilization of alkoxides vs oxoalkoxides and/or reduction of the polymerization of metal alkoxides.

We now report the synthesis and molecular structure of $[N(C_2H_4O)(C_2H_4OH)_2]_2Ba \cdot 2EtOH$, the first structurally characterized barium alkoxide.

EXPERIMENTAL

All manipulations were routinely performed under argon using Schlenk tubes and vacuum line techniques with solvents purified by standard methods. Triethanolamine was dried over molecular sieves. ^1H and ^{13}C NMR and IR spectra were recorded using Bruker AC-200 and IR-FTS 45 spectrometers, respectively. IR spectra were obtained as Nujol mulls. Mass spectra were recorded on a R10-10 Ribermag spectrometer by chemical ionization techniques. Analytical data were obtained from the Centre de Microanalyses du CNRS.

Synthesis of $[N(C_2H_4O)(C_2H_4OH)_2]_2Ba \cdot 2EtOH$

Bis-triethanolamine barium was obtained by reacting metallic barium (1.57 g, 11 mmol) with triethanolamine (4.92 g, 33 mmol) in a mixture of toluene and THF (60 cm^3, 1:1 in volume). After refluxing for 24 h, all the metal had dissolved and the reaction medium was evaporated. Extraction of the oily residue was performed with ethanol and crystals suitable for X-ray analysis (soluble in acetone or alcohols) were obtained on cooling (3.63 g, 65%). Microanalysis: Found: C, 36.0; H, 7.5; N, 5.4. Calc. for $C_{16}H_{40}O_8N_2Ba$: C, 36.5; H, 7.7; N, 5.3%. IR (Nujol, cm^{-1}): 3130 ν(OH), 1348, 1298, 1261, 1249, 1161, 1107s; 1101, 1084, 1047, 1024 ν(C—O), 974, 903, 878, 730, 580; 540 sh, 490, 395 ν(Ba—O), 274. ^1H NMR (CD_3OD, ppm): 1.22 (t, $J = 7$ Hz), 6H, 2.66 (t, $J = 5.1$ Hz), 12H, 3.66 (q, $J = 7$ Hz), 4H, 3.76 (t, $J = 5.1$ Hz), 12H. $^{13}C\{^1H\}$ NMR (CD_3OD): 18 (CH_3), 58 (OCH_2)(EtOH), 57.8 (NCH_2), 60 (OCH_2). MS (*m/z*, IE): $Ba(OH)(OHC_2H_4)_3N$ (7%), $BaNOC_3H_4$ (25%), BaC_2 (16%), $NC_6H_{12}O_3$ (6%), $NC_4H_{10}O$ (15%), C_2H_4O (100%).

The same product was obtained by reacting the precipitate resulting from the reaction between metallic barium and ethanol with triethanolamine at room temperature.

Crystallographic studies

A crystal suitable for X-ray (grown from crystallization in ethanol) was mounted in a Lindeman capillary and set on a CAD4 Enraf–Nonius diffractometer at room temperature. Accurate unit cell dimensions and crystal orientation matrix were obtained from least-squares refinements of 25 reflections. Two standard reflections were monitored periodically; they showed no change during data collection. Crystallographic data and other pertinent information are summarized in Table 1. Corrections were made for Lorenz, polarization and absorption effects.[9]

Computations were performed using CRYSTALS adapted on a Microvax II.[10] Atomic form factors for neutral Ba, N, O, C and H atoms were obtained from ref. 11. The structure was solved by heavy-atom techniques. The barium atom was located at the origin from unsharpened Patterson. The heavy-atom phasing did not distinguish between the three possible space groups *C*2, *Cm* or *C*2/*m*. In each case, the subsequent F_o syntheses indicated the carbon, nitrogen and oxygen atoms. However, the use of *Cm* or *C*2/*m* implied a disordered model with carbon atoms of the CH_2 groups of the triethanolamine molecule in statistical distribution with respect to the mirror plane. Moreover, *F*-tests showed that the space group should not be centrosymmetric. These results led us to continue refinements in the *C*2 group. Two molecules of ethanol of crystallization were found in a difference synthesis. The two carbon atoms of the ethyl group were statistically distributed between two sites related by a pseudo-two-fold axis. The disordered ethanol molecules were constrained to chemically reasonable dimensions [O—C 1.48(1), C—C 1.52(1), O—C—C 109(1) Å]. All hydrogen atoms, except those in the ethanol (H4) molecules, were found in a difference map. However, only the coordinates of the hydrogen atoms attached to oxygen were refined, but the O—H distances of the triethanolamine ligand were constrained at 1.0 Å with an e.s.d. of 0.1 Å. These hydrogen atoms were given an overall isotropic temperature factor. All other hydrogen atoms were introduced in the refinements as calculated contributors. Their coordinates were recalculated after each cycle, and they were attributed isotropic thermal parameters 20% higher than those of the carbon atoms to which they are attached. Anisotropic temperature factors were introduced for all the non-hydrogen atoms. Least-squares refinements with approximation to the normal matrix were carried out by minimizing the function $\Sigma w(|F_o| - |F_c|)^2$, where F_o and F_c are the observed and calculated structure factors. The cri-

Table 1. Summary of crystallographic data of $Ba[(OC_2H_4)(OHC_2H_4)_2N]_2 \cdot 2EtOH$

Compound	$C_{16}H_{40}N_2O_8Ba$
Molecular weight	525.8
Crystal system	Monoclinic
Space group	$C2$
a (Å)	14.324(2)
b (Å)	8.270(1)
c (Å)	10.618(2)
α (°)	90
β (°)	116.75(1)
Γ (°)	90
V (Å^3)	1123
Z	2
Density (calc.) (g cm^{-3})	1.56
Crystal dimensional (mm)	$0.3 \times 0.2 \times 0.2$
$F(000)$ (e$^-$)	540
Diffractometer	CAD4 ENRAF NONIUS
Radiation	Mo-K_α
Linear absorption coefficient (cm^{-1})	18.06
Scan type	ω–2θ
2θ range (°)	$3 < 2\theta < 56$
Scan width	$1.0 + 0.34 \tan\theta$
Data collected	1508
Number of variables	152
Unique data used [$F_o^2 > 3\sigma(F_o^2)$]	1435
Absorption corrected by	DIFABS[9]
$R = \Sigma([F_o]-[F_c])/\Sigma[F_o]$	0.0231
$R_w = \Sigma w([F_o]-[F_c])^2/w[F_o]^2)^{1/2}$	0.0257
Weighting scheme[a]	$w = w'[1-(\Delta F/6\sigma(F)^2]^2$
Coefficient for the Chebyshev series	6.52, −6.19, 4.80

[a] $w' = 1/\Sigma^3 ArTx(X)$ where 3 is the number of coefficients of Ar for a Chebyshev series, for which X is F_o/F_c(max).[4]

teria for a satisfactory complete analysis were the ratio of the rms shift to the standard deviation being less than 0.1, and no significant features appearing in the final difference map.

Atomic coordinates and thermal parameters are given as supplementary material.

RESULTS AND DISCUSSION

Bis-triethanolaminato barium was obtained by refluxing metallic barium and triethanolamine with toluene:THF as a solvent, according to eq. (1). Purification was achieved by crystallization in ethanol. Addition of triethanolamine to the insoluble material obtained by reacting barium with ethanol and thus alcoholysis provides another route to $[N(C_2H_4O)(C_2H_4OH)_2]_2Ba \cdot 2EtOH$

$$Ba + 2N(C_2H_4OH)_3 \xrightarrow{\text{toluene/THF}} [N(C_2H_4O)(C_2H_4OH)_2]_2Ba + H_2 \quad (1)$$

By contrast with other barium alkoxides, this new compound was relatively air stable, suggesting that triethanolamine acts as a polydentate encapsulating ligand. The structure was established by X-ray crystallography. The compound corresponds to an ethanol solvate $[N(C_2H_4O)(C_2H_4OH)_2]_2Ba \cdot 2EtOH$; the structure of the $[N(C_2H_4O)(C_2H_4OH)_2]_2Ba$ moiety is shown in Fig. 1. Selected bond lengths and angles are listed in Table 2. The barium atom is surrounded by a core of oxygen atoms with Ba—O distances of 2.73(1), 2.753(3) and 2.78(1) Å, corresponding to Ba—O as well as Ba—O(H) bonds. The observed Ba—N distance is 3.009(3) Å. These data are in agreement with the values reported for other barium derivatives in which triethanolamine generally acts as a neutral ligand,[12] the coordination sphere being completed by ligands such as acetates or nitrophenols. The triethanolamine ligand is thus tetradentate, with a transannular Ba—N coordination bond; the clearly pyramidal nitrogen atom (ΣC—N—C

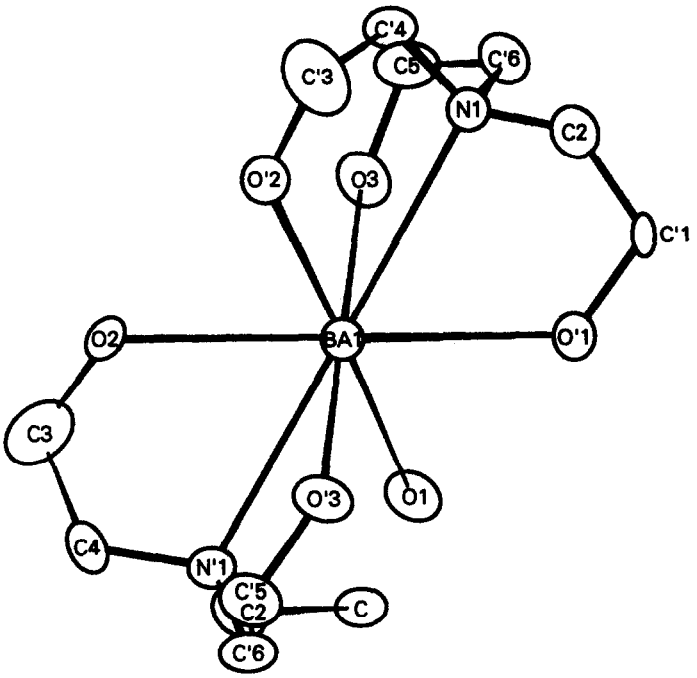

Fig. 1. ORTEP view of the $[N(C_2H_4O)(C_2H_4OH)_2]_2Ba$ moiety of $[N(C_2H_4O)(C_2H_4OH)_2]_2Ba \cdot 2EtOH$ showing the atom numbering scheme. The hydrogen atoms of the hydroxyl groups could not be located. Atoms labelled ′ are related by a C_2 axis.

Table 2. Interatomic distances (Å) and bond angles (°) of $[N(C_2H_4O)(C_2H_4OH)_2]_2Ba \cdot 2EtOH$

Bond lengths (Å)			
Ba(1)—O(1)	2.73(1)	Ba(1)—O(3)	2.753(3)
Ba(1)—O(2)	2.78(1)	Ba(1)—N(1)	3.009(3)
Bond angles (°)			
O(1)—Ba(1)—O(1)′[a]	85.3(5)	N(1)—Ba(1)—O(1)′	121.8(5)
O(2)—Ba(1)—O(1)	96.4(1)	N(1)—Ba(1)—O(2)	59.2(5)
O(2)—Ba(1)—O(1)′	178.2(5)	N(1)—Ba(1)—O(2)′	119.4(5)
O(2)—Ba(1)—O(2)′	81.8(5)	N(1)—Ba(1)—O(3)	59.48(8)
O(3)—Ba(1)—O(1)	96.7(4)	N(1)—Ba(1)—O(3)′	120.53(8)
O(3)—Ba(1)—O(1)′	83.3(4)	N(1)—Ba(1)—N(1)′	178.4(9)
O(3)—Ba(1)—O(2)	96.2(4)		
O(3)—Ba(1)—O(2)′	83.8(4)	Ba(1)—O(1)—C(1)	124.7(7)
O(3)—Ba(1)—O(3)′	180.0(9)	Ba(1)—O(2)—C(2)	126.6(11)
N(1)—Ba(1)—O(1)	59.6(4)	Ba(1)—O(3)—C(3)	124.3(3)
Hydroxyls and hydrogen bonding			
Bond lengths (Å)			
O(1)···H(4)	1.4(1)	O(4)—H(4)	1.1(1)
O(2)···H(3)	1.71(7)	O(2)—H(2)	0.81(8)
O(4)···H(2)	1.74(8)	O(3)—H(3)	0.86(7)
Bond angles (°)			
O(4)—H(4)···O(1)	171.2(5)	O(4)···H(2)—O(2)	170.5(6)
O(4)···H(3)—O(3)	161.7(6)		

[a] Atoms labelled ′ are related by a two-fold axis.

angles = 330.1°) supports this interpretation, the barium atom being octacoordinated. Such a high coordination number is in agreement with the results obtained for other barium–oxygen derivatives where nine- or 10-coordination is common.[12–14]

The range of the Ba—O, Ba—O(H) distance is rather small (2.73–2.78 Å) and the metal–oxygen distances compare well with the sum of the covalent radii (≈ 2.71 Å). The Ba—O—C angles are quite comparable (125.2° av.) probably as a result of the small variation in the Ba—O distances and of the constrained triethanolamine ligand.

All oxygen atoms of the triethanolamine moiety have short contacts (2.54 Å) implying hydrogen bonding with two lattice-ethanol molecules (located ≈ 4.80 Å away from the metal). In fact, intermolecular hydrogen-bonding between the alcohol functionalities both on ethanol and on the coordinated triethanolamine is responsible for the formation of an extensive two-dimensional network, as shown in Fig. 2. The lattice-ethanol molecules build the network and each alcohol is linked via hydrogen-bonding to three different $[N(C_2H_4O)(C_2H_4OH)_2]_2Ba$ molecules, which thus have all their six oxygen centres involved in hydrogen-bonding. This two dimensional network thus spreads out along the *a* and *b* axis, the different layers stack along the *c* axis; there is no interaction between successive layers. The various hydrogen-bonds imply O4(EtOH) is unsymmetrical and nearly linear (161.7–171.2°). The O···H distances are quite short [1.4(1) to 1.74(8) Å], the acidity of the alcohol functionality of the triethanolamine molecule being enhanced by coordination to a very electropositive metal. The shortest interaction is observed between O1 and H4, thus supporting O1 as the alkoxide donor site of the coordinated triethanolamine ligand. The small range in the values of the O···H interactions suggests that the hydroxyl functionality is nearly as potent a donor for hydrogen-bonding as the alkoxide ligand, as observed for instance in $Nb_2Cl_4(OMe)_4(MeOH)_2 \cdot 2MeOH$.[15,16]

Molecular triethanolamine derivatives of various elements have been reported in the literature.[17] They have generally been obtained by exchange reactions starting from alkyls, amides or alkoxides. Reaction (1) seems to be the first example of a synthesis directly from a metal. Solid-state structural information on ethanolamine derivatives is limited to some examples of Group V elements[18] and the aluminum compound $\{[N(C_2H_4O)_3]Al_2Me_3\}_2$.[19] $[N(C_2H_4O)(C_2H_4OH)_2]_2Ba \cdot 2EtOH$ is, to the best of our knowledge, the first example of a homoleptic metal triethoxyaminate which has been structurally characterized.

$[N(C_2H_4O)(C_2H_4OH)_2]_2Ba \cdot 2EtOH$ displays a broad ν(O—H) stretch characteristic of hydrogen-bonding in the IR spectrum at 3130 cm^{-1}. The

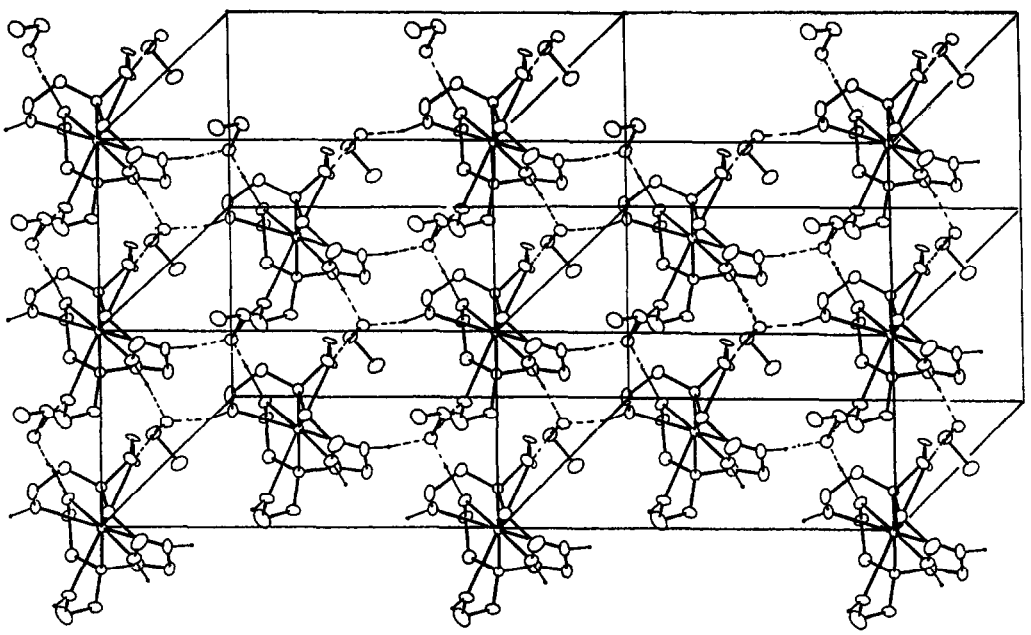

Fig. 2. Projection onto the *a*, *b* plane showing the two-dimensional hydrogen-bonding network of $[N(C_2H_4O)(C_2H_4OH)_2]_2Ba \cdot 2EtOH$. The representation covers four unit cells; only plan (110) is shown and there are no interactions between plans. Only one position of the ethyl chain of the alcohol has been represented for better clarity.

NMR (^1H and ^{13}C) spectra were obtained in methanol-d_4 solution and the exchange of ethanol by methanol is observed. While most barium alkoxides form precipitates by hydrolysis, $[N(C_2H_4O)(C_2H_4OH)_2]_2Ba \cdot 2EtOH$ is converted into stable gels by the addition of excess water to its ethanol solutions. The formation of the gel network is probably assisted by hydroden-bonding, as observed in the solid state. $[N(C_2H_4O)(C_2H_4OH)_2]_2Ba \cdot 2EtOH$ is also volatile as shown by mass spectrometry. However, the existence of an extensive two-dimensional network due to hydrogen-bonding requires conditions which are too drastic for MOCVD applications, and the overall properties are more appropriate for spray-pyrolysis.

Acknowledgement—We thank the CNRS-PIRMAT for financial support.

REFERENCES

1. L. G. Hubert-Pfalzgraf, *New J. Chem.* 1987, **11**, 663.
2. (a) L. G. Hubert-Pfalzgraf, M. C. Massiani, R. Papiernik and O. Poncelet, *Proc. EURO CVD-7. Editions de Physique* 1989, **50**, C5-981; (b) D. C. Bradley, *Chem. Rev.* 1989, **89**, 1317.
3. (a) C. N. R. Rao and B. Raveau, *Acc. Chem. Res.* 1989, **22**, 106; (b) S. Nomura, L. Toyama and K. Kaneta, *Jap. J. Appl. Phys.* 1982, **21**, L624.
4. P. P. Phule, S. Raghavan and S. H. Risbud, *J. Am. Ceram. Soc.* 1987, **70**, C108.
5. T. Labrize and L. G. Hubert-Pfalzgraf, to be published.
6. K. G. Caulton, M. H. Chisholm, S. R. Drake and K. Folting, *J. Chem. Soc., Chem. Commun.* 1990, 1349.
7. (a) T. Monde, H. Kosuka and S. Sakka, *Chem. Lett.* 1988, 287; (b) K. Jones, T. J. Davies, H. G. Emblem and P. Parks, *Better Ceramics Through Chemistry* II, *Mater. Res. Soc. Proc.* 1986, **73**, 111. (Edited by C. J. Brinker, D. E. Clark and D. R. Ulrich), Vol. 73, p. 11 (1986). MRS, Pittsburgh.
8. K. Kuroda, Y. Tanaka, Y. Sugahara and C. Kato, *Better Ceramics Through Chemistry* III, *Mater. Res. Soc. Proc.* (Edited by C. J. Brinker, D. E. Clark and D. R. Ulrich), p. 575 (1988). MRS, Pittsburgh.
9. (a) N. Walker and D. Stuart, *Acta Cryst.* 1983, **A39**, 159; (b) E. Prince, *Mathematical Techniques in Crystallography*. Springer Verlag, Berlin (1982).
10. D. T. Cromer and W. Waber, *International Tables for X-ray Crystallography*, Vol. IV. Kynoch Press, Birmingham (1974) (Present distributor D. Reidel, Dordrecht).
11. D. J. Watkins, J. R. Carruthers and P. W. Betteridge, *Crystals User Guide*. Chemical Crystallography Laboratory, University of Oxford, U.K. (1985).
12. (a) J. A. Kanters, W. J. Y. Smeets, K. Venkatasubralmanian and N. S. Poona, *Acta Cryst.* 1984, **C40**, 1701; (b) J. A. Konters, A. dé Koster, A. Schonten, K. Venkatasubramanian and N. S. Poova, *Acta Cryst.* 1985, **C41**, 1585.
13. N. N. Sauer, E. Garcia, K. V. Salazar, R. R. Ryan and J. A. Martin, *J. Am. Chem. Soc.* 1990, 1524.
14. I. Gautier-Luneau and A. Mosset, *J. Solid State Chem.* 1988, **73**, 4036.
15. F. A. Cotton, M. P. Diebold and W. J. Roth, *Inorg. Chem.* 1987, **26**, 3319.
16. B. Vaartstra, J. C. Huffman, P. S. Gradeff, L. G. Hubert-Pfalzgrad, J. C. Daran, S. Parraud, K. Yunlu and K. G. Caulton, *Inorg. Chem.* 1990, **29**, 3126 and refs therein.
17. D. C. Bradley, R. C. Mehrotra and D. P. Gaur, *Metal Alkoxides*. Academic Press, New York (1978).
18. F. Kober, *Zeit. Chem.* 1980, **20**, 49.
19. M. D. Healy and A. R. Barron, *J. Am. Chem. Soc.* 1989, **111**, 398.

Polyhedron Vol. 10, No. 17, pp. 2051–2055, 1991
Printed in Great Britain

0277–5387/91 $3.00+.00
© 1991 Pergamon Press plc

BIS-PAEONOLIMINATOCOPPER(II)

E. R. J. SILLANPÄÄ*

Department of Chemistry and Biochemistry, University of Turku, SF 20500, Turku 50, Finland

and

ADNAN AL-DHAHIR and R. D. GILLARD*

School of Chemistry and Applied Chemistry, University of Wales, College of Cardiff, P.O. Box 912, Cardiff CF1 3TB, Wales, U.K.

(*Received* 17 *January* 1991; *accepted* 23 *May* 1991)

Abstract—Aqueous ammonia, "paeonol" (2-hydroxo-4-methoxy-acetophenone) and copper(II) salts readily form the neutral bis-iminatocopper(II) complex, a new compound. The solid contains the *trans* isomer, with four-coordinated copper(II). Bis-paeonolatocopper(II) itself exists as a dihydrate and as the anhydrate which is at least dimorphic.

Such *ortho*-substituted phenols as salicylaldehyde (**Ia**; R = R¹ = H; X = O) or acetophenone (**Ib**; R¹ = H; R = CH_3; X = O) are classical chelating agents.[1] Paeonol (**Ic**; R = CH_3, R¹ = OCH_3; X = O, whose trivial name derives from its one-time use in perfumery) is the derivative of acetophenone, substituted by methoxyl at the 4-position.

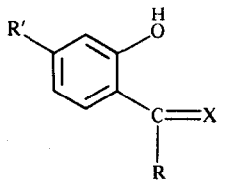

(I)

Pfeiffer studied[2,3] its chelating properties with several metals, including copper(II). The stoichiometries then reported (denoting paeonol as HP) included: CuP_2, $CuP_2 \cdot C_6H_5NH_2$ and $CuP_2 \cdot$ pyridine.

In preliminary work,[4] some of the detail was not reproduced. We now describe the formation and structure of a new brown product, the bis-complex of the diimine (**Id**, R = CH_3, R¹ = OCH_3, X = NH):

$$Cu^{2+} + 2C_9H_9O_3 \longrightarrow Cu(C_9H_8O_3)_2 + 2H^+$$
$$\downarrow 2NH_3$$
$$Cu(C_9H_{10}NO_2)_2 + 2H_2O.$$

EXPERIMENTAL

Paeonol (2-hydroxy-4-methoxyacetophenone) from Aldrich had, after recrystallization, a m.p. of 51°C. Electronic spectra were recorded with a Perkin–Elmer Lambda 5 spectrophotometer. IR spectra were recorded with a Perkin–Elmer IR 783 spectrophotometer using KBr discs (0.8 mg of compound dispersed in 0.06 g KBr, giving a disc 0.2 mm thick). Magnetic moments were measured with a Gouy balance. Melting points were measured using glass capillaries, and are uncorrected.

Bis-paeonolatocopper(II) was made essentially by the method[2] of Pfeiffer *et al.*, omitting ethanol. The green product had μ_{eff} = 1.7 BM at 13°C (Gouy balance). It was dissolved in the minimum of warm chloroform (spectrosol grade), filtered and kept for 1–2 weeks in an atmosphere of acetone, when crystals formed. The whole process was repeated. Depending upon conditions, three distinct solids

* Authors to whom correspondence should be addressed.

(all green) were obtained. These were square plates of dihydrate (m.p. 260° often with bright luminescence), hexagons (m.p. 245–247°), trigonal prisms or needles (m.p. 254°), or a mixture. Recrystallizing the original solid product from either CH_2Cl_2 or benzene yielded only needles.

IR spectra and analysis showed that the square plates are dihydrated. Found: C, 51.1, 51.2; H, 5.0, 5.4. Calc. for $Cu(C_9H_9O_3)_2 \cdot 2H_2O$: C, 50.3; H, 5.2%. Found (for needles) [mol. mass (mass spec) 394]: C, 54.6; H, 4.68. Calc. for $Cu(C_9H_9O_3)_2$ (mol. mass 393.88): C, 54.9; H, 4.6%. Although the samples were apparently beautifully crystalline, no diffraction spots could be observed. In chloroform, the compound obeyed the Beer–Lambert law, and the derived values for molar extinction coefficients at band maxima are: 647 (ε50) and 550 (ε45) nm. The dihydrate showed IR absorption at (KBr discs, in cm^{-1}) 3480m, 3340sh, 3220sh, 3080sh, 3000w, 2960w, 2940w, 2900sh, 2840w, 1665vw, 1610vs, 1570vs, 1510vs, 1490sh, 1460m, 1430s, 1410sh, 1390s, 1350vw, 1335w, 1260sh, 1250vs, 1220s, 1180m, 1160w, 1140s, 1070s, 1030sh, 1020m, 990m, 970w, 940vw, 870w, 860m, 850m, 790m, 780vw, 750m, 740sh, 660vw, 630sh, 620sh, 610s, 590vw, 500w, 460wm and 390w.

Bis-paeonoliminatocopper(II)

This brown complex (red–purple when crystalline) was prepared by gently heating bis-paeonolatocopper(II) in an excess of concentrated ammonia (sp.gr. 0.88) to complete dissolution. The procedure used in recrystallizing bis-paeonolatocopper(II) was then applied. The ultimate product appeared as homogeneous prismatic needles, m.p. 254°. It showed IR absorptions (KBr discs in cm^{-1}) at 3340m, 3200vw, 3100vw, 3060vw, 3000vw, 2970vw, 2840w, 1600vs, 1525vs, 1500sh, 1480wm, 1450w, 1430s, 1410w, 1365vw, 1350sh, 1330wm, 1280vs, 1260w, 1220vs, 1190vw, 1170s, 1155vs, 1130vw, 1065m, 1040m, 1025s, 990s, 970vw, 915vw, 870vw, 840m, 820s, 770vw, 750w, 725w, 660sh, 645m, 600m, 580sh, 510wm, 460w and 400w. Found [mol. mass (mass spec) 392]: C, 54.5, 54.6; H, 5.2, 5.11; N, 7.0, 7.2. Calc. for $Cu(C_9H_{10}O_2N)_2$ (mol. mass 391.914): C, 55.2; H, 5.1; N, 7.1%.

Unlike bis-paeonolatocopper(II), the visible spectrum of this complex in chloroform revealed only one band at 563 nm. This system obeys the Beer–Lambert law, with $\varepsilon = 78.3$.

The crystals used in the X-ray structural determination were from ethanolic solution: pertinent details of methods are summarized in Table 1 and selected intramolecular bond distances and angles are in Tables 2 and 3. Tables of coordinates of atoms, and of related quantities, and of torsion angles, intramolecular distances and structure factors have been deposited as supplementary results.

DISCUSSION

The properties of the red–brown product strongly suggest that it is a monomeric bis-iminatochelate. It has $\mu_{eff} = 1.76$ BM at 13°, its analyses and molecular ion (m/z 392) agree, and it obeys the Beer–Lambert law with a small extinction coefficient (78). The IR spectrum shows a single sharp absorption at 3340 cm^{-1} (NH). A second major difference from the bis-paeonolatocomplex (which has strong bands at 1610 and 1570 cm^{-1}) is

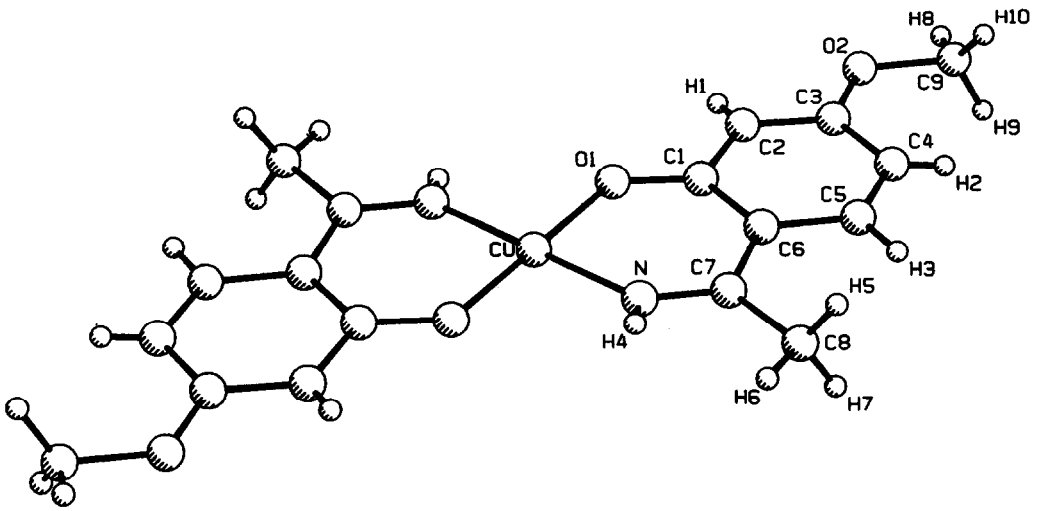

Fig. 1. The molecular structure of bis-paeonoliminatocopper(II).

Table 1. Crystal properties and details of collection of results and of the refinement of the structure

(a) Crystal	
Empirical formula	$C_{18}H_{20}N_2O_4Cu$
Formula weight	391.92
Crystal colour, habit	Brown, bar
Crystal dimensions (mm)	$0.150 \times 0.200 \times 0.300$
Crystal system	Monoclinic
Number of reflections used for unit cell determination (2θ range)	25 (20.9–34.2°)
Omega scan peak width at half-height	0.15
Lattice parameters:	$a = 6.154(3)$ Å
	$b = 18.092(8)$ Å
	$c = 7.540(3)$ Å
	$\beta = 100.39(4)°$
	$V = 826(1)$ Å^3
Space group	$P2_1/c$ (No. 14)
Z value	2
$F(000)$	406
μ(Mo-K_α)	13.49 cm^{-1}
(b) Intensity measurements	
Diffractometer	Rigaku AFC5s
Radiation	Mo-K_α ($\lambda = 0.71069$ Å)
Temperature	23°C
Take-off angle	6.0°
Detector aperture	6.0 mm horizontal
	6.0 mm vertical
Crystal to detector distance	40.0
Scan type	ω–2θ
Scan rate	32.0° min^{-1} (in omega) (2 rescans)
Scan width	$(1.63 + 0.30 \tan\theta)°$
$2\theta_{max}$	50.0°
Number of reflections measured	Total: 1655
	Unique: 1513 ($R_{int} = 0.081$)
Corrections	Lorentz–polarization
	Absorption (trans. factors: 0.92–1.00)
	Decay (−25.00% decline)
(c) Structure solution and refinement	
Structure solution	Direct methods
Refinement	Full-matrix least-squares
Function minimized	$\Sigma w(\|F_o\| - \|F_c\|)^2$
Least-squares weights	$4F_o^2/\sigma^2(F_o^2)$
p-factor	0.03
Anomalous dispersion	All non-hydrogen atoms
Number of observations [$I > 3.00\sigma(I)$]	752
Number of variables	145
Reflection/parameter ratio	5.19
Residuals: R; R_w	0.057; 0.060
Goodness of fit indicator	1.61
Maximum shift/error in final cycle	0.01
Maximum peak in final diff. map	0.72 e$^-$ Å^{-3}
Minimum peak in final diff. map	−0.43 e$^-$ Å^{-3}

Table 2. Selected intramolecular distances (Å)

Cu—O(1)	1.924(6)	N—H(4)	0.67(9)
Cu—N	1.915(8)	O(2)—C(3)	1.35(1)
O(1)—C(1)	1.30(1)	O(2)—C(9)	1.45(1)
N—C(7)	1.29(1)		

the presence of only one strong band at 1600 cm^{-1}. The red–brown colour is typical[5] of a bis-iminato complex of *o*-hydroxy substituted acetophenones (**I**; R ≠ H). The corresponding salicylaldehyde derivatives (**I**; R = H) are, in general,[5] green.

The single most noteworthy feature of the molecular structure is the proof that this involves a four-coordinated copper(II) ion, doubly chelated by the imine (**Id**) of paeonolate. The environment of the copper ion is closely planar and is almost square. The isomer which is *trans* about the copper(II) ion has crystallized, although this fact need not comment on the equilibrium between geometric isomers in solution. Of all environments for copper(II) ions in crystals, the square and planar is probably the least common.

The formation of the imine from ammonia and the substituted *o*-hydroxyacetophenone is not unexpected.[6] Indeed, one of the earliest observations (150 years ago) of a reaction of a coordinated ligand was for salicylaldehyde (**Ia**) and ammonia. In the presence of nickel(II). Ettling[6a] found this to give the bis complex of the imine (**Id**; R = R' = H; X = NH). However, while complexed salicylaldimines form readily[5b] from salicylaldehydes and ammonia, the corresponding ketimines of the *o*-hydroxyacetophenones do not form nearly so easily.

Such chelated imines are, nevertheless, well enough known. **Id** is also formed in poor and variable yield from the reaction with dioxygen of the complexes of Schiff bases of type (**II**), where the

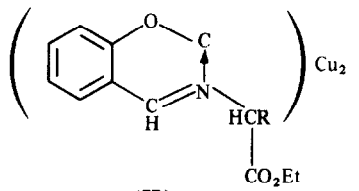

(**II**)

Schiff base is derived from leucine[7] [R = CH_2 $CH(CH_3)_2$] or from valine[8] [R = $CH(CH_3)_2$]. However, structural studies of imines are rare. The present work seems also to be the first crystallographic study of any derivative of paeonol, though again the composition and properties of its complex compounds with cobalt, such as Co

Table 3. Selected intramolecular angles (°)

Atoms	Angle	Atoms	Angle
O(1)—Cu—O(1)	180.00	Cu—N—C(7)	130.8(6)
O(1)—Cu—N	91.8(3)	Cu—N—H(4)	122(9)
O(1)—Cu—N	88.2(3)	C(7)—N—H(4)	107(9)
Cu—O(1)—C(1)	127.5(6)	C(3)—O(2)—C(9)	116.7(7)

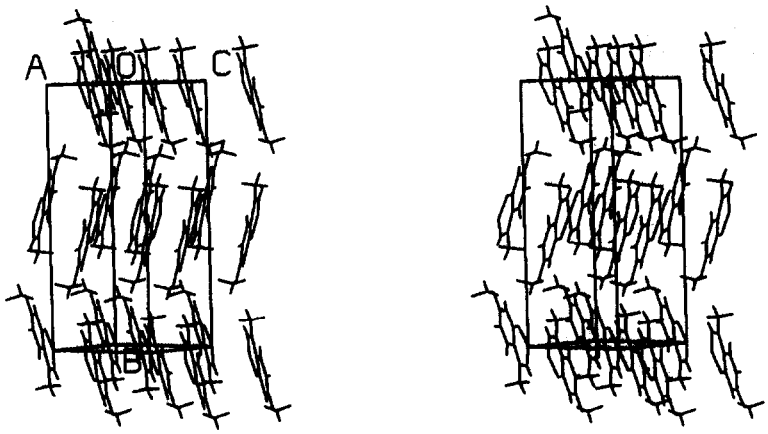

Fig. 2. A view of the crystal packing.

(paeonolate)$_3 \cdot CHCl_3$ and salts of [Coen$_2$ (paeonolate)]$^{2+}$ are well-established, as are structures (by diffraction) of complex compounds of copper(II) with the archtypal salicylaldehyde (Hsal), e.g. [Cu(sal)$_2$][9] and [Cu(1,10-phen) (sal)](NO_3).[10]

Finally, the "adduct" of aniline with bis-paeonolatocopper(II) made by Pfeiffer and his students seems likely to be a similar imine complex. Their pyridine adduct may well be more closely akin to the five-coordinated species Cu(acac)$_2 \cdot$ B formed by N-heterocycles (B = pyridine,[11] quinoline[12]) with such copper(II) bis-β-diketonates as bis-2,4-pentane-dionatocopper(II), "copper acetylacetonate".

REFERENCES

1. M. Calligaris and L. Randaccio, in *Comprehensive Coordination Chemistry* (Edited by G. Wilkinson, R. D. Gillard and J. A. McCleverty), Vol. 2, p. 15. Pergamon Press, Oxford (1987).
2. P. Pfeiffer, S. Golther and O. Angern, *Chem. Ber.* 1927, **60B**, 305.
3. P. Pfeiffer, E. Buchholz and O. Bauer, *J. Prakt. Chem.* 1931, **129**, 163 (esp. p. 177).
4. R. A. Wiggins and R. D. Gillard, unpublished work (1970).
5. (a) R. P. Houghton and D. J. Pointer, *J. Chem. Soc.* 1964, 3302; (b) Personal communication, 1990–1, from Dr R. P. Houghton of Cardiff.
6. (a) C. Ettling, *Liebigs Ann.* 1840, **35**, 265; (b) F. R. Duke, *Ind. Eng. Chem. Anal.* 1944, **16**, 750; (c) M. M. Jones, *"Ligand Reactivity and Catalysis"*, p. 22. Academic Press, New York (1968); (d) D. St. C. Black, in *Comprehensive Coordination Chemistry* (Edited by G. Wilkinson, R. D. Gillard and J. A. McCleverty), Vol. 1, p. 415 (esp. p. 434) and Vol. 6, (esp. p. 156). Pergamon Press, Oxford (1987).
7. P. Pfeiffer, W. Offerman and H. Werner, *J. Prakt. Chem.* 1942, **159**, 313.
8. (a) R. D. Gillard and R. Wootton, *J. Chem. Soc. B*, 1970, 364; (b) R. Wootton, PhD thesis, UKC (1968); (c) Remarkably, the analogous compounds of nickel(II) also undergo this oxidation by aerial dioxygen.
9. A. J. McKinnon, T. N. Water and A. Hall, *J. Chem. Soc.* 1964, 3290.
10. X. Solans, L. Ruiz-Rameriz, L. Gasque and J. L. Brianso, *Acta Cryst.* 1987, **C43**, 428.
11. D. Graddon and E. C. Watton, *J. Inorg. Nucl. Chem.* 1961, **21**, 49.
12. (a) J. D. Main Smith and G. T. Morgan, *J. Chem. Soc.* 1926, 912; (b) R. D. Gillard and G. Wilkinson, *J. Chem. Soc.* 1963, 5399.

Polyhedron Vol. 10, No. 17, pp. 2057–2064, 1991
Printed in Great Britain

0277–5387/91 $3.00+.00
© 1991 Pergamon Press plc

THE MoO_3–ETHYLENEDIAMINE SYSTEM. SYNTHESIS, THERMAL BEHAVIOUR AND CRYSTAL STRUCTURE OF A NOVEL BINUCLEAR MOLYBDENUM(VI) OXOCOMPLEX, $(enH_2)[O_3Mo—O—Mo(en)O_3]$

PASCUAL ROMÁN,* ANTONIO LUQUE and JUAN M. GUTIÉRREZ-ZORRILLA

Departamento de Química Inorgánica, Universidad del País Vasco, Apartado 644, 48080 Bilbao, Spain

and

SANTIAGO GARCÍA-GRANDA

Departamento de Química Física y Analítica, Facultad de Química, Universidad de Oviedo, 33071 Oviedo, Spain

(*Received* 21 *January* 1991; *accepted* 23 *May* 1991)

Abstract—A new binuclear molybdenum(VI) oxocomplex, ethylenediammonium trioxomolybdate(VI)-μ-oxotrioxoethylenediaminemolybdate(VI), with the formula $(enH_2)[O_3Mo—O—Mo(en)O_3]$ (**1**), has been synthesized. Thermal degradation of the compound to the oxide MoO_3 has been studied by means of thermoanalytical methods. The IR spectrum confirms the presence of the ethylenediammonium cation and the complex anion. The crystal structure of the title compound was determined by X-ray diffraction methods. The crystal contains $[O_3Mo—O—Mo(en)O_3]^{2-}$ anions and ethylenediammonium cations. The molybdenum atoms in the complex anion, show two different coordination geometries which produce a structure formed by a tetrahedral $[MoO_4]$ and an octahedral $[MoO_4N_2]$ sharing an oxygen atom. The ethylenediamine has two functions, it acts as a bidentate ligand and as a cation in the complex salt.

Recently, there has been much interest in the chemistry of oxocomplexes of molybdenum due to their structural similarity to the active sites of certain molybdoenzymes.[1] The biological activity of molybdenum mostly involves the molybdenum(VI) state, the coordination chemistry of which is based to a large extent on oxocomplexes which are of importance for their role in oxidation catalysed by metals.[2] Polydentate ligands have played a key role in the development of modern coordination chemistry and interest in these ligands has been heightened by the realization that they have the potential of providing a controlled coordination sphere to the metal which may mimic the function of the protein in metalloenzymes. On the other hand, the coordination chemistry of polyoxomolybdates complexes containing organic ligands has received considerable attention by virtue of their interest as models for the investigation of the interactions between organic substrates and catalytic metal oxide surfaces in heterogeneous catalysis employing solid molybdenum oxides.[3] They also have relevance in the catalytic photo-oxidation of organic compounds.[4]

In view of this wide interest and as a part of our general research programme on oxocomplexes of molybdenum, vanadium and tungsten with polydentate amines in aqueous solution,[5,6] we report in this paper the preparation, chemical characterization, thermal behaviour and the crystal structure and bonding of a new binuclear molybdenum(VI) oxocomplex with the formula $(enH_2)[O_3Mo—O—Mo(en)O_3]$ (**1**). Interestingly, compound **1** may be classified into two different types of compounds: (a) as a part of the family of

* Author to whom correspondence should be addressed.

molybdenum(VI) oxocomplexes, and also (b) as a polyoxomolybdate, as it derives from the dimolybdate anion, $[Mo_2O_7]^{2-}$.[7]

Several polymolybdates containing fluoro-,[8] oxygen-[9] and nitrogen-donating ligands[10,11] have been prepared and structurally characterized in the last 10 years. In most of them two sites of the polymolybdate core are occupied only by the ligand L.

EXPERIMENTAL

Molybdenum trioxide and ethylenediamine were purchased from Merck and were used without further purification. Carbon, nitrogen and hydrogen analyses were performed on a Perkin–Elmer 240 C-, H-, N-analyser. Molybdenum was determined thermogravimetrically as MoO_3 after thermal decomposition of the sample in an atmosphere of argon and oxygen. IR spectra were recorded in the 4000–250 cm^{-1} range from KBr dishes on an IR BECKMAN 4240 spectrophotometer. Differential analysis (DTA) and thermogravimetric (TG) analyses were measured simultaneously on a SETARAM TAG 24 S 16 instrument under an argon and oxygen atmosphere with a heating rate of 5°C min^{-1}.

Synthesis of $(enH_2)[O_3Mo—O—Mo(en)O_3]$

Ethylenediammonium trioxomolybdate(VI)-μ-oxotrioxoethylenediaminemolybdate(VI), $(enH_2)[O_3Mo—O—Mo(en)O_3]$ (**1**), was prepared by direct reaction between molybdenum trioxide (1.84 g, 12.8 mmol) and ethylenediamine (2 cm^3, 29.89 mmol) dissolved in distilled water (75 cm^3), by heating and refluxing at 100°C for 5 h, as described in reaction (1). Colourless crystals of **1** suitable for X-ray analysis were obtained by slow evaporation at room temperature. The crystals were filtered off, washed with water, ether and ethanol, and then dried in air. Crystals were found to be stable to air, light and X-ray exposure. Yield 67%. Found: C, 11.2; H, 4.3; N, 13.0; Mo, 44.8. Calc. for $C_4H_{18}Mo_2N_4O_7$: C, 11.3; H, 4.3; N, 13.1; Mo, 45.0%.

$$MoO_3 + C_2H_8N_2(exc) \xrightarrow[H_2O,\,100°C]{pH = 8.7} (enH_2)[O_3Mo—O—Mo(en)O_3]. \quad (1)$$

Crystallographic data collection and structural refinement

Data collection was carried out on an Enraf Nonius CAD4 four circle diffractometer at 295 K with a graphite monochromator and Mo-K_α radiation. A prismatic single crystal with approximate dimensions $0.45 \times 0.40 \times 0.13$ mm was selected and used for intensity measurements. Unit-cell parameters were obtained from a least-squares fitting of the setting angles for 25 reflections in the range $13 < \theta < 16°$. Intensity data were collected using the ω–2θ scanning technique with Miller indices running from 0 to 13 for h, from 0 to 10 for k and from -25 to 25 for l. During data collection, two reference reflections (4 4 0 and 4 2 -10) were monitored after every 100 reflections and every 7200 s to check for drifts in electronics, radiation damage, variations in X-ray tube intensity, crystal stability and counter response. No crystal decay was observed during the data collection process. Data were corrected for Lorentz and polarization effects. Scattering factors for neutral atoms and anomalous dispersion corrections for all non-hydrogen atoms were taken from the *International Tables for X-ray Crystallography* (1974).[12] The position of molybdenum atoms were located on a Patterson map, the remaining non-hydrogen atoms of the structure were located on successive Fourier syntheses. An empirical absorption correction following the DIFABS procedure[13] was applied to data refined with isotropic displacement parameters. Anisotropic refinement was carried out by full-matrix least-squares analysis. A convenient weighting scheme[14] of the type $w = w_1 \times w_2$ with $w_1 = 1/(8.06 - 27.98 \sin\theta/\lambda + 25.96 \sin^2\theta/\lambda)^2$ and $w_2 = k/(a + b|F_o|)^2$ was used to obtain flat dependence in $\langle w\Delta^2 F\rangle$ vs $\langle \sin\theta/\lambda\rangle$ and vs $\langle F_o\rangle$; the coefficients used were $k = 0.55$; $a = 1.14$, $b = 0.00$ for $|F_o| \leqslant 26$; $a = 0.47$, $b = 0.02$ for $26 < |F_o| \leqslant 51$; $a = 0.88$, $b = 0.01$ for $51 < |F_o| \leqslant 67$; $a = -0.98$, $b = 0.04$ for $67 < |F_o| \leqslant 107$; $a = -0.17$, $b = 0.03$ for $|F_o| > 107$. A Fourier difference synthesis revealed the positions of all the hydrogen atoms close to those expected on geometrical grounds and they were kept fixed as isotropic contributors. Most calculations were carried out using the XRAY 76 system[15] running on a Micro VAX II computer. The details of the crystal data are collected in Table 1. Final atomic positional and thermal parameters, together with observed and calculated structure factors, have been deposited as supplementary material with the Editor, from whom copies are available on request. Atomic coordinates have also been submitted to the Cambridge Crystallographic Data Centre.

RESULTS AND DISCUSSION

Spectroscopic characterization

The IR spectrum of compound **1** shows two peaks at 3390 and 3300 cm^{-1} and they are attribu-

table to N—H stretching vibrations of ammonium groups. There are two strong bands at 3210 and 3140 cm^{-1} due to the $—NH_2$ group of ethylenediamine, shifted towards lower wave numbers by the involvement of the nitrogen atoms of the ligand in coordination.[16] In the 900–810 cm^{-1} region the spectrum displays a complicated pattern of intense bands associated with the symmetric and asymmetric Mo=O stretching vibrations[17] and consistent with the presence of chemically distinct Mo=O moieties. Between 800 and 650 cm^{-1} there is a group of bands which can be assigned to the stretching of the nearly linear Mo—O_b—Mo group.[18]

Thermal analyses

Compound **1** is stable up to approximately 198°C. Its thermal decomposition starts with an endothermic step in the temperature range 198–232°C, corresponding to a mass loss observed in the TG and DTG curves of 6.72%. This first decomposition step is followed by one exothermic process between 232 and 252°C. Both of the two steps are overlapped in the DTG curve. In the DTA curve there are three other exothermic processes in relation with different oxidation processes between 235 and 450°C. A constant weight is achieved above 450°C after losing 32.80% of the original weight. This constant weight indicates that MoO_3 has been formed. This solid product was identified by its X-ray power diffraction pattern and IR spectrum. Thermal decomposition for the whole process can be expressed by reaction (2). It is supposed that unidentified intermediate compounds are oxidized between 198–450°C as shown by reaction (3). Figure 1 shows the thermal decomposition of compound **1**.

$$(enH_2)[O_3Mo—O—Mo(en)O_3] \xrightarrow{\Delta} 2MoO_3 + 2(en) + H_2O \quad (2)$$

$$(en) \xrightarrow{[O]} NO_x + CO_2 + H_2O. \quad (3)$$

X-ray structure determination

The structural analysis reveals that the crystal is composed of discrete complex dianions, $[O_3Mo—O—Mo(en)O_3]^{2-}$, and ethylenediammonium cations, $(enH_2)^{2+}$. The contents of the unit cell and some neighbouring species are shown in Fig. 2, while Fig. 3 shows the structure of the complex dianion and the cation together with the atomic numbering scheme. This kind of associ-

Table 1. Crystal and refinement data of $(enH_2)[O_3Mo—O—Mo(en)O_3]$

Formula	$(enH_2)[O_3Mo—O—Mo(en)O_3]$
Formula weight	426.09
Crystal system	Monoclinic
Space group	*Cc*
a (Å)	9.404(1)
b (Å)	7.406(1)
c (Å)	17.795(1)
β (°)	99.91(1)
V (Å^3)	1220.9(2)
Z	4
ρ_x (g cm^{-3})	2.32
ρ_{calc} (g cm^{-3})	2.31(1)
μ (cm^{-1})	20.362
F(000)	840
Temperature (K)	295(1)
Radiation Mo-K_α (λ = 0.71069 Å)	Graphite-monochromated
Scan type	ω–2θ
θ (°)	2–30
Recorded reflections	1887
Observed reflections [$I > 3\sigma(I)$]	1785
Refined parameters	152
$(\Delta/\sigma)_{max}$	0.03
$(\Delta/\sigma)_{aver}$	0.004
$(\Delta\rho)_{max}$ (e Å^{-3})	1.10
R	0.028
R_w	0.033

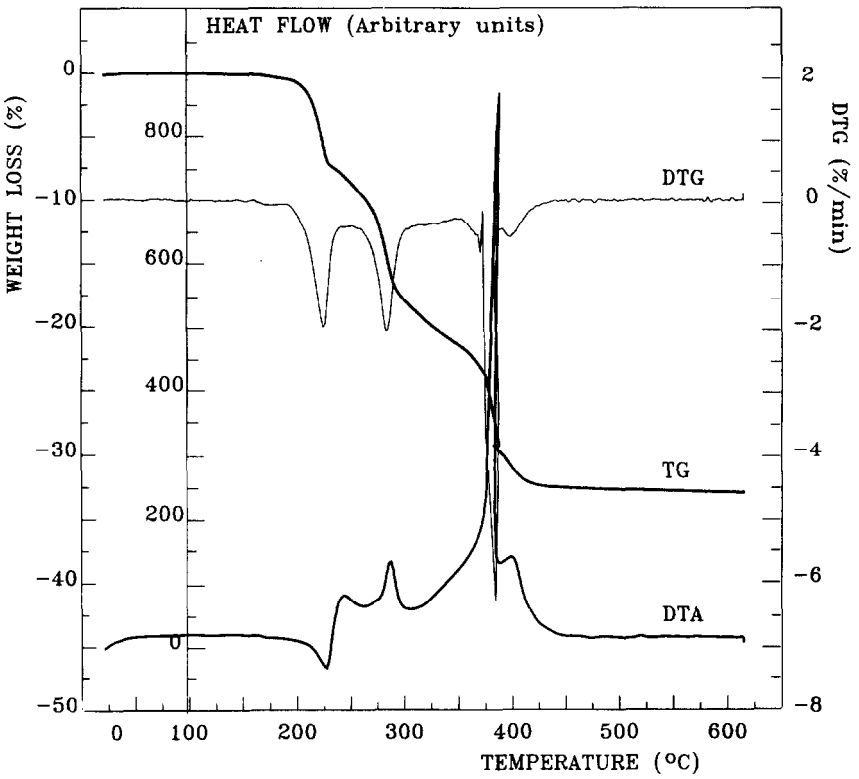

Fig. 1. TG, DTG and DTA curves for compound **1**.

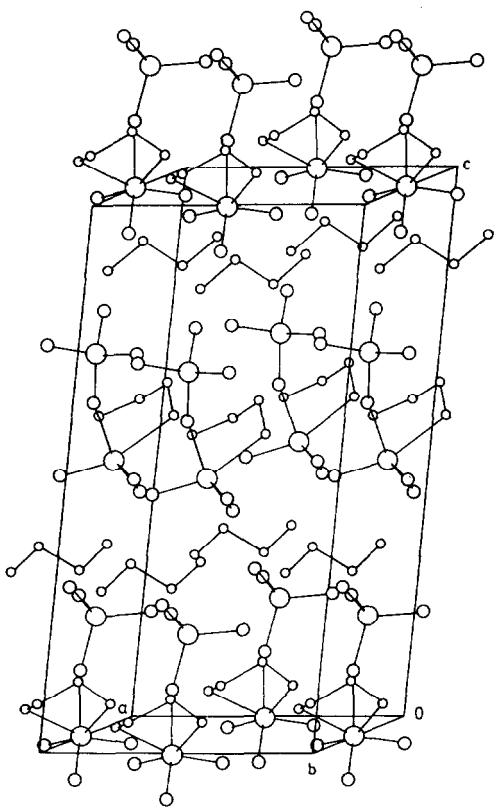

Fig. 2. A view of the unit cell of $(enH_2)[O_3Mo—O—Mo(en)O_3]$.

ation has been found in a different complex with composition $(enH_2)[Cr^{III}(en)F_4]Cl$.[19]

The dianion comprises the asymmetric $[O_3Mo(\mu\text{-}O)Mo(L)O_3]$ core, which, to the best of our knowledge, has not been crystallographically characterized previously. The asymmetry gives rise to non-equivalent molybdenum coordination geometries. Molybdenum (**1**) displays a distorted octahedral $[MoO_4N_2]$ coordination through ligation to three terminal oxo groups, to two diamine nitrogen atoms, and to a bridging oxo group. In contrast, molybdenum (**2**) exhibits tetrahedral $[MoO_4]$ coordination via bonding to three terminal oxygen atoms and to the bridging oxo group. Thus, the overall structure of the anion may be viewed as an octahedron and a tetrahedron which are linked together by a bridging oxygen atom vertex. Bond lengths and bond angles in both coordination polyhedra in the anion are listed in Table 2. Although non-equivalent metal sites are not uncommon in binuclear systems of molybdenum(III) and (V), binuclear complexes of molybdenum(VI) usually exhibit symmetrical structures.

The bonding parameters associated with the tetrahedral $[MoO_4]$ unit are unexceptional. However, several other features of the geometry of the $[MoO_4N_2]$ unit merit discussion. In $[MoO_4N_2]$ the Mo=O bond lengths range from 1.747(4) to

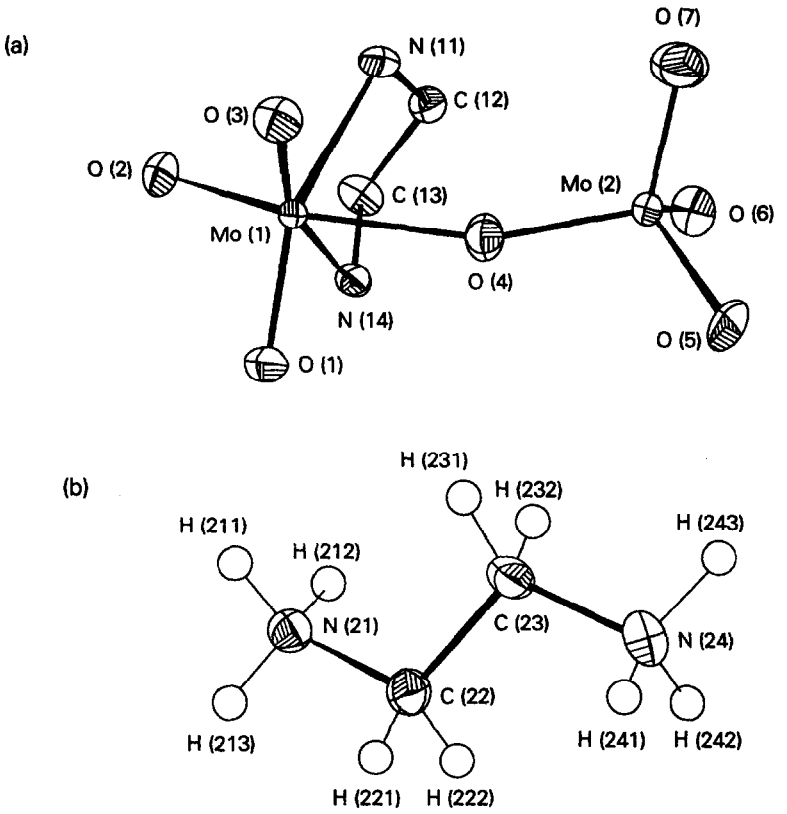

Fig. 3. ORTEP view of the structure of (a) the $[O_3Mo—O—Mo(en)O_3]^{2-}$ anion and (b) the $(enH_2)^{2+}$ cation, showing the atom-labelling scheme.

1.764(4) Å, those in $[MoO_4]$ from 1.737(5) to 1.770(4) Å. These values agree very well with those found in other molybdenum(VI) oxocomplexes[20] or in discrete[7] and polymeric[20,21] dimolybdate anions with molybdenum–oxygen double bonds. The long Mo—N distances [2.317(4) and 2.348(5) Å], in the *trans* positions with respect to the Mo=O bonds, indicate weak interactions, reflecting the absence of a strong electrostatic component to the bonding; a common observation for interactions between molybdenum(VI) and neutral base ligands.[6,18] There is a significant inequality of the bond angles O(2)—Mo(1)—N(11) [84.6(2) Å] and O(4)—Mo(1)—N(11) [76.1(2) Å] involving terminal oxygen atoms and a bridging oxygen atom. This reflects stronger repulsion from the Mo=O bond compared to the Mo—O_b bond. The most significant structural feature of the anion is the presence of non-equivalent molybdenum-bridging oxo distances of 2.129(4) Å for Mo(1)—O(4) and 1.799(4) Å for Mo(2)—O(4), due to the strong influence of the terminal oxo group O(2) and the negligible *trans* influence of terminal oxygen atoms in the distorted tetrahedron $[MoO_4]$. A similar lengthening is shown in polymeric dimolybdate anions which are built by $[MoO_6]$ and $[MoO_4]$ groups linked together by sharing a corner.[20,22] The Mo—O_b—Mo angle is 161.6(3)° and it is indicative of some electronic delocalization which is usually an important factor in the presence of photochemical properties of this type of compound.[23] The distance between the molybdenum atoms of the dianion is 3.8772(4) Å, which is consistent with the absence of Mo—Mo interactions, as expected for a binuclear Mo^{VI}-d^0 complex, and contrasts with the distance of *ca* 2.80 Å observed for oxocomplexes of molybdenum(V), where metal–metal bonding is invoked.[24] The nitrogen atoms are *cis* to each other in the ethylenediamine ligand, giving a gauche configuration [dihedral angle between the N(11)—C(12)—C(13) and N(14)—C(13)—C(12) planes, 54.6(5)°] similar to that observed previously.[25] The ethylenediammonium cation is nearly planar [dihedral angle 178.7(4)°] with *trans* nitrogen atoms. Bond distances and bond angles in the ligand do not significantly differ from those for the cation (Table 2). Nevertheless, N—C and C—C bond distances, and N—C—C bond angles are generally slightly bigger in the ethylenediammonium cation compared to the ethylenediamine ligand.

Table 2. Selected values and bond lengths (Å) and bond angles (°) for compound **1**

Anion			
Mo(1)—O(1)	1.747(4)	Mo(2)—O(4)	1.799(4)
Mo(1)—O(2)	1.764(4)	Mo(2)—O(5)	1.759(4)
Mo(1)—O(3)	1.755(4)	Mo(2)—O(6)	1.770(4)
Mo(1)—O(4)	2.129(4)	Mo(2)—O(7)	1.737(5)
Mo(1)—N(11)	2.348(5)		
Mo(1)—N(14)	2.317(4)	Mo(1)···Mo(2)	3.8872(4)
O(1)—Mo(1)—O(2)	104.6(2)	O(4)—Mo(2)—O(5)	109.4(2)
O(1)—Mo(1)—O(3)	106.2(2)	O(4)—Mo(2)—O(6)	110.4(2)
O(1)—Mo(1)—O(4)	89.2(2)	O(4)—Mo(2)—O(7)	109.8(2)
O(1)—Mo(1)—N(11)	157.7(2)	O(5)—Mo(2)—O(6)	106.8(2)
O(1)—Mo(1)—N(14)	87.7(2)	O(5)—Mo(2)—O(7)	110.0(2)
O(2)—Mo(1)—O(3)	102.8(2)	O(6)—Mo(2)—O(7)	110.4(2)
O(2)—Mo(1)—O(4)	156.0(2)		
O(2)—Mo(1)—N(11)	84.6(2)	Mo(1)—O(4)—Mo(2)	161.6(3)
O(2)—Mo(1)—N(14)	84.3(2)		
O(3)—Mo(1)—O(4)	91.8(2)		
O(3)—Mo(1)—N(11)	91.1(2)		
O(3)—Mo(1)—N(14)	161.9(2)		
O(4)—Mo(1)—N(11)	76.1(2)		
O(4)—Mo(1)—N(14)	76.6(2)		
N(11)—Mo(1)—N(14)	72.8(2)		
Ethylenediamine		Ethylenediammonium	
N(11)—C(12)	1.479(6)	N(21)—C(22)	1.485(7)
C(12)—C(13)	1.509(8)	C(22)—C(23)	1.520(6)
C(13)—N(14)	1.479(7)	C(23)—N(24)	1.475(7)
N(11)—C(12)—C(13)	109.4(4)	N(21)—C(22)—C(23)	109.9(4)
C(12)—C(13)—N(14)	107.7(4)	C(22)—C(23)—N(24)	109.3(4)

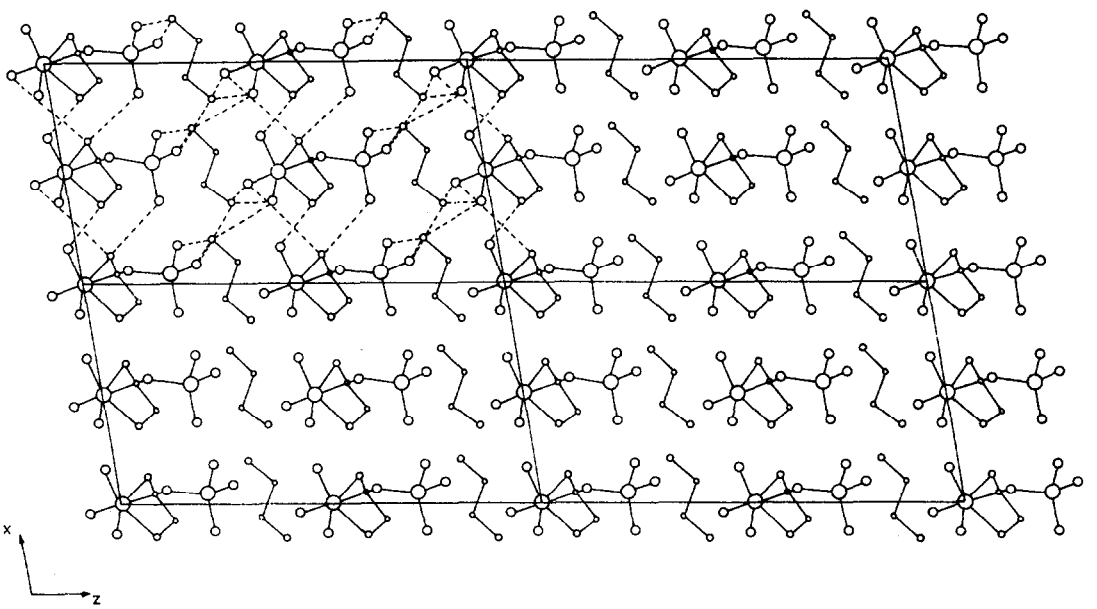

Fig. 4. Projection of the crystal structure of $(enH_2)[O_3Mo—O—Mo(en)O_3]$ in the ac plane showing the hydrogen-bonding network (N···O).

Table 3. Hydrogen contacts of $(enH_2)[O_3Mo—O—Mo(en)O_3]$

Bond type		X—H	X···O	H···O	< X—H···O
N(11)—H(111)···O(1)	(1)	1.00	2.915(5)	2.07	141.1
N(14)—H(141)···O(7)	(2)	1.00	3.090(5)	2.36	129.4
N(14)—H(142)···O(3)	(2)	1.00	2.990(6)	2.01	166.4
N(21)—H(211)···O(6)	(3)	1.00	2.826(6)	1.87	158.8
N(21)—H(212)···O(5)	(4)	1.00	2.732(6)	1.76	162.2
N(21)—H(213)···O(2)	(5)	1.00	2.842(6)	1.91	150.4
N(24)—H(241)···O(3)	(6)	1.00	2.839(6)	1.86	166.4
N(24)—H(242)···O(2)	(7)	1.00	2.898(6)	1.95	158.5
N(24)—H(243)···O(6)	(8)	1.00	2.847(6)	1.95	149.0
		1.00			
C(22)—H(221)···O(1)	(6)	1.00	3.257(7)	2.32	154.9
C(22)—H(222)···O(2)	(7)	1.00	3.351(7)	2.59	132.5
C(22)—H(222)···O(3)	(5)	1.00	3.250(6)	2.58	124.0
C(23)—H(231)···O(7)	(4)	1.00	3.475(7)	2.51	161.2
C(23)—H(232)···O(5)	(8)	1.00	3.261(6)	2.59	124.6
C(23)—H(232)···O(6)	(3)	1.00	3.308(7)	2.56	131.7

Symmetry codes

(1)	$-1/2+x$,	$1/2+y$,	z	(5)	$1/2+x$,	$-1/2+y$,	$1+z$
(2)	$1/2+x$,	$1/2+y$,	z	(6)	x,	y,	$1+z$
(3)	x,	$1-y$,	$1/2+z$	(7)	x,	$-1+y$,	$1+z$
(4)	x,	$-y$,	$1/2+z$	(8)	$-1/2+x$,	$1/2-y$,	$1/2+z$

The crystal packing in this structure is formed by zig-zag parallel chains along the c axis following a sequence ...acac... (where a = anion and c = cation). These chains are placed in two different x levels: $x = 0$ and $x = 1/2$. While the complex anion is nearly situated in the (100) plane, the ethylenediammonium cation is located along the [100] direction. The projection of the crystal structure in the ac plane showing the hydrogen bonding network (N···O) is given in Fig. 4. The crystal structure is stabilized by electrostatic interactions and the presence of an extended hydrogen bond network. Each anion is connected by three $N_a \cdots O$ hydrogen bonds with neighbouring anions from chains at different x levels and the same z level. The ethylenediammonium cation forms $N_c \cdots O$ hydrogen bonds with anions of its own chain and of different chains. The closest approach distances that are suitably orientated to permit hydrogen contacts are listed in Table 3.

It is interesting to note that $N_a \cdots O$ (2.91–2.99 Å) hydrogen bonds between anions are longer than $N_c \cdots O$ (2.73–2.90 Å) hydrogen bonds. In the structure there also are some relatively short $C_c \cdots O$ (3.25–3.47 Å) hydrogen contacts between the oxygen atoms of anions and the carbon atoms of cations. No doubt all the C—H···O contacts cannot be considered as hydrogen bonds, but they do indicate some degree of polarization and the role of this type of interactions in a series of organic and inorganic compounds has also been examined in the literature.[26,27]

Acknowledgements—Three of the authors (P.R., A.L. and J.M.G.-Z.) wish to thank Iberduero, S.A. for financial support.

REFERENCES

1. R. C. Bray and G. N. George, *Biochem. Soc. Trans.* 1985, **13**, 560; G. N. George, R. C. Bray and S. P. Cramer, *Biochem. Soc. Trans.* 1986, **14**, 651; S. Purohit, A. Puasad-Koley and S. Ghosh, *Polyhedron* 1990, **9**, 881.
2. J. K. Kochi, in *Organometallic Mechanisms and Catalysis*, Ch. 2. Academic Press, New York (1978); M. S. Reynolds, J. M. Berg and R. H. Holm, *Inorg. Chem.* 1984, **23**, 3057.
3. V. W. Day and W. G. Klemperer, *Science* 1985, **228**, 533; S. Liu, S. N. Shaikh and J. Zubieta, *Inorg. Chem.* 1987, **26**, 4303; S. Liu, S. N. Shaikh and J. Zubieta, *Inorg. Chem.* 1988, **27**, 3064; V. W. Day, W. G. Klemperer, C. Schwart and R.-C. Wang, in NATO ASI Series C, Vol, 231: *Molecular Approaches to Surface Catalysis* (Edited by J.-M. Basset *et al.*), p. 173. Kluwer, Dordrecht (1988); S. Liu, L. Ma, D. McGowty and J. Zubieta, *Polyhedron* 1990, **9**, 1541.
4. T. Yamase, *J. Chem. Soc., Dalton Trans.* 1985, 2585; T. Yamase, *Polyhedron* 1986, **5**, 79; M. M.

Williamson, D. A. Bouchard and C. L. Hill, *Inorg. Chem.* 1987, **26**, 1436.
5. A. Luque, PhD Thesis. Universidad del País Vasco, Spain (1990).
6. P. Román, A. Luque and J. M. Gutiérrez-Zorrilla, *Acta Cryst.* 1991, **C47**, 188.
7. V. W. Day, M. F. Frederich, W. G. Klemperer and W. Shum, *J. Am. Chem. Soc.* 1977, **99**, 6146.
8. B. Kamenar, B. Kaitner and N. Strukan, *Acta Cryst.* 1990, **C46**, 2249.
9. M. Isobe, F. Marumo, T. Yamase and T. Ikawa, *Acta Cryst.* 1978, **B34**, 2728; R. Adams, W. G. Klemperer and R.-S. Liu, *J. Chem. Soc., Chem. Commun.* 1979, 256; B. Kamenar, B. Korpar-Colig, M. Penavic and M. Cindric, *J. Chem. Soc., Dalton Trans.* 1990, 1125.
10. E. M. McCarron III, J. F. Whitney and D. B. Chase, *Inorg. Chem.* 1984, **23**, 3275.
11. B. Kamenar, M. Penavic and B. Markovic, *Acta Cryst.* 1988, **C44**, 1521.
12. *International Tables for X-ray Crystallography*, Vol. IV. (Present distributor: D. Reidel, Dordrecht). Kynoch Press, Birmingham (1974).
13. N. Walker and D. Stuart, *Acta Cryst.* 1983, **A39**, 158.
14. M. Martínez-Ripoll and F. H. Cano, PESOS. Program for the automatic treatment of weighting schemes for least-squares refinement. Instituto Rocasolano, CSIC, Serrano 119, 28006, Madrid, Spain (1975).
15. J. M. Stewart, P. A. Machin, C. W. Dickinson, H. L. Ammon, H. Heck and H. Flack, The XRAY 76 System. Tech. Rep. TR-446. Computer Science Centre, University of Maryland, College Park, Maryland, U.S.A. (1976).
16. P. S. Roy and K. Wieghardt, *Inorg. Chem.* 1987, **26**, 1885.
17. C. Bustos, O. Burckhardt, R. Schrebler, D. Carrillo, A. M. Arif, A. H. Cowley and C. M. Nunn, *Inorg. Chem.* 1990, **29**, 3996; S. Liu, L. Ma, D. McGowty and J. Zubieta, *Polyhedron* 1990, **9**, 1541; R. N. Mohanty and K. C. Dash, *Polyhedron* 1990, **9**, 1011.
18. T. C. Hsieh, S. N. Shaikh and J. Zubieta, *Inorg. Chem.* 1987, **26**, 4079; L. Ma, S. Liu and J. Zubieta, *Polyhedron* 1989, **8**, 1571; N. W. Alcock, M. Dudek, R. G. Grybos, E. Hodorowicz, A. Kanas and A. Samatus, *J. Chem. Soc., Dalton Trans.* 1990, 707.
19. C. Díaz, A. Seguí, J. Ribas, X. Solans, M. Font-Altaba, A. Solans and J. Casabó, *Trans. Metal. Chem.* 1984, **9**, 469.
20. S. Liu and J. Zubieta, *Polyhedron* 1988, **7**, 1129.
21. R. M. Gatehouse, *J. Less-common Metal.* 1977 **54**, 283.
22. I. Knöpnadel, H. Hartl, W. D. Hunnius and J. Fuchs, *Angew. Chem. Int. Edn* 1974, **13**, 823.
23. T. Yamase, H. Naruke and Y. H. Sasaki, *J. Chem. Soc., Dalton Trans.* 1990, 1678.
24. J. Zubieta, E. Block, G. Ofori-Okai and K. Lang, *Inorg. Chem.* 1990, **29**, 4595.
25. A. J. Jircitano, R. F. Henry and R. R. Hammond, *Acta Cryst.* 1990, **C46**, 1799.
26. R. Taylor and O. Kennard, *J. Am. Chem. Soc.* 1982, **104**, 5063.
27. P. Román, J. M. Gutiérrez-Zorrilla, A. Luque and M. Martínez-Ripoll, *Z. Kristallogr.* 1988, **184**, 175.

Polyhedron Vol. 10, No. 17, pp. 2065–2068, 1991
Printed in Great Britain

0277–5387/91 $3.00+.00
© 1991 Pergamon Press plc

2-ARYLTELLUROETHANOLS AND THEIR MERCURY(II), PALLADIUM(II) AND PLATINUM(II) ALKOXIDES CHELATED THROUGH TELLURIUM—SYNTHESIS AND SPECTRA

AJAI K. SINGH* and S. THOMAS

Department of Chemistry, Indian Institute of Technology, New Delhi 110 016, India

(*Received* 22 *October* 1990; *accepted* 23 *May* 1991)

Abstract—The sodium salt of 2-aryltelluroethanol (**1**) (aryl = 4-$MeOC_6H_4$ or 4-$EtOC_6H_4$), which was synthesized by the reaction of $HOCH_2CH_2Cl$ with $ArTe^-Na^+$ (generated *in situ* by borohydride reduction of the appropriate Ar_2Te_2), reacts with $HgCl_2$, $PdCl_2$ and K_2PtCl_4 in 1 : 1 molar ratio resulting in alkoxides of stoichiometry $[MCl(1\text{-}H)_2]_2$. The chelation through tellurium has been supported by proton NMR spectra and in the case of mercury(II) complexes, by ^{13}C NMR spectra also. The presence of ν[M—Cl(bridging)] in the range 200–270 cm^{-1} supports the dimeric formulation for these alkoxides based on chlorine bridges. The ArTe group does not significantly affect the hydrogen bonding pattern of the ethanol. The CH_2 rocking vibrations suggest that **1** exists in the complexes in the *gauche* conformation.

The interest in hybrid organotellurium ligands has been growing since the mid-eighties.[1] Recently, syntheses of several interesting (Te, N) donors[2] and their ligation behaviour have been reported. In the repertoire of (Te, O) ligands there are few compounds as only the ligation of aryltelluroacetic acid[3] and 2-(4-ethoxyphenyltelluro)benzoate[4] has been attempted so far. However, synthetic routes[1d,5] are available for structures **2**–**7**, which may act as (Te, O) donors. Continuing our investigations on hybrid organotellurium ligands, we have synthesized 2-aryltelluroethanols (**1**) and investigated their mercury(II), palladium(II) and platinum(II) alkoxides. The results are reported in the present paper. The alkoxides of palladium(II)[6] and platinum(II)[7] are rare. Recently some chelate stabilized alkoxoplatinum(II) complexes have been synthesized by Pringle *et al.*[8–10] by reacting $Ph_2PCH_2CR_2OH$ (R = H or Me) with a variety of platinum(II) moieties. In the absence of chelate stabilization alkoxides of platinum(II) are extremely moisture-, oxygen- and temperature-sensitive, decomposing to the hydride *via* β-hydrogen elimination or depositing the metal(0). The palladium(II) and platinum(II) alkoxides of **1** have been found to be quite stable and moisture-insensitive, most probably due to the formation of a chelate ring through tellurium. Thus, the present investigations of 2-aryltelluroethanols not only extend to the repertoire of (Te, O) donors but also enlarge the very limited number of examples known of alkoxypalladium(II)/platinum(II) complexes.

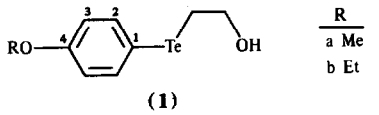

(1)

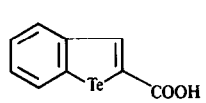

(2)

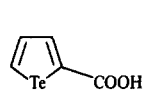

(3)

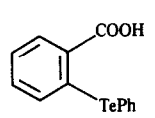

(4)

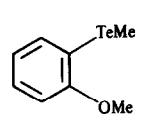

(5)

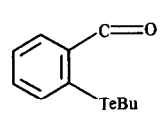

(6)

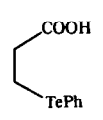

(7)

EXPERIMENTAL

Published methods[11] were used to synthesize bis(4-methoxyphenyl) and bis(4-ethoxyphenyl)

* Author to whom correspondence should be addressed.

ditellurides. Tellurium was estimated by a standard method.[12] The carbon, hydrogen and nitrogen analyses were carried out using a Perkin–Elmer elemental analyser, 240C. The ^1H and $^{13}C\{^1H\}$ NMR spectra in $CDCl_3$ and DMSO-d_6 were recorded at 25°C on a JEOL FX-100 FT-NMR spectrometer at 99.55 and 25 MHz, respectively. IR spectra (of Nujol mulls between CsI windows or KBr/CsI discs) in the range 200–4000 cm^{-1} were recorded on a Nicolet 5DX FT-IR spectrometer. Far-IR spectra (up to 50 cm^{-1}) were recorded in polyethylene on a Perkin–Elmer Far-IR spectrometer, model 1700X. Electronic spectra were recorded on a Hitachi UV–vis spectrometer, model 300.

Synthesis of 2-*aryltelluroethanols* (**1**)

Bis(4-methoxyphenyl) or bis(4-ethoxyphenyl) ditelluride (10 mmol) was dissolved in ethanol (30 cm^3). Sodium borohydride (1 g) dissolved in 1 N NaOH (50 cm^3) was added dropwise to the solution of ditelluride under an oxygen-free dinitrogen atmosphere until it became light yellow. 2-Chloroethanol (1.61 g, 20 mmol) dissolved in ethanol (5 cm^3) was added to this light yellow solution. The mixture was refluxed for 1 h with stirring under a nitrogen atmosphere, cooled and poured into excess water. The aqueous mixture was acidified with dilute acetic acid and extracted using chloroform. The evaporation of chloroform produced a deep yellow liquid. The results of elemental analyses and spectral data are given below.

1a: Analysis. Found: C, 36.6; H, 5.6. Calc. for $C_9H_{12}O_2Te$: C, 38.1; H, 5.6%. NMR (^1H, $CDCl_3$, 25°C): δ 2.20 (bs, OH), 2.88–3.01 (t, 2H, $TeCH_2$), 3.72–3.79 (t, 5H, OCH_2+OCH_3), 6.67–6.76 (d, 2H, ArH *ortho* to Te), 7.61–7.70 (d, 2H, ArH *meta* to Te); ($^{13}C\{^1H\}$, $CDCl_3$, 25°C): δ, 13.3 ($TeCH_2$), 55.3 (OCH_3), 63.0 ($HOCH_2$), 99.6 (C_1), 115.2 (C_3, C_5), 141 (C_2, C_6), 159.8 (C_4).

1b: Analysis. Found: C, 39.2; H, 5.9. Calc. for $C_{10}H_{14}O_2Te$: C, 40.3; H, 6.0%. NMR (^1H, $CDCl_3$, 25°C): δ, 1.30–1.44 (q, 3H, CH_3), 2.89 (bs, OH), 3.69–3.87 (t, 2H, $TeCH_2$), 3.94–4.08 (m, 4H, OCH_2), 6.06–6.79 (d, 2H, ArH *ortho* to Te), 7.59–7.68 (d, 2H, ArH *meta* to Te); ($^{13}C\{^1H\}$, $CDCl_3$, 25°C): δ, 12.9 (CH_3), 14.7 ($TeCH_2$), 58.2 (OCH_2), 63.2 ($HOCH_2$), 99.1 (C_1), 115.6 (C_3, C_5), 140.8 (C_2, C_6), 158.9 (C_4).

Synthesis of mercury(II) *alkoxides of* **1**

1a or **1b** (1 mmol) was dissolved in methanol (20 cm^3). Sodium metal (1 mmol) dissolved in methanol (8–10 cm^3) was added to a solution of **1** and stirred for 30 min. Mercury(II) chloride (1 mmol) dissolved in methanol (5–10 cm^3) was stirred with this mixture for 2 h. The pale yellow precipitate formed was filtered, washed thoroughly with a cold methanol and water (9:1) mixture and dried *in vacuo*. The results of the elemental analyses, m.p.s and spectral data are recorded below.

$[HgCl(\mathbf{1a}\text{-H})]_2$: m.p. 238–40°C (d). Analysis. Found: C, 21.3; H, 3.0; Te, 26.2; Hg, 38.6; Cl, 6.9. Calc. for $C_9H_{11}O_2TeHgCl$: C, 20.8; H, 2.9; Te, 24.6; Hg, 38.6; Cl, 6.8%. NMR (^1H, DMSO-d_6, 25°C): δ, 2.52 (t, 2H, $TeCH_2$), 6.84–6.93 (d, 2H, ArH *ortho* to Te), 7.33–7.41 (d, 2H, ArH *meta* to Te).

$HgCl(\mathbf{1b}\text{-H})]_2$: m.p. 226°C (d). Analysis. Found: C, 23.0; H, 3.1; Te, 24.7; Hg, 36.1; Cl, 6.4. Calc. for $C_{10}H_{13}O_2TeHgCl$: C, 22.5; H, 3.2; Te, 24.0; Hg, 37.6; Cl, 6.7%. NMR (^1H, DMSO-d_6, 25°C): δ, 1.25–1.39 (t, 3H, CH_3), 2.22–2.50 (t, 2H, $TeCH_2$), 6.37–7.14 (d, 2H, ArH *ortho* to Te), 7.62–7.85 (d, 2H, ArH *meta* to Te).

Synthesis of palladium(II) *alkoxides of* **1**

The sodium salt of **1a** or **1b** (0.05 mmol) was prepared as described above and mixed with solid $PdCl_2$ (0.5 mmol). The mixture was stirred for 2 h at room temperature (25°C) in a nitrogen atmosphere. When the $PdCl_2$ dissolved completely, the volume of the mixture was reduced. The precipitate thus formed was filtered, washed with cold methanol and dried *in vacuo*. The results of the elemental analyses, m.p.s and NMR data are given below.

$[PdCl(\mathbf{1a}\text{-H})]_2$: m.p. 98°C (d). Analysis. Found: C, 25.0; H, 3.5; Te, 31.1; Cl, 8.9. Calc. for $C_9H_{11}O_2TePdCl$: C, 25.4; H, 3.5; Te, 31.0; Cl, 8.3%. NMR (^1H, DMSO-d_6, 25°C): δ, 2.08–2.51 (t, 2H, $TeCH_2$), 6.94–7.58 (d, 2H, ArH *ortho* to Te), 7.82–8.38 (d, 2H, *meta* to Te).

$[PdCl(\mathbf{1b}\text{-H})]_2$: m.p. 114°C (d). Analysis. Found: C, 27.0; H, 4.2; Te, 29.8; Cl, 8.0. Calc. for $C_{10}H_{13}O_2TePdCl$: C, 27.4; H, 3.9; Te, 29.1; Cl, 8.1%. NMR (^1H, DMSO-d_6, 25°C): δ, 1.25–1.38 (t, 3H, CH_3), 2.50–2.80 (t, 2H, $TeCH_2$), 6.71–7.08 (d, 2H, ArH *ortho* to Te), 7.58–7.92 (d, 2H, ArH *meta* to Te).

Synthesis of platinum(II) *alkoxides of* **1**

A methanolic solution of the sodium salt of **1a** or **1b** (0.5 mmol) was prepared by the procedure described above and mixed with a solution of K_2PtCl_4 (0.5 mmol) (in approx. 5 cm^3 of water). The mixture was stirred for 3 h until it became reddish-brown and a precipitate started to appear. The vol-

ume of the solution was reduced to half. The resulting precipitate was filtered, thoroughly washed with cold methanol and dried *in vacuo*. The m.p. results of elemental analyses and NMR data are given below.

[PtCl(**1a**-H)]$_2$: m.p. 98°C (d). Analysis. Found: C, 20.6; H, 3.1; Te, 25.1; Cl, 7.0. Calc. for $C_9H_{11}O_2TePtCl$: C, 21.0; H, 2.9; Te, 24.9; Cl, 6.9%. NMR (^{1}H, DMSO-d$_6$, 25°C): δ, 2.38–2.52 (t, 2H, $TeCH_2$), 6.66–6.91 (d, 2H, ArH *ortho* to Te), 7.47–7.62 (d, 2H, ArH *meta* to Te).

[PtCl(**1b**-H)]$_2$: m.p. 132°C (d). Analysis. Found: C, 22.6; H, 3.4; Te, 23.9; Cl, 6.0. Calc. for $C_{10}H_{13}O_2TePtCl$: C, 22.7; H, 3.2; Te, 24.2; Cl, 6.7%. NMR (^{1}H, DMSO-d$_6$, 25°C): δ, 1.25–1.38 (t, 3H, CH_3), 2.50–2.92 (t, 2H, $TeCH_2$), 6.81–7.11 (d, 2H, ArH *ortho* to Te), 7.65–8.01 (d, 2H, ArH *meta* to Te).

The signals of OCH_2, OCH_3 and CH_2O^- protons in the ^{1}H NMR spectra of all the complexes were found to merge with the DMSO signals.

RESULTS AND DISCUSSION

2-Aryltelluroethanols (**1a–b**) and their metal complexes were synthesized by the following reactions.

$$HO(CH_2)_2Cl \xrightarrow{ArTe^-Na^+} HO(CH_2)_2TeAr \xrightarrow{Na} NaO(CH_2)_2TeAr \xrightarrow{M(II)} ClM\overline{O(CH_2)_2TeAr_2} \quad (1)$$

(Ar = 4-$MeOC_6H_4$ or 4-$EtOC_6H_4$, M = Hg, Pd or Pt).

The ^{1}H and ^{13}C NMR of **1a** and **1b**, authenticated by elemental analyses, were found to be characteristic. The OH signal in the ^{1}H NMR spectra appears at a position very close to that of ethanol (δ, 2.26 ppm), suggesting that the intermolecular hydrogen bonding of ethanol is not greatly disturbed by substituting its CH_3 group with $ArTeCH_2$. The ν(OH) in the IR spectra occurs as a broad band around 3200 cm^{-1}, which corresponds to the results of the ^{1}H NMR. The regions in the IR spectra generally assigned to the CH_2 rocking mode have bands around 925, 815 and 720 cm^{-1}, which suggest that **1a** and **1b** probably exist in both *trans* and *gauche* forms,[13] at least in the free liquid. Tellurium shields the carbon atoms linked to it and therefore, C_1 and CH_2 protons (even those iinked to OH) appear in ^{13}C NMR upfield.

Mercury(II), palladium(II) and platinum(II) complexes of **1a** and **1b** were found to be fairly air-stable and soluble only in polar solvents like DMSO and DMF, contrary to the ligands which were found to be fairly soluble in $CHCl_3$, CH_3CN, CH_3OH and C_6H_6. All of these complexes are diamagnetic and cannot be synthesized by the direct reaction of metal halides with **1a** or **1b**. The electronic spectra of the alkoxides of palladium and platinum in DMSO exhibit a band around 26 kK, which seems to have major contribution from the $^1A_{1g} \rightarrow {}^1B_{1g}$ transition characteristic of square planar geometry of palladium/platinum.

On comparing the ^{1}H NMR spectra of the ligands **1a** and **1b** with those of the metal alkoxides, taking into account the solvent effect, it appears that the protons of the CH_2Te group undergo deshielding of the order 0.5–1.2 ppm. This probably appears because the negative charge on oxygen is greater in the complexes than in the ligand (**1a** or **1b**), which in turn has an overall shielding effect on the —CH_2CH_2— backbone. The ring protons of **1a** and **1b** exhibit deshielding (0.2–0.8 ppm) on complexation with palladium/platinum(II), which is probably due to the engagement of tellurium in the coordination. The deshielding of protons *ortho* to tellurium also occurs in complexation of **1** with mercury(II) but its magnitude is ~ 0.2 ppm, probably due to the weak nature of the Hg—Te bond relative to the Pd/Pt—Te bond. The dimeric nature of all the complexes is supported by the occurrence of ν[M—Cl(bridging)] vibrations around 200, 270 and 260 cm^{-1} respectively for mercury, palladium and platinum. The absence of ν(OH) in the IR spectra and an OH signal in ^{1}H NMR spectra lends further support that **1** behaves as a uninegative and bidentate ligand in its present complexes. Based on these observations, structure **8** may be proposed for these alkoxides with the presumption that the geometry around mercury is tetrahedral and square planar around palladium/platinum. Since the ν[M—Cl (bridging)] band in the IR spectra of Pd^{II}/Pt^{II} complexes does not exhibit any splitting, it is reasonable to assume they are centrosymmetric. Moreover, ^{1}H NMR spectra of palladium(II) and platinum(II) complexes do not have additional signals, ruling out the possibility that they are mixtures of centrosymmetric *trans* and *cis* isomers (**8**).

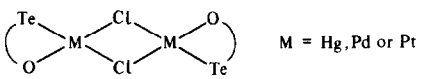

(**8**)

The CH_2 rocking vibrations in the IR spectra of all the present complexes appear in the ranges 920–880 and 820–805 cm^{-1}, suggesting that probably the two CH_2 groups of **1a** or **1b** adopt a *gauche* conformation.[8] To further support the ligation of **1** with the three metals through tellurium, com-

parison of ^{13}C NMR spectra of these complexes with those of the ligands was not possible due to inadequate solubility of the former for recording the NMR, except in the case of [HgCl(**1b**-H)]$_2$. The ^{13}C NMR spectrum of this complex exhibits signals[14] at δ 14.4 (CH_3), 24.5 ($TeCH_2$), 58.8 (OCH_2), 63.3 (CH_2O^-), 102.0 (C_1), 115.8 (C_3), 139.2 (C_2) and 159.6 (C_4) ppm. The $TeCH_2$ and C_2 signals appear to be deshielded ($\sim$ 12 and 2.5 ppm, respectively) with respect to the corresponding signals of **1b**, supporting the involvement of tellurium in coordination with at least mercury(II). Attempts to synthesize pure samples of alkoxides of the composition M(**1**-H)$_2$ have not yet succeeded. Similarly we have failed so far in growing crystals of the present alkoxides, suitable for single crystal X-ray work.

REFERENCES

1. (a) H. J. Gysling, *The Chemistry of Organic Selenium and Tellurium Compounds* (Edited by S. Patai and Z. Rappoport), Ch. 18, p. 815. John Wiley, New York (1986); (b) H. J. Gysling and H. R. Luss, *Organometallics* 1984, **3**, 596; (c) N. I. Al-Salim, T. A. Hamor and W. R. McWhinnie, *J. Chem. Soc., Chem. Commun.* 1986, 453; (d) T. Kemmitt and W. Levason, *Organometallics* 1989, **8**, 1303.
2. (a) A. K. Singh, V. Srivastava and B. L. Khandelwal, *Polyhedron* 1990, **9**, 495, 851; (b) B. L. Khandelwal, A. K. Singh, V. Srivastava, D. C. Povey and G. W. Smith, *Polyhedron* 1990, **9**, 2041.
3. A. K. Singh, S. Thomas and B. L. Khandelwal, *J. Coord. Chem.* 1990, **21**, 71.
4. N. I. Al-Salim and W. R. McWhinnie, *Inorg. Chim. Acta* 1989, **155**, 213.
5. (a) J. L. Piette and M. Renson, *Bull. Soc. Chim. Belges* 1970, **79**, 353; 1971, **80**, 521; (b) F. Fringuelli and A. Taticchi, *J. Chem. Soc., Perkin Trans. I* 1972, 199; (c) J. L. Piette, P. Thibaut and M. Renson, *Tetrahedron* 1978, **34**, 655; (d) K. Y. Abid, N. I. Al-Salim, M. Greaves, W. R. McWhinnie, A. A. West and T. A. Hamor, *J. Chem. Soc., Dalton Trans.* 1989, 1697.
6. C. F. J. Barnard and M. J. H. Russell, *Comprehensive Coordination Chemistry* (Edited by G. Wilkinson, R. D. Gillard and J. A. McCleverty), Vol. 5, p. 1113. Pergamon Press, London (1987); F. Glocking and E. H. Brooks, *Prepr. Div. Pet. Chem., Am. Chem. Soc.* 1969, **14**, B135; F. A. White, *J. Chem. Soc. (A)* 1971, 143.
7. (a) N. W. Alcock, A. W. G. Platt and P. G. Pringle, *Inorg. Chim. Acta* 1987, **128**, 215; H. E. Bryndza, J. C. Calabrese, M. Marsi, D. C. Roe, W. Tam and J. F. Bercaw, *J. Am. Chem. Soc.* 1986, **108**, 4805; (c) R. T. Boere and C. J. Willis, *Inorg. Chem.* 1985, **24**, 1059; (d) H. E. Bryndza, S. A. Kretchmor and T. H. Tulip, *J. Chem. Soc., Chem. Commun.* 1985, 977; (e) M. A. Bennett, G. B. Robertson, P. O. Whimp and T. Yoshida, *J. Am. Chem. Soc.* 1973, **95**, 3028; (f) A. B. Goel, S. Goel and D. G. Vanderveer, *Inorg. Chim. Acta* 1981, **54**, 2169; (g) H. E. Bryndza, *Organometallics* 1985, **4**, 406.
8. N. W. Alcock, A. W. G. Platt and P. Pringle, *J. Chem. Soc., Dalton Trans.* 1987, 2273.
9. N. W. Alcock, A. W. G. Platt and P. G. Pringle, *Inorg. Chim. Acta* 1987, **128**, 215.
10. N. W. Alcock, A. W. G. Platt and P. G. Pringle, *J. Chem. Soc., Dalton Trans.* 1989, 139.
11. K. J. Irgolic and R. A. Zingaro, *Organomet. React.* 1971, **2**, 117.
12. F. H. Kruse, R. F. Sanftner and J. F. Suttle, *Analyt. Chim. Acta* 1953, **25**, 500.
13. K. Nakamoto, *Infrared and Raman Spectra of Inorganic and Coordination Compounds*, 4th edn, p. 201. John Wiley, New York (1986).
14. R. K. Chadha and J. M. Miller, *J. Chem. Soc., Dalton Trans.* 1982, 117.

Polyhedron Vol. 10, No. 17, pp. 2069–2073, 1991
Printed in Great Britain

0277–5387/91 $3.00+.00
© 1991 Pergamon Press plc

DYNAMICAL NMR STUDIES ON THALLIUM(III) MESO-TETRAPHENYLPORPHYRIN ACETATE

JYH-CHING CHEN, HUEY-SHWU JANG and JYH-HORUNG CHEN*

Department of Chemistry, National Chunghsing University, Taichung, Taiwan 40227, R.O.C.

and

LIAN-PIN HWANG

Department of Chemistry, National Taiwan University and Institute of Atom and Molecular Science, Academia Sinica, Taipei, Taiwan, R.O.C.

(*Received* 18 *March* 1991; *accepted* 20 *May* 1991)

Abstract—It is shown from the proton resonances spectra of thallium(III) meso-tetraphenylporphyrin acetate that the intermolecular exchange of the acetato group has an activation energy of 4.1 kcal mol^{-1} in CD_2Cl_2. In the slow exchange region, the methyl and carbonyl carbons of the acetato group are observed at 18.8 ppm [with $^3J(Tl—^{13}C)$ coupling constant 280 Hz] and 174.9 ppm [with $^2J(Tl—^{13}C)$ coupling constant 235 Hz], respectively, at −90°C. The phenomenon of the rotation of phenyl groups in the complex from the angle 90–60° relative to the N_4 plane to approximately 0° was identified and examined by using ^{13}C and ^1H NMR spectroscopy at various temperatures.

Thallium(III) meso-tetraphenylporphyrin acetate, Tl(tpp)(OAc), (shown in Fig. 1) is a compound suitable for dynamical NMR studies. It is believed that Tl(tpp)(OAc) has a coordination number of five, rather than six, because the thallium atom is displaced out of the porphyrin plane by about 0.9 Å.[1–4]

In an NMR study of Tl(tpp)(OAc), Abraham *et al.*[5–7] have reported that the methyl protons of the apical acetate ligand were observed as a sharp singlet at $\delta = -0.03$ ppm, with no evidence of coupling of the thallium nuclei with the acetate group. Neither the carbonyl nor methyl signals of the acetate ligand in the ^{13}C NMR spectra was found. However, all other ^{13}C signals in the porphyrin were clearly observed. Hence, they surmised that this effect might be due to the broadening of the ^{13}C signal through an exchange process involving the apical ligand. In the present communication, the proton and ^{13}C NMR spectra of Tl(tpp)(OAc) in solution at low temperatures are examined to confirm the previous inference and to determine the value of the activation energy for the exchange process. Furthermore, an abnormal conformation change at low temperatures has been detected.

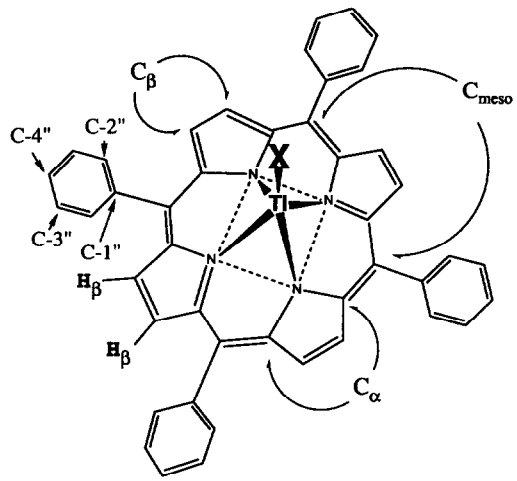

where X=OAc

Fig. 1. Structure of the Tl(tpp)(OAc) complex.

On cooling a 0.05 M solution of Tl(tpp)(OAc) in CD_2Cl_2 (Fig. 2), the methyl proton signal, which

* Author to whom correspondence should be addressed.

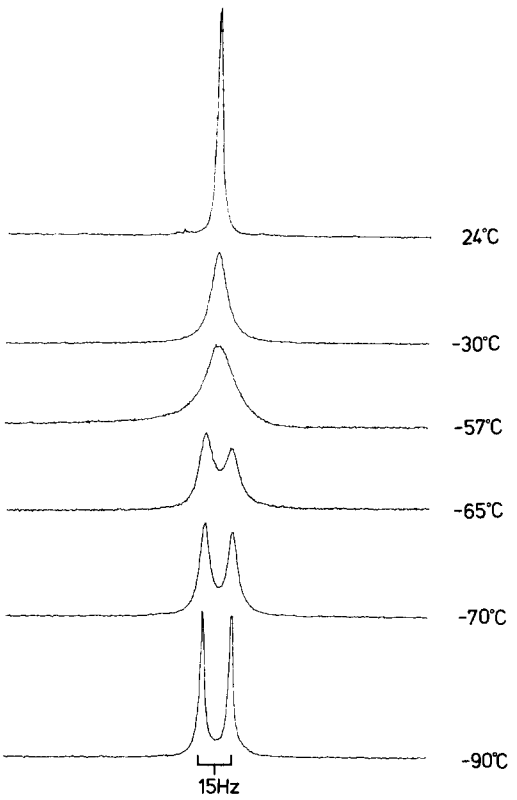

Fig. 2. 300 MHz ^{1}H NMR spectra of the axial acetato protons in Tl(tpp)(OAc) in CD_2Cl_2 at various temperatures.

displays a single peak at room temperature (δ = 0.06 ppm), broadens (temperature of coalescence, T_c −57°C) and finally splits into two peaks with a separation of 14.7 Hz. The process is completely reversible, and the results measured at 300 MHz confirm the separation as a coupling ^4J(Tl—H) rather than a chemical-shift difference. The rate process is treated as a simple two-site exchange rate process and the use of the usual coalescence analysis yields the exchange rate of 32.65 s^{-1} at −57°C, which corresponds to an activation energy (E_a) of 4.1 kcal mol^{-1}.

^{13}C NMR data for Tl(tpp)(OAc) at different temperatures is shown in Table 1. At −90°C (or −75°C), because the intermolecular exchange is extremely slow, methyl and carbonyl carbons of the acetato group are observed at 18.8 ppm [with ^3J(Tl—^{13}C) coupling constant 280 Hz] and 174.9 ppm [with ^2J(Tl—^{13}C) coupling constant 235 Hz], respectively. At 24°C, the rate of intermolecular exchange of the acetato ligand is 352 Hz. The exchange rate is comparable with the coupling frequency of Tl—^{13}C, i.e. 258±23 Hz. In this intermediate exchange region, the signals are broadened beyond detection. Hence, no signal of the axial ^{13}C has been found at 24°C.

The abnormal conformation change due to the rotation of the phenyl group in the complex is also observed from the ^{13}C and ^{1}H NMR spectra at different temperatures. The temperature variation of the c-2″ carbon spectrum of Tl(tpp)(OAc) is shown in Fig. 3 as from a doublet of doublets at 24°C to a triplet at −90°C. This indicates that the dihedral angles between the mean plane of the porphyrin skeleton and the planes of the four phenyl groups vary from a range of 90–60° [3,8] to about 0°. Consequently, the two ortho carbons in the same phenyl group become more equivalent and the inner peaks of doublet of doublets merge together with decreasing temperature. Also, the steric hindrance between the phenyl groups and β-pyrrole increases. It causes the β-pyrrole proton to shift downfield by about 39 Hz from 9.07 ppm at 24°C to 9.20 ppm at −90°C. All other phenyl protons are shifted downfield about 16±5 Hz (shown in Table 2). Furthermore, the chemical shift of C_α (and *c*-1″) shifts upfield about 53 Hz from 150.5 (or 142.4) ppm to 149.8 (or 141.7) ppm (shown in Table 1). Those effects are also evidenced from 2D NOESY at −90°C and 24°C as shown in Figs 4(a) and (b), respectively. Figure 4(a) indicates that there is a strong through space steric interaction between the protons of β-pyrrole and the phenyl protons, while in Fig. 4(b), there is only a weak through space interaction between the protons of β-pyrrole and *ortho* phenyl protons but no signal indicates the interaction between the protons of β-pyrrole and other phenyl protons. All these observations show that, as the temperature decreases, the phenyl groups rotate from the planes at the angle of 90–60°

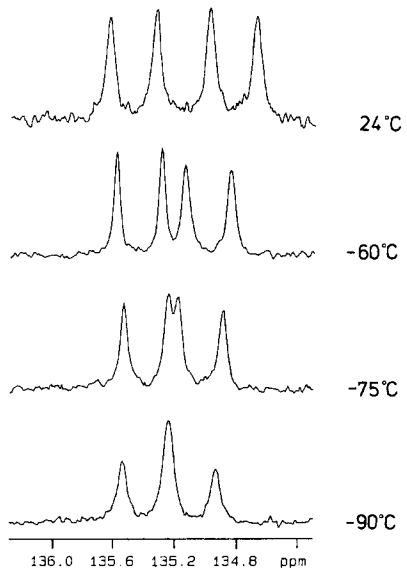

Fig. 3. Temperature dependence of chemical shifts for the C-2″ carbons of Tl(tpp)(OAc) in CD_2Cl_2.

Table 1. ^{13}C chemical shifts (δ) and thallium–carbon coupling constant (J) in Hertz of Tl(tpp)(OAc) in CD_2Cl_2[a]

Temperature (°C)	C_α	C_β	C_{meso}	C-1″	C-2″	C-3″	C-4″	COC*H$_3$	C*OCH$_3$
Room temperature[b]	149.3 (17)	131.8 (120)	121.6 (147)	141.1 (27)	133.8 (22) 134.6 (18)	126.1	127.3	—	—
24	150.5 (18)	132.9 (118)	122.7 (148)	142.4 (27)	134.8 (25) 135.5 (23)	127.2	128.4	—	—
−60	150.1 (18)	133.1 (118)	122.7 (148)	142.0 (28)	135.0 (22) 135.4 (22)	127.4	128.4	—	—
−75	149.9 (17)	133.1 (118)	122.5 (148)	141.8 (28)	135.0 (22) 135.4 (22)	127.3	128.3	18.8 (279)	174.8 (234)
−90	149.8 (17)	133.1 (118)	122.5 (148)	141.7 (28)	135.1 (23) 135.4 (23)	127.3	128.3	18.8 (280)	174.9 (235)

[a] Chemical shifts in ppm relative to TMS. Values in parentheses beneath are J(Tl—^{13}C) coupling constants in Hertz.
[b] From ref. 6.

relative to the N_4 plane to the planes approximately parallel to it.

EXPERIMENTAL

Dynamic NMR spectroscopy

Proton and ^{13}C NMR spectra were recorded on a Varian VXR-300 spectrometer in dichloromethane-d_2, locked on solvent deuterium, and referenced to the residual solvent peak. The temperature of the spectrometer probe was calibrated by the shift difference of methanol resonance in the ^1H NMR spectrum.

Preparation of Tl(tpp)(OAc)

Tl(tpp)(OAc) was prepared as described elsewhere.[5,9] It was dissolved in CD_2Cl_2 to give a concentration of 0.05 M for the NMR measurement.

Table 2. Proton chemical shifts (δ) and thallium–proton coupling constant J in Hertz for the Tl(tpp)(OAc) complex in CD_2Cl_2 in the absence of the axial ligand[a]

Temperature (°C)	H_β(β-pyrrole)	o-phenyl	m,p-phenyl
Room temperature[b]	9.02 (64 Hz)	8.31, 8.08	7.73
24	9.07 (63 Hz)	8.35, 8.18	7.82
−90	9.20 (64 Hz)	8.38, 8.25	7.88

[a] Chemical shifts in ppm relative to TMS. Values in parentheses beneath are J(Tl—H) coupling constants in Hertz.
[b] From ref. 5.

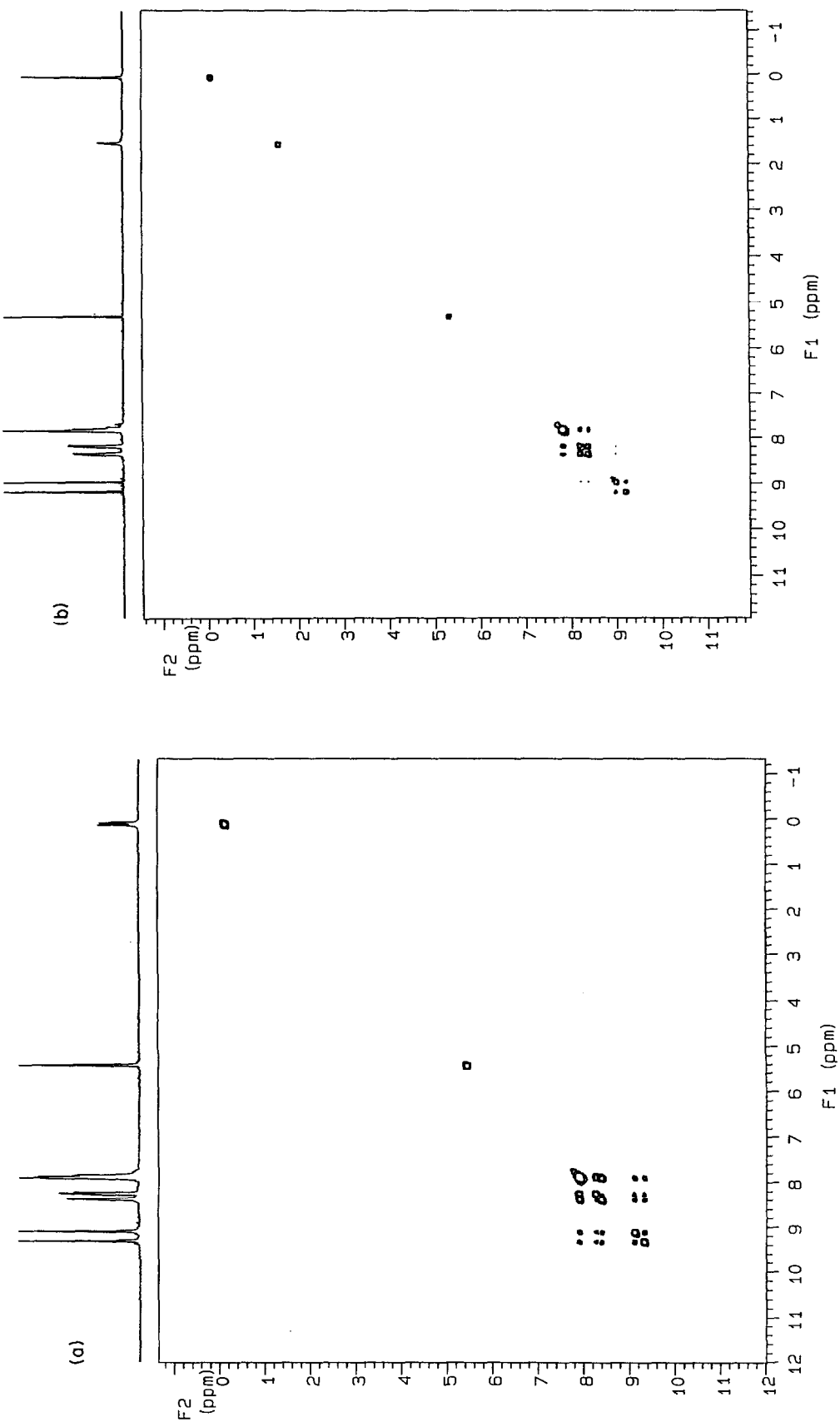

Fig. 4. 2H NOESY spectra for Tl(tpp)(OAc) in CD_2Cl_2 at temperatures of (a) −90°C and (b) 24°C.

Acknowledgments—Financial support of the National Research Councils of the R.O.C. under Grant NSC 80-0208-M005-13 is gratefully acknowledged. The authors wish to thank Dr T. Y. Chau for the help in preparing the Tl(tpp)(OAc). Special thanks to Dr Fung E. Hong for illuminating discussions.

REFERENCES

1. R. N. Butler, *Chem. Rev.* 1984, **84**, 249.
2. K. Henrick, R. W. Matthews and P. A. Tasker, *Inorg. Chem.* 1977, **16**, 3293.
3. F. Brady, K. Henrick and R. W. Matthews, *J. Organomet. Chem.* 1981, **210**, 281.
4. J. F. Hinton, K. R. Metz and R. W. Briggs, *Prog. NMR Spectrosc.* 1988, **20**, 423.
5. R. J. Abraham, G. H. Barnett and K. M. Smith, *J. Chem. Soc., Perkin Trans. I*, 1973, 2142.
6. R. J. Abraham, G. E. Hawkes, M. F. Hudson and K. M. Smith, *J. Chem. Soc., Perkin Trans. II*, 1975, 204.
7. R. J. Abraham, G. E. Hawkes and K. M. Smith, *Tetrahedron Lett.* 1975, 1999.
8. J. L. Hoard, *Porphyrins and Metalloporphyrins* (Edited by K. M. Smith), Elsevier, Amsterdam (1976).
9. P. Rothemund and A. R. Menotti, *J. Am. Chem. Soc.* 1948, **70**, 1808.

Polyhedron Vol. 10, No. 17, pp. 2075–2078, 1991
Printed in Great Britain

0277–5387/91 $3.00+.00
© 1991 Pergamon Press plc

SYNTHESIS AND CHARACTERIZATION OF *TRANS*-$[Co(NH_3)_4(NH_2CH_3)L]^{3+}$ [L = $(CH_3)_2SO$ OR $(CH_3)_2NCHO$] COMPLEXES

BEATRIZ SIENRA* and ADRIANA MASSAFERRO

Cátedra de Química Inorgánica, Facultad de Química, Av. General Flores 2124, C.C. 1157, Montevideo, Uruguay

(*Received* 19 *February* 1991; *accepted* 5 *April* 1991)

Abstract—*Trans*-$[Co(NH_3)_4(NH_2CH_3)(CH_3)_2SO]^{3+}$ and *trans*-$[Co(NH_3)_4(NH_2CH_3)(CH_3)NCHO]^{3+}$ ions are prepared by Ag^+-induced solvolysis of *trans*-$[Co(NH_3)_4(NH_2CH_3)X]^{2+}$ (X = Cl or Br) complexes in dimethylsulphoxide or dimethylformamide. The complexes were characterized by electronic, IR and ^1H magnetic resonance spectroscopy. Both, dimethylsulphoxide and dimethylformamide are bonded through the oxygen atom. The *trans*-complexes obtained are not contaminated with the *cis*-isomers.

Complexes of the type *trans*-$[Co(NH_3)_4(NH_2CH_3)L]$ have been prepared previously with uninegative (L = Cl, Br, ONO_2, NO_2, ONO),[1–3] binegative (L = OCO_2)[4] and neutral (L = OH_2)[4] substituents. In all cases, the methylamine ligand has been introduced in the coordination sphere making use of the strong *trans*-labilizing influence of the sulphito group.[5] It appeared to be useful to prepare some complexes with neutral ligands (other than water) and this paper describes the synthesis of such complexes with dimethylsulphoxide (dmso) and dimethylformamide (dmf). An obvious route, by analogy with the synthesis of the corresponding pentaamines,[6,7] was to heat *trans*-$[Co(NH_3)_4(NH_2CH_3)OH_2](ClO_4)_3$ in dmso or dmf. Nevertheless, following this procedure Balt *et al.*[8] obtained a mixture of *cis*- and *trans*-$[Co(NH_3)_4(^{15}NH_3)dmso]^{3+}$ from the *trans*-$[Co(NH_3)_4(^{15}NH_3)OH_2]^{3+}$ complex. Another possibility was to try substitution of the labile *trans*-$[Co(NH_3)_4(NH_2CH_3)OSO_2CF_3]^{2+}$ ion. However, the *trans*-$[Co(NH_3)_4(^{15}NH_3)OSO_2CF_3]^{2+}$ complex has not been obtained pure (9% *cis* impurity,[9] 13% *cis* impurity).[10] Therefore, we tried the Ag^+-induced solvolysis of *trans*-$[Co(NH_3)_4(NH_2CH_3)Cl]^{2+}$ or *trans*-$[Co(NH_3)_4(NH_2CH_3)Br]^{2+}$ complexes, reactions which were expected to take place with retention of the *trans* configuration.

EXPERIMENTAL

Preparation of trans-$[Co(NH_3)_4(NH_2CH_3)dmso](ClO_4)_3$ *and* trans-$[Co(NH_3)_4(NH_2CH_3)dmso]Br_3$

Solutions of *trans*-$[Co(NH_3)_4(NH_2CH_3)Cl](ClO_4)_2$ (5 g) in dmso (4 cm^3) and $AgClO_4 \cdot H_2O$ (2.87 g) in dmso (4 cm^3) were mixed and kept at room temperature for *ca* 24 h. The silver chloride precipitate was removed and the filtrate washed with ethanol (25 cm^3). Ether (600 cm^3) was slowly added with vigorous stirring. Upon standing, an oily, red dmso phase settled. The ether phase was decanted off and the oily residue dissolved in 95% ethanol (40 cm^3). The complex was precipitated by the addition of ether (200 cm^3), filtered, washed with ethanol and ether and air dried. The product was recrystallized from water by adding concentrated $HClO_4$ (**CAUTION**) and cooling. The red–violet crystals were collected, washed as before and vacuum dried. Yield 20%.

A saturated solution of the perchlorate salt in water was treated with a concentrated aqueous solution of LiBr and cooled in an ice bath. The product was recrystallized in the same manner.

The complex may be also obtained from *trans*-$[Co(NH_3)_4(NH_2CH_3)Br](ClO_4)_2$, by following the same procedure. The rate of solvolysis of this complex is greater than that of the *trans*-chloro ion.

* Author to whom correspondence should be addressed.

Table 1. The electronic absorption spectra of $[Co(NH_3)_4(NH_2R)X]$ complexes[a]

X	R	λ_{max} (nm)	ε_{max} ($M^{-1}cm^{-1}$)	λ_{max} (nm)	ε_{max} ($M^{-1}cm^{-1}$)	Reference
dmso	H	515	61.3	351	63.7	15
	CH_3	522	64.6	353	67.5	[b]
dmf	H	506	79.4	348	69.2	17
	CH_3	510	78.0	349	71.0	[b]

[a] For R = CH_3, the complexes have the *trans* configuration.
[b] This work.

Preparation of trans-$[Co(NH_3)_4(NH_2CH_3)dmf](ClO_4)_3$

Solutions of *trans*-$[Co(NH_3)_4(NH_2CH_3)Cl](ClO_4)_2$ (5 g) in dmf (20 cm^3) and $AgClO_4 \cdot H_2O$ (2.87 g) in dmf (4 cm^3) were mixed and kept at room temperature for *ca* 24 h. The silver chloride precipitate was discarded and the filtrate treated with ethanol to precipitate a red–violet solid. After cooling in an ice bath, the crystals were collected, washed with ethanol and ether and air dried. The complex was recrystallized from water by adding concentrated $HClO_4$ and cooling on ice. Yield 30%. Alternatively the compound may be prepared from the *trans*-bromo complex.

Chemicals

The precursor complexes *trans*-$[Co(NH_3)_4(NH_2CH_3)Cl](ClO_4)_2$ and *trans*-$[Co(NH_3)_4(NH_2CH_3)Br](ClO_4)_2$ were prepared by reported methods.[1,2] Other reagents used were AR grade.

Apparatus

UV–vis spectra were recorded on a Shimadzu 210 UV spectrophotometer; IR spectra on a Perkin–Elmer IR 283 instrument; and ^1H NMR spectra were obtained using a Varian T 60 spectrometer.

RESULTS AND DISCUSSION

In this section the *trans*-$[Co(NH_3)_4(NH_2CH_3)L]$ ions are abbreviated as $CoBr^{2+}$, $Co(dmso)^{3+}$, etc.

Both $CoCl^{2+}$ or $CoBr^{2+}$ perchlorates, treated at room temperature with an equivalent amount of $AgClO_4$ in dmso or dmf, produce the corresponding $Co(solvent)^{3+}$ complexes. Therefore, the Ag^+-induced solvolysis reactions take place with stereochemical retention, as expected.

The complexes so obtained and recrystallized, were characterized by elemental analysis* and by their electronic, IR and ^1H magnetic resonance spectra. The latter, especially, gives conclusive evidence of the geometry and purity of the complexes.

The visible absorption maxima of the $Co(dmso)^{3+}$ and $Co(dmf)^{3+}$ ions show a minor shift to longer wavelengths compared with the parent pentaamines (Table 1), in addition to an increase of the molar absorptivity coefficients. These features have been observed in other methylamine complexes[1,2] and were interpreted in terms of a decrease of the crystal-field parameter.[11] Furthermore, the visible spectra of the complexes are indicative of a CoN_5O chromophore, which indicates that dmso and dmf coordinate through the oxygen atom.[7]

The IR spectra of the bromide salt (in KBr and Nujol mull) of both complexes are in good agreement with those reported for the corresponding pentaamines (Table 2). In the $Co(dmso)^{3+}$ complex, the S—O band is identified at 940 cm^{-1}, while in free dmso it appears at 1055 cm^{-1}. Such shifting has been considered as indicating coordination through the oxygen atom.[12] The carbonyl stretching frequency, which appears at 1681 cm^{-1} in free dmf, is shifted to 1650 cm^{-1} in the $Co(dmf)^{3+}$ complex, which indicates that dmf coordinates through the oxygen atom.[13]

The ^1H NMR spectra of both complexes are in agreement with those reported for the corresponding pentaamines (Table 3).[11,14–17] The position of the (NH_3+NH_2) and the *trans*-CH_3 (methylamine) proton resonances are consistent with a CoN_5O coordination entity. In O-bonded *trans*-methylaminetetraamminecobalt(III) complexes, the (NH_3+NH_2) resonance occurs at δ 3.83–3.92 ppm and that of *trans*-CH_3 at δ 1.45–1.63

*Found: Co, 11.1; Cl, 19.8; N, 13.2. $C_3Cl_3CoH_{23}N_5O_{13}S$ requires: Co, 11.0; Cl, 19.9; N, 13.1%. Found: Co, 11.3; Cl, 19.9; N, 16.0. $C_4Cl_3CoH_{24}N_6O_{13}$ requires: Co, 11.1; Cl, 20.1; N, 15.9%.

Table 2. Some IR spectral data for $[Co(NH_3)_4(NH_2R)X]$ complexes[a]

X	R	NH_3 δ_d	NH_3 δ_s	NH_3 ρ_r	dmso ν(S—O)	dmf ν(C=O)	Reference
dmso	H	1625, 1585	1330	830	940	—	21
	CH_3	1625, 1580	1340	840	940	—	[b]
dmf	H	1600	1315	830	—	1655	11
	CH_3	1625, 1600	1300	840	—	1650	[b]

[a] Data in cm^{-1}. For R = CH_3, the complexes have the *trans* configuration. Abbreviations: ν, stretching; δ_d, degenerate deformation; δ_s, symmetric deformation; ρ_r, rocking.
[b] This work.

Table 3. ^1H NMR chemical shifts observed for $[Co(NH_3)_4(NH_2R)X]$ complexes[a]

		Chemical shifts (ppm)					
X	R	CH_3 (trans)	NH_3	CH_3 (dmso)	CH_3 (dmf)	HCO	Reference
dmso	H	—	3.87	2.72	—	—	15
	CH_3	1.45	3.83	2.72	—	—	[b]
dmf	H	—	3.86	—	2.90, 3.08	7.40	11
	CH_3	1.57	3.92	—	2.90, 3.10	7.47	[b]

[a] Downfield from internal tms. The perchlorate salts were in d_6-dmso solution. For R = CH_3, the complexes have the *trans* configuration.
[b] This work.

ppm.[2–4] Furthermore, the appearance of a doublet for N—CH_3 in the ^1H NMR spectrum of free dmf, has been interpreted as due to restricted rotation about the OC—N< bond, as a result of partial double bonding involving the nitrogen lone pair of electrons.[18,19] The retention of this doublet in the spectrum of the $Co(dmf)^{3+}$ ion implies that such double bonding is retained, prohibiting coordination of the nitrogen atom to the metal.

The ^1H NMR spectra of both complexes also enable the assignment of their absolute configurations. It has been shown[1,2] that the position of the methyl triplet of the methylaminetetraamminecobalt(III) complexes may be employed for this purpose: the *cis* complexes present the methyl resonance at lower field (δ 2 ppm for CoN_5O complexes) than the corresponding *trans* isomers. This allows us to establish the isomeric purity of the compounds obtained, since the spectra show a single methyl triplet, in a position corresponding to a methyl group *trans* to an O-bonded ligand.

Finally, the ^1H NMR spectra confirm the absence of an aqua complex (a possible impurity) because the characteristic sharp Co—OH_2 resonance at δ 5.6 ppm is not present. This method for the detection of the aqua complex impurity is quite sensitive if a high cobalt concentration is used (the perchlorate salts provide the desired solubility).[20]

Acknowledgement—The authors are indebted to Professor E. Umpiérrez for recording the IR spectra and for stimulating discussions.

REFERENCES

1. S. Balt, H. J. Gamelkoorn, C. R. Píriz Mac-Coll and W. E. Renkema, *Transition Met. Chem.* 1984, **9**, 224.
2. B. Sienra, A. Massaferro and C. R. Píriz Mac-Coll, *Z. Anorg. Allg. Chem.*, in press.
3. A. Massaferro, M. Queirolo and B. Sienra, unpublished work.
4. S. Balt, M. W. G. De Bolster and C. R. Píriz Mac-Coll, *Z. Anorg. Allg. Chem.* 1985, **529**, 235.
5. D. A. Buckingham, I. I. Olsen and A. M. Sargeson, *J. Am. Chem. Soc.* 1967, **89**, 5129.
6. C. R. Píriz Mac-Coll and L. Beyer, *Inorg. Chem.* 1973, **12**, 7.
7. E. S. Gould, *J. Am. Chem. Soc.* 1965, **87**, 4730.

8. S. Balt, H. J. Gamelkoorn and W. E. Renkema, *J. Chem. Soc., Dalton Trans.* 1983, 2415.
9. S. Balt and H. J. Gamelkoorn, *J. Chem. Soc., Dalton Trans.* 1985, 659.
10. N. E. Brasch, D. A. Buckingham, C. R. Clark and K. S. Finnie, *Inorg. Chem.* 1989, **28**, 4567.
11. R. J. Balahura and R. B. Jordan, *J. Am. Chem. Soc.* 1970, **92**, 1533.
12. K. Nakamoto, *Infrared and Raman Spectra of Inorganic and Coordination Compounds*, 3rd edn. John Wiley, New York (1978).
13. E. W. Randall, C. M. Yoder Silcox and J. J. Zuckerman, *Inorg. Chem.* 1966, **5**, 2240.
14. D. A. Buckingham, W. Marty and A. M. Sargeson, *Inorg. Chem.* 1974, **13**, 2165.
15. N. E. Dixon, W. G. Jackson, W. Marty and A. M. Sargeson, *Inorg. Chem.* 1982, **21**, 688.
16. N. E. Dixon, W. G. Jackson, M. J. Lancaster, G. A. Lawrence and A. M. Sargeson, *Inorg. Chem.* 1981, **20**, 470.
17. D. A. Buckingham, J. Macb. Harrowfield and A. M. Sargeson, *J. Am. Chem. Soc.* 1974, **96**, 1726.
18. W. D. Phillips, *J. Chem. Phys.* 1955, **23**, 1363.
19. H. Guttowsky and C. H. Holm, *J. Chem. Phys.* 1956, **25**, 1228.
20. D. A. Buckingham, P. J. Cresswell, A. M. Sargeson and W. G. Jackson, *Inorg. Chem.* 1981, **20**, 1647.
21. T. V. O'Halloran and J. M. Malin, *Inorg. Nucl. Chem.* 1979, **41**, 117.

Polyhedron Vol. 10, No. 17, pp. 2079–2081, 1991
Printed in Great Britain

0277-5387/91 $3.00+.00
© 1991 Pergamon Press plc

COMMUNICATION

DISTORTION POTENTIAL FOR MOLECULAR MECHANICS CALCULATION OF PLASTICITY OF COPPER(II) COORDINATION: AN APPROXIMATION

J. SABOLOVIĆ and N. RAOS*

Institute for Medical Research and Occupational Health, University of Zagreb, Ksaverska cesta 2, 41001 Zagreb, Croatia, Yugoslavia

and

Kj. RASMUSSEN

Chemistry Department A, Building 207, The Technical University of Denmark, DK-2800 Lyngby, Denmark

(*Received* 20 *May* 1991; *accepted* 25 *June* 1991)

Abstract—A new, simpler definition is proposed for the distortion coordinate β, defining the empirical potential which was introduced earlier (J. Sabolović and N. Raos, *Polyhedron* 1990, **9**, 1277) in order to reproduce the shapes of distorted coordination polyhedra of tetracoordinated copper(II) complexes. A simpler definition of β, proposed in this communication, facilitates its implementation in the programme for conformational analysis. No significant difference in the structure parameters obtained with the old and the new expression for β was observed. The new function also has a slight advantage in reducing the computational time and accelerating the convergence.

In an attempt to reproduce accurately the shape of (distorted) coordination polyhedra of tetracoordinated copper(II) complexes, we proposed three kinds of models suitable for molecular mechanics calculations: (1) a "dummy" atom model;[1,2] (2) models with distortion potential;[3,4] and (3) a model based on coulombic interactions.[5] Models (2) and (3) reproduced fairly well the planar/tetrahedral distortion as observed in crystal structures of copper(II) bis-chelates with naturally occurring amino acids and their N-alkylated derivatives.[4–6]

In our first paper dealing with the distortion potential,[3] the new potential was defined as:

$$V(\beta) = \tfrac{1}{2}k_\beta(\beta-\beta_0)^2; \qquad (1)$$

where k_β and β_0 (= 180°) are empirical parameters and β is a distortion coordinate defined as an angle between bisectors of two opposite valence angles (Fig. 1).

For the implementation of a new internal coordinate in the existing programme[7,8] it was necessary to define two "dummy" atoms (denoted as Y and Y′, Fig. 1) with the coordinates:

$$x_{iY} = \tfrac{1}{2}(x_{iO}+ax_{iN}) \quad i = 1,2,3; \qquad (2)$$

where x_{iO} and x_{iN} stood for Cartesian coordinates of two (oxygen and nitrogen) atoms in a chelate ring. Variable a was the ratio of Cu—O and Cu—N bond lengths:

$$a = \frac{b_{MO}}{b_{MN}}. \qquad (3)$$

Such an expression for the distortion angle β is rather complicated, especially when calculation of the first and second derivatives of V_β with respect to Cartesian coordinates (necessary for energy minimization) and derivatives of observables with

* Author to whom correspondence should be addressed.

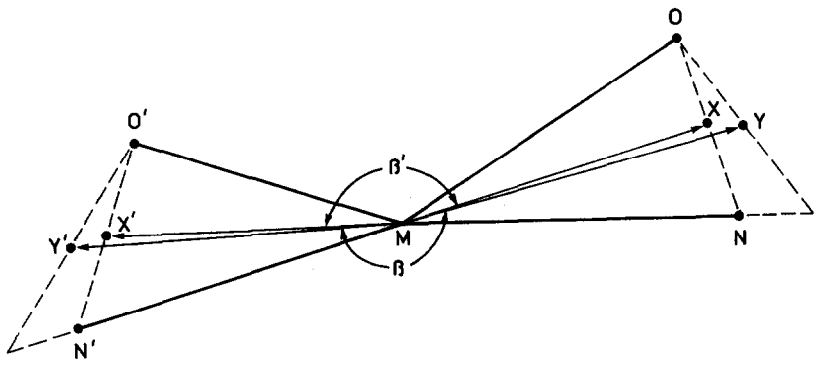

Fig. 1. Definition of distortion angles in tetracoordinated chelates with amino acids. Angle β is defined as an angle Y—M—Y′ and its approximation, distortion angle β' as an angle X—M—X′. M denotes the central atom and X, X′, Y and Y′ are "dummy" atoms needed for construction. The atoms marked with ′ belong to the same chelate ring.

respect to energy function parameters (for optimization of empirical parameters) are needed. Therefore, we investigated a simpler definition of the distortion coordinate (β', Fig. 1) by putting $a = 1$ in eq. (2). The approximation seems to be sound because for copper(II)-aminoacidates, Cu—O and Cu—N bond lengths are virtually constant and $b_{MO} \approx b_{MN}$.

The new function was checked on 12 conformations of bis(N,N-dimethylvalinato)copper (II). The implementation of the new function in the computer programme for conformational analysis produced a reduction, although not an essential one, in computation time (about 1–2% for typical runs with 80 steepest descent and up to 25 Newton–Raphson iterations) and a slightly faster convergence (average 11.1 vs 12.1 Newton–Raphson iterations).

The next test of the validity of the approximate calculation of the distortion angle was to prove if both expressions for the distortion potential yielded comparable results for the most critical internal coordinates (Table 1). The values for the bond lengths around copper for both expressions were virtually identical (mean difference 3.25×10^{-5} Å, $\sigma = 2.49 \cdot 10^{-4}$ Å; for all Cu—O and Cu—N bonds), differing by less than typical experimental error in X-ray analysis. Comparison of the angles yielded slightly higher values (Table 1) which were still in the range of typical experimental error. Also, it has to be noted that no systematic error in any internal coordinate was observed: all mean differences fitted very well in the range of the standard deviations.

From the discussion presented above we can therefore conclude that the new expression for the distortion angle produces essentially the same results and, in addition to being better fitted for implementation in a programme for conformational analysis, it has a slight advantage in reducing the computation time and accelerating the convergence.

Table 1. Comparison of the most critical internal coordinates as calculated with the two functions (the new and the old one) for distortion potential[a]

Internal coordinate	Mean difference (new–old)	Standard deviation	Range
Cu—O	0.0001	0.0003	−0.0005–0.0007
Cu—O′	−0.0001	0.0003	−0.0006–0.0007
Cu—N	0.0001	0.0002	−0.0005–0.0002
Cu—N′	0.0000	0.0002	−0.0005–0.0003
O—Cu—O	−0.124	0.236	−0.623–0.855
N—Cu—N	0.175	0.165	−0.004–0.413
O—Cu—N	0.003	0.008	−0.006–0.022
O′—Cu—N′	0.001	0.008	−0.006–0.020
O′—Cu—N	−0.010	0.031	−0.052–0.043
O—Cu—N′	0.008	0.034	−0.053–0.059

[a] Bond lengths are expressed in Å and angles in degrees. The conformers involved are: 6-6LL, 5-5LL, 2-2LL, 3-3LL, 4-4LL, 1-1LL, 4-6LL, 1-6LL, 3-6LL, 1-4LL, 3-3LL and 4-6DL, according to our notation[9] (L and D denote the ligand configuration). The calculations were performed by using our Model 5.[4]

REFERENCES

1. N. Raos, S. R. Niketić and Vl. Simeon, *J. Inorg. Biochem.* 1982, **16**, 1.
2. N. Raos and Vl. Simeon, *Croat. Chem. Acta* 1985, **58**, 127.
3. J. Sabolović, N. Raos and Kj. Rasmussen, *Croat. Chem. Acta* 1989, **62**, 495.
4. J. Sabolović and N. Raos, *Polyhedron* 1990, **9**, 1277.

5. J. Sabolović and N. Raos, *Polyhedron* 1990, **9**, 2419.
6. N. Kaitner, N. Paulić and N. Raos, *J. Coord. Chem.* 1991, **22**, 269.
7. S. R. Niketić and Kj. Rasmussen, *The Consistent Force Field: A Documentation, Lecture Notes in Chemistry*, Vol. 3. Springer, Berlin (1977).
8. Kj. Rasmussen, *Potential Energy Functions in Conformational Analysis, Lecture Notes in Chemistry*, Vol. 37. Springer, Berlin (1985).
9. N. Raos and Vl. Simeon, *Croat. Chem. Acta* 1983, **56**, 79.

Polyhedron Vol. 10, No. 17, pp. 2083–2087, 1991
Pergamon Press plc. Printed in Great Britain

BOOK REVIEWS

Introduction to Cluster Chemistry. By D. Michael, P. Mingos and David J. Wales. Prentice-Hall, 1990, ISBN 0-413-499049-9 (hardback), xv + 318 pp.

Cluster chemistry has been one of the most spectacular growth areas in the whole inorganic field, aided by advances in synthetic techniques and in particular the mushroom growth in X-ray diffraction studies. Gradually, but less spectacularly, this has been undergirded by a framework describing the bonding in these compounds.

This book provides a timely overview of the whole area of clusters—both metals and non-metals. It is modestly claimed to be an introduction to the area, but in reality is far more than that. Overview, yes, but in no way superficial, as a review of the contents indicate.

The first chapter is a review-length survey of cluster chemistry (71 pp.). It looks at the relationship between metal–metal distance and bond order, and the part played by bridging ligands; bond-enthalpy data; kinetic and steric factors—before launching into a survey of cluster types across the Periodic Table—from Chevrel phases to gold–phosphine clusters, polyhedral boranes to iron–sulphur clusters (does anyone known *why* some ferredoxins have two irons in the cluster, some three and some four?). One valuable feature of the book is the use of information boxes strategically placed in the text; many appear in this chapter summarizing synthetic routes without interrupting the flow of the structural systematization. The book is intended to function as a teaching tool and is amply supplied with questions at the end of this and the other chapters, many of these relating to clusters in the recent literature.

Chapter 2 and succeeding chapters are concerned with the electronic structure of clusters, beginning with an outline of the polyhedral skeletal electron pair theory (PSEPT), but without assuming that the reader already knows the principles of electron-counting. Similarities between non-metal and metal clusters are stressed. Ideas like the isolobal principle and Lipscombe's styx method are touched on in Chapter 2, whilst Chapter 3 traces the Tensor Surface Harmonic Theory (TSH) and its application to clusters, beginning with analogies to the Huckel treatment of polyenes then translating this to spherical functions. The theory is successively applied to σ, π and δ orbitals, first as an outline in Chapter 3 then more fully in succeeding chapters. Thus, Chapter 4 considers clusters like the gold–phosphine systems where radial bonding predominates and σ bonding interactions can be considered in isolation; both types, those with and without interstitial atoms are discussed. MO schemes are set out for various cluster geometries and structures related to the number of valence electrons available. Chapter 5 treats the clusters where the p orbitals are sufficiently low-lying in energy to be involved so that σ and π interactions have to be considered, beginning with boranes and carboranes, but later linking with transition-metal clusters like polynuclear carbonyls. The following chapter looks at skeletal rearrangements. Here, as elsewhere, the book seeks to develop useful analogies, introducing the reader to the principles via the familiar application of the Woodward–Hofmann rules. Chapter 7 turns to bonding in condensed and high-nuclearity clusters, treated mainly by electron-counting (the reader will probably find it useful, here, as elsewhere, to refer to the review by Mingos and May in the recent book, *The Chemistry of Metal Cluster Complexes*). Various clusters are analysed depending on how they are joined together whilst the capping principle is considered and illustrated in terms of Group Theory. Finally, Chapter 8 looks at those clusters where δ orbitals need to be specifically considered, basically those of the early d-block metals where they may be incompletely occupied, and where the less contracted d-orbitals overlap more fully. The book is completed with an index, and there are handy little summaries of the number of electrons associated with common metals and ligands, and of the PSEPT rules on the endpapers.

About the only important cluster not represented is buckminsterfullerene, (growth industry of 1990–1991), though the authors cannot be blamed for not anticipating it! I think that this book will be widely used by researchers, teachers and students. It will interest the synthesist, the structural chemist, the spectroscopist and the theoretician with its encompassing scope. If you have to have one book on clusters, this is surely it.

Bonding and Structure (Structural Principles in Inorganic and Organic Chemistry). By N. W. Alcock. Ellis Horwood, Chichester, 1990, ISBN 0-13-465253-3 (hardback), 0-13-465246-0 (paperback), 321 pp., £16.95.

This book is intended as an undergraduate text. Its style is conceptual rather than extensively mathematical and serves as a very readable introduction to the subject.

The book is made up of three sections. The first two chapters form an introduction, in which the electronegativities of the two atoms in the bond are used to predict bond type, and the techniques giving quantitative information on structure are examined, with emphasis on diffraction methods and EXAFS. Section two, Chapters 3–5, is devoted to metallic, ionic and covalent

Polyhedron Vol. 10, No. 17, pp. 2083–2087, 1991
Pergamon Press plc. Printed in Great Britain

BOOK REVIEWS

Introduction to Cluster Chemistry. By D. Michael, P. Mingos and David J. Wales. Prentice-Hall, 1990, ISBN 0-413-499049-9 (hardback), xv + 318 pp.

Cluster chemistry has been one of the most spectacular growth areas in the whole inorganic field, aided by advances in synthetic techniques and in particular the mushroom growth in X-ray diffraction studies. Gradually, but less spectacularly, this has been undergirded by a framework describing the bonding in these compounds.

This book provides a timely overview of the whole area of clusters—both metals and non-metals. It is modestly claimed to be an introduction to the area, but in reality is far more than that. Overview, yes, but in no way superficial, as a review of the contents indicate.

The first chapter is a review-length survey of cluster chemistry (71 pp.). It looks at the relationship between metal–metal distance and bond order, and the part played by bridging ligands; bond-enthalpy data; kinetic and steric factors—before launching into a survey of cluster types across the Periodic Table—from Chevrel phases to gold–phosphine clusters, polyhedral boranes to iron–sulphur clusters (does anyone known *why* some ferredoxins have two irons in the cluster, some three and some four?). One valuable feature of the book is the use of information boxes strategically placed in the text; many appear in this chapter summarizing synthetic routes without interrupting the flow of the structural systematization. The book is intended to function as a teaching tool and is amply supplied with questions at the end of this and the other chapters, many of these relating to clusters in the recent literature.

Chapter 2 and succeeding chapters are concerned with the electronic structure of clusters, beginning with an outline of the polyhedral skeletal electron pair theory (PSEPT), but without assuming that the reader already knows the principles of electron-counting. Similarities between non-metal and metal clusters are stressed. Ideas like the isolobal principle and Lipscombe's styx method are touched on in Chapter 2, whilst Chapter 3 traces the Tensor Surface Harmonic Theory (TSH) and its application to clusters, beginning with analogies to the Huckel treatment of polyenes then translating this to spherical functions. The theory is successively applied to σ, π and δ orbitals, first as an outline in Chapter 3 then more fully in succeeding chapters. Thus, Chapter 4 considers clusters like the gold–phosphine systems where radial bonding predominates and σ bonding interactions can be considered in isolation; both types, those with and without interstitial atoms are discussed. MO schemes are set out for various cluster geometries and structures related to the number of valence electrons available. Chapter 5 treats the clusters where the p orbitals are sufficiently low-lying in energy to be involved so that σ and π interactions have to be considered, beginning with boranes and carboranes, but later linking with transition-metal clusters like polynuclear carbonyls. The following chapter looks at skeletal rearrangements. Here, as elsewhere, the book seeks to develop useful analogies, introducing the reader to the principles via the familiar application of the Woodward–Hofmann rules. Chapter 7 turns to bonding in condensed and high-nuclearity clusters, treated mainly by electron-counting (the reader will probably find it useful, here, as elsewhere, to refer to the review by Mingos and May in the recent book, *The Chemistry of Metal Cluster Complexes*). Various clusters are analysed depending on how they are joined together whilst the capping principle is considered and illustrated in terms of Group Theory. Finally, Chapter 8 looks at those clusters where δ orbitals need to be specifically considered, basically those of the early d-block metals where they may be incompletely occupied, and where the less contracted d-orbitals overlap more fully. The book is completed with an index, and there are handy little summaries of the number of electrons associated with common metals and ligands, and of the PSEPT rules on the endpapers.

About the only important cluster not represented is buckminsterfullerene, (growth industry of 1990–1991), though the authors cannot be blamed for not anticipating it! I think that this book will be widely used by researchers, teachers and students. It will interest the synthesist, the structural chemist, the spectroscopist and the theoretician with its encompassing scope. If you have to have one book on clusters, this is surely it.

Bonding and Structure (Structural Principles in Inorganic and Organic Chemistry). By N. W. Alcock. Ellis Horwood, Chichester, 1990, ISBN 0-13-465253-3 (hardback), 0-13-465246-0 (paperback), 321 pp., £16.95.

This book is intended as an undergraduate text. Its style is conceptual rather than extensively mathematical and serves as a very readable introduction to the subject.

The book is made up of three sections. The first two chapters form an introduction, in which the electronegativities of the two atoms in the bond are used to predict bond type, and the techniques giving quantitative information on structure are examined, with emphasis on diffraction methods and EXAFS. Section two, Chapters 3–5, is devoted to metallic, ionic and covalent

bonding respectively in their "pure" forms. Metallic structures are analysed in packing of spheres whilst physical properties are related to electronic structure (the Schrödinger equation is given as an appendix). The principal ionic structures are delineated and ionic radii on various scales discussed; binding forces lead into lattice energies, treated qualitatively and quantitatively. Bonding in covalent compounds is discussed in terms of MO theory, starting with simple species like H_2 and H_2^+, then going on to cases like CH_4 and C_2H_2. The VSEPR method is applied to molecular shapes. After a discussion of covalent radii and the factors affecting them, Chapter 5 is concluded with a section on MO schemes for π-bonded systems like N_2, CO and O_2, relating the schemes to PE spectra.

Section three of the book is entitled "Real Bonds and Real Compounds", though it does begin with a chapter on metals(!) that develops the themes already established to trends in the structures of metals and alloys as well as interstitial compounds. Chapter 7, "The Accompaniment of Covalent Bonding", is devoted to van der Waals forces, donor–acceptor bonding (with a valuable classification of donors and acceptors), hydrogen bonding and secondary bonding. Chapter 8 views metal complexes from both the crystal field and MO viewpoints, including CFSE, the spectrochemical series and Jahn–Teller effects. The following chapter begins with an examination of the extent of *d*-orbital involvement in covalent compounds, using various molecules such as the xenon fluorides as vehicles. The boron hydrides and borane anions receive detailed examination and classification into structurally related families and Wade's rules are explained. There is a taste of metal clusters and a rather more extended treatment of delocalized and aromatic systems; a two-page outline of Huckel calculations is appended.

Chapter 10 runs to only 25 pages, but will be of great interest to many readers, as it includes within its compass a range of topical substances—warm superconductors, non-linear optical materials, superionic conductors, ferroelectrics, stabilized zirconia... Chapter 11 contains more important compounds—especially semiconductors. The concept of partial ionic bonding in NaCl and ZnS structures is explored as are layer structures ($CrCl_3$, $CdCl_2$) intercalated compounds and, continuing the theme of layer structures, molecular metals (TTF:TCNQ). The chapter concludes with silicates and modified metals.

The book is completed with tables of covalent, van der Waals, metallic and ionic radii.

This book has many points in its favour. It is very readable and contains much in it that is of use to pre-University students and their teachers as well. Each chapter has a list of useful books and articles for further reading whilst information "boxes" summarizing important concepts are strategically placed throughout the text. Illustrations are clear and liberally used. There are a number of misprints in the text (notably Fig. 7.5); on a personal level, I'd like to have seen a list of structures of all the elements, not just transition metals, and a formula index could have been useful. This text nicely complements existing books like D. W. Smith's *Inorganic Substances*, and D. A. Johnson's *Some Thermodynamic Aspects of Inorganic Chemistry* and will thus be bought by many inorganic chemists and also, I think, many others.

Organometallics in Organic Synthesis 2. Edited by H. Werner and G. Erker. Springer, Berlin, 1989, ISBN 3-540-50531-8, x+322 pp., DM 94.

Readers of the German literature will be aware of the suspicion that their publications are not known as well as in the West as they should. This volume is one of the attempts to rectify this situation! It consists of 17 papers presented at the second of a series of symposia on "Organic Synthesis via Organometallics". The majority of the papers are by Germans, but the international flavour is supplied by contributions from Swiss, Dutch, Austrian, Japanese and American laboratories.

One great advantage of this kind of publication is that it enables one to get an overview of an area of research activity that is not easily obtained by regular perusal of the literature. Different reviewers will choose to highlight different selections of articles; for me, the keynote lecture (G. Wilke) featured useful landmarks, such as Sabatier's discovery of catalytic hydrogenation (1897), as well as some striking syntheses via organo-nickel compounds. Several of the articles featured enantioselective syntheses—that by H. Werner featuring the chiral cyclamen blossom and another plant of traditional use to inorganic chemists (hops) as well as syntheses using chiral phosphine complexes. The recent syntheses and use of di-Grignard reagents in the preparation of metallacyclobutanes and their role in organic synthesis are discussed by F. Bickelhaupt. Some interesting observations on the choice of transition metal alkyls as organic reagents are made by Th. Kauffmann.

Not the least significant point in the collection is the high proportion of the research carried out in inorganic chemistry departments; clearly organic chemistry is too important to be left to organic chemists!

Gmelin Handbook of Inorganic Chemistry. Tungsten. Supplement Volume A3, Physical Properties (continued). 8th edn. Springer, Berlin, 1989, ISBN 3-540-93594-0, xiv+274 pp., DM 1260.

The previous Supplementary Volume, A2, initiated coverage of the physical properties of this element. The present volume extends the properties of bulk tungsten (electronic structure, bonding, lattice dynamics and some crystallographic properties having been dealt with earlier) commencing with deformation properties of both single crystals and polycrystalline specimens. Mechanisms for this are considered at some length, and differences between the two types of specimens noted.

bonding respectively in their "pure" forms. Metallic structures are analysed in packing of spheres whilst physical properties are related to electronic structure (the Schrödinger equation is given as an appendix). The principal ionic structures are delineated and ionic radii on various scales discussed; binding forces lead into lattice energies, treated qualitatively and quantitatively. Bonding in covalent compounds is discussed in terms of MO theory, starting with simple species like H_2 and H_2^+, then going on to cases like CH_4 and C_2H_2. The VSEPR method is applied to molecular shapes. After a discussion of covalent radii and the factors affecting them, Chapter 5 is concluded with a section on MO schemes for π-bonded systems like N_2, CO and O_2, relating the schemes to PE spectra.

Section three of the book is entitled "Real Bonds and Real Compounds", though it does begin with a chapter on metals(!) that develops the themes already established to trends in the structures of metals and alloys as well as interstitial compounds. Chapter 7, "The Accompaniment of Covalent Bonding", is devoted to van der Waals forces, donor–acceptor bonding (with a valuable classification of donors and acceptors), hydrogen bonding and secondary bonding. Chapter 8 views metal complexes from both the crystal field and MO viewpoints, including CFSE, the spectrochemical series and Jahn–Teller effects. The following chapter begins with an examination of the extent of *d*-orbital involvement in covalent compounds, using various molecules such as the xenon fluorides as vehicles. The boron hydrides and borane anions receive detailed examination and classification into structurally related families and Wade's rules are explained. There is a taste of metal clusters and a rather more extended treatment of delocalized and aromatic systems; a two-page outline of Huckel calculations is appended.

Chapter 10 runs to only 25 pages, but will be of great interest to many readers, as it includes within its compass a range of topical substances—warm superconductors, non-linear optical materials, superionic conductors, ferroelectrics, stabilized zirconia... Chapter 11 contains more important compounds—especially semiconductors. The concept of partial ionic bonding in NaCl and ZnS structures is explored as are layer structures ($CrCl_3$, $CdCl_2$) intercalated compounds and, continuing the theme of layer structures, molecular metals (TTF:TCNQ). The chapter concludes with silicates and modified metals.

The book is completed with tables of covalent, van der Waals, metallic and ionic radii.

This book has many points in its favour. It is very readable and contains much in it that is of use to pre-University students and their teachers as well. Each chapter has a list of useful books and articles for further reading whilst information "boxes" summarizing important concepts are strategically placed throughout the text. Illustrations are clear and liberally used. There are a number of misprints in the text (notably Fig. 7.5); on a personal level, I'd like to have seen a list of structures of all the elements, not just transition metals, and a formula index could have been useful. This text nicely complements existing books like D. W. Smith's *Inorganic Substances*, and D. A. Johnson's *Some Thermodynamic Aspects of Inorganic Chemistry* and will thus be bought by many inorganic chemists and also, I think, many others.

Organometallics in Organic Synthesis 2. Edited by H. Werner and G. Erker. Springer, Berlin, 1989, ISBN 3-540-50531-8, x+322 pp., DM 94.

Readers of the German literature will be aware of the suspicion that their publications are not known as well as in the West as they should. This volume is one of the attempts to rectify this situation! It consists of 17 papers presented at the second of a series of symposia on "Organic Synthesis via Organometallics". The majority of the papers are by Germans, but the international flavour is supplied by contributions from Swiss, Dutch, Austrian, Japanese and American laboratories.

One great advantage of this kind of publication is that it enables one to get an overview of an area of research activity that is not easily obtained by regular perusal of the literature. Different reviewers will choose to highlight different selections of articles; for me, the keynote lecture (G. Wilke) featured useful landmarks, such as Sabatier's discovery of catalytic hydrogenation (1897), as well as some striking syntheses via organo-nickel compounds. Several of the articles featured enantioselective syntheses—that by H. Werner featuring the chiral cyclamen blossom and another plant of traditional use to inorganic chemists (hops) as well as syntheses using chiral phosphine complexes. The recent syntheses and use of di-Grignard reagents in the preparation of metallacyclobutanes and their role in organic synthesis are discussed by F. Bickelhaupt. Some interesting observations on the choice of transition metal alkyls as organic reagents are made by Th. Kauffmann.

Not the least significant point in the collection is the high proportion of the research carried out in inorganic chemistry departments; clearly organic chemistry is too important to be left to organic chemists!

Gmelin Handbook of Inorganic Chemistry. Tungsten. Supplement Volume A3, Physical Properties (continued). 8th edn. Springer, Berlin, 1989, ISBN 3-540-93594-0, xiv+274 pp., DM 1260.

The previous Supplementary Volume, A2, initiated coverage of the physical properties of this element. The present volume extends the properties of bulk tungsten (electronic structure, bonding, lattice dynamics and some crystallographic properties having been dealt with earlier) commencing with deformation properties of both single crystals and polycrystalline specimens. Mechanisms for this are considered at some length, and differences between the two types of specimens noted.

bonding respectively in their "pure" forms. Metallic structures are analysed in packing of spheres whilst physical properties are related to electronic structure (the Schrödinger equation is given as an appendix). The principal ionic structures are delineated and ionic radii on various scales discussed; binding forces lead into lattice energies, treated qualitatively and quantitatively. Bonding in covalent compounds is discussed in terms of MO theory, starting with simple species like H_2 and H_2^+, then going on to cases like CH_4 and C_2H_2. The VSEPR method is applied to molecular shapes. After a discussion of covalent radii and the factors affecting them, Chapter 5 is concluded with a section on MO schemes for π-bonded systems like N_2, CO and O_2, relating the schemes to PE spectra.

Section three of the book is entitled "Real Bonds and Real Compounds", though it does begin with a chapter on metals(!) that develops the themes already established to trends in the structures of metals and alloys as well as interstitial compounds. Chapter 7, "The Accompaniment of Covalent Bonding", is devoted to van der Waals forces, donor–acceptor bonding (with a valuable classification of donors and acceptors), hydrogen bonding and secondary bonding. Chapter 8 views metal complexes from both the crystal field and MO viewpoints, including CFSE, the spectrochemical series and Jahn–Teller effects. The following chapter begins with an examination of the extent of *d*-orbital involvement in covalent compounds, using various molecules such as the xenon fluorides as vehicles. The boron hydrides and borane anions receive detailed examination and classification into structurally related families and Wade's rules are explained. There is a taste of metal clusters and a rather more extended treatment of delocalized and aromatic systems; a two-page outline of Huckel calculations is appended.

Chapter 10 runs to only 25 pages, but will be of great interest to many readers, as it includes within its compass a range of topical substances—warm superconductors, non-linear optical materials, superionic conductors, ferroelectrics, stabilized zirconia... Chapter 11 contains more important compounds—especially semiconductors. The concept of partial ionic bonding in NaCl and ZnS structures is explored as are layer structures ($CrCl_3$, $CdCl_2$) intercalated compounds and, continuing the theme of layer structures, molecular metals (TTF:TCNQ). The chapter concludes with silicates and modified metals.

The book is completed with tables of covalent, van der Waals, metallic and ionic radii.

This book has many points in its favour. It is very readable and contains much in it that is of use to pre-University students and their teachers as well. Each chapter has a list of useful books and articles for further reading whilst information "boxes" summarizing important concepts are strategically placed throughout the text. Illustrations are clear and liberally used. There are a number of misprints in the text (notably Fig. 7.5); on a personal level, I'd like to have seen a list of structures of all the elements, not just transition metals, and a formula index could have been useful. This text nicely complements existing books like D. W. Smith's *Inorganic Substances*, and D. A. Johnson's *Some Thermodynamic Aspects of Inorganic Chemistry* and will thus be bought by many inorganic chemists and also, I think, many others.

Organometallics in Organic Synthesis 2. Edited by H. Werner and G. Erker. Springer, Berlin, 1989, ISBN 3-540-50531-8, x+322 pp., DM 94.

Readers of the German literature will be aware of the suspicion that their publications are not known as well as in the West as they should. This volume is one of the attempts to rectify this situation! It consists of 17 papers presented at the second of a series of symposia on "Organic Synthesis via Organometallics". The majority of the papers are by Germans, but the international flavour is supplied by contributions from Swiss, Dutch, Austrian, Japanese and American laboratories.

One great advantage of this kind of publication is that it enables one to get an overview of an area of research activity that is not easily obtained by regular perusal of the literature. Different reviewers will choose to highlight different selections of articles; for me, the keynote lecture (G. Wilke) featured useful landmarks, such as Sabatier's discovery of catalytic hydrogenation (1897), as well as some striking syntheses via organo-nickel compounds. Several of the articles featured enantioselective syntheses—that by H. Werner featuring the chiral cyclamen blossom and another plant of traditional use to inorganic chemists (hops) as well as syntheses using chiral phosphine complexes. The recent syntheses and use of di-Grignard reagents in the preparation of metallacyclobutanes and their role in organic synthesis are discussed by F. Bickelhaupt. Some interesting observations on the choice of transition metal alkyls as organic reagents are made by Th. Kauffmann.

Not the least significant point in the collection is the high proportion of the research carried out in inorganic chemistry departments; clearly organic chemistry is too important to be left to organic chemists!

Gmelin Handbook of Inorganic Chemistry. Tungsten. Supplement Volume A3, Physical Properties (continued). 8th edn. Springer, Berlin, 1989, ISBN 3-540-93594-0, xiv+274 pp., DM 1260.

The previous Supplementary Volume, A2, initiated coverage of the physical properties of this element. The present volume extends the properties of bulk tungsten (electronic structure, bonding, lattice dynamics and some crystallographic properties having been dealt with earlier) commencing with deformation properties of both single crystals and polycrystalline specimens. Mechanisms for this are considered at some length, and differences between the two types of specimens noted.

Recrystallization is examined, together with the factors affecting the kinetics.

Mechanical properties are next reviewed; successively density, elasticity and anelasticity, plasticity, hardness and ductility. This section of the book involves some 70 pages of text. This is one of the areas in which Gmelin is much more than simply a handbook of inorganic chemistry and would particularly repay study by many engineers and metallurgists.

In the next 40 pages there is a comprehensive account of thermal properties. Tungsten is well known to chemists as the element with the highest melting point; it appears that a value of 3695 K represents the best accepted current value. Other properties critically treated include heat capacity, diffusion, conductance and expansion. A similar amount is given over to electrical properties, particularly conduction. Bulk tungsten is a superconductor below 0.015 K but in thin films superconducting transition temperatures up to 6.1 K have been reported.

The final two sections give an overview of magnetic and optical properties. Here as throughout the book, there is extensive coverage of the Soviet literature, not the least useful feature of the Gmelin system. This particular volume is likely to be more generally useful to scientists from a wide range of disciplines than the more narrowly chemical parts of the Handbook.

The Chemistry of Metal Cluster Complexes. Edited by D. F. Shriver, H. D. Kaesz and R. D. Adams. Verlag Chemie, New York, Weinheim and Cambridge, 1990, ISBN 1-56081-012-2, 439 pp., price not stated.

This important book is the first of a series on the chemistry of organo-metallic clusters. It consists of a balanced collection of reviews by experts in the field, covering bonding, syntheses, reactions of ligands, cluster rearrangements, and catalysis with last, but by no means least, a review of the review literature.

Not the least striking advance in cluster chemistry has been the development of theories to account for the range—undreamed of 25 years ago—of cluster geometries. D. M. P. Mingos and A. S. May survey the classes of cluster compounds; their classification of cluster geometries in order of nuclearity permits some interesting comparisons to be drawn (perhaps a brief introduction to electron counting would make this a little more friendly to the novice). The meat of the chapter lies in the exposition of the Polyhedral Skeletal Electron Pair Theory in its application to clusters. It is pointed out that the "rules" for correlating structures of polyhedra with numbers of electrons are soundly based on large numbers of structures, as well as receiving theoretical justification. The Tensor Surface Harmonic Theory approach is outlined; similarities between isostructural borane and metal cluster fragments leading to the use of isolobal relationships are pointed out. Clusters that do not follow the "rules" are analysed.

The methodology of cluster synthesis is outlined by R. D. Adams. The importance of ligand removal from coordinatively saturated metal compounds as a jumping-off point for cluster synthesis is examined. This can include abstraction of coordinated CO as well as the use of complexes containing labile ligands (e.g. THF)—"lightly stabilized" species that can participate in cluster build-up under mild conditions. Bridge-assisted, metal–metal exchange and other routes are duly considered, along with the more traditional photolytic and (more robust) thermolytic methods. D. J. Darensbourg summarizes substitution reactions in clusters, pointing out the importance of this to an understanding of catalytic processes. He examines examples of the dissociative, associative and interchange pathways, along with different ways in which metal–metal bond dissociation can affect the cluster. The role of isotopic labelling—either metal isotope or ^{13}CO—is discussed.

Cluster-assisted ligand transformations are the subject of G. Lavigne's chapter, pointing out that clusters now offer gentler reaction conditions and a greater degree of control over route. He summarizes ideal conditions—an ideal combination difficult to realise in practice—for a catalytically active cluster. A number of trinuclear clusters are chosen from the iron triad where a range of routes are used to activate the cluster—photochemically or with a suitable nucleophile, for example. Transformations of ligands with a variety of hetero-atoms (P, S, O, and N) as well as of CO and carbon-containing fragments are all considered.

Fluxionality was of course observed first in mononuclear organometallics; here B. F. G. Johnson and A. Rodgers point out that rearrangement of clusters does not just involve ligand positional change but also motion of metal atoms. The normal modes of clusters have to be considered, including librational modes. There is a useful little section for the newcomer on electron counting in clusters and another discussing the relationship between structural studies in the solid state and solution with the timescale of the process. Some case histories [$Fe_3(CO)_{12}$ and $Co_4(CO)_{12}$] are given within the context of isomerization, and a section considers fragmentational routes. Clusters have been considered to be possible models for metal surfaces in heterogeneous catalysis, so that not the least interest in cluster complexes lies in their catalytic potential, explored by W. L. Gladfelter and K. J. Roesselet. In a relatively short chapter, they examine the ability of carbonyl and hydridocarbonyl clusters to catalyse the water–gas shift reaction, olefin hydrogenation, isomerization and hydroformylation, and oxidations. The hydrogenation of CO is a reaction with great industrial appeal—the most promising systems seem to be those running at high temperature and pressure; it is pointed out that under these conditions there is scope for cluster formation, reorganization and breakdown. There would seem to be much scope for the study of activated clusters to permit low-temperature, low-pressure pathways. Much also remains to be done in establishing the

Recrystallization is examined, together with the factors affecting the kinetics.

Mechanical properties are next reviewed; successively density, elasticity and anelasticity, plasticity, hardness and ductility. This section of the book involves some 70 pages of text. This is one of the areas in which Gmelin is much more than simply a handbook of inorganic chemistry and would particularly repay study by many engineers and metallurgists.

In the next 40 pages there is a comprehensive account of thermal properties. Tungsten is well known to chemists as the element with the highest melting point; it appears that a value of 3695 K represents the best accepted current value. Other properties critically treated include heat capacity, diffusion, conductance and expansion. A similar amount is given over to electrical properties, particularly conduction. Bulk tungsten is a superconductor below 0.015 K but in thin films superconducting transition temperatures up to 6.1 K have been reported.

The final two sections give an overview of magnetic and optical properties. Here as throughout the book, there is extensive coverage of the Soviet literature, not the least useful feature of the Gmelin system. This particular volume is likely to be more generally useful to scientists from a wide range of disciplines than the more narrowly chemical parts of the Handbook.

The Chemistry of Metal Cluster Complexes. Edited by D. F. Shriver, H. D. Kaesz and R. D. Adams. Verlag Chemie, New York, Weinheim and Cambridge, 1990, ISBN 1-56081-012-2, 439 pp., price not stated.

This important book is the first of a series on the chemistry of organo-metallic clusters. It consists of a balanced collection of reviews by experts in the field, covering bonding, syntheses, reactions of ligands, cluster rearrangements, and catalysis with last, but by no means least, a review of the review literature.

Not the least striking advance in cluster chemistry has been the development of theories to account for the range—undreamed of 25 years ago—of cluster geometries. D. M. P. Mingos and A. S. May survey the classes of cluster compounds; their classification of cluster geometries in order of nuclearity permits some interesting comparisons to be drawn (perhaps a brief introduction to electron counting would make this a little more friendly to the novice). The meat of the chapter lies in the exposition of the Polyhedral Skeletal Electron Pair Theory in its application to clusters. It is pointed out that the "rules" for correlating structures of polyhedra with numbers of electrons are soundly based on large numbers of structures, as well as receiving theoretical justification. The Tensor Surface Harmonic Theory approach is outlined; similarities between isostructural borane and metal cluster fragments leading to the use of isolobal relationships are pointed out. Clusters that do not follow the "rules" are analysed.

The methodology of cluster synthesis is outlined by R. D. Adams. The importance of ligand removal from coordinatively saturated metal compounds as a jumping-off point for cluster synthesis is examined. This can include abstraction of coordinated CO as well as the use of complexes containing labile ligands (e.g. THF)—"lightly stabilized" species that can participate in cluster build-up under mild conditions. Bridge-assisted, metal–metal exchange and other routes are duly considered, along with the more traditional photolytic and (more robust) thermolytic methods. D. J. Darensbourg summarizes substitution reactions in clusters, pointing out the importance of this to an understanding of catalytic processes. He examines examples of the dissociative, associative and interchange pathways, along with different ways in which metal–metal bond dissociation can affect the cluster. The role of isotopic labelling—either metal isotope or ^{13}CO—is discussed.

Cluster-assisted ligand transformations are the subject of G. Lavigne's chapter, pointing out that clusters now offer gentler reaction conditions and a greater degree of control over route. He summarizes ideal conditions—an ideal combination difficult to realise in practice—for a catalytically active cluster. A number of trinuclear clusters are chosen from the iron triad where a range of routes are used to activate the cluster—photochemically or with a suitable nucleophile, for example. Transformations of ligands with a variety of hetero-atoms (P, S, O, and N) as well as of CO and carbon-containing fragments are all considered.

Fluxionality was of course observed first in mononuclear organometallics; here B. F. G. Johnson and A. Rodgers point out that rearrangement of clusters does not just involve ligand positional change but also motion of metal atoms. The normal modes of clusters have to be considered, including librational modes. There is a useful little section for the newcomer on electron counting in clusters and another discussing the relationship between structural studies in the solid state and solution with the timescale of the process. Some case histories [$Fe_3(CO)_{12}$ and $Co_4(CO)_{12}$] are given within the context of isomerization, and a section considers fragmentational routes. Clusters have been considered to be possible models for metal surfaces in heterogeneous catalysis, so that not the least interest in cluster complexes lies in their catalytic potential, explored by W. L. Gladfelter and K. J. Roesselet. In a relatively short chapter, they examine the ability of carbonyl and hydridocarbonyl clusters to catalyse the water–gas shift reaction, olefin hydrogenation, isomerization and hydroformylation, and oxidations. The hydrogenation of CO is a reaction with great industrial appeal—the most promising systems seem to be those running at high temperature and pressure; it is pointed out that under these conditions there is scope for cluster formation, reorganization and breakdown. There would seem to be much scope for the study of activated clusters to permit low-temperature, low-pressure pathways. Much also remains to be done in establishing the

similarities and differences between mononuclear and cluster systems.

Clusters have spawned a considerable literature, collected together by M. I. Bruce in the final chapter. It has, besides a bibliography of reviews, a handy table of all organometallic cluster syntheses listed in *Inorganic and Organometallic Syntheses* and *Brauer's Handbook*, plus an author index to the reviews.

The book is finished off with both a subject index and an excellent formula index, arranged in order of nuclearity.

There is much in this volume that will result in it being read, and reread, by organometallic and, one hopes, organic chemists.

Ultrasound in Synthesis (Reactivity and Structure: Concepts in Organic Chemistry, Volume 27). Steven V. Ley and Caroline M. R. Low. Springer-Verlag, Berlin, 1989, ISBN 3-540-51023-0, x+133 pp., DM 128.

One of the spin-offs of the age of the instant everything was the application of the microwave oven to chemical synthesis. This slim volume examines a technique that has been around for rather longer, yet is only just starting to be taken seriously.

I fear that the series title will be sufficient to ensure that this volume is read largely by specialists in the chemistry of the element carbon. This would be unfortunate, for whole chapters devoted to organolithium and organomagnesium compounds are of just as much interest to organometallic chemists, let alone that on transition metal carbonyls.

The volume is directed to the synthetic utility of the technique; for this reason there is a long opening section covering practical considerations. Most workers so far have used laboratory cleaning baths, but this book points out the advantages of using ultrasonic probes directly immersed in the reaction vessel. Cells have been developed that allow reactions to be carried out under an inert atmosphere or at moderate pressures. Reaction rates at ambient temperatures can be considerably greater than under reflux without sonic stimulation. It is important to avoid the use of chlorinated solvents as this can mean the release of Cl_2 or HCl. Untrasound liberates OH and H radicals from water, thus producing hydrogen peroxide, so that redox reactions are often encountered in aqueous systems.

Ultrasound considerably shortens the induction time in generating Grignard reagents, probably through removing adsorbed water from the metal surface; very active magnesium hydride can also be made. Potential for one-pot organometallic synthesis is also revealed. A highlight of the lithium chapter is the application to rapid synthesis of lithium diisopropylamide and alkyl- and aryllithiums in high yield in wet technical grade THF! Succeeding chapters treat compounds of other alkali metals and organozinc compounds. The applications to transition metal catalysts have so far been little explored, but a long section reveals many pathways for organic synthesis with iron carbonyls.

A very interesting read; there are many possibilities here for organometallic chemists—the possibility of high yield, rapid syntheses avoiding refluxing, to name but one.

Gmelin Handbook of Inorganic Chemistry. Manganese D7 (Coordination Compounds). Springer-Verlag, 1990, ISBN 3-540-93602-5, DM 1335.

Gmelin coverage of manganese complexes is well-advanced. Since 1979, successive volumes have dealt with complexes of most oxygen- and nitrogen-donor ligands, this volume continuing this coverage with complexes of nitriles and related ligands. Most of it is, however, taken up with complexes of sulphur, selenium and tellurium ligands (mainly the former).

Though less fashionable than the corresponding iron complexes, widely studied as models for the active sites of ferredoxins and other iron–sulphur proteins, manganese forms a wide variety of complexes of these ligands—with both mono- and bidentate ligands, in oxidation states +2, +3 and +4; with "non-innocent" dithiolene ligands, a wider range of formal oxidation states is encountered. Dithiocarbamates and related complexes have been especially studied, the manganese(III)tris complexes undergoing one electron oxidation and reduction to the corresponding cationic manganese(IV) and anionic manganese(II) compounds. Other ligands treated include thioamides and thioureas; for consistency, sulphoxides are dealt with in this volume although they are generally believed to bind to manganese through the oxygen.

As usual with Gmelin, there are clear tabulations of material and a thorough ligand formula index. Much of the literature cited is obscure or inaccessible, making these volumes helpful in these days of cuts in journal subscriptions. It is a measure of the depth of information retrieval that one learns that the manganese(II) complex of saccharin is less sweet than saccharin itself, but leaves a bitter aftertaste in the throat!

Gmelin Handbook of Inorganic Chemistry. Organoiron Compounds, Part B17. Springer-Verlag, 1990, ISBN 3-540-93601-7, DM 1873.

Like Gaul, the Gmelin treatment of the organometallic chemistry of iron falls into three parts. The ferrocene family is in series A, other mononuclear compounds in series B and compounds with more than one iron atom in series C.

Coverage of the compounds with pentahapto ligands bound to iron began in part B11; this volume begins with

similarities and differences between mononuclear and cluster systems.

Clusters have spawned a considerable literature, collected together by M. I. Bruce in the final chapter. It has, besides a bibliography of reviews, a handy table of all organometallic cluster syntheses listed in *Inorganic and Organometallic Syntheses* and *Brauer's Handbook*, plus an author index to the reviews.

The book is finished off with both a subject index and an excellent formula index, arranged in order of nuclearity.

There is much in this volume that will result in it being read, and reread, by organometallic and, one hopes, organic chemists.

Ultrasound in Synthesis (Reactivity and Structure: Concepts in Organic Chemistry, Volume 27). Steven V. Ley and Caroline M. R. Low. Springer-Verlag, Berlin, 1989, ISBN 3-540-51023-0, x+133 pp., DM 128.

One of the spin-offs of the age of the instant everything was the application of the microwave oven to chemical synthesis. This slim volume examines a technique that has been around for rather longer, yet is only just starting to be taken seriously.

I fear that the series title will be sufficient to ensure that this volume is read largely by specialists in the chemistry of the element carbon. This would be unfortunate, for whole chapters devoted to organolithium and organomagnesium compounds are of just as much interest to organometallic chemists, let alone that on transition metal carbonyls.

The volume is directed to the synthetic utility of the technique; for this reason there is a long opening section covering practical considerations. Most workers so far have used laboratory cleaning baths, but this book points out the advantages of using ultrasonic probes directly immersed in the reaction vessel. Cells have been developed that allow reactions to be carried out under an inert atmosphere or at moderate pressures. Reaction rates at ambient temperatures can be considerably greater than under reflux without sonic stimulation. It is important to avoid the use of chlorinated solvents as this can mean the release of Cl_2 or HCl. Untrasound liberates OH and H radicals from water, thus producing hydrogen peroxide, so that redox reactions are often encountered in aqueous systems.

Ultrasound considerably shortens the induction time in generating Grignard reagents, probably through removing adsorbed water from the metal surface; very active magnesium hydride can also be made. Potential for one-pot organometallic synthesis is also revealed. A highlight of the lithium chapter is the application to rapid synthesis of lithium diisopropylamide and alkyl- and aryllithiums in high yield in wet technical grade THF! Succeeding chapters treat compounds of other alkali metals and organozinc compounds. The applications to transition metal catalysts have so far been little explored, but a long section reveals many pathways for organic synthesis with iron carbonyls.

A very interesting read; there are many possibilities here for organometallic chemists—the possibility of high yield, rapid syntheses avoiding refluxing, to name but one.

Gmelin Handbook of Inorganic Chemistry. Manganese D7 (Coordination Compounds). Springer-Verlag, 1990, ISBN 3-540-93602-5, DM 1335.

Gmelin coverage of manganese complexes is well-advanced. Since 1979, successive volumes have dealt with complexes of most oxygen- and nitrogen-donor ligands, this volume continuing this coverage with complexes of nitriles and related ligands. Most of it is, however, taken up with complexes of sulphur, selenium and tellurium ligands (mainly the former).

Though less fashionable than the corresponding iron complexes, widely studied as models for the active sites of ferredoxins and other iron–sulphur proteins, manganese forms a wide variety of complexes of these ligands—with both mono- and bidentate ligands, in oxidation states +2, +3 and +4; with "non-innocent" dithiolene ligands, a wider range of formal oxidation states is encountered. Dithiocarbamates and related complexes have been especially studied, the manganese(III)tris complexes undergoing one electron oxidation and reduction to the corresponding cationic manganese(IV) and anionic manganese(II) compounds. Other ligands treated include thioamides and thioureas; for consistency, sulphoxides are dealt with in this volume although they are generally believed to bind to manganese through the oxygen.

As usual with Gmelin, there are clear tabulations of material and a thorough ligand formula index. Much of the literature cited is obscure or inaccessible, making these volumes helpful in these days of cuts in journal subscriptions. It is a measure of the depth of information retrieval that one learns that the manganese(II) complex of saccharin is less sweet than saccharin itself, but leaves a bitter aftertaste in the throat!

Gmelin Handbook of Inorganic Chemistry. Organoiron Compounds, Part B17. Springer-Verlag, 1990, ISBN 3-540-93601-7, DM 1873.

Like Gaul, the Gmelin treatment of the organometallic chemistry of iron falls into three parts. The ferrocene family is in series A, other mononuclear compounds in series B and compounds with more than one iron atom in series C.

Coverage of the compounds with pentahapto ligands bound to iron began in part B11; this volume begins with

similarities and differences between mononuclear and cluster systems.

Clusters have spawned a considerable literature, collected together by M. I. Bruce in the final chapter. It has, besides a bibliography of reviews, a handy table of all organometallic cluster syntheses listed in *Inorganic and Organometallic Syntheses* and *Brauer's Handbook*, plus an author index to the reviews.

The book is finished off with both a subject index and an excellent formula index, arranged in order of nuclearity.

There is much in this volume that will result in it being read, and reread, by organometallic and, one hopes, organic chemists.

Ultrasound in Synthesis (Reactivity and Structure: Concepts in Organic Chemistry, Volume 27). Steven V. Ley and Caroline M. R. Low. Springer-Verlag, Berlin, 1989, ISBN 3-540-51023-0, x+133 pp., DM 128.

One of the spin-offs of the age of the instant everything was the application of the microwave oven to chemical synthesis. This slim volume examines a technique that has been around for rather longer, yet is only just starting to be taken seriously.

I fear that the series title will be sufficient to ensure that this volume is read largely by specialists in the chemistry of the element carbon. This would be unfortunate, for whole chapters devoted to organolithium and organomagnesium compounds are of just as much interest to organometallic chemists, let alone that on transition metal carbonyls.

The volume is directed to the synthetic utility of the technique; for this reason there is a long opening section covering practical considerations. Most workers so far have used laboratory cleaning baths, but this book points out the advantages of using ultrasonic probes directly immersed in the reaction vessel. Cells have been developed that allow reactions to be carried out under an inert atmosphere or at moderate pressures. Reaction rates at ambient temperatures can be considerably greater than under reflux without sonic stimulation. It is important to avoid the use of chlorinated solvents as this can mean the release of Cl_2 or HCl. Untrasound liberates OH and H radicals from water, thus producing hydrogen peroxide, so that redox reactions are often encountered in aqueous systems.

Ultrasound considerably shortens the induction time in generating Grignard reagents, probably through removing adsorbed water from the metal surface; very active magnesium hydride can also be made. Potential for one-pot organometallic synthesis is also revealed. A highlight of the lithium chapter is the application to rapid synthesis of lithium diisopropylamide and alkyl- and aryllithiums in high yield in wet technical grade THF! Succeeding chapters treat compounds of other alkali metals and organozinc compounds. The applications to transition metal catalysts have so far been little explored, but a long section reveals many pathways for organic synthesis with iron carbonyls.

A very interesting read; there are many possibilities here for organometallic chemists—the possibility of high yield, rapid syntheses avoiding refluxing, to name but one.

Gmelin Handbook of Inorganic Chemistry. Manganese D7 (Coordination Compounds). Springer-Verlag, 1990, ISBN 3-540-93602-5, DM 1335.

Gmelin coverage of manganese complexes is well-advanced. Since 1979, successive volumes have dealt with complexes of most oxygen- and nitrogen-donor ligands, this volume continuing this coverage with complexes of nitriles and related ligands. Most of it is, however, taken up with complexes of sulphur, selenium and tellurium ligands (mainly the former).

Though less fashionable than the corresponding iron complexes, widely studied as models for the active sites of ferredoxins and other iron–sulphur proteins, manganese forms a wide variety of complexes of these ligands—with both mono- and bidentate ligands, in oxidation states +2, +3 and +4; with "non-innocent" dithiolene ligands, a wider range of formal oxidation states is encountered. Dithiocarbamates and related complexes have been especially studied, the manganese(III)tris complexes undergoing one electron oxidation and reduction to the corresponding cationic manganese(IV) and anionic manganese(II) compounds. Other ligands treated include thioamides and thioureas; for consistency, sulphoxides are dealt with in this volume although they are generally believed to bind to manganese through the oxygen.

As usual with Gmelin, there are clear tabulations of material and a thorough ligand formula index. Much of the literature cited is obscure or inaccessible, making these volumes helpful in these days of cuts in journal subscriptions. It is a measure of the depth of information retrieval that one learns that the manganese(II) complex of saccharin is less sweet than saccharin itself, but leaves a bitter aftertaste in the throat!

Gmelin Handbook of Inorganic Chemistry. Organoiron Compounds, Part B17. Springer-Verlag, 1990, ISBN 3-540-93601-7, DM 1873.

Like Gaul, the Gmelin treatment of the organometallic chemistry of iron falls into three parts. The ferrocene family is in series A, other mononuclear compounds in series B and compounds with more than one iron atom in series C.

Coverage of the compounds with pentahapto ligands bound to iron began in part B11; this volume begins with

those compounds where there is additionally an η^2-ligand and two others such as CO, CS, RNC or a carbene. Subsequently, one moves to the $(C_5H_5)Fe$ compounds where the other ligands are allyls (and other trihapto systems), tetra- and pentahapto rings exemplified by the ferrocene analogue $(C_5H_5)Fe(C_5H_4N)$. The volume concludes with acyclic pentadienyls ("open sandwiches") and $(C_5H_5)Fe$ derivatives of pentahapto ligands with six or more ring carbons.

"Gmelin" would be most useful if it were just an aid to literature searching, a kind of catalogue. It is, however, very much more than this, as the literature is carefully sifted. Within families of related compounds, synthetic routes are analysed, and compounds listed with full and clear tabulations of physical properties and spectroscopic data. These tables feature structural formulae of each compound described, so that one is in no doubt, as well as presenting fuller diagrams where the molecular structure has been determined. There are both ligand and formula indexes, so that, all in all, an area containing a bewildering variety of very similar-looking compounds is reduced to order.

The literature is surveyed to the end of 1987, with quite a few references subsequent to that date.

Felixstowe College, **SIMON COTTON**
Felixstowe IP11 7NQ, U.K.

Polyhedron Vol. 10, No. 18, pp. 2089–2093, 1991
Printed in Great Britain

0277–5387/91 $3.00+.00
© 1991 Pergamon Press plc

REDUCTION OF WCl_6 BY ALLYLTRIMETHYLSILANE. A CONVENIENT METHOD TO PREPARE $WCl_5(OEt_2)$ AND SOME OTHER DERIVATIVES OF WCl_5

CHRISTINA PERSSON and CARLAXEL ANDERSSON*

Inorganic Chemistry I, Chemical Center, University of Lund,
P.O. Box 124, S 22100 Lund, Sweden

(*Received* 1 *May* 1990; *accepted* 25 *June* 1991)

Abstract—WCl_6 was reacted with excess allyltrimethylsilane in diethyl ether solution at low temperature. The main product in the reaction was shown to be $WCl_5(OEt_2)$ which was isolated as black–green air- and moisture-sensitive crystals. $WCl_5(OEt_2)$ was reacted with different Lewis bases, e.g. pyridine and 9-fluorenone to yield the new compounds WCl_5 (pyridine) and WCl_5(9-fluorenone). The latter most likely being an oxygen bonded complex.

Tungsten is one of the transition metals that can be used as a catalyst for the metathesis of olefins.[1,2] Well-defined tungsten based metathesis catalysts, e.g. isolated tungsten carbene complexes have been developed in recent years.[3–5] An active but poorly defined catalyst can also be prepared *in situ* by reacting WCl_6 with an alkylating co-catalyst, e.g. alkyl-tin, alkyl-lithium or alkyl-alumina reagents.[2] Considerable efforts have been devoted to elucidate the nature of the active catalyst in these latter systems, i.e. to determine the actual oxidation state of the metal and the ligands in the coordination sphere of the metal. The reduction of tungsten(VI) as an important reaction path when alkyl-tin reagents are used as co-catalysts has been demonstrated[6,7] and the reducing properties of $SnBu_4$ have also been used[8] to prepare WCl_5 from WCl_6.

Allyltrimethylsilane has been found to undergo slow self-metathesis and fast cross-metathesis without an added co-catalyst.[9,10] Likewise ring-opening polymerizations have been performed using WCl_6/allyltrimethylsilane as the catalyst system.[11,12]

A mechanism involving metalla-carbene and metalla-cyclobutane complexes is the accepted mechanism of the metathesis reaction.[2] How an initiating metalla-carbene is formed in the system of WCl_6/allyltrimethylsilane is still an unanswered question. Based on the organic products propene and chlorotrimethylsilane, found after reaction of WCl_6 with allyltrimethylsilane, suggestions involving double allylation of tungsten and subsequent α-hydrogen transfer and propene elimination have been put forward as a route to form a carbene.[13,14] As indicated by the other organic products, allylchloride and 1,5-hexadiene, reductive elimination reactions are in this case competing reactions not leading to an active carbene but to reduced tungsten.

In the course of a project aiming at the metathesis of functionalized olefins we have continued the study of allyltrimethylsilane and its reactions with WCl_6 to eventually identify or isolate tungsten-σ-allyl or carbene complexes in the reaction mixture. Based on the observed reduction of tungsten(VI) by tetra-alkyl-tin compounds[6–8] or by cyclic olefins[15,16] we have also considered reduced tungsten as a likely product of the reaction. The work presented here describes the isolation and the identification of $WCl_5(OEt_2)$ and some complexes of tungsten(V).

RESULTS AND DISCUSSION

Reaction between WCl_6 *and allyltrimethylsilane*

The treatment of WCl_6 partly dissolved in diethyl ether at −25°C with excess (4 equiv.) allyltrimethylsilane leads to a colour change in the solution and a dissolution of the undissolved WCl_6.

* Author to whom correspondence should be addressed.

After *ca* 2 h a green precipitate is formed. Continued reaction overnight leads to a dark orange solution and a fluffy green precipitate (**I**). Schlenk filtration to remove the precipitate gives a clear solution. Slow evaporation at low temperature (−30°C) of the ether solvent leads to the deposition of large black–green crystals (**II**) with a metallic lustre. Several crops with the same appearance can be isolated in this way. GC-MS analysis of the organic evaporate reveals the presence of unreacted allyltrimethylsilane together with propene, allylchloride, chlorotrimethylsilane and 1,5-hexadiene. No attempt was made to quantify the relative amount of these products. The relative amount of the green (**I**) and black–green (**II**) materials varies from one experiment to another but in no case does the amount of **I** exceed more than 10% of the total isolated solid material. Both the isolated solids are extremely air- and moisture-sensitive which precludes full spectroscopic characterizations and a precise elemental analysis.

Since direct spectroscopic and analytical methods gave no decisive information on the composition of the solids indirect methods to characterize the major product **II** were sought for. In the search for more stable adducts, reduced tungsten, i.e. tungsten(V) or (IV) was considered as the likely parent compound.

Tungsten(IV) has been isolated as its THF adduct,[17] $WCl_4(THF)_2$, and tungsten(IV) also forms isolable complexes with other Lewis bases, e.g. pyridine[18–20] and bipyridine.[21] Chloro complexes of tungsten(IV), e.g. WCl_6^{2-} are also known.[18] Tungsten(V) forms stable chloro complexes[22] but no simple stable Lewis base adducts besides WCl_5(bipyridine).[8] A brief note[23] describing some benzoic ester derivative is also known.

Complexes with nitrogen donor ligands

Compound **II** dissolves in neat pyridine. An orange solution is thus obtained which within 45 min deposits a small amount of an orange solid. Heating the mixture at reflux results in a dark red solution and more of the orange solid (**III**). After isolation of the solid from the hot solution the elemental anslysis and the IR spectrum reveals that this is the known *trans*-WCl_4(pyridine)$_2$.

Treatment of an etheral solution of **II** with one equiv. of pyridine at room temperature results in immediate darkening of the solution. Within a few minutes stirring a dark green precipitate (**IV**) forms. No definite conclusion as to the formulation of (**IV**) is obtained by elemental analysis.

Comparing the IR spectra of **III** and **IV** disclose similarities, i.e. coordinated pyridine in both substances as demonstrated by the three bands at 444, 683 and 1607 cm^{-1} in the spectrum of **III** and at 440, 680 and 1607 cm^{-1} in the spectrum of **IV**, but also differences in the region of metal halide vibrations. In the spectrum of **III** an intense band at 311 cm^{-1} is present, which is most likely the W—Cl stretch in a *trans*(*D4h*) arrangement of the two chloride ligands, while in the spectrum of **IV** two intense bands at 348 and 322 cm^{-1} are present.

On addition of allyltrimethylsilane (1.3 equiv.) to an ether solution of **II** at room temperature before the addition of pyridine (1 equiv.) a dark solution is obtained. From this solution dark black–green crystals (**V**) separate within minutes. Elemental analysis of this product is in accordance with the formula WCl_5(pyridine).

The IR spectrum of **V** is in many respects similar to the spectra of **III** and **IV**. The bands at 438, 687 and 1607 cm^{-1} showing coordinated pyridine are almost unshifted relative to those of **III** and **IV**. One intense band at 334 cm^{-1}, a shoulder at 350 cm^{-1} and a medium band at 392 cm^{-1} are present in the metal halide stretching region.

If it is considered that pyridine in its reaction with high valent metal ions possesses reducing properties[24,25] as well as complexing properties, the formation of the products **III**, **IV** and **V** can be rationalized. Excess pyridine and heating promotes the reduction to tungsten(IV) as in **III**, while stoichiometric amounts of pyridine at room temperature bring about only partial reduction leading to some kind of mixed tungsten(V)/(IV) product (**IV**) with coordinated pyridine. The isolation of analytically pure WCl_5(pyridine), which is a rare example of tungsten(V) nitrogen-coordinated complex, when allyltrimethylsilane is used as a co-reactant is most likely due to some kind of stabilizing effect of the olefin prohibiting the reduction to tungsten(IV). WCl_5(pyridine) is soluble in solvents such as toluene, benzene and chlorobenzene. In all these solvents red solutions are obtained, but the parent compound cannot be recovered.

As is the case with pyridine, bipyridine reacts with an ether solution of **II** at room temperature to yield a yellow–brown precipitate analysing approximately to a mixture of WCl_5(bipyridine) and WCl_4(bipyridine). This is in accordance with the observation in the case of pyridine and further studies were therefore not pursued. An impure compound of the formula WCl_5(bipyridine) was prepared recently[8] and described as being brick-red.

Chloro-complexes

Compound **II** dissolves in CH_2Cl_2 to produce a clear green solution. On addition of tetra-

phenylarsonium chloride in CH_2Cl_2 a red–brown solution is obtained. Within minutes of stirring a brown solid deposits. Brown crystals (**VI**) are isolated by cooling to −30°C and subsequent filtration. The elemental analysis and the IR spectrum shows that this is the known[22] $[WCl_6][AsPh_4]$. In a similar way the green tetramethylammonium salt is obtained.

The formation of the hexachloro coordinated anion WCl_6^- from (**II**) is strong evidence that (**II**) is a chloro complex of tungsten(V), most likely the ethyl ether adduct $WCl_5(OEt_2)$. A high excess of Cl^- has been observed to induce reduction of metal halides[24] but we are convinced that this is not the case in the present study.

Complexes with oxygen donors

Having reached a likely formulation of (**II**) we found it interesting to try to substitute diethyl ether by other oxygen donors.

On dissolution of **II** in THF by dropwise addition of THF to solid **II** heat is evolved and a yellow suspension is initially obtained. Further addition of THF gives a clear green solution. On continued stirring of this solution at room temperature it gradually changes to finally reach a turquoise colour. By reducing the volume and cooling to −25°C very air-sensitive turquoise crystals of **VII** deposit. The elemental analysis and IR spectrum reveal that this is $WOCl_3(THF)_2$. Precedence for oxygen abstraction reactions from THF can be found[26] although hexamethyldisiloxane seems to be the preferred reagent for this kind of reaction.[8,27] Other oxygen donors react differently. We have studied the reaction of **II** with 9-fluorenone, an example outside the ether class.

Dropwise addition of 9-fluorenone in CH_2Cl_2 into a solution of **II** in the same solvent gives an immediate precipitation of a dark solid. Isolation by filtration gives green–black crystals (**VIII**) which analyse for WCl_5(9-fluorenone). The formation of this compound does not necessarily implicate that 9-fluorenone is a better donor than diethyl ether with respect to tungsten(V). The low solubility of the fluorenone adduct shifts the equilibrium towards the formation of the fluorenone adduct.

All the reactions described and the products isolated in these reactions clearly demonstrate that the parent compound (**II**) must be WCl_5, probably as its diethyl ether solvate. Further proof for this is found in the UV spectrum of **II**. This spectrum shows an absorbance maximum at 298 nm which is in accordance with published data.[28] The reactions carried out also show that care must be taken if adduct formation is used as a method to characterize an unknown compound.

The reaction between WCl_6 and allyltrimethylsilane is in our opinion a convenient entry into tungsten(V) chemistry, easier than the older high temperature methods[29–33] to use. The method is easily applicable for the synthesis of quantities of about 10 g. The solubility of $WCl_5(OEt_2)$ in organic solvents makes this useful as a precursor for other tungsten(V) compounds.

Regarding the actual mechanism by which WCl_5 is formed in the present case, this is still an open question. The results presented here do not allow a distinction between direct reduction and a reaction path involving allylation of WCl_6 and subsequent reductive elimination as suggested in earlier studies. A direct reduction can proceed via chlorine radical transfer from WCl_6 to allyltrimethylsilane resulting in WCl_5, chlorotrimethylsilane and an allyl radical. Further reactions as dimerization of allyl radicals, recombination of allyl and chlorine radicals and hydrogen abstraction from a hydrogen source in the system could equally well, as the indirect reduction, explain the organic products 1,5-hexadiene, allylchloride and propene. The present study reveals, however, no formation of tungsten(IV), which must form in a mono-molecular reductive elimination from tungsten(VI).

EXPERIMENTAL

General procedures and chemicals

All preparations and reactions were carried out under an atmosphere of dried nitrogen or argon using conventional Schlenk techniques. Solvents were dried and stored over activated molecular sieves. Allyltrimethylsilane (Janssen Chimica) was distilled prior to use and stored over activated molecular sieves. Tetraphenylarsoniumchloride (Merck) was dried over Sicapent *in vacuo*. Tetramethylammoniumchloride was dried by vacuum treatment at 50°C for 48 h. 2,2-bypiridine (Merck) was recrystallized from ethanol prior to drying over Sicapent *in vacuo*. Tungsten hexachloride (Janssen Chimica) was purified from the volatile impurities by a continuous nitrogen flow at 120°C. Tungsten was determined gravimetrically as WO_3. Chlorine was determined by Mohr titration. Elemental analyses were done by Mikro Kemi AB, Uppsala, Sweden. IR spectra were recorded on a PE 580B spectrometer or on a Nicolet 20 SXC FT-IR spectrometer as Nujol or Fluorolube mulls between CsI windows or as CsI tablets. UV spectra were recorded in standard Schlenk tubes using a Guided

Wave, Model 260 fibre optic spectrophotometer equipped with an adjustable probe head.

Preparations

(1) *(Diethyl ether)pentachlorotungsten* (**II**). Allyltrimethylsilane (11 cm^3, 69 mmol) was added to a suspension of WCl_6 (6.8 g, 17.1 mmole) in diethyl ether (200 cm^3) at $-25°C$. Upon continuous stirring of the cold mixture WCl_6 gradually dissolved and after 24 h a clear solution and a green precipitate were obtained. The green solid (0.5 g) was separated by Schlenk filtration. Cooling the solution to $-25°C$ and concentration to *ca* 70 cm^3 afforded the first crop (1.9 g) of large black–green crystals. Further concentration to *ca* 20 cm^3 afforded 2.5 g and additional concentration afforded another 0.4 g. Total yield = 4.8 g (64%).

IR: W—Cl 315(s), 351(sh) cm^{-1} and coordinated ether, 1013 and 999 cm^{-1}. Found: Cl, 40.7. Calc.: Cl, 40.7%.

(2) *Bis(pyridine)tetrachlorotungsten* (**III**). **II** (0.45 g, 1 mmol) was dissolved in pyridine (25 cm^3) to give a clear orange solution. After stirring for 45 min at room temperature a small amount of an orange solid was formed. Heating the reaction mixture under reflux for 1.5 h afforded a dark red solution and an orange solid. The solid was isolated by filtering the hot mixture. The solid was washed with 3×5 cm^3 ether and dried *in vacuo*. Isolated yield = 0.20 g.

Found: C, 25.1; H, 2.1; N, 5.8; Cl, 27.7; W, 37.5. $C_{10}H_{10}N_2Cl_4W$ requires: C, 24.8; H, 2.1; N, 5.8; Cl, 29.3; W, 38.0%.

IR: W—Cl 311(s), 330(sh) cm^{-1} and coordinated pyridine, 1607, 683, 444 cm^{-1}.

(3) *(Pyridine)pentachlorotungsten* (**V**). **II** (0.75 g, 1.7 mmol) was dissolved in diethyl ether (30 cm^3) and the solution was filtered to give a clear solution. To this solution 0.36 cm^3 (2.3 mmol) of allyltrimethylsilane was added followed by an addition of 0.16 cm^3 (2 mmol) of pyridine. The solution darkened and dark crystals separated at once. The crystals were collected by filtration and dried *in vacuo*. The crystals were stable in air for a short period.

Found: C, 13.9; H, 1.0; N, 3.2; Cl, 39.0; W, 41.0. $C_5H_5NCl_5W$ requires: C, 13.6; H, 1.1; N, 3.2; Cl, 40.3; W, 41.8%.

IR: W—Cl 334(s), 350(sh), 392(mw) cm^{-1} and coordinated pyridine, 1607, 687 and 438 cm^{-1}.

(4) *Tetraphenylarsonium hexachlorotungstate*(V) (**VI**). Tetraphenylarsoniumchloride (0.8 g, 1.9 mmol) dissolved in CH_2Cl_2 (20 cm^3) was added dropwise to **II** (0.9 g, 2.1 mmol) dissolved in CH_2Cl_2 to give a red solution. After stirring for some minutes a brown solid deposited. Cooling to $-30°C$ and filtration afforded a brown solid (0.6 g). An additional 0.6 g was obtained by addition of CCl_4 (10 cm^3) to the filtrate. The solid can be recrystallized by dissolution in CH_2Cl_2 and precipitated by the addition of CCl_4. Total isolated yield = 1.2 g (81%). M.p. = 255°C (lit.[22] 253–256°C).

Found: C, 36.8; H, 2.5; Cl, 26.3; W, 23.3. $C_{24}H_{20}Cl_6AsW$ requires: C, 36.9; H, 2.6; Cl, 27.3; W, 23.6%.

IR: W—Cl 315(s), 332(sh), 350(m) and 385(w) cm^{-1}.

(5) *Bis(tetrahydrofuran)trichlorooxotungsten* (**VII**). THF (30 cm^3) was added dropwise to solid **II** (0.45 g, 1 mmol). On addition, heat was evolved and an initial yellow suspension was obtained which on further addition gave a green homogeneous solution. Further stirring at room temperature gave a turquoise solution. Reducing the volume to one third of the original volume and cooling to $-25°C$ for 3 days afforded turquoise air-sensitive crystals. These were separated, washed with diethyl ether and dried *in vacuo*.

Found: C, 20.3; H, 3.2; Cl, 23.3. $C_8H_{16}Cl_3OW$ requires: C, 21.3; H, 3.6; Cl, 23.6%.

IR: W—Cl 325(s), 351(m) cm^{-1}; W=O 998(vs), 1003(sh) cm^{-1} and coordinated THF, 1047 cm^{-1}.

(6) *(9-Fluorenone)pentachlorotungsten* (**VIII**). Fluorenone (0.54 g, 3 mmol) dissolved in CH_2Cl_2 (10 cm^3) was added dropwise to a solution of **II** (1.3 g) in CH_2Cl_2 (15 cm^3), whereupon a dark solid deposited. The black–green crystals were separated by filtration and washed repeatedly with diethyl ether before drying *in vacuo*.

Found: C, 29.5; H, 1.6; Cl, 32.5. $C_{12}H_6Cl_5OW$ requires: C, 28.8; H, 1.5; Cl, 32.7%.

IR (Fluorolube): C=O 1550(s,br) cm^{-1}; W—Cl 334(s), 385(m) cm^{-1}.

Acknowledgements—Financial support from STU (Swedish Board for Technical Development) and from SJFR (Swedish Council for Forestry and Agricultural Research) is greatfully acknowledged.

REFERENCES

1. (a) V. Dragutan, A. T. Balaban and M. Dimonic, *Olefin Metathesis and Ring-Opening Polymerization of Cyclic Olefins*. Wiley Interscience, New York (1985); (b) K. J. Ivin, *Olefin Metathesis*. Academic Press, London (1983).
2. R. H. Grubbs, *Comprehensive Organometallic Chemistry* (Edited by G. Wilkinson, F. G. A. Stone and E. W. Abel), Vol. 8, Ch. 54. Pergamon Press, New York (1982).
3. G. Schoettle, J. Kress and J. A. Osborn, *J. Chem. Soc., Chem. Commun.* 1989, 1062.

4. R. R. Schrock, J. S. Murdzek, G. C. Bazan, J. Robbin, M. DiMare and M. O'Regan, *J. Am. Chem. Soc.* 1990, **112**, 3875.
5. R. R. Schrock, R. T. DuPue, J. Feldman, K. B. Yap, D. C. Yang, D. M. Davis, L. Park, M. DiMare, M. Schofield, J. Anhans, E. Walborsky, E. Ritt, C. Krüger and P. Betz, *Organometallics* 1990, **9**, 2262.
6. E. Thorn-Csanyi, *Die Angew. Makromol. Chemie* 1981, **94**, 181.
7. E. Thorn-Csanyi and H. Timm, *J. Molec. Catal.* 1985, **28**, 37.
8. W. A. Herrman, W. R. Thiel and E. Herdweck, *Chem. Ber.* 1990, **23**, 271.
9. M. Berglund, C. Andersson and R. Larsson, *J. Organomet. Chem.* 1985, **292**, C15.
10. M. Berglund, C. Andersson and R. Larsson, *J. Organomet. Chem.* 1986, **314**, 61.
11. I. A. Oreshkin, L. I. Redkina, I. L. Kershenbaum, G. M. Chernenko, K. L. Makovetsky, I. L. Tinyakova and B. A. Golgopolsk, *Eur, Polym. J.* 1977, **13**, 447.
12. B. A. Dolgoplosk, *J. Molec. Catal.* 1982, **15**, 193.
13. I. S. Akhrem, D. V. Avetisyan, R. S. Vartanyan, K. G. Shakhatuni and M. E. Volpin, *Izv. Akad. Nauk. SSSR, Ser. Khim.* 1975, **24**, 2327.
14. I. Ya. Ostrovskaya, L. I. Redkina and K. L. Makovetsky, *Izv. Akad. Nauk. SSSR, Ser. Khim.* 1980, **29**, 2650.
15. L. Castellani and M. C. Gallazzi, *Trans. Metal Chem.* 1985, **10**, 194.
16. E. Thorn-Csanyi, M. Kessler, B. Löwer and H. Timm, *J. Molec. Catal.* 1991, **65**, 261.
17. W. Grahlert and K.-H. Thiele, *Z. Anorg. Allg. Chem.* 1971, **383**, 144.
18. C. D. Kennedy and R. D. Peacock, *J. Chem. Soc.* 1963, 3392.
19. D. G. Blight and D. L. Kepert, *J. Chem. Soc. A* 1968, 534.
20. J. V. Brencic, B. Ceh and P. Segedin, *Z. Anorg. Allg. Chem.* 1979, **454**, 181.
21. J. Quirk and G. Wilkinson, *Polyhedron* 1982, **1**, 209.
22. R. N. Dickinson, S. E. Feil, F. N. Collier, W. W. Horner, S. M. Horner and S. Y. Tyree, *Inorg. Chem.* 1964, **3**, 1600.
23. H. Funk and H.-R. Hoppe, *Z. Chem.* 1968, **8**, 31.
24. R. A. Walton, *Progress in Inorganic Chemistry*, Vol. 16, Ch. 1. Interscience, New York (1972).
25. P. M. Boorman, N. N. Greenwood, M. A. Hildon and R. V. Parish, *J. Chem. Soc. A* 1968, 2002.
26. G. W. A. Fowles and J. L. Frost, *J. Chem. Soc. A* 1967, 671.
27. V. C. Gibson, T. P. Kee and A. Shaw, *Polyhedron* 1990, **9**, 2293.
28. B. Löwer, Doctoral Thesis. Universität Hamburg, Hamburg (1981).
29. W. Blitz and C. Fendius, *Z. Anorg. Allg. Chem.* 1928, **172**, 385.
30. T. M. Brown and E. L. McCann, *Inorg. Chem.* 1968, **7**, 1227.
31. E. L. McCann, *Inorg. Synth.* 1971, **13**, 150.
32. B. G. Korshunov and V. N. Bezuerskaya, *Zh. Neorg. Khim.* 1967, **12**, 3270.
33. P. C. Crouch, G. W. A. Fowles and R. A. Walton, *J. Inorg. Nucl. Chem.* 1970, **32**, 329.

Polyhedron Vol. 10, No. 18, pp. 2095–2103, 1991
Printed in Great Britain

0277–5387/91 $3.00+.00
© 1991 Pergamon Press plc

SYNTHESIS OF A NEW SERIES OF IRON COMPLEXES $Fe(C_5H_5)(CO)(EPh_3)SCOR$, $Fe(Bu^t\text{-}C_5H_4)(CO)(EPh_3)SCOR$ AND $Fe(1,3\text{-}Bu^t\text{-}C_5H_3)(CO)(PPh_3)SCOR$ (E = P, As, Sb) THROUGH PHOTOLYTIC CO-SUBSTITUTION. STUDY OF THE EFFECT OF R, E AND Cp-SUBSTITUENTS ON THE CO-SUBSTITUTION REACTIONS*

IBRAHIM JIBRIL,† MAHMOUD EL-HINNAWI and MOHAMMAD EL-KHATIB

Department of Chemistry, Yarmouk University, Irbid, Jordan

(*Received* 20 *December* 1990; *accepted* 21 *June* 1991)

Abstract—A series of new half-sandwich iron thiocarboxylate derivatives $FeCp'(CO)(EPh_3)SCOR$ [$Cp' = C_5H_5$, $Bu^t\text{-}C_5H_4$, $1,3\text{-}Bu^t\text{-}C_5H_3$; E = P, As, Sb; R = CH_3, $C(CH_3)_3$, C_6H_5, $2\text{-}(O_2N)\text{-}C_6H_4$, $3,5\text{-}(O_2N)_2\text{-}C_6H_3$] has been prepared and characterized through photolytic CO-substitution reactions. The reaction times of these photolytic CO-substitution reactions reveal that these reactions are strongly influenced by the substituents on the Cp ring, R group of the thiocarboxylate moiety and the donor atom E of EPh_3.

The photolytic reactions between the half-sandwich iron complexes $FeCp(CO)_2X$ (X = halides, alkyls, SiR_3, SnR_3, SR) and ER_3 ligands ($E = P$, As, Sb) were commonly applied to prepare the CO-substituted complexes $FeCp(CO)(ER_3)X$. A thermal reaction was also used for the same preparation.[1–10]

The types and yields of the CO-substituted product obtained from any of these reactions are mainly determined by the nature of X and the type of ER_3 ligands. For example, the ionic species $[FeCp(CO)_2ER_3]X$ (X = halide) and the acetyl product $FeCp(CO)(ER_3)COCH_3$ ($X = CH_3$) are among the important products of such reactions.[1–5]

Reactions of $FeCp(CO)_2X$ (X = I, Br) with PMe_3 give $FeCp(CO)(PMe_3)X$, the ionic species $[FeCp(PMe_3)_3]X$ and $[FeCp(CO)_2(PMe_3)]X$ depending on the type of the solvent.[10] Moreover, the irradiation time, the molar ratios of the reactants, the reaction temperature, the nature of the transition metal in the complex and the wavelength range for the UV irradiation are also important factors in determining the type and yield of the different products obtained from a certain reaction.[4,6,11]

The effect of Cp substituents on the rate of thermal CO-substitution reactions has recently been studied on complexes $(C_5H_4X)Rh(CO)_2$ (x = NO_2, CF_3, Cl, H, CH_3 and $N(CH_3)_2$).[12] The study showed that the rate increases as the electron-withdrawing ability of the Cp substituent increases. The effect of electron-donating substituents on the Cp-ring is limited to $(C_5(CH_3)_5)Rh(CO)_2$, which decreases the rate of CO-substitution by 10^{-3} relative to the parent compound but some of this decrease is due to steric factors.[12]

On the other hand, a variety of photochemical deactivation pathways for the mononuclear intermediates $CpFe(CO)X$ have been reported. These include CO dissociation, homolytic or heterolytic metal–X bond cleavage, intramolecular isomerization and interligand rearrangements.[13]

In this study, we carried out the photolytic CO-substitution reactions of a series of new iron dicarbonyl cyclopentadienyl thiocarboxylates, $FeCp(CO)_2SCOR$ where R = CH_3 (**1**), $(CH_3)_3$-C (**2**), C_6H_5 (**3**), $2\text{-}O_2NC_6H_4$ (**4**) and $3,5\text{-}(NO_2)_2C_6H_3$ (**5**)[14,15] with EPh_3 (E = P, As, Sb) in THF at 0°C.

The photolytic CO-substitution reactions with some tert-butyl-substituted cyclopentadienyl derivatives of the iron thiocarboxylate complexes $Fe(Bu^t\text{-}C_5H_4)(CO)_2SCOR$ [R = CH_3 (**6**), C_6H_5 (**7**), $3,5\text{-}(O_2N)_2\text{-}C_6H_3$ (**8**)] and $Fe(1,3\text{-}Bu^t_2\text{-}C_5H_3)(CO)_2SCOR$ [R = CH_3 (**9**), C_6H_5 (**10**), $3,5\text{-}(O_2N)_2\text{-}C_6H_3$ (**11**)][16] are also included in this study.

* Dedicated to the memory of Dr Mahmoud A. El-Hinnawi.

† Author to whom correspondence should be addressed.

The cyclopentadienyl iron thiocarboxylates[1–5] and the tert-butylcyclopentadienyl iron thiocarboxylates[6–8] react with EPh_3 (E = P, As, Sb) to give exclusively the mono-CO-substituted derivatives $Fe(C_5H_5)(CO)(EPh_3)SCOR$ and $Fe(Bu^t\text{-}C_5H_4)(CO)(EPh_3)SCOR$, while the ditert-butylcyclopentadienyl iron thiocarboxylates[9–11] react only with PPh_3 to give the mono-CO-substituted derivatives $Fe(1,3\text{-}Bu^t\text{-}C_5H_3)(CO)(PPh_3)SCOR$ and fail to react with $AsPh_3$ and $SbPh_3$.

EXPERIMENTAL

All reactions and manipulations of chemicals were performed under nitrogen. Solvents were dried and purified by distillation. The thiocarboxylate iron complexes $FeCp(CO)_2SCOR$ (**1–5**), were prepared as described previously.[14,15] The thiocarboxylate derivatives $Fe(Bu^t\text{-}C_5H_4)(CO)_2SCOR$ (**6–8**) and $Fe(1,3\text{-}Bu^t\text{-}C_5H_3)(CO)_2SCOR$ (**9–11**) were prepared as previously reported.[16] A high-pressure mercury lamp (HANAU, 240–600 nm) was used for photolysis. IR spectra were recorded on a Pye–Unicam SP3-100 spectrophotometer. ^1H NMR spectra were recorded on Bruker WP80SY spectrometer with TMS as internal standard. Elemental analyses were performed by M-H-W Laboratories, Phoenix Arizona, U.S.A.

General procedure for the photolytic reaction of $FeCp(CO)_2SCOR$ *with* EPh_3 (E = P, As, Sb)

A THF solution (100 cm^3) of the iron thiocarboxylate complex $FeCp'(CO)_2SCOR$ (usually 1.0 mmol) together with excess (1.5–2.0 mmol) EPh_3 was irradiated at 0°C (ice-bath). The reaction was monitored by IR spectroscopy and irradiation continued until the reaction had gone to completion. This is identified by the disappearance of the two ν(CO) stretching bands in the ranges 2060–2028 and 1998–1980 cm^{-1} that correspond to the two terminal carbonyls in the starting material $FeCp(CO)_2SCOR$, and the appearance of a single ν(CO) stretching band in the range 1954–1915 cm^{-1} that corresponds to the carbonyl group of the CO-substituted products $FeCp'(CO)EPh_3SCOR$.

All reactions gave only the mono-CO-substituted products and no other derivatives were observed. The products were separated by column chromatography (Silica 70–230 mesh). The column was eluted first with 1 : 10 (V/V) ether/n-hexane to isolate the unreacted EPh_3 and then with 1 : 2 (V/V) ether/n-hexane to separate the product. The products were recrystallized from CH_2Cl_2/hexane. The reaction times and the yields are presented in Table 1. Spectroscopic data are presented in Tables 2 and 3. Colours, melting points and elemental analysis are shown in Tables 4 and 5.

Table 1. Reaction time data and product yields for the photolytic CO-substitution reactions of $FeCp(CO)_2SCOR$ (**1–5**), $Fe(Bu^t\text{-}C_5H_4)(CO)_2SCOR$ (**6–8**) and $Fe(1,3\text{-}Bu^t_2\text{-}C_5H_3)(CO)_2SCOR$ (**9–11**) with EPh_3 (E = P, As, Sb)

	P compounds (**1a–11a**)		As compounds (**1b–8b**)		Sb compounds (**1c–8c**)	
Compound (R/E)	Reaction time (min)	(% yield)	Reaction time (min)	(% yield)	Reaction time (min)	(% yield)
1 CH_3	115	65	153	40	275	55
2 $(CH_3)_3C$	139	62	195	32	280	48
3 C_6H_5	158	75	215	45	295	62
4 $2\text{-}O_2N\text{-}C_6H_4$	80	85	155	60	195	71
5 $3,5\text{-}(O_2N)_2\text{-}C_6H_3$	30	90	75	73	86	75
6 CH_3	150	55	225	35	280	46
7 C_6H_5	175	68	205	61	295	60
8 $3,5\text{-}(NO_2)_2\text{-}C_6H_3$	90	72	168	53	215	46
9 CH_3	243	28	—	—	—	—
10 C_6H_5	370	22	—	—	—	—
11 $3,5\text{-}(NO_2)_2\text{-}C_6H_3$	185	24	—	—	—	—

Table 2. IR and ^{1}H NMR spectra for Fe(Cp)(CO)(PPh_3)SCOR (**1a–5a**), Fe(CP)(CO)($AsPh_3$)SCOR (**1b–5b**) and FeCp(CO)($SbPh_3$)SCOR (**1c–5c**)

Compound (R)	IR (CH_2Cl_2) (cm^{-1})	^{1}H NMR ($CDCl_3$) [δ(ppm)]
1a CH_3	1950(vs)^h, 1610(s)^k, 1475m, 1340m, 1140m, 1107m, 1092s, 988w, 944(m)^p	2.30(s, 3H, CH_3) 4.52(d, 5H, C_5H_5) 7.44(m, 15H, PPh_3)
2a $C(CH_3)_3$	1945(vs)^h, 1595(s)^k, 1472m, 1354m, 1090m, 1042m, 943(s)^p, 825m	1.13[s, 9H, $C(CH_3)_3$] 4.51(d, 5H, C_5H_5) 7.46(m, 15H, PPh_3)
3a C_6H_5	1950(vs)^h, 1589(s)^k, 1566s, 1477m, 1428w, 1165s, 1090w, 922(s)^p	4.58(d, 5H, C_5H_5) 7.43(m, 15H, PPh_3) 7.55(m, 3H, *m, p*-Ar-H) 7.99(m, 2H, *o*-Ar-H)
4a 2-(O_2N)-C_6H_4	1948(vs)^h, 1586(s)^k, 1520(s)^q, 1345(s)^q, 1195s, 945(s)^p, 890m	4.60(d, 5H, C_5H_5) 7.43(m, 18H, Ar-H and PPh_3) 7.83(m, 1H, *o*-Ar-H)
5a 3,5-$(O_2N)_2$-C_6H_3	1945(vs)^h, 1598(s)^k, 1540(s)^q, 1338(s)^q, 938(s)^p, 890m	4.63(d, 5H, C_5H_5) 7.42(m, 15H, PPh_3) 9.04(m, 3H, Ar-H)
1b CH_3	1943(vs)^h, 1608(s)^k, 1476m, 1343w, 1105w, 944(m)^p	2.28(s, 3H, CH_3) 4.59(s, 5H, C_5H_5) 7.36(m, 15H, $AsPh_3$)
2b $C(CH_3)_3$	1940(vs)^h, 1595(s)^k, 1360w, 943(s)^p, 830m	1.09[s, 9H, $C(CH_3)_3$] 4.59(s, 5H, C_5H_5) 7.35(m, 15H, $AsPh_3$)
3b C_6H_5	1945(vs)^h, 1587(s)^k, 1565s, 1476m, 1192s, 1175s, 1080m, 921(s)^p, 840m	4.66(s, 5H, C_5H_5) 7.36(m, 20H, Ar-H and $AsPh_3$)
4b 2-(O_2N)-C_6H_4	1942(vs)^h, 1590(s)^k, 1522(s)^q, 1342(s)^q, 1190s, 937(s)^p, 825s	4.71(s, 5H, C_5H_5) 7.41(m, 1H, *o*-Ar-H) 7.81(s, 18H, Ar-H and $AsPh_3$)
5b 3,5-$(O_2N)_2$-C_6H_3	1942(vs)^h, 1595(s)^k, 1540(s)^q, 1340(s)^q, 941(s)^p, 890m	4.71(s, 5H, C_5H_5) 7.41(m, 15H, $AsPh_3$) 8.99(s, 3H, Ar-H)
1c CH_3	1934(vs)^h, 1590(s)^k, 1480w, 1385m, 1123m, 1008m, 935(m)^p, 825m	2.01(s, 3H, CH_3) 4.65(s, 5H, C_5H_5) 7.52(m, 15H, $SbPh_3$)
2c $C(CH_3)_3$	1932(vs)^h, 1575(s)^k, 1583m, 1390m, 1370m, 1078m, 937(s)^p, 838m	0.86[s, 9H, $C(CH_3)_3$] 4.63(s, 5H, C_5H_5) 7.48(m, 15H, $SbPh_3$)
3c C_6H_5	1938(vs)^h, 1597(s)^k, 1655s, 1212m, 1080m, 929(s)^p, 847m	4.72(s, 5H, C_5H_5) 7.52(m, 20H, Ar-H and $SbPh_3$)
4c 2-(O_2N)-C_6H_4	1933(vs)^h, 1560(s)^k, 1525(s)^q, 1341(s)^q, 1195, 945(s)^p, 835s	4.82(s, 5H, C_5H_5) 7.41(m, 18H, *m, p*-Ar-H and $SbPh_3$) 7.89(m, 1H, *o*-Ar-H)
5c 3,5-$(O_2N)_2$-C_6H_3	1938(vs)^h, 1558(s)^k, 1535(s)^q, 1338(s)^q, 1095s, 944(s)^p	4.77(s, 5H, C_5H_5) 7.49(m, 15H, $SbPh_3$) 8.67(d, 2H, *o*-Ar-H) 8.91(t, H, *p*-Ar-H)

s: strong, vs: very strong, m: medium, w: weak. Superscripts: h = ν(C≡O), k = ν(C═O), p = ν(C···S), q = ν(N═O).

Table 3. IR and ^{1}H NMR spectra for Fe(Bu^t-C_5H_4)(CO)(PPh_3)SCOR (**6a–8a**), Fe(Bu^t-C_5H_4)(CO)($AsPh_3$)SCOR (**6b–8b**), Fe(Bu^t-C_5H_4)(CO)($SbPh_3$)SCOR (**6c–8c**) and Fe(1,3-Bu^t-C_5H_3)(CO)(PPh_3)SCOR (**9a–11a**)

Compound (R)	IR (CH_2Cl_2) (cm^{-1})	^{1}H NMR ($CDCl_3$) [δ(ppm)]
6a CH_3	1943(vs)[h], 1601(s)[k], 1480w, 1432w, 946(s)[p]	1.35[s, 9H, $C(CH_3)_3$] 2.24(s, 3H, CH_3) 3.25, 4.16 (two m, 2H, C_5H_4) 4.79(m, 2H, C_5H_4) 7.39(m, 15H, PPh_3)
7a C_6H_5	1948(vs)[h], 1598(s)[k], 1528m, 1430m, 1090s, 925(s)[p]	1.36[s, 9H, $C(CH_3)_3$] 3.45, 4.25, 4.81, 4.93 (four m, 4H, C_5H_4) 7.72(m, 15H, PPh_3) 7.97(m, 5H, Ar-H)
8a 3,5-$(O_2N)_2$-C_6H_3	1945(s)[b], 1558(s)[k], 1525(s)[q], 1335(s)[q], 1090s, 942(s)[p]	1.36[s, 9H, $C(CH_3)_3$] 3.81, 4.18, 4.83, 4.98 (four m, 4H, C_5H_4) 7.40(m, 15H, PPh_3) 8.91(m, 3H, Ar-H)
6b CH_3	1938(vs)[h], 1609(s)[k], 1450m, 1109m, 942(m)[p], 846m	1.30[s, 9H, $C(CH_3)_3$] 2.14(s, 3H, CH_3) 3.75, 4.21, 4.84, 5.09 (four m, 4H, C_5H_4) 7.69(m, 15H, $AsPh_3$)
7b C_6H_5	1941(vs)[h], 1600(s)[k], 1435m, 1094s, 946(s)[p]	1.33[s, 9H, $C(CH_3)_3$] 3.85, 4.20, 4.91, 5.03 (four m, 4H, C_5H_4) 7.54(m, 15H, $AsPh_3$) 7.94(m, 5H, Ar-H)
8b 3,5-$(O_2N)_2$-C_6H_3	1937(vs)[h], 1595(s)[k], 1530(s)[q], 1342(s)[q], 1098m, 910(m)[p]	1.33[s, 9H, $C(CH_3)_3$] 4.11, 4.21, 5.01, 5.20 (four m, 4H, C_5H_4) 7.38(m, 15H, $AsPh_3$) 8.73(d, 2H, *o*-Ar) 8.90(t, 1H, *p*-Ar)
6c CH_3	1928(vs)[h], 1598(s)[k], 1438m, 964(s)[p], 840m	1.32[s, 9H, $C(CH_3)_3$] 1.96(s, 3H, CH_3) 4.09, 4.34, 4.72, 4.94 (four m, 4H, C_5H_4) 7.44(m, 15H, $SbPh_3$)
7c C_6H_5	1930(vs)[h], 1585(s)[k], 1530m, 1435m, 1090s, 925(s)[p]	1.36[s, 9H, $C(CH_3)_3$] 4.05, 4.12, 4.78, 5.01 (four m, 4H, C_5H_4) 7.35(m, 20H, Ar-H and $SbPh_3$)
8c 3,5-$(O_2N)_2$-C_6H_3	1936(vs)[h], 1595(s)[k], 1535(s)[q], 1345(s)[q], 1090s, 932(s)[p]	1.36[s, 9H, $C(CH_3)_3$] 4.27, 4.39, 5.08, 5.11 (four m, 4H, C_5H_4) 7.43(m, 15H, $SbPh_3$) 8.63(d, 2H, *o*-Ar-H) 8.89(t, 1H, *p*-Ar-H)
9a CH_3	1928(vs)[h], 1602(s)[k], 1572m, 945(m)[p]	1.31, 1.81 [two s, 18H, $C(CH_3)_3$] 2.23(s, 3H, CH_3) 2.63, 4.73 (two m, 2H, 4.5-C_5H_3) 4.4(t, 1H, 2-C_5H_3) 7.46(m, 15H, PPh_3)
10a C_6H_5	1917(vs)[h], 1588(s)[k], 1090m, 1061m, 948(s)[p]	1.15, 1.34 [two s, 18H, $C(CH_3)_3$] 2.60, 4.48 (two m, 2H, 4.5-C_5H_3) 4.60(t, 1H, 2-C_5H_3) 7.56(m, 15H, PPh_3) 8.05(m, 5H, Ar-H)

Table 3—*continued*

Compound (R)	IR (CH_2Cl_2) (cm^{-1})	^1H NMR ($CDCl_3$) [δ(ppm)]
11a 3,5-$(O_2N)_2$-C_6H_3	1915(vs)[h], 1598(s)[k], 1530(s)[q], 1341(s)[q], 1093m, 940(m)[p]	1.15, 1.35 [two s, 18H, $C(CH_3)_3$] 2.55, 4.44 (two m, 2H, 4.5-C_5H_3) 4.60(t, 1H, 2-C_5H_3) 7.55(m, 15H, PPh_3) 8.02(t, 1H, *p*-Ar-H) 8.10(d, 2H, *o*-Ar-H)

s: strong, vs: very strong, m: medium, w: weak. Superscripts: h = ν(C≡O); k = ν(C═O); p = ν(C···S); q = ν(N═O).

Table 4. Melting points, colours and elemental analysis for the complexes $FeCp(CO)(PPh_3)SCOR$ (**1a–5a**), $FeCp(CO)(AsPh_3)SCOR$ (**1b–5b**) and $FeCp(CO)(SbPh_3)SCOR$ (**1c–5c**)

Compound	M.p. (°C)	Colour	Elemental analysis (%) C	H	S	N
1a CH_3	146–146	Red	63.5	5.0	6.4	—
			(64.2)	(4.7)	(6.6)	—
2a $C(CH_3)_3$	144–145	Red	65.6	5.6	5.8	—
			(65.9)	(5.5)	(6.0)	—
3a C_6H_5	156–158	Red–brown	67.7	4.6	5.6	—
			(66.9)	(4.6)	(5.8)	—
4a 2-(O_2N)-C_6H_4	166–167	Orange–red	62.8	4.1	5.4	2.3
			(62.7)	(4.0)	(5.4)	(2.4)
5a 3,5-$(O_2N)_2$-C_6H_3	148–149	Red	58.2	3.4	4.9	4.2
			(58.3)	(3.6)	(5.0)	(4.4)
1b CH_3	121–122	Red	58.9	4.5	6.1	—
			(58.9)	(4.3)	(6.0)	—
2b $C(CH_3)_3$	>200 (dec)	Orange–red	60.9	5.2	5.6	—
			(60.8)	(5.1)	(6.0)	—
3b C_6H_5	126–127	Dark–red	62.9	4.3	5.5	—
			(62.8)	(4.2)	(5.4)	—
4b 2-(O_2N)-C_6H_4	141–142	Red	58.1	4.0	4.9	2.2
			(58.4)	(3.8)	(5.0)	(2.2)
5b 3,5-$(O_2N)_2$-C_6H_3	161–162	Red	54.7	3.6	4.9	4.1
			(54.5)	(3.4)	(4.7)	(4.1)
1c CH_3	86–87	Violet	54.3	4.0	5.0	—
			(54.1)	(4.0)	(5.6)	—
2c $C(CH_3)_3$	102–103	Violet	55.9	4.8	4.9	—
			(56.2)	(4.7)	(5.2)	—
3c (C_6H_5)	124–125	Violet	58.1	3.7	5.0	—
			(58.1)	(3.9)	(5.0)	—
4c 2-(O_2N)-C_6H_4	146–147	Violet	53.9	4.0	4.6	2.1
			(54.4)	(3.5)	(4.7)	(2.0)
5c 3,5-$(O_2N)_2$-C_6H_3	155–156	Violet	51.5	3.0	4.5	3.9
			(51.0)	(3.2)	(4.4)	(3.8)

Values in parentheses are calculated, the others are found values.

Table 5. Melting points, colours and elemental analyses for the complexes $Fe(Bu^t\text{-}C_5H_4)(CO)(CO)(PPh_3)SCOR$ (**6a–8a**), $Fe(Bu^t\text{-}C_5H_4)(CO)(AsPh_3)SCOR$ (**6b–8b**), $Fe(Bu^t\text{-}C_5H_4)(CO)(SbPh_3)SCOR$ (**6c–8c**) and $Fe(1.3\text{-}Bu^t\text{-}C_5H_3)(CO)(PPh_3)SCOR$ (**9a–11a**)

Compound	M.p. (°C)	Colour	Elemental analysis (%) C	H	S	N
6a CH_3	124–125	Red	66.4	5.7	5.9	—
			(66.8)	(5.7)	(4.8)	—
7a C_6H_5	129–130	Red	69.5	5.5	5.3	—
			(69.4)	(5.4)	(5.0)	—
8a $3,5\text{-}(O_2N)_2\text{-}C_6H_3$	152–153	Red	60.6	4.8	4.5	4.1
			(60.5)	(4.5)	(4.6)	(4.0)
6b CH_3	89–90	Red	60.4	5.3	4.5	—
			(57.0)	(4.7)	(4.2)	—
7b C_6H_5	111–112	Red	46.8	5.1	4.9	—
			(46.8)	(5.1)	(5.0)	—
8b $3,5\text{-}(O_2N)_2\text{-}C_6H_3$	128–129	Red	56.9	4.2	4.3	3.8
			(56.8)	(4.3)	(4.3)	(3.8)
6c CH_3	105–106	Red	56.9	4.9	5.1	—
			(56.8)	(5.0)	(5.1)	—
7c C_6H_5	107–108	Red	60.4	4.8	4.6	—
			(60.2)	(4.5)	(4.7)	—
8c $3,5\text{-}(O_2N)_2\text{-}C_6H_3$	137–138	Red	53.5	4.0	4.1	3.1
			(53.5)	(4.0)	(4.2)	(3.7)
9a CH_3	117–118	Red	67.9	6.4	5.2	—
			(68.2)	(6.5)	(5.4)	—
10a C_6H_5	136–137	Red–brown	70.7	6.0	4.8	—
			(70.9)	(6.2)	(4.8)	—
11a $3,5\text{-}(O_2N)_2\text{-}C_6H_3$	108–109	Red	62.3	5.1	4.2	—
			(62.4)	(5.2)	(4.3)	—

Values in parentheses are calculated, the others are found values.

RESULTS AND DISCUSSION

The photolytic CO-substitution reactions of the thiocarboxylate compounds **1–11** with excess EPh_3 (E = P, As, Sb) were carried out in THF at 0°C. Cooling was necessary to minimize decomposition and to obtain reasonable reactions rates. The photolytic reactions conducted in this study result exclusively in the formation of the mono-CO-substituted derivatives $FeCp(CO)(EPh_3)SCOR$, $FeCp^*(CO)(EPh_3)SCOR$ and $FeCp^{**}(CO)(PPh_3)$-SCOR [$Cp = \eta^5\text{-}C_5H_5$, $Cp^* = \eta^5\text{-}(Bu^t\text{-}C_5H_4)$, $Cp^{**} =$

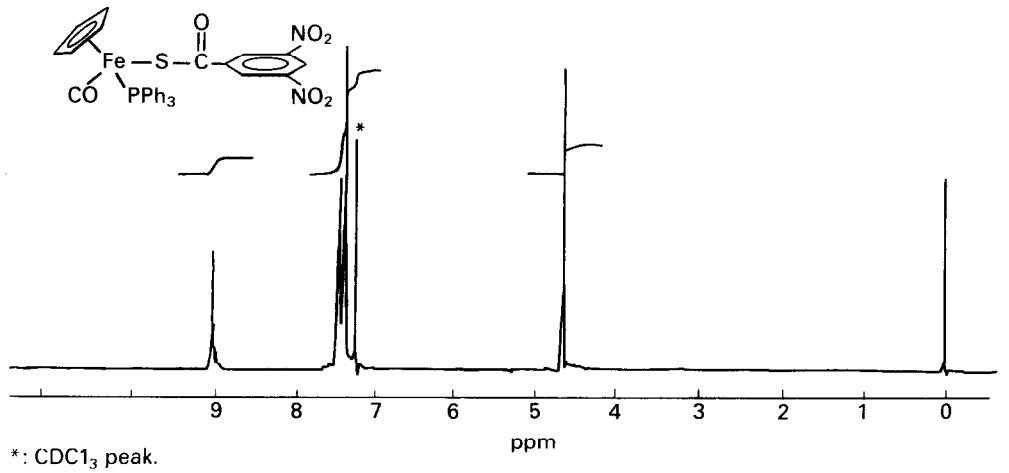

*: $CDCl_3$ peak.

Fig. 1. ^1H NMR spectra of $Fe(C_5H_5)(CO)(PPh_3)SCO(3,5\text{-}(NO_2)_2C_6H_3$.

η^5-(1,3-Bu^t_2-C_5H_3)], as shown in eqs (1), (2) and (3), respectively.

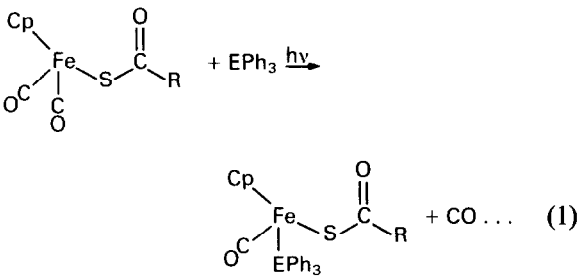

(1)

Compound (R/E)	P	As	Sb
1 CH_3	**1a**	**1b**	**1c**
2 $C(CH_3)_3$	**2a**	**2b**	**2c**
3 C_6H_5	**3a**	**3b**	**3c**
4 2-$(O_2N)_2$-C_6H_4	**4a**	**4b**	**4c**
5 3,5-$(O_2N)_2$-C_6H_3	**5a**	**5b**	**5c**

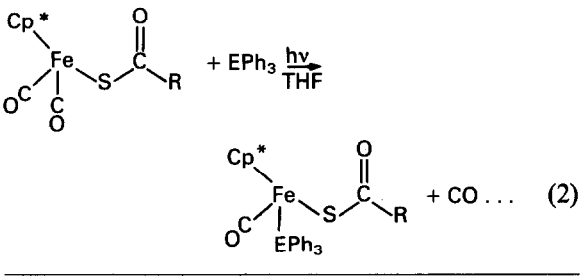

(2)

Compound (R/E)	P	As	Sb
6 CH_3	**6a**	**6b**	**6c**
7 C_6H_5	**7a**	**7b**	**7c**
8 3,5-$(O_2N)_2$-C_6H_4	**8a**	**8b**	**8c**

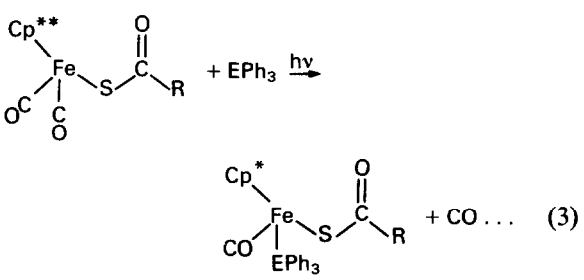

(3)

Compound (R/E)	P
9 CH_3	**9a**
10 C_6H_5	**10a**
11 3,5-$(O_2N)_2$-C_6H_3	**11a**

The synthesized complexes were characterized by elemental analysis, IR and ^{1}H NMR spectra. The ^{1}H NMR spectra of all complexes (Tables 2 and 3) show the characteristic protons in their expected chemical shift regions. Selected ^{1}H NMR spectra for $Fe(C_5H_5)(CO)(PPh_3)SCO(3,5\text{-}(NO_2)_2C_6H_3$, $Fe(Bu^t\text{-}C_5H_4)(CO)(AsPh_3)SCOCH_3$ and $Fe(Bu^t_2\text{-}C_5H_3)(CO)(PPh_3)SCO(3,5\text{-}NO_2)_2C_6H_3$ are shown in Figs 1, 2 and 3, respectively. Assignment of the protons of the different ligands is based on reported literature.[16]

The IR spectra for the CO-substituted complexes are presented in Tables 2 and 3. The spectra of all complexes show one strong terminal CO stretching band and another two bands in the ranges 1525–1610 and 920–950 cm^{-1}, characteristic of the C=O and (C—S) bonds of the S-bonded thiocarboxylate group.[17]

The value of the CO stretching frequency in these complexes is influenced by EPh_3 and the Cp substituents. Thus, ν(CO) for complexes having the same *R* and cyclopentadienyl ligand follows the order $PPh_3 > AsPh_3 > SbPh_3$. This trend is attributed to the increase in the Fe $d\pi$–π^*CO back-donation in going from PPh_3 to $SbPh_3$ because the π-acceptor ability of these ligands is of the order $PPh_3 > AsPh_3 > SbPh_3$.[18] Moreover, ν(CO) for complexes having the same R and EPh_3 follows the order Cp > Cp* > Cp**. This observation could be attributed to the σ-donor strength of the cyclopentadienyl ligand which increases on going from Cp to Cp**. Therefore, alkyl substitution on the Cp ring leads to an increase in the electron density around the iron atom and consequently the Fe $d\pi$–π^*CO back-donation increases.

As mentioned earlier, all the photolytic reactions conducted in this study afforded exclusively the mono-CO-substituted derivatives, FeCp'(CO)(EPh_3)SCOR (Cp' = Cp, Cp*, Cp**). Neither the ionic [FeCp$(CO)_2$-(EPh_3)]SCOR nor the disubstituted [FeCp$(EPh_3)_2$SCOR] products were observed in any of the reactions tried. This could be attributed to the presence of a strong Fe—S bond and to the steric repulsion of the thiocarboxylate moiety with the entering group (EPh_3).

Table 1 shows the product yields and the reaction time data for these photolytic CO-substitution reactions. The reaction time data shows clearly the dependence of these reactions on three major factors, namely, the donor atom E of the reactant EPh_3, the R group of the thiocarboxylate moiety and the substituents on the cyclopentadienyl ligand.

As far as the donor atom E of EPh_3 is concerned, the study shows that the substitution reaction rate follows the order $PPh_3 > AsPh_3 > SbPh_3$. This result is consistent with the previously reported observations.[19] It could be attributed to the nucleophilicity and π-accepting ability of the EPh_3 ligands

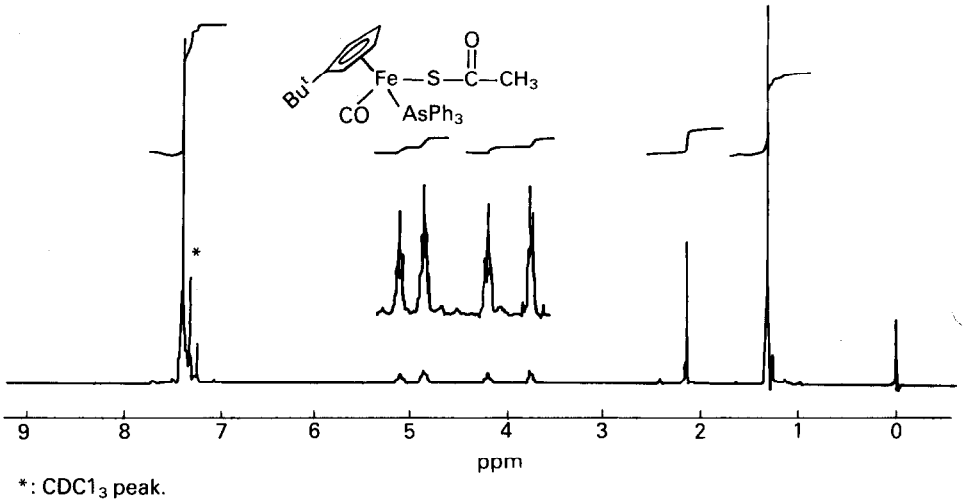

*: $CDCl_3$ peak.

Fig. 2. ^1H NMR spectra of $Fe(Bu^t\text{-}C_5H_4)(CO)(AsPh_3)SCOR$.

that are in the order $PPh_3 > AsPh_3 > SbPh_3$.[10]

Considering the effect of the R group of the SCOR moiety, the reaction time data show that the reaction rate follows the order $3,5\text{-}(O_2N)_2\text{-}C_6H_3 > 2\text{-}(O_2N)\text{-}C_6H_4 > CH_3 > C(CH_3) > C_6H_5$. It seems that the reaction time decreases as the electronegativity of R increases, except for C_6H_5. This result could be related to a decrease in the Fe—(CO) bond strength as a result of decreasing the electron density on the sulphur atom and consequently increasing Fe $d\pi$–S $d\pi$ back-donation and decreasing the electron donation from Fe to CO(π^*).[14,15] However, a mechanistic study using additional R groups is certainly necessary to get a clear picture and to come out with reliable conclusions about the effect of R in these reactions.

This study also shows that the tert-butyl substituents on the Cp ring influence the substitution reactions. The reaction time data indicate that the rates of the CO-substitution reactions with PPh_3 follow the order Cp > Cp* > Cp**. Both steric and electronic effects of the tert-butyl groups might be considered in explaining this order.

Finally, the steric effects of the tert-butyl substituents seem to be the most important factor that explains the absence of any product in the reactions of $FeCp^{**}(CO)_2SCOR$ with the bulky $AsPh_3$ and $SbPh_3$ which have a larger cone angle than PPh_3.[17,20]

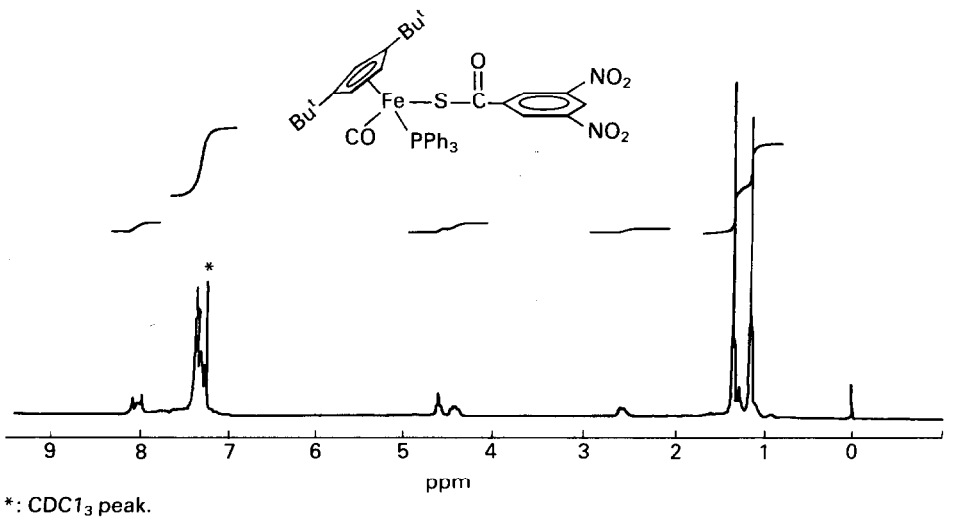

*: $CDCl_3$ peak.

Fig. 3. ^1H NMR spectra of $Fe(Bu^t_2\text{-}C_5H_3)(CO)(PPh_3)SCO(3,5\text{-}NO_2)_2C_6H_3$.

Acknowledgement—Financial support from Yarmouk University is gratefully acknowledged.

REFERENCES

1. P. M. Treichel, R. L. Shubkin, K. W. Barnett and D. Reichard, *Inorg. Chem.* 1966, **5**, 1177.
2. R. J. Hanines, A. L. due Preez and T. L. Marais, *J. Organomet. Chem.* 1971, **28**, 405.
3. D. A. Brown, H. J. Lyons, A. R. Manning and J. M. Rowley, *Inorg. Chim. Acta.* 1969, **3**, 346.
4. V. N. Pandey, *Inorg. Chim. Acta.* 1977, **22**, L39.
5. K. W. Barnett and P. M. Treichel, *Inorg. Chem.* 1966, **6**, 294.
6. C. R. Folkes and A. J. Rest, *J. Organomet. Chem.* 1977, **136**, 355.
7. H. G. Alt, M. E. Erechner, B. M. Janson and U. Thewalt, *Z. Naturforsch.* 1982, **37b**, 1109.
8. H. U. Wekel and W. Malisch, *J. Organomet. Chem.* 1984, **264**, C10.
9. G. Thum and W. Malisch, *J. Organomet. Chem.* 1984, **264**, C5.
10. P. M. Treichel and D. A. Komar, *J. Organomet. Chem.* 1981, **206**, 77.
11. E. M. Thorsteinson and F. Basolo, *J. Am. Chem. Soc.* 1980, **90**, 2531.
12. M. Cheong and F. Basolo, *Organometallics* 1988, **7**, 2041.
13. D. G. Alway and K. W. Barnett, *Inorg. Chem.* 1978, **17**, 2826.
14. M. A. El-Hinnawi and A. M. Al-Ajlouni, *J. Organomet. Chem.* 1987, **332**, 321.
15. M. A. El-Hinnawi, A. M. Al-Ajlouni, J. S. Abu-Nasser, A. K. Powell and H. Vahrenkamp, *J. Organomet. Chem.* 1989, **359**, 79.
16. M. A. El-Hinnawi, M. El-Khatib, I. Jibril and S. T. Abu-Orabi, *Synth. React. Inorg. Met.-Org. Chem.* 1989, **19**, 809.
17. M. O. Albers and J. Coville, *J. Organomet. Chem.* 1982, **232**, 261.
18. V. V. Savant, J. Gapalakrishnan and C. C. Patel, *Inorg. Chem.* 1977, **9**, 748.
19. G. G. Moor and R. B. Trego, *Tetrahedron* 1962, **18**, 205.
20. C. A. Tolman, *Chem. Rev.* 1977, **77**, 313.

Polyhedron Vol. 10, No. 18, pp. 2105–2110, 1991
Printed in Great Britain

0277–5387/91 $3.00+.00
© 1991 Pergamon Press plc

REDUCTION OF $Cl_2Sn[Fe(CO)_2(\eta^5\text{-}C_5H_5)]_2$ WITH LITHIUM TO FORM $\{:Sn[Fe(CO)_2(\eta^5\text{-}C_5H_5)]_2\}$

Z. DUAN, D. LEI and M. J. HAMPDEN-SMITH*

Department of Chemistry and Center for Micro-Engineered Ceramics, University of New Mexico, Albuquerque, NM 87131, U.S.A.

(*Received* 3 *April* 1991; *accepted* 18 *June* 1991)

Abstract—The reduction of $Cl_2Sn[Fe(CO)_2(\eta^5\text{-}C_5H_5)]_2$ (**1**) with lithium has been investigated. A species with one tin–tin bond, as shown by ^{119}Sn NMR spectroscopy, believed to be $[(\eta^5\text{-}C_5H_5)(CO)_2Fe]ClSn—SnCl[Fe(CO)_2(\eta^5\text{-}C_5H_5)]$ (**2**), is formed as an intermediate. Further reduction results in the formation of $\{:Sn[Fe(CO)_2(\eta^5\text{-}C_5H_5)]_2\}$ (**3**), which has been characterized by spectroscopic and analytical methods and is monomeric in benzene solution, as determined by cryoscopic molecular weight determination. The reactivity of **2** and **3** are discussed.

The synthesis of oligomers of the lower members of the Group 14 elements has been the subject of much study in recent years. Principally, three different synthetic approaches have been utilized to prepare oligomeric organo-germanium and organo-tin species. Linear organo-tin oligomers have been prepared in a stepwise fashion by the reaction of organo-stannyl anions with organo-tin halides.[1] Tin(II) halides have been reacted with Grignard reagents to form, oxidative coupling, a number of interesting spiro-cyclic organo-tin oligomers,[2–4] and the alkali metal-induced reduction of organo-germanium and tin halides has also resulted in the formation of a fascinating series of spiro-cyclic organo-germanium and tin species.[5–8] Other methods have also been used less widely, including thermolysis,[9] photolysis[10,11] and electrochemical reduction reactions.[12,13] We have recently demonstrated that the reduction of transition-metal substituted organo-halo germanes with lithium is an effective route for the formation of Ge—Ge bonds and that the substituent $[Fe(CO)_2(\eta^5\text{-}C_5H_5)]$ is inert to the reaction conditions.[14] However, there are surprisingly few examples of heavy Group 14 oligomers containing transition metal substituents. Pannell and co-workers have studied the synthesis and reactivity of transition-metal substituted organo-silyl compounds for many years[15] and have recently prepared some germanium and tin analogues. Mackay *et al.*[16–18] and Whitmore *et al.*[19] have prepared many examples of Group 14 elements containing transition-metal carbonyl clusters, and Lappert *et al.*[20] have prepared many species containing transition metal–Group 14 element bonds, but few examples contain Group 14–Group 14 elements bonds. We report here our findings on the reductive coupling of the transition-metal substituted halo-stannane, $Cl_2Sn[Fe(CO)_2(\eta^5\text{-}C_5H_5)]_2$.

EXPERIMENTAL

General procedures

All manipulations were carried out under an atmosphere of dry (4 Å molecular sieves), deoxygenated (MnO) nitrogen.[21] Hydrocarbon solvents were dried and distilled from sodium benzophenone ketyl and stored under nitrogen over molecular sieves. Deuterated NMR solvents were dried over 4 Å molecular sieves and stored under nitrogen. The starting material, $[Fe(CO)_2Cp]_2SnCl_2$, was prepared by the reaction of $SnCl_2$ (Aldrich) with $[Fe(CO)_2Cp]_2$ (Aldrich) using the method of Bonati and Wilkinson.[22] NMR spectra were recorded on a Bruker AC-250 NMR spectrometer. ^1H NMR chemical shifts were referenced to the protio impurity of the deuterated solvent, and ^{13}C NMR chemical shifts were referenced to the central ^{13}C

* Author to whom correspondence should be addressed.

NMR resonance of the deuterated solvent. ^{119}Sn NMR data were referenced to external Me_4Sn using the high frequency = positive sign convention. IR spectra were recorded on a Perkin–Elmer 1620 FTIR spectrometer. Mass spectral data were recorded on a Finnegan mass spectrometer. Elemental analyses were performed by Oneida Research Services.

Syntheses

(1) *Reaction condition A.* $Cl_2Sn[Fe(CO)_2(\eta^5\text{-}C_5H_5)]_2$ (0.52 g, 0.96 mmol) (**1**) was placed in a 250 cm^3 Schlenk flask and dissolved in 20 cm^3 of THF. An excess of lithium metal was added (15.3 mg, 2.2 mmol) and the mixture stirred at room temperature for 22 h. Immediately after the addition of lithium, the solution changed from orange to deep burgundy–red (3 h) and finally to red–brown after 22 h. During the reaction, samples were removed periodically in order to monitor the reaction by ^{1}H NMR spectroscopy, and the presence of an intermediate **2** was observed. After stirring for 22 h the volatile components were removed *in vacuo* to leave a red–brown residue, which was extracted with 3×20 cm^3 of toluene and filtered. The washings were combined, and the toluene was removed *in vacuo*. The residue was then washed with 4×10 cm^3 of n-pentane, dried *in vacuo* and weighed. The product (**3**) was isolated (0.225 g, 0.48 mmol) in 50% yield.

(2) *Reaction condition B.* A similar reaction was carried out on a larger scale where $Cl_2Sn[Fe(CO)_2(\eta^5\text{-}C_5H_5)]_2$ (2.00 g, 3.8 mmol) was dissolved in 80 cm^3 of THF in a 250 cm^3 Schlenk flask, and 80 mg (11 mmol) of lithium was added. The mixture was stirred at room temperature for a total of 36 h (when the reaction was complete). The volatile components were removed *in vacuo* to leave a red–brown residue, which was extracted with 4×20 cm^3 of benzene, filtered and the solvent removed *in vacuo* to give a red–brown solid. The product (1.80 g, 3.8 mmol) was obtained in quantitative yield.

Characterization data for **2**: ^{1}H NMR data (23°C, 250 MHz, C_6D_6): 4.66 ppm, s, $J(^{119,117}Sn—^1H) = 7.5$ Hz; (η^5-C_5H_5); ^{13}C NMR (23°C, 62.9 MHz, C_6D_6): 83.6 ppm, s, (η^5-C_5H_5); ^{13}CO was not observed; ^{119}Sn NMR data (23°C, 93.3 MHz, C_6D_6): 689.6 ppm, s, $J(^{119}Sn—^{117}Sn) = 2981$ Hz, 7.4%.

Characterization data for **3**: ^{1}H NMR data (23°C, 250 MHz, C_6D_6): 4.56 ppm, s, $J(^{119,117}Sn—^1H) = 5$ Hz (η^5-C_5H_5); ^{13}C NMR data (23°C, 62.9 MHz, C_6D_6): 84.5 ppm, s (η^5-C_5H_5); 215.5 ppm, s, $J(^{119}Sn—^{13}C) = 95$ Hz, CO; ^{119}Sn NMR data (23°C, 93.3 MHz, C_6D_6): 889.9 ppm, s. No change in line width was observed upon cooling to 183 K, but chemical shift changes were as follows (C_7D_8): 293 K, 887.5 ppm; 243 K, 894.7 ppm; 213 K, 899.5 ppm; 183 K, 904.4 ppm. IR data (KBr disc, cm^{-1}): 2007(s), 1964(s, br), 1915(s), 1429(w), 1413(w), 1001(w), 840(m), 637(m), 574(s), 512(m). Cryoscopic molecular weight determination (C_6H_6): molecular weight was measured at two different concentrations, 0.018 M and 0.033 M. The values were 437 ± 44 and 532 ± 35 Daltons, respectively. The calculated value for $\{Sn[Fe(CO)_2(\eta^5\text{-}C_5H_5)]_2\}$ is 473 Daltons. Each value was determined by three measurements: Mass spectral data (70 eV): 474, M, 3%, $[SnFe_2(CO)_4(\eta^5\text{-}C_5H_5)_2]^+$; 446, M, 5%, $[SnFe_2(CO)_3(\eta^5\text{-}C_5H_5)_2]^+$; 416, M, 10%, $[SnFe_2(CO)_2(\eta^5\text{-}C_5H_5)_2]^+$; 388, M, 5%, $[SnFe_2(CO)(\eta^5\text{-}C_5H_5)_2]^+$; 360, M, 18%, $[SnFe_2(\eta^5\text{-}C_5H_5)_2]^+$; 295, M, 21%, $[SnFe_2(\eta^5\text{-}C_5H_5)]^+$ and/or $Fe_2(CO)_2(\eta^5\text{-}C_5H_5)_2$; 296, M. 8%, $[Fe_2(CO)(\eta^5\text{-}C_5H_5)_2]^+$; 242, M, 5%, $[Fe_2(\eta^5\text{-}C_5H_5)_2]^+$; 186, 100%, $[Fe(\eta^5\text{-}C_5H_5)_2]^+$; 121, 80%, $[Fe(\eta^5\text{-}C_5H_5)]^+$; 91, 63%; 56, 58%, Fe^+. Two other peaks of higher mass were also observed: 650, 12%, M; 509, 18%, M. The letter "M" indicates that more than one peak was found centred around the value of m/z quoted. For a number of these fragments marked "M", the intensity ratio of the peaks corresponded very closely to the isotope ratio expected for the combination $SnFe_2$ (especially $m/z = 474$, 446, 416, and 390). Found: C, 35.9; H, 2.1; N, 0.0. Calc. for $C_{14}H_{10}O_4Fe_2Sn$: C, 35.5; H, 2.1%. Different reaction performed under reaction conditions B; Found: C, 35.84; H, 1.72; N, 0.00%.

(3) *Reaction of 3 with ethyl iodide.* Compound **3** (120 mg) was dissolved in 10 cm^3 of benzene, and 0.7 cm^3 (an excess) of ethyl iodide was added. The mixture was stirred for 30 min, but no change was observed. The volatile components was removed *in vacuo*, and ^{1}H NMR spectroscopy revealed that **3** was recovered unchanged. ^{119}Sn NMR spectroscopy exhibited a resonance at the chemical shift of authentic **3**, which remained a singlet during a gated decoupling experiment.

(4) *Reaction of 3 with pyridine.* The final product (**3**) (0.104 g, 0.2 mmol) was dissolved in 10 cm^3 of toluene, and 3.5 cm^3 (44 mmol, a large excess) of pyridine was added. The solution was stirred at room temperature for 1 h and the volatile components removed *in vacuo*. ^{119}Sn and ^{1}H NMR showed that no pyridine was present and that **3** was recovered unchanged.

(5) *Reaction of a mixture of 2 and 3 with isobutyl magnesium chloride.* $Cl_2Sn[Fe(CO)_2(\eta^5\text{-}C_5H_5)]_2$ (0.52 g, 0.96 mmol) was dissolved in 50 cm^3 of THF in a 100 ml Schlenk flask and lithium was added (9.6 g). The reaction mixture was monitored by ^{1}H

NMR spectroscopy and allowed to react until all the starting material had been consumed and a mixture of **2** and **3** remained. After 5 h, the ^1H NMR resonance of **1** was barely detectable. At this stage, the volatile components were removed *in vacuo*, and the deep red–brown residue was extracted with 13 cm^3 of toluene, washed with 4 cm^3 of toluene, the washings combined, and the flask placed in the freezer at −10°C. After 30 h, only a very small amount of microcrystalline material was formed. A small portion (3.5 cm^3) of this solution was removed for other experiments. The ratio of **2** : **3** in the remaining 13.5 cm^3 was found to be 28 : 72 by integration of the respective ^1H NMR cyclopentadienyl resonances. To half of this solution was added approximately 0.1 cm^3 of an ether solution of 2 M isobutyl magnesium chloride; a slight excess, assuming **2** contains two chloride substituents per molecule. The mixture was stirred for 1 h at room temperature during which time the solution turned deep red. The volatile components were removed *in vacuo*, and the residue was extracted with three 10 cm^3 portions of toluene extracted with three 10 cm^3 portions of toluene. ^1H NMR spectroscopy of the crude toluene extract showed that **3** was still present, but the cyclopentadienyl resonance of **2** had disappeared and a new resonance at 4.45 ppm was present in approximately the ratio relative to **3** as the original mixture of **2** : **3**.

RESULTS

The reaction of $[(\eta^5\text{-}C_5H_5)(CO)_2Fe]_2SnCl_2$ (**1**) with lithium metal results in the smooth formation of a reactive intermediate (**2**) and a final product (**3**), which analyses correctly as $\{Sn[Fe(CO)_2(\eta^5\text{-}C_5H_5)]_2\}_n$ according to eq. (1). Intermediate **2** is quantitatively converted into **3** by lithium after **1** has been completely consumed.

$$\underset{\mathbf{1}}{[(\eta^5\text{-}C_5H_5)(CO)_2Fe]_2SnCl_2} \xrightarrow{Li} \underset{\mathbf{2}}{[\text{intermediate}]} \xrightarrow{Li} \underset{\mathbf{3}}{\{Sn[Fe(CO)_2(\eta^5\text{-}C_5H_5)]_2\}_n} \quad (1)$$

This reaction is conveniently monitored by ^1H NMR spectroscopy by removing small aliquots of the reaction mixture at various intervals, removing the solvent *in vacuo*, and dissolving the residue in a deuterated solvent (benzene-d_6). Under the reaction conditions A, as described in the Experimental, the reaction of **1** with lithium metal for 3 h results in the formation of a deep burgundy–red solution, and ^1H NMR spectroscopy reveals that three cyclopentadienyl-containing species exist. These three species have ^1H NMR chemical shifts of 4.29, 4.54 and 4.66 ppm in the relative ratios 1 : 8.2 : 6, respectively. The ^1H NMR chemical shift of 4.29 ppm is consistent with the cyclopentadienyl resonance of the starting material (**1**), while 4.54 ppm is observed to be the chemical shift of the cyclopentadienyl resonance of the final product (**3**). All three resonances exhibit coupling to a single type of NMR-active tin nuclei (^{119}Sn: $I = 1/2$, natural abundance = 8.58%; ^{117}Sn: $I = 1/2$, natural abundance = 7.61%) with coupling constants of approximately 5 Hz. After 6 h, the starting material was barely detectable, and the resonances at 4.54 and 4.66 ppm were present in the integrated ratios 1 : 0.6, respectively. As the reaction proceeds further, the resonance at 4.54 ppm grows at the expense of the resonance at 4.66 ppm until, after 22 h, only the cyclopentadienyl resonance at 4.54 ppm is observed. ^{119}Sn NMR spectroscopy of the reaction mixture after 6 h reveals the presence of two ^{119}Sn NMR resonances. One resonance at 892.1 ppm corresponds to the resonance of the final product, while the other resonance occurs at 689.6 ppm and exhibits coupling to ^{117}Sn, where $J(^{119}Sn—^{117}Sn) = 2981$ Hz corresponding to $J(^{119}Sn—^{119}Sn) = 3119$ Hz with an integrated relative intensity that is consistent with the presence of one Sn—Sn bond (see Fig. 1). When the same reaction is carried out under slightly different conditions (Experiment B), the relative concentration of the NMR resonances at 4.66 ppm (^1H NMR) and 689.6 ppm (^{119}Sn NMR) increase, corresponding to intermediate **2**.

Elemental analysis of the final product of reductive coupling (**3**) is consistent with the empirical formula $\{Sn[Fe(CO)_2(\eta^5\text{-}C_5H_5)]_2\}_n$. Cryoscopic molecular weight determinations performed at two different concentrations indicate that **3** is monomeric in benzene solution. Confirmation that the Sn—Fe bond is intact in **3** comes from ^{13}C NMR spectroscopy of the carbonyl ligands in which coupling to both ^{119}Sn and ^{117}Sn is observed where $J(^{119}Sn—^{13}C) = 95$ Hz. In comparison, we have observed that $^2J(^{119}Sn—^{13}C) = 149$ Hz for the carbonyl ligands of **1** (see Fig. 2). The ^1H, ^{13}C and ^{119}Sn NMR spectra of both **2** and **3** are temperature invariant over the range 343–183 K. The IR spectrum of **3** is analogous to that of **1** and $[(\eta^5\text{-}C_5H_5)(CO)_2Fe]_2$. Unfortunately, attempts to isolate the intermediate (**2**) free of either starting material or final product have been unsuccessful. Attempts to monitor this reaction by UV–vis spectroscopy were irreproducible probably as a result of the photolytic lability of these compounds. We did not observe any reaction between **3** and either

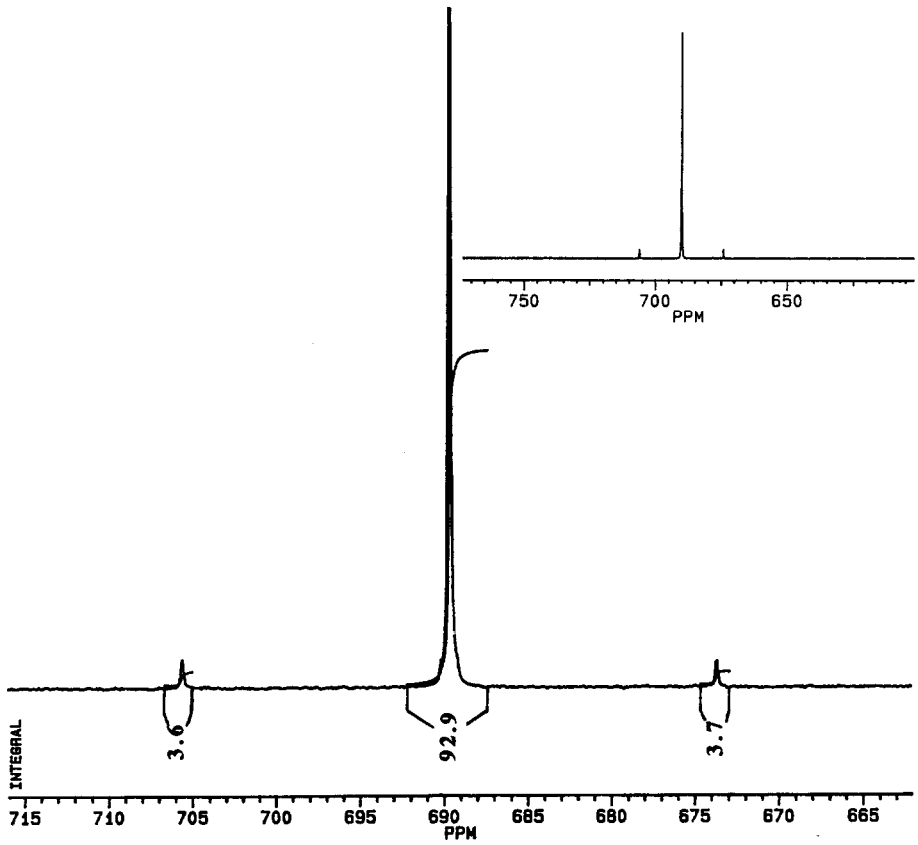

Fig. 1. Proton decoupled ^{119}Sn NMR spectrum of intermediate **2**, showing the ^{117}Sn satellite corresponding to the presence of one tin–tin bond.

ethyl iodide or pyridine under the conditions described in the Experimental. However, **2** reacted with isobutyl magnesium chloride.

DISCUSSION

The goal of this work is to explore the reductive coupling of transition-metal substituted halo-stannanes as a method for the formation of transition-metal substituted oligostannanes. In analogous reactions involving cyclopentadienyldicarbonyl-ferrio-substituted germanium species, we have shown that lithium-induced reductive coupling of Ge—Ge bonds occurs and that the $[Fe(CO)_2Cp]$ moiety is inert to these reaction conditions.[14] A control experiment was conducted according to eq. (2)

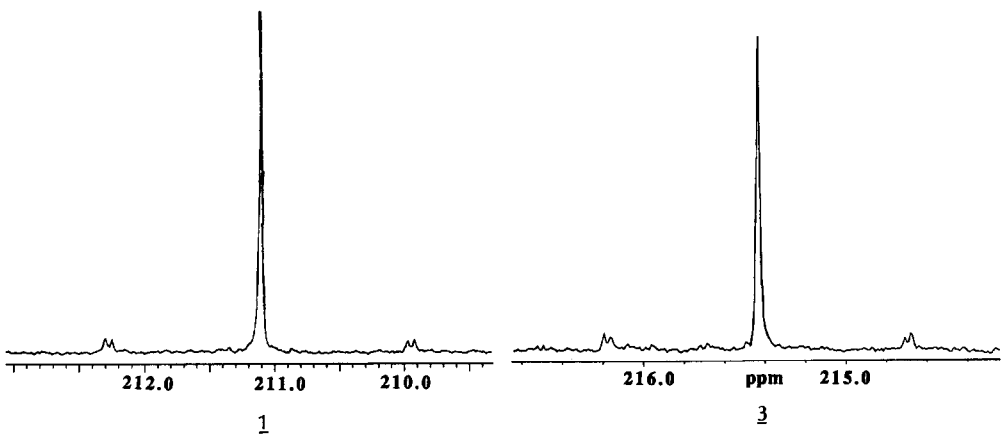

Fig. 2. Proton decoupled ^{13}C NMR spectra of the carbonyl region of **1** and **3**, showing the coupling to ^{117}Sn and ^{119}Sn.

$$[\eta^5\text{-}C_5H_5(CO)_2Fe]R_2GeCl + Li \xrightarrow{THF} 1/2\{[\eta^5\text{-}C_5H_5(CO)_2Fe]R_2Ge\}_2 + LiCl \quad (2)$$

in which the presence of a Ge—Ge bond was conclusively established by single crystal X-ray diffraction. In the present work, the reductive coupling of $Cl_2[SnFe(CO)_2(\eta^5\text{-}C_5H_5)]_2$ appears to follow a different course in which a species containing one tin–tin bond and $[Fe(CO)_2Cp]$ substituents is formed as an intermediate *en route* to isolation of $\{Sn[Fe(CO)_2(\eta^5\text{-}C_5H_5)]_2\}$. We propose that the most likely possibility for the identity of intermediate **2** is 1,2-dichloro-1,1,2,2-tetra(cyclopentadienyldicarbonylferrio)ditin, as shown in eq. (3).

$$\underset{\mathbf{1}}{Cl_2Sn[Fe(CO)_2(\eta^5\text{-}C_5H_5)]_2} \xrightarrow{Li} \underset{\mathbf{2}}{[(\eta^5\text{-}C_5H_5)(CO)_2Fe]_2ClSn—ClSn[Fe(CO)_2(\eta^5\text{-}C_5H_5)]_2} \xrightarrow{Li} \underset{\mathbf{3}}{\{Sn[Fe(CO)_2(\eta^5\text{-}C_5H_5)]_2\}} \quad (3)$$

The fact that **2** contains a tin–tin bond is clearly demonstrated by ^{119} Sn NMR spectroscopy where the tin–tin coupling constant is in the range expected. Unfortunately, since **2** has not been isolated, pure analytical data are not available. However, the presence of Sn—Cl bonds in **2** is consistent with the observations that, in the absence of lithium, solutions containing a mixture of **2** and **3** do not change (in the absence of light) and that **2** reacts with isobutyl magnesium chloride, whereas **3** does not. 1,2-dibromo-1,1,2,2-tetra(pentacarbonylmanganio)ditin has previously been unambiguously characterized[23] as the product of the reaction of $H_2Sn_2[Mn(CO)_5]_2$ with CBr_4.[24] Unfortunately, there are no NMR data available for these species for comparison to **2**.

In the presence of lithium, **2** reacts further to form the heavy metal carbene analogue (**3**) in preference to either an oligomeric tin species or a distannylene. All characterization data for **3** are consistent with the presence of a monomeric heavy carbene analogue, $\{:Sn[Fe(CO)_2(\eta^5\text{-}C_5H_5)]_2\}$, in solution. The possibility that the final product (**3**) exists as an equilibrium mixture of a number of different species is inconsistent with the variable temperature NMR data, where no changes were observed (assuming the rates of exchange are the same order as the NMR time scale). The presence of isocarbonyl–tin bonds was recently observed in similar tin species such as $\{Fe(CO)_3(\mu\text{-}CO)Sn[Fe(CO)_2(\eta^5\text{-}C_5H_5)]_2\}$-(O, Sn), but can be ruled out in the case of **3** as a result of the lack of an IR band in the vicinity of 1866 cm^{-1} in the solid state.[20] Other examples of transition-metal substituted stannylenes have been claimed,[25,26] such as $\{Sn[M(CO)_3(\eta^5\text{-}C_5H_5)]_2\}$, where M = Mo and W, but they have been refuted.[27] However, authentic examples of transition-metal substituted plumbenes have been prepared and unambiguously characterized, such as $\{Pb[Mo(CO)_3(\eta^5\text{-}C_5H_5)]_2\}$.[25] It is worth noting that, in the absence of a Lewis base (such as THF), the bis(metallaplumbene exists as a dimer with isocarbonyl bridges and two types of cyclopentadienyl NMR resonances. Attempts to isolate the base stabilized adduct of **3** $\{:Sn[Fe(CO)_2(\eta^5\text{-}C_5H_5)]_2 \cdot py$, were unsuccessful. This is consistent with the observation that **3** is not isocarbonyl bridged in the solid state.

Other examples of $[E(M'L_n)_2]$, where E = a lower Group 14 element, have been prepared and authenticated by single crystal X-ray diffraction, but are best considered as derivatives of Ge^{IV} or Pb^{IV}.[28–33] This chemistry has been extensively reviewed recently.[34–37]

Summary

The reductive coupling of $Cl_2Sn[Fe(CO)_2(\eta^5\text{-}C_5H_5)]_2$ with lithium metal in THF solution results in the formation of a species containing one tin–tin bond believed to be $[(\eta^5\text{-}C_5H_5)(CO)_2Fe]Cl\,Sn—SnCl[Fe(CO)_2(\eta^5\text{-}C_5H_5)]$ which, upon further reduction, forms $\{Sn[Fe(CO)_2(\eta^5\text{-}C_5H_5)]_2\}$ rather than transition-metal substituted tin oligomers.

Acknowledgements—We thank the Sandia University Research Program for financial support, the Research Allocation Committee (UNM), Dr Dan Doughty for helpful discussions, Eva Quesnell for typing this manuscript, and the NSF Chemical Instrumentation Program for the purchase of a low-field NMR spectrometer.

REFERENCES

1. S. Adams and M. Drager, *Angew. Chemie, Int. Edn Engl.* 1987, **26,** 1255.
2. L. R. Sita and R. D. Bickerstaff, *J. Am. Chem. Soc.* 1989, **111,** 6454.
3. L. R. Sita and R. D. Bickerstaff, *J. Am. Chem. Soc.* 1989, **111,** 3769.
4. L. R. Sita and I. Kiroshita, private communication.
5. Y. Kabe, M. Kwoda, Y. Honda, O. Yamashita, T. Kawase and S. Masamune, *Angew. Chemie, Int. Edn Engl.* 1988, **27,** 1725.
6. M. Kwoda, Y. Kabe, M. Hashimoto and S. Masamune, *Angew. Chemie, Int. Edn Engl.* 1988, **27,** 1727.
7. M. Weidenbruch, F.-T. Grimm, S. Pohl and W. Saak, *Angew. Chemie, Int. Edn Engl.* 1989, **28,** 198.
8. A. Sekiguchi, C. Kabuta and H. Sakwai, *Angew. Chemie, Int. Edn Engl.* 1989, **28,** 55.
9. H. Matsumoto, K. Higuchi, Y. Hashino, H. Koike,

Y. Naoi and Y. Nagai, *J. Chem. Soc., Chem. Commun.* 1988, 1083.
10. J. Park, S. Batcheller and S. Masamune, *J. Organomet. Chem.* 1989, **367,** 39.
11. W. Ando and T. Tsumwaya, *J. Chem. Soc., Chem. Commun.* 1987, 1514.
12. See e.g. W. G. Boboski and A. L. Allred, *J. Organomet. Chem.* 1975, **88,** 73.
13. C. Combes, R. J. P. Corrie, G. Dabosi, B. J. L. Herner and M. Martineau, *J. Organomet. Chem.* 1984, **270,** 141.
14. G. Barsuaskas, D. Lei, M. J. Hampden-Smith and E. N. Duesler, *Polyhedron* 1990, **9,** 773.
15. K. H. Pannell, J. M. Rozell and C. Hernandez, *J. Am. Chem. Soc.* 1989, **111,** 4482 and refs therein.
16. S. Anema, J. A. Audett, K. M. Mackay and B. K. Nicholson, *Dalton Trans.* 1988, 2629.
17. S. G. Anema, K. M. Mackay and B. K. Nicholson, *Inorg. Chem.* 1989, **28,** 3158.
18. J. A. Audett and K. M. Mackay, *J. Chem. Soc., Dalton Trans.* 1988, 2635.
19. K. H. Whitmire, C. B. Lagrone, M. R. Churchill, J. C. Fettinger and B. M. Robinson, *Inorg. Chem.* 1987, **26,** 3491.
20. P. B. Hitchcock, M. F. Lappert and M. J. McGeary, *Organometallics* 1990, **9,** 884 and refs therein.
21. D. F. Shriver and M.A. Drezden, *The Manipulation of Air-Sensitive Compounds*, 2nd edn, p. 78. Wiley-Interscience, New York (1986).
22. F. Bonati and G. Wilkinson, *J. Chem. Soc. A* 1964, 179.
23. A. L. Spek, K. D. Bos, F. J. Bulton and J. G. Noltes, *Inorg. Chem.* 1976, **15,** 339.
24. K. D. Bos, E. J. Bulton and J. G. Noltes, *J. Organomet. Chem.* 1975, **92,** 33.
25. P. B. Hitchcock, M. F. Lappert and M. J. Michalczyk, *J. Chem. Soc., Dalton Trans.* 1987, 2635.
26. P. G. Harrison and S. R. Stobart, *J. Chem. Soc., Dalton Trans.* 1973, 940.
27. M. F. Lappert and P. P. Power, *J. Chem. Soc., Dalton Trans.* 1985, 51.
28. H.-J. Kneuper, E. Herdweck and W. Herrman, *J. Am. Chem. Soc.* 1987, **109,** 2508.
29. G. Huttner, A. Weber, B. Segworth, O. Scheidsteger, H. Long and L. Zsolnai, *J. Organomet. Chem.* 1985, **282,** 331.
30. O. Scheidsteger, G. Huttner, K. Dehnicke and J. Pebler, *Angew. Chemie, Int. Edn Engl.* 1985, **24,** 428.
31. D. Melzer and E. Weiss, *J. Organomet. Chem.* 1984, **263,** 67.
32. W. Gade and E. Weiss, *J. Organomet. Chem.* 1981, **213,** 451.
33. N. M. Kostic and R. Fenske, *J. Organomet. Chem.* 1982, **233,** 337.
34. W. Herrmann, *Angew. Chemie, Int. Edn. Engl.* 1986, **25,** 56.
35. W. Petz, *Chem. Rev.* 1986, **86,** 1019.
36. M. S. Holt, W. C. Wilson and J. H. Nelson, *Chem. Rev.* 1989, **89,** 11.
37. M. F. Lappert and R. S. Rowe, *Coord. Chem. Rev.* 1990, **100,** 267.

Polyhedron Vol. 10, No. 18, pp. 2111–2121, 1991
Printed in Great Britain

0277–5387/91 $3.00+.00
© 1991 Pergamon Press plc

CADMIUM HALIDE COMPLEXES WITH PYRIDINE-N-OXIDE, AND THEIR CRYSTAL STRUCTURES

MARK NIEUWENHUYZEN, WARD T. ROBINSON* and CUTHBERT J. WILKINS*
Chemistry Department, University of Canterbury, Christchurch, New Zealand

(*Received* 4 *March* 1991; *accepted* 18 *June* 1991)

Abstract—Cadmium chloride and bromide form crystalline pyridine-N-oxide (pyo) complexes $[\{(CdCl_2)_3(pyo)_2\}_n]$ (**1**) and an isomorphous pair $[\{CdX_2(pyo)\}_n]$, X = Cl (**2A**), Br (**2B**). X-ray analysis of their structures shows them to have layer lattices arising from removal of a proportion of CdX_2 units from the cadmium halide structures. There is retention of six-coordination through insertion of pyo bridges. The pyo rings overlie the voids created by removal of the cadmium centres. Complexes **2A** and **2B** have the chromium chloride connectivity. The cadmium iodide lattice is more readily degraded and a series of compounds having increasing pyo content is formed; *viz* $[\{CdI_2(pyo)\}_n]$ (**3**) (an already known chain polymer), $[\{(CdI_2)_2(pyo)_3\}_n]$ (**4**), $[\{CdI_2(pyo)_2\}_2]$ (**5**), and $[Cd(pyo)_6]^{2+}$ $[CdI_4]^{2-}$ (**6**). Compound **4** is a chain polymer with mixed iodo- and oxo-bridges, and alternating five- and six-coordinated cadmium centres. Compound **5** is a pyo-bridged dimer with five-coordinate cadmium. In both **4** and **5** pyo plays both bridging and terminal roles. There is a methanolate derivative of **5**, $[\{CdI_2(pyo)_2(MeOH)\}_2]$ (**5A**), with six-coordinate cadmium. The structures show the ease with which cadmium moves between five- and six-coordination, as well as the breaking of the Cd—I bond. In these structures cadmium shows no evidence of any disposition towards the strong digonal bonding characteristic of mercury(II).

Cadmium halides form a wide range of coordination complexes,[1,2] with variety promoted not only by ligand characteristics,[3] but also by the ready variation in coodination number and stereochemistry permitted by the d^{10} configuration of a cadmium centre. With monodentate ligands of low steric demand, e.g. pyridine[4] or formamide,[5] formation of $CdX_2 \cdot L_2$ compounds having linear halogen-bridged chain structures with six-coordinate cadmium are common. There are also a few zigzag or double chain structures formed by $CdCl_2 \cdot L$ derivatives, as with methylurea[6] or water[7] in the monohydrate. In these, there is fusion of a pair of single chains by way of triple bridging provided by half the chlorine atoms. This triple bridging offsets the lower ligand : halide ratio and maintains the six-coordination. If a ligand itself were to have bridging properties there might be other variations.

The high polarity of the N—O bond in pyridine-N-oxide (pyo) means that it has both bridging capacity and the ability to promote ionization[8] through the formation of cations $[M(pyo)_6]^{n+}$. It is known to form cadmium halide derivatives $(CdCl_2)_3(pyo)_2$ (**1**), $CdBr_2(pyo)$ (**2B**) and $CdI_2(pyo)$ (**3**), all with low pyo : halide ratios.[9] The structures of the first two have remained unknown, but the last has been shown to have a polymeric chain structure of yet another type with bridges formed alternately by a pair of iodine atoms and a pair of oxygen atoms.[10] The cadmium is five-coordinate, with terminal linkage to the remaining iodine. With this interesting behaviour there seemed a case for closer examination of the behaviour of pyo towards cadmium halides, and determination of the structures of other derivatives.

It was confirmed first, that compounds **1**, **2B** and $CdCl_2(pyo)$ (**2A**), which is isomorphous with **2B**, are the only crystalline products obtainable from the chloride and bromide under our conditions. The

* Authors to whom correspondence should be addressed.

Table 1. Cadmium halide complexes with pyridine-N-oxide

	Compound	Structural type
1	$[\{(CdCl_2)_3(pyo)_2\}_n]$[a]	Polymeric sheet[b]
2A	$[\{CdCl_2(pyo)\}_n]$[c]	Polymeric sheet[b]
2B	$[\{CdBr_2(pyo)\}_n]$[a]	Polymeric sheet[b]
3	$[\{CdI_2(pyo)\}_n]$[a,d]	Chain polymer[e]
4	$[\{(CdI_2)_2(pyo)_3\}_n]$	Chain polymer[b,e]
5	$[\{CdI_2(pyo)_2\}_2]$	Bi-nuclear molecule[e]
5A	$[\{CdI_2(pyo)_2(MeOH)\}_2]$	Bi-nuclear molecule[b]
6	$[Cd(pyo)_6]^{2+}[CdI_4]^{2-}$	Ionic

[a] Compound already known.
[b] Six-coordinate cadmium.
[c] Isomorphous with **2B**.
[d] Structure previously reported.
[e] Five-coordinate cadmium.

Table 2. Analyses (%)[a]

Compound	C	H	N
1[b]	16.5(16.2)	1.35(1.36)	3.7(3.7)
1[c]	16.3(16.2)	1.32(1.36)	3.5(3.7)
2A	21.4(21.6)	1.63(1.80)	5.2(5.0)
2B	16.5(16.35)	1.40(1.37)	3.8(3.8)
3	13.1(13.0)	1.02(1.09)	3.1(3.0)
4	17.8(17.7)	1.38(1.49)	4.2(4.1)
4[d,e]	18.0(17.7)	1.42(1.49)	4.2(4.1)
5	21.7(21.6)	1.92(1.81)	5.15(5.0)

[a] Calculated values in parentheses.
[b] Primary crop.
[c] Recrystallized plates, from which diffractometer sample was obtained.
[d] Acicular form from ethanol.
[e] I, 50.4 (51.0)%.

compounds have layer lattices with ligand bridges, which represent only modifications of the parent CdX_2[11] structure. With cadmium iodide on the other hand, there is more complete degradation of the lattice and increase in the pyo : CdI_2 reactant ratio produces a succession of derivatives **3**, **4**, **5** and **6**, as listed in Table 1. There is a methanolate (**5A**) akin to **5**.

EXPERIMENTAL

Preparations

The compounds were obtained by direct reaction of the halide with pyo in ethanol or methanol. Ligand : halide ratios were varied between equimolecular and 12 : 1, or greater. Methanol provided greater solubility for the parent cadmium halide and faster reaction. It was suitable for the preparation of **1**, **2A**, **2B** and **4**, but ethanol was preferable for **5** and essential for **3** and **6**. Preparation of all cadmium iodide derivatives is, however, prone to complication through the initial appearance of non-equilibrium phases (and some irreproducibility), evidently through lack of requisite nucleation for the equilibrium phases. For recovery, crystals were rinsed with triethoxymethane and dry ether, and dried under a nitrogen stream. Analytical compositions of products are given in Table 2.

$[\{(CdCl_2)_3(pyo)_2\}_n]$ (**1**). With modification of the earlier procedure,[9] pyo (2 mM) in methanol was added to $CdCl_2 \cdot 2.5H_2O$ (2 mM) in boiling methanol (100 cm^3) containing triethoxymethane (4 cm^3). The solution was boiled, filtered, and evaporated to *ca* 40 cm^3. A mass of fine crystals (elongated plates) appeared. Larger single crystals suited to diffractometry were obtained as single or clustered plates by evaporating the mother liquor to half volume and allowing crystallization at *ca* 5°.

$[\{CdCl_2(pyo)\}_n]$ (**2A**). Using a similar procedure, but with the pyo : halide ratios not less than 6 : 1, and boiling for 1 h, analytically pure **2A** separated in finely divided form. Larger crystals were not obtainable, but structural identity with the bromide (**2B**) is shown by powder diffraction data (Table 3).

$[\{CdBr_2(pyo)\}_n]$ (**2B**). The primary product from methanol[9] was finely divided, but recrystallization from dilute solution gave clear (leaf-like) plates, but rather inferior for structure analysis. Variation of reactant ratios did not lead to different products.

$[\{CdI_2(pyo)\}_n]$ (**3**). Clear acicular crystals were obtained from ethanol.[9,10] Use of methanol usually gave **4** and/or **5**, but occasionally large tabular crystals of **3** slowly appeared. The identity of such mor-

Table 3. X-ray powder *d* values for **2A** and **2B**[a]

2A	**2B**	**2A**	**2B**
9.92(100)	9.99(100)	3.29(41)	3.27(24)
5.91(58)	6.09(11), 5.98(14)	3.23(41)	
		3.10(23)	3.20(20)
5.58(32)[b]	5.51(40)	2.98(34)	2.98(18)
5.10(22), 4.98(29)	5.22(8)	2.80(22)	2.85(14)
		2.65(16), 2.61(33)	2.68(19)
4.51(19)	4.61(11)		
4.35(29)[b]	4.33(10)	2.56(27)	2.56(13)

[a] Relative intensities in parentheses.
[b] Value for **2A** greater than for **2B**.

Table 4. Crystal data, experimental conditions and refinement

	$[\{(CdCl_2)_3(pyo)_2\}_n]$ (1)	$[\{CdBr_2(pyo)\}_n]$ (2B)	$[\{(CdI_2)_2(pyo)_3\}_n]$ (4)	$[\{CdI_2(pyo)_2\}_2]$ (5)	$[\{CdI_2(pyo)_2(MeOH)\}_2]$ (5A)	$[Cd(pyo)_6]^{2+}[CdI_4]^{2-}$ (6)
M	739.9	367.3	508.7	556.4 ("monomer")	588.4	1302.4
Crystal size (mm)	$0.32\times0.28\times0.10$	$0.50\times0.28\times0.10$	$0.41\times0.20\times0.10$	$0.75\times0.35\times0.12$	$0.4\times0.4\times0.15$	$0.25\times0.1\times0.1$ (*ca*)
Crystal system	Orthorhombic	Triclinic	Orthorhombic	Triclinic	Orthorhombic	Triclinic
Space group (Z)	*Pbca* (8)	$P\bar{1}$(2)	*Pbca*(8)	$P\bar{1}$(2)	*Pbca*(8)	$P\bar{1}$(2)
a (Å)	7.672(5)	6.641(9)	13.442(14)	7.747(8)	12.397(4)	10.006(7)
b (Å)	11.102(17)	6.888(8)	15.455(7)	11.086(9)	15.742(6)	9.891(6)
c (Å)	22.653(18)	10.309(2)	23.181(12)	10.513(8)	17.119(8)	20.941(23)
α (°)	90	71.63(13)	90	64.38(6)	90	78.04(7)
β (°)	90	82.08(14)	90	74.29(8)	90	84.51(7)
γ (°)	90	65.58(9)	90	66.57(7)	90	80.03(5)
U (Å^3)	1929.5(3.5)	407.5(1.1)	4815(6)	741.6(1.2)	3340.8(2.5)	1993.2(3.0)
$D_c(D_m)^a$	2.55(2.47)	3.00(2.90)	2.81(2.69)	2.49(2.42)	2.34	2.17(2.10)
F(000)	1384	336	3664	508	2176	1216
μ (cm^{-1}), Mo-K_α	41.15	123.2	68.58	55.52	49.7	41.74
Range h	0–10	−10 to 10	0–17	0–10	0–12	0–12
Range k	0–14	−10 to 10	0–20	−14 to 14	0–22	−12 to 12
Range l	0–27	0–15	0–29	−12 to 13	0–24	−25 to 25
Unique reflections	1983	2092	4422	2609	3003	7020
Reflections used	1073 ($I > 3\sigma I$)	1599 ($I > 3\sigma I$)	2878 ($I > 3\sigma I$)	2139 ($I > 2\sigma I$)	2150 ($I > 2\sigma I$)	5828 ($I > 2\sigma I$)
Transmission range	0.883–0.487	0.725–0.119	0.947–0.475	1.000–0.560	0.738–0.528	0.708–0.615
Parameters refined	106	91	239	154	175	436
Weighting (g)	0.0009	0.0006	0.00021	0.00047	0.00016	0.00016
Residual density (e Å^{-3})	1.32, −1.32	2.80, −3.31[b]	1.77, −1.67	1.60, −1.15	0.95, −1.12	0.97, −1.04
$R(R')$	0.0481 (0.0583)	0.0552 (0.0661)	0.0435 (0.0400)	0.0429 (0.0478)	0.0370 (0.0313)	0.0339 (0.0351)

[a] D_c at 150 K; D_m at room temperature.

[b] The high residuals are in the vicinity of cadmium and bromine.

phologically different crystals was provided by cell parameters on a broken fragment.

$[\{(CdI_2)_2(pyo)_3\}_n]$ (**4**). This product, usually in admixture with **5**, crystallized from methanol solutions having pyo : CdI_2 in the wide range 1 : 1 to 6 : 1, e.g. pyo (1.5 mM) and CdI_2 (1 mM) in 12 cm^3. The clear crystals were diamond-like with bevelled edges. They were readily distinguished and separated from those of **5** under the microscope. Surprisingly, this product was also obtained (though now in acicular form) from ethanol containing very high pyo : CdI_2 ratios (18 : 1). Its appearance over such varying pyo concentrations shows its crystal nucleation can occur preferentially.

$[\{CdI_2(pyo)_2\}_2]$ (**5**) *and* $[Cd(pyo)_6]^{2+}[CdI_4]^{2-}$ (**6**). Clustered crystals of **5** together with individual prisms suitable for diffraction separated from solutions containing pyo (3 mM) and CdI_2 (0.5 mM) in boiling ethanol (10 cm^3). Dissolution was not complete, but clear crystals separated from the mother liquor.

Crystals of **6** slowly separated when a solution obtained by boiling pyo (5–6 mM) and CdI_2 (0.5 mM) in ethanol (12 cm^3) was allowed to stand.

The methanolate $[\{CdI_2(pyo)_2(MeOH)\}_2]$ (**5A**). Crystallization of this phase from methanol is favoured by reduced temperature, but can be prejudiced by prior crystallization of **5**. Cadmium iodide (0.035 mM) and pyo (7.0 mM, large excess) dissolved in boiling methanol (10 cm^3) gave crystals of **5** at room temperature. However, over a period of 4 weeks there was growth of clear tabular crystals of **5A**. The dry crystals are unstable in air at room temperature, probably due to superficial loss of methanol.

X-ray structure determination. The general procedure was as peviously described.[12] Crystals were held at *ca* 150 K, and ω scans were used. The usual scan speed was 4.88° min^{-1}, over the 2θ range 4–50 or 60°. Details on crystal data, other experimental conditions etc. are given in Table 4. Heavy atoms were located from Patterson maps, and other atoms from difference Fourier syntheses. Hydrogen atoms were introduced at idealized positions, but in **5A**, where the hydrogen atoms appeared, the position of the hydroxylic proton was allowed to refine. The function minimized in the least-squares refinement, with anisotropic thermal parameters, was $\Sigma w(|F_o| - |F_c|)^2$, and reflection weights $w = [\sigma^2|F_o| - g|F_o|^2]^{-1}$. The SHELXTL package[13] was used for data reduction and structure solution.

The more significant bond lengths and angles are listed in Table 5. Additional material available from the Cambridge Crystallographic Data Centre com-

Table 5. Bond lengths (Å) and bond angles (°)

$[\{(CdCl_2)_3(pyo)_2\}_n]$ (**1**)

Cd(1)—Cl(2)	2.576(4)	Cd(1)—O	2.248(8)
Cd(1)—Cl(3)	2.644(4)	Cd(2)—O	2.329(8)
Cd(2)—Cl(1)	2.599(4), 2.592(4)	O—N	1.362(13)
Cd(2)—Cl(2)	2.541(4)	N—C	1.334(16) av
Cd(2)—Cl(3)	2.717(4), 2.681(4)	Cd(1)···Cd(2)	3.855, 3.841

Cd(1)—Cl(3)—Cd(2)	92.0(1), 92.3(1)	Cd(1)—O—Cd(2)	114.8
Cd(2)—Cl(2)—Cd(2)	96.0(1)	Cd(1)—O—N	121.6(6)
Cl(1)—Cd(1)—Cl(3)	85.2(1)	Cd(2)—O—N	121.6(6)
Cl(1)—Cd(2)—Cl(3)	85.8(1), 86.4(1)	O—N—C(1)	122.0(9)
	159.5(1)	O—N—C(5)	115.5(11)
Cl(3)—Cd(1)—O	77.2(2), 102.3(2)		

$[\{CdBr_2(pyo)\}_n]$ (**2B**)

Cd—Br(1)/Br(1)′[a]	2.722(1), 2.764(1)	O—N	1.338(10
Cd—Br(2)/Br(2)′[a]	2.774(1), 2.691(1)	N—C(1)	1.335(12)
Cd—O/O′[a]	2.353(9), 2.304(10)	N—C(5)	1.345(15)

Br(1)—Cd—Br(1)′	82.3(1)	Cd—O—Cd	115.1(2)
Br(2)—Cd—Br(2)′	86.1(1)	Cd—Br(1)—Cd	97.7(1)
O—Cd—O′	64.8(3)	Cd—Br(2)—Cd	93.9(1)
O—Cd—Br(1)	161.2(2)	Cd—O—N	122.1(8)
O′—Cd—Br(2)′	153.8(2)	O—N—C(1)	118.4(9)
Br(1)′—Cd—Br(2)	170.9(1)	O—N—C(5)	118.7(7)

Ring inclinations to layer plane: Cd—O—Cd′—O′, 57.7; Cd—Br(1)—Cd′—Br(1)′, 58.7; Cd—Br(2)—Cd′—Br(2)′, 68.5; pyo ring, 85.6°.

$[\{(CdI_2)_2(pyo)_3\}_n]$ **(4)**

Cd(1)—I(1)[b]	2.801(1)	Cd(1)—I(4)[b,c]	2.736(1)
Cd(1)—I(2)[d]	2.972(1)	Cd(2)—I(2)[d,c]	2.776(1)
Cd(1)—I(3)[d]	3.309(1)	Cd(2)—I(3)[d,c]	2.776(1)
Cd(1)—O(1)[d]	2.321(7)	Cd(2)—O(1)[d,e]	2.357(8)
Cd(1)—O(3)[d]	2.374(8)	Cd(2)—O(3)[d,e]	2.438(8)
Cd(1)—O(2)[b]	2.286(9)	O(2)—N(2)	1.330(12)

I(1)—Cd(1)—O(1)	165.6(2)	I(2)—Cd(2)—I(3)	114.5(1)[b,c]
I(1)—Cd(1)—O(2)	1.58.6(2)	I(2)—Cd(2)—I(4)	117.9(1)[b,c]
I(3)—Cd(1)—O(3)	160.2(2)	I(3)—Cd(2)—I(4)	127.7(1)[b,c]
O(1)—Cd(2)—O(3)	166.7(3)[b,d]	Cd(1)—O(2)—N(2)	119.4(6)

Cd(1)—I(2)—Cd(2)—O(3) ring angles: 80.3, 85.2, 83.5, 108.0, respectively
Cd(1)—I(3)—Cd(2)—O(1) ring angles: 75.4, 85.4, 79.2, 115.5, respectively

$[\{CdI_2(pyo)_2\}_2]$ **(5)**

Cd—I(1)	2.736(1)	Cd—O(2)	2.307(8)
Cd—I(2)	2.745(1)	O(2)—N(2)	1.335(9)
Cd—O(1)	1.385(6)		
Cd—O(1)′	2.270(6)	Cd···Cd	3.57

I(1)—Cd—I(2)	125.8(1)	I(2)—Cd—O(1)′	114.5(2)
O(1)—Cd—O(2)	152.0(2)	Cd—O(2)—N(2)	117.4(6)
O(1)—Cd—O(1)′	69.3(3)	Cd—O(1)—N(1)	116.8(4)
Cd—O(1)—Cd′	110.7(3)	Cd′—O(1)—N(1)	125.4(4)
I(1)—Cd—O(1)′	118.4(2)		

Ring inclinations to Cd—O(1)—Cd′—O(1)′: pyo(N1), 54.2°, pyo (N2), 45.7°.

$[Cd(pyo)_6]^{2+}[CdI_4]^{2-}$ **(6)**

Cd(1)—I(1)	1.805(1)	Cd(2)—O(1)	2.263(4)
Cd(1)—I(2)	2.764(1)	Cd(2)—O(2)	2.241(4)
Cd(1)—I(3)	2.797(1)	Cd(1)—O(3)	2.278(4)
Cd(1)—I(4)	2.772(1)	Cd(3)—O(4)	2.280(4)
O—N	1.332 av	Cd(3)—O(5)	2.276(4)
		Cd(3)—O(6)	2.269(4)

I—Cd—I	range 106.1(1)–116.9(1)
O—Cd—O	range 86.4(2)–95.5(2)
Cd—O—N	range 114.7(4)–125.7(3); 120.2 av

$[\{CdI_2(pyo)_2(MeOH)\}_2]$ **(5A)**

Cd—I(1)	2.783(1)	O(3)—C(3)	1.404(10)
Cd—I(2)	2.823(1)	O(1)—N(1)	1.348(7)
Cd—O(1)	2.343(5)	O(2)—N(2)	1.339(8)
Cd—O(1)′	2.365(5)	O(3)—H(3)	0.78 (0.12)
Cd—O(2)	2.387(5)	Cd···Cd	3.948
Cd—O(3)	2.369(5)	O(2)···O(3)	2.715

I(1)—Cd—I(2)	103.1	Cd—O(1)—Cd′	114.0(2)
O(1)—Cd—O(1)′	66.0(2)	Cd—O(3)—C(3)	128.3(5)
O(1)—Cd—I(1)	157.6(1)	Cd—O(1)—N(1)	120.4(4)
O(1)′—Cd—I(2)	164.9(1)	Cd′—O(1)—N(1)	125.6(4)
O(2)—Cd—O(3)	148.0(2)	Cd—O(2)—N(2)	129.5(4)

Plane inclinations to Cd—O(1)—Cd′—O(1)′: mean-plane Cd, Cd′, O(2), O(2)′, O(3), O(3)′, 89.4; pyo (N1) ring, 83.0; pyo(N2) ring, 71.2; mean-plane C(3), O(3), H(3), 55.8.

[a] Symmetry-related atoms of the bridging rings: Br(1)′, $1-x$, $-y$, $1-z$; Br(2)′, $-x$, $1-y$, $1-z$; O′, $1-x$, $1-y$, $1-z$.
[b] Terminal.
[c] tbp equatorial positions.
[d] Bridging.
[e] tbp apical positions.

prises atom coordinates, thermal parameters and remaining bond lengths and angles.

RESULTS AND DISCUSSION

Comments on the structures of individual compounds

The structures show that at the lower pyo : CdX_2 ratios, pyo engages in bridging before terminal bonding develops. This ligand bridging can be by pyo pairs (as in **2**, **3** and **5**) or through mixed bridging with halide (as in **1** and **4**). This compatibility of the O and X atoms for bridging metal centres arises from the ease with which the atoms can accommodate bond angle variations.[12,14] It would also seem to reflect the prior existence in solution of halide-bridged species which can become ligand stabilized.

$[\{(CdCl_2)_3(pyo)_2\}_n]$ (**1**) *and* $[\{CdX_2(pyo)\}_2]$ (**2A**), (**2B**). These layer lattice structures both relate to the "parent" CdX_2 structure,[11] but not directly to one another. In the layer lattice of **1** there are two different octahedral cadmium environments. Cd(1) is linked diametrically to a pair of simple-bridging Cl(2) atoms, a pair of triple-bridging Cl(3) atoms, and a pair of bridging ligands, as in Fig. 1. Coordination around Cd(2) is provided by two Cl(1) atoms, one Cl(2), two Cl(3) and a ligand bridge. The Cl(2)/Cl(3) combination provides bridging to a Cd(1) centre, ligand/Cl(3) to a second Cd(1), and the two equivalent Cl(1)/Cl(3) combinations to two different Cd(2) centres.

In an atom row in the A···A′ direction there are seen to be alternating Cd(1) and Cd(2) centres, but in the adjacent parallel rows the Cd(1) atoms are omitted at the positions marked *. The ligand rings extend across the voids. There are thus twice as many Cd(2) as Cd(1) centres, and the ligand count is two-thirds of the total of cadmium centres. The Cd(1) atoms within each layer are coplanar, with z coordinates 0.5, but the conjunction of simple and triple-bridging causes the Cd(2) atoms to lie alternately 1.82 Å above and below this 002 plane. The complexity of the Cd—Cl bonding accounts for the inadequacy of IR evidence towards indication of the structure.[9]

In **2A**/**2B** the layer structure is more simple. The cadmium atoms all lie in the one plane and their six-coordination is provided by two pairs of bridging halogen atoms and one pair of bridging ligand oxygen atoms. In relation to the CdX_2 structure there is omission of every third cadmium centre (together with two corresponding bridging halogens) along

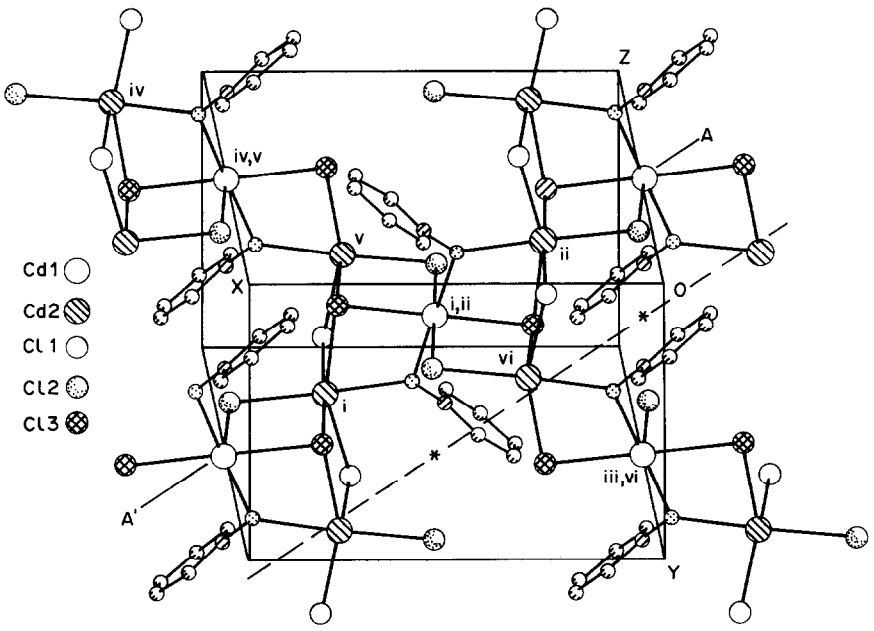

Fig. 1. A single layer for **1** as viewed nearly in the [011] direction. The origin is at the lower rear right of the cell. The z coordinates of Cd(1) atoms are 0.5, but those of alternate Cd(2) are 0.42 and 0.58, respectively. Unoccupied Cd(1) positions (as compared with a $CdCl_2$ lattice) are indicated by *. Symmetry codes shown for cadmium atoms are: (i) x, y, z; (ii) $1-x, 1-y, 1-z$; (iii) $\frac{1}{2}-x, \frac{1}{2}+y, z$; (iv) $\frac{1}{2}+x, \frac{1}{2}-y, 1-z$; (v) $1\frac{1}{2}-x, y-\frac{1}{2}, z$; (vi) $x-\frac{1}{2}, 1\frac{1}{2}-y, 1-z$.

diagonals in the B—B′ direction as seen in Fig. 2. All bridging atoms are thereby reduced to a two-way rather than a triple-bridging role. The "missing" halogen bridges are replaced by ligand oxygen bridges. The connectivity so developed corresponds precisely with that in the chromium trichloride structure.[11b,15] Pairs of pyo rings are disposed above and below the voids arising from cadmium omission, as with **1**. The rings projecting from the layers provide the relatively few approaches (to Br) which are mainly responsible for inter-layer cohesion. Even so, the Br—C(H) inter-layer closest approaches, 3.7(3.0)–3.75(3.1) Å, are slightly longer than the intra-layer approaches, *ca* 3.6(2.8) Å. The weak cohesion would seem to underlie not only the poor crystal development, but also the probability of a small degree of layer misplacement. We have observed that for different crystals the cell parameters c and β are variable. On one crystal the c value, which is determined by inter-layer spacing, was 10.381 Å (cf. 10.309 in Table 4).

It will be noticed that the *trans* disposition of the ligands around Cd(1) in **1** contrasts with the *cis* disposition of the ligand pair in the **2A/2B** structure, the configuration having to meet the demands of bridging in each case. Therefore, while structures **1**, **2A/2B** provide octahedral bonding arrangements which carry increasing ligand content, they do not represent a strictly progressive structural sequence.

$[\{CdI_2(pyo)\}_n]$ (**3**) *and* $[\{CdI_2)_2(pyo)_3\}_n]$ (**4**). As compared with the foregoing polymeric layer structures, the chain structure of **3** indicates, not unexpectedly, that the CdI_2 lattice is more readily degraded than the $CdCl_2/CdBr_2$ lattices. The five-fold cadmium coordination approximating to trigonal bipyramidal (tbp) has received comment.[10]

The chain structure of **4**, Fig. 3, with non-equivalent atoms (oxygen and iodine) paired for bridging contrasts with the equivalent-pair bridging in **3**. The increased ligand content of solutions suited to crystallization of **4** has resulted in the appearance of six-coordinated cadmium centres alternating with five-coordinated along the chain. Iodine and oxygen occupy diametrically opposite positions in the (distorted) octahedron around Cd(1). The Cd(2) environment again approaches tbp, with relatively weak bonding to the ligand oxygen atoms in the apical positions. Going on the chain geometry, it seems to be this tbp bonding influence that underlies the alteration in bridging structure in **4** as compared with **3**.

Within the cell of **4**, the chains lie in the [010] direction. As to be expected, chain packing is determined both by chain conformation and the dis-

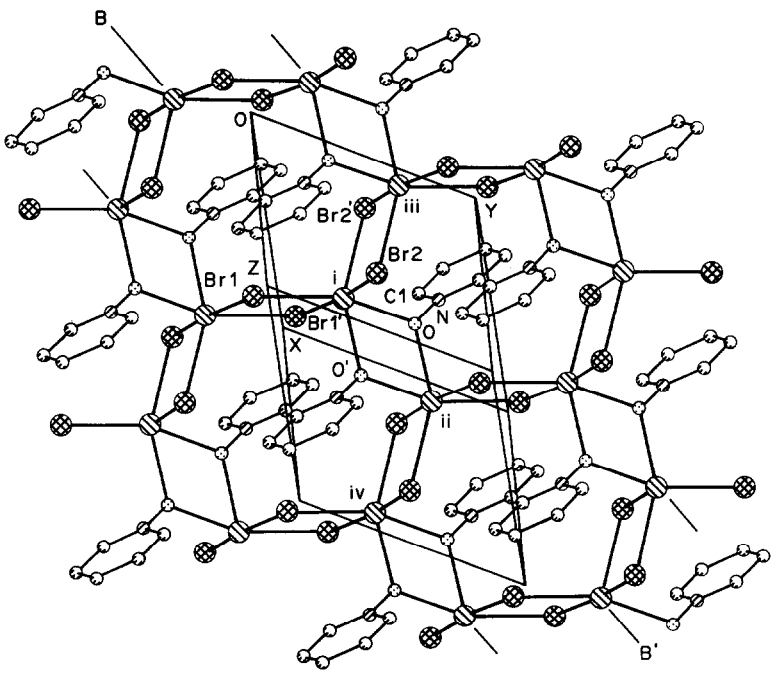

Fig. 2. A single layer of **2** as seen looking towards the [101] direction, with the origin at the top rear left. The disposition of the ligand rings above and below the voids is evident. Symmetry cores for the cadmium centres are: (i) x, y, z; (ii) $1-x, 1-y, 1-z$; (iii) $-x, 1-y, 1-z$; (iv) $x+1, y, z$.

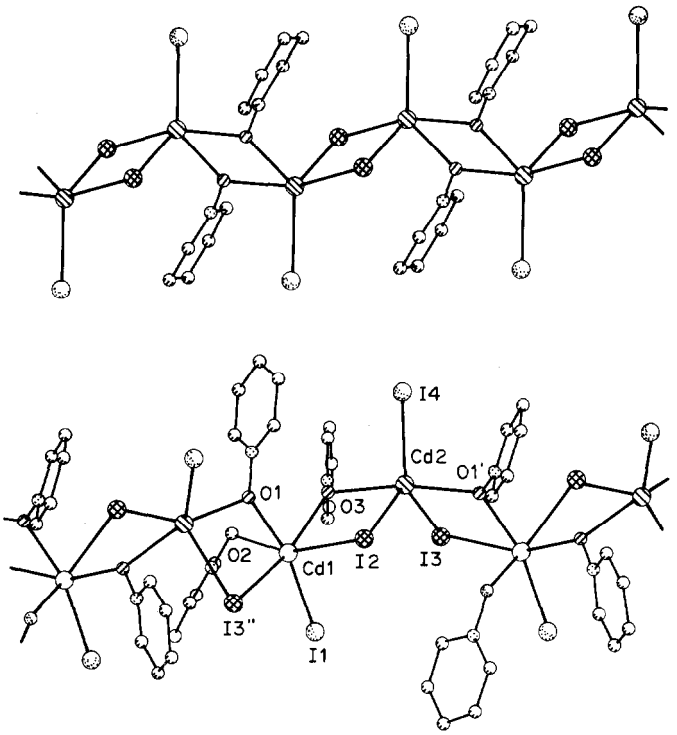

Fig. 3. The chain structures of **3** (upper) and **4** (lower), showing the differing bridging. The structure of **3** is replotted from coordinates given in ref. 10. In **4** there is an alternation of six-coordinate Cd(1) and five-coordinate Cd(2) centres. Bridging oxygen atoms occupy apical positions, and three iodine atoms (two of them bridging) are in equatorial positions around Cd(2). The repeat distance, parallel to the *y* axis of the cell, extends over two asymmetric units.

position of the pyo rings. The shortest inter-chain C—I approaches are 3.8–4.0 Å.

$[\{CdI_2(pyo)_2\}_2]$ (**5**) *and* $[\{CdI_2(pyo)_2(MeOH)\}_2]$ (**5A**). In **5** the coordination is seen to have reverted to five (Fig. 4), although conversion back to the six-coordinate methanolate (**5A**) occurs quite readily. The higher pyo proportion has caused the polymeric chain to break into binuclear molecules. The cadmium environment is still best considered as tbp, even though the O_1—Cd—O_2 angle has fallen to

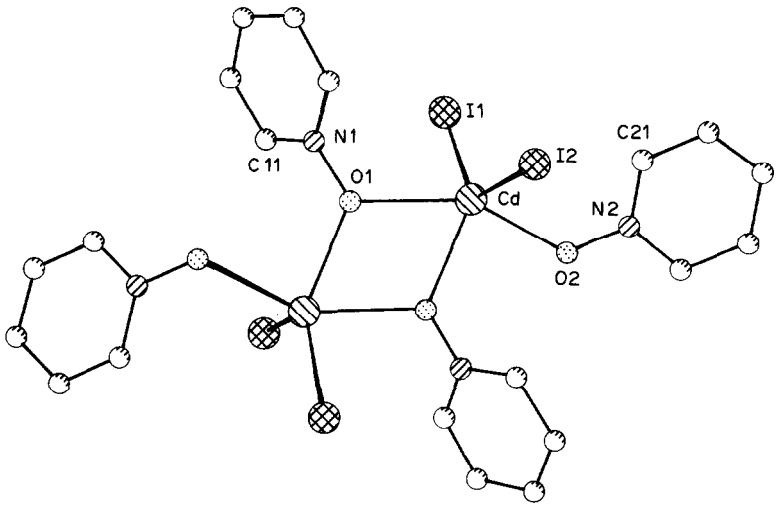

Fig. 4. The centrosymmetric molecule of **5**, with bridging and terminal pyo ligands. With the O(1)—Cd—O(2) angle 152°, O(1) and O(2) lie towards apical positions.

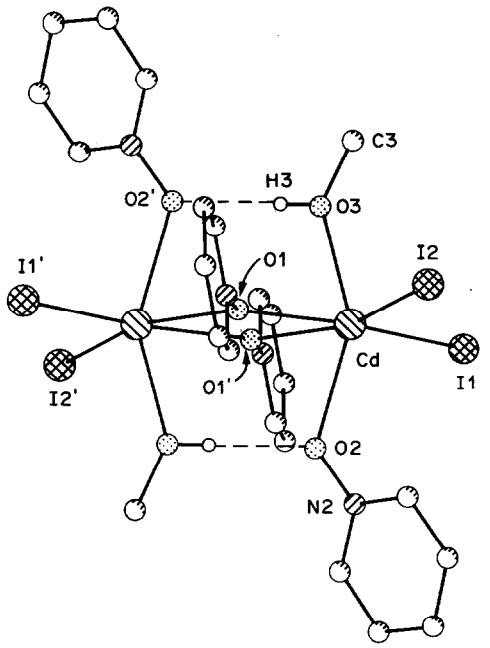

Fig. 5. The centrosymmetric molecule of **5A** with the cadmium centres now in six-coordination through methanol addition. The effect of the hydrogen-bonding on the ligand dispositions is evident.

152°, through the bridging constraint exerted on O(1). The structure of this compound is analogous to that developed by copper(II) halide complexes with pyo.[16]

The structure of **5A** in relation to **5**, with its retention of centrosymmetrical bridging is apparent from Fig. 5. The O(3) and O(2)′ atoms of coordinated methanol and pyo are bent towards each other at 2.715 Å, and hydrogen-bonding which the methanol proton provides between them augments the ligand bridging. This proton position is refined at 0.78 (0.12) Å from O(3), and 0.20 Å from the O(3)—O(2)′ vector. (The displacement is almost parallel to the Cd, Cd′, O(1), O(1)′ meanplane and towards the O(1)′ side.) The O(3)—H(3)—O(2)′ angle of 161° is below the 168° limit which would correspond to e.s.d. values. Thus, there seems to be a real deviation from linearity, probably through constraint from the methanol molecule. The hydrogen-bonding lengthens the O(2)—Cd bond; at 2.387 Å it is longer than the Cd—O(1) and Cd—O(1)′ bridge bonds. The torsion angle between N(2)—O(2) and the I(1)—Cd—I(2) angle bisector is small (4.5° towards I(1)), but that between C(3)—O(3) and the bisector is much larger (32° towards I(1)).

$[Cd(pyo)_6]^{2+}[CdI_4]^{2-}$ (**6**). The cell content is shown in Fig. 6. In the extended structure each iodine makes nearest approaches (I—C, 3.7–4.0 Å; I—H, 3.1–3.4 Å) to rings from four different cations. Through their mutual interaction, both cation and anion are somewhat distorted from regular coordination (see Table 5), although the cation ligands do approach a centrosymmetric array. The Cd—I bond length (2.785 Å av) is slightly longer than the

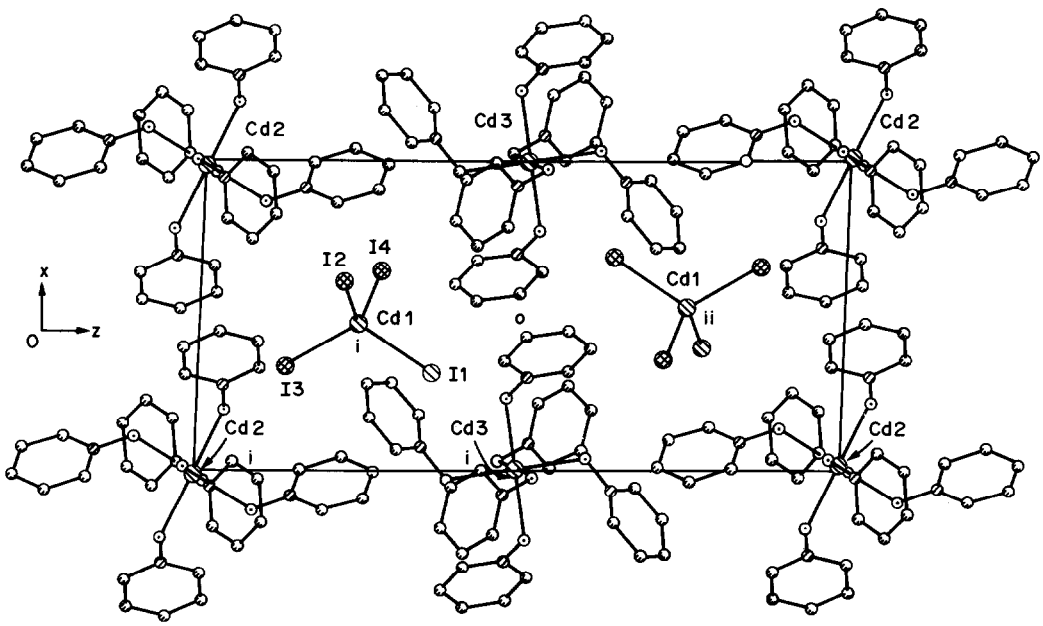

Fig. 6. The triclinic cell of **6** viewed along the *y* axis. Cd(2) and Cd(3) have the *y* coordinate 0.5, while the Cd(1) anion centres (i) and (ii) have $y = 0.0520$ and 0.9480, respectively. Disposition of the ligands about Cd(2) and Cd(3) approximates to centrosymmetric.

terminal Cd—I lengths in neutral five-coordinate structures.

Remarks on cadmium halide behaviour

The formation of these structures is seen as a consequence of the progressive ease of disruption of the Cd—X bonds with the heavier halogens. With the chlorides, the formation of **1** involves relatively small degradation of the $CdCl_2$ lattice. The structure retains some three-way bridging which provides six-coordination for cadmium even with the low pyo : $CdCl_2$ ratio. Excess ligand and a longer reaction time are needed to produce **2A**, where three-way bridging has been eliminated. With $CdBr_2$, on the other hand, no product with triple-bridging could be obtained, and **2B** remained the only product, whether using either higher or lower pyo : $CdBr_2$ ratios.

Cadmium iodide produces no layer lattice deriative, **3** being formed even using the lowest pyo : CdI_2 ratios. The chain structure of **3** occurs as a component of the **2A**/**2B** structure, as can be seen along the top boundary of Fig. 2. Here, in the bromide the chains are linked laterally through equivalent halogen-pair bridges. In place of such inter-chain bridging in the iodide, the halogen remains terminal, with the cadmium in five-coordination.

With the iodide derivatives as a class, there is evidence of greater halide mobility and ease of switching between five- and six-coordination. The lower Cd—I bond strength[17] and larger steric requirement of iodine are relevant—along with the low field of force associated with the large d^{10} cadmium centre. The development of varied bridging modes, and the appearance of non-equilibrium phases which can tip completely the initial course of crystallization are in themselves evidence of halide mobility.[18] The ionic compound **6** comprises the separately known $[Cd(pyo)_6]^{2+}$[19] and $[CdI_4]^{2-}$[1] (Fig. 6). Several factors will control the crystallization of such a compound, but in so far as both breaking and formation of Cd—I bonds are involved, it remains that lattice energy must be impotant in stabilization.

Significance of cadmium bond lengths in tbp and octahedral structures

The structure of **4** permits useful comparison of bond lengths of the octahedral Cd(1) and the tbp Cd(2) (see Table 5). The bridging atoms O(1) and O(3) are linked apically to Cd(2), while the bridging I(1) and I(2) are in equatorial positions, along with the terminal I(4). The Cd(2)—O bonds are longer, while the Cd(2)—I are shorter than their counterparts with Cd(1). This is in line with the normal relationships between tbp and octahedral bond lengths in comparable situations.[20,21] Its particular significance for cadmium lies in confirming the strong distinction between cadmium and mercury(II) coordination. Mercury is characterized by its preference for strong (and relatively short) diagonal bonding at the expense of bonding in other directions.[22] It is evident that cadmium shows no such tendency. This contrast between mercury and cadmium is further emphasized by the very large bond length disparities between $HgCl_2(pyo)$[10] and the present **2B** structure, despite their otherwise matching connectivities.

Acknowledgements—X-ray powder diffractograms were kindly run by Mr John Hastie. We are also indebted to Mr Mark Inder and Ms Jan Wikaira for their varied assistance. Laboratory facilities were provided by the University of Canterbury and through the New Zealand Universities research fund.

REFERENCES

1. D. G. Tuck, *Rev. Inorg. Chem.* 1979, **1**, 209.
2. Cambridge Crystallographic Data Base.
3. H. Strasdeit, W. Saak, S. Pohl, W. L. Driessen and J. Reedijk, *Inorg. Chem.* 1988, **27**, 1557; S. S. Al-Inaid, N. B. Buttrus, C. Eaborn, P. B. Hitchcock, J. D. Smith and K. Tabakkoli, *J. Chem. Soc., Chem. Commun.* 1988, 1389.
4. H. Paulus, *Z. Anorg. Allg. Chem.* 1969, **369**, 38.
5. A. Mitschler, J. Fischer and R. Weiss, *Acta Cryst.* 1967, **22**, 236.
6. M. Nardelli, L. Coghi and G. Azzani, *Gazz. Chim. Ital.* 1958, **88**, 235.
7. L. Leligny and J. C. Monier, *Acta Cryst.* 1974, **B30**, 305.
8. N. M. Karayannis, L. L. Pytlewski and C. M. Mikulski, *Coord. Chem. Rev.* 1973, **11**, 93.
9. G. Schmauss and H. Specker, *Z. Anorg. Allg. Chem.* 1968, **363**, 113.
10. G. Sawitski and H.-G. von Schnering, *Chem. Ber.* 1974, **107**, 3266.
11. (a) L. Pauling and J. Sherman, *Z. Krist.* 1937, **96**, 481; (b) A. F. Wells, *Structural Inorganic Chemistry*, 3rd edn, p. 147. Oxford University Press, London (1962).
12. W. T. Robinson, C. J. Wilkins and Zhang Zeying, *J. Chem. Soc., Dalton Trans.* 1990, 219.
13. G. N. Sheldrick, SHELTXL, Integrated System for Solving, Refining and Displaying Crystal Structures from Diffraction Data, versions 4.1 (1985) and PC (1990) for graphics. Siemens, Madison, Wisconsin.
14. M. Nieuwenhuyzen, W. T. Robinson and C. J. Wilkins, *Polyhedron* 1990, **9**, 2315.
15. N. Wooster, *Z. Krist.* 1930, **74**, 363.
16. D. R. Johnson and W. H. Watson, *Inorg. Chem.*

1971, **6**, 1281; A. D: Mighell, C. W. Reismann and A. Santoro, *Acta Cryst.* 1972, **B28**, 126.
17. J. E. Huheey, *Inorganic Chemistry*, Appendix F. Harper and Row, London (1975).
18. I. G. Dance, R. G. Gabbutt and D. C. Craig, *Inorg. Chem.* 1987, **26**, 3732.
19. J. Reedijk, *Rec. Trav. Chim.* 1969, **88**, 499.
20. R. J. Gillespie, *Molecular Geometry*, Ch. 4. Van Nostrand Reinhold, London (1972).
21. W. T. Robinson, C. J. Wilkins and Zhang Zeying, *J. Chem. Soc., Dalton Trans.* 1988, 2187.
22. L. E. Orgel, *An Introduction to Transition Metal Chemistry*, p. 66. Methuen, London (1960).

Polyhedron Vol. 10, No. 18, pp. 2123–2129, 1991
Printed in Great Britain

0277–5387/91 $3.00+.00
© 1991 Pergamon Press plc

H^+ ADDITION TO THE HETEROATOMIC CoP_3 CLUSTER. SYNTHESIS OF THE RADICAL CoP_3^+ CLUSTER AND ELECTROCHEMICAL STUDY

MASSIMO DI VAIRA and PIERO STOPPIONI*

Dipartimento di Chimica, Università di Firenze, Via Maragliano 77, 50144 Firenze, Italy

and

STEFANO MIDOLLINI

Istituto ISSECC, CNR, Via J. Nardi 39, 50132 Firenze, Italy

and

FRANCO LASCHI and PIERO ZANELLO

Dipartimento di Chimica, Università di Siena, Pian dei Mantellini 44, 53100 Siena, Italy

(*Received* 28 *February* 1991; *accepted* 18 *June* 1991)

Abstract—Treatment of a dichloromethane suspension of [(triphos)CoP_3] [triphos = 1,1,1-tris(diphenylphosphinomethyl)ethane] with CF_3SO_3H affords a compound of formula [(triphos)CoP_3H]$(CF_3SO_3)_2 \cdot (H_5O_2)$. An X-ray crystallographic analysis of the compound has provided evidence for one hydrogen atom bridging a Co—P edge of the CoP_3 core of the metal cation, which crystallizes with one oxonium ion, two $CF_3SO_3^-$ counterions, and one water molecule, all interlinked via a net of hydrogen bonds. The NMR data for the [(triphos)CoP_3H]$^+$ cation suggest that the H^+ electrophilic addition involves both the P_3 group and the metal atom. Additional information on the physical properties of the CoP_3 cluster has been obtained by investigating its electrochemical behaviour and synthesizing the [(triphos)CoP_3]$^+$ cation, containing the radical cluster CoP_3^+, through the oxidation of the parent [(triphos)CoP_3] compound.

The neutral compounds [(triphos)MP_3] [triphos = 1,1,1-tris(diphenylphosphinomethyl)ethane; M = Co, Rh, Ir] which has a pseudotetrahedral core formed by three unsubstituted phosphorus atom and one cobalt group metal, stabilized by the tripod tridentate ligand triphos,[1] exhibit distinct reactivity on the electron rich phosphorus atoms. The heteroatomic polarized MP_3 core interacts with various transition metal fragments through one phosphorus atom,[2] a P—P edge[3] or the P_3 triangular face,[4] depending on the nature of the metal–ligand system provided by the reactant. The reactivity of the above neutral compounds towards various isolobal fragments has recently been considered. The R^+ (R = CH_3,[5] Et[6]) organic groups add to a phosphorus atom of the MP_3 core producing notable distortions in its geometry. The $AuPR_3^+$ fragments upon interaction with a P—P edge of the MP_3 group undergo labilization of the phosphine ligand,[7] with a departure from the behaviour both in solution[8] and toward metal clusters[9] of the gold(I) phosphine halides. Finally, the HgY^+ fragments (Y = Me, Ph) add to a P—P edge in the [(triphos)MP_3] (M = Co, Rh) compounds,[3] producing minor modifications of the core.

It was therefore of interest to examine the reactions of the [(triphos)MP_3] compounds with H^+, which is isolobal with Me^+, Et^+, $AuPR_3^+$ and

* Author to whom correspondence should be addressed.

HgY^+ but presents a smaller steric hindrance. It was also expected that useful complementary information could be obtained by studying the redox properties of the CoP_3 cluster.

EXPERIMENTAL

All reactions and manipulations were performed under an atmosphere of oxygen-free nitrogen. Solvents were freshly distilled under nitrogen from the appropriate drying agents immediately before use. Electronic spectra were obtained using a Perkin–Elmer Lambda 9 spectrometer. Magnetic susceptibilities were measured by the Faraday method with an automated magnetometer DMS-5. The ^{31}P and ^1H NMR spectra were obtained in CD_2Cl_2 using a VARIAN VXR 300 spectrometer operating at 121.4 and 300.1 MHz and are referred to external 85% H_3PO_4 and internal TMS, respectively. The materials and the apparatus used for EPR spectroscopy and electrochemistry have been described elsewhere.[10] The potential values refer to an aqueous calomel electrode (SCE). Analytical data for carbon, hydrogen and cobalt were obtained in the Microanalytical Laboratory of the Department of Chemistry; phosphorus and sulphur elemental analyses were performed by Mykroanalytisches Labor Pascher, Remagen, F.R.G. [(triphos)CoP_3][2] and $[(C_5H_5)_2Fe]PF_6$[11] were prepared as previously described; CF_3SO_3H (Aldrich) was used as supplied. All the compounds were collected on a sintered-glass frit, in a closed system, and washed with benzene and light petroleum (b.p. 40–70°C) in turn before being dried under a stream of nitrogen.

Synthetic procedures

Synthesis of the compounds. [(triphos)CoP_3H]$(CF_3SO_3)_2\cdot(H_5O_2)$. Neat CF_3SO_3H (0.8 mmol) was added to a dichloromethane suspension (40 cm^3) of [(triphos)CoP_3] (0.31 g, 0.4 mmol). Quick dissolution of the solid, with concomitant change in the colour of the solution to orange, was observed. The resulting solution was stirred at 0°C for 2 h. Orange crystals of the compound were obtained by addition of benzene and slow concentration. The compound crystallizes, as found from the X-ray analysis, with water molecules whose amount, mainly assigned in accordance with the results of the structural investigation (see below), well agrees with the elemental analyses (yield 80%). Found: C, 46.6; H, 4.1; Co, 5.3; P, 16.5; S, 5.7. [(triphos)CoP_3H]$(CF_3SO_3)_2\cdot(H_5O_2)$, $C_{43}H_{45}CoF_6O_8P_6S_2$, requires: C, 46.4; H, 4.1; Co, 5.3; P, 16.7; S, 5.8%. ^1H NMR: δ −13.75 (1H, br, $\nu_{1/2}$ 15 Hz), 1.90 (3H, s, CCH_3), 2.70 (6H, s, PCH_2), 7.70 (30H, m, arom. H).

[(triphos)CoP_3]PF_6. Solid $[(C_5H_5)_2Fe]PF_6$ (0.17 g, 0.5 mmol) was added to a dichloromethane suspension (50 cm^3) of [(triphos)CoP_3] (0.39 g, 0.5 mmol). Immediate dissolution of the solid, with concomitant change in colour of the solution to deep red, was observed. The solution was stirred at room temperature for a few minutes and n-hexane (50 cm^3) was added. The resulting solution was concentrated under vacuum at room temperature until a red oil separated. Dark red microcrystals of the compound were obtained on leaving the system overnight (yield 70%). Found: C, 52.9; H, 4.2; Co, 6.1. [(triphos)CoP_3]PF_6, $C_{41}H_{39}CoF_6P_7$, requires: C, 53.4; H, 4.3; Co, 6.4%.

X-ray crystal structure

Diffraction data for [(triphos)CoP_3H]$(CF_3SO_3)_2\cdot(H_5O_2)$. The determination of lattice constants and the intensity data collection were performed using a crystal with dimensions $0.20\times0.30\times0.80$ mm, which was coated with paraffin in order to prevent slow decomposition. An Enraf–Nonius CAD4 diffractometer and Mo-K_α radiation ($\lambda = 0.71069$ Å) were used for all operations, which were performed at room temperature. Lattice constants were determined by least-squares refinement of the angular settings of 22 reflections with $20 \leqslant 2\theta \leqslant 24°$.

Crystal data. $C_{43}H_{45}CoF_6O_8P_6S_2$, $M_r = 1112.73$, monoclinic, $a = 17.968(5)$, $b = 20.823(6)$, $c = 13.326(3)$ Å, $\beta = 103.15(2)°$, $U = 4855(2)$ Å^3, $Z = 4$, $D_c = 1.522$ g cm^{-3}, $F(000) = 2280$, μ(Mo-K_α) = 7.00 cm^{-1}, space group $P2_1/n$.

The intensities of the $\pm h$, $+k$, $+l$ reflections were measured in the range $5 \leqslant 2\theta \leqslant 46°$ in the ω–2θ scan mode with a scan width of $(0.90+0.35\tan\theta)°$ and variable 3–8° min^{-1} scan speed. No crystal decay was observed. Of the total 6750 reflections recorded, 4102 having $I > 3\sigma(I)$ were used for structure determination. Intensity data were corrected for Lorentz and polarization effects and, at isotropic convergence after the structure was solved, they were corrected for absorption by an empirical procedure.[12] The principal computer programs used in the crystallographic calculations are listed in refs 12–14.

Crystal structure determination. The structure was solved by heavy-atom procedures. In the least-squares refinement the function $\Sigma w(|F_o|-|F_c|)^2$ was minimized with final weights $w = [\sigma^2(F_o)+0.0005F_o^2]^{-1}$. The scattering factors for the neutral atoms and the anomalous dispersion correction for cobalt were taken from ref. 15. In

the final refinement the cobalt and phosphorus atoms, as well as all those forming the $CF_3SO_3^-$ anions and the oxygen atoms of the water molecules were assigned anisotropic thermal parameters, whereas the other atoms were refined isotropically. The phenyl groups of the triphos ligand were refined as rigid bodies with idealized geometry. Hydrogen atoms of the triphos ligand were introduced in calculated positions (C—H = 1.00 Å) with temperature factors 20% larger than those of the respective carbon atoms, the methyl group of the ligand being refined as a rigid body, but the hydrogen atoms in the solvate molecules as well as that one considered to be present in the CoP_3 cluster could not be clearly located on ΔF maps and were not introduced in the model. Refinement converged at $R = 0.066$ and $R_w = 0.074$. The highest peaks in the final ΔF map, with heights < 0.7 e Å^{-3} could not be assigned definite meaning. The largest shift/error ratios in the final cycles were < 0.03. Final atomic positional and thermal parameters, bond lengths and angles and F_o/F_c values have been deposited as supplementary material with the Editor, from whom copies are available on request. Atomic coordinates have also been submitted to the Cambridge Crystallographic Data Centre.

RESULTS AND DISCUSSION

Treatment of a dichloromethane solution of [(triphos)CoP_3] with CF_3SO_3H in stoichiometric ratios ranging from 1 : 1 to 1 : 3, affords after the addition of benzene a compound of the formula [(triphos)CoP_3H]$(CF_3SO_3)_2 \cdot (H_5O_2)$. The best yield is obtained for the 1 : 2 ratio of the reagents, in accordance with the formula of the final compound. This is mildly air-sensitive and soluble in chloroform and dichloromethane. It decomposes quickly, even under nitrogen, in nucleophilic solvents such as acetone, alcohols and ethers, yielding the parent [(triphos)CoP_3]. This behaviour is indicative of a weak interaction between the H^+ and the heteroatomic cluster. Although the synthetic procedures were carried out using dry reagents and solvents, the final compound crystallized invariably with $(H_5O_2)CF_3SO_3$; it is likely that the small amount of water was introduced with the inert gas into the solution.

The structure of the compound, as revealed by the X-ray analysis, is formed by [(triphos)CoP_3H]$^+$ and $H_5O_2^+$ cations, and $CF_3SO_3^-$ anions. A view of the metal cation appears in Fig. 1. Although hydrogen atoms, in particular those in the $H_5O_2^+$ ion or the CoP_3 cluster, could not be safely located, there is convincing structural evidence, as discussed below, of their presence and therefore for the validity of the formula assigned to the compound. In particular, each $H_5O_2^+$ cation forms hydrogen bonds to four anions as in the structures of $(H_5O_2)CF_3SO_3$[16] and $(H_5O_2)_2SO_4$,[17] although the present network of hydrogen bonds, involving a centrosymmetric cluster of two $H_5O_2^+$ and four $CF_3SO_3^-$ ions (Fig. 2), is less extended than the two-[16] or three-dimensional[17] networks existing in the other two structures, probably due to the presence of the large metal cation in the present one. In close agreement with the structures already mentioned, the distance between the oxygen atoms in $H_5O_2^+$ [O(7)···O(8) = 2.43(1) Å] is shorter than the distances [2.53–2.71 Å] formed by the same

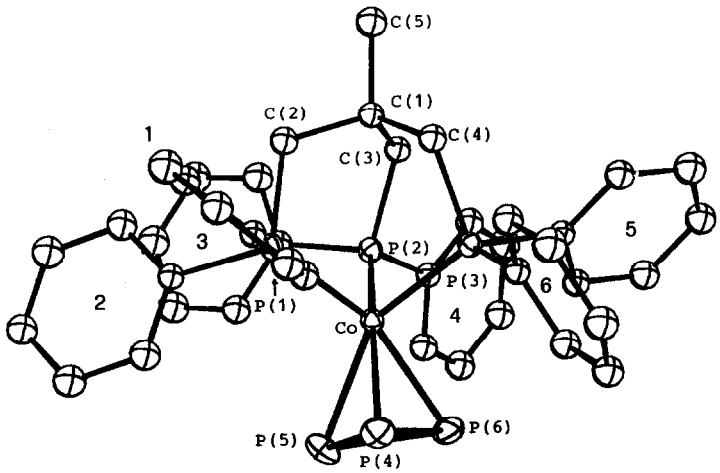

Fig. 1. Perspective view of the [(triphos)CoP_3H]$^+$ cation in the structure of [(triphos)CoP_3H]$(CF_3SO_3)_2 \cdot (H_5O_2)$, with 20% probability ellipsoids. Phenyl groups are numbered but their carbon atoms are not labelled for clarity.

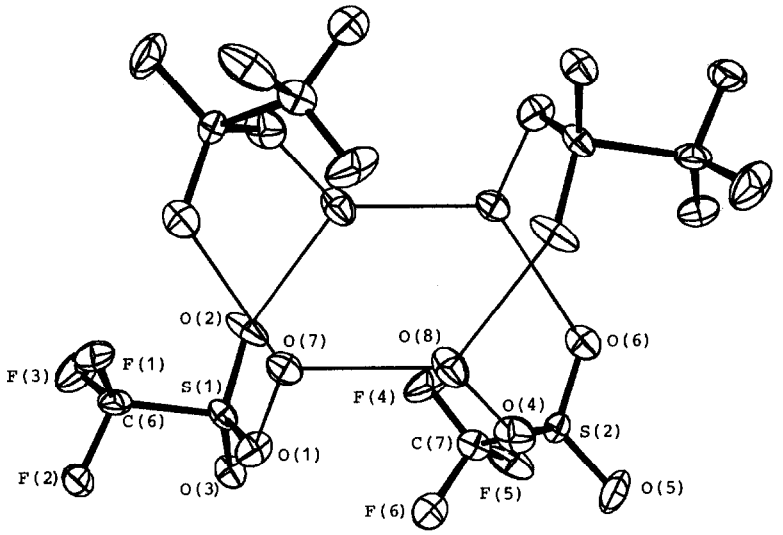

Fig. 2. View of the centrosymmetric cluster formed by two $(H_5O_2)^+$ cations and four $CF_3SO_3^-$ anions in the structure of $[(triphos)CoP_3H](CF_3SO_3)_2 \cdot (H_5O_2)$. Only symmetry-independent atoms are labelled. Hydrogen bond interactions are marked by light lines.

oxygens with those of the anions to which they are hydrogen bonded; moreover, each oxygen atom in $H_5O_2^+$ is pyramidal, with 102–125° angles between the directions to its hydrogen-bonded neighbours. The dimensions of the $CF_3SO_3^-$ anions closely agree with those already reported.[16] The main difference between the geometry of the $[(triphos)CoP_3H]^+$ cation and that of the neutral parent $[(triphos)CoP_3]$ is due to lengthening of a Co—$P(P_3)$ bond from the 2.301(1) Å value, which is identical by symmetry for the three bonds of this type in the parent complex, to 2.396(2) Å (Table 1). The other two Co—$P(P_3)$ distances are only slightly larger (by 0.015 Å, in the mean) in the cation, as are the Co—P(triphos) distances (by 0.027 Å), whereas the dimensions of the P_3 ring are substantially unchanged.

The above structural data suggest that the added H^+ ion should lie close, in the solid, to the region of a Co—$P(P_3)$ bond. A rationalization for this was sought by performing extended Hückel calculations[18] with the CACAO set of programs.[19] According to the highest overlap population and FMO energy-matching criteria, the Co—P edges of the CoP_3 cluster were better points of attack for H^+ than the P—P edges or the face centres. Moreover, only under the assumption of Co—P activation the experimental trend in bond lengths, essentially consisting in elongation of one Co—P bond, could be anticipated on the basis of the distribution of the overlap population values. In such a position the H^+ ion has similar bonding opportunities to the P_3 group as those available to CH_3^+ in the $[(triphos)Co(MeP_3)]^+$ cation,[5] but it is bound

Table 1. Selected bond distances (Å) and angles (°) for the compound $[(triphos)CoP_3H](CF_3SO_3)_2 \cdot (H_5O_2)$

Co—P(1)	2.220(2)	Co—P(6)	2.309(2)
Co—P(2)	2.218(2)	P(4)—P(5)	2.128(4)
Co—P(3)	2.200(2)	P(4)—P(6)	2.143(3)
Co—P(4)	2.324(2)	P(5)—P(6)	2.134(4)
Co—P(5)	2.396(2)		
P(1)—Co—P(2)	90.9(1)	P(5)—Co—P(6)	53.9(1)
P(1)—Co—P(3)	94.8(1)	P(5)—P(4)—P(6)	60.0(1)
P(2)—Co—P(3)	92.0(1)	P(4)—P(5)—P(6)	60.4(1)
P(4)—Co—P(5)	53.6(1)	P(4)—P(6)—P(5)	59.7(1)
P(4)—Co—P(6)	55.1(1)		

in addition to the metal atom, forming essentially a Co—H—P three-centre bond; the latter possibility is prevented by steric factors on CH_3^+,[5] which is forced to lie on the opposite side of the P_3 plane with respect to that presumably occupied by the smaller H^+ in the present structure. Bonding within the P_3 group is predicted to be little affected.

The room temperature ^1H NMR spectrum of the compound exhibits the triphos signals with the expected shifts and a high field broad resonance ($\delta = -13.75$) whose intensity and shift are consistent with the presence of one hydride hydrogen atom. Such resonance remains substantially unchanged down to the lowest temperature reached ($-90°C$). The $^{31}P\{^1H\}$ NMR spectrum exhibits two broad and well-separated resonances ($\delta = 28.21$, $\nu_{1/2} = 82$ Hz; $\delta = -296.49$, $\nu_{1/2} = 70$ Hz) having a 1 : 1 intensity ratio. The two resonances, strongly affected by the cobalt quadrupole moment, remain essentially unchanged down to $-90°C$. The lower field signal is assigned to the phosphorus atoms of the triphos ligand and the higher field signal to the unsubstituted phosphorus atoms; the latter signal, which is not affected by proton coupling, occurs at higher field than that found for the parent [(triphos)CoP_3] ($\delta = -276.21$).[20] The high field shift of the P_3 signal in the present compound was unexpected, as such resonance moves considerably downfield on going from the neutral [(triphos)MP_3] (M = Co, Rh, Ir) compounds to the cationic [(triphos)MP_3]BF_4 (M = Ni, Pd, Pt) compounds,[20] which are isoelectronic to [(triphos)MP_3] and to the present derivative. Moreover, it has been observed that also the addition of CH_3^+ to a phosphorus atom of the MP_3 core,[5] or the insertion of the isolobal $AuPR_3^+$ or HgY^+ fragments into one of its P—P edges[3,7] yield low field shifts of the P_3 signal. Finally, a particularly notable low field shift is observed when the addition yields an azide-like P_3 chain.[6] The high field shift exhibited by the unsubstituted phosphorus atoms in the present compound might then be accounted for by an unprecedented type of interaction with the rest of the structure undergone by the P_3 group, such as that suggested above, consisting of a three-centre bond and two "normal" Co—P bonds. In such an arrangement, according to the results of the structural investigation and of the EH calculations, bonding within the P_3 ring is similar to that existing in the parent cluster, but the overall interaction of the ring with the metal centre is smaller than in the CoP_3 case. Finally, hydrogen exchange between the three Co—P bonds and rotation in solution of the P_3H group with respect to the pseudo three-fold axis of the cation may be responsible for the absence of P—H coupling in the spectrum.

Since the H^+ addition should reduce to some extent the availability of electrons to the CoP_3 skeleton, it was considered interesting to study the electrochemical behaviour of [(triphos)CoP_3]. Cyclic voltammetry of [(triphos)CoP_3] in dichloromethane solution shows two successive anodic steps: the first one exhibits features of chemical reversibility (Fig. 3), whereas the second one, lacking any associated response in the reverse scan, is very close to the solvent discharge. Controlled potential coulometry in correspondence to the first oxidation process ($E_w = +0.5$ V) shows that it involves a one-electron molecule. Analysis[10] of the relevant cyclic voltammetry response with scan rate varying from 0.02

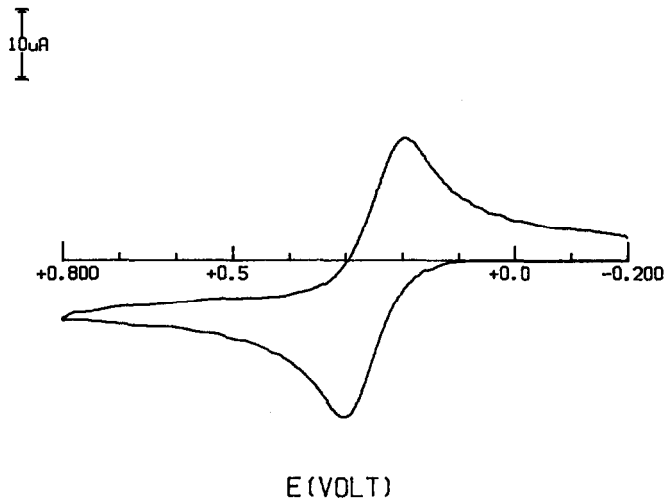

Fig. 3. Cyclic voltammetric response recorded at a platinum electrode in a CH_2Cl_2 solution containing [(triphos)CoP_3] (1.51×10^{-3} mol dm^{-3}) and $[NBu_4]ClO_4$ (0.2 mol dm^{-3}). Scan rate 0.2 V s^{-1}.

to 10.24 V s^{-1} shows that: (i) the peak current ratio i_{pc}/i_{pa} is constantly equal to unity; (ii) the peak-to-peak separation (ΔE_p) progressively increases from 82 to 444 mV; (iii) the current function $i_{pa}v^{-1/2}$ remains substantially constant. On considering that, under the same experimental conditions, the one electron oxidation of ferrocene ($E^{\circ\prime} = +0.45$ V) displays a similar trend in ΔE_p, one can assume that the [(triphos)CoP_3]$^{0/+}$ redox change involves a substantially reversible electron transfer ($E^{\circ\prime} = +0.24$ V). The stability of the electrogenerated monocation [(triphos)CoP_3]$^+$ is not limited to the time scale of cyclic voltammetry (tenths of a second): it is stable also over the longer times of macroelectrolysis, as proved by the relevant cyclic voltammogram, which is complementary to that shown in Fig. 3. The solution turns from yellow to deep red in the course of this process.

The electrogenerated [(triphos)CoP_3]$^+$ was characterized by EPR spectroscopy. The liquid nitrogen ($T = 100$ K) X-band EPR spectrum of the paramagnetic species in dichloromethane solution shows an unresolved anisotropic structure, with axial symmetry [$g_\parallel = 2.228+0.005$, $g_\perp = 2.012+0.005$; $g_{calc} = 1/3(g_\parallel+g_\perp) = 2.084+0.005$]. At 300 K the absorption line splits into a well-resolved hyperfine octuplet (Fig. 4) as a result of the magnetic interaction of the unpaired electron with the cobalt nucleus ($I = 7/2$). The isotropic parameters are $g = 2.086+0.005$ and $a = 27.7+0.5$, in good agreement with the low temperature g value. The spectral parameters are therefore consistent with the metal character of the unpaired electron.

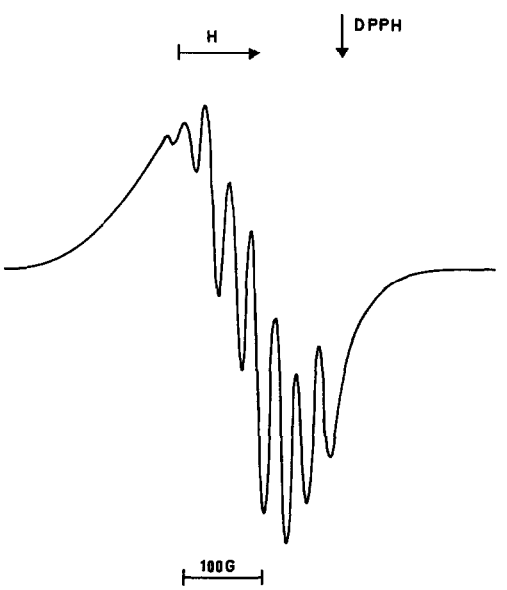

Fig. 4. X-band EPR spectrum recorded at room temperature on a CH_2Cl_2 solution of [(triphos)CoP_3]$^+$.

In view of the electrochemical results the synthesis of a compound containing the CoP_3^+ radical cluster was undertaken. [$(C_5H_5)_2$Fe]PF_6 was chosen as a mild oxidizing agent. When a quantitative amount of [$(C_5H_5)_2$Fe]PF_6 is added to [(triphos)CoP_3] in CH_2Cl_2 a rapid reaction occurs and a dark red microcrystalline compound of formula [(triphos)CoP_3]PF_6 is obtained upon addition of n-hexane. The compound which is stable under nitrogen both in the solid state and in chlorinated solvents solution exhibits a room temperature magnetic moment of 2.2 μ_B. The EPR data for the compound agree with those found for the electrogenerated species. The electronic spectrum of the complex, which exhibits two absorption maxima at 800 and 380 nm and a shoulder at 480 nm, is typical for low spin hexacoordinate cobalt(II).

In conclusion, the data available for the oxidized species suggest that the one-electron oxidation involves removal of one electron from a metal orbital in [(triphos)CoP_3]. Metal orbitals are also involved in the H^+ addition to a definitely larger extent than in any of the previously performed additions to atoms or insertions into P—P bonds of MP_3 clusters.[3,7] However, the amount of charge transferred in the present H^+ addition should be less than that removed by the one-electron oxidation process; moreover, different MOs are likely to be involved in the two processes.

Acknowledgements—We are grateful to Dr C. Mealli for providing the CACAO set of programs. We thank the Italian Ministero dell' Università e della Ricerca Scientifica e Tecnologica for financial support.

REFERENCES

1. M. Di Vaira and L. Sacconi, *Angew. Chem. Int. Edn Engl.* 1982, **21**, 330.
2. C. A. Ghilardi, S. Midollini, A. Orlandini and L. Sacconi, *Inorg. Chem.* 1980, **19**, 301.
3. M. Di Vaira, D. Rovai and P. Stoppioni, *Polyhedron* 1990, **9**, 2477.
4. M. Di Vaira, S. Midollini and L. Sacconi, *J. Am. Chem. Soc.* 1979, **101**, 1757; C. Bianchini, M. Di Vaira, A. Meli and L. Sacconi, *J. Am. Chem. Soc.* 1981, **103**, 1448.
5. G. Capozzi, L. Chiti, M. Di Vaira, M. Peruzzini and P. Stoppioni, *J. Chem. Soc., Chem. Commun.* 1986, 1799.
6. A. Barth, G. Huttner, M. Fritz and L. Zsolnai, *Angew. Chem. Int. Edn Engl.* 1990, **29**, 929.
7. M. Di Vaira, M. Peruzzini and P. Stoppioni, *J. Chem. Soc., Dalton Trans.* 1990, 109.
8. R. J. Puddephatt, *Topics in Inorganic and General*

Chemistry (Edited by R. J. H. Clark), Vol. 16, The Chemistry of Gold, p. 54. Elsevier, Amsterdam (1978); S. J. Berners-Price, P. S. Jarrett and P. J. Sadler, *Inorg. Chem.* 1987, **26**, 3074.
9. S. S. D. Brown, P. J. McCarthy, I. D. Salter, P. A. Bates, M. B. Hursthouse, I. J. Colquhoun, W. McFarlane and M. Murray, *J. Chem. Soc., Dalton Trans.* 1988, 2787.
10. E. Bouwman, W. L. Driessen, J. Reedijk, C. Smykalla, J. M. M. Smits, P. T. Beurskens, F. Laschi and P. Zanello, *Inorg. Chem.* 1990, **29**, 4881.
11. J. C. Smart and B. L. Pinsky, *J. Am. Chem. Soc.* 1980, **102**, 1009.
12. N. Walker and D. Stuart, *Acta Cryst., Sect. A* 1983, **39**, 158.
13. G. M. Sheldrick, "SHELX 76" System of Computing Programs. University of Cambridge, Cambridge, U.K. (1976).
14. C. K. Johnson, ORTEP-II, Report ORNL-5138. Oak Ridge National Laboratory, Tennessee (1976).
15. *International Tables for X-ray Crystallography*, Vol. 4. Kynoch Press, Birmingham (1974).
16. R. G. Delaplane, J. O. Lundgren and I. Olovsson, *Acta Cryst., Sect B* 1975, **31**, 2202.
17. T. Kjällman and I. Olovsson, *Acta Cryst., Sect. B* 1972, **28**, 1692.
18. R. Hoffmann, *Angew. Chem. Int. Edn Engl.* 1982, **21**, 711.
19. C. Mealli and D. M. Proserpio, *J. Chem. Edn* 1990, **67**, 3399.
20. M. Di Vaira, L. Sacconi and P. Stoppioni, *J. Organomet. Chem.* 1983, **250**, 183.

Polyhedron Vol. 10, No. 18, pp. 2131–2136, 1991
Printed in Great Britain

0277–5387/91 $3.00+.00
© 1991 Pergamon Press plc

SYNTHESIS AND PROPERTIES OF COORDINATION COMPLEXES OF ACRYLONITRILE, METHACRYLONITRILE AND *CIS/TRANS*-CROTONONITRILE WITH THE CHLORIDES BCl_3, $TiCl_4$, $SnCl_4$ AND $SbCl_5$

M. A. I. EL-ERIAN, P. G. HUGGETT and K. WADE*

Chemistry Department, University of Durham, Science Laboratories, South Road, Durham DH1 3LE, U.K.

and

J. R. JENNINGS

ICI Chemicals and Polymers Limited, Research and Technology Department, Wilton Centre, Middlesbrough, Cleveland TS6 8JE, U.K.

(*Received* 21 *May* 1991; *accepted* 6 *June* 1991)

Abstract—The coordination complexes of acrylonitrile, $CH_2{=}CHCN$, methacrylonitrile, $CH_2{=}CMeCN$, and *cis/trans* crotononitrile, $MeCH{=}CHCN$, with a series of metal and metalloid chlorides, MCl_n, where M = Ti^{IV}, Sn^{IV}, B^{III} and Sb^{V}, have been prepared and the coordination is shown to be σ-bonded through the nitrogen "lone pair" to the metal centre. The olefinic protons of the 1:1 complexes of $TiCl_4$ and $SnCl_4$, on coordination, show an upfield shift in the ^1H NMR spectra. Electrical conductivity measurements in nitrobenzene solution show all the addition compounds of $SnCl_4$ and $TiCl_4$ to be non-electrolytes and therefore non-ionic. Consistent with this observation, all of the compounds except for the $SbCl_5$ complex are volatile at room temperature while the 2:1 complexes of $TiCl_4$ with acrylonitrile and methacrylonitrile tend to dissociate in the vapour phase into the 1:1 complex and free ligand. The IR spectra of the complexes have also been studied and in all cases the cyanide stretching frequency increases, showing coordination occurs through the nitrile group.

Addition complexes of nitriles with metallic and organometallic compounds have been known for many years.[1–4] Coordination is normally via the lone pair of electrons on the nitrogen atom and it was observed that on coordination, the IR stretching frequency of the nitrile group always increased. The magnitude of the increase correlated broadly with the strength of the metal–nitrogen bond and clearly reflects strong coupling between the stretching vibrations of the co-linear C≡N and N→M bonds. Acrylonitrile is an interesting nitrile in that, potentially, it is bifunctional and can offer coordination through either the nitrile group or the C=C group, particularly when complexed with transition metals. This gives rise to several possible different structural types and the existence of the three shown in Fig. 1 has been well established.

Other modes of coordination such as via the π-electrons of the nitrile group are also possible, as has been discussed previously.[5]

The coordination chemistry of acrylonitrile has been the subject of recent review,[5] but the coordination chemistry of its methyl derivatives, methacrylonitrile and the isomers of crotononitrile has received relatively little study. The copper(I) derivative $CuBrNCCMe:CH_2$ has been prepared[6] and shown by X-ray diffraction to consist of a chain of bromine-bridged copper atoms in tetrahedral coordination with the other two sites occupied by

* Author to whom correspondence should be addressed.

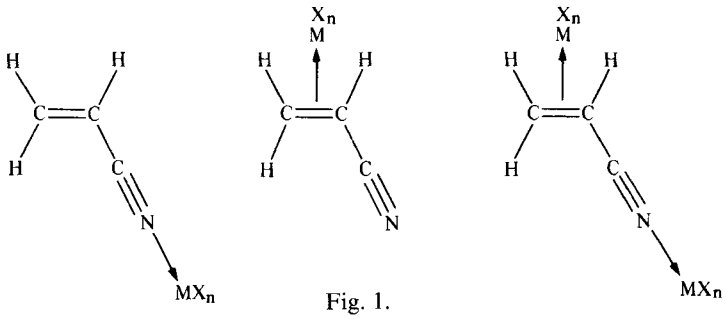

Fig. 1.

methacrylonitrile molecules, σ-bonded through the nitrogen "lone pairs". The π-bonded product analogous to $Cu_2Cl_2(CH_2CHCN)$ was not obtained from the reaction mixture, even with excess methacrylonitrile. Similarly, while bis(acrylonitrile) nickel is a well-characterized compound[7] containing π-bonded olefinic groups, no analogues have been prepared from either methacrylonitrile or crotononitrile.[8] Furthermore, while acrylonitrile itself is known to form stable complexes, anomalous behaviour has been observed[9,10] in its interaction with germanium and silicon tetrachlorides, in which a net repulsion was observed in mixtures of the nitrile and the chloride. The present work was therefore commenced to explore further the coordination chemistry of both methacrylonitrile and crotononitrile for comparison with the coordination chemistry of acrylonitrile itself.

EXPERIMENTAL

Starting materials

Tin tetrachloride, titanium tetrachloride, antimony pentachloride and boron trichloride were obtained commercially and purified by distillation. Acrylonitrile was purified by refluxing with calcium hydride for at least 6 h and then fractionally distilled onto freshly activated 3 Å molecular sieves. This treatment removed the stabilizer, so it was necessary to store the acrylonitrile in the dark to prevent photo-initiated polymerization. Both methacrylonitrile and the mixed isomers of crotononitrile were used without further purification other than standing over freshly activated 3 Å molecular sieves. Nitrobenzene was distilled from P_4O_{10}, and both benzene and pentane were dried over sodium wire. Experimental techniques included the use of a conventional vacuum line, a nitrogen-filled glove box and a dry nitrogen line.

Preparation of metal complexes

Since the methods used for the preparation of the complexes of acrylonitrile and its derivatives are similar, the experiments described below are classified according to the metal chloride used. The term L is used universally to denote acrylonitrile, methacrylonitrile or crotononitrile. Analytical data are given in Table 1.

Preparation of $TiCl_4 \cdot 2L$. Titanium tetrachloride (*ca* 2.5 cm^3) was added by syringe to the ligand (10 cm^3) in a cooled nitrogen-filled flask. A yellow suspension formed which was dissolved in excess ligand by warming with a hair-drier to yield a clear solution. On standing for 15 min and cooling, yellow crystals were deposited from solution which were collected on a filter and washed with cold ligand. The product was dried in a stream of dry nitrogen.

Preparation of $TiCl_4 \cdot L$. Titanium tetrachloride (*ca* 5 cm^3) was added slowly by syringe to a well stirred 1 : 1 stoichiometric solution of the nitrile in benzene (40 cm^3) at room temperature. The solution deposited a yellow microcrystalline solid which was filtered, washed with cold benzene and dried in a stream of nitrogen.

Preparation of $BCl_3 \cdot L$. Boron trichloride (*ca* 5 g) was condensed under reduced pressure into a flask cooled by liquid nitrogen. Pure nitrogen was admitted and dry pentane (30 cm^3) was added by syringe. The mixture was warmed to room temperature to dissolve the boron trichloride uniformly in the pentane. The solution was then cooled in liquid nitrogen and an equivalent molar weight of the ligand was added by syringe. On warming to room temperature, a white solid was obtained which was filtered, washed in dry pentane, and dried in a stream of nitrogen.

Preparation of $SbCl_5 \cdot L$. Antimony pentachloride (*ca* 4 cm^3) was added by syringe to the ligand (10 cm^3) in a flask cooled to liquid nitrogen temperature. On warming to room temperature, a very strongly exothermic reaction occurred, forming a precipitate which was redissolved on warming to obtain a clear yellow solution. On cooling, the solution deposited a white crystalline solid which was recovered by filtration, washed with cold ligand and dried as before.

Preparation of $SnCl_4 \cdot 2L$. Stannic chloride (4

Table 1. Analytical data for the nitrile–metal chloride addition complexes

Compound	Found %C	%H	%N	%Cl	Required %C	%H	%N	%Cl
$TiCl_4$·ACN	15.9	1.7	5.5	54.3	14.8	1.2	5.8	58.5
$TiCl_4$·2ACN	24.5	2.4	9.6	47.8	24.3	2.0	9.6	48.0
$TiCl_4$·MCN	19.1	3.1	5.4	51.2	18.7	2.0	5.5	55.3
$TiCl_4$·2MCN	28.3	3.2	8.1	41.3	29.6	3.1	8.6	43.8
$TiCl_4$·CNN	20.1	2.5	5.6	52.6	18.7	1.9	5.5	55.3
$TiCl_4$·2CNN	29.2	3.5	3.7	40.3	29.6	3.1	3.7	43.8
$SnCl_4$·2ACN	19.2	2.1	7.5	38.8	19.6	1.6	7.6	38.7
$SnCl_4$·2MCN	24.0	3.6	7.1	37.0	24.2	2.5	7.1	35.8
$SnCl_4$·2CNN	23.4	3.1	6.2	33.9	24.2	2.5	7.1	35.8
BCl_3·ACN	18.3	1.1	8.2	54.3	21.2	1.8	8.2	62.6
BCl_3·MCN	26.1	2.5	7.7	57.0	26.1	2.7	7.6	57.8
BCl_3·CNN	24.8	2.7	7.4	54.0	26.1	2.7	7.6	57.8
$SbCl_5$·ACN	11.6	1.2	4.4	48.9	10.2	0.9	4.0	50.4
$SbCl_5$·MCN	12.5	1.7	3.6	47.4	13.1	1.4	3.8	48.5
$SbCl_5$·CNN	13.3	1.3	4.1	45.5	13.1	1.4	3.8	48.5

ACN, MCN and CNN represent acrylonitrile, methacrylonitrile and crotononitrile, respectively.

cm^3) was added by syringe to the ligand (20 cm^3) in a flask cooled to −196°C. On warming to room temperature, a white precipitate was formed immediately, which was dissolved by warming. On cooling, white crystals were deposited which were recovered and dried as in the previous example.

RESULTS AND DISCUSSION

Some 15 complexes have been prepared from acrylonitrile and its methyl derivatives, crotononitrile and methacrylonitrile, with the chlorides BCl_3, $TiCl_4$, $SnCl_4$ and $SbCl_5$. Their analytical data (Table 1) are consistent with the formation of 1 : 1 addition complexes, though in the case of $TiCl_4$ and $SnCl_4$, a 2 : 1 stoichiometry can also be obtained. Vapour pressures were measured manometrically at room temperature using a cathetometer. Details are given in Table 2. With the exception of the antimony complex, the adducts are volatile crystalline solids and they are all extremely sensitive to air or moisture. The boron complex had the lowest vapour pressure of the volatile adducts, consistent with the strong Lewis acid properties of boron trichloride, and the tin complex proved to be the least stable of the series, though still contrasting strongly with the silicon and germanium derivatives[9,10] which showed no tendency for complex formation. The 2 : 1 complexes of $TiCl_4$ with acrylonitrile and methacrylonitrile show a tendency to dissociate on heating *in vacuo* to the 1 : 1 complex and free ligand. The methacrylonitrile complex appeared to be more thermally stable than its acrylonitrile analogue as shown by a higher temperature required to effect this dissociation.

Electrical conductivity measurements

While many coordination compounds are simple covalent adducts between donor and acceptor mol-

Table 2. Vapour pressure data for the nitrile–metal chloride addition complexes

Metal complex	Vapour pressure at 20°C (mm Hg) CH_2=CHCN	CH_2=CMeCN	MeCH=CHCN
$SbCl_5$·L	0.00	0.00	0.00
BCl_3·L	1.01	0.59	0.52
$TiCl_4$·2L	1.34	3.41	1.15
$TiCl_4$·L	2.52	2.95	3.68
$SnCl_4$·L	3.12	8.31	0.22

ecules, coordination complexes of polychlorometallic compounds have a tendency to form ionic compounds typified by species such as $[L_2MCl_2]^{2+}[MCl_6]^{2-}$ and which, clearly, have a significant electrical conductivity in solution,[11] usually in the range 100–200 Ω^{-1} cm^2 mol^{-1} and 20–30 Ω^{-1} cm^2 mol^{-1} for 1:1 electrolytes. To assess whether the titanium and tin compounds of this study were ionic in nature, the electrical conductivities of the relevant compounds in nitrobenzene solution were measured using a conductivity cell and a PTI-18 digital conductivity meter. All of the conductivities lay in the range 0.8–1.9 Ω^{-1} cm^2 mol^{-1}, showing these complexes to be non-electrolytes and hence simple donor/acceptor adducts.

IR spectra

IR spectra of all the complexes as Nujol mulls were recorded across the frequency range 4000–200 cm^{-1}, using Perkin–Elmer 477 and 577 spectrometers. The assignments of the most diagnostic bands for free acrylonitrile,[12] methacrylonitrile[13] and crotononitrile,[14] together with their coordination complexes are given in Table 3. The shifts in the absorption frequencies of the nitrile bond, the olefinic stretch and the out-of-plane deformation of the olefinic hydrogens upon coordination to the metal centre are also given in Table 2. The importance of these shifts is that they indicate a change in the force constant in the functional group upon coordination, from which the mode of coordination of the ligand can be determined.

All of the adducts show an increase in the nitrile stretching frequency in the range 22–89 cm^{-1}. This indicates strongly that the nitrile group is involved in the coordination. The largest shifts in frequency, which ranged from75–89 cm^{-1}, were observed for the complexes formed by the strongest Lewis acid (and that of lowest molecular mass), boron trichloride which presumably formed the strongest M—N bond. In general, the largest shifts (37–89 cm^{-1}) were also observed for the parent ligand, acrylonitrile. The smallest shifts were observed for methacrylonitrile (22–75 cm^{-1}), possibly for steric rather than electronic reasons and no particular trends were detected for the other metals, or within the 1:1 and 1:2 complexes. The increase in frequency described in this work is in good agreement with other published data[5] on acrylonitrile complexes known to coordinate through the nitrogen where the increase lies in the range 14–61 cm^{-1}.

Stretching frequencies for the C=C bond are also given in Table 3. In each complex, there is a small decrease in the stretching frequency ranging from 3 to 21 cm^{-1}. When acrylonitrile is coordinated via the π-electrons of the C=C group, the stretching frequency of the C—C unit always falls significantly as the new bond order approaches unity. For example,

Table 3. IR data for derivatives of acrylonitrile and their complexes

Compound	ν(C≡N) (cm^{-1})	ν(C=C) (cm^{-1})	$\delta\nu$(C≡N) (cm^{-1})	$\delta\nu$(C=C) (cm^{-1})
CH_2=CHC≡N (ACN)	2223	1608	—	—
BCl_3·ACN	2312	1596	89	−12
$SnCl_4$·2ACN	2270	1605	47	−3
$SbCl_5$·ACN	2260	1600	37	−8
$TiCl_4$·2ACN	2265	1600	42	−8
$TiCl_4$·ACN	2270	1597	47	−11
CH_2=CMeC≡N (MCN)	2233	1629	—	—
BCl_3·MCN	2308	1608	75	−1
$SnCl_4$·2MCN	2255	1610	22	−19
$SbCl_5$·MCN	2270	1620	37	−9
$TiCl_4$·2MCN	2265	1613	32	−16
$TiCl_4$·MCN	2255	1608	22	−21
MeCH=CHC≡N (CNN)	2223	1635	—	—
BCl_3·CNN	2300	1620	77	−15
$SnCl_4$·2CNN	2255	1628	32	−7
$SbCl_5$·CNN	2255	1622	32	−13
$TiCl_4$·2CNN	2250	1621	27	−14
$TiCl_4$·CNN	2250	1622	27	−13

Table 4. IR spectral data for the CH_2 out of plane deformation modes

Compound	$\tau(CH_2)$ (cm^{-1})	$\omega(CH_2)$ (cm^{-1})	δ cm^{-1}
$CH_2{=}CHC{\equiv}N$	962	962	0
$BCl_3 \cdot ACN$	945	996	51
$SnCl_4 \cdot 2ACN$	960	990	30
$SbCl_5 \cdot ACN$	960	—	—
$TiCl_4 \cdot 2ACN$	955	985	30
$TiCl_4 \cdot ACN$	953	986	33

Table 5. ^1H NMR data for acrylonitrile complexes

Compound	Centre of multiplet	Shift from ACN
$CH_2{=}CHC{\equiv}N$ (ACN)	5.53	
$BCl_3 \cdot ACN$	4.66	−0.87
$SbCl_5 \cdot ACN$	4.25	−1.28
$SnCl_4 \cdot ACN$	4.83	−0.70
$TiCl_4 \cdot ACN$	4.04	−1.49
$SnCl_4 \cdot 2ACN$	4.90	−0.63
$TiCl_4 \cdot 2ACN$	4.79	−0.74

in bis (acrylonitrile) nickel, a shift of 162 wave numbers from 1608 to 1446 cm^{-1} was observed.[15] Typical shifts lie in the range 106–168 cm^{-1}. It is clear, therefore, that any π-bonding contribution to these complexes is minimal. The twisting $\tau(CH_2)$ and wagging $\omega(CH_2)$ modes, also diagnostic for the mode of coordination of acrylonitrile,[16] were observed in the spectrum of the acrylonitrile derivatives and are listed in Table 4. The shifts are also consistent with coordination via the nitrogen lone pair and the magnitude of the observed splitting confirms boron trichloride to be the strongest Lewis acid of the series under study.

Nuclear magnetic resonance spectra

^1H NMR spectra were recorded on the complexes in benzene solution using a Varian A60/56D spectrometer, operating at 60 Mhz and with tetramethylsilane as the external reference standard. Under normal resolution, the olefinic protons of free acrylonitrile give rise to an ABC-pattern of peaks centred about 6.0 ppm downfield from TMS.[17] Coordination of acrylonitrile through the nitrogen usually results in a small downfield shift of 0.1–0.5 ppm in the resonance from the α-hydrogen, due to the electron-withdrawing effect of the Lewis acid. The effect on the resonance of the β-hydrogen is less well-defined and the shift can be either way.[18] The changes in the ^1H NMR spectrum of acrylonitrile when coordinated to the metal chlorides of this study are summarized in Table 5. A complex pattern of overlapping peaks was obtained for each compound, the centres of which were in the range 4.04–4.83 ppm downfield from TMS. This corresponds to each signal arising from the protons of the vinyl group having been shifted upfield by 0.63–1.49 ppm on coordination to the metal chloride.

In comparison with previous work on nitrogen-bonded acrylonitrile complexes, the magnitudes of the shifts of these compounds are significantly greater and more importantly, are in the opposite direction. Similar upfield shifts, but of a smaller magnitude are also seen in the complexes of methacrylonitrile and crotononitrile, as shown in Tables 6 and 7.

This suggests the presence of some interaction between the C=C π-system and either the metal complex or the metal chloride itself. There is also some evidence for partial dissociation of the nitrile ligand. The 1 : 1 and 2 : 1 complexes of all three nitriles were prepared from stannic chloride and titanium tetrachloride. The upfield shift relative to

Table 6. ^1H NMR data for methacrylonitrile complexes

Compound	CH_3	H_{cis}	H_{trans}	ΔCH_3	ΔH_{cis}	ΔH_{trans}
$CH_2{=}CMeC{\equiv}N$ (MCN)	1.60	5.30	5.40			
$BCl_3 \cdot MCN$	0.92	4.93	—	−0.68	−0.37	
$SbCl_5 \cdot MCN$	0.82	4.67	4.83	−0.78	−0.63	−0.57
$SnCl_4 \cdot MCN$	1.06	4.83	4.98	−0.54	−0.47	−0.42
$TiCl_4 \cdot MCN$	0.80	4.52	4.82	−0.80	−0.78	−0.58
$SnCl_4 \cdot 2MCN$	1.23	5.00	5.16	−0.37	−0.30	−0.24
$TiCl_4 \cdot 2MCN$	1.10	4.88	5.08	−0.50	−0.42	−0.32

Table 7. ^{1}H NMR data for crotononitrile complexes

Compound	CH_3	H_{cis}	H_{trans}	ΔCH_3	ΔH_{cis}	ΔH_{trans}
$CH_3CH{=}CHC{\equiv}N$ (CNN)	1.53	4.79	5.89	—	—	—
$BCl_3 \cdot CNN$	1.12	4.07	5.67	−0.41	−0.72	−0.22
$SbCl_5 \cdot CNN$	0.79	3.55	5.29	−0.74	−1.24	−0.60
$SnCl_4 \cdot CNN$	1.11	4.18	5.72	−0.42	−0.61	−0.17
$TiCl_4 \cdot CNN$	1.00	4.08	5.70	−0.53	−0.71	−0.19
$SnCl_4 \cdot 2CNN$	1.32	4.44	5.83	−0.21	−0.35	−0.06
$TiCl_4 \cdot 2CNN$	1.14	4.26	5.67	−0.39	−0.53	−0.22

the free ligand is always greater for the 1 : 1 complex than for the 1 : 2 complex and this is consistent with a dissociation process, in solution, of the 2 : 1 complex into the 1 : 1 adduct and the free nitrile:

$$MCl_4 \cdot 2L \underset{-Bz}{\overset{+Bz}{\rightleftharpoons}} L + MCl_4 \cdot L \underset{-Bz}{\overset{+Bz}{\rightleftharpoons}} 2L + MCl_4.$$

Such a mixture would then be expected to show the signals arising from the weighted mean of the chemical shifts of the free and complexed ligand. Such a dissociative process also offers a possible explanation for the upfield shift displayed by the nitrile protons on coordination, since the olefinic bond would then be able to interact with any coordinative unsaturation generated by dissociation. It was also observed that the chemical shift of the olefinic protons decreased in the sequence:

$$CH_2{=}CHCN > CH_3CH{=}CHCN \sim CH_2{=}C(CH_3)CN.$$

This reflects the order of stability for the complexes of acrylonitrile and its methyl derivatives with metal halides where it appears that the bulk of the methyl group is sufficient to inhibit the degree of coodination.

Acknowledgements—Financial support from ICI and SERC through the CASE scheme (PGH) and from the British Council (MAIE-E) is gratefully acknowledged.

REFERENCES

1. I. R. Beattie, *Q. Rev. Chem. Soc.* 1963, **17**, 382.
2. B. N. Storhoff and H. C. Lewis, *Coord. Chem. Rev.* 1977, **23**, 1.
3. D. F. Shriver and B. Swanson, *Inorg. Chem.* 1971, **10**, 1354.
4. J. R. Jennings, J. E. Lloyd and K. Wade, *J. Chem. Soc.* 1965, 5083.
5. S. J. Bryan, P. G. Hugget, K. Wade, J. A. Daniels and J. R. Jennings, *Coord. Chem. Rev.* 1982, **44**, 149.
6. M. Massaux, G. Ducreux, R. Chevalier and M. T. Le Bihan, *Acta Cryst.* 1978, **B34**, 1863.
7. G. N. Schrauzer, *J. Am. Chem. Soc.* 1959, **81**, 5310.
8. M. Herberhold, *Metal Complexes*, Vol. II, Part 1, p. 290. Elsevier Publishing Company, Amsterdam (1972).
9. J. A. Daniels, J. R. Jennings, P. G. Huggett and K. Wade, *Inorg. Nucl. Chem. Lett.* 1978, **14**, 445.
10. P. G. Huggett, K. Manning and K. Wade, *J. Inorg. Nucl. Chem.* 1980, **42**, 665.
11. W. J. Geary, *Coord. Chem. Rev.* 1971, **7**, 81.
12. F. Halverson, R. F. Stamm and J. J. Whalen, *J. Chem. Phys.* 1948, **16**, 808.
13. J. Bragin, K. L. Kizerand and J. R. Durig, *J. Molec. Spectrosc.* 1971, **38**, 289.
14. J. R. Durig, C. K. Tong, C. W. Hawley and J. Bragin, *J. Phys. Chem.* 1971, **75**, 44.
15. G. N. Schrauzer and H. P. Fritz, *Chem. Ber.* 1961, **94**, 650.
16. W. Kuran, S. Pasynkiewicz, Z. Florjanczyk and E. Lusztyk, *Makromol. Chem.* 1976, **177**, 2627.
17. A. G. Moritz, *Molec. Phys.* 1971, **20**, 945.
18. R. D. Foust and P. C. Ford, *J. Am. Chem. Soc.* 1972, **94**, 5686.

Polyhedron Vol. 10, No. 18, pp. 2137–2143, 1991
Printed in Great Britain

0277–5387/91 $3.00+.00
© 1991 Pergamon Press plc

COMPLEXES OF RUTHENIUM(II) AND (III) DERIVED FROM O,N-DONOR LIGANDS, AND THEIR EFFICIENCY AS CATALYTIC OXIDANTS FOR ALCOHOLS

AHMED M. EL-HENDAWY

Chemistry Department, Faculty of Science, Damietta, Egypt

(*Received* 1 *May* 1991; *accepted* 4 *June* 1991)

Abstract—The new complexes $[Ru^{II}Cl_2(PPh_3)_2L]$ (L = benzoic hydrazide, bhz; substituted derivatives, R-bhz; R = *p*-Cl, *p*-CH_3, *o*-NH_2 and phenylacetic hydrazide) and $[Ru^{III}X_2(AsPh_3)_2L']$ (L′ = monoanions of 8-hydroxyquinoline, 8-hq; *o*-aminophenol; 2-amino-3-hydroxypyridine; X = Cl or Br) have been isolated. They were characterized by spectroscopic techniques and their redox behaviour was studied by cyclic voltammetry. The ruthenium(III) complexes were found to be more effective catalysts than those of ruthenium(II) for the oxidation of primary alcohols to aldehydes and of secondary alcohols to ketones in the presence of N-methylmorpholine-N-oxide as co-oxidant. Turnovers reached 400 with the catalyst $[Ru^{III}Cl_2(AsPh_3)_2(8\text{-hq})]$.

The interaction of dichlorotris(triphenylphosphine)ruthenium(II) with the sodium salts of various Schiff bases, L, derived from aliphatic dianions and β-diketones or aromatic aldehydes gives the octahedral species *trans*-$[Ru^{II}L_n(PPh_3)_m]$ ($n = 1, 2$; $m = 2$).[1] Pentacoordinated ruthenium(II) complexes have been prepared when isonicotinoyl hydrazone derivatives of β-diketones or salicylaldehyde reacted with $[RuCl_2(PPh_3)_3]$ in the presence of sodium hydride.[2] Recently, we have isolated and characterized $[M^{III}Cl_2(PPh_3)_2L']$ [M = Ru, Os; L′ = O,O-donor ligand(−1)].[3–5] We have been interested in the oxidation chemistry of *trans*-dioxoruthenium(VI) complexes[6–9] and also ruthenium(II) and (III) complexes containing triphenylphosphine.[3,10]

We now report the preparation of the new complexes $[Ru^{II}Cl_2(PPh_3)_2(bhz')]$ [bhz′ = benzoic hydrazide (bhz), $PhCONHNH_2$; substituted benzoic hydrazides, R-$PhCONHNH_2$, where R = *p*-Cl, *p*-CH_3, *o*-NH_2 and phenylacetic hydrazide (phachz), $PhCH_2CONHNH_2$] and $[Ru^{III}X_2(AsPh_3)_2L]$ [L = monoanions of 8-hydroxyquinoline (8-hq), *o*-aminophenol (*o*-amph), 2-amino-3-hydroxypyridine (amhpy); X = Cl or Br]. We also report their spectroscopic and electrochemical behaviour and study the catalytic oxidation of alcohols by such complexes in the presence of N-methylmorpholine-N-oxide (NMO) as co-oxidant.

RESULTS AND DISCUSSION

Reaction of $[RuCl_2(PPh_3)_3]$ with different hydrazide derivatives (bhz′) in refluxing methanol under nitrogen yields yellow precipitates within 0.5–2 h. The ruthenium(III) complexes of 8-hydroxyquinoline, *o*-aminophenol and 2-amino-3-hydroxypyridine were made from $[RuX_3(AsPh_3)_2MeOH]$ (I) (X = Cl, Br) by refluxing methanolic solutions of I with the appropriate ligand for 1–2 h. We have reported previously the synthesis of $[Os^{III}Cl_2(PPh_3)_2L]$ (L = O,O-donor ligand(−1))[4,5] starting with $[OsCl_3(PPh_3)_2MeOH]$. The analytical data (Table 1) indicate that these complexes have the formulae $[Ru^{II}Cl_2(PPh_3)_2(bhz')]$, $[Ru^{III}Cl_2(AsPh_3)_2L]$ (L = 8-hq, *o*-amph, amhpy) and $[Ru^{III}Br_2(AsPh_3)_2(8\text{-hq})]$. The ruthenium(II) hydrazide complexes are air-sensitive since their colour changes on exposure to air, while the other ruthenium(III) complexes are air-stable. All the complexes are only soluble in CH_2Cl_2 and their molar conductivities are very low.

The hydrazide complex $[RuCl_2(PPh_3)_2(bhz')]$ was found to be diamagnetic at room temperature; the other complexes are paramagnetic and their magnetic moments lie in the range 1.65–2.15 BM (Table 2), close to the spin-only value (1.73 BM) for one unpaired electron. This suggests the low-spin $d^5(t_{2g})^5$

Table 1. Analytical and spectroscopic data for complexes

Compound	Colour	Analysis Found (Calc.), % C	H	N	IR data, wavenumbers (cm^{-1}) ν(C═O)	$\delta(NH_2)$	ν(Ru—N)	ν(Ru—Cl)	Other bands	UV-vis data, λ_{max} (nm) (ε, $M^{-1}\,cm^{-1}$)
$[RuCl_2(PPh_3)_2(bhz)]$	Yellow	61.6 (62.2)	4.4 (4.6)	3.3 (3.4)	1636vs	1605s	424m	320m		481(665), 350(2300), 295(6950)
$[RuCl_2(PPh_3)_2(p\text{-Cl bhz})]$	Yellow	59.2 (59.5)	4.1 (4.3)	2.9 (3.2)	1636vs	1602s	423m	322m		474(890), 376(2400), 295(10,780)
$[RuCl_2(PPh_3)_2(p\text{-Me bhz})]$	Yellow	62.1 (62.4)	4.5 (4.7)	3.2 (3.3)	1633s	1615sh 1590m	425m	323m		479(1180), 345(4200), 295(13,750)
$[RuCl_2(PPh_3)_2(o\text{-}NH_2\text{ bhz})]$	Yellowish-brown	60.6 (60.9)	4.3 (4.6)	4.7 (5.0)	1624vs	1590s	424m	322m		486(440), 347(6850), 276sh(9100)
$[RuCl_2(PPh_3)_2(phachz)]$	Yellow	62.0 (62.4)	4.4 (4.7)	3.2 (3.3)	1631vs	1574s	422m	323m		470(250), 378(480), 273(6200), 234(31,140)
$[RuCl_2(AsPh_3)_2(8\text{-hq})]$	Yellowish-green	58.2 (58.2)	3.8 (3.9)	1.5 (1.5)	1279m[a]			323s	405w	775(1030), 445sh, 380(6300), 260sh(30,130), 225(45,030)
$[RuBr_2(AsPh_3)_2(8\text{-hq})]$	Yellowish-brown	52.9 (53.2)	3.3 (3.5)	1.3 (1.4)	1274m[a]			260w[b]	405w	795(570), 430(4300), 360(4955), 230(37,880)
$[RuCl_2(AsPh_3)_2(o\text{-amph})]$	Purple	56.4 (56.5)	3.9 (4.0)	1.5 (1.6)		1615m	473s	324s	1271m	555(3820), 455(3200), 285(17,240), 225(30,970)
$[RuCl_2(AsPh_3)_2(amhpy)]$	Deep purple	54.9 (55.1)	3.8 (3.9)	3.0 (3.1)		1618m	475s	323m	1223m 1294m	

[a] Due to ν(C—O).
[b] Due to ν(Ru—Br).

Table 2. Magnetic moments, ESR parameters and voltammetric data of the complexes

Compound	μ_{eff} (BM)[a]	g-values			Voltammetric data (V) Reduction			Oxidation			Scan rate (mV s^{-1})
		g_x	g_y	g_z	$E_{p,c}$	$E_{p,a}$	ΔE	$E_{p,c}$	$E_{p,a}$	ΔE	
$[RuCl_2(PPh_3)_2(bhz)]$	D				—			+0.46	+0.54	0.080	20, 50, 100
$[RuCl_2(PPh_3)_2(p\text{-Cl bhz})]$	D				—			+0.50	+0.58	0.080	20, 50, 100
$[RuCl_2(PPh_3)_2(p\text{-Me bhz})]$	D				—			+0.47	+0.55	0.080	20, 50, 100
$[RuCl_2(PPh_3)_2(o\text{-}NH_2bhz)]$	D				—			+0.44	+0.52	0.080	20, 50, 100
$[RuCl_2(PPh_3)_2(phachz)]$	D				—				+1.34		20, 50, 100
$[RuCl_2(AsPh_3)_2(8\text{-hq})]$	2.12	2.49	2.26	1.94	−0.48	−0.56	0.080	+0.67	+0.84	0.170	10, 20
$[RuBr_2(AsPh_3)_2(8\text{-hq})]$	2.15				−0.46	−0.53	0.070	+0.64	+0.82	0.180	10, 20
$[RuCl_2(AsPh_3)_2(o\text{-amph})]$	1.69	2.49	2.16	1.71	−0.80	—	—	+0.49	+0.56	0.070	10, 20, 50
$[RuCl_2(AsPh_3)_2(amhpy)]$	1.85	2.56	2.03	1.68	−0.74	—	—	+0.50	+0.56	0.060	10, 20, 50

[a] D = diamagnetic.

configuration for the ruthenium(III) ion in an octahedral environment, as is the case for other ruthenium(III) and osmium(III) complexes.[3-5,11]

The IR spectra of the complexes showed bands due to triphenylphosphine, arsine and coordinated L. Characteristic bands of L are shifted to lower wavenumbers. The strong bands around 1630 and 1600 cm^{-1} observed in the ruthenium(II) complexes of hydrazides are tentatively assigned to the ν(C=O) and $\delta(NH_2)$ vibrations which appear near 1660 and 1600 cm^{-1} in the free hydrazide ligands. This confirms the participation of both the carbonyl oxygen and the amino nitrogen atoms of hydrazide ligands in coordination. The $\delta(NH_2)$ band has been shifted near 1615 cm^{-1} for the complexes $[Ru^{III}Cl_2(AsPh_3)_2L]$ (L = *o*-amph, amhpy). Distinct bands at 1279 and 1274 cm^{-1} were found in the complexes $[RuX_2(AsPh_3)_2(8\text{-hq})]$ (X = Cl, Br), which are consistent with the phenolic ν(C—O) vibration[12,13] which was observed at 1286 cm^{-1} in the free ligands (H8-hq). We could not assign such bands in $[Ru^{III}Cl_2(AsPh_3)_2L]$ (L = *o*-amph, amhpy) due to the presence of ν(C—N) modes in this region. A new band has been found near 425 or 473 cm^{-1} in the complexes which probably arises from the ν(Ru—N) modes as previously assigned for metal–nitrogen vibrations.[14,15] The bands near 320 cm^{-1} are likely to be due to ν(Ru—Cl), similar to those found in $[MCl_2(PPh_3)_2L]$ [M = Ru, Os; L = O,O-donor ligands(−1)].[3-5] A weak band at 260 cm^{-1} was observed for the complex $[RuBr_2(AsPh_3)_2(8\text{-hq})]$ which is probably due to ν(Ru—Br), as found for *trans*-$[RuBr_2(py)_4]$.[7] In the complex $[RuCl_2(AsPh_3)_2(amhpy)]$, no bands were observed for ν(Ru—py) as found with $[RuCl_2(py)_4]$ and $[RuCl_2L_4]$ (L = *o*-aminopyridine) at 294 and 306 cm^{-1}, respectively.[16] This suggests that the coordination of the ligand (amhpy) involves only the amino and hydroxyl groups as with the complex $[RuCl_2(AsPh_3)_2(o\text{-amph})]$. The most important IR bands are listed in Table 1. The air sensitivity of the ruthenium(II) complexes and the deep colours of the ruthenium(III) complexes make them all unsuitable for Raman studies.

Electronic spectra and electron spin resonance

The UV–vis spectra of the ruthenium(II) complexes in de-aerated CH_2Cl_2 solution (Table 1) showed a broad band near 475 nm. This is assigned to metal–ligand charge-transfer transitions, $t_2(Ru) \rightarrow \pi^*(L)$, similar to those found for $[Ru^{II}(bipy)_2A][ClO_4]$ [A = arylazo-oximato ligand(−1)].[17] The band in the region 375–345 nm could arise from $X \rightarrow t_2$ (X = Cl) transitions.[4,18,19] The bands below 300 nm are of the interligand $\pi \rightarrow \pi^*$ type.[5,20] The spectra of ruthenium(III) complexes in CH_2Cl_2 show bands above 550 nm of high intensity, attributed to ligand(π)→metal(d) transitions,[20-23] and the other bands observed (Table 1) are similarly assigned as in the ruthenium(II) complexes above.

The ESR spectra of the solid samples of the ruthenium(III) complexes were carried out at −170°C, cold nitrogen gas was passed over the sample tube for cooling. The spectrum of each complex (Fig. 1 as a representative example) shows three g-values (Table 2) in agreement with a low-symmetry of the ligand field similar to the g-values for *mer*-$[RuCl_3(AsPh_3)_3]$[24] and $[Ru^{III}Cl(Salen)(PPh_3)]$ [H_2Salen = N,N - ethylenebis(Salicylaldimine)].[25] We have recently[4] shown that the complex $[OsCl_2(PPh_3)_2L]$ [L = hexafluoroacetylacetonate ion(−1)] had a similar type of ESR spectrum with C_2 symmetry, so we suggest the structure below for

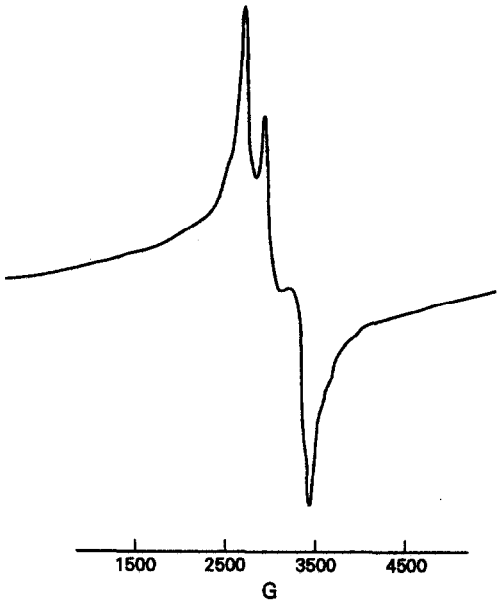

Fig. 1. ESR spectrum of $[RuCl_2(AsPh_3)_2(8\text{-hq})]$.

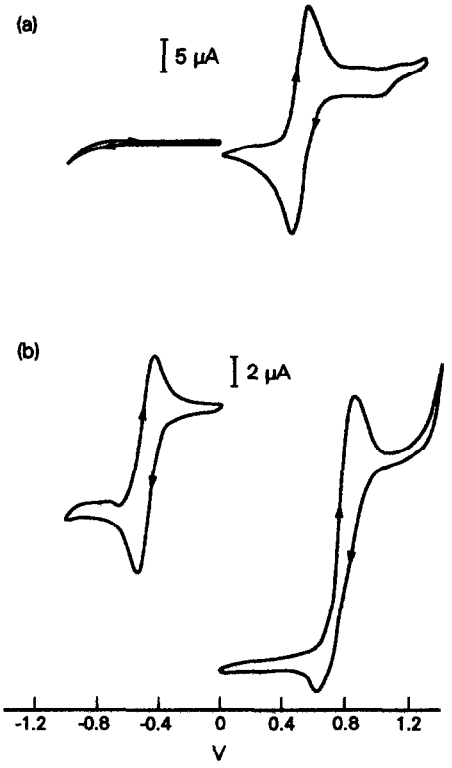

Fig. 2. Cyclic voltammogram in CH_2Cl_2 with 0.1 M $(Bu^n_4N)PF_6$ as supporting electrolyte; volts vs silver electrode: (a) $[RuCl_2(PPh_3)_2(bhz)]$ ($\sim 10^{-3}$ M), scan rate 50 mV s^{-1}; (b) $[RuBr_2(AsPh_3)_2(8\text{-hq})]$ ($\sim 10^{-3}$ M), scan rate 10 mV s^{-1}.

our ruthenium(III) complexes $[RuCl_2(AsPh_3)_2L']$ [L' = O,N-donor ligand(−1)] of C_s symmetry.

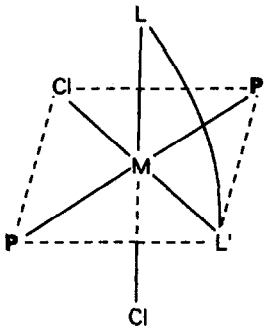

[M = Os, P = PPh_3, L–L' = O,O-donor ligand (−1)[4]; M = Ru, P = $AsPh_3$, L–L' = O,N-donor ligand (−1)]

Redox properties

The electrochemical properties of the complexes were investigated by cyclic voltammetry. Voltammetric data vs the silver electrode for 0.1 M $Bu^n_4NPH_6$-CH_2Cl_2 solutions are presented in Table 2. The voltammogram of the hydrazide complexes $[Ru^{II}Cl_2(PPh_3)_2(bhz')]$ reveals only an oxidation wave in each (ΔE = 70–80 mV) which corresponds to a Ru^{II}/Ru^{III} oxidation. The peak separation (ΔE) for each complex is close to that anticipated for a Nernstian one electron process (59 mV);[26] no other peaks could be observed at negative potentials. For $[RuCl_2(PPh_3)_2(bhz)]$, a representative example [Fig. 2(a)] shows only a quasi-reversible one electron oxidation wave, $E_{1/2}$ = +0.50 V, ΔE = 80 mV. The presence of such oxidation waves seems to be typical of ruthenium(II) complexes, e.g. $[Ru^{II}(Salen)(PPh_3)_2]$[27] and $[Ru^{II}(bipy)_2A][ClO_4]$ (HA = arylazo-oxime).[17] The irreversible peak of oxidation found for $[Ru^{II}Cl_2(PPh_3)_2(phachz)]$ was typically observed for $[Ru^{II}Cl_2(HA)]$ at +1.2 V and also explained as being due to a Ru^{II}/Ru^{III} oxidation.[28]

The complexes $[Ru^{III}X_2(AsPh_3)_2(8\text{-hq})]$ (X = Cl, Br) show a pair of cathodic and anodic peaks in each complex [Fig. 2(b)]. The reversible wave at a negative potential (ΔE = 60–70 mV) is presumably assigned to Ru^{III}/Ru^{II} reduction, similar to that found for $[M^{III}Cl_2(PPh_3)_2L]$ [M = Ru, Os; L = O,O-donor ligand(−1)][3,4] and $[Ru^{III}(Salen)(PPh_3)(py)][ClO_4]$.[29] The other couple of peaks at positive potentials have heights double those of the corresponding reduction, ΔE = 170–180 mV. This probably arises from the oxidation of ruthenium(III) to higher oxidation states [e.g. Ru^V], as similarly found for the presence of an irreversible peak at +1.26 V in $[Ru^{III}Cl_2(PPh_3)_2(acac)]$.[4] A small shift to a more negative potential was

observed for the reduction wave of $[RuCl_2(AsPh_3)_2(8\text{-hq})]$ compared with that of the analogous bromo complex, since we expect that the bromo complex is more readily reduced as reported for $[Os^{III}X_2(PPh_3)_2L]$ (X = Cl, Br; HL = 2-hydroxypyridine, 2-hydroxy-6-methylpyridine and picolinic acid).[30] The complexes $[Ru^{III}Cl_2(AsPh_3)_2L']$ (L′ = *o*-amph, amhpy) show an irreversible cathodic peak and a reversible wave of oxidation, corresponding to Ru^{III}/Ru^{II} reduction and Ru^{III}/Ru^{IV} oxidation, respectively.

For scan rates (SR) between 10–100 mV s^{-1}, the ratio $i_p/(SR)^{1/2}$ (i_p = peak current) was constant and the ratio of anodic to cathodic peak current is one, the peak separation being independent of the scan rate. This indicates that the electron transfer is reversible or approaches reversibility and the mass transfer is limited.

Catalytic oxidation

In attempts to find new ruthenium(II) and ruthenium(III) complexes that act as efficient catalysts in the presence of excess NMO for selective oxidation of primary alcohols to aldehydes and secondary alcohols to ketones, we have used the present new complexes for such catalytic oxidation. It has been reported that the complexes $[RuCl_2(PPh_3)_3]$[10] and $Ru^{III}Cl_2(PPh_3)_2(acac)]$[3] (**II**) in the presence of excess NMO are good catalytic oxidants for alcohols with turnovers 50–100. Table 3 summarizes our results for catalytic oxidations by $[Ru^{II}Cl_2(PPh_3)_2(bhz)]$ (**III**) and $[Ru^{III}Cl_2(AsPh_3)_2(8\text{-hq})]$ (**IV**) for alcohols with NMO as the co-oxidant. The oxidations were carried out at room temperature in dichloromethane solution from which water was removed using powdered molecular sieves. There was no detectable oxidation of the alcohols with NMO present only in the absence of a ruthenium complex. Primary alcohols were oxidized to aldehydes and secondary alcohols to ketones with both higher yields and turnovers. The ruthenium(II) catalyst **III** has turnovers (60–80) similar to those obtained by **II**[3] while complex **IV** is far superior to the other catalysts,[3,5,10] achieving turnovers of 400. Both the present catalysts **III** and **IV** are more effective towards oxidation of unsaturated alcohols, e.g. cinnamyl alcohol. The oxidation of cinnamyl alcohol was also carefully carried out using $[RuCl_2(PPh_3)_2(bhz'')]$/NMO [bhz″ = substituted hydrazides; *p*-Cl bhz(**III′**), *p*-Me bhz(**III″**)] instead of **III** under the same conditions; the yield of the aldehyde was 68, 64 and 61% for the catalysts **III′**, **III** and **III″**, respectively. Although the $E_{1/2}$ values of the oxidation waves for the different hydrazide ruthenium(II) complexes are close, it is clear from the oxidation of cinnamyl alcohol that a coordinating hydrazide which contains an electron attracting group (*p*-Cl bhz) increases the rate of oxidation contrary to that obtained with the electron repelling group (*p*-Me bhz). Catalytic oxidation for *p*-methoxybenzyl alcohol by

Table 3. Catalytic oxidation of alcohols by $[RuCl_2(AsPh_3)_2(8\text{-hq})]$/NMO

Alcohol	Product[a]	Time (h)	Yield (%)	Turnover[b]
p-methoxybenzyl	A	2.5	94	400
	A	2	93	80
	A[c]	3[c]	92[c]	105[c]
	(A)	(2.5)	(95)	(200)
piperonyl	A	2.5	83	250
	A	3	79	70
	(A)	(3)	(91)	(200)
cinnamyl	A	4	75	400
	A	2.5	64	70
α-tetralol	K	3	76	400
	K	2	92	65
benzohydrol	K	3	89	200
benzyl	A	3	94	220
	A	2	95	60

Underlined data refer to oxidation by $[RuCl_2(PPh_3)_2(bhz)]$/NMO and those between parentheses are by $[RuCl_2(AsPh_3)_2(o\text{-amph})]$/NMO.

[a] A = corresponding aldehyde, K = corresponding ketones.

[b] Turnover = moles of product/moles of catalyst.

[c] Oxidation carried out under nitrogen.

$[RuCl_2(PPh_3)_2(bhz)]$ was also carried out under nitrogen, and a better yield of the corresponding aldehyde was obtained. This indicates that the oxidations by **III** were not assisted aerobically as are those effected by $[Ru_2^{VI}O_6(py)_4]$,[8] and indeed the optimum condition of oxidation is to perform it under nitrogen since these ruthenium(II) complexes are air-sensitive.

The complex $[Ru^{III}Cl_2(AsPh_3)_2(o\text{-amph})]$(**V**) was also used for oxidation of piperonyl and *p*-methoxybenzyl alcohols; the yield of the corresponding aldehyde (turnovers 200, Table 3) is lower than that given by **IV**. It is of interest to note that the catalyst $[RuCl_2(AsPh_3)_2(8\text{-hq})]$ (**IV**) is more efficient than the other ruthenium(III) complexes (e.g. **V**). This can be concluded from the difference in their electrochemical behaviour at positive potentials, since complex **IV** shows an oxidation wave of current height twice that of complex **V**, as suggested above due to the oxidation of Ru^{III} to higher oxidation states of ruthenium, possibly Ru^{V} and Ru^{III} to Ru^{IV}, respectively. Also, catalyst **IV** is much better than the reported $[RuCl_2(PPh_3)_2acac]$ for the oxidation of alcohols; this probably arises from the appearance of an oxidation wave for **IV** ($\Delta E = 170$ mV) instead of the only anodic peak observed at positive potentials for the acetylacetonate complex **II**. We believe that the presence of such an oxidation wave in **IV** reflects the reason for the more efficient catalysis cycle of oxidation and consequently the higher turnovers given (reached 400).

EXPERIMENTAL

Preparation of complexes

Benzoic acid hydrazide and its substituted derivatives were prepared according to the procedures described earlier.[31]

Preparation of $[Ru^{II}Cl_2(PPh_3)_2(bhz)]$. Complex $[RuCl_2(PPh_3)_3]$[32] (**VI**) (0.48 g, 0.5 mmol) was added under nitrogen to a degassed methanolic solution (10 cm^3) containing benzoic acid hydrazide (0.1 g, 0.75 mmol). The mixture was refluxed on a steam bath where the dark crystals of **VI** dissolved rapidly, followed by the separation of a yellow precipitate. Heating was continued for 0.5 h under nitrogen. The precipitate was filtered off, washed with a little degassed methanol and ether, and dried *in vacuo*.

A similar procedure was used to prepare the other hydrazide complexes in which reflux was continued for 1–2 h. Evaporation of some methanolic solution occurred by passing nitrogen gas through to separate out the products at the end of the reaction.

Preparation of $[Ru^{III}Cl_2(AsPh_3)_2(8\text{-hq})]$. Complex $[RuCl_3(AsPh_3)_2MeOH]$[32] (**I**) was used as a starting material. A solution of **I** (0.21 g, 0.25 mmol) in methanol (100 cm^3) was refluxed, then the ligand (H 8-hq) (0.05 g, 0.35 mmol) added. The mixture was refluxed for 1 h after which time, good yellowish-green microcrystals were obtained, filtered off, washed with methanol and then ether and dried *in vacuo*. The analogous bromo complex was similarly prepared from $[RuBr_3(AsPh_3)_2MeOH]$[32] and reflux continued for 2 h.

The same procedure was used to synthesize the complexes of *o*-aminophenol and 2-amino-3-hydroxypyridine.

Catalytic oxidation by $[RuCl_2(AsPh_3)_2(8\text{-hq})]$ (**IV**)

The oxidation of *p*-methoxybenzyl alcohol is typical. To a solution of *p*-methoxybenzyl alcohol (1 mmol) was added NMO (3 mmol) in CH_2Cl_2 (20 cm^3) and 2.5×10^{-3} mmol of compound **IV**. The solution was stirred for 2.5 h in the presence of 4 Å molecular sieves (0.5 g). The mixture was evaporated to dryness and extracted with ether (2×25 cm^3). The combined ethereal extracts were filtered and evaporated to give *p*-methoxybenzaldehyde which was characterized and quantified as its 2,4-dinitrophenylhydrazone derivative.

The same experiment was carried out using $[RuCl_2(PPh_3)_2(bhz)]$ and $[RuCl_2(AsPh_3)_2(o\text{-amph})]$ in place of **IV**.

IR spectra were measured on a Perkin–Elmer 883 or FT 1720 instrument as liquid paraffin mulls between CsI plates and KBr discs. ESR spectra were recorded with a Varian E-12 spectrometer. The electronic spectra were measured on a Philips PU 8740 UV–vis spectrophotometer or a Varian 634 model. Cyclic voltammetric studies were carried out on a potentiostat/wave generator (Oxford Electrodes) using a platinum working electrode and silver reference electrode in conjunction with a Philips PM 8043 X-Y recorder. Magnetic measurements were made on a Johnson Matthey magnetic susceptibility balance.

Acknowledgements—We thank the Royal Society for support, Drs W. P. Griffith and J. F. Gibson for helpful advice and also Johnson Matthey Ltd for the loan of hydrated ruthenium trichloride.

REFERENCES

1. J. R. Thornback and G. Wilkinson, *J. Chem. Soc., Dalton Trans.* 1978, 110.
2. S. A. Pardhy, K. Joseph, S. Gopinathan and C. Gopinathan, *Polyhedron* 1985, **4**, 307.
3. A. M. El-Hendawy and M. S. El-Shahawi. *Polyhedron* 1989, **8**, 2813.
4. A. M. El-Hendawy, *Polyhedron* 1990, **9**, 2309.

5. A. M. El-Hendawy, *Inorg. Chim. Acta* 1991, **179**(2), 223.
6. A. M. El-Hendawy, W. P. Griffith, B. Piggott and D. J. Williams, *J. Chem. Soc., Dalton Trans.* 1988, 1983.
7. A. M. Al-Hendawy, W. P. Griffith, M. N. Moussa and F. I. Taha, *J. Chem. Soc., Dalton Trans.* 1989, 901.
8. A. C. Dengel, A. M. El-Hendawy, W. P. Griffith, C. O'Mahoney and D. J. Williams, *J. Chem. Soc., Dalton Trans.* 1990, 737.
9. A. C. Dengel, W. P. Griffith, A. M. El-Hendawy and J. M. Jolliffe, *Polyhedron* 1990, **9**, 1751.
10. K. B. Sharpless, K. Akashi and K. Oshima, *Tetrahedron Lett.* 1976, 2503.
11. J. Chatt, G. J. Leigh, D. M. Mingos and R. Paske, *J. Chem. Soc.* (*A*) 1968, 2636.
12. J. E. Kovacic, *Spectrochim. Acta* 1967, **23A**, 183.
13. M. R. Mohmoud and M. T. El-Haty, *J. Inorg. Nucl. Chem.* 1980, **42**, 349.
14. V. B. Rana, S. K. Sahni, S. P. Gupta and S. K. Sangal, *J. Inorg. Nucl. Chem.* 1977, **39**, 1098.
15. M. P. Teotia, J. N. Gurtu and V. B. Rana, *J. Inorg. Nucl. Chem.* 1980, **42**, 821.
16. J. D. Gilbert, D. Rose and G. Wilkinson, *J. Chem. Soc.* (*A*) 1970, 2765.
17. A. R. Chakravarty and A. Chakravorty, *J. Chem. Soc., Dalton Trans.* 1983, 961.
18. S. M. Tetrick and R. A. Walton, *Inorg. Chem.* 1984, 379.
19. G. M. Bryant and J. E. Fergussion, *Aust. J. Chem.* 1971, **24**, 275.
20. C. J. Hawkins and T. A. Kabanos, *Inorg. Chem.* 1989, **28**, 1084.
21. S. P. Cooper, Y. B. Koh and K. N. Raymond, *Inorg. Chem.* 1982, **104**, 5092.
22. R. B. Von Dreele and R. C. Fay, *J. Am. Chem. Soc.* 1972, **94**, 7935.
23. T. W. Hambley, C. J. Hawkins and T. A. Kabanos, *Inorg. Chem.* 1987, **26**, 3740.
24. G. Mercati and F. Morazzoni, *Gazz. Chim. Ital.* 1979, **109**, 161.
25. K. S. Murray, A. M. van den Bergen and B. O. West, *Aust. J. Chem.* 1978, **31**, 203.
26. R. Nicholson and I. Shain, *Analyt. Chem.* 1964, **36**, 706.
27. H. Doine, F. F. Stephens and R. D. Cannon, *Bull. Chem. Soc. Japan* 1985, **58**, 1327.
28. A. R. Chakravarty, A. Chakravorty, F. A. Cotton, L. R. Falvello, B. K. Ghosh and M. Tomas, *Inorg. Chem.* 1983, **22**, 1892.
29. W. H. Leung and C. M. Che, *Inorg. Chem.* 1989, **28**, 4619.
30. J. E. Armstrong and R. A. Walton, *Inorg. Chem.* 1983, **22**, 1545.
31. A. I. Vogel, *A Text-book of Practical Organic Chemistry*. Longman, London (1972).
32. T. A. Stephenson and G. Wilkinson, *J. Inorg. Nucl. Chem.* 1966, **28**, 945.

Polyhedron Vol. 10, No. 18, pp. 2145–2152, 1991
Printed in Great Britain

0277–5387/91 $3.00+.00
© 1991 Pergamon Press plc

FURTHER STUDIES OF $Mo_3(\mu_3\text{-}I)(\mu_3\text{-}H)(\mu\text{-}I)_3I_3L_3$ CLUSTER SPECIES: COMPOUNDS WITH L = PEt_3 AND PPh_3

ALFREDO BURINI, F. ALBERT COTTON* and JOANNA CZUCHAJOWSKA

Department of Chemistry and Laboratory for Molecular Structure and Bonding, Texas A&M University, College Station, TX 77843, U.S.A.

(*Received* 17 *April* 1991; *accepted* 4 *June* 1991)

Abstract—The chemistry leading to the isolation of $Mo_3HI_7L_3$ compounds has been re-examined. Although yields of the species with L = THF could not be improved, crystalline samples of compounds with L = PPh_3 (**1**) and PEt_3 (**2**) have been obtained and characterized by X-ray crystallography and ^1H NMR spectra. The NMR spectra (1,3,3,1 quartets for ^1H) provide conclusive evidence for the presence of the μ_3-H ligand. The principal crystallographic data are: (**1**): orthorhombic space group *Pnma*, $a = 20.726(3)$, $b = 21.704(1)$, $c = 20.05(1)$ Å; $V = 9020$ Å^3; $Z = 4$; d_{calc}, 1.672 g cm^{-3}; $R = 0.0361$, $R_w = 0.0533$ for 423 parameters and 4935 observed data [$F_o^2 > 3\sigma(F_o^2)$]. (**2**): orthorhombic space group *Pbca*, $a = 20.877(8)$, $b = 16.951(5)$, $c = 24.007(4)$ Å; $V = 8495$ Å^3; $Z = 8$; $d_{calc} = 2.508$ g cm^{-3}; $R = 0.0343$, $R_w = 0.0495$ for 296 parameters and 4655 observed data [$F_o^2 > 3\sigma(F_o^2)$]. NMR (^1H in C_6D_6) data: (**1**) $\delta = -5.01$, $^2J(HP) = 36$ Hz; (**2**) $\delta = -2.26$, $^2J(HP) = 39$ Hz.

The preparation and structural characterization of a new type of triangular metal atom cluster species, $Mo_3(\mu_3\text{-}I)(\mu_3\text{-}H)(\mu\text{-}I)_3I_3L_3$ were reported from this laboratory a few years ago.[1] Four compounds, with L = RCN or THF, were structurally characterized by X-ray crystallography. The presence of the μ_3-H atom, which could not be observed in any of the structures, was supported by an NMR signal (−10.3 ppm for the compound with L = PhCN), by the diamagnetism of the compounds and by a molecular orbital calculation. Further studies have now been carried out and are reported here. As will be seen, the present results provide conclusive evidence for the presence of the μ_3-H atom and for its location on the molecular three-fold axis.

EXPERIMENTAL

Materials and methods

All manipulations were carried out under an atmosphere of purified argon using standard Schlenk techniques. The solvents were carefully purified by conventional methods and freshly distilled under dinitrogen prior to use. Chemicals were purchased from the following sources: $Mo(CO)_6$, Aldrich; I_2, Baker; phosphines, Strem. All chemicals were used without further purification. The compounds $Mo(CO)_3(\eta^6\text{-}C_6H_5CH_3)$,[2] $MoI_2(CO)_3(CH_3CN)_2$[3] and $MoI_3(THF)_3$[4] were prepared according to the literature; $Mo_3HI_7(THF)_3$ was prepared according to the literature method[1] or by the procedure reported below. Instruments used were: IR, Perkin-Elmer 783; UV–vis, Cary 17; ^1H NMR, Varian XL-200; ^{31}P NMR, Varian XL-400; elemental analyses were by Galbraith Laboratories, Knoxville, Tennessee.

Preparation of intermediate **A**

This substance was prepared from $Mo(CO)_3(\eta^6\text{-}C_6H_5CH_3)$ by the method described by Cotton and Poli.[1] From 1.50 g of starting material, a yield of 1.60 g of dry **A** was obtained.

Preparation of intermediate **B** *from* $MoI_2(CO)_3(CH_3CN)_2$

Using $MoI_2(CO)_3(CH_3CN)_2$ instead of $Mo_2I_4(CO)_8$, a material which appears to be similar

* Author to whom correspondence should be addressed.

(with CH_3CN ligands instead of THF ligands) to Cotton and Poli's "sample A" was obtained. $MoI_2(CO)_3(CH_3CN)_2$ (0.4 g, 0.77 mmol) was dissolved in benzene (30 cm^3) to afford a brown solution, and this was warmed to reflux temperature. After 2 h a dark brown precipitate was filtered off, washed with benzene and dried *in vacuo*; yield 0.250 g (sample **B**). The IR spectrum (Nujol mull, cm^{-1}) of this compound shows two medium bands at 2308 and 2278 due to coordinated CH_3CN.

Preparation of $Mo_3HI_7(PPh_3)_3$ *from* **A**

Intermediate **A** (0.290 g) was suspended in THF (20 cm^3). Ph_3P (0.200 g, 0.76 mmol) was added and the stirred mixture was warmed to reflux temperature. After 20 h a dark brown solution and a brown precipitate were formed. The brown precipitate, separated by filtration, washed with THF and dried *in vacuo*, did not show any peaks in the IR spectrum; yield 0.150 g. The solution was evaporated to dryness and the oily mixture obtained was washed with hexane. The crude product obtained was extracted with benzene (10 cm^3) and the solution was then filtered through Celite and layered with hexane (30 cm^3). Brown crystals and some brown microcrystalline material were obtained after 3 days. A single crystal from this batch was used for the X-ray analysis. The microcrystalline compound shows the same spectroscopic properties as the larger crystals; yield 30 mg. Found: C, 37.8; H, 2.8. Calc. for $C_{66}H_{58}I_7Mo_3P_3$: C, 37.4; H, 2.8%. ^1H NMR (C_6D_6):[5] δ −5.01 (q, η^3-*H*, ^2J(HP) = 36 Hz), 7.10–8.05 (m, Ar*H*). The UV–vis spectrum in CH_2Cl_2 solution is shown in Fig. 1.

Preparation of $Mo_3HI_7(PPh_3)_3$ *from* **B**

Intermediate **B** (0.250 g) was added to THF (20 cm^3). Most of the solid dissolved to form a dark brown solution. Ph_3P was added and the reaction mixture was warmed to reflux temperature. After about 20 h the reaction mixture was filtered through Celite, and the brown solution obtained was evaporated to dryness. The crude compound was washed with hexane and then extracted with benzene (25 cm^3). The benzene solution was filtered through Celite, concentrated *in vacuo* to about 10 cm^3, and layered with hexane (25 cm^3). A few brown crystals were formed after a few days. These were characterized to be $Mo_3HI_7(Ph_3P)_3$ by their spectroscopic properties.

Reaction between **A** *and* PEt_3

Intermediate **A** (0.200 g) was suspended in THF (20 cm^3), PEt_3 (0.1 cm^3, 0.68 mmol) was added by syringe, and the reaction was stirred at room temperature. After about 3 h most of **A** dissolved giving an emerald green solution and a brown insoluble residue. The reaction was checked by TLC using a silica gel plate and a 1:1 mixture of THF/hexane 1:1 as eluant. The chromatography showed two main spots, a blue one at RF = 0.7 and a yellow one at RF = 0.5. There was no spot corresponding to the spot of a sample of $Mo_3HI_7(PEt_3)_3$ used as a reference. After the reaction mixture was stirred overnight, without any changes being observed, it was evaporated to dryness and the residue extracted with hexane (15 cm^3). The blue solution obtained was concentrated to about 2 cm^3 *in vacuo*. After 2 days at −20°C blue crystals were recovered from the solution. The spectroscopic properties of this sample were in accord with the known compound $Mo_2I_4(PEt_3)_4$.[4] The residue left after extraction with hexane was dissolved in THF (20 cm^3), the solution filtered and layered with hexane (30 cm^3). After a few days yellow crystals were obtained. These were characterized by IR spectroscopy to be $[MoI_4(PEt_3)_2][HPEt_3]$.[4]

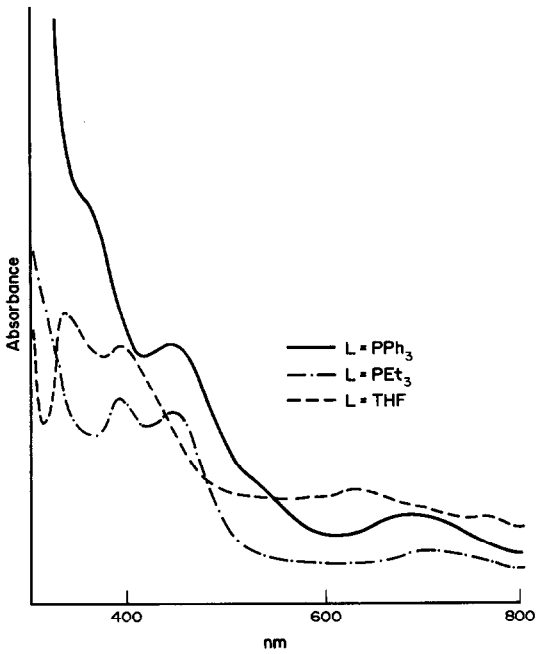

Fig. 1. A comparison of UV–vis spectra for the trinuclear clusters $Mo_3HI_7L_3$ (L = THF, PEt_3, PPh_3). The absorbance is given on an arbitrary scale.

Reaction between **B** *and* PEt_3

Intermediate **B** and PEt_3 were permitted to react as in the procedure described above for the reaction between **A** and PEt_3. Analogous results were obtained.

Preparation of $Mo_3HI_7(THF)_3 \cdot THF$ *from* $MoI_3(THF)_3$

To a suspension of $MoI_3(THF)_3$ (0.50 g, 0.72 mmol) in THF (20 cm^3), toluene (1 cm^3) and $Mo(CO)_6$ (0.024 g, 0.09 mmol) were added. The stirred mixture was warmed to reflux temperature. After 22 h a brown solution and some unreacted starting material were obtained. The solution was filtered through Celite. The presence of the trinuclear cluster $Mo_3HI_7(THF)_3$ was detected by the UV–vis spectrum of the solution. From this solution dark cuboidal crystals were obtained after 2 days. These were found to be $Mo_3HI_7(THF)_3$ by UV–vis spectroscopy and by their reactivity with PEt_3 (see below). Yield: 0.025 g (6%). The mother liquor, checked by UV–vis spectroscopy, showed neither the presence of further $Mo_3HI_7(THF)_3$ nor were there any absorption bonds indicative of $Mo_2I_4(THF)_4$ or other quadruply bonded species.

Preparation of $Mo_3HI_7(PEt_3)_3$

$Mo_3HI_7(THF)_3 \cdot THF$ (20 mg, 6.8 μmol) was suspended in THF (3 cm^3). A small amount of the solid dissolved to afford a green solution. PEt_3 (0.1 cm^3, 0.68 mmol) was added by syringe, and the reaction was stirred at room temperature. All the starting material slowly went into solution and the colour of this turned from green to brown in about 1 h. The reaction mixture was stirred for an additional 2 h, filtered through Celite and concentrated to about 1 cm^3 *in vacuo*. After cooling to -20°C for 1 day dark plate crystals formed. One of the crystals was used for the X-ray analysis. The conversion was almost quantitative. ^1H NMR (C_6D_6):[5] δ -2.26 (q, η^3-*H*, $^2J(HP) = 39$ Hz), 0.92 (dt, C*H*$_3$, $^3J(HP) = 14$ Hz, $^2J(HH) = 7$ Hz), 1.91 (qu, C*H*$_2$, $^2J(HP) = {}^3J(HH) = 7$ Hz). The $^{31}P\{^1H\}$ NMR spectrum was run in a THF solution to which a few drops of C_6D_6 were added. The ^{31}P shift referenced to 85% H_3PO_4 was δ -5.63. The UV–vis spectrum in THF solution is shown in Fig. 1.

X-ray crystallography

The structures of $Mo_3HI_7(PPh_3)_3 \cdot 4C_6H_6 \cdot C_4H_8O$ (**1**) and $Mo_3HI_7(PEt_3)_3 \cdot 2C_4H_8O$ (**2**) were determined by standard procedures for this laboratory.[6] Data collection and reduction were carried out by standard methods with the use of well-established computational procedures.[7] Crystallographic and procedural data for both are summarized in Table 1. Complete tables of crystal positional parameters, further details of data collection and refinement, bond distances, bond angles, anisotropic displacement parameters and structure factors are available as supplementary material.

Compound (**1**)

A dark brown, block-shaped crystal of $Mo_3HI_7(PPh_3)_3 \cdot 4C_6H_6 \cdot C_4H_8O$ was mounted on the tip of a glass fibre using epoxy resin. The reduced cell dimensions indicated that the crystal belonged to the orthorhombic crystal system, and this was verified by axial photography. No correction for decay was necessary. Azimuthal scans of six reflections with Eulerian angle χ near 90° were used as the basis for an empirical absorption correction.[8] After averaging the equivalent reflections there remained 6850 unique data and 4842 reflections with $F_o^2 \geqslant 3\sigma(F_o)^2$. On the basis of systematic absences the space group could be either *Pnma* or $Pn2_1a$. Using *Pnma*, we employed the direct-methods program in SHELXS-86[9] which led to the location of the molybdenum, iodine and phosphorus atoms. The atoms Mo(1), I(1), I(122), I(22), μ_3-H, P(1), C(121), C(124) and H(124) were found to lie on a mirror plane while atoms Mo(2), I(2), I(12) and P(2) lie off the mirror and thus all other atoms are generated by symmetry. After a sequence of alternating least-squares cycles and difference Fourier maps all carbon atoms belonging to the phenyl rings were located, in addition to four molecules of the interstitial solvent benzene and one of THF. Two of the benzene molecules lie on a mirror plane. At this stage most of the atoms were refined anisotropically to give acceptable values of R and R_w. A difference Fourier map now revealed a small amount of electron density above the centre of the Mo_3 unit; this was assigned as a hydrogen atom. Subsequent refinement including the hydrogen atoms in the phenyl groups was carried out using SHELXS-76[10] to give $R = 0.0361$ and $R_w = 0.0533$. The central part and the entire molecule of $Mo_3HI_7(PPh_3)_3$ are shown in Figs 2 and 3, respectively.

Compound (**2**)

A brown–orange, plate crystal of $Mo_3HI_7(PEt_3)_3 \cdot 2C_4H_8O$ was shown to be of good quality by polarized light microscopy. It was mounted on the tip of a glass fibre using Apiezon grease. All procedures for collection and reduction of data are described previously (see Table 1). On the basis of systematic absences the space group was determined to be *Pbca*. The entire molecule was located using the direct-methods program in SHELX-86.[9] The subsequent development of the structure was done by an alternating sequence of least-squares

Table 1. Crystal data for compounds **1** and **2**

Compound	**1**	**2**
Formula	$C_{76}H_{72}I_7Mo_3OP_3$	$C_{22}H_{54}I_7Mo_3O_1P_3$
Formula weight	2270.49	1603.75
Space group	*Pnma* (62)	*Pbca* (61)
Syst. absences	$0kl, k+l \neq 2n$; $hk0, h \neq 2n$; $h00, h \neq 2n$; $0k0, k \neq 2n$; $00l, l \neq 2n$	$0kl, k \neq 2n$ $h0l, l \neq 2n$ $hk0, h \neq 2n$
a (Å)	20.726(3)	20.877(8)
b (Å)	21.704(1)	16.951(5)
c (Å)	20.05(1)	24.007(4)
α (°)	90	90
β (°)	90	90
γ (°)	90	90
V (Å^3)	9020(7)	8495(7)
Z	4	8
d_{calc} (g cm^{-3})	1.672	2.508
Crystal size (mm)	0.5 × 0.4 × 0.3	0.4 × 0.3 × 0.1
μ(Mo-K_α) (cm^{-1})	28.597	60.174
Data collection instrument	ENRAF-NONIUS CAD4	ENRAF-NONIUS CAD4
Radiation monochromated In incident beam (λ, Å)	0.70930	0.70930
Orientation reflections:		
Number, range (2θ, deg.)	25; $20 \leqslant 2\theta \leqslant 34$	25; $22 \leqslant 2\theta \leqslant 30$
Temperature (°C)	+5	−50
Scan method	ω	ω
Data collection range (2θ, deg.)	$4 \leqslant 2\theta \leqslant 45$	$4 \leqslant 2\theta \leqslant 48$
No. unique data, total with $F_o^2 > 3\sigma(F_o^2)$	6850, 4935	6633, 4655
No. parameters refined	423	296
Transmission factor, % maximum, minimum	99.97, 75.64	100, 33
R[a]	0.0361	0.0343
R_w[b]	0.0533	0.0495
Quality of fit indicator[c]	1.26	1.14
Largest shift/esd, final cycle	0.249	0.046
Largest peak (e Å^{-3})	0.74	0.77

[a] $R = \Sigma||F_o|-|F_c||/\Sigma|F_o|$.
[b] $R = [\Sigma w(|F_o|-|F_c|)^2]^{1/2}$; $w = 1/\sigma^2[|F_o|]$.
[c] Quality-of-fit = $[\Sigma w|F_o|-|F_c|^2/(N_{obs}-N_{par})]^{1/2}$.

refinement and difference Fourier maps. Supplementary data has been deposited.*

RESULTS AND DISCUSSION

We have found that the previously described reactions leading to $Mo_3HI_7L_3$ species are reproducible. Unfortunately we have been unable to make substantial improvement in the very small yields of the trinuclear products. We have introduced several hydride sources, $(n\text{-}C_4H_9)_2SnH$, NaH, $NaBH_4$, into the reactions which produce intermediate solutions **A** and **B**, but this has not helped. We have also tried to carry out reaction (1) which, on paper, is perfectly stoichiometric, but it does not go under any known conditions. However, we found an alternative way to prepare $Mo_3HI_7(THF)_3$ (see Experimental) following reaction (2), but the best yield was only 6%.

* *Supplementary material available.* A fully labelled drawing of **1**, tables of positional parameters for **1** and **2**, full tables of anisotropic thermal parameters and molecular dimensions and listings of observed and calculated structure factors (total pages 79).

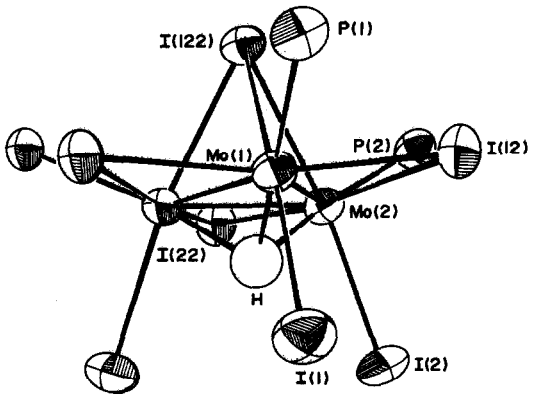

Fig. 2. An ORTEP view of the central core of the trinuclear cluster $Mo_3HI_7(PPh_3)_3$ (**1**). The carbon atoms are omitted for clarity. Atoms are represented by 50% probability ellipsoids.

$$3MoI_2(CO)_3(CH_3CN)_2 + HI(g) \xrightarrow{\text{benzene}} Mo_3HI_7(CH_3CN)_3 + 9CO + 3CH_3CN \quad (1)$$

$$8MoI_3(THF)_3 + Mo(CO)_6 + 3\text{solv-H} \xrightarrow{\text{THF/toluene}} 3Mo_3HI_7(THF)_3 + 6CO + 3\text{solv-I} \quad (2)$$

The presence of $Mo(CO)_6$ in the reaction system is essential since when $MoI_3(THF)_3$ was refluxed alone a brown solution was obtained for which the UV–vis spectrum did not show the cluster species. $Mo_2I_6(THF)_4$ or $Mo_2I_6(THF)_3$, analogous to the corresponding chlorine and bromide compounds,[11] was probably formed. The source of H^- and the fate of the lost iodine are not known; we have suggested in eq. (2) that the solvent plays a role in both these parts of the process, but this is only a speculation. One conclusion that might be drawn from the ineffectiveness of the added hydride is that the slow and limited formation of the products may not be solely restricted by availability of the hydride ligand, but also by the process of forming the Mo_3 cluster itself.

We have found that the compound in which $L = PPh_3$ can be obtained by direct reaction of PPh_3 with the intermediates **A** and **B**. Although this direct approach failed for PEt_3, it was possible to obtain the PEt_3 compound by first isolating $Mo_3HI_7(THF)_3$ and then displacing the THF ligands. This would probably be a fairly general route to the $Mo_3HI_7L_3$ species when L is any ligand other than THF. However, this route will become important only if the preparation of $Mo_3HI_7(THF)_3$ can be substantially improved.

The structures of compounds **1** and **2** are very similar to those previously determined for com-

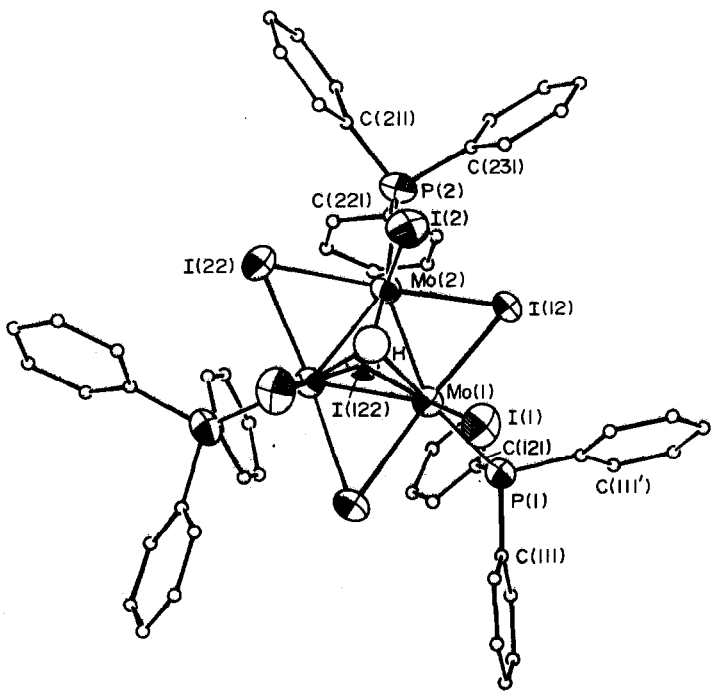

Fig. 3. An ORTEP top view of the $Mo_3HI_7(PPh_3)_3$ molecule (**1**). The ellipsoids represent thermal displacements and are drawn at the 50% probability level. Carbon atoms are represented by spheres of arbitrary size.

Table 2. Selected bond distances (Å) and bond angles (degrees) for $Mo_3HI_7(PPh_3)_3 \cdot 3C_6H_6 \cdot C_4H_8O$

Mo(1)—Mo(2)	2.581(1)	Mo(2)—I(122)	2.7968(8)	P(1)—C(121)	1.81(1)
Mo(1)—I(122)	2.787(1)	Mo(2)—I(2)	2.6916(9)	P(2)—C(211)	1.823(6)
Mo(1)—I(1)	2.682(1)	Mo(2)—I(12)	2.7696(8)	P(2)—C(221)	1.814(6)
Mo(1)—I(12)	2.7653(4)	Mo(2)—I(22)	2.7692(9)	P(2)—C(231)	1.831(6)
Mo(1)—P(1)	2.653(3)	Mo(2)—P(2)	2.656(2)		
Mo(2)—Mo(2′)	2.5884(9)	P(1)—C(111)	1.820(7)		
Mo(2)—Mo(1)—Mo(2′)	60.18(3)	Mo(1)—Mo(2)—I(12)	62.11(2)	I(12)—Mo(2)—I(22)	169.36(3)
Mo(2)—Mo(1)—I(122)	62.66(3)	Mo(1)—Mo(2)—I(22)	121.74(3)	I(12)—Mo(2)—P(2)	84.58(5)
Mo(2)—Mo(1)—I(1)	108.42(3)	Mo(1)—Mo(2)—P(2)	138.79(5)	I(22)—Mo(2)—P(2)	87.34(5)
Mo(2)—Mo(1)—I(12)	62.28(2)	Mo(2)—Mo(2′)—I(122)	62.44(2)	Mo(1)—I(122)—Mo(2)	55.08(2)
Mo(2)—Mo(1)—P(1)	139.93(5)	Mo(2)—Mo(2′)—I(2′)	108.51(3)	Mo(2)—I(122)—Mo(2′)	55.13(2)
I(122)—Mo(1)—I(1)	169.36(4)	Mo(2)—Mo(2′)—I(12′)	121.83(3)	Mo(1)—I(12)—Mo(2)	55.60(3)
I(122)—Mo(1)—I(12)	87.51(2)	Mo(2)—Mo(2′)—I(22)	62.14(2)	Mo(2)—I(22)—Mo(2′)	55.73(2)
I(122)—Mo(1)—P(1)	94.23(7)	Mo(2)—Mo(2′)—P(2′)	141.34(5)	Mo(1)—P(1)—C(111)	118.6(2)
I(1)—Mo(1)—I(12)	93.23(2)	I(122)—Mo(2)—I(2)	169.44(3)	Mo(1)—P(1)—C(121)	106.9(4)
I(1)—Mo(1)—P(1)	96.40(7)	I(122)—Mo(2)—I(12)	87.23(2)	C(111)—P(1)—C(121)	105.1(3)
I(12)—Mo(1)—I(12′)	170.15(4)	I(122)—Mo(2)—I(22)	86.52(3)	Mo(2)—P(2)—C(211)	121.7(2)
I(12)—Mo(1)—P(1)	85.95(2)	I(122)—Mo(2)—P(2)	94.65(5)	Mo(2)—P(2)—C(221)	105.9(2)
Mo(1)—Mo(2)—Mo(2′)	59.91(2)	I(2)—Mo(2)—I(12)	93.84(3)	Mo(2)—P(2)—C(231)	118.3(2)
Mo(1)—Mo(2)—I(122)	62.26(3)	I(2)—Mo(2)—I(22)	93.89(3)	C(211)—P(2)—C(221)	103.9(2)
Mo(1)—Mo(2)—I(2)	109.07(3)	I(2)—Mo(2)—P(2)	95.92(5)	C(211)—P(2)—C(231)	100.2(3)
				C(221)—P(2)—C(231)	104.9(3)

Numbers in parentheses are estimated standard deviations in the least significant digits.

pounds of the same general formula, $Mo_3HI_7L_3$, where L represents THF or an RCN molecule. Tables 2 and 3 present the principal bond distances and angles for **1** and **2**, respectively. Table 4 gives a compilation of the Mo—Mo, Mo—I and Mo—L distances in all compounds. The Mo—Mo distances in the phosphine complexes are slightly longer than those in the complexes with the harder ligands (*ca* 0.06 Å). In the structure of **1** a small bump of electron density was found approximately where

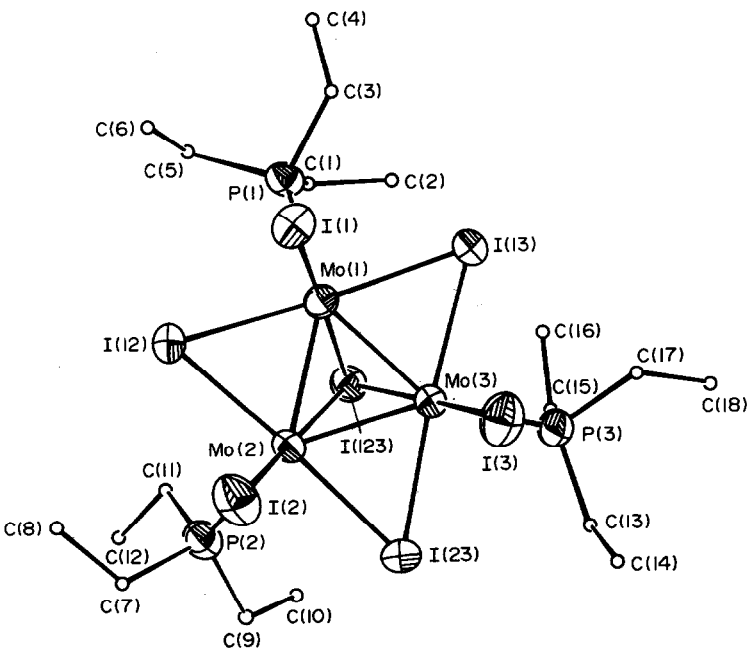

Fig. 4. An ORTEP top view of the $Mo_3HI_7(PEt_3)_3$ molecule (**2**). The ellipsoids represent thermal displacements and are drawn at the 50% probability level. Carbon atoms are represented by spheres of arbitrary size.

Table 3. Selected bond distances (Å) and bond angles (degrees) for $Mo_3HI_7(PEt_3)_3 \cdot C_4H_8O$

I(1)—Mo(1)	2.687(1)	I(123)—Mo(1)	2.798(1)	P(1)—C(1)	1.82(1)
I(2)—Mo(2)	2.695(1)	I(123)—Mo(2)	2.797(1)	P(1)—C(3)	1.82(1)
I(3)—Mo(3)	2.688(1)	I(123)—Mo(3)	2.806(1)	P(1)—C(5)	1.83(1)
I(12)—Mo(1)	2.769(1)	Mo(1)—Mo(2)	2.585(1)	P(2)—C(7)	1.79(2)
I(12)—Mo(2)	2.765(1)	Mo(1)—Mo(3)	2.592(1)	P(2)—C(9)	1.81(2)
I(13)—Mo(1)	2.769(1)	Mo(1)—P(1)	2.607(3)	P(2)—C(11)	1.87(2)
I(13)—Mo(3)	2.769(1)	Mo(2)—Mo(3)	2.590(1)	P(3)—C(13)	1.83(1)
I(23)—Mo(2)	2.758(1)	Mo(2)—P(2)	2.604(3)	P(3)—C(15)	1.86(1)
I(23)—Mo(3)	2.756(1)	Mo(3)—P(3)	2.615(3)	P(3)—C(17)	1.83(1)
Mo(1)—I(12)—Mo(2)	55.70(3)	I(12)—Mo(1)—Mo(3)	121.98(4)	I(2)—Mo(2)—Mo(1)	111.60(4)
Mo(1)—I(13)—Mo(3)	55.81(3)	I(12)—Mo(1)—P(1)	87.17(7)	I(2)—Mo(2)—Mo(3)	111.42(4)
Mo(2)—I(23)—Mo(3)	56.03(3)	I(13)—Mo(1)—I(123)	90.50(3)	I(2)—Mo(2)—P(2)	93.38(8)
Mo(1)—I(123)—Mo(2)	55.03(3)	I(13)—Mo(1)—Mo(2)	122.10(4)	I(12)—Mo(2)—I(23)	171.74(4)
Mo(1)—I(123)—Mo(3)	55.10(3)	I(13)—Mo(1)—Mo(3)	62.08(3)	I(12)—Mo(2)—I(123)	88.02(3)
Mo(2)—I(123)—Mo(3)	55.06(3)	I(13)—Mo(1)—P(1)	87.10(7)	I(12)—Mo(2)—Mo(1)	62.22(3)
I(1)—Mo(1)—I(12)	91.39(3)	I(123)—Mo(1)—Mo(2)	62.47(3)	I(12)—Mo(2)—Mo(3)	122.21(4)
I(1)—Mo(1)—I(13)	90.75(3)	I(123)—Mo(1)—Mo(3)	62.60(3)	I(12)—Mo(2)—P(2)	85.68(7)
I(1)—Mo(1)—I(123)	174.24(4)	I(123)—Mo(1)—P(1)	94.29(7)	I(23)—Mo(2)—I(123)	88.16(3)
I(1)—Mo(1)—Mo(2)	112.24(4)	Mo(2)—Mo(1)—Mo(3)	60.03(3)	I(23)—Mo(2)—Mo(1)	121.94(4)
I(1)—Mo(1)—Mo(3)	113.23(4)	Mo(2)—Mo(1)—P(1)	140.43(7)	I(23)—Mo(2)—Mo(3)	61.95(3)
I(1)—Mo(1)—P(1)	91.39(7)	Mo(3)—Mo(1)—P(1)	139.42(7)	I(23)—Mo(2)—P(2)	87.27(7)
I(12)—Mo(1)—I(13)	173.93(4)	I(2)—Mo(2)—I(12)	92.48(4)	I(123)—Mo(2)—Mo(1)	62.50(3)
I(12)—Mo(1)—I(123)	87.93(3)	I(2)—Mo(2)—I(23)	92.21(4)	I(123)—Mo(2)—Mo(3)	62.64(3)
I(12)—Mo(1)—Mo(2)	62.08(3)	I(2)—Mo(2)—I(123)	172.91(5)	I(123)—Mo(2)—P(2)	93.71(7)
Mo(1)—Mo(2)—Mo(3)	60.12(3)	I(23)—Mo(3)—I(123)	88.03(4)	C(1)—P(1)—C(5)	99.0(5)
Mo(1)—Mo(2)—P(2)	139.04(8)	I(23)—Mo(3)—Mo(1)	121.75(4)	C(3)—P(1)—C(5)	103.5(5)
Mo(3)—Mo(2)—P(2)	140.06(8)	I(23)—Mo(3)—Mo(2)	62.03(3)	Mo(2)—P(2)—C(7)	116.6(6)
I(3)—Mo(3)—I(13)	90.71(4)	I(23)—Mo(3)—P(3)	87.55(7)	Mo(2)—P(2)—C(9)	117.9(7)
I(3)—Mo(3)—I(23)	91.46(4)	I(123)—Mo(3)—Mo(1)	62.30(3)	Mo(2)—P(2)—C(11)	109.9(6)
I(3)—Mo(3)—I(123)	174.08(4)	I(123)—Mo(3)—Mo(2)	62.31(3)	C(7)—P(2)—C(9)	102.4(9)
I(3)—Mo(3)—Mo(1)	113.27(4)	I(123)—Mo(3)—P(3)	95.48(8)	C(7)—P(2)—C(11)	107.0(9)
I(3)—Mo(3)—Mo(2)	112.34(4)	Mo(1)—Mo(3)—Mo(2)	59.85(3)	C(9)—P(2)—C(11)	101.7(9)
I(3)—Mo(3)—P(3)	90.39(8)	Mo(1)—Mo(3)—P(3)	139.92(8)	Mo(3)—P(3)—C(13)	118.3(5)
I(13)—Mo(3)—I(23)	174.11(4)	Mo(2)—Mo(3)—P(3)	141.25(8)	Mo(3)—P(3)—C(15)	115.1(4)
I(13)—Mo(3)—I(123)	90.36(3)	Mo(1)—P(1)—C(1)	115.8(4)	Mo(3)—P(3)—C(17)	113.2(4)
I(13)—Mo(3)—Mo(1)	62.11(3)	Mo(1)—P(1)—C(3)	113.2(4)	C(13)—P(3)—C(15)	97.9(6)
I(13)—Mo(3)—Mo(2)	121.95(4)	Mo(1)—P(1)—C(5)	118.7(4)	C(13)—P(3)—C(17)	104.8(6)
I(13)—Mo(3)—P(3)	86.96(7)	C(1)—P(1)—C(3)	104.6(5)	C(15)—P(3)—C(17)	105.7(6)

Numbers in parentheses are estimated standard deviations in the least significant digits.

Table 4. Comparison of the Mo—Mo, Mo—I and Mo—L distances in $Mo_3HI_7L_3$ compounds

	THF	MeCN	PhCN	PPh_3	$PPEt_3$
Mo(1)—Mo(2)	2.509(2)	2.541(1)	2.525(3)	2.581(1)	2.585(1)
Mo(2)—Mo(2′)	2.507(2)	2.539(1)	2.527(3)	2.588(1)	2.590(1), 2.592(1)
Mo(1)—I(122)	2.830(2)	2.789(2)	2.805(3)	2.787(1)	2.798(1)
Mo(2)—I(122)	2.830(2)	2.795(1)	2.826(2)	2.797(1)	2.806(1), 2.797(1)
Mo(1)—I(12)	2.787(2)	2.790(1)	2.790(2)	2.765(0)	2.769(1)
Mo(2)—I(12)	2.795(2)	2.786(1)	2.771(2)	2.770(1)	2.765(1), 2.758(1)
Mo(2)—I(22)	2.798(2)	2.806(1)	2.785(2)	2.769(1)	2.769(1), 2.756(1)
Mo(1)—I(1)	2.685(3)	2.715(2)	2.674(4)	2.682(1)	2.687(1)
Mo(2)—I(2)	2.691(2)	2.706(1)	2.672(2)	2.692(1)	2.695(1), 2.688(1)
Mo(1)—L(1)	2.27(2)	2.183(14)	2.22(2)	2.653(3)	2.607(3)
Mo(2)—L(2)	2.232(14)	2.202(9)	2.15(2)	2.656(2)	2.604(3), 2.615(3)

the μ_3-H atom is expected to be. This is the only structure in which such an observation was made. However, when this was included in the refinement with variable positional parameters it moved somewhat away from the three-fold axis, although it remained in the crystallographic mirror plane.

The most important contribution of the present work is the rigorous demonstration that these clusters contain a hydrogen atom located so that it is coupled equally to all three phosphorus atoms in the $Mo_3HI_7(PR)_3$. The signals for hydride ions in the ^1H NMR spectra of compounds **1** and **2** are located at -5.01 and -2.26 ppm, respectively. These are both 1,3,3,1 quartets and the coupling constants ^2J(H—P) are 36 Hz when L = PPh_3 and 39 Hz when L = PEt_3. The values of ^2J(H—P) are unusually low for PR_3 *trans* to hydrogen; others are known to be in the range 90–180 Hz. This may be due to the low bond order (1/3) of the M—H bonds to the hydride ligand. However, the chemical shifts and the coupling constants are close to those found in the trinuclear iridium clusters $[IrH_2(PCy_3)Py]_3(\mu_3\text{-}H)(BF_4)_2$.[12] The presence of the solvent molecules in the crystal structure of compound **1** was confirmed by ^1H NMR only for two molecules of benzene. The same results were given from the elemental analyses (see Experimental). The absence of one benzene molecule and one THF molecule is due to the fact that the samples used in these cases had been pumped *in vacuo* overnight. The $^{31}P\{^1H\}$ NMR of compound **2** shows a singlet at -5.63 ppm due to the triethyl phosphine ligand in agreement with the presence of three equivalent phosphorus atoms in the trinuclear cluster.

The UV–vis spectra of compounds **1** and **2** are shown in Fig. 4 together with that of $Mo_3HI_7(THF)_3$ in THF solution; they show a blue shift going from L = PR_3 to L = THF with bands at 710, 445, 395 (L = PEt_3), 680, 445, 360 (L = PPh_3), 640, 395 and 340 nm (L = THF).

Acknowledgements—We thank the National Science Foundation for general support and the Consiglio Nazionale delle Ricerche (Italy) for support to A.B. Drs L. R. Falvello and R. Luck are also thanked for their interest and assistance.

REFERENCES

1. F. A. Cotton and R. Poli, *J. Am. Chem. Soc.* 1988, **110**, 830.
2. W. Strohmeier, *Chem. Ber.* 1961, **94**, 3337.
3. A. Barbati, F. Calderazzo, R. Poli and P. F. Zanazzi, *J. Chem. Soc., Dalton Trans.* 1986, 2569.
4. F. A. Cotton and R. Poli, *Inorg. Chem.* 1987, **26**, 1514.
5. s = singlet, dt = double triplet, q = quartet, qu = quintet, m = multiplet.
6. (a) A. Bino, F. A. Cotton and P. E. Fanwick, *Inorg. Chem.* 1979, **18**, 3558; (b) F. A. Cotton, B. A. Frenz, G. Deganello and A. Shaver, *J. Organomet. Chem.* 1973, **50**, 227.
7. Crystallographic computing was done on a Local Area VAX Cluster, employing the VAX/VMS V5.3 computer.
8. A. C. T. North, D. C. Phillips and F. S. Matthews, *Acta Cryst., Sect. A.* 1968, **24**, 351.
9. G. M. Sheldrick, "SHELXS-86". Institut für Anorganische Chemie der Universität, Göttingen, F.R.G. (1986).
10. G. M. Sheldrick, "SHELXS-76". University of Cambridge, England (1976).
11. R. Poli and H. D. Mui, *J. Am. Chem. Soc.* 1990, **112**, 2446.
12. D. F. Chodosh, R. H. Crabtree, H. Felkin, S. Morehouse and G. E. Morris, *Inorg. Chem.* 1982, **21**, 1307.

Polyhedron Vol. 10, No. 18, pp. 2153–2161, 1991
Printed in Great Britain

0277–5387/91 $3.00+.00
© 1991 Pergamon Press plc

SYNTHESIS AND CHARACTERIZATION OF SOME BIMETALLIC PLATINUM–RHODIUM COMPLEXES. CRYSTAL STRUCTURE OF $[(PhC{\equiv}C)Pt(\mu\text{-dppm})_2(\mu\text{-}N_2C_3Br_3)Rh(CO)]PF_6$

JEFFREY C. DePRIEST and CLIFTON WOODS*

Department of Chemistry, The University of Tennessee, Knoxville, TN 37996-1600, U.S.A.

(*Received* 4 *February* 1991; *accepted* 4 *June* 1991)

Abstract—The addition of pyrazolate ions to $[ClPt(\sigma,\eta\text{-}C{\equiv}CPh)(\mu\text{-dppm})_2Rh(CO)]PF_6$ (dppm = bis(diphenylphosphino)methane) produces the complexes $[(PhC{\equiv}C)Pt(\mu\text{-Z})(\mu\text{-dppm})_2Rh(CO)]PF_6$ (Z = pyrazolate derivative). The use of the 3-methyl-5-trifluoromethylpyrazolate ion gives a mixture of the two isomers that contain the unsymmetrical pyrazolate ligand in its two possible orientations. The addition of *t*-BuNC to the complexes $[(PhC{\equiv}C)Pt(\mu\text{-Z})(\mu\text{-dppm})_2Rh(CO)]PF_6$ leads to substitution of the CO by *t*-BuNC. The complexes $[(CN)Pt(\mu\text{-Z})(\mu\text{-dppm})_2Rh(CO)]PF_6$ were prepared in a similar manner from $[(CN)_2Pt(\mu\text{-dppm})_2Rh(CO)Cl]$. The dapm analogues $[(CN)Pt(\mu\text{-35mpz})(\mu\text{-dapm})_2Rh(L)]PF_6$ [dapm = (diphenylarsino)(diphenylphosphino)methane; 35mpz = 3,5-dimethylpyrazolate; L = CO, *t*-BuNC] and the complex [*cis*-$ClPt(\mu\text{-35mpz})(\mu\text{-dapm})_2$-*trans*-$Rh(CO)]PF_6$ have also been prepared and characterized. $[(PhC{\equiv}C)Pt(\mu\text{-345Bpz})(\mu\text{-dppm})_2Rh(CO)]PF_6$ (345Bpz = 3,4,5-tribromopyrazolate) crystallizes in the triclinic space group $P\bar{1}$ with $a = 10.351(5)$, $b = 14.707(6)$, $c = 22.445(10)$ Å, $\alpha = 94.78(3)°$, $\beta = 98.56(4)°$, $\gamma = 107.68(3)°$, $V = 3189(2)$ Å^3 and $Z = 2$ at 298 K. The structure was refined to an *R* value of 0.0405 using 8382 unique reflections and 740 parameters. The structure consists of the platinum and rhodium atoms in square planar environments, each with two *trans* phosphorus atoms and a nitrogen atom from the pyrazolate ligand. The fourth ligand coordinated to the platinum atom is a terminal phenylacetylide ion and the fourth ligand coordinated to the rhodium atom is a terminal carbon monoxide.

Bis(diphenylphosphino)methane (dppm) has been a convenient ligand for the construction of binuclear transition-metal complexes. Though complexes of the ligand (diphenylarsino)(diphenylphosphino)methane (dapm) have been much less studied, dapm offers most of the same features as dppm. We have recently investigated several of the chemical, electrochemical and structural aspects of pyrazolato-bridged dirhodium complexes of both of these ligands.[1] In order to gain better insights into factors affecting bonding modes and chemical, electrochemical and structural features of dppm and dapm bimetallic complexes, we have expanded our investigations to include pyrazolato-bridged heterodinuclear transition-metal complexes that contain *trans* dppm and dapm bridging ligands. Herein we describe the synthesis and characterization of several such platinum–rhodium complexes listed in Table 1.

EXPERIMENTAL

Materials

Pyrazole (Hpz), 4-methylpyrazole (H4mpz) and 3,5-dimethylpyrazole (H35mpz) were purchased from Aldrich Chemicals. 4-Bromo-3,5-dimethylpyrazole (H4B35mpz) was obtained from Pfaltz and Bauer and 3,4,5-tribromopyrazole (H345Bpz)[2] and 3-methyl-5-trifluoromethylpyrazole (Hmtmpz) were prepared by a reported procedure.[3] Bis(diphenylphosphino)methane (dppm) was purchased from Strem and phenylacetylene was purchased from Aldrich and both were used without further purification. (Diphenylarsino)(diphenylphosphino)

* Author to whom correspondence should be addressed.

Table 1. Compound identification

Compound No.	Compound
1	$[ClPt(\mu\text{-}C_2Ph)(\mu\text{-dppm})_2Rh(CO)]PF_6$
2	$[(PhC_2)Pt(\mu\text{-35mpz})(\mu\text{-dppm})_2Rh(CO)]PF_6$
3	$[(PhC_2)Pt(\mu\text{-4mpz})(\mu\text{-dppm})_2Rh(CO)]PF_6$
4	$[(PhC_2)Pt(\mu\text{-pz})(\mu\text{-dppm})_2Rh(CO)]PF_6$
5	$[(PhC_2)Pt(\mu\text{-4B35mpz})(\mu\text{-dppm})_2Rh(CO)]PF_6$
6	$[(PhC_2)Pt(\mu\text{-345Bpz})(\mu\text{-dppm})_2Rh(CO)]PF_6$
7	$[(PhC_2)Pt(\mu\text{-mtmpz})(\mu\text{-dppm})_2Rh(CO)]PF_6$
8	$[(PhC_2)Pt(\mu\text{-35mpz})(\mu\text{-dppm})_2Rh(t\text{-BuNC})]PF_6$
9	$[(PhC_2)Pt(\mu\text{-4B35mpz})(\mu\text{-dppm})_2Rh(t\text{-BuNC})]PF_6$
10	$[(CN)_2Pt(\mu\text{-dppm})_2Rh(CO)Cl]$
11	$[(CN)Pt(\mu\text{-35mpz})(\mu\text{-dppm})_2Rh(CO)]PF_6$
12	$[(CN)Pt(\mu\text{-4B35mpz})(\mu\text{-dppm})_2Rh(CO)]PF_6$
13	$[(CN)Pt(\mu\text{-345Bpz})(\mu\text{-dppm})_2Rh(CO)]PF_6$
14	$[(CN)Pt(\mu\text{-35mpz})(\mu\text{-dppm})_2Rh(t\text{-BuNC})]PF_6$
15	$[(CN)Pt(\mu\text{-4B35mpz})(\mu\text{-dppm})_2Rh(t\text{-BuNC})]PF_6$
16	$[Pt(CN)_2(dapm\text{-}P)_2]$
17	$[(CN)_2Pt(\mu\text{-dapm})_2Rh(CO)Cl]$
18	$[(CN)Pt(\mu\text{-35mpz})(\mu\text{-dapm})_2Rh(CO)]PF_6$
19	$[(CN)Pt(\mu\text{-35mpz})(\mu\text{-dapm})_2Rh(t\text{-BuNC})]PF_6$
20	$[cis\text{-}Cl_2Pt(\mu\text{-dapm})_2\text{-}trans\text{-}Rh(CO)Cl]$
21	$[cis\text{-}ClPt(\mu\text{-35mpz})(\mu\text{-dapm})_2\text{-}trans\text{-}Rh(CO)]PF_6$
22	$[trans\text{-}ClPt(\mu\text{-35mpz})(\mu\text{-dapm})_2\text{-}trans\text{-}Rh(CO)]PF_6$

methane,[4] $Pt(CN)_2(dppm)_2$[5] and $PtCl_2(dapm)_2$[6] were prepared by literature procedures.

Preparation of $[Pt(dppm)_2]Cl_2$

This compound was initially prepared from $PtCl_2(COD)$ and dppm.[7] The following method was used in subsequent preparations. Solutions of dppm (2.5371 g, 6.60 mmol) in 10 cm^3 of CH_2Cl_2 and K_2PtCl_4 (1.1694 g, 2.81 mmol) in distilled water were mixed and refluxed for *ca* 3 h during which time the water layer changed from red to colourless and the CH_2Cl_2 changed from colourless to light green. The CH_2Cl_2 layer was separated from the water layer and the product was precipitated from the CH_2Cl_2 layer as a white powder upon the addition of diethyl ether. The yield was quantitative.

Preparation of $[ClPt(\sigma,\eta\text{-}C{\equiv}CPh)(\mu\text{-dppm})_2Rh(CO)]PF_6$ (**1**)

A modification of the procedure of Hutton *et al.*[8] was used to prepare **1**. To a solution of $Pt(dppm)_2Cl_2$ (1.7569 g, 1.70 mmol) in acetone was added solid $AgC_2H_3O_2$ (0.2834, 1.70 mmol) and phenylacetylene, (0.1529 g, 8.50 mmol). The resulting yellow suspension was stirred in darkness for 2 h, after which an acetone solution of $Rh_2(CO)_4Cl_2$ (0.3300 g, 0.85 mmol) was slowly added dropwise. After the mixture was stirred for 1/2 h, during which time the colour changed from dark yellow to orange, solid NH_4PF_6 (2.7674 g, 17.70 mmol) was added and the mixture was stirred for an additional 10 h. The mixture was filtered and the red filtrate was evaporated to dryness. The product was recrystallized twice from CH_2Cl_2/diethyl ether and dried *in vacuo*. The yield was 80%.

Preparation of $[(PhC{\equiv}C)Pt(\mu\text{-}Z)(\mu\text{-dppm})_2Rh(CO)]PF_6$ (**2**, Z = 35mpz; **3**, Z = 4mpz; **4**, Z = pz; **5**, Z = 4B35mpz; **6**, Z = 345Bpz; **7**, Z = mtmpz)

Method 1. To a solution of **1** (0.300 g, 0.217 mmol) in 40 cm^3 of acetone, a solution prepared by adding 2.72 cm^3 of 0.08 M KOH in methanol to 35mpz (0.0210 g, 0.217 mmol) was added dropwise. After the solution was stirred for 20 min, during which time the colour changed from orange to reddish-orange, it was evaporated to dryness. The product was recrystallized from CH_2Cl_2/diethyl ether. The yellow–orange product was dried *in vacuo*. The yield was 83%.

Method 2 (Z = 35mpz, 4mpz, pz). Solid 35mpz (0.1049 g, 1.085 mmol) was added to an acetone solution of **1** (0.300 g, 0.217 mmol). The solution

was stirred for 1 h, during which time the colour changed from orange to reddish-orange. The solution was evaporated to dryness and the product was recrystallized from CH_2Cl_2/diethyl ether and dried *in vacuo*. The yield was 83%.

Preparation of [(PhC≡C)Pt(μ-Z)(μ-dppm)$_2$Rh(*t*-BuNC)]PF_6 (**8**, Z = 35mpz; **9**, Z = 4B35mpz)

To a stirred solution of **2** (0.125 g, 0.091 mmol) in 40 cm^3 of acetone cooled to 0°C, 0.011 cm^3 (0.100 mmol) of *t*BuNC was added dropwise. The colour changed from orange to red and after the solution was stirred for 20 min, the volume was reduced to 8 cm^3 on a rotary evaporator. The light orange solid that was obtained upon the addition of diethyl ether was recrystallized from acetone/diethyl ether and dried *in vacuo*. The yield was 90%.

Preparation of [(CN)Pt(μ-Z)(μ-dppm)$_2$Rh(CO)]PF_6 (**11**, Z = 35mpz; **12**, Z = 4B35mpz; **13**, Z = 345Bpz)

To a solution of **10** (0.159 g, 0.134 mmol) dissolved in 5 cm^3 of CH_2Cl_2 and 100 cm^3 of acetone, solid NH_4PF_6 (0.044 g, 0.27 mmol) was added and the resulting suspension was stirred for 1 h. A methanol solution of KOH (0.076 g, 0.134 mmol) and 35mpz (0.026 g, 0.27 mmol) was added dropwise and the resulting mixture was stirred for 2 h. The yellow solution was evaporated to dryness and the residue was dissolved in CH_2Cl_2 and filtered. Diethyl ether was added to the filtrate and a light yellow solid was recovered and recrystallized four times from CH_2Cl_2/diethyl ether. The yield was 50%.

Found: C, 48.9; H, 4.1. Calc. for **11** $C_{57}H_{51}F_6N_3OP_5PtRh$: C, 50.3; H, 3.8%.

Preparation of [(CN)Pt(μ-Z)(μ-dppm)$_2$Rh(*t*-BuNC)]PF_6 (**14**, Z = 35mpz; **15**, Z = 4B35mpz)

Compound **11** (0.201 g, 0.150 mmol) was dissolved in 40 cm^3 of freshly distilled CH_2Cl_2 and 40 cm^3 of freshly distilled methanol and cooled to 0°C. After the solution was purged with pre-purified argon, *t*-BuNC (0.0135 g, 0.165 mmol) was added dropwise. The solution changed from orange to dark red and was stirred for 15 min. After the solution was evaporated to dryness, the red solid was recrystallized from degassed acetone/diethyl ether. The yield was 75%.

Found: C, 52.8; H, 4.4. Calc. for **14**, $C_{60}H_{60}F_6N_4P_5PtRh$: C, 51.7; H, 4.3%.

Preparation of [Pt(CN)$_2$(dapm-P)$_2$] (**16**)

$PtCl_2$(dapm-*P*)$_2$ (0.260 g, 0.231 mmol) was dissolved in 10 cm^3 of CH_2Cl_2, after which 50 cm^3 of absolute ethanol was added. To this solution a solution of NaCN (0.0225 g, 0.463 mmol) dissolved in 100 cm^3 of ethanol was added dropwise. The resulting solution was stirred for 15 min and evaporated to *ca* one-third the original volume on a rotary evaporator. The product which precipitated upon the addition of diethyl ether was recrystallized from CH_2Cl_2/diethyl ether. The yield was 87%.

Found: C, 56.4; H, 4.2. Calc. for **16**, $C_{52}H_{44}As_2N_2P_2Pt$: C, 56.6; H, 4.0%.

Preparation of [(CN)$_2$Pt(μ-dapm)$_2$Rh(CO)Cl] (**17**)

To a stirred solution of $Rh_2(CO)_4Cl_2$ (0.0386 g, 0.099 mmol) dissolved in 10 cm^3 of CH_2Cl_2 cooled to 0°C, was added dropwise a solution of **16** (0.219 g, 0.198 mmol) dissolved in 10 cm^3 of CH_2Cl_2. After the solution was stirred for 30 min, it was evaporated to dryness on a rotary evaporator. The orange residue was recrystallized from CH_2Cl_2/diethyl ether and dried *in vacuo*. The yield was 78%.

Found: C, 50.2; H, 3.5. Calc. for **17**, $C_{53}H_{44}As_2ClN_2OP_2PtRh$: C, 50.1; H, 3.5%.

Preparation of [(CN)Pt(μ-5mpz)(μ-dapm)$_2$Rh(CO)]PF_6 (**18**)

The same procedure used to prepare **11** was used to prepare **18** from **17** (0.104 g, 0.082 mmol), NH_4PF_6 (0.0266 g, 0.164 mmol), KOH (0.0046 g, 0.082 mmol) and 35mpz (0.0158 g, 0.082 mmol). The yield was 78%.

Found: C, 46.8; H, 3.7. Calc. for **18**, $C_{57}H_{51}As_2F_6N_3OP_3PtRh$: C, 47.2; H, 3.5%.

Preparation of [(CN)Pt(μ-35mpz)(μ-dapm)$_2$Rh(*t*-BuNC)]PF_6 (**19**)

Compound **19** was prepared from **18** by the same procedure used to prepare **14**. Typical quantities were 119 mg (0.081 mmol) of **18** and 7.44 mg (0.090 mmol) of *t*-BuNC. The yield was 85%.

Found: C, 47.8; H, 4.2. Calc. for **19**, $C_{60}H_{60}As_2F_6N_4P_3PtRh$: C, 48.7; H, 4.0%.

Preparation of [cis-ClPt(μ-35mpz)(μ-dapm)$_2$-trans-Rh(CO)]PF_6 (**21**)

Solid NH_4PF_6 (0.015 g, 0.091 mmol) was added to a solution of **20** (0.117 g, 0.091 mmol) in 10 cm^3 of CH_2Cl_2 and 40 cm^3 of acetone. In a separate flask, 35mpz (0.013 g, 0.14 mmol) and KOH (0.0051 g,

0.090 mmol) were combined and allowed to stand for 5 min. The latter solution was added dropwise to the former mixture and the resulting mixture was stirred for 20 min at 0°C. Stirring was continued while the mixture warmed to room temperature. The solvent was removed via a rotary evaporator and the resulting solid was treated with freshly distilled CH_2Cl_2 and filtered. Anhydrous diethyl ether/hexanes (50/50) was added until precipitation was complete. The product was dried *in vacuo*. The yield was 70%.

Found: C, 46.1; H, 3.8. Calc. for **21**, $C_{56}H_{51}As_2ClF_6N_2OP_3PtRh$: C, 46.1; H, 3.5%.

Physical measurements

^{31}P NMR spectral data were obtained on CH_2Cl_2 solutions with a JEOL FX90Q spectrometer operating at 36.21 MHz. The external reference was 85% H_3PO_4. IR data were obtained on Nujol mulls between polyethylene sheets with the use of a Digilab FTS-20C/V Fourier transform spectrometer. UV–vis data were obtained on CH_2Cl_2 solutions with the use of a Cary 219 spectrophotometer. Spectroscopic data are listed in Table 2. Elemental analyses were performed by Galbraith Laboratories, Knoxville, TN.

Structure determination for [(PhC≡C)Pt(μ-345Bpz)(μ-dppm)$_2$Rh(CO)]PF_6 (**6**)

Crystallographic data are listed in Table 3. Intensity measurements were made on a Siemens R3m/V diffractometer at room temperature. Refined unit-cell parameters were derived by least-squares treatment of diffractometer setting angles of 20 reflec-

Table 2. Spectral data

	NMR[a]					IR[b]			UV–vis[a]
Compound No.	δ(Pt—P) (ppm)	^1J(Pt—P) (Hz)	δ(Rh—P) (ppm)	^1J(Rh—P) (Hz)	N (Hz)	ν(C≡C)	ν(CO) (cm^{-1})	ν(NC)	λ(ε) nm (M^{-1} cm^{-1})
1	0.58	2358.4	19.02	112.3	31.7	2040(w)	1983(s)		425(3200)
2	4.08	2646.5	20.40	129.3	44.0	2129(w)	1983(s)		435(14,680), 350(6000)
3	6.44	2666.0	21.31	129.4	46.4	2126(w)	1983(s)		438(14,600), 352(5400)
4	6.77	2658.7	21.51	127.0	46.4	2122(w)	1983(s)		437(15,200), 350(6300)
5	3.60	2634.3	19.69	127.0	44.0	2122(w)	1983(s)		435(13,400), 350(5000)
6	2.80	2607.4	17.74	127.0	39.1	2133(w)	1987(s)		431(12,000), 350(5300)
7a	3.81	2644.1	18.62	127.0	41.5	2129(w)	1987(s)[c]		
7b	1.52	2617.2	[d]						
8	1.39	2707.5	18.01	136.7	44.0			2122(s)	453(14,000), 371(4200)
9	0.92	2695.3	18.01	136.7	44.0			2106(s)	454(14,000), 370(4300)
10	−0.90	2529.3	18.62	127.0	44.0		1975(s)	2129(m)	426(7400)
11	0.59	2404.8	19.46	129.4	34.2		1992(s)	2120(m)	427(9100)
12	0.72	2397.5	19.29	127.0	34.2		1991(s)	2123(m)	426(8600)
13	0.78	2369.4	19.43	127.0	36.6		1989(s)	2124(m)	428(8700)
14	−0.43	2500.0	16.57	148.5	54.0			2141(s)	450(6100)
15	−0.43	2500.0	16.60	146.5	51.0			2140(s)	450(6300)
16	7.92	2324.2						2135(s)	
17	3.47	2509.8					1973(s)	2129(m)	416(7500)
	1.12	3037.1	25.92	148.9[e]					
18	2.46	2392.6					1991(s)	2120(m)	417(8100)
	0.98	2902.8	23.43	149.0[e]					
19	3.20	2483.0						2140(s)	452(7200)
	2.20	3063.0	21.75	168.9[e]					
21	7.04	4050.2	[f]				1979(s)		
	−0.03	3004.0							

[a] NMR and UV–vis data were obtained on dichloromethane solutions.

[b] IR data were obtained on Nujol mulls between thin sheets of polyethylene.

[c] These values are for the mixture of isomers **7a** and **7b**.

[d] The NMR peaks for the rhodium-bound phosphorus atoms in the minor isomer were partially masked by those of the major isomer and the chemical shifts could not be measured accurately.

[e] HT isomer.

[f] ^2J(P—P) = 19.5 Hz.

Table 3. Crystallographic data for [(PhC≡C)Pt(μ-345Bpz)(μ-dppm)$_2$Rh(CO)]PF_6

Molecular formula	$C_{62}H_{49}Br_3F_6N_2OP_5PtRh$
fw	1644.5
Space group	$P\bar{1}$
Z	2
a (Å)	10.351(5)
b (Å)	14.707(6)
c (Å)	22.445(10)
α (°)	94.78(3)
β (°)	98.56(4)
γ (°)	107.68(3)
V (Å^3)	3189(2)
d_{calc} (g/cm^3)	1.713
Radiation type; wavelength (Å)	Mo; 0.71073
Temperature (K)	298
Absorption coefficient (cm^{-1})	45.11
R (%)	4.05
R_w (%)	4.64

tions. The intensities of three check reflections were monitored every 50 reflections and no significant variations in intensities were observed during the data collection. The intensity data were corrected for Lorentz and polarization effects. An empirical absorption correction, based on the φ dependence of the intensities of four reflections with χ *ca* 90° (T_{max} : T_{min} = 0.958 : 0.759), was applied to the intensity data.

The crystal structure was solved by heavy atom (Patterson and difference Fourier) methods.[9] Full-matrix least-squares adjustment of positional and anisotropic temperature factor parameters, with hydrogen atoms included at their calculated position during final iterations, converged to $R = 0.0405$ ($R_w = 0.0464$). The asymmetric unit contains one cation and one-half of two slightly distorted PF_6^- ions. The phosphorus atoms of the PF_6^- ions lie on crystallographic inversion centres, thus resulting in site occupation numbers for P5 and P6 of 0.5. Additional details of data collection and refinement are found in supplementary materials.*

RESULTS AND DISCUSSION

The dppm-bridged complexes **2–6** were synthesized by the addition of the potassium salt of the appropriate pyrazole to **1**. In the cases of the 35mpz, 4mpz and the pz complexes, the pyrazoles can be used directly to obtain the desired product. Hutton *et al.*[8] have shown that **1** contains a phenylacetylide ligand that is σ-bonded to the platinum and weakly π-bonded to the rhodium. The addition of a pyrazolate ion results in the loss of the terminal chloride ion on the platinum and the conversion of PhC≡C$^-$ from weakly bridging to terminal. The pyrazolate ions bridge the two metal atoms to form new unsymmetrical A-frame complexes.

The $^{31}P\{^1H\}$ NMR spectrum of **2** is shown in Fig. 1 and is typical of the spectra of **1–6**. The NMR data are found in Table 2. The bimetallic cations exhibit two ^{31}P resonances. The phosphorus atoms bonded to rhodium (^{103}Rh, 100%, I = 1/2) have chemical shifts in the range 17.4–21.5 ppm and ^1J(Rh—P) values in the range 112–127 Hz. The phosphorus atoms bonded to platinum exhibit chemical shifts in the range 0.58–6.8 ppm and ^1J(Pt—P) values (^{195}Pt, 33.4%, I = 1/2) in the range 2666–2358 Hz.

The ^{195}Pt satellites and the main resonance due to the phosphorus atoms bonded to the non-magnetic platinum atoms appear as virtual triplets. We denote the separation of the outer peaks of the triplets as *N*, following the designation of Shaw *et al.*,[8] where *N* is defined as ^2J(P—P) + ^4J(P—P). The resonances of the phosphorus atoms bonded to rhodium appear as a multiplet which might be described as a pair of virtual triplets with each triplet sandwiched by two weak outer peaks. These outer peaks probably result from weak second-order effects ascribed to the AA′BB′MX spin system.

* *Supplementary material available*: Table S1 (details of data collection, structure solution, and refinement) (3 pages), Table S2 (non-hydrogen atomic positions) (2 pages), Table S3 (hydrogen atom positions), Table S4 (bond distances), Table S5 (bond angles) (2 pages), Table S6 (anisotropic thermal parameters) (2 pages), Table S7 (observed and calculated structure factors) (30 pages).

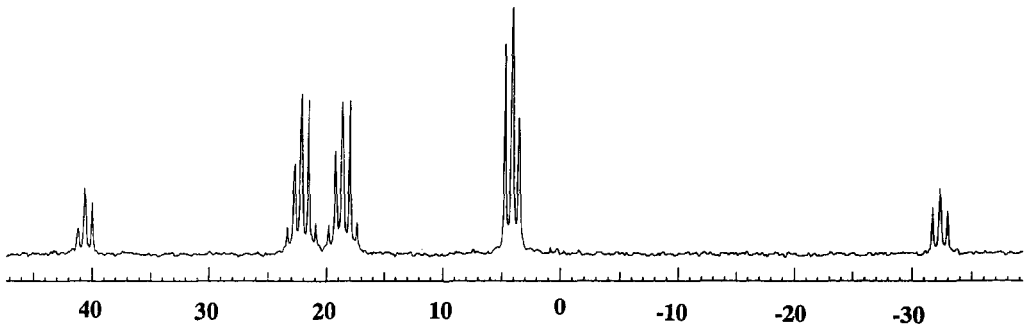

Fig. 1. ^{31}P NMR spectrum of $[(PhC_2)Pt(\mu\text{-}35mpz)(\mu\text{-}dppm)_2Rh(CO)]PF_6$ (**2**).

The IR spectra of **2–6** exhibit $\nu(C{\equiv}C)$ values about 85 cm^{-1} higher than that found in **1**. This is consistent with the conversion of the semi-bridging phenylacetylide ligand in **1** to a terminal ligand in **2–6**.

The reaction of the 3-methyl-5-trifluoromethylpyrazolate ion (mtmpz) with **1** gives **7**, whose ^{31}P NMR spectrum is shown in Fig. 2. The spectrum indicates the presence of two products. Since mtmpz is an unsymmetrical ligand, the two donor sites would be expected to exhibit different basicities, possibly resulting in different phosphorus resonances for the isomers **7a** and **7b**. Through induc-

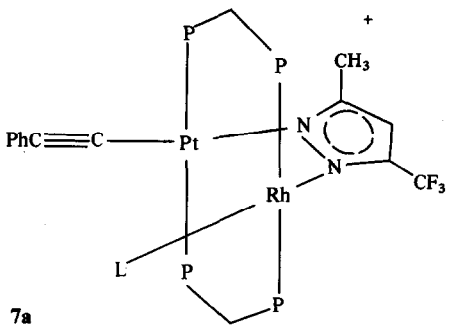

7a

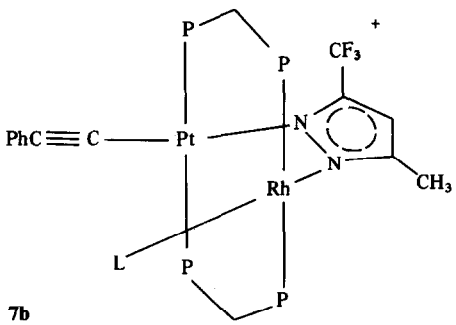

7b

tive effects, the donor nitrogen on the side of the heterocyclic ring with the CF_3 group might be expected to be less basic than the one on the side with CH_3. Perusal of the Pt—P chemical shift and coupling constant data in Table 2 reveals the general trend that J(Pt—P) and δ(Pt—P) decrease as the substituents on the ring become more electronegative. Assuming that this trend holds for the unsymmetrical ligand mtmpz, the platinum-bound phosphorus atom would exhibit lower J and δ values when the nitrogen on the same side of the ring as the CF_3 group is coordinated to the platinum. This analysis leads to the assignment of the minor isomer, with δ(Pt—P) of 1.52 ppm and J(Pt—P) of 2617 Hz, as **7b**, and the dominant isomer as **7a**, with chemical shift and coupling constant values of 3.81 ppm and 2644 Hz, respectively.

The assignment of **7a** and **7b** as the major and minor isomers, respectively, is also consistent with bonding preferences based on hard–soft acid–base (HSAB) principles. The softer platinum should prefer the nitrogen closest to the electron donating substituent, in this case the CH_3 group; thus, based on HSAB theory the dominant isomer is again predicted to be **7a**.

The addition of one equiv of *t*-BuNC to **2** and **5** results in the substitution of CO by *t*-BuNC to give **8** and **9**, respectively. Attempts to prepare the *t*-BuNC complexes of **3**, **4** and **6** resulted in a mixture of complexes that we were unable to separate. The $^{31}P\{^1H\}$ NMR spectra of **8** and **9** are similar to those of **1–6** and the NMR data are found in Table 2.

Treatment of **10** with the appropriate pyrazolate ions leads to complexes **11–13**. The addition of one equiv of *t*-BuNC to **11** and **12** leads to the replacement of CO to give **14** and **15**, respectively. This substitution results in an increase in the metal–phosphorus NMR coupling constants. This effect is attributed to the increase in electron density at the

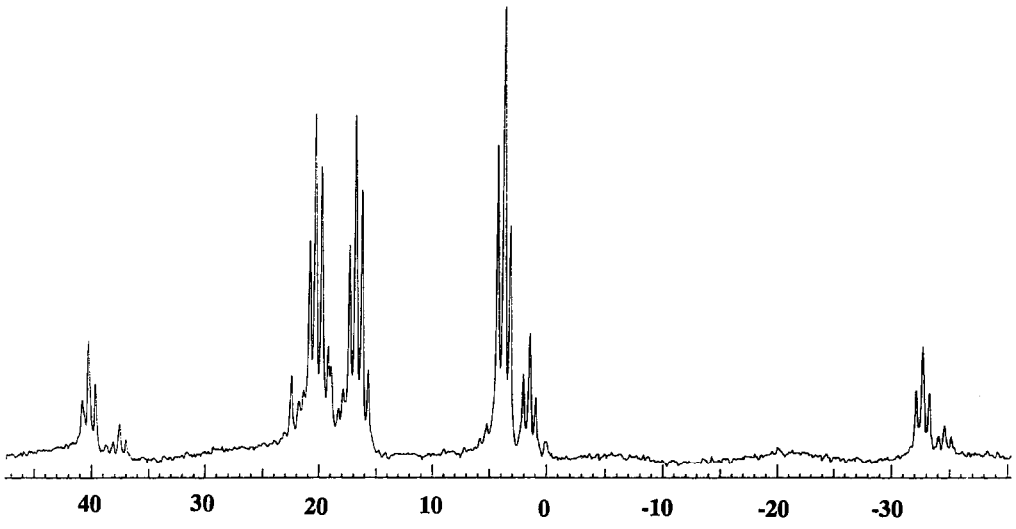

Fig. 2. ^{31}P NMR spectrum of $[(PhC_2)Pt(\mu\text{-mtmpz})(\mu\text{-dppm})_2Rh(CO)]PF_6$ (7).

metal and is consistent with the general observation that one-bond metal–phosphorus coupling constants increase with a decrease in oxidation state of the metal. It is generally accepted that *t*-BuNC is a better σ-donor and poorer π-acceptor than CO, thus placing more electron density on the rhodium and more electron density on the platinum through redistribution of electron density by the ligands.

The ν(CO) values of **11**–**13** show an increase over that of **10**. This can be interpreted as a decrease in the antibonding electron density on the CO and thus, a decrease in the π-backbonding involving the rhodium and CO. The Cl in **10** is acting as a better π-donor than is the pyrazolate ion in **11**–**13**. The replacement of one CN on platinum with the pyrazolate results in a slight decrease in the stretching frequency of the remaining CN ligand. This suggests that the pyrazolate is a slightly poorer π-acceptor than CN.

Dapm complexes

When a solution of *cis*-$Cl_2Pt(dapm\text{-}P)_2$ is treated with NaCN, complex **16**, $(CN)_2Pt(dapm\text{-}P)_2$, is formed. The value of 2324 Hz measured for ^1J(Pt—P) is typical of coupling constants observed for *trans* phosphorus atoms bonded to a platinum atom.[10] The dppm analogue *trans*-$Pt(CN)_2(dppm)_2$ has been shown to be fluxional at 25°C with exchange of bound and unbound phosphorus atoms.[5] Complex **16** does not appear to be fluxional since its ^{31}P NMR resonances are sharp and well defined, features that suggest that the species is not fluxional or that if exchange does occur, it is very rapid at 25°C.

Complex **17** is prepared by reacting 1 equiv of **16** with 1/2 equiv of $Rh_2(\mu\text{-}Cl)_2(CO)_2$. Several isomers are possible for **17**. One isomer has the two phosphorus atoms bound to the platinum and is designated the head-to-head (HH) isomer. The head-to-tail (HT) isomer has a phosphorus atom and an arsenic atom coordinated to platinum. The $^{31}P\{^1H\}$ NMR spectrum clearly indicates that both isomers are present, with the HH isomer being the dominant one. Since **16** was shown by NMR to exist only as the phosphorus-bound HH isomer, dissociation of a dapm ligand must have occurred during the formation of **17** in order for the HT isomer to form. The dissociation of the dapm ligands leads to the possible formation of a second HH isomer of **17** in which the two phosphorus atoms are coordinated to the rhodium atom. However, the ^{31}P NMR spectrum confirms the absence of this isomer.

The addition of 35mpz to **17** produces **18** whose $^{31}P\{^1H\}$ NMR spectrum is similar to that of **17** and also indicates the presence of HH and HT isomers. The isomeric mixture is maintained upon the addition of *t*-BuNC to **18** to form **19**.

Structural characterization of complex **20** indicated that a square planar *trans*-$Rh(CO)ClAs_2$ unit is connected to a *cis*-$PtCl_2P_2$ unit via two dapm bridges such that the two metals are separated by 3.043 Å.[11] Since our investigations indicate that the pyrazolate ions are poorer π-donors than chloride,

we thought that the replacement of a platinum-bound Cl with the pyrazolate ions might favour the arrangement that has the Cl *trans* to the pyrazolate and the phosphorus atoms *trans* to each other. Complex **21** exhibits a $^{31}P\{^{1}H\}$ NMR spectrum that consists of two equally intense doublets with chemical shifts of 7.04 and −0.03 ppm. The chemical shift values and the presence of two sets of satellite doublets due to coupling to ^{195}Pt, indicate that **21** contains two types of platinum-bound phosphorus atoms. These data indicate that the *cis* disposition of phosphorus atoms about the platinum is maintained during the conversion of **20**–**21**.

Several products were shown to result when **20** was refluxed in $CHCl_3$.[10] Among those products was an isomer of **20** that results from the transfer of a Cl from the platinum unit to the rhodium unit. The resulting species has a metal–metal bond, and has the phoshorus atoms bound to the platinum and the arsenic atoms bound to the rhodium in *trans* positions. Because of the bidentate nature of the pyrazolate ions, complex **21** was not expected to undergo the type of thermal isomerization observed for **20** that led to the formation of the metal–metal bond. When **21** was heated in $CHCl_3$ for 2 h, no colour change was observed; however, a single peak at 6.37 ppm accompanied by ^{195}Pt satellites, with a J value of 2598 Hz, did appear in the $^{31}P\{^{1}H\}$ NMR spectrum. The single phosphorus NMR peak and a value of 2598 Hz for ^{1}J(Pt—P) are features that are consistent with the isomer of **21** that is formulated as [*trans*-ClPt(μ-35mpz)(μ-dapm)$_2$-*trans*-Rh(CO)]PF_6, (**22**). Though the conversion of **21** to **22** appeared to be clean, i.e. no other phosphorus-containing species were evident from the NMR, the conversion was not complete, even after heating for at least 12 h. Based on relative intensities, it was estimated that there was about a 20–30% conversion. Attempts to separate the two isomers were unsuccessful.

Structure of [(PhC≡C)Pt(μ-345Bpz)(μ-dppm)$_2$ Rh(CO)]PF_6 (**6**)

As shown in Fig. 3 and revealed by the data listed in Tables 3 and 4, the solid-state structure of **6** consists of a platinum atom and a rhodium atom, Pt(1) and Rh(1), bridged by two transoid dppm ligands and a 3,4,5-tribromopyrazolate anion. The platinum atom is also coordinated to a terminal phenylacetylide ligand and the rhodium is coordinated to a terminal CO. The methylene bridges of the dppm ligands are folded over the 345Bpz bridging ligand. This orientation minimizes the steric interactions of the phenyl groups with the 345Bpz ligand since the phenyl rings on the side with 345Bpz flair outward, thus, creating a more open environment for the bridging 345Bpz ligand. The platinum and rhodium atoms are in approximate square planar environments with the least-squares plane through Rh(1), P(1), P(3), N(1) and C(1) making an angle of 70.8° with the one through Pt(1), P(2), P(4), N(2) and C(4). The Pt—P bond distances and the Rh—P bond distances are essentially the same (Table 4), as are the Pt—N and Rh—N distances. The Pt · · · Rh separation of 3.265 Å suggests that there is no metal–metal bond.[11] Other selected bond distances and angles are found in Table 4.

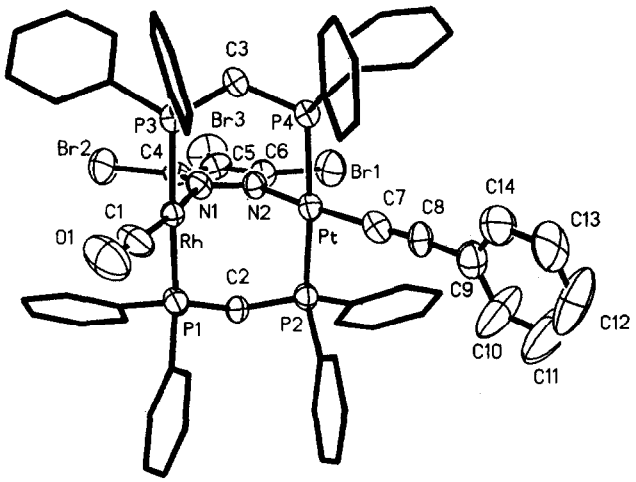

Fig. 3. Structure of [(PhC≡C)Pt(μ-345Bpz)(μ-dppm)$_2$Rh(CO)]$^+$ (cation of **6**) showing 50% thermal ellipsoids (hydrogen atoms and phenyl carbon atoms in dppm are omitted for clarity).

Table 4. Selected bond distances and angles for [(PhC≡C)Pt (μ-345Bpz)(μ-dppm)$_2$Rh(CO)]PF_6

Distances (Å)			
Pt—P(2)	2.327(3)	Pt—P(4)	2.330(3)
Pt—N(2)	2.070(9)	Pt—C(7)	1.971(12)
Rh—P(1)	2.334(3)	Rh—P(3)	2.321(3)
Rh—N(1)	2.078(8)	Rh—C(1)	1.807(12)
P(1)—C(2)	1.836(8)	P(2)—C(2)	1.841(10)
P(3)—C(3)	1.843(8)	P(4)—C(3)	1.835(10)
N(1)—N(2)	1.356(10)	O(1)—C(1)	1.171(15)
C(7)—C(8)	1.177(17)		
Angles (°)			
P(2)—Pt—P(4)	175.4(1)	P(2)—Pt—N(2)	87.8(2)
P(4)—Pt—N(2)	89.6(2)	P(2)—Pt—C(7)	91.0(3)
P(4)—Pt—C(7)	91.3(3)	N(2)—Pt—C(7)	169.3(3)
P(1)—Rh—P(3)	172.1(1)	P(1)—Rh—N(1)	84.9(2)
P(3)—Rh—N(1)	87.2(2)	P(1)—Rh—C(1)	94.0(4)
P(3)—Rh—C(1)	93.7(4)	N(1)—Rh—C(1)	171.4(5)
Rh—P(1)—C(2)	113.0(3)	Pt—P(2)—C(2)	110.3(3)
Pt—P(4)—C(3)	111.7(3)	Rh—N(1)—N(2)	114.0(7)
Rh—N(1)—C(6)	136.7(6)	Pt—N(2)—N(1)	120.7(6)
Pt—N(2)—C(8)	131.4(7)	Rh—C(1)—O(1)	175.6(13)
P(1)—C(2)—P(2)	116.5(5)	P(3)—C(3)—P(4)	115.5(5)
Pt—C(7)—C(8)	176.3(8)		

Acknowledgements—The authors wish to thank Research Corporation for support of this work and Johnson Matthey, Inc for a generous loan of rhodium trichloride.

REFERENCES

1. C. J. Janke, L. J. Tortorelli, J. L. E. Burn, C. A. Tucker and C. Woods, *Inorg. Chem.* 1986, **25**, 4597; L. J. Tortorelli, C. Woods and A. T. McPhail, *Inorg. Chem.* 1990, **29**, 2726; C. Woods, L. J. Tortorelli, D. P. Rillema, J. L. E. Burn and J. C. DePriest, *Inorg. Chem.* 1989, **28**, 1673.
2. *Chem. Abstr.* 1975, **82**, 112068C.
3. Trofimenko, *J. Am. Chem. Soc.* 1967, **89**, 3165.
4. P. D. Enlow and C. Woods, *Organometallics* 1983, **2**, 64.
5. F. S. M. Hassan, D. P. Markham, P. G. Pringle and B. L. Shaw, *J. Chem. Soc., Dalton Trans.* 1985, 279.
6. A. L. Balch, R. R. Guimerans, J. Linehan and F. E. Wood, *Inorg. Chem.* 1985, **24**, 2021.
7. M. P. Brown, J. R. Fisher, R. Hill, R. J. Puddephatt and K. R. Seddon, *Inorg. Chem.* 1981, **20**, 3516.
8. A. T. Hutton, R. C. Langrick, D. M. McEwan, P. G. Pringle and B. L. Shaw, *J. Chem. Soc., Dalton Trans.* 1985, 2121.
9. G. M. Sheldrick, SHELXTL PLUS, version 4.1. Siemens Analytical X-ray Instruments, Inc. Madison, WI (1990).
10. A. L. Balch, R. R. Guimerans, J. Linehan, M. M. Olmstead and D. E. Oram, *Organometallics* 1985, **4**, 1445.
11. R. R. Guimerans, F. E. Wood and A. L. Balch, *Inorg. Chem.* 1984, **23**, 1307.

Polyhedron Vol. 10, No. 18, pp. 2163–2169, 1991
Printed in Great Britain

0277–5387/91 $3.00+.00
© 1991 Pergamon Press plc

A NOVEL AMINO ACID RACEMIZATION IN VITAMIN B_6-AMINO ACID SCHIFF BASE COPPER COMPLEXES: CRYSTAL STRUCTURES OF AQUO (5′-PHOSPHOPYRIDOXYLIDENE-DL-TYROSINATO) COPPER(II) $3.5H_2O$ AND AQUO (5′-PHOSPHOPYRIDOXYLIDENE-DL-PHENYLALANINATO) COPPER(II) $2.5H_2O$

I. I. MATHEWS and H. MANOHAR*

Department of Inorganic and Physical Chemistry, Indian Institute of Science, Bangalore 560 012, India

(*Received* 4 *February* 1991; *accepted* 23 *May* 1991)

Abstract—A novel racemization observed in the Vitamin B_6-amino acid Schiff base complexes, aquo (5′-phosphopyridoxylidene-L-tyrosinato) copper(II) and aquo (5′-phosphopyridoxylidene-L-phenylalaninato) copper(II) is described. The racemization taking place in solution under mild acidic conditions (pH 5–6) was confirmed by CD studies and the products were characterized by single crystal X-ray diffraction. The structures of both complexes show almost parallel orientation of the aromatic side chain and the pyridoxal π-system. The activation of the αC—H group due to the intermolecular π–π interaction is probably the reason for the unusual racemization observed.

Amino acid racemization reactions are of interest in peptide synthesis,[1] geochronology,[2] geothermometry[2] and nutrition.[3] A number of mechanisms have been put forward to explain the diverse nature of these reactions.[2b,4a,5] Neuberger,[5a] in 1948, first proposed that the mechanism involves the removal of the α-hydrogen of the amino acid resulting in the formation of a planar carbanion. Stabilization of this incipient carbanion transition state controls the rate of racemization. This could result from a number of factors[5] that alter the enthalpy and entropy of the transition state, such as inductive and resonance effects, solvation and neighbouring group participation, and steric effects (resulting from both intra- and intermolecular interactions).

Metal complexes of both transition and non-transition metal ions (except nickel[4c]) are known to catalyse racemization.[4c,5d] Metal ions through coordination, can stabilize the intermediate carbanion.[6]

The pyridoxal-amino acid Schiff bases are well known for their catalytic activity in racemization reactions.[7] These studies have received special attention because pyrixodal phosphate-amino acid Schiff bases have been proposed as intermediates in enzymatic racemization reactions.[8] Aromatic amino acids show increased reactivity in these reactions.[9] NMR studies and semi-empirical calculations[9,10] have shown that stabilization of the π-system of the Schiff base due to the π–π interaction with the aromatic ring plays an important role. These studies were done at pH values (*ca* 12.3) which were far from physiological pH. Studies on metal complexes of amino acid Schiff bases have shown that racemization takes place under basic conditions after heating.[11]

Here we report an interesting racemization observed in the copper complexes of pyridoxal phosphate (PLP) with L-tyrosine (I) and L-phenylalanine (II). This study shows that racemization in these systems takes place under acidic conditions, close to physiological pH. The products of racemization were characterized by single crystal X-ray analysis. CD studies show slow racemization in solution.

* Author to whom correspondence should be addressed.

EXPERIMENTAL

PLP and amino acids were obtained from the Sigma Chemical Company. Methanol (AR grade), $Cu(NO_3)_2 \cdot 3H_2O$ and NaOH were procured from BDH India Limited. The circular dichroism (CD) spectra were recorded in the range 280–470 nm using a J-500A spectropolarimeter attached to a DP-501N data processor.

Preparation of complexes

The Schiff base ligand was first prepared by treating PLP with the corresponding L-amino acid at room temperature. The pH was adjusted to *ca* 4.5 by adding 0.1 M NaOH. The resultant Schiff base was immediately treated with metal salt solution and the final pH was adjusted to *ca* 4.6.

CD spectra

The CD spectra for the complexes were recorded immediately after mixing, after 1, 6, 18 and 23 days. The spectra were also recorded for DL-amino acid Schiff base complexes prepared under identical conditions for comparison.

X-ray structure determination

Details regarding data collection and processing are presented in Table 1. The data were corrected for Lorentz and polarization effects, and for absorption[12] effects for complex **II**.

The structures were solved by conventional Patterson and Fourier techniques and refined by full-matrix least-squares treatment.[13] Hydrogen atoms were located from difference electron density maps.

Table 1. Summary of crystallographic data

	Complex **I**	*Complex* **II**
Mol. formula	$CuC_{17}O_{12.5}N_2H_{26}P$	$CuC_{17}O_{10.5}N_2H_{24}P$
Mol. wt	552.73	518.73
Crystal system	Triclinic	Triclinic
Space group	$P\bar{1}$	$P\bar{1}$
a (Å)	8.634(2)	8.777(3)
b (Å)	11.827(2)	11.736(4)
c (Å)	11.981(1)	12.188(4)
α (°)	94.07(1)	97.55(2)
β (°)	109.57(1)	108.72(2)
γ (°)	103.40(1)	103.36(2)
V (Å^3)	1106	1127
Z	2	2
F(000)	572	536
ρ (calc.) (g cm^{-3})	1.659	1.528
ρ (obs.) (g cm^{-3})[a]	1.68	1.54
Diffractometer	CAD4	CAD4
Radiation	Graphite-monochromated Mo-K_α (0.71073 Å)	
Temperature (°C)	21	21
Reflections measured	$\pm h, \pm k, +l$	$\pm h, \pm k, +l$
Scan type	$\omega/2\theta$	$\omega/2\theta$
θ range (°)	1.0–27.0	1.0–26.0
Observed unique reflections	4117 [$I > 2.0\sigma(I)$]	2177 [$I > 2.5\sigma(I)$]
Crystal size (mm)	$0.30 \times 0.16 \times 0.14$	$0.22 \times 0.12 \times 0.08$
Absorption coefficient (cm^{-1})	11.54	11.24
Transmission coefficient		0.98–1.09[b]
Weighting scheme (w)	$[\sigma^2(F_o)+0.0000F_o^2]^{-1}$	$[\sigma^2(F_o)+0.000435F_o^2]^{-1}$
R[c]	0.043	0.073
R_w[d]	0.050	0.072

[a] By flotation in $CHCl_3+CHBr_3$.
[b] Normalized to an average of unity.
[c] $R = \Sigma \|\|F_o\| - \|F_c\|\| / \Sigma |F_o|$.
[d] $R_w = [\Sigma w(\|\|F_o\| - \|F_c\|\|)^2 / \Sigma |F_o|^2]^{1/2}$.

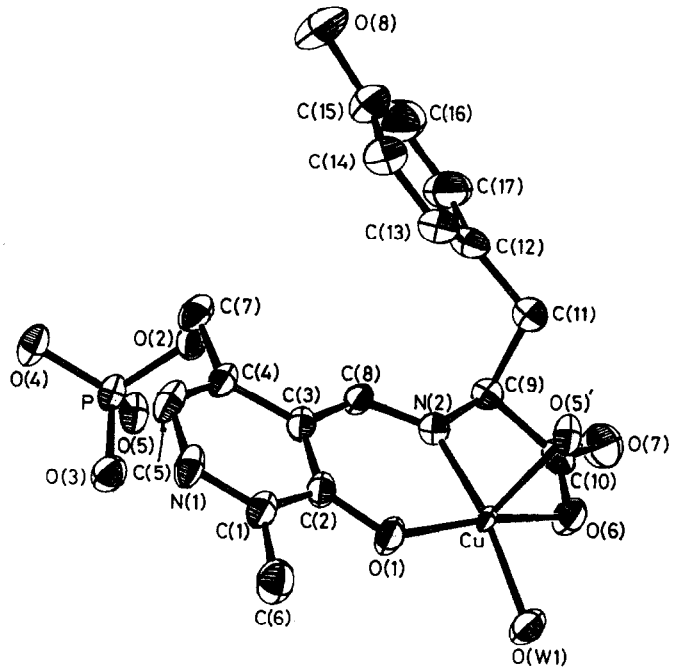

Fig. 1. ORTEP[14] diagram of complex I with thermal ellipsoids at 50% probability, showing the atom-labelling scheme.

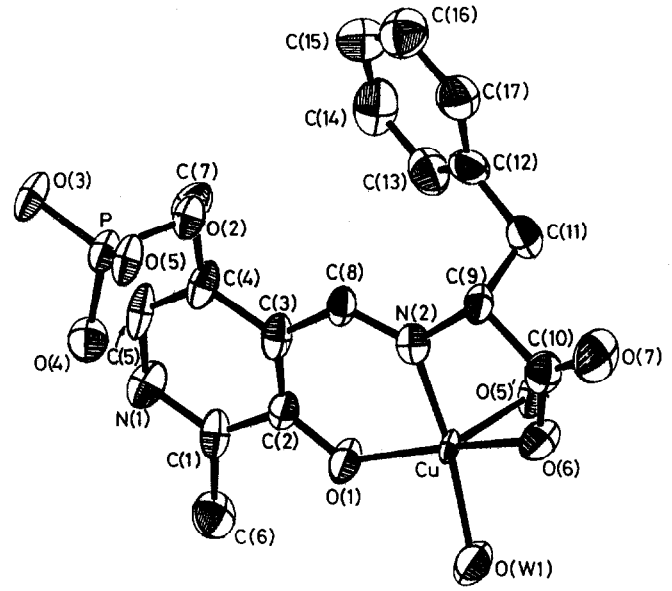

Fig. 2. ORTEP diagram of complex II with thermal ellipsoids at 50% probability, showing the atom-labelling scheme.

RESULTS AND DISCUSSION

The molecular structures of complexes I and II, including atom labelling, are shown in Figs 1 and 2, respectively. The structure of complex I closely resembles that prepared using DL-tyrosine as the starting material.[15]

In the structures of both complexes I and II,* copper(II) has a distorted square-pyramidal geometry. The tetradentate Schiff base exists as a

*This structure was previously solved[16] by photographic methods to a final R factor of 0.145 for 1177 observed reflections, but the coordinates were neither published nor deposited with the Cambridge Data Centre. The low accuracy of the structure is probably due to the reported difficulty of obtaining good single crystals. No experimental details of the synthesis are available. However, we presume that the authors used the DL-compound for their preparation since there is no mention of racemization in the paper.

divalent anion with the phenolate and carboxylate groups deprotonated and the pyridine nitrogen and the phosphate group protonated. The copper ion is coordinated by the Schiff base through the phenolate oxygen O(1), carboxylate oxygen O(6) and imino nitrogen N(2), and the fourth basal donor is a water molecule O(W1). The axial position is occupied by the phosphate oxygen O(5′) from a neighbouring molecule, thus resulting in a one-dimensional polymer. The bond lengths and bond angles (selected values in Table 2) are unexceptional. In both structures centrosymmetrically related molecules run in a zigzag fashion parallel to the *a*-axis. The benzene ring makes dihedral angles of 31.4 and 23.5° with the basal plane, in structures **I** and **II**, respectively. The planarity of the pyridoxal π-system is indicated by the torsion angle 2.0° (**I**) of the aldimine plane H(8)—C(8)—N(2)—C(9) (3.0° in **II**). The molecules are held together in the lattice by hydrogen-bonds and van der Waals interactions.

The crystallization of these complexes in a centrosymmetric space group confirms racemization of the amino acid. Furthermore, the crystals failed to show second harmonic generation when irradiated with a laser beam.

The racemization of amino acids under acidic conditions is unusual, more so for the following reasons. (i) The crystal structures of the copper(II)-salicylaldehyde (a model for PLP) Schiff base complexes of L-phenylalanine[17] and L-tyrosine[18] prepared under acidic conditions do not show racemization. (ii) The copper(II) complexes of these amino acids are also stable to racemization.[19] (iii) The preparation of the reduced Schiff base involving PLP and L-tyrosine carried out under basic conditions[20a] did not result in racemization, as confirmed by X-ray studies.[20b]

It is reported[5b] that environmental factors, as well as structural changes are critical to racemization. Furthermore, as mentioned in the Introduction, π–π interactions may play an important role in these reactions. Therefore, a comparison of X-ray structures of these complexes is of interest. Both complexes showed approximately parallel orientation of the pyridoxal π-system and the aromatic side chain of the amino acid (Fig. 3) [C(8)···C(12) = 3.099, C(8)···C(13) = 3.173, N(2)···C(12) = 3.057 and N(2)···C(13) = 3.403 Å, for complex **I** and 3.046, 3.024, 3.006 and 3.248 Å, respectively, for complex **II**]. A perfect overlapping is probably hindered by the packing effects. This, in conjunction with the NMR results,[9] suggests that a better overlap is possible in solution. The higher temperature factors shown by phenyl ring atoms may be an indication of its mobility. A plausible pathway for the reaction in solution could be given as follows. In the complex, the π–π interaction stabilizes the delocalization in the pyridoxal π-system resulting in the activation of αC—H. This eventually leads to its removal probably by water.[22] The resultant planar carbanion is open to attack by a proton on either side resulting in racemization.

The CD spectra of these complexes were recorded to study the racemization in solution. The spectral changes taking place immediately after mixing are shown in Fig. 4. The CD spectra for the DL-compounds and the L-compounds do not show any

Table 2. Coordinating distances (Å) and angles (°) with their e.s.d.s in parentheses (first line: complex **I**, second line: complex **II**

Cu—O(W1)	1.956(2)	Cu—O(6)	1.983(2)
	1.972(8)		1.980(7)
Cu—O(1)	1.905(2)	Cu—O(5′)	2.263(2)
	1.913(7)		2.269(7)
Cu—N(2)	1.930(2)		
	1.923(9)		
O(W1)—Cu—O(1)	86.5(1)	O(1)—Cu—O(6)	165.0(1)
	86.9(3)		164.6(3)
O(W1)—Cu—N(2)	166.0(1)	O(1)—Cu—O(5′)	103.4(1)
	165.7(3)		102.9(3)
O(W1)—Cu—O(6)	93.4(1)	N(2)—Cu—O(6)	83.6(1)
	93.5(3)		83.5(3)
O(W1)—Cu—O(5′)	96.9(1)	O(5′)—Cu—N(2)	96.8(1)
	96.6(3)		97.6(3)
O(1)—Cu—N(2)	92.9(1)	O(5′)—Cu—O(6)	91.5(1)
	92.3(3)		92.4(3)

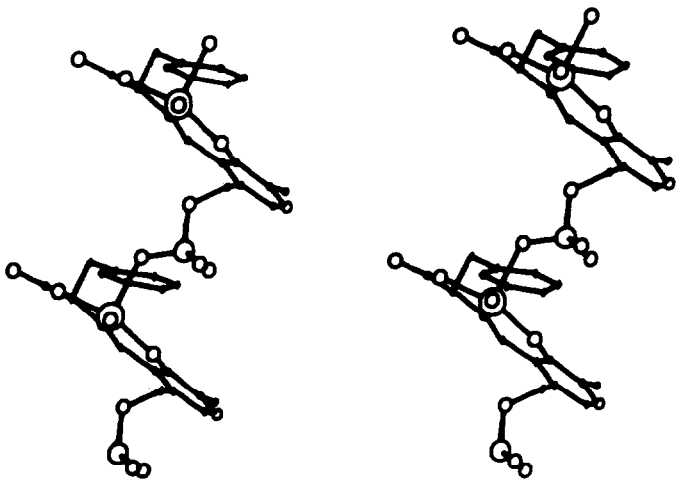

Fig. 3. Stereoscopic[21] view of complex II.

bands after 23 days. The intensity of the peak around 380 nm in Fig. 4 increases with time, indicating the formation of a Schiff base metal complex. Both L-tyrosine and L-phenylalanine showed similar changes. Figure 5 shows the spectra of these complexes after 1, 6 and 18 days. The spectral changes indicate slow racemization. The suggestion of the removal of the proton by water is supported by the fact that complete racemization could be effected in 18 days when water is used as the solvent, whereas a water/methanol mixture showed incomplete racemization for the same period (Figs 5 and 6).

It is reported[11a] for a solution of Cu—PLP—L-phenylalanine complex that racemization is the major reaction at pH *ca* 9.6 and transamination predominates at pH *ca* 5. Since aldimine and ketimine are in equilibrium through transamination some racemization can occur through this equilibrium. However, the isolation of a racemic mixture in good yields (~ 75%) in the present study under acidic conditions is unexpected. The removal of

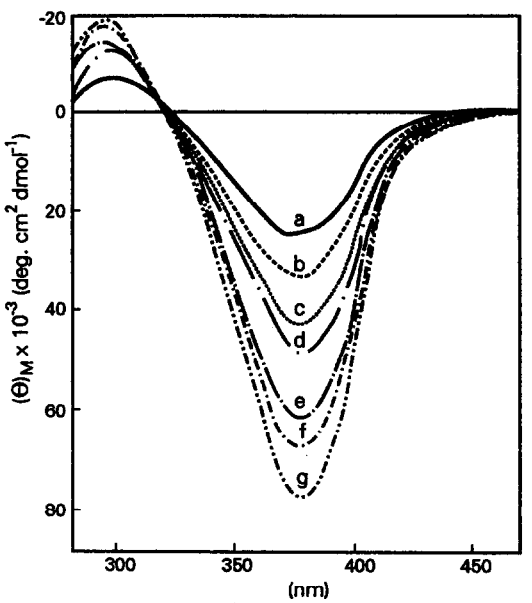

Fig. 4. Circular dichroism spectra of Cu(PLP-L-phenylalanine) complex at different time intervals (concentration 1×10^{-3} M, cell path 0.1 cm): (a)—— ~ 20 min after mixing of the reactants; (b) – – – – after ~ 24 min; (c) ···· after ~ 29 min; (d) ·——·——· after ~ 32 min; (e) ·—·—· after ~ 45 min; (f) ·–·–· after ~ 54 min; (g) –···–···– after 1 h.

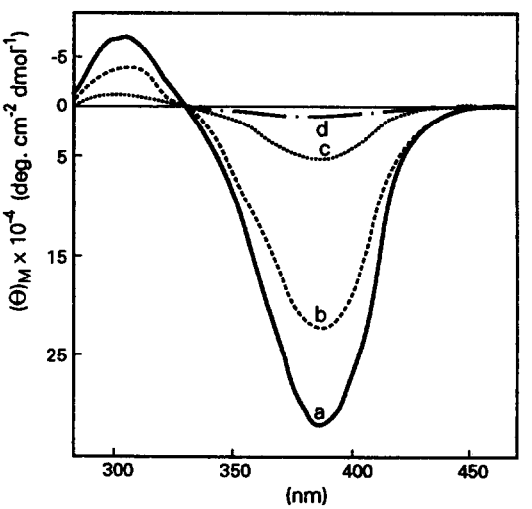

Fig. 5. CD spectra of Cu(PLP-L-phenylalanine) complex (concentration 1×10^{-3} M; cell path 0.1 cm): (a)—— in water ~ 1 day after mixing; (b) – – – – in water after ~ 6 days; (c) ···· in aqueous methanol after ~ 18 days; (d) –·–·– in water after ~ 18 days.

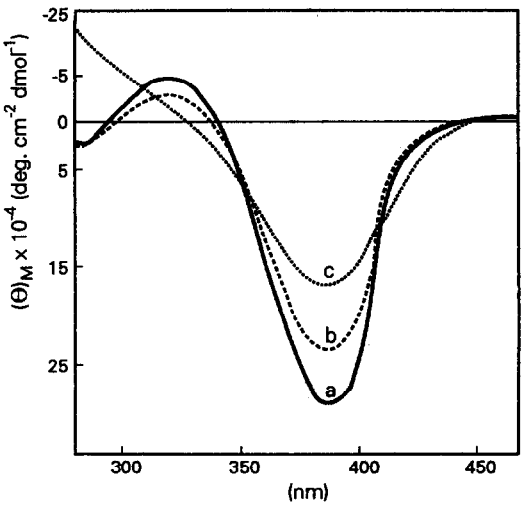

Fig. 6. Circular dichroism spectra of Cu(PLP-L-tyrosine) complex after ~ 6 days (concentration 1×10^{-3} M; cell path 0.1 cm): (a) —— in aqueous methanol at pH ~ 4.2; (b) ---- in water at pH ~ 4.3; (c) ···· in aqueous methanol at pH ~ 8.5.

the DL-complex due to crystallization may be the driving force for the L to D conversion. This is supported by the fact that the isolation of the DL-complex as single crystals could be achieved in 5–6 days, whereas the CD changes do not show that amount of conversion during the same period.

CONCLUSION

This paper describes an unusual racemization under mild acidic conditions observed in two Vitamin B_6/amino acid Schiff base metal complexes. The CD studies show slow racemization for the complexes in solution. The analysis of products by single crystal X-ray analysis confirms the role of intramolecular interactions proposed in amino acid racemization.[5b] These results could be extended to explain the unexpected racemization reactions of amino acids bound to dipeptides and proteins.[23]

Acknowledgement—We thank the Chairman, Molecular Biophysics Unit, for the use of the spectropolarimeter. The help rendered by S. V. Balasubramanian and D. S. Seetharaman in the CD measurements is gratefully acknowledged.

Listings of positional and thermal parameters of all atoms, bond distances and angles, least-squares planes, selected torsional angles, possible hydrogen-bonds and intermolecular short contacts, and observed and calculated structure factors (63 pages) have been deposited with the Cambridge Crystallographic Data Centre.

REFERENCES

1. J. Kovacs, *The Peptides, Analysis, Synthesis and Biology* (Edited by E. Gross and J. Meinhofer), Vol. 2, pp. 486–567. Academic Press, New York (1980).
2. (a) J. L. Bada and R. A. Schroeder, *Naturwiss.* 1975, **62**, 71; (b) G. G. Smith, K. M. Williams and D. M. Wonnacott, *J. Org. Chem.* 1978, **43**, 1; (c) *Biogeochemistry of Amino Acids* (Edited by P. E. Hare, T. C. Hoering and K. King, Jr). Wiley (1980); (d) J. L. Bada, *Ann. Rev. Earth Planet Sci.* 1985, **13**, 241.
3. M. Friedman and M. R. Gumbmann, *J. Nutr.* 1984, **114**, 2089.
4. (a) G. S. Reddy, G. V. Reddy and G. G. Smith, *Inorg. Chim. Acta* 1989, **166**, 55; (b) J. L. Bada, *Chemistry and Biochemistry of Amino Acids* (Edited by G. C. Barret), pp. 399–414. Chapman and Hall, London (1985); (c) G. G. Smith, A. Khatib and G. S. Reddy, *J. Am. Chem. Soc.* 1983, **105**, 293.
5. (a) A. Neuberger, *Adv. Protein Chem.* 1948, **4**, 298; (b) G. G. Smith and G. V. Reddy, *J. Org. Chem.* 1989, **54**, 4529; (c) W. E. Keyes, R. E. Caputo, R. D. Willett and J. I. Legg, *J. Am. Chem. Soc.* 1976, **98**, 6939; (d) G. G. Smith and Beatriz Silva de Sol, *Science* 1980, **207**, 765.
6. (a) A. Pasini and L. Casella, *J. Inorg. Nucl. Chem.* 1974, **36**, 2133; (b) A. Dempse and D. A. Phipps, *Inorg. Chim. Acta* 1979, **36**, L425.
7. (a) H. C. Dunathan, *Adv. Enzymol.* 1971, **35**, 79; (b) *Chemical and Biological Aspects of Pyridoxal Catalysis* (Edited by E. E. Snell, P. M. Fasella, A. E. Braunstein and A. Rossi-Fanelli). Interscience, New York (1963).
8. (a) P. Ayengar and E. Robert, *J. Biol. Chem.* 1952, **197**, 453; (b) *Pyridoxal Catalysis: Enzymes and Model Systems* (Edited by E. E. Snell, A. E. Braunstein, E. S. Severin and Yu. M. Torchinsky). Interscience, New York (1968).
9. M.-D. Tsai, H. J. R. Weintraub, S. R. Byrn, C.-J. Chang and H. G. Floss, *Biochemistry* 1978, **17**, 3183.
10. M.-D. Tsai, S. R. Byrn, C.-J. Chang, H. G. Floss and H. J. R. Wientraub, *Biochemistry* 1978, **17**, 3177.
11. (a) J. Olivard, D. E. Metzler and E. E. Snell, *J. Biol. Chem.* 1952, **199**, 669; (b) G. N. Weinstein, M. J. O'Connor and R. H. Holm, *Inorg. Chem.* 1970, **9**, 2104; (c) M. Ando and S. Emoto, *Bull. Chem. Soc. Japan* 1969, **42**, 2624.
12. A. C. T. North, C. C. Phillips and F. S. Mathews, *Acta Cryst.* 1968, **24**, 351.
13. G. M. Sheldrick, SHELX-76, Program for Crystal Structure Determination. University of Cambridge, Cambridge, U.K. (1976).
14. C. K. Johnson, ORTEP II, Program for Thermal Ellipsoid Plotting. Oak Ridge National Laboratory, Oak Ridge, Tennessee (1976).
15. I. I. Mathews and H. Manohar, *Inorg. Chem.* 1991, **30**, 2181.
16. G. A. Bentley, J. M. Waters and T. N. Waters, *J. Chem. Soc., Chem. Commun.* 1968, 988.
17. R. Hamalainen, U. Turpeinen, M. Ahlgren and M. Rantala, *Acta Chem. Scand.* 1978, **A32**, 549.

18. R. Hamalainen, M. Ahlgren, U. Turpeinen and M. Rantala, *Acta Chem. Scand.* 1978, **A32**, 235.
19. S. H. Laure, *Aust. J. Chem.* 1967, **20**, 2609.
20. (a) M. Ikawa, *Arch. Biochem. Biophys.* 1972, **118**, 497; (b) A. Mangia, M. Nardelli, G. Pelizzi, C. B. Voltattoni, A. Orlacchio and C. Turamo, *J. Chem. Soc., Perkin II* 1975, 60.
21. S. Motherwell and W. Clegg, PLUTO, Program for Drawing Crystal and Molecular Structures. University of Cambridge, Cambridge, U.K. (1978).
22. (a) P. M. Masten and M. Friedman, *ACS Symposium Series No.* 123, 1080, 165; (b) J. L. Bada, *Chemistry and Biochemistry of Amino Acids* (Edited by G. C. Barret), pp. 408–409. Chapman and Hall, London (1975).
23. (a) N. Kriausakul and R. M. Mitterer, *Biogeochemistry of Amino Acids* (Edited by P. E. Hare, T. C. Hoering and K. King), p. 283. Wiley, New York (1980); (b) S. Steinberg and J. L. Bada, *Science* 1981, **213**, 544; (c) R. Liardon and R. Jost, *Int. J. Peptide Protein Res.* 1981, **18**, 500; (d) J. L. Bada, *Interdicip. Soc. Rev.* 1982, **7**, 30.

Polyhedron Vol. 10, No. 18, pp. 2171–2177, 1991
Printed in Great Britain

0277–5387/91 $3.00+.00
© 1991 Pergamon Press plc

THE YTTRIUM CHLORIDE-1,10-PHENANTHROLINE INTERACTION: SYNTHESIS AND X-RAY CRYSTAL STRUCTURE OF THE COMPLEX $[Y(OH)(H_2O)_2(phen)_2]_2Cl_4 \cdot 2(phen) \cdot MeOH$

M. D. GRILLONE

Department of Chemical Engineering, University of Palermo, Viale delle Scienze, 90128 Palermo, Italy

and

F. BENETOLLO*

Institute of Chemistry and Technology of Radioelements, C.N.R., Corso Stati Uniti 4, 35020 Padova, Italy

and

G. BOMBIERI

Institute of Pharmaceutical Chemistry, University of Milano, Viale Abruzzi 42, 20131 Milano, Italy

(*Received* 16 *January* 1991; *accepted* 23 *May* 1991)

Abstract—Investigations on the reaction between $YCl_3 \cdot H_2O$ and phen (1,10-phenanthroline) led to the isolation of the title compound. The synthesis, IR and X-ray structural characterization are described. The crystal contains centrosymmetric binuclear dications $[Y_2(phen)_4(\mu\text{-}OH)_2(H_2O)_4]^{4+}$, uncoordinated chloride anions, two clathrated phen molecules and a disordered methanol molecule. The yttrium ions are eight-coordinated with square antiprismatic geometry to the nitrogen atoms of two phen molecules, to bridging hydroxyl groups and to two water molecules. The $Y \cdots Y^I$ separation in the dimer is 3.651(2) Å.

Among the isolated complexes of Y^{III} and of the lanthanide ions, those with O-donors are significantly more common than those with N-donors. Little is known about the structure of complex species with N-donor bidentate ligands such as 1,10-phenanthroline (phen) and 2,2′-bipyridine (bpy), the nature of which has been mainly examined by their solid-state IR spectra.[1–3] They have been reported to contain a lanthanide/ligand stoichiometry ranging from 1 : 1 to 1 : 4, depending on the counter-ion associated with the starting lanthanide compound in the interaction.[2–5]

Our interest in the coordination ability of yttrium(III) towards N-donors led us to examine the interaction of its compounds with phen. From the $YCl_3 \cdot H_2O$/phen system, we obtained the title complex species in crystals suitable for X-ray analysis. Such a system had been found to afford the compound $Y(phen)_2Cl_3 \cdot zH_2O$.[2]

Preliminary results of our study and of the crystallographic characterization of the title complex have been communicated,[6] and herein we report them in detail.

EXPERIMENTAL

Phen monohydrate (Fluka or Merck) was recrystallized from water, while the other reactants and solvents, reagent grade (Stream Chemical, C.

* Author to whom correspondence should be addressed.

Erba, Fluka), were used as received. The analytical data were determined in our laboratory, and the IR spectra of Nujol mulls (CsI plates) were recorded on a Perkin–Elmer model 1430 instrument.

Synthesis of the title compound

$YCl_3 \cdot 6H_2O$ (1 mmol) was added to a stirred methanolic solution of phen $\cdot H_2O$ (6–7 mmol, in *ca* 15 cm^3); the resulting solution was warmed to 50–60°C for *ca* 30 min and then filtered. The filtrate was evaporated under reduced pressure to dryness to give a white sticky residue which was dissolved in methanol (10 cm^3). Me_2CO was then added (*ca* 4 cm^3), and the solution was allowed to stand at room temperature for *ca* 8 days, during which time the product separated in a good crystalline form in *ca* 40% yield. The crystals were washed twice with drops of Me_2CO and allowed to dry to air. Found: C, 56.3; H, 4.3; N, 10.7; Y, 12.0; Cl, 9.4. Calc. for $C_{73}H_{62}N_{12}Y_2Cl_4O_7$: C, 57.0; H, 4.1; N, 10.9; Y, 11.5; Cl, 9.2%. The compound was slowly soluble in methanol, but less so in ethanol; it did not separate from methanol solutions even if very concentrated, and appeared air-stable at room temperature in the solid state.

Crystal data

$C_{73}H_{62}N_{17}O_7Y_2Cl_2$, $Mr = 1539.28$, triclinic $P\bar{1}$ (confirmed by structure determination), $a = 13.970(3)$, $b = 11.398(3)$, $c = 10.818(2)$ Å, $\alpha = 102.07(4)$, $\beta = 94.96(4)$, $\gamma = 86.75(4)°$, $Z = 1$, $V = 1676.8(8)$ $Å^3$, $D_{calc} = 1.49$ Mg m^{-3}, λ(Mo-K_α) = 0.71069 Å, μ(Mo-K_α) = 18.85 cm^{-1}, $F(000) = 786$, room temperature; final conventional R value is 0.0367 ($R_w = 0.0374$). A pale green–yellow crystal (dimensions $0.20 \times 0.28 \times 0.41$ mm) was used for data collection on a Philips PW1100 automated diffractometer with monochromated Mo-K_α radiation, 2θ scan technique $2\theta_{max} = 52°$. Twenty-five reflections $10 \leqslant \theta \leqslant 14°$ were used for cell dimension refinement. Index ranges measured h −17 to 17, k −13 to 13, l 0 to 13, with two reflections (−2 −3 1 and 2 3 1) measured after every 180 min of X-ray exposure time. There was no significant fluctuation on intensities other than those expected from Poisson statistics. The scan width was 1.20°, scan speed 0.30 s and the total background measuring time was 20 s. The total number of reflections measured was 6963; 4676 reflections having $I \geqslant 3\sigma(I)$, were used in the analysis and corrected for Lorentz and polarization effects and for absorption;[7] no corrections were made for extinction. The structure was solved by using three-dimensional Patterson and Fourier techniques and refined by full-matrix least-squares techniques with anisotropic thermal parameters assigned to all the non-hydrogen atoms (except CH_3OH). Hydrogen atoms were located by difference Fourier maps and refined isotropically. Refinement converged to $R = 0.0367$, $R_w = 0.0374$, $S = 1.27$ weights, $w = 1/[\sigma^2(F_o) + 0.000587(F_o)^2]$, $\Delta/\sigma < 0.04$, residual electron density ± 0.4 e $Å^{-3}$. (Scattering factors were taken from the International Tables for X-Ray Crystallography (1974),[8] with anomalous dispersion terms corrected for Y.) Data processing and computation were carried out using the SHELX 76 program package[9] and molecular illustrations were drawn with ORTEP[10] and PLUTO.[11] Supplementary material (tables of atomic coordinates, atomic vibrations and calculated structure amplitudes) has been deposited with the Editor.

RESULTS AND DISCUSSION

$YCl_3 \cdot 6H_2O$ was allowed to interact with phen under conditions involving salt : ligand molar ratios from 1 : 3 to 1 : 9, reaction solvents such as ethanol or methanol, Me_2CO, THF (tetrahydrofuran), or solvent mixtures, and temperatures from 25 to 60°C. In most cases, the separation of the complex compounds occurred when the reaction was carried out in methanol or ethanol, and Me_2CO or toluene or 2-PrOH was added subsequently. Clear evidence for the formation of another complex species in addition to the title one was obtained by IR spectroscopy. Often, this, as yet, uncharacterized species separated as the first crop of crystals from ethanol–toluene mixtures. The title species was the second crop from those mixtures but it was the main reaction product separating from methanol–Me_2CO.

Isolation of pure samples of the title compound in a good crystalline form occurred when $YCl_3 \cdot 6H_2O$ was allowed to interact with phen at 1 : 6–1 : 7 molar ratios in methanol at *ca* 50°C, with Me_2CO added to the reaction solution.

The solid-state (Nujol mull) IR spectrum of these samples in the 1800–200 cm^{-1} region—where more or less marked alterations of the ligand bands upon coordination can mainly be observed (a)—is shown in Fig. 1, compared to the similar IR spectrum of the free phen monohydrate (b).

As can be seen, the changes from the free ligand consist of multiple splittings, shifts and intensity changes of its bands, but, as known for the phen complexes of alkali and transition metal ions, it is difficult to interpret the spectra satisfactorily in terms of the structure of the complex species, or to relate them to changes in bonding in the ligand. Bands in the 1650–1400 cm^{-1} region (attributed to

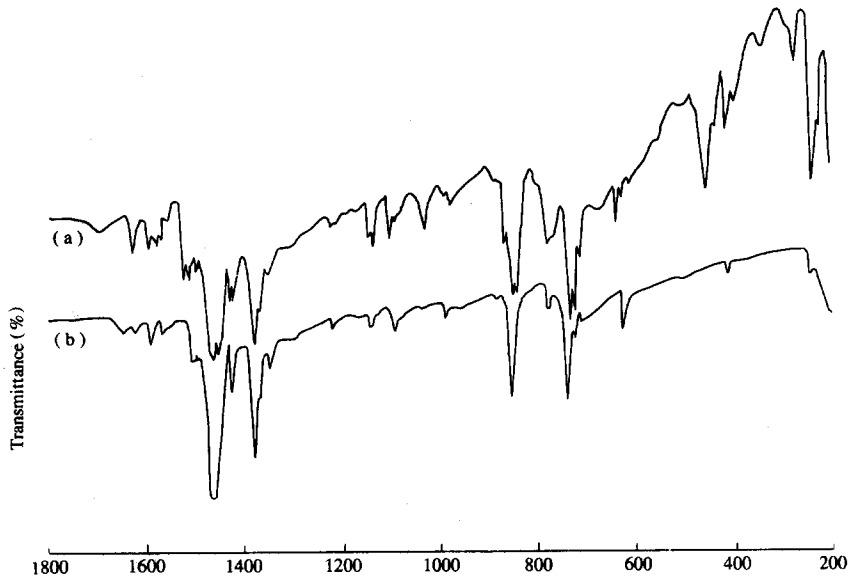

Fig. 1. IR spectra of Nujol mulls: (a) $\{[Y(OH)(H_2O)_2(phen)_2]_2Cl_4 \cdot 2phen\} \cdot MeOH$, and (b) the phen monohydrate.

ring vibrations) undergo splitting and shift to higher frequencies.[1,12,13] Similar shifts occur for bands between 1250 and 1100 cm^{-1}, while those between 1050 and 700 cm^{-1} shift to lower frequencies with splitting of the two strong bands at 850 and 738 cm^{-1} (out-of-plane hydrogen deformation vibrations) and at 852–843 and 732–725 cm^{-1}, respectively. The low-frequency region (650–200 cm^{-1}) appears to be interesting. As is known, ν(MN) (between 400 and 200 cm^{-1}) and other metal-sensitive vibrations may be found in this region.[14] However, besides bands due to coordinated OH ions and water molecules, bands due to the ligand also can be observed (see Fig. 1); those of the free phen at 620, 412 and 240 cm^{-1} shift to higher frequencies. Thus, band assignment for ν(MN) appears difficult; in agreement with another study,[2] the band at 280 cm^{-1} is tentatively assigned to this stretching vibration.

Figure 2 shows the structure of the complex; selected bond distances and angles are summarized in Table 1. Two yttrium(III) ions are bridged by two μ-OH groups; the cation possesses crystallographically required symmetry C_i. Each yttrium ion is eight-coordinate and the coordination geometry is best described as square antiprismatic, but a loss of planarity in the tetrahedral sense of the "squares" indicates that the structure is on the geometric pathway to being dodecahedron. Each of the two squares consists of two phenanthroline nitrogen atoms and two water molecules in one case and of the symmetrically-related hydroxyl oxygens in the second square.

The least-square planes through the "squares" show the following deviations from planarity: first square N(1), N(2), O(2), O(3), −0.060(4), 0.058(4), −0.064(4) and 0.066(4) Å; second square N(21), N(22), O(1), O(11) 0.051(4), −0.053(4), −0.049(3) and 0.048(3) Å, respectively; the dihedral angle between the two best-squares planes is 3.52(9)°. The rotation of one square with respect to the second is about 50°. This relatively regular coordination polyhedron is due to the fact that the only constraint on the polyhedron geometry is due to the coordination of phenanthroline nitrogens as they are at the rigid distances of 2.698(5) Å for N(1)···N(2) and 2.706(5) Å for N(21)···N(22). The two coordination polyhedrons share the hydroxyl edge. Least-squares planes through the phenanthroline ligands indicate distortion from planarity for the two coordinated to the metal in the ranges of −0.104(4)–0.194(5) Å for the N(1)···N(2) ligand and −0.176(5)–0.089(4) Å for the N(21)···N(22) ligand. The third uncoordinated phenanthroline ligand [N(31)···N(32)] is rather flat, with deviations from planarity ranging from −0.051(6) to 0.048(7) Å and with a N(31)···N(32) distance of 2.735(5) Å which is longer with respect to the coordinated ligands. Examination of bond distances in the coordination polyhedron shows that the hydroxyl bridge is rather symmetric: Y—O(1) 2.218(3) Å being not much different from Y—O(1)^{I} 2.233(3) Å (^{I} $-x, -y, -z$); while the Y—O_{water} distances are significantly longer: Y—O(2) 2.357(3) Å and Y—O(3) 2.386(3) Å. These values can be compared to the Y—O_{water} distances

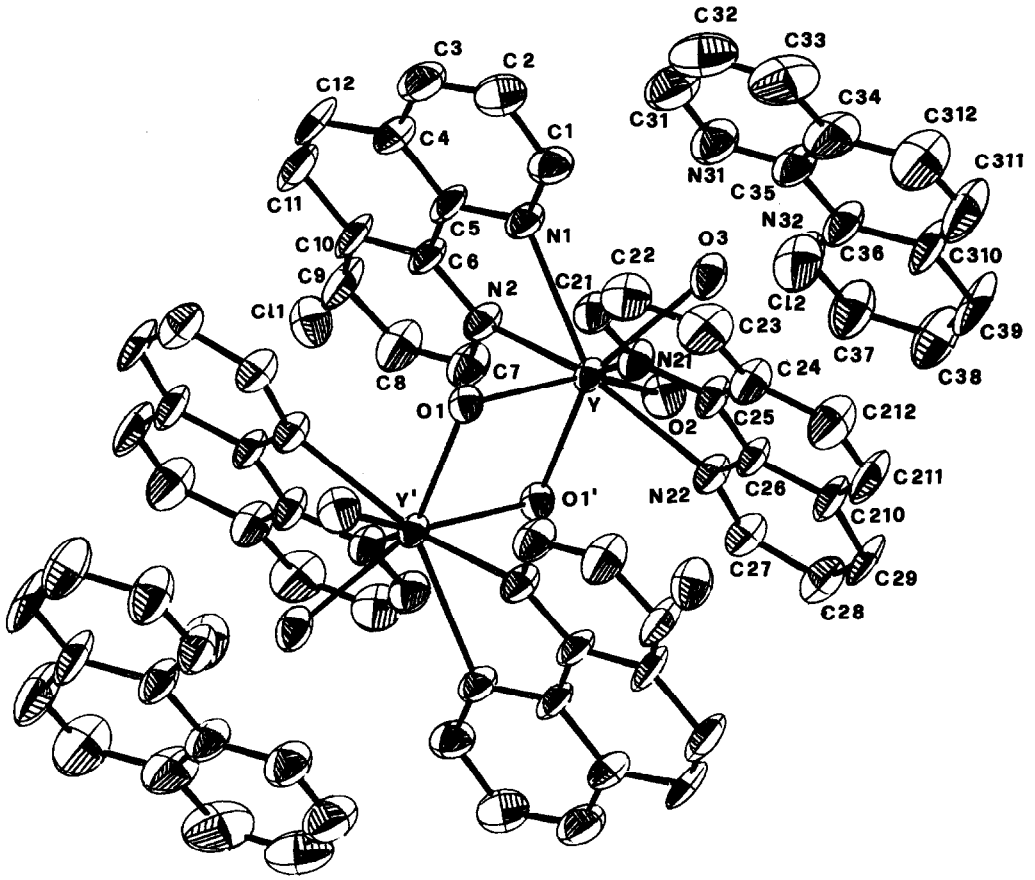

Fig. 2. ORTEP drawing of $\{[Y(OH)(H_2O)_2(phen)_2]_2Cl_4 \cdot 2phen\}$ with the atom numbering system. (Thermal ellipsoids are at 50% probability level.)

Table 1. Selected bond distances (Å) and angles (°) with e.s.d.s in parentheses

Selected bond lengths (Å)			
Y—O(1)	2.218(3)	Y—O(2)	2.357(3)
Y—O(1)^I	2.233(3)	Y—O(3)	2.386(3)
Y—N(1)	2.587(3)	Y—N(2)	2.567(3)
Y—N(21)	2.577(3)	Y—N(22)	2.543(3)
N(1)—C(1)	1.323(4)		
N(1)—C(5)	1.370(5)	N(2)—C(6)	1.353(4)
N(2)—C(7)	1.325(4)	C(1)—C(2)	1.405(6)
C(2)—C(3)	1.359(6)	C(3)—C(4)	1.401(6)
C(4)—C(5)	1.400(5)	C(4)—C(12)	1.449(6)
C(5)—C(6)	1.436(5)	C(6)—C(10)	1.412(5)
C(7)—C(8)	1.403(6)	C(8)—C(9)	1.339(6)
C(9)—C(10)	1.406(6)	C(10)—C(11)	1.430(6)
C(11)—C(12)	1.325(7)	N(21)—C(21)	1.330(4)
N(21)—C(25)	1.369(4)	C(21)—C(22)	1.396(5)
C(22)—C(26)	1.358(4)	N(22)—C(27)	1.339(5)
C(22)—C(23)	1.358(6)	C(23)—C(24)	1.404(6)
C(24)—C(25)	1.407(5)	C(24)—C(212)	1.433(6)
C(25)—C(26)	1.436(5)	C(26)—C(210)	1.410(5)
C(27)—C(28)	1.397(6)	C(28)—C(29)	1.363(6)
C(29)—C(210)	1.399(6)	C(210)—C(211)	1.428(6)
C(211)—C(212)	1.330(6)		
N(32)—C(36)	1.364(5)	N(32)—C(37)	1.319(6)
N(31)—C(31)	1.327(6)	N(31)—C(35)	1.351(5)

Table 1—*continued*

C(31)—C(32)	1.395(7)	C(32)—C(33)	1.365(9)
C(33)—C(34)	1.388(7)	C(34)—C(35)	1.405(6)
C(34)—C(312)	1.443(8)	C(35)—C(36)	1.437(5)
C(36)—C(310)	1.407(6)	C(37)—C(38)	1.394(7)
C(38)—C(39)	1.356(7)	C(39)—C(310)	1.389(6)
C(310)—C(311)	1.439(7)	C(311)—C(312)	1.312(8)

Selected bond angles (°)

N(21)—Y—N(22)	63.8(1)	N(2)—Y—N(22)	151.1(1)
N(2)—Y—N(21)	145.1(2)	N(1)—Y—N(22)	142.9(1)
N(1)—Y—N(21)	85.0(1)	N(1)—Y—N(2)	63.1(1)
O(3)—Y—N(22)	79.1(1)	O(3)—Y—N(21)	74.1(1)
O(3)—Y—N(2)	107.0(2)	O(3)—Y—N(1)	73.1(1)
O(2)—Y—N(22)	79.7(1)	O(2)—Y—N(21)	134.6(2)
O(2)—Y—O(3)	75.4(1)	O(2)—Y—N(1)	114.1(1)
O(1)—Y—N(21)	73.3(1)	O(1)—Y—N(22)	111.8(1)
O(1)—Y—N(1)	79.0(1)	O(2)—Y—N(2)	81.0(1)
	78.8(1)	Y—O(1)—Y^1	110.2(2)
O(1)—Y—O(3)	142.4(1)		
O(1)—Y—O(2)	142.7(1)	Y—N(1)—C(5)	116.4(3)
Y—N(1)—C(1)	124.1(3)	C(1)—N(1)—C(5)	118.0(4)
Y—N(2)—C(7)	122.9(3)	Y—N(2)—C(6)	118.1(2)
C(6)—N(2)—C(7)	117.8(4)	N(1)—C(1)—C(2)	122.8(4)
C(1)—C(2)—C(3)	119.2(5)	C(2)—C(3)—C(4)	119.9(5)
C(3)—C(4)—C(12)	123.9(4)	C(3)—C(4)—C(5)	117.5(4)
C(5)—C(4)—C(12)	118.5(4)	N(1)—C(5)—C(4)	122.5(4)
C(4)—C(5)—C(6)	119.7(4)	N(1)—C(5)—C(6)	117.6(4)
N(2)—C(6)—C(5)	117.6(4)	C(5)—C(6)—C(10)	119.5(4)
N(2)—C(6)—C(10)	122.8(4)	N(2)—C(7)—C(8)	122.9(4)
C(7)—C(8)—C(9)	119.4(4)	C(8)—C(9)—C(10)	120.2(5)
C(6)—C(10)—C(9)	116.7(4)	C(9)—C(10)—C(11)	124.0(4)
C(6)—C(10)—C(11)	119.2(4)	C(10)—C(11)—C(12)	121.1(5)
C(4)—C(12)—C(11)	121.7(5)	Y—N(21)—C(25)	118.1(2)
Y—N(21)—C(21)	124.5(3)	C(21)—N(21)—C(25)	117.1(3)
N(21)—C(21)—C(22)	123.2(4)	Y—N(22)—C(27)	122.5(3)
Y—N(22)—C(26)	119.5(3)	C(26)—N(22)—C(27)	117.3(4)
C(21)—C(22)—C(23)	120.0(4)	C(22)—C(23)—C(24)	118.9(4)
C(23)—C(24)—C(212)	122.9(4)	C(23)—C(24)—C(25)	117.9(4)
C(25)—C(24)—C(212)	119.1(4)	N(21)—C(25)—C(24)	122.6(4)
C(24)—C(25)—C(26)	119.7(4)	N(21)—C(25)—C(26)	117.6(3)
N(22)—C(26)—C(25)	117.8(4)	C(25)—C(26)—C(210)	119.2(3)
N(22)—C(26)—C(210)	122.9(4)	N(22)—C(27)—C(28)	123.1(4)
C(27)—C(28)—C(29)	119.5(5)	C(28)—C(29)—C(210)	119.4(5)
C(26)—C(210)—C(29)	117.8(4)	C(29)—C(210)—C(211)	123.3(4)
C(26)—C(210)—C(211)	118.9(4)	C(210)—C(211)—C(212)	122.0(5)
C(24)—C(212)—C(211)	12.9(5)	C(36)—N(32)—C(37)	117.6(4)
C(31)—N(31)—C(35)	116.2(4)	N(31)—C(31)—C(32)	125.6(5)
C(31)—C(32)—C(33)	117.0(5)	C(32)—C(33)—C(34)	120.2(5)
C(33)—C(34)—C(312)	122.0(5)	C(33)—C(34)—C(35)	118.2(5)
C(35)—C(34)—C(312)	119.7(5)	N(31)—C(35)—C(34)	122.7(4)
C(34)—C(35)—C(36)	119.0(4)	N(31)—C(35)—C(36)	118.3(4)
N(32)—C(36)—C(35)	118.8(4)	C(35)—C(36)—C(310)	119.7(4)
C(32)—C(36)—C(310)	121.4(4)	N(32)—C(37)—C(38)	124.2(5)
C(37)—C(38)—C(39)	118.3(5)	C(38)—C(39)—C(310)	119.9(5)
C(36)—C(310)—C(39)	118.5(4)	C(39)—C(310)—C(311)	122.9(5)
C(36)—C(310)—C(311)	118.6(5)	C(310)—C(311)—C(312)	122.2(6)
C(34)—C(312)—C(311)	120.6(6)		

varying from 2.327(8) to 2.40(1) Å for the $[Y(OH_2)_7(OHMe)]^{3+}$ complex cation.[15] This significant difference in the yttrium oxygen distances allows us to distinguish between the hydroxyl and the water oxygen. In fact, a short distance has been attributed to the yttrium OH^- distance. This was also confirmed by the localization of one hydrogen on O(1). The yttrium–nitrogen bond distances have values comparable to those found in the hexanitrogen macrocycles, $YMAC(NCS)_3$,[16] $[YMAC(CH_3COO)_2]^+$[17] and $[YMAC(H_2O)(CH_3COO)]^{2+}$,[17] evidencing once more the prevalent electrostatic nature of the bonds to the yttrium ion. Distances where yttrium is enclosed in a macrocycle (which, for this reason, must have dimensions suitable for enclosing the metal ion), are similar to those with chelating ligands such as the phenanthrolines. The $Y\cdots Y^I$ bond distance of 3.651(2) Å seems to exclude any metal···metal interaction.

The crystal packing shown in Fig. 3 is dominated by hydrogen bond interactions. The dimeric cationic units $[Y(phen)_2(H_2O)_2\mu OH]_2^{2+}$, are connected via hydrogen bonding to the chlorine anions and to the two centrosymmetrically-related clathrated phenanthroline. In fact, the $O(3)_{water}$ links $N(32)^{II}$ (^{II} x, y, $1+z$) via hydrogen bonds: O(3)—H(115) 0.90(4) Å, O(3)···$N(32)^{II}$ 2.757(4), H(115)···$N(32)^{II}$ 1.93(5), O(3)—H(115)···$N(32)^{II}$ 153(4)°. The hydroxyl oxygen O(1) is 3.221(4) Å apart from Cl(1), O(1)—H(111) 0.61(4) Å, H(111)···Cl(1) 2.63(4), O(1)—H(111)···Cl(1) 163(4)°; $O(2)_{water}$ at 2.976(3) Å from $Cl(1)^{III}$ (^{III} $-x$, $-y$, $-z-1$) O(2)—H(113) 1.12(5) Å, H(113)···$Cl(1)^{III}$ 1.87(5) Å, O(2)—H(113)···$Cl(1)^{III}$ 169(4)°. Cl(2) makes short contacts with O(2) and O(3) belonging to the coordinated water molecules; the values are 3.018(4) and 3.174(4), respectively.

In addition, as already observed for $[K(phen)_3][Cr_2(CO)_{10}(\mu\text{-}H)]$,[18] coordinated and uncoordinated phen molecules are rather parallel and the angles between the planes of the different phen moieties are $phen_1$–$phen_2$ 12.6(1)°, $phen_2$–$phen_3$ 9.0(1)° and $phen_1$–$phen_3$ 12.5(1)°. The different phens bear several contact distances less than 3.6 Å. In particular, $phen_1$ faces $phen_2^I$ on one side and $phen_1^{IV}$ on the other side (^{IV} $-x$, $1-y$, $-z$), while $phen_2$ is between $phen_3^{II}$ and $phen_1^I$.

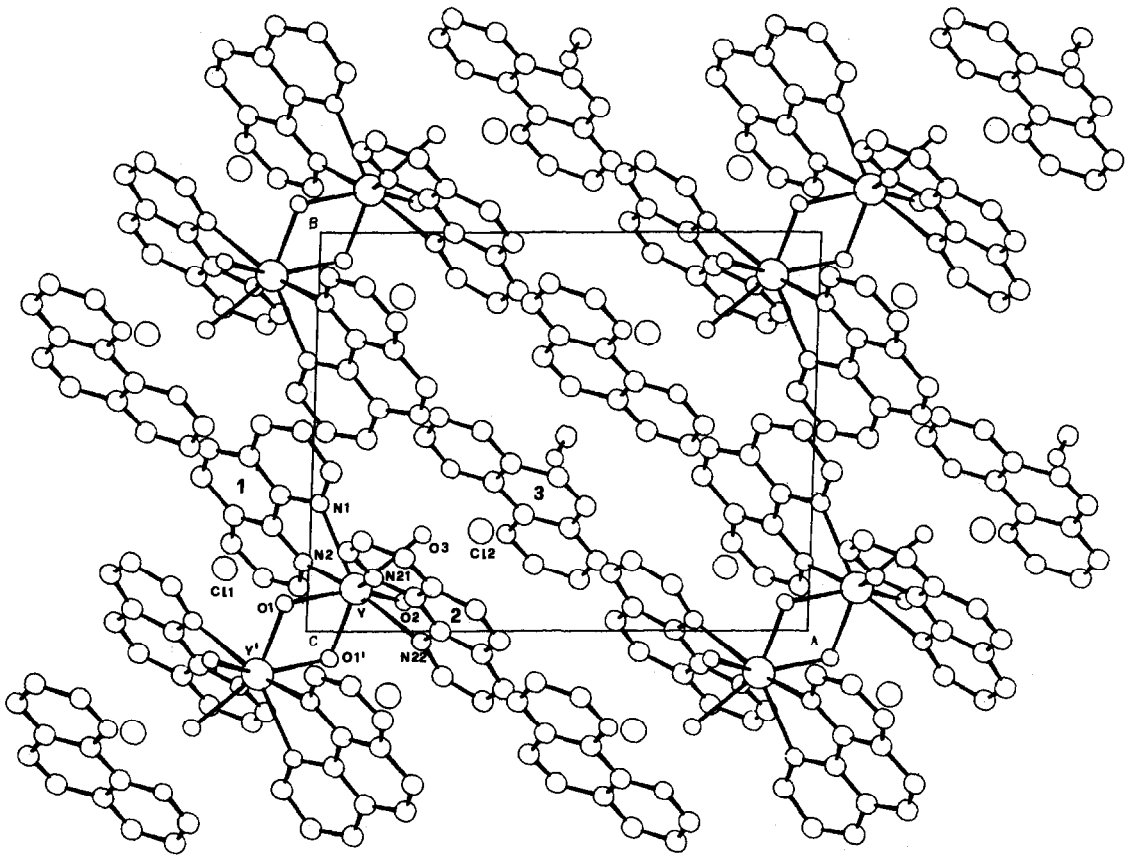

Fig. 3. Cell content viewed down the *c* axis.

Additional short contacts involve $phen_3$ and $phen_3^{V}$ (^{V} $1-x$, $1-y$, $-1-z$). This molecular packing gives rise to columns developing along the [1 1 1] crystallographic direction. These graphitic type interactions, found also in the structure of the free phen,[19] could also be indicative in the case of dipole–dipole interactions among coordinated (in the dimers) and uncoordinated phen molecules.

REFERENCES

1. S. P. Sinha, *Spectrochim. Acta* 1964, **20**, 879.
2. J. R. Ferraro, L. J. Basile and D. L. Kovacic, *Inorg. Chem.* 1966, **5**, 391.
3. D. M. Czakis-Sulikowska and J. Radwanska-Doczekalska, *J. Monatsh. Chem.* 1987, **117**, 783 and ref therein.
4. F. A. Hart and F. P. Laming, *J. Inorg. Nucl. Chem.* 1964, **26**, 579.
5. W. R. McWhinnie and J. D. Miller, *Adv. Inorg. Chem. Radiochem.* 1969, **12**, 135.
6. M. D. Grillone, F. Benetollo and G. Bombieri, *Proc. XXVIIth. Int. Conf. Coord. Chem.* 1989, W106.
7. A. C. T. North, D. C. Phillips and F. S. Mathews, *Acta Cryst.* 1968, **A24**, 351.
8. *International Tables for X-Ray Crystallography*, Vol. IV. (Present distributor Kluxer Academic Publishers, Dordrecht.) Kynoch Press, Birmingham (1974).
9. G. M. Sheldrick, SHELX76, Program for crystal structure determination. University of Cambridge, U.K. (1976).
10. C. K. Johnson, ORTEP, Report ORNL-5138. Oak Ridge National Laboratory, Tennessee (1976).
11. W. D. S. Motherwell and W. Clegg, PLUTO, Program for plotting molecular and crystal structures. University of Cambridge, U.K. (1978).
12. A. A. Schilt and R. C. Taylor, *J. Inorg. Nucl. Chem.* 1959, **9**, 211.
13. M. D. Grillone and M. A. Nocilla, *Inorg. Nucl. Chem. Letters* 1978, **14**, 49.
14. K. Nakamoto, *Infrared and Raman Spectra of Inorganic and Coordination Compounds*, 4th edn. Wiley, New York (1986).
15. R. G. Rogers, L. K. Kurihara and E. J. Voss, *Inorg. Chem.* 1987, **26**, 2360.
16. G. Bombieri, F. Benetollo, A. Polo, L. De Cola, W. T. Hawkins and L. M. Vallarino, *Polyhedron* 1989, **8**, 2157.
17. G. Bombieri, F. Benetollo, W. T. Hawkins, A. Polo and L. M. Vallarino, *Polyhedron* 1989, **8**, 1923.
18. G. Bombieri, G. Bruno, M. D. Grillone and G. Polizzotti, *J. Organomet. Chem.* 1984, **273**, 69.
19. S. Nishigaki, H. Yoshioka and K. Nakatsu, *Acta Cryst.* 1978, **B34**, 875.

Polyhedron Vol. 10, No. 18, pp. 2179–2184, 1991
Printed in Great Britain

0277–5387/91 $3.00+.00
© 1991 Pergamon Press plc

COPPER(II) CHROMATE AND DICHROMATE COMPLEXES WITH POLYPYRIDINES. PHYSICOCHEMICAL AND REACTIVITY STUDIES

MARIA CIEŚLAK-GOLONKA* and ADAM BARTECKI

Institute of Inorganic Chemistry and Metallurgy of Rare Elements, Technical University of Wrocław, 50-370 Wrocław, Poland

and

JULIA JEZIERSKA

Institute of Chemistry, University of Wrocław, 50-383 Wrocław, Poland

(*Received* 26 *November* 1990; *accepted* 8 *May* 1991)

Abstract—Copper chromate and dichromate complexes with 2,2′-bipyridyl and 1,10-phenanthroline were synthesized and characterized (UV–vis, IR, FIR, ESR and thermal data). The coordination of the anion in the chromate complexes was proposed from the IR data. The ESR data for the powdered samples reflect both $d_{x^2-y^2}$ and d_{z^2} ground states for the copper ion whereas the glassy solution spectra exhibit only the former. The presence of the chromium(V) ion in the spectra of the complexes dissolved in the water–ethylene glycol mixture is discussed.

Recently, we have reported on the formation of silver(I) chromate complexes with some heterocyclic bases.[1] It was found that in some cases the chromate ion acts as a bidentate ligand forming bridge complexes with the silver ion. The aim of the present paper was to extend this investigation to a new series of copper(II) chromate and dichromate coordination compounds of the type $Cu(HB)_xA$, where HB denotes heterocyclic bases as 2,2′-bipyridine (bpy) and 1,10-phenanthroline (phen) and A represents the CrO_4^{2-} or $Cr_2O_7^{2-}$ ions. Recently, similar compounds have been used in organic syntheses as milder and more efficient reagents than $KMnO_4$ or $K_2Cr_2O_7$.[2–5] Moreover, potent carcinogenic and mutagenic properties of the chromium(VI) ion found in biological systems both *in vivo* and *in vitro*,[6–10] require further detailed studies on the interaction of this ion with various simple and complex cations. Preliminary results on the biological activity of the complexes obtained in this study show that they are less mutagenic than simple alkali metal chromates.[11]

* Author to whom correspondence should be addressed.

EXPERIMENTAL

Reagent grade chemicals were used in all experiments. Stoichiometries of the solid compounds obtained were established by microanalysis which gave satisfactory results. Complexes of the following formulae have been prepared for the first time: $Cu(bpy)_2CrO_4 \cdot 2H_2O$, $[Cu(bpy)_2]_2CrO_4Cl_2 \cdot 2H_2O$, $[Cu(bpy)_2]_2CrO_4(NO_3)_2 \cdot 4H_2O$, $Cu(phen)_2CrO_4 \cdot 2H_2O$, $Cu(bpy)Cr_2O_7$, $Cu(bpy)_2Cr_2O_7$ and $Cu(phen)_2Cr_2O_7$. Generally, the compounds were formed during the reaction of the methanolic solution of ligand previously mixed with a water solution of K_2CrO_4, and a water solution of the respective copper salt: $CuSO_4$, $CuCl_2$ and $Cu(NO_3)_2$. Dichromate complexes were formed from a mixture of CrO_3 and $CuSO_4$ to which a methanolic solution of ligand was added. The precipitates were washed with water and dried over $CaCl_2$. The chromate complexes were formed as dark green crystals whereas the dichromate complexes were light green powders. The presence of water in the complex molecules was additionally checked by thermal (TG, DTG, DTA) studies. For comparison purposes $CuCrO_4$ was also obtained.

(1) $CuCrO_4$

This compound was prepared[12] by the reaction of $CuSO_4$ (0.2 M) and K_2CrO_4 (0.2 M). The precipitate was allowed to stay overnight in the mother liquid and filtered off.

(2) $Cu(bpy)_2CrO_4 \cdot 2H_2O$

A methanolic solution of 2,2′-bipyridine (50 cm^3, 0.75 M) was added dropwise upon stirring to the same amount of 0.25 M K_2CrO_4 solution. This was mixed with 0.25 M $CuSO_4$ (45 cm^3). The resulting dark green solution was evaporated to approximately 1/3 of its initial volume and left to stand overnight. The obtained crystals were washed and dried (*vide supra*).

(3) $[Cu(bpy)_2]_2CrO_4Cl_2 \cdot 2H_2O$ *and* (4) $[Cu(bpy)_2]_2CrO_4(NO_3)_2 \cdot 4H_2O$

These compounds were prepared as for (2) but using $CuCl_2$ and $Cu(NO_3)_2$ for (3) and (4), respectively.

(5) $Cu(phen)_2CrO_4 \cdot 2H_2O$

Prepared as for (2) but using $CuSO_4$ (40 cm^3, 0.25 M) and a methanolic solution of 1,10-phenanthroline (0.75 M).

(6) $Cu(bpy)Cr_2O_7$

A solution of $CuSO_4$ (100 cm^3, 0.2 M) was added to the solution of CrO_3 (100 cm^3, 0.2 M). The resulting solution was warmed and finally bpy in methanol (100 cm^3, 0.25 M) was added dropwise. The brownish precipitate was formed immediately.

(7) $Cu(bpy)_2Cr_2O_7$

Prepared as for (6) but using only 80 cm^3 of $CuSO_4$ (0.2 M).

(8) $Cu(phen)_2Cr_2O_7$

Prepared as for (6) but using 100 cm^3 of phenanthroline solution (0.25 M).

IR spectra were recorded on a Perkin-Elmer 180 (50–3500 cm^{-1}) spectrophotometer in KBr pellets, Nujol mulls and 1,3-hexachlorobutadiene sandwiched between AgBr plates. FIR spectra were obtained in Nujol mulls sandwiched between polyethylene plates.

UV–vis spectra were recorded on a double beam Hitachi 356 spectrophotometer in the 200–850 nm spectral range in Li_2CO_3 pellets and water, methanol, DMF and formamide solutions and on a Beckmann UV 5240 instrument in the 400–2400 nm spectral range in MgO pellets.

ESR spectra were recorded using a JEOL JES-ME-X band spectrometer with a nuclear magnetometer MJ 110R and microwave frequency meter JES-SH-30X. The ESR spectra were measured for the solutions of the concentration *ca* 1.5×10^{-3} M for the dichromate complexes and *ca* 3.5×10^{-3} for the chromate complexes. In the redox experiments the concentration of all reagents [$K_2Cr_2O_7$, bpy, $Cu(bpy)Cr_2O_7$ and $Cu(ClO_4)_2$] dissolved in the mixture of 40% ethylene glycol and 60% water was the same and equal to 1.25×10^{-3} M.

Thermal analyses (TG, DTG, DTA) were carried out simultaneously on a MOM derivatograph (Budapest Company). The final decomposition products were examined by the X-ray diffraction technique (DRON-2 diffractomter).

WARNING: Complexes decompose violently on heating.

RESULTS AND DISCUSSION

IR spectra

On coordination as a monodentate $OCrO_3$ ligand the tetrahedral symmetry of the chromate ion can be lowered to C_{3v} whereas in the case of a bidentate O_2CrO_2 coordination it is lowered to C_{2v}.[13] In this study (Table 1) similar to other data,[14,15] we were able to observe all splittings resulting from the symmetry lowering except those of v_4 vibrations which can be explained by their low intensity. The number of bands in the Cr—O stretching frequencies region (800–950 cm^{-1}) and their very strong intensities point to the bidentate chromate coordination in the complexes. The C_{2v} local environment of the chromium ion can be additionally elucidated by the comparison of the Cr—O stretching frequency region of copper chromate and the dichromate complexes of the $Cu(phen)_2A$ type. As they are practically similar and because the dichromate anion (C_{2v}) has less coordination tendency than the chromate ion,[16–18] we conclude that in our case the chromate has indeed the C_{2v} symmetry.

For the assumed O_2CrO_2 coordination, the vibrations associated with the OCrO bridge or

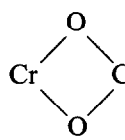

ring can be expected. Unfortunately, the "IR criterion" is not able to distinguish between

Table 1. Band positions (in cm^{-1}) assigned to the Cr—O vibrations in copper(II) chromate complexes

	ν_1	ν_2	ν_3	ν_4	ν_{as}(CuOCr)
$Cu(bpy)_2CrO_4 \cdot 2H_2O$	812	830 855 890	310	360	775
$[Cu(bpy)_2]_2CrO_4Cl_2 \cdot 2H_2O$	815	860 895 940	312	360	770
$[Cu(bpy)_2]_2CrO_4(NO_3)_2 \cdot 4H_2O$	805	830 900 920		370	760
$Cu(phen)_2CrO_4 \cdot 2H_2O$	(810)	(900) 935v.br	304	360	775

these two types of coordination.[19] However, the known crystallographic data for Cu—L—CrO_4 (L—NH_3, OH^-, py)[20,21] and other metal–chromate systems[22–25] show that the chromate ion acts exclusively as a bidentate bridging ligand. In the *ca* 750 cm^{-1} region a strong band is observed which can be assigned to the CrOCu bridge vibration, in accordance with known CrOCr,[26] AgOCr,[1] CoOCr[27] and perhaps accidently, FeOFe ones.[28]

The complexation effect can be also pronounced in the IR spectra *via* copper–nitrogen vibrations (strong bands at 260–310 cm^{-1}) and the absorption in the 1700–1800 cm^{-1} region indicative for the coordination modes of the nitrate group.[29] One single band at 1741 cm^{-1} shows that in the spectrum of **4** the ionic nitrate is present. The coordination of (bpy) and (phen) is observed through splitting and shifting (20–30 cm^{-1}) of the stretching and ring deformation vibrations.

ESR spectra

The ESR spectra of the complexes under study can be divided into three types (Table 2):

(1) Spectra with a line shape characteristic of at least two g values, with $g_\parallel > g_\perp$ [$Cu(bpy)Cr_2O_7$, $Cu(phen)_2CrO_4$, $Cu(phen)_2Cr_2O_7$].

(2) Spectra with a line shape which is the reverse of that of (1), with $g_\parallel < g_\perp$ [$Cu(bpy)_2Cr_2O_7$, $[Cu(bpy)_2]_2CrO_4Cl_2$ and $Cu(bpy)_2CrO_4$].

(3) Spectrum with a broad isotropic line, $[Cu(bpy)_2]_2CrO_4(NO_3)_2$.

Type (1) spectra are consistent with the $d_{x^2-y^2}$ ground state of copper(II) ion with a decreasing

Table 2. Important spectroscopic data for studied complexes. (Wave numbers in cm^{-1}, diffuse reflectance spectra in MgO pellets, the g parameters obtained from ESR spectra for the solid samples, in the parentheses the g values measured at 77K. Crystal water in the formulae has been omitted)

	d–d	ν (Cu—N)	g	
$Cu(bpy)_2CrO_4$	9800sh, 12,500	293, 260	$g_\perp$	2.170 (2.166)
			$g\|\|$	2.072 (2.066)
$[Cu(bpy)_2]_2CrO_4Cl_2$	10,300sh, 13,500	288, 270	$g_\perp$	2.166 (2.166)
			$g_\parallel$	2.035 (2.035)
$[Cu(bpy)_2]_2CrO_4(NO_3)_2$	10,300sh, 13,300	290, 270	g_{av}	2.122
$Cu(phen)_2CrO_4$	10,200sh, 13,300	305, 260	$g_\perp$	2.063 (2.053)
			$g_\parallel$	2.182 (2.174)
$Cu(bpy)Cr_2O_7$	12,700sh, 14,700	282	$g_\perp$	2.064 (2.061)
			$g_\parallel$	2.288 (2.282)
$Cu(bpy)_2Cr_2O_7$	12,900	310, 268	$g_\perp$	2.131 (2.131)
			$g_\parallel$	2.027 (2.027)
$Cu(phen)_2Cr_2O_7$	13,600sh, 15,100	268	$g_\perp$	2.060 (2.056)
			$g_\parallel$	2.111 (2.098)

tetragonal distortion in these three complexes. It should be noted that the spectrum of the complex with one bipyridyl ligand exhibits the greatest anisotropy of the g values suggesting the largest tetragonal distortion being close to the square planar stereochemistry.

The g values of the type (2) spectra suggest the d_{z^2} as the ground state. The observed raising of the g values above 2.00 could be caused by distortion of regular geometry associated with d_{z^2} ground state, i.e. trigonal bipyramidal or *cis*-octahedral or lower symmetries.[30] For the chromate complexes of type (2) this increase is even greater than for the dichromate and can be additionally caused by the exchange coupling between two copper(II) ions bridged with the OCrO grouping.

For $[Cu(bpy)_2]_2CrO_4(NO_3)_2$ (type 3) a broad, isotropic ESR spectrum is observed. The most common reason for this type of line shape is the exchange coupling between copper(II) ions[31] and this is reasonable on the grounds of the bridging ability of the chromate ion.

It has been found[32] that in water–ethylene glycol solutions of $Cubpy_2(ClO_4)_2$ and $Cubpy_2(NO_3)_2$ the ESR spectra in the glasses may be attributed mainly to the 1:1 and 1:3 (Cu:bpy) disproportionation species. Our data (Table 3, Fig. 1) show that: (a) tetragonally distorted copper(II) species ($d_{x^2-y^2}$) are exclusively formed in solution; (b) 1:3 (Cu:bpy) species can be found in the chromate complexes. The nine-line pattern of the superhyperfine splitting of $Cu(bpy)_2CrO_4$ spectrum [Fig. 1(d)] is associated with four nitrogen atoms coordinating in the xy plane. As the coordination of two (bpy) or (phen) molecules in plane seems to be unlikely from steric factors, three bidentate ligands arranged in the *cis*-octahedral stereochemistry may provide four nitrogen atoms to be close to the plane; and (c) mixture of 1:1 and 1:3 species is present in $Cu(bpy)_2Cr_2O_7$ and $Cu(phen)_2Cr_2O_7$ complexes immediately after dissolution of the compound. For $Cu(bpy)Cr_2O_7$, only the 1:1 form has been observed. However, after a few days only the species characteristic of the 1:3 form was found [Fig. 1(c)].

Table 3. ESR parameters for the complexes dissolved in 40% ethylene glycol–60% water solutions at 77 K. In parentheses data for the spectra measured after few days

Complex	$g_\parallel$	$A_\parallel$ (cm^{-1})
$Cu(bpy)_2CrO_4$	2.265	169
$[Cu(bpy)_2]_2CrO_4Cl_2$	2.262	169
$[Cu(bpy)_2]_2CrO_4(NO_3)_2$	2.266	167
$Cu(phen)_2CrO_4$	2.268	168
$Cu(bpy)Cr_2O_7$	2.308	170
	(2.261)	(174)
$Cu(bpy)_2Cr_2O_7$	2.309	172
	2.260	173
$Cu(phen)_2Cr_2O_7$	2.312	167
	2.264	173

The dynamical process (c) connected with the change of the coordination sphere of the cation are characteristic of the dichromate complexes and can be associated with the $Cr_2O_7^{2-}/CrO_4^{2-}$ equilibria (we have observed pH increasing with time).

No such change appears for $Cu(phen)_2SO_4$ which supports the above conclusion.

Apparently, a mode of copper coordination depending upon the chromate or dichromate ion causes the different effects of these anions on the copper(II)–polypyridine equilibria in the water–glycol solutions.

Although various compounds of biological relevance[33] as well as other organic species[34] were studied as reducing agents for chromium(VI), only a few experiments have been done with complexes other than alkali metal chromates and dichromates.[35] The possibility of applying our complexes as mild and selective oxidizers[36] encouraged us to study the interaction of $Cu(bpy)Cr_2O_7$ with ethylene glycol and compare the results with those for $K_2Cr_2O_7$. The additional signals observed at $g = 1.981$ (77 K and room temperature) in a water–ethylene glycol mixture (Fig. 1) can be assigned[37] to chromium(V) complexes formed in the process of glycol oxidation with chromium(VI). Observation of the intensity of ESR signals indicated that in the copper(II) complex, in comparison to potassium chromate, the concentration of chromium(V) is smaller and kinetically less stable. Furthermore, our ESR studies showed that copper(II) ions and (bpy) studied separately, have a diminishing effect on the formation and life time of the chromium(V) species. Further investigation of the oxidation ability of copper(II) chromate and dichromate complexes is in progress.

Electronic spectra

Data on ligand field bands are compiled in Table 2. In general, the tetragonal symmetry, on the basis of ESR data, for the complexes with $d_{x^2-y^2}$ copper(II) ground state can be interpreted by assuming three electronic d–d transitions. The electronic spectra of the chromate complexes exhibit a fairly intense ($\varepsilon \sim 200\ M^{-1}\ cm^{-1}$) broad band at *ca* 13,000 cm^{-1} (requiring a further Gaussian analysis) with a more or less pronounced low energy shoulder at 9000–10,000 cm^{-1}).

Studying the complexes with d_{z^2} copper(II)

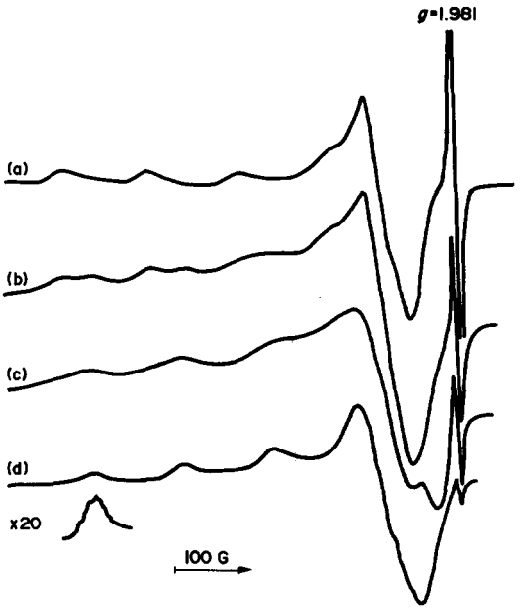

Fig. 1. ESR spectra in 40% ethylene glycol–60% water solutions at 77 K. (a) $Cu(bpy)Cr_2O_7$ freshly dissolved. (b) $Cu(bpy)Cr_2O_7$ after 1 day. (c) $Cu(bpy)Cr_2O_7$ after 2 days. (d) $Cu(bpy)_2CrO_4$. The ESR signals at $g = 1.981$ are due to the chromium(V) species. The decrease of the signals characteristic of chromium(V) from (a) to (c) is observed.

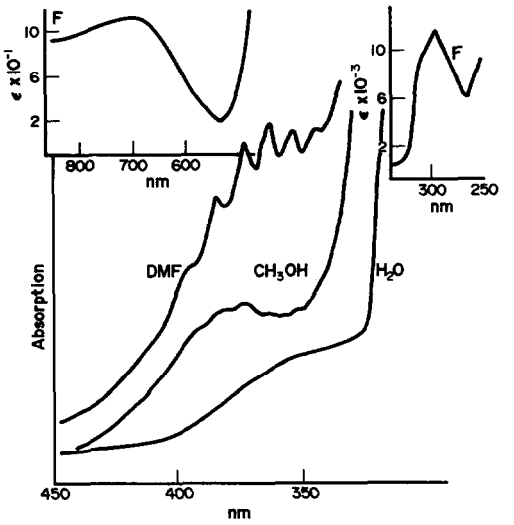

Fig. 2. Electronic spectra of $Cu(bpy)_2CrO_4 \cdot 2H_2O$ in formamide (F), dimethylformamide (DMF), methanol (CH_3OH) and water (H_2O).

ground state, Hathaway and co-workers[38] have found, that the electronic spectra can be used to distinguish between trigonal bipyramidal and *cis*-octahedral coordination modes. The former coordination exhibits one band at *ca* 12 kK whereas the latter is characterized by two bands of approximately equal intensity separated by 3–5 kK. In this case the band maximum at 13 kK with a shoulder at about 3 kK to lower energy may be associated with the *cis*-distorted octahedral geometry.

An intense absorption in the region 350–420 nm (*ca* 28,500–24,000 cm^{-1}) can be seen in the spectra. In this region, the oxygen–chromium CT transitions with characteristic vibrational fine structure attributed to the ν_s(Cr—O) totally symmetric vibrations is observed. The strong disturbance of the structure (Fig. 2) can be explained by the solute–solvent interactions (e.g. hydrogen bonds when formamide or water is used) operating in the systems. The position of the CT bands due to intra-anion transitions for chromate and dichromate anions did not change significantly upon complexation.

Unlike the Cr—O charge transfer transitions, the π–π^* very intense intra-ligand transitions are 200–1000 cm^{-1} bathochromatically shifted upon complexation.

Unfortunately, we were not able to find electronic transitions attributable to the oxo bridge. These bands can be obscured by more intense (e.g. O—Cr CT) electronic bands.

Thermal data

Preliminary results on thermal analysis show that all complexes except $[Cu(bpy)_2]_2CrO_4Cl_2 \cdot 2H_2O$ and $Cu(phen)_2CrO_4 \cdot 2H_2O$ are **explosive** on heating in air. Moreover, $Cu(bpy)Cr_2O_7$ appears to react very violently also in an inert atmosphere. In nitrogen atmosphere the complexes decompose through several stages with the liberation of a non-stoichiometric amount of organic ligand. The final decomposition product in 1000°C was found to be copper(I) metachromite-$CuCrO_2$.

Acknowledgements—The authors are indebted to Miss A. Słowikowska, for help in preparation of the compounds. Mrs M. Raczko, M. Kruk and K. Płuzinska are acknowledged for recording electronic and IR spectra. We also thank the Polish Academy of Science for financial assistance.

REFERENCES

1. M. Cieślak-Golonka, A. Bartecki and M. Raczko, *Polyhedron* 1988, 7, 601.
2. H. Firouzabadi, B. Vessal and M. Naderi, *Tetrahedron Lett.* 1982, **23**, 1847; and refs therein.
3. H. Firouzabadi, M. Naderi, A. Sardarian and B. Vessal, *Synth. Comm.* 1983, **13**, 611.
4. H. Firouzabadi, A. R. Sardarian and H. Gharbi, *Synth. Comm.* 1984, **14**, 89.

5. H. Firouzabadi and A. R. Sardarian, *Synthesis* 1986, **11**, 946.
6. P. H. Connett and K. E. Wetterhahn, *Struct. Bond.* 1983, **54**, 94.
7. V. Bianchi and A. G. Levis, *Toxicol. Environm. Chem.* 1987, **15**, 1.
8. S. C. Rossi, N. Gorman and K. E. Wetterhahn, *Chem. Res. Toxicol.* 1988, **1**, 101.
9. R. B. Hayes, *Sci. Total Environ.* 1988, **71**, 331.
10. A. Kortenkamp, Z. Ozolins, D. Beyersmann and P. O'Brien, *Mut. Res.* 1989, **216**, 19.
11. K. Szyba, private communication.
12. *Gmelin Handbuch für Anorgische Chemie*, Vol. 60, p. 1221. Verlag Chemie, GMBH, Weinheim/Bergstr (1965).
13. K. Nakamoto, *Infrared and Raman Spectra of Inorganic and Coordination Compounds*, 3rd edn. Wiley–Interscience, New York (1978).
14. J. Casabo, J. Ribas and J. M. Coronas, *J. Inorg. Nucl. Chem.* 1976, **38**, 886.
15. J. Ribas, J. Casabo and J. M. Coronas, *J. Chem. Educ.* 1977, **54**, 321.
16. C. Puglisi, *J. Inorg. Nucl. Chem.* 1970, **32**, 692.
17. M. Cieślak-Golonka, *Coord. Chem. Rev.* 1991, **109**, 223.
18. M. Cieślak-Golonka, *Pol. J. Chem.* 1990, **64**, 443.
19. B. J. Hathaway, *Comprehensive Coordination Chemistry*, Vol. 2, p. 41, 3. Pergamon Press, Oxford (1987).
20. B. M. Gatehouse and L. W. Guddat, *Acta Cryst.* 1987, **C43**, 1445.
21. W. Bengsch, N. Seferiadis and H. R. Oswald, *Inorg. Chim. Acta* 1987, **126**, 113.
22. V. Debelle, P. Gravereau and A. Hardy, *Acta Cryst.* 1974, **B30**, 2185.
23. A. M. Domingo and G. M. Sheldrick, *J. Chem. Soc., Dalton Trans.* 1974, 477.
24. P. Chaudhuri, M. Winter, K. Wieghardt, S. Ghering, W. Hasse, B. Nuber and J. Weiss, *Inorg. Chem.* 1988, **27**, 1564.
25. S. Drueke, K. Wieghardt, B. Nuber, J. Weiss, H. P. Fleischhauer, S. Ghering and W. Haase, *J. Am. Chem. Soc.* 1989, **111**, 8622.
26. H. Stammreich, D. Bassi, O. Sala and H. C. Siebert, *Spectrochim. Acta* 1958, **13**, 1972.
27. R. Coomber and W. P. Griffith, *J. Chem. Soc.* (*A*) 1968, 1112.
28. A. Spool, I. D. Williams and S. J. Lippard, *Inorg. Chem.* 1985, **24**, 2156.
29. A. B. P. Lever, E. Mantovani and B. S. Rameswamy, *Can. J. Chem.* 1971, **49**, 1957.
30. B. J. Hathaway, I. M. Proctor, R. C. Slade and A. A. G. Tomlinson, *J. Chem. Soc.* (*A*) 1969, 2219.
31. B. J. Hathaway and A. A. G. Tomlinson, *Coord. Chem. Rev.* 1969, **5**, 1.
32. F. A. Walker and H. Sigel, *Inorg. Chem.* 1972, **11**, 1162.
33. M. Branca, A. Dessi, H. Kozłowski, G. Micera and M. V. Serra, *Febs Lett.* 1989, **57**, 52.
34. M. Mitewa, P. R. Bontchev and V. Bojinov, *Inorg. Nucl. Chem. Lett.* 1972, **8**, 51.
35. P. Bontchev, M. Mitewa, K. Kabassov and A. Malinovski, *Inorg. Nucl. Chem. Lett.* 1975, **11**, 799.
36. R. Rusek and M. Cieślak-Golonka, unpublished results.
37. M. Mitewa, A. Malinowski, P. R. Bontchev and K. Kabassov, *Inorg. Chim. Acta* 1974, **8**, 17.
38. I. M. Procter, B. J. Hathaway, D. E. Billing, R. Dudley and P. Nicholls, *J. Chem. Soc.* (*A*) 1969, 1192.

Polyhedron Vol. 10, No. 18, pp. 2185–2189, 1991
Printed in Great Britain

0277–5387/91 $3.00+.00
© 1991 Pergamon Press plc

COORDINATION COMPLEXES OF ACETYLFERROCENE-m-NITROBENZOYLHYDRAZONE WITH LANTHANIDES

ZHAO GANG†

Chemistry Department, Chengdu University of Science and Technology, Chengdu 610065, China

and

MA YONGXIANG

Chemistry Department, Lanzhou University, Lanzhou 730000, China

(*Received* 18 *March* 1991; *accepted* 3 *May* 1991)

Abstract—The coordination complexes of acetylferrocene-m-nitrobenzoylhydrazone(HL) with lanthanide elements, LnL_3 (where Ln = lanthanide), have been prepared by the reaction of HL with the metal(III) chlorides in acetonitrile. The data of elemental analyses, IR, UV, NMR, molar conductance, TG and DTA show that the ligand coordinates in the enolic form with a molar ratio of 3 : 1. The complexes are non-electrolytes in DMF, and are more thermostable than their ligands due to the formation of chelate rings.

Metal aroylhydrazones are known to possess biological activity and are potent inhibitors for many enzymatic reactions. The coordination chemistry of aroylhydrazines and related compounds was the subject of extensive studies.[1–6] Acid hydrazones can coordinate to metal ions in (a) the enolic form or (b) the keto form. In general, they coordinate to

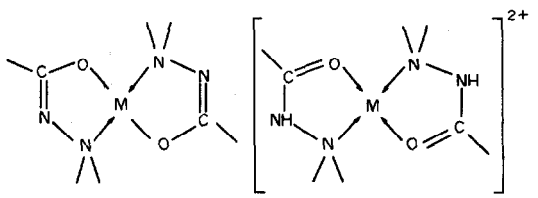

(a) (b)

central ions in the keto form when complexing with metal chlorides, nitrates, sulphates and thiocyanates etc.,[1] but in the enolic form with metal acetates in ethanol. In an earlier communication[7] we reported that HL coordinated with yttrium (III) and lanthanide(III) chloride in the keto form. In this paper, these complexes, coordinated in the enolic form, are prepared through the reaction of hydrazone with metal chlorides rather than metal acetates.

EXPERIMENTAL

Methods and materials

Acetylferrocene was prepared according to the method in the literature.[8] The lanthanide chlorides were reagent grade chemicals and m-nitrobenzoylhydrazine was analytical reagent grade. Acetylferrocene-m-nitrobenzoylhydrazone was also prepared according to the literature.[7]

Syntheses of lanthanide chelates

Lanthanide(III) chloride (0.20 mmol) was dissolved in 40 cm^3 of acetonitrile with heating. 20 cm^3 of acetylferrocene-m-nitrobenzoylhydrazone solution (0.80 mmol) in acetonitrile containing 2 cm^3 of triethyl orthoformate were added dropwise into the above solution. The mixture was maintained under reflux for 8 h. The precipitate was separated, filtered on cooling, washed several times with cold acetonitrile and ether and dried to constant weight *in vacuo* to give the pure product, yield > 72%. The physical properties and elemental analyses of these

† Author to whom correspondence should be addressed.

Table 1. Decomposition points and elemental analyses of the complexes

Complex	Formula	Decomposition point (°C)	Elemental analysis: found (calc.) (%) C	H	N
I	LaL_3[a]	293	52.8(52.3)	3.7(3.7)	9.8(9.6)
II	CeL_3	297	52.0(52.2)	3.7(3.7)	9.8(9.6)
III	PrL_3	292	52.3(52.2)	3.7(3.7)	9.6(9.6)
IV	NdL_3	290	52.4(52.1)	3.6(3.7)	9.7(9.6)
V	SmL_3	290	51.6(51.8)	3.7(3.7)	9.5(9.5)
VI	EuL_3	297	51.3(51.8)	3.8(3.7)	9.2(9.5)
VII	GdL_3	299	51.9(51.5)	3.5(3.6)	9.7(9.5)
VIII	TbL_3	293	51.5(51.5)	3.6(3.6)	9.4(9.5)
IX	DyL_3	292	51.5(51.3)	3.7(3.6)	9.6(9.5)
X	HoL_3	297	51.4(51.2)	3.7(3.6)	9.5(9.4)
XI	ErL_3	290	51.2(51.2)	3.8(3.6)	9.4(9.4)
XII	TmL_3	294	51.9(51.1)	3.4(3.6)	9.7(9.4)
XIII	YbL_3	293	50.7(50.9)	3.7(3.6)	9.4(9.4)
XIV	LuL_3	295	50.6(50.9)	3.7(3.6)	9.2(9.4)

[a] $L = C_5H_5FeC_5H_4C(CH_3)=N-N=C(O-)-C_6H_4-NO_2$—m.

complexes are listed in Table 1 along with their formulae.

Physical measurements

IR spectra were recorded using a Nicolet 5DX spectrometer using KBr discs in the 400–4000 cm^{-1} region. UV spectra were recorded on a Shimadzu-240 spectrophotometer, using DMF solution in the 200–500 nm region. PMR spectra were obtained on a FT-80A spectrometer using deuterodimethyl sulphoxide as a solvent and TMS as the internal reference. Electrolytic conductance measurements were made with a DDS-IIA molar conductometer and DMF as a solvent at 25°C. Thermal characterization studies were carried out with a Du Pont 1090 thermal analyser in a nitrogen atmosphere.

RESULTS AND DISCUSSION

The complexes of lanthanide elements with acetylferrocene-m-nitrobenzoylhydrazone are amorphous brown powders. These are insoluble in petroleum ether, benzene and water, sparingly soluble in diethyl ether, but soluble in methanol, ethanol, DMF and DMSO. These chelates are hygroscopic. Their elemental analyses show that $LnCl_3$ forms complexes with the loss of chloride ions and that they conform to the formula LnL_3. The reaction solvent acetonitrile promotes the enolization of the ligand.[7]

IR spectra

The important IR frequencies of the ligand and its complexes along with their relative assignments are given in Table 2. The IR spectra of these complexes show significant changes when compared with those of the parent ligand. It can be seen that the bands due to N—H and C=O stretching vibrations and δ(N—H) are not observed in the spectra of these complexes. Instead, new bands are observed around 1607 cm^{-1} and 1246 cm^{-1} which can be assigned to the stretching vibrational modes of conjugate —C=N—N=C—[9] and C—O[10] groups. It is shown that the ligand undergoes enolization in acetonitrile and then reacts with the lanthanide ions to form complexes, accompanied by the release of chloride ions. It is also found that the ν(C=N) band is shifted to a lower frequency by *ca* 20 cm^{-1} while the ν(N—N) band is shifted to a higher frequency by *ca* 27 cm^{-1}. These observations support the coordination through the azomethine nitrogen atom. In addition, the characteristic frequencies of ferrocenyl appear around 3089, 1389, 1102 and 813 cm^{-1}. The bands of m-nitrobenzoyl are observed at 3176, 1597, 1576, 1475 and 713 cm^{-1}.

UV spectra

The UV spectra of the ligand and its complexes in methanol are shown in Fig. 1. It can be seen that

Table 2. Important IR absorption bands of the ligand and its complexes (cm^{-1})

Compound	ν(C=N—N=C)	ν(C=N)	δ(N—H)	ν(C—O)	ν(N—N)
HL[a]	—	1542vs	1529vs	—	1000w
I	1607s	1520vs	—	1246m	1028w
II	1610m	1520s	—	1246m	1026w
III	1610m	1520s	—	1246m	1026w
IV	1608s	1520vs	—	1246m	1027w
V	1607s	1520vs	—	1247m	1027w
VI	1610s	1520vs	—	1246m	1027w
VII	1610m	1522s	—	1246m	1027w
VIII	1610s	1521s	—	1245m	1027w
IX	1609s	1520vs	—	1245m	1027w
X	1607s	1520vs	—	1245m	1027w
XI	1607s	1520vs	—	1245m	1027w
XII	1607s	1520vs	—	1245m	1027w
XIII	1607s	1520vs	—	1245m	1027w
XIV	1610s	1520vs	—	1245m	1027w

vs = very strong, s = strong, m = medium, w = weak, br = broad, sh = shoulder.

[a] ν(N—H), 3335 br, m; ν(C=O) 1658 sh.

the UV spectra of all the complexes are similar, but they are different from that of the ligand. The band at 298 nm in the ligand is attributed to a band (π–π^* transition) but in the complexes, a bathochromic shift of 30–40 nm is observed. It is possible that the *f*-orbitals of the metal atom and the *p*-orbital of the ligand overlap to form a greater conjugate system after enolizing and complexing. The formation of the greater conjugate system makes the energy level difference between the π and π^* orbitals, i.e. π–π^* transition energy required, decrease. These factors led to the bathochromic shift of the K band in the complexes. The band at *ca* 363 nm is typical of the internal transition of the ligand in the complex and therefore assigned to the —C=N—N=C—O$^-$ fragment of the complex. The ligand and complexes exhibit broad and weak bands around 430 nm, which are due to charge-transfer from iron to either the non-bonding or the anti-bonding orbitals on the cyclopentadienyl rings.[11]

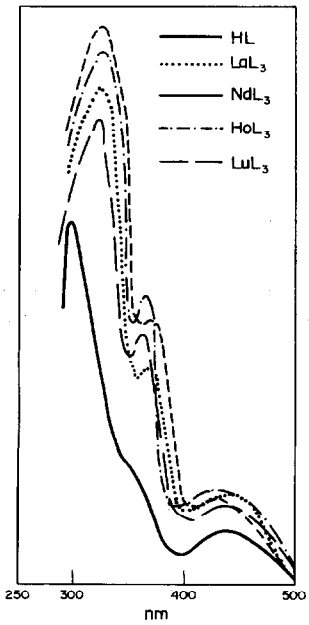

Fig. 1. The UV spectra of the ligand and its complexes.

PMR spectra

The PMR spectra of the ligand and its complexes have been investigated using DMSO as a solvent. Because lanthanides have a tendency to maintain unpaired electron spins, which interact with the nuclei (protons), the H-signals of these complexes are broadened and very weak, except for La^{III} and Lu^{III} complexes. The PMR data of the ligand and two complexes are listed in Table 3. The free ligand exhibits a peak due to the N—H proton at 10.9 ppm, which disappears on deuteration with D_2O. In the spectra of the lanthanide complexes, however, the N—H signal disappears as expected for the enol form. In the spectra of the complexes, the methyl proton suffers some deshielding and gives rise to a signal between 2.45–2.60 ppm, which is shifted downfield by 0.18–0.33 ppm compared to that of the parent ligand. These results indicate that the coordination of the ligand with the lanthanide ions involves the enol form of the ligand.

Table 3. PMR chemical shifts (δ, ppm) of the ligand and some complexes

Compound	CH_3	Ferrocenyl group		C_6H_4	N—H
		Unsubstituted	Substituted		
HL	2.27(s)	4.25(s)	4.42, 4.72	7.81–8.70(m)	10.91(s)
LaL_3	2.45(s)	4.25(s)	4.43, 4.75	7.82–8.74(m)	—
LuL_3	2.60(s)	4.22(s)	4.42, 4.70	7.78–8.80(m)	—

s = singlet, m = multiplet.

Molar conductance

Dissolving the lanthanide complexes in DMF produced a deep brown solution. The molar conductance values (Table 4) of the complexes in DMF lie in the range 17–42 Ω^{-1} cm^2 mol^{-1}. A comparison of these values with those previously reported in the literature[12] shows the non-electrolytic nature of the complexes in DMF.

Thermal analysis

Thermal analyses of the ligand and its complexes show that an explosive decomposition occurs when heated to an appropriate temperature which is due to the presence of the nitro group on phenyl. Hence, the weight loss is difficult to measure accurately. However, TG and DTA measurements of the ligand indicate melting at 186°C and the beginning of decomposition at 190°C, then an **explosive decomposition** at about 243°C. It is interesting to note that the complexes are more thermostable than the ligand. All the complexes decomposed explosively above 327°C.

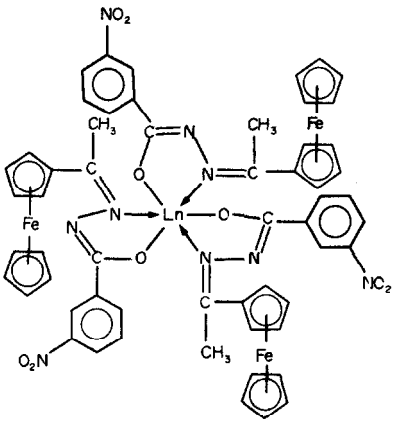

Fig. 2. Proposed structure for the complexes.

Table 4. Molar conductances of the complexes in DMF at 25°C

Complex	Conc. (10^{-3} mol)	λ_m (Ω^{-1} cm^2 mol^{-1})
I	0.98	42
II	0.94	37
III	0.99	38
IV	0.99	41
V	1.07	25
VI	1.05	17
VII	0.99	30
VIII	0.98	21
IX	1.02	25
X	1.09	23
XI	1.04	40
XII	0.91	29
XIII	0.97	18
XIV	0.93	25

Conclusions

Acetylferrocene-m-nitrobenzoylhydrazone is a bidentate ligand, three molecules of which coordinate with one molecule of lanthanide(III) chloride through its nitrogen atom in azomethine, and its oxygen atom in the enolic form in acetonitrile, accompanied by the release of three chloride ions; their coordination numbers are equal to six. Therefore, we suggest a plausible structure for our complexes as shown in Fig. 2.

Acknowledgement—We thank Chengdu University of Science and Technology for the financial support.

REFERENCES

1. M. F. Iskander, L. El. Sayed and M. A. Lasheen, *Inorg. Chim. Acta* 1976, **16**, 147.
2. S. R. Patil, U. N. Kantak and D. N. Sen, *Inorg. Chim. Acta* 1982, **63**, 261; 1983, **68**, 1.

3. Z. Gang, L. Feng, X. Jishan and M. Yongxiang, *Polyhedron* 1988, **7**, 393.
4. M. Yongxiang and Z. Gang, *Inorg. Chim. Acta* 1988, **144**, 265.
5. Z. Gang and M. Yongxiang, *Chin. Sci. Bull.* 1989, **34**, 566.
6. M. Yongxiang and Z. Gang, *Polyhedron* 1988, **7**, 1101.
7. M. Yongxiang, Z. Tongjun and Z. Gang, *Lanthanide Actinide Res.* 1988, **2**, 235.
8. P. J. Graham, R. V. Lindsey, G. W. Parshall, M. L. Peterson and G. M. Whitman, *J. Am. Chem. Soc.* 1957, **79**, 3416.
9. R. G. R. Bacon and W. S. Lindsay, *J. Chem. Soc.* 1958, 1382.
10. K. Nagano, H. Kinoshita and A. Hirakawa, *Chem. Pharm. Bull., Tokyo* 1964, **12**, 1198.
11. M. Rosenblum, J. O. Santer and W. G. Jowells, *J. Am. Chem. Soc.* 1963, **85**, 1450.
12. W. J. Geary, *Coord. Chem. Rev.* 1971, **71**, 81.

Polyhedron Vol. 10, No. 18, pp. 2191–2201, 1991
Printed in Great Britain

0277–5387/91 $3.00+.00
© 1991 Pergamon Press plc

ROLE OF THE LIGANDS IN AFFECTING THE STOICHIOMETRY AND THE RATE OF REACTIONS BETWEEN PLATINUM(IV) AND PLATINUM(II) COMPLEXES

ARNALDO PELOSO

Dipartimento di Chimica Inorganica, Metallorganica ed Analitica, Universita' di Padova, Via Marzolo 1, 35131 Padua, Italy

(*Received* 4 *January* 1991, *accepted* 15 *April* 1991)

Abstract—The stoichiometries and the rates of the reactions between *trans*-$[Pt(en)(N\text{-}N)Cl_2]^{2+}$ and $[Pt(en)(N'\text{-}N')]^{2+}$ in the presence of bromide ions have been studied in aqueous solutions (N-N and N′-N′ = en, 1,3-pn, 1,2-pn, meen, dmen, tmen). The platinum(IV) reaction product is either *trans*-$[Pt(en)(N\text{-}N)Br_2]^{2+}$ or *trans*-$[Pt(en)(N'\text{-}N')Br_2]^{2+}$, depending on the bulkiness of N-N and N′-N′. The reaction rates obey a pseudo-first-order rate law with $k_{obs} \approx \{k_c[Br^-]+k_d[Br^-]^2\}[Pt(en)(N'\text{-}N')^{2+}]$. The ligands significantly affect the rates, mainly via their steric hindrance. An increase of the steric hindrance near the platinum(IV) centre only moderately enhances its reactivity towards reduction, whereas a strong lowering of the reactivity of platinum(II) towards oxidation is caused by an increase of the steric hindrance of the ligands coordinated to this atom centre. The quantitative kinetic effect displayed by changes of such ligands either on platinum(IV) or on platinum(II) complexes is also dependent on the particular platinum(II) or platinum(IV) complex used as the standard reducing or oxidizing reagent. An explanation of the observed behaviour is suggested in terms of an atom-transfer redox mechanism.

The rates of inner-sphere redox reactions between platinum(IV) and platinum(II) complexes are known to be affected by non-labile ligands coordinated to the central metal atom.[1-3] However, scarce attention has been so far devoted to establish whether reaction rates are more sensitive to changes of ligands coordinated to platinum(IV) or to platinum(II) complexes.

In order to shed some light on this field, a kinetic investigation has been carried out in aqueous solutions on the reactions between *trans*-$[Pt(en)(N\text{-}N)Cl_2]^{2+}$ and $[Pt(en)(N'\text{-}N')]^{2+}$ complexes in the presence of bromide ions [N-N and N′-N′ = ethylenediamine (en), 1,3-propylenediamine (1,3-pn), 1,2-propylenediamine (1,2-pn), N-methylethylenediamine (meen), N,N-dimethylethylenediamine (dmen), N,N,N′,N′-tetramethylethylenediamine (tmen)].

EXPERIMENTAL

Materials

Platinum(II) compounds of the type $[Pt(en)(N\text{-}N)]Cl_2$ were prepared by treating aqueous suspensions of $[Pt(N\text{-}N)Cl_2]$ with a small excess of ethylenediamine and heating at 60–80°C until clear, colourless solutions were obtained. The solutions were evaporated almost to dryness *in vacuo* and the crude material recovered was dissolved in a small portion of either water or methanol. After the addition of charcoal, the resulting solutions were warmed and filtered. Subsequent addition of either acetone or acetonitrile caused the separation of the required products as colourless or very pale yellow flakes or microcrystals (Table 1). Diperchlorates, $[Pt(en)(N\text{-}N)](ClO_4)_2$ (N-N = 1,3-pn, 1,2-pn, meen and dmen), were obtained by treating very concentrated cold aqueous solutions of dichloride analogue with either concentrated perchloric acid or saturated solutions of sodium perchlorate. Platinum(IV) compounds of the type *trans*-$[Pt(en)(N\text{-}N)Cl_2]Cl_2$ were obtained by conventional oxidation of the platinum(II) parents in aqueous solutions with hydrogen peroxide and hydrochloric acid. The solutions were heated on a water-bath for at least 30 min, after which they were evaporated almost to dryness *in vacuo*. The required products were recovered from

Table 1. Elemental analyses of platinum(II) and platinum(IV) complexes

Complex	C (%) Calc.	C (%) Found	H (%) Calc.	H (%) Found	N (%) Calc.	N (%) Found
Platinum(II) complexes						
$[Pt(en)_2]Cl_2$	12.4	12.3	4.2	4.1	14.5	14.4
$[Pt(en)(1,3\text{-pn})](ClO_4)_2$	11.3	11.3	3.4	3.5	10.6	10.5
$[Pt(en)(1,2\text{-pn})](ClO_4)_2$	11.3	11.2	3.4	3.4	10.6	10.5
$[Pt(en)(1,2\text{-pn})]Cl_2$	15.0	15.2	4.6	4.7	14.0	13.9
$[Pt(en)(meen)](ClO_4)_2$	11.3	11.4	3.4	3.4	10.6	10.6
$[Pt(en)(meen)]Cl_2$	15.0	15.2	4.6	4.7	14.0	14.0
$[Pt(en)(dmen)](ClO_4)_2$	13.3	13.3	3.7	3.7	10.3	10.3
$[Pt(en)(tmen)]Cl_2$	21.7	21.6	5.4	5.7	12.6	12.5
Platinum(IV) complexes						
$[Pt(en)_2Cl_2]Cl_2 \cdot 2H_2O$	9.7	9.7	4.1	4.0	11.3	11.3
$[Pt(en)(1,3\text{-pn})Cl_2]Cl_2 \cdot 2H_2O$	11.8	11.6	4.3	4.3	11.0	10.9
$[Pt(en)(1,2\text{-pn})Cl_2]Cl_2 \cdot 2H_2O$	11.8	11.6	4.3	4.3	11.0	10.9
$[Pt(en)(meen)Cl_2]Cl_2 \cdot 1/2H_2O$	12.5	12.3	4.0	3.9	11.6	11.6
$[Pt(en)(dmen)Cl_2]Cl_2 \cdot 2H_2O$	13.8	13.8	4.6	4.4	10.7	10.6
$[Pt(en)(tmen)Cl_2]Cl_2 \cdot 2H_2O$	18.1	18.2	4.9	4.9	10.5	10.7

the obtained crude materials as described above for platinum(II) complexes.

Reagent grade sodium bromide and perchlorate were dried before use. Doubly-distilled water was used to prepare stock solutions of the reactants.

Reaction products

Spectrophotometric investigations showed that the *trans*-$[Pt(en)(N\text{-}N)Cl_2]^{2+}$ complexes examined in this paper react with bromide ions both in the absence and in the presence of added platinum(II) complexes, leading to a reaction product which displays an absorption band with a maximum (λ_{max}) located in the 320–338 nm wavelength range (Table 2), and consistent with the formation of a *trans*-dibromo (ethylenediamine) (diamine) platinum (IV) complex.[4,5] The platinum(IV) reaction product for the reactions carried out in the absence of added platinum(II), as well as in the cases in which platinum(IV) and the added platinum(II) complexes contain the same diamines, is invariably *trans*-$[Pt(en)(N\text{-}N)Br_2]^{2+}$. Such behaviour is rather common for these kinds of reactions.[1,4-6] In the cases investigated here the formation of the named dibromoplatinum(IV) complexes is supported by the verified identity of the value of λ_{max} determined for the exhausted reaction mixtures (Table 2) with that of authentic *trans*-$[Pt(en)(N\text{-}N)Br_2]^{2+}$ complexes [i.e.: 320 (en[4] and 1,2-pn), 321 (1,3-pn), 322 (meen), 327 (dmen) or 338 nm (tmen[5])]. In many cases, two isosbestic points occurred at the correct wavelengths expected for the conversion of the starting dichloroplatinum(IV) complex into the dibromoplatinum(IV) analogue {e.g. (at $[Br^-] = 0.10$ mol dm^{-3}): 281 and 271 (N-N = en), 281 and 275 (1,3-pn), 280 and 272 (1,2-pn), 282 and 273 nm (meen)}. However, the location of these isosbestic points has not been considered as strong evidence for the general identification of the reaction products since they were found to be strongly dependent on the bromide ion concentration (see below). The values of λ_{max} for the exhausted reaction mixtures for reactions between platinum(IV) and platinum(II) complexes containing different diamines allowed to deduce the nature of the reaction product only for the cases reported in Table 2. The exact nature of the platinum(IV) reaction products for the reactions between platinum(IV) and platinum(II) complexes containing only primary diamines or meen could not be established owing to the almost identical values of λ_{max} exhibited by the pair of possible reaction products {i.e. *trans*-$[Pt(en)(N\text{-}N)Br_2]^{2+}$ and *trans*-$[Pt(en)(N'\text{-}N')Br_2]^{2+}$}.

In all the cases in which the reaction products were identified, it was found that the absorbance of the exhausted reaction mixture at a given bromide ion concentration was consistent with quantitative conversion of the starting platinum(IV) complex into the particular dibromoplatinum(IV) complex reported in Table 2. However, it was observed that the absorbance value of an exhausted reaction mixture is higher for a higher bromide ion concentration, even though the wavelength of the absorb-

Table 2. Wavelength (λ_{max}, nm) of the maximum absorbance (near UV region) for exhausted reaction mixtures of *trans*-$[Pt(en)(N\text{-}N)Cl_2]^{2+}$ and $[Pt(en)(N'\text{-}N')]^{2+}$ complexes in NaBr (0.2 M)

	$[Pt(en)(N'\text{-}N')]^{2+}$					
trans-$[Pt(en)(N\text{-}N)Cl_2]^{2+}$	$[Pt(en)_2]^{2+}$	$[Pt(en)(1,3\text{-pn})]^{2+}$	$[Pt(en)(1,2\text{-pn})]^{2+}$	$[Pt(en)(meen)]^{2+}$	$[Pt(en)(dmen)]^{2+}$	$[Pt(en)(tmen)]^{2+}$
$[Pt(en)_2Cl_2]^{2+}$	320	321	320	321	320	320
$[Pt^{IV}$ reaction product$]\rightarrow$	$[Pt(en)_2Br_2]^{2+}$	—	—	—	$[Pt(en)_2Br_2]^{2+}$	$[Pt(en)_2Br_2]^{2+}$
$[Pt(en)(1,3\text{-pn})Cl_2]^{2+}$	320	321	320	321	320	321
$[Pt^{IV}$ reaction product$]\rightarrow$	–	$[Pt(en)(1,3\text{-pn})Br_2]^{2+}$	—	—	$[Pt(en)(1,3\text{-pn})Br_2]^{2+}$	$[Pt(en)(1,3\text{-pn})Br_2]^{2+}$
$[Pt(en)(1,2\text{-pn})Cl_2]^{2+}$	320	321	320	321	321	320
$[Pt^{IV}$ reaction product$]\rightarrow$	—	—	$[Pt(en)(1,2\text{-pn})Br_2]^{2+}$	—	$[Pt(en)(1,2\text{-pn})Br_2]^{2+}$	$[Pt(en)(1,2\text{-pn})Br_2]^{2+}$
$[Pt(en)(meen)Cl_2]^{2+}$	319	322	320	322	321	322
$[Pt^{IV}$ reaction product$]\rightarrow$	—	—	—	$[Pt(en)(meen)Br_2]^{2+}$	$[Pt(en)(meen)Br_2]^{2+}$	$[Pt(en)(meen)Br_2]^{2+}$
$[Pt(en)(dmen)Cl_2]^{2+}$	319	321	320	321	327	329
$[Pt^{IV}$ reaction product$]\rightarrow$	$[Pt(en)_2Br_2]^{2+}$	$[Pt(en)(1,3\text{-pn})Br_2]^{2+}$	$[Pt(en)(1,2\text{-pn})Br_2]^{2+}$	$[Pt(en)(meen)Br_2]^{2+}$	$[Pt(en)(dmen)Br_2]^{2+}$	$[Pt(en)(dmen)Br_2]^{2+}$
$[Pt(en)(tmen)Cl_2]^{2+}$	319	321	320	321	328	338
$[Pt^{IV}$ reaction product$]\rightarrow$	$[Pt(en)_2Br_2]^{2+}$	$[Pt(en)(1,3\text{-pn})Br_2]^{2+}$	$[Pt(en)(1,2\text{-pn})Br_2]^{2+}$	$[Pt(en)(meen)Br_2]^{2+}$	$[Pt(en)(dmen)Br_2]^{2+}$	$[Pt(en)(tmen)Br_2]^{2+}$

ance maximum does not change. As a consequence, the location of isosbestic points which accompany the progress of many reactions is dependent on the bromide ion concentration. The observed behaviour is not connected with the occurrence of only incomplete reactions. In fact, addition of sodium bromide to exhausted reaction mixtures was found to cause a sudden increase in the absorbance even at the wavelengths where isosbestic points were observed, which is evidence against the occurrence of an incomplete reaction. On the other hand, such behaviour is a rather common feature for cationic platinum(IV) complexes[5,7] and has not been further investigated.

Kinetics

Stock solutions of the reactants were prepared by weight in aqueous, acidic solutions ($HClO_4$, pH 3.0), an ionic strength of 0.50 mol dm^{-3} being ensured by the addition of the required amount of $NaClO_4$. The reactions were started by mixing appropriate volumes of thermostatted stock solutions of the reactants in 1 cm silica cells maintained in the thermostat-controlled cell compartment of a Lambda 5 UV–vis Perkin–Elmer spectrophotometer. The progress of the reactions was followed by scanning the absorption spectrum of the reacting mixture in the 360–250 nm region at appropriate time intervals. Fast reactions were followed by recording the absorbance against time at a constant wavelength (near 250–260 or 320–340 nm, dependent on both the concentration and type of complexes used). Under kinetic conditions the starting concentration of platinum(IV) complexes was always less than 1×10^{-4} mol dm^{-3} and usually at least 10 times lower than that of the interacting platinum(II) complexes. The concentration ranges explored for platinum(II) complexes and bromide ions are listed in Table 3. It was usually found that the reactions obey a pseudo-first-order rate law for at least two half-lives. Pseudo-first-order rate constants, k_{obs}, were evaluated from the gradient of plots of log $(A_\infty - A_t)$ against time (A_t and A_∞ are the absorbances of the reacting mixture at time t and at the end of the reaction, respectively, at a given wavelength). Some experiments were also performed using comparable concentrations of platinum(IV) and platinum(II) complexes. It was found that a first-order rate law operates even in these cases provided that the platinum(IV) reaction product contains the same diamines as its dichloroplatinum(IV) parent.

Pseudo-first-order rate constants obtained from replicate kinetic runs were usually found to agree to better than 5%. At least 12 kinetic runs were carried out at each temperature explored, using different concentrations of platinum(II) complexes and bromide ions.

RESULTS

The data in Table 3 imply that the reactions studied in this paper display either stoichiometry (1) or (2) dependence on the ligands bonded to the starting platinum(IV) and platinum(II) complexes:

$$trans\text{-}[Pt(en)(N\text{-}N)Cl_2]^{2+} + 2Br^- \xrightarrow{\text{Added } Pt^{II} \text{ complex}} trans\text{-}[Pt(en)(N\text{-}N)Br_2]^{2+} + 2Cl^- \quad (1)$$

$$trans\text{-}[Pt(en)(N\text{-}N)Cl_2]^{2+} + [Pt(en)(N'\text{-}N')]^{2+} + 2Br^- \longrightarrow [Pt(en)(N\text{-}N)]^{2+} + trans\text{-}[Pt(en)(N'\text{-}N')Br_2]^{2+} + 2Cl^- . \quad (2)$$

According to Table 3, stoichiometry (1) is operating for all the reactions between platinum(IV) and platinum(II) complexes containing identical diamines. It must be acknowledged that such stoichiometry is rather common for reactions of this type[1] and, in particular, it has been known for a long time for N-N = en[8] and tmen[5]. Stoichiometry (2) invariably occurs when N-N in *trans*-$[Pt(en)(N\text{-}N)Cl_2]^{2+}$ bears a larger number of N-methyl groups than N′-N′ in $[Pt(en)(N'\text{-}N')]^{2+}$ [i.e. (a) N-N = dmen or tmen; N′-N′ = en, 1,3-pn, 1,2-pn, meen; (b) N-N = tmen, N′-N′ = dmen]. Conversely, stoichiometry (1) occurs when the N-N ligand on platinum(IV) contains a lower number of N-methyl groups than N′-N′ on platinum(II) [i.e. (a) N-N = en, 1,3-pn, 1,2-pn, meen; N′-N′ = dmen, tmen; (b) N-N = dmen, N′-N′ = tmen]. Such behaviour for reactions between platinum(IV) and platinum(II) complexes does not appear to have been previously observed, and its occurrence will be rationalized below. The stoichiometry for the reactions between platinum(IV) and platinum(II) complexes containing only primary diamines or meen cannot be inferred from any identification of the platinum(IV) reaction products. Nevertheless, stoichiometry (2) is likely to occur since in the absence of other driving forces the concentration of the starting platinum(II) complex should control the predominating dibromoplatinum(IV) complex which is formed. Under the experimental conditions chosen, the reactions studied obey a pseudo-first-order rate law whose k_{obs}

Table 3. Explored concentration ranges of $[Pt(en)(N'\text{-}N')]^{2+}$ and NaBr for the reactions between *trans*-$[Pt(en)(N\text{-}N)Cl_2]^{2+}$ and $[Pt(en)(N'\text{-}N')]^{2+}$ in the presence of NaBr ($I = 0.50$ mol dm^{-3})

N-N	N′-N′	Conc. range (mol dm^{-3}) of $[Pt(en)(N'\text{-}N')]^{2+}$	Conc. range (mol dm^{-3}) of NaBr	N-N	N′-N′	Conc. range (mol dm^{-3}) of $[Pt(en)(N'\text{-}N')]^{2+}$	Conc. range (mol dm^{-3}) of NaBr
en	en	2.09×10^{-4}–6.27×10^{-4}	3.33×10^{-3}–3.67×10^{-2}	meen	en	3.88×10^{-4}–1.16×10^{-3}	2.00×10^{-3}–1.47×10^{-2}
	1,3-pn	2.96×10^{-4}–8.88×10^{-4}	3.33×10^{-3}–3.67×10^{-2}		1,3-pn	2.36×10^{-4}–6.48×10^{-4}	3.33×10^{-3}–3.67×10^{-2}
	1,2-pn	3.17×10^{-4}–9.52×10^{-4}	3.33×10^{-3}–3.67×10^{-2}		1,2-pn	3.55×10^{-4}–1.07×10^{-3}	1.33×10^{-3}–3.67×10^{-2}
	meen	3.40×10^{-4}–1.02×10^{-3}	3.33×10^{-3}–3.67×10^{-2}		meen	1.15×10^{-4}–5.88×10^{-4}	3.33×10^{-3}–1.67×10^{-1}
	dmen	2.66×10^{-4}–7.97×10^{-4}	3.33×10^{-2}–3.67×10^{-1}		dmen	4.53×10^{-4}–1.36×10^{-3}	6.67×10^{-3}–5.33×10^{-2}
	tmen	1.23×10^{-3}–5.69×10^{-3}	5.00×10^{-2}–3.17×10^{-1}		tmen	7.94×10^{-4}–2.38×10^{-3}	5.00×10^{-2}–3.17×10^{-1}
1,3-pn	en	3.88×10^{-4}–1.16×10^{-3}	3.33×10^{-3}–3.67×10^{-2}	dmen	en	2.73×10^{-4}–7.63×10^{-4}	6.00×10^{-3}–8.33×10^{-2}
	1,3-pn	1.20×10^{-4}–3.78×10^{-4}	6.67×10^{-3}–7.67×10^{-2}		1,3-pn	2.27×10^{-4}–5.45×10^{-4}	3.33×10^{-3}–3.67×10^{-2}
	1,2-pn	3.55×10^{-4}–1.07×10^{-3}	6.00×10^{-3}–6.00×10^{-2}		1,2-pn	2.94×10^{-4}–8.81×10^{-4}	3.33×10^{-3}–3.67×10^{-2}
	meen	4.55×10^{-4}–1.37×10^{-3}	3.33×10^{-3}–3.67×10^{-2}		meen	2.38×10^{-4}–6.88×10^{-4}	3.33×10^{-3}–3.67×10^{-2}
	dmen	2.88×10^{-4}–5.76×10^{-4}	3.33×10^{-2}–3.67×10^{-1}		dmen	2.41×10^{-4}–1.45×10^{-3}	3.33×10^{-3}–3.81×10^{-1}
	tmen	7.71×10^{-4}–2.31×10^{-3}	5.00×10^{-2}–3.17×10^{-1}		tmen	1.03×10^{-3}–4.14×10^{-3}	3.33×10^{-2}–3.67×10^{-1}
1,2-pn	en	3.88×10^{-4}–1.16×10^{-3}	3.33×10^{-3}–3.67×10^{-2}	tmen	en	2.12×10^{-4}–6.68×10^{-4}	3.33×10^{-3}–3.82×10^{-2}
	1,3-pn	2.87×10^{-4}–6.57×10^{-4}	3.33×10^{-3}–3.67×10^{-2}		1,3-pn	1.72×10^{-4}–4.82×10^{-4}	2.00×10^{-3}–1.47×10^{-2}
	1,2-pn	2.51×10^{-4}–8.27×10^{-4}	3.33×10^{-3}–3.83×10^{-1}		1,2-pn	2.48×10^{-4}–7.26×10^{-4}	1.33×10^{-3}–1.47×10^{-2}
	meen	2.37×10^{-4}–7.24×10^{-4}	3.33×10^{-3}–3.67×10^{-2}		meen	2.37×10^{-4}–6.43×10^{-4}	1.33×10^{-3}–1.47×10^{-2}
	dmen	8.80×10^{-4}–3.52×10^{-3}	3.33×10^{-3}–3.67×10^{-2}		dmen	2.45×10^{-4}–6.33×10^{-4}	3.33×10^{-2}–3.83×10^{-1}
	tmen	1.18×10^{-3}–5.56×10^{-3}	5.00×10^{-2}–3.17×10^{-1}		tmen	4.34×10^{-4}–1.30×10^{-3}	3.33×10^{-2}–3.87×10^{-1}

Table 4. Rate constants [see eq. (3)] and activation parameters[a] for the reactions between *trans*-$[Pt(en)(N\text{-}N)Cl_2]^{2+}$ and $[Pt(en)(N'\text{-}N')]^{2+}$ complexes in the presence of NaBr ($I = 0.50$ mol dm^{-3})

Platinum(II) complex	Platinum(IV) complex	t (°C)	k_c (dm^6 mol^{-2} s^{-1})	ΔH_c^* (kJ mol^{-1})	ΔS_c^* (J K^{-1} mol^{-1})	k_d (dm^9 mol^{-3} s^{-1})
$[Pt(en)_2]^{2+}$	*trans*-$[Pt(en)_2Cl_2]^{2+}$	25.0	4.72×10^2			—
		35.0	6.46×10^2	20.2	−126	—
		45.0	8.40×10^2			—
	trans-$[Pt(en)(1,3\text{-}pn)Cl_2]^{2+}$	25.0	5.85×10^2			—
		35.0	7.86×10^2	19.0	−128	—
		45.0	1.01×10^3			—
	trans-$[Pt(en)(1,2\text{-}pn)Cl_2]^{2+}$	25.0	3.75×10^2			—
		35.0	5.19×10^2	24.1	−115	—
		45.0	7.38×10^2			—
	trans-$[Pt(en)(meen)Cl_2]^{2+}$	25.0	6.63×10^2			—
		35.0	9.05×10^2	19.5	−126	—
		45.0	1.16×10^3			—
	trans-$[Pt(en)(dmen)Cl_2]^{2+}$	25.0	2.73×10^3			—
		35.0	3.48×10^3	13.8	−133	—
		45.0	4.16×10^3			—
	trans-$[Pt(en)(tmen)Cl_2]^{2+}$	25.0	8.16×10^3			—
		35.0	1.04×10^4	15.8	−117	—
		45.0	1.30×10^4			—
$[Pt(en)(1,3\text{-}pn)]^{2+}$	*trans*-$[Pt(en)_2Cl_2]^{2+}$	25.0	2.58×10^2			—
		35.0	3.44×10^2	19.7	−133	—
		45.0	4.53×10^2			—
	trans-$[Pt(en)(1,3\text{-}pn)Cl_2]^{2+}$	25.0	3.50×10^2			—
		35.0	4.74×10^2	21.3	−125	—
		45.0	6.40×10^2			—
	trans-$[Pt(en)(1,2\text{-}pn)Cl_2]^{2+}$	25.0	2.51×10^2			—
		35.0	3.48×10^2	21.1	−128	—
		45.0	4.57×10^2			—
	trans-$[Pt(en)(meen)Cl_2]^{2+}$	25.0	4.07×10^2			—
		35.0	5.41×10^2	19.8	−129	—
		45.0	7.17×10^2			—
	trans-$[Pt(en)(dmen)Cl_2]^{2+}$	25.0	1.87×10^3			—
		35.0	2.34×10^3	13.0	−139	—
		45.0	2.77×10^3			—
	trans-$[Pt(en)(tmen)Cl_2]^{2+}$	25.0	5.17×10^3			—
		35.0	6.05×10^3	8.9	−144	—
		45.0	6.91×10^3			—
$[Pt(en)(1,2\text{-}pn)]^{2+}$	*trans*-$[Pt(en)_2Cl_2]^{2+}$	25.0	2.88×10^2			—
		35.0	3.84×10^2	19.0	−134	—
		45.0	4.97×10^2			—
	trans-$[Pt(en)(1,3\text{-}pn)Cl_2]^{2+}$	25.0	3.42×10^2			—
		35.0	4.63×10^2	19.7	−130	—
		45.0	6.02×10^2			—
	trans-$[Pt(en)(1,2\text{-}pn)Cl_2]^{2+}$	25.0	2.16×10^2			2.5×10^2
		35.0	2.94×10^2	20.3	−132	3.4×10^2
		45.0	3.86×10^2			3.1×10^2
	trans-$[Pt(en)(meen)Cl_2]^{2+}$	25.0	3.68×10^2			—
		35.0	5.08×10^2	22.9	−119	—
		45.0	7.01×10^2			—
	trans-$[Pt(en)(dmen)Cl_2]^{2+}$	25.0	1.61×10^3			—
		35.0	2.01×10^3	15.0	−133	—
		45.0	2.51×10^3			—
	trans-$[Pt(en)(tmen)Cl_2]^{2+}$	25.0	4.61×10^3			—
		35.0	5.69×10^3	12.8	−132	—
		45.0	6.81×10^3			—

Platinum(II) complex	Platinum(IV) complex	t (°C)	k_c (dm^6 mol^{-2} s^{-1})	ΔH_c^* (kJ mol^{-1})	ΔS_c^* (J K^{-1} mol^{-1})	k_d (dm^9 mol^{-3} s^{-1})
$[Pt(en)(meen)]^{2+}$	*trans*-$[Pt(en)_2Cl_2]^{2+}$	25.0	4.54×10^{2}			—
		35.0	6.16×10^{2}	21.6	−122	—
		45.0	8.37×10^{2}			—
	trans-$[Pt(en)(1,3\text{-pn})Cl_2]^{2+}$	25.0	5.10×10^{2}			—
		35.0	6.86×10^{2}	19.2	−129	—
		45.0	8.86×10^{2}			—
	trans-$[Pt(en)(1,2\text{-pn})Cl_2]^{2+}$	25.0	3.33×10^{2}			—
		35.0	4.66×10^{2}	21.6	−124	—
		45.0	6.13×10^{2}			—
	trans-$[Pt(en)(meen)Cl_2]^{2+}$	25.0	5.46×10^{2}			9.7×10^{2}
		35.0	7.37×10^{2}	19.2	−128	1.4×10^{3}
		45.0	9.49×10^{2}			2.1×10^{3}
	trans-$[Pt(en)(dmen)Cl_2]^{2+}$	25.0	2.48×10^{3}			—
		35.0	3.13×10^{3}	13.0	−136	—
		45.0	3.66×10^{3}			—
	trans-$[Pt(en)(tmen)Cl_2]^{2+}$	25.0	5.62×10^{3}			—
		35.0	6.74×10^{3}	10.4	−138	—
		45.0	7.80×10^{3}			—
$[Pt(en)(dmen)]^{2+}$	*trans*-$[Pt(en)_2Cl_2]^{2+}$	25.0	1.48×10^{1}			2.27×10^{1}
		35.0	2.02×10^{1}	22.2	−148	3.29×10^{1}
		45.0	2.77×10^{1}			4.75×10^{1}
	trans-$[Pt(en)(1,3\text{-pn})Cl_2]^{2+}$	25.0	1.22×10^{1}			1.03×10^{1}
		35.0	1.83×10^{1}	27.4	−132	1.40×10^{1}
		45.0	2.61×10^{1}			1.77×10^{1}
	trans-$[Pt(en)(1,2\text{-pn})Cl_2]^{2+}$	25.0	1.05×10^{1}			—
		35.0	1.58×10^{1}	27.7	−133	—
		45.0	2.26×10^{1}			—
	trans-$[Pt(en)(meen)Cl_2]^{2+}$	25.0	1.82×10^{1}			—
		35.0	2.65×10^{1}	25.4	−136	—
		45.0	3.70×10^{1}			—
	trans-$[Pt(en)(dmen)Cl_2]^{2+}$ [b]	25.0	2.66×10^{1}			3.2×10^{1}
		35.0	3.98×10^{1}	29.4	−119	4.2×10^{1}
		45.0	5.98×10^{1}			6.0×10^{1}
	trans-$[Pt(en)(tmen)Cl_2]^{2+}$	25.0	9.18×10^{1}			7.8×10^{1}
		35.0	1.33×10^{2}	27.0	−117	1.1×10^{2}
		45.0	1.94×10^{2}			1.3×10^{2}
$[Pt(en)(tmen)]^{2+}$	*trans*-$[Pt(en)_2Cl_2]^{2+}$	25.0	5.4×10^{-1}			4.8×10^{-1}
		35.0	7.7×10^{-1}	22.9	−173	7.5×10^{-1}
		45.0	1.03			1.11
	trans-$[Pt(en)(1,3\text{-pn})Cl_2]^{2+}$	25.0	4.6×10^{-1}			5.0×10^{-1}
		35.0	6.8×10^{-1}	26.4	−163	7.6×10^{-1}
		45.0	9.6×10^{-1}			1.2
	trans-$[Pt(en)(1,2\text{-pn})Cl_2]^{2+}$	25.0	4.3×10^{-1}			9.6×10^{-1}
		35.0	6.1×10^{-1}	25.7	−166	1.5
		45.0	8.8×10^{-1}			2.2
	trans-$[Pt(en)(meen)Cl_2]^{2+}$	25.0	9.75×10^{-1}			2.08
		35.0	1.33	22.9	−168	2.72
		45.0	1.86			3.35
	trans-$[Pt(en)(dmen)Cl_2]^{2+}$	25.0	1.80×10^{-1}			(0.1 ± 0.1)
		35.0	2.86×10^{-1}	31.7	−153	—
		45.0	4.29×10^{-1}			—
	trans-$[Pt(en)(tmen)Cl_2]^{2+}$	25.0	1.71×10^{-1}			1.3×10^{-1}
		35.0	3.14×10^{-1}	41.4	−120	2.0×10^{-1}
		45.0	5.27×10^{-1}			2.9×10^{-1}

[a] Estimated errors (from average errors in the rate constants) : ±4 kJ mol^{-1} (ΔH_c^*) and ±12 J K^{-1} mol^{-1} (ΔS_c^*).
[b] At $I = 6.5\times10^{-2}$ mol dm^{-3}: $k_c = 2.33\times10^{1}$ (25°C), 3.75×10^{1} (35°C), 5.34×10^{1} dm^6 mol^{-2} s^{-1} (45°C); $\Delta H_c^* = 30.3$ kJ mol^{-1}; $\Delta S_c^* = -117$ J K^{-1} mol^{-1}.

is shown in relationship (3):

$$-\frac{d[[Pt(en)(N\text{-}N)Cl_2]^{2+}]}{[[Pt(en)(N\text{-}N)Cl_2]^{2+}]\,dt} = k_{obs} = \{k_c[Br^-] + k_d[Br^-]^2\}[[Pt(en)(N'\text{-}N')]^{2+}]. \quad (3)$$

Actually, very small rate terms which are independent of the concentration of either platinum(II) {i.e. $k_a[Br^-]$} or bromide ions {i.e. $k_b[[Pt(en)(N'\text{-}N')]^{2+}]$} could be evidenced in some cases when very low concentrations of platinum(II) or bromide ions were used. However, their contribution to the overall rate was usually within the experimental errors when the reactions were carried out in the presence of added platinum(II) complexes and using not very low bromide ion concentrations. Only in the case of the reactions of *trans*-$[Pt(en)(N\text{-}N)Cl_2]^{2+}$ (N-N ≠ tmen)]$^{2+}$ was the k_a rate term always found to be important owing to the poor ability of the named platinum(II) complex to promote the reactions. However, in the evaluation of the k_c and k_d values reported in Table 4, care was taken for the albeit small contribution of the k_a and k_b rate terms. Only activation parameters related to k_c are reported in Table 4, the k_d values being too inaccurate (not better than 5%) to give reliable activation parameters.

DISCUSSION

The results obtained suggest that the reactions occur basically by the well-known atom-transfer redox mechanism (4).[1,2,9,10] In the form depicted by eqs (4a)–(4d) such a mechanism is specifically referred to the reaction path responsible of the k_c rate term, but it can be adjusted to also explain the k_d rate term (see below) (as well as the k_a and k_b rate terms).

$$[Pt(en)(N'\text{-}N')]^{2+} + Br^- \overset{K}{\rightleftharpoons} [Pt(en)(N'\text{-}N')Br]^+ \quad (4a)$$

$$[Pt(en)(N\text{-}N)Cl_2]^{2+} + [Pt(en)(N'\text{-}N')Br]^+ \overset{k_1}{\underset{k_2}{\rightleftharpoons}} [Cl(en)(N\text{-}N)Pt\text{-}Cl\text{-}Pt(en)(N'\text{-}N')Br]^{3+} \quad (4b)$$

$$[Cl(en)(N\text{-}N)Pt\text{-}Cl\text{-}Pt(en)(N'\text{-}N')Br]^{3+} \xrightarrow{k_3} [Pt(en)(N\text{-}N)]^{2+} + Cl^- + [Pt(en)(N'\text{-}N')ClBr]^{2+} \quad (4c)$$

$$[Pt(en)(N'\text{-}N')ClBr]^{2+} + Br^- \xrightarrow{Fast,\ [Pt(en)(N'\text{-}N')]^{2+}} Cl^- + [Pt(en)(N'\text{-}N')Br_2]^{2+}. \quad (4d)$$

The reaction steps depicted here give an account of the reactions displaying stoichiometry (2) as well as of those displaying stoichiometry (1) provided that N-N and N′-N′ are the same. In order to account for stoichiometry (1) of reactions involving platinum(IV) complexes bearing N-N ligands less bulky than N′-N′ coordinated to the starting platinum(II) complex, the subsequent fast reaction (4e) can be confidently suggested to occur:

$$[Pt(en)(N'\text{-}N')Br_2]^{2+} + [Pt(en)(N\text{-}N)]^{2+} \xrightarrow{Fast,\ Br^-} [Pt(en)(N'\text{-}N')]^{2+} + [Pt(en)(N\text{-}N)Br_2]^{2+}. \quad (4e)$$

Some remarks support the reliability of such a proposal. Firstly, data are available[11] which indicate that hindering ligands thermodynamically stabilize platinum(II) over platinum(IV). On this basis only, the occurrence of reaction (4e) is extensively favoured when the N′-N′ ligands are much more hindered than N-N so that *trans*-$[Pt(en)(N\text{-}N)Br_2]^{2+}$ will be the actual product of the overall reaction. Secondly, such a reaction step is expected to be very fast even if the concentration of the $[Pt(en)(N\text{-}N)]^{2+}$ intermediate is very low, if for no other reason than because a bromide ion acts as the bridging atom.[1,2]

Relationship (5) is the rate law expression for reaction mechanism (4) and is fully consistent with that related to the k_c rate term if relationship (6) is accepted:

$$-\frac{d[[Pt(en)(N\text{-}N)Cl_2]^{2+}]}{[[Pt(en)(N\text{-}N)Cl_2]^{2+}]\,dt} = \frac{k_1k_3}{k_2+k_3}K[Pt(en)(N'\text{-}N')]^{2+}][Br^-] \quad (5)$$

$$k_c = \frac{k_1k_3}{k_2+k_3}K \approx \frac{k_1}{k_2}k_3K. \quad (6)^*$$

The second-order dependence on the bromide ions related to the k_d rate term has been previously observed in some cases and ascribed[1] to a reaction path involving a Pt^{IV}, Br^- ion pair in step (4b) instead of *trans*-$[Pt(en)(N\text{-}N)Cl_2]^{2+}$. Although such an interpretation is attractive, it should be recalled that second-order dependencies on halide ion concentration have been found many times lately in the oxidation reactions of cationic platinum(II) complexes,[12–14] even when the oxidizing agent is not adequate (e.g. $IrCl_6^{2-}$),[14] to form ion pairs with anions. A reaction path involving a $Pt(en)(N'\text{-}N')Br^+$, Br^- ion pair in (4b) would pro-

* The simplification adopted takes into account the fact that the atom-transfer redox act (k_3 rate term) is likely rate determining.

vide a reason for the occurrence of a second-order dependence of the rate on Br^- and cannot be ruled out in a tentative explanation of the k_d rate term.

An examination of the effect of the ligands on the rates will be restricted to the k_c reaction path.

The data in Table 4 unequivocably indicate that a change of the ligands coordinated to platinum(IV) and/or to platinum(II) has a kinetic effect on the rates of the reactions studied in this paper. However, it is generally found that platinum(IV) or platinum(II) complexes containing only primary diamines react very similarly. Therefore, neither the expansion of the chelate ring (on going from en to 1,3-pn) nor the replacement of a hydrogen atom by a methyl group on the carbon next to the H_2N group (on going from en to 1,2-pn) play an important part in the reactivity of both platinum(IV) towards reduction and platinum(II) towards oxidation. Conversely, the replacement of hydrogen atoms on nitrogen by methyl groups has a definite effect on the rates. Such an effect appears to be qualitatively larger (though in the opposite direction) when N-methyl groups are contained in platinum(II) rather than in platinum(IV) complexes. Moreover, it appears that the observed effect is quantitatively dependent on the particular platinum(II) or platinum(IV) chosen as standard reducing or oxidizing reagent, respectively. Thus, the relative reactivity trends shown in Table 5 are observed at 25°C either for the reductions of platinum(IV) complexes [Table 5(A)] or for the oxidation of platinum(II) complexes [Table 5(B)], as a function of the particular platinum(II) or platinum(IV) complex used as reductant or oxidant, respectively.

A simple explanation of such behaviour is difficult, since a guess of the activation parameters, even once their limited reliability is considered, shows that the reactivity trend found for the reduction of *trans*-$[Pt(en)(N\text{-}N)Cl_2]^{2+}$ complexes is largely associated with changes of the enthalpy of activation, whereas changes of the entropy of activation appear to be very important in establishing the reactivity trends for the oxidation of $[Pt(en)(N'\text{-}N')]^{2+}$ complexes, at least when platinum(IV) complexes containing primary diamines are used as oxidizing agents. Many factors may participate in causing the observed trends, in particular solvation changes connected with the replacement of hydrophilic hydrogen groups on nitrogen by hydrophobic methyl groups and changes of steric hindrance caused by the N-methyl groups which are located near the central metal atom. However, many results previously reported in several papers were satisfactorily accounted for by assuming that steric hindrance has a prevailing part in affecting the reactivity of both platinum(IV) complexes towards reduction[3,5,13] and platinum(II) complexes towards oxidation,[3,13,15–18] including platinum(II)[18,19] and platinum(IV)[5] complexes containing en, meen, dmen, and tmen as ligands. On the other hand, the role of steric hindrance in affecting the rates of redox reactions is fully recognized.[20–27] Changes in steric hindrance near the metal atom centres can be reasonably suggested to be responsible for the reactivity trends estab-

Table 5. (A) Relative reactivity for the reduction of *trans*-$[Pt(en)(N\text{-}N)Cl_2]^{2+}$

Platinum(II) reducing complex	Relative reactivity trend as a function of N—N			
	en	meen	dmen	tmen
$[Pt(en)_2]^{2+}$	1.0	1.4	5.8	17
$[Pt(en)(meen)]^{2+}$	1.0	1.2	5.5	12
$[Pt(en)(dmen)]^{2+}$	1.0	1.2	1.8	6.2
$[Pt(en)(tmen)]^{2+}$	1.0	1.8	3.3×10^{-1}	3.2×10^{-1}

Table 5. (B) Relative reactivity for the oxidation of $[Pt(en)(N'\text{-}N')]^{2+}$

Platinum(IV) oxidizing complex	Relative reactivity trend as a function of N'—N'			
	en	meen	dmen	tmen
trans-$[Pt(en)_2Cl_2]^{2+}$	1.0	9.6×10^{-1}	3.1×10^{-2}	1.1×10^{-3}
trans-$[Pt(en)(meen)Cl_2]^{2+}$	1.0	8.2×10^{-1}	2.7×10^{-2}	1.5×10^{-3}
trans-$[Pt(en)(dmen)Cl_2]^{2+}$	1.0	9.1×10^{-1}	9.7×10^{-3}	6.6×10^{-5}
trans-$[Pt(en)(tmen)Cl_2]^{2+}$	1.0	6.9×10^{-1}	1.1×10^{-2}	2.1×10^{-5}

lished in this paper and the following discussion will be centred on this hypothesis.

According to mechanism (4) the experimental rate constant, k_c, is a composite function of [see eq. (6)]: (a) the stability of the five-coordinate platinum(II) adduct, $[Pt(en)(N'\text{-}N')Br]^+$, accounted for by the stability constant K (step 4a), (b) the thermodynamic tendency of the interacting platinum complexes to form the bridged precursor, accounted for by k_1/k_2 (step 4b), and (c) the feasibility of the atom-transfer redox path, accounted for by k_3 (step 4c). A convenient starting point for a discussion is to consider the reactivity trends of platinum(IV) complexes during the reduction by a common platinum(II) complex. The benefit is that in such cases the stability constant of the five-coordinated complex, K, is the same for the entire sequence of reactions, so that observed changes of reactivity should be related only to changes in k_1/k_2 and/or k_3. As far as changes of the diamine in *trans*-$[Pt(en)(N\text{-}N)Cl_2]^{2+}$ are concerned, it can be expected that the formation of the bridged precursor becomes thermodynamically more difficult on increasing the number of N-methyl groups on the diamine, owing to the hampering steric interactions arising between these groups and the ligands bonded to the approaching platinum(II) complex. As far as the k_3 atom-transfer redox step is concerned, it should be recognized that rearrangement of the first coordination sphere (and solvation sphere) of both platinum(IV) and platinum(II) complexes plays a predominant part in the attainment of the transition state configuration of this reaction step. On this basis, it can be reasonably expected that this redox step becomes progressively more favoured on increasing the tendency of platinum(IV) to convert into platinum(II), since a lower rearrangement of the coordination sphere round platinum(IV) will be required [the reducing platinum(II) reactant should play a minor part as it is kept constant]. On the other hand, it should be recalled that (a) increasing steric hindrance near the metal atom stabilizes platinum(II) over platinum(IV)[11] and (b) it is a rather common feature that a redox reaction is kinetically and thermodynamically favoured in the same direction.[10] Therefore, the k_3 term (step 4c) should increase with increasing steric hindrance of N-N in *trans*-$[PtCl_2(en)(N\text{-}N)]^{2+}$. In conclusion, an increase of the steric hindrance near the platinum(IV) centre is expected to cause a decrease of the k_1/k_2 value and an increase of the k_3 term. Experimentally, it is found that the reactivity of platinum(IV) complexes towards reduction by a given platinum(II) complex increases smoothly with the steric hindrance caused by N-N, at least as far as platinum(II) complexes containing non-bulky diamines are considered [however, for platinum(II) complexes containing a very bulky diamine such as tmen the order is somewhat reversed]. Therefore, it can be concluded that in these cases the most commonly observed reactivity trend of platinum(IV) complexes is mainly ascribable to the fact that the positive effect of the driving forces on step (4c) caused by steric hindrance normally exceeds the opposite effect connected with the concomitant destabilization of the bridged precursor. The large important kinetic role played by steric hindrance in the stability of the bridged precursor can be envisaged by comparing the rate constants of the reactions between platinum(IV) and platinum(II) complexes containing identical diamines (e.g. N-N = N'-N' = en, meen, dmen, tmen). In such cases, the atom-transfer redox step (k_3) should scarcely be affected by changes of the ligands since the tendency of platinum(IV) to convert to platinum(II) should be essentially balanced by the opposing tendency of platinum(II) to convert into platinum(IV). On the other hand, the stability constant of the five-coordinated platinum(II), K, should also not change significantly on changing the diamine. Therefore, in the cases above, changes in stability of the bridged precursor, k_1/k_2, should be mostly responsible for any reactivity changes. The relative rates on changing N-N at 25°C are of the order: en (1.0) $\sim$ meen (1.1) $>$ dmen (5.6×10^{-2}) $>$ tmen (3.6×10^{-4}). Therefore, for the above considerations, such a sharp decrease should be ascribed to the destabilizing effect caused by steric hindrance on the bridged intermediate precursor formation. The relative stability of the bridged intermediate is likely to also have a strong part in determining the sequence of reactivity of the series of platinum(II) complexes studied on oxidation by a given platinum(IV) complex. In such cases each of the K, k_1/k_2 and k_3 terms may in principle be affected by changes in the ligands on platinum(II). However, the stability constant of $[Pt(en)(N'\text{-}N')Br]^+$ should not be affected much by changes in the diamine since the steric hindrance should not significantly obstruct the approach of Br^- and even the acceptor ability of platinum(II) should not be affected by changes in ligands of similar basicity. Conversely, the stability of the bridged precursor should decrease by the increasing steric hindrance of the diamine on platinum(II). On the other hand, the atom-transfer redox step should be disfavoured by increasing steric hindrance since (see above) the latter hampers the conversion of platinum(II) to platinum(IV). Therefore, in such cases an increase in steric hindrance near platinum(II) would lead to a decrease of both k_1/k_2 and k_3, thus leading to a decrease in the

experimental rate constant, k_c, which has just been found experimentally.

We can now try to account also for the above-mentioned higher effect displayed by changes in steric hindrance on platinum(II) rather than in platinum(IV) complexes. In fact, when the replaced diamine is linked to platinum(II) both k_1/k_2 and k_3 change in the same direction causing the greatest overall effect, whereas when the replacement is performed on the platinum(IV) complex these terms tend to balance each other, causing the lowest overall effect. Moreover, since a similar dichotomous behaviour should also operate in the contribution of enthalpies and entropies of steps (4b) and (4c) on the experimental enthalpies and entropies of activation, a reasonable justification of the fact that the entropy and enthalpy of activation have a different weight when diamine changes are performed on platinum(IV) rather than on platinum (II) complexes is found.

Finally, it was noticed above that the relative reactivity trends are also dependent on the particular platinum(II) or platinum(IV) complex used as the standard reducing or oxidizing reagent, respectively. This behaviour indicates that the steric hindrances of platinum(IV) and platinum(II) do not behave as mutually independent factors, i.e. they are not additive parameters. This is possibly due to the fact that the Pt^{IV}—Cl—Pt^{II} bridge in the bridged precursors is not symmetric, resembling the cation of Wolfram's red salt in which the Pt^{IV}—Cl bond length is much shorter than that of Pt^{II}—Cl.[28,29] This means that the extent of the interactions between the ligands bonded to platinum(IV) and platinum(II) (and between the ligands and the transferring chloride group) will be dependent on the reciprocal sites where the ligands are located.

Acknowledgement—This work was supported by the Ministero dell'Universita' e della Ricerca Scientifica e Technologica.

REFERENCES

1. W. R. Mason, *Coord. Chem. Rev.* 1972, **7**, 241.
2. A. Peloso, *Coord. Chem. Rev.* 1973, **10**, 123.
3. A. Peloso, *J. Chem. Soc., Dalton Trans.* 1984, 249.
4. A. J. Poë, *J. Chem. Soc.* 1963, 183.
5. A. J. Poë and D. H. Vaughan, *J. Am. Chem. Soc.* 1970, **92**, 7537.
6. A. Peloso, *Gazz. Chim. Ital.* 1970, **100**, 188.
7. H. Ito, J. Fujita and K. Saito, *Bull. Chem. Soc. Japan* 1969, **42**, 1286.
8. R. C. Johnson and F. Basolo, *J. Inorg. Nucl. Chem.* 1960, **13**, 36.
9. F. Basolo and R. G. Pearson, *Mechanisms of Inorganic Reactions*, Ch. 6. Wiley, New York (1967).
10. R. D. Cannon, *Electron Transfer Reactions*, Ch. 5. Butterworths, London (1980).
11. N. N. Zheligovskaya, N. Kamalov and S. I. Spitsyn, *Bull. Acad. Sci., USSR* 1975, **24**, 2289.
12. A. Peloso and M. Basato, *J. Chem. Soc., Dalton Trans.* 1972, 2040.
13. A. Peloso, *J. Chem. Soc., Dalton Trans.* 1979, 1160.
14. A. Peloso, *J. Chem. Soc., Dalton Trans.* 1987, 1473.
15. F. Basolo, M. L. Morris and R. G. Pearson, *Discuss. Faraday Soc.* 1960, **29**, 80.
16. A. Peloso, *J. Chem. Soc., Dalton Trans.* 1983, 1285.
17. A. Peloso, *Gazz. Chim. Ital.* 1985, **115**, 625.
18. A. Peloso, *J. Chem. Soc., Dalton Trans.* 1988, 1577.
19. A. Peloso, *Gazz. Chim. Ital.* 1988, **118**, 787.
20. A. Peloso, *Gazz. Chim. Ital.* 1990, **120**, 61.
21. Yan-i Wang and E. S. Gould, *J. Am. Chem. Soc.* 1969, **91**, 4998.
22. K. Ohashi, *Bull. Chem. Soc. Japan* 1972, **45**, 947.
23. J. C. Chen and E. S. Gould, *J. Am. Chem. Soc.* 1973, **95**, 5539.
24. Fu-Ren, F. Fan and E. S. Gould, *Inorg. Chem.* 1974, **13**, 2639.
25. C. A. Koval, R. L. A. Pravata and C. M. Reidsema, *Inorg. Chem.* 1974, **23**, 545.
26. G. Costa, A. Puxeddu, C. Tavagnacco and R. Dreos-Garlatti, *Inorg. Chim. Acta* 1984, **89**, 65.
27. T. W. Hambley, *Inorg. Chem.* 1988, **27**, 2496.
28. M. B. Robin and P. Day, *Adv. Inorg. Chem. Radiochem.* 1967, **10**, 247.
29. M.-H. Whangbo and M. J. Foshee, *Inorg. Chem.* 1981, **20**, 113.

Polyhedron Vol. 10, No. 18, pp. 2203–2215, 1991
Printed in Great Britain

0277–5387/91 $3.00+.00
© 1991 Pergamon Press plc

SYNTHESIS, STRUCTURE AND MOLECULAR ORBITAL STUDIES OF A SERIES OF CUBANE-TYPE TETRANUCLEAR MOLYBDENUM (TUNGSTEN) CLUSTERS WITH $[S_2P(OC_2H_5)_2]^-$ AS LIGANDS

LU SHAO-FANG,* HUANG JIAN-QUAN,† ZHUANG HONG-HUI, LI JUN-QIAN,† WU DING-MING, HUANG ZI-XIANG, LU CAN-ZHONG, HUANG JIN-LING† and LU JIA-XI

Fujian Institute of Research on the Structure of Matter, Academia Sinica, Fuzhou Laboratory of Structural Chemistry, The Department of Chemistry, Fuzhou University, Fuzhou, Fujian 350002, R.O.C.

(*Received* 17 *October* 1990; *accepted* 5 *April* 1991)

Abstract—The synthetic route, structural features and qualitative results of molecular orbital calculations for 10 cubane-type tetranuclear molybdenum (tungsten) clusters with $S_2P(OC_2H_5)_2$(dtp) as the ligand are summarized. There are two cluster cores, $[Mo_4S_4]$ and $[Mo_4OS_3]$, in the structures of a series of the compounds. Two isomer configurations—α and β—exist for both cubane cores which possess very similar total energies. The difference between the α and β configurations lies only in the coordinating fashion of the dtp ligands to the molybdenum (tungsten) atoms. A characteristic feature of these M—S tetranuclear cluster compounds is that a change in the number of electrons of $\{Mo_4\}$ from 10 to 12 does not affect the fundamental cubane-like molecular configuration. This may be attributed to the effect of symmetry of the cluster structure and the nature of the ligand on the electronic structure of the compounds.

During the past decade, with the exploration of biochemical systems in life processes, the chemistry of cubane-type tetranuclear metal clusters has grown at an enormous rate,[1–5] since the M_4S_4 complexes may act as the active centre in these processes. Our recent research on cubane clusters with dtp ligands [dtp = $S_2P(OC_2H_5)_2$] of $[M_4S_3X(dtp)_6]^n$ (M = Mo or W; X = S or O; $n = 0$ or -1) is summarized here and includes the synthetic route, structural features, as well as the qualitative results of the molecular orbital (MO) calculations for 10 compounds. These clusters are listed as follows:

α-$Mo_4OS_3(\mu$-dtp$)_3$(dtp$)_3$ (1)

α-$Mo_4OS_3(\mu$-dtp$)_3$(dtp$)_3 \cdot 3CH_3CN$ (2)

α-$Mo_4XS_3(\mu$-dtp$)_3$(dtp$)_3$ (3)

(X = S, O; the occupancy factor is about 60% for S)

β-$Mo_4OS_3(\mu$-dtp$)_2$(dtp$)_4$ (4)

β-$Mo_4S_4(\mu$-dtp$)_2$(dtp$)_4$ (5)

β-$Mo_4S_4(\mu$-OAc$)_2$(dtp$)_4$ (6)

β-$Mo_4S_4(\mu$-OAc$)_2$(dtp$)_4 \cdot H$ (7)

β-$Mo_4S_4(\mu$-OAc$)_2$(dtp$)_4 \cdot H \cdot (CH_3)_2CO$ (8)

β-$W_4S_4(\mu$-dtp$)_2$(dtp$)_4$ (9)

α-$W_4S_4(\mu$-dtp$)_3$(dtp$)_3$ (10)

EXPERIMENTAL

The following instruments were used in this work: IR, Perkin–Elmer 577 spectrophotometer, KBr plate; UV–vis absorption, UV-300 Shimadzu recording spectrophotometer, DMSO as the solvent; ^{1}H NMR, VARIAN FT-80A spectrometer; ESR, ER-420 spectrometer, powder specimen; XPS, NP-3G spectrometer (Shenyang Scientific Instrument Factory, Chinese Academy of Sciences),

* Author to whom correspondence should be addressed.
† Invited Professor at Fuzhou University.

radiation source: Mg-K_α (1253.6 eV), 15 kV, 5 mA; cyclic voltammograms, CV-1b cyclic voltammograph and an X–Y recorder; X-ray crystallography, Enraf–Nonius CAD-4 diffractometer. Other details may be found in the related references.

RESULTS AND DISCUSSION

Synthetic route

The spontaneous self-assembly synthesis from the mononuclear molybdenum (tungsten) compounds

The reactions are as follows:

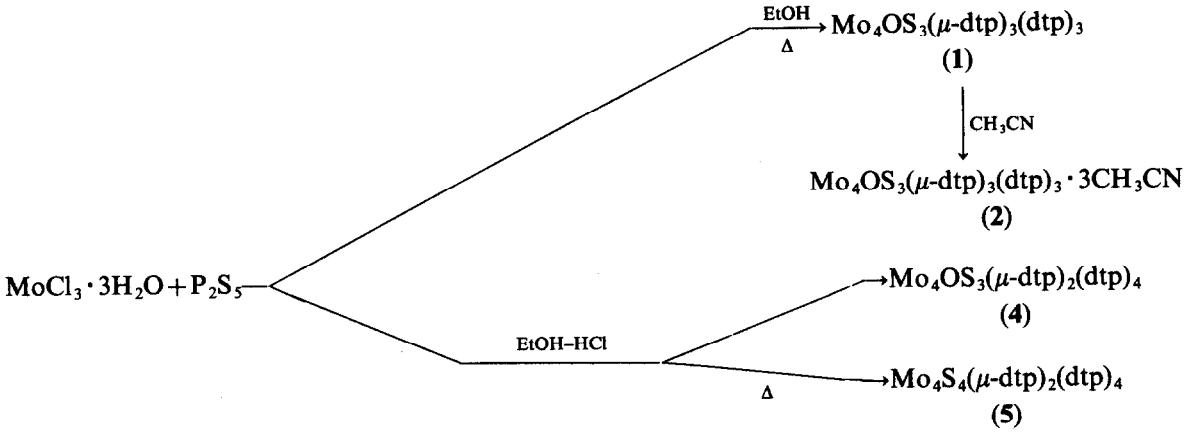

$$Mo(CO)_6 + MoCl_5 \xrightarrow[\Delta]{EtOH,\ P_2S_5} Mo_4XS_3(\mu\text{-dtp})_3(dtp)_3 \quad (X = 40\%\ O + 60\%\ S) \qquad (3)$$

$$W(CO)_6 + Na_2WO_4 \xrightarrow[\Delta]{EtOH,\ P_2S_5} W_4S_4(\mu\text{-dtp})_2(dtp)_4 \qquad (9)$$

$$K_3W_2Cl_9(aq.) \xrightarrow{\text{Ion exchange}} H_3W_2Cl_9 \xrightarrow{P_2S_5,\ EtOH} W_4S_4(\mu\text{-dtp})_3(dtp)_3. \qquad (10)$$

Although the spontaneous self-assembly synthesis is an effective method in the discovery and preparation of new cluster compounds, it has obvious limitations. Firstly, the success of obtaining a new cluster is sometimes only achieved by accident. Secondly, except for compounds **1** and **5**, poor reproducibility and low yields occur in the other synthesis.

The designed syntheses from some polynuclear molybdenum cluster compounds

(1) By direct ligand substitution of a Mo_4 cluster:

$$Mo_4S_4(\mu\text{-dtp})_2(dtp)_4 \xrightarrow{NaOAc} Mo_4S_4(\mu\text{-OAc})_2(dtp)_4$$
(5) (6)

or (2) by a [3 + 1] reaction mode via $[Mo_3S_4]^{4+} + Mo$:

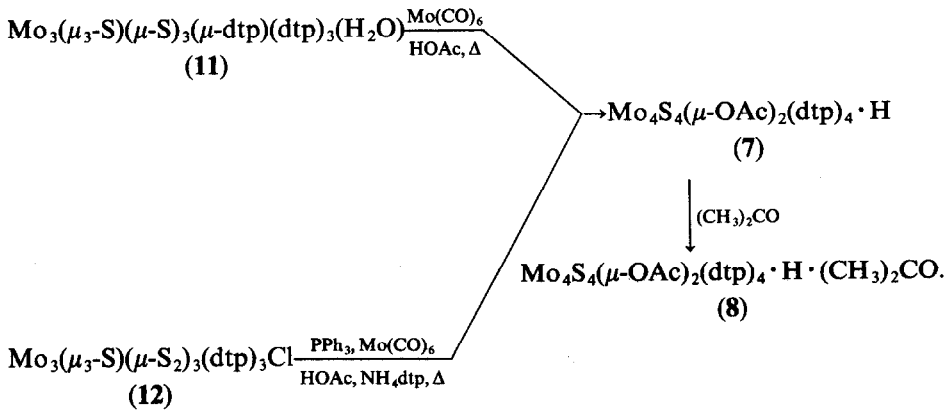

In route (1) it is reasonable to suppose that cluster **6** can be obtained by OAc selective substitution of two bridging dtp from six dtp ligands in cluster **5**, since the OAc^- ligand can only be used as a bridging bidentate ligand in Mo_4 cluster compounds. In route (2), our proposal is (1) the successful synthesis of **6** by a [3 + 1] mode using **11**[26] is dependent on the choice of oxidation state of the added molybdenum cluster. On consideration of **11**, e.g. $[Mo_3S_4]^{4+}$, our attempted synthesis is the reaction of $Mo(CO)_6$ with HOAc to form $Mo_2(OAc)_4$, thereby containing the adduct according to $[Mo_3S_4]^{4+} + Mo^{2+} \rightarrow [Mo_4S_4]^{6+}$ (**6**). (2) When **12**[27] is used as the reactant in a [3 + 1] reaction, the addition of PPh_3 as a desulphurizing reagent changes (μ-S_2) into μ-S; at the same time a dtp ligand is added. The other reaction conditions are similar to those with compound **11**. However, it is shown from the structural analysis that the actual product in the above two reactions is **7**, i.e. $[Mo_4S_4]^{5+}$. One more hydrogen atom is present in **7** than in **6**, which is probably due to the reduction by $Mo(CO)_6$, but the reaction details are not yet clear.

Compared with the spontaneous self-assembly method, this designed synthesis of new cluster compounds from known clusters has the advantages of good reproducibility, high yields and product prediction.

The structural feature

The molecular configuration

The four basic molecular structures of the compounds are shown in Fig. 1. It can be seen that the Mo_4 core displays distorted tetrahedral geometry and contains six Mo—Mo bonds. The μ_3 ligands cap the faces of the Mo_4 tetrahedron (three of which are sulphido atoms and the fourth is a sulphido or oxygen atom) to form the Mo_4XS_3 (M = Mo or W; X = O or S) cubane-type cluster atom. Although many cluster compounds containing the "$[Mo_4S_4]$" core have been reported,[11] the $[Mo_4OS_3]$ core was first discovered by us, and contains the mixed S/O cuboidal Mo_4 species.[28,29]

There are also six dtp bidentate ligands in the

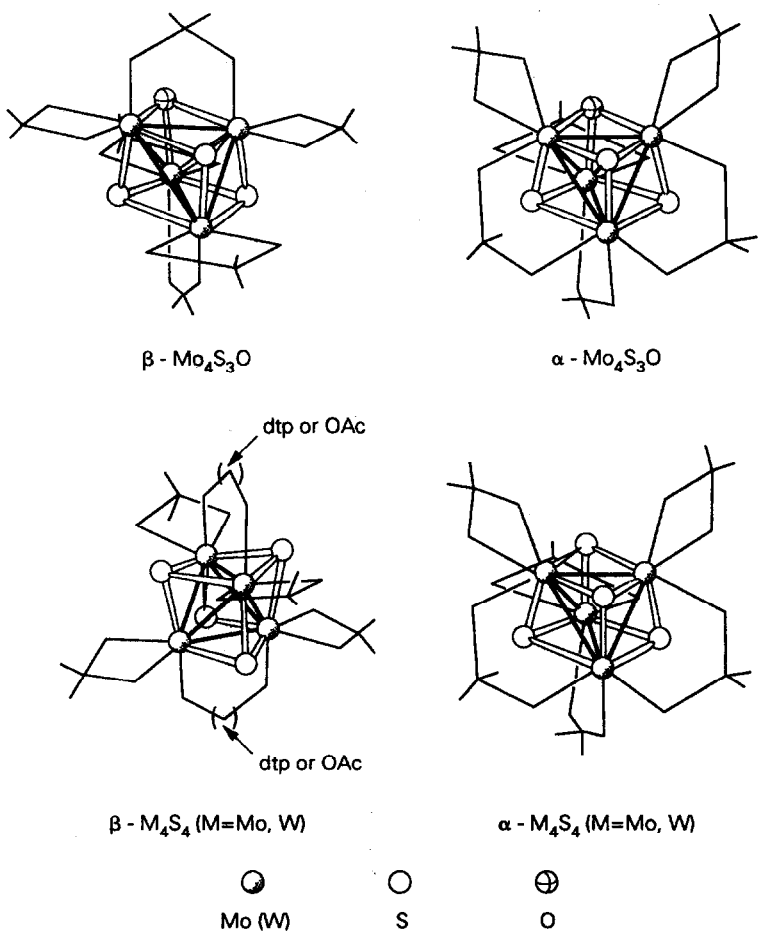

Fig. 1.

Table 1. The main structural data for 10 tetranuclear molybdenum (tungsten) cluster compounds

Compound	Space group	Unit cell parameters	The number of electrons in [Mo_4] (Mo oxidation state)	The symmetry of the core	Mo—Mo bond (Å)	Mo—μ_3S(μ_3-O) bond (Å) (W)	$\{Mo_4\}$ volume (Å)^3	Magnetism	Reference
α-$Mo_4OS_3(\mu$-dtp$)_3$(dtp$)_3$ (**1**)	$P\bar{1}$	$a = 13.387(3)$ Å $\alpha = 72.84(2)°$ $b = 13.997(4)$ Å $\beta = 87.92(3)°$ $c = 16.281(3)$ Å $\gamma = 84.87(2)°$ $V = 2903.2$ Å^3 $Z = 2$	58 (3.5)	C_{3v}	2.716(1) 2.704(2) 2.706(1) 2.837(1) 2.847(1) 2.838(1)	Mo—μ_3-S 2.350 Mo—μ_3O 2.050	2.512		16
α-$Mo_4OS_3(\mu$-dtp$)_3$(dtp$)_3 \cdot 3CH_3CN$ (**2**)	$R3$	$a = b = c = 12.852(3)$ Å $\alpha = \beta = \gamma = 108.37(2)°$ $V = 1697.3$ Å^3 $Z = 1$	58 (3.5)	C_{3v}	2.831(1) × 3 2.700(1) × 3	$\overline{\text{Mo—}\mu_3\text{S}}$ 2.356 Mo—μ_3O 2.036	2.486		17
α-$Mo_4XS_3(\mu$-dtp$)_3$(dtp$)_3$ (**3**) (X = S, 60% and O, 40%)	$P\bar{1}$	$a = 14.031(4)$ Å $\alpha = 92.15(3)°$ $b = 13.372(2)$ Å $\beta = 72.91(3)°$ $c = 16.270(8)$ Å $\gamma = 95.20(2)°$ $V = 2905.4$ Å^3 $Z = 2$	58 (3.5)	C_{3v}	2.736(2) 2.723(1) 2.732(1) 2.861(1) 2.863(1) 2.875(1)	Mo—μ_3S 2.346 Mo—μ_3X 2.248	2.581		18
β-$Mo_4OS_3(\mu$-dtp$)_2$(dtp$)_4$ (**4**)	$P2_1/n$	$a = 13.689(2)$ Å $b = 30.903(4)$ Å $\beta = 93.07(1)°$ $c = 14.212(2)$ Å $V = 6003$ Å^3 $Z = 4$	58 (3.5)	C_{2v}	2.673(1) 2.748(1) 2.758(1) 2.821(1) 2.818(1) 2.811(1)	Mo—μ_3S 2.344 Mo—μ_3O 2.005	2.511		19

β-$Mo_4S_4(\mu\text{-dtp})_2(dtp)_4$ (**5**)	$P2/n$	$a = 12.827(3)$ Å $b = 17.206(3)$ Å $\beta = 97.12(2)°$ $c = 13.507(2)$ Å $V = 2958.0$ Å^3 $Z = 2$	58 (3.5)	D_{2d}	2.746(4) 2.808(5) 2.856(3) × 2 2.865(3) × 2	Mo—μ_3S	2.333	2.679		20
β-$Mo_4S_4(\mu\text{-OAc})_2(dtp)_4$ (**6**)	$P2/c$	$a = 13.176(4)$ Å $b = 11.699(3)$ Å $\beta = 116.11(3)°$ $c = 18.526(4)$ Å $V = 2564$ Å^3 $Z = 2$	58 (3.5)	D_{2d}	2.739(2) 2.748(2) 2.665(2) × 2 2.879(2) × 2	Mo—μ_3S	2.343	2.486	Paramagnetic	21
β-$Mo_4S_4(\mu\text{-OAc})_2(dtp)_4 \cdot H$ (7)	$Pcab$	$a = 18.90(2)$ Å $b = 21.678(4)$ Å $c = 24.491(4)$ Å $V = 10031(7)$ Å^3 $Z = 8$	59 (3.25)	D_{2d}	2.685(1) 2.707(1) 2.765(1) 2.772(1) 2.969(1) 2.969(1)	Mo—μ_3S	2.354	2.606	Paramagnetic	22
β-$Mo_4S_4(\mu\text{-OAc})_2(dtp)_4 \cdot H \cdot (CH_3)_2CO$ (**8**)	$P2/n$	$a = 17.271(3)$ Å $b = 11.985(3)$ Å $\beta = 105.94(1)°$ $c = 13.061(2)$ Å $V = 2599(2)$ Å^3 $Z = 2$	59 (3.25)	D_{2d}	2.750(1) 2.761(1) 2.696(1) × 2 2.972(1) × 2	Mo—μ_3S	2.357	2.610	Paramagnetic	23
β-$W_4S_4(\mu\text{-dtp})_2(dtp)_4$ (**9**)	$P2/n$	$a = 12.807(3)$ Å $b = 17.195(5)$ Å $\beta = 97.33(2)°$ $c = 13.488(3)$ Å $V = 2946(7)$ Å^3 $Z = 2$	58 (3.5)	D_{2d}	2.756(5) 2.773(4) 2.834(3) × 2 2.846(3) × 2	W—μ_3S	2.35	2.629		24
α-$W_4S_4(\mu\text{-dtp})_3(dtp)_3$ (**10**)	$P\bar{1}$	$a = 14.063(5)$ Å $\alpha = 92.06(3)°$ $b = 16.289(4)$ Å $\beta = 95.24(3)°$ $c = 13.377(3)$ Å $\gamma = 73.06(2)°$ $V = 2919(3)$ Å^3 $Z = 2$	58 (3.5)	C_{3v}	2.749 2.872 2.879 2.742 2.747 2.896	W—μ_3S	2.355	2.629		25

cluster molecule. Their coordination can be divided into two different categories, α and β, according to the time order of discovery. In the cluster molecule of the α-type, three of the dtp groups are terminal ligands where the remaining three are bridging ligands. On the other hand, the β-type has four terminal chelating dtp and two bridging dtp or OAc ligands for molybdenum atoms. The structures of the already known compounds $Mo_4S_4(dtc)_6$ [dtc = $S_2CN(CH_3)_2$][30] and $Mo_4S_4(Et_2PS_2)_6$[31] belong to the β-type, while the α-type was also first discovered in our work.

Our synthetic experiments indicate that in the preparation of "Mo_4" clusters from mononuclear molybdenum compounds by the spontaneous self-assembly method, the $[Mo_4OS_3]^{6+}$ core tends to be the α-type whereas as for $[Mo_4S_4]^{6+}$, the formation of the β-type is favourable.

Important structural data

Table 1 summarizes the main structural data for the 10 compounds obtained by X-ray crystallography.

As shown in Table 1, the crystal structures of compounds **1**, **3** and **10** (all α-type core) belong to the triclinic system. However, the solvated cluster compound **2** has crystallographically imposed C_{3v} symmetry. So far, there are only two examples of cubane-type Mo_4 clusters possessing trigonal symmetry; the other example is $[Mo_4S_4(SCN)_{12}]$ discovered by Cotton.[3]

As for most of the β-type Mo_4 cluster crystals, they belong to the monoclinic or orthorhombic system.

The cubane-type cluster cores $[Mo_4OS_3]$ *and* $[Mo_4S_4]$

Mo—Mo *bond lengths and the volume of the* $[Mo_4]$ *tetrahedron*

In earlier studies on the trinuclear Mo—S cluster compounds, it was found that replacement of μ_3-S by μ_3-O for a pair of μ_3-S and μ_3-O trimolybdenum cluster analogue compounds tends to shorten the Mo—Mo distances. For example, the average Mo—Mo bond lengths of $Mo_3(\mu_3\text{-}S)(\mu\text{-}S)_3(dtp)_4 \cdot$Oxazole and $Mo_3(\mu_3\text{-}O)(\mu\text{-}S)_3(dtp)_4 \cdot$Oxazole[32] are 2.760 and 2.638 Å, respectively, with a difference of about 0.12 Å (as shown at the end of Table 2).

On account of our successful preparations of a series of $[Mo_4OS_3]$ and $[Mo_4S_4]$ clusters with dtp as ligands it is thus possible to compare the influence of μ_3-S and μ_3-O on the Mo—Mo bond, not only within the Mo_3 cluster analogue compounds but also within a single Mo_4 framework. The Mo—Mo bond lengths of the representative Mo_4 clusters are listed in Table 2.

Table 2. The Mo—Mo and Mo—μ_3-X bond distances (Å) for six tetranuclear molybdenum clusters

Clusters	Mo—Mo 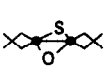	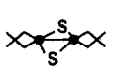	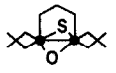	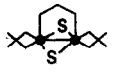	Mo—μ_3-S (av.)	Mo—μ_3-O (av.)
α-$Mo_4OS_3(\mu\text{-}dtp)_3(dtp)_3 \cdot 3CH_3CN$ (**2**)	2.831 × 3			2.700 × 3	2.356	2.036
β-$Mo_4OS_3(\mu\text{-}dtp)_2(dtp)_4$ (**4**)	2.821 2.818	2.748 2.758	2.811	2.673	2.344	2.005
α-$Mo_4XS_3(\mu\text{-}dtp)_3(dtp)_3$ (**3**)	2.863 2.866 2.880			2.738 2.733 2.728	2.346	(60%μ_3-S 40%μ_2-O) 2.248
β-$Mo_4S_4(\mu\text{-}dtp)_2(dtp)_4$ (**5**)		2.856 × 2 2.865 × 2		2.746 2.808	2.333	
β-$Mo_4S_4(\mu\text{-}OAc)_2(dtp)_4$ (**6**)		2.739 2.748 2.879 × 2		2.665 × 2	2.343	
β-$Mo_4S_4(\mu\text{-}OAc)_2(dtp)_4 \cdot H$ (**7**)		2.772 2.765 2.969 × 2		2.685 2.707	2.354	
$Mo_3(\mu_3\text{-}O)(\mu\text{-}S)_3(dtp)_4 \cdot$oxazole	2.628	2.642	2.644	2.638(av.)		2.027
$Mo_3(\mu_3\text{-}S)(\mu\text{-}S)_3(dtp)_4 \cdot$oxazole	2.752	2.760	2.767	2.760(av.)	2.337	

A comparison of the structural geometry and the Mo—Mo bond lengths of these compounds indicates that both the capping μ_3 ligand and the edge-bridging μ-dtp or μ-OAc ligands are two important factors in affecting the Mo—Mo bond.

Let us first discuss the influence of the bridging bidentate ligand on the Mo—Mo bond distances. In **5**, the average Mo—Mo distance between the two dtp bridged molybdenum atoms is 2.777 Å, whereas that for the four remaining, unbridged Mo—Mo bonds is 2.861 Å (they differ by 0.084 Å). Similarly, in **6**, the μ-OAc bridged Mo—Mo mean value of 2.655 Å is 0.146 Å shorter than the unbridged value of 2.811 Å. It can be seen, therefore, that the presence of bridging dtp or OAc results in the shortening of the Mo—Mo distances, i.e. the Mo—Mo interaction is increased. In addition, the OAc ligand has a stronger effect than the dtp ligand. These effects are very similar to those discussed previously in trinuclear molybdenum clusters.

The influence of μ_3-S and μ_3-O on Mo—Mo bonds in a Mo_4 core is also considered. In **2**, the mean value of three μ_3-O bridged Mo—Mo bonds is 2.831 Å, while that of the other three μ_3-S and μ-dtp bridged Mo—Mo bonds is 2.700 Å (a difference of 0.131 Å). On the other hand, in **4**, the average distance of the two μ_3-S/μ_3-O bridged Mo—Mo bonds is 0.067 Å longer than that of the μ_3-S/μ_3-S bridged molybdenum atoms, whereas that of the μ_3-O and μ-dtp bridged Mo—Mo bond is 0.138 Å longer than that of the μ_3-S and μ-dtp bridged Mo—Mo bond. Thus, it can be seen that in a $[Mo_4]$ core, the μ_3-S/μ_3-O bridged Mo—Mo bonds are always longer than those bridged by μ_3-S/μ_3-S atoms. This result is contrary to that in trinuclear molybdenum clusters, as shown in Table 2.

It is interesting to note that although the μ_3-O bridged Mo—Mo bonds are longer than the μ_3-S bridged bonds in the same molecule, in the $[Mo_4OS_3]$ core, the average value of the six Mo—Mo bond lengths is shorter than in $[Mo_4S_4]$, while the volume of the Mo_4 tetrahedra is still smaller. For instance, in the $[Mo_4OS_3]$ core of **4**, the average Mo—Mo bond is 2.772 Å and the $[Mo_4]$ volume 2.511 $Å^3$, whereas in the $[Mo_4S_4]$ core of **5**, the values are 2.883 and 2.679 $Å^3$, respectively.

Determination of IR and UV spectra

By using clusters **1** and **5** as representatives of $[Mo_4OS_3]$ and $[Mo_4S_4]$ cores, respectively, the measurement of their IR and UV spectra has been carried out. The selected results are as follows: ν(Mo—μ_3-O) (**1**), 590(m) (cm^{-1}); ν(Mo—μ_3-S) (**5**), 440–457(br), 300–360(w) (cm^{-1}). UV–vis absorption: $[Mo_4OS_3]$ (**1**), 240nm(s), 250nm(s), 330nm(br), 420nm(m), 540nm(br); $[Mo_4S_4]$ (**5**), 240nm(s), 350nm(m), 540nm(br), 675nm(w).

In the $[Mo_4OS_3]$ core, splitting of the peaks (240 and 250; 330 and 420) occurs, which correspond to the peaks at 240 and 350 nm in the spectrum of $[Mo_4S_4]$, owing to the lower symmetry caused by the substitution of one μ_3-S ligand by μ_3-O (see Fig. 2).

The number of bonding electrons in Mo_4 *clusters*

As has been mentioned above, when cluster **6** is synthesized by the [3+1] reaction mode, i.e. β-$Mo_4S_4(\mu\text{-}OAc)_2(dtp)_4$, it can be seen from the structural analysis that the resulting product is **7** rather than **6**, i.e. β-$Mo_4S_4(\mu\text{-}OAc)_2(dtp)_4 \cdot H$. Although the position of this hydrogen atom cannot be determined by X-ray crystal structural analysis, it is valid to say that the hydrogen atom does exist based on a variety of spectroscopic data.

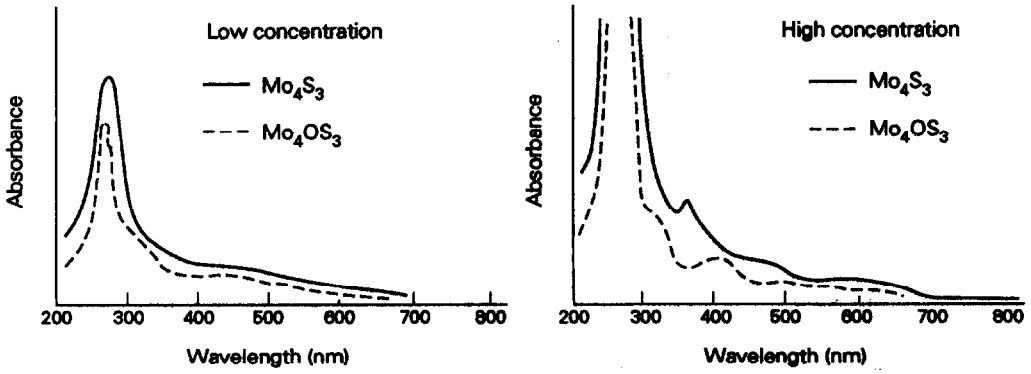

Fig. 2. Comparison of the electronic absorption spectra of $[Mo_4OS_3]^{6+}$ and $[Mo_4S_4]^{6+}$ in DMSO solutions.

Table 3. The Mo—Mo bond distances and number of electrons in [Mo_4]

Compounds	n	Number of electrons in [Mo_4]	Molybdenum oxidation state	Average Mo—Mo bond (Å)
$[Mo_4S_4(edta)_2]^{n-}$	2	10	3.5	2.826
	3	11	3.25	2.807
	4	12	3	2.783
$[Mo_4S_4(\eta\text{-}C_5H_4Pr^i)_4]^{n+}$	2	10	3.5	2.749
	1	11	3.25	2.856
	0	12	3	2.887
$[Mo_4S_4(\mu\text{-}OAc)_2(dtp)_4]^{n-}$	0 (**6**)	10	3.5	2.763
	1 (**7**)	11	3.25	2.811
	1 (**8**)	11	3.25	2.808

The interrelation of Mo—Mo *distances and the number of electrons in* Mo_4

In the two sets of Mo_4 clusters $[Mo_4S_4(\eta\text{-}C_5H_4Pr^i)_4]^{n+}$ ($n = 0, 1, 2$)[33] and $[Mo_4S_4(edta)_2]^{n-}$ ($n = 2, 3, 4$),[34] the Mo—Mo distances vary in a regular way with the number of electrons (10–12) in Mo_4 (see Table 3).

Although the variation of Mo—Mo distances as a function of the number of electrons from 10, 11 to 12 is different, the interrelationship between them is certainly present. As soon as the structural analysis indicates that a difference between the average Mo—Mo bond lengths in clusters **7** and **8** and those in cluster **6** occurs, we are aware that this may be due to the difference in the number of electrons in {Mo_4}. In {Mo_4} of **6**, there are only 10 electrons, while in **7** and **8**, {Mo_4} contains 11 electrons with corresponding total electron numbers of 58 and 59, respectively. Thus it may be deduced that a hydrogen ion must be present in the structures of **7** and **8** to achieve the electroneutrality.

The characterization of ^{1}H *NMR, ESR, XPS and cyclic voltammograms*

In order to further distinguish the differences between **6** and **7** (**8**), ^{1}H NMR, ESR, XPS and cyclic voltammograms were used under the same experimental conditions for the characterization of these compounds.

^{1}H *NMR*. It can be seen from Fig. 3 that an additional hydrogen resonance for **7** appears at 1.75 ppm which then disappears by rapid exchange with deuterium. Thus it may be considered as an active hydrogen in **7**.

ESR. The ESR parameters for **6** and **7** are given in Table 4.

It can be seen from Table 4 that the g factors of **6** and **7** (**8**) are significantly different from each other although they are all paramagnetic. This indicates that the electronic structures of **6** and **7** are also different.

XPS (*X-ray photoelectron spectroscopy*). All the measurements were performed with the Ag(3*d*) lines (373.89 eV, 367.9 eV) as the reference. The resolution is 0.1 eV and the relative binding energies can be measured to an accuracy of 0.05 eV. The electron binding energies of $Mo_3S_4(dtp)_4(H_2O)$ (here Mo is in the +4 oxidation state) are also given for comparison (Table 5).

It can be seen that binding energies of **7** are somewhat less than those of **6** (for $3d_{3/2}$ and $3d_{5/2}$): the oxidation state of molybdenum in **7** is +3.25 which is lower than that of **6**. The number of electrons in {Mo_4} in **6** and **7** is therefore 10 and 11, respectively.

Table 4. The ESR spectral parameters

Specimen	Temperature (K)	g_1	g_2	g_3
$Mo_4S_4(OAc)_2(dtp)_4$ (**6**)	289	2.79	2.29	~ 1.98
	77	2.37	2.14	1.98
$Mo_4S_4(OAc)_2(dtp)_4 \cdot H$ (**7**)	289	2.15	1.97	
	77	2.00	1.95	1.92

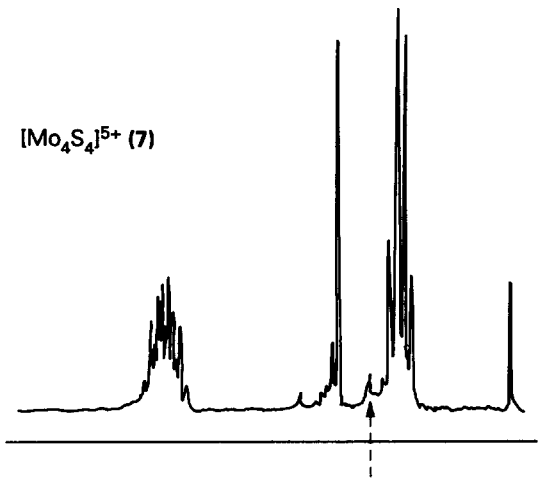

Fig. 3.

Cyclic voltammograms (see Fig. 4). Both the cyclic voltammograms of **7** and **6** have two quasi-reversible waves. The E_p values of **7** are shifted to more positive values than those of **6**, indicating that **7** is more readily reduced than **6**.

To sum up, it can be concluded that the structures of cluster compounds **6** and **7**, prepared by different synthetic routes, are very similar but their Mo—Mo electron numbers are different. This is a common phenomenon in many transition metal–sulphur cubane systems. This means that in this type of cluster molecules, the gain or loss of one or two electrons can still maintain the fundamental molecular configuration. It is also shown that the cubane-like configuration $[Mo_4S_4]$ may act as a reservoir of electrons for redox chemistry. It is on account of the discovery of the property of $[Fe_4S_4]$ ferredoxins as donors or acceptors of electrons in nature that the research on cubane-like metal cluster compounds has attracted great attention and made much progress.

The molecular orbital calculations

In order to elucidate the structural law mentioned above, an analysis of the electronic structure will be provided in this section. A systematic molecular orbital calculation has been carried out using the SCC–EHMO method,[35] developed by Hoffmann *et al.* on several typical clusters (**1**, **4**, **5**, **6** and **7**). The results of these calculations are provided to discuss the following three aspects.

The reason which causes the elongation of the Mo—Mo *bond lengths bridged by the* μ_3-O *atom in the* $[Mo_4OS_3]$ *core*

(1) *The effect of* d–pπ *conjugate interaction.* As is expected from the calculation of the multiple centre *d–p*π bond,[36,37] the OOP (Orbital Overlap Population) between the d_M (non-bonding *d* orbital) and *p*π (S or O lone-pair orbital) makes a significant contribution to the ROP (Reduced Overlap Population) between the metal and bridging atoms in the cluster. The ratio of OOP to ROP for the tetranuclear cluster is about 15–20%. In the α-type $[Mo_4OS_3]$ core (see Fig. 5), owing to the stronger Mo—S—Mo *d–p*π interaction than in Mo—O—Mo, the Mo(1)—S bond length is usually shorter than that of Mo(2)—S, 2.34 and 2.39 Å, respectively. Moreover, more *p*π electrons are transferred to the Mo(1)—S bond. According to the rule of bonding electron-pair repulsive interactions, the

Table 5. The binding energies (eV)

Sample	$3d_{3/2}$	$3d_{5/2}$	Oxidation state of molybdenum
$Mo_3S_4(dtp)_4(H_2O)$	233.65	230.95	+4
$Mo_4S_4(OAc)_2(dtp)_4$ (**6**)	232.21	229.05	+3.5
$Mo_4S_4(OAc)_2(dtp)_4 \cdot H$ (**7**)	232.04	228.84	+3.25

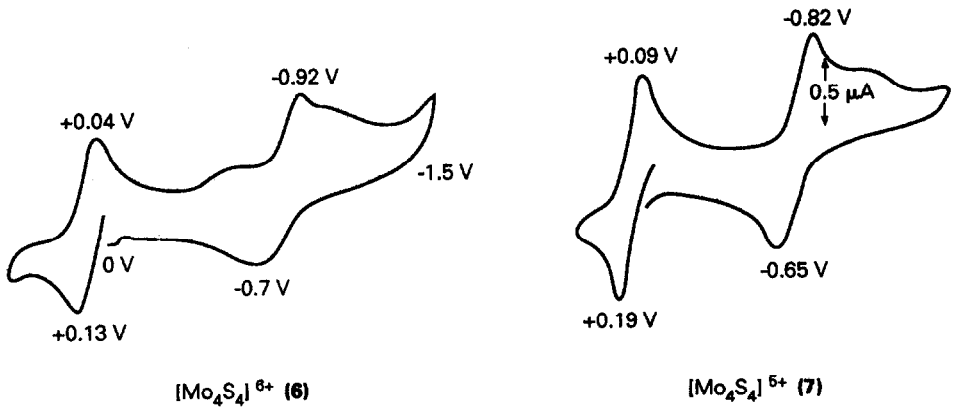

Fig. 4. Cyclic voltammograms (100 mV s^{-1}) of $[Mo_4S_4]^{6+}$ (**6**) and $[Mo_4S_4]^{5+}$ (**7**) (2 mM) in DMF solution containing 0.1 M Bu_4NClO_4 as the supporting electrolyte, peak potential vs SCE.

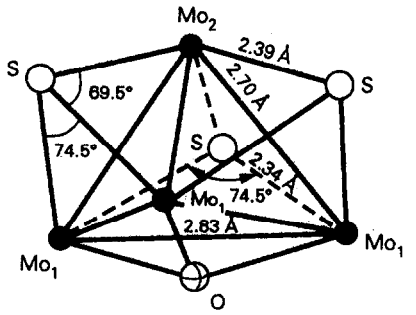

Fig. 5. The structural unit of the α-$[Mo_4OS_3]$ core.

Mo(1)—S—Mo(1) angle (74.5°) is greater than the Mo(2)—S—Mo(1) angle (69.5°). All this is consistent with the results from the X-ray structure analysis. As a consequence, the Mo(1)—Mo(1) bond length is longer than the Mo(1)—Mo(2) bond length.

(2) *The effect of the* μ_3-O *charge.* In general, the greater electronegativity of the oxygen atom increases the Mo—O—Mo bond angle. In the case of $[Mo_4OS_3]$, there is a considerably great negative charge on μ_3-O and therefore the Mo—O—Mo angle is extremely large (see Table 6). Thus, we can see that although the Mo—O bond length is roughly the same as those in other clusters, the charge effect is enough to cause the marked lengthening of the Mo(1)—Mo(1) bonds.

(3) *The pull effect of the bridging* dtp *ligand.* The bridging dtp ligand can actually pull two molybdenum atoms closer together, which results in the shortening of the Mo—Mo bonds.

By comparison, the above two effects (1) and (2) are the dominant factors in the lengthening of the Mo—Mo bond distances (as shown in Table 7). It can be seen from the table that in the β-type $[Mo_4OS_3]$ core, the order of distances is:

$$(\text{Mo—Mo})_{\mu_3\text{-S}+\mu_3\text{-O}+\mu\text{-dtp}} < (\text{Mo—Mo})_{\mu_3\text{-S}+\mu_3\text{-S}}$$
$$2.811\,\text{Å} \qquad 2.753\,\text{Å}$$

$$(\text{Mo—Mo})_{\mu_3\text{-S}+\mu_3\text{-O}+\mu\text{-dtp}} > (\text{Mo—Mo})_{\mu_3\text{-S}+\mu_3\text{-S}+\mu\text{-dtp}}$$
$$2.811\,\text{Å} \qquad 2.673\,\text{Å}.$$

Table 7 also lists the ROP values of various Mo—Mo bonds bridged by different ligands in the α- and β-type $[Mo_4OS_3]$ cores.

The relationship between the number of bonding electrons in M—M *and* M—M *bond lengths*

In the clusters where each metal atom is approximately octahedrally coordinated, according to the

Table 6. Some characterization data of μ-O in Mo clusters

Clusters	Net charge (μ_3,μ_2-O)	Angle (°) (Mo—O—Mo)	Distance (Å) (Mo—O)	Distance (Å) (Mo—Mo bridged by O)
$Mo_2O_4(SO_2NC_5H_{10})_2$	−0.2960	83.1	1.932	2.562
$[Mo_3O_2Cl_3]^{3+}$	−0.0564	73.9	2.130	2.560
$[Mo_4OS_3]^{6+}$ (α)	−1.20	88	2.037	2.831
$[Mo_4OS_3]^{6+}$ (β)	−1.21	89	2.005	2.820

Table 7. The Mo—Mo distances (Å) and ROP in α and β $[Mo_4OS_3]$ cores

Clusters	α-$Mo_4OS_3(dtp)_6$		β-$Mo_4OS_3(dtp)_6$			
Mo—Mo (Å)	2.700	2.831	2.673	2.753	2.811	2.820
ROP (Mo—Mo)	0.1845	0.0737	0.2616	0.1905	0.0946	0.0859
Bridge	μ_3-S+μ_3-S +μ-dtp	μ_3-S+μ_3-O	μ_3-S+μ_3-S +μ-dtp	μ_3-S+μ_3-S	μ_3-S+μ_3-O +μ-dtp	μ_3-S+μ_3-O

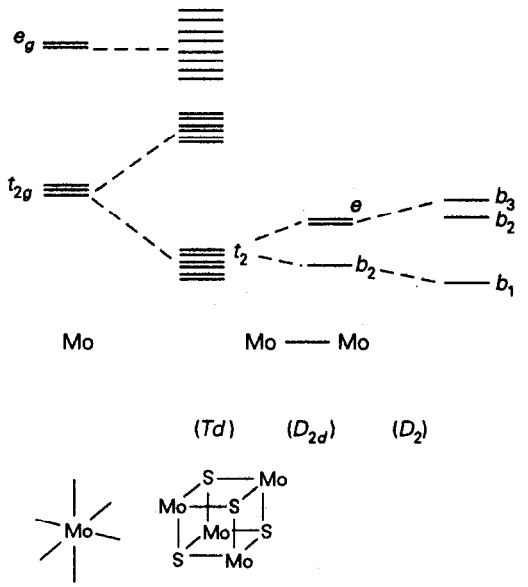

Fig. 6. Qualitative molecular orbital energy level scheme.

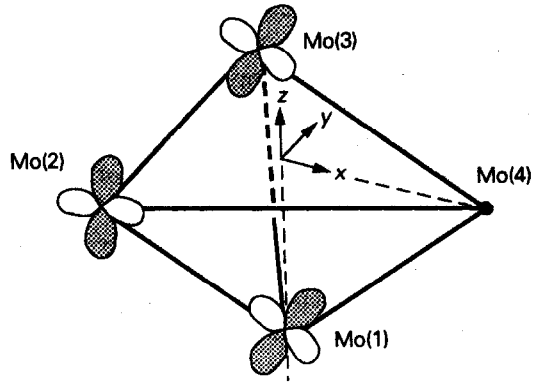

Fig. 7. The weak Mo—Mo π*-antibonding orbital of $[Mo_4S_4(OAc)_2(dtp)_4]^-$.

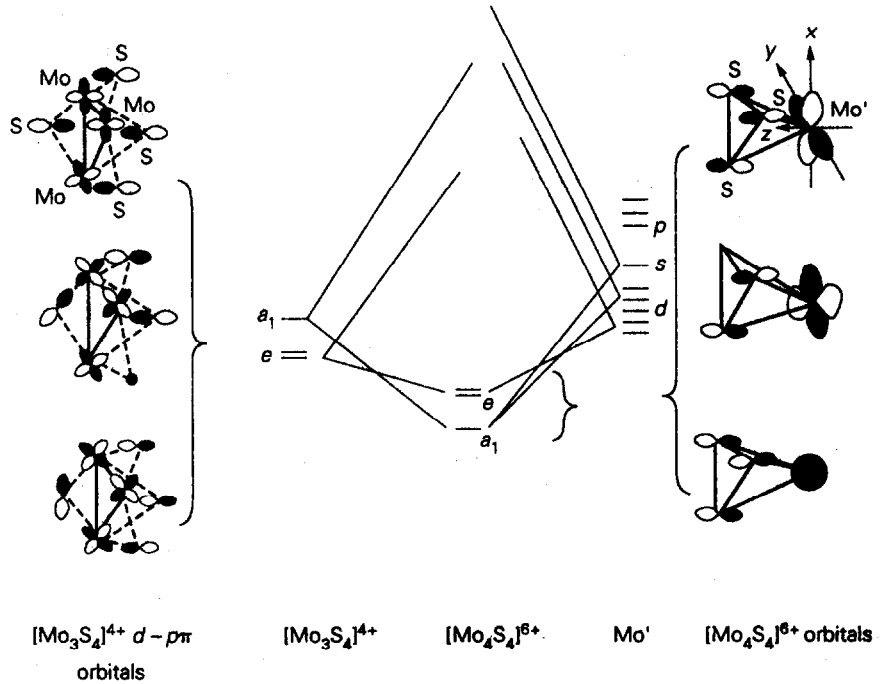

Fig. 8. Correlation diagram showing the interaction of $[Mo_3S_4]^{4+}$ with $Mo(CO)_6$ to form $[Mo_4S_4]^{6+}$.

cluster valence electron (CVE) scheme, 60 electrons will lead to a completely bonded metal tetrahedron in the case of ideal T_d symmetry, of which 12 electrons occupy the six M_4 cluster bonding orbitals, for instance $Mo_4S_4(CN)_{12}$.[2] In many circumstances, however, the $[Mo_4S_4]$ configuration often distorts from T_d to some extent and thus the t_2 orbital (HOMO) of the tetranuclear cluster under T_d symmetry will be split into $e+b_2$ orbitals for D_{2d} symmetry or $b_1+b_2+b_3$ orbitals for D_2 symmetry (as shown in Fig. 6).[38]

It is known from the calculations that the three highest occupied energy levels are -10.26, -10.28 and -10.42 eV, respectively, for $[Mo_4S_4(OAc)_2(dtp)_4]^-$. Since the HOMO is degenerate (having a very small energy difference), both the 10-electron and 11-electron systems may be paramagnetic. Meanwhile, owing to the weak Mo—Mo π^*-antibonding of the HOMO orbital (Mo d_{xy}–d_{xy}, see Fig. 7), the Mo—Mo bond length of **7** (11-electron cluster) is, on the contrary, longer than that of **6** (10-electron cluster). This reason may also explain the difficulty in obtaining the $[Mo_4S_4(\mu\text{-}OAc)_2(dtp)_4]^{2-}$ complex.

The formation mechanism of **7** *by the* [3 + 1] *reaction mode*

It is found from the calculations that it is the σ interaction between the μ_2-S $p\pi$ orbital of $Mo_3S_4(dtp)_4(H_2O)$ and the valence orbitals of $Mo(CO)_6$ that leads to the $[Mo_4S_4]$ cluster, as shown in Fig. 8 (for the sake of convenience in the description, the structure of the $[Mo_4S_4]$ cluster core can be approximately considered as C_{3v} symmetry with Mo′ lying on the z axis, which is perpendicular to the $\{Mo_3\}$ plane).

Clearly, it can be seen that the effect of a multiple centre d–$p\pi$ bond can not only lead to the unusual stability of the $[Mo_3S_4]$ core,[39,40] but speed up the addition reaction as well.

Acknowledgements—This investigation was supported by the Science Foundation of the Chinese Academy of Sciences and the Fuzhou Laboratory of Structural Chemistry, Fujian Institute of Research on the Structure of Matter. The authors would like to thank Professor Wu Qiang-Jin for his technical assistance and Professor Fang Yi-Xiong for his careful examination of the translated manuscript.

REFERENCES

1. J-Q. Huang, J-L. Huang and M-Y. Shang, *Youji Huaxue* 1985, **6**, 450.
2. A. Muller, R. Jostes, W. Eltzner, C. S. Nie, E. Diemann, H. Bogge, M. Zimmermann, M. Dartmann, U. Reinsch-vogell, S. Che, S. J. Cyvin and B. N. Cyvin, *Inorg. Chem.* 1985, **24**, 2872.
3. F. A. Cotton, M. P. Diebold, Z. Dori, R. Llusar and W. Schwotzer, *J. Am. Chem. Soc.* 1985, **107**, 6735.
4. F. A. Cotton, Z. Dori, R. Llusar and W. Schwotzer, *Inorg. Chem.* 1986, **25**, 3529.
5. T. Shibahara, H. Akashi and H. Kuroya, *J. Am. Chem. Soc.* 1986, **108**, 1342.
6. T. Shibahara and H. Kuroya, *J. Coord. Chem.* 1988, **18**, 233.
7. T. Shibahara, H. Akashi and H. Kuroya, *J. Am. Chem. Soc.* 1988, **110**, 3313.
8. T. Shibahara, T. Yamamoto, H. Kanadani and H. Kuroya, *J. Am. Chem. Soc.* 1987, **109**, 3495.
9. T. Sugano, T. Shibahara, H. Kobayashi, N. Uryv and M. Kinoshita, *Bull. Chem. Soc. Jpn.* 1988, **61**, 1785.
10. M. Martinez, Bee-Lean Ooi and A. G. Sykes, *J. Am. Chem. Soc.* 1987, **109**, 4615.
11. P. D. Williams and M. D. Curtis, *Inorg. Chem.* 1986, **25**, 4562.
12. Suzanne Harris, *Inorg. Chem.* 1987, **26**, 4278.
13. X-T. Wu, Y-F. Zhang and S-W. Du, *Acta Cryst.* 1989, **C45**, 1070.
14. R. E. Palermo, R. Singh, K. Bashkin and R. H. Holm, *J. Am. Chem. Soc.* 1984, **106**, 2600.
15. S. A. Duraj, M. T. Andras and B. Rihter, *Polyhedron* 1989, **8**, 2763.
16. D-M. Wu, J-L. Huang and J-Q. Huang, *Wuzi Huaxue* 1985, **1**, 32.
17. S-F. Lu, J-Q. Huang and J-L. Huang, *Acta Chimica Sinica* 1985, **4**, 300.
18. S-F. Lu, Y-H. Lin, J-Q. Huang and J-L. Huang, *Kexue Tongbao* 1986, **31**, 1609.
19. H-H. Zhuang, results to be published.
20. X-M. Zhang, Master Thesis Fujian Institute of Research on the Structure of Matter, Chinese Academy of Sciences, Fuzhou (1985).
21. Y-H. Lin and J-Q. Huang, results to be published.
22. S-F. Lu, J-Q. Huang, Z-X. Huang and J-L. Huang, *Jiegou Huaxue*, to be published.
23. S-F. Lu, J-Q. Huang, Z-X. Huang, Q-J. Wu, W-Z. Chen, G-T. Lu, Q-L. Sun and J-L. Huang, *Inorg. Chim. Acta* 1990, **176**, 35.
24. S-F. Lu and H-H. Zhuang, results to be published.
25. S-C. Lin and G. Chen, *Jiegou Huaxue* 1990, **9**, 111.
26. X-T. Lin, Y-H. Lin, J-Q. Huang and J-L. Huang, *Kexue Tongbao* 1986, **7**, 509.
27. M-Y. Shang, J-L. Huang and J-X. Lu, *Sci. Sin., Ser. B.* 1984, 687.
28. H. Akashi, T. Shibahara, T. Narahara, H. Tsuru and H. Kuroya, *Chem. Letts.* 1989, **132**, 129.
29. A. Deeg, H. Keck, A. Kruse, W. Kuchen and H. Wunderlich, *Z. Naturforsch.* 1988, **43b**, 1541.
30. T. C. W. Mak, K. S. Jasim and C. Chieh, *Inorg. Chem.* 1985, **24**, 1587.
31. H. Keck, A. Kruse, W. Kuchen, J. Mathow and H. Wunderlich, *Z. Naturforsch.* 1987, **42b**, 1373.
32. S-F. Lu, M-Y. Shang, J-Q. Huang, J-L. Huang and J-X. Lu, *Sci. Sin., Ser. B.* 1988, 147.
33. J. A. Bandy, C. E. Davies, J. C. Green, M. L. H.

Green, K. Prout and D. P. S. Rodgers, *J. Chem. Soc., Chem. Commun.* 1983, 1395.
34. T. Shibahara, H. Kuroya, K. Matsumoto and S. Ooi, *Inorg. Chim. Acta* 1986, **116**, L25.
35. C. Wilker and R. Hoffmann, PROGRAM ICON8 (1981).
36. J-Q. Li, *J. Mol. Struct.* 1988, **181**, 185.
37. J-Q. Li, *Exploration of Nature* (*Chinese*) 1988, **7**, 81.
38. S. Harris, *Polyhedron* 1989, **8**, 2843.
39. J-Q. Huang, S-F. Lu, M-Y. Shang, X-T. Lin, M-D. Huang, Y-H, Lin, D-M. Wu, H-H. Zhuang, J-L. Huang and J-X. Lu, *Jiegou Huaxue* 1987, **6**, 219.
40. W-D. Cheng, Q-E. Zhang, J-S. Huang and J-X. Lu, *Polyhedron* 1989, **8**, 2785.

Polyhedron Vol. 10, No. 18, pp. 2217–2219, 1991
Printed in Great Britain

0277–5387/91 $3.00+.00
© 1991 Pergamon Press plc

COMMUNICATION

PREPARATION AND SPECTROSCOPIC CHARACTERIZATION OF CAESIUM HEXACHLOROPHOSPHATE

ALAN S. MUIR

Department of Chemistry, Royal Holloway and Bedford New College, Egham Hill, Egham, Surrey TW20 0EX, U.K.

(*Received* 5 *April* 1991; *accepted* 19 *July* 1991)

Abstract—The first alkali-metal hexachlorophosphate, $Cs^+PCl_6^-$, was prepared and characterized by elemental analysis, solid-state ^{31}P NMR, IR and Raman spectroscopies. The thermodynamic stability of alkali-metal hexachlorophosphates is briefly discussed.

The hexafluorophosphate and hexachlorophosphate anions are both well-known and have been characterized as essentially octahedral species by X-ray diffraction[1,2] and a variety of spectroscopic techniques.[3,4] However, the hexabromophosphate anion is unknown, as indeed is the trigonal bipyramidal (molecular) form of PBr_5: this presumably results from steric factors. Mixed chlorofluorophosphate anions have also been reported, as well as a variety of pseudo halogen-substituted anions: ^{31}P and ^{19}F NMR spectroscopy have proved particularly useful in identifying such species in solution.[5–10] Alkali-metal hexafluorophosphates have been known for some time[11] but until now hexachlorophosphates were only known with large polyatomic cations[4,12,13] and *none* of the related alkali-metal salts have been reported. Thermodynamic calculations for the decomposition reactions [eq. (1)] using the Kapustinskii–Yatsimirskii approach have indicated that such species are of borderline stability,[12,13] with values of $\Delta G_R^{\ominus}$ for $K^+PCl_6^-$ and $Cs^+PCl_6^-$ of *ca* -38 and -6 kJ mol^{-1}, respectively.

$$MPCl_6(c) \longrightarrow MCl(c) + PCl_5(c) \quad (M = K, Cs) \qquad (1)$$

EXPERIMENTAL

All manipulations were carried out in an atmosphere of dry nitrogen. Chemicals of the best available commercial grade were used without further purification, although CsCl, RbCl and KCl were dried by warming to *ca* 100°C *in vacuo* for several hours. $Cs^+PCl_6^-$ was prepared typically as follows: hydrogen chloride gas (dried by passage through concentrated H_2SO_4) was condensed onto a mixture of CsCl (2.00 g, 1.20×10^{-2} mol) and $PCl_4^+PCl_6^-$ (2.50 g, 1.19×10^{-2} mol) by immersing the reaction vessel in liquid nitrogen. HCl liquefaction was achieved by warming to *ca* -95°C with a toluene/nitrogen slush-bath and the reaction mixture was agitated for 15 min. The HCl was then permitted to evaporate over $2\frac{1}{2}$ h by controlled warming. The resulting off-white solid was dried by pumping. Chlorine was analysed by potentiometric titration: Found: Cl, 56.3. $CsPCl_6$ requires: Cl, 56.5%.

Raman spectra were recorded using a Coderg PHO spectrometer with excitation at 514.5 nm provided by a Coherent Radiation Argon Ion laser; samples were contained in sealed capillaries. IR spectra were recorded using a Perkin–Elmer 983 spectrometer; CsI plates were used and samples were prepared either as Nujol mulls or as finely-ground solids. Solid-state MAS ^{31}P NMR spectra were recorded using a Bruker MSL 300 spectrometer operating at 121.5 MHz.

RESULTS AND DISCUSSION

The IR and Raman wavenumbers obtained for $Cs^+PCl_6^-$ are presented in Table 1, along with appropriate data for some previously known hex-

Table 1. IR and Raman spectroscopic data (cm^{-1}) for some hexachlorophosphates

Complex	Reference	Modes $\nu_1(A_{1g})$	$\nu_2(E_g)$	$\nu_3(T_{1u})$	$\nu_4(T_{1u})$	$\nu_5(T_{2g})$	$\nu_6(T_{2u})$
$Cs^+PCl_6^-$	Current study	359(s)	268, 277 (m)	440(vs)	286(w)	250, 240 (m)	Inactive
$PCl_4^+PCl_6^-$	Current study	360(s)	279(m)	N.R.	N.R.	240(w)	Inactive
$Et_4N^+PCl_6^-$	4	360(s)	283(m/w)	444(vs)	285(w)	238(w)	Inactive
$pyH^+PCl_6^-$	4	357(s)	275(m)	444(vs)	285(w)	240(w)	Inactive

N.R. = not recorded.

achlorophosphates. The agreement is good although there are some small shifts: for an octahedral MX_6^- species three Raman active (A_{1g}, E_g, T_{2g}) and two IR (T_{1u}) modes are predicted and observed. The Raman spectrum is shown in Fig. 1 and some splittings are seen in the degenerate modes: E_g (268 and 277 cm^{-1}) and T_{2g} (250 and 240 cm^{-1}). The IR spectrum recorded as a Nujol mull showed additional bands at 588 and 336 cm^{-1} due to $POCl_3$ impurities arising from sample

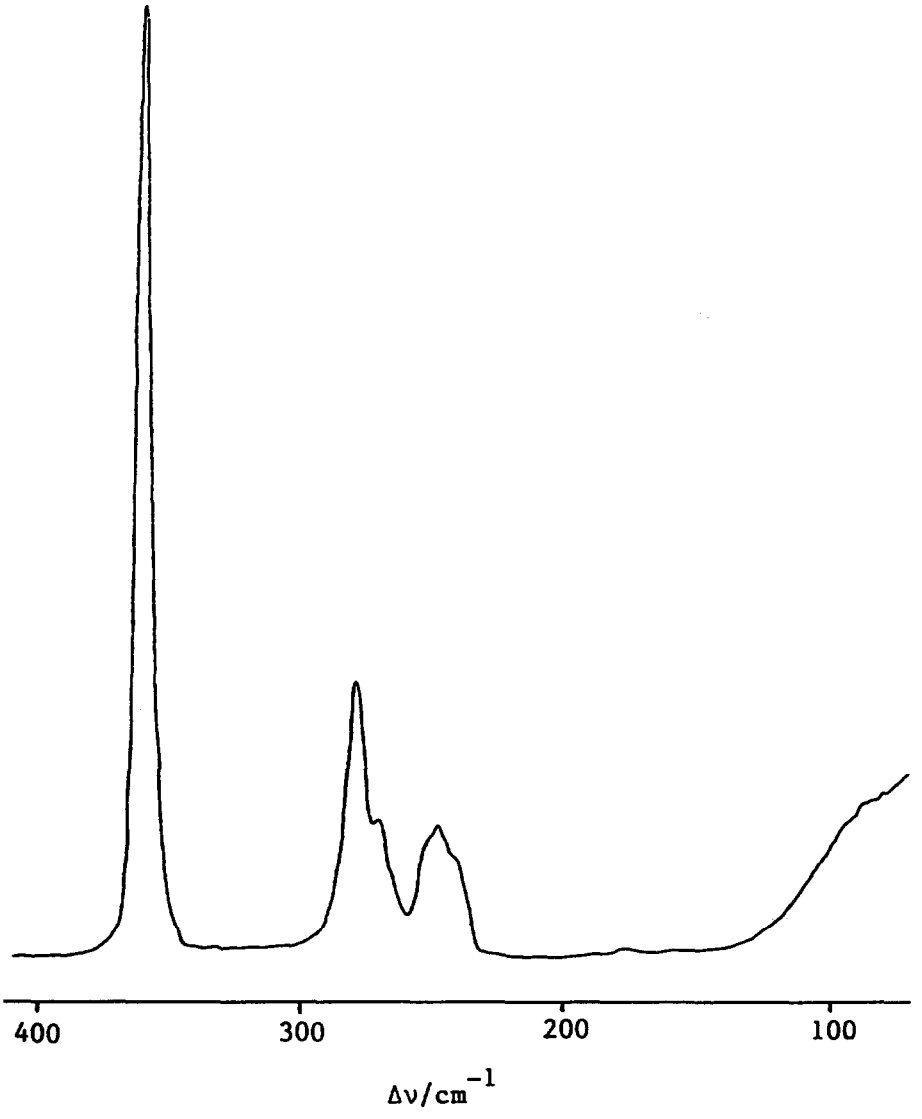

Fig. 1. Raman spectrum of $Cs^+PCl_6^-$.

decomposition, although these did not obscure the PCl_6^- modes at 440 and 286 cm^{-1}. The ^{31}P MAS NMR spectrum of $Cs^+PCl_6^-$ showed a single resonance at −294.7 ppm ($\Delta\nu_{1/2} = 30$ Hz) in accord with previous measurements of hexachlorophosphate salts.[14] The relatively narrow line width is consistent with considerable ionic motion within the system.

When a sample of $Cs^+PCl_6^-$ sealed in a long (6 cm) capillary tube was heated to *ca* 220°C for 1 h in a melting point apparatus, a sublimate was observed at the cool end of the tube: the Raman spectrum of this showed bands at 178, 242, 253, 279, 359, 457 and 656 cm^{-1} indicative of phosphorus pentachloride[15] as confirmed by comparison with the spectrum of an authentic sample of $PCl_4^+PCl_6^-$. No Raman signals were obtained from the residue; thus, the decomposition in Eq. (2) may be predicted.

$$Cs^+PCl_6^-(c) \xrightarrow{\Delta} \underset{\text{residue}}{CsCl(c)} + [PCl_5(g) \rightleftharpoons PCl_3(g) + Cl_2(g)] \longrightarrow \underset{\text{sublimate}}{PCl_4^+PCl_6^-(c)} \quad (2)$$

However, all attempts to prepare the analogous $K^+PCl_6^-$ and $Rb^+PCl_6^-$ salts by a similar process involving anhydrous HCl failed, yielding only the starting materials, although a similar reaction between CsF and PCl_2F_3 in acetonitrile at ambient temperature has been shown[6] to yield the salt $Cs^+PCl_4F_2^-$ in admixture with $Cs^+PF_6^-$. This reflects the calculated borderline thermodynamic stability for the alkali-metal hexachlorophosphates and suggests that the stability of $Cs^+PCl_6^-$ derives from kinetic factors. Moreover, on the basis of cation size, the failure to isolate either a potassium or rubidium salt indicates that the title compound is probably unique as a metallic hexachlorophosphate.

Acknowledgements—The author thanks Dr P. N. Gates for helpful discussions and Mr D. Butler (University of London Intercollegiate Research Service) for obtaining the NMR spectra.

REFERENCES

1. H. Bode and H. Clausen, *Z. Anorg. Allg. Chem.* 1951, **265**, 229.
2. H. Preiss, *Z. Anorg. Allg. Chem.* 1971, **380**, 51.
3. G. M. Begun and A. C. Rutenberg, *Inorg. Chem.* 1967, **6**, 2212.
4. I. R. Beattie, T. Gilson, K. Livingston, V. Fawcett and G. A. Ozin, *J. Chem. Soc. A* 1967, 712.
5. K. B. Dillon, R. J. Lynch, R. N. Reeve and T. C. Waddington, *J. Inorg. Nucl. Chem.* 1974, **36**, 815 and refs therein.
6. H. W. Roesky, *Angew. Chem. Int. Edn* 1967, **6**, 363.
7. Y. A. Buslaev, E. G. Il'in and M. N. Shcherbakova, *Dokl. Akad. Nauk S.S.S.R. Ser Khim.* 1984, **219**, 1154 and refs therein.
8. L. Kolditz, I. Beierlein, W. Wieker and A. R. Grimmer, *Z. Chem.* 1968, **8**, 226.
9. K. B. Dillon and A. W. G. Platt, *J. Chem. Soc., Dalton Trans.* 1983, 1159 and refs therein.
10. K. B. Dillon and A. W. G. Platt, *J. Chem. Soc., Chem. Commun.* 1983, 1089.
11. D. E. C. Corbridge, *Phosphorus. An Outline of its Chemistry, Biochemistry and Technology*, 2nd edn., Elsevier, Amsterdam (1980).
12. H. D. B. Jenkins, K. P. Thakur, A. Finch and P. N. Gates, *Inorg. Chem.* 1982, **21**, 423.
13. A. Finch, P. N. Gates, S. I. Nwankwo and M. Stephens, *Thermochim. Acta* 1980, **41**, 387.
14. K. B. Dillon, P. N. Gates, R. K. Harris, A. S. Muir and A. Root, *Spectrochim. Acta A* 1991, **47**, 831.
15. A. Finch, P. N. Gates, H. D. B. Jenkins and K. P. Thakur, *J. Chem. Soc., Chem. Commun.* 1980, 579.

Polyhedron Vol. 10, No. 18, pp. 2221–2223, 1991
Printed in Great Britain

0277–5387/91 $3.00+.00
© 1991 Pergamon Press plc

COMMUNICATION

SOLVOLYSIS OF THE DIFLUORO(1,10-PHENANTHOLINE)BORONIUM CATION IN DMSO: A ^{11}B AND ^{19}F NMR STUDY

KLAUS R. KOCH* and SUSANNE MADELUNG

Department of Chemistry, University of Cape Town, P. Bag Rondebosch, Cape Town 7700, South Africa

(*Received* 9 *April* 1991; *accepted* 25 *June* 1991)

Abstract—The salts $[LLBF_2]^+BF_4^-$, where LL = 1,10-phenantholine and 2,2′-bipyridine, undergo solvolysis in DMSO solution. The rate of solvolysis of the difluoro(1,10-phenantholine)boronium cation may conveniently be followed by means of ^{11}B and ^{19}F NMR. In contrast, the difluoro(2,2′-bipyridine)boronium cation appears to be rapidly solvolysed on dissolution, highlighting the differences in stabilities of these two boronium cations.

A considerable number of stable cationic boron complexes involving the interaction of monodentate Lewis bases with alkyl- and halogenoboranes have been prepared and characterized.[1–3] The stabilities of these boronium complexes vary greatly depending on the nature of the Lewis base and the substituent on the boron atom.[3] Despite the fact that the first stable cationic chelate boronium complex had been reported in 1906,[4] relatively few complexes involving neutral bi- and polydentate Lewis bases have been reported. Rund *et al.* prepared and characterized a series of complexes of the type $[LLBX_2]^+BX_4$, where $X = F^-$, Cl^- and LL = 1,10-phenantholine, 2,2′-bipyridine.[5] We have had cause to examine the chemistry of similar complexes in solution, and here report the unexpected solvolysis of the difluoro(1,10-phenantholine)boronium cation, $[(phen)BF_2]^+$, in dimethylsulphoxide (DMSO) solution as followed by ^{11}B and ^{19}F NMR.

The complexes $[(phen)BF_2]BF_4$ (**1**) and $[(bipy)BF_2]BF_4$ (**2**) may conveniently be prepared by treatment of a solution of the ligand in anhydrous ether/acetone with the appropriate amount of $(C_2H_5)_2O \cdot BF_3$, at room temperature under dry nitrogen. The salts **1** and **2** precipitate as essentially pure colourless solids and were used without further purification. For **1**: Found: C, 45.4; H, 2.7; N, 9.0. Calc. for $C_{12}H_7N_2B_2F_6$: C, 45.8; H, 2.2; N, 8.9%. For **2**: Found: C, 40.6; H, 2.7; N, 9.5. Calc. for $C_{10}H_8N_2B_2F_6$: C, 41.2; H, 2.8; N, 9.6%.

Examination of the 64.1 MHz ^{11}B NMR spectrum of a freshly prepared solution of **1** in dry DMSO-d_6 shows three resonances: a broad peak at 9.12 ppm, a well defined triplet centred at 2.15 ppm [$J(^{19}F—^{11}B) = 12.5$ Hz], and a sharp single line at 0.75 ppm relative to external $(C_2H_5)_2O \cdot BF_3$. After *ca* 18 min, the broad peak at 9.12 ppm had disappeared and a new resonance at 1.5 ppm appeared. The intensity of the latter resonance grew with the concomitant disappearance of the triplet at 2.15 ppm. After *ca* 19 h, only two resonances at 1.5 and 0.75 ppm were observed; no further changes occurred over a 48 h period. Resolution enhancement of the resonance at 1.5 ppm shows that it has the structure of a poorly resolved quartet, ascribed to $^1J(^{19}F—^{11}B) = 5 \pm 1$ Hz (Fig. 1). The time dependence of the ^{11}B NMR spectrum of **1** is mirrored by the 188.15 MHz ^{19}F spectrum, which initially shows four ^{19}F resonances at −63.35 ppm [unsymmetrical quartet, $J(^{10/11}B—^{19}F) = 12$–14 Hz] and −65.75 ppm (broad, unresolved peak) and two sharp single resonances in the ratio 1:4 at −67.79 and −67.85 ppm, respectively. The resonance at −63.35 ppm disappeared, while the peak at −65.75 ppm grew more intense according to a similar time scale observed in the ^{11}B NMR spectrum. The two resonances at −67.79 and −67.85 ppm did not

* Author to whom correspondence should be addressed.

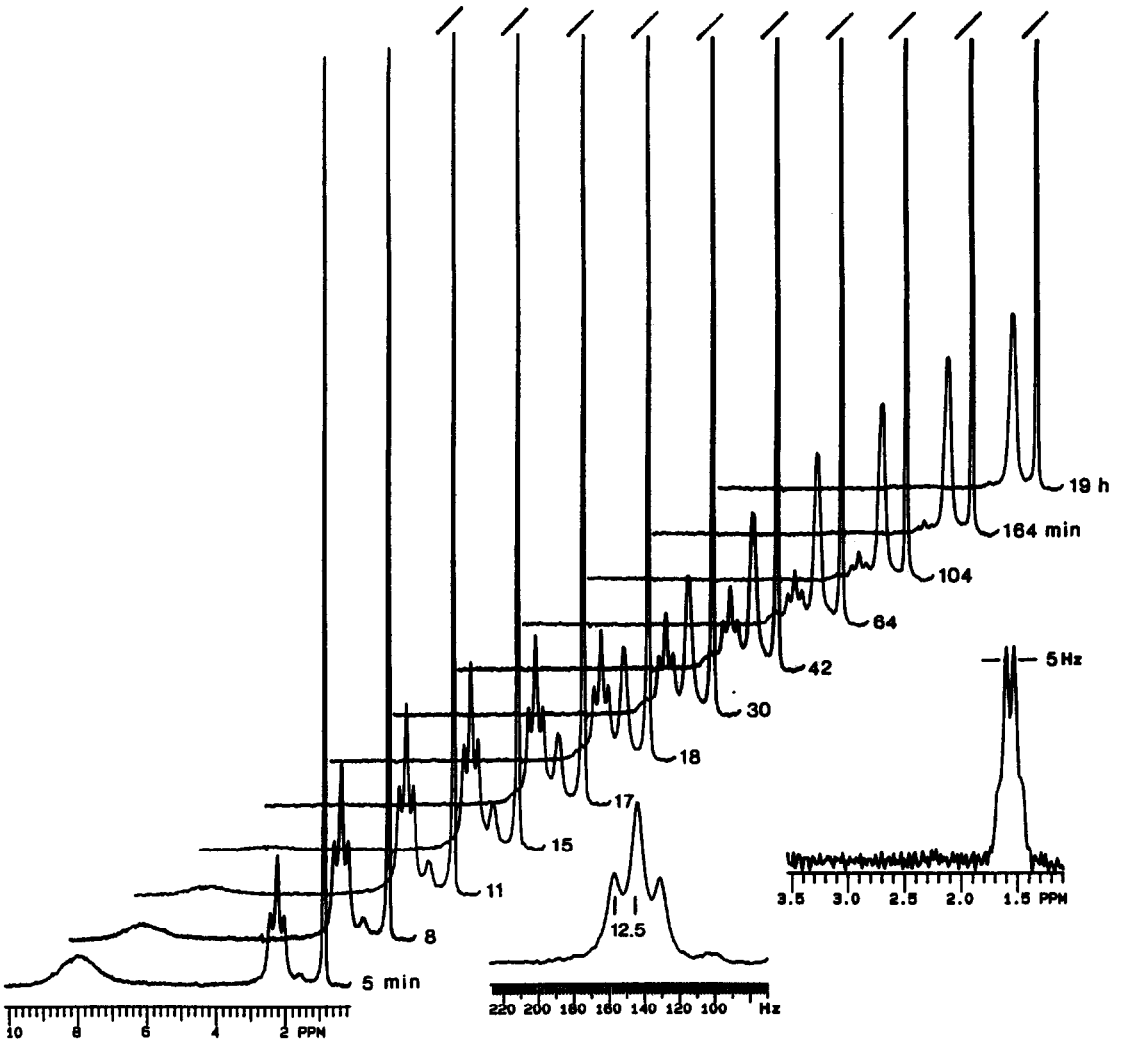

Fig. 1. The ^{11}B NMR spectra of $[(phen)BF_2]\cdot BF_4$ in DMSO-d_6 as a function of time. The resonances at 2.15 and 1.55 ppm are shown in expansion showing resolved $^{19}F—^{11}B$ coupling.

change significantly and may be assigned to the BF_4^- anion, showing the characteristic $^{10}B/^{11}B$ isotope shift of *ca* 0.05 ppm.[6]

By contrast, the ^{11}B and ^{19}F spectra of fresh solutions of **2** did not show a similar time dependence as that observed for **1**. The ^{11}B spectrum obtained is almost identical to that obtained for **1** after 19 h, consisting of a poorly resolved quartet at 1.6 ppm [$^1J(^{19}F—^{11}B) = 4$–5 Hz] and a single resonance at 0.8 ppm. The corresponding ^{19}F spectrum of **2** shows resonances at −65.76 ppm (poorly resolved multiplet) and at −67.78 and −67.84 ppm (ratio 1 : 4).

These spectra clearly show that solvolysis of the boronium *cations* $[(phen)BF_2]^+$ (**3**) and $[(bipy)BF_2]^+$ (**4**) occurs in DMSO-d_6 solution. The rate of solvolysis of **3** is sufficiently slow to be conveniently monitored by means of NMR spectroscopy, whilst for **4** this phenomenon occurs much more rapidly on dissolution of **2**. Based on the analysis of the spectra shown in Fig. 1, we proposed the assignments given in Table 1.

It should be noted that our assignments differ to those of Rund *et al.*[5] These authors reported identical ^{11}B shifts for both **1** and **2**, assigning the resonance at 1.2 ppm to BF_4^- and that at 0.6 ppm to the respective boronium cation. This suggests that solvolysis had already taken its course by the time the ^{11}B NMR spectra was recorded. Moreover, the reported shift values are different to our assignments, despite using the conventional external ^{11}B reference,[7] $(C_2H_5)_2O\cdot BF_3$, as did Rund and coworkers. This discrepancy highlights the importance of proper referencing to avoid confusion. We recorded the ^{11}B and ^{19}F NMR spectra of tetra-*n*-butylammonium tetrafluoroborate in DMSO-d_6,

Table 1.

Species	$\delta(^{11}B)$ (ppm[a])	$^1J(^{19}F—^{11}B)$ (Hz)	$\delta(^{19}F)$[b]
$[(phen)BF_2]^+$	2.15	12.5	−63.35
BF_4^-	0.75	n.r.[c]	−67.79
			−67.85
$BF_3 \cdot DMSO$	1.55	~ 5	−65.35
[c]	9±0.5	n.r.	Not obs.
$[(bipy)BF_2]^+$	Not obs.	—	—
BF_4^-	0.80	n.r.[d]	−67.78
			−67.84
$BF_3 \cdot DMSO$	1.60	~ 5	−65.76

[a] Shifts are relative to external $(C_2H_5)_2O \cdot BF_3$ at 25°C.
[b] Shifts relative to 50% v/v CF_3COOH/D_2O at 25°C.
[c] Species uncertain but could be $[(phen)BF_3]$ in view of the line width of this resonance.
[d] Not resolved, < 1.2 Hz, see ref. 8.

finding a single resonance at 0.73 ppm and −67.93/−67.98 ppm, respectively. Addition of $(C_2H_5)_2O \cdot BF_3$ to some DMSO-d_6 gave a broad signal at 1.47 ppm and −65.71 pm for ^{11}B and ^{19}F, respectively.

In conclusion, we find that the boronium cations **3** and **4** show markedly different stabilities to solvolysis in DMSO-d_6, although in both cases the chelating Lewis base is effectively displaced from the coodination sphere of the boronium cation. We postulate that a highly reactive intermediate $BF_2(DMSO)_2^+$ presumably reacts with BF_4^- to yield the neutral $DMSO \cdot BF_3$ species:

$$[(phen)BF_2]^+ \xrightarrow{DMSO} phen + BF_2(DMSO)_2^+$$

$$BF_2(DMSO)_2^+ + BF_4^- \longrightarrow 2BF_3 \cdot DMSO.$$

The substantial differences in the rates of solvolysis for cations **3** and **4** is an interesting example of the dependence of the stabilities of these boronium cations on subtle differences in the nature of the two chelating ligands involved. Presumably the rigidity of the 1,10-phenantholine as compared to the 2,2′-bipyridine chelate confers added stability to the boronium cation **3**.

Acknowledgements—We are grateful to the University of Cape Town and the F.R.D. for financial assistance.

REFERENCES

1. O. P. Shitov, S. L. Ioffe, V. A. Tartakovskii and S. S. Novikov, *Russ. Chem. Rev.* 1970, **39**, 905.
2. B. M. Mikhailov, *Pure Appl. Chem.* 1977, **49**, 749.
3. J. Emri and B. Györi, in *Comprehensive Coordination Chemistry* (Edited by G. Wilkinson, R. D. Gillard and J. A. McCleverty), Vol. 3, p. 97. Pergamon, Oxford (1987).
4. W. Dilthey, *Liebigs Ann. Chem.* 1906, **344**, 300.
5. D. D. Axtell, A. C. Cambell, P. C. Keller and J. V. Rund, *J. Coord. Chem.* 1976, **5**, 129.
6. R. J. Gillespie and J. S. Hartman, *Can. J. Chem.* 1967, **45**, 859.
7. C. Brevard and P. Granger, *Handbook High Resolution Multinuclear NMR*, p. 88. Wiley, New York (1981).
8. R. J. Gillespie, J. S. Hartman and M. Parekh, *Can. J. Chem.* 1968, **46**, 1601.

Polyhedron Vol. 10, No. 19, pp. 2225–2227, 1991
Printed in Great Britain

0277–5387/91 $3.00+.00
© 1991 Pergamon Press plc

SYNTHESIS, IR SPECTRA AND X-RAY CRYSTAL STRUCTURE OF DINITRATO(N,N′-DIMETHYL-1,2-ETHANEDIAMINE)COPPER(II)

D. GOMEZ DE ANDEREZ

Department of Chemistry, University of Los Andes, Merida, Venezuela

and

A. K. MUKHERJEE

Department of Physics, Jadavpur University, Calcutta 700 032, India

and

S. KONER and N. RAY CHAUDHURI*

Department of Inorganic Chemistry, Indian Association for the Cultivation of Science, Jadavpur, Calcutta 700 032, India

(*Received* 20 *February* 1991; *accepted* 25 *June* 1991)

Abstract—Blue crystals of $[Cu(NN'dmen)(NO_3)_2]$ (where NN′dmen = N,N′-dimethyl-1,2-ethanediamine) were prepared and its structure was determined by single crystal X-ray crystallography. In this complex both the nitrates are mono-coordinated to the copper in *cis* positions. The IR spectra and magnetic susceptibility are reported.

The combination bands of the ν_1 symmetric stretching mode and the doubly-degenerate in-plane bending mode of nitrate ions, which appear in the 1700–1800 cm^{-1} region in the IR spectra of metallic complexes have been used for structural diagnosis.[1–3] This is very useful for a nitrato complex containing other organic ligands as the IR bands of the common organic ligands are almost absent in this region. An ionic nitrate group gives rise to a relatively strong and sharp combination frequency while the coordinated nitrate groups give two frequencies.[3,4] In the bidentate coordination mode the separation between the two frequencies is wider than that in the monodentate coordinating mode.[4] Single crystal X-ray analysis of $[Cu(N,N'dmen)(NO_3)_2]$ (N,N′dmen = N,N′-dimethyl-1,2-ethanediamine) was undertaken to establish these IR spectral evidences. Moreover, additional knowledge of the structure of the complexes that may exist in solution is of potential importance in understanding the intermediate in the stability studies and in the ligand exchange reactions in solution.

EXPERIMENTAL

High purity N,N′-dimethyl-1,2-ethanediamine was purchased from Fluka AG and used as received. All the other chemicals used were of AR grade.

Preparation of the complex

$Cu(NO_3)_2 \cdot 3H_2O$ (1 mmol) was dissolved in methanol (10 cm^3). Diamine (1 mmol) was then added to the $Cu(NO_3)_2$ solution with stirring. The solution was allowed to evaporate slowly until fine blue crystals formed. Found: C, 17.5; H, 4.6; N, 20.2; Cu, 23.2. Calc. for $C_4H_{12}N_4CuO_6$: C, 17.4; H, 4.4; N, 20.3; Cu, 23.0%. $\mu_{eff} = 1.84$ B.M.; $\lambda_{max} = 592, 701(sh)$ nm.

* Author to whom correspondence should be addressed.

Physical measurements

The equipment employed for IR spectra (in KBr discs and in Nujol), electronic spectra, elemental analysis and magnetic measurements was the same as described in an earlier report.[1]

Crystal data

$C_4H_{12}N_4CuO_6$, $M_r = 275.7$, tetragonal, space group $P4_12_12$, $a = b = 8.797(2)$, $c = 12.957(3)$ Å, $V = 1002.7(4)$ Å^3, $Z = 4$, (Mo-K_α) = 21.99 cm^{-1}, $D_c = 1.826$ g cm^{-3}, $T = 293$ K.

Data collection, structure solution and refinement

A single crystal ($0.35 \times 0.20 \times 0.15$ mm) was mounted on a glass fibre with epoxy glue. Unit cell dimensions and Laue class were determined from precession photographs. Final cell parameters were obtained by least-squares analyses of the diffractometer angle settings of 25 well-centred reflections having $20 < 2\theta < 35°$. Intensity data were collected on a Hilger–Watt four circle diffractometer (graphite monochromatized Mo-K_α radiation, $\lambda = 0.71073$ Å) using a ω–2θ scan. Of 664 unique data collected up to $2\theta_{max} = 50°$, 438 with $|F_o| > 3\sigma(F_o)$ were considered observed and were used in structure refinement. Intensities of three standard reflections monitored after every 50 measurements during data collection showed no significant change. Data were corrected for Lorentz–polarization factors. An empirical absorption correction[5] was applied using ψ-scan data.

The structure was solved by Patterson and successive Fourier synthesis and refined by full-matrix least-squares using SHELX76[6] with anisotropic thermal parameters for all non-hydrogen atoms, while the hydrogen atoms were kept fixed with isotropic temperature factors in their calculated positions. The final $R[= \Sigma||F_o|-|F_c||/\Sigma|F_o|]$ and $R_w = [\Sigma w(|F_o|-|F_c|)^2/\Sigma w|F_o|^2]^{1/2}$ values were 0.030 and 0.031, respectively, using $w^{-1} = \sigma^2(F) + 0.0018|F|^2$. The maximum/minimum peak heights in the final difference Fourier synthesis were 0.48 and -0.31 e Å^{-3}, respectively. Maximum shift/e.s.d. in the final cycle of refinement was 0.005. Neutral atom scattering factors were used.[7] All computations were carried out on Vax cluster system at the University of York, England during the author's (DGA, AKM) stay there.

RESULTS AND DISCUSSION

An ORTEP[8] drawing of the complex showing the atom labelling scheme is shown in Fig. 1. Selected bond lengths and angles are listed in Table 1. The asymmetric unit contained half of the complex with copper lying on a crystallographic two-fold axis. Four major ligand atoms (N(2), N(22), O(1), O(12)) around copper form an approximate square-planar arrangement with one bidentate N,N′-dimethyl-1,2-ethanediamine molecule and two monodentate nitrate ions in a *cis* configuration. Weak coordination of the two symmetry related positions of O(3) [^{1}O(3) at 0.7679, 0.8695, 0.7002 and ^{2}O(3) at 0.8695, 0.7679, 0.2998; Cu—^{1}O(3) = Cu—^{2}O(3) = 2.673(4) Å] completes a distorted octahedron. As expected the IR spectrum, for both the nitrates being coordinated to the metal atom via one oxygen atom, of the complex [Cu(N,N′dmen)(NO$_3$)$_2$] taken in KBr (Fig. 2)

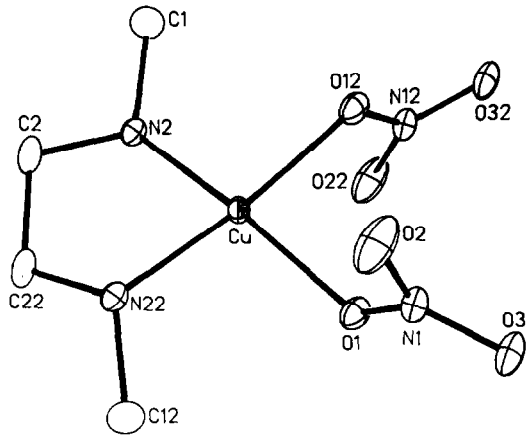

Fig. 1. ORTEP plot of [Cu(N,N′dmen)(NO$_3$)$_2$] with labelling of the non-hydrogen atoms.

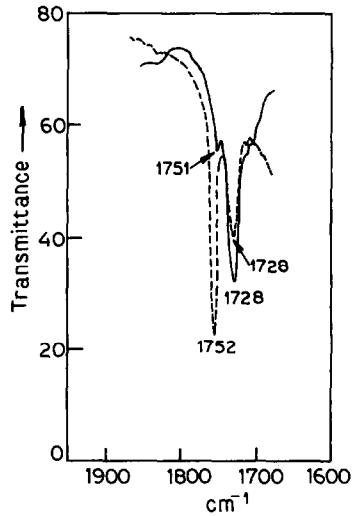

Fig. 2. IR spectra showing the change of band ratio when taken in Nujol (——) and KBr (– – –).

Table 1. Selected bond lengths (Å) and bond angles (°)

Cu—N(2)	2.000(3)	Cu—O(1)	1.993(3)
N(2)—C(1)	1.482(6)	N(2)—C(2)	1.479(6)
N(1)—O(1)	1.293(5)	N(1)—O(2)	1.234(6)
N(1)—O(3)	1.223(5)		
N(2)—Cu—O(1)	165.5(1)	N(2)—Cu—N(22)	86.6(1)
N(2)—Cu—O(12)	95.5(1)	O(1)—Cu—O(12)	86.1(1)
Cu—O(1)—N(1)	119.3(2)	Cu—N(2)—C(1)	119.6(3)
O(1)—N(1)—O(2)	119.2(4)	O(1)—N(1)—O(3)	117.9(4)
O(2)—N(1)—O(3)	122.9(4)		

showed two absorption bands at 1752 and 1728 cm^{-1} with a separation of 24 cm^{-1}. The intensity ratio of the two peaks is reversed when the spectrum is taken in Nujol mulls (Fig. 2). Probably due to exchange of NO_3 ions with Br ions of KBr the IR band which appears at 1752 cm^{-1} overlaps the ionic nitrate band and increases the intensity. The displacements of N(2) and N(22) atoms from the least-squares plane through N(2), N(22), Cu, O(1) and O(12) are $\pm 0.258(4)$ Å, whilst the corresponding values for O(1) and O(12) are $\pm 0.246(4)$ Å, respectively. The nitrate group is essentially planar, the maximum displacement of any atom from the least-squares plane through N(1), O(1), O(2) and O(3) being 0.003(5) Å and almost perpendicular to the plane defined by Cu, N(2), N(22), O(1) and O(12) atoms [the dihedral angle between the two planes is 88.0(2)°]. The distances Cu—O(1) 1.993(3) Å and Cu—N(2) 2.000(3) Å are comparable to those observed in similar systems.[9,10] The magnetic moment of the complex [Cu,(N,N′dmen)$(NO_3)_2$] is 1.84 B.M. at 20°C.

It is to be noted that the structure of the title complex is interesting as both the nitrate ions are coordinated with copper(II) at the *cis* position which is apparently unfavourable due to inter-anionic repulsion.[11]

Acknowledgements—The authors wish to thank Professor J. R. Helliwell, Department of Chemistry, University of Manchester, U.K. for helpful discussions and Mr Suranjan Bhanjachoudhury for the ORTEP plot done at the National Single Crystal Diffractometer Facility, Department of Inorganic Chemistry, Indian Association for the Cultivation of Science, Calcutta. We are also grateful to the Department of Physics, University of York, U.K. for allowing two of the authors (DGA, AKM) to use the X-ray diffractometer facility.

REFERENCES

1. S. Koner, A. Ghosh and N. Ray Chadhuri, *J. Chem. Soc., Dalton Trans.* 1990, 1563.
2. S. Koner, A. Ghosh and N. Ray Chaudhuri, *Trans. Metal Chem.* 1991, **16**, 397.
3. Y. Ihara, Y. Fukuda and K. Sone, *Inorg. Chem.* 1987, **26**, 3745.
4. A. B. P. Lever, E. Mantovani and B. S. Ramaswamy, *Can. J. Chem.* 1971, **49**, 1957.
5. A. C. T. North, D. C. Phillips and E. S. Mathews, *Acta Cryst.* 1968, **24A**, 351.
6. G. M. Sheldrick, SHELX76, Program for Crystal Structure Determination. University of Cambridge, England (1976).
7. *International Tables for X-ray Crystallography*, Vol. IV. Kynoch Press, Birmingham (1974).
8. C. K. Johnson, ORTEP, Report ORNL-3794. Oak Ridge National Laboratory, Oak Ridge, Tennessee (1965).
9. P. Murray-Rust, J. Murray-Rust and R. M. Clay, *Acta Cryst.* 1980, **B36**, 452.
10. J. M. Latour, S. S. Tandon and D. C. Povey, *Acta Cryst.* 1989, **C45**, 7.
11. N. F. Curtis and Y. M. Curtis, *Inorg. Chem.* 1965, **4**, 804.

Polyhedron Vol. 10, No. 19, pp. 2229–2233, 1991
Printed in Great Britain

0277–5387/91 $3.00+.00
Pergamon Press plc

SYNTHESIS OF NEW RUTHENIUM(III) AND RHODIUM(III) DERIVATIVES OF THE PYRIDYL-2-DIETHYLPHOSPHONATE LIGAND. EVIDENCE FOR ARBUZOV-LIKE DEALKYLATION OF THE PHOSPHONATE MOIETY

YOUNG-SHEN HUANG and BRUNO CHAUDRET*

Laboratoire de Chimie de Coordination du CNRS, Unité No. 8241 liée par Convention à l'Université Paul Sabatier et à l'Institut National Polytechnique de Toulouse, 205 route de Narbonne, 31077 Toulouse Cédex, France

and

JACQUES BELLAN and MARIE-ROSE MAZIERES

Laboratoire de Chimie des Molécules Phosphorées, URA CNRS No. 454 and Laboratoire de Chimie Pharmaceutique, Université Paul Sabatier, 118 route de Narbonne, 31062 Toulouse Cédex, France

(*Received* 18 *February* 1991; *accepted* 25 *June* 1991)

Abstract—The reaction of $K_2RuCl_5 \cdot H_2O$ with $(C_5H_4N)P(O)(OEt)_2(L)$ yields the anionic complex $K\{RuCl_2[OP(O)(OEt)(C_5H_4N)]_2\}$ (**4**). One ethyl group of L has been eliminated in an Arbuzov-type reaction. This compound is stable and unreactive (no reaction with imidazole, pyridine, tert-butyl-pyridine, 18-crown-6, PMETA). The reactions of (**4**) with zinc, aluminium or $NaBH_4$ do not lead to reduction of the metal centre but to further dealkylation of L. In contrast, the reactions of L with $MCl_3 \cdot 3H_2O$ produce the new fluxional compounds MCl_3L_2 [M = Ru (**6**), M = Rh (**7**)] containing one bidentate and one monodentate ligand.

Organometallic chemistry of higher oxidation states is attracting increased attention at the present time. Thus, if low oxidation state organometallic chemistry has been extensively studied for the past 20 years,[1] it is only recently that interest has been shown for the reactivity of high oxidation derivatives. Bottomley *et al.* have explored the chemistry of early transition metal oxo-cyclopentadienyl clusters,[2] whereas the discovery by Hermann *et al.* of the complex $(C_5Me_5)ReO_3$ and of its rich reactivity[3] has stimulated a new impetus for the study of such complexes. Attempts to prepare similar ruthenium derivatives in our group have led to new hydrido oxo clusters.[4] However, these compounds are very stable and fairly unreactive which led us to look for new systems containing hard donor ligands.

Recently Taqui Kahn *et al.* described the remarkable reactivity of the ruthenium(III) complex $K[Ru(Hedta)Cl] \cdot 2H_2O$ for reactions as different as hydrogenation, carbonylation and oxidation of hydrocarbons including alkanes.[5]

Furthermore, porphyrin complexes of ruthenium were shown to be able to catalytically oxidize hydrocarbons using molecular oxygen as oxidants.[6] Kläui has used a cobalt complex containing phosphonato groups as a ligand containing oxygen donor groups analogous to cyclopentadienyl. This ligand led to the preparation of both low and high oxidation state derivatives.[7]

In the search for new ligand systems able to accommodate high oxidation state derivatives in the

* Author to whom correspondence should be addressed.

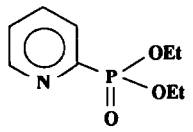

Fig. 1. Structure of the ligand.

chemistry of ruthenium but also to link to medium oxidation state precursors, we considered pyridine phosphonato compounds.[8]

This paper describes our first results with this ligand, namely $P(O)(OEt)_2(C_5H_4N)$ (L; Fig. 1).

RESULTS AND DISCUSSION

The ligand was reacted with two ruthenium complexes: $K_2RuCl_5(H_2O)$ (**1**), since this is a well-defined mononuclear compound,[9] and $RuCl_3 \cdot 3H_2O$ (**2**) as well as $RhCl_3 \cdot 3H_2O$ (**3**).

(1) *Reactions with* $K_2RuCl_5(H_2O)$

Compound **1** reacts slowly with L in refluxing methanol to give a yellow solution from which a new compound (**4**) is obtained as a yellow powder upon the addition of diethyl ether. Compound **4** is air-stable, soluble in water and polar solvents (methanol, acetone) and is a 1 : 1 conductor in methanol ($\Lambda_M = 80\ \Omega^{-1}\ cm^2\ mol^{-1}$). The ruthenium-containing moiety is most probably anionic since no reaction was observed with $NaBPh_4$ in methanol. However, we equally failed to observe a reaction with $(PPh_4)^+$ probably because of a strong interaction of K^+ with oxygen.

Complex **4** is paramagnetic and shows a magnetic moment of 1.90 μB, in agreement with the presence of one single electron and thus of a d^7 ruthenium(III) configuration. Furthermore, the EPR spectra, whether recorded at room temperature as a powder or at 100 K in CH_2Cl_2, show two signals corresponding to $g_\perp$ at 2.4465 and $g_\parallel$ at 1.9964. This is in agreement with the presence of a C_2 axis.

This symmetry of the molecule is confirmed by NMR. Only one peak is observed on the ^{31}P NMR spectrum at δ 2.26 ppm, whereas the ^{13}C NMR spectrum shows the methylene groups of the phosphonate moiety at δ 65 ppm (t, $J(CH) = 161$ Hz), the methyl groups at δ 17 ppm (q, $J(CH) = 140$ Hz) and the pyridine carbons as five broad peaks at δ 156 (d, $J(CH) = 184$ Hz), 145 (s), 141 (d, $J(CH) = 184$ Hz), 130 (d, $J(CH) = 182$ Hz) and129 ppm ($J(CH) = 180$ Hz). The ^1H NMR spectra only show broad peaks near δ 0.9, 1.4, 4.4 and 7.58 ppm.

The IR spectra show as their most salient feature an intense broad band at 1226 cm^{-1} which is attributed to P=O stretching. This is not due to the free ligand [ν(P=O) 1255 cm^{-1}], but a more important shift of this bond would be expected in the case of direct coordination of this functionality to ruthenium. The P—O stretching frequency is observed at 1025 cm^{-1}.

In summary, we propose for **4** the formula $K[RuCl_2\{(C_5H_4N)PO(O)(OEt)\}_2] \cdot MeOH$ (see Scheme 1). This results from the spectroscopic data described above [symmetrical ruthenium(III) structure, equivalence of the phosphorus and carbons,

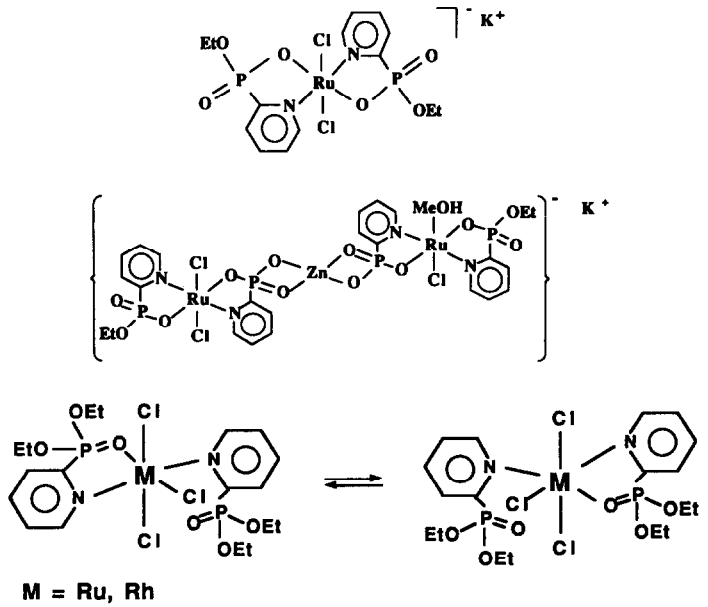

Scheme 1. Proposed structure for complexes **4**–**7**.

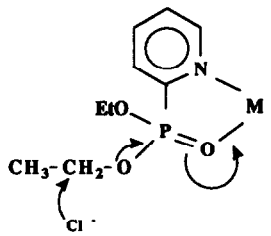

Scheme 2. Proposed mechanism for the dealkylation reaction.

non-coordination of P=O groups] and the conductivity and microanalytical data (C, H, N, P, Cl, O, Ru).

The mechanism for the formation of **4** could involve firstly the substitution of chloride groups by the pyridine phosphonate ligand and then a dealkylation, Arbuzov-type reaction. Such a mechanism has been recently demonstrated during the formation of $[(\eta^5\text{-}C_5H_5)(CO)_2Fe\{P(CO)(NR_2)_n(OR')_{2-n}\}]$ ($n = 1, 2$).[10] Thus, one Cl^- liberated during the substitution could react on one ethyl group of the coordinated pyridine phosphonate ligand to give EtCl and the formation of a sigma Ru—O bond (see Scheme 2).

Reactivity of complex (**4**)

Cation exchange. Since it proved difficult to crystallize complex **4**, cation exchange reactions were attempted with PPh_4Cl and PPNCl. In neither case did a reaction occur. Similarly, no reaction was observed when the crown ether 18-crown-6 or a tridentate amine (PMETA) were added to **4** in methanol. This tends to prove that the potassium cation is strongly associated with the P—O groups of the ligands.

Substitution. In order to render the complex more reactive substitution reactions were attempted with the ligand showing a strong σ-donor character such as imidazole, pyridine and tert-butyl-pyridine. These reactions failed whether carried out in the presence or absence of silver triflate, thus demonstrating the low reactivity of the complex.

Reduction. Reduction reactions were attempted with the hope of leading to neutral and thus more tractable and reactive species. These reactions were attempted with zinc, $Al/HgCl_2$ and $NaBH_4$ in methanol. The reaction occurs rapidly in all three cases to lead to red paramagnetic ruthenium(III) derivatives. Only in the case of zinc was a crystalline material isolated in high yield (**5**). As for **4**, two gyromagnetic constants are observed in EPR ($g_\parallel = 2.225$; $g_\perp = 2.049$). Three ν(P=O) stretches are observed by IR spectroscopy (1261, 1224 and 1165 cm^{-1}) corresponding to three different environments for the phosphonato groups. The ν(P—O) vibration is found at 1025 cm^{-1} as for **4**.

The ^{31}P NMR spectrum shows a broad peak centred at δ 32.9 ppm and the ^1H NMR is broad and similar to that of **4** but reveals the presence of methanol and water in the crystals.

A tentative structure is deduced from microanalysis on eight elements (C, H, N, P, Cl, K, O, Ru) and is shown on Scheme 1. Unfortunately again, the crystals were not found suitable for X-ray analysis. Nevertheless, this result demonstrates the inertness of the ruthenium(III) core in this compound, perhaps because of the lack of a vacant site, and the preferential reactivity of the phosphonato group.

(2) *Reactions of* $C_5H_4NP(O)(OEt)_2(L)$ *with* $MCl_3 \cdot 3H_2O$ (M = Ru, Rh)

Since the lack of reactivity of complex **4** could be attributed to its ligand saturation, anionic character and to the formation of a strong interaction between the potassium cation and the phosphonato ligand, we attempted the preparation of neutral or even possibly cationic derivatives. This chemistry was extended to rhodium which should lead to diamagnetic complexes which are easier to characterize.

Reaction with $RuCl_3 \cdot 3H_2O$. The reaction of $RuCl_3 \cdot 3H_2O$ with two equiv. of L in refluxing methanol yields a yellow solution from which a yellow powder is obtained after the appropriate work-up.

The new complex (**6**) is air-stable, non-conducting in methanol and paramagnetic. Thus, it only shows one broad peak in EPR at $g = 2.3877$, in agreement with a ruthenium(III) formulation.

The IR spectrum shows a very broad band centred at 1160 cm^{-1} and attributed to a coordinated P=O group. A shoulder is visible at 1220 cm^{-1} which could be attributed to a non-coordinated P=O functionality. The P—O stretch is observed as a broad band near 1030 cm^{-1}.

Finally, the ^{31}P NMR spectrum shows two peaks at δ 71.5 and 63.1 ppm, while the ^1H NMR spectrum is broad.

These data together with microanalytical data (C, H, N, Cl) are in agreement with the proposed formulation (see Scheme 1). Some water remains present in the complex and is detected by IR and ^1H NMR. The ruthenium atom remains coordinated to three chloride groups, one bidentate and one monodentate pyridine phosphonate ligand.

It is not entirely clear which end of L coordinates preferentially to ruthenium. IR evidence suggests that it is the pyridine end; furthermore, many pyridine compounds of ruthenium(III) are known.

M = Rh. In order to shed some light on the preceding result, the same reaction was carried out with $RhCl_3 \cdot 3H_2O$. The reaction is similar to that of ruthenium yielding a new complex (**7**) as an air-stable orange powder. The IR spectrum shows, as in (**6**), two bands at 1155 and 1200 cm^{-1} for coordinated and non-coordinated P=O groups.

The ^{31}P NMR spectrum shows at room temperature two broad peaks centred at δ 2.80 and 29.0 ppm. Upon cooling the solution down to 183 K, the peak at δ 2.80 ppm does not move but becomes sharper, whereas the one at δ 29.0 ppm splits into two peaks at δ 28.7 and 30.0 ppm. This result demonstrates a slow exchange between the two pyridine phosphonato ligands at room temperature. The peak near δ 2 ppm is attributed to the non-coordinated phosphonato moiety.

The ^1H NMR spectrum shows two types of ethoxy ligand (methyl groups at δ 1.27 and 1.47 ppm; methylene groups at δ 4.25 and 4.40 ppm). One of these signals is found close to the value in the free ligand (1.43 and 4.31 ppm). Multiplets between δ 7.73 and 9.55 ppm are attributed to the pyridine protons.

As for **6**, the microanalysis of complex **7** favours the formulation $RhCl_3L_2 \cdot 2H_2O$, which is in agreement with the spectroscopic data.

CONCLUSION

We describe in this paper the preparation of new complexes of ruthenium(III) or rhodium(III) of the pyridine diethylphosphonate ligand. This ligand associating a good σ-donor ligand (pyridine) with a good π-donor ligand (phosphonate) could be of great interest for the preparation of new, high oxydation state transition-metal derivatives. We give evidence for the easy dealkylation of the phosphonate in an Arbuzov-type process. The resulting complex is very stable and totally inert. This process is possible because of the existence of free chloride ions in the reaction mixture.

In contrast, complexes **6** and **7** resulting from the reaction of L with $MCl_3 \cdot 3H_2O$ (M = Ru, Rh) are trichlorides for which no evidence for the dissociation of chloride groups have been found.

The reactivity of these new compounds deserves further investigation.

EXPERIMENTAL

General

Microanalyses were performed in the laboratory. All manipulations were carried out under dry argon using standard Schlenk-tube techniques. The solvents were degassed and distilled before use. IR spectra were recorded in the solid state as Nujol mulls or KBr discs on a Perkin–Elmer 983 spectrometer. NMR spectra were recorded on Bruker WH90, WM250 or AC200 spectrometers operating in the Fourier transform mode.

$RuCl_3 \cdot 3H_2O$ and $RhCl_3 \cdot 3H_2O$ were purchased from Johnson Matthey Ltd. $K_2RuCl_5 \cdot H_2O$[9] was prepared according to published procedures. The ligand $(C_5H_4N)P(O)(OEt)_2$ was prepared by a modified literature procedure.[11]

$K[RuCl_2\{(C_5H_4N)PO(O)(OEt)\}_2] \cdot MeOH$ (**4**). Pyridyl-2-diethyl phosphonate (L) (0.23 g, 1.07 mmol) dissolved in absolute ethanol (20 cm^3) was added dropwise to a solution of $K_2RuCl_5 \cdot H_2O$ (0.2 g, 0.53 mmol) in methanol (20 cm^3) for 2 h at room temperature.

The reaction mixture was then refluxed for 48 h yielding a light yellow solution and a very small amount of white precipitate. The filtrate was then concentrated. Addition of diethyl ether caused the precipitation of a light yellow powder which was washed three times with 20 cm^3 positions of diethyl ether and dried *in vacuo*; yield: 63%. Attempts at recrystallization in various solvents were unsuccessful. Found: C, 30.0; H, 3.6; N, 5.2; P, 10.8; Cl, 10.0; O, 19.6; Ru, 17.1. Calc. for $C_{15}H_{22}O_7N_2Cl_2P_2KRu$: C, 29.3; H, 3.6; N, 4.5; P, 10.1; Cl, 11.5; O, 18.2; Ru, 16.4%.

$K[Ru_2Cl_3\{(C_5H_4N)PO(O)(OEt)\}_2\{(C_5H_4N)PO_2(O)\}_2ZnCH_3OH]CH_3OH \cdot H_2O$ (**5**). Excess zinc powder (0.3 g) was added to methanol. The colour of the reaction solution changed rapidly from yellow to red. After 10 min stirring at room temperature, the red solution was then concentrated. Addition of diethyl ether yielded a red precipitate which was washed with three portions of diethyl ether; yield: 85%. Found: C, 26.3; H, 3.3; N, 4.5; P, 9.3; Cl, 8.4; K, 2.5; O, 19.9. Calc. for $C_{26}H_{36}O_{15}N_4Cl_3P_4KZnRu_2$: C, 26.4; H, 3.0; N, 4.7; P, 10.5; Cl, 9.0; K, 3.3; O, 20.3%.

$RuCl_3[(C_5H_4N)P(O)(OEt)_2]_2 \cdot 2H_2O$ (**6**). Pyridyl 2-diethylphosphonate (0.25 g, 1.04 mmol) was added to $RuCl_3 \cdot 3H_2O$ (0.15 g, 0.57 mmol) and refluxed for 24 h yielding a yellow–orange solution. The solution was then evaporated to dryness and washed twice with ether; yield: 80%. Samples for analysis were obtained by redissolution in methanol and reprecipitation using diethyl ether. Found: C, 32.4; H, 5.1; N, 3.5; Cl, 15.0. Calc. for $RuC_{18}H_{32}N_2O_8Cl_3P_2$: C, 32.1; H, 4.7; N, 4.1; Cl, 15.8%.

$RhCl_3[(C_5H_4N)P(O)(OEt)_2]_2 \cdot 2H_2O$ (**7**). As for **6** using $RhCl_3 \cdot 3H_2O$ (0.25 g, 0.98 mmol) pyridil-2-diethylphosphonate (0.41 g, 1.9 mmol), a light orange precipitate was obtained; yield: 80%. Found: C, 31.2; H, 4.0; N, 4.6; Rh, 15.6. Calc. for

$RhC_{18}H_{32}N_2O_8Cl_3P_2$: C, 32.0; H, 4.7; N, 4.1; Rh, 15.2%.

Acknowledgements—We thank Professors M. Sanchez and R. Poilblanc for helpful discussions and CNRS for support.

REFERENCES

1. See: G. Wilkinson, F. G. A. Stone and E. W. Abel (Editors), *Comprehensive Organometallic Chemistry*, Vols 4–6. Pergamon Press, Oxford (1982).
2. F. Bottomley and L. Satin, *Adv. Organomet. Chem.* 1988, **28**, 339.
3. W. A. Herrmann, *Angew. Chem., Int. Edn Engl.* 1988, **27**, 1297.
4. X. D. He, B. Chaudret, F. Lahoz and J. A. Lopez, *J. Chem. Soc., Chem. Commun.* 1990, 958.
5. (a) M. M. Taqui Kahn, S. B. Halligudi and H. R. Abdi, *J. Molec. Catal.* 1988, **48**, 7; (b) 1988, **48**, 313; (c) 1988, **48**, 325; (d) M. M. Taqui Kahn, R. S. Shukla and A. Prakash Rao, *Inorg. Chem.* 1989, **28**, 452; (e) M. M. Taqui Kahn, H. C. Bajaj and M. R. H. Siddiqui, *J. Molec. Catal.* 1988, **44**, 279.
6. J. T. Groves and K. H. Ahn, *Inorg. Chem.* 1987, **26**, 3831.
7. W. Kläui, *Angew. Chem., Int. Edn. Engl.* 1990, **29**, 627.
8. J. J. Bulot, E. E. Aboujaoude, N. Collignon and P. Savignac, *Phosphorus and Sulphur* 1984, **21**, 197.
9. R. Charonnat, *Ann. Chim. (Paris)* 1931, **16**, 40.
10. H. Nakazawa, Y. Kadoi and K. Miyoshi, *Organometallics* 1989, **8**, 2851.
11. (a) J. K. Kim and J. B. Bunnett, *J. Am. Chem. Soc.* 1979, **35**, 7644; (b) P. Page, J. Bellan, M. R. Mazières, M. Sanchez and B. Chaudret, in preparation.

Polyhedron Vol. 10, No. 19, pp. 2235–2239, 1991
Printed in Great Britain

0277–5387/91 $3.00+.00
© 1991 Pergamon Press plc

TUNGSTEN(V) DIMERIC COMPLEXES WITH ETHYL XANTHATE

R. LOZANO,† J. ROMAN, F. DE JESUS and E. ALARCON

Departamento de Química Inorgánica y Bioinorgánica, Facultad de Farmacia, Universidad Complutense, 28040 Madrid, Spain

(*Received* 16 *November* 1990; *accepted* 25 *June* 1991)

Abstract—The chemical, spectroscopic and magnetic properties of a number of oxo- and sulphido-bridged tungsten(V) oxo-complexes with ethyl xanthate as a ligand are described. The following formulae are assigned to the complexes: $W_2O_3(LL)_4$, $W_2O_4(LL)_2$, $W_2O_2S_2(LL)_2$, $W_2O_3S(LL)_2$. IR and electronic spectra of these compounds are modified by the introduction of sulphur atoms into the bridge system. The low magnetic moments observed are due either to an interaction through the bridging atoms or to a direct spin–spin interaction, according to a dimer structure with monoxo, dioxo, disulphido and oxo-sulphido bridges. The thermal behaviour has also been studied by differential scanning calorimetry (DSC) and thermogravimetric analysis (TGA). The results are discussed on the basis of the structural information available to tungsten complexes.

The relevance to bioinorganic chemistry of molybdenum and tungsten and also to heterogeneous catalysis has been stressed several times in the literature.[1–6]

Although the chemistry of oxo-molybdenum(V) species is dominated by binuclear complexes, curiously, similar binuclear oxo-complexes of tungsten(V) are not known in general. However, we have recently reported the study and characterization of tungsten(V) dimeric complexes with dithiocarbamate and oxine as ligands.[7–11]

The object of the present study has been to obtain binuclear complexes of tungsten(V) with ethyl xanthates as ligands.

The systematic changes upon bridge modification are useful in characterizing the compounds and in clarifying assignments of W—O and W—S bridge stretching frequencies.

These complexes were characterized by IR and electronic spectroscopy, magnetic susceptibility measurements and analytical data. The results obtained permit us to assign the following formulae to the complexes: $W_2O_3(LL)_4$, $W_2O_4(LL)_2$, $W_2O_2S_2(LL)_2$, $W_2O_3S(LL)_2$.

† Author to whom correspondence should be addressed.

EXPERIMENTAL

(1) *Materials*

$Na_2WO_4 \cdot 2H_2O$ was a Merck commercial product and used as supplied. Potassium ethyl xanthate was prepared by the direct reaction of potassium hydroxide with carbon disulphide and ethanol, and was recrystallized from water: ethanol. The solvents used to prepare and recrystallize the complexes were from Carlo Erba or Merck. The solutions for absorption spectra were prepared using dimethylsulphoxide (DMSO), spectral grade (Merck–Uvasol).

(2) *Analytical procedures*

Elemental analysis were performed on a Perkin–Elmer model 240B elemental analyser.

Tungsten was determined by atomic absorption with a Perkin–Elmer model 430 atomic absorption spectrophotometer, after the complexes had been decomposed with a 1:1 mixture of concentrated nitric and sulphuric acid.

Analytical data are collected in Table 1. Results conform to the proposed formula.

Table 1. Analytical data and magnetic moments of tungsten(V) oxo-complexes

Compound		C (%)	H (%)	S (%)	W (%)	μ (B.M.)
$W_2O_3(C_2H_5OCS_2)_4$	Found	15.9	2.0	28.6	40.5	0.60
	Calc.	16.0	2.2	28.4	40.9	
$W_2O_4(C_2H_5OCS_2)_2$	Found	11.1	1.3	19.7	55.1	0.18
	Calc.	10.7	1.5	19.0	54.6	
$W_2O_2S_2(C_2H_5OCS_2)_2$	Found	10.3	1.3	19.0	52.2	0.00
	Calc.	10.2	1.4	18.1	52.1	
$W_2O_3S(C_2H_5OCS_2)_2$	Found	11.0	1.3	18.7	53.6	0.10
	Calc.	10.4	1.4	18.6	53.3	

(3) *Methods*

Magnetic susceptibility was determined by the Gouy method at room temperature using a Mettler H-51 AR balance and a type C Newport electromagnet. Molar susceptibilities have been corrected for diamagnetism. Table 1 shows the data.

The IR spectra were measured on a Perkin–Elmer recording spectrophotometer model 283. The samples were run as KBr pellets. Important IR absorption peaks for the compounds are listed in Table 2.

Near UV–vis spectra were measured in the range 220–1000 nm, on a Beckman recording spectrophotometer model 554 using complex solutions in DMSO. The results obtained are given in Table 3.

Thermogravimetric analysis and differential scanning calorimetry were performed between 25 and 600°C on a Mettler TA 3000 system fitted with a Mettler TG-50 thermobalance, and a Mettler DSC-20 differential scanning calorimeter. The scanning rate used was 2°C min^{-1} and samples of *ca* 5 mg were used, so as to render insignificant the temperature non-uniformity within the sample. An aluminium pan was used. Two different atmospheres were used: between 25–400°C a dynamic nitrogen atmosphere, and between 400–600°C a dynamic oxygen atmosphere to allow oxidation to WO_3. The instrument calibration was checked periodically with standard samples of indium (99.99% purity). Several runs were made.

(4) *Preparation of the complexes*

$W_2O_3(S_2COC_2H_5)_4$. $Na_2WO_4 \cdot 2H_2O$ (3.3 g, 10 mmol) was dissolved in 30 cm^3 of water and depolymerized with 2 N NaOH. Another solution of potassium ethyl xanthate (3.25 g, 20 mmol) in 60 cm^3 of water was prepared. A solution of sodium dithionite (1 g) was added, and it was refluxed at 60°C for 15 min, changing from yellow to green. Glacial acetic acid was added dropwise and with vigorous stirring until reaching pH = 5.

A brown solid precipitated which was filtered with heat and *in vacuo* to obtain a brown powder which was then washed with a benzene and petroleum ether mixture and dried over P_4O_{10}. Yield: 63%.

$W_2O_4(S_2COC_2H_5)_2$. A solution of $Na_2WO_4 \cdot$

Table 2. IR absorption maxima of tungsten(V) oxo-complexes

Compound	ν(C=S)	ν(C—S)	ν(W=O)	ν(W—O_b)	ν(W—S_b)	ν(W—O—C)
$W_2O_3(C_2H_5OCS_2)_4$	1260	1080	932	ν_a 820 ν_s 450	—	1160
$W_2O_4(C_2H_5OCS_2)_2$	1210	1050	943	ν_a 810 ν_s 436	—	1120
$W_2O_2S_2(C_2H_5OCS_2)_2$	1225	1055	940	—	ν_a 471 ν_s 372	1130
$W_2O_3S(C_2H_5OCS_2)_2$	1230	1065	935	ν_a 817 ν_s 445	ν_s 463 ν_s 358	1137

Table 3. Electronic absorption spectra of tungsten(V) oxo-complexes

Compound	ν (cm^{-1})	ε ($M^{-1}\,cm^{-1}$)	Transition
$W_2O_3(C_2H_5OCS_2)_4$	15,503	55	$^2B_2 \rightarrow {}^2E(I)$
	16,556	213	$^2B_2 \rightarrow {}^2B_1$
	21,413	3640	Charge transfer
	23,752	6228	Charge transfer
	30,303	10,453	Intraligand
	33,898	17,604	Intraligand
	40,000	32,912	Intraligand
$W_2O_4(C_2H_5OCS_2)_2$	15,455	154	$^2B_2 \rightarrow {}^2E(I)$
	16,583	706	$^2B_2 \rightarrow {}^2B_1$
	21,276	5114	Charge transfer
	23,696	8723	Charge transfer
	30,120	14,520	Intraligand
	33,333	22,719	Intraligand
	40,816	48,065	Intraligand
$W_2O_2S_2(C_2H_5OCS_2)_2$	15,432	131	$^2B_2 \rightarrow {}^2E(I)$
	16,583	504	$^2B_2 \rightarrow {}^2B_1$
	21,276	6173	Charge transfer
	22,123	3249	Charge transfer
	23,809	7983	Charge transfer
	30,303	11,654	Intraligand
	32,258	27,473	Intraligand
	35,714	35,245	Intraligand
$W_2O_3S(C_2H_5OCS_2)_2$	15,455	95	$^2B_2 \rightarrow {}^2E(I)$
	16,611	489	$^2B_2 \rightarrow {}^2B_1$
	21,367	4140	Charge transfer
	22,222	3834	Charge transfer
	23,809	9213	Charge transfer
	30,120	13,724	Intraligand
	32,051	22,054	Intraligand
	38,167	39,515	Intraligand

$2H_2O$ (3.30 g, 10 mmol) dissolved in 40 cm^3 of water was prepared. 2 N NaOH was added until reaching pH 10 and the solution was then heated by boiling for 10 min.

A second solution of potassium ethyl xanthate (1.65 g, 10 mmol) dissolved in 40 cm^3 of water was then prepared. The two solutions were combined and the resulting one was yellow in colour. A solution of sodium dithionite (0.5 g) in water (20 cm^3) was added to it and the resultant solution was refluxed for 10 min, giving a green coloured solution. Lastly, 2 N HCl was added dropwise with continuous stirring until reaching pH 2 whereupon a brownish precipitate was obtained which was washed with a benzene and petroleum ether mixture and dried over P_4O_{10}. Yield: 57%.

$W_2O_2S_2(S_2COC_2H_5)_2$. $Na_2WO_4 \cdot 2H_2O$ (3.3 g, 10 mmol) was dissolved in water (50 cm^3) and a concentrated sodium hydroxide solution was added. The solution was heated by boiling for 10 min to avoid polymerization.

At the same time potassium ethyl xanthate (1.64 g, 10 mmol) was dissolved in water (40 cm^3). This solution was added to the previous one and a new solution of sodium dithionite (1 g) in water (40 cm^3) was added. The resulting solution was refluxed for 10 min, changing colour from yellow to green. Hydrogen sulphide was passed through the resulting solution with simultaneous cooling in a freezing mixture for *ca* 30 min. Glacial acetic acid was added dropwise until reaching pH = 6 and total precipitation then occurred. The solution was filtered and a brownish residue was obtained which was washed repeatedly with a benzene and petroleum ether mixture and dried over P_4O_{10}. Yield: 61%.

$W_2O_3S(S_2COC_2H_5)_2$. A solution of sodium tungstate (3.3 g, 10 mmol) in water (50 cm^3) was prepared, concentrated boiling NaOH (10 cm^3) was

added and HCl (dropwise) until reaching pH = 2. Another solution of sodium dithionite (1 g) in water (40 cm^3) was added to the previous one. The resulting solution was heated gently for 15 min. Once cooled, hydrogen sulphide was then bubbled slowly through the solution for *ca* 60 min changing the solution to a dark brown colour.

Another solution of potassium ethyl xanthate (1.65 g, 10 mmol) in water (40 cm^3) was prepared. The two solutions were combined and refluxed for 15 min. Glacial acetic acid was then added dropwise until reaching pH = 5 and a total precipitation then occurred. The solid obtained was washed with a benzene and petroleum ether mixture and dried over P_4O_{10}. Yield: 63%.

DISCUSSION

According to the results of the analytical, magnetic (Table 1) and spectroscopic data, the synthesized oxocomplexes are dimeric.

(1) *Magnetic properties*

The magnetic moments found for the complexes are low (0.00–0.60 BM). This is probably due to an interaction through the bridged atoms or the possible formation of a direct metal–metal bond.[7-14]

(2) *IR spectra*

The IR spectra show, in all cases, a strong band in the range 932–940 cm^{-1}, which was attributed to the vibration of the symmetric stretching mode of the terminal W=O bond (Table 2).

In the complexes with monoxo-, dioxo- and oxo-sulphido bridges, the bands corresponding to the W—O—W bridge were assigned to 810–820 cm^{-1} and the vibration of the antisymmetric and symmetric stretching modes, of the W—O bridge bond were assigned to the bands between 436–450 cm^{-1}.

Another two bands, which appear in the IR spectra of the complexes with disulphido and oxo-sulphido bridges in the regions 463–471 and 358–372 cm^{-1}, can be attributed to the vibration of the antisymmetric and symmetric stretching mode, respectively, of the W—S bridge bond.

All the complexes studied exhibit two bands in the IR spectra in the 1120–1160 cm^{-1} region, attributable to a W—O—C bond.

In the IR spectra two vibrational stretching modes for the C—S bond appear, one corresponding to the C=S and the other to the C—S bond, as proved by Cotton *et al.*[15] The band corresponding to the C=S bond is assigned to the 1210–1260 cm^{-1} region while the C—S band appears in the 1050–1080 cm^{-1} region.

(3) *Visible and UV spectra*

The electronic spectra (Table 3) for all the complexes present two bands in the 15,432–15,503 and 16,556–16,611 cm^{-1} regions, which were attributed to *d–d* transitions. The two bands were assigned to $^2B_2 \rightarrow {}^2E(I)$ and $^2B_2 \rightarrow {}^2B_1$ transitions, respectively, for a distorted octahedral structure[16] for the monoxo bridge complexes and for a square-pyramidal structure[17] for the complexes with dioxo-, disulphido- and oxo-sulphido bridges.

In the visible region we can detect two other bands between 21,000 and 23,000 cm^{-1} that were attributed to charge-transfer transitions.

In the complexes with disulphido and oxo-sulphido bridges, another band appears in the visible region at 22,000 cm^{-1} that can be attributed to a charge transfer:

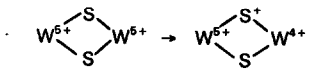

as has been observed in other transition metal complexes with a sulphur bridge.[18,19] The electronic spectra show, in the UV region, three other bands at 30,000, 32,000 and 38,000 cm^{-1}. The electronic spectra of potassium etylxanthate also exhibit three bands at the same wavelength.[20] The differences are not significant. We can attribute these bands to intraligand transitions, $n \rightarrow \pi^*$, $\pi \rightarrow \pi^*$ and $n \rightarrow \sigma^*$, respectively.

(4) *Thermal studies*

The study of the thermal decomposition of tungsten(V) complexes has been made by thermogravimetric and differential scanning calorimetry analysis (Table 4).

The processes observed for the complexes can be schematized as:

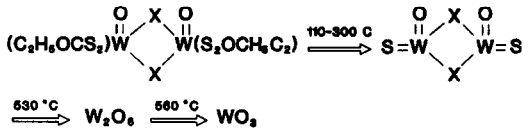

Scheme 1.

All the intermediary species have been identified by elemental analysis and IR spectra.

A strong exothermic process was detected between 575 and 600°C for all the compounds without weight loss in the TG curves, which can be attributed to WO_3 formation.

Table 4. Thermal data of tungsten(V) oxo-complexes

Compound	T(°C)	Weight loss % Found (Calc.)	Identified product
$W_2O_3(C_2H_5OCS_2)_4$	115–212	47.02 (46.66)	$W_2O_3S_2$[a]
	357–523	4.09 (3.33)	W_2O_6
	573–612	—	WO_3
$W_2O_4(C_2H_5OCS_2)_2$	132–305	27.32 (26.40)	$W_2O_4S_2$
	363–558	6.82 (6.45)	W_2O_6
	589–632	—	WO_3
$W_2O_2S_2(C_2H_5OCS_2)_2$	123–262	25.31 (25.79)	$W_2O_3S_3$
	372–543	10.03 (9.37)	W_2O_6
	583–682	—	WO_3
$W_2O_3S(C_2H_5OCS_2)_2$	165–297	24.34 (25.21)	$W_2O_2S_4$
	345–498	11.43 (12.12)	W_2O_6
	578–675	—	WO_3

[a] Not identified.

Acknowledgements—The authors gratefully acknowledge support from the Comisión Interministerial de Ciencia y Tecnología (MAT88-0646-CO3-03).

REFERENCES

1. E. I. Stiefel, *Prog. Inorg. Chem.* 1977, **22**, 1.
2. B. K. Burgess, D. B. Jacobs and E. I. Stiefel, *Biochim. Biophys. Acta* 1980, **614**, 196.
3. Z. Dori, *Prog. Inorg. Chem.* 1981, **28**, 293.
4. R. Lozano, A. L. Doadrio and A. Doadrio, *Polyhedron* 1982, **1**, 163.
5. C. Sharp and A. G. Sykes, *Inorg. Chem.* 1988, **27**, 501.
6. R. Lozano, J. Román, F. De Jesús and E. Alarcón, *Trans. Metal Chem.* 1990, **15**, 141.
7. R. Lozano, A. L. Doadrio, E. Alarcón, J. Román and A. Doadrio, *Rev. Chim. Minér.* 1983, **20**, 109.
8. R. Lozano, E. Alarcón, A. L. Doadrio and A. Doadrio, *Polyhedron* 1983, **2**, 435.
9. R. Lozano, E. Alarcón, A. L. Doadrio and A. Doadrio, *Polyhedron* 1984, **3**, 25.
10. R. Lozano, E. Alarcón, J. Román and A. Doadrio, *Rev. Chim. Minér.* 1984, **21**, 177.
11. R. Lozano, J. Román and F. De Jesús, *Polyhedron* 1989, **7**, 947.
12. F. A. Cotton, S. M. Morehouse and J. S. Wood, *Inorg. Chem.* 1964, **3**, 1063.
13. L. Ricard, C. Martin, R. Wiest and R. Weiss, *Inorg. Chem.* 1975, **14**, 2300.
14. L. Ricard, J. Stienne, J. Karagiannidis, P. Toledano, J. Fisher and A. Mitschler, *J. Coord. Chem.* 1974, **3**, 277.
15. H. B. Blake, F. A. Cotton and J. S. Wood, *J. Am. Chem. Soc.* 1964, **86**, 3024.
16. C. J. Ballhausen and H. B. Gray, *Molecular Orbital Theory*. Benjamin, New York (1965).
17. H. B. Gray and C. B. Hare, *Inorg. Chem.* 1962, **1**, 363.
18. I. G. Dance and A. E. Landers, *Inorg. Chem.* 1979, **18**, 3487.
19. A. Kay and P. C. H. Mitchell, *J. Chem. Soc. A.* 1970, 2421.
20. M. L. Sankaranarayana and C. Patel, *Acta Chem. Scand.* 1965, **19**, 1113.

Polyhedron Vol. 10, No. 19, pp. 2241–2253, 1991
Printed in Great Britain

0277–5387/91 $3.00+.00
© 1991 Pergamon Press plc

SYNTHESIS AND REACTIONS OF TERT-BUTYLIMIDO COMPLEXES OF RHENIUM. X-RAY CRYSTAL STRUCTURES OF $[(ReNBu^t)_2(OSiMe_3)]_2(\mu\text{-}O)(\mu\text{-}OSiMe_3)(\mu\text{-}O_2CCF_3)$, $Re(NBu^t)_3PPh_2$ AND $[Re(NBu^t)_3(NH_2Bu^t)]O_3SCF_3$

VAHÉ SABOONCHIAN, ANDREAS A. DANOPOULOS, ANGEL GUTIERREZ, GEOFFREY WILKINSON* and DAVID J. WILLIAMS*

Johnson Matthey and Chemical Crystallography Laboratories, Chemistry Department, Imperial College, London SW7 2AY, U.K.

(*Received* 23 *May* 1991; *accepted* 25 *June* 1991)

Abstract—The reactions of $Re(NBu^t)_3Cl$ with NaC_5H_5, AgX (X = BF_4, PF_6 and CF_3CO_2) and with $SbCl_5$ lead to the loss of an NBu^t group, and the formation of bis tert-butylimido compounds, respectively, $[Re(NBu^t)_2(\eta^1\text{-}C_5H_5)]_2(\mu\text{-}O)(\mu\text{-}C_5H_4)$, $[(Bu^tN)_2(Cl)Re(\mu\text{-}F)(\mu\text{-}NBu^t)Re(NBu^t)(\mu\text{-}F)]_2X$ (X = BF_4 and PF_6), $[Re(NBu^t)_2]_2(\mu\text{-}OSiMe_3)(\mu\text{-}O_2CCF_3)$ and $[Re(NBu^t)_2Cl_2(MeCN)_2]SbCl_6$. The interaction between $Re_3(NBu^t)_4(O)_5(OSiMe_3)_3$ and AgO_2CCF_3 produces a species, $[Re(NBu^t)_2(OSiMe_3)]_2(\mu\text{-}O)(\mu\text{-}OSiMe_3)(\mu\text{-}O_2CCF_3)$, in which the μ-$OReO_3$ group in the starting material is replaced by μ-O_2CCF_3. Protonation of $Re(NBu^t)_3(NHBu^t)$ by CF_3SO_3H produces the cation $[Re(NBu^t)_3(NH_2Bu^t)]^+$ in which the amine can be replaced by PPh_3. Reactions of $Re(NBu^t)_3X$, where X = Cl or $OSiMe_3$ are replaced by NR_2, PR_2, $NPPh_3$ and $C_4H_3N_2$, are described. Deprotonation of $Re(NBu^t)_3PH(mes)$, mes = $2,4,6\text{-}Me_3C_6H_2$, by Bu^tLi gives the known compound $[Re(NBu^t)_2(\mu\text{-}NBu^t)]_2$ and a new cyclotriphosphane, $(Pmes)_3$.

The structures of compounds listed in the title have been determined by X-ray diffraction. The $[Re(NBu^t)_2(OSiMe_3)]_2(\mu\text{-}O)(\mu\text{-}OSiMe_3)(\mu\text{-}O_2CCF_3)$ structure has crystallographic C_s symmetry with a planar Re_2O_2 ring; Re···Re separation is 3.25 Å. The bridging acetate has a significantly enlarged O—C—O angle of 134°. The $[Re(NBu^t)_3(NH_2Bu^t)]O_3SCF_3$ structure has tetrahedral geometry at rhenium with noticeably differing Re—N distances which correlate to the Re—N—C angles. The $Re(NBu^t)_3PPh_2$ compound has tetrahedral geometry at rhenium and a pyramidal geometry at phosphorus. The Re—P distance is 2.445(2) Å.

In previous papers[1–3] on tris tert-butylimido compounds of rhenium(VII) we have characterized the aryls[1] $Re(NBu^t)_3Ar$, Ar = $2\text{-}MeC_6H_4$, $2,6\text{-}Me_2C_6H_3$ and $2,4,6\text{-}Me_3C_6H_2$(mes) and determined the X-ray crystal structure of the mesityl.[2] The structures of the compounds $Re(NBu^t)_3X$, where X = Cl and $OSiMe_3$, were also determined and the chloride converted to the amido species $Re(NBu^t)_3(NHBu^t)$, which in turn was deprotonated by Bu^nLi to give $Li(tmed)Re(NBu^t)_4$, where tmed = $Me_2NCH_2CH_2NMe_2$.[3] Recently, the arylimido methyl, $Re(NAr)_3CH_3$, where Ar = $2,6\text{-}Pr^iC_6H_3$, was synthesized, as were the compounds $Re(NBu^t)_3R$, where R = Me, Et, σ-C_3H_5 and C≡CPh.[4]

We now describe some unusual reactions of $Re(NBu^t)_3X$, where X = Cl[3] and $OSiMe_3$[5], in which an imido group is removed leading to bis tert-butylimido compounds. Substitution of the siloxide group gives dialkyl- or diarylamido and phosphido species. The amido compound $Re(NBu^t)_3(NHBu^t)$ on protonation gives the cation $[Re(NBu^t)_3(NH_2Bu^t)]^+$ as its trifluoromethane sulphonate.

Analytical and physical data for new compounds are given in Table 1.

* Authors to whom correspondence should be addressed.

Table 1. Analytical and physical data for new compounds

Compound	Colour	m.p. (°C)	Analyses[a] C	H	N	Other
(1) $Re_2(NBu^t)_4(O)(C_5H_5)_2(C_5H_4)$	Orange	104–5	41.0 (42.9)	5.7 (5.9)	6.3 (6.4)	
(2) $Re_2(NBu^t)_4(O)(OSiMe_3)_3(O_2CCF_3)$	Yellow	113–115	28.2 (30.1)	5.0 (6.0)	5.3 (5.3)	6.0 (F) (5.7)
(3) $Re_2(NBu^t)_4(OSiMe_3)(O_2CCF_3)$	Yellow	70–72	28.8 (29.4)	5.2 (5.3)	6.2 (6.5)	5.8 (O) (5.6)
(4) $[Re_4(NBu^t)_8Cl_2F_4]BF_4$	Yellow	> 200	24.1 (24.8)	4.5 (4.6)	7.1 (7.2)	
(5) $[Re_4(NBu^t)_8Cl_2F_4]PF_6$	Yellow	> 200	23.2 (23.9)	4.3 (4.5)	7.5 (7.0)	10.8 (F) (11.8)
(6) $[Re(NBu^t)_2Cl_2(MeCN)_2]SbCl_6$	Orange–red	146 dec.	17.9 (17.7)	3.0 (3.0)	7.0 (7.0)	34.3 (Cl) (34.8)
(7) $[Re(NBu^t)_3(NH_2Bu^t)]O_3SCF_3$	Yellow	145–8	33.2 (32.9)	6.1 (6.1)	8.9 (9.0)	
(8) $[Re(NBu^t)_3(PPh_3)]O_3SCF_3$	Orange	158–60	45.5 (45.9)	5.1 (5.2)	4.9 (5.2)	
(9) $Re(NBu^t)_3(NMe_2)$	Yellow	oil	38.1 (37.9)	7.5 (7.5)	12.4 (12.6)	
(10) $Re(NBu^t)_3(NPh_2)$	Yellow	62–3	52.0 (51.0)	6.6 (6.6)	9.6 (9.9)	
(11) $Re(NBu^t)_3(PPh_2)$	Orange	50–2	49.3 (49.3)	6.4 (6.4)	7.3 (7.2)	5.5 (P) (5.3)
(12) $Re(NBu^t)_3[P(SiMe_3)_2]$	Yellow	65–6	37.8 (37.5)	7.9 (7.9)	7.1 (7.3)	5.5 (P) (5.4)
(13) $Re(NBu^t)_3[PH(mes)]$	Yellow	85	45.5 (45.8)	7.1 (7.1)	7.4 (7.6)	
(14) $Re(NBu^t)_3(NPPh_3)$	Yellow	161–3	53.4 (53.3)	6.3 (6.3)	8.2 (8.3)	4.8 (P) (4.7)
(15) $Re(NBu^t)_3(C_3H_3N_2)$	Orange–red	150–152	37.8 (38.6)	6.5 (6.5)	15.0 (15.0)	

[a] Calculated values in parentheses. Mass spectra are given in the Experimental.

RESULTS AND DISCUSSION

(1) *Reactions leading to bis tert-butylimido compounds*

In attempts to convert $Re(NBu^t)_3(OSiMe_3)$ to the chloride[3] it was observed that interactions with $SOCl_2$ and PCl_3 gave the bis imidotrichloride $Re(NBu^t)_2Cl_3$. We now describe other, different reactions leading to the removal of an NBu^t group.

(a) *Interaction of* $Re(NBu^t)_3Cl$ *and* NaC_5H_5. It was stated by Herrmann *et al.*[4] that all attempts to react $Re(NBu^t)_3(OSiMe_3)$ with C_5H_5M (M = Na, Tl, $SnBu^n_3$) or C_5Me_5M (M = K, MgCl, Li) were unsuccessful. The reaction of $Re(O)_3OSiMe_3$ with C_5H_5Na in THF gives only low yields (*ca* 5%) of $Re(O)_3(\eta^5\text{-}C_5H_5)$, characterized by analysis and spectra.*

The interaction between $Re(NBu^t)_3Cl$ in Et_2O and NaC_5H_5 in THF leads to air-sensitive crystals from hexane of the orange compound **1**, whose X-ray crystal structure has been determined[6] as that shown in Structure I. The bridging $C_5H_4^{2-}$ group

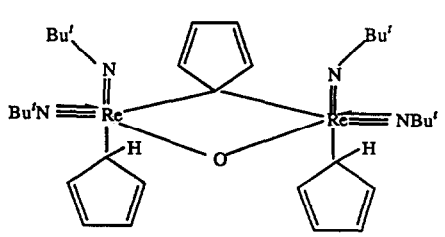

I

* P. G. Edwards and G. Wilkinson, unpublished work, 1979.

is unique; other types of μ-C_5H_4 moieties are, however, known (see ref. 6). The ^{1}H NMR spectra over a certain temperature range confirmed the fluxionality of the η^1-C_5H_5 groups in **1**, although the slow exchange limit could not be reached at −90°C.

Any mechanism for the synthesis of the compound has to account for the loss of a NBu^t group from each metal atom and for the presence of the bridging oxygen. A possibility is given in Scheme 1 where the first step is the formation of a σ-C_5H_5 compound (**A**). While similar substitution by various Cp nucleophiles in $Re(NBu^t)_3(OSiMe_3)$ has been claimed as impossible on steric and electronic grounds,[4] it is likely that lowered crowding in the chloride compared to the siloxide, coupled with the formation of NaCl rather than $NaOSiMe_3$, can drive the substitution to completion. The intermediate **A** of Scheme 1 could be in a tautomeric equilibrium with the alkylidene **B** from which the tert-butylimido group can be removed by NaCp to give **C** and $NaNHBu^t$. Reaction (iv) competing with (iii) could be a base-initiated (i.e. $NaNHBu^t$) cycloelimination reaction of tetrahydrofuran leading to **D** with the loss of tert-butylamine and butadiene. Interaction of **C** and **D** would then lead to the isolated species with the μ-C_5H_4 group 1.

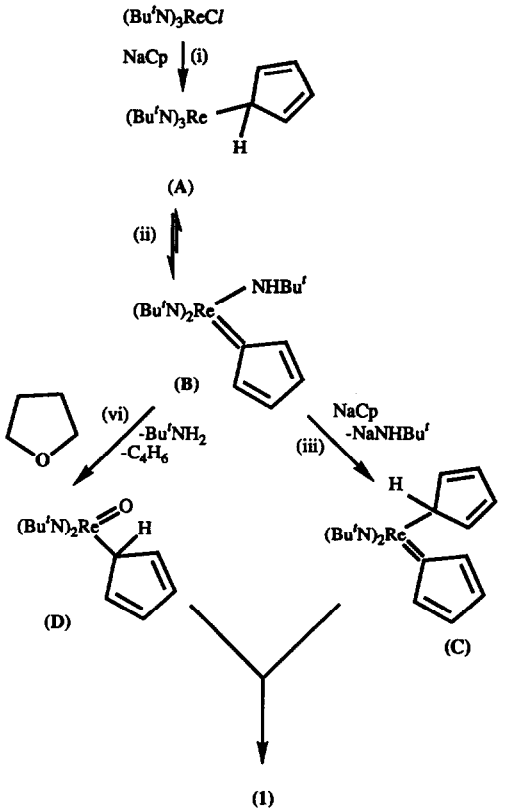

Scheme 1. Possible route to synthesis of compound **1**.

(b) *Interaction of tert-butylimido siloxides with* AgO_2CCF_3. The rhenium siloxides, $[Re(NBu^t)_2(OSiMe_3)]_2(\mu\text{-}OSiMe_3)(\mu\text{-}O)(\mu\text{-}OReO_3)$ (Structure **II**), together with $Re(NBu^t)_3(OSiMe_3)$ were obtained[5] from the interaction between $ReO_3(OSiMe_3)$ and $Bu^tNH(SiMe_3)$, the former on using a deficiency of the amine. The structure of dimer **II** was earlier determined by X-ray diffraction.[7] Another dimer,[2] $Re_2(NBu^t)_3Br(O)(mesityl)(CH_2Me_2C_6H_2O)$ which has μ-O and μ-NBu^t groups, has been characterized crystallographically.

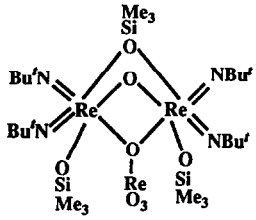

II

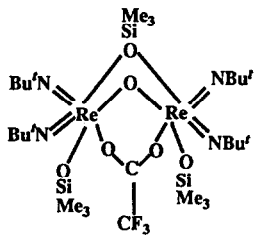

III

Although first obtained in low yield by interaction of $Re(NBu^t)_3Cl$ and AgO_2CCF_3, compound **2** was subsequently made by the more rational procedure of the interaction between Nugent's triply-bridged species and silver trifluoroacetate, which leads to substitution of the μ-$OReO_3$ group by μ-O_2CCF_3. The orange crystalline compound **2** was shown by X-ray crystallography to have structure **III**. The structure is shown in Fig. 1; data in Table 2.

The molecule has crystallographic C_s symmetry about a plane bisecting the Re(1)···Re(1′) vector and passing through the bridging μ-O and the O_2CCF_3 and $OSiMe_3$ groups. The geometry at each rhenium atom is distorted octahedral with inter-bond angles in the ranges 73–104° and 151–171°. The angles subtended at rhenium by O(1), O(3) and O(4) are significantly contracted from 90°, whereas those formed by N(1), O(2) and N(2) are noticeably enlarged. The former are a consequence of satisfying the Re···Re separation and ligand bridging constraints and the latter of accommodating the bulky facially-substituted NBu^t and $OSiMe_3$ groups. The strain of bridging between the two rhenium centres by the O_2CCF_3 ligand is reflected in a significant enlargement of the O(4)—C(14)—

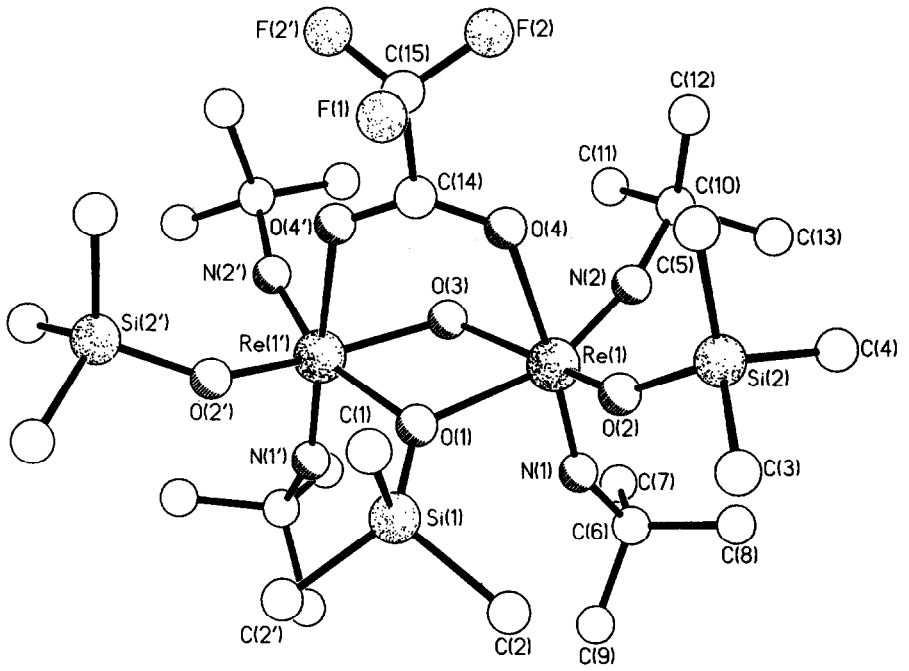

Fig. 1. The structure of $[(Bu^tN)_2(Me_3SiO)Re]_2(\mu\text{-}O)(\mu\text{-}OSiMe_3)(\mu\text{-}O_2CCF_3)$.

O(4′) angle, 134(2)°. With the exception of the Re(1)—O(4) distance [2.32(1) Å], which is significantly longer than that observed for Re—O in e.g. acetates or formates, the remaining Re—O and Re—N distances are normal. The central Re_2O_2 ring is planar to within 0.007 Å and the transannular Re···Re and O···O distances are 3.25 and 2.41 Å, respectively. The angles at N(1) and N(2) are both appreciably bent [152.5(12) and 165.4(13)°, respectively] and consistent with two doubly-bound NBu^t groups. There is marked enlargement of the angle at O(2), 145.3(8)°, compared with that to Si at O(1), 131.0(3)°. These values are virtually identical to those reported for the closely related structure by Nugent and Harlow.[7]

It may be noted that structures **I**, **II** and **III** are

Table 2. Bond lengths (Å) and angles (°) for (**2**) with e.s.d.s in parentheses

Re(1)—O(1)	2.160(11)	Re(1)—O(2)	1.935(12)
Re(1)—O(3)	1.900(10)	Re(1)—O(4)	2.322(9)
Re(1)—N(1)	1.731(9)	Re(1)—N(2)	1.693(14)
Si(1)—O(1)	1.647(19)	O(3)—Re(1′)	1.900(10)
Si(2)—O(2)	1.618(13)		
O(1)—Re(1′)	2.160(11)		
O(4)—C(14)	1.232(14)		

O(1)—Re(1)—O(2)	85.9(5)	O(1)—Re(1)—O(3)	72.6(6)
O(2)—Re(1)—O(3)	151.0(6)	O(1)—Re(1)—O(4)	79.3(4)
O(2)—Re(1)—O(4)	75.6(4)	O(3)—Re(1)—O(4)	81.4(5)
O(1)—Re(1)—N(1)	93.1(5)	O(2)—Re(1)—N(1)	99.4(5)
O(3)—Re(1)—N(1)	100.9(6)	O(4)—Re(1)—N(1)	171.1(5)
O(1)—Re(1)—N(2)	160.3(5)	O(2)—Re(1)—N(2)	101.0(6)
O(3)—Re(1)—N(2)	94.0(7)	O(4)—Re(1)—N(2)	84.5(5)
N(1)—Re(1)—N(2)	103.8(5)	Re(1)—O(1)—Si(1)	131.0(3)
Re(1)—O(1)—Re(1′)	97.4(7)	Re(1)—O(3)—Re(1′)	117.3(10)
Re(1)—O(2)—Si(2)	145.3(8)	Re(1)—N(1)—C(6)	152.5(12)
Re(1)—O(4)—C(14)	125.3(12)		
Re(1)—N(2)—C(10)	165.4(13)		
O(4)—C(14)—O(4′)	133.6(20)		

quite similar being bis-imido species with different bridging groups. The IR and NMR spectra are in accord with the structures. Thus, for **2** the ^{1}H NMR data indicate terminal NBu^t groups and both terminal and bridging $OSiMe_3$ groups with the correct intensity ratios, while there is a single ^{19}F resonance for the μ-O_2CF_3 group. The IR spectra show typical bands for the μ-carboxylate and the other groups except that the μ-O frequency is uncertain due to other bands in this region.

The interaction between $Re(NBu^t)_3(OSiMe_3)$ and silver trifluoroacetate also leads to a bis imido species, presumably by initial electrophilic attack of Ag^+ on a bent imido group; the reaction is evidently complicated and the yield is not quantitative. On the basis of analytical and spectroscopic data, product **3** has structure **IV**; crystals suitable for X-ray study could not be obtained. The compound has rhenium in the V oxidation state corresponding to the loss of an imido group from rhenium(VII). The IR and NMR data are similar to those of **2**.

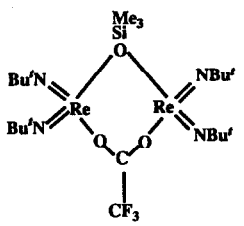

IV

(c) *Interaction of* $Re(NBu^t)_3Cl$ *with* $AgBF_4$ *and* $AgPF_6$. The interaction between $Re(NBu^t)_3Cl$ and $AgBF_4$ (or $AgPF_6$) is sensitive to the nature of the solvent used and the order of addition of reactants. Crystalline products (**4**, **5**) were obtained only when the reaction was carried out in CH_2Cl_2 and with the addition of the imido compound to the solvent salt in excess.

The salts thus obtained both have a cation with the tetrameric structure shown in Structure V. This structure is based on analytical and spectroscopic data and an incomplete X-ray study[8] of the BF_4^- salt. The latter confirmed the tetrameric structure with the rhenium atoms having distorted square-pyramidal geometry, but the refinement was hindered by disorder problems.

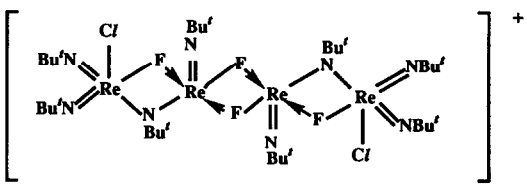

V

As in the reaction of the siloxide with AgO_2CCF_3, reduction occurred since the cation contains rhenium atoms formally in oxidation states IV (inner) and VII (outer). This structure with a linear chain of four metal atoms resembles that of a neutral tert-butylimido(oxo)osmium(VI) compound, $[(Bu^tN)_2Os(\mu\text{-}NBu^t)_2Os(NBu^t)(\mu\text{-}O)]_2$.[9] Since both **4** and **5** are diamagnetic, metal–metal bonding or electron spin coupling via the bridge groups in the cation is evident. The ^{1}H NMR spectrum (CD_2Cl_2) of the cation shows two Bu^tN groups in a 1 : 1 ratio at 25°C, but on cooling there is initial broadening and finally collapse of these peaks at $T_c = -70$°C. Further cooling to −90°C does not allow observation of the slow exchange limit. The data suggest that at higher temperatures the two internal NBu^t and μ-NBu^t groups are exchanging positions very rapidly and the two peaks observed are due to "external" and "internal" imido groups. There is only a single ^{19}F resonance for the bridging fluoride groups at all temperatures.

(d) *Interaction of* $Re(NBu^t)_3Cl$ *and* $SbCl_5$ *in* MeCN. This reaction also leads to the loss of an NBu^t group and the formation of the rhenium(VII) complex $[Re(NBu^t)_2Cl_2(MeCN)_2]SbCl_6$ (**6**). The complex could be formed by chlorination of an NBu^t group by $SbCl_5$, similar to the conversion of $Re(NBu^t)_3(OSiMe_3)$ to $Re(NBu^t)_2Cl_3$ noted above [and to the reaction of Cl_2 with $Cr^{VI}(NBu^t)_2Cl_2$ which leads[10] to $Cr^V(NBu^t)Cl_3$], and possibly Bu^tNCl_2. An alternative route is the following:

$$Re(NBu^t)_3Cl + SbCl_5 \longrightarrow Re(NBu^t)_3{}^+SbCl_6{}^-$$

$$Re(NBu^t)_3{}^+ + SbCl_5 + 2MeCN \longrightarrow [Re(NBu^t)_2Cl_2(MeCN)_2]^+ + Bu^tN{=}SbCl_3.$$

Although $Bu^tN{=}SbCl_3$ is not known it would be similar to $Bu^tN{=}TaCl_3$.

Compound **6** is also available essentially quantitatively by chloride abstraction in refluxing MeCN according to the stoichiometry:

$$Re(NBu^t)_2Cl_3 + 2MeCN + SbCl_5 \longrightarrow [Re(NBu^t)_2Cl_2(MeCN)_2]SbCl_6.$$

The salt crystallizes from MeCN as large, deep orange–red crystals that are soluble in MeCN, THF, CH_2Cl_2 and $CHCl_3$; it is a 1 : 1 electrolyte in MeCN. The IR spectrum shows two stretches for the *cis* nitriles at 2292 and 2319 cm^{-1} that are above the value for free MeCN (2255 cm^{-1}), indicating the absence of M—N π-bonding (which may lower the CN stretching frequency[13]) as can be expected with the high oxidation state of rhenium.

Although an X-ray study confirmed the general features, difficulties in refinement due to disorder

problems preclude detailed discussion. The IR and NMR spectra, which show equivalence of the NBu^t groups, suggest an octahedral structure with *cis*-MeCN and Bu^tN groups and *trans*-chlorines.

Attempts to isolate the triply-coordinated ion $[Re(NBu^t)_3]^+$ have been unsuccessful. The interaction between $Re(NBu^t)_3Cl$ in CH_2Cl_2 and $AlCl_3$ leads to $Re(NBu^t)_2Cl_3$ (cf. above) as the only rhenium-containing product and there is no evidence for $[Re(NBu^t)_3]AlCl_4$. An aluminium-containing product appears to be $[AlCl(NBu^t)]_n$ for which analogues, e.g. $[AlCl(NPr^i)]_6$ are known.[11] The attempted removal of Bu^tNH_2 from the cation $[(Bu^tN)_3Re(NH_2Bu^t)]^+$ by refluxing its salt (described below) in toluene[12] also failed.

(2) *Protonation of* $Re(NBu^t)_3(NHBu^t)$

The interaction of this amide[3] with trifluoromethanesulphonic acid leads to the specific protonation of the amido nitrogen atom and the formation of the cation $[(Re(NBu^t)_3NH_2Bu^t]^+$, which is isolated as the triflate (**7**). The basicity of the amido nitrogen will be greater than that of the imido nitrogens since the lone pairs on the latter are involved in π-bonding $Bu^tN{=}Re$ to a greater extent than is the case for $Bu^tHN{=}Re$. Similar behaviour has been observed for $W(NBu^t)_2(NHBu^t)_2$, where $NHBu^t$ protonation of the amido ligand gives *cis,cis,trans*-$W(NBu^t)_2(\eta^1\text{-}OTf)_2(NH_2Bu^t)_2$.[14] The rhenium compound is a 1 : 1 electrolyte in CH_2Cl_2 or MeCN, although after *ca* 5 min reaction with MeCN begins to occur. The cationic nature contrasts with the structure of the tungsten compound, which has oxygen-bound η^1-triflate groups, possibly due to the reluctance of rhenium(VII) to be five- or six-coordinate when three bulky NBu^t groups are present. The compound is readily hydrolysed by moisture. The IR spectrum of the solid has a band at 1250 cm^{-1} assignable to $CF_3SO_3^-$.[15]

The X-ray crystal structure of the cation is shown in Fig. 2, data is given in Table 3. The geometry at rhenium deviates from tetrahedral with the angles subtended by N(1) and N(2) and by N(3) and N(4), both contracted at 102° whilst the remainder are all slightly enlarged at 113°. There are marked differences in the Re—N bond lengths which range from 1.724(8) Å for N(1) to 1.849(9) Å for N(2). There are concomitant differences in the degree of bending at nitrogen, ranging from 164.6(8)° at N(1) to 139.8(7)° at N(2). In fact, the relationship between Re–N distance and angle at nitrogen is almost linear. The dominance of the scattering by the rhenium atom coupled with the disorder in the F_3CSO_3 anion prevented the location of the NH_2 hydrogen atoms. However, the length of the Re—N(2) bond and the associated angle at nitrogen indicates N(2) as the most likely site for protonation. This conclusion is further strengthened by inspection of the packing of the anion and cation in the crystal (Fig. 3). Here we see that one of the oxygen atoms [O(2)] of the anion is inserted into a cleft between N(2) and N(1) in the cation at a distance of 3.06 Å from N(2).

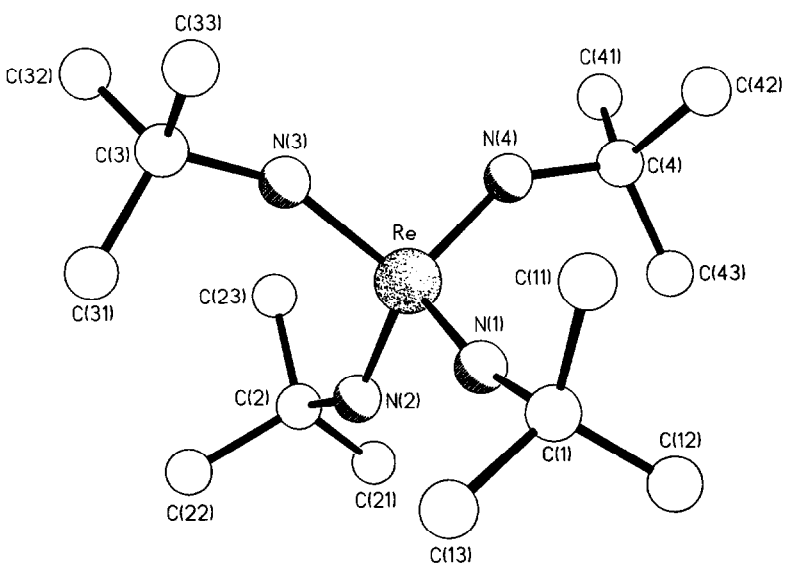

Fig. 2. The structure of the $[Re(NBu^t)_3(NH_2Bu^t)]^+$ ion in the trifluoromethanesulphonate.

Table 3. Bond lengths (Å) and angles (°) for (7) with e.s.d.s in parentheses

Re—N(1)	1.724(8)	Re—N(2)	1.849(9)
Re—N(3)	1.761(10)	Re—N(4)	1.805(10)
N(1)—Re—N(2)	102.2(4)	N(1)—Re—N(3)	113.0(4)
N(2)—Re—N(3)	113.5(5)	N(1)—Re—N(4)	113.2(5)
N(2)—Re—N(4)	113.2(4)	N(3)—Re—N(4)	102.1(5)
Re—N(1)—C(1)	164.6(8)	Re—N(2)—C(2)	139.8(7)
Re—N(3)—C(3)	152.6(8)	Re—N(4)—C(4)	146.0(8)

This is compatible with the formation of a weak cation···anion N—H···O hydrogen bond [the N(1)···O(2) distance is 3.7 Å]; N(3) and N(4) are not approached in this way.

Attempts to substitute the Bu^tNH_2 ligand with various bases such as PMe_3 or PMe_2Ph by reactions in CH_2Cl_2 solution gave mixtures. However, triphenylphosphine gave the salt $[Re(NBu^t)_3(PPh_3)]O_3SCF_3$ (**8**).

Attempts to obtain the hydride $ReH(NBu^t)_3$ by action of NaH or KH on $[Re(NBu^t)_3(NH_2Bu^t)]^+$ in THF gave only the neutral amido complex by deprotonation. Similarly, thermal decompositions of alkyls such as $Re(NBu^t)_3Et$[4] or $Re(NBu^t)_3(O^iPr)$ and treatment of $Re(NBu^t)_3Cl$ with various hydrides, boro- and aluminohydrides also failed, as did the reaction of H_2 in the presence of Et_3N in hexane.

(3) *Substitution reactions of* $Re(NBu^t)_3X$, X = Cl *or* $OSiMe_3$

(a) *Dialkyl- and arylimido compounds.* The interaction of $Re(NBu^t)_3Cl$ and $LiNMe_2$ in Et_2O leads to the dimethylamido complex **9** as a yellow, high-boiling oil. A similar reaction using the siloxide gave a red solution from which no well-defined product could be isolated. However, the siloxide and $LiNPh_2$ react cleanly to give $Re(NBu^t)_3(NPh_2)$ (**10**) as yellow crystals. Both amides are moderately air- and moisture-sensitive. It is of interest that while the oxo analogue $ReO_3[N(mes)_2]$, whose crystal structure was determined, was formed by interaction of $ReO_2(mes)_2$ with nitric oxide via an oxygen transfer to rhenium and a double aryl migration to the nitrogen atom,[16] the reaction of $Re(NBu^t)_2(mes)_2$ with NO gives $[Re(NBu^t)(O)(mes)(\mu\text{-}O)]_2$ and $Bu^tN{=}Nmes$.[2]

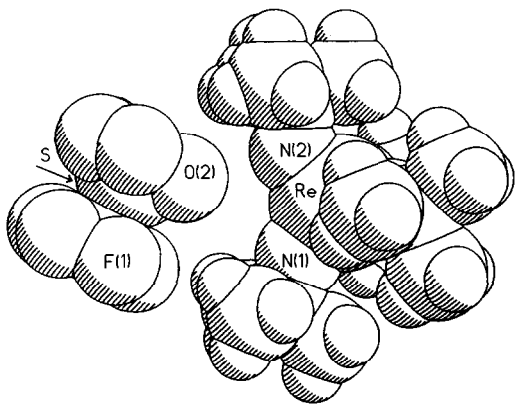

Fig. 3. Space-filling representation of the cation and anion in $[Re(NBu^t)_3(NH_2Bu^t)]SO_3CF_3$.

In the ^1H NMR spectrum of $Re(NBu^t)_3(NPh_2)$ there are two multiplets for the aromatic protons (centred at 7.00 and 7.23 ppm). There is no temperature dependency from −90 to +100°C unlike that found in $ReO_3[N(mesityl)_2]$.[16] For the dimethylamido complex the methyl resonance occurs at 3.35 ppm as a singlet.

(b) *Dialkyl and arylphosphido complexes.* There is a marked difference between the reactivities of $Re(NBu^t)_3X$ (X = Cl or $OSiMe_3$) and those of lithium phosphido reagents. Reaction of the chloride with $LiPPh_2$ gives $[Ph_2P]_2$ as the only identifiable product; this was characterized by its NMR spectrum ($^{31}P\{^1H\}$ = 15.12 ppm in C_6D_6) and m.p. (120°C).[17] $Re(NBu^t)_3(OSiMe_3)$ reacts cleanly with $LiPR_2$ (R = Ph, $SiMe_3$) and LiPH(mes) in Et_2O at −78°C to give the corresponding phosphido complexes: $Re(NBu^t)_3PPh_2$ (**11**), $Re(NBu^t)_3P(SiMe_3)_2$ (**12**) and $Re(NBu^t)_3PH(mes)$ (**13**). The diphenylphosphido complex is obtained as an oil from hexane, but can be crystallized from MeCN as a yellow crystalline solid in *ca* 40% yield. The complexes $Re(NBu^t)_3P(SiMe_3)_2$ and $Re(NBu^t)_3PH(mes)$ are obtained as yellow–orange solids from hexane in yields of *ca* 60 and 45%, respec-

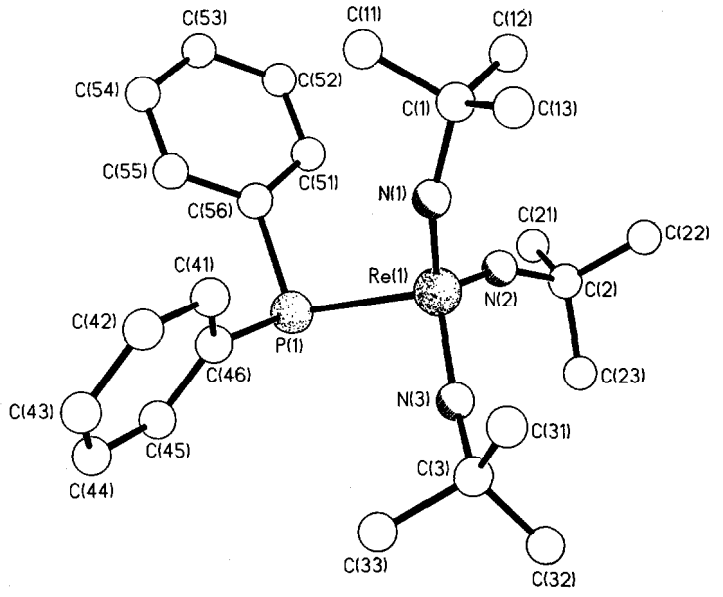

Fig. 4. The structure of $Re(NBu^t)_3(PPh_2)$.

tively. All three compounds have low melting points, are soluble in all common organic solvents, and are moderately air- and moisture-sensitive.

The structure of the diphenylphosphido compound **11** is shown in Fig. 4; data are in Table 4. The compound crystallizes with two crystallographically-independent molecules in the asymmetric unit. Both molecules have nearly identical conformations, the only major difference being in the orientation of one of the tert-butyl groups [C(2)]. The geometry at rhenium is distorted tetrahedral with angles ranging from 99.7(2) to 115.2(3)° in one molecule and from 99.3(3) to 116.2(3)° in the other. The Re—N distances do not differ significantly and are in the range 1.732(7)–1.748(8) Å. The angles at nitrogen reflect an almost equal degree of bending with values between 153.2(6) and 158.7(7)°. It is interesting to note that these values fit the bond length/angle correlation observed above in the $[Re(NBu^t)_3(NH_2Bu^t)]^+$

Table 4. Bond lengths (Å) and angles (°) for (**11**) with e.s.d.s in parentheses

Re(1)—N(1)	1.745(7)	Re(1)—N(2)	1.748(8)
Re(1)—N(3)	1.732(7)	Re(1)—P(1)	2.446(2)
P(1)—C(46)	1.853(8)	P(1)—C(56)	1.852(7)
Re(1′)—N(1′)	1.743(6)	Re(1′)—N(2′)	1.744(7)
Re(1′)—N(3′)	1.732(7)	Re(1′)—P(1′)	2.445(2)
P(1′)—C(46′)	1.856(6)	P(1′)—C(56′)	1.834(7)

N(1)—Re(1)—N(2)	114.1(4)	N(1)—Re(1)—N(3)	114.8(3)
N(2)—Re(1)—N(3)	115.2(3)	N(1)—Re(1)—P(1)	107.6(2)
N(2)—Re(1)—P(1)	103.2(2)	N(3)—Re(1)—P(1)	99.7(2)
Re(1)—N(1)—C(1)	154.9(7)	Re(1)—N(2)—C(2)	156.1(6)
Re(1)—N(3)—C(3)	157.0(7)	Re(1)—P(1)—C(46)	102.9(2)
Re(1)—P(1)—C(56)	104.6(2)	C(46)—P(1)—C(56)	102.2(3)
N(1′)—Re(1′)—N(2′)	114.5(3)	N(1′)—Re(1′)—N(3′)	116.2(3)
N(2′)—Re(1′)—N(3′)	115.3(3)	N(1′)—Re(1′)—P(1′)	100.8(2)
N(2′)—Re(1′)—P(1′)	107.9(2)	N(3′)—Re(1′)—P(1′)	99.3(3)
Re(1′)—N(1′)—C(1′)	158.7(7)	Re(1′)—N(2′)—C(2′)	153.2(6)
Re(1′)—N(3′)—C(3′)	154.1(7)	Re(1′)—P(1′)—C(46′)	102.6(2)
Re(1′)—P(1′)—C(56′)	104.2(2)	C(46′)—P(1′)—C(56′)	104.4(3)

cation. The two Re—P distances are 2.446(2) and 2.445(2) Å and the angles at phosphorus are all less than tetrahedral ranging between 102.2(3) and 104.6(2)°. The pyramidal geometry at phosphorus is in agreement with the NMR data given below.

Terminal dialkyl or aryl phosphido complexes are relatively rare;[18] for rhenium there is the homoleptic anion,[18c] $[Re(PCy_2)_4]^-$, where Cy = cyclohexyl. The IR and NMR spectra of **11** are in accord with the structure found in the crystal. The ^1H NMR spectrum shows two multiplets (centred at 7.86 and 7.14 ppm) for the aromatic protons and a singlet for the NBu^t protons (at 1.26 ppm); there is no temperature dependency from −90 to +100°C. The ^{31}P NMR spectrum shows a quintet centred at −8.78 ppm, due to the coupling of the four *ortho*-hydrogen nuclei on the phenyl rings with the ^{31}P nucleus (^4J(P—H) = 7 Hz); decoupling the proton resonances gives a sharp singlet at −8.78 ppm. The shifts are in the region characteristic for M—PR_2 single-bonded compounds with pyramidal geometry.[18c]

For $Re(NBu^t)_3P(SiMe_3)_2$, the $SiMe_3$ protons are split into a doublet by the phosphorus nucleus (^3J(P—H) = 4.5 Hz). The $^{31}P\{^1H\}$ NMR spectrum has a singlet at −212.33 ppm. The ^1H NMR spectrum of $Re(NBu^t)_3PH(mes)$ shows a doublet centred at 5.37 ppm for the phosphido proton (^1J(P—H) = 195 Hz). The same coupling constant is observed in the ^{31}P NMR spectrum of the complex where the doublet is centred at −153.1 ppm.

Attempts to deprotonate $Re(NBu^t)_3P(H)(mes)$ (**13**) in the hope of obtaining a phosphinidine[19] species, $[(Bu^tN)_3Re{=}P(mes)]^-$, by interaction with Bu^{t}Li in hexane or MeLi in Et_2O or by refluxing in toluene with Et_3N were unsuccessful. Although deprotonation occurs, other reactions followed and the only rhenium-containing species isolated was the rhenium(VI) dimer $[Re(NBu^t)_2(\mu\text{-}Bu^tN)]_2$, whose structure has been determined.[3] From the reaction of **13** with one equiv. of Bu^{n}Li in hexane the only other product that could be isolated was a colourless, crystalline solid that has been found to be the new cyclophosphane $[P(2,4,6\text{-}Me_3C_6H_2)]_3$.

Cyclophosphanes, $(PR)_n$ (n = 3–6), are known.[20–22] The trimers, with bulky R groups have two of the R groups on one side of the P_3 plane. The $^{31}P\{^1H\}$ spectrum of $(Pmes)_3$ has two singlets at −111.20 and −118.35 ppm in a 2:1 ratio that are in close agreement with values reported for similar compounds.

The mechanism of this reaction leading to the formation of the rhenium(VI) dimer and the cyclophosphane is not clear. The oily, lithium-containing residue has eluded characterization. It is of interest that phosphinidine intermediates have been proposed[22] in the synthesis of metal compounds such as $[(CO)_5Cr]_3(PBu)_3$.

(c) *Phosphiniminato compound.* The interaction between $Re(NBu^t)_3Cl$ and a slight excess of $LiNPPh_3$ in refluxing toluene gives the phosphiniminato complex $Re(NBu^t)_3(N{=}PPh_3)$ (**14**). The resonance form Re—$\ddot{N}$=PPh_3 rather than others such as $Re^-{=}N^+{=}PPh_3$ appears to be the main contributor since the IR band at 1094 cm^{-1} is at the lower limit of the ν(P—N) region (1052–1200 cm^{-1}) for such complexes.[23a] The only other related rhenium(VII) compound is $Re[N(2,6\text{-}^iPr_2C_6H_3)]_3(N{=}PPh_3)$, whose X-ray structure was recently reported: it was made by the interaction between Ph_3PNReO_3 and the aryl isocyanate.[23b]

(d) *Pyrazolate.* The interaction of $Re(NBu^t)_3Cl$ with the sodium salt of pyrazole in THF gives $Re(NBu^t)_3(C_3H_3N_2)$ (**15**). The mass spectrum indicates that the compound is monomeric in the gas phase; the ^1H NMR spectra shows a singlet for the NBu^t protons and an ABC pattern for the $C_3H_3N_2$ protons; the ratio is 9:1 as expected.

EXPERIMENTAL

The general techniques and instruments used have been described.[3,24] All compounds and operations were carried out under purified nitrogen, argon or *in vacuo*. Commercial chemicals were from Aldrich. NMR spectra (250 MHz) are in ppm (δ) in C_6D_6 unless otherwise stated and referenced to Me_4Si (^1H), $CFCl_3$ (^{19}F) and external H_3PO_4 (^{31}P). IR spectra (in cm^{-1}) are in Nujol mulls. Electron impact mass spectra (m/z) show isotropic envelopes for the rhenium-containing ions but only peaks corresponding to those with ^{187}Re (62.5%) are listed.

The compounds $Re(NBu^t)_3(OSiMe_3)$[5] and $Re(NBu^t)_3Cl$[3] were made as described. The previously undescribed tert-butoxide and isopropoxide have been made from the chloride as below.

The reagents $LiNMe_2$, $LiNPh_2$, $LiPPh_2$ and LiP(H)(mes) were prepared by the standard method of interaction of the corresponding amine or phosphine with one equiv. of Bu^{n}Li in hexane at −78°C. $LiP(SiMe_3)_2$ was prepared by the interaction of $P(SiMe_3)_3$ with Bu^{n}Li in THF at −40°C. $LiN{=}PPh_3$ was prepared from $HN{=}PPh_3$[25] and one equiv. of Bu^{n}Li in toluene at −78°C. The sodium salt of pyrazole was made by adding a suspension of NaH in THF to a solution of pyrazole at −78°C; the solution was stirred for 30 min at room temperature, filtered, evaporated and the residue washed with hexane (3 × 30 cm^3).

Tris(tert-butylimido)tert-butoxo)- and -(isopropoxo) rhenium(VII)

To a mixture of $Re(NBu^t)_3Cl$ (0.44 g, 1 mmol) and $KOBu^t$ (0.11 g, 1 mmol) at −20°C was added cold Et_2O (20 cm^3); the yellow solution was allowed to warm and was then stirred for 15 h at ambient temperature. After filtration and removal of the solvent, extraction with hexane (5 cm^3) and cooling gave yellow needles. Yield: 0.34 g, 71%; m.p. 55–56°C. Found: C, 40.7; H, 7.6; N, 9.0%. M.S. 473 (18%), $Re(NBu^t)_3(OBu^t)$; 402 (100%), $Re(NBu^t)_2(OBu^t)$. NMR: ^1H: 1.34 (s, 27H, OBu^t); 1.25 (s, 9H, OBu^t).

The *isopropoxide* was made similarly. Yield: *ca* 82%, b.p. 100–120° at *ca* 0.15 mm Hg. M.S. 457 (M^+), 442 (M—Me); 400 (M—$Me_2C{=}CH_2$); 386 (M—NBu^t). IR: 1220 cm^{-1}, $ReNBu^t$. NMR: ^1H: 1.35 (*s*, 27H, $NCMe_3$); 1.30 (d, 6H, Me_2CH); 450 (sept., ^1H, $CHMe_2$).

Bis[bis(tert-butylimido)(η^1-cyclopentadienyl)rhenium (VII)](μ-oxo)(μ-cyclopentadienylidene) (**1**)

To $ReCl(NBu^t)_3$ (0.45 g, 1 mmol) in Et_2O (20 cm^3) at −78°C was added a THF solution of NaC_5H_5 (1.12 cm^3 of 0.98 M solution, 1.1 mmol) and the mixture was allowed to warm to ambient temperature when the colour changed from orange to brown. After stirring for 1 h the volatiles were removed *in vacuo* and the residue extracted with hexane (3 × 10 cm^3); the orange extracts were concentrated and cooled (−20°C, 12h) to give orange prisms. Yield: 0.065 g, 15%. M.S. 736(1), $Re_2(NBu^t)_4(O)(C_5H_5)$; 458 (45), $Re(NBu^t)_2(C_5H_5)_2$; 443 (100), $Re(NBu^t)(C_5H_5)-CH_3$; 410 (32), $Re(NBu^t)_2(O)(C_5H_5)$. NMR: ^1H (20°C, CD_2Cl_2): 1.35 (s, 18H) and 1.32 (s, 18H) $NCMe_3$; 5.85 (m, 4H, μ-C_5H_4); 6.2 (s, 8H, η^1-C_5H_5).

Bis[bis(tert-butylimido)(trimethylsiloxo)rhenium(VII)] (μ-oxo)-(μ-trimethylsiloxo)(μ-trifluoroacetato) (**2**)

To a suspension of AgO_2CCF_3 (0.11 g, 0.5 mmol) in THF (30 cm^3) at −78°C was added a solution of $Re_3(NBu^t)_4(O)_5(OSiMe_3)_3$[5] (0.45 g, 0.38 mmol) in THF (20 cm^3). After stirring at room temperature (12 h) the solution was evaporated and extracted with hexane (2 × 20 cm^3). Concentration (10 cm^3) and cooling (−20°C) gave yellow crystals, some of X-ray quality. Yield: 0.18 g (44%). IR: 1682 (ν_{asym} OCO); 1454 (ν_{sym} OCO); 1203 (NBu^t). The values of the symmetric and asymmetric carboxylate stretches and the separation $\Delta = 228\ cm^{-1}$ are similar to those in other bridged trifluoroacetates.[26] NMR ($CDCl_3$): ^1H: 1.42 (s, 26H, NBu^t); 0.25 (s, 9H, μ-$OSiMe_3$); 0.13 (s, 18H, $OSiMe_3$). ^{19}F: 57.72 (s).

Bis[bis(tert-butylimido)rhenium(V)](μ-trimethylsiloxo) (μ-trifluoroacetato) (**3**)

To a suspension of AgO_2CCF_3 (0.2 g, 1.27 mmol) in THF (30 cm^3) at −78°C was added a solution of $Re(NBu^t)_3(OSiMe_3)$ (0.5 g, 1.02 mmol) in THF (10 cm^3). After warming and stirring at room temperature for *ca* 18 h, the solution was evaporated *in vacuo* and the residue extracted with hexane (2 × 20 cm^3). Concentration (to 10 cm^3) of the filtered extract and cooling (−20°C) gave a yellow crystalline solid. Yield: 0.57 g, 65%. IR: 1674, 1450 cm^{-1} (asym and sym νOCO, $\Delta = 224\ cm^{-1}$); 1208 (NBu^t). NMR ($CDCl_3$): ^1H: 1.44 (s, 36H, NBu^t); 0.13 (s, 9H, $OSiMe_3$). ^{19}F: 60.18 (s).

Bis[bis(tert-butylimido)chlororhenium(VII)(μ-tert-butylimido)(μ-fluoro)(tert-butylimido)rhenium(IV)(μ-fluoro)]tetrafluoroborate (**4**) *and hexafluorophosphate* (**5**)

To a solution of $AgBF_4$ (0.15 g, 0.76 mmol) or $AgPF_6$ (0.19 g, 0.75 mmol) in CH_2Cl_2 (15 cm^3) was added $Re(NBu^t)_3Cl$ (0.3 g, 0.7 mmol) in CH_2Cl_2 (20 cm^3) when a white precipitate (AgCl) formed immediately. After stirring in the dark for 4 h, the volatiles were removed *in vacuo* and the residue washed with Et_2O (3 × 20 cm^3). Extraction of the residue with CH_2Cl_2 (2 × 10 cm^3) and concentration to 2–3 cm^3, followed by layering with Et_2O gave yellow prisms after *ca* 24 h at room temperature. Yield: *ca* 20%. NMR ($CDCl_3$): ^1H: 1.65 (terminal NBu^t); 1.61 (internal and bridge NBu^t). ^{19}F: BF_4^- salt, −150 (BF_4^-); −126 (μ-F). ^{19}F: PF_6^- salt, −75 (d, J(P—F) = 713 Hz, equatorial F of PF_6^-); −80 (d, J(P—F) = 986 Hz, axial F of PF_6^-); −135 (μ-F).

Bis(tert-butylimido)dichlorobis(acetonitrile)rhenium (VII)hexachloroantimonate(V) (**6**)

To $Re(NBu^t)_3Cl$ (0.4 g, 0.92 mmol) in MeCN (30 cm^3) was added $SbCl_5$ (1 cm^3 of 1 M solution in CH_2Cl_2) and the solution refluxed (*ca* 12 h) and evaporated. The residue was washed with Et_2O (2 × 30 cm^3) and extracted into MeCN (2 × 10 cm^3); concentration and cooling gives bright orange–red crystals. Further crops may be obtained from the supernatant. Overall yield: 0.54 g (72%). Conductivity (MeCN): $\Lambda_M = 111\ \Omega^{-1}\ cm^2\ mol^{-1}$. IR:

2319, 2292 (MeCN); 1200 (NBu^t); 337 vs ($SbCl_6^-$). NMR: ^1H: 1.64 (s, Bu^tN); 2.22 (s, MeCN).

The compound is obtained similarly from stoichiometric amounts of $Re(NBu^t)_2Cl_3$[27] and $SbCl_5$ in MeCN with an essentially quantitative yield.

Tris(tert-butylimido)(tert-butylamine)rhenium(VII) *trifluoromethanesulphonate* (**7**)

To a solution of $Re(NBu^t)_3(NHBu^t)$[3] (0.5 g, 1.05 mmol) in Et_2O (30 cm^3) at −78°C was added dropwise with stirring a pre-cooled solution of CF_3SO_3H (0.1 cm^2, 1.17 mmol in 20 cm^3 Et_2O). The yellow solution was stirred for 1 h and then allowed to warm slowly. The yellow precipitate was collected, washed with Et_2O (2 × 10 cm^3) and crystallized from CH_2Cl_2–Et_2O (1:2) at −20°C as yellow prisms. Yield: 0.29 g, 45%. IR: 3177 (H_2NBu^t); 1250 ($CF_3SO_3^-$); 1210 (NBu^t). NMR ($CDCl_3$): ^1H: 1.45 (s, 27H, NBu^t); 1.39 (s, 9H, H_2NBu^t). ^{19}F: −82.0. Conductivity (CH_2Cl_2): Λ_M = 141 Ω^{-1} cm^2 mol^{-1} (cf. $Bu^n{}_4NPF_6$ under the same conditions, Λ_M = 145 Ω^{-1} cm^2 mol^{-1}.

Tris(tert-butylimido)(triphenylphosphine)rhenium (VII)*trifluoromethanesulphonate* (**8**)

To a solution of the above amine complex (0.2 g, 0.32 mmol) in CH_2Cl_2 (20 cm^3) was added PPh_3 (0.1 g, 0.4 mmol) when the colour changed from yellow to orange. After stirring for 2 h the volatiles were moved *in vacuo* and the residue washed with Et_2O (3 × 30 cm^3) and recrystallized as orange needles from CH_2Cl_2 after addition of Et_2O at −20°C. Yield: 0.14 g, 55%. IR: 1255 (CF_3SO_3); 1210 (NBu^t). NMR ($CDCl_3$): ^1H: 1.25 (s, 27H, NBu^t); 7.3 (m, 15H, PPh_3). $^{31}P\{^1H\}$: 34.83. ^{19}F: −79.0.

Tris(tert-butylimido)(dimethylamido)rhenium(VII) (**9**)

To a solution of $Re(NBu^t)_3Cl$ (0.45 g, 1.03 mmol) in Et_2O (20 cm^3) at −78°C was added a cold suspension of $LiNMe_2$ (0.07 g, 1.4 mmol) in Et_2O (30 cm^3). After warming and stirring at room temperature for 5 h the solution was evaporated and the residue extracted with hexane (2 × 5 cm^3). Evaporation of the extract left a yellow oil which was distilled under high vacuum at *ca* 150°C. Yield: 0.16 g, 35%. M.S. 444 (M); 429 (M—Me); 373 (M—NBu^t). IR: 1211 (NBu^t). NMR: ^1H: 3.35 [s, 6H, $N(Me)_2$], 1.37 (s, 27H, NBu^t).

Tris(tert-butylimido)(diphenylamido)rhenium(VII)(**10**)

As above but using $Re(NBu^t)_3(OSiMe_3)$ (0.42 g, 0.86 mmol) in Et_2O (20 cm^3) and $LiNPh_2$ (0.19 g, 1.10 mmol) in Et_2O (30 cm^3). Concentration of the hexane extract and cooling (−20°C) gave yellow crystals. Yield: 0.26 g, 53%. M.S. 568 (M); 553 (M—Me); 497 (M—Bu^tN). IR: 1200 (NBu^t). NMR: ^1H: 7.00–7.23 (m, 10H, NPh_2); 1.29 (s, 27H, NBu^t).

Tris(tert-butylimido)(diphenylphosphido)rhenium(VII) (**11**)

As above but using $Re(NBu^t)_3(OSiMe_3)$ (0.51 g, 1.04 mmol) in Et_2O (20 cm^3) and $LiPPh_2$ (0.25 g, 1.30 mmol) in Et_2O (30 cm^3). The hexane extracted (30 cm^3) was evaporated and the residue crystallized from MeCN to give an orange–yellow crystalline solid. Yield: 0.24 g, 40%. M.S. 585 (M); 570 (M—Me); 555 (M—2Me); 514 (M—Bu^tN). IR: 1211 (NBu^t). NMR: ^1H: 7.14, 7.86 (m, 10H, PPh_2); 1.26 (s, 27H, NBu^t). ^{31}P: −8.78 [quin. ^4J(P—H) = 7 Hz; coupling to four *o*-H on C_6H_5 rings]. $^{31}P\{^1H\}$: −8.78 (s).

Tris(tert-butylimido)[bis(trimethylsilyl)phosphido]rhenium(VII) (**12**)

As above from $Re(NBu^t)_3(OSiMe_3)$ (0.55 g, 1.13 mmol) in Et_2O (20 cm^3) and $Li[P(SiMe_3)_2]$ (0.26 g, 1.41 mmol) in Et_2O (20 cm^3). Concentration of the hexane extract (20 cm,[3]) and work-up gave a yellow crystalline solid. Yield: 0.28 g, 43%. M.S. 577 (M); 562 (M—Me); 520 (M—Bu^t); 504 (M—$SiMe_3$); 406 (M—3 × Bu^t); 333 (M—3 × Bu^tSiMe_3). IR: 1211 (NBu^t). NMR: ^1H: 1.37 (s, 27H, NBu^t); 0.49 (d, 18H, $SiMe_3$, ^3J(P—H) = 4.5 Hz). $^{31}P\{^1H\}$: −212.33 (s).

Tris(tert-butylimido)(mesitylphosphido)rhenium(VII) (**13**)

As above from $Re(NBu^t)_3(OSiMe_3)$ (0.639 g, 1.29 mmol) but using LiPH(mesityl) (6.25 g, 1.58 mmol). The product is obtained from hexane as yellow crystals. Yield: 60%. M.S. 551 (M); 536 (M—Me); 478 (M—Me, HBu^t); 463 (M—2Me, Bu^t, H); 431 (M—mesityl, H). IR: 2328 (P—H), 1211 (NBu^t). NMR: ^1H: 1.27 (s, 27H, NBu^t); 2.16 (s, 3H, *p*-CH_3); 2.65 (s, 6H, *o*-CH_3); 5.37 [d, 1H, P—H, ^1J(P—H) = 195 Hz]; 6.78 (s, 2H, C_6H_2). $^{31}P\{^1H\}$: −153.16 (s). ^{31}P: −153.1, 155.79 (d, J(P—H) = 195 Hz).

The interaction of stoichiometric amounts of **13**

and Bu^nLi in hexane gave yellow $[(Re(NBu^t)_2(\mu\text{-}NBu^t)]_2$,[3] identified by m.p. and ^1H NMR spectrum, and colourless $(Pmesityl)_3$, which crystallized first, in yields 10–20%. Found: C, 71.5; H, 8.0; P, 20.5. Calc. for $C_{27}H_{33}P_3$: C, 72.0; H, 7.4; P, 20.6%. M.S. 450 (M); 330 (M—mesityl—H); M 302 [M—$(mesP)_2$]. For NMR see text.

Tris(tert-butylimido)(triphenylphosphineiminato)rhenium(VII) (**14**)

To $Re(NBu^t)_3Cl$ (0.38 g, 0.87 mmol) in toluene (20 cm^3) was added $LiN{=}PPh_3$ (0.30 g, 1.06 mmol) in toluene (20 cm^3) and the solution refluxed for 12 h. After evaporation the residue was extracted into hexane (2×30 cm^3) which was filtered, concentrated and cooled to give an orange–brown powder. Recrystallization from Et_2O gave a yellow crystalline solid. Yield: 0.2 g, 33%. M.S. 676 (M); 661 (M—Me); 646 (M—2Me); 605 (M—Bu^t); 400 (M—$NPPh_3$). IR: 1206 (NBu^t). NMR: ^1H: 7.02, 7.44 (m, 15H, Ph); 1.44 (s, 27H, NBu^t). $^{31}P\{^1H\}$: 15.28 (s).

Tris(tert-butylimido)pyrazolatorhenium(VII) (**15**)

To a solution of $Re(NBu^t)_3Cl$ (0.56 g, 1.29 mmol) in THF (20 cm^3) at −78°C was added a cold solution of sodium pyrazolate (from pyrazole and NaH in THF; 0.15 g, 1.67 mmol) in THF (30 cm^3). After warming and stirring at room temperature (18 h) the solution was evaporated and extracted with hexane (2×20 cm^3). Concentration (to 5 cm^3), filtration and cooling (−20°C) gave orange–red crystals. Yield: 0.19 g, 32%. M.S. 464 (M—3H), 449 (M—3H—CH_3); 393 (M—3H—NBu^t). NMR ($CDCl_3$): ^1H: 7.18 (m, 1H, C_4H_3N); 7.59 (m, 1H, C_4H_3N); 5.95 (m, 1H, C_4H_3N); 1.53 (s, 27H, NBu^t).

X-ray crystallography

All three compounds were air-sensitive and were sealed in Lindemann glass capillaries under argon. Crystal data: (**2**) $C_{27}H_{63}F_3N_4O_6Re_2Si_3$, M = 1053.5, monoclinic, a = 9.895(1), b = 22.603(4), c = 10.383(1) Å, β = 109.77(1)°, V = 2185 $Å^3$, space group $P2_1/m$, Z = 2 (the complex has crystallographic C_s symmetry), D_c = 1.60 g cm^{-3}, copper radiation, λ = 1.54178 Å, μ(Cu-K_α) = 115 cm^{-1}, F(000) = 1040. Data were measured on a Nicolet R3m diffractometer with Cu-K_α radiation (graphite monochromator) using ω-scans. A crystal of dimensions $0.03\times0.18\times0.38$ mm was used. 3046 independent reflections ($2\theta \leqslant 116°$) were measured, of which 2252 had $|F_o| > 3\sigma(|F_o|)$, and were considered to be observed. The data were corrected for Lorentz and polarization factors; a numerical absorption correction (face-indexed crystal) was applied; maximum and minimum transmission factors were 0.677 and 0.141. The structure was solved by the heavy-atom method. The non-hydrogen atoms were refined anisotropically. The positions of the hydrogen atoms were idealized, C—H = 0.96 Å, assigned isotropic thermal parameters, U(H) = 0.08, and allowed to ride on their parent carbon atoms. The methyl groups were refined as rigid bodies. Refinement was by full-matrix least-squares to R = 0.064, R_w = 0.058 [$w^{-1} = \sigma^2(F)+0.00050F^2$]. The maximum and minimum residual electron densities in the final ΔF map were 2.32 and −1.87 e $Å^{-3}$, respectively. The mean and maximum shift/errors in the final refinement were 0.000 and 0.000, respectively. Computations were carried out on an Eclipse S140 computer using the SHELXTL program system and on an IBM 386 PC using SHELXTL PC.

Crystal data: (**7**) $C_{17}H_{38}F_3N_4O_3ReS$, M = 621.8, monoclinic, a = 15.495(5), b = 11.208(5), c = 16.034(11) Å, β = 105.48(4)°, V = 2684 $Å^3$, space group $P2_1/a$, Z = 4, D_c = 1.54 g cm^{-3}, copper radiation, λ = 1.54178 Å, μ(Cu-K_α) = 96 cm^{-1}, F(000) = 1240. Data were measured as above for a crystal of dimensions $0.17\times0.20\times0.33$ mm. 3625 independent reflections ($2\theta \leqslant 116°$) were measured, of which 2969 had $|F_o| > 3\sigma(|F_o|)$, and were considered to be observed. The data were corrected for Lorentz and polarization factors; an empirical absorption correction (ellipsoidal) based on 309 azimuthal measurements was applied; maximum and minimum transmission factors were 0.367 and 0.206. The structure was solved by the heavy-atom method. The non-hydrogen atoms were refined anisotropically. The triflate ion was disordered about the C—S axis and was refined with two rigid body orientations for both the CF_3 and SO_3 groups. The amine hydrogen atoms could not be located. The positions of the remaining hydrogen atoms were idealized, C—H = 0.96 Å, assigned isotropic thermal parameters, U(H) = $1.2U_{eq}$(C), and allowed to ride on their parent carbon atoms. The methyl groups were refined as rigid bodies. Refinement was by block-cascade full-matrix least-squares to R = 0.046, R_w = 0.045 [$w^{-1} = \sigma^2(F)+0.00054F^2$]. The maximum and minimum residual electron densities in the final ΔF map were 0.75 and −0.61 e $Å^{-3}$, respectively. The mean and maximum shift/error in the final refinement were 0.047 and 0.465, respectively. Computations were carried out as above.

Crystal data: (**11**) $C_{24}H_{37}N_3PRe$, M = 584.8, triclinic, a = 10.430(2), b = 10.319(3), c = 26.227(10) Å, α = 91.23(3), β = 94.23(3), γ = 99.30(2)°, V = 2776 $Å^3$, space group $P\bar{1}$, Z = 4 (2 crystallo-

graphically-independent molecules), $D_c = 1.40$ g cm^{-3}, copper radiation, $\lambda = 1.54178$ Å, μ(Cu-K_α) = 90 cm^{-1}, $F(000) = 1168$. Data were measured as above on a crystal of dimensions $0.17 \times 0.23 \times 0.26$ mm. 7485 independent reflections ($2\theta \leqslant 116°$) were measured, of which 5868 had $|F_o| > 3\sigma(|F_o|)$ and were considered to be observed. The data were corrected for Lorentz and polarization factors; a numerical absorption correction (face-indexed crystal) was applied; maximum and minimum transmission factors were 0.352 and 0.105. The structure was solved by the heavy-atom method. The non-hydrogen atoms were refined anisotropically. The phenyl rings together with their hydrogen atoms were refined as idealized rigid bodies. The methyl groups were also refined as idealized rigid bodies with a common refined-free variable isotropic thermal parameter for each tert-butyl group. Refinement was by blocked full-matrix least-squares to $R = 0.043$, $R_w = 0.047$ [$w^{-1} = \sigma^2(F) + 0.00147F^2$]. The maximum and minimum residual electron densities in the final ΔF map were 0.89 and -0.79 e Å^{-3}, respectively. The mean and maximum shift/error in the final refinement were 0.000 and 0.000, respectively. Computations were carried out as above.

Acknowledgements—We thank the SERC for a studentship (V.S.), the Universidad Complutense, Madrid for study leave (A.G.) and the SERC for support and provision of X-ray facilities.

REFERENCES

1. C. J. Longley, P. D. Savage, G. Wilkinson, B. Hussain and M. B. Hursthouse, *Polyhedron* 1988, **7**, 1079.
2. A. Gutierrez, G. Wilkinson, B. Hussain-Bates and M. B. Hursthouse, *Polyhedron* 1990, **9**, 2081.
3. A. A. Danopoulos, C. J. Longley, G. Wilkinson, B. Hussain and M. B. Hursthouse, *Polyhedron* 1989, **8**, 2657.
4. W. A. Herrmann, G. Weichselbaumer, R. A. Paciello, R. A. Fischer, E. Herdtwecks, J. Okuda and D. W. Marz, *Organometallics* 1990, **9**, 489.
5. W. A. Nugent, *Inorg. Chem.* 1983, **22**, 965.
6. A. A. Danopoulos, G. Wilkinson and D. J. Williams, *J. Chem. Soc., Chem. Commun.* 1991, 181.
7. W. A. Nugent and R. L. Harlow, *J. Chem. Soc., Chem. Commun.* 1979, 1105.
8. B. Hussain-Bates and M. B. Hursthouse, private communication.
9. A. A. Danopoulos, G. Wilkinson, B. Hussain-Bates and M. B. Hursthouse, *J. Chem. Soc., Dalton Trans.* 1991, 269.
10. A. A. Danopoulos, B. Hussain-Bates, M. B. Hursthouse, W-H. Leung and G. Wilkinson, *J. Chem. Soc., Dalton Trans.* 1991, 2051.
11. F. A. Cotton and G. Wilkinson, *Advanced Inorganic Chemistry*, 5th edn, p. 227. John Wiley, New York (1988); M. Veith, *Chem. Rev.* 1990, **90**, 3.
12. C. J. Burns and R. A. Andersen, *J. Organomet. Chem.* 1987, **325**, 31.
13. R. E. Clarke and P. C. Ford, *Inorg. Chem.* 1970, **9**, 227.
14. A. A. Danopoulos, G. Wilkinson, B. Hussain-Bates and M. B. Hursthouse, *Polyhedron* 1989, **8**, 2947; *J. Chem. Soc., Dalton Trans.* 1990, 2753.
15. cf. N. E. Dixon, W. G. Jackson, M. A. Lancaster, G. A. Lawrence and A. M. Sargeson, *Inorg. Chem.* 1981, **20**, 1470; P. V. Bernhardt and G. A. Lawrence, *Polyhedron* 1987, **6**, 1875.
16. B. S. McGilligan, J. Arnold, G. Wilkinson, B. Hussain-Bates and M. B. Hursthouse, *J. Chem. Soc., Dalton Trans.* 1990, 2465.
17. (a) G. M. Kosolapoff and L. Maier, *Organic Phosphorus Compounds*, p. 383. John Wiley, New York (1972); (b) D. G. Dick, R. Rouseau and D. W. Stephen, Interaction of $(R_2N)_3TiCl$ and $LiPR'_2$ also gives $P_2R'_4$ and Ti^{III} amides, *Can. J. Chem.* 1990, **69**, 357.
18. (a) F. A. Cotton and G. Wilkinson, *Advanced Inorganic Chemistry*, 5th edn, p. 440. John Wiley, New York (1988); (b) R. T. Baker, J. F. Whitney and S. S. Wreford, *Organometallics* 1983, **2**, 1049; (c) R. T. Baker, P. J. Krusic, T. H. Tulip, J. C. Calabrese and S. S. Wreford, *J. Am. Chem. Soc.* 1983, **105**, 6763; R. T. Baker, J. C. Calabrese and T. E. Glassman, *Organometallics* 1988, **7**, 1889; (d) E. Heyn and V. Müller, *Z. Naturforsch* 1989, **44**, 1538, [$Cp_2Zr(PHmes)_2$]; (e) A. Handler, P. Peringer and E. P. Müller, *J. Chem. Soc., Dalton Trans.* 1990, 3725 (Pt).
19. A. H. Cowley, B. Pellerin, J. L. Atwood and S. G. Bott, *J. Am. Chem. Soc.* 1990, **112**, 6734; B. Bohra, P. B. Hitchcock, M. F. Lappert and W.-P. Leung, *Polyhedron* 1989, **8**, 1884.
20. M. Baudler, (a) *Pure Appl. Chem.* 1980, **52**, 755; (b) *Angew. Chem., Int. Edn Engl.* 1982, **21**, 492; (c) *Phosphorus and Sulphur* 1983, **18**, 57.
21. J. Hahn, M. Baudler, C. Krüger and Y.-H. Tsay, *Z. Naturforsch., Teil B* 1982, **37B**, 797.
22. J. Borm, G. Hüttner and O. Orama, *J. Organomet. Chem.* 1986, **306**, 29.
23. (a) K. Dehnicke and J. Strähle, *Polyhedron* 1989, **8**, 707; B. F. G. Johnson, B. L. Haymore and J. L. Dilworth, *Comprehensive Coordination Chemistry* (Edited by G. Wilkinson, R. D. Gillard and J. A. McCleverty), Vol. 2, p. 124. Pergamon Press, Oxford (1987); (b) H. W. Roesky, D. Hesse, M. Holtemeyer and G. M. Sheldrick, *Chem. Ber.* 1991, **124**, 757.
24. A. A. Danopoulos, A. C. C. Wong, G. Wilkinson, B. Hussain and M. B. Hursthouse, *J. Chem. Soc., Dalton Trans.* 1990, 315.
25. L. Birkhofer, A. Ritter and P. Richter, *Chem. Ber.* 1963, **96**, 2750.
26. see G. R. Fraucnhoff, S. R. Wilson and J. R. Shapley, *Inorg. Chem.* 1991, **30**, 78 and refs therein.
27. D. S. Edwards, L. V. Biondi, J. W. Ziller, M. R. Churchill and R. R. Schrock, *Organometallics* 1983, **2**, 1505.

Polyhedron Vol. 10, No. 19, pp. 2255–2263, 1991
Printed in Great Britain

0277–5387/91 $3.00+.00
© 1991 Pergamon Press plc

A LINEAR TRINUCLEAR CHROMIUM(III) COMPLEX WITH MIXED THIOLATE/ALKOXIDE LIGATION: PREPARATION AND PROPERTIES OF $(PPh_4)_2(Na)[Cr_3(SCH_2CH_2O)_6]$

JOHN R. NICHOLSON† and GEORGE CHRISTOU‡

Department of Chemistry, Indiana University, Bloomington, IN 47405, U.S.A.

and

RU-JI WANG and JOHN C. HUFFMAN

Molecular Structure Center, Indiana University, Bloomington, IN 47405, U.S.A.

and

HSIU-RONG CHANG and DAVID N. HENDRICKSON‡§

School of Chemical Sciences, University of Illinois, Urbana, IL 61801, U.S.A.

(*Received* 24 *April* 1991; *accepted* 20 *June* 1991)

Abstract—The reaction between $CrCl_3(THF)_3$, NaOEt and 2-hydroxyethanethiol ($hetH_2$) gave the complex $(PPh_4)_2Na[Cr_3(het)_6]$ (**1**) as a highly crystalline solid in good yield. Analytical data and structural characterization show the presence also of solvate molecules, one of which is an EtOH group, and another which may be a second EtOH or a H_2O molecule hydrogen-bonded to an Et_2O group; the true formulation is thus **1**·2EtOH or **1**·EtOH·H_2O·Et_2O, or a combination. Complex **1**·EtOH·solvent crystallizes in monoclinic space group $P2_1/n$ with (at −155°C): $a = 23.605(24)$, $b = 17.390(14)$, $c = 17.668(20)$ Å, $\beta = 107.09(4)°$, $Z = 4$ and $V = 6931.98$ Å^3. The structure was solved and refined using 4350 unique data with $F > 3.0\sigma(F)$ collected in the range $6° \leqslant 2\theta \leqslant 45°$. Final values of $R(R_w)$ were 10.98 (10.75)%. The high values of $R(R_w)$ are a consequence of the limited number of strong reflections and the large number of independent atoms arising from the presence of two independent PPh_4^+ cations and two independent anions, both lying on inversion centres. As a result, not all atoms were refined anisotropically; the uncertainty in the identity of the disordered second solvate molecule was also detrimental. The two anions are essentially superimposable. The three chromium(III) atoms are linearly disposed (Cr···Cr, ~2.7 Å) with each Cr_2 pair bridged by oxygen atoms from three het^{2-} groups whose sulphur atoms are terminally ligated. The inversion centre at the central chromium leads to idealized S_6 symmetry with distorted octahedral geometry at each metal. Variable-temperature, solid-state magnetic susceptibility data were collected in the temperature range 2–300 K. The effective magnetic moment, μ_{eff} per Cr_3, decreases from 4.77 μ_B at 299.9 K to 3.71 μ_B at 75.0 K, is then almost constant to 8.0 K and then decreases to 3.16 μ_B at 2.08 K. The data were least-squares fit to the theoretical expression derived for isotropic exchange

† UK SERC/NATO Postdoctoral Fellow.

‡ Authors to whom correspondence should be addressed.

§ Present address: Department of Chemistry, 0506, University of California at San Diego, La Jolla, CA 92093-0506, U.S.A.

interactions between three $S = 3/2$ centres. The fitting parameters were found to be $J = -37.7\ cm^{-1}$, $J' = 0\ cm^{-1}$ and $g = 1.90$, where J refers to interactions between adjacent chromium(III) centres and J' to the interaction between the terminal chromium(III) centres. The metals are thus antiferromagnetically coupled and the complex has an $S = 3/2$ ground state. The structure of the anion of **1** is compared to that found for the $[Cr_3(E_4)_6]^{3-}$ (E = Se, Te) complexes which also possess a linear Cr_3 unit and tetra-atomic chelating ligands.

Over the last few years, we have been involved in developing the thiolate chemistry of the early transition metals. Much of our work to-date has been concentrated on manganese[1] and vanadium,[2] and a variety of species of different nuclearities and oxidation levels have been obtained. Technical advantage has resulted from the use of either chelating or sterically-bulky thiolate ligands to inhibit polymerization and lead to tractable materials. The use of ethane-1,2-dithiolate (edt^{2-}) has been particularly beneficial. With vanadium(III), an unusual tetra-bridged, metal–metal bonded species $[V_2(edt)_4]^{2-}$ results.[2,3] The unusual nature of the vanadium(III) species prompted us to wonder what the product with chromium(III) would be. As reported by others,[3b] chromium(III) forms a complex with the empirical formula $\{(NMe_4)[Cr(edt)]\}_n$ that could not be obtained in a form suitable for crystallography. Our own efforts along these lines with the same anion proved equally fruitless. In the hope of obtaining better crystals, the related chelate 2-hydroxyethanethiol ($hetH_2$)[4] was employed, and the product was successfully characterized as $[Cr_3(het)_6]^{3-}$, suggesting the edt^{2-} complex may be of similar nuclearity and structure. More importantly, however, $[Cr_3(het)_6]^{3-}$ turned out to be the first example of a linear Cr_3^{III} unit, and it has been reported in preliminary form.[5] The prototypical nature of this complex also prompted magnetochemical studies, and the full details of this combined work are described herein.

EXPERIMENTAL

Syntheses

All manipulations were carried out under a dinitrogen atmosphere using standard anaerobic techniques and apparatus. Solvents were degassed by repeated vacuum/nitrogen cycles. Reagents were obtained commercially and used as received except $CrCl_3(THF)_3$, which was prepared as described elsewhere.[6]

Sodium metal (0.50 g, 21.7 mmol) was dissolved in EtOH (80 cm^3) with stirring and 2-hydroxyethanethiol (0.75 cm^3, 10.7 mmol) added by syringe. The septum cap on the flask was then briefly removed under a positive pressure of nitrogen, solid $CrCl_3(THF)_3$ (2.0 g, 5.3 mmol) was added in one portion, and the septum cap replaced and the flask subjected to vacuum/nitrogen cycles to remove any admitted air. The solid slowly dissolved on stirring to give a deep, blue–green solution and a fine white powder of NaCl. After stirring the solution for 2 h at room temperature, solid PPh_4Br (4.5 g, 10.7 mmol) was added as above and the solution stirred for a further 10 min. The solution was filtered and the filtrate allowed to sit undisturbed for 3 days at room temperature. Large dark green, rectangular-shaped crystals were obtained. These were collected by filtration, washed with 1:1 $EtOH/Et_2O$ (3×7 cm^3) and dried *in vacuo*; yield 40–45% based on chromium. The same procedure employing an increased het^{2-} : Cr ratio of 3:1 gave the same product in comparable yield. A sample from a reaction employing the latter ratio provided the crystal employed for the X-ray structural investigation. Found: C, 54.7; H, 5.9; P, 4.4. Calc. for $C_{60}H_{64}O_6P_2S_6NaCr_3 \cdot C_2H_5OH \cdot H_2O$: C, 54.0; H, 5.3; P, 4.5. Calc. for $C_{60}H_{64}O_6P_2S_6NaCr_3 \cdot (C_2H_5OH)_2$: C, 54.6; H, 5.4; P, 4.4. Calc. for $C_{60}H_{64}O_6P_2S_6NaCr_3 \cdot C_2H_5OH \cdot H_2O \cdot (C_2H_5)_2O$: C, 54.6; H, 5.7; P, 4.3%.

X-ray crystallography and structure solution

Data were collected on a Picker four-circle diffractometer using standard low-temperature facilities; details of the diffractometry, low-temperature facilities and computational procedures employed by the Molecular Structure Centre are available elsewhere.[7] Data collection parameters are summarized in Table 1. A systematic search of a limited hemisphere of reciprocal space located a set of diffraction maxima with monoclinic symmetry and systematic absences corresponding to the unique monoclinic space group $P2_1/n$, an alternate

Table 1. Crystallographic data for complex **1**

$C_{62}H_{72}O_8P_2S_6NaCr_3$[a]	Space group $P2_1/n$
$M_r = 1378.53$	$T = -155°C$
$a = 23.605(24)$ Å	$\lambda = 0.71069$ Å
$b = 17.390(14)$ Å	Range $6° \leqslant 2\theta \leqslant 45°$
$c = 17.668(20)$ Å	Unique data 9045
$\beta = 107.09(4)°$	Observed data 4350
$V = 6931.98$ Å^3	$F > 3.0\sigma(F)$
$Z = 4$	$R = 10.98\%$
$\rho_{calc.} = 1.321$ g cm^{-3}	$R_w = 10.75\%$
$\mu = 7.226$ cm^{-1}	

[a] For the formulation $(PPh_4)_2Na[Cr_3(het)_6]\cdot EtOH\cdot H_2O$.

setting of $P2_1/c$. Following data collection, routine data processing and averaging of equivalent reflections, a set of 9045 unique reflections was obtained, of which 4350 were considered observed based on the $F > 3.0\sigma(F)$ criterion. The structure was solved by a combination of direct methods (MULTAN) and standard Fourier techniques. The asymmetric unit consists of two independent anions, each lying on a centre of inversion, one sodium and two PPh_4^+ cations situated in general positions, one well-behaved EtOH solvate molecule and atoms assigned to a second solvate molecule. Because of the large number of independent atoms and the small number of observed reflections, only the non-hydrogen atoms of the anions, the sodium and the two phosphorus atoms were refined with anisotropic thermal parameters. The PPh_4^+ carbon atoms and the non-hydrogen atoms of the well-behaved EtOH molecule were refined isotropically. At this point, a difference Fourier map was used to identify the second solvate molecule. One peak was a reasonable distance from the sodium for assignment as an oxygen atom, O(54), and it refined well as such. In addition, there were six peaks clustered near O(54), but the closest was at 3.134 Å. These peaks were included as carbon atoms with isotropic thermal parameters in the final refinement cycles. Due to limitations imposed by the number of data and independent atoms, a search for a better fitting model for the poorly-behaved second solvate group(s) was not considered warranted. No hydrogen atoms were included in the final cycles. Final discrepancy indices are included in Table 1. The formula and molecular weight in Table 1 are those for $(PPh_4)_2Na[Cr_3(het)_6]\cdot EtOH\cdot H_2O$, the formulation employing only those atoms in the structure solution which are well-behaved and are at chemically-reasonable distances (*vide infra*).

Other measurements

Variable-temperature magnetic susceptibility data were collected on a Series 800 VTS-50 SQUID susceptometer operating at a magnetic field strength of 10 kG. Diamagnetic corrections were estimated from Pascal's constants for the formula $\mathbf{1}\cdot EtOH\cdot H_2O$ and subtracted from the experimental susceptibility data to obtain the molar paramagnetic susceptibility of the compound. This was then least-squares fit[8] to the appropriate theoretical expression. Solution magnetic moments were obtained in $(CD_3)_2SO$ using the Evans NMR method on a Bruker 300 MHz instrument; a co-axial NMR tube was employed and the frequency separation was measured for the two peaks of the hexamethyldisiloxane internal reference. A diamagnetic correction (Pascal's constants) was employed.

RESULTS AND DISCUSSION

Synthesis and structure

The procedure to complex **1** involves readily-available starting materials and leads to good yields of crystalline product. Treatment of $CrCl_3(THF)_3$ with two or more equiv. of $2Na/hetH_2$ leads to fairly rapid formation of a blue–green solution from which the product slowly crystallizes on addition of a PPh_4^+ salt. Even in the presence of sufficient phosphonium salt, the crystalline material contained one Na^+ cation, which can be rationalized as due to lattice energy effects; the Na^+ is interacting with the anion as will be described below. The formation of a bridged 2:1 ligand:chromium product is a consequence of the preference of the alkoxide oxygens to bridge rather than occupy terminal positions; the formation of non-mononuclear products with het^{2-} has also been observed by us in vanadium(IV) chemistry.[4]

The crystal structure and the analytical data for complex **1** indicate the presence of solvate molecules bound to the Na^+ cation. One molecule is clearly an EtOH, refining well albeit with fairly large thermal parameters. The other molecule is less clear. One atom, O(54), is 2.378 Å from the Na^+, similar to 2.289 Å for the Na—O(EtOH) interaction. Six other peaks, refined as carbon atoms, were also located and one possible interpretation is that these belong to severely disordered ethyl carbons of a second EtOH group. However, none is within 3 Å of O(24) and while this may be an artifact of the model, it is also possible that it is not EtOH. An alternative possibility is that the six peaks are from a disordered Et_2O molecule that is hydrogen-bonded to a H_2O molecule [O(24)]. Based on ana-

lytical data, the formulations **1**·2EtOH and **1**·EtOH·H_2O·Et_2O are both equally acceptable, or indeed a combination of the two.

The structure of the anion is shown in Figs 1 and 2 and selected structural parameters are listed in Table 2. The complex contains two independent anions, each lying on an inversion centre. The two anions are distinguished in Table 2 by the A and B suffixes. Each anion consists of a linear array of three chromium(III) atoms with Cr···Cr separations of 2.677(4) and 2.684(4) Å for anions A and B. Each pair of chromium atoms is bridged by three μ-oxygen atoms from three het^{2-} ligands whose sulphur atoms are terminally ligated. The unit thus consists of three face-sharing octahedra, with the central Cr1 possessing a CrO_6 ligation environment and Cr2 and Cr2′ possessing a CrO_3S_3 environment. The bridges are distinctly asymmetrical, the O—Cr1 distances 1.968(11)–1.989(12) Å being noticeably shorter than O–Cr2 distances, 2.023(13)–2.041(12) Å. All Cr—S distances are essentially identical, 2.023(13)–2.041(12) Å. The inversion centre at Cr1 and the disposition of the chelate rings affords idealized S_6 symmetry to the anions, and a view approximately down the S_6 axis is provided in Fig. 2.

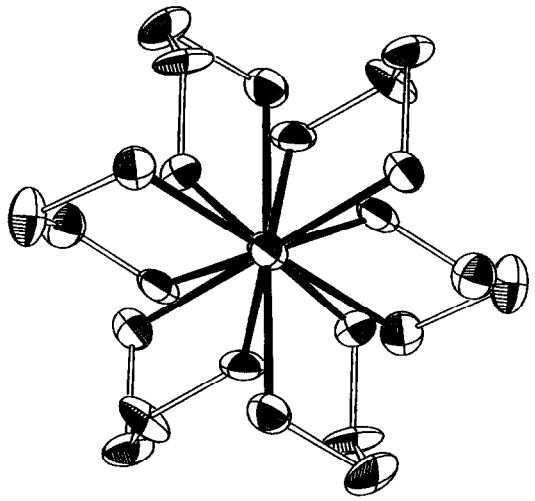

Fig. 2. View of the anion of complex **1** approximately down the Cr_3 axis emphasizing the idealized S_6 symmetry.

The structures of the two independent anions are extremely similar (Table 3) and also extremely similar to that reported for $[Cr_3(E_4)_6]^{3-}$ (E = Se, Te)[9] where E_4^{2-} serves to replace the similarly tetraatomic SCCO backbone of het^{2-} in **1**. The $[Cr_3(E_4)_6]^{3-}$ ions also lie on inversion centres and have idealized S_6 symmetry. Selected structural parameters of **1** and $[Cr_3(E_4)_6]^{3-}$ are compared in Table 3. The major difference is the Cr···Cr separations which are much shorter in **1** (~2.68 Å) than in the chalcogenide-bridged species (>3.2 Å). Note, however, that the Cr1—X_b—Cr_2 angle in the $[Cr_3(E_4)_6]^{3-}$ complexes is slightly *more* acute (~77.5°) than in **1** (~84°) suggesting the increased Cr···Cr separations in the former are merely the consequence of the larger bridging atoms and the correspondingly longer Cr—X_b distances.

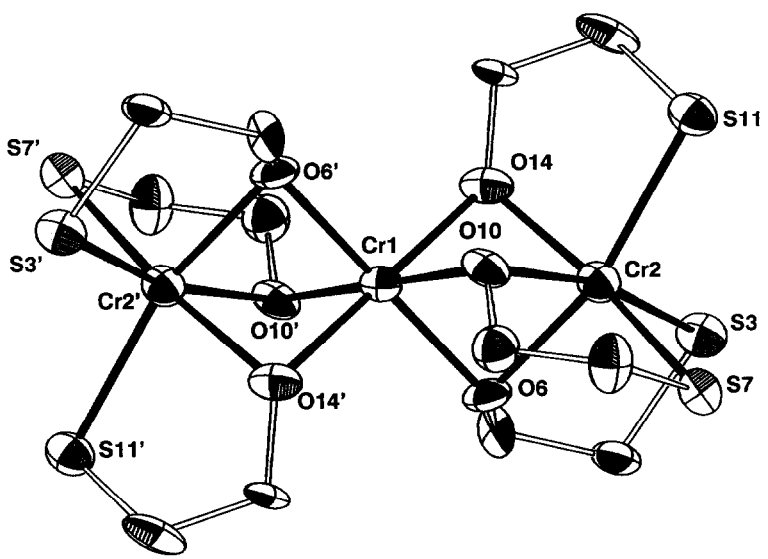

Fig. 1. ORTEP representation of one of the independent anions of complex **1** at the 50% probability level. Primed and unprimed atoms are related by the inversion centre at Cr1. Carbon atoms are numbered consecutively from S to O.

Table 2. Selected bond distances (Å) and angles (deg)

		Bonds	
Cr(1A)···Cr(2A)	2.677(4)	Cr(1B)···Cr(2B)	2.684(4)
Cr(1A)—O(6A)	1.968(11)	Cr(1B)—O(6B)	1.985(12)
Cr(1A)—O(10A)	1.968(12)	Cr(1B)—O(10B)	1.971(11)
Cr(1A)—O(14A)	1.989(12)	Cr(1B)—O(14B)	1.970(11)
Mean	1.975(10)	Mean	1.975(7)
Cr(2A)—S(3A)	2.365(6)	Cr(2B)—S(3B)	2.367(6)
Cr(2A)—S(7A)	2.358(6)	Cr(2B)—S(7B)	2.358(6)
Cr(2A)—S(11A)	2.369(6)	Cr(2B)—S(11B)	2.356(6)
Mean	2.364(5)	Mean	2.360(5)
Cr(2A)—O(6A)	2.030(12)	Cr(2B)—O(6B)	2.023(13)
Cr(2A)—O(10A)	2.027(11)	Cr(2B)—O(10B)	2.025(12)
Cr(2A)—O(14A)	2.023(13)	Cr(2B)—O(14B)	2.041(12)
Mean	2.027(3)	Mean	2.030(8)
		Angles	
O(6A)—Cr(1A)—O(10A)	98.3(5)	O(6B)—Cr(1B)—O(10B)	99.4(5)
O(6A)—Cr(1A)—O(14A)	80.6(5)	O(6B)—Cr(1B)—O(14B)	81.4(5)
O(10A)—Cr(1A)—O(14A)	98.2(5)	O(10B)—Cr(1B)—O(14B)	81.9(5)
Mean	92.4(83)	Mean	87.6(84)
S(3A)—Cr(2A)—S(7A)	94.28(21)	S(3B)—Cr(2B)—S(7B)	96.72(23)
S(3A)—Cr(2A)—S(11A)	95.67(21)	S(3B)—Cr(2B)—S(11B)	95.48(24)
S(7A)—Cr(2A)—S(11A)	97.66(21)	S(7B)—Cr(2B)—S(11B)	95.93(23)
Mean	95.87(139)	Mean	96.04(51)
S(3A)—Cr(2A)—O(6A)	86.7(4)	S(3B)—Cr(2B)—O(6B)	85.6(4)
S(3A)—Cr(2A)—O(14A)	98.8(4)	S(3B)—Cr(2B)—O(10B)	98.4(4)
S(7A)—Cr(2A)—O(6A)	99.0(4)	S(7B)—Cr(2B)—O(10B)	87.0(4)
S(7A)—Cr(2A)—O(10A)	86.9(4)	S(7B)—Cr(2B)—O(14B)	98.5(4)
S(11A)—Cr(2A)—O(10A)	98.6(3)	S(11B)—Cr(2B)—O(6B)	98.2(4)
S(11A)—Cr(2A)—O(14A)	84.6(4)	S(11B)—Cr(2B)—O(14B)	86.5(4)
Mean	92.4(64)	Mean	92.4(60)
S(3A)—Cr(2A)—O(10A)	165.4(3)	S(3B)—Cr(2B)—O(14B)	164.3(4)
S(7A)—Cr(2A)—O(14A)	166.5(4)	S(7B)—Cr(2B)—O(6B)	165.4(4)
S(11A)—Cr(2A)—O(6A)	162.9(4)	S(11B)—Cr(2B)—O(10B)	165.4(4)
Mean	164.9(15)	Mean	165.0(5)
O(6A)—Cr(2A)—O(10A)	78.8(5)	O(6B)—Cr(2B)—O(10B)	78.5(5)
O(6A)—Cr(2A)—O(14A)	78.4(5)	O(6B)—Cr(2B)—O(14B)	78.8(5)
O(10A)—Cr(2A)—O(14A)	79.6(5)	O(10B)—Cr(2B)—O(14B)	78.9(5)
Mean	78.9(5)	Mean	78.7(2)
Cr(1A)—O(6A)—Cr(2A)	84.0(4)	Cr(1B)—O(6B)—Cr(2B)	84.1(5)
Cr(1A)—O(10A)—Cr(2A)	84.1(4)	Cr(1B)—O(10B)—Cr(2B)	84.4(4)
Cr(1A)—O(14A)—Cr(2A)	83.7(5)	Cr(1B)—O(14B)—Cr(2B)	84.0(4)
Mean	83.9(2)	Mean	84.2(2)

The short Cr···Cr separation (~2.68 Å) in **1** appears to be a consequence of the three RO^- bridges. As noted above, three chalcogenide (Se, Te) bridges give >3 Å separations in trinuclear species, as do the $(\mu\text{-O})(\mu\text{-O}_2\text{CR})_2$ bridges across each chromium pair in the triangular $[Cr_3O(O_2CR)_6]^+$-containing species.[10,11] For dinuclear chromium(III) species, single O^{2-} or OH^- bridges give very long (>3.6 Å) separations and large (135°) Cr—O—Cr angles,[12] whereas two OH^- or OR^- bridges give Cr···Cr separations in the *ca* 2.9–3.1 Å and Cr—O—Cr angles in the *ca* 95–104° range.[13] Only in the complex $[LCr(\mu\text{-OH})_3CrL]^{3+}$ (L = 1,4,7-trimethyl-1,4,7-triazacyclononane)[14] are the Cr···Cr separations [2.642(2) Å] and Cr—O—Cr angles [84.1(3)°] comparable to those in **1**. Similarly, short M···M separations are found in $[(NH_3)_3Co(OH)_3$

Table 3. Structural comparisons (Å, deg) between complex **1** and $[Cr_3(E_4)_6]^{3-}$ (E = Se, Te)

Parameter[a,b]	1(A)	1(B)	E = Se	E = Te
Cr···Cr	2.677(4)	2.684(4)	3.207	3.41(1)
Cr1—X_b	1.975	1.975	2.587	2.734
Cr2—X_b	2.027	2.030	2.530	2.744
Cr2—X_t	2.364	2.360	2.467	2.689
Cr1—X_b—Cr2	83.9	84.2	77.6	77.3

[a] Cr1 and Cr2 labelled as in Fig. 1; for $[Cr_3(E_4)_6]^{3-}$, the central and terminal chromium atoms were originally labelled Cr2 and Cr1, respectively.

[b] Quoted values represent the mean of S_6 symmetry-related parameters: b = bridging, t = terminal, X = O, S, Se or Te.

$Co(NH_3)_3]^{3+}$ [2.565(6) Å][15] and mixed valence $[LFe(OH)_3FeL]^{2+}$ [2.509(6) Å].[16]

The Na^+ cation in **1** is ligated to oxygen atoms O(S1) and O(S4) of the two solvent groups, and is also bound to four sulphur atoms, S7 and S11 of anion A, and S3 and S7 of anion B. The Na···S interactions are in the range 2.842–3.02 Å, typical for Na···S(thiolate) interactions.[17] The Na^+ ion is distorted octahedral and serves to link the two independent anions and give an extended network in the solid state.

One would not expect the Na^+ anion interactions within the solid state to remain intact on dissolution in good donor solvents such as MeCN or DMSO. However, to probe whether the anion maintains its trinuclear nature in solution, a magnetic moment determination in $(CD_3)_2SO$ was performed (Evans method). For a ~1.6 mM solution at 22.6°C, a magnetic moment of 4.68 μ_B per Cr_3 (2.70 μ_B per Cr) was obtained. This is similar to the solid-state value of 4.77 μ_B (*vide infra*) supporting retention of the trinuclear structure in solution. Disruption into mononuclear units would be expected to give 3.87 μ_B per Cr (d^3 spin-only value).

The visible spectrum of complex **1** has been recorded in DMF solution. Two broad bands are observed at wavelengths of 504 and 671 nm with extinction coefficients (ε_M/Cr_3; L mol^{-1} cm^{-1}) of 560 and 505, respectively. These features resemble those expected for isolated chromium(III) ions in near-octahedral fields and may be assigned to the $^4A_{2g} \rightarrow {}^4T_{1g}$ and $^4A_{2g} \rightarrow {}^4T_{2g}$ transitions.[10] Interpretation of the electronic spectra of weakly exchange-coupled metal aggregates in terms of the *d–d* transitions of the individual metal ions has been shown to be an acceptable approximation.[10] Particularly related to the present case are the spectra of trinuclear $Cr_3O(O_2CMe)_6(H_2O)_3^+$; these are also antiferromagnetically coupled (*vide infra*) and display spectra very similar to that of **1**.[10] The two inequivalent types of chromium(III) environments in **1** and the significant lowering of symmetry from octahedral are probably the cause of the broadness in the bands of **1**; the bands representing envelopes of several components. The exchange interactions are almost certainly the origin of the intensity enhancements seen for **1**, the ε_M values being somewhat higher than normally observed for chromium(III).

Magnetic susceptibility studies

Variable-temperature solid-state magnetic susceptibility studies were performed on powdered samples in the temperature range 2–300 K. The formulation $\mathbf{1} \cdot EtOH \cdot H_2O$ was employed in calculating the moles of material employed; use of other formulations as described above affects the values given below only slightly ($\leqslant 1\%$), comparable with the intrinsic experimental and fitting uncertainties. The effective magnetic moment per trinuclear complex, μ_{eff}/Cr_3, decreases from 4.77 μ_B at 299.9 K to 3.71 μ_B at 75.0 K, is then almost constant, decreasing to only 3.54 μ_B at 8.0 K, and then decreases more sharply to 3.16 μ_B at 2.08 K (Fig. 3). The 299.9 K value corresponds to 2.75 μ_B per chromium, significantly less than the spin-only value for a chromium(III) (d^3) centre (3.87 μ_B) and indicating the presence of intramolecular antiferromagnetic exchange interactions. The approximate plateau in the μ_{eff} vs T plot is suggestive of an $S = 3/2$ ground state (spin-only value, 3.87 μ_B/Cr_3).

The general spin-Hamiltonian describing the isotropic exchange interaction for a linear trinuclear complex is given by eq. (1).

$$\hat{H} = -2(J_{12}\hat{S}_1 \cdot \hat{S}_2 + J_{12'}\hat{S}_1 \cdot \hat{S}_{2'} + J_{22'}\hat{S}_2 \cdot \hat{S}_{2'}) \quad (1)$$

The pairwise magnetic exchange interactions

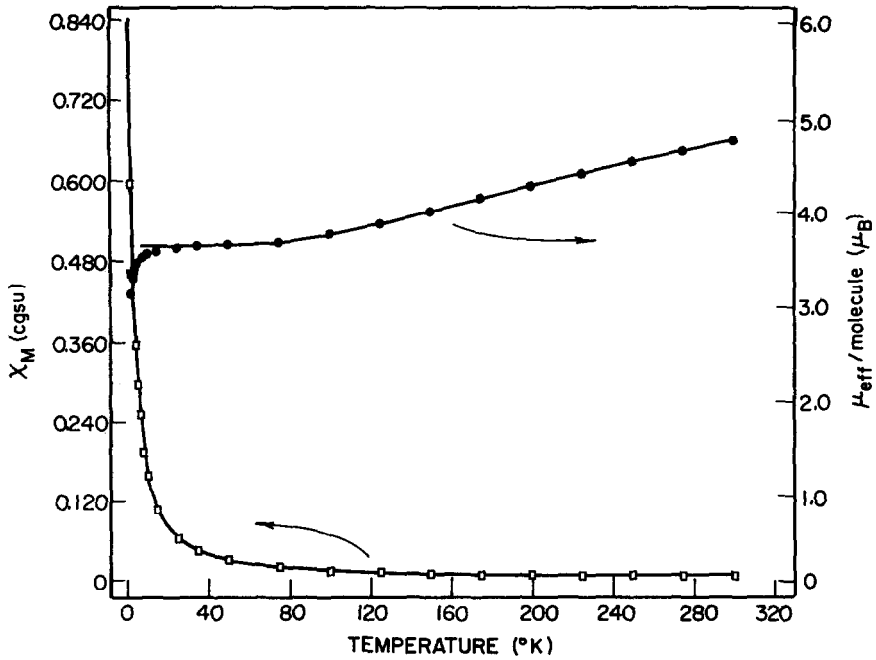

Fig. 3. Plots of the molar paramagnetic susceptibility, χ_M (□), and effective magnetic moment per trinuclear complex, μ_{eff}/Cr_3 (●), vs temperature for a polycrystalline sample of complex **1**·EtOH·H_2O. The solid lines result from a least-square fit of the data to the appropriate theoretical expression. See the text for fitting parameters.

between the central Cr1 and each of the terminal atoms Cr2 and Cr2′ must be identical by symmetry, such that $J_{12} = J_{12'} = J$. The spin-Hamiltonian of eq. (1) can therefore be simplified so that in eq. (2),

$$\hat{H} = -2J(\hat{S}_1 \cdot \hat{S}_2 + \hat{S}_1 \cdot \hat{S}_{2'}) - 2J'(\hat{S}_2 \cdot \hat{S}_{2'}), \quad (2)$$

where $J' = J_{22'}$. For complex **1**, $S_1 = S_2 = S_{2'} = 3/2$. The eigenvalues of the spin-Hamiltonian [eq. (2)] can be determined by using the Kambe vector coupling method[18a] with the coupling scheme $\hat{S}^* = \hat{S}_2 + \hat{S}_{2'}$, and $\hat{S}_T = \hat{S}^* + \hat{S}_1$. The energies of the spin states, which are eigenfunctions of the Hamiltonian in this coupling scheme, are given by eq. (3), where $S = S_1 = S_2 = S_{2'} = 3/2$. The overall degeneracy of this spin system is 64, made up of 12 spin states ranging from $S_T = 1/2$ to 9/2.

$$E = -J[S_T(S_T+1) - S^*(S^*+1) - S(S+1)] - J'[S^*(S^*+1) - 2S(S+1)] \quad (3)$$

A theoretical expression for the molar paramagnetic susceptibility χ_M vs temperature dependence was derived using eq. (3) and the Van Vleck equation;[18b] this expression was employed to fit the experimental χ_M vs T data, and a fit was obtained with $J = -37.7$ cm^{-1}, $J' = 0$ cm^{-1} and $g = 1.90$, with temperature-independent paramagnetism (TIP) held constant at 200×10^{-6} cgsu. No paramagnetic impurity correction term (PAR) was needed. The fit is shown as a solid line in Fig. 3. The zero value of J' is reasonable given the large separation between Cr2 and Cr2′. The ground state with these values of J and J' is a quartet $S_T = 3/2$ state with a doublet $S_T = 1/2$ first excited state and a sextet $S_T = 5/2$ second excited state at ~ 113 cm and ~ 189 cm^{-1} in energy above the $S_T = 3/2$ ground state. The $S_T = 3/2$ ground state is thus fairly isolated from the nearest excited states, and this rationalizes the plateau observed in Fig. 3 in the 8–75 K temperature range, essentially all molecules being in the ground state. The sharp decrease in μ_{eff} below 8.0 K is not predicted by the theoretical model employed (Fig. 3). This low-temperature behaviour may be due to either zero field splitting (ZFS) within the $S_T = 3/2$ ground state or to *intermolecular* antiferromagnetic exchange interactions. ZFS with a positive ZFS parameter D would yield a decrease in the observed value of μ_{eff} as the higher M_S states of the $S_T = 3/2$ manifold become depopulated with decreasing temperature. Alternatively, the Na^+ cation linking the anions (*vide supra*) could be mediating weak inter-anion antiferromagnetic exchange interactions which would again decrease μ_{eff} at very low temperatures. Since these effects, whatever their origin, only manifest them-

selves in the very low temperature region, it was not considered warranted or necessary to pursue a more sophisticated model.

The sign and magnitude of the exchange interactions observed for complex **1** may be compared to those determined for many other di- and trinuclear chromium(III) complexes. In the vast majority of cases, dinuclear Cr_2^{III} complexes have been found to exhibit intramolecular antiferromagnetic exchange interactions with J values in the -0.6 to -55.5 cm^{-1} range.[13] In very few cases have weak ($J = 2.2$ cm^{-1}) ferromagnetic interactions been observed.[19] For triply-bridged Cr_2^{III} species, antiferromagnetic interactions have again been observed; for the $[Cr(\mu\text{-}X)_3Cr]^{3+}$-containing complexes ($X = Cl^-$, Br^-), J values are in the 0 to -8 cm^{-1} range.[20] In contrast, $[LCr(OH)_3CrL]^{3+}$ has a significantly stronger antiferromagnetic exchange interaction ($J = -64$ cm^{-1})[21] consistent with the three shorter Cr—O bonds and better π-bonding oxygen bridges facilitating the super-exchange interaction. For trinuclear systems, antiferromagnetic interactions have been observed in the triangular $[Cr_3(\mu_3\text{-}O)]^{7+}$-containing species with J values in the -9.3 to -19.7 cm^{-1} range.[10] The value of $J = -37.7$ cm^{-1} determined for complex **1** is thus reasonable in both sign and magnitude, the relatively strong nature of the interaction being consistent with the number of bridging oxygen atoms between each Cr_2 pair.

Additional comparison can be made between complex **1** and three other linear Cr_3^{III} species. Two of these $[Cr_3(E_4)_6]^{3-}$ (E = Sc, Tc) were described above; the third is $Cr_3(lig)_2$ (lig = 1,5-diphenyl-1,3,5-pentanetrionato) which has not been structurally characterized but is assumed linear due to ligand restrictions.[22] In all four complexes, exchange interactions between adjacent chromium(III) ions are antiferromagnetic but the J value for complex **1** (-37.7 cm^{-1}) is significantly greater than those for the E = Se (-10.8 cm^{-1}), E = Te (-5.3 cm^{-1}) and lig^{2-} (-6.0 cm^{-1}) complexes. Again, these differences are consistent with the differing nature and number of bridging atoms. Interestingly, only for complex **1** does the least-squares fit give a $J' = 0$ value for interactions between the terminal chromium(III) atoms; for the other complexes J' is in the range $+1.44$ to -1.35 cm^{-1}.

Supplementary material available. Complete listings of atomic coordinates, thermal parameters, bond distances and angles, the derived susceptibility vs temperature equation, and experimental and calculated magnetic susceptibility data (10 pages): tables of observed and calculated structure factors (12 pages). Ordering information is given on any current masthead page.

Acknowledgements—This work was supported by NSF Grants 8507748 and 8808019 (to G. C.) and NIH Grant HL 13652 (to D. N. H.). We thank the Camille and Henry Dreyfus Foundation for a Teacher–Scholar Grant and the Alfred P. Sloan Foundation for a Research Fellowship (to G. C.). We also thank Eduardo Libby for assistance with figure preparation.

REFERENCES

1. (a) J. L. Seela, J. C. Huffman and G. Christou, *J. Chem. Soc., Chem. Commun.* 1985, 58; (b) G. Christou and J. C. Huffman, *J. Chem. Soc., Chem. Commun.* 1983, 558; (c) J. L. Seela, K. Folting, R.-J. Wang, J. C. Huffman, G. Christou, H.-R. Chang and D. N. Henderickson, *Inorg. Chem.* 1985, **24**, 4456.
2. (a) R. W. Wiggins, J. C. Huffman and G. Christou, *J. Chem. Soc., Chem. Commun.* 1983, 1313; (b) J. K. Money, J. R. Nicholson, J. C. Huffman and G. Christou, *Inorg. Chem.* 1986, **25**, 4072; (c) J. K. Money, J. C. Huffman and G. Christou, *Inorg. Chem.* 1985, **24**, 3297; (d) J. K. Money, K. Folting, J. C. Huffman, D. Collison, J. Temperley, F. E. Mabbs and G. Christou, *Inorg. Chem.* 1986, **25**, 4583; (e) J. K. Money, J. C. Huffman and G. Christou, *J. Am. Chem. Soc.* 1987, **109**, 2210; (f) J. K. Money, J. C. Huffman and G. Christou, *Inorg. Chem.* 1988, **27**, 507; (g) J. R. Rambo, J. C. Huffman, G. Christou and O. Eisenstein, *J. Am. Chem. Soc.* 1989, **111**, 8027; (h) D. D. Heinrich, K. Folting, J. C. Huffman, J. G. Reynolds and G. Christou, *Inorg. Chem.* 1991, **30**, 300.
3. (a) T. Costa, J. R. Dorfman, K. S. Hagen and R. H. Holm, *Inorg. Chem.* 1983, **22**, 4091; (b) Ch. Pulla Rao, J. R. Dorfman and R. H. Holm, *Inorg. Chem.* 1986, **25**, 428; (c) G. Henkel, K. Greiwe and B. Krebs, *Angew. Chem., Int. Edn Engl.* 1985, **24**, 117; (d) D. Szeymies, B. Krebs and G. Henkel, *Angew. Chem., Int. Edn Engl.* 1983, **22**, 885; (e) J. R. Dorfman and R. H. Holm, *Inorg. Chem.* 1983, **22**, 3179.
4. J. R. Nicholson, J. R. Rambo, J. C. Huffman, H.-R. Chang, D. N. Hendrickson and G. Christou, submitted for publication.
5. J. R. Nicholson, R.-J. Wang, J. C. Huffman, G. Christou, H.-R. Chang and D. N. Hendrickson, *J. Chem. Soc., Chem. Commun.* 1985, 1781.
6. J. P. Collman and E. T. Kittleman, *Inorg. Synth.* 1966, **8**, 149.
7. M. H. Chisholm, K. Folting, J. C. Huffman and C. C. Kirkpatrick, *Inorg. Chem.* 1984, **23**, 1021.
8. J. P. Chandler, "Program 66", Quantum Chemistry Program Exchange. Indiana University, Bloomington, Indiana.
9. W. A. Flomer, S. C. O'Neal, W. T. Pennington, D. Jeter, A. W. Cordes and J. W. Kolis, *Angew. Chem., Int. Edn Engl.* 1988, **27**, 1702.
10. R. D. Cannon and R. P. White, *Prog. Inorg. Chem.* 1988, **36**, 195 and refs therein.
11. (a) S. C. Chang and G. A. Jeffrey, *Acta Cryst.* 1970,

B26, 673; (b) T. Glowiak, M. Kubiak and B. Jezowska-Trebiatowska, *Bull. Acad. Polon. Sci. Ser. Chim.* 1977, **33**, 3106; (c) B. N. Figgis and G. B. Robertson, *Nature (Lond.)* 1965, **205**, 694; (d) E. Gonzalez-Vergara, J. Hegenauer, P. Saltman, M. Sabat and J. A. Ibers, *Inorg. Chim. Acta* 1982, **66**, 115.

12. (a) M. Yevitz and J. A. Stanko, *J. Am. Chem. Soc.* 1971, **93**, 1512; (b) K. Kaas, *Acta Cryst., Sect. B* 1979, **B25**, 596 and 1603; (c) D. J. Hodgson and E. Pedersen, *Inorg. Chem.* 1980, **19**, 3116; (d) J. T. Veal, D. Y. Jeter, J. C. Hempel, R. P. Eckberg, W. E. Hatfield and D. J. Hodgson, *Inorg. Chem.* 1973, **12**, 2928; (e) S. J. Cline, J. Glerup, D. J. Hodgson, G. S. Jensen and E. Pedersen, *Inorg. Chem.* 1981, **20**, 2229; (f) J. Ferguson and H. U. Gudel, *Aust. J. Chem.* 1973, **26**, 505 and 513.
13. (a) K. Michelsen, E. Pedersen, S. R. Wilson and D. J. Hodgson, *Inorg. Chim. Acta* 1982, **63**, 141; (b) J. T. Veal, W. E. Hatfield and D. J. Hodgson, *Acta Cryst., Sect. B* 1973, **B29**, 12; (c) R. P. Scaringe, P. Singh, R. P. Eckberg, W. E. Hatfield and D. J. Hodgson, *Inorg. Chem.* 1975, **14**, 1127; (d) A. Bentler, H. U. Güdel, T. R. Snellgrove, G. Chapuis and K. Schenk, *J. Chem. Soc., Dalton Trans.* 1979, 983; (e) S. J. Cline, R. P. Scaringe, W. E. Hatfield and D. J. Hodgson, *J. Chem. Soc., Dalton Trans.* 1977, 1662; (f) K. Kaas, *Acta Cryst.* 1976, **B32**, 2021; (g) J. T. Veal, W. E. Hatfield, D. Y. Jeter, J. C. Hempel and D. J. Hodgson, *Inorg. Chem.* 1973, **12**, 342; (h) E. D. Estes, R. P. Scaringe, W. E. Hatfield and D. J. Hodgson, *Inorg. Chem.* 1976, **15**, 1179; (i) E. D. Estes, R. P. Scaringe, W. E. Hatfield and D. J. Hodgson, *Inorg. Chem.* 1977, **16**, 1605; (j) H. R. Fischer, J. Glerup, D. J. Hodgson and E. Pedersen, *Inorg. Chem.* 1982, **21**, 3063; (k) S. J. Cline, E. Pedersen and D. J. Hodgson, *Inorg. Chem.* 1979, **18**, 796; (l) R. P. Scaringe, W. E. Hatfield and D. J. Hodgson, *Inorg. Chem.* 1977, **16**, 1601; (m) R. P. Scaringe, W. E. Hatfield and D. J. Hodgson, *Inorg. Chim. Acta* 1977, **22**, 175; (n) S. J. Cline, D. J. Hodgson, S. Kallesoe, S. Larsen and E. Pedersen, *Inorg. Chem.* 1983, **22**, 637; (o) H. R. Fischer, D. J. Hodgson and E. Pedersen, *Inorg. Chem.* 1984, **23**, 4755; (p) G. Sradanov, R. Herak, D. J. Radanovic and D. S. Veselinovic, *Inorg. Chim. Acta* 1980, **38**, 37; (q) H. R. Fischer, D. J. Hodgson, K. Michelsen and E. Pedersen, *Inorg. Chim. Acta* 1984, **88**, 143; (r) H. Oki and H. Yoneda, *Inorg. Chem.* 1981, **20**, 3875; (s) P. Andersen, K. M. Neilson and A. Petersen, *Acta Chem. Scand.* 1984, **A38**, 593; (t) M. A. Heinrichs, D. J. Hodgson, K. Michelsen and E. Pedersen, *Inorg. Chem.* 1984, **23**, 3174.
14. K. Wieghardt, P. Chaudhuri, B. Nuber and J. Weiss, *Inorg. Chem.* 1982, **21**, 3086.
15. T. Laier and J. Springborg, *Acta Chem. Scand., Ser. A* 1981, **A35**, 145.
16. S. Drueke, P. Chaudhuri, K. Pohl, K. Wieghardt, X.-Q. Ding, E. Bill, A. Sawaryn, A. X. Trautwein, H. Winkler and S. J. Gurman, *J. Chem. Soc., Chem. Commun.* 1989, 59.
17. J. K. Money, J. C. Huffman and G. Christou, *Inorg. Chem.* 1985, **24**, 3297.
18. (a) K. Kambe, *J. Phys. Soc. Japan* 1950, **5**, 48; (b) J. H. Van Vleck, *The Theory of Electric and Magnetic Susceptibilities*. Oxford University Press, London (1932).
19. R. P. Scaringe, W. E. Hatfield and D. J. Hodgson, *Inorg. Chem.* 1977, **16**, 1600.
20. (a) R. Saillant and R. A. Dal, *Inorg. Chem.* 1968, **7**, 1606; (b) I. E. Grey and P. W. Smith, *Aust. J. Chem.* 1971, **24**, 73.
21. D. E. Bolster, P. Gutlich, W. E. Hatfield, S. Kremer, E. W. Muller and K. Wieghardt, *Inorg. Chem.* 1983, **22**, 1725.
22. L. L. Borer, R. Horsma, O. A. Rajan and E. Sinn, *Inorg. Chem.* 1986, **25**, 3652.

Polyhedron Vol. 10, No. 19, pp. 2265–2272, 1991
Printed in Great Britain

0277–5387/91 $3.00+.00
© 1991 Pergamon Press plc

CYCLOMETALLATION OF N,N-DIMETHYL-FURAN-2(AND 3)-CARBOSELENOAMIDE WITH PALLADIUM(II), RHODIUM(III) AND RUTHENIUM(II)

MATSUO NONOYAMA*

Coordination Chemistry Laboratories, Institute for Molecular Science, Okazaki National Research Institutes, Myodaiji, Okazaki 444, Japan

and

KIYOKO NONOYAMA

Konan Junior College, Omatsubara, Takaya-cho, Konan, Aichi 483, Japan

(*Received* 13 *May* 1991; *accepted* 25 *June* 1991)

Abstract—Freshly prepared N,N-dimethyl-furan-2(and 3)-carboselenoamide [abbreviated as H(C-E), or as Hafs and Hbfs, respectively] was cyclopalladated with lithium tetrachloropalladate in methanol giving PdCl(C-E), which reacted with tri-n-butylphosphine (PBu_3) and 4-t-butylpyridine (tbp) to give the adducts PdCl(C-E)(PBu_3) and PdCl(C-E)(tbp), respectively. The iodo analogues were also prepared. Spectroscopic characterization revealed that the furan ring of H(C-E) is cyclopalladated and the selenium atom of the selenoamide group is coordinated to form a five-membered palladaselenaheterocycle. The cyclopalladation of Hbfs occurs exclusively at position 2 of the furan ring. The two selenoamides are cyclorhodated with trichlorobis(tri-n-butylphosphine)rhodium(III) in refluxing toluene to give $RhCl_2$(C-E)$(PBu_3)_2$. The bromo analogues are similarly obtained. Hbfs is similarly cycloruthenated with dichlorotricarbonylruthenium(II) in refluxing 2-methoxyethanol to afford RuCl(bfs)$(CO)_2$, but Hafs is not cycloruthenated under the same conditions. This fact suggests that Hbfs is more reactive towards cyclometallation than Hafs.

Cyclometallated compounds are now recognized as being potentially useful starting materials for organic synthesis and applications to organic synthesis are now becoming a subject of rapidly growing interest.[1] Most of the applications reported concern cyclometallated benzene derivatives and little has been studied regarding such applications of heterocycles, because of a deficiency in the knowledge of cyclometallated heterocycles.[2] This requires investigation for cyclometallation of heterocycles and we have recently been interested in this subject.

An N,N-dimethylthiocarbamoyl group was previously shown to be a good auxiliary substituent which promotes cyclometallation of heterocycles such as furan[3,4] and thiophene.[5] The study is now extended to those heterocycles substituted with a homologous N,N-dimethylselenocarbamoyl group. The cyclometallation with a selenium donor as an auxiliary group is, to the best of our knowledge, the first example. In this paper the results of cyclometallation of N,N-dimethyl-furan-2(and 3)-carboselenoamide (abbreviated as Hafs and Hbfs, respectively) are described and the results of the thiophene derivatives will be separately reported elsewhere. The preliminary report has already appeared.[6]

RESULTS AND DISCUSSION

N,N-dimethyl-furan-2(and 3)-carboselenoamide (Hafs and Hbfs) were obtained by the reaction of the corresponding carboxamides with phenyldichlorophosphine selenide and characterized spectroscopically (Tables 1 and 2).[6] The selenoamides

* Author to whom correspondence should be addressed.

Table 1. ^1H and $^{31}P\{^1H\}$ NMR spectra (δ ppm from tetramethylsilane and 85% H_3PO_4, respectively) of the complexes[a] (coupling constants are given in parentheses in Hz), and ν(C—N) and ν(M—X) bands (cm^{-1}) of the IR spectra (Nujol mulls)

Complex	4-H	5-H	$N(CH_3)_2$	^{31}P	ν(C—N)	ν(M—X)
Hafs[b]	6.43dd (1.8, 3.5)	7.52dd (0.9, 1.8)	3.37, 3.62		1513	
PdCl(afs)[c]	7.20br	7.93d (1.8)	3.59, 3.73		1589	281 241
PdBr(afs)[c]	7.20br	7.92d (1.8)	3.59, 3.71		1594	
PdCl(afs)(PBu_3)	6.45d (1.8)	7.56t (1.8)	3.62, 3.71	13.6 (130)[d]	1572	299
PdI(afs)(PBu_3)					1577	
trans-(C, I)	6.49d (1.8)	7.67t (1.7)	3.67, 3.72	12.2 (133)[d]		
cis-(C, I)	7.47dd (1.8, 2.4[e])	7.55t (1.8)	3.60, 3.67	−1.4		
PdCl(afs)(tbp)					1581	307
trans-(C, Cl)	5.91d (1.8)	[f]	3.60, 3.69			
cis-(C, Cl)	7.26d (1.8)	7.49d (1.8)	3.60, 3.73			
PdI(afs)(tbp)	7.57br	7.43br	3.58, 3.71		1578	
$RhCl_2$(afs)(PBu_3)$_2$	7.24br	7.65d (1.5)	3.55, 3.71	1.4 (86.3)[g]	1558	236 212
$RhBr_2$(afs)(PBu_3)$_2$	7.35br	7.65d (1.5)	3.53, 3.68	−3.7 (86.3)[g]	1560	
Hbfs[h]	6.54dd (0.9, 1.7)	7.36dd (1.5, 1.7)	3.31, 3.64		1522	
PdCl(bfs)[c]	6.71d (2.2)	7.77d (2.2)	3.62		1577 1597	304 240
PdBr(bfs)[c]	6.72d (2.2)	7.79d (2.2)	3.62		1576 1595	
PdCl(bfs)(PBu_3)	6.38d (2.2)	7.44dd (2.2, 1.1[e])	3.58, 3.66	17.0 (124)[d]	1567	305
PdI(bfs)(PBu_3)	6.44d (2.2)	7.53dd (2.2, 1.1[e])	3.60, 3.63	15.3 (126)[d]	1575	
PdCl(bfs)(tbp)					1572	297
trans-(C, Cl)	6.37d (2.4)	7.33d (2.4)	3.61, 3.66			
cis-(C, Cl)	6.37d[f] (2.4)	7.48d (2.4)	3.66[f]			
PdI(bfs)(tbp)	6.35d (2.2)	7.40d (2.2)	3.60, 3.64		1578	
$RhCl_2$(bfs)(PBu_3)$_2$	6.63d (2.3)	7.71d (2.3)	3.56	5.0 (86.3)[d]	1549	240 215
$RhBr_2$(bfs)(PBu_3)$_2$	6.62d (2.4)	7.72d (2.4)	3.61	0.1 (84.5)[d]	1550	
RuCl(bfs)$(CO)_2$[c,i]	6.89d (2.2)	7.97d (2.2)	3.64, 3.68		1566 1578	295 273
RuCl(bfs)$(CO)_2$(PBu_3)	6.54dd (2.2, 0.7[e])	7.70dd (2.2, 1.1[e])	3.55, 3.67	6.1	1557	287
RuCl(bfs)$(CO)_2$(etpb)	6.56dd (2.2, 1.1[e])	7.69t (2.1)	3.58, 3.68	119.4	1559	295

[a] Only the signals due to Hafs and Hbfs are given in this table. $CDCl_3$ was used as a solvent unless otherwise noted. The signals of $N(CH_3)_2$ are singlets, br = broad, d = doublet, and t = triplet.
[b] The 3-H signal is at 7.19 ppm (dd) (J = 3.5, 0.9 Hz).
[c] Dimethyl sulphoxide-d_6 is used as a solvent.
[d] $^2J(^{31}P—^{77}Se)$.
[e] $J(^1H—^{31}P)$.
[f] Overlapped with other signals.
[g] $^1J(^{31}P—^{103}Rh)$.
[h] The 2-H signal is at 7.72dd (0.9, 1.5).
[i] Accompanied with several weak signals.

Table 2. $^{13}C\{^1H\}$ NMR spectra of the complexes [δ ppm against tetramethylsilane and figures in parentheses are J(P—C) in Hz][a]

Complex	2-C	3-C	4-C	5-C	C=S	$N(CH_3)_2$
Hafs	155.1	118.9	112.2	143.2	187.4 [207][b]	48.5, 45.4
PdCl(afs)[c]	150.7	143.8	118.1	145.8	173.4	47.1, 43.6
PdBr(afs)[c]	150.4	144.0	119.1	145.6	174.0	47.0, 43.5
$PdCl(afs)(PBu_3)_2$	154.8 (2.4)	144.2 (3.8)	120.2 (10.4)	145.0 (3.1)	179.5 (3.8)	48.3, 44.0 (3.8)
$PdI(afs)(PBu_3)_2$						
trans-(C, I)	154.2 (2.1)	148.1 (2.4)	119.8 (10.1)	145.9 (2.8)	181.0 (3.5)	48.4, 44.0 (4.1)
cis-(C, I)	153.9 (2.1)	156.1 (144)	126.9 (3.5)	146.9 (7.6)	177.4 (10.4)	47.9, 44.1
PdCl(afs)(tbp)[c]						
trans-(C, Cl)	[d]					
cis-(C, Cl)	151.9	147.0	121.5	145.1	175.7	47.1, 44.1
PdI(afs)(tbp)[c]	150.5	149.7	128.9	145.9	177.3	47.6, 44.0
$RhCl_2(afs)(PBu_3)_2$	151.2 [3.8][e]	167.0 [31.1][e] (9.2)	121.8	145.6	177.3	46.5, 43.6
$RhBr_2(afs)(PBu_3)_2$	150.5 [4.1][e]	166.1 [32.8][e] (9.6)	123.2	145.8	177.9	46.4, 43.7
Hbfs	141.3	131.6	110.0	142.4	194.2 [207][b]	47.9, 44.8
PdCl(bfs)[c]	177.8	131.9	108.4	145.0	183.1	48.1, 45.1
PdBr(bfs)[c]	178.7	131.6	108.3	145.1	183.4	48.1, 45.1
$PdCl(bfs)(PBu_3)$	185.1 (5.9)	135.5 (2.4)	108.5	144.2 (3.1)	189.0 (2.4)	49.2, 45.2 (3.8)
$PdI(bfs)(PBu_3)$	188.2 (6.6)	134.6 (2.4)	108.0	144.5 (2.8)	189.5 (2.4)	49.3, 45.7 (3.8)
PdCl(bfs)(tbp)[c]						
trans-(C, Cl)	187.1	131.9	108.3	144.4	187.2	48.7, 45.5
cis-(C, Cl)	[d]					48.4, 45.5
PdI(bfs)(tbp)[c]	184.0	131.8	108.1	145.4	187.5	48.8, 45.9
$RhCl_2(bfs)(PBu_3)_2$	200.0 [37.3][e] (10.7)	131.6 [4.1][e]	109.0	146.4	187.5	47.5, 45.3
$RhBr_2(bfs)(PBu_3)_2$	200.5 [39.4][e] (10.7)	130.8 [4.1][e]	108.6	146.6	188.2	47.3, 45.3
$RuCl(bfs)(CO)_2$[c,f]	190.5	132.8	109.6	148.2	185.1	48.4, 45.7
$RuCl(bfs)(CO)_2(PBu_3)$[f]	194.7 (8.0)	133.2 (5.5)	108.5	148.2 (5.5)	189.4 (7.3)	48.5, 45.6
$RuCl(bfs)(CO)_2(etbp)$[f]	190.9 (14.2)	133.3 (8.3)	108.7	148.3 (9.3)	189.4 (10.7)	48.6, 45.9

[a] Only the signals due to Hafs and Hbfs are given in this table. Solvents are the same as those used for ^1H NMR measurements. Signals for which no coupling constant is given are singlets.

[b] $^1J(^{13}C—^{77}Se)$.

[c] Measured in the presence of tris(acetylacetonato)chromium(III) as a relaxation reagent.

[d] Low concentration prevented identification of signals.

[e] $J(^{13}C—^{103}Rh)$.

[f] $\delta(^{13}C)$ of CO is 191.8, 201.3; 195.1(8.6), 213.2(90.5); 191.7(15.6), 209.8ppm(154.8 Hz) in order of listing.

reacted with lithium tetrachloropalladate in methanol to give, PdCl(afs) and PdCl(bfs), respectively, for which we have already proposed structures **I** and **II**.

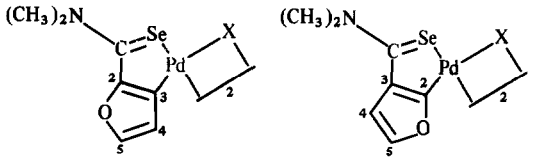

I **II**

These palladium complexes reacted with tri-n-butylphosphine (PBu_3) and 4-t-butylpyridine (tbp) to give the adducts as shown in Table 3. Metathesis of these complexes with excess lithium iodide in acetone afforded the iodo complexes (Table 3). The IR spectra of these complexes (Table 1) reveal that the selenoamide group is coordinated through a selenium atom:[7] the ν(C—N) bands are in the same region as those of the parents. The appearance of ν(Pd—Cl) is an indication of the coordination of chlorine donors.

The ^{1}H, ^{13}C{^{1}H} and ^{31}P{^{1}H} NMR spectral results are summarized in Tables 1 and 2. The ^{1}H and ^{13}C spectral patterns essentially resemble those of the parents, suggesting that the cyclopalladated skeletons are retained in these adducts. The ^{1}H and ^{13}C spectral patterns and the ^{31}P chemical shift of PdCl(afs)(PBu_3) are very similar to those of the corresponding thioamide analogue PdCl(aft)(PBu_3) (Haft = N,N-dimethyl-furan-2-carbothioamide) reported previously,[3] to which a *trans*-(C, Cl) arrangement was assigned (cf. structure **III**) (in this

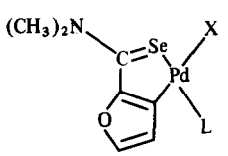

III, *trans*-(C,X)

notation C represents a metallated carbon atom). For the present complex the *trans*-(C, Cl) geometry is further confirmed by the value $^2J(^{31}P—^{77}Se) = 129.9$ Hz, which is in the range reported for a *trans*-(P, Se) arrangement.[8]

The ^{1}H, ^{13}C and ^{31}P NMR spectra of PdI(afs)(PBu_3) reveal that in a $CDCl_3$ solution two isomers exist in a ratio of 57:43 (the ratio is estimated based on the integration intensity of the ^{1}H NMR spectrum). The more abundant isomer shows spectra similar to those of the above mentioned PdCl(afs)(PBu_3), to which a *trans*-(C, X) geometry (**III**) was assigned. The ^{31}P chemical shift of the minor isomer is at a significantly high field to indicate that the phosphorus donor is coordinated *trans* to a carbon donor with a strong *trans* influence[9] which is also consistent with a large J(P—C) value of 3-C (Table 2). A *cis*-(C, X) geometry (structure **IV**) is suited for this; phosphorus and selenium donor

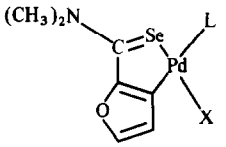

IV, *cis*-(C,X)

atoms are, as a matter of course, in a *cis* relation showing no P—Se coupling. The remarkable downfield shift of the 4-H of the furan ring is also consistent with this arrangement because the 4-H is in proximity to the bulky iodo donor which induces a downfield shift for a nearby proton.[10]

The ^{1}H and ^{13}C NMR spectra of PdCl(afs)(tbp) in $CDCl_3$ solution show the presence of two isomers in the ratio 17:83. The chemical shift of the 4-H of the furan ring is very different between the isomers and very informative (Table 1). In the minor isomer the 4-H is shielded while in the major isomer the 4-H is deshielded relative to that of free Hafs. The difference is explained as follows. In the former case the 4-H is placed in the shielding region of the pyridine ring ligated perpendicularly to the coordination plane; structure **III** (L = tbp; X = Cl) is assigned to this isomer. In the latter case the 4-H deshielding is caused by the nearby located chloro donor[10] in a similar manner as for the above *cis*-(C, I)-PdI(afs)(PBu_3) (structure **IV**: L = tbp; X = Cl). The NMR spectral patterns of PdI(afs)(tbp) are essentially similar to those of the major isomer of PdCl(afs)(tbp) and a *cis*-(C, I) geometry is suitable for this iodo complex. The halogen-dependent chemical shift of 4-H (7.26 ppm for X = Cl and 7.57 ppm for X = I) is consistent with the arrangement where the 4-H is situated near the halogen X.[10]

The ^{1}H and ^{13}C NMR spectra of PdX(bfs)(PBu_3) (X = Cl, I) are similar to those of the parent compound and show the absence of isomerism. The ^{31}P chemical shifts and ^2J(P—Se) values of the two are similar to those of *trans*-(C, X)-PdX(afs)(PBu_3) and structure **V** (X = Cl, I; L = PBu_3) is proposed for the two. For the corresponding thiophene analogue this geometry has been confirmed by X-ray analysis.[11] PdI(bfs)(tbp) exists as a single species but in the case of PdCl(bfs)tbp, two isomers are detected in the ratio 71:29. The structures of these are assumed

Table 3. Yields, m.p.s and analytical results of the complexes

Complex[a]	Yield (%)	M.p.[b] (°C)	Analysis: Found (Calc.) (%) C	H	N
Hafs	55	37–38	41.5 (41.6)	4.4 (4.5)	7.0 (6.9)
Hbfs	66	27–28	41.6 (41.6)	4.5 (4.5)	6.9 (6.9)
PdCl(afs)	93	228 (dec.)	24.5 (24.5)	2.3 (2.3)	4.1 (4.1)
PdBr(afs)	93	235 (dec.)	21.6 (21.7)	2.1 (2.1)	3.6 (3.6)
$PdCl(afs)(PBu_3)$	65	147–149	41.8 (41.8)	6.6 (6.5)	2.6 (2.6)
$PdI(afs)(PBu_3)$	74	113–116	35.6 (35.8)	5.5 (5.5)	2.1 (2.2)
PdCl(afs)(tbp)	55	253 (dec.)	40.2 (40.2)	4.1 (4.4)	5.9 (5.9)
PdI(afs)(tbp)	45	242 (dec.)	33.6 (33.7)	3.4 (3.7)	5.0 (4.9)
$RhCl_2(afs)(PBu_3)_2$	77	184–186	47.7 (47.7)	8.1 (8.0)	1.8 (1.8)
$RhBr_2(afs)(PBu_3)_2$	68	186–189	42.7 (42.8)	7.2 (7.2)	1.5 (1.6)
$RuCl_2(Hafs)_2(CO)_2$	79	217 (dec.)	30.3 (30.4)	2.9 (2.9)	4.4 (4.4)
PdCl(bfs)	99	235 (dec.)	24.5 (24.5)	2.4 (2.3)	4.1 (4.1)
PdBr(bfs)	99	250 (dec.)	21.6 (21.7)	2.1 (2.1)	3.6 (3.6)
$PdCl(bfs)(PBu_3)$	81	152–153	41.8 (41.8)	6.4 (6.5)	2.5 (2.6)
$PdI(bfs)(PBu_3)$	77	90–91	35.8 (35.8)	5.5 (5.5)	2.2 (2.2)
PdCl(bfs)(tbp)	75	230 (dec.)	40.1 (40.2)	4.5 (4.4)	5.8 (5.9)
PdI(bfs)(tbp)	64	235 (dec.)	33.6 (33.7)	3.4 (3.7)	4.9 (4.9)
$RhCl_2(bfs)(PBu_3)_2$	77	230 (dec.)	47.9 (47.8)	8.0 (8.0)	1.8 (1.8)
$RhBr_2(bfs)(PBu_3)_2$	70	223–227	43.0 (42.9)	7.2 (7.2)	1.6 (1.6)
$RuCl(bfs)(CO)_2$	80	205 (dec.)	26.9 (27.5)	1.8 (2.0)	3.5 (3.6)
$RuCl(bfs)(CO)_2(PBu_3)$	30	111–115	42.5 (42.3)	5.8 (5.9)	2.1 (2.3)
$RuCl(bfs)(CO)_2(etpb)$	61	245 (dec.)	32.4 (32.4)	3.4 (3.4)	2.5 (2.5)

[a] Abbreviations: Hafs = N,N-dimethyl-furan-2-carboselenoamide, Hbfs = N,N-dimethyl-furan-3-carboselenoamide, PBu_3 = tri-n-butylphosphine, tbp = 4-t-butyl-pyridine and etpb = 4-ethyl-2,6,7-trioxa-1-phosphabicyclo[2.2.2]octane.

[b] dec. = decomposition.

based on the ^1H chemical shifts of the tbp ligand: when tbp is coordinated *cis* to a carbon donor the 2-H chemical shift is at a lower field than that when tbp is *trans* to a carbon donor. This relationship has been confirmed for the above mentioned afs complexes as well as the furan and thiophene thioamide analogues reported previously. The 2-H chemical shift of tbp of the major isomer is at 8.80 ppm, while that of the minor one is at 8.61 ppm. The major isomer has a *trans*-(C, Cl) structure (V)

Table 4. Relative abundance[a] of *trans*-(C, X) and *cis*-(C, X) isomers of PdX(C-E)(L) (C-E = aft, bft, afs and bfs)[b]

C-E\L/X	tbp/C	tbp/I	PBu_3/Cl	PBu_3/I
aft	*trans* 18%		*trans* 100%	*trans* 82%
	cis 82%	*cis* 100%		*cis* 18%
bft	*trans* 67%		*trans* 100%	*trans* 100%
	cis 33%	*cis* 100%		
afs	*trans* 17%		*trans* 100%	*trans* 57%
	cis 83%	*cis* 100%		*cis* 43%
bfs	*trans* 71%		*trans* 100%	*trans* 100%
	cis 29%	*cis* 100%		

[a] Relative abundance was estimated based on the integration intensities of the ^1H NMR spectra in $CDCl_3$ solutions at ambient temperature.
[b] C represents a palladated carbon atom.

and the minor is *cis*-(C, Cl) (**VI**). The spectral pat-

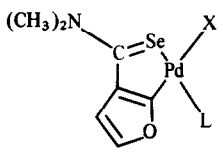

V, *trans*-(C,X)

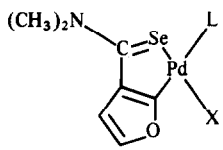

VI, *cis*-(C,X)

tern of the iodo complex is very similar to that of the minor isomer and a *cis*-(C, I) geometry is suggested for the iodo analogue. The structure of the corresponding thiophene selenoamide derivative has been confirmed by X-ray analysis to have a *cis*-(C, I) geometry.[11]

The isomerism found for these palladium complexes is similar to that for the corresponding thioamide analogues (Table 4) showing that Cl and PBu_3 ligands prefer a *trans*-(C, X) arrangement to a *cis* one, whilst I and tbp ligands prefer *cis*-(C, X) to *trans*-(C, X). A similar preference also exists in the isomerism of cyclopalladated N,N-dimethylferrocenecarbothioamide[12] and N,N-dimethylthiophene-2(and 3)-carbothioamide[5] derivatives. We are now seeking the cause of the isomerism.

The two selenoamides were cyclorhodated with $RhX_3(PBu_3)_2$ in refluxing toluene to form RhX_2(afs)$(PBu_3)_2$ and RhX_2(bfs)$(PBu_3)_2$ (X = Cl, Br). The IR spectra show selenium-coordination of a selenoamide group[7] and the coordination of chlorine donors is apparent from the presence of ν(Rh—Cl) bands (Table 1). The ^{31}P NMR spectra indicate that the two PBu_3 ligands are equivalent and the ^1J(Rh—P) values reveal that the two phosphorus donors are coordinated *trans* to each other. The ^1H and ^{13}C spectral patterns are essentially similar to those of the above palladium complexes except that the ^{13}C signals of the 3-C (afs) and 2-C (bfs) of the furan ring appear as a doublet [^1J(Rh—C)] of triplets [^2J(P—C)] (Table 2). These data are consistent with structures **VII**(afs) and **VIII** (bfs). The thioamide analogue Haft[3] is not cyclo-

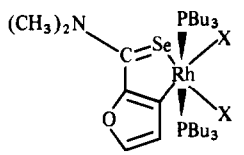

VII

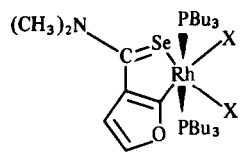

VIII

rhodated with $RhCl_3(PBu_3)_2$ in the same conditions employed here, suggesting that the auxiliary ability of an N,N-dimethyl-selenocarbamoyl group should be superior to that of the corresponding thioamide analogue.

The reactivity of Hafs and Hbfs toward $RuCl_2(CO)_3$ in hot 2-methoxyethanol is very different: Hafs gave only the adduct $RuCl_2$(Hafs)$_2(CO)_2$ while Hbfs was cycloruthenated to afford RuCl(bfs)$(CO)_2$ (Table 3). The former is hardly soluble in common solvents preventing measurement of an NMR spectrum, but the IR spectrum (Nujol mull) reveals selenium coordination of the selenoamide group [ν(C—N) = 1537, 1571 cm^{-1}] and *cis*-coordination of the two CO groups [ν(CO): 1966, 2037 cm^{-1}] as well as the two chlorine donors [ν(Ru—Cl) = 298, 268 cm^{-1}].

The IR spectrum of RuCl(bfs)$(CO)_2$ shows strong ν(CO) bands at 2064, 2049 and 1986br cm^{-1}. The ^1H NMR spectrum of a $CDCl_3$ solution was complicated and that of a dmso-d_6 solution showed

one set of main signals (Table 1), accompanied by several weak signals suggesting the presence of isomers. The complex reacted with phosphorus donors to give the adducts (Table 3). The ^1H and ^{13}C NMR spectra (Tables 1 and 2) are essentially similar to those discussed above to confirm cyclometallation of Hbfs. The large ^2J(P—C) observed for one CO group reveals that the CO and phosphorus donors are coordinated *trans* to each other. The IR spectra of the two show two strong ν(CO) bands [2033, 1962 (PBu_3); 2056, 1996 (etpb)] to suggest *cis*-coordination of the two CO groups. Structure **IX**

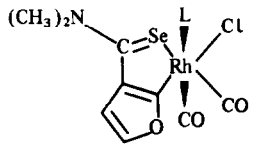

IX

(L = PBu_3, etpb) is tentatively proposed but X-ray analysis will be required for confirmation.

EXPERIMENTAL

Measurements

NMR spectra were recorded on Hitachi R-90H (^1H, 90 MHz; ^{13}C, 22.6 MHz; ^{31}P, 36.4 MHz) and Jeol PMX-60 (^1H, 60 MHz) spectrometers. Chemical shifts (δ ppm) were relative to internal tetramethylsilane (^1H, ^{13}C) and to external 85% H_3PO_4 (^{31}P). IR spectra (Nujol mulls) were measured on Jasco IR-A3 and Hitachi EPI-L spectrometers.

Synthesis

Yields, m.p.s, and analytical results are summarized in Table 3.

N,N-Dimethyl-furan-2(and 3) carboselenoamide. The two selenoamides were prepared according to the method reported in the literature.[13] The reaction time employed was 6 h and the two oily amides became an orange solid in the freezer,

PdX(C-E) (X = Cl, Br; C-E = afs, bfs). To a methanol solution (30 cm^3) of lithium tetrachloro (bromo) palladate, prepared *in situ* from palladium(II) chloride (1 mmol) and lithium chloride (2 mmol) (4 mmol of lithium bromide), was added Hafs (Hbfs) (1 mmol) and the mixture was stirred overnight at room temperature. A brown precipitate was collected, washed with methanol and dried in air.

PdCl(afs)(PBu_3). To a suspension of PdCl(afs) (1 mmol) in dichloromethane (30 cm^3) was added PBu_3 (1 mmol) and the mixture was stirred until it became almost clear. To the concentrated solution was added n-hexane in small portions and an initially precipitated brown material was filtered off. Further addition of n-hexane gave a yellow precipitate, which was filtered, washed with n-hexane and dried in air. The iodo analogue was obtained upon metathesis of the chloro complex with excess lithium iodide in acetone. The other palladium complexes were similarly prepared (tbp was used in a two-fold excess and the addition of a few drops of tbp was required in the metathesis reaction with lithium iodide).

RhX_2(C-E)(PBu_3)$_2$ (X = Cl, Br; C-E = afs, bfs). A mixture of $RhX_3(PBu_3)_2$ (1 mmol) and Hafs (Hbfs) (1 mmol) in toluene (30 cm^3) was refluxed with stirring for 6 h and evaporated to dryness under reduced pressure. The residue was dissolved in dichloromethane and the solution was filtered. To the filtrate was added n-hexane and the mixture was then concentrated to a small volume to precipitate yellow crystals, which were collected, washed with n-hexane and dried in air.

$RuCl_2(Hafs)_2(CO)_2$ *and* RuCl(bfs)$(CO)_2$. A mixture of $RuCl_2(CO)_3$ (1 mmol) and Hafs(Hbfs) (1 mmol) in 2-methoxyethanol (30 cm^3) was stirred under reflux for 3 h. Upon cooling the reaction mixture, $RuCl_2(Hafs)_2(CO)_2$ precipitated as a yellow powder, which was collected, washed with ethanol and dried in air. In order to isolate RuCl(bfs)$(CO)_2$, the reaction mixture was evaporated under reduced pressure to near dryness and addition of ethanol to the mixture resulted in the precipitation of a light brown powder, which was similarly treated.

RuCl(bfs)$(CO)_2$(L) (L = PBu_3, etpb). The adducts were prepared in a similar manner as for the above palladium phosphine complexes.

REFERENCES

1. A. D. Ryabov, *Synthesis* 1985, 233.
2. I. Omae, *Organometallic Intramolecular Coordination Compounds*. Elsevier, Amsterdam (1986).
3. M. Nonoyama, *Inorg. Chim. Acta* 1989, **157**, 9.
4. M. Nonoyama, *Trans. Metal Chem.* 1990, **15**, 366.
5. H. Mizuno and M. Nonoyama, *Polyhedron* 1990, **9**, 1287.
6. M. Nonoyama and K. Nonoyama, *Polyhedron* 1989, **8**, 2517.
7. K. Jensen and P. H. Nielsen, *Acta Chem. Scand.* 1966, **20**, 597.

8. V. K. Jain and S. Kannan, *J. Organomet. Chem.* 1991, **405**, 265.
9. J. M. Vila, M. Gayoso, J. J. Fernandez, J. M. Ortigueira and A. Suarez, *Polyhedron* 1990, **9**, 2741.
10. A. Albinati, A. Affolter and R. S. Pregosin, *Organometallics* 1990, **9**, 379.
11. H. Mizuno, M. Kita, M. Nonoyama and J. Fujita, submitted.
12. M. Nonoyama and K. Hanamura, *J. Organomet. Chem.* 1991, **407**, 271.
13. J. P. Michael, D. H. Reid, B. G. Rose and R. A. Speirs, *J. Chem. Soc., Chem. Commun.* 1988, 1494.

Polyhedron Vol. 10, No. 19, pp. 2273–2281, 1991
Printed in Great Britain

0277–5387/91 $3.00+.00
© 1991 Pergamon Press plc

SYNTHESIS AND REACTIONS OF DIMOLYBDENUM(II,II), DIRUTHENIUM(II,III) AND DICOPPER(II,II) COMPLEXES CONTAINING UNSATURATED ALIPHATIC CARBOXYLATE BRIDGING LIGANDS: X-RAY CRYSTAL STRUCTURE OF $[Ru_2(\mu\text{-}O_2C(CH_3)C{=}CH_2)_4Cl]$

MALACHY McCANN,* ANDREW CARVILL, PAULINE GUINAN, PAULA HIGGINS, JAMES CAMPBELL, HELEN RYAN and MAUREEN WALSH

Department of Chemistry, St. Patrick's College, Maynooth, Co. Kildare, Ireland

and

GEORGE FERGUSON* and JOHN GALLAGHER

Department of Chemistry and Biochemistry, University of Guelph, Ontario, Canada NIG 2W1

(*Received* 25 *February* 1991; *accepted* 17 *June* 1991)

Abstract—Metathesis reactions were used to prepare dimolybdenum(II,II), diruthenium (II,III) and dicopper(II,II) tetra-μ-carboxylato complexes containing unsaturated aliphatic carboxylate ligands (O_2CR) {R^1 = $HC{=}CH_2$, R^2 = $(CH_3)C{=}CH_2$, R^3 = $H_2CHC{=}CH_2$, R^4 = C_7H_9, R^5 = C_8H_{11}}. The X-ray crystal structure of $[Ru_2(\mu\text{-}O_2C(CH_3)C{=}CH_2)_4Cl]$ (**9**) shows that there are two independent centrosymmetric Ru_2L_4 dimers in the unit cell, bridged by chlorine atoms to form an infinite polymeric chain. Principal dimensions are Ru—Ru 2.287(1) and 2.290(1) Å, Ru—Cl 2.555(2) and 2.572(2) Å, Ru—Cl—Ru 118.29(7)°. The terminal ethylene ($=CH_2$) and methyl ($-CH_3$) groups of the ligand are mutually disordered. The bicyclo[2.2.1]hept-5-ene-2-carboxylato complexes $[Mo_2(\mu\text{-}O_2CR^4)_4]$ (**3**), $[Ru_2(\mu\text{-}O_2CR^4)_4Cl]$ (**8**) and $[Cu_2(\mu\text{-}O_2CR^4)_4]\cdot 2H_2O$ (**14**) were also synthesized by the Diels–Alder [4+2] cycloaddition reaction of cyclopentadiene with the respective propenoato complexes, $[Mo_2(\mu\text{-}O_2CR^1)_4]\cdot 0.5H_2O$ (**2**), $[Ru_2(\mu\text{-}O_2CR^1)_4Cl]\cdot 2HO_2CR^1$ (**7**) and $[Cu_2(\mu\text{-}O_2CR^1)_4]\cdot 2H_2O$ (**13**). The bicyclo[2.2.1]hept-5-ene-2-methyl-2-carboxylato complex, $[Ru_2(\mu\text{-}O_2CR^5)_4Cl]$ (**10**), was prepared by a similar cycloaddition route from $[Ru_2(\mu\text{-}O_2CR^2)_4Cl]$ (**9**). No Diels–Alder adducts were formed when cyclopentadiene was reacted with $[Mo_2(\mu\text{-}O_2CR^2)_4]\cdot 0.5H_2O$ (**4**), $[Cu_2(\mu\text{-}O_2CR^2)_4]\cdot 2H_2O$, $[Cu_2(\mu\text{-}O_2CR^3)_4]\cdot 2H_2O$ and $[Ru_2(\mu\text{-}O_2CR^3)_4Cl]$ (**11**).

Although much has been written about the chemistry of bimetallic complexes containing saturated alkyl carboxylate bridging ligands[1a,2] relatively little is known about complexes containing the anions of unsaturated aliphatic carboxylic acids. A family of dicopper(II,II) complexes of the general formula $[Cu_2(\mu\text{-}O_2C(H_2C)_nHC{=}CR^1R^2)_4L_x]$ (R^1 = H, CH_3; R^2 = H, CH_3; n = 0, 1, 2, 3; L = heterocyclic nitrogen ligand or PPh_3; x = 0, 2) have been prepared and their magnetic properties studied.[3–6] Mononuclear copper(II) complexes of the formula $[Cu(O_2C(H_2C)_nHC{=}CH_2)_2(py)_2]$ (n = 0, 1, 2) were made by reacting the respective dicopper(II,II) complexes, $[Cu_2(\mu\text{-}O_2C(H_2C)_nHC{=}CH_2)_4$, with pyridine.[3] Resnik and Douglas[7] carried out a polarographic and potentiometric investigation of the effect of the variation of the structural features of unsaturated carboxylic acids (2-butene-1,4-dicarboxylic, 3-butenoic, *trans*-2-butenoic and *cis*-

* Authors to whom correspondence should be addressed.

and *trans*-butenedioic acid) on the stability of complexes formed with Cu^{II}, Cu^{I}, Ag^{I} and Zn^{II}. The crystal structures of the *trans*-2-butenoate complexes $[M_2(\mu\text{-}O_2CHC{=}CH(CH_3))_4(\text{quinoline})_2]$ (M = Cu,[8] Zn[9]) have been described. Mono-, di- and trinuclear cobalt(II) complexes of the formula $[Co_n(O_2C(R^3)C{=}CR^2R^1)_{2n}L_2]$ (R^1 = H, CH_3; R^2 = H, CH_3; R^3 = H, CH_3; L = sterically hindered amine; n = 1, 2, 3) were prepared by reacting $CoCO_3$ with the unsaturated carboxylic acid in the presence of controlled amounts of amine.[10] In addition, homo- and heterotrinuclear *trans*-2-butenoate complexes of the formula $[Zn_3(O_2CHC{=}CH(CH_3))_6L^1{}_2]$[11] and $[MZn_2(O_2CHC{=}CH(CH_3))_6L^2{}_2]$[12] ($L^1$ = quinoline; $L^2 = L^1$, 6-methylquinoline; M = Mn, Co, Ni, Zn, Cd, Mg, Ca, Sr) have also been prepared and structurally characterized. *Trans*-$[Pt(O_2C(H_2C)_n(R)C{=}CH_2)H(\text{tricyclohexylphosphine})_2]$ (R = CH_3, n = 0; R = H, n = 1) complexes have been synthesized by the oxidative addition of 2-methylpropenoic and 3-butenoic acids to $[Pt(cod)_2]$ (cod = 1,5-1,5-cyclooctadiene),[13] and in these complexes the carboxylate ligand is bonded to the metal by only one of its oxygen atoms. Furthermore, Carmona *et al.*[14] have reacted mononuclear ethylene complexes, *trans*-$[M(C_2H_4)_2(PCH_3)_4]$ (M = Mo, W), with carbon dioxide under mild conditions to give binuclear propenoic acid complexes, $[M_2(HO_2CHC{=}CH_2)_2(C_2H_4)_2(PCH_3)_4]$, and the structure of the dimolybdenum complex was determined by X-ray analysis. Chelating 3-butenoate (via the olefin moiety and one carboxyl oxygen) has been inferred in catalytic cycles for rhodium-catalysed C—C coupling of allenes with 3-butenoic acid,[15] and also in the catalysis of C—C bond formation reactions by nickel complexes.[16] Polymeric dimolybdenum(II,II)[17] and monomeric cobalt(III)[18] complexes containing unsaturated dicarboxylate ligands are also known. In this paper we report on the synthesis of a range of new dimolybdenum(II,II) and diruthenium(II,III) complexes containing unsaturated carboxylato ligands, and the structure of the diruthenium complex $[Ru_2(\mu\text{-}O_2C(CH_3)C{=}CH_2)_4Cl]$ (**9**) is described. In addition, the reactivity of the pendant C=C groups of the new complexes [and analogous dicopper(II,II) complexes] with cyclopentadiene was investigated.

RESULTS AND DISCUSSION

Routes to the bimetallic molybdenum, ruthenium and copper complexes containing unsaturated carboxylato ligands are summarized in Scheme 1, and selected IR data are listed in Table 1. In general,

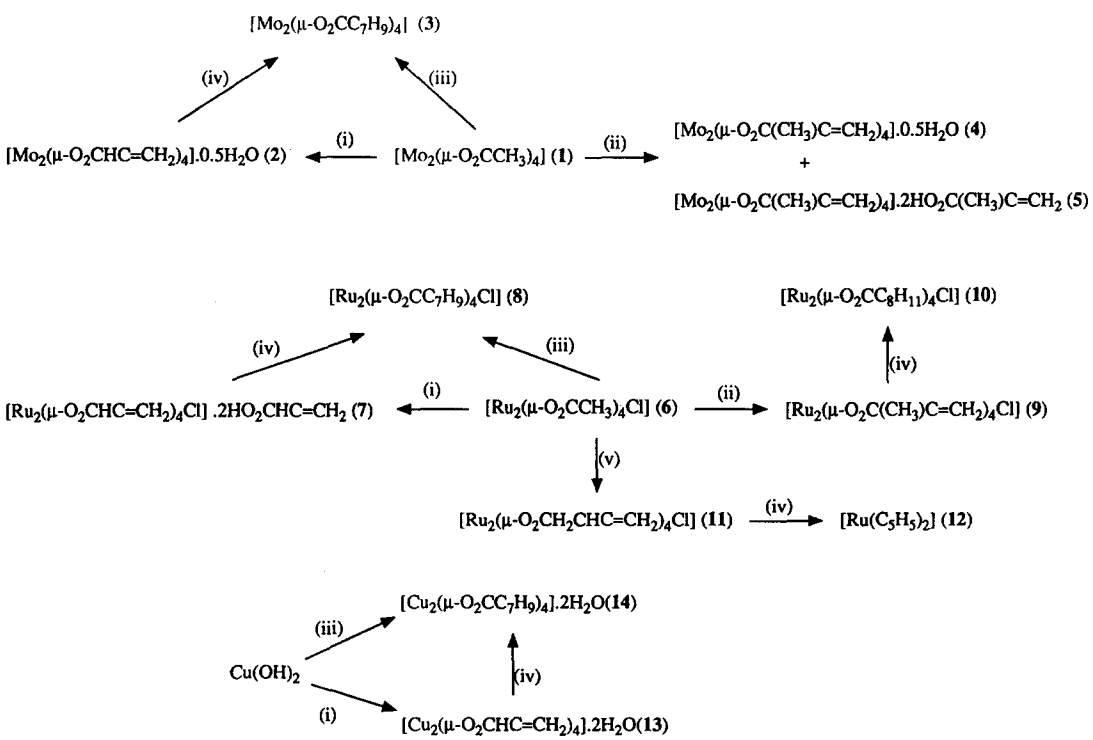

Scheme 1. (i) $CH_2{=}CHCO_2H$, (ii) $CH_2{=}C(CH_3)CO_2H$, (iii) $C_7H_9CO_2H$, (iv) cyclopentadiene, (v) $CH_2{=}CHCH_2CO_2H$.

Table 1. Selected IR data (cm^{-1}) for the bridging carboxylate ligands of the complexes (KBr disc)[a]

Complex	$\nu_{asym}(CO_2)$	$\nu_{sym}(CO_2)$	$\nu(C{=}C)$
$[Mo_2(\mu\text{-}O_2CHC{=}CH_2)_4]\cdot 0.5H_2O$ (**2**)	1484s	1430s	1637m
$[Mo_2(\mu\text{-}O_2CC_7H_9)_4]$ (**3**)	1500s	1420s	1625w
$[Mo_2(\mu\text{-}O_2C(CH_3)C{=}CH_2)_4]\cdot 0.5H_2O$ (**4**)	1480s	1415s	1637w
$[Mo_2(\mu\text{-}O_2C(CH_3)C{=}CH_2)_4]\cdot 2HO_2C(CH_3)C{=}CH_2$ (**5**)[a,c]	1490s	1410s	1637w
$[Ru_2(\mu\text{-}O_2CHC{=}CH_2)_4Cl]\cdot 2HO_2CHC{=}CH_2$ (**7**)[b,d]	1430[e]		1635m
$[Ru_2(\mu\text{-}O_2CC_7H_9)_4Cl]$ (**8**)	1420[e]		1630w
$[Ru_2(\mu\text{-}O_2C(CH_3)C{=}CH_2)_4Cl]$ (**9**)	1440s	1410s	1635m
$[Ru_2(\mu\text{-}O_2CC_8H_{11})_4Cl]$ (**10**)	1435s	1400s	1630w
$[Ru_2(\mu\text{-}O_2CH_2CHC{=}CH_2)_4Cl]$ (**11**)	1450s	1410s	1635m
$[Cu_2(\mu\text{-}O_2CC_7H_9)_4]\cdot 2H_2O$ (**14**)	1580s	1415s	1640m

[a] s = strong, b = broad, w = weak, m = medium.
[b] $\nu(OH)_{s,b}$ of acid 2500–3500 cm^{-1}.
[c] $\nu(C{=}O)$ of acid molecules 1690 cm^{-1}.
[d] $\nu(C{=}O)$ of acid molecules 1725 cm^{-1}.
[e] Separate $\nu_{asym}(CO_2)$ and $\nu_{sym}(CO_2)$ bands were not distinguishable in the broad band centred around this value.

the new unsaturated carboxylato complexes were found to be much more soluble in organic solvents than their saturated precursors. The dimolybdenum(II,II) parent complex (**1**) was treated with a large excess of the incoming unsaturated acid for conversion to the respective tetra-substituted product. In the case of the parent diruthenium(II,III) acetato complex (**6**), two successive metathesis cycles with the incoming unsaturated acid were required to procure complete conversion to the pure tetra-substituted product. The mass spectra of the ruthenium products obtained after only one methathesis cycle showed that the solids were mixtures. In addition to the ion fragment which corresponded to the fully-substituted product ($[Ru_2(\mu\text{-}O_2CR)_4]^+$) {R = unsaturated carboxylate ligand}, fragments attributable to partially-substituted species (e.g. $[Ru_2(\mu\text{-}O_2CCH_3)(\mu\text{-}O_2CR)_3]^+$) were also observed. Mixed-carboxylate product mixtures indicative of incomplete carboxylate exchange have previously been reported for substitution reactions involving diruthenium,[19] dirhodium[20] and dimolybdenum[21,22] complexes. Attempts to prepare the neutral, dimolybdenum tetra-μ-3-butenoate complex $[Mo_2(\mu\text{-}O_2CH_2CHC{=}CH_2)_4]$ by reacting $[Mo_2(\mu\text{-}O_2CR)_4]$ (R = CH_3, C_6H_5) with excess 3-butenoic acid in methanol were unsuccessful, and in each case the only product recovered was a brown, insoluble molybdenum-oxo complex.*

Two methods were used to prepare each of the unsaturated bicyclocarboxylato complexes (**3**), (**8**) and (**14**), with the most direct route being the reaction of *endo*-bicyclo[2.2.1]hept-5-ene-2-carboxylic acid ($C_7H_9CO_2H$) with **1**, **6** and copper(II) hydroxide, respectively. The second method involved the reaction of cyclopentadiene (*ca* 20°C) with the respective tetra-μ-propenoato complexes **2**, **7** and **13**. This latter method features four Diels–Alder [4+2] cycloaddition reactions on each molecule of **2**, **7** and **13**, with each of the propenoato ligands behaving as a dienophile (Scheme 2). The diruthenium(II,III) bicyclo[2.2.1]hept-5-ene-2-methyl-2-carboxylato complex (**10**) was also obtained in high yield by the Diels–Alder route (**9** → **10**). Surprisingly, the 2-methylpropenoato molybdenum complex (**4**) and its copper analogue, $[Cu_2(\mu\text{-}O_2C(CH_3)C{=}CH_2)_4]\cdot 2H_2O$,† both failed to give a Diels–Alder adduct with cyclopentadiene, and essentially unreacted starting complexes were recovered in each case. Whereas the synthesis of complex **10** was accomplished at *ca* 20°C, the usual Diels–Alder method for preparing bicyclo[2.2.1]hept-5-ene-2-methyl-2-carboxylic acid from 2-methylpropenoic acid and cyclopentadiene requires much more forcing conditions (e.g. 2 h at 150°C in a sealed tube[23]). On comparing the reactivities of free 2-methylpropenoic acid and complex **9** towards cyclopentadiene it might be argued that the inductive effect of the Ru_2^{5+} core of **9** enhances the reactivity

* The IR spectrum of the brown solid contained prominent Mo-oxo bands at 740 and 470 cm^{-1} and a broad band in the region 2700–3700 cm^{-1} (O—H and hydrogen-bonding). Analytical data: Found: C, 15.7; H 2.4%.

† This complex was made using the same general procedure outlined in ref. 3 except that freshly prepared copper(II) hydroxide was used instead of basic copper carbonate.

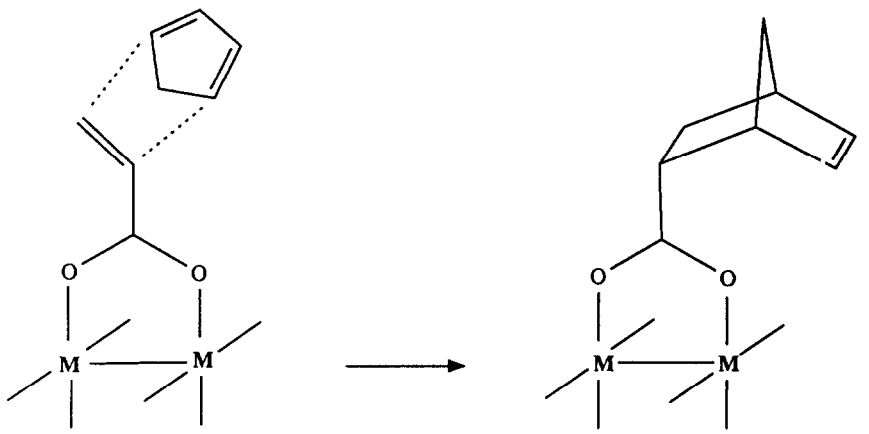

M = Mo, Ru, Cu

Scheme 2.

of the C=C group of the 2-methylpropenoate ligand towards cycloaddition (i.e. activates the dienophiles). Under the same reaction conditions the Mo_2^{4+} core of **4** and the Cu_2^{4+} core of $[Cu_2(\mu\text{-}O_2C(CH_3)C{=}CH_2)_4]\cdot 2H_2O$ do not appear to have the same activating power as their Ru_2^{5+} analogue. In addition to any beneficial inductive effects that may be operative in the above Diels–Alder reactions there may also be a contribution from the localized "ordered" nature of the complexed dienophiles. Having the four dienophiles bonded to the metal centres via their carboxylate groups confines their movement and effectively compresses them in the same way as the "macroscopic" application of external pressure. As the [4+2] cycloaddition reaction has a negative volume of activation this "ordering" effect should help to raise the ground-state energy of the dienophiles relative to the transition state, thereby lowering the activation energy.[24]

No Diels–Alder adducts were formed on reacting cyclopentadiene (*ca* 20°C) with the 3-butenoate complexes $[Cu_2(\mu\text{-}O_2CH_2CHC{=}CH_2)_4]\cdot 2H_2O$* and **11**. In the latter case ruthenocene (**12**) was isolated from the reaction mixture after prolonged standing. This formation of ruthenocene can be compared to the reaction of $[Mo_2(\mu\text{-}O_2CCH_3)_4]$ with sodium cyclopentadienide to give a molybdenocene dimer containing a bridging fulvalene ligand, $(\eta^5{:}\eta^5\text{-}C_{10}H_8)[(\eta^5\text{-}C_5H_5)MoH]_2$.[25] The apparent lack of reactivity of the copper and ruthenium 3-butenoate complexes towards cycloaddition is not totally surprising since the presence of the methylene group between the olefinic and carboxylate functions of the β,γ-unsaturated 3-butenoate ligand will have a significant deactivating effect on the dienophile. Alder and Windemuth[26] reported that the addition of cyclopentadiene to 3-butenoic acid, to give bicyclo[2.2.1]hept-5-ene-2-acetic acid, was indeed much slower (affected at 170–180°C) than that to propenoic acid. Furthermore, Sallerno *et al.*[27] have recently reported the rhodium-catalysed reaction of 3-butenoic acid with cyclopentadiene to give bicyclo[2.2.1]hept-5-ene-2-acetic acid.

The crystal structure of $[Ru_2(\mu\text{-}O_2C(CH_3)C{=}CH_2)_4Cl]$ (**9**) consists of two independent centrosymmetric Ru_2L_4 dimers which are linked by a bridging chlorine atom, to form a polymeric chain (Fig. 1). Table 2 lists the principal dimensions. Each ruthenium atom has octahedral coordination with Ru(1)—Ru(1) 2.287(1), Ru(2)—Ru(2) 2.290(1), Ru(1)—Cl 2.555(2), Ru(2)—Cl 2.572(2), Ru—O 2.006(5)–2.026(5), mean 2.018(5) Å, Ru(1)—Ru(1)—Cl 177.99(5), Ru(2)—Ru(2)—Cl 174.28(5) and Ru(1)—Cl—Ru(2) 118.29(7)°. These dimensions are similar to those observed in several other determinations of the type Ru_2L_4Cl (where L is a carboxylate ligand).[1b] Unlike complex **9** there is no disorder in the unsaturated *trans*-2-butenoate ligands in the complexes $[M_2(\mu\text{-}O_2CHC{=}CH(CH_3))_4(\text{quinoline})_2]$ (M = Cu,[8] Zn[9]).

EXPERIMENTAL

Literature methods were used to prepare $[Mo_2(\mu\text{-}O_2CCH_3)_4]$ (**1**),[29] $[Ru_2(\mu\text{-}O_2CCH_3)_4Cl]$ (**6**),[30] $[Cu_2(\mu\text{-}O_2CHC{=}CH_2)_4]\cdot 2H_2O$ (**13**)* and *endo*-bicyclo[2.2.1]hept-5-ene-2-carboxylic acid.[31] Reac-

* See footnote † to p. 2275.

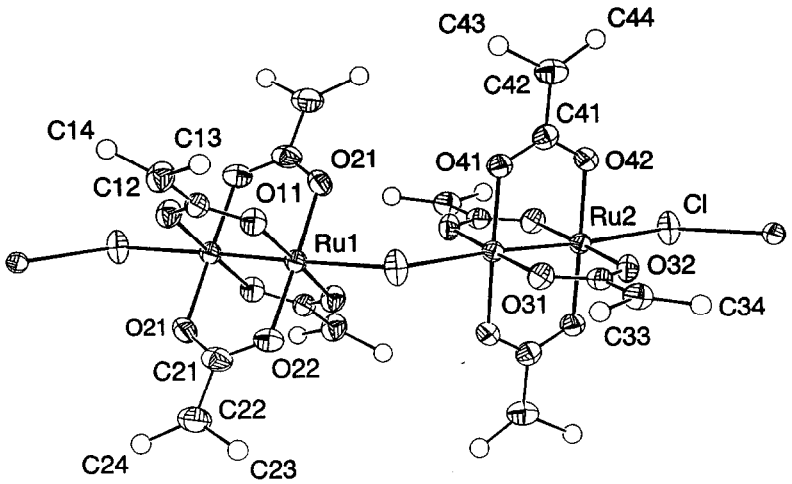

Fig. 1. A view of the $Ru_2(\mu\text{-}O_2C(CH_3)C{=}CH_2)_4Cl$ polymeric chain with our numbering scheme. The sites of the disordered $=CH_2$ and $-CH_3$ groups are shown as spheres of arbitrary size.[28]

tions were carried out in the air except in the case of the molybdenum complexes which were conducted under nitrogen using standard Schlenk techniques. In general, the molybdenum samples were found to be very air and moisture sensitive. Elemental analyses were performed by the Microanalytical Laboratory, University College Cork, Ireland. IR spectra were recorded in the region 4000–200 cm^{-1} on a Perkin–Elmer 783 grating spectrometer, and UV–vis spectra were run on a Milton Roy Spectronic 3000 Array. Solid-state, room temperature magnetic susceptibility measurements were made on a Johnson Matthey Magnetic Susceptibility Balance, and mass spectra were obtained using an AEI MS30 instrument equipped with an MSS Data System.

Crystallography

Crystals of **9** suitable for X-ray analysis were obtained by slow evaporation of a methanol solution at ambient temperatures. The crystal chosen was a dark red block of approximate dimensions $0.22 \times 0.12 \times 0.18$ mm.

Crystal data for $C_{16}H_{20}O_8ClRu_2$ (**9**), $M_r = 577.9$, monoclinic, space group $P2_1/a$, $a = 9.062(2)$, $b = 17.815(4)$, $c = 12.792(2)$ Å, $\beta = 92.69(2)°$, $V = 2063(2)$ $Å^3$, $Z = 4$, $D_x = 1.86$ g cm^{-3}, $\mu = 16.0$ cm^{-1}, $F(000) = 1140$, graphite monochromatized λ (Mo-K_α) = 0.71073 Å, $T = 15°C$. 5028 reflections were measured on a CAD4 diffractometer ($2\theta_{max} = 54°$), 4919 were unique and 2871 had $I > 3\sigma(I)$. Lorentz, polarization and empirical absorption corrections were applied. The structure was solved using the Patterson heavy-atom method. All non-hydrogen atoms except the terminal ethylene and methyl carbons were refined anisotropically. The terminal ethylene ($=CH_2$) and methyl ($-CH_3$) groups of the $CH_3{-}C{=}CH_2$ fragment were mutually disordered. This disorder was treated (using the DFIX option in SHELX76)[32] by fixing each of the eight terminal carbon atom positions with site occupancy of 0.5 at 1.34 Å (for ethylene) and site occupancy of 0.5 at 1.50 Å (for methyl) from the relevant C*n*2 carbon (n = 1–4) at appropriate angles. The methyl and ethylene hydrogens were placed geometrically (C—H 0.95 Å) with 0.5 occupancy; the methyl hydrogens were allowed to rotate around the C—C axis, in order to adopt the most favoured conformation. Refinement (with weights derived from coupling statistics) by full-matrix least-squares calculations converged with $R = 0.038$ and $R_w = 0.056$ for the 2871 observed reflections. The final refinement cycle included 332 variable parameters, maximum shift error of 0.01. The final difference map had no chemically significant features. Full details of the analysis are available from the Cambridge Crystallographic Data Centre or from the authors.

$[Mo_2(\mu\text{-}O_2CHC{=}CH_2)_4]\cdot 0.5H_2O$ (**2**)

To a suspension of complex **1** (0.24 g, 0.56 mmol) in dry benzene (15 cm^3) was added propenoic acid (3.0 g, 43.7 mmol). The resulting yellow–brown solution was stirred at room temperature for 4 h during which time the yellow product gradually precipitated. The solid was filtered off, washed with n-hexane and dried *in vacuo*; yield: 0.19 g (70%). Found: C, 29.1; H, 2.6. Calc.: C, 29.5; H, 2.7%. The complex was soluble in all common organic solvents except n-hexane.

Table 2. Molecular dimensions

(a) Bond lengths (Å)

Ru(1)—Ru(1) (I)	2.287(1)	O(11)—C(11)	1.269(8)
Ru(1)—Cl	2.555(2)	O(12)—C(11)	1.270(8)
Ru(1)—O(11)	2.024(5)	O(21)—C(21)	1.265(9)
Ru(1)—O(12) (I)	2.015(5)	O(22)—C(21)	1.294(9)
Ru(1)—O(21)	2.006(5)	O(31)—C(31)	1.275(8)
Ru(1)—O(22) (I)	2.026(5)	O(32)—C(31)	1.272(8)
Ru(2)—Ru(2) (II)	2.290(1)	O(41)—C(41)	1.269(9)
Ru(2)—Cl	2.572(2)	O(42)—C(41)	1.271(9)
Ru(2)—O(31)	2.011(4)	C(11)—C(12)	1.493(10)
Ru(2)—O(32) (II)	2.018(5)	C(21)—C(22)	1.496(11)
Ru(2)—O(41)	2.018(5)	C(31)—C(32)	1.503(9)
Ru(2)—O(42) (II)	2.022(5)	C(41)—C(42)	1.506(10)

(b) Bond angles (°)

Ru(1) (I)—Ru(1)—Cl	177.99(5)	O(31)—Ru(2) (II)—O(42)	90.2(2)
Ru(1) (I)—Ru(1)—O(11)	89.6(1)	O(32) (II)—Ru(2)—O(41)	89.4(2)
Ru(1) (I)—Ru(1) (I)—O(12)	88.8(1)	O(32) (II)—Ru(2) (II)—O(42)	90.3(2)
Ru(1) (I)—Ru(1)—O(21)	89.0(1)	O(41)—Ru(2) (II)—O(42)	178.4(2)
Ru(1) (I)—Ru(1) (I)—O(22)	89.9(2)	Ru(1)—Cl—Ru(2)	118.29(7)
Cl—Ru(1)—O(11)	91.0(1)	Ru(1)—O(11)—C(11)	118.8(4)
Cl—Ru(1) (I)—O(12)	90.7(1)	Ru(1) I)—O(12)—C(11)	120.0(4)
Cl—Ru(1)—O(21)	89.1(1)	Ru(1)—O(21)—C(21)	120.4(5)
Cl—Ru(1) (I)—O(22)	92.0(2)	Ru(1) (I)—O(22)—C(21)	117.6(4)
O(11)—Ru(1) (I)—O(12)	178.2(2)	Ru(2)—O(31)—C(31)	120.1(4)
O(11)—Ru(1)—O(21)	89.2(2)	Ru(2) (II)—O(32)—C(31)	119.1(4)
O(11)—Ru(1) (I)—O(22)	90.0(2)	Ru(2)—O(41)—C(41)	119.0(4)
O(12) (I)—Ru(1)—O(21)	91.4(2)	Ru(2) (II)—O(42)—C(41)	119.3(4)
O(12) (I)—Ru(1) (I)—O(22)	89.3(2)	O(11)—C(11)—O(12)	122.8(6)
O(21)—Ru(1) (I)—O(22)	178.7(2)	O(11)—C(11)—C(12)	119.6(6)
Ru(2) (II)—Ru(2)—Cl	174.28(5)	O(12)—C(11)—C(12)	117.4(6)
Ru(2) (II)—Ru(2)—O(31)	88.8(1)	O(21)—C(21)—O(22)	123.1(7)
Ru(2) (II)—Ru(2) (II)—O(32)	89.5(1)	O(21)—C(21)—C(22)	119.2(7)
Ru(2) (II)—Ru(2)—O(41)	89.5(1)	O(22)—C(21)—C(22)	117.7(7)
Ru(2) (II)—Ru(2) (II)—O(42)	88.9(1)	O(31)—C(31)—O(32)	122.4(6)
Cl—Ru(2)—O(31)	85.9(1)	O(31)—C(31)—C(32)	118.5(6)
Cl—Ru(2) (II)—O(32)	95.8(1)	O(32)—C(31)—C(32)	119.1(6)
Cl—Ru(2)—O(41)	92.6(1)	O(41)—C(41)—O(42)	123.2(6)
Cl—Ru(2) (II)—O(42)	89.0(1)	O(41)—C(41)—C(42)	118.8(6)
O(31)—Ru(2) (II)—O(32)	178.3(2)	O(42)—C(41)—C(42)	117.9(6)
O(31)—Ru(2)—O(41)	90.1(2)		

The atoms of the disordered $=CH_2$ and $-CH_3$ groups were assigned fixed geometry, C—C 1.34 and 1.50(2) Å, and 120° bond angles.

The roman numerals refer to the following equivalent positions; (I) $-x, -y, -z$ and (II) $= -x, -y, 1-z$.

$[Mo_2(\mu\text{-}O_2CC_7H_9)_4]$ (**3**)

Method (*a*). A mixture of **1** (0.25 g, 0.58 mmol), *endo*-bicyclo[2.2.1]hept-5-ene-2-carboxylic acid (1.1 g, 7.9 mmol) and dry methanol (15 cm^3) was stirred at room temperature for 12 h. The volume of the suspension was then reduced to *ca* 5 cm^3 by evaporation under high vacuum (without heating). The yellow product was filtered off, washed with ice-cold methanol and n-hexane, and then dried *in vacuo*. The solid was recrystallized from dry methanol; yield: 0.36 g (84%).

Method (*b*). Complex **2** (0.22 g, 0.45 mmol), cyclopentadiene (2 cm^3) and methanol (15 cm^3) were stirred together at room temperature for 4 days. The product precipitated when the solution was concentrated to low volume (no heating). The solid was recovered as in method (a); yield: 0.17 g

(51%). Found: C, 51.6; H, 4.8. Calc.: C, 51.9; H, 4.9%.

$[Mo_2(\mu\text{-}O_2C(CH_3)C{=}CH_2)_4]\cdot 0.5H_2O$ (**4**) and $[Mo_2(\mu\text{-}O_2C(CH_3)C{=}CH_2)_4]\cdot 2(HO_2C(CH_3)C{=}CH_2)$ (**5**)

Complex **1** (0.24 g, 0.56 mmol) and 2-methylpropenoic acid (3.0 g, 35.3 mmol) were stirred together in dry methanol (20 cm^3) at room temperature for 3 h. During the course of the reaction a yellow solid (**4**) precipitated. The solid was filtered off, washed with n-hexane and dried *in vacuo*; yield: 0.26 g, (86%). The remaining yellow–brown filtrate was rotary evaporated at 30°C to *ca* 10 cm^3 and the flask was then sealed under nitrogen. After a short time complex **5** precipitated as yellow microcrystals and these were recovered in the same manner as with complex **4**; yield: 0.04 g (10%). Found: C, 35.5; H, 3.9. Calc.: C, 35.6; H, 3.74. (**5**) C, 41.9; H, 4.7; C, 40.9; H, 4.6%. Both complexes were soluble in all common organic solvents except n-hexane.

Note: complex **5** was also made from **4** as follows. Complex **4** (0.17 g, 0.31 mmol) was added to a mixture comprising 2-methylpropenoic acid (10 cm^3), acetone (5 cm^3) and acetonitrile (5 cm^3). The resulting brown solution was sealed under nitrogen and after 24 h crystals of complex **5** formed. The solid was recovered in the same manner as described above.

$[Ru_2(\mu\text{-}O_2CHC{=}CH_2)_4Cl]\cdot 2(HO_2CHC{=}CH_2)$ (**7**)

Complex **6** (0.95 g, 2.0 mmol) and propenoic acid (5.5 g, 77 mmol) were stirred together in methanol (50 cm^3) at room temperature, and after 72 h all of the solid had dissolved to give a dark brown solution. The solution was rotary evaporated (without heating) to *ca* 5 cm^3 and then ethyl acetate (20 cm^3) was slowly added. The resulting solution was concentrated by rotary evaporation until the brown product just began to precipitate. n-Hexane (30 cm^3) was then slowly added causing a total precipitation of the product. The solid was filtered off, washed several times with diethylether and dried *in vacuo*. The brown solid was then redissolved in a fresh solution of propenoic acid (5.5 g) in methanol (40 cm^3) and the mixture was stirred for a further 72 h. The resulting red–brown solution was rotary evaporated to *ca* 5 cm^3, and the product was reprecipitated using the ethyl acetate/n-hexane method described above; yield: 0.92 g (69%). Found: C, 32.5; H, 2.8; Cl, 4.7. Calc.: C, 32.5; H, 3.0; Cl, 5.3%; m.p. = 257°C (dec); μ_{eff} = 4.0 B.M. per Ru_2; λ_{max} = 435 nm (ε = 623 $dm^3\ mol^{-1}\ cm^{-1}$ in MeOH).

$[Ru_2(\mu\text{-}O_2CC_7H_9)_4Cl]$ (**8**)

All operations were carried out at room temperature.

Method (a). Complex **6** (0.474 g, 1.0 mmol), methanol (40 cm^3) and *endo*-bicyclo[2.2.1]hept-5-ene-2-carboxylic acid (2.2 g, 16 mmol) were stirred together for 72 h. This brown solution was then evaporated under high vacuum to give a red–black tar. Ethyl acetate (25 cm^3) was added and the solution then concentrated to *ca* 5 cm^3. Slow addition of n-hexane (*ca* 40 cm^3) induced precipitation of the brown product. The solid was filtered off, washed with n-hexane and dried *in vacuo*. The solid was redissolved in a fresh mixture of methanol (40 cm^3) and *endo*-bicyclo[2.2.1]hept-5-ene-2-carboxylic acid (2.2 g, 16 mmol) and allowed to stir for a further 72 h. The solution was again concentrated to a tar and the beige product was recovered using the same ethyl acetate/n-hexane procedure as described above; yield: 0.62 g (79%).

Method (b). Complex **7** (0.3 g, 0.45 mmol), methanol (30 cm^3) and freshly distilled cyclopentadiene (2 cm^3) were stirred together for 20 h. The solution was concentrated to a low volume using high vacuum. Ethyl acetate (20 cm^3) was added and the solution was again concentrated using high vacuum. The resulting dark red tar was stirred thoroughly with n-hexane (40 cm^3). The beige solid which precipitated was filtered off, washed with n-hexane and dried *in vacuo*; yield: 0.34 g (96%). Found: C, 48.3; H, 4.7; Cl, 4.0. Calc.: C, 48.9; H, 4.6; Cl, 4.5%; m.p. = 270°C (dec); μ_{eff} = 4.0 B.M. per Ru_2; λ_{max} = 431 nm (ε = 642 $dm^3\ mol^{-1}\ cm^{-1}$ in MeOH).

$[Ru_2(\mu\text{-}O_2C(CH_3)C{=}CH_2)_4Cl]$ (**9**)

The same method was followed as for the preparation of complex **7** using 2-methylpropenoic acid instead of propenoic acid. In addition, 80 cm^3 of methanol was used instead of 40 cm^3. The product formed as a dark brown solid; yield: 0.94 g (81%). Found: C, 33.5; H, 3.8; Cl, 5.8. Calc.: C, 33.2; H, 3.5; Cl, 6.1%; m.p. = 280°C (dec); μ_{eff} = 3.9 B.M. per Ru_2; λ_{max} = 440 nm (ε = 598 $dm^3\ mol^{-1}\ cm^{-1}$ in MeOH). Crystals suitable for X-ray analysis were obtained by slow evaporation of a solution of (**9**) in 10% 2-methylpropenoic acid in methanol.

$[Ru_2(\mu\text{-}O_2CC_8H_{11})_4Cl]$ (**10**)

The same procedure was followed as for the preparation of complex **8** [method (b)] using complex **9** instead of complex **7**. The product was recovered as a dark beige solid; yield: 0.29 g (76%). Found:

C, 49.4; H, 4.9; Cl, 4.2. Calc.: C, 51.3; H, 5.3; Cl, 4.2%; m.p. = 250–280°C (dec); μ_{eff} = 4.0 B.M. per Ru_2; λ_{max} = 428 nm (ε = 620 dm^3 mol^{-1} in MeOH).

$[Ru_2(\mu\text{-}O_2CH_2CHC{=}CH_2)_4Cl]$ (**11**)

The same method was followed as for the preparation of complex **7** using 3-butenoic acid instead of propenoic acid. The product formed as a dark brown solid; yield: 0.80 g (69%). Found: C, 33.2; H, 3.5; Cl, 5.9. Calc.: C, 33.2; H, 3.5; Cl, 6.1%; m.p. = 242°C (dec); μ_{eff} = 3.9 B.M. per Ru_2; λ_{max} = 432 nm (ε = 713 dm^3 mol^{-1} cm^{-1} in MeOH).

$[Ru(C_5H_5)_2]$ (**12**)

Complex **11** (0.11 g, 0.2 mmol) was dissolved in methanol (5 cm^3). Freshly distilled cyclopentadiene (0.5 cm^3) was added and the resulting solution was left to stand for *ca* 3 months. Pale yellow crystals of ruthenocene (**12**) formed in low yield. Found: C, 52.0; H, 4.3. Calc.: C, 51.9; H, 4.3%; m/z = 232 $\{Ru(C_5H_5)_2^+\}$.

$[Cu_2(\mu\text{-}O_2CC_7H_9)_4]\cdot 2H_2O$ (**14**): *Method (a)*

Freshly prepared $Cu(OH)_2$ (0.2 g, 2.1 mmol) was added to a solution of *endo*-bicyclo[2.2.1]hept-5-ene-2-carboxylic acid (1.1 g, 8.0 mmol) in methanol (20 cm^3) and the resulting solution was stirred at room temperature for 96 h. Unreacted $Cu(OH)_2$ was removed by filtration and the filtrate was concentrated by rotary evaporation to a blue oil. Ethyl acetate (10 cm^3) was added and the solution was again reduced to a low volume. Diethyl ether (3 cm^3) and n-hexane (3 cm^3) were sequentially added and a pale blue solid (**a**) precipitated. Solid **a** was filtered off, washed with diethylether and dried *in vacuo*; yield: 0.17 g. The original filtrate was stored at *ca* 4°C for 12 h. Over this period a blue complex (**14**) precipitated. The solid was filtered off, washed with diethylether, and allowed to air dry; yield: 0.25 g (33%).

Method (b): Complex **13** (0.2 g, 0.45 mmol) was dissolved in diethylether (100 cm^3) and freshly distilled cyclopentadiene (5 cm^3) was added. The solution was stirred at 20°C for 24 h. Another 5 cm^3 of cyclopentadiene was added and the mixture was stirred for a further 24 h. More cyclopentadiene (5 cm^3) was added and the mixture stirred for another 48 h. A pale blue solid (**b**) was filtered off, washed with diethylether and then dried in air; yield: 0.04 g. The original filtrate was concentrated by rotary evaporation to a blue oil. n-Hexane (5 cm^3) was then added and the mixture stored at 4°C overnight. Complex **14** precipitated and was recovered as outlined in method (a); yield: 0.18 g (56%). Found for (**14**): C, 54.0; H, 5.5. Calc: C, 54.0; H, 5.7%; m.p. = 240°C (dec) (colour change at 120°C); μ_{eff} = 1.9 B.M. per Cu_2 (1.3 B.M. per Cu); λ_{max} = 674 nm (ε = 8900 dm^3 mol^{-1} cm^{-1} in MeCN).

Note: We have not, as yet, been able to establish the identity of the insoluble, paramagnetic, pale blue solids (**a**) and (**b**), and work on this is currently in progress.

Acknowledgements—We thank Johnson Matthey plc for the loan of ruthenium trichloride, and NSERC Canada for financial support.

REFERENCES

1. (a) F. A. Cotton and R. A. Walton, *Multiple Bonds Between Metal Atoms*. Wiley, New York (1982); (b) Table 5.2.2., page 196.
2. R. C. Mehrotra and R. Bohra, *Metal Carboxylates*. Academic Press, London (1983).
3. B. J. Edmondson and A. B. P. Lever, *Inorg. Chem.* 1965, **4**, 1608.
4. J. Mrozinski and E. Heyduk, *Pol. J. Chem.* 1982, **56**, 683.
5. J. Mrozinski and E. Heyduk, *Pol. J. Chem.* 1983, **57**, 375.
6. J. Mrozinski and E. Heyduk, *J. Coord. Chem.* 1984, **13**, 291.
7. R. K. Resnik and B. E. Douglas, *Inorg. Chem.* 1963, **2**, 1246.
8. M. Bukowska-Stryzewska, J. Skoweranda, E. Heyduk and J. Morzinski, *Inorg. Chim. Acta* 1983, **73**, 207.
9. W. Clegg, I. R. Little and B. P. Straughan, *J. Chem. Soc., Dalton Trans.* 1986, 1283.
10. I. R. Little, B. P. Straughan and P. Thornton, *J. Chem. Soc., Dalton Trans.* 1986, 2211.
11. W. Clegg, I. R. Little and B. P. Straughan, *J. Chem. Soc., Chem. Commun.* 1985, 73.
12. W. Clegg, I. R. Little and B. P. Straughan, *Inorg. Chem.* 1988, **27**, 1916.
13. T. Yamamoto, K. Sano and A. Yamamoto, *Chem. Lett.* 1982, 907.
14. R. Alvarez, E. Carmona, D. J. Cole-Hamilton, A. Galindo, E. Gutierrez-Puebla, A. Monge, M. L. Poveda and C. Ruiz, *J. Am. Chem. Soc.* 1985, **107**, 5529.
15. G. Salerno, C. Gallo, G. P. Chiusoli and M. Costa, *J. Organomet. Chem.* 1986, **317**, 373.
16. U. Bersillin, M. Catellani, G. P. Chiusoli, W. Giroldini and G. Salerno, *Fundam. Res. Homog. Catal.* 1979, **3**, 893.
17. R. J. Mureinik *J. Inorg. Nucl. Chem.* 1976, **38**, 1275.
18. R. T. M. Fraser, *Nature* 1964, **202**, 691.
19. E. B. Boyar, P. A. Harding, S. D. Robinson and C. P. Brock, *J. Chem. Soc., Dalton Trans.* 1986, 1771.

20. J. L. Bear, J. Kichens and M. R. Wilcott III, *J. Inorg. Nucl. Chem.* 1971, **33**, 3479.
21. M. McCann and H. Ryan, *Inorg. Chim. Acta* 1987, **133**, 11.
22. D. J. Santure and A. P. Sattelberger, *Inorg. Chem.* 1985, **24**, 3477.
23. J. S. Meek and W. B. Trapp, *J. Am. Chem. Soc.* 1957, **79**, 3909.
24. P. A. Grieco, J. J. Nunes and M. D. Gaul, *J. Am. Chem. Soc.* 1990, **112**, 4595.
25. J. C. Smart and C. J. Curtis, *Inorg. Chem.* 1978, **17**, 3290.
26. K. Alder and E. Windemuth, *Ber.* 1938, **71B**, 1939.
27. G. Salerno, F. Gigliotti and G. P. Chiusoli, *J. Organomet. Chem.* 1986, **314**, 231.
28. C. K. Johnson, ORTEPII, Report ORNL-5138. Oak Ridge National Laboratory, Tennessee, U.S.A. (1976).
29. T. A. Stephenson, E. Bannister and G. Wilkinson, *J. Chem. Soc.* 1964, 2538.
30. R. W. Mitchell, A. Spencer and G. Wilkinson, *J. Chem. Soc., Dalton Trans.* 1973, 846.
31. K. Alder and G. Stein, *Ann.* 1934, **514**, 197.
32. G. Sheldrick, SHELX76, A program for crystal structure analysis. University of Cambridge.

Polyhedron Vol. 10, No. 19, pp. 2283–2291, 1991
Printed in Great Britain

0277–5387/91 $3.00+.00
© 1991 Pergamon Press plc

SYNTHESIS OF NEW DIMOLYBDENUM(II,II) DI-μ-CARBOXYLATO DICATIONIC AND DIANIONIC COMPLEXES, AND THEIR USE AS POLYMERIZATION CATALYSTS

MALACHY McCANN† and PAULINE GUINAN

Chemistry Department, St. Patrick's College, Maynooth, Co. Kildare, Ireland

(*Received* 29 *April* 1991; *accepted* 21 *June* 1991)

Abstract—The dicationic complex salt *cis*-$[Mo_2(\mu\text{-}O_2CCH_3)_2(MeCN)_6][BF_4]_2$ (**1**), reacts with an excess of unsaturated carboxylic acid (RCO_2H) to give a family of new dicationic salts, $[Mo_2(\mu\text{-}O_2CR)_2(MeCN)_4][BF_4]_2 \cdot xH_2O$ [R = $HC{=}CH_2$ (**2**), $(CH_3)C{=}CH_2$ (**4**), $H_2CCHC{=}CH_2$ (**6**), $(CH_3)HCH_2CHC{=}CH_2$ (**7**), C_7H_9 (**8**); x = 1 or 2]. Complex **1** also reacts with Et_4NBr to give the dianionic salt $(Et_4N)_2[Mo_2(\mu\text{-}O_2CCH_3)_2Br_4]$ (**9**). Complexes **1**, **4** and **9** catalyse the room temperature polymerization of bicyclo[2.2.1]hept-2-ene. $EtAlCl_2$ was employed as a co-catalyst in these reactions. The dicationic salts **1**, **2** and **4** also catalyse the room temperature polymerization of cyclopentadiene, but the dianionic salt **9** is inactive towards this monomer.

A large number of dimolybdenum(II,II) complexes of the general formula $[Mo_2(\mu\text{-}O_2CR)_4]$ have been made using saturated alkyl and aryl carboxylate ligands.[1] We have recently described the synthesis of a range of Mo_2^{4+}, Cu_2^{4+} and Ru_2^{5+} tetra-μ-carboxylato complexes containing unsaturated alkyl carboxylate ligands, and demonstrated how the pendant C=C functions of the complexed ligands could react with cyclopentadiene to form the respective Diels–Alder cycloaddition adducts.[2] In this paper we describe the synthesis of some dimolybdenum(II,II) dicationic complexes containing two unsaturated carboxylate ligands, and the preparation of a new di-μ-acetato dianionic complex. The use of these complexes as catalysts for the polymerization of bicyclo[2.2.1]hept-2-ene and cyclopentadiene is also reported.

RESULTS AND DISCUSSION

Two different research groups have independently prepared and structurally characterized the red dimolybdenum(II,II) salt *cis*-$[Mo_2(\mu\text{-}O_2CCH_3)_2(MeCN)_6][BF_4]_2$ (**1**), the complex dication having the structure shown below.[3a,b] Earlier, Drago and Telser[3c] reported the synthesis of the closely related salts $[Mo_2(\mu\text{-}O_2CCH_3)_2(MeCN)_4][CF_3SO_3]_2$ and $[Mo_2(\mu\text{-}O_2CCH_3)_2(MeCN)_5][BF_3OH]_2$, which contain four and five MeCN ligands, respectively.

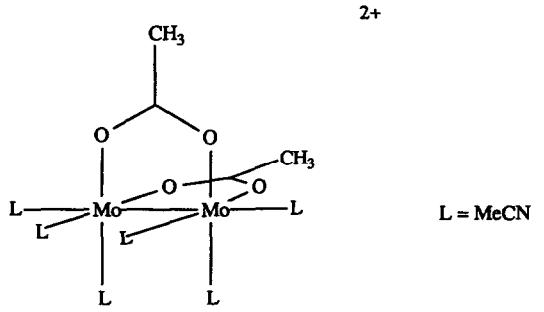

We have employed **1** as the starting material for the preparation of a series of similar dicationic complexes containing two unsaturated carboxylate ligands. Solutions of **1** in MeCN were reacted with an excess of the unsaturated carboxylic acid so as to replace the two acetate ligands with unsaturated carboxylate ligands (Scheme 1). Two successive metathesis cycles were usually required for complete substitution of the acetate by the new carboxylate ligand. The dications of the new salts have the common formula $[Mo_2(\mu\text{-carboxylate})_2(MeCN)_4]^{2+}$, and given that the structural data for

† Author to whom correspondence should be addressed.

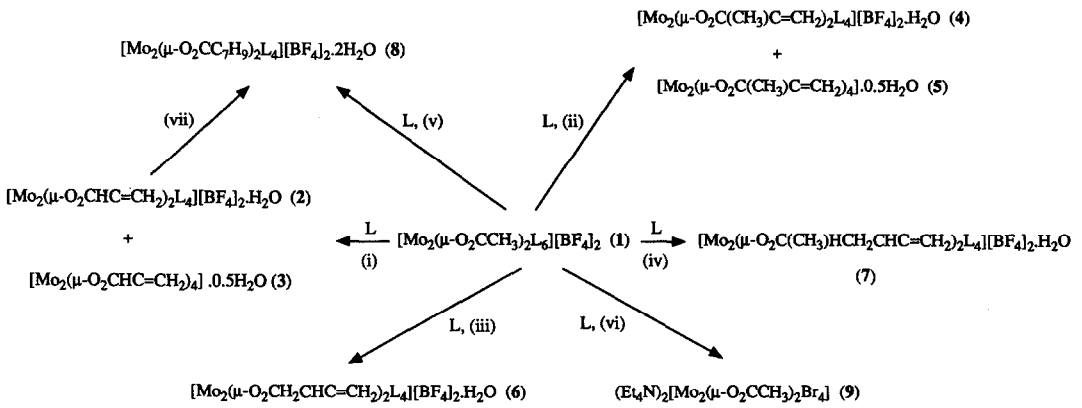

Scheme 1. L = MeCN, (i) $CH_2{=}CHCO_2H$, (ii) $CH_2{=}C(CH_3)CO_2H$, (iii) $CH_2{=}CHCH_2CO_2H$, (iv) $CH_2{=}CHCH_2CH(CH_3)CO_2H$, (v) $C_7H_9CO_2H$, (vi) Et_4NBr, (vii) cyclopentadiene.

1 show the four Mo—N (equatorial) distances to be considerably shorter than the two Mo—N (axial) distances,[3a,b] it is reasonable to assume that the four MeCN ligands in the present complexes are bonded equatorially to the bimetallic core.

During the synthesis of the di-μ-propenoato and di-μ-2-methylpropenoato salts **2** and **4** small amounts of the respective neutral tetra-μ-propenoato and tetra-μ-2-methylpropenoato complexes (**3** and **5**) also formed. Pure samples of **3** and **5** have previously been obtained in high yield by reacting $[Mo_2(\mu\text{-}O_2CCH_3)_4]$ with an excess of the respective unsaturated acid.[2] It is interesting to note that when $[Mo_2(\mu\text{-}O_2CCH_3)_4]$ was reacted with the longer chain unsaturated acids 3-butenoic acid and 2-methylpent-4-enoic acid, the tetrasubstituted complexes $[Mo_2(\mu\text{-}O_2CH_2CHC{=}CH_2)_4]$ and $[Mo_2(\mu\text{-}O_2C(CH_3)HCH_2CHC{=}CH_2)_4]$ did not form, and only Mo–oxo complexes were recovered.[4] However, when the same two long-chain unsaturated acids were reacted with salt **1**, the metathesis products **6** and **7** were recovered in high yield and, again, none of the corresponding neutral tetra-μ-carboxylato complexes formed. The di-μ-bicyclo[2.2.1]hept-5-ene-2-carboxylato complex **8** was synthesized by reacting the propenoato complex **2** with a large excess of cyclopentadiene (cpd). Some polycyclopentadiene (pcpd) also formed during the reaction (discussed later). The conversion of **2** to **8** occurs via a Diels–Alder cycloaddition reaction of the type mentioned previously.[2] Complex **8** was also prepared by reacting **1** directly with *endo*-bicyclo[2.2.1]hept-5-ene-2-carboxylic acid ($C_7H_9CO_2H$). Finally, when a solution of **1** in MeCN was reacted with Et_4NBr, the red salt **9** formed, which contains the complex dianion $[Mo_2(\mu\text{-}O_2CCH_3)_2Br_4]^{2-}$.

The IR spectra of the new di-μ-carboxylato salts have $\nu_{asym}(CO_2)$ and $\nu_{sym}(CO_2)$ bands at frequencies consistent with those expected for bridging carboxylates, and a ν(C=C) band was also evident for the complexes (except **8**) containing unsaturated carboxylate ligands (Table 1). Weak bands attributable to the MeCN ligands were present at *ca* 2280 cm^{-1}. In the spectrum of the dianionic complex **9** the acetate $\nu(CO_2)$ bands were at frequencies similar to those found in the spectrum of the structurally characterized diacetate **1**, and a strong ν(Mo—Br) band[5,6] was observed at 268 cm^{-1}.

Although the ^1H NMR spectra of the new salts (Table 1) did show peaks attributable to the different hydrogen atoms of the ligands not much structural information on the complexes was forthcoming due to the complexity of the observed splitting patterns. The spectrum of a DMSO-d_6 solution of the dianionic complex **9** contained two distinct methyl (CH_3CO_2) resonances at 1.93 and 2.00 ppm in a ratio of *ca* 9:1. The presence of two signals suggests that in solution there are two different species present. This type of behaviour was similar to that observed for $CDCl_3$ solutions of the neutral complex $[Mo_2(\mu\text{-}O_2CCH_3)Cl_3(PMe_3)_3]\cdot 0.75THF$.[7] An acetonitrile solution of complex **9** was prepared under anaerobic conditions and its electronic absorption spectrum immediately recorded (Fig. 1, $t = 0$). A single visible peak corresponding to the metal–metal $\delta \rightarrow \delta^*$ transition[1] was present at 540 nm ($\varepsilon \approx 838$ dm^3 mol^{-1} cm^{-1}). This spectrum was similar to that reported for methanol solutions of the closely related dianions $[Mo_2(\mu\text{-}O_3SCH_3)_2Br_4]^{2-}$ ($\lambda_{max} = 522$ nm)[6] and $[Mo_2(\mu\text{-}O_2CCH_3)_2Cl_4]^{2-}$ ($\lambda_{max} = 495$ nm).[9] A solution of **9** was allowed to slowly air-oxidize and the spectrum was recorded at intervals up to $t = 24$ h,

Table 1. IR[a,b] and ^{1}H NMR[c,d] data for the complexes[e]

Complex	IR $\nu_{asym}(CO_2)$	IR $\nu_{sym}(CO_2)$	IR $\nu(C{=}C)$	^{1}H NMR
$[Mo_2(\mu\text{-}O_2CCH_3)_2L_6][BF_4]_2$ (**1**)[f]	1500	1400		1.98(s) CH_3CN; 2.9(s) CH_3
$[Mo_2(\mu\text{-}O_2CHC{=}CH_2)_2L_4][BF_4]_2 \cdot H_2O$ (**2**)	1490	1435	1635	1.98(s) CH_3CN; 6.0–7.3(m) $CH_2{=}CH$
$[Mo_2(\mu\text{-}O_2C(CH_3)C{=}CH_2)_2L_4][BF_4]_2 \cdot H_2O$ (**4**)	1472	1412	1620	1.98(s) CH_3CN; 2.25(dd) CH_3; 5.9(m), 6.4(m) $CH_2{=}C$
$[Mo_2(\mu\text{-}O_2CH_2CHC{=}CH_2)_2L_4][BF_4] \cdot H_2O$ (**6**)	1505	1420	1640	1.98(s) CH_3CN; 3.9–4.1(m) CH_2; 5.2–5.6(m) $CH_2{=}CH$; 6.0–6.6(m) $CH_2{=}CH$
$[Mo_2(\mu\text{-}O_2C(CH_3)HCH_2CHC{=}CH_2)_2L_4][BF_4]_2 \cdot H_2O$ (**7**)	1500	1425	1640	1.98(s) CH_3CN; 1.55(d) CH_3; 2.5–3.0(m) CH_2CH; 3.4(tq) CH_3CH; 5.1–5.4(m) $CH_2{=}CH$; 5.7–6.3(m) $CH_2{=}CH$
$[Mo_2(\mu\text{-}O_2CC_7H_9)_2L_4][BF_4]_2 \cdot 2H_2O$ (**8**)	1490	1422	[g]	1.98(s) CH_3CN; 1.4–2.5(m), 2.8–4.1(m); 6.0–6.9(m) $CH{=}CH$
$(Et_4N)_2[Mo_2(\mu\text{-}O_2CCH_3)_2Br_4]$ (**9**)[h]	1515	1438		[i] 1.93(s); 2.0(s) CH_3

[a] KBr disc.
[b] Values in cm^{-1}.
[c] CD_3CN solutions: values in ppm.
[d] (s) singlet, (d) doublet, (dd) doublet of doublets, (tq) triplet of quartets, (m) multiplet.
[e] L = MeCN.
[f] See ref. 5.
[g] $\nu(C{=}C)$ not visible.
[h] $\nu(Mo{-}Br)$ 268 cm^{-1}.
[i] Solvent = DMSO-d_6.

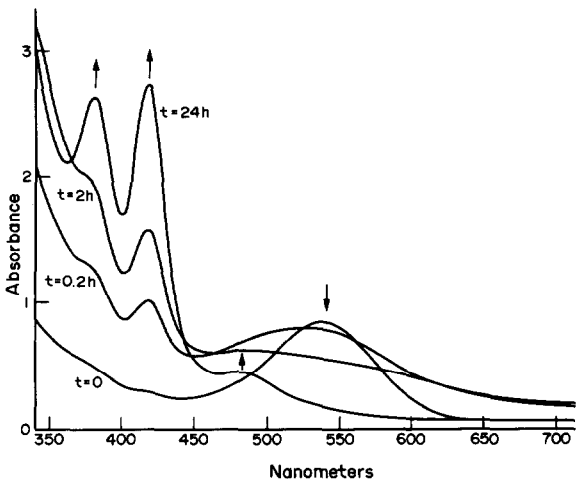

Fig. 1.

at which time the 540 nm peak had completely disappeared and three new absorption peaks had grown (481, 419 and 382 nm). The disappearance of the 540 nm peak signifies the rupture of the Mo—Mo δ bond.

In conclusion, it is thought that in the solid state the new dicationic complexes are essentially isostructural with **1** [Fig. 2(a)]. It should be mentioned that these complexes could also have a *trans* configuration [Fig. 2(b)]. The dianion, $[Mo_2(\mu\text{-}O_2CCH_3)_2Br_4]^{2-}$, is thought to be structurally similar to the known dianions $[Mo_2(\mu\text{-}O_3SCH_3)_2X_4]^{2-}$ (X = Cl, Br, I)[6] and $[Mo_2(\mu\text{-}O_2CCH_3)_2Cl_4]$.[2-9] The X-ray crystal structure of the latter dianion showed the two acetates to be *trans*. Possible *cis* and *trans* structures for $[Mo_2(\mu\text{-}O_2CCH_3)_2Br_4]^{2-}$ are illustrated in Figs 1(c) and (d).

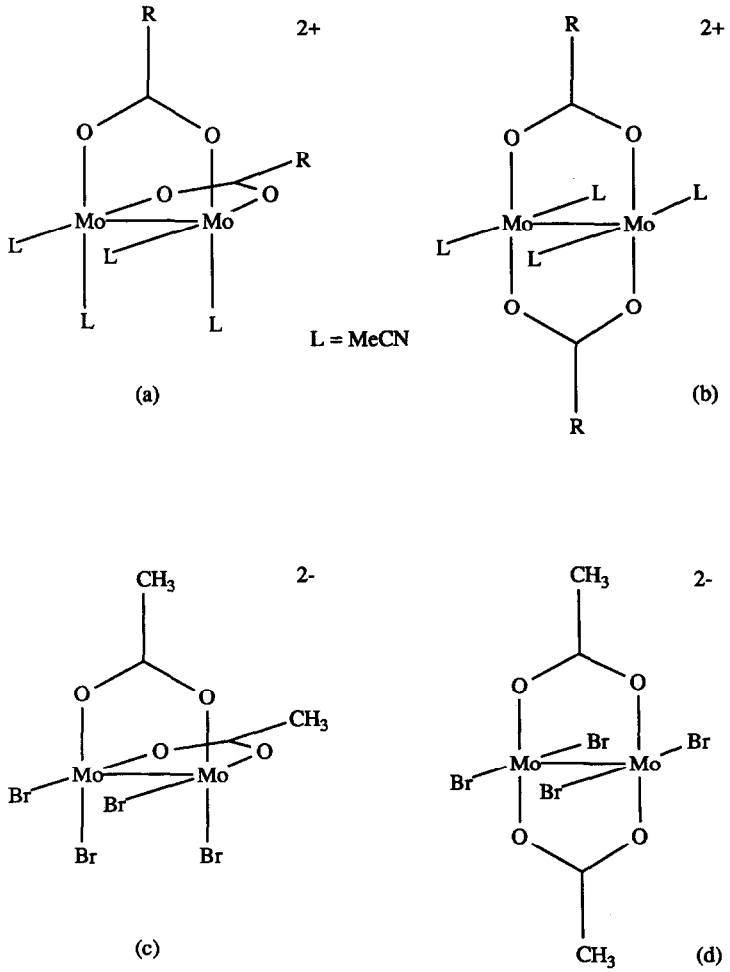

Fig. 2. (a) and (b) Possible structures for the new dications $[Mo_2(\mu\text{-}O_2CR)_2L_4]^{2+}$ [R = HC═CH$_2$ (**2**), (CH$_3$)C═CH$_2$ (**4**), H$_2$CCHC═CH$_2$ (**6**), R = (CH$_3$)HCH$_2$CHC═CH$_2$(**7**), C$_7$H$_9$ (**8**); L = MeCN]. (c) and (d) Possible structures for the dianion, $[Mo_2(\mu\text{-}O_2CCH_3)_2Br_4]^{2-}$.

Polymerization catalysis

(1) *Bicyclo*[2.2.1]*hept-2-ene*(*norbornene*). In 1981 Lamotte *et al.*[10] reacted aluminium isopropoxide with $[Mo_2(\mu\text{-}O_2CCH_3)_4]$ to give $[Mo_2(\mu\text{-}O_2CCH_3)_2\{\mu\text{-}(OCH(CH_3)_2)_2Al(OCH(CH_3)_2\}_2]$, the X-ray crystal structure of which showed *trans* acetates and *trans* aluminium isopropoxides. Later, Diefenbach reported that dimolybdenum(II,II) carboxylato complexes in the presence of aluminium, titanium or zirconium alkoxides were good catalysts for the metathesis of alkynes.[11] Furthermore, he prepared and characterized complexes of the type $[Mo_2(O_2CR)_2\{Al(p\text{-}OC_6H_4Cl)_4\}_2]$ [R = CH_3, $C(Me)_3$, CF_3], and subsequently showed that they also catalysed alkyne metathesis reactions. Earlier, we had shown that the neutral and anionic dimolybdenum(II,II) complexes $[Mo_2(\mu\text{-}O_2CR)_4]$ (R = CH_3, CF_3) and $K_4[Mo_2Cl_8]$ are good metathesis catalysts for ring-opening polymerization reactions.[12,13] For example, each of the catalyst/co-catalyst systems $[Mo_2(\mu\text{-}O_2CCH_3)_4]/EtAlCl_2$ and $K_4[Mo_2Cl_8]/EtAlCl_2$ polymerized bicyclo[2.2.1]hept-2-ene and 1-methylbicyclo[2.2.1]hept-2-ene at 20°C, and $[Mo_2(\mu\text{-}O_2CCF_3)_4]$ polymerized the same monomers even in the absence of a co-catalyst.

The dicationic complexes **1** and **4** and the dianionic complex **9**, when used in the presence of $EtAlCl_2$ as a co-catalyst, catalysed (0.28 mol % catalyst) the room temperature ring-opening polymerization of bicyclo[2.2.1]hept-2-ene to give poly(1,3-cyclopentylene-vinylene) (pcpv). When the reaction solvent was changed from toluene to acetonitrile no polymerization occurred.[14] From the ^{13}C NMR spectra of the polymers the fraction of double bonds in the polymer chain with *cis* character (σ_c) was calculated.[12,13] The close similarity in

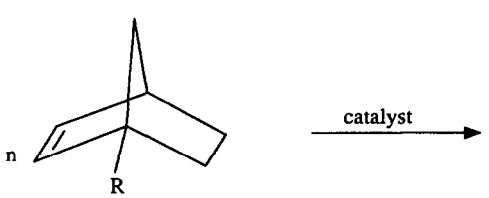

(R = H, Me)

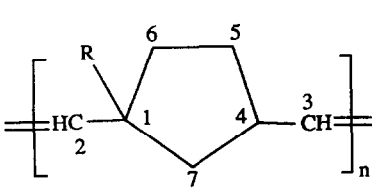

the values of σ_c (*ca* 0.36) found for the three pcpv samples indicates that changing the ligands on the dimolybdenum(II,II) core does not cause a significant change in the stereochemistry of the double bonds in the polymer chain.

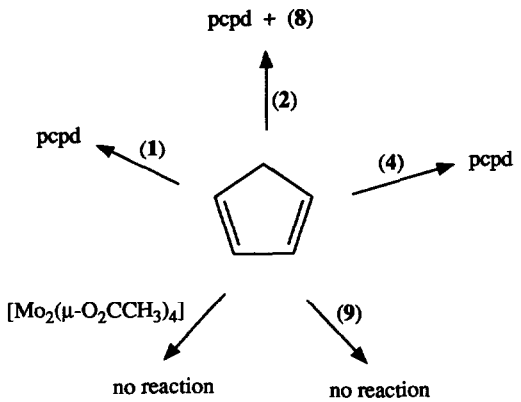

Scheme 2. pcpd = polycyclopentadiene.

(2) *Cyclopentadiene*. We have recently described how some neutral dimolybdenum(II,II), dicopper(II,II) and diruthenium(II,III) complexes containing four unsaturated carboxylate ligands react with excess cyclopentadiene to give the respective Diels–Alder cycloaddition adducts.[2] No polycyclopentadiene (pcpd) formed during these reactions. The results of reactions of some of the present complex salts with excess cyclopentadiene in acetonitrile at room temperature are outlined in Scheme 2. A 0.09 mol % solution of **4** rapidly catalysed the addition polymerization of cyclopentadiene, with the pcpd precipitating as a white solid (yield: 35%). Unchanged **4** was subsequently recovered from the reaction filtrate. Although **1** also catalysed the formation of pcpd (yield: 8%), it was not as active as **4**. Complex **2** was even less active than **1** and only a very small amount of pcpd was obtained. Furthermore, the Diels–Alder cycloaddition adduct **8** was isolated in high yield from the filtrate of the latter reaction (Scheme 1). The dianionic complex **9** failed to react with cyclopentadiene, and unchanged **9** was recovered. In addition, no pcpd formed when the neutral complex $[Mo_2(\mu\text{-}O_2CCH_3)_4]$ was reacted (either as a suspension in acetonitrile or as a solution in hot methanol) with cyclopentadiene.

Although there are many examples known where non-transition metal Lewis acids have been used as catalysts of the polymerization of cyclopentadiene,[15] there are only a few cases in which transition metal complexes [other than those of titanium(IV)] have been employed,[16] and it is generally thought that all of these catalysts cause the polymerization to proceed via a cationic mechanism.[17–19] Normally, the pcpd obtained from these literature reactions is soluble[20] in $CHCl_3$ and from

their NMR spectra[15,21] it was deduced that these addition polymers contain both 1,4- and 1,2-structural units. Furthermore, it has been shown that the 1,4- and 1,2-content of the polymers is generally dependent on the type of catalyst used, solvent and temperature.[17] Unfortunately, the insolubility of the pcpd obtained using the present complex salts prohibited detailed structural characterization by NMR spectroscopy. However, the IR spectra of these insoluble polymers were identical to those illustrated in the literature[15] for soluble poly-1,4-/1,2-cyclopentadiene.

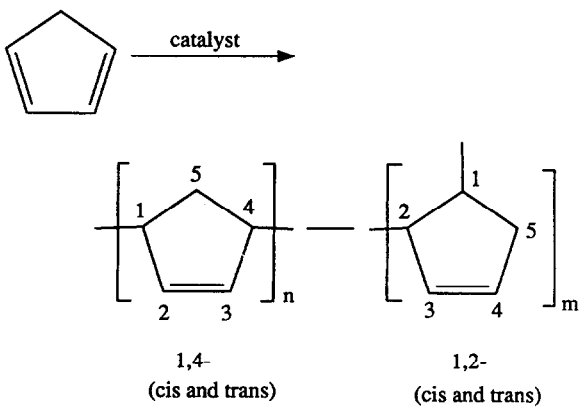

Assuming that the present polymers are comprised of 1,4- and 1,2-units a possible cationic addition mechanism for their formation can be visualized (Scheme 3). ^1H and ^{13}C NMR studies on complex **1**[3b] have shown that the MeCN ligands are labile, and we have further demonstrated here that they are readily replaced by bromide ions (formation of **9**). Thus, a first step in the polymerization process is likely to be the displacement of one or more MeCN ligands by cyclopentadiene to give species (a). The cyclopentadiene molecule may bond to either one or both (i.e. bridging) molybdenum atoms of the bimetallic core to give the carbocation (**b**), which itself may isomerize to (**c**).[23] Addition of cyclopentadiene molecules to (**b**) and (**c**) will give rise to separate 1,2-pcpd and 1,4-pcpd, respectively. A single polymer molecule containing a mixture of 1,2- and 1,4-units in the chain can form if there is isomerization of either (**b**) or (**c**) during polymerization (Scheme 4).

Given the close similarity in both the structural and electronic properties of the complex dications of salts **1**, **2** and **4** it is difficult to understand the large differences observed in their catalytic activity towards cyclopentadiene. The inactivity of salt **9** is probably attributable to the fact that the dianion $[Mo_2(\mu\text{-}O_2CCH_3)_2Br_4]^{2-}$ can be viewed as a Lewis base and, as such, would effectively repel the electron-rich cyclopentadiene molecule. The neutral complex $[Mo_2(\mu\text{-}O_2CCH_3)_4]$ also failed to catalyse the polymerization of cyclopentadiene, suggesting that it too is not a strong enough Lewis acid for diene activation.

EXPERIMENTAL

All reactions were carried out under nitrogen using dry solvents. Standard Schlenk techniques were employed during the preparation of the molybdenum complexes. Although all of the complex salts were air-sensitive the dicationic salts appeared to be considerably more sensitive than the dianionic salt. Literature methods were used to prepare *cis*-$[Mo_2(\mu\text{-}O_2CCH_3)_2(MeCN)_6][BF_4]_2$ (**1**),[3b] $[Mo_2(\mu\text{-}O_2CCH_3)_4]$[24] and *endo*-bicyclo[2.2.1]hept-5-ene-2-carboxylic acid.[25] Ethylaluminiumdichloride was used as a 25% solution in hexane. IR spectra were recorded in the region 4000–200 cm^{-1} on a Perkin–Elmer 783 grating spectrometer, and electronic spectra were run on a Milton Roy Spectronic 3000 Array. ^1H NMR spectra of solutions of the complexes (in $CDCl_3$ or DMSO-d_6, and under nitrogen) and ^{13}C NMR of bicyclo[2.2.1]hept-2-ene polymers (in $CDCl_3$) were recorded using a Bruker AC 80 spectrometer. Elemental analyses were performed by the Microanalytical Laboratory, University College, Cork, Ireland.

$[Mo_2(\mu\text{-}O_2CCH{=}CH_2)_2(MeCN)_4][BF_4]_2 \cdot H_2O$ (**2**) *and* $[Mo_2(\mu\text{-}O_2CHC{=}CH_2)_4] \cdot 0.5H_2O$ (**3**)*

A solution of complex **1** (0.36 g, 0.49 mmol) and propenoic acid (0.5 g, 6.9 mmol) in acetonitrile (20 cm^3) was stirred at room temperature for 12 h, and the resulting light red solution was then reduced under high vacuum (at 20°C) to *ca* 1 cm^3. Addition of toluene (40 cm^3) induced the formation of a dense red oil. The upper yellow liquid was decanted off and fresh toluene (20 cm^3) and acetonitrile (3 cm^3) was added to the red oil. The mixture was stirred vigorously and the crude product **2** eventually precipiated as a red solid. The solid was filtered off, washed with toluene (2 × 20 cm^3) and dried *in vacuo*. The solid was then redissolved in a fresh solution of propenoic acid (0.5 g, 6.9 mmol) in acetonitrile (20 cm^3) and stirred at room temperature for a further 3 h. The red complex was then reprecipitated from the oil form as described above; yield: 0.2 g

* Microanalytical and IR data for complexes **3** and **5** corresponded with that reported in ref. 2 for these complexes.

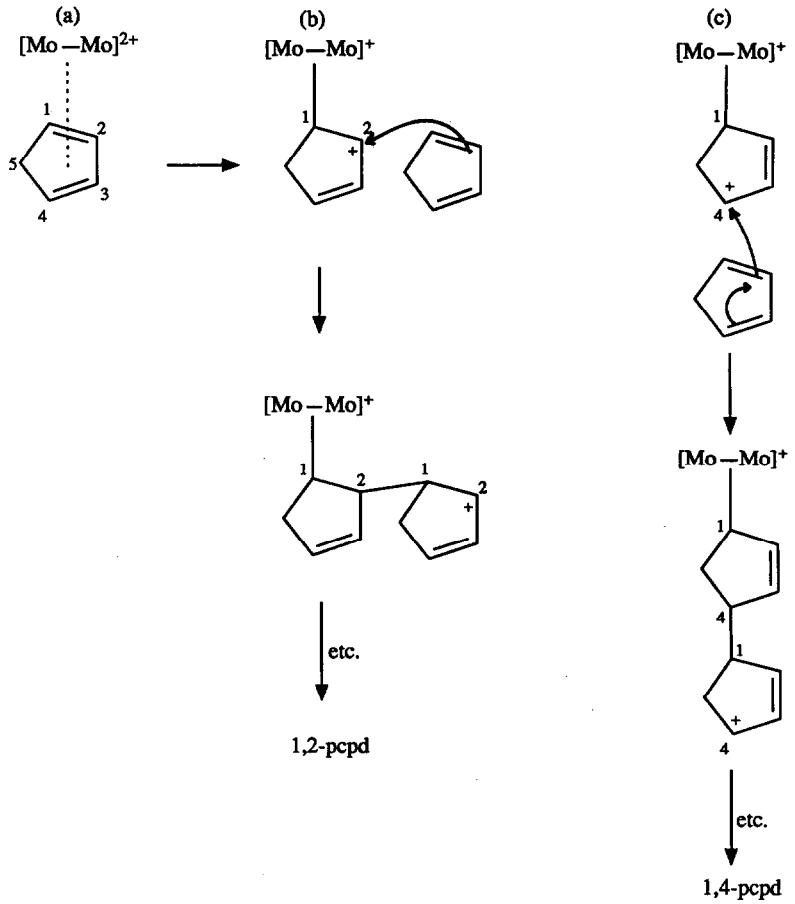

Scheme 3. [Mo—Mo] = $[Mo_2(\mu\text{-}O_2CR)_2(MeCN)_x]$, R = CH_3,$HC{=}CH_2$, $(CH_3)C{=}CH_2$, $x < 6$.

(59%). The combined reaction filtrates (yellow liquid and toluene washings) were concentrated to low volume under high vacuum (at 20°C) and the yellow solid **3** precipitated; yield: 0.05 g (21%). (**2**): Found: C, 24.5; H, 2.8; N, 7.7. Calc.: C, 24.4; H, 2.9; N, 8.1%.

$[Mo_2(\mu\text{-}O_2C(CH_3)C{=}CH_2)_2(MeCN)_4][BF_4]_2 \cdot H_2O$ (**4**) *and* $[Mo_2(\mu\text{-}O_2C(CH_3C{=}CH_2)_4] \cdot 0.5H_2O$ (**5**)*

Using 2-methylpropenoic acid these complexes (red and yellow coloured, respectively) were prepared and recovered by the same method as described for **2** and **3**; yield (**4**): (76%). Found: C, 26.2; H, 3.6; N, 7.9. Calc.: C, 26.8; H, 3.4; N, 7.8%.

$[Mo_2(\mu\text{-}O_2CH_2CHC{=}CH_2)_2(MeCN)_4][BF_4]_2 \cdot H_2O$ (**6**)

Using 3-butenoic acid this red complex was prepared and recovered by the same method as

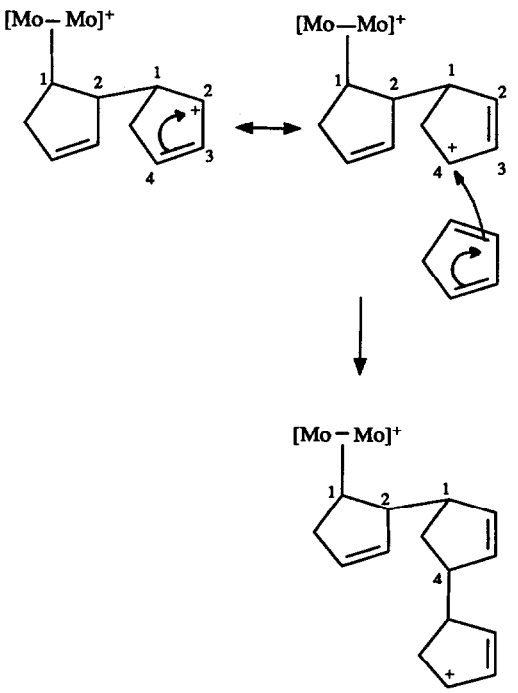

Scheme 4.

described for **2**; yield: (80%). Found: C, 26.9; H, 3.6; N, 7.4. Calc.: C, 26.8; H, 3.4; N, 7.8%.

$[Mo_2(\mu\text{-}O_2C(CH_3)HCH_2CHC{=}CH_2)_2(MeCN)_4][BF_4]_2 \cdot H_2O$ (**7**)

Using 2-methylpent-4-enoic acid this red complex was prepared and recovered by the same method as described for **2**; yield: (93%). Found: C, 31.3; H, 4.1; N, 7.7. Calc.: C, 31.0; H, 4.2; N, 7.2%.

$[Mo_2(\mu\text{-}O_2CC_7H_9)_2(MeCN)_4][BF_4]_2 \cdot 2H_2O$ (**8**)

Method (a). Using *endo*-bicyclo[2.2.1]hept-5-ene-2-carboxylic acid this red complex was prepared and recovered by the same method as described for **2**; yield: (68%).

Method (b). Complex **2** (0.17 g, 0.25 mmol) and cyclopentadiene (0.4 g, 6.1 mmol) were stirred together in acetonitrile (20 cm^3) at room temperature for 24 h. A small amount of white pcpd solid was filtered off and complex (**8**) was subsequently recovered from the filtrate using the method outlined for the isolation of **2**; yield: 0.14 g (70%). Found: C, 34.3; H, 4.1; N, 7.1. Calc.: C, 34.3; H, 4.1; N, 6.7%.

$(Et_4N)_2[Mo_2(\mu\text{-}O_2CCH_3)_2Br_4]$ (**9**)

To a solution of **1** (0.33 g, 0.45 mmol) in acetonitrile (20 cm^3) was added tetraethylammonium bromide (0.57 g, 2.1 mmol), and this resulted in an immediate red to dark purple colour change. The solution was stirred for 0.5 h and the solvent was then removed using high vacuum. Ethanol (30 cm^3) was added and the resulting suspension was stirred for 1.5 h. The red product was removed by filtration and then resuspended in fresh ethanol (10 cm^3) and stirred for another 10 min. The solid was filtered off, washed with ethanol (3 × 5 cm^3) and then dried *in vacuo*; yield: 0.23 g (57%). Found: C, 26.9; H, 5.4; N, 3.2; Br, 36.2. Calc.: C, 27.0; H, 5.2; N, 3.1; Br, 35.9%. Complex **9** gives an orange solution in MeOH and DMSO, and a purple solution in MeCN.

Polymerization reactions

All polymerization reactions were performed at room temperature and under nitrogen. Typical polymerization procedures are outlined below.

Polymerization of bicyclo[2.2.1]hept-2-ene

Bicyclo[2.2.1]hept-2-ene (0.5 g, 5.3 mmol) was dissolved in dry toluene (1 cm^3) and the dimolybdenum(II,II) salt (0.015 mmol) was added. Ethylaluminiumdichloride solution (0.5 cm^3, 0.33 mmol) was then added and this resulted in rapid polymer formation (as indicated by an increase in solution viscosity). The mixture was then allowed to stand at room temperature for 1 h. Ethanol (*ca* 25 cm^3) was added and the precipitated polymer (pcpv) was washed several times with small volumes of ethanol. The wet solid was then dissolved in chloroform (*ca* 75 cm^3), and the resulting polymer solution was dripped into ethanol (300 cm^3) containing concentrated hydrochloric acid (0.2 cm^3) causing the polymer to reprecipitate as a fine white solid. This solid was filtered off, washed with ethanol and dried *in vacuo* for 1 h at room temperature. A solution of the polymer in $CDCl_3$ was then characterized using ^{13}C NMR spectroscopy. For example, using complex **4** as catalyst, 40 mg of pcpv was obtained. Polymer σ_c values (in parentheses) obtained using the various catalysts were as follows: **1** (0.36), **4** (0.36), **9** (0.35).

Polymerization of cyclopentadiene

A solution of the dimolybdenum(II,II) complex salt (0.036 mmol) and cyclopentadiene (2.6 g, 39.4 mmol) in acetonitrile (5 cm^3) was stirred for 72 h during which time the white pcpd gradually precipitated. The solid was filtered off, washed with acetonitrile and dried *in vacuo*. For example, using complex **4** as catalyst pcpd was formed in 35% yield. The pcpd formed in these reactions was insoluble in all common organic solvents. The polymers discoloured slightly on standing.

REFERENCES

1. F. A. Cotton and R. A. Walton, *Multiple Bonds Between Metal Atoms*, Ch. 8.3. Wiley, New York (1982).
2. M. McCann, A. Carvill, P. Guinan, P. Higgins, J. Campbell, H. Ryan, M. Walsh, G. Ferguson and J. Gallagher, *Polyhedron* 1991, **10**, 2273.
3. (a) F. A. Cotton, A. H. Reid Jr and W. Schwotzer, *Inorg. Chem.* 1985, **24**, 3965; (b) W. Clegg, G. Pimblett and C. D. Garner, *Polyhedron* 1986, **5**, 31; (c) J. Telser and R. S. Drago, *Inorg. Chem.* 1984, **23**, 198.
4. When $[Mo_2(\mu\text{-}O_2CCH_3)_4]$ was reacted with 3-butenoic acid a brown Mo–oxo solid formed (see ref. 2). Under similar experimental conditions 2-methylpent-4-enoic acid also produced a brown Mo–oxo complex. Analytical data: Found: C, 23.32; H, 3.60. The two brown solids had similar IR spectra.
5. E. Hochberg and E. H. Abbott, *Inorg. Chem.* 1978, **17**, 506.

6. J. San Filippo, H. J. Sniadoch and R. L. Grayson, *Inorg. Chem.* 1974, **13**, 2121.
7. P. A. Bates, A. J. Nielson and J. M. Waters, *Polyhedron* 1987, **6**, 2111.
8. Although the authors of references 3(a) and 3(b) reported the synthesis and X-ray crystal structure of complex **1** they did not report the IR band positions for the carboxylate groups or the NMR peak positions for the ligands. As an aid to structural assignment for the complexes described in this work we report some relevant IR and NMR data for **1** in Table 1.
9. W. Clegg, C. D. Garner, S. Parkes and I. B. Walton, *Inorg. Chem.* 1979, **18**, 2250.
10. J. Lamotte, O. Oideberg, L. Dupont and P. Durbut, *Cryst. Struct. Comm.* 1981, **10**, 59.
11. S. P. Diefenbach, U.S. Patent 4,704,377 (1987).
12. J. G. Hamilton, K. J. Ivin, M. McCann and J. J. Rooney, *Makromol. Chem.* 1985, **186**, 1477.
13. K. J. Ivin, D. T. Laverty and J. J. Rooney, *Makromol. Chem.* 1977, **178**, 1545.
14. Diefenbach reported that alkyne metathesis did not occur when acetonitrile was used as the reaction solvent (see ref. 11).
15. C. Aso, T. Kunitake and Y. Ishimoto, *J. Polym. Sci. A-1* 1968, **6**, 1163.
16. R. V. Honeychuck, P. V. Bonnesen, J. Farahi and W. H. Hersh, *J. Org. Chem.* 1987, **562**, 5293 and refs therein.
17. C. Aso, T. Kunitake and Y. Ishimoto, *J. Polym. Sci. A-1* 1968, **6**, 1175.
18. C. Aso, T. Kunitake, K. Ito and Y. Ishimoto, *J. Polym. Sci. Polym. Lett.* 1966, **4**, 701.
19. J.-P. Vairon and P. Sigwalt, *Bull. Soc. Chim. Fr.* 1971, 559.
20. When $[(Me_3P)(CO)_3(NO)W\text{-}FSbF_5]$ was used as a catalyst to polymerize a solution of cyclopentadiene in ether a soluble pcpd product was obtained. However, when dichloromethane was used as the reaction solvent an insoluble form of pcpd precipitated (see ref. 16). Similarly, $[WCl_4(OCH(CH_2Cl)_2\text{-}Al(C_2H_5)Cl\text{-}THF]$ polymerizes cyclopentadiene in THF and in toluene to give soluble and insoluble pcpd, respectively (see ref. 21).
21. A. V. Orlov, Yu. B. Korshak, M. A. Tlenkopachev and E. A. Robas, *Dokl. Akad. Nauk SSSR* 1988, **300**, 138.
22. It is not possible to estimate the relative ratio of 1,4-: 1,2-units in the polymer from the IR spectrum (see ref. 15).
23. Initially, species (**c**) would be expected to be more stable than (**b**) as the two positive charges in the latter are closer together, but as the polymer chain grows this repulsive feature becomes less important as the two charges get further apart.
24. T. A. Stephenson, E. Bannister and G. Wilkinson, *J. Chem. Soc.* 1964, 2538.
25. K. Alder and G. Stein, *Ann.* 1934, **514**, 197.

Polyhedron Vol. 10, No. 19, pp. 2293–2299, 1991
Printed in Great Britain

0277-5387/91 $3.00+.00
© 1991 Pergamon Press plc

THE CHEMISTRY OF β-DIKETONATE COPPER(I) COMPOUNDS—III. THE SYNTHESIS OF (β-DIKETONATE) Cu(1,5-COD) COMPOUNDS, THE SOLID STATE STRUCTURE AND DISPROPORTIONATION OF HEXAFLUOROACETYLACETONATO (1,5-CYCLOOCTADIENE)COPPER(I), (hfac)Cu(1,5-COD)

K. M. CHI, H.-K. SHIN, M. J. HAMPDEN-SMITH* and E. N. DUESLER

Department of Chemistry, Center for Micro-Engineered Ceramics, University of New Mexico, Albuquerque, NM 87131, U.S.A.

and

T. T. KODAS*

Department of Chemical Engineering, Center for Micro-Engineered Ceramics, University of New Mexico, Albuquerque, NM 87131, U.S.A.

(*Received* 17 *April* 1991; *accepted* 18 *June* 1991)

Abstract—The compounds (β-diketonate)Cu(1,5-COD) have been prepared by the reaction between $[(1,5\text{-COD})CuCl]_2$ and Na(β-diketonate) for β-diketonate = hexafluoroacetylacetonate (hfac), trifluoroacetylacetonate (tfac) and acetylacetonate (acac) and 1,5-COD = 1,5-cyclooctadiene. These compounds were characterized spectroscopically and (hfac)Cu(1,5-COD) was characterized, in the solid state, by single-crystal X-ray diffraction. Crystal data: empirical formula, $C_{13}H_{13}CuF_6O_2$; crystal system, monoclinic; space group, $P2_1/c$; $a = 10.011(2)$, $b = 9.777(3)$, $c = 15.658(3)$ Å and $\beta = 107.88(2)°$ and $Z = 4$. The coordination of the copper centre is best described as "3+1" with an asymmetrically coordinated 1,5-COD ligand where the Cu—C(6)═C(7) centroid and Cu—C(10)═C(11) centroid distances are 1.953 and 2.418 Å, respectively. The quantitative disproportionation, according to the equation $2(hfac)Cu(1,5\text{-COD}) \rightarrow Cu + Cu(hfac)_2 + 2(1,5\text{-COD})$ to produce copper metal and volatile by-products, was observed at 200°C.

The chemistry of copper(II) β-diketonate compounds and their Lewis base adducts has been investigated extensively.[1] However, the chemistry of copper(I) β-diketonate compounds has received much less attention. Stable Lewis base adducts of copper(I) β-diketonates with amines,[2] isonitriles,[3] phosphines,[3,4] olefins[5] and carbon monoxide[5] have been prepared, with the general formula (β-diketonate)CuL_n, where $n = 1$ or 2. That the unligated copper(I) acetylacetonate moiety is unstable with respect to disproportionation was quantitatively demonstrated for the ammonia derivative (acetylacetonate)$Cu(NH_3)_{2.5}$.[2]

$$2(acac)Cu(NH_3)_{2.5} \longrightarrow Cu + Cu(acac)_2 + 5NH_3 \quad (1)$$

More recently, it has been shown, qualitatively, that the carbonyl derivative, (hfac)Cu(CO), will evolve carbon monoxide and also undergo a similar disproportionation reaction to produce copper metal and Cu(II)$(hfac)_2$.[5] In principle, this disproportionation reaction could be used as a method to deposit thin films of copper by chemical vapor deposition (CVD) for applications in semicon-

* Authors to whom correspondence should be addressed.

ductor metallization. To take advantage of this reaction for CVD purposes, it is important that the copper-containing precursor be volatile, thermally inert at room temperature and susceptible to thermally-induced disproportionation at elevated temperatures. To avoid impurity contamination in the film, the disproportionation products should be thermally inert at the deposition reaction temperature and volatile so they can be easily removed from the system.

We have recently reported the first evidence for such a thermally-induced disproportionation mechanism during CVD of copper in a series of copper(I) β-diketonate compounds, (β-diketonate)Cu(PMe_3).[6,7] Here we report the synthesis and spectroscopic characterization of the compounds (β-diketonate)Cu(1,5-COD) (where 1,5-COD = 1,5-cyclooctadiene and β-diketonate = hexafluoroacetylacetonate, hfac; trifluoroacetylacetonate, tfac; acetylacetonate, acac),the single-crystal X-ray diffraction structure of (hfac)Cu(1,5-COD) and the quantitative disproportionation of (hfac)Cu(1,5-COD) at elevated temperatures.

EXPERIMENTAL

(1) *Syntheses*

All manipulations were carried out *in vacuo* or under an inert atmosphere using Schlenk techniques as previously described.[8] All β-diketones were purchased from Aldrich Chemical Company, and were stored over 4 Å molecular sieves. The sodium salts of the β-diketones were prepared by a method previously described.[9] 1,5-cyclooctadiene was purchased from Aldrich Chemical company and distilled under nitrogen prior to use and stored over 4 Å molecular sieves.

Elemental analyses were performed by Ms R. Ju at the University of New Mexico, Department of Chemistry. NMR data were recorded on a Bruker AC-250P NMR spectrometer using the protio impurities of the deuterated solvents as references for the ^1H NMR and the ^{13}C resonance of the solvents as reference for ^{13}C NMR spectroscopy. Temperatures were calibrated with either ethylene glycol or methanol. IR data were recorded on a Perkin–Elmer Model 1620 FTIR spectrophotometer. Mass spectra were recorded on a Finnegan GC-mass spectrometer.

The preparation of $[CuCl(1,5\text{-}COD)]_2$ was carried out under reaction conditions different from those described in the literature[10] that are described below. The preparation of (hfac)Cu(1,5-COD) and (tfac)Cu(1,5-COD) compounds was carried out under analogous conditions. The preparation of (hfac)Cu(1,5-COD) is described here in detail as a representative example. The compound (acac)Cu(1,5-COD) was prepared using a similar procedure at lower temperature (−78°C) and could not be isolated, but was identified spectroscopically at low temperature.

(a) *Preparation of* $[CuCl(1,5\text{-}COD)]_2$. A slight excess of 1,5-cyclooctadiene (19.4 g, 0.18 mol, 22 cm^3) was added slowly to a slurry of CuCl (14.8 g, 0.15 mol) in 150 cm^3 of benzene by syringe. When the addition was complete, the solution was stirred in a warm water bath (40°C) for 2 h. Removal of volatile components gave an analytically pure, white powder $[CuCl(1,5\text{-}COD)]_2$ (24.6 g, 79% yield). NMR data: ^1H (C_6D_6, 20°C) δ(ppm) 1.14 (s, br, 8H, CH_2), 5.64 (s, br, 4H, CH). $^{13}C\{^1H\}$ δ(ppm) 28.3 (s, CH_2), 124.2 (s, CH) ppm. IR data (KBr disc, cm^{-1}): 3040(w), 2949(m), 2920(m), 2878(s), 2826(m), 1551(w), 1474(m), 1426(s), 1344(w), 1238(m), 1186(w), 1082(w), 993(w), 957(w), 849(w), 818(m), 744(s), 715(m), 649(m), 480(w), 409(w). Elemental analysis data: Found: C, 46.2; H, 6.0. Calc. for $C_{16}H_{24}Cl_2Cu_2$: C, 46.4; H, 5.8%.

(b) *Preparation of* (hfac)Cu(1,5-COD). The compounds $[CuCl(1,5\text{-}COD)]_2$ (5.20 g, 12.55 mmol) and an excess of Na(hfac) (5.9 g, 25.64 mmol) were placed in a 250 cm^3 Schlenk flask. Addition of 100 cm^3 of Et_2O immediately gave a yellow solution. After 1 h stirring and removal of solvent, a greenish-yellow solid was obtained. Extraction of the product with pentane (150 cm^3) followed by filtration and removal of solvent gave bright yellow crystalline (hfac)Cu(1,5-COD) (6.62 g, 69.5% yield). The compound was sublimed at 65°C under reduced pressure (100 mtorr).

(c) *Spectroscopic data for* (β-diketonate)Cu(1,5-COD) *compounds*:

(hfac)Cu(1,5-COD)

NMR data: ^1H (C_6D_6, 20°C) δ(ppm) 1.80 (s, br, 8H, CH_2 in 1,5-COD), 5.07 (s, br, 4H, CH in 1,5-COD), 6.17 (s, 1H, CH in hfac). $^{13}C\{^1H\}$ δ(ppm) 28.0 (s, CH_2 in 1,5-COD), 89.0 (s, CH in hfac), 115.0 (s, CH in 1,5-COD), 118.5 (q, CF_3 in hfac, J(C—F) = 286.2 Hz), 177.8 ($CF_3C{=}O$ in hfac, J(C—F) = 33.6 Hz). IR data (KBr disc, cm^{-1}): 2953(w), 2892(w), 2842(w), 1637(s), 1593(m), 1553(m), 1526(m), 1483(s), 1432(m), 1345(w), 1259(s), 1210(s), 1142(s), 1097(m), 997(w), 810(w), 796(m), 747(m), 725(w), 671(m), 585(m), 528(w). Mass spectral data (70 eV, m/z): 477, 7%, $[Cu(hfac)_2]^+$; 441, 2%, $[(hfac)Cu_2(1,5\text{-}COD)]^+$;

408, 23%, $[(hfac)Cu(O_2C_2CHCF_3)]^+$; 378, 46%, $[(hfac)Cu(1,5\text{-}COD)]^+$; 339, 23%, $[(hfac)Cu(O_2C_2CH)]^+$; 279, 5%, $[Cu(1,5\text{-}COD)_2]^+$; 201, 51%, $[Cu(O_2C_2CHCF_3)]^+$; 171, 98%, $[Cu(1,5\text{-}COD)]^+$; 117, 26%, $[Cu(C_4H_6)]^+$; 108, 8%, $[1,5\text{-}COD]^+$; 93, 10%, $[C_7H_9]^+$; 80, 35%, $[C_6H_8]^+$; 79, 37%, $[C_6H_7]^+$; 69, 8%, $[CF_3]^+$; 67, 100%, $[C_5H_7]^+$; 63, 35%, $[Cu]^+$; 54, 95%, $[C_4H_6]^+$. Elemental analysis data: Found: C, 41.1; H, 3.48. Calc. for $C_{13}H_{13}O_2F_6Cu$: C, 41.2; H, 3.5%.

(tfac)Cu(1,5-COD)

NMR data: ^1H (C_6D_6, 20°C) δ(ppm) 1.73 (s, 3H, CH_3 in tfac), 1.96 (br, s, 8H, CH_2 in 1,5-COD), 5.11 (br, 2, 4H, CH in 1,5-COD), 5.71 (s, 1H, CH in tfac). $^{13}C\{^1H\}$ δ(ppm) 28.2 (s, CH_2 in 1,5-COD), 29.0 (s, CH_3 in tfac), 94.5 (s, CH in tfac), 112.9 (s, CH in 1,5-COD), 120.0 (q, CF_3 in tfac, J(C—F) = 286 Hz), 171.0 (q, $CF_3C{=}O$ in tfac, J(C—F) = 31.1 Hz), 197.6 (s, $CH_3C{=}O$ in tfac). IR data (KBr disc, cm^{-1}): 2951(w), 2924(w), 2894(w), 2842(w), 1623(s), 1553(m), 1517(m), 1473(m), 1427(m), 1365(s), 1285(s), 1226(s), 1180(s), 1126(s), 941(w), 857(m), 775(s), 742(m), 730(m), 654(w), 600(w), 577(m), 518(w), 419(w). Mass spectral data (70 eV, m/z): 369, 16%, $[Cu(tfac)_2]^+$; 354, 2%, $[(tfac)Cu(O_2C_2CHCF_3)]^+$; 327, 12%, $[(tfac)Cu(OCCH_2CF_3)]^+$; 324, 5%, $[(tfac)Cu(1,5\text{-}COD)]^+$; 300, 14%, $[(tfac)Cu(O_2C_2CHCH_3)]^+$; 285, 2%, $[(tfac)Cu(O_2C_2CH)]^+$; 231, 9%, $[Cu(O_2C_2CHCH_3)_2]^+$; 216, 3%, $[Cu(tfac)]^+$; 201, 2%, $[Cu(O_2C_2CHCF_3)]^+$; 171, 7%, $[Cu(1,5\text{-}COD)]^+$; 147, 19%, $[Cu(O_2C_2CHCH_3)]^+$; 108, 8%, $[1,5\text{-}COD]^+$; 93, 10%, $[C_7H_9]^+$; 80, 30%, $[C_6H_8]^+$; 79, 35%, $[C_6H_7]^+$ 67, 91%, $[C_5H_7]^+$; 54, 100%, $[C_4H_6]^+$. Found: C, 47.4; H, 4.8. Calc. for $C_{13}H_{16}O_2F_3Cu$: C, 48.1; H, 5.0%.

(acac)Cu(1,5-COD)

NMR data ^1H (toluene-d_8, −30°C) δ(ppm) 5.41 (br, s, CH in 1,5-COD), 5.30 (s, CH in acac), 2.11 (br, s, CH_2 in 1,5-COD), 1.95 (s, CH_3 in acac). (−45°C) δ(ppm) 5.43 (br, s, CH in 1,5-COD), 5.31 (s, CH in acac), 2.09 (br, s, CH_2 in 1,5-COD), 1.97 (s, CH_3 in acac). (−60°C) δ(ppm) 5.48 (br, s, CH in 1,5-COD), 5.30 (s, CH in acac), 2.07 (br, s, CH_2 in 1,5-COD), 1.97 (s, CH_3 in acac).

(2) *Thermally induced disproportionation of* (hfac)Cu(1,5-COD)

The thermally-induced decomposition of (hfac)Cu(1,5-COD) was studied in a reactor which consisted of a glass tube, closed at one end with a Kontes tap at the other end. The Kontes tap was attached to a liquid nitrogen cooled U-trap with rubber tubing and the U-trap was attached to a vacuum pump via a Schlenk line. A similar apparatus has been described previously, in detail.[11] A number of thermal decomposition experiments were conducted, and a typical example is described below.

The compound (hfac)Cu(1,5-COD) (370 mg, 0.98 mmol) was placed in the closed end of a glass tube in a nitrogen-filled dry-box and the glass tube attached to the U-trap. The whole apparatus was evacuated (~100 mtorr) and the glass tube placed in two furnaces such that (hfac)Cu(1,5-COD) was heated to 70°C and the remainder of the glass tube was heated to 200°C under dynamic vacuum. The (hfac)Cu(1,5-COD) evaporated from the 70°C zone into the hotter zone where thermal decomposition occurred resulting in copper film formation. After all the (hfac)Cu(1,5-COD) had evaporated, the reaction products were collected and characterized. The compound $Cu(hfac)_2$ was isolated from the cold portion between the hot zone and the U-trap, and 1,5-COD was isolated from the U-trap. The calculated (assuming quantitative disproportionation) and observed amounts of reaction products were as follows: Copper, calc. 30.8 mg, 0.49 mmol; obs. 33.1 mg, 0.52 mmol. $Cu(hfac)_2$: calc. 233.3 mg, 0.49 mmol; obs. 223.8 mg, 0.51 mmol. 1,5-COD: calc. 91.0 mg, 0.98 mmol; obs. 80.0 mg, 0.86 mmol. No isomerization of 1,5-COD was observed.

(3) *Crystallographic data for* (hfac)Cu(1,5-COD)

Yellow crystals of (hfac)Cu(1,5-COD) were grown at low temperature from n-pentane solution. The crystal was mounted in a capillary under a nitrogen atmosphere at 219 K and transferred to a goniostat where it was cooled to 243 K. Crystal data are summarized in Table 1. A total of 2565 independent reflections were measured in the range $2.0 < 2\theta < 50°$ on Siemens R3m/V diffractometer using Mo-K_α(λ = 0.71073 Å) radiation. The data was solved by direct methods using full-matrix least-squares refinement. All hydrogen atoms were visible in a difference Fourier synthesis phased on non-hydrogen parameters. All hydrogens were refined anisotropically with fixed Us set to 1.25 U(equiv.) of parent atoms and non-hydrogen atoms were refined anisotropically in the final cycles. A final difference Fourier map was essentially featureless, with the largest amplitude of 1.70 e $Å^{-3}$. The final agreement factors were $R = 0.0730$ and $R_w = 0.0769$ for 1928 reflections having $F > 3.0\ \sigma(F)$. The relevant bond lengths and angles are presented in Tables 2 and 3, respectively.

Table 1. Summary of crystal data

Empirical formula	$C_{13}H_{13}CuF_6O_2$
Colour of crystal	Pale yellow
Crystal dimensions (mm)	$0.345 \times 0.414 \times 0.460$
Space group	$P2_1/c$
Temperature	248 K
Cell dimensions	
a (Å)	10.011(2)
b (Å)	9.777(3)
c (Å)	15.658(3)
β (°)	107.88(2)
Z (molecules/unit cell)	4
Volume (Å^3)	1457.6(6)
Calculated density (g cm^{-3})	1.726
Wavelength (Mo-K_α)	0.71073
Molecular weight	378.8
Linear absorption correction (mm^{-1})	1.568
Scan speed (deg min^{-1})	Variable 6.00–30.00
2θ range	2.0–50.0°
Total number of reflections	5320
Number of unique intensities	2565
Number of intensities with $F > 3.00\sigma F$	1928
Goodness of fit for last cycle	1.87
$R(F)$	7.30
$R_w(F)$	7.69

Table 2. Selected bond lengths

Cu—O(1)	1.999 (6)	Cu—O(2)	2.001 (4)
Cu—C(6)	2.049 (6)	Cu—C(7)	2.089 (7)
Cu—C(10)	2.466 (8)	Cu—C(11)	2.550 (7)
O(1)—C(1)	1.247 (7)	C(1)—C(2)	1.371 (9)
C(1)—C(4)	1.525 (11)	C(2)—C(3)	1.393 (10)
C(3)—O(2)	1.241 (8)	C(3)—C(5)	1.518 (10)
C(4)—F(1)	1.263 (9)	C(4)—F(2)	1.278 (8)
C(4)—F(3)	1.299 (11)	C(5)—F(4)	1.283 (10)
C(5)—F(5)	1.269 (12)	C(5)—F(6)	1.375 (12)
C(6)—C(7)	1.367 (11)	C(6)—C(13)	1.504 (10)
C(7)—C(8)	1.522 (12)	C(8)—C(9)	1.536 (10)
C(9)—C(10)	1.506 (12)	C(10)—C(11)	1.331 (10)
C(11)—C(12)	1.503 (9)	C(12)—C(13)	1.520 (10)

RESULTS AND DISCUSSION

The compounds (hfac)Cu(1,5-COD) and (tfac)Cu(1,5-COD) have previously been synthesized by the reaction of 1,5-COD and hfacH with Cu_2O, although no spectroscopic characterization data or reaction yields were reported.[5] In this work, (β-diketonate)Cu(1,5-COD), (β-diketonate) = hfac and tfac were prepared and isolated from the reaction of the corresponding sodium salt of the β-diketone with $[(1,5\text{-COD})CuCl]_2$. The compound (acac)Cu(1,5-COD) was also prepared by this method at −78°C, but it is thermally unstable even at 0°C. This species has been identified in solution by NMR spectroscopy at low temperatures by carrying out the above reaction in a deuterated solvent.

While (tfac)Cu(1,5-COD) has relatively limited thermal stability at room temperature, (hfac)Cu(1,5-COD) exists as a thermally stable, volatile, yellow solid, and is suitable for CVD of copper.[12] This species was characterized further by single-crystal X-ray diffraction at −30°C. Crystal data are presented in Table 1. An ORTEP plot is shown in Fig. 1 together with relevant bond distances and angles in Tables 2 and 3, respectively. Unlike many

Table 3. Selected bond angles

O(1)—Cu—O(2)	93.3 (2)	O(1)—Cu—C(6)	108.5 (3)
O(2)—Cu—C(6)	149.8 (3)	O(1)—Cu—C(7)	146.5 (2)
O(2)—Cu—C(7)	115.4 (2)	C(6)—Cu—C(7)	38.6 (3)
O(1)—Cu—C(10)	113.8 (2)	O(2)—Cu—C(10)	94.0 (2)
C(6)—Cu—C(10)	95.7 (3)	C(7)—Cu—C(10)	82.5 (3)
O(1)—Cu—C(11)	93.4 (2)	O(2)—Cu—C(11)	119.3 (2)
C(6)—Cu—C(11)	80.8 (3)	C(7)—Cu—C(11)	87.4 (3)
C(10)—Cu—C(11)	30.7 (2)	Cu—O(1)—C(1)	122.6 (5)
O(1)—C(1)—C(2)	128.4 (7)	O(1)—C(1)—C(4)	113.7 (6)
C(2)—C(1)—C(4)	117.8 (6)	C(1)—C(2)—C(3)	124.6 (6)
C(2)—C(3)—O(2)	128.4 (6)	C(2)—C(3)—C(5)	118.1 (6)
O(2)—C(3)—C(5)	113.4 (7)	Cu—O(2)—C(3)	122.4 (5)
C(1)—C(4)—F(1)	112.8 (7)	C(1)—C(4)—F(2)	115.4 (6)
F(1)—C(4)—F(2)	109.0 (8)	C(1)—C(4)—F(3)	109.9 (7)
F(1)—C(4)—F(3)	106.0 (8)	F(2)—C(4)—F(3)	102.9 (7)
C(3)—C(5)—F(4)	116.2 (8)	C(3)—C(5)—F(5)	114.3 (8)
F(4)—C(5)—F(5)	112.0 (7)	C(3)—C(5)—F(6)	107.7 (6)
F(4)—C(5)—F(5)	102.4 (8)	F(5)—C(5)—F(6)	102.4 (9)
Cu—C(6)—C(7)	72.3 (4)	Cu—C(6)—C(13)	107.6 (4)
C(7)—C(6)—C(13)	128.8 (7)	Cu—C(7)—C(6)	69.1 (4)
Cu—C(7)—C(8)	111.7 (4)	C(6)—C(7)—C(8)	125.1 (7)
C(7)—C(8)—C(9)	115.9 (6)	C(8)—C(9)—C(10)	115.8 (7)
Cu—C(10)—C(9)	96.5 (5)	Cu—C(10)—C(11)	78.1 (5)
C(9)—C(10)—C(11)	127.6 (7)	Cu—C(11)—C(10)	71.1 (4)
Cu—C(11)—C(12)	100.6 (4)	C(10)—C(11)—C(12)	126.4 (7)
C(11)—C(12)—C(13)	114.5 (6)	C(6)—C(13)—C(12)	116.3 (6)

examples of copper(I) olefin compounds,[10,13–17] (hfac)Cu(1,5-COD) is monomeric in the solid state with the central copper atom coordinated by the bidentate hfac ligand (O—Cu—O = 93.3(2)°) and the bidentate, but asymmetric 1,5-COD ligand [C(10)—C(11) centroid–Cu—C(6)—C(7) centroid = 86.2°]. The angles and distances within the hfac ligand, and its coordination to copper(I) are similar to other examples of β-diketonate copper(I)

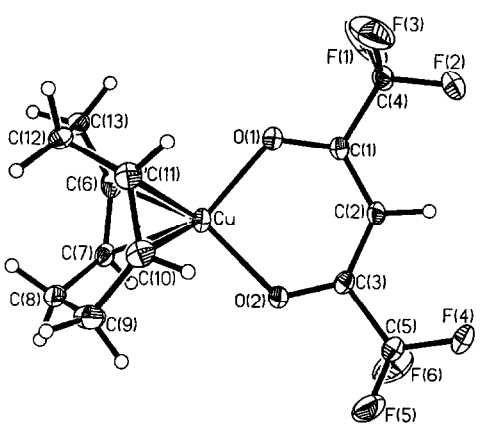

Fig. 1. ORTEP plot of (hfac)Cu(1,5-COD) emphasizing the symmetrical bonding of the hfac ligand to the copper(I) centre.

species we have previously characterized.[3,9,11] The most notable structural feature is the asymmetry in coordination of the 1,5-COD ligand which exhibits Cu—C(6)=C(7) centroid and Cu—C(10)=C(11) centroid distances of 1.953 and 2.418 Å, respectively. This asymmetry is similar to but more pronounced than that previously observed for [(1,5-COD)CuCl]$_2$[10] where the copper double-bond centroid distances were 2.05 and 2.22 Å. Consistent with the copper–carbon bond length asymmetry, C(10)—C(11) is shorter [1.33(1) Å] than C(6)—C(7) [1.37(1) Å]. These C=C bond distances are in the range normally attributed to unactivated, coordinated alkenes. Other angles and distances within the 1,5-COD ligand are as expected. The asymmetry of the 1,5-COD ligand coordination is emphasized in the view shown in Fig. 2 where the copper atom lies 0.267 Å below the O(1), O(2), C(6), C(7) plane. The coordination environment of copper is considerably distorted from tetrahedral and is probably better described as "3+1" coordination. This description emphasizes the observation that one of the double bonds is weakly coordinated to the copper centre which would otherwise possess approximately trigonal planar coordination geometry.

In solution, all three (β-diketonate)Cu(1,5-COD)

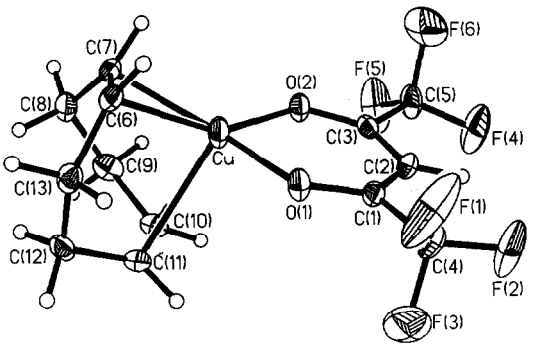

Fig. 2. ORTEP plot of (hfac)Cu(1,5-COD) emphasizing the asymmetry of the coordination of the 1,5-cyclooctadiene ligand to the copper(I) centre.

compounds exhibit one type of olefinic and aliphatic 1,5-COD ^{1}H and ^{13}C NMR resonances, respectively, even at -90°C in toluene-d_8 solutions. This is most surprising for (tfac)Cu(1,5-COD), containing the asymmetric tfac ligand, where two types of vinylic ^{13}C and ^{1}H resonances, respectively, were expected. We observed a similar phenomenon for $[(1,5\text{-COD})CuCl]_2$. This is in contrast to the corresponding rhodium complex $[(1,5\text{-COD})RhCl]_2$ which exhibits three types of 1,5-COD ^{1}H NMR resonances.[18,19] Based on the solid-state structural data we believe that it is most likely that the 1,5-COD ligand is labile and undergoes dynamic rearrangement in solutions of (hfac)Cu(1,5-COD). It is noteworthy that addition of 1,5-COD to a toluene-d_8 solution of (hfac)Cu(1,5-COD) results in rapid exchange between free and coordinated 1,5-COD at room temperature on the ^{1}H NMR time scale. The addition of hfacH to a toluene-d_8 solution of (hfac)Cu(1,5-COD) results in slow exchange with coordinated hfac on the ^{1}H NMR time scale at room temperature. The activation barrier of $\Delta G^{\dagger} = 14.1(+/-0.5)$ kcal mol^{-1} was estimated from the coalescence temperature (308 K) of the methine protons.

Experiments to probe the thermally-induced disproportionation of (hfac)Cu(1,5-COD) have been carried out in which the volatile by-products can be trapped and characterized. A sample of (hfac)Cu(1,5-COD) was heated to 70°C in one end of a glass reactor, with a geometry similar to that previously described,[11] under dynamic vacuum (10^{-2} torr) and evaporated into a hotter zone maintained at 200°C. The compound (hfac)Cu(1,5-COD) completely thermally decomposed under these conditions to yield copper on the hot walls of the reactor, copper(II)$(hfac)_2$ on the cold reactor walls after the hot zone and 1,5-COD in the cold trap.* The compound 1,5-COD was characterized by NMR and mass spectroscopy and $Cu(hfac)_2$ was characterized by mass spectroscopy and elemental analysis. No other products were observed and the disproportionation reaction according to eq. (2) was quantitative by mass balance within the estimated limits of experimental error.

$$2(\text{hfac})\text{Cu}(1,5\text{-COD}) \longrightarrow \text{Cu} + \text{Cu}(\text{hfac})_2 + 2(1,5\text{-COD}) \quad (2)$$

Other reports of disproportionation of copper(I) species have appeared in the literature such as copper(I) aryloxides,[20] but this has recently been disputed.[21]

Further experiments are underway to explore the influence of the copper ligands on the disproportionation reaction and to probe the mechanism of the ligand exchange reactions in this system.

Crystallographic Data. Complete listings of bond distances and bond angles have been deposited with the Editor at Queen Mary College and atomic positional parameters are available from the Director, Cambridge Crystallographic Data Centre.

Acknowledgements—We thank Motorola for funding, the NSF Chemical Instrumentation program for the purchase of a low-field NMR spectrometer and TTK acknowledges support from the Presidential Young Investigator award No. CTS9058538.

REFERENCES

1. A. R. Seidle, in *Comprehensive Coordination Chemistry* (Edited by G. Wilkinson, R. D. Gillard and J. A. McCleverty), Ch. 15A. Pergamon Press, Oxford (1987).
2. R. Nast, R. Mohr and C. Schultze, *Chem. Ber.* 1963, **96**, 2127.
3. H.-K. Shin, M. J. Hampden-Smith, T. T. Kodas and E. N. Duesler, *Polyhedron* 1991, **10**, 645.
4. D. Gibson, B. F. G. Johnson and J. Lewis, *J. Chem. Soc.* 1970, 367.
5. G. Doyle, K. A. Eriksen and D. Van Engen, *Organometallics* 1985, **4**, 830.
6. H.-K. Shin, K. M. Chi, M. J. Hampden-Smith, T. T. Kodas, M. Paffett and J. D. Farr, *Angew. Chem. Adv. Mater.* 1991, **3**, 246.
7. H.-K. Shin, K. M. Chi, M. J. Hampden-Smith, T. T. Kodas, M. Paffett and J. D. Farr, in *Chemical Perspectives of Microelectronic Materials II, Mat. Res. Soc., Symp. Proc.*, Vol. 204, p. 421. Materials Research Society, Pittsburgh, U.S.A. (1991).
8. M. J. Hampden-Smith, D. S. Williams and A. L. Rheingold, *Inorg. Chem.* 1990, **29**, 4076.
9. H.-K. Shin, K. M. Chi, J. Farkas, M. J. Hampden-

* Copper metal was characterized by Auger electron spectroscopy. No inpurities were found within the detection limits (~1%).

Smith, T. T. Kodas and E. N. Duesler, *Inorg. Chem.*, in press, 1991.
10. J. H. van de Hende and W. C. Baird Jr, *J. Am. Chem. Soc.* 1963, **85**, 1009.
11. H.-K. Shin, M. J. Hampden-Smith, T. T. Kodas, M. Paffett and J. D. Farr, Mat. Res. Soc., Spring Meeting, Symposium J (1990).
12. K. M. Chi, H.-K. Shin, J. W. Garvey, M. J. Hampden-Smith, T. T. Kodas, J. D. Farr and M. F. Paffett, *J. Mater. Res.*, submitted.
13. (cyclooctene)$_3$(CuCl)$_2$; P. Ganis, U. Lepore and E. Martuscelli, *J. Phys. Chem.* 1970, **74**, 2439.
14. [(norbornadiene)CuCl]$_4$; N. C. Baenziger, H. L. Haight and J. R. Doyle, *Inorg. Chem.* 1964, **3**, 1535.
15. (COT)(CuCl)$_2$; N. C. Baenziger, G. F. Richards and J. R. Doyle, *Inorg. Chem.* 1964, **11**, 1529.
16. [Cu(OOCCF$_3$)]$_4$(C$_6$H$_6$)$_2$; P. F. Rodesiler and E. L. Amma, *J. Chem. Soc., Chem. Commun.* 1974, 599.
17. Cu(HBpz$_3$)(cyclohexene)CuCl; J. S. Thompson and J. F. Whitney, *Acta Cryst.* 1984, **C40**, 756.
18. T. A. Wark, E. A. Gulliver, M. J. Hampden-Smith and A. L. Rheingold, *Inorg. Chem.* 1990, **29**, 4360.
19. T. A. Wark and M. J. Hampden-Smith, manuscript in preparation.
20. P. Fiaschi, C. Floriani, M. Pasquali, A. Chiesi-villa and C. Guastini, *Inorg. Chem.* 1986, **25**, 462.
21. K. G. Caulton, G. Davies and E. M. Holt, *Polyhedron* 1990, **9**, 2319.

Polyhedron Vol. 10, No. 19, pp. 2301–2308, 1991
Printed in Great Britain

0277–5387/91 $3.00+.00
© 1991 Pergamon Press plc

PREPARATION AND CHARACTERIZATION OF TRIPLY-BRIDGED DINUCLEAR COPPER(II) COMPLEXES CONTAINING THE $[Cu_2(\mu\text{-OH})(\mu\text{-X})(\mu\text{-OAc})]^+$ CORE (X = Cl, Br), AND THE CRYSTAL STRUCTURE OF $[Cu_2(OH)Cl(OAc)(bpy)_2](ClO_4)\cdot H_2O$

SPIROS P. PERLEPES,* JOHN C. HUFFMAN, and GEORGE CHRISTOU†

Department of Chemistry and Molecular Structure Center, Indiana University, Bloomington, IN 47405, U.S.A.

(*Received* 12 *March* 1991; *accepted* 18 *June* 1991)

Abstract—Synthetic procedures are described that allow access to complexes containing the cation $[Cu_2(\mu\text{-OH})(\mu\text{-X})(\mu\text{-O}_2\text{CMe})(bpy)_2]^+$ (X = Cl, Br). Reaction mixtures consisting of CuX_2, bpy, OH^-, $MeCO_2^-$ and ClO_4^- ($X = Cl^-$) in $MeOH/H_2O$ give blue solutions from which the products $[Cu_2(OH)Cl(O_2CMe)(bpy)_2](ClO_4)\cdot H_2O$ (**1**) and $[Cu_2(OH)Br(O_2CMe)(bpy)_2]Br\cdot H_2O$ (**4**) can be obtained in good yield. Complex **1** may also be prepared from the known complexes $[Cu_2(OH)(H_2O)(O_2CMe)(bpy)_2](ClO_4)_2$ (**2**) and $Cu_2(OH)_2(bpy)_2(ClO_4)_2$ (**3**). Complex **1** crystallizes in monoclinic space group $P2_1/n$ with (at −175°C) $a = 8.434(1)$, $b = 16.074(2)$, $c = 9.430(1)$ Å, $\beta = 98.09(1)°$, $Z = 2$ and $V = 1265.83$ Å^3. The structure was solved by direct methods (MULTAN) and refined to values of conventional indices $R(R_w)$ of 3.38 (3.54)% using 1499 unique reflections with $F > 2.33\sigma(F)$. The structure of the cation consists of a triply-bridged pair of five-coordinate copper(II) atoms. One of the bridging ligands is a *syn,syn* $\eta^1:\eta^1:\mu_2$ acetate group, the others being the Cl^- and OH^- ions; a terminal bpy molecule completes five-coordination at each metal. The Cu···Cu separation is 2.957(1) Å. The metal coordination geometry is best described as distorted square-pyramidal with the Cl^- ligand occupying the apical site for each metal. The oxygen atom of the water molecule is hydrogen-bonded to the OH^- hydrogen. Recrystallization of **1** from warm water yields **3** in 20% yield; addition of $NaClO_4$ to the solution increases the yield to 40%. Complex **1** in warm water containing one equiv. of $NaClO_4$ and one equiv. of NaOH also gives **3** (yield 73%). The thermal decomposition, room temperature μ_{eff} values, and electronic and IR spectra of **1** and **4** are discussed in terms of the nature of bonding and structure of **1**.

The bridged dinuclear structure $M_2(O_2CR)_4L_2$, first documented in 1953 for copper(II) acetate monohydrate,[1] is ubiquitous in modern coordination chemistry. It is found not only for carboxylates of many transition elements,[2] but also for dimers containing a wide variety of other triatomic bridging ligands.[3] This structural type is associated with a spectrum of metal–metal interactions[4] ranging from no interactions, weak spin-pairing in the copper(II) carboxylates, various orders of metal–metal bonding, to the "super-short" metal–metal bonds. The axial groups are normally monodentate ligands but they may represent inter-dimer association into a polymeric structure[5] or may be absent.[6]

Only a few attempts have been made to incorporate chelating ligands (mainly tridentate), instead of monodentate ones into the $Cu_2(O_2CMe)_4$ structural unit.[7–14] In all cases, dimeric[7–11,13] or polymeric[12,14] complexes with a smaller number of acetate ligands and interesting structural and magnetic characteristics have been obtained. A matter of interest is how much versatility there is in the type of bridging found in copper(II) acetate and whether other small bridging ligands can be incorporated together with acetate bridges in the same complex.

In recent years, we have been investigating the

* On sabbatical leave from the University of Ioannina, Ioannina, Greece.

† Author to whom correspondence should be addressed.

reactions between 3*d* metal carboxylates and N,N- and O,N-bidentate ligands. Most of our efforts have been concentrated in manganese[15] and iron,[16] but we recently extended our efforts to copper and have found that the reactions of $Cu_2(O_2CMe)_4(H_2O)_2$ with chelating 2,2′-bipyridine (bpy) lead to a wide variety of products[17] with bridging units not previously observed in Cu_2^{4+} chemistry. In extending the above work, attempts have been made to prepare a trinuclear complex with the $[Cu_3(\mu_3\text{-}OR)(\mu\text{-}O_2CR')_3]^{2+}$ core, as this structural unit has not yet been identified in copper(II) chemistry.[18] Initial attempts have instead led to interesting dinuclear complexes containing three bridging ligands; the properties of these species are described in this report.

EXPERIMENTAL

Starting materials

All manipulations were performed under aerobic conditions using materials as received; water was distilled in-house. The complex $[Cu_2(OH)(H_2O)(O_2CMe)(bpy)_2](ClO_4)_2$ (**2**) was available from previous work.[17] $Cu_2(OH)_2(bpy)_2(ClO_4)_2$ was prepared as described.[19a] *Caution*: Perchlorate salts are potentially explosive. Although no detonation tendencies have been observed in our work, caution is advised and handling of only small quantities is recommended.

Compound preparation

(1) *Preparation of* $[Cu_2(OH)Cl(O_2CMe)(bpy)_2](ClO_4)\cdot H_2O$ (**1**). *Method A*. To a stirred pale green solution of $CuCl_2$ (0.67 g, 5.0 mmol) in MeOH (25 cm^3) was added bpy (0.78 g, 5.0 mmol) in small portions to give a green precipitate of the known compound $CuCl_2(bpy)$.[19b] This was collected by filtration and dissolved in H_2O (70 cm^3). The resulting blue solution was stirred while an aqueous solution (10 cm^3) containing NaOH (0.07 g, 1.7 mmol), NaO_2CMe (0.41 g, 5.0 mmol) and $NaClO_4$ (0.41 g, 3.3 mmol) was added. The solution soon began to deposit violet–blue microcrystals. The flask was stored at ambient temperature overnight, and the precipitate was collected by filtration, washed with H_2O and Et_2O and dried *in vacuo*; yield, 0.82 g (49% based on available copper). Found: C, 39.4; H, 3.2; N, 8.1; Cl, 10.5. Calc. for $C_{22}H_{22}N_4O_8Cl_2Cu_2$: C, 39.5; H, 3.3; N, 8.4; Cl, 10.6%. IR spectrum (Nujol mull, cm^{-1}): 3450mb, 3365mb, 1601s, 1576m, 1551sb, 1445sh, 1319m, 1312m, 1252m, 1171m, 1157m, 1082vsb, 1055m, 1019m, 978w, 932w, 918w, 897w, 810w, 768vs, 731s, 663m, 650sh, 623s, 545w, 488m, 459m, 417m. Magnetic moment per copper(II) (Faraday method): 2.03 μ_B at 26°C. Solid-state (diffuse reflectance) electronic spectrum: λ_{max}, nm; 340sh, 370, 670, 710sh. Electronic spectrum in MeCN: λ_{max}, nm (ε_M/Cu_2, L mol^{-1} cm^{-1}); 685 (165). Using 0.67 g (5.0 mmol) of $CuCl_2$, 0.78 g (5.0 mmol) of bpy, 0.10 g (2.5 mmol) of NaOH, 0.21 g (2.5 mmol) of NaO_2CMe and 0.31 g (2.5 mmol) of $NaClO_4$, the above synthetic procedure again yielded complex **1**; yield, 1.05 g (63%).

Method B. A slurry of $[Cu_2(OH)(H_2O)(O_2CMe)(bpy)_2](ClO_4)_2$[17] (**2**) (0.25 g, 0.34 mmol) in H_2O (10 cm^3) was treated with solid NaCl (0.04 g, 0.68 mmol). No noticeable colour change occurred. The reaction mixture was stirred for 1 h at 50°C. After cooling to room temperature, the blue solid was collected by filtration, washed with H_2O and Et_2O, and dried *in vacuo*; yield, 0.16 g (70%). The product had IR and electronic spectra identical with those detailed under method A.

Method C. To a slurry of $Cu_2(OH)_2(bpy)_2(ClO_4)_2$[19a] (**3**) (0.67 g, 1.0 mmol) in H_2O (10 cm^3) was added glacial MeCOOH (0.06 cm^3, 1.0 mmol). A noticeable colour change from lavender to blue occurred. To this were added solid NaCl (0.08 g, 1.4 mmol) and MeOH (3 cm^3). The reaction mixture was stirred for 1 h at 40°C. The resulting blue solid was collected by filration, washed with H_2O and Et_2O, and dried *in vacuo*; yield, 0.56 g (84%). The product was identical on spectroscopic examination with **1** prepared by method A.

(2) *Preparation of* $[Cu_2(OH)Br(O_2CMe)(bpy)_2]Br\cdot H_2O$ (**4**). To a stirred dark brown solution of $CuBr_2$ (1.12 g, 5.0 mmol) in MeOH (25 cm^3) was slowly added solid bpy (0.78 g, 5.0 mmol) in small portions to give a pale brown precipitate of $CuBr_2(bpy)$. This was collected by filtration and dissolved in H_2O (105 cm^3). The resulting blue solution was stirred while an aqueous solution (10 cm^3) containing NaOH (0.10 g, 2.5 mmol) and $NaO_2CMe\cdot 3H_2O$ (0.34 g, 2.5 mmol) was added. The dark blue solution was left at ambient temperature. The pale blue, microcrystalline powder that formed was collected by filtration, washed with H_2O and Et_2O (not added to the filtrate) and dried *in vacuo* over silica gel; yield, 0.65 g (38%). Overnight storage of the filtrate at 4°C yielded a second crop of microcrystals of **4**, which were isolated as above; overall yield *ca* 60%. Found: Cu, 18.6; Br, 23.3; H_2O, 2.5. Calc. for $C_{22}H_{22}N_4O_4Br_2Cu_2$: Cu, 18.3; Br, 23.0; H_2O, 2.6%. IR spectrum (KBr pellet, cm^{-1}): 3440mb, 2265sb, 1607m, 1597vs, 1558m, 1487m, 1467m, 1438s, 1430sh, 1319m, 1312m, 1250m, 1169m, 1153m, 1098m, 1069w, 1057w,

1041w, 1022s, 1010s, 942w, 907sh, 890m, 802w, 764vs, 728s, 652w, 575mb, 484mb, 460m, 413m. Magnetic moment per copper(II) (Faraday method): 2.16 μ_B at 23°C. Solid-state (diffuse reflectance) electronic spectrum: λ_{max}, nm: 342, 375, 665, 705sh. Attempts to isolate the ClO_4^- or PF_6^- salt of $[Cu_2(OH)Br(O_2CMe)(bpy)_2]^+$ led to mixtures of $[Cu_2(OH)Br(O_2CMe)(bpy)_2]Br \cdot H_2O$ and $[Cu_2(OH)Br(O_2CMe)(bpy)_2]Y \cdot H_2O$ ($Y = ClO_4$ or PF_6), as deduced from analytical data and IR spectroscopy.

(3) *Conversion of complex* **1** *to complex* **3**

(i) A slurry of complex **1** (0.30 g, 0.45 mmol) in H_2O (20 cm^3) was stirred at 50°C for 45 min. A colour change from blue to lavender occurred. After cooling the mixture to room temperature, the solid was collected by filtration, washed with H_2O and Et_2O, and dried *in vacuo*; yield, 0.06 g (20% based on copper). The identity of the product was deduced by IR spectral comparison with authentic material. An identical procedure but with added $NaClO_4$ (0.06 g, 0.50 mmol) leads to an increased yield of **3**, 0.12 g (40%).

(ii) To a slurry of complex **1** (0.30 g, 0.45 mmol) in H_2O (20 cm^3) was added solid $NaClO_4$ (0.06 g, 0.50 mmol), followed by addition of a solution of NaOH (0.18 g, 0.45 mmol) in H_2O (10 cm^3). An immediate colour change from blue to lavender occurred. The reaction mixture was stirred for 15 min at 50–60°C and the resulting solid was collected by filtration, washed with H_2O and Et_2O, and dried *in vacuo*; yield, 0.22 g (73%). The product had an IR spectrum identical with that of compound **3**.

X-ray crystallographic studies

Crystals suitable for crystallography were grown by careful layering of a green solution of **1** (0.2 g) in DMF (15 cm^3) with Et_2O (25 cm^3) at room temperature. Data were collected on a Picker four-circle diffractometer at −175°C; details of the diffractometry, low-temperature facilities and computational procedures employed by the Molecular Structure Centre are available elsewhere.[20] Data collection parameters are summarized in Table 1.

The structure was solved by a combination of direct methods (MULTAN) and Fourier techniques and refined by full-matrix least-squares. A systematic search of a limited hemisphere of reciprocal space located a set of diffraction maxima with symmetry and systematic absences corresponding to a

Table 1. Crystallographic data collection and refinement parameters for $[Cu_2(OH)Cl(O_2CMe)(bpy)_2]ClO_4 \cdot H_2O$ (**1**)

Formula	$C_{22}H_{22}N_4O_8Cl_2Cu_2$
Formula weight	668.46
Space group	$P2_1/n$
Temperature (°C)	−175
a (Å)	8.434(1)
b (Å)	16.074(2)
c (Å)	9.430(1)
β (°)	98.09(1)
V (Å^3)	1265.83
Z	2
ρ_{calc} (g cm^{-3})	1.754
Crystal dimensions (mm)	0.25 × 0.25 × 0.25
Radiation (λ, Å)	Mo-K_α (0.71069)
Absorption coefficient (cm^{-1})	19.512
2θ range (°)	6.00–45.00
Scan speed (deg min^{-1})	4.0
Scan width (°)	2.0 + dispersion
Take-off angle (°)	2.0
Data collected	3354
Unique data	1710
Data with $F > 2.33\sigma(F)$	1499
Averaging R	0.025
R	0.0338
R_w	0.0354
Goodness of fit for last cycle	1.063

monoclinic space group, $P2_1$ or $P2_1/m$. Subsequent solution and refinement of the structure confirmed the centrosymmetric choice, $P2_1/m$. All non-hydrogen atoms were readily located and refined with anisotropic thermal parameters. All hydrogen atoms were clearly visible in a subsequent difference Fourier map; these atoms were included in the final cycles and refined isotropically. The final difference Fourier map was essentially featureless, the largest peak being 0.45 e $Å^{-3}$. The two largest peaks were located in the vicinity of the perchlorate ion. No absorption correction was deemed necessary. Final discrepancy indices R and R_w are included in Table 1.

Physical measurements

IR spectra were recorded as Nujol mulls between CsI plates or KBr discs using a Nicolet 510P Fourier transform spectrometer or a Perkin–Elmer Model 283 spectrophotometer. Solid-state (diffuse reflectance, 890–330 nm) and solution (800–350 nm) electronic spectra were recorded on Varian 634 and Hewlett–Packard 4450A instruments, respectively. Magnetic susceptibilities were measured at room temperature by the Faraday method with a Cahn–Ventron RM-2 balance standardized with HgCo$(SCN)_4$. The molar susceptibilities were corrected for the diamagnetism of the constituent atoms using Pascal's constants. TG/DTG data were obtained with a DuPont R90 instrument equipped with a 951 thermogravimetric analyser in a nitrogen gas flow (50 $cm^3\ min^{-1}$); sample weights of 5–10 mg and heating rates of 1 and 5°C min^{-1} were used.

Analytical procedures

Elemental analyses for **1** were performed at the Microanalytical Laboratory, Department of Chemistry, Manchester University, England. For the bromide determination, samples of **4** were decomposed in 2 M HNO_3; the total bromides were determined potentiometrically with a standard 0.1 M $AgNO_3$ solution, using a Corning–Eel Model 12 potentiometer with calomel and sulphide-selective electrodes.[21] Copper(II) was estimated gravimetrically as copper(II) quinaldate.[22] The amount of water in **4** was determined from the TG pattern.

RESULTS AND DISCUSSION

Syntheses

In our development of Cu^{II}/RCO_2^-/bpy chemistry,[17] we had employed $Cu_2(O_2CMe)_4(H_2O)_2$ and Cu:bpy ratios of 1:1 (a 1:2 ratio is known to produce mononuclear $[Cu(O_2CMe)(bpy)_2]^+$ complexes);[23] all the synthetic methods used led to dinuclear complexes.[17] In extending this chemistry, we considered it of interest to try to prepare trinuclear complexes. These are far less common than are dinuclear copper(II) systems and limited to two structural types,[24] i.e. linear and triangular; they also present interesting structural and magnetic features.[24–30] Recently, we tried to prepare a linear trimer of the formula $Cu_3(O_2CMe)_6(bpy)_2$, like the Mn^{II} analogue,[28] employing a Cu^{II}:bpy ratio of 1.5:1; however, the reaction instead led to $[Cu_2(O_2CMe)_4(bpy)_2]\cdot 2H_2O$ and $[Cu_4(O_2CMe)_4(bpy)_2]_n$.[17] In this work, the influence of added OH^- ($Cu:OH^- = 3:1$) was investigated, wondering whether a product with a $[Cu_3(\mu_3\text{-}OH)(\mu\text{-}O_2CMe)_3]^{2+}$ core might be attainable. An MeOH/H_2O (*ca* 1:3) reaction mixture containing $CuCl_2$. bpy, NaOH, NaO_2CMe and $NaClO_4$ in a 3:3:1:3:2 molar ratio gave a blue solution from which the dinuclear complex **1** was isolated in good yield. The crystal structure of **1** identified the complex to be triply-bridged $[Cu_2(OH)Cl(O_2CMe)(bpy)_2](ClO_4)\cdot H_2O$. Whether Cu_3 species are present in the reaction solution is unclear and difficult to ascertain given the presence of paramagnetism. Nevertheless, as **1** is the first triply-bridged dinuclear copper(II) complex containing three *different* anionic bridging ligands, we decided to pursue the study of this new family of complexes further and a higher yield of **1** was subsequently obtained by changing the $Cu:OH^-$ ratio from 3:1 to 2:1 [eq. (1)].

$$2CuCl_2 + 2bpy + OH^- + MeCO_2^- + ClO_4^- \xrightarrow{MeOH/H_2O} \underset{\mathbf{1}}{[Cu_2(OH)Cl(O_2CMe)(bpy)_2](ClO_4)\cdot H_2O} + 3Cl^- \quad (1)$$

Complex **1** may also be prepared from the complexes $[Cu_2(OH)(H_2O)(O_2CMe)(bpy)_2](ClO_4)_2$ (**2**) and $Cu_2(OH)_2(bpy)_2(ClO_4)_2$ (**3**). Reaction of **2** with an excess of NaCl in H_2O at 50°C gave a clean and high-yield conversion to **1**, emphasizing the lability to substitution of the weakly-bound, bridging aqua group.[17] This reaction is summarized in eq. (2).

$$\underset{\mathbf{2}}{[Cu_2(OH)(H_2O)(O_2CMe)(bpy)_2](ClO_4)_2} + Cl^- \xrightarrow{H_2O} \underset{\mathbf{1}}{[Cu_2(OH)Cl(O_2CMe)(bpy)_2](ClO_4)\cdot H_2O} + ClO_4^- \quad (2)$$

In addition, treatment of **3** with one equiv. of acetic acid in H_2O at 40°C, followed by addition of a slight excess of NaCl led to clean, high-yield

isolation of **1** [eq. (3)], presumably by protonation

$$\underset{\mathbf{3}}{Cu_2(OH)_2(bpy)_2(ClO_4)_2} + MeCO_2H + Cl^- \xrightarrow{H_2O/MeOH} \underset{\mathbf{1}}{[Cu_2(OH)Cl(O_2CMe)(bpy)_2](ClO_4)\cdot H_2O} + ClO_4^- \quad (3)$$

of an OH^- bridge followed by binding of the generated $MeCO_2^-$ and substitution of the bridging aqua ligand by the chloro group. This transformation of **3** to **1** is reversible. Recrystallization of **1** from warm water (~50°C) yielded **3** in 20% yield based on copper; the yield is ClO_4^- limited, however, and addition of $NaClO_4$ to the mixture [eq. (4)] increases the yield of isolated **3**

$$2\underset{\mathbf{1}}{[Cu_2(OH)Cl(O_2CMe)(bpy)_2](ClO_4)\cdot H_2O} + 2NaClO_4 \xrightarrow{H_2O} \underset{\mathbf{3}}{2Cu_2(OH)_2(bpy)_2(ClO_4)_2} + 2MeCO_2H + 2NaCl \quad (4)$$

to 40%. Complex **1** in H_2O containing $NaClO_4$ (one equiv.) and NaOH (one equiv.) also gives **3** (73% isolated yield) at 50–60°C.

The access to $[Cu_2(\mu\text{-}OH)(\mu\text{-}Cl)(\mu\text{-}O_2CMe)]^+$ species from $CuCl_2$ suggested that the reaction system might be capable of extension to other CuX_2 salts (X = halide). The above procedure but with $CuBr_2$ was found to successfully yield the $[Cu_2(\mu\text{-}OH)(\mu\text{-}Br)(\mu\text{-}O_2CMe)]^+$ species in good overall yield [eq. (5)].

$$2CuBr_2 + 2bpy + OH^- + MeCO_2^- \xrightarrow{MeOH/H_2O} \underset{\mathbf{4}}{[Cu_2(OH)Br(O_2CMe)(bpy)_2]Br\cdot H_2O} + 2Br^- \quad (5)$$

Efforts to isolate the ClO_4^- or PF_6^- salt of $[Cu_2(OH)Br(O_2CMe)(bpy)_2]^+$ led to mixtures of **4** and $[Cu_2(OH)Br(O_2CMe)(bpy)_2]Y\cdot H_2O$ ($Y = ClO_4$ or PF_6), due to the low solubility of the bromide salt.

Description of structure

An ORTEP projection of the cation of complex **1** is given in Fig. 1. An ORTEP plot of the inner coordination sphere about the Cu_2 core for the same complex is depicted in Fig. 2. The important structural parameters are listed in Table 2.

The structure of **1** consists of a dinuclear triply-bridged cation lying on a crystallographic mirror plane, a molecule of water of crystallization and a well-separated perchlorate anion; the latter will not be further discussed. The cations are well separated

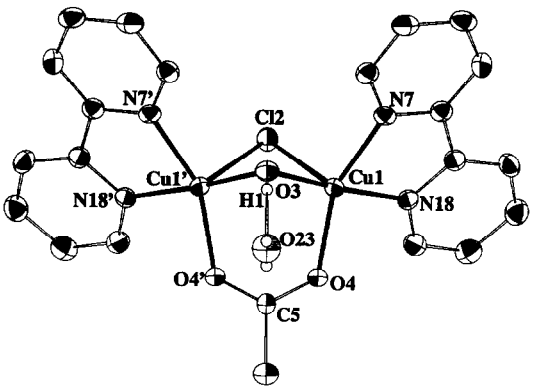

Fig. 1. ORTEP representation of the cation of complex **1** at the 50% probability level. Bipyridine carbon atoms are labelled consecutively from N7. The unlabelled acetate carbon atom is C6. OH^- and H_2O hydrogen atoms are included as spheres of arbitrary size.

from each other. The acetate group is in the familiar bidentate *syn,syn* $\eta^1:\eta^1:\mu_2$-bridging mode; a terminal bpy molecule completes five-coordination at each metal atom. The Cu···Cu separation in **1** is noticeably shorter than in dinuclear triply-bridged copper(II) complexes containing three or two acetato bridges (2.96 vs 3.15–3.40 Å), presumably due to the greater number of mono-atomic bridges.

The metal coordination geometry may be described as distorted square-pyramidal with the chloro ligand occupying the apical position at each metal; this is particularly emphasized by Fig. 2. Analysis of the shape-determining angles using the approach of Addison *et al.*[31] yields a value for trigonality index, τ, of 0.40 for the copper ($\tau = 0$ and 1.09 for square-pyramidal and trigonal bipyramidal geometry, respectively). Thus, the geometry about Cu(1) and Cu(1′) is significantly distorted,

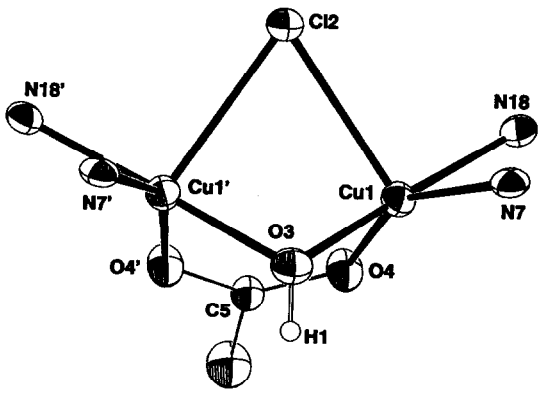

Fig. 2. ORTEP representation of the inner coordination sphere of the Cu_2 core for complex **1**.

Table 2. Selected bond distances (Å) and angles (deg) for complex **1**

		Distances	
Cu(1)···Cu(2)	2.957(1)	Cu(1)—O(3)	1.920(3)
Cu(1)—Cl(2)	2.557(1)	Cu(1)—O(4)	1.971(3)
Cu(1)—N(7)	2.012(3)	O(3)—H(1)	0.81(7)
Cu(1)—N(18)	1.998(4)	O(23)···H(1)	2.02(7)
		Angles	
Cu(1)—Cl(2)—Cu(1′)	70.6(1)	N(18)—Cu(1)—O(4)	89.7(1)
Cu(1)—O(3)—Cu(1′)	100.7(2)	N(18)—Cu(1)—O(3)	175.4(2)
Cl(2)—Cu(1)—N(7)	102.8(1)	O(4)—Cu(1)—O(3)	94.2(2)
Cl(2)—Cu(1)—N(18)	96.4(1)	Cu(1)—O(4)—C(5)	127.1(3)
Cl(2)—Cu(1)—O(4)	105.0(1)	Cu(1′)—Cu(1)—Cl(2)	54.7(1)
Cl(2)—Cu(1)—O(3)	85.0(1)	Cu(1′)—Cu(1)—N(18)	144.0(1)
N(7)—Cu(1)—N(18)	80.6(2)	Cu(1′)—Cu(1)—N(7)	123.0(1)
N(7)—Cu(1)—O(4)	151.4(1)	Cu(1)—Cu(1)—O(4)	79.7(1)
N(7)—Cu(1)—O(3)	94.9(2)	O(23)···H(1)—O(3)	171.0(6)

and the four atoms N(7), N(18), O(4) and O(3) defining the basal plane deviate from that plane by an average of 0.22 Å [maximum deviation by N(18), 0.233 Å]; Cu(1) lies 0.245 Å out of the least-squares basal plane towards Cl(2). The dihedral angle between the two CuN_2O_2 planes is 60.6°.

The bond lengths to the bridging hydroxo and acetate oxygens and to the two bpy nitrogen atoms are typical.[17,32] The distance Cu(1)—Cl(2) [2.557(1) Å] and the acute angle Cu(1)—Cl(2)—Cu(1′) [70.6(1)°] are both very similar to those observed in other dinuclear, square-pyramidal copper(II) complexes sharing a common μ_2-Cl^- apex;[33] the bond from the copper to the bridging apical chloro ligand is longer than that to bridging basal chloro ligands (~2.3 Å).[34]

The oxygen atom O(23) of the water molecule hydrogen-bonds to the OH^- hydrogen H(1) [O(3)—H(1), 0.81(7) Å; H(1)···O(23), 2.02(7) Å; O(23)···H(1)—O(3), 171(6)°]. No evidence of inter-cation hydrogen bonds was found.

Complex **1** represents the first structurally characterized example of a triply-bridged, dinuclear copper(II) complex containing three different anionic bridging ligands. Another triply-bridged Cu_2 complex is somewhat structurally related to compound **1** in that it has three different anionic bridging ligands: $[Cu_2(OH)(ClO_4)L]^+$ [35] [L = the monoanion of 2,6-bis(N-(2-pyridylmethyl) formidoyl)-4-methylphenol]; in this complex, however, the third bridging ligand is provided by the aryloxide oxygen of the pentadentate binucleating L.

Some other triply-bridged Cu_2 complexes with three different bridging ligands (two anionic, one neutral) should be mentioned at this point: (i) $[Cu_2(\mu\text{-OH})(\mu\text{-X})LX_2]$ [X = Cl, Br; L = binucleating phthalazine or pyridazine ligands[36] and 2,7-bis(2-pyridyl)-1,8-naphthyridine][33] are also the only other examples of dinuclear copper(II) complexes bridged by both equatorial OH^- and apical X^-. (ii) The MeOH inclusion compound $[Cu_2(\mu\text{-OH})(\mu\text{-}O_2CMe)(L—L)](ClO_4)_2 \cdot MeOH$[37] (L—L = a binucleating tetradentate hexaimidazole ligand) and complex **2**[17] are also the only other examples of Cu_2 complexes bridged by *one* OH^- and *one* $MeCO_2^-$.

The structure of the cation of **1** shows some similarity to that of $[Cu_2(OH)(H_2O)(O_2CMe)(bpy)_2]^{2+}$ [17] (**2**); obviously, the replacement of μ_2-H_2O by μ_2-Cl^- at the common apical position has little structural effect. However, the cations of **2** form infinite chains as a result of hydrogen-bonding interactions with the ClO_4^- counter-ions,[17] while **1** is an isolated dinuclear species with only an intramolecular hydrogen bond.

Thermal decomposition of **1** *and* **4**, *IR and electronic spectroscopy*

The thermal decomposition of **1** and **4** was studied using TG/DTG techniques. We first comment on the dehydration process. The TG curve of **1** shows a one-step, first mass loss between 75 and 100°C, which corresponds exactly to the release of the water content (Found: 2.7. Calc.: 2.7%). The low temperature of H_2O loss shows that this is not coordinated. A TG plateau is present from 105 to 202°C. The anhydrous complex decomposes in four steps, as revealed by the appearance of four DTG maxima, between 205 and 280°C and in a slower process between 280 and 670°C. The absence of TG plateaux during decomposition indicates that stable intermediates are not formed. The final, thermally-

stable residue is CuO (Found 23.4. Calc. 23.8%). The thermal decomposition of **4** is completely analogous.

The room temperature μ_{eff} values of **1** and **4** would appear to exclude strong antiferromagnetic coupling, but it is difficult to rule out weak antiferromagnetic interactions. In fact, both complexes are likely either weakly antiferromagnetically- or ferromagnetically-coupled, due to the "non-complementarity"[38,39] of $MeCO_2^-$ and OH^- orbitals with $d_{x^2-y^2}$ magnetic orbitals. It is interesting to note that all Cu_2^{II} systems bridged by one $R'CO_2^-$ and one RO^- (R = H, alkyl) are known to be weakly antiferromagnetic or ferromagnetic.[17,37-39]

Complexes **1** and **4** possess very similar solid-state electronic spectra, supporting similar structures for their cations. Both exhibit two LMCT transitions[40] in the 375–340 nm range and *d–d* transitions at lower energies. The *d–d* frequencies are fairly typical of distorted square-pyramidal structures.[34,40] The *d–d* spectrum of **1** in dry MeCN is different from the solid-state spectrum, indicating structural changes upon dissolution and/or cation–solvent interactions.

In the IR spectra, complexes **1** and **4** exhibit bands at ~3450 and 3365 cm^{-1}, assigned to $\nu(OH^-)$ and $\nu(H_2O)$, respectively;[41] their broadness and low frequency are both indicative of hydrogen bonding. The $\nu_{as}(COO)$ and $\nu_s(COO)$ bands of **1** and **4** are at 1558–1551 and 1445–1438 cm^{-1}, respectively; the difference Δ [$\Delta = \nu_{as}(COO) - \nu_s(COO)$; 106 cm^{-1} for **1**, 120 cm^{-1} for **2**] is less than that for NaO_2CMe (164 cm^{-1}), as expected for the bidentate bridging mode of carboxylate ligation.[42]

Acknowledgements—Support from the National Science Foundation (CHE 8808019) is gratefully acknowledged. We thank Eduardo Libby for technical assistance and Sheyi Wang for help with figure preparation.

REFERENCES

1. J. N. van Nieker and F. R. L. Schoening, *Acta Cryst.* 1953, **6**, 227.
2. For a tabulation, see: Y. B. Koh and G. C. Christoph, *Inorg. Chem.* 1979, **18**, 1122.
3. F. A. Cotton and R. A. Walton, *Multiple Bonds Between Metal Atoms*. Wiley and Sons, New York (1982).
4. L. C. Porter, M. H. Dickman and R. J. Doedens, *Inorg. Chem.* 1983, **22**, 1962 and refs therein.
5. J. S. Valentine, A. J. Silverstein and Z. G. Soos, *J. Am. Chem. Soc.* 1974, **96**, 97.
6. M. Kato and Y. Muto, *Coord. Chem. Rev.* 1988, **92**, 45.
7. A. M. Greenaway, C. J. O'Connor, J. W. Overman and E. Sinn, *Inorg. Chem.* 1981, **20**, 1508.
8. J.-P. Costes, F. Dahan and J.-P. Laurent, *Inorg. Chem.* 1985, **24**, 1018.
9. S. J. Brown, X. Tao, D. W. Stephan and P. K. Mascharak, *Inorg. Chem.* 1986, **25**, 3377.
10. N. A. Bailey, D. E. Fenton, J. R. Tate and P. M. Thomas, *J. Chem. Soc., Dalton Trans.* 1985, 1471.
11. R. Hämäläinen, M. Ahlgrén and U. Turpeinen, *Acta. Cryst. Sect. B* 1982, **B38**, 1577.
12. B. Chiari, J. H. Helms, O. Piovesana, T. Tarantelli and P. F. Zanazzi, *Inorg. Chem.* 1986, **25**, 870.
13. B. Chiari, J. H. Helms, O. Piovesana, T. Tarantelli and P. F. Zanazzi, *Inorg. Chem.* 1986, **25**, 2408.
14. B. Chiari, O. Piovesana, T. Tarantelli and P. F. Zanazzi, *Inorg. Chem.* 1988, **27**, 3246.
15. (a) G. Christou, *Acc. Chem. Res.* 1989, **22**, 328 and refs therein; (b) E. Libby, K. Folting, J. C. Huffman and G. Christou, *J. Am. Chem. Soc.* 1990, **112**, 5354.
16. (a) J. B. Vincent, J. C. Huffman, G. Christou, Q. Li, M. A. Nanny, D. N. Hendrickson, R. H. Fong and R. H. Fish, *J. Am. Chem. Soc.* 1988, **110**, 6898; (b) J. K. McKusker, J. B. Vincent, E. A. Schmitt, M. L. Mino, K. Shin, D. K. Coggin, P. M. Hagen, J. C. Huffman, G. Christou and D. N. Hendrickson, *J. Am. Chem. Soc.* 1991, **113**, 3012.
17. (a) G. Christou, S. P. Perlepes, E. Libby, K. Folting, J. C. Huffman, R. J. Webb and D. N. Hendrickson, *Inorg. Chem.* 1990, **29**, 3657; (b) S. P. Perlepes, E. Libby, J. C. Huffman and G. Christou, submitted for publication.
18. (a) M. Angaroni, G. A. Ardizzoia, T. Beringhelli, G. La Monica, D. Gatteschi, N. Masciocchi and M. Moret, *J. Chem. Soc., Dalton Trans.* 1990, 3305; (b) F. B. Hulsberger, R. W. M. ten Hoedt, G. C. Verschoor, J. Reedijk and A. L. Spek, *J. Chem. Soc., Dalton Trans.* 1983, 539.
19. (a) W. R. McWhinnie, *J. Chem. Soc.* 1964, 2959; (b) K. Hyde, *J. Inorg. Nucl. Chem.* 1969, **31**, 934.
20. M. H. Chisholm, K. Folting, J. C. Huffman and C. C. Kirkpatrick, *Inorg. Chem.* 1984, **23**, 1021.
21. W. E. Bazzelle, *Anal. Chim. Acta* 1971, **54**, 29.
22. A. I. Vogel, *A Text-Book of Quantitative Inorganic Analysis*, 3rd edn, pp. 497–499. Longman, London (1969).
23. B. J. Hathaway, N. Ray, D. Kennedy, N. O'Brien and B. Murphy, *Acta Cryst.* 1980, **B36**, 1371.
24. B. J. Hathaway, *Comprehensive Coordination Chemistry* (Edited by G. Wilkinson, R. D. Gillard and J. A. McCleverty), Ch. 53, pp. 635–636. Pergamon Press, Oxford (1987).
25. K. Smolander and K. Leisto, *Inorg. Chim. Acta* 1990, **169**, 151.
26. H. Okawa, M. Koikawa, S. Kida, D. Luneau and H. Oshio, *J. Chem. Soc., Dalton Trans.* 1990, 469 and refs therein.
27. H. Muhonen and W. E. Hatfield, *Acta Chem. Scand.* 1986, **A40**, 41.
28. A. Schake, J. C. Huffman and G. Christou, unpublished results.
29. C. Benelli, A. Caneschi, D. Gatteschi, O. Guillou and L. Pardi, *Inorg. Chem.* 1990, **29**, 1750.
30. R. J. Doedens, *Prog. Inorg. Chem.* 1976, **21**, 209.

31. A. W. Addison, T. N. Rao, J. Reedijk, J. V. Rijn and G. C. Verschoor, *J. Chem. Soc., Dalton Trans.* 1984, 1349.
32. M. S. Haddad, S. R. Wilson, D. J. Hodgson and D. N. Hendrickson, *J. Am. Chem. Soc.* 1981, **103**, 384 and refs therein.
33. W. R. Tikkanen, C. Krüger, K. D. Bomben, W. L. Jolly, W. C. Kaska and P. C. Ford, *Inorg. Chem.* 1984, **23**, 3633.
34. K. D. Karlin, A. Farooq, J. C. Hayes, B. I. Cohen, T. M. Rowe, E. Sinn and J. Zubieta, *Inorg. Chem.* 1987, **26**, 1271.
35. C. J. O'Connor, D. Firmin, A. K. Pant, B. R. Babu and E. D. Stevens, *Inorg. Chem.* 1986, **25**, 2300.
36. For a tabulation, see L. K. Thompson, F. L. Lee and E. J. Gabe, *Inorg. Chem.* 1988, **27**, 39.
37. W. B. Tolman, R. L. Rardin and S. J. Lippard, *J. Am. Chem. Soc.* 1989, **111**, 4532.
38. V. McKee, M. Zvagulis and C. A. Reed, *Inorg. Chem.* 1985, **24**, 2914.
39. Y. Nishida and S. Kida, *J. Chem. Soc., Dalton Trans.* 1986, 2633 and refs therein.
40. A. B. P. Lever, *Inorganic Electronic Chemistry*, 2nd edn, pp. 356, 553–572, 636–638. Elsevier, Amsterdam (1984).
41. K. Nakamoto, *Infrared and Raman Spectra of Inorganic and Coordination Compounds*, 4th edn, pp. 147–150, 227–233, 251–253. Wiley, New York (1986).
42. G. B. Deacon and R. J. Phillips, *Coord. Chem. Rev.* 1980, **33**, 227.

Polyhedron Vol. 10, No. 19, pp. 2309–2316, 1991
Printed in Great Britain

0277–5387/91 $3.00+.00
Pergamon Press plc

MIXED ALKOXIDE-ANILIDE d^3–d^3 DIMERS OF MOLYBDENUM AND TUNGSTEN. THE X-RAY CRYSTAL STRUCTURES OF $M_2(OBu^t)_4(HNPh)_2(H_2NPh)_2$ (M = Mo, W)

MALCOLM H. CHISHOLM,* IVAN P. PARKIN, WILLIAM E. STREIB and KIRSTEN S. FOLTING

Department of Chemistry and Molecular Structure Center, University of Indiana, Bloomington, IN 47405, U.S.A.

(*Received* 26 *February* 1991; *accepted* 18 *June* 1991)

Abstract—The reactions in diethyl-ether/hexane solutions between aniline and $M_2(OBu^t)_6$ (M = Mo, W) produce $M_2(OBu^t)_4(HNPh)_2(H_2NPh)_2$ in high yield (79–85%) as red–black crystals. The compounds are air-sensitive, soluble in aromatic hydrocarbon solvents, and exhibit dynamic NMR behaviour. The IR spectra show ν(N—H) at 3320 and 3100 cm^{-1}, corresponding to aniline and anilide N—H stretches, respectively. The X-ray crystal structures of $M_2(OBu^t)_4(HNPh)_2(H_2NPh)_2$ are isomorphous for molybdenum and tungsten and reveal eclipsed four-coordinate, essentially planar ends supporting a metal–metal triple bond. Some important bond lengths and angles for $W_2(OBu^t)_4(HNPh)_2(H_2NPh)_2$ ($Mo_2(OBu^t)_4(NHPh)_2(NH_2Ph)_2$ in parentheses) are as follows (at −169°C and −168°C): M—M 2.3225(8) [2.2538(7)], M—O = 1.93 (1.94) (ave), 1.98 (1.96) (ave), M—N (amide) 1.97 (ave) [1.99 (ave)], M—N (amine) 2.37 Å (ave) [2.36 Å (ave)].

There is now an extensive group of $X_3M{\equiv}MX_3$ compounds where M = Mo and W = X = alkyl (β-H stabilized), NMe_2, OR, SAr′ and SeAr′ (Ar′ = mesityl).[1–4] The $M_2(OR)_6$ complexes are coordinatively unsaturated and depending upon the steric requirements of R may reversibly pick up Lewis bases to form $M_2(OR)_6L_2$ complexes (L = pyridine, amine or tertiary phosphine).[5] The general synthesis of $M_2(OR)_6$ compounds involves the addition of an alcohol to the $M_2(NMe_2)_6$ compound[6] [eq. (1)].

$$M_2(NMe_2)_6 + 6ROH \xrightarrow[\text{hydrocarbon}]{} M_2(OR)_6 + 6HNMe_2 \quad (1)$$

In a number of cases reaction (1) yields dimethylamine adducts $M_2(OR)_6(HNMe_2)_2$ because the equilibrium reaction (2) lies well to the right for the specific combination of R and L, e.g. M = Mo, R = $SiMe_3$, L = $HNMe_2$[7] and M = W, R = Pr^i, CH_2Bu^t, L = $HNMe_2$.[8,9]

$$M_2(OR)_6 + 2L \rightleftharpoons M_2(OR)_6L_2 \quad (2)$$

We describe here reactions involving the addition of aniline to $M_2(OBu^t)_6$ compounds which, contrary to the general reaction shown in eq. (2), proceed to give displacement of tert-butanol and formation of anilide ligands. This provides a rare, and possibly the first example of the replacement of an alkoxide by an amide [eq. (3)].[9]

$$L_nM\text{-}OR + HNR'R'' \longrightarrow L_nM\text{-}NR'R'' + ROH \quad (3)$$

RESULTS AND DISCUSSION

Synthesis

The reactions of excess (> 6 fold) aniline or 3,5 dimethylaniline with $M_2(OBu^t)_6$ (M = Mo, W) in hexane/diethyl-ether solution at room temperature produce red crystals of $M_2(OBu^t)_4(HNPh)_2(H_2NPh)_2$ in high yield (79–85%) [eq. (4)].

$$M_2(OBu^t)_6 + 4H_2NAr \xrightarrow{\text{hexane/ether}} M_2(OBu^t)_4(NHAr)_2(NH_2Ar)_2 + 2HOBu^t \quad (4)$$

(M = Mo, W; Ar = C_6H_5, C_6H_5-3,5-Me_2)

* Author to whom correspondence should be addressed.

The product starts to precipitate from the reaction on standing at room temperature approximately 5 min after mixing the solutions. [Following the reaction by ^{1}H NMR (in benzene-d_6) indicates the formation of HOBu^t but no other intermediate compounds.] The reaction proceeds with less than four equivalents of aniline, though unreacted $M_2(OBu^t)_6$ is obtained with the yields reduced accordingly. No detectable reaction occurs between 2,6-dimethylaniline and $M_2(OBu^t)_6$. Probably steric factors deny access to a potential coordination site in $M_2(OBu^t)_6$.

The $M_2(OBu^t)_4(NHPh)_2(NH_2Ph)_2$ complexes are air-sensitive in both solution and the solid state, decomposing to brown oils. They have relatively low decomposition points (90–114°C), probably due to the ready loss of the Lewis base aniline ligands. For this reason they are not sublimable without decomposition. The $M_2(OBu^t)_4(NHPh)_2(NH_2Ph)_2$ complexes are not light sensitive. They are soluble in aromatic hydrocarbon solvents but only sparingly soluble in ethereal or aliphatic solvents.

Spectroscopic characterization

The compounds $M_2(OBu^t)_4(NHPh)_2(NH_2Ph)_2$ were characterized by IR, microanalysis, ^{1}H NMR, melting points and X-ray crystallography. The IR spectra were run as KBr pressed discs which gave the expected ^{t}BuO and aniline/anilide vibrations. The molybdenum/tungsten analogues of $M_2(OBu^t)_4(NHC_6H_5)_2(NH_2C_6H_5)_2$ have essentially identical spectra. The IR spectra revealed two types of N—H stretching vibrations:[10] $\nu = 3350$ and 3100 cm^{-1}. The higher frequency vibration is attributable to a ν(N—H) of the NH_2 group on the Lewis base aniline ($\nu = 3280$ cm^{-1} for aniline) and the lower frequency due to a ν(N—H) of the anilide ligands.

The ^{1}H NMR spectra of $M_2(OBu^t)_4(NHPh)_2(NH_2Ph)_2$ are temperature dependent. At very low temperature (−75°C) along with the expected ^{t}BuO$^{\ominus}$ and aniline/anilide aromatic proton resonances there are three singlets at $\delta = 11.85$, 9.40 and 4.75 ppm of equal intensity. These latter resonances are due to the protons on aniline and anilide nitrogens. The peaks at 9.40 and 4.75 ppm can be reasonably assigned to the diastereotopic protons on the aniline nitrogen. One proton is bridging across the M—M core to an adjacent ^{t}BuO$^{\ominus}$ ligand whilst the other proton is pointing away from the M—M multiple bond (see Fig. 1). Presumably the resonance at 9.40 is due to the proton involved in this hydrogen bridge as similar low-field shifts for bridging OH protons have been observed in analogous $M_2(OAr)_4(OBu^t)_2(HOBu^t)_2$ (M = Mo, W; Ar = C_6H_5, C_6H_4-4-Me) complexes.[11] The lower frequency resonance at 4.75 ppm is likely due to the other protons on the aniline. This is further supported by spin saturation transfer experiments at −75°C that reveal the $\delta = 4.75$ and $\delta = 9.40$ ppm resonances are in slow chemical exchange. Irradiation at one resonance causes a > 90% reduction in signal intensity at the other resonance. This is most easily achieved by a slow (on the NMR time-scale) exchange between the two aniline protons, due to O···H hydrogen-bond breakage and rotation about the M—N aniline bond. The peak at $\delta = 11.85$ ppm is unaffected (less than 10% reduction) by these decoupling experiments at low temperature.

The resonance at $\delta = 11.85$ is thus assigned to the anilide protons. It occurs at lower field than the ArNH_2 resonances because it is anisotropically deshielded both by the formal nitrogen–metal multiple bond and its close vicinity to the M—M triple bond.[12]

Raising the temperature from −75°C to room temperature alters the ^{1}H NMR spectra of $W_2(OBu^t)_4(NHPh)_2(NH_2Ph)_2$. The single peak at $\delta = 11.85$ broadens at −45 to −35°C but sharpens from −15 to 25°C. The peaks at 9.4 and 4.75 ppm are broadened and then lost into the baseline at −35°C and subsequently a peak grows at around 4.6 ppm from −30 to 0°C. This new peak has an integration of four compared to that at 11.85 ppm of two. This implies that it is due to the protons on the aniline ligand which are equivalent above −30°C. In turn this suggests that the aniline ligands are freely dissociated into solution above −30°C as the weighted average of the signal falls at 4.6 ppm rather than at 7.1 ppm, the expected value if a rotation about the M—N bond were making the protons on the aniline equivalent. The aniline nitrogen protons shift to lower frequency with higher temperature such that they occur at $\delta = 3.8$ ppm at 25°C, 3.4 ppm at 65°C and $\delta = 3.2$ ppm at 95°C. Free aniline has for H_2NPh $\delta = 3.2$ ppm. Thus, at 95°C, little aniline is coordinated to the metal. However, in the intermediate regime from 0 to 95°C this resonance is higher than the free value. The aniline is undergoing a fast equilibrium of the type shown in Scheme 1. At high temperatures the equilibrium lies in favour of $W_2(OBu^t)_4(NHPh)_2$ and aniline.

Addition of aniline to an NMR tube of $W_2(OBu^t)_4(NHPh)_2(NH_2Ph)_2$ in toluene gave at low temperature (−75°C) the resonances at 11.85, 9.40 and 4.75 ppm, as well as that for free aniline at 3.5 ppm (PhNH_2). At room temperature irradiation at the aniline resonance of $\delta = 3.8$ ppm

does not cause any diminishing of the anilide peak at $\delta = 11.8$ ppm, thus indicating that the anilide and aniline N—*H* protons are not undergoing chemical exchange at a measurable rate. At temperatures between 0 and +95°C only one resonance for the H_2NPh protons is observed and the resonance is shifted to higher field upon addition of successive aliquots of aniline, and with increasing temperature indicating that all the aniline in solution spends some time on the dimetallic core.

The anilide N—*H* proton is split into three resonances of unequal intensity on raising the temperature above 0°C. Upon raising the temperature one signal decreases in intensity as the other two increase. At 95°C two peaks of equal intensity are observed at 11.8 and 10.9 ppm. On cooling the sample from 95°C this interconversion is fully reversible such that at 0°C only a peak at 11.85 ppm is observed. This process could be due to a mixture of eclipsed (i.e. N—H···O bonded) and staggered conformers (anti and gauche) of $W_2(NHPh)_2(OBu^t)_4$ with the latter being favoured at high temperatures. At 75°C decoupling of the aniline NH_2 protons at $\delta = 3.5$ ppm does cause a reduction of *ca* 50% in the intensity of the two peaks at $\delta = 11.8$ and 10.9 ppm, thus indicating at higher temperatures the aniline and anilide protons are undergoing a slow exchange.

The variable temperature ^{1}H NMR spectra of $Mo_2(OBu^t)_4(NHPh)_2(NH_2Ph)_2$ and $W_2(OBu^t)_4(NHC_6H_3Me_2)_2(NH_2C_6H_5)_2$ showed very similar behaviour. The proposed dynamic processes are illustrated in Scheme 1.

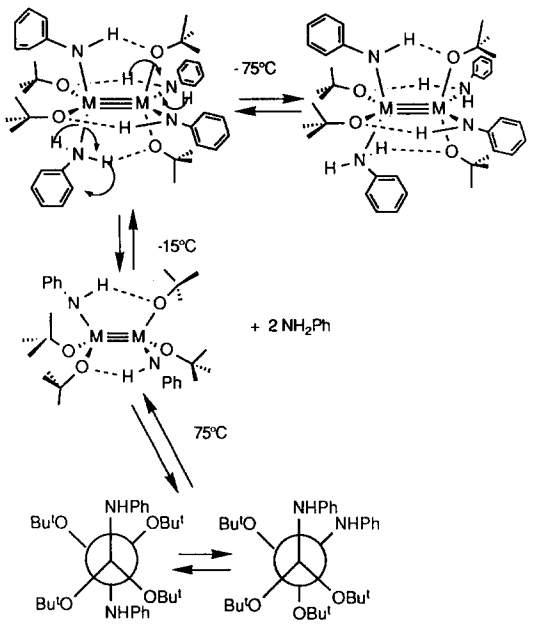

Scheme 1.

Crystallographic studies of $M_2(OBu^t)_4(HNPh)_2(H_2NPh)_2$

Crystals suitable for X-ray diffraction were grown from a hexane/ether reaction solution of $M_2(OBu^t)_6$ and aniline at room temperature. The molecular structure of $Mo_2(OBu^t)_4(HNPh)_2(H_2NPh)_2$ is shown in Figs 1 and 2 viewed perpendicular and parallel to the M—M vector, respectively. The selected bond lengths and angles for $M_2(OBu^t)_4(HNPh_2)_2(H_2NPh)_2$ (M = Mo, W) are shown in Table 1 and crystallographic data collection parameters are given in Table 2.

The structures of the molybdenum and tungsten $M_2(OBu^t)_4(HNPh)_2(H_2NPh)_2$ complexes are isomorphous with all bond angles and lengths (within the 3σ criteria) being equivalent apart from M—M = 2.2538(7) Å for M = Mo and 2.3225(8) Å for M = W. These distances are typical for M—M triple bonds uniting four coordinate metal atoms.[5,8]

The $M_2(OBu^t)_4(NHPh)_2(NH_2Ph)_2$ molecule adopts an eclipsed conformation in the solid state with two essentially square planar ends being joined by a metal–metal triple bond. The eclipsed geometry is sterically unfavourable in dimetallic systems because of non-bonded repulsions between groups on either end of the multiple bond. The observed eclipsed geometry is likely due to the presence of four hydrogen bonds bridging the dinuclear centre. The hydrogens were located in the X-ray analysis for $Mo_2(OBu^t)_4(NHPh)_2(NH_2Ph)_2$ and were refined isotropically (see Table 3).

The metal–nitrogen distances, 1.98 (ave) and 2.38 Å (ave), clearly indicate two types of coordinated nitrogen ligands. The Lewis base aniline has a weak M—N bond. Indeed this M—N distance, 2.38 Å (ave), is longer than in $W_2(OPr^i)_6py_2$ at 2.26 Å,[5] and is the longest measured first-row Lewis base to metal distance in any $M_2(OR)_6L_2$ complex.[5] The other M—N distance of 1.98 Å (ave) is consistent with a deprotonated aniline. It is only slightly longer than the M—N distances in $M_2(NMe_2)_6$ and $M_2(NMe_2)_4R_2$ complexes [1.94 Å (ave)] and indicates a significant degree of M—N $d\pi$–$p\pi$ bonding.[1]

The M—O distances of 1.95 Å (ave) in $M_2(OBu^t)_4(PhNH)_2(PhNH_2)_2$ are typical of those in other $M_2(OR)_6L_2$ complexes.[5]

The ligands in $M_2(OBu^t)_4(NHPh)_2(NH_2Ph)_2$ are disposed such that the $^tBuO^{\ominus}$ groups are *trans* to each other on each tungsten. The two O—M—O units are nearly mutually perpendicular to each other. This is probably caused by steric requirements, with the $^tBuO^{\ominus}$ ligands being bulkier than the aniline/anilide ligands. However, this arrangement also maximizes the hydrogen bonding between neighbouring groups across the multiple

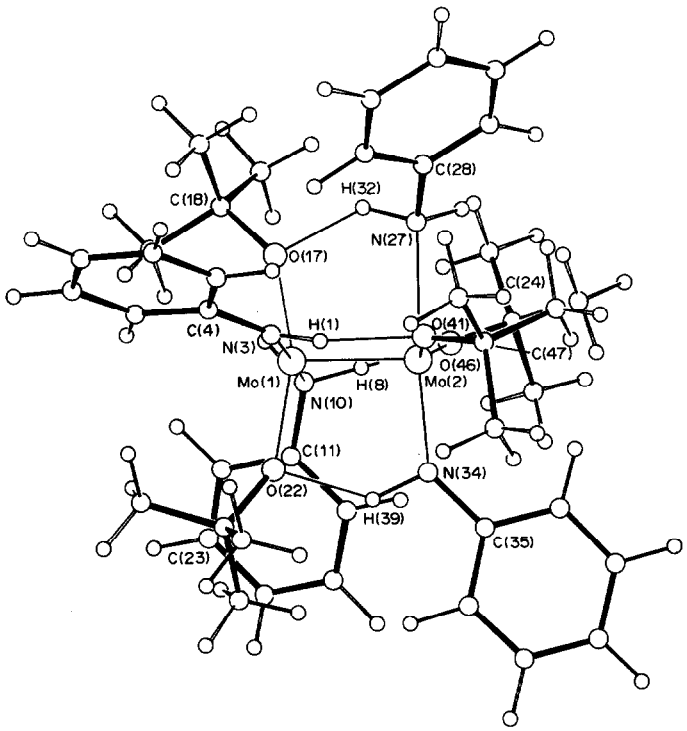

Fig. 1. A ball-and-stick drawing of the $Mo_2(OBu^t)_4(NHPh)_2(NH_2Ph)_2$ molecule showing the atom number scheme used in the tables and the NH···O hydrogen bonding across the M—M bond.

bond. Interestingly the anilines are on the same side of the molecule. To complement this, the geometry is distorted from the idealized eclipsed geometry with the OBu^t groups being closer to the aniline groups than the anilides at each tungsten centre, resulting in the O—M—O angle of 152.9°.

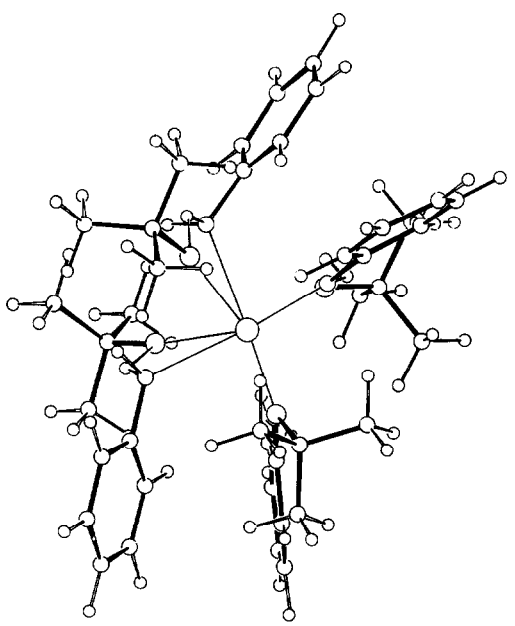

Fig. 2. A view of the $Mo_2(OBu^t)_4(NHPh)_2(NH_2Ph)_2$ molecule looking down the M—M bond emphasizing the near eclipsed geometry that results from the hydrogen bonding across the M—M bond.

The non-bonded N···O distances between *syn* groups across the M—M bond range from 2.69 to 2.77 Å. This is indicative of hydrogen bonding.[13] The hydrogens were located in the molybdenum structure and can be inferred for the tungsten analogue because of the isostructural nature of the complexes. The atoms M, M, N and O for the anilides and alkoxide ligands that are involved in hydrogen bonding lie in a plane. As a result of this hydrogen bonding the M—M—O angles (99.3° ave) and the M—M—N angles at 94° (ave) and 91° (ave) for the anilide and aniline nitrogens, respectively, are all smaller than the M—M—N/O angles in $M_2(OR)_6$ and $M_2(NMe_2)_6$ complexes.

Concluding remarks

The aminolysis reaction reported here is a very rare example of reaction (3). Normally the reverse reaction is observed and is driven by the greater strength of the M—OR bond relative to M—NR′R″. Aminolysis does not occur with cyclohexylamine, dimethylamine or methylamine. It appears to be restricted to aniline. This may be a reflection of the pKa of the amine.[14] However, hydrogen bonding is clearly a contributing factor in stabilizing the $M_2(OBu^t)_4(NHAr)_2(NH_2Ar)_2$

Table 1. Selected bond lengths and angles for $M_2(OBu^t)_4(HNPh)_2(H_2NPh)_2$ (M = Mo, W)

	M	
	Mo	W
M(1)—M(2)	2.2538(7)	2.3225(8)
M(1)—O(17)	1.933(4)	1.939(7)
M(1)—O(22)	1.978(5)	1.956(7)
M(1)—N(3)	1.976(6)	1.984(9)
M(1)—N(10)	2.381(5)	2.359(9)
M(2)—O(41)	1.926(4)	1.930(7)
M(2)—O(46)	1.979(4)	1.974(7)
M(2)—N(27)	1.970(6)	1.989(8)
M(2)—N(34)	2.366(6)	2.354(8)

	M			M	
	Mo	W		Mo	W
M(2)—M(1)—O(17)	99.16(13)	98.67(20)	O(41)—M(2)—O(46)	151.95(18)	153.2(3)
M(2)—M(1)—O(22)	100.70(14)	100.05(22)	O(41)—M(2)—N(27)	100.67(22)	100.6(3)
M(2)—M(1)—N(3)	93.87(17)	94.10(25)	O(41)—M(2)—N(34)	82.39(19)	82.9(3)
M(2)—M(1)—N(10)	90.06(15)	90.00(21)	O(46)—M(2)—N(27)	96.60(21)	96.1(3)
O(17)—M(1)—O(22)	152.15(18)	153.2(3)	O(46)—M(2)—N(34)	78.31(19)	78.7(3)
O(17)—M(1)—N(3)	100.87(20)	100.5(3)	N(27)—M(2)—N(34)	173.13(22)	173.3(3)
O(17)—M(1)—N(16)	83.01(19)	83.5(3)	M(1)—O(17)—C(18)	132.8(4)	132.1(6)
O(22)—M(1)—N(3)	97.08(21)	97.1(3)	M(1)—O(22)—C(23)	141.1(4)	140.3(6)
O(22)—M(1)—N(10)	77.65(19)	77.5(3)	M(2)—O(41)—C(24)	144.3(4)	144.5(7)
N(3)—M(1)—N(10)	173.95(22)	172.8(3)	M(2)—O(46)—C(47)	143.7(4)	143.2(7)
M(1)—M(2)—O(41)	100.80(14)	100.16(21)	M(1)—N(3)—C(4)	138.0(5)	138.0(8)
M(1)—M(2)—O(46)	99.67(13)	99.35(22)	M(1)—N(10)—C(11)	127.9(4)	127.0(7)
M(1)—M(2)—N(27)	94.53(16)	94.34(26)	M(2)—N(27)—C(28)	135.1(5)	135.0(7)
M(1)—M(2)—N(34)	90.91(15)	90.57(21)	M(2)—N(34)—C(35)	123.4(4)	123.1(7)

Table 2. Crystallographic data collection parameters

Empirical formula	$C_{40}H_{62}Mo_2N_4O_4$	$C_{40}H_{62}W_2N_4O_4$
Colour of crystal	Black	Red
Crystal dimensions (mm)	$0.16 \times 0.24 \times 0.32$	$0.10 \times 0.12 \times 0.24$
Space group	$P2_1/n$	$P2_1/n$
Cell dimensions		
Temperature (°C)	−169	−168
a (Å)	11.754(2)	11.759(3)
b (Å)	22.726(5)	22.738(7)
c (Å)	15.548(3)	15.563(5)
β (°)	91.81(1)	91.98(2)
Z (molecules/cell)	4	4
Volume (Å^3)	4151.06	4158.81
Calculated density (gm cm^{-3})	1.368	1.646
Wavelength (Å)	0.71069	0.71069
Molecular weight	854.83	1030.65
Linear absorption coefficient (cm^{-1})	6.298	56.873
Detector to sample distance (cm)	22.5	22.5
Sample to source distance (cm)	23.5	23.5
Average omega scan width at half height	0.25	0.25
Scan speed (deg min^{-1})	6.0	6.0
Scan width (deg+dispersion)	1.8	1.7
Individual background (s)	6	6
Aperture size (mm)	3.0×4.0	3.0×4.0
2θ range (deg)	6–45	6–45
Total number of reflections collected	6407	7322
Number of unique intensities	5458	5470
Number with $F > 3.0\sigma(F)$	4255	4448
$R(F)$	0.0486	0.0411
$R_w(F)$	0.0454	0.0390
Goodness of fit for the last cycle	0.995	0.982
Maximum delta/sigma for last cycle	0.11	0.09

Table 3. Hydrogen bonding in $Mo_2(OBu^t)_4(HNPh)_2(H_2NPh)_2$

	Distance	Sigma
O(41)—N(3)	2.75	0.007
N(3)—H(1)	0.88	0.091
O(41)—H(1)	1.98	0.091
O(46)—N(10)	2.69	0.007
N(10)—H(8)	1.07	0.109
O(46)—H(8)	1.71	0.110
O(17)—N(27)	2.72	0.007
N(27)—H(32)	0.66	0.127
O(17)—H(32)	2.07	0.128
O(22)—N(34)	2.77	0.007
N(34)—H(38)	0.95	0.088
O(22)—H(39)	1.93	0.121

molecules relative to say $M_2(OBu^t)_6(NH_2Ar)_2$. Given that reactions of type (3) are equilibria involving proton transfer, it is quite likely that the hydrogen bonding more than compensates for the difference in expected M—OR and M—NHR bond strengths.

EXPERIMENTAL

All reactions were performed under dry nitrogen atmospheres by standard Schlenk techniques. Solvents were dried and deoxygenated by standard methods. ^1H NMR spectra were recorded at 299.60 MHz on a Varian XL 300 in $C_6D_5CD_3$ and are referenced to residual protio toluene at $\delta = 2.09$ ppm. IR spectra were obtained as pressed KBr discs on a Perkin–Elmer 283 spectrophotometer. $M_2(OBu^t)_6$ (M = Mo, W) compounds were prepared according to literature procedures.[15] Aniline and 3,5-dimethylaniline were purchased from Aldrich Chemical Company and were used as supplied. Microanalysis were provided by Oneida Research Services, Whiteboro, New York.

$M_2(OBu^t)_4(NHAr)_2(NH_2Ar)_2$ [M = Mo, Ar = C_6H_5; M = W, Ar = C_6H_5, 3,5-$Me_2C_6H_3$]

The same general procedure was adopted for all compounds, illustrated here for $W_2(OBu^t)_4(HNPh)_2(NH_2Ph)_2$.

To $W_2(OBu^t)_6$ (0.200 g, 0.248 mmol) dissolved in hexane (15 cm^3) at room temperature was added dropwise a solution of aniline (0.140 g, 1.48 mmol) in hexane (5 cm^3)/diethyl-ether (5 cm^3). The solution was allowed to stand at room temperature and after 5 min red crystals were precipitated. After 24 h the filtrate was removed and the red crystals washed with hexane (15 cm^3) and diethyl-ether (5 cm^3) and dried briefly *in vacuo*. Obtained $W_2(OBu^t)_4(HNPh)_2(NH_2Ph)_2$ (0.190 g, 0.185 mmol, 75%).

Found: C, 47.0; H, 6.4; N, 5.5. Calc.: C, 46.6; H, 6.1; N, 5.4%.

Found: C, 49.1; H, 6.4; N, 4.8. Calc. for $W_2(NHC_6H_4Me)_2(NH_2C_6H_4Me)_2(OBu^t)_4$: C, 48.6; H, 6.4; N, 5.1%.

$W_2(OBu^t)_4(NHPh)_2(NH_2Ph)_2$: ^1H NMR (C_6D_6, 15°C): δ: 11.85 (s, 2H), 7.15 (m, 4H), 7.06 (m, 8H), 6.72 (m, 4H), 6.42 (m, 4H), 4.21 (s, 4H), 1.52 (s, 6H), 1.48 (s, 6H), 1.32 (s, 24H).

$Mo_2(OBu^t)_4(NHC_6H_5)_2(NH_2C_6H_5)_2$ (in benzene at 25°C): δ: 12.8 (s, 2H), 7.15 (m, 4H), 7.06 (m, 8H), 6.69 (m, 4H), 6.42 (m, 4H), 4.21 (m, 4H), 1.56 (s, 13H), 1.36 (m, 23H).

$W_2(OBu^t)_4(NHC_6H_3Me_2)_2(NH_2C_6H_3Me_2)_2$ (in toluene at 25°C): δ: 12.1 (s, 2H), 6.85 (s, 4H), 6.65 (s, 4H), 6.25 (s, 4H), 4.20 (s, 4H), 2.41 (s, 8H), 2.23 (s, 16H), 1.63 (s, 36H).

IR data

$W_2(OBu^t)_4(HNPh)_2(H_2NPh)_2$. ν (cm^{-1}) 3350m, 3130m, 3060m, 3020m, 2945s, 2910s, 2880sh, 2840sh, 1585vs, 1570sh, 1480vs, 1460vs, 1372s, 1368s, 1350vs, 1310w, 1260vs, 1220s, 1215vs, 1070s, 1048s, 1015s, 985m, 955s, 930vs, 900w, 855vs, 815m, 795m, 760s, 745s, 680s, 670s, 600m, 545m, 535m, 525m, 510m, 470m, 380m, 350m.

$Mo_2(OBu^t)_4(HNPh)_2(H_2NPh)_2$. ν (cm^{-1}) 3360m, 3090m, 3060m, 3030m, 2940s, 2900sh, 2880sh, 2840sh, 1585vs, 1475vs, 1460vs, 1375m, 1370sh, 1350vs, 1260vs, 1220m, 1165vs, 1065s, 1025vs, 988m, 930vs, 895sh, 850vs, 810w, 790s, 760s, 745vs, 680vs, 660vs, 600m, 540m, 525m, 510m, 465m, 400w, 395w, 350m.

$W_2(OBu^t)_4(HNC_6H_3Me_2)_2(H_2NC_6H_3Me_2)_2$. ν (cm^{-1}) 3340m, 3135m, 3020m, 2945m, 2900s, 2845m, 1590vs, 1480m, 1460m, 1410m, 1370m, 1350s, 1310s, 1255m, 1225m, 1165s, 1150s, 1060m, 1030m, 1020, 990w, 960s, 945vs, 890w, 855w, 823m, 820s, 760m, 700s, 685m, 650m, 540m, 465m, 410w, 360sh, 350m, 300w, 285w, 275w.

Single crystal X-ray studies

General operating procedures and a listing of programs have been reported.[16]

$Mo_2(OBu^t)_4(NH_2Ph)_2(NHPh)_2$. A suitable small single crystal was selected from the bulk sample using inert atmosphere handling techniques. The

crystal was transferred to the goniostat where it was cooled to −169°C for characterization and data collection. A systematic seach of a limited hemisphere of reciprocal space yielded a set of reflections that exhibited monoclinic symmetry (2/*m*). The systematic extinction of *h*0*l* reflections for $h+l = 2n+l$ and of 0*k*0 for $k = 2n+l$ uniquely identified the space group as $P2_1/n$. Data collection was undertaken as detailed in Table 2. A total of 6407 reflections (including space group extinctions and standard reflections) were collected in the given range. Following the usual data reduction and averaging of equivalent reflections a unique set of 5458 reflections was obtained. The *R* value for the averaging was 0.05 for 696 reflections measured more than once. A plot of the four standard reflections measured every 400 reflections showed no significant trends. No correction for absorption was applied ($\mu = 6.3$). Unit cell dimensions were determined for 66 unique reflections having 2θ values between 21 and 31°.

The structure was solved using a combination of direct methods and Fourier techniques. The two molybdenum atoms were located in the initial *E*-map and the remaining non-hydrogen atoms were located in a difference map. Following initial refinement all of the hydrogen atoms associated with the nitrogen atoms were located as well as almost all other hydrogen atoms. All hydrogen atoms were then introduced in idealized positions. Full-matrix least-squares refinement was completed using anisotropic thermal parameters on all non-hydrogen atoms and individual isotropic thermal parameters on the hydrogen atoms. The final *R* value was 0.049 and $R_w(F)$ was 0.045. Reflections having $R < 3.0\sigma(F)$ were given zero weight during the refinement.

The final difference Fourier was essentially featureless, the largest peak being 0.71 e Å^{-3} in the vinicity of C(16).

$W_2(OBu^t)_4(NHPh)_2(NH_2Ph)_2$. A crystal of suitable size was mounted in a nitrogen atmosphere glove bag using silicone grease, and then transferred to a goniostat where it was cooled to −168°C for characterization and data collection. A search of a limited hemisphere of reciprocal space revealed intensities with Laue symmetry and systematic absences consistent with the space group $P2_1/n$, which was later confirmed by the successful solution of the structure. Following complete intensity data collection and correction for absorption, data processing gave a residual of 0.031 for the averaging of 1064 unique intensities which had been measured more than once. Four standards measured every 300 data showed no significant trends.

The structure is isomorphous with the molybdenum complex. It was solved independently using a combination of direct methods (MULTAN-78) and Fourier techniques. The tungsten positions were obtained from an initial *E*-map. The remainder of the non-hydrogen atoms were found in subsequent iterations of least-squares refinement and difference Fourier calculation. Hydrogen atoms were included in calculated positions but were not refined. Hydrogen thermal parameters were fixed at one plus the isotropic thermal parameters of the atom to which it was bonded. The number of hydrogen atoms on each nitrogen was obvious from the W—N distances (1.98 Å for W—NH— and 2.35 Å for W—NH_2—), which was consistent with the earlier work.

In the final cycles of refinement the non-hydrogen atoms were varied with anisotropic thermal parameters to a value of $R(F) = 0.041$. The final difference map was reasonably clean, the largest peak being a tungsten residual of 1.2 e Å^{-3}.

Acknowledgements—We thank the National Science Foundation for support. I.P.P. thanks the SERC (U.K.) for a NATO fellowship.

REFERENCES

1. M. H. Chisholm, *Angew. Chem., Int. Edn Engl.* 1988, **25**, 21; *Acc. Chem. Res.* 1990, **23**, 419.
2. F. Huq, W. Mowat, A. Shortland, A. C. Skapski and G. Wilkinson, *J. Chem. Soc., Chem. Commun.* 1971, 1079.
3. M. H. Chisholm, J. F. Corning and J. C. Huffman, *Inorg. Chem.* 1984, **23**, 754.
4. M. H. Chisholm, I. P. Parkin, J. C. Huffman and W. E. Streib, *J. Chem. Soc., Chem. Commun.* 1990, **13**, 921; *Polyhedron* 1990, **9**, 2941.
5. M. Akiyama, M. H. Chisholm, F. A. Cotton, M. W. Extine, D. A. Haitko, D. Little and P. E. Fanwick, *Inorg. Chem.* 1979, **18**, 2321; M. H. Chisholm, *Polyhedron* 1983, **2**, 681.
6. M. H. Chisholm, J. C. Huffman and C. A. Smith, *J. Am. Chem. Soc.* 1986, **108**, 222.
7. M. H. Chisholm, F. A. Cotton, M. W. Extine and W. W. Reichert, *J. Am. Chem. Soc.* 1978, **100**, 153.
8. M. J. Chetcuti, M. H. Chisholm, J. C. Huffman and J. Leonelli, *J. Am. Chem. Soc.* 1983, **105**, 292.
9. M. H. Chisholm and I. P. Rothwell, *Comprehensive Coordination Chemistry*, Vol. 2, pp. 161 and 235. Pergamon Press (1987).
10. A. J. Gordeń and R. A. Ford (Editors), *The Chemists Companion. A Handbook of Practical Data Techniques and References*, p. 83. J. Wiley, New York (1972).
11. M. H. Chisholm and I. P. Parkin, results to be published.
12. M. H. Chisholm and F. A. Cotton, *Acc. Chem. Res.* 1978, **11**, 356.

13. P. Schuster, G. Zundel and C. Sandorfy, *The Hydrogen Bond.* Amsterdam, North Holland (1970).
14. Compare kPa for $ArNH_2$ of 3–5 with pKa for RNH_2 of 10–11. J. March, in *Advanced Organic Chemistry*, 3rd edn. Wiley and Sons, New York (1985).
15. M. H. Chisholm, F. A. Cotton, C. A. Murillo and W. W. Reichert, *Inorg. Chem.* 1977, **16**, 1801.
16. M. H. Chisholm, K. Folting, J. C. Huffman and C. C. Kirkpatrick, *Inorg. Chem.* 1984, **24**, 1021.

Polyhedron Vol. 10, No. 19, pp. 2317–2329, 1991
Printed in Great Britain

0277–5387/91 $3.00+.00
© 1991 Pergamon Press plc

AN ALTERNATIVE MECHANISM FOR THE FORMATION OF THE COBALT(III) MOLYBDATE CATION, $Co(NH_3)_5MoO_4^+$

MICHAEL R. GRACE*† and PETER A. TREGLOAN

Inorganic Chemistry Section, School of Chemistry, University of Melbourne, Parkville, Victoria 3052, Australia

(*Received* 7 *March* 1991; *accepted* 5 *June* 1991)

Abstract—An alternative mechanism is proposed for the formation of $Co(NH_3)_5MoO_4^+$ from $Co(NH_3)_5H_2O^{3+}$ and MoO_4^{2-} in slightly basic solution (pH 7.1–8.0). The observed second-order rate dependence upon $[MoO_4^{2-}]$ may be explained by $HMoO_4^-$ acting as a proton-donating catalyst, in contrast to the previously postulated mechanism involving the formation of dimeric molybdenum(VI) species. An increase in reaction rate was also caused by the addition of other protonated anions (HCO_3^-, $H_2PO_4^-$) to the reaction solution, thus supporting the contention of a general proton-assisted mechanism. No evidence of dimeric molybdenum(VI) was found.

Taylor has reported that the formation of $Co(NH_3)_5MoO_4^+$ from MoO_4^{2-} and $Co(NH_3)_5OH^{2+}$, in the pH range 7.1–8.0, could be conveniently followed using the stopped-flow technique.[1] It was also found that the complexation reaction, given in eq. (1), showed a greater than first-order dependence upon $[MoO_4^{2-}]$.

$$Co(NH_3)_5OH_2^{3+} + MoO_4^{2-} \underset{}{\overset{k_f}{\rightleftharpoons}} Co(NH_3)_5MoO_4^+ + H_2O \quad (1)$$

The forward rate constant, k_f, has four terms, according to eq. (2):

$$k_f = k_a + k_b[H^+] + k_c[MoO_4^{2-}] + k_d[H^+][MoO_4^{2-}]; \quad (2)$$

where: $k_a = 96 \pm 7\ M^{-1}\ s^{-1}$, $k_b = (1.1 \pm 0.2) \times 10^9\ M^{-2}\ s^{-1}$, $k_c = (2.2 \pm 0.2) \times 10^3\ M^{-2}\ s^{-1}$ and $k_d = (1.02 \pm 0.05) \times 10^{11}\ M^{-3}\ s^{-1}$ at 25°C and $\mu = 1.0$ M ($NaClO_4$).

Taylor also noted that the rate of reaction was consistent with substitution at the molybdenum(VI) rather than cleavage of the inert cobalt(III)–oxygen bond. It was suggested that the pathways k_a and k_b correspond to the reaction of $HMoO_4^-$ with $Co(NH_3)_5OH_2^{3+}$ and $Co(NH_3)_5OH^{2+}$, respectively. The second-order $[MoO_4^{2-}]$ dependence for paths k_c and k_d was ascribed to a reaction involving the dimolybdate species $Mo_2O_8^{4-}$, $HMo_2O_8^{3-}$ or $H_2Mo_2O_8^{2-}$, depending upon the active cobalt(III) entity, in order to conform to the observed acid dependence.

The dimolybdate anion, $Mo_2O_7^{2-}$, has been isolated from acetonitrile solution as the $(n\text{-}C_4H_9)_4N^+$ salt, containing corner-shared MoO_4^{2-} tetrahedra.[2] However, $Mo_2O_7^{2-}$ has never been detected in aqueous solution, although a recent study by Cruywagen and Heyns[3] reported evidence of the protonated species $HMo_2O_7^-$ under mildly acidic conditions ($2.3 \leqslant pH \leqslant 6.1$). The discrete dimeric species, $Mo_2O_5(H_2O)_6^{2+}$, has been identified as the major component of molybdate solutions in 2–6 M $HClO_4$ and HNO_3 by ^{95}Mo NMR and Raman spectroscopy.[4] The structure involves two molybdenum(VI) centres bridged by a single oxygen. Two terminal oxygens and three aquo ligands constitute an octahedral environment around each molybdenum ion. However, the existence of an aqueous dimeric molybdenum(VI) species, under normal conditions, must remain tentative since another recent potentiometric study[5] found no molybdate oligomers between monomers and the heptameric series $Mo_7O_{24}H_n^{(6-n)-}$ ($n = 0$, 1, 2 and 3).

The major objective of the present study was to reinvestigate the complexation between MoO_4^{2-}

* Author to whom correspondence should be addressed.
† Present address: Chemistry Department, University of Calgary, Calgary, Alberta, Canada T2N 1N4.

and $Co(NH_3)_5OH_2^{3+}$ in basic solution, in order to investigate Taylor's postulated reaction between cobalt(III) ions and dimeric molybdenum(VI) species. The presence (or absence) of a term involving dimolybdate in the rate expression could then be used as independent evidence for its existence and assist in the continuing development of the models used to describe molybdenum(VI) speciation in acid solution.

We thought that the second order term in $[MoO_4^{2-}]$ might also arise from $HMoO_4^-$ acting as a general acid catalyst. Consequently, the effect of a range of anions upon the rate of the complexation reaction was also examined.

EXPERIMENTAL

Materials

$[Co(NH_3)_5OH_2](ClO_4)_3$ was prepared by established methods.[6,7] UV–vis spectra were in good agreement with those reported previously.[7,8] $Na_2MoO_4 \cdot 2H_2O$ (May & Baker, LR) was twice recrystallized from base solution (pH $\approx$ 11). Triethylanolamine (Ajax, LR) was distilled *in vacuo*. Na_2HPO_4 (Ajax, AR), $NaHCO_3$ (BDH, Analar), Na_2SO_4 (BDH, Analar) and NaOH (Ajax, AR) were used without further purification. Twice distilled, once deionized water was used throughout

Both equilibrium and kinetic measurements were performed in the presence of 0.1 M triethanolamine in order to buffer the solutions at the required pH and prevent the formation of polymeric molybdenum(VI) species.[1] Solutions were adjusted to the desired pH by addition of either 2 M $HClO_4$ or 2 M NaOH. These solutions showed negligible drift in pH (< 0.05 pH) units) over a period of several months.

The synthesis of $[Co(NH_3)_5MoO_4](ClO_4)$ involved mixing slightly alkaline 0.05 M solutions ($8 \leqslant pH \leqslant 9$) of MoO_4^{2-} and $Co(NH_3)_5OH^{2+}$ at 50–60°C in the presence of *ca* 0.5 M $NaClO_4$. The mixed solution was maintained at this temperature for a further 15 min. The pink solid formed upon cooling was filtered and then washed with ice-cold water, CH_3CH_2OH and then $(CH_3CH_2)_2O$ and dried at 60°C for several hours. The crude complex was recrystallized from a minimum of hot ($\approx$ 80°C) water at pH 8, filtered, washed and dried as above. Yields were typically 30–40%.

The analysis of NH_3 content has been described previously.[9] For $[Co(NH_3)_5MoO_4](ClO_4)$: Found: 20.6. Calc.: 21.1%. The residue after product decomposition was filtered and the molybdenum concentration in the filtrate was determined gravimetrically as $MoO_2(C_9H_6ON)_2$ after complexation with 8-hydroxyquinoline.[10] Found: 23.5. Calc.: 23.8%.

Physical methods

All pH* measurements were performed using a Radiometer GK2401C combined glass electrode, in which the saturated KCl reference solution was replaced with 1 M NaCl to prevent the precipitation of $KClO_4$ at the liquid junction. The electrode was calibrated daily with a series of acid ($HClO_4$, pH 2–3.5, μ = 1.0 M) and base (NaOH, pH 11–12.5, μ = 1.0 M) standards. The slope of the pH vs electrode potential plot was typically 0.059 ± 0.002 V per pH unit.

Absorbance measurements were performed on a Varian Techtron 635D UV–vis spectrophotometer, using a cell block thermostatted to 25.0 ± 0.1°C. Spectra were recorded in a quartz mixing cell (Hellma, 238-QS) which is divided into two equal path-length compartments by a thin wall; a hole at the top of this wall allows mixing of the two reactant solutions. Consequently any absorbance change upon mixing can be directly attributed to chemical reaction.

IR spectra were recorded as KBr discs on a Jasco 302 IR spectrometer. Raman spectra were obtained using a Spex Ramalog 5 Raman spectrometer interfaced with an M6800 microcomputer. During Raman studies of molybdate/phosphate solutions, $NaClO_4$ was added to each solution to maintain an ionic strength of 1.0 M and also provide an intensity calibration for each spectrum [at $\nu_1(ClO_4^-) = 935$ cm^{-1}]. HCl was used to obtain the desired solution pH.

Diffuse reflectance spectra were recorded over the range 340–750 nm on a Beckman DK-2A spectrophotometer ($BaSO_4$ reference). Variable temperature magnetochemical measurements were performed over the range 210–350 K on a thermostatted Gouy balance, calibrated with $Hg[Co(NCS)_4]$. Diamagnetic corrections were applied according to König.[11]

Rate measurements

The formation of $Co(NH_3)_5MoO_4^+$ from MoO_4^{2-} and $Co(NH_3)_5OH_2^{3+}$ was followed spectrophotometrically at 550 nm, using the stopped-flow technique. The cobalt(III) concentration was maintained at 0.0020 M,† whilst $[MoO_4^{2-}]$ was

* The term "pH", used throughout this paper, refers to the quantity $-\log_{10}[H^+]$.

† All concentrations are at the "instant of mixing" = stock concentration/2.

varied between 0.010 and 0.100 M. All rate measurements were made at an ionic strength of 1.0 M ($NaClO_4$) and at 25.0 ± 0.1°C over the pH range 7.1–8.0.

A stopped-flow apparatus, designed and constructed within the Chemistry Department at Melbourne University, was used to perform kinetic experiments with half-lives ranging from 10 ms to several minutes. The molybdate and cobalt(III) reactant solutions were drawn into 2 cm^3 glass, gas-tight drive syringes (Hamilton, 1002-TEFLL) from plastic reserve syringes via three-way taps (Hamilton, No. 86727). A kinetic experiment ("run") was initiated by triggering a solenoid-controlled pneumatic drive, which forced fresh reactant solutions through a Kel-F mixer[12] and into the observation chamber. Up to 20 runs can be recorded before refilling the drive syringes.

The observation cell consists of either: (a) a "straight-through" 2 mm internal diameter quartz tube where the light-beam passes through the tube at a 90° angle, or (b) a "Z-shape" 18 mm path-length chamber in a Kel-F block, enclosed into the brass stopped-flow block by quartz windows. Choice of cell is governed by the magnitude of the absorbance change and the intensity of the transmitted light. Optically dense solutions necessitated using the short path-length tube to ensure adequate signal-to-noise response of the photomultiplier detection system.

The stopped-flow unit is encased in a brass block through which thermostatted water is circulated, allowing temperatures between 7 and 45°C to be maintained to within 0.05°C. A Hewlett Packard 34740A platinum resistance thermometer is inserted into a cavity in the brass casing to enable temperature resolution of 0.01°C. All reactant solutions were thermostatted within the drive syringes for 20 min to ensure thermal equilibration.

A 100 W quartz–halogen lamp, powered by a Hewlett Packard Model 6286A supply, provided the light source for the spectrophotometric detection of reaction progress. A Czerny–Turner design Spex type 1670 Minimate monochromator was used to select the required wavelength. The light source is focussed onto the entrance slit of the monochromator with a quartz lens. An adjustable diaphragm shutter, mounted on the lens, enables the light beam to be blocked between measurements to minimize any photolytic side reactions. The transmitted light from the observation cell is detected by a photomultiplier (RCA type 1P28).

All optical detection components are mounted on an optical rail (Oriel), with the light source, quartz lens, entrance and exit slits of the monochromator and the photomultiplier at the same height as the observation cell of the stopped-flow apparatus.

The difference between the output voltage from the photomultiplier and an adjustable constant voltage source is amplified (Analog Devices AD521J) to maximize the reaction signal change in the range −2.5 to 2.5 V (the bipolar limits of the analogue to digital converter). A passive RC type circuit is used to remove high-frequency noise. The filtered signal is simultaneously displayed by oscilloscope and sampled by the AR11 analogue subsystem of a PDP-11/10-S minicomputer (or an M6802 microcomputer) and stored for subsequent analysis.

Each stopped-flow run consisted of collecting 200 voltage/time data pairs at a specified sampling rate, waiting a predetermined interval and then collecting a further 20 data pairs, representing reaction equilibrium. The sampling rate was usually chosen so that 200 data pairs covered 95% of the total reaction amplitude.

The collection and preliminary analysis of stopped-flow data were performed under the control of the BASIC program RDATA, developed within this laboratory. This program allowed the collection of up to 20 runs for each set of reactant solutions with the capability to maximize the signal-to-noise ratio. Pseudo first-order rate constants for each run and the signal-average could be calculated by either a simple integrated rate expression or by the Guggenheim method.[13]

RESULTS

Characterization of $[Co(NH_3)_5MoO_4](ClO_4)$

IR and Raman spectra were used to ascertain the coordination mode of the molybdate species in $[Co(NH_3)_5MoO_4](ClO_4)$. Table 1 lists the principal observed IR and Raman frequencies for this compound and for $[Co(NH_3)_5MoO_4]Cl$, $[Co(NH_3)_4MoO_4]NO_3$, $[Co(NH_3)_5Cl]MoO_4$ and free MoO_4^{2-}, reported by Coomber and Griffith.[14] Fundamental Raman frequencies for MoO_4^{2-} and ClO_4^-, measured from solid samples of Na_2MoO_4 and $NaClO_4$, are also included.

The ν_1 symmetric stretch of the MoO_4^{2-} moiety can be used to discriminate between alternate modes of coordination. The observed ν_1 frequencies for $[Co(NH_3)_5MoO_4](ClO_4)$, 912 (IR) and 909 cm^{-1} (R), are in excellent agreement with the values cited for $[Co(NH_3)_5MoO_4]Cl$, thus indicating monodentate, inner-sphere coordination to the cobalt(III) ion. Not surprisingly, the frequencies of the perchlorate anion are similar in the cobalt(III) complex and in $NaClO_4$, indicating no significant

Table 1. Principal IR and Raman frequencies for cobalt(III) molybdate complexes

Complex		$\delta_{as}(NH_3)$	$\delta_s(NH_3)$	$\rho(NH_3)$	ν(Co—N)	$\nu_1(ClO_4)$	$\nu_3(ClO_4)$	$\nu_4(ClO_4)$	$\nu_1(MoO_4)$	$\nu_3(MoO_4)$	$\nu_4(MoO_4)$	Reference
Free MoO_4^{2-}	(R)	—	—	—	—	—	—	—	897	841	338	14
	(R)	—	—	—	—	—	—	—	896	840	332	This work
ClO_4^-	(R)	—	—	—	—	935	1090	634	—	—	—	This work
$[Co(NH_3)_5MoO_4]Cl$		1625m	1320s	830s	495w	—	—	—	910s	877vs	350m	14
			1295sh		449w					833vs		
$[Co(NH_3)_4MoO_4]NO_3$		1620s	1290s	830s	501w	—	—	—	920s	865vs	371m	14
									845vs			
$[Co(NH_3)_5Cl]MoO_4$		1590m	1312m	825s	503w	—	—	—	893w	825s,br	335s	14
				1293m		495w						
$[Co(NH_3)_5MoO_4](ClO_4)$	(R)	1625m	1317s	835s	494w	—	1080vs	620s	912s,sh	870vs,br	—	This work
			1295sh		450vw					840vs		
						938	—	—	909	—	—	This work

All frequencies are in cm^{-1}. (R) signifies Raman measurements. $\nu_{1\to4}(MoO_4)$: Molybdate fundamental frequencies are defined by Nakamoto.[15]

interaction between the cobalt(III) and ClO_4^- in the solid.

The UV–vis spectrum of $[Co(NH_3)_5MoO_4](ClO_4)$ was recorded by diffuse reflectance from the solid to avoid complications arising from concurrent rapid aquation to MoO_4^{2-} and $Co(NH_3)_5OH_2^{3+}$ when the complex is dissolved in solution. The spectrum has absorbance maxima at 360 and 525 nm, corresponding to the $^1T_{2g} \leftarrow {}^1A_{1g}(\nu_2)$ and $^1T_{1g} \leftarrow {}^1A_{1g}(\nu_1)$ electronic transitions, respectively.

The effective magnetic moment, μ_{eff}, of $[Co(NH_3)_5MoO_4](ClO_4)$ at 298 K was determined as 0.54 B.M. This value is consistent with a wide variety of low-spin cobalt(III) compounds with moments ranging from 0 to 1 B.M.,[11,16] including the analogous monodentate chromate complex, $[Co(NH_3)_5CrO_4](ClO_4)$, which has a μ_{eff} of 0.62 B.M.[9] As was observed with the chromato species, the non-zero magnetic moment for the d^6 cobalt(III) complex can be explained by temperature-independent paramagnetism, where there is a coupling of the ground and excited states under the influence of the applied magnetic field. This contention is supported by the invariance of the molar susceptibility ($\chi_M = 1.55 \pm 0.05 \times 10^{-9}$ m^3 mol^{-1}) over the temperature range 210–350 K. The molybdate moiety would also most probably be contributing to the observed μ_{eff}, since applying diamagnetic corrections to the uncorrected susceptibilities for Na_2MoO_4 and K_2MoO_4 yield room temperature, magnetic moments of 0.33 and 0.34 B.M., respectively (again arising from temperature-independent paramagnetism).[11]

Equilibrium measurements

As noted by Taylor in his original determination of K_1, the equilibrium constant describing the complexation given in eq. (1), mixing solutions of $Co(NH_3)_5OH_2^{3+}$ and molybdenum(VI) under slightly basic conditions results in a rapid intensification of the purple colour. Figure 1 shows spectra from a mixing cell experiment illustrating the total absorbance change resulting from the complexation reaction. Taylor attributed this absorbance enhancement to the formation of $Co(NH_3)_5MoO_4^+$. This proposal is supported by the close similarity in absorbance maxima between the aqueous spectrum (λ_{max} = 365 and 525 nm) and the diffuse reflectance measurements on $[Co(NH_3)_5MoO_4](ClO_4)$ in this study (λ_{max} = 360 and 525 nm).

The evaluation of K_1 involved analysis of the absorbance changes at 540, 550 and 560 nm (corresponding to the wavelengths of maximum change) using the Benesi–Hildebrand method[17]

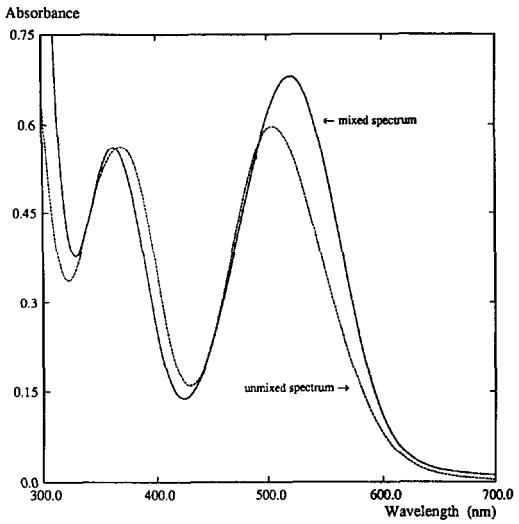

Fig. 1. The effect of complexation upon the UV–vis spectrum of $Co(NH_3)_5OH^{2+}$ and MoO_4^{2-} at 25°C and 1.0 M ionic strength.

with the molybdate concentration in large excess. Calculations were performed according to Taylor and resulted in an average value for K_1 of 960 ± 80 M^{-1} at 25°C and 1.0 M ionic strength (cf. 475 ± 30 M^{-1}).[1]

Kinetic measurements

The acid dependence of the reaction was measured over the pH range 7.1–8.0. Lower pH values and higher molybdate concentrations were avoided to minimize formation of isopolymolybdate species.[18]

All reaction transients were first-order for at least five half-lives. The observed rate constants, k_{obs}, and the relevant reaction conditions are listed in Table 2. Data analysis involved the determination of the forward rate constant, k_f, and its resolution into the four terms given in eq. (2).

Plots of k_f vs $[MoO_4^{2-}]$ were linear at all pH values indicating a second-order dependence upon $[MoO_4^{2-}]$. The slope and intercept terms, shown in Table 3, correspond to the molybdate-dependent and -independent pathways in the forward rate law. Plotting these slope and intercept terms against $[H^+]$ yields the four individual rate constants in Taylor's rate expression.[1] The resultant values for k_a, k_b, k_c and k_d are included in Table 3. The agreement between the two studies is very reasonable if the constants are recalculated using molybdenum(VI) stock concentrations, rather than those at the "instant of mixing".

Table 2. Experimental parameters and observed first-order rate constants for the $Co(NH_3)_5OH^{2+}/MoO_4^{2-}$ complexation reaction at 25°C and 1.0 M ionic strength

pH	$[MoO_4^{2-}]$ (M)	k_{obs} (s^{-1})	Error
7.17	0.05	17.1	0.7
	0.10	53.8	4.6
	0.075	35.1	1.8
	0.025	6.39	0.31
	0.01	1.94	0.08
	0.0375	11.5	0.3
	0.0175	3.77	0.19
7.73	0.05	3.61	0.12
	0.10	9.84	0.28
	0.075	6.15	0.19
	0.025	1.44	0.07
	0.01	0.49	0.05
	0.0375	2.41	0.07
	0.0175	0.93	0.03
7.43	0.05	7.03	0.33
	0.10	21.8	1.2
	0.075	13.94	0.50
	0.025	2.93	0.17
	0.01	1.02	0.05
	0.0375	4.78	0.21
	0.0175	1.93	0.07
7.92	0.05	1.96	0.09
	0.10	5.17	0.20
	0.075	3.33	0.15
	0.025	0.87	0.07
	0.01	0.3	0.05
	0.0375	1.37	0.10
	0.0175	0.57	0.05

All measurements were made at 25.0 ± 0.1°C, 1.0 M ionic strength ($NaClO_4$) and with a total cobalt(III) concentration of 0.002 M. Solutions were buffered with 0.1 M triethanolamine. Quoted errors are one standard deviation and are derived from the signal-averaged reaction transient. Concentrations are at the "instant of mixing".

Catalysis of $Co(NH_3)_5MoO_4^+$ *formation*

As mentioned in the introductory remarks, it is possible that the observed second-order dependence upon $[MoO_4^{2-}]$ may be due to general acid catalysis of complex formation, presumably by $HMoO_4^-$. In order to test this hypothesis, various potential catalysts (Na_2HPO_4, $NaHCO_3$ and Na_2SO_4) were added to the molybdate solution prior to the stopped-flow run.

The potential catalyst was mixed with the molybdate solution since SO_4^{2-}, CO_3^{2+} and PO_4^{3-} all form complexes with $Co(NH_3)_5OH^{2+}$ in alkaline

Table 3. Evaluation of second- and third-order rate constants for the formation of $Co(NH_3)_5MoO_4^+$

(a) Results of the k_f versus $[MoO_4^{2-}]$ plots

pH	Slope	Intercept	Correction coefficient
7.17	$(3.42\pm0.13)\times10^4$	467 ± 37	0.9960
7.43	$(2.02\pm0.08)\times10^4$	379 ± 25	0.9954
7.73	$(1.65\pm0.05)\times10^4$	233 ± 19	0.9941
7.92	$(1.20\pm0.06)\times10^4$	161 ± 26	0.9949

(b) Results of plots of molybdate-dependent and -independent paths versus $[H^+]$

	Molybdate-independent path	Molybdate-dependent path	Reference
Intercept	k_a ($M^{-1}s^{-1}$)	k_c ($M^{-2}s^{-1}$)	
	123 ± 23	$(8.52\pm0.60)\times10^3$	This work
	166 ± 16	$(2.26\pm0.19)\times10^3$	This work[a]
	96 ± 7	$(2.2\pm0.2)\times10^3$	1
Slope	k_b ($M^{-2}s^{-1}$)	k_d ($M^{-3}s^{-1}$)	
	$(5.74\pm0.73)\times10^9$	$(3.64\pm0.23)\times10^{11}$	This work
	$(3.02\pm0.47)\times10^9$	$(8.12\pm0.68)\times10^{10}$	This work[a]
	$(1.1\pm0.2)\times10^9$	$(1.02\pm0.05)\times10^{11}$	1
Correction coefficient	0.9567	0.9730	This work
	0.9461	0.9656	This work[a]

[a] Calculated using stock $[MoO_4^{2-}]$ rather than "instant of mixing" concentrations.

solution.[19] Before assessing the effect of these anions upon the rate of $Co(NH_3)_5MoO_4^+$ formation, some preliminary experiments, designed to determine any direct reaction between these anions and MoO_4^{2-}, were performed. This precaution was deemed essential, since the ability of molybdenum(VI) to form heteropolymolybdate species, including heterophosphates, in acidic solution is well known.[20] Murata and Ikeda have used Raman spectroscopy to follow the formation of the 12-molybdophosphate species, $PMo_{12}O_{40}^{3-}$.[21]

These brief investigations involved quantitatively monitoring the intensity of the Raman ν_1 symmetric stretch of MoO_4^{2-} at 897 cm^{-1}, upon the addition of increasing concentrations of the proposed catalytic species. The formation of any molybdenum(VI)–anion complex would result in a loss of MoO_4^{2-} tetrahedral symmetry and a consequent diminution in the ν_1 peak intensity. In all cases, the concentration of free molybdate was greater than 99% of total molybdenum(VI), even with "catalyst" concentrations in 10-fold excess. A realistic estimate for the accuracy of this technique is $\pm1\%$, thus trace amounts of a molybdo–anion complex would not be detected. Pettersson[22] determined the speciation of molybdophosphates at 25°C over the pH range 3–9. At low pH, the total molybdenum(VI) concentration was comprised almost solely of complex molybdenum-phosphate species, but above pH 7, only MoO_4^{2-} was detected. The combined results of these two studies suggest that the concentration of possible molybdophosphate species at pHs higher than 7.2 would be negligibly small.

(a) *The effect of* SO_4^{2-} *addition.* The effect of SO_4^{2-} upon the rate of $Co(NH_3)_5MoO_4^+$ formation was assessed by adding Na_2SO_4 to a 0.10 M MoO_4^{2-} stock solution prior to mixing with 0.0040 M cobalt(III) at pH 7.54. The results of these experiments are summarized in Table 4(a) and show that SO_4^{2-} has only a marginal effect upon k_{obs}.

(b) *The effect of* HPO_4^{2-} *addition.* In view of the small rate enhancement caused by the addition of sodium sulphate to the reactant system, a preliminary stopped-flow experiment was performed, under identical solution conditions, using 0.025 M Na_2HPO_4. The resultant reaction was too fast for accurate detection using the stopped-flow technique. The concentration of HPO_4^{2-} was then reduced by a factor of 50 and the reaction transient

Table 4. General catalysis of $Co(NH_3)_5MoO_4^+$ formation at 25°C and $\mu = 1.0$ M

(a) Catalysis by SO_4^{2-}

pH	$[Co^{III}]$ (M)	$[MoO_4^{2-}]$ (M)	$[SO_4^{2-}]^a$ (M)	k_{obs} (s^{-1})
7.54	0.0020	0.050	0	5.05±0.13
			0.0025	5.57±0.22
			0.025	6.22±0.22
			0.100	6.59±0.45

(b) Catalysis by HPO_4^{2-}

pH	$[Co^{III}]$ (M)	$[MoO_4^{2-}]$ (M)	$[HPO_4^{2-}]^a$ $\times 10^3$ (M)	k_{obs} (s^{-1})
7.35	0.0020	0.050	0	11.5±0.6
			0.25	18.1±1.2
			0.50	21.3±0.9
			0.75	27.7±2.5
			1.00	31.3±1.5
7.54			0	5.01±0.18
			0.50	11.6±0.3
			1.00	18.7±1.0
			1.75	25.3±1.2
			2.50	37.3±3.1
			25.0	Too fast
7.84			0	4.33±0.23
			0.50	7.28±0.26
			1.00	11.5±0.8
			1.75	15.9±0.7
			2.50	20.7±1.8

(c) The effect of $[NaHCO_3]$ upon the rate of complex formation

pH	$[Co^{III}]$ (M)	$[MoO_4^{2-}]$ (M)	$[HCO_3^-]^a$ $\times 10^3$ (M)	k_{obs} (s^{-1})
7.25	0.0020	0.025	0	5.62±0.06
			1.25	7.96±0.12
			2.50	10.3±0.4
			3.75	12.6±0.5
			5.00	14.6±0.5
7.50			0	2.53±0.06
			1.25	4.67±0.14
			2.50	6.8±0.2
			3.75	8.6±0.2
			5.00	10.9±0.4
7.81			0	1.38±0.05
			3.13	5.4±0.2
			6.25	10.1±0.9
			9.38	14.4±0.5
			12.5	19.3±1.5

[a] Refers to the added concentrations of Na_2SO_4, Na_2HPO_4 and $NaHCO_3$ at the "instant of mixing".

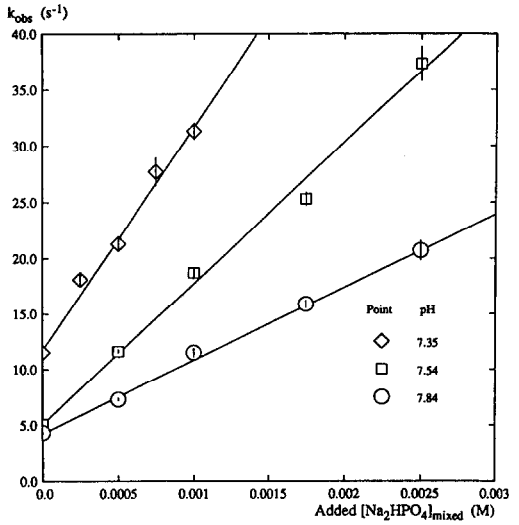

Fig. 2. The effect of pH and total phosphate concentration on the rate of $Co(NH_3)_5OH^{2+}/MoO_4^{2-}$ complexation at 25°C and 1.0 M ionic strength. $[Co^{III}] = 0.0020$ M. $[MoO_4^{2-}] = 0.050$ M.

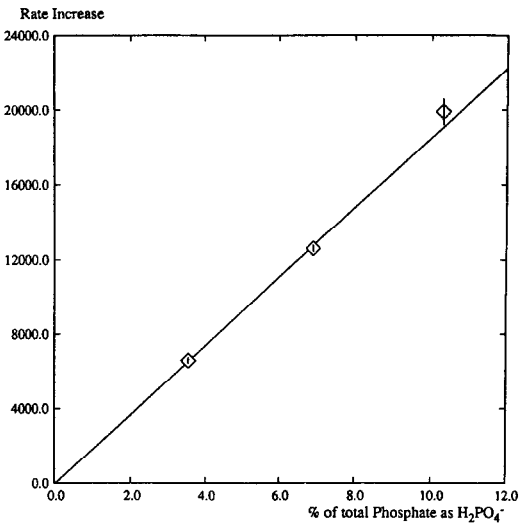

Fig. 3. The catalytic activity of $H_2PO_4^-$ on the rate of $Co(NH_3)_5OH^{2+}/MoO_4^{2}$ complexation at 25°C and 1.0 M ionic strength. $[Co^{III}] = 0.0020$ M. $[MoO_4^{2-}] = 0.050$ M.

showed that even at 5×10^{-4} M, this species doubled the rate of $Co(NH_3)_5MoO_4^+$ formation. Further stopped-flow runs were then conducted to determine the dependence of this rate enhancement upon the concentration of added Na_2HPO_4 and the solution pH. Solution conditions and the observed first-order rate constants for these experiments are listed in Table 4(b).

Figure 2 shows that rate enhancement is linearly dependent upon Na_2HPO_4 at a given pH, but also that the degree of enhancement is acid dependent. The slope of the plot at each pH is a measure of "catalytic activity". The results of the linear analysis of these plots are presented in Table 5.

In the pH range 7–8, phosphate solutions contain both HPO_4^{2-} and $H_2PO_4^-$. The relative proportions of these species are determined by the deprotonation equilibria:

$$H_2PO_4^- \overset{K_a}{\rightleftharpoons} HPO_4^{2-} + H^+.$$

A value of 6.40 ± 0.06 was determined for pK_a at 25.0°C and $\mu = 1.0$ M ($NaClO_4$), by potentiometric titration with NaOH in CO_2-free water, using the automatic titration equipment described elsewhere.[23] This value is in good agreement with the 6.46 ± 0.02 quoted by Smith and Martell under the same conditions.[24]

Figure 3 shows a plot of the catalytic activity vs the percentage of total phosphate as $H_2PO_4^-$. It is apparent from this plot that rate enhancement is linearly dependent upon $[H_2PO_4^-]$ and also, that this species is the only detectable catalyst in solution.

Complications arising from anation reactions between the cobalt(III) and phosphate species in the stopped-flow chamber were not expected since these processes occur by slow cobalt–oxygen bond fission.[25] Hence, $Co(NH_3)_5MoO_4^+$ formation would be essentially complete before any cobalt(III) phosphate complexation occurs.

(c) *The effect of* HCO_3^- *addition.* The addition reaction of CO_2 to $Co(NH_3)_5OH^{2+}$ occurs over the same time frame as the molybdate complexation process[26] and hence poses a potential interference to the desired reaction sequence (due to competition

Table 5. Determination of the pH dependence of Na_2HPO_4 catalytic efficiency on the rate of $Co(NH_3)_5OH_2^{3+}/MoO_4^{2-}$ complexation at 25°C and 1.0 M ionic strength

pH	$[H^+] \times 10^8$	% of Na_2HPO_4 as $H_2PO_4^-$	Slope (catalytic activity)	Intercept	Correction coefficient
7.35	4.47	10.30	19900 ± 1400	11.7 ± 0.6	0.9956
7.54	2.88	6.90	12600 ± 420	5.1 ± 0.1	0.9978
7.84	1.45	3.55	6580 ± 340	4.2 ± 0.2	0.9976

Table 6. Determination of the pH dependence of $NaHCO_3$ catalytic efficiency on the rate of $Co(NH_3)_5OH_2^{3+}/MoO_4^{2-}$ complexation at 25°C and 1.0 M ionic strength

pH	$[H^+] \times 10^8$	% of carbonate as H_2CO_3	% of carbonate as HCO_3^- [1]	Slope	Intercept	Correction coefficient
7.25	5.62	1.15×10^{-2}	94.47	1830±62	5.63±0.06	0.9998
7.50	3.16	6.62×10^{-3}	96.27	1655±45	2.54±0.06	0.9996
7.81	1.55	3.26×10^{-3}	96.88	1363±37	1.37±0.09	0.9994

between MoO_4^{2-} and CO_2 for the cobalt(III) ions). However, the nature of the Co^{III}/MoO_4^{2-} complexation reaction and a careful choice of experimental parameters enables some very informative, semi-quantitative results to be obtained. Taylor found that with $[Mo^{VI}]$ in large excess, the rate of $Co(NH_3)_5MoO_4^+$ formation was independent of $[Co^{III}]$ and observations during preliminary stopped-flow runs in this work indicated that the presence of $NaHCO_3$ had no obvious effect on the reaction transient for this process. The transients were first-order for at least five half-lives and also showed no diminution in absorbance change during reaction upon increased bicarbonate concentration. There was also no indication of a second, first-order transient corresponding to $Co(NH_3)_5CO_3^+$ formation. By limiting the lowest pH solutions to 7.25, the amount of dissolved CO_2 was kept below 5% of the total carbonate concentration and the ratio of MoO_4^{2-} to CO_2 was never less than 2000.

It was found that the presence of $NaHCO_3$ in solution during stopped-flow runs substantially increased the rate of $Co(NH_3)_5MoO_4^+$ formation. Solutions were prepared from CO_2-free water in a nitrogen-filled glove-box. The results of the catalysis experiments are summarized in Table 4(c). The catalytic activity of $NaHCO_3$ was determined in an identical manner to the phosphate system and the linear fit parameters to the k_{obs} vs $[NaHCO_3]$ plots are given in Table 6.

The determination of the active catalytic species is complicated by extensive carbonate speciation and potential reaction with $Co(NH_3)_5OH^{2+}$. Over the pH range studied, CO_3^{2-}, HCO_3^-, H_2CO_3 and dissolved CO_2 are all present in solution. The relationship between these species and the cobalt(III) reaction products is shown in the following equilibrium scheme:

$$H_2O + CO_2 \overset{K_1}{\rightleftharpoons} H_2CO_3 \overset{K_2}{\rightleftharpoons} H^+ + HCO_3^- \overset{K_3}{\rightleftharpoons} H^+ + CO_3^{2-}$$

$$Co(NH_3)_5OH^{2+} \Big\| K_E$$

$$Co(NH_3)_5HCO_3^{2+} \overset{K_H}{\rightleftharpoons} Co(NH_3)_5CO_3^+ + H^+$$

The deprotonation equilibrium involving HCO_3^- and CO_3^{2-} has been well-characterized with a pK_3 value of 9.57 at 25°C and $\mu = 1.0$ M.[24] Dissolved CO_2 and H_2CO_3 are in an equilibrium heavily favouring CO_2, to the extent that the equilibrium constants K_1 and K_2 are normally combined into one apparent pK_{app} for the "deprotonation of CO_2"[26] ($pK_{app} = 6.02$ at 25°C and $\mu = 1.0$ M[24]). A limited amount of work has been done on resolving K_{app} into its K_1 and K_2 components. van Eldik and Palmer report values for these constants of 2.28×10^{-3} and 4.6×10^{-4} M, respectively in 0.5 M NaCl.[27] In the absence of values at 1.0 M $NaClO_4$, these results were used, in combination with K_3, to calculate preliminary carbonate speciation in the molybdate solutions, at the pH values used in this study. The close agreement between the resultant K_{app} value at $\mu = 0.5$ M NaCl[26] and the 1.0 M $NaClO_4$ value indicates that the error introduced by this procedure would be negligible in comparison to the inherent errors in the measurement of the observed rate constants and the effects of cobalt(III)–carbonato complexation. The calculated percentages of total carbonate as H_2CO_3 and HCO_3^- at the "instant of mixing" are included in Table 6.

The plot of catalytic activity against apparent percentage H_2CO_3, shown in Fig. 4, demonstrates that although the doubly protonated species appears to be the major catalyst for the formation of $Co(NH_3)_5MoO_4^+$, the large positive intercept term indicates that another species, most probably HCO_3^-, is also responsible for some rate-enhancing effect. As there is considerable doubt as to the actual concentrations of these species, no further attempt was made to accurately quantify these effects.

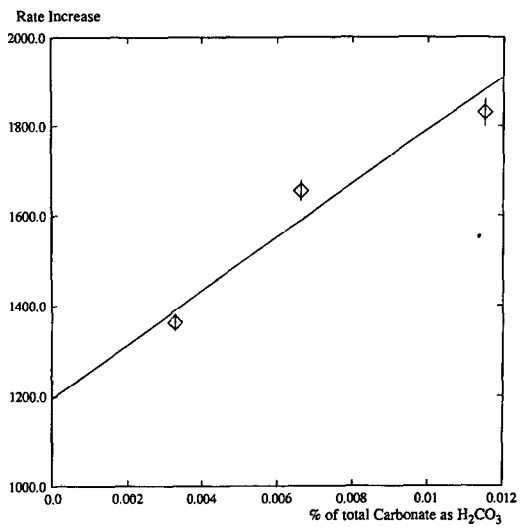

Fig. 4. The catalytic activity of H_2CO_3 on the rate of $Co(NH_3)_5OH^{2+}/MoO_4^{2-}$ complexation at 25°C and 1.0 M ionic strength. $[Co^{III}] = 0.0020$ M. $[MoO_4^{2-}] = 0.050$ M.

DISCUSSION

The reinvestigation of the pH and molybdate dependence for the formation of $Co(NH_3)_5MoO_4^+$, resulted in an expression for the forward rate term which corresponded exactly with that proposed by Taylor[2] [eq. (2)]. After allowing for a plausible difference, by a factor of two, in evaluating the MoO_4^{2-} concentration (stock or "instant of mixing"), the individual second- and third-order rate constants comprising this term were also in good agreement. However, after consideration of the catalytic effect of several protonated anions, an alternative reaction scheme can be proposed to account for the apparent second-order dependence upon $[MoO_4^{2-}]$, observed in both studies. Scheme 1, shown below, involves direct reaction between the cobalt(III) and MoO_4^{2-} species and also requires proton donation from an external "acid catalyst". The resultant rate expression from this scheme also conforms to the observed pH and concentration dependences expressed in eq. (2).

The catalytic species, HA, may be any moiety in solution capable of proton donation to the molybdate to assist in water elimination. In this scheme, the reaction between cobalt(III) and MoO_4^{2-}, observed by Taylor, is catalysed by $HMoO_4^-$ in solution. Although the concentration of $HMoO_4^-$ constitutes less than 0.1% of the total molybdate, it is still present at levels 100–1000 times higher than $[H^+]$. The added catalysts $H_2PO_4^-$, H_2CO_3 and possibly HCO_3^- contribute to the total solution "pool" of proton-donating species.

If the mechanism involves rate-determining proton-transfer and water departure, then the degree of rate enhancement should reflect the acidity of the proton which migrates to the molybdenum(VI) hydroxy group. The slope of the catalytic activity plot is a direct measure of the effectiveness of that species to increase the rate of $Co(NH_3)_5MoO_4^+$ formation. The slope of the plot for H_2CO_3, $(6.0 \pm 0.9) \times 10^4$, is much greater than that for $H_2PO_4^-$, $(1.9 \pm 0.1) \times 10^3$, which can be attributed to the greater acidity of the carbonate species. The slope estimate for H_2CO_3 is a lower limit since no account was taken of the effect of $Co(NH_3)_5CO_3^+$ formation upon carbonate speciation. Clearly, the existence of any correlation between the pK_a of the proton-donating anion and the catalytic efficiency of the species, based only upon two anions, must remain speculative. Further investigation using a wide variety of substitution-inert, proton-donating species may help clarify this situation. It might also be expected that a second-order dependence upon cobalt(III) concentration would be observed with this species in excess over $[MoO_4^{2-}]$. In addition, $Co(NH_3)_5OH_2^{3+}$ would be the likely catalyst due to the greater acidity of the aquo ligand's proton relative to the $Co(NH_3)_5OH^{2+}$ proton. Another advantage of using excess cobalt(III) is that the complications arising from $HMoO_4^-$ catalysis could be minimized.

Path (b) in Scheme 1 involves the initial formation of the protonated complex, $Co(NH_3)_5HMoO_4^{2+}$, followed by rapid deprotonation to $Co(NH_3)_5MoO_4^+$. It has been demonstrated that the incorporation of a $Co(NH_3)_5$ group into the coordination sphere of various oxo anions

(a) $Co(NH_3)_5OH_2^{3+} + MoO_4^{2-} \rightleftharpoons Co(NH_3)_5MoO_4^+ + H_2O$,

(b) $Co(NH_3)_5OH_2^{3+} + HMoO_4^- \rightleftharpoons Co(NH_3)_5MoO_4^+ + H_2O + H^+$,

(c) $Co(NH_3)_5OH^{2+} + MoO_4^{2-} + HA \rightleftharpoons Co(NH_3)_5MoO_4^+ + H_2O + A^-$,

(d) $Co(NH_3)_5OH_2^{3+} + MoO_4^{2-} + HA \rightleftharpoons Co(NH_3)_5MoO_4^+ + H_2O + HA$.

Scheme 1. Various possible reaction paths for the formation of $Co(NH_3)_5MoO_4^+$.

(AsO_4^{3-}, PO_4^{3-}, SeO_3^{3-}, CrO_4^{2-}) dramatically enhances the acidity of any ionizable protons on that anion.[28-31] It is therefore assumed that the pK_a of $Co(NH_3)_5HMoO_4^{2+}$ will be significantly lower than $HMoO_4^-$ itself (3.92 at 25°C and $\mu = 1.0$ M[5]) and consequently, at pH values above 7, the concentration of the protonated product would be negligible.

The almost complete indifference of the reaction rate to added SO_4^{2-} suggests that the catalysis involves proton transfer. It may be argued that the very small dependence of k_{obs} upon increasing sulphate concentration [Table 4(a)] is due to trace amounts of HSO_4^-, but it is equally plausible that this dependence is simply a medium effect resulting from the relatively high concentrations of added Na_2SO_4 (up to 0.1 M). Taylor noted that changing the electrolyte from $NaClO_4$ to $LiClO_4$ caused a marked decrease in k_{obs}. It is interesting to note that the addition of Na_2SO_4 did not retard the complexation reaction as was observed with the formation of Co(tetren)HSO_3^{2+}.[22] This decrease in rate upon addition of SO_4^{2-} was attributed to the formation of unreactive $\{Co(tetren)OH_2^{3+} \cdots SO_4^{2-}\}$ ion pairs.

Unfortunately, definitive assignment of reaction pathways to the terms in the rate expression is impossible due to the inherent proton ambiguities. Paths (a) and (d) in Scheme 1 may be rewritten as reactions involving $Co(NH_3)_5OH^{2+}$ and $HMoO_4^-$, as proposed by Taylor. It is believed that the reaction between Co—OH and $HMoO_4^-$ is more likely than Co—OH_2 and MoO_4^{2-}, since the latter option requires transfer of both protons from the aquo ligand to a molybdenum(VI) oxygen, whereas only one transfer to the molybdenum(VI) hydroxo ligand is necessary from $Co(NH_3)_5OH^{2+}$. Conversely, significant ion-pairing and internal hydrogen-bonding would favour the +3/−2 reaction. Paths (a) and (b) may also be expressed in terms of external proton donation or catalysis as shown below:

(e) $Co(NH_3)_5OH^{2+} + MoO_4^{2-} + H^+ \rightleftharpoons Co(NH_3)_5MoO_4^+ + H_2O$

(f) $Co(NH_3)_5OH_2^{3+} + MoO_4^{2-} + H^+ \rightleftharpoons Co(NH_3)_5MoO_4^+ + H_2O + H^+$.

The attractive feature of this last proposal is that paths (e) and (f) are identical to the general catalysis paths (c) and (d) (except that HA is now specifically H^+) and therefore, only two reactions are required to describe the entire complexation process.

Figure 5 depicts possible transition states for the various pathways proposed for the complexation

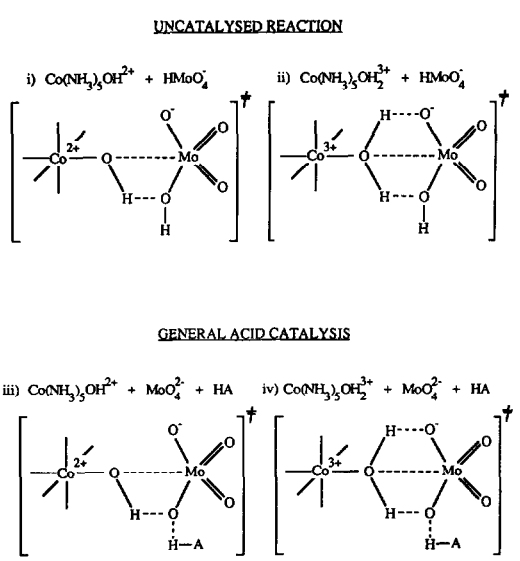

Fig. 5. Proposed transition states for cobalt(III) molybdate complexation.

process. The $HMoO_4^-$ anion has been assigned as the reactive molybdenum(VI) species in the uncatalysed reactions on the basis of the proton-transfer argument discussed above, and also to allow direct comparison with other molybdate substitution processes which are all expressed in terms of this protonated species. The specific proton-catalysed reaction pathways are incorporated into the general acid terms (iii) and (iv), where HA = H^+. The rate constants for the formation of transition states (i)–(iv) are given by:

(i) $k_1 = k_a \times K_H/K_{HM} = 6.6 \times 10^4\ M^{-1}\ s^{-1}$
(ii) $k_2 = k_b/K_{HM} = 1.3 \times 10^6\ M^{-1}\ s^{-1}$
(iii) $k_3 = k_c \times K_H = 2.1 \times 10^{10}\ M^{-3}\ s^{-1}$
(iv) $k_4 = k_d = 3.6 \times 10^{11}\ M^{-3}\ s^{-1}$;

where K_H and K_{HM} are the acidity constants for $Co(NH_3)_5OH_2^{3+}$ (4.79×10^{-7} at 25°C and $\mu = 1.0$ M[10]) and $HMoO_4^-$, respectively.

The rate constants, k_1 and k_2, for the uncatalysed reaction of $HMoO_4^-$ with $Co(NH_3)_5OH^{2+}$ and $Co(NH_3)_5OH_2^{3+}$, respectively, are much lower than for a series of bidentate ligands, shown in Table 7, where the second-order rate constants falls in the range $(0.4\text{–}2.0) \times 10^8\ M^{-1}\ s^{-1}$. These faster reactions have all been attributed to ligand addition processes where the molybdenum(VI) centre expands its coordination to six and Mo—O bond cleavage is unnecessary. Although the reaction of $HMoO_4^-$ with H_2EDTA^{2-} forms an octahedral molybdenum(VI) complex, the slow rate of reaction results from the necessity to break one Mo—O bond.

Table 7. Second-order rate constants for complexation with $HMoO_4^-$ at 25°C[a]

Ligand (L)	Rate constant ($M^{-1}\,s^{-1}$)	Product	Denticity number of L	Reference
$Co(NH_3)_5OH^{2+}$	6.6×10^4	MoO_3L^+	1	This work
$Co(NH_3)_5OH_2^{3+}$	1.3×10^6	MoO_3L^+	1	This work
H_2EDTA^{2-}	2.3×10^5	$MoO_3L_3^{2-}$	3	33
$Oxine^-$	1.5×10^8	$MoO_2(OH)_2L_2^-$	2	34
$(Oxine)SO_3^{2-}$	4.0×10^7	$MoO_2(OH)_2L_2^{2-}$	2	35
$Hcatechol^-$	1.9×10^8	$MoO_2(OH)_2L_2^{2-}$	2	36

[a] Adapted from ref. 1.

A comparison of the rate constants for the two uncatalysed processes (k_1 and k_2), reveals that complexation occurs more quickly with $Co(NH_3)_5OH_2^{3+}$ than the corresponding hydroxo species. The importance of ion-pairing in this reaction scheme was dismissed in the previous study,[1] by analogy with the weak outer-sphere interaction between $Co(NH_3)_6^{3+}$ and MoO_4^{2-}. However, the formation of hydrogen-bonding contacts between the anions $HSeO_3^-$ or $HCrO_4^-$ and $Co(NH_3)_5OH_2^{3+}$ resulted in values for the ion-pairing constant, K_{os}, of between 6 and 8 M^{-1}.[31,37] Even allowing for an order of magnitude difference between K_{os} values for the $+3/-1$ and $+2/-1$ ion-pairs, the intrinsic rate constant for the reaction with the aquo species is still twice that for the cobalt(III) hydroxo ligand. Thus, the effect of increased hydrogen bonding in the transition state and greater proton acidity for reaction with $Co(NH_3)_5OH_2^{3+}$ slightly outweighs the higher nucleophilicity of the hydroxo ligand in $Co(NH_3)_5OH^{2+}$, in determining the more reactive cobalt(III) species towards $HMoO_4^-$.

Even with the absence of supporting activation parameters for this reaction, it still seems reasonable that, in view of the associative nature of the MoO_4^{2-}–oxygen exchange reaction,[38] the extent of bond formation in the complexation transition state outweighs bond breaking. Consequently, changing the nature of the inert cation substituting into the molybdenum coordination sphere should affect the rate of complex formation.

CONCLUSION

Whilst the form of the rate law for the complexation reaction between MoO_4^{2-} and aquo- and hydroxo-pentamminecobalt(III) cations in basic solution is consistent with a previous proposal for the existence of dimeric molybdenum(VI) species, general anion catalysis experiments show that an alternative mechanism is likely. The observed rate of reaction is enhanced by anionic species capable of proton donation to the molybdenum(VI) hydroxo ligand, thereby facilitating water elimination from the transition state. The apparent second-order dependence upon $[MoO_4^{2-}]$ may be explained by the involvement of $HMoO_4^-$ in proton donation. Consequently, this study found no definitive evidence for the formation of molybdenum dimers in slightly basic solution.

Proton ambiguities preclude definitive identification of reactant species in aqueous solution. An investigation into the direct reaction of MoO_4^{2-} with $Co(NH_3)_5OH_2^{3+}$ or $Co(NH_3)_5OH^{2+}$ in an aprotic solvent may prove beneficial in this regard.

Acknowledgement—M.R.G. is grateful to the Australian Government for the assistance of a Commonwealth Postgraduate Research Award.

REFERENCES

1. R. S. Taylor, *Inorg. Chem.* 1977, **16**, 116.
2. V. W. Day, M. F. Fredrich, W. G. Klemperer and W. J. Shum, *J. Am. Chem. Soc.* 1977, **99**, 6146.
3. J. J. Cruywagen and J. B. B. Heyns, *Inorg. Chem.* 1987, **26**, 2569.
4. M. J. Taylor and J. M. Coddington, Conference Abstract M25, XXVII International Conference on Coordination Chemistry, Queensland, Australia (1989).
5. P. L. Brown, M. E. Shying and R. N. Sylva, *J. Chem. Soc., Dalton Trans.* 1987, 2149.
6. F. Basolo and R. K. Murmann, *Inorg. Synth.* 1953, **4**, 171.
7. R. van Eldik and G. M. Harris, *Inorg. Chem.* 1980, **19**, 880.
8. W. E. Jones and T. W. Swaddle, *Can. J. Chem.* 1967, **45**, 2647.
9. B. F. Abrahams, M. R. Grace, B. F. Hoskins and P. A. Tregloan, *Inorg. Chem. Acta* 1991, **182**, 135.
10. A. I. Vogel, *Textbook of Quantitative Inorganic Analysis*, 4th edn. Longmans, London (1978).

11. E. König, *Magnetic Properties of Transition Metal Compounds*, Vol. 2. Springer-Verlag, Berlin (1966).
12. Q. H. Gibson and L. Milnes, *Biochem. J.* 1964, **91**, 161.
13. A. A. Frost and R. G. Pearson, *Kinetics and Mechanism*, 2nd edn. John Wiley and Sons, New York (1961).
14. R. Coomber and W. P. Griffith, *J. Chem. Soc. A* 1968, 1128.
15. K. Nakamoto, *Infrared and Raman Spectra of Inorganic and Coordination Compounds*, 3rd edn. Wiley-Interscience, New York (1978).
16. E. König and G. König, *Magnetic Properties of Transition Metal Compounds*, Supplement 2. Springer-Verlag, Berlin (1979).
17. H. A. Benesi and J. H. Hildebrand, *J. Am. Chem. Soc.* 1949, **71**, 2703.
18. C. F. Baes Jr and R. E. Mesmer, *The Hydrolysis of Cations*. Wiley-Interscience, New York (1976).
19. W. G. Jackson, C. N. Hookey, M. L. Randall, P. Comba and A. M. Sargeson, *Inorg. Chem.* 1984, **23**, 2473.
20. For example: A. Yagasaki, I. Andersson and L. Pettersson, *Inorg. Chem.* 1987, **26**, 3926.
21. K. Murata and S. Ikeda, *Polyhedron* 1987, **6**, 1681.
22. L. Pettersson, *Acta Chem. Scand.* 1971, **25**, 1958.
23. A. Campisi and P. A. Tregloan, *Inorg. Chim. Acta* 1985, **100**, 251.
24. R. M. Smith and A. E. Martell, *Critical Stability Constants*, Vol. 4. Plenum Press, New York (1976).
25. S. F. Lincoln and D. R. Stranks, *Aust. J. Chem.* 1968, **21**, 37.
26. E. Chaffee, T. S. Dasgupta and G. M. Harris, *J. Am. Chem. Soc.* 1973, **95**, 4169.
27. R. van Eldik and D. A. Palmer, *J. Soln Chem.* 1982, **11**, 339.
28. *Stability Constants of Metal-Ion Complexes*, IUPAC Chemical Data Series, No. 21. Pergamon Press, Oxford (1982).
29. T. A. Beech, N. C. Lawrence and S. F. Lincoln, *Aust. J. Chem.* 1973, **26**, 1877.
30. A. D. Fowless and D. R. Stranks, *Inorg. Chem.* 1977, **16**, 1271.
31. M. R. Grace and P. A. Tregloan, manuscript in preparation.
32. A. C. Dash, A. A. El-Awady and G. M. Harris, *Inorg. Chem.* 1981, **20**, 3160.
33. D. S. Honig and K. Kustin, *J. Am. Chem. Soc.* 1973, **95**, 5525.
34. P. F. Knowles and H. Diebler, *Trans. Faraday Soc.* 1968, **84**, 977.
35. H. Diebler and R. E. Timms, *J. Chem. Soc. A.* 1971, 273.
36. K. Kustin and S.-T. Liu, *J. Am. Chem. Soc.* 1976, **98**, 2487,
37. A. D. Fowless and D. R. Stranks, *Inorg. Chem.* 1977, **16**, 1276.
38. H. Gamsjäger and R. K. Murmann, *Advances in Inorganic and Bioinorganic Mechanisms* (Edited by A. G. Sykes), Vol. 2. Academic Press, London (1983).

Polyhedron Vol. 10, No. 19, pp. 2331–2335, 1991
Printed in Great Britain

0277–5387/91 $3.00+.00
© 1991 Pergamon Press plc

COORDINATION OF COPPER(II) IONS BY α,β-DEHYDRO-DIPEPTIDES. POTENTIOMETRIC AND SPECTROSCOPIC STUDY

M. JEŻOWSKA-BOJCZUK and H. KOZŁOWSKI*

Institute of Chemistry, University of Wrocław, F. Joliot-Curie 14, 50-383 Wrocław, Poland

and

I. SOVAGO

Institute of Inorganic and Analytical Chemistry, University of Debrecen, H 4010-Debrecen, Hungary

and

Z. KUBICA, B. RZESZOTARSKA and L. SMEŁKA

Institute of Chemistry, Pedagogical University of Opole, 45-052 Opole, Poland

(*Received* 7 *February* 1991; *accepted* 23 *May* 1991)

Abstract—Potentiometric and spectroscopic data have shown that the double bond within dehydro-peptides considerably affects their behaviour as ligands relative to their saturated parents, with proton and copper(II) ions.

α,β-Dehydro-amino acids, or by convention Δ-amino acids, are unsaturated analogues of the respective α-amino acids. They exhibit various biological activities and specific structural properties important for many biomolecules.[1–4]

The (*Z*) isomers of Δ-amino acids are much more common than the (*E*) isomers, which were found only for Δ-His and Δ-Ile in a few antibiotics.[2] These structural as well as chemical features which are characteristic for Δ-amino acids should also be critical for their coordination abilities compared to the parent peptides. In this work we present the potentiometric and spectroscopic data for a series of copper(II) complexes with α,β-dehydro-dipeptides and the respective saturated dipeptides.

EXPERIMENTAL

Ligands

α,β-Dehydro-dipeptides were synthesized according to refs 5–8 and Gly-Δ-Leu and Gly-Δ-Phe had the (*Z*) configuration. Gly–Ala and Gly–Phe were obtained from the corresponding protected dipeptides via successive saponification of methyl esters and hydrogenation of the benzyloxycarbonyl groups. Analytical data of the free peptides were in agreement with those from the literature.[9] Gly–Leu came from Fluka. The purities and the exact concentrations of ligands in solution were determined by the Gran method.[10]

Potentiometric studies

The stability constants of the proton and copper(II) complexes of the ligands were determined by pH-metric titrations of 5 cm^3 samples in the pH range 3–10. The concentration of copper(II) chloride stock solution was measured gravimetrically via precipitation of the oxinate. The ligand concentration was 4×10^{-3} mol dm^{-3}, the metal to ligand ratios were 0:1, 1:1, 1:2 or 1:4, and the ionic strength was adjusted to 0.2 mol dm^{-3} (KCl). The titrations were performed with KOH solution of a known concentration (*ca* 0.2 mol dm^{-3}). The pH was measured at 298 ± 0.1 K with a radiometer pHM 64 instrument with a GK2301

* Author to whom correspondence should be addressed.

combined electrode. The electrode system was calibrated by the method described by Irving *et al.*[11] to convert the pH-meter readings to hydrogen ion concentrations. The stability constants $\beta_{pqr} = [M_pA_qH_r]/[M]^p[A]^q[H]^r$ were calculated from the pH-metric titration curves with a PSEQUAD computer program.[12]

Spectroscopic studies

Absorption spectra were recorded on a Beckman UV 5240 spectrophotometer and circular dichroism (CD) spectra on an automatic JASCO J-20 spectropolarimeter. EPR spectra were taken on a RADIOPAN SE/X spectrometer at 120 K and 9.3 GHz. The copper(II) ion concentration in the solutions measured was adjusted to 3×10^{-3} and the metal to ligand ratio of 1 : 3.

RESULTS AND DISCUSSION

Protonation constants (pK values) for the ligands investigated are given in Table 1. There are two protonation steps (*ca* pH 3 and 7–8) which clearly correspond to proton dissociation from the carboxyl and the amino groups, respectively. The appearance of a double bond at the C-terminal α-carbon slightly decreases the basicity of the amino group compared to the relative parent peptides. This may suggest that some electronic density is transferred from the amino nitrogen into the conjugated double bond system of the Δ-residue. The acidity of the carboxyl group increases for Δ-Ala dipeptides and decreases for dipeptides with another Δ-residue. This indicates that the α,β-double bond alone stabilizes the carboxylate anion in the system studied similarly in acrylic acid (pKa 4.26) compared to propionic acid (pKa 4.87). The (*Z*)-side-chain of the Δ-residue exerts a destabilizing effect as with the (*Z*)-substituent in α,β-dehydro-acids.

Table 1. Proton dissociation constants for dehydrodipeptides and some of their saturated counterparts; $T = 298$ K, $I = 0.2$ mol dm^{-3}

Peptide	pK (NH_3^+)	pK (COOH)	log β
Gly–Ala	8.15	3.10	11.25
Gly–Leu	8.18	3.16	11.34
Gly–Phe	8.09	2.99	11.08
Gly-Δ-Ala	7.97	2.83	10.80
Val-Δ-Ala	7.77	2.85	10.62
Phe-Δ-Ala	7.35	2.85	10.20
Gly-Δ-Leu	8.06	3.47	11.53
Gly-Δ-Val	8.15	3.65	11.80
Gly-Δ-Phe	8.00	3.17	11.17

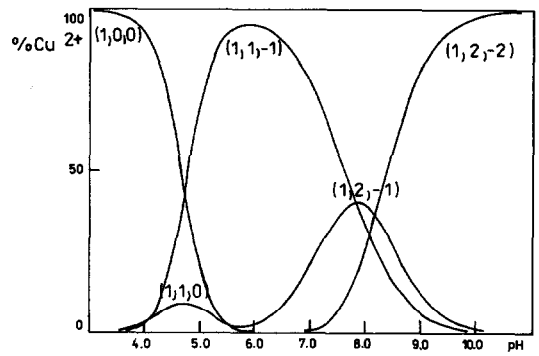

Fig. 1. Concentration distribution curves of the complexes present in the copper(II) Gly-Δ-Leu solution for ligand concentration 4×10^{-3} mol dm^{-3} and 1 : 3 metal to ligand ratio

All investigated dehydro-dipeptides form stable complexes with copper(II) ions and the stability constants (Fig. 1, Table 2) derived from potentiometric titrations could be obtained with a high level of accuracy. The binding modes seem to be the same as in ordinary dipeptides, i.e. the coordination starts at the amino nitrogen and then follows to the amide and the carboxyl groups. This coordination is seen clearly from the spectroscopic data (Table 3).

Copper(II) complexes with X-Δ-Ala

The CD spectra of Phe-Δ-Ala or Val-Δ-Ala complexes exhibit distinct bands characteristic of the amine and amide nitrogen to metal charge transfer transitions indicating the involvement of both nitrogens in the metal ion coordination. Also, ESR and absorption spectra gave good evidence for the species formed (Tables 2 and 3). The species distribution obtained for X-Δ-Ala systems is similar to that for the Gly–Ala system, but the stability constants of complexes with dehydro-peptides are distinctly higher (Table 2). The second deprotonation, i.e. proton dissociation from $CuAH_{-1}$ species occurs around pH 9. The product could be either $CuAH_{-2}$ or CuA_2H_{-2} species. However, the pK value of this process being around 9.2 corresponds precisely to the values obtained for saturated dipeptides for which the hydrolysis (the formation of $CuAH_{-2}$) was proved undoubtedly.[13] Also, in the stability constant calculations the best fit was gained with the $CuAH_{-2}$ complex rather than the CuA_2H_{-2} species. The formation of the former complex at the higher pH range is supported by the absorption spectra which do not change dras-

Table 2. Stability constants ($\log\beta$) of copper(II) complexes of dehydro-dipeptides and some of their saturated counterparts; $T = 298$ K, $I = 0.2$ mol dm^{-3}

Peptide	CuA	$CuAH_{-1}$	CuA_2H_{-1}	CuA_2H_{-2}	$CuAH_{-2}$	$Cu_2A_2H_{-3}$	pK_2-CuA	pK_1^{amid}	$\log K^{CuAH}_{CuA_2H_{-1}}$	pK_2^{amid}
Gly–Ala	5.73	1.52	4.89	—	−7.80	−4.05	2.42	4.21	3.37	—
Gly–Leu	5.75	1.03	4.28	—	−8.17	−4.73	2.43	4.72	3.25	—
Gly–Phe	5.58	1.76	4.94	—	−7.44	−3.48	2.51	3.82	3.18	—
Gly-Δ-Ala	5.63	3.23	6.29	—	−6.04	−0.82	2.34	2.40	3.06	—
Val-Δ-Ala	5.84	3.22	5.53	—	−6.02	—	1.93	2.62	2.31	—
Phe-Δ-Ala	6.22	3.34	5.82	—	−5.86	—	1.13	2.88	2.48	—
Gly-Δ-Leu	5.27	1.22	4.50	−3.67	—	—	2.79	4.05	3.28	8.17
Gly-Δ-Val	5.70	0.82	4.23	−4.02	—	—	2.45	4.88	3.41	8.25
Gly-Δ-Phe	5.40	2.03	5.45	−1.94	—	—	2.60	3.37	3.42	7.39

Table 3. Spectroscopic data for copper(II) complexes of dehydro-dipeptides

Species	EPR $A_\parallel$[G]	EPR $g_\parallel$	Absorption λ nm (ε)	CD λ nm ($\Delta\varepsilon$)	
Gly-Δ-Ala					
$CuAH_{-1}$	183	2.25	632 (120)		
$CuAH_{-2}$	170	2.23	620 (120)		
Val-Δ-Ala					
$CuAH_{-1}$	182	2.25	640 (83)	650 (−0.57)	B+E
				325 (+1.00)	$N^- \rightarrow Cu$
				265 (−1.82)	$NH_2 \rightarrow Cu$
$CuAH_{-2}$	164	2.24	610 (82)	625 (−0.55)	B
				540 (−0.62)	E
				320 (−0.81)	$N^- \rightarrow Cu$
				270 (+4.04)	$NH_2 \rightarrow Cu$
CuA_2H_{-2}[a]	206	2.18			
Phe-Δ-Ala					
$CuAH_{-1}$	182	2.25	625 (120)	645 (+0.24)	B+E
				325 (+0.35)	$N^- \rightarrow Cu$
				263 (−8.69)	$NH_2 \rightarrow Cu$
$CuAH_{-2}$	170	2.23	620 (125)	662 (+0.24)	B
				sh535 (−0.03)	$E(\Gamma_a)$
				493 (−0.06)	$E(\Gamma_b)$
				263 (−9.39)	$NH_2 \rightarrow Cu$
CuA_2H_{-2}[a]	200	2.19			
Gly-Δ-Val					
CuA	142	2.34	762 (30)		
$CuAH_{-1}$	176	2.25	625 (172)		
CuA_2H_{-1}	170	2.23			
CuA_2H_{-2}	200	2.19	510 (273)		
Gly-Δ-Leu					
CuA	140	2.34	760 (20)		
$CuAH_{-1}$	178	2.25	640 (100)		
CuA_2H_{-1}	167	2.23			
CuA_2H_{-2}	200	2.19	505 (130)		
Gly-Δ-Phe					
CuA	142	2.35	770 (20)		
$CuAH_{-1}$	177	2.25	640 (124)		
CuA_2H_{-2}	201	2.19	520 (153)		

[a] Too low concentration to be clearly observed in CD or absorption spectra.

sh = shoulder.

tically when $CuAH_{-1}$ transforms into $CuAH_{-2}$. The formation of the CuA_2H_{-2} complex with four nitrogens bound to the metal ion should shift the *d–d* transition band to a much higher energy (500–550 nm)[14,15] than that observed for the species discussed, i.e. 620 nm (Table 3). Moreover, only slight variation of the ESR parameters (Table 3) excludes the CuA_2H_{-2} species.[15,16] At very high pH the formation of the latter complex is likely but it is never a dominating species in the solution.

Copper(II) *complexes with Gly-Δ-X ligands*

This group of molecules with X = Leu, Val or Phe, in which a Δ-amino acid residue contains the (*Z*)-side chain, behaves differently than those containing a Δ-Ala residue. There is no pronounced increase in stability of the complexes compared to usual dipeptides (Table 2). However, these ligands give the CuA_2H_{-2} species at pH 7–9 (Fig. 1). The pKs of the formation of the complexes are well below 9.2 (7.4–8.2), excluding the hydrolysis process characteristic of X-Δ-Ala complexes. The parameters of the ESR spectra and the absorption spectra with the *d–d* bands around 500 nm (Table 3) clearly indicate the formation of the four-nitrogen complexes, i.e. the CuA_2H_{-2} species with a $2\times\{NH_2,N^-\}$ coordination mode. The formation of the latter complexes is rather unique for the Gly-Δ-X peptides, although it is possible to observe this kind of species for saturated dipeptides in an extremely high excess of ligand (a 50 : 1 molar ratio). In the latter case the stabilities are about three to five orders lower[17] than those obtained here for Δ-dipeptides. The formation constants collected in Table 2 also indicate the strong impact of the nature of the (*Z*)-side-chain on the stability of the CuA_2H_{-2} species. The weakest complex results from the ligand containing the Δ-Val residue with a methyl group. A slightly stronger complex is formed with Gly-Δ-Leu with an isopropyl group and the strongest one with Gly-Δ-Phe dipeptide with the phenyl side-chain.

CONCLUSIONS

α,β-Dehydro-dipeptides coordinate to cupric ions (similarly to saturated dipeptides) with, however, considerably different stabilities. The stabilities for the X-Δ-Ala complexes are distinctly higher than those of the respective complexes with parent saturated ligands which can derive from the maximal degree of electronic conjugation in the planar $CONH—C(=CH_2)COOH$ moiety.[18–23]

The stabilities of the complexes with the Gly-Δ-X dipeptides (X = Val, Leu and Phe), of which X contains a (*Z*) substituent, are only slightly higher than those of the parent ligands. The formation of the unique CuA_2H_{-2} species is observed. Among the Δ-residues with a (*Z*) substituent, the highest degree of conjugation in the CONH—C=C fragment has been found for Δ-Phe and the lowest for Δ-Val residues.[20] This explains the influence of these side-chains on the stability of the CuA_2H_{-2} complexes.

Acknowledgements—This work was supported by the Polish Ministry of National Education (Projects RP.II.13.1.5. and UPB/112/91/P) and the Hungarian Academy of Sciences (Project 240/86). The authors wish to thank I. Huse and H. Szyszuk for technical help.

REFERENCES

1. K. Noda, Y. Shimonigashi and N. Izumiya, in *The Peptides. Analysis, Synthesis, Biology* (Edited by E. Gross and J. Meienhofer), Vol. 5, p. 285. Academic Press, New York (1983) and refs therein.
2. B. Rzeszotarska, Z. Kubica and J. Tarnawski, *Post. Biochem.* 1987, **33**, 533 and refs therein.
3. U. Schmidt, A. Lieberknecht and J. Wild, *Synthesis* 1988, 159 and refs therein.
4. T. P. Singh, P. Narula and H. C. Patel, *Acta Cryst. Sect. B* 1990, **46**, 539 and refs therein.
5. M. Makowski, B. Rzeszotarska, Z. Kubica and P. Wieczorek, *Liebigs Ann. Chem.* 1984, 920.
6. M. Makowski, B. Rzeszotarska, L. Smełka and Z. Kubica, *Liebigs Ann. Chem.* 1985, 1457.
7. L. Smełka, B. Rzeszotarska, G. Pietrzynski and Z. Kubica, *Liebigs Ann. Chem.* 1988, 485.
8. L. Smełka, B. Rzeszotarska and Z. Kubica, *Liebigs Ann. Chem.*, in press.
9. K. R. Rao, S. M. Birmbaum, R. B. Kingsley and G. P. Greenstein, *J. Biol. Chem.* 1952, **198**, 507.
10. G. Gran, *Acta Chem. Scand.* 1950, **29**, 599.
11. H. Irving, M. G. Miles and L. D. Pettit, *Anal. Chim. Acta* 1967, **38**, 475.
12. L. Zékány and I. Nagypál, in *Computational Methods for the Determination of Stability Constants* (Edited by D. Leggett). Plenum Press, New York (1985).
13. H. Sigel and R. B. Martin, *Chem. Rev.* 1982, **82**, 385.
14. B. Decock-Le Reverend, F. Liman, C. Livera, L. D. Pettit, S. Pyburn and H. Kozłowski, *J. Chem. Soc., Dalton Trans.* 1988, 887.
15. G. Formicka-Kozłowska, H. Kozłowski and B. Jeżowska-Trzebiatowska, *Inorg. Chim. Acta* 1977, **25**, 1.
16. T. Szabo-Planca, G. Peintler, A. Rockenbauer, M. Gyor, M. Varga-Fabian, L. Institorisz and L. Balá-spiri, *J. Chem. Soc., Dalton Trans.* 1989, 1925.
17. E. Farkas and T. Kiss, *Polyhedron* 1989, **8**, 2463.
18. D. Ajó, G. Granozzi, E. Tondello, A. Del Pra and G. Zanotti, *J. Chem. Soc., Perkin Trans.* II 1979, 927.

19. D. Ajó, G. Granozzi, E. Ciliberto and I. Fragalá, *J. Chem. Soc., Perkin Trans.* II 1980, 483.
20. D. Ajó, M. Casarin, G. Granozzi, H. C. J. Ottenheijm and R. Plate, *Recl. Trav. Chim. Pays-Bas* 1984, **103**, 365.
21. K. H. Ongania, G. Granozzi, V. Busetti, M. Casarin and D. Ajó, *Tetrahedron* 1985, **41**, 2015.
22. J. A. Mayoral, C. Cativiela, M. P. Lopez, D. Ajó and F. DeZuane, *J. Crystallogr. Spectrosc. Res.* 1989, **19**, 993.
23. G. Pietrzyński, Z. Kubica and B. Rzeszotarska, in *Peptides 1990, Proc. 21th Eur. Pept. Symp., Platja d'Aro 1990* (Edited by E. Giralt and D. Andreau). Escom Science Publishers B.V., Leiden (1991).

Polyhedron Vol. 10, No. 19, pp. 2337–2340, 1991
Printed in Great Britain

0277–5387/91 $3.00+.00
© 1991 Pergamon Press plc

INVESTIGATIONS INTO THE REACTION OF S_4N_4 WITH $[PPh_4]_2[Pd_2Cl_6]$. THE X-RAY CRYSTAL STRUCTURES OF $[PPh_4]_2[Pd_2(\mu\text{-}S_2N_2)Cl_6]$ AND $[PPh_4][Pd_2(\mu\text{-}S_3N_2)Cl_4]$

PAUL F. KELLY, ALEXANDRA M. Z. SLAWIN, DAVID J. WILLIAMS and J. DEREK WOOLLINS*

Department of Chemistry, Imperial College of Science, Technology and Medicine, South Kensington, London SW7 2AY, U.K.

(*Received* 14 *January* 1991; *accepted* 23 *May* 1991)

Abstract—S_4N_4 reacts with $[PPh_4]_2[Pd_2Cl_6]$ (**1**) in CH_2Cl_2 to give a mixture of $[PPh_4]_2[Pd_2(\mu\text{-}S_2N_2)Cl_6]$ (**2**) and $[PPh_4]_2[Pd_2(\mu\text{-}S_3N_2)Cl_4]$ (**3**). X-ray crystallography reveals (**2**) to contain neutral S_2N_2 as a bridging ligand whilst (**3**) constitutes only the second example of a complex of the bridging $S_3N_2^{2-}$ ligand.

There is currently great interest in the coordination chemistry of sulphur–nitrogen ligands such as the now well-established $S_2N_2^{2-}$, S_3N^- and $S_2N_3^{3-}$[1] anions as well as rarer species such as $S_3N_2^{2-}$ which has only been observed in two complexes. In $[Pd_2(\mu\text{-}S_3N_2)(S_3N)_2]$ which is prepared in very low yield from the reaction of $PdCl_2$ with S_4N_4 in methanol, the sulphur–nitrogen ligand is symmetrical and bridges the two palladium centres *via* its sulphur atoms.[2] In contrast, the ligand in $[Cp_2Ti(S_3N_2)]$ that is obtained from the reaction of $Cp_2Ti(CO)_2$ with S_4N_4 in thf, is asymmetric (—SSNSN—) and chelate.[3] In addition to complexes of anionic ligands, complexes containing neutral S_2N_2 rings and S_4N_4 cages are also known. The S_2N_2 complexes exhibit bridging coordination through nitrogen in complexes of the type $(S_2N_2)\cdot 2SbCl_5$[4] and $(S_2N_2)\cdot 2CuCl_2$.[5]

Although there have been a wide range of reactions performed on Group 8–10 metal halides, most have made use of polar solvents because of the poor solubility of the metal halides in non-polar solvents. Previous work showed that S_4N_4 reacts with both the binuclear chloro-bridged platinum species $[PtCl_2(PMe_2Ph)]_2$[6] and with the anionic species $[Pt(C_2H_4)Cl_3]^-$[7] (which acts as a source of coordinatively unsaturated $[PtCl_3]^-$) to give platinum(IV) complexes of $S_4N_4^{2-}$. Here we report on the reaction of the binuclear chloro-bridged species $[Pd_2Cl_6]^{2-}$ (present as the tetraphenyl phosphonium salt) with S_4N_4 in CH_2Cl_2. The X-ray structures of the two products are reported.

EXPERIMENTAL

Reactions were performed in an inert atmosphere (nitrogen) using standard Schlenk techniques; $[PPh_4]_2[Pd_2Cl_6]$ (**1**) was prepared by the reaction of $[PPH_4]Cl$ with $Na_2[PdCl_4]$ (1 : 1) in water, followed by recrystallization from CH_2Cl_2/toluene.

In a typical reaction **1** (0.11 g, 0.1 mmol) and S_4N_4 (37 mg, 0.2 mmol) were mixed as solids and then CH_2Cl_2 (50 cm^3) was added with stirring to give a golden brown solution. After a few hours stirring this had changed to a very dark red colour which gradually lightened over the next 48 h. At this point the volume of the solution was reduced to a few cm^3 *in vacuo* and the solution was transferred to a 10 mm diameter tube where it was layered with pentane. Slow diffusion of the pentane for 48 h resulted in the growth of two types of well-formed crystals, dark brown and light orange in colour. These were separated from each other manually; X-ray crystallography revealed the brown compound to be $[PPh_4]_2[Pd_2(\mu\text{-}S_2N_2)Cl_6]$ (**2**) (yield 45 mg, 38%—microanalysis). Found: C, 46.7; H, 3.1; N, 2.2. Calc.: C, 48.2; H, 3.4; N, 2.4%. The orange species was found to be $[PPh_4]_2[Pd_2(\mu\text{-}S_3N_2)Cl_4]$ (**3**) (yield 15 mg, 13%—microanalysis). Found: C, 48.5; H, 3.1; N, 2.3. Calc.: C, 49.8; H, 3.5; N, 2.4%.

* Author to whom correspondence should be addressed.

Crystal data. $C_{48}H_{40}Cl_6N_2P_2Pd_2S_2$ (**2**), M = 1196.5, triclinic, $a = 9.577(1)$, $b = 9.760(2)$, $c = 14.518(3)$ Å, $\alpha = 81.41(2)$, $\beta = 72.15(1)$, $\gamma = 83.65(1)°$, $U = 1274$ Å^3, space group $P\bar{1}$, $Z = 1$ (the molecule is disposed about a centre of symmetry), D_c 1.56 g cm^{-3}. μ(Cu-K_α) = 105 cm^{-1}, $\lambda = 1.54178$ Å, $F(000) = 598$.

Crystal data. $C_{48}H_{40}Cl_4N_2P_2Pd_2S_3$ (**3**), M = 1157.6, monoclinic, $a = 9.634(1)$, $b = 34.973(6)$, $c = 14.664(4)$ Å, $\beta = 98.21(2)°$, $U = 4890$ Å^3, space group $P2_1/c$, $Z = 4$, $D_c = 1.57$ g cm^{-3}. μ(Cu-K_α) = 102 cm^{-1}, $\lambda = 1.54178$ Å, $F(000)$ = 2320.

Data collection and processing for **2** *and* **3**

Nicolet R3m diffractometer, ω-scan method ($2\theta \leqslant 116°$), graphite monochromated Cu-K_α radiation; 3446 and 6603 independent measured reflections, 2987 and 4969 observed [$|F_o| > 3\sigma(|F_o|)$], corrected for Lorentz and polarization factors; empirical absorption correction (ellipsoidal) based on 284 azimuthal scans for **2** and a numerical absorption correction (face indexed crystal) for **3**; the maximum and minimum transmission factors were 0.448 and 0.347 for **2** and 0.588 and 0.236 for **3**.

Structure analysis and refinement

The structures were solved by direct methods and all the non-hydrogen atoms refined anisotropically. In **2** the phenyl groups were refined as rigid bodies. The hydrogen atoms were idealized (C—H = 0.96 Å), assigned isotropic thermal parameters, $U(H) = 1.2U_{eq}(C)$, and allowed to ride on their parent carbons. Refinement was by block-cascade full-matrix least squares to $R = 0.048$, 0.057 ($R = \Sigma[|F_o| - |F_c|]/\Sigma|F_o|$), $R_w = 0.051$, 0.049 ($w^{-1} = \sigma^2(F) + 0.00068F^2$ and $0.00015F^2$) for **2** and **3**, respectively. The maximum and minimum residual electron densities in the final ΔF map for **2** and **3** were 0.74, 0.69 and −0.98, −0.82 e Å^{-3} and the mean and maximum shifts/error in the final refinement cycles were 0.001, 0.004 and 0.004, 0.018, respectively. Computations were carried out on an Eclipse S140 computer using the SHELXTL program system.[8]

RESULTS AND DISCUSSION

When $[PPh_4]_2[Pd_2Cl_6]$ (**1**) is stirred with S_4N_4 in CH_2Cl_2 at room temperature the chloro bridge is disrupted and replaced by a neutral bridging S_2N_2 ligand to give $[PPh_4]_2[Pd_2(\mu\text{-}S_2N_2)Cl_6]$ (**2**) as the initial product. A longer reaction time also leads to further disruption of the Pd—Cl framework giving $[PPh_4]_2[Pd_2(\mu\text{-}S_3N_2)Cl_4]$ (**3**) in addition to **2**. Compound **2** is the first example of an S_2N_2 complex of a group 10 metal, whilst **3** is the first example of a complex of bridging $S_3N_2^{2-}$ to be prepared in reasonable yield (13%). The two complexes are obtained as a mixture of irregular brown crystals (**2**) and well-formed orange needles (**3**). Both types are large enough to allow efficient separation by hand and hence good yields of both complexes can be obtained; similarly both types of crystal were of sufficient quality to allow analysis by X-ray crystallography.

The X-ray structure of **2** (Fig. 1, Table 1) shows that the S_4N_4 cage has been cleaved to give S_2N_2 which is coordinated via both nitrogens, in a centrosymmetric arrangement, to two $PdCl_3^{2-}$ units. The anion is virtually planar with the maximum deviation from planarity for S(1) of 0.06 Å. The geometry of the S_2N_2 ring is not significantly different from that observed in other single crystal studies[1] having transannular S···S and N···N distances of 2.44 and 2.22 Å, respectively. The Pd—Cl distances are in the range 2.282(2)–2.342(2) Å, the shortest being for Pd—Cl *trans* to nitrogen. Interestingly, the Pd—N bond length [1.959(6) Å] is substantially shorter than the values observed for PdS_2N_2 rings in $[Pd(S_2N_2H)(PMe_2Ph)_2]BF_4$[9] [2.031(6) Å] and $Pd(S_2N_2H)(L—L')$ [(L—L') =

Table 1. Selected bond lengths (Å) and angles (°) for **2**

Pd—Cl(1)	2.342(2)	Pd—Cl(2)	2.282(2)
Pd—Cl(3)	2.303(2)	Pd—N(1)	1.959(6)
N(1)—S(1)	1.657(7)	N(1)—S(1′)	1.642(6)
Cl(1)—Pd—Cl(2)	96.2(1)	Cl(1)—Pd—Cl(3)	169.4(1)
Cl(2)—Pd—Cl(3)	94.3(1)	Cl(1)—Pd—N(1)	85.1(2)
Cl(3)—Pd—N(1)	84.3(2)	Pd—N(1)—S(1)	130.3(3)
Pd—N(1)—S(1′)	134.1(4)	S(1)—N(1)—S(1′)	95.6(3)
N(1)—S(1)—N(1′)	84.4(3)		

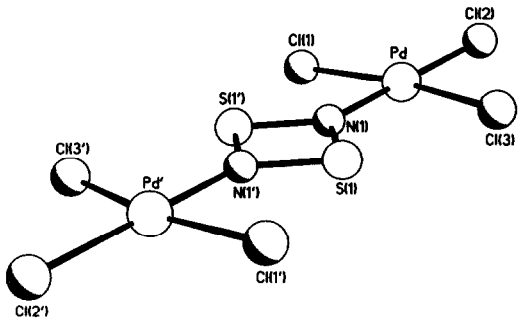

Fig. 1. The X-ray crystal structure of the anion in **2**.

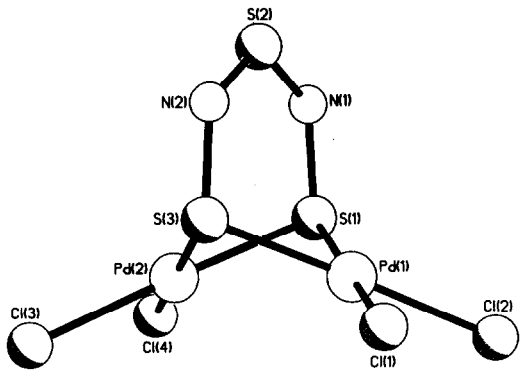

Fig. 2. The X-ray crystal structure of the anion in **3**.

acetophenone 2.104(6), N,N-dimethylhydrazone 2.064(6) Å].[10]

An unusual feature of the geometry about palladium in **2** is the significant contraction from 180° of the Cl(1)—Pd—Cl(3) angle [169.4(1)°], the two chlorine atoms being bent towards the sulphur atoms of the S_2N_2 ring. The Cl(1)···S(1′) and Cl(3)···S(1) distances are 3.13 and 2.99 Å, respectively. These distances are substantially less than the sum of the van der Waals radii and coupled with the overall planarity are indicative of an electrostatic interaction between S($\delta+$) and Cl($\delta-$). The associated Cl(1)···Cl(2) and Cl(2)···Cl(3) distances are 3.44 and 3.36 Å, respectively. This type of interaction has also been observed in $(SbCl_5)_2S_2N_2$ (**4**),[4] $(AlCl_3)_2S_2N_2$[11] (**5**) and $[MoCl_4(NSCl)]_2S_2N_2$[12] (**6**). In **4** and **6** the Cl—M—Cl angles are 161, 158.5° (M = Sb, Mo) and 171, 172° for the units which are coplanar and orthogonal respectively, to the S_2N_2 ring. In **4** and **6** the Cl—M—Cl angles are 161 and 158.5° (M = Sb, Mo) for the groups which are coplanar to the S_2N_2 ring, whereas the out-of-plane Cl—M—Cl angles are 171 and 172°. In **4** the Cl···S distance is 3.18 Å. In **5**, which contains distorted pyramidal $AlCl_3$ groups, the shortest intramolecular Cl···S distance is 3.06 Å (the analogous S···Br distance for the bromo compound is 3.15 Å).[13] Clearly, there is a strong attractive interaction between sulphur and the halogen atoms in these systems. We are currently investigating this effect further.

Within the crystal of **2**, the anions form stepped layers (interplanar step separation 0.8 Å) with Cl(3)···Cl(3″) 3.50 Å; there are no other significant intermolecular interactions.

The X-ray structure of **3** (Fig. 2, Table 2) reveals a different cleavage pattern of the S_4N_4 with formation of a bridging $S_3N_2^{2-}$ ligand. This bridges two $PdCl_2^{2-}$ units with coordination through sulphur. The anion has approximate non-crystallographic C_{2v} symmetry and the $Pd_2S_3N_2$ frag-

Table 2. Selected bond lengths (Å) and angles (°) for **3**

Pd(1)—Cl(1)	2.366(2)	Pd(1)—Cl(2)	2.370(2)
Pd(1)—S(1)	2.280(2)	Pd(1)—S(3)	2.272(2)
Pd(2)—Cl(3)	2.367(2)	Pd(2)—Cl(4)	2.350(2)
Pd(2)—S(1)	2.266(2)	Pd(2)—S(3)	2.279(2)
S(1)—N(1)	1.645(8)	S(2)—N(1)	1.563(8)
S(2)—N(2)	1.576(8)	S(3)—N(2)	1.638(7)
Cl(1)—Pd(1)—Cl(2)	95.1(1)	Cl(3)—Pd(2)—Cl(4)	96.0(1)
Cl(1)—Pd(1)—S(1)	173.3(1)	Cl(1)—Pd(1)—S(3)	89.3(1)
Cl(2)—Pd(1)—S(1)	90.6(1)	Cl(2)—Pd(1)—S(3)	175.2(1)
S(1)—Pd(1)—S(3)	85.1(1)	S(1)—Pd(2)—S(3)	85.3(1)
Cl(3)—Pd(2)—S(1)	175.2(1)	Cl(3)—Pd(2)—S(3)	90.9(1)
Cl(4)—Pd(2)—S(1)	88.0(1)	Cl(4)—Pd(2)—S(3)	172.0(1)
Pd(1)—S(3)—N(2)	107.0(3)	Pd(2)—S(3)—N(2)	106.1(3)
Pd(1)—S(1)—Pd(2)	79.8(1)	Pd(1)—S(3)—Pd(2)	79.7(1)
Pd(1)—S(1)—N(1)	105.7(3)	Pd(2)—S(1)—N(1)	106.9(3)
S(1)—N(1)—S(2)	127.1(5)	N(1)—S(2)—N(2)	119.1(4)
S(2)—N(2)—S(3)	126.8(5)		

Table 3. Vibrational frequencies (cm^{-1}) of the M—S—N groups in **3**, **6** and **7**

3	6	7
1018	1033	
	988	1007
	694	702/692
643	626	
	514	511
		479
387	387	
309		
291		
277		

ment has very similar geometry to that observed in $Pd_2(S_3N_2)(S_3N)_2$ (**6**)[2] with two short and two long S—N bonds and an apical angle at S(2) of 119.4°. The Pd—S distances in **3** [2.266(2)–2.280(2) Å] are significantly shorter than those in (**6**) [2.335(5)–2.354(5) Å], reflecting the difference in the *trans* ligand. The transannular Pd···Pd and S···S distances in **3** are 2.92 and 3.08 Å, respectively. Viewed from the S(1)···S(3) axis the coordination planes are equally inclined from the S_3N_2 plane (119°) and inclined by 121° to each other. There is a noticeable deviation from planarity for both $PdCl_2S_2$ units due to a 4.5° twist of the $PdCl_2$ planes with respect to the PdS_2 planes. There are no significant intermolecular contacts. It is somewhat surprising, in view of the near optimal bite geometry of the $S_3N_2^{2-}$ ligand that so few examples have been reported.

The most prominent features of the IR spectra of **2** and **3** are the bands due to $[PPh_4]^+$, although a number of medium strength vibrations associated with the S—N ligand can be identified in each case. Table 3 compares the IR spectrum of **3** with that of **6** and the related species $Pd(S_3N)_2$ (**7**).[14] The spectrum of **6** is more complex than that of **3** due to the presence of the two S_3N^- ligands; however, comparison with the spectrum of **7** enables the bands due to the latter groups to be identified, namely those at 988, 694 and 514 cm^{-1}. The remaining vibrations, at 1033, 626 and 387 cm^{-1}, compare well with those at 1018, 643 and 387 cm^{-1} in **3** and can be assigned as ν(S—N) and δ(S—N). The low frequency bands in **3**, which are not seen in **6**, can be assigned to Pd—Cl stretches. The IR spectrum of **2** contains medium strength bands at 877, 436, 340 and 282 cm^{-1}; comparison with $(SbCl_5)_2S_2N_2$ and $(SbCl_5)S_2N_2$[15] which show bands at 818/461 and 800/459 cm^{-1}, respectively, indicates that the two high frequency bands are due to S—N vibrations and the others to Pd—Cl stretches.

Acknowledgements—We are grateful to the Wolfson foundation for support and to Johnson Matthey for loans of precious metals. J.D.W. is currently the Sir Edward Frankland Fellow of the Royal Society of Chemistry.

REFERENCES

1. T. Chivers and F. Edelmann, *Polyhedron* 1986, **5**, 1661.
2. U. Thewalt, *Z. Naturforsch.* 1982, **37B**, 276.
3. C. G. Marcellus, R. T. Oakley, W. T. Pennington and A. W. Cordes, *Organometallics* 1986, **5**, 1395.
4. R. L. Patton and K. N. Raymond, *Inorg. Chem.* 1969, **8**, 2426.
5. U. Thewalt and B. Muller, *Z. Anorg. Allg. Chem.* 1980, **462**, 214.
6. M. B. Hursthouse, M. Motevalli, P. F. Kelly and J. D. Woollins, *Polyhedron* 1989, **8**, 997.
7. P. S. Belton, P. F. Kelly, R. N. Sheppard and J. D. Woollins, in preparation.
8. G. M. Sheldrick, SHELXTL, An Integrated System for Solving, Refining and Displaying Crystal Structures from Diffraction Data. University of Gottingen.
9. R. Jones, P. F. Kelly, D. J. Williams and J. D. Woollins, *J. Chem. Soc., Dalton Trans.* 1988, 803.
10. C. A. O'Mahoney, I. P. Parkin, D. J. Williams and J. D. Woollins, *J. Chem. Soc., Dalton Trans.* 1989, 1179.
11. U. Thewalt and M. Burger, *Angew. Chem., Int. Edn Engl.* 1982, **21**, 634.
12. U. Kynast, P. Klingelhofer, U. Muller and K. Dehnicke, *Z. Anorg. Allg. Chem.* 1984, **515**, 61.
13. U. Thewalt and K. Holl, *Z. Naturforsch.* 1984, **39B**, 145.
14. J. D. Woollins, *Metal Complexes Containing Sulphur–Nitrogen Ligands*, PhD thesis. University of East Anglia, 1979.
15. R. L. Patton and W. L. Jolly, *Inorg. Chem.* 1969, **8**, 1389.

Polyhedron Vol. 10, No. 19, pp. 2341–2345, 1991
Printed in Great Britain

0277–5387/91 $3.00+.00
© 1991 Pergamon Press plc

SYNTHESIS AND MOLECULAR STRUCTURE OF THE FIVE-COORDINATE ZIRCONIUM COMPLEX $(CH_3C_5H_4)_2ZrCl(\alpha\text{-}C_{10}H_7COO)$

ZHI-QIANG WANG,* SHI-WEI LU and HE-FU GUO

Dalian Institute of Chemical Physics, Academia Sinica, Dalian 116023, P.R.C.

and

NING-HAI HU and YONG-SHENG LIU

Changchun Institute of Applied Chemistry, Academia Sinica, Changchun, P.C.C

(*Received* 10 *December* 1990; *accepted* 20 *May* 1991)

Abstract—Bis(methylcyclopentadienyl)chloro(α-naphthoyloxy)zirconium, $(CH_3C_5H_4)_2ZrCl(\alpha\text{-}C_{10}H_7COO)$, has been synthesized by the reaction between $(MeCp)_2ZrCl_2$ and equimolar sodium α-naphthoate in toluene at room temperature. The molecular structure of the title complex was determined by X-ray diffraction. The molecules have a five-coordinate bent metallocene structure in which the α-naphthoxyligand is bidentate [Zr—O, 2.317(2), 2.260(2) Å]. The remaining distances are [Zr—Cl, 2.521(1) Å; Zr—C, 480-2, 565 Å; Zr—cent—$CH_3C_5H_4$ 2.217 and 2.230 Å].

Most zirconium metallocene derivatives determined by X-ray diffraction have four-coordinate, 16-electron molecular structures.[1] A limited number of five-coordinate, 18-electron zirconium metallocenes have also been reported.[2–9] More recently, the structures of $Cp_2ZrCl(OOCCH_2CH_2COFc)$,[10] $[Cp_2Zr(\mu\text{-}OCOC_6H_4OCO)]_3$[11] and $[Cp_2Zr(\mu\text{-}OCOC{\equiv}COCO)_n$[12] have been reported, but aromatic carboxyl derivatives of analogous mononuclear zirconium metallocene have not as yet. As part of continuing studies on the substituted cyclopentadienyl titanium group metallocenes,[13] we report here the synthesis and molecular structure of a new five-coordinate, 18-electron complex, $(CH_3C_5H_4)_2ZrCl(C_{10}H_7COO)$.

EXPERIMENTAL

Preparation of $(CH_3C_5H_4)_2ZrCl(\alpha\text{-}C_{10}H_7COO)$

The title complex was prepared by the reaction of equimolar amounts of $(CH_3C_5H_4)_2ZrCl_2$ with anhydrous sodium α-naphthoxyl in toluene for 12 h under nitrogen. The reaction mixture was filtered to remove NaCl. The volume of the filtrate was reduced by vacuum distillation and *n*-hexane was added to crystallize the product. Recrystallization from toluene–hexane solvent afforded colourless crystals; the solid melted at 102–104°C; yield was 84%. Found: C, 60.0; H, 4.5. Calc. for $(CH_3C_5H_4)_2ZrCl(\alpha\text{-}C_{10}H_7COO)$: C, 60.6; H, 4.6%. ^1H NMR (ppm): 2.12(CH_3); 6.08(C_5H_4); 7.40–9.20($C_{10}H_7$). IR(KBr pellets) (cm^{-1}): 3110m, 3060m, 2938w; ν(C—H); 1585s, 1472s, (C=C); 1520s, ν_{asym} OCO; 1450s, ν_{sym} OCO; 1155m, 1038s, 880s, 800s, 780s, δ(C—H).

X-ray structure determination

Cell parameters were determined on a Nicolet R3m/E, four-circle diffractometer with graphite-monochromated Mo-K_α radiation (0.71073 Å) from 19 centred reflections ($3 < 2\theta < 55°$). Details of the crystal parameters along with data collection and structure refinement are summarized in Table 1. Intensity data were corrected for Lorentz and polarization effects but not for absorption.

* Author to whom correspondence should be addressed.

Table 1. Crystal and refinement data

Compound	$(CH_3C_5H_4)_2ZrCl(C_{10}H_7CO_2)$
Molecular weight	456.09
a (Å)	6.814(1)
b (Å)	12.371(3)
c (Å)	12.465(3)
α (°)	95.86(2)
β (°)	104.54(1)
γ (°)	74.18(2)
V (Å^3)	977.9(4)
Space grpup	$P\bar{1}$
Z	2
D_{calc} (g cm^{-3})	1.55
μ (cm^{-1})	7.0 (Mo-K_α)
Crystal size (mm)	$0.16\times0.24\times0.36$
Scan mode	ω
Scan width (°)	1.2
Scan speed (° min^{-1})	5.33
2θ Range (°)	3–55
Unique data measured	4460
Unique data used	3080 ($I > 3\sigma(I)$)
No. of variables	295
Weighting scheme	$w = [\sigma^2(F_o)+0.0001(F_o)^2]^{-1}$
R^a	0.040
R^a	0.036
(Δ/σ)	0.40
$\Delta\rho_{max}$ (e Å^{-3})	0.38

[a] $R = \Sigma||F_o|-|F_c||/\Sigma F_o$; $R_w = [\Sigma w(F_o-|F_c|)^2/\Sigma wF_o^2]^{1/2}$.

The structure was solved by heavy-atom methods and refined by block-diagonal least-squares methods, minimizing the function $\Sigma w(|F_o|-|F_c|)^2$. Non-hydrogen atoms were assigned anisotropic thermal parameters. All hydrogen atoms, except those of the two methyl groups, were located on a difference map and refined with isotropic temperature factors ($U = 0.06$ Å^2).

The hydrogen atoms of the methyl groups were introduced at calculated positions. The final R and R_w values were 0.040 and 0.036 for 3080 observed reflections. All calculations were performed using

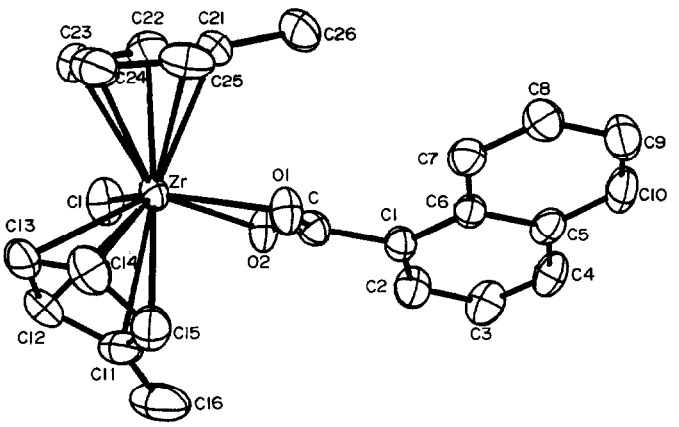

Fig. 1. Molecular structure of $(\eta\text{-}CH_3C_5H_4)_2ZrCl(\alpha\text{-}C_{10}H_7COO)$.

Table 2. Important bond distances and bond angles in $(\eta\text{-}CH_3C_5H_4)_2ZrCl(\alpha\text{-}C_{10}H_7COO)$

Bond distances (Å)					
Zr—Cl	2.251(1)	Zr—Cp_1'	2.217	Zr—O1	2.317(2)
Zr—O2	2.260(2)	Zr—Cp_2'	2.230	Zr—C11	2.550(4)
Zr—C12	2.539(4)	Zr—C13	2.484(4)	Zr—C14	2.480(5)
Zr—C15	2.527(5)	Zr—C21	2.565(4)	Zr—C22	2.536(4)
Zr—C23	2.484(4)	Zr—C24	2.512(4)	Zr—C25	2.522(4)
O1—C	1.259(5)	O2—C	1.269(5)	Zr—C	2.676(3)
C11—C16	1.491(6)	C21—C26	1.502(6)	C—C1	1.497(4)
C11—C12	1.402(5)	C11—C15	1.408(7)	C12—C13	1.390(6)
C13—C14	1.393(6)	C14—C15	1.398(5)		
Bond angles (°)					
Cl—Zr—O1	134.8(1)	Cl—Zr—O2	78.6(1)		
O1—Zr—O2	56.3(1)	Cp_1'—Zr—Cp_2'	130.0		
Cp_1'—Zr—Cl	101.3	Cp_2'—Zr—Cl	101.5		
Cp_1'—Zr—O1	98.3	Cp_2'—Zr—O1	96.1		
Cp_1'—Zr—O2	112.7	Cp_2'—Zr—O2	115.1		
O1—C—O2	117.2(3)	O1—C—C1	123.2(3)		
O2—C—C1	119.6(3)	O1—Zr—C	28.1(1)		
Zr—O2—C	94.4(2)	O2—Zr—C	28.2(1)		
Zr—O1—C	92.0(2)				

Cp_1' and Cp_2' are defined as centroids of C11, C12, C13, C14, C15 rings and C21, C22, C23, C24, C25 rings, respectively.

the SHELXTL program system on an Eclipse S/140 computer.

RESULTS AND DISCUSSION

A perspective view of the molecule $(CH_3C_5H_4)_2ZrCl(\alpha\text{-}C_{10}H_7COO)$, showing the atom-numbering scheme, is displayed in Fig. 1. The important bond distances and bond angles are given in Table 2.

Molecules of the title complex have the bent metallocene geometry, with the zirconium atom attached to a chlorine atom, a bidentate α-naphthoxyl ligand and two symmetrically bound η-$CH_3C_5H_4$ ligands. The zirconium atom has a coordination number of 5, if each η-$CH_3C_5H_4$ group is considered to occupy a single coordination site. The η-$CH_3C_5H_4$ rings are in a staggered conformation, as shown in Fig. 2. Both η-$CH_3C_5H_4$ rings are planar, with displacements of the carbon atom from the mean planes of the ligands being <0.0169 Å (cf. Table 3). The angle between the normals and the planes of the two η-$CH_3C_5H_4$ ligands (126.4°) is slightly smaller than the (centroid $CH_3C_5H_4$)-Zr-(centroid $CH_3C_5H_4$) angle (130.0°), indicating that Zr-(centroid $CH_3C_5H_4$) vectors are not orthogonal to the planes of the η-$CH_3C_5H_4$ ligands. The 10 Zr—C distances are not uniform (2.480–2.565 Å) due to the methyl group on the cyclopentadienyl rings. The values of the Zr—C distances are slightly longer than those of the analogous cyclopentadienyl–zirconium structures.[10] The distances from the zirconium atom to the centroids of the $CH_3C_5H_4$ group rings are 2.217 and 2.230 Å.

Due to crowding in the coordination environment the Zr—Cl bond length [2.521(1) Å] is significantly longer than the distance in four-coordinate zirconocenes[1] (2.441 Å) or in six-coordinate $(MeCp)ZrCl_3(thf)_2$ (2.473–2.493 Å).[14] Compared with the more crowded five-coordinate complexes (cf. Table 4), the Zr—Cl distances in carboxylate derivatives of cyclopentadienyl–zirconium are slightly shorter than those in other derivatives.

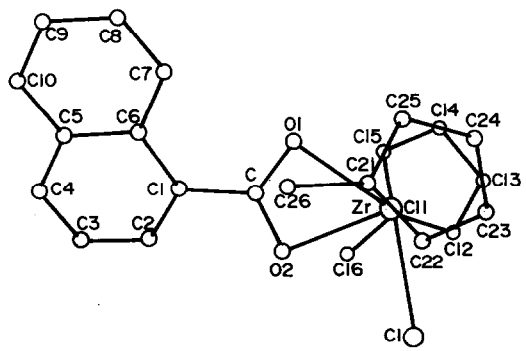

Fig. 2. Projection of the title complex on the equatorial plane by the atoms Zr, O1, O2 and C.

Table 3. Least-squares mean planes of the form $AX+BY+CZ = D$ where X, Y and Z are orthogonalized coordinates

Plane number	atoms	A	B	C	D
1	Zr, O1, O2, C	0.1413	0.2217	0.9648	3.2223
2	C11, C12, C13, C14, C15	−0.3006	0.2314	0.9253	0.0000
3	C21, C22, C23, C24, C25	0.5891	0.2052	0.7815	5.9468
4	C1, C2, C3, C4, C5, C6, C7, C8, C9, C10	−0.1035	−0.2086	0.9725	0.9206

	Atoms and their displacement from planes (Å)
Plane 1	Zr(0.005), O1(−0.0102), O2(−0.0104), C(0.0156)
Plane 2	C11(0.0111), C12(−0.0097), C13(0.0044), C14(0.0027), C15(−0.0085)
Plane 3	C21(0.0019), C22(0.0085), C23(−0.0159), C24(0.0171), C25(−0.0116)
Plane 4	C1(0.0205), C2(0.0391), C3(−0.0130), C4(−0.0265), C5(−0.0113), C6(−0.0299), C7(−0.0271), C8(0.0001), C9(0.00263), C10(0.0219)

Dihedral angles between planes					
Plane	Plane	Dihedral	Plane	Plane	Dihedral
1	2	25.6°	1	3	28.0°
1	4	28.7°	2	3	53.6°
2	4	28.0°	3	4	49.0°

Table 4. The important data of five-coordinate zirconocene complexes

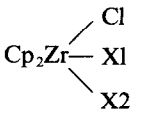

Complex	X1	X2	Zr—X1	Zr—X2	Zr—Cl	Zr—Cp	Cp—Zr—Cp	Cl—Zr—X2	Reference
$Cp_2ZrCl(S_2CNEt_2)$	S	S	2.635(2)	2.723(2)	2.556(2)	2.22	129.4	137.5	2
$Cp_2ZrCl(SOCNMe_2)$	S	O	2.641(2)	2.249(4)	2.550(2)	2.23	128.5	138.1	4
$Cp_2ZrCl(O_2NCMe_2)$	O	O	2.218(2)	2.230(2)	2.536(1)	2.23	127.5	134.5	5
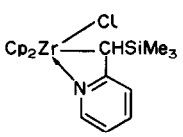	C	N	2.38(1)	2.34(6)	2.564(2)	2.26	127.8	138.4	6
$Cp_2ZrCl(OCOC_2H_4COFc)$	0	0	2.248(3)	2.287(3)	2.518(1)				10
$(MeCp)_2ZrCl(C_{10}H_7CO_2)$	0	0	2.260(2)	2.317(2)	2.521(1)	2.22–2.23	130.0	134.8	This work

The naphthoxyl is coordinated to zirconium in a bidentate mode. The Zr—O distances are 2.317 and 2.260 Å, respectively. The Zr—O bond distances are not equal, indicating that the coordinating ability of the two oxygens in the naphthoxyl are different. The C—O bond distances, which are larger than the normal C=O distance (1.22 Å), are also different (C—O1, 1.259 Å; C—O2, 1.269 Å). The Zr—O bond lengths in the title complex are longer than those in $Cp_2ZrCl(OOCCH_2CH_2COFc)$[10] due to steric congestion, but the bond angles Cl—Zr—O, Zr—O—C and O—Zr—O in the two complexes are almost the same.

REFERENCES

1. C. E. Holloway, I. M. Walker and M. Melnik, *J. Organomet. Chem.* 1987, **321**, 143.
2. M. E. Silver, O. Einsenstein and R. C. Fay, *Inorg. Chem.* 1983, **22**, 759.
3. T. D. Tilley, *Organometallics* 1985, **4**, 1452.
4. M. E. Silver and R. C. Fay, *Organometallics* 1983, **2**, 44.
5. B. N. Diel and H. Hope, *Inorg. Chem.* 1986, **25**, 4448.
6. S. I. Bailey, D. Colgan, L. M. Engelhardt, W.-P. Leung, R. I. Papasergio, C. L. Raston and A. H. White, *J. Chem. Soc., Dalton Trans.* 1986, 603.

7. H. Takaya, M. Yamakawa and K. Mashima, *J. Chem. Soc., Chem. Commun.* 1983, 1283.
8. U. Thewalt and W. Lasser, *J. Organomet. Chem.* 1984, **276**, 341.
9. W. Lasser and U. Thewalt, *J. Organomet. Chem.* 1986, **302**, 201.
10. M. Yongxiang, Z. Ying, W. Xin and M. Chunlin, *Polyhedron* 1989, **8**, 929.
11. U. Thewalt, S. Klima and K. Berhalter, *J. Organomet. Chem.* 1988, **342**, 303.
12. U. Thewalt and T. Guthner, *J. Organomet. Chem.* 1989, **361**, 309.
13. Z. Yaokun, W. Zhiqiang, W. Xin and Z. Ying, *Polyhedron* 1990, **9**, 783.
14. G. Erker, C. Sarter, M. Albrecht and S. Dehnicke, *J. Organomet. Chem.* 1990, **382**, 89.

Polyhedron Vol. 10, No. 19, pp. 2347–2349, 1991
Printed in Great Britain

0277–5387/91 $3.00+.00
© 1991 Pergamon Press plc

COMMUNICATION

PHOTOCHEMISTRY OF PHENYL-SUBSTITUTED DIGERMANOXANE. FIRST DIRECT OBSERVATION OF GERMOXY RADICALS PROBED BY LASER FLASH PHOTOLYSIS

KUNIO MOCHIDA,* CHIE YOSHIZAWA and SATOSHI TOKURA

Department of Chemistry, Faculty of Science, Gakushuin University, 1-5-1 Mejiro, Tokyo 171, Japan

and

MASANOBU WAKASA and HISAHARU HAYASHI

The Institute of Physical and Chemical Research, Wako, Saitama 351-01, Japan

(*Received* 8 *July* 1991; *accepted* 12 *August* 1991)

Abstract—Laser flash photolysis of the phenyl-substituted digermanoxanes $(Ph_nMe_{3-n}Ge)_2O$ (n = 1–3) results in Ge—O bond homolysis to give germyl radicals and germoxy radicals.

The chemistry of polysiloxanes and polygermanoxanes has recently become of interest because of their importance as electric conductors, photoresistors, liquid crystals and new materials.[1,2] However, the study of polygermanoxanes is very much limited compared with that of polysiloxanes. Herein we describe the first laser flash photolysis studies on aryl-substituted digermanoxanes, $(Ph_nMe_{3-n}Ge)_2O$ (**1–3**, n = 1–3, respectively). The photolysis of phenylated digermanoxanes causes germanium–oxygen bond homolysis to give germyl radicals and germoxy radicals.

Laser flash photolysis (λ = 266 nm, pulse width 5 ns, power 10 mJ pulse^{-1})[3] of **1–3** (10^{-3} M) in cyclohexane at 293 K gave a transient absorption around 360 nm for **1**, and two separated absorptions at both *ca* 320–330 nm and 360 nm for **2** and **3**, as shown in Fig. 1.[4,5] Careful examination of the transient peak of **1** shows that this is composed of two components (λ_{max} = *ca* 320 and 360 nm). The transient peak at *ca* 320 nm arising from **1** cannot be observed apparently because of its much smaller molar coefficient than that of the other transient peak at λ_{max} = 360 nm.[6]

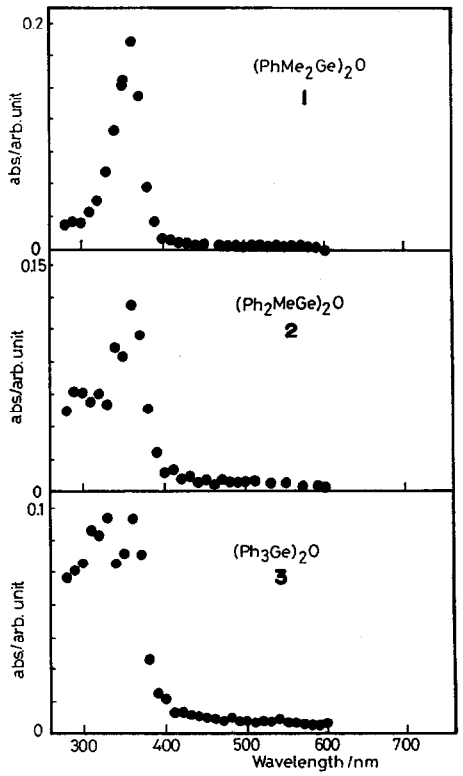

Fig. 1. Transient absorption at 200 ns after photoexcitation of $(Ph_nMe_{3-n}Ge)_2O$ (**1–3**, n = 1–3, respectively) in the degassed cyclohexane solution at 293 K.

* Author to whom correspondence should be addressed.

Table 1. Rate constants for the disappearance of the transients produced by photolysis of the germanoxanes in cyclohexane at 293 K

Compound	λ_{max} (nm)	k/ε (s^{-1} cm)[a]	Rate constant (M^{-1} s^{-1}) O_2	CCl_4	Diene
$(PhMe_2Ge)_2O$	360 nm	6.5×10^{6}[b]	2.3×10^{9}	Not quenched	2.0×10^{9}
(1)	320 nm (s)	9.1×10^{6}[c]	2.0×10^{9}	1.1×10^{8}	—[d]
$(Ph_2MeGe)_2O$	360 nm	1.3×10^{7}[b]	2.2×10^{9}	Not quenched	1.4×10^{9}
(2)	320 nm (s)	8.2×10^{6}[c]	1.2×10^{9}	2.0×10^{8}	—[d]
$(Ph_3Ge)_2O$	360 nm	2.5×10^{7}[b]	2.6×10^{9}	Not quenched	2.0×10^{9}
(3)	330 nm	7.3×10^{6}[c]	1.1×10^{9}	1.2×10^{8}	—[d]

[a] k is the rate constant of second-order decay and ε is the corresponding molar extinction coefficient.
[b] At 370 nm.
[c] At 330 nm.
[d] The absorption is too weak to determine the rate constant.

The transient peaks at shorter wavelength are reasonably assigned to those of the aryl-substituted germyl radicals, $Ph_nMe_{3-n}Ge^{\cdot}$ (n = 1–3), from comparison of spectral characteristics with those of the germyl radicals reported.[4-7] The transient from **1–3** in cyclohexane decayed with second-order kinetics, suggesting the dimerization of germyl radicals to give digermenes. The experimentally determined decay constants of these transients are summarized in Table 1. The assignment of the shorter wavelength transient is futher substantiated by quenching experiments with carbon tetrachloride, oxygen and 2,3-dimethyl-1,3-butadiene. Addition of carbon tetrachloride, an effective radical scavenger,[8] quenched the transient absorption as shown in Table 1.

$$Ph_nMe_{3-n}Ge^{\cdot} + CCl_4 \rightarrow Ph_nMe_{3-n}GeCl + {}^{\cdot}CCl_3$$
$$(n = 1\text{–}3)$$

The quenching rate constants observed agreed with the values reported for the germyl radicals.[4-7] Similarly, oxygen quenched the shorter wavelength very rapidly, as shown in Table 1. The laser flash photolysis of **1–3** in cyclohexane containing oxygen was also performed. The transients at shorter wavelength disappeared, resulting in the build-up of transient peaks at the longer wavelength.

On the other hand, the transient at the longer wavelength in Table 1 may be assigned to that of a germoxy radical by comparing its spectral properties with that generated by laser flash photolysis of germyl-t-butylperoxide ($R_3GeOOBu^t$) and **1–3** in cyclohexane containing oxygen. The photolysis of germyl-t-butylperoxides is well known to give germoxy and t-butoxy radicals.[9]

$$R_3GeOOBu^t \xrightarrow{h\nu} R_3GeO^{\cdot} + {}^{\cdot}OBu^t$$

These transients arising from **1–3** in cyclohexane decayed with second-order kinetics, suggesting the dimerization of germoxy radicals to give digermyl peroxides. The transient from **1–3** in cyclohexane in the presence of a large excess of 2,3-dimethyl-1,3-butadiene and oxygen decayed with pseudo first-order kinetics, and the rate constants obtained are shown in Table 1.

The values of k/ε in Table 1 increase in the order: $Ph_3Ge^{\cdot} < Ph_2MeGe^{\cdot} < PhMe_2Ge^{\cdot}$ for the phenylated germyl radicals, and $PhMe_2GeO^{\cdot} < Ph_2MeGeO^{\cdot} < Ph_3GeO^{\cdot}$ for the phenylated germoxy radicals, respectively. The trend for the germyl radicals may reflect the steric environments around the germanium atom. On the other hand, the trend for the germoxy radicals may be explained by the electronic effect of triorganogermyl groups on the oxygen atom due to the longer Ge—O bond length.

Along with the laser flash photolysis experiments, product studies were carried out by photolysing **1–3** (0.04 M) in cyclohexane with a 110 W low-pressure mercury arc lamp (spiral type) at room temperature for 8–10 h under argon. Unidentified, high molecular weight compounds containing germanium (mol. wt = *ca* 4000) were formed.[10] The cyclohexane solution of **1–3** containing CCl_4 was similarly irradiated for 1 h to give the corresponding chlorogermanes in unexpectedly high yields (168, 200 and 185% for **1**, **2** and **3**, respectively).

$$(Ph_nMe_{3-n}Ge)_2O \xrightarrow{h\nu}$$
$$Ph_nMe_{3-n}Ge^{\cdot} + {}^{\cdot}OGePh_nMe_{3-n}$$
$$2Ph_nMe_{3-n}Ge^{\cdot} \longrightarrow (Ph_nMe_{3-n}Ge)_2$$
$$2Ph_nMe_{3-n}GeO^{\cdot} \longrightarrow (Ph_nMe_{3-n}GeO)_2$$
$$n = 1\text{–}3$$

Scheme 1.

These results are best rationalized by a homolytic scission of the germanium–oxygen bonds of the digermanoxanes **1–3**, as described in Scheme 1. Judging from the yields of the chlorogermanes produced by the photolysis of digermanoxanes **1–3** in cyclohexane containing CCl_4, germyl radicals, which abstract chlorine atoms from CCl_4, may be effectively formed by the photolysis of digermylperoxides.

The bathochromic shift of the observed germoxy radicals relative to that of the corresponding carbon analogue, such as the butoxy radical (λ_{max} = 320 nm), may be explained by a contribution in part by the Ge=O resonance structure as follows:

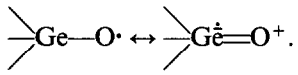

Acknowledgement—This research was supported in part by the Ministry of Education, Science and Culture (Grant-in-Aid on Priority Area No. 02231227).

REFERENCES

1. H. Sakurai, *Synthesis and Application of Polysilanes*. CMC, Tokyo (1990).
2. G. Meyer and D. Wohrle, *Makro. Chem.* 1974, **175**, 714.
3. Y. Sakaguchi, H. Hayashi and S. Nagakura, *J. Phys. Chem.* 1982, **86**, 3177.
4. K. Mochida, I. Yoneda and M. Wakasa, *J. Organomet. Chem.* 1990, **399**, 53; M. Wakasa, I. Yoneda and K. Mochida, *J. Organomet. Chem.* 1989, **366**, C1.
5. K. Mochida, M. Wakasa, Y. Nakadaira, Y. Sakaguchi and H. Hayashi, *Organometallics* 1988, **7**, 1869; K. Mochida, M. Wakasa, Y. Sakaguchi and H. Hayashi, *Bull. Chem. Soc.* 1991, **54**, 1889.
6. K. Mochida, M. Wakasa, Y. Sakaguchi and H. Hayashi, *J. Am. Chem. Soc.* 1987, **109**, 7942.
7. K. Mochida, M. Wakasa, S. Ishizaka, M. Kotani, Y. Sakaguchi and H. Hayashi, *Chem. Lett.* 1985, 1709.
8. H. Sakurai, K. Mochida, A. Hosomi and F. Mita, *J. Organomet. Chem.* 1972, **38**, 275.
9. P. Riviere, M. R. Baudet and J. Satge, in *Comprehensive Organometallic Chemistry* (Edited by G. Wilkinson, F. G. A. Stone and E. W. Abel), Ch. 10. Pergamon Press, New York (1982).
10. K. Mochida, M. Wakasa, Y. Sakaguchi and H. Hayashi, *Nippon Kagaku Kaishi* 1987, 1171.

Polyhedron Vol. 10, No. 19, pp. 2351–2352, 1991
Printed in Great Britain

0277–5387/91 $3.00+.00
© 1991 Pergamon Press plc

COMMUNICATION

METAL REPLACEMENT REACTIONS OF MIXED-METAL CUBANE-TYPE CLUSTERS $[Mo_3MS_4(H_2O)_{10}]^{4+}$ (M = Fe, Ni)

TAKASHI SHIBAHARA,* TATSUNOBU ASANO and GENTA SAKANE

Department of Chemistry, Okayama University of Science, 1-1 Ridai-cho, Okayama 700, Japan

(*Received* 18 *March* 1991; *accepted* 19 *July* 1991)

Abstract—Mixed-metal cubane-type clusters with Mo_3MS_4 cores (M = Fe, Ni) react with Cu^{2+}: $[Mo_3MS_4(aq)]^{4+} + Cu^{2+} \rightarrow [Mo_3CuS_4(aq)]^{4+} + M^{2+}$, in a new type of reaction involving the replacement of the metal atom in the metal cluster by another metal.

Many ligand substitution reactions of mono- and polynuclear coordination compounds have been reported,[1,2] however, no reports have appeared on metal substitution reactions of metal clusters. Recently we synthesized and characterized mixed-metal cubane-type clusters with Mo_3MS_4 cores (M = Fe, Co, Ni, Cu, Sn, Hg).[3] These reactions can be regarded as reductive additions of metals to the core Mo_3S_4 of the incomplete cubane-type aqua cluster $[Mo_3S_4(H_2O)_9]^{4+}$ (**A**). We report here the reaction of mixed-metal cubane-type clusters $[Mo_3MS_4(H_2O)_{10}]^{4+}$ (M = Fe, Ni) with some divalent and trivalent metal ions.

All procedures were carried out under a dinitrogen atmosphere at room temperature. Six kinds of experiments have been carried out. Experiment 1: reaction of $[Mo_3FeS_4(H_2O)_{10}]^{4+}$ (**B**) with Cu^{2+} ions proceeded as follows. Immediately after $CuCl_2$ was added to **B** (5.75×10^{-4} M in 1 M HCl; $Cu^{2+}/\mathbf{B} = 10$), the characteristic peaks at 464 and 512 nm in the electronic spectrum of **B** grew to give a larger peak at 480 nm, indicating the formation of the $Mo_3CuS_4(aq)^{4+}$ cluster (**C**)[3c] as shown in Fig. 1. Experiment 2: upon the addition of $CuCl_2$ to $[Mo_3NiS_4(H_2O)_{10}]^{4+}$ (**D**; 8.55×10^{-4} M in 1 M HCl; $Cu^{2+}/\mathbf{D} = 10$), the peak at 686 nm in the electronic spectrum of **D** disappeared and the peak at 498 nm shifted towards shorter wavelengths with increasing intensity in 15 h which also indicated the formation of cluster **C** (Fig. 2). Mixing either **B** with Ni^{2+} (Experiment 3: $Ni^{2+}/\mathbf{B} = 10$) or **D** with Fe^{2+}

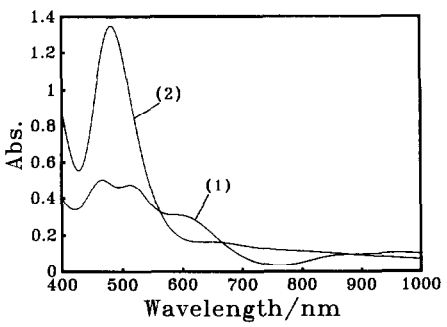

Fig. 1. Spectral change by the reaction of $[Mo_3FeS_4(H_2O)_{10}]^{4+}$ (**B**) with Cu^{2+}. (1) Spectrum containing only **B**. (2) Spectrum taken after 1 min from mixing **B** with Cu^{2+}.

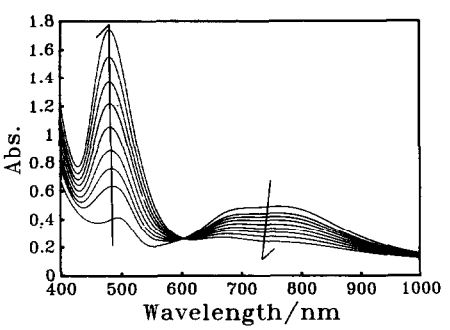

Fig. 2. Spectral changes by the reaction of $[Mo_3NiS_4(H_2O)_{10}]^{4+}$ (**D**) with Cu^{2+}. Spectra taken after 1, 30, 60, 105, 180, 285, 405, 600 and 930 min from mixing **D** with Cu^{2+}. The arrows show the directions of changes of absorbances.

* Author to whom correspondence should be addressed.

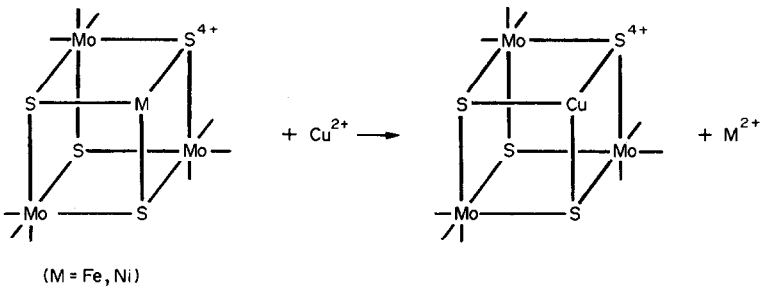

(M = Fe, Ni)

Scheme 1. Reaction of mixed-metal cubane-type clusters $[Mo_3MS_4(H_2O)_{10}]^{4+}$ (M = Fe, Ni) with Cu^{2+}.

(Experiment 4: Fe^{2+}/**D** = 10) resulted in the formation of **A** 3 weeks from mixing, and neither the formation of **D** in the former nor that of **B** in the latter was observed. Mixtures **B** and R^{3+} (Experiment 5: R = Pr, Nd, Sm, Eu, Tb, Dy, Ho) and **D** and R^{3+} (Experiment 6: R = La, Ce, Nd, Eu) were followed spectrophotometrically and column-chromatographically, however, no signs of the formation of clusters with Mo_3RS_4 cores were observed.

The reaction of the mixed-metal cubane-type clusters **B** (or **D**) with Cu^{2+} to give **C** can be shown by Scheme 1. This is the reaction in which one of the metal atoms in the metal cluster is replaced by another metal. The magnitude of the solubility products is of the order: La_2S_3 (10^{-13} M^5) > FeS (10^{-18} M^2) > NiS (10^{-19}–10^{-27} M^2) ≫ CuS (10^{-40} M^2).[4] The results of Experiments 1–6 can be explained by the affinity of metals for bridging sulphurs, which could be expressed by the order Cu—S ≫ Ni—S > Fe—S > R—S.

The aqua cluster **B** is very unstable towards air oxidation[3a] and decomposes to give **A** and Fe^{2+} even under a dinitrogen atmosphere in a couple of weeks,[5] whilst **D** is fairly stable towards air oxidation and the absorption spectrum does not change at all under a dinitrogen atmosphere. The result of Experiment 4 can be explained by the following equilibrium: $\mathbf{D}+Fe^{2+} \rightleftharpoons \mathbf{B}+Ni^{2+}$. The very small amount of **B** thus formed, which cannot be detected spectrophotometrically, decomposes to give **A** and Fe^{2+}. The magnitude of the pseudo first-order rate constants of the substitution reactions ($\mathbf{B}+Cu^{2+}$: $k_{obs} > 1$ s^{-1} at *ca* 25°C; $\mathbf{D}+Cu^{2+}$: $k'_{obs} \approx 5 \times 10^{-5}$ s^{-1} at *ca* 25°C) can also be explained by the difference in affinities of metals for bridging sulphurs.

REFERENCES

1. D. W. Margerum, G. R. Cayley, D. C. Weatherburn and G. K. Pagenkopf, *Coordination Chemistry* (Edited by A. E. Martell), ACS Monograph 174, Vol. 2, Ch. 1. American Chemical Society, Washington, DC (1978).
2. For example, (a) D. Coucouvanis, A. Toupadakis, S.-M. Koo and A. Hadjikyriacou, *Polyhedron* 1989, **8**, 1705; (b) P. E. Palermo, R. Singh, J. K. Bashkin and R. H. Holm, *J. Am. Chem. Soc.* 1984, **106**, 2600.
3. For example, (a) Mo_3FeS_4: T. Shibahara, H. Akashi and H. Kuroya, *J. Am. Chem. Soc.* 1986, **108**, 1342; (b) Mo_3NiS_4: T. Shibahara, M. Yamasaki, H. Akashi and T. Katayama, *Inorg. Chem.* 1991, **30**, 2693; (c) Mo_3CuS_4: T. Shibahara, H. Akashi and H. Kuroya, *J. Am. Chem. Soc.* 1988, **110**, 3313; (d) Mo_3SnS_4: H. Akashi and T. Shibahara, *Inorg. Chem.* 1989, **28**, 2906.
4. (a) Other datum: Ce_2S_3 (10^{-10} M^5); (b) *Critical Stability Constants Vol. 4, Inorganic complexes* (Edited by R. M. Smith and A. E. Martell), p. 76. Plenum Press, New York (1976); (c) *Stability Constants of Metal-Ion Complexes*, Section I (Edited by L. G. Sillen), Special Publication No. 17, p. 217. The Chemical Society, London (1964).
5. Reaction of $[Mo_3FeS_4(H_2O)_{10}]^{4+}$ (**B**) with O_2 has been reported very recently: P. W. Dimmock and A. G. Sykes, *J. Chem. Soc., Dalton Trans.* 1990, 3101.

Polyhedron Vol. 10, No. 20/21, pp. 2353–2370, 1991
Printed in Great Britain

0277–5387/91 $3.00+.00
© 1991 Pergamon Press plc

POLYHEDRON REPORT NUMBER 40

THE STRUCTURES OF COMPOUNDS CONTAINING SELENIUM–NITROGEN AND TELLURIUM–NITROGEN BONDS

MÁR BJÖRGVINSSON and HERBERT W. ROESKY*

Institut für Anorganische Chemie, Universität Göttingen, Tammannstrasse 4, W-3400 Göttingen, F.R.G.

CONTENTS

1. INTRODUCTION 2353
2. EARLY STRUCTURAL INVESTIGATIONS 2354
3. SELENIUM–NITROGEN AND TELLURIUM–NITROGEN HETEROCYCLES . . . 2354
4. AMIDE DERIVATIVES OF SELENIUM AND TELLURIUM 2363
5. IMIDE DERIVATIVES OF SELENIUM AND TELLURIUM 2367
6. CONCLUSIONS 2368

1. INTRODUCTION

Over the past few decades a large number of sulphur–nitrogen (S—N) compounds have been prepared and structurally characterized.[1] The S—N compounds display a variety of structures ranging from simple amides and imides to ring and cage structures. Many S—N rings and cages are stabilized through extensive π-bonding and the binary S—N cations can be rationalized as being aromatic systems.[2–4] In particular, this was evident from the metallic-like character of the $(SN)_n$ polymer and the fact that it becomes a super-conductor at low temperature.[5] This discovery further stimulated interest in S—N compounds and they have been one of the most active areas of inorganic research.

In view of the rich chemistry of S—N compounds, one might have expected an analogous diversity for their related selenium–nitrogen (Se—N) and tellurium–nitrogen (Te—N) compounds. This, however, has not been realized and until about a decade ago, only relatively few Se—N compounds[6] and even fewer Te—N compounds[7] had been characterized, some of which decompose slowly or even explosively. For example, three inorganic Se—N compounds Se_4N_4,[8] Ag_3SeO_3N[9] and $[K^+]_3[(SeO_2N)_3{}^{3-}]$,[10] which had been structurally characterized, can explode violently. Furthermore, even simple classes of compounds such as amides or imides of selenium and tellurium were, with few exceptions, unknown. It is therefore not surprising that the consensus developed among many chemists that compounds containing Se—N and Te—N bonds were generally unstable.

Probably a significant factor in destabilizing the formation of Se—N and Te—N compounds is the weakening or absence of π-bonding involving the heavier main-group elements. Consequently, it is to be expected that only a few Se—N and even fewer Te—N analogues of the many π-bonded S—N ring systems can exist.

* Author to whom correspondence should be addressed.

However, the "Achilles' heel" in the preparation of new Se—N and Te—N compounds has been the lack of suitable stable precursors, such as S_4N_4 in the preparation of a large number of S—N compounds. Thus, although Wöhler and Espenschied[11] reported in 1869 that Se_4N_4 was more easily prepared than S_4N_4, it also had a much greater tendency to detonate and consequently limits its use in synthesis. The poorly characterized Te_3N_4 and Te_4N_4 are even more explosive.[7] Most Se—N and Te—N compounds which have been reported were synthesized by reacting amines, persilylated amines or lithium amides with chalcogen halides or oxides.

In the last decade an increasing number of Se—N and Te—N compounds have been reported and the detailed structure determined for many of them. Some of these compounds have related S—N partners but the properties of others show interesting differences and often have novel structures. Furthermore, along these developments few new Se—N and Te—N synthetic precursors have been prepared. In light of this recent important progress in inorganic Se—N and Te—N chemistry, we will in this manuscript review the structures of these compounds.

2. EARLY STRUCTURAL INVESTIGATIONS

Only 100 years after its first preparation, a crystalline sample of Se_4N_4 could be prepared by ammonolysis of $SeBr_4$ in liquid ammonia at high temperature and pressure.[12] Subsequent X-ray crystallographic studies showed that the crystals consisted of approximately body-centred cubic packing of cage-like Se_4N_4 molecules (**1**).[8]

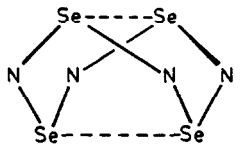

1

The average Se—N atomic distances in Se_4N_4 (179 pm) are significantly shorter than Pauling's single bond distance (186 pm),[13] indicating multiple bonding over the eight-membered ring. The relatively long intramolecular Se—Se distances (average 275 pm) complete the cage-like structure of the molecule. The approximately body-centred cubic packing of the Se_4N_4 is believed to be due to relatively short intermolecular parallelogram-type Se···N secondary interactions (296–345 pm; van der Waals Se···N = 350 pm[13]). Undoubtedly, these strong Se···N intermolecular contacts are responsible for the insolubility of Se_4N_4 in all common solvents.

A number of selenamide anions are formed from ammonolysis of SeO_2F_2 or SeO_3 and some of their salts have been isolated.[6,14,15] The detailed structures of Ag_3SeO_3N[9] and $[K^+]_3[(SeO_2N)_3^{3-}]$[10] have been determined. The former compound showed the presence of tetrahedrally-shaped SeO_3N^{3-} anions ($\mathbf{2}^{3-}$) with a very short Se—N distance (167 pm). However, the short Ag—N distances (218 pm) suggested covalent Ag—N bonds.[9] The latter compound contained a relatively flat Se—N six-membered ring, $(SeO_2N)_3^{3-}$ ($\mathbf{3}^{3-}$), in a chair conformation. The average Se—N distance (177 pm) of $\mathbf{3}^{3-}$ and the ring flatness indicated some π-electron delocalization over the ring.

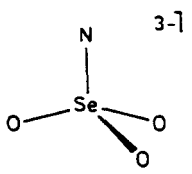

$\mathbf{2}^{3-}$

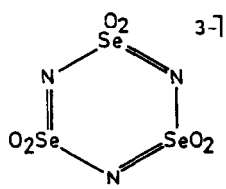

$\mathbf{3}^{3-}$

3. SELENIUM–NITROGEN AND TELLURIUM–NITROGEN HETEROCYCLES

3.1. *Five-membered heterocycles*

3.1.1. *Inorganic heterocycles.* One of the first well-characterized inorganic five-membered rings containing a Se—N bond was reported by Gillespie *et al.*[16]

$$S_4N_4 + [Se^{2+}][AsF_6^-]_2 \longrightarrow [(SN_2Se_2)_2^{2+}][AsF_6^-]_2 \quad (1)$$

The two SN_2Se_2-rings form a dimer in the lattice, $[SN_2Se_2]_2^{2+}$($\mathbf{4}_2^{2+}$), with relatively long Se—Se intermolecular bond distances. Passmore *et al.* have recently prepared and structurally characterized the isostructural all-selenium analogue, $[SeN_2Se_2]_2^{2+}$ ($\mathbf{5}_2^{2+}$, Fig. 1), using Se_4N_4 instead of S_4N_4, or by oxidizing Se_4N_4 directly with AsF_5.[17] Furthermore, when Se_4N_4 was treated with excess AsF_5 in SO_2, the AsF_6^- salt of the new $SeN_2Se_2^{2+}$ cation ($\mathbf{6}^{2+}$) could be isolated.[17]

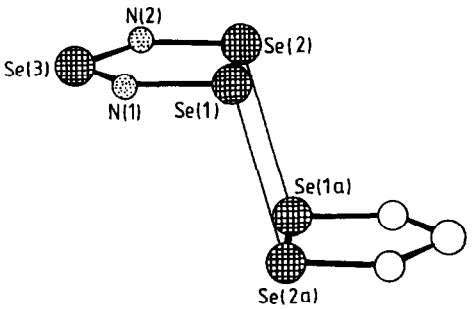

Fig. 1. Crystal structure of $[SeN_2Se_2]_2^{2+}$ ($\mathbf{5}_2^{2+}$).

Recently the mixed sulphur/selenium analogues of the $SN_2S_2Cl^+$ cation, $SN_2Se_2Cl^+$ ($\mathbf{7}^+$)[18] and SN_2SSeCl^+ ($\mathbf{8}^+$)[19,20] [eqs (2)–(4)], have been characterized.

$$Se(NSO)_2 \xrightarrow{AsF_5} [\mathbf{4}_2^{2+}][AsF_6^-]_2 \xrightarrow[SO_2]{Cl_2} [SN_2Se_2Cl^+][AsF_6^-] \quad (2)$$

$$Se_2Cl_2 + S_3N_3Cl_3 \xrightarrow{SO_2} S_2N_2SeCl_2 \quad (3)$$

$$Se + [SN^+][AlCl_4^-] \xrightarrow{CH_2Cl_2} [SN_2SSeCl^+][AlCl_4^-] \quad (4)$$

Interestingly, $S_2N_2SeCl_2$ contained both an ionic pair $\mathbf{8}^+Cl^-$ and the neutral $S_2N_2SeCl_2$ molecule in the same lattice.[19] Both ring cations $\mathbf{7}^+$ and $\mathbf{8}^+$ are nearly planar and have the chlorine atoms bonded to selenium.

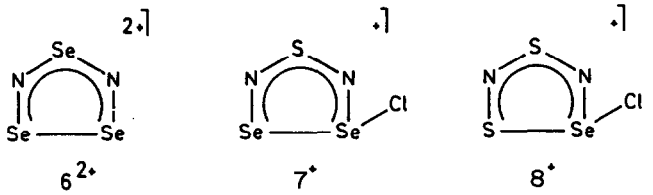

$\mathbf{6}^{2+}$ $\mathbf{7}^+$ $\mathbf{8}^+$

The relatively short Ch—N (Ch=S/Se) distances in the $\mathbf{4}_2^{2+}$–$\mathbf{8}^+$ cations (Table 1), are consistent with π-electron ring delocalization. However, all the ring Ch—Ch distances correspond to single-bond distances. Perhaps the delocalization system indicated above is more appropriate for these rings rather than a full ring delocalization.

In a search to prepare new low-dimensional conducting materials, Oakley *et al.* have characterized a series of 1,2,3,5-diselenadiazolium cations, $(Ph)CN_2Se_2^+$ ($\mathbf{9}^+$)[21] and p-$C_6H_4(CN_2Se_2)_2^{2+}$ ($\mathbf{10}^{2+}$),[22] by reacting the appropriate persilylated benzamidine with $SeCl_4$ in the presence of a reducing agent, $SbPh_3$ [eq. (5)].

$$\underset{T = SiMe_3}{Ph—C(NT)(NT_2)} + 2(SeCl_4/SbPh_3) \longrightarrow (Ph)CN_2Se_2^+ \quad (5)$$

By metathesis with $NO^+PF_6^-$, the PF_6^- salts could be isolated and their structures determined.[21,22] Like their isovalent analogue $\mathbf{6}^{2+}$, the five-membered rings of $\mathbf{9}^+$ and $\mathbf{10}^{2+}$ are planar and formally have an aromatic 6π-electron system. The Se—Se distances in $\mathbf{9}^+$ and $\mathbf{10}^{2+}$ are significantly shorter than those of $\mathbf{6}^{2+}$, presumably owing to the smaller carbon atoms in the rings.

Complexes $\mathbf{9}^+$ and $\mathbf{10}^{2+}$ can be chemically reduced by $SbPh_3$ to give the formal 7π-electron diselenadiazyl radicals $\mathbf{9}^\circ$ and $\mathbf{10}^{\circ\circ}$.[21,23] Careful purification by sublimation isolated the crystalline materials. Like their isovalent analogues $\mathbf{4}_2^{2+}$ and $\mathbf{5}_2^{2+}$, the radicals form dimers, $\mathbf{9}_2$ and $\mathbf{10}_2$, with

Table 1. The bond distances of the ChN_2Ch_2 five-membered heterocycles

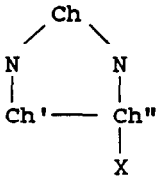

Cation	Ch	Ch′	Ch″	X	Average bond lengths (pm)[a] Ch—N	Ch′—N	Ch″—N	Ch′—Ch″	Ch—X	Ref.
$\mathbf{4}_2^{2+}$ [b]	S	Se	Se	Se	156	176	176	235	314	16
$\mathbf{5}_2^{2+}$ [b]	Se	Se	Se	Se	170	176	176	240	314	17
$\mathbf{6}^{2+}$	Se	Se	Se		169	174	174	233		17
$\mathbf{7}^{+}$	S	Se	Se	Cl	156	177	177	238	[c]	18
$\mathbf{8}^{+}$	S	S	Se	Cl	157	165	179	228	225	19
$\mathbf{8}^{+}$	S	S	Se	Cl	156	163	174	229	219	20

[a] For reference the following are Pauling's single-bond values (pm):[13] 174 (S—N), 186 (Se—N), 221 (S—Se), 234 (Se—Se), 214 (Se—Cl).

[b] Also an identical Ch′—X bond.

[c] Value not given.

long intermolecular Se—Se distances (Table 2). However, the dimeric CN_2Se_2-rings are in eclipsed configurations ($\mathbf{9}_2$, Fig. 2). Furthermore, a network of Se · · · Se contacts between the dimers, resulting from secondary interactions, was also present in the crystals.

Table 2. The bond lengths of the CN_2Se_2 five-membered heterocycles

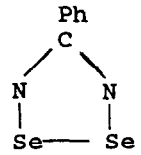

Compound	Average bond lengths (pm) C—N	N—Se	Se—Se	Se—Se′[a]	Ref.
$[\mathbf{9}^{+}][PF_6^{-}]$	136	176	226		21
$\mathbf{9}_2$	132	178	234	325	21
$[\mathbf{10}^{2+}][SbF_6^{-}]_2$	132	173	226		22
$\mathbf{10}_2$	130	179	234	327	23

[a] The dimers' inter-ring Se—Se distances.

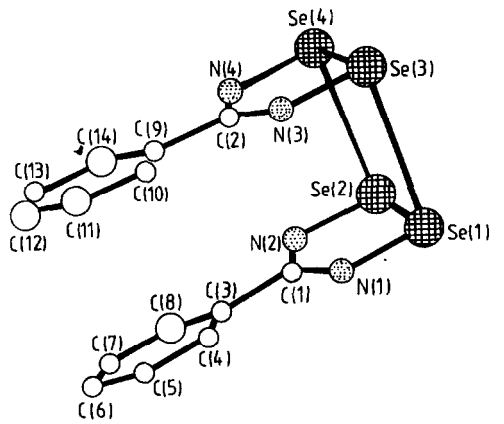

Fig. 2. Crystal structure of the dimer $(PhCN_2Se_2)_2$ ($\mathbf{9}_2$).

A novel series of five-membered platinum(II) heterocycles (**11**–**13**$^+$) has been prepared and characterized by Woollins and co-workers.[24–27]

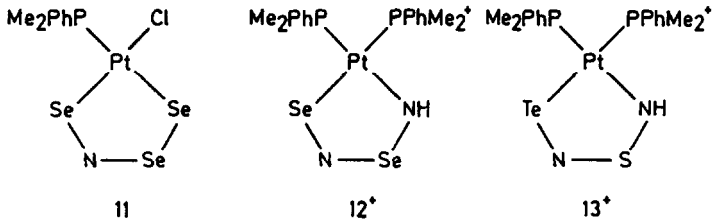

Complex **11** was isolated by chromatography of the mixture from the reaction between Se_4N_4 and $PtCl_2(PMe_2Ph)_2$ in $CHCl_3$.[24] [**12**$^+$]Cl^- was, however, isolated after treating the reaction mixture with PMe_2Ph.[25] The BF_4^- salt of **13**$^+$ was prepared by treating $Pt(TeSN_2)(PMe_2Ph)_2$ with HBF_4,[26] which in turn had been isolated from the reaction of $PtCl_2(PMe_2Ph)_2$ with the poorly characterized $Te_3SN_2Cl_2$.[27] The mixed sulphur/selenium analogue of **13**$^+$, $[Pt(SeSN_2H)(PMe_2Ph)_2^+][BF_4^-]$ (**14**$^+$[BF_4^-]), has also been characterized.[28]

The Pt^{II} heterocycles can formally be described as resulting from the coordination of Se_3N^-, $Se_2N_2H^-$ (Fig. 3) and $TeSN_2H^-$ anions to platinum(II).[24–25] Structural analysis revealed the planar nature of the rings and indicated a multiple bond character within the anion fragments (Table 3). This is consistent with the formal 6π-electron system for the anion fragments (or the whole ring). The significant resonance structures illustrating this are given below for **12**$^+$ (Scheme 1).

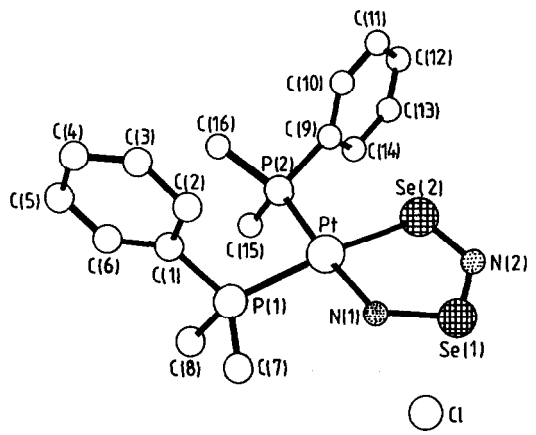

Fig. 3. Molecular structure of $[(PhMe_2P)_2PtSe_2N_2H^+]Cl^-$ (**12**); the hydrogen atoms are omitted for clarity.

Table 3. The bond lengths of the platinum compounds

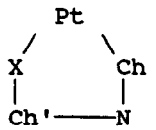

Compound	Ch	Ch′	X	Bond lengths (pm) Ch—N	Ch′—N	Ch′—X	Pt—X	Pt—Ch	Ref.
14$^+$	Se	S	NH	183	151	160	203	240	28
13$^+$	Te	S	NH	199	153	157	205	255	26
12$^+$	Se	Se	NH	179	172	176	202	241	25
11	Se	Se	Se	181	171	228	239	230	24

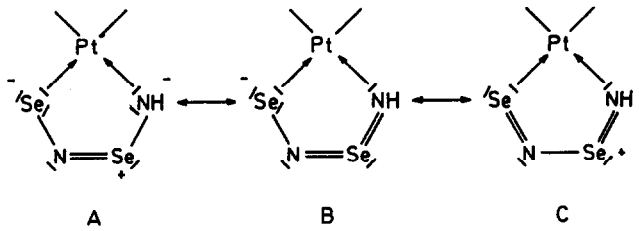

A B C

Scheme 1.

3.1.2. *Organic heterocycles.* Although it is only in the last decade that five-membered Se—N and Te—N inorganic heterocycles have been synthesized, the first five-membered organic Se—N ring was prepared more than 100 years ago by Hinsberg.[29] Hinsberg prepared benzo-1,2,5-selenadiazole (**15**), piazselenol, by simply treating SeO_2 with *o*-diaminobenzene. This reaction is a general synthetic route for other benzo-1,2,5-selenadiazoles and has proved to be an excellent method for analytical determination of selenium.[30] The parent 1,2,5-selenadiazole, $(CH)_2N_2Se$ (**16**), was first prepared about 15 years ago[31,32] and a number of other derivatives have been synthesized.[33]

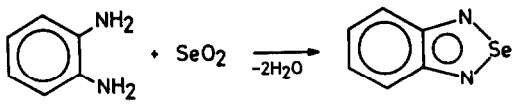

15 (6)

The first organic Te—N heterocycle 1,2,5-telluradiazole, $(CH)_2N_2Te$ (**17**), was synthesized by treating **16** with EtMgBr, followed by the addition of $TeCl_4$ [eq. (7)].[30]

$$(CH)_2N_2Se \xrightarrow[(2)\ TeCl_4]{(1)\ EtMgBr} (CH)_2N_2Te \qquad (7)$$

Compound **17** shows striking stability, being stable in air even when heated on a hot plate![34]

The first preliminary structural investigation of selenadiazole was done on piazselenol.[35] However, it is only in the last decade that the detailed molecular structure has been determined for a number of benzo- and 1,2,5-chalcogenadiazoles (**16–22**),[36–43] as well as the related naphtodiazaselen (**23**).[44]

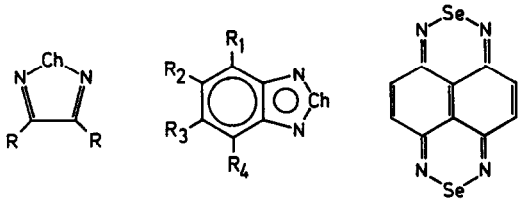

23

Ch	R	
Se	H	16
Se	Ph	18
Te	H	17

Ch	R_1/R_4	R_2/R_3	
Se	4H		15
Se	O		19
Se	$C(CN)_2$	N_2Se	20
Se	N_2S	(R_1,R_2)	21
Te			22

The Ch—N distances of these compounds (Table 4) indicate only a small multiple-bond character (single-bond lengths: Se—N 186, Te—N 205 pm).[13] Therefore, the 1,2,5-chalcogenadiazoles, as well as the benzo derivatives, show an increasing importance of resonance structure B in Scheme 2.

Table 4. The interatomic distances and bond angles of 1,2,5-chalcogenadiazoles of selenium and tellurium

Compound	Ch	Average distances (pm) and bond angles (°) Ch—N	N—C	C—C	Se···N	NSeN	Ref.
18	Se	181	130	144	295	92	36
15	Se	178	132	144	315	95	37
15	Se	179	132	145	269	93	38
21	Se	179	132	145	293	93	41
19	Se	180	132	143	295[a]	94	39
20	Se	178	132	144	294[b]	93	40
23[c]	Se	181	128			103	44
17	Te	202	127	142	276	83	42
22	Te	202	130	147	283	84	43

[a] Se···O secondary contacts.
[b] Coordination by CN groups.
[c] A six-membered ring.

A B

Scheme 2.

Furthermore, the importance of B follows the order Te > Se, consistent with the weakening of π-bonds for the heavier elements.

The high polarity of the Ch—N bonds in these compounds relative, for example, to the related seleno- and tellurophenes, is evident from the physicochemical properties and the presence of short Ch···N intermolecular interactions in their crystals.[34] Thus, intermolecular Ch_2N_2 parallelograms, similar to those in Se_4N_4,[8] are often formed. A higher polymerization of the parallelograms can take place resulting in a planar (**17**) or a ladder-type (**22**) polymer (Scheme 3).

Electrophilic groups such as H^+[38] or $M(CO)_5$ (M = Cr, Mo, W)[45] coordinate to the nitrogen atoms of the 1,2,5-selenadiazole rings. However, reaction with $(Ph_3P)_2Pt(C_2H_4)$ resulted in a Se—N bond insertion to give the near-planar six-membered ring $C_4N_4SePt(PPh_3)_2$ (**24**, Fig. 4).

The benzo-isochalcogenazoles of selenium (**25**) and tellurium (**26**) have been determined.[47] However, the structures of other organic Se—N heterocycles such as 1,2,3-selenadiazole (**27**)[48] and

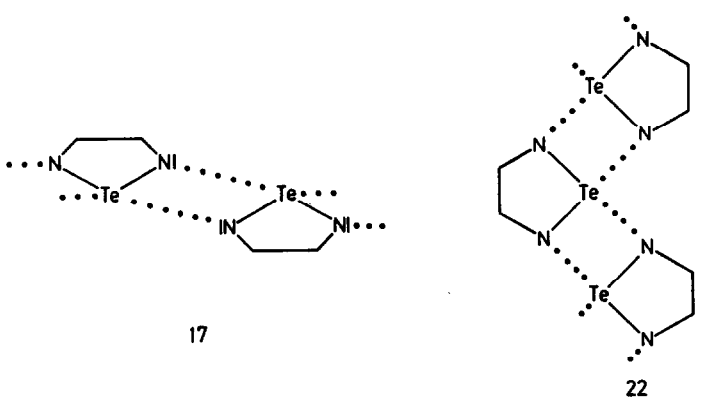

17 22

Scheme 3.

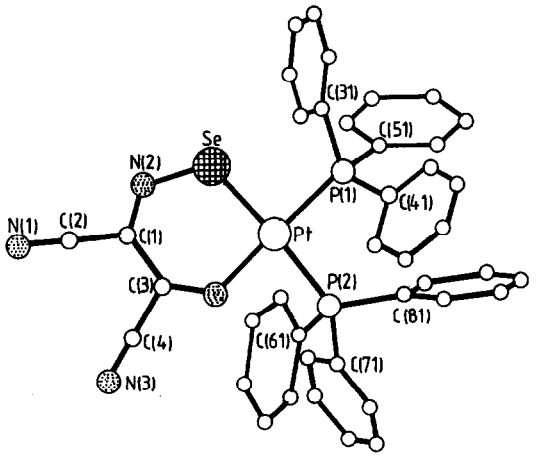

Fig. 4. Molecular structure of $C_4N_4SePt(PPh_3)_2$ (**24**) in the crystal.

tetraazaselenapentalene (**28**)[49] have not been studied in detail. Organic Se—N heterocycles have previously been reviewed.[50–52]

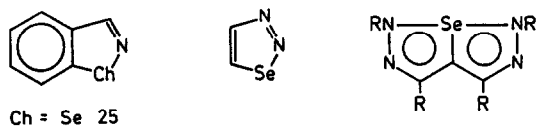

3.2. *Six-membered heterocycles*

Recently a number of transition-metal cyclometallaphosphazenes have been characterized in our laboratory.[53] The first structurally characterized cycloselenaphosphazene $N(Ph_2P)_2N_2SeCl$ (**29**) was synthesized by reacting $[ClPh_2PNPPh_2Cl^+]Cl^-$ with the thermally unstable $Se(=NSiMe_3)_2$.[54,55]

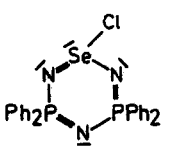

29

The series resulting from successive replacement of Ph_2P groups with PhC groups $N(PPh_2)(CPh)N_2SeCl$ (**30**)[56] and $N(CPh)_2N_2SeCl$ (**31**)[57] have also been structurally characterized.

The six-membered rings **29–31** are all nearly planar and the rings' short interatomic distances (Table 5) are further consistent with a 6π-electron ring delocalization. However, a more appropriate description of **30** and **31** is to represent them as hybrids of a "normal" π-system and a phosphazene π-system, i.e. replacing Ph_2P with PhC successively fuses Dewar's cyclophosphazene π-electron "islands".[58] The Se—Cl distances in **29–31** are all significantly longer than Pauling's single bond distance (214 pm).

Reduction of **31** gave an eclipsed Se—Se bonded dimer $\mathbf{31}_2$, similar to $\mathbf{9}_2$ and $\mathbf{10}_2$.[57] However, reduction of **30** did not give a Se—Se bonded dimer but two rings linked together by a Se—N bond, $(NPh_2PNPhCNSe)$—$(NSeCPhNPPh_2)$ ($\mathbf{30}_2$).[55] The selenium-bonded ring is analogous to **30** where the chlorine atom has been replaced by the —$NSeCPhNPPh_2$ ring.

Compound **31** was prepared from the six-membered $HN(CPh)_2N_2SeCl_2$ (**32**) ring by careful heating to affect HCl elimination. Structural investigation of **32** showed the ring to have a relatively flat boat-like conformation.[59] However, the Se—N distance (181 pm) indicated a small π-bond character.

Table 5. Bond distances of inorganic Se—N heterocyclic six-membered rings

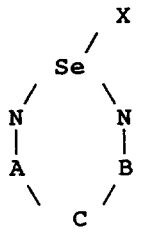

Compound	A	B	C	X	Se—N	N—A	N—B	A—C	B—C	Se—X	Ref.
29	PPh_2	PPh_2	N	Cl	173	164	164	158	158	234	54
30	PPh_2	CPh	N	Cl	174	164	134	161	132	234	56
31	CPh	CPh	N	Cl	176	135	135	135	135	235	57
$\mathbf{31}_2$	CPh	CPh	N		178	134	134	135	135	279	57
$\mathbf{30}_2$	PPh_2	CPh	N	[a]	174	163	133	159	134	199	55
32	CPh	CPh	NH	C12	181	130	130	138	138	241	59

[a] Bonded to a nitrogen atom of a similar ring.

3.3. *Other heterocycles*

Shreeve *et al.* have prepared Si_2N_4Se (**33**) and Sn_2N_4Se (**34**) spiro heterocycles.[60]

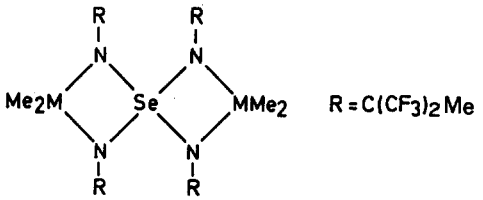

However, the detailed molecular structures have not been determined.

Eight-membered and 15-membered Se—N rings, $Se_6(NCMe_3)_2$ (**35**) (Fig. 5) and $Se_9(NCMe_3)_6$ (**36**) (Fig. 6), were isolated from the reaction of $LiN(CMe_3)SiMe_3$ with $SeOCl_2$ or Se_2Cl_2 in a 1 : 1 molar ratio.[61] The rings' Se—N distances (average 184 pm) fall within the range of single-bond lengths. Interestingly, three short intramolecular Se···Se contacts are present in **36**.

The eight-membered $(Ph_2P)_2N_4Se_2Me_2$ ring (**37**) was obtained from the reaction of $Ph_2P(NT)(NT_2)$ (T = $SiMe_3$) with $MeSeCl_3$.[62] The ring has a chair configuration with the SeMe

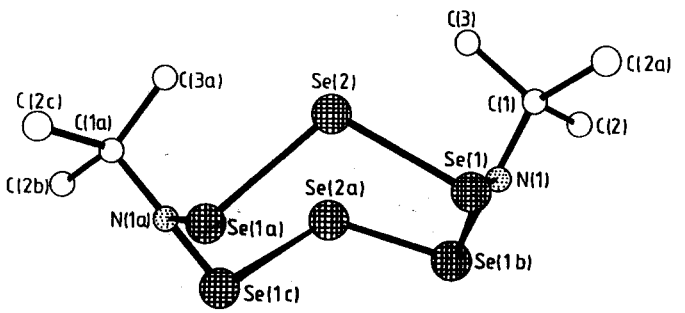

Fig. 5. Molecular structure of the eight-membered ring $Se_6(NCMe_3)_2$ (**35**); the hydrogen atoms are omitted for clarity.

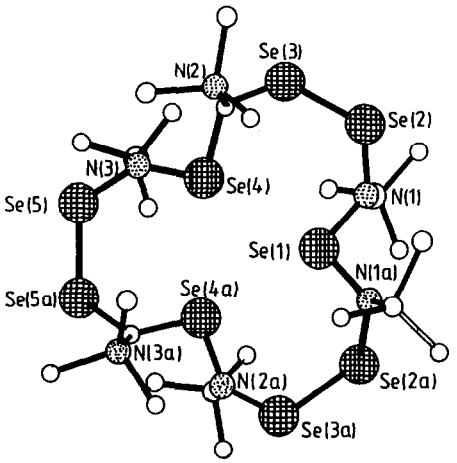

Fig. 6. Molecular structure of the 15-membered Se—N ring (**36**); the hydrogen atoms are omitted.

groups above and below the plane formed by the P_2N_4 atoms (Fig. 7). The ring Se—N bonds are relatively short (178 pm).

A novel cage-like structure, $N[Te(NSN)Cl]_3 \cdot 3DMF$ (**38**) was formed when $TeCl_4$ was treated with $S(=NSiMe_3)_2$ and the product recrystallized from DMF.[63] The unique nitrogen atom is bonded to three tellurium(IV) atoms which in turn are bridged by NSN and Cl groups (Fig. 8). The Te—N distances of 205–207 pm (N) and 202–207 pm (NSN) correspond to single-bond lengths. The overall geometry around tellurium is octahedral with an additional DMF molecule coordinating to the lone-pair side.

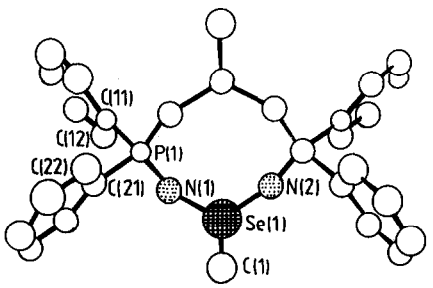

Fig. 7. Molecular structure of the eight-membered ring $(Ph_2P)_2N_4Se_2Me_2$ (**37**) without hydrogen atoms.

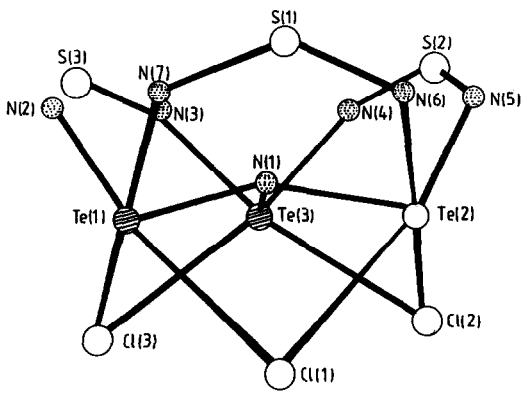

Fig. 8. Molecular structure of $N[Te(NSN)Cl]_3 \cdot 3DMF$ (**38**) without solvent molecules.

4. AMIDE DERIVATIVES OF SELENIUM AND TELLURIUM

4.1. *Amide derivatives of selenium*(IV) *and tellurium*(IV) *chlorides*

Both the mono- and bis-N=PPh_3 substituted derivatives of selenium and tellurium tetrachloride, $(Ph_3PN)ChCl_3$ [Ch = Se (**39**),[64] Te (**40**)[65]] and $(Ph_3PN)_2ChCl_2$ [Ch = Se (**41**),[64] Te (**42**)[66]], can be prepared by reacting $Ph_3PNSiMe_3$ with chalcogen tetrachlorides [eq. (8)].

$$n\,Ph_3PNSiMe_3 + ChCl_4 \longrightarrow (Ph_3PN)_nChCl_{4-n} \quad (8)$$
$$n = 1,2 \qquad Ch = Se, Te$$

The related selenamide $(Me_2S(O)=NPPh_2=N)_2SeCl_2$ (**43**) has also been prepared by a similar reaction.[67]

Compounds **41**–**43** all have the same geometry around selenium with the ligand's nitrogen atoms in the equatorial plane and the chlorine atoms in axial positions. However, the Ch—N distances are short, indicating a high multiple-bonding character, but the Ch—Cl bonds are very long (Table 6). Furthermore, contrary to the predictions of the VSEPR rules for AX_4E systems,[68] the chlorine atoms are bent away from the nitrogen atoms.

Table 6. The bond distances (pm) and bond angles (°) of $(AN)_2Ch^{IV}Cl_2$ (Ch = Se/Te)

Compound	A	Ch	Ch—N	Ch—Cl	ClChCl	Ref.
32	CPh[a]	Se	181	241	174	59
41	PPh_3	Se	174	260	150	64
43	PPh_2X[b]	Se	170	265	154	67
42	PPh_3	Te	192	260	163	66

[a] Part of a ring.
[b] X = —$NSO(Me)_2$.

The long Ch—Cl distances suggest very ionic Ch—Cl bonds such that one extreme view of describing **41**–**43** would be a coordination of Cl^- anions to a π-electron stabilized $(R_3PN)_2Ch^{2+}$ cation (Scheme 4).

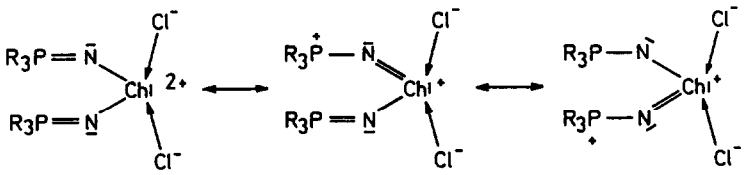

Scheme 4.

The bending of the $ChCl_2$ fragment would then be a result of the coordination of Cl^- anions to the lone-pair side of the chalcogen atom. This would be consistent with the coordination of anions towards the metal cation lone-pair side observed for a number of other main-group halides.[69]

An alternative rationalization for the ChN_2Cl_2 geometry is to consider the chalcogen atom lone-pair to be more spread out in the equatorial plane to have the multiple Ch—N bonds perpendicular to the ChN_2 plane. The directional character of the multiple Ch—N bond would then repel the Ch—Cl bond pairs away more effectively.

A similar directional repulsion effect of multiple bonds has been invoked to account for the bending of the axial Xe—F bonds of XeO_2F_2 (an AX_4E type system) towards the xenon lone pair.[70] Consistent with this description is the bending of $ChCl_2$ which is much larger for the strong π-donating R_3PN ligands than for weaker π-donors such as, for example, in **32**.

Compound **39** forms chlorine-bridged dimers in the solid state (Fig. 9) with a very short Se—N bond distance (168 pm).[64] The two Se—Cl bridge distances are also very long (263 and 298

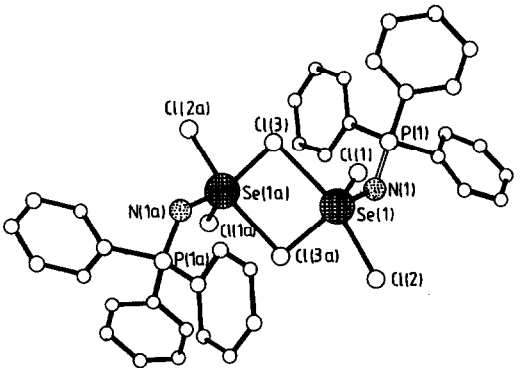

Fig. 9. Molecular structure of the $Ph_3PNSeCl_3$ (**39**) dimer without hydrogen atoms.

pm) and probably very ionic. Thus, the structure of the dimer can be described as ylene (or ylide) pyramidal cations, $SeCl_2(NPPh_3)^+$, coordinated by two Cl^- anions, approximately *trans* to the cation's Se—Cl bonds.

Compound **40** is also present as the dimer in the solid state (Fig. 10) but, unlike **39**, forms a planar four-membered Te_2N_2 ring with short (200 pm) and long (228 pm) Te—N distances.[65] The geometry around the tellurium atom is approximately ψ-octahedral, but with the two chlorine atoms perpendicular to the Te_2N_2 plane bent away from the shorter Te—N bond towards the tellurium lone pair.

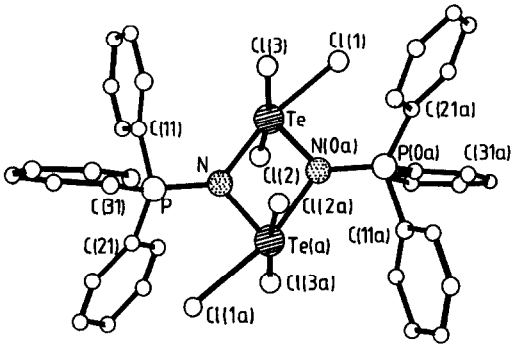

Fig. 10. Molecular structure of the $Ph_3PNTeCl_3$ (**40**) dimer without hydrogen atoms.

The reaction of $PhC(NT)(NT_2)$ (T = $SiMe_3$) with $TeCl_4$ gave the monomeric $PhC(NT)_2TeCl_3$ (**44**).[71] Compound **44** also has a short Te—N bond (210 pm) and a longer intramolecular Te—N adduct-type bond (219 pm). However, the two Te—N bonds are more equivalent in **44** and the tellurium atom has the expected ψ-octahedral geometry. The reaction of $PhC(NT)(NT_2)$ with $RSeCl_3$ (R = Me, Ph) resulted in an oxidation of the ligand and gave a near-planar diazine (**45**) with two N—Se bonds (181–182 pm).[72] Like **44**, **45** is also stabilized by intramolecular Se—N contacts (265 pm) and formally forms a fused five-membered ring system. Analogous intramolecular donor contacts have been observed in organic seleno-imines.[73,64]

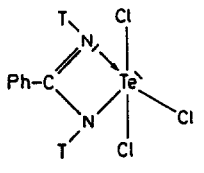

44

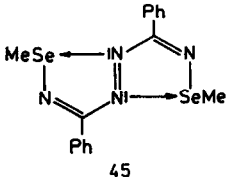

45

4.2. *Other amide derivatives of selenium and tellurium*

Foss *et al.* have isolated and structurally characterized a series of diaminopolyselanes, $Se_n[N(CH_2)_4O]$ and $Se_4[N(CH_2)_5]$ [n = 2 (**46**), 3 (**47**), 4 (**48**)].[74,76] Compounds **46–48** were formed

when the amines were heated over selenium powder and PbO_2. They all have a chain-like geometry with Se—N distances (184–185 pm) in the single-bond range.

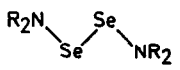

46

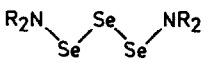

47

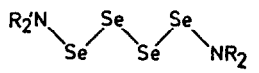

48

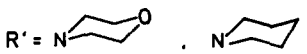

As in **46–48** where nitrogen is bonded to one selenium(II) atom, the **35** and **36** rings are amines with nitrogen bonded to two selenium(II) atoms. An amine with nitrogen bonded to three selenium(II) atoms, $N[SeCF_3]_3$ (**49**), has been characterized from electron diffraction studies.[77] The Se—N distances (184 pm) correspond to a single bond but the Se—N—Se bond angle (119°) is relatively large.

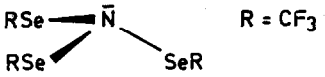

49

Seppelt and co-workers have prepared a large number of H_2NTeF_5 derivatives.[78] Thus, starting from H_2NTeF_5 or $H(SiMe_3)NTeF_5$, compounds with TeF_5 groups bonded to nitrogen containing groups such as N=C=O (**50**), N=S=O (**51**), NCl_2 (**52**), $N{=}SF_2$ (**53**), $N{=}SeF_2$ (**54**), $N{=}PF_3$ (**55**) and $N{=}WCl_4$ (**56**) have been isolated.

Structural analysis showed **56** to be a chlorine-bridged dimer with an almost linear Te—N—W skeleton (Te—N—W 173°, Te—N 198 pm).[78] The Se—N—W skeleton of the recently characterized $Cl_5WNSeMe^-$ (**57**$^-$) anion was likewise near-linear (Se—N—W 174°, Se—N 181 pm).[79] Another metal complex H_2NTeF_5-derivative, $Hg[N(CF_3)TeF_5]_2$ (**58**), had a Te—N distance of 201 pm.[80]

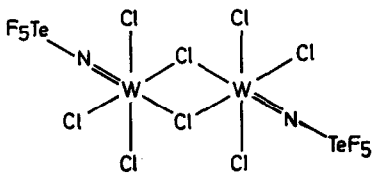

56

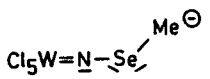

57$^-$

The molecular structure of **50** and its selenium analogue, O=C=$NSeF_5$ (**58**), have been determined from electron diffraction studies.[81] The Se—N distance (178 pm) of **58** is 7 pm shorter than Pauling's single bond distance but **50** was found to have a surprisingly short Te—N distance (186 pm).

Haas *et al.* have prepared [eqs (9) and (10)] and characterized the bis(sulphinylamido)chalcogens $Ch(N{=}S{=}O)_2$[Ch=Se (**59**), Te (**60**)].[82,83]

$$Se_2Cl_2 + 2Me_3SiNSO \xrightarrow[-2Me_3SiCl,\ 1/8Se_8]{CH_2Cl_2} Se(NSO)_2 \qquad (9)$$

$$(t\text{-}BuMe_2Si)_2Te + 2ClNSO \xrightarrow[-2t\text{-}BuMe_2SiCl]{CH_2Cl_2} Te(NSO)_2 \qquad (10)$$

The Ch—N distances of 183 (selenium) and 204 pm (tellurium) fall within the single-bond range

and the N—Ch—N bond angles are 92° and 87°, respectively. A similar geometry was found for the recently characterized (2,4,6)$(CF_3)_3C_6H_2SeN{=}S{=}O$ (**54**) (Se—N 185 pm, C—Se—N 93°).[84]

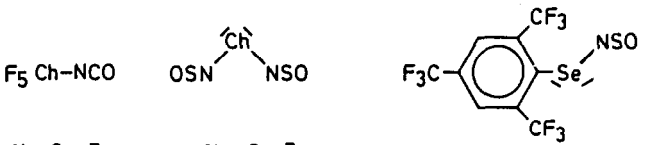

Ch = Se, Te — Ch = Se, Te

58, 50 — 59, 60 — 61

$(Me_2N)_2SeO$ (**55**) could be prepared by reacting Me_2NH with $SeOCl_2$ at low temperature [eq. (11)].[85] By standing at room temperature **55** decomposes to give $Se(NMe_2)_2$ (**56**) and oxygen gas [eq. (11)].

$$SeOCl_2 + 4Me_2NH \xrightarrow[-2Me_2NH_2Cl]{-20^\circ C} (Me_2N)_2SeO \xrightarrow[-\frac{1}{2}O_2]{25^\circ C} Se(NMe_2)_2 \qquad (11)$$

However, very few other bisaminochalcogen compounds, $(R_2N)_2Ch$, of selenium and tellurium have been reported. Recently the bis(trimethylsilyl)amide (NT_2) derivatives of selenium and tellurium $Ch(NT_2)_2$ [Ch = Se (**57**)[86,87] Te (**58**)[87]] were prepared in high yields [eqs (12) and (13)].

$$Se_2Cl_2 + LiNT_2 \xrightarrow[-2LiCl,\ 1/8Se_8]{} Se(NT_2)_2 \qquad (12)$$

$$TeCl_4 + 4LiNT_2 \xrightarrow[-4\,LiCl]{} Te(NT_2)_2 \qquad (13)$$

$T = SiMe_3$

In order to prepare **58** and to prevent formation of elemental tellurium, $TeCl_4$ had to be added to four equivalents of $LiNT_2$. It is likely that **58** is formed by a radical mechanism. The tert-butyltrimethylsilylamide ($NTCMe_3$) derivatives $Ch(NT(CMe_3))_2$ [Ch = Se (**59**), Te (**60**)] were prepared by identical procedures.[88]

Low temperature structural analyses of **57**–**60** showed the expected V-shaped geometry of the ChN_2 groups (Fig. 11). However, unlike **57** and **59**, **58** and **60** form dimers in the crystals (Fig. 12) with relatively short Te···Te contact distances [Te···Te 377 (**58**) and 423 pm (**60**); van der Waals Te···Te 420 pm[13]].

In a study of the coordination properties of **58** to metal cations, the AsF_6^- salt of the dark blue tellurium(III) radical cation $Te(NT_2)_2^{\circ+}$ (**61**$^{\circ+}$) was isolated.[81] Radical **61**$^{\circ+}$ was formed when **58** was treated with Ag^+AsF_6 [eq. (14)].

$$Te(NT_2)_2 + Ag^+AsF_6^- \xrightarrow[-Ag^\circ]{CH_2Cl_2} [Te(NT_2)_2{}^{\circ+}][AsF_6^-] \qquad (14)$$

Low temperature structural analysis showed **61**$^{\circ+}$ to be monomeric with two relatively short Te···F interionic contacts (Fig. 13). The short Te—N distances (average 197 pm) of **61**$^{\circ+}$ and the changes

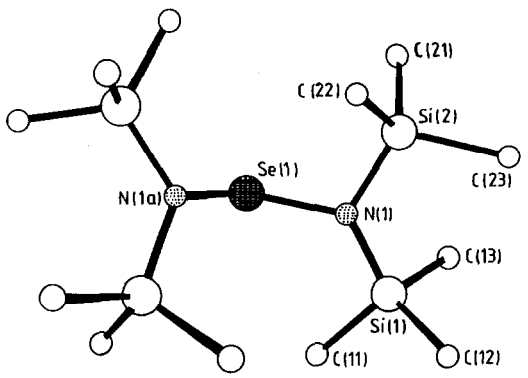

Fig. 11. Molecular structure of $Se[N(SiMe_3)_2]_2$ (**57**) without hydrogen atoms.

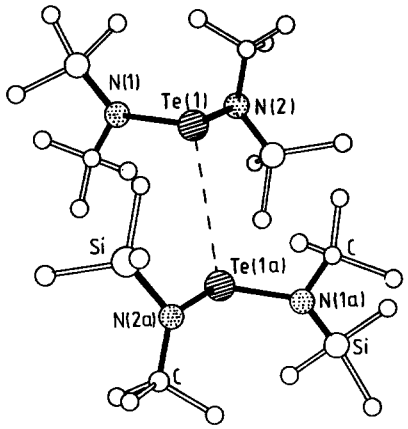

Fig. 12. Molecular structure of the $Te[N(SiMe_3)CMe_3]_2$ (**60**) dimer without hydrogen atoms.

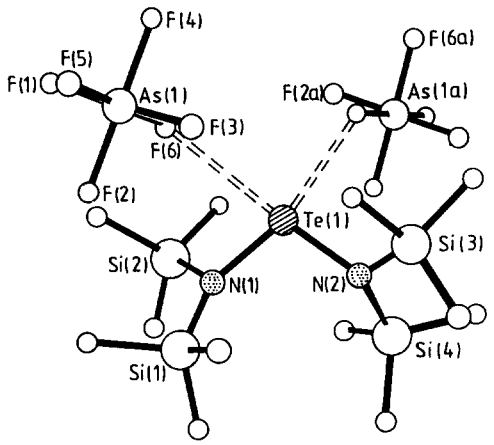

Fig. 13. Crystal structure of $[Te(N(SiMe_3)_2)_2{}^{\circ+}][AsF_6^-]$ (**61**$^{\circ+}$) with Te···F interionic contacts.

in the NT_2 groups geometries correlate well with the back-bonding model of the ligands' nitrogen atom lone pairs onto the positively charged tellurium atom. ESR solution studies of **61**$^{\circ+}$ indicated that the unpaired electron is localized in a *p*-orbital on tellurium.

5. IMIDE DERIVATIVES OF SELENIUM AND TELLURIUM

A large number of organo-selenimides, $R_2Se{=}NR'$, and a few organo tellurimides, $R_2Te{=}NR'$, are known and have been used for some time in organic synthesis (for a recent review on organo Se—N and Te—N compounds see ref. 52). However, only the detailed structure of $Ph_2Se{=}NSO_2Ph$ (**62**),[90] $(p\text{-}MeC_6H_4)_2Se{=}NSO_2C_6H_4(p\text{-}Me)$ (**63**)[64] and $((p\text{-}MeO)C_6H_4)_2Te{=}NSO_2C_6H_4(p\text{-}Me)$ (**64**)[91] have been determined. The chalcogen atoms in **62–64** are three-coordinated and have the expected pyramidal structure. The structures of the Se—N [182 (**62**) and 179 pm (**63**)] and Te—N (198 pm) compounds **62–64** are best described by the resonance form B. (Scheme 5).

The first binary Te—N cation $Te(N_3)_3{}^+$ (**65**$^+$) has a pyramidal structure with tellurium bonded

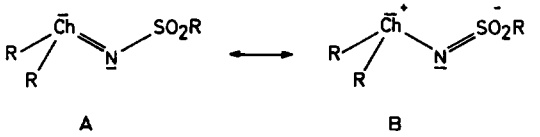

Scheme 5.

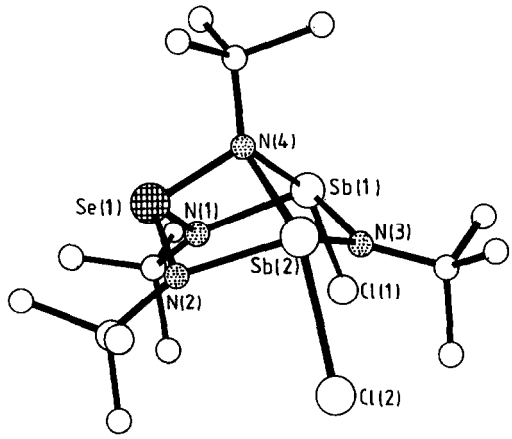

Fig. 14. Molecular structure of $SeSb_2Cl_2(NCMe_3)_4$ (**66**) without hydrogen atoms.

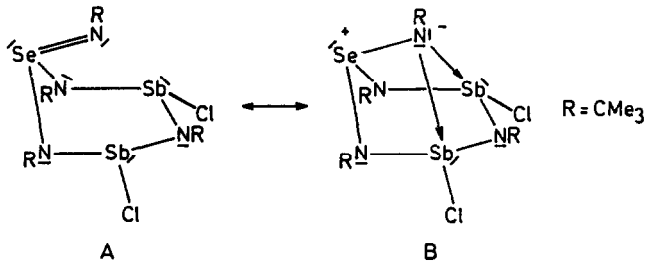

Scheme 6.

to three nearly linear N_3 groups (Te—N 199 pm).[92] Complex 65^+ was found to be analogous to tellurium halide cations, TeX_3^+,[92] so would then correspond to an ylide.

Recently the first all-nitrogen bonded seleniumimide $SeSb_2Cl_2(NCMe_3)_4$ (**66**, Fig. 14) was characterized in our laboratory.[93] Compound **66** consists of a six-membered SeN_2Sb_2N ring with a N—Se bonded non-ring $NCMe_3$ group coordinating further to the antimony atoms. The seleniumimide is thus stabilized by the Sb—N adduct bond as indicated in Scheme 6. The three Se—N distances are nearly equal (179–183 pm) and do not indicate high multiple bonding.

The thermally unstable selenium diimide $Se(=NSiMe_3)_2$ (**67**)[94] was used in the synthesis of **29**. Other selenium diimides such as $Se(=NSO_2C_6H_4(p\text{-}Me))_2$ (**68**)[95] have been used for some time in organic synthesis. However, no structures have been determined.

6. CONCLUSIONS

From the many Se—N and Te—N compounds which have been characterized in the last decade, it is evident that they are not in general unstable but show a relatively rich chemistry. In particular, the introduction of new synthetic precursors such as **57–60** will further stimulate progress in this area. Moreover, the characterization of the novel cages **38** and **66** strongly suggests that Se—N and Te—N compounds can have structures quite different from the known S—N compounds. Due to the low thermal stabilibity of Se—N and Te—N compounds, they might function as precursors for the generation of II/VI semi-conductors at low temperatures.

Acknowledgements—We thank J. Schimkowiak for making the drawings for us and the Alexander von Humbolt Foundation for a fellowship to M.B. Support by the Deutsche Forschungsgemeinschaft is gratefully acknowledged.

REFERENCES

1. Sulfur–nitrogen compounds. In *Gmelin Handbook of Inorganic Chemistry*, Parts 1–5. Berlin, Springer-Verlag (1977, 1985, 1987, 1990).

2. H. G. Heal, *The Inorganic Heterocyclic Chemistry of Sulfur, Nitrogen and Phosphorus*. Academic Press, New York (1980).
3. H. W. Roesky, *Adv. Inorg. Chem. Radiochem.* 1979, **22**, 240.
4. T. Chivers and R. T. Oakley, *Top. Curr. Chem.* 1982, **102**, 117.
5. M. M. Labes, P. Love and L. F. Nichols, *Chem. Rev.* 1979, **79**, 1.
6. Selenium. *Gmelin Handbook of Inorganic Chemistry*, Vol. B1, p. 321. Springer-Verlag, Berlin (1981).
7. Tellurium. *Gmelin Handbook of Inorganic Chemistry*, Vol. B1, p. 151. Springer-Verlag, Berlin (1976).
8. H. Bärnighausen, T. von Volkman and J. Jander, *Acta Cryst.* 1966, **21**, 571.
9. J. K. Fawcett, V. Kocman, S. C. Nyburg and R. J. O'Brien, *J. Chem. Soc., Chem. Commun.* 1969, 1198.
10. V. Kocman and J. Rucklidge, *Acta Cryst.* 1974, **B30**, 6.
11. F. Wöhler and R. Espenschied, *Liebigs Ann.* 1859, **109**, 375.
12. J. Jander and V. Doetsch, *Chem. Ber.* 1960, **93**, 561.
13. L. Pauling, *The Nature of the Chemical Bond*, 3rd edn, Ch. 7. Cornell University Press, Ithaca, New York (1960).
14. (a) A. Engelbrecht and F. Clementi, *Monatsh. Chem.* 1961, **92**, 555; 570; (b) A. Engelbrecht, *Monatsh. Chem.* 1961, **92**, 1269; 1273.
15. K. Dostál and J. Krejci, *Z. Anorg. Allg. Chem.* 1958, **296**, 29.
16. R. J. Gillespie, J. P. Kent and J. F. Sawyer, *Inorg. Chem.* 1981, **20**, 4053.
17. E. G. Awere, J. Passmore, P. S. White and T. Klapötke, *J. Chem. Soc., Chem. Commun.* 1989, 1415.
18. A. Haas and J. Kasprowski, *Chimia* 1988, **42**, 343.
19. R. J. Gillespie, J. P. Kent and J. F. Sawyer, *Inorg. Chem.* 1990, **29**, 1251.
20. A. Apblett, T. Chivers and J. F. Fait, *Inorg. Chem.* 1990, **29**, 1643.
21. P. D. B. Belluz, A. W. Cordes, E. M. Kristof, P. V. Kristof, S. W. Liblong and R. T. Oakley, *J. Am. Chem. Soc.* 1989, **111**, 9276.
22. A. W. Cordes and R. T. Oakley, *Acta Cryst.* 1990, **C46**, 699.
23. A. W. Cordes, R. C. Haddon, R. T. Oakley, L. F. Schneemeyer, J. V. Waszczak, K. M. Young and N. M. Zimmerman, *J. Am. Chem. Soc.* 1991, **113**, 582.
24. P. F. Kelly, A. M. Z. Slawin, D. J. Williams and J. D. Woollins, *J. Chem. Soc., Chem. Commun.* 1989, 408.
25. P. F. Kelly, I. P. Parkin, A. M. Z. Slawin, D. J. Williams and J. D. Woollins, *Angew. Chem.* 1989, **101**, 1052; *Angew. Chem., Int. Edn Engl.* 1989, **28**, 1047.
26. P. F. Kelly, A. M. Z. Slawin, D. J. Williams and J. D. Woollins, *Polyhedron* 1990, **9**, 2659.
27. A. V. Zibarev, G. G. Furin and G. G. Yakobson, *Acad. Sci. USSR Chem. Ser.* 1985, **34**, 2571; *Izv. Akad. Nauk SSSR, Ser. Khim.* 1985, **12**, 2774.
28. C. A. O'Mahoney, I. P. Parkin, D. J. Williams and J. D. Woollins, *Polyhedron* 1989, **8**, 2215.
29. O. Hinsberg, *Ber. Deutsch. Chem. Ges.* 1889, **22**, 862.
30. J. F. Alicina and J. A. Kowald, in *Organic Selenium Compounds Their Chemistry and Biology* (Edited by D. L. Klayman and W. H. Günther), Ch. 17, pp. 1050–1081. John Wiley & Sons, New York (1973).
31. L. M. Weinstock, P. Davis, D. M. Mulvey and J. C. Schaeffer, *Angew. Chem.* 1967, **79**, 315; *Angew. Chem. Int. Edn Engl.* 1967, **6**, 364.
32. V. Bertini, *Angew. Chem.* 1967, **79**, 530; *Angew. Chem., Int. Edn. Engl.* 1967, **6**, 563.
33. V. Bertini and F. Lucchesini, *Synthesis* 1979, 979.
34. V. Bertini and F. Lucchesini, *Synthesis* 1982, 681.
35. P. V. Luzzati, *Acta Cryst.* 1951, **4**, 193.
36. M. Mellini and S. Merlino, *Acta Cryst.* 1976, **B32**, 1074.
37. A. C. Gomes, G. Biswas, A. Banerjee and W. L. Duax, *Acta Cryst.* 1989, **C45**, 73.
38. A. Gieren, T. Hübner, V. Lamm, R. Neidlein and D. Droste, *Z. Anorg. Allg. Chem.* 1985, **523**, 33.
39. N. L. Klimasenko, L. A. Chetkina and G. A. Golder, *J. Struct. Chem.* 1973, **14**, 469.
40. T. Suzuki, C. Kabuto, Y. Yamashita, G. Saito, T. Mukai and T. Miyashi, *Chem. Lett.* 1987, 2285.
41. A. Gieren, H. Betz, T. Hübner and V. Lamm, *Z. Naturforsch.* 1984, **39b**, 485.
42. V. Bertini, P. Dapporto, F. Lucchesini, A. Sega and A. De Munno, *Acta Cryst.* 1984, **C40**, 653.
43. R. Neidlein and D. Knecht, *Z. Naturforsch.* 1987, **42b**, 84.
44. A. Gieren, V. Lamm, R. C. Haddon and M. L. Kaplan, *J. Am. Chem. Soc.* 1980, **102**, 5070.
45. W. Kaim and S. Kohlmann, *Inorg. Chim. Acta* 1985, **101**, L21.
46. H. W. Roesky, T. Gries, H. Hofmann, J. Schimkowiak, P. G. Jones, K. Meyer-Bäse and G. M. Sheldrick, *Chem. Ber.* 1986, **119**, 366.
47. H. Campsteyn, L. Dupont, J. Lamotte-Brasseur and M. Vermeire, *J. Heterocycl. Chem.* 1978, **15**, 745.
48. I. Lalezari, A. Shafiee and M. Yalpani, *J. Org. Chem.* 1971, **36**, 2836.
49. M. Perrier and J. Vialle, *Bull. Soc. Chim. Fr. II* 1979, 205.
50. E. Bulka in ref. 30, Ch. 11C, pp. 459–496.
51. I. Lalezari and A. Shafiee, *Adv. Heterocycl. Chem.* 1979, **24**, 109.

52. G. Kirsch and L. Christiaens, in *The Chemistry of Organic Selenium and Tellurium Compounds* (Edited by S. Patai), Ch. 11, pp. 421–461. John Wiley & Sons, New York (1987).
53. (a) H. W. Roesky, K. V. Katti, U. Seseke, M. Witt, E. Egert, R. Herbst and G. M. Sheldrick, *Angew. Chem.* 1986, **98**, 447; *Angew. Chem., Int. Edn Engl.* 1986, **25**, 477; (b) H. W. Roesky, K. V. Katti, U. Seseke, H.-G. Schmidt, E. Egert, R. Herbst and G. M. Sheldrick, *J. Chem. Soc., Dalton Trans.* 1987, 847; (c) K. V. Katti, U. Seseke, M. Witt and H. W. Roesky, *Phosphorus and Sulfur* 1987, **30**, 421.
54. A. W. Cordes, K. Bestari and R. T. Oakley, *Acta Cryst.* 1990, **C46**, 504.
55. K. Bestari, A. W. Cordes, R. T. Oakley and K. M. Young, *J. Am. Chem. Soc.* 1990, **112**, 2249.
56. H. W. Roesky, U. Scholz and M. Noltemeyer, *Z. Anorg. Allg. Chem.* 1989, **576**, 255.
57. R. T. Oakley, R. W. Reed, A. W. Cordes, S. L. Craig and J. B. Graham, *J. Am. Chem. Soc.* 1987, **109**, 7745.
58. M. J. S. Dewar, E. A. C. Lucken and M. A. Whitehead, *J. Chem. Soc.* 1960, 2423.
59. A. W. Cordes, R. T. Oakley and R. W. Reed, *Acta Cryst.* 1986, **C42**, 1889.
60. T. Kitazume and J. M. Shreeve, *Inorg. Chem.* 1977, **16**, 2040.
61. H. W. Roesky, K. L. Weber and J. W. Bats, *Chem. Ber.* 1984, **117**, 2686.
62. T. Chivers, D. D. Doxsee and J. F. Fait, *J. Chem. Soc., Chem. Commun.* 1989, 1703.
63. H. W. Roesky, J. Münzenberg and M. Noltemeyer, *Angew. Chem.* 1990, **102**, 73; *Angew. Chem., Int. Edn Engl.* 1990, **29**, 61.
64. H. W. Roesky, K. L. Weber, U. Seseke, W. Pinkert, M. Noltemeyer, W. Clegg and G. M. Sheldrick, *J. Chem. Soc., Dalton Trans.* 1985, 565.
65. J. Münzenberg, M. Noltemeyer and H. W. Roesky, *Chem. Ber.* 1989, **122**, 1915.
66. H. W. Roesky, J. Münzenberg, R. Bohra and M. Noltemeyer, *J. Organomet. Chem.*, submitted.
67. F. Schrumpf, H. W. Roesky and M. Noltemeyer, *Z. Naturforsch.* 1990, **45b**, 433.
68. R. J. Gillespie, *Molecular Geometry*. van Norstrand Rheinhold, London (1972).
69. J. F. Sawyer and R. J. Gillespie, *Prog. Inorg. Chem.* 1986, **34**, 65.
70. I. Hargittai and M. Hargittai, *Symmetry Through the Eyes of a Chemist*, p. 138. VCH Publishers, New York (1986).
71. E. Hey, C. Ergezinger and K. Dehnicke, *Z. Naturforsch.* 1989, **44b**, 205.
72. V. Chandrasekhar, T. Chivers, J. F. Fait and S. S. Kumaravel, *J. Am. Chem. Soc.* 1990, **112**, 5373.
73. A. Atkinson, A. G. Brewster, S. V. Ley, R. S. Osborn, D. Rogers, D. J. Williams and K. A. Woode, *J. Chem. Soc., Chem. Commun.* 1977, 325.
74. O. Foss and V. Janickis, *J. Chem. Soc., Chem. Commun.* 1977, 833.
75. O. Foss and V. Janickis, *J. Chem. Soc., Dalton Trans.* 1980, 620.
76. O. Foss and V. Janickis, *J. Chem. Soc., Dalton Trans.* 1980, 628.
77. A. Haas, *J. Fluor. Chem.* 1986, **32**, 415.
78. H. Hartl, P. Huppmann, D. Lentz and K. Seppelt, *Inorg. Chem.* 1983, **22**, 2183.
79. D. Fenske, A. Frankenau and K. Dehnicke, *Z. Naturforsch.* 1990, **45b**, 427.
80. J. S. Thrasher, J. B. Nielsen, S. G. Bott, D. J. McClure, S. A. Morris and J. L. Atwood, *Inorg. Chem.* 1988, **27**, 570.
81. H. Oberhammer, K. Seppelt and R. Mews, *J. Molec. Struct.* 1983, **101**, 325.
82. A. Haas and J. Kasprowski, *Chimia* 1987, **41**, 340.
83. A. Haas and R. Pohl, *Chimia* 1989, **43**, 261.
84. N. Bertel, H. W. Roesky, F. T. Edelmann, M. Noltemeyer and H.-G. Schmidt, *Z. Anorg. Allg. Chem.* 1990, **586**, 7.
85. R. Paetzold and E. Rönsch, *Z. Anorg. Allg. Chem.* 1965, **338**, 22.
86. A. Haas and J. Kasprowski, *Chimia* 1990, **44**, 57.
87. M. Björgvinsson, H. W. Roesky, F. Pauer, D. Stalke and G. M. Sheldrick, *Inorg. Chem.* 1990, **29**, 5140.
88. M. Björgvinsson, H. W. Roesky, F. Pauer, D. Stalke and G. M. Sheldrick, *Eur. J. Solid State Inorg. Chem.*, submitted.
89. M. Björgvinsson, T. Heinze, H. W. Roesky, F. Pauer, D. Stalke and G. M. Sheldrick, *Angew. Chem.*, in press.
90. N. G. Furmanova, R. G. Gerr, V. P. Krasnov and V. I. Naddaka, *J. Struct. Chem.* 1985, **25**, 821.
91. N. G. Furmanova, V. I. Naddaka and V. P. Krasnov, *J. Struct. Chem.* 1981, **22**, 574.
92. J. P. Johnson, G. K. MacLean, J. Passmore and P. S. White, *Can. J. Chem.* 1989, **67**, 1687.
93. M. Björgvinsson, H. W. Roesky, F. Pauer, D. Stalke and G. M. Sheldrick, *Chem. Ber.*, submitted.
94. F. Fockenberg and A. Haas, *Z. Naturforsch.* 1986, **41b**, 413.
95. K. B. Sharpless, T. Hori, L. K. Truesdale and C. O. Dietrich, *J. Am. Chem. Soc.* 1976, **98**, 269.

Polyhedron Vol. 10, No. 20/21, pp. 2371–2375, 1991
Printed in Great Britain

0277–5387/91 $3.00+.00
© 1991 Pergamon Press plc

ETA-6 BONDING OF BENZENE TO POTASSIUM IN $[(C_6H_6)KOSiMe_2Ph]_4$

GARY R. FUENTES, PAUL S. COAN, WILLIAM E. STREIB and KENNETH G. CAULTON*

Department of Chemistry and Molecular Structure Center, Indiana University, Bloomington, IN 47405, U.S.A.

(*Received* 29 *April* 1991; *accepted* 16 *July* 1991)

Abstract—Reaction of KH with $PhMe_2SiOH$ in toluene, followed by recrystallization from benzene, gives $[(C_6H_6)KOSiMe_2Ph]_4$, characterized by elemental analysis, ^1H and ^{29}Si NMR and X-ray diffraction. The molecule is a cubane tetramer of rigorous S_4 symmetry, in which the KO_3 coordination environment is supplemented by η^6-binding of one benzene to each potassium. Crystal data (−169°C): $a = 12.972(2)$, $b = 18.006(2)$ Å, with $Z = 8$ in space group $I\bar{4}$.

There has been considerable recent activity in the field of siloxide (R_3SiO^-) chemistry. Metals have included lanthanides[1] and actinides,[2] transition metals,[3–8] alkaline earths[9] and also alkali metals.[10] The alkali metal chemistry shows the siloxide to be a suitable bridging, as well as terminal ligand, and reveals the common occurrence of the cubane tetramer $[M^I(\mu_3\text{-}OSiR_3)]_4$ structural motif. The curious feature of the cubane structure is that metal coordination number three gives a trigonal pyramidal, rather than the predicted (VSEPR theory) planar structure. It would be anticipated that the pyramidal geometry would leave the metal with enhanced electrophilic character, and the cubane tetramers are in fact found to bind Lewis bases, when these are available. We report here the course of potassium siloxide chemistry when conventional Lewis bases are strictly excluded.

EXPERIMENTAL

Materials and procedures

All manipulations were performed using standard Schlenk techniques either *in vacuo* or in an atmosphere of nitrogen or using a nitrogen-filled glovebox. Solvents used (toluene and benzene) were dried over potassium/benzophenone ketyl. These solvents were distilled under nitrogen and subsequently subjected to freeze–evacuate–thaw cycles prior to use. The reagents KH and Me_2PhSiH were obtained commercially (Aldrich). Potassium hydride was purified by washing repeatedly with hexane, followed by drying *in vacuo*. Dimethylphenyl silane was hydrolysed under buffered conditions to yield the corresponding silanol, $Me_2PhSiOH$,[11] which was then vacuum distilled and subsequently subjected to freeze–evacuate–thaw cycles prior to use.

Physical measurements

^1H and ^{29}Si NMR spectra were recorded on a Nicolet NT360 and a Bruker AM500 (^1H at 361 MHz, ^{29}Si at 99.4 MHz) spectrometer, respectively. These spectra were referenced to $SiMe_4$. Elemental analysis was performed by Oneida Research Services, Inc. Combustion aides were used in an effort to discourage carbide formation.

$[KOSiMe_2Ph]_n$, 1

A 100 cm^3 Schlenk flask was charged with KH (0.74 g, 18.5 mmol) and toluene (15 cm^3). This solution was chilled to 0°C, whereupon $Me_2PhSiOH$ (2 cm^3, 12.3 mmol) in toluene (15 cm^3) was added via cannula. H_2 evolution was observed during the period of addition. After addition of all the $Me_2PhSiOH$, the reaction mixture was allowed to stir for 10 h at

* Author to whom correspondence should be addressed.

Table 1. Crystallographic data for $[(C_6H_6)KOSiMe_2Ph]_4$

Chemical formula	$C_{56}H_{68}K_4O_4Si_4$
a (Å)	12.972(2)
b (Å)	18.006(2)
V (Å^3)	3030.08
Z	8
Formula weight	268.47
Space group	$I\bar{4}$
T (°C)	−169
λ (Å)	0.71069
ρ_{calcd} (g cm^{-3})	1.177
μ(Mo-K_α) (cm^{-1})	4.08
R	0.0374
R_w	0.0420

room temperature. After filtration through a 2 cm thick plug of Celite to remove unreacted KH, the solution was concentrated, whereupon a white crystalline solid formed on the sides of the flask. The crystalline solid fractured to a white powder upon removal of all solvent under vacuum. Per cent yield: 89%. ^{1}H NMR (C_6D_6): δ 7.56 (dd, 7.8 Hz, 1.5 Hz, 2H, *ortho*); 7.42 (dd, apparent triplet, 7.8 Hz, 2H, *meta*); 7.29 (tt, 7.3 Hz, 1.5 Hz, 1H, *para*); 2.88 (s, 6H, Me). ^{29}Si NMR (C_6D_6): δ −21.25. Found: C, 50.3; H, 6.1. Calc. for $C_8H_{11}SiOK$: C, 50.5; H, 5.8%.

$[KOSiMe_2Ph]_4 \cdot 4C_6H_6$, 2

A 20 cm^3 Schlenk flask was charged with approximately 0.50 g of $KOSiMe_2Ph$. Approximately 2 cm^3 of benzene was added via cannula. The solution was heated briefly in order to dissolve all of the $KOSiMe_2Ph$. Upon cooling, large colourless crystals precipitated. These were suitable for X-ray analysis.

X-ray structure determination

A crystal of suitable size was cleaved from a large piece of the sample. The crystal was mounted using silicone grease and was transferred to a goniostat where it was cooled to −169°C for characterization and data collection[12] (see Table 1). An initial search of a limited hemisphere of reciprocal space revealed an I-centred tetragonal lattice. Following complete intensity data collection, the Laue symmetry and the lack of any additional systematic absences limited the space group to $I4$, $I\bar{4}$, or $I4/m$. Four standards measured every 300 data showed no significant trends. No correction was made for absorption.

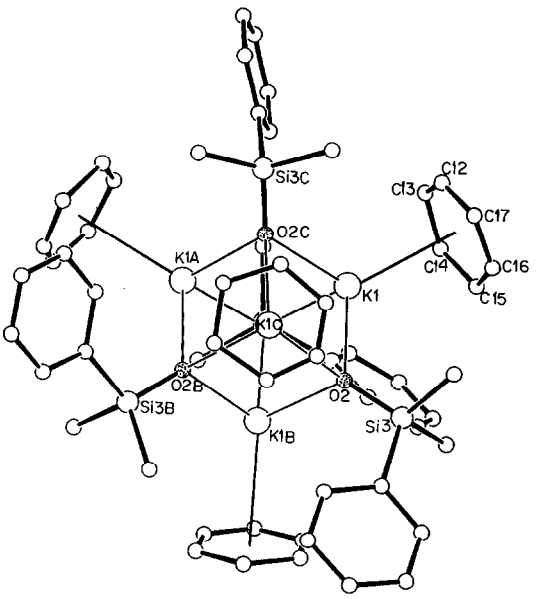

Fig. 1. ORTEP drawing of the non-hydrogen atoms of $[(C_6H_6)KOSiMePh]_4$ showing selected atom labelling. O2A is eclipsed by K1C. Oxygens are stippled.

The structure was solved using a combination of direct methods (MULTAN78) and Fourier techniques when space group $I\bar{4}$ was chosen. The positions of the K, O and Si atoms were obtained from an E-map and the remaining non-hydrogen atoms

Table 2. Fractional coordinates and isotropic thermal parameters[a] for $[(C_6H_6)KOSiMe_2Ph]_4$

	$10^4 x$	$10^4 y$	$10^4 z$	10 B_{iso}
K(1)	5421(1)	1325.6(5)	3251.5(4)	20
O(2)	6391(2)	−435(2)	3196(1)	22
Si(3)	7393(1)	−683(1)	3664(1)	25
C(4)	7901(3)	−2022(3)	3447(2)	25
C(5)	7296(3)	−2730(3)	3057(2)	29
C(6)	7633(3)	−3724(3)	2904(2)	33
C(7)	8612(4)	−4026(3)	3135(2)	36
C(8)	9227(3)	−3346(4)	3514(2)	38
C(9)	8877(3)	−2355(3)	3665(2)	31
C(10)	7127(5)	−647(3)	4690(2)	48
C(11)	8482(3)	238(3)	3485(4)	55
C(12)	5100(7)	3142(9)	4459(10)	123
C(13)	5295(7)	3679(4)	3888(7)	97
C(14)	6318(7)	3628(4)	3571(3)	68
C(15)	7039(3)	3022(4)	3956(3)	41
C(16)	6709(5)	2518(4)	4584(3)	54
C(17)	5730(9)	2617(9)	4812(4)	104

[a] Isotropic values for those atoms refined anisotropically are calculated using the formula given by W. C. Hamilton, *Acta Cryst.* 1959, **12**, 609.

Table 3. Selected bond distances (Å) and angles (deg) for $[(C_6H_6)KOSiMe_2Ph]_4$

K(1)—O(2)A	2.6082(23)	K(1)—C(16)	3.308(6)
K(1)—O(2)	2.6092(22)	K(1)—C(17)	3.296(9)
K(1)—O(2)C	2.6218(23)	C(12)—C(13)	1.268(18)
Si(3)—O(2)	1.5822(22)	C(12)—C(17)	1.240(17)
K(1)—C(12)	3.233(14)	C(13)—C(14)	1.445(12)
K(1)—C(13)	3.265(7)	C(14)—C(15)	1.404(9)
K(1)—C(14)	3.256(6)	C(15)—C(16)	1.376(8)
K(1)—C(15)	3.294(5)	C(16)—C(17)	1.340(12)
O(2)—K(1)—O(2)A	89.26(7)	K(1)B—O(2)—Si(3)	124.11(13)
O(2)A—K(1)—O(2)C	88.99(7)	K(1)—O(2)—Si(3)	123.60(12)
O(2)—Si(3)—C(4)	111.18(14)	C(13)—C(12)—C(17)	125.9(10)
O(2)—Si(3)—C(10)	111.57(20)	C(12)—C(13)—C(14)	118.6(7)
O(2)—Si(3)—C(11)	113.40(19)	C(13)—C(14)—C(15)	116.3(6)
K(1)B—O(2)—K(1)C	90.67(7)	C(14)—C(15)—C(16)	117.7(5)
K(1)—O(2)—K(1)C	87.24(7)	C(15)—C(16)—C(17)	120.1(7)
K(1)—O(2)—K(1)B	90.95(7)	C(12)—C(17)—C(16)	121.4(9)
K(1)C—O(2)—Si(3)	128.82(12)		

were obtained from subsequent iterations of least-squares refinement and difference Fourier calculation. Hydrogen atoms were included in fixed calculated positions with thermal parameters fixed at one plus the isotropic thermal parameter of the carbon to which they were bonded. In the final cycles of least-square refinement, the non-hydrogen atoms were varied with anisotropic thermal parameters. The final difference map was essentially featureless, the largest residual peak being 0.3 e $Å^{-3}$. The results of the structure determination are shown in Tables 2 and 3 and Figs 1 and 2.

RESULTS

Solid-state structures of $[(C_6H_6)KOSiMe_2Ph]_4$

The X-ray diffraction study reveals a tetrameric molecule with a crystallographic S_4 axis (Figs 1 and 2). The rotational conformation about the O—Si bond leaves the $SiMe_2Ph$ group staggered with respect to the OK_3 group. The independent K—O distances within the cube are nearly identical at 2.61 (twice) and 2.62 Å (once), in spite of the pattern of silicon substituents which breaks any rigorous

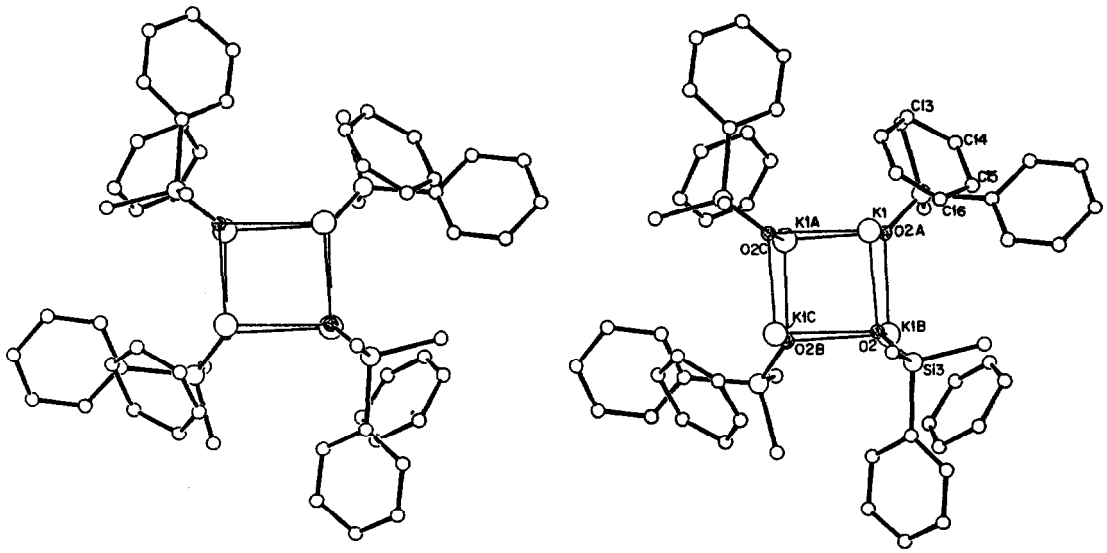

Fig. 2. Stereo ORTEP drawing of the non-hydrogen atoms of $[(C_6H_6)KOSiMe_2Ph]_4$, viewed down the crystallographic S_4 axis. Oxygens are stippled.

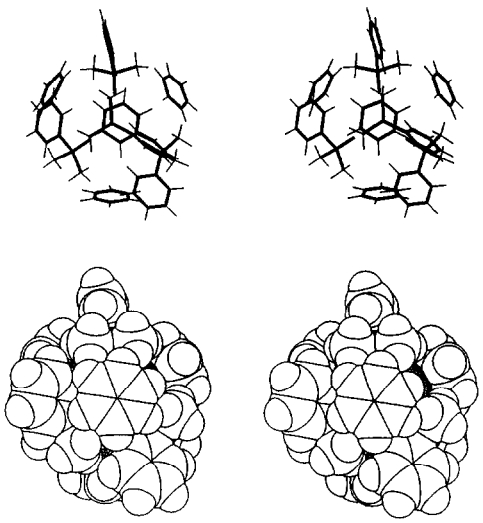

Fig. 3. Stereo stick figure and space-filling drawings of $[(C_6H_6)KOSiMe_2Ph]_4$, with d(C—H) fixed at 1.05 Å. View is perpendicular to the plane of the benzene ring in the foreground.

threefold symmetry. The pattern of placement of these substituents puts the four phenyl rings over a belt of four faces of the cube, leaving two opposite faces unshielded by these phenyl rings. The angles at the corners of the cube (either K or O) are all $90 \pm 2.8°$.

The most interesting revelation of the solid-state structure determination is the occurrence of η^6-binding of one benzene to every potassium. The K—C distances vary by less than 5 esd's and average 3.275 Å.[13] It is evident from a space-filling drawing (Fig. 3) that the tetramer has room to accommodate η^6-binding of benzene because the siloxide bears two small substituents (i.e. methyl). If the siloxide were the more commonly employed $OSiPh_3$, benzene coordination would probably be precluded. It is equally evident from Fig. 3 that ring substituents will weaken the binding of arene to potassium. It is therefore understandable that crystals grown from toluene readily lose solvent and fracture, while those grown from benzene are more stable.

DISCUSSION

This report emphasizes the reality of binding of organic π-electron systems to alkali metals when no better donors are available and when the alkali metal is both sterically accessible and electronically "prepared". The latter term refers here to a three-coordinate potassium which is pyramidal, and thus has more than one hemisphere of its surroundings unoccupied. The present work shows that such binding can occur even in the absence of the back bonding found in transition metal/arene compounds, and also in the absence of Coulomb attraction found in K^+/carbanion compounds. The K—C bond length found here is not much longer than it is in (TMEDA)K(fluorenide)[14] (3.06–3.68 Å). Another relevant comparison material is the potassium/graphite intercalate KC_8, where the K—C distance is 3.06 Å.[15] In $K_8(OSiPh_3)_8(DME)_3$, there is a K—C_{ipso} distance of 3.08 Å.[16] Potassium ion/arene interactions have been reported by the groups of Atwood[17,18] and of Schaverien,[19] and the K—C distances (which range from 3.31 to 3.59 Å) have been reviewed.[19]

We feel that K/arene binding is ubiquitous. Thus, while it has been reported[20] that $K_2[\mu\text{-}N(SiMe_3)_2]_2 \cdot 2$toluene has a bent two-coordinate geometry at potassium (i.e. KN_2), we have calculated the K/toluene distances and find that six K—C (ring) separations range from 3.19 to 3.36 Å. This compound is therefore an unrecognized example of precisely the η^6-benzene binding phenomenon we report in $[(C_6H_6)KOSiMe_2Ph]_4$. A hard Lewis acid like K^+ thus has an affinity even for as soft a donor as an arene π-system. Finally, it bears mention that benzene solutions of alkali metal compounds with low metal coordination numbers are also likely to exhibit this same K/arene binding.

Acknowledgements—This work was supported by the Department of Energy and the taxpayers of the state of Indiana. We also thank Scott Horn for skilled technical assistance.

Supplementary material available: Crystallographic details and anisotropic thermal parameters (3 pages) and observed and calculated structure factors (5 pages). Ordering information is given on any current masthead page.

REFERENCES

1. P. S. Gradeff, K. Yunlu, A. Gleizes and J. Gally, *Polyhedron* 1989, **8**, 100.
2. M. Porchia, N. Brianese, U. Casellato, F. Ossola, G. Rossetto, P. Zanella and R. Graziani, *J. Chem. Soc., Dalton Trans.* 1989, 677.
3. G. A. Sigel, R. A. Bartlett, D. Decker, M. M. Olmstead and P. P. Power, *Inorg. Chem.* 1987, **26**, 1773.
4. E. A. Babaian, D. C. Hrncir, S. G. Bott and J. L. Atwood, *Inorg. Chem.* 1986, **25**, 4818.
5. Y. Do, E. D. Simhon and R. H. Holm, *Inorg. Chem.* 1985, **24**, 1831 and refs therein.
6. L. D'Ornelas, A. Choplin, J. M. Basset, L.-Y. Hsu and S. Shore, *Nouv. J. Chim.* 1985, **9**, 155.

7. S. G. Bott and A. C. Sullivan, *J. Chem. Soc., Chem. Commun.* 1988, 1577.
8. G. S. Kim, D. A. Keszler and C. W. DeKock, *Inorg. Chem.* 1991, **30**, 574.
9. K. G. Caulton, M. H. Chisholm, S. R. Drake and W. E. Streib, *Angew. Chem., Int. Edn Engl.* 1990, **29**, 1483.
10. A. Naiini, S. R. Drake, M. H. Chisholm, J. C. Huffman and W. E. Streib, *Polyhedron* 1991, **10**, 337.
11. G. H. Barnes and N. E. Daughenbaugh, *J. Org. Chem.* 1966, **31**, 885.
12. J. C. Huffman, L. N. Lewis and K. G. Caulton, *Inorg. Chem.* 1990, **19**, 1840.
13. Since the thermal parameters of some of the benzene carbons suggest some librational motion or modest disorder, the esd's are probably underestimated.
14. R. Zerger, W. Rhine and G. D. Stucky, *J. Am. Chem. Soc.* 1974, **96**, 5441.
15. S. S. Solin, *Adv. Chem. Phys.* 1982, **49**, 455.
16. M. J. McGeary, K. Folting, W. E. Streib, J. C. Huffman and K. G. Caulton, submitted.
17. J. L. Atwood and S. K. Seale, *J. Organomet. Chem.* 1976, **114**, 107.
18. J. L. Atwood, K. D. Crissinger and R. D. Rogers, *J. Organomet. Chem.* 1978, **155**, 1.
19. C. J. Schaverien and J. B. van Mechelen, *Organometallics* 1991, **10**, 1704.
20. P. G. Williard, *Acta Cryst.* 1988, **C44**, 270.

Polyhedron Vol. 10, No. 20/21, pp. 2377–2380, 1991
Printed in Great Britain

0277–5387/91 $3.00+.00
© 1991 Pergamon Press plc

AN ASED–MO CALCULATION OF THE ENERGY LEVELS OF A COPPER(III) COMPLEX: THE (BIS(MALEONITRILEDITHIOLATO)COPPER(III))$^-$ COMPLEX ANION

MUNIME LUNDEEN

Division of Chemistry, Ataturk Egitim Fakultesi, Marmara University, Fikirtepe 81040, Istanbul, Turkey

(*Received* 14 *June* 1991; *accepted* 9 *July* 1991)

Abstract—The molecular orbitals of bis(maleonitriledithiolato)copper(III)$^-$ were calculated by the ASED–MO method. The empty molecular orbital with 25% $3d_{x^2-y^2}$ (Cu) orbital character also has 41% 3*s*, 3*p*, 3*d* (S) and 34% 2*s*, 2*p* (C, N) atomic orbital character. Empty antibonding π_v (S) levels are below this molecular orbital. The HOMO is a π_v (S) level which has 26% $3d_{xz+yz}$ character. An almost pure π_h (S) level is below the HOMO and is followed by the b_{2g} (π^*), π_v (S), π_h (S), b_{4g} (π^*), a_{1g} (σ^*), and b_{3g} (π^*) molecular orbitals. The $\sigma \rightarrow \sigma^*$ transitions from the $\sigma_{C\text{-}S}$ molecular orbitals to the empty molecular orbital with 25% $3d_{x^2-y^2}$ (Cu) atomic orbital contribution in it, which is fully allowed, is calculated to have an average oscillator strength of 1.40.

Copper(III) coordination complexes are not very common. They are expected to have square planar coordination around the copper(III) ion.[1] The crystal and molecular structure of the tetrabutylammonium salt of bis(maleonitriledithiolato) copper(III) complex anion was published by Forrester, Zalkin and Templeton[2] in 1964. We have used the ASED–MO method[3] to calculate the energy levels of this square planar copper(III) complex anion.

PROCEDURE

The ASED–MO method is a semi-empirical method which has given as good results as or better results than HF or CI calculations in the calculation of molecular properties such as equilibrium force constants, k_e, equilibrium bond lengths, R_e, and bond dissociation energies, D_e, of the first-row transition-metal diatomic oxides[3c] and sulphides.[3d] The method produces the overlap integrals, S_{ij}, using analytical approximation to Slater–HF atomic orbitals with atomic orbital exponents which are input. The resonance integrals which are obtained semi-empirically as interaction energies,

$$H_{ij} = -1.125 \cdot (H_{ii}+H_{jj}) \cdot S_{ij} \cdot e^{-0.13R}, \quad (i \neq j)$$

differ from the usual EH approximation in the value of the multiplier of the product of the overlap integral, S_{ij}, between the atoms and the Coulomb energies, H_{nn}, of the atoms, and in having an additional multiplier, $e^{-0.13R}$.[3d] The calculation takes into account repulsions between atoms with their electronic shells around their nuclei by including a term which describes the "bond charge density", which is not symmetric around either nucleus. This term, labelled E_{npf} (potential energy describing the "non-perfectly following" electron density in the bonding region),[3] is approximated by:

$$E_{npf} = \sum_i n_i \cdot e_i^{ab} - \sum_i n_i \cdot e_i^a \cdot \sum_j n_j \cdot e_j^b,$$

where n_i and n_j = the occupation numbers of two-electron orbitals i on atom a and j on atom b, e_i^a and e_j^b = the appropriate Coulomb energies of atoms a and b, e_i^{ab} = the two-body interaction energy, which is calculated by setting the total potential energy, E, at the equilibrium bond distance equal to the sum of a potential energy term, in which the electron density follows the nucleus perfectly, (E_{pf}), and a second term, (E_{npf}), which does not follow the nucleus perfectly. The sum over the i two-electron orbitals is usually taken over the more electronegative atom.[3c,d]

The atomic orbital exponents for the H, C, N and S were obtained from Clementi and Raimondi[4a] and are reported in refs 3a and 5. The 4*s*, 4*p* and double-zeta 3*d* exponents for copper were taken from the work of Richardson *et al.*[4b,c] The exponents for copper are reported in refs 3c and 3d. The valence state ionization energy for the 4*p* atomic orbital of copper is taken as the smallest value for the $4s \rightarrow 4p$ excitation energy in Moore's tables of atomic energy levels.[4d] All other Coulomb energies were taken from Lotz.[4e]

An idealized geometry was used for the complex ion. The sulphur donor atoms were placed along *x* and *y* axes at 2.15 Å bond distances. This bond distance is slightly shorter than the reported average copper(III)–sulphur bond distance of 2.170 Å.[2]

RESULTS AND DISCUSSION

The energy levels of nd^8 square planar complexes have been calculated by Chatt *et al.*,[6] Fenske *et al.*[7] and Gray and Ballhausen.[8] Three LF transitions, two of which may be observed, and several CT transitions are expected.[6-8] If the ligand donor atoms have pi electrons, as in the case of the cyanide ion, an orbitally forbidden CT transition may take place from the occupied $3d_{xy}$ orbital of the metal ion to the lowest energy unoccupied orbital on the ligand with weak intensity.[8] Intense CT transitions are expected from the filled $3d_{z^2}$ and $3d_{xz}$ or $3d_{yz}$ orbitals of the metal ion to the lowest energy unoccupied pi orbitals of the ligands.[8]

The square planar complex anion, bis(maleonitriledithiolato)copper(III)$^-$, has an extended pi system. The four sulphur donor atoms are soft ligands which have large lone-pair electron lobes. Presumably, the square planar copper(III) complex forms so that the lone-pair electrons can participate in the extended pi system. The expected order of the energies of the 3*d* orbitals of the metal ion is $3d_{x^2-y^2} > 3d_{xy} > 3d_{z^2} > 3d_{xz}$, $3d_{yz}$.[8] Because the Coulomb energy of the 3*d* orbital of the copper in the ASED–MO calculation is almost equal to the Coulomb energy of the 3*p* orbital of the sulphur donor (Lotz's[4e] values were used for the Coulomb energies of the orbitals of sulphur), resonance occurs between the atomic orbitals of the metal and the atomic orbitals of the ligand.[3d] The results are shown in Table 1 and require comment.

1. The $3d_{x^2-y^2}$ orbital on the copper which is directed at the sulphur donors is raised in energy above the empty ligand pi orbitals and it is about 2 eV above the highest occupied molecular orbital. The $3d_{x^2-y^2}$ orbital shows significant mixing of the π_v orbitals on the sulphur donors.

2. There are two empty orbitals below the $3d_{x^2-y^2}$ orbital. One of these shows some mixing of the $3d_{yz}$ and $-3d_{xz}$ orbitals of the copper into the π_v orbitals on the sulphur donors. The lower energy empty orbitals are antibonding π_v orbitals on the sulphur donors. These two molecular orbitals are separated by 0.05 eV and are about 0.62 to 0.67 eV above the highest occupied molecular orbital.

3. The highest occupied molecular orbital shows considerable mixing of the $3d_{xz}$ and $3d_{yz}$ orbitals on the copper into the ligand π_v orbitals which have antibonding pi C—S character. This molecular orbital and the filled molecular orbital lying next in energy derive mostly from ligand lone-pair orbitals. In contrast to the highest occupied molecular orbital, the next filled molecular orbital shows no mixing of the 3*d*(Cu) orbitals in it. These two lower-energy filled molecular orbitals appear to be stabilized somewhat by very small coefficients of bonding pi C—N interactions.

4. The order of the energies of the filled 3*d* orbitals on the copper(III) ion is: $3d_{xy} > 3d_{yz-xz} > 3d_{z^2} > 3d_{xz+yz}$. The $3d_{xy}$ orbital has a small amount of sigma overlap with the π_h orbitals on the sulphur donors derived from $3p_y$ atomic orbitals.

5. There are two filled molecular orbitals between the $3d_{xy}$ (Cu) orbital and the $3d_{yz-xz}$ combination of copper orbitals. Of these two molecular orbitals, the lower energy one has some $4p_z$ (Cu) character so that this molecular orbital is a bonding pi Cu—S molecular orbital. The higher energy molecular orbital has no copper atomic orbital character (ignoring very small positive coefficients of the $4p_x$ and $4p_y$ atomic orbitals of the copper). It has bonding pi C—S character (as well as very small amounts of bonding pi C—C and C—N character). It is derived from the π_h orbitals on the sulphur donors.

6. It may be noted that the choice of the *xy*-plane as the equatorial plane about the copper(III) ion with the sulphur donors along the *x*- and *y*-axes in D_{4h} symmetry has led to the construction of two orbitals on the copper, $3d_{xz+yz}$ and $3d_{yz-xz}$, which are not degenerate. The $3d_{yz-xz}$ combination which shows pi overlap with the pi S—C—C system has the higher energy. The lower-energy $3d_{xz+yz}$ orbital has some bonding pi Cu—S character.

7. Just below the 3*d* orbitals of the copper are the π_h orbitals on the sulphur donors which show some bonding sigma Cu—S character. The $3d_{x^2-y^2}$ (Cu) and $-3d_{xy}$, $3d_{z^2}$, $-4s$ atomic orbitals on copper are mixed into these molecular orbitals.

8. The next two molecular orbitals are π_v orbitals on the sulphur donors, one of which has no copper atomic orbital character in it. This orbital, which is at higher energy, has bonding pi C—C—S character. The molecular orbital at lower energy has

Table 1. The energy levels of the bis(maleonitriledithiolato)copper(III)$^-$ anion

Level	Energy (eV)	Atomic orbitals of copper and sulphur which make the largest contributions to the MO
b_{1g} (σ^*)	+1.9852	25% x^2-y^2 (Cu); 35% (s, x, y) (S); 6% $3d$ (S)
π_v^* (S)	+0.6731	9% $yz-xz$ (Cu); 34% z (S); 2% $3d$ (S)
π_v^* (S)	+0.6207	36% z (S); 2% $3d$ (S)
π_v (S)	0.0	26% $yz+xz$ (Cu); 62% z (S); 1% $3d$ (S)
π_h (S)	−0.9725	1% (x, y) (Cu); 96% (s, x, y) (S)
b_{2g} (π^*)	−0.9733	59% xy (Cu); 8% z^2 (Cu); 1% s (Cu); 26% (s, x, y) (S)
π_v (S)	−0.9734	2% z (Cu); 80% z (S)
π_h (S)	−1.0749	1% (x, y) (Cu); 91% (s, x, y) (S)
b_{4g} (π^*)	−1.1756	74% $yz-xz$ (Cu); 4% z (S); 1% $3d$ (S)
a_{1g} (σ^*)	−1.2330	82% z^2 (Cu); 13% xy (Cu); 3% s (Cu)
b_{3g} (π^*)	−1.7432	72% $yz+xz$ (Cu); 4% z (S); 1% $3d$ (S)
π_h (S)	−1.9199	28% x^2-y^2 (Cu); 69% (s, x, y) (S)
π_h (S)	−2.0835	2% s (Cu); 7% z^2 (Cu); 26% xy (Cu); 58% (s, x, y) (S)
π_v (S)	−2.1336	57% z (S)
π_v (S)	−2.5012	18% $yz-xz$ (Cu); 56% z (S)
σ_{C-S}	−2.9541	53% x^2-y^2 (Cu); 27% (s, x, y) (S)
σ_{C-S}	−3.4861	5% (x, y) (Cu); 53% (s, x, y) (S)
σ_{C-S}	−3.5541	1% (x, y) (Cu); 54% (s, x, y) (S)
σ_{C-S}	−4.5630	5% s (Cu); 1% z^2 (Cu); 1% xy (Cu); 42% (s, x, y) (S)

$3d_{yz-xz}$ (Cu) character mixed into it. This molecular orbital has some bonding pi C—C—S—Cu character. The molecular orbitals which are bonding sigma C—S orbitals are below the sulphur lone-pair and $3d$ (Cu) orbitals. Mixed into these sigma C—S molecular orbitals are either $3d$ (Cu) or $4p_x$ (Cu), $4p_y$ (Cu) orbitals.

We expect that transitions from the sigma C—S molecular orbitals to the empty $3d_{x^2-y^2}$ (Cu) orbital will be allowed $\sigma \rightarrow \sigma^*$ transitions which have high intensity. These transitions are calculated to be at about 39,840 (I), 44,131 (II), 44,680 (III) and 52,818 (IV) cm^{-1}. The orbital to which these transitions are made has non-zero coefficients of sulphur donor orbitals. Approximate oscillator strengths of the transitions from these sigma C—S molecular orbitals to the empty $3d_{x^2-y^2}$ (Cu) level may be calculated using simplified wavefunctions for the excited state and the initial state. Using the $3p_x$ and $3p_y$ atomic orbitals of the sulphur donors for the ligand wavefunction, ϕ_L, and the $4p_x$ and $4p_y$ atomic orbitals of the copper for the metal wavefunction, ϕ_M, the total wavefunction is taken to be equal to $\Phi = c_M \cdot \phi_M \pm c_L \cdot \phi_L$. The wavefunction for the excited state is taken as the linear combination of the $3d_{x^2-y^2}$ atomic orbital of the copper and the $3s$, $3p_x$, $3p_y$ atomic orbitals of the sulphur donors. The wavefunction for the initial state is for one of the four sigma C—S levels and has coefficients mostly for the ligand $3s$, $3p$ and $3p_y$ orbitals. The sigma carbon–sulphur molecular orbital labelled (I) has a large amount of $3d_{x^2-y^2}$ (Cu) character, the molecular orbital labelled (II) has substantial $4p_x$ (Cu) and $4p_y$ (Cu) character, and the molecular orbital labelled (IV) has substantial $4s$ (Cu) character. The dipole moment integral, D, was evaluated for transitions from each of these levels to the empty $3d_{x^2-y^2}$ (Cu) level (which contains significant contributions from the $3s$, $3p_x$ and $3p_y$ (S) atomic orbitals) using the expression:[9,10]

$$D = \langle \Psi' | \mathbf{R} | \Psi \rangle \approx c' \cdot c \cdot \sum_{\alpha=1}^{4} \left(\sum_{m_l=-1}^{+1} c'_{\alpha_{m_l}} \cdot c_{m_l} \cdot \langle \Phi'_{\alpha_{m_l}} | \mathbf{R} | \phi_{\alpha_{m_l}} \rangle \right),$$

which was set equal to:

$$D = \sum_{\alpha=1}^{\alpha=4} \sum_{m_l=-1}^{+1} c'_{\alpha_{m_l}} \cdot c_{\alpha_{m_l}} \cdot |\mathbf{R}| \cdot \langle \phi'_{\alpha_{m_l}} \cdot \phi_{\alpha_{m_l}} \rangle,$$

where the primed coefficients and wavefunctions apply to the excited state and $|\mathbf{R}|$ is taken as the scalar value, 2.15 Å, which is the copper(III)–sulphur bond length used in the calculations.[2] The theoretical value for the oscillator strength, f(theoretical), is obtained using the formula:

$$f(\text{theoretical}) = 1.085 \times 10^{11} \cdot (\bar{\nu}_{\text{final state}} - \bar{\nu}_{\text{initial state}}) \cdot |D|^2.$$[9]

The values of f(theoretical) which are calculated for electronic transitions from the molecular orbitals labelled levels I, II, III and IV, respectively, to the

$3d_{x^2-y^2}$ (Cu) orbital are 3.486, 2.002, 0.048 and 0.060. Thus, the average value of the oscillator strength for these four transitions is about 1.40.

The energy levels of the bis(maleonitriledithiolato)copper(III)$^-$ complex ion have not been reported previously. Eisenberg, Ibers, Clark and Gray[11] calculated the energy levels of the bis(maleonitriledithiolato)nickel(II)$^{2-}$ complex ion and found the following ordering of the $3d$ (Ni) atomic orbitals: $3d_{xy} > 3d_{x^2-y^2} > 3d_{yz} > 3d_{z^2} > 3d_{xz}$. Aside from the reversal of the positions of the $3d_{x^2-y^2}$ and $3d_{xy}$ atomic orbitals of the nickel(II) ion, which arises from the choice of the x and y axes to bisect the sulphur donor—copper—sulphur donor bonds in the chelate loop, the order given for nickel(II) agrees with the order we give for copper(III). The planar complex anions of Co^{III} and Ni^{III} with the same ligand each have an intense band in the near-IR which is not observed in bis(maleonitriledithiolato)nickel(II)$^{2-}$ and in bis(maleonitriledithiolato)copper(III)$^-$ complex ions.[12] The free maleonitriledithiol ligand has a $\pi_v \rightarrow \pi_v^*$ band at about 29,500 cm^{-1} which is observed at 31,700 cm^{-1} ($\varepsilon = 24{,}000$ cm^{-1}) in the nickel(II) complex ion.[11] This work reports that the π_v orbitals of the sulphur donors appear in the molecular orbitals below the empty $3d_{x^2-y^2}$ (Cu) orbital and, therefore, the transition observed in the free ligand should go to one of these two molecular orbitals which are calculated to be at about 0.673 and 0.621 eV in this ASED–MO calculation. Thus, we assigned the $\pi_v \rightarrow \pi_v^*$ transition of the ligand at 25,604 cm^{-1} and the $\sigma \rightarrow \sigma^*$ transition at 40,000–53,000 cm^{-1}. The latter transitions are fully allowed transitions from the $\sigma_{C\text{-}S}$ molecular orbital to the empty molecular orbital with $3d_{x^2-y^2}$ (Cu) character.

Acknowledgements—A Collaborative Research Grant from NATO is gratefully acknowledged. I am indebted to Professor Alfred B. Anderson for the fruitful and very pleasant 3 weeks spent in the campus of Case Western Reserve University in Cleveland, Ohio in July 1990.

REFERENCES

1. (a) D. W. Margerum, K. L. Chelappa, F. P. Bossu and G. L. Bruce, *J. Am. Chem. Soc.* 1975, **97**, 6894; (b) M. P. Youngblood and D. W. Margerum, *Inorg. Chem.* 1980, **19**, 3068; (c) J. M. Anast, A. W. Hamburg and D. W. Margerum, *Inorg. Chem.* 1983, **22**, 2139; (d) P. R. Sharp and A. J. Bard, *Inorg. Chem.* 1983, **22**, 3462; (e) L. Fabrizzi, A. Perotti and A. Poggi, *Inorg. Chem.* 1983, **22**, 1411.
2. J. D. Forrester, A. Zalkin and D. H. Templeton, *Inorg. Chem.* 1964, **3**, 1507.
3. (a) A. B. Anderson, *Inorg. Chem.* 1976, **15**, 2598; (b) A. B. Anderson, *Inorg. Chem.* 1976, **15**, 2601; (c) A. B. Anderson, R. W. Grimes and S. Y. Hong, *J. Phys. Chem.* 1987, **91**, 4245; (d) A. B. Anderson, S. Y. Hong and J. L. Smialek, *J. Phys. Chem.* 1987, **91**, 4250.
4. (a) E. Clementi and D. L. Raimondi, *J. Chem. Phys.* 1963, **38**, 2686; (b) J. W. Richardson, W. C. Nieuwpoort, R. R. Powell and W. F. Edgell, *J. Chem. Phys.* 1962, **36**, 1057; (c) J. W. Richardson, R. R. Powell and W. C. Nieuwpoort, *J. Chem. Phys.* 1963, **38**, 796; (d) C. E. Moore, *Atomic Energy Levels*, NBS Circ. No. 467, National Bureau of Standards, U.S. Government Printing Office, Washington, D.C. (1958); (e) W. Lotz, *J. Opt. Soc. Am.* 1970, **60**, 206.
5. D. E. Nikles, A. B. Anderson and F. L. Urbach. In *Copper Coordination Chemistry: Biochemical and Inorganic Perspectives* (Edited by K. D. Karlin and J. Zubieta), pp. 203–222. Adenine Press, New York (1983).
6. J. Chatt, G. A. Gamlen and L. E. Orgel, *J. Chem. Soc.* 1958, 486.
7. R. F. Fenske, D. S. Martin Jr and K. Rudenberg, *Inorg. Chem.* 1962, **3**, 441.
8. H. B. Gray and C. J. Ballhausen, *J. Am. Chem. Soc.* 1963, **85**, 260.
9. C. J. Ballhausen and H. B. Gray, *Molecular Orbital Theory*, Ch. 5, W. A. Benjamin Inc., New York, Amsterdam (1965).
10. A. A. Gewirth and E. I. Solomon, *J. Am. Chem. Soc.* 1988, **110**, 3811.
11. R. Eisenberg, J. A. Ibers, R. J. H. Clark and H. B. Gray, *J. Am. Chem. Soc.* 1964, **86**, 113.
12. A. Davison, N. Edelstein, R. H. Holm and R. H. Maki, *Inorg. Chem.* 1963, **2**, 1227.

Polyhedron Vol. 10, No. 20/21, pp. 2381–2388, 1991
Printed in Great Britain

0277–5387/91 $3.00+.00
© 1991 Pergamon Press plc

REARRANGEMENTS OF THE UNSATURATED LIGAND 1,1-BIS(DIPHENYLPHOSPHINOMETHYL)ETHENE AND ITS CHALCOGENIDES AND GROUP VI METAL CARBONYL COMPLEXES

JONATHAN L. BOOKHAM*

Department of Chemical and Life Sciences, Newcastle upon Tyne Polytechnic, Ellison Building, Newcastle upon Tyne, NE1 8ST, U.K.

and

WILLIAM McFARLANE

Department of Chemistry, University of Newcastle upon Tyne, Newcastle upon Tyne, NE1 7RU, U.K.

(*Received* 23 *May* 1991; *accepted* 9 *July* 1991)

Abstract—In contrast to the behaviour of other unsaturated organophosphines, treatment of the new ligand $(Ph_2PCH_2)_2C{=}CH_2$ with Ph_2PH in the presence of $KOBu^t$ does not result in addition to the double bond; instead, an allylic rearrangement occurs to give *cis* and *trans* $Ph_2PCH{=}C(CH_3)CH_2PPh_2$ in a 3:7 ratio. In the case of $(Ph_2P(E)CH_2)_2C{=}CH_2$ [E = S, Se] only the *trans* isomer is obtained from this reaction, while under similar conditions $(CO)_4M(Ph_2PCH_2)_2C{=}CH_2$ [M = Cr, Mo, W] yields only a *cis* product in which the two phosphorus atoms remain chelated. The products of these and related reactions are characterized by elemental analysis and ^{13}C and ^{31}P NMR spectroscopy.

The base-catalysed addition of primary and secondary phosphines to activated carbon–carbon multiple bonds is an established route to secondary and tertiary phosphines respectively.[1–5] Activation by one[6] or two (geminally related)[7] Ph_2P groups is of especial interest because the products are then polyphosphines that are important as polydentate ligands, a simple example being $(Ph_2P)_2CHCH_2PPh_2$ which can be formed by the addition of Ph_2PH to $(Ph_2P)_2C{=}CH_2$ as in eq. (1).

(1)

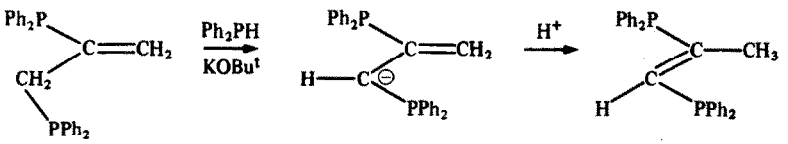

(2)

Furthermore, the activating ability of the Ph_2P group(s) is retained or even enhanced when phosphorus is coordinated to a metal atom or is in a higher oxidation state, as in the $Ph_2P(E)$ [E = O, S, Se] moiety.[8]

It is unclear whether any activating ability is retained when a CH_2 group is inserted between Ph_2P and the multiple bond since there is now also the possibility of an allylic rearrangement (double bond migration) which is normally the favoured pathway, and which would probably proceed via a carbanion intermediate as in eq. (2).

However, when the two phosphorus atoms of the starting olefin are coordinated to the same metal atom, two products are obtained in this reaction—the rearranged olefin with the two coordinated

* Author to whom correspondence should be addressed.

Ph_2P groups mutually *cis* at the double bond, and also the expected triphosphine $Ph_2PCH_2CH(PPh_2)CH_2PPh_2$ with two of its phosphorus atoms coordinated and one free.[9] It is clear then that in this case the double bond is still activated towards addition, but this may be due to the presence of the remaining adjacent Ph_2P group, and in order to test this possibility we have studied the corresponding behaviour of 1,1-bis(diphenylphosphinomethyl)ethene (**1**) and its metal complexes and dichalcogenides. For this system the simple addition reaction would lead to the new ligand $(Ph_2PCH_2)_3CH$.

Table 1. Melting points and analytical data for new compounds

Compound	M.p. (°C)	%C Found	%C Calc.	%H Found	%H Calc.
1	85	78.5	79.2	6.3	6.2
2	129	68.6	68.8	5.5	5.4
3	135	58.0	57.7	4.5	4.5
4a	209	65.3	65.3	4.6	4.4
4b	207	60.7	60.8	4.0	4.1
4c	215	53.3	53.4	3.6	3.6
10	161	68.6	68.8	5.5	5.4
11	146	57.4	57.7	4.3	4.5
7a	234	65.1	65.3	4.5	4.4
7b	226	60.6	60.8	4.2	4.1
7c	242	53.5	53.4	3.7	3.6

RESULTS AND DISCUSSION

1 was prepared in *ca* 70% yield by the reaction between the readily available 3-chloro-2-chloromethylprop-1-ene and $NaPPh_2$ in refluxing liquid ammonia. It was isolated as white crystals which can be handled in air but which may be oxidized on prolonged exposure. Microanalytical data and melting points are given in Table 1.

The molecular structure of **1** is confirmed by its ^{31}P and ^{13}C NMR spectra which are summarized in Tables 2–7. The equivalent phosphorus(III) atoms have $\delta(^{31}P) = -18.3$ ppm which may be compared with a value of -16 ppm calculated from group contributions.[10] The carbons of the chemically equivalent CH_2 groups are each part of an AA'X [A,A' = ^{31}P, X = ^{13}C] spin system, but since the coupling $^4J(^{31}P^{31}P)$ is very small their ^{13}C resonances appear as a doublet of doublets at $\delta = 38$ ppm with splittings of 7.3 and 15.3 Hz that correspond very closely to the actual AX and A'X couplings and which are assigned to $^3J(^{31}P—^{13}C)$ and $^1J(^{31}P—^{13}C)$ respectively on the basis of com-

Table 2. ^{31}P, ^{77}Se, ^{95}Mo and ^{183}W NMR data for the new species

Compound[a]	$\delta(^{31}P_A)$[b] (ppm)	$\delta(^{31}P_X)$[b] (ppm)	$J(P_AP_X)$ (Hz)	$\delta(M)$ (ppm)	$^1J(P_AM)$ (Hz)	$^1J(P_XM)$ (Hz)
1	−18.3	—	–	—	—	—
2	+39.0	—	–	—	—	—
3	+31.2	—	–	−321.1[c]	731.2[d]	—
4a	+46.2	—	–	158[e]	134[f]	—
4b	+21.4	—	–	—	—	—
4c	+7.7	—	–	+314[g]	227.1[h]	—
5	−13.8	−31.6	3.1	—	—	—
6	−17.4	−28.4	5.5	—	—	—
7a	+62.4	+35.6	41.5	—	—	—
7b	+47.0	+17.4	30.5	+126[e]	134[f]	134[f]
7c	+31.5	−1.5	24.4	+268[g]	244.1[h]	222.2[h]
8	+38.3	+28.1	5.5	—	—	
9	+27.7	+16.7	6.1	[j]	745.8[d]	717.8[d]
10	+40.0	+28.3	9.8	—	—	—
11	+32.9	+18.5	9.7	[j]	738.5[d]	714.3[d]

[a] As *ca* 10% solutions in $CDCl_3$.
[b] To high frequency of 85% H_3PO_4.
[c] $\delta(^{77}Se)$ relative to $SeMe_2 = 0.0$ ppm.
[d] M = ^{77}Se.
[e] To high frequency of $Mo(CO)_6$.
[f] ±3 Hz, M = ^{95}Mo.
[g] To high frequency of $W(CO)_6$.
[h] M = ^{183}W.

Table 3. ^{13}C NMR data for the ligands in the symmetrical species **1**, **2**, **3** and **4a–4c**

Compound	$\delta(^{13}C_1)^a$ (ppm)	$N(C_1P)$ (Hz)	$\delta(^{13}C_2)^a$ (ppm)	$^2J(C_2P)$ (Hz)	$\delta(^{13}C_3)^a$ (ppm)	$^3J(C_3P)$ (Hz)
1	38.0	8.0	141.0	8.2	115.5	10.1
2	40.8	53.4	130.8	9.2	122.5	10.5
3	40.5	45.8	130.8	8.5	123.2	10.6
4a	42.4	19.8	137.9	0.0	118.6	8.1
4b	42.6	19.8	138.0	0.0	119.4	8.8
4c	42.9	23.4	138.0	0.0	119.9	8.8

[a] To high frequency of Me_4Si.
[b] As *ca* 10% solutions in $CDCl_3$.
[c] $N = {}^1J(^{31}P—^{13}C)+{}^3J(^{31}P—^{13}C)$.

parison with similar molecules. The olefinic CH_2 and C groups are symmetrically related to two phosphorus atoms and their ^{13}C spectra are simple triplets which were assigned by ^{13}C-{^1H} gated decoupling experiments.

1 reacted with elemental sulphur or selenium in refluxing benzene to give the corresponding dichalcogenides (**2**) and (**3**) [see Scheme 1] as air-stable white solids. These have ^{31}P and ^{13}C NMR spectra with the same basic structure as those of **1**, but with changes in the chemical shifts and coupling constants of the magnitudes and in the directions expected[11] to accompany the $P^{III} \rightarrow P^{V}$ transformation, and with ^{77}Se satellites in the ^{31}P spectrum of **3**.

With the group VI metal hexacarbonyls in refluxing diglyme (2,5,8-trioxanonane) **1** gave the corresponding metal tetracarbonyl chelate complexes (**4a–c**) are pale yellow air-stable crystals whose melting points and analytical data are in Table 1. Their ^{31}P chemical shifts correspond well with those calculated using established[12] values of coordination chemical shifts for chromium, molybdenum and tungsten tetracarbonyl complexes with six-membered chelate rings. The values of $\delta(^{95}Mo)$, $^1J(^{95}Mo^{31}P)$, $\delta(^{183}W)$ and $^1J(^{183}W^{31}P)$

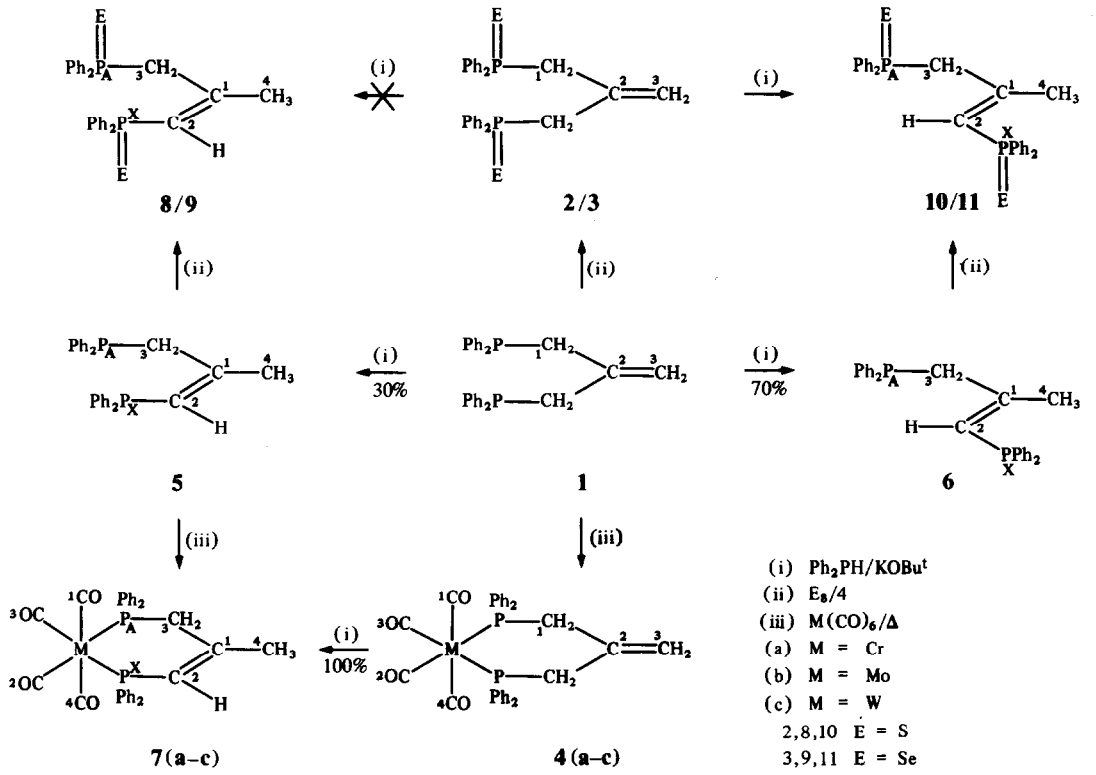

Scheme 1.

Table 4. ^{13}C NMR data for the ligands in the unsymmetrical species, **5–11**[a]

Compound	$\delta(^{13}C_1)$[b] (ppm)	$^2J(C_1P_A)$ (Hz)	$^2J(C_1P_X)$ (Hz)	$\delta(^{13}C_2)$[b] (ppm)	$^3J(C_2P_A)$ (Hz)	$^1J(C_2P_X)$ (Hz)	$\delta(^{13}C_3)$[b] (ppm)	$^1J(C_3P_A)$ (Hz)	$^3J(C_3P_X)$ (Hz)	$\delta(^{13}C_4)$[b] (ppm)	$^3J(C_4P_A)$ (Hz)	$^3J(C_4P_X)$ (Hz)
5	152.2	7.9	26.2	125.2	6.1	6.1	36.5	15.9	24.4	27.3	10.4	6.5
6	150.6	7.3	26.9	125.7	8.1	8.1	42.7	16.5	6.1	21.6	7.9	24.4
7a	151.4	0.9	11.0	121.3	11.7	33.3	35.8	15.4	13.2	31.0	3.3	11.3
7b	151.0	1.0	10.7	121.4	11.0	33.7	36.7	14.7	12.8	30.7	2.7	11.0
7c	151.6	2.2	9.5	121.2	10.3	38.8	36.9	19.0	11.7	31.0	2.9	11.7
8	154.2	0.0	7.3	120.9	9.8	86.6	38.3	51.9	8.5	28.9	3.1	15.9
9	150.9	2.4	8.5	124.8	9.8	86.6	46.3	49.4	16.5	23.9	1.2	8.5
10	154.1	0.0	6.1	121.0	10.4	78.1	38.1	46.4	9.1	28.6	3.6	15.9
11	150.5	3.3	9.0	124.2	10.4	78.7	46.2	42.1	17.1	23.9	1.8	9.2

[a] As *ca* 10% solutions in $CDCl_3$.
[b] To high frequency of Me_4Si.

Table 5. ^{13}C NMR data for the carbonyl groups of the complexes **4a–4c** and **7a–7c**[a]

Compound	$\delta(^{13}CO_1)$[b] (ppm)	$^2J(CP_A)$ (Hz)	$^2J(CP_X)$ (Hz)	$\delta(^{13}CO_2)$[b] (ppm)	$^2J(CP)_{cis}$ (Hz)	$^2J(CP)_{trans}$ (Hz)	$\delta(^{13}CO_3)$[b] (ppm)	$^2J(CP)_{cis}$ (Hz)	$^2J(CP)_{trans}$ (Hz)
4a	221.7	13.6	—	226.7	[c]	[c]	—	—	—
4b	210.8	8.8	—	215.5	[d]	[d]	—	—	—
4c	203.1	7.0	—	206.3	[e]	[e]	—	—	—
7a	221.2	13.7	13.7	227.7	13.9	4.4	227.2	11.7	5.9
7b	210.3	8.4	8.4	216.6	9.5	27.1	216.1	7.7	23.1
7c	202.6	6.6	6.6	207.1	6.6	24.9	206.5	5.1	22.7

[a] As *ca* 10% solutions in $CDCl_3$.
[b] To high frequency of Me_4Si.
[c] $N(^{13}C^{31}P) = {}^2J(CP)_{cis} + {}^2J(CP)_{trans} = 18.3$ Hz.
[d] $N(^{13}C^{31}P) = {}^2J(CP)_{cis} + {}^2J(CP)_{trans} = 15.3$ Hz.
[e] $N(^{13}C^{31}P) = {}^2J(CP)_{cis} + {}^2J(CP)_{trans} = 16.1$ Hz.

Table 6. ^{13}C NMR data for the phenyl groups of the symmetrical species **1–4c**[a]

Compound	$\delta(^{13}C_i)$[b] (ppm)	$N(C_iP)$[c] (Hz)	$\delta(^{13}C_o)$[b] (ppm)	$N(C_oP)$[c] (Hz)	$\delta(^{13}C_m)$[b] (ppm)	$N(C_mP)$[c] (Hz)	$\delta(^{13}C_p)$[b] (ppm)	$N(C_pP)$[c] (Hz)
1	138.9	14.6	133.2	18.9	128.7	7.3	128.9	< 1.0
2	132.7	79.7[e]	131.7	10.4	128.9	12.2	131.8	3.1
3	131.5	71.4[f]	132.3	10.2	128.9	11.9	132.0	2.4
4a	138.5	36.6	132.6	10.3	128.8	8.8	130.2	< 1.0
4b	138.5	34.4	132.7	11.7	128.9	8.8	130.2	< 1.0
4c	138.0	41.0	132.8	11.7	128.9	9.5	130.4	< 1.0

[a] As *ca* 10% solutions in $CDCl_3$.
[b] *i* = *ipso*, *o* = *ortho*, *m* = *meta*, *p* = *para*.
[c] $N(C_iP) = {}^nJ(C_iP) + {}^mJ(C_iP')$.
[d] To high frequency of TMS.
[e] $^1J(C_iP) = 81.2$ Hz, $^5J(C_iP) = -1.5$ Hz.
[f] $^1J(C_iP) = 73.2$ Hz, $^5J(C_iP) = -1.8$ Hz.

also accord with those expected[13] for this type of complex, and the ^{13}C spectra show the presence of axial and equatorial carbonyl groups in a 2 : 2 ratio.

In its reaction with Ph_2PH in the presence of $KOBu^t$ **1** has the potential to undergo either an addition reaction to yield the known triphosphine $(Ph_2PCH_2)_3CH$ or a double bond migration (an allylic rearrangement). In fact, under a range of conditions the result was invariably a mixture of the *cis* and *trans* rearrangement products (**5** and **6**) (see Scheme 1) in a *ca* 3 : 7 ratio. This mixture was a viscous oil from which **5** and **6** could not be obtained in analytically pure forms. However, it was possible to purify them sufficiently to record their individual NMR spectra. The ^{13}P spectrum (see Table 2) of each of these shows an AX spin system with values of $\delta(^{31}P_A)$ and $\delta(^{31}P_X)$ near −15 and −30 ppm as expected[14] for Ph_2PCH_2—R and Ph_2PCH_2=CR_2 fragments respectively, and small values of $J(^{31}P^{31}P)$ as expected for a four-bond coupling. In the ^{13}C spectra (Table 4) the multiplicities were assigned by gated ^{13}C-{^1H} decoupling experiments, and selective ^{13}C-{^{31}P} decoupling experiments were used to assign the various ^{31}P—^{13}C coupling constants. The couplings $^2J(^{31}P_A{}^{13}C_1)$, $^2J(^{31}P_X{}^{13}C_1)$, $^3J(^{31}P_A{}^{13}C_2)$, $^1J(^{31}P_X{}^{13}C_2)$, $^1J(^{31}P_A{}^{13}C_3)$, and $^3J(^{31}P_A{}^{13}C_4)$ can be expected to be substantially independent of the geometry at the double bond and indeed are very similar in **5** and **6**. In contrast $^3J(^{31}PC : C^{13}C)$ is known[15] to be characteristically large when the coupled nuclei are *cis* and small when they are *trans*; the values of 24.4 and 6.5 Hz for this coupling in **5** and **6** respectively therefore lead us confidently to assign to these isomers *cis* and *trans* geometries respectively. This conclusion is supported by the ability of **5** *but not* **6** to form chelate metal complexes (*vide infra*).

The 3 : 7 mixture of **5** and **6** reacted with elemental sulphur or selenium to yield respectively the disulphides **8** and **10** and the diselenides **9** and **11**, the 3 : 7 isomer ratio being retained in the products in each case. In each case the major [i.e. **10** or **11**] isomer was isolated by fractional crystallization as a white air-stable solid (analytical data and melting points in Table 1) and had NMR spectra that confirmed its structure. In particular, the values of $\delta(^{31}P)$ are in the expected regions, and the values of $J(^{31}P$—$^{13}C)$ are *ca* 50 Hz for P^V bound to sp^3-hybridized carbon and *ca* 80 Hz for P^V bound to sp^2-hybridized carbon. It was also possible to obtain most of the NMR parameters of **8** and **9** and these too confirmed the proposed structures. Insufficient is known about the stereochemical dependence of $^3J(^{31}P^VC : C^{13}C)$ to use this coupling to establish the geometry at the double bond, but the nature of the reaction of P^{III} with chalcogen and the retention of the 3 : 7 isomer ratio indicate that no isomerization will have occurred, and that **8** and **9** have the *cis* geometry and **10** and **11** the *trans*.

It was also found that the disulphide **2** reacted with Ph_2PH in the presence of $KOBu^t$ to yield *exclusively* the *trans* isomer **10**. Furthermore, in this reaction no replacement of $Ph_2P(S)$ by Ph_2P occurred, thus confirming that these isomerizations are true allylic rearrangements. Quantitative rearrangement behaviour was also observed when the complexes **4a–4c** were treated with Ph_2PH/$KOBu^t$, the *cis* products **7a–7c** being isolated as air-stable pale yellow crystals (melting points and elemental analyses in Table 1). This is in contrast to the situation found for the *cis* $M(CO)_4$ [M = Cr,

Table 7. ^{13}C NMR data for the phenyl groups in the unsymmetrical complexes **7a–7c**[a]

Compound		$\delta(^{13}C_i)$[c] (ppm)[b]	$^1J(C_iP)$ (Hz)	$^3J(C_iP)$ (Hz)	$\delta(^{13}C_o)$[c] (ppm)[b]	$^2J(C_oP)$[d] (Hz)	$\delta(^{13}C_m)$[c] (ppm)[b]	$^3J(C_mP)$[d] (Hz)	$\delta(^{13}C_p)$[c] (ppm)	$^4J(C_pP)$[d] (Hz)
7a	A	137.6	31.9	1.9	132.2	11.0	128.9	8.8	130.0	1.8
7a	X	138.3	38.1	2.6	132.3	10.6	129.0	9.2	130.3	1.8
7b	A	137.4	30.4	0.9	132.4	11.7	129.0	8.8	130.1	1.5
7b	X	138.1	36.3	1.8	132.5	12.8	129.1	9.5	130.4	1.5
7c	A	137.3	35.9	1.5	132.6	11.0	129.1	8.8	130.4	2.2
7c	X	138.0	41.8	2.9	132.7	12.5	129.2	9.5	130.7	2.2

[a] As *ca* 10% solutions in $CDCl_3$.
[b] To high frequency of Me_4Si.
[c] i = *ipso*, o = *ortho*, m = *meta*, p = *para*.
[d] Longer range couplings all < 0.5 Hz.

Mo, W] complexes of $Ph_2PC(CH_2PPh_2)=CH_2$ where either addition of a Ph_2P group or rearrangement can occur. The complexes **7a–7c** can also be prepared by the reaction in refluxing diglyme of the 3:7 mixture of **5** and **6** with a 30% equivalent of $M(CO)_6$. This process leaves **6** essentially unaltered and further confirms the assignment of a *cis* geometry to **5**. The use of a larger amount of $M(CO)_6$ again yields **7a–7c**, but in addition di- and polymeric species are formed as a result of coordination by **6** which is unable to form monometallic chelates.

The structures of **7a–7c** are fully confirmed by their NMR spectra (Table 2–6). These show three ^{13}CO resonances with 2:1:1 intensity ratios, arising from two equivalent axial and two inequivalent equatorial carbonyl groups. The ligand backbone ^{13}C resonances are at chemical shift positions close to those found in the corresponding *cis* species **5**, **8** and **9**, and the apparently unaltered values of $^1J(^{31}P^{13}C)$ upon coordination in reality conceal an algebraic increase of *ca* 32 Hz because of a change of sign from −16 Hz in **5** to *ca* +16 Hz in **7a–7c**.

The values of $^2J(^{31}P_A{}^{31}P_X)$ of 41.5, 30.5, and 24.4 Hz for **7a**, **7b** and **7c** respectively are close to those found by Grim[16] as the metal-mediated contributions in unstrained chelate rings for Cr, Mo and W, and thus confirm that any four-bond backbone component can be disregarded.

The overall pattern of these reactions is summarized in Scheme 1 and it is clear that for $(Ph_2P(E)CH_2)_2C=CH_2$ [E = lone pair, S, Se, $M(CO)_4/2$] treatment with Ph_2PH in the presence of $KOBu^t$ leads exclusively to a rearrangement reaction with the double bond migrating to a position closer to one of the Ph_2P groups, and that addition does not occur at room temperature. The stereochemistry of such rearrangements depends upon the relative thermodynamic stability of the products since the *cis* and *trans* isomers share a common intermediate. For E = lone pair the rearrangement is 70% selective for the *trans* product; for E = S, Se it is 100% selective for the *trans* product; and for E = $M(CO)_4/2$ the *cis* product is formed exclusively. This pattern therefore represents the relative stabilities of the (feasible) products and is probably sterically determined—in the last case by necessity, and in the first and second by the moderate and somewhat greater sizes of the Ph_2P and $Ph_2P(E)$ groups respectively.

Finally, it should be noted that all of the products of these rearrangement reactions have a double bond with a single adjacent (and therefore potentially activating) Ph_2P group and yet Ph_2PH does not add to them under our conditions. This we attribute to the presence of relatively bulky sub-

stituents on the olefinic carbon atoms which make attack difficult. In the case of $(Ph_2P)_2C:CHR$ the addition of Ph_2PH becomes substantially slower when R is changed from H to CH_3.[15]

EXPERIMENTAL

NMR spectra were measured on a JEOL FX90 Q multinuclear spectrometer at 2.1 T in CH_2Cl_2 or $CDCl_3$ solutions in 10-mm o.d. spinning tubes. Solvents were dried and deaerated by standard procedures and all manipulations were conducted under an atmosphere of dry dinitrogen or ammonia. For the complexes the procedure used for the chromium congener is given in each case; identical methods were used with molybdenum and tungsten and their proton NMR data are given in that order following the corresponding chromium parameter.

1,1-*Bis(diphenylphosphinomethyl)ethene* (**1**)

Triphenylphosphine (65.5 g, 0.25 mol) in tetrahydrofuran (thf) (200 cm^3) was added over 0.5 h to a stirred solution of sodium (11.5 g, 0.5 mol) in refluxing anhydrous ammonia (1000 cm^3). Solid ammonium bromide (24.5 g, 0.25 mol) was then added over 0.5 h to a give a bright red solution to which 3-chloro-2-chloromethylprop-1-ene (15.6 g, 0.125 mol) in thf (50 cm^3) was added dropwise over 0.75 h. The solution became cream-coloured and after removal of ammonia and thf by evaporation the residue was extracted with diethylether (2×200 cm^3). The combined extracts were dried over anhydrous sodium sulphate and the solvent was removed under vacuum to give a viscous oil. On addition of ethanol (200 cm^3) and storage at $-20°C$ for 24 h a white solid crystallized. Recrystallization of this from methanol (150 cm^3)/dichloromethane (50 cm^3) at $-20°C$ gave the product as colourless crystals in 68% yield. ^1H NMR: ($CDCl_3$) δ(—CH_2—) 3.01 ppm, complex multiplet, 4H; δ(=CH_2) 4.74 ppm, complex multiplet, 2H; $\delta(C_6H_5)$ 7.0–7.5 ppm, complex overlapping multiplets, 20H.

Cis *and* trans-1,3-*bis(diphenylphosphino)*-2-*methylpropene* (**5**, **6**)

To a solution of **1** (10.0 g, 24 mmol) and diphenylphosphine (0.2 g, 1 mmol) in dry thf (50 cm^3) was added potassium tert-butoxide (0.05 g, catalytic amount). The solution was stirred until ^{31}P NMR indicated quantitative conversion into a 3:7 mixture of **5** and **6** (*ca* 2 h) and the solvent was then removed under vacuum. Methanol (50 cm^3) was added to the residue which then yielded a colourless oil upon standing at $-20°C$ for 24 h. After the methanolic mother liquor had been decanted the crude product was dissolved in dichloromethane (20 cm^3) and methanol (80 cm^3) was added to the resulting solution. After standing at $-20°C$ for 24 h the mother liquor was decanted and the oily product was washed with cold methanol (2×200 cm^3) and vacuum dried to give an air-sensitive viscous oil containing the isomers **5** and **6** in a 3:7 ratio. Yield: 88%. Attempts to separate the isomers by fractional distillation were unsuccessful.

^1H NMR: ($CDCl_3$): (**5**); $\delta(CH_3)$ 1.92 ppm, broad singlet, 3H; $\delta(CH_2)$ 3.39 ppm, multiplet, 2H; δ(CH) 5.84 ppm, multiplet, 1H; $\delta(C_6H_5)$ 6.9–7.5 ppm, complex overlapping multiplets, 20H. (**6**); $\delta(CH_3)$ 2.05 ppm, broad singlet, 3H; $\delta(CH_2)$ 2.96 ppm, broad singlet, 2H; δ(CH) 5.64, broad singlet, 1H; $\delta(C_6H_5)$ 6.9–7.5 ppm, complex overlapping multiplets, 20H.

1,1-*Bis(diphenylphosphinomethyl(ethene*-P,P′-*disulphide* (**2**)

A solution of **1** (4.2 g, 10 mmol) in benzene (30 cm^3) containing elemental sulphur (1 g; excess) was stirred at room temperature for 2 h and then refluxed for 0.1 h. After filtration of the cooled solution, methanol (30 cm^3) was added to the filtrate to give a white solid which was recrystallized from methanol (30 cm^3)/dichloromethane (50 cm^3) to give the product as air-stable colourless crystals in 90% yield.

^1H NMR: ($CDCl_3$): δ(—CH_2—) 3.53 ppm, complex multiplet, 4H; δ(=CH_2) 4.64 ppm, complex multiplet, 2H; $\delta(C_6H_5)$ 7.3–7.8 ppm, complex overlapping multiplets, 20H.

1,1-*Bis(diphenylphosphinomethyl(ethene*-P,P′-*diselenide* (**3**)

This compound was prepared in a similar manner to the disulphide **2** using elemental selenium and a reflux period of 2 h. The product was isolated as air-stable colourless crystals in 86% yield.

^1H NMR: ($CDCl_3$): δ(—CH_2—) 3.80 ppm, complex multiplet, 4H; δ(=CH_2) 4.59 ppm, complex multiplet, 2H; $\delta(C_6H_5)$ 6.9–7.9 ppm, complex overlapping multiplets, 20H.

Cis[1,1-*bis(diphenylphosphinomethyl)ethene*-P,P′]*tetracarbonylchromium*(0) (**4a**)

A mixture of hexacarbonylchromium (4.4 g, 20 mmol) and **1** (8.4 g, 20 mmol) in diglyme (50 cm^3) was heated under reflux for 2 h. Methanol (50 cm^3) was added to the cooled and filtered solution to yield a yellow solid which was recrystallized from

methanol (50 cm^3)/dichloromethane (30 cm^3) to give the product as air-stable yellow crystals in 75% yield.

^1H NMR: ($CDCl_3$): $\delta(CH_3)$ 1.36, 1.28, 1.30 ppm, $^4J(H_{methyl}H_{olefinic})$ 1.2, 1.6, 1.7 Hz, $^4J(H_{methyl}{}^{31}P_A)$ 0, 0, 0 Hz, $^4J(H_{methyl}{}^{31}P_X)$ 1.2, 1.6, 1.7 Hz, $^4J(H_{methyl}H_{aliphatic})$ 0, 0, 0 Hz; $\delta(CH_2)$ 2.60, 2.65, 2.87 ppm, $^2J(H^{31}P_A)$ 8.3, 7.8, 8.5 Hz. $^4J(H^{31}P_X)$ 0, 0, 0 Hz, 2H; δ(CH) 5.98, 5.89, 5.83 ppm, $^4J(H^{31}P_A)$ 2.9, 4.4, 4.0 Hz, $^2J(H^{31}P_X)$ 2.9, 4.4, 5.4 Hz, 1H; $\delta(C_6H_5)$ 7.0–7.7, 7.0–7.7, 7.0–7.7 ppm, complex overlapping multiplets, 20H.

Trans-1,3-*bis*(*diphenylphosphino*)-2-*methylprop*-1-*ene*-P,P′-*disulphide* (**10**)

Potassium tert-butoxide (0.05 g, catalytic amount) was added to a solution of **2** (4.9 g, 10 mmol) and diphenylphosphine (0.5 g, catalytic amount) in thf (50 cm^3). The mixture was stirred for 24 h, its volume was reduced to 25 cm^3 at the pump and methanol (50 cm^3) was then added to give a white crude solid which was recrystallized from methanol (30 cm^3)/dichloromethane (15 cm^3) to give the product as air-stable pale yellow crystals in 74% yield.

^1H NMR: ($CDCl_3$): $\delta(CH_3)$ 1.83 ppm, $^4J(H_{methyl}H_{olefinic})$ 0.9 Hz, $^4J(H_{methyl}{}^{31}P_A)$ 2.9 Hz, $^4J(H_{methyl}{}^{31}P_X)$ 2.9 Hz, 3H; $\delta(CH_2)$ 2.93 ppm, $^2J(H^{31}P_A)$ 14.4 Hz, 2H; δ(CH) 6.01 ppm, $^2J(H^{31}P_X)$ 21.5 Hz, $^4J(H^{31}P_A)$ 5.4 Hz, 1H; $\delta(C_6H_5)$ 6.0–8.0 ppm, complex overlapping multiplets, 20H.

Trans-1,3-*bis*(*diphenylphosphino*)-2-*methylprop*-1-*ene*-P,P′-*diselenide* (**11**)

This compound was prepared using an identical method to that for the disulphide **10** starting from the corresponding diselenide **3**. The product was isolated as air-stable colourless crystals in 78% yield.

^1H NMR: ($CDCl_3$): $\delta(CH_3)$ 1.76 ppm, $^4J(H_{methyl}H_{olefinic})$ 1.4 Hz, $^4J(H_{methyl}{}^{31}P_A)$ 3.0 Hz, $^4J(H_{methyl}{}^{31}P_X)$ 3.0 Hz, 3H; $\delta(CH_2)$ 3.09 ppm, $^2J(H^{31}P_A)$ 14.4 Hz, 2H; δ(CH) 6.04 ppm, $^2J(H^{31}P_X)$ 21.0 Hz, $^4J(H^{31}P_A)$ 5.4 Hz, 1H; $\delta(C_6H_5)$ 6.9–8.1 ppm, complex overlapping multiplets, 20H.

Acknowledgements—We thank the SERC and the Leverhulme Trust for support.

REFERENCES

1. R. B. King and P. N. Kapoor, *J. Am. Chem. Soc.* 1969, **91**, 5191.
2. R. B. King, J. C. Cloyd Jr and P. N. Kapoor, *J. Chem. Soc., Perkin Trans.* 1973, **1**, 2226.
3. R. B. King and and J. C. Cloyd Jr, *J. Am. Chem. Soc.* 1975, **97**, 46.
4. J. L. Bookham, W. McFarlane and I. J. Colquhoun, *J. Chem. Soc., Dalton Trans.* 1988, 503.
5. J. L. Bookham, W. McFarlane, I. J. Colquhoun and M. Thornton-Pett, *J. Organomet. Chem.* 1988, **354**, 313.
6. R. B. King and P. N. Kapoor, *J. Am. Chem. Soc.* 1971, **93**, 4158.
7. J. L. Bookham, W. McFarlane and I. J. Colquhoun, *J. Chem. Soc., Chem. Commun.* 1986, 1041.
8. G. R. Cooper, F. Hassan, B. L. Shaw and M. Thornton-Pett, *J. Chem. Soc., Chem. Commun.* 1985, 2353.
9. J. L. Bookham and W. McFarlane, *J. Chem. Soc., Dalton Trans.* 1990, 489.
10. S. O. Grim, W. McFarlane and E. F. Davidoff, *J. Org. Chem.* 1967, **32**, 781.
11. I. J. Colquhoun and W. McFarlane, *J. Chem. Soc., Dalton Trans.* 1982, 1915.
12. G. T. Andrews, I. J. Colquhoun and W. McFarlane, *Polyhedron* 1983, **2**, 783.
13. G. T. Andrews, I. J. Colquhoun, W. McFarlane and S. O. Grim, *J. Chem. Soc., Dalton Trans.* 1982, 2353.
14. S. O. Grim, R. P. Molenda and J. D. Mitchell, *J. Org. Chem.* 1980, **45**, 250.
15. J. L. Bookham and W. McFarlane, *Polyhedron* 1988, **7**, 239.
16. S. O. Grim, R. C. Barth, J. D. Mitchell and J. Delgaudio, *Inorg. Chem.* 1977, **16**, 1776.

Polyhedron Vol. 10, No. 20/21, pp. 2389–2397, 1991
Printed in Great Britain

0277–5387/91 $3.00+.00
© 1991 Pergamon Press plc

EARLY STAGES OF THE HYDROLYSIS OF CHROMIUM(III) IN AQUEOUS SOLUTION—VIII. KINETICS OF DIMERIZATION OF DEPROTONATED FORMS OF DOUBLY BRIDGED DIMER

MICHAEL R. GRACE and LEONE SPICCIA†

Department of Chemistry, Monash University, Clayton, Victoria 3168, Australia

(*Received* 26 *April* 1991; *accepted* 9 *July* 1991)

Abstract—The dimerization of the doubly bridged hydrolytic dimer of Cr^{III} to give tetramer has been followed in the pH range 3.4–5.0, using a pH stat facility. Acid is liberated as the reaction proceeds and initial rates were estimated from the volume of base added to maintain constant pH with time. The reaction was followed only over the first 8% of dimer conversion to ensure that tetramer was the major product. The pH dependence of k_{obs} has been successfully fitted to an expression which assumes the predominance of three reaction pathways:

$$Cr_2(\mu\text{-}OH)_2(OH)^{3+} + Cr_2(\mu\text{-}OH)_2(OH)^{3+} \longrightarrow \text{tetramer}\quad k_{11} = (2.18 \pm 0.21) \times 10^{-4}\,M^{-1}\,s^{-1};$$

$$Cr_2(\mu\text{-}OH)_2(OH)_2^{2+} + Cr_2(\mu\text{-}OH)_2(OH)^{3+} \longrightarrow \text{tetramer}\quad k_{21} = (5.2 \pm 3.2) \times 10^{-3}\,M^{-1}\,s^{-1};$$

$$Cr_2(\mu\text{-}OH)_2(OH)_2^{2+} + Cr_2(\mu\text{-}OH)_2(OH)_2^{2+} \longrightarrow \text{tetramer}\quad k_{22} = (0.83 \pm 0.08)\,M^{-1}\,s^{-1}.$$

Each deprotonation of dimer affords rate enhancements of 25–160 fold which are in keeping with previous observations for the dimerization of Cr^{3+} and result primarily from labilization of the primary coordination sphere of Cr^{III} on deprotonation of the aquo ligands. The marginally faster overall rate of dimerization of dimer compared with Cr^{3+} is attributed to the greater acidity of dimer and does not result from a greater reactivity of its deprotonated forms.

The conversion of divalent and trivalent metal ions into polynuclear species and, ultimately, polynuclear metal hydroxides involves a complicated sequence of hydrolytic processes. Because these processes occur concurrently, it is often difficult to obtain reliable measurements of discrete polymerization rates. As a consequence, information about the mechanism of these reactions is generally lacking.

In the case of Fe^{3+},[1] measurements of the rate of dimerization of $FeOH^{2+}$ to give $[Fe_2(\mu\text{-}OH)_2]^{4+}$ (eq. 1) have shown that the forward reaction ($k_{11} = 630\ M^{-1}\ s^{-1}$ at 25°C) is faster than the reverse reaction ($k_{-11} = 0.4\ s^{-1}$) for $[FeOH^{2+}] > 0.001$ M. Hence, the equilibrium constant indicates that dimer formation is favoured under these conditions.

$$FeOH^{2+} + FeOH^{2+} \underset{k_{-11}}{\overset{k_{11}}{\rightleftharpoons}} Fe_2(\mu\text{-}OH)_2^{4+}. \quad (1)$$

Furthermore, it has been estimated that formation of dimer from $FeOH^{2+}$ is about 10 orders of magnitude faster than from Fe^{3+}. This is in keeping with the faster rates of substitution observed on deprotonation of Fe^{3+}.[1]

Recent work on the dimerization of Cr^{3+} [2] has shown that several pathways contribute to the reaction rates (eqs 2–4), their relative effect being determined primarily by solution pH.

$$CrOH^{2+} + CrOH^{2+} \longrightarrow \text{dimer} \quad (2)$$

$$CrOH^{2+} + Cr(OH)_2^{+} \longrightarrow \text{dimer} \quad (3)$$

$$Cr(OH)_2^{+} + Cr(OH)_2^{+} \longrightarrow \text{dimer}. \quad (4)$$

The results showed a systematic increase in dimerization rate with degree of deprotonation of the

† Author to whom correspondence should be addressed.

Cr^{III} aquo ion, consistent with the faster rate of H_2O exchange on $CrOH^{2+}$ compared with Cr^{3+}.[3]

We report here the kinetics of dimerization of the hydrolytic dimer of Cr^{III}, $[Cr_2(\mu\text{-}OH)_2]^{4+}$, to give tetramer (eq. 5) measured over the pH range 3.4–5.0, $T = 298.2$ K and $I = 1.0$ M ($NaClO_4$)

$$Cr_2(\mu\text{-}OH)_2(OH)_r^{(4-r)+} \longrightarrow Cr_4(\mu\text{-}OH)_6(OH)_s^{(6-5)+} + mH^+ \quad (5)$$

using a pH-stat technique. The work is part of a continuing effort aimed at developing a kinetic scheme for the propagation of polymerization in partially neutralized solutions of Cr^{3+}.

EXPERIMENTAL

Materials

$[Cr_2(\mu\text{-}OH)_2(OH_2)_8](CH_3)_3C_6H_2SO_3)_4 \cdot 4H_2O$ was prepared as described in the literature.[4] Dimer solutions in perchlorate media were obtained by reaction of Cr metal with perchloric acid (under nitrogen) to give Cr^{2+} followed by air oxidation to produce dimer, which was subsequently purified by ion-exchange chromatography. Sodium perchlorate and 70% perchloric acid (Merck p.a.) were used as received. Imidazole (Fluka p.a.) was twice recrystallized from ethanol. All aqueous solutions were prepared using deionized, distilled water and those used in pH measurements were also degassed to remove dissolved CO_2.

Instruments and methods

Solution pH values and pH-stat kinetics were measured on a Metrohm 605 pH meter connected to a Metrohm 665 Dosimat autoburette using a Ross combined glass electrode (Orion). The electrode was calibrated against standard $HClO_4$ (pH 2–3, $I = 1.0$ M ($NaClO_4$)) and allowances for differences in ionic mobility were made by applying a Henderson correction. All pH measurements were carried out at $I = 1.0$ M ($NaClO_4$) and a temperature of 298.2 ± 0.1 K, maintained by circulating water through a double-walled reaction vessel from a waterbath fitted with a Haake D8 thermostat and Haake D12 compressor. A slow, continuous flow of N_2 was maintained through the solutions to prevent the absorption of CO_2. Kinetic experiments were conducted with exclusion of light since this has been shown to accelerate the polymerization reactions of Cr^{III}.[2]

The determination of the first two hydrolysis constants of the doubly bridged dimer (K_{D1} and K_{D2}) at $I = 1.0$ M ($NaClO_4$) was performed as described by Stünzi and Marty.[5] The dimer solution was chromatographically purified just prior to measurement and degassed by N_2 before and during the potentiometric titration.

The pH meter and Dosimat were interfaced to a Pericom AT computer through an IEEE interface package (IO tech). This system enabled direct computer acquisition of kinetic data which could then be conveniently analysed using the statistical package SYSTAT.[6]

The chromium content of salts and solutions was determined spectrophotometrically following conversion to CrO_4^{2-}.[5]

Kinetics

The dimer solutions used in kinetic experiments were prepared by either: (i) dissolution of the dimer mesitylene sulphonate in a solution containing 0.01 M $HClO_4$ and sufficient $NaClO_4$ to give $I = 1.0$ M; or (ii) elution of dimer from ion-exchange columns with a 0.01 M $HClO_4$/0.99 M $NaClO_4$ solution since this gave a solution with $I = 1.00(\pm 0.03)$ M. An aliquot of either of these solutions was introduced into the reaction vessel and allowed to reach thermal equilibrium. After electrode stabilization (10 min) a moderately concentrated imidazole solution (0.2 M, $I = 1.0$ M) was added slowly by graduated pipette until the solution pH was close to the desired value. Vigorous stirring was necessary during this addition to avoid localized areas of high pH, which could result in artificially rapid polymerization of the dimer. The computer-controlled titration system was then used to obtain the commencing pH, via addition of more dilute base solution (0.02 M imidazole, $I = 1.0$ M) and to follow the dimerization reaction by measuring the volume of base required to maintain constant pH as a function of time. The reaction was typically followed for 5–8% conversion of dimer.

Product analysis

At the completion of (and sometimes during) data acquisition, aliquots of solutions were taken from the reaction vessel, acidified to pH 2, diluted to $I < 0.1$ M and absorbed onto Sephadex SP C25 ion-exchange columns. The products were then eluted as described by Stünzi and Marty[5] and the chromium content of each fraction determined. For a typical experiment at pH = 3.80, the following product distribution was obtained: dimer, 92.1%; tetramer, 7.3%; higher oligomers, < 0.6%. Analysis of the reaction mixtures as dimerization progressed showed an almost constant amount of higher oligomers (< 0.8%).

RESULTS AND DISCUSSION

In the pH range 3.4–5.0, homogeneous solutions of the Cr^{III} doubly bridged dimer slowly polymerize, initially forming tetramer, followed by further reaction to higher oligomers and the precipitation of polymeric hydroxides. The structure of the dimer (**1**)[7] and the proposed structure of the "open" form of the tetramer (**2**)[5] are shown in Fig. 1. The work presented here concerns only the conversion of dimer into tetramer. Thus, it was important to establish the conditions for following this reaction without interference from subsequent polymerization processes.

The acid dissociation constants of dimer (K_{D1}, K_{D2}) and tetramer (K_{T1}, K_{T2}) can be used to determine whether dimerization releases or consumes protons. The proton balance for the reaction (eq. 5) is given by eq. (6):

$$m = 1 + \frac{s}{2} - r, \tag{6}$$

where

$$r = \frac{\{K_{D1}[H^+]^{-1} + 2K_{D1}K_{D2}[H^+]^{-2}\}}{\{1 + K_{D1}[H^+]^{-1} + K_{D1}K_{D2}[H^+]^{-2}\}} = \frac{[Cr_2(OH)_3^{3+}] + 2[Cr_2(OH)_4^{2+}]}{[\text{dimer}]_T} \tag{7}$$

$$s = \frac{\{K_{T1}[H^+]^{-1} + 2K_{T1}K_{T2}[H^+]^{-2}\}}{\{1 + K_{T1}[H^+]^{-1} + K_{T1}K_{T2}[H^+]^{-2}\}} = \frac{[Cr_4(OH)_7^{5+}] + 2[Cr_4(OH)_8^{4+}]}{[\text{tetramer}]_T}. \tag{8}$$

Values of K_{D1} ($= \{2.14 \pm 0.05\} \times 10^{-4}$ mol dm^{-3}) and K_{D2} ($= \{1.48 \pm 0.07\} \times 10^{-6}$ mol dm^{-3}) used in the calculation of r throughout kinetic analysis were determined as part of this work, while K_{T1} and K_{T2} were taken from ref. 5. Terms involving higher dissociation constants of dimer (K_{D3}, K_{D4}) and tetramer (K_{T3}, K_{T4}, ...) have been neglected as they are expected to make minimal contribution at pH < 5. This is reasonable since the observed difference between the first two dissociation constants of Cr^{III} oligomers of 1–2 pH units[5] is expected to continue for subsequent successive deprotonations of dimer and tetramer. Furthermore, pK_{a3} values for several Cr^{III} amine complexes have been found to be greater than 8.[8]

Although m was found to vary with pH, the values were always positive (Table 1) indicating that the conversion of dimer into tetramer liberates H^+. Thus, reaction could be followed by monitoring the release of H^+ as a function of time.

Product analyses

Product analyses have shown that tetramer is the dominant product formed in the early stages of reaction (< 8% conversion of dimer), although small amounts of higher oligomers (< 0.8%) were found in all reaction mixtures. The proportion of these higher oligomers remained constant throughout each experiment indicating that they were formed at the commencement of the reaction when mildly concentrated base (0.2 M imidazole) is added to rapidly adjust solution pH to the desired value. Regions of relatively high base concentrations (pH > 5) can form for short periods of time which could give rise to multiply deprotonated forms of dimer which, as will be shown later, polymerize at much faster rates than fully protonated dimer and could therefore transform it into polynuclear species. At pH > 5, the "active" dimer hydroxide, $Cr_2(\mu\text{-}OH)_2(OH)_4(OH_2)_4 \cdot xH_2O$, could also form, but as equilibrium pH is established throughout the reaction mixture it would redissolve regenerating deprotonated forms of the dimer. Since substitution is not involved, this process does not lead to polynuclear species.

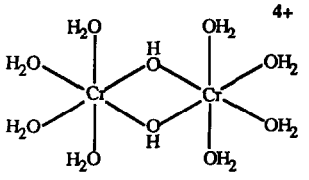

1 Dimer

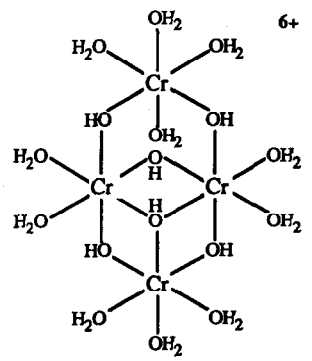

2 Proposed Tetramer Structure

Fig. 1. Structures of the dimer (**1**) and open tetramer (**2**).

Table 1. Experimental parameters and observed rate constants for the dimerization of DBD at 25.0±0.1°C and I = 1.0 M ($NaClO_4$)

pH	[Dimer]$_t$ ($\times 10^3$ M)	V_0 (cm^3)	m[a]	k_{obs}[b,c] ($M^{-1}s^{-1}$)	$k^{\#}$[c,d] ($\times 10^{12}$)
3.401	20.43	26.41	1.0979	$(3.27\pm0.21)\times10^{-5}$	42.2±3.6
3.421	9.473	27.05	1.0901	$(3.34\pm0.14)\times10^{-5}$	37.1±2.4
3.489	7.221	27.35	1.0623	$(4.16\pm0.21)\times10^{-5}$	27.8±2.1
3.515	19.46	28.13	1.0511	$(3.69\pm0.18)\times10^{-5}$	20.4±1.5
3.518	9.197	22.97	1.0498	$(5.20\pm0.23)\times10^{-5}$	28.1±2.0
3.575	8.786	27.52	1.0243	$(7.32\pm0.33)\times10^{-5}$	26.2±1.9
3.594	9.147	22.38	1.0156	$(7.49\pm0.30)\times10^{-5}$	23.5±1.6
3.624	19.69	23.02	1.0017	$(7.21\pm0.32)\times10^{-5}$	18.3±1.3
3.712	9.393	27.28	0.9600	$(7.47\pm0.34)\times10^{-5}$	10.3±0.8
3.715	7.625	27.65	0.9586	$(6.13\pm0.30)\times10^{-5}$	8.30±0.68
3.803	19.52	23.22	0.9167	$(1.03\pm0.05)\times10^{-4}$	7.78±0.65
3.817	9.376	27.33	0.9101	$(1.21\pm0.07)\times10^{-4}$	8.34±0.78
3.824	8.984	28.05	0.9068	$(1.10\pm0.07)\times10^{-4}$	7.24±0.73
3.884	17.61	27.90	0.8791	$(1.43\pm0.07)\times10^{-4}$	6.42±0.56
3.917	9.352	27.40	0.8642	$(1.42\pm0.07)\times10^{-4}$	5.19±0.46
3.983	8.369	29.52	0.8355	$(2.30\pm0.12)\times10^{-4}$	5.60±0.53
3.987	9.059	23.32	0.8338	$(2.08\pm0.10)\times10^{-4}$	4.94±0.45
4.020	17.33	28.00	0.8201	$(2.70\pm0.12)\times10^{-4}$	5.26±0.46
4.112	16.57	28.05	0.7846	$(2.91\pm0.13)\times10^{-4}$	3.31±0.30
4.121	9.443	27.30	0.7814	$(3.68\pm0.19)\times10^{-4}$	3.98±0.39
4.192	8.920	26.43	0.7572	$(4.64\pm0.25)\times10^{-4}$	3.36±0.35
4.211	17.23	28.15	0.7512	$(4.47\pm0.22)\times10^{-4}$	2.91±0.29
4.213	8.833	27.56	0.7506	$(6.08\pm0.35)\times10^{-4}$	3.92±0.42
4.313	9.231	27.76	0.7224	$(7.05\pm0.37)\times10^{-4}$	2.64±0.28
4.315	17.81	28.40	0.7219	$(8.52\pm0.46)\times10^{-4}$	3.16±0.34
4.414	8.135	27.95	0.6996	$(1.47\pm0.09)\times10^{-3}$	3.24±0.38
4.434	4.761	23.01	0.6957	$(1.37\pm0.09)\times10^{-3}$	2.73±0.33
4.500	4.747	23.08	0.6842	$(1.66\pm0.11)\times10^{-3}$	2.37±0.29
4.505	8.940	23.63	0.6835	$(1.67\pm0.10)\times10^{-3}$	2.32±0.27
4.534	7.414	27.97	0.6792	$(1.98\pm0.13)\times10^{-3}$	2.39±0.30
4.596	7.670	28.01	0.6712	$(2.57\pm0.17)\times10^{-3}$	2.29±0.29
4.607	7.272	28.33	0.6699	$(2.32\pm0.15)\times10^{-3}$	1.96±0.25
4.623	9.195	25.25	0.6682	$(2.93\pm0.27)\times10^{-3}$	2.29±0.35
4.625	4.755	23.04	0.6679	$(3.03\pm0.21)\times10^{-3}$	2.35±0.31
4.699	4.747	22.53	0.6610	$(3.44\pm0.24)\times10^{-3}$	1.88±0.25
4.720	2.353	27.00	0.6593	$(4.14\pm0.32)\times10^{-3}$	2.05±0.29
4.809	4.739	23.12	0.6531	$(5.32\pm0.40)\times10^{-3}$	1.75±0.25
4.832	2.315	27.44	0.6516	$(7.18\pm0.58)\times10^{-3}$	2.13±0.31
4.916	4.745	23.69	0.6466	$(8.23\pm0.66)\times10^{-3}$	1.68±0.25
4.929	2.388	27.17	0.6459	$(9.75\pm0.83)\times10^{-3}$	1.88±0.29
4.984	4.743	23.10	0.6424	$(1.00\pm0.08)\times10^{-2}$	1.53±0.23
5.005	2.349	27.04	0.6409	$(1.22\pm0.11)\times10^{-2}$	1.70±0.28

[a] Defined in eq. (6).
[b] Eq. (12).
[c] Quoted errors are one standard deviation.
[d] Eq. (13).

In summary, product analyses have shown that tetramer is the only significant product formed in the early stages of polymerization of the Cr^{III} hydrolytic dimer. Thus, rate constants can be obtained by the initial rates method successfully used to study the dimerization of Cr^{3+}.[2]

Determination of k_{obs}

The kinetic scheme for conversion of dimer into tetramer is complicated by the presence of several deprotonated forms of the dimer. Over the pH range 3.4–5.0, $Cr_2(OH)_2^{4+}$, $Cr_2(OH)_3^{3+}$ and $Cr_2(OH)_4^{2+}$ are expected to be the dominant species although $Cr_2(OH)_5^{+}$ and $Cr_2(OH)_6$ could also be present albeit in extremely low concentrations. Thus, dimerization may occur through many pathways:

$$Cr_2(OH)_2^{4+} + Cr_2(OH)_2^{4+} \xrightarrow{k_{00}} \text{Tetramer}$$

$$Cr_2(OH)_3^{3+} + Cr_2(OH)_2^{4+} \xrightarrow{k_{10}} \text{Tetramer}$$

$$Cr_2(OH)_4^{2+} + Cr_2(OH)_2^{4+} \xrightarrow{k_{20}} \text{Tetramer}$$

$$Cr_2(OH)_5^{+} + Cr_2(OH)_2^{4+} \xrightarrow{k_{30}} \text{Tetramer}$$

$$Cr_2(OH)_6^{0} + Cr_2(OH)_2^{4+} \xrightarrow{k_{40}} \text{Tetramer}$$

$$Cr_2(OH)_3^{3+} + Cr_2(OH)_3^{3+} \xrightarrow{k_{11}} \text{Tetramer}$$

$$Cr_2(OH)_4^{2+} + Cr_2(OH)_3^{3+} \xrightarrow{k_{21}} \text{Tetramer}$$

$$Cr_2(OH)_5^{+} + Cr_2(OH)_3^{3+} \xrightarrow{k_{31}} \text{Tetramer}$$

$$Cr_2(OH)_6^{0} + Cr_2(OH)_3^{3+} \xrightarrow{k_{41}} \text{Tetramer}$$

$$Cr_2(OH)_4^{2+} + Cr_2(OH)_4^{2+} \xrightarrow{k_{22}} \text{Tetramer}$$

$$Cr_2(OH)_5^{+} + Cr_2(OH)_4^{2+} \xrightarrow{k_{32}} \text{Tetramer}$$

$$Cr_2(OH)_6^{0} + Cr_2(OH)_4^{2+} \xrightarrow{k_{42}} \text{Tetramer}$$

$$Cr_2(OH)_5^{+} + Cr_2(OH)_5^{+} \xrightarrow{k_{33}} \text{Tetramer}$$

$$Cr_2(OH)_6^{0} + Cr_2(OH)_5^{+} \xrightarrow{k_{43}} \text{Tetramer}$$

$$Cr_2(OH)_6^{0} + Cr_2(OH)_6^{0} \xrightarrow{k_{44}} \text{Tetramer.}$$

The rate law which combines all these pathways is given by:

$$-\frac{1}{2}\frac{d[dimer]}{dt} = k_{00}[Cr_2(OH)_2^{4+}]^2 + k_{10}[Cr_2(OH)_3^{3+}][Cr_2(OH)_2^{4+}] + k_{20}[Cr_2(OH)_4^{2+}][Cr_2(OH)_2^{4+}] + \ldots \quad (9)$$

Since the concentrations of all dimeric species present in solution are related by the appropriate acid dissociation constants, this expression may be rewritten as:

$$\frac{-d[dimer]}{dt} = 2k_{obs}[dimer]_T^2,$$

where

$$k_{obs} = (\{k_{00} + k_{10}K_{D1}[H^+]^{-1} + k_{20}K_{D1}K_{D2}[H^+]^{-2} + \ldots\}/\{1 + K_{D1}[H^+]^{-1} + K_{D1}K_{D2}[H^+]^{-2} + K_{D1}K_{D2}K_{D3}[H^+]^{-3} + K_{D1}K_{D2}K_{D3}K_{D4}[H^+]^{-4}\}^2). \quad (10)$$

Measurements of the pK_as of dimer indicate that mono- and doubly-deprotonated dimers are the only conjugate bases of dimer present in significant concentrations in the pH range 3.4–5.0. Hence, the last two terms in the denominator may be neglected.

As the reaction proceeds, the solution volume increases as dilute base is added to maintain constant pH, which is accounted for in the kinetic analysis by incorporating a volume dependent term (eq. 11).

$$\frac{-d[dimer]}{dt} = 2k_{obs}[dimer]_T^2 + [dimer]_T\frac{dV}{(V_0+V)}. \quad (11)$$

In eq. (11), V_0 is the initial volume of the reaction mixture and V is the volume base added at time t. Following the derivation developed for the dimerization of Cr^{3+},[2] the following expression is obtained:

$$k_{obs} = \frac{1}{2t}\left(\frac{V}{[dimer]_0V_0 - \frac{V}{m}([B]+[H^+])}\left\{\frac{[B]+[H^+]}{m[dimer]_0} + 1\right\} + \frac{m}{([B]+[H^+])}\ln\left[1 - \frac{V([B]+[H^+])}{m[dimer]_0V_0}\right]\right), \quad (12)$$

where $[dimer]_0$ is the dimer concentration at $t = 0$, [B] is the base concentration and m is given by eq. (6). If the volume of base consumed is small, this expression simplifies to:

$$V\left[\frac{m[dimer]_0 + [B] + [H^+]}{2m[dimer]_0^2V_0}\right] = k_{obs}t. \quad (13)$$

Consequently, the volume of added base becomes a linear function of time. Plots of V against time were found to be linear for at least the initial 8% conversion of dimer under all experimental con-

ditions. Values of k_{obs} were determined by linear least-squares analysis and are listed in Table 1.

Reaction reversibility

The rate law (eq. 9) assumes that dimerization is irreversible. This aspect requires examination since the interpretation of k_{obs} would be complicated by the existence of back reactions which convert tetramer into dimer. Reaction reversibility may be ascertained from the stability constants of dimer and tetramer. The dimerization reaction may be represented as:

$$\text{dimer} + \text{dimer} \underset{k_r}{\overset{k_f}{\rightleftharpoons}} \text{tetramer}. \quad (14)$$

whereupon the rate law becomes:

$$-\frac{d[\text{dimer}]}{2dt} = k_f[\text{dimer}]^2 - k_r[\text{tetramer}]. \quad (15)$$

The equilibrium constant for the reaction is given by:

$$K = \frac{k_f}{k_r} = \frac{[\text{tetramer}]}{[\text{dimer}]^2} = \frac{\{[Cr_4(OH)_6^{6+}] + [Cr_4(OH)_7^{5+}] + [Cr_4(OH)_8^{4+}]\}}{\{[Cr_2(OH)_2^{4+}] + [Cr_2(OH)_3^{3+}] + [Cr_2(OH)_4^{2+}]\}^2} \quad (16)$$

which with the use of the stability constants[5] of dimer ($\beta_{22} = [Cr_2(OH)_2^{4+}][H^+]^2/[Cr^{3+}]^2 = 10^{-5.25}$) and tetramer ($\beta_{46} = [Cr_4(OH)_6^{6+}][H^+]^6/[Cr^{3+}]^4 = 10^{-13.86}$) simplifies to:

$$K = \frac{\beta_{46}\{1 + K_{T1}[H^+]^{-1} + K_{T1}K_{T2}[H^+]^{-2}\}}{\beta_{22}^2[H^+]^2\{1 + K_{D1}[H^+]^{-1} + K_{D1}K_{D2}[H^+]^{-2}\}^2}. \quad (17)$$

Note that the equilibrium constant is pH dependent and that higher pK_as of dimer and tetramer have been ignored as they would have negligible effect in the pH range 3.4–5.0. Mass conservation at constant volume requires that $[\text{dimer}]_0 = [\text{dimer}] + 2[\text{tetramer}]$. It can then be shown that:

$$-\frac{d[\text{dimer}]}{2dt} = k_f\left[[\text{dimer}]^2 - \frac{([\text{dimer}]_0 - [\text{dimer}])}{2K}\right]. \quad (18)$$

Thus, the reaction is effectively irreversible if:

$$\frac{2K[\text{dimer}]^2}{([\text{dimer}]_0 - [\text{dimer}])} \gg 1. \quad (19)$$

Since the reaction was followed for < 8% dimer conversion this condition is met if:

$$R = \frac{2K(0.92)^2[\text{dimer}]_0}{0.08} = 21.2K[\text{dimer}]_0 \gg 1. \quad (20)$$

For the range of pH and [dimer] over which the reaction was followed, the smallest R value of 1800 was obtained at pH = 3.42 and $[\text{dimer}]_0 = 9.5 \times 10^{-3}$ M. Clearly, the back reactions make little contribution to the reaction rate and the observed reaction is essentially irreversible.

Dimerization rate constants

Rearrangement of eq. (10) and collection of all terms with the same power in H^+ gives the following expression for k^*:

$$k^* = k_{obs}\{1 + K_{D1}[H^+]^{-1} + K_{D1}K_{D2}[H^+]^{-2}\}^2 = a_0 + a_1[H^+]^{-1} + a_2[H^+]^{-2} + \cdots + a_8[H^+]^{-8}, \quad (21)$$

where, for example, $a_0 = k_{00}$, $a_1 = k_{10}K_{D1}$, $a_2 = k_{11}K_{D1}^2 + k_{20}K_{D1}K_{D2}$, etc.

As in the previous work on the dimerization of Cr^{3+},[2] the significant terms in $[H^+]^n$ have been identified from a plot of $\log k^*$ against $\log[H^+]$. The plot gives slopes of −2.3, −3.3 and −3.7 at pH = 3.6, 4.0 and 4.8, respectively. These limiting slopes indicate that the important terms in the expression for k^* are those with powers in H^+ of −2, −3 and −4. Integer values were not obtained in this analysis because more than one process will contribute to the overall rate at a particular pH. In the expression for k^*, the corresponding parameters a_2, a_3 and a_4 are in fact composite values, namely $a_2 = k_{11}K_{D1}^2 + k_{20}K_{D1}K_{D2}$, $a_3 = k_{21}K_{D1}^2K_{D2} + k_{30}K_{D1}K_{D2}K_{D3}$ and $a_4 = k_{22}K_{D1}^2K_{D2}^2 + k_{31}K_{D1}^2K_{D2}K_{D3} + k_{40}K_{D1}K_{D2}K_{D3}K_{D4}$. However, it is expected that all pathways where the dimer reactants differ by two or more deprotonations (k_{30}, k_{31}, k_{40}, etc.) will not be significant because: (i) the separations between measured and predicted pK_a values for dimer are such that significant concentration of both species would not be present at the same pH; and (ii) as the reactants approach, rapid proton transfer would occur to the dimer species with the highest degree of deprotonation. Based on these considerations, the expression for k^* was simplified to:

$$k^{\#} = \frac{k^*[H^+]^4}{K_{D1}^2} = k_{11}[H^+]^2 + k_{21}K_{D2}[H^+] + k_{22}K_{D2}^2. \quad (22)$$

Values of $k^{\#}$ are included in Table 1. Weighted† least-squares analysis of the $k^{\#}$ vs $[H^+]$ data gave

† Weighting scheme: $w(i) = 1/\sigma_{k_i}^2{}^{\#}$.

the following rate constants: $k_{11} = (2.18 \pm 0.21) \times 10^{-4}$, $k_{21} = (5.2 \pm 3.2) \times 10^{-3}$, $k_{22} = 0.83 \pm 0.08$ M^{-1} s^{-1}. Attempts were made to fit expressions involving other terms in $[H^+]^n$, but in all cases systematic deviations were found between the calculated and measured values of $k^{\#}$. For example, a model with rate constants k_{10}, k_{11}, k_{21} gave a poor fit at pH > 4.5 while one which allowed only for k_{21} and k_{22} gave a poor fit at pH < 3.8.

Interpretation of dimerization rate constants

The mechanism of conversion of dimer into tetramer is difficult to ascertain for a number of reasons:

(i) Since the reaction was followed for < 8% conversion of dimer, the detection of intermediates which may be present in very low concentrations is extremely difficult. Furthermore, these intermediates may undergo relatively rapid intramolecular processes (e.g. singly bridged dimer, a possible intermediate, is converted into Cr^{3+} at pH < 0 and doubly bridged dimer at pH > 1) which would make their isolation virtually impossible. Chromatographic analysis provided no evidence for the existence of such intermediates.

(ii) Cleavage of tetramer does not produce dimer but rather gives quantitative yields of trimer and monomer.[5] Hence, the often more accessible cleavage reactions provide little insight into the mechanism of tetramer formation.

From the structure of the dimer (**1**) and proposed structure of the "open" tetramer (**2**), plausible reaction mechanisms may be postulated. One such mechanism is given in Scheme 1. This scheme is only intended to represent a reasonable sequence of bond making and breaking stages. The actual order of processes and the specific ligands involved in the formation of the tetramer remain unknown.

Even though the full mechanism of formation is not known, the rate constants can be rationalized by assuming that they reflect the initial dimerization process and not subsequent intramolecular rearrangements to give the most stable form of tetramer. This is reasonable since the interconversion between open (**2**) and closed (**3**) forms of tetramer, depicted in Scheme 1, is much faster ($k = 0.1$–4 s^{-1})[9] than the dimerization rates reported here. During dimerization of Cr^{3+}, conversion of mononuclear Cr^{III} species into singly bridged forms of dimer has been shown to be much slower than subsequent intramolecular ring closure to give doubly bridged dimer. The slower rate of intermolecular dimerization, *cf.* intramolecular processes, probably results from the need to bring the positively charged reactants into close proximity before reaction can occur.

The pH dependence of k_{obs} has been fitted to an expression comprising three rate constants, k_{11}, k_{21} and k_{22}, which represent the following dimerization reactions:

$$Cr_2(\mu\text{-}OH)_2(OH)^{3+} + Cr_2(\mu\text{-}OH)_2(OH)^{3+} \longrightarrow \text{tetramer} \quad k_{11} = (2.18 \pm 0.21) \times 10^{-4}\,M^{-1}\,s^{-1}$$

$$Cr_2(\mu\text{-}OH)_2(OH)_2^{2+} + Cr_2(\mu\text{-}OH)_2(OH)^{3+} \longrightarrow \text{tetramer} \quad k_{21} = (5.2 \pm 3.2) \times 10^{-3}\,M^{-1}\,s^{-1}$$

$$Cr_2(\mu\text{-}OH)_2(OH)_2^{2+} + Cr_2(\mu\text{-}OH)_2(OH)_2^{2+} \longrightarrow \text{tetramer} \quad k_{22} = (0.83 \pm 0.08)\,M^{-1}\,s^{-1}.$$

Substantial rate increases (25- and 160-fold, respectively) accompany each deprotonation of dimer. These rate enhancements are similar to those reported for the dimerization of Cr^{3+}. The rate constants are a combination of the "true" dimerization constants and the ion-pair association constants (K_{IP}) for bringing the positively charged reactants together. Since deprotonation effectively reduces the charge on the reactants, both K_{IP} and the overall rate constants should increase with the degree of deprotonation, as is observed. In addition, deprotonation is known to labilize the aquo ligands in the Cr^{III} coordination sphere and this could also account for the observed rate enhancements. Such accelerations have been observed for the conversion of SBD into DBD,[10] where little variation in ion-pairing constants is anticipated. For example, ring closure within doubly deprotonated SBD, $HOCr\text{-}OH\text{-}CrOH^{3+}$, was found to be 25 times faster than within mono-deprotonated SBD, $Cr\text{-}OH\text{-}CrOH^{4+}$.

In principle, ion-pairing constants can be estimated from the Fuoss and Davies equations and the "true" dimerization rate constants calculated. For the dimerization of Cr^{3+}, such a treatment gives corrected rate constants ($k'_{11} = 0.047$, $k'_{21} = 1.0$ and $k'_{22} = 17$ s^{-1}) which show a constant, *ca* 20-fold increase in rate with each deprotonation. This compares particularly well with the 25-fold rate enhancement reported for ring closure within SBD. However, closer inspection reveals that the corrected dimerization constants are faster than the corresponding ring closure reactions of SBD. This situation probably arises because only electrostatic interactions are considered in the calculation of K_{IP} and it is well known for metal aquo complexes in aqueous solution that H-bonding interactions (both between the metal ions and with the solvent) can have dramatic effects on ion-association. For ex-

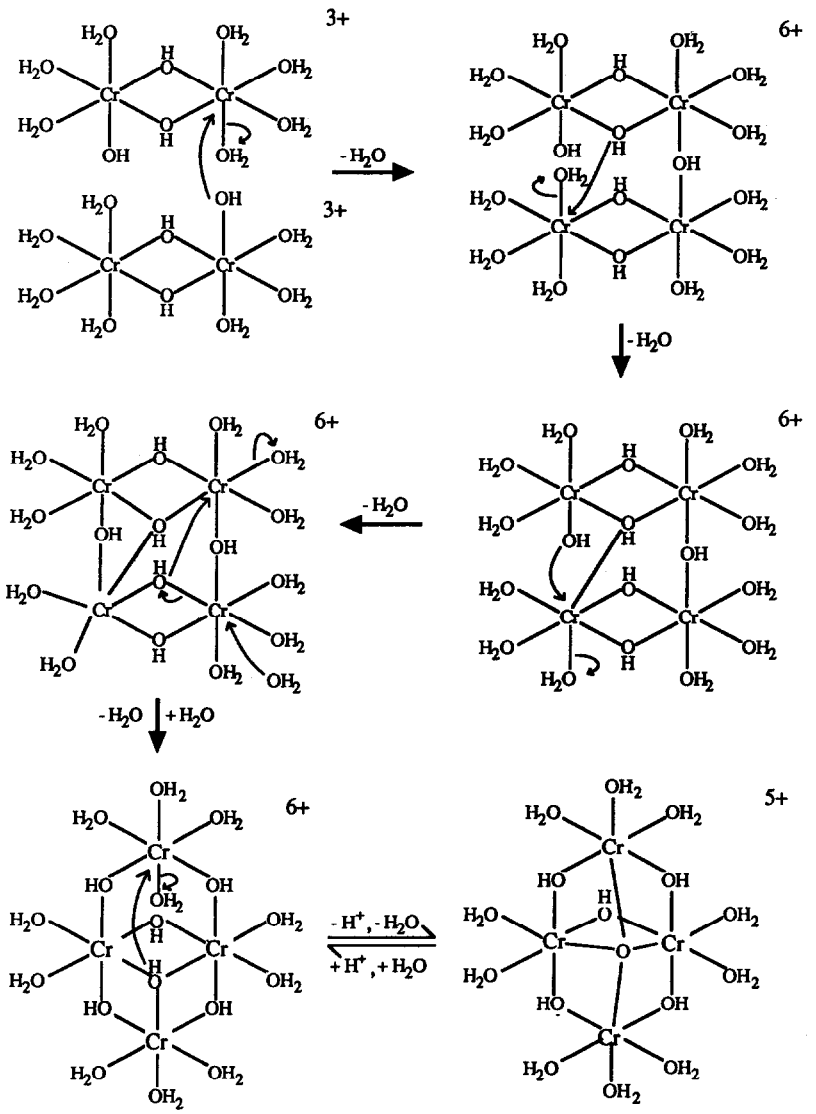

2 Proposed 'Open' Tetramer Structure

3 Proposed 'Closed' Tetramer Structure

Scheme 1. A possible reaction sequence for the formation of tetramer from deprotonated forms of dimer.

ample, the existence of H-bonding in both solution and solid state has been confirmed for several complexes of the type *cis*- and *trans*-$[A_4M(OH_2)(OH)]^{2+}$.[11,12] As the degree of deprotonation increases (i.e. charge decreases) H-bonding between the ions is expected to become more important while interactions with the solvent are expected to weaken. Thus, realistic ion-pairing constants may be much larger than those predicted from the Fuoss–Davies treatment and consequently, the corrected rate constants significantly slower than those estimated above. Given these complications and the fact that the calculation of K_{IP} for interaction between deprotonated forms of dimer would need to account for the non-spherical nature of the ions this treatment was not applied to the current study.

Although k_{obs} for the conversion of dimer into tetramer is larger is 1.3–6 times faster than for the dimerization of Cr^{3+} over the pH range studied, the rate constants for each reaction pathway (k_{11}, etc.) are either equal or greater for the Cr^{3+} case. The faster overall rate of dimerization of dimer can be attributed to the higher acidity of this oligomer, cf. Cr^{3+}. It was anticipated that the presence of bridging OH groups in the dimer, in addition to terminal OH groups, would result in a more labile Cr^{III} coordination sphere than in the case of conjugate of Cr^{3+} which contain only terminal OH groups. However, the reactants are of higher charge

in the case of dimer and this should reduce the ability of the species to come together and undergo dimerization. Knowledge of the rates of other substitution reactions of dimer such as solvent exchange and anation (Cl^-, SCN^-, etc.) would assist in this interpretation. Preliminary kinetic measurements on the sulphate anation of dimer indicate that the singly deprotonated form, $Cr_2(OH)_3^{3+}$, reacts at least an order of magnitude faster than fully protonated $Cr_2(OH)_2^{4+}$.[13]

Acknowledgement—This work was supported by the Australian Research Council.

REFERENCES

1. W. Schneider, *Comments Inorg. Chem.* 1984, **3**, 205.
2. F. P. Rotzinger, H. Stünzi and W. Marty, *Inorg. Chem.* 1986, **25**, 489.
3. F.-C. Xu, R. Krouse and T. W. Swaddle, *Inorg. Chem.* 1985, **24**, 267.
4. T. Merakis, A. Murphy, L. Spiccia, A. Beguin and W. Marty, *Helv. Chim. Acta* 1989, **72**, 993.
5. H. Stünzi and W. Marty, *Inorg. Chem.* 1983, **22**, 2145.
6. L. Wilkinson, SYSTAT: The System for Statistics. SYSTAT Inc., Evanston, Illinois (1988).
7. L. Spiccia, H. Stoeckli-Evans, W. Marty and R. Giovanoli, *Inorg. Chem.* 1987, **26**, 474.
8. J. Springborg, *Adv. Inorg. Chem.* 1988, **32**, 55.
9. H. Stünzi, F. P. Rotzinger and W. Marty, *Inorg. Chem.* 1984, **23**, 2160.
10. L. Spiccia and W. Marty, *Polyhedron* 1991, **10**, 619.
11. M. Ardon and A. Bino, *Struct. Bonding* 1987, **65**, 1.
12. M. Ardon, A. Bino and K. Michelsen, *J. Am. Chem. Soc.* 1987, **109**, 1986.
13. M. R. Grace and L. Spiccia, manuscript in preparation.

Polyhedron Vol. 10, No. 20/21, pp. 2399–2403, 1991
Printed in Great Britain

0277–5387/91 $3.00+.00
© 1991 Pergamon Press plc

SYNTHESIS AND CHARACTERIZATION OF THORIUM(IV) AND DIOXOURANIUM(VI) COMPLEXES OF 4-[N(2-HYDROXY-1-NAPHTHALIDENE)AMINO]ANTIPYRINE*

R. K. AGARWAL† and JAI PRAKASH

Department of Chemistry, Lajpat Rai Postgraduate College, Sahibabad-201 005, Ghaziabad, India

(*Received* 20 *February* 1991; *accepted* 9 *July* 1991)

Abstract—Some complexes of thorium(IV) and dioxouranium(VI) with the Schiff base of 2-hydroxy-1-naphthaldehyde condensed with 4-aminoantipyrine (HNAAP) with the general composition $[ThX_4(HNAAP)_2]$ (X = Cl, Br, NO_3 or NCS), $[ThX_4(HNAAP)_3]$ (X = I or ClO_4), $[UO_2X_2(HNAAP)_2]$ (X = Cl, Br, I, NO_3, NCS or CH_3COO) or $[UO_2(ClO_4)_2(HNAAP)_3]$ have been synthesized and characterized by elemental analyses, conductivity, molecular weight, magnetism and IR spectra. The neutral bidentate ligand coordinates through the azomethine nitrogen and the carbonyl oxygen. IR data also reveal that the perchlorate groups are ionic, the thiocyanate groups are N-bonded while the nitrate groups are bi-covalently bonded. The probable coordination number of Th(IV) is 6, 8 or 12 and of U(VI) is 8 or 10 depending on the nature of anions. Thermal properties are also discussed.

The coordination behaviour of thorium(IV) and dioxouranium(VI) is peculiar because of their inherent capacity to form compounds with coordination numbers of six or higher. The variation in coordination number (6 to 12) observed in the actinide complexes may be attributed to steric factors and electrostatic forces of attaction and repulsion, rather than bond orientation by the well-shielded 5*f*-orbitals of the metal ion.[1–4]

During the last 10 years, there has been considerable interest in the coordination chemistry of Schiff bases with actinide metal ions and a number of publications have appeared in the literature.[5] The ligand derived from condensation of 4-aminoantipyrine with 2-hydroxy-1-naphthaldehyde, i.e. 4-[N-(2-hydroxy-1-naphthalidene)amino]antipyrine (HNAAP) (**I**) is of interest because it is capable of acting as a bidentate or a tridentate ligand depending on whether or not the functional group —OH is involved in coordination. This work reports the isolation and structure elucidation of the complexes of HNAAP with Th^{4+} and UO_2^{2+}.

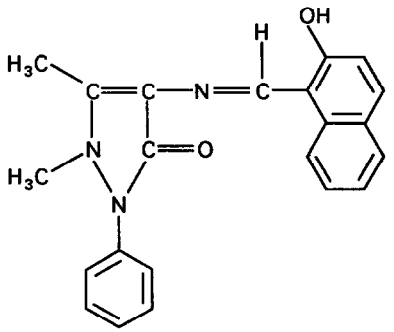

HNAAP (**I**)

EXPERIMENTAL

Hydrated thorium(IV) nitrate and dioxouranium (VI) nitrate were B.D.H. reagents. Thorium(IV) halides and perchlorates were prepared by established methods.[6,7] The dioxouranium(VI) salts were prepared by an established method.[8] The Schiff base was synthesized as follows. A solution of 1-hydroxy-2-naphthaldehyde (1 mmol) in absolute ethanol (50 cm^3) was mixed with 4-aminoantipyrine (1.1 mmol) in the same solvent and the mixture was refluxed for 2 h. On cooling a yellow crystalline product was separated, which was filtered off and

* Presented at IXth Annual Conference of Indian Council of Chemists, Gulbarga University, Gulbarga (India), 21–23 December 1990.

† Author to whom correspondence should be addressed.

recrystallized in the same solvent. (Yield *ca* 75%; colour—dark yellow; m.p. 201°C.)

Synthesis of the complexes

Crystalline complexes of thorium(IV) and dioxouranium(VI) of the Schiff base were isolated by one of the following methods:

(a) A methanolic solution of the metal salt was added to the Schiff base solution in the same solvent with heating and the reaction mixture was refluxed for 2 h. The solid compound was obtained after partial evaporation under a fan. This was filtered, washed with methanol and dried *in vacuo* over P_4O_{10}.

(b) To a solution of metal salt in ethyl acetate was added the ligand in the same solvent and the reaction mixture was refluxed for 1 h and left overnight at room temperature. The fine crystalline product so obtained, was filtered, washed with ethyl acetate and finally dried *in vacuo* over P_4O_{10}.

(c) To a solution of the metal salt in isopropyl alcohol was added a hot solution of the ligand in the same solvent. In some cases, the desired complex was obtained immediately, but in others it was necessary to reflux the reaction mixture for 1–2 h. On cooling at room temperature the desired solid product was filtered off washed with isopropyl alcohol and dried *in vacuo* over P_4O_{10}.

All the physical measurements and analyses were performed as reported earlier.[8,9]

RESULTS AND DISCUSSION

The interaction of thorium(IV) and dioxouranium(VI) salts with 4-[(*N*-2-hydroxy-1-naphthalidene) amino]-antipyrine (HNAAP) results in the formation of $[ThX_4(HNAAP)_n]$ (X = Cl, Br, NCS or NO_3, $n = 2$; X = I or ClO_4, $n = 3$) and $[UO_2X_2(HNAAP)_n]$ (X = Cl, Br, I, NCS, NO_3 or CH_3COO, $n = 2$; X = ClO_4, $n = 3$). The analytical data are recorded in Tables 1 and 2. All the complexes are quite stable and can be stored for long periods except $[ThI_4(HNAAP)_3]$ which decomposes slowly at room temperature with evolution of iodine vapour. Among the thorium(IV) complexes, the chloro, bromo, nitrato and thiocyanato complexes are non-electrolytes (Tables 1 and 2) in $PhNO_2$, whereas the iodo and perchlorato complexes dissociate in this solvent. The iodo complex appears to be a 1:2, while the perchlorato complex is a 1:4 electrolyte. The uranyl complexes $[UO_2X_2(HNAAP)_2]$ (X = Cl, Br, I, NO_3, NCS or CH_3COO) are all essentially non-electrolytes in $PhNO_2$. The conductance value for the perchlorato complex $[UO_2(HNAAP)_3](ClO_4)_2$ suggests ionic perchlorate groups, the presence of which was further confirmed by the IR spectra. Data on the molecular weights of the complexes in $PhNO_2$ are given in Tables 1 and 2, along with values calculated on the basis of established formula of the complexes. The ground states of uranyl and thorium compounds contain no unpaired electrons, the compounds are therefore weakly diamagnetic as observed by others.[10]

IR spectra and the nature of coordination

The IR spectral band assignments for HNAAP and its complexes are shown in Table 3. The ligand has bands around 3000 cm^{-1} [ν(OH)], at 1640 cm^{-1} [ν(C=O)] and 1590 cm^{-1} [ν(C=N)]. In the com-

Table 1. Analytical, conductivity and molecular weight data of Th(IV) complexes of HNAAP

Complex	m.p. (°C)	Found (Calc.) % Th	C	H	N	Anion	Mol. wt Found (Calc.)	Ω_M (ohm^{-1} cm^2 mol^{-1})
$[ThCl_4(HNAAP)_2]$	211	22.0 (21.3)	48.1 (48.5)	3.4 (3.5)	7.6 (7.7)	12.6 (13.0)	1076 (1088)	4.3
$[ThBr_4(HNAAP)_2]$	200	18.9 (18.3)	41.3 (41.7)	2.9 (3.0)	6.5 (6.6)	24.4 (25.3)	1257 (1266)	4.7
$[ThI_4(HNAAP)_3]$	201	13.5 (12.8)	43.3 (43.7)	3.1 (3.1)	6.8 (6.9)	27.1 (28.0)	601 (1811)	51.9
$[Th(NO_3)_4(HNAAP)_2]$	191	20.2 (19.4)	43.9 (44.2)	3.0 (3.2)	11.6 (11.7)	—	1185 (1194)	3.9
$[Th(NCS)_4(HNAAP)_2]$	> 260	20.4 (19.7)	48.4 (48.9)	3.1 (3.2)	11.8 (11.9)	19.0 (19.7)	1165 (1178)	4.1
$[Th(ClO_4)_4(HNAAP)_3]$	191	14.3 (13.6)	46.1 (46.6)	3.3 (3.3)	7.3 (7.4)	22.5 (23.4)	338 (1701)	98.7

Table 2. Analytical, conductivity and molecular weight data of UO_2(VI) complexes of HNAAP

Complex	m.p. (°C)	Found (Calc.) % U	C	H	N	Anion	Mol. wt Found (Calc.)	Ω_M (ohm^{-1} cm^2 mol^{-1})
$[UO_2Cl_2(HNAAP)_2]$	> 240	23.2 (22.5)	49.0 (50.0)	3.5 (3.6)	7.8 (8.0)	6.1 (6.7)	1049 (1055)	3.7
$[UO_2Br_2(HNAAP)_2]$	229	21.7 (20.8)	45.2 (46.1)	3.2 (3.3)	7.2 (7.3)	13.0 (14.0)	1136 (1144)	4.1
$[UO_2I_2(HNAAP)_2]$	> 260	20.0 (19.2)	41.8 (42.6)	3.0 (3.1)	6.7 (6.8)	19.9 (20.5)	1231 (1238)	5.3
$[UO_2(NO_3)_2(HNAAP)_2]$	> 260	22.3 (21.5)	46.7 (47.6)	3.3 (3.4)	7.5 (7.6)	—	1101 (1108)	4.9
$[UO_2(NCS)_2(HNAAP)_2]$	201	22.4 (21.6)	49.3 (50.2)	3.4 (3.4)	7.5 (7.6)	10.0 (10.5)	1092 (1100)	4.7
$[UO_2(ClO_4)_2(HNAAP)_3]$	211	16.1 (15.4)	50.6 (51.4)	3.6 (3.7)	8.1 (8.2)	12.3 (12.9)	510 (1540)	52.7
$[UO_2(CH_3COO)_2(HNAAP)_2]$	226	22.3 (21.6)	51.4 (52.3)	3.3 (3.4)	7.5 (7.6)	—	1094 (1102)	4.5

Table 3. Partial IR bands (cm^{-1}) of Th(IV) and UO_2(VI) complexes of HNAAP

Compound	ν(OH)	ν(C=O)	ν(C=N)	ν(M—O) ν(M—N)
HNAAP	3055w 3020w	1640vs 1635vs	1590vs	—
$[ThCl_4(HNAAP)_2]$	3055w 3025w	1598s 1582s	1542s	400w 370w
$[ThBr_4(HNAAP)_2]$	3060w 3022w	1602s 1590s	1545s	405m 380w
$[ThI_4(HNAAP)_3]$	3055w 3020w	1598s 1580s	1540m	400w 365w
$[Th(NO_3)_4(HNAAP)_2]$	3055w 3020w	1605s,br 1590sh	1530s,br	410m 370w
$[Th(NCS)_4(HNAAP)_2]$	3055w 3020w	1605s 1580m	1542m	415w 352w
$[Th(ClO_4)_4(HNAAP)_3]$	3060w 3022w	1600s 1585m	1540s	405m 370w
$[UO_2Cl_2(HNAAP)_2]$	3055w 3025w	1602s 1590s	1540s	402m 380w
$[UO_2Br_2(HNAAP)_2]$	3055w 3020w	1602s 1590s	1542s	400w 370w
$[UO_2I_2(HNAAP)_2]$	3060w 3022w	1600s 1592s	1545s	402m 370w
$[UO_2(NO_3)_2(HNAAP)_2]$	3055w 3020w	1610sh 1598s	1545s	418m 355m
$[UO_2(NCS)_2(HNAAP)_2]$	3060w 3022w	1605s	1550m	400w 365w
$[UO_2(ClO_4)_2(HNAAP)_3]$	3060w 3020w	1600s	1542s	405w 370w
$[UO_2(CH_3COO)_2(HNAAP)_2]$	3058w 3025w	1605vs 1582s	1530s	390s 315w

plexes, the hydroxyl frequency appears at the same region as in the free ligand. The carbonyl frequency occurs in the 1605–1580 cm^{-1} region and the azomethine frequency in the 1545–1530 cm^{-1} region, indicating that these two groups are involved in bonding. Thus HNAAP in these complexes acts as neutral bidentate ligand. In the far IR region metal–ligand vibrations are tentatively assigned in 410–330 cm^{-1} to ν(M—O) and ν(M—N) modes.[8,9]

The strong ν_3 and ν_4 bands in the spectra of perchlorato complexes occur at 1085 and 620 cm^{-1} respectively, showing the ionic character of the perchlorato groups.[11,12] The ν(C—N) frequency in the actinide thiocyanate complexes lies at *ca* 2020 cm^{-1} and the ν(C—S) frequency falls in the 828–760 cm^{-1} region strongly suggesting N-bonded NCS.[13,14] The ν_3, i.e. δ(NCS) frequency also occurs at *ca* 465 cm^{-1}. The IR spectra of the nitrato complexes show the absence of ν_3 bands at *ca* 1360 cm^{-1} due to ionic nitrate.[15] The bidentate nature of covalent nitrato groups in $Th(NO_3)_4 \cdot 2HNAAP$ has been established by comparing the IR bands at *ca* 1530 (ν_4), 1290 (ν_1), 1030 (ν_2), 808 (ν_6), 740 (ν_3) and 695 (ν_5) cm^{-1} with the spectral bands of $Th(NO_3)_4 \cdot 5H_2O$ at 1520, 1290, 1030, 808, 745 and 715 cm^{-1} respectively.[16,17] In $UO_2(NO_3)_2 \cdot 2HNAAP$ the nitrate groups also seem to be bidentate since the IR frequencies at *ca* 1510 (ν_4), 1280 (ν_1), 1025 (ν_2), 828 (ν_6), 745 (ν_3) and 714 (ν_5) cm^{-1} in this complex due to this group occur almost at the same frequencies as reported earlier.[15,18,19] The complex $[UO_2(CH_3COO)_2(HNAAP)_2]$ is monomeric in nature and the IR data show two bands at 1550 and 1470 cm^{-1} region attributed to ν_{asym}COO and ν_{sym}COO respectively.[20] In this complex the acetate groups are bicovalently bonded.

In all the dioxouranium(VI) complexes, the ν_1 and ν_3 modes of O=U=O are assigned in the ranges 835–825 and 930–925 cm^{-1} respectively[21] (Table 4). Wilson's G–F matrix method[22] was used to determine the stretching and interaction force constants from which the U—O bond distances were calculated following Badger's formula.[23] It is apparent from the calculated data that the U—O bond length decreases with the increase in the value of symmetric stretching frequency (ν_1).[24] A plot of ($\nu_1 + \nu_3$) vs force constants gave a straight line. The U—O bond distances in dioxouranium salts generally range from 1.60 to 1.92 Å depending on the nature of the equatorial ligands.[25] The calculated values of the U—O bond distances in the present complexes are close to 1.73–1.74 Å (Table 4).

Thermal behaviour

The TG and DT curves of thorium(IV) complexes do not show the presence of water molecules either in or out of the coordination sphere. The halo and nitrato complexes decompose endothermically while the perchlorato complexes decompose exothermically[26] with a **slight explosion and evolution of smoke**[26]**—caution.** The TG curves of chloro, bromo and thiocyanato complexes indicate that in the first step, only one mol of ligand has been lost, while at *ca* 475°C, the remaining ligand mole is lost. Finally at *ca* 620°C, oxohalide and oxothiocyanate formation takes place. The thorium(IV) nitrate complexes decompose in the 300–450°C temperature region, losing both ligand molecules. Finally, ThO_2 is obtained as residual mass at *ca* 650°C. The TG curve of $[Th(HNAAP)_3](ClO_4)_4$ shows that the complex starts to decompose at 260°C and continues up to 625°C, after which ThO_2 remains. From the pyrolysis curve it is clear that no stable intermediate perchlorate complex has been formed in this species.

The TG and DT curves of the uranyl(VI) com-

Table 4. Uranyl frequencies (cm^{-1}), force constants and U—O bond distances of dioxouranium(VI) complexes of HNAAP

Complex	ν_1 (cm^{-1})	ν_3 (cm^{-1})	U—O force constant (mdynes $Å^{-1}$)	Force constant due to interaction between bonds (mdynes $Å^{-1}$)	Calc. U—O bond distance (Å)
$[UO_2Cl_2(HNAAP)_2]$	832	925	6.82	−0.29	1.74
$[UO_2Br_2(HNAAP)_2]$	827	930	6.82	−0.37	1.74
$[UO_2I_2(HNAAP)_2]$	825	927	6.78	−0.36	1.74
$[UO_2(NO_3)_2(HNAAP)_2]$	830	928	6.82	−0.33	1.74
$[UO_2(NCS)_2(HNAAP)_2]$	830	925	6.80	−0.31	1.74
$[UO_2(ClO_4)_2(HNAAP)_3]$	835	930	6.88	−0.31	1.74
$[UO_2(CH_3COO)_2(HNAAP)_2]$	832	930	6.86	−0.33	1.74

plexes clearly indicate the absence of water molecules in the complexes. All the pyrolysis curves behave similarly and show that the decomposition of these complexes have started at 270°C and are completed at *ca* 470°C. The break in the curves in the 270–325°C temperature region indicates that at this stage only 1 mol of ligand has been lost (22–23%) for the halo, nitrato and perchlorato complexes. In the temperature range 430–470°C there is an additional decrease in weight due to loss of all the ligand molecules. The oxide U_3O_8 is formed around 625°C via the formation of UO_3, following which there is no measurable change in weight.[27]

Stereochemistry and the structure of the complexes

The preferred coordination number of thorium(IV) is 6 or 8, but higher coordination numbers have also been observed.[28] In $[Th(HNAAP)_2X_4]$ (X = Cl, Br or NCS) and $[Th(HNAAP)_3I_2]I_2$ the coordination number of Th^{IV} is 8. The conductance, molecular weight and IR data show that in the perchlorate complex, all the four perchlorato groups are present outside the coordination sphere and hence Th^{IV} is six-coordinated in this complex. In $[Th(HNAAP)_2(NO_3)_4]$, the coordination number of Th^{IV} is 12.

In $[UO_2(HNAAP)_2X_2]$ (X = Cl, Br, I or NCS), the coordination number of uranium is 8. In $[UO_2(HNAAP)_3](ClO_4)_2$, both the perchlorato groups are ionic in nature, thus in this complex uranium is octa-coordinated. The IR data of $[UO_2(HNAAP)_2(NO_3)_2]$ and $[UO_2(HNAAP)_2(CH_3COO)_2]$ suggest bidentate nature of nitrate and acetate ligands in these complexes. Thus in these complexes the coordination number of uranium(VI) is 10.

Acknowledgement—One of the authors (RKA) is thankful to the University Grants Commission, New Delhi, for financial support of this work.

REFERENCES

1. W. H. Zachariasen, *Acta Cryst.* 1954, **7**, 795.
2. A. F. Wells, *Structural Inorganic Chemistry*, 3rd edn. Oxford University Press, London (1968).
3. S. J. Lippard, *Progress in Inorganic Chemistry* (Edited by F. A. Cotton), Vol. 8. Wiley, New York (1967).
4. J. C. Taylor, M. H. Mueller and R. L. Hittermann, *Acta Cryst.* 1966, **20**, 842; G. Shanker, R. R. Premkumar and S. K. Ramaligam, *Polyhedron* 1986, **5**, 991.
5. Jai Prakash, Physico-chemical investigations of some actinide coordination compounds, Ph.D. thesis (1990).
6. P. Ramamurthy and C. C. Patel, *J. Inorg. Nucl. Chem.* 1963, **25**, 310.
7. V. V. Savant and C. C. Patel, *J. Less Common Metals*, 1971, **24**, 459.
8. A. K. Srivastava, S. Sharma and R. K. Agarwal, *Inorg. Chim. Acta* 1982, **61**, 235.
9. R. K. Agarwal, A. K. Srivastava and T. N. Srivastava, *Trans. Met. Chem.* 1980, **5**, 95.
10. S. C. Rastogi, Studies of the stereochemistry of high coordination compounds of oxozirconium(IV), dioxouranium(VI) and thorium(IV) involving some oxygen and nitrogen donor ligands, Ph.D. thesis, Meerut University (1985).
11. S. K. Madan and A. M. Donohue, *J. Inorg. Nucl. Chem.* 1966, **28**, 1303.
12. P. Ramamurthy and C. C. Patel, *Can. J. Chem.* 1964, **42**, 856.
13. Z. M. S. Al-Kazaz, K. W. Bagnall and D. Brown, *J. Inorg. Nucl. Chem.* 1973, **35**, 150.
14. J. L. Burmeister, *Coord. Chem. Rev.* 1966, **1**, 205; 1968, **3**, 225.
15. B. M. Gatehouse, S. E. Livingstone and R. S. Nyholm, *J. Chem. Soc.* 1957, 4222.
16. J. R. Ferraro and A. Walker, *J. Chem. Phys.* 1966, **45**, 550.
17. J. C. Taylor, M. H. Mueller and R. L. Hitterman, *Acta Cryst.* 1966, **20**, 842.
18. G. Topping, *Spectrochim. Acta* 1965, **21**, 1743.
19. J. I. Bullock, *J. Inorg. Nucl. Chem.* 1967, **29**, 2257.
20. I. S. Ahuja, C. L. Yadava and S. Tripathi, *Asian J. Chem.* 1989, **1**, 195.
21. P. A. Vigato, U. Casellato and M. Vidali, *Gazz. Chim.* (Ital.) 1971, **107**, 61.
22. L. B. Wilson, *J. Chem. Phys.* 1939, **7**, 1047; 1941, **9**, 76.
23. R. M. Badger, *J. Chem. Phys.* 1934, **2**, 128; 1935, **3**, 710.
24. C. L. Garga, S. D. Gupta and K. V. Narasimhan, *Ind. J. Pure Appl. Phys.* 1970, **8**, 108.
25. W. H. Zachariasen, *Acta Cryst.* 1954, **7**, 783.
26. A. K. Srivastava, M. Srivastava and R. K. Agarwal, *Ind. Engng Chem. Products Res. Dev.* 1982, **21**, 135.
27. W. W. Wendlandt, *J. Inorg. Nucl. Chem.* 1957, **5**, 118.
28. B. C. Smith and M. A. Wassef, *J. Chem. Soc. A* 1968, 1817.

Polyhedron Vol. 10, No. 20/21, pp. 2405–2415, 1991
Printed in Great Britain

0277–5387/91 $3.00+.00
Pergamon Press plc

PREPARATION AND PROPERTIES OF COMPLEXES OF LANTHANIDE(III) SALTS WITH N-(2-PYRIDYL) PYRIDINE-2′-CARBOXAMIDE

THEODOROS F. ZAFIROPOULOS*

Department of Chemistry, University of Patras, Rio, Patras, Greece

and

JOHN C. PLAKATOURAS and SPIROS P. PERLEPES*

Department of Chemistry, University of Ioannina, 451 10 Ioannina, Greece

(*Received* 12 *December* 1990; *accepted* 4 *July* 1991)

Abstract—New complexes of the general formulae $[Ln(LH)_2(NCS)_3(H_2O)]$ (Ln = La–Eu), $[Ln(LH)_2(NCS)_3]$ (Ln = Gd–Yb), $[Ln(LH)_3(OClO_3)](ClO_4)_2$ (Ln = La–Gd), $[Ln(LH)_3](ClO_4)_3$ (Ln = Tb–Yb), $[Ln(LH)_2(ONO_2)_2](NO_3)$ (Ln = La–Yb) and $[Ln(LH)(ONO_2)_3]$ (Ln = La, Pr, Nd, Sm, Eu), where LH = N-(2-pyridyl)pyridine-2′-carboxamide, have been isolated. The complexes were characterized by elemental analyses, conductivity measurements, X-ray powder patterns, thermal methods, magnetic susceptibilities and spectroscopic (IR, ^1H NMR, electronic diffuse reflectance and solid state emission *f–f* spectra) studies. All the data are discussed in terms of the nature of the bonding and the possible structural types. The 1:2 and 1:3 complexes appear to be monomeric, while polymeric structures are assigned for the 1:1 nitrato compounds. The LH molecule behaves as a bidentate ligand in the monomeric complexes, bonding through the amide oxygen and N(1′). The amide oxygen and both pyridine residues are coordinated in the 1:1 nitrato complexes.

In recent publications,[1–3] we have reported our efforts towards the preparation and study of lanthanide(III) complexes with amidic ligands, as such complexes have received little attention.[4–10] Our main work to-date has concentrated on the use of ligands which have both amide and carboxylate groups as potential donor sites. With the exception of the monoanion of iso-orotic acid,[3] the neutral amide group of the ligands used remained uncoordinated on complexing with Ln^{III} in aqueous media, despite the fact that this interaction would be stabilized by the formation of stable chelate rings. This is partly because the O_{amide} atom is only weakly basic, and so metal binding is weak, and partly because of competition by the stronger aqua and —COO^- ligands. In agreement with this, when H_2O is driven off by heating then coordination of the amide oxygen does occur; the coordinative unsaturation, after the removal of the coordinated water molecules, leads to the neutral amide group coordination.

In extending the above work, we considered it important to use synthetic conditions and ligands which would favour direct amide coordination. Obvious conditions for our goal were the absence of water from the reaction mixtures and use of weakly coordinating counter-ions, i.e. ClO_4^-. We also felt that the lack of readily ionizable oxygen-based groups, i.e. —OH and —COOH, from the ligands and incorporation of nitrogen-based donor sites might allow access to species with coordinated amide groups. We herein report the results of this effort, the reactions of lanthanide(III) salts with N-(2-pyridyl)pyridine-2′-carboxamide, abbreviated as LH, to give interesting complexes with amide coor-

* Authors to whom correspondence should be addressed.

dination.

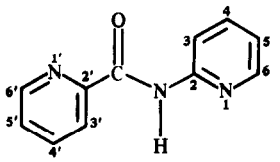

I, LH

The ligands LH and L^- have been shown[11] to coordinate to transition metal ions in several modes, largely determined by the nature of the metal ion and anion present and preparative conditions.

EXPERIMENTAL

Materials and methods

The salts $LnCl_3 \cdot nH_2O$, $Ln(ClO_4)_3 \cdot nH_2O$ and $Ln(NO_3)_3 \cdot nH_2O$ ($n = 6$, 7) were obtained from Aldrich, Fluka and Ventron. Lanthanide oxides of 99.9% purity were purchased from Johnson Matthey and Co. The anhydrous perchlorates were prepared by slowly heating the hydrates at 1.0 Torr, as suggested by Forsberg and Moeller.[12] Hydrated perchlorates of the lighter lanthanides lost water readily at 200°C without hydrolytic decomposition. With the heavier lanthanides, however, the 250°C temperature required for complete dehydration caused hydrolytic conversion at about half of the hydrated compound to an insoluble product;[12] the anhydrous perchlorate was easily removed by extraction with anhydrous MeCN. Aliquots of solutions of the anhydrous salts in MeCN were analysed by dilution with water and titration with standard 0.01 M EDTA, using xylenol orange as indicator. Anhydrous nitrates were prepared by direct reaction of the oxides with liquid nitrogen (IV) oxide.[12] MeCN and Et_2O were dried by distillation from CaH_2 and Na/benzophenone, respectively. The ligand LH was synthesized as described earlier.[11] Metal, carbon, hydrogen and nitrogen analyses were performed by conventional volumetric and microanalytical methods. The amount of water present in the complexes $[Ln(LH)_2(NCS)_3(H_2O)]$ (Ln = La–Eu) was also confirmed from the TG patterns. **Caution:** Perchlorate salts are potentially explosive. Although no detonation tendencies have been observed with our compounds, caution is advised and handling of only small quantities is recommended. Physicochemical measurements and spectroscopic techniques were carried out by published methods.[13,14]

Complex preparation

For the preparation of the isothiocyanato complexes an ethanolic solution of potassium thiocyanate (6.0 mmol, 15 cm^3), warmed to *ca* 50°C, was slowly added to an ethanolic solution of the appropriate lanthanide(III) chloride hexahydrate (2.0 mmol, 10 cm^3). The resulting mixture was stirred at 50°C for 10 min and then allowed to cool to room temperature, whereupon the precipitated potassium chloride was removed by filtration. The filtrate was mixed with a warm solution of LH (4.0 mmol) in absolute EtOH (15 cm^3) and precipitation occurred over 25–30 min. All precipitates were collected by filtration immediately after 1 h stirring at 50°C, washed with absolute EtOH and Et_2O and dried *in vacuo* over silica gel.

For the preparation of the perchlorate complexes, the anhydrous lanthanide(III) perchlorate (3.0 mmol) was dissolved in MeCN (25 cm^3) in the presence of triethyl*ortho*formate (TEOF, 5 cm^3) as dehydrating agent. The solution so obtained was added to a vigorously stirred, warm solution of LH (9.0 mmol) in MeCN (60 cm^3). Solid product formation was rather rapid (10 min), but completely stoichiometric products and satisfactory yields were obtained after the reaction mixtures were heated under reflux for 1–2 h. The mixtures were filtered while hot and the solids obtained were washed with hot MeCN and *n*-hexane and dried *in vacuo* over P_4O_{10}.

For the preparation of the 1 : 2 nitrate complexes $[Ln(LH)_2(ONO_2)_2](NO_3)$ to 1.0 mmol of the hydrated lanthanide(III) nitrate in 20 cm^3 of warm absolute EtOH was added 10 cm^3 of TEOF and the solution was refluxed overnight. This solution was added slowly to a solution of LH (2.0 mmol) in warm absolute EtOH (15 cm^3). The resulting solution was stirred at 45°C for 2 h. Solid products were deposited during this time, which were collected by filtration, washed copiously with hot absolute EtOH and Et_2O and dried *in vacuo* over P_4O_{10}.

The reactions for the preparation of the 1:1 nitrato complexes $[Ln(LH)(ONO_2)_3]$ (Ln = La, Pr, Nd, Sm, Eu) were carried out under rigorously anhydrous conditions. All manipulations were effected in a gloved box which was flushed constantly with dry nitrogen and which contained anhydrous P_4O_{10} as a desiccant. The complexes were prepared by dissolving 2.0 mmol of the appropriate anydrous nitrate in 10 cm^3 of MeCN and adding a solution of *ca* 1.8 mmol of LH in 20 cm^3 of MeCN. Precipitation of the product occurred immediately. The reaction mixtures were stirred for several hours (exact time not critical) and the solids were collected by filtration, washed with warm MeCN and Et_2O and dried *in vacuo* from 24 to 48 h before evaluation. No preparation of the Ce^{III} complex was attempted. Attempts to obtain complexes with the nitrates of lanthanide elements

heavier than europium resulted in non-stoichiometric solids; only Er^{III} gave repeatedly a solid with the formula $Er(LH)(NO_3)_3$. MeCN, which decomposed when removal of MeCN was attempted.

Efforts to prepare complexes with other stoichiometries were unsuccessful; in most cases the same complexes (those described in Tables 1, 2 and 3) were again isolated.

RESULTS AND DISCUSSION

Physical properties of the complexes

The formulae of the compounds, ligand : metal salt molar ratios used for the preparation of the complexes, yields, colours, molar conductivity values, effective magnetic moments and bonding parameters are given in Tables 1–3. Analytical data are summarized in Table 4. The complexes **40–44** are insoluble in all common organic solvents, while **1–39** are soluble only in DMF and DMSO. Because of the insolubility of the complexes in suitable solvents, we could not grow crystals for single-crystal X-ray structural studies. The Λ_M values of **14–20**, **21–26** and **27–29** in DMSO are in accord with these groups of complexes being formulated as 1 : 2, 1 : 3 and 1 : 1 electrolytes,[15] respectively. The X-ray powder diffraction patterns indicate the formation of six groups of isostructural compounds.

The first group includes the complexes **1–6**, the second the complexes **7–13**, the third the complexes **14–20**, the fourth the complexes **21–26**, the fifth the complexes **27–39** and the sixth group includes the compounds **40–44**. The patterns of the last group show a much smaller number of diffraction lines than for the complexes of the fifth group, suggesting polynuclear arrangements.[16] The room temperature effective magnetic moments of the complexes show little deviation from the Van Vleck theoretical values.

The thermal decomposition of the complexes prepared was studied in the 30–650°C region using TG/DTG, DTA and DSC techniques. The detailed thermal study of the complexes will be described in a subsequent paper.[17] As preliminary results we herein report that: (i) the water molecule present in

Table 1. Preparative data, colours, conductivity data, effective magnetic moments and bonding parameters of the complexes of lanthanide(III) isothiocyanates with LH

No.	Complex	Ligand : metal salt[a]	Yield (%)	Colour	Λ_M[b,c] (S cm^2 mol^{-1})	μ_{eff}[d] (BM)	$\bar{\beta}$[e]	δ (%)[e]	$b^{1/2}$[e]
1	$[La(LH)_2(NCS)_3(H_2O)]$	1 : 1, 2 : 1, 4 : 1	53	white	7	dia			
2	$[Ce(LH)_2(NCS)_3(H_2O)]$	2 : 1	57	pale brown	13	2.29			
3	$[Pr(LH)_2(NCS)_3(H_2O)]$	1 : 1, 2 : 1, 3 : 1	61	greenish	26	3.47	0.996[f]	+0.40[f]	0.045[f]
4	$[Nd(LH)_2(NCS)_3(H_2O)]$	1 : 1, 2 : 1	59	pale lilac	14	3.56	0.995[g]	+0.50[g]	0.050[g]
5	$[Sm(LH)_2(NCS)_3(H_2O)]$	1 : 1, 2 : 1, 5 : 1	70	cream	22	1.67	0.997[h]	+0.30[h]	0.039[h]
6	$[Eu(LH)_2(NCS)_3(H_2O)]$	2 : 1	64	white	7	3.46			
7	$[Gd(LH)_2(NCS)_3]$	1 : 1, 2 : 1	67	pale yellow	9	8.00			
8	$[Tb(LH)_2(NCS)_3]$	1 : 1, 2 : 1	56	white	14	9.62			
9	$[Dy(LH)_2(NCS)_3]$	2 : 1, 4 : 1	43	pale yellow	21	10.48			
10	$[Ho(LH)_2(NCS)_3]$	1 : 1, 2 : 1, 3 : 1	66	pale orange	30	10.74	0.994[i]	+0.60[i]	0.055[i]
11	$[Er(LH)_2(NCS)_3]$	1 : 1, 2 : 1	68	peach	18	9.67	0.993[j]	+0.70[j]	0.059[j]
12	$[Tm(LH)_2(NCS)_3]$	2 : 1	57	pale green	17	7.38			
13	$[Yb(LH)_2(NCS)_3]$	3 : 1	49	white	9	4.39			

[a] Molar ratio.
[b] Values of molar conductivity for 10^{-3} M solutions in DMSO at 25°C.
[c] The conductivities of most solutions change with time.
[d] Per metal ion at room temperature.
[e] Calculated for the Pr^{III}, Nd^{III}, Sm^{III}, Ho^{III} and Er^{III} complexes from their solid state *f–f* spectra.
[f] Calculated from the $^3H_4 \rightarrow {}^1D_2$, $^3P_0$, $^3P_1$ and $^3P_2$ transitions.
[g] From the $^4I_{9/2} \rightarrow {}^4F_{5/2}$, $^2H_{9/2}$, ($^4F_{7/2}$, $^4S_{3/2}$), $^2H_{11/2}$, ($^4G_{5/2}$, $^2G_{7/2}$), ($^2K_{13/2}$, $^4G_{7/2}$, $^4G_{9/2}$), $^2K_{15/2}$, ($^2G_{9/2}$, $^2D_{3/2}$, $^2P_{3/2}$), $^4G_{11/2}$ and ($^2P_{1/2}$, $^2D_{5/2}$) transitions.
[h] From the $^6H_{5/2} \rightarrow {}^4M_{15/2}$, $^4I_{13/2}$, (^6P, $^4P)_{5/2}$, $^6P_{3/2}$ and $^6P_{7/2}$ transitions.
[i] From the $^5I_8 \rightarrow {}^5F_5$, ($^5S_2$, $^5F_4$), $^5F_3$, $^5F_2$, $^3K_8$, ($^5G_6$, $^5F_1$) and $^3H_6$ transitions.
[j] From the $^4I_{15/2} \rightarrow {}^4F_{9/2}$, $^4S_{3/2}$, $^2H_{11/2}$, $^4F_{7/2}$, $^4F_{5/2}$, $^4F_{3/2}$, (^2G, ^4F, $^2H)_{9/2}$ and $^4G_{11/2}$ transitions.
dia = diamagnetic.

Table 2. Preparative data, colours, conductivity data, effective magnetic moments and bonding parameters[a,b] of the complexes of lanthanide(III) perchlorates with LH

No.	Complex	Ligand : metal salt[c]	Yield (%)	Colour	Λ_M[d] (S cm^2 mol^{-1})	μ_{eff}[e] (BM)	$\bar{\beta}$	δ (%)	$b^{1/2}$
14	$[La(LH)_3(OClO_3)](ClO_4)_2$	2:1, 3:1, 4:1	71	white	76	dia			
15	$[Ce(LH)_3(OClO_3)](ClO_4)_2$	3:1	69	off-white	74	2.34			
16	$[Pr(LH)_3(OClO_3)](ClO_4)_2$	3:1, 4:1	68	pale green	69	3.50	1.002	−0.20	—
17	$[Nd(LH)_3(OClO_3)](ClO_4)_2$	2:1	64	pale lilac	71	3.54	1.000	0	0
18	$[Sm(LH)_3(OClO_3)](ClO_4)_2$	2:1, 3:1	66	cream	68	1.66	0.998	+0.20	0.031
19	$[Eu(LH)_3(OClO_3)](ClO_4)_2$	3:1	71	white	70	3.36			
20	$[Gd(LH)_3(OClO_3)](ClO_4)_2$	3:1	69	white	73	7.96			
21	$[Tb(LH)_3](ClO_4)_3$	2:1, 3:1, 4:1	59	cream	106	9.86			
22	$[Dy(LH)_3](ClO_4)_3$	3:1	68	white	102	10.34			
23	$[Ho(LH)_3](ClO_4)_3$	3:1, 4:1	73	pale yellow	99	10.70	0.996	+0.40	0.045
24	$[Er(LH)_3](ClO_4)_3$	2:1, 3:1	65	pale pink	107	9.61	0.994	+0.60	0.055
25	$[Tm(LH)_3](ClO_4)_3$	3:1	68	pale green	96	7.60			
26	$[Yb(LH)_3](ClO_4)_3$	3:1	65	white	98	4.44			

[a] Calculated for the Pr^{III}, Nd^{III}, Sm^{III}, Ho^{III} and Er^{III} complexes from their solid state *f–f* spectra.
[b] Calculated from the *f–f* transitions shown as footnotes in Table 1.
[c] Molar ratio.
[d] Values of molar conductivity for 10^{-3} M solutions in DMSO at 25°C.
[e] Per metal ion at room temperature.

Table 3. Preparative data, colours, conductivity data, effective magnetic moments and bonding parameters[a,b] of the complexes of lanthanide(III) nitrates with LH

No.	Complex	Ligand : metal salt[c]	Yield (%)	Colour	Λ_M[d] (S cm^2 mol^{-1})	μ_{eff}[e] (BM)	$\bar{\beta}$	δ (%)	$b^{1/2}$
27	$[La(LH)_2(ONO_2)_2](NO_3)$	2:1, 3:1	66	white	36	dia			
28	$[Ce(LH)_2(ONO_2)_2](NO_3)$	2:1	74	pale brown	34	2.55			
29	$[Pr(LH)_2(ONO_2)_2](NO_3)$	2:1, 3:1	61	green	33	3.58	1.003	−0.30	—
30	$[Nd(LH)_2(ONO_2)_2](NO_3)$	2:1	66	pale violet	36	3.62	1.001	−0.10	—
31	$[Sm(LH)_2(ONO_2)_2](NO_3)$	3:1	76	cream	32	1.54	0.999	+0.10	0.022
32	$[Eu(LH)_2(ONO_2)_2](NO_3)$	2:1, 3:1	70	white	40	3.57			
33	$[Gd(LH)_2(ONO_2)_2](NO_3)$	2:1, 3:1	70	white	34	7.97			
34	$[Tb(LH)_2(ONO_2)_2](NO_3)$	3:1	63	white	37	9.57			
35	$[Dy(LH)_2(ONO_2)_2](NO_3)$	2:1	68	cream	35	10.54			
36	$[Ho(LH)_2(ONO_2)_2](NO_3)$	2:1	64	yellowish	32	10.48	0.996	+0.40	0.045
37	$[Er(LH)_2(ONO_2)_2](NO_3)$	2:1	68	white–pink	30	9.57	0.997	+0.30	0.039
38	$[Tm(LH)_2(ONO_2)_2](NO_3)$	2:1	60	pale green	33	7.49			
39	$[Yb(LH)_2(ONO_2)_2](NO_3)$	2:1, 3:1	70	white	34	4.41			
40	$[La(LH)(ONO_2)_3]$	0.9:1	92	white	i	dia			
41	$[Pr(LH)(ONO_2)_3]$	0.8:1	93	pale green	i	3.61	0.991	+0.91	0.067
42	$[Nd(LH)(ONO_2)_3]$	0.9:1	97	pale lilac	i	3.70	0.990	+1.01	0.071
43	$[Sm(LH)(ONO_2)_3]$	0.9:1	94	pale yellow	i	1.61	0.988	+1.21	0.077
44	$[Eu(LH)(ONO_2)_3]$	0.9:1	96	off-white	i	3.50			

[a,b,c,d,e] See footnotes in Table 2.
i = insoluble.

Table 4. Analytical data (%)[a] of the complexes

No.	Ln	C	H	N
1	18.8(19.0)	41.3(41.2)	2.8(2.8)	17.7(17.3)
2	19.0(19.2)	40.6(41.1)	2.9(2.8)	17.4(17.3)
3	19.4(19.3)	40.8(41.0)	2.6(2.8)	17.3(17.2)
4	20.0(19.6)	41.0(40.9)	2.7(2.8)	17.5(17.2)
5	20.6(20.3)	40.8(40.5)	2.5(2.7)	17.3(17.0)
6	20.4(20.5)	40.6(40.4)	2.8(2.7)	17.0(17.0)
7	21.9(21.5)	41.4(41.1)	2.4(2.5)	17.6(17.3)
8	22.0(21.7)	40.9(41.0)	2.6(2.5)	17.4(17.2)
9	22.4(22.1)	41.1(40.8)	2.5(2.5)	17.3(17.2)
10	22.4(22.4)	40.9(40.7)	2.6(2.5)	16.5(17.1)
11	22.9(22.6)	40.5(40.6)	2.6(2.5)	16.8(17.0)
12	23.5(22.8)	40.8(40.5)	2.7(2.5)	16.9(17.0)
13	23.7(23.2)	40.1(40.3)	2.5(2.4)	17.2(16.9)
14	13.7(13.4)	38.5(38.3)	2.5(2.6)	12.3(12.2)
15	12.9(13.5)	38.4(38.3)	2.6(2.6)	12.5(12.2)
16	14.0(13.6)	38.0(38.2)	2.6(2.6)	11.9(12.2)
17	13.8(13.9)	38.6(38.1)	2.8(2.6)	12.1(12.1)
18	14.4(14.4)	38.3(37.9)	2.4(2.6)	12.1(12.1)
19	15.1(14.5)	37.8(37.8)	2.5(2.6)	12.2(12.0)
20	14.3(14.9)	37.2(37.6)	2.9(2.6)	12.3(12.0)
21	14.7(15.1)	37.7(37.6)	2.6(2.6)	11.8(12.0)
22	15.1(15.4)	37.2(37.4)	2.5(2.6)	11.9(11.9)
23	16.2(15.6)	37.3(37.4)	2.3(2.6)	12.1(11.9)
24	16.4(15.7)	38.0(37.3)	2.5(2.6)	12.0(11.9)
25	15.8(15.9)	37.4(37.2)	2.7(2.6)	12.0(11.8)
26	15.9(16.2)	37.6(37.1)	2.6(2.5)	11.7(11.8)
27	19.4(19.2)	36.5(36.5)	2.4(2.5)	17.3(17.4)
28	18.7(19.3)	36.8(36.5)	2.6(2.5)	17.7(17.4)
29	19.6(19.4)	36.4(36.4)	2.6(2.5)	17.6(17.4)
30	20.7(19.8)	36.8(36.3)	2.7(2.5)	17.2(17.3)
31	21.0(20.5)	35.7(36.0)	2.5(2.5)	16.8(17.2)
32	20.3(20.6)	35.7(35.9)	2.5(2.5)	16.9(17.1)
33	20.5(21.2)	[b]	[b]	[b]
34	22.1(21.4)	[b]	[b]	[b]
35	21.6(21.8)	35.5(35.4)	2.5(2.4)	16.9(16.9)
36	22.4(22.0)	35.4(35.3)	2.3(2.4)	17.0(16.8)
37	22.0(22.3)	35.2(35.2)	2.4(2.4)	16.7(16.8)
38	23.1(22.4)	35.1(35.0)	2.6(2.4)	16.8(16.7)
39	22.7(22.8)	[b]	[b]	[b]
40	26.8(26.5)	25.4(25.2)	1.7(1.7)	15.7(16.0)
41	27.4(26.8)	24.8(25.1)	1.8(1.7)	15.9(16.0)
42	28.0(27.2)	[b]	[b]	[b]
43	28.3(28.1)	24.8(24.7)	1.8(1.7)	16.0(15.7)
44	27.9(28.3)	24.5(24.6)	1.6(1.7)	15.6(15.6)

[a] Calculated values in parentheses.
[b] No data available.

1–6 is coordinated to the lanthanide ions, (ii) the thermal decomposition of **27–32** occurs in two steps:

$$[Ln(LH)_2(ONO_2)_2][NO_3) \xrightarrow{N_2} \underset{\textbf{27–32}}{} [Ln(LH)(ONO_2)_3] + \uparrow LH \quad (1)$$

40–44, $[Ce(LH)(ONO_2)_3]$

$$[Ln(LH)(ONO_2)_3] \xrightarrow{N_2}$$

Lanthanide(III) oxide + gaseous products (2)

and (iii) the thermal decomposition of some anhydrous isothiocyanato complexes occurs also in two steps, but with a different stoichiometry:

$$2[Ln(LH)_2(NCS)_3] \xrightarrow{N_2} [Ln_2(LH)_3(NCS)_6] + \uparrow LH \quad (3)$$

10–14

$$[Ln_2(LH)_3(NCS)_6] \xrightarrow{N_2}$$

Lanthanide(III) oxide/sulphide(?) + gaseous products (4)

IR spectra

Tables 5 and 6 give diagnostic IR bands; in these tables only selected representative complexes are listed. In the ν(O—H)$_{water}$ region, the spectra of **1–6** show one medium sharp band at 3495–3470 cm^{-1} attributed to the presence of coordinated water.[18]

The IR spectrum of LH shows the characteristic bands of a *trans* secondary, hydrogen-bonded, amide with two chemically non-equivalent 2-pyridyl residues.[11] The absence of large systematic shifts of the ν(N—H) and amide V bands in the spectra of the complexes, in comparison with these bands in LH, confirms the inability of the amide nitrogen to participate in coordination, if non-deprotonated. The amide I band shifts to a lower frequency, while the amide II and III bands shift to higher frequencies; these shifts indicate amide-O coordination.[19]

It is well known that the IR spectra of complexes containing ligands with two pyridine residues may be reliably used as a guide to pyridine coordination and the criteria employed have been adequately discussed.[20–26] The careful study of multiplicity and shifts of mid- and far-IR bands associated with internal modes of vibration of the pyridine rings, can lead to fairly clear structural conclusions. The bands of interest, mostly affected by coordination, are the four ν(C=N) and ν(C=C) bands observed between 1610 and 1410 cm^{-1}, the ring breathing mode near 1000 cm^{1}, an out-of-plane CH deformation near 770 cm^{-1} and the two in-plane and out-of-plane ring deformation bands at *ca* 600 and 400 cm^{-1}, respectively.[20–25] These characteristic bands of the pyridine ring are doubled in the spectrum of LH, due to the presence of two non-equivalent pyridine residues, i.e. C_5H_4NCO— and C_5H_4NNH—. The complexes can be divided into two series on the basis of their IR spectra. The first series complexes (**40–44**) have spectra in which almost all of the key ring bands indicative of metal

Table 5. Diagnostic IR[a] bands (cm^{-1}) of LH and some selected representative lanthanide(III) complexes

Assignment[b]	LH	3	10	17	24	32	42
ν(O—H)$_{coord.\ water}$		3485m					
ν(N—H)	3321mb	3255mb	3260mb	3275wb	3265mb	3245mb	3250mb
Amide I[c]	1676vs	1637s	1633vs	1635vs	1629s	1640vs	1639vs
Amide II[d]	1511s	1520m	1519s	1522s	1518m	1520m	1519m
Rings' stretching vibrations, i.e. ν(C=N) and ν(C=C)	1589m, 1580m, 1561s, 1552m, 1482m, 1466m, 1433s, 1414s	1603s, 1580m, 1573m, 1554sh, 1506s, 1468s, 1444s, 1417m	1604s, 1578s, 1570s, 1553m, 1504m, 1464m, 1451s, 1416m	1597s, 1578s, 1572m, 1551m, 1499m, 1465s, 1448m, 1413m	1598s, 1579s, 1574s, 1552m, 1500m, 1466m, 1450m, 1414sh	1602m, 1580s, 1573s, 1554sh, 1505sb,[g] 1472m, 1446m, 1420m	1605s, 1588mb, 1569s, 1560m, 1498s,[g] 1478m, 1450sh, 1432vs
Amide III[d]	1214m	1227m	1226w	1222m	1221m	1226w	1230m
Ring breathing modes	995s, 986m	1027m, 996s	1028m, 995s	1032m, 998s	1031s, 995s	1027m, 1000s	1022s, 1012m
Out-of-plane CH def.	775s, 758m	766vs, 757s	764vs, 758s	763vs, 756m	764vs, 757m	766vs, 759m	746m, 735s
Amide V[e]	684sb	689mb	687mb	689s, 682sh	688s, 681sh	687sb	685mb
δ(Py) in-plane	620s, 596s	647m, 601s	648m, 600s	651sb,[f] 599m	649s, 602w	652s, 603w	644s, 625m
δ(Py) out-of-plane	407m, 400m	419m, 399m	420m, 400w	420m, 402m	423m, 403m	426m, 402w	432m, 417m

[a] Fourier-transform IR spectra.
[b] Assignments of the amide bands of LH and some complexes were assisted by deuterium isotopic substitution.
[c] ν(C=O).
[d] In secondary amides these bands arise from ν(C—N) and δ(NH) modes.
[e] π(NH).
[f] Overlapping with the $\nu_3(A_1)$ band of the monodentate C_{3v} perchlorato group.
[g] Overlapping with the $\nu_1(A_1)$ band of the bidentate C_{2v} nitrato groups.
Py = pyridine ring.

Table 6. Characteristic isothiocyanate, perchlorate and nitrate IR[a] bands (cm^{-1}) for some selected representative lanthanide(III) complexes of LH

Assignment	3	10	17	24	32	42
Isothiocyanate bands						
ν(CN)	2073vs	2075vs, 2067s				
ν(CS)	799m	802m				
δ(NCS)	475m	479w				
Perchlorate bands						
$\nu_4(E)$			1144s			
$\nu_3(F_2)$			1092sb	1088sb		
$\nu_1(A_1)$			1034s			
$\nu_2(A_1)$			931m			
$\nu_3(A_1)$[+δ(Py) in-plane]			651sb			
$\nu_5(E)$[+$\nu_4(F_2)$]			628sb			
$\nu_4(F_2)$				630s		
Nitrate bands[a]						
$\nu_1(A_1)$						1577m
$\nu_1(A_1)$[+ring stretch. vibr.]					1505sb	1498s
$\nu_3(E')$					1385sb	
$\nu_4(B_2)$					1292s	1303m, 1293s
$\nu_2(A_1)$					1017s	1015s
$\nu_6(B_1)$					829m	840m, 825m
$\nu_6(B_1)$[+$\nu_2(A_2'')$]					829m	
$\nu_5(B_2)$						723m, 700w
$\nu_5(B_2)$[+$\nu_4(E')$]					707wb	

[a] The $\nu_3(A_1)$ mode of the C_{2v} nitrato groups was not assigned because the region at *ca* 750 cm^{-1} is obscured by strong bands of the coordinated organic ligand.

coordination are doubled. Since these bands are significantly shifted from their positions in the free ligand spectrum (the shift is to higher frequencies for the ν(C=N) and ν(C=C) vibrations, the ring breathing mode and the δ(Py) modes), the implication is that both pyridine-N atoms are coordinated.[20-25] Ring bands of the coordinated ligand in the spectra of the second series complexes (**1–39**) are again doubled, one band being nearly coincident with the corresponding one of the free ligand and the other occurring at a different frequency; these results have been interpreted in terms of the presence of both coordinated and non-coordinated pyridine residues on the same ligand molecule.[20,23-26]

The spectra of **1–13** exhibit the ν(CN), ν(CS) and δ(NCS) modes all in the regions characteristic of terminal N-bonded isothiocyanato groups.[27] In the spectra of **21–26** both the $\nu_3(F_2)$ and $\nu_4(F_2)$ modes of the ClO_4^- group, appearing at *ca* 1090 and 630 cm^{-1}, remain unsplit, showing that the perchlorate groups are present in these complexes only as ionic species.[27] Apart from the T_d ClO_4^- frequencies already observed in the **21–26** series, the spectra of **14–20** show a number of additional anion vibrations, the number and the frequencies of which are indicative of the simultaneous presence of monodentate C_{3v} perchlorato groups.[27,28] In the spectra of **27–39** the frequencies of the bands assigned as vibrational modes of the nitrate groups suggest the simultaneous presence of ionic and coordinated nitrates. The appearance of a strong and broad band at *ca* 1380 cm^{-1} ($\nu_3(E')$) confirms the presence of ionic D_{3h} nitrates.[29] The other vibrational nitrate fundamentals suggest chelating bidentate nitrato groups, as the separation of the two highest frequency bands is large (*ca* 210 cm^{-1}); [27,29] the possibility of bridging nitrato groups is ruled out, because the highest frequency nitrato mode appears below 1550 cm^{-1}.[29] The non-appearance of the $\nu_3(E')$ band in the spectra of **40–44** shows that ionic nitrates are absent. However, these spectra are very complex in the regions of the coordinated nitrate vibrations, and support a complex structure with possible bidentate chelating and bridging nitrato groups being simultaneously involved.[30]

Electronic spectra

The electronic diffuse reflectance spectra of the complexes involve mainly intraligand and *f–f* tran-

sitions. The values of the bonding parameters $\bar{\beta}$(nephelauxetic ratio), δ(Sinha's parameter) and $b^{1/2}$ (covalent factor) of the Pr^{III}, Nd^{III}, Sm^{III}, Ho^{III} and Er^{III} complexes (Tables 1–3), calculated from the solid state *f–f* spectra by standard equations,[31–33] indicate that the interaction between the trivalent lanthanides and the ligands is essentially electrostatic and that there is a very small participation of 4*f* orbitals in bonding.[31–33]

The shape and fine structure of the same *hypersensitive f–f* bands for Nd^{III}, Ho^{III} and Er^{III} have been related to coordination number.[34] For Nd^{III} four transitions are sensitive to coordination environment but one, the $^4I_{9/2} \rightarrow {}^4G_{5/2}$, $^2G_{7/2}$ at about 590 nm, is particularly so. By comparing the spectra of standard Nd^{III} compounds with those of our complexes in the region of the above-mentioned transition, it is concluded that **4** and **30** are eight-coordinated, **17** is seven-coordinated and **42** is nine-coordinated.[34,35] Analogous studies[34,36] for the Ho^{III} (in the region of the *hypersensitive* $^5I_8 \rightarrow {}^5G_6$, $^5F_1$ transition at about 450 nm) and Er^{III} (in the region of the *hypersensitive* $^4I_{15/2} \rightarrow {}^2H_{11/2}$ transition at about 530 nm) complexes demonstrate that **10** and **11** are seven-coordinated, **23** and **24** are six-coordinated, while **36** and **37** are either eight- or seven-coordinated.

The details of the observed low temperature, solid state, fluorescence spectra of the Eu^{III} complexes are given in Table 7. Of primary interest are the transition manifolds, $^5D_0$ to $^7F_0$, $^5D_0$ to $^7F_1$, and $^5D_0$ to $^7F_2$, since these transitions are normally intense and may give vital clues as to the site symmetry around the Eu^{III} ion. Band assignments and the determination of crystal field site symmetries by the examination of Eu^{III} fluorescence band splittings were made by methods described elsewhere.[37,38]

The fluorescence spectrum of **19** shows a single band at 579.5 nm, associated with the $^5D_0 \rightarrow {}^7F_0$ transition. The exhibition of this line is consistent with the following site symmetries:[39] C_n, C_s and $C_{n'v}$ ($n = 2, 3, 4, 6$; $n' = 1, 2, 3, 4, 6$). The magnetic-dipole-allowed $^5D_0 \rightarrow {}^7F_1$ transition consists of two medium components at 590.0 and 592.5 nm. Two intense lines at 612.5 and 616.0 nm and one shoulder at a lower frequency arise from the electric-dipole allowed $^5D_0 \rightarrow {}^7F_2$ transition. The absence of an inversion centre is confirmed by the larger intensities of the transitions to the $J = 2$ and $J = 4$ sublevels, with respect to the intensity of the transition to the $J = 1$ sublevel.[40] The number of transitions to the $J = 0$, 1, 2 and 4 sublevels, appearing in the emission spectrum of **19**, is exactly the same as that theoretically expected in C_{3v} symmetry, where 1, 2, 3 and 5 transitions to $J = 0$, 1, 2 and 4 respectively are allowed.[37,40] Therefore, we believe that the C_{3v}

Table 7. Solid state fluorescence spectra[a,b] (nm) of the Eu^{III} complexes of LH

Assignment	**6**	**19**	**32**	**44**
$^5D_0 \rightarrow {}^7F_0$	579.0w	579.5w	580.0vw	580.5w
$^5D_0 \rightarrow {}^7F_1$	590.0m, 592.0m, 595.5w	590.0m, 592.5m	589.5m, 592.0m, 596.0w	591.0m, 594.0m
$^5D_0 \rightarrow {}^7F_2$	612.5vs, 615.0s, 619.5s, 624.0sh	612.5s, 616.0s, 621.5sh	611.5s, 613.0m	615.5vs, 616.5s, 620.0m
$^5D_0 \rightarrow {}^7F_3$	650wb[c]	648.0w, 651.0sh, 653.5w	654.5w[c]	651.5wb, 658.5vwb
$^5D_0 \rightarrow {}^7F_4$	682.0vw, 688.5sh, 691.5m, 694.0sh, 696.5w, 700.0s	683.5sh, 688.5sh, 692.5m, 696.5w, 700.0vs	691.5vw[c]	682.5wb, 687.0vwb, 696.0vw, 701.5vw

[a] Obtained at liquid nitrogen temperature by exciting with near-UV radiations.
[b] Emission originates almost totally from the $^5D_0$ excited state (bands associated with $^5D_{1,2} \rightarrow {}^7F_{o,1,2}$ transitions are very weak).
[c] Poorly resolved band.

site symmetry is the most consistent for Eu^{III} in **19**. This site symmetry, together with the physical and other spectral data obtained for this complex (see conclusions), allow us to assign a seven-coordinate structure, corresponding to a capped octahedron.[37,41]

The $^5D_0 \rightarrow {}^7F_0$ transition is allowed in **6** and appears as a medium line at 579.0 nm. The degeneracy of the $^7F_{1,2}$ sublevels is removed and three and four components of the $^5D_0 \rightarrow {}^7F_1$ and $^5D_0 \rightarrow {}^7F_2$ transitions, respectively, appear in the relative regions. This spectral pattern suggests C_{2v} site symmetry for Eu^{III} in this compound.[37,40] The $^5D_0 \rightarrow {}^7F_3$ transition appears as a weak broad band and does not show clearly its components, but the $^5D_0 \rightarrow {}^7F_4$ transition exhibits six components between 682.0 and 700.0 nm (in C_{2v} symmetry seven transitions to $J = 4$ are allowed). This site symmetry, together with the other data obtained for **6**, let us assign an eight-coordinate structure, corresponding to a bicapped trigonal prism.[37,41]

Assignment of **32** is slightly more difficult. The $^5D_0 \rightarrow {}^7F_0$ transition at 580.0 nm can be considered as symmetry-forbidden, the spectrum exhibiting a line the intensity of which is clearly less than 0.5% the most intense $^5D_0 \rightarrow {}^7F_2$ transition; this would rule out C_n, C_s and $C_{n'v}$ site symmetries.[38] There are only two well-resolved $^5D_0 \rightarrow {}^7F_1$ features in the 590 nm region with a weak diffuse feature at about 597 nm. The two $^5D_0 \rightarrow {}^7F_2$ features in the 610 nm region have an intensity region of about 2:1. This situation corresponds best to D_{2d} symmetry[38,42] and dodecahedral geometry.[41]

The last compound to be considered is **44**. This compound is weakly fluorescent at room temperature, but fluoresces strongly at 77 K. The emission spectrum of the solid complex shows a weak line at 580.5 nm associated with the $^5D_0 \rightarrow {}^7F_0$ transition. The two $^5D_0 \rightarrow {}^7F_1$ features at about 590 nm have nearly the same intensity. Two lines at 612.5 and 613.5 nm arise from the $^5D_0 \rightarrow {}^7F_2$ transition; their splitting is relatively small and indicates that these two lines originate from an E-component.[43] A strong line at 616.0 nm is also associated with this transition. The above features correspond with what would be expected from C_{4v} symmetry.[38,43] To the physical and other spectral data for **44** let us assign a nine-coordinate structure (see later); we may consider the C_{4v} site symmetry as the one most consistent with the data, corresponding to a mono-capped square antiprism.[41]

^{1}H *NMR spectra*

Table 8 gives the ^{1}H NMR chemical shifts for the free ligand and its diamagnetic La^{III} complexes in DMSO-d_6 (downfield from TMS). The study was based on comparisons with a number of related ligands and complexes,[11,14,19,44–49] on deuterium exchange and on resonance decoupling experiments.

Table 8. ^{1}H NMR (300 MHz) spectral data (δ, ppm) of LH and its diamagnetic La^{III} complexes[a] in DMSO-d_6

Assignment[b]	LH	1	14	27
—CO—NH—	10.40sb	10.44sb	10.43sb	10.37sb
Water		3.70sb		
H_3	8.22d	8.29mt	8.26mt	8.21d
H_4	7.83t	7.86mt	7.85mt	7.90t
H_5	7.25t	7.26mt	7.33mt	7.31t
H_6	8.42d	8.48mt	8.47mt	8.41d
$H_{3'}$	8.09d	8.18mt	8.14mt	8.06d
$H_{4'}$	7.93t	8.05mt	7.97mt	8.01t
$H_{5'}$	7.74t	7.80mt	7.71mt	7.79t
$H_{6'}$	8.72d	9.04mt	8.99mt	9.14d

[a] The spectrum of **40** could not be recorded because of its low solubility.

[b] Assignments for individual ring protons were assisted by resonance decoupling studies.

s = singlet; d = doublet; t = triplet; mt = multiplet; b = broad.

The variable-temperature ^{1}H NMR spectrum of LH has been interpreted[11,46–49] in terms of the structure shown in **I** with a *trans* amide group and *trans* pyridine rings. The appearance of the H_3 signal at a considerably low field has been rationalized[11] as the result of long range deshielding by the amide carbonyl group which is *cis* to, and approximately coplanar with, the 2-aminopyridine ring; in **I** the carbonyl group exerts its maximum deshielding effect. The observed conformational preference can be explained by the strong dipole–dipole interactions between the aminopyridine ring and the amide bond;[48,49] this stabilization also hinders rotation about the N_{amide}—C_{ring} bond.

In the spectra of the diamagnetic complexes **1**, **14** and **27**, the amide proton undergoes only a marginal shift to indicate the non-involvement of the amide-N atom in coordination. The signal of the 6′-pyridyl hydrogen shifts downfield compared with that of LH, suggesting that the N(1′) atom of the picolinamide unit is coordinated to La^{III}.[50] The shift observed for the 6-pyridyl hydrogen is insignificant (0.01–0.06 ppm), indicating that the N(1) atom of the aminopyridine unit remains non-coordinated in the complexes. If N(1) coordination had occurred, i.e. coordinating behaviour **II**, the H_3 signal would have shifted to a much higher field because on N(1), O_{amide} chelation LH must have changed its configuration from **I** to **II**;[49] the H_3 atom in **II** is no

longer deshielded by the carbonyl group. The δ value of H_3 is almost unchanged from that in LH, which rules out **II**.

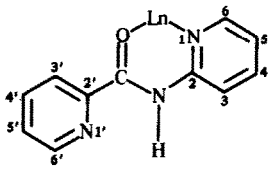

II

From the overall study presented it is concluded that in complexes **1–39** LH behaves as a bidentate chelating N(1′), O_{amide} ligand giving monomeric complexes, while the amide oxygen and both pyridine residues are coordinated in the 1 : 1 nitrato complexes **40–44** yielding polymeric compounds. A coordination number of eight is assigned to **1–6** with the participation of three terminal isothiocyanato ligands and one water molecule in the coordination sphere of Ln^{III}; bicapped trigonal prismatic structures are proposed for these complexes taking into account that **1–5** are isostructural with the Eu^{III} compound (**6**), which has a solid state emission spectrum indicative of this geometry. Physical and spectroscopic data suggest that the complexes **7–13** consist of the coordination entity $[Ln(O_{amide})_2(N(1'))_2(N_{NCS})_3]$; our data do not permit differentiation between pentagonal bipyramidal, capped octahedral, capped trigonal prismatic or trigonal base–tetragonal base structures. Seven-coordination attained by three bidentate LH ligands and one monodentate perchlorato group is assigned to **14–20**; capped octahedral structures are proposed for these complexes bearing in mind that **14–18** and **20** are isostructural with the Eu^{III} compound **19**, which has an emission *f–f* spectrum indicative of this structure. There is little doubt that the compounds **21–26** consist of the six-coordinate $[Ln(O_{amide})_3(N(1'))_3]^{3+}$ coordination sphere and three ionic perchlorates. Physical and spectroscopic data suggest that the complexes **27–39** consist of the coordination entity $[Ln(O_{amide})_2(N(1'))_2(O_{nitrato})_4]^+$ formed by two chelating LH ligands and two bidentate chelating nitrato groups; dodecahedral geometries with a D_{2d} site symmetry for the Ln^{III} ions are assigned to these complexes taking into account that **27–31** and **33–39** are isostructural with $[Eu(LH)_2(ONO_2)_2](NO_3)$ (**32**) which has a solid state emission *f–f* spectrum characteristic of this site symmetry and geometry. Finally, a coordination number of nine and a monocapped square antiprismatic structure with a C_{4v} site symmetry for the metal ion are assigned to the complexes **40–44**, both from physical and spectroscopic data, with bidentate chelating and bridging nitrato groups being simultaneously involved.

The present work demonstrates the utility of amides as coordinating ligands for lanthanide complexes. Our systematic investigation of the Ln^{III}/LH reaction system has confirmed our belief that a variety of amide-coordinated Ln^{III} complexes are capable of existence and that this area may yet prove to be as extensive as that developed for transition metal/amide chemistry.[51] Work in progress at the time of writing is providing neutral, water-soluble, Gd^{III} complexes with chelating amidic ligands, which are currently evaluated as contrast agents for magnetic resonance imaging (MRI).[7] This work will be described in a subsequent report.

Acknowledgements—Some of the spectroscopic material of this work was obtained at the Laboratorium Anorganische Scheikunde, Rijksuniversitair Centrum Antwerpen, Belgium; we wish to thank Prof. H. O. Desseyn for this convenience. We thank Mr P. Kirkos for technical assistance.

REFERENCES

1. S. P. Perlepes, V. Lazaridou and J. M. Tsangaris, *Synth. React. Inorg. Met.-Org. Chem.* 1989, **19**, 841.
2. V. Lazaridou, S. P. Perlepes, J. M. Tsangaris and Th. F. Zafiropoulos, *J. Less-Common Met.* 1990, **158**, 1.
3. S. P. Perlepes, V. Lazaridou, B. S. Sankhla and J. M. Tsangaris, *Bull. Soc. Chim. France* 1990, **127**, 597.
4. G. Condorelli, A. Seminara and A. Musumeci, *J. Inorg. Nucl. Chem.* 1974, **36**, 3763.
5. C. Airoldi, F. S. Dias, G. F. De Sa and J. G. Espinola, *J. Inorg. Nucl. Chem.* 1978, **40**, 1537.
6. N. Rajasekar and S. Soundararajan, *J. Inorg. Nucl. Chem.* 1981, **43**, 977.
7. M. S. Konings, W. C. Dow, B. D. Love, K. N. Raymond, S. C. Quay and S. M. Rocklage, *Inorg. Chem.* 1990, **29**, 1488 and references cited therein.
8. E. E. Castelano and R. W. Becker, *Acta Cryst. B* 1981, **37**, 61.
9. S. P. Perlepes and A. G. Galinos, *J. Less-Common Met.* 1984, **96**, 69.
10. Th. F. Zafiropoulos, S. P. Perlepes and J. M. Tsangaris, *J. Coord. Chem.* 1985, **14**, 87.
11. S. P. Perlepes, Th. Kabanos, V. Hondrellis and J. M. Tsangaris, *Inorg. Chim. Acta* 1988, **150**, 13.
12. J. H. Forsberg and T. Moeller, *Inorg. Chem.* 1969, **8**, 883.
13. S. P. Perlepes, P. Jacobs, H. O. Desseyn and J. M. Tsangaris, *Spectrochim. Acta* 1987, **43A**, 771.
14. V. Hondrellis, S. P. Perlepes, Th. A. Kabanos and J. M. Tsangaris, *Synth. React. Inorg. Met-Org. Chem.* 1988, **18**, 83.
15. W. J. Geary, *Coord. Chem. Rev.* 1971, **7**, 81.
16. A. Seminara, S. Giuffrida, G. Bruno, G. Siracusa

and G. Condorelli, *J. Inorg. Nucl. Chem.* 1979, **41**, 701.
17. S. P. Perlepes, J. C. Plakatouras, Th. F. Zafiropoulos and H. O. Desseyn, to be submitted.
18. L. S. Gelfand, F. J. Iaconianni, L. L. Pytlewski, A. N. Speca, C. M. Mikulski and N. M. Karayannis, *J. Inorg. Nucl. Chem.* 1980, **42**, 377.
19. R. L. Chapman, F. S. Stephens and R. S. Vagg, *Inorg. Chim. Acta* 1981, **52**, 161.
20. D. A. Baldwin, A. B. P. Lever and R. V. Parish, *Inorg. Chem.* 1969, **8**, 107.
21. M. Keeton, A. B. P. Lever and B. S. Ramaswamy, *Can. J. Chem.* 1970, **48**, 3185.
22. M. Keeton and A. B. P. Lever, *Inorg. Chem.* 1971, **10**, 47.
23. M. Nonoyama, *J. Inorg. Nucl. Chem.* 1975, **37**, 59.
24. R. Grzeskowiak, C. Whatley and M. Goldstein, *Spectrochim. Acta* 1975, **31A**, 1577.
25. R. Grzeskowiak and M. Goldstein, *Inorg. Chim. Acta* 1979, **33**, L153.
26. E. Rivarola, A. Silvestri, G. Alonzo, R. Barbiery and R. H. Herber, *Inorg. Chim. Acta* 1985, **99**, 87.
27. K. Nakamoto, *Infrared and Raman Spectra of Inorganic and Coordination Compounds*, 4th edn, pp. 121–25, 130–37, 251, 253–57, 283–87. Wiley, New York (1986).
28. R. P. Scholer and A. E. Merbach, *Inorg. Chim. Acta* 1975, **15**, 15.
29. U. Casellato, P. A. Vigato and M. Vidali, *Coord. Chem. Rev.* 1981, **36**, 183.
30. S. P. Perlepes, D. Nicholls and M. R. Harrison, *Inorg. Chim. Acta* 1985, **102**, 61.
31. C. K. Jorgensen, *Modern Aspects of Ligand Field Theory*, p. 293. North-Holland, Amsterdam (1971).
32. S. P Sinha, *Spectrochim. Acta* 1966, **22**, 57.
33. D. E. Henrie and G. R. Choppin, *J. Chem. Phys.* 1968, **49**, 477.
34. D. G. Karraker, *Inorg. Chem.* 1967, **6**, 1863; 1968, **7**, 473.
35. J. I. Bullock and H.-A. Tajmir-Riahi, *Inorg. Chim. Acta* 1980, **38**, 141, and references cited therein.
36. K. Iftikhar and N. Ahmad, *Aust. J. Chem.* 1983, **36**, 695.
37. J. H. Forsberg, *Coord. Chem. Rev.* 1973, **10**, 195.
38. G. M. Murray, L. L. Pesterfield, N. A. Stump and G. K. Schweitzer, *Inorg. Chem.* 1989, **28**, 1994.
39. A. Musumeci, R. P. Bonomo, V. Cucinotta and A. Seminara, *Inorg. Chim. Acta* 1982, **59**, 133.
40. J.-C. G. Bunzli and J.-R. Yersin, *Helv. Chim. Acta* 1982, **65**, 2498.
41. S. P. Sinha, *Struct. Bonding (Berlin)* 1976, **25**, 69.
42. A. Seminara, A. Musumeci and A. Chisari, *Inorg. Chim. Acta* 1984, **82**, 173.
43. A. Seminara, A. Musumeci and S. Calogero, *J. Inorg. Nucl. Chem.* 1980, **42**, 1208.
44. S. P. Perlepes, Th. Kabanos, V. Lazaridou and J. M. Tsangaris, *Inorg. Chim. Acta* 1986, **117**, 27.
45. V. Hondrellis, Th. Kabanos, S. P. Perlepes and J. M. Tsangaris, *Inorg. Chim. Acta* 1987, **136**, 1.
46. M. Nonoyama, S. Tomita and K. Yamasaki, *Inorg. Chim. Acta* 1975, **12**, 33.
47. V. Scheller-Krattiger, K. H. Scheller, E. Sinn and R. B. Martin, *Inorg. Chim. Acta* 1982, **60**, 45.
48. R. F. C. Brown, L. Radom, S. Sternhell and I. D. Rae, *Can. J. Chem.* 1968, **46**, 2577.
49. J. Bould and B. J. Brisdom, *Inorg. Chim. Acta* 1976, **19**, 159.
50. M. Nonoyama, *Trans. Met. Chem.* 1982, **7**, 281.
51. H. Sigel and R. B. Martin, *Chem. Rev.* 1982, **82**, 385.

Polyhedron Vol. 10, No. 20/21, pp. 2417–2421, 1991
Printed in Great Britain

0277–5387/91 $3.00+.00
© 1991 Pergamon Press plc

SYNTHESIS AND STRUCTURE OF DIMETHOXYETHANE-DICHLORODIOXO-TUNGSTEN(VI)—A HIGHLY SOLUBLE DERIVATIVE OF TUNGSTEN DIOXODICHLORIDE

KLAUS DREISCH, CARLAXEL ANDERSSON* and CLAES STÅLHANDSKE

Department of Inorganic Chemistry, Chemical Center, University of Lund, P.O. Box 124, S 221 00 Lund, Sweden

(*Received* 25 *April* 1991; *accepted* 2 *July* 1991)

Abstract—$WOCl_4$ reacted with hexamethyldisiloxane at room temperature in the presence of ethyleneglycol dimethylether (dme) giving the white crystalline compound, WO_2Cl_2(dme) (80% yield) and its structure was determined by X-ray diffraction. The structure, which is isomorphous with MoO_2Cl_2(dme), is built up of discrete molecules with a distorted octahedral geometry, the tungsten atom coordinates two oxygens in *cis* positions, two dme oxygen atoms and two chlorine atoms.

High oxidation state organometallic chemistry is of great current interest.[1,2] Compounds of this family are active catalysts in the olefin metathesis reaction[3–5] and they serve as model compounds for the active catalyst in the industrially important propylene ammonoxidation reaction.[6] Typical hard donors, e.g. oxo, imido or alkoxy, which can stabilize the high oxidation state of the central atom, are recurrent auxiliary ligands in these complexes. The role of the oxo-ligand as a spectator in metathesis catalysts has been discussed.[7] By reaction with aryl or alkyl isocyanates metal-oxo complexes are conveniently converted into metal-imido complexes.[8]

A recent method to convert metal-chloro complexes to metal-oxo complexes involves the reaction with hexamethyldisiloxane as an oxygen transfer reagent.[9–11] Metal sulphido complexes have also been prepared in a similar way using hexamethyldisilthiane as the transfer reagent.[11] The preparations of different Lewis base adducts $WO_2Cl_2L_2$ have been described[12] and more recent reports include the preparation of the acetonitrile adduct[11] and the bipyridine adduct.[13] The bromo complex WO_2Br_2(bpy) has been successfully alkylated in THF suspension.[14,15] With a soluble adduct of WO_2Cl_2 at hand a more straightforward method than the existing one[16] to prepare the complex Cp*WO_2Cl (Cp* = η^5-permethyl cyclopentadienyl) can be foreseen. In the course of a program directed towards the development of new homogeneous catalysts for the metathesis of functionalized olefins we have considered tungsten–oxo complexes as suitable starting materials for further synthesis. In our search for soluble adducts, $WO_2Cl_2L_2$, compatible with alkylating agents, e.g. alkyl-tin, alkyl-lithium or Grignard reagents we have considered various ethers since ethers, especially dimethoxyethane (dme), have been used as ligands in the preparation of tungsten alkylidene complexes[5] and we present here the synthesis and the crystal structure of WO_2Cl_2(dme).

RESULTS AND DISCUSSION

Preparation of WO_2Cl_2(dme)

Hexamethyl disiloxane reacts with an equimolar amount of $WOCl_4$ suspended in CH_2Cl_2 to give a light yellow solid. The IR spectrum of this solid shows two very strong and broad absorption bands at 853 and 817 cm^{-1} indicative of bridging oxo groups. Additional absorption bands at 1250 and 1000 cm^{-1} which can be assigned[17] to siloxide groups are also present. Based on these IR observations a likely formulation of this intermediate is a highly polymeric tungsten complex, $[W(O)Cl_3(OSiMe_3)]_x$. After addition of excess dme most of the suspended solid is dissolved. The title compound is

* Author to whom correspondence should be addressed.

obtained as white needles from the filtrate by the addition of diethylether and cooling to −30°C.

The dissolution of the initially formed solid on addition of dme indicates the formation of an ether adduct, $[W(O)Cl_3(OSiMe_3)(dme)]$, as the next step in the reaction sequence. Further elimination of $ClSiMe_3$ from this intermediate to give the isolated product is probably facilitated by the presence of the second oxygen atom of the dme ligand in the coordination sphere of the tungsten atom. This method of preparation is essentially the same as that applied in the preparation of $WO_2Cl_2(bpy)$ using the chelating dme ligand instead of bipyridine,[13] with the exception that the bipyridine adduct is insoluble in the reaction mixture. In our hands the preparation of the bipyridine adduct gave the desired compound mixed with varying amounts of $WOCl_3(bpy)$ as indicated by the tungsten oxo vibration $\nu(W{=}O)$ at 972 cm^{-1} in the IR spectrum and by the green colour of the product. This problem is, however, circumvented by letting the reaction between $WOCl_4$ and hexamethyldisiloxane proceed until all the $WOCl_4$ is consumed before bipyridine is added. In the case of dme no reduction of W^{VI} is observed and the isolated product is pure $WO_2Cl_2(dme)$. Alternatively, the reversed reaction order can be used: $WOCl_4$ dissolved in dme/CH_2Cl_2 reacts within half a day with an equimolar amount of hexamethyl disiloxane to give a decolourized solution from which the product can be isolated as given above. The rate of product formation using this method greatly depends on the amount of dme added, decreasing markedly by increasing the dme/$WOCl_4$ ratio. It has been shown[18] that dme reacts with $WOCl_4$ in $CHCl_3$ solution to form an octahedrally coordinated tungsten etherate which reacts further by cleavage of a carbon–oxygen bond to form a tungsten alkoxide complex. Under the reaction conditions given in the Experimental this side reaction is, however, appreciably slower (approx. 3 days) than the chloride/oxide exchange by hexamethyl disiloxane (approx. half a day) and no product from this side reaction is observed.

The two methods presented give products which are indistinguishable by IR or analytical means. The complex prepared is very soluble in donating organic solvents, e.g. thf, dme, dmf and acetonitrile. The solubility of $WO_2Cl_2(dme)$ in CH_2Cl_2 is appreciably high (0.4 M) in contrast to the low solubility in $CHCl_3$. This high solubility is somewhat surprising since the analogous bipyridine complex is virtually insoluble in the same solvents.

$MoO_2Cl_2(dme)$ has been prepared by reaction of solid MoO_2Cl_2 with dme.[19] Attempted preparation of $WO_2Cl_2(dme)$ *via* direct reaction of dme with solid WO_2Cl_2 did not lead to any dissolution of WO_2Cl_2 although the reaction was continued for 5 weeks.

This indicates that the barrier for breaking up the polymeric network of solid WO_2Cl_2 is so high that a direct synthesis is not feasible. The presence of the dme ligand in the coordination sphere of the metal in the step forming the second metal–oxo bond is therefore probably of importance. ^1H and ^{13}C spectra of $WO_2Cl_2(dme)$ in neat thf or acetonitrile show that the dme ligand is labile. The dme ligand is completely substituted in thf while in acetonitrile both the solvated complexes exist in equilibrium, indicating a difference in complex strength for N and O donors. Contrary to the reported[20] lack of reactivity of uncomplexed WO_2Cl_2 with $^tBuNH(SiMe_3)$ we find that WO_2Cl_2(dme) reacts readily with $^tBuNH_2$ and $^tBuNH(SiMe_3)$ to hitherto not fully characterized tungsten amido/imido complexes.[21]

Attempts to exchange the dme ligand in the complex for two thf ligands give a white product with bands at 1040 and 847 cm^{-1} in its IR spectrum as expected for coordinated thf.[22] In addition the presence of a strong broad band at 725 cm^{-1} in the IR spectrum reveals bridging oxo-groups. The analytical data [Found (Calc.) W, 50.3 (51.2); Cl, 19.2 (19.7); C, 13.9 (13.4); H, 2.4 (2.1)%] for this compound are close to the formula $WO_2Cl_2(thf)$ and this formulation is also supported by the bridging oxo group as observed by IR. Whether this oxo bridged structure exists in thf solution or if it is formed as a consequence of a loss of thf during the isolation of the complex is not known. A decreased solubility in thf after the initial isolation indicates that a loss of thf with subsequent formation of oxo bridges might occur.

The structure of $WO_2Cl_2(dme)$

The $WO_2Cl_2(dme)$ molecule with atomic numbering is shown in Fig. 1 and selected bond distances

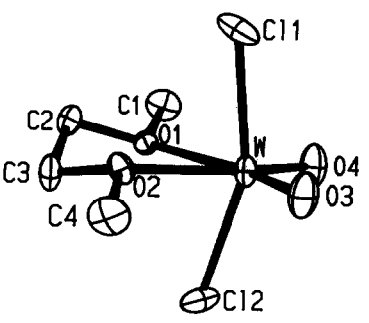

Fig. 1. A perspective view of the $WO_2Cl_2(dme)$ molecule.

Table 1. Selected bond distances (Å) and angles (°) for WCl_2O_3 (dme)

Bond distances (Å)			
W—O(3)	1.69(1)	O(1)—C(1)	1.44(1)
W—O(4)	1.69(1)	O(1)—C(2)	1.46(1)
W—O(1)	2.253(7)	C(2)—C(3)	1.49(2)
W—O(2)	2.292(8)	O(2)—C(3)	1.44(1)
W—Cl(1)	2.344(4)	O(2)—C(4)	1.45(2)
W—Cl(2)	2.344(3)		

Bond angles (°)			
O(1)—W—O(2)	70.5(3)	W—O(1)—C(1)	120.5(7)
O(2)—W—O(3)	91.9(4)	W—O(1)—C(2)	117.2(7)
O(3)—W—O(4)	105.1(5)	O(1)—C(2)—C(3)	107.1(9)
O(4)—W—O(1)	92.5(4)	O(2)—C(3)—C(2)	107.4(10)
Cl(1)—W—Cl(2)	157.6(2)	W—O(2)—C(3)	115.2(7)
		W—O(2)—C(4)	119.6(8)

and angles are presented in Table 1. The structure is isomorphous with MoO_2Cl_2(dme).[19] The W^{VI} atom has a distorted octahedral coordination, with the two oxide ions and the two oxygen atoms of the dme ligand forming the equatorial plane and with the chlorine atoms at the apices. The four oxygen atoms are almost coplanar with the tungsten atom in the plane. The oxide ions are *cis* oriented, as also suggested from theoretical calculations,[23] with both W=O bond distances of 1.69(1) Å and an angle O=W=O of 105.1°. The W=O bond distance is close to the mean value of 1.709 Å, recently calculated from other dioxo complexes.[24] The tungsten–oxygen bond distances to the dme ligand are 2.253(7) and 2.292(8) Å, respectively, and the angle O—W—O is 70.5°.

Two chlorine atoms at 2.344(4) Å complete the octahedron around tungsten. Both chlorine atoms are bent towards the dme ligand resulting in a Cl—W—Cl angle of 157.6°. This deviation from linearity is in agreement with extended Hückel calculations[25] on the octahedrally coordinated Mo^{VI} dioxo complex, $H_4MoO_2^{2-}$.

Comparison with the closely related structure, WO_2Cl_2(bpy),[9] shows significantly longer W=O bonds in the bpy derivate (1.745(3), 1.792(2) Å). The bond distance W—Cl and the bond angle Cl—W—Cl are, however, similar in the two compounds.

EXPERIMENTAL

All manipulations were carried out on a vacuum line using standard Schlenk techniques under an atmosphere of dry nitrogen.

$WOCl_4$ was prepared by the method of Gibson,[9] CH_2Cl_2, $O(C_2H_5)_2$ (Merck), $O(SiMe_3)_2$ and ethyleneglycol dimethylether (dme) (Jansen) were distilled and dried using activated molecular sieves (4 Å) before use.

Tungsten analysis was done gravimetrically as WO_3, chloride analysis was done argentometrically according to Mohr's method. Analysis for C, H were done by Ilse Beetz, Mikroanalytishes Laboratorium, Kronach, Germany.

IR spectra (Nujol mulls between CsI plates) were recorded using a Nicolet 20SXC spectrometer. ^1H, ^{13}C NMR spectra in $CDCl_3/CH_2Cl_2$ solution were recorded using a Varian XL 300 spectrometer.

X-ray crystallography

A crystal of the title compound was enclosed in a Lindemann capillary to prevent it from air and moisture. The space group, $P2_1/n$, was uniquely determined from systematic absences. Unit cell parameters were derived from least-squares fit of angular settings of 50 reflexions ($18° < 2\theta < 30°$). The data were corrected for a linear decrease of 17% during the data collection and for Lorentz, polarization and absorption effects, the latter by an empirical method.[26] Some crystal data are collected in Table 2.

The structure was solved by direct methods (MULTAN80), which gave the positions of the tungsten atom and the two chlorine atoms. The remaining non-hydrogen atoms were located from subsequent difference Fourier synthesis. In the final least-squares refinement all non-hydrogen atoms were refined with anisotropic thermal parameters. The hydrogen atoms of the methylene groups were

Table 2. Crystal and data collection parameters for WCl_2O_2(dme)

Crystal data	
Formula	$WC_4H_{10}Cl_2O_4$
Molecular weight	376.88
Size (mm)	$0.12 \times 0.15 \times 0.22$
Space group	$P2_1/n$
a (Å)	7.196(2)
b (Å)	11.328(4)
c (Å)	12.040(3)
β (°)	92.95(2)
V (Å^3)	980.2(3)
D_c (g cm^{-3})	2.55
μ(Mo-K_α) (cm^{-1})	116
Temperature (°C)	23
Data collection and structure refinement	
Diffractometer	CAD4
Radiation	Mo-K_α (λ = 0.71073 Å)
Data collection ($2\theta_{max}$)	56
Monochromator	Graphite
Scan mode	ω–2θ
Independent refl.	2359
Observed refl. ($I > 3\sigma(I)$)	1399
Weighting scheme (w^{-1})	$\sigma^2(F_o)+(0.03F_o)^2+3.0$
R	0.037
R_w	0.049
$\Delta(\rho_{max})$ (e Å^{-3})	1.05

included with fixed positional parameters at calculated positions (d(C—H) = 0.95 Å).

Synthesis of WO_2Cl_2(dme)

Method 1. To a suspension of freshly sublimed $WOCl_4$ (6.43 g, 18.8 mmol) in 100 cm^3 CH_2Cl_2 is added $(Me_3Si)_2O$ (3.20 g, 19.8 mmol). The orange crystals are slowly consumed to give a yellow solution. After approximately 1.5 h stirring a light yellow solid precipitates. Ethylene glycol dimethylether (dme) (2.54 g, 28.2 mmol) is added and the reaction mixture is stirred overnight and filtered (G4-frit) to remove the brownish residue which has formed. The clear filtrate is then concentrated at room temperature on the vacuum-line. When pure white crystals begin to precipitate diethylether (100 cm^3) is added. After cooling overnight at −30°C the white crystals formed are collected on a filter, washed once with 20 cm^3 of diethylether and dried *in vacuo*. Yield: 6.11 g, 86%.

Method 2. To a suspension of freshly sublimed $WOCl_4$ (14.24 g, 41.7 mmol) in 170 cm^3 CH_2Cl_2 is added dme (4.88 g, 54.2 mmol). After 5 min stirring $WOCl_4$ is completely dissolved. To the orange solution is added $(Me_3Si)_2O$ (7.10 g, 43.8 mmol) and the reaction mixture is vigorously stirred about 6 h at room temperature. The reaction is completed when the solution is decolourized having only a faint yellowish tint. The clear solution is concentrated on the vacuum-line until white crystals begin to precipitate, 150 cm^3 diethylether is added and the reaction mixture is kept at −30°C for one day. After filtering, the white crystals are washed with diethylether (3×20 cm^3) and dried *in vacuo*. Yield: 12.22 g, 77.8%.

IR data (Nujol, CsI; cm^{-1}): 1279w, 1245w, 1193w, 1155vw, 1108vw, 1078s, 1018vs,br, 976s, 933vs, 862s, 821m, 415w, 402sh, 376vw, 349m, 339m,br, 272w, 257m.

NMR data (300 MHz, 1 : 4 mixture of *d*-chloroform and methylenchloride, 298 K): ^{1}H: 4.09 (s, O-CH_3) and 4.04 (s, CH_2-O), ^{13}C-{^{1}H}: 71.70 (CH_2-O) and 65.45 (O-CH_3). Elemental analysis for $C_4H_{10}Cl_2O_4W$: Found (Required): C, 12.0 (12.7); H, 2.6 (2.7); Cl, 18.9 (18.8); W, 48.7 (48.8)%.

Acknowledgements—Financial support from STU (Swedish Board for Technical Development) and from SJFR (Swedish Council for Forestry and Agricultural Research) is gratefully acknowledged.

REFERENCES

1. W. A. Herrmann, *Comments Inorg. Chem.* 1988, **7**, 73.
2. W. A. Herrmann, *Angew. Chem., Int Edn Engl.* 1988, **27**, 1297.
3. G. Schoettle, J. Kress and J. A. Osborn, *J. Chem. Soc., Chem. Commun.* 1989, 1062.
4. R. R. Schrock, J. S. Murdzek, G. C. Bazan, J. Robbins, M. DiMare and M. O'Regan, *J. Am. Chem. Soc.* 1990, **112**, 3875.
5. R. R. Schrock, R. T. DePue, J. Feldman, K. B. Yap, D. C. Yang, D. M. Davis, L. Park, M. DiMare, M. Schofield, J. Anhaus, E. Walborsky, E. Evitt, C. Krüger and P. Betz, *Organometallics* 1990, **9**, 2262.
6. D. M. T. Chan and W. A. Nugent, *Inorg. Chem.* 1985, **24**, 1422.
7. A. K. Rappe and W. A. Goddard III, *J. Am. Chem. Soc.* 1982, **104**, 448.
8. W. A. Nugent and B. L. Haymore, *Coord. Chem. Rev.* 1980, **31**, 123.
9. V. C. Gibson, T. P. Kee and A. Shaw, *Polyhedron* 1988, **7**, 579.
10. V. C. Gibson, A. Shaw and D. N. Williams, *Polyhedron* 1989, **8**, 549.
11. V. C. Gibson, T. P. Kee and A. Shaw, *Polyhedron* 1990, **9**, 2293.
12. B. J. Brisdon, *Inorg. Chem.* 1967, **6**, 1791.
13. W. A. Herrman, W. R. Theil and E. Herdweck, *Chem. Ber.* 1990, **123**, 271.
14. C. Zhang, X. Zhang, N. Liu and G. N. Schrautzer, *Organometallics* 1990, **9**, 1307.

15. C. Zhang, E. O. Schlemper and G. N. Schrautzer, *Organometallics* 1990, **9**, 1016.
16. J. W. Faller and Y. Ma, *J. Organomet. Chem.* 1988, **340**, 59.
17. H. Bürger, *Organomet. Chem. Rev. A* 1968, **3**, 425.
18. G. A. W. Fowles, D. A. Rice and K. J. Shanton, *J. Chem. Soc., Dalton Trans.* 1978, 1658.
19. B. Kamenar, M. Penavic, B. Korpar-Colig and B. Markovic, *Inorg. Chim. Acta* 1982, **65**, L245.
20. W. A. Nugent and R. L. Harlow, *Inorg. Chem.* 1980, **19**, 777.
21. K. Dreisch and C. Andersson, to be published.
22. P. C. Crouch, G. W. A. Fowles, P. R. Marshall and R. A. Walton, *J. Chem. Soc. A* 1968, 1634.
23. K. Tatsumi and R. Hoffman, *Inorg. Chem.* 1980, **19**, 2656.
24. J. M. Mayer, *Inorg. Chem.* 1988, **27**, 3899.
25. D. C. Brower, J. L. Templeton and D. M. P. Mingos, *J. Am. Chem. Soc.* 1987, **109**, 5203.
26. N. Walker and D. Stuart, *Acta Cryst.* 1983, **A39**, 158.

Polyhedron Vol. 10, No. 20/21, pp. 2423–2435, 1991
Printed in Great Britain

0277–5387/91 $3.00+.00
© 1991 Pergamon Press plc

UNEXPECTED REACTION OF $[Ni(CO)_{4-n}(R_2PCl)_n]$ ($n = 1, 2$; R = Bu^t, Cy, Ph) WITH $Na_2[Fe_2(CO)_8]$. SYNTHESIS AND ELECTRONIC STRUCTURE OF THE ANIONS $[Fe_2(\mu\text{-CO})(CO)_6(\mu\text{-PR}_2)]^-$ AND THEIR REACTIONS WITH H^+ AND $[M(PPh_3)]^+$ (M = Cu, Ag, Au)

BERNHARD WALTHER,* HELMUT HARTUNG, HANS-C. BÖTTCHER, UTE BAUMEISTER and UWE BÖHLAND

Department of Chemistry, Martin Luther University, Halle-Wittenberg, Weinbergweg 16, O-4050 Halle/S., Germany

and

JOACHIM REINHOLD and JOACHIM SIELER

Department of Chemistry, University of Leipzig, Talstr. 35, O-7010 Leipzig, Germany

and

JEAN LADRIERE

Inorganic and Nuclear Chemistry Laboratory, University of Louvain, 2, Chemin du Cyclotron, B-1348 Louvain-la-Neuve, Belgium

and

HANS-MARTIN SCHIEBEL

Department of Organic Chemistry, Technical University Braunschweig, Hagenring 30, W-3300 Braunschweig, Germany

(*Received* 23 *April* 1991; *accepted* 2 *July* 1991)

Abstract—Treatment of $[Ni(CO)_{4-n}(R_2PCl)_n]$ ($n = 1, 2$; R = Bu^t, Cy, Ph) with $Na_2[Fe_2(CO)_8]$ gave, depending on n and R, either the doubly phosphido-bridged complexes $[Fe_2(CO)_6(\mu\text{-PR}_2)_2]$ or the anions $[Fe_2(\mu\text{-CO})(CO)_6(\mu\text{-PR}_2)]^-$. These anions can also be obtained by the reaction of $[Fe(CO)_4(PR_2)]^-$ with either $[Fe_2(CO)_9]$ or $[Fe(CO)_5]$ via the intermediate $[Fe_2(CO)_8(\mu\text{-PR}_2)]^-$. The electronic structure of the anions $[Fe_2(\mu\text{-CO})(CO)_6(\mu\text{-PR}_2)]^-$ has been studied by an EHT calculation which supports their ambident oxygen- or metal-nucleophilicity. The metal-centred nucleophilic reactions of the anion $[Fe_2(\mu\text{-CO})(CO)_6(\mu\text{-PBu}^t_2)]^-$ with H^+ and $[M(PPh_3)]^+$, (M = Cu, Ag, Au), respectively, are described. The new complexes have been characterized by various spectroscopic methods and the structure of $[Fe_2\{\mu\text{-Ag}(PPh_3)\}(\mu\text{-CO})(CO)_6(\mu\text{-PBu}^t_2)]$ has been established by X-ray analysis.

Phosphido-bridged di-iron anions of type $[Fe_2(\mu\text{-CO})(CO)_6(\mu\text{-PR}_2)]^-$ first reported by Osterloh[1] in 1982 (R = Ph), obviously offer a wealth of reactivity. Baker *et al.*[2–4] have recently reported oxidation with $[Fecp_2][BF_4]$ to give a new family of 33e dinuclear radicals $[Fe_2(CO)_7(\mu\text{-PR}_2)]$, which has been extensively investigated by electron spin resonance and molecular orbital studies, ligand substitution reactions as well as structural and electrochemical studies. The same authors described

* Author to whom correspondence should be addressed.

substitution reactions which lead by opening the iron–iron bond to disubstituted di-iron complexes $NEt_4[Fe_2(CO)_6L_2(\mu\text{-}PPh_2)]$ ($L = PPh_3$, PMe_3, $P(OMe)_3$). Photolysis of these complexes results in ligand loss and formation of the substituted anionic complexes $NEt_4[Fe_2(\mu\text{-}CO)(CO)_5L(\mu\text{-}PPh_2)]$ and $NEt_4[Fe_2(\mu\text{-}CO)(CO)_4L_2(\mu\text{-}PPh_2)]$, respectively. We expect these anions to have ambident nucleophilic reactivity as described in structures A and B.

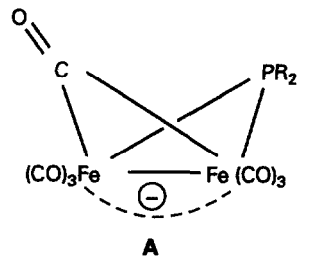

A

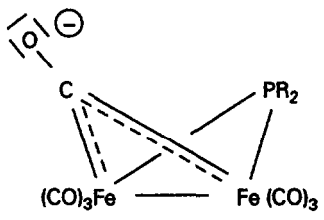

B

Osterloh[1] found that the oxygen-based nucleophilic reaction with $[R_3O][BF_4]$ afforded alkoxymethylidine complexes $[Fe_2(CO)_6(\mu\text{-}COR)(\mu\text{-}PPh_2)]$ which isomerized on heating into the acyl complexes $[Fe_2(CO)_6(\mu\text{-}\eta^2\text{-}COR)(\mu\text{-}PPh_2)]$.

In this paper we show that the reaction of chlorophosphane-substituted nickel carbonyl complexes with the di-iron octacarbonyl dianion does not give heteronuclear iron–nickel complexes but gives either $[Fe_2(CO)_6(\mu\text{-}PR_2)_2]$ or $Na[Fe_2(\mu\text{-}CO)(CO)_6(\mu\text{-}PR_2)]$. A new synthesis of the di-iron anions $[Fe_2(CO)_7(\mu\text{-}PR_2)]^-$ is presented. The metal-based nucleophilic reactions of the anionic complex $Na[Fe_2(\mu\text{-}CO)(CO)_6(\mu\text{-}PBu^t_2)]$ with the electrophilic agents H^+ and $[M(PPh_3)]^+$ (M = Cu, Ag, Au) to yield the hydride complex and the triangular Fe_2M clusters of the coinage metals, respectively, are described. The structure of the Fe_2Ag cluster has been determined by X-ray crystal analysis. In order to come to a better understanding of the bonding properties of the di-iron anions an EHMO calculation on the model anion $[Fe_2(\mu\text{-}CO)(CO)_6(\mu\text{-}PH_2)]^-$ has been performed.

EXPERIMENTAL

All reactions were performed under oxygen-free argon using conventional Schlenk techniques. Solvents were dried over molecular sieves or over sodium/benzophenone ketyl and distilled under argon prior to use. Melting points were recorded in sealed capillaries under argon and are uncorrected. Starting materials were either commercially available or were prepared according to literature procedures: Bu^t_2PCl,[5] Cy_2PCl,[6] Ph_2PCl,[7] Me_2PCl,[8] $Na_2[Fe_2(CO)_8]$,[9] $Na_2[Fe(CO)_4]\cdot 1.5C_4H_8O_2$,[10] [PPN]Cl,[11] $[\{CuCl(PPh_3)\}_4]$,[12] $[\{AgCl(PPh_3)\}_4]$,[13] $[AuCl(PPh_3)]$.[14]

IR spectra were obtained using an IR 71 of VEB Carl Zeiss Jena. ^1H and ^{31}P NMR spectra were recorded on the Bruker spectrometers WP 200 (^1H at 200.1 MHz, ^{31}P at 81.0 MHz) and AC 80 (^1H at 80.1 MHz, ^{31}P at 32.4 MHz). Chemical shift references are the absolute frequencies of Me_4Si (^1H) and external 85% H_3PO_4(aq)(^{31}P), respectively. Positive shifts are to lower field. The EI mass spectra were obtained with a Hewlett Packard spectrometer 5995 A. FAB MS were obtained with a Finnigan MAT 8430 instrument (Bremen, Germany). Xenon was used for neutral beam production with a beam energy of 8 kV. 3-Nitrobenzylalkohol (NBA) and 2-nitro-*n*-octylether (NOE), respectively, were used as liquid matrix. Mössbauer spectra were recorded at room temperature using a constant acceleration spectrometer with a source of ^{57}Co in rhodium. All isomer shifts are quoted relative to natural iron at room temperature. Absorbers containing less than 10 mg cm^{-2} of natural iron were used for all spectra. The spectra have been fitted to Lorentzian line shapes using an iterative least-squares program. The intensity of the quadrupole doublets were constrained to be equal which is a good assumption for a powdered random sample. The relative proportions of the different components were calculated from peak areas, assuming that all iron species have similar Lamb–Mössbauer factors, which could give rise to an inaccuracy of $\pm 5\%$.

$[Ni(CO)_{4-n}(R_2PCl)_n]$ (**1a–c**, **2a,b**)

These complexes were synthesized according to the procedure used by Ehrl and Vahrencamp[15] for the synthesis of $[Ni(CO)_3(Me_2PCl)]$ by stirring *ca* 10 mmol $[Ni(CO)_4]$ with R_2PCl in the appropriate molar ratio (**1** : 1 : 2 ; **2** : 1 : 1) in diethylether, usually at room temperature in the dark for 1 h (**2**) and 3 h (**1**), respectively. Only the synthesis of **1a** requires refluxing for an additional 4 h after having stirred the mixture for 1 h at room temperature. The CO evolution was monitored by gas volumetric measurements. Subsequently, all volatile materials were removed *in vacuo*, and the residue was dissolved in a minimum quantity of pentane (*ca* 5–10

cm^3). The cold solvent was decanted off, and the white crystals were dried *in vacuo*, keeping them cold and in the dark. The yield is about 80%. Complexes **1** and **2** proved to be fairly unstable both thermally and photolytically and have to be stored below 0°C. $[Ni(CO)_3(Ph_2PCl)]$ appeared too unstable for separation. The analytical and physical data are summarized in Table 1.

Reaction of $[Ni(CO)_2(Bu^t_2PCl)_2]$ (**1a**) *with* $Na_2[Fe_2(CO)_8]$

Complex **1a** (0.48 g, 1 mmol) was added to a suspension of $Na_2[Fe_2(CO)_2]$ (0.38 g, 1 mmol) in 20 cm^3 THF and stirred in the dark at room temperature for 5 h. The deep red–brown mixture was filtered and the solvent was removed *in vacuo*. The sticky residue became microcrystalline by stirring in pentane. After repeated extractions with small amounts of pentane until the solvent remained colourless, the crystals were collected by filtration and dried *in vacuo*. Yield 0.48 g Na[**3a**] (~ 100%). Characterization s. below. The other reactions, summarized in eq. (1), were carried out similarly.

Preparation of Na(K,PPN)[**3a–d**]

(A) An equimolar amount of R_2PCl (0.36 g Bu^t_2PCl, 0.46 g Cy_2PCl, 0.43 g Ph_2PCl, 0.19 g Me_2PCl) was added dropwise to a suspension of 0.69 g (2 mmol) $Na_2[Fe(CO)_4]\cdot 1.5$ dioxane in 30 cm^3 THF, and the mixture was stirred for 2 h. The bright yellow solution changed colour to red–brown after the addition of $[Fe(CO)_5]$ (0.27 cm^3, 2 mmol) or $[Fe_2(CO)_9]$ (0.72 g, 2 mmol), respectively. On stirring for 24 h, the solution was irradiated (Hg lamp) for 5 h. During this time the colour turned deep brown. The reaction mixture was subsequently evaporated to dryness under reduced pressure and the residue suspended in 20 cm^3 pentane, filtered and then washed with an additional 20 cm^3 pentane. After drying *in vacuo* the microcrystalline pyrophoric solids Na(K)[**3a–d**] (yield nearly 100%) were used directly for further reactions, or were dissolved in 10 cm^3 degassed methanol, filtered and the filtrate treated with 1.15 g (2.1 mmol) [PPN]Cl. The resulting crystals of PPN[**3a–d**] were collected by filtration, washed with methanol and dried *in vacuo*.

(B) A solution of 0.72 g (2 mmol) $[Fe_2(CO)_9]$ and an equimolar amount of R_2PH (0.37 g Bu^t_2PH, 0.37 g Ph_2PH) in 30 cm^3 THF were stirred at room temperature for 2 h. The solvent and the $[Fe(CO)_5]$ formed during reaction were removed *in vacuo*, and the residue was redissolved in 30 cm^3 THF. This solution was treated with an excess of KH (*ca* 0.1 g) for 2 h, giving a deep red solution of K[$Fe(CO)_4(PR_2)$] which was filtered and handled after addition of 0.72 g (2 mmol) $[Fe_2(CO)_9]$ as described above. The yields were similar to method A. Complexes Na(K)[**3a–d**] were highly air sensitive in both solid state and solution whereas PPN[**3a–d**] are stable as solids but moderately air sensitive in solution.

Table 1. Analytical and physical data of $[Ni(CO)_{4-n}(R_2PCl)_n]$ (n = 2, **1a–c**; n = 1, **2a,b**)

Compound	M.p. (dec.) (°C)	Analytical data[a] C	H	Cl	P	NMR data (ppm)[b] ^1H	^{31}P	IR ν(CO) (cm^{-1})
1a $[Ni(CO)_2(Bu^t_2PCl)_2]$	97–101	45.2 (45.4)	7.0 (6.8)	14.6 (14.9)	13.1 (13.0)	1.33d[c]	177.26s	2000(s), 1942(s)[e]
1b $[Ni(CO)_2(Cy_2PCl)_2]$	101–104	53.4 (53.8)	7.9 (7.6)	12.2 (12.2)	10.4 (10.6)		154.5s	2011(s), 1950(s)[e]
1c $[Ni(CO)_2(Ph_2PCl)_2]$	99–101	55.7 (56.1)	4.0 (3.6)	12.5 (12.8)	11.1 (11.1)		110.0s	2004(s), 1946(s)[e]
2a $[Ni(CO)_3(Bu^t_2PCl)]$	~ 10	41.0 (40.8)	5.4 (5.6)	11.2 (11.0)	9.3 (9.6)	1.05d[d]	175.95s	2065(s), 1990(s), 1985(s)[f]
2b $[Ni(CO)_3(Cy_2PCl)]$	48–50	47.9 (48.0)	6.3 (5.9)	10.0 (9.4)	8.2 (8.2)		150.0s	2075(s), 1990(s), 1955(d)[f]

[a] Calculated figures in parentheses.
[b] ^1H: C_6D_6; ^{31}P: C_6D_6.
[c] $^3J(PH)$ 13.6 Hz.
[d] $^3J(PH)$ 14.9 Hz.
[e] Nujol mull.
[f] Pentane.

Table 2. Analytical and physical data of PPN[**3a–d**]

Compound		Colour	Yield, g (%)	M.p. (dec.) (°C)	Analytical data[a] C	H	N	P
PPN[**3a**]	$PPN[Fe_2(CO)_7(\mu\text{-}PBu^t_2)]$	brick-red	1.60 (80)	138–140	61.6	4.9	1.4	9.6
					(61.8)	(4.9)	(1.4)	(9.4)
PPN[**3b**]	$PPN[Fe_2(CO)_7(\mu\text{-}PCy_2)]$	brown	1.25 (60)	134–136	63.8	4.7	1.4	9.3
					(63.3)	(5.0)	(1.3)	(8.9)
PPN[**3c**]	$PPN[Fe_2(CO)_7(\mu\text{-}PPh_2)]$	deep red	1.64 (80)	121–123	63.1	4.1	1.5	8.9
					(64.6)	(3.9)	(1.3)	(9.0)
PPN[**3d**]	$PPN[Fe_2(CO)_7(\mu\text{-}PMe_2)]$	orange–yellow	1.10 (60)	130–135	59.1	4.2	1.6	10.4
					(59.5)	(4.0)	(1.5)	(10.0)
4a	$[Fe_2(CO)_7(H)(\mu\text{-}PBu^t_2)]$	deep red	0.34 (75)	89	40.0	4.5		6.4
					(39.7)	(4.2)		(6.8)
5	$[Fe_2(\mu\text{-}CuPPh_3)(CO)_7(\mu\text{-}PBu^t_2)]$	red–violet	0.20 (25)	146–148	50.6	4.3		7.6
					(50.9)	(4.3)		(7.9)
6	$[Fe_2(\mu\text{-}AgPPh_3)(CO)_7(\mu\text{-}PBu^t_2)]$	red–violet	0.42 (51)	172–175	48.3	4.1		7.2
					(48.1)	(4.0)		(7.5)
7	$[Fe_2(\mu\text{-}AuPPh_3)(CO)_7(\mu\text{-}PBu^t_2)]$	red–violet	0.57 (62)	179–182	43.0	3.7		6.4
					(43.4)	(3.6)		(6.8)

[a] Calculated figures in parentheses.

These complexes are well soluble in THF and CH_2Cl_2 but not in diethylether and hexane. Analytical and physical data of PPN[**3a–d**] are given in Table 2.

$[Fe_2(CO)_7(H)(\mu\text{-}PBu^t_2)]$ (**4a**)

A solution of $Na[Fe_2(CO)_7(\mu\text{-}PBu^t_2)]$ (**3a**) (0.48 g, 1 mmol) and CH_3COOH (0.12 g, 2 mmol) in *ca* 20 cm^3 THF was rigorously stirred for 30 min. Subsequently, the solvent was removed *in vacuo*, and the residue was three times extracted with 10 cm^3 pentane. The combined extracts were filtered and evaporated *in vacuo* until 5 cm^3 remained. Deep red crystals of **4a** were obtained at −78°C. Further details are given in Table 2.

$[Fe_2(CO)_7(H)(\mu\text{-}PPh_2)]$ (**4c**)

The solution of NEt_4[**3c**] (0.62 g, 1 mmol) and CF_3COOH (0.23 g, 2 mmol) in 30 cm^3 THF was stirred for 3 h. The solvent was removed *in vacuo* and the residue was extracted three times with 10 cm^3 pentane. Evaporation of the filtered pentane extracts gave a deep red oily material (m.p. < −40°C) which was characterized by spectroscopic means.

Air-oxidation of complex **4c**

Dried air was bubbled through a THF solution of **4c** for 1 h. The solution was filtered, and the solvent was removed *in vacuo*. The residue was three times extracted with pentane, and the combined extracts were reduced *in vacuo* to 5 cm^3. $[Fe_2(CO)_6(\mu\text{-}OH)(\mu\text{-}PPh_2)]$ crystallized at −78°C. M.p. 123°C (dec.). IR (hexane, cm^{-1}): 2073 (vs), 2070 (m, sh), 2033 (vs), 2000 (s), 1994 (s), 1984 (s, sh), 1977 (vs). ^1H NMR (CD_2Cl_2): δ −2.16 (d, ^3J(PH) 11.8 Hz, FeH), 7.5 (m, Ph). ^{31}P NMR ($CHCl_3$): δ 121.8 s.

$[Fe_2\{\mu\text{-}M(PPh_3)\}(\mu\text{-}CO)(CO)_6(\mu\text{-}PBu^t_2)]$ (M = Cu, **5**; Ag, **6**; Au, **7**)

The suspension of Na[**3a**] (0.72 g, 1.5 mmol) and $[MCl(PPh_3)]$ (0.36 g (Cu), 0.41 g (Ag), 0.5 g (Au), 1 mmol) in 30 cm^3 THF was stirred at room temperature in the dark for 5 (Cu), 4 (Ag), and 3 (Au) h, respectively. After filtration, the solution was evaporated to dryness, the residue washed with pentane, and repeatedly extracted with small amounts of diethylether until the ether remains nearly colourless. Complexes **5–7** crystallize from these solutions at −30°C. **5** and **6** require purification by repeated recrystallization from pentane/diethylether mixture. For further details and analytical data see Table 2.

X-ray analysis of **6**

Crystal data. $C_{33}H_{33}AgFe_2O_7P_2$, F.W. = 823.1, triclinic, space group $P\bar{1}$, a = 12.714(2), b = 14.667(2), c = 10.121(2) Å, α = 96.79(1), β =

113.14(1), γ = 88.68(1)°, V = 1722.6(4) Å^3, Z = 2, D_{calc} = 1.59 g cm^{-3}, $F(000)$ = 832, λ(Mo-K_α) = 0.71069 Å, μ(Mo-K_α) = 15.2 cm^{-1}.

Measurements. A red cubic crystal with approximate dimensions 0.15 × 0.15 × 0.15 mm was mounted in a glass capillary. All measurements were done on a Rigaku AFC6R diffractometer with graphite monochromated Mo-K_α radiation at 296 K. Cell constants and orientation matrix were obtained from a least-squares treatment of the setting angles for 25 reflections in the range 37.8 < 2θ < 43.2°. Intensity data were measured using the ω–2θ scan technique up to 50° in 2θ. A total of 6334 reflections delivered a set of 6036 unique intensity data (R_{int} = 0.039), 4026 of them were considered observed ($I \geq 3.00\sigma(I)$). Lorentz and polarization corrections were applied during the process of data reduction.

Solution and refinement of the structure. The structure was solved by direct methods[16,17] and refined by full-matrix least-squares techniques with anisotropic displacement parameters for the non-H atoms. The displacement parameters of the H-atoms all found in a difference map were refined isotropically. For the refinement 9.17 reflections/parameter were available. The applied weighting scheme was based on counting statistics and included a factor to downweight the intense reflections. The final R was 0.048 (R_w = 0.056). A final difference map had maximum peak heights of 1.11 and −1.31 e Å^{-3}, respectively. The maximum shift/error ratio in the last 1.s. cycle was 0.01. Scattering factors including corrections for anomalous dispersion effects were taken from ref. 18. All calculations were performed using the TEXSAN[19] crystallographic software package of Molecular Structure Corporation. Tables of atomic coordinates and displacement parameters, lists of observed and calculated structure factors as well as a complete list of bond lengths and angles have been deposited with the editor, atomic coordinates also with the Cambridge Crystallographic Data Centre.

RESULTS AND DISCUSSION

Synthesis

In an attempt to prepare the electron precise heteronuclear cluster $[Fe_2Ni(CO)_8(\mu\text{-}PBu^t_2)_2]$ by "bridge-assisted" synthesis from $[Ni(CO)_2(Bu^t_2PCl)_2]$ (**1a**) and $Na_2[Fe_2(CO)_8]$ in tetrahydrofurane we unexpectedly obtained the di-iron anion $[Fe_2(\mu\text{-}CO)(CO)_6(\mu\text{-}PBu^t_2)]^-$ (**3a**) as the sodium salt Na[**3a**]. This result prompted further investigation of the reaction of $[Ni(CO)_{4-n}(R_2PCl)_n]$ (n = 2, **1**; n = 1, **2**) with $Na_2[Fe_2(CO)_8]$. Thus, complexes **1b,c** gave under analogous conditions the well-known neutral bis(phosphido)-bridged di-iron complexes $[Fe_2(CO)_6(\mu\text{-}PR_2)_2]$. On the other hand, treatment of the monosubstituted nickel carbonyl complexes **2** with $Na_2[Fe_2(CO)_8]$ showed no reaction with **2a** and the formation of Na[**3b**] from **2b**, respectively. The reactions discussed are summarized in eq. (1).

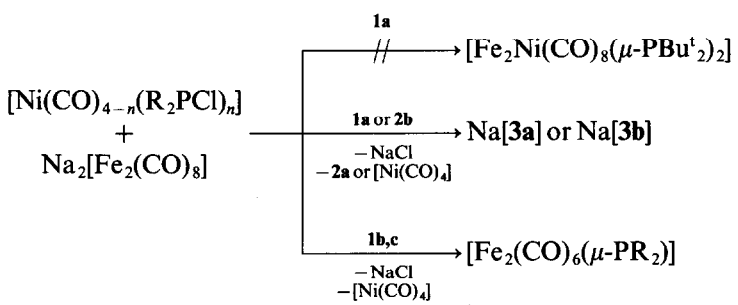

(1)

R	Bu^t	Cy	Ph	Me
	a	b	c	d

(throughout this work)

These reactions show (i) distinct differences in the reactivity of $[Ni(CO)_{4-n}(R_2PCl)_n]$ with $Na_2[Fe_2(CO)_8]$ depending on n and R and (ii) that they neither provide heteronuclear FeNi complexes nor a general procedure for the phosphido-bridged di-iron anions **3**.

The mechanism of these reactions remains unknown. However, in summary, one or two ligand exchange steps of R_2PCl for CO occur to give $[Ni(CO)_{5-n}(R_2PCl)_{n-1}]$ and Na[**3**] or $[Fe_2(CO)_6(\mu\text{-}PR_2)_2]$. The latter two products are formed by conversion of R_2PCl into the R_2P^- ligand through

NaCl elimination. The $[Ni(CO)_{5-n}(R_2PCl)_{n-1}]$ by-products were either detected *in situ* by ^{31}P NMR ($n = 2$) or by IR spectroscopy ($n = 1$) as constituents of the volatile material obtained by evacuation of the reaction mixture. $NEt_4[Fe_2(\mu\text{-}CO)(CO)_6(\mu\text{-}PPh_2)]$, obviously an anionic complex of type **3**, had already been synthesized by Osterloh[1] in 1982 by treatment of $(NEt_4)_2[Fe_2(CO)_8]$ with Ph_2PCl via $NEt_4[Fe_2(CO)_8(\mu\text{-}PPh_2)]$ as an isolable intermediate. This procedure has later been used by Baker *et al.*[3] for the *in situ* preparation of the di-iron anions **3** with R = Et, Ph, Cy, Bu^t. To our knowledge, the preparation and characterization of these anionic di-iron complexes have not yet been published. This, together with the poor yields of anions **3** [isolated as bis(triphenylphosphane)immonium (PPN^+) salts] we obtained by reacting R_2PCl with $Na_2[Fe_2(CO)_8]$ (PPN[**3a**] 45%, PPN[**3b**] zero %, PPN[**3c**] 10%), lead us to suggest a synthetic method on the basis of the anion $[Fe(CO)_4(PR_2)]^-$ as outlined in eq. (2).

$$\begin{array}{l} Na_2[Fe(CO)_4] + R_2PCl \xrightarrow[-NaCl]{} \\ [Fe(CO)_4(R_2PH)] + KH \xrightarrow[-H_2]{} \end{array} \xrightarrow{THF,\ r.t.,\ 2h} [Fe(CO)_4(PR_2)]^- \qquad (2)$$

$$[Fe(CO)_4(PR_2)]^- \xrightarrow{24\,h;\ +[Fe_2(CO)_9]\ -[Fe(CO)_5],\ \text{or}\ +[Fe(CO)_5],} [Fe_2(CO)_8(\mu\text{-}PR_2)]^- \xrightarrow[-CO]{hv,\ 5h} Na(K)[\mathbf{3a\text{–}d}] \xrightarrow[-Na(K)Cl]{PPNCl} PPN[\mathbf{3a\text{–}d}]$$

The protonation reaction of anionic binuclear complexes and clusters has been frequently employed to produce neutral hydride complexes. Accordingly, complex Na[**3a**] reacts at room temperature in THF with acetic acid to afford crystalline $[Fe_2(\mu\text{-}CO)(CO)_6(H)(\mu\text{-}PBu^t_2)]$ (**4a**) in good yield.

Although the spectroscopic data of complex **4a** (see below) do not allow a decision concerning the coordination mode of the hydride ligand (terminal or bridging) the observed high-field shift for this ligand in the ^1H NMR spectrum gives evidence for a direct iron–hydrogen bond. This result is of interest in the light of the reports on related complexes in the literature. In 1972 Treichel *et al.*[20] reported the synthesis of complexes $[Fe_2(CO)_6(\mu\text{-}H)(\mu\text{-}PR_2)]$ (R = Me, Et, Ph) and one year later found by X-ray analysis of the complex $[Fe_2(CO)_6(\mu\text{-}OH)\{\mu\text{-}P(p\text{-}C_6H_4Me)_2\}]$ that these compounds actually bear a bridging hydroxy ligand.[21] The origin of the oxygen atom remained unknown. Osterloh[1] described, that the reaction of NEt_4[**3c**] with $HBF_4 \cdot OEt_2$ in THF gave the same complex $[Fe_2(CO)_6(\mu\text{-}OH)(\mu\text{-}PPh_2)]$ as reported,[20,21] and noted that the mechanism by which this complex is formed is not known.

These results stimulated further investigation of these complexes. Contrary to the μ-PBu^t_2-bridged anion **3a** the μ-PPh_2-bridged complexes $Na(NEt_4)$ [**3c**] do not react with acetic acid but react readily with CF_3COOH to result under anaerobic conditions a deep red oily material. All attempts to crystallize this compound have failed until now. On the basis of the spectroscopic data, this complex is assigned an analogous constitution $[Fe_2(\mu\text{-}CO)(CO)_6(H)(\mu\text{-}PPh_2)]$ (**4c**) to that of the hydride complex **4a**.

Evidence that the above-mentioned μ-OH bridged complexes were formed by air-oxidation of the hydride complexes in the course of their preparation[1,20] comes from the systematic oxidation of the hydride **4c**. Bubbling dry air through a THF solution of this hydride for 1 h gave orange–red $[Fe_2(CO)_6(\mu\text{-}OH)(\mu\text{-}PPh_2)]$ which was identified by identical IR, ^1H and ^{31}P NMR data with those previously reported.[1,20]

Treatment of the THF solution of Na[**3a**] with the electrophilic complexes $[\{MCl(PPh_3)\}_n]$ (M = Cu, Ag, $n = 4$; M = Au, $n = 1$) yielded the triangular 46e clusters $[Fe_2\{\mu\text{-}M(PPh_3)\}(\mu\text{-}CO)(CO)_6(\mu\text{-}PBu^t_2)]$ (M = Cu, **5**; Ag, **6**; Au, **7**) as deep red–violet crystals. Similar coinage metal clusters have very recently been reported by another group.[22]

Spectroscopy

The new complexes were characterized by elemental analysis (see Experimental) as well as by IR, ^1H, $^{31}P\{^1H\}$ NMR (Table 3), and mass spec-

Table 3. Spectroscopic data of complexes PPN[**3a–d**] and **4a,c**

Complex		IR (cm^{-1})[a]		^{1}H NMR		^{31}P NMR	
		ν(t-CO)	ν(μ-CO)	δ (ppm)	$^{2/3}J$(PH), Hz	δ (ppm)	^3J(PP), Hz
PPN[**3a**]	PPN[$Fe_2(CO)_7(\mu\text{-}PBu^t_2)$]	2000(vs), 1952(vs,br), 1902(s,br), 1880(w)	1720(vs)	1.43d(PBu^t_2)[b] 7.6br(PPN)	13.0	239.5s[b]	
PPN[**3b**]	PPN[$Fe_2(CO)_7(\mu\text{-}PCy_2)$]	2004(vs), 1950(vs), 1914(s), 1888(s)	1724(vs)			160.2s[b]	
PPN[**3c**]	PPN[$Fe_2(CO)_7(\mu\text{-}PPh_2)$]	2016(vs), 1964(vs,br), 1928(s), 1904(w), 1892(w)	1724(vs)			125.3s[b]	
PPN[**3d**]	PPN[$Fe_2(CO)_7(\mu\text{-}PMe_2)$]	2008(vs), 1956(s), 1920(s), 1904(vs), 1880(vw)	1716(vs)	1.85d(PMe_2)[c] 6.9br(PPN)	8.6	100.0[b]	
4a	[$Fe_2(CO)_7(H)(\mu\text{-}PBu^t_2)$]	2074(vs), 2040(vs), 2004(s), 1996(s), 1984(vs)	1804(vs)	1.14d(PBu^t_2)[d] −10.7d(HFe)	13.0 51.0	206.0s[e]	
4c	[$Fe_2(CO)_7(H)(\mu\text{-}PPh_2)$]			−10.0d(HFe)[d]	54.1	166.0[e]	
5	[$Fe_2(\mu\text{-}CuPPh_3)(CO)_7(\mu\text{-}PBu^t_2)$]	2032(vs), 1988(s), 1972(s), 1952(w), 1934(s), 1922(s)	1756(vs)	1.35d(PBu^t_2)[d]	13.8	239.5d(PBu^t_2)[e] 0.2br(PPh_3)	10.4
6	[$Fe_2(\mu\text{-}AgPPh_3)(CO)_7(\mu\text{-}PBu^t_2)$]	2028(vs), 1986(m), 1966(s), 1948(w), 1932(s)	1744(vs)	1.4d(PBu^t_2)[d]	13.8	251.3(PBu^t_2)[e,g] 10.63dd(PPh_3)[h] 10.23dd(PPh_3)[h]	9.25
7	[$Fe_2(\mu\text{-}AuPPh_3)(CO)_7(\mu\text{-}PBu^t_2)$]	2036(vs), 2000(s), 1968(m), 1956(w), 1940(s,br)	1766(vs)	1.36d(PBu^t_2)[d]	13.5	243.5d(PBu^t_2)[e] 52.8d(PPh_3)	20.3

[a] Nujol mull.
[b] $CDCl_2$.
[c] CH_2Cl_2.
[d] C_6D_6.
[e] C_6H_6.
[f] CD_2Cl_2.
[g] Pseudo-triplet, ^2J(AgP) 12.4 Hz (av.).
[h] $J(^{109}AgP)$ 482.8 Hz, $J(^{107}AgP)$ 418.0 Hz.

troscopy. The structure of $[Fe_2\{\mu\text{-}Ag(PPh_3)\}(\mu\text{-}CO)(CO)_6(\mu\text{-}PBu^t_2)]$ (**6**) was determined by X-ray structure determination.

The FAB mass spectra of the anionic complexes PPN[**3a–d**] show in the spectra of the positive ions the $(PPN)^+$ with high abundance (100%). The spectra are nearly matrix-free and display only a few fragments of low abundance (< 10%). In the negative ion mode the characteristic feature of FAB–MS is obtained, i.e. superposition of matrix and sample spectra. The signals of the anions **3a–d** were recorded with a relative abundance in the range of 20–60%. Successive loss of up to three carbonyl ligands is the only degradation process that can be observed. In all cases, for this fragmentation the same course of intensity is displayed, the $(3\text{-}CO)^-$ ion being the most abundant peak. In order to produce this ion it is likely that the bridging carbonyl ligand is being lost to generate a fragment having a formal iron–iron double bond. Ions of the type $(M+3)^-$ and $(M+PPN)^+$, respectively, could not be detected.

Among the ν(CO) bands of complexes PPN [**3a–c**] that near 1720 cm^{-1} indicates a μ-CO ligand. Similar anions with other bridging ligands have been reported recently, and all of them show a band in the $\nu(\mu\text{-CO})$ region.[23] The ^{31}P NMR spectra reveal two signals; one at δ 21.0 for the PPN cations, and the other one at low field indicative of phosphido groups bridging a metal–metal bond.[24–26]

The EI mass spectrum of the hydride complex **4a** shows the molecular peak at $m/z = 454$ followed by a sequence of seven peaks arising from the successive loss of all carbonyl ligands. The remaining fragment ion $HFe_2(PBu^t_2)^+$ ($m/z = 258$) appears with relatively high intensity (8.65%), and fragments further by either loss of Bu^t ($m/z = 57$, base peak) or isobutene $C_4H_8^+$ ($m/z = 56 \triangleq Fe^+$) to leave the fragment ions $HFe_2(PBu^t)^+$ ($m/z = 201$) and $H_2Fe_2(PBu^t)^+$ ($m/z = 202$), respectively. The ^{31}P NMR spectrum displays a singlet at low field again indicating that the phosphido ligand bridges the iron–iron bond. The ^1H NMR spectrum consists of two doublets, one for the protons of the μ-PBu^t_2 ligand and the other one at high field for the hydride ligand. The similarity of the structures of **4a** and **4c** is particularly supported by the signals of the hydride ligands at δ *ca* −10 ppm in the ^1H NMR spectra. For the complex $[Fe_2(CO)_6(\mu\text{-}OH)(\mu\text{-}PPh_2)_2]$ proton signals at δ −2.40 ppm (J(PH) 11.5 Hz)[1] and −2.58 ppm (J(PH) 11.0 Hz),[20] respectively, had been assigned to the μ-OH ligand.

The position of the hydride ligand in complexes **4a,c** could not be elucidated with certainty. Therefore it seemed meaningful to investigate the related coinage metal complexes due to the observation that in almost all clusters where structural comparisons are available the $Au(PPh_3)$ unit occupies a similar position to that of the isolobal hydrido ligand in the related hydrido compound.[27]

The coinage metal clusters **5–7** exhibit a similar band pattern in the ν(CO) region of the IR spectra as do both the starting di-iron anion **3a** and the hydride complex **4a**. Thus five bands appear for terminal CO groups and one for a bridging CO ligand. Due to the positive $M(PPh_3)$ moiety, these bands are shifted to higher wave numbers by about 30 cm^{-1} compared with those of the anionic complex PPN[**3a**]. This could be interpreted in terms of a decrease in the electron density on the iron atoms.

The $^{31}P\{^1H\}$ NMR spectra are as expected, showing one μ-PBu^t_2 environment at low field and one PPh_3 environment. The phosphorus resonance of the PPh_3 ligand coordinated to the M atom appears as a doublet ^3J(PP) for complex **7**, and is split into two double doublets for complex **6** due to both the coupling with ^{109}Ag and ^{107}Ag as well as the ^3J(PP) coupling; for complex **5** this resonance is broad because of the quadrupole moment of the copper nucleus.[28] Accordingly, the signal of the μ-PBu^t_2 ligand appears as a doublet for complexes **5** and **7** ^3J(PP); for complex **6** this resonance appears as a pseudo-triplet due to the superposition of the two double doublets expected from the couplings ^3J(PP) and ^2J(AgP).

The molecular ion of the Fe_2Cu cluster **5** can only be observed in the FAB spectrum of the positive ions. The spectrum is dominated by the matrix and the radical cation $(M)^{+\bullet}$. **5** is detected with less than 5% at m/z 788. Compared with the spectra of complexes **3a–d**, the course of fragmentation is somewhat different. In this case the $(M\text{-}CO)^{+\bullet}$ and the $(M\text{-}3CO)^{+\bullet}$ ions are of very low intensity whereas $(M\text{-}4CO)^{+\bullet}$ provide the base peak in the upper range of the spectrum.

The ^{57}Fe Mössbauer data of compounds PPN[**3a**] and **5–7** are collected in Table 4. The spectra consist of one quadrupole-split doublet corresponding to two equal iron sites which is fully consistent with the crystal structure of the Fe_2Ag cluster **6**. PPN[**3a**] may be thought of as derived from $[Fe_2(CO)_9]$ by replacing two bridging carbonyls by one bridging $Bu^t_2P^-$ ligand. The quadrupole splitting of the anionic complex PPN[**3a**] is roughly three times that observed for $[Fe_2(CO)_9]$ (0.42)[29] but still of the magnitude for a compound with a distorted octahedral environment.[30] A more appropriate description of the coordination sphere around the iron atoms is, ignoring the metal–metal bond, the distorted square pyramid as shown by the X-

Table 4. Room temperature Mössbauer data of complexes PPN[**3a**], **5–7**

	Complex	δ (mm s^{-1})	ΔE_q (mm s^{-1})	Γ (mm s^{-1})	I (%)
PPN[**3a**]	$PPN[Fe_2(CO)_7(\mu\text{-}PBu^t_2)]$	−0.117	1.290	0.271	65.4[a]
5	$[Fe_2(\mu\text{-}CuPPh_3)(CO)_7(\mu\text{-}PBu^t_2)]$	−0.078	0.986	0.261	100
6	$[Fe_2(\mu\text{-}AgPPh_3)(CO)_7(\mu\text{-}PBu^t_2)]$	−0.050	0.967	0.250	82.07[b]
7	$[Fe_2(\mu\text{-}AuPPh_3)(CO)_7(\mu\text{-}PBu^t_2)]$	−0.050	1.006	0.245	100

[a] Impurity: δ −0.334, ΔE_q 0.847, Γ 0.616, I 34.6.
[b] Impurity: δ +0.10, ΔE_q 0.492, Γ 0.27, I 17.93.

ray crystal structure analysis of $NEt_4[Fe_2(\mu\text{-}CO)(CO)_6(\mu\text{-}PPh_2)]$.[1] The lower isomeric shift of the anion compared with $[Fe_2(CO)_9]$ (0.16)[29] reflects a higher s-electron density on the iron atoms. This is most likely to be caused by an increased s-electron density through phosphorus-to-iron σ-donation although a decrease in the shielding of the s-electrons by decreasing the $3d$ electron density through increased π-back donations should also be taken into account. On going from the anionic complex PPN[**3a**] to the coinage metal complexes **5–7** an increase of the isomeric shift is observed. This reflects a decrease in the s-electron density which is qualitatively in accord with the 3c–2e bond description of the $Fe_2(\mu\text{-}Ag)$ core as discussed below.

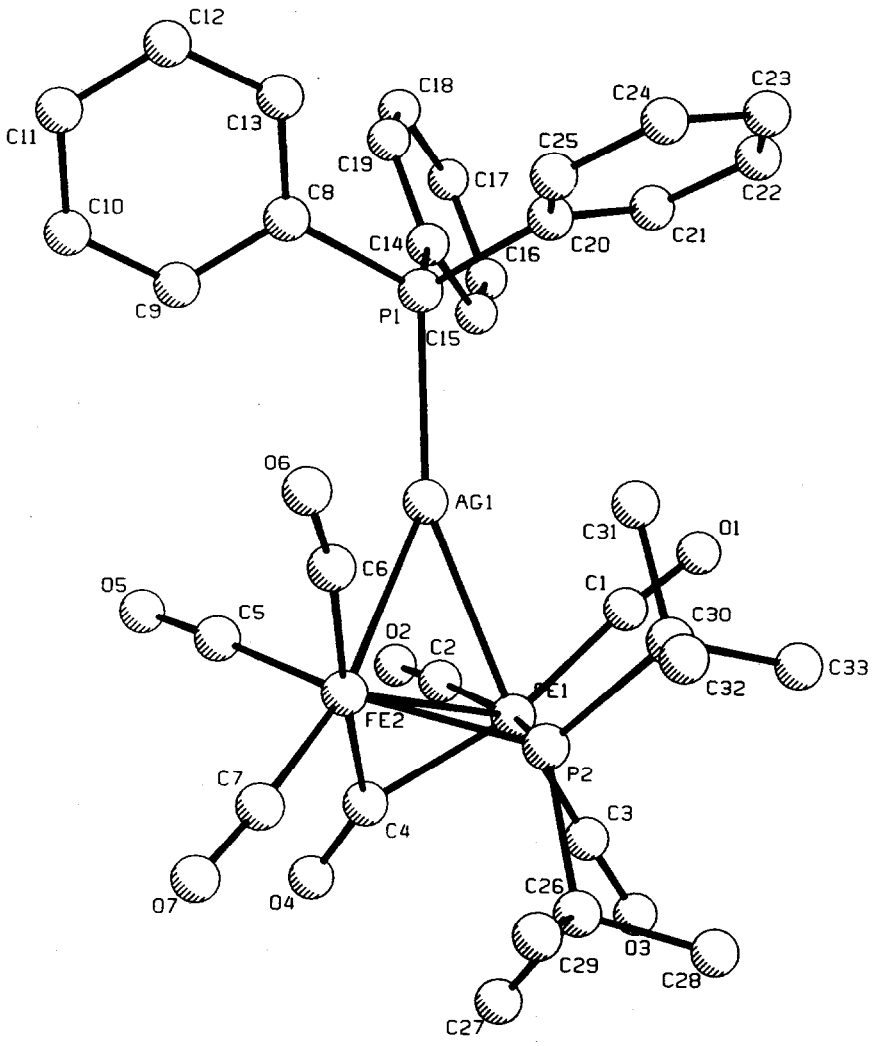

Fig. 1. Molecular structure of **6**.

The structure of $[Fe_2\{\mu\text{-}Ag(PPh_3)\}(\mu\text{-}CO)(CO)_6(\mu\text{-}PBu^t_2)]$ **(6)**

Figure 1 shows the molecular structure of **6** with the atomic numbering scheme. Selected bond lengths and angles are given in Table 5.

The core of the molecule consists of a trinuclear cluster built up of two iron atoms and a silver atom which are positioned at the corners of an almost equilateral triangle. The Fe—Fe bond is double-bridged by both a di-tert.-butylphosphido ligand and a carbonyl group. Besides, the Ag atom is coordinated by a triphenylphosphane ligand and to each iron atom three terminal CO groups are attached. Apart from the organic substituents at the P atoms, the molecule has, in rather good approximation, C_s symmetry with a mirror plane containing atoms Ag, C(4), O(4), P(1) and P(2).

The structure of **6** strongly resembles that of the cation in $[Fe_2(\mu\text{-}Ag)(CO)_6\{\mu\text{-}CHC(NHCH_3)(C_6H_5)\}\mu\text{-}PPh_2)]ClO_4 \cdot C_6H_6 \cdot C_6H_5CH_3$[31] with the only relevant difference that the iron atoms are bridged by a carbonyl group instead of a μ-η^1-alkylidene ligand. Bond lengths in the Fe_2Ag triangles (Ag—Fe(1) = 2.685(1), Ag—Fe(2) = 2.703(1), Fe(1)—Fe(2) = 2.682(1) Å for the cation,[31] for **6** cf. Table 5) are substantially the same and differ by less than 0.03 Å. The Fe—P(2) distances within the phosphido bridge of **6** are about 0.05 Å longer compared with those of the cation and accordingly the Fe(1)—P(2)—Fe(2) angle is more acute by 2.6°. The Ag—P bond length in **6** (2.404(2) Å) is in the range normally observed in silver phosphane complexes (e.g. 2.414(4) Å in $[cp(CO)_2Mo\{\mu\text{-}Ag(PPh_3)\}(\mu\text{-}PPh_2)Mn(CO)_4]$[32]).

The three planes defined by the two iron atoms and one of the corresponding atoms bridging them make the following angles: Fe(1), Fe(2), Ag/Fe(1), Fe(2), P(2) 110.8°, Fe(1), Fe(2), Ag/Fe(1), Fe(2), C(4) 134.5°, Fe(1), Fe(2), Ag/Fe(1), Fe(2), C(4) 114.7°. Surprisingly, the interplanar angle between the planes including the ligator atoms with the most

Table 5. Selected bond lengths (Å) and angles (°) in **6** with estimated standard deviations in parentheses

Ag—Fe(1)	2.693(1)	Fe(1)—C(1)	1.817(7)
Ag—Fe(2)	2.670(1)	Fe(1)—C(2)	1.770(9)
Fe(1)—Fe(2)	2.656(1)	Fe(1)—C(3)	1.749(8)
Ag—P(1)	2.404(2)	Fe(1)—C(4)	1.985(7)
Fe(1)—P(2)	2.271(2)	Fe(2)—C(4)	1.942(7)
Fe(2)—P(2)	2.274(2)	Fe(2)—C(5)	1.809(9)
		Fe(2)—C(6)	1.787(8)
		Fe(2)—C(7)	1.767(7)

Fe(1)—Ag—Fe(2)	59.36(2)	Ag—Fe(2)—Fe(1)	60.75(3)
Fe(1)—Ag—P(1)	154.70(5)	Ag—Fe(2)—P(2)	88.05(5)
Fe(2)—Ag—P(1)	145.23(6)	Ag—Fe—C(4)	97.4(2)
Ag—Fe(1)—Fe(2)	59.89(3)	Ag—Fe(2)—C(5)	74.2(2)
Ag—Fe(1)—P(2)	87.55(6)	Ag—Fe(2)—C(6)	74.2(2)
Ag—Fe(1)—C(1)	71.5(3)	Ag—Fe(2)—C(7)	167.7(3)
Ag—Fe(1)—C(2)	79.1(3)	Fe(1)—Fe(2)—P(2)	54.20(5)
Ag—Fe(1)—C(3)	169.6(2)	Fe(1)—Fe(2)—C(4)	48.1(2)
Ag—Fe(1)—C(4)	95.6(2)	Fe(1)—Fe(2)—C(5)	101.7(3)
Fe(2)—Fe(1)—P(2)	54.30(5)	Fe(1)—Fe(2)—C(6)	125.5(2)
Fe(2)—Fe(1)—C(1)	123.3(2)	Fe(1)—Fe(2)—C(7)	131.2(3)
Fe(2)—Fe(1)—C(2)	104.5(2)	P(2)—Fe(2)—C(4)	82.0(2)
Fe(2)—Fe(1)—C(3)	130.4(2)	P(2)—Fe(2)—C(5)	155.5(3)
Fe(2)—Fe(1)—C(4)	46.8(2)	P(2)—Fe(2)—C(6)	97.9(3)
P(2)—Fe(1)—C(1)	98.9(2)	P(2)—Fe(2)—C(7)	101.8(3)
P(2)—Fe(1)—C(2)	158.8(3)	C(4)—Fe(2)—C(5)	83.6(3)
P(2)—Fe(1)—C(3)	97.8(3)	C(4)—Fe(2)—C(6)	171.6(3)
P(2)—Fe(1)—C(4)	81.2(2)	C(4)—Fe(2)—C(7)	91.3(3)
C(1)—Fe(1)—C(2)	92.5(3)	C(5)—Fe(2)—C(6)	93.4(4)
C(1)—Fe(1)—C(3)	98.8(4)	C(5)—Fe(2)—C(7)	98.3(4)
C(1)—Fe(1)—C(4)	167.1(3)	C(6)—Fe(2)—C(7)	96.9(4)
C(2)—Fe(1)—C(3)	98.0(4)	Fe(1)—P(2)—Fe(2)	71.51(6)
C(2)—Fe(1)—C(4)	83.8(3)		
C(3)—Fe(1)—C(4)	94.0(3)		

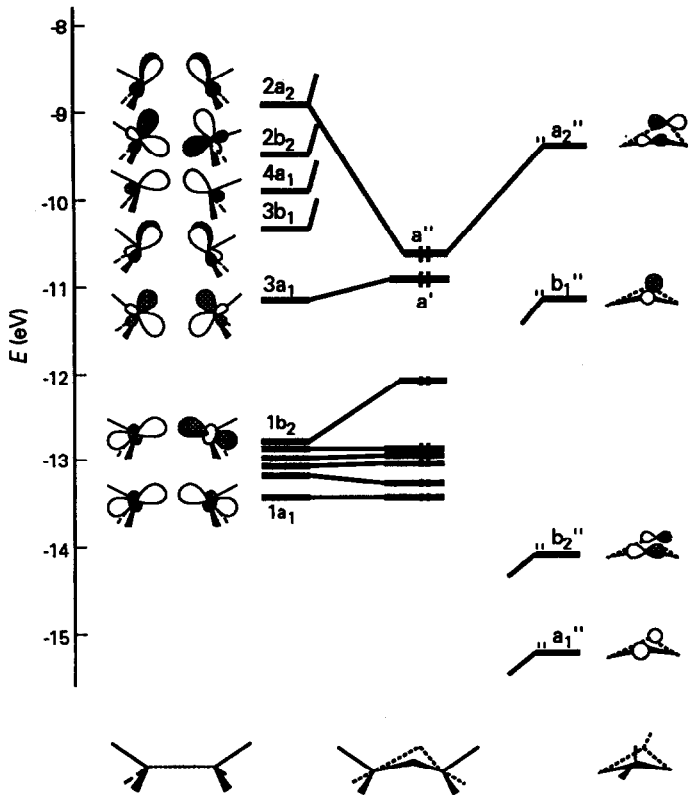

Fig. 2. Molecular orbital diagram of the anion $[Fe_2(\mu\text{-}CO)(CO)_6(\mu\text{-}PH_2)]^-$ build up from a $Fe_2(CO)_6$ fragment and the two bridging ligands CO and PH_2^-. The orbitals of both fragments have been donated according to the point group C_{2v} to make clear the orbital interactions. The orbitals of the anion itself have been donated according to C_s.

bulky substituents (Ag, P(2)) is the smallest. A comparison between the terminal CO groups and the μ-CO with regard to their bond lengths gives the expected result: the former have longer C—O distances (mean value 1.146(8) Å compared with C(4)—O(4) = 1.191(8) Å) but shorter Fe—C distances.

The six Fe—C—O angles expected to be nearby 180° can be classified into two groups: four with values of about 176° and two (at C(1) and C(7)) with stronger deviations from linearity (about 170°). The latter belong to CO groups in *trans*-position to C(4) and the bend might arise from the influence of the triphenyl-phosphane substituent at the silver atom.

The crystal packing consists of isolated molecules without special intermolecular contacts. Preliminary X-ray investigations of the analogous clusters **5** and **7** gave no indication of isomorphism with **6**.

* Standard parameters were used for the calculations. The geometries for the models match that of the X-ray diffraction studies reported in ref. 1 and in the present paper.

Molecular orbital calculations

The ambident nucleophilic reactivity of the anions $[Fe_2(\mu\text{-}CO)(CO)_6(\mu\text{-}PR_2)]^-$ as described in the resonance formulae A and B should be reflected in the electronic structure of the compound. Therefore, we carried out Extended Hückel molecular orbital calculations[33,34] to examine the sources for this ambivalence.*

Figure 2 shows the molecular orbital diagram of the anion built up from the well-known $Fe_2(CO)_6$ fragment[35] and the two bridging ligands CO and PH_2^-, the latter being a model for the phosphido ligands PR_2^-. The di-iron fragment orbitals $2a_2$, $2b_2$, $4a_1$ and $3b_1$ interact with the symmetric and antisymmetric combinations of the σ and π orbitals of the coordinating atoms to form four metal-bridge bonds. Caused by the different energetic position of the phosphido orbitals and the CO orbitals the symmetric combinations of the ligand orbitals are mainly localized at the phosphorus, whereas the antisymmetric combinations are mainly CO in character. The two highest occupied anion orbitals a'' and a' are schematically shown in Fig. 3. The

Fig. 3. The two highest occupied anion orbitals.

HOMO a'' is the bonding combination between the orbitals $2a_2$ of the di-iron fragment and the π^* orbital of the carbonyl ligand. It represents one of the four metal-bridge bonds. The orbital a' is not influenced by interactions with the bridging ligands. It is considered to indicate the bent Fe—Fe bond in the anion, resembling that described for the $[Fe_2(CO)_6(\mu\text{-}PR_2)_2]$ system.[36,37] Both orbitals a' and a'', can act as donor orbitals towards nucleophiles. Figure 4 represents the metal-based reactivity against a "third bridging ligand" $[M(PR_3)]^+$ with a d^{10}-configurated metal ion M^+ (M = Cu, Ag, Au). The LUMO of $[M(PR_3)]^+$ is a σ-acceptor orbital that interacts with the anion orbital a' to form one additional metal-bridge bond. This description of the bonding within the Fe_2M core of complexes **5–7** is in accordance with the bonding situation in heteronuclear gold-metal clusters containing a μ-bridging $Au(PR_3)$ fragment which is generally said to involve a three-centre two-electron bond between the two metal atoms and the gold atom.[38] Thus, the 46 electron count of these triangular clusters follows from the electron deficiency of this bond.

Although the structure of the hydride complex $[Fe_2(\mu\text{-}CO)(CO)_6(H)(\mu\text{-}PBu^t_2)]$ (**4a**) could not be ascertained, this complex might have a similar molecular and electronic structure as discussed for complexes **5–7** due to the isolobal analogy of H^+ and $[M(PPh_3)]^+$ (M = Cu, Ag, Au).

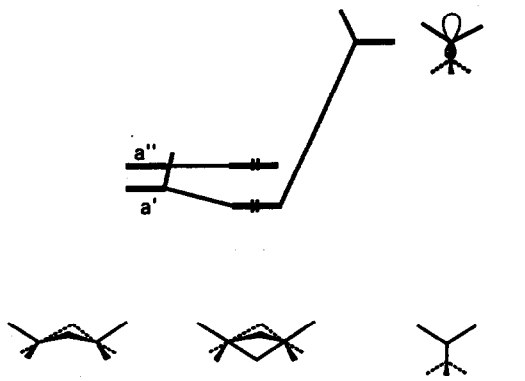

Fig. 4. Schematic plot of the bonding interaction between the anion orbital a' and the LUMO of a bridging $[M(PR_3)]^+$ group (M = Cu, Ag, Au).

The oxygen-based nucleophilicity of anions **3** is understandable by inspecting orbital a'' (Fig. 3). This orbital can be considered to be mainly an oxygen lone pair orbital that is able to donate electronic density from oxygen into the acceptor orbital of e.g. a CR_3^+ group. This is confirmed by the net charges (Mulliken population analysis) of the atoms in the anion model compound: q(Fe) = 0.22, $q(PH_2)$ = 0.02, $q(C_{term})$ = 0.67 (mean value), $q(O_{term})$ = −0.78 (mean value), $q(C_{bridge})$ = 0.20, $q(O_{bridge})$ = −1.03, i.e. the carbonyl bond in the bridging CO is highly polar corresponding to formula **B**.

Acknowledgements—B.W. thanks Dr E. P. Kyba, Fort Worth, Texas, for providing a copy of parts of T. Osterloh's thesis, and Dr R. T. Baker, Wilmington, Delaware, for comments concerning the synthesis of complexes **3**.

REFERENCES

1. W. T. Osterloh, Ph.D. thesis. University of Texas, Austin, TX (1982); University Microfilms International Ann Arbor, MI (1982).
2. R. T. Baker, J. C. Calabrese, P. J. Krusic, M. J. Therien and W. C. Trogler, *J. Am. Chem. Soc.* 1988, **110**, 8392.
3. R. T. Baker, P. J. Krusic, J. C. Calabrese and D. C. Roe, *Organometallics* 1986, **5**, 1506.
4. P. J. Krusic, R. T. Baker, J. C. Calabrese, J. R. Morton, K. F. Preston and Y. LePage, *J. Am. Chem. Soc.* 1989, **111**, 1262.
5. M. Field, O. Stelzer and R. Schmutzler, *Inorg. Synth.* 1973, **14**, 4.
6. K. Issleib and W. Seidel, *Chem. Ber.* 1959, **92**, 2681.
7. M. P. Brown and H. B. Silver, *Chem. Ind.* 1961, 24.
8. G. W. Parshall, *Inorg. Synth.* 1974, **15**, 191.
9. J. P. Collmann, R. G. Finke, P. L. Matlock, R. Wahren, R. G. Komoto and J. J. Baumann, *J. Am. Chem. Soc.* 1978, **100**, 1119.
10. R. G. Finke and T. N. Sorrell, *Org. Synth.* 1980, **59**, 102.
11. J. K. Ruff and W. J. Schlientz, *Inorg. Synth.* 1974, **15**, 84.
12. G. Costa, E. Reisenhofer and L. Stefani, *J. Inorg. Nucl. Chem.* 1965, **27**, 2581.
13. A. Pernick and M. Ardon, *J. Am. Chem. Soc.* 1975, **97**, 1256.
14. A. Davison and J. E. Ellis, *J. Organomet. Chem.* 1972, **36**, 113.
15. W. Ehrl and H. J. Vahrenkamp, *J. Organomet. Chem.* 1963, **63**, 389.
16. C. J. Gilmore, *J. Appl. Cryst.* 1984, **17**, 42.
17. P. T. Beurskens, W. P. Bosman, H. M. Doesburg, R. O. Gould, Th. E. M. van den Hark, P. A. J. Prick, J. H. Nordiik, G. Beurskens and V. Parthasarathi, DIRDIF, Direct methods for difference structures (Technical report 1984/1), Crystallography Laboratory, Toernooiveld, Netherlands (1984).

18. *International Tables for X-ray Crystallography*, Vol. IV, p. 71. The Kynoch Press, Birmingham, England (1974).
19. TEXSAN-TEXRAY *Structure Analysis Package*, Molecular Structure Corporation (1985).
20. P. M. Treichel, W. K. Dean and W. M. Douglas, *Inorg. Chem.* 1972, **11**, 1609.
21. P. M. Treichel, W. K. Dean and J. C. Calabrese, *Inorg. Chem.* 1973, **12**, 2908.
22. M. Ferrer, R. Reina, O. Rossell, M. Seco and X. Solans, *J. Chem. Soc., Dalton Trans.* 1991, 347.
23. D. Seyferth, G. B. Womack, C. M. Archer and J. C. Dewan, *Organometallics* 1980, **8**, 430.
24. P. E. Garrou, *Chem. Rev.* 1981, **81**, 229.
25. A. J. Carty, *Adv. Chem. Res.* 1982, **196**, 163.
26. G. L. Geoffroy, *Organometallics* 1983, **2**, 53.
27. I. D. Salter, *Adv. Organomet. Chem.* 1989, **29**, 249.
28. B. Delavaux, B. Chandret, F. Dahan and R. Poilblanc, *J. Organomet. Chem.* 1986, **317**, 69.
29. T. C. Gibb, R. Greatrex and N. N. Greenwood, *J. Chem. Soc. A* 1968, 890.
30. T. C. Gibb, R. Greatrex, N. N. Greenwood and D. T. Thompson, *J. Chem. Soc. A* 1967, 1663.
31. G. N. Mott, N. J. Taylor and A. J. Carty, *Organometallics* 1983, **2**, 447.
32. A. D. Horton, M. J. Mays, T. Adatia and M. McPartlin, *J. Chem. Soc., Dalton Trans.* 1988, 1683.
33. R. Hoffmann and W. N. Lipscomb, *J. Chem. Phys.* 1962, **36**, 2179.
34. R. Hoffmann, *J. Chem. Phys.* 1963, **39**, 1397.
35. R. H. Summerville and R. Hoffmann, *J. Am. Chem. Soc.* 1979, **101**, 3821.
36. B. K. Teo, M. B. Hall, R. F. Fenske and L. F. Dahl, *Inorg. Chem.* 1975, **14**, 3103.
37. E. L. Anderson, T. P. Fehlner, A. E. Foti and D. R. Salahub, *J. Am. Chem. Soc.* 1980, **102**, 7422.
38. K. P. Hall and D. M. P. Mingos, *Prog. Inorg. Chem.* 1984, **32**, 277.

Polyhedron Vol. 10, No. 20/21, pp. 2437–2450, 1991
Printed in Great Britain

0277–5387/91 $3.00+.00
© 1991 Pergamon Press plc

SUBSTITUTED METAL CARBONYLS—XVIII. RHENIUM 1,1′-BIS(DIPHENYLPHOSPHINO)FERROCENE (DPPF) COMPLEXES DERIVED FROM $[Re_2(CO)_9]$. CRYSTAL STRUCTURES OF TWO ISOMORPHOUS PENTAMETALLIC $[M_2(CO)_9]_2(\mu$-dppf) (M = Mn, Re) AND TRIMETALLIC $Re_2(CO)_9$(dppfO) COMPLEXES

T. S. A. HOR,* H. S. O. CHAN, K.-L. TAN,† L.-T. PHANG and Y. K. YAN

Departments of Chemistry and †Physics, Faculty of Science,
National University of Singapore, Kent Ridge 0511, Singapore

and

L.-K. LIU* and Y.-S. WEN

Institute of Chemistry, Academia Sinica, Taipei 11529, Taiwan, R.O.C.

(*Received* 9 *April* 1991; *accepted* 2 *July* 1991)

Abstract—Amine oxide-assisted decarbonylation of $Re_2(CO)_{10}$ in the presence of 1,1′-bis(diphenylphosphino)ferrocene (dppf) produces, under different conditions, $[Re_2(CO)_9]_2$ (μ-dppf) (**1**), $Re_2(CO)_9(\eta^1$-dppf) (**5**) and its oxidation product $Re_2(CO)_9(\eta^1$-dppfO) (**7**). **1** undergoes an oxidative bridge-scission with Me_3NO to give **7**. X-ray crystallographic analysis of **1** and $[Mn_2(CO)_9]_2(\mu$-dppf) (**2**), included for comparison, revealed that the two molecules are isomorphous, each taking the form of an open and "linear" tetranuclear complex supported alternately by M—M bonds and a "half eclipsed" dppf bridge. Complex **7**, which is trimetallic, consists of dppf (mono)oxide coordinated to $[Re_2(CO)_9]$ through the phosphine site. X-ray Photoelectron Spectra revealed the existence of the chemically inequivalent Re and P sites within the same molecule. The chemically distinct Re centres in **1**, **5**, **7** and $Re_2(CO)_9(CH_3CN)$ are differentiable by their Re($4f_{7/2}$) and Re($4f_{5/2}$) binding energies.

Thermal decarbonylation of substituted metal carbonyls is a subject of our recent interest.[1] Phosphine substitution of $Re_2(CO)_{10}$ almost invariably yields $Re_2(CO)_{10-n}(PR_3)_n$ ($n \leqslant 3$)[2] or the intramolecularly bridged $Re_2(CO)_{10-2n}(P—P)_n$ ($n \leqslant 2$)[3] when diphosphines are used. Most of these substitutions were photo-induced and hence competed with the notorious metal—metal bond homolysis. Some of the supposedly dinuclear complexes so formed have in fact been subsequently found to be mononuclear and/or paramagnetic in the form of the hydrido, orthometallated and oxidized products.[4] As a result of our continued efforts to use amine oxide to create different functional metalloligands from the basic metalloligand 1,1′-bis(diphenylphosphino)ferrocene (dppf), we report in this paper that under a mild synthetic condition, a heterometallic complex, $[Re_2(CO)_9]_2(\mu$-dppf) (**1**), was isolated in good yield in the reaction between $Re_2(CO)_{10}$ and dppf. The molecular structure of the analogous $[Mn_2(CO)_9]_2(\mu$-dppf)[5] (**2**) is also included for comparative purpose. These polynuclear complexes though supported by M—M bonds do not have the usual deltahedral structures and hence can only be loosely defined as "open clusters". Whilst the structures of diaxial $Re_2(CO)_8(PMe_2Ph)_2$[6] and a series of $Re_2(CO)_{10-n}(CNR)_n$[7] complexes have been reported, to date there are no X-ray structural data on the analogous Re(0) diphosphine complexes. Most of the structural reports of dppf complexes in the literature have

* Authors to whom correspondence should be addressed.

centred on the ligand in its chelating mode.[8] The present paper, however, emphasizes the bridging nature of the phosphine.

Our isolation of a series of Re complexes with different nuclearities and phosphines in different electronic environments have enabled us to explore the use of X-ray Photoelectron Spectroscopy (XPS) in the study of these Re complexes in their solid state. Though established as a surface technique, XPS has been widely applied as a probe to the chemical and electronic properties of metal complexes. Earlier reports in the applications of XPS in organometallics were devoted mainly to the study of phosphine coordination.[9] Progress however has been inhibited by the general insensitivity of the core binding energies (b.e.s) of phosphorus atoms to different electronic environments.[10] Over the years the effect on metal b.e.s of ligand changes have also attracted considerable attention,[11] including the Re complexes.[9b,12] Reported herein are some of the XPS data which complement the solution results obtained in NMR spectroscopy.

EXPERIMENTAL

General

All reactions were performed under pure dry argon using standard Schlenk techniques. Preparations of $Mn_4(CO)_{18}(dppf)$[5] and $Re(CO)_5Br$[27] were described previously. Reaction of $Re_2(CO)_{10}$ with dppf in thf/CH_3CN mixture led to the isolation of $Re_2(CO)_9(NCCH_3)$ in 52% yield. Preparation of $Re_2(CO)_9(NCCH_3)$ has been reported.[2d,14] Precoated silica plates of layer thickness 0.25 mm were obtained from Merck. The general procedures and instruments used were as described in our earlier reports.[28] The TG and DSC experiments were conducted by use of a Du Pont 9900 thermal analyser under similar conditions as reported.[29] Core level spectra were obtained on a VG ESCA/SIMSLAB MK II spectrometer using Mg–K_α radiation, operating ρn a fixed retardation of 40 and covered the energy regions for all the elements present in the samples. The sample in powder form was sprinkled onto a double-sided Scotch tape mounted onto a standard VG holder. The binding energies were referenced to the hydrocarbon component in the C_{1s} envelope defined at 285.0 eV to compensate for surface charging. The b.e. of each core ionization peak was determined from a symmetric curve fit of the band and is estimated to have an uncertainty of ± 0.2 eV. Sample stoichiometries were checked and confirmed by their core level peak intensities. Deconvolution of the overlapping spectral components were performed on VG softwares. In the simulated spectrum each pair of $Re(4f_{7/2})$ and Re $(4f_{5/2})$ lines is restrained to have an intensity ratio of 4:3 and the spin orbital splitting to be 2.4 ± 0.1 eV. No strenuous effort was made to resolve the P(2*p*) sub-levels. Elemental analyses were performed by the analytical service of this department. The presence of solvate molecules in the sample crystals was confirmed by NMR analysis. The solvent inclusion property of many dppf complexes has been noted in the literature.[30] In reactions in which unreacted dppf ligand was recovered, the experimental yields were calculated based on the ligand consumed.

$Re_4(CO)_{18}(\mu\text{-dppf})\ 0.5\ CH_2Cl_2\ 0.5\ C_6H_{14}$ (1)

A quantity of 35 cm^3 of thf was added to a solution of $Me_3NO \cdot 2H_2O$ (0.051 g, 0.46 mmol) in 1 cm^3 of methanol at room temp. The resultant solution was then slowly transferred into a continuously stirred solution of $Re_2(CO)_{10}$ (0.305 g, 0.47 mmol) in 15 cm^3 of thf, at room temp., via a PTFE transfer tube. The yellow solution so formed was stirred *in vacuo* for 30 min. Two-thirds of the solvent was then removed *in vacuo* and the remaining solution was stirred at room temp. for a further 15 min. Solid dppf (0.128 g, 0.23 mmol) was added and the resultant orange solution was stirred for 50 min under argon. The solvent was removed and the orange solid redissolved in a minimum quantity of CH_2Cl_2 and chromotographed on silica t.l.c. plates. Elution with CH_2Cl_2–hexane (1:4) yielded three orange bands, the second and third of which were converted into the first when left in CH_2Cl_2 solution for 1 week. Recrystallization of the combined extracts from CH_2Cl_2–hexane mixture yielded 0.244 g (59%) of $Re_4(CO)_{18}(\mu\text{-dppf})\ 0.5\ CH_2Cl_2\ 0.5\ C_6H_{14}$ (1). Found: C, 35.2; H, 1.9; P, 3.5. $C_{55.5}H_{36}ClFeO_{18}P_2Re_4$ requires C, 35.3; H, 1.9; P, 3.3%; ν_{max}(CO) 2106m, 2033m, 2000vs, 1970s, 1935vs cm^{-1} ($CHCl_3$); $\delta_H(CDCl_3)$ 7.49–7.36 (m, 20 H, Ph), 5.29 (s, 1H, CH_2Cl_2), 4.36 (t, 4 H, CpH_β), 3.99 (m, 4 H, CpH_α), 1.26 (s(br), 4H, hexane), 0.88 (m, 3 H, hexane); $\delta_P(CDCl_3)$ 5.79 (s).

Complex 1 can be stripped of its occluded solvent by heating the solid at 155°C under argon for 20 min. Found: C, 34.8; H, 1.4; Fe, 3.1. Calc. for $C_{52}H_{28}FeO_{18}P_2Re_4$: C, 34.6; H, 1.6; Fe, 3.1%.

$Re_2(CO)_9(dppf)$ (5)

A quantity of 35 cm^3 of thf was added to a solution of $Me_3NO \cdot 2H_2O$ (0.051 g, 0.46 mmol) in a minimum amount of MeOH at room temp. The resultant solution was slowly transferred into a continuously stirred solution of $Re_2(CO)_{10}$ (0.305 g,

0.47 mmol) in thf (15 cm^3) via a PTFE transfer tube. The yellow solution so formed was stirred *in vacuo* for ½ h, after which two-thirds of the solvent was removed *in vacuo*. The remaining solution was stirred for a further 15 min before it was slowly transferred to a solution of dppf (0.311 g, 0.56 mmol) in thf (12 cm^3). The resultant orange solution was stirred under argon for about 1 h. Half of the solvent was then removed and stirring was continued for 50 min. The solution was evaporated to dryness and the orange residue redissolved in a minimum quantity of CH_2Cl_2 and chromatographed on silica t.l.c. plates. Elution with CH_2Cl_2–hexane (3 : 17) followed by further recrystallization from CH_2Cl_2–MeOH mixture yielded the orange $Re_2(CO)_9$(dppf) (0.254 g, 54%). Found: C, 43.4; H, 2.1; P, 6.1; Fe, 4.4. $C_{43}H_{28}FeO_9P_2Re_2$ requires C, 43.8; H, 2.4; P, 5.3; Fe, 4.7%. ν_{max}(CO) 2106m, 2033m, 1997vs, 1960m, 1935s cm^{-1} ($CHCl_3$); δ_H($CDCl_3$) 7.41–7.35 (m, 10 H, Ph), 7.27–7.15 (m, 10 H, Ph), 4.45 (t, 2 H, coord. CpH_β), 4.19 (t, 2 H, free CpH_β), 4.11 (m, 2 H, coord. CpH_α), 3.83 (q, 2 H, free CpH_α); δ_P($CDCl_3$) 5.65 (s, $P_{coord.}$), −16.96 (s, P_{free}). The yield is very sensitive to experimental conditions and can fluctuate in the range 20–60%. The compound is also invariably contaminated with varying quantities of **1**, from which it is difficult to separate by t.l.c. Unreacted dppf (0.090 g, 0.16 mmol) was also isolated.

$[Re_2(CO)_9(Ph_2P(C_5H_4)Fe(C_5H_4)PMePh_2)]^+I^-$ (6)

MeI (1 cm^3, 16.1 mmol) was added to a diethyl ether suspension (3.5 cm^3) of **5** (0.045 g, 0.038 mmol). The resultant orange solution was stirred for 2½ h at room temp., during which a tan–orange solid gradually precipitated. The residue that remained after removal of the solvent was washed with hexane (3 × 5 cm^3) and characterized to be **6**. (0.049 g, 97%). Ready decomposition of this compound upon isolation precludes an accurate microanalysis; ν_{max}(CO) 2107w, 2040w, 1999vs, 1960m, 1934m cm^{-1} ($CHCl_3$); δ_H($CDCl_3$) 7.71 (m, 5 H, Ph), 7.62 (m, 5 H, Ph), 7.43 (m, 10 H, Ph), 4.93 (t, 2 H, Me-P-CpH_β), 4.56 (q, 2 H, Re-P-CpH_β), 4.36 (q, 2 H, Me-PCpH_α), 4.24 (m, 2 H, Re-P-CpH_α), 3.05 (d, 3H, P-CH_3, $^2J_{P-H}$ 13.2 Hz), δ_P($CDCl_3$), 24.37 (s, H_3C—P), 5.52 (s, Re—P).

$Re_2(CO)_9(Ph_2P(C_5H_4)Fe(C_5H_4)P(O)Ph_2)$ (7)

A quantity of 25 cm^3 of thf was added to a solution of $Me_3NO \cdot 2H_2O$ (0.004 g, 0.036 mmol) in a minimum quantity of MeOH. Solid **1** (0.066 g, 0.035 mmol) was introduced and the resultant solution was refluxed under argon for 7½ h. Two-thirds of the solvent was removed and the remaining solution was refluxed for another 4 h giving a brownish-orange solution together with a little black powdery solid. The solvent was evaporated off and the residue extracted with CH_2Cl_2 and chromatographed on silica t.l.c. plates. Elution by hexane–CH_2Cl_2 (1 : 1) moved only a single orange band of unreacted **1** (0.022 yielded, on recrystallization from CH_2Cl_2/hexane mixture, $[Re_2(CO)_9\{Ph_2P(C_5H_4)Fe(C_5H_4)P(O)Ph_2\}] \cdot H_2O$ (0.014 g, 50% based on **1** consumed). Found: C, 43.0; H, 2.5; P, 5.5; Fe, 4.3. $C_{43}H_{30}FeO_{11}P_2Re_2$ requires C, 42.6; H, 2.5; P, 5.1; Fe, 4.6%; ν_{max} 2106m, 2033m, 1998vs, 1970m, 1936s, (CO)($CHCl_3$) and 1121w (PO) cm^{-1} (KBr); δ_H($CDCl_3$) 7.66–7.35 (m, 20 H, Ph), 4.87 (t, 2 H, O=P—CpH_β), 4.28 (q, 2 H, Re—P—CpH_β), 4.13 (m, 2 H, O=P—CpH_α), 4.05 (q, 2 H, Re—P—CpH_α); δ_P($CDCl_3$) 28.40 (s, O=P), 5.72 (s, Re—P).

Complex **7** could also be obtained from the reaction of $Re_2(CO)_{10}$, dppf and $Me_3NO \cdot 2H_2O$ in 2 : 1 : 2 molar ratio in a single pot in thf, or oxidation of **5** with H_2O_2 in CH_3CN in *ca* 6 and 33% yields respectively.

$Fe(C_5H_4P(O)Ph_2)_2$ 0.5 CH_2Cl_2 (10)

Preparation of this complex has been reported in the literature.[31] The following procedure was preferred for its convenience and higher yield.

30% aqueous H_2O_2 (2 cm^3, 17.65 mmol) was added to a suspension of dppf (0.840 g, 1.52 mmol) in CH_3CN (60 cm^3) at room temp. The resultant orange suspension was stirred for 1½ h at room temp., and evaporated to dryness *in vacuo*. The residual brownish orange solid was recrystallized from EtOH and then from CH_2Cl_2/*n*-hexane to yield tan–orange crystals of **10** (0.640 g, 67%). Found: C, 66.0; H, 4.8; Fe, 8.9. Calc. for $C_{34.5}H_{29}ClFeO_2P_2$: C, 65.8; H, 4.6; Fe, 8.9%; ν_{max}(P=O) 1191vs cm^{-1} (KBr); δ_H($CDCl_3$), 7.61 (m, 4 H, Ph), 7.45 (m, 16 H, Ph), 5.29 (s, 1 H, CH_2Cl_2), 4.71 (q, 4 H, CpH_β), 4.26 (q, 4 H, CpH_α); δ_P($CDCl_3$) 28.27 (s).

$Re(CO)_3$(dppf)Br (11)

Dppf (0.162 g, 0.29 mmol) was added to a solution of $Re(CO)_5Br$ (0.120 g, 0.29 mmol) in acetone (7 cm^3) and thf (10 cm^3) at room temp. The resultant mixture was vigorously stirred as solid $Me_3NO \cdot 2H_2O$ (0.064 g, 0.58 mmol) was added. The orange solution was stirred *in vacuo* for 2 h at room temp. before it was evaporated under vacuum. The product was taken up in CH_2Cl_2 and chromatographed on silica t.l.c. plates. Elution with

CH_2Cl_2/hexane (7:13) followed by recrystallization from CH_2Cl_2/MeOH mixture yielded chrome-yellow crystals of **11** (0.171 g, 65%). Found: C, 49.1; H, 3.1; P, 7.0; Fe, 6.2; Br, 8.7. $C_{37}H_{28}BrFeO_3P_2Re$ requires C, 49.1; H, 3.1; P, 6.8; Fe, 6.2; Br, 8.7%. ν_{max}(CO) 2038s, 1960m, 1902m cm^{-1} ($CHCl_3$); δ_H($CDCl_3$) 7.70 (m, 8 H, Ph), 7.42 (m, 12 H, Ph), 4.95 (m, 2 H, Cp), 4.39 (m, 2 H, Cp), 4.31 (s, 4 H, Cp); δ_P($CDCl_3$) 0.27 (s).

Crystallography

Large orange single crystals of complex $[Re_2(CO)_9]_2(\mu$-dppf)·solvate (**1**) and $[Mn_2(CO)_9]_2(\mu$-dppf)·thf (**2**) were grown from CH_2Cl_2/hexane and thf/EtOH mixtures respectively at 5°C. Single crystals suitable for X-ray diffraction were mounted inside a lithium glass capillary for preliminary characterization and intensity data collection. The crystallographic data and refinement details of **1** and **2** are listed in Table 1. A single crystal of $Re_2(CO)_9(Ph_2P(C_5H_4)P(O)Ph_2)\cdot H_2O$ (**7**) was mounted on top of a glass fibre for preliminary characterization. At this stage one of the cell edges was found to be longer than 35 Å. The diffraction spots would not be well resolved if using Mo–K_α radiation. Hence the intensity data were collected employing Cu–K_α radiation, taking a necessary weak point of high absorption coefficient.

The structures of **1** and **2** were solved by direct methods MULTAN and were found to be isomorphous. The ferrocenyl Fe atom was located along a two-fold axis. Hence only one-half of the molecule is crystallographically independent. The crystal structures were found to have disordered solvate molecules around a crystallographic two-fold axis. For complex **1**, the solvate molecule seemed to be a disordered CH_2Cl_2. Yet as reasonable models of CH_2Cl_2 could not be constructed, C_{41}–C_{44} per acentric unit were refined to cover scattering due to the electron densities in the solvate region. For complex **2**, the electron density distribution conformed to a thf molecule. The molecular drawings of **1** are shown in Fig. 1 whilst **2** is isomorphous to **1**. Final atomic fractional coordinates and selected bond distances and angles for **1** and **2** are listed in Table 2(a) and (b) respectively.

The structure of **7** was solved also by direct methods MULTAN. With $Z = 8$, there are two independent molecules per asymmetric unit. Included in the crystal structure is one hydrate for one $Re_2(CO)_9$(dppfO), linked in a hydrogen bonding system.

All hydrogen atoms were fixed as isotropic μ values in the final cycles of least-squares refinement. The non-hydrogen atoms, except for the hydrate oxygen atoms, were varied anisotropically. The atomic scattering curves of Re, Fe, Mn, P, O, C and H were taken from *International Tables for X-ray Crystallography*, Volume IV. Computations were carried out on a microVAX 3600 with NRCC package.[32]

RESULTS AND DISCUSSION

Synthesis and properties

Reaction between $Re_2(CO)_{10}$ and dppf does not proceed under thermal conditions (refluxing thf). The presence of Me_3NO, however, leads to rapid oxidative decarbonylation of the former thereby facilitating phosphine substitution. The most obvious intermediate for the formation of the title complexes is $M_2(CO)_9(\eta^1$-dppf). Evidence for the Mn complex has recently been obtained. The Re analogue **5** can also be isolated when excess dppf is used. The ^{31}P-NMR of **5** shows a characteristic high field singlet together with the low-field signal assignable to the axial-coordinated phosphine. The nucleophilicity of the pendant phosphine is demonstrated by its ready methylation with CH_3I to give $[Re_2(CO)_9(\eta^1$-$Ph_2P(C_5H_4)Fe(C_5H_4)PMePh_2)]I$ (**6**). Complex **5** can be oxidized by H_2O_2 to give $Re_2(CO)_9(\eta^1$-$Ph_2P(C_5H_4)Fe(C_5H_4)P(O)Ph_2)$ (**7**), which was also isolated as a minor product in a one-pot reaction of $Re_2(CO)_{10}$, dppf and Me_3NO (2:1:2) in thf but best prepared from **1** in its oxidative bridge-scission reaction with Me_3NO in refluxing thf. Such oxygen transfer from an amine oxide to a stable bridging phosphine in preference to a carbonyl carbon was unexpected and unprecedented. This oxygen migratory reaction may possibly be facilitated by a nucleophilic attack of Me_3NO on the coordinate phosphorus site. The ability for the ferrocenyl moiety to dissipate excess charge in the transition state, an idea not dissimilar to that proposed for bridging carbonyls,[13] possibly renders the phosphine phosphorus more electrophilic than the carbonyl carbon. An alternative mechanism which requires the cleavage of the Re—P bond prior to oxygen transfer is deemed to be less likely in view of the inertness of free dppf towards Me_3NO at room temperature, and the kinetic stability of the Re—P bond, as exemplified by the fact that complex **1** is robust even when refluxed with dppf in hexane.

The negligible shift for the ^{31}P NMR signal due to the coordinated phosphorus atom from **5** to **6** and **7** and in fact between **1** and **5** suggests that there is negligible electronic interaction across the dppf backbone in these complexes. The title

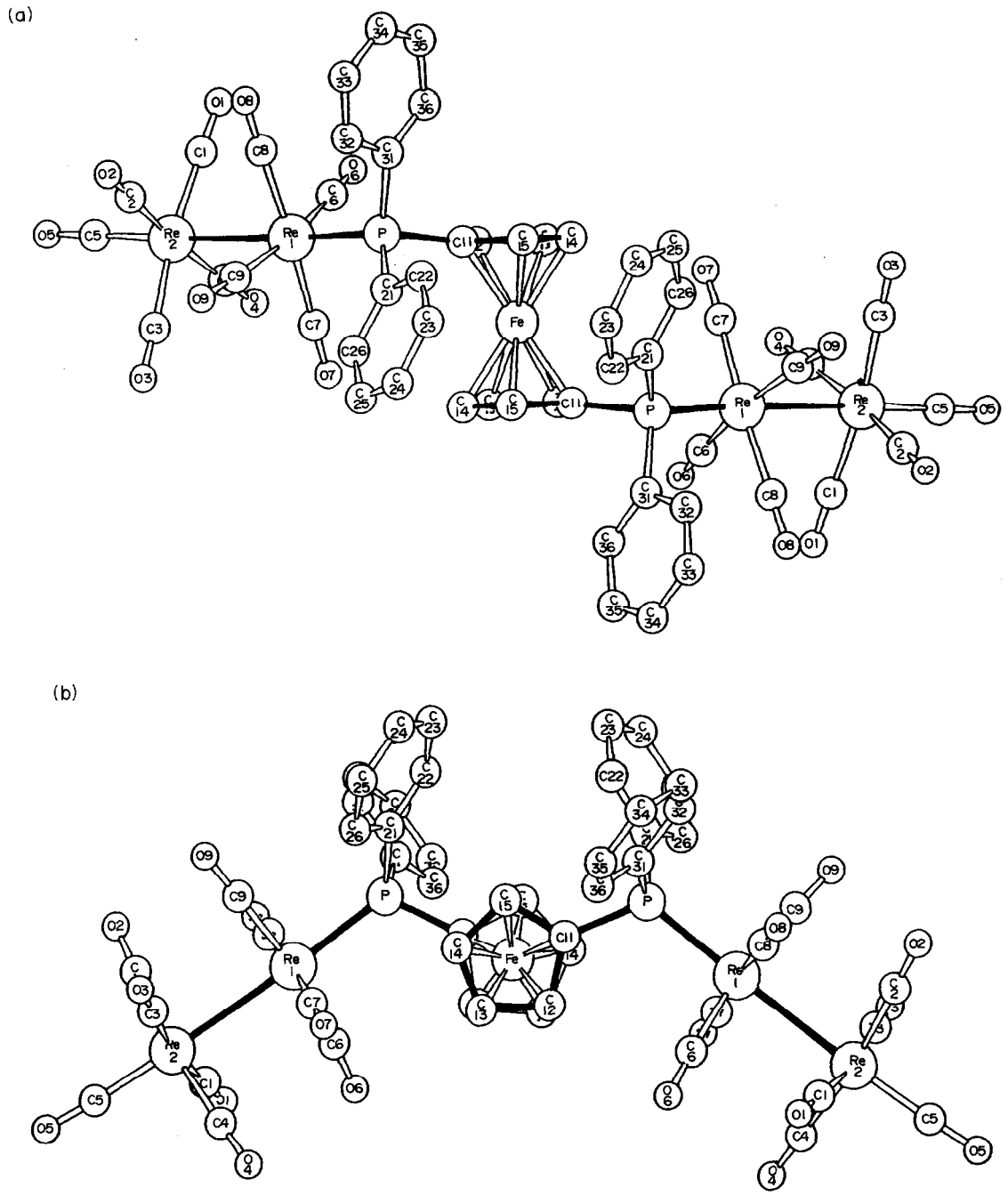

Fig. 1. (a) SCHAKAL plot of $[Re_2(CO)_9]_2(\mu$-dppf) (**1**) (hydrogen atoms omitted for clarity). (b) Top view on the phosphinocyclopentadienyl ring showing its "half-eclipsed" form and the relative orientation of the $[Re_2(CO)_9]$ moieties.

complex **1** is not formed when the preparation is carried out in CH_3CN, in which case $Re_2(CO)_9(CH_3CN)$[2d,14] (**8**) is isolated as the major product. The substitutional inertness of **8** has been documented.[14] The effect of amine oxide in these reactions is particularly significant when one considers the recent photo-induced synthesis of $Mn_2(CO)_8(\mu$-dppf) and $Mn_2(CO)_8Cl_2(\mu$-dppf),[17] neither of which was apparent under our experimental conditions in the synthesis of **2**. Thermogravimetric and Differential Scanning Calorimetric analyses of **1** and **2** revealed their release of trapped solvents at *ca* 154 and 124°C and decomposition of the complexes at *ca* 183 and 182°C respectively. Like the Gp 6 dimeric $M_2(CO)_{10}(\mu$-dppf), both complexes are resistant to further decarbonylation by Me_3NO

Table 1. Crystallographic data and refinement details for $[M_2(CO)_9]_2(dppf)$ (M=Re (**1**) and Mn (**2**)) and $Re_2(CO)_9(dppfO)$

	$[Re_2(CO)_9]_2(dppf)\cdot(solvate)$	$[Mn_2(CO)_9]_2(dppf)\cdot(thf)$
Crystal system	Orthorhombic	Orthorhombic
Space group[a]	$P2_12_12$	$P2_12_12$
a (Å)	14.330(1)	14.290(2)
b (Å)	23.053(6)	22.289(5)
c (Å)	9.307(1)	9.218(3)
β (deg)	—	—
V (Å^3)	3074.4(9)	2936.0(13)
Empirical formula	$C_{52}H_{28}FeO_{18}P_2Re_4$+solv[b]	$C_{52}H_{28}FeMn_4O_{18}P_2$+thf
Crystal dimensions (mm)	$0.49\times0.29\times0.31$	$0.41\times0.08\times0.20$
FW	1899.47	1350.44
Z	2	2
F(000)	1776	1360
D_{calc} (g cm^{-3})	2.15	1.53
μ (mm^{-1})	8.30	1.17
λ (Å)	0.70930	0.70930
2θ (max)	49.8	50.0
Diffractometer	Nonius CAD4	Nonius CAD4
Scan mode	$\theta/2\theta$	$\theta/2\theta$
Data ranges	$0<h<17$, $0<k<27$, $0<l<11$	$0<h<16$, $0<k<26$, $0<l<10$
Unique reflections	3054	2928
Observations	2704 $I>2.0\sigma(I)$	2098 $I>2.5\sigma(I)$
Absorption corrections	Yes	Yes
Trans factors	0.439–1.000	0.923–1.000
Total atoms	57	60
Parameters	364	372
Weights	counting-statistics	counting-statistics
Weight modifier	0.0100	0.0100
R_f	0.034	0.036
R_w	0.045	0.038
Goodness of fit	2.15	1.30
Max shift/σ	0.961[c]	0.013
Peaks in D-map (e Å^{-3})		0.390
high	1.140[d]	−0.270
low	−1.440	

	$Re_2(CO)_9dppfO\cdot H_2O$
Crystal system	Monoclinic
Space group[a]	$P2/c$
a (Å)	20.556(3)
b (Å)	12.811(1)
c (Å)	35.622(5)
β (deg)	104.76(1)
V (Å^3)	9071.1(20)
Empirical formula	$C_{34}H_{28}FeO_{10}P_2Re_2\cdot H_2O$
Crystal dimensions (mm)	$0.26\times0.12\times0.20$
FW	1212.91
Z	8
F(000)	4656
D_{calc} (g cm^{-3})	1.78
μ (mm^{-1})	13.52
λ (Å)	1.54056
2θ (max)	120.0
Diffractometer	Rigaku AFC5R

Table 1—*continued.*

	$Re_2(CO)_9dppfO \cdot H_2O$
Scan mode	$\theta/2\theta$
Data ranges	$-23 < h < 22$
	$0 < k < 14$
	$0 < l < 40$
Unique reflections	13499
Observations	8858 $I > 2.0\sigma(I)$
Absorption corrections	Yes
Trans factors	0.655–1.000
Total atoms	174
Parameters	1054
Weights	counting-statistics
Weight modifier	0.0100
R_f	0.073[e]
R_w	0.092
Goodness of Fit	2.27
Max shift/σ	0.310
Peaks in D-map (e Å^{-3})	
high	1.740[f]
low	−1.060

[a] The parameter η was checked so that the space group conformed to the correct polarity: 1.00(8).

[b] The solvate molecule is probably disordered CH_2Cl_2 and/or *n*-hexane. As reasonable models of either CH_2Cl_2 or *n*-hexane could not be constructed, C_{41}–C_{44} per asymmetric unit are refined so that contribution of electron densities in the solvate region to the scattering is included.

[c] 0.961, for a parameter in solvate region. 0.008, for $[Re_2(CO)_9]_2$(dppf) parameters.

[d] The highest residual peaks are 1.0–1.2 Å next to Re atoms.

[e] Block-diagonal least-squares reiterations were employed to convergence.

[f] The highest peaks are next to Re atoms at *ca* 1.0–1.1 Å.

at room temperature. No higher substituted products were evident in the preparative reactions of **1** and **2**. The chemical stability of **1** is further demonstrated by its inertness towards S_8 and dppf in refluxing *n*-hexane.

Crystal and molecular structures

In view of the subtleties in the conformational variations of dppf as a ligand, and the lack of structural data for monosubstituted $Re_2(CO)_9(PR_3)$ or its polynuclear analogues in the literature, the X-ray structural analyses for $[Re_2(CO)_9]_2(\mu$-dppf)·solvate (**1**), $[Mn_2(CO)_9]_2(\mu$-dppf)·thf (**2**), and $Re_2(CO)_9(Ph_2P(C_5H_4)Fe(C_5H_4)P(O)Ph_2) \cdot H_2O$ (**7**) were carried out. Single crystals of **1** were obtained from CH_2Cl_2/hexane mixture at 5°C. The crystals of **2** which were suitable for X-ray analysis were grown from thf/EtOH mixture at the same temperature. The molecular structure of **1** is shown in Fig. 1(a). Crystallographic data of **1** and **2** are given in Table 1(a) and (b). Some pertinent molecular data are listed in Tables 2(a) and (b). **2** crystallizes with an occluded thf molecule. ^{1}H NMR spectra of **1** indicates its solvation with hexane and CH_2Cl_2 but the X-ray data only revealed a disordered C_4 entity. The molecules are structurally isomorphous, each consisting of a dppf molecule axially and singly bridging between two $M_2(CO)_9$ moieties with the ferrocenyl iron atom being located on a two-fold axis. These polymetallic complexes are thus supported by two metal—metal bonds and a dppf bridge. The general features of this dppf bridge is similar to that reported earlier for $M_2(CO)_{10}(\mu$-dppf) (M = Cr (**3**), Mo (**4**))[15] with a few notable differences. Whereas the P···Fe···P′ for the Group 6 dimers is virtually linear (Ave. 172.4(3)°), it narrows substantially to 140.56(11)° for **1** and 140.29(6)° for **2**. Accordingly, the P···P′ separation is shortened from an average of 7.068(3) Å in the Cr and Mo dimers to 6.689(4) Å in **1** and 6.697(4) Å in **2**. Related to this M···M shortening is the near-eclipsed ferrocenyl rings in **1** (twist angle = 12.7°) (Fig. 1b) and **2** (12.6°) and near-staggered configuration in **3** and **4** (average angular deviation from the eclipsed configuration is 28.4°).

Table 2. (a) Selected bond lengths (Å) and angles (deg) for $[Re_2(CO)_9]_2(dppf)$

Atom—atom	Length (Å)	Atom—atom—atom	Angle (deg)
Fe—C(11)	2.05(2)	Re(2)—Re(1)—P	177.32(9)
Fe—C(12)	2.05(2)	Re(2)—Re(1)—C(6)	84.7(4)
Fe—C(13)	2.06(2)	Re(2)—Re(1)—C(7)	88.4(4)
Fe—C(14)	2.05(2)	Re(2)—Re(1)—C(8)	86.5(5)
Fe—C(15)	2.05(1)	Re(2)—Re(1)—C(9)	85.4(5)
Re(1)—Re(2)	3.0537(9)	P—Re(1)—C(6)	96.2(4)
Re(1)—P	2.382(3)	P—Re(1)—C(7)	94.1(4)
Re(1)—C(6)	1.98(2)	P—Re(1)—C(8)	91.0(5)
Re(1)—C(7)	1.97(2)	P—Re(1)—C(9)	93.6(5)
Re(1)—C(8)	1.98(2)	C(6)—Re(1)—C(7)	90.0(7)
Re(1)—C(9)	1.97(2)	C(6)—Re(1)—C(8)	89.0(8)
Re(2)—C(1)	1.98(2)	C(6)—Re(1)—C(9)	169.7(7)
Re(2)—C(2)	1.99(2)	C(7)—Re(1)—C(8)	174.9(6)
Re(2)—C(3)	2.01(2)	C(7)—Re(1)—C(9)	92.4(7)
Re(2)—C(4)	2.00(2)	C(8)—Re(1)—C(9)	87.8(7)
Re(2)—C(5)	1.94(2)	Re(1)—Re(2)—C(1)	85.2(5)
P—C(11)	1.84(1)	Re(1)—Re(2)—C(2)	83.6(5)
P—C(21)	1.82(2)	Re(1)—Re(2)—C(3)	86.0(5)
P—C(31)	1.84(1)	Re(1)—Re(2)—C(4)	88.6(5)
O(1)—C(1)	1.15(3)	Re(1)—Re(2)—C(5)	176.5(6)
O(2)—C(2)	1.12(2)	C(1)—Re(2)—C(2)	90.8(7)
O(3)—C(3)	1.13(3)	C(1)—Re(2)—C(3)	171.1(7)
O(4)—C(4)	1.12(2)	C(1)—Re(2)—C(4)	88.2(8)
O(5)—C(5)	1.17(2)	C(1)—Re(2)—C(5)	93.6(8)
O(6)—C(6)	1.13(2)	C(2)—Re(2)—C(3)	89.7(8)
O(7)—C(7)	1.13(2)	C(2)—Re(2)—C(4)	172.2(7)
O(8)—C(8)	1.14(2)	C(2)—Re(2)—C(5)	93.2(8)
O(9)—C(9)	1.15(2)	C(3)—Re(2)—C(4)	90.0(8)
		C(3)—Re(2)—C(5)	95.3(8)
		C(4)—Re(2)—C(5)	94.6(8)
		Re(1)—P—C(11)	118.7(5)
		Re(1)—P—C(21)	119.2(5)
		Re(1)—P—C(31)	111.1(5)

The title complexes otherwise show normal substituent-induced ring distortions[16] and a displacement of the phosphorus atoms from the plane of the Cp ring, by 0.22(3) Å for **1** and 0.235(13) Å for **2**, away from the iron centre.

Single crystals of **7** were grown from CH_2Cl_2/hexane mixture at 5°C. Two crystallographically independent molecules were located and are shown in Fig. 2. Crystallographic data are given in Table 1(c), and some molecular data summarized in Table 2(c).

Each complex molecule co-crystallizes with a water molecule, which is hydrogen-bonded to the phosphoryl oxygen of the dppfO ligand ($O(1)\cdots O(2) = 2.81(4)$ Å; $O(3)\cdots O(4) = 2.64(7)$ Å). The hydrates are also linked among themselves by hydrogen bonds. The behaviour of free phosphine oxide co-crystallizing with hydrogen-bonding molecules has been documented and elegantly applied to optical resolutions[17] and as crystallizing aids.[18]

Complex **7** consists of a dppfO molecule axially coordinated through the phosphine to a $Re_2(CO)_9$ moiety. The phosphoryl group is pendant with its P atom coplanar with the attached Cp ring. The phosphine P on the other hand is displaced from the Cp plane away from the Fe centre by 0.22(3) Å (0.24(4) Å for the other crystallographically independent molecule) presumably due to the steric bulk of the dimetal entity. The P—O length of 1.432(16) Å (1.494(15) Å) is normal for a P=O bond.[19]

The general structural characteristics of the ferrocenyl and dirhenium nonacarbonyl fragments closely resemble those of **1** and warrant no special mention. Some conformational differences can, however, be noted, e.g. the twist angle of 17.2(15)

Table 2. (b) Selected bond lengths (Å) and angles (deg) for $[Mn_2(CO)_9]_2 \cdot (dppf)$

Atom—atom	Length (Å)	Atom—atom—atom	Angle (deg)
Fe—C(11)	2.058(7)	Mn(2)—Mn(1)—P	179.61(7)
Fe—C(12)	2.039(7)	Mn(2)—Mn(1)—C(6)	85.88(24)
Fe—C(13)	2.054(8)	Mn(2)—Mn(1)—C(7)	86.70(23)
Fe—C(14)	2.048(7)	Mn(2)—Mn(1)—C(8)	87.4(3)
Fe—C(15)	2.042(7)	Mn(2)—Mn(1)—C(9)	84.8(3)
Mn(1)—Mn(2)	2.933(2)	P—Mn(1)—C(6)	94.49(25)
Mn(1)—P	2.276(2)	P—Mn(1)—C(7)	93.14(23)
Mn(1)—C(6)	1.836(9)	P—Mn(1)—C(8)	92.7(3)
Mn(1)—C(7)	1.826(8)	P—Mn(1)—C(9)	94.9(3)
Mn(1)—C(8)	1.844(9)	C(6)—Mn(1)—C(7)	90.4(4)
Mn(1)—C(9)	1.828(8)	C(6)—Mn(1)—C(8)	87.9(4)
Mn(2)—C(1)	1.82(1)	C(6)—Mn(1)—C(9)	169.8(3)
Mn(2)—C(2)	1.86(1)	C(7)—Mn(1)—C(8)	174.0(4)
Mn(2)—C(3)	1.86(1)	C(7)—Mn(1)—C(9)	93.1(4)
Mn(2)—C(4)	1.84(1)	C(8)—Mn(1)—C(9)	87.7(4)
Mn(2)—C(5)	1.787(9)	Mn(1)—Mn(2)—C(1)	83.9(3)
P—C(11)	1.815(7)	Mn(1)—Mn(2)—C(2)	84.7(3)
P—C(21)	1.832(7)	Mn(1)—Mn(2)—C(3)	86.1(3)
P—C(31)	1.821(8)	Mn(1)—Mn(2)—C(4)	88.4(3)
O(1)—C(1)	1.15(1)	Mn(1)—Mn(2)—C(5)	177.9(3)
O(2)—C(2)	1.13(1)	C(1)—Mn(2)—C(2)	91.0(4)
O(3)—C(3)	1.12(1)	C(1)—Mn(2)—C(3)	169.7(4)
O(4)—C(4)	1.14(1)	C(1)—Mn(2)—C(4)	88.0(4)
O(5)—C(5)	1.15(1)	C(1)—Mn(2)—C(5)	95.3(4)
O(6)—C(6)	1.15(1)	C(2)—Mn(2)—C(3)	90.3(4)
O(7)—C(7)	1.15(1)	C(2)—Mn(2)—C(4)	173.1(4)
O(8)—C(8)	1.13(1)	C(2)—Mn(2)—C(5)	93.5(4)
O(9)—C(9)	1.15(1)	C(3)—Mn(2)—C(4)	89.5(4)
		C(3)—Mn(2)—C(5)	94.7(4)
		C(4)—Mn(2)—C(5)	93.4(4)
		Mn(1)—P—C(11)	118.5(3)
		Mn(1)—P—C(21)	119.14(23)
		Mn(1)—P—C(31)	110.82(24)

Table 2. (c) Selected bond lengths and angles for $Re_2(CO)_9dppfO \cdot H_2O$

Atom—atom	Length (Å)	Atom—atom—atom	Angle (deg)
Re(1)—Re(2)	3.052(1)	Re(2)—Re(1)—P(1)	177.84(13)
Re(1)—P(1)	2.390(5)	Re(2)—Re(1)—C(11)	88.4(6)
Re(1)—C(11)	1.96(2)	Re(2)—Re(1)—C(12)	85.4(5)
Re(1)—C(12)	2.05(2)	Re(2)—Re(1)—C(13)	82.6(6)
Re(1)—C(13)	1.92(2)	Re(2)—Re(1)—C(14)	86.9(6)
Re(1)—C(14)	1.99(2)	P(1)—Re(1)—C(11)	90.2(6)
Re(2)—C(15)	1.96(2)	P(1)—Re(1)—C(12)	92.9(5)
Re(2)—C(16)	2.00(3)	P(1)—Re(1)—C(13)	98.8(6)
Re(2)—C(17)	2.05(2)	P(1)—Re(1)—C(14)	94.8(6)
Re(2)—C(18)	2.00(2)	C(11)—Re(1)—C(12)	88.9(9)
Re(2)—C(19)	1.85(3)	C(11)—Re(1)—C(13)	170.9(9)
Re(3)—Re(4)	3.049(1)	C(11)—Re(1)—C(14)	90.2(9)
Re(3)—P(3)	2.381(5)	C(12)—Re(1)—C(13)	89.1(9)
Re(3)—C(71)	2.09(3)	C(12)—Re(1)—C(14)	172.3(8)
Re(3)—C(72)	1.98(2)	C(13)—Re(1)—C(14)	90.7(9)

Table 2. (c)—*continued.*

Atom—atom	Length (Å)	Atom—atom—atom	Angle (deg)
Re(3)—C(73)	1.98(2)	Re(1)—Re(2)—C(15)	86.0(6)
Re(3)—C(74)	1.99(3)	Re(1)—Re(2)—C(16)	85.3(6)
Re(4)—C(75)	2.09(3)	Re(1)—Re(2)—C(17)	83.4(5)
Re(4)—C(76)	1.94(3)	Re(1)—Re(2)—C(18)	85.1(6)
Re(4)—C(77)	2.09(3)	Re(1)—Re(2)—C(19)	179.3(8)
Re(4)—C(78)	1.92(4)	C(15)—Re(2)—C(16)	87.8(12)
Re(4)—C(79)	1.96(3)	C(15)—Re(2)—C(17)	91.5(10)
Fe(1)—C(41)	2.05(2)	C(15)—Re(2)—C(18)	171.0(9)
Fe(1)—C(42)	2.02(2)	C(15)—Re(2)—C(19)	94.6(10)
Fe(1)—C(43)	2.02(2)	C(16)—Re(2)—C(17)	168.6(8)
Fe(1)—C(44)	1.99(2)	C(16)—Re(2)—C(18)	92.2(12)
Fe(1)—C(45)	2.03(2)	C(16)—Re(2)—C(19)	94.3(10)
Fe(1)—C(46)	2.04(2)	C(17)—Re(2)—C(18)	86.7(11)
Fe(1)—C(47)	2.04(2)	C(17)—Re(2)—C(19)	97.0(9)
Fe(1)—C(48)	2.04(2)	C(18)—Re(2)—C(19)	94.4(10)
Fe(1)—C(49)	2.04(2)	Re(4)—Re(3)—P(3)	175.93(13)
Fe(1)—C(50)	2.04(2)	Re(4)—Re(3)—C(71)	87.8(5)
Fe(2)—C(101)	2.06(2)	Re(4)—Re(3)—C(72)	82.3(6)
Fe(2)—C(102)	2.09(2)	Re(4)—Re(3)—C(73)	87.8(6)
Fe(2)—C(103)	2.10(2)	Re(4)—Re(3)—C(74)	81.9(6)
Fe(2)—C(104)	2.02(2)	P(3)—Re(3)—C(71)	91.9(5)
Fe(2)—C(105)	2.05(2)	P(3)—Re(3)—C(72)	93.6(6)
Fe(2)—C(106)	2.05(2)	P(3)—Re(3)—C(73)	96.3(6)
Fe(2)—C(107)	2.02(2)	P(3)—Re(3)—C(74)	98.2(6)
Fe(2)—C(108)	2.06(2)	C(71)—Re(3)—C(72)	87.7(8)
Fe(2)—C(109)	2.05(2)	C(71)—Re(3)—C(73)	90.1(8)
Fe(2)—C(110)	2.04(2)	C(71)—Re(3)—C(74)	169.5(8)
P(1)—C(21)	1.82(2)	C(72)—Re(3)—C(73)	169.9(8)
P(1)—C(31)	1.81(2)	C(72)—Re(3)—C(74)	88.8(9)
P(1)—C(41)	1.76(2)	C(73)—Re(3)—C(74)	91.7(9)
P(2)—O(2)	1.43(2)	Re(3)—Re(4)—C(75)	86.4(6)
P(2)—C(46)	1.79(2)	Re(3)—Re(4)—C(76)	87.8(7)
P(2)—C(51)	1.77(2)	Re(3)—Re(4)—C(77)	87.9(6)
P(2)—C(61)	1.80(2)	Re(3)—Re(4)—C(78)	86.0(7)
P(3)—C(81)	1.80(2)	Re(3)—Re(4)—C(79)	178.2(8)
P(3)—C(91)	1.89(2)	C(75)—Re(4)—C(76)	89.9(9)
P(3)—C(101)	1.82(2)	C(75)—Re(4)—C(77)	89.4(9)
P(4)—O(4)	1.49(2)	C(75)—Re(4)—C(78)	172.3(9)
P(4)—C(106)	1.79(2)	C(75)—Re(4)—C(79)	94.0(10)
P(4)—C(111)	1.87(2)	C(76)—Re(4)—C(77)	175.7(9)
P(4)—C(121)	1.84(2)	C(76)—Re(4)—C(78)	89.9(11)
O(11)—C(11)	1.13(3)	C(76)—Re(4)—C(79)	90.5(11)
O(12)—C(12)	1.08(3)	C(77)—Re(4)—C(78)	90.1(11)
O(13)—C(13)	1.12(3)	C(77)—Re(4)—C(79)	93.9(10)
O(14)—C(14)	1.12(3)	C(78)—Re(4)—C(79)	93.7(11)
O(15)—C(15)	1.14(3)	Re(1)—P(1)—C(21)	111.3(6)
O(16)—C(16)	1.10(3)	Re(1)—P(1)—C(31)	118.1(6)
O(17)—C(17)	1.09(3)	Re(1)—P(1)—C(41)	116.5(6)
O(18)—C(18)	1.11(3)	O(2)—P(2)—C(46)	113.2(10)
O(19)—C(19)	1.21(4)	O(2)—P(2)—C(51)	115.5(10)
O(71)—C(71)	1.08(3)	O(2)—P(2)—C(61)	112.5(10)
O(72)—C(72)	1.15(3)	Re(3)—P(3)—C(81)	112.6(6)
O(73)—C(73)	1.12(3)	Re(3)—P(3)—C(91)	119.3(6)
O(74—C(74)	1.15(3)	Re(3)—P(3)—C(101)	118.5(7)
O(75)—C(75)	1.06(3)	O(4)—P(4)—C(106)	115.5(10)
O(76)—C(76)	1.14(3)	O(4)—P(4)—C(111)	114.4(10)
O(77)—C(77)	1.07(3)	O(4)—P(4)—C(121)	112.4(9)
O(78)—C(78)	1.20(4)		
O(79)—C(79)	1.11(3)		

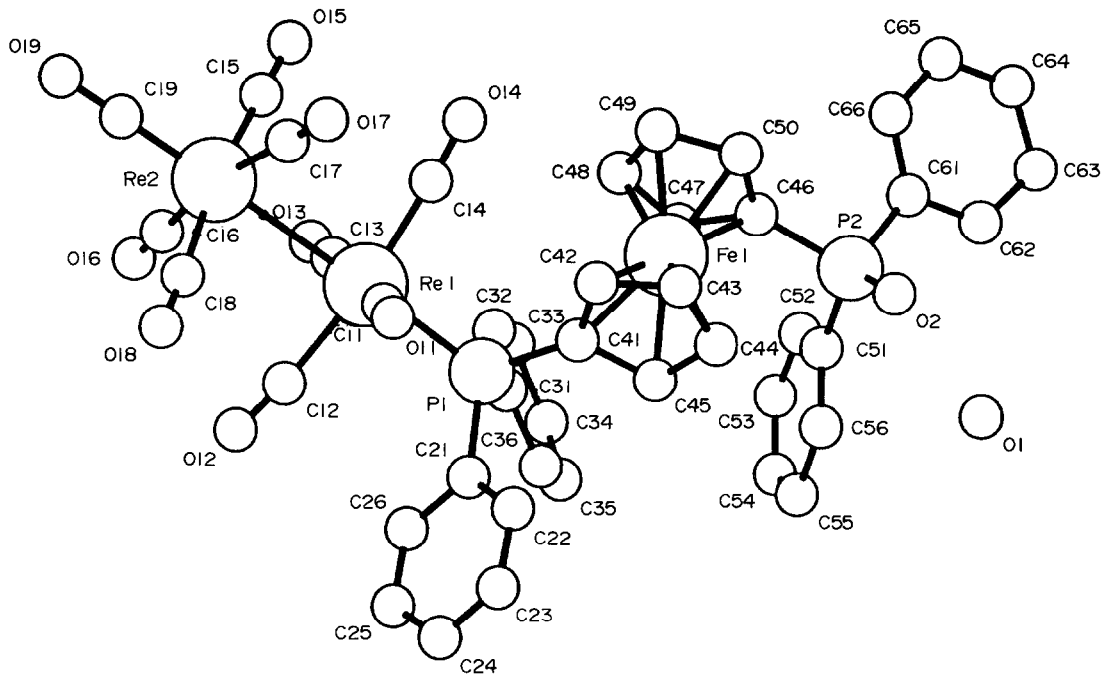

Fig. 2. SCHAKAL plot of $Re_2(CO)_9(dppfO)\cdot H_2O$ (7) (hydrogen atoms omitted for clarity) showing two crystallographically independent molecules.

(20.2(15)°), which orientates the molecule to midway between being idealized eclipsed and staggered. A torsional (C(41)–Cent(1)–Cent(2)–C(46)) twist of 127.0(12)° (122.1(13)°) is also substantially smaller than that found in free dppf[20] and other open-bridged systems[21] including complexes **1**–**4** and consequentially the intramolecular P···P separation (6.369(7) Å (6.342(8) Å) and P···Fe···P angle (133.5(2)° (131.7(2)°) are decreased.

XPS studies

Table 3 summarizes some b.e.s observed in the multinuclear XPS spectra of the compounds studied. Complexes with inequivalent phosphorus atoms generally show a peak broadening of *ca* 0.3 eV in their P(2*p*) spectra. Such broadening, which has been observed in some Gp 6 carbonyls substituted by dppf in a unidentate coordination mode,[22] allows the extraction of a doublet of Gaussian components. A typical P(2*p*) photoelectron spectrum is that of **5** which is shown in Fig. 3. The high energy shift in **5** of 0.9 eV from the dangling site to the coordinated phosphorus reflects the net electron drift P → M upon coordination of the phosphine. Although there is a general consensus[9,9e,10a,10c,10d] that phosphine coordination does not alter the P(2*p*) b.e. because of the counter-balance of σ and π electron drifts, a similar high-energy shift has been reported in a few monophosphine complexes.[23] In these literature cases however, comparisons are made on *different* complexes, the accuracy of which depends on the reliability of the reference peaks.

Just as the b.e.s for free dppf **9**, (131.1(1.8)) and a dangling dppf site in **5** (131.15(1.90)) is virtually

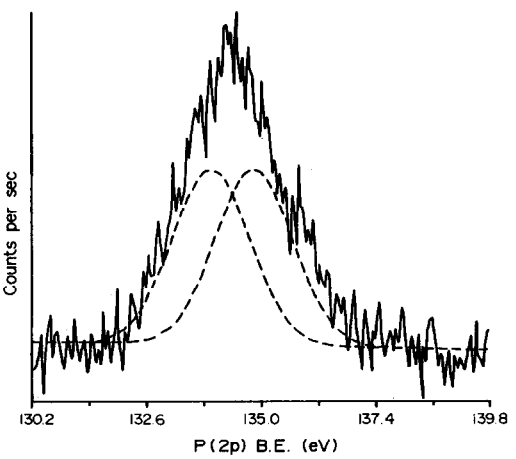

Fig. 3. Experimental (——) and deconvoluted (----) P(2*p*) X-ray Photoelectron Spectra of $Re_2(CO)_9(dppf)$ (**5**) showing the high and low energy bands corresponding to the coordinated and pendant phosphine groups.

Table 3.[a] XPS data listing the core level binding energies (eV)

Complex	P(2*p*)	Re(4$f_{7/2}$)	Re(4$f_{5/2}$)	Others
$[Re_2(dppf)_9](\mu\text{-dppf})$ (**1**)	131.9(2.05)	41.5(1.85)	43.9(1.85)	708.5(2.00)[b]
	—	42.2(1.85)	44.5(1.85)	
$Re_2(CO)_9(dppf)$ (**5**)	131.15(1.90)	41.55(1.85)	43.9(1.85)	708.35(1.95)[b]
	132.05(1.90)	42.15(1.85)	44.5(1.85)	
$Re_2(CO)_9(dppfO)$ (**7**)	131.85(2.00)	41.5(1.80)	43.9(1.80)	708.5(1.75)[b]
	132.6(2.00)	42.15(1.80)	44.5(1.80)	
$Re_2(CO)_9(CH_3CN)$ (**8**)	—	41.7(1.90)	44.1(1.90)	400.85(1.90)[c]
	—	42.3(1.90)	44.7(1.90)	
dppf (**9**)	131.1(1.8)	—	—	708.5(1.4)[b]
$dppfO_2$ (**10**)	132.55(1.95)	—	—	708.3(1.65)[b]
$Re(CO)_3(dppf)Br$ (**11**)	131.85(1.85)	41.9(1.85)	44.25(1.85)	68.5(2.00)[d]
				708.55(1.60)[b]
$Re(CO)_5Br$ (**12**)	—	43.0(1.90)	45.35(1.90)	69.25(2.00)[d]
$Re_2(CO)_{10}$ (**13**)	—	42.35(1.90)	44.7(1.90)	—

[a] Core level binding energies are referenced to hydrocarbon peak at 285.0 eV; full-width half-maximum values given in parentheses; [b] Fe(2$p_{3/2}$); [c] N(1s); [d] Br(3$d_{5/2}$).

indistinguishable, the values for $Fe(C_5H_4P(O)Ph_2)_2$ ($dppfO_2$) (**10**), (132.55(1.95) eV) and the phosphoryl group (132.6(2.00)) are comparable. Midway between these values lie the coordinated phosphines, as shown in **1**, **5** and $Re(CO)_3(dppf)Br$ (**11**). These subtle but significant differences in the P(2*p*) shifts are in full accord with the structural and chemical differences of these systems. The similarity in the P(2*p*) b.e.s of the metal-bound phosphorus in **1**, **5** and **11**, which lie within a narrow range of 0.2 eV, however suggests a rather restricted use in the P(2*p*) core b.e. in the differentiation of the different ligation mode of the phosphine, or the identification of the oxidation state of the metal centre upon which the phosphine is attached. However, comparison of the XPS and ^{31}P NMR shift data revealed a trend showing that the highest b.e. was registered for the most deshielded phosphoryl nucleus and the lowest the most shielded pendant phosphorus. A similar correlation has been recently observed in a Mo–W mixed-metal system in which the ^{31}P NMR shift is related to the metal b.e. though in this case the phosphorus b.e.s are relatively insensitive.[24]

For the nine Re(0) and Re(I) species examined, the Re(4$f_{7/2}$) b.e.s fall in the range of 41.5–43.0 eV, a region generally observed for Re(I)–Re(IV) complexes.[10b,12b,i 2d,12e] The lowest b.e. is found in **1** and **5**, both of which possess a tetracarbonyl rhenium moiety monosubstituted by a phosphine group. Such a relatively low value is expected in view of the zero oxidation state of the metal coupled with the substitution of a π acceptor by a strong σ donor.[25] The high value found in $Re(CO)_5Br$ (**12**), is explained by the strong electron demand on the Re(I) centre by the COs in the pentacarbonyl moiety. Carbonyl substitution in $Re_2(CO)_{10}$ (**13**), invariably leads to a drop in the Re(4*f*) b.e.

A significant feature of the Re(4*f*) spectra of **1**, **5**, **7** and **8** is that, for each, the broad Re(4$f_{7/2}$) peak of FWHM = 2.00–2.05 eV can be deconvoluted into a doublet of equal intensity (FWHM = 1.80–1.90 eV) separated by 0.6–0.7 eV. The equally broad Re(4$f_{5/2}$) peaks can be similarly deconvoluted. Mononuclear, e.g. **11** and **12** and symmetrical dinuclear, e.g. **13** complexes have generally sharper Re(4*f*) bands. A typical spectrum obtained in **1** is illustrated in Fig. 4. The higher energy bands, attributed to the $Re(CO)_5$ fragment, lie within 0.2 eV of the bands from the parent $Re_2(CO)_{10}$ (**13**), This implies that only a marginal increase in electronic charge on the neighbouring metal occurs upon carbonyl substitution on one of the Re atoms. The deconvolution into two Re(4$f_{7/2}$) and two Re(4$f_{5/2}$) peaks provides strong evidence for the existence of two chemically differentiable Re centres with equal statistical distribution in these four tri- and penta-metallic Re complexes.

CONCLUSION

Most of the substitution chemistry of $Re_2(CO)_{10}$ is based on the substitutionally labile $Re(CO)_5$ unit. As demonstrated in this report and some other recent studies,[6,26] the pathway involving homolysis of the Re—Re bond can be bypassed under less stringent experimental conditions. The resultant dirhenium species provides a building block in poly-

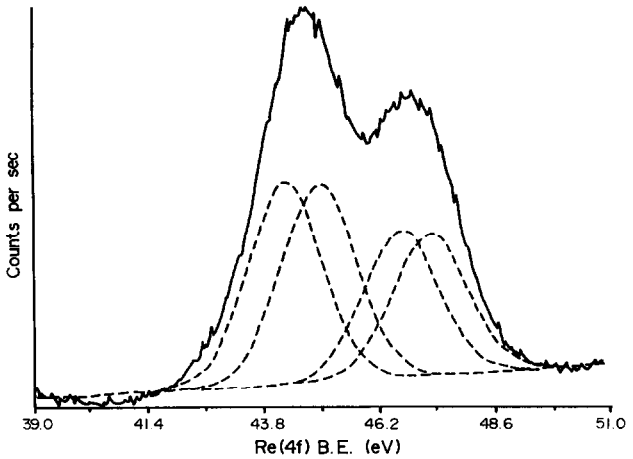

Fig. 4. Experimental (——) and deconvoluted (----) Re(4*f*) X-ray Photoelectron Spectra of $[Re_2(CO)_9]_2(\mu$-dppf) (**1**), showing the two sets of doublets of 1 : 1 intensity.

metallic synthesis. The feasibility of these metal aggregates as synthons to linear clusters and A-frame molecules attracts our current attention.

Acknowledgements—Financial supports from the National University of Singapore (NUS) (RP850030) and Academia Sinica, Taipei, are gratefully acknowledged. L.T.P. and Y.K.Y. extend their appreciation to NUS for a scholarship award. Technical assistance from Y.-P. Leong is much indebted.

REFERENCES

1. Part 17, T. S. A. Hor and L.-T. Phang, *Thermochim. Acta* 1991, **178**, 287.
2. (a) K.-W. Lee and T. L. Brown, *Organometallics* 1985, **4**, 1030; (b) P. O. Nubel and T. L. Brown, *J. Am. Chem. Soc.* 1984, **106**, 644; (c) P. O. Nubel and T. L. Brown, *J. Am. Chem. Soc.* 1982, **104**, 4955; (d) U. Koelle, *J. Organomet. Chem.* 1978, **155**, 53; (e) D. J. Cox and R. Davis, *J. Organomet. Chem.* 1980, **186**, 347; (f) D. J. Cox and R. Davis, *Inorg. Nucl. Chem. Lett.* 1977, **13**, 301; (g) D. J. Cox and R. Davis, *J. Organomet. Chem.* 1980, **186**, 339; (h) D. Sonnenberger and J. D. Atwood, *J. Am. Chem. Soc.* 1980, **102**, 3484; (i) A. M. Stolzenberg and E. L. Muetterties, *J. Am. Chem. Soc.* 1983, **105**, 822; (j) D. G. DeWit, J. P. Fawcett and A. Po, *J. Chem. Soc., Dalton Trans.* 1976, 528; (k) J. T. Moelwyn-Hughes, A. W. B. Garner and N. Gordon, *J. Organomet. Chem.* 1971, **26**, 373.
3. (a) K.-W. Lee, W. T. Pennington, A. W. Cordes and T. L. Brown, *Organometallics* 1984, **3**, 404; (b) K.-W. Lee and T. L. Brown, *Organometallics* 1985, **4**, 1025.
4. (a) J. A. Armstead, D. J. Cox and R. Davis, *J. Organomet. Chem.* 1982, **236**, 213; (b) N. M. Boag and H. D. Kaesz, in *Comprehensive Organometallic Chemistry* (Edited by G. Wilkinson, F. G. A. Stone and E. W. Abel), Vol. 4, Ch. 30, p. 161. Pergamon Press, Oxford (1982).
5. T. S. A. Hor and L.-T. Phang, *J. Organomet. Chem.* 1990, **390**, 345.
6. G. W. Harris, J. C. A. Boeyens and N. J. Coville, *J. Chem. Soc., Dalton Trans.* 1985, 2277.
7. (a) G. W. Harris, J. C. A. Boeyens and N. J. Coville, *Organometallics* 1985, **4**, 914; (b) G. W. Harris and N. J. Coville, *Organometallics* 1985, **4**, 908; (c) M. O. Albers, J. C. A. Boeyens, N. J. Coville and G. W. Harris, *J. Organomet. Chem.* 1984, **260**, 99; (d) D. J. Robinson, G. W. Harris, J. C. A. Boeyens and N. J. Coville, *J. Chem. Soc., Chem. Commun.* 1984, **19**, 1307.
8. (a) T. M. Miller, M. S. Wrighton and K. J. Ahmed, *Inorg. Chem.* 1989, **28**, 2347; (b) C. E. Housecroft, S. M. Owen, P. R. Raithby and B. A. M. Shaykh, *Organometallics* 1990, **9**, 1617, and references therein.
9. (a) W. E. Morgan, W. J. Stec, R. G. Albridge and J. R. Van Wazer, *Inorg. Chem.* 1971, **10**, 926; (b) J. R. Blackburn, R. Nordberg, F. Stevie, R. G. Albridge and M. M. Jones, *Inorg. Chem.* 1970, **9**, 2374; (c) W. E. Swartz, Jr, J. K. Ruff and D. M. Hercules, *J. Am. Chem. Soc.* 1972, **94**, 5227; (d) P. A. Grutsch, M. V. Zeller and T. P. Fehlner, *Inorg. Chem.* 1973, **12**, 1431; (e) C. A. Tolman, W. M. Riggs, W. J. Linn, C. M. King and R. C. Wendt, *Inorg. Chem.* 1973, **12**, 2770.
10. (a) S. O. Grim and L. J. Matienzo, *Inorg. Chem.* 1975, **14**, 1014; (b) G. L. Leigh and W. Bremser, *J. Chem. Soc., Dalton Trans.* 1972, 1216; (c) C. D. Cook, K. Y. Wan, U. Gelius, K. Hamrin, G. Johansson, E. Olsson, H. Siegbahn, C. Nordling and K. Siegbahn, *J. Am. Chem. Soc.* 1971, **93**, 1904; (d) G. Kumar, J. R. Blackburn, R. G. Albridge, W. E. Moddeman and M. M. Jones, *Inorg. Chem.* 1972, **11**, 296; (e) T. H. Lee, W. L. Jolly, A. A. Bakke, R. Weiss and J. G. Verkade, *J. Am. Chem. Soc.* 1980, **102**, 2631.

11. (a) R. D. Feltham and P. Brant, *J. Am. Chem. Soc.* 1982, **104**, 641; (b) B. J. Brisdon, W. S. Mialki and R. A. Walton, *J. Organomet. Chem.* 1980, **187**, 341; (c) B. J. Brisdon, G. F. Griffin, J. Pierce and R. A. Walton, *J. Organomet. Chem.* 1981, **219**, 53; (d) W. M. Riggs, *Analyt. Chem.* 1972, **44**, 830.
12. (a) B. Folkesson, *Acta Chem. Scand.* 1973, **27**, 287; (b) J. Chatt, C. M. Elson, N. E. Hooper and G. J. Leigh, *J. Chem. Soc., Dalton Trans.* 1975, 2392; (c) P. Brant, D. J. Salmon and R. A. Walton, *J. Am. Chem. Soc.* 1978, **100**, 4424; (d) P. Brant, H. D. Glicksman, D. J. Salmon and R. A. Walton, *Inorg. Chem.* 1978, **17**, 3203; (e) J. R. Ebner and R. A. Walton, *Inorg. Chem.* 1975, **14**, 2289.
13. (a) S. C. Avanzino and W. L. Jolly, *J. Am. Chem. Soc.* 1976, **98**, 6505; (b) J.-K. Shen, Y.-C. Gao, Q.-Z. Shi and F. Basolo, *Organometallics* 1989, **8**, 2144.
14. L. K. Peterson, R. S. Dhami and F. Wada, *Synth. React. Inorg. Met. Org. Chem.* 1983, **13(3)**, 291.
15. T. S. A. Hor, L.-T. Phang, L.-K. Liu and Y.-S. Wen, *J. Organomet. Chem.* 1990, **397**, 29.
16. (a) L.-K. Liu, S.-K. Yeh and C.-C. Lin, *Bull. Inst. Chem. Acad. Sin.* 1988, **35**, 45; (b) A. L. Bandini, G. Banditelli, M. A. Cinellu, G. Sanna, G. Minghetti, F. Demartin and M. Manassero, *Inorg. Chem.* 1989, **28**, 404.
17. H. Takaya, K. Mashima, K. Koyano, M. Yagi, H. Kumobayashi, T. Taketomi, S. Akutagawa and R. Noyori, *J. Org. Chem.* 1986, **51**, 629.
18. (a) M. C. Etter and P. W. Baures, *J. Am. Chem. Soc.* 1988, **110**, 639; (b) E. G. Bent, R. Schaeffer, R. C. Haltiwanger and A. D. Norman, *J. Organomet. Chem.* 1989, **364**, C25.
19. (a) G. M. Kosolapoff and L. Maier, *Organic Phosphorus Compounds*, Vol. 3, pp. 418–419. Wiley-Interscience, New York (1972); (b) G. Ruban and V. Zabel, *Cryst. Struct. Commun.* 1976, **5**, 671.
20. U. Casellato, D. Ajó, G. Valle, B. Corain, B. Longato and R. Graziani, *J. Crystallogr. Spec. Res.* 1988, **18(5)**, 583.
21. S. Onaka, A. Mizuno and S. Takagi, *Chem. Lett.* 1989, 2037.
22. H. S. O. Chan, T. S. A. Hor, L.-T. Phang and K. L. Tan, *J. Organomet. Chem.* 1991, **407**, 353.
23. M. Pelavin, D. N. Hendrickson, J. M. Hollander and W. L. Jolly, *J. Phys. Chem.* 1970, **74**, 1116.
24. R. T. Carlin and R. E. McCarley, *Inorg. Chem.* 1989, **28**, 280.
25. (a) D. T. Clark and D. B. Adams, *J. Chem. Soc., Chem. Commun.* 1971, 740; (b) D. T. Clark and D. B. Adams, *Chem. Phys. Lett.* 1971, **10**, 121; (c) M. Barbar, J. A. Connor, I. H. Hillier and V. R. Saunders, *J. Chem. Soc., Chem. Commun.* 1971, 682; (d) J. Chatt and G. J. Leigh, *Angew. Chem., Int. Edn Engl.* 1978, **17**, 400.
26. (a) R. K. Menon and T. L. Brown, *Inorg. Chem.* 1989, **28**, 1370; (b) K.-W. Lee, W. T. Pennington, A. W. Cordes and T. L. Brown, *J. Am. Chem. Soc.* 1985, **107**, 631; (c) M. O. Albers, N. J. Coville and E. Singleton, *J. Chem. Soc., Chem. Commun.* 1982, 96.
27. S. P. Schmidt, W. C. Trogler and F. Basolo, *Inorg. Synth.* 1985, **23**, 41.
28. (a) T. S. A. Hor and L.-T. Phang, *J. Organomet. Chem.* 1989, **373**, 319; (b) T. S. A. Hor and L.-T. Phang, *J. Organomet. Chem.* 1990, **381**, 121.
29. (a) T. S. A. Hor, H. S. O. Chan, Y.-P. Leong and M.-M. Tan, *J. Organomet. Chem.* 1989, **373**, 221; (b) H. S. O. Chan, T. S. A. Hor, J. R. Lusty, K. H. Lim and C. S. M. Chiam, *J. Therm. Anal.* 1988, **34**, 121.
30. For example, I. R. Butler, W. R. Cullen, T.-J. Kim, S. J. Rettig and J. Trotter, *Organometallics* 1985, **4**, 972.
31. J. J. Bishop, A. Davison, M. L. Katcher, D. W. Lichtenberg, R. E. Merrill and J. C. Smart, *J. Organomet. Chem.* 1971, **27**, 241.
32. E. J. Gabe, F. L. Lee and Y. Le Page, in *Crystallographic Computing 3: Data Collection, Structure Determination, Proteins, and Databases* (Edited by G. M. Sheldrick, C. Krueger and R. Goddard), pp. 167–174. Clarendon Press, Oxford (1985).

Polyhedron Vol. 10, No. 20/21, pp. 2451–2455 1991
Printed in Great Britain

0277–5387/91 $3.00+.00
© 1991 Pergamon Press plc

SYNTHESIS AND CRYSTAL STRUCTURE OF THE DIMERIC COMPOUND DI-μ-AZIDE-BIS(2,2′:6′,2″-TERPYRIDINE) DICOPPER(II) HEXAFLUOROPHOSPHATE

M. I. ARRIORTUA,* M. K. URTIAGA, M. INSAUSTI,† J. L. MESA† and T. ROJO†

Departamentos de Mineralogía-Petrología y †Química Inorgánica, Facultad de Ciencias, Universidad del País Vasco, Apdo. 644, E-48080 Bilbao, Spain

(*Received* 8 *April* 1991; *accepted* 2 *July* 1991)

Abstract—The title compound of formula $[Cu(terpy)(N_3)]_2(PF_6)_2$ (with terpy = 2,2′:6′,2″-terpyridine) has been synthesized and its crystal structure solved at room temperature by X-ray diffraction methods. The structure consists of $[Cu_2(terpy)_2(N_3)_2]^{2+}$ dimeric cations and non-coordinated hexafluorophosphate anions. The copper(II) ions are five-coordinate linked to three nitrogen atoms of the tridentate terpy ligand and two nitrogen atoms of the azide groups. The geometry of the coordination polyhedron is near to regular square pyramidal. Within the binuclear unit, the copper(II) ions are bridged by two azide groups in an end-on fashion. The Cu—Cu separation is 3.313(2) Å, and the Cu—N—Cu bridging angle is 96.3(3)°.

In recent years extensive studies have been directed toward the synthesis and properties of transition metal azide complexes.[1] The interest in the azide anion in coordination chemistry lies, in part, on the marked ability of this pseudohalide to act as a bridging ligand. The azide ligand can bridge two metallic ions either in a symmetrical "end-to-end" fashion or in an "end-on" fashion.[2,3] Among structurally characterized di-μ-azide-bridged complexes of copper, the type "end-on" bridge has been found in the polymeric $[Cu(bpy)(N_3)_2]$[4] (bpy = 2,2′-bipyridine) and dimeric $[Cu_2(N_3)_4(C_{16}H_{34}N_2O_6)(H_2O)]$[5] complexes; while the type "end-to-end" bridge has been reported in the dimeric $[Cu_2(PPh_3)_4(N_3)_2]$ compound.[6] Both kinds of bridging occur in the polymeric copper(II) azide.[7] We are studying some azide-compounds with general formula $[ML_{III}(N_3)_2]$ or $[ML_{III}(N_3)](PF_6)$; where M is Cu or Ni and L_{III} is a tridentate rigid ligand, as 2,2′:6′,2″-terpyridine, pyridine-2-aldehyde 2′-pyridylhydrazone and N-(6-methyl-2-pyridylmethylene)-2-(2-pyridyl) ethylamine.[8–11] In this publication, we present the crystal structure of a new dimeric copper(II) "end-on" azide complex, with formula $[Cu(terpy)(N_3)]_2(PF_6)_2$.

*Author to whom correspondence should be addressed.

EXPERIMENTAL

Synthesis of $[Cu(terpy)(N_3)](PF_6)$

A warm aqueous solution (20 cm^3) of 0.20 g (0.525 mmol) of $[Cu(terpy)(N_3)_2]$ complex,[8] was treated with a KPF_6-saturated aqueous solution. After stirring a green solid precipitate was obtained. Crystallization of this product from a saturated aqueous solution yielded a few crystals, which were isolated by vacuum filtration and utilized for the X-ray crystal structure determination. The powder pattern of the solid precipitate obtained together with the crystals, shows the existence of other phases, which have vitiated a study of the physical properties. The elemental analysis of the crystals gives the following results: Found: C, 36.4; H, 2.2; N, 17.1. Calc. for $[Cu(C_{15}H_{11}N_3)(N_3)](PF_6)$: C, 36.9; H, 2.3; N, 17.4%.

X-ray data collection and structure determination

A well-formed prismatic crystal with dimensions $0.28 \times 0.10 \times 0.16$ mm was selected for the X-ray study. Preliminary cell dimensions and space group symmetry were obtained from Weissenberg and oscillation photographs. The same crystal was mounted on an Enraf–Nonius CAD-4 diffrac-

tometer equipped with graphite-monochromatized Mo-K_α radiation. Accurate cell constants were determined from least-squares refinement of the setting angles of 25 reflections with $14 \leqslant 2\theta \leqslant 25°$.

Crystal data: $[Cu(C_{15}H_{11}N_3)(N_3)](PF_6)$, $M = 483.9$, $P2_1/n$, $a = 10.149(2)$, $b = 15.593(2)$, $c = 11.694(4)$ Å, $\beta = 103.57(2)°$, $V = 1799(9)$ Å^3, $Z = 4$, $D_m = 1.79(2)$, $D_x = 1.79$ g cm^{-3}, $\lambda(\text{Mo-}K_{\alpha 1}) = 0.7107$ Å, $\mu(\text{Mo-}K_\alpha) = 14.47$ cm^{-1}, $F(000) = 956$, $T = 294$ K. Density was measured by flotation in a chloroform/1,1,2,2-tetrabromoethene mixture.

A total of 7122 reflections were measured ($2\theta \leqslant 50°$; $0 \leqslant h \leqslant 12$; $0 \leqslant k \leqslant 18$; $-13 \leqslant l \leqslant 13$) with the variable-speed $\omega/2\theta$ scan technique. 1902 reflections were considered observed with $I \geqslant 3\sigma(I)$, and used in the determination of the structure. Examination of three standard reflections [(−2−5−2), (−1−4−2), (43−3)] monitored after each 2 h, showed no substantial intensity decay. Lorentz and polarization corrections were applied, but no corrections for absorption. The structure was solved by direct methods with MULTAN 84 system,[12] and refined by full-matrix least-squares, using the SHELX 76 program.[13] The function minimized was $\Sigma w[|F_o| - |F_c|]^2$, where $w = [\sigma^2(F_o) + 0.002907(F_o)^2]^{-1}$. Positions of the hydrogen atoms were computed and refined with an overall isotropic thermal parameters and anisotropy for the remaining atoms. The final R was 0.057 ($R_w = 0.061$) for all observed reflections. At the end of the refinement the maximum peak in the final ΔF map was 0.71 e Å^{-3}. Scattering factors were taken from the *International Tables of X-Ray Crystallography*.[14] All calculations were carried out on a Microvax Computer at the computer centre of the Basque University. The geometric calculations were performed with XANADU[15] and molecular illustrations were drawn with SCHAKAL 88.[16] Further details are presented as Supplementary data, together with atomic coordinates, thermal parameters, bond lengths and angles, mean average planes and structure factors.

RESULTS AND DISCUSSION

Table 1 shows some selected bond distances and angles of the compound. The local copper(II) environment in the dimeric cation is presented in Fig. 1, with the labelling scheme used. Figure 2 shows a stereoscopic view of packing of the molecules in the unit cell.

The structure consists of cationic $[Cu_2(terpy)_2(N_3)_2]^{2+}$ units and non-coordinated hexafluorophosphate anions. The dimeric complex cation is built by two $[Cu(terpy)(N_3)]^+$ units, linked through two azide groups in an end-on fashion, and related by a crystallographic inversion centre.

The geometry of the coordination sphere around the copper(II) ion can be described as distorted square pyramidal. The basal positions are occupied by the three nitrogens of the terpyridine ligand

Table 1. Selected bond distances (Å) and angles (°) in the $[Cu(C_{15}H_{11}N_3)(N_3)](PF_6)$ complex, with e.s.d.s in parentheses

Coordination polyhedron, azide and hexafluorophosphate groups					
Cu—N(1)	2.030(8)	Cu—N(2)	1.933(6)	Cu—N(3)	2.005(7)
Cu—N(4)	1.954(7)	Cu—N(4)^i	2.469(6)	Cu—Cu^i	3.313(2)
N(1)—C(1)	1.33(1)	N(1)—C(5)	1.36(1)	C(5)—C(6)	1.46(1)
N(2)—C(6)	1.35(1)	N(2)—C(10)	1.32(1)	C(10)—C(11)	1.48(1)
N(3)—C(11)	1.37(1)	N(3)—C(15)	1.34(1)	N(4)—N(5)	1.20(1)
N(5)—N(6)	1.15(1)	P—F(1)	1.572(9)	P—F(2)	1.44(2)
P—F(3)	1.48(1)	P—F(4)	1.54(2)	P—F(5)	1.48(1)
P—F(6)	1.49(2)				
N(1)—Cu—N(2)	80.1(3)	N(1)—Cu—N(3)	158.5(3)		
N(1)—Cu—N(4)	95.9(3)	N(2)—Cu—N(4)	173.8(3)		
N(2)—Cu—N(3)	80.1(3)	N(3)—Cu—N(4)	104.4(3)		
N(4)^i—Cu—N(1)	92.2(2)	N(4)^i—Cu—N(2)	91.7(2)		
N(4)^i—Cu—N(3)	96.8(2)	N(4)^i—Cu—N(4)	83.7(2)		
Cu—N(4)—Cu^i	96.3(3)	Cu—N(4)—N(5)	129.4(5)		
N(4)—N(5)—N(6)	174.5(8)				
Mean values of the terpy ligand					
C—C	1.39(4)	C—N	1.34(2)		
C—C—C	122(4)	C—N—C	120(2)		

$i = 1-x, -y, 1-z$.

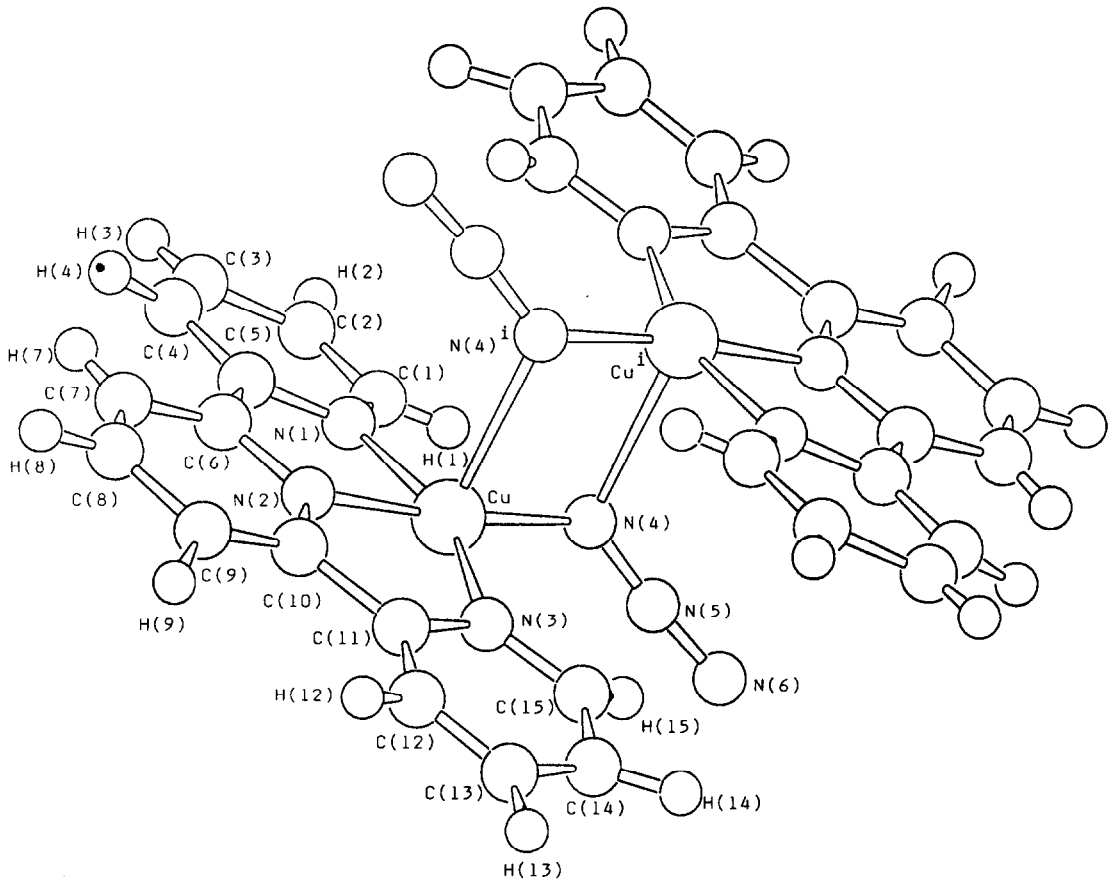

Fig. 1. Molecular structure of the dimeric cation $[Cu_2(C_{15}H_{11}N_3)_2(N_3)_2]^{2+}$.

[Cu—N(1), N(2), N(3); 2.030(8), 1.933(6), 2.005(7) Å, respectively] and one N-azide group [Cu—N(4), 1.954(7) Å]. The apical site is occupied by the other N-azide ligand [Cu—N(4)^i = 2.469(6) Å; $i = 1-x, -y, 1-z$], belonging to the other half of the dimer. The average value of the angles N apical—Cu—N basal is 91(5)°, while the *trans*-basal angles, N(1)—Cu—N(3) and N(2)—Cu—N(4) are 158.5(3) and 173.8(3)°, respectively. The basal atoms are coplanar within ±0.11 Å and the copper(II) ion is practically situated in this mean basal plane (the displacement is 0.03 Å). The departure of these angles from the ideal values of a regular square pyramid is due to the rigid nature of the tridentate ligand. The distortion of the coordination polyhedron from trigonal bipyramid (Δ = 0) towards a regular square pyramid (Δ = 1), has been calculated by quantification of the Muetterties and Guggenberger description.[17,18] The value obtained, Δ = 0.91 (Table 2), is in good agreement with a topology near to regular square pyramidal.

The bridging network Cu_2N_2 is planar due to the

Table 2. Dihedral angles (°) and distortion (Δ) for the coordination polyhedron of the title compound, compared to the ideal geometries trigonal bipyramid (TBP) and regular square pyramid (SP_r)

Dihedral angle	TBP	[CuN(1)N(2)N(3)N(4)N(4)^i]		SP_r
δa_1	101.5	N(4)N(2)N(3)N(4)^i	127.9	121.8
δa_3	101.5	N(2)N(3)N(4)N(4)^i	119.9	121.8
δa_4	101.5	N(4)N(2)N(1)N(4)^i	126.4	121.8
δa_6	101.5	N(2)N(1)N(4)N(4)^i	119.6	121.8
δa_2	101.5	N(2)N(3)N(4)^{i}N(4)	75.2	73.9
δa_5	101.5	N(1)N(4)N(4)^{i}N(3)	89.6	73.9
δe_1	53.1	N(1)N(2)N(4)^{i}N(3)	67.4	73.9
δe_2	53.1	N(2)N(1)N(4)^{i}N(4)	73.6	73.9
δe_3	53.1	N(1)N(2)N(4)N(3)	12.0	0
Δ	0	0.91		1

$\Delta = |[(\delta a_1 + \delta a_3 + \delta a_4 + \delta a_6) - 406.0]/182.7| + |[(\delta a_2 + \delta a_5) - 203.0]/248.4| + |[(\delta e_1 + \delta e_2) - 106.2]/187.2| + |(53.1 - \delta e_3)/477.9|$.

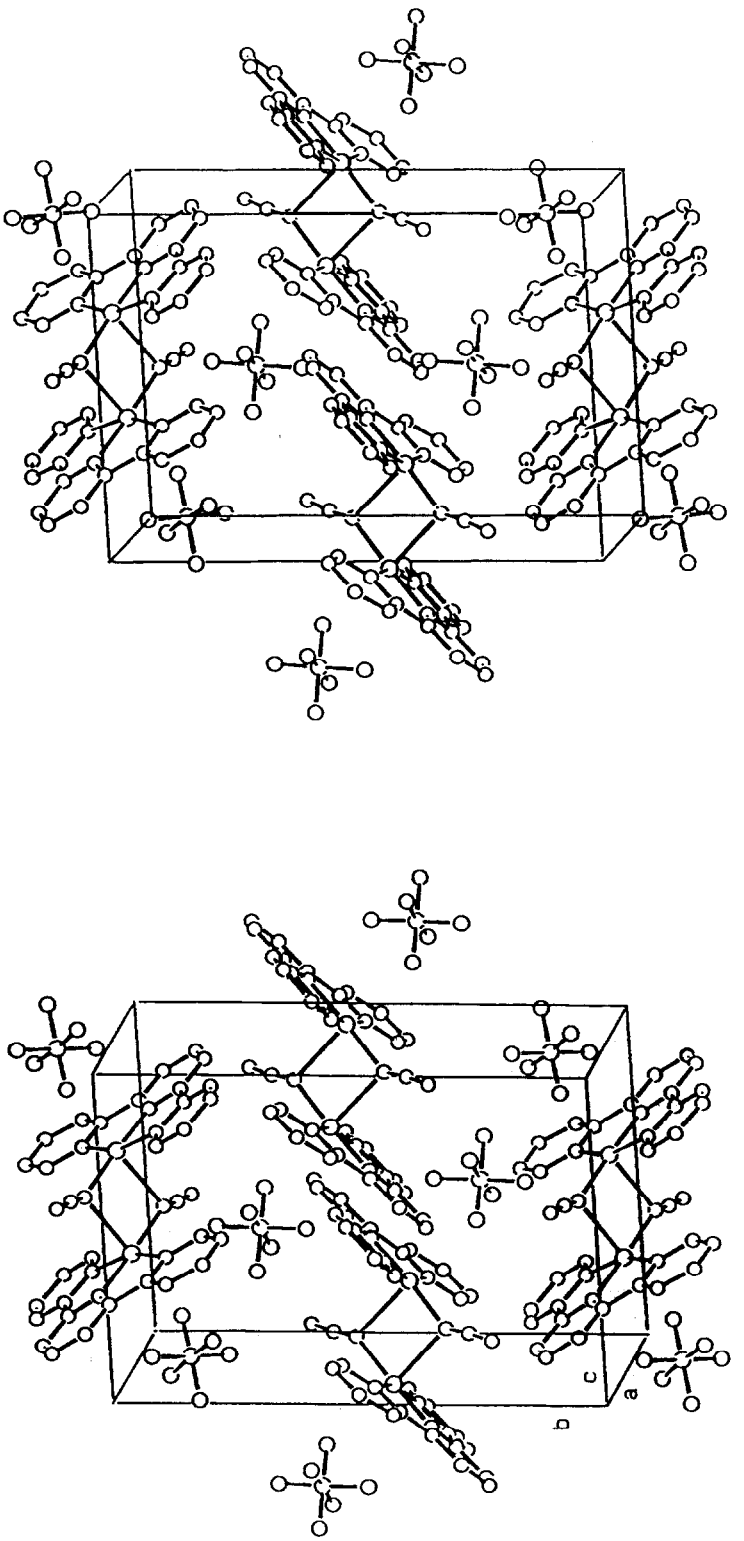

Fig. 2. Stereoscopic view of the molecules in the unit cell.

presence of a crystallographic inversion centre in the dimer. The intradimeric Cu—Cu distance is 3.313(2) Å, and the bridging angle Cu—N(4)—Cu^{i} is equal to 96.3(3)°. The end-on azide group is found to be linear within experimental error [angle N(4)—N(5)—N(6) is 174.5(8)°]. The value for the angle Cu—N(4)—N(5) [129.4(5)°] lies within the expected range for the angle of a trigonally hybridized nitrogen.[19] The N(4)—N(5) and N(5)—N(6) bond lengths are 1.20(1) and 1.15(1) Å, respectively. The values obtained for both bond distances and angles in the tridentate terpy ligand are in good agreement with those given in the literature.[20-22]

Acknowledgements—This work was financially supported in part by a grant of the Universidad del País Vasco (O.P.V. 130.310-E049/90) which we gratefully acknowledge.

REFERENCES

1. A. M. Golub, H. Kohler and V. V. Skopenko, *Chemistry of Pseudohalides*, p. 28. Elsevier, Amsterdam (1986).
2. R. D. Willet, D. Gatteschi and O. Kahn, *Magneto-structural Correlations in Exchange-Coupled Systems*, NATO ASI Series, p. 57. Reidel, Dordrecht, Holland (1985).
3. M. Charlot, O. Kahn, M. Chaillet and C. Larrieu, *J. Am. Chem. Soc.* 1986, **108**, 2574.
4. G. W. Bushnell and M. A. Khan, *Can. J. Chem.* 1974, **52**, 3125.
5. J. Commarmond, P. Plumere, J. M. Lehn, Y. Agnus, R. Louis, K. Weiss, O. Khan and I. Morgensten, *J. Am. Chem. Soc.* 1982, **104**, 6330.
6. R. F. Ziolo, A. P. Gaughan, Z. Dori, C. G. Pierpont and R. Eisenberg, *Inorg. Chem.* 1971, **10**, 1289.
7. R. Soderquist, *Acta Cryst.* 1968, **B24**, 450.
8. J. Vía, M. I. Arriortua, T. Rojo, J. L. Mesa and A. García, *Bull. Soc. Chim. Belg.* 1989, **98**, 179.
9. M. I. Arriortua, R. Cortés, L. Lezama, T. Rojo, X. Soláns and M. Font-Bardía, *Inorg. Chim. Acta* 1990, **174**, 263.
10. T. Rojo, L. Lezama, R. Cortés, J. L. Mesa, M. I. Arriortua and G. Villeneuve, *J. Magnet. Magn. Mater.* 1990, **83**, 519.
11. T. Rojo, J. I. R. Larramendi, I. Durán, J. L. Mesa, J. Vía and M. I. Arriortua, *Polyhedron* 1990, **9**, 2693.
12. P. Main, G. Germain and M. M. Woolfson, MULTAN 84. A System of Computer Programs for the Automatic Solution of Crystal Structures from X-ray Diffraction Data. University of York, U.K. and Louvain, Belgium (1984).
13. G. M. Sheldrick, SHELX 76. Program for Crystal Structure Determination. University of Cambridge, U.K. (1976).
14. *International Tables for X-ray Crystallography*, Vol. 4, pp. 72–79. Kynoch Press, Birmingham (1974).
15. P. Roberts and G. M. Sheldrick, XANADU. Program for Torsion Angle, Mean Plane and Libration Correction Calculations. University of Cambridge, U.K. (1975).
16. E. Ketler, SCHAKAL 88. A Fortran Program for the Graphic Representation of Molecular and Crystallographic Models. University of Freiburg (1988).
17. E. L. Muetterties and L. J. Guggenberger, *J. Am. Chem. Soc.* 1988, **7**, 1383.
18. J. L. Mesa, M. I. Arriortua, L. Lezama, J. L. Pizarro, T. Rojo and D. Beltrán, *Polyhedron* 1988, **7**, 1383.
19. Z. Dori and R. F. Ziolo, *Chem. Rev.* 1973, **73**, 247.
20. T. Rojo, M. I. Arriortua, J. Ruiz, J. Darriet, G. Villeneuve and D. Beltrán, *J. Chem. Soc., Dalton Trans.* 1987, 285.
21. T. Rojo, J. L. Mesa, M. I. Arriortua, J. M. Savariault, J. Galy, G. Villeneuve and D. Beltrán, *Inorg. Chem.* 1988, **27**, 3904.
22. T. Rojo, R. Cortés, L. Lezama, J. L. Mesa, J. Vía and M. I. Arriortua, *Inorg. Chim. Acta* 1989, **165**, 91.

Polyhedron Vol. 10, No. 20/21, pp. 2457–2461, 1991
Printed in Great Britain

0277–5387/91 $3.00+.00
© 1991 Pergamon Press plc

THE FORMATION OF MOLECULAR COMPOUNDS IN THE REACTION BETWEEN $[MgCl_2(THF)_2]$ AND $[MoCl_3O(THF)_2]$. CRYSTAL STRUCTURE OF $[\{MoCl_4O(THF)\}_2Mg(THF)_4]\cdot CH_2Cl_2$

PIOTR SOBOTA,* JOLANTA EJFLER, TADEUSZ PŁUZIŃSKI and TADEUSZ LIS

Institute of Chemistry, University of Wrocław, 14, F. Joliot-Curie, 50-383 Wrocław, Poland

(*Received* 21 *March* 1991; *accepted* 2 *July* 1991)

Abstract—The interaction of $[MgCl_2(THF)_2]$ with $[MoCl_3O(THF)_2]$ in 1 : 1 and 1 : 2 ratios in CH_2Cl_2 gave the paramagnetic complexes $[(THF)_3Mg(\mu\text{-}Cl)_3MoCl_2O]$ **I** and $[\{MoCl_4O(THF)\}_2Mg(THF)_4]\cdot CH_2Cl_2$ **II** (THF, tetrahydrofuran). In complex **I**, the molybdenum and magnesium atoms are octahedrally surrounded by three bridging chlorine atoms and terminal oxo-oxygen and two chlorine atoms and by three THF molecules, respectively. Complex **II** consists of Mg^{2+} ions coordinated by four THF molecules and two *trans*-$[MoCl_4O(THF)]^-$ anions coordinated to an Mg atom by oxo O-atoms.

In a previous paper we described the synthesis and properties of the product formed during reaction between $[MgCl_2(THF)_2]$ and $[MoCl_3O(THF)_2]$ in tetrahydrofuran.[1]

$$[MgCl_2(THF)_2]+2[MoCl_3O(THF)_2]\xrightarrow{THF}[Mg(THF)_6][MoCl_4O(THF)]_2 \quad (1)$$

$$2[MgCl_2(THF)_2]+[MoCl_3O(THF)_2]\xrightarrow{THF}[Mg_2(\mu\text{-}Cl)_3(THF)_6][MoCl_4O(THF)] \quad (2)$$

The Mo^{5+} ion is a stronger Lewis acid than Mg^{2+} (reactions 1 and 2) removes chloride ions from $[MgCl_2(THF)_2]$. The formation of $[Mg(THF)_6]^{2+}$, $[Mg_2(\mu\text{-}Cl)_3(THF)_6]^+$, $[MgCl(THF)_5]^+$ and $[MgCl_4]^{2-}$ ions from $[MgCl_2(THF)_2]$ under the influence of transition metal chlorides MCl_n in THF is well documented.[1–4] However, in less polar solvents the formation of the molecular compounds could be expected. Here we describe the results of the study of reaction between $[MgCl_2(THF)_2]$ and $[MoCl_3O(THF)_2]$ in 1 : 1 and 1 : 2 molar ratios in CH_2Cl_2 and the crystal structure of complex $[\{MoCl_4O(THF)\}_2Mg(THF)_4]\cdot CH_2Cl_2$ **II**.

EXPERIMENTAL

Reactions were carried out under dinitrogen using dried solvents and conventional Schlenk apparatus. The complexes $[MoCl_3O(THF)_2]$ and $[MgCl_2(THF)_2]$ were obtained by literature methods.[5,6] ESR spectra were obtained on an SE type X spectrometer, variable temperature (4.2–298 K). Magnetic susceptibility measurements were determined by the Faraday method. IR spectra were obtained using a Perkin–Elmer spectrometer (values in cm^{-1}).

Tris(tetrahydrofuran)magnesium - tri - μ - chloro-oxodichloromolybdenum(V). $[MoCl_3O(THF)_2]$ (1.32 g, 3.64 mmol) was dissolved in 40 cm^3 of CH_2Cl_2 and $[MgCl_2(THF)_2]$ (0.87 g, 3.66 mmol) was suspended in 50 cm^3 of CH_2Cl_2. The solutions were mixed and the stirring was continued until the compounds dissolved. The solution was filtered off and the volume was reduced *in vacuo* to *ca* 50 cm^3. The solution was exposed to slow diffusion of n-hexane. After 24 h green crystals appeared which were filtered off, and washed with n-hexane (3 × 10 cm^3). Yield: 1.5 g, 77.8%. Found: C, 27.1; H, 4.5; Cl, 33.6; Mo, 18.0; Mg, 4.5. $C_{12}H_{24}Cl_5MgMoO_4$ requires: C, 27.2; H, 4.6; Cl, 33.5; Mo, 18.1; Mg, 4.6%; IR ν(Mo=O) 980 (s); other bands: 298 (m), 350 (s), 680 (w), 742 (s), 870 (s), 922 (w), 996 (m), 1020 (vs), 1176 (w), μ_{eff} = 1.6 μ_B (77–298 K), ESR, g = 1.950.

Trans - *bis*[trans - *tetrachloro-oxo(tetrahydrofuran)molybdenio(V)*-O] - *tetrakis(tetrahydrofuran) magnesium dichloromethane.* $[MoCl_3O(THF)_2]$ (3.9 g, 10.8 mmol) was dissolved in 60 cm^3 of CH_2Cl_2 and $[MgCl_2(THF)_2]$ (1.3 g, 5.4 mmol) was sus-

* Author to whom correspondence should be addressed.

pended in 40 cm^3 of CH_2Cl_2. The solutions were mixed and the stirring was continued until the compounds dissolved. The solution was filtered off and the volume was reduced *in vacuo* to *ca* 50 cm^3. After 24 h the green–yellow crystals which were obtained by slow diffusion of *n*-hexane into the solution were filtered off, and washed with *n*-hexane (3×10 cm^3). Yield: 4.6 g, 83.2%. Found: C, 28.8; H, 4.9; Cl, 34.0; Mo, 18.5; Mg, 2.5. $C_{25}H_{50}Cl_{10}MgMo_2O_8$ requires: C, 28.6; H, 4.8; Cl, 33.8; Mo, 18.3; Mg, 2.3%; IR ν(Mo=O) 946 (s), other bands: 278 (m), 316 (m), 354 (vs), 678 (w), 698 (w), 864 (vs), 920 (s), 1018 (vs), 1046 (w), $\mu_{eff} = 2.1$ μ_B (4.2–298 K); ESR, g (1.975, 1.969, 1.906).

The green crystalline compound **II** on heating above 373 K or *in vacuo* (6 h, 10^{-3} hPa) lost CH_2Cl_2 and collapsed to a green–yellow powder. Found: C, 29.8; H, 4.9; Cl, 30.0; Mo, 19.5; Mg, 2.5. $C_{24}H_{48}Cl_8MgMo_2O_8$ requires: C, 29.9; H, 5.0; Cl, 29.4; Mo, 19.9; Mg, 2.5%.

X-ray crystal structure determination

Specimens ($0.5 \times 0.5 \times 1.0$ mm) for **I** and ($0.8 \times 0.8 \times 0.35$ mm) for **II** were cut from larger crystals and sealed in capillaries. For both crystals intensity data were recorded on a Syntex $P2_1$ automated diffractometer using graphite-monochromatized Mo–K_α radiation. Intensities were measured using a 2θ–ω scan technique up to $2\theta = 66°$ and to $2\theta = 52°$ for **I** and **II**, respectively. The intensities of two standard reflections, monitored after every 50 intensity scans, showed no evidence of crystal decay. 2745 [4000] reflections were collected, of which 2069 [3827] [$I > 3\sigma(I)$] were used for the structure analysis for **I** and **II**, respectively. (For **II** only reflections above background were measured.) The data were corrected for background attenuation and polarization effects. For **II** an absorption correction following the DIFABS procedure[7] was applied; minimum and maximum corrections were 0.897 and 1.059, respectively.

Structure determination and refinement

Both structures were solved by direct methods using the SHELXS program.[8] In the case of **I** preliminary Weissenberg photographs showed $P6_3$ or $P6_3/m$ space groups. The non-centrosymmetric space group was assumed, in which Mo and Mg atoms lie on a three-fold axis. This situation is only possible when an oxo O and two terminal Cl atoms bonded to an Mo atom are statistically disordered. Furthermore, because of a so-called structural *trans* effect observed in monooxo complexes[9] the Mo atom also should be slightly disordered around the three-fold axis. This was visible in the large values of B_{11} and B_{22} temperature factors for Mo atoms. Since the positions of O and two terminal Cl atoms are very similar (by symmetry) it was not possible to uniquely distinguish their positions. Therefore no attempt was made to find the detailed crystal structure of this complex. The refinement stopped at $R = 0.07$ for 994 reflections with $I > 3$ (**I**). The principal interatomic distances are: Mg—O 2.03(1), Mg—Cl 2.55(1) and Mg···Mo 3.39(1) Å. In the case of **II** all heavy atoms were found from direct methods and H-atoms were included in geometrically calculated positions with d(C—H) = 1.08 Å. Full-matrix least-squares refinements were carried out on the positional and anisotropic thermal parameters of all the non-hydrogen atoms. Least-squares refinement converted with $R = \Sigma[|F_o| - |F_c|]/\Sigma|F_o| = 0.035$ and $R' = (\Sigma w \Delta F^2 / \Sigma w F_o^2)^{1/2} = 0.0408$; where $w = 1/\sigma^2(F_o)$. Neutral-atom scattering factors were taken from ref. 10. The scattering factors for Mo, Mg, Cl, O and C were corrected for real and imaginary components. A final difference map showed features in the range -0.26 to $+0.32$ eÅ^{-3}. A summary of crystallographic data for compounds **I** and **II** is given in Table 1.

Atomic coordinates, displacement factor coefficients and the list of F_o/F_c values have been deposited as supplementary data with the Editor, from whom copies are available on request. Atomic coordinates have been deposited with the Cambridge Crystallographic Data Centre.

RESULTS AND DISCUSSION

Synthesis and structure of [$(THF)_3Mg(\mu\text{-}Cl)_3MoCl_2O$]

The interaction of bis(tetrahydrofuran)magnesium dichloride with [$MoCl_3O(THF)_2$] in 1:1 molar ratio in dichloromethane leads to good yields of the green crystalline complex **I** of the above stoichiometry

$$[MoCl_3O(THF)_2] + [MgCl_2(THF)_2] \xrightarrow[CH_2Cl_2]{} \underset{\mathbf{I}}{[(THF)_3Mg(\mu\text{-}Cl)_3MoCl_2O]} + THF. \quad (3)$$

The IR spectrum in Nujol shows the expected bands due to ν(COC) of coordinated THF molecules at 1020 (s) and 870 (s) cm^{-1} and sharp bands at 980 (s) and 350 (s) cm^{-1} due to ν(Mo=O) and ν(Mo—Cl), respectively; by comparison with the $[Mg_2(\mu\text{-}Cl)_3(THF)_6]^+$ cation[1] the peak at 298 cm^{-1} attributed to ν(Mg—O). The crystalline compound **I** is very reactive, undergoing immediate de-

Table 1. Crystallographic information for compounds **I** and **II**

(a) Crystal data for $[(THF)_3Mg(\mu\text{-}Cl)_3MoCl_2O]$ **I**
Chemical formula: $C_{12}H_{24}Cl_5MgMoO_4$
$fw = 529.8$
Unit cell dimensions: $a = 11.126(5)$ Å, $c = 10.148(5)$ Å
$V = 1087.9(9)$ Å^3
$Z = 2$
Space group: $P6_3$
$\lambda = 0.71069$ Å
$T = 303(2)$ K
$D_{calc} = 1.617(2)$ g cm^{-3}
$D_{meas} = 1.622$ g cm^{-3} (by flotation)
$\mu = 12.4$ cm^{-1}

(b) Crystal data for $[\{MoCl_4O(THF)\}_2Mg(THF)_4]\cdot CH_2Cl_2$ **II**
Chemical formula: $C_{24}H_{48}Cl_8MgMo_2O_8\cdot CH_2Cl_2$
$fw = 1049.4$
Unit cell dimensions: $a = 10.87(2)$ Å, $b = 15.65(2)$ Å, $c = 26.36(3)$ Å, $\beta = 101.40(8)°$
$V = 4409(5)$ Å^3
$Z = 4$
Space group: $P2_1/c$
$\lambda = 0.71069$ Å
$T = 298(2)$ K
$D_{calc} = 1.581(3)$ g cm^{-3}
$D_{meas} = 1.584$ g cm^{-3} (by flotation)
$\mu = 12.1$ cm^{-1}
$R(F_o) = 0.035$
$R_w(F_o) = 0.0408$

composition on exposure either to air or moisture but is stable in a closed flask in the solid state and in solution of CH_2Cl_2 under N_2. It is soluble in halogenated solvents, insoluble in hydrocarbons and unstable in THF because the magnesium easily undergoes solvation and the salt $[Mg(THF)_6][MoCl_4O(THF)]_2$ is formed immediately. The compound **I** is paramagnetic, with $\mu_{eff} = 1.6\ \mu_B$ and the ESR spectra in frozen CH_2Cl_2/toluene solution and in the solid state are typical of Mo^{5+} complexes.[1] The molecular structure of **I** was shown by spectroscopic methods to contain molybdenum and magnesium atoms surrounded octahedrally by three bridging Cl atoms and terminal oxo-oxygen and two Cl atoms and three THF molecules, respectively as depicted schematically in Scheme 1.

The course of reactions (1) and (2) in THF is different and the salts $[Mg(THF)_6][MoCl_4O(THF)]_2$ and $[Mg_2(\mu\text{-}Cl)_3(THF)_6][MoCl_4O(THF)]$ are formed. The $[(THF)_3Mg(\mu\text{-}Cl)_3Mg(THF)_3]^+$ cation arises in the reaction:

$$[MgCl_2(THF)_2]+[MgCl(THF)_5]^+ \xrightarrow{THF} [(THF)_3Mg(\mu\text{-}Cl)_3Mg(THF)_3]^+. \quad (4)$$

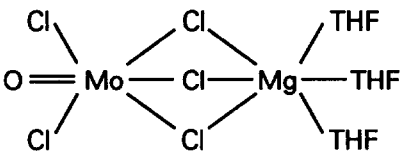

Scheme I. Schematic structure of the $[(THF)_3Mg(\mu\text{-}Cl)_3MoCl_2O]$ molecule.

This cation is stable only in the solid state and is the component of other salts, e.g. $[Mg_2(\mu\text{-}Cl)_3(THF)_6][TiCl_5(THF)]$[11] or $[Mg_2(\mu\text{-}Cl)_3(THF)_6][MoCl_4O(THF)]$.[1]

Synthesis and structure of $[\{MoCl_4O(THF)\}_2Mg(THF)_4]\cdot CH_2Cl_2$

This compound is readily obtained in high yield by interaction of $[MgCl_2(THF)_2]$ with $[MoCl_3O(THF)_2]$ in a 1 : 2 molar ratio in CH_2Cl_2:

$$2[MoCl_3O(THF)_2]+[MgCl_2(THF)_2] \xrightarrow{CH_2Cl_2} [\{(THF)Cl_4MoO\}_2Mg(THF)_4]\cdot CH_2Cl_2. \quad (5)$$
II

Complex **II** is soluble in halogenated solvents, insoluble in hydrocarbons and unstable in THF. The IR spectrum in Nujol shows stretching modes at 1040 (sh), 1018 (vs), 864 (vs, br) cm^{-1} attributed to ν(COC) and sharp band at 946 cm^{-1} due to ν(Mo=O) which is shifted to lower frequences compared to ν(Mo=O) 980 cm^{-1} found in the $[MoOCl_4(THF)]^-$ anion.[1] The band at 353 (vs) cm^{-1} is assigned to Mo—Cl stretching and at 330 (s) and 278 (m) cm^{-1} to Mg—O vibrations.[1] The stoichiometry of **II** and the shifting of the ν(Mo=O) band to lower frequencies by 34 cm^{-1} in comparison to the $[MoCl_4O(THF)]^-$ ion[1] suggested that the $[MoCl_4O(THF)]^-$ unit was coordinated by solvated magnesium Mg^{2+} and this formation is confirmed by the X-ray study. The structure of the $[\{MoCl_4O(THF)\}_2Mg(THF)_4]$ molecule is in Fig. 1 and some important molecular geometry parameters are given in Table 2. The magnesium atom is octahedrally coordinated by four tetrahydrofuran molecules and two $[MoCl_4O(THF)]^-$ units by O-atoms in *trans* positions. The Mg—O(1,2) bond lengths 2.159(6) and 2.175(5) Å are longer than the respective Mg—O distances of 2.11(1), 2.09(1) Å in $[(ReMe_4O)Mg_2(THF)_4]$[12] and $[\{o\text{-}C_6H_4(CH_2)_2WO\}_2Mg(THF)_4]$.[13] Viewing along the Mo—Mg—Mo axis, the $Mg(THF)_4$ units look like a system of propellers, although each of the THF ligands has a different conformation. The THF molecules containing O(3) and O(4) atoms have

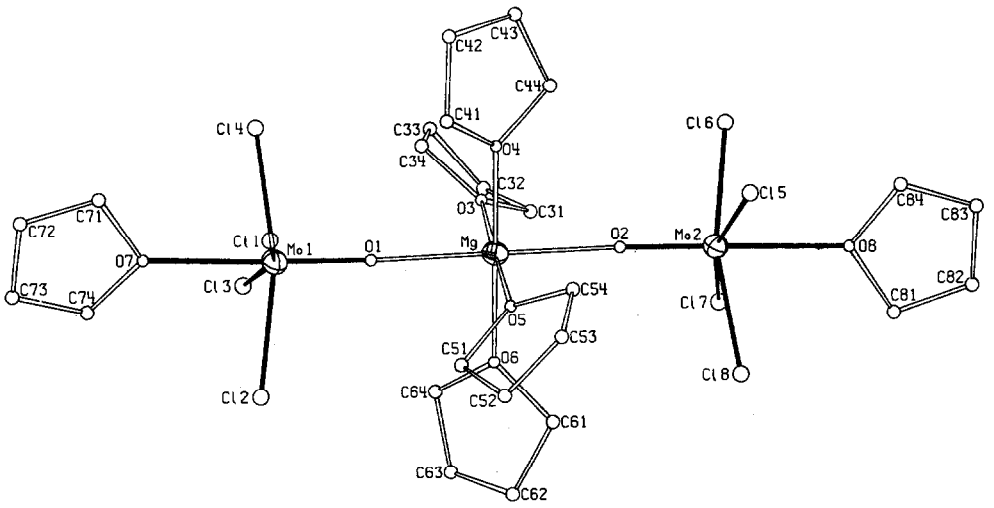

Fig. 1. View of $[\{MoCl_4O(THF)\}_2Mg(THF)_4]$ molecule.

conformations between twist and envelope with asymmetric C(31), C(32) and O(4), C(41) atoms, respectively. The THF molecule with O(6) atom has the twist conformation with C(61) and C(62) atoms moved below and above the plane of the ring, respectively. An envelope conformation is found for THF molecule containing O(5), with atom C(52) displaced from the best plane. The THF ring with atom O(7) is planar and this means that its conformation is an average of different conformations or equivalent ones with mirror symmetry relationships. High temperature factors give additional support for this supposition. The conformation of the tetrahydrofuran molecule with atom O(8) is a distorted envelope. The O(8) atom is deflecting much more as in the typical envelope case.

Complex **II** is paramagnetic with temperature (4.2–298 K) independent μ_{eff} *ca* 2.1 μ_B per two molybdenum centres (the plot of $1/\chi$ against T gives a straight line of slope passing through the origin). The 2.1 μ_B value is too low for two d^1 unpaired electrons of Mo^{5+} (2.83 μ_B), but we do not know

Table 2. Selected bond distances (Å) and angles (°) with standard deviations in parentheses for **II**

Mg—O(1)	2.155(5)	Mo(1)—O(1)	1.674(5)	Mo(2)—O(2)	1.679(5)
Mg—O(2)	2.170(5)	Mo(1)—O(7)	2.276(5)	Mo(2)—O(8)	2.325(5)
Mg—O(3)	2.063(5)	Mo(1)—Cl(1)	2.361(2)	Mo(2)—Cl(5)	2.353(2)
Mg—O(4)	2.055(5)	Mo(1)—Cl(2)	2.359(2)	Mo(2)—Cl(6)	2.352(2)
Mg—O(5)	2.057(5)	Mo(1)—Cl(3)	2.348(2)	Mo(2)—Cl(7)	2.358(2)
Mg—O(6)	2.047(5)	Mo(1)—Cl(4)	2.357(2)	Mo(2)—Cl(8)	2.362(2)
O(1)—Mg—O(2)	179.3(2)	O(1)—Mo(1)—O(7)	178.6(2)	O(2)—Mo(2)—O(8)	179.2(2)
O(1)—Mg—O(3)	90.0(2)	O(1)—Mo(1)—Cl(1)	97.6(2)	O(2)—Mo(2)—Cl(5)	98.3(2)
O(1)—Mg—O(4)	90.7(2)	O(1)—Mo(1)—Cl(2)	97.6(2)	O(2)—Mo(2)—Cl(6)	97.8(2)
O(1)—Mg—O(5)	90.7(2)	O(1)—Mo(1)—Cl(3)	97.7(2)	O(2)—Mo(2)—Cl(7)	97.8(2)
O(1)—Mg—O(6)	89.1(2)	O(1)—Mo(1)—Cl(4)	96.3(2)	O(2)—Mo(2)—Cl(8)	97.0(2)
O(2)—Mg—O(3)	89.5(2)	O(7)—Mo(1)—Cl(1)	81.9(2)	O(8)—Mo(2)—Cl(5)	82.5(2)
O(2)—Mg—O(4)	89.8(2)	O(7)—Mo(1)—Cl(2)	83.6(2)	O(8)—Mo(2)—Cl(6)	82.5(2)
O(2)—Mg—O(5)	89.7(2)	O(7)—Mo(1)—Cl(3)	82.9(2)	O(8)—Mo(2)—Cl(7)	81.5(2)
O(2)—Mg—O(6)	90.4(2)	O(7)—Mo(1)—Cl(4)	82.5(2)	O(8)—Mo(2)—Cl(8)	82.6(2)
O(3)—Mg—O(4)	89.4(3)	Cl(1)—Mo(1)—Cl(2)	88.3(1)	Cl(5)—Mo(2)—Cl(6)	89.2(1)
O(3)—Mg—O(5)	178.7(3)	Cl(1)—Mo(1)—Cl(3)	164.7(1)	Cl(5)—Mo(2)—Cl(7)	163.9(1)
O(3)—Mg—O(6)	90.8(2)	Cl(1)—Mo(1)—Cl(4)	89.1(1)	Cl(5)—Mo(2)—Cl(8)	89.6(1)
O(4)—Mg—O(5)	89.5(3)	Cl(2)—Mo(1)—Cl(3)	88.9(1)	Cl(6)—Mo(2)—Cl(7)	89.1(1)
O(4)—Mg—O(6)	179.7(3)	Cl(2)—Mo(1)—Cl(4)	166.1(1)	Cl(6)—Mo(2)—Cl(8)	165.1(1)
O(5)—Mg—O(6)	90.2(2)	Cl(3)—Mo(1)—Cl(4)	90.1(1)	Cl(7)—Mo(2)—Cl(8)	88.0(1)
Mg—O(1)—Mo(1)	177.7(3)	Mg—O(2)—Mo(2)	177.6(3)		

the reason. It is noteworthy that for linear trimetallic complexes where the central metal is diamagnetic antiferromagnetic interactions between the d^1 centres have been observed.[14]

The structure and bond lengths and angles of the $[MoCl_4O(THF)]^-$ units are similar to those found in $[Mg(THF)_6][MoCl_4O(THF)]_2$ and $[Mg_2(\mu\text{-}Cl)_3(THF)_6][MoCl_4O(THF)]$ salts.[1,15,16] Other tetrahydrofuran-solvated magnesium molecular species such as $[(THF)_4Mg(\mu\text{-}Cl)_2FeCl_4]$[17] and $[\{(Me_3P)_3CoN_2\}_2Mg(THF)_4]$[18] are also known.

The adducts of oxo-oxygen molybdenum species like $[MoCl_4O(THF)]^-$ with Lewis acids were unknown. Note, that the $[\{(THF)Cl_4MoO\}_2Mg(THF)_4]$ complex could be obtained only in halogenated solvents because in THF $[Mg(THF)_6][MoCl_4O(THF)]_2$ and $[Mg_2(\mu\text{-}Cl)_3(THF)_6][MoClO_4(THF)]$ compounds are formed (reactions 1 and 2). However, the compounds $[(ReMe_4O)_2Mg(THF)_4]$ and $[\{o\text{-}C_6H_4(CH_2)_2WO\}_2Mg(THF)_4]$ arise in reactions of Grignard reagent or MgR_2 with Re_2O_7 or WCl_4O in tetrahydrofuran.[13,14] Hence it follows that molybdenum oxo-oxygen Mo=O is a weaker base than similar oxo-oxygens of Re=O and W=O because the oxo-oxygen of Mo=O does not form an adduct with Mg^{2+} in THF.

Acknowledgement—This work was supported financially by MEN, grant no. 255.

REFERENCES

1. P. Sobota, T. Płuziński and T. Lis, *Z. Anorg. Allg. Chem.* 1986, **533**, 215.
2. P. Sobota, T. Płuziński, J. Utko and T. Lis, *Inorg. Chem.* 1989, **28**, 2217.
3. P. Sobota, T. Płuziński and T. Lis, *Bull. Pol. Acad. Sci. Chem.* 1985, **33**, 491.
4. P. Sobota, *Pure Appl. Chem.* 1989, **61**, 861.
5. K. Feenan and G. W. A. Fowells, *Inorg. Chem.* 1965, **4**, 310.
6. E. C. Ashby and R. C. Arnott, *J. Organomet. Chem.* 1968, **14**, 1.
7. N. Walker and D. Stuart, *Acta Cryst. A* 1983, **39**, 158.
8. G. M. Sheldrick, SHELXS 86, Program for Crystal Structure Solution. University of Göttingen, Fed. Rep. Ger. (1986).
9. T. Głowiak, in *Problemy i metody chemii koordynacyjnej* (Edited by P. W. Naukowe), p. 253. Warszawa (1981).
10. *International Tables for X-Ray Crystallography*, Vol. 4. Kynoch Press, Birmingham (1974).
11. P. Sobota, J. Utko and T. Lis, *J. Chem. Soc., Dalton Trans.* 1984, 2077.
12. S. Stavropoulos, P. G. Edwards and G. Wilkinson, *J. Chem. Soc., Dalton Trans.* 1985, 2167.
13. M. F. Lappert, C. L. Raston, G. L. Rowbottom, B. W. Skelton and A. H. White, *J. Chem. Soc., Dalton Trans.* 1984, 883.
14. D. Sekutowsky, R. Jungst and G. D. Stucky, *Inorg. Chem.* 1978, **17**, 1848.
15. E. M. Shustorovich, M. A. Porai-Koshits and A. Yu. Buslaew, *Coord. Chem. Rev.* 1975, **17**, 1.
16. H. Bird and W. A. Wickramasinghe, *Can. J. Chem.* 1981, **59**, 2879.
17. P. Sobota, T. Płuziński and T. Lis, *Polyhedron* 1984, **3**, 45.
18. R. Hammer, H. F. Klein, V. Schubert, A. Frank and G. Huttner, *Angew. Chem., Int. Edn Engl.* 1976, **15**, 612.

Polyhedron Vol. 10, No. 20/21, pp. 2463–2464, 1991
Printed in Great Britain

0277–5387/91 $3.00+.00
© 1991 Pergamon Press plc

SYNTHESIS, CHARACTERIZATION AND STEREOCHEMISTRY OF BIS(ACETYLACETONATO) DIISOTHIOCYANATO SILANE

SURAJ P. NARULA,* RAVI SHANKAR, BALWANT KAUR and SAJEEV SONI

Department of Chemistry, Panjab University, Chandigarh-160014, India

(*Received* 12 *December* 1990; *accepted* 2 *July* 1991)

Abstract—A hexacoordinated monomeric silicon(IV) complex, $(acac)_2Si(NCS)_2$ [where acac = $(CH_3COCHCOCH_3)^-$] was isolated and characterized by elemental analyses, IR, multinuclei (^1H, ^{13}C and ^{29}Si) NMR spectral data. Initially the complex has the *cis*-structure in solution which changes to an equilibrium mixture (1.8 : 1) of *cis* and *trans* isomers at room temperature in 24 h.

Only a few neutral hexacoordinated complexes of silicon with 1,3-diketonate ligands have been reported[1–4] and their stereochemical lability studied by dynamic NMR spectroscopy and kinetic measurements.[5–9] Amongst the known complexes of the type $(acac)_2SiR_2$, the complexes where R=Cl or Ph, adopt the *trans* structure[3,4] while for R=OAc, it exists in the *trans* form but isomerizes in solution to give an equilibrium mixture of *cis–trans* isomers.[5,6] The heterosubstituted complexes, $(acac)_2SiR'R''$ (where R'=Cl and R''=Me or Ph) exist in non-rigid *cis* form in solution.[7] However, there is no report on the acetylacetonates with other substituents on the silicon atom. Therefore, isolation and characterization of a new homo-substituted bis(acetylacetonato) diisothiocyanato silane, $(acac)_2Si(NCS)_2$ was undertaken and results are reported herein.

EXPERIMENTAL

All operations were carried out under an oxygen-free dry nitrogen atmosphere. Solvents were dried by conventional methods. Silicon tetrachloride (Fluka) was distilled before use.

IR spectra were recorded as Nujol mulls using NaCl/polyethylene optics on a Perkin–Elmer 1430 ratio recording spectrophotometer. ^1H, ^{13}C and ^{29}Si NMR in $CDCl_3$ taking TMS as internal reference were recorded on a Bruker (AM 500) 500 MHz instrument at TIFR (Bombay, India). Elemental analyses of the samples were obtained using a Carlo Erba Strumentazione (Italy) elemental analyser-Model 1106. Mass spectra were recorded on V-G micromass MM 70/70F double focusing spectrometer. Molecular weight of the complex was determined cryoscopically in nitrobenzene.

Preparative methods

Diethoxy/di-n-propoxy diisothiocyanato silanes were prepared by a method already known in literature.[10] The purity of these compounds was checked by elemental analyses, IR, ^1H, ^{13}C and ^{29}Si NMR spectral data.

Preparation of bis(acetylacetonato) diisothiocyanato silane

Acetylacetone (2.0 g, 0.02 mol) in THF was added dropwise to diethoxy/di-*n*-propoxy diisothiocyanato silane (2.34/2.62 g, 0.01 mol) in the same solvent and the mixture was stirred for 15 h at room temperature. The clear solution so obtained was concentrated and n-hexane was added to it. A white solid was precipitated out in each case which was filtered, washed with n-hexane and dried *in vacuo*. The solid was recrystallized in aceto-nitrile/n-hexane mixture. Yield 1.8 g, 53%, m.p. 122–124°C (decomp.). Found: C, 41.8; H, 4.0; N, 8.1; S, 18.4; Si, 7.9. Calc. for $C_{12}H_{14}N_2O_4S_2Si$: C, 42.1; H, 4.1; N, 8.2; S, 18.7; Si, 8.2%. Mol. wt. Found 368; required 342. MS (70 eV): *m/z* (rela-

* Author to whom correspondence should be addressed.

tive intensity %) 284 (100) [M^+—NCS], 243(9.5) [M^+—acac], 226(25.2) [M^+—2NCS], 59(64.9) $[HNCS]^+$.

RESULTS AND DISCUSSION

Bis(acetylacetonato) diisothiocyanato silane is is obtained from the reaction of dialkoxy diisothiocyanato silane with acetylacetone as,

$$(RO)_2Si(NCS)_2 + 2acacH \xrightarrow{THF} (acac)_2Si(NCS)_2 + 2ROH.$$
$$(R = Et \text{ or } n\text{-}Pr)$$

Elemental analyses and cryoscopically determined molecular weight conform to the above composition. The compound is a white hygroscopic solid, soluble in organic polar solvents. It decomposes on prolonged standing even under inert atmosphere. Mass spectrum of the compound shows no molecular ion $[M]^+$ peak, but the base peak at *m/z* 284 corresponds to the ion [M^+—NCS]. Conductance of its millimolar solution in acetonitrile ($\Lambda_0 = 14.0$ ohm^{-1} cm^2 mol^{-1}) suggests its non-electrolytic nature.

Spectral data

IR spectrum reveals negative spectral shift of ~ 75 cm^{-1} in the ν CO mode (1550 cm^{-1}) of the compound as compared to the free ligand. In metal–acetylacetonates, this change is attributed to the ligand acting as a bidentate monoanion.[1] The ν CN mode at 2110–2100 cm^{-1} has a positive spectral shift ($\sim$20–25 cm^{-1}) relative to the reactants. This may be due to change in phase/predominant N≡C—S$^{\delta-}$ structure[11] in the complex. The ν CS and δ NCS modes at 720 and 460 cm^{-1} respectively are practically unchanged.

The ^{1}H NMR spectrum of the freshly prepared solution of the title compound in $CDCl_3$ reveals two well-resolved signals at 2.2 and2.3 ppm showing non-equivalent methyl groups in the complex. This non-equivalence can be rationalized on the basis of C_{2v} symmetry of the *cis* structure of the molecule. The methyne proton appears as a singlet at 6.0 ppm. However, after 30 min, two additional signals at 2.1 and 5.7 ppm emerge and grow with time reaching a constant concentration after 24 h. These signals integrate protons in the ratio 6:1. This time-dependent change in the spectral pattern may point to the stereochemical lability of the compound in solution. By analogy with the reported δ ^{1}H NMR values of metal acetylacetonates,[12] the signals at 2.1 and 5.7 ppm may be assigned to CH_3 and CH group protons respectively of the *trans* isomer of the compound. The appearance of only one methyl signal is in agreement with D_{2h} symmetry of the *trans* isomer. On the basis of proton integration of various signals in 1-day-old solution, *cis*: *trans* ratio on the equilibrated sample is found to be 1.8:1.

^{13}C NMR data [*cis*: 25.8, 25.7 (CH_3); 102.9 (CH); 193.1, 192.9 (CO) ppm and *trans*, 24.7 (CH_3); 100.6 (CH); 191.9 (CO) ppm] reveal three signals (two for *cis* and one for *trans*) for the methyl and three signals for the carbonyl carbons in the 1-day-old solution of the compound. As expected[9] only a single resonance is observed for each methyne carbon of *cis* and *trans* isomers. Only one signal is observed for the isothiocyanate carbon at 133.5 ppm.

The ^{29}Si NMR spectrum of the *cis* and *trans* mixture in solution exhibits signals at -199.3 and -214.0 ppm. These values are consistent with the six coordinated silicon atoms in both the compounds.[13]

From the above data, it may be concluded that bis(acetylacetonato) diisothiocyanato silane in solution exists initially as the *cis* isomer but is equilibrated to a *cis–trans* mixture (1.8:1) after 24 h. This is a rare observation in the homo-substituted bis(acetylacetonato) silanes.

Acknowledgements—RS and SS are grateful to UGC (New Delhi) and CSIR (New Delhi) respectively for financial assistance.

REFERENCES

1. R. West, *J. Am. Chem. Soc.* 1958, **80**, 3246.
2. R. M. Pike and R. R. Luono, *J. Am. Chem. Soc.* 1965, **87**, 1403.
3. K. M. Taba and W. V. Dohlhoff, *J. Organomet. Chem.* 1985, **280**, 27.
4. D. W. Thompson, *Inorg. Chem.* 1969, **8**, 2015.
5. R. M. Pike and R. R. Luongo, *J. Am. Chem. Soc.* 1966, **88**, 2972.
6. C. L. Holloway, R. R. Luongo and R. M. Pike, *J. Am. Chem. Soc.* 1966, **88**, 2060.
7. N. Serpone and K. A. Hersh, *J. Organomet. Chem.* 1975, **84**, 177.
8. J. A. Cella and J. D. Mitchell, *J. Organomet. Chem.* 1983, **244**, C-5.
9. D. T. Haworth, G. Yu Lin and C. A. Wilkie, *Inorg. Chim. Acta* 1980, **40**, 119.
10. H. H. Anderson, *J. Am. Chem. Soc.* 1950, **72**, 193.
11. M. A. Mullins and C. Curran, *Inorg. Chem.* 1968, **7**, 2584.
12. J. A. S. Smith and E. J. Wilkins, *J. Chem. Soc.* (*A*) 1966, 1749.
13. J. A. Cella, J. D. Cargioli and E. A. Williams, *J. Organomet. Chem.* 1980, **186**, 13.

Polyhedron Vol. 10, No. 20/21, pp. 2465–2470, 1991
Printed in Great Britain

0277–5387/91 $3.00+.00
© 1991 Pergamon Press plc

MIXED LIGAND COMPLEXES OF RUTHENIUM(III)EDTA WITH NUCLEOSIDES

BADAR TAQUI KHAN† and K. ANNAPOORNA

Department of Chemistry, Osmania University, Hyderabad 500 007, India

(*Received* 22 *October* 1990; *accepted* 28 *June* 1991)

Abstract—Mixed ligand complexes of ruthenium(III)edta with nucleosides, adenosine, guanosine, xanthosine, inosine, cytidine and uridine were synthesized and characterized by elemental analysis, IR spectra, electronic spectra, ^{1}H NMR, ESR and by polarography. Based on the above data it is proposed that the purine nucleosides, adenosine, guanosine, xanthosine and inosine coordinate to the metal ion through N_7 and the pyrimidine nucleoside uridine coordinates to the metal ion through N_3, however cytidine forms a chelate coordinating to the metal ion through N_3 and C_2O.

$K[Ru(edta\text{-}H)Cl]\cdot 2H_2O$ is a well-known complex and its mixed ligand complexes with σ-donor and π-acceptor ligands have been widely studied both in solution and solid state.[1–6] In these mixed ligand complexes edta can act as a pentadentate or a tetradentate ligand leaving one or two coordination positions on the metal ion. Nucleosides which are constituents of nucleic acid form many mixed ligand complexes with platinum group metal ions.[7–15] In our earlier studies we have reported mixed ligand complexes of Ru(III)edta with purines and pyrimidines.[5,6] In the present investigation mixed ligand complexes of ruthenium(III)edta with nucleosides were synthesized and characterized by various physicochemical methods.

EXPERIMENTAL

Materials

Hydrated ruthenium trichloride and nucleosides were purchased from Johnson Matthey Company and Sigma Chemical Company (U.S.A.). The disodium salt of ethylenediaminetetraaceticacid was obtained from BDH chemicals. Solvents used were of high purity and distilled before use.

Synthesis

$K[Ru(edta\text{-}H)Cl]\cdot 2H_2O$, complex **1** was prepared by the method of Ezerskaya and Solovykh[16] as modified by Diamantis and Dubrawski.[17] $K_2[RuCl_5(H_2O)]$ was prepared by a modified method of Mercer and Buckley[18] used as the starting material in the above preparation.

Physical measurements

Elemental analysis of complexes were obtained from the Central Drug Research Institute (Lucknow, India). Potassium analysis was done by flame photometry. Conductivity data were measured on a digital conductivity meter No. DI 909. IR and electronic spectra of the complexes were recorded on Shimadzu IR 435 and UV-160 respectively. Far IR spectra were recorded at RSIC IIT Madras. ^{1}H NMR and ^{13}C NMR spectra were recorded on Jeol 500 MHz spectrometer at TIFR Bombay. Electron paramagnetic resonance spectra were recorded on a Bruker ESP 300 X band instrument at CSMCRI, Bhavnagar, on a Princeton Applied Research Electrochemical Instrument equipped with a precision *X–Y* recorder. A PAR 174, polarographic analyser was used to record dc and differential pulse polarograms.

Preparation of complexes

(2) Potassium(ethylenediaminetetraacetato)adenosine ruthenate(III)
(3) Potassium(ethylenediaminetetraacetato)guanosine ruthenate(III)
(4) Potassium(ethylenediaminetetraacetato)xanthosine ruthenate(III)

† Author to whom correspondence should be addressed.

(5) Potassium(ethylenediaminetetraacetato)inosine ruthenate(III)
(6) Potassium(ethylenediaminetetraacetato)cytidine ruthenate(III)
(7) Potassium(ethylenediaminetetraacetato)uridine ruthenate(III) hexahydrate.

Potassium chloroethylenediaminetetraacetatoruthenate(III) (0.4 mM) dissolved in water was added to a hot solution of the ligand (0.4 mM) (adenosine, guanosine, xanthosine, inosine, cytidine, uridine) in water, when the yellow colour of the solution changed to either red (adenosine, guanosine, xanthosine) or deep yellow (inosine, cytidine, uridine). The pH of the solution was between 3 and 4. The solution was refluxed for 12–16 h in an atmosphere of pure nitrogen and the completion of the reaction was checked by TLC which indicated the presence of a single substance. The solution was concentrated to one-fourth of its volume and was precipitated with ethanol/acetone. The complex was filtered, washed with acetone/water mixture, finally with acetone and was then vacuum dried. The complexes are soluble in water.

RESULTS AND DISCUSSION

The analytical and conductivity data of the complexes are presented in Table 1. The conductivity values in DMSO correspond to 1 : 1 electrolytes.[19] The conductivity in water, however, is much higher than that expected for a 1 : 1 electrolyte. The conductivity values in aqueous solution continuously change and attain an equilibrium value after a long time. This is because of the extensive hydrolysis of the complexes in solution around pH 3–4. The equilibrium in solution is complicated and the solution becomes acidic with increase in hydrolysis as tested by pH measurements. The conductivity of complex **1** is also high because of the dissociation of a proton from an uncoordinated carboxylic acid group and hydrolysis of the metal ion.[3]

The IR spectra of the complexes show the N—H and C—H stretching vibrations due to the coordinated ligand in the region 3100–2950 cm^{-1}. In complex **1** K[Ru(edta-H)Cl]·$2H_2O$ a sharp peak at 1720 cm^{-1} and a broad peak at 1650 cm^{-1} shows the presence of uncoordinated and coordinated carboxylate groups of edta respectively. On complexation the peak at 1720 cm^{-1} disappears, indicating the absence of free COOH group in these complexes. In complexes **2**, **3** and **6** a broad peak at 1640 cm^{-1} is due to the overlap of NH_2 deformation modes of the secondary ligand and also due to the coordinated carboxylate group of edta. The $\nu C{=}O$ stretching frequency of coordinated cytidine in complex **6** shifts to a lower frequency by 20 cm^{-1} and is observed at 1680 cm^{-1} indicating that the $\nu C{=}O$ group is involved in coordination to the metal ion. The $\nu C{=}C$ and $\nu C{=}N$ stretching frequencies of the complexes were shifted to a lower frequency by 30–50 cm^{-1} as compared to the frequencies of the nucleosides observed around 1600–1450 cm^{-1}, indicating the involvement of

Table 1. Analytical and conductivity data of complexes

Complex no.	Complex	Analysis[a] % Carbon	% Hydrogen	% Nitrogen	% Potassium	Molar conductivity at 30° in mhos cm^{-2} H_2O	DMSO
1	K[Ru(edta-H)Cl]·$2H_2O$	24.2 (24.0)	3.3 (3.4)	5.5 (5.6)	7.7 (7.8)	326	18
2	K[Ru(edta)(ado)]	34.0 (34.5)	3.6 (3.6)	13.7 (14.1)	5.4 (5.6)	289	17
3	K[Ru(edta)(guo)]·$2H_2O$	31.5 (32.1)	3.8 (3.8)	13.9 (13.1)	5.1 (5.2)	230	16
4	K[Ru(edta)(xan)]	33.2 (33.7)	3.3 (3.4)	11.4 (11.8)	5.4 (5.5)	319	16
5	K[Ru(edta)(ino)]·H_2O	33.2 (33.6)	3.6 (3.6)	12.3 (11.8)	5.5 (5.5)	355	15
6	K[Ru(edta)(cyd)]	33.2 (33.9)	3.6 (3.7)	10.0 (10.4)	5.7 (5.8)	254	24
7	K[Ru(edta)(urd)]·$6H_2O$	29.0 (29.2)	4.7 (4.6)	7.0 (7.2)	5.0 (5.0)	366	27

[a] Calculated values in parentheses.

ring nitrogens in coordination to the metal ion. The νM—N and νM—O stretching frequencies are observed around 500 and 400 cm^{-1} respectively in these complexes indicating that edta coordinates to the metal ion through oxygen and nitrogen.

The electronic spectral absorption bands and their assignments for the complexes are shown in Table 2. The weak bands in the 500–800 nm region observed in some of the complexes are *d–d* transitions of Ru^{III} with some MLCT character.

The NMR spectra were recorded on a high-resolution spectrometer, as the spectra could not be recorded on a low-resolution spectrometer, because of the paramagnetism of Ru^{III}. A representative spectrum is given in Fig. 1. The NMR spectral data of complex **1** are given in Table 3. In complex **1** edta is pentadentate and the sixth position is occupied by a chloride. The ^1H NMR spectrum of complex **2** shows a downfield shift in C_2H and C_8H proton by 0.13 and 0.54 ppm respectively as compared to the ligand. Since the downfield shift in C_8H proton is more than C_2H proton, it is inferred that adenosine coordinates to metal ion through N_7. The $^{13}C[^1H]$ NMR spectrum of complex **2** also supports the coordination of adenosine to the metal ion through N_7. In the ^{13}C NMR of adenosine, the resonances are as follows: $C_2 = 152.85$; $C_4 = 148.97$; $C_5 = 119.28$; $C_6 = 156.02$; $C_8 = 140.05$ and in the complex the resonances are as follows: $C_2 = 152.85$; $C_4 = 149.0$; $C_5 = 120.01$; $C_6 = 156.12$; $C_8 = 142.67$.

Table 2. Electronic spectral data of ruthenium(III)edta mixed ligand complexes and secondary ligands

Complex no.	Ligand/complex	Absorption maxima λ_{max} (nm)	ε_{max} (M^{-1} cm^{-1})	Transition	
1	K[Ru(edta-H)Cl·$2H_2O$	283	2.71×10^3	LMCT	
		350	5.8×10^2	*d–d*	
	Adenosine	259	1.1×10^4	π–π^*	
2	K[Ru(edta)(ado)]	261	2.57×10^4	LMCT	adenosine
		357	2.18×10^3	LMCT	edta
		800	7.5×10	*d–d*	Ru^{III}
	Guanosine	259	9.47×10^3	π–π^*	
3	K[Ru(edta)(guo)]·$2H_2O$	238	1.59×10^4	LMCT	guanosine
		275	1.14×10^4	LMCT	
		354	1.45×10^3	LMCT	edta
		748	7.1×10	*d–d*	Ru^{III}
	Xanthosine	263	1.05×10^4	π–π^*	
4	K[Ru(edta)(Xan)]	265	1.08×10^4	LMCT	xanthosine
		354	8.2×10^2	LMCT	edta
		962	4×10	*d–d*	Ru^{III}
	Inosine	248	1.14×10^4	π–π^*	
5	K[Ru(edta)(ino)]·H_2O	248	1.69×10^4	LMCT	inosine
		354	1.250×10^3	LMCT	edta
		778	4.5×10^2	*d–d*	Ru^{III}
		976	2.44×10^2	*d–d*	
	Cytidine	271	1.07×10^4	π–π^*	
6	K[Ru(edta)(Cyd)]	275	7.41×10^3	LMCT	cytidine
		354	1.25×10^3	LMCT	edta
		753	4.69×10^2	*d–d*	Ru^{III}
		974	2.43×10^2	*d–d*	
	Uridine	262	1.05×10^4	π–π^*	
7	K[Ru(edta)(urd)]·$6H_2O$	280	4.54×10^3	LMCT	uridine
		357	1.02×10^3	LMCT	edta
		408	3.00×10^2	*d–d*	Ru^{III}

Table 3. ^{1}H NMR spectral data of ruthenium(III)edta mixed ligand complexes and secondary ligands

Complex no.	Complex/ligand	Purine nucleoside		Pyrimidine nucleoside		edta protons			Ribose protons				
		C_2H	C_8H	C_5H	C_6H	N—CH_2—CH_2N	CH_2COO^- (Free)	CH_2COO (Coordinated)	C'_1H	C'_2H	C'_3H	C'_4H	C'_5H
1	K[Ru(edta-H)Cl]·$2H_2O$					3.26; 3.48	3.68	4.00					
	Adenosine	8.15	8.36	—	—	—	—	—	6.40	2.65	4.63	4.19	3.90
2	K[Ru(edta)(ado)]	8.28	8.90	—	—	3.3; 3.43	3.52	3.80	6.4	2.60	4.60	3.90	3.70
	Guanosine	—	7.80	—	—	—	—	—	5.68	4.72	4.43	4.35	3.92
3	K[Ru(edta)(guo)]·$2H_2O$	—	8.21	—	—	3.38; 3.54	3.7	3.86	5.74	4.70	4.38	4.24	4.08
	Xanthosine	—	8.00	—	—	—	—	—	5.80	5.3	4.80	4.20	3.85
4	K[Ru(edta)(xan)]	—	8.30	—	—	2.8; 3.6	4.1	4.2	5.80	5.35	4.70	4.40	4.00
	Inosine[a]	8.11	8.22	—	—	—	—	—	5.89	—	—	—	—
5	K[Ru(edta)(ino)]H_2O[a,b]	8.10	9.10	—	—	3.0 to 4.0	—	—	6.05	—	—	—	—
	Cytidine	—	—	5.70	7.78	—	—	—	5.91	4.32	4.32	3.65	3.96
6	K[Ru(edta)(cyd)]	—	—	6.47	8.34	2.95; 3.26	3.9	4.01	6.01	4.30	4.30	—	4.21
	Uridine	—	—	5.80	7.80	—	—	—		3.82 to 5.90			
7	K[Ru(edta)(urd)]·$6H_2O$[b]	—	—	6.22	7.84		3.00 to 4.20			3.60 to 6.00			

[a] Solvent: D_2O/DMSO–d_6 (values are given in ppm).
[b] Ribose protons could not be resolved.

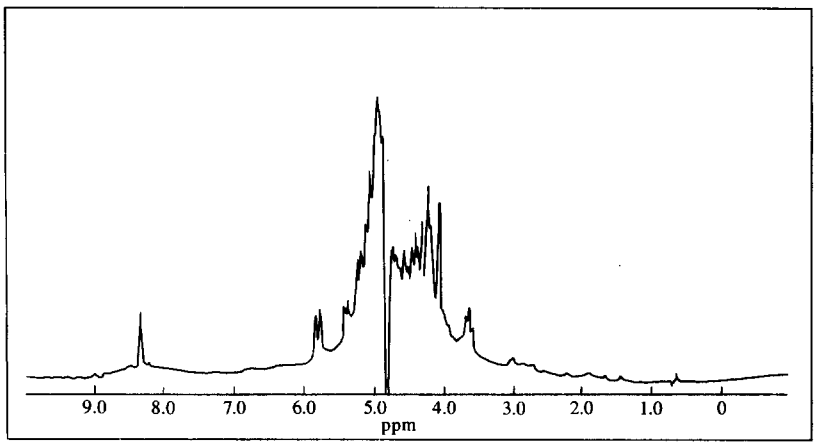

Fig. 1. ^1H NMR spectrum of K[Ru(edta)(xanthosine)].

Since there is a downfield shift in C_8 carbon by 2.62 ppm as compared to resonances in the ligand, the complexation of adenosine to metal ion through N_7 is supported. The ^1H NMR spectra of complexes **3**, **4** and **5** show a downfield shift in C_8H proton by 0.41, 0.30 and 0.88 ppm respectively, indicating that guanosine, xanthosine and inosine coordinate to the metal ion through N_7 in these complexes. The ^1H NMR spectrum of complex **6** shows a downfield shift in C_5H and C_6H protons by 0.77 and 0.56 ppm respectively as compared to the ligand, inferring that cytidine coordinates to the metal ion through N_3 and C_2O. The ^1H NMR spectrum of complex **7** shows a downfield shift in C_5H proton by 0.42 ppm showing that uridine coordinates to the metal ion through N_3. The ribose protons are observed as distinct peaks in the region 2.5 and 6.5 ppm, shown in Table 3 and the edta protons resonate between 3 and 4 ppm.

The electron paramagnetic resonance spectra of the complexes in general show rhombic or isotropic distortions. Complexes **1** and **2** show compressed rhombic distortions with g values 2.37, 2.32 and 1.94; and 2.40, 2.30, 1.99; $g_{av} = 2.23$ respectively. Complexes **3**, **6** and **7** also show rhombic distortions with g values 2.56, 2.30, 1.89, $g_{av} = 2.26$; 2.39, 2.38, 1.94, $g_{av} = 2.21$ and 2.36, 2.26, 2.11, $g_{av} = 2.24$ respectively. Complex **4** shows isotropic distortion with one g value at 2.10.

The electrochemical data of the complexes are given in Table 4. The differential pulse polarogram of complexes show a single peak for the Ru^{3+}/Ru^{2+} couple supporting the formation of 1 : 1 complexes. In these complexes the potentials are more positive as compared to complex **1**, indicating the drift of electron density from metal to the nucleoside ligand, which acts as a weak π-acid. This is further supported by weak MLCT bands around 500 to 800 nm in the electronic spectra of the complexes.

Based on analytical and spectroscopic data, the structures for complexes **2**, **3**, **4** and **5** are shown in Fig. 2, where edta is pentadentate and the ligands coordinate to metal ion through N_7 in these complexes. The structure for complex **6** is shown in Fig. 3, where edta is tetradentate and cytidine acts as a bidentate ligand coordinating to the metal ion

Table 4. Electrochemical data for ruthenium(III)edta mixed ligand complexes

Sl. no.	Complex	$E_{1/2}$ values		
		Ru^{3+}/Ru^{2+}	Ru^{2+}/Ru^{+}	$(H^+/\frac{1}{2}H_2)$
1	$K[Ru(edta\text{-}H)Cl]\cdot 2H_2O$	−0.220	−0.842	−1.012
2	K[Ru(edta)(ado)]	−0.183	—	−0.990
3	$K[Ru(edta)(guo)]\cdot 2H_2O$	−0.206	−0.624	−1.017
4	K[Ru(edta)(xan)]	−0.183	−0.538	−0.735
5	$K[Ru(edta)(ino)]\cdot H_2O$	−0.175	—	−1.080
6	K[Ru(edta)(cyd)]	−0.222	−0.820	−1.041

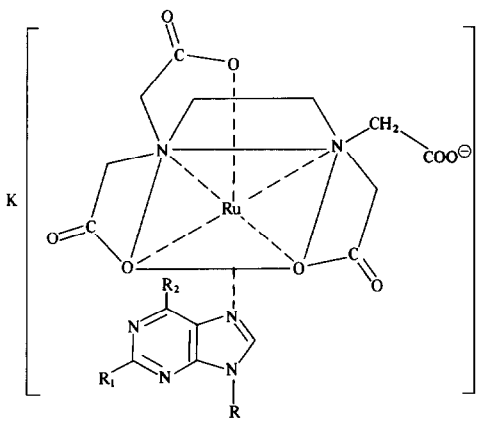

Fig. 2. (a) Structure of K[Ru(edta)(ado)] $R_1 = H$; $R_2 = NH_2$; R = Ribose. (b) Structure of K[Ru(edta)(guo)]$2H_2O$ $R_1 = NH_2$; $R_2 = OH$; R = Ribose. (c) Structure of K[Ru(edta)(xan)] $R_1 = OH$; $R_2 = OH$; R = Ribose. (d) Structure of K[Ru(edta)(ino)]H_2O $R_1 = H$; $R_2 = OH$; R = Ribose.

through N_3 and C_2O. Complex **7** is a monomer with edta as pentadentate and uridine coordinating to the metal ion through N_3.

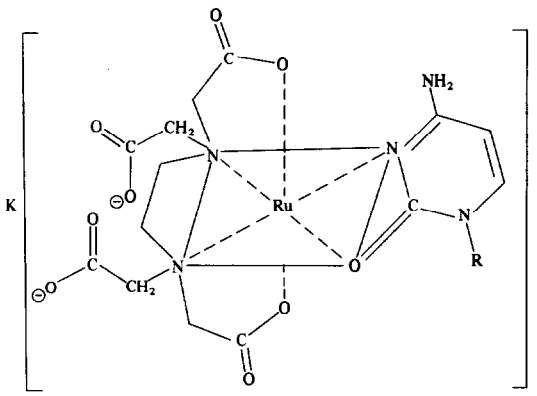

Fig. 3. Structure of K[Ru(edta)(cyd)]; R = Ribose.

Acknowledgement—Miss K. Annapoorna (Research Associate) is grateful to CSIR, New Delhi, for financial assistance.

REFERENCES

1. A. A. Diamantis and J. V. Dubrawski, *Inorg. Chem.* 1983, **22**, 1934.
2. T. Matsubara and C. Creutz, *Inorg. Chem.* 1979, **18**, 1956.
3. M. M. Taqui Khan, A. Hussain, G. Ramachandraiah and M. A. Moiz, *Inorg. Chem.* 1986, **25**, 3023.
4. (a) N. A. Ezerskaya and T. P. Solovykh, *Zh. Neorg. Khim.* 1966, **11**, 1855; (b) *Ibid.*, 1966, **11**, 2197; (c) *Ibid.*, 1967, **12**, 2922; (d) *Ibid.*, 1966, **11**, 1462; (e) *Ibid.*, 1968, **13**, 186; (f) *Ibid.*, 1966, **11**, 2569.
5. Badar Taqui Khan and K. Annapoorna, *Inorg. Chim. Acta* 1990, **176**, 241.
6. Badar Taqui Khan and K. Annapoorna, *Inorg. Chim. Acta* 1990, **171**, 157.
7. Badar Taqui Khan, A. Gaffuri, P. Nageswara Rao and S. M. Zakeeruddin, *Polyhedron* 1987, **6**, 387.
8. Badar Taqui Khan, A. Gaffuri and M. R. Somayajulu, *Ind. J. Chem.* 1981, **20A**, 189.
9. A. I. Stetsenka and E. S. Dimitrivea, Translated from: *Koord. Khim.* 1977, **8**, 1240.
10. R. W. Gellert and R. Bau, *J. Am. Chem. Soc.* 1975, **97**, 28.
11. P. Chang Kong and T. Theophanides, *Inorg. Chem.* 1975, **3**, 5.
12. A. B. Robins, *Chem. Biol. Interact* 1973, **6**, 35.
13. N. Hadjiliadis and T. Theophanides, *Inorg. Chim. Acta* 1976, **16**, 77.
14. T. Theophanides, *Rev. Latinoam. Quim.* 1971, **2**, 1.
15. G. Peumatikakis, N. Hadjiliadis and T. Theophanides, *Inorg. Chem.* 1978, **17**, 4.
16. N. A. Ezerskaya and T. P. Solovykh, *Russ. J. Inorg. Chem.* 1966, **11**, 991.
17. A. A. Diamantis and J. V. Dubrawski, *Inorg. Chem.* 1981, **20**, 1142.
18. E. E. Mercer and R. R. Buckley, *Inorg. Chem.* 1965, **4**, 1692.
19. W. J. Geary, *Coord. Chem. Rev.* 1971, **7**, 81.

Polyhedron Vol. 10, No. 20/21, pp. 2471–2474, 1991
Printed in Great Britain

0277–5387/91 $3.00+.00
© 1991 Pergamon Press plc

SYNTHESIS AND NMR SPECTROSCOPY OF THE FIVE-COORDINATE PLATINUM(II) COMPLEXES [Pt(pp_2-P,P′,P″)(dppmE-P,E)]$(O_3SCF_3)_2$ [pp_2 = $PhP(CH_2CH_2PPh_2)_2$, dppmE = $Ph_2PCH_2P(E)Ph_2$, E = S, Se]

ANDREAS HANDLER and PAUL PERINGER*

Institut für Anorganische und Analytische Chemie der Universität Innsbruck, Innrain 52a, A-6020 Innsbruck, Austria

and

ERNST P. MÜLLER

Institut für Organische und Pharmazeutische Chemie der Universität Innsbruck, Innrain 52a, A-6020 Innsbruck, Austria

(*Received* 9 *July* 1990; *accepted* 28 *June* 1991)

Abstract—The title compounds were generated by the reaction between [$Ptpp_2Cl_2$, dppmE] and TlO_3SCF_3. On the basis of solution ^{31}P, ^{77}Se and ^{195}Pt NMR spectroscopic data, a square-pyramidal structure is proposed with the chalcogen atom in the apical position. In contrast, [Pt(pp_2-P,P′,P″)(dppmO-P)]$(O_3SCF_3)_2$ is four-coordinate. The reaction between $Ptpp_2Cl_2$ and $dppmSe_2$ involves a selenium transfer yielding the *cis* and *trans* isomers of [$PtPhP(CH_2CH_2PPh_2)(CH_2CH_2P(Se)Ph_2$-P,P′)(dppmSe-P,Se)]$(O_3SCF_3)_2$, which are also accessible from [Pt(pp_2-P,P′,P″)(dppmSe-P,Se)]$(O_3SCF_3)_2$ and elemental selenium.

There has been recent interest in platinum(II) coordination complexes with the bidentate mixed Group 15/Group 16 ligands dppmE and $dppmE_2$ (E = O, S, Se) and their anions.[1–5] We report here on the reaction of $Ptpp_2Cl_2$ with dppmE and $dppmE_2$. The former reaction is shown to yield the five-coordinate platinum(II) complexes [Pt(pp_2-P,P′,P″)(dppmE-P,E)]$^{2+}$ (E = S, Se), involving a P_4S or P_4Se donor set.

The vast majority of platinum(II) complexes are square planar, five-coordination is less common. Species of the type $[PtP_4L]^{2+}$ or $[PtP_4X]^+$, i.e. platinum coordinated to four phosphorus donor atoms and one neutral or anionic ligand have been previously reported: $[PtQPCl]^+$ [QP = tris-(*o*-diphenylphosphinophenyl)phosphine], the first compound with a PtP_4Cl core, was reported in 1963.[6] $[Pt(POMe_3)_5]^{2+}$ and $[Pt(PEt_3)_4H]^+$, representing the first complexes involving PtP_5 and PtP_4H cores, were reported in 1973 and 1976.[7–9] Five-coordinate platinum complexes with a PtP_4Hg core have been reported recently.[10]

Reaction of $Ptpp_2Cl_2$ *and* dppmSe

$Ptpp_2Cl_2$[11] reacts with dppmSe[12] and TlO_3SCF_3 according to eq. (1).

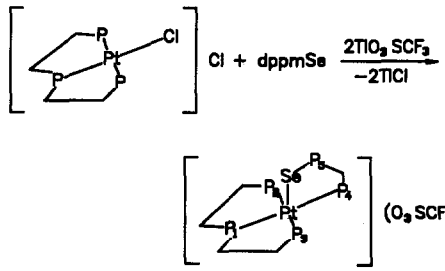

1 (1)

Product **1** was isolated as yellow crystals, readily soluble in polar organic solvents. On the basis of solution ^{31}P, ^{77}Se and ^{195}Pt NMR spectroscopic data, the structure of cation **1** is proposed to be

*Author to whom correspondence should be addressed.

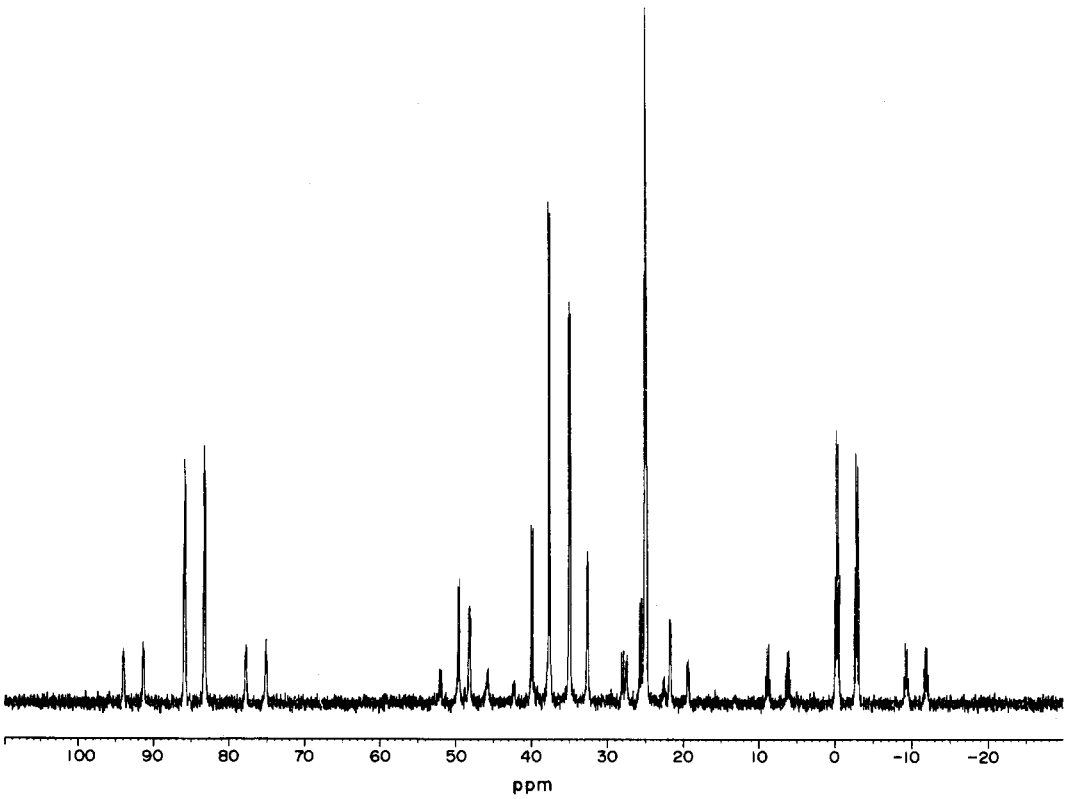

Fig. 1. $^{31}P\{^{1}H\}$ NMR spectrum of **1** (121.4 MHz).

square pyramidal with the selenium atom in an apical position as will be outlined below.

Nuclear magnetic resonance of **1**

^{195}Pt *NMR.* The ^{195}Pt NMR spectrum consists of a dddd signal flanked by ^{77}Se satellites. The Pt—P and Pt—Se coupling constants are in the range of one-bond couplings indicating four phosphorus atoms and one selenium atom coordinated to platinum.

^{31}P *NMR.* The ^{31}P NMR spectrum recorded at 223 K (Fig. 1) shows the presence of five inequivalent phosphorus atoms. The central phosphorus atom of the pp_2 ligand is easily identifiable by its high chemical shift. Its resonance is split by a large two-bond coupling involving the directly bound phosphorus of the dppmSe ligand. A large two-bond coupling is also observed between the terminal phosphorus atoms of the pp_2 ligand. Large $^{2}J(PP)$ couplings indicate the P_1PtP_4 and P_2PtP_3 angles to be near 180°. This requirement is fulfilled in a square pyramidal-like geometry as indicated in eq. (1). The inequivalence of the terminal phosphorus atoms of the pp_2 ligand (Fig. 1) may originate from a twisted conformation of the PtdppmSe chelate ring:* molecular structures of PtdppmS and PtdppmO chelate rings showed the phosphine sulphide and phosphine oxide phosphorus atoms to be out of the coordination plane.[2] An analogous conformation of the PtdppmSe ring would cause inequivalent environments of the terminal phosphorus atoms of the pp_2 ligand. This is sketched below using the positional parameters of a PtdppmS ring.[2] The

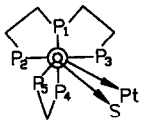

inequivalent terminal phosphorus atoms should render the central phosphorus atom of the pp_2 ligand and the platinum centre to be chiral. Despite the two chiral centres only one set of ^{31}P NMR parameters could be resolved, indicating the absence of NMR identification of the stereoisomers according to whether the phenyl group on the central phosphorus of the pp_2 ligand and the selenium atom are mutually *cis* or *trans*. *Cis–trans* isomers

* However, it is unlikely that the barrier to interconversion of the two twisted conformations of the chelate ring will be high enough for this; we thank the referee for pointing this out.

have been reported for some iridium[13] and rhodium[14] complexes of PhP(CH$_2$CH$_2$CH$_2$PCy$_2$)$_2$ (Cy = Cyclohexyl) or ^{t}BuP(CH$_2$CH$_2$CH$_2$PPh$_2$)$_2$, whilst other complexes involving the same metals and ligands only one isomer was observed.

At ambient temperature, the signals of the terminal phosphorus atoms of the pp$_2$ ligand are broadened, indicating a process which interchanges the chemical shifts of these phosphorus atoms.

The phosphine selenide signal is flanked by ^{77}Se satellites. The ^{77}Se—^{31}P coupling (624 Hz) is reduced from that of free dppmSe and this is typical for the coordination of phosphine selenides.[1-3] The chemical shifts of the directly-coordinated phosphorus of dppmSe and the phosphine-selenide phosphorus atom are at −4.0 and 27.5 ppm in comparison with a range of 18.1–24.4 and 32.1–44.1 ppm for other PtdppmSe chelate rings.[1-4] These two parameters were found to depend strongly on the nature of the ligands in the *trans* position in square-planar complexes.[2,4] Since selenium in the apical position has no *trans* ligand, this may account for the anomalous behaviour.

^{77}Se *NMR*. The selenium signal at −371 ppm relative to Me$_2$Se consists of a doublet due to the one bond ^{77}Se—^{31}P coupling and is flanked by ^{195}Pt satellites. The resonance is at lower frequencies in comparison with free dppmSe. By contrast, all selenium shifts of PtdppmSe coordination compounds appear at higher frequencies.[1-3]

Table 1. NMR data of [Ptpp$_2$(dppmE)](O$_3$SCF$_3$)$_2$[a]

	E = O	E = S	E = Se
δP1	93.8	86.9	82.1
δP2	41.6	39.6	35.9
δP3	41.6	32.4	31.4
δP4	2.3	−2.6	−4.0
δP5	26.0	34.8	22.4
δPt	−5126[b]	−4817[c]	−4862[c,d]
J(PtP1)	2157	2043	1967
J(PtP2)	2444	2886	2918
J(PtP3)	2444	3038	3211
J(PtP4)	2602	2330	2192
J(P1P3)	6	7	10
J(P1P4)	303	315	320
J(P1P5)	3	13	16
J(P2P3)		298	286
J(P2P4)	23	24	27
J(P2P5)	[e]	[e]	3
J(P3P4)	23	17	20
J(P3P5)	[e]	[e]	[e]
J(P4P5)	[e]	15	21
T (K)	300	223	223

[a] The labelling scheme is shown in eq. (1); solvent CH_2Cl_2/CH_3OH; chemical shifts in ppm to high frequency of 85% H_3PO_4 or 1 M Na_2PtCl_6; coupling constants in Hz.
[b] ddt (d = doublet, t = triplet).
[c] dddd.
[d] *J*(PtSe) 432.
[e] Not resolved.

Reactions of Ptpp$_2$Cl$_2$ *with* dppmS *and* dppmO

The yellow complex [Ptpp$_2$dppmS](O$_3$SCF$_3$)$_2$ (**2**) was obtained analogously to eq. (1). The NMR characteristics (Table 1) parallel that of **1** so that a five-coordinate structure [Pt(pp$_2$-P,P′,P″)(dppmS-P,S)](O$_3$SCF$_3$)$_2$ is proposed by analogy. In contrast, [Ptpp$_2$dppmO](O$_3$SCF$_3$)$_2$ (**3**) is colourless and the NMR data (Table 1) provide no evidence for the coordination of oxygen to platinum. This can be rationalized in view of the poorer donor abilities of the hard oxygen in comparison to the soft sulphur and selenium.

Reaction of Ptpp$_2$Cl$_2$ *with* dppmE$_2$ (E = Se, S, O)

The reaction of Ptpp$_2$Cl$_2$, dppmSe$_2$ and TlO$_3$SCF$_3$ was anticipated to result in the coordination of dppmSe$_2$ in a mono- or bidentate manner. Instead, one selenium atom of dppmSe$_2$ is transferred to the pp$_2$ ligand and a mixture of **4** and **5** [eq. (2)] is formed. A similar selenium migration has been observed previously.[4] The same products are obtained upon reaction of **1** with elemental selenium. It is interesting to note that the pp$_2$–selenide ligand present in **4** and **5** does not exist out of the

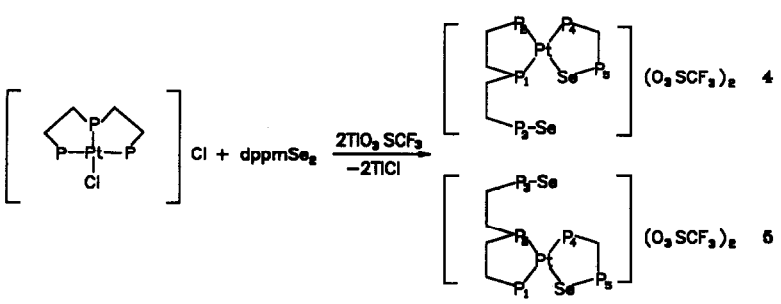

(2)

platinum coordination sphere: the reaction of pp_2 with 1 meq selenium yields the isomer $Ph(Se)P(CH_2CH_2PPh_2)_2$ according to the higher basicity of the central phosphorus atom.

Complexes **4** and **5** were characterized by ^{31}P NMR spectroscopy (see the Experimental). Complexes **4** and **5** are formed in a ratio of 1:1.3 as estimated by the integration of the ^{31}P NMR spectrum. We were unable to separate **4** and **5**. It is not known if this is due to the similarity of the compounds or to rapid isomerization on the preparative time scale. Down to 233 K, there is no evidence for the coordination of the phosphine selenide to platinum. There is no reaction of $Ptpp_2Cl_2$ and $dppmS_2$ or $dppmO_2$ according to eq. (2).

EXPERIMENTAL

$Ptpp_2Cl_2$ and $dppmE_n$ ($n = 1, 2$; E = O, S, Se) were prepared by published procedures.[11,12] All manipulations were performed under dinitrogen in dried solvents. The NMR spectra were recorded on Bruker WP-80 and AM 300 spectrometers. The chemical analyses were performed by the Institut für Physikalische Chemie der Universität Wien.

$[Ptpp_2(dppmSe)](O_3SCF_3)_2$ (**1**)

A solution of TlO_3SCF_3 (77.8 mg, 0.22 mmol) in methanol (0.3 cm^3) was added dropwise with stirring to $Ptpp_2Cl_2$ (80.1 mg, 0.1 mmol) and dppmSe (46.3 mg, 0.1 mmol) in CH_2Cl_2/MeOH (0.5+0.5 cm^3). After 10 min, the solvent was removed *in vacuo* and the residue was extracted with dichloromethane (1 cm^3) and filtered in order to remove TlCl and excess TlO_3SCF_3. The solvent was removed *in vacuo*. The resulting powder was suspended in methanol and dissolved by dropwise addition of dichloromethane. Slow evaporation yielded yellow crystals of **1**. Found: C, 49.1; H, 3.6. Calc. for $C_{61}H_{55}F_5O_6P_5PtS_2Se$: C, 49.1; H, 3.7%.

$[Ptpp_2(dppmS)](O_3SCF_3)_2$ (**2**)

This was prepared in an analogous method. Found: C, 50.7; H, 3.8. Calc. for $C_{61}H_{55}F_6O_6P_5PtS_3$: C, 50.7; H, 3.8%.

$[Ptpp_2(dppmO)](O_3SCF_3)_2$ (**3**)

This was also prepared analogously. Found: C, 50.4; H, 3.9. Calc. for $C_{61}H_{55}F_6O_7P_5PtS_2 \cdot 0.5CH_2Cl_2$: C, 50.2; H, 3.8%.

$[Pt(PhP)(CH_2CH_2PPh_2)(CH_2CH_2P(Se)Ph_2)(dppmSe)](O_3SCF_3)_2$ (**4**, **5**)

TlO_3SCF_3 (77.8 mg, 0.22 mmol) in CH_3OH (0.1 cm^3) was added to a solution of $Ptpp_2Cl_2$ (80.1 mg, 0.1 mmol) and $dppmSe_2$ (54.2 mg, 0.1 mmol) in CH_2Cl_2/MeOH (0.5+0.5 cm^3). The resulting suspension was stirred for 1 h and filtered to remove precipitated TlCl.

^{31}P NMR data (the labelling scheme is shown in eq. 2): **4**: δP1 57.3, δP2 48.9, δP3 39.7, δP4 27.9, δP5 38.2; J(PtP1) 2311, J(PtP2) 30.48, J(PtP4) 2406; J(P1P2) 6, J(P1P3) 55, J(P1P4) 330, J(P1P5) 35, J(P2P4) 15, J(P2P5) 6, J(P4P5) 48; J(SeP3) 732.

5: δP1 54.7, δP2 46.9, δP3 38.3, δP4 26.0, δP5 35.9; J(PtP1) 2328, J(PtP2) 3038, J(PtP4) 2386; J(P1P2) 6, J(P1P4) 336, J(P1P5) 35, J(P2P3) 43, J(P2P4) 15, J(P2P5) 6, J(P4P5) 48; J(SeP3) 730.

$PhP(Se)(CH_2CH_2PPh_2)_2$

Elemental selenium (7.9 mg, 0.1 mmol) was added to a solution of pp_2 (53.5 mg, 0.1 mmol) in CH_2Cl_2 (0.5 cm^3). The mixture was stirred until a clear solution was obtained.

^{31}P NMR data: δP 42.2, −14.1; J(PP) 42; J(SeP) 727.

REFERENCES

1. R. Colton and J. Ebner, *Inorg. Chem.* 1989, **28**, 1559.
2. D. E. Berry, J. Browning, K. R. Dixon and R. W. Hilts, *Can. J. Chem.* 1988, **66**, 1272.
3. R. Colton, S. Ebner and B. F. Hoskins, *Inorg. Chem.* 1988, **27**, 1993.
4. P. Peringer and J. Schwald, *J. Chem. Soc., Chem. Commun.* 1986, 1625.
5. J. Browning, G. W. Bushnell, K. R. Dixon and A. Pidcock, *Inorg. Chem.* 1983, **22**, 2226.
6. J. G. Hartley, L. M. Venanzi and D. C. Goodall, *J. Chem. Soc.* 1963, 3930.
7. J. P. Jesson and P. Meakin, *Inorg. Nucl. Chem. Lett.* 1973, **7**, 1221.
8. P. Meakin and J. P. Jesson, *J. Am. Chem. Soc.* 1974, **96**, 5751.
9. A. D. English, P. Meakin and J. P. Jesson, *J. Am. Chem. Soc.* 1976, **98**, 422.
10. A. Handler, P. Peringer and E. P. Müller, *J. Organomet. Chem.* 1990, **389**, C23.
11. R. B. King, P. N. Kapoor and R. N. Kapoor, *Inorg. Chem.* 1971, **10**, 1841.
12. S. O. Grim and E. D. Walton, *Inorg. Chem.* 1980, **19**, 1982.
13. C. Yang, S. M. Socol, D. J. Kountz, D. W. Meek and R. Glaser, *Inorg. Chim. Acta* 1986, **114**, 119.
14. L. Dahlenburg, N. Höck and H. Berke, *Chem. Ber.* 1988, **121**, 2083.

Polyhedron Vol. 10, No. 20/21, pp. 2475–2476, 1991
Printed in Great Britain

0277–5387/91 $3.00+.00
© 1991 Pergamon Press plc

A RAPID AND CONVENIENT SYNTHESIS OF TETRAKIS(TRIPHENYLPHOSPHINE)PALLADIUM(0) AND -PLATINUM(0) COMPLEXES BY PHASE-TRANSFER CATALYSIS

MARCELLA IOELE, GIANCARLO ORTAGGI,* MARCO SCARSELLA and GIANCARLO SLEITER*

Centro CNR di Studio sui Meccanismi di Reazione e Dipartimento di Chimica, Università "La Sapienza", P.le Aldo Moro 2, 00185 Roma, Italy

(*Received* 22 *April* 1991; *accepted* 25 *June* 1991)

Abstract—The tetrakis(triphenylphosphine)palladium(0) and -platinum(0) complexes can be prepared with good yields from the corresponding dichlorobis(triphenylphosphine)palladium(II) and platinum(II) complexes using phase-transfer catalysis. A hypothesis on the mechanism is reported.

Tetrakis(triphenylphosphine)palladium(0) (**1**) and -platinum(0) (**2**) are the most commonly used complexes both as starting materials for the preparation of organometallic complexes of these two metals, and for their catalytic effects in many reactions.

For example, **1** is an extremely versatile catalyst for alkene additions and oligomerizations, coupling of organic halides and organometallic carbonylations;[1] **2** catalyses the hydrosilylation of olefins, cleavage of Si—C bonds, carbonylation, hydrogenation and isomerization of olefins.[2]

Although the two complexes are not very stable in the solid state, especially when exposed to air, they are commercially available and may be prepared by several methods, e.g. (a) the action of hydrazine on an alcoholic suspension of bis(triarylphosphine)dihalogenopalladium or -platinum in the presence of an excess of phosphine;[3,4] (b) the action of an excess of triarylphosphine on freshly precipitated palladium oxide;[4] (c) the reaction of an excess of triphenylphosphine with a hot concentrated solution of palladium nitrate;[4] and (d) from chloroplatinate(II), triphenylphosphine and ethanolic potassium hydroxide.[5]

Generally, the two complexes are prepared either by Fitton's modification of the procedure of Malatesta and Angoletta or, more conveniently, by the method of Takahashi.[6]

The method reported by Coulson[7] would presumably be the current one of choice. Now we report a quite general, facile and convenient preparation of **1** and **2** which employs the phase-transfer catalysis, as outlined by the following equations:

$$(Ph_3P)_2MCl_2 + 3Ph_3P + NaOH \xrightarrow[1.5\,M\,NaOH]{THF,\ Bu_4N^+(HSO_4)^-} (Ph_3P)_4M + Ph_3PO + NaCl + HCl$$

M = Pd or Pt.

To a suspension of dichlorobis(triphenylphosphine)palladium(II) (0.17 g, 0.24 mmol) and triphenylphosphine (0.25 g, 0.96 mmol) in peroxide-free THF (10 cm^3) are added 1.5 M NaOH (10 cm^3) and $Bu_4N^+(HSO_4^-)$ (0.01 g) as a phase-transfer catalyst. The mixture is stirred at 25°C for 24 h; then the aqueous layer is removed and the organic yellow phase is evaporated at 40°C *in vacuo*.

The yellow residue is treated with absolute ethanol (5 cm^3), the suspension stirred at 60°C for 20 min, filtered and the solution kept at −15°C for 30 min. Bright-yellow crystals precipitated, that were filtered under argon, washed once with a little cold absolute ethanol (*ca* 1 cm^3) and dried *in vacuo*. Yield: 0.24 g (84%); m.p. 110–115°C (dec.) [lit.[8] m.p. 109–115°C (dec.); lit.[9] m.p. 104–106°C (dec.); lit.[7a] m.p. 116°C (dec.)]. IR, ^1H and ^{13}C NMR spec-

* Authors to whom correspondence should be addressed.

org. $(Ph_3P)_2MY_2 + OH^- \xrightarrow{slow} (Ph_3P)_2M(Y)OH + Y^-$

interface $Q^+HSO_4^- + Na^+OH^-$ $Q^+OH^- + Na^+HSO_4^-$

aq. Na^+OH^- $Na^+HSO_4^-$

Scheme 1.

tra were identical to those of a specimen prepared according to Coulson's method and of a commercial sample (Fluka).

The same procedure adopted for the preparation of $(Ph_3P)_4Pt$ gave compound **2** in 87% yield; m.p. 158–160°C (dec.) [lit.[10] m.p. 159–160°C (dec.)] with the spectroscopic properties identical to those of an authentic specimen.

The reaction mechanism probably involves the transport of OH^- ions in the organic phase to form $L_2M(Cl)OH$ by nucleophilic substitution, followed by the rapid substitution of the second chloride by PPh_3 and, according to the general mechanistic scheme, by reductive elimination of a proton and triphenylphosphine oxide.

The triphenylphosphine (in excess) reacts with the coordinatively unsaturated L_2M complex to shift the dissociation equilibrium toward L_4M which precipitates.

Acknowledgements—We want to thank Ms A. Stella and Ms G. Gigli for carefully typewriting the manuscript.

REFERENCES

1. M. Fieser, *Reagents for Organic Synthesis*, Vol. 8, p. 472. J. Wiley, New York (1983).
2. (a) H. Watanaba, M. Aaki, N. Sakurai, K. Watanaba and Y. Nagai, *J. Organomet. Chem.* 1978, **160**, C1; (b) I. S. Akhrem, R. S. Vartanyan, N. M. Chistovalova, E. I. Mysov and M. E. Vol'pin, *Izv. Akad. Nauk. SSSR, Ser. Kim.* 1976, 2069.
3. L. Malatesta and C. Cariello, *J. Chem. Soc.* 1957, 2323.
4. L. Malatesta and M. Angoletta, *J. Chem. Soc.* 1957, 1186.
5. W. Ransey and R. Foster, *Organomet. Chem. Rev. A* 1970, **6**, 119.
6. Personal communications from Dr P. Fitton and Dr Y. Takahashi (see ref. 8).
7. (a) D. R. Coulson, *Inorganic Synthesis*, Vol. XIII, p. 121. McGraw-Hill, New York (1972); (b) D. R. Coulson, *Inorg. Synthesis*, Vol. XI, p. 105. McGraw-Hill, New York (1968).
8. J. M. Townsend, J. D. Reingold, M. C. R. Kenday and T. A. Spencer, *J. Org. Chem.* 1975, **40**, 2976.
9. E. O. Fischer and H. Werner, *Chem. Ber.* 1962, **95**, 703.
10. J. McAvay, *Inorg. Synth.* 1969, **11**, 105.

Polyhedron Vol. 10, No. 20/21, pp. 2477–2481, 1991
Printed in Great Britain

0277–5387/91 $3.00+.00
© 1991 Pergamon Press plc

MANGANESE(II) COMPLEX OF A HYDRAZONE LIGAND DERIVED FROM PYRUVIC ACID AND 4-PYRIDINE CARBOXYLIC ACID HYDRAZIDE—SYNTHESIS AND CRYSTAL STRUCTURE

WANG LIUFANG, ZHU YING,* YANG ZHENGYIN and WU JIGUI

Department of Chemistry, Lanzhou University, Lanzhou 730000, P.R.C.

and

WANG QI

Lanzhou Institute of Chemical Physics, Chinese Academy of Sciences, Lanzhou 730000, P.R.C.

(*Received* 18 *February* 1991; *accepted* 25 *June* 1991)

Abstract—A hydrazone ligand (H_2PAPH) derived from pyruvic acid and 4-pyridine carboxylic acid hydrazide and its manganese(II) complex have been synthesized and X-ray diffraction analysis of the complex was carried out. The crystal is monoclinic, space group $P2_1/n$, with unit-cell dimensions $a = 11.252(1)$, $b = 9.828(2)$, $c = 13.708(2)$ Å, $\beta = 66.03(1)°$ and $V = 1385.2$ Å^3, $Z = 4$, $D_c = 2.812$ g cm^{-3}, $F(000) = 1216$, μ(Mo-K_α) = 18.506 cm^{-1}. The structure was solved by the heavy-atom technique from 2417 observed, independent reflections recorded at 293 K and refined to a final $R = 0.028$. The manganese atom has a distorted octahedral coordination with two *trans* water molecules in axial sites and an NO_3 donor set from hydrazone ligands (H_2PAPH) in the equatorial plane. The complex has a polymeric structure. The crystal structure also contains 2.5 water molecules of crystallization, which are involved in a hydrogen-bonding network in the crystal packing. The complex has been also characterized by elemental analysis and IR spectra.

For their chelating capability and pharmacological activity, the chemical properties of hydrazones have received special attention and have been extensively investigated in several research fields.[1–5]

It is well-known that Schiff base complexes with metals have some biological activity, such as anticancer and anti-tumor activity. Because hydrazones are similar to Schiff base chelating agents, we were interested in synthesizing a hydrazone ligand (H_2PAPH) derived from pyruvic acid and 4-pyridine carboxylic acid hydrazine and its complexes with metals to examine their structure, properties and biological activity.

This paper is one of a series on our investigation of metal complexes with H_2PAPH, and describes the synthesis, IR spectra and X-ray crystal structure of manganese(II) complexes with H_2PAPH.

EXPERIMENTAL

Preparations

The hydrazone ligand (H_2PAPH) was prepared by refluxing pyruvic acid (2 g, 23 mmol) and 4-pyridine carboxylic acid hydrazide (3 g, 22 mmol) (1 : 1 molar ratio) in absolute ethanol solution for 6 h. The solution was filtered on cooling and the solid was washed with distilled water and dried *in vacuo* at 80°C. A white powder was obtained; yield, 4.3 g (95%); m.p. 222–3°C. Found: C, 48.1; H, 5.0; N, 18.4. Calc.: C, 48.0; H, 4.9; N, 18.7%.

A saturated $MnSO_4$ solution (1 g) was added to NaOH solution to precipitate $Mn(OH)_2$. The

*Author to whom correspondence should be addressed.

precipitate was filtered and washed with distilled water to separate $MnSO_4$. $Mn(OH)_2$ was then added to a solution of H_2PAPH (0.5 g) in distilled water (30 cm^3). After stirring for 5 h at room temperature, the solution turned yellow (pH = 7). The solution was filtered and the solid was dried *in vacuo* at 80°C (light-yellow powder); yield: 0.5 g (77%). The complex was recrystallized from distilled water to afford orange crystals. Found: C, 35.3; H, 3.6; N, 13.7; Mn, 18.0. Calc.: C, 35.6; H, 3.7; N, 13.5; Mn, 17.5%.

Structure determination

A transparent orange crystal ($0.52 \times 0.37 \times 0.26$ mm) was mounted on an Enraf–Nonius CAD-4 diffractometer. The unit cell was measured by centring 25 reflections ($9 \leqslant \theta \leqslant 16°$) and refined by least-squares. Graphite-monochromated Mo-K_α radiation was used. Intensities were measured with a ω–2θ scan technique (scan width: $0.5+0.35\tan\theta$), θ range: $1 \leqslant \theta \leqslant 26°$ ($h = -13$ to 13; $k = 0$–12; $l = 0$–16). 2765 independent reflections were collected, of which 2417 were considered observed ($I > 3\sigma(I)$). Lorentz and polarization, but no absorption, corrections were made.

The manganese atom was located from a Patterson synthesis and the remaining non-hydrogen atoms from Fourier synthesis. The structure was refined isotropically and the anisotropically by least-squares refinement. The function minimized was $\Sigma w(|F_o|-|F_c|)^2$, where $w = 1$. All hydrogen atoms were located from a difference synthesis, and refined with an overall isotropic thermal parameter. The final R factor was 0.028 ($R_w = 0.030$), $(\Delta/\sigma)_{max} = 0.01$ and the final difference-Fourier map showed peaks being less than 0.39 e $Å^{-3}$.

Atomic scattering factors were taken from ref. 6. All calculation were carried out on a PDP 11/44 computer using the SDP package.[7]

RESULTS AND DISCUSSION

Selected interatomic distances and bond angles are in Table 1.

Crystal structure of $[Mn(H_2PAPH)(OH_2)_2]\cdot 2.5H_2O$

Chemical analysis of the manganese(II) complex suggested the formula $Mn(H_2PAPH)(OH_2)_2$. Structure analysis shows that there is one complex unit $Mn(H_2PAPH)(OH_2)_2$ and 2.5 lattice water molecules in the asymmetric unit. The structure of the complex is shown in Fig. 1 and a diagram showing the unit-cell contents is given in Fig. 2.

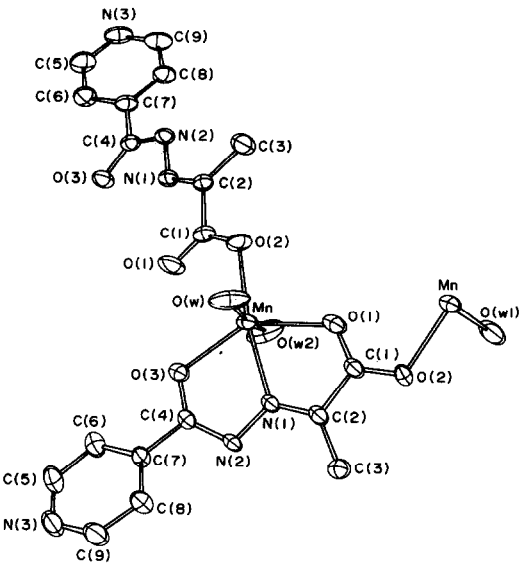

Fig. 1. Structure of the title compound showing the atomic numbering.

The coordination sphere about manganese is a slightly distorted octahedron, with three oxygen atoms and one nitrogen of the H_2PAPH ligands in the equatorial positions and two oxygen atoms of two water molecules occupying axial sites. Valency angles at manganese show significant distortions from an ideal octahedral arrangement. Two of four angles subtended at manganese by adjacent equatorial atoms are smaller than 90°, their range being 70.47(6)–71.06(6)°, while the other two are larger, range 99.61(5)–118.87(6)°. The range of equatorial to axial angles is 84.61(7)–95.75(7)°, and the inter-axial angle is reduced from a theoretical value of 180° to 170.85(6)°.

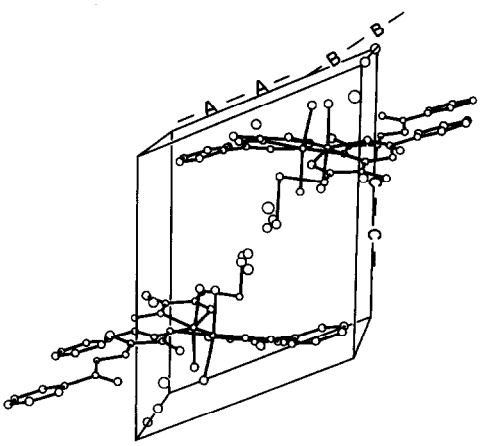

Fig. 2. Cell packing diagram.

Table 1. Selected distances (Å) and angles (°) of $Mn(H_2PAPH)(OH_2)_2$

(a) Coordination sphere of Mn

Mn—O(1)	2.255(2)	Mn—N(1)	2.214(1)
Mn—O(2)	2.137(1)	Mn—O(w1)	2.180(2)
Mn—O(3)	2.200(1)	Mn—O(w2)	2.217(2)

O(1)—Mn—O(2)	99.61(5)	O(2)—Mn—O(3)	118.87(6)
O(1)—Mn—N(1)	71.06(7)	O(3)—Mn—N(1)	70.47(6)
O(w1)—Mn—O(w2)	170.85(6)		

(b) Ligand

O(1)—C(1)	1.249(2)	C(1)—C(2)	1.514(3)
O(2)—C(1)	1.261(3)	C(2)—C(3)	1.486(3)
O(3)—C(4)	1.279(2)	C(4)—C(7)	1.498(3)
N(1)—N(2)	1.384(2)	C(5)—C(6)	1.383(4)
N(1)—C(2)	1.281(3)	C(6)—C(7)	1.387(3)
N(2)—C(4)	1.322(3)	C(7)—C(8)	1.390(3)
N(3)—C(5)	1.330(3)	C(8)—C(9)	1.383(3)
N(3)—C(9)	1.332(4)		

O(1)—C(1)—O(2)	124.0(2)	O(3)—C(4)—C(7)	118.2(2)
O(1)—C(1)—C(2)	118.6(2)	N(2)—C(4)—C(7)	115.0(2)
O(2)—C(1)—C(2)	117.5(2)	N(3)—C(5)—C(6)	123.3(2)
N(1)—C(2)—C(1)	112.2(2)	C(5)—C(6)—C(7)	118.8(2)
N(1)—C(2)—C(3)	126.4(2)	C(6)—C(7)—C(8)	118.3(2)
N(2)—N(1)—C(2)	119.4(2)	C(7)—C(8)—C(9)	118.4(2)
N(1)—N(2)—C(4)	108.7(1)	N(3)—C(9)—C(8)	123.6(2)
O(3)—C(4)—N(2)	126.8(2)		

(c) Hydrogen bonding

D—H···A	Symmetry code	D···A	D—H	H···A	D—H···A
O(w1)—H(w1)···N(2)	i	2.994	0.831	2.175	169.1
O(w1)—H(w1′)···N(3)	ii	2.705	0.723	1.986	173.2
O(w2)—H(w2)···O(w3)	iii	2.650	0.850	1.813	167.4
O(w3)—H(w3)···O(2)	iv	2.801	0.788	2.018	172.3
O(w3)—H(w3′)···O(3)	v	2.944	0.768	2.213	159.6
O(w4)—H(w4)···O(3)	vi	2.963	0.851	2.117	172.2
O(w4)—H(w4′)···O(w5)	vii	2.944	0.745	2.208	169.4
O(w5)—H(w5)···O(4)	viii	2.731	0.931	1.957	139.0

i: $1/2+x, 1/2-y, z-1/2$;
ii: $1/2-x, 1/2-y, 1(1/2)-z$;
iii: $1/2+x, 1/2-y, 1/2+z$;
iv: $1-x, 1-y, 1-z$;
v: $1/2+x, 1/2-y, 1/2+z$;
vi: x, y, z;
vii: $-x, 1-y, -z$.

The N(1), O(1), O(2), O(3) and manganese atoms are nearly co-planar with a maximum displacement from the least-square planes of 0.017 Å. With regard to the Mn—O bonds, the three equatorial distances are Mn—O(1) 2.255, Mn—O(2) 2.137 and Mn—O(3) 2.204 Å, while the axial distances are 2.180(2) and 2.217(2) Å. The shortest Mn—O bond is that between the manganese and oxygen atoms of the carboxyl group in the adjacent H_2PAPH ligand. The observed Mn—N(1) bond distance is 2.214(1) Å. Compared with the complexes of other hydrazones with manganese, the mean Mn—O (2.199 Å) and Mn—N (2.214 Å) bond distances of our complex are slightly shorter than those reported in the literature (as shown in Table 2). This is due to the effect of the coordinated oxygen of the carboxyl group.

The carboxyl group in the H_2PAPH ligands cause a polymeric structure, in which two oxygen atoms and one nitrogen coordinated to the manganese(II) atom are from a H_2PAPH ligand while another oxygen is from the carboxyl group of an adjacent H_2PAPH ligand (symmetry code: $1.5-x, y-1/2. 1.5-z$). In other words, two oxygen atoms of the

Table 2. Comparison of structure parameters in manganese complexes with hydrazone

	Mn-Leq	Mn-Lax	C(4)—O(3)	C(4)—N(2)	C(2)—N(1)	N(1)—N(2)	C(4)—C(7)
1	2.199[a] 2.214[b]	2.199[a]	1.279	1.322	1.281	1.384	1.498
2	2.190[a] 2.281[b]	2.202	1.270	1.326	1.274	1.386	1.496
3	2.253[a] 2.306[b]	2.258	1.225	1.364	1.279	1.385	1.478
4	2.304[a] 2.327[b]	2.189	1.245	1.375	1.287	1.369	1.478
5	2.212[a] 2.271[b]	2.300	1.23	1.370	1.27	1.38	1.475

Complex: **1**, this work; **2**, $Mn(dappc)\cdot 9H_2O$;[2] **3**, $[Mn(H_2dapb)(OH)_2Cl]Cl$;[3] **4**, $[Mn(HL)(OH_2)_2Cl]Cl\cdot H_2O$;[4] **5**, $[Mn(H_2dapb)(CH_3OH)Cl]Cl\cdot H_2O$.[5]

[a] Oxygen donor atom.

[b] Nitrogen donor atom.

carboxyl group in each H_2PAPH ligand bond to two manganese(II) atoms, respectively, resulting in polymer formation. Because two carboxyl oxygens take part in coordination, the bond lengths between carbon and the two carboxyl oxygen atoms are quite close: C(1)—O(1) 1.249(3) and C(1)—O(2) 1.261(3) Å. This is similar to other polymeric structures involving the carboxyl oxygen of manganese complexes.[8,9]

The H_2PAPH ligand and manganese form two five-membered chelate rings. The data in Table 3 show that the five-membered chelate rings are almost in a plane, so the atoms in the chelating rings constitute a conjugated system. Because of conjugation, it appears that the double bonds become longer and single bonds shorter than in the manganese complex with hydrazone reported in the literature. Thus, compared to the manganese(II) complex with hydrazone listed in Table 2, the C(4)—O(3) double bond distance of the title complex is longer than the corresponding C—O bond distances in other manganese(II) hydrazone complexes, and the C(4)—N(2) single bond distance is correspondingly shorter. This shows that the O(3)—C(4)—N(2) group becomes more enolized. The pyridine ring is planar, but this and the two five-membered chelate rings are not co-planar, the dihedral along C(1)—C(4) angle being 26.4° (shown in Table 3).

The molecular packing is dominated by an extensive system of hydrogen bonds between the oxygen and nitrogen atoms of the H_2PAPH ligand and hydrogen atoms of uncoordinated water molecules. Detailed data on hydrogen bonds are summarized in Table 1.

IR spectra—The IR absorption bands which appear at 3451 [ν(N—H)], 1546 [δ(N—H)] and 1286 cm^{-1} [δ(O—H)] in free H_2PAPH disappear in the complex, indicating that the carboxyl oxygen and hydrazide nitrogen atom are coordinated to the metal atom and have lost their hydrogen atoms. The vibration assigned to ν(C—O) of the hydrazide in the complex is at 1307 cm^{-1} instead of ν(C=O) at 1623 cm^{-1} in the free ligand, and the ν(C—N) (at 1452 cm^{-1}) band shifts towards a higher ($\Delta\nu$ 58 cm^{-1}) frequency. It can be attributed to the pres-

Table 3. Planar fragments of the complex

Plane 1 $(-0.4358)x+0.2590y+(-0.8620)z+12.706=0$

Atom	C(1)	C(2)	N(1)	N(2)	C(4)	O(1)	O(2)	O(3)	Mn
Δ (Å)	0.020	0.006	−0.013	0.005	0.048	−0.003	0.004	−0.019	−0.003

Plane 2 $(-0.1206)x+(-0.0280)y+(-0.9923)z+11.5071=0$

Atom	C(4)	C(5)	C(6)	C(7)	C(8)	C(9)	N(3)
Δ (Å)	0.004	−0.005	0.010	−0.012	−0.003	0.009	−0.003

Dihedral angle 26.4°

ence of the 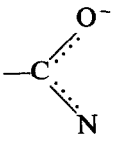 group, suggesting the coordination of the amide-oxygen atom in its enolic form.

Acknowledgement—This work was supported by the National Science Foundation of China.

REFERENCES

1. P. K. Rastogi, S. K. Sahni, V. B. Rana and S. K. Dua, *J. Coord. Chem.* 1978, **8**, 97.
2. C. Pelizzi, G. Pelizzi, G. Predieri and S. Resola, *J. Chem. Soc., Dalton Trans.* 1982, 1349.
3. C. Lorenzini, C. Pelizzi, G. Pelizzi and G. Predieri, *J. Chem. Soc., Dalton Trans.* 1982, 721.
4. C. Pelizzi, G. Pelizzi and P. Tarasconi, *J. Chem. Soc., Dalton Trans.* 1985, 215.
5. C. Pelizzi, G. Pelizzi, G. Prederi and F. Vitali, *J. Chem. Soc., Dalton Trans.* 1985, 2387.
6. *International Tables for X-ray Crystallography*, Vol. IV. Kynoch Press, Birmingham (1974).
7. B. A. Frenz, *Enraf–Nonius Structure Determination Package*, SDP Users Guide. Version of April 1983, Enraf–Nonius, Delft, The Netherlands (1983).
8. C. H. L. Kennard, G. Smith, E. J. O'Reilly and P. T. Manoharan, *Inorg. Chem. Acta* 1984, **82**, 35.
9. J. P. Guptu and R. Ram, *Ind. J. Phys.* 1977, **51**, 223.

Polyhedron Vol. 10, No. 20/21, pp. 2483–2486, 1991
Printed in Great Britain

0277–5387/91 $3.00+.00
© 1991 Pergamon Press plc

SYNTHESES, X-RAY STRUCTURE AND PROPERTIES OF (η^5-CYCLOPENTADIENYL)RUTHENIUM(II) COMPLEXES OF PYRIDYL-2-HYDRAZONE LIGANDS

SISIR K. MANDAL and AKHIL R. CHAKRAVARTY*

Department of Inorganic and Physical Chemistry, Indian Institute of Science, Bangalore 560 012, India

(*Received* 5 *February* 1991; *accepted* 25 *June* 1991)

Abstract—Complexes of the formulae [(η-Cp)Ru(PPh_3)(η^2-PPH)]Cl and [(η-Cp)Ru(PPh_3)(py)(η^1-PPH)]Cl were prepared by reacting pyridyl-2-phenylhydrazone [PPH, C_5H_4N-2-CH=NNHPh] with (η-Cp)Ru(PPh_3)$_2$Cl and (η-Cp)Ru(PPh_3)(py)Cl, respectively. In these complexes the PPH ligand displays bidentate chelating and unidentate modes of bonding. The molecular structure of [(η-Cp)Ru(PPh_3)(η^2-PPH)](ClO_4)·CH_2Cl_2 was determined by X-ray crystallography. In this complex the metal is bonded to the N-pyridyl and N-imine atoms of the chelating ligand. ^{1}H NMR spectral data suggests that PPH is bonded to ruthenium through the pyridine moiety of the PPH ligand in [(η-Cp)Ru(PPh_3)(py)(η^1-PPH)]Cl.

Recent developments in the chemistry of monocyclopentadienylruthenium(II) complexes containing PPh_3 facial ligand(s) have shown[1–3] that the electron-rich nature of the {(η-Cp)Ru(II)} fragment leads to the formation of a variety of complexes with primarily π-acceptor ligands. The reactivity study of nitrogen-donor ligands with this moiety is largely confined to heterocyclic bases.[4,5] We have investigated the ligational behaviour of the pyridyl-2-phenylhydrazone (PPH, C_5H_4N-2-CH=NNHPh) ligand with (η-Cp)Ru(PPh_3)$_2$Cl (**1**) and (η-Cp)Ru(PPh_3)(py)Cl (**2**). It is observed that while PPH undergoes the chelating mode of bonding on reaction with **1**, it acts as a unidentate ligand when reacted with **2**. Herein, we report the synthesis and properties of two complexes, [(η-Cp)Ru(PPh_3)(η^2-PPH)]Cl (**3**) and [(η-Cp)Ru(PPh_3)(py)(η^1-PPH)]Cl (**4**). Complex **3**, as a perchlorate salt, was characterized by X-ray crystallography.

EXPERIMENTAL

Materials and methods

Dry benzene was used as a solvent. The reactions were carried out under a dinitrogen atmosphere using the Schlenk technique. The precursor complexes (η-Cp)Ru(PPh_3)$_2$Cl and (η-Cp)Ru(PPh_3)(py)Cl were made by following literature procedures.[5,6] The ligand was obtained by reacting pyridine-2-carboxaldehyde (Fluka) and phenylhydrazine (Merck) in ethanol at 0°C. The yellow crystalline PPH thus obtained was washed with cold ethanol and dried *in vacuo* over P_4O_{10}. Elemental analysis was performed on a Heraeus CHN—O rapid elemental analyser. ^{1}H NMR spectra were recorded in $CDCl_3$ on a Bruker WH-270 MHz spectrometer using tetramethylsilane (TMS) as a standard.

Preparation of [(η-Cp)Ru(PPh_3)(η^2-PPH)]Cl (**3**)

A benzene solution (20 cm^3) containing (η-Cp)Ru(PPh_3)$_2$Cl (200 mg, 0.28 mmol) and PPH (200 mg, 0.99 mmol) was heated under reflux for 24 h. On cooling the solution to 25°C, an orange–yellow crystalline precipitate was obtained. The product was filtered, washed with benzene and dried *in vacuo* over P_4O_{10} (yield: 70%). The complex was found to be stable in air and light; m.p. = 165–170°C (decomposition). Found: C, 62.9; H, 4.9; N, 5.9. Calc.: C, 63.6; H, 4.7; N, 6.3%. ^{1}H NMR [δ, ppm, $CDCl_3$]: 4.87 [s, 5H], 6.88 [d, 4H, J = 7 Hz], 7.15–7.58 [m, 20H], 8.86 [d, 1H, J = 6 Hz],

* Author to whom correspondence should be addressed.

11.40 [s, 1H] (s, singlet; d, doublet; m, complex multiplet; J of H—H).

Preparation of [(η-Cp)Ru(PPh_3)(py)(η^1-PPH)]Cl (**4**)

This complex was prepared following the above procedure using (η-Cp)Ru(PPh_3)(py)Cl as a precursor complex (yield: 70%). Complex **4** has stability similar to **3**; m.p. = 190°C (decomposition). Found: C, 64.1; H, 4.8; N, 7.2. Calc.: C, 64.9; H, 4.9; N, 7.5%. ^{1}H NMR [δ, ppm, $CDCl_3$]: 4.86 [s, 5H], 6.89 [q, 4H, J = 7 Hz], 7.15–8.06 [m, 24H], 8.54 [d, 1H, J = 6 Hz], 8.85 [d, 1H, J = 6 Hz], 11.37 [s, 1H] (q, quintet).

Crystallographic analysis

Complex **3** was converted to a perchlorate salt for crystallization since the chloro analogue did not form crystals suitable for X-ray diffraction. Single crystals of the perchlorate salt of cationic **3** were obtained from a dichloromethane solution of the complex layered with n-hexane in a Schlenk tube under a dinitrogen atmosphere. A reddish coloured prismatic crystal of 0.1 × 0.2 × 0.3 mm dimensions was mounted on a glass fibre using epoxy cement. Unit cell and intensity data were obtained using an Enraf–Nonius CAD4 diffractometer with graphite-monochromatized Mo-K_α radiation following standard procedures. The structure was solved and all non-hydrogen atoms were located by conventional heavy-atom and difference Fourier methods. Refinements were made by the full-matrix least-square procedure. The metal and chlorine atoms, carbon atoms of the Cp ring and all nitrogen atoms were refined anisotropically leaving remaining atoms at the isotropic stage. The convergence was obtained by applying a weighting scheme of the form weight (w) = $1.4387/[\sigma^2(F)+0.000620(F)^2]$. The perchlorate anion was found to be disordered showing a highest peak of 1.24 e Å^{-3} located in the final-difference Fourier map. Other electron densities were < 1.0 e Å^{-3}. All calculations were carried out using a DEC 1090 computer with SHELX[7] programs at the computer centre of the Indian Institute of Science. Complete tables of structure factors, anisotropic thermal parameters and complete lists of bond distances and angles (16 pages) have been deposited with the Editor. Positional parameters and isotropic thermal parameters have been forwarded to the Director of the Cambridge Crystallographic Data Centre.

Crystal data for [(η-Cp)Ru(PPh_3)(η^2-PPH)](ClO_4)·CH_2Cl_2. Formula = $C_{36}H_{33}N_3O_4PCl_3Ru$, M = 873.79, monoclinic, $P2_1$, a = 9.853(2), b = 13.679(3), c = 13.179(2) Å, β = 90.99(2)°, V = 1776.2 Å^3, Z = 2, D_c = 1.63 g cm^{-3}, λ = 0.7107 Å, μ(Mo-K_α) = 6.35 cm^{-1}, $F(000)$ = 818, I = 18°C, 2804 reflections with $I \geqslant 1.5\sigma(I)$, data collection range (2θ) = 4–50°, R = 0.0611, R_w = 0.0614, g = 0.000620, largest shift/e.s.d. = 0.097.

RESULTS AND DISCUSSION

The precursor complexes **1** and **2** were found to react with pyridyl-2-hydrazone (PPH, C_5H_4N-2-CH=NNHPh) to form complexes **3** and **4**, respectively [eqs (1) and (2)]. Characterization of the complexes was done using elemental analytical and ^{1}H NMR spectroscopic techniques.

(η-Cp)Ru(PPh_3)$_2$Cl(**1**) + PPH ⟶ [(η-Cp)Ru(PPh_3)(η^2-PPH)]Cl(**3**) (1)

(η-Cp)Ru(PPh_3)(py)Cl(**2**) + PPH ⟶ [(η-Cp)Ru(PPh_3)(py)(η^1-PPH)]Cl(**4**) (2)

In the ^{1}H NMR spectra of (**3**) and (**4**), the Cp ring protons display a sharp singlet at δ 4.9. The presence of η-Cp, PPh_3 and PPH in a 1:1:1 ratio is observed from the peak integrations of the ^{1}H NMR spectra of **3**. The peak at δ 11.40 could be assigned to the NH proton of the PPH ligand as it undergoes D_2O exchange. The doublet observed at δ 8.86 is assigned to the *ortho*-proton of the pyridine ring in PPH. The spectral pattern in the range δ 7.15–7.58 is complex. A singlet resonance observed at δ 7.58 could be due to the CH proton of the imine group. In **4**, the NH proton appears at δ 11.37. As in **3**, the doublet observed at δ 8.85 could be from the *ortho*-proton of the pyridine moiety in the η^1-PPH ligand. The spectral pattern of **4** in the aromatic region is complex. Peak integrations, however, show a ratio of 5:31 for Cp: other protons in **4**. The spectral features, shown in Fig. 1, are indicative of the presence of both pyridine and η^1-PPH ligands besides one PPh_3 in **4**.

Complex **3** as a perchlorate salt with one CH_2Cl_2 molecule as a solvent of crystallization was structurally characterized by X-ray crystallography. The cationic complex is shown in Fig. 2. Selected bond distances and angles for **3** are given in Table 1. The coordination geometry of ruthenium is essentially octahedral. While one face of the octahedron is occupied by a η^5-Cp ring, the other three facial sites have PPh_3 and a bidentate chelating PPH ligand.

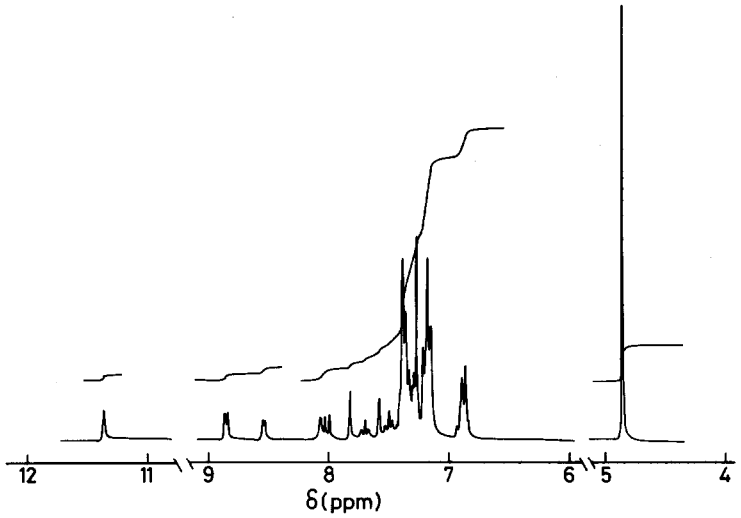

Fig. 1. ^{1}H NMR spectrum of **4** in $CDCl_3$.

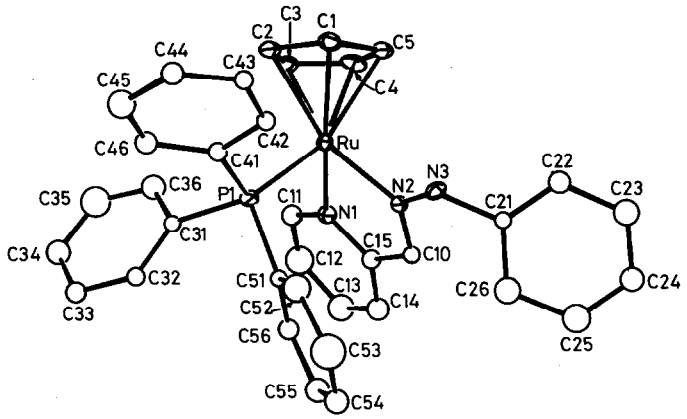

Fig. 2. A perspective view of $[(\eta\text{-Cp})Ru(PPh_3)(\eta^2\text{-PPH})]^+$ showing the atom labelling scheme.

Table 1. Selected bond distances (Å) and bond angles (°) for $[(\eta\text{-Cp})Ru(PPh_3)(\eta^2\text{-PPH})](ClO_4)\cdot CH_2Cl_2$ with e.s.d.s in parentheses

Bond distances (Å)			
Ru—P(1)	2.321(3)	P(1)—C(41)	1.808(8)
Ru—N(1)	2.089(7)	C(1)—C(2)	1.447(12)
Ru—N(2)	2.058(6)	C(2)—C(3)	1.425(12)
Ru—C(1)	2.219(9)	C(3)—C(4)	1.428(13)
Ru—C(2)	2.200(8)	C(4)—C(5)	1.410(12)
Ru—C(3)	2.175(8)	C(1)—C(5)	1.456(13)
Ru—C(4)	2.200(9)	C(10)—N(2)	1.320(10)
Ru—C(5)	2.207(9)	N(2)—N(3)	1.396(9)
P(1)—C(31)	1.833(8)	C(10)—C(15)	1.418(11)
P(1)—C(51)	1.835(8)	C(21)—N(3)	1.443(9)
Bond angles (°)			
P(1)—Ru—N(1)	92.9(2)	C(10)—N(2)—N(3)	120.6(6)
P(1)—Ru—N(2)	89.7(2)	C(21)—N(3)—N(2)	119.8(6)
N(1)—Ru—N(2)	75.9(3)	Ru—P(1)—C(31)	116.3(3)
C(10)—C(15)—N(1)	116.1(7)	Ru—P(1)—C(41)	114.2(3)
C(15)—C(10)—N(2)	114.2(7)	Ru—P(1)—C(51)	115.6(3)

The average Ru—C(η-Cp) distance of *ca* 2.2 Å is similar to that found[1,2,8] in other monocyclopentadienylruthenium(II) complexes. The PPH ligand is bonded through the pyridine and imino nitrogen atoms. The Ru—N(1) distance is found to be marginally longer than the Ru—N(2) distance. This suggests that the Ru—N(py) and Ru—N(imine) bonds are essentially of equal strength.

The isolation of **3** and **4** from two closely related precursor complexes shows that the PPh_3 substitution by the pyridine moiety is the initial step in the former case. This is again evidenced from the fact that both **1** and **2** are unreactive towards benzaldehydephenylhydrazone (PhCH=NNHPh) which has a similar chromophore to that in PPH. The formation of a chelate ring in **3** is facilitated by the removal of a facile PPh_3 ligand of **1**, whilst the imino-nitrogen is unable to form a chelate ring when reacted with **2** since the presence of PPh_3 and py ligands in **2** reduces the electron density on the metal as well as the steric constraints on the coordination geometry.

Acknowledgement—We thank the Department of Science and Technology, Government of India, for financial support.

REFERENCES

1. S. G. Davies, J. P. Mcnally and A. J. Smallridge, *Adv. Organomet. Chem.* 1990, **30**, 1.
2. M. O. Albers, D. J. Robinson and E. Singleton, *Coord. Chem. Rev.* 1987, **79**, 1.
3. M. A. Bennet, M. I. Bruce and T. W. Matheson, *Comprehensive Organometallic Chemistry* (Edited by G. Wilkinson), Vol. 4, pp. 759–776. Pergamon, Oxford (1982).
4. R. Uson, L. A. Oro, M. A. Ciriano, M. M. Naval, M. C. Apreda, C. Foces-foces, F. H. Cano and S. Garcia-Blanco, *J. Organomet. Chem.* 1983, **256**, 331.
5. R. F. N. Ashok, M. Gupta, K. S. Arulsamy and U. C. Agarwala, *Inorg. Chim. Acta* 1985, **98**, 161.
6. M. I. Bruce, C. Hameister, A. G. Swincer and R. C. Wallis, *Inorg. Synth.* 1982, **21**, 78.
7. G. M. Sheldrich, SHELX76, A Program for Crystal Structure Determination. Cambridge University Press, Cambridge (1976).
8. S. K. Mandal and S. R. Chakravarty, *Ind. J. Chem.* 1990, **29A**, 1169.

Polyhedron Vol. 10, No. 20/21, pp. 2487–2493, 1991
Printed in Great Britain

0277–5387/91 $3.00+.00
© 1991 Pergamon Press plc

DECARBOXYLATION IN THE REACTIONS OF $O^{-\cdot}$ WITH METAL CARBONYL COMPLEXES IN THE GAS PHASE

STEVEN L. VanORDEN and STEVEN W. BUCKNER†

Department of Chemistry, University of Arizona, Tucson, AZ 85721, U.S.A.

(*Received* 30 *March* 1991; *accepted* 25 *June* 1991)

Abstract—The gas phase reactions of $O^{-\cdot}$ with some first row transition metal complexes have been investigated using Fourier transform ion-cyclotron resonance spectroscopy. $O^{-\cdot}$, generated by dissociative electron capture from N_2O, reacts with $M(CO)_x$ (M = V, Cr, Fe) and manganese(methylcyclopentadienyl)$(CO)_3$ to generate $ML(CO)_{n-1}^-$, exclusively. Thermochemical arguments indicate the products cannot be generated by a simple dissociative electron-transfer mechanism, but must result from loss of CO_2. Although the reactions that generate the metal anion complexes and CO_2 are > 95 kcal mol^{-1} exothermic, the metal carbonyl anion products do not subsequently decompose indicating non-statistical energy disposal in the products. The order of relative rate constants for the reactions of the homoleptic carbonyl complexes [$k^{II}(O^{-\cdot}/V(CO)_6) > k^{II}(O^{-\cdot}/Cr(CO)_6) > k^{II}(O^{-\cdot}/Fe(CO)_5)$] and the product energy disposal results support an addition/elimination mechanism.

Although gas-phase inorganic chemistry has been a very active field during the past two decades,[1,2] there have been relatively few studies on the reactions of negative ions with neutral transition metal complexes. The reactions which have been investigated have mainly focused on nucleophilic addition reactions with carbonyl complexes. Foster and Beauchamp investigated the reactions of F^- and $C_2H_5O^-$ with $Fe(CO)_5$ in an ion-cyclotron resonance spectrometer,[3] and found both anions to react via pathway (1).

$$A^- + Fe(CO)_5 \longrightarrow Fe(CO)_3A^- + 2CO \quad (1)$$

Subsequently, Squires and co-workers have investigated the reactions of varous bare[4] and solvated[5] anions with $Fe(CO)_5$ which proceed via a variety of reaction pathways including electron transfer, direct attachment, hydride abstraction, proton transfer and nucleophilic attachment with the loss of various ligands. The final products obtained in their flowing afterglow reactor are different than those obtained in the low-pressure environment of the ICR spectrometer due to quenching of some reactive intermediates by the helium buffer gas. These intermediates are crucial to understanding the overall nucleophilic activation mechanism, shown in Scheme I. Initially, the nucleophile attacks the carbonyl carbon to form a metal–acyl anionic complex. This activated complex can

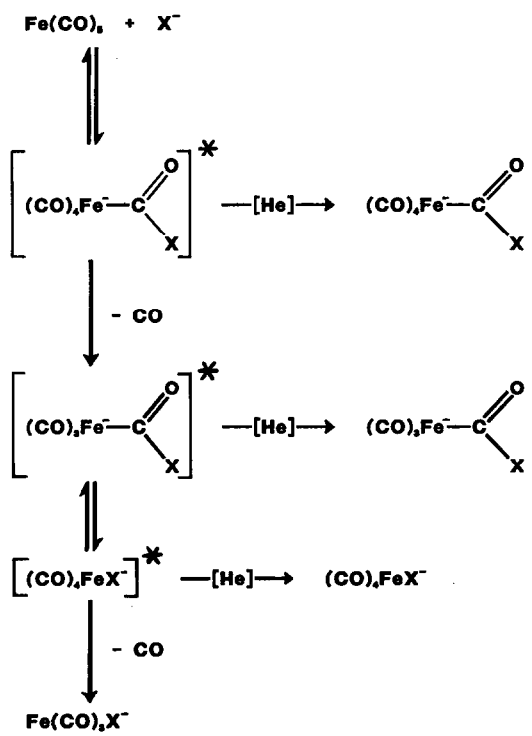

Scheme I.

† Author to whom correspondence should be addressed.

dispose of its excess energy by collision with a neutral molecule as in the high-pressure flow reactor studies, or by the loss of a carbonyl. If the reactive complex loses a carbonyl the unsaturated metal centre forms an M—X bond by migratory deinsertion. In turn, this excited complex can also be quenched by collision with a neutral molecule under high-pressure conditions or decompose by loss of another carbonyl group.

A recent study of nucleophilic activation of metal carbonyl complexes has been directed toward developing an understanding of the homogeneously catalysed water–gas shift reaction (WGSR) and, in particular, the generation of CO_2 in this process.[6] There have been proposals that CO_2 is generated either by decomposition of a carboxylic acid anion $[M(CO)_{x-1}(COOH)^-]$ or the conjugate base metallocarboxylate $[M(CO)_{x-1}(COO)^{2-}]$.[7] The recent gas-phase work investigating this problem has focused on the formation and decomposition of isolated metal carboxylic acid anions.[6] These results have indicated that a large barrier exists to decarboxylation of these species, with decomposition of $Fe(CO)_4(COOH)^-$ occurring exclusively by loss of CO.

In the present work we report on the interactions of the highly reactive anion $O^{-\cdot}$[8] with a variety of neutral metal complexes studied by Fourier transform ion-cyclotron resonance mass spectrometry. The present study was undertaken in an effort to generate gas-phase metallocarboxylates by an addition mechanism similar to Scheme I, and study their decomposition pathways. We observe these gas-phase metallocarboxylates to decompose exclusively via the loss of CO_2. The relationship of metallocarboxylates to the WGSR has been previously discussed.[7,9]

EXPERIMENTAL

All experiments were performed on a Fourier transform ion-cyclotron resonance mass spectrometer recently constructed in our laboratory.[9,10] The trapping cell is a single chamber with dimensions $2.75 \times 1.375 \times 1.375$ in. All reagent gases are admitted into the reaction chamber via Varian variable leak valves. The chamber is pumped by a 6 in. Alcatel diffusion pump backed by an Alcatel rough pump. Pressures are monitored with a Granville–Phillips 271 ionization gauge. Base pressures in the chamber are $\sim 1 \times 10^{-9}$ torr. The magnetic field is supplied by a Varian electromagnet with the field regulated at ~ 0.7 T. The trapping cell and experimental pulse sequences are controlled by a Nicolet FTMS-2000 computer.

Typical reagent gas pressures (nitrogen equivalent) were $\sim 3 \times 10^{-5}$ torr (N_2O) with $\sim 2 \times 10^{-7}$ torr of the metal complex. $O^{-\cdot}$ was generated by N_2O dissociative electron capture, as shown in reaction (2).[11] Electrons were introduced in a 5 ms 3 mA pulse of 8 eV electrons. Stray electrons remaining in the trapping cell after the initial electron beam pulse undergo efficient dissociative electron attachment by the metal carbonyl complexes, [see eq. (3)].[12]

$$N_2O + e^-(8\,eV) \longrightarrow O^{-\cdot} + N_2 \qquad (2)$$

$$e^- + M(CO)_x \longrightarrow M(CO)_{x-1}^- + CO \qquad (3)$$

To verify that the metal containing anion products were due to ion–molecule reactions and not reaction (3), all ions present in the cell were ejected 35 ms after the electron beam pulse. In a delay period (from 20 to 100 ms) after the ejection pulse, no ions were produced. This indicates that 35 ms after the electron beam pulse, no electrons remained in the cell to be attached by the reagent gases. The 35 ms delay was retained in the experimental sequence to eliminate trapped electrons and serve as a thermalization period for the $O^{-\cdot}$ (~ 40 collisions of $O^{-\cdot}$ with neutrals in the ICR cell). Swept double-resonance ejection pulses were used to isolate $O^{-\cdot}$ after the 35 ms formation and cooling periods, and prior to reaction with the metal complex of interest.[13] NO^-, generated by the reaction of $O^{-\cdot}$ with background N_2O, was continuously ejected during the reaction period to prevent direct electron transfer from NO^- (electron affinity = 20 meV) to the metal carbonyl complexes.

For measurement of the relative rate constants for the reactions of $O^{-\cdot}$ with the metal carbonyls it was necessary to determine relative ion gauge sensitivities for the neutral complexes. Obtaining absolute rates for reactions (4)–(6), which would allow determination of absolute ion gauge sensitivities for the metal carbonyls, is not feasible in our instrument due to difficulties in determining absolute ion abundances. However, by simultaneously measuring the relative intensities for $V(CO)_5^-$, $Cr(CO)_5^-$ and $Fe(CO)_4^-$ generated in reactions (4)–(6) and comparing these with the respective literature rate constants of 1.6×10^{-8} cm^3 molecule^{-1} s^{-1}, 2.8×10^{-8} cm^3 molecule^{-1} s^{-1} and 1.1×10^{-8} cm^3 molecule^{-1} s^{-1},[12] it is possible to determine the relative ion gauge sensitivities. For the reactions discussed below the relative rate constants were determined using the uncorrected ion gauge pressure reading and dividing by the relative ion gauge sensitivity.

$$V(CO)_6 + e^- \longrightarrow V(CO)_5^- + CO \qquad (4)$$

$$Cr(CO)_6 + e^- \longrightarrow Cr(CO)_5^- + CO \quad (5)$$

$$Fe(CO)_5 + e^- \longrightarrow Fe(CO)_4^- + CO \quad (6)$$

N_2O was obtained commercially from Matheson. All metal complexes were obtained commercially and used as supplied except for multiple freeze-pump-thaw cycles which were used to remove non-condensible gases.

RESULTS

Under the present low-pressure conditions, $O^{-\cdot}$ reacts with $Fe(CO)_5$, $Cr(CO)_6$, $V(CO)_6$ and $Mn(Me\text{-}Cp)(CO)_3$ (Me-Cp = methylcyclopentadienyl) via pathways (7) and (8), while $O^{-\cdot}$ does not react with ferrocene and cobaltocene. Nucleophilic attack on metallocenes has been observed in solution. Figure 1 shows mass spectra corresponding to reaction (7). The relative rate constants for the reactions of the homoleptic carbonyl complexes are shown in Table 1.

$$O^{-\cdot} + M(CO)_x \longrightarrow M(CO)_{x-1}^- + [CO + O] \quad (7)$$

(M = Fe, Cr, V)

$$Mn(Me\text{-}Cp)(CO)_3 + O^{-\cdot} \longrightarrow Mn(Me\text{-}Cp)(CO)_2^- + [CO + O] \quad (8)$$

The neutral products from reactions (7) and (8) are not detected in the mass spectrum but can be inferred from thermochemical considerations. For $Fe(CO)_5$, dissociative electron attachment is exothermic by 14 ± 10 kcal mol^{-1}.[15] Consideration of the high electron affinity of oxygen[16] makes a simple electron transfer mechanism, as in reaction (9), endothermic by $\sim 20 \pm 10$ kcal mol^{-1}. Reaction (10), which results in the formation of CO_2, is exothermic by 106 ± 10 kcal mol^{-1}. Energetics for reactions (7) and (8) are shown in Table 2 and indicate that CO_2 is generated as the neutral product.[17-20]

$$O^{-\cdot} + Fe(CO)_5 \longrightarrow Fe(CO)_4^- + CO + O \quad \Delta H_{rxn} = 20 \pm 10 \text{ kcal mol}^{-1} \quad (9)$$

Table 1. Rate constants for reaction (4)[a,b]

Neutral	Relative rate constant for reaction with $O^{-\cdot}$[c]	Rate constant for dissociative electron attachment by metal carbonyl[d]
$V(CO)_6$	1.0 ($\pm$0.5)	6×10^{-8}
$Cr(CO)_6$	0.31 ($\pm$0.16)	3×10^{-7}
$Fe(CO)_5$	0.17 ($\pm$0.08)	2×10^{-7}

[a] All rates in cm^3 molecule^{-1} s^{-1}.

[b] Collision frequency for the ion–molecule encounters is 3.5×10^{-9} cm^3 molecule^{-1} s^{-1} based on $\alpha(M(CO)_x) = 33$ Å^3.[14]

[c] Relative rate constants are corrected for relative ion gauge sensitivities for the neutral metal complexes.

[d] See ref. 12.

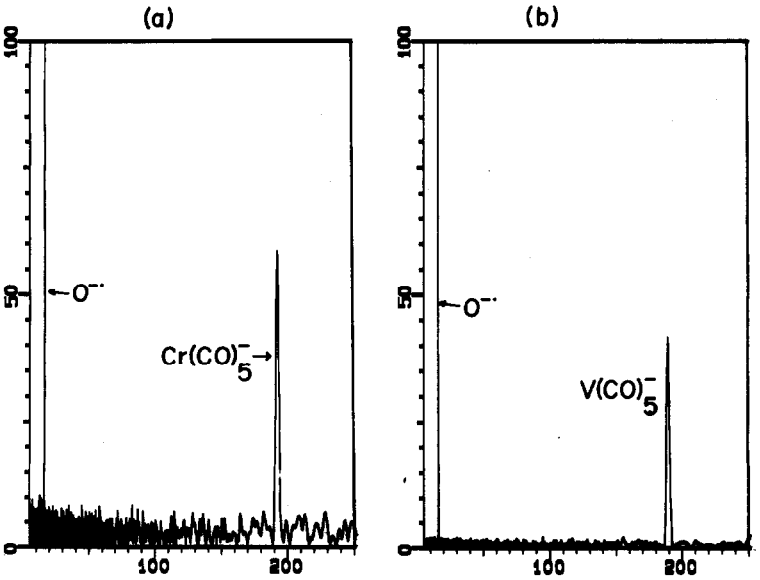

Fig. 1. (a) Mass spectrum of the reaction of $O^{-\cdot}$ with $Cr(CO)_6$. NO^-, generated in the reaction of $O^{-\cdot}$ with N_2O, was continuously ejected. (b) Mass spectrum corresponding to the reaction of $O^{-\cdot}$ with $V(CO)_6$.

Table 2. Energetics for the reaction of $O^{-\cdot}$ with metal complexes[a]

Reaction	ΔH_{rxn} (CO+O as neutral products)	ΔH_{rxn} (CO_2 as neutral product)	D[M(CO)$_{x-2}$CO][17]	CO_2 internal energy	Total product internal energy
$O^{-\cdot}+Fe(CO)_5$	20 ± 12	-106 ± 12[14]	<33	~ 56	$\lesssim 89\pm12$
$O^{-\cdot}+Cr(CO)_6$	19 ± 5	-107 ± 5[18]	$<62, >35$	~ 56	$\lesssim 118\pm12$
$O^{-\cdot}+V(CO)_6$	29 ± 15	-97 ± 15[19]	NA		
$O^{-\cdot}+Mn(Me\text{-}Cp)(CO)_3$	29 ± 15	-97 ± 15[19]	NA		

[a] All energies in kcal mol^{-1}.

$$O^{-\cdot}+Fe(CO)_5 \longrightarrow Fe(CO)_4^- + CO_2$$
$$\Delta H_{rxn} = -106\pm10\,\text{kcal mol}^{-1} \quad (10)$$

The reactions of $O^{-\cdot}$ contrast those of many previously-studied nucleophiles (see Scheme I), since the incoming oxygen atom is lost as part of the neutral product.[4,21] Also, Mn(Me-Cp)(CO)$_3$ reacts with the nucleophiles NH_2^- [$\Delta H_{acid}(NH_3) = 403.6$ kcal mol^{-1}][22] and F^- [$\Delta H_{acid}(HF) = 371.5$ kcal mol^{-1}] via deprotonation with no nucleophilic activation at the carbonyl.[23] However, $O^{-\cdot}$, which has a proton affinity between F^- and NH_2^- [$\Delta H_{acid}(OH^-) = 381$ kcal mol^{-1}], reacts via decarboxylation [reaction (8)] with no proton transfer observed. In contrast to reaction (8), solution studies of the reactions of Mn(Me-Cp)(CO)$_3$ with closed shell anions indicate nucleophilic attack occurs preferentially at the hydrocarbon.[24]

$$Mn(Me\text{-}Cp)(CO)_3 + (F^-, NH_2^-) \longrightarrow Mn(C_6H_6)(CO)_3^- + (HF, NH_3) \quad (11)$$

DISCUSSION

An interesting aspect of the $O^{-\cdot}$ reactions is that the metal carbonyl anion products are not observed to undergo subsequent decomposition, even though the reactions with $O^{-\cdot}$ are more than 95 kcal mol^{-1} exothermic. Recent photo-dissociation studies performed in our laboratory have indicated D(Fe(CO)$_3^-$—CO) $<$ 33 kcal mol^{-1} and 35 kcal mol^{-1} $<$ D(Cr(CO)$_4^-$—CO) $<$ 62 kcal mol^{-1}[18] (see Table 2). The lack of further carbonyl loss from the ionic products generated in reaction (7) indicates the metal carbonyl-anion products are generated with less internal energy than the first metal anion–carbonyl binding energy. Therefore, a large portion of the reaction exothermicity must appear as excitation of CO_2 and/or as relative translational energy of the products. From simple energy randomization considerations the above result is unexpected. For example, in the Cr(CO)$_6$ reaction the product metal carbonyl complex [Cr(CO)$_5^-$] has 27 vibrational modes while the CO_2 has only four vibrational modes. Additionally, the metal complex product has many low-frequency vibrational modes which are not present for CO_2. This will result in a higher density of states for Cr(CO)$_5^-$. Both of these contributions indicate that, based on simple statistical considerations, Cr(CO)$_5^-$ should be generated with a much higher internal excitation than CO_2. Given the high exothermicities for the reactions shown in Table 2 ($> 97\pm15$ kcal mol^{-1}) the metal complexes produced in reactions (7) and (8) would be expected to undergo further decarbonylation.

Similar behaviour has recently been observed by Hack and Rossing in the reaction of triplet oxygen atoms with Cr(CO)$_6$.[25] Interestingly, this reaction also proceeds with the exclusive loss of CO_2, reaction (12). This reaction is quite exothermic [$\Delta H_{rxn}(12) = -90$ kcal mol^{-1}]. The decomposition of Cr(CO)$_5$ only requires 40 kcal mol^{-1}, suggesting that Cr(CO)$_4$ should be generated. However, kinetic evidence suggests the Cr(CO)$_5$ product generated in reaction (12) does not decompose. In their study the only product directly observed in the gas phase was CO_2. Thus, the lack of fragmentation of the nascent Cr(CO)$_5$ was not based on direct observations. The results are, however, consistent with the present results for the reactions of $O^{-\cdot}$ where the metal complexes are not observed to decompose.

$$O(^3P) + Cr(CO)_6 \longrightarrow Cr(CO)_5 + CO_2 \quad (12)$$

There are two reasonable mechanisms which can account for the apparent non-statistical partitioning of exothermicity into the products of reactions (7) and (8). The first is an addition/elimination mechanism. A second mechanism, initiated by electron transfer, is also consistent with the product energy distributions.

Scheme II shows a possible radical addi-

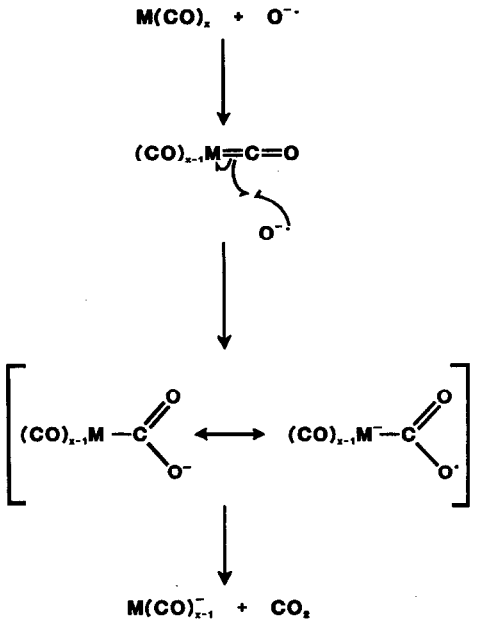

Scheme II.

tion/elimination mechanism for the reaction of $O^{-\cdot}$ with the metal complexes. Previous studies of nucleophilic addition to metal carbonyls have involved closed shell nucleophiles. However, for $O^{-\cdot}$ the highest occupied orbital will contain the unpaired electron, and initial addition involves this orbital. It is likely that the reaction of the radical $O(^3P)$ studied by Hack and Rossing involves this mechanism.[25] The intermediate metallocarboxylate which is generated can decompose via the loss of CO_2. The decomposition involves elimination of a highly bent CO_2 from the complex. Structures for a variety of metallocarboxylate anions and metallocarboxylic acid anions have been obtained and the O—C—O bond angles are generally close to 120°.[7,26] Assuming a bond angle of 120° for the present complexes, the nascent CO_2 would be formed with a *ca* 120° bend, which corresponds to vibrational excitation of the order 56 kcal mol^{-1} in the bending mode.[27,28] Upon decomposition it is likely that the metal carbonyl-anion products will also be generated in a distorted geometry. However, the metal carbonyl anions are highly fluxional with low barriers to isomerization (i.e. square pyramidal to trigonal bipyramidal) and thus, the internal energies associated with the geometric distortions of the carbonyl anion products will be very small.

Given the bond dissociation energies for the metal carbonyl complexes shown in Table 2 along with the observation that the product ions do not undergo loss of CO, less than 62 kcal mol^{-1} must be deposited into the $Cr(CO)_5^-$ product from the energy partitioning to be consistent with our results. Assuming CO_2 contains 56 ± 12 kcal mol^{-1} of vibrational excitation implies a total of $< 118 \pm 12$ kcal mol^{-1} is deposited into internal excitation of the products for the $Cr(CO)_6$ reaction, which is within experimental error of the reaction exothermicity. This is also the case for the $O^{-\cdot}/Fe(CO)_5$ reaction; the sum of the upper limit on the internal excitation of $M(CO)_{x-1}^-$ and the vibrational excitation of CO_2 expected for an addition/elimination mechanism is very close (within experimental error) to the reaction exothermicity. Thus, this mechanism is consistent with the absence of fragmentation of the metal carbonyl-anion products.

An alternative to the addition mechanism involves electron transfer within the nascent ion-induced dipole complex. Recently, many reactions, including ligand switching,[29-31] halogen atom transfer,[32] and small group transfer reactions,[33] have been shown to be initiated by electron transfer in the collision complex. The basic mechanism is shown in Scheme III. After formation of the ion-neutral collision complex, dissociative electron transfer can occur from $O^{-\cdot}$ to the metal carbonyl. As discussed above, direct dissociative electron transfer with the formation of O, CO and $M(CO)_{x-1}^-$ is endothermic. However, the ion-induced dipole complexation energy ($\sim$ 15 kcal mol^{-1}) can facilitate an intermediate electron transfer to generate an $[O \cdots CO \cdots M(CO)_{x-1}^-]$ complex. Within this complex, O and CO can combine to generate $(CO_2)^*$. This produces the complex $[M(CO)_{x-1}^- \cdots (CO_2)^*]$, with the energy localized in the CO_2 moiety. The complex will decompose before full energy redistribution can occur. This mechanism would also result in most of the reaction exothermicity partitioned into vibrational exci-

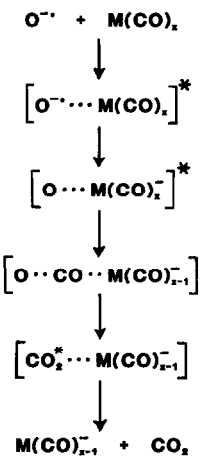

Scheme III.

tation of CO_2, while $M(CO)_{x-1}^-$ would be generated with little internal excitation, which is consistent with the absence of fragmentation of $M(CO)_{x-1}^-$.

Both of the proposed reaction mechanisms, addition/elimination and electron transfer, are consistent with the available reaction energetics and the observed metal-carbonyl energy disposal and suggest most of the reaction exothermicity will be channelled into CO_2 excitation. Previous studies of electron transfer initiated reactions have observed a correlation between the rate constant for thermal electron attachment for the incoming neutral (in the present study this would correspond to $M(CO)_x$) with the rate constant for the ion–molecule reaction under study.[32] A comparison of the relative rate constants for the metal-carbonyl reactions with the rate for dissociative electron capture by the corresponding metal carbonyl, shown in Table 1, clearly demonstrates that a correlation does not exist, suggesting the electron transfer process is not important for the present reactions. The present results suggest that the gas-phase $M(CO)_x(CO_2)^-$ (M = V, Cr, Fe), generated by nucleophilic addition, decompose preferentially by the loss of CO_2, with no loss of CO observed.

Summary

The reactions of O^- with $V(CO)_6$, $Cr(CO)_6$, $Fe(CO)_5$ and $Mn(Me\text{-}Cp)(CO)_3$ proceed with the production of $M(CO)_{x-1}^-$ and vibrationally excited CO_2. Two mechanisms have been considered for this reaction which account for the apparent non-statistical energy disposal in the reaction products: an addition/elimination mechanism where the CO_2 is generated in a bent configuration, and an intermediate electron-transfer mechanism in which CO_2 is produced by recombination of O and CO within the collision complex. Kinetic data show no correlation with the rate for thermal electron attachment by the metal-carbonyl complex, suggesting the electron transfer mediated process is not operative for these reactions.

Finally, $M(CO)_{x-1}(COO)^-$ (M = V, Cr, Fe) generated in the gas phase by nucleophilic attack, decompose exclusively by decarboxylation. This is in contrast to previous studies of the metallocarboxylic acid anions, $M(CO)_{x-1}(COOH)^-$ which decompose exclusively via decarbonylation, reactions (13).[6]

$$M(CO)_x + OH^- \longrightarrow M(CO)_{x-1}OH^- + CO \quad (13)$$

Acknowledgements—Made to the donors of the Petroleum Research Fund administered by the American Chemical Society for partial support of this work and to Bell laboratories for an equipment donation. We thank Professor R. N. McDonald for helpful comments.

REFERENCES

1. For a review of gas phase anionic metal chemistry, see: R. R. Squires, *Chem. Rev.* 1987, **87**, 623.
2. Representative publications in this area include: (a) R. N. McDonald and E. K. Chowdhury, *Organometallics* 1986, **5**, 1187; (b) D. E. Richardson, C. S. Christ, P. Sharpe and J. E. Eyler, *Organometallics* 1987, **6**, 1819; (c) T. Prusse, C. B. Lebrilla, T. Drewello and H. Schwarz, *J. Am. Chem. Soc.* 1988, **110**, 5986; (d) D. A. Peake and M. L. Gross, *Analyt. Chem.* 1985, **57**, 115; (e) D. B. Jackson and B. S. Freiser, *J. Am. Chem. Soc.* 1985, **107**, 72; (f) L. Sanders, S. Hanton and J. C. Weisshaar, *J. Phys. Chem.* 1987, **91**, 5145; (g) J. Allison and B. D. Radecki, *J. Am. Chem. Soc.* 1984, **106**, 946; (h) J. Allison and D. P. Ridge, *J. Am. Chem. Soc.* 1979, **101**, 4998; (i) M. A. Hanratty, L. L. Beauchamp, A. J. Illies, P. Van Koppen and M. T. Bowers, *J. Am. Chem. Soc.* 1988, **110**, 1; (j) D. Wang and R. R. Squires, *Organometallics* 1987, **5**, 905; (k) J. L. Elkind and P. B. Armentrout, *J. Phys. Chem.* 1986, **90**, 5736; (l) J. J. Klaassen and D. B. Jacobson, *J. Am. Chem. Soc.* 1988, **110**, 974.
3. M. S. Foster and J. L. Beauchamp, *J. Am. Chem. Soc.* 1975, **97**, 4808.
4. K. R. Lane, L. Sallans and R. R. Squires, *J. Am. Chem. Soc.* 1986, **108**, 4368.
5. K. R. Lane and R. R. Squires, *J. Am. Chem. Soc.* 1986, **108**, 7187.
6. (a) K. R. Lane, L. Sallans and R. R. Squires, *Inorg. Chem.* 1984, **23**, 1999; (b) K. R. Lane, R. E. Lee, L. Sallans and R. R. Squires, *J. Am. Chem. Soc.* 1984, **106**, 5767.
7. (a) P. C. Ford and A. J. Rokicki, *Adv. Organomet. Chem.* 1988, **28**, 139; (b) R. G. Pearson and H. Mauermann, *J. Am. Chem. Soc.* 1982, **104**, 500; (c) in the condensed phase the isolated carboxylic acid of iron, $(Cp)(PPh_3)(CO)FeCOOH$ has been observed to decarboxylate under mild heating whereas the conjugate base, $(Cp)(PPh_3)(CO)FeCOO^-$ does not decompose up to 100°C, see: N. Grice, S. C. Kao and R. Pettit, *J. Am. Chem. Soc.* 1979, **101**, 1627; (d) D. J. Darensbourg, M. Y. Darensbourg, N. Walker, J. A. Froelich and H. L. C. Barros, *Inorg. Chem.* 1979, **18**, 1401.
8. (a) D. K. Bohme and L. B. Young, *J. Am. Chem. Soc.* 1970, **92**, 3301; (b) A. P. Bruins, A. J. Ferrer-Correia, A. G. Harrison, K. R. Jennings and R. K. Mitchum, *Adv. Mass Spectrosc.* 1976, **7A**, 355; (c) A. G. Harrison and K. R. Jennings, *J. Chem. Soc., Faraday Trans.* 1976, **72**, 1601; (d) G. E. Streit, *J. Phys. Chem.* 1982, **86**, 2321; (e) J. C. Kleingeld and N. M. M. Nibbering, *Tetrahedron* 1984, **40**, 2789; (e) J. H. J. Dawson and N. M. M. Nibbering, *Lect. Notes Chem.* 1978, **7**, 146; (f) C. L. Johlman and C.

L. Wilkins, *J. Am. Chem. Soc.* 1985, **107**, 327; (g) H. Van Der Wel and N. M. M. Nibbering, *Int. J. Mass Spec. Ion Proc.* 1986, **72**, 145; (h) J. J. Grabowski and S. J. Melly, *Int. J. Mass Spec. Ion Proc.* 1987, **81**, 147; (i) J. M. Van Doren, S. E. Barlow, C. H. Depuy and V. M. Bierbaum, *J. Am. Chem. Soc.* 1987, **109**, 4412; (j) P. K. Chou and S. R. Kass, *J. Am. Chem. Soc.* 1991, **113**, 697.

9. Decarboxylation has been proposed for (diphos) $(CO)_3MnCOO^-$, see: D. J. Darensbourg and J. A. Froelich, *Inorg. Chem.* 1978, **11**, 3300; 1978, 413.
10. (a) M. B. Comisarow and A. G. Marshall, *Chem. Phys. Lett.* 1974, **25**, 282; (b) C. L. Johlman, R. L. White and C. L. Wilkins, *Mass Spec. Rev.* 1983, **2**, 389; (c) M. L. Gross and D. L. Rempel, *Science* 1984, **226**, 261; (d) A. G. Marshall, *Accts Chem. Res.* 1985, **18**, 316; (e) S. W. Buckner and S. L. VanOrden, *Organometallics* 1990, **9**, 1093.
11. R. Marx, G. Mauclaire, F. C. Fehsenfeld, D. B. Dunkin and E. E. Ferguson, *J. Chem. Phys.* 1973, **58**, 3267.
12. P. M. George and J. L. Beauchamp, *J. Chem. Phys.* 1982, **76**, 2959.
13. M. B. Comisarow, G. Parisod and V. Grassi, *Chem. Phys. Lett.* 1978, **57**, 413.
14. G. Giomousius and D. P. Stevenson, *J. Chem. Phys.* 1958, **29**, 294.
15. R. N. McDonald and P. L. Schell, *Organometallics* 1988, **7**, 1806.
16. D. M. Neumark, K. R. Lykke, T. Anderson and W. C. Lineberger, *Phys. Rev. A* 1985, **32**, 1890.
17. Supplementary thermochemical information taken from: S. G. Lias, J. E. Bartmess, J. F. Liebman, J. L. Holmes, R. D. Levin and W. G. Mallard, *J. Phys. Chem. Ref. Data* 1988, **17**, suppl. 1.
18. B. T. Cooper and S. W. Buckner, in preparation.
19. An electron affinity of 52 ± 4 kcal mol^{-1} for $Cr(CO)_5$ is estimated based on data from: L. Sallans, K. R. Lane, R. R. Squires and B. S. Freiser, *J. Am. Chem. Soc.* 1985, **107**, 4379 [$EACr(CO)_5 > 2.3$ eV]; R. N. McDonald and P. L. Schell, *Organometallics* 1988, **7**, 1820 [$EACr(CO)_5 < 2.4 \pm 0.3$ eV]. Combined with $DCr(CO)_5CO = 36.8$ kcal mol^{-1} from: G. P. Smith, *Polyhedron* 1988, **7**, 1605, indicates thermal electron attachment by $Cr(CO)_6$ is 15 ± 5 kcal mol^{-1} exothermic.
20. From the observation of slow dissociation attachment of thermal energy electrons by $V(CO)_6$ and $Mn(Me\text{-}Cp)(CO)_3$ we estimate the following:

$$V(CO)_6 + e^- \longrightarrow V(CO)_5^- + CO$$
$$\Delta H_{rxn} = -5 \pm 15 \text{ kcal mol}^{-1}$$

$$Mn(Me\text{-}Cp)(CP)_3 + e^- \longrightarrow Mn(Me\text{-}Cp)(CO)_2^- + CO$$
$$\Delta H_{rxn} = -5 \pm 15 \text{ kcal mol}^{-1},$$

for use in determination of the $I^{-\cdot}$/metal complex reaction exothermicities.
21. CO_2 loss has recently been reported in the reactions of some metal-carbonyl anions with O_2, see: K. R. Lane, L. Sallans and R. R. Squires, *J. Am. Chem. Soc.* 1984, **106**, 2719; D. L. Bricker and D. H. Russell, *J. Am. Chem. Soc.* 1987, **109**, 3910; and references 14 and 29.
22. Proton affinities were taken from: J. E. Bartmess and R. T. McIver, in *Gas Phase Ion Chemistry* (Edited by M. R. Bowers), Vol. 2, Ch. 11. Academic Press, New York (1979).
23. Cl^- [$\Delta H_{acid}(HCl) = 333$ kcal mol^{-1}] is unreactive with $Mn(Me\text{-}Cp)(CO)_3$ due to its lower proton affinity. Coupling this with reaction (11) can be used to bracket the gas phase acidity of the manganese complex, yielding 333 kcal mol^{-1} < [$\Delta H_{acid}(Mn(Me\text{-}Cp)(CO)_3$] < 372 kcal mol^{-1}. Proton transfer has also recently been observed for $Mn(C_5H_5)(CO)_3$, see: R. R. Squires, in *Gas Phase Inorganic Chemistry* (Edited by D. H. Russell). Plenum Press, New York (1989).
24. S. G. Davies, M. L. H. Green and D. M. P. Mingos, *Tetrahedron* 1978, **34**, 3047.
25. W. Hack and A. Rossing, *Chem. Phys. Lett.* 1990, **171**, 547.
26. G. Fachinetti, C. Floriani and P. F. Zanazzi, *J. Am. Chem. Soc.* 1978, **100**, 7405.
27. The internal energy of CO_2 bent at 120° was approximated using the equation:

$$\text{Energy} = 0.5k(\Delta x)^2,$$

where Δx is the displacement of either oxygen atom from the equilibrium position. The force constant k, can be calculated from the frequency of the bending mode 667 cm^{-1} (ν_2). A factor of two was introduced into the reduced mass due to the symmetry of the molecule. This equation places an upper limit on the internal energy of the nascent CO_2. Using a similar approach, an angle of 115° corresponds to 64 kcal mol^{-1} while an angle of 125° corresponds to 47 kcal mol^{-1}. Due to uncertainties in the CO_2 geometry at the transition state and effects due to anharmonicity, limits on product CO_2 internal energy have been set at ± 12 kcal mol^{-1}.
28. Decarboxylation of organic carboxylates in the gas phase had recently been shown to proceed with an activation barrier equal to the reaction endothermicity. This implies CO_2 is produced with little or no vibrational excitation at the CID threshold for the organic molecules. See: S. T. Graul and R. R. Squires, *J. Am. Chem. Soc.* 1990, 112, 2517.
29. Y. H. Pan and D. P. Ridge, *J. Am. Chem. Soc.* 1989, **111**, 1150.
30. R. N. McDonald and P. L. Schell, *Organometallics* 1988, **7**, 1820.
31. S. L. VanOrden, R. M. Pope and S. W. Buckner, *Organometallics* 1991, **10**, 1089.
32. M. T. Jones, R. N. McDonald, P. L. Schell and M. H. Ali, *J. Am. Chem. Soc.* 1989, **111**, 5983.
33. (a) S. W. McElvaney and J. Allison, *Organometallics* 1986, **5**, 416; (b) S. W. McElvaney and J. Allison, *Organometallics* 1986, **5**, 1219.

Polyhedron Vol. 10, No. 20/21, pp. 2495–2500, 1991
Printed in Great Britain

0277–5387/91 $3.00+.00
© 1991 Pergamon Press plc

TRIAMMINE COBALT(III)-L-MALATE. MALATE ION AS A TRIDENTATE LIGAND

SERGIO BUNEL,* CARMEN IBARRA and VICTOR CALVO

Departmento de Quimica Inorganica y Analitica, Facultad de Ciencias Quimicas y Farmaceuticas, Universidad de Chile, Casilla 233, Santiago, Chile

and

ANDREI BLASKÓ, CLIFFORD A. BUNTON* and NANCY L. KEDER

Department of Chemistry, University of California, Santa Barbara, CA 93106, U.S.A.

(*Received* 21 *January* 1991; *accepted* 18 *June* 1991)

Abstract—The crystal structure of the title compound has been determined from single crystal X-ray diffraction data. There is little angle strain in the complex which has two carboxylate ions and one alkoxide ion bound to cobalt(III). These conclusions agree with IR, CD and NMR spectral data except that ^1H coupling constants show that the conformation of the malate ligand differs slightly in solid and solution. The three ammonia ligands have different ^1H chemical shifts and different rates of hydrogen exchange in D_2O.

The reaction of the L-malate ion with a tetraamine *cis*-diaquo complex of cobalt(III) at pH 7 gives a crystalline product whose empirical formula is $[Co(NH_3)_3$-L-malate$]\cdot 2H_2O$ (**1**). It is non-ionic, based on conductivity and chemical analysis, suggesting that cobalt binds to a tridentate malate trianion through two carboxylate and one alkoxide oxygen.[1] Such a structure is consistent with the CD spectra in solution and the IR spectra of the solid. There is considerable evidence, based largely on spectroscopic or analytical evidence, for binding of alkoxide ions in complexes of hydroxyacids.[2] For example, mixed bis-phenanthroline-malate complexes of Co^{III}—CO_2^- and —O^- form a five-membered ring with hydrogen bonding of the second carboxylic residue to the alkoxide oxygen.[3] The X-ray diffraction evidence on copper(II)-tartrate complexes demonstrates complexing to the alkoxide oxygen.[4] Some of these complexes are polynuclear and in others the metal is bound to one alkoxide and one carboxylate group. Sugars form ammine complexes with cobalt(III) but binding is by hydroxyl rather than alkoxide groups.[5]

The proposed structure of **1** is reasonable, but unproven; chemical analysis, for example, is consistent with the malate ion acting as a bidentate ligand and with OH^- complexed to cobalt(III). We therefore examined the structure in solution by NMR spectroscopy and in the crystal by X-ray diffraction.

RESULTS AND DISCUSSION

Structure in the crystal

The L-malate trianion is bound to the cobalt atom through O(1A), O(2A) and O(4A) forming five- and six-membered rings; the numbering scheme is shown in Fig. 1. O(4B) of the L-malate ligand is hydrogen bonded to water, $H_2O(9)$, which is hydrogen bonded to the other water molecule, $H_2O(8)$. Hydrogen bonds between water solvates related by the 2_1 axes parallel to the *c* axis result in helical "chains" of molecules along the *c* direction. Hydrogen bonds between water and O(2A) of the L-malate related by the 2_1 axes parallel to the *b* axis result in interactions between the "chains".

Bond lengths and angles between heavy atoms are given in Table 1. (Values in parentheses are the number of standard deviations.) Complete bond distances and angles are included in the Supplementary Material. Bond angles about cobalt are

* Authors to whom correspondence should be addressed.

Table 1. Selected bond distances and angles for Co $(NH_3)_3$(L-malate)·$2H_2O$

Distance (Å)	
Co(1)—O(1A)	1.926(2)
Co(1)—O(2A)	1.887(2)
Co(1)—O(4A)	1.926(2)
Co(1)—N(5)	1.938(2)
Co(1)—N(6)	1.970(2)
Co(1)—N(7)	1.947(2)
C(1)—O(1A)	1.288(3)
C(1)—O(1B)	1.241(3)
C(1)—C(2)	1.535(4)
C(2)—O(2A)	1.415(3)
C(2)—C(3)	1.528(4)
C(3)—C(4)	1.521(4)
C(4)—O(4A)	1.282(3)
C(4)—O(4B)	1.238(3)
Angle (°)	
O(1A)—Co(1)—O(2A)	85.6(1)
O(1A)—Co(1)—O(4A)	89.7(1)
O(1A)—Co(1)—N(5)	176.1(1)
O(1A)—Co(1)—N(6)	94.3(1)
O(1A)—Co(1)—N(7)	89.3(1)
O(2A)—Co(1)—O(4A)	91.8(1)
O(2A)—Co(1)—N(5)	90.5(1)
O(2A)—Co(1)—N(6)	177.6(1)
O(2A)—Co(1)—N(7)	91.6(1)
O(4A)—Co(1)—N(5)	90.3(1)
O(4A)—Co(1)—N(6)	85.8(1)
O(4A)—Co(1)—N(7)	176.4(1)
N(5)—Co(1)—N(6)	89.6(1)
N(5)—Co(1)—N(7)	90.8(1)
N(6)—Co(1)—N(7)	90.8(1)
Co(1)—O(1A)—C(1)	109.9(2)
Co(1)—O(2A)—C(2)	105.1(1)
Co(1)—O(4A)—C(4)	129.3(2)
O(1A)—C(1)—O(1B)	123.9(3)
O(1A)—C(1)—C(2)	115.1(2)
O(1B)—C(1)—C(2)	121.1(2)
O(2A)—C(2)—C(1)	109.2(2)
O(2A)—C(2)—C(3)	110.7(2)
C(1)—C(2)—C(3)	109.4(2)
C(2)—C(3)—C(4)	113.6(2)
O(4A)—C(4)—O(4B)	121.0(2)
O(4A)—C(4)—C(3)	120.1(2)
O(4B)—C(4)—C(3)	118.9(2)

close to 90°, and those for carbon and oxygen of the malate ligand are close to values typical of tetrahedral and trigonal centres, corresponding to little angle strain in the malate ligand. Figure 1 shows the structure of the complex and Fig. 2 shows it looking down the C(2)—C(3) bond.

Bond lengths of cobalt are *ca* 1.9 and 1.95 Å to oxygen and nitrogen, respectively (Table 1). The malate residue is also relatively unstrained. The bond lengths of cobalt to oxygen and nitrogen are similar to those in L-glutamate bis(ethylenediamine)cobalt(III) perchlorate[8] except that this has a slightly shorter bond of 1.87 Å between the cobalt and alkoxide oxygen. Bonds of cobalt to alkoxide oxygens are shorter than to carboxylate oxygens, pointing to a stronger interaction. Complexes of cobalt(III) with the bidentate malate or tartrate ion typically involve one alkoxide and one carboxylate ligand rather than two carboxylate ligands.[3]

The new results fit earlier evidence[1] that structures are similar in the solid and solution and formation of a complex with a tridentate malate trianion forces chirality on the cobalt centre.

NMR spectra

There are four well-defined ^{13}C signals (^1H decoupled) of the complex at 75.4 and 39.3 ppm corresponding to the methine and methylene carbons, respectively, and two signals of the carboxyl carbon at 179 and 190 ppm.[9] We measured T_1 values for the carboxyl carbons in order to assign the signals, and values are: 2.63 (190 ppm) and 6.41 s (179 ppm). We assume that the carboxyl residue [C(4)] in a six-membered ring (Fig. 1) will have a higher mobility and a higher T_1 than the carboxyl residue [C(2)] in a five-membered ring. On this basis we assign the signal at 190 ppm to C(1) and that at 179 ppm to C(4).

There are two methylene (2.4 and 2.6 ppm) and one methine (3.7 ppm) signals in the ^1H NMR spectrum in D_2O with extensive vicinal and geminal coupling and each set of signals is a doublet of doublets (Fig. 3). The chemical shifts (δ, ppm) and coupling constants (J, Hz) are shown in Scheme 1. We have to consider the assignments of the methylene hydrogens H(3A) and H(3B) on C(3) and their coupling with the methine hydrogen on C(2) (Fig. 3). The view of the crystal structure down the C(2)—C(3) bond (Fig. 2) shows that in the solid methine and methylene hydrogens are in an approximately staggered conformation with dihedral angles of *ca* 60°. This conformation should lead to very similar low vicinal coupling constants between the methine hydrogen and each of the methylene hydrogens,[10] but instead we have very different coupling constants of $J \approx 6$ and 1 Hz (Scheme 1). This result suggests that the complex has slightly different geometries in the crystal and in solution, with a change in the dihedral angles due to rotation about the C(2)—C(3) bond (Fig. 2). Probably the H(2A)—H(3A) dihedral angle decreases from *ca* 60° in the crystal and that for H(2A)—H(3B) correspondingly increases. The coupling constants approximately fit a Karplus

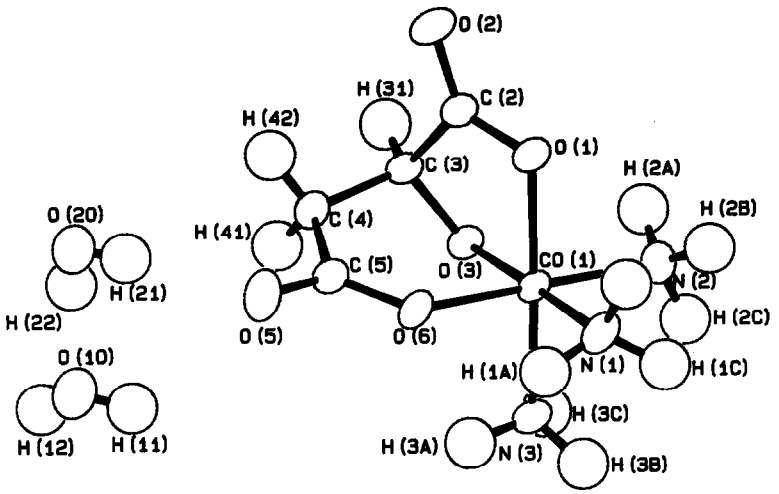

Fig. 1. ORTEP[6] drawing of the structure of $Co(NH_3)_3$(L-malate)·$2H_2O$ (1) showing the atomic numbering scheme;[7] ellipsoids are drawn at 50% probability level.

relation[10] if the H(2A)—H(3A) dihedral angle decreases in solution to 20–30° and that for H(2A)—H(3B) increases to 90–100°. This rotation changes the geometry of the six-membered ring in the complex. An alternative possibility is that rotation reduces the H(2A)—H(3B) dihedral angle (Fig. 2). Inspection of models and molecular mechanics calculations (Experimental) suggests that a decrease in the H(2A)—H(3A) bond angle is preferred (Experimental).

The conformation of the six-membered ring of the malate ligand in the crystal is probably governed in part by hydrogen bonding (Fig. 1 and Supplementary Material). These packing constraints disappear in solution permitting the observed rotation about the C(2)—C(3) bond. In addition, hydrogen bonds to water molecules in the crystal differ from those in solution. Changes in conformation on going from the solid to aqueous solution are understandable, for example, intramolecular hydrogen bonds in hydrogen malate and hydrogen phthalate ion are unsymmetrical in water, but symmetrical in the crystal.[11]

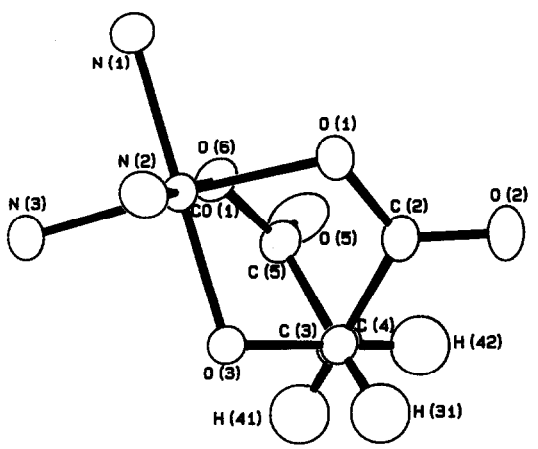

Fig. 2. ORTEP[6] drawing of $Co(NH_3)_3$(L-malate)·$2H_2O$ (1) looking down the C(3)—C(4) bond; ellipsoids drawn at 50% probability level. Solvate waters and ammonia hydrogens have been eliminated for clarity. Atom labels modified with PLOTMD.[7]

Hydrogens of the ammonia ligands give broad, well-separated, signals (Fig. 3). Exchange with D_2O is relatively slow, and different for the three ammonias. The spectra of freshly prepared and 1-day-old solutions are compared in Figs 3A and B. There is little exchange for N—H signals at 3.43 ppm, more for those at 2.91 ppm and extensive exchange for those at 2.76 ppm. There is also line-broadening, in part due to the replacement of NH by ND. Exchange and line-broadening were very evident after 6 days and new signals appeared because of the decomposition of the complex which would generate paramagnetic cobalt(II) and cause line-broadening.

The ^1H coupling constants in the NMR spectrum of L-malate dianion (Scheme 1) fit a conformation with *anti*-carboxylate residues as shown in a Newman projection (**2**).

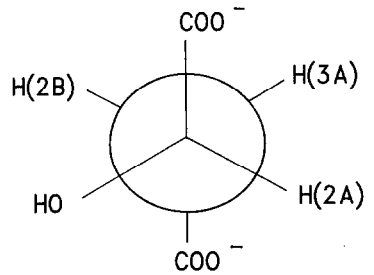

2

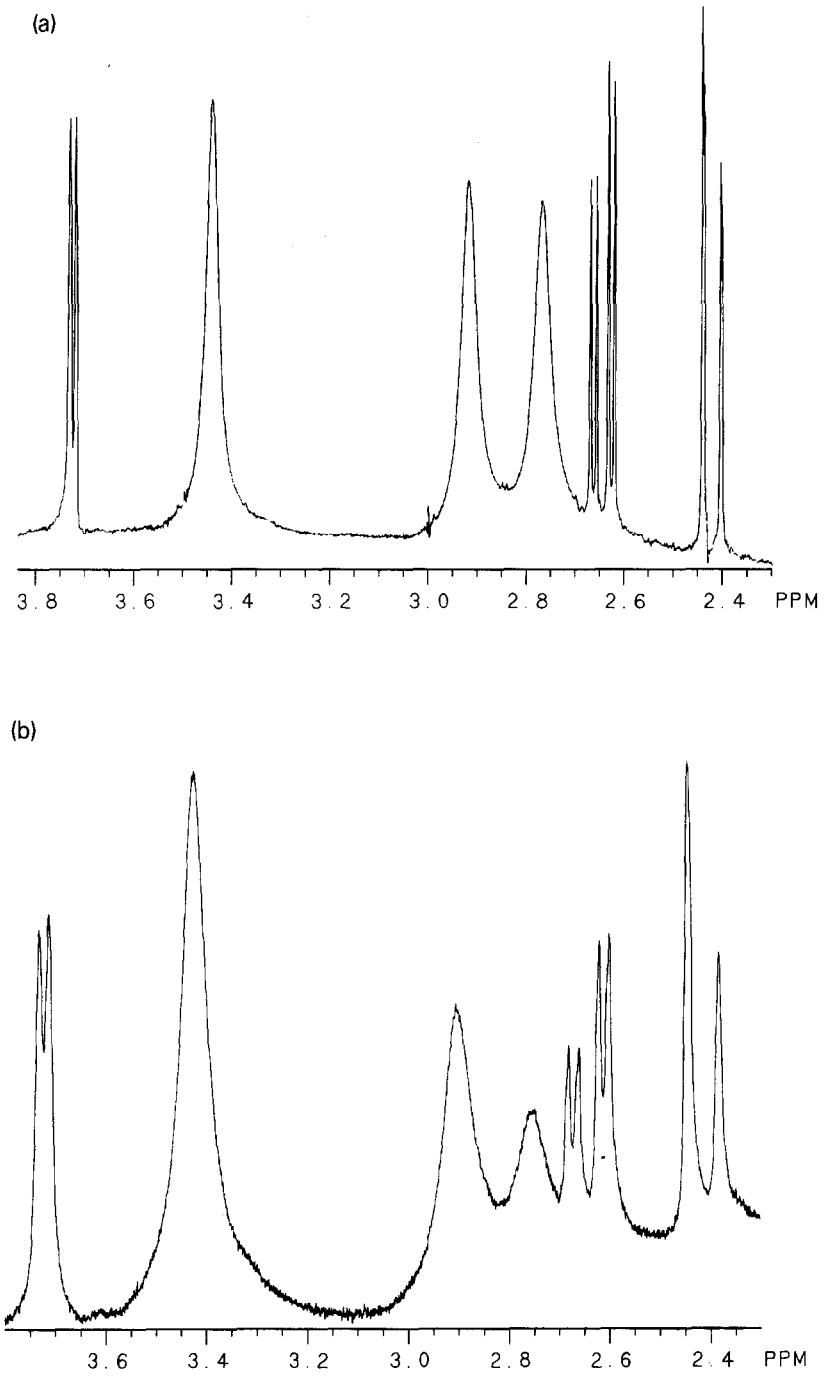

Fig. 3. ^{1}H NMR spectra of 0.01 M **1** in D_2O, (a) fresh solution, (b) after 1 day.

EXPERIMENTAL

Materials

The preparation and characterization of triammine cobalt(III)-L-malate has been described.[1] Single crystals were obtained by slow recrystallization from water.

Crystal data

$Co(NH_3)_3(C_4H_3O_5)\cdot 2H_2O$, $M = 2.77.12$ g mol^{-1}, $D_c = 1.73$ g cm^{-3}, $F(000) = 5.44$, μ(Mo-K_α) = 16.31 cm^{-1}, orthorhombic, $a = 9.6983(3)$, $b = 14.2528(4)$, $c = 7.6901(2)$ Å, $V = 1063(3)$ Å^3, $Z = 4$, space group $P2_12_12_1$ (no. 19), red–violet, crystal dimensions $0.50 \times 0.30 \times 0.25$ mm.

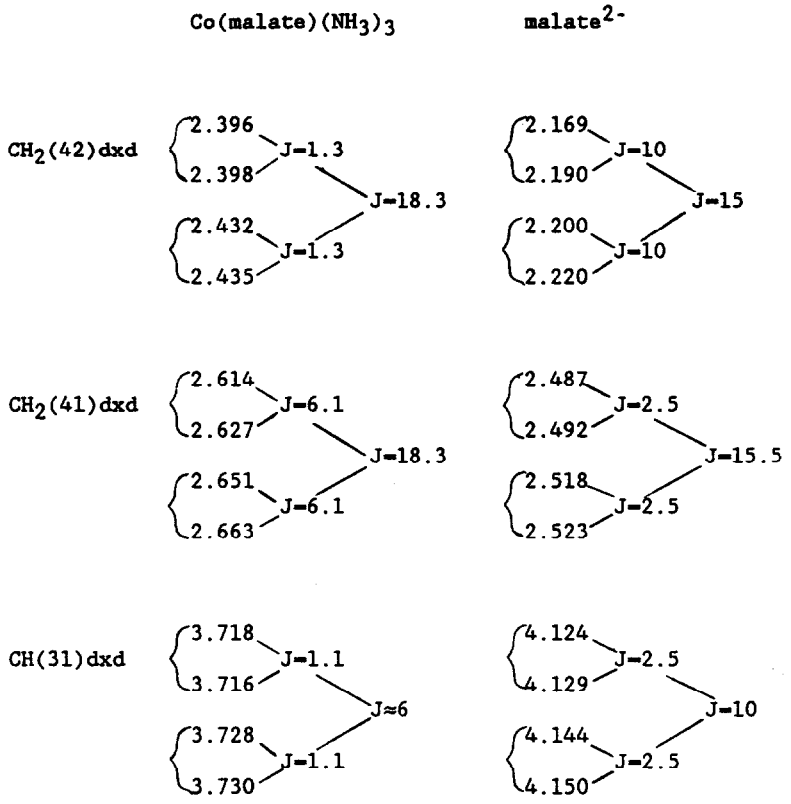

Scheme 1.

Structure determination

Diffraction data were obtained on a Huber four-circle diffractometer automated by Crystal Logic, Inc. (Mo-K_α, $l = 0.71073$ Å, graphite monochromator, room temperature, $2\theta_{max} = 65°$, θ–2θ scan mode). Measurement of the $+h$, $+k$, $+1$ and $-h$, $-k$, -1 quadrants yielded a total of 4452 reflections of which 3994 [$I > 3\sigma(I)$] were used in the refinement. Lorentz, polarization and analytical[12] absorption corrections were applied to the data.

The structure was solved by direct methods (SHELXS)[13] and difference Fourier syntheses. Full-matrix, least-squares refinement was carried out using a locally modified version of the UCLA Crystallographic Computing Package.[14] All least-squares refinements computed the agreement factors R and R_w according to:

$$R = \Sigma||F|F_o| - |F_c||/\Sigma(|F_o|)$$

$$R_w = [\Sigma(\omega(|F_o| - |F_c|)^2)/\Sigma(\omega)|F_o|^2)^{1/2};$$

where F_o is the observed structure factor, F_c is the calculated structure factor, and $\omega = 1/(\sigma(F_o))^2$.

Scattering factors and corrections for anomalous dispersion were taken from the International Tables for X-ray Crystallography.[15] Positions and anisotropic thermal parameters were allowed to vary for all non-hydrogen atoms. Hydrogens were assigned thermal parameters of 0.05 Å^2, those of the solvent water molecules were located in difference maps and their positions allowed to refine; those bonded to nitrogen or carbon were fixed at calculated positions. The final refinement of 148 parameters converged at $R = 0.046$ and $R_w = 0.060$ with EOF = 1.98. The final difference map contained no significant features.

The chiral molecule crystallizes in the enantiomorphic space group $P2_12_12_1$, uniquely determined by the systematic absences: $h00$, $h = 2n+1$; $0k0$, $k = 2n+1$; 001, $1 = 2n+1$. The Friedel pairs were not averaged due to anomalous dispersion effects. Confirmation of the L-malate complex as the correct enantiomer was made by refining the D-malate enantiomer (obtained by coordinate inversion) as described above which converged at $R = 0.057$ and $R_w = 0.078$.

Full details of data collection, atomic coordi-

nates, thermal parameters, full bond length and angle data, and observed and calculated structure factors have been deposited as supplementary material with the Editor, from whom copies are available on request.

NMR spectra

The ^1H and ^{13}C spectra were determined in D_2O at 25°C in a GN500 spectrometer. Freshly made solutions were used except for the examination of NH exchange. The solutions were kept in the dark. We used a 2D ^1H homonuclear shift correlation (COSY) to confirm the ^1H assignments.

There was only one signal of $^{59}Co^{16}$ in D_2O at -2445.5 ppm relative to that of $Co(acac)_3$ in CD_3OD (0 ppm). These measurements were made at 25°C on a GN300 spectrometer.

The ^{13}C T_1 data were obtained by the inversion recovery method[17] on a GN500 spectrometer at 25°C.

Molecular modelling

We used the Chem-X program[18] to model the structure of the complex based on minimization of the free energy. However, the predicted lengths of the Co—O(1A) and Co—O(2A) bonds are respectively longer and shorter by *ca* 0.4 Å than the crystallographic values probably because the program attempts to eliminate strain in the five-membered ring of the complex and does not consider effects of hydrogen bonding to water molecules.

Supplementary material for $Co(NH_3)_3$(L-malate)·$2H_2O$. Table I, complete crystallographic data; Table II, atomic positions; Table III, anisotropic thermal parameters; Table IV, complete bond distances; Table V, complete bond angles; Table VI, hydrogen bonding interactions; Table VII, observed and calculated structure factors.

Acknowledgements—This work was supported by the Fondo Nacional de Ciencias (FONDECYT), project 230, by the Departamento Tecnico de Investigacion, Universidad de Chile, project Q 2741-8823 and by the National Science Foundation (Organic Chemical Dynamics and International Programs). This support is gratefully acknowledged.

REFERENCES

1. S. Bunel, C. Ibarra, V. Calvo and L. Larrea, *Bol. Soc. Chil. Quim.* 1990, **35**, 137.
2. (a) R. A. Haines and D. W. Bailey, *Inorg. Chem.* 1975, **14**, 1310; (b) A. Tatehata, *Inorg. Chem.* 1978, **17**, 725; (c) K. S. Rajan and A. E. Martell, *J. Inorg. Nucl. Chem.* 1967, **29**, 463.
3. J. S. Chambers, R. D. Gillard, P. A. Williams and R. S. Vagg, *Inorg. Chim. Acta* 1983, **72**, 263.
4. C. K. Prout, J. R. Carruthers and F. J. C. Rossotti, *J. Chem. Soc. A* 1971, 3336.
5. (a) S. Bunel and C. Ibarra, *Polyhedron* 1985, **4**, 1537; (b) S. Bunel, C. Ibarra, V. Calvo and E. Moraga, *Polyhedron* 1989, **8**, 2023.
6. C. K. Johnson, ORTEP-II, ORNL-5138. Oak Ridge, Tennessee (1976).
7. H. L. Ammon, J. Luo and G. L. Gilliland, *J. Appl. Cryst.* 1989, **22**, 186.
8. R. D. Gillard, N. C. Payne and G. B. Robertson, *J. Chem. Soc. A* 1970, 2579.
9. E. Pretsch, J. Seibl, W. Simon and T. Clerc, *Spectral Data for Structure Determination of Organic Compounds*, 2nd Edn. Springer, New York (1989).
10. R. M. Silberstein, G. C. Bassler and T. C. Morrill, *Spectrometric Identification of Organic Compounds*, 4th Edn, Ch. 4. Wiley, New York (1981).
11. C. L. Perrin and J. D. Thoburn, *J. Am. Chem. Soc.* 1989, **111**, 8010.
12. W. R. Busing and H. A. Levy, *Acta Cryst.* 1957, **10**, 180.
13. G. M. Sheldrick, C. Krueger and R. Goddard, *Crystallographic Computing 3*, p. 175. Oxford University Press (1985).
14. C. E. Strouse, UCLA Crystallographic Computing Package. Department of Chemistry, UCLA, LA.
15. *International Tables for X-ray Crystallography*, Vol. IV. Kynoch Press, Birmingham, U.K. (1974).
16. W. Hackbusch, H. H. Rupp and K. Wieghardt, *J. Chem. Soc., Dalton Trans.* 1975, 1015.
17. R. Freeman, S. P. Kempsell and M. H. Levitt, *J. Magn. Reson.* 1980, **38**, 453.
18. Chemical Design Ltd, Chem-X program. Oxford, U.K. (1989).

Polyhedron Vol. 10, No. 20/21, pp. 2501–2509, 1991
Printed in Great Britain

0277–5387/91 $3.00+.00
© 1991 Pergamon Press plc

SULPHIDES OF THE PLATINUM GROUP ELEMENTS—12.[1] BIS(TETRAPHENYLPHOSPHONIUM) PENTAKAIDEKAKISSULPHIDO PLATINATES(IV)

P. S. CARTWRIGHT and R. D. GILLARD*

School of Chemistry and Applied Chemistry, University of Wales, College of Cardiff, P.O. Box 912, Cardiff CF1 3TB, Wales, U.K.

and

E. R. J. SILLANPAA*

Department of Chemistry and Biochemistry, University of Turku, SF 20500, Turku 50, Finland

and

JUSSI VALKONEN

Department of Chemistry, University of Jyvaskyla, Jyvaskyla, Finland

(*Received* 16 *January* 1991; *accepted* 23 *May* 1991)

Abstract—Synthetic routes to tetraphenylphosphonium salts of $[PtS_x]^{2-}$ are outlined, where $x = 15$ or 18. Generally, $(PPh_4)_2[Pt(S_5)_3]$ is formed most readily.

The compound $[(C_6H_5)_4P]_2[PtS_{15}]$, always solvated, has been obtained by synthesis in acetonitrile (sulphur, triethylamine, H_2S and $[PPh_4]_2[PtCl_6]$) and by metathesis (in DMF) from the known hydrated ammonium compound

$$(NH_4)_2[Pt(S_5)_3]2H_2O + 2[Ph_4P]Br \longrightarrow (Ph_4P)_2[Pt(S_5)_3] \cdot DMF + 2NH_4Br,$$

and from the dismutation (in acetone)

$$3PtS_{17}^{2-} \longrightarrow PtS_{15}^{2-} + 2PtS_{18}^{2-}.$$

X-ray diffraction shows that crystals obtained from DMF and acetone are the solvated salts $[Ph_4P]_2 \cdot [Pt(S_5)_3] \cdot S$, with solvent molecules (S) uncoordinated. In both, the three platinopentathian rings related by a three-fold axis of the anion have the chair conformation. Molecules of the solvent are located between the anion and cation.

Platinum group elements have high affinities for sulphur, manifest in many ways. Heated platinum crucibles commonly embrittle when their contents include sulphur or its compounds. Processes of magmatic concentration often produce[2] a mineralogical association of platinum, palladium and rhodium with sulphides. Platinum metals form stable compounds with ions S_x^{2-}, i.e. sulphides ($x = 1$) and oligosulphides ($2 \leqslant x \leqslant 6$). These include many minerals, such as braggite (PdS), laurite (RuS), cooperite (PtS), bowie-ite (PtIrRhS), sulrhodite (RhS) and erlichmanite (Os, S). New examples exist,[3] like kashinite (Ir, Rh, S), formulated as $(Ir, Rh)_2S_3$.

In the context of geochemistry, of flotation and surface modification of ores and of helping to provide reproducible phases with defined properties, we have been evaluating combinations obtainable from dissolution of heavy metal sulphides in such aqueous systems as yellow ammonium sulphide.

* Authors to whom correspondence should be addressed.

Even recent discussions[4] of the mobility of platinum in aqueous media are in terms of platinum(II) and unidentate S_x^{2-}, whereas the oxidizing power of S_x^{2-} with $x > 4$ and the chelate effect actually combine to make chelated species containing platinum(IV), such as $Pt(S_5)_3^{2-}$, dominant. In much the same way, the early assumption that treatment of compounds of rhodium(III) with stannous salts gave the reduced state rhodium(I) has needed revision, since anions $[Rh(SnCl_3)_nCl_{6-n}]^{3-}$ are isolable.[5]

In addition to the $[PtS_{15}]^{2-}$ ion of Hofmann and Höchtlen,[6] and the remarkable[1k] $[Pt(S_6)_3]^{2-}$ ion, with three seven-membered rings, it was possible to prepare the $[PtS_{17}]^{2-}$ anion (which resolved[1a] spontaneously upon crystallization) as its ammonium salt dihydrate. This finding prompted further investigation of the platinum polysulphide system. We hoped to exercise control over stoichiometry during the synthesis, leading to the selective preparation of $[PtS_x]^{2-}$ ions ($12 \leqslant x \leqslant 21$), wholly inorganic dissymmetric anions.

Most platinum polysulphides have been synthesized from aqueous ammonia. We have in addition studied two other routes. The main solvent now used to prepare polysulphide solutions containing S_x^{2-} of known average x was acetonitrile and the base was NEt_3. We mixed such solutions formed via eq. (1) with an acetonitrile-soluble platinum(IV) compound, according to eq. (2) (where $4 \leqslant x \leqslant 7$).

$$2NEt_3 + H_2S + \frac{(x-1)}{8}S_8 \longrightarrow S_x^{2-} + 2NEt_3H^+ \quad (1)$$

$$(PPh_4)_2[PtCl_6] + 3S_x^{2-} \longrightarrow (PPh_4)_2[Pt(S_x)_3] + 6Cl^- \quad (2)$$

Rauh and associates made polysulphide solutions of a given sulphur chain length by another method.[7] Lithium, or its sulphide, is dissolved in non-aqueous solvents containing sulphur according to equations (3) or (4), respectively:

$$2Li + \frac{x}{8}S_8 \longrightarrow Li_2S_x \quad (3)$$

$$Li_2S + \frac{(x-1)}{8}S_8 \longrightarrow Li_2S_x. \quad (4)$$

Such solutions were also treated with the platinum(IV) salt to give polysulphides.

Our results are given here, with the crystal and molecular structure of the most frequently crystallized product, $(PPh_4)_2[Pt(S_5)_3]$, as two of its many solvates.

EXPERIMENTAL

Electronic spectra were measured with Cary 17, Unicam SP8000 and Perkin–Elmer λ-5 spectrometers, calibrated for wavelength and absorbance with holmium oxide and acidified potassium dichromate, respectively. IR spectra (some are given in Table 1) were recorded, as mulls, using a Perkin–Elmer 783 spectrometer. All solvents were of reagent grade. Acetonitrile was dried at reflux over calcium hydride, ethanol at reflux over magnesium and THF at reflux over sodium/benzophenone or sodium–potassium alloy.

$[PPh_4]_2[PtCl_6]$: $K_2[PtCl_6]$ (1.0 g) was dissolved in hot water (75 cm^3) and a solution of $[PPh_4]Br$ (2.25 g) in hot water (100 cm^3) was slowly added. The resulting orange precipitate was collected by filtration, washed with cold water and dried at 70°C for 12 h. The filtrate, kept cold for 12 h, yielded more orange precipitate which was treated in the same fashion. The total yield was 1.95 g (85%). Found: C, 52.5; H, 3.5. Calc. for $C_{48}H_{40}Cl_6P_2Pt$: C, 53.0; H, 3.7%. Tetraphenylphosphonium bromide was analysed to check the method. Found: C, 65.8; H, 5.3. Calc. for $C_{24}H_{20}BrP$: C, 65.9; H, 5.0%.

Table 1. IR spectra of some tetraphenylphosphonium salts[a]

$[PtCl_6]^{2-}$	S_7^{2-}	$[PtS_{15}]^{2-}$	$[Br^-]$
1583m	1580m	1582m	1582m
1188m	1185m	1182m	1181m
1165m	1165m	1163m	1158m
1105s	1108s	1108s	1103s
995m	995m	995m	994m
762m	760m		768m
752m	750m	750m	755m
			696m
688s	688s	688s	688s
615w	618w	615w	622w
528s	528s	528s	528s
465w	460w		463w
	450w	455m	
		440w	430w
		410w	
	395m	400m	
		385m	
		370w	
321s[b]			

[a] Recorded as Nujol mulls.

[b] cf. the Pt—Cl stretch of $(R_4N)_2[PtCl_6]$ at 324 cm^{-1}.[8]

Preparation of ditetraphenylphosphonium heptasulphide: $(PPh_4)_2S_7$

Sulphur (265 mg, 1.0 mmol) was added with dry MeCN (50 cm^3), PPh_4Br (1.33 g, 3.2 mmol) and NEt_3 (0.46 cm^3, 3.3 mmol) to a triple-necked flask. The solution was first degassed (nitrogen gas flow) for 5 min, then H_2S (Kipps apparatus) was bubbled through for 30 min, followed by dinitrogen bubbled slowly through for 2 h. The solution was stored cold (refrigerator) over two nights, and red crystals formed. These were collected and washed with ether: yield, 0.33 g. Found: C, 63.9; H, 4.00. Calc. for $C_{48}H_{40}P_2S_7$: C, 63.8; H, 4.5%. The single crystal unit cell parameters were $a = 1105$, $b = 1858$, $c = 1205$ pm, $\alpha = 74.56$, $\beta = 68.97$, $\gamma = 87.73°$ and $V = 2.223$ nm^3. The known cell parameters for $(PPh_4)_2S_7$ arc[9] $a = 1104$, $b = 1859$, $c = 1204$ pm, $\alpha = 74.58$, $\beta = 69.05$, $\gamma = 87.76°$ and $V = 2.220$ nm^3.

Preparation of $(PPh_4)_2[PtS_x]$ (x = 12–21)

The results are collected in Table 2.

The polysulphide solutions were prepared according to eqs (1) and (2).

(1) *Aerobic syntheses.* A typical attempted preparation is described (actually for $(PPh_4)_2[PtS_{12}]$). For PtS_{15}, PtS_{18} and PtS_{21} systems, the absolute amounts of base and $(PPh_4)_2[PtCl_6]$ were varied, keeping the same molar proportions using 100 mg elemental sulphur in each synthesis.

Elemental sulphur (0.100 g, 0.39 mmol) was added, with dried MeCN (50 cm^3) and NEt_3 (0.29 cm^3, 2.09 mmol) to a 100 cm^3 Erlenmeyer flask. H_2S was bubbled through the mixture for 2 min, after which all the sulphur dissolved to give a brownish-red solution. A 25 cm^3 aliquot was added to a solution of $(PPh_4)_2[PtCl_6]$ (0.189 g, 0.17 mmol), in MeCN (20 cm^3). A stopper was placed in the reaction flask and it was left at room temperature.

After 12 h, all the flasks contained some solid. Only the $[PtS_{15}]^{2-}$ system gave reasonable crystals; these were collected by decantation and washed with a little MeCN, then ether (final mass = 75 mg). After a further 6 weeks, more brown solids had separated which did not analyse as pure polysulphide complexes of platinum.

Further experiments were done using different mixed solvents. (i) To sulphur (1.25 g) and NEt_3 (3.0 cm^3) were added dry MeCN (35 cm^3) and dry ethanol (35 cm^3) and H_2S (from a Kipps apparatus) was bubbled through the mixture for 2 min, by which time all the sulphur had dissolved. Some of this solution (5.0 cm^3) was added to a solution of $(PPh_4)_2[PtCl_6]$ (100 mg) in MeCN (20 cm^3). The red crystals which formed after 12 h were separated and washed three times with toluene and ether.

(ii) Experiment (i) was slightly modified: bench reagents were used, and ethanol was replaced by THF. After 12 h, a mixture of sulphur and red polysulphide crystals was isolated. The product was washed well with toluene, then ether.

(2) *Anaerobic synthesis.* Typical preparations, actually for $(Ph_4P)_2[Pt(S_5)_3]$, are described.

(i) In MeCN: (a) dry MeCN (100 cm^3) was added to sulphur (2.04 g) in a triple-necked flask. The mixture was degassed (vacuum line) and oxygen-free NEt_3 (3.4 g) was added. H_2S was slowly bubbled through the mixture which was kept at −10°C (methanol–solid carbon dioxide bath) for 20 min, with continuous stirring, until all the sulphur had dissolved to give a deep red solution. The solution (A) was allowed to warm slowly to room temperature.

A 10 cm^3 aliquot of this solution (A) was added to a deoxygenated (nitrogen bubbler) solution of $(PPh_4)_2[PtCl_6]$ (0.200 g, 0.18 mmol) in MeCN (10 cm^3) and the mixture cooled (refrigerator). After 3 days, the red leafy crystals were separated and washed with ether (yield: 0.232 g, 93%).

The remaining polysulphide solution (A) was kept under nitrogen at room temperature for 13 days, then a 5 cm^3 aliquot was added to $(PPh_4)_2[PtCl_6]$ (0.100 g) in MeCN (10 cm^3). The solution was stored (refrigerator) for 12 h and the resultant red crystals were isolated and washed with THF and ether (yield: 0.110 g, 88%).

(b) Elemental sulphur (0.256 g, 1.0 mmol) was added to a triple-necked flask containing $(PPh_4)Br$ (1.677 g, 4.0 mmol) and NEt_3 (0.404 g, 4.0 mmol) in dry MeCN (50 cm^3). The mixture was cooled to approximately −30°C (methanol–solid carbon dioxide) and degassed (vacuum) three times. H_2S was bubbled through the stirred solution for about 5 s, causing an immediate green colouration, the solution soon becoming red. Further 5 s additions of H_2S were carried out at intervals of 10 min for 1 h, by which time all the sulphur had dissolved to give a red solution. This was stored under nitrogen for 12 h in the refrigerator. Red crystals (200 mg) were filtered off and washed with a little THF and ether.

The "hexa- and heptasulphide" analogues were prepared in a similar fashion, varying the amounts of starting materials according to eq. (1). The small, red spherical crystals obtained for "S_6^{2-}" and the red, acicular crystals filtered from the "S_7^{2-}" preparation were collected as above.

(ii) In mixed solvent: sulphur (2.5 g) was added to premixed THF (35 cm^3), MeCN (35 cm^3) and NEt_3 (6.0 cm^3). The new mixture was degassed and

Table 2. Summary of preparation of polysulphido complexes of platinum from $(PPh_4)_2[PtCl_6]$

Stoichiometry,[a] x, (in $[Pt(S_x)_3]^{2-}$)	Solvent[b]	O_2 free	Method	Yield (% based on Pt)	Microanalysis[c] C	H	S[d]	Comment
5	MeCN	×	NEt_3 as base	32	42.6	3.9	—	Low yield of $(PPh_4)_2[PtS_{15}]$
5	MeCN/ethanol	×	NEt_3 as base[e]	60	42.7	2.8	—	Reasonable yield of pure $(PPh_4)_2[PtS_{15}]$
5	MeCN/THF bench solvents	×	NEt_3 as base[e]	50	44.8	3.7	—	Impure product when solvents are not dry
5	MeCN		NEt_3 as base, S_5^{2-} solution prepared at −10°C	93	44.1	3.4	35.6	Good yields of $(PPh_4)_2[PtS_{15}]$
			S_5^{2-} solution used 13 days later	88	42.1	2.9	35.5	
5	MeCN/THF		(i) NEt_3 as base	85	42.7	3.4	—	Good synthesis of $(PPh_4)_2[PtS_{15}]$
			(ii) 5 h later	84	42.0	3.1	—	
6	MeCN		(i) NEt_3 as base, S_6^{2-} solution prepared	75[f]	43.1	3.1	37.8	$(PPh_4)_2[PtS_{15}]$ prepared, not $[PtS_{18}]^{2-}$
			(ii) Degassed S_6^{2-} and treated with H_2S	94[f]	36.3	3.6	—	Impure product which recrystallizes to give pure $(PPh_4)_2[PtS_{15}]$
			(iii) Product of (ii) recrystallized from DMF/THF/ether	80	42.6	2.7	—	
5	MeCN	×	$2Li + \frac{5}{5}S_8 \longrightarrow Li_2S_5$	Low	24.9	2.4	—	$(PPh_4)_2[PtS_{15}]$ obtained in low yield, by recrystallizing a very impure crude product.

[a] Defined by the preparative ratio of sulphur to platinum.
[b] All solvents dried unless stated otherwise.
[c] Calc. for $(PPh_4)_2[PtS_{15}]$: C, 42.6; H, 3.0; S, 35.5%. $(PPh_4)_2[PtS_{18}]$: C, 39.7; H; 2.8; S, 39.7%.
[d] Sulphur analysis by oxidation to the sulphate (H_2O_2) and titration vs barium(II).
[e] H_2S from cylinder except in these two cases, when it was from a Kipps apparatus.
[f] Based on $[PtS_{18}]^{2-}$.

H_2S was slowly bubbled for 25 min until all the sulphur dissolved. Some (4.0 cm^3, 1.12 mmol) of this polysulphide solution (P) was added to a deoxygenated solution of $(PPh_4)_2[PtCl_6]$ (0.200 g, 0.18 mmol) in MeCN (25 cm^3). After standing for 12 h (refrigerator), red crystals (0.21 g, 85%) were isolated and washed with THF and ether.

The remaining polysulphide solution (P) was kept for 5 h under nitrogen at room temperature and the above experiment repeated to yield 0.210 g of similar red crystals (84%) (see Table 2).

(iii) From attempted synthesis of $(PPh_4)_2[PtS_{18}]$: a mixture of sulphur (2.05 g, 8.0 mmol), NEt_3 (3.6 cm^3, 25.6 mmol) and MeCN (100 cm^3) was degassed twice at −5°C (methanol–solid carbon dioxide). H_2S was slowly bubbled for 30 min, during which time the temperature rose to 15°C. (After 5 min bubbling, all the sulphur had dissolved—however a fluffy brown solid formed which re-dissolved upon further addition of H_2S.) (a) The resulting solution (F) was stirred under nitrogen for 2 h and added (10 cm^3) to a solution of $(PPh_4)_2[PtCl_6]$ (0.20 g, 0.185 mmol) in MeCN (5 cm^3). After 12 h in the cold, red crystals, similar in appearance to $(PPh_4)_2[PtS_{15}]$, (0.200 g, 74%—based on $(PPh_4)_2[PtS_{18}]$) were isolated and washed with THF, toluene and ether (see Table 2). (b) The remaining polysulphide solution (F) was degassed three times at −10°C to remove any excess of H_2S, and yellow crystals appeared. H_2S was therefore passed into the mixture until all solids dissolved. 10 cm^3 of this new solution was added to a solution of $(PPh_4)_2[PtCl_6]$ (0.166 g) in MeCN (5 cm^3). After 2 weeks in the refrigerator, yellow–red crystals (X) were separated and washed with ethanol, benzene and ether (yield: 0.208 g, 94%—based on $(PPh_4)_2[PtS_{18}]$). Because of its microanalysis (low carbon, high hydrogen), the substance, X (53 mg) was dissolved in DMF (2 cm^3) and THF (2 cm^3) was added. After 5 days in the refrigerator, 19 mg of red crystals were separated by filtration. Diethyl ether (1 cm^3) was added to the filtrate; after 3 days in the refrigerator, a further 23 mg of red crystals were isolated. (Total yield from recrystallization of X was 42 mg, 80%.)

(3) *Using lithium reagents.* Solutions of lithium sulphides in acetonitrile were made up following eqs (3) and (4) of the text, to give $x \doteq 5$. The polysulphide solutions were added to solutions of $(PPh_4)_2[PtCl_6]$ in acetonitrile. Reaction (4) gave no useful products, whereas path (3) gave a brown-black material. This crude $(PPh_4)_2PtS_x$ (30 mg) was dissolved in DMF (1.0 cm^3). The solution was kept for 3 days in the refrigerator, diethyl ether (1.0 cm^3) was added and after a further 2 days in the refrigerator, red crystals (15 mg) were separated by filtration and washed with ether. Further addition of ether to the filtrate gave only a trace of brown substance.

X-ray analyses of bis(tetraphenylphosphonium) tris(pentasulphido)platinate(IV) *mono solvates*

The crystals of $(PPh_4)_2Pt(S_5)_3$, isolated from the DMF solution of "$(PPh_4)_2PtS_{18}$" and the DMF solution of $(PPh_4)_2PtS_x$ (made from lithium sulphides) were studied by X-ray methods. Crystals from both samples had the same unit cell within experimental error. The intensity data set was collected for a crystal obtained from the lithium sulphide source. The crystal structure of the compound isolated from DMF showed it to be a DMF solvate. During our earlier work,[1k] crystals were isolated from the aged and dismuted acetone solution of $(NH_4)_2PtS_{17}\cdot 2H_2O$. These had almost the same unit cell as those recrystallized from DMF. An intensity data set was also collected for this crystal, isolated from acetone. It has the same molecular structure, according to X-ray measurements, but is an acetone solvate.

Single-crystal measurements were carried out with an Enraf-Nonius CAD4 diffractometer using Mo-K_α radiation. The data obtained were corrected for Lorentz and polarization effects.

Crystal properties for $(PPh_4)_2Pt(S_5)_3\cdot$DMF (**1**): $M_r = 1427.87$; space group $P1$; $a = 1185.3(11)$, $b = 1335.3(7)$, $c = 1930.3(15)$ pm; $\alpha = 95.77(1)°$; $\beta = 93.76(3)°$; $\gamma = 105.64(2)°$; $Z = 2$; $V = 2.913$ nm^3; μ(Mo-K_α) = 30.4 cm^{-1} and $T = 296$ K.

Crystal properties for $(PPh_4)_2Pt(S_5)_3\cdot$acetone (**2**): $M_r = 1412.94$; space group $P1$; $a = 1172.3(11)$, $b = 1337.3(7)$, $c = 1937.4(15)$ pm; $\alpha = 96.03(5)°$; $\beta = 94.57(7)°$; $\gamma = 104.79(6)°$; $Z = 2$; $V = 2.903$ nm^3; μ(Mo-K_α) = 30.5 cm^{-1} and $T = 296$ K.

The intensities of two check reflections of **1** and **2** showed no loss of intensity. Of 8174 independent reflections of **1**, 5422 having $I > 2.5\sigma(I)$ were accepted as observed. Of 6439 independent reflections of **2**, 2907 having $I > 2.5\sigma(I)$ were accepted as observed.

The structures were solved by direct methods, which gave positional parameters for platinum and sulphur atoms. The atomic scattering factors and anomalous dispersion correction factors for heavy atoms were taken from the International Tables.[10] The structure was refined with Pt and P atoms having anisotropic and O, N, C and H atoms isotropic temperature factors, respectively. Phenyl groups were refined as rigid units. An empirical absorption correction was applied. The C—H hydrogen positions were calculated assuming the C—H distances to be 95 pm.

The refinements led to a final $R = 0.048$ ($R_w = 0.051$) for **1** and $R = 0.062$ ($R_w = 0.043$) for **2**. The weighting scheme was based on sigma weights. For both compounds, the largest residual electron densities (1.5 e $Å^{-3}$) were near the sulphur atoms [S(11), S(12), S(13)]. Temperature parameters of the same atoms were also large. Crystallographic calculations were performed with the TEXSAN programs.[11] Figures were drawn with PLUTO[12] and ORTEP[13].

RESULTS AND DISCUSSION

Results of the synthetic work are displayed in Table 2. Orange $(PPh_4)_2[PtCl_6]$ was prepared in good yield (see Experimental) and was soluble in acetonitrile.

Attempts to prepare platinum polysulphides from pure acetonitrile solutions in the presence of oxygen were, on the whole, unsuccessful. However, some crystals of $(PPh_4)_2[PtS_{15}]$ were obtained in low yield (see Table 2).

Reaction of lithium sulphide with sulphur in acetonitrile [eq. (3)] and subsequent addition of $(PPh_4)_2[PtCl_6]$ gave no useful products. However, if lithium sulphide was replaced by lithium [eq. (4)], a brownish-black material was obtained. Analysis showed that this was not pure $(PPh_4)_2[PtS_x]$. However, when this crude substance was recrystallized from DMF (see Experimental), red crystals were obtained which analysed (C, H) for "$(PPh_4)_2[PtS_{17}]$" (see Table 2). Nevertheless, the X-ray structure determination proved this compound in fact to be $(PPh_4)_2[PtS_{15}]\cdot(H_3C)_2NCHO$ with molecules of the solvent DMF occupying gaps in the structure. Dismutation in acetone gave $(PPh_4)_2[Pt(S_5)_3]\cdot$acetone.

Preparation of $(PPh_4)_2[PtS_n]$ *complexes under nitrogen*

When the sulphide solution (stoichiometry "S_5") was prepared in acetonitrile in the absence of dioxygen and added to a deoxygenated solution of $(PPh_4)_2[PtCl_6]$ in the same solvent, a high yield (93%) of $(PPh_4)_2[PtS_{15}]$ resulted (see Table 2). When the polysulphide solution used was stored under nitrogen for 13 days and the experiment repeated, similar leafy, red crystals formed in 88% yield. The crystals made in acetonitrile were not good enough for X-ray work. The compound is insoluble in water and all common solvents except DMSO and DMF; in fact, boiling in concentrated sodium hydroxide causes no dissolution and hence no decomposition. $(PPh_4)_2[PtS_{15}]$ slowly decomposes in DMF: a fresh solution has maximal absorption at 390 nm ($\varepsilon = 10{,}800$ dm^3 mol^{-1} cm^{-1}) and 310 nm ($\varepsilon = 17{,}800$); a solution 3 days old shows considerable broadening of these bands and the apparent extinction coefficients drop to 5530 and 12,430 dm^3 mol^{-1} cm^{-1}, respectively).

Preparation of $(PPh_4)_2S_7$

When $(PPh_4)Br$ was added to a polysulphide solution prepared in dry MeCN ("S_5^{2-}" stoichiometry) in the absence of any metal ion, red crystals formed within 12 h. From preliminary X-ray studies, this compound is the known $(PPh_4)_2S_7$, which Coucouvanis and his colleagues prepared[7] also from MeCN solutions. Microanalyses of compounds prepared as $(PPh_4)_2S_6$ and $(PPh_4)_2S_7$ show these to be different (or decomposed) materials, and whose composition is not understood. The compounds are insoluble in water, diethyl ether, toluene and triethylamine, but dissolve in polar organic solvents to give unstable blue/green solutions, which lose all colour if left at room temperature in air for several minutes. The cause of such blue colours has been much debated,[14] most workers agreeing that it is the S_3^- ion radical which is responsible.

Structures of bis(tetraphenylphosphonium)tris(pentasulphido)platinate(IV) *mono solvates*

The molecular structures of both studied crystals consist of PPh_4^+ cations and $Pt(S_5)_3^{2-}$ anions with the solvent molecules in the holes formed by the ions. The structural parameters of the cation are normal. The S_5^{2-} ligands are coordinated to platinum(IV) ions in a bidentate way, forming three six-membered rings around the platinum ion (Fig. 1). The bonding parameters of the anions in both compounds are very much the same (see Table 3). The Pt—S bond distances are of the same order as in other compounds of the $[Pt(S_5)_3]^{2-}$ anion.[1k,15,16]

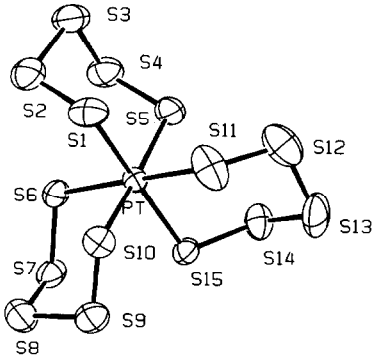

Fig. 1. The structure and labelling of the ion $[Pt(S_5)_3]^{2-}$ in **1** and **2**.

Table 3. Bond distances (pm) and bond angles (°) of $Pt(S_5)_3^{2-}$ anions

Distances

	(1)	(2)		(1)	(2)
Pt—S(1)	238.4(3)	241.2(6)	S(1)—S(2)	202.6(5)	203(1)
Pt—S(5)	237.6(4)	234.5(8)	S(2)—S(3)	206.7(6)	212(1)
Pt—S(6)	238.1(3)	236.6(6)	S(3)—S(4)	206.3(5)	209(1)
Pt—S(10)	239.5(4)	245.7(7)	S(4)—S(5)	201.9(3)	201.7(9)
Pt—S(11)	241.8(4)	244(1)	S(6)—S(7)	201.5(5)	201.9(9)
Pt—S(15)	238.9(3)	237.3(5)	S(7)—S(8)	203.0(5)	204(1)
			S(8)—S(9)	205.9(5)	202(1)
			S(9)—S(10)	199.4(5)	196(1)
			S(11)—S(12)	203.1(6)	198(1)
			S(12)—S(13)	209.5(6)	210(1)
			S(13)—S(14)	208.1(6)	210(1)
			S(14)—S(15)	202.3(5)	199.1(9)

Angles

	(1)	(2)		(1)	(2)
S(1)—Pt—S(5)	91.1(1)	91.3(2)	Pt—S(1)—S(2)	110.6(2)	111.1(4)
S(1)—Pt—S(6)	93.4(1)	92.9(2)	S(1)—S(2)—S(3)	104.9(2)	105.3(4)
S(1)—Pt—S(10)	83.6(1)	83.2(1)	S(2)—S(3)—S(4)	100.8(2)	99.3(4)
S(1)—Pt—S(11)	83.9(1)	83.5(3)	S(3)—S(4)—S(5)	107.3(2)	107.7(4)
S(1)—Pt—S(15)	173.1(1)	172.6(2)	S(4)—S(5)—Pt	109.2(2)	110.3(4)
S(5)—Pt—S(6)	91.2(1)	90.5(2)	Pt—S(6)—S(7)	108.8(1)	108.8(3)
S(5)—Pt—S(10)	174.2(1)	174.1(2)	S(6)—S(7)—S(8)	108.7(2)	108.9(4)
S(5)—Pt—S(11)	93.3(1)	93.9(3)	S(7)—S(8)—S(9)	100.1(2)	100.5(4)
S(5)—Pt—S(15)	93.3(1)	93.6(2)	S(8)—S(9)—S(10)	105.2(2)	106.8(4)
S(6)—Pt—S(10)	91.6(1)	92.1(2)	S(9)—S(10)—Pt	111.4(2)	110.3(4)
S(6)—Pt—S(11)	174.8(1)	174.4(3)	Pt—S(11)—S(12)	111.0(2)	113.6(5)
S(6)—Pt—S(15)	91.9(1)	92.6(2)	S(11)—S(12)—S(13)	108.1(2)	112.3(6)
S(10)—Pt—S(11)	83.7(1)	83.2(3)	S(12)—S(13)—S(14)	99.2(2)	100.1(4)
S(10)—Pt—S(15)	91.7(1)	91.6(2)	S(13)—S(14)—S(15)	107.5(2)	108.5(4)
S(11)—Pt—S(15)	90.5(1)	90.6(2)	S(14)—S(15)—Pt	110.6(2)	111.4(3)

The values of the chelate S—Pt—S angles in $Pt(S_5)$ units range from 90.5 to 92.1°. These values are very near to the values[1k] of 90.9–92.8(2)° of the corresponding S—Pt—S angles in the anionic PtS_5 units of $(NH_4)_2[Pt(S_5)_3]\cdot 2H_2O$.

The torsion angles within PtS_5-rings (S = 1–5), (S = 6–10) and (S = 11–15) are in Table 4. They vary from 57.4(5) to 79.9(1)°. The greatest deviations from the normal chair-type six-membered bonding parameters occur in the third chelate ring in **2**. The residual electron densities and high temperature parameters of S(11), S(12) and S(13) suggest that there might be some disorder in this chelate ring. However, none of these sulphur-atoms refined in two positions. The six-membered rings are flexible. The packing forces may induce the ring to have a certain conformation: the presence of the different solvent molecules in the unit cells may be the underlying reason for that. The packing of **1** is shown in Fig. 2.

The bond angles within the chelate rings are all between 91–93°, and rather remarkably, in a structure ostensibly free of strain, the angles made at platinum by opposite sulphur ligand atoms are all between 173–4°. The same feature, apparent departure from linearity (in strain-free compounds of octahedral metal ions) of the angles along the *x*, *y* and *z* axes, is even clearer in the related salt[1k] $(PPh_4)_2[Pt(S_6)_3]$, where these angles are all about 169°. Such apparent deviations from expected linearity in angles at thio-ligated ions are not without precedent (cf. proustite, Ag_3AgS_3 and pyrargite, Ag_3SbS_3, where the bond angles at the two coordinated silver are 165°).

Conclusion

Speciation in polysulphide solutions arises from complicated equilibria sensitive to solvent, to the base used, and to the presence of dioxygen. The particular S_x^{2-} species (i) concentrated in, and (ii) isolated from such complicated solutions by a given metal ion depends markedly on the metal ion and/or cation present and on relative solubilities, e.g.

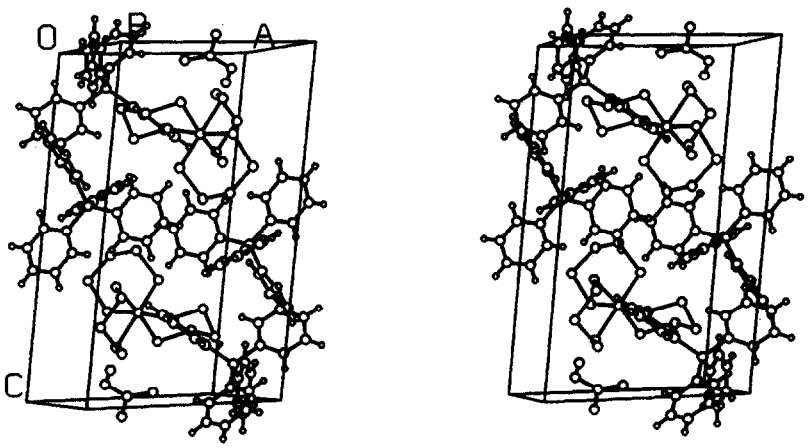

Fig. 2. Views of the packing in **1**.

$[AuS_9]^-$,[17] $[PPh_4]_2S_7$[9] and $[PPh_4]_2[PtS_x]$ ($x = 15$ for most reactions here, employing a wide range of conditions; 17[1c] or 18[1k]). When the combined effect of these factors can be predicted, a whole series of new anions $[MS_x]^{n-}$ or salts C_aS_x (C = cation) could be prepared. The situation is, naturally, further enriched by elements of kinetic control and by the presence of ligands other than oligosulphides. For example, both platinum(II) and platinum(IV) are most readily obtained, homoleptic, with S_5^{2-}: in the presence of phosphines, however, S_4^{2-} is selected (at least in the crystallizing solid), in $[(R_3P)_2PtS_4]$.

Table 4. Torsion angles within chelate rings of solvates

Atom 1 2 3 4	(1)[a]	(2)[a]
Pt—S(1)—S(2)—S(3)	−77.1(3)	−76.0(5)
S(1)—S(2)—S(3)—S(4)	74.2(3)[b]	73.3(5)
S(2)—S(3)—S(4)—S(5)	−75.5(3)	−75.3(5)
S(3)—S(4)—S(5)—Pt	76.5(2)	78.1(5)
S(4)—S(5)—Pt—S(1)	−62.3(2)	−62.2(4)
S(5)—Pt—S(1)—S(2)	64.2(2)	63.0(4)
Pt—S(6)—S(7)—S(8)	76.0(2)	75.3(4)
S(6)—S(7)—S(8)—S(9)	−76.7(2)	−75.9(4)
S(7)—S(8)—S(9)—S(10)	74.7(2)	75.5(5)
S(8)—S(9)—S(10)—Pt	−76.5(2)	−75.9(4)
S(9)—S(10)—Pt—S(6)	62.4(2)	61.3(4)
S(10)—Pt—S(6)—S(7)	−59.3(2)	−58.3(3)
Pt—S(11)—S(12)—S(13)	−75.4(3)	−68.7(6)
S(11)—S(12)—S(13)—S(14)	72.8(3)	66.5(6)
S(12)—S(13)—S(14)—S(15)	−74.1(3)	−70.8(5)
S(13)—S(14)—S(15)—Pt	78.6(2)	79.9(4)
S(14)—S(15)—Pt—S(11)	−62.6(2)	−62.6(4)
S(15)—Pt—S(11)—S(12)	61.2(2)	57.4(5)

[a] These columns describe the two independent anions within the solvates (**1**) (DMF) and (**2**) (acetone).

[b] The sign is positive if, when looking from atom 2 (here S(2)) towards atom 3 (here S(3)), clockwise motion of atom 1 (here S(1)) would superimpose it upon atom 4 (here S(4)).

Deposited material

For $(PPh_4)Pt(S_5)_3 \cdot DMF$ (**1**). Positional parameters and B(eq); U values; intramolecular distances; torsion or conformational angles; intermolecular distances observed and calculated structure factors.

For $(PPh_4)_2Pt(S_5)_3 \cdot Acetone$ (**2**). Similar tables.

REFERENCES

1. For Part 11 see R. D. Gillard and E. R. J. Sillanpaa, "Stability of Minerals" (Mineralogical Society's Winter Meeting). London (1989). Abstract volume, 30: earlier parts of this series are: (a) Part 1, R. D. Gillard and F. L. Wimmer, *J. Chem. Soc., Chem. Comm.* 1978, 936; (b) Part 2, R. D. Gillard and F. L. Wimmer, *XIII Mendeleev Congress of the Russian Chemical Society*, p. 42. Baku (1981); (c) Part 3, R.D. Gillard, F. G. Riddell and F. L. Wimmer, *J. Chem. Soc., Chem. Comm.* 1982, 332; (d) Part 4, R. D. Gillard, *Chem. Brit.* 1984, **20**, 1022; (e) Part 5, R. D. Gillard, F. L. Wimmer and J. P. G. Richards, *J. Chem. Soc., Dalton Trans.* 1985, 253; (f) Part 6, E. H. M. Evans, J. P. G. Richards, R. D. Gillard and F. L. Wimmer, *Nouv. J. Chim.* 1986, **19**, 783; (g) Part 7, S. C. Termes, A. N. Buckley and R. D. Gillard, *Inorg. Chim. Acta* 1987, **126**, 79; (h) Part 8, Peter Cartwright, R. D. Gillard, Reijo Sillanpaa and Jussi Valkonen, *Polyhedron* 1987, **6**, 1775; (j) Part 9, R. D. Gillard, A. N. Buckley, H. J. Wouterlood and P. S. Cartwright, *Inorg. Chim. Acta* 1988, **141**, 77;

(k) Part 10, Reijo Sillanpaa, P. S. Cartwright and R. D. Gillard, *Polyhedron* 1988, **7**, 1801.
2. *Geo-Platinum* 87 (Edited by H. M. Pritchard, P. J. Potts, J. F. W. Bowles and S. J. Cribb). Elsevier Applied Sciences, London (1987).
3. V. D. Begizov, E. N. Zav'yalov, N. S. Rudacherskii and L. N. Vyal'Sov, *Zapiski Vsesoyuznogo Mineralogicheskogo Obschechestva* 1985, **114**, 622: *Min. Abs.* 1987, **87M/1349**, 143.
4. B. W. Mountain and S. A. Wood, ref. 2, p. 57.
5. H. Moriyama, *J. Chem. Soc., Dalton Trans.* 1981, 639.
6. K. A. Hofmann and F. Höchtlen, *Chem. Ber.* 1903, **36**, 3090; 1904, **37**, 245.
7. R. D. Rauh, F. S. Shuker, J. M. Marston and S. B. Brummer, *J. Inorg. Nucl. Chem.* 1977, **39**, 1761.
8. D. A. Felly and M. L. Good, *Spectrochim. Acta* 1972, **28**, 1529.
9. M. G. Kanatzidis, N. C. Baenziger and D. Coucouvanis, *Inorg. Chem.* 1985, **24**, 24.
10. *International Tables for X-ray Crystallography*, Vol. 4. Kynoch Press, Birmingham (1974).
11. TEXSAN, *Single Crystal Structure Analysis Software*, Version 5.0. Molecular Structure Corporation, The Woodlands, Texas (1989).
12. W. D. S. Motherwell and W. Clegg, PLUTO78, *A Program for Plotting Crystal and Molecular Structures*. University of Cambridge, U.K. (1978).
13. C. K. Johnson, ORTEP-II, *A Fortran Thermal-ellipsoid Plot Program for Crystal Structure Illustrations*. Report ORNL-5138. Oak Ridge National Laboratory, Tennessee (1976).
14. P. Dubois, J. P. Lelier and G. Lepoutre, *Inorg. Chem.* 1988, **27**, 1883.
15. P. E. Jones and L. Katz, *Acta Cryst.* 1967, **25B**, 745; 1972, **28B**, 3438.
16. M. Spangenberg and W. Bronger, *Z. Naturforsch. B* 1978, **33**, 482.
17. G. Marbach and J. Strahle, *Angew. Chem. Int. Edn Engl.* 1984, **23**, 246.

Polyhedron Vol. 10, No. 20/21, pp. 2511–2518, 1991
Printed in Great Britain

0277–5387/91 $3.00+.00
© 1991 Pergamon Press plc

COMPLEXES OF LAWSONE WITH URANIUM, MOLYBDENUM, RUTHENIUM AND OSMIUM, AND THEIR USE AS ORGANIC OXIDANTS

AHMED M. EL-HENDAWY

Chemistry Department, Faculty of Science, Damietta, Egypt

(*Received* 8 *March* 1991; *accepted* 3 *May* 1991)

Abstract—The new complexes *trans*-$[UO_2(NQ)_2]$, *cis*-$[MoO_2(NQ)_2]$ and $[M^{III}Cl_2(EPh_3)_2NQ]$ (M = Ru, E = As; M = Os, E = P; HNQ = lawsone, 2-hydroxyl-1,4-naphthoquinone) have been prepared. They were characterized by spectroscopic techniques and investigated by cyclic voltammetry. The complex $[RuCl_2(AsPh_3)_2NQ]$ was found to be a more efficient catalyst than that of the osmium complex for the oxidation of primary alcohols to aldehydes and of secondary alcohols to ketones in the presence of N-methylmorpholine-N-oxide as co-oxidant.

Quinones play an important role in many biological electron-transfer processes, particularly in respiration and photosynthesis.[1] Some of these reactions are catalysed by metal ions such as copper, iron, manganese and molybdenum, although mechanistic aspects of these interactions have not been fully elucidated.[2] During these processes, quinones are reversibly reduced to either semiquinone radical anions or dianionic catechol with concomitant oxidation of the metal ions. Lawsone (HNQ) is the 2-hydroxy-1,4-naphthoquinone pigment found in the leaves of *Lawsonia alba* ("Henna"). Preparation and characterization of its complexes with divalent copper, cobalt, nickel, zinc and lead have been investigated.[3] High-spin ferrous complexes of the type $[Fe^{II}L_2(H_2O)_2]$ (L = anion of lawsone, NQ or its C-3 substituted derivatives, R-NQ; R = CH_3, Cl, I, Br, NO_2) have been studied.[4] More recently[5] the X-ray crystal structure of the complex $[Fe^{II}(NQ)_2(H_2O)_2]$ has been determined, showing that the bound lawsone ligands are in their fully oxidized form and the coordination centres are the C-2 phenolate and the C-1 carbonyl oxygen atoms.

We now report the preparation of the new complexes: *trans*-$[UO_2(NQ)_2]$, *cis*-$[MoO_2(NQ)_2]$ and $[M^{III}Cl_2(EPh_3)_2NQ]$ (M = Ru, E = As; M = Os, E = P). We also report their spectroscopic and electrochemical behaviour and study the catalytic oxidation of alcohols by ruthenium and osmium complexes in the presence of N-methylmorpholine-N-oxide (NMO) as co-oxidant, since $[Ru^{III}Cl_2(PPh_3)_2acac]$ and $[Os^{III}Cl_2(PPh_3)_2SQ]$ (SQ = semiquinone of catechol) have been used previously.[6,7]

RESULTS AND DISCUSSION

Reaction of lawsone with both uranyl acetate $UO_2(CH_3COO)_2 \cdot 2H_2O$ and $MoO_2(acac)_2$ in refluxing ethanol for 2–4 h gives dark reddish-brown and dark brown products, respectively. The ruthenium and osmium complexes were made from $[MCl_3(EPh_3)_2MeOH]$ (M = Ru, E = As; M = Os, E = P) since the complex $[OsCl_3(PPh_3)_2MeOH]$ was reported to be a precursor for the synthesis of $[OsCl_3(PPh_3)_2L]$ (L = O,O-donor ligand (−1) or semiquinone anion).[7,8] Analytical data (Table 1) indicate that these complexes have the formula $[MO_2(NQ)_2]$ (M = U or Mo) and $[M^{III}Cl_2(EPh_3)_2NQ]$ (M = Ru, E = As; M = Os, E = P). Uranium and molybdenum complexes are soluble only in DMSO, but the other complexes are soluble in dichloromethane in which their molar conductivities are very low. The magnetic moment at room temperature, μ_{eff} of the ruthenium and osmium complexes are 1.83 and 2.12 BM, respectively, near the spin-only value corresponding to one unpaired electron, suggesting the low-spin d^5 $(t_{2g})^5$ configuration for the ruthenium(III) or osmium(III)

Table 1. Analytical and vibrational spectroscopic data for the complexes

Compound	Colour	Analysis Found (Calc.) (%) C	H	IR data, wavenumbers (cm^{-1})[a] ν(C=O) free	ν(C=O) chelated	ν(C—O)	ν(C=C)[b]	Other bands	Assignments
Lawsone (HNQ)				1682m 1675s	1640s[c] 1643s[c]	1222m	1580m 1579m	3190m,b	ν(O—H)
trans-$[UO_2(NQ)_2]$	Reddish-brown	38.7 (39.0)	1.5 (1.6)	1640m 1624m	1585s 1567m	1248s	1570sh 1559m	928s 826s	$\nu_{as}(UO_2)$ $\nu_s(UO_2)$
cis-$[MoO_2(NQ)_2]$	Deep brown	50.2 (50.6)	2.2 (2.1)	1630m	1587s	1273m	1560m	958s 920s	$\nu_s(MoO)_2$ $\nu_{as}(MoO_2)_2$
$[RuCl_2(AsPh_3)_2NQ]$ (IV)	Black	57.2 (57.6)	3.5 (3.7)	1622s	1558s	1242m	1548sh 1538m	329s	ν(Ru—Cl)
$[OsCl_2(PPh_3)_2NQ]$ (III)	Dark blue	57.3 (57.6)	3.6 (3.7)	1620m	1578m	1300m	1558s	320m	ν(Os—Cl)

[a] Raman data underlined.
[b] Activated by carbonyl.
[c] Refer to hydrogen-bonded carbonyl.

ion in an octahedral environment. These values are similar to those found for previously reported ruthenium(III) and osmium(III) complexes.[6,8]

Vibrational spectra

The IR spectra of lawsone shows a medium broad band at 3190 cm^{-1} due to the ν(O—H) vibration, as previously mentioned;[4b] this band, as expected, is not observed in the complexes. Raman spectra of the solid of the free ligand display strong bands at 1675 and 1643 cm^{-1} similar to those found in the IR spectra at 1682 and 1640 cm^{-1} attributable to the free carbonyl and the hydrogen-bonded carbonyl.[3,9] In the complexes, both of the two carbonyl vibrations are shifted to lower wavenumbers, as found for lawsonato and substituted lawsonato iron(II) complexes.[4] The hydrogen-bonded carbonyl band in the ligand is more greatly shifted in our complexes and appears in the region 1590–1560 cm^{-1}. This shifted carbonyl band was found to activate the adjacent C=C skeletal in-plane vibration of the conjugated aromatic ring and these activated C=C vibrations can be seen in the region 1570–1540 cm^{-1}, at lower wavenumbers compared with those of the free ligand. The ν(C—O) vibration at 1222 cm^{-1} in lawsone is shifted upwards by *ca* 20–80 cm^{-1} in our complexes due to increase in the bond order.[4b] This confirms the participation of C-1 carbonyl and C-2 hydroxyl in coordination. Raman spectra of $[UO_2(NQ)_2]$ in DMSO contains a strong band at 826 cm^{-1} which is likely to arise from the symmetric stretch of $\nu_s(UO_2)$ of the *trans*-O=U=O moiety, with the strong IR band at 928 cm^{-1} being assigned to $\nu_{as}(UO_2)$. For the molybdenum complex, strong IR bands are found at 920 and 958 cm^{-1}, assigned to asymmetric and symmetric stretches, respectively, of the *cis*-MoO_2 unit as in other complexes of this type.[10–12] The deep colours of the complexes other than the uranyl complex makes them unsuitable for Raman studies. In the ruthenium and osmium complexes, besides the bands representing triphenylphosphine, arsine or coordinated lawsonate anion (NQ), strong bands were observed at 329 and 320 cm^{-1}, likely to be due to ν(Ru—Cl) and ν(Os—Cl) vibrations, respectively, and similar to those observed for $[M^{III}Cl_2(PPh_3)_2L]$ (L = O,O-donor ligand (−1); M = Ru, Os).[6,8] The most important vibrational bands for lawsone and its complexes are listed in Table 1.

^{1}H and ^{13}C NMR spectra

The ^{1}H and ^{13}C shifts are listed and assigned in Table 2; the numbering scheme for the carbon nuclei of lawsone is shown in Fig. 1. It has been

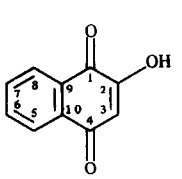

Fig. 1. 2-Hydroxy-1,4-naphthoquinone (HNQ), with atom numbering scheme.

Table 2. NMR, UV–vis spectroscopic and voltammetric data for lawsone and complexes

Compound	NMR data[a] and UV–vis data	Solvent	Voltammetric data (V)						Scan rate ($mV\ s^{-1}$)
			Reduction			Oxidation			
			$E_{p,c}$	$E_{p,a}$	ΔE	$E_{p,c}$	$E_{p,a}$	ΔE	
Lawsone (HNQ)	^1H: 6.15(s, H_3), 7.79(q, $H_{6,7}$), 7.90(d, H_5), 7.95(d, H_8)	$(CD_3)_2SO$	−0.58	—					10
			−1.40	−1.24	0.160				
	11.63(b, H—O)		−0.60[b]	—					100[b]
			−1.43[b]	−1.36[b]	0.070[b]				
	^{13}C: C-1 C-2 C-3 C-4 C-5 C-6 C-7 C-8 C-9 C-10	$(CD_3)_2SO$							
	181 159.3 111 184.3 125 134 133 125.7 130.3 131.7								
2-Methoxy-1,4-naphthoquinone[c]	180 160.4 109.9 184.7 126.1 134.3 133.3 126.6 131.1 132	$CDCl_3$							
trans-$[UO_2(NQ)_2]$	189.5 171 112.7 184 125.3 134.5 132 126 133.5 131.5	$(CD_3)_2SO$	−0.40	−0.32	0.080				20, 50
			−1.45	—					
	^1H: 6.10(s, H_3), 7.8(m, $H_{6,7}$), 7.95(d, H_5), 8.08(d, H_8)	$(CD_3)_2SO$							
	UV–vis data, λ_{max}, nm (ε, $M^{-1}\ cm^{-1}$):								
$[RuCl_2(AsPh_3)_2NQ]$ **(IV)**	758(4493), 623(3003), 508(2002), 311(20,712), 280sh(30,468)		−0.60	−0.52	0.080	+0.32	+0.38	0.060	20, 50, 100
			−0.84	−0.77	0.070	—	+1.04		
	249sh(36,100)								
$[OsCl_2(PPh_3)_2NQ]$ **(III)**	693(5508), 640(5423), 555sh(3593), 515sh(3008), 293sh(9605)		−0.54	−0.47	0.070	+0.32	+0.40	0.080	10, 20, 50
			−0.68	−0.62	0.060	+0.84	+0.92	0.080	
	254(41,019), 224(56,500)		−1.31	−1.24	0.070	—	—		

[a] Shifts in ppm relative to $(CH_3)_4Si$.
[b] Reference 27.
[c] Reference 18.

reported earlier that in lawsone the hydroxyl signal was not observed,[13] but a broad signal (in $CDCl_3$) at δ 7.42 ppm was seen by others[14] suggesting a dimeric and polymeric association of lawsone. In our hands lawsone in $(CD_3)_2SO$ showed a broad signal at δ 11.63 ppm typical of intramolecular hydrogen bond formation,[15] similar to that found for juglone (5-hydroxy-1,4-naphthoquinone) and plumbagin (2-methyljuglone) at δ 12.3 ppm.[14] The H_3 proton appears as a sharp singlet while the $H_{6,7}$ protons appear as a multiplet. The H_5 and H_8 protons each give a doublet at δ 7.90 and 7.95 ppm, respectively. For the uranium complex $[UO_2(NQ)_2]$, the hydroxyl signal disappeared and there is relatively little difference in the spectral pattern, but a shift to higher field is observed for the H_3 proton although it is only slightly consistent with electron withdrawal by the metal causing decreased electron density in the olefinic double bond; similar effects are observed more in catecholato complexes.[12,16]

The ^{13}C NMR spectrum of the ligand has not been fully and correctly assigned,[17] and on the basis of ^{13}C NMR data of 2-methoxy-1,4-naphthoquinone and other derivatives[18] we could assign the spectra of lawsone and of its uranyl complex as listed in Table 2. The only two resonances to undergo major shifts are C-1 and C-2 (about 10 ppm) to lower field, those nuclei adjacent to oxygen-donor atoms of carbonyl and hydroxyl groups; as observed in the complexes of catechols,[12,16] catecholamine,[10] tropolone[19] and maltol.[20] There is a similar but smaller consequential shift for C-3 and C-9 (see Table 2). We were unable to measure the NMR spectra of the molybdenum complex owing to its low solubility.

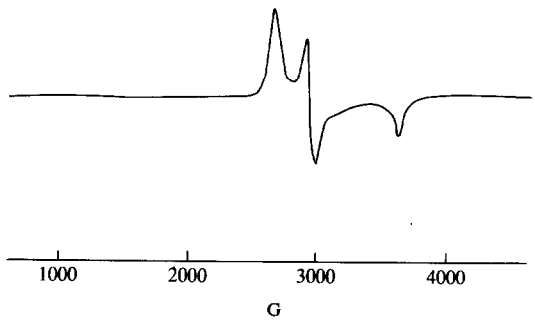

Fig. 2. ESR spectrum of **IV**.

over the sample tube. The spectrum (Fig. 2) shows three g-values in agreement with the low symmetry of the ligand-field with $g_x = 2.49$, $g_y = 2.24$ and $g_z = 1.81$, similar to the g-values for *mer*-$[RuCl_3(AsPh_3)_3]$[25] and $[Ru^{III}(Salen)(PPh_3)Cl]$ [H_2Salen = N,N′-ethylenebis(salicylaldimine)].[26] Recently[8] we have shown that the complex $[OsCl_2(PPh_3)_2L]$ (L = hexafluoroacetylacetonate) (**A**) has a similar type of ESR spectrum, and therefore we suggest structure **B** for our present ruthenium complex of C_2 symmetry, which is similar to that of complex **A**.[8]

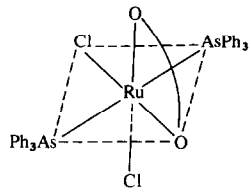

(B)

(O—O = NQ)

Electronic and ESR spectra

The UV–vis spectra of ruthenium and osmium complexes in dichloromethane solution (Table 2) contained high intensity bands above 500 nm assigned to ligand(π) → metal(d) charge-transfer. The band around 300 nm or the shoulder (in the osmium complex) has been assigned to metal(d) → ligand(π^*) charge-transfer.[21–24] The d–d electronic transition band of lower intensity that has been observed[6] around 600 nm in the complexes $[Ru^{III}Cl_2(PPh_3)_2L]$ [L = O,O-donor ligand (−1)], is therefore expected to receive a large contribution from the intense charge-transfer bands.[4b] The ligand π–π^* transitions occur at 280[7,24] and 254 nm for ruthenium and osmium complexes, respectively.

The ESR spectrum in dichloromethane frozen glasses of the complex $[RuCl_2(AsPh_3)_2NQ]$ (**IV**) (concentration 5×10^{-3} M) was measured at 77 K; cooling was by means of cold nitrogen gas passed

Redox properties

The electrochemical properties of the complexes were investigated by cyclic voltammetric techniques (Table 2). The voltammograms of lawsone, its ruthenium and osmium complexes were recorded on 0.1 M $Bu^n_4NPF_6$–CH_2Cl_2 solutions (potentials vs the Ag electrode). Lawsone exhibits an irreversible cathodic peak, $E_{p,c} = -0.58$ V, and a quasi-reversible wave of reduction, $E_{1/2} = -1.32$ ($\Delta E = 160$ mV), similar to those obtained in 0.1 M $Bu^n_4NClO_4$–DMSO solution.[27] The cathodic peak corresponds to the one-electron reduction of the quinone to the semiquinone anion (**C**), while the reduction wave arises from the conversion of semiquinone to the catecholate dianion (**D**).[4b,28,29] Lawsone can be represented by the tautomeric form of o-quinone (o-Q) which undergoes one-electron reduction to both the **C** and **D** forms shown in Scheme 1.

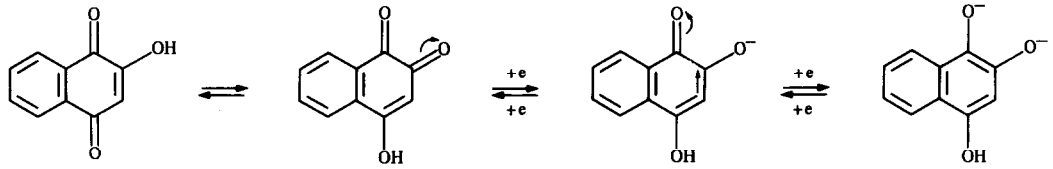

Scheme 1.

The complex $[UO_2(NQ)_2]$ shows only a quasi-reversible reduction wave, $E_{1/2} = -0.36$ V ($\Delta E =$ 80 mV), and an irreversible reduction peak, $E_{p,c} = -1.45$ V; these could be attributed to reduction of the coordinated lawsone to forms **C** and **D**, respectively. Uranyl acetate under the same conditions does not show any peaks corresponding to reduction or oxidation, nor does the complex $[MoO_2(NQ)_2]$. In the ruthenium complex $[RuCl_2(AsPh_3)_2NQ]$ (**IV**), two redox waves of reduction were found, $E_{1/2} = -0.56$ V ($\Delta E = 80$ mV) and -0.81 V ($\Delta E = 70$ mV), due to *o*-Q/SQ and SQ/Cat reductions, respectively. At positive potentials there is an oxidation wave of similar peak height to those of the reduction waves, arising from a Ru^{III}/Ru^{IV} oxidation. An irreversible anodic oxidation peak is also observed, $E_{p,a} = +1.04$ V, similar to that found for $[RuCl_2(PPh_3)_2acac]$ (**I**),[8] confirming the formation of higher oxidation states of ruthenium other than ruthenium(IV).

For $[OsCl_2(PPh_3)_2NQ]$ (**III**), the voltammogram (Fig. 3) shows three redox waves for reduction and another two for oxidation, each of similar peak height. The peak separation (ΔE) is close to that anticipated for a Nernstian one-electron process (59 mV).[30] The two oxidation waves at positive potentials may presumably be assigned to Os^{III}/Os^{IV} and Os^{IV}/Os^{V} oxidations, since the first redox wave was similarly found for osmium(III) complexes, e.g. $[OsCl_2(PPh_3)_2L]$ [L = O,O-donor ligand (-1)],[7,8] $[OsCl_3(PPh_3)py_2]$[31] and $[Os^{III}X_2(PPh_3)_2L']$ (X = Cl, Br; HL′ = 2-hydroxypyridine and picolinic acid).[32] The first reduction wave, $E_{1/2} = -0.51$ V ($\Delta E = 70$ mV), appears to be similar to those observed for the Os^{III}/Os^{II} reduction of osmium(III) complexes.[8,31,32] The other two reduction waves at more negative potentials are typical of *o*-Q/SQ and SQ/Cat reductions, as in the complexes $[Fe(NQ')_2(H_2O)_2]$ (NQ′ = NQ, R-NQ).[4b] These latter two redox waves are shifted to more negative potentials in the osmium complex than in the ruthenium complex. This reflects a decrease in the acidity of the osmium(II) species (**E**) compared with that of the ruthenium(III) complex (**F**), since the 5*d* electrons in the third-row transition element, osmium, are less tightly held by the nucleus than the 4*d* electrons in its congener, ruthenium, and also the difference in oxidation states of osmium(II) and ruthenium(III). So we expect that **IV** will be more oxidizing than the corresponding osmium complex (because it is more difficult to detach electrons from ruthenium). The formation of species **E** and **F** is shown below.

For scan rates (SR) between 10 and 100 mV s^{-1}, the ratio $i_p/(SR)^{1/2}$ (i_p = peak current) was constant and the ratio of anodic to cathodic peak current is one, the peak separation being independent of the scan rate. This indicates that the electron transfer is reversible or approaches reversibility and that mass transfer is limited. The stabilities of different oxidation states of ruthenium and osmium and coordinated NQ, SQ or Cat in the complexes are reflected by the reversibility of these processes (Scheme 2).

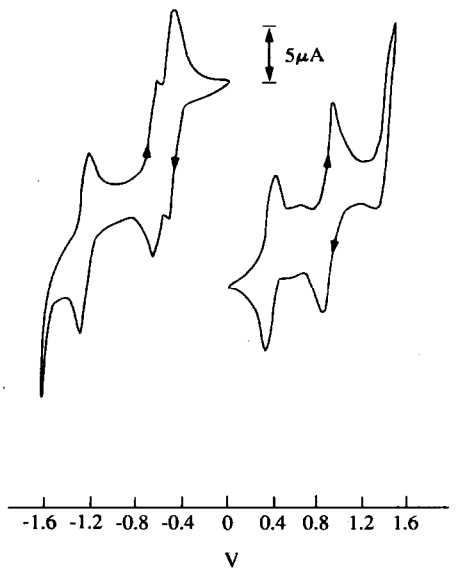

Fig. 3. Cyclic voltammogram in dichloromethane with 0.1 M $(Bu^n_4N)PF_6$ as supporting electrolyte (V vs silver electrode, scan rate 50 mV s^{-1}) for **III** ($\sim 10^{-3}$ M).

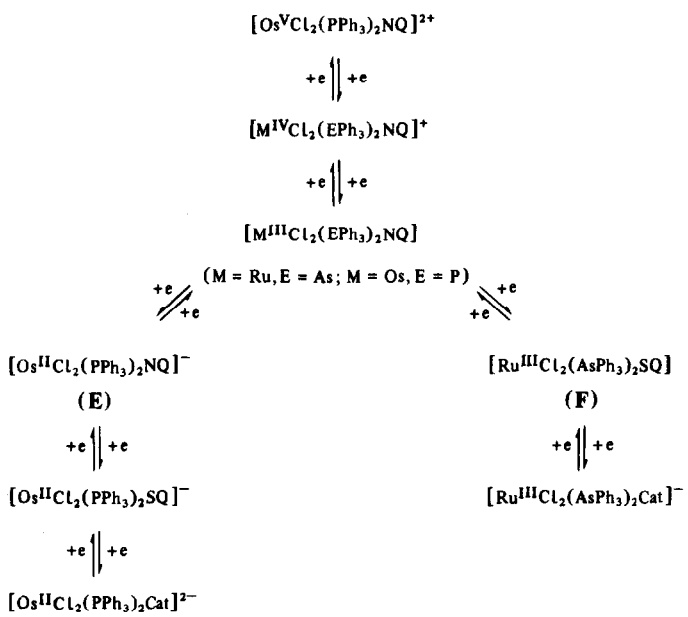

Scheme 2.

Catalytic oxidations

In our continuing work to develop new ruthenium(III) and osmium(III) complexes[6–8] as catalytic oxidants in the presence of excess NMO for selective oxidation of primary alcohols to aldehydes and secondary alcohols to ketones, we used the present, new complexes of ruthenium and osmium for such catalytic oxidation. The complex [Ru^{III}Cl$_2$(PPh$_3$)$_2$acac] (**I**) was found[6] to be a good oxidant for alcohols but the analogous osmium complex[8] showed only weak oxidation of alcohols. In Table 3 we summarize our results for catalytic oxidations by [M^{III}Cl$_2$(EPh$_3$)$_2$NQ] (M = Ru, E = As; M = Os, E = P) in the presence of NMO as the co-oxidant. The oxidations were carried out at room temperature in dichloromethane solution, from which water was removed using powdered molecular sieves. In no case was there detectable oxidation of an alcohol in the presence of NMO but in the absence of a ruthenium or osmium complex. Primary alcohols were oxidized to aldehydes and secondary alcohols to ketones with both higher yields and turnovers, similar to oxidations carried out previously using ruthenium complex **I** and [Os^{III}Cl$_2$(PPh$_3$)$_2$SQ][7] (**II**). In the case of unsaturated alcohols, e.g. cinnamyl alcohol, a lower yield of the corresponding aldehyde was produced by the osmium complex than was given by the ruthenium catalyst. A similar effect was noted for the catalytic oxidation by **II**[7] and by (4-t-But$_4$-pyH)$_2$[RuO$_2$Cl$_4$] in the presence of a greater excess of Et$_4$NCl.[33]

From Table 3 we notice that oxidations by [OsCl$_2$(PPh$_3$)$_2$NQ] (**III**) need more time for completion than oxidations by the ruthenium complex, which is expected as suggested above by the cyclic voltammetric data. Complex **III** can act as a real catalyst for such oxidations since the blue solution of the reaction mixture does not change at all during the reaction time. The osmium complex **III** is much more efficient towards oxidation compared with [OsCl$_2$(PPh$_3$)$_2$acac][8] but is similar to **II**. Also, the ruthenium complex [RuCl$_2$(AsPh$_3$)$_2$NQ] (**IV**) is a better oxidant than **I**. We believe that a possible reason for the efficiency of our present ruthenium and osmium complexes is due to the ability of the coordinated lawsone ligand, NQ, to be reduced to the semiquinone and catechol forms, as shown by the cyclic voltammetric behaviour of these complexes. The catalytic cycle of oxidation is activated by the presence of osmium(III) and ruthenium(III) in the complexes, which are being oxidized, respectively, to osmium(IV), osmium(V) and to ruthenium(IV) and its other higher oxidation states.

EXPERIMENTAL

Preparation of the complexes

Preparation of trans-[UO$_2$(NQ)$_2$]. To a hot solution of uranyl acetate, UO$_2$(CH$_3$COO)$_2$·2H$_2$O (0.42 g, 1 mmol), in ethanol (20 cm^3) was added 2-hydroxy-1,4-naphthoquinone (HNQ) (0.44 g, 2.5

Table 3. Catalytic oxidation of alcohols by $[MCl_2(EPh_3)_2NQ]$ (M = Ru, E = As; M = Os, E = P)/NMO

Alcohol	Product[a]	Time (h)	Yield (%)	Turnovers[b]
p-Methoxybenzyl	A	2	97	80
	A	5	81	100
Benzyl	A	3	87	80
	A	24	95	120
Piperonyl	A	3	94	100
	A	5	79	40
	A	20	91	120
Benzohydrol	K	2	84	50
	K	20	72	40
α-Tetralol	K	2	94	50
	K	24	93	60
Cinnamyl	A	2	91	60
	A	24	39	50

Underlined data refer to oxidation by $[OsCl_2(PPh_3)_2NQ]$/NMO.
[a] A = corresponding aldehyde, K = corresponding ketones.
[b] Turnovers = moles of product/moles of catalyst.

mmol) in ethanol (10 cm^3). The mixture was refluxed for 2 h on a steam bath, when a reddish-brown precipitate separated out, which was washed with hot ethanol and ether, and dried *in vacuo*. A similar procedure was used to prepare *cis*-$[MoO_2(NQ)_2]$ in which $MoO_2(acac)_2$ (prepared by the literature method[34]) replaced $UO_2(CH_3COO)_2 \cdot 2H_2O$ and a deep brown precipitate was obtained after 4 h reflux.

Preparation of $[RuCl_2(AsPh_3)_2NQ]$ (**IV**). The complex $[RuCl_3(AsPh_3)_2MeOH]$ (**V**)[35] was used as the starting material. A solution of **V** (0.21 g, 0.25 mmol) in methanol (100 cm^3) was refluxed, then the ligand (HNQ) (0.07 g, 0.4 mmol) added. The mixture was refluxed for 2 h and a dark solution was obtained, which was evaporated on a steam bath to near dryness. The residue was evaporated with hot methanol, washed carefully with methanol (3×10 cm^3) and then ether, and dried *in vacuo*.

Preparation of $[OsCl_2(PPh_3)_2NQ]$ (**III**). The complex was prepared from $[OsCl_3(PPh_3)_2MeOH]$, which was synthesized as reported previously.[8] A solution of $[OsCl_3(PPh_3)_2MeOH]$ (0.42 g, 0.5 mmol) in methanol (140 cm^3) was refluxed for 30 min on a steam bath until the solution became slightly dark yellow, followed by the addition of the ligand (HNQ) (0.13 g, 0.75 mmol). A reddish, then purple and finally blue solution was obtained, and after continuing reflux for 2 h, nice dark blue microcrystals were precipitated, filtered off, washed with methanol and ether, and dried *in vacuo*.

Catalytic oxidation by $[RuCl_2(AsPh_3)_2NQ]$ (**IV**)

The oxidation of piperonyl alcohol is typical. To a solution of piperonyl alcohol (1 mmol) was added NMO (3 mmol) in dichloromethane (20 cm^3) and 10^{-2} mmol of compound **IV**. The solution was stirred for 3 h in the presence of 4 Å molecular sieves (0.5 g). The mixture was evaporated to dryness and extracted with ether (2×25 cm^3). The combined ethereal extracts were filtered and evaporated to give piperonal, which was characterized and quantified as its 2,4-dinitrophenylhydrazone derivative.

The same experiment was carried out using $[OsCl_2(PPh_2)_2NQ]$ in place of **IV** above. The solution of the reaction mixture maintains its blue coloration and requires more time for completion (as in Table 3).

IR spectra were measured on a Perkin–Elmer 883 or FT 1720 instrument as liquid paraffin mulls between CsI plates and as KBr discs. Raman spectra were measured on a Spex Ramalog 5 instrument with a Coherent Radiation Innova 90 krypton-ion laser with excitation at 5682 Å (yellow), as a spinning disc with a KBr base for the solid sample of lawsone, and excitation at 6471 Å (red) for a DMSO solution of the uranyl complex in a sealed capillary. NMR spectra were measured on a Bruker WM-250 spectrometer. The electronic spectra were measured on a Philips PU 8740 UV–vis spectrophotometer or Varian 634 model. ESR spectra were recorded with a Varian E-12 spectrometer. Cyclic voltammetric

studies were carried out on a potentiostat/wave generator (Oxford Electrodes) using a platinum working electrode and silver reference electrode in conjunction with a Philips PM 8043 X–Y recorder. Magnetic measurements were made on a Johnson Matthey magnetic susceptibility balance.

Acknowledgements—I thank the Royal Society for support, Drs W. P. Griffith and J. F. Gibson for helpful advice, and also Johnson Matthey Ltd for the loan of platinum metals. I thank the University of London Intercollegiate Research Service (ULIRS) for the Raman spectra.

REFERENCES

1. (a) R. H. Thomson, *Naturally Occurring Quinones*. Academic Press, New York (1971); (b) R. A. Morton, *Biochemistry of Quinones*. Academic Press, New York (1965).
2. R. M. Buchanan and C. G. Pierpont, *Coord. Chem. Rev.* 1981, **38**, 45.
3. R. S. Bottei and C. P. McEachern, *J. Inorg. Nucl. Chem.* 1970, **32**, 2653.
4. (a) S. Padhye, P. Garge and M. P. Gupta, *Inorg. Chim. Acta* 1988, **152**, 37; (b) P. Garge, S. Padhye and J. P. Tauchagues, *Inorg. Chim. Acta* 1989, **157**, 239.
5. P. Garge, R. Chikate, S. Padhye, J. M. Savariault, P. Loth and J. P. Tauchagues, *Inorg. Chem.* 1990, **29**, 3315.
6. A. M. El-Hendawy and M. S. El-Shahawi, *Polyhedron* 1989, **8**, 2813.
7. A. M. El-Hendawy, *Inorg. Chim. Acta* 1991, **179**, 223.
8. A. M. El-Hendawy, *Polyhedron* 1990, **9**, 2309.
9. H. Kido, W. C. Fernelius and C. G. Haas Jr, *Analyt. Chim. Acta* 1960, 116.
10. A. M. El-Hendawy, W. P. Griffith and C. A. Pumphrey, *J. Chem. Soc., Dalton Trans.* 1988, 1817.
11. A. M. El-Hendawy and W. P. Griffith, *Inorg. Chim. Acta* 1989, **160**, 67.
12. A. M. El-Hendawy, W. P. Griffith, C. A. O'Mahoney and D. J. Williams, *Polyhedron* 1989, **8**, 519.
13. R. E. Moore and P. J. Scheuer, *J. Org. Chem.* 1966, **31**, 3272.
14. S. B. Padhye and B. A. Kulkarni, *J. Mag. Reson.* 1974, **16**, 150.
15. S. N. Viaogradov and R. H. Linnel, *Hydrogen Bonding*. Van Nostrand Reinhold, New York (1971).
16. W. P. Griffith, C. A. Pumphrey and T. A. Rainey, *J. Chem. Soc., Dalton Trans.* 1986, 1125.
17. H. Yano, M. Yamasaki, Y. Shimomura, M. Iwasaki, M. Ohta, Y. Furuno, K. Kouno, Y. Ono and Y. Ueda, *Chem. Pharm. Bull.* 1980, **28**, 1207.
18. G. Hofle, *Tetrahedron* 1977, **33**, 1963.
19. W. P. Griffith, C. A. Pumphrey and A. C. Skapski, *Polyhedron* 1987, **6**, 891.
20. S. J. Greaves and W. P. Griffith, *Polyhedron* 1988, **7**, 1973.
21. S. P. Cooper, Y. B. Koh and K. N. Raymond, *Inorg. Chem.* 1982, **104**, 5092.
22. R. B. Von Dreele and R. C. Fay, *J. Am. Chem. Soc.* 1972, **94**, 7935.
23. T. W. Hambley, C. J. Hawkins and T. A. Kabanos, *Inorg. Chem.* 1987, **26**, 3740.
24. C. J. Hawkins and T. A. Kabanos, *Inorg. Chem.* 1989, **28**, 1084.
25. G. Mercati and F. Morazzoni, *Gazz. Chim. Ital.* 1979, **109**, 161.
26. K. S. Murray, A. M. van den Bergen and B. O. West, *Aust. J. Chem.* 1978, **31**, 203.
27. V. Arancibia and M. Bodini, *An. Quim.* 1986, **82**, 309.
28. J. S. Jaworski, E. Lesniewska and M. K. Kalinowski, *J. Electroanalyt. Chem.* 1979, **105**, 329.
29. M. E. Peover, *J. Chem. Soc.* 1962, 4540.
30. R. Nicholson and I. Shain, *Analyt. Chem.* 1964, **36**, 706.
31. D. J. Salmon and R. A. Walton, *Inorg. Chem.* 1978, **17**, 2379.
32. J. E. Armstrong and R. A. Walton, *Inorg. Chem.* 1983, **22**, 1545.
33. A. C. Dengel, W. P. Griffith, A. M. El-Hendawy and J. M. Jolliffe, *Polyhedron* 1990, **9**, 1751.
34. G. J. J. Chen, J. W. McDonald and W. E. Newton, *Inorg. Chem.* 1976, **15**, 2612.
35. T. A. Stephenson and G. Wilkinson, *J. Inorg. Nucl. Chem.* 1966, **28**, 945.

Polyhedron Vol. 10, No. 20/21, pp. 2519–2521, 1991
Printed in Great Britain

0277–5387/91 $3.00+.00
© 1991 Pergamon Press plc

COMMUNICATION

THE SYNTHESIS, SPECTROSCOPIC PROPERTIES AND REACTIONS WITH NEUTRAL DONOR LIGANDS OF THE NOVEL SIX DIFFERENT LIGAND MOLYBDENUM(II) COMPLEX [MoCl($GeCl_3$)(CO)(NCMe)(PPh_3)(η^2-MeC_2Me)]

PAUL K. BAKER* and DAFYDD ap KENDRICK

Department of Chemistry, University of Wales, Bangor, Gwynedd LL57 2UW, Wales, U.K.

(*Received* 12 *July* 1991; *accepted* 30 *July* 1991)

Abstract—The seven-coordinate complex [MoCl($GeCl_3$)$(CO)_2$$(NCMe)_2$($PPh_3$)] reacts with an excess of but-2-yne in CH_2Cl_2 at room temperature to give the six different ligand compound [MoCl($GeCl_3$)(CO)(NCMe)(PPh_3)(η^2-MeC_2Me)] (**1**) in good yield. Solid-state ^{13}C NMR spectroscopy suggests that the but-2-yne ligand is donating four electrons to the molybdenum in **1**. Preliminary studies of the reaction chemistry of **1** with neutral donor ligands are also described.

Many attempts to prepare octahedral complexes with six different monodentate ligands attached have been made with little success. Hitherto, no examples of molybdenum(II) or tungsten(II) complexes of this type have been made. We have been studying the chemistry of the seven-coordinate complexes [$MI_2(CO)_3(NCMe)_2$] (M = Mo or W)[1] with donor ligands[2] and alkynes.[3] In our attempt to potentially increase the number of different ligands attached to the metal, more recently we have been investigating the reactions with donor ligands[4] of the seven-coordinate compound [MoCl($GeCl_3$)$(CO)_3(NCMe)_2$]. This is prepared in high yield by reacting the zero-valent trisacetonitrile compound [$Mo(CO)_3(NCMe)_3$][5] *in situ* with $GeCl_4$. In this communication we report the preparation of the first example of a six different monodentate ligand molybdenum(II) complex [MoCl($GeCl_3$)(CO)(NCMe)(PPh_3)(η^2-MeC_2Me)] (**1**), and describe preliminary reports of its reaction chemistry.

Reaction of [MoCl($GeCl_3$)$(CO)_2$$(NCMe)_2$($PPh_3$)] and a four-fold excess of but-2-yne in CH_2Cl_2 at room temperature affords the dark green complex [MoCl($GeCl_3$)(CO)(NCMe)(PPh_3)(η^2-MeC_2Me)] (**1**) in greater than 70% yield. Complex **1** is particularly sensitive to water, and is also air-sensitive and can only be stored for a few days under nitrogen. It is soluble in polar solvents such as CH_2Cl_2, $CHCl_3$ and acetonitrile, but insoluble in hydrocarbon solvents and diethyl ether. Compound **1** has been fully characterized by elemental analysis (C, H and N), IR, ^1H and solid-state ^{13}C NMR spectroscopy.† Many attempts were made to grow suitable single crystals of **1** for X-ray analysis without success.

The IR spectrum of **1** shows, as expected, a broad single carbonyl band at 1975 cm^{-1}, and a weak asymmetric doublet due to coordinated acetonitrile at $\nu(N{\equiv}C)$ = 2313 and 2286 cm^{-1}. A very weak band at 1684 cm^{-1} due to coordinated but-2-yne is observed, which is at a considerably lower wavenumber compared to uncoordinated but-2-yne suggesting there is considerable back-donation of elec-

* Author to whom correspondence should be addressed.

† Selected data for compound (1): Found: C, 43.2; H, 3.5; N, 1.4. $C_{25}H_{24}NOCl_4PGeMo$ requires: C, 43.2; H, 3.5; N, 2.0%. IR ($CHCl_3$) ν(CN) = 2313 (w) and 2286 (w) cm^{-1}; ν(CO) = 1975 (s) cm^{-1}; $\nu(C{\equiv}C)$ = 1684 (w) cm^{-1}. ^1H NMR (25°C) (CD_2Cl_2) 7.4 (m, 15H, Ph-H), 3.0 (vbrs, 6H, ≡C*Me*), 2.35 (s, 3H, NC*Me*) ppm. ^{13}C NMR (25°C, solid) 228.98 (bs, C≡C), 200.86 (bs, C≡O), 131.18 (bm, $CH_3C{\equiv}N$), 23.18 (vbrs, $CH_3C{\equiv}C$), 4.53 (bs. $CH_3C{\equiv}N$).

tron density from filled metal *d* orbitals to empty π^* orbitals on the but-2-yne. The solid-state ^{13}C NMR spectrum shows a broad alkyne carbon (C≡C) resonance at 228.98 ppm which suggests[6] that the but-2-yne ligand is utilizing both of its filled $p\pi$ orbitals and donating four-electrons to the molybdenum. It is difficult to postulate a structure for **1** from the spectroscopic data, and there are at least 30 (15 diastereomers, each one with an enantiomer) possible isomers for this compound. The ^{31}P NMR spectrum ($CDCl_3$, +25°C) of **1** shows a number of resonances, and hence confirms the existence of several different isomers in solution. The ^1H NMR spectrum of **1** from 243–308 K shows a very broad resonance at $\delta = 3.0$ ppm due to the but-2-yne methyl resonances which may again suggest several isomers for this complex.

The reaction chemistry of **1** is diverse, and some reactions with neutral donor ligands are given in Scheme 1. For example, **1** reacts with an equimolar amount of PPh_3 in CH_2Cl_2 at room temperature to afford the dark green acetonitrile displaced product $[MoCl(GeCl_3)(CO)(PPh_3)_2(\eta^2\text{-}MeC_2Me)]$ in good yield. All the new complexes described in Scheme 1 have been characterized by elemental analysis (C, H and N), IR, ^1H, and in selected cases ^{13}C NMR spectroscopy.*

Variable-temperature ^1H NMR studies were carried out on the complex $[MoCl(GeCl_3)(CO)(PPh_3)_2(\eta^2\text{-}MeC_2Me)]$. These studies suggested that the but-2-yne ligand was undergoing rapid propeller-like rotation at room temperature (298 K) (single resonance for the but-2-yne methyl groups at δ = 2.45 ppm), whereas at 228 K two different but-2-yne methyl resonances were observed at $\delta = 2.32$ and 2.40 ppm. Using the equation[7] $\Delta G^{\ddagger} = \pi\Delta\nu h/\sqrt{2}K_BT_C$ ($\Delta\nu = 24.22$ Hz, $T_C = 239$ K), the barrier to but-2-yne rotation of $[MoCl(GeCl_3)(CO)(PPh_3)_2(\eta^2\text{-}MeC_2Me)]$ was calculated to be 50.4 kJ mol^{-1}. This value is typical of other calculated values for dihaloalkyne complexes of molybdenum(II) or tungsten(II) of the type $[MX_2(CO)L_2(\eta^2\text{-}MeC_2Me)]$.[3c-d,8] After many attempts, no suitable single crystals for X-ray crystallography have been grown of the products shown in Scheme 1.

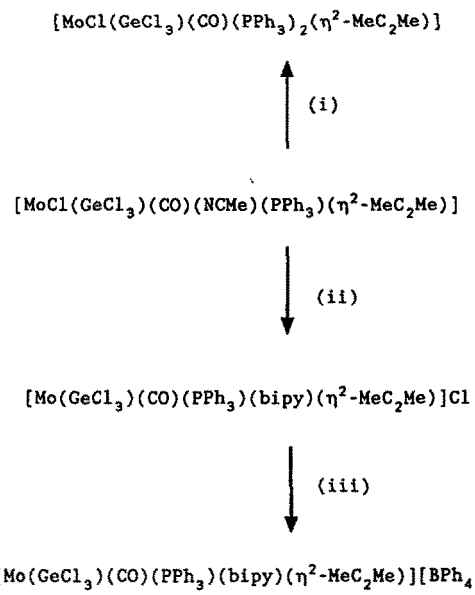

Scheme 1. Reagents: (i) PPh_3 in CH_2Cl_2 at room temperature for 24 h; (ii) bipy in CH_2Cl_2 at room temperature for 1 h; (iii) $Na[BPh_4]$ in NCMe at room temperature for 24 h.

* Selected data for $[MoCl(GeCl_3)(CO)(PPh_3)_2(\eta^2\text{-}MeC_2Me)]$. Found: C, 54.2; H, 3.8. $C_{41}H_{36}OCl_4GePMo$ requires: C, 53.7; H, 4.0%. IR ($CHCl_3$) ν(CO) = 1973 (s), ν(C≡C) = 1682 (w) cm^{-1}. ^1H NMR [25°C, $(CD_3)_2CO$], 7.4 (s, 30H, Ph—H); 2.45 (s, 6H, ≡C*Me*). Selected data for $[Mo(GeCl_3)(CO)(PPh_3)(bipy)(\eta^2\text{-}MeC_2Me)]Cl$. Found: C, 49.2; H, 4.0; N, 3.2. $C_{33}H_{29}N_2OCl_4GePMo$ requires: C, 48.8; H, 3.9; N, 3.4%. IR ($CHCl_3$) ν(CO) = 1948 (s), ν(C≡C) = 1687 (w) cm^{-1}. ^1H NMR [25°C, $(CD_3)_2CO$] 9.55 (d, 2H, bipy), 8.5 (m, 4H, bipy), 7.8 (d, 2H, bipy), 7.35 (m, 15H, Ph-H), 3.0 (d, 6H, ≡C*Me*). Selected data for $[Mo(GeCl_3)(CO)(PPh_3)(bipy)(\eta^2\text{-}MeC_2Me)][BPh_4]$. Found: C, 62.2; H, 4.8; N, 2.6. $C_{57}H_{49}N_2OCl_4GeBPMo$ requires: C, 62.5; H, 4.5; N, 2.6%. IR (CO) = 1956 (s) cm^{-1}. ^1H NMR [25°C, $(CD_3)_2CO$]: 9.7 (d, 2H, bipy), 8.4 (m, 4H, bipy), 7.9 (d, 2H, bipy), 7.5 (m, 35H, Ph), 3.05 (d, 6H, ≡C*Me*).

REFERENCES

1. P. K. Baker, S. G. Fraser and E. M. Keys, *J. Organomet. Chem.* 1986, **309**, 319.
2. (a) P. K. Baker and S. G. Fraser, *J. Organomet. Chem.* 1987, **329**, 209; (b) P. K. Baker, S. G. Fraser and M. G. B. Drew, *J. Chem. Soc., Dalton Trans.* 1988, 2729; (c) P. K. Baker, S. G. Fraser and D. ap Kendrick, *J. Chem. Soc., Dalton Trans.* 1991, 131.
3. (a) E. M. Armstrong, P. K. Baker and M. G. B. Drew, *Organometallics* 1988, **7**, 319; (b) P. K. Baker, E. M. Armstrong and M. G. B. Drew, *Inorg. Chem.* 1988, **27**, 2287; (c) E. M. Armstrong, P. K. Baker, M. E. Harman and M. B. Hursthouse, *J. Chem. Soc., Dalton Trans.* 1989, 295; (d) P. K. Baker, E. M. Armstrong and M. G. B. Drew, *Inorg. Chem.* 1989, **28**, 2406; (e) P. K. Baker, K. R. Flower, M. G. B. Drew and G. Forsyth, *J. Chem. Soc., Dalton Trans.* 1989, 1903; (f) E. M. Armstrong, P. K. Baker, K. R. Flower and M. G. B. Drew, *J. Chem. Soc., Dalton Trans.* 1990, 2535.

4. P. K. Baker and D. ap Kendrick, unpublished results.
5. D. P. Tate, W. R. Knipple and J. M. Augl, *Inorg. Chem.* 1962, **1**, 433.
6. J. L. Templeton and B. C. Ward, *J. Am. Chem. Soc.* 1980, **102**, 3288.
7. (a) H. S. Gutowsky and C. H. Holm, *J. Chem. Phys.* 1956, **25**, 1228; (b) A. Allerhand, H. S. Gutowsky, J. Jones and R. A. Meinzer, *J. Am. Chem. Soc.* 1966, **88**, 3185.
8. (a) J. L. Davidson and G. Vasapollo, *J. Chem. Soc., Dalton Trans.* 1985, 2239; (b) P. B. Winston, S. J. N. Burgmayer, T. L. Tonker and J. L. Templeton, *Organometallics* 1986, **5**, 1707.

Polyhedron Vol. 10, No. 22, pp. 2523–2527, 1991
Printed in Great Britain

0277–5387/91 $3.00+.00
© 1991 Pergamon Press plc

PALLADIUM A-FRAME COMPLEXES CONTAINING CARBOXYLATO LIGANDS. SYNTHESIS OF $[Pd_2(O_2CR)_2\{\mu\text{-}C_2(CO_2Me)_2\}(\mu\text{-}Ph_2PCH_2SCH_2Ph)_2]$ AND NMR EVIDENCE OF THE ENANTIOTOPIC FACE IN THE SIDE-BY-SIDE COMPLEX $[Pd_2Cl_2(\mu\text{-}Ph_2PCH_2SCH_2Ph)_2]$

YOSHIO FUCHITA* and KAZUHIKO ARIMA

Laboratory of Chemistry, College of General Education, Kyushu University, Ropponmatsu, Chuo-ku, Fukuoka 810, Japan

and

YOSHIHISA OHTA and KATSUMA HIRAKI

Department of Industrial Chemistry, Faculty of Engineering, Nagasaki University, Bunkyo-machi, Nagasaki 852, Japan

(*Received* 24 *June* 1991; *accepted* 22 *July* 1991)

Abstract—The A-frame complex $[Pd_2Cl_2\{\mu\text{-}C_2(CO_2Me)_2\}(\mu\text{-}Ph_2PCH_2SCH_2Ph)_2]$, obtained by the reaction between the side-by-side complex $[Pd_2Cl_2(\mu\text{-}Ph_2PCH_2SCH_2Ph)_2]$ (**1**) and dimethyl acetylenedicarboxylate, reacts with silver acetate and silver benzoate to give $[Pd_2(O_2CR)_2\{\mu\text{-}C_2(CO_2Me)_2\}(\mu\text{-}Ph_2PCH_2SCH_2Ph)_2]\cdot 3H_2O$ [R = Me (**3**), Ph (**4**)]. Similar reactions with silver salts of (*S*)- and racemic-2-phenylpropionic acid afford $[Pd_2(O_2CHMePh)_2\{\mu\text{-}C_2(CO_2Me)_2\}(\mu\text{-}Ph_2PCH_2SCH_2Ph)_2]$ [(*S*)- (**5**), racemic- (**6**)]. The NMR spectra of **5** and **6** show diastereoisomeric signal splitting, elucidating the presence of the enantiotopic face in **1**.

We[1] have previously reported the synthesis of the side-by-side complex $[Pd_2Cl_2(\mu\text{-}Ph_2PCH_2SCH_2Ph)_2]$ (**1**) and the A-frame complex $[Pd_2Cl_2\{\mu\text{-}C_2(CO_2Me)_2\}(\mu\text{-}Ph_2PCH_2SCH_2Ph)_2]$ (**2**) containing the unsymmetrical bidentate ligand (benzylthiomethyl)diphenylphosphine. In these complexes, two bidentate ligands are coordinated in a head-to-tail fashion. Different from the side-by-side complexes such as $[Pd_2Cl_2(\mu\text{-}Ph_2PCH_2PPh_2)_2]$[2] and $[Pd_2Cl_2(\mu\text{-}Ph_2AsCH_2AsPh_2)_2]$[3] which contain symmetrical bidentate ligands, it has been pointed out that the side-by-side complexes involving unsymmetrical bidentate ligands like **1** or $[Pd_2Cl_2(\mu\text{-}Ph_2PPy)_2]$ have enantiotopic faces if the ligands are coordinated in the head-to-tail mode.[4] Scheme 1 demonstrates the presence of the enantiotopic face in the head-to-tail type of complex which affords chiral A-frames by reaction with a molecule X. We now report the preparation of some dicarboxylato derivatives of **2** and demonstrate by NMR the presence of the enantiotopic face in the side-by-side complex **1**.

RESULTS AND DISCUSSION

Analytical and physical data and NMR spectral data of the complexes obtained in this study are listed in Table 1 and 2, respectively.

Preparation of the dicarboxylato complexes $[Pd_2(O_2CR)_2\{\mu\text{-}C_2(CO_2Me)_2\}(\mu\text{-}Ph_2PCH_2SCH_2Ph)_2]$

As previously reported,[1] the A-frame complex $[Pd_2Cl_2\{\mu\text{-}C_2(CO_2Me)_2\}(\mu\text{-}Ph_2PCH_2SCH_2Ph)_2]$ (**2**) was easily obtained by the reaction of the side-by-side complex $[Pd_2Cl_2(\mu\text{-}Ph_2PCH_2SCH_2Ph)_2]$ (**1**) with dimethyl acetylenedicarboxylate. Complex **2** reacted with two equivalents of silver acetate to give $[Pd_2(O_2CMe)_2\{\mu\text{-}C_2(CO_2Me)_2\}(\mu\text{-}Ph_2PCH_2SCH_2Ph)_2]\cdot 3H_2O$ (**3**). The IR spectrum of **3** exhibited

* Author to whom correspondence should be addressed.

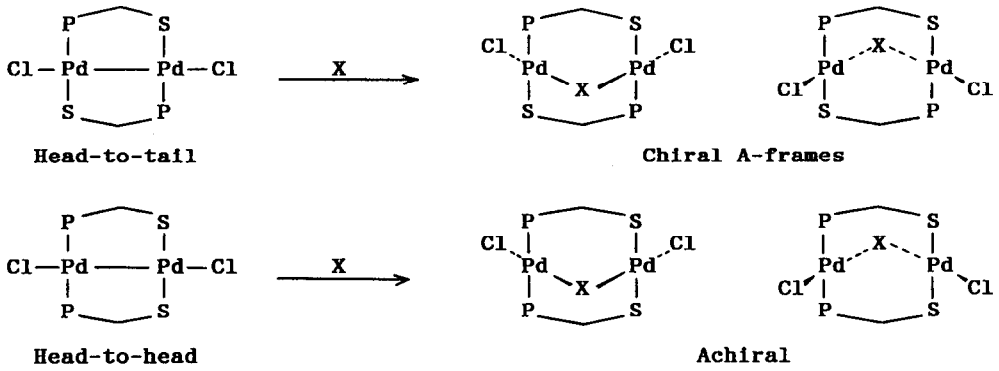

Scheme 1. Chirality of A-frame complexes derived from the head-to-tail type side-by-side complex $[Pd_2Cl_2(\mu\text{-}Ph_2PCH_2SCH_2Ph)_2]$ (**1**).

characteristic bands due to the terminal acetato ligand[5] at 1575 and 1370 cm^{-1}, together with the ν(COO) frequencies of the ester group in the μ-$C_2(CO_2Me)_2$ moiety. As for the ^1H NMR spectrum (in $CDCl_3$), **3** showed a similar spectrum as compared with **2**,[1] except for a new signal at δ 1.55 assignable to the acetatomethyl resonance. These facts suggested that **3** was the diacetato derivative of **2**, but its elemental analysis also suggested the presence of three molecules of water. Actually, the ^1H NMR spectrum in water-free C_6D_6 confirmed that **3** contained three molecules of water. Similarly, **2** reacted with silver benzoate to give $[Pd_2(O_2CPh)_2\{\mu\text{-}C_2(CO_2Me)_2\}(\mu\text{-}Ph_2PCH_2SCH_2Ph)_2]\cdot 3H_2O$ (**4**) which also contained three molecules of water. These water molecules might be incorporated between two carboxylato groups by hydrogen bonding. Complexes **3** and **4** did afford good crystals in solution for X-ray structural analysis, but the crystals rapidly became turbid when they were exposed to the air.

It is well established that palladium(II) acetate is a good cyclometallating reagent in comparison with palladium(II) chloride or the palladium(II) chloride–sodium acetate system.[6-8]. In addition, we have found that benzyl sulphide easily reacts with palladium(II) acetate to afford cyclopalladated complexes.[9,10] Complex **3** is a good candidate for the preparation of cyclometallated A-frame complexes as it has both the acetato ligand and benzyl sulphide group. However, **3** could not be converted into a desired cyclometallated complex under the conditions of refluxing in benzene or dioxane.

Silver salts of (*S*)- and racemic-2-phenylpropionic acids also reacted with **2** to produce the bis(2-phenylpropionato) complexes $[Pd_2(O_2CCHMePh)_2\{\mu\text{-}C_2(CO_2Me)_2\}(\mu\text{-}Ph_2PCH_2SCH_2Ph)_2]$ [(*S*)- (**5**), racemic- (**6**)], but in these cases ^1H NMR spectra and elemental analyses showed they contained no water.

Table 1. Yields, melting points and analytical data

Complex	Yield (%)	Melting point[a] (°C)	Analysis (%)[b] C	H
3	78	137	51.4 (51.3)	4.6 (4.8)
4	64	196	55.4 (55.6)	4.7 (4.9)
5	30	180	58.9 (59.2)	4.8 (4.8)
6	35	185	58.5 (59.2)	4.8 (4.8)

[a] With decomposition.
[b] Calculated values in parentheses.

NMR spectroscopic evidence of the presence of an enantiotopic face in the side-by-side complex $[Pd_2Cl_2(\mu\text{-}Ph_2PCH_2SCH_2Ph)_2]$ (**1**)

As shown in Scheme 2, the side-by-side complex **1** has an enantiotopic face and the resulting A-frame complex (**2**) consists of two enantiomers, **2**-(R^p) and **2**-(S^p). In the 400 MHz ^1H NMR spectrum of **5**, two sets of signals with comparable intensities were observed for the resonance of the 2-phenylpropionato ligand (Me: δ 1.07 and 1.18) and the μ-$C_2(CO_2Me)_2$ moiety (MeO: δ 3.05 and 3.08) due to the formation of a mixture of two diastereoisomeric complexes. These two diastereoisomers have the configurations, S^c-R^p-S^c and S^c-S^p-S^c (Scheme 2; superscript c abbreviates the asymmetric carbon atom of the 2-phenylpropionato ligand and superscript p abbreviates the chirality of the plane). The methyl groups of the 2-phenylpropionato ligands as well as the methyl groups of the μ-$C_2(CO_2Me)_2$ moiety in each isomer are equivalent. Moreover, the 162 MHz $^{31}P\{^1H\}$ NMR spectrum of **5** showed two signals at δ 22.06 and 22.23 owing to equivalent phosphorus atoms in each diastereoisomeric complex.

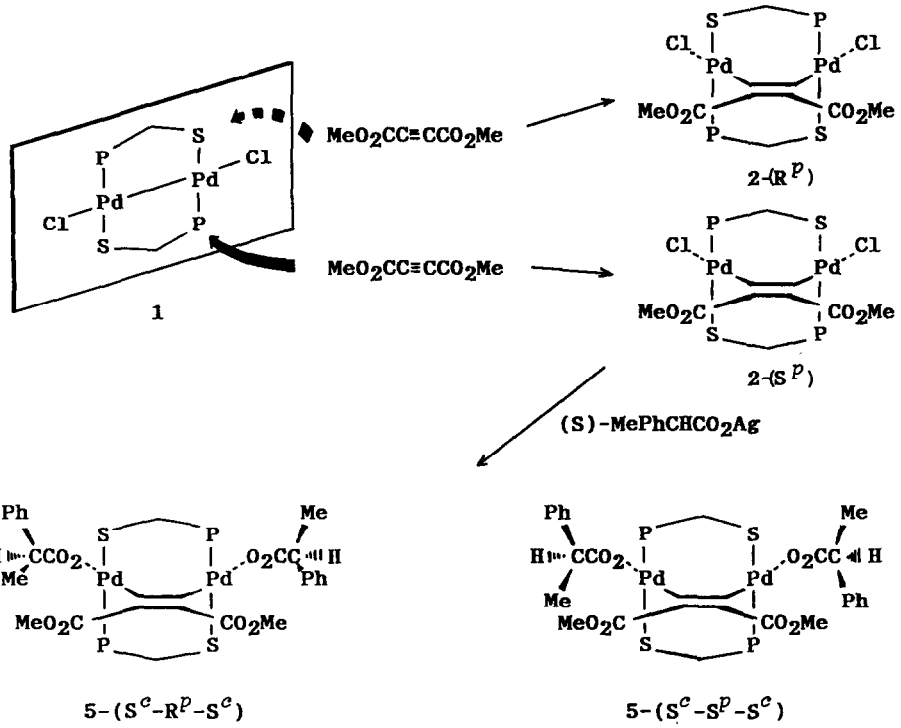

Scheme 2. Enantiotopic face in **1**, two enantiomers of **2** and two diastereoisomeric complexes of **5** derived from the reaction of **2** and silver (*S*)-2-phenylpropionate (superscript c abbreviates asymmetric carbon atom and superscript p abbreviates the plane of chirality).

On the other hand, when racemic silver 2-phenylpropionate is used, the resulting complex (**6**) must be composed of six isomers; S^c-S^p-S^c, R^c-R^p-R^c, R^c-S^p-R^c, S^c-R^p-S^c, R^c-S^p-S^c and R^c-R^p-S^c. In these isomers, three pairs **A**(S^c-S^p-S^c and R^c-R^p-R^c), **B**(R^c-S^p-R^c and S^c-R^p-S^c) and **C**(R^c-S^p-S^c and R^c-R^p-S^c) are enantiomers to each other and are equivalent in NMR spectrometry. The formation probability of pair **C** is twice as much as that of **A** or **B**, as the diastereoisomers having the configurations S^c-S^p-R^c and S^c-R^p-R^c are the same as the isomers R^c-S^p-S^c and R^c-R^p-S^c, respectively, of pair **C**. As for the two phenylpropionatomethyl groups, they are equivalent in pair **A** or **B** but are non-equivalent in pair **C**. Consistent with the above consideration, the observed ^{1}H NMR spectrum of **6** exhibited four methyl signals for the 2-phenylpropionato ligand at δ 1.04, 1.07, 1.19 and 1.20 with equal intensities. Concerning the methyl resonance of the μ-$C_2(CO_2Me)_2$ moiety, three singlets were observed at δ 3.05, 3.06 and 3.08; the signal at δ 3.08 is ascribed to a coincidence of two signals by comparison of intensities. Furthermore, the $^{31}P\{^1H\}$ NMR spectrum of **6** showed four signals at δ 24.85, 22.06, 22.41 and 22.54 due to equivalent phosphorus atoms of each pair **A** and **B**, and two non-equivalent phosphorus atoms of pair **C**.

In conclusion, we report that the enantiotopic face in **1** has been revealed by NMR spectroscopy by comparing its diastereoisomeric derivatives **5** and **6**. The separation of diastereoisomers and their application to asymmetric synthesis are under investigation.

EXPERIMENTAL

General procedures and apparatus were the same as reported in a previous publication from our laboratory.[11] Complex **2** was prepared as described.[1] (*S*)- and racemic-$MePhCHCO_2H$ and silver acetate were commercially available and were used without purification.

Preparations of silver salts of benzoic acid and 2-phenylpropionic acids

These compounds were prepared by a method similar to that of Matthews *et al.*[12] and were obtained as white microcrystals. $PhCO_2Ag$: yield 80%; m.p. 292°C (decomp.). Found: C, 36.4; H, 2.2. $C_7H_5AgO_2$ requires: C, 36.7; H, 2.2%. Racemic-$MePhCHCO_2Ag$: yield 54%; m.p. 245°C (decomp.). Found: C, 41.9; H, 3.5. $C_9H_9AgO_2$

Table 2. NMR spectral data

Complex	^{1}H NMR[a]	^{31}P NMR[b]
3[c]	1.55 (s, *Me*CO_2), 1.89 (s, H_2O), 2.77 [ddd, ^2J(HH) = 11.6 Hz, J(PH) = 11.7, 6.8 Hz, PCH_2S], 2.98 (s, CO_2Me), 3.26 [dd, ^2J(HH) = 11.6 Hz, J(PH) = 5.7 Hz, PCH_2S], 4.31 [d, ^2J(HH) = 13.9 Hz, SCH_2Ph], 4.59 [d, ^2J(HH) = 13.9 Hz, SCH_2Ph], 7.1–8.1 (m, Ph)	20.85(s)
4	1.82 (s, H_2O), 2.74 [ddd, ^2J(HH) = 12.0 Hz, J(PH) = 12.0, 7.1 Hz, PCH_2S], 3.14 (s, CO_2Me), 3.27 [dd, ^2J(HH) = 12.0 Hz, J(PH) = 5.3 Hz, PCH_2S], 4.16 [d, ^2J(HH) = 13.7 Hz, SCH_2Ph], 4.56 [d, ^2J(HH) = 13.7 Hz, SCH_2Ph], 7.05–8.05 (m, Ph)	25.96(s)
5	1.07 [d, ^3J(HH) = 7.0 Hz, CH*Me*Ph], 1.18 [d, ^3J(HH) = 7.0 Hz, CH*Me*Ph], 2.57 [q, ^3J(HH) = 7.0 Hz, C*H*MePh], 2.68 [q, ^3J(HH) = 7.0 Hz, C*H*MePh], 3.05 (s, CO_2Me), 3.08 (s, CO_2Me), 3.17 [ddd, ^2J(HH) = 11.6 Hz, J(PH) = 11.6, 5.8 Hz, PCH_2S], 3.18 [ddd, ^2J(HH) = 11.6 Hz, J(PH) = 11.6, 5.8 Hz, PCH_2S], 3.38 [dd, ^2J(HH) = 11.6 Hz, J(PH) = 5.8 Hz, PCH_2S], 3.39 [dd, ^2J(HH) = 11.6 Hz, J(PH) = 5.8 Hz, PCH_2S], 3.85 [d, ^2J(HH) = 13.2 Hz, SCH_2Ph], 3.87 [d, ^2J(HH) = 13.2 Hz, SCH_2Ph], 4.28 [d, ^2J(HH) = 13.2 Hz, SCH_2Ph], 4.31 [d, ^2J(HH) = 13.2 Hz, SCH_2Ph], 6.9–8.0 (m, Ph)	22.06(s) 22.23(s)
6	1.04 [d, ^3J(HH) = 7.0 Hz, CH*Me*Ph], 1.07 [d, ^3J(HH) = 7.0 Hz, CH*Me*Ph], 1.19 [d, ^3J(HH) = 7.0 Hz, CH*Me*Ph], 1.20 [d, ^3J(HH) = 7.0 Hz, CH*Me*Ph], 2.6 (c, C*H*MePh), 3.05 (s, CO_2Me), 3.06 (s, CO_2Me), 3.08 (s, CO_2Me), 3.15 [ddd, ^2J(HH) = 11.5 Hz, J(PH) = 11.5, 5.7 Hz, PCH_2S], 3.16 [ddd, ^2J(HH) = 11.5 Hz, J(PH) = 11.5, 5.7 Hz, PCH_2S], 3.17 [ddd, ^2J(HH) = 11.5 Hz, J(PH) = 11.5, 5.7 Hz, PCH_2S], 3.19 [ddd, ^2J(HH) = 11.5 Hz, J(PH) = 11.5, 5.7 Hz, PCH_2S], 3.379 [dd, ^2J(HH) = 11.5 Hz, J(PH) = 5.7 Hz, PCH_2S], 3.385 [dd, ^2J(HH) = 11.5 Hz, J(PH) = 5.7 Hz, PCH_2S], 3.395 [dd, ^2J(HH) = 11.5 Hz, J(PH) = 5.7 Hz, PCH_2S], 3.404 [dd, ^2J(HH) = 11.5 Hz, J(PH) = 5.7 Hz, PCH_2S], 3.79 [d, ^2J(HH) = 13.6 Hz, SCH_2Ph], 3.84 [d, ^2J(HH) = 13.6 Hz, SCH_2Ph], 3.87 [d, ^2J(HH) = 13.6 Hz, SCH_2Ph], 3.90 [d, ^2J(HH) = 13.6 Hz, SCH_2Ph], 4.21 [d, ^2J(HH) = 13.6 Hz, SCH_2Ph], 4.32 [d, ^2J(HH) = 13.6 Hz, SCH_2Ph], 4.41 [d, ^2J(HH) = 13.6 Hz, SCH_2Ph], 6.9–8.0 (m, Ph)	21.85(s) 22.06(s) 22.41(s) 22.54(s)

[a] Recorded in $CDCl_3$ solution at 400 MHz and 30°C. Chemical shifts (δ) in ppm relative to $SiMe_4$. s = singlet, d = doublet, dd = doublet of doublets, ddd = doublet of doublets of doublets, m = multiplets, c = complex.

[b] Recorded in $CDCl_3$ solution at 162 MHz and 35°C. Chemical shifts (δ) in ppm relative to external 85% H_3PO_4.

[c] In C_6D_6: 1.33 (s, H_2O), 1.97 (s, *Me*CO_2), 2.74 [ddd, ^2J(HH) = 11.6 Hz, J(PH) = 11.7, 6.9 Hz, PCH_2S], 2.95 (s, CO_2Me), 3.44 [dd, ^2J(HH) = 11.6 Hz, J(PH) = 5.3 Hz, PCH_2S], 4.51 [d, ^2J(HH) = 13.7 Hz, SCH_2Ph], 4.93 [d, ^2J(HH) = 13.7 Hz, SCH_2Ph], 6.9–8.1 (m, Ph).

requires: C, 42.1; H, 3.6%. (*S*)-MePhCHCO$_2$Ag: yield 77%; m.p. 247°C (decomp.). Found: C, 42.0; H, 3.5. $C_9H_9AgO_2$ requires: C, 42.1; H, 3.6%. These compounds are almost insoluble in common organic solvents and ^{1}H NMR data could not be obtained.

Synthesis of the dicarboxylato complexes [$Pd_2(O_2CR)_2\{\mu$-$C_2(CO_2Me)_2\}(\mu$-$Ph_2PCH_2SCH_2Ph)_2$] (**3**–**6**)

The preparation of all the dicarboxylato complexes was quite similar and a typical example is shown. (*S*)-MePhCHCO$_2$Ag (0.053 g, 0.206 mmol) was added to a dichloromethane solution (20 cm^3) of **2**, and the mixture was stirred for 1 day at room temperature. The resulting suspension was filtered and evaporated to dryness *in vacuo*. The residue was extracted with ether and diluted with hexane. The mixture was left standing for 1 day in a refrigerator to give **5** as yellow microcrystals (0.036 g, 30%).

REFERENCES

1. Y. Fuchita, K. I. Hardcastle, K. Hiraki and M. Kawatani, *Bull. Chem. Soc. Japan* 1990, **63**, 1961.
2. P. G. Pringle and B. L. Shaw, *J. Chem. Soc., Dalton Trans.* 1983, 889.
3. G. B. Jacobsen and B. L. Shaw, *J. Chem. Soc., Dalton Trans.* 1987, 151.
4. J. P. Farr, M. M. Olmstead, C. H. Hunt and A. L. Balch, *Inorg. Chem.* 1981, **20**, 1182.

5. T. A. Stephenson, S. M. Morehouse, A. R. Powell, J. P. Heffer and G. Wilkinson, *J. Chem. Soc.* 1965, 3632.
6. K. Hiraki, Y. Fuchita and K. Takechi, *Inorg. Chem.* 1981, **20**, 4316.
7. K. Hiraki, Y. Fuchita and T. Uchiyama, *Inorg. Chim. Acta* 1983, **69**, 187.
8. K. Hiraki, Y. Fuchita, M. Nakashima and H. Hiraki, *Bull. Chem. Soc. Japan* 1986, **59**, 3073.
9. Y. Fuchita, K. Hiraki, T. Yamaguchi and T. Maruta, *J. Chem. Soc., Dalton Trans.* 1981, 2405.
10. K. Hiraki, Y. Fuchita and Y. Kage, *J. Chem. Soc., Dalton Trans.* 1984, 99.
11. Y. Fuchita, Y. Ohta, K. Hiraki, M. Kawatani and N. Nishiyama, *J. Chem. Soc., Dalton Trans.* 1990, 3767.
12. F. W. Matthews, G. G. Warren and J. H. Michell, *Analyt. Chem.* 1950, **22**, 514.

Polyhedron Vol. 10, No. 22, pp. 2529–2533, 1991
Printed in Great Britain

0277–5387/91 $3.00+.00
© 1991 Pergamon Press plc

HALOGENOCOMPLEXES OF COPPER(II) IN ANHYDROUS PROPAN-2-OL

S. DALI and F. BENGHANEM

Institut de Chimie, Université de Sétif, 19000 Sétif, Algérie

and

M. A. KHAN

Faculté de Pharmacie, Université d'Angers, 49100 Angers, France

and

J. MEULLEMEESTRE and F. VIERLING*

Laboratoire de Chimie Physique, URA 405 CNRS, EHICS, Université Louis Pasteur, 1 rue Blaise Pascal, F-67008 Strasbourg Cedex, France

(*Received* 26 *March* 1991; *accepted* 22 *July* 1991)

Abstract—Solutions of copper(II) halides in propan-2-ol were investigated spectrophotometrically at 25°C and at constant ionic strength. For the chlorides as well as the bromides four mononuclear complexes are present in the solutions and their overall stability constants were calculated as $\log\beta_{CuCl^+} = 5.7$, $\log\beta_{CuCl_2} = 8.6$, $\log\beta_{CuCl_3^-} = 10.2$, $\log\beta_{CuCl_4^{2-}} = 10.6$, and $\log\beta_{CuBr^+} = 6.1$, $\log\beta_{CuBr_2} = 8.4$, $\log\beta_{CuBr_3^-} = 10.2$, $\log\beta_{CuBr_4^{2-}} = 10.7$. Electronic spectra of all the species present in the solution were calculated; the tetrahalogenocuprate CuX_4^{2-} has D_{2d} symmetry.

A comparative study of the thermodynamic stabilities of these complexes in alcohols shows a tendency of stability as an increasing function of number of carbon atoms in the alcohol.

In this paper we present the results of a spectrophotometric study of the copper(II) halide complexes in propan-2-ol with a view to determine the solvent effects on the thermodynamic and spectroscopic properties of these complexes in alcohols. An exhaustive bibliography of copper(II) halogenocomplexes in aqueous as well as in organic solutions has already been reported in our earlier publications,[1,2] we shall therefore limit our bibliographic references to studies carried out in alcoholic medium only.

There are hardly any quantitative studies in alcohols reported in the literature. In one of the earlier works, Kosower *et al.*[3] who observed six absorption bands propose the existence of six bromocomplexes in ethanol. Barnes and Hume[4] have identified the absorption maximum at 625 nm in ethanol as that of the tribromocuprate. Furlani and co-workers have discussed the configurations of the tetrahalogenocuprates as D_{2d} or D_{4h} in different organic solvents.[5,6]

Our results of the studies of these complexes in methanol[1] and ethanol[2] have shown the presence of four mononuclear complexes in both the alcohols. Overall stability constants as well as individual electronic spectra of all species were calculated and the structures in solution of the tetracoordinated complexes were discussed. We now report the results of the copper(II) halide complexes in propan-2-ol. The successive equilibria, the simplified representation of which does not take into account the solvated character of the copper(II) in the inner coordination sphere, $Cu^{2+} + jX^- \rightleftarrows CuX_j^{(j-2)-}$ (X = Cl, Br), were studied at 25°C and at constant ionic strength maintained at 1 mol dm^{-3}. Overall

* Author to whom correspondence should be addressed.

stability constants, β_j, for the species present were calculated using experimental data of absorption measurements in the UV, vis and the near-IR regions and these parameters in turn were used to calculate the individual electronic spectrum of the species. We do emphasize that β_j are apparent stability constants, calculated in the approximation of no occurrence of ion-pairing of the different species present in the non-aqueous medium.

EXPERIMENTAL

Anhydrous propan-2-ol, Merck p.a., was used. Stock solutions were prepared from $Cu(ClO_4)_2 \cdot 6H_2O$, $LiClO_4$, LiCl, (Fluka) and LiBr (Merck p.a.). Copper solution was titrated against EDTA using murexide as an indicator.[7] Ionic strength was kept constant at 1 mol dm^{-3} with the help of lithium perchlorate. Ligand concentrations were kept higher in order to eliminate the possibilities of formation of plurinuclear complexes on the one hand and favour the formation of highly coordinated complexes such as CuX_4^{2-} on the other hand.

Since copper(II) halide solutions are not very stable, especially the bromide solutions, all measurements were made immediately after the addition of the last reactant. The experimental conditions, in short, were identical to those in studies in methanol and ethanol in order to make a uniform comparison.

RESULTS AND DISCUSSION

Experimental spectra

Figures 1 and 2 represent the experimental spectra of copper(II) chlorides and bromides, respectively.

In the case of chloride solutions the free solvated copper ion seems to have its absorption maximum at *ca* 240 nm. As soon as small quantities of ligand are added an absorption band at 270 nm appears and progressively shifts to 290 nm for $C \geqslant 0.004$ mol dm^{-3}. For ligand concentrations higher than 0.008 mol dm^{-3} a shoulder peak is noticed at *ca* 250 nm, and for still higher concentrations a large band centred at 390 nm is observed along with isobestic points at 264, 308 and 366 nm. In the near-IR region, Cu^{2+} has its characteristic absorption at 800 nm which, as the ligand is added, shifts regularly until 960 nm. For solutions of higher concentrations a large band appears at about 1100 nm.

In the bromide solutions, even at very dilute ligand concentrations, a maximum is observed at 310 nm which for $C > 0.02$ mol dm^{-3} splits in two:

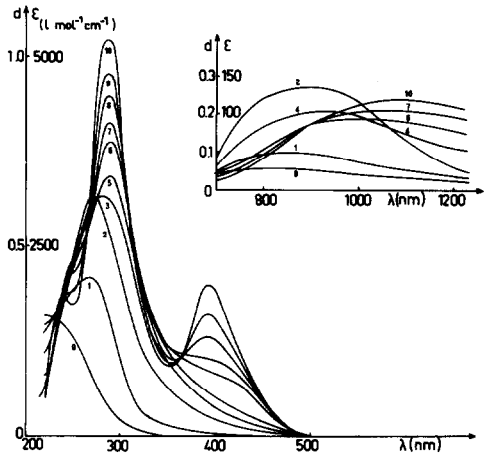

Fig. 1. Absorption spectra of copper(II) in lithium chloride–perchlorate isopropanolic mixtures. $B = 1 \times 10^{-3}$ M, $l = 0.2$ cm (UV–vis), 2 cm (near-IR). Spectra/$[Cl^-]_0$: 0/0; 1/0.001; 2/0.002; 3/0.004; 4/0.008; 5/0.01; 6/0.04; 7/0.08; 8/0.20; 9/0.40; 10/1.0.

one at 280 and the other at 350 nm. The absorption band at 280 nm undergoes a hypsochromic shift to 270 nm. In the vis spectrum there are two large bands at 510 and 640 nm. Finally in the IR region, the absorption maximum of the copper ion at 800 nm is progressively shifted with the addition of bromide ions from 860 to 940 nm in a quite similar way to the chloride system. For $C > 0.08$ mol dm^{-3} this maximum shifts from 940 to 1100 nm, which is probably due to the change in configuration of the tetracoordinated complex.

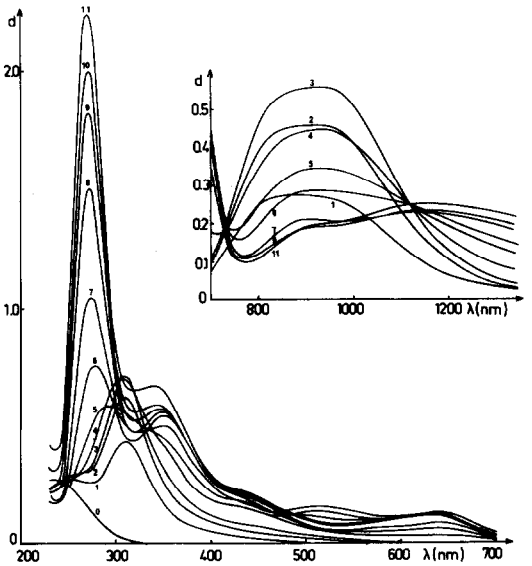

Fig. 2. Absorption spectra of copper(II) in lithium bromide–perchlorate isopropanolic mixtures. $B = 1 \times 10^{-3}$ M; $l = 0.2$ cm (UV–vis), 2 cm (near-IR). Spectra/$[Br^-]_0$: 0/0; 1/0.001; 2/0.002; 3/0.003; 4/0.010; 5/0.02; 6/0.04; 7/0.10; 8/0.20; 9/0.40; 10/0.80; 11/1.0.

Numerical analysis and stability constants

A matrix rank treatment, based on the method of Hugus and El Awady was used to determine the minimum number of absorbing species in the solution.[8] These calculations were carried out on an experimental data set of $N \times L = 400$ absorption measurements for the chlorides (number of wavelength $L = 16$, number of solutions $N = 25$) and 392 measurements ($N = 14$, $L = 28$) for the bromides. The details of the mathematical expressions used for calculations have already been given in our earlier publications.[9,10]

For both the systems, results indicate the presence of at least three complexes. Taking into account these results and the fact that experimental conditions are such that the formation of plurinuclear complexes is negligible, theoretical models for three and four mononuclear complexes, i.e. CuX^+, CuX_2, CuX_3^- and CuX^+, CuX_2, CuX_3^- and CuX_4^{2-}, respectively, were tested and their results summarized in Table 1.

Several initial assumptions are used for the thermodynamic basis of the stability constant of a complex in this kind of non-aqueous solutions:

(1) A stabilization of the ionic environment of the metal is obtained by addition of concentrated electrolytes which do not interfere in the coordination process between metal and ligand. The activity coefficients of the different reacting species will be stabilized in constant ionic strength medium as they are in aqueous solutions. Their values will certainly differ from one non-aqueous medium to another, but it is demonstrated that the ratio of the activity coefficients of the species inherent in superposed equilibria will be constant.

(2) Protic solvents such as propan-2-ol are classified as weakly dissociating solvents having a good ionizing ability according to the dielectric constant values of the pure solvents lying over 20: introducing strong electrolyte mixtures within the medium will certainly, despite constant ionic strength, modify the value of this parameter and consequently the dissociating property of the solvent; but the impact of this variation should be negligible for the solvation energies of the free ions as for the complexes. In such a medium the complexes will be present as ions which is not the case in molecular solvents (acetic acid[11] or tetrahydrofuran[12]) where all the species are ion-pairs or ion-aggregates. The assumption is made that in protic solvents such as propan-2-ol the formation of ion-pairs is not taken into account in the numerical analysis and the calculation of the constants β_j. This condition could only be considered if the association constants and activity coefficients of all species involved in the superposed equilibria are known: but these quantities are impossible to measure simultaneously.

(3) Transferring the ionic strength concept to this non-aqueous medium with the assumption of the activity coefficients stabilization, the interpretation of the superposed equilibria in non-aqueous solutions is possible: it leads to "apparent stability constants" which can be used as "thermodynamic parameters". The zero of the thermodynamic constants of complexation could be obtained through equilibria investigations at different constant ionic strengths and extrapolation to zero ionic strength of the obtained apparent stability constants.

It is seen that in both cases the standard deviation for all measurements in the whole spectrum region, σ_t, is better for models with four than the models with three complexes. Adding to this the fact that

Table 1. Overall stability constants, β_j, for copper(II) chloro- and bromocomplexes for [1, 2, 3] and [1, 2, 3, 4] models

Complexes	β_j	[1, 2, 3]	[1, 2, 3, 4]
$CuCl^+$	β_1	1.6×10^5	1.8×10^5
$CuCl_2$	β_2	2.3×10^8	4.1×10^8
$CuCl_3^-$	β_3	4.2×10^9	1.4×10^{10}
$CuCl_4^{2-}$	β_4	—	3.7×10^{10}
σ_{UV-vis}		0.071	0.031
σ_{IR}		0.147	0.119
σ_t		0.118	0.089
$CuBr^+$	β_1	8.8×10^2	1.3×10^6
$CuBr_2$	β_2	3.5×10^4	2.6×10^8
$CuBr_3^-$	β_3	4.1×10^5	1.6×10^{10}
$CuBr_4^{2-}$	β_4	—	5.1×10^{10}
σ_{UV-vis}		0.114	0.067
σ_{IR}		0.088	0.088
σ_t		0.104	0.076

Table 2. Coordinates of experimental and calculated isobestic points for [1, 2, 3] and [1, 2, 3, 4] models: λ_{iso} [nm] (ε_{iso} [$dm^3\ mol^{-1}\ cm^{-1}$])

	Experimental	Calculated [1, 2, 3]	Calculated [1, 2, 3, 4]
Chlorides	264 (2600)	266 (2860)	263 (2560)
	308 (3250)	310 (2800)	307 (3320)
	365 (1050)	362 (980)	365 (1080)
Bromides	486 (675)	500 (640)	485 (680)
	590 (580)	595 (575)	590 (580)

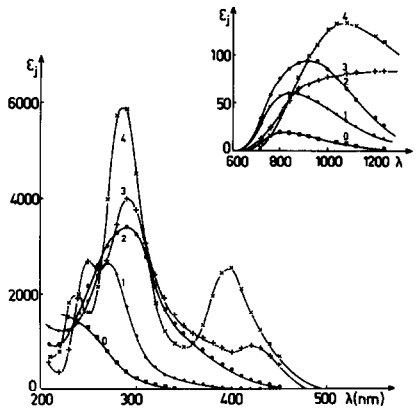

Fig. 3. Calculated electronic spectra of copper(II) chlorocomplexes in anhydrous isopropanol solutions: $Cu(^{i}PrOH)_4^{2+}$ [0]; $CuCl^+$ [1]; $CuCl_2$ [2]; $CuCl_3^-$ [3]; $CuCl_4^{2-}$ [4].

the calculated and experimental isobestic points are in harmony in the case of four complexes (Table 2), we postulate the presence of CuX^+, CuX_2, CuX_3^- and CuX_4^{2-} in propan-2-ol.

With the help of the overall stability constants already determined, we calculated the individual electronic spectra of all species present in the solution. This is represented in Figs 3 and 4 and the principal absorption bands are summarized in Table 3.

Both the tetracoordinated complexes have their *d–d* transitions at about 1100 nm, a position which is commonly admitted to be due to a flattened tetrahedron and assigned to D_{2d} symmetry.[13,14]

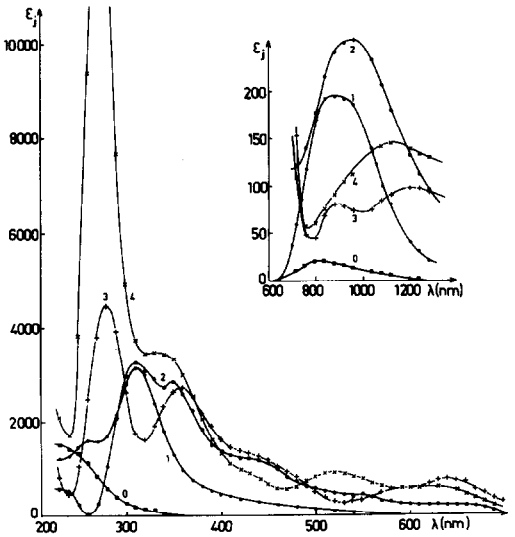

Fig. 4. Calculated electronic spectra of copper(II) bromocomplexes in anhydrous isopropanol solutions: $[Cu(^{i}PrOH)_4^{2+}$ [0]; $CuBr^+$ [1]; $CuBr_2$ [2]; $CuBr_3^-$ [3]; $CuBr_4^{2-}$ [4].

Table 3. Principal absorption bands of all species present in propan-2-ol

	Chlorocomplexes λ_{max} [nm] (ε_{max} [dm^3 mol^{-1} cm^{-1}])	Bromocomplexes λ_{max} [nm] (ε_{max} [dm^3 mol^{-1} cm^{-1}])
Cu^{2+}	<225 (1800)	<225 (1800)
	800 (22)	800 (22)
CuX^+	270 (2650)	310 (3180)
	840 (60)	870 (195)
CuX_2	290 (3440)	260 (1600)
		310 (3300)
		440 (1200)
	920 (95)	960 (256)
CuX_3^-	250 (2680)	280 (4450)
	292 (4000)	360 (2750)
	420 (940)	440 sh
		640 (800)
		880 (80)
	1120 (82)	1200 (98)
CuX_4^{2-}	240 (2000)	270 (13440)
	285 (5000)	340 (3450)
	396 (2550)	520 (920)
		620 sh
	1080 (135)	1120 (140)

The distribution curves of the copper(II) complexes are very similar in the chloride and bromide systems: the degree of formation of the chlorocomplexes confirms the superposition of equilibria for both systems: whatever the ligand concentration there is a simultaneous presence of at least two complexes.

For a comprehensive comparison in alcohols of stabilities and electronic spectra more than three

Table 4. Log β_j of the copper(II) halogeno-complexes in the three alcohols

	Solvent		
Complexes	Methanol	Ethanol	Isopropanol
$CuCl^+$	2.5	3.3	5.7
$CuCl_2$	4.2	6.0	8.6
$CuCl_3^-$	5.4	7.8	10.2
$CuCl_4^{2-}$	5.7	8.3	10.6
$CuBr^+$	3.7	5.0	6.1
$CuBr_2$	5.6	7.8	8.4
$CuBr_3^-$	6.3	9.2	10.2
$CuBr_4^{2-}$	6.3	10.3	10.7

solvents are necessary, therefore a similar study in butanol is desirable and has already been undertaken in our laboratory. This may permit us to establish a few empirical laws in R-OH type solvents. Nevertheless, a tentative comparison of thermodynamic stabilities in the three alcohols, *viz* methanol, ethanol and propan-2-ol is given in Table 4.

A study of the relative stabilities of the chlorides and bromides in the three alcohols brings into prominence two major aspects: (1) in a given solvent the bromides are generally more stable than the chlorides; and (2) the stability of any specific complex increases from methanol to propanol, i.e. the stability of these complexes is directly proportional to the number of carbon atoms in the alcohol.

If this empirical rule is confirmed by the results of our study of these complexes in butanol it can be presumed that an approximate value of the stability constants of the copper(II) halogenocomplexes in the R-OH type solvents can be predicted theoretically.

Acknowledgement—We thank Arno Wedel, Graduate Student at the University of Bonn (Germany) for his contribution to the experimental part of this work performed in our laboratory and sponsored by the European Exchange Program of the I.A.E.S.T.E. and the Franco-German Youth Office.

REFERENCES

1. M. A. Khan, J. Meullemeestre, M. J. Schwing and F. Vierling, *Inorg. Chem.* 1989, **28**, 3306.
2. S. Chafaa, T. Douadi, M. A. Khan, J. Meullemeestre, M. J. Schwing and F. Vierling, *New J. Chem.* 1991, **15**, 39.
3. E. M. Kosower, R. L. Martin and V. M. Meloche, *J. Am. Chem. Soc.* 1957, **79**, 1509.
4. J. C. Barnes and D. N. Hume, *Inorg. Chem.* 1963, **2**, 444.
5. C. Furlani and G. Morpurgo, *Theor. Chim. Acta* 1963, **1**, 102.
6. L. Sestili, C. Furlani, A. Ciani and F. Garbassi, *Electrochem. Acta* 1970, **15**, 225.
7. H. A. Flaschka, *EDTA Titrations*, p. 82. Pergamon Press, Oxford (1964).
8. Z. Z. Hugus and A. A. El Awady, *J. Phys. Chem.* 1971, **75**, 2957.
9. M. Elleb, J. Meullemeestre, M. J. Schwing and F. Vierling, *Inorg. Chem.* 1980, **19**, 2699.
10. F. Vierling, M. J. Schwing and J. Meullemeestre, *Spectra 2000* 1982, **79**, 10.
11. M. A. Khan, J. Meullemeestre, M. J. Schwing and F. Vierling, *Polyhedron* 1990, **9**, 2613.
12. C. Amuli, J. Meullemeestre, M. J. Schwing and F. Vierling, *Inorg. Chem.* 1983, **22**, 3567.
13. B. Morosin and E. C. Lingafelter, *Acta Cryst.* 1960, **13**, 807.
14. B. Morosin and E. C. Lingafelter, *J. Phys. Chem.* 1961, **65**, 50.

Polyhedron Vol. 10, No. 22, pp. 2535–2539, 1991
Printed in Great Britain

0277–5387/91 $3.00+.00
© 1991 Pergamon Press plc

TRIMETHYLSTANNANE DERIVATIVES OF COBALT(I); SYNTHESIS AND NMR SPECTROSCOPY. THE CRYSTAL STRUCTURES OF $[Co(Me_3Sn)(CO)_3L]$ ($L = PPh_3$, $AsPh_3$)

CHRISTA LOUBSER, JAN L. M. DILLEN and SIMON LOTZ*

Department of Chemistry, University of Pretoria, Pretoria 0002, South Africa

(*Received* 21 *January* 1991; *accepted* 22 *July* 1991)

Abstract—The Na/Hg reductive cleavage of the cobalt—cobalt bond in $Co_2(CO)_6L_2$ ($L = PPh_3$, $P(OPh)_3$, $AsPh_3$) and subsequent reaction with Me_3SnCl, afforded the five-coordinate complexes $Co(Me_3Sn)(CO)_3L$ ($L = PPh_3$, $P(OPh)_3$, $AsPh_3$). The intermediate sodium salts $Na[Co(CO)_3L]$ are unstable and were not isolated. The ^{31}P, ^{119}Sn, ^{13}C and ^{1}H NMR spectra were recorded and are discussed. Crystal structure analyses of $[Co(Me_3Sn)(CO)_3L]$ ($L = PPh_3$, $AsPh_3$) revealed, in both cases, a trigonal bipyramidal geometry with the trimethyl tin and the triphenyl phosphine/arsine in the two axial positions.

While preparing new Co^{I} compounds, we investigated the possibility of using complexes of the type $[Co(Me_3Sn)(CO)_3L]$ as useful starting materials. Compounds with Co—Sn bonds have been the subject of much interest,[1] particularly with respect to the nature of the metal—metal bond.

In $[Co(Me_3Sn)(CO)_3L]$, R and L were usually limited to triphenyl phosphine,[2,3] mainly because of the ease with which the $[Co(R_3Sn)(CO)_3PPh_3]^-$ anion is generated and handled. We found that the analogous triphenyl phosphite and triphenyl arsine anions could be prepared similarly, i.e. by cleaving the respective dimer $[Co(CO)_3L]_2$ ($L = P(OPh)_3$, $AsPh_3$), followed by stabilization with Me_3SnCl.

Here, a facile synthetic method for the preparation of $Co(Me_3Sn)(CO)_3L$ [$L = PPh_3$ (**1**), $P(OPh)_3$ (**2**), $AsPh_3$ (**3**)] in good yield and high purity is outlined, and the X-ray crystal structures of **1** and **3** discussed.

EXPERIMENTAL

Synthesis

Compounds **1**, **2** and **3** were prepared by cleaving the respective dimer $[Co(CO)_3L]_2$ [$L = PPh_3$, $P(OPh)_3$, $AsPh_3$] with a sodium amalgam according to eq. (1),

$$[Co(CO)_3L]_2 \xrightarrow[THF]{Na/Hg} 2Na[Co(CO)_3L], \quad (1)$$

whereupon the anions were treated with Me_3SnCl to form the desired products:

$$Na[Co(CO)_3L] + Me_3SnCl \longrightarrow Co(Me_3Sn)(CO)_3L. \quad (2)$$

Products were confirmed with the aid of elemental analyses and IR spectra, the results of which, together with the detailed synthetic procedures, are to be published elsewhere.[4]

NMR spectroscopy

NMR spectra were recorded on a Bruker AC300 instrument at 30°C. Deuterated solvents were degassed before use and samples prepared under N_2. Spectra were obtained at 300 (^{1}H), 75.5 (^{13}C), 121.5 (^{31}P) and 111.9 (^{119}Sn) MHz, respectively.

Crystal data: collection and analysis

$C_{24}H_{24}CoO_3PSn$ (**1**), $M = 568.96$, $a = 9.849(3)$, $b = 9.955(3)$, $c = 13.610(4)$ Å, $\alpha = 98.64(2)$, $\beta = 107.43(3)$, $\gamma = 95.620(3)°$, $U = 1244.2$ Å^3, space group $P\bar{1}$, $Z = 2$, $D_c = 1.52$ g cm^{-3}. Colourless paralleleopipeds, $\mu(Mo\text{-}K_\alpha) = 17.6$ cm^{-1}, $F(000) = 566$.

$C_{24}H_{24}CoO_3AsSn$ (**3**), $M = 612.91$, $a = 9.840(2)$, $b = 10.025(3)$, $c = 13.758(1)$ Å, $\alpha = 99.606(2)$,

* Author to whom correspondence should be addressed.

$\beta = 107.814(1)$, $\gamma = 94.8(2)°$, $U = 1260.8$ Å^3, space group $P\bar{1}$, $Z = 2$, $D_c = 1.62$ g cm^{-3}. Colourless pyramids, μ(Mo-K_α) = 28.3 cm^{-1}, $F(000) = 604$.

Diffraction data were collected at ambient temperature with an Enraf–Nonius CAD4 diffractometer using graphite monochromated Mo-K_α radiation. Unit cell dimensions were obtained from a least squares fit of 25 centred reflections. Data were measured using a variable scan speed, with a maximum of 3.30° min^{-1} (5.49 in the case of **3**) and a minimum corresponding to a 60 s measuring time per reflection. A $\omega:2\theta$-scan was employed. The horizontal aperture was fixed at 1.3 mm and the vertical slit at 4 mm. The ω-scan angle changed as $0.51 + 0.34 \tan\theta(°)$ ($0.42 + 0.34 \tan\theta$ for **3**). Intensity checks were carried out every hour and orientation control every 200 reflections. Data were corrected for Lorentz and polarization effects, and for absorption using an empirical method involving ψ-scans.

The crystal structure was solved by Patterson and subsequent Fourier methods and refined anisotropically with a full matrix method using $1/\sigma^2(F)$ weights. Hydrogen atoms were placed on calculated positions ($r_{CH} = 1.08$ Å, $\angle$**HCH** = 109.5°) and refined riding on their associated carbon atom with a common isotropic temperature factor $U = 0.11(1)$ Å^2 ($U = 0.121(4)$ Å^2 for **3**). Final residuals were $R = 0.084$ and $R_W = 0.051$ for 3028 reflections and 281 variables ($R = 0.042$ and $R_W = 0.026$ for 5046 reflections and 281 variables in the case of **3**). Computations were carried out using the SHELXTL program system.[5] The maximum residual electron densities in the final ΔF maps were 1.5 and 0.47 eÅ^{-3}.

RESULTS AND DISCUSSION

Synthesis

Although cleavage of $[Co(CO)_3PPh_3]_2$ was only accomplished after 16 h, $[Co(CO)_3L]_2$ [L = $P(OPh)_3$, $AsPh_3$] only required 20 min to be cleaved completely. This difference is merely thought to be a consequence of the low solubility of $[Co(CO)_3PPh_3]_2$.

Interestingly, although the triphenyltin analogues of **1** and **2** [i.e. $Co(Ph_3Sn)(CO)_3L$, L = PPh_3, $P(OPh)_3$] were previously prepared,[2,6] no triphenyl arsine analogue existed. In fact, a search of the literature did not reveal any compounds of the type $[Co(R_3M)(CO)_3AsR'_3]$ (R = Me, Ph; M = Si, Ge, Sn; R′ = Me, Ph).

A literature search revealed that, contrary to our results, Hieber and Lindner[7] had reported that their attempts to cleave the dimer $[Co(CO)_3AsPh_3]_2$ merely led to decomposition and the recovery of $AsPh_3$ amongst other products. We found that the successful preparation of the unstable salt Na[Co $(CO)_3AsPh_3$] crucially depended on the rigorous exclusion of air and moisture, its swift manipulation, and finally the rapid addition of Me_3SnCl.

NMR spectroscopy

^{1}H NMR data for **1**, **2** and **3** appear in Table 1, while ^{13}C, ^{31}P and ^{119}Sn NMR data are shown in Table 2. ^{1}H and ^{13}C NMR resonances could be assigned unambiguously by way of inspection. The methyl protons of **1**, **2** and **3** are observed as sharp singlets, with that of the triphenylphosphite deriva-

Table 1. ^{1}H NMR data for **1**, **2** and **3**[a]

	Phenyl H			Methyl H		
	$\delta(H_o)$	$\delta(H_m)$	$\delta(H_p)$	δ(H)	$^2J(^{119}SnH)$	$^2J(^{117}SnH)$
1	7.60 (m, 6H)	6.97 (m, 9H)		0.72 (s, 9H)	48.0	
2[b]	7.31 (d, 6H)	7.03 (t, 6H)	6.87 (t, 3H)	0.45 (s, 9H)	50.0	
3	7.58 (m, 6H)	6.98 (m, 9H)		0.73 (s, 9H)	50.6	49.0

[a] In benzene-d_6; chemical shifts in ppm relative to TMS; coupling constants in Hz.

[b] $^3J(H_pH_m) = 7.4$; $^3J(H_oH_m) = 7.9$; $^4J(H_oH_p) < 1$.

Table 2. Selected bond lengths (Å) and angles (°) in **1** and **3**

Bond/angle	1	3
Co—Sn	2.574(2)	2.565(1)
Co—P/As	2.197(3)	2.289(1)
Co—C_1	1.78(2)	1.758(5)
Co—C_2	1.79(2)	1.758(5)
Co—C_3	1.699(13)	1.734(5)
C_1—O_1	1.13(2)	1.146(5)
C_2—O_2	1.11(2)	1.132(5)
C_3—O_3	1.171(13)	1.139(5)
Sn—methyl C[a]	2.14	2.12
P/As—ring C[b]	1.808	1.933
Sn—Co—C_1	85.3(4)	84.2(1)
Sn—Co—C_2	85.8	86.5(1)
Sn—Co—C_3	84.6(4)	83.3(1)
Sn—Co—P/As	177.9(1)	177.6
C_1—Co—C_2	117.5(8)	118.5(2)
C_1—Co—C_3	121.7(7)	119.7(2)
C_2—Co—C_3	118.8(7)	119.2(2)
Co—C_1—O_1	177.7(12)	178.1(5)
Co—C_2—O_2	178.0(2)	177.9(4)
Co—C_3—O_3	177.5(14)	178.3(4)

[a] Average of Sn—C_4, Sn—C_5, Sn—C_6.
[b] Average of P/As—C_7, P/As—C_{13}, P/As—C_{19}.

tive occurring 0.3 ppm downfield from those of **1** and **3**.

The slight upfield shift of the methyl carbons relative to the carbons of Me_3SnCl [$\delta(^{13}C) = 5.4$ ppm] on the ^{13}C spectrum, is indicative of the absence of a major movement of electron density across the Co—Sn bond. This supports the suggestion that this bond is of a covalent and not a donor/acceptor nature.[8] Observed $^1J(SnC)$ coupling constants fall in the range 265–280 Hz (average values are given as resolution does not always permit distinction between ^{117}Sn and ^{119}Sn). Earlier NMR studies unfortunately often lack coupling constant details,[9,10] but more recently values ranging from 280 to 320 Hz were reported for $[Co(Ph_3Sn)(CO)_3L]$ (L = carbene).[11,12] The carbonyl carbons in **1**, **2** and **3** occur in the vicinity of 200 ppm (Table 2) and were difficult to detect, presumably due to broadening caused by ^{59}Co.

The $^{31}P\{^1H\}$ spectra of **1** and **2** each consist of a singlet with $\Delta\nu_{\frac{1}{2}} = 50$ Hz (**1**) and 160 Hz (**2**). The spectrum of **1** (Fig. 1) displays the $^{117}Sn/^{119}Sn$-satellites as broad shoulders on either side of the ^{31}P resonance. An accurate value for $^2J(PSn)$ was however, obtained from the well resolved doublet on the $^{119}Sn\{^1H\}$ spectrum.

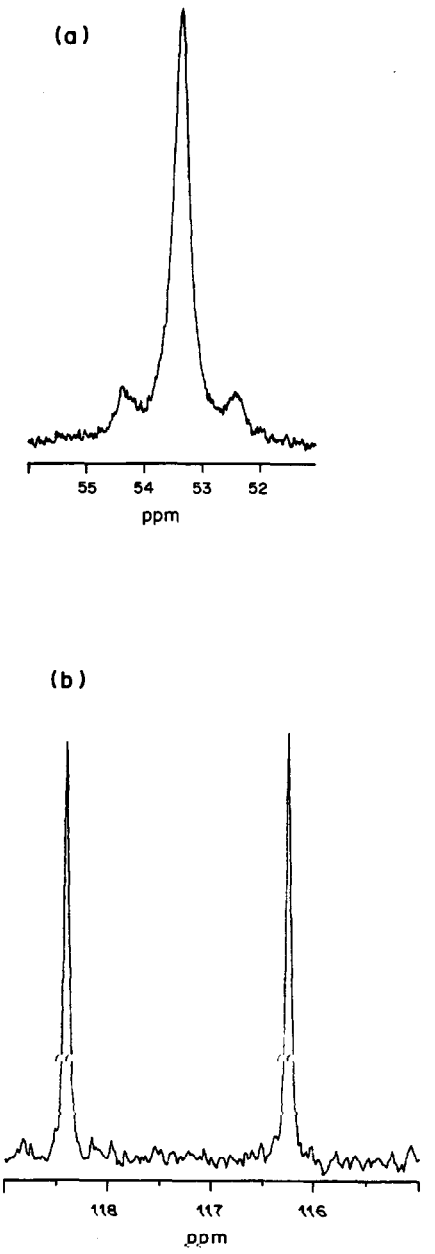

Fig. 1. (a) $^{31}P\{^1H\}$ NMR spectrum of **1** showing the Sn-satellites; (b) $^{119}Sn\{^1H\}$ NMR spectrum of **1** as a result of coupling with ^{31}P.

^{119}Sn spectra were well-resolved. The Sn nucleus seemingly uninfluenced by the neighbouring ^{59}Co nucleus. The sensitivity of the Sn nucleus towards the group occupying the *trans* position (L), is obvious from the decrease in ^{119}Sn chemical shift as electron density is moved away from L and the metal centre towards the three carbonyl groups (for the unsubstituted $Co(Me_3Sn)(CO)_3L$ (L = CO), $\delta(^{119}Sn) = 151$ ppm). The ^{119}Sn chemical shift therefore is a useful measure of the nucleophilicity of the $[Co(CO)_3L]^-$ anion.

Table 3. $^{13}C\{^1H\}$, $^{31}P\{^1H\}$ and $^{119}Sn\{^1H\}$ NMR data[a] for **1**, **2** and **3**

Compound	$Sn(CH_3)_3$[b]	$\delta(^{13}C)$, phenyl carbons				CO[e]	$\delta(^{31}P)$	$\delta(^{119}Sn)$	$^2J(PSn)$[f]
		C_i	C_o	C_m	C_p				
1	−2.8[c]	135.4(d)	133.4(d)	128.8(d)	130.5(s)	201.7(br)	53.4	117.3(d)	240.8
	$^1J(SnC) = 267.2$	$^1J(PC) = 44.4$	$^2J(PC) = 11.7$	$^3J(PC) = 10.2$	$^4J(PC) = 0$				
2	−3.1[d]	151.5(d)	122.1(d)	130.0(s)	125.7(s)	199.5(br)	130.6(br)	136.2(d)	418.7
	$^1J(SnC) = 278.2$	$^2J(PC) = 5.9$	$^3J(PC) = 4.3$	$^4J(PC) = 0$	$^5J(PC) = 0$				
3	−2.6	136.3(s)	132.8(s)	129.3(s)	130.3(s)	201.6(br)			
	$^1J(^{119}SnC) = 276$	—	—	—	—		—	143.6(s)	—
	$^1J(^{117}SnC) = 263$								

[a] Obtained in benzene-d_6; $\delta(^{13}C)$ in ppm relative to solvent ($\delta = 128.00$ ppm); $\delta(^{31}P)$ in ppm relative to 85% H_3PO_4; $\delta(^{119}Sn)$ in ppm relative to Me_4Sn; coupling constants in Hz.

[b] $^1J(SnC)$ is the average of $^1J(^{119}SnC)$ and $^1J(^{117}SnC)$.

[c] $^3J(PC) = 3.0$ Hz.

[d] $^3J(PC) = 5.5$ Hz.

[e] $^2J(PC)$ cannot be obtained due to extensive broadening of the CO resonance by ^{59}Co.

[f] Coupling constants obtained from $^{119}Sn\{^1H\}$ spectra.

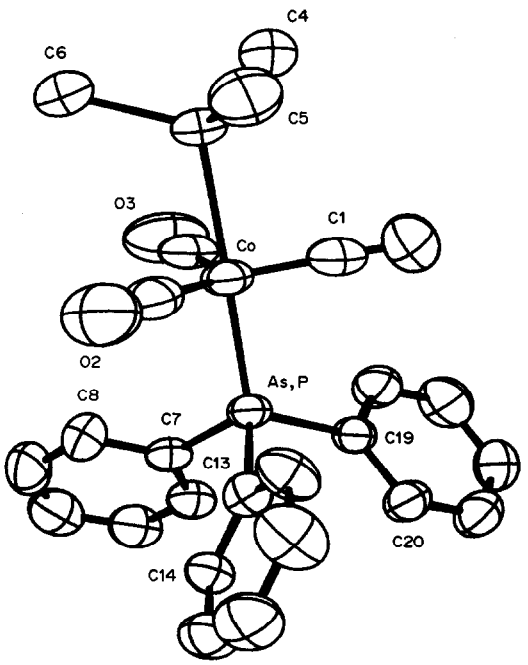

Fig. 2. The X-ray structure of **1** and **3**, showing the numbering of the atoms.

Structural determinations

The X-ray structures of **1** and **3** are shown in Fig. 2, with selected bond lengths and angles in Table 3. In both cases the Co atom forms the centre of a near-perfect trigonal bipyramid with the three carbonyl groups occupying the three equatorial sites. The three phenyl rings and the three methyl groups are eclipsed and are staggered with respect to the three CO groups. The Co atom and the three CO groups are not coplanar; the Co lies at a distance of 0.146(2) Å (**1**) and 0.162(1) Å (**3**), respectively, below the plane. This observed "bending" of the carbonyl ligands towards the $SnMe_3$ moiety has been observed for various compounds containing a transition metal–tin bond—the degree of bending is commonly thought to increase with decreasing bulkiness of the groups on Sn.[8]

In support of the covalent nature of the Co—Sn bond, the Co—Sn distance has been found to decrease on replacement of the organic substituents on Sn by halogens or oxygen.[8] Expectedly therefore, the length of this bond remains uninfluenced by the *trans* ligand, and a Co—Sn bond length of 2.574(2) Å and 2.565(1) Å was respectively measured for **1** and **3**. These values fall well within the limits obtained from a statistical calculation using the CSDS[14] which reveals a mean Co—Sn bond length of 2.58(5) Å for 34 different bonds. A comparison with the structure of the analogous $Co(Ph_3Sn)(CO)_3PPh_3$[15] will also become possible once a more detailed structural analysis is completed.

CONCLUSION

The stability of the compounds $[Co(X)(CO)_3L]$ decreases in the order $X = Ph_3Sn > Me_3Sn$ and $L = PPh_3 > AsPh_3 > P(OPh)_3$. The greater reactivity of the less bulky trimethyltin derivatives (as a result of the weaker (Co—Sn bond) could provide an entry into the synthesis of new compounds with carbonyls in the equatorial plane which, for the purpose of modification, are more accessible.

Acknowledgement—SL and JLMD wish to acknowledge financial assistance by the Foundation for Research Development, Pretoria.

REFERENCES

1. K. M. Mackay and B. K. Nicholson, in *Comprehensive Organometallic Chemistry* (Edited by E. W. Abel, F. G. A. Stone and G. Wilkinson), Vol. 6, pp. 1083–1090. Pergamon Press, Oxford (1981).
2. M. D. Curtis, *Inorg. Chem.* 1972, **11**, 802.
3. R. D. Gorsich, *J. Am. Chem. Soc.* 1962, **84**, 2486.
4. C. Loubser and S. Lotz, *Inorg. Synth.* 1992, **29**, accepted for publication.
5. G. M. Sheldrick, SHELXTL, An integrated system for solving, refining and displaying crystal structures from diffraction data. University of Göttingen, FRG (1978); Revision 4.1 (August 1983).
6. L. M. Bower and M. B. H. Stiddard, *J. Chem. Soc. (A)* 1968, 706.
7. W. Hieber and E. Lindner, *Chem. Ber.* 1961, **94**, 1417.
8. B. Y. K. Ho and J. J. Zuckerman, *J. Organomet. Chem.* 1973, **49**, 1 and refs. therein.
9. D. H. Harris, M. F. Lappert, J. S. Poland and W. McFarlane, *J. Chem. Soc., Dalton Trans.* 1975, 311.
10. V. S. Petrosyan, *Progr. NMR Spectrosc.* 1977, **11**, 115.
11. A. C. Filippou, E. O. Fischer and H. G. Alt, *J. Organomet. Chem.* 1987, **30**, 325.
12. A. C. Filippou, E. O. Fischer and G. Muller, *J. Organomet. Chem.* 1987, **329**, 223.
13. J. K. Stalick and J. A. Ibers, *J. Organomet. Chem.* 1970, **22**, 213.
14. Cambridge Structural Database System.
15. B. Ziolkowska, *Rozniki Chem.* 1969, **43**, 1781.

Polyhedron Vol. 10, No. 22, pp. 2541–2549, 1991
Printed in Great Britain

0277–5387/91 $3.00+.00
© 1991 Pergamon Press plc

SPECTROSCOPIC AND MAGNETIC PROPERTIES OF HIGH SPIN CHROMIUM(II) AND COPPER(II) COMPLEXES WITH BIDENTATE α,α′-DIIMINE LIGANDS: 2,2′-PYRIDYLBENZIMIDAZOLE; 2,2′-PYRIDYLIMIDAZOLE AND 2,2′-PYRIDYLIMIDAZOLINE

BALTAZAR DE CASTRO,* CRISTINA FREIRE, DEOLINDA DOMINGUES and JOÃO GOMES

Departamento de Química, Faculdade de Ciências do Porto, P-4000 Porto, Portugal

(*Received* 22 *February* 1991; *accepted* 11 *July* 1991)

Abstract—Synthesis and physical properties of chromium(II) and copper(II) complexes of general formula $[M(L\text{-}L')Cl_2]$ are reported, where L-L′ is one of the bidentate α,α′-diimine ligands: 2,2′-pyridylbenzimidazole; 2,2′-pyridylimidazole; 2,2′-pyridylimidazoline. The chromium(II) complexes are high spin and spectroscopic data suggest a polymeric hexacoordinate distorted chloride bridged structure; the IR active bands in the region 350–250 cm^{-1} have been assigned to Cr—N and Cr—Cl stretching vibrations. The spectroscopic, EPR and magnetic data for the copper(II) compounds suggest that they are structurally similar to the chromium(II) compounds.

The complexes formed by α,α′-diimine ligands, such as 2,2′-bipyridine (bipy), 1,10-phenanthroline (phen) and related ligands with bivalent transition metals ions have been extensively investigated and several examples of mono-, bis- and tris-diimine complexes have been thoroughly characterized.[1] For chromium(II), most of the known complexes with these ligands have two or three diimines bound to the metal,[2,3] and the few examples of mono-diimine compounds occur with halides or pseudo-halides and possess polymeric hexacoordinate distorted coordination geometries.[3,4]

As part of a more general investigation on the coordination chemistry of chromium(II)[5] we report the synthesis and characterizaton of chromium(II) complexes of the type $[Cr(L\text{-}L')Cl_2]$, where L-L′ is one of the following bidentate α,α′-diimine ligands: 2,2′-pyridylbenzimidazole (pyb); 2,2′-pyridylimidazole (pyi) and 2,2′-pyridylimidazoline (pyim).

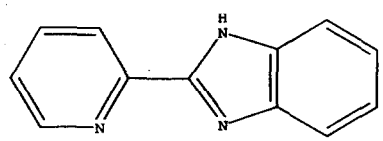

pyb

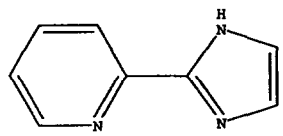

pyi

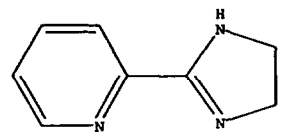

pyim

It is also generally observed that most high-spin chromium(II) complexes are structurally similar to the analogous copper(II) compounds as revealed by X-ray powder diffraction data,[6–8] an observation that has been attributed to the occurrence of Jahn–Teller distortions for both metal ions. This fact prompted us to prepare copper(II) complexes with the same ligands and stoichiometry, $[Cu(L\text{-}L')Cl_2]$, that are more amenable to be studied than the extremely air-sensitive chromium(II) compounds,

* Author to whom correspondence should be addressed.

and to obtain indirect indications on the coordination geometry of the chromium complexes.

EXPERIMENTAL

Materials

Metallic chromium (electrolytic grade) was from Fluka Balzers and copper chloride dihydrate from Merck; all other reagents were from Aldrich and used without further purification, except for ethylenediamine (Merck) that was freshly distilled prior to use. The solvents (Merck; *pro analysi*) were dried over molecular sieves (Merck) and thoroughly degassed before use.

Preparation of compounds

(a) *Ligands.* The ligands 2,2′-pyridylbenzimidazole (pyb), 2,2′-pyridylimidazole (pyi) and 2,2′-pyridylimidazoline (pyim) were prepared and purified by literature methods.[9,10] The ligands were characterized by their ^{1}H NMR spectra and melting points. (Observed and literature values for the melting points—for pyi: 133–135 and 134–135°C;[9] for pyb: 218–220 and 216–219°C;[10] and for pyim: 95–97 and 96–98°C.[10])

(b) *Dichloro(α′-diimine)chromium* (II) *complexes.* All manipulations involving chromium(II) compounds were carried out under dry nitrogen using standard Schlenk techniques. Hydrated chromium(II) chloride was prepared by dissolving chromium metal in dilute hydrochloric acid.[11] All complexes were prepared by treating hot ethanolic solutions of $CrCl_2$ with ethanolic solutions of the ligands in a stoichiometric amount. For the complex $[Cr(pyi)Cl_2]$, 1.2 g of $CrCl_2 \cdot H_2O$ in 20 cm^3 of hot ethanol were reacted with a solution of 1.0 g of pyi in 20 cm^3 of hot ethanol and the resulting solution was then cooled in an ice bath. The microcrystalline solids that formed immediately were collected by filtration, washed with cold diethyl ether and dried by continuous pumping for several hours. Yields of purified complexes ranged from 50 to 70%. These brown compounds are air- and moisture-sensitive, and change colour to green in a few hours when exposed to air, but are stable for several weeks when kept in sealed tubes under dry nitrogen.

(c) *Dichloro(α′-diimine)copper*(II) *complexes.* These complexes were prepared similarly by treating hot solutions of $CuCl_2 \cdot 2H_2O$ (1 g) in ethanol (20 cm^3) with ethanolic solutions of the ligands in a stoichiometric amount. The resulting bright green complexes, collected and dried as described above for the chromium(II) compounds with a yield of 70–90%, are moisture sensitive.

Physical measurements

Analysis. Elemental analysis (C, H, N) were performed at the Microanalytical Laboratory, University of Manchester. Copper and chromium were determined by adding an excess of EDTA (Merck; Titrisol) and back titrating the excess of EDTA with standard calcium solutions (Merck; Titrisol) using a Ca^{2+} selective electrode. Chloride was titrated potentiometrically with silver nitrate using a Cl^- selective electrode. The analytical data are summarized in Table 1.

Visible–IR spectra. Visible and NIR spectra (solution and Nujol mulls) of the copper(II) and chromium(II) complexes were recorded at room temperature on a Cary 17 DX spectrophotometer.

IR spectra. IR spectra were recorded in a Philiphs PU-1800 FTIR spectrophotometer. In the region from 4000 to 300 cm^{-1} the spectra were obtained using KBr pellets or Nujol mulls between KBr plates. For the region 600–200 cm^{-1} CsI pellets of Nujol mulls between polyethylene plates were used.

Conductivity measurements. Conductivity measurements for solutions of the Cu^{II} complexes were carried out with a Metrohm E-518 conductivity meter at 25°C for 10^{-3} M solutions in dimethylformamide (dmf) and methanol (MeOH).

Magnetic measurements. Magnetic susceptibility measurements on powdered solids in sealed tubes were carried out by the Gouy method, from room to liquid nitrogen temperature. The apparatus, calibrated with $Hg[Co(NCS)_4]$, was supplied by Newport Instruments. The magnetic moments were corrected for diamagnetism by using Pascal's constants and for temperature independent paramagnetism, TIP = 0.75 mm^3 mol^{-1} for copper(II).[12]

EPR spectra. EPR spectra were obtained with an X-band Varian E109 spectrometer (9 GHz) equipped with a variable-temperature accessory. The spectra were calibrated with diphenylpicrylhydrazyl (dpph; $g = 2.0037$); the magnetic field was calibrated by use of Mn^{2+} in MgO. The spectra were recorded at −140°C using sealed quartz tubes.

RESULTS AND DISCUSSION

The chromium compounds are soluble or partially soluble in the majority of coordinating solvents (water, dimethyl sulphoxide, *N*,*N*′-dimethylformamide, methanol) but their solutions are dark green, except in dmf where the solutions remain brown. The copper complexes are not soluble in most solvents, being partially soluble in methanol, dmf, $(CH_3)_2SO$ and water.

Table 1. Magnetic data and elemental analyses

Complex	μ_{eff}[a] (BM) 298 K	97 K	Curie–Weiss Law θ[a] (K)	10^5 C[b]	g	Analyses (%)[c] C	H	N	Cr	Cu	Cl⁻	Colour
[illegible]	4.67	4.66	−1	3.44		42.8	3.5	12.4	15.5		21.0	Dark
						(42.9)	(3.3)	(12.5)	(15.5)		(21.1)	brown
$Cr(pyi)Cl_2 \cdot 1/2\,H_2O$	4.57	4.11	−38	3.71		34.5	3.0	15.0	18.9		25.5	Brown
						(34.7)	(2.9)	(15.2)	(18.8)		(25.6)	
[illegible]	4.78	4.33	−34	3.97		33.6	3.5	13.9	17.8		24.7	Dark
						(33.4)	(3.8)	(14.6)	(18.0)		(24.6)	brown
$Cu(pyb)Cl_2$	1.79	1.80	2	0.51	2.07	43.2	2.7	12.5		19.1	21.3	Green
						(43.7)	(2.8)	(12.8)		(19.3)	(21.5)	
$Cu(pyi)Cl_2$	1.81	1.85	6	0.51	2.08	34.5	2.5	15.0		22.5	25.1	Green
						(34.4)	(2.5)	(15.0)		(22.7)	(25.4)	
$Cu(pyim)Cl_2$	1.88	1.90	6	0.54	2.14	34.4	3.2	14.9		22.9	25.0	Green
						(34.1)	(3.2)	(14.9)		(22.6)	(25.2)	

[a] Calculated from $\mu_{eff} = 797.8\,(\chi_A T)^{1/2}$ and the Curie–Weiss law, $\chi_A^{-1} \propto (T-\theta)$.
[b] Values in $m^3\ mol^{-1}$ K.
[c] Calculated values are given in parentheses.

Compounds of $[Cr(L\text{-}L)Cl_2]$

Magnetic data. The observed room temperature magnetic moments are somewhat below the spin-only values expected for systems with four unpaired electrons ($\mu \approx 4.83$ BM) and their values for $[Cr(pyi)Cl_2]$ and $[Cr(pyim)Cl_2]$ decrease with decreasing temperature. The Curie–Weiss law is obeyed for all complexes down to 97 K, although for $[Cr(pyb)Cl_2]$ the value of $\theta \cong 0$ (Table 1).

The magnetic moments for monomeric, tetrahedral high-spin chromium complexes are assumed to be greater than the spin only value and to show a marked temperature dependence,[13] as expected from a T_2 ground state. Our data do not fit this pattern, as the room temperature magnetic moments are smaller than the spin-only value and thus rule out tetrahedral coordination for the chromium complexes reported in this work.

The observed magnetic behaviour is similar to those found in other high-spin chromium(II) complexes of general formula $[Cr(L\text{-}L')X_2]$, where L-L′ is a bidentate ligand and X a halide,[3,4,14] for which a polymeric species with a hexacoordinate sphere around the chromium was asserted. Assuming that a similar structure applies to our complexes, the magnetic moment dependence with temperature can be attributed to antiferromagnetic interaction between chromium atoms. A superexchange mechanism involving chlorine bridges between the metal ions can account for partial spin coupling and is consistent with the proposed polymeric structure. Although for $[Cr(pyb)Cl_2]$ the value of $\theta \cong 0$, a polymeric structure is also assumed, due to the similarity of the spectroscopic data with those of the other two chromium(II) complexes (*vide infra*).

Electronic spectra. The band maxima are presented in Table 2; the electronic spectra of the complexes in Nujol (Fig. 1A) show two bands in the region 450–600 nm (22,200–16,700 cm^{-1}) and a weaker one at ≈750 nm (13,300 cm^{-1}). This behaviour is typical of distorted high-spin six-coordinate chromium(II) complexes,[3,4,6,8,14,15] where the low energy (distortion) band is associated with transitions between the components of the ^5E ground state ($^5B_1 \rightarrow {}^5A_1$), and the higher energy (main) bands is assigned to superimposed $^5B_1 \rightarrow (^5B_2, {}^5E)$ transitions. The main bands, although affected by stereochemical distortions of the complex, are mainly determined by the ligand field strength, and their values are similar to those of polymeric hexacoordinate species with monoamine bidentate ligands and chloride.[3,4]

The complexes prepared, dissolve readily in water, methanol and other hydroxylic solvents, but the resulting solutions are dark green. The electronic spectra of the complexes in these solutions (Fig. 1B) show new high intensity bands in the region from 1250 to 400 nm (25,000–8000 cm^{-1}). These spectra show identical bands to those observed in Nujol mulls and in solution for the low-spin complexes $[Cr(L\text{-}L')_3]Cl_2$, with the same ligands (L-L′) used in our study.[5] This observation implies the existence of low-spin complexes in

Table 2. Solution and Nujol electronic spectra of the $Cr(L\text{-}L')Cl_2$ complexes[a]

Complex	Absorption bands (cm^{-1})						Solvent
$Cr(pyb)Cl_2 \cdot H_2O$	20,100(sh)		15,310				Nujol
	20,100		15,450				dmf
		17,240	14,490		9430[b]	8620	$(CH_3)_2SO$
	21,730	16,660	14,380	13,330[b]	9520	8330	Methanol
	21,500	16,800	15,030	13,330[b]	9250	8360	Water
$Cr(pyi)Cl_2 \cdot 1/2\,H_2O$	22,800(sh)	20,000(sh)		13,330			Nujol
	22,700	20,100		13,500			dmf
		17,200		13,690	10,100	9090	$(CH_3)_2SO$
	21,970	16,000	14,280[b]	13,330	10,200	9170	Methanol
	21,730	16,000	14,280[b]	13,600	10,300	9210	Water
$Cr(pyim)Cl_2 \cdot H_2O$	20,500(sh)	18,200(sh)	14,200(sh)				Nujol
	21,000	18,400	14,000				dmf
		17,100	13,880	13,150		9250	$(CH_3)_2SO$
	20,400	16,390	14,080[b]	12,980[b]	10,100[b]	9090	Methanol
	20,830	16,260	13,880[b]	12,820[b]	10,100[b]	9090	Water

[a] The molar extinction coefficients for the solution spectra are not reported as the high reactivity of these species prevents their determination.

[b] These absorption bands were obtained by spectral deconvolution.

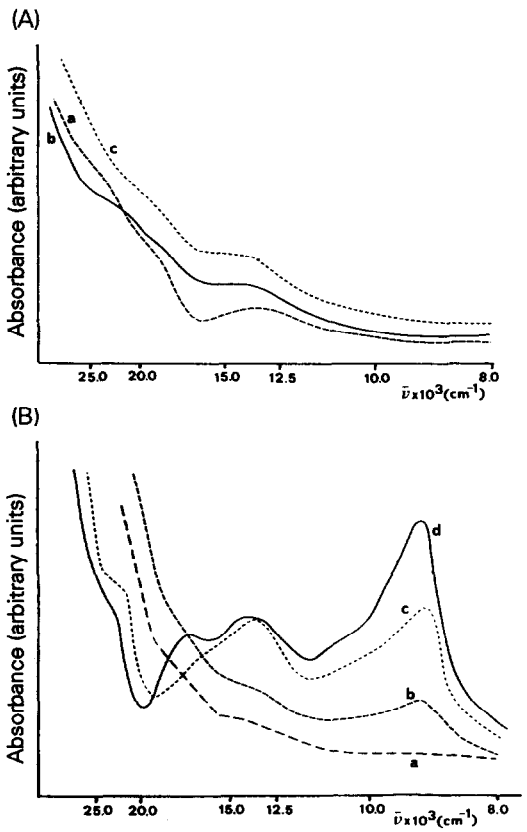

Fig. 1. Electronic specta of $Cr(L\text{-}L')Cl_2$ complexes. (A) Nujol spectra: (a) $Cr(pyi)Cl_2$; (b) $Cr(pyim)Cl_2$; (c) $Cr(pyb)Cl_2$. (B) Solution spectra of $Cr(pyi)Cl_2$ in: (a) dmf; (b) $(CH_3)_2SO$; (c) H_2O and (d) MeOH. The molar extinction coefficients are not reported as the high reactivity of the chromium(II) species prevents their determination.

hydroxylic solvents and provides spectral evidence for the disproportion of monoamine complexes in solution.

$$3/n[Cr(L\text{-}L')Cl_2]_n \rightleftharpoons [Cr(L\text{-}L')_3]Cl_2 + [CrCl_2].$$

The dissolution of these complexes in hydroxylic solvents breaks the halogen bridges and the polymeric structure is destroyed. Similar behaviour has been observed for the analogous complexes with *o*-phenanthroline, where no bands from $CrCl_2$ are observed in the spectra, since the absorption coefficients of $CrCl_2$ are negligible relative to that of the low spin complex.

The observation that solution spectra in $(CH_3)_2SO$ keep some of the features of the Nujol spectra but also exhibit new intense bands, suggests the existence in solution of some of the original species, thus implying only a partial breakdown of the solid structure. Also, as the spectra in dimethylformamide are similar to that obtained in Nujol, it is also conceivable that the solid structure must be retained to a large extent in solution.

IR spectra. Information on metal–ligand stretching vibrations for high-spin chromium(II) complexes is very scarce[16–19] and no data for complexes with bidentate α,α'-diimines and halogens were found in the literature. Larkworthy *et al.* reported IR data for several high-spin chromium(II) chlorocomplexes with pyridine derivatives and assigned the strong band at $\approx$320–330 cm^{-1} to the stretching vibration Cr—Cl, and the less intense band at 270–290 cm^{-1} to the stretching

vibration Cr—N. In these complexes the halogens are bridging the chromium atoms and one ν(Cr—N) vibration and two IR active ν(Cr—Cl) vibrations are expected for these polymeric compounds. The other ν(Cr—Cl) band was assumed to occur at *ca* 160 cm^{-1}, but in the spectra[17] of $[Cr(4\text{-mepy})_2X_2]$, a band at 280 cm^{-1} observed for the chloro-complex was shifted to 251 cm^{-1} when the chlorine was replaced by bromine. It is conceivable that this latter band is also ν(Cr—Cl). For octahedral monomeric complexes with the same ligands (L) and axial terminal halogen atoms $[CrL_4X_2]$, the stretching vibrations Cr—Cl are observed at a much lower frequency ($\approx$150 cm^{-1}), but the stretching Cr—N showed little or no variation. This result is observed for metal ions with Jahn–Teller effect, where long axial bond lengths are expected, thus shifting ν(Cr—Cl) to lower frequencies.[20–22]

To assign the IR spectra of our complexes, the spectra were compared with those of analogous compounds with bromide.[23] The observed stretching frequencies for the chloro and bromo complexes in the region 400–200 cm^{-1} are listed in Table 3, and typical IR spectra are shown in Fig. 2A.

For $[Cr(pyb)Cl_2]$ and $[Cr(pyi)Cl_2]$ the spectra show one strong anion dependent band at $\approx$330 cm^{-1}, that is shifted by *ca* 50 and 30 cm^{-1}, respectively, when the halogen is replaced by bromide (Table 3). Halogen replacement also shifts the band at 305 cm^{-1} of $[Cr(pyb)Cl_2]$ to 249 cm^{-1}; and for $[Cr(pyi)Cl_2]$ the band at 295 cm^{-1} is shifted to 260 cm^{-1}, thus allowing an unambiguous assignment of these two bands to ν(Cr—Cl). The bands at 322 and 305 cm^{-1} for $[Cr(pyb)Cl_2]$ and for $[Cr(pyi)Cl_2]$, respectively, are anion independent and are assigned to ν(Cr—N).

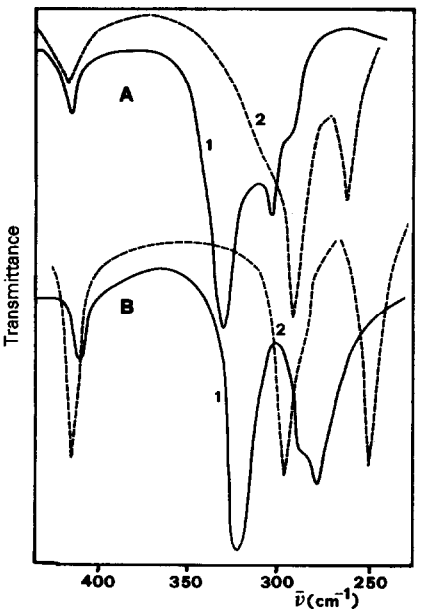

Fig. 2. IR spectra of $M(pyi)X_2$ complexes. (A) (1) $Cr(pyi)Cl_2$; (2) $Cr(pyi)Br_2$. (B) (1) $Cu(pyi)Cl_2$; (2) $Cu(pyi)Br_2$.

As the complex $[Cr(pyim)Br_2]$ could not be prepared, ν(Cr—X) was not assigned by halogen substitution, but as ν(Cr—N) are not strongly ligand dependent, the bands at 336 cm^{-1} and at 305 cm^{-1} are assigned to ν(Cr—Cl), and the one at 278 cm^{-1} is then assigned to ν(Cr—N).

The similarity of high energy band ν(Cr—Cl) in our complexes with those of other chromium(II)[17] complexes with polymeric structure also provides evidence for the postulated structure of our complexes, where asymmetric halogen bridges take place with two short and two long bonds.

Table 3. IR spectra of $Cr(L\text{-}L')X_2$ and $Cu(L\text{-}L')X_2$ complexes

	IR bands, ν (cm^{-1})					
	X = Cl			X = Br[a]		
Complex	(M—N)	(M—Cl)		(M—N)	(M—Br)	
$Cr(pyb)X_2$	322	332	305	322	283	249
$Cr(pyi)X_2$	305	329	295	310	291	260
$Cr(pyim)X_2$	278	335	305	[b]	[b]	[b]
$Cu(pyb)X_2$	322	304	282	321	291	249
$Cu(pyi)X_2$	285	322	280	287	297	249
$Cu(pyim)X_2$	258	304	277	264	289	247

[a] From ref. 33.

[b] The complex could not be prepared.

Compounds of $[Cu(L\text{-}L')Cl_2]$

Contrasting with chromium complexes, the known stereochemistries for copper complexes of general formula $[Cu(L\text{-}L')X_2]$ or $[CuL_2X_2]$ are much more diverse, and the choice of the correct one can hardly be accomplished without X-ray data from single crystals.[1,24] However, combination of spectroscopic and magnetic data, allows for some insight into the stereochemistry of the copper complexes studied.

EPR data. Powdered samples of the pure complexes exhibit at low temperature, EPR spectra that are all different (Fig. 3A and Table 4). For $[Cu(pyi)Cl_2]$ the spectrum is of the rhombic type with three g values; for $[Cu(pyb)Cl_2]$ only two g values are obtained (axial type); and for $[Cu(pyim)Cl_2]$ a pseudo-isotropic spectrum is obtained. No hyperfine splitting with copper or with the ligand nuclei (^{14}N or $^{35,37}Cl$) are observed, probably due to dipole–dipole or exchange interaction. As no signal at half field ($\Delta M_s = \pm 2$) is observed for any spectra, the existence of dimeric structures bridged either by the α,α′-diimine ligand or by the halogen, can be ruled out. However several structures are still possible, monomeric (pseudo-tetrahedral) and polymeric; the latter situation may include doubly halogen-bridged hexacoordinate structure, and singly halogen-bridged five-coordinate complexes. Polycrystalline EPR data do not allow for a clear-cut distinction between monomeric (pseudo-tetrahedral) and polymeric geometries.

Better resolution was achieved in copper-doped (α,α-diimine) cadmium dichloride compounds, for which axial type EPR spectra with coupling to copper in the low field region ($I = 3/2$; four bands) are observed (Fig. 3B). For $[Cu(pyb)Cl_2]$ a hyperfine structure is also observed in the high field region. The structures of these (α,α′-diimine) cadmium dichlorides are not known, but those of [Cd(mpyb)Cl_2], where mpyb is 2-(4′-methyl-2′-pyridyl)benzimidazole, and of other compounds of general formula $[Cd(L\text{-}L')Cl_2]$ with bidentate diimine ligands, are polymeric distorted hexacoordinate with bridging halogens.[25] This coordination geometry must be imposed on the dopant copper complexes and the values of $G = (g_\parallel - 2)/(g_\perp - 2) = 4$ are indicative of a $d_{x^2-y^2}$ ground state for these pseudo-octahedral complexes.[26] For the doped complexes, the g values are invariant within experimental error, suggesting similar electronic properties. However there is a difference between the $A_\parallel$ values of the $[Cu(pyb)Cl_2]$ and the other two complexes; this may be interpreted as resulting from stronger stereochemical distortions imposed for the complex with the bulkier ligand. Indeed, $g_\parallel$ and

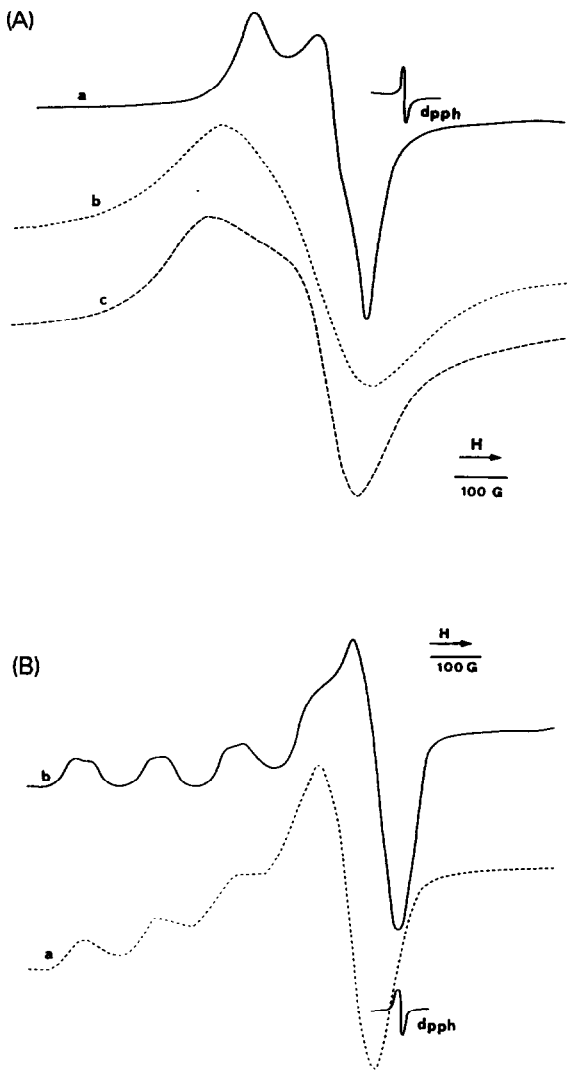

Fig. 3. EPR spectra of $Cu(L\text{-}L')Cl_2$ complexes. (A) Powder spectra: (a) $Cu(pyi)Cl_2$; (b) $Cu(pyim)Cl_2$; (c) $Cu(pyb)Cl_2$. (B) (a) Cu/doped $Cd(pyi)Cl_2$; (b) $Cu(pyi)Cl_2$ in dmf.

$A_\parallel$ values seem relatively insensitive to strong axial perturbations, but rather sensitive to in-plane distortions for hexacoordinate species.[1]

Frozen solution EPR spectra of the pure complexes in dmf (Fig. 3B) and methanol show two sets of bands that must be due to the existence of at least two different species in solution, indicating the compounds to have undergone some structural changes when in the solvents (see below electronic spectra and conductivity data). All spectra show coupling to copper in the low field region and to the nitrogen atoms in the high field region.

IR spectra. To assign the IR spectra of our complexes, the analogous bromo complexes were also prepared. The observed stretching frequencies for the chloro and bromo complexes in the region

Table 4. EPR data for $Cu(L\text{-}L')Cl_2$ complexes

Complex		g_1[a]	g_2[a]	g_3	g_{av}	$A_\parallel$	G[b]
$Cu(pyb)Cl_2$	powder	2.23	2.07		2.12		
	Cu/Cd[c]	2.29	2.07		2.14	133	4.1
	dmf	[d]					
	MeOH	2.30	2.07		2.15	162	4.1
$Cu(pyi)Cl_2$	powder	2.20	2.10	2.05	2.12		
	Cu/Cd[c]	2.28	2.07		2.14	143	4.0
	dmf	[d]					
	MeOH	[d]					
$Cu(pyim)Cl_2$	powder	2.12			2.12		
	Cu/Cd[c]	2.28	2.07		2.14	140	4.0
	dmf	[d]					
	MeOH	[d]					

[a] In methanol and in the doped cadmium complex, $g_\parallel$ is $g_\parallel$ and g_2 is $g_\perp$, except for $Cu(pyim)Cl_2$ whose powder spectrum is pseudo-isotropic.

[b] Calculated as $G = (g_\parallel - 2)/(g_\perp - 2)$.[25]

[c] Cu/Cd refer to EPR data for copper doped (α,α'-diimine) cadmium dichloride compounds.

[d] EPR data show that there are more than one complex in solution, see Fig. 3B.

400–200 cm^{-1} are listed in Table 3, and typical IR spectra are shown in Fig. 2B.

For $[Cu(pyb)X_2]$ and $[Cu(pyim)X_2]$ three bands are observed for both halo complexes. One of them (at 322 and 258, respectively for the pyb and pyim complexes) is invariant with halogen substitution and is attributable to ν(Cu—N). The other two are anion dependent and have been assigned to ν(Cu—X). The complexes $[Cu(pyi)X_2]$ show also two well-resolved bands that are anion dependent and assigned to ν(Cu—X), and partially superimposed on these bands the anion independent on assigned to ν(Cu—N) can also be observed. Absorptions assignable to ν(Cu—N) fall in the region 320–250 cm^{-1}, typical of copper(II) complexes with aromatic nitrogen ligands, and increase with the aromatic character of the diimine ligand.

The ν(Cu—Cl) bands lie in the frequency range indicative of terminally bound chlorides in pseudo-tetrahedral compounds (320–280 cm^{-1}),[27] although for polymeric hexacoordinate copper complexes with two nitrogen donor atoms the values observed for bridging chlorides lie in the same region, well above the expected values for bridging chlorides in other late first transition divalent metal complexes, that appear below 250 cm^{-1}. This anomalous behaviour has been attributed to asymmetric M—X—M bonds caused by the Jahn–Teller effect in d^9 systems, and as copper–halogen stretching frequencies are highly dependent on bond lengths, values ranging from 400 to 240 cm^{-1} have been observed for distorted polymeric hexacoordinate compounds.[22]

The spectra of $[Cu(bipy)X_2]$ and of $[Cu(phen)X_2]$, whose structure is known to be polymeric hexacoordinate, show three sets of strong or medium intensity bands in the region 320–220 cm^{-1} that have been assigned to ν(Cu—N) and to ν(Cu—X) (two bands).[28] The similarity of our ligands to bipy and phen, and of the IR spectra of our copper complexes with those of bipy and phen, lend some support to propose a polymeric distorted hexacoordinate structure for the complexes reported. Nevertheless, a polymeric tetragonally distorted five-coordinate structure could not be excluded for all the complexes, as two different types of Cu—Cl bonds (one short and one long) are also expected for this geometry.[29]

Magnetic data. The Curie–Weiss law is obeyed in the temperature range studied for all compounds with very small and positive Weiss constants, with room temperature magnetic moments (Table 1) lying in the range 1.8–1.9 BM, higher than the spin-only value.[13] Both results provide no evidence for significant magnetic interaction between copper atoms, in the temperature range used, despite the postulated polymeric (hexacoordinate) structure. The g values calculated from the magnetic data show reasonable agreement with those of g_{av} obtained by EPR.

Electronic spectra. The visible/NIR spectra in Nujol (Table 5) show the usual *d–d* type unsymmetrical band, with maxima at *ca* 12,500–14,500 cm^{-1} tailing into the near IR,[14] and with energies

Table 5. Nujol, solution electronic spectra and conductivity data of $Cu(L\text{-}L')Cl_2$ complexes

Complex	Electronic spectra, ν (cm^{-1})					Conductivities, Λ_M ($S\ cm^2\ mol^{-1}$)	
	Nujol	dmf	$(CH_3)_2SO$	CH_3OH	H_2O	dmf	CH_3OH
$Cu(pyb)Cl_2$	12,820	12,820	12,820	13,510	13,890	15.9	73.6
$Cu(pyi)Cl_2$	14,700	13,510	13,340	13,890	14,090	22.2	73.9
$Cu(pyim)Cl_2$	13,340	13,700	13,340	14,090	14,290	25.0	84.4

The values of Λ_M ($S\ cm^2\ mol^{-1}$) in methanol are: 80–115 for 1:1 electrolytes and 160–220 for 1:2 electrolytes, respectively; in dmf the values for 1:1 electrolytes are 60–90, and for 1:2 electrolytes 130–170.[30]

comparable to that of $[Cu(phen)Cl_2]$.[30] This broad band is likely due to several overlapping transitions that are not well resolved, although a deconvolution into two broad bands seems obvious, and assuming D_{4h} symmetry, the unsymmetrical band are assigned to $^2B_{1g} \rightarrow (^2B_2, {}^2E)$ transitions.

Solution electronic spectra show marked variation in band maxima and spectral width, suggesting that the postulated bridges are partially broken in solution, corroborating the EPR data that more than one species are present in solution. As the possible structures in solution are not known, no attempts to deconvolute the unsymmetrical band were made, since possible overlap of bands from different species are possible. Nevertheless, the band maximum show a red shift for dmf and $(CH_3)_2SO$, and a hypsochromic shift for the hydroxylic solvents (water and methanol). The latter shifts are indicative of appreciable chloride substitution by the solvent molecules yielding a stronger ligand field. The red shift can be explained by noting that dmf and $(CH_3)_2SO$ are less effective in disrupting the halogen bridges, and that the resulting species could then involve weaker axial coordination to the solvent molecules, thus rendering the total ligand field weaker than in the polymeric structures.

Conductivity data. The molar conductivity values (Table 5) for dmf solutions of the compounds (*ca* 10^{-3} M) are indicative of non-electrolyte behaviour, but as EPR and electronic spectroscopy data show, the complexes undergo structural changes in solutions through incorporation of solvent molecules in the coordinating sphere of the metal.

The conductivity data for methanol solutions are in the lower limit for 1:1 electrolyte type behaviour,[31] and suggests partial release of chloride ions into solution and an extensive disruption of the polymeric structure. As the EPR spectra also indicate the presence of at least two species in solution, in this solvent it is possible that some chloride ligands are replaced by solvent molecules, also supported by the large changes induced in their electronic spectra.

CONCLUDING REMARKS

The structural characterization of the chromium(II) compounds posed no ambiguities and hexacoordinate polymeric structures with Jahn–Teller distortions were proposed based on magnetic and spectroscopic data.

For copper a bewildering range of structural types is known for complexes of the general formulation $Cu(L\text{-}L')X_2$ or CuL_2X_2,[24,32,33] and it has proved difficult to predict even gross structural features in these complexes in the absence of crystallographic data. In the lack of relationships between structural characteristics and spectroscopic and magnetic properties for these types of copper(II) complexes, the non-availability of X-ray data raises severe difficulties in obtaining structural information for our complexes. Nevertheless, by comparing the data for our complexes with those of other copper(II) complexes with similar ligands and with known structures, we were able to suggest for the complexes reported a hexacoordinated polymeric skeleton, similar to that observed for the analogous chromium(II) complexes.

Acknowledgement—This work was supported by Instituto Nacional de Investigação Científica (INIC, Lisboa) through contract no. 89/EXA/3.

REFERENCES

1. *Comprehensive Coordination Chemistry* (Edited by G. Wilkinson, R. D. Gillard and J. A. McCleverty),

Vol. 2 and 5. Pergamon Press, New York (1987).
2. A. Earnshaw, L. F. Larkworthy, K. C. Patel, K. S. Patel, R. L. Carlin and E. G. Terezakis, *J. Chem. Soc. A* 1966, 511.
3. A. Earnshaw, L. F. Larkworthy and K. C. Patel, *J. Chem. Soc. A* 1970, 1840.
4. A. Earnshaw, L. F. Larkworthy, K. C. Patel and B. J. Tucker, *J. Chem. Soc., Dalton Trans.* 1977, 2209.
5. B. Castro and C. Freire, *Synth. React. Inorg. Met.-Org. Chem.* 1990, **20**, 1.
6. L. F. Larkworthy and B. J. Tucker, *Inorg. Chim. Acta* 1987, **134**, 95.
7. L. F. Larkworthy and M. H. O. N. Richardson, *Inorg. Chim. Acta* 1978, **28**, 251.
8. L. F. Larkworthy and J. M. Tabatabai, *Inorg. Chim. Acta* 1977, **21**, 265.
9. B. Chiswell, F. Lions and B. S. Mornis, *Inorg. Chem.* 1964, **3**, 110.
10. J. L. Walter and H. Freiser, *Analyt. Chem.* 1954, **26**, 217.
11. (a) W. A. Knight and E. M. Rich, *J. Chem. Soc. (Lond.)* 1911, **99**, 87; (b) H. Lux and G. Illman, *Chem. Ber.* 1958, **91**, 2143.
12. E. Maarschall, A. Botterman, S. Veta and A. Miedema, *Physica* 1969, **41**, 473.
13. F. E. Mabbs and D. J. Machin, *Magnetism and Transition Metal Complexes*. Chapman, London (1973).
14. A. B. P. Lever, *Inorganic Electronic Spectroscopy*, 2nd edn. Elsevier, New York (1984).
15. A. Earnshaw, L. F. Larkworthy and K. C. Patel, *J. Chem. Soc. A* 1968, 2276.
16. F. Mani and G. Scapacci, *Inorg. Chim. Acta* 1976, **16**, 163.
17. M. M. Khamar, L. F. Larkworthy and M. H. O. N. Richardson, *Inorg. Chim. Acta* 1978, **28**, 245.
18. L. F. Larkworthy and M. H. O. N. Richardson, *Inorg. Chim. Acta* 1980, **40**, 217.
19. F. Mani and R. Morassi, *Inorg. Chim. Acta* 1979, **36**, 63.
20. R. J. H. Clark and C. S. Williams, *Inorg. Chem.* 1965, **4**, 350.
21. D. M. Adams and P. J. Lock, *J. Chem. Soc. A* 1967, 620.
22. R. H. Nuttall, *Talanta* 1968, **15**, 157.
23. B. Castro, C. Freire and D. Domingues, unpublished results. It must be mentioned that the compound $[Cr(pyim)Br_2]$ could not be prepared.
24. M. Melnik, *Coord. Chem. Rev.* 1982, **47**, 249.
25. M. Masssacesi, M. Biddau, G. Devoto, E. Barni and P. Savarino, *Inorg. Chim. Acta* 1984, **82**, 27.
26. B. J. Hathaway and D. E. Billing, *Coord. Chem. Rev.* 1970, **5**, 143.
27. K. Nakamoto, *Infrared and Raman Spectra of Inorganic and Coordination Compounds*, 4th edn. Wiley, New York (1986).
28. R. E. Wilde and T. K. K. Srinivasan, *J. Inorg. Nucl. Chem.* 1973, **35**, 1017.
29. R. A. Bream, E. D. Ester and D. J. Hodgson, *Inorg. Chem.* 1975, **14**, 1672.
30. N. Ray, S. Tyagi and B. Hathaway, *J. Chem. Soc., Dalton Trans.* 1982, 143.
31. W. J. Geary, *Coord. Chem. Rev.* 1971, **7**, 81.
32. W. E.Marsh, T. L. Bowman, W. E. Hatfield and D. J. Hodgson, *Inorg. Chim. Acta* 1982, **59**, 19.
33. W. E. Marsh, D. E. Eggleston, W. E. Hatfield and D. J. Hodgson, *Inorg. Chim. Acta* 1983, **70**, 137.

Polyhedron Vol. 10, No. 22, pp. 2551–2557, 1991
Printed in Great Britain

0277–5387/91 $3.00+.00
© 1991 Pergamon Press plc

ELECTRON PARAMAGNETIC RESONANCE STUDY ON RADIATION REDUCTION OF DIRHODIUM(II) $[Rh_2(O_2CR)_4]$ AND $[Rh_2Cl_2(O_2CR)_2(N—N)_2]$ COMPLEXES

F. PRUCHNIK,* A. JEZIERSKI and E. KALECIŃSKA

Institute of Chemistry, University of Wrocław, 50-383 Wrocław, Poland

(*Received* 10 *April* 1991; *accepted* 9 *July* 1991)

Abstract—Rhodium(II) complexes $[Rh_2(O_2CR)_4L_2]$ and $[Rh_2Cl_2(O_2CR)_2(N—N)_2]$ (R = H, Me, (*S*)-PhCHOH, (N—N) = 2,2′-bipyridine, 1,10-phenanthroline, L = solvent) in various solvents were reduced using ^{60}Co γ-rays. The resulting unstable species were detected and characterized by EPR spectroscopy. The main products of reduction were axially symmetric complexes containing the Rh_2^{3+} core: $[Rh_2(O_2CR)_4L_2]^-$ and $[Rh_2Cl(O_2CR)_2(N—N)_2L]$.

The chemistry of dirhodium(II) complexes continues to attract considerable attention. The studies on these compounds have developed due to the interest in the theory of the electronic structure of clusters with the single metal–metal bond, their spectroscopic properties, reactivity and their practical application.[1–4] Binuclear rhodium(II) complexes are effective catalysts in reduction of olefins and ketones and in the oxidation of alkenes and alkylaromatic hydrocarbons. They are catalysts for silylation, for cyclopropanation of olefins with diazo compounds, for photocatalytic decomposition of water, etc.

The majority of the rhodium(II) complexes contain bridging ligands: $[Rh_2(\mu\text{-}X)_4L_2]$ (L = Lewis base, X = $RCOO^-$, R′NC(R)O, R′(NC(R)NR′, 2-C_5H_4NNR, RNNNR, 2-C_5H_4NO, etc.) (Fig. 1). The compounds containing either a lower number of bridges, *e.g.* $[Rh_2(\mu\text{-}X)_3L_4]^+$,[5] $[Rh_2X_2(\mu\text{-}OOCR)_2(N—N)_2]$[4,6–11] or containing no bridging ligands, *e.g.* $[Rh_2(dmgH)_4]$, $[Rh_2L_{10}]^{4+}$[3,12] are also known. Dimeric complexes containing the $[Rh_2]^{4+}$ core undergo one-electron transfer reactions giving compounds with $[Rh_2]^{3+}$[13–17] or $[Rh_2]^{5+}$ cores.[2,3,18–21] The dirhodium(II,III) species with the oxygen-containing ligands are easily formed and may be reduced to the parent dirhodium(II) compounds using electrochemical methods,[2,3,18,19] while the singly reduced $Rh_2^{II,I}$ are irreversible and unstable.[13,14] Relatively stable dirhodium(II,I) complexes containing nitrogen ligands: $[Rh_2(R'NCRNR')_4]^-$,[15] $[Rh_2(\mu\text{-}R'NCRNR')_2(CO)_3L]^+$,[16] $[Rh_2(\mu\text{-}RNNNR)_2(CO)_2L_2]^+$,[16] $[Rh_2(\mu\text{-}RNNNR)_2(CO)L(bpy)]^+$[16] and $[Rh_2(\mu\text{-}pz)_2(cod)_2]^+$[17] have been prepared and investigated. Spectroscopic studies suggest the delocalized bonding in the mixed valence complexes containing the $[Rh_2]^{3+}$ core.[13–17]

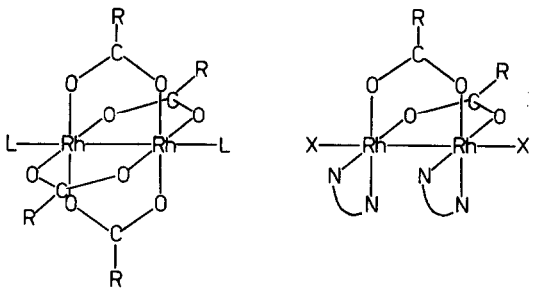

Fig. 1. Scheme of the investigated complexes.

Eastland and Symons have found that $[Rh_2(O_2CCH_3)_4]$ and $[Rh_2(O_2CCF_3)_4]$ complexes may be reduced by radiolysis in CD_3OD using ^{60}Co γ-rays.[13] We have used this method for the reduction of $[Rh_2(O_2CH)_4]$ and $[Rh_2(O_2CCHOHC_6H_5)_4]$.[14]

In this paper we detail the reduction of the $[Rh_2(O_2CR)_4]$ (R = H, $CHOHC_6H_5$) and $[Rh_2Cl_2(O_2CR)_2(N—N)_2]$ complexes (R = H, CH_3, $CHOHC_6H_5$; N—N = 2,2′-bypiridine (bpy), 1,10-phenanthroline (phen)).

Eastland and Symons have found[13] that the initial reduction product was $[Rh_2(O_2CCH_3)_4(solv)_2]^-$, an axially symmetric anion with the electron located in an antibonding $\sigma^*(d_{z^2})$ orbital. Annealing above 77 K gave the other substances; the proposed reactions and assignments of compounds are as follows:[13]

* Author to whom correspondence should be addressed.

$$[Rh_2(\mu\text{-}O_2CCH_3)_4(CD_3OD)_2] \xrightarrow[CD_3OD]{^{60}Co\ \gamma\text{-rays}} [Rh_2(\mu\text{-}O_2CCH_3)_4(CD_3OD)_2]^- \quad \mathbf{I}, g_\perp = 2.24$$

$$\longrightarrow [Rh_2(\mu\text{-}O_2CCH_3)_2(O_2CCH_3)_2(CD_3OD)_2]^- \longrightarrow \mathbf{II}, g_x = 2.248, g_y = 2.240, A_\perp = 0.35\ \text{mT}$$

$$\longrightarrow [(CD_3OD)(CH_3COO)Rh(\mu\text{-}O_2CCH_3)Rh(O_2CCH_3)_2(CD_3OD)]^- \longrightarrow \mathbf{III}, g_x = 2.32, g_y = 2.25, g_z = 2.006$$

$$\longrightarrow [Rh(O_2CCH_3)_2(CD_3OD)_n] + [Rh(O_2CCH_3)_2(CD_3OD)_m]^- \quad \mathbf{IV}, g_x = 2.57$$

In this work we have used similar assignments (I–IV) for the reaction products of our above-mentioned complexes.

EXPERIMENTAL

The complexes

$[Rh_2(O_2CCHOHC_6H_5)_4(H_2O)_2]$,[7] $[Rh_2(O_2CCH_3)_4(H_2O)_2]$,[22] $[Rh_2Cl_2(O_2CH)_2(bpy)_2]\cdot 4H_2O$,[6,8] $[Rh_2Cl_2(O_2CH)_2(phen)_2]$,[6,8] $[Rh_2Cl_2(O_2CCHOHC_6H_5)_2(bpy)_2]\cdot 2H_2O$,[7] $[Rh_2Cl_2(O_2CCH_3)_2(bpy)_2]$[6], $[Rh_2Cl_2(O_2CCH_3)_2(phen)_2]\cdot(H_2O)$[6,23] and $Na_4[Rh_2(CO_3)_4]\cdot 2.5H_2O$[12] were prepared by published procedures.

Synthesis of $[Rh_2(O_2CH)_4(H_2O)_2]$

A mixture, containing $Na_4[Rh_2(CO_3)_4]\cdot 2.5H_2O$ (1 mmol, 0.583 g) and 8.5 cm^3 6% HCOOH was heated at 100°C for 30 min. The product precipitated as a green solid was filtered off, washed with water, then with methanol and dried *in vacuo*; yield 0.27 g (65%).

Radiation reduction of the complexes

The solution of complexes were prepared in methanol, deuterated methanol and deuterated acetone in an argon atmosphere and frozen in liquid nitrogen. The samples were irradiated at 77 K in a ^{60}Co source with doses of 7–11 kGy.

EPR spectra were obtained in JES-ME (Jeol) and SE (Radiopan) X-band spectrometers. The nuclear magnetometer MJ (Radiopan) and EPR standards were used. After measurement at 77 K the samples were annealed to various temperatures and then re-cooled to 77 K for further measurements. The spectra were analysed by the method described earlier.[24]

RESULTS

Radiation reduction of $[Rh_2(O_2CCHOHC_6H_5)_4(H_2O)_2]$ was carried out in CH_3OH, CD_3OD, C_2D_5OD and CD_3COCD_3 solutions. The best results were obtained for CD_3OD solution because of the solubility of the complex and relatively simple EPR spectrum of γ-irradiated CD_3OD. In the EPR spectra of γ-irradiated samples the following paramagnetic species were detected: solvated electrons, organic free radicals, D (or H) atoms and rhodium complexes (Figs 2–4).

A single narrow line characteristic of solvated electrons strongly decreases with temperature increase, and decreases with increase of microwave power. Characteristic lines for radicals: $^{\bullet}CD_2OD$, $^{\bullet}CDO$ and $^{\bullet}CD_3$ (in CD_3OD, and analogous ones in other solvents) were also found.

The paramagnetic rhodium complexes detected in sample containing tetraformatodirhodium and tetramandelatodirhodium were attributable to electron capture species $[Rh_2(O_2CR)_4L_2]^-$ (L = solvent molecule). The initial species observed after irradiation at 77 K had a strong EPR signal with $g_\perp = 2.230$ and $g_\perp = 2.241$ for the formato and mandelato complexes, respectively. The line shape indicated that the signal is a perpendicular feature. The associated parallel feature expected at *ca* $g = 2.00$ was never observed being covered by intense free radicals and solvated electrons signals in that region (Figs 2 and 3). All attempts to detect the parallel line for the rhodium complexes have failed because of the lower stability of the complexes in comparison with that of the organic free radicals in the γ-irradiated solutions. Apart from the $[Rh_2(O_2CR)_4L_2]^-$ complexes, the monomeric complexes $[Rh(O_2CH)_2L]$ ($g_1 = 2.532$, $g_2 = 2.064$, $g_3 = 2.00$) and $[Rh(O_2CCHOHC_6H_5)_2L]$ ($g_1 = 2.512$, $g_2 = 2.046$, $g_3 = 2.00$) were formed (Figs 2 and 3).

Reduction of the $[Rh_2Cl_2(O_2CR)_2(N{-}N)_2]$ complexes gave paramagnetic compounds with $g_\perp$ values at *ca* 2.190–2.195 ($g_\parallel$ is hidden beneath the intense solvent radical lines) (Fig. 4). In the EPR spectrum of $[Rh_2Cl_{2-n}(O_2CCHOHC_6H_5)_2(bpy)_2(CD_3OD)_n]^{(n-1)+}$ the perpendicular feature at $g_\perp = 2.190$ showed a poorly resolved triplet ($A_\perp = 0.7$ mT). After annealing of the samples

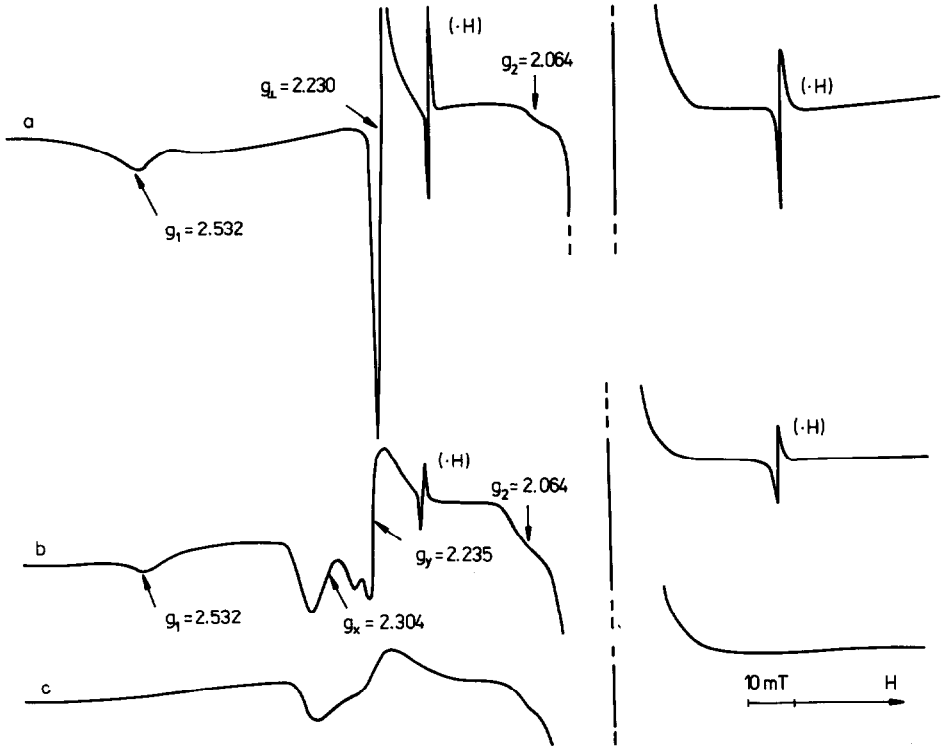

Fig. 2. EPR spectra of γ-irradiated $[Rh_2(O_2CH)_4]$ in CD_3OD. Initial concentration of the rhodium complex 2×10^{-3} M. Dose 7.7 kGy. Microwave frequency 9.112 GHz. (a) At 77 K, gain 2×10^2; (b) at 77 K after annealing at 130 K, gain 1.6×10^3; (c) at 150 K, gain 1.6×10^4.

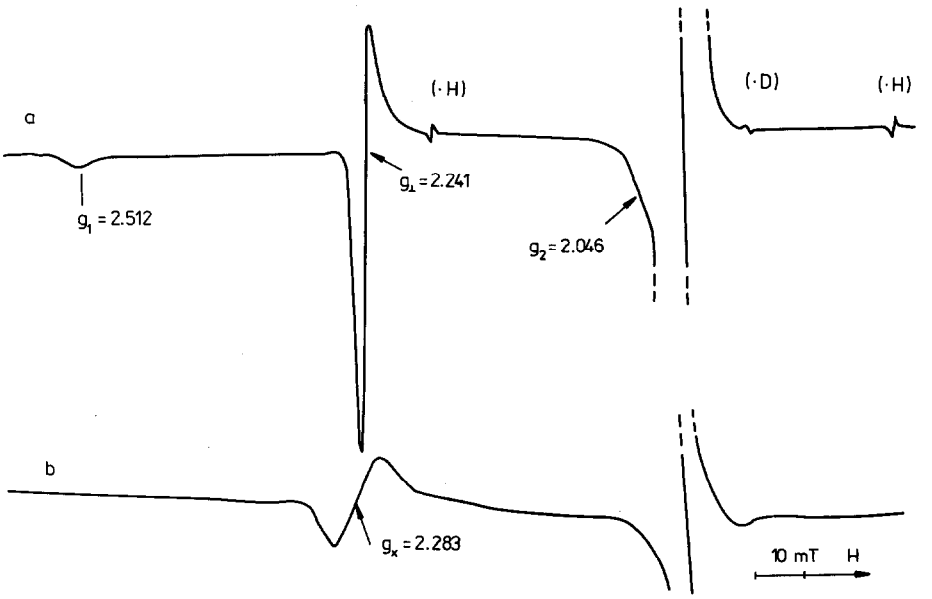

Fig. 3. EPR spectra of γ-irradiated $[Rh_2(O_2CCHOHC_6H_5)_4]$ in C_2D_5OD. Initial concentration of the rhodium complex 1×10^{-2} M. Dose 11.3 kGy. Microwave frequency 9.110 GHz. (a) At 77 K, gain 1×10^2; (b) at 77 K after annealing at 130 K, gain 1.25×10^4.

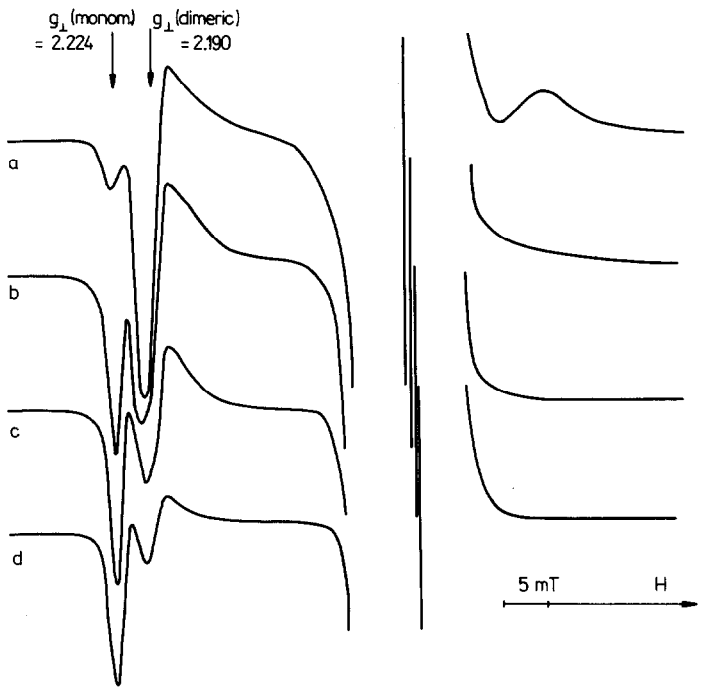

Fig. 4. Temperature dependence of the EPR spectra of the γ-irradiated $[Rh_2Cl_2(O_2C\text{-}CHOHC_6H_5)_2(bpy)_2]$ in CD_3OD. Initial concentration of the rhodium complex 10^{-3} M. Dose 11.5 kGy. Microwave frequency 9.188 GHz, gain 2×10^3. (a) At 77 K; (b) at 112 K, (c) at 125 K, (d) at 145 K.

new signals with g in the region 2.22–2.23 were detected. These signals gained intensity on annealing at the expense of the features at $g_\perp = 2.19$ (Figs 4 and 5). Weak signals at $g = 1.92$, 1.97, 2.18 and 2.28 were also detected. Their intensity is 30–40 times lower as compared with the signals with $g_\perp = 2.190$–2.195. After annealing above the melting point of CD_3OD, the samples containing $[Rh_2Cl_2(O_2CR)_2(N\text{—}N)_2]$ complexes show a relatively intense signal at 2.003, line width 0.6 mT.

The γ-irradiated solid samples of $[Rh_2Cl_2(O_2OCCHOHC_6H_5)_2(bpy)_2]\cdot 2H_2O$ and $[Rh_2Cl_2(O_2CH)_2(bpy)_2]\cdot 4H_2O$ (at room temperature, dose 560 kGy) show at room temperature the stable signals at $g = 2.200$ and $g = 2.220$, respectively.

DISCUSSION

The tetracarboxylato complexes

The signals with $g_\perp$ at *ca* 2.23–2.24 observed for solutions of $[Rh_2(O_2CH)_4(solv)_2]$ and $[Rh_2(O_2CCHOHC_6H_5)_4(solv)_2]$ γ-irradiated at 77 K in anion forming solvents (Figs 2 and 3) are assigned to axially symmetric radical anions, $[Rh_2(O_2CR)_4(solv)_2]^-$. The $g_\perp$ values are very close to that obtained for $[Rh_2(O_2CCH_3)_4(solv)_2]^-$.[13]

In the samples of the mandelato and formato complexes the paramagnetic monomeric rhodium(II) complexes with $g_1 \approx 2.5$ are present (Figs 2 and 3) at 77 K. Annealing of the samples yields the new signal at about $g = 2.3$ analogous to the form III described in ref. 13 (Figs 2 and 3).

These data indicate that the formato- and mandelatodirhodium complexes, contrary to the acetatodirhodium complex[13] during the reduction give both axially symmetric anions $[Rh_2(\mu\text{-}O_2CR)_4(CD_3OD)_2]^-$ and monomers $[Rh(O_2CR)_2(CD_3OD)_n]$. Therefore in the case of these complexes the γ-rays cause not only the reduction of $[Rh_2]^{4+}$ core to the $[Rh_2]^{3+}$ core but also splitting of the Rh—Rh bond.

On the basis of the EPR spectra the following mechanisms of radiation of the $[Rh_2(O_2CR)_4L_2]$ complexes could be proposed as in Scheme 1.

The observed differences between the formato and mandelato complexes described in Schemes 1 and 2, and the acetato complex (described in ref. 13) could be explained on the basis of different redox properties of these complexes. The oxidation potentials $E_{1/2}$ for $[Rh_2(O_2CCH_3)_4(DMF)_2]$, $[Rh_2(O_2CCHOHC_6H_5)_4(DMF)_2]$ and $[Rh_2(O_2CH)_4(DMF)_2]$ are 0.990, 1.170 and 1.215, respectively.[10] The stability of the $[Rh_2(O_2CR)_4L_2]$ complexes depends on the dissociation con-

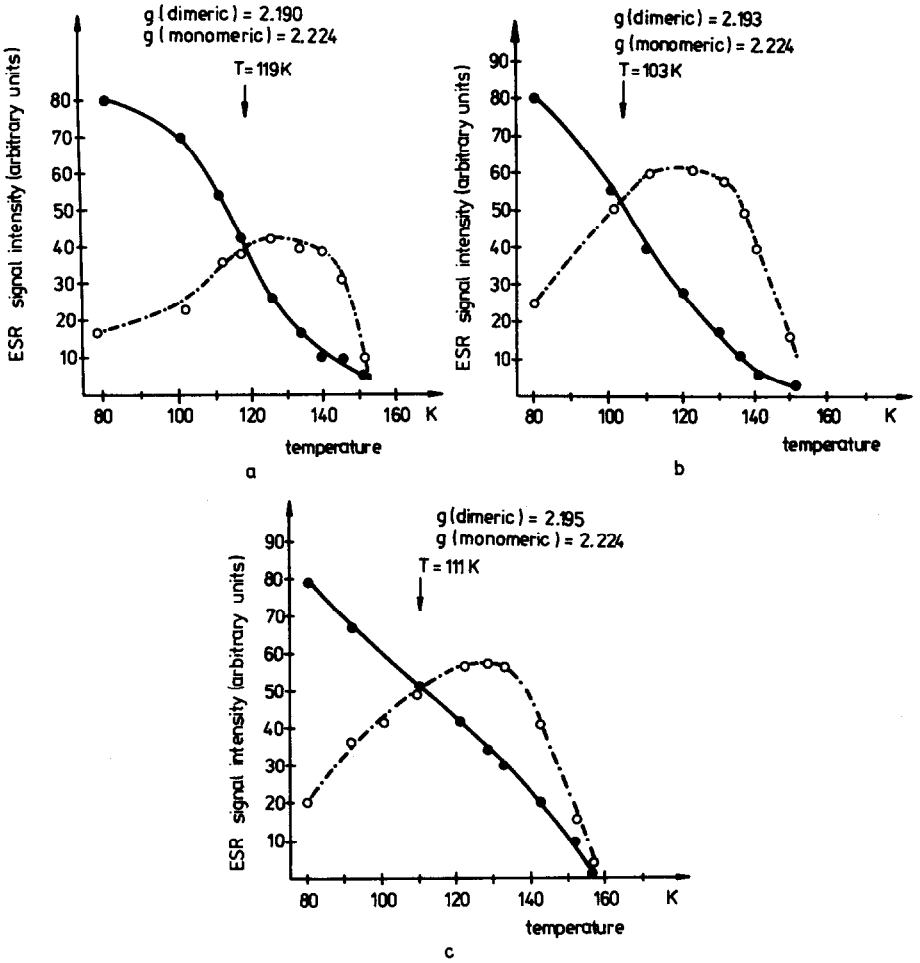

Fig. 5. Temperature dependence of "monomeric" ($g = 2.224$) and "dimeric" ($g = 2.19$) EPR lines for $[Rh_2Cl_2(O_2CR)_2(bpy)_2]$ complexes. Solvent: CD_3OD. Microwave frequency 9.2 GHz. Other comments: see text. Filled circles (solid lines)—the "dimeric" lines ($g = 2.19$); open circle (dashed lines)—the "monomeric" lines ($g = 2.224$). (a) $[Rh_2Cl_2(O_2CCHOHC_6H_5)_2(bpy)_2]$, initial concentration of the rhodium complex 10^{-3} M. (b) $[Rh_2Cl_2(O_2CCH_3)_2(bpy)_2]$, initial concentration of the rhodium complex 10^{-4} M. (c) $[Rh_2Cl_2(O_2C)_2(bpy)_2]$, initial concentration of the rhodium complex 5×10^{-4} M.

stants of the RCOOH acids. This is evidenced by the linear relationship of the half-wave potentials and dissociation constants K_{RCOOH}. The reduction potentials $E_{p,c}$ for $[Rh_2(O_2CR)_4L_2]$ complexes also increase in the same order: $O_2CCH_3 < O_2CCHOHC_6H_5 < O_2CH$. In the case of $Rh_2(O_2CCF_3)_4$ the reduction is favoured by about 0.5 V compared to the acetato complexes.[25] These

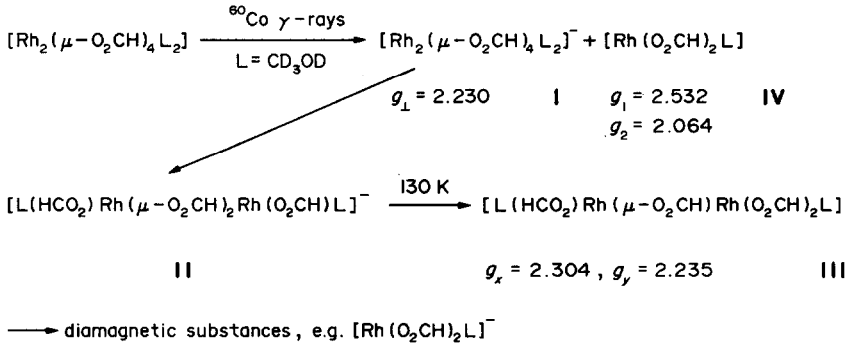

Scheme 1.

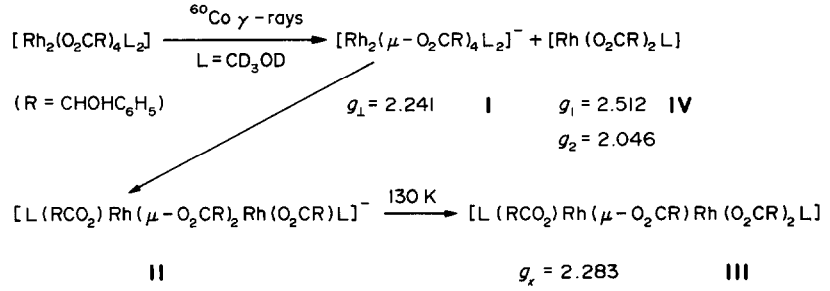

Scheme 2.

relationships indicate that electron-withdrawing substituents help to stabilize the higher oxidation state of the metal. Therefore, the formato and mandelato $[Rh_2^{I,II}(O_2CR)_4L_2]^-$ complex anions probably undergo disproportionation giving mononuclear rhodium(II) and rhodium(I) compounds opposed to the acetato complex. The strength of the Rh—Rh bond in these complexes is almost the same, since Rh—Rh distances for $[Rh_2(O_2CCH_3)_4(H_2O)_2]$, $[Rh_2(O_2CCHOHC_6H_5)_4(C_2H_5OH)_2]$ and $[Rh_2(O_2CH)_4(H_2O)_2]$ differ only slightly (these are 238.56, 238.6 and 238 pm, respectively.[1-4,26]

The complexes containing nitrogen ligands, $[Rh_2Cl_2(O_2CR)_2(N—N)_2]$

In these complexes chloro ligands are coordinated along the Rh—Rh axis (Fig. 1). The Rh—Cl bond is weak because of the long Rh—Cl distance, *ca* 251 pm. In solutions of these complexes the Cl ligands may be replaced by solvent molecules (Lewis bases), *e.g.* $[Rh_2Cl(O_2CR)_2(N—N)_2(solv)]^+$. This was proved by conductivity measurements of these complexes in water and alcohol solutions.[7]

The $[Rh_2Cl_{2-n}(O_2CR)_2(N—N)_2(solv)_n]^{n+}$ complexes are reduced with ^{60}Co γ-rays in solvents giving radicals (mainly $^{\cdot}CD_2OD$). The products are two types of paramagnetic compounds with g values in the range 2.190–2.195 and 2.22–2.23. The EPR data indicate that the $[Rh_2]^{4+}$ core is reduced to $[Rh_2]^{3+}$. In the case of the mandelato complex with 2,2′-bipyridine the dominant product is most likely $[Rh_2Cl_{2-n}(O_2CCHOHC_6H_5)_2(bpy)_2(CD_3OD)_n]^{(n-1)+}$ with $g = 2.190$. This line is a perpendicular feature with poorly resolved splitting with A about 0.7 mT due to two ^{103}Rh nuclei. The similar g values are observed for analogous $[Rh_2Cl_{2-n}(O_2CR)_2(N—N)_2(CD_3OD)_n]^{(n-1)+}$ complexes (N—N = 2,2′-bipyridine, 1,10-phenanthroline, R = H, CH_3).

Annealing of the samples in the temperature range 77–145 K leads to a decrease of the signal at $g = 2.19$ and an increase of the signal at $g = 2.22$ (Fig. 5). The complexes with $g = 2.22$ are probably monomeric rhodium(II) compounds and they arise from dimers. Stability of the dimeric complexes with $[Rh_2]^{3+}$ core decreases in the series: $O_2CCH_3 > O_2CCHOHC_6H_5 > O_2CH$, *i.e.* with the increase of the dissociation constants of the parent carboxylic acids RCOOH (1.85×10^{-5}, 1.4×10^{-4} and 1.77×10^{-4}, respectively). The oxidation potentials $E_{p,a}$ for the $[Rh_2Cl_{2-n}(O_2CR)(bpy)_2(DMF)_n]^{n+}$ complexes increase in the same order: 1.15, 1.145 and 1.160 V for R = CH_3, $CHOHC_6H_5$ and H, respectively.[27] Therefore, the rate of disproportionation reaction of $[Rh_2]^{3+}$ core with formation of Rh^{II} and Rh^{I} mononuclear complexes should decrease in the order: $O_2CH > O_2CCHOHC_6H_5 > O_2CCH_3$. According to this order the highest concentration of $[RhCl_x(O_2CR)(bpy)(CD_3OD)_y]^{y+}$ $(x+y=1)$ were found at *ca* 110–120 K for acetato, *ca* 125–130 K for mandelato and 125–135 K for formato complex (Fig. 5).

On the basis of the experimental data the following scheme of reaction proceeding during the γ-radiolysis of solutions of $[Rh_2Cl_2(O_2CR)_2(N—N)_2]$ complexes can be proposed:

$$[Rh_2Cl_2(\mu\text{-}O_2CR)_2(N—N)_2] \xrightarrow[L = CD_3OD]{^{60}Co\ \gamma\text{-rays}} [Rh_2Cl_{2-n}(\mu\text{-}O_2CR)_2(N—N)_2L_n]^{n+}$$

$$\longrightarrow [Rh_2Cl_{2-n}(\mu\text{-}O_2CR)_2(N—N)_2L_n]^{(n-1)+} + \text{small amount of monomer IV}$$

$$g_\perp = 2.190\text{–}2.195 \quad \mathbf{I}$$

(annealing 77–145 K)

$$\longrightarrow [RhCl_x(O_2CR)(N—N)L_y]^{y+} \quad (x+y=1)$$

$$g = 2.22 \quad \mathbf{IV}$$

The EPR spectra showed that in the primary products of γ-radiolysis small quantities of unidentified paramagnetic substances with g parameters 1.92, 1.97, 2.18 and 2.28 are present.

Among them monomeric rhodium(II) five- or six-coordinate complexes and dimeric complexes with the $[Rh_2]^{3+}$ core without bridging carboxylato ligands may be postulated. In the samples containing products of γ-radiolysis of the $[Rh_2Cl_2(O_2CR)_2(N{-}N)_2]$ complexes annealed to the melting point of the solvent (CD_3OD), a relatively strong signal at $g = 2.003$ and line width 0.6 mT has been observed. These signals should be assigned to rhodium(0) complexes, $[RhCl_x(O_2CR)_y(N{-}N)L]^-$ $(x+y=1)$ with the unpaired electron in the π^* orbital of 2,2′-bipyridine or 1,10-phenanthroline molecules. Similar signals were observed for [M(chel)(N—N)] and $[M(N{-}N)_2]$ (chel = 1,5-cyclooctadiene, 2,5-norboranadiene, (N—N) = bpy, phen, 4,7-Ph_2-phen, 2,2′-bipyrazine) with an electron located in the π^* orbital.[28,29]

It is noteworthy that all results obtained for the $[Rh_2Cl_2(O_2CR)_2(N{-}N)_2]$, (N—N) = 1,10-phenanthroline, are practically the same as those obtained for (N—N) = bpy; g parameters for both types of complexes are the same within the limits of experimental error.

REFERENCES

1. F. A. Cotton and R. A. Walton, *Multiple Bonds Between Metal Atoms*. Wiley Interscience, New York (1982); F. A. Cotton and R. A. Walton, *Structure Bonding* 1985, **62**, 1.
2. E. B. Boyar and S. D. Robinson, *Coord. Chem. Rev.* 1983, **50**, 109.
3. T. R. Felthouse, *Prog. Inorg. Chem.* 1982, **29**, 73.
4. F. P. Pruchnik, *Pure Appl. Chem.* 1989, **61**, 795.
5. I. B. Baranovskii, M. A. Golubichaya, L. M. Dikareva and R. N. Shchelokov, *Zhurn. Neorg. Khim.* 1984, **29**, 1520.
6. F. Pruchnik and M. Zuber, *Rocznicki Chem.* 1977, **51**, 1813.
7. F. Pruchnik, B. R. James and P. Kvintovics, *Can. J. Chem.* 1986, **64**, 936.
8. T. Głowiak, H. Pasternak and F. Pruchnik, *Acta Cryst.* 1987, **C43**, 1036.
9. F. Pruchnik, J. Hanuza, K. Hermanowicz, K. Wajda-Hermanowicz, H. Pasternak and M. Zuber, *Spectrochim. Acta* 1989, **45A**, 835.
10. A. Szymaszek and F. Pruchnik, *Polyhedron* 1990, **9**, 1135.
11. H. Pasternak, E. Lancman and F. Pruchnik, *J. Mol. Cat.* 1985, **29**, 13.
12. C. R. Wilson and H. Taube, *Inorg. Chem.* 1975, **14**, 405; 1975, **14**, 2276.
13. G. W. Eastland and M. C. R. Symons, *J. Chem. Soc., Dalton Trans.* 1984, 2193.
14. E. Kalecińska, A. Jezierski, J. Kaleciński, F. Pruchnik and B. Jeżowska-Trzebiatowska, *Radiat. Phys. Chem.* 1990, **36**, 109.
15. J. C. Le, M. Y. Chavan, L. K. Chau, J. L. Bear and K. M. Kadish, *J. Am. Chem. Soc.* 1985, **107**, 7195.
16. N. G. Connelly and G. Garcia, *J. Chem. Soc., Chem. Commun.* 1987, 246; N. G. Connelly, G. Garcia, M. Gilbert and J. S. Stirling, *J. Chem. Soc., Dalton Trans.* 1987, 1403; N. C. Connelly, C. J. Finn, M. J. Freeman, A. G. Orpen and J. Stirling, *J. Chem. Soc., Chem. Commun.* 1984, 1025.
17. D. O. Fjeldsted and S. R. Stobart, *J. Chem. Soc., Chem. Commun.* 1985, 908; C. Woods, L. J. Tortelli, D. P. Rillema, J. L. E. Burn and J. C. DePriest, *Inorg. Chem.* 1989, **28**, 1673.
18. T. Kawamura, H. Katayama and T. Yamabe, *Chem. Phys. Lett.* 1986, **130**, 20.
19. R. S. Drago, R. Cosmano and J. Telser, *Inorg. Chem.* 1984, **23**, 3120.
20. J. L. Bear, C. L. Yao, F. J. Capdevielle and K. M. Kadish, *Inorg. Chem.* 1988, **27**, 3782.
21. P. Piraino, G. Bruno, S. Lo Schiavo, F. Laschi and P. Zanello, *Inorg. Chem.* 1987, **26**, 2205.
22. G. A. Rempel, P. Ledzdins, H. Smith and G. Wilkinson, *Inorg. Synth.* 1972, **13**, 90.
23. T. Głowiak, M. Zuber and F. Pruchnik, *Polish J. Chem.*, in press.
24. P. Chmielewski and A. Jezierski, *Polyhedron* 1988, **7**, 25.
25. K. Das, K. M. Kadish and J. L. Bear, *Inorg. Chem.* 1978, **17**, 930.
26. P. A. Agaskar, F. A. Cotton, L. R. Falvello and S. Han, *J. Am. Chem. Soc.* 1986, **108**, 1214.
27. A. Szymaszek and F. P. Pruchnik, submitted for publication.
28. W. A. Fordyce, K. H. Pool and G. A. Crosby, *Inorg. Chem.* 1982, **21**, 1027.
29. H. Caldararu, M. K. DeArmond, K. W. Hanck and V. E. Sahini, *J. Am. Chem. Soc.* 1976, **98**, 4455.

Polyhedron Vol. 10, No. 22, pp. 2559–2565, 1991
Printed in Great Britain

0277–5387/91 $3.00+.00
© 1991 Pergamon Press plc

RUTHENIUM(III) SCHIFF BASE CHLORO AND CARBONYL COMPLEXES: SYNTHESIS, CHARACTERIZATION AND EPR STUDIES

M. M. TAQUI KHAN,* D. SRINIVAS, R. I. KURESHY and N. H. KHAN

Discipline of Coordination Chemistry and Homogeneous Catalysis,
Central Salt and Marine Chemicals Research Institute, Bhavnagar 364 002, India

(*Received* 18 *March* 1991; *accepted* 9 *July* 1991)

Abstract—The synthesis and characterization of stable ruthenium(III) Schiff base chloro and carbonyl complexes with the axial ligands chloro (Cl), imidazole (Im) and 2-methylimidazole (2-MeIm) are reported. The Schiff bases were synthesized by the interaction of naphthaldehyde with amines such as *o*-phenylenediamine, ethylenediamine, propylenediamine and diethylenetriamine. The geometry around ruthenium in these complexes is psuedooctahedral. The complexes are low-spin $4d^5$ (S = 1/2) and display characteristic EPR spectra in the powder samples and in frozen solutions at 298 and 77 K. The EPR data and EHMO calculations on model complexes indicate that the d_{xy} orbital lies above d_{xz} and d_{yz} orbitals.

Studies on carbonyl complexes of ruthenium are confined so far to the low-valent oxidation state of ruthenium with only a few reports available on Ru^{III} carbonyl complexes.[1,2] Several ruthenium complexes are known as homogeneous catalysts in carbonylation, hydroformylation and oxo reactions.[3–7] With the intention of synthesizing high valent stable ruthenium complexes and to study their catalytic activity, we initiated work on some Ru^{III} Schiff base chloro and carbonyl complexes derived from aldehydes, namely salicylaldehyde and picolinaldehyde and several amines.[8,9] Some of these complexes were found to be good homogeneous catalysts in the reductive carbonylation of nitrobenzene to phenylurethane by a phosgene-free route[10] and in the oxidation reaction of cyclohexene to its epoxide.[11]

In continuation of our earlier work,[8–11] we now report the synthesis and characterization of a new class of Ru^{III} Schiff base chloro (**1a–10a**) and carbonyl (**1b–10b**) complexes of the type $[RuLX(Cl)]^m$ and $[RuLX(CO)]^n$, respectively, where L = Schiff base, namely bis(naphthaldehyde)-*o*-phenylenediimine (naphoph), bis(naphthaldehyde)ethylenediimine (naphen), bis(naphthaldehyde)propylenediimine (naphprop) and bis(naphthaldehyde)diethylenetriimine (naphdien); $m = -1$ and $n = 0$ for $X = Cl^-$; $m = 0$ and $n = 1$ for X = Im and 2-MeIm (Structure 1). The geometry around ruthenium in these complexes is distorted octahedral with naphoph, naphen and naphprop coordinating as tetradentate ligands and naphdien as a pentadentate ligand.

The complexes were characterized by analytical data and spectroscopic (UV–visible, IR and EPR), magnetic susceptibility and differential pulse polarographic (DPP) techniques. The EPR spectroscopy is used as a probe to study the molecular distortions caused by the substituents on the Schiff bases and on axial ligands (X) and the catalytic activity of the complexes. Extended Hückel Molecular Orbital (EHMO) calculations were performed on model chloro and carbonyl complexes to estimate the electronic ground state wave function and MO energy level scheme.

EXPERIMENTAL

Preparation of the complexes

Ruthenium(III) Schiff base chloro complexes, $K[Ru(naphoph)Cl_2]$ (**1a**), [Ru(naphoph)(Im)Cl] (**2a**), [Ru(naphoph)(2-MeIm)Cl] (**3a**), $K[Ru(naphen)Cl_2]$ (**4a**), [Ru(naphen)(Im)Cl] (**5a**), [Ru(na-

* Author to whom correspondence should be addressed.

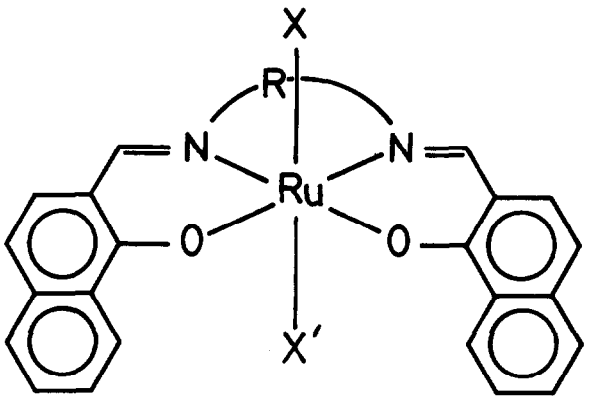

Complex No.	X'	X	R
1a, 2a, 3a	Cl	Cl, Im, 2-MeIm	$-(C_6H_4)-$
1b, 2b, 3b	CO		
4a, 5a, 6a	Cl	Cl, Im, 2-MeIm	$-(CH_2)_2-$
4b, 5b, 6b	CO		
7a, 8a, 9a	Cl	Cl, Im, 2-MeIm	$-(CH(CH_3)CH_2)-$
7b, 8b, 9b	CO		
10a	Cl	N of R	$-(C_2H_4)NH(C_2H_4)-$
10b	CO		

Structure 1

phen)(2-MeIm)Cl] (**6a**), K[Ru(naphprop)Cl_2] (**7a**), [Ru(naphprop)(Im)Cl] (**8a**), [Ru(naphprop)(2-MeIm)Cl] (**9a**) and [Ru(naphdien)Cl] (**10a**) were prepared according to the reported procedure.[12]

The carbonyl complexes, [Ru(naphoph)(Cl)(CO)] (**1b**), [Ru(naphoph)(Im)(CO)]Cl (**2b**), [Ru(naphoph)(2-MeIm)(CO)]Cl (**3b**), [Ru(naphen)(Cl)(CO)] (**4b**), [Ru(naphen)(Im)(CO)]Cl (**5b**), [Ru(naphen)(2-MeIm)(CO)]Cl (**6b**), [Ru(naphprop)(Cl)(CO)] (**7b**), [Ru(naphprop)(Im)(CO)]Cl (**8b**), [Ru(naphprop)(2-MeIm)(CO)]Cl (**9b**) and [Ru(naphdien)(CO)]Cl (**10b**) were synthesized from their respective parent chloro complexes **1a**–**10a**.

Carbon monoxide was bubbled through the methanolic solutions of the parent complexes (2 mM) for about 10 h under constant stirring. Except complexes **1b**, **4b** and **7b**, for the rest of the carbonyl complexes the above reaction mixture was concentrated and precipitated by the addition of dry diethyl ether. The complexes were recrystallized from dry diethyl ether and ethyl acetate. The carbonyl complexes thus obtained were dried *in vacuo* over $CaCl_2$.

In the cases of complexes **1b**, **4b** and **7b**, KCl was filtered off, the filtrates were concentrated and the complexes were precipitated and recrystallized in the same way as discussed above. Naphoph complexes **1b**–**3b** were dark brown while the rest of the carbonyl complexes were dark green in colour (yield: 60–70%). All the chemicals and solvents used were of AR grade and purified further prior to use.

Physical measurements

Microanalyses (C, H, N) of the complexes were done by a Carlo Erba 1106 elemental analyser. Solution electrical conductivity was measured at

298 K by using a Digisun Electronics Conductivity bridge. IR spectra were obtained at 298 K on a Nicolet 200 SXV FT-IR instrument as Nujol mulls/KBr pellets. Electronic spectra were recorded in DMF solutions on a Shimadzu Model UV-160 spectrophotometer. DPP data were recorded at 298 K on a Princeton Applied Research Model 174 electrochemical system.

Magnetic moment of the solid complexes were measured by a PAR model 155 vibrating sample magnetometer. The complex $Hg[Co(SCN)_4]$ was used as a calibrant and the experimental magnetic moments were corrected for diamagnetism. EPR spectra were recorded on a Bruker X-band spectrometer using 100 kHz field modulation. The organic free radical DPPH was used as a field marker ($g = 2.0036$). Experiments were conducted in powder samples as well as in solutions at 298 and 77 K.

Molecular orbital calculations

MO calculations were performed by using the EHMO method described by Hoffmann.[13] The off-diagonal elements were calculated by a weighted Wolfberg–Helmholz formula,[14] with the Hückel constant of 1.65. The input parameters such as Coulomb integrals and orbital exponents for Ru, Cl, O, N and H were taken from ref. 15.

In the present Schiff base complexes such as complex **1a** one has to deal with a basis set containing 173 AOs to evaluate the MOs and their energies. As the program cannot handle such large molecules, calculations were performed on model chloro and carbonyl complexes in which the bridging group between N and O (Structure 1) was replaced by =CH—CH=CH— and that between N atoms was replaced by a NH group. As the crystal structures of the complexes are not known average Ru^{III}-ligand distances were assumed (Ru—Cl = 2.36, Ru—O = 2.03, Ru—N = 2.11, N—H = 1.0, C—H = 1.09 Å, N—Ru—O = 96° and N_1—Ru—N_2 = 84°). The Schiff base ligand was assumed to be in the *xy* plane and the *z*-axis coincides with the Cl—Ru—X axis. The Ru—C≡O bond was assumed linear with Ru—C = 1.84 Å and C≡O = 1.13 Å.

RESULTS AND DISCUSSION

The analytical data for the solid Ru^{III} Schiff base carbonyl complexes **1b–10b** are listed in Table 1. The freshly prepared DMF solutions of complexes **2b**, **3b**, **5b**, **6b**, **8b** and **9b** (1 mM) are 1:1 electrolytes while the rest of the carbonyl complexes are non-electrolytes.

In the IR spectra of the complexes a band at 1625–1635 cm^{-1} due to the azomethine group of the ligands undergoes shift to lower frequency (1590–1610 cm^{-1}) after complexation indicating the coordination of imine nitrogen to ruthenium.[16,17] The ν(Ru—Cl) band is more intense than ν(Ru—N) band and occurs around 320 cm^{-1} in all the complexes. Imidazole and 2-methylimidazole complexes show additional bands near 620 and 1000 cm^{-1} for the coordinated Im and 2-MeIm groups, respectively. The IR spectra of solid carbonyl complexes are characterized by an intense ν(C≡O) band in the range 1940–1980 cm^{-1} (Table 1) which was completely absent in the parent chloro complexes.[12] This band for free CO occurs at 2155 cm^{-1}. The shift in ν(C≡O) on coordination is consistent with those reported earlier.[9]

The electronic absorption spectra for complexes **1b–10b** are almost similar to those for the parent chloro complexes **1a–10a** except for some changes in peak intensities and positions.[12] Intense bands around 270, 305 and 345 nm in the UV region (Table 1) are assigned to the π–π^* and n–π^* transitions of the Schiff base ligand. The latter band undergoes a hypsochromic shift in all the complexes due to coordination of the Schiff base ligand to ruthenium. Three resolved and moderately intense CT bands appear in the range 420–760 nm. Some of the *d–d* bands are masked by the CT bands in this region.

The DPP of complexes **1b–10b** under dropping mercury electrode consists of a single Ru^{III}/Ru^{II} reduction couple. The equatorial and axial ligands have a significant effect on the $E_{1/2}$ values (Table 1). The $-E_{1/2}$ values for complexes **1b–10b** vary with the Schiff bases in the order naphoph > naphprop > naphen > naphdien and with the axial ligands in the order Im > 2-MeIm > Cl^-. A similar trend in $E_{1/2}$ values with the axial ligands was also observed with the other Ru^{III} Schiff base complexes reported earlier.[9] Though 2-MeIm is more basic than Im, large negative $E_{1/2}$ values for Im complexes compared to that for 2-MeIm complexes could be due to the intermolecular H-bonding in the former case than in the latter.

The magnetic moment (μ_{eff}) for all the chloro and carbonyl complexes as powder samples at 298 K falls in the range 1.97–2.08 μ_B corresponding to a single unpaired electron.

The EPR spectra for complexes **1a–10a** and **1b–10b**, as powders at 298 K consist of three partially resolved *g* features characteristic of the +3 oxidation state for ruthenium with the unpaired electron in one of the t_2 orbitals and a low-symmetry crystal field around ruthenium. The EPR lines at 298 K are broad probably due to short spin–lattice relaxation time and intermolecular spin exchange

Table 1. Elemental analysis, IR data, $E_{1/2}$ values for the Ru^{III}/Ru^{II} reduction couple and UV–visible spectral data for Ru^{III} Schiff base carbonyl complexes

Complex no.	Elemental analysis[a] (%) C	H	N	$\nu(C\equiv O)$[b] (cm^{-1})	$E_{1/2}$[c] Ru^{III}/Ru^{II}	Electronic spectral data[d] λ_{max} (nm) (ε, $M^{-1}\,cm^{-1}$)
1b	60.0 (60.1)	3.0 (3.1)	4.3 (4.8)	1970	−0.54	760(1490), 559(3505), 471(4935), 345(8550)[e] 317(1900), 269(11,790)
2b	62.1 (62.9)	3.1 (3.5)	9.0 (9.2)	1980	−0.59	715(2920), 555(3498), 469(5080), 346(7848), 310(6740), 268(7220)
3b	63.2 (63.3)	3.3 (3.9)	8.3 (8.9)	1980	−0.56	735(2970), 545(3445),[e] 348(74,100), 309(4800), 278(12,500)
4b	56.3 (56.6)	3.1 (3.4)	5.2 (5.3)	1965	−0.48	620(1670), 550(13,700),[e] 453(23,900), 375(8320), 273(56,900)
5b	59.1 (59.8)	3.1 (3.8)	9.3 (10.0)	1970	−0.56	690(2420), 550(935), 420(1755),[e] 319(3950), 259(12,500)
6b	60.1 (60.4)	4.0 (4.0)	9.1 (9.7)	1945	−0.54	624(4100), 553(19,200), 394(2755),[e] 315(6710), 270(13,500)
7b	57.1 (57.4)	3.2 (3.5)	5.0 (5.1)	1950	−0.54	670(2020), 550(18,550), 450(5003), 420(14,405), 339(8523), 290(53,200)
8b	60.2 (60.5)	3.4 (3.8)	9.1 (9.7)	1970	−0.62	624(4130), 555(936), 420(14,160),[e] 319(3950), 279(58,275)
9b	63.1 (63.3)	3.4 (3.9)	8.0 (8.9)	1975	−0.59	660(1900), 550(29,900), 425(20,710),[e] 362(37,200), 259(12,502)
10b	60.0 (60.4)	4.0 (4.1)	7.3 (7.8)	1980	−0.53	653(1800), 554(29,350), 410(2510),[e] 340(8250), 305(1250)

[a] Found (Calc).
[b] In KBr pellets at 298 K.
[c] Dropping mercury electrode is the working electrode; solvent is DMF, supporting electrode is tetrabutyl ammonium perchlorate (0.1 M), the standard electrode is Ag/AgCl.
[d] Solvent is DMF.
[e] Shoulder.

interaction. Cooling the samples to 77 K narrowed the lines. No hyperfine coupling due to ruthenium could be observed. The absence of ruthenium hyperfine features was observed also by several investigators.[18,19] The g-values at 77 K listed in Table 2 are slightly different from those at 298 K indicating the depopulation of paramagnetic excited J states which have become thermally inaccessible at low temperatures.

The EPR spectra of the carbonyl complexes as frozen DMF solutions are similar to those for their powder samples at 77 K. However, the spectra for the chloro complexes at 77 K vary considerably with the solvent indicating that Ru^{III} chloro complexes are unstable in solution while the carbonyl complexes are quite stable. The instability of the chloro complexes could be attributed to the lability of the Ru—Cl bond that dissociates in solution to form solvated species. As the chloro complexes are not stable in solution, we had restricted our study only to solid complexes in the latter part of the section. Representative EPR spectra of the complexes are shown in Fig. 1.

The EPR data on powder samples, at 77 K, were analysed using the approach developed by Hill[20] and successfully applied to a number of low-spin d^5 systems by several investigators.[9,18,19] The details of the calculation were discussed elsewhere.[9] In the presence of low-symmetry (tetragonal, Δ and rhombic, V) distortions and spin–orbit coupling, the six T_2 orbitals of a low-spin d^5 configuration split into three Kramers' doublets. The ground state doublet is composed of t_2 functions, $|+1\rangle = -(d_{xz}+id_{yz})/\sqrt{2}$, $|\xi\rangle = id_{xy}$ and $|-1\rangle = (d_{xz}-id_{yz})/\sqrt{2}$, with admixture coefficients a, b and c, respectively.

For a particular g values set two solutions, (1) $g_z < g_x$ and g_y; g_x, g_y and g_z are positive and (2) $g_z < g_x$ and g_y; g_x and g_y are positive while g_z is negative, were found to be physically reasonable. The covalency parameter, k for solution 1 was less then 1.0 while it was greater than 1 for solution 2. The distortion parameters (Δ and V) and excitation

Table 2. g values,[a] MO coefficients, delocalization parameter, distortion parameters and excitation energies of ruthenium(III) Schiff base chloro and carbonyl complexes at 77 K

Complex no.	g_x	g_y	g_z	a	b	c	k	Δ/λ	V/λ	$\Delta E_1/\lambda$	$\Delta E_2/\lambda$
1a	2.377	2.132	1.919	0.116	0.992	0.042	0.877	7.547	−5.886	4.707	10.634
1b	2.340	2.112	1.876	0.149	0.988	0.047	0.660	5.700	−3.954	3.849	7.871
2a	2.416	2.112	1.845	0.164	0.985	0.058	0.709	5.355	−4.196	3.409	7.655
2b	2.348	2.115	1.881	0.145	0.988	0.047	0.685	5.878	−4.167	3.919	8.148
3a	2.465	2.105	1.823	0.174	0.983	0.066	0.732	5.193	−4.402	3.161	7.602
3b	2.344	2.125	1.897	0.134	0.990	0.043	0.729	6.308	−4.366	4.237	8.666
4a	2.451	2.181	1.758	0.209	0.977	0.048	0.707	3.902	−2.112	3.007	5.251
4b	2.352	2.195	1.805	0.190	0.981	0.030	0.659	4.130	−1.520	3.472	5.200
5a	2.382	2.167	1.845	0.167	0.985	0.040	0.718	4.885	−2.665	3.675	6.454
5b	2.365	2.132	1.845	0.167	0.985	0.046	0.662	4.967	−3.094	3.556	6.740
6a	2.398	2.132	1.897	0.132	0.990	0.047	0.825	6.646	−5.159	4.184	9.389
6b	2.390	2.156	1.843	0.167	0.985	0.044	0.714	4.925	−2.918	3.597	6.614
7a[b]		2.096					1.072				
7b	2.373	2.105	1.860	0.157	0.986	0.054	0.670	5.529	−4.183	3.579	7.817
8a	2.365	2.086	1.855	0.161	0.985	0.058	0.634	5.521	−4.425	3.458	7.930
8b	2.357	2.132	1.855	0.162	0.986	0.045	0.667	5.135	−3.190	3.669	6.948
9a	2.415	2.066	1.887	0.136	0.989	0.066	0.752	7.408	−7.749	3.677	11.431
9b	2.373	2.149	1.863	0.156	0.987	0.043	0.720	5.301	−3.226	3.811	7.127
10a	2.425	2.160	1.866	0.152	0.987	0.046	0.810	5.577	−3.773	3.817	7.662
10b	2.390	2.100	1.924	0.111	0.993	0.050	0.884	8.620	−8.252	4.604	12.872

[a] Estimated error in g_1, g_2, g_3 is ± 0.008.

[b] Isotropic spectrum was observed and k was calculated by using the expression $g_{av} = 2/3(2k+1)$.

energies from the ground Kramers' doublet to excited doublets (ΔE_1 and ΔE_2) were larger for solution 1 than for solution 2. However, a molecular model for the complexes (Structure 1) and extended π-delocalization of the Schiff base ligand indicate that the covalency parameter must be less than 1 and distortions and excitation energies must be large. It is therefore concluded that solution 1 gives the correct ground state wave function. The MO admixture coefficients, covalency, distortion parameters and excitation energies corresponding to solution 1 for all the complexes are listed in Table 2. EHMO calculations on chloro and carbonyl complexes (vide infra) support these results.

It is clear from Table 2 that the tetragonal splitting, Δ, is larger than the rhombic splitting, V and further both these parameters are larger than the spin–orbit coupling constant (λ).* The positive value for Δ/λ for all the complexes and the larger MO coefficient for d_{xy} orbital, b, than 'a' and 'c' indicate that in the absence of spin–orbit coupling d_{xy} lies above ($d_{xz} + id_{yz}$) orbitals resulting in the ground state electronic configuration $d_{xz}^2 d_{yz}^2 d_{xy}^1$. The value for Δ is in general larger for carbonyl complexes than for chloro complexes. It is pertinent to note that Ru^{III} chloro complexes derived from salicylaldehyde have a d_{xz}/d_{yz} ground state while their carbonyl analogues have a d_{xy} ground state.[9] However, in the present case the stabilization of d_{xz}/d_{yz} orbitals for both chloro and carbonyl complexes could be because of the additional π-interaction in the naphthaldehyde group.

The parameters k, Δ/λ and $\Delta E_i/\lambda$ ($i = 1$ and 2) change with the basicity of the axial ligands in the order 2-MeIm > Im > Cl^-. The value of k is smaller for carbonyl complexes than for chloro complexes indicating that the Ru—CO bond is more covalent than Ru—Cl bond. This is because of the difference in the nature of binding of Cl^- and CO (Cl^- is a σ-donor whereas CO is a π-acceptor). As the $d\pi$ orbitals (assuming z-axis coincides with Ru—Cl or Ru—CO bond) are filled in these complexes they can donate electron density to the $p\pi$ orbitals of CO whereas the $p\pi$ orbitals of Cl^- cannot donate electron density to the metal $d\pi$ orbitals leading to a labile Ru—Cl bond. The value of k

* The spin–orbit coupling constant (λ) for the Ru^{III} ion is 1150 cm^{-1}. In complexes it is assumed to be 1000 cm^{-1}.

Table 3. Molecular orbital energy and wave function for model ruthenium(III) chloro and carbonyl complexes

MO[a]	Orbital energy (eV)	Wave function[b]
		Ru^{III} Chloro Complex
37	−11.140	$-0.93d_{xz}(Ru)+0.11p_x(C11-C12)+0.15d_{xz}(C11+C12)$
38	−11.101	$-0.93d_{yz}(Ru)+0.11p_y(C11-C12)+0.15d_{yz}(C11+C12)+0.10(O1-O2)$
39	−11.030	$0.97d_{x^2-y^2}(Ru)+0.10d_{xy}(Ru)+0.12p_y(O1-O2)$
40	−9.962	$-0.68d_{z^2}(Ru)-0.19p_z(C11-C12)-0.44d_{z^2}(C11+C12)-0.10p_y(N1-N2)$
41, 42	−9.490, −9.461	Ligand orbitals
43	−9.371	$-0.97d_{xy}(Ru)-0.21p_x(N1-N2)-0.20p_y(N1+N2)-0.10p_x(O1-O2)+0.17p_y(O1+O2)$
		Ru^{III} Carbonyl Complex
38	−11.465	$0.82d_{xz}(Ru)+0.09p_x(Cl)-0.14d_{xz}(Cl)+0.37p_x(C)-0.25p_x(O)$
39	−11.435	$0.81d_{yz}(Ru)+0.09p_y(Cl)-0.14d_{yz}(Cl)+0.38p_y(C)-0.25p_y(O)$
40	−11.047	$-0.97d_{x^2-y^2}(Ru)-0.10d_{xy}(Ru)-0.12p_y(O1-O2)$
41	−9.827	$0.41d_{z^2}(Ru)-0.12p_z(Cl)+0.84d_{z^2}(Cl)-0.12s(C)+0.09p_z(C)$
42–47	−9.675, −9.461	Chlorine and ligand orbitals
48	−9.374	$0.95d_{xy}(Ru)+0.17d_{xy}(Cl)-0.11d_{yz}(Cl)-0.21p_x(N1-N2)-0.19p_y(N1+N2)$

[a] The HOMOs for chloro and carbonyl complexes are 39th and 40th MOs respectively. The symmetry at the site of ruthenium is as low as C_{2v}.

[b] Atoms O1 and O2 belong to Schiff base; C and O belong to carbonyl group.

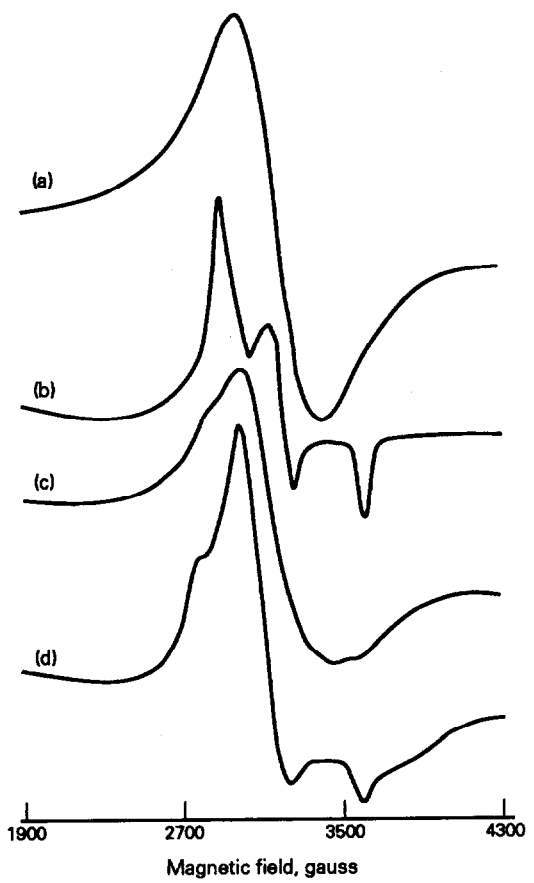

Fig. 1. X-band EPR spectra of K[Ru(naphprop)Cl_2] **7a** and [Ru(naphprop)(Cl)(CO)] **7b** complexes at 77 K. (a) **7a** as powder sample, (b) frozen acetone solution of **7a**, (c) **7b** as powder sample, and (d) frozen DMF solution of **7b**.

varies with the Schiff bases in the order salicylaldehyde > picolinaldehyde > naphthaldehyde. This suggests that the naphthaldehyde Schiff base complexes reported in this investigation are more stable than salicylaldehyde and picolinaldehyde complexes reported elsewhere.[9] Because of the higher stability of the naphthaldehyde Schiff base complexes they are less active catalytically than salicylaldehyde and picolinaldehyde complexes.[10]

EHMO calculations

The HOMO in both chloro and carbonyl complexes is predominantly a $d_{x^2-y^2}$ orbital.* The wave functions for a few MOs above and below the HOMO along with their energies are listed in Table 3. It is obvious from Table 3 that replacement of Cl^- by CO has lowered the energy of d_{xz} and d_{yz} orbitals while that of $d_{x^2-y^2}$ is unaltered. The d_{z^2} and d_{xy} orbitals are more destabilized in the case of carbonyl complexes. Ruthenium d_{xz} and d_{yz} orbitals involve an antibonding interaction with $p\pi$ orbitals of Cl^- and CO. The $d\pi$–$p\pi$ interaction is more in the case of carbonyl complexes than in chloro complexes (the coefficients for $d\pi$ orbitals are smaller in the case of carbonyl complexes than in the chloro complexes) leading to more stabilized d_{xz} and d_{yz}

* The $d_{x^2-y^2}$ orbital in EHMO calculation is the same as the d_{xy} orbital discussed in the EPR provided the coordinate system used in EHMO calculation is rotated by 45° about z-axis.

orbitals in carbonyl complexes. It is therefore expected that the replacement of Cl^- by CO group increases the axial and crystal field splittings. EPR results on chloro and carbonyl complexes are consistent with this observation (the value for the axial distortion Δ is more for carbonyl complexes than for chloro complexes). A similar behaviour in the energy level ordering was observed for the chloro and carbonyl complexes of ferrous porphyrins.[21]

REFERENCES

1. M. Schröder and T. A. Stephenson, in *Comprehensive Coordination Chemistry* (Edited by G. Wilkinson), Vol. 4, Chapter 45, p. 277. Pergamon Press, New York (1987).
2. A. J. Hewitt, J. H. Holloway, P. D. Peacock, J. B. Raynor and I. L. Willon, *J. Chem. Soc., Dalton Trans.* 1978, 579.
3. M. M. Taqui Khan and A. E. Martell, *Homogeneous Catalysis by Metal Complexes*, Vol. I and II. Academic Press, New York (1974).
4. G. N. Schrauzer (Ed.), *Transition Metals in Homogeneous Catalysis*. Marcel Dekker Inc., New York (1971).
5. A. E. Shilov (Ed.), *Fundamental Research in Homogeneous Catalysis*, Vol. I. Gordon and Breach, New York (1986).
6. G. Süss-Fink and G. F. Schmidt, *J. Mol. Catal.* 1987, **42**, 361; T. Squarez and B. Fontal, *ibid.* 1985, **32**, 191.
7. M. M. Taqui Khan, S. B. Halligudi and S. H. R. Abdi, *J. Mol. Catal.* 1988, **44**, 179; *ibid.* 1988, **45**, 215; M. M. Taqui Khan, S. A. Samad and M. R. H. Siddiqui, *J. Mol. Catal.* 1989, **53**, 23.
8. M. M. Taqui Khan, Ch. Sreelatha, S. A. Mirza, G. Ramachandraiah and S. H. R. Abdi, *Inorg. Chim. Acta* 1988, **154**, 103.
9. M. M. Taqui Khan, D. Srinivas, R. I. Kureshy and N. H. Khan, *Inorg. Chem.* 1990, **29**, 2320.
10. M. M. Taqui Khan, S. B. Halligudi, S. Shukla and Z. A. Shaikh, *J. Mol. Catal.* 1990, **57**, 301 and 307.
11. M. M. Taqui Khan, S. A. Mirza, A. Prakash Rao and Ch. Sreelatha, *J. Mol. Catal.* 1988, **44**, 107.
12. M. M. Taqui Khan, N. H. Khan, R. I. Kureshy and A. B. Boricha, *Inorg. Chim. Acta* 1990, **174**, 175.
13. R. Hoffmann, *J. Chem. Phys.* 1963, **39**, 1397; R. Hoffmann and W. N. Lipscomb, 1962, **37**, 177.
14. S. P. McGlynn, L. G. Vanquickenborne, M. Kinoshita and D. G. Carroll, *Introduction to Applied Quantum Chemistry*. Holt, Reinhart and Winston, New York (1972).
15. K. Tatsumi and R. Hoffmann, *J. Am. Chem. Soc.* 1981, **103**, 3328.
16. L. J. Boucher, *J. Inorg. Nucl. Chem.* 1974, **36**, 531; L. J. Boucher and M. O. Farrel, *ibid.* 1973, **35**, 3731.
17. F. M. Ashmawy, R. M. Issa, S. A. Amer, C. A. McAuliffe and R. V. Parish, *J. Chem. Soc., Dalton Trans.* 1986, 421.
18. A. Hudson and M. J. Kennedy, *J. Chem. Soc. A* 1969, 1116; J. B. Raynor and B. G. Jeliazkowa, *J. Chem. Soc., Dalton Trans.* 1982, 1185.
19. A. R. Chakravarty and A. Chakravorty, *J. Chem. Soc., Dalton Trans.* 1982, 615; N. Bag, G. K. Lahiri, S. Bhattacharya, L. R. Felvello and A. Chakravorty, *Inorg. Chem.* 1988, **27**, 4396.
20. N. J. Hill, *J. Chem. Soc., Faraday Trans.* 1972, 427.
21. M. Zerner, M. Gouterman and H. Kobayashi, *Theoret. Chim. Acta* 1966, **6**, 363.

Polyhedron Vol. 10, No. 22, pp. 2567–2571, 1991
Printed in Great Britain

0277-5387/91 $3.00+.00
© 1991 Pergamon Press plc

SYNTHESIS AND CHARACTERIZATION OF THORIUM(IV) AND DIOXOURANIUM(VI) COMPLEXES OF PENTAMETHYLENE SULPHOXIDE

R. K. AGARWAL* and JAI PRAKASH

Postgraduate Department of Chemistry, Lajpat Rai Postgraduate College, Meerut University, Sahibabad-201 005, Ghaziabad, India

(*Received* 20 *February* 1991; *accepted* 9 *July* 1991)

Abstract—Some thorium(IV) and dioxouranium(VI) complexes with pentamethylene sulphoxide (PMSO) of the general composition $[ThX_4(PMSO)_n]$ (X = Cl, Br, NO_3 or NCS, $n = 2$; X = I, $n = 4$; X = ClO_4, $n = 6$) and $[UO_2X_2(PMSO)_n]$ (X = Cl, Br, I, NO_3, NCS or CH_3COO, $n = 2$; X = ClO_4, $n = 4$) were synthesized and characterized by IR, conductivity, molecular weight and analytical techniques. In all the complexes the PMSO is coordinated to the metal ion via its oxygen donor atom. The thermal properties of the complexes are also reported.

We have previously synthesized some actinide complexes of several sulphoxides, namely tetramethylene sulphoxide,[1–3] dibenzyl sulphoxide[4,5] and methyl phenyl sulphoxide.[6] In this paper we report our results on thorium(IV) and dioxouranium(VI) complexes of pentamethylene sulphoxide $(CH_2)_5SO$.

EXPERIMENTAL

Materials

Thorium(IV) nitrate and uranyl(VI) nitrate were obtained from B.D.H. Crystalline thorium(IV) perchlorate[7] and ThX_4 (X = Cl, Br, I or NCS)[8] were prepared by known methods. Other uranyl(VI) salts were prepared as reported earlier.[9] The ligand PMSO was obtained from Aldrich Chemical Co. and was used as received. All the solvents were of AnalaR grade.

Synthesis of the complexes

All the thorium(IV) and uranyl(VI) complexes of PMSO were prepared by the following methods.

(i) An acetone solution of the metal salt was added slowly to the constantly stirred PMSO solution in acetone at *ca* 8–10°C. After stirring the reaction mixture for 30 min, the complex separated almost quantitatively and was washed by decanting with acetone to free it from adhering ligand, filtered and dried *in vacuo* over P_4O_{10}.

(ii) A methanolic solution of the respective metal salt was treated with the calculated amount of PMSO (in the same solvent) with constant stirring at 10°C. After stirring the reaction mixture for 30 min, an excess of anhydrous diethyl ether was added to the mixture giving a precipitate which was filtered, washed with methanol and finally with diethyl ether and dried *in vacuo* over fused $CaCl_2$.

(iii) An isopropanol solution of the metal salt was treated with a solution of PMSO in ethyl acetate. The reaction mixture was cooled to *ca* 10°C and on stirring for *ca* 30 min, the solid product was obtained which was filtered, washed with ethyl acetate and isopropyl alcohol mixture. Finally it was washed with petroleum ether and dried as above.

All the analyses and physical measurements were performed as reported previously.[9]

RESULTS AND DISCUSSION

The interaction of various thorium(IV) and dioxouranium(VI) salts with pentamethylene sulphoxide (PMSO) resulted in the formation of the type $[ThI_4(PMSO)_n]$ (X = Cl, Br, NO_3 or NCS, $n = 2$; X = I, $n = 4$; X = ClO_4, $N = 6$) and $[UO_2X_2$

* Author to whom correspondence should be addressed.

Table 1. Analytical, conductivity and molecular weight data of Th(IV) complexes of PMSO

Complex	M.p. (°C)	Found (Calc.) % Th	C	H	S	Anion	Ω_M (ohm^{-1} cm^2 mol^{-1})	Electrolytic nature	Average mol. wt. (formula weight)
$[ThCl_4(PMSO)_2]$	240	38.3 (38.0)	19.0 (19.7)	3.2 (3.3)	10.7 (10.5)	23.4 (23.3)	5.3	Non-electrolyte	617 (610)
$[ThBr_4(PMSO)_2]$	236	29.9 (29.4)	14.8 (15.2)	2.4 (3.3)	8.4 (8.1)	40.8 (40.6)	6.0	Non-electrolyte	781 (788)
$[ThI_2(PMSO)_4]I_2$	245	19.3 (19.1)	19.3 (19.8)	3.2 (3.3)	10.7 (10.6)	42.2 (41.9)	52.6	1:2	415 (1212)
$[Th(NO_3)_4(PMSO)_2]$	> 260	32.6 (32.4)	16.2 (16.7)	2.7 (2.8)	9.3 (8.9)	—	3.9	Non-electrolye	712 (716)
$[Th(NCS)_4(PMSO)_2]$	> 250	33.4 (33.1)	23.3 (24.0)	2.8 (2.8)	27.6 (27.4)	33.3 (33.1)	4.1	Non-electrolyte	707 (700)
$[Th(PMSO)_6](ClO_4)_4$	200d	17.5 (17.3)	26.0 (26.9)	4.4 (4.5)	14.5 (14.3)	29.9 (29.7)	98.9	1:4	271 (1338)

$(PMSO)_n]$ (X = Cl, Br, I, NO_3, NCS or CH_3COO, $n = 2$; X = ClO_4, $n = 4$). The elemental analyses of these complexes are presented in Tables 1 and 2.

In order to understand the nature of the complexes in solutions, their electrical conductivities were determined in nitrobenzene. The results are presented in Tables 1 and 2. In the case of the thorium(IV) complexes, the molar conductances of the perchlorate and iodide complexes show the presence of 1:4 and 1:2 electrolytes respectively. Thus in the perchlorate complex all four perchlorate groups are present outside the coordination sphere whilst in the case of the iodide complex only two of the four iodide groups may be ionic in nature. The molar conductances of all the uranyl(VI) complexes (except the perchlorate complex) of PMSO fall in the range 3.2–5.1 Ω^{-1} cm^2 mol^{-1} indicate that the complexes are non-electrolytes. In the case of the perchlorate complex the value corresponds to 52.5 indicating the 1:2 electrolytic nature of this complex. Data on the molecular weight of the complexes in freezing nitrobenzene are given in Tables 1 and 2 along with the formula weight. The thorium(IV) and uranyl(VI) complexes are either

Table 2. Analytical, conductivity and molecular weight data of uranyl(VI) complexes of PMSO

Complex	M.p.	Found (Calc.) % U	C	H	S	Anion	Ω_M (ohm^{-1} cm^2 mol^{-1})	Electrolytic nature	Average mol. wt. (formula weight)
$[UO_2Cl_2(PMSO)_2]$	252d	41.4 (41.2)	20.5 (20.8)	3.4 (3.5)	11.2 (11.1)	12.4 (12.3)	4.1	Non-electrolyte	569 (577)
$[UO_2Br_2(PMSO)_2]$	250d	35.9 (35.7)	17.7 (18.0)	2.9 (3.0)	9.7 (9.6)	23.9 (24.0)	3.9	Non-electrolyte	630 (636)
$[UO_2I_2(PMSO)_2]$	245	31.5 (31.3)	15.5 (15.8)	2.5 (2.6)	8.2 (8.4)	33.1 (33.4)	5.1	Non-electrolyte	723 (736)
$[UO_2(NO_3)_2(PMSO)_2]$	> 260	37.9 (37.8)	18.6 (19.0)	3.1 (3.2)	10.3 (10.1)	—	3.2	Non-electrolyte	619 (630)
$[UO_2(NCS)_2(PMSO)_2]$	> 260	38.4 (38.3)	22.8 (23.1)	2.0 (2.1)	20.7 (20.6)	18.3 (18.6)	4.1	Non-electrolyte	612 (622)
$[UO_2(PMSO)_4](ClO_4)_2$	237	25.4 (25.3)	24.9 (25.5)	4.1 (4.2)	13.8 (13.6)	20.7 (21.1)	52.5	1:2	310 (941)
$[UO_2(CH_3COO)_2(PMSO)_2]$	250d	38.4 (38.1)	14.9 (15.3)	3.6 (3.7)	10.4 (10.2)	—	4.6	Non-electrolyte	617 (624)

diamagnetic or weakly paramagnetic depending upon the diamagnetism of the other ions and the surrounding ligand field.[10]

Infrared spectra and the nature of coordination

In the spectra of PMSO, two absorptions associated with S=O and C—S stretching modes undergo significant shift on coordination.[11] S=O stretching frequency in free PMSO appears as a strong absorption at 1022 cm^{-1},[12] which disappears on complex formation and a new band of enhanced intensity appears in the 980–950 cm^{-1} region (Table 3) showing coordination of PMSO to the metal ion through its oxygen atom.[12] The other important absorption in the spectra of sulphoxide is the C—S stretching vibration which has been identified in free PMSO at 660 cm^{-1}.[12] This absorption undergoes a slight positive shift on complexation (Table 3). A negative shift of the S=O stretching frequency and shift of the C—S stretching frequency towards higher wave number are indicative of the decrease in the double bond character of the S=O bond. ν(M—O) stretching vibrations occur at *ca* 400 cm^{-1}[5,6] and the CSO deformation modes appear in the 380–340 cm^{-1} region. A distinct difference between δ' symmetric and δ'' antisymmetric CSO absorption is an indication of electron donation from the oxygen atom of the sulphoxide molecule.

The ν(M—Cl) (M = Th or U) vibration has been assigned in 270–255 cm^{-1} region in thorium(IV) and uranyl(VI) chloride complexes of PMSO.[13] In the spectra of $[Th(PMSO)_6](ClO_4)_4$ and $[UO_2(PMSO)_4](ClO_4)_2$ the very strong ν_3 and ν_4 infrared bands appear at *ca* 1080 and *ca* 620 cm^{-1} respectively for perchlorate ions, indicating that tetrahedral symmetry is maintained and the perchlorate ions are not bonded to the thorium(IV) or uranyl(VI) ions.[14] In the complex $[Th(NO_3)_4(PMSO)_2]$ the absence of the ν_3 band of ionic nitrate (D_{3h}) around 1360 cm^{-1} and the occurrence of two strong bands at *ca* 1525 and 1300 cm^{-1} suggest the strong covalent nature of the NO_3^- ion.[15] The bidentate nature of the nitrato groups in the complex has been established by comparing the spectral bands of the complex with those of $Th(NO_3)_4 \cdot 5H_2O$.[16] In $[Th(PMSO)_4(NO_3)_4]$, the NO_3^- vibrations occur at 1525 (ν_1), 1300 (ν_4), 1040 (ν_2), 815 (ν_6) and 750 cm^{-1} (ν_3/ν_5) while in $Th(NO_3)_4 \cdot 5H_2O$ the corresponding bands occur at 1520, 1290, 1030, 808, 745 and 715 cm^{-1} respectively. The nitrate groups in $[UO_2(PMSO)_2(NO_3)_2]$ complex appears to be bidentate since the IR bands due to this group occur almost in the same region as in case of reported bidentate complexes.[17] The C—N stretching frequency in $[Th(PMSO)_2(NCS)_4]$ and $[UO_2(PMSO)_2(NCS)_2]$ appears in 2060–2050 cm^{-1} region, which lies on the border line for distinguishing between sulphur and nitrogen bonding in the thiocyanate,[18] although the high relative intensity of the band in all cases suggests that the thiocyanate groups are nitrogen bonded.[19] The ν(C—S) frequency observed at *ca* 780 and δ(NCS) at *ca* 480 cm^{-1} further confirm the N-bonding to

Table 3. Important IR bands (cm^{-1}) of Th(IV) and UO_2(VI) complexes of PMSO

Complex	ν(S=O)	ν(C—S)	δ'_{sym}CSO	δ''_{asym}CSO	$\Delta(\delta'-\delta'')$	ν(M—O)
PMSO	1022vs	660s	—	—	—	—
$[ThCl_4(PMSO)_2]$	970vs	675m	3702	350s	20	400m
$[ThBr_4(PMSO)_2]$	960vs	670m	375s	355s	20	405m
$[ThI_2(PMSO)_2]I_2$	965vs	672m	360s	345s	15	400m
$[Th(NO_3)_4(PMSO)_2]$	950s	675m	375m	350m	25	400m
$[Th(NCS)_4(PMSO)_2]$	980s	670m	365m	350m	15	405m
	950s					
$[Th(PMSO)_6](ClO_4)_4$	960s	675m	370s	350s	20	410m
	940s					
$[UO_2Cl_2(PMSO)_2]$	970vs	675m	365m	350m	15	415m
$[UO_2Br_2(PMSO)_2]$	975vs	670m	375m	360m	15	410m
$[UO_2I_2(PMSO)_2]$	970s	672m	370m	350m	20	400m
$[UO_2(NO_3)_2(PMSO)_2]$	980s	680m	350s	320m	30	420m
	950s					
$[UO_2(NCS)_2(PMSO)_2]$	965vs	675m	370m	350m	20	405m
$[UO_2(PMSO)_4](ClO_4)_2$	970s	670m	370s	345m	25	415m
$[UO_2(CH_3COO)_2(PMSO)_2]$	960s	682m	360s	340m	20	405m

the metal atom.[20] The IR spectrum of $UO_2(CH_3COO)_2 \cdot 2PMSO$ shows bands at *ca* 1540, 1420 and 665 cm^{-1} which are assigned to νOCO asymmetric, νOCO symmetric and δOCO modes, respectively, due to coordinated acetato group.[21] On the basis of previous reports, it is concluded that the acetate groups coordinate in a bidentate chelating fashion with the uranyl acetate.[22]

The other notable feature in the stretching frequency of U=O bond in uranyl(VI) compounds before and after complexation. The stretching frequency (*ca* 950 cm^{-1}) falls about 20–25 cm^{-1} after complexing with the ligand due to lowering of d_π–p_π interaction in the U=O bond which is supported by the observations of McGlynn and coworkers.[23]

Thermal studies

The TG and DT curves of the Th(IV) complexes of PMSO do not show the presence of water. In the DT curve of $[Th(PMSO)_6](ClO_4)_4$, one sharp exothermic peak at *ca* 202°C is obtained. At this temperature the compound **decomposes violently due to the oxygen content of the perchlorate group.**[24]—**Caution.** TG analysis of that complex shows that it is stable up to 195°C, beyond which the decomposition starts and is completed at *ca* 510°C. At this temperature the residual mass corresponds to ThO_2. In the halo complexes, *i.e.* chloro, bromo and thiocyanato complexes the decomposition process is completed in two steps. In the first step, the complexes lose both the ligand molecules as shown by the break in the TG curve and the endo peak in the DT curve. The final product is oxohalide in these cases. In the nitrato complex the two coordinated ligands are lost between 210 and 280°C and finally at *ca* 505°C, metal oxide is obtained as an end product.

The thermograms of the uranyl(VI) complexes indicate virtually no change in weight up to 175°C. At 175–240°C, a loss of 27–31% is observed which corresponds to a loss of 1.5 mol of ligand, PMSO, followed by a further loss of 37–41° at 265–340°C showing the complete loss of PMSO molecules leaving a residue of UO_3. The oxide U_3O_8 was finally formed at *ca* 610°C. Above this temperature there is no observable change in weight.[25]

Stereochemistry of the complexes

(a) *Thorium*(IV) *complexes.* The conductance and molecular weight data concluded that chloro, bromo and thiocyanato complexes are non-electrolytes and hence all the anionic ligands are present in the coordination sphere, but in the iodo complex, the two iodine atoms and in the perchlorate complex, all the four perchlorate groups are present outside the coordination sphere. Hence the coordination number six has been suggested in these complexes. In the $[Th(NO_3)_4(PMSO)_2]$ complex the presence of four bidentate nitrate groups and the additional two unidentate PMSO molecules produces a coordination number of ten for the thorium(IV) atoms.[26]

(b) *Uranyl*(VI) *complexes.* The complex $[UO_2(NO_3)_2(PMSO)_n]$ may be considered to have an eight-coordinated uranium atom with six-ligand atoms (two oxygens from the two ligand molecules and four oxygens from two bidentate nitrate groups) in a plane perpendicular to the linear OUO group.[27] In $[UO_2(CH_3COO)_2(PMSO)_2]$ the monodentate nature of PMSO and bidentate chelating acetato groups, an eight-coordinated (all oxygen atoms) structure with six oxygens (four from two bidentate chelating acetato ligands and two from monodentate organic ligand PMSO) around the linear uranyl group is assigned. In uranyl(VI) halo and thiocyanato complexes, the coordination number six has been suggested. In the perchlorato complex, the conductance and molecular weight data suggested the ionic nature of perchlorate ions and thus both the perchlorate ions are present outside the coordination sphere. In this complex, the uranium(VI) atom is surrounded by six oxygen atoms.

Acknowledgement—The authors are thankful to the University Grants Commission, New Delhi (India) for financial support for this work.

REFERENCES

1. R. K. Agarwal, T. N. Srivastava and A. K. Srivastava, *Transition Met. Chem.* 1980, **5**, 95.
2. R. K. Agarwal and A. K. Srivastava, *Thermochim. Acta* 1982, **56**, 247.
3. R. K. Agarwal, Lakshman Singh and Pravesh Kumar, *J. Inst. Chemists (India)* 1989, **61**, 15.
4. R. K. Agarwal, Pravesh Kumar and H. K. Rawat, *Thermochim. Acta* 1985, **88**, 397.
5. R. K. Agarwal and Pravesh Kumar, *J. Ind. Chem. Soc.* 1986, **63**, 565.
6. R. K. Agarwal, Pitam Singh and Lakshman Singh, *Synth. React. Inorg. Met.-Org. Chem.* 1991.
7. P. Ramamurthy and C. C. Patel, *J. Inorg. Nucl. Chem.* 1963, **25**, 310.
8. V. V. Savant and C. C. Patel, *J. Less Common Metals* 1971, **24**, 459.
9. A. K. Srivastava, Shashi Sharma and R. K. Agarwal, *Inorg. Chim. Acta* 1982, **61**, 235.
10. E. D. Eastman, L. Brewer, L. A. Bromley, P. W. Gilles and N. L. Lofgren, *J. Am. Chem. Soc.* 1950, **72**, 4019.
11. F. A. Cotton, R. Francis and W. D. Horrocks Jr, *J. Phys. Chem.* 1960, **64**, 1534.

12. J. Gopalakrishnan and C. Patel, *J. Sci. Ind. Res.* 1968, **27**, 475.
13. Z. M. S. Al-Kazaz and K. W. Bagnal, *J. Inorg. Nucl. Chem.* 1973, **35**, 1493.
14. V. Krishnan and C. C. Patel, *J. Inorg. Nucl. Chem.* 1964, **26**, 2201.
15. C. C. Addison and N. Logan, *Adv. Inorg. Chem. Radiochem.* 1964, **6**, 95.
16. J. R. Ferraro and A. Walker, *J. Chem. Phys.* 1966, **45**, 550.
17. J. I. Bullock, *J. Inorg. Nucl. Chem.* 1967, **29**, 2257.
18. A. Sabatini and I. Bertini, *Inorg. Chem.* 1965, **4**, 1655; 1966, **5**, 1025.
19. C. Pecile, *Inorg. Chem.* 1966, **5**, 210.
20. J. L. Burmeister, *Coord. Chem. Rev.* 1966, **1**, 205; 1968, **3**, 225.
21. K. Nakamoto, *Infrared and Raman Spectra of Inorganic and Coordination Compounds.* Wiley, Interscience, New York (1977).
22. I. S. Ahuja, Raghuvir Singh and R. Sriramnlu, *Trans. Met. Chem.* 1978, **3**, 193.
23. S. P McGlynn, J. K. Smith and W. C. Neely, *J. Chem. Phys.* 1961, **35**, 105.
24. A. K. Srivastava, M. Srivastava and R. K. Agarwal, *Ind. Engng Chem. Prod. Res. Dev.* 1982, **21**, 135.
25. W. W. Wendlandt, *J. Inorg. Nucl. Chem.* 1957, **5**, 118; 1959, **9**, 136.
26. B. C. Smith and M. A. Wassef, *J. Chem. Soc. A* 1968, 1817.
27. E. Glueckauf and H. A. C. Mackay, *Nature* 1950, **165**, 594.

Polyhedron Vol. 10, No. 22, pp. 2573–2585, 1991
Printed in Great Britain

0277–5387/91 $3.00+.00
© 1991 Pergamon Press plc

REACTIONS OF $Mo_2(O_2CMe)_4$ WITH AMINES AND DIAMINES: A STRUCTURAL AND THERMAL STUDY OF STEPWISE ACETATE DISPLACEMENT AND HYDROGEN BONDING

BRYAN W. EICHHORN*

Department of Chemistry and Biochemistry, University of Maryland, College Park, MD 20742, U.S.A.

and

MICHAEL C. KERBY*
Exxon Research and Development Laboratories, P.O. Box 2226, Baton Rouge, LA 70821, U.S.A.

and

KAZI J. AHMED
Department of Chemistry, University of Vermont, Burlington, VT 05405, U.S.A.

and

JOHN C. HUFFMAN
Molecular Structure Center, Indiana University, Bloomington, IN 47405, U.S.A.

(*Received* 5 *June* 1991; *accepted* 5 *July* 1991)

Abstract—$Mo_2(O_2CMe)_4$ (**1**) reacts with the neat bidentate diamines $Me(H)NCH_2CH_2N(H)Me$ (*N,N'*-dmed), $H_2NCH_2CH_2CH_2NH_2$ (pda), $H_2NCH_2CH_2NMe_2$ (*N,N*-dmed), and $H_2NCH_2CH_2N(H)Me$ (*N*-med) to form the compounds $^1_\infty[Mo_2(O_2CMe)_4(N,N'\text{-dmed})]$ (**4**), $^1_\infty[Mo_2(O_2CMe)_4(pda)]$ (**5**), $\{[Mo_2(O_2CMe)_3(N,N\text{-dmed})_2]^+[(O_2CMe)]^-\}_2$ (**6**), and $\{[Mo_2(O_2CMe)_3(N\text{-med})_2]^+[(O_2CMe)]^-\}_2 \cdot N\text{-med}$ (**7**), respectively. Compounds **4**–**7** possess Mo—Mo quadruple bonds (Mo—Mo = 2.11(2) Å, ave) and weak axial Mo—N bonds (Mo—N_{ax} = 2.7(1) Å, ave). Compound **4** exhibits a kinked, one-dimensional chain structure comprising $Mo_2(O_2CMe)_4$ units linked by *N,N'*-dmed ligands. The amine hydrogens are weakly hydrogen-bonded to adjacent O_2CMe oxygens (N···O = 3.09(9) Å). Compound **5** crystallizes in a linear one-dimensional chain structure with a four-fold disorder in the pda chain. Conversely, compounds **6** and **7** display structures resulting from acetate displacement from the Mo_2 centre. Each Mo atom possesses a chelating diamine with the —NH_2 group bound in the equatorial position previously occupied by the displaced acetate moiety. Two $[Mo_2(O_2CMe)_3(diamine)_2]^+$ units are linked together via hydrogen bonding between the equatorial —NH_2 diamine hydrogens and the oxygens of the displaced acetate groups. The polar monoamines $MeNH_2$ and NH_3 do not affect acetate displacement presumably due to their inability to overcome entropic effects of the bidentate acetate ligands. Compounds **4**–**7** expel the diamine ligands in the solid state and reform crystalline **1** (XRD). The temperatures of amine expulsions occur at or below the boiling points of the pure diamine liquids. Crystal data for **4** at 20°C: triclinic, $P\bar{1}$, a = 8.784(3); b = 12.945(6), c = 8.663(3) Å; α = 91.73(3)°, β = 97.23(3)°, γ = 101.45(4)°;

* Authors to whom correspondence should be addressed.

$V = 956.2$ Å^3, $d_{calc} = 1.79$ g cm^{-3} and $Z = 2$. For **5** at 25°C: tetragonal, $P4_2/m$, $a = 7.852(2)$ Å, $c = 14.382(2)$; $V = 886.7$ Å^3; $d_{calc} = 1.88$ g cm^{-3} and $Z = 2$. For **6** at −155°C: monoclinic, $P2_1/c$, $a = 14.367(2)$, $b = 10.011(4)$, $c = 17.246(7)$ Å; $\beta = 95.92(2)°$, $V = 2467$ Å^3, $d_{calc} = 1.627$ g cm^{-3} and $Z = 2$. For **7** at −95°C: triclinic, $P\bar{1}$, $a = 12.988(10)$, $b = 15.881(12)$, $c = 12.963(10)$ Å, $\alpha = 105.77(3)°$, $\beta = 101.83(4)°$, $\gamma = 81.95(3)°$, $V = 2508$ Å^3; $d_{calc} = 1.653$ g cm^{-3} and $Z = 2$.

The substitutional lability of carboxylate ligands in dinuclear tetracarboxylate complexes can be correlated with the M—M molecular orbital configuration and parallels the crystal field models describing ligand substitution at mononuclear centres.[1] We have recently been investigating the reactivity of $Mo_2(O_2CMe)_4$ (**1**) with pure amines in the absence of additional co-solvents to assess the factors affecting acetate displacement and the ligand/structure/reactivity relationships of the resulting complexes. Our previous studies involving reactions of **1** with ethylenediamine (en)[2] and tetramethylethylenediamine (tmed)[3] showed that two markedly different products were obtained with significantly different properties.[2–5] The non-polar tmed ligand reacts with **1** to form a weakly associated, one-dimensional polymer of formula $^1_\infty[Mo_2(O_2CMe)_4(tmed)]$ (**2**) comprising unperturbed Mo_2 units linked head-to-tail by tmed ligands as shown by structure **I**. The reaction between **1** and neat en, however, yields an unusual ion-paired complex of formula $[Mo_2(O_2CMe)_2(en)_4]^{2+}[(O_2CMe)_2]^{2-} \cdot$ en (**3**) in which two of the acetate ligands of the parent Mo_2 complex are displaced from the Mo_2 coordination sphere by two spanning en ligands. The displaced acetate ions are in turn hydrogen bonded to the amine hydrogens of the spanning en ligands. Two additional en ligands are axially coordinated as shown by structure **II** below. Both **2** and **3** thermally decompose in the solid state to reform crystalline **1** upon expulsion of the diamine ligands.[2,3] A similar thermal instability was noted for the py complex $Mo_2(O_2CMe)_4(py)_2$.[6,7]

We are interested in determining what factors govern acetate displacement in these systems and how acetate displacement enhances reactivity at the Mo_2 (M≡M) centre. In this paper, we describe the reactions of **1** with bidentate diamines of polarity intermediate to those of tmed and en —namely Me(H)NCH$_2$CH$_2$N(H)Me (*N,N'*-dmed), H$_2$NCH$_2$CH$_2$CH$_2$NH$_2$ (pda), Me$_2$NCH$_2$CH$_2$NH$_2$ (*N,N*-dmed), and Me(H)NCH$_2$CH$_2$NH$_2$ (*N*-med). The latter two diamines react with **1** to form unusual coupled monocationic complexes of formula $\{[Mo_2(O_2CMe)_3(diamine)_2]^+[(O_2CMe)]^-\}_2$ whereas the former two produce one-dimensional chain structures similar to that observed for **2**. Polar monoamines NH_3 and $MeNH_2$ presumably form axial Lewis base adducts and do not affect acetate displacement.

EXPERIMENTAL

General procedures

All reactions and sample manipulations were conducted under N_2 (g) using standard Schlenk techniques and Vacuum Atmospheres Co. glovebox systems. The TGA data were obtained using a DuPont Thermal Analyst 2000 Thermogravimetric system. The samples were run under an He or Ar purge at a heating rate of 10°C min^{-1}. The powder X-ray diffraction data were collected using a Rigaku VS-DXR 3000 X-ray diffractometer. The $Mo_2(O_2CMe)_4$ residues in the TGA experiments were identified by comparisons of their X-ray diffractograms with that of an authentic sample. Elemental analyses were performed by Schwarzkopf Microanalytical Laboratories, Woodside, NY. All sample preparations for microanalysis were conducted in a glovebox.

Syntheses $Mo_2(O_2CMe)_4$ and $Mo_2(O_2CCF_3)_4$ were prepared by published methods.[8] *N,N*-Dimethylethylenediamine (*N,N*-dmed), 1,3-diaminopropane (pda), *N,N'*-Dimethylethylenediamine

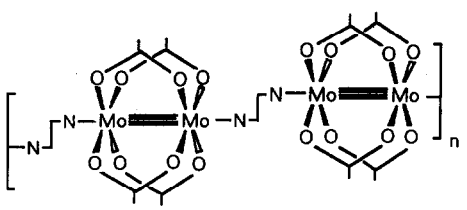

I

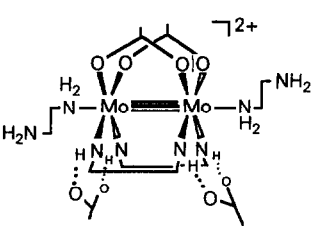

II

(*N,N'*-dmed), and monomethylethylenediamine (*N*-med) were deoxygenated and stored over 4 Å molecular sieves under an N_2 atmosphere. NH_3 and $NMeH_2$ were distilled from Na immediately prior to use.

$^1_\infty[Mo_2(O_2CMe)_4(N,N'\text{-dmed})]$ (**4**). $Mo_2(O_2CMe)_4$ (100 mg, 0.234 mmol) and *N,N'*-dmed (2 cm^3) were combined in a Schlenk reaction vessel. The mixture was gently warmed until all the $Mo_2(O_2CMe)_4$ dissolved producing a pale yellow solution. After cooling to room temperature, the solution was filtered through a fine frit. Crystallization started immediately after filtration. The mixture was cooled to 5°C and, after 16 h, small yellow crystals of **4** separated from solution and were isolated by removing the solution and drying briefly *in vacuo* (crystalline yield: 72.7 mg, 0.141 mmol, 60%). Found: C, 27.9; H, 4.7; N, 5.4. Calc. for $Mo_2C_{12}H_{24}N_2O_8$: C, 27.9; H, 4.7; N, 5.4%.

$^1_\infty[Mo_2(O_2CMe)_4(pda)]$ (**5**). A procedure similar to that described for **4** was employed. $Mo_2(O_2CMe)_4$ (120 mg, 0.28 mmol) was dissolved in 2 cm^3 of pda and warmed to 50°C to produce a red solution. Pale yellow crystals of **5** were isolated and dried *in vacuo* (crystalline yield: 46 mg, 33%). Found: C, 26.4; H, 4.4; N, 5.4. Calc. for $Mo_2C_{11}H_{22}N_2O_8$: C, 26.3; H, 4.4; N, 5.6%.

$\{[Mo_2(O_2CMe)_3(N,N\text{-dmed})_2]^+[(O_2CMe)]^-\}_2$ (**6**). To a vial in the drybox was added $Mo_2(O_2CMe)_4$ (100 mg, 0.23 mmol) and *N,N*-dmed (2 cm^3). The solution was warmed to 50°C producing a light orange solution. The mixture was cooled to room temperature and concentrated to *ca* 1 cm^3 total volume and filtered. After 12 h, light orange crystals of **6** were separated from the solution and were isolated by filtration (crystalline yield: 86 mg, 62%). The crystals used in the X-ray study were not subjected to vacuum due to the ease of solvent loss from this complex. Found: C, 31.7; H, 6.2; N, 9.3. Calc. for $Mo_2C_{16}H_{36}N_4O_8$: C, 31.8; H, 6.0; N, 9.3%.

$\{[Mo_2(O_2CMe)_3(N\text{-med})_2]^+[(O_2CMe)]^-\}_2 \cdot$ N-med (**7**). A 20 cm^3 glass vial was charged with $Mo_2(O_2CMe)_4$ (100 mg, 0.23 mmol) and *N*-med (2 cm^3) in the drybox. The mixture was warmed to *ca* 50°C producing an orange solution. The solution was slowly cooled to room temperature and concentrated *in vacuo* to *ca* 1 cm^3 total volume. After 12 h, orange cube-shaped crystals separated from solution and were isolated by filtration (crystalline yield: 80 mg, 56%). The crystals used in the X-ray study were not subjected to vacuum due to the ease of solvent loss from this complex. Found: C, 30.3; H, 6.3; N, 11.6. Calc. for $Mo_2C_{15.5}H_{36}N_5O_8$: C, 30.4; H, 5.9; N, 11.4%.

$Mo_2(O_2CMe)_4 + NH_3$ *and* $MeNH_2$. In a typical experiment, $Mo_2(O_2CMe)_4$ (100 mg, 0.23 mmol) was placed in a 9-mm pyrex tube that was fitted with a Cajon vacuum adaptor. The tube was then attached to a vacuum line and evacuated. Gaseous NH_3 was then condensed onto Na in a 250 cm^3 three neck flask fitted with a dry ice/acetone condenser and refluxed for *ca* 30 min. The characteristic blue solution was observed. The amine (*ca* 4 cm^3) was then distilled into the pyrex tube charged with $Mo_2(O_2CMe)_4$. The tube was then frozen at −198°C, evacuated, and sealed with a torch. The mixture was warmed to room temperature *behind a shield in a hood* whereupon the solution turned pale yellow. Upon warming to 60°C, the solution turned golden yellow. After 24 h at 60°C, the mixture was cooled to −15°C for 1 week during which time chunky yellow crystals formed. Attempts to isolate the crystals by crushing the pyrex tube inside a piece of tygon tubing and allowing the NH_3 to evaporate under N_2 at 0°C were unsuccessful. The crystals decomposed to powdery yellow $Mo_2(O_2CMe)_4$ (XRD) before they could be isolated. Attempts to allow the NH_3 to evaporate in the air resulted in a brown–black residue.

$Mo_2(O_2CCF_3)_4 + NH_3$. The procedure described for $Mo_2(O_2CMe)_4 + NH_3$ was employed. Upon thawing, the $NH_3/Mo_2(O_2CCF_3)_4$ solutions turned bright red. The colour faded to orange red upon warming to room temperature. No solids were isolated from these reactions.

Crystallography

Complete listings of fractional coordinates and anisotropic thermal parameters, bond distances and angles, full crystallographic summaries and a listing of observed and calculated structure factors for **4**, **5**, **6**, and **7** have been deposited with the Editor as supplementary data.*

$^1_\infty[Mo_2(O_2CMe)_4(N,N'\text{-dmed})]$ (**4**). A pale yellow crystal was glued inside a glass capillary and sealed under N_2. Cell constants and an orientation matrix were obtained from least-squares refinement using 23 setting angles between 6° and 23° in 2θ. No systematic absences or symmetry were observed suggesting a triclinic space group. Subsequent solution and refinement of the structure in space group $P\bar{1}$ (#2) confirmed the choice.

Of the 4390 reflections collected between 5° and 54° in 2θ, 3946 were unique. Only the 2678 reflections with $I > 3\sigma(I)$ were used in the solution and

* Atomic coordinates have also been deposited with the Cambridge Crystallographic Data Centre for inclusion in their Data Base. Copies are also available, on request, from the Editor at Indiana University.

refinement of the structure. Lorentz and polarization corrections were applied. The data were corrected for decay but no absorption correction was applied. The two Mo atoms were located using direct methods (MULTAN 78). The remaining atoms were located using a combination of difference Fourier syntheses and full-matrix least-squares refinements. A few of the hydrogen atoms were visible in the later difference maps and the remainder were placed at idealized positions with d(C—H) = 0.95 Å and d(N—H) = 0.92 Å. All non-hydrogen atoms were refined anisotropically and the hydrogen atoms included as fixed atom contributors in the final cycles of refinement.

The final difference map was essentially featureless showing three peaks of approximately 1 e Å^{-3} around an acetate oxygen. No other peaks were observed above background. The final residuals were $R(F) = 0.055$ and $R_w(F) = 0.070$.

$^{1}_{\infty}$[$Mo_2(O_2CMe)_4$(pda)] (**5**). A well-formed yellow crystal of approximate dimension 0.25 × 0.25 × 0.30 mm was mounted under nitrogen inside a capillary which was then sealed with epoxy resin. The cell constants and orientation matrix for data collection were based on 25 carefully centred reflections in the range $20° < 2\theta < 30°$. Acceptable ω scans of some strong low angle reflections were obtained. ω–2θ scans over the 2θ range 4.5–65° produced 1678 unique reflections, of which 1163 ($I > 3\sigma(I)$) were used for structure refinement. The data were consistent with the tetragonal space groups $P4_2$ and $P4_2/m$. Successful solution and refinement of the structure in $P4_2/m$ (no. 84) confirmed that the centric space group was the correct choice. The structure was solved by a combination of direct methods and heavy atom Fourier techniques (Siemens SHELXTL PLUS crystallographic package). Full-matrix least-squares refinement was carried out with anisotropic thermal parameters for all non-hydrogen atoms. The hydrogen atoms were placed in calculated positions. Due to positional disorder, C(3) (two-fold disordered) and C(4) (four-fold disordered) were assigned partial structure occupancies of 50 and 25%, respectively, and the C—N and C—C distances fixed at idealized values [C—C = 1.54 Å, C—N = 1.45 Å]. Refinement converged at $R = 0.0466$ and $R_w = 0.0496$. The maximum shift/ESD in the last cycle of refinement was less than 0.02 and the maximum residual electron density in the final difference Fourier map was <0.85 e Å^{-3}. No absorption correction was applied.

{[$Mo_2(O_2CMe)_3$(N,N-dmed)$_2$]$^+$[(O_2CMe)]$^-$}$_2$ (**6**). A suitable crystal was located and transferred to the goniostat using inert atmosphere handling techniques and cooled to −155°C for characterization and data collection. General operating conditions have been described elsewhere.[9]

A systematic search of a limited hemisphere of reciprocal space located a set of diffraction maxima with symmetry and systematic absences uniquely determining the space group as the monoclinic $P2_1/c$. Subsequent solution and refinement of the structure confirmed this choice.

Data were collected using a continuous θ–2θ scan with fixed backgrounds. Of the 5373 total reflections collected in the range $6° < 2\theta < 45°$, 3227 were unique and the 2710 with $I > 2.33\sigma(I)$ were used in the refinement of the structure. Lorentz and polarization corrections were applied but an absorption correction was not necessary and not applied.

The structure was solved by a combination of direct methods (MULTAN78) and Fourier techniques. A difference Fourier synthesis revealed the location of some, but not all, hydrogen atoms. All hydrogen atom positions were therefore calculated using idealized geometries and d(C—H) = 0.95 Å. These calculated positions were fixed for the final cycles of refinement. A final difference Fourier was featureless, with the largest peak being 0.65 e Å^{-3}. The final residuals were $R(F) = 0.064$ and $R_w(F) = 0.066$.

{[$Mo_2(O_2CMe)_3$(N-med)$_2$]$^+$[(O_2CMe)]$^-$}$_2$·N-med (**7**). A suitable crystal was located and transferred to the goniostat using inert atmosphere handling techniques and cooled to −95°C for characterization and data collection. General operating conditions have been described elsewhere.[9] Initial attempts to cool the sample to lower temperatures resulted in a catastrophic phase transition.

A systematic search of a limited hemisphere of reciprocal space located a set of diffraction maxima with no symmetry or systematic absences, indicating a triclinic space group. Subsequent solution and refinement of the structure confirmed the centrosymmetric $P\bar{1}$.

Data were collected in the usual manner using a continuous θ–2θ scan with fixed backgrounds. Data were reduced to a unique set of intensities and associated sigmas. Lorentz and polarization corrections were applied. No absorption correction was performed. A total of 10,552 reflections were collected; of which 6574 were unique. Only the 5524 unique reflections with $I > 2.33\sigma(I)$ were used in the solution and refinement of the structure.

The structure was solved by a combination of direct methods (MULTAN78) and Fourier techniques. A difference Fourier synthesis revealed the location of some, but not all, hydrogen atoms. All hydrogen atoms positions were therefore calculated using idealized geometries and d(C—H) =

0.95 Å. These calculated positions were fixed for the final cycles of refinement. There were eight peaks in the latter difference maps that corresponded to the disordered *N*-med solvate molecule. These peaks were all refined as carbon atoms and included as fixed atom contributors in the final cycles of refinement. A final difference Fourier was featureless, with the largest peak being 0.45 e A^{-3}. The final residuals were $R(F) = 0.051$ and $R_w(F) = 0.055$.

RESULTS

Syntheses

$Mo_2(O_2CMe)_4$ dissolves in neat diamines *N,N'*-dmed and pda to form yellow or red–yellow solutions that, upon concentration, produce air-sensitive, pale yellow crystals of $^1_\infty[Mo_2(O_2CMe)_4(\text{diamine})]$ complexes [where diamine = *N,N'*-dmed (**4**); pda (**5**)] in 60 and 33% yields, respectively (eq. 1). Compounds **4** and **5** exhibit chain structures (Figs 1 and 2) and have been characterized by thermal gravimetric analysis (TGA), IR, elemental analysis and single-crystal X-ray diffraction.

$$Mo_2(O_2CMe)_4 + \text{heat diamine} \rightarrow {}^1_\infty[Mo_2(O_2CMe)_4(\text{diamine})] \quad (1)$$

(**4**) diamine = *N,N'*-dmed

(**5**) diamine = pda

The diamines *N,N*-dmed and *N*-med react

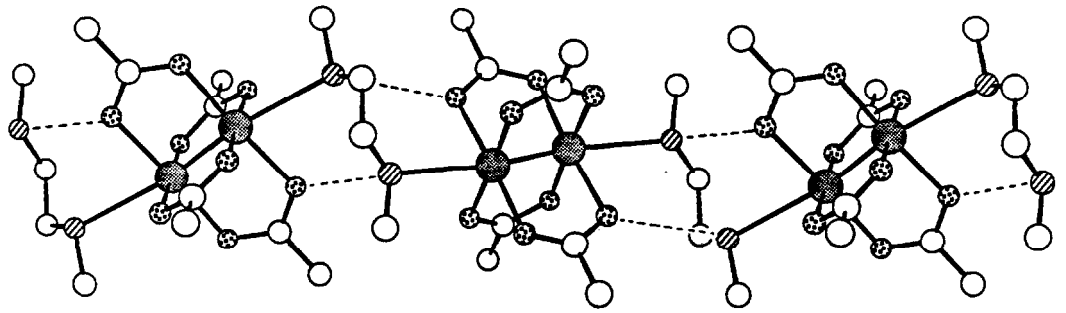

Fig. 1. Ball-and-stick drawing* of the kinked chain structure of $^1_\infty[Mo_2(O_2CMe)_4(N,N'\text{-dmed})]$ (**4**). The dotted lines represent the N—H···O hydrogen bonds.

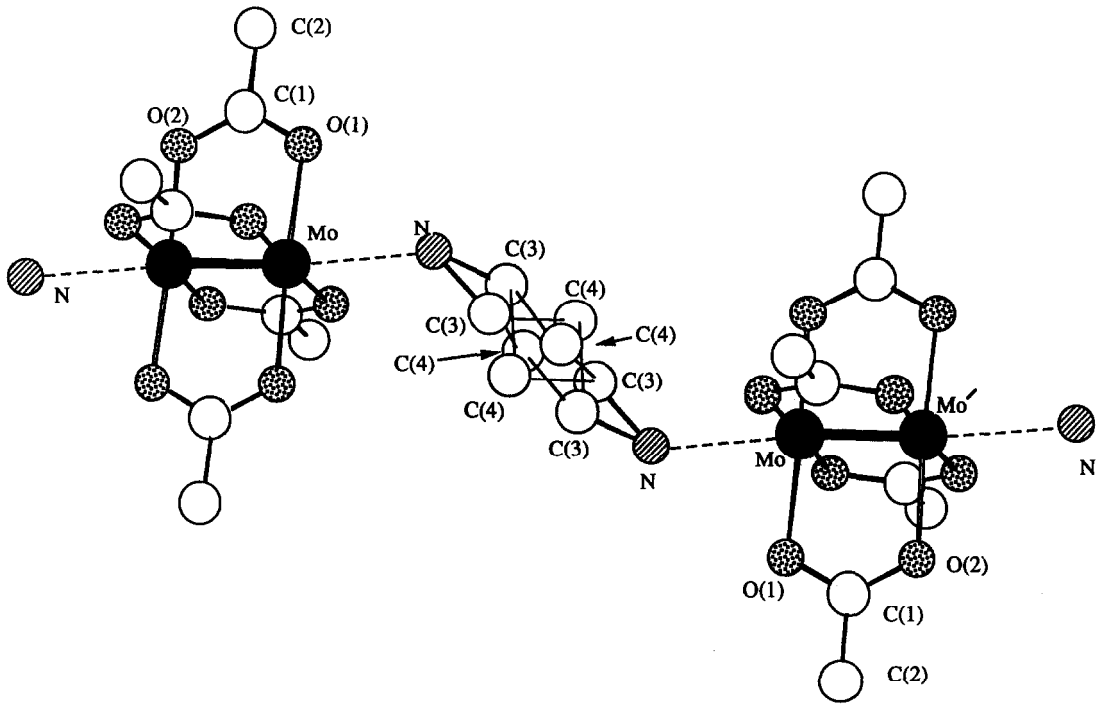

Fig. 2. Ball-and-stick drawing* of the chain structure of $^1_\infty[Mo_2(O_2CMe)_4(pda)]$ (**5**). The disordered sites of C(3) and C(4) are included.

* A combination of the Tektronix CaCHE system and CHEM-3D were used for generating ball-and-stick figures.

with $Mo_2(O_2CMe)_4$ upon gentle warming (*ca* 50°C) to form clear, pale orange solutions. Upon cooling to 30°C, air-sensitive pale orange–yellow crystals of formula $\{[Mo_2(O_2CMe)_3(diamine)_2]^+[(O_2CMe)]^-\}_2 \cdot x$ diamine precipitate from solution [where diamine = *N,N*-dmed; $x = 0$, (**6**); diamine = *N-med*, $x = 1.0$, (**7**)] in 62 and 56% yield, respectively (eq. 2).

$$Mo_2(O_2CMe)_4 + \textit{neat}\ Me(R)NCH_2CH_2NH_2 \rightarrow \{[Mo_2(O_2CMe)_3(Me(R)NCH_2CH_2NH_2)_2]^+[(O_2CMe)]^-\}_2 \cdot xMe(R)NCH_2CH_2NH_2 \quad (2)$$

(**6**) *N,N*-dmed (R = Me), $x = 0$

(**7**) *N*-med (R = H), $x = 1.0$.

Compounds **6** and **7** have similar structures comprising two Mo_2 units linked together via hydrogen bonding (Figs 3 and 4, respectively) and will be discussed in detail in the next section. Both compounds are air sensitive and decompose at room temperature even when stored under an inert atmosphere. The complexes have been characterized by TGA, IR, elemental analysis and single crystal X-ray diffraction.

$Mo_2(O_2CMe)_4$ also dissolves in liquid ammonia (*ca* 5 mg cm^{-3} at 25°C) and liquid $MeNH_2$ (*ca* 12 mg cm^{-3}) to form golden yellow solutions that yield large, air-sensitive, chunky crystals upon cooling to −15°C. When the solvent is removed (evaporated) under N_2 at 0°C, the crystals decomposed almost instantly leaving powdery $Mo_2(O_2CMe)_4$. The yel-

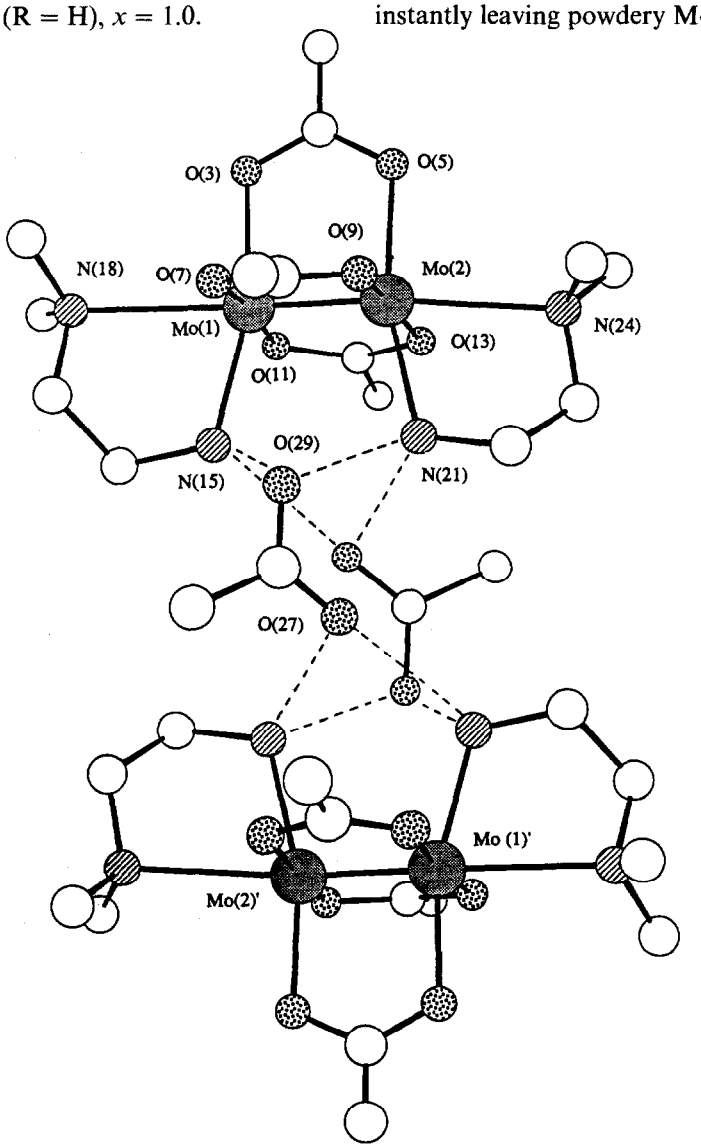

Fig. 3. Ball-and-stick representation* of the $\{[Mo_2(O_2CMe)_3(N,N\text{-dmed})_2]^+[(O_2CMe)]^-\}_2$ complex (**6**). All hydrogen atoms have been omitted for clarity. The dotted lines denote N—H···O bonding interactions.

* See footnote to p. 2577.

low crystals are presumably axial bis-amine adducts of formula $Mo_2(O_2CMe)_4L_2$ [where $L = NH_3$, $MeNH_2$] but are too unstable to isolate [cf. $Mo_2(O_2CMe)_4(py)_2$].[6,7] Heating the solutions to 60°C did not affect a colour change.

$Mo_2(O_2CCF_3)_4$ readily dissolves in liquid ammonia (*ca* 30 mg cm^{-3} at 25°C) forming bright red solutions at −77°C that fade to orange–red at room temperature. No products have been isolated from these reactions.

Solid state structures

A ball-and-stick drawing of the *N,N'*-dmed chain complex $^1_\infty[Mo_2(O_2CMe)_4(N,N'\text{-dmed})]$ (**4**) is shown in Fig. 1. A summary of the crystallographic data is given in Table 1 and selected bond distances and angles are given in Table 2.

The one-dimensional chain structure of **4** consists of $Mo_2(O_2CMe)_4$ units linked head-to-tail by axially bound *N,N'*-dmed ligands. As in the related $^1_\infty[Mo_2(O_2CMe)_4(tmed)]$ complex **2**,[3] the $Mo_2(O_2CMe)_4$ fragment of **4** is virtually unperturbed by the axial amine ligands with an Mo—Mo distance of 2.101(1) Å (ave) and Mo—O distances of 2.12(2) Å (ave). For comparison, the Mo—Mo and Mo—O distances in the parent complex **1** are 2.093(1) Å and 2.119(5) Å (ave), respectively.[10] The axial Mo—N contacts in **4** are characteristically long at 2.69 Å (ave) [Mo(1)—N(1) = 2.73(1) Å,

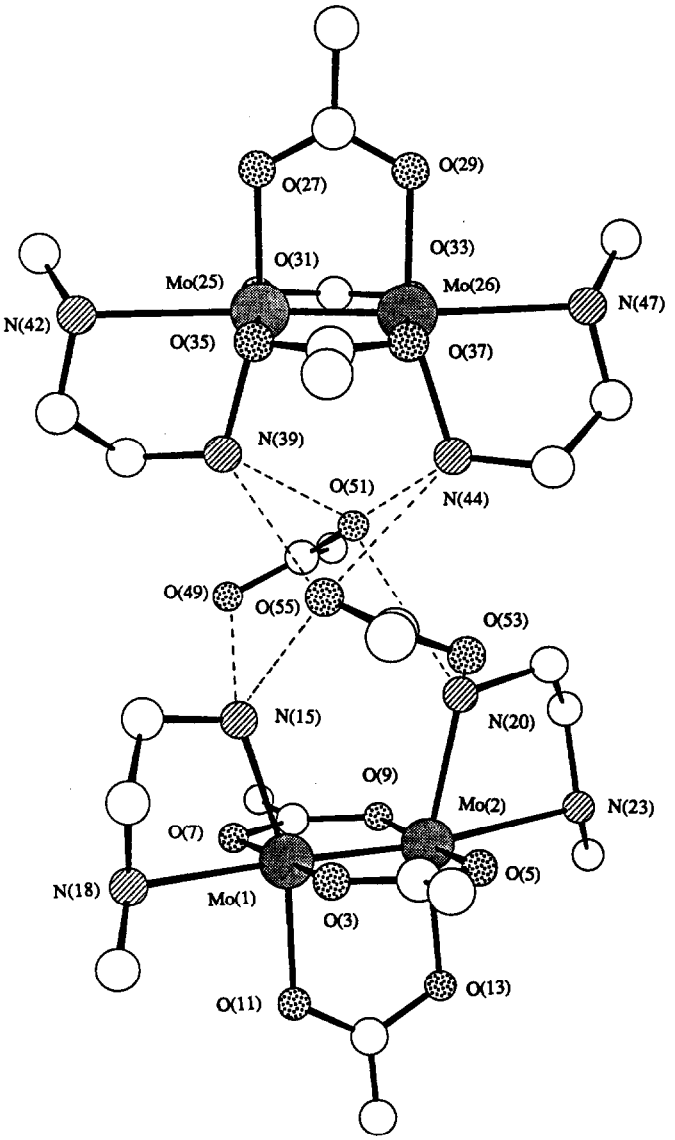

Fig. 4. Ball-and-stick representation* of the $\{[Mo_2(O_2CMe)_3(N\text{-med})_2]^+[(O_2CMe)]^-\}_2 \cdot N\text{-med}$ complex (**7**). All hydrogen atoms have been omitted for clarity. The dotted lines denote N—H···bonding interactions.

* See footnote to p. 2577.

Table 1. Summary of crystallographic data for **4–7**

Compound[a]	**4**	**5**	**6**	**7**
Empirical formula	$Mo_2C_{12}H_{24}O_8N_2$	$Mo_2C_{11}H_{22}O_8N_2$	$Mo_4C_{32}H_{72}N_8O_{16}$	$Mo_4C_{28}H_{64}N_8O_{16}$
Space group	$P\bar{1}$	$P4_2/m$	$P2_1/c$	$P\bar{1}$
Temperature (°C)	20	25	−155	−95
Cell dimensions:				
a (Å)	8.784(3)	7.852(2)	14.367(5)	12.988(10)
b (Å)	12.945(6)	7.852(2)	10.011(4)	15.881(12)
c (Å)	8.663(3)	14.382(2)	17.246(7)	12.963(10)
α (°)	91.73(3)	90	90	105.77(3)
β (°)	97.23(3)	90	95.92(2)	101.83(4)
γ (°)	101.45(4)	90	90	81.95(3)
Z (molecules cell^{-1})	2	2	2	2
Volume (Å^3)	956.2	886.7	2467.31	2508.43
Calculated density (g cm^{-3})	1.79	1.88	1.627	1.653
Wavelength (Å)	0.71073	0.71073	0.71069	0.71069
Molecular weight (amu)	516.21	502.13	604.36	1248.71
Linear absorption coefficient (cm^{-1})	13.2	14.2	10.353	10.213
$R(F)$	0.055	0.047	0.064	0.051
$R_w(F)$	0.076	0.050	0.066	0.055

[a] Compound **4** is $^1_\infty[Mo_2(O_2CMe)_4(N,N'\text{-dmed})]$, **5** is $^1_\infty[Mo_2(O_2CMe)_4(pda)]$, **6** is $\{[Mo_2(O_2CMe)_3(N,N\text{-dmed})_2]^+[(O_2CMe)]^-\}_2$ and **7** is $\{[Mo_2(O_2CMe)_3(N\text{-med})_2]^+[(O_2CMe)]^-\}_2 \cdot N\text{-med}$.

Mo(2)—N(2) = 2.642(9) Å] and display slight deviations from linearity [Mo(1)′—Mo(1)—N(1) = 166.6(2)°; Mo(2)′—Mo(2)—N(2) = 171.2(2)°] which is typical for these types of compounds.[2,3,11]

The unusual structural feature in **4** is the weak hydrogen bonding between amine hydrogens of the *N,N′*-dmed ligand and the acetate oxygens on neighbouring $Mo_2(O_2CMe)_4$ fragments [N(1)—O(1) = 3.1(1) Å, N(2)—O(7) = 3.08(9) Å]. Even though the N···O separations are somewhat

Table 2. Selected bond distances (Å) and angles (°) for $^1_\infty[Mo_2(O_2CMe)_4(N,N'\text{-dmed})]$ (**4**)

Bond distances			
Mo(1)—Mo(1)′	2.101(1)	Mo(2)—O(3)	2.12(1)
Mo(1)—O(5)	2.088(9)	Mo(2)—O(4)	2.13(1)
Mo(1)—O(6)	2.116(9)	Mo(2)—O(2)	2.642(9)
Mo(1)—O(7)	2.132(8)	N(1)—C(9)	2.45(2)
Mo(1)—O(8)	2.110(9)	N(1)—C(10)	1.47(2)
Mo(1)—N(1)	2.73(1)	N(1)—C(12)	1.45(2)
Mo(2)—Mo(2)′	2.102(1)	N(2)—C(9)	1.45(2)
Mo(2)—O(1)	2.13(1)	N(2)—C(10)	2.48(2)
Mo(2)—O(2)	2.130(9)	N(2)—C(11)	1.45(2)
Bond angles			
Mo(1)—Mo(1)—O(5)	93.0(2)	O(6)—Mo(1)—O(8)	176.9(3)
Mo(1)—Mo(1)—O(6)	91.8(2)	O(6)—Mo(1)—N(1)	94.4(3)
Mo(1)—Mo(1)—O(7)	89.9(2)	O(7)—Mo(1)—O(8)	89.0(3)
Mo(1)—Mo(1)—O(8)	91.3(2)	O(7)—Mo(1)—N(1)	78.0(3)
Mo(1)—Mo(1)—N(1)	166.6(2)	O(8)—Mo(1)—N(1)	82.7(3)
O(5)—Mo(1)—O(6)	89.9(3)	Mo(2)—Mo(2)—O(1)	91.1(2)
O(5)—Mo(1)—O(7)	176.6(3)	Mo(2)—Mo(2)—O(2)	91.6(2)
O(5)—Mo(1)—O(8)	89.3(3)	Mo(2)—Mo(2)—O(3)	91.7(2)
O(5)—Mo(1)—N(1)	98.9(3)	Mo(2)—Mo(2)—O(4)	92.9(2)
O(6)—Mo(1)—O(7)	91.6(3)	Mo(2)—Mo(2)—N(2)	171.2(2)

longer than normal,[12] these hydrogen bonding interactions impart a kink in chain structure that effectively doubles the unit cell relative to the tmed complex **2**. The structural differences between **2** and **4** are best illustrated by examining Newman projections of the two complexes viewed down the ethylene C—C bonds of the diamine backbones. The tmed complex **2** adopts the more stable *anti* conformation **III** which maximizes the distance between neighbouring Mo_2 units. Compound **4**, however, adopts a *gauche* conformation, **IV**, to bring the amine hydrogens and the acetate oxygens within hydrogen bonding distances. The conformational strain that results from the steric interaction of the two [NMe(H)Mo_2] groups is apparently compensated by the formation of the two hydrogen bonds—even though the interactions appear to be weak.

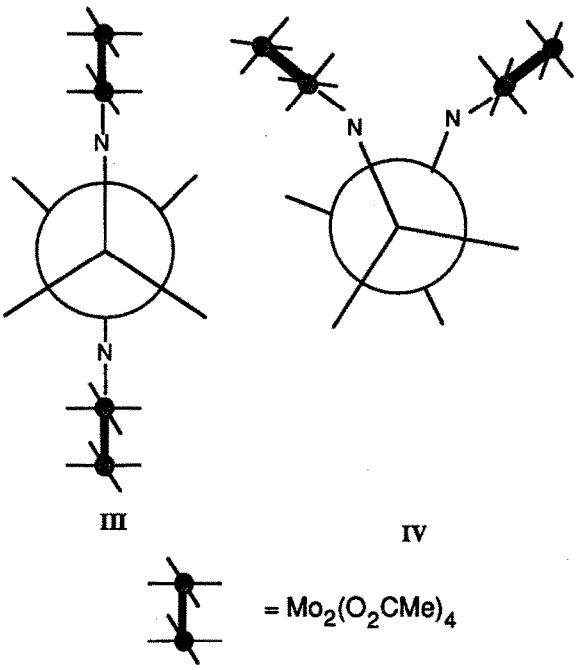

A ball-and-stick drawing of $^1_\infty[Mo_2(O_2CMe)_4(pda)]$ (**5**) is shown in Fig. 2 and a listing of selected bond distances and angles is given in Table 3. A summary of the crystallographic data is given in Table 1.

Compound **5** adopts a chain structure similar to that observed for the tmed complex **2**. The complex is tetragonal, space group $P4_2/m$, with Mo(1) and N(1) located in the (001) mirror plane. There is a two-fold disorder of C(3) about the mirror plane and a four-fold disorder of C(4) about the crystallographic inversion centre at 1/2, 1/2, 0 and (001) mirror plane. The rest of the complex was well behaved with typical Mo—Mo, Mo—O and O—C bonds and a characteristically long Mo—N bond length of 2.636(11) Å.

Ball-and-stick drawings of the *N,N*-dmed complex (**6**) and *N*-med complex (**7**) are shown in Figs 3 and 4, respectively. Selected bond distances and angles are given in Table 4 and 5. Summaries of the crystallographic data are presented in Table 1.

The gross structural features of compounds **6** and **7** are quite similar. Compound **6** is monoclinic, space group $P2_1/c$, with a crystallographic inversion centre that relates the two Mo_2 fragments within the Mo_4 core. Compound **7**, however, crystallizes in the triclinic space group $P\bar{1}$ and contains the entire Mo_4 complex in the asymmetric unit. With the exception of the methyl groups on the *N*-med ligands and the relative conformations of one of the chelate rings, the two Mo_2(*N*-med)$_2$ fragments are related by a pseudo centre of inversion. The lattice of the *N*-med complex **7** is also solvated with *ca* one disordered *N*-med molecule per Mo_4 formula unit.

Both **6** and **7** contain two Mo_2 subunits with Mo—Mo quadruple bonds [Mo—Mo = 2.12(1) Å (ave)] and three spanning acetate ligands with typical Mo—O distances [Mo—O = 2.12(1) Å (ave)].[13] Each metal atom possesses a chelating diamine ligand that occupies one axial [Mo—N = 2.63(3)

Table 3. Selected bond distances (Å) and angles (°) for $^1_\infty[Mo_2(O_2CMe)_4(pda)]$ (**5**)

Bond distances			
Mo—Mo′	2.103(1)	O(2)—C(1)	1.268(7)
Mo—O(1)	2.127(4)	C(1)—C(2)	1.497(9)
O(1)—C(1)	1.279(7)	N(1)—C(3)	1.451(20)
Mo—N(1)	2.636(11)	C(3)—C(4)	1.542(32)
Mo—O(2)	2.117(4)		
Bond angles			
Mo—Mo′—N(1)	174.8(3)	Mo—Mo′—O(2)	92.2(1)
O(1)—Mo—N(1)	85.0(2)	Mo—Mo′—O(1)	91.3(1)
Mo—N(1)—C(3)	129.9(11)	O(2)—Mo—N(1)	91.5(2)
N(1)—C(3)—C(4)	107.6(16)		

Table 4. Selected bond distances (Å) and angles (°) for $\{[Mo_2(O_2CMe)_3(N,N\text{-dmed})_2]^+[(O_2CMe)]^-\}_2$ (**6**)

Bond distances			
Mo(1)—Mo(2)	2.1238(16)	O(5)—C(4)	1.269(16)
Mo(1)—O(3)	2.124(8)	O(7)—C(8)	1.276(15)
Mo(1)—O(7)	2.142(8)	O(9)—C(8)	1.260(15)
Mo(1)—O(11)	2.102(8)	O(11)—C(12)	1.280(14)
Mo(1)—N(15)	2.224(9)	O(13)—C(12)	1.259(14)
Mo(1)—N(18)	2.660(9)	O(27)—C(28)	1.229(15)
Mo(2)—O(5)	2.122(9)	O(29)—C(28)	1.273(15)
Mo(2)—O(9)	2.107(9)		
Mo(2)—O(13)	2.150(8)	N(15)—O(29)	2.95(2)
Mo(2)—N(21)	2.240(10)	N(15)—O(27)′	2.95(2)
Mo(2)—N(24)	2.642(9)	N(21)—O(29)	2.92(2)
O(3)—C(4)	1.273(16)	N(21)—O(27)′	3.00(2)

Bond angles			
Mo(2)—Mo(1)—O(3)	91.38(24)	Mo(1)—Mo(2)—N(24)	169.9(3)
Mo(2)—Mo(1)—O(7)	90.38(22)	O(5)—Mo(2)—O(9)	93.2(3)
Mo(2)—Mo(1)—O(11)	92.89(22)	O(5)—Mo(2)—O(13)	92.9(3)
Mo(2)—Mo(1)—N(15)	103.99(25)	O(5)—Mo(2)—N(21)	165.3(3)
Mo(2)—Mo(1)—N(18)	171.5(3)	O(9)—Mo(2)—O(13)	173.5(3)
O(3)—Mo(1)—O(7)	93.2(3)	O(9)—Mo(2)—N(21)	85.5(4)
O(3)—Mo(1)—O(11)	92.7(3)	O(13)—Mo(2)—N(21)	88.0(4)
O(3)—Mo(1)—N(15)	164.6(3)	Mo(1)—O(3)—C(4)	116.7(8)
O(7)—Mo(1)—O(11)	173.2(3)	Mo(2)—O(5)—C(4)	116.5(8)
O(7)—Mo(1)—N(15)	86.1(3)	Mo(1)—O(7)—C(8)	116.4(7)
O(11)—Mo(1)—N(15)	87.3(4)	Mo(2)—O(9)—C(8)	116.6(7)
Mo(1)—Mo(2)—O(5)	91.76(25)	Mo(1)—O(11)—C(12)	117.4(7)
Mo(1)—Mo(2)—O(9)	92.49(23)	Mo(2)—O(13)—C(12)	118.6(8)
Mo(1)—Mo(2)—O(13)	89.58(22)	Mo(1)—N(15)—C(16)	112.4(7)
Mo(1)—Mo(2)—N(21)	102.94(25)	Mo(2)—N(21)—C(22)	112.7(7)

Å (ave)] and one equatorial [Mo—N = 2.23(1) Å (ave)] site. The axial Mo—N contacts are long relative to the equatorial Mo—N bonds and show slight deviations from linearity [Mo—Mo—N ≈ 170°] but are somewhat shorter than the axial Mo—N contacts in related compounds [cf. 2.68(4) Å in **4**, 2.7(2) Å in **3**, and 2.73(1) Å in **2**].[2,3] The equatorial Mo—N bond distances are typical for Mo—N dative bonds [cf. 2.22(2) Å in **3**] but the nitrogens are bent out of the equatorial plane. This distortion is illustrated by obtuse Mo—Mo—N_{eq} bond angles [104(2)° for **6** and 105(2)° for **7**] relative to the nearly ideal 91(1)° (ave) Mo—Mo—O angles observed for the coordinated acetates.

In **6** and **7**, the acetate ions that were displaced from the Mo_2 coordination spheres are hydrogen bonded to the NH_2 hydrogens of the diamine ligands. Four NH_2 groups and two acetate ions form a hydrogen bonding network that links the two Mo_2 subunits together. In compound **6**, the four Mo atoms are rigorously coplanar due to the crystallographic inversion centre whereas the two Mo_2 units in **7** are twisted relative to each other (dihedral Mo—Mo—Mo—Mo = 19.3°) producing a "cogging" effect. As a result, the Mo_2 moieties are closer together in **7** (Mo_2 midpoint to Mo_2 midpoint = 7.96 Å) than in **6** (Mo_2 midpoint to Mo_2 midpoint = 8.84 Å).

The hydrogen bonding networks in **6** and **7** are also somewhat dissimilar. In **6**, the displaced acetate ion O—O vectors are perpendicular to the Mo_2 vectors. This arrangement allows each oxygen atom to form two N—H···O hydrogen bonds (N···O separations less than 3.0 Å). Both N—H···O bonds to a given oxygen involve equatorial amine hydrogens on the same Mo_2 fragment. In contrast, the O—O vectors in **7** are twisted towards a parallel orientation relative to the Mo_2 fragments. This conformation allows one oxygen on each displaced acetate to form three N—H···O hydrogen bonds whereas the other oxygen only forms one. All significant N···O contacts are between 2.95 and 3.1 Å except one long contact of 3.16(2) Å involving N(39) and O(51) (see Tables 4 and 5).

Interestingly, the least Lewis basic nitrogens of the diamines, the NH_2 groups, occupy the equa-

Table 5. Selected bond distances (Å) and angles (°) for $\{[Mo_2(O_2CMe)_3(N\text{-med})_2]^+[(O_2CMe)]^-\}_2 \cdot N\text{-med}$ (7)

Bond distances			
Mo(1)—Mo(2)	2.1296(19)	Mo(25)—N(42)	2.613(9)
Mo(1)—O(3)	2.153(5)	Mo(26)—O(29)	2.126(6)
Mo(1)—O(7)	2.112(5)	Mo(26)—O(33)	2.124(5)
Mo(1)—O(11)	2.118(6)	Mo(26)—O(37)	2.108(5)
Mo(1)—N(15)	2.248(7)	Mo(26)—N(44)	2.219(7)
Mo(1)—N(18)	2.619(9)	Mo(26)—N(47)	2.624(9)
Mo(2)—O(5)	2.100(5)		
Mo(2)—O(9)	2.133(6)	N(20)—O(53)	3.02(2)
Mo(2)—O(13)	2.130(5)	N(44)—O(55)	3.01(2)
Mo(2)—N(20)	2.233(6)	N(39)—O(55)	2.96(2)
Mo(2)—N(23)	2.604(9)	N(15)—O(55)	2.98(2)
Mo(25)—Mo(26)	2.1220(20)	N(15)—O(49)	3.00(2)
Mo(25)—O(27)	2.126(6)	N(20)—O(51)	3.00(2)
Mo(25)—O(31)	2.122(6)	N(39)—O(51)	3.16(2)
Mo(25)—O(35)	2.134(5)	N(44)—O(51)	3.07(2)
Mo(25)—N(39)	2.211(7)		
Bond angles			
Mo(2)—Mo(1)—O(3)	88.58(15)	Mo(26)—Mo(25)—O(27)	91.15(16)
Mo(2)—Mo(1)—O(7)	93.04(16)	Mo(26)—Mo(25)—O(31)	91.93(16)
Mo(2)—Mo(1)—O(11)	91.80(16)	Mo(26)—Mo(25)—O(35)	90.24(15)
Mo(2)—Mo(1)—N(15)	105.12(17)	Mo(26)—Mo(25)—N(39)	107.17(17)
Mo(2)—Mo(1)—N(18)	163.6(1)	Mo(26)—Mo(25)—N(42)	169.1(1)
O(3)—Mo(1)—O(7)	177.84(21)	O(27)—Mo(25)—O(31)	90.90(23)
O(3)—Mo(1)—O(11)	90.99(22)	O(27)—Mo(25)—O(35)	93.68(22)
O(3)—Mo(1)—N(15)	92.18(23)	O(27)—Mo(25)—N(39)	161.63(22)
O(7)—Mo(1)—O(11)	90.39(22)	O(31)—Mo(25)—O(35)	174.90(21)
O(7)—Mo(1)—N(15)	86.02(23)	O(31)—Mo(25)—N(39)	87.16(24)
O(11)—Mo(1)—N(15)	162.86(22)	O(35)—Mo(25)—O(35)	87.78(23)
Mo(1)—Mo(2)—O(5)	93.78(16)	Mo(25)—Mo(26)—O(29)	91.19(16)
Mo(1)—Mo(2)—O(9)	89.76(15)	Mo(25)—Mo(26)—O(33)	90.77(16)
Mo(1)—Mo(2)—O(13)	90.60(15)	Mo(25)—Mo(26)—O(37)	92.75(15)
Mo(1)—Mo(2)—N(20)	105.41(17)	Mo(25)—Mo(26)—N(44)	104.18(18)
Mo(1)—Mo(2)—N(23)	168.1(1)	Mo(25)—Mo(26)—N(47)	176.4(1)
O(5)—Mo(2)—O(9)	176.03(20)	O(29)—Mo(26)—O(33)	90.63(22)
O(5)—Mo(2)—O(13)	90.39(21)	O(29)—Mo(26)—O(37)	93.47(22)
O(5)—Mo(2)—N(20)	88.83(23)	O(29)—Mo(26)—N(44)	164.59(23)
O(9)—Mo(2)—O(13)	91.37(21)	O(33)—Mo(26)—O(37)	174.54(21)
O(9)—Mo(2)—N(20)	88.50(22)	O(33)—Mo(26)—N(44)	90.33(24)
O(13)—Mo(2)—N(20)	163.99(22)	O(37)—Mo(26)—N(44)	84.77(24)

torial positions in both **6** and **7**. Intuitively, one might expect the more Lewis basic, alkylated nitrogens (—NMeH for *N*-med, —NMe_2 for *N*,*N*-dmed) to occupy the equatorial positions where strong metal–ligand interactions occur and maximum Mo—N bonding could be realized.[1] However, if the —NH_2 groups were removed from the equatorial positions, the hydrogen-bonding network that couples the two Mo_2 fragments together would be compromised.

Thermal decomposition studies

Crystalline samples of **4**, **6** and **7** decompose thermally, in inert atmospheres, to form crystalline $Mo_2(O_2CMe)_4$ at temperatures less than 120°C. TGA studies showed diamine expulsions at temperatures at or below the boiling points of the pure diamine ligands.* In addition, diamine loss from the *N*-med complex **7** occurs in two steps, whereas the two dmed complex **4** and **6** show single step diamine losses (see Figs 5 and 6). Powder X-ray diffractograms of the brown–yellow 120°C

* Boiling points of the diamine ligands found in the **4**, **6** and **7** and the corresponding TGA expulsion temperatures (first derivative maximum) in parentheses: *N*,*N*-dmed, 104–106°C (98°C); *N*,*N*′dmed, 119°C (105°C); *N*-med, 114–116°C (110°C, ave).

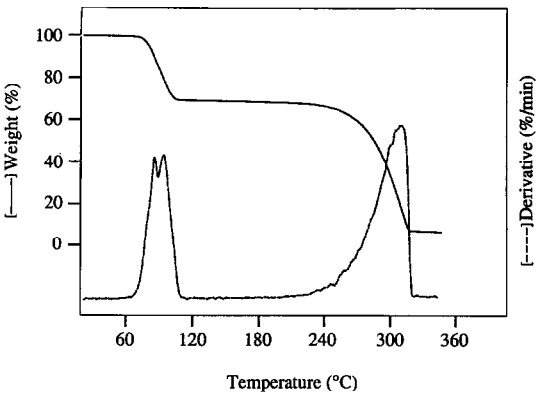

Fig. 5. TGA trace (solid line) and first derivative (dotted line) for the $\{[Mo_2(O_2CMe)_3(N\text{-med})_2]^+[(O_2CMe)]^-\}_2 \cdot N$-med complex (7) showing the two-step N-med loss.

residues from the TGA experiments showed only $Mo_2(O_2CMe)_4$. The slight discolouration [$Mo_2(O_2CMe)_4$ is pale yellow] is likely due to the partial oxidation of the air-sensitive amine complexes during TGA sample preparation, which is conducted in the air. Small amounts of an amorphous black residue (<15%) remain in the TGA pan after sublimation of the $Mo_2(O_2CMe)_4$ is complete ($T > 300$°C). As previously noted,[2] slower heating rates seem to increase the amount of final residue produced. The identity of this material is currently unknown.

The two-step N-med loss during the thermal treatment of **7** suggests that the solvate molecule and coordinated ligands are expelled separately. It is tempting to speculate that the solvate N-med molecule might be expelled before the coordinated N-med ligands, but we currently do not have quantitative data to support this hypothesis. However, a similar three-step diamine elimination was observed from the en complex **3**, which has two types of en ligands as well as an en solvate molecule.[2] The number of N-med solvate molecules in the lattice of the N-med complex **7** was determined by elemental analysis (one N-med per Mo_4), although TGA studies suggested only *ca* 0.7 N-med solvate molecules per Mo_4 unit. The lower N-med content observed in the TGA experiments probably results from partial desolvation of the complex during sample preparation.

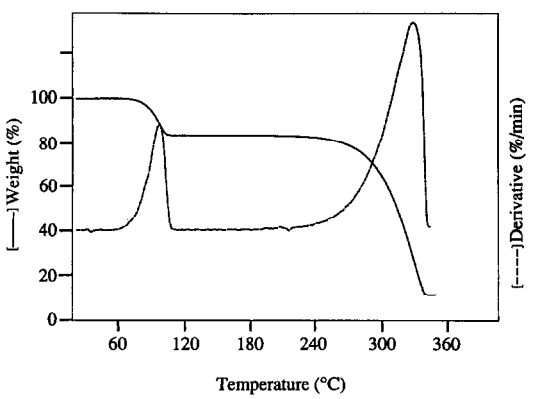

Fig. 6. TGA trace (solid line) and first derivative (dotted line) for the $^1_\infty[Mo_2(O_2CMe)_4(N,N'\text{-dmed})]$ complex (**4**) showing the simple one-step diamine elimination processes.

Table 6. Selected IR data for compounds **4**, **5**, **6** and **7**

Compound	ν_{asym}(OCO) (cm^{-1})	ν_{sym}(OCO) (cm^{-1})
4	1530	1429
5	1530	1432
6	1582, 1527	1430, 1383
7	1569, 1529	1430, 1387

It is interesting to note that the displaced acetate ions in **6** and **7** must migrate *ca* 4 Å to recoordinate to the Mo_2 centre during the amine expulsion process. A similar phenomenon occurs in the thermal decomposition of **3**.[2]

The thermal behaviour of **5** appears to follow the same decomposition pathway but was not studied in detail.

IR spectroscopic studies

The IR bands for the acetate O—C—O vibrations from solid state samples (KBr pellets) are listed in Table 6. For the coupled monocations **6** and **7**, two sets of acetate vibrations are observed which correspond to the two types of acetate moieties present in the complexes—coordinated and displaced. The chain complexes **4** and **5**, however, show only one set of acetate bands which is consistent with the presence of only bound acetate ligands.[2,3,13]

DISCUSSION

Pale yellow crystals of the weakly associated one-dimensional chain complexes $^1_\infty[Mo_2(O_2CMe)_4$(diamine)] are formed in good yield [where diamine = N,N'-dmed (**4**); pda (**5**)] from concentrated solutions of $Mo_2(O_2CMe)_4$ (**1**) dissolved in the respective pure diamine. In contrast, solutions of **1** dissolved in N,N-dmed and N-med precipitate monocationic complexes that are coupled, via hydrogen bonding, to form the tetrameric

compounds **6** and **7** of general formula $\{[Mo_2(O_2CMe)_3(diamine)_2]^+[(O_2CMe)]^-\}_2$. For each Mo_2 fragment, one acetate ligand is displaced by two diamine ligands in both of the latter complexes. Pale yellow crystals of *proposed* formula $Mo_2(O_2CMe)_4(L)_2$ [where $L = NH_3$ or $MeNH_2$] are formed from concentrated yellow solutions of $Mo_2(O_2CMe)_4$ dissolved in the neat amine [cf. $Mo_2(O_2CMe)_4(py)_2$],[6,7] however, these complexes were too unstable to fully characterize. The amines that form only axial adducts (tmed, *N,N'*-dmed, $MeNH_2$, and NH_3) form pale yellow solutions with $Mo_2(O_2CMe)_4$ whereas amines that displace acetates (en, *N*-med, *N,N*-dmed) form orange–red to red solutions. The red colour observed in the reaction of $Mo_2(O_2CMe)_4$ with pda suggests that extensive acetate displacement occurs in solution even though the resulting crystalline complex **5** has an unperturbed $Mo_2(O_2CMe)_4$ core. Similar colour changes occur in the reactions of $Mo_2(O_2CCF_3)_4$ with phosphine in which displaced carboxylates were observed.[14,15]

It is interesting to correlate the structures of compounds **2–7** with the functionalities of the diamine ligands. As the polarity and number of amine hydrogens increase in a diamine, the extent of acetate displacement increases. Of particular interest is the comparison of the *N,N'*-dmed and the *N,N*-dmed complexes **4** and **6**, respectively, in which acetate displacement is observed in the latter but not in the former. It appears that an $—NH_2$ function is necessary for acetate displacement in order to stabilize the displaced acetate ions in the solid state through hydrogen bonding. Furthermore, the $—NH_2$ functions prefer equatorial sites on the Mo_2 centre as maximum hydrogen bonding is realized in this conformation. Even though acetate displacement appears to occur in the $Mo_2(O_2CMe)_4$/pda system in solution, a suitable H-bonding network may not be available to stabilize the displaced acetates in the solid state and the axial adduct **5** is isolated instead.

A related reaction[16] between $Mo_2(O_2CCF_3)_4$ and 2,2′-bipyridyl yielded a charge-separated complex of proposed formula $[Mo_2(O_2CCF_3)_3(2,2'\text{-bipyridyl})]^+[O_2CCF_3]^-$ which would presumably have a core structure similar to those of **6** and **7** although hydrogen bonding and axial ligation would be absent in the former.

Entropic effects (ΔS_0) in the $Mo_2(O_2CMe)_4$–amine systems also appear to be important in acetate displacement in that methyl amine and liquid ammonia apparently do not affect acetate displacement even though they are as polar and would have Mo—N bond strengths similar to those found in **3**, **6** and **7**. It seems plausible that only the diamines capable of neutralizing the standard entropy effects of the bidentate, spanning acetate groups can promote acetate displacement.

Acknowledgements—This work was funded in part by Exxon Research and Engineering Company. B.W.E. acknowledges the Department of Chemistry and Biochemistry, University of Maryland, and the Donors of The Petroleum Research Fund, administered by the American Chemical Society, for partial support of this research. The authors wish to thank Mr Cahit Eylem for assistance with the X-ray data collection and Ms Karen Jones for assistance with the TGA experiments.

REFERENCES

1. J. M. Casas, R. H. Cayton and M. H. Chisholm, *Inorg. Chem.* 1991, **30**, 358.
2. B. W. Eichhorn, M. C. Kerby, R. C. Haushalter and K. P. C. Vollhardt, *Inorg. Chem.* 1990, **29**, 723.
3. M. C. Kerby, B. W. Eichhorn, J. A. Creighton and K. P. C. Vollhardt, *Inorg. Chem.* 1990, **29**, 1319.
4. M. C. Kerby, B. W. Eichhorn, L. Doviken and K. P. C. Vollhardt, *Inorg. Chem.* 1991, **30**, 156.
5. B. W. Eichhorn, R. C. Haushalter, B. Wilson and F. A. Cotton, *Inorg. Chem.* 1988, **27**, 4084.
6. T. A. Stephenson, E. Bannister and G. Wilkinson, *J. Chem. Soc.* 1964, 2538.
7. F. A. Cotton and J. G. Norman Jr, *J. Am. Chem. Soc.* 1972, **94**, 5697.
8. A. B. Brignole and F. A. Cotton, *Inorg. Synth.* 1972, **13**, 81.
9. M. H. Chisholm, K. Folting, J. C. Huffman and C. C. Kirkpatrick, *Inorg. Chem.* 1984, **23**, 1021.
10. (a) E. W. Abel, A. Singh and G. Wilkinson, *J. Chem. Soc.* 1959, 3097; (b) D. Lawton and R. Mason, *J. Am. Chem. Soc.* 1965, **87**, 921.
11. (a) F. A. Cotton, A. H. Reid and W. Schwotzer, *Inorg. Chem.* 1985, **24**, 3965; (b) C. D. Garner, G. Pimblett and W. Clegg, *J. Chem. Soc., Dalton Trans.* 1986, 1257.
12. J. E. Huheey, *Inorganic Chemistry—Principles of Structure and Reactivity*, 3rd edn. Harper & Row, New York (1983).
13. F. A. Cotton and R. A. Walton, *Multiple Bonds Between Metal Atoms*. Wiley, New York (1982).
14. K. Teramoto, Y. Sasaki, K. Migita, M. Iwaizumi and K. Saito, *Bull. Chem. Soc. Japan* 1979, **52**, 446.
15. G. S. Girolami, V. V. Mainz and R. A. Anderson, *Inorg. Chem.* 1980, **19**, 805.
16. C. D. Garner and R. G. Senior, *J. Chem. Soc., Dalton Trans.* 1976, 1041.

Polyhedron Vol. 10, No. 22, pp. 2587–2596, 1991
Printed in Great Britain

0277–5387/91 $3.00+.00
© 1991 Pergamon Press plc

PROTOLYTIC EQUILIBRIA IN AQUEOUS CONCENTRATED SOLUTIONS OF ORTHOPHOSPHATES

LIBERATO CIAVATTA,* MAURO IULIANO, RAFFAELLA PORTO and ERMANNO VASCA

Dipartimento di Chimica dell'Università, Via Mezzocannone, 4, 80134 Napoli, Italy

(*Received* 9 *November* 1990; *accepted* 4 *July* 1991)

Abstract—The protolytic equilibria, in solutions prepared to contain 3 M Na^+ ions by adding $NaClO_4$, have been studied at 25°C by potentiometric methods using glass or hydrogen half-cells. Most of the experiments (glass electrode) have been carried out in $Na(ClO_4, H_2PO_4)$ media where the phosphate molar concentration ranged from 0.1 to 3. A few experiments (hydrogen electrode) have been made in $Na(ClO_4, HPO_4)$ media at the phosphorus(V) levels of 0.3 and 1 M. The potentiometric data are consistent with the presence in solution of dimers, $H_n(PO_4)_2^{n-6}$, with n ranging from 1 to 6, as well as of the usual monomeric species. The formation constants are found to vary significantly as orthophosphates replace ClO_4^- ions of the medium. This phenomenon is ascribed to strong short-range interactions of the polar $H_2PO_4^-$ and HPO_4^{2-} ions with other species, even negatively charged ones, in evident contrast with the Brønsted principle.

For several metal orthophosphates, such as the Ca^{2+}, Mg^{2+}, Fe^{2+}, Zn^{2+} salts, which are of interest in geochemistry, oceanography, water pollution and other fields where phosphates are widely found and in large quantity, a low degree of complexation in solution is indicated by scanty and contradictory literature data.[1,2] This implies that in these systems equilibrium analysis, strictly correlated to the presence of detectable amounts of reaction products, can be reliably performed only considering concentrated reagent solutions. In this connection it is essential to establish the formation and equilibrium constants of the protolytic species that become important in phosphate solutions of concentration exceeding 0.1 M.

Though monomeric species prevail, there is some evidence by various authors, Table 1, that dimers may form in concentrated solutions. The main source of uncertainty that can be envisaged in the assessment of polynuclear complexes from the reviewed data in concentrated solutions, is the neglect of the effects of medium changes, occurring as inert ions of the medium are replaced for a large part by phosphate species. Since the polynuclear complexes are of low stability, even small medium changes may seriously influence their stoichiometry and formation constants. It was, therefore, thought worth a reinvestigation of the system by more appropriate experimental conditions and calculation procedures.

In this work the protolytic equilibria have been studied at 25°C by potentiometric titrations employing glass or hydrogen electrodes in cells without transference. All the solutions were prepared to contain 3 M Na^+ ions by adding $NaClO_4$. The measurements with the glass elecrode were carried out in $Na(ClO_4, H_2PO_4)$ media where the phosphorus(V) concentration ranged from 0.1 to 3 M. The experiments with the hydrogen half-cell were made in 0.3 and 1 M Na_2HPO_4. In order to avoid the implications connected with medium changes, data pertaining to a given phosphate level were considered separately according to the principle of the self-medium method.[11] Since glass and hydrogen electrodes cannot be calibrated in the absence of reaction products on the self-medium scale, formal standard potentials of the employed cells were adjusted simultaneously with other parameters (equilibrium constants) in the treatment of experimental data by minimizing procedures with a high-speed computer.

* Author to whom correspondence should be addressed.

Table 1. Survey of previous work on the formation equilibria of the $H_n(PO_4)_2^{n-6}$ species. Temperature 25°C (37 in ref. 5)

Author	Medium	Concentration range	Method	n	Equilibrium constant
Selvaratnam and Spiro[3]	dilute	0.02–0.093M	trans. num.	5	3[a]
Elmore *et al.*[4]	dilute	0.1–10 m	various	6	0.3[b]
				5	1.26[a]
Childs[5]	0.15MKNO$_3$	(2–12) mM	EMF	4	5.6[c]
				3	2.7[d]
Hietanen *et al.*[6]	3MNa(ClO$_4$)	1–3 M	EMF	5	23.4[e]
				3	6.5×10^{-7}[f]
Ferroni *et al.*[7]	3MK(Cl)	0.1–1 M	EMF	4	0.42[c]
				3	4.4×10^{-7}[f]
Ferroni *et al.*[8]	3MK(Cl)	0.05–2 M	EMF	6	0.41[g]
				5	2.4×10^{-2}[b]
				4	2.7×10^{-3}[h]
Ferroni *et al.*[9]	3MK(Cl)	0.05–2 M	EMF	2	0.18[i]
Ivakin and Voronova[10]	3MNa(Cl)	0.02–1 M	EMF	5	1.45×10^{2}[e]
				4	0.73[c]
				3	4.9×10^{6}[j]

[a] $H_3PO_4+H_2PO_4^- \leftrightarrows H_5(PO_4)_2^-$.
[b] $H_6(PO_4)_2 \leftrightarrows H_5(PO_4)_2^- + H^+$.
[c] $2H_2PO_4^- \leftrightarrows H_4(PO_4)_2^{2-}$.
[d] $H_2PO_4^- + HPO_4^{2-} \rightleftarrows H_3(PO_4)_2^{3-}$.
[e] $2H_2PO_4^- + H^+ \leftrightarrows H_5(PO_4)_2^-$.
[f] $2H_2PO_4^- \leftrightarrows H_3(PO_4)_2^{3-} + H^+$.
[g] $2H_3PO_4 \leftrightarrows H_6(PO_4)_2$.
[h] $H_5(PO_4)_2^- \leftrightarrows H_4(PO_4)_2^{2-} + H^+$.
[i] $2HPO_4^{2-} \leftrightarrows H_2(PO_4)_2^{4-}$.
[j] $2HPO_4^{2-} + H^+ \leftrightarrows H_3(PO_4)_2^{3-}$.

EXPERIMENTAL

(A) *Chemicals and analysis*

Stock solutions of *orthophosphoric acid*, prepared from a B.D.H. AnalaR product, were standardized gravimetrically, as $MgNH_4PO_4\cdot6H_2O$, by the method described by Winkler,[12] and potentiometrically by acid-base titration, using a glass electrode. Strong base was generated by constant-current coulometry. The potentiometric analyses were performed at 25°C with solutions made to contain 3 M $NaClO_4$. The presence of the inert electrolyte allowed the preliminary calibration of the apparatus in terms of concentrations. Since K_{a1} and K_{a2}, the first and second acid constant of H_3PO_4, are exactly known under the chosen experimental conditions,[13] the total phosphate concentration, C_P, could be calculated for each point of the titration from relationship (1) which was

$$C_P[1+(K_{a2}/[H^+]-[H^+]/K_{a1})/\{1+[H^+]/K_{a1}+K_{a2}/[H^+]\}] = [H^+]+C_B, \quad (1)$$

derived by assuming H_3PO_4 as monoprotic. C_B stands for concentration of strong base. It is apparent from (1) that the most accurate values of C_P can be evaluated from measurements in the vicinity of $[H^+] = (K_{a1}K_{a2})^{1/2}$, when the term in brackets approaches one and $[H^+]$ becomes sufficiently small compared with the strong base concentration. Values of C_P calculated in the $[H^+]$ range 2×10^{-3} to 10^{-5} M coincided to within 0.1% or better.

The results of analyses by the independent procedures agreed to within 0.1%.

Sodium dihydrogen phosphate, $NaH_2PO_4\cdot2H_2O$, Bakers p.a., was crystallized once from water. Stock solutions were analysed gravimetrically in two different ways: (a) as described for H_3PO_4 (b) by

drying at 120°C to constant weight. The results agreed to within 0.2%.

The level of protolytic impurities (H_3PO_4 or HPO_4^{2-}) contaminating this salt was ascertained potentiometrically with the procedure described above. An exactly known amount of $HClO_4$ was added to a 0.01 M NaH_2PO_4 solution and the excess of acid was back-titrated. The concentration of $HClO_4$ established potentiometrically coincided with that introduced to better than 0.1%. On the basis of this result we estimate the concentration of impurities introduced by NaH_2PO_4 3 molar to be less than 10^{-3} M.

Disodium hydrogen phosphate, $Na_2HPO_4 \cdot 12H_2O$, Bakers p.a., was recrystallized twice from water. The solutions were standardized gravimetrically, as described for NaH_2PO_4, and acidimetrically through potentiometric titrations to the $H_2PO_4^-$ equivalent point, using a glass electrode. The procedure illustrated for H_3PO_4 analyses was adopted to establish the end-point. The results by different methods of analysis coincided to within 0.1%.

Sodium perchlorate was obtained as described by Biedermann.[14] *Perchloric acid* solutions, prepared by dilution of a Merck p.a. product, were analysed with an accuracy of 0.1% using $KHCO_3$ and Tl_2CO_3 as standard and methyl red as visual indicator. *Sodium chloride*, Bakers p.a. and *sodium bromide*, Merck p.a., before use, were ignited at 360°C in Pt crucibles.

Nitrogen and *hydrogen* gases were taken from commercial cylinders and were passed through 1 M H_2SO_4, 1 M NaOH, 0.1 M Cr(II) chloride, water and 3 M $NaClO_4$.

(B) *Potentiometric measurements*

The experiments in $Na(ClO_4, H_2PO_4)$ media were carried out with cell (G)

$$-\text{Ag/AgCl/solution S/glass electrode}+ \quad \text{(G)}$$

where test solution S had the general composition in molar units: NaCl (0.02), $H_3PO_4(C_0)$, $NaH_2PO_4(C_1)$, $Na_2HPO_4(C_2)$, $NaClO_4(2.98-C_1-2C_2)$. The C_1 levels chosen were 0.1, 0.3, 1 and 3. In each run the total phosphate concentration, $C_P = C_o+C_1+C_2$, was kept constant, except for the highest level when the condition $C_P = 3+C_0-C_2$ was fulfilled. The quantity C_0-C_2 (the analytical concentration excess of hydrogen ions counting $H_2PO_4^-$ and H_2O as zero level) was made to vary by adding H_3PO_4 or Na_2HPO_4. To avoid large medium changes the C_0-C_2 values never exceeded the limits between 0.2 and −0.2 M.

During the measurements a vigorous stream of purified and presaturated nitrogen gas was led through S to preserve it from atmospheric contamination.

The EMF data of cell (G), E_G, as a function of C_0-C_2 are the basis of the calculations.

The measurements in $Na(ClO_4, HPO_4)$ solutions were made with cell (H)

$$-\text{Pt/H}_2\text{(g)/solution S*/AgBr/Ag}+ \quad \text{(H)}$$

where solution S* = $NaBr(C_{Br})$, $NaH_2PO_4(C_1)$, $Na_2HPO_4(C_2)$, $Na_3PO_4(C_3)$, $NaClO_4(3-C_{Br}-C_1-2C_2-3C_3)$. Owing to the limited solubility of Na_2HPO_4 the highest C_P in S* was 1. Values lower than 0.3 M were not included in the present study in consideration of little information on polynuclear species from dilute solutions.

In each titration the quantity C_1-C_3, the analytical concentration excess of hydrogen ions assuming HPO_4^{2-} and H_2O as zero level, was decreased stepwise by coulometric generation of OH^- ions. A known volume, V_o dm^3, of starting solution S_0^*: $NaBr(C_{Br}^0)$, $NaH_2PO_4(C_1^0)$, $Na_2HPO_4(C_2^0)$, $NaClO_4(3-C_{Br}^0-C_1^0-2C_2^0)$, prepared under an inert nitrogen atmosphere, formed the liquid phase of the electrolysis cell (E)

$$-\text{Pt/solution S}_0^*\text{/Ag}+ \quad \text{(E)}$$

and the acidity was decreased by connecting (E) to a constant-current supply. By assuming that only the following electrode reactions occur: $H_2O+e \rightarrow OH^- + (1/2)H_2(g)$ at the cathode and $Ag+Br^- \rightarrow AgBr+e$ at the anode, after the passage of w F, $[Br^-]$ and C_1-C_3 can be calculated as C_{Br}^0-w/V_0 and C_1^0-w/V_0, respectively. The calculations of the next section are founded on $E_H^*(C_1-C_3)$ data, where $E_H^* = E_H+0.05916\log([Br^-]p_{H_2}^{-(1/2)})$, E_H is the EMF of cell (H) and p_{H_2} is the partial pressure of hydrogen.

(C) *Apparatus*

During the EMF measurements the cell assembly was immersed in a silicone oil thermostat kept at 25.00±0.02°C. Ag–AgCl and Ag–AgBr electrodes were prepared according to Brown.[15] Glass electrodes, type EA 109 supplied by Metrohm, acquired a constant potential, within 10 min after the addition of reagents, which remained unchanged to $\pm 5\times10^{-5}$ V for several hours. Lightly platinized Pt nets served as hydrogen electrodes. They took as a rule more than 1 h to reach a steady potential which afterwards did not change by more than $\pm 5\times10^{-5}$ V for 12 h. A Pt gauze, boiled in 1:1 HNO_3, formed the cathode of cell (E).

The EMF values of (G) and (H), E_G and E_H respectively, were measured with a precision of 1×10^{-5} V by a computer controlled data acqui-

sition unit 3421 A, furnished by Hewlett–Packard. The constant-current source of the coulometric circuit was a 6186C DC, manufactured by Hewlett–Packard.

DATA AND CALCULATIONS

The experimental data $E_G((C_0-C_2), C_P)$ and $E^*_H((C_1-C_3), C_P)$, given in Tables 2 and 3, are the basis of the following treatment. First the measurements in $NaClO_4$–NaH_2PO_4 media are considered.

The EMF of cell (G) at 25°C can be written as in eq. (2)

$$E_G = E_{0G}+0.05916\log([Cl^-][H^+]y_H y_{Cl}) = E_{0G}+0.05916\log(K_{a1}[Cl^-][H_3PO_4] \times [H_2PO_4^-]^{-1}y_0 y_{Cl} y_1^{-1}), \quad (2)$$

in which E_{0G} is a constant in each run, K_{a1} is the first protolysis constant of H_3PO_4 and y stands for activity coefficient. y_0 and y_1 refer, respectively, to H_3PO_4 and $H_2PO_4^-$. The standard states are so chosen that the activity coefficients tend to unity as the composition of solution S approaches 3 M $NaClO_4$.

At a given C_P, since $(C_0-C_2)/[Na^+]$ never exceeded ± 0.07, the composition of the test solutions changed only slightly in the course of a titration. Consequently, we may regard it as a good approximation to assume the constancy of the activity coefficients. Thus, eq. (2) for any particular self-medium can be expressed as eq. (3)

$$E_G = E'_{0G}+0.05916\log[H^+] = E''_{0G}+0.05916\log([H_3PO_4]/[H_2PO_4^-]), \quad (3)$$

where E'_{0G} includes y_H, y_{Cl} and $[Cl^-] = 0.02$, whereas $E''_{oG} = E_{0G}+0.05916\log(K_{a1}[Cl^-]y_0 y_{Cl} y_1^{-1})$. The constants E'_{0G} and E''_{0G} are not directly determinable, since $[H^+]$ and $[H_3PO_4]/[H_2PO_4^-]$ are not explicitly expressible in function of analytical concentrations in a self-medium. They, however, can be estimated along with other parameters in the calculations by high-speed computer programs. It was found that E'_{0G} is strongly correlated with K_{a1} which is not known in the media in question. On the contrary, rapidly converging results could be arrived at by choosing the $[H_3PO_4]/[H_2PO_4^-]$ ratio as the independent variable.

By assuming that the reagents H_3PO_4 and $H_2PO_4^-$ form a series of complexes of general composition $(H_3PO_4)_p(H_2PO_4)_q^{q-}$, the analytical concentration excess of H^+, C_0-C_2, can be written as eq. (4), neglecting $[OH^-]$,

$$C_0-C_2 = [H^+]+\Sigma p[(H_3PO_4)_p(H_2PO_4)_q^{q-}] = [H^+]+\Sigma pK_{pq}[H_3PO_4]^p[H_2PO_4^-]^q y_0^p y_1^q y_{pq}^{-1}, \quad (4)$$

in which K_{pq} and y_{pq} stand, respectively, for the formation constant and for the activity coefficient of the (p, q) species. At a given phosphate level the activity coefficients are approximately constant and the equilibrium condition is described as well by the quotient Q_{pq} defined by (5)

$$Q_{pq} = K_{pq}y_0^p y_1^q y_{pq}^{-1}. \quad (5)$$

Introduction of $[H_3PO_4]$, expression (6) deduced from (3), into (4) yields (8)

$$[H_3PO_4] = [H_2PO_4^-]\,\text{antilog}((E_G-E''_{0G})/0.05916) = [H_2PO_4^-]\chi_0 x \quad (6)$$

$$\chi_0 = \text{antilog}(-E''_{0G}/0.05916) \quad (7)$$

$$C_0-C_2 = Q_{1,-1}\chi_0 x+\Sigma pQ_{pq}\chi_0^p x^p[H_2PO_4^-]^{(p+q)}. \quad (8)$$

Notice how H^+ in our symbolism is the $(1, -1)$ species with a formation constant $K_{1,-1}$ corresponding to the first protolysis constant of H_3PO_4.

From the stoichiometric condition one has finally

$$C_P = \Sigma(p+q)Q_{pq}\chi_0^p x^p[H_2PO_4^-]^{(p+q)}. \quad (9)$$

Values of (p, q) and of Q_{pq} for the predominating reaction products were determined by processing the experimental data with the generalized least-squares procedure Letagrop.[16] The sum (10), where

$$U = \Sigma(((C_0-C_2)-(C_0-C_2)_{calc})/(C_0-C_2))^2 \quad (10)$$

$(C_0-C_2)_{calc}$ is a value calculated with a given set of constants, was minimized. As adjustable parameters we considered the equilibrium constants as well as χ_0 for each titration. A satisfactory explanation of the data was found by assuming: H^+, HPO_4^{2-}, $H_6(PO_4)_2$, $H_5(PO_4)_2^-$, $H_4(PO_4)_2^{2-}$ and $H_3(PO_4)_2^{3-}$. Agreement factors of less than 0.5% were calculated with this scheme and gave a measure of the fit. Furthermore, the standard deviation of E''_{0G}, usually less than 10^{-4} V, matches well the reproducibility of the EMF of cell (G). On the other hand, significantly higher minima were found with other models including an equal number of species. The Q_{pq} values of Table 4a are averages from parallel runs. In the estimation of the uncertainties the accumulated errors arising from 3 times the standard deviation and from the highest deviations by the averages of Q_{pq}s found in various titrations, have all been taken into account.

Table 2. Survey of measurements in $NaClO_4$–NaH_2PO_4 media. E_G, the EMF of cell (G), in mV, as a function of the analytical concentration excess of H^+, C_0-C_2, at various C_P

$E_G((C_0-C_2)\times 10^3)$

$C_P = 0.100$

(a) 20.35 (−38.99); 26.25 (−34.04); 32.38 (−29.25); 39.22 (−24.59); 46.04 (−20.06); 54.45 (−15.65); 64.37 (−11.37); 77.74 (−7.20); 86.05 (−5.16); 99.40 (−3.15); 119.19 (−1.16); 150.57 (0.72); 173.97 (2.74); 187.42 (4.65); 196.09 (6.54); 203.44 (8.40); 213.75 (12.05); 221.41 (15.61); 227.32 (19.09); 232.39 (22.48); 236.85 (25.78); 240.84 (29.01); 244.19 (32.16); 247.58 (35.24); 250.45 (38.25); 253.27 (41.19); 255.83 (44.07); 257.97 (46.60).

(b) 8.50 (−49.84); 18.17 (−41.34); 27.94 (−33.24); 38.36 (−25.52); 46.30 (−20.32); 53.91 (−16.00); 61.68 (−12.49); 68.76 (−9.73); 77.72 (−7.03); 89.37 (−4.37); 108.89 (−1.75); 145.01 (0.814); 175.14 (3.34); 191.01 (5.82); 200.70 (8.26); 216.86 (14.19); 227.21 (19.88).

(c) 7.72 (−50.73); 17.71 (−41.96); 26.37 (−34.71); 35.37 (−27.80); 44.54 (−21.66); 55.00 (−15.85); 70.25 (−9.32); 81.28 (−6.48); 99.09 (−3.28); 133.08 (−0.31); 171.61 (2.54); 190.47 (5.45); 202.37 (8.51); 210.03 (11.20); 218.99 (15.26); 227.46 (20.20).

$C_P = 0.300$

(a) 29.03 (−99.49); 32.97 (−91.49); 36.05 (−85.47); 40.85 (−76.50); 45.51 (−68.34); 50.67 (−59.92); 57.09 (−50.37); 64.48 (−40.73); 73.00 (−31.27); 80.36 (−24.61); 89.40 (−18.00); 98.29 (−13.01); 109.07 (−8.48); 121.62 (−4.68); 145.41 (0.525); 165.36 (4.90); 180.76 (9.975); 196.69 (18.49); 201.32 (21.91).

(b) 29.07 (−98.32); 35.15 (−87.11); 42.90 (−72.76); 52.05 (−57.68); 58.82 (−47.91); 66.04 −38.81); 74.44 (−29.90); 83.62 (−22.07); 94.74 (−14.88); 108.87 (−8.52); 124.27 (−3.94); 144.92 (0.43); 164.37 (4.74); 180.42 (10.07); 191.24 (15.44); 200.35 (21.58); 207.54 (27.79); 214.22 (34.82).

$C_P = 1.000$

(a) 82.83 (−99.63); 91.31 (−77.24); 98.14 (−61.94); 104.88 (−48.99); 111.16 (−38.64); 117.55 (−29.57); 123.23 (−22.52); 128.79 (−16.39); 135.29 (−9.93); 141.97 (−3.78); 148.41 (1.95); 155.10 (8.02); 161.32 (14.07); 167.55 (20.77); 172.82 (27.17); 178.21 (34.62); 183.62 (43.19); 188.75 (52.54).

(b) 82.75 (−99.63); 88.18 (−84.87); 93.81 (−71.17); 9.20 (−59.49); 104.63 (−49.16); 109.65 (−40.75); 114.72 (−33.20); 119.44 (−26.87); 124.16 (−21.22); 129.13 (−15.82); 134.39 (−10.58); 139.87 (−5.46); 145.61 (−0.329); 151.88 (5.27); 158.16 (11.16); 165.59 (18.80); 172.90 (27.51); 179.21 (36.38); 184.32 (44.69); 188.00 (51.39).

$C_P = 3.000+C_0-C_2$

(a) 101.89 (−195.3); 110.65 (−148.2); 119.92 (−104.7); 129.69 (−64.63); 137.60 (−35.26); 144.19 (−11.57); 147.32 (0.00); 152.24 (18.12); 156.28 (33.82); 160.40 (50.95); 164.27 (68.69); 170.11 (98.09); 176.39 (135.9); 180.10 (161.7); 184.00 (192.7).

(b) 180.10 (161.3); 175.26 (128.0); 169.59 (94.61); 162.83 (61.05); 147.50 (0.00); 150.60 (11.50); 145.71 (−6.54); 142.50 (−18.19); 137.18 (−37.09); 124.69 (−84.55); 115.96 (−122.3); 109.94 (−151.5); 101.58 (−196.5).

Table 3. Survey of the $E_H^*(C_1-C_3)$ data in $NaClO_4$–Na_2HPO_4 solutions. E_H^*, in mV, is equal to $E_H+59.16\log([Br^-]p_H^{-1/2})$, where E_H is the EMF of cell (H)

$E_H^*((C_1-C_3)\times 10^3)$

$C_P = 0.300$

478.99 (40.91); 482.55 (38.23); 484.96 (35.54); 487.32 (33.01); 490.00 (30.33); 492.84 (27.65); 495.96 (24.96); 499.24 (22.28); 503.01 (19.59); 507.09 (16.91); 511.88 (14.23); 517.41 (11.54); 524.19 (8.86); 533.50 (6.18); 545.38 (3.49); 553.81 (2.00); 561.62 (0.810); 574.20 (−0.979); 582.08 (−2.17); 590.52 (−3.66); 602.16 (−6.35); 610.74 (−9.03); 617.43 (−11.72); 622.88 (−14.40); 627.67 (−17.08); 631.58 (−19.76); 635.15 (−22.45); 638.39 (−25.13); 641.32 (−27.81); 643.94 (−30.50); 648.89 (−35.86).

$C_P = 1.000$

(a) 539.07 (37.62); 541.25 (34.98); 543.47 (32.34); 545.34 (29.69); 547.33 (27.05); 549.88 (24.41); 552.69 (21.76); 555.48 (19.12); 559.25 (16.48); 566.76 (11.19); 570.85 (8.55); 575.67 (5.90); 580.44 (3.26); 583.18 (1.79); 589.38 (−1.15); 591.52 (−2.32); 594.26 (−3.79); 599.06 (−6.43); 603.55 (−9.08); 607.87 (−11.72); 611.90 (−14.36); 615.78 (−17.01); 618.29 (−19.65).

(b) 537.77 (40.26); 539.89 (37.62); 542.00 (34.99); 544.20 (32.36); 546.21 (29.72); 548.48 (27.09); 551.07 (24.46); 553.86 (21.82); 556.79 (19.19); 560.10 (16.56); 563.59 (13.93); 567.41 (11.29); 571.61 (8.66); 576.19 (6.03); 580.97 (3.395); 583.81 (1.93); 586.11 (0.763); 592.56 (−2.16); 595.40 (−3.63); 600.28 (−6.26); 604.80 (−8.89); 609.01 (−11.52); 612.80 (−14.16); 616.26 (−16.79); 619.00 (−19.42); 621.82 (−22.05); 624.55 (−24.68); 627.05 (−27.32); 629.39 (−29.95); 634.00 (−35.21).

Concerning the interpretation of the $E_H^*((C_1-C_3))$ data we assumed as reagents $H_2PO_4^-$ and HPO_4^{2-} and a series of $(H_2PO_4)_q(HPO_4)_r^{(q+2r)-}$ species with equilibrium constants for their formation K'_{qr}. For a given C_P, taking as a good approximation the constancy of the activity coefficients, one has

$$E_H^* = E'_{0H} - 0.05916\log[H^+]$$
$$= E''_{0H} - 0.05916\log([H_2PO_4^-]/[HPO_4^{2-}]) \quad (11)$$

where E'_{0H} and E''_{0H} are constants. Furthermore,

Table 4. Calculated values of the equilibrium quotients

(a) The Q_{pq} values in $NaClO_4$–NaH_2PO_4 media

C_P	H^+ $-\log Q_{1,-1}$	HPO_4^{2-} $-\log Q_{-1,2}$	$H_5(PO_4)_2^-$ $\log Q_{11}$	$H_3(PO_4)_2^{3-}$ $-\log Q_{-1,3}$	$H_4(PO_4)_2^{2-}$ $-\log Q_{02}$	$H_6(PO_4)_2$ $-\log Q_{20}$
0.1	1.79(1)	4.46(2)	0.43(3)	4.15(3)	1.2(2)	0.0(2)
0.3	1.77(1)	4.62(1)	0.41(2)	4.14(1)	1.2(1)	0.0(1)
1.0	1.60(2)	4.99(1)	0.198(2)	4.23(1)	1.5(1)	0.0(1)
3	1.3(1)	6.4(2)	−0.16(2)	4.25(1)	1.46(1)	0.13(8)
0	1.80(3)	4.38(2)	0.45(5)	4.15(5)	1.2(2)	0.0(2)

(b) The Q'_{qr} values in $NaClO_4$–Na_2HPO_4 media

C_P	PO_4^{3-} $-\log Q'_{-1,2}$	$H_3(PO_4)_2^{3-}$ $-\log Q'_{11}$	$H(PO_4)_2^{5-}$ $-\log Q'_{-1,3}$	$H_4(PO_4)_2^{2-}$ $-\log Q'_{20}$	$H_2(PO_4)_2^{4-}$ $-\log Q'_{02}$
0.3	4.82(1)	−0.41(1)	4.68(1)	2.1 max	2.1 max
1.0	4.38(3)	1.03(8)	6.1(2)	1.5(2)	0.8 max
0	(4.57)	(−0.2)		(1.2)	

the equilibrium condition is described also by the quotient Q'_{qr} defined in (12)

$$Q'_{qr} = K'_{qr} y_1^q y_2^r y_{qr}^{-1}, \qquad (12)$$

where y_{qr} and y_2 are the activity coefficients of the (q, r) species and HPO_4^{2-} respectively.

Values of E''_{0H} and of Q'_{qr} of the predominating complexes were sought for by minimizing the sum: $\Sigma(((C_1-C_3)-(C_1-C_3)_{calc})/(C_1-C_3))^2$, where $(C_1-C_3)_{calc}$ is a value calculated with a certain set of parameters. The results of computations, summarized in Table 4b, indicate the formation of $H_2(PO_4)_2^{4-}$ and $H(PO_4)_2^{5-}$ in addition to PO_4^{3-}, $H_4(PO_4)_2^{2-}$ and $H_3(PO_4)_2^{3-}$. The standard deviation of E''_{0H} amounted in any case to about 10^{-4} V which gives a measure of the agreement between the data and the proposed model.

In Figs 1, 2 and 3 the distributions of various species as a function of the analytical concentration excess of H^+ ions for three different C_P values are shown. Even at the lowest phosphate level investigated the dimers $H_5(PO_4)_2^-$ and $H_3(PO_4)_2^{3-}$ acquire concentrations of about 5% of C_P and are, consequently, not completely negligible.

Effect of medium changes on formation quotients

The variations of the equilibrium quotients in Table 4, as phosphate species replace ClO_4^- ions, are surprising and large according to the specific interaction theory, SIT,[17] founded on the Brønsted principle. This assumes as negligible short-range forces, and interaction coefficients between ions of the same charge sign. Consequently, since all the constants, except $Q_{1,-1}$ and Q_{20}, refer to equilibria among only anions, they should undergo no appreciable change at constant Na^+ concentrations and for the limited variations of ionic strength when $H_2PO_4^-$ is substituted by other phosphate species. This phenomenon led us to revise Brønsted's postulate. While for spherically symmetric ions, as Na^+, Ca^{2+}, Cl^-, ClO_4^-, the principle is strictly valid,

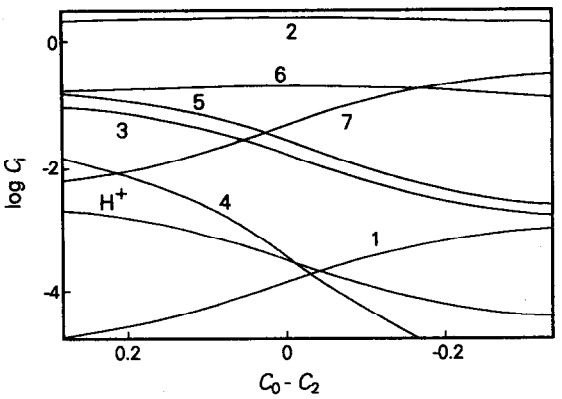

Fig. 2. Log c_i plotted as a function of the analytical concentration excess of H^+, C_0-C_2, for a 3 M $Na(H_2PO_4)$ medium with $C_P = 3+C_o-C_2$. The curves have been calculated with the quotients of the fourth row of Table 4a. Species and numbers as in Fig. 1.

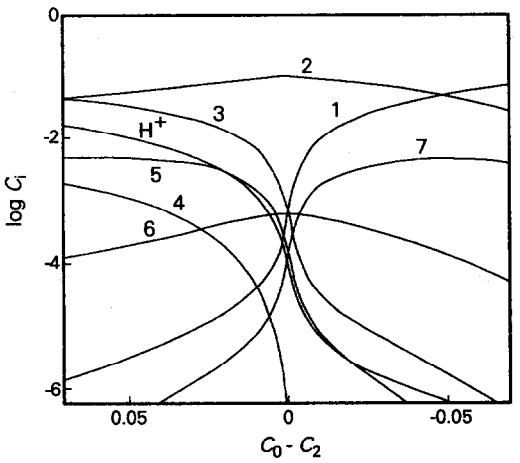

Fig. 1. Log c_i plotted as a function of the analytical concentration excess of H^+, C_0-C_2, for a 3 M $Na(ClO_4, H_2PO_4)$ medium with $C_P = 0.1$. The curves have been calculated with the quotients of the first row of Table 4a. Numbers refer to: HPO_4^{2-} (1); $H_2PO_4^-$ (2), H_3PO_4 (3); $H_6(PO_4)_2$ (4); $H_5(PO_4)_2^-$ (5); $H_4(PO_4)_2^{2-}$ (6); $H_3(PO_4)_2^{3-}$ (7).

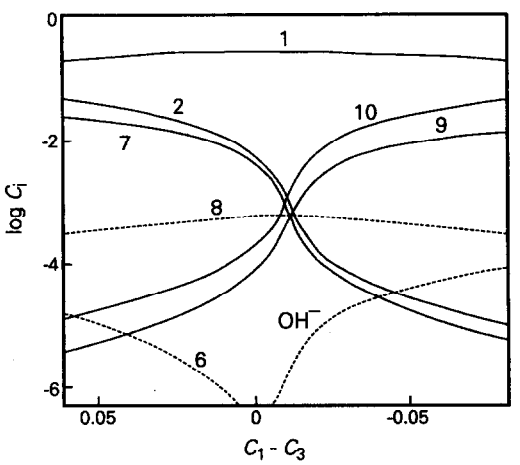

Fig. 3. Log c_i plotted as a function of the analytical concentration excess of H^+, C_1-C_3, in a 3 M $Na(ClO_4, HPO_4)$ medium with $C_P = 0.3$. The curves have been calculated with the quotients in the first row of Table 4b. Dotted curves have been traced by assuming the max values of Q'_{20} and Q'_{02}; the OH^- concentration has been estimated using $pK_w = 14.22$ and $pK_{a3}(H_3PO_4) = 10.85$ valid in 3 M $NaClO_4$. Species and numbers as in Fig. 1; in addition: $H_2(PO_4)_2^{4-}$ (8); $H(PO_4)_2^{5-}$ (9) and PO_4^{3-} (10).

it would apply not correctly for polar ions and molecules, as $H_2PO_4^-$ and HPO_4^{2-}, whose positive pole has the chance to come near a negatively charged ion. This is consistent with the tendency of $H_2PO_4^-$ to dimerize and to associate with HPO_4^{2-}. Thus short-range interactions set in to produce interaction coefficients significantly different from zero.

The remarkable effect on $Q_{-1,2}$ in $NaClO_4$–NaH_2PO_4 mixtures and on all the equilibria in Na_2HPO_4 media is an indication of a large interaction coefficient between $H_2PO_4^-$ and HPO_4^{2-}, and prompted the following estimation of its magnitude. Owing to the lack of information on several parameters necessary for a rigorous treatment, we made the approximations:

(i) pure NaH_2PO_4 solutions, though according to our findings contain a certain amount of $H_5(PO_4)_2^-$, $H_4(PO_4)_2^{2-}$ and $H_3(PO_4)_2^{3-}$, are assumed to be composed of Na^+ and $H_2PO_4^-$ ions;

(ii) ionic strength variations of $NaClO_4$–NaH_2PO_4 mixtures of constant total molarity, caused by the replacement of $H_2PO_4^-$ by phosphate ions of higher charge, are considered to be negligible.

For a "pure" 3 M NaH_2PO_4 solution, which is 3.41 molal as calculated from the density values compiled by Weast,[18] one finds, by introducing in eq. (5) of ref. 17 the osmoric coefficient, 0.691, listed by Robinson and Stokes,[19] an interaction coefficient of -0.057 molal^{-1}. This is related to interaction coefficients, b, of the constituent ions by means of (13):

$$-0.057 = b(Na^+, H_2PO_4^-) + (1/2)b(Na^+, Na^+) + (1/2)b(H_2PO_4^-, H_2PO_4^-). \quad (13)$$

If the Brønsted principle is valid $b(Na^+, Na^+) = b(H_2PO_4^-, H_2PO_4^-) = 0$. On the other hand, setting $b(Na^+, Na^+) = 0$ and $b(Na^+, H_2PO_4^-) = b(Na^+, ClO_4^-) \simeq 0$, in consideration of identical charges and comparable sizes, one gets $b(H_2PO_4^-, H_2PO_4^-) = -0.11$ molal^{-1}. The combination of this value with the dependence of the various Q_{pq} on the medium composition allows the estimation of other interaction coefficients and, consequently, of the activity coefficients.

A $NaClO_4$–NaH_2PO_4 mixture of constant total molarity has also a constant molality on account of the almost coincident densities of equimolar $NaClO_4$ and NaH_2PO_4 solutions. Thus, molal activity coefficients are practically equal to molar ones in our medium scale. Neglecting the effect of ionic strength variations, when $H_2PO_4^-$ ions are substituted by other phosphate species, one obtains from eq. (1) of ref. 17 for the activity coefficient of the i species:

$$\log y_i = (b(i, H_2PO_4^-) - b(i, ClO_4^-))1.16C_P, \quad (14)$$

where b is expressed in molal^{-1} and 1.16 is the molality/molarity ratio of the medium constituents. Setting $b(H_2PO_4^-, ClO_4^-) = 0$, $\log y_1 = -0.13C_P$. This and $b(Cl^-, H_2PO_4^-) = b(Cl^-, ClO_4^-) = 0$ allow an estimate of $\log y_0 = -0.13C_P$ from the variation of E''_{0G} with C_P. Introduction of y_1 and y_0 in the expression of $Q_{-1,2}$ yields finally $\log y_2 = 0.56\ C_P$. From the dependence of other equilibrium quotients on C_P we find: $\log y_H = -0.18C_P$; $\log y_{20} = -0.63C_P$; $\log y_{11} = -0.26C_P$; $\log y_{02} = -0.14C_P$; $\log y_{-1,3} = -0.22C_P$.

The most interesting result of the above computations is the large and positive value of $b(H_2PO_4^-, HPO_4^{2-}) = 0.48$ molal^{-1}. Evidently the ions come so near when forming $H_3(PO_4)_2^{3-}$ that appreciable repulsive short-range forces set in to yield a large interaction coefficient. On the contrary, negative coefficients for all the other interactions may suggest attractive forces prevailing over repulsive ones. Finally, the linear dependence on C_P of $\log y_i$ permits extrapolation of the various quotients to the inert 3 M $NaClO_4$. The extrapolated values are given in Table 4.

The following K_{a1} and K_{a2}/K_{a1} values ($K_{1,-1}$ and $K_{-1,2}$ in our terminology) have been determined under identical experimental conditions but with transference cells:

$-\log K_{a1}$	$-\log(K_{a2}/K_{a1})$	Authors
1.89(1)	4.38(1)	Baldwin and Sillén[13]
1.83(3)	4.41(4)	Pettersson[20]
1.88(5)	4.40(6)	Havel and Högfeldt[21]

The agreement with data of Table 4 is as good as can be expected, with the exception of K_{a1} proposed by Baldwin and Sillén. We have not been able to explain the discrepancy; probably the accuracy of this constant is overestimated.

The interpretation of data in $NaClO_4$–Na_2HPO_4 solutions is more complicated due to the variation of the ionic strength and consequently of the interaction coefficients as ClO_4^- is replaced by HPO_4^{2-}. Then extrapolation of the Q'_{qr} values to the inert 3 M $NaClO_4$ medium is more uncertain. This point is illustrated by taking into account $K'_{-1,2}$, $K'_{1,1}$ and K'_{20}, evaluated from the results in $NaClO_4$–NaH_2PO_4 media, and included in Table 4b (line corresponding to $C_P = 0$). Clearly, Q'_{qr}s go through maxima or minima so the estimation of variable interaction coefficients on the basis of two or three data points is made difficult.

In conclusion, though the data in $NaClO_4$–

Na_2HPO_4 mixtures cannot be rationalized in terms of interaction coefficients, the results are of practical importance; the presence of $H_3(PO_4)_2^{3-}$ and $H_4(PO_4)_2^{2-}$ is confirmed and the new species $H(PO_4)_2^{5-}$ is demonstrated.

DISCUSSION

Equilibrium data give only the charge of the species and the number of phosphorus atoms but not the amount of water. So there is no way to distinguish, say, the $H_6(PO_4)_2$ species and pyrophosphoric acid $H_4P_2O_7$. A plausible proof can, however, be found by the comparison of the present results with the protolysis constants of the pyrophosphoric acid system.

The constant for $2H_3PO_4 \leftrightarrows H_4P_2O_7 + H_2O$, as calculated from free energy values published by US NBS,[22] is about $10^{-2.79}$ at 25°C in dilute solution. If one disregards large salting effects by $NaClO_4$, the concentration of $H_4P_2O_7$ attained in our solutions less than 10^{-4} M which is the detection level of the experimental procedure. As a consequence, K_{20} of Table 4 refers to the formation of bonds which are different from the oxygen bridge between the phosphorus atoms in pyrophosphoric acid. As additional proof we may consider the acidity constants of $H_6(PO_4)_2$ and $H_4P_2O_7$, given in Table 6. The pK_a values of $H_6(PO_4)_2$ were deduced from Table 4 and their large errors are mostly due to the rather uncertain K_{02}, K_{20} and K'_{20}s. The constants for $H_4P_2O_7$ are those determined by Näsänen as quoted by Smith and Martell.[23] Clearly, the constants differ significantly; therefore, we are measuring on something of a diverse nature to the pyrophosphate system.

There is sufficient information to expect in the dimeric species hydrogen bonds which, according to Emsley's criteria,[24] may be strong as in many other bisoxo-anions such as $H(NO_3)_2^-$, $H(CO_3)_2^{3-}$, $H(RCO_2)_2^-$. Bond lengths, O···O, of about 250 ± 10 pm, found by X-ray scattering in concentrated H_3PO_4 solutions[25] as well as in solid $KH_5(PO_4)_2$,[26] KH_2PO_4[27] and $(pClC_6H_4O)_2PO_2H$,[28] are a clear indication of strong hydrogen bonding. Evidence comes also from continua in the IR spectra of H_3PO_2, H_3PO_3 and H_3PO_4 solutions[29] and from IR and NMR data of K- and NaH_2PO_2 solutions in carboxylic acids.[30] A further suggestion is the bond energy of 58 kJ mol^{-1} for the adduct $Ph_3PO \cdots HCO_2CCl_3$.[31]

Structures I, II and III, with 1, 2 and 3 hydrogen

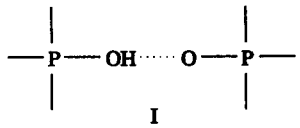

I

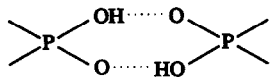

II

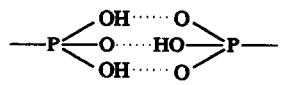

III

bonds, respectively, can be envisaged for the $H_n(PO_4)_2^{n-6}$ complexes. For $H(PO_4)_2^{5-}$ I is self-evident. For both $H_6(PO_4)_2$ and $H_2(PO_4)_2^{4-}$ either I or II is plausible, whilst $H_5(PO_4)_2^-$, $H_4(PO_4)_2^{2-}$ and $H_3(PO_4)_2^{3-}$ may assume each of the structures. Assignments have been attempted, Table 5, on the

Table 5. Probable structures of the dimers

Species	Structure	Evidence	Ref.
$H_6(PO_4)_2$	II	X-ray diffraction in 58mH_3PO_4	25
$H_5(PO_4)_2^-$	III	Isotope effect in the nuclear magnetic relaxation of ^{31}P in 6 M H_3PO_4[a]	32
$H_4(PO_4)_2^{2-}$	II	Trend in dimerization and acidity constants[b]	This work
$H_3(PO_4)_2^{3-}$	III	Trend in dimerization and acidity constants[b]	This work
$H_2(PO_4)_2^{4-}$	II	Trend in dimerization and acidity constants[b]	This work

[a] In these solutions $H_5(PO_4)_2^-$ prevails over H_3PO_4 and $H_6(PO_4)_2$ assuming the compositional estimates by Elmore *et al.*[4]

[b] See text.

Table 6. Comparison of pK_a values for $H_6(PO_4)_2$ and pyrophosphoric acid, $H_4P_2O_7$, at 25°C in 3 M $NaClO_4$

	$H_6(PO_4)_2$	$H_4P_2O_7$
pK_{a1}	1.35(25)	~ 0
pK_{a2}	3.45(25)	1.4
pK_{a3}	4.75(25)	5.29
pK_{a4}	~ 8.5	7.17
pK_{a5}	~ 8.7	—

basis of some literature data and of trends in dimerization constants as well as in pK_as of $H_6(PO_4)_2$.

The formation constants of $H_6(PO_4)_2$, $H_4(PO_4)_2^{2-}$ and $H_2(PO_4)_2^{4-}$ from, respectively, H_3PO_4, $H_2PO_4^-$ and HPO_4^{2-}, taking into due consideration the increasing electrostatic repulsion in the order $H_2(PO_4)_2^{4-} > H_4(PO_4)_2^{2-} > H_6(PO_4)_2$, are nearly comparable. Hence, all these species should have the same structure, *i.e.* II. Similarly, K_{11} matches well the constant for $H_2PO_4^- + HPO_2^{2-} \rightleftarrows H_3(PO_4)_2^{3-}$ so that structure III fits $H_3(PO_4)_2^{3-}$ as $H_5(PO_4)_2^-$.

The above assignments are supported by the sequence of pK_as of $H_6(PO_4)_2$. Suppose that this acid on loosing its protons does not change the configuration II. On the basis of electrostatic considerations the succession $pK_{a1} \simeq pK_{a2} \ll pK_{a3} \simeq pK_{a4}$ would result. As a matter of fact, the removal of a proton from $H_5(PO_4)_2^-$ with structure II would involve a negative charge far away to have $pK_{a1} \simeq pK_{a2}$. The third proton, on the other hand, would be given off from a tetrahedron that already has a negative charge to cause $pK_{a3} \gg pK_{a2}$. The same would apply to the fourth proton to have $pK_{a3} \simeq pK_{a4}$. The observed trend, Table 6, suggests on the contrary that $H_5(PO_4)_2^-$ and $H_3(PO_4)_2^{3-}$ have more stable structures, III, than neighbouring species with less stable configurations, as II.

Acknowledgement—This work has been financially supported by MURST, Rome.

REFERENCES

1. L. G. Sillén and E. A. Martell, *Stability Constants.* The Chemical Society, London, Spec. Pub. N.17 (1964) and N.25 (1971).
2. E. Högfeldt, *Stability Constant.* Pergamon Press, Oxford (1982).
3. M. Selvaratnam and M. Spiro, *Trans. Farad. Soc.* 1965, **61**, 360.
4. K. L. Elmore, J. D. Hatfield, R. L. Dunn and A. D. Jones, *J. Phys. Chem.* 1965, **69**, 3520.
5. C. W. Childs, *J. Phys. Chem.* 1969, **73**, 2956.
6. S. Hietanen, L. G. Sillén and E. Högfeldt, *Chem. Scripta* 1973, **3**, 23.
7. G. Ferroni, G. Antonetti, R. Romanetti and J. Galea, *Bull. Soc. Chim. France* 1973, 3269.
8. G. Ferroni, J. Galea, G. Antonetti and R. Romanetti, *Bull. Soc. Chim. France* 1974, 2695.
9. G. Ferroni, *Bull. Soc. Chim. France* 1974, 2698.
10. A. A. Ivakin and E. M. Voronova, *Russ. J. Inorg. Chem.* 1973, **18**, 465.
11. S. Hietanen and L. G. Sillén, *Acta Chem. Scand.* 1959, **13**, 533.
12. L. W. Winkler, *Ausgewählte Untersuchungsverfahren für das chemisches Laboratorium.* Enke Verlag, Stuttgart (1936).
13. W. G. Baldwin and L. G. Sillén, *Arkiv Kemi* 1969, **31**, 391.
14. G. Biedermann, Dissertation. *Svensk Kem. Tid.* 1964, **76**, 362.
15. A. S. Brown, *J. Am. Chem. Soc.* 1934, **56**, 646.
16. L. G. Sillén and B. Warnqvist, *Arkiv Kemi* 1969, **31**, 315.
17. L. Ciavatta, *Ann. Chim. (Rome)* 1980, **70**, 551.
18. R. C. Weast, *Handbook of Chemistry and Physics*, 56th Ed (1975–76). CRC Press, Cleveland, Ohio.
19. R. A. Robinson and R. H. Stokes, *Electrolyte Solutions.* Butterworths, London (1959).
20. L. Pettersson, *Acta Chem. Scand.* 1971, **25**, 1959.
21. J. Havel and E. Högfeldt, *Chem. Scripta* 1974, **5**, 164.
22. D. D. Wagman, W. H. Evans, V. B. Parker, R. H. Schumm, I. Halow, S. M. Bailey, K. L. Churney and R. L. Nuttal, *J. Phys. Chem. Ref. Data* 1982, **11**, suppl. 2, 1.
23. R. M. Smith and E. A. Martell, *Critical Stability Constants, Vol. 4, Inorganic Complexes.* New York, Plenum Press (1976).
24. J. Emsley, *Chem. Soc. Rev.* 1980, **9**, 91.
25. D. L. Wertz and G. A. Cook, *J. Sol. Chem.* 1985, **14**, 41.
26. E. Philippot and O. Lindqvist, *Acta Chem. Scand.* 1971, **25**, 512.
27. D. W. Jones and D. W. J. Cruickshank, *Z. Krist.* 1961, **116**, 101.
28. M. Calleri and J. C. Speakman, *Acta Cryst.* 1964, **17**, 1097.
29. M. Leuchs and G. Zundel, *Can. J. Chem.* 1979, **57**, 487.
30. J. H. Clark, J. Emsley and T. B. Middleton, *J. Chem. Soc., Dalton Trans.* 1979, 1693.
31. D. Hadži and J. Rajnvajn, *J. Chem. Soc. Faraday I* 1973, **69**, 151.
32. H. S. Kielman and J. C. Leyte, *Ber. Buns. Phys. Chem.* 1975, **79**, 1201.

Polyhedron Vol. 10, No. 22, pp. 2597–2603, 1991
Printed in Great Britain

0277–5387/91 $3.00+.00
© 1991 Pergamon Press plc

THE STRUCTURES OF *anti*-αβ-AZIDO- AND ISOTHIOCYANATO-{1,9-BIS(2′-PYRIDYL)-2,5,8-TRIAZANONANE}COBALT(III) PERCHLORATE AND *anti*-αβ-ISOTHIOCYANATO-{1,11-BIS(2′-PYRIDYL)-2,6,10-TRIAZAUNDECANE}COBALT(III) PERCHLORATE

DEREK A. TOCHER and MARTIN L. TOBE*

Christopher Ingold Laboratories, University College London, 20 Gordon Street, London WC1H 0AJ, U.K.

and

MADALENA HUMANES

Centro Electroquimica e Cinetica da Universitade de Lisboa no Instituto Rocha Cabral, Lisboa, Portugal

(*Received* 10 *April* 1991; *accepted* 2 *July* 1991)

Abstract—X-ray diffraction analyses have been made on single crystals of [Co(picdien)(N_3)](ClO_4)$_2$, [Co(picdien)(NCS)](ClO_4)$_2$·H_2O, and [Co(picditn)(NCS)](ClO_4)$_2$·H_2O, (picdien = 1,9-bis(2′-pyridyl)-2,5,8-triazanonane; picditn = 1,11-bis(2′-pyridyl)-2,6,10-triazaundecane) in order to see if there is any structural reason for the fact that the proton acidity of the [Co(picdien)(NCS)]$^{2+}$ cation is much greater than that of the other complexes. Both NCS complexes have the *anti*-αβ configuration and the ligand is N-bonded. The *anti*-αβ configuration of the N_3 complex is also confirmed. The strain at the central meridional amine nitrogen in the picdien complex which increases the C—N—C angle to 115–116° is relieved by the larger ring size in the picditn analogues and it is suggested that this accounts for the difference in the acidity of analogous picdien and picditn complexes.

In a recent paper we examined the kinetics of the reaction, [Co(L_5)X]$^{2+}$ + OH^- → [Co(L_5)(OH)]$^{2+}$ + X^- (L_5 = picdien, picditn; X = NCS, N_3 and NO_2) and showed that, when L_5 = picdien and X = NO_2 or NCS, the rate law takes the form, $k_{obs} = ab[OH^-]/(1+b[OH^-])$ (OH^- is sufficiently more concentrated than the complex to ensure first-order kinetics; k_{obs} is the first-order rate constant) and the rate becomes almost independent of [OH^-] at concentrations greater than 0.05 mol dm^{-3}. The solvolyses of the other complexes follow the usual rate law, $k_{obs} = k_{OH}[OH^-]$.[1] In order to see whether the change in behaviour was the result of a change in stereochemistry on going from the picdien to the picditn system, the structures of the thiocyanato complexes have been determined by X-ray diffraction. The [Co(picdien)(N_3)]$^{2+}$ complex, predicted from its ^{1}H NMR spectrum to have the *anti*-αβ configuration, has also been examined in order to confirm this.

EXPERIMENTAL

Preparations

The complexes were prepared by previously reported methods.[2]

Details of the crystal structure determination

Crystals of [Co(picdien)(N_3)](ClO_4)$_2$ (**I**), were grown by dissolving the complex in dimethylformamide and diluting the solution with aqueous perchloric acid (0.1 mol dm^{-3}), those of [Co(picdien)(NCS)](ClO_4)$_2$·H_2O (**II**), and [Co(picditn)(NCS)](ClO_4)$_2$·H_2O (**III**), were obtained by

* Author to whom correspondence should be addressed.

slowly evaporating aqueous solutions of the complexes in desiccators. In all cases only one type of crystal could be observed under the microscope. Suitable single crystals were mounted on glass fibres with Araldite.

All geometric and intensity data were taken from these crystals using an automated four-circle diffractometer (Nicolet R3mV) equipped with a graphite monochromated Mo-K_α radiation (λ = 0.71073 Å) source. Important crystallographic data are collected in Table 1.

The lattice vectors were identified by application of the automatic indexing routine of the diffractometer to the positions of [30], [34], [23] reflections, respectively, for the three complexes, taken from rotation photographs and centred by the diffractometer. The ω–2θ technique was used to measure [4525], [8986], [4954] reflections for the three compounds in the range $5° < 2\theta < 50°$, of which [4018], [8243], [4431] respectively were unique. Three standard reflections, remeasured every 97 scans showed no significant loss of intensity during data collection. The data were corrected for Lorentz and polarization effects, and empirically for absorption.

(I) *anti*-$\alpha\beta$-[Co(picdien)(N_3)](ClO_4)$_2$

The 3111 unique data with $I \geqslant 1.5\sigma I$ were used in the structure solution and refinement in the space group $P2_1/n$. The structure was solved by direct methods. Alternating cycles of least-squares refinement and difference Fourier synthesis led to the complete solution of the structure. The asymmetric unit cell contains one complex cation and

Table 1. Some crystallographic data

Compound	I[a]	II	III
Formula	$C_{16}H_{23}N_8O_8Cl_2Co$	$C_{17}H_{25}N_6O_9SCl_2Co$	$C_{19}H_{29}N_6O_9SCl_2Co$
f_w	585.28	619.33	647.4
Space group	$P2_1/n$	$P\bar{1}$	$P2_1/c$
a (Å)	9.884(2)	10.799(2)	10.220(2)
b (Å)	10.052(2)	14.566(3)	10.960(3)
c (Å)	23.177(5)	16.853(4)	23.322(6)
α (deg)	90.0	68.41(2)	90.0
β (deg)	93.38(2)	84.81(2)	95.55(2)
γ (deg)	90.0	88.05(2)	90.0
V (Å^3)	2299	2454	2600
Z	4	4	4
F(000)	1200	1272	1336
d_{calc} (g cm^{-3})	1.69	1.63	1.65
Crystal size (mm)	0.40 × 0.45 × 0.08	0.40 × 0.20 × 0.10	0.38 × 0.15 × 0.08
μ(Mo-K_α) (cm^{-1})	10.4	10.6	10.0
Data collection instrument,	Nicolet R3m/V		
Radiation,	Mo (λ = 0.71073 Å)		
Orientation reflections:			
No.; range (2θ)	30; $18 \leqslant 2\theta \leqslant 28°$	34; $10.4 \leqslant 2\theta \leqslant 26.2°$	23; $9.0 \leqslant 2\theta \leqslant 20.1°$
Temp (°C)	19	19	18
No. of unique data	4018	8243	4431
Total with $I \geqslant 2.5\sigma I$	3050	3706	2404
No. of parameters	343	349	343
R[b]	0.0536	0.0868	0.0636
R_w[c]	0.0619	0.0886	0.0679
Weighting scheme $w^{-1} = \sigma^2(F) + g(F)^2$			
g	0.003235	0.000522	0.000989
Largest shift/ESD in final cycle	0.11	0.004	0.001
Largest peak (e Å^{-3})	0.53	1.06	0.75

[a] I = $\alpha\beta$-*anti*-[Co(picdien)(N_3)](ClO_4)$_2$; II = $\alpha\beta$-*anti*-[Co(picdien)(NCS)](ClO_4)$_2$·H_2O, III = $\alpha\beta$-*anti*-[Co(picditn)(NCS)](ClO_4)$_2$·H_2O.

[b] $R = \Sigma[|F_o| - |F_c|]/\Sigma|F_o|$.

[c] $R_w = \Sigma[|F_o| - |F_c|] \cdot w^{1/2}(\Sigma|F_o|w^{1/2})$.

two perchlorate anions, one of which is disordered between two orientations with O(5) common to both and 50% occupancy of each set of atoms {O(6), O(7) and O(8)} and {O(9), O(10) and O(11)}. With the exception of the perchlorate oxygens, which were refined isotropically, all of the non-hydrogen atoms were refined anisotropically. The hydrogens of the pyridyl groups were idealized to trigonal planar positions with C—H = 0.96 Å (U = 0.08 Å^2), while the aliphatic hydrogens and amine protons were idealized to tetrahedral positions with the same dimensions. The final least-squares cycle included 343 parameters for 3050 variables ($I \geqslant 2.5\sigma I$) and gave $R = 0.0536$ and $R_w = 0.0619$ and did not shift any parameter by more than 0.11 times its ESD. The final difference Fourier contained two peaks of 0.5 e Å^{-3} within one of the perchlorate ions but was otherwise featureless.

A selection of bond lengths and angles is listed in Table 2.

In the complex cation, Fig. 1, the cobalt is coordinated octahedrally to six nitrogens. The pentadentate ligand adopts the $\alpha\beta$ configuration and the proton on the "flat" nitrogen N(4) points towards the opposite side of the molecule to the azido ligand. The azide group is linear N(6)—N(7)—N(8) = 176.1(5)° and the bond angle Co—N(6)—N(7) = 116.7(3)°, making the azido group lie over one of the pyridine rings. The disordered perchlorate ion, $[Cl(2)O_4]^-$ is held in place by hydrogen bonding between O(5) and N(3) via H(300) and O(8) [O(10)] and N(2) vis H(200).

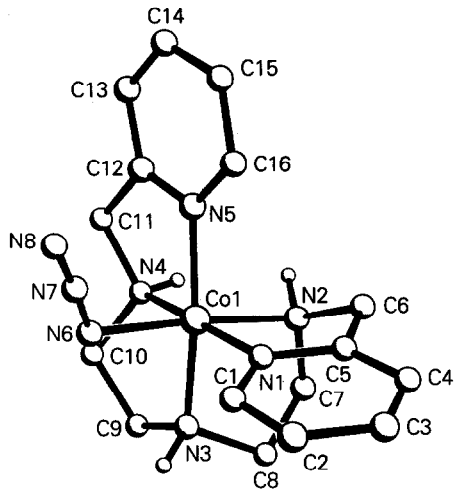

Fig. 1. A view of the *anti*-$\alpha\beta$-$[Co(picdien)(N_3)]^{2+}$ cation showing the numbering scheme. Apart from the three amine protons, all hydrogens have been omitted for clarity.

(II) $\alpha\beta$-*anti*-$[Co(picdien)(NCS)](ClO_4)_2 \cdot H_2O$

The 4360 unique data with $I \geqslant 1.5\sigma I$ were used in the structure solution and refinement in space group $P\bar{1}$. A Patterson projection showed two heavy (Co) atoms in the asymmetric unit and all the non-hydrogen atoms could be identified from the Fourier difference map after the first refinement. There was no disorder among the perchlorate oxygens.

Because of the larger number of atoms in the asymmetric unit and in order to maintain a ratio of variables to parameters of approximately 10, only the Co, Cl and N—C—S atoms were refined anisotropically. The hydrogen atoms were placed in idealized positions as before. The final least-squares cycle included 349 parameters for 3706 variables ($I \geqslant 2.5\sigma I$) and gave $R = 0.0869$, $R_w = 0.0886$ and did not shift any parameter by more than 0.004 times its ESD. Selected bond lengths and angles are given in Table 3.

Table 2. Some bond lengths (Å) and bond angles (°) for *anti*-$\alpha\beta$-$[Co(picdien)(N_3)](ClO_4)_2$

Co(1)—N(1)	1.956(4)	Co(1)—N(2)	1.982(4)
Co(1)—N(3)	1.954(4)	Co(1)—N(4)	1.929(4)
Co(1)—N(5)	1.937(4)	Co(1)—N(6)	1.956(4)
N(6)—N(7)	1.208(6)	N(7)—N(8)	1.146(6)
N(1)—Co(1)—N(2)	83.4(2)	N(1)—Co(1)—N(3)	91.5(2)
N(2)—Co(1)—N(3)	86.8(2)	N(1)—Co(1)—N(4)	176.6(2)
N(2)—Co(1)—N(4)	93.9(2)	N(3)—Co(1)—N(4)	86.1(2)
N(1)—Co(1)—N(5)	97.9(2)	N(2)—Co(1)—N(5)	94.8(2)
N(3)—Co(1)—N(5)	170.6(2)	N(4)—Co(1)—N(5)	84.5(2)
N(1)—Co(1)—N(6)	93.4(2)	N(2)—Co(1)—N(6)	175.0(2)
N(3)—Co(1)—N(6)	89.3(2)	N(4)—Co(1)—N(6)	89.1(2)
N(5)—Co(1)—N(6)	89.5(2)	C(10)—N(4)—C(11)	114.6(4)
Co(1)—N(6)—N(7)	116.7(3)	N(6)—N(7)—N(8)	176.1(5)

Table 3. Some bond lengths (Å) and bond angles (°) for *anti*-αβ-[Co(picdien)(NCS)][ClO_4)$_2$·H_2O

Co(1)—N(1)	1.940(10)	Co(2)—N(7)	1.954(10)
Co(1)—N(2)	1.971(11)	Co(2)—N(8)	1.939(10)
Co(1)—N(3)	1.928(14)	Co(2)—N(9)	1.951(14)
Co(1)—N(4)	1.918(11)	Co(2)—N(10)	1.909(10)
Co(1)—N(5)	1.939(10)	Co(2)—N(11)	1.954(13)
Co(1)—N(6)	1.909(11)	Co(2)—N(12)	1.922(12)
S(1)—C(17)	1.587(14)	S(2)—C(34)	1.606(14)
N(6)—C(17)	1.150(18)	N(12)—C(34)	1.158(18)
N(1)—Co(1)—N(2)	83.2(4)	N(7)—Co(2)—N(8)	83.0(4)
N(1)—Co(1)—N(3)	94.0(5)	N(7)—Co(2)—N(9)	93.4(5)
N(2)—Co(1)—N(3)	86.3(5)	N(8)—Co(2)—N(9)	86.8(5)
N(1)—Co(1)—N(4)	176.5(4)	N(7)—Co(2)—N(10)	176.4(4)
N(2)—Co(1)—N(4)	93.3(4)	N(8)—Co(2)—N(10)	93.4(4)
N(3)—Co(1)—N(4)	85.4(5)	N(9)—Co(2)—N(10)	85.9(5)
N(1)—Co(1)—N(5)	96.0(5)	N(7)—Co(2)—N(11)	96.0(5)
N(2)—Co(1)—N(5)	95.9(5)	N(8)—Co(2)—N(11)	94.3(5)
N(3)—Co(1)—N(5)	169.9(5)	N(9)—Co(2)—N(11)	170.6(4)
N(4)—Co(1)—N(5)	84.6(5)	N(10)—Co(2)—N(11)	84.7(5)
N(1)—Co(1)—N(6)	93.1(5)	N(7)—Co(2)—N(12)	93.3(5)
N(2)—Co(1)—N(6)	174.4(6)	N(8)—Co(2)—N(12)	176.1(5)
N(3)—Co(1)—N(6)	89.9(5)	N(9)—Co(2)—N(12)	92.2(6)
N(4)—Co(1)—N(6)	90.4(5)	N(10)—Co(2)—N(12)	90.2(5)
N(5)—Co(1)—N(6)	88.6(5)	N(11)—Co(2)—N(12)	87.3(5)
C(10)—N(4)—C(11)	116.3(12)	C(27)—N(10)—C(28)	115.6(12)
Co(1)—N(6)—C(17)	167.1(10)	Co(2)—N(12)—C(34)	166.4(12)
S(1)—C(17)—N(6)	176.8(14)	S(2)—C(34)—N(12)	178.9(15)

The asymmetric unit consists of a pair of enantiomeric complex cations, shown in Fig. 2, together with four perchlorate ions and two water molecules. The cobalt is octahedrally coordinated to six nitrogens and the ligand adopts the *anti*-αβ configuration. The nitrogen bound thiocyanato ligand is essentially linear, N—C—S = 176.8(14)° and 178.9(15)°, but the Co—N—C angle is significantly bent, 167.1(10)° and 166.4(12)°.

The two water molecules are linked by a strong hydrogen bond O(17)···O(18) = 2.69 Å and O(18) is also bound to N(10) by hydrogen bonding

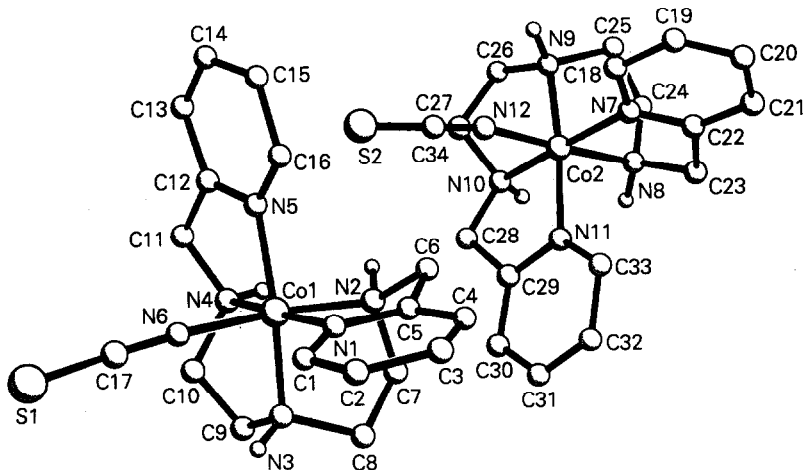

Fig. 2. A view of an enantiomeric pair of *anti*-αβ-[Co(picdien)(NCS)]$^{2+}$ cation showing the numbering scheme. Apart from the three amine protons, all hydrogens have been omitted for clarity.

through H(100) {O(18)···N(10) = 2.76 Å} and to the perchlorate oxygen, O(10) {O(18)···O(10) = 2.86 Å}. Longer interactions are to be found between N(9) and O(5) (2.97 Å), N(4) and O(14) (3.02 Å), and N(3) and O(2) (3.04 Å). These all serve to fix the perchlorate ions in rigid positions. The distinction between the enantiomeric cations lies in their relationship to these hydrogen bonding interactions. The complex cation containing Co(1) is linked to $[Cl(1)O_4]^-$ by O(2)···N(3) and $[Cl(4)O_4]^-$ by O(14)···N(4), while that containing Co(2) is bound to $[Cl(3)O_4]^-$ by O(5)···N(9) and one water of crystallization by O(18)···N(10). The other perchlorate $[Cl(2)O_4]^-$ is bound to O(18) by O(10)···O(18).

(III) $\alpha\beta$-*anti*-[Co(picditn)(NCS)]$(ClO_4)_2 \cdot H_2O$

The 3061 unique data with $I \geqslant 1.5\sigma I$ were used in the structure solution and refinement in space group $P2_1/c$. The cobalt atom was located by a Patterson projection and all the non-H atoms could be identified from the Fourier difference map after the first refinement. All non-hydrogen atoms except the oxygens of the perchlorate and the water of crystallization were refined anisotropically. There was no disorder in either of the perchlorate ions. Hydrogen atoms were idealized as described above. The final least-squares cycle included 343 parameters for 2404 variables ($I \geqslant 2.5sI$) and gave $R = 0.0636$, $R_w = 0.0679$ and did not shift any parameter by more than 0.001 times its ESD. Selected bond lengths and angles are collected in Table 4.

The asymmetric unit contains one cation, shown in Fig. 3, two perchlorate anions and one water of crystallization. The cobalt is octahedrally coordinated to six nitrogens and the ligand adopts the *anti*-$\alpha\beta$ configuration.

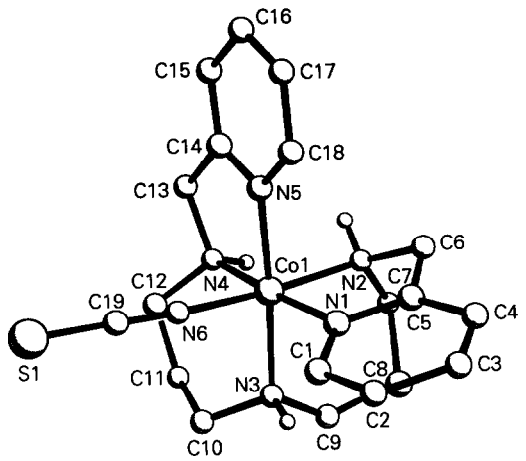

Fig. 3. A view of the *anti*-$\alpha\beta$-$[Co(picditn)(NCS)]^{2+}$ cation showing the numbering scheme. Apart from the three amine protons, all hydrogens have been omitted for clarity.

Hydrogen bonding between O(1) and N(4) {O(1)···N(4) = 2.99 Å} and O(8) and N(3) {O(8)···N(3) = 2.97 Å} anchor the perchlorate anions to the amine groups of the complex and N(2) is hydrogen bonded to the water molecule {N(2)···O(9) = 2.89 Å}.

RESULTS AND DISCUSSION

All three complexes have the same *anti*-$\alpha\beta$ configuration and so the difference in the amine acidities of the picdien and picditn NCS complexes, which both have the ligand bound to Co by N, cannot be ascribed to an isomeric difference. The Co—N—C—S sequence is closer to linearity in the picditn complex (Co—N—C = 175.8(9)°, N—C—S = 178.8(9)°) than it is in the analogous

Table 4. Some bond lengths (Å) and bond angles (°) for *anti*-$\alpha\beta$-[Co(picditn)(NCS)]$(ClO_4)_2 \cdot H_2O$

Co(1)—N(1)	1.957(8)	Co(1)—N(2)	1.964(7)
Co(1)—N(3)	2.035(8)	Co(1)—N(4)	1.970(8)
Co(1)—N(5)	1.955(8)	Co(1)—N(6)	1.913(8)
S(1)—C(19)	1.592(10)	N(6)—C(19)	1.163(13)
N(1)—Co(1)—N(2)	83.9(3)	N(1)—Co(1)—N(3)	89.2(3)
N(2)—Co(1)—N(3)	96.5(3)	N(1)—Co(1)—N(4)	176.9(3)
N(2)—Co(1)—N(4)	93.3(3)	N(3)—Co(1)—N(4)	92.5(3)
N(1)—Co(1)—N(5)	92.6(3)	N(2)—Co(1)—N(5)	87.1(3)
N(3)—Co(1)—N(5)	176.1(3)	N(4)—Co(1)—N(5)	85.7(3)
N(1)—Co(1)—N(6)	92.4(3)	N(2)—Co(1)—N(6)	171.9(4)
N(3)—Co(1)—N(6)	90.6(3)	N(4)—Co(1)—N(6)	90.2(3)
N(5)—Co(1)—N(6)	85.9(3)	C(12)—N(4)—C(13)	108.6(7)
S(1)—C(19)—N(6)	178.8(9)		

Table 5. The effect of ring strain on C—N bond lengths and C—N—C bond angles

(i) $\alpha\beta$-[Co(picdien)X]$^{n+}$ [a]

X	*anti*-Cl[4]	*syn*-Br[5]	*anti*-Br[6]	*syn*-NO_2[6]	*anti*-NCS	*anti*-N_3	*anti*-H_2O[7]
Co—N(4)[b]	1.92(2)	1.94(1)	1.929(7)	1.906(8)	1.91(1)	1.929(4)	1.919(7)
ave Co—N	1.97(2)	1.96(1)	1.951(7)	2.000(8)	1.95(1)	1.968(4)	1.948(7)
C—N(4)—C	116(2)	119(1)	116(1)	118(1)	116(1)	114.6(4)	119.2(8)

(ii) $\alpha\beta$-[Cr(picdien)Cl]$^{2+}$ [8]

Co—N(4)	2.032(3)
ave Co—N	2.078(3)
C—N(4)—C	116.1(3)

(iii) $\alpha\beta$-[Co(picditn)X]$^{2+}$

	anti-Cl	*anti*-ONO[10]	*anti*-NCS
Co—N(4)	1.96(1)	1.97(1)	1.970(8)
ave Co—N	1.97(1)	1.98(1)	2.000(8)
C—N(4)—C	108(1)	110(1)	108.6(7)

[a] For X = *anti*-H_2O, $n = 3$, otherwise $n = 2$.

[b] In some of the references the numbering sequence of the ligand is reversed, i.e. N(4) is labelled N(2).

picdien species, {average Co—N—C—S = 166.7°}. The M—N—C angle in *N*-bonded thiocyanate is frequently close to 180° but there are many examples where this angle lies between 160 and 170°.[3] The distortion in this case may arise from packing considerations and is unlikely to affect the acidity of the *trans* N—H group. The N—C and C—S bond lengths are within the range of those reported for other *N*-bonded thiocyanato complexes.

The effect of changing from two linked five-membered rings in picdien to two linked six-membered rings in picditn can be seen at N(4) which is the central atom in a meridional set of three donors. Two meridional five-membered rings produce noticcable strain at the linking donor which results in significant shortening of the Co—N bond and a widening of the C—N—C bond angle, Table 5. This has been found for all complexes of the type, $\alpha\beta$-[Co(picdien)X]$^{n+}$ examined, X = *anti*-Cl,[4] *syn*-[5] and *anti*-Br,[6] *syn*-NO_2,[6] *anti*-OH_2,[7] *anti*-N_3 and *anti*-NCS and also for *anti*-$\alpha\beta$-[Cr(picdien)Cl]$^{2+}$.[8] The effect of the release in strain caused by the presence of an adjacent six-membered ring in the $\alpha\beta$-[Co(picditn)X]$^{n+}$ complexes has been less thoroughly studied but in the cases where X = *anti*-Cl,[9] *anti*-ONO,[10] and *anti*-NCS, the Co—N(4) bond length is close to the average of the HN—Co bond lengths and the C—N—C bond angle is much closer to that of a regular tetrahedron (109.4°). It the N(4)—H(400) amine group was the site of the most acidic proton it might be possible to account for the differences in the acidities of the picdien and picditn complexes in terms of the stabilisation of the amido base through the release of the steric strain which is present in the picdien complex and absent in the picditn analogue. The large increase in acidity in going from the $\alpha\beta$-*anti*-[Co(picdien)(N_3)]$^{2+}$ cation to $\alpha\beta$-*anti*-[Co(picdien)(NCS)]$^{2+}$ and $\alpha\beta$-*syn*-[Co(picdien)(NO_2)$^{2+}$ is not easy to explain. We are reluctant to place any significance on the observation that the C—N(4)—C angle is smaller in the azido complex as the effect is not far enough outside experimental error to be statistically significant. Previously,[1] we argued in favour of a stabilization of the conjugate-base when X was a π-acceptor, such as, -NO_2 and -NCS through interaction between this ligand and the *trans* amido group acting as a π-donor. This would require N(2)—H(200) to be the most acidic amine group. We are therefore unable, at this time, to provide a single explanation of all the facts.

Proton exchange studies, now in progress,[10] show that the rate constants for the exchange of the most labile protons lie in the range 10^8 to 10^9 dm^3 mol^{-1} s^{-1} and there is no simple relationship between the magnitudes of these rate constants and the acidities of the complexes. Since deprotonation is approaching diffusion control, it is not unreasonable to find

that the rate constant for reprotonation becomes sensitive to the nature of the complex. These results will be reported elsewhere in due course.

Additional material consisting of lists of positional parameters, complete collection of bond lengths and angles, structure factors, thermal parameters and H-atom parameters has been deposited.

Acknowledgements—We thank the SERC for providing funds for the purchase of the diffractometer.

REFERENCES

1. E. Ahmed, M. L. Tobe and M. Humanes, *J. Chem. Soc., Dalton Trans.* 1990, 2175.
2. E. Ahmed, C. Chatterjee, C. J. Cooksey, M. L. Tobe, G. Williams and M. Humanes, *J. Chem. Soc., Dalton Trans.* 1989, 645.
3. J. Burmeister, *Chemistry and Biochemistry of Thiocyanic Acid* (Edited by A. A. Newman), Chap. 2, p. 70. Academic Press, London (1975).
4. G. Bombieri, E. Forsellini, A. Del Pra and M. L. Tobe, *Inorg. Chim. Acta* 1981, **51**, 177.
5. G. Bombieri, E. Forsellini, A. Del Pra, M. L. Tobe and C. Chatterjee, *Inorg. Chim. Acta* 1983, **68**, 205.
6. G. Bombieri, E. Forsellini, A. Del Pra, M. L. Tobe, C. Chatterjee and C. J. Cooksey, *Inorg. Chim. Acta* 1983, **75**, 93.
7. G. Bombieri, A. Polo, F. Benetello, M. L. Tobe, M. Humanes and C. Chatterjee, *Acta Cryst.* 1987, **C43**, 1866.
8. V. Ugalde-Saldivar, M. A. Luna-Canut, M. E. Sosa-Torres, M. J. Rosales-Hoz, R. A. Toscano and M. L. Tobe, *J. Chem. Soc., Dalton Trans.* 1990, 3629.
9. G. Bombieri, E. Forsellini, A. Del Pra and M. L. Tobe, *Inorg. Chim. Acta* 1980, **40**, 71.
10. L. Tang and M. L. Tobe, to be submitted.

Polyhedron Vol. 10, No. 22, pp. 2605–2609, 1991
Printed in Great Britain

0277–5387/91 $3.00+.00
© 1991 Pergamon Press plc

ELECTROSYNTHESIS OF TRANSITION METAL FLUORO COMPLEXES BY THE DISSOLUTION OF A SACRIFICIAL METAL ANODE

M. C. CHAKRAVORTI,* GAMPA. V. B. SUBRAHMANYAM and D. BANDYOPADHYAY

Department of Chemistry, Indian Institute of Technology, Kharagpur-721 302, India

(*Received* 15 *June* 1990; *accepted* 28 *June* 1991)

Abstract—A general method for the electrosynthesis of anionic fluoro complexes of transition metals has been developed by the oxidation of sacrificial metal anodes in 20% HF medium at room temperature and at an applied potential of 2–8 V. Some mixed-valent complexes, e.g. $Fe_2F_5 \cdot 2H_2O$ and $Fe_2F_5 \cdot 7H_2O$, have also been obtained by the same method. $K_2[MnF_5] \cdot H_2O$ was obtained by subsequent electrolytic oxidation of the Mn(II) fluoro complex obtained *in situ* in the first step. The method is rapid and gives a good yield with high purity.

Electrochemical synthesis in which a sacrificial metal anode is dissolved in the presence of an electrolyte containing an appropriate ligand is an established way for the electrolytic synthesis of a variety of metal complexes[1] in a single step. The process uses the metals directly, and thus contamination of the product by the anions, which is often encountered in chemical methods using the metal salts, is absent. The method is rapid and highly selective. Thiocyanato complexes of a large number of metals have been prepared by the dissolution of metal anodes in a solution containing HSCN.[2,3] The chloro complex, $[CoCl_4]^{2-}$ has been prepared[4] by using a cobalt anode in the presence of hydrochloric acid. We have also reported[5] a very convenient electrosynthesis of $K_2[MoOF_5]$ using a molybdenum anode. We have now extended our studies with various transition metals and demonstrated that the procedure can be used as a general method for the preparation of a wide variety of fluoro complexes of different metals in various oxidation states from aqueous medium. The results are presented in this communication. Some complexes in higher oxidation state, e.g. $K_2[MnF_5] \cdot H_2O$, can be prepared by a two step electrolysis—the first step resulting in the formation *in situ* of the complex in the normal oxidation state by the dissolution of the sacrificial metal anode, followed by electrolytic oxidation of the complex using inert platinum electrodes. The fluoro complexes reported in this communication are already known. Some of these are remarkable in having a variety of structures and physical properties. Many of these were prepared earlier from a non-aqueous medium or by reactions in the solid state at high temperature. The present method uses an aqueous medium at room temperature. Pure metals which are not strongly electropositive dissolve in aqueous hydrofluoric acid slowly even at higher temperature, but the application of an electrical potential increases the rate of dissolution at room temperature.

EXPERIMENTAL

The metals were in the form of rods, lumps, chips or foils and were mostly 99.8% pure. Titanium powder was pressed to make pellets. A few metals (e.g. chromium and manganese) were first deposited on a platinum foil by the electrolysis of their salt solutions and these were subsequently used as the anode. Other chemicals were of AR/GR quality from reputable manufacturers.

The electric power was supplied by a dc power supply (Aplab, India). A milliammeter was connected into the circuit in cases where the current was very feeble. The electrolytic cell was a tall form of polythene beaker (100 cm^3) fitted with a rubber

* Author to whom correspondence should be addressed.

stopper through which four holes were made. The appropriate metal rods which formed the anode were inserted through a hole. In cases where metal lumps, foils or pellets were used, these were fused onto a platinum wire which was inserted through the hole. Chromium and manganese were previously deposited onto a platinum foil sealed to a platinum wire which served as the anode. In all cases a platinum foil (about $1 \times 1 \times 0.15$ cm) connected to a platinum wire served as the cathode and was introduced through the second hole. Two polythene tubes were introduced through the other two holes. These allowed input and exit of nitrogen where it was necessary to carry out electrolysis in the absence of air.

Fluorine was analysed by titration with $Th(NO_3)_4$ after fusing the complex with sodium hydroxide, or steam distillation of fluorosilicic acid.[6] Potassium and caesium were determined by atomic absorption using a Pye Unicom instrument (SP-2900). Other metals were analysed by standard titrimetric or gravimetric methods. Reflectance spectra were recorded using a Shimadzu UV spectrophotometer (No. 3100) against barium sulphate. Infrared spectra were recorded in CsI pellets using a Perkin–Elmer instrument (No. 883). Magnetic susceptibility was measured by the Gouy method using $Hg[Co(NCS)_4]$ as calibrant. Diamagnetic corrections were taken from a standard source.[7] X-ray powder diffraction patterns were obtained with a Philip's diffractometer (PW 1729) employing nickel filtered Cu-K_α radiation.

Preparation of the complexes

$M_2[TiF_6]$, $M_2[VOF_4]$, $K_3[CrF_6]$, $K[MnF_3]$, $M_3[FeF_6]$, $M[CoF_3]$, $M[NiF_3]$, $Cs_2[NbOF_5]$ *and* $K_2[TaF_7]$ *where* M = K *or* Cs. Each electrolysis was carried out using 10 cm^3 hydrofluoric acid (20%). The details of the experimental conditions are given in Table 1. After electrolysis, the solution was filtered to free it from any disintegrated metal particles (when an iron anode was used, a yellow deposit was also obtained from which $Fe_2F_5 \cdot 7H_2O$ and $Fe_2F_5 \cdot 2H_2O$ could be prepared). The potassium and the caesium salts were precipitated by adding concentrated solutions of KF and CsF in HF (20%). The complexes were separated by fil-

Table 1. Experimental conditions for the electrochemical synthesis of the complexes

Compound	Initial voltage (V)	Initial current (A)	Time of electrolysis (h)	Amount of metal oxidized (g)	Yield (g)	(%)	E_F (mol F^{-1})
$K_2[TiF_6]$	5	0.50	2.0	0.400	1.5[b]	75	0.22
$Cs_2[TiF_6]$	5	0.50	2.0	0.400	2.9[b]	81	0.22
$K_2[VOF_4]$	3	0.35	2.0	0.306	1.0[b]	74	0.23
$Cs_2[VOF_4]$	3	0.35	2.0	0.306	1.9[b]	74	0.23
$K_3[CrF_6]$	2	0.04	3.0	0.085	0.3	65	0.36
$K[MnF_3]$	2	0.05	2.0	0.100	0.2	55	0.49
$K_3[FeF_6]$	8	0.45	2.0	0.600[a]	1.1		
$Fe_2F_5 \cdot 7H_2O$					1.5		
$Fe_2F_5 \cdot 2H_2O$					1.0		
$K[CoF_3]$	5	0.30	3.0	0.780	1.3	63	0.39
$Cs[CoF_3]$	5	0.31	3.0	0.800	2.7	82	0.39
$K[NiF_3]$	4	0.05	2.5	0.180	0.3	63	0.65
$Cs[NiF_3]$	4	0.05	2.5	0.180	0.5	66	0.65
$K_2[NbOF_5] \cdot H_2O$	5	0.40	2.0	0.555	1.3[b]	74	0.20
$K_2[TaF_7]$	3	0.20	2.0	0.540	1.0[b]	82	0.19
$K_2[MnF_5] \cdot H_2O$	2(20)[c]	0.05(1.0)[c]	2.0(3.0)[c]	0.100	0.3	68	

[a] Total amount of iron oxidized in one experiment, out of which the yields of $K_3[FeF_6]$, $Fe_2F_5 \cdot 7H_2O$ and $Fe_2F_5 \cdot 2H_2O$ are recorded separately.

[b] The compounds were precipitated immediately on the addition of MF. In other cases the compounds were crystallized out on evaporation in a desiccator over concentrated H_2SO_4.

[c] Values in parentheses refer to the subsequent electrolytic oxidation of the initially formed M(II) complex.

tering under suction and dried by pressing between the folds of filter paper and then keeping in a desiccator over KOH. For the calculation of electrochemical efficiency (number of moles of metal dissolved per faraday of electricity passed) the anodes were weighed before and after the electrolysis.

$Fe_2F_5 \cdot 7H_2O$ *and* $Fe_2F_5 \cdot 2H_2O$. The residue which was obtained during the electrolysis using an iron anode, was digested with 10 cm^3 HF (20%) on a steam bath until it dissolved almost completely. The hot solution was quickly filtered and the filtrate was divided into two parts. One part gave a deposit of $Fe_2F_5 \cdot 7H_2O$ on cooling, while the other gave a precipitate of $Fe_2F_5 \cdot 2H_2O$ on evaporation over a steam bath until the volume was reduced to half. These were separated and dried as described above.

$K_2[MnF_5] \cdot H_2O$. After 2 h of electrolysis, the manganese anode was replaced by a platinum foil electrode and electrolysis was continued for a further 2 h. Finally, the potassium salt was obtained by the addition of a concentrated solution of KF in HF (20%).

RESULTS AND DISCUSSION

Our studies show that fluorides of many transition metals can be easily prepared from aqueous HF at room temperature. The applied voltage is low

Table 2. Physicochemical data for the complexes

Compound	μ_{eff} at 300 K, BM	Bands in electronic spectra (cm^{-1})	X-ray powder diffraction data,[a] d (Å)	Bands in IR spectra (cm^{-1})
$K_2[TiF_6]$	diamag		2.3(100), 3.31(90), 4.58(80), 9.15(60), 2.17(60), 2.10(40), 2.85(30), 1.70(30)	580
$K_3[CrF_6]$	4.10	15,000, 15,900, 16,400, 23,400, 36,300	3.00(100), 4.95(80), 4.31(80), 2.51(60), 2.18(60), 2.14(60), 1.76(60)	544, 500, 296
$K[MnF_3]$	5.87	19,000, 22,900, 25,000, 29,800, 32,900	2.89(100), 2.09(65), 1.70(30), 4.14(25), 2.41(14)	426, 300
$K_3[FeF_6]$	5.73	14,200, 19,700, 25,400, 28,800, 30,200	3.00(100), 2.15(40), 4.96(30), 1.76(30), 4.30(20), 1.52(10). 2.50(10), 1.66(10)	580. 484, 310, 275
$K[CoF_3]$	3.90	16,400, 19.420	3.90(100), 2.00(70), 1.66(35), 4.08(25), 2.35(14), 1.30(12), 1.82(12), 1.09(10)	485, 384, 276
$K[NiF_3]$	2.36	15,200, 21,400, 25,000	2.85(100), 2.00(65), 4.00(30), 1.65(30), 1.41(25), 2.32(12), 1.80(12), 12.70(10)	485, 450, 255
$Cs_2[VOF_4]$	1.90	15,800, 23,800		990.486
$Cs_2[NbOF_5]$	diamag		3.65(100), 3.52(90), 3.59(90), 2.52(30), 4.00(25), 4.25(18), 2.38(16)	980, 460
$K_2[TaF_7]$	diamag		5.10(100), 3.45(45), 4.29(40), 3.35(40), 3.19(40), 4.51(30), 2.00(18), 2.11(14), 2.56(10)	530
$Fe_2F_5 \cdot 7H_2O$	7.89	9500, 11,000, 21,700	4.72(100), 4.23(100), 3.83(80), 3.48(80), 3.28(80), 2.74(80), 2.50(80), 2.43(80), 1.86(80)	470, 303, 280, 260
$Fe_2F_5 \cdot 2H_2O$	7.35	7900, 9600, 15,000, 20,500, 25,500	5.65(100), 3.20(80), 5.00(60), 3.65(60), 3.20(60), 3.10(60), 2.85(60), 1.85(60)	500, 336, 300
$K_2[MnF_5] \cdot H_2O$	3.41	12,500, 18,200, 21,200	5.8(100), 5.91(60), 2.96(25), 2.90(25), 3.30(10), 2.21(10), 2.6(8), 2.38(8)	580, 417, 290

[a] Values in parentheses are the intensities.

(2–8 V) and the yield is very good (about 60–85% based on the amount of metal oxidized). The main reactions taking place at the electrodes are:

$$2H^+ + 2e \longrightarrow H_2 \text{ (at cathode)}$$

$$M - ne \longrightarrow M^{+n} \text{ (at anode)}$$

which is evident from the observed electrochemical efficiency. A slight deviation of the electrochemical efficiency (Table 1) from the theoretical value of $1/n$ is ascribed to some disintegration of the metal anode and slight fluctuation of the current during electrolysis.

Anodic dissolution of the metals was also studied in a stream of nitrogen. The products however, were identical with those obtained in air using metal anodes. With titanium, a purple solution was initially obtained, which ultimately gave the same Ti(IV) compound. It appears that a Ti(III) fluoro complex is initially formed, which was subsequently oxidized during the working up.

All the compounds gave satisfactory analytical results of alkali metal, fluoride and the respective transition metals. The oxidation number of Mn in $K_2[MnF_5]\cdot H_2O$ determined iodometrically was +3.0. The observed magnetic moments of the compounds (see Table 2) were in agreement with those reported in the literature.[8–11] The X-ray powder diffraction data of many of the compounds are available in the X-ray powder diffraction file. Our data (Table 2) for these compounds were in excellent agreement with the recorded values. The band positions in the electronic spectra of the complexes are given in Table 2. These also compare well with the literature values.[8,11,12] The IR spectral data of only a few of the compounds were reported earlier.[8,13,14] The positions of the important IR spectral bands of the compounds are recorded in Table 2. The M—F stretching frequency occurs around 500 cm^{-1} for all the compounds of the type $[MF_6]^{n-}$ and also for $[TaF_7]^{2-}$, $[VOF_4]^{2-}$, $[NbOF_5]^{2-}$ and $K_2[MnF_5]\cdot H_2O$. A comparison of the vibrational spectra of these diverse types of species is very difficult. However, some characteristic features may be noted. The increase in the position of ν_3 in $[CrF_6]^{3-}$ compared to $[FeF_6]^{3-}$ is in keeping with the trend generally found among the hexafluoro complexes. The higher value of the ν_3 in $[TiF_6]^{2-}$ compared to that in $[CrF_6]^{3-}$ is again in agreeement with the expected trend. The relatively lower Ta—F band position in the spectra of $[TaF_7]^{2-}$ is attributed to an increased coordination number of the metal. The spectra of $[NiF_3]^-$ and $[CoF_3]^-$ are very similar. In these two complexes and also in $[MnF_3]^-$ the M—F vibration occurs at a lower frequency which is probably due to a —F—M—F—M—F— type of interaction in the complexes.[8,15,16] The spectrum of $K_2[MnF_5]\cdot H_2O$, which contains both bridging and terminal fluoride,[17] gives a number of bands in the region 600–250 cm^{-1}. The mixed-valent complexes $Fe_2F_5\cdot 2H_2O$ and $Fe_2F_5\cdot 7H_2O$ have been widely studied.[10,11,18,19] While the former contains fluoride bridges, the latter is represented as $[Fe(H_2O)_6][FeF_5(H_2O)]$. In keeping with these structures their spectra also give a number of bands in the above region. The spectra of the two oxo complexes $[VOF_4]^{2-}$ and $[NbOF_5]^{2-}$ give the characteristic M=O bands in the region 970–1000 cm^{-1}, in addition to M—F bands.

In recent years there has been growing interest in the synthesis of coordination compounds starting directly from metals.[20–22] Many metals are readily available in more than 99.8% purity. As stated earlier, the metals may also be previously deposited on a platinum foil by electrolysis of their salt solutions. The method, therefore serves as a general one for the electrosynthesis of fluoro complexes from aqueous medium at room temperature.

REFERENCES

1. V. A. Konev, V. Yu. Kukushkin and Yu. N. Kukushkin, *Russ. J. Inorg. Chem.* 1986, **31**, 838.
2. D. G. Tuck, M. J. Taylor and C. Oldham, *Inorg. Chim. Acta* 1985, **100**, L9.
3. M. C. Chakravorti and G. V. B. Subrahmanyam, unpublished work.
4. C. Oldham and D. G. Tuck, *J. Chem. Edn.* 1982, **59**, 420.
5. M. C. Chakravorti and D. Bandyopadhyay, *Polyhedron* 1988, **7**, 1135.
6. G. Charlot and D. Bezier, English translation by R. C. Murray, *Quantitative Inorganic Analysis*, p. 425. Methuen and Co., London (1957).
7. J. Lewis and R. G. Wilkins, *Modern Coordination Chemistry*, p. 403. Interscience, New York (1960).
8. R. Colton and J. H. Canterford, *Halides of the First Row Transition Metals*, pp. 194, 237, 242, 245, 295, 370, 469. Wiley, New York (1969).
9. R. S. Nyholm and A. G. Sharpe, *J. Chem. Soc.* 1952, 3579; 1957, 563.
10. E. G. Walton, P. J. Corvan, D. B. Brown and P. Day, *Inorg. Chem.* 1976, **15**, 1737.
11. E. G. Walton, D. B. Brown, H. Wong and W. M. Reiff, *Inorg. Chem.* 1977, **16**, 2425.
12. A. B. P. Lever, *Inorganic Electronic Spectroscopy*, pp. 419, 481, 508. Elsevier, Amsterdam (1984).
13. D. F. Evans and P. A. W. Dean, *J. Chem. Soc. A.* 1967, 698.
14. R. D. Peacock and D. W. A. Sharp, *J. Chem. Soc.* 1958, 2762.
15. M. N. Bhattacharjee, M. K. Chaudhuri, M. Devi

and Y. Khriesavilie, *J. Chem. Soc., Dalton Trans.* 1987, 1055.
16. I. Nawagawa, A. Tsuchida and T. Shimanouchi, *J. Chem. Phys.* 1967, **47**, 982.
17. A. J. Edwards, *J. Chem. Soc. A* 1971, 2654.
18. K. J. Gallagher and M. R. Ottaway, *J. Chem. Soc., Dalton Trans.* 1975, 978.
19. W. Hall, S. Kim, J. Zubieta, E. G. Walton and D. B. Brown, *Inorg. Chem.* 1977, **10**, 1884.
20. P. L. Timmis, *Adv. Inorg. Radiochem.* 1972, **14**, 121.
21. G. A. Ozin and A. Vander Volt, *Prog. Inorg. Chem.* 1975, **19**, 105.
22. D. G. Tuck, *Pure Appl. Chem.* 1979, **51**, 2005.

Polyhedron Vol. 10, No. 22, pp. 2611–2616, 1991
Printed in Great Britain

0277–5387/91 $3.00+.00
© 1991 Pergamon Press plc

REACTIVITY OF THE COMPLEXES $Mo(CO)_3(\eta^2\text{-NN})(\eta^1\text{-dppm})$ (NN = bpy, phen, dmp) WITH HgX_2 (X = Cl, Br, I, CN, SCN). FORMATION OF TRIMETALLIC Mo—Hg—Mo AND BIMETALLIC Mo—Hg COMPLEXES

M. CANO* and J. A. CAMPO

Departamento de Química Inorgánica, Facultad de Ciencias Químicas,
Universidad Complutense, 28040-Madrid, Spain

(*Received* 10 *May* 1991; *accepted* 28 *June* 1991)

Abstract—The reactions of the complexes $[Mo(CO)_3(\eta^2\text{-NN})(\eta^1\text{-dppm})]$ [NN = 2,2′-bipyridyl (bpy), 1,10-phenanthroline (phen), 2,9-dimethyl-1,10-phenanthroline (dmp); dppm = bis(diphenylphosphino)methane] with HgX_2 (X = Cl, Br, I, CN, SCN) led to three types of compounds $[Mo(CO)_3(\eta^2\text{-NN})(X)]_2Hg$ (NN = bpy, phen; X = Cl, Br, CN, SCN. NN = dmp; X = CN), $[Mo(CO)_3(\eta^2\text{-NN})(\mu\text{-dppm})HgI]HgI_3$ (NN = bpy, phen; X = I) and $[Mo(CO)_3(\eta^2\text{-dmp})(HgX)(X)]$ (X = Cl, Br, I, SCN), depending on the NN-ligand and the mercuric derivative employed. The formation of the trinuclear complexes $[Mo(CO)_3(\eta^2\text{-NN})(X)]_2Hg$ is favoured over the expected bimetallic derivatives, in which two metals are bridged by the dppm ligand. Bimetallic compounds are obtained when bulky ligands are present, such as dmp bonded to a molybdenum atom or I bonded to mercury, and only in the latter case is a Mo—Hg complex bridged by dppm obtained.

Heterobimetallic complexes containing a transition metal bonded to mercury are of current interest, especially because some of these have been used as intermediates in organic and organometallic synthesis. Complexes containing constraining ligands such as $Ph_2PCH_2PPh_2$ [bis(diphenylphosphino)methane, dppm] are of special interest since proximity effects involved in bridging behaviour can be used to favour formation of the metal–metal bond.[1] However, dppm bridged systems involving molybdenum and mercury have not been described and we are interested in the study of this type of compound.

On the other hand it has been established that complexes of the type $[Mo(CO)_3(\eta^2\text{-dppm})(\eta^1\text{-dppm})]$ [dppm = bis(diphenylphosphino)methane] in their reactions with transition metal derivatives are able to form dinuclear heterobimetallic complexes bridging two metals by the dppm ligand.[2,3] However, no bimetallic derivatives were obtained from the reaction of $[Mo(CO)_3(\eta^2\text{-dppm})(\eta^1\text{-dppm})]$ with HgX_2 (X = Cl, SCN) (although Mo—Hg bonded species have been suggested as intermediates) and new dicarbonyl molybdenum-complexes were formed by elimination of mercury.[4]

In a previous communication, we have reported the behaviour of the related $[Mo(CO)_3(\eta^2\text{-bpy})(\eta^1\text{-dppm})]$ complex towards some metal derivatives. Molybdenum–metal complexes were formed in all cases, and in particular a trinuclear compound $[Mo(CO)_3(\eta^2\text{-bpy})(Cl)]_2Hg$ was obtained in the reaction with $HgCl_2$.[5]

As an extension of the above results we have studied the reactions of $[Mo(CO)_3(\eta^2\text{-NN})(\eta^1\text{-dppm})]$ [NN = 2,2′-bipyridyl (bpy), 1,10-phenanthroline (phen), 2.9-dimethyl-1,10-phenanthroline (dmp)] with HgX_2 (X = Cl, Br, I, CN, SCN), in an attempt to form new heterobimetallic Mo—Hg complexes with dppm as bridge.

RESULTS AND DISCUSSION

The spectroscopic and analytical data of the isolated compounds are summarized in Tables 1 and 2.

* Author to whom correspondence should be addressed.

Table 1. Analytical, conductivity and IR data for the complexes $[Mo(CO)_3(\eta^2\text{-NN})(X)]_2Hg$, $[Mo(CO)_3(\eta^2\text{-NN})(\mu\text{-dppm})HgI]HgI_3$ and $[Mo(CO)_3(\eta^2\text{-dmp})(HgX)(X)]$

Compound (Colour)	Analyses (%)[a] C	H	N	Λ_m[b] (ohm^{-1} cm^2 mol^{-1})	ν_{CO}[c] (cm^{-1})
$[Mo(CO)_3(\eta^2\text{-bpy})(Cl)]_2Hg$ (Yellow-orange)	32.9 (33.1	1.6 1.7	5.8 6.0)	13.2	1978sh 1950s 1935s 1850sh 1835vs
$[Mo(CO)_3(\eta^2\text{-phen})(Cl)]_2Hg$ (Orange)	35.9 (36.4	1.6 1.6	5.5 5.7)	9.4	1978m 1940vs 1888sh 1848s 1820vs
$[Mo(CO)_3(\eta^2\text{-dmp})(HgCl)(Cl)]$ (Orange)	30.7 (31.0	1.6 1.9	4.0 4.2)	13.5	1978vs 1895sh 1870s
$[Mo(CO)_3(\eta^2\text{-bpy})(Br)]_2Hg$ (Orange)	29.7 (30.1	1.3 1.6	5.2 5.4)	12.5	1975sh 1952s 1938s 1855sh 1838vs
$[Mo(CO)_3(\eta^2\text{-phen})(Br)]_2Hg$ (Orange)	32.8 (33.4	1.4 1.5	5.0 5.2)	10.2	1974m 1942s 1850s 1825vs
$[Mo(CO)_3(\eta^2\text{-dmp})(HgBr)(Br)]$ (Orange)	26.9 (27.3	1.3 1.6	3.5 3.7)	14.2	1978vs 1870s
$[Mo(CO)_3(\eta^2\text{-bpy})(\mu\text{-dppm})HgI]HgI_3$ (Yellow)	27.7 (28.0	1.5 1.9	1.7 1.7)	52.0	1968vs 1872sh 1852vs
$[Mo(CO)_3(\eta^2\text{-phen})(\mu\text{-dppm})HgI]HgI_3$ (Yellow)	28.8 (29.0	1.6 1.8	1.8 1.7)	43.2	1965vs 1878sh 1852vs
$[Mo(CO)_3(\eta^2\text{-dmp})(HgI)(I)]$ (Yellow)	24.0 (24.3	1.2 1.4	3.1 3.3)	10.3	1975s 1870s
$[Mo(CO)_3(\eta^2\text{-bpy})(NCS)]_2Hg$ (Orange)	33.9 (34.0	1.6 1.6	8.0 8.5)	17.6	1982vs 1950vs 1905sh 1882s 1840vs 2090sh(ν_{CN}) 2075s(ν_{CN})
$[Mo(CO)_3(\eta^2\text{-phen})(NCS)]_2Hg$ (Orange)	36.8 (37.1	1.5 1.6	7.8 8.1)	14.7	1975s 1950vs 1872vs 1855s 2095s(ν_{CN}) 2060sh(ν_{CN})
$[Mo(CO)_3(\eta^2\text{-dmp})(HgSCN)(SCN)]$ (Orange-yellow)	32.1 (32.4	1.5 1.7	7.6 8.0)	15.0	1978vs 1900s 1862vs 2098s(ν_{CN})

Table 1—*continued*

Compound (Colour)	Analyses (%)[a] C	H	N	Λ_m[b] (ohm^{-1} cm^2 mol^{-1})	ν_{CO}[c] (cm^{-1})
$[Mo(CO)_3(\eta^2\text{-bpy})(CN)]_2Hg$ (Yellow)	36.0 (36.4	1.6 1.7	8.9 9.1)	12.5	1995s 1975vs 1898sh 1870vs 1845vs 2105w(ν_{CN})
$[Mo(CO)_3(\eta^2\text{-phen})(CN)]_2Hg$ (Orange-yellow)	39.2 (39.6	1.5 1.7	8.4 8.7)	15.2	1988vs 1960vs 1895sh 1862vs 2105m(ν_{CN})
$[Mo(CO)_3(\eta^2\text{-dmp})(CN)]_2Hg$ (Orange-yellow)	41.7 (42.1	2.2 2.4	8.0 8.2)	9.5	1985s 1960s 1890vs 1870sh 2105w(ν_{CN})

[a] Found; (calculated).
[b] In dimethylformamide solutions 10^{-3} M.
[c] In KBr pellets; vs = very strong, s = strong, m = medium, w = weak, sh = shoulder.

Table 2. NMR data for $[Mo(CO)_3(\eta^2\text{-NN})(\mu\text{-dppm})HgI]HgI_3$

NN	δ (^{1}H) (ppm) (CH_2 in dppm)	δ (^{31}P) (ppm)	$^2J_{P-P}$ (Hz)
bpy	4.45br[a]	30.0br, 48.7br[b] 29.6d, 49.0d[a]	149
phen	4.21br[b]	26.3br, 44.4br[b]	

[a] In $(CD_3)_2CO$ solution at −20°C.
[b] In $(CD_3)_2CO$ solution at room temperature.
br = broad; d = doublet.

(a) *Reactivity of* $[Mo(CO)_3(\eta^2\text{-NN})(\eta^1\text{-dppm})]$ (NN = bpy, phen) *with* HgX_2 (X = Cl, Br)

The $[Mo(CO)_3(\eta^2\text{-NN})(\eta^1\text{-dppm})]$ complex (NN = bpy, phen) reacts with mercury(II) halide, HgX_2 (X = Cl, Br), in a 1:1 or 1:2 molar ratio at room temperature and no CO evolution is observed. The solids isolated are insoluble in common solvents and they have been characterized as a mixture of $[Mo(CO)_3(\eta^2\text{-NN})(X)]_2Hg$ and $HgX_2 \cdot n$dppm.

The IR spectra of the solids show in the carbonyl region the characteristic pattern of bands of $[Mo(CO)_3(\eta^2\text{-bpy})(X)]_2Hg$ complexes;[5,6] however, absorptions attributed to coordinated dppm ligand are also observed, and suggest the presence of $HgX_2 \cdot n$dppm (NN = bpy, phen; X = Cl, Br).

In order to confirm our hypothesis we studied compounds of the type $HgX_2 \cdot n$dppm, synthesized by direct reactions between HgX_2 and dppm. New products, characterized as $HgX_2 \cdot n$dppm (X = Cl, $n = 1/3$; X = Br, $n = 1$) were isolated and all of these were insoluble in common solvents.[7]

The ^{31}P-NMR spectra of the above compounds, registered in DMSO-d_6, show a singlet (X = Cl, $\delta = 2.25$ ppm; X = Br, $\delta = 2.00$ ppm) with their corresponding mercury satellites.[7] These signals appear at the same position as those observed for the solids formed in the reactions referred to above, and confirm the suggested presence of the adducts $HgX_2 \cdot n$dppm in the products of these reactions.

On this basis we thought that a 2:1 (Mo:Hg) stoichiometry for the reaction between the molybdenum complex $[Mo(CO)_3(\eta^2\text{-NN})(\eta^1\text{-dppm})]$ and HgX_2 could yield the trinuclear derivative exclusively. We have carried out these 2:1 reactions and the products isolated were characterized as the expected complexes $[Mo(CO)_3(\eta^2\text{-NN})(X)]_2Hg$. This fact indicates that the dppm ligand is always liberated from the starting molybdenum complex and that the formation of $HgX_2 \cdot n$dppm compounds occurs when an excess of HgX_2 with respect to the 2:1 molar ratio of the reaction is employed.

The above trinuclear complexes had already been obtained by reactions of $[Mo(CO)_3(\eta^2\text{-NN})(L)]$ (L = N-, P- or S-donor ligands) with HgX_2.[6,8-12] For these reactions, an insertion of $Mo(CO)_3(\eta^2\text{-NN})$ groups into Hg—X bonds had been proposed.[6]

(b) *Reactivity of* $[Mo(CO)_3(\eta^2\text{-NN})(\eta^1\text{-dppm})]$ (NN = bpy, phen) *with* HgX_2 (X = CN, SCN)

In order to establish if the insertion of $Mo(CO)_3(\eta^2\text{-NN})$ groups into the Hg—X bonds is dependent on the X groups bonded to the mercury atom, we have studied the reactivity of $[Mo(CO)_3(\eta^2\text{-NN})(\eta^1\text{-dppm})]$ (NN = bpy, phen) with $Hg(CN)_2$ and $Hg(SCN)_2$.

The reactions have been carried out in the same conditions used with the mercury halides described above. In all cases, the isolated products have been characterized as the complexes $[Mo(CO)_3(\eta^2\text{-NN})(X)]_2Hg$ (NN = bpy, phen; X = CN, SCN). Additional $Hg(CN)_2$ molecules are present in the final compounds obtained when a 1:2 (Mo:Hg) stoichiometric ratio was employed.

The IR spectra of the compounds show a pattern of carbonyl absorptions similar to that observed in the compounds $[Mo(CO)_3(\eta^2\text{-bpy})(X)]_2Hg$,[5,6] which is characteristic of the skew configuration of the carbonyl groups round the Mo—Hg—Mo linkage.[13]

The ν_{CN} frequencies appear in the same region as those observed in complexes containing the CN and SCN groups bonded to the molybdenum atom[4,14-16] and is consistent with the analytical data. A formulation as $[Mo(CO)_3(\eta^2\text{-NN})(X)]_2Hg$ (NN = bpy, phen; X = CN, SCN) was proposed for our compounds. The low values of the ν_{CN} frequencies observed for the compounds $[Mo(CO)_3(\eta^2\text{-NN})(CN)]_2Hg$ (NN = bpy, phen) have been attributed to a pseudobridging character of the CN groups in these complexes.[17]

The elimination of the dppm ligand of the starting molybdenum complexes is revealed by spectroscopic data, and the formation of the soluble compounds $HgX_2 \cdot n$dppm (X = CN, SCN)[7] has been probed from the solution reaction when a 1:2 (Mo:Hg) molar ratio has been used.

On another occasion we have shown that $Mo(CO)_3(\eta^2\text{-NN})$ groups are formed in these reactions with elimination of the dppm ligand. These moieties with 16-electrons round the molybdenum atom are inserted into the Hg—X bonds giving the 18-electron configuration in the stable $[Mo(CO)_3(\eta^2\text{-NN})(X)]_2Hg$ (X = CN, SCN) derivatives.

(c) *Reactivity of* $[Mo(CO)_3(\eta^2\text{-NN})(\eta^1\text{-dppm})]$ (NN = bpy, phen) *with* HgI_2

The reactions of $[Mo(CO)_3(\eta^2\text{-NN})(\eta^1\text{-dppm})]$ (NN = bpy, phen) with HgI_2 have been studied in analogous conditions that those above described in (a) and (b). No influence of the stoichiometric ratio is observed and new products formulated as $[Mo(CO)_3(\eta^2\text{-NN})(\mu\text{-dppm})HgI]HgI_3$ (NN = bpy, phen) are obtained.

The IR spectra show three carbonyl bands, shifted to higher frequencies than those of the starting complexes, consistent with an increase in the formal oxidation state of molybdenum atom. Absorptions of the NN and dppm ligands are also observed in their characteristic regions.

The new compounds are soluble in some polar solvents such as ethanol, methanol or acetone. The molar conductivity (Λ_m) measurements in acetone and dimethyl formamide solutions indicate the ionic character of these compounds. The values of Λ_m are slightly lower than those expected for 1:1 electrolytes which could be attributed to a low ionic mobility of the species present.

The ^{31}P-NMR spectra of the new complexes in acetone-d_6 at room temperature show two broad signals due to the coordinated phosphorus atoms. At −20°C, the signals appear as doublets with phosphorus–phosphorus couplings (Table 2). These results are in agreement with an inequivalence of the two phosphorus atoms of the coordinated dppm ligand. This fact eliminates the possibility of the formation of adducts of the type $HgI_2 \cdot n$dppm in these reactions.[7] No mercury satellites are observed and a tentative assingment of the signals was made, with the signal at higher field being assigned to the phosphorus atom coordinated to the molybdenum and the signal at lower field attributed to the phosphorus atom bonded to the mercury.[18]

The above results together with the analytical data suggest for these compounds a formulation of the type $[Mo(CO)_3(\eta^2\text{-NN})(\mu\text{-dppm})HgI]HgI_3$ (NN = bpy, phen). A possible structural form is shown in Fig. 1.

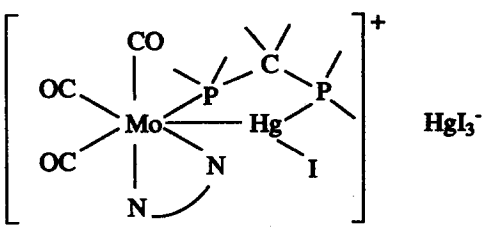

Fig. 1. Proposed structural form for $[Mo(CO)_3(\eta^2\text{-NN})(\mu\text{-dppm})HgI]HgI_3$ (NN = bpy, phen). (P—C—P = dppm.)

(d) *Reactivity of* $[Mo(CO)_3(\eta^2\text{-dmp})(\eta^1\text{-dppm})]$ *with* HgX_2 (X = Cl, Br, I, CN, SCN)

Related reactions between the complexes $[Mo(CO)_3(\eta^2\text{-dmp})(\eta^1\text{-dppm})]$ and HgX_2 (X = Cl, Br, I, CN, SCN) have been studied. In the starting molybdenum complex we have introduced dmp as the NN-ligand, which is more basic and presents more demanding steric effects than the others.

Surprisingly, compounds of the type $[Mo(CO)_3(\eta^2\text{-dmp})(HgX)(X)]$ (X = Cl, Br, I, SCN) were isolated, and only products of double insertion of the type $[Mo(CO)_3(\eta^2\text{-dmp})(CN)]_2Hg$ were obtained in the reaction with $Hg(CN)_2$. This different behaviour could be attributed to the low stability of the Mo—Hg—CN bonds.[19]

CONCLUSIONS

Formation of trinuclear complexes of the type $[(\eta^2\text{-NN})(CO)_3(X)Mo—Hg—Mo(X)(CO)_3(\eta^2\text{-NN})]$ appears to be favoured by reaction between $[Mo(CO)_3(\eta^2\text{-NN})(L)]$ and HgX_2; even when L is a PP-ligand coordinated in a monodentate form as η^1-dppm this behaviour is not modified, and the expected bimetallic complexes in which two metals are bridging by dppm ligand are not formed.

Particular results are obtained when bulky ligands are present, such as in the case of dmp bonded to molybdenum or I bonded to mercury, and bimetallic derivatives are formed in these cases. An intermediate species as in Fig. 2 is proposed to explain the formation of the final cationic compound $[Mo(CO)_3(\eta^2\text{-NN})(\mu\text{-dppm})HgI]^+$. This fact does not occur when the NN-ligand is dmp, probably due to the greater electronic and steric properties of this ligand.

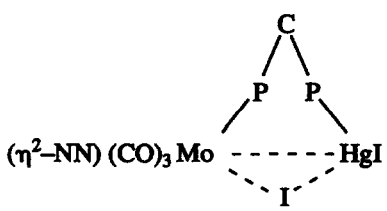

Fig. 2.

EXPERIMENTAL

(a) *General*

All reactions were carried out under oxygen-free dry nitrogen. Analytical grade solvents were used. The $[Mo(CO)_3(\eta^2\text{-NN})(\eta^1\text{-dppm})]$ (NN = bpy, phen, dmp) complexes were prepared as previously described.[18] C, H and N analyses were carried out by Elemental Micro-Analysis Laboratories Ltd. (Devon, U.K.). IR spectra were recorded on a Perkin–Elmer 1300 spectrophotometer with KBr pellets. The NMR spectra were recorded on a Varian XL-300 spectrometer at room temperature and −20°C, operated at 299.95 MHz for ^1H and 121.42 MHz for ^{31}P, with $(CH_3)_4Si$ as internal standard for ^1H and 85% phosphoric acid as external standard for ^{31}P; the solvents used were $(CD_3)_2CO$ and $(CD_3)_2SO$. Conductance measurements were performed in dimethylformamide solutions at room temperature.

(b) *Reactions*

Preparation of $[Mo(CO)_3(\eta^2\text{-NN})(X)]_2Hg$ (NN = bpy, phen; X = Cl, Br). 0.1 mmol of HgX_2 was added to a solution of $[Mo(CO)_3(\eta^2\text{-NN})(\eta^1\text{-dppm})]$ (0.2 mmol) in dichloromethane (15 cm^3). The mixture was stirred for 1 h and the precipitate formed was filtered off, washed with dichloromethane and petroleum ether (b.p. 40–60°C) and dried *in vacuo*.

Preparation of $[Mo(CO)_3(\eta^2\text{-NN})(X)]_2Hg$ (NN = bpy, phen; X = CN, SCN). 0.12 mmol of HgX_2 was added to a solution of $[Mo(CO)_3(\eta^2\text{-NN})(\eta^1\text{-dppm})]$ (0.24 mmol) in dichloromethane (15 cm^3). The mixture was stirred for 30 min for $Hg(SCN)_2$ and 2 h for $Hg(CN)_2$. The solid formed was filtered off, washed with petroleum ether (b.p. 40–60°C) and dried *in vacuo*.

Preparation of $[Mo(CO)_3(\eta^2\text{-NN})(\mu\text{-dppm})HgI]HgI_3$ (NN = bpy, phen). 0.5 mmol of HgI_2 was added to a solution of $[Mo(CO)_3(\eta^2\text{-NN})(\eta^1\text{-dppm})]$ (0.25 mmol) in dichloromethane (15 cm^3). A colour change was observed immediately (from violet to yellow-orange) and the formation of a yellow precipitate occurred. The mixture was stirred for 15 min, and the solid was filtered off, washed with petroleum ether (b.p. 40–60°C) and dried *in vacuo*.

Preparation of $[Mo(CO)_3(\eta^2\text{-dmp})(HgX)(X)]$ (X = Cl, Br, I, SCN). 0.5 mmol of HgX_2 was added to a solution of $[Mo(CO)_3(\eta^2\text{-dmp})(\eta^1\text{-dppm})]$ (0.25 mmol) in dichloromethane (10 cm^3). A colour change was observed quickly (from violet to orange). The compounds were obtained by precipitation with petroleum ether (b.p. 40–60°C) after 5–10 min of stirring. The compound obtained with $Hg(SCN)_2$ precipitated in the reaction medium. The solids were filtered off, washed with petroleum ether (b.p. 40–60°C) and dried *in vacuo*.

Acknowledgement—Financial support for this work from the Comisión Asesora de Investigación Científica y Técnica (CAICYT) is gratefully acknowledged (Project No. 367/84).

REFERENCES

1. B. Chaudret, B. Delavaux and R. Poilblanc, *Coord. Chem. Rev.* 1988, **86**, 191.
2. E. E. Isaacs and W. A. G. Graham, *Inorg. Chem.* 1975, **14**, 2560.
3. A. Blagg, P. G. Pringle and B. L. Shaw, *J. Chem. Soc., Dalton Trans.* 1987, 1495 and refs therein.
4. A. Blagg, A. T. Hutton and B. L. Shaw, *Polyhedron* 1987, **6**, 95.
5. M. Cano, J. A. Campo, P. Ovejero and J. V. Heras, *Inorg. Chim. Acta* 1990, **170**, 139.
6. P. Correa, M. E. Vargas and J. Granifo, *Polyhedron* 1987, **6**, 1781.
7. M. Cano and J. A. Campo, unpublished results.
8. M. P. Pardo and M. Cano, *J. Organomet. Chem.* 1983, **247**, 293.
9. M. A. Lobo, M. F. Perpiñán, M. P. Pardo and M. Cano, *J. Organomet. Chem.* 1983, **254**, 325.
10. M. Panizo and M. Cano, *J. Organomet. Chem.* 1984, **266**, 247.
11. M. P. Pardo and M. Cano, *J. Organomet. Chem.* 1984, **270**, 311.
12. A. López, M. Panizo and M. Cano, *J. Organomet. Chem.* 1986, **311**, 145.
13. R. D. Fischer and K. Noack, *J. Organomet. Chem.* 1969, **16**, 125.
14. D. M. Adams, *Metal-Ligand and Related Vibrations.* Edward Arnold, London (1967).
15. R. Bhattacharyya, G. Prashad Bhattacharjee and A. Mohan Saha, *Polyhedron* 1985, **4**, 583, and refs therein.
16. R. Bhattacharyya and G. Prashad Bhatacharjee, *J. Chem. Soc., Dalton Trans.* 1983, 1593.
17. M. M. Kubicki, R. Kergoat, J. E. Guerchais, C. Bois and P. L'Haridon, *Inorg. Chim. Acta* 1980, **43**, 17.
18. M. Cano, J. A. Campo, V. Pérez-García, E. Gutiérrez-Puebla and C. Alvarez-Ibarra, *J. Organomet. Chem.* 1990, **382**, 397.
19. T. A. George, *J. Organomet. Chem.* 1971, **33**, C13.

Polyhedron Vol. 10, No. 22, pp. 2617–2628, 1991
Printed in Great Britain

0277–5387/91 $3.00+.00
© 1991 Pergamon Press plc

MOLYBDENUM AND TUNGSTEN(VI) BIMETALLIC ALKOXIDES. DECOMPOSITION ACCOMPANIED BY DIALKYLETHER ELIMINATION

N. Ya. TUROVA,* V. G. KESSLER* and S. I. KUCHEIKO

M.V. Lomonosov Moscow State University, Chair of Inorganic Chemistry, 117234 Moscow, U.S.S.R.

(*Received* 25 *January* 1991; *accepted* 18 *June* 1991)

Abstract—Conductometric titration curves of $MO(OR)_4$ and $MO_2(OR)_2$ (M = Mo, W; R = Et, ^{i}Pr, C_2H_4OMe) by sodium (or lithium) alkoxides have ultimately proved the existence of the (1 : 1) bimetallic complexes in alcohol solutions. Upon evaporation of the solvents from the solutions, decomposition of the complexes occurs, accompanied by the elimination of ether, resulting in the precipitation of Na_2MoO_4; the molybdenum derivatives decompose more readily than the corresponding tungsten species. Under special conditions the crystals of $[NaWO(OEt)_5(EtOH)_2]_2$ (**I**) and $[NaMo_2O_4(OR)_5(ROH)]_2$ [R = ^{i}Pr (**VI**), Et (**VIII**)] complexes have been isolated. $[NaMoO_2(OC_2H_4OMe)_3]_2$ (**XI**) proved to be the only stable complex. Solubility isotherms in the systems $WO(OEt)_4$-$M(OEt)_n$-EtOH and $MoO_2(OC_2H_4OMe)_2$-$M(OC_2H_4OMe)_n$-$MeOC_2H_4OH$ (M = Na, Bi) were measured which allowed us to establish the regions of stability of the complexes. The nature of the M—O bonding in the synthesized bimetallic complexes is discussed on the basis of their crystal structures and IR spectra.

The intensive study of the chemistry of the double metal alkoxides during the last 20 years has practically left untouched the derivatives of the elements of Group VI.[1] Alkoxotungstates(V), $M^IW(OR)_6$ (R = Et, Ph), are known;[2,3] partially methylated isopolymolybdates, e.g. $Na_4[Mo_8O_{24}(OMe)_4]\cdot 8MeOH$, $[MePh_3P]_2[Mo_4O_{10}(OMe)_6]$, $[Mg(MeOH)_6]^{2+}$ $[Mg_2Mo_8O_{22}(MeO)_6(MeOH)_4]^{2-}\cdot 6MeOH$ are presently being studied.[4–6]

This paper reports the study of the bimetallic alkoxide derivatives of the two series of molybdenum and tungsten alkoxides $MO(OR)_4$ and $MO_2(OR)_2$ (R = Et, ^{i}Pr, C_2H_4OMe). The properties and structures of these complexes as well as the data on the solubility diagrams in the systems $MO_n(OR)_{6-2n}$-$M'(OR)_m$-ROH (M = Mo, W; M′ = Na, Bi) are of practical importance insofar as they may be used in oxide materials preparation; it is worth noting that they are readily available and far more stable than the derivatives of molybdenum and tungsten in the lower oxidation states.[7–9]

* Authors to whom correspondence should be addressed.

EXPERIMENTAL

All experiments were performed under a dry argon flow. The solvents were dried using conventional techniques. The initial molybdenum and tungsten alkoxides—$MoO(OR)_4$, $MoO_2(OR)_2$, $W(OR)_6$, $WO(OR)_4$ and $WO_2(OR)_2$—were synthesized from the corresponding chlorides and oxychlorides[10–12] or by anodic oxidation of the metals in absolute alcohol in the presence of conductive additives.[13]

Molybdenum and tungsten contents were determined gravimetrically in the form of MO_3. The hydroxides were precipitated from the solutions by hot HNO_3 (1 : 1) and washed on the filters with water and calcined at 400°C. Sodium content was calculated from the difference between the mass of the incombustible residue (in the course of organic microanalysis) and the MO_3 content in the sample, as determined gravimetrically. Solubility in the three-component systems has been studied by analytical methods. The solid phases were identified analytically as well as by means of X-ray powder analysis. Equilibrium was achieved after isothermal

saturation of the solutions by the solid phase in no more than 2 h.

IR spectra were measured with a Perkin–Elmer 580 IR spectrometer. ^{95}Mo NMR spectra were registered with a CXP-300 Bruker instrument, using a frequency of 1956 MHz.

Interaction of molybdenum (tungsten) alkoxides with M^IOR

Solid $WO(OEt)_4$ (1.64 g, 4.31 mmol) was introduced into a concentrated solution of Na (0.1 g, 4.34 mmol) in 5.4 cm^3 of EtOH (Na : W = 1.05 : 1.0) at 50–60°C. Slowly cooling the solution precipitated transparent, colourless crystals of **I** which readily release alcohol to form **II**. In an analogous manner **III** was obtained by evaporating the solutions containing $WO_2(OEt)_2$ and NaOEt. **XI** was obtained from solutions of $MoO_2(OC_2H_4OMe)_2$ and $NaOC_2H_4OMe$ in methoxyethanol. While **IV** precipitated from the freshly prepared solutions containing $WO(OEt)_4$ and LiOEt, **V** crystallized from solutions stored for 7 days. In order to obtain **VI**, sodium (0.11 g, 4.93 mmol) was dissolved in 100 cm^3 of a hexane/^{i}PrOH (1 : 1 by volume) mixture and after cooling and vigorous stirring $MoO(OPr^i)_4$ paste (3.54 g, 10.18 mmol) was introduced into the solution. The light-yellow solution thus obtained was stored for 1 day (in order to ensure that decomposition with the elimination of R_2O was completed). The solvent was then evaporated off *in vacuo* and the residue was recrystallized from 20 cm^3 of ^{i}PrOH; yield = 4.71 g (~73%).

Compound **VIII** was synthesized in the same manner as **VI** from sodium and molybdenum ethoxides. In the synthesis of **IX**, LiOEt and $MoO(OEt)_4$ or $MoO_2(OEt)_2$ were used. A colourless solution containing 7.2 mmol of each component in 30 cm^3 of EtOH was concentrated to a volume of 4 cm^3 and cooled to 0°C. The precipitated residue was isolated by centrifugation and dried *in vacuo*. Complex **IX** (0.82 g), poorly soluble in alcohol, was obtained (yield ~42%).

Reactions of alcohol interchange

Heating compound **VI** in EtOH solution at 50°C for 1 h (the operation was repeated twice, each time the solvent was evaporated) resulted in the formation of **VIII** with a quantitative yield. Liquid $MoO(OC_2H_4OMe)_4$ was synthesized from the alcohol interchange of $MoO(OEt)_4$ with an excess of methoxyethanol; EtOH and the excess of $MeOC_2H_4OH$ were evaporated *in vacuo*. Storage for 1–2 days resulted in crystallization of the liquid in accordance with the following scheme:

$$MoO(OC_2H_4OMe)_4 \longrightarrow MoO_2(OC_2H_4OMe)_2(\mathbf{X}) + (MeOC_2H_4)_2O.$$

The synthesis of **XII**—$Bi(OEt)_3$ (2 g, 5.8 mmol, which was obtained from the exchange of $BiCl_3$ with NaOEt[14]) was dissolved in $MeOC_2H_4OH$ (50 cm^3). The solvent was subsequently evaporated *in vacuo* (10^{-2} mm Hg) at 60–70°C. Analytical data for all the synthesized compounds as well as the IR spectral data for the range of M—O stretching vibrations are summarized in Table 1.

RESULTS AND DISCUSSION

Conductometry titration in alcohol solutions was used in order to determine the composition of the complexes formed between molybdenum and tungsten alkoxides and alkaline metal alkoxides. Interaction between $MoO(OR)_4$ (R = Et, ^{i}Pr) or $MoO_2(OR)_2$ (R = Et, C_2H_4OMe) and M^IOR (M^I = Li, Na) gave a break on the conductivity curve at the molar ratio M^I : Mo = 1 : 1 [Fig. 1(a)]. Titration of $W(OEt)_6$ with NaOEt solution gave a monotonous increase in conductivity, indicating the absence of interactions between the alkoxides in solution and is in good agreement with the coordination saturation of the metal atom in the octahedral $W(OR)_6$ molecule. Titration of $WO(OEt)_4$ and $WO_2(OEt)_2$ by sodium and lithium ethoxides gave breaks at the ratio of M^I : W = 1 : 1, which indicates the formation of complexes with the same composition as in the case of the molybdenum derivatives. It is worth noting that the interaction between NaOEt and $WO_2(OEt)_2$ occurs with time [Fig. 1(b), curves 2a and c]. When measurements were taken every 15 min (curve 2c) after the addition of NaOEt solution, the maximum of the curve smooths off and the character of the curve does not differ from that of the $WO(OEt)_4$ titration curve (curve 3). Presumably, the formation of quite stable associates from $WO_2(OEt)_2$ molecules[12] hinders the quick interaction with sodium alkoxides to form bimetallic complexes.

Upon evaporation of the alcohol from the solutions of the freshly prepared complexes with the composition W : M^I = 1 : 1 transparent crystals of $[NaWO(OEt)_5(EtOH)_2]_2$ (**I**) (readily losing the solvating alcohol), glasses of $NaWO_2(OEt)_3$ (**III**) and $LiWO_2(OEt)_3$ (**V**) and the amorphous powder $LiWO(OEt)_5$ (**IV**) were isolated.

Attempts to isolate the analogous bimetallic molybdenum ethoxides on evaporation of the solvent from the alcohol solutions containing $MoO(OEt)_4$ or $MoO_2(OEt)_2$ and M^IOEt in the ratio of 1 : 1 failed: Li_2MoO_4 and Na_2MoO_4 (high-tem-

Table 1. Analysis data, IR spectra and appearance of the isolated compounds

Complex	Analysis Found (Calc.) (%) W(Mo)	C	H	IR	Appearance
$NaWO(OEt)_5 \cdot 2EtOH$ (I)	35.6	29.5	5.0	—	Colourless crystals eliminating
	(34.1)	(31.1)	(6.8)	—	EtOH at $T \geqslant 20°C$
$NaWO(OEt)_5$ (II)[a,b]	41.3	26.4	5.3	930m, 895vs,	Powder, m.p. 78–80°C
	(41.1)	(26.8)	(5.6)	620s, 585s	
$NaWO_2(OEt)_3$ (III)[b]	49.0	19.3	4.1	930vs, 900vs,	Glass
	(49.2)	(19.2)	(4.0)	610m, 580s, 540m, 440w	
$LiWO(OEt)_5$ (IV)	42.9	26.9	5.6	830vs, b, 625s, b,	Powder
	(42.6)	(27.8)	(5.8)	580s	
$LiWO_2(OEt)_3$ (V)	50.8	20.7	4.3	945v, 890v, s,	Glass
	(51.4)	(20.1)	(4.2)	600v, b, 550sh	
$NaMo_2O_4(OPr^i)_5(^iPrOH)]_2$ (VI)	30.7	34.2	6.9	980s, 930s,	Light-yellow crystals (de-
	(30.3	(31.1)	(6.9)	910s, 885vs, 840m, 815m, 620m, br, 565m, 530m, 525m, 480m, νOH 3440s	composition 80–100°C)
$NaMo_2O_4(OPr^i)_5(EtOH)$ (VII)	31.0	32.9	6.7	—	As above
	(31.0)	(32.9)	(6.6)		
$NaMo_2O_4(OEt)_5(EtOH)$ (VIII)	34.7	27.0	5.7	—	As above
	(35.1)	(26.2)	(5.6)		
$LiMoO_2(OEt)_3$ (IX)[c]	35.7	27.1	5.7	—	Blueish powder
	(35.6)	(26.7)	(5.6)		
$MoO_2(OC_2H_4OMe)_2$ (X)	33.8	26.6	5.3	945m, 910v,	Crystals, colourless to light
	(34.5)	(25.9)	(5.0)	830m, 580m, 565vs, 540m	yellow, m.p. 102–105°C (with decomposition)
$[NaMoO_2(OC_2H_4OMe)_3]_2$ (XI)	25.4	28.8	5.9	960vw, 905vs,	Colourless crystals, m.p.
	(25.5)	(28.7)	(5.6)	885vs, 825s, 605s, 520m, 480sh, 450w	170–173°C (with de-composition)
$Bi(OC_2H_4OMe)_3$ (XII)	Bi—47.5	25.2	5.0	900v, 840m,	Yellow dense liquid or crystals
	(48.1)	(25.9)	(4.8)	580sh, 545vs	(from hexane), m.p. 45–48°C

[a] The X-ray powder diffraction pattern cannot be indexed in unit cell parameters obtained in the course of the X-ray single crystal study of I and differs from the patterns of the initial compounds $WO(OEt)_4$ and NaOEt, d(Å): 9.94(10), 9.12(55), 8.67(50), 8.35(100), 6.15(30), 5.37(25), 5.13(20), 4.82(15), 4.75(15), 4.62(15), 4.21(35), 3.74(10), 3.30(10), 3.16(10), 3.08(10).

[b] In the mass spectrum of III the fragmentation products of $W(OR)_6$ and $WO(OR)_4$ are registered. The latter are likely to be formed due to disproportionation of $WO_2(OEt)_2$.

[c] X-ray powder diffraction pattern of IX, d(Å): 9.06(20), 8.43(100), 6.56(50), 6.33(40), 4.04(20), 3.77(10), 3.71(20)— differs from that of LiOEt and $MoO_2(OEt)_2$.[10]

perature hexagonal and cubic phases, respectively) precipitated from the solutions. Their formation is due to the following reactions:

$$MoO(OEt)_4 + 2M^IOEt \longrightarrow M^I_2MoO_4 \downarrow + 3Et_2O$$

$$MoO_2(OEt)_2 + 2M^IOEt \longrightarrow M^I_2MoO_4 \downarrow + 2Et_2O.$$

The elimination of diethyl ether was detected by gas–liquid chromatography. The quantitative precipitation of $M^I_2MoO_4$ occurred in accordance with the stoichiometry provided the composition of the reacting solutions was $M^I : Mo = 2 : 1$.

Decomposition with the elimination of ether is to a certain extent characteristic of the simple molybdenum alkoxides as well. Thus, $MoO(OR)_4$ (R = Et, ^{i}Pr), especially in its "young" (the least associated) forms, completely transfers into $MoO_2(OR)_2$ for several days. The process occurs equally in pure $MoO(OR)_4$, in solution or in the gas phase.[10] Among tungsten alkoxides, decomposition

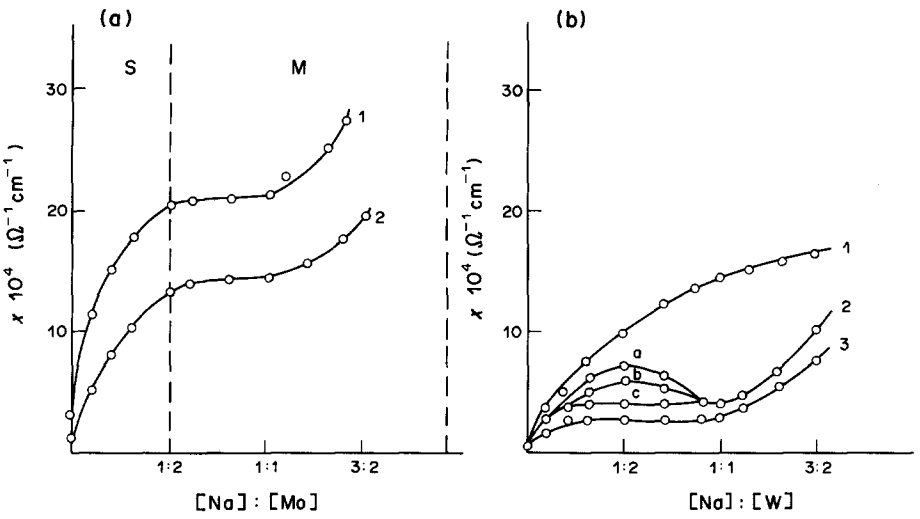

Fig. 1. Conductometric titration curves in alcohols: 0.05 M solutions of $MoO(OR)_4$ [R = Et(1), ^{i}Pr(2)] by 0.1 M solutions of NaOR (S—region of stability of solutions, M—region of slow decomposition with precipitation of Na_2MoO_4) (a); 0.02 M solutions of $W(OEt)_6$ (1), $WO_2(OEt)_2$ (2) and $WO(OEt)_4$ (3) by 0.02 M solution of NaOEt (b).

of this type was only described for $W(OBu\text{-}t)_6$ on its formation.[11] Among the bimetallic derivatives such a reaction has also been registered for $Cs[Nb(OEt)_nF_{6-n}]$.[15]

Stability of solutions containing both molybdenum and alkaline metal alkoxides depends considerably on the ratio of the components. Thus, if Li : Mo $\leqslant$ 2 : 1, precipitation of Li_2MoO_4 occurs only on refluxing the solutions. Partial evaporation of the solvent from solutions containing $MoO(OEt)_4$ or $MoO_2(OEt)_2$ and LiOEt in the ratio of Li : Mo = 1 : 1 isolated the complex with the composition $LiMoO_2(OEt)_3$. Solutions containing NaOR and $MoO(OR)_4$, with its composition within the S area [Fig. 1(a)] where Na : Mo $\leqslant$ 1 : 2, are quite stable. In the interval of the Na : Mo ratio (1 : 2)–(2 : 1) (M region) the rate of Na_2MoO_4 precipitation is low; however, further increase of the NaOR content accelerates the precipitation drastically. Careful partial evaporation of solutions with Na : Mo $\leqslant$ 1 : 2 with cooling results in crystallization of $NaMo_2O_4(OR)_5 \cdot ROH$ [R = ^{i}Pr (**VI**), Et (**VIII**)]. They are formally bimetallic derivatives of the alkoxides of the $MoO_2(OR)_2$ series [while $MoO(OR)_4$ alkoxides were introduced], but they cannot be obtained by direct synthesis: $MoO_2(OPr^i)_2$ does not exist in the individual state; interaction of $MoO_2(OEt)_2$ with NaOEt results in precipitation of Na_2MoO_4 even if the molybdenum derivative is in a considerable excess. The methoxyethoxide derivative $NaMoO_2(OC_2H_4OMe)_3$ (**XI**) is the only stable bimetallic complex of the series.

Decomposition with the elimination of ether has also been registered in the case of alkoxytungstates, but it occurs under severe conditions. Thus, after evaporation of alcohol from the $LiWO(OEt)_5$ solutions stored for 7 days, transparent glass-like $LiWO_2(OEt)_3$ (**V**) was left. The prolonged refluxing of solutions with Li : W $\leqslant$ 2 : 1 results in precipitation of hexagonal Li_2WO_4. In excess LiOEt (>2 : 1), Li_2WO_4 precipitates from solutions already at ambient temperature; a further increase of LiOEt content up to the value of 4 : 1 results in crystallization of the cubic Li_4WO_5.

On dissolution in alcohol **I** decomposes slowly with the elimination of ether and crystallization of cubic Na_2WO_4. In the 5% solution the reaction was complete in 12 h [the analogous solution of "$NaMoO(OEt)_5$" decomposes with the precipitation of Na_2MoO_4 in 1 h]. The yield of Na_2WO_4 precipitating from the 30% solution does not exceed 20% for 6 months. These facts suggest analogous decomposition in the course of the electrochemical synthesis of tungsten alkoxides, where bimetallic alkoxides are formed as a result of the interaction of alkoxides with the conductive additive. Refluxing the 5% solution of $WO(OEt)_4$ containing the conductive additive $[R_4N]X$ (under the conditions simulating electrolysis[13]) for 48 h yields a mixture of the initial alkoxide (40%) and $WO_2(OEt)_2$ (60%). Thus, formation of $WO(OR)_4$, $WO_2(OR)_2$ and ultimately oxotungstates (e.g. $[R_4N]_2W_6O_{19}$) is associated with decomposition of $W(OR)_6$—the first products of anodic oxidation of

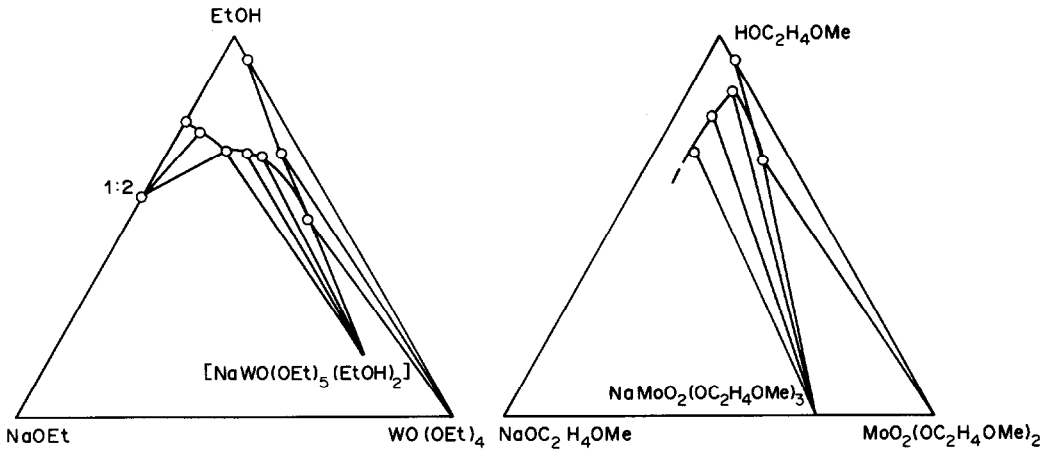

Fig. 2. Solubility diagrams for the systems NaOEt-$WO(OEt)_4$-EtOH and $NaOC_2H_4OMe$-$MoO_2(OC_2H_4OMe)_2$-$MeOC_2H_4OH$ at 25°C.

the metal. It is interesting that solutions containing both $WO(OPr^i)_4$ and $NaOPr^i$ are already stable up to the ratio of Na : W ⩽ 4 : 1 (afterwards Na_2WO_4 crystallizes), which makes them promising for application in oxide preparations.

Conditions of formation of bimetallic complexes have also been studied in the course of the investigation into solubility isotherms in the systems NaOEt-$WO(OEt)_4$-EtOH and $NaOC_2H_4OMe$-$MoO_2(OC_2H_4OMe)_2$-$MeOC_2H_4OH$ at 25°C (Fig. 2). In both systems solid complexes of the composition 1 : 1 exist, which is in good agreement with the data of the conductometric titrations. In the solubility diagrams the wide crystallization regions of the complexes are symmetrical relative to the section ROH-complex; they are located on one side of this section. Equilibrium in the first system is in fact metastable: it may be realized only in the case of a high concentration of the components (⩽ 30%) in solution, i.e. under the conditions where decomposition with precipitation of Na_2WO_4 occurs very slowly. At the same time $NaMoO_2(OC_2H_4OMe)_3$, in contrast to all other alkoxomolybdates, is quite stable even in the presence of a considerable excess of the alkaline alkoxide (which is indefinitely soluble in methoxyethanol).

Preparation of solutions containing both alkoxides of molybdenum or tungsten and bismuth is of special interest in oxide applications as far as a series of oxide materials with useful properties are known in the systems Bi_2O_3-WO_3 and Bi_2O_3-MoO_3. It proved possible to plot the branches corresponding to the crystallization of the components in the system $Bi(OEt)_3$-$WO(OEt)_4$-EtOH (Fig. 3); however, their location along the sections corresponding to Bi:W ratios of 3:2 and 1:1 suggest formation

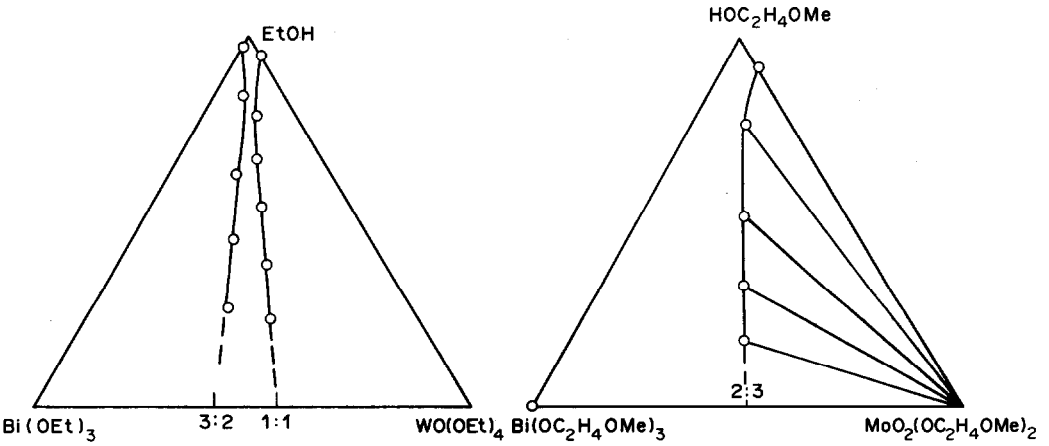

Fig. 3. Solubility diagrams for the systems $Bi(OEt)_3$-$WO(OEt)_4$-EtOH and $Bi(OC_2H_4OMe)_3$-$MoO_2(OC_2H_4OMe)_2$-$MeOC_2H_4OH$ at 25°C.

of the complexes of such compositions in solutions.[16] Diagrams of this kind are well-known in cases where bimetallic complexes exist in solution but cannot be isolated as solids [e.g. in systems $M(OR)_n$-$Fe(OR)_3$].[17] Interaction of $Bi(OEt)_3$ with $MoO(OEt)_4$ or $MoO_2(OEt)_2$ in EtOH at any reagent ratio results in the precipitation of $Bi_2O_3 \cdot nMoO_3$, although all of them have pseudo cubic structures with $a \sim 5.6$ Å (that is why they could not be identified by X-ray), and the composition of the precipitates differs in a wide range. The methoxyethoxide solutions containing bismuth and molybdenum proved to be stable. There was only one solid phase found in the $MoO_2(OC_2H_4OMe)_2$-$Bi(OC_2H_4OMe)_3$-HOC_2H_4OMe molybdenum methoxyethoxide system; its crystallization branch is located along the section with a Bi : Mo ratio of 2 : 3 (which suggests the formation of a complex with this composition in solution). $Bi(OC_2H_4OMe)_3$ is soluble indefinitely. It is clear from Fig. 3 that concentrated solutions with Mo : Bi ratios 3 : (2-∞) are stable, and diluted solutions (concentration up to ~15%) at any Mo : Bi ratio.

Among the isolated complexes the most interesting are crystalline sodium alkoxomolybdates and tungstates. $NaMo_2O_4(OR)_5 \cdot ROH$ [R = ^{i}Pr (**VI**), Et (**VIII**)] are golden-yellow crystals. They readily eliminate alcohol in dry atmosphere and are especially sensitive to moisture, soluble in benzene and poorly soluble in hexane. Compound **VIII** is extremely unstable: on dissolution in alcohol it decomposes with the precipitation of Na_2MoO_4. At the same time, **VI** is absolutely stable towards alcohol. The equilibrium values of solubility may be achieved by different means of saturation, which suggest that its molecular composition is constant either in the solid state or in solution (quite unusual for simple and complex metal alkoxides).[18,19] The solubility enthalpy ~3.5 kcal mol^{-1} (0–50°C) has been calculated by the Shrëder technique. The solubility polytherm in ^{i}PrOH (Fig. 4) is interrupted at ~80°C (due to the decomposition of the complex, accompanied by dark-red colouring of the solution).

The high stability of **VI** is noteworthy: refluxing a solution of **XI** with excess EtOH results only in the substitution of the solvating alcohol molecule with the formation of $NaMo_2O_4(OPr^i)_5 \cdot EtOH$ (**VII**). However, addition of $NaOPr^i$ to the alcohol solution of **VI** immediately results in the precipitation of Na_2MoO_4 in accordance with the following scheme:

$$NaMo_2O_4(OPr^i)_5 \cdot {}^i PrOH + 3NaOPr^i \longrightarrow 2Na_2MoO_4 + 4{}^i Pr_2O + {}^i PrOH.$$

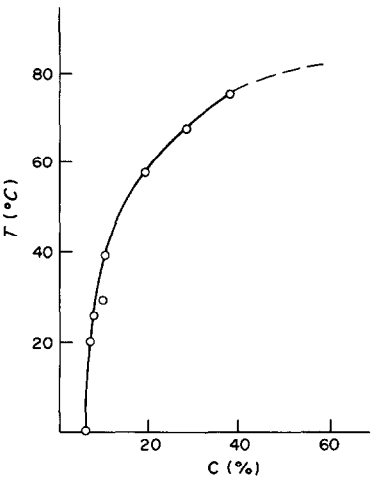

Fig. 4. Solubility polytherm of $[NaMo_2O_4(OPr^i)_5 (^iPrOH)]_2$ (**VI**) in ^{i}PrOH.

The unstable $NaMoO_2(OPr^i)_3$ is presumably formed as an intermediate in the course of this transformation (cf. Fig. 1A).

The X-ray structural study of **VI** has shown that its crystals are formed from centrosymmetric dimeric molecules of $[NaMo_2O_4(OPr^i)_5(^iPrOH)]_2$ (Fig. 5).[20] In each of the two monomeric fragments, one may distinguish a pair of molybdenum atoms [Mo(1) and Mo(2)] which are linked via three RO-bridges: one which is bidentate [RO(3)], bonded only to molybdenum atoms and two which are tridentate [RO(1) and RO(2)], bonded to the sodium atom as well. Along with two μ_3-O alkoxide groups the sodium atom is also coordinated by one μ_2-bridging O(4) atom belonging to the ^{i}PrO-group, bonded only to the Mo(1) atom. The fourth and fifth coordination sites of the sodium atom environment are occupied by the O(10) atom, belonging to the monodentate molecule of the solvating ^{i}PrOH, and the "molybdenyl" oxygen atom O(9′) which is bonded to the Mo(2) atom of the second part of the dimeric molecule.

The $[Mo_2O_4(OPr^i)_5]$ fragment is analogous in its structure to the widely spread group of the type $[M_2X_9]$, which consists of two octahedra with a common face. Fragments of such type are characteristic of clusters in low oxidation states (e.g. in numerous molybdenum and tungsten alkoxides[21]), or in bimetallic complexes of molybdenum(VI) derivatives of the polyatomic aliphatic alcohol mannitol—$Na[Mo_2O_5(\mu_3\text{-}O)_3(OH)C_6H_8(OH)_2]$[22] —and the diatomic phenolpyrocatechin—$(NH_4)_2[Mo_2O_5(C_6H_4O_2)_2] \cdot 2H_2O$.[23] The Mo—Mo bond lengths in these fragments are 3.140 and 3.135 Å, respectively. The peculiarity of the structure of the derivative we studied with a considerably elongated

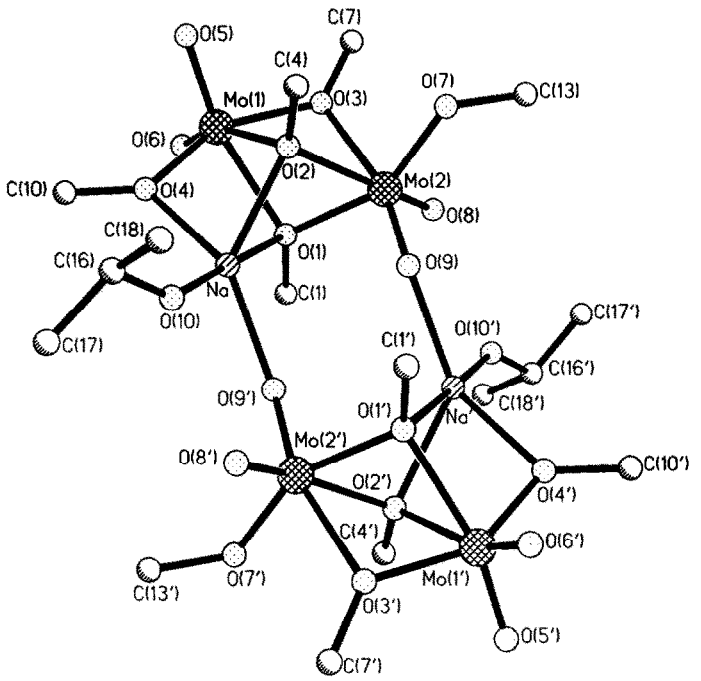

Fig. 5. Molecular structure of $[NaMo_2O_4(OPr^i)_5(^iPrOH)]_2$ (**VI**).

Mo—Mo distance [3.245(1) Å] is that the OR groups which are the residues of the monoatomic alcohol act as bridges. It is interesting to compare the structure of the dimeric fragment in **VI** with the structure of $[W(OBu^t)_2(=NPh)]_2(\mu\text{-}O)(\mu\text{-}OBu^t)_2$. In the latter molecule the two metal atoms are kept together not only by the two μ-OR groups but by oxo-bridges as well.[24] The metal–metal distance is considerably shorter (3.059 Å) and bond angles at the bridging oxygen atoms are much smaller than in **VI** [$\sim 89°$ in comparison with 93.6(1), 96.8(1), 99.6(1)°], presumably due to the presence of the bridging oxo-ligand.

Both molybdenum atoms in the molecule have considerably distorted octahedral surrounding. The different functions of the oxygen atoms in the structure ("molybdenyl", alkoxide terminal, μ_2- and μ_3-bridging) correspond to a considerable difference in the Mo—O values [from 1.690(3) to 2.279(2) Å]. However, in all cases the sums of the bond lengths located in *trans*-positions towards each other in fact coincide (3.90–3.97 Å) (which is usual for the structures of molybdenum compounds[25]). The coordination polyhedron of the sodium atom may be described as a tetrahedron [NaO(2)O(4)O(9)O(10)] (Na—O 2.197–2.999 Å), with one additional and more remote O(1) atom [2.487(3) Å] located over one of its faces. Alternatively, this polyhedron may be treated as a distorted trigonal bipyramid [O(10)NaO(1) 178.8(1)°] with considerably unequal axial distances.

The "active" hydrogen atom on the O(10) atom in **VI** participates in intramolecular hydrogen-bonding, O(10)—H···O(8′) [O(10)—H 0.68(5), H···O(8′) 2.19(5) Å, O(10)—H···O(8′) angle is 166(3)°], which results in the formation of the six nuclear chelate cycle HO(10)NaO(9)Mo(2′)O(8′). Complex **VI** presumably preserves its structure in benzene solution. In the ^{95}Mo NMR spectra there are two lines of approximately equal intensities, +74 and +3 ppm (relative to MoO_4^{2-}), which suggest the existence of molybdenum atoms of two types in the ratio of 1 : 1.

Crystal **I** is built up of dimeric centrosymmetric molecules $[NaWO(OEt)_5(EtOH)_2]_2$ (Fig. 6).[26] Two pairs of atoms, tungsten and sodium, are connected via two μ_3- and four μ_2-bridging alkoxide groups. Such structures formed by four octahedra with common edges (metal atoms belong to one plane) are known for a series of simple as well as double metal alkoxides, e.g. $[Ti(OR)_4]_4$ (R = Me, Et),[27] $[W(OEt)_4]_4$,[28] $[LiNb(OEt)_5(OH)]_2$[29] and $[Mo_4O_{10}(OMe)_6]^{2-}$.[5] While in $[Ti_4(OR)_{16}]$ or $[LiNb(OEt)_5(OH)]_2$ the increase in coordination number of the OR-group results in subsequent elongation of M—O bonds and a decrease in the values of MOC bond angles,[29] in **I** all the bond lengths and bond angles are of approximately the same order.

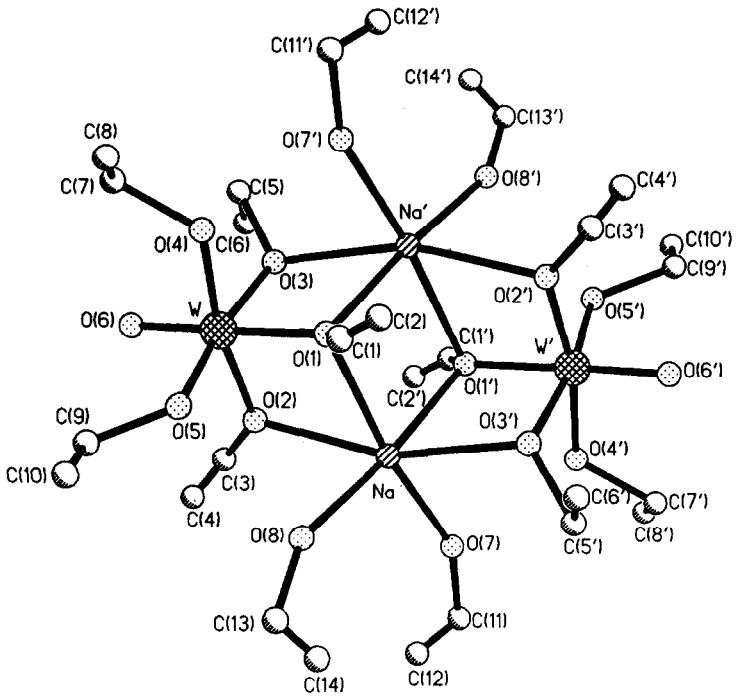

Fig. 6. Molecular structure of $[NaWO(OEt)_5(EtOH)_2]_2$ (I).

Indeed, the distances between tungsten and the μ_2-bridging alkoxide O atoms [W—O(2) 1.94(2) and W—O(3) 1.99(2) Å] in fact coincide with the distances between W and O atoms of the terminal groups [W—O(4) 1.97(2) and W—O(5) 1.98(2) Å]. Small elongation of the distance between tungsten and the μ_3-bridging oxygen atom to the value of W—O(1) 2.03(2) Å in comparison with the above-mentioned bond lengths does not substantially exceed the experimental error. The mean value of bond angles is 126°. This situation may be easily explained by the ionic character of the bonds between the sodium atom and the $[WO(OR)_5]$ fragment. In this case all OR groups at the tungsten atom are essentially terminal. Indeed the values for the Na—OR bond lengths in this complex (2.47–2.52 Å) indicate its ionic character, and thus complex **I** (in contrast to **VI**) should be regarded as an ionic salt: $[Na(EtOH)_2]_2^+[WO(OEt)_5]_2^-$. Cations and anions are combined into a quite strong ionic pair, not only by the Na···O interaction but also [as far as it can be be anticipated from the O(7)···O(4) 2.71(2) and O(8)···O(5) 2.90(2) Å distances] by hydrogen bonds [O(7')—H···O(4) and O(8)—H···O(5)].

Compound **I** is the second example after $WO(OBu\text{-}t)_4 \cdot THF$[30] among the known structures of the alkoxide derivatives of tungsten(VI) with a terminal oxo-group: usually tungsten alkoxides have the W=O···W chains in their structures.[31] Stability of the "tungstyl" in **I** is probably ensured by the coordination saturation of the tungsten atom in the $[WO(OEt)_5]^-$ anion.

The discussed structure of **I** allows us to make certain suggestions concerning the extreme instability of the bimetallic complexes of molybdenum with the Na : Mo ratio 1 : 1. Assuming the analogy between the structures of **I** and of $NaMoO(OR)_5$. which are unknown in the solid state, it may be anticipated that the coordination sphere of the molybdenum atom contains five terminal OR groups. In accordance with the mechanism of decomposition of alkoxides occurring with the elimination of ether,[32] this complex must be extremely unstable:

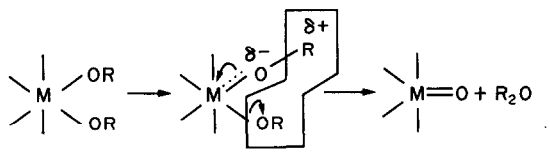

Indeed, attempts to isolate this in the solid state have resulted in the precipitation of Na_2MoO_4.

$MoO(OR)_4$ are oligomers with bridging OR groups, which allow them to exist in the free state for a certain, although not long, period of time. These compounds may be stabilized by polymerization (by the introduction of small amounts of NaOR). It may be suggested that the anion $[MoO(OR)_5]^-$ formed on the introduction of

NaOR (alkoxide groups of the latter possess high electron-donor properties) attacks the neutral $MoO(OR)_4$ molecules causing the chain growth, and thus leading to the polymolybdate anions of the following type:

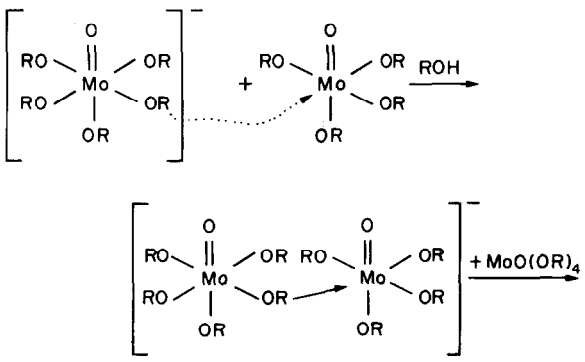

This mechanism is analogous to that described earlier[18] for polymerization of the oligomeric Al, Fe, Ti alkoxides with alcohols [the electron-donor properties of the latter proved, however, insufficient to cause "ageing" of $MoO(OR)_4$]. Stability of molecule **VI** towards decomposition with the elimination of ether is presumably ensured by the existence in the structure of the minimal number of terminal OR groups (only two) per four molybdenum atoms.

Overall, the process occurring in the interaction of $MoO(OR)_4$ with NaOR may be expressed by the scheme represented in Fig. 7.

The structures of complexes **I** and **VI** are of interest in connection with the widely discussed problem

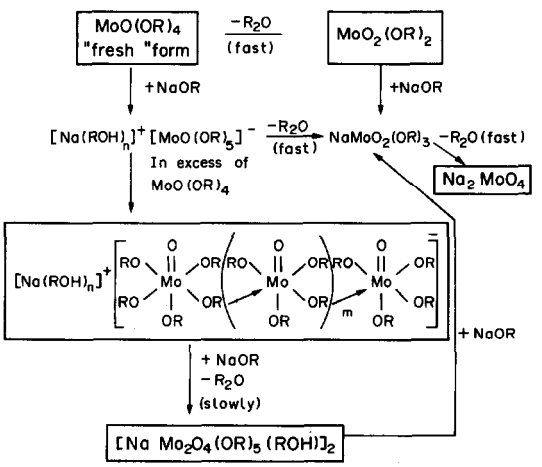

Fig. 7. Scheme of transformations occurring in the interaction of $MoO(OR)_4$ with NaOR (R = Et, ^{i}Pr). Compounds isolated as individual species are enclosed in boxes.

concerning the nature of double metal alkoxides ("Meerwein salts"). The properties of most of the complexes in this class as well as the data on their crystal structures,[1] e.g. $Li[Cr\{OCH(OBu^t)_2\}_4]\cdot THF$, $Li[Fe\{OCH(OBu^t)_2\}_4]\cdot {}^tBu_2CHOH$ and $[LiNb(OEt)_5(OH)]_2$, indicate their molecular nature.[29,33,34] On the other hand $Na[B(OMe)_4]\cdot MeOH\cdot 1.5\ H_2O$,[35] $[R_4N][W(OPh)_6]$[3] and $Na_2[Mo_6(OMe)_6(\mu_3\text{-}X)_8](MeOH)_{10}$, where X = Cl, OMe,[36] as well as the above mentioned methylated molybdates[4-6] contained in their structures, can isolate cations and anions of alkoxometallates in agreement with the ideas developed by Meerwein.[37] Structures **I** and **VI** allow us to return to the discussion of this problem. Comparison of the three shortest Na—O distances (2.20–2.30 Å) in molecule **VI** with those known for the alkoxides NaOMe, $NaOBu^t$ (2.24–2.32 Å)[38,39] and ionic structures (NaOH, Na_2O, Na_2SO_4, $Na[B(OMe)_4]\cdot MeOH\cdot 1.5\ H_2O$, Na···O 2.39–2.47 Å[35,40]) suggests that the short bonds in **VI** are at least partially covalent. Distortion of the planar surroundings of the oxygen atom which is coordinated by sodium may also be regarded as an indirect argument supporting this suggestion. Thus, the sum of the bond angles at the O(3) atom [μ_2-bridge between Mo(1) and Mo(2)] is 358.8°, whereas at the O(1) and O(2) atoms [μ_3-bridges between Mo(1), Mo(2) and Na] the MoOC angles are 348.4 and 339.9°, respectively. Thus, both oxygen atoms, especially O(2), which form a shorter bond with sodium than O(1) [2.299(3) and 2.487(3) Å] are displaced from the plane. The O(4) atom, which forms only three bonds [with Na, Mo(1) and C(10)], and O(3) have almost planar surroundings: the sum of the bond angles is 358.8°.

The manner in which the alkaline metal atom is adjusted to the dimeric fragment of the $[Mo_2(OR)_9]$ type in molecule **VI** is analogous to that known, for instance, for $KU_2(OBu^t)_9$, in which potassium coordinates two oxygen atoms of μ-OR groups and one oxygen atom of the terminal OR groups belonging to different uranium atoms.[41] However, the K—O bonds, judging by the bond lengths (~2.93–2.97 Å), are ionic. The oxygen atoms are located in the base of the tetragonal pyramid with the potassium atom at its apex.

The bimetallic methoxyethoxide derivative $NaMoO_2(OC_2H_4OMe)_3$ (**XI**) is built up of dimeric centrosymmetric molecules (Fig. 8),[42] analogous in structure to **I**. However, the positions of the sodium atoms in molecule **XI** are occupied by the tungsten atoms in **I** and alternatively, Mo in **XI** is equivalent to sodium in **I**. In contrast to **I**, $Ti_4(OR)_{16}$ and other structural analogues, molecules of **XI** are linked into infinite chains by pairs of asymmetric

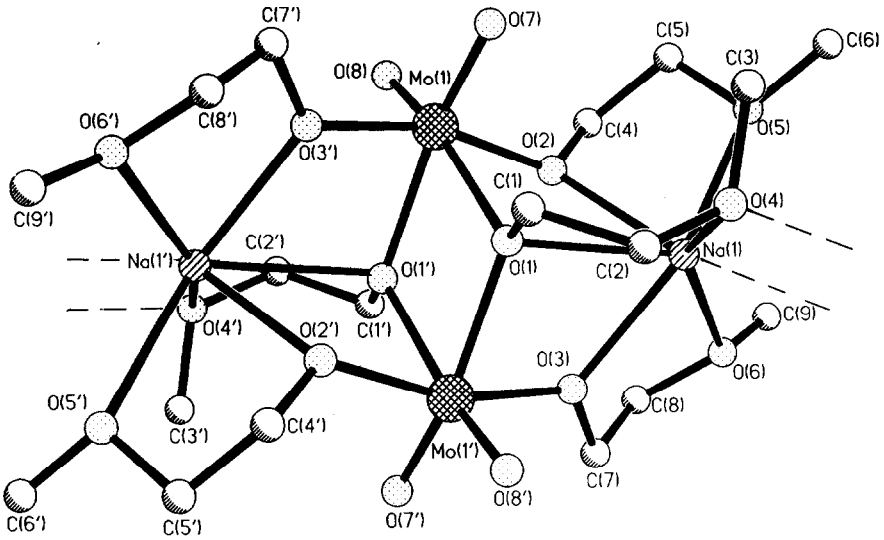

Fig. 8. Molecular structure of $[NaMoO_2(OC_2H_4OMe)_3]_2$ (**XI**).

bridges which are formed by the ether oxygen atoms O(4) and O(4′) of one of the three methoxyethoxide groups. In general, the skeleton of the tetranuclear fragment $[Na_2Mo_2O_4(OC_2H_4OMe)_6]$ is similar in its structure to the cation $[Mg_4(OC_2H_4OMe)_6(MeOC_2H_4OMe)_2]^{2+}$:[43] the alkoxide oxygen atoms form bridges (μ_2 and μ_3) and the ether oxygen atoms form monodentate bridges [with the exception of O(4)]. These are part of the coordination sphere of sodium atoms thus forming chelate cycles round them. The molybdenum atoms are also attached due to the enhanced coordination number of the alkoxide oxygen atoms. The tridentate O(1) and O(1′) are located at distances of 2.255(3) and 2.162(3) Å from molybdenum, respectively, while the bidentate O(2) and O(3) are at the distances of 1.964(3) and 1.975(3) Å. Two terminal oxo-groups complete the molybdenum octahedron (Mo=O ~ 1.705 Å). The lengths of the Mo—O bonds located in the *trans* position are 3.86–3.96 Å.

A highly distorted seven-vertex polyhedron surrounding the sodium atom consists of three alkoxide oxygens [tridentate O(1), two bidentate oxygens O(2) and O(3) at the distances of 2.689(3), 2.341(4) and 2.308(4) Å, respectively] and three ether oxygens—O(4), O(5) and O(6) (with bond lengths 2.493–2.529 Å). The seventh place is occupied by the ether oxygen atom O(4′) of the neighbouring four-nuclear molecule at a distance of 2.881(4) Å, which, however, exceeds the length of the chemical bond Na—O. The Na—O (alkoxide) bond lengths in **XI** are close to those values in **VI** and NaOR; this fact together with the dependence of the Mo—O bond lengths on the coordination of oxygen indicates the molecular character of the bimetallic methoxyethoxide derivative (**XI**). The absence of the terminal OR groups and the formation of chelate cycles presumably ensure high stability of the complex towards decomposition with the elimination of ether.

The structure of **XI** differs from the structures of the known methoxyethoxides of bismuth and yttrium[44–46] by the absence of the terminal OR groups and should be close to that of $Ba_2Cu_2(\mu_3\text{-}OC_2H_4OMe)_4(acac)\cdot 2MeOC_2H_4OH$,[47] which is presumably due to the tendency of sodium and barium to chelate to polyoxoligands.

The structural data discussed above are in a good agreement with the IR spectra of bimetallic complexes. Thus, the IR spectra of **VI** contains bands corresponding to the vibrations of the two terminal (620 cm^{-1}), four bidentate (of two types) and four tridentate alkoxide groups (525, 530, 565 cm^{-1}); *cis*-MoO_2 (~930, 980 cm^{-1}); free (~910 cm^{-1}) and sodium-bonded (~885 cm^{-1}) "molybdenyls" Mo=O, and the band (OH) of the solvating alcohol (3440 cm^{-1}). The spectrum of **I** could not be registered due to quick desolvation with the formation of $NaWO(OEt)_5$ (**II**), which appears to be a result of condensation with the formation of new Na···O···W or Na—OR—W bridges (analogous to Na···O—Mo and Na—OR—Mo in structure **VI**). The spectra of **II** contain the only band (895 cm^{-1}) in the region corresponding to vibrations of W=O bonds and two bands corresponding to bridging and terminal OR groups (620 and 585 cm^{-1}). Thus, the formation of bridges by the terminal W=O seems the most probable variant. The

only W—OR band (600 cm^{-1}) in the spectra of $WO(OEt)_4$ and $WO_2(OEt)_2$ splits into two (620 and 585 cm^{-1}) in the spectra of **II** and $NaWO_2(OEt)_3$ (**III**), probably due to the existence of bridging along side the terminal alkoxides. The absorption bands corresponding to vibrations in the units of W=O···W chains in the crystal structure of $WO(OEt)_4$-*trans* $[WO_2(OEt)_4]_\infty$ (795 cm^{-1}) or

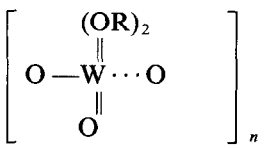

(880 cm^{-1}) shift in the amorphous $WO_2(OEt)_2$ in the direction of high-frequencies (~900–930 cm^{-1}) as a result of complex formation occurring with the rupture of asymmetric bridges and building of structures with presumably molecular character. On the other hand, in the IR spectra of $MoO_2(OR)_2$ (**X**), the associates of which contain bridges of both types —Mo···O···Mo and Mo—OR—Mo, no drastic changes were seen in the character of the IR spectra when formation of complexes with NaOR occurs. The crystalline $MoO_2(OC_2H_4OMe)_2$ is the only exception. All its oxogroups are terminal (945, 910 cm^{-1}) and $MeOC_2H_4O$ groups take part in the formation of the chelate cycles (565 cm^{-1}).[42] In $NaMoO_2(OC_2H_4OMe)_2$, ν(Mo=O) only slightly shifts in the low-frequency direction and ν(Mo—OR) splits into 605, 520 and 480 cm^{-1}.

Acknowledgement—The authors would like to express their gratitude to the student A. V. Korolev for his experimental assistance, Dr M. A. Fedotov (Institute of Catalysis of the Siberian branch of the Academy of Sciences of the U.S.S.R.) for the measurements of the ^{95}Mo NMR spectra and Dr A. I. Belokon' (State Institute of Chemical Technology of the Organometallic Compounds) for the measurements of the mass spectra of the alkoxides studied.

REFERENCES

1. K. G. Caulton and L. G. Hubert-Pfalzgraf, *Chem. Rev.* 1990, **90**, 969.
2. W. J. Reagan and C. H. Brubaker, *Inorg. Chem.* 1970, **9**, 827.
3. J. J. Davies, J. F. Gibson, A. C. Skapski and G. Wilkinson, *Polyhedron* 1982, **1**, 641.
4. E. M. McCarron and R. L. Harlow, *Acta Cryst.* 1984, **C40**, 1140.
5. S. Liu, S. N. Shaikh and J. Zubieta, *Inorg. Chem.* 1987, **26**, 4303.
6. M. Yu. Antipin, Yu. T. Struchkov and A. K. Shilova, *Metalloorganich. khimiya* 1989, **2**, 331; *J. Chem. Soc., Chem. Commun.* 1989, **1**, 1467.
7. I. E. Obvintseva, M. I. Yanovskaya, S. I. Kucheiko and N. Ya. Turova, *Izv. An SSSR, Neorg. Mater.* 1988, **24**, 790; 1989, **25**, 90, 1805.
8. M. I. Yanovskaya, I. E. Obvintseva and S. Yu. Stefanovich, The VII International Meeting on Ferroelectricity, Abstract p. 445. Saarbrüken (1989).
9. M. I. Yanovskaya, I. E. Obvintseva and V. G. Kessler, *J. Non-Cryst. Solids* 1990, **124**, 155.
10. N. Ya. Turova and V. G. Kessler, *Zh. Obzch. Khim.* 1990, **60**, 113.
11. S. I. Kucheiko, N. Ya. Turova and N. I. Kozlova, *Koord. Khimiya* 1985, **11**, 1521, 1656.
12. S. I. Kucheiko, N. Ya. Turova and O. M. Soloveichik, *Zh. Obzch. Khim.* 1985, **55**, 2353.
13. S. I. Kucheiko, N. Ya. Turova and V. A. Shreider, *Zh. Obzch. Khim.* 1985, **55**, 2396.
14. S. I. Kucheiko, V. G. Kessler and N. Ya. Turova, *Koord. Khimiya* 1987, **13**, 1043.
15. Yu. A. Buslaev and Yu. V. Kokunov, *Izv. AN SSSR, Neorg. Mater.* 1968, **4**, 537.
16. N. Ya. Turova, *Koord. Khimiya* 1984, **10**, 1165.
17. T. V. Rogova, N. Ya. Turova and N. I. Kozlova, *Koord. Khimiya* 1986, **12**, 762.
18. N. Ya. Turova, T. V. Rogova and N. I. Kozlova, *Koord. Khimiya* 1983, **9**, 1244.
19. N. Ya. Turova and N. I. Kozlova, *Koord. Khimiya* 1982, **8**, 653.
20. V. G. Kessler, N. Ya. Turova and A. I. Yanovsky, *Zh. Obshch. Khim.* 1990, **60**, 2769.
21. M. H. Chisholm, *New J. Chem.* 1987, **11**, 459.
22. B. Hedman, *Acta Cryst.* 1977, **B33**, 3077.
23. V. V. Tkachev and L. O. Atovmjan, *Koord. Khimiya* 1976, **2**, 110.
24. F. A. Cotton and E. S. Shamshoum, *J. Am. Chem. Soc.* 1984, **106**, 3222.
25. M. A. Poray-Koshitz and L. O. Atovmjan, *Crystallography and Stereochemistry of the Coordination Compounds of Molybdenum*, M., "Nauka" (1974).
26. A. I. Yanovsky, V. G. Kessler, N. Ya. Turova and Yu. T. Struchkov, *Koord. Khimiya* 1991, **17**, 54.
27. D. A. Wright and D. Williams, *Acta Cryst.* 1968, **B24**, 1107.
28. M. H. Chisholm, J. C. Huffman and K. Folting, *J. Am. Chem. Soc.* 1981, **103**, 6093.
29. A. I. Yanovsky, E. P. Turevskaya, N. Ya. Turova and Yu. T. Struchkov, *Koord. Khimiya* 1985, **11**, 110.
30. F. A. Cotton and E. S. Shamshoum, *J. Organomet. Chem.* 1985, **296**, 55.
31. N. I. Kozlova, V. G. Kessler and N. Ya. Turova, *Koord. Khimiya* 1989, **15**, 1524.
32. D. C. Bradley, B. N. Chakravarti and A. K. Chatterjee, *J. Chem. Soc.* 1958, 99.
33. M. Bochmann, G. Wilkinson, G. B. Young and M. B. Hursthouse, *J. Chem. Soc., Dalton Trans.* 1980, 1863.
34. P. G. Edwards, G. Wilkinson and M. B. Hursthouse, *J. Chem. Soc., Dalton Trans.* 1980, 2467.
35. G. Heller and G. Horbat, *Z. Naturforsch.* 1977, **B32**, 989.

36. M. H. Chisholm, J. A. Heppert and J. C. Huffman, *Polyhedron* 1984, **3**, 475.
37. H. Meerwein und T. Bersin, *Ann.* 1929, **476**, 113.
38. E. Weiss, *Z. Anorg. Allg. Chem.* 1964, **332**, 197.
39. J. Davies, J. Kopf and E. Weiss, *Acta Cryst.* 1982, **B32**, 2251.
40. I. Narai-Sabo, *Inorganic Crystallography*. Academy of Sciences of Hungary, Budapest (1969).
41. F. A. Cotton and W. Schwotzer, *Inorg. Chem.* 1984, **23**, 4211.
42. V. G. Kessler, N. Ya. Turova and A. I. Yanovsky, *Medeleev Commun.* 1991, 1N3.
43. E. A. Sadurski, W. H. Ilsley and R. D. Thomas, *J. Am. Chem. Soc.* 1978, **100**, 7761.
44. M. C. Massiani, R. Papernik and L. G. Hubert-Pflalzgraf, *J. Chem. Soc., Chem. Commun.* 1990, 301.
45. M. A. Matchett, M. Y. Chiang and W. E. Buhro, *Inorg. Chem.* 1990, **29**, 358.
46. O. Poncelet, L. G. Hubert-Pfalzgraf, J.-C. Duran and R. Astier, *J. Chem. Soc., Chem. Commun.* 1989, 1846.
47. N. N. Sauer, E. Garcia and K. V. Salazar, *J. Am. Chem. Soc.* 1990, **112**, 1524.

Polyhedron Vol. 10, No. 22, pp. 2629–2640, 1991
Printed in Great Britain

0277–5387/91 $3.00+.00
© 1991 Pergamon Press plc

THE CHARACTERIZATION OF $[HSe]^-$ AND $[Se_x]^{2-}$ IONS BY ^{77}Se NMR

JOHN CUSICK and IAN DANCE*

School of Chemistry, University of New South Wales, PO Box 1, Kensington, NSW 2033, Australia

(*Received* 26 *March* 1991; *accepted* 20 *May* 1991)

Abstract—Preparative reactions for the ions Se^{2-}, HSe^- and $[Se_x]^{2-}$ in protic and aprotic solvent systems are established, and these ions in solution have been characterized by the most informative probe, ^{77}Se NMR. Fully reduced solutions in DMF contain HSe^- for which δ_{Se} ranges between -530 and -390 ppm (vs Me_2Se) depending strongly on solvent and temperature: $^1J(Se—H) = 26$ Hz. Although HSe^- and Se^{2-} are in fast equilibrium, there is no *direct* NMR evidence for the conjugate strong base Se^{2-} in any of these solutions, and it is predicted that $\delta_{Se}(Se^{2-}) < -650$ ppm. There is no NMR evidence for $[Se_2]^{2-}$, which is believed to disproportionate to HSe^- plus $[Se_x]^{2-}$ ($x > 2$) or $Se_{(s)}$. The polyselenide ions $[Se_x]^{2-}$, $x = 3$–6, all exist in DMF, and the resonances for all selenium atoms in each of these ions have been observed and assigned. Using α, β, γ to signify selenium positions relative to the equivalent ends of the chain, the $\delta_{Se}(\alpha)$, $\delta_{Se}(\beta)$, $\delta_{Se}(\gamma)$ data [in DMF plus 38% (vol) EtOH, 230°K] are: $[Se_3]^{2-}$, 193, 214, -; $[Se_4]^{2-}$, 256, 581, -; $[Se_5]^{2-}$, 354, 570, 868; $[Se_6]^{2-}$, 404, 636, 807. The chemical shifts of the Se(α) in these ions are very responsive to the solvent proticity, becoming more negative in the range DMF → ethanol, while the Se(β) atoms respond much less, and the effect at the Se(γ) atoms is small and can be in the other direction. Protic solvents retard the selenium exchange reactions of polyselenide ions. Comparative analysis is made of the δ_{Se} values for related compounds of type XSe^- or with chains of selenium atoms. There is no NMR evidence for ions with $x > 6$. The spirocyclic ion $[Se(Se_5)_2]^{2-}$ is formed from $[Se_x]^{2-}$ with many oxidants, including NO_3^- in DMF, and possesses only one exchanging ^{77}Se resonance at 720 ppm.

Although monoselenide (Se^{2-} and HSe^-) and polyselenide (Se_x^{2-}) salts with alkali and some transition metals have been known as solid compounds for some time, it is only recently that non-aqueous solvents have been used to expand the range of equilibria and compounds accessible.[1–22] This has paralleled more extensive development of polysulphide and metal polysulphide chemistry in non-aqueous media.[23]

The characterized crystalline salts of polyselenide ions (not containing transition and post-transition metals) are listed in Table 1, together with the preparative reactions and the characterization data. Despite this large amount of information about isolated compounds, uncertainty surrounds knowledge of the species and their interconversions in solution. This occurs because electronic and vibrational spectra are not unambiguously definitive. The electronic spectra of polyselenide ions in liquid ammonia contain multiple overlapping absorptions.[24] We have used ^{77}Se NMR to investigate $[Se_x]^{2-}$ ions and their metal complexes, because this technique can probe individual selenium atoms. The advantages of ^{77}Se NMR are the wide chemical shift range of *ca* 3000 ppm, the consequent dynamic range of 10^{-2}–10^{-5} s for access to interconversion reactions, and the ability to make measurements over a substantial temperature range. It has been claimed[2] that ^{77}Se NMR signals cannot be observed for $[Se_x]^{2-}$ ions in DMF solution because paramagnetic monoanions $[Se_x]^-$ are present, but we do observe the ^{77}Se NMR of $[Se_x]^{2-}$ in DMF, and report our results here. We also report new results on the preparation and redox interconversions of polyselenide ions.

* Author to whom correspondence should be addressed.

Table 1. Crystalline salts of polyselenide ions (compounds containing transition metals and post-transition metals are excluded)

Polyselenide ion Cation	Preparative reactions	Crystallization solvent	Characterization data	Reference
$[Se_2]^{2-}$ Na^+	Se + Na, in NH_3	NH_3	Crystal structure	25
$[Se_3]^{2-}$ $[CH_3(CH_2)_{15}NMe_3]^+$	Na_2Se_2 + 10Se, in ethanol	Ethanol	CHN analysis	26
$[Se_4]^{2-}$ $Ph_3PNPPh_3^+$	Cs_3TaSe_4	CH_3CN	Crystal structure	27
$[Se_4]^{2-}$ $[Ba(en)_4]^{2+}$ en	Ba + Se, in ethylenediamine	Ethylenediamine	Crystal structure	28
$[Se_4]^{2-}$ $[Ba(2,2,2\text{-crypt})]^{2+}$	$BaBiSe_3$ + 2,2,2-crypt	Ethylenediamine	Crystal structure	29
$[Se_5]^{2-}$ Ph_4P^+	Side product from $Na_2Se_x + PtCl_2 + Ph_4PCl$	DMF	Crystal structure	16
	Unplanned product from Zr + $Zr(OEt)_4$ + Se + Ph_4PCl + $(OctMe_2Si)_2Se$	DMF/ether	Crystal structure, IR	30
$[Se_5]^{2-}$ $[Cs(18\text{-crown-}6)_2]^+$	Cs_3TaSe_4	CH_3CN	Crystal structure	27
$[Se_5]^{2-}$ Cs^+	Cs + Se, in NH_3	NH_3	Crystal structure	31a
$[Se_5]^{2-}$ Rb^+	Se + Na, in NH_3	NH_3	Crystal structure	31b
$[Se_5]^{2-}$ $[CH_3(CH_2)_{15}NMe_3]^+$	Na_2Se_2 + 10Se, in ethanol	Ethanol	CHN analysis	26
$[Se_6]^{2-}$ Bu_4N^+	Na_2Se_6, in H_2O	Water	Crystal structure, vibrational spectra, electronic spectra	32
$[Se_6]^{2-}$ Et_4N^+	Na_2Se + 10Se, in ethanol	Ethanol	CHN analysis	26
$[Se_6]^{2-}$ $[CH_3(CH_2)_{13}NMe_3]^+$	Na_2Se + 10Se, in ethanol	Ethanol	Crystal structure	26
$[Se_7]^{2-}$ $[CH_3(CH_2)_{15}NMe_3]^+$	Na_2Se + Se, in ethanol	Ethanol	CHN analysis	26
$[Se_8]^{2-}$ $[CH_3(CH_2)_{13}NMe_3]^+$	Na_2Se + Se, in ethanol	Ethanol	CHN analysis	26
$[Se_9]^{2-}$ $[CH_3(CH_2)_{13}NMe_3]^+$	Na_2Se + Se, in ethanol	Ethanol	CHN analysis	26
$[Se_{11}]^{2-}$ Ph_4P^+	$Na_2Se_5 + I_2$, in DMF, $Na_2Se_5 + AuCl_3$, in DMF	DMF	Crystal structure, two crystal forms, spirocyclic $[Se(Se_5)_2]^{2-}$	13
$[Se_{11}]^{2-}$ Ph_4P^+			Crystal structure	33
$[Se_{10}]^{2-}$	Li + Se in DMF	DMF	Crystal structure	34
$[Se_{16}]^{4-}$ Cs^+	Cs_2CO_3 + Se, in MeOH at 160°C	MeOH	Crystal structure, Se_6 cycle with two Se_5 chains connected to one square planar selenium	22

EXPERIMENTAL

Materials, solvents and general methods

All preparations were performed under N_2(g). DMF was purified by treatment with 4A molecular sieves for several days, followed by vacuum distillation. Solvents were deoxygenated before use. The selenium used was the black powder.

Preparation of solid compounds

NaHSe, *eq.* (1).[35] Selenium powder (1.0 g, 13 mmol) was stirred with absolute ethanol (20 cm^3) cooled with ice. Solid $NaBH_4$ (1.0 g, 26 mmol) was added gradually with stirring, causing the vigorous and exothermic evolution of hydrogen. The mixture became brown and then colourless. On completion the ethanol was distilled out leaving a white solid. $B(OC_2H_5)_3$ was not separated from NaHSe.

$$NaBH_4 + Se + 3C_2H_5OH \longrightarrow NaHSe + B(OC_2H_5)_3 + 3H_2. \quad (1)$$

$(Bu_4N)_2[Se_6]$. A flask fitted with a low temperature condenser was charged with selenium powder (2.0 g, 25 mmol) and liquid NH_3 (30 cm^3). Sodium (0.20 g, 8.7 mmol) was added and the mixture stirred until all sodium had dissolved to form a dark green solution. After removal of the NH_3, water (20 cm^3) was added to form a dark green solution, which was cooled to 0°C and treated with a cooled solution of Bu_4NBr (2.73 g, 8.5 mmol) in water (10 cm^3). The dark green needles that formed at 0°C were filtered, washed with cold water, and dried *in vacuo*. Yield 3.3 g (81%). The solid, which is oxidized to selenium after several hours exposure to air, was identified by its powder diffraction. This reaction has been successfully scaled up tenfold.

$(Ph_4P)_2[Se_5]$. The procedure of the previous reaction was followed, using selenium powder (5.0 g, 63 mmol), NH_3 (40 cm^3 liquid) and Na (0.58 g, 25 mmol), generating a dark green solution after stirring for 40 min. After removal of the NH_3 to leave a red–brown solid, water (100 cm^3) was added to form a dark red solution, which was cooled to 0°C and treated with a cooled solution of Ph_4PBr (10.6 g, 25 mmol) in ethanol (50 cm^3). The black–brown needles that formed at 0°C were filtered, washed with cold water, and dried *in vacuo*. Yield 8.2 g (88%). The compound was characterized by single crystal diffraction analysis.[36]

$(Ph_4P)_2[Se(Se_5)_2]$. To a flask fitted with a low temperature condenser was added selenium powder (5.0 g, 63 mmol) and liquid NH_3 (40 cm^3). Sodium (0.58 g, 25 mmol) was added and the mixture stirred for 40 min, generating a dark green solution. After removal of the NH_3 to leave a red–brown solid, DMF (80 cm^3) was added and the mixture stirred to complete dissolution. $NaNO_3$ (1.08 g, 13 mmol) and Ph_4PBr (5.3 g, 13 mmol) were added, and the stirring was continued for 30 min to generate an olive green solution. After filtration, THF (80 cm^3) was layered onto the solution which was stored at *ca* 0°C. After 2 days black crystals had formed. They were collected, washed with THF, and vacuum dried. Yield 1.06 g. The product was identified by powder X-ray diffraction, and by complete crystal structure determination.[37]

Preparations of solutions for NMR

NaHSe *in aqueous solution.*[35] $NaBH_4$ (1.0 g, 26 mmol) in water (10 cm^3) was stirred into a suspension of selenium (1.0 g, 13 mmol) in water (10 cm^3), at room temperature. After 10 min the H_2 evolution had ceased and the selenium had dissolved completely to yield a pale grey solution.

NaHSe *in ethanol solution.* Following Klayman and Griffin[35] eq. (1), excess $NaBH_4$ was used in this reaction. Cold absolute ethanol (20 cm^3) was added with stirring to a mixture of selenium (1.0 g, 13 mmol) and $NaBH_4$ (0.58 g, 15 mmol), and the mixture cooled during the vigorous evolution of hydrogen. A colourless solution resulted.

NaHSe *in DMF solution.* The ethanol was distilled from the previous solution, yielding a white solid which was dissolved in DMF (20 cm^3) to generate a colourless solution.

"Na_2Se_2" *in aqueous solution.* Following Klayman and Griffin[35] $NaBH_4$ (1.0 g, 26 mmol) in water (10 cm^3) was added with stirring to selenium (1.0 g, 13 mmol) suspended in water (10 cm^3) at room temperature. After the initial vigorous reaction had subsided, a further portion of selenium (1.0 g, 13 mmol) was added, the mixture stirred for 15 min, and then briefly heated to complete the reactive dissolution of the selenium, yielding a dark red–brown solution. After storage at 0°C for 16 h a black precipitate formed, but the solution was still strongly coloured.

"Na_2Se_2" *in ethanol solution, eq.* (2).[35] Absolute ethanol (100 cm^3) was added with stirring to selenium (3.0 g, 38 mmol) and $NaBH_4$ (1.0 g, 26 mmol) cooled with ice. After the initial reaction had subsided the mixture was heated at reflux for 1.5 h, while the N_2 flush gas containing H_2Se was passed through aqueous lead acetate, yielding PbSe (1.15 g, 4.0 mmol). The dark red–brown reaction solution formed a small amount of black precipitate on storage at 0°C.

$$2NaBH_4 + 3Se + 6C_2H_5OH \longrightarrow Na_2Se_2 + H_2Se + 2B(OC_2H_5)_3 + 6H_2. \quad (2)$$

"Na_2Se_x" *in DMF solution*, $x = 3$–6. The general procedure is the same for all compounds, so the description of Na_2Se_4 only is presented in detail. A two-necked flask was charged with selenium powder (1.0 g, 13 mmol), fitted with a low temperature condenser, and NH_3 (30 cm^3 liquid) was condensed into the flask. Sodium (0.15 g, 6.3 mmol) was then added against a N_2 stream, and the reaction mixture was stirred at $< -60°C$ for about 1 h until the dissolution of sodium was complete. The solution colour changed from initial blue though various colours to dark brown. The NH_3 was evaporated, leaving a dark coloured solid which was dried *in vacuo* for a further 1.2 h. The solid was then dissolved in freshly distilled and degassed DMF (15 cm^3) at room temprature, generating a dark brown coloured solution.

Preparative data for other solutions are presented as: nominal composition "Na_2Se_x"; amount of sodium; amount of selenium; volume (cm^3) of NH_3 and colour; volume (cm^3) of DMF and colour. "Na_2Se_3"; 0.21 g (9.1 mmol); 1.0 g (12.7 mmol); 30, green; 15, brown–red. "Na_2Se_4", 0.15 g (6.5 mmol); 1.0 g (12.7 mmol); 30, brown; 15, brown. "Na_2Se_5", 0.12 g (5.2 mmol); 1.0 g (12.7 mmol); 30, green; 15, green. "Na_2Se_6", 0.097 g (4.2 mmol); 1.0 g (12.7 mmol); 30, green; 15, green. "Na_2Se_7", 0.17 g (7.4 mmol); 2.0 g (25 mmol); 50, green; 20, green. "Na_2Se_8", 0.15 g (6.5 mmol); 2.0 g (25 mmol); 50, green; 20, green. "Na_2Se_9", 0.13 g (5.6 mmol); 2.0 g (25 mmol); 50, green; 20, green. "Na_2Se_{10}", 0.12 g (5.2 mmol); 2.0 g (25 mmol); 50, green; 20, green. "Na_2Se_{11}", 0.11 g (4.4 mmol); 2.0 g (25 mmol); 50, green; 20, green. Very small amounts of unreacted selenium were removed.

Attempts to use this procedure to generate a solution of Na_2Se_2 in DMF generated white solids that would not dissolve in DMF, and were abandoned.

NMR

The ^{77}Se spectra were measured at 57.2 MHz with a Bruker CXP300 spectrometer, using a 10 mm broadband probe. The spectra were recorded at temperatures in the range *ca* $-60°C$–$27°C$.[38] A 40° pulse (20 μs) was used, with a pulse delay of 1 s. Natural line widths at half height range from 13–90 Hz. Chemical shifts, positive with high frequency, are relative to Me_2Se. A saturated solution of Na_2SeO_3 in H_2O was used as the secondary chemical shift reference, set as 1253 ppm (at 300 K) relative to the primary standard of neat Me_2Se = 0 ppm.[39,40]

RESULTS

HSe^- *and* Se^{2-}

We have used ^{77}Se NMR to characterize this pair of ions, the shortest members of the $[Se_x]^{2-}$ series. The spectra of several solutions are shown in Fig. 1, and all chemical shift data are presented in Table 2. The spectrum of the aqueous solution obtained

Table 2. ^{77}Se NMR data for solutions containing Se_1 species

Solution	Temperature (°K)	Chemical shift (ppm)[a]	Resonance characteristics
NaHSe in water (0.63 M)	300	−529	Doublet, $^1J(^{77}Se—^1H)$ = 26 Hz
NaHSe in ethanol (0.63 M)	300	−518	Singlet, 30 Hz (fwhh[b])
NaHSe in DMF (0.63 M)	300	−447	Singlet, 55 Hz fwhh
	260	−404	
	ca 245	−397	
	ca 235	−393	
NaHSe in *ca* 30% ethanol/DMF	300	−462	Doublet, *ca* 16 Hz splitting, fwhh *ca* 13 Hz
NaHSe in *ca* 45% ethanol/DMF	300	−475	Doublet, *ca* 19 Hz splitting, fwhh *ca* 20 Hz
NaHSe in *ca* 50% ethanol/DMF	300	−482	fwhh *ca* 90 Hz
NaHSe in *ca* 30% water/DMF	300	−477	fwhh *ca* 54 Hz
"Na_2Se_2" in water	300	−527	
"Na_2Se_2" in ethanol	300	−518	25 Hz doublet just resolved
	260	−514	25 Hz double resolved
	ca 245	−511	25 Hz doublet well resolved
	ca 235	−509	25 Hz doublet well resolved

[a] Reference $SeMe_2$.
[b] fwhh = full width at half height.

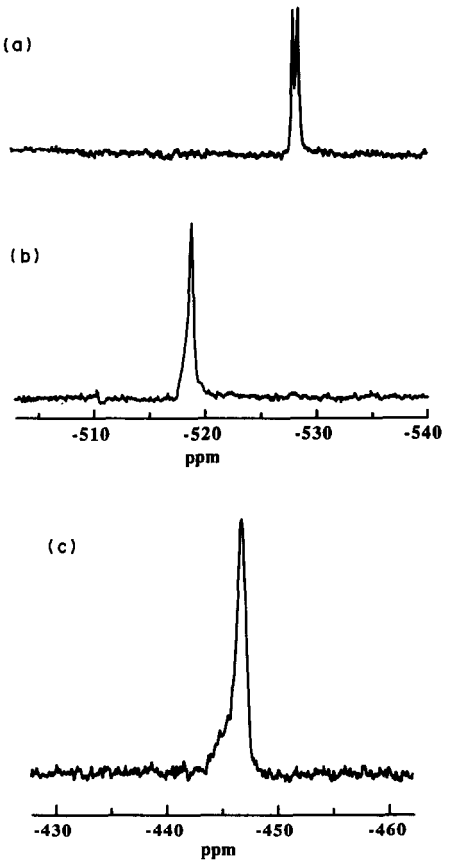

Fig. 1. ^{77}Se NMR spectra of solutions of NaHSe (*ca* 0.63 M) in (a) H_2O, (b) ethanol, and (c) DMF, at 300°K.

by BH_4^- reduction of selenium is a doublet, at $\delta_{Se} = -528$ ppm (300°K). The splitting of *ca* 26 Hz is presumed to be ^1J(Se—H) coupling because it is comparable with the value of 60.8 ± 0.1 Hz for H_2Se[41] and values of 38–61 Hz for RSeH.[42] Addition of NaOH, in attempt to deprotonate the HSe^-, causes instead the crystallization of a solid believed to be Na_2Se:[43,44] addition of Et_3N did remove the splitting, but moved the resonance to −519 ppm. However this experiment is not decisive, because the amount of Et_3N required to be equivalent to the high concentration of HSe^- is not miscible with the aqueous phase: the high proportion of Et_3N probably causes a medium effect in the chemical shift, as discussed below. Further, the K_a data for H_2Se in water[45] indicate that Et_3N would not be sufficiently basic to deprotonate HSe^- in water. Because K_a (HSe^-) is expected to be even smaller in aprotic solvents than the value of 10^{-15} in water, it is most probable that in all of our solutions the principal species is HSe^-. The resonances for solutions of HSe^-/Se^{2-} formed by other means and in other solvents are all at least 20 Hz wide at half height, and the ^1J(Se—H) coupling is generally poorly resolved, if at all. We recognise that some of the line broadening (up to 60 Hz) may be caused by minor amounts of Se^{2-} in fast exchange with HSe^-. However, the spectra are reproduceable, indicating that adventitious base in these unbuffered solutions is not influential. In the absence of definite evidence to the contrary, we presume that the species present in all of our fully reduced (colourless) solutions is HSe^-, despite the limited observation of the ^1J(Se—H) coupling.

Solutions of HSe^- prepared by borohydride reduction in ethanol showed only a sharp singlet at $\delta_{Se} = -519$ ppm (300°C), while in DMF the resonance is shifted substantially to −447 ppm. This is a medium influence on the chemical shift, which is similar in magnitude to the medium influences observed for Br^- and other halide ions,[46,47] and correlates with the thermodynamic activation of small anions in aprotic media.[48–50] Chemical shifts for *uncharged* organoselenium compounds are solvent dependent by up to 50 ppm[51] and it is known that other properties of anions are affected more by solvent proticity than are uncharged analogs. The δ_{Se} data for HSe^- in DMF/ethanol and DMF/water mixtures are intermediate between the extremes, confirming that these variations in chemical shifts are due to anion solvation.

The temperature dependence of δ_{Se} for HSe^- in DMF is large, *ca* −1 ppm per degree.

$[Se_2]^{2-}$

This ion has not been well characterized in solution. The reaction of selenium and equimolar sodium in NH_3 yielded a bright red solution and a white solid, but not a homogeneous product.[52] Literature procedures for generation of $[Se_2]^{2-}$ in solution, including reduction of selenium by BH_4^- in water (eq. 3) or ethanol (eq. 2),[35] or by reduction with sodium in DMF,[53] were assessed only through further reactions of the solutions, which were consistent with substantial yields of $[Se_2]^{2-}$ in the reduction stage. Therefore we have measured the ^{77}Se NMR of the solutions formed in ethanol or water by BH_4^- reduction, and found that in both cases there is a single resonance at the same δ_{Se} as the HSe^- solutions described above.[54] This result is consistent with our observations (see Experimental) that the amount of H_2Se formed is less (*ca* 1/3) than predicted for reaction (2), and the fact that the solutions deposited some elemental selenium on standing, indicating disproportionation. The resonance from the ethanol solution at −518 ppm is a doublet with the same 26 Hz splitting as observed for NaHSe in water. Thus we have no NMR evidence for $[Se_2]^{2-}$ in aqueous or ethanolic solution.

$$4NaBH_4 + 2Se + 2H_2O \longrightarrow 2NaHSe + Na_2B_4O_7 + 14H_2 \quad (3a)$$

$$Na_2B_4O_7 + 2NaHSe + 2Se + 5H_2O \longrightarrow 2Na_2Se_2 + 4H_3BO_3. \quad (3b)$$

When equimolar sodium and selenium were reacted in DMF at 90°C a dark red solution was obtained, which showed two equal intensity selenium resonances at 598 and 347 ppm (*ca* 220 K). This is consistent with the presence of $[Se_4]^{2-}$ (see below), and thus it appears that there is disproportionation of $[Se_2]^{2-}$ to $[Se_4]^{2-}$ and probably $[HSe]^-$. When the "Na_2Se_2" formed by reaction of the elements in NH_3(l) is treated with DMF there is not complete dissolution but instead formation of white and black solids which we interpret as disproportionation to Na_2Se and Se.

Na_2Se_x *in solution*

Solutions with nominal compositions Na_2Se_x, $x = 3$–11, and concentrations of approximately 0.3 M were prepared by reaction of sodium and selenium in NH_3(l) followed by removal of solvent and redissolution in DMF. The "Na_2Se_4" solution was brown, "Na_2Se_3" was green in NH_3 but brown in DMF, while the other "Na_2Se_x" solutions were green. All solutions were highly susceptible to oxidation by O_2, precipitating selenium on exposure to air of less than 5 s. Therefore rigorous techniques were used throughout.

None of these solutions showed ^{77}Se resonances at 300°K, and it was necessary to reduce the temperatures to *ca* 240°K in order to obtain satisfactory spectra. This temperature effect is illustrated in Fig. 2 with the spectra from the solution "Na_2Se_5" at different temperatures. There is a collection of resonances which appear for solutions "Na_2Se_3", "Na_2Se_4", "Na_2Se_5" and "Na_2Se_6", but we have not been able to detect any resonances for the solutions "Na_2Se_x", $x > 6$. We have scanned the chemical shift range 2100 to −500 ppm, at room temperature and low temperatures, with no evidence of additional resonances. Although all of the solutions are in the slow exchange regime, the slow exchange limit for polyselenide interconversions is below the accessable measurement temperatures.

The resonances for "Na_2Se_3", "Na_2Se_4", "Na_2Se_5" and "Na_2Se_6" are shown diagrammatically in Fig. 3. Clearly there exists more than one $[Se_x]^{2-}$ ion in some of these solutions, but the resonances belonging to each of the species $[Se_3]^{2-}$, $[Se_4]^{2-}$, $[Se_5]^{2-}$ and $[Se_6]^{2-}$ can be assigned unequivocally. Referring to Fig. 3, the resonances at 251 and 192 ppm (intensity ratio 2:1) are due to $[Se_3]^{2-}$; the equal intensity lines at 591 and 301 ppm are due to $[Se_4]^{2-}$, those at 860, 603 and 448 ppm (relative intensities 1:2:2) are due to $[Se_5]^{2-}$, while the equal intensity resonances at 798, 681 and 497 ppm are due to $[Se_6]^{2-}$.[55]

We have not been able to detect ^nJ(Se—Se) coupling satellites that would assist with the assignment of the resonances: the intensities of the satellites at

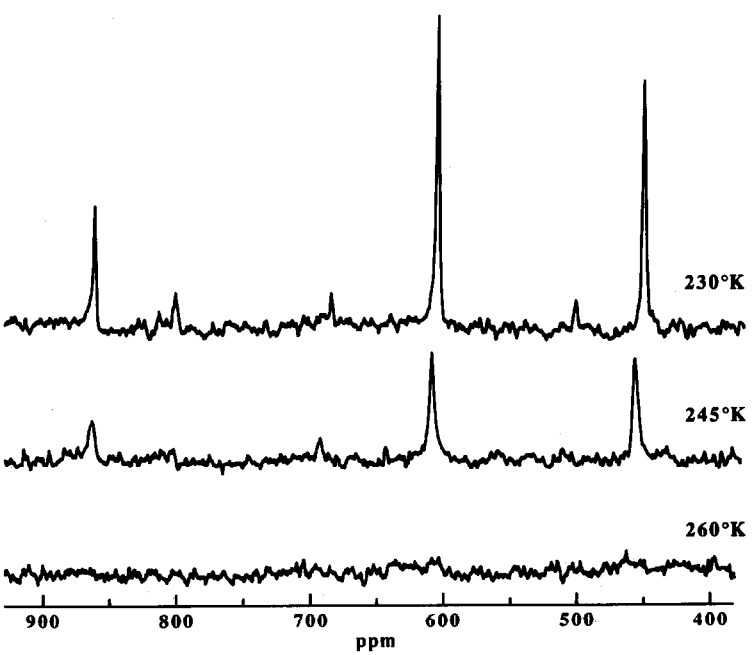

Fig. 2. ^{77}Se NMR spectra of "Na_2Se_5" in DMF at the temperatures marked.

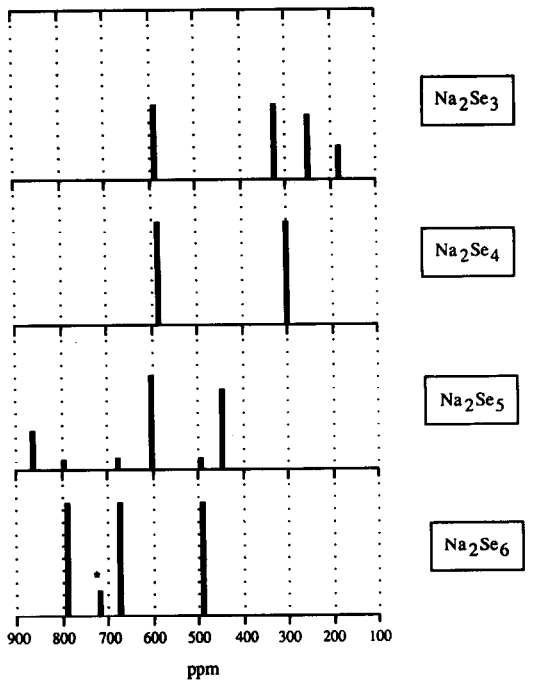

Fig. 3. Diagram of the ^{77}Se NMR resonance positions and intensities for solutions of nominal compositions Na_2Se_x in DMF at 230 K.

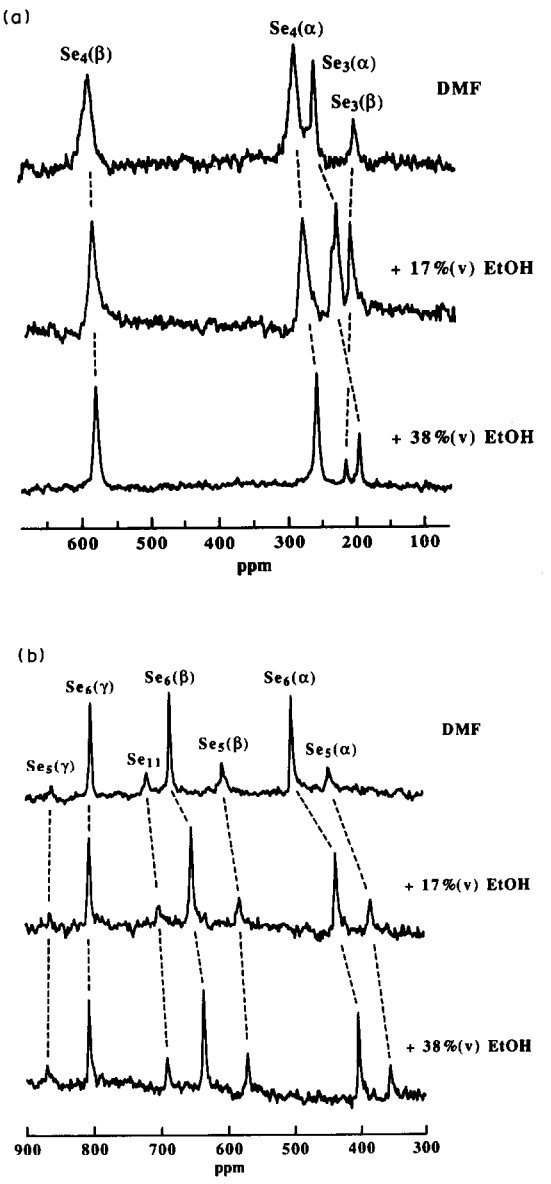

Fig. 4. Diagram of the ^{77}Se resonance positions (at 230 K) for (a) solutions containing a mixture of $[Se_3]^{2-}$ and $[Se_4]^{2-}$ and (b) solutions containing a mixture of $[Se_5]^{2-}$ and $[Se_6]^{2-}$, in DMF/ethanol in the proportions marked.

natural abundance are low (*ca* 5%), and the expected coupling magnitudes of 20–120 Hz[56,57] are less than the line-widths of our resonances.

Only for $[Se_3]^{2-}$ will the relative intensity data allow unambiguous assignment of resonances to the individual selenium atoms in the $[Se_x]^{2-}$ ions. In order to obtain experimental information on the assignments of the resonances in the other $[Se_x]^{2-}$ ions we have deployed solvent influences. As already described, the chemical shifts of ^{77}Se in HSe^- anions are strongly dependent on solvent proticity. Like all instances of solvent proticity on anion activity,[48–50] this effect is proportional to the negative charge density on the affected atoms. Therefore the solvent influences on chemical shifts in $[Se_x]^{2-}$ ions indicate the charge densities at the various selenium atoms. The chemical shifts of the resonances in a solution containing $[Se_3]^{2-}$ and $[Se_4]^{2-}$ [Fig. 4(a)] and a solution containing $[Se_5]^{2-}$ and $[Se_6]^{2-}$ [Fig. 4(b)] vary in different ways as the proportion of ethanol in DMF is increased.

We use the notation α, β, γ, to signify positions of selenium atoms relative to the chain ends in $[Se_x]^{2-}$, and quote data for solutions in DMF and 50% DMF/ethanol. In $[Se_3]^{2-}$ the 257 ppm resonance (α) in DMF shifts to 193 ppm with increasing solvent proticity, while the 194 ppm resonance (β) moves slightly in the other direction to 214 ppm: the effect is greatest on first addition of ethanol to DMF. This is entirely consistent with the assignments based on resonance intensities, and with the assumption that the negative charge density on $[Se_3]^{2-}$ is greater at the terminal α selenium atoms. This validates the assignment principle that can be applied to other $[Se_x]^{2-}$ ions, namely that as the negative charge density on selenium diminishes with distance from the terminal selenium atoms the chemical shifts (at least in protic media) become less negative. For $[Se_4]^{2-}$ the high chemical shift decreases by only 8 ppm with addition of ethanol, while the other δ_{Se} decreases by 29 ppm, thereby

Table 3. Chemical shifts for $[Se_x]^{2-}$ ions in DMF plus 38% (vol) EtOH

$[Se_x]^{2-}$ ion	$\delta_{Se}(\alpha)$ ppm	$\delta_{Se}(\beta)$ ppm	$\delta_{Se}(\gamma)$ ppm
$[Se_3]^{2-}$	193	214	—
$[Se_4]^{2-}$	256	581	—
$[Se_5]^{2-}$	354	570	868
$[Se_6]^{2-}$	404	636	807

identifying the equal intensity lines as β and α, respectively. For $[Se_5]^{2-}$ the highest δ_{Se} line increases by 7 ppm, the intermediate line decreases by 34 ppm, and the lower δ_{Se} decreases by 89 ppm, indicating the assignments Se(γ), Se(β), Se(α), respectively, for these lines. In the case of $[Se_6]^{2-}$ the solvent effects are similarly impressive, and allow similar assignments: the highest δ_{Se} line increases by 5 ppm and is assigned Se(γ), the intermediate δ_{Se} line decreases by 47 ppm and is assigned Se(β), while the lowest δ_{Se} line decreases by 95 ppm and is assigned Se(α). Note that the relationship $\delta_{Se}(\gamma) > \delta_{Se}(\beta) > \delta_{Se}(\alpha)$ applies for all $[Se_x]^{2-}$ ions, but is valid for $[Se_3]^{2-}$ only when the chemical shifts are those of protic solvents. Chemical shift assignments standardized to the solution in DMF containing 38% EtOH are presented in Table 3.

In general the line-widths of the $[Se_x]^{2-}$ resonances decrease as ethanol is added and the solvent proticity increases. This is interpreted as indicating retardation of polyselenide exchange reactions on addition of ethanol, consistent with the normal lowering of the kinetic activity of anions with increased solvent proticity.

$(Ph_4P)_2[Se_5]$ *and* $(Bu_4N)_2[Se_6]$

There have been two reports of the crystal structure of $(Ph_4P)_2[Se_5]$, from crystals obtained accidentally from an irrational reaction[30] or as a side product.[16] We provide here a direct preparation of this compound. We determined the crystal structure of our preparation before the publication of the results of others,[19,30] but report only the essential results here. There are some distinctive differences between the unit cell dimensions obtained in the three independent measurements, listed for ref. 30, ref. 16 and this work, respectively: a = 9.573, 9.615, 9.617; b = 16.945, 17.122, 17.092; c = 13.563, 13.788, 13.724 Å, β = 105.29, 105.18, 105.18°. The residual R is substantially lower for our structure than for the other two. It is interesting to compare the Se—Se distances in $[Se_5]^{2-}$ as obtained in the three independent determinations: the four Se—Se distances along the chain, listed for ref. 30, ref. 16 and this work, are 2.316, 2.355, 2.366, 2.314; 2.326, 2.345, 2.321; 2.308, 2.360, 2.354, 2.310 Å. Thus two of the determinations are in agreeement with the chemical notion that the Se(α)—Se(β) bonds are slightly (*ca* 0.04 Å) shorter than the Se(β)—Se(γ) bonds. The ^{77}Se NMR spectrum of $(Ph_4P)_2[Se_5]$ dissolved in DMF contains the resonances of $[Se_5]^{2-}$ and $[Se_6]^{2-}$, indicative of some disproportionation. Low solubility at low temperature restricted our measurement of the ^{77}Se NMR spectrum of $(Bu_4N)_2[Se_6]$.

$[Se(Se_5)_2]^{2-}$

We first observed the crystallization of the Ph_4P^+ salt of this unusual polyselenide anion during attempts to prepare polyselenide complexes of oxidising metal ions, including gold(III) and bismuth (III), and with some non-oxidising metal salts such as $Cr(NO_3)_3$. Subsequently $(Ph_4P)_2[Se(Se_5)_2]$ was characterized crystallographically by Krebs *et al.*[33] During preparation and characterization of metal polysulphide complexes in aprotic media we observed that nitrate salts in DMF caused elongation of the polysulphide chain, an oxidative process.[58] Therefore we tested $NaNO_3$ as an oxidant for polyselenides in DMF, and found that it converted $[Se_5]^{2-}$ to $[Se(Se_5)_2]^{2-}$ and can be used as a convenient oxidant in the preparation of $(Ph_4P)_2[Se(Se_5)_2]$. The use of gold(III) or I_2 for oxidation of $[Se_5]^{2-}$ to $[Se(Se_5)_2]^{2-}$ has been reported by Kanatzidis and Huang.[13] In the preparations of metal polyselenide complexes in DMF and other aprotic solvents it is important to recognise that $[Se_x]^{2-}$ can be readily oxidised by both cations and oxidising counter anions present.

Solutions containing the $[Se(Se_5)_2]^{2-}$ ion do not display an informative ^{77}Se NMR spectrum. At low temperature (*ca* 235 K) in DMF there is a broad (1000 Hz) resonance at 720 ppm. This resonance appears also in solutions of other $[Se_x]^{2-}$ ions that have undergone partial oxidation. Four NMR distinct selenium sites are expected, but despite extensive searches (2100 to −500 ppm) only the one broad resonance has been located. The one resonance observed does move to lower frequency and sharpen slightly on addition of ethanol. The magnitude of the solvent dependence of the chemical shift is similar to that of the Se(β) atoms in the noncyclic $[Se_x]^{2-}$ ions.

DISCUSSION

Although Se^{2-} and HSe^- are the simplest selenide species, their δ_{Se} characteristics had not pre-

viously been well established. Odom *et al.* observed a resonance at −511 ppm for a solution of H_2Se plus excess NH_3 in D_2O[44] which was interpreted without supporting evidence as being Se^{2-} in equilibrium with a minor amount of HSe^-. Lyons and Young[59] measured a single resonance at −670 ppm for a 3 M solution of K_2Se in 0.1 M KOH. We discuss our δ_{Se} data in the context of that collected in Table 4 for other species in the general classes XSe^- and XSeH.

In general δ_{Se} becomes more negative with the negative charge on selenium.[39,40,42] By extrapolation of $\Delta\delta_{Se}$ for deprotonation of RSeH, from R = Pr^i, Et, Me, a value of δ_{Se} for aqueous HSe^- would be estimated (from δ_{Se} for aqueous H_2Se) at $-288 - ca\ 200) = ca\ -490$ ppm. This approximate estimate is entirely consistent with the observations in Table 4, and with our interpretation of the sample of $(NH_4)_2Se$ in D_2O[44] as containing $NH_4^+ + HSe^- + NH_3$. The question remains open about the chemical shift for Se^{2-}, which is likely to exist as such only in aprotic basic media. The solution of K_2Se in aqueous 0.1 M KOH listed in Table 4 would be expected to contain the $HSe^- \rightleftharpoons Se^{2-}$ equilibrium, with HSe^- dominant since pK_2 for $H_2Se = 15$.[45] By general extrapolation using the H_2Se, HSe^-, $MeSe^-$ data in Table 4, $\delta_{Se}(Se^{2-})$ might be expected to be at least as negative as −700 ppm, and probably closer to −800 ppm. The most negative δ_{Se} recorded is the value −736 for $H_3SiSe^-Li^+$.[63]

We have established unambiguously that the four polyselenide ions $[Se_3]^{2-}$, $[Se_4]^{2-}$, $[Se_5]^{2-}$ and $[Se_6]^{2-}$ exist in solution (thus dispelling earlier claims[24] of the non-existence of $[Se_5]^{2-}$), and in equilibrium, but we have no evidence for the existence of $[Se_2]^{2-}$ in DMF solution. Kanatzidis[2] has claimed that polyselenide ions dissociate to paramagnetic polyselenide radicals, eq. (4), in solution. However the assignment[2] of the 610 nm absorption in solutions of polyselenide ions to polyselenide radicals is incorrect: such electronic absorptions had previously been attributed to the polyselenide ions.[24] Although the poor NMR spectroscopic state of the polyselenide solutions at ambient temperatures could be due to paramagnetic broadening, there is no evidence of concomitant paramagnetic shifting, and we consider that the dissociation (4) in solution occurs to a very small extent that does not interfere with the recording of ^{77}Se NMR.

$$[Se_x]^{2-} \rightleftharpoons [Se_y]^- + [Se_{x-y}]^- . \qquad (4)$$

As expected, polyselenide ions are reponsive to solvent proticity in various ways, including the selenium exchange dynamics and the selenium chemical shifts. The magnitude of the effect is dependent on the location of the selenium atom in the polyselenide chain, and its negative charge density. We have no evidence that the solvent dependence involves dissociation into radicals.

In Fig. 5 are charted δ_{Se} values for selenium atoms in four types of polyselenium chains, (a) $[Se_x]^{2-}$ and (b) Oct^n—Se_x—Oct^n which are acyclic,[64] (c) selected (d^{10}) M(Se_4) chelate rings,[19,65] and (d) cyclic $S_{8-x}Se_x$.[66] Our δ_{Se} values for selenium atoms in the

Table 4. ^{77}Se chemical shift data for species XSe^- and XSeH

Compound	State	δ_{Se}	Reference, comments
H_2Se	Liquid	−226	41, 42, 60
H_2Se	1.0 M in D_2O	−288	44
NaHSe	H_2O	−528	This work
NaHSe	Ethanol	−519	This work
NaHSe	DMF	−447	This work
$(NH_4)_2Se$, interpreted as $NH_4^+ + HSe^- + NH_3$	D_2O, prepared as solution of H_2Se, excess NH_3 in D_2O	−511	44
K_2Se	In 0.1 M aqueous KOH	−670	59
MeSeH	Neat, $CDCl_3$	−116, −130	42
$MeSe^-Na^+$	H_2O	−332	42
EtSeH	Liquid	42	42
$EtSe^-Na^+$	H_2O	−150	42
Pr^{i}SeH	Liquid	159	42
$Pr^iSe^-Na^+$	H_2O	9	42
$NCSe^-K^+$	0.5 M in ethanol	−322	61
$(H_3Si)_2Se$	Liquid	−666	62
$H_3SiSe^-Li^+$		−736	63, this species is involved in an unspecified fast exchange

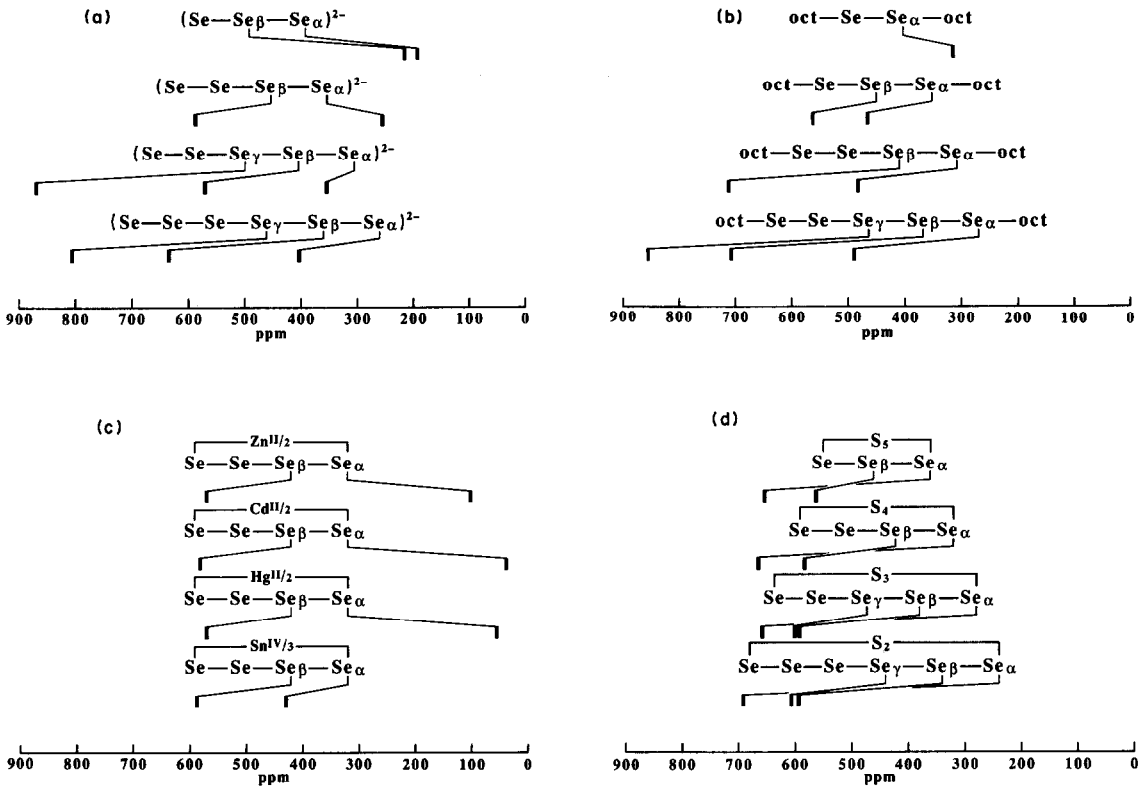

Fig. 5. Comparative chart of the ^{77}Se chemical shifts in four classes of polyselenium chains: (a) $[Se_x]^{2-}$; (b) $Oct^n—Se_x—Oct^n$; (c) $M(Se_4)$; and (d) $S_{8-x}Se_x$. The thick lines mark the chemical shift values.

polyselenide chains $[Se_x]^{2-}$ of various lengths provide the best reference for comparable δ_{Se} data from polyselenium chains R—Se_x—R with various terminating groups R. Discussing the $[Se_x]^{2-}$ data first, it can be seen that the weighted average chemical shift moves non-linearly to higher frequency as the length of the chain increases, consistent with decreased average negative charge per selenium atom. The changes in $\delta_{Se}(\alpha)$ with x in the $[Se_x]^{2-}$ series are more regular than the changes in $\delta_{Se}(\beta)$. The $\delta_{Se}(\alpha)$ values and the $\delta_{Se}(XSe^-)$ values (Table 4) are entirely consistent with the general notion that the negative charge on the terminal selenium atoms of $[Se_x]^{2-}$ is about 0.5. It is not clear why $\delta_{Se}(\gamma)$ in $[Se_5]^{2-}$ is more negative than $\delta_{Se}(\gamma)$ in $[Se_6]^{2-}$, although different torsional angles at the centre of the longer chain may be responsible. It should be remembered that these selenium chemical shift tensors are very probably quite anisotropic, and that an average chemical shift only is accessible here. Further, the influence of solvent environment is sufficient to interchange the two average chemical shifts in $[Se_3]^{2-}$. In the series $Oct^n—Se_x—Oct^n$ it is the internal selenium atoms that move more than $\delta_{Se}(\alpha)$ to larger chemical shift as x increases. We note that the δ_{Se} patterns for comparable chains $[Se_x]^{2-}$ and $Oct^n—Se_x—Oct^n$ are similar, with the δ_{Se} for $[Se_x]^{2-}$ less positive, and with the differences more pronounced for the shorter chains.

Finally we analyse the data (Fig. 5) for the cyclic polyselenide chains, closed by sulphur atoms or d^{10} metal atoms.[67] In the four MSe_4 ($M = Zn^{II}$, Cd^{II}, Hg^{II}, Sn^{IV}) chelate rings the $\delta_{Se}(\beta)$ are virtually the same (*ca* 580 ppm) as that in $[Se_4]^{2-}$, and the $\delta_{Se}(\alpha)$ are metal dependent. In the polyselenium compounds where the eight-membered cycle is completed by sulphur atoms there is little polarity and limited disperson of the selenium chemical shifts. The $\delta_{Se}(\beta)$ (and $\delta_{Se}(\gamma)$) are also close to 580 ppm as they are in the metal–chelate rings, but the $\delta_{Se}(\alpha)$ are anomalously larger. This could be due to the reversed polarity of the Se(α)—S bonds compared with Se(α)—C or Se(α)—M.

SUMMARY

The principal results from this investigation are:

(1) Fully reduced solutions of selenium in DMF contain HSe^- for which δ_{Se} ranges between −530 and −390 ppm (vs Me_2Se) depending strongly on solvent and temperature;

(2) Solutions of $[Se_x]^{2-}$ can be prepared by partial

reduction, and, for $x = 3$–6, confirmed and characterized by ^{77}Se NMR;

(3) There is no NMR evidence for the occurrence of $[Se_2]^{2-}$, which is believed to disproportionate in these solutions;

(4) δ_{Se} values for selenium atoms in $[Se_x]^{2-}$ ions are proportional to distance from the end of the chain $[\delta_{Se}(\gamma) > \delta_{Se}(\beta) > \delta_{Se}(\alpha)]$, and inversely proportional to negative charge density;

(5) δ_{Se} values for selenium atoms in $[Se_x]^{2-}$ ions are influenced by solvation with more protic solvents giving less positive δ_{Se}: the solvation dependence magnitudes are $\delta_{Se}(\alpha) > \delta_{Se}(\beta) > \delta_{Se}(\gamma)$, in proportion to negative charge density at selenium.

(6) Atom exchange in $[Se_x]^{2-}$ is relatively fast at room temperature, and is retarded by protic solvents.

(7) $[Se(Se_5)_2]^{2-}$, a common oxidation product of $[Se_x]^{2-}$, can be identified by ^{77}Se NMR, but not fully characterized because the ion appears to be undergoing exchange which is NMR-fast.

Acknowledgements—This search is supported by the Australian Research Council. We are grateful to Dr J. Hook for assistance in obtaining the NMR spectra. J.C. acknowledges the award of an Australian Postgraduate Award.

REFERENCES

1. M. A. Ansari and J. A. Ibers, *Coord. Chem. Rev.* 1990, **100**, 223.
2. M. G. Kanatzidis, *Comments Inorg. Chem.* 1990, **10**, 161.
3. R. M. W. Wardle, S. Bhaduri, C.-N. Chau and J. A. Ibers, *Inorg. Chem.* 1988, **27**, 1747.
4. R. M. W. Wardle, C. H. Mahler, C.-N. Chau and J. A. Ibers, *Inorg. Chem.* 1988, **27**, 2790.
5. M. G. Kanatzidis and S.-P. Huang, *J. Am. Chem. Soc.* 1989, **111**, 760.
6. R. M. H. Banda, J. Cusick, M. L. Scudder, D. C. Craig and I. G. Dance, *Polyhedron* 1989, **8**, 1995.
7. R. M. H. Banda, J. Cusick, M. L. Scudder, D. C. Craig and I. G. Dance, *Polyhedron* 1989, **8**, 1999.
8. J. Cusick, M. L. Scudder, D. C. Craig and I. G. Dance, *Polyhedron* 1989, **8**, 1139.
9. J. Cusick, M. L. Scudder, D. C. Craig and I. G. Dance, *Aust. J. Chem.* 1990, **43**, 209.
10. G. Kräuter, F. Weller and K. Dehnicke, *Z. Naturforsch.* 1989, **44b**, 444.
11. Y-J. Lu, M. A. Ansari and J. A. Ibers, *Inorg. Chem.* 1989, **28**, 4049.
12. M. A. Ansari and J. A. Ibers, *Inorg. Chem.* 1989, **28**, 4068.
13. M. G. Kanatzidis and S.-P. Huang, *Inorg. Chem.* 1989, **28**, 4667.
14. M. G. Kanatzidis and S.-P. Huang, *Angew. Chem. Int. Ed. Engl.* 1989, **28**, 1513.
15. S. C. O'Neal, W. T. Pennington and J. W. Kolis, *Canad. J. Chem.* 1989, **67**, 1981.
16. G. Kräuter, K. Dehnicke and D. Fenske, *Chemiker-Zeitung* 1990, **114**, 7.
17. S.-P. Huang, S. Dhingra and M. G. Kanatzidis, *Polyhedron* 1990, **9**, 1389.
18. G. Kräuter, M.-L. Ha-Eierdanz, U. Müller and K. Dehnicke, *Z. Naturforsch.* 1990, **45b**, 695.
19. M. A. Ansari, C. H. Mahler, G. S. Chorghade, Y.-J. Lu and J. A. Ibers, *Inorg. Chem.* 1990, **29**, 3832.
20. S. C. O'Neal, W. T. Pennington and J. W. Kolis, *Inorg. Chem.* 1990, **29**, 4134.
21. M. G. Kanatzidis and J.-H. Liao, *J. Am. Chem. Soc.* 1990, **112**, 7400.
22. W. S. Sheldrick and H. G. Braunbeck, *Z. Naturforsch.* 1989, **44b**, 1397.
23. A. Müller and E. Diemann, *Adv. Inorg. Chem.* 1987, **31**, 89.
24. K. W. Sharp and W. H. Koehler, *Inorg. Chem.* 1977, **16**, 2258.
25. H. Von Föppl, E. Busmann and F.-K. Frorath, *Z. Anorg. Allg. Chem.* 1962, **314**, 12.
26. F. Weller, J. Adel and K. Dehnicke, *Z. Anorg. Allg. Chem.* 1987, **548**, 125.
27. N. E. Brese, C. R. Randall and J. A. Ibers, *Inorg. Chem.* 1988, **27**, 940.
28. T. König, B. Eisenmann and H. Schafer, *Z. Naturforsch.* 1982, **37b**, 1245.
29. T. König, B. Eisenmann and H. Schafer, *Z. Anorg. Allg. Chem.* 1983, **498**, 99.
30. C-N. Chau, R. M. W. Wardle and J. A. Ibers, *Acta Cryst.* 1988, **C44**, 883.
31. (a) U. Kretschmann and P. Böttcher, *Z. Naturforsch.* 1985, **40b**, 895; (b) P. Böttcher, *Z. Krist.* 1979, **150**, 65.
32. R. G. Teller, L. J. Krause and R. C. Haushalter, *Inorg. Chem.* 1983, **22**, 1809.
33. B. Krebs, E. Lührs, L. Stork and R. Willmen, *Abstract* 08.2-5, *Congress of the International Union of Crystallography*, Perth, Australia (1987).
34. D. Fenske, G. Kräuter and K. Dehnicke, *Angew. Chem. Int. Ed. Engl.* 1990, **29**, 390.
35. D. L. Klayman and T. S. Griffin, *J. Am. Chem. Soc.* 1973, **95**, 197.
36. Crystal data: space group $P2_1$, $a = 9.617$, $b = 17.092$, $c = 13.725$ Å, $\beta = 105.18°$, 3223 observed reflections ($I/\sigma(I) > 3$), Mo-K_α radiation, $R = 0.026$.
37. Two crystal forms of this compound were analysed: Form A: composition $(Ph_4P)_2Se_{11}$, space group $P2_1/c$, $a = 12.869$, $b = 14.818$, $c = 15.780$ Å, $\beta = 121.93°$, $Z = 2$, 2191 observed reflections ($I/\sigma(I) > 3$), Mo-K_α radiation, $R = 0.051$. Form B: composition $(Ph_4P)_2Se_{11}$, space group $P2_1/c$, $a = 9.961$, $b = 13.883$, $c = 19.137$ Å, $\beta = 107.93°$, $Z = 2$, 1920 observed reflections ($I/\sigma(I) > 3$), Mo-K_α radiation, $R = 0.039$.
38. The lower temperatures quoted are reproduceable but uncertain (5°) due to incomplete thermal calibration of the probe.
39. R. K. Harris and B. E. Mann, *NMR and the Periodic Table*. Academic Press, London (1978).

40. J. Mason, *Multinuclear NMR*, Ch. 15. Plenum Press, New York (1987).
41. H. J. Jacobsen, A. J. Zozulin, P. D. Ellis and J. D. Odom, *J. Mag. Res.* 1980, **38**, 219.
42. W. McFarlane and R. J. Wood, *J. Chem. Soc., Dalton Trans.* 1972, 1397.
43. Na_2Se prepared by reaction of sodium and selenium in $NH_3(l)$ has very low solubility in water. This was also reported by Odom *et al.*[44]
44. J. D. Odom, W. H. Dawson and P. D. Ellis, *J. Am. Chem. Soc.* 1979, **101**, 5815.
45. $K_1 = 1.3 \times 10^{-4}$: H. Hagisawa, *Bull. Inst. Phys. Chem. Res. Tokyo* 1941, **20**, 384; *Chem. Abs.* 1942, **36**, 1231; and $K_2 = 10^{-15}$: R. H. Wood, *J. Am. Chem. Soc.* 1958, **80**, 1559.
46. J. Mason, *Multinuclear NMR*, Ch. 17. Plenum Press, New York (1987).
47. T. R. Stengle, Y.-C. E. Pan and C. H. Langford, *J. Am. Chem. Soc.* 1972, **94**, 9037.
48. A. J. Parker, *Chem. Rev.* 1969, **69**, 1.
49. R. Alexander, A. J. Parker, J. H. Sharp and W. E. Waghorne, *J. Am. Chem. Soc.* 1972, **94**, 1148.
50. C. Reichardt, *Solvents and Solvent Effects in Organic Chemistry*, 2nd Edn. VCH Publishers (1988).
51. S. W. Carr and R. Colton, *Aust. J. Chem.* 1981, **34**, 35.
52. This was observed also by Sharp and Koehler.[24]
53. D. J. Sandman, G. W. Allen, L. A. Acampora, J. C. Stark, S. Jansen, M. T. Jones, G. J. Ashwell and B. M. Foxman, *Inorg. Chem.* 1987, **26**, 1664.
54. The range -860 to $+820$ ppm was scanned.
55. There are relatively small variations in the resonance positions due to differences in temperature and solvent.
56. P. Pekonen, Y. Hiltunen, R. S. Laitinen and T. A. Pakkanen, *Inorg. Chem.* 1990, **29**, 2770.
57. P. Pekonen, Y. Hiltunen and R. S. Laitinen, *Acta Chem. Scand.* 1989, **43**, 914.
58. (a) H. R. M. Banda, I. G. Dance, T. D. Bailey, D. C. Craig and M. L. Scudder, *Inorg. Chem.* 1989, **28**, 1862; (b) T. D. Bailey, H. R. M. Banda, D. C. Craig, I. G. Dance, I. N. L. Ma and M. L. Scudder, *Inorg. Chem.* 1991, **30**, 187.
59. L. E. Lyons and T. L. Young, *Aust. J. Chem.* 1986, **39**, 511.
60. T. Birchall, R. J. Gillespie and S. L. Vekris, *Canad. J. Chem.* 1965, **43**, 1672.
61. W. H. Pan and J. P. Fackler Jr, *J. Am. Chem. Soc.* 1978, **100**, 5783.
62. D. E. J. Arnold, J. S. Dryburgh, E. A. V. Ebsworth and D. W. H. Rankin, *J. Chem. Soc., Dalton Trans.* 1972, 2518.
63. S. Cradock E. A. V. Ebsworth, D. W. H. Rankin and W. J. Savage, *J. Chem. Soc., Dalton Trans.* 1976, 1661.
64. H. Eggert, O. Nielsen and L. Henriksen, *J. Am. Chem. Soc.* 1986, **108**, 1725.
65. J. Cusick and I. G. Dance, to be published.
66. R. S. Laitinen and T. A. Pakkanen, *Inorg. Chem.* 1987, **26**, 2598.
67. The data for polyselenide chelate rings including d^n ($n \neq 0$, 10) transition metals do not fit these patterns.[19,65]

Polyhedron Vol. 10, No. 22, pp. 2641–2645, 1991
Printed in Great Britain

0277–5387/91 $3.00+.00
© 1991 Pergamon Press plc

COMMUNICATION

THE X-RAY CRYSTAL STRUCTURE OF $Na_2[Ph_2PSe_2]_2 \cdot THF \cdot 5H_2O$—A POLYMER CONTAINING SIX-MEMBERED SODIUM–WATER RINGS AND SODIUM COORDINATED BY SELENIUM

MARK J. PILKINGTON, ALEXANDRA M. Z. SLAWIN, DAVID J. WILLIAMS and J. DEREK WOOLLINS*

Department of Chemistry, Imperial College, London SW7 2AY, U.K.

(*Received* 9 *July* 1991; *accepted* 21 *August* 1991)

Abstract—Na_xSe_y, prepared by the reaction of sodium and selenium in liquid ammonia, has been reacted with Ph_2PCl in THF/ethanol to give a mixture of Ph_2PSeH, $Ph_2P(Se)OP(Se)Ph_2$ and the title compound (**5**) which was characterized by X-ray crystallography. Compound **5** consists of a central polymeric core built up of $Na(H_2O)_6$ and $Na(H_2O)_3(thf)(Se)$ units with additional hydrogen-bonded $Ph_2PSe_2^-$ anions.

We have recently reported[1,2] on the syntheses of four- and five-membered P–Se rings such as $(PhPSe)_2Se_2$ (**1**), $(PhP)_3Se_2$ (**2**), $(PhP)_4Se$ (**3**) and $(PMe)_4Se_3$ (**4**). Compound **1** undergoes reaction[3] with $PtCl_2(PR_3)_2$ to give complexes containing the bidentate $[PhPSe_3]^{2-}$ ligand. This observation prompted us to investigate the synthesis of Ph_2PSe_2H and its deprotonated anion $Ph_2PSe_2^-$ as a preliminary to studying its coordination chemistry. To our knowledge, although the coordination chemistry of phosphates and thiophosphates is well-developed there have been no reports on the analogous selenium chemistry. Here, we report on the X-ray crystal structure of $Na_2[Ph_2PSe_2]_2 \cdot THF \cdot 5H_2O$ (**5**).

A number of workers have described[4–6] the use of liquid ammonia solutions for the preparation of Na_xE_y (E = S, Se, Te). We have investigated the usefulness of these solutions for the preparation of P—Se heterocycles. Thus, for example, dissolution of sodium (10 mmol) in liquid ammonia (10 cm^3) at −78°C followed by addition of grey selenium (5 mmol) gives an intensely coloured solution. If this solution is allowed to warm to room temperature and the ammonia evaporated off the remaining solid may be suspended in THF and reacted with $PhPCl_2$ at reflux to give **2**. However, this reaction is not particularly reproducible, in part at least, because of the first stage giving a mixture of products together with unreacted sodium metal. Furthermore, varying the molar ratio of sodium to selenium does not improve the efficiency or the utility of the reaction with $PhPCl_2$.

We have also attempted the reaction of Na_xSe_y with Ph_2PCl in THF and here again the reactions are not readily reproducible. Some improvement in the reproducibility is obtained if the second stage of the reaction is performed in a mixture of THF and ethanol since the ethanol destroys any residual sodium. Thus, sodium (35 mmol) and selenium (50 mmol) were combined in liquid (10 cm^3) ammonia at −78°C and stirred together for 1 h before the reaction was warmed to room temperature and the ammonia evaporated off. A mixture of THF (15 cm^3) and ethanol (10 cm^3) was added followed by Ph_2PCl (35 mmol) and the reaction was stirred at room temperature overnight. ^{31}P NMR analysis of the reaction mixture revealed the presence of $Ph_2P(Se)H$ (δ = 6.4 ppm, comparable with the reported value[7]) and $Ph_2P(Se)OP(Se)Ph_2$ (δ = 84.5 ppm) together with a number of other species.

* Author to whom correspondence should be addressed.

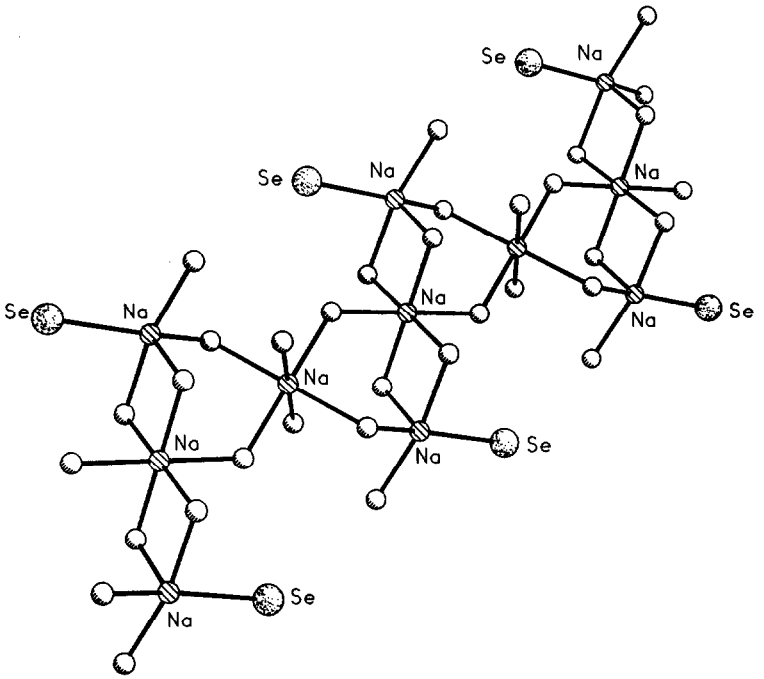

Fig. 1. The X-ray structure of the central polymeric core in **5** showing the octahedral and distorted trigonal bipyramidal sodium environments.

Addition of hexane enabled the isolation of crystals of (5) suitable for X-ray analysis.*

The X-ray analysis reveals a polymeric structure consisting of a central core of fused and spiro Na_3O_3 rings (Fig. 1). The sodium atoms are linked by water molecules; two of the sodium atoms, which are octahedrally coordinated by six water molecules, lie on independent crystallographic centres of symmetry, the third is in a general position and has distorted trigonal bipyramidal coodination. This latter sodium atom has three *facial* water molecules, the other two sites being occupied by a THF and a selenium atom from one of the $Ph_2PSe_2^-$ anions. The other $Ph_2PSe_2^-$ anion is linked (Fig. 2) to the central polymeric core via pairs of O—H···Se hydrogen bonds [Se(1)···O(2) 3.42, Se(2)···O(3) 3.38, Se(1)···H—O(2) 172°, Se(2)···H—O(3) 173°]. Within the asymmetric unit (Fig. 3) the Na—OH_2 distances are in the range 2.347(4)–2.497(4) Å (Table 1) with the Na—O(THF) distance [2.388(4) Å] also being within this range. The Na—Se distance is, as expected, significantly longer [2.984(2) Å]. The P—Se bond lengths in the hydrogen-bonded anion are equivalent [2.156(1), 2.152(1) Å] and intermediate to the two distances in the other anion which are significantly different from each other [P(2)—Se(3) 2.142(1), P(2)—Se(4) 2.161(1) Å]. Surprisingly, the shortest P—Se bond is for the sodium-bound selenium atom; the non-coordinate selenium atom Se(4) only having a long range contact to a water oxygen atom O(3′) of 3.55 Å. The closest contact of a proton of O(3′) to Se(4) is 2.61 Å, cf. H···Se distances of 2.46 and 2.43 Å for Se(1) and Se(2), respectively.

The observation of six-membered $Na_3(H_2O)_3$ rings is not especially surprising and we believe that these rings could be readily built up into extended 2-D and 3-D arrays. Perhaps the most surprising feature in the structure of **5** is the formation of an Na—Se bond with shortening of the P—Se bond

*Crystal data (**5**), $C_{28}H_{38}O_6P_2Se_4Na_2$, $M = 894.4$, triclinic, $a = 8.709(2)$, $b = 15.158(5)$, $c = 15.676(3)$ Å, $\alpha = 68.37(2)$, $\beta = 74.12(2)$, $\gamma = 77.06(2)°$, $U = 1833$ Å^3, space group $P\bar{1}$, $Z = 2$, $D_c = 1.62$ g cm^{-3}, μ(Cu-K_α) = 63.2 cm^{-1}, $F(000) = 884$. Crystal dimensions 0.13 × 0.40 × 0.60 mm. Data were measured on a Nicolet R3m diffractometer with graphite monochromated Cu-K_α radiation using ω-scans. The structure was solved by direct methods and refined anisotropically using absorption corrected data (maximum and minimum transmission factors 0.438 and 0.098, respectively) to give $R = 0.046$, $R_w = 0.051$ for 4526 independent observed reflections [$|F_o| > 3\sigma(|F_o|)$, $2\theta \leqslant 116°$]. The atomic coordinates are available on request from the Director of the Cambridge Crystallographic Data Centre, University Chemical Laboratory, Lensfield Rd, Cambridge CB2 1EW. Any request should be accompanied by a full literature citation for this communication.

Table 1. Bond lengths (Å) and angles (°) with esds in parentheses

P(1)—Se(1)	2.156(1)	P(1)—Se(2)	2.152(1)
P(1)—C(1)	1.832(6)	P(1)—C(7)	1.832(4)
P(2)—Se(3)	2.142(1)	P(2)—Se(4)	2.161(1)
P(2)—C(13)	1.848(4)	P(2)—C(19)	1.828(6)
Se(3)—Na(1)	2.984(2)	C(13)—C(14)	1.372(6)
O(1)—C(25)	1.419(7)	O(1)—C(28)	1.399(7)
O(1)—Na(1)	2.388(4)	Na(1)—O(2)	2.348(4)
Na(1)—O(4)	2.442(3)	Na(1)—O(6′)	2.347(4)
Na(2)—O(2)	2.497(4)	Na(2)—O(3)	2.433(3)
Na(2)—O(5)	2.431(3)	Na(2)—O(2′)	2.497(4)
Na(2)—O(3′)	2.433(3)	Na(2)—O(5′)	2.431(3)
Na(3)—O(3)	2.451(4)	Na(3)—O(4)	2.431(3)
Na(3)—O(6)	2.349(3)	Na(3)—O(3″)	2.451(4)
Na(3)—O(4′)	2.431(3)	Na(3)—O(6′)	2.349(3)
O(6)—Na(1′)	2.347(4)		
Se(1)—P(1)—Se(2)	117.4(1)	Se(1)—P(1)—C(1)	107.7(2)
Se(2)—P(1)—C(1)	110.1(2)	Se(1)—P(1)—C(7)	109.0(1)
Se(2)—P(1)—C(7)	108.6(2)	Se(4)—P(2)—C(19)	108.4(1)
Se(3)—P(2)—Se(4)	116.0(1)	Se(3)—P(2)—C(13)	109.1(2)
Se(4)—P(2)—C(13)	107.5(1)	Se(3)—P(2)—C(19)	110.2(1)
P(2)—Se(3)—Na(1)	92.7(1)	C(25)—O(1)—C(28)	107.1(4)
C(25)—O(1)—Na(1)	121.6(4)	C(28)—O(1)—Na(1)	121.5(4)
O(1)—C(25)—C(26)	108.2(6)	C(25)—C(26)—C(27)	107.7(7)
C(26)—C(27)—C(28)	108.6(7)	O(1)—C(28)—C(27)	107.5(6)
Se(3)—Na(1)—O(1)	97.9(1)	Se(3)—Na(1)—O(2)	162.1(1)
O(1)—Na(1)—O(2)	89.5(1)	Se(3)—Na(1)—O(4)	93.4(1)
O(1)—Na(1)—O(4)	168.1(2)	O(2)—Na(1)—O(4)	80.8(1)
Se(3)—Na(1)—O(6′)	91.0(1)	O(1)—Na(1)—O(6′)	87.3(2)
O(2)—Na(1)—O(6′)	105.7(2)	O(4)—Na(1)—O(6′)	88.7(1)
O(2)—Na(2)—O(3)	93.3(1)	O(2)—Na(2)—O(5)	91.5(1)
O(3)—Na(2)—O(5)	88.1(1)	O(2)—Na(2)—O(2′)	180.0
O(3)—Na(2)—O(2′)	86.7(1)	O(5)—Na(2)—O(2′)	88.5(1)
O(2)—Na(2)—O(3′)	86.7(1)	O(3)—Na(2)—O(3′)	180.0
O(5)—Na(2)—O(3′)	91.9(1)	O(2′)—Na(2)—O(3′)	93.3(1)
O(2)—Na(2)—O(5′)	88.5(1)	O(3)—Na(2)—O(5′)	91.9(1)
O(5)—Na(2)—O(5′)	180.0	O(2′)—Na(2)—O(5′)	91.5(1)
O(3′)—Na(2)—O(5′)	88.1(1)	O(3)—Na(3)—O(4)	90.5(1)
O(3)—Na(3)—O(6)	93.9(1)	O(4)—Na(3)—O(6)	91.1(1)
O(3)—Na(3)—O(3″)	180.0	O(4)—Na(3)—O(3″)	89.5(1)
O(6)—Na(3)—O(3″)	86.1(1)	O(3)—Na(3)—O(4′)	89.5(1)
O(4)—Na(3)—O(4′)	180.0	O(6)—Na(3)—O(4′)	88.9(1)
O(3″)—Na(3)—O(4′)	90.5(1)	O(3)—Na(3)—O(6′)	86.1(1)
O(4)—Na(3)—O(6′)	88.9(1)	O(6)—Na(3)—O(6′)	180.0
O(3″)—Na(3)—O(6′)	93.9(1)	O(4′)—Na(3)—O(6′)	91.1(1)
Na(1)—O(2)—Na(2)	112.1(1)	Na(2)—O(3)—Na(3)	126.2(1)
Na(1)—O(4)—Na(3)	89.0(1)	Na(3)—O(6)—Na(1′)	93.4(1)

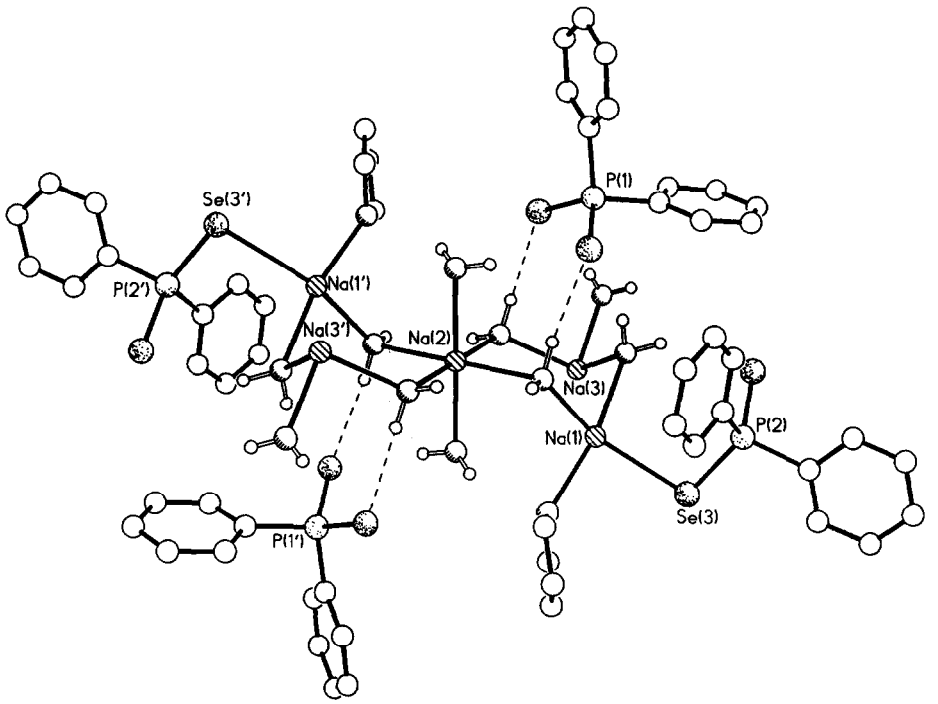

Fig. 2. Part of the structure of **5** showing the hydrogen bonding of the non-coordinated $Ph_2PSe_2^-$ anion to the central polymeric core.

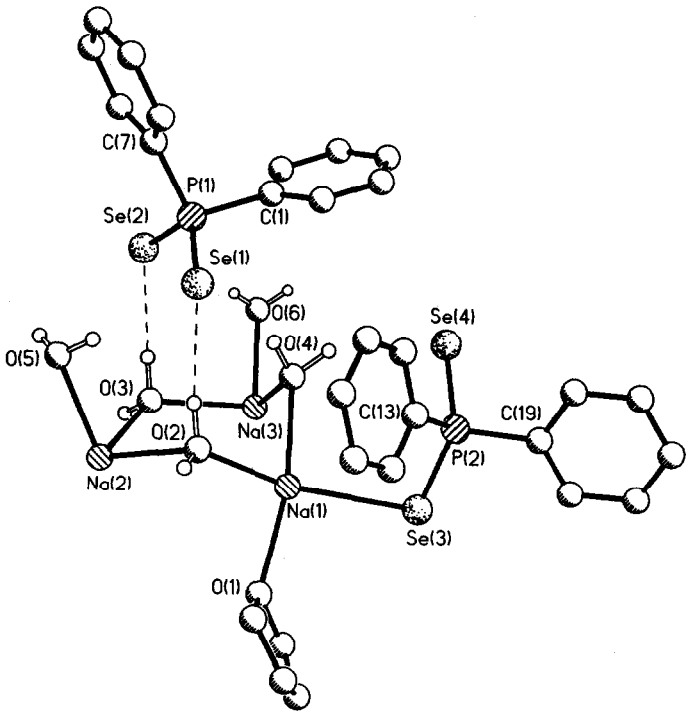

Fig. 3. The asymmetric unit in **5** giving the numbering scheme.

and further studies into the generality of this observation are in progress.

Acknowledgements—JDW and MJP are grateful to SERC for the award of an earmarked studentship and to the Wolfson Foundation for support. JDW is currently the Sir Edward Frankland Fellow of the Royal Society of Chemistry.

REFERENCES

1. M. J. Pilkington, A. M. Z. Slawin, D. J. Williams, P. T. Wood and J. D. Woollins, *Heteroatom* 1990, **1**, 351.
2. S. W. Hall, M. J. Pilkington, A. M. Z. Slawin, D. J. Williams and J. D. Woollins, *Polyhedron* 1991, **10**, 261.
3. I. P. Parkin, M. J. Pilkington, A. M. Z. Slawin, D. J. Williams and J. D. Woollins, *Polyhedron* 1990, **9**, 987.
4. S. C. O'Neal and J. W. Kolis, *Inorg. Chem.* 1989, **28**, 2780.
5. S. C. O'Neal and J. W. Kolis, *J. Am. Chem. Soc.* 1988, **110**, 1971.
6. J. W. Kolis, *Coord. Chem. Rev.* 1990, **105**, 195 and refs therein.
7. W. McFarlane and S. S. Rycroft, *J. Chem. Soc., Chem. Commun.* 1972, 902.

Polyhedron Vol. 10, No. 22, pp. 2647–2650, 1991
Printed in Great Britain

0277-5387/91 $3.00+.00
© 1991 Pergamon Press plc

COMMUNICATION

SYNTHESIS AND X-RAY CRYSTAL STRUCTURE OF $Re_4(NBu^t)_8(\mu\text{-}O)_2(\mu_3\text{-}O)_2(OSO_2CF_3)_4$

HON-WAH LAM, GEOFFREY WILKINSON* and DAVID J. WILLIAMS*

Johnson Matthey and Chemical Crystallography Laboratories, Chemistry Department, Imperial College, London SW7 2AY, U.K.

(*Received* 22 *July* 1991; *accepted* 21 *August* 1991)

Abstract—Interaction of $Re(NBu^t)_3(NHBu^t)$ and CF_3SO_3H in Et_2O leads to the known $[Re(NBu^t)_3(NH_2Bu^t)]O_3SCF_3$ but also to a low yield, presumably via a competitive reaction, of a red compound, $Re_4(NBu^t)_8(\mu\text{-}O)_2(\mu_3\text{-}O)_2(OSO_2CF_3)_4$, whose X-ray crystal structure has been determined.

The structure has a Re_4O_4 core comprising oxo-bridged, five- and six-coordinate rhenium centres. The six-coordinate rhenium centres have *cis* oriented oxo, NBu^t and $\eta^1\text{-}O_3SCF_3$ ligands; the five-coordinate centres have pairs of NBu^t and μ_3-O ligands and a μ-O ligand.

In previous papers we have described the synthesis and X-ray crystal structures of binuclear oxo-bridged rhenium compounds, e.g. $[Re(NBu^t)_2(OSiMe_3)]_2(\mu\text{-}O)(\mu\text{-}OSiMe_3)(\mu\text{-}O_2CCF_3)$.[1] We now report the synthesis of a tetrameric neutral species $Re_4(NBu^t)_8(\mu\text{-}O)_2(\mu_3\text{-}O)_2(OSO_2CF_3)_4$ (**1**).

In the synthesis[1b] of $[Re(NBu^t)_3(NHBu^t)]O_3SCF_3$ by interaction of CF_3SO_3H with $Re(NBu^t)_3(NHBu^t)$ in diethylether it was noted that after removal of the yellow precipitate of the triflate, the filtrate had an orange colour and gave an orange oil after the removal of volatiles. Extraction of the oil with diethylether and work-up led to red crystals of **1** whose crystal structure has been determined (see below). It is not clear whether a competitive reaction, which involves not only loss of one NBu^t group from the rhenium atom but also the formation of μ-O groups is associated with adventitious water or comes from cleavage of diethylether. The materials used were all thoroughly dried and reactions carried out under dry nitrogen or *in vacuo*. Thus, the oxo groups could arise by the well known acid cleavage of ethers,[2] *viz*

$$Et_2O + HSO_3CH_3 \longrightarrow EtSO_3CF_3 + EtOH,$$

followed by the reaction at the metal centre:

$$L_nRe + EtOH \longrightarrow L_nRe + C_2H_4 + H_2O,$$

and hydrolysis of the imido rhenium species by water.

The structure has crystallographic C_i symmetry with an approximately planar (maximum deviation 0.2 Å) Re_4O_4 core comprising oxo-bridged five- and six-coordinate rhenium centres (Fig. 1; Table 1 gives main bond lengths and angles). Re(1) has distorted octahedral symmetry with pairs of *cis*-oriented oxo, NBu^t and O_3SCF_3 ligands. The angles at Re(1) are in the ranges 74–105° and 156–164°, the enlargements from 90° being due to accommodating the bulky NBu^t and O_3SCF_3 groups. The two Re—NBu^t bonds are of the same length, 1.718(7) Å to N(1) and 1.711(7) Å to N(2). However, the angles at nitrogen differ significantly, with that *trans* to O_3SCF_3 appreciably bent [157.6(7)°], whilst that *trans* to one of the oxo bridges, N(2), is almost linear [172.0(7)°]. There is also a marked difference in the two Re—O_3SCF_3 bond lengths; that *trans* to μ-O is significantly shorter [2.084(6) Å] than that *trans* to NBu^t [2.272(7) Å].

The geometry at Re(2) can be considered as either distorted trigonal bipyramidal with the oxygens O(1) and O(2) of the oxo bridges as the apical atoms and the two NBu^t ligands and the symmetry related bridging oxo oxygen O(2′) as the equatorial components; Re(2), N(4), N(3) and O(2′) are co-planar to within 0.03 Å. Alternatively, the arrangement may be visualized as distorted square pyramidal

* Authors to whom correspondence should be addressed.

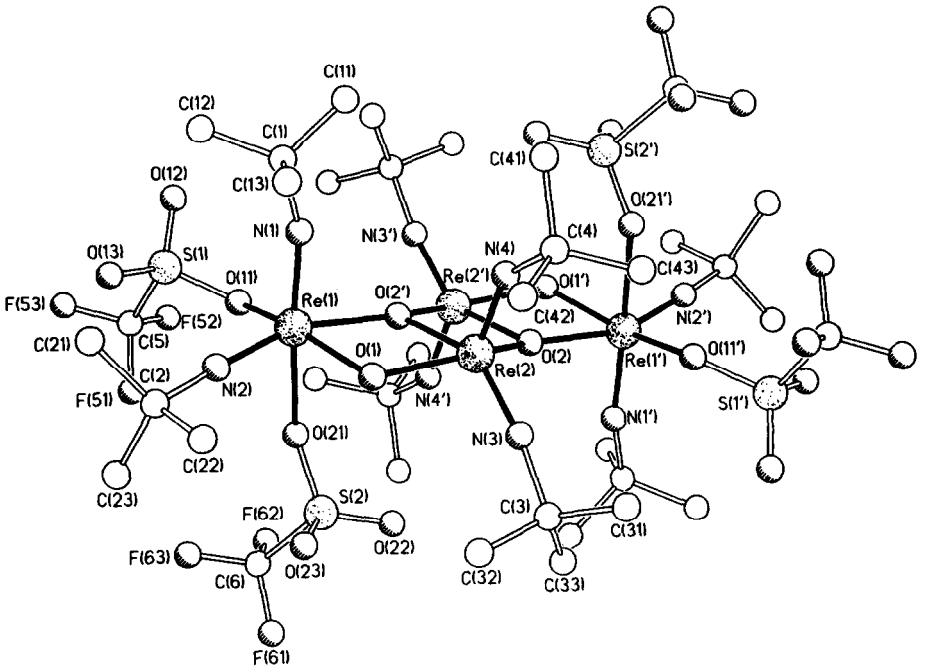

Fig. 1. The structure of $Re_4(NBu^t)_8(\mu\text{-}O)_2(\mu_3\text{-}O)_2(OSO_2CF_3)_4$ (**1**).

with O(2), O(2′), O(1), N(3) and Re(2) forming the base and N(4) the apex (Fig. 2). In this configuration Re(2) lies 0.5 Å above the basal plane towards N(4). The two Re—NBu^t bonds differ significantly, with that "*trans*" to μ_3-O to N(3) 1.684(7) Å, noticeably shorter than that to the apical N atom N(4), 1.724(7) Å. Furthermore, the angle at N(3), 171.8(6)° is very much closer to linear than that to N(4), 143.9(6)°. There are marked asymmetries in the Re—O—Re bridges with Re—O distances rang-

Table 1. Selected bond lengths (Å) and bond angles (°)

Re(1)—O(1)	1.911(5)	Re(1)—N(1)	1.718(7)
Re(1)—N(2)	1.711(7)	Re(1)—O(11)	2.084(6)
Re(1)—O(21)	2.272(7)	Re(1)—O(2′)	2.156(6)
O(1)—Re(2)	1.928(6)	Re(2)—O(2)	1.943(6)
Re(2)—N(3)	1.684(7)	Re(2)—N(4)	1.724(7)
Re(2)—O(2′)	2.094(5)		

O(1)—Re(1)—N(1)	101.3(3)	O(1)—Re(1)—N(2)	93.3(3)
N(1)—Re(1)—N(2)	105.0(4)	O(1)—Re(1)—O(11)	155.6(3)
N(1)—Re(1)—O(11)	94.8(3)	N(2)—Re(1)—O(11)	100.2(3)
O(1)—Re(1)—O(21)	85.9(2)	N(1)—Re(1)—O(21)	164.3(3)
N(2)—Re(1)—O(21)	88.2(4)	O(11)—Re(1)—O(21)	74.4(2)
O(1)—Re(1)—O(2′)	73.6(2)	N(1)—Re(1)—O(2′)	90.4(3)
N(2)—Re(1)—O(2′)	161.6(3)	O(11)—Re(1)—O(2′)	88.1(2)
O(21)—Re(1)—O(2′)	78.2(2)	Re(1)—O(1)—Re(2)	112.5(3)
Re(1)—N(2)—C(2)	172.0(7)	Re(1)—N(1)—C(1)	157.6(7)
Re(1)—O(11)—S(1)	128.6(4)	Re(1)—O(21)—S(2)	132.6(4)
O(1)—Re(2)—O(2)	143.6(2)	O(1)—Re(2)—N(3)	95.1(3)
O(2)—Re(2)—N(3)	100.4(3)	O(1)—Re(2)—N(4)	100.7(3)
O(2)—Re(2)—N(4)	106.0(3)	N(3)—Re(2)—N(4)	106.7(3)
O(1)—Re(2)—O(2′)	74.7(2)	O(2)—Re(2)—O(2′)	73.3(3)
N(3)—Re(2)—O(2′)	143.5(3)	N(4)—Re(2)—O(2′)	109.6(3)
Re(2)—O(2)—Re(1′)	154.6(3)	Re(2)—O(2)—Re(2′)	106.7(3)
Re(1′)—O(2)—Re(2′)	97.4(2)	Re(2)—N(3)—C(3)	171.8(6)
Re(2)—N(4)—C(4)	143.9(6)		

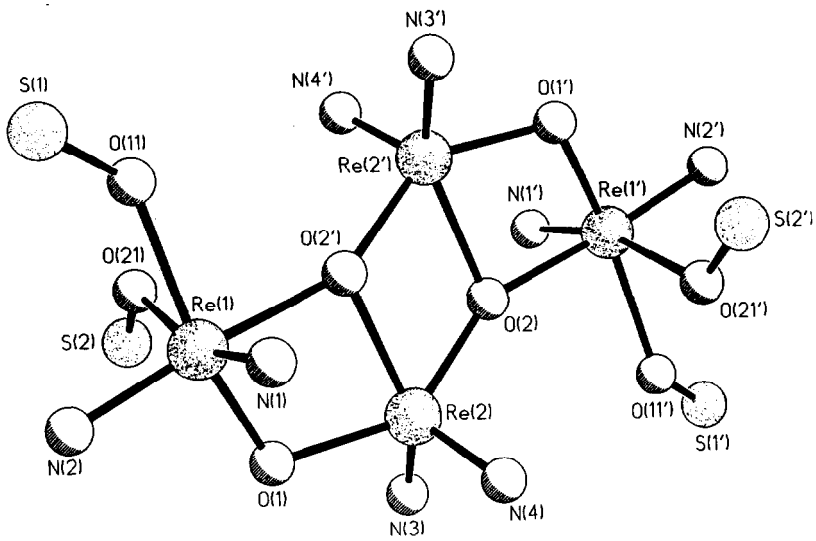

Fig. 2. Core structure of **1** showing geometries about rhenium.

ing between 1.911(5) Å for Re(1)—O(1) to 2.156(6) Å for Re(1)—O(2). There is no obvious rationale to this though overall the μ-O distances are shorter than the μ_3-O distances. The central Re_2O_2 ring is planar with transannular Re—Re and O—O distances of 3.24 and 2.41 Å, respectively, whereas the outer Re_2O_2 rings are slightly folded with fold angles of 12° about the O(1)—O(2′) axis and 17° about Re(1)—Re(2). In the latter the transannular Re—Re and O—O distances are 3.19 and 2.44 Å.

There are no important non-bonded intermolecular interactions.

The NMR and IR spectra of **1** are not particularly instructive other than bands for NBu^t and CF_3SO_3 and some bands below 1000 cm^{-1} that could be oxo stretches. Unidentate trifluoromethane sulphonate compounds have been characterized.[3]

EXPERIMENTAL

The general procedures and instruments were as previously.[1b] Solvents were dried by standard methods and all operations were carried out under purified nitrogen or argon.

The procedure[1b] for synthesis of $[Re(NBu^t)_3(NH_2Bu^t)]O_3SCF_3$ was followed using $Re(NBu^t)_3(NHBu^t)$ (0.5 g, 1.06 mmol) in Et_2O (20 cm^3) and CF_3SO_3H (3.0 cm^3 of 0.35 M solution in Et_2O, 1.06 mmol) at −78°C. After stirring (1 h) and warming to room temperature with stirring for a further 12 h, the yellow precipitate of the triflate was collected and the mother liquor evaporated in vacuum to leave an orange oil. This was extracted with Et_2O (10 cm^3) which was filtered, concentrated and cooled (−20°C) to yield red crystals. Yield: *ca* 10%; m.p. 159–160°. NMR, ^1H ($CDCl_3$); δ 1.68s, NBu^t. IR: (Nujol mull): 1260 (Re=NBu^t), 1189 (CF_3SO_3) cm^{-1}.

X-ray crystallography

Crystal data: $C_{36}H_{72}F_{12}N_8O_{16}Re_4S_4$, $M = 1974.1$, monoclinic, $a = 12.530(4)$, $b = 16.264(5)$, $c = 15.990(8)$ Å, $\beta = 94.91(3)°$, $V = 3247$ $Å^3$, space group $P2_1/n$, $Z = 2$ (the molecule is disposed about a centre of symmetry), $D_c = 2.02$ g cm^{-3}, copper radiation, $\lambda = 1.54178$ Å, μ(Cu-K_α) = 163 cm^{-1}, $F(000) = 1888$. Data were measured on a Nicolet R3m diffractometer with Cu-K_α radiation (graphite monochromator) using ω-scans. A crystal of dimensions $0.17 \times 0.23 \times 0.41$ mm sealed under argon in a Lindemann glass capillary was used. 4386 independent reflections ($2\theta \leqslant 116°$) were measured, of which 3799 had $|F_o| > 3\sigma(|F_o|)$, and were considered to be observed. The data were corrected for Lorentz and polarization factors; a numerical absorption correction (face-indexed crystal) was applied; maximum and minimum transmission factors 0.192 and 0.047. The structure was solved by the heavy atom method. The non-hydrogen atoms were refined anisotropically. The positions of the hydrogen atoms were idealized, C—H = 0.96 Å, assigned isotropic thermal parameters, $U(H) = 1.2U_{eq}(C)$, and allowed to ride on their parent carbon atoms. The methyl groups were refined as rigid bodies. Refinement was by blocked full-matrix least-squares to $R = 0.036$, $R_w = 0.035$ [$w^{-1} = \sigma^2(F) + 0.00050F^2$]. The maximum and minimum

residual electron densities in the final ΔF map were 1.37 and -1.29 e $Å^{-3}$, respectively. The mean and maximum shift/error in the final refinement were 0.004 and 0.027, respectively. Computations were carried out on an IBM PS/2 model 70 PC using the SHELXTL PC program system. Full supplementary material has been deposited.

Acknowledgements—We thank the Croucher Foundation, Hong Kong for a Fellowship (W-H. Lam) and the SERC for provision of X-ray facilities.

REFERENCES

1. (a) A. A. Danopoulos, G. Wilkinson and D. J. Williams, *J. Chem. Soc., Chem. Commun.* 1991, 181; (b) V. Saboonchian, A. A. Danopoulos, A. Gutierrez, G. Wilkinson and D. J. Williams, *Polyhedron* 1991, **10**, 2241.
2. J. March, *Advanced Organic Chemistry: Reactions, Mechanisms and Structures*, pp. 327–344. McGraw-Hill, New York (1968).
3. A. A. Danopoulos, G. Wilkinson, B. Hussain-Bates and M. B. Hursthouse, *J. Chem. Soc., Dalton Trans.* 1990, 2753; *Polyhedron* 1989, **8**, 2947.

Polyhedron Vol. 10, No. 23/24, pp. 2651–2657, 1991
Printed in Great Britain

0277–5387/91 $3.00+.00
© 1991 Pergamon Press plc

SYNTHESES AND ELECTROCHEMISTRY OF SOME TRANSITION METAL COMPLEXES WITH 2-MERCAPTOPYRIDINE N-OXIDE AND CRYSTAL STRUCTURE OF BIS(2-MERCAPTOPYRIDINE N-OXIDE)NICKEL(II)

XUETAI CHEN, YONGHAN HU, DAXU WU, LINGHONG WENG and BEISHENG KANG*

Fuzhou Laboratory of Structural Chemistry and Fujian Institute of Research on the Structure of Matter, Chinese Academy of Sciences, Fuzhou, Fujian 350002, China

(*Received* 19 *July* 1991; *accepted* 27 *August* 1991)

Abstract—The complexes $M(mpo)_n$ (M = Mn, Ni, $n = 2$; M = Fe, Co, $n = 3$) (Hmpo = 2-mercaptopyridine N-oxide) were prepared by reacting the appropriate metal chloride with either Nampo or dtpo [2,2-dithiobis(pyridine N-oxide)] in the presence of sodium methoxide. The structure of the complex $Ni(mpo)_2$ was determined by X-ray diffraction. The nickel atom is in a square planar environment of two mpo^- ligands in the *cis* configuration. The four complexes were investigated by physicochemical methods especially by ^1H NMR spectroscopy and cyclic voltammetry.

Transition-metal thiolato complexes have been of interest for the simulation of many metallo-enzymes where the thiolato group mimics the ligation of cysteinyl residues in proteins. Recently we have studied a series of transition metal complexes with 1,2-bidentate sulphur-containing ligands such as 2-mercaptophenol (H_2mp)[1–5] and 2-mercapto-3-pyridinol (H_2mpp),[6] of which H_2mp has been found to be a multifunctional ligand in its ligation to transition metal atoms with versatile coordination modes.[5] It would be interesting to learn if other bidentate ligands with simultaneous oxido and sulphido donor atoms may exhibit similar but not identical coordination behaviour with respect to their varied aromatic rings. The coordination chemistry of metal complexes with the ligand 2-mercaptopyridine N-oxide (Hmpo) has scarcely been studied[7–8] in spite of their potential biological activities,[9] whereas those with amine N-oxide have been described and reviewed extensively.[10–11] The syntheses and physicochemical characterizations of complexes $M(mpo)_n$ (M = Mn, Ni, $n = 2$; M = Fe, Co, $n = 3$) and crystal structure of $Ni(mpo)_2$ are described in this paper following the report of the crystal structure of $Co(mpo)_3 \cdot CH_3CN$.[12]

EXPERIMENTAL

Materials and methods

All solvents were reagent grade and dried with molecular sieves. Sodium 2-mercaptopyridine N-oxide (Nampo), 2,2′-dithiobis(pyridine N-oxide) (dtpo) and metal chlorides were all commercially available and used without further purification.

Physical measurements were performed on the following instruments: IR, Perkin–Elmer 577 spectrophotometer (solids in KBr pellets); ^1H NMR, Varian FT-80A spectrometer (SIMEQ program for spectrum simulation); cyclic voltammetry, Longjin Model 8511B potentiostat (a Pt-inlay working electrode, Pt-wire auxiliary electrode and SCE reference electrode); mass spectra, Finnigan MAT 312 (or 8230) GC/MS/DS mass spectrometer (EI or FAB mode); X-ray crystallography, MSC/Rigaku diffractometer.

Preparations of complexes

$Mn(mpo)_2$ (**1**). To a solution of Nampo (0.60 g, 4.0 mmol) in 50 cm^3 of DMF/MeOH (2:1) was

* Author to whom correspondence should be addressed.

added solid $MnCl_2 \cdot 4H_2O$ (0.40 g, 2.0 mmol). The mixture was stirred for 4 h and filtered. The green filtrate was stored at 5°C for several days to give the green powder of **1** (yield: 70%), which was collected, washed with THF and dried *in vacuo*. Found: Mn, 17.5; S, 19.3. Calc. for $C_{10}H_8MnN_2O_2S_2$: Mn, 17.9; S, 20.9%. IR (KBr): 3040(w), 1585(m), 1530(m), 1450(s), 1405(s), 1265(w), 1255(w), 1230(w), 1195(s), 1180(s), 1150(m, C—S), 1140(s, C—S), 1085(s, N—O), 1025(w), 825(s), 780(m), 750(s), 705(s), 615(m), 585(s), 550(m), 435(w), 360(s), 345(w), 280(w), cm^{-1}. MS (EI): 307 (M^+).

Fe(mpo)$_3$ (**2**). Route 1: A mixture of anhydrous $FeCl_2$ (0.10 g, 0.79 mmol), dtpo (0.30 g, 1.19 mmol) and NaOMe (0.043 g, 0.80 mmol) in 20 cm^3 of MeOH was stirred for 19 h and filtered. The dark blue filtrate was stored at 5°C to give dark microcrystals of **2** (yield: 67%), which was collected and dried *in vacuo*. Found: Fe, 13.0; S, 21.8. Calc. for $C_{15}H_{12}FeN_3N_3O_3S_3$: Fe, 12.9; S, 20.1%. IR (KBr): 3040(w), 1600(m), 1540(m), 1460(s), 1420(m), 1265(w), 1230(w), 1200(m), 1160(m, C—S), 1145(m, C—S), 1090(s, N—O), 1030(w), 830(s), 765(s), 750(s), 715(s), 610(s), 560(m), 515(w), 440(w), 340(m), 260(m) cm^{-1}. MS (FAB): 434 ($M^+ + H$).

Route 2: A mixture of $FeCl_3 \cdot 6H_2O$ (0.065 g, 0.24 mmol) and Nampo (0.11 g, 0.73 mmol) in 50 cm^3 of acetone/methanol (1:2) was stirred for 1 h to give a deep blue solution with some precipitates, which was then filtered. The filtrate was stored at 5°C to give dark blue microcrystals. The precipitate was recrystallized from DMF/^{i}PrOH to give deep blue microcrystals also (total yield: 75%). Their IR spectra are identical to that obtained by route 1.

Co(mpo)$_3$ (**3**). Route 1: A mixture of $CoCl_2 \cdot 6H_2O$ (0.15 g, 0.63 mmol), dtpo (0.32 g, 1.27 mmol) and NaOMe (0.07 g, 1.3 mmol) in 40 cm^3 of MeOH/MeCN (1:1) was stirred for 18 h and filtered. The dark brown filtrate was stored at 5°C for several days to give large black block crystals of **3**·CH_3CN (yield: 63%), which were collected and dried *in vacuo*. Found: C, 43.1; H, 3.3; Co, 13.0; N, 11.2; S, 19.2. Calc. for $C_{17}H_{15}CoN_4O_3S_3$: C, 42.7; H, 3.2; Co, 12.3; N, 11.7; S, 20.1%. IR (KBr): 3040(w), 1595(m), 1535(s), 1450(s), 1400(s), 1260(m), 1230(s), 1175(s), 1150(s, C—S), 1130(s, C—S), 1085(s, N—O), 1030(w), 1020(m), 815(s), 745(s), 705(s), 610(s), 570(w), 500(w), 430(m), 380(m), 335(m) cm^{-1}. MS (FAB): 438 ($M^+ + H$).

Route 2: A mixture of anhydrous $CoCl_2$ (0.2 g, 1.54 mmol), Nampo (0.23 g, 1.53 mmol) in 30 cm^3 of THF was stirred for 21 h and filtered. The greenish brown filtrate was stored at 5°C to give microcrystals (total yield: 78%), which were collected. The IR spectrum is identical to that obtained by route 1 except for the absorptions of CH_3CN.

Ni(mpo)$_2$ (**4**). Route 1: To a suspension of dtpo (0.38 g, 1.5 mmol) in 50 cm^3 of MeOH/MeCN (1:1) was added $NiCl_2 \cdot 6H_2O$ (0.24 g, 1.0 mmol). The mixture was stirred for a while and added to NaOMe (0.10 g, 1.85 mmol). After stirring for 20 h, the solution developed a brown colour and was then filtered. The filtrate gave deep brown prism crystals of **4** (yield: 60%) on standing at 5°C, which were collected by filtration. Found: C, 38.8; H, 2.9; N, 8.6; Ni, 18.0; S, 19.9. Calc. for $C_{10}H_8N_2NiO_2S_2$: C, 38.6; H, 2.6; N, 9.0; Ni, 18.9; S, 20.6%. IR (KBr): 3040(w), 1595(m), 1545(s), 1480(w), 1455(s), 1410(m), 1270(w), 1250(s), 1180(s), 1150(sh, C—S), 1140(m, C—S), 1085(s, N—O), 1050(w), 1030(w), 825(s), 745(s), 710(s), 695(w), 665(m), 630(s), 430(m), 395(m), 335(m), 275(m) cm^{-1}. MS (EI): 310 (M^+).

Route 2: A mixture of $NiCl_2 \cdot 6H_2O$ (0.48 g, 2 mmol) and Nampo (0.60 g, 4.0 mmol) in 80 cm^3 of MeOH/MeCN (3:5) was stirred for 15 h and filtered. The precipitate was recrystallized from DMF to give brown prism crystals of **4** and the filtrate was stored at 5°C to give **4** also (total yield: 87%). The IR spectra and crystal parameters are identical to that obtained by route 1.

X-ray crystallography

Crystal data for **4**. $C_{10}H_8N_2NiO_2S_2$, Mr = 311.03, monoclinic, space group $P2_1/n$, a = 8.769(4), b = 13.627(4), c = 9.857(3) Å, β = 97.76(3)°, V = 1167.1 Å^3, Z = 4, D_c = 1.770 g cm^{-3}, μ = -22.1 cm^{-1}, $F(000)$ = 632.

A single crystal of **4** with the dimensions 0.25 × 0.3 × 0.2 mm obtained from the reaction solution of route 1 was mounted on a MSC/Rigaku diffractometer with Mo-K_α (λ = 0.71069 Å) radiation and graphite monochromator. A total of 2854 reflections were collected in the range of $2° \leqslant 2\theta \leqslant 54.1°$ in the ω–2θ scan mode and corrected for anisotropic decay, LP factors and absorptions empirically. The systemic absence ($h0l$, $h+l = 2n$; $0k0$, $k = 2n$) indicated the space group to be $P2_1/n$ exclusively. The 2133 unique reflections with $I \geqslant 3\sigma(I)$ were used for structure determination. The structure was solved by direct methods on a VAX 11/785 computer with the SDP program package and refined by full-matrix least-squares procedures with anisotropic thermal parameters for all non-hydrogen atoms. The hydrogen atoms were added to the structure factor calculations but not refined. The final R value is 0.034 and the R_w value is 0.037 with w = 1.

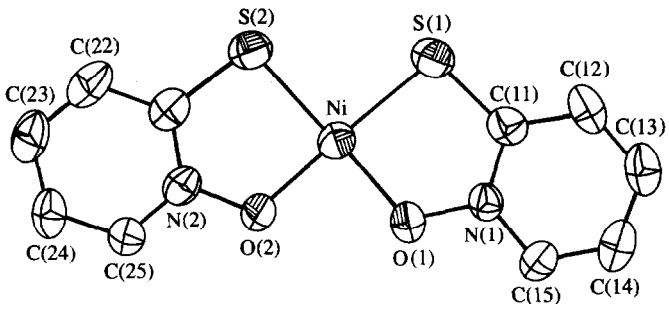

Fig. 1. ORTEP diagram of the structure of **4**.

RESULTS AND DISCUSSION

Synthetic studies

Complexes **1**–**4** were obtained by treatment of the respective metal chloride with Nampo in the appropriate organic solvent (route 2). This procedure is different from that reported by Robinson[8] which was performed in aqueous medium. All these complexes except **1**, can also be synthesized by the reaction of metal chlorides with the organic disulphide dtpo under strongly basic conditions (route 1). Considering the possibility of hetero-cleavage of the disulphide in cobalt(III) disulphide systems[13] in the presence of a strong base, we believe that route 1 might involve the cleavage of dtpo in the presence of base to form mpo^- and then the latter coordinates to the metal atoms. But, the possibility of coordination of dtpo to the metal atoms first and then by base hydrolysis to give the products is not excluded. However, the reaction of $MnCl_2 \cdot 6H_2O$ with dtpo forms only insoluble and inextractable materials which were not further studied.

It is interesting to note that these complexes can be prepared whether under a dinitrogen atmosphere or not and are stable in air. Until now, we have not been able to prepare similar complexes with the oxidation states nickel(III), manganese(III), iron(II) and cobalt(II). Unlike this, many 1,2-dithiolenes such as benzenedithiolate or toluenedithiolate[14–15] can stabilize both divalent and tervalent metal ions. This observation agrees well with the electrochemical behaviour of these complexes (*vide infra*).

Structure description

The structure of complex **4** is shown in Fig. 1 and selected bond lengths and bond angles are given in Table 1. The molecule has a nickel atom in the centre of the nearly square plane of NiS_2O_2 with the oxido and sulphido atoms from the two mpo^- ligands in *cis* configuration. The whole molecule exhibits a pseudo-C_{2v} symmetry with the C_2 axis passing through the nickel atom and the mid-points of S(1)---S(2) and O(1)---O(2). The Ni^{II}—S bond lengths of av. 2.132 Å are somewhat

Table 1. Selected bond distances (Å) and bond angles (°) for complex **4**

Ni—S(1)	2.136(1)	S(2)—C(21)	1.343(4)
Ni—S(2)	2.129(1)	O(1)—N(1)	1.348(4)
Ni—O(1)	1.868(3)	O(2)—N(2)	1.351(4)
Ni—O(2)	1.864(3)	N(1)—C(11)	1.342(5)
S(1)—C(11)	1.710(4)	N(2)—C(21)	1.343(4)
S(1)—Ni—S(2)	92.81(4)	Ni—S(2)—C(21)	97.0(1)
S(1)—Ni—O(1)	89.67(8)	Ni—O(1)—N(1)	115.9(3)
S(1)—Ni—O(2)	177.43(9)	Ni—O(2)—N(2)	116.6(2)
S(2)—Ni—O(1)	177.37(8)	O(1)—N(1)—C(11)	120.4(3)
S(2)—Ni—O(2)	89.45(8)	O(2)—N(2)—C(21)	119.4(4)
O(1)—Ni—O(2)	88.1(2)	S(1)—C(11)—N(1)	117.2(3)
Ni—S(1)—C(11)	96.8(1)	S(2)—C(21)—N(2)	117.4(3)

shorter than those terminal values reported for $[Ni_2(Hmp)_2(mp)_2]^{2-}$[4] (av. 2.160 Å), $[Ni_2(SCH_2CH_2S)_3]^{3-}$[16] (av. 2.185 Å), $[Ni_3(edt)_4]^{2-}$[16] (av. 2.189 Å) and $[Ni_3(SCH(CH_3)CH_2S)_4]^{2-}$[17] (av. 2.168 Å). To our knowledge, nickel complexes with the Ni—O bond in a square planar arrangement are relatively rare[4,18–22] and even the four-coordinate analogues[20] with amine N-oxide have not been investigated by X-ray diffraction analysis. The Ni—O bond of av. 1.866 Å agrees well with those in $[Ni_2(mpH)_2(mp)_2]^{2-}$[4] (av. 1.852 Å), $[Ni_3(SCH(CH_3)COO)_4]^{2-}$[18] (av. 1.875 Å) and Ni(enac)[19] (H_2enac = 4,9-dimethyl-5,8-diazadodeca-4,8-diene-2,11-dione) (av. 1.857 Å), but evidently is shorter than those in $Ni(acac)_2$[21] (acac = acetylacetonate) (av. 2.01 Å), $NiBr_2(S(CH_2CH_2OH)_2)$[22] (av. 2.046 Å) or in six-coordinate complexes with amine N-oxide such as $[Ni(pyO)_6](BrO_3)_2$[23] (pyO = pyridine N-oxide) (2.062 Å) and $[Ni(PyO)_2(2,4\text{-pentanedionate})_2]$[24] (av. 2.096 Å). The relatively short C—S distances (av. 1.712 Å) as also observed in $Co(mpo)_3$[12] (1.716 Å) show partial double bond character as they are nearly 0.1 Å shorter than the normal covalent distance (1.81 Å)[13] for a single bond. The bite distance (O---S) of av. 2.823 Å is similar to those in $Co(mpo)_3$[12] and within the range for a series of metal complexes[1–5,12] with 1,2-bidentate sulphur-containing ligands. The two bite angles O—Co—S are nearly equivalent and close to 90°, as in $Co(mpo)_3$.[12] The two five-membered rings NiS(1)O(1)N(1)C(11) and NiS(2)O(2)N(2)C(21) are nearly planar with maximum deviations of 0.0176 and 0.0285 Å, respectively. The Ni—S—C angles of av. 96.9° and Ni—O—N angles of av. 116.3° show the bonding orbitals of the sulphur atom are mainly of *p* character while those of oxygen atom sp^2 character, almost the same as those in mpH_2 ligated complexes.[3]

Spectroscopic studies

The IR absorptions of bonds C—S and N—O agree well with those reported in the literature.[8,25] It has been substantiated by X-ray diffraction analysis (*vide supra*) that the rather short C—S bond exhibits some double bond character. The free ligand (Hmpo) may exist in two tautomeric forms (thiol or thione) and has been established to be in the thione form predominantly.[25] When the sulphur atom is coordinated to metal atoms, it is not extraordinary that the C—S absorptions persist in the range 1160–1130 cm^{-1} as that of the free ligand (1142 cm^{-1}).[25]

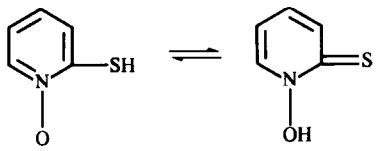

thiol ⇌ thione

The ^1H NMR spectra of **1** and **2** in DMSO solution showed a paramagnetic nature with line-broadening and/or shifting of peaks to low field and only broad signals at 24 and 7.58 ppm can be assigned to the mpo^- ligands in **1** and **2**, respectively, in addition to the signals of the solvents. The ^1H NMR spectra of **3** and **4** shown in Figs 2a and 2c, respectively, are similar and showed the diamagnetic nature. The protons of mpo^- appear at 6.5–7.5

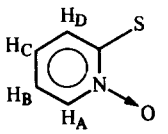

($H_B \sim H_D$) and 8.5 ppm (H_A) as a multiplet and a doublet, respectively. The simulated spectra of **3** and **4** based on the parameters listed in Table 2 are shown in Figs 2b and 2d, respectively. The consistancy of experimental spectra with simulated ones indicates the correctness of these assignments. The downfield shift of H_A is in agreement with those of the parent pyridine (8.5 ppm) or pyO (8.1 ppm).[26]

Electrochemical properties

Complexes **1–4** are all electroactive and exhibit interesting redox properties by cyclic voltammetric

Table 2. Proton chemical shifts (ppm) and coupling constants (Hz) of mpo^- in **3** and **4**

Compound	Chemical shift (ppm) A	B	C	D	Coupling constant (Hz) AB	AC	AD	BC	BD	CD
3	8.52	7.08	7.30	7.49	6.5	1.2	0.5	7.2	1.8	8.0
4	8.48	7.05	7.34	7.45	6.5	1.2	0.5	7.2	1.8	8.0

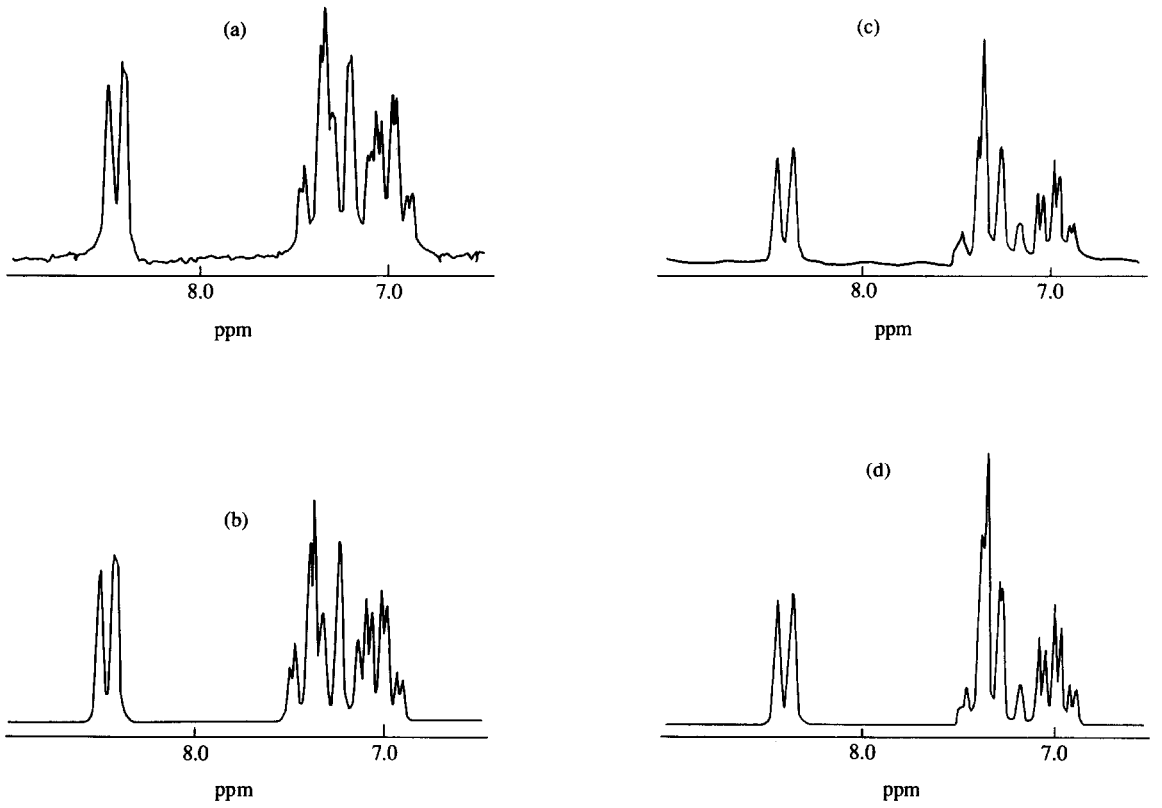

Fig. 2. ^{1}H NMR spectra. (a) Experimental spectrum of **3** in DMSO; (b) simulated spectrum of **3**; (c) experimental spectrum of **4** in DMSO; (d) simulated spectrum of **4**.

studies. As shown in Fig. 3a, the cyclic voltammogram of the DMF solution of **1** in the interval of $-0.5 \sim 1.0$ V (all potential values vs SCE) shows two reversible redox processes ($i_{pa}/i_{pc} \approx 1$) with the $E_{1/2}$ values of 0.48 and -0.04 V and the peak separations ΔE of 70 and 80 mV, respectively, which can be attributed to the following one-electron processes:

$$Mn(mpo)_2^- \underset{+e}{\overset{-e}{\rightleftharpoons}} Mn(mpo)_2 \underset{+e}{\overset{-e}{\rightleftharpoons}} Mn(mpo)_2^+.$$

This redox behaviour of **1** is quite different from manganese complexes with other 1,2-bidentate sulphur-containing ligands. For example, the redox wave at -0.67 V for $Mn(tdt)_2^-/Mn(tdt)_2^{2-}$ [15] is much more negative than the corresponding wave of **1**. Therefore, $Mn(mpo)_2$ is stable in air while $Mn(tdt)_2^{2-}$ is easily oxidized by air to $Mn(tdt)_2^-$.

The cyclic voltammogram of **2** (Fig. 3b) in DMF exhibits one quasi-reversible reduction couple for $Fe(mpo)_3/[Fe(mpo)_3]^-$ at $E_{1/2}$ of -0.53 V with ΔE of 70 mV and $i_{pa}/i_{pc} \approx 1$.

The DMF solution of **3** (Fig. 3c) shows one irreversible reduction at -0.80 V and an irreversible oxidation at -0.25 V, respectively. The former may account for the fact that the reduced species undergoes degradation and/or chemical reactions in the time-scale of CV measurements.

The reversible redox couple with $E_{1/2}$ of -1.30 V (ΔE of 100 mV, $i_{pa}/i_{pc} = 1$) in the CV diagram of **4** (Fig. 3d) corresponds to the electron-transfer process $Ni(mpo)_2/[Ni(mpo)_2]^-$. Unlike this, many nickel complexes of 1,2-dithiolene exhibit one-electron oxidation for the couple $[Ni(L)_2]^-/[Ni(L)_2]^{2-}$.

In addition to the aforementioned redox waves, all the four complexes exhibit an irreversible wave (0.88, 0.93, 1.05 and 0.85 V for **1**, **2**, **3** and **4**, respectively) for the oxidation of the bound ligand mpo^- to dtpo, which is not an electroactive species.

In summary, the coordination properties of the mpo^- ligand are shown in this unusual redox behaviour and in the high selectivity to the stabilization of oxidation states. It may be caused by the electronic nature of mpo^- in which the N-oxide bond is highly polarizable and the total charge is less negative compared to other 1,2-bidentate sulphur-containing ligands.

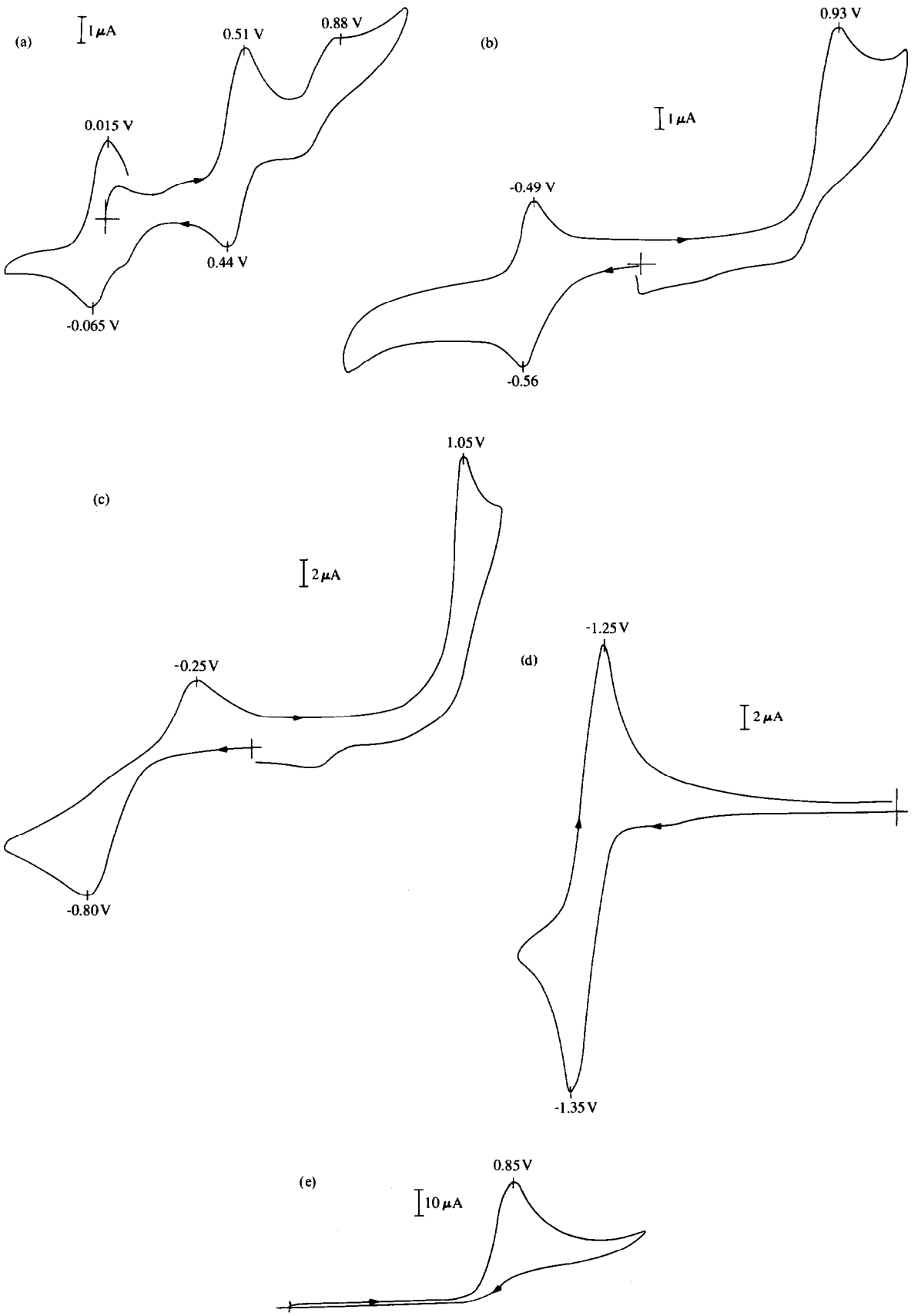

Fig. 3. Cyclic voltammograms in DMF, V vs SCE, 0.1 M of Bu_4NBF_4 as electrolyte, scan rate 100 mV s^{-1}. (a) **1**; (b) **2**; (c) **3**; (d) and (e) **4**.

Acknowledgements—This work is supported by NNSF, NSFCAS, and FNSF. The helpful experimental assistantship of Cai, S.H. and Cai, Y. B. and the members of the X-ray analysis group and the chemical analysis group in our institute are greatly appreciated.

REFERENCES

1. B. S. Kang, L. H. Weng, D. X. Wu, F. Wang, Z. Guo and H. Q. Liu, *Inorg. Chem.* 1988, **27**, 1128.
2. B. S. Kang, L. H. Weng, D. X. Wu, L. R. Huang, F. Wang, Z. Guo and H. Q. Liu, *Inorg. Chim. Acta* 1988, **148**, 147.
3. B. S. Kang, L. H. Weng, H. Q. Liu, D. X. Wu, L. R. Huang, C. Z. Lu, J. H. Cai, X. T. Chen and J. X. Lu, *Inorg. Chem.* 1990, **29**, 4873.
4. X. T. Chen, H. Q. Liu, L. H. Weng, L. R. Huang, D. X. Wu, X. J. Lei and B. S. Kang, *J. Coord. Chem.* 1991, **22**, 109.
5. B. S. Kang, X. T. Chen, L. H. Weng, L. R. Huang, C. Z. Lu and J. X. Lu, *Science in China* (chi.) *Ser. B.* 1991, 18.
6. X. T. Chen, L. H. Weng and B. S. Kang, *Jiegou Huexue* **10**, 227.
7. J. L. Davison, P. L. Preston and M. V. Russo, *J. Chem. Soc., Dalton Trans.* 1983, 783.
8. M. A. Robinson, *J. Inorg. Nucl. Chem.* 1964, **26**, 1277.
9. F. E. Pansy, H. Stander, W. L. Koerber and R. Donovick, *Proc. Soc. Expl. Biol. Med.* 1953, **82**, 122.
10. R. G. Garvey, J. H. Nelson and R. O. Ragsdale, *Coord. Chem. Rev.* 1968, **3**, 375.
11. N. M. Karayannis, L. L. Pytlewslei and C. M. Milkulski, *Coord. Chem. Rev.* 1973, **11**, 93.
12. Y. H. Hu, L. H. Weng, X. T. Chen, L. R. Huang, D. X. Wu and B. S. Kang, *Acta Cryst. C*, 1991, to be published.
13. J. D. Lydon, R. C. Elder and E. Deutsch, *Inorg. Chem.* 1982, **21**, 3186.
14. C. Mahadevan, *J. Cryst. Spectrosc. Res.* 1986, **16**, 347.
15. K. Greiwe, B. Krebs and G. Henkel, *Inorg. Chem.* 1989, **28**, 3713.
16. J. R. Nicholson, G. Christou, J. C. Huffman and K. Folting, *Polyhedron* 1987, **6**, 863.
17. X. T. Chen, B. S. Kang, L. H. Weng, L. R. Huang, H. Q. Liu, D. X. Wu, X. J. Lei, M. C. Hong and J. X. Lu, *Trans. Met. Chem.*, to be published.
18. S. G. Ronsenfield, M. L. Wong, D. W. Stephan and P. K. Mascharak, *Inorg. Chem.* 1987, **26**, 4119.
19. C. C. Lin, S. X. Liu, S. Shi, X. Z. You, X. C. Wang and S. H. Zeng, *Jiegou Huaxue* 1990, **9**, 133.
20. M. K. Mohan, J. C. Khera, S. G. Mittal and A. K. Srivastava, *Gazz. Chim.* 1978, **108**, 523.
21. G. J. Bullen, R. Mason and P. Pauling, *Inorg. Chem.* 1965, **4**, 456.
22. M. R. Udupa and B. Krebs, *Inorg. Chim. Acta* 1981, **52**, 215.
23. A. Paduan-Filho, E. Sinn, R. D. Chirico and R. L. Carlin, *Inorg. Chem.* 1981, **20**, 2688.
24. W. D. Horrocks Jr, D. H. Templeton and A. Zalkin, *Inorg. Chem.* 1968, **7**, 1552.
25. R. A. Jones and A. R. Katritzsky, *J. Chem. Soc.* 1960, 2937.
26. R. A. Abramovitch and J. B. David, *J. Chem. Soc. B* 1966, 1137.

Polyhedron Vol. 10, No. 23/24, pp. 2659–2663, 1991
Printed in Great Britain

0277–5387/91 $3.00+.00
© 1991 Pergamon Press plc

TRANSITION METAL COMPLEXES OF THE SCHIFF BASES DERIVED FROM S-ALKYLDITHIOCARBAZATE WITH 2-PYRIDINECARBOXALDEHYDE N-OXIDE—III. SYNTHESES, PROPERTIES AND STRUCTURES OF MONONUCLEAR NICKEL(II) COMPLEXES

SHAOHUA GOU,* XIAOZENG YOU and ZHENG XU

Coordination Chemistry Institute, Nanjing University, Nanjing, P.R.C.

and

ZHONGYUAN ZHOU and KAIBE YU

Chengdu Center of Analysis and Determination, Academia Sinica, Chengdu, P.R.C.

(*Received* 4 *January* 1991; *accepted* 5 *August* 1991)

Abstract—A series of mononuclear nickel(II) complexes of two tridentate ligands, S-methyl- and S-benzyl-β-N-(pyridine N-oxide-2-ylmethylidene)dithiocarbazate (SMPDH and SBPDH), were prepared and their magnetic properties, electronic and IR spectra were obtained. Both square planar and octahedral configurations were defined among these complexes. The crystal structure of [Ni(SMPD)ImH]ClO_4 was determined by X-ray diffraction, and showed that the nickel atom lies in a square planar coordination environment.

We have studied copper(II) complexes of S-R-β-N-(pyridine N-oxide-2-ylmethylidene)dithiocarbazate (R = methyl, benzyl),[1,2] since these compounds may exhibit antibacterial and antitumour activities like other transition metal complexes of ligands containing sulphur and nitrogen atoms.[3,4] We report here a series of mononuclear nickel(II) complexes of the above two ligands with or without additional ligands.

EXPERIMENTAL

Preparation of the nickel(II) *complexes*

Complexes **1–4**. $Ni(ClO_4)_2 \cdot 6H_2O$ (1 mmol) dissolved in ethanol (10 cm^3) was added to a hot ethanol solution (50 cm^3) of ligand (1 mmol) (SMPDH or SBPDH). The above solution was heated under reflux for 5 min, then imidazole (2 mmol) or pyridine in ethanol (5 cm^3) was added. The mixture was kept refluxing for a further 10 min, and filtered when hot. Brown crystals were obtained when the filtrate was kept at room temperature.

Complexes **5–8**. A solution of $Ni(NO_3)_2 \cdot 6H_2O$ (1 mmol) in ethanol (10 cm^3) was added into a solution of ligand (1 mmol) (SMPDH or SBPDH) in ethanol (50 cm^3). The mixed solution was refluxed for 5 min and then NaN_3 or NaSCN in (1 mmol) of ethanol/water (10 cm^3) (1 : 1) was added. The resulting solution was kept refluxing for a further 10 min and brown crystals appeared after the solution was cooled to room temperature.

Complexes **9–10**. A solution of ligand (SMPDH or SBPDH) in hot ethanol (50 cm^3) and $NiCl_2 \cdot 6H_2O$ (1 mmol) in ethanol (10 cm^3) were mixed and refluxed; brown crystals soon appeared.

Complexes **11–12**. A solution of ligand (1 mmol) (SMPDH or SBPDH) in hot ethanol (50 cm^3) was mixed with a solution of $Ni(OAc)_2 \cdot 4H_2O$ or $Ni(NO_3)_2 \cdot 6H_2O$ (1 mmol) in 10 cm^3 ethanol. After the mixture was refluxed for 10 min, brown crystals were obtained.

Table 1 lists the data on yields and elemental analyses for all complexes.

Spectroscopic measurements

Electronic absorption spectra were recorded in acetonitrile for complexes **1–10** and in DMF for

* Author to whom correspondence should be addressed.

Table 1. Yields and elemental analyses

No.	Compound	Formula	Yield (%)	Analyses (%) (Found/Calc.) C	H	N
1	[Ni(SMPD)ImH](ClO$_4$)	$NiC_{11}H_{12}N_5ClO_5S_2$	84	29.0	2.3	14.7
				29.2	2.7	15.5
2	[Ni(SMPD)Py](ClO$_4$)	$NiC_{13}H_{13}N_4ClO_5S_2$	80	33.7	2.8	11.8
				33.7	2.8	12.1
3	[Ni(SBPD)ImH](ClO$_4$)	$NiC_{17}H_{16}N_5ClO_5S_2$	80	38.6	2.6	13.1
				39.1	3.0	13.3
4	[Ni(SBPD)Py](ClO$_4$)	$NiC_{19}H_{17}N_4ClO_5S_2$	75	42.8	3.2	10.6
				42.3	3.2	10.4
5	[Ni(SMPD)N$_3$]	$NiC_8H_8N_6OS_2$	46	29.2	2.4	25.3
				29.4	2.5	25.7
6	[Ni(SMPD)SCN]	$NiC_9H_8N_4OS_3$	82	31.2	2.2	15.5
				31.5	2.3	16.3
7	[Ni(SBPD)N$_3$]	$NiC_{14}H_{12}N_6OS_2$	85	42.0	2.9	20.2
				41.7	3.0	20.9
8	[Ni(SBPD)SCN]	$NiC_{15}H_{12}N_4OS_3$	89	43.3	2.5	13.7
				43.0	2.9	13.4
9	[Ni(SMPD)Cl]	$NiC_8H_8N_3ClOS_2$	95	30.0	2.4	12.9
				30.0	2.5	13.1
10	[Ni(SBPD)Cl]	$NiC_{14}H_{12}N_3ClOS_2$	91	42.3	2.9	10.6
				42.4	3.0	10.6
11	[Ni(SMPD)$_2$]·H$_2$O	$NiC_{16}H_{18}N_6O_3S_4$	72	36.2	3.1	15.5
				36.3	3.4	15.9
12	[Ni(SBPD)$_2$]	$NiC_{28}H_{24}N_6O_2S_4$	92	50.2	3.7	12.8
				50.7	3.6	12.7

complexes **11**–**12** on a Shimadzu 240 spectrophotometer. IR spectra (4000–100 cm^{-1}) were obtained as solid KBr pellets on a 170SX FT-IR instrument. Magnetic susceptibilities were measured routinely in the solid state at 283.3 K using a Gouy balance with [Ni(en)$_3$]S$_2$O$_3$ as calibrant.

Selected spectroscopic data and corrected magnetic moments of the complexes are given in Table 2.

X-ray data collection and structure determination of [Ni(SMPD)ImH]ClO$_4$

A brown–red single crystal (0.15 × 0.4 × 0.5 mm) developed in a CH$_3$CN–(C$_2$H$_5$)$_2$O (1 : 5) solution of the complex was measured with an R3M/E four-circle diffractometer. The data obtained were corrected for Lorentz and polarization effects. The

Table 2. Data of magnetic moments, electronic and IR spectra

No.	μ_{eff} (R.T., BM)	*d*–*d* band (nm)	ν(C=N)	ν(C—S)	ν(N—O) (cm^{-1})	ν(Cl—O)	ν(characteristic)
1		Undetermined	1448vs	1044w	1205w	1103vs	3278m (N—H)
2		Undetermined	1439vs	1045w	1205w	1088vs	
3		Undetermined	1452vs	1037w	1201m	1090vs	3307m (N—H)
4		Undetermined	1448vs	1037w	1205m	1084vs	
5		Undetermined	1441s	1030m	1194w		2027s (N≡N)
6		Undetermined	1442s	1047m	1200w		2091s (C≡N)
7		Undetermined	1442s	1034m	1198w		2033s (N≡N)
8		Undetermined	1436s	1036m	1197w		2109s (C≡N)
9		Undetermined	1433s	1029s	1191m		281s (Cl—Ni)
10		Undetermined	1429s	1044s	1194w		286s (Cl—Ni)
11	3.31	590	1398s	1044s	1193m		
12	3.86	562	1406s	1037s	1195m		

experimental details and crystal data are as follows: $NiC_{11}H_{12}ClN_5O_5S_2$: $M_r = 452.51$, space group $P2_1/n$; $a = 9.744(2)$, $b = 10.859(2)$, $c = 16.377(6)$ Å; $\beta = 97.47(2)°$; $Z = 4$; $V = 1718.10$ Å^3; $D_c = 1.75$ g cm^{-3}; λ(Mo-K_α) = 0.71073 Å; $\mu = 15.52$ cm^{-1}; $F(000) = 892$; $T = 293$ K.

The structure was solved by direct methods (SHELXTL 4.1), and refined by least-squares techniques to an R value of 0.0398 for 1976 [$I > 3\sigma(I)$] independent reflections with 275 variables. Hydrogen atoms were refined with isotropic parameters. Scattering factors were taken from the International Tables.[5] Final atomic coordinates and equivalent isotropic temperature factors as well as lists of F_o/F_c values form the supplementary material deposited with the Editor.

RESULTS AND DISCUSSION

In general, *d–d* bands of nickel(II) complexes with planar structures appear in the neighbourhood of 500 nm, but these absorptions were not determined in the electronic spectra of complexes **1–10**. The reason is that the strong charge-transfer absorptions of the ligands containing sulphur atoms, appearing at lower wavenumbers,[6] have overlapped the *d–d* bands of the nickel(II) ions. Absorptions of 590 and 562 nm in complexes **11** and **12**, assigned to the $^3A_{2g} - {}^3T_{1g}$ transition of metal ions with octahedral configurations,[7] indicate that the two complexes are non-planar. The magnetic data reveal complexes **1–10** are diamagnetic, as expected for planar structures of these complexes. However, magnetic moments of complexes **11** and **12** are 3.31 and 3.86 BM respectively, suggesting that the geometry around the nickel atom is octahedral.

The IR spectra of complexes **1–10** are similar to those of reported tetracoordinated copper(II) complexes.[1] Both ν(C=N) and ν(N—O) of the ligands decrease and ν(C—S) appears upon complex formation. Complexes **1–4** have a very strong band at approx. 1090 cm^{-1}, assigned to ν(Cl—O) of ClO_4^- groups. Complexes **1** and **3** also have bands at 3278 and 3307 cm^{-1} assigned to ν(N—H) owing to the presence of imidazole rings. Sharp bands at about 2030 cm^{-1} without splitting are observed in complexes **5** and **7** due to the unsymmetric stretching vibrations of the N_3^- groups.[8] Analogously, SCN^- groups in complexes **6** and **8** show the stretching vibrations of C≡N bonds near 2100 cm^{-1}. Both ν(N≡N) and ν(C≡N) are within the normal range of wavenumbers,[9] indicating the single coordination mode of N_3^- or SCN^- groups to nickel(II) ions, consistent with literature reports.[10] Usually, the coordination of SCN^- groups to nickel(II) ions involves Ni—N bonding rather than Ni—S bonding, but this may be changed.[9] It is difficult to decide here whether an Ni—N or an Ni—S bond is preferred. ν(Ni—Cl) of complexes **9** and **10** is observed at *ca* 280 cm^{-1},[11] and ν(Ni—S) at *ca* 385 cm^{-1} in their far IR spectra.

In the IR spectra of complexes **11** and **12**, neither the absorptions of the CH_3COO^- anion at 1560 and 1461 cm^{-1} [9] nor those of the NO_3^- anion in the range 800–850 cm^{-1} [12] are observed. Except the characteristic bands of the ligand, these also demonstrate the octahedral configuration among nickel ions and confirm the result derived from the magnetic data and electronic spectra. A broad absorption in the range 3000–3500 cm^{-1} is also observed in complex **11**, which is attributed to the water of crystallization.

We can conclude from above discussions that the configuration of complexes **1–10** is tetracoordinated planar and that of complexes **11** and **12** is hexacoordinated octahedral (shown as Structs I and II).

The crystal structure of [Ni(SMPD)ImH]ClO_4 has been determined by X-ray diffraction (see Fig. 1 showing the atomic numbering scheme). Figure 2 is a view of the unit cell content. Geometric data are presented in Table 3.

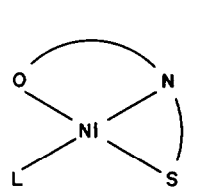

I

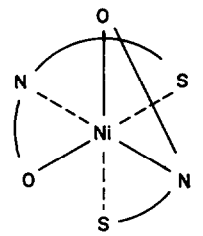

II

L = Additional ligands

This structure is isomorphous with that of the reported [Cu(SMPD)ImH]ClO_4.[1] The nickel atom is coordinated via O(1), N(3) and S(1) of the ligand as well as N(1) of the imidazole molecule, and located in the centre of the plane composed of four coordination atoms (maximum deviation: 0.0325 Å). Bond lengths of M—S, M—N and M—O in [Ni(SMPD)ImH]ClO_4 are shorter than analogous bonds in [Cu(SMPD)ImH]ClO_4, suggesting the higher stability of the nickel(II) complex with the ligand; however, they are nearly equivalent to corresponding distances in [Ni(SMPD)Py]ClO_4.[13] The maximum difference in coordination bond distances between [Ni(SMPD)ImH]ClO_4 and [Ni(SMPD)Py]ClO_4 is the Ni—N bond (arising from additional ligand) [the former is 1.888(4) Å and latter 1.912(4) Å], depending on the bulk of the additional ligands—imidazole and pyridine rings.

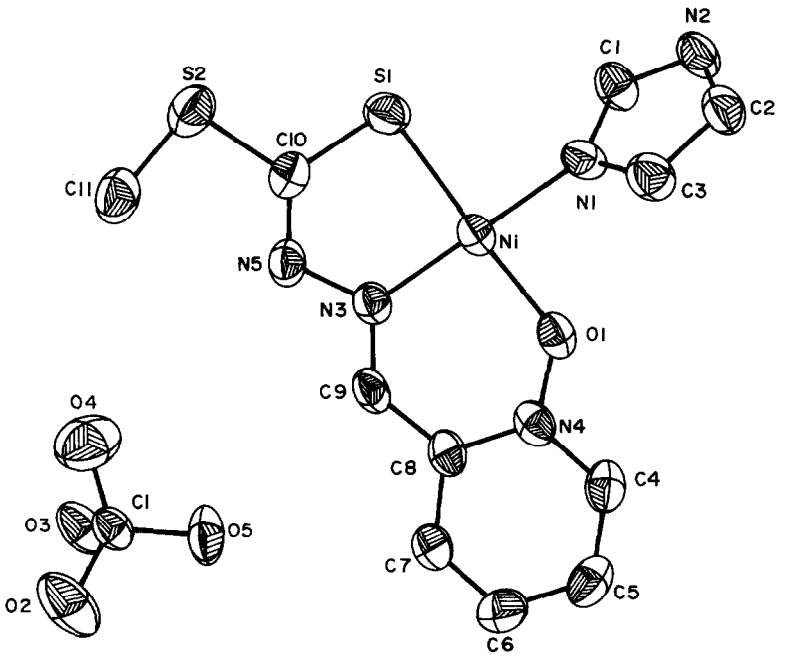

Fig. 1. X-ray crystal structure of $[Ni(SMPD)ImH]ClO_4$.

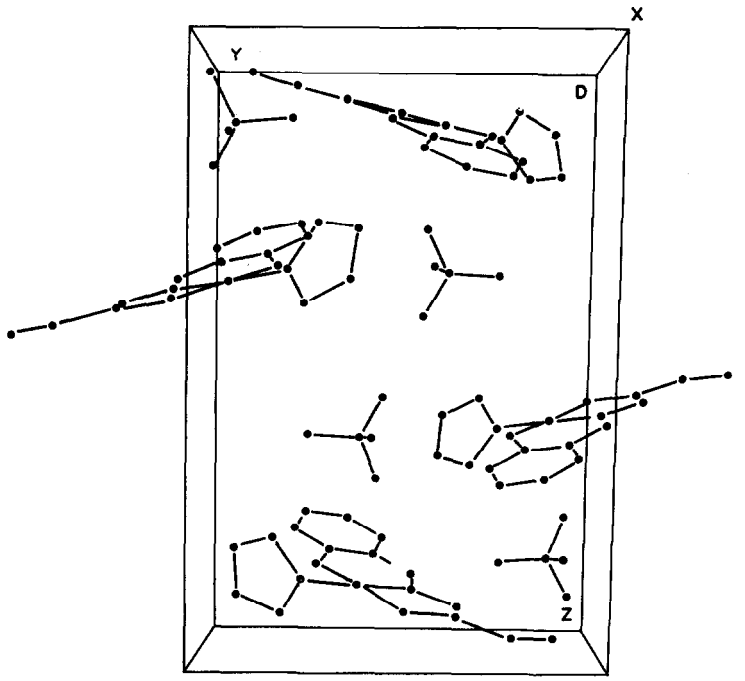

Fig. 2. A view of the unit cell.

Table 3. Selected bond lengths (Å) and bond angles (°) of [Ni(SMPD)ImH]ClO_4

Ni—S(1)	2.143(1)	Ni—N(1)	1.888(4)
Ni—N(3)	1.840(3)	Ni—O(1)	1.860(3)
S(1)—C(10)	1.724(5)	S(2)—C(10)	1.741(5)
N(4)—O(1)	1.331(4)	S(2)—C(11)	1.792(6)
N(3)—N(5)	1.407(5)	N(3)—C(9)	1.281(5)
N(5)—C(10)	1.300(6)	C(8)—C(9)	1.444(6)

S(1)—Ni—N(1)	91.5(1)	S(1)—Ni—N(3)	87.7(1)
N(1)—Ni—N(3)	178.0(2)	S(1)—Ni—O(1)	177.0(1)
N(1)—Ni—O(1)	86.1(1)	N(3)—Ni—O(1)	94.7(1)
Ni—S(1)—C(10)	95.2(1)	C(10)—S(2)—C(11)	102.3(2)
Ni—N(1)—C(1)	129.1(3)	Ni—N(1)—C(3)	125.1(3)
Ni—N(3)—N(5)	122.1(2)	Ni—N(3)—C(9)	125.4(3)
N(5)—N(3)—C(9)	112.5(3)	Ni—O(1)—N(4)	126.4(2)
N(3)—N(5)—C(10)	110.3(3)	S(1)—C(10)—S(2)	116.4(2)
S(1)—C(10)—N(5)	124.0(3)	S(2)—C(10)—N(5)	119.5(3)
O(1)—N(4)—C(8)	123.0(3)	O(1)—N(4)—C(4)	115.4(3)
N(4)—C(8)—C(9)	122.5(4)	C(7)—C(8)—C(9)	119.8(4)
N(3)—C(9)—C(8)	126.1(4)		

Like [Cu(SMPD)ImH]ClO_4, the imidazole ring and the plane consisting of Ni, S(1), O(1), N(1), N(3) have a dihedral angle (125.1°) which decreases spatial repulsion, to result in low symmetry of the whole molecule.

REFERENCES

1. S. H. Gou, X. Z. You, Z. Xu, K. B. Yu and Z. Y. Zhou, *Polyhedron* 1990, **9**, 2981.
2. S. H. Gou, X. Z. You, Z. Xu, Z. Y. Zhou and K. B. Yu, *Polyhedron* 1991, **10**, 1363.
3. D. L. Klayman, J. P. Scovil, J. F. Bartosevich and J. Bruce, *J. Med. Chem.* 1983, **26**, 35 and refs therein.
4. M. A. Ali and S. E. Livingstone, *Coord. Chem. Rev.* 1974, **13**, 101.
5. *International Tables for X-ray Crystallography*, Vol. 4. Kynoch Press, Birmingham (1974).
6. J. S. Dwivedi and U. Agarwala, *Ind. J. Chem.* 1972, **10A**, 657.
7. M. T. H. Tarafder, M. A. Mah, R. N. Bose and M. A. Ali, *J. Inorg. Nucl. Chem.* 1981, **43**, 315.
8. J. Lorosch, H. Paulus and W. Hause, *Inorg. Chim. Acta* 1985, **106**, 101.
9. K. Nakamoto, *Infrared and Raman Spectra of Inorganic and Coordination Compounds*, 3rd edn. John Wiley & Sons, New York (1978).
10. A. E. Landers and D. J. Phillips, *Inorg. Chim. Acta* 1984, **85**, 77.
11. A. Sabatini and L. Sacconi, *J. Am. Chem. Soc.* 1964, **86**, 17.
12. A. Addison, W. Hendrick and H. M. Reedijr, *Inorg. Chem.* 1981, **20**, 103.
13. Z. Y. Zhou, K. B. Yu, S. H. Gou, X. Z. You and Z. Xu, *Polyhedron* 1991, **10**, 37.

Polyhedron Vol. 10, No. 23/24, pp. 2665–2672, 1991
Printed in Great Britain

0277–5387/91 $3.00+.00
© 1991 Pergamon Press plc

LIGAND FIELD ANALYSIS OF METAL–OXYGEN INTERACTIONS—I. TRIS(OXALATO)COBALTATE(III)

SNEŽANA ZARIĆ and S. R. NIKETIĆ*†

Department of Chemistry, Faculty of Science, University of Belgrade, Studentski trg 16, P.O. Box 550, YU-11001 Belgrade, Yugoslavia

(*Received* 10 *July* 1991; *accepted* 1 *August* 1991)

Abstract—Ligand field analysis of $[Co(ox)_3]^{3-}$ has been performed using the angular overlap model (AOM) approach. The metal–oxygen interactions were treated as locally anisotropic. Experimental spectra were well reproduced by the calculations in which the Trees' correction was included. The effect of geometrical distortions on the calculated energies of ligand field states has been investigated.

Our previous[1,2] study of tris(aminocarboxylato) cobalt(III) complexes revealed that the differences in the electronic structure between complexes with five-membered glycinato and six-membered β-alaninato chelate rings are a consequence of different torsional angles around M—O bonds (due to the non-planarity of β-Ala rings) rather than of different chelate (N—M—O) angles. The observation led us to propose a hypothesis about the anisotropy of the M—O interaction involving the carboxylato oxygen ligator. This model offered, therefore, the possibility to relate the conformation of a chelate ring to the electronic structure of the coordination complex.

To investigate further this relationship in structures with flexible metal chelate rings, we sought for other examples of chelate complexes containing coordinated carboxylato oxygen(s), in which the influence of chelate ring conformation is expected to be observable via the anisotropy of M—O interactions.

Tris(oxalato) complexes chosen for this study[3] do not offer wide structural variations with respect to the ring conformation. Nevertheless, as shown in this paper on $[Co(ox)_3]$ structures, and in the next paper on $[Cr(ox)_3]$ structures, small structural deformations of the $M(ox)_3$ skeleton are capable of producing significant changes in calculated energies of the ligand field states.

Another reason for our choice is that tris(oxalato) complexes offer a possibility to investigate the extent of transferability of ligand field parameters across the series of chromophores $MN_{6-3n}O_{3n}$ for $n = 0$, 1, 2. In the previous study[2] on tris(aminocarboxylato) complexes (chromophore MN_3O_3) we used the AOM parameters for nitrogen optimized on the MN_6 chromophore. Here we wanted to determine whether the AOM parameters for oxygen are transferable to the MO_6 chromophore as well.

COMPUTATIONAL METHODS

This ligand field analysis is based on the angular overlap model (AOM) approach.[4–7] Here we shall briefly examine geometry relationships for tris(oxalato) structures which are of importance for the AOM analysis. Then we shall outline some extensions of the AOM model used in this as well as in the following[8] work.

Trigonal dihedral geometry definition

The overall coordination geometry of a regular (D_3) trigonal dihedral tris(bidentate) structure is completely defined by any two of the three geometrical descriptors: chelate angle (α), tilt angle (θ) or twist angle (ω) (see e.g. Fig. 2 in Ref. 2). In the so-called trigonal orientation (i.e. z-axis coinciding with the molecular C_3 axis, and the x-axis bisecting the chelate angle, α) the geometry of the metal coordination sphere may be completely defined by, e.g.

* Author to whom correspondence should be addressed.
† E-mail address: ⟨xpmfh01@yubgss21.bitnet⟩.

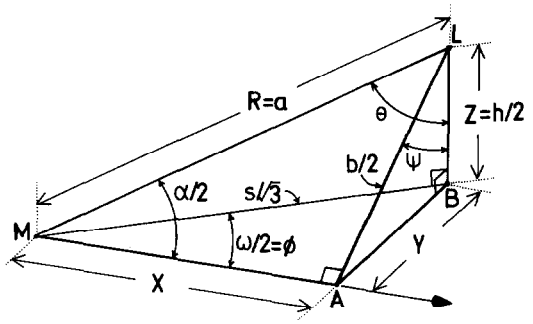

Fig. 1. Rectangular tetrahedron defined by the position of one of the ligator atoms (L) in a trigonally oriented D_3 tris(bidentate) structure showing the relationships between various geometry descriptors. Angles α, θ and ω are defined in the text. Line L-A is equal to a half of the bite distance L-L, and line L-B is a half of the octahedron height (h). M-B is likewise related to the length of the octahedron side (s) through a factor of $\sqrt{3}$. Angle ψ shown on this figure is the pitch angle (octahedral value = 35.5°) and not the ψ(AOM) (octahedral value = 45°).

the two spherical polar coordinates of one of the ligators on a sphere the radius of which corresponds to the unit M—L distance. Several workers[9-16] have commented on various relations between α, θ and ω angles or other (simple or derived) geometry descriptors and ligator (either spherical polar or Cartesian) coordinates. However, it is possible to derive all these and many other relationships between geometry descriptors of a trigonal dihedral tris(bidentate) structure by considering the trigonometry of a rectangular tetrahedron (Fig. 1) defined by the position of one of the ligator atoms in a trigonally oriented structure.

Any regular (i.e. D_3 or C_3) tris(bidentate) structure can easily be brought into a trigonal orientation and compared to other similar structures. The situation is less straightforward for the structures which lack any symmetry. Indeed, all reported crystal structures of the $M(ox)_3$ ion, except one (see below), are unsymmetrical. Therefore, any attempt to define their structural deformations must assume some kind of averaging of the geometrical descriptors. There are essentially two methods for doing this.

In cases of small deviations from C_3 symmetry, it is possible to define average values of chelate and other relevant bond angles[2,4,13] and to derive average twist angles (ω) irrespective of molecular orientation. Alternatively, it is possible to find the best trigonal orientation[10,11] of a low symmetry structure which gives an ω and a pair of θ angles ("upper" and "lower") for each chelate ring. We prefer the latter method because it retains the original structural information and, at the same time, allows for various levels of averaging if and when necessary.

Trigonal deformations in $M(ox)_3$ *structures*

Five-membered M(oxalato) chelate rings are either nearly planar or deformed in an irregular way. Accordingly, in assessing the effects of structural variations in $M(ox)_3$ structures on the results of AOM analysis, it is equally important to consider the modes of departure from the regular octahedral symmetry of the coordination polyhedron. For that reason we have analysed geometries of $M(ox)_3$ ions as reported in published crystal structure determinations.

From the CSD[17] we have extracted data on 30 crystal structure determinations of $M(ox)_3$ ions. Except in one case (PNIOCO, space group $P2_13$ allowing for C_3 symmetry of the complex anion), all the structures belong to space groups which permit at most C_1 and/or C_2 site symmetries, but $M(ox)_3$ ions in all of them were of C_1 symmetry! In order to find the values of θ and ω for these $M(ox)_3$ structures we have adopted the following procedure. Mid-points between ligator atoms belonging to the same chelate rings (three points) and those between ligators on the opposite trigonal faces on adjacent chelate rings (another three points) were located. Eulerian rotations were then applied iteratively, keeping the metal atom in the origo, so that the sum of squares of the displacements of all the six points from the xy-plane is minimized. In this orientation the axis perpendicular to the xy-plane and passing through the atom (i.e. z-axis) is taken as the best C_3 molecular axis. Angles θ and ω for each chelate ring were calculated with respect to this C_3 axis. Subsequent smoothing of the structure may be performed in two steps: by averaging the ω angles to get C_3 symmetry, and by averaging the θ angles to get D_3 symmetry. This method may be regarded as an elaboration of the twist angle definition ϕ[6] of Flandera and Lingafelter.[11] It is numerically stable and yields the smallest variation in ω and θ angles among the chelate rings.

Among many possible bivariate relationships of the geometrical descriptors of tris(bidentate) structures we have found that a plot of ω vs θ yields the most illustrative overview of the $M(ox)_3$ deformations (Fig. 2). It shows that most of the structures follow the relationship $\cos(\omega/2) = \cos(\alpha/2)\sin(\theta)$. Furthermore, metal ions of similar ionic radii have approximately similar α angles. Therefore, the points in the θ–ω plot belonging to the same metal atom or those with similar ionic radii, follow the

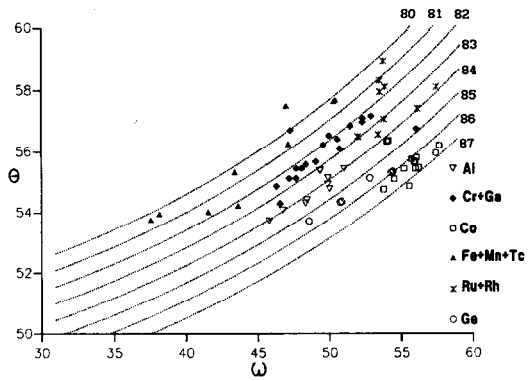

Fig. 2. X-ray structures of $[M(ox)_3]^{3-}$ ions on the θ–ω plot showing that most of the structures approximately follow the relationship $\cos(\omega/2) = \cos(\alpha/2)/\sin(\theta)$, and that metal ions of similar ionic radii have approximately similar α angles. The dotted lines correspond to constant values of α, indicated in the upper right corner of the graph. All data extracted from CSD[17] are shown.[18]

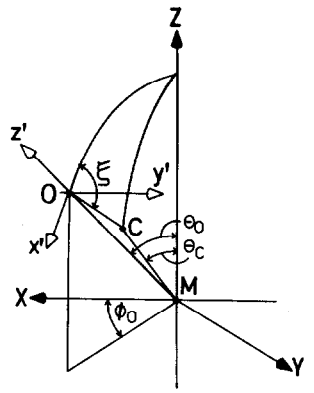

Fig. 3. The spherical trigonometry relationships of the triangle defined by projecting the positions of the oxygen ligator, O, and the neighbouring carbonyl carbon, C, onto the unit sphere around the metal atom. Spherical angle ξ is subtended by the O—C line and the x-axis of the local coordinate system on the oxygen ligator. Therefore, $\psi(\text{AOM}) = \text{abs}(\pi/2 - \xi)$.

α = const. lines (shown as dotted lines in the background on Fig. 2). A full account of the analysis of all 30 $M(ox)_3$ structures is available elsewhere.[18] Here we give only a summary of the structures of five $[Co(ox)_3]$ complexes (Table 1).

Definition and specification of ψ angles

The AOM model which takes into account the anisotropy of an M—L bond requires the specification of the ψ angle[5] in addition to the spherical polar angles which define the position of L on a unit sphere. The angle ψ is related to the torsional angle at the M—L bond. However, while the torsional angle is invariant with respect to molecular orientations, the ψ angle depends also on the spherical polar coordinates of the ligator L.

One way to evaluate the angle ψ is to locate the coordinates of a ligand atom directly connected to the ligator. In the present case it is the carbonyl carbon, C_k. Atoms M, O and C_k define a nodal plane for the π-type orbital on the oxygen ligator. The angle between this plane and the xz-plane of the local coordinate system on O, ξ, can be defined on the basis of spherical trigonometry relationships of the triangle defined by projecting the positions of O and C_k onto the unit sphere around the metal atom (see Fig. 3):

$$\cos(\psi(\text{AOM})) = \cos(\theta) \times \sqrt{\{[\cos 2(\theta) + \cos 2(\alpha/2) \times \tan 2(\omega/2)][1 + \tan 2(\omega/2)]\}}.$$

The angle ψ(AOM) has a value of 45° for the O_h symmetry. It should be distinguished from the pitch

Table 1. Selected structural data on $[Co(ox)_3]^{3-}$ complexes

CSD Refcode[a]	Space group	Chelate angle (α)			Average values α	θ	ω
DAZVUV	$C2/c$	86.072	86.750	86.328	86.38	55.81	56.36
DAZWEG	$P3_12_1$	86.478	86.525	86.678	86.56	55.48	55.81
PNIOCO	$P2_13$	84.269	84.269	84.269	84.27	56.36	54.08
QQQCMAa	P-1	86.768	86.304	86.368	86.48	55.42	55.55
QQQCMAb	P-1	86.202	86.235	87.299	86.58	55.38	55.61

[a] Refcodes:
DAZVUV—monoclinic $K_3[Co(ox)_3] \cdot 2H_2O$.[43]
DAZWEG—Λ-$K_3[Co(ox)_3] \cdot 2H_2O$.[43]
PNIOCO—$K[Ni(o\text{-phen})_3][Co(ox)_3] \cdot 2H_2O$.[40]
QQQCMAa—rac-$K_3[Co(ox)_3] \cdot H_2O$ (Struct. A).[43]
QQQCMAb—rac-$K_3[Co(ox)_3] \cdot H_2O$ (Struct. B).[43]

(or tilt) angle, ψ[19,20] (O_h value = 35.5°), which is related to the angles θ and α (or ω) in the trigonal orientation of an idealized (D_3) tris(bidentate) geometry (as shown in Fig. 1):

$$\psi = \pi/2 - \arccos[\cos(\theta)/\sin(\alpha/2)]$$
$$= \pi/2 - \arctan[\tan(\theta) \times \sin(\omega/2)].$$

The latter expression or variants thereof have been sometimes imprecisely cited in connection with the definition of ψ(AOM).[14]

Computational model for the AOM analysis

The basic computational method for AOM analysis used in this work has been described.[2] In addition, for the purpose of the present study, we have adopted two extensions to the AOM procedure. They are related to the Trees' correction, and to the explicit treatment of the second coordination sphere. The former is applied both for cobalt(III) and chromium(III) complexes, and the latter only in the case of $[Cr(ox)_3]^{3-}$ in a crystal environment.

It has been repeatedly demonstrated[21-24] that the so-called Trees' correction[25-28] affects the calculated energies both for the free and for coordinated transition metal ions, so that the agreement between calculated and experimental energies becomes improved.

Trees' correction is introduced in the following form:

$$\langle \alpha SLJM|H(Trees)|\alpha'S'L'J'M'\rangle$$
$$= \delta(S,S')\delta(L,L')\delta(J,J')\delta(M,M')$$
$$\times \{[L(L+1) - 6n]\alpha + \beta Q\};$$

where α and β are the empirical parameters and Q the total seniority operator.[28] For transition metals treated in this study the contribution involving parameter β is negligible. α is treated as an empirically adjustable parameter[23,29,30] with a value ranging from 20 to 110 cm^{-1}.

The other extension of the AOM analysis is related to the inclusion of atoms of the second coordination sphere. Careful inspection of crystal structures of different $M(ox)_3$ ions shows that some counter-ions or polar molecules may influence the crystal field around the central transition metal atom. This influence may be two-fold. Counter-ions may interact with ligand atoms causing small steric and/or electronic deformations which are reflected onto M—L interactions. Furthermore, in some $M(ox)_3$ structures, there are counter-ions which are located close to the C_3 (or pseudo-C_3) molecular axis at short distances from the atom M, and thus may have a direct effect on it.

We have treated selected counter-ions from the outer coordination sphere in the same way as ligator atoms. Their positions (in spherical polar coordinates with respect to the global coordinate system of M) were determined from the crystallographic data. Their influence on M is small, therefore, only e_σ parameters are retained. Their magnitudes are roughly estimated on the basis of the well-known relationships between AOM and crystal-field parameters.[31-33]

RESULTS AND DISCUSSION

Best-fit ligand field parameters

The basis for the ligand field analysis of tris (oxalato)cobaltate(III) ion was the structural data on five complexes retrieved from the Cambridge Structural Database[17] (Table 1) and optical spectra. The latter are room temperature solution spectra which provide positions of the low-lying singlet bands[34-36] and, in one case,[37] of the first triplet transition. Single crystal spectra[38] correspond to $[Co(ox)_3]$ doped in $NaMg[Al(ox)_3]\cdot 9H_2O$, the crystal structure of which is not known.

For the optimization of crystal field parameters the recent spectral data[39] for singlet transitions, and reported[37] triplet transitions, were used. The geometrical model was, therefore, the C_3 average structure derived from four out of five crystal structure geometries. The average values of descriptors were: $\alpha = 86.5$, $\theta = 55.52$ and $\omega = 55.83$ degrees. The structure of $K[Ni(o\text{-phen})_3][Co(ox)_3]\cdot 2H_2O$[40] was omitted since it deviated from all the other structures for more than 3(σ) in most of the structural parameters relevant to this study.

The scarcity of spectroscopic data for $[Co(ox)_3]^{3-}$ limits the number of parameters that could be optimized simultaneously in an AOM calculation. Since our intention was to investigate the transferability of AOM parameters for oxygen, we chose to fix e_σ and e_π parameters for the carboxylate oxygen at the values optimized previously[2] on tris(aminocarboxylato)cobalt(III) complexes. The spin-orbit coupling constant was likewise taken over from the previous[2] study as an upper limit for cobalt(III) suggested by Wilson and Solomon.[41] Inter-electron repulsion parameters F_2 and F_4 were optimized to fit the singlet and triplet spectra in the following way. The baricentre of the A_2 and E_a trigonal components was fitted to the position of the first singlet "*d–d*" band, and the E_b component alone to the second singlet "*d–d*" band. However, it was not possible to reproduce the experimentally

Table 2. Results of ligand field analysis on $[Co(ox)_3]^{3-}$

Level	Exptl (cm^{-1})	Calc.[a] (cm^{-1})
$^3T_{1g}$	8300[b]	8760
$^3T_{2g}$	12,700[b]	12,180
$^1T_{1g}$	16,610[c]	16,600[d]
$^1T_{2g}$	23,750[c]	23,740[e]

[a] $F_2 = 1130\ cm^{-1}$, $F_4 = 107\ cm^{-1}$, $\alpha(\text{Trees}) = 11\ cm^{-1}$, $\zeta = 600\ cm^{-1}$, $e(\sigma) = 7400\ cm^{-1}$, $e(\pi c) = 1700\ cm^{-1}$ and $e(\pi s) = 0$.

[b] Ref. 37.

[c] Ref. 39.

[d] Baricentre of A_2 (16,480 cm^{-1}) and E_a (16,670 cm^{-1}).

[e] E_b component. The $^1A_1$ component is calculated at 23,830 cm^{-1}.

observed $^3T_{1g}$ transition. Substantial improvement was achieved by inclusion of the Trees' parameter α in the optimization simultaneously with F_2 and F_4. The best parameter set is shown in Table 2.

The resultant Trees' parameter is rather small compared to the value reported[42] for the free cobalt(III) ion (70 cm^{-1}) although it is expected to be reduced.[22]

Effects of structural deformations

With the optimized parameters we have next studied deformations of the $M(ox)_3$ structures. There are essentially two sources for structural variations. First, they are trigonal deformations of the coordination polyhedron, characterized by deviations of global geometry descriptors (α, θ and ω) from their regular trigonal dihedral (D_3) values, both with and without retention of the C_3 axis. Second, deformations may be due to various departures from planarity of the five-membered oxalato metal chelate rings.

Deformations of the coordination polyhedron

Trigonal elongations or compressions are characteristic deformations of tris(bidentate) structures. Since α, θ and ω angles are not independent, changes in, e.g. α are accompanied by simultaneous changes in either θ or ω angles.

Simulation of deformations of α on a model structure can, therefore, be effected either at θ = const. or at ω = const. In both cases an inversion in the order of trigonal components (A and E) of the $^1T_{1g}$ and $^1T_{2g}$ states takes place at $\alpha = 90°$. However, the order is opposite in the cases of θ = const. and ω = const. These results are shown in Fig. 4.

The order of trigonal components calculated for the average crystal structure of C_3 symmetry is $A_2 < E_a < E_b < A_1$. Since the value for θ in this structure is close to octahedral [$\theta(O_h) = 54.7°$], the order of trigonal components of $^1T_{1g}$ is $A_2 < E_a$, as predicted by the model structure with θ = const.

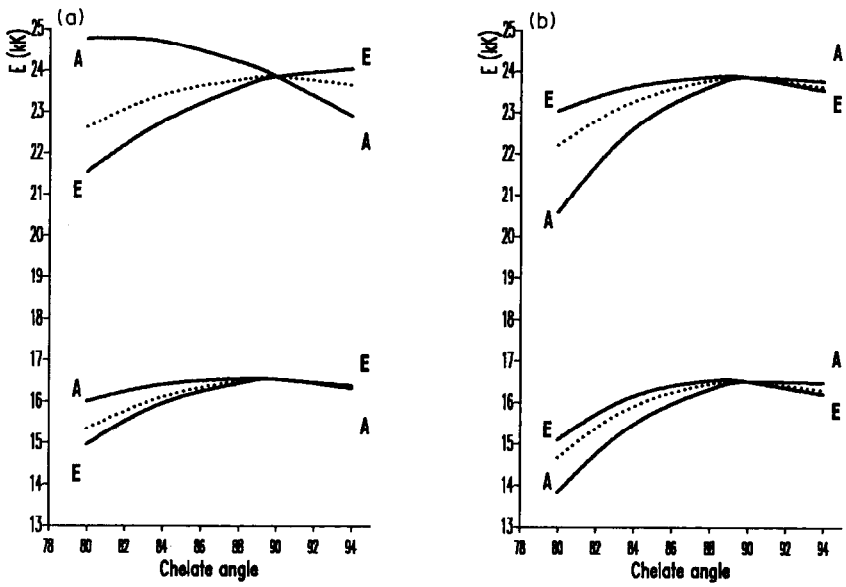

Fig. 4. The influence of trigonal deformations on the positions and splittings of singlets transitions. (a) Simultaneous change of α and θ at $\omega = 60°$. (b) Simultaneous change of α and ω at $\theta = 54.74°$. Baricentres are shown as dotted lines. For both diagrams the best-fit parameter set was used: $F_2 = 1123\ cm^{-1}$, $F_4 = 108\ cm^{-1}$, $\zeta = 600\ cm^{-1}$, $\alpha(\text{Trees}) = 11\ cm^{-1}$, $e(\sigma) = 7400\ cm^{-1}$ and $e(\pi c) = 1700\ cm^{-1}$.

Table 3. Results of ligand field analysis[a] on X-ray structures[b] of $[Co(ox)_3]$ complexes

Level in O_h	Crystal structures PNIOCO	QQQCMAa	QQQCMAb	DAZWEG	DAZVUV	Average struct.[c]
$^1T_{1g}$	16,120 E_a	16,370[d]	16,310 E_a	16,380[d]	16,180 E_a	16,480 A_2
	16,450 A_2		16,550 A_2		16,760 A_2	16,660 E_a
$^1T_{2g}$	23,260 E_b	23,360 A_1	23,720[d]	23,420 A_1	23,240 A_1	23,750 E_b
	24,140 A_1	23,920 E_b		23,870 E_b	23,990 E_b	23,830 A_1

[a] Best-fit parameter set from Table 2.
[b] For Refcodes see Table 1.
[c] Average of all crystal structures (except PNIOCO) with imposed C_3 symmetry axis.
[d] Baricentre (large mixing of A and E states).

The order of trigonal components for $^1T_{2g}$ is more susceptible to the changes of the angle θ, and is difficult to predict when both ω and θ are distorted.

The results of calculations on the individual crystal structures are presented in Table 3. All structures, except PNIOCO, are unsymmetrically distorted. For PNIOCO the order of trigonal components is the same as reported[38] for the NaMg salt, but different from that calculated for the average crystal structure with C_3 symmetry.

In certain cases the reduction of symmetry affects the calculations so that the expected degeneracies of the energy levels are removed and the eigenvectors appear to be composed of mixtures of functions transforming as A and E. Notwithstanding this uncertainty, it is evident that the order of trigonal components is sensitive to small structural deformations of the coordination octahedron in $[Co(ox)_3]$ complexes. In order to circumvent the problem of symmetry assignment of the calculated eigenvectors, we have fitted each crystal structure to a model of C_3 symmetry. The results (Table 4) again show that the order of trigonal components is sensitive to the structural variations which remain after C_3 averaging. Furthermore, comparison of the results in the cases of structures DAZVUV and QQQCMA, shows that the results are sensitive to lowering of symmetry as well.

The structure PNIOCO is different from the other four not only with respect to the symmetry but also with respect to the shape of the chelate rings. The angle α in PNIOCO is the smallest [84.3° as compared to 86.50(33)° for the other four structures] and the chelate ring puckering is the highest (the torsional angle O—C—C—O is 24.0° as compared to 8.8° in average for DAZWEG, and 1.2° in average for the other structures).

Qualitatively different results are obtained for PNIOCO if the chelate rings in this structure are made planar. Therefore, we argue that the chelate ring puckering (in addition to the overall deformations of the coordination octahedron) are affecting the calculated energy levels. In order to estimate the effect of chelate ring puckering we have studied two idealized modes of ring deformations: envelope and skew-boat puckering (see Fig. 5).

In the envelope puckering, torsional angles around M—O bonds become different from zero

Table 4. Results of ligand field analysis[a] on $[Co(ox)_3]$ complexes derived from crystal structures[b] by imposing C_3 symmetry

Level	PNIOCO	PNIOCO[c]	QQQCMAa	QQQCMAb	DAZWEG	DAZVUV
$^1T_{1g}$	16,190 E_a	16,190 A_2	16,280 A_2	16,280 A_2	16,300 A_2	16,360 A_2
	16,590 A_2	16,410 E_a	16,500 E_a	16,500 E_a	16,500 E_a	16,490 E_a
$^1T_{2g}$	23,350 E_b	23,530 E_b	23,755[d]	23,740 A_1	23,750 E_b	23,680 E_b
	24,280 A_1	23,900 A_1		23,760 E_b	23,770 A_1	23,940 A_1

[a] Best-fit parameter set from Table 2.
[b] See Table 1.
[c] Chelate rings forced to planar conformation.
[d] Accidental degeneracy.

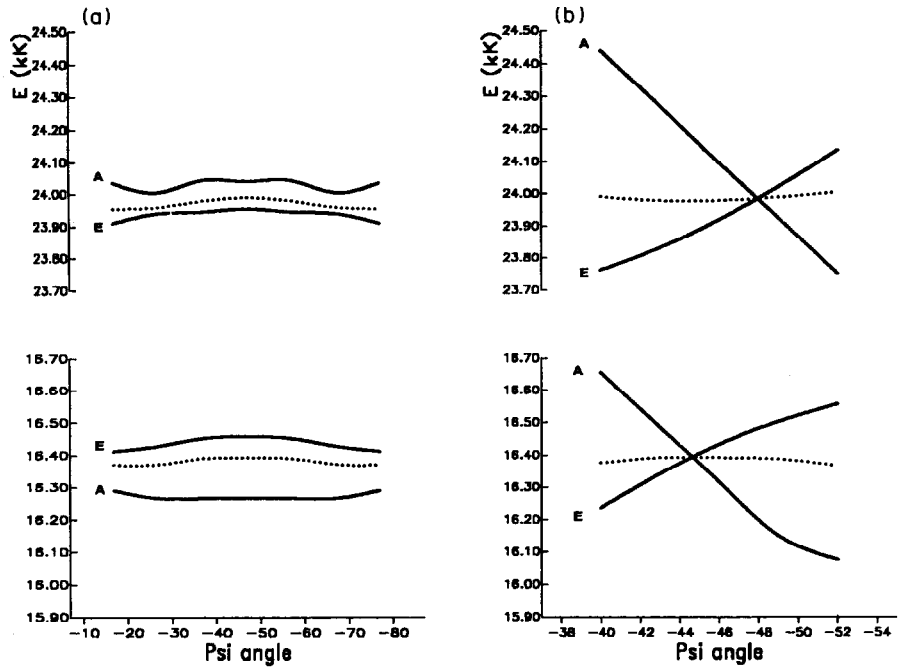

Fig. 5. The influence of the chelate ring conformation on the positions and splittings of singlets transitions. (a) Envelope type of ring puckering with ψ angles of the opposite sign. (b) Skew-boat type of ring puckering with ψ angles of the same sign. Baricentres are shown as dotted lines. For both diagrams the best-fit parameter set was used: $F_2 = 1123\ cm^{-1}$, $F_4 = 108\ cm^{-1}$, $\zeta = 600\ cm^{-1}$, $\alpha(\text{Trees}) = 11\ cm^{-1}$, $e(\sigma) = 7400\ cm^{-1}$ and $e(\pi c) = 1700\ cm^{-1}$.

and opposite in sign, whereas the value for the O—C—C—O torsion remains close to zero. This puckering mode does not change the order of trigonal components and has a very small influence on the calculated energies (Fig. 5). On the other hand, the skew-boat puckering, characterized by substantial departure from planarity in the O—C—C—O fragment and small torsional angles around M—O bonds of the same sign, greatly influences the trigonal splitting and the order of trigonal components (Fig. 5). The skew-boat mode of puckering, present in PNIOCO, explains therefore, the difference between the results obtained with the strict crystal structure and the one corresponding to the planar rings. Furthermore, in the latter case, the results are qualitatively similar to those for the other crystal structures. Angle θ is closest to its octahedral value in one of the structures of QQQCMA (column 3 in Table 4). There the order of trigonal components of the "second" band is $A_1 < E_b$ as expected from Fig. 4 for the case $\alpha < 90°$. In all other crystal structures the variation in θ is more pronounced and the opposite order, $E_b < A_1$, is obtained. The other of the two structures of QQQCMA (column 2 in Table 4) shows deformations both in θ and in ω in such a way that their effect is compensated and practically no splitting of $^1T_{2g}$ is obtained.

CONCLUSIONS

The results of AOM analysis on idealized (D_3) geometries are shown to differ appreciably from those obtained on the basis of the real geometries. This raises the question of necessity to use real geometries in AOM calculations, or at least to consider the effects of possible structural deformations when analysing spectral data for systems which are not fully characterized in terms of their structures.

Furthermore, it was shown that chelate ring conformation is an important structural feature in ligand field studies. In $[Co(ox)_3]$ structures, it is manifested in terms of deviations of oxalato metal chelate rings from planarity. They influence AOM results through the changes in α, θ and ω angles, as well as in the torsional angles around metal–ligand bonds.

Finally, it was shown that the AOM parameter may be treated as transferable across the series of chromophores $CoN_{6-3n}O_{3n}$, $n = 0, 1, 2$. The $e_{\varsigma\lambda}$ parameters for nitrogen were successfully taken over from $[Co(NH_3)_6]^{3+}$ to $[Co(Gly/\beta\text{-}Ala)_3]$, and those for oxygen from $[Co(Gly/\beta\text{-}Ala)_3]$ to $[Co(ox)_3]^{3-}$. The electron repulsion parameters optimized with such a choice for $e_{\varsigma\lambda}$ parameters yielded reasonable numerical values, which were within the limits for CoN_6 and CoO_6 chromo-

phores. However, they do not fit the interpolated values, i.e. the "rule of average environment" is not applicable to electron repulsion parameters.

Acknowledgements—This work was supported by the Serbian Research Fund. Computer resources were generously made available by the Serbian State Institute of Statistics (RZS) through the Computer Laboratory of the University of Belgrade.

REFERENCES

1. W. Urland and S. R. Niketić, *Chem. Phys. Lett.* 1986, **129**, 592.
2. S. R. Niketić and W. Urland, *Polyhedron* 1987, **6**, 947.
3. Parts of this work were described in: (a) S. Zarić and S. R. Niketić, p. 165. First Yugoslav Conference on Molecular Sciences, Zagreb, Yugoslavia (May 1986). (b) S. Zarić, N. Mutić and S. R. Niketić, paper O24, p. 588. Sixth Yugoslav–Italian Crystallographic Conference, Pula, Yugoslavia (May 1989). (c) S. Zarić, M.Sc. Thesis, University of Belgrade, Yugoslavia (1990).
4. C. E. Schaffer and C. K. Jorgensen, *Math. fys. Medd. Dan. Vid. Selsk* 1965, **34**, 13.
5. C. E. Schaffer, *Struct. Bond.* 1968, **5**, 68.
6. C. E. Schaffer, *Pure Appl. Chem.* 1970, **24**, 361.
7. C. E. Schaffer, *Struct. Bond.* 1973, **14**, 69.
8. S. Zarić and S. R. Niketić, *Polyhedron* 1991, **10**, 2673.
9. A. Avdeev and J. P. Fackler Jr., *Inorg. Chem.* 1975, **14**, 2002.
10. K. R. Dymrock and G. J. Palenik, *Inorg. Chem.* 1975, **14**, 1220.
11. M. A. Flandera and E. C. Lingafelter, *Inorg. Chem.* 1976, **15**, 750.
12. D. L. Kepert, *Inorg. Chem.* 1972, **11**, 1561.
13. D. L. Kepert, *Progr. Inorg. Chem.* 1977, **23**, 1.
14. E. Larsen and G. N. La Mar, *J. Chem. Educ.* 1974, **51**, 633.
15. K. N. Raymond, S. S. Isled, L. D. Brown, F. R. Franczek and J. H. Nibert, *J. Am. Chem. Soc.* 1976, **95**, 1767.
16. E. I. Stiefel and G. F. Brown, *Inorg. Chem.* 1972, **11**, 434.
17. Cambridge Structural Database. For description see, e.g. (a) F. H. Allen, S. Bellard, M. D. Brice, B. A. Cartwright, A. Doubleday, H. Higgs, T. Hummelnik, B. G. Hummelnik-Peters, O. Kennard, W. D. S. Motherwell, J. R. Rogers and D. G. Watson, *Acta Cryst.* 1973, **B35**, 2331; (b) F. H. Allen, O. Kennard and R. Taylor, *Accts Chem. Res.* 1983, **16**, 146.
18. S. Zarić and S. R. Niketić, to be submitted.
19. L. H. Pignolet, *Top. Curr. Chem.* 1975, **56**, 91.
20. B. G. Thomas, M. L. Morris and R. L. Hilderbrandt, *Inorg. Chem.* 1978, **17**, 2901.
21. J. Ferguson and D. L. Wood, *Austral. J. Chem.* 1970, **23**, 861.
22. P. E. Hoggard, *Coord. Chem. Rev.* 1986, **70**, 85.
23. P. E. Hoggard and K.-W. Lee, *Inorg. Chem.* 1988, **27**, 2335.
24. M. Gerloch and R. C. Slade, *Ligand Field Parameters*. Cambridge University Press, Cambridge (1973).
25. R. E. Trees, *Phys. Rev.* 1951, **83**, 756.
26. R. E. Trees, *Phys. Rev.* 1951, **84**, 1089.
27. R. E. Trees, *Phys. Rev.* 1952, **85**, 382.
28. C. K. Jorgensen, *Modern Aspects of Ligand Field Theory*. Elsevier/North-Holland, Amsterdam (1971).
29. N. D. Fenton and M. Gerloch, *Inorg. Chem.* 1987, **26**, 3273.
30. K.-W. Lee and P. E. Hoggard, *Inorg. Chem.* 1988, **27**, 907.
31. M. Kibler, G. Grenet and R. Chatterjee, *J. Luminesc.* 1979, **18/19**, 609.
32. P. J. Steenkamp and J. W. Gonsalves, *Austral. J. Chem.* 1980, **33**, 1705.
33. M. Kibler, *Austral. J. Chem.* 1982, **35**, 231.
34. C. K. Jorgensen, *Adv. Phys. Chem.* 1963, **5**, 33.
35. A. J. McCaffery, S. F. Mason and R. E. Ballard, *J. Chem. Soc.* 1965, 2883.
36. R. D. Gillard, D. J. Shepherd and D. A. Tarr, *J. Chem. Soc., Dalton Trans.* 1976, 594.
37. V. S. Sastri and C. H. Langford, *Can. J. Chem.* 1969, **47**, 4237.
38. T. S. Piper and R. L. Carlin, *J. Chem. Phys.* 1961, **35**, 1809.
39. R. Bramley, M. Brorson, A. M. Sargerson and C. E. Schaffer, *J. Am. Chem. Soc.* 1985, **107**, 2780.
40. K. R. Butler and M. R. Snow, *J. Chem. Soc.* (*A*) 1971, 565.
41. R. B. Wilson and E. I. Solomon, *J. Am. Chem. Soc.* 1980, **102**, 4085.
42. J. Ferguson, *Prog. Inorg. Chem.* 1970, **12**, 159.
43. H. Okazaki, Y. Kushi and H. Yoneda, *J. Am. Chem. Soc.* 1985, **107**, 4183.

Polyhedron Vol. 10, No. 23/24, pp. 2673–2681, 1991
Printed in Great Britain

0277–5387/91 $3.00+.00
© 1991 Pergamon Press plc

LIGAND FIELD ANALYSIS OF METAL–OXYGEN INTERACTIONS—II. TRIS(OXALATO)CHROMATE(III)

SNEŽANA ZARIĆ and S. R. NIKETIĆ*†

Department of Chemistry, Faculty of Science, University of Belgrade, Studentski trg 16, P.O. Box 550, YU-11001 Belgrade, Yugoslavia

(*Received* 10 *July* 1991; *accepted* 1 *August* 1991)

Abstract—Ligand field analysis of $[Cr(ox)_3]^{3-}$ has been performed using the angular overlap model (AOM) approach. The metal–oxygen interactions were treated as locally anisotropic. The Trees' correction and the explicit treatment of the second coordination sphere were included. A set of parameters was derived which reproduces both the quartet bands and sharp doublet lines. Relationships between structural and spectral data were investigated.

In the previous paper of this series[1(a)] we have reported our studies on the tris(oxalato) cobaltate(III) ion in an attempt to examine the nature of metal–oxygen interactions, and to determine the extent of transferability of ligand-field parameters across the series of chromophores $MO_{6-3n}N_{3n}$, $n = 0, 1, 2$.

Already in the initial stages of that work we turned our attention also to chemically analogous chromium(III) complexes. In addition to offering the possibility to extend the range of systems on which we intended to investigate the above-mentioned hypotheses, $[Cr(ox)_3]^{3-}$ presents a textbook example for ligand field studies.[2,3] The latter is due to its rich and characteristic electronic absorption features.

It is therefore not surprising that $[Cr(ox)_3]^{3-}$ has been widely investigated both experimentally and theoretically. Thus, while our work was in progress (parts are described in Ref. 1(b)) Schmidtke *et al.* have published an analysis of the quartet spectra[4] and the doublet spectra[5] of $[Cr(ox)_3]^{3-}$. Also, among several examples in a review on sharp line spectra, Hoggard[6] commented on the results of an AOM analysis of $[Cr(ox)_3]^{3-}$. The paper[4] attempted to explain the observed large trigonal splitting of tris(oxalato) and tris(acetylacetonato) chromate(III) ions (the latter being of almost regular octahedral coordination) using the non-additive AOM approach due to the phase-coupling in the π-conjugated chelate rings. However, it was shown[4] that such an approach is not required for the analysis of oxalato chelates.

* Author to whom correspondence should be addressed.
† E-mail address: ⟨xpmfh01@yubgss21.bitnet⟩.

METHODS

Computational procedures employed in this work are based on the AOM formalism[7–10] and complete matrix diagonalization methods.[11,12] They have been fully described previously.[13] Extensions to the AOM treatment used in the study of $[Cr(ox)_3]^{3-}$ were outlined in the preceeding paper.[1(a)]

RESULTS AND DISCUSSION

In the ligand field analysis of $[Cr(ox)_3]^{3-}$ we have first optimized the parameters on quartet spectra. Then we have proceeded to fit the doublets spectra starting with those parameters. At this stage, we refined the parameters and introduced necessary extensions to the model in order to reproduce the spin-forbidden transitions and their splittings. This, eventually, led us to formulate the best parameter set and the conditions required to fit the whole optical spectrum of $[Cr(ox)_3]^{3-}$.

Quartet spectrum of $[Cr(ox)_3]^{3-}$

Development of parameters. As in the case of Co^{III},[1(a)] the basis for the ligand field analysis of $[Cr(ox)_3]^{3-}$ was X-ray structural data[14] on the following five complexes: $(NH_4)_3[Cr(ox)_3]\cdot 2H_2O$,[15] $K_3[Cr(ox)_3]\cdot 3H_2O$,[16] $(Me_4N)_3[Cr(ox)_3]\cdot$

Table 1. Selected structural data on $[Cr(ox)_3]^{3-}$ complexes

CSD Refcode[a]	Space group	Chelate angle (α)			Average values α	θ	ω
AMOXCR	$P\bar{1}$	84.835	84.221	80.036	82.36	56.31	50.35
CROXKH	$P2_1/c$	82.475	82.513	81.749	82.25	55.52	47.85
DITFER	$P\bar{1}$	82.427	82.352	82.201	82.33	57.08	52.51
SOXCRP	$C2/c$	82.428	82.799	82.244	82.49	55.99	49.79
FEPCOS	$P\bar{1}$	82.371	82.073	82.000	82.15	56.23	49.81

[a] Refcodes:
AMOXCR—$(NH_4)_3[Cr(ox)_3]\cdot 2H_2O$,[15]
CROXKH—$K_3[Cr(ox)_3]\cdot 3H_2O$,[16]
DITFER—$(Me_4N)_3[Cr(ox)_3]\cdot H_2O$,[17]
SOXCRP—$Na_3[Cr(ox)_3]\cdot 5H_2O$,[18]
FEPCOS—$(NH_4)_3[Cr(ox)_3]\cdot 3H_2O$.[19]

H_2O,[17] $Na_3[Cr(ox)_3]\cdot 5H_2O$,[18] and $(NH_4)_3[Cr(ox)_3]\cdot 3H_2O$,[19] (Table 1), as well as the spectral data on $[Cr(ox)_3]^{3-}$.[20-23]

Commonly observed quartet spectra consist of two broad maxima at around 17.5 kK ($^4T_{2g}$) and 24.5 kK ($^4T_{1g}$). Trigonal splitting of the first spin-allowed band is observed[20,21,23] as $^4A_1 < {}^4E_a$ in the monocrystal polarized spectra of Cr^{III} doped in $NaMg[Al(ox)_3]\cdot 9H_2O$. Qualitatively similar splitting was inferred from the analysis of CD spectra.[24,25] The symmetry-forbidden $^4A_2$ component of the second ($^4T_{1g}$) band has been observed,[4,21] due to vibronic coupling, as a weak band in polarized spectra.

Due to the fact that the crystal structure of $NaMg[Al(ox)_3]\cdot 9H_2O$, the host lattice for all published solid-state electronic spectra of $[Cr(ox)_3]^{3-}$, is not known, we have chosen an idealized average geometry of $[Cr(ox)_3]^{3-}$ as a starting point for ligand-field analysis. The trigonal model structure was obtained by averaging over 12 oxalato rings from the four crystal structure determinations, and imposing the C_3 symmetry. This average structure is characterized by: $\alpha = 82.315°$, $\theta = 56.22°$, $\omega = 50.06°$, and $\psi = 50.01°$.

Preliminary calculations with different crystal structure geometries and idealized trigonal geometries showed that the positions and the order of trigonal components, as well as the extent of trigonal splitting, is dependent on small structural variations and on the presence or absence of a C_3 axis.

Therefore, we have set the following weighting criteria for parameter optimization. Highest relative weight was ascribed to the order of trigonal components of the "first" quartet band, taken as $^4A_1 < {}^4E_a$, as found both in the solid-state optical spectra[20,21,23] and in the solution CD spectra.[24,25] In the same way we have treated the position of the baricentre and the ^4E_b component of $^4T_{1g}(O_h)$. The magnitude of trigonal splitting, the order of the components of the "second" quartet band, and the position of the $^4A_2$ component of $^4T_{1g}(O_h)$ were given lower weight in the fitting procedure.

During the optimization the values of F_2, F_4, e_σ and e_π were allowed to vary. It was found that the results are quite insensitive with respect to the variation of the spin-orbit parameter. Therefore, its value was fixed at 115 cm^{-1} in agreement with previous studies.[4] The position of the $^4T_{2g}$ baricentre is sensitive to e_σ and e_π parameters, and the order of trigonal components depends upon e_π. Second quartet band is dependent on F_2 and F_4 as well. The best parameter set for quartet spectra (Table 2) yielded for cubic crystal-field parameter,

Table 2. Comparison of experimental and calculated quartets spectra of $[Cr(ox)_3]^{3-}$complexes (in cm^{-1})

Level	Exptl		Calc.[a]
$^4A_1$	17630[b]	17608[c]	17710
^4E_a	18060	18101	18020
Baricentre	17917	17937	17920
^4E_b	23830	23856	23840
$^4A_2$[d]	25160	25155	23910[e]

[a] $F_2 = 1035$ cm^{-1}, $F_4 = 94$ cm^{-1}, $e(\sigma) = 6570$ cm^{-1}, $e(\pi c) = 650$ cm^{-1}, $e(\pi s) = 0$, $\zeta = 115$ cm^{-1}.
[b] $NaMg[Cr(ox)_3]\cdot 9H_2O$ at 25 K.[21]
[c] 1.5% $[Cr(ox)_3]^{3-}$ in $NaMg[Al(ox)_3]\cdot 9H_2O$ at 77 K.[23]
[d] Forbidden transition.
[e] This value shifts towards higher energies with the parameter set optimized on the whole spectrum and also with inclusion of the outer coordination sphere into AOM calculation (see Table 6).

10 Dq, 18410 cm^{-1}, and for Racah electrostatic parameters: $C = 3290\ cm^{-1}$ and $B = 565\ cm^{-1}$.

Effects of structural deformations. Three characteristic modes[1] of trigonal deformations (θ = const., ω = const., and α = const.) were simulated on the idealized model of $[Cr(ox)_3]^{3-}$. Their effect is shown on Fig. 1.

The average of 12 ox chelate rings from four crystal structures of $[Cr(ox)_3]^{3-}$ with imposed C_3-axis can be classified as belonging to the θ = const.

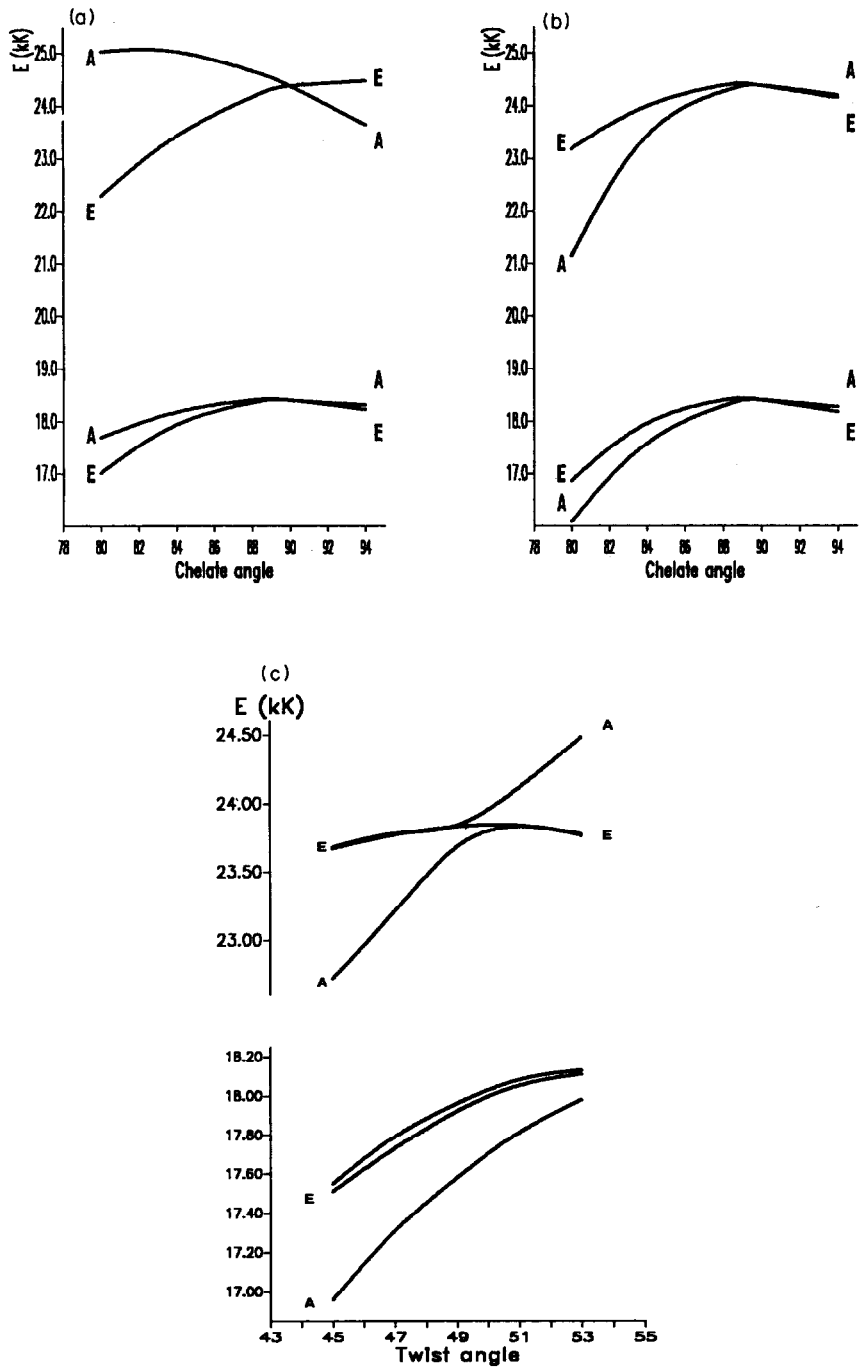

Fig. 1. The influence of characteristic modes of trigonal deformations on the calculated positions of trigonal components of the quartet bands. (a) Simultaneous change of α and θ at $\omega = 60°$. (b) Simultaneous change of α and ω at $\theta = 54.74°$. (c) Simultaneous change of θ and ω at $\alpha = 82.31°$. For all diagrams the best-fit parameter set for quartets spectra was used: $F_2 = 1035\ cm^{-1}$, $F_4 = 94\ cm^{-1}$, $\zeta = 115\ cm^{-1}$, $e(\sigma) = 6570\ cm^{-1}$, and $e(\pi c) = 650\ cm^{-1}$.

type of deformation. For that structure, analysis from Fig. 1 predicts the order $^4A_1 < {}^4E_a$, which is actually observed both in polarized crystal spectra[20,21,4] and in solution CD spectra.[24,25]

Another class of structural deformations is the one in which the trigonal symmetry is removed. In order to study the low symmetry deformations as found in actual crystal structures, we performed calculations on exact crystal structure geometries, on the same geometries with imposed C_3-symmetry, and with both the C_3-symmetry and with chelate rings constrained into planar conformations. The results (Table 3) indicate that both the baricentre positions and the order of trigonal components are indeed highly sensitive to these deformations.

Unfortunately, AOM results on actual crystal structure geometries are difficult to interpret because of extensive mixing of A and E components in both quartet bands ($^4T_{2g}$ and $^4T_{1g}$). If we assign symmetries to the trigonal components on the basis of clustering of the energy levels, we see that the experimentally established order ($A_1 < E_a < E_b < A_2$) is not the same for all structures. The question as to whether these differences are due to trigonal deformations of $[Cr(ox)_3]$ framework or to the lowering of symmetry (to C_1), or perhaps, to chelate ring puckering, is difficult to answer due to the impossibility to decouple different types of structural deformations which often show opposite effects on the energies of ligand-field states.

The order of trigonal components of the second quartet band ($^4T_{1g}$) appears to be most sensitive upon all kinds of structural deformations. In addition, this order for both quartet bands can be influenced by the changes in chelate ring conformation as shown in Fig. 2 for the skew-boat type[1(a)] of ring puckering.

Idealized structures derived from X-ray structures (by imposing C_3 symmetry and chelate-ring planarity) generally show the "correct" order of LF

Table 3. Results of ligand-field analysis[a] on crystal structures and idealized (trigonal) structures derived from X-ray data of $[Cr(ox)_3]^{3-}$ complexes (in cm^{-1})

	Crystal structures[b]				
Level	DITFER	SOXCRP	AMOXCR	CROXKH	FEPCOS
$^4T_{2g}$	17380[c]	17620[c]	17240[c]	17410[c]	17620[c]
	17960	17870	17650	17630	17800
	18690	17990	17940	17930	18020
$^4T_{1g}$	23600 E	23620[c]	23400[c]	23390[c]	23600[c]
		23800	23550	23600	23800
	24750 A	23910	23760	23880	23910

	Idealized structures				
Level	DITFER[d]	DITFER[e]	SOXCRP[d]	SOXCRP[e]	AMOXCR[d]
$^4T_{2g}$	18050[f]	18060[f]	17710 A	17670 A	17620 A
			17980 E	18000 E	17980 E
$^4T_{1g}$	23740 E	23800 E	23840[f]	23840[f]	23820[f]
	24500 A	24380 A			

	Idealized structures				
Level	AMOXCR[e]	CROXKH[d]	CROXKH[e]	FEPCOS[d]	FEPCOS[e]
$^4T_{2g}$	17710 A	17480 A	17430 A	17840[f]	17650 A
	18010 E	17820 E	17850 E		17930 E
$^4T_{1g}$	23870[f]	23490 A	23430 A	23650 E	23750 E
		23760 E	23800 E	24040 A	23860 A

[a] Best-fit parameter set from Table 2.

[b] Structures defined in Table 1.

[c] Symmetry assignment was not possible due to extensive mixing of A and E functions. All calculated values are given.

[d] Trigonal symmetry imposed.

[e] Trigonal symmetry and planar chelate rings.

[f] Baricentre.

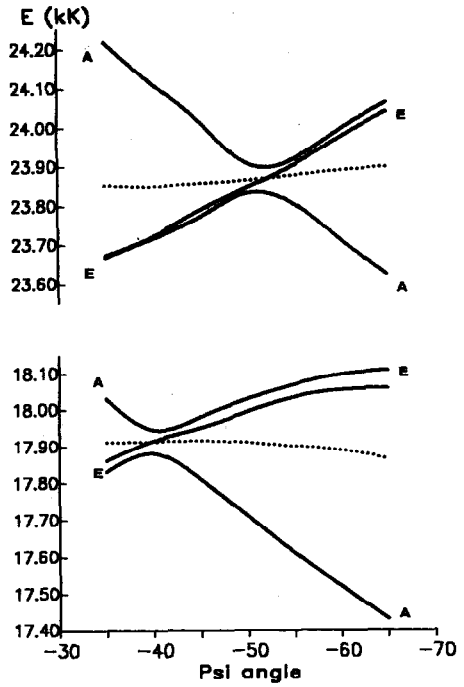

Fig. 2. The influence of the skew-boat type[1(a)] of puckering of all three chelate rings in $[Cr(ox)_3]^{3-}$ structure on the positions and splittings of quartets transitions. The best-fit parameter set for the whole spectrum was used: $F_2 = 1118.5$ cm^{-1}, $F_4 = 71.7$ cm^{-1}, $\zeta = 115$ cm^{-1}, α(Trees) = 230 cm^{-1}, $e(\sigma) = 6540$ cm^{-1}, and $e(\pi c) = 600$ cm^{-1}.

levels ($A_1 < E_a < E_b < A_2$). An exception is CROXKH[16] where it is reversed for $^4T_{1g}$. This is interpreted as being due to high relative degree of trigonal elongation of this structure (the lowest values of ω and θ; Table 1). On the other hand, idealized structures of DITFER[17] and AMOXCR,[15] which are trigonally compressed—or, at least, less elongated than CROXKH (see Table 1) show the "correct" order of ligand-field levels.

The comparison of the present results with the calculations of Schmidtke *et al.*[4] is interesting. These authors[4] have analysed $[Cr(ox)_3]^{3-}$ on the basis of their electronic spectrum [17.3, 17.5, 24.3 and 24.6 kK assigned to $^4A_1$, ^4E_a, ^4E_b and $^4A_2$, respectively] which is characterized by substantially smaller trigonal splittings compared to the previously reported spectra.[20–23] Using their parametrization, with isotropic treatment of Cr–O interactions, we obtained a good fit to the experimental spectrum when the actual X-ray geometry of CROXKH[16] was used in the calculation. However, neither the anisotropic model nor the smoothing of the CROXKH structure into the C_3 geometry, could account for the above spectral data.[4] On the other hand our parametrization based on the anisotropic AOM model, is able to reproduce well the experimental data on the solid state spectra,[21,23] on the average geometry of all crystal structures, as well as on the smoothed geometries of most of the crystal structures except for the trigonally elongated CROXKH.

Therefore the proposition[4] that $[Cr(ox)_3]$ is subjected to a trigonal compression in the host lattice of $K_3[Al(ox)_3]$ is in agreement with our results—but only if other sources of structural deformations are disregarded (as is clearly evident from the α = const. diagram of Fig. 1). However, we argue that other types of deformations, such as symmetry lowering, and chelate-ring puckering, (the latter clearly evident from Fig. 2) are equally important, and that without further structural data on [Cr/Al $(ox)_3$] systems it is not possible to extract unequivocal conclusions from the AOM results.

Doublet spectrum of $[Cr(ox)_3]^{3-}$

Development of parameters. The lowest energy spin-forbidden transitions in $[Cr(ox)_3]^{3-}$ can be detected even in aqueous solution spectra.[2,26] However, only the low-temperature spectra of monocrystals,[20,21] luminescent spectra,[22] and recent excitation spectra[23] provide accurate experimental details to identify components of ^2E, $^2T_{1g}$, and $^2T_{2g}$ that arise from the lowering of symmetry of the chromophore and from spin-orbit coupling.

For the optimization of LF parameters we have, therefore, used the data from low-temperature luminescent[22] and excitation[23] spectra of doublet transitions measured for 1% $[Cr(ox)_3]$ in $K_3[Al(ox)_3]\cdot 9H_2O$ host lattice, and the geometry corresponding to the crystal structure of $K_3[Cr(ox)_3]$. The inconsistency of such an approach may be due to the possible deformations of $[Cr(ox)_3]$ moiety in the host lattice and to the temperature effects (room temperature X-ray study vs low temperature spectral study). However, Coleman[23] assumed that differences between solid state spectra of pure Cr^{III} salts and their 1% solid solutions in isomorphous Al^{III} salts are not significant.

The LF and AOM parameters optimized on quartets spectra do not reproduce the positions of doublets at all. But it has been shown before[27] that it is impossible to fit spin-forbidden and spin-allowed transitions with the same interelectron repulsion parameters. Therefore, we first attempted to optimize F_2 and F_4 on doublets spectra keeping $e_{\zeta\lambda}$ parameters at their previously obtained (best-fit) values. This attempt failed also. Doublets spectra were indeed excellently reproduced (e.g. as in Table 4) only if all parameters were subjected to optimization. However, the parameter set that emerged

from such a refinement (see Table 4) proved to be unacceptable for quartets spectra. The improved parameter set which could simultaneously account for quartet and doublet transitions was eventually obtained after introduction of the Trees' correction, as will be discussed below.

^2E splitting. In spin-forbidden spectra of $[Cr(ox)_3]^{3-}$ below 15 kK a ^2E transition is identified[21] with ^2E splitting varying over two orders of magnitude[22] in different $[Cr(ox)_3]^{3-}$ salts (see Table 5). This splitting is ascribed[22,23] to spin-orbit coupling and its relative magnitude to lattice effects.

A number of recent examples from the literature[5,28-31] point to the difficulties in interpreting ^2E splitting in Cr^{III} complexes and to various attempts to reproduce it in LF analyses with the help of, e.g. Trees' correction,[31] second coordination sphere,[31] differential orbital expansion,[27] symmetry limited π-orbital expansion,[29] etc. but with limited success.

Using arbitrarily assumed values for electron repulsion parameters Hoggard[6] postulated that the ^2E splitting has to be much larger than experimentally deduced[22] and that the supposed ^2E splitting reported by Coleman[22] is in fact due to the existence of non-equivalent sites or to vibronic coupling. In contrast, our study showed that it is possible to account for the observed[22] splitting of ^2E within the present AOM approach.

The splitting of ^2E is very sensitive to the changes in the $e(\pi c)$ parameter. It is not at all sensitive to F_2 and F_4 which determine the difference between ^2E and the other doublet states. Therefore it appears not to be necessary to fit $\Delta E(^2E - {}^2T_{1g})$ difference with $e(\pi s)$ parameter as was done by Hoggard.[6] The spin-orbit parameter does not have much influence on the ^2E splitting, so it was not optimized in this study. Trees' parameter, α, which was introduced in order to correct the calculated position of $^2T_{2g}$, increases slightly the splitting of ^2E. Last, the skew-boat type[1] of chelate-ring puckering (but not the envelope type) also increases ^2E splitting.

Calculated ^2E splittings in the cases for which the X-ray crystal structures were available, are given in Table 5. These results show that both the magnitude and the trend within the series of $[Cr(ox)_3]^{3-}$ salts has been well reproduced. Lower calculated values for ^2E splitting than the experimental ones[22,23] are justifiable on the grounds that the present AOM treatment includes only the static contributions to splittings.

Markedly smaller ^2E splitting obtained for the mean idealized structure (with D_3 symmetry) indicates that this spectral detail is particularly sensitive to symmetry lowering deformations such as those found in crystal structures of tris(oxalato) chromates(III). Another geometrical factor that presumably influences the ^2E splitting is the trigonal compression. In the series of investigated $[Cr(ox)_3]^{3-}$ structures the potassium salt CROXKH shows the highest trigonal elongation and the largest ^2E splitting. It is smaller in the case of trigonally less-elongated SOXCRP and AMOXCR. In fact, the splitting is a result of various simultaneous structural deformations (including also the chelate-ring conformation) and is difficult to rationalize on the basis of individual contributions

Table 4. Comparison of experimental and calculated doublets spectra of $[Cr(ox)_3]^{3-}$ complexes (in cm^{-1})

Level	Exptl		Calc.[a]
^2E	14443[b]		14440
	14525		14527
	15187[d]	15210[d]	15171
$^2T_{1g}$	15272	15384	15264
	15305	15421	15319
	20508[c]	20522[d]	20491
$^2T_{2g}$	20596	20688	20588
	20628	20702	20772

[a] $F_2 = 1205\ cm^{-1}$, $F_4 = 88.2\ cm^{-1}$, $e(\sigma) = 4020\ cm^{-1}$, $e(\pi c) = 650\ cm^{-1}$, $e(\pi s) = 0$, $\zeta = 115\ cm^{-1}$.

[b] 1% $[Cr(ox)_3]^{3-}$ in $K_3[Al(ox)_3] \cdot 3H_2O$ at 77 K.[22]

[c] 1% $[Cr(ox)_3]^{3-}$ in $K_3(Al(ox)_3] \cdot 3H_2O$ at 77 K.[23]

[d] 1.5% $[Cr(ox)_3]^{3-}$ in $MaMg[Al(ox)_3] \cdot 9H_2O$ at 77 K.[23]

Table 5. ^2E Splittings in $[Cr(ox)_3]^{3-}$ salts (in cm^{-1})

Cation	Ref.[a]	Exptl	Calc.[b]	Calc.[c]
NaMg	20	21	—[d]	—
NaMg	21	20	—	—
NaMg	22	20	—	—
Na_3	22	34	25	24
$(NH_4)_3$	22	46	34	38
$(NH_4)_3$	—	—	27	31
K_3	22	82	82	82
$(Me_4N)_3$	—	—	75	35
D_3[e]	—	—	12	15

[a] References are given for experimental Δ^2E reports only.

[b] Best parameter set for the whole spectrum: $F_2 = 1118.5\ cm^{-1}$, $F_4 = 71.7\ cm^{-1}$, $e(\sigma) = 6540\ cm^{-1}$, $e(\pi c) = 600\ cm^{-1}$, $e(\pi s) = 0$, $\zeta = 115\ cm^{-1}$. α(Trees) $= 230\ cm^{-1}$ (see Table 6).

[c] Best parameter set for doublets spectra: $F_2 = 1205\ cm^{-1}$, $F_4 = 88.2\ cm^{-1}$, $e(\sigma) = 4020\ cm^{-1}$, $e(\pi c) = 650\ cm^{-1}$, $e(\pi s) = 0$, $\zeta = 115\ cm^{-1}$.

[d] Crystal structure not known.

[e] Structure of $[Cr(ox)_3]$ averaged to D_3 symmetry.

taken in turn. A good example is DITFER, which shows highest trigonal compression (Table 1) and yet it yields ^2E splitting comparable to AMOXCR or SOXCRP. The explanation for such a result may be sought in different chelate-ring conformations between DITFER and AMOXCR or SOXCRP, as well as in different "degree of departure from C_3 symmetry" in addition to trigonal deformations.

$^2T_1$ and $^2T_2$ states. Spin-forbidden transitions to the components of $^2T_{1g}$ and $^2T_{2g}$ were described by several authors[20,21,23,26] who disagree in detailed assignments.

Our calculations show that F_2 and F_4 do influence the baricentres of $^2T_1$ and $^2T_2$, but that variations in $e_{\zeta\lambda}$ are particularly insignificant. Good fits to both ^2T states are possible only with Trees' correction (as shown below). Splittings of ^2T states are well-reproduced with the parameter set optimized on all doublets. Splittings are influenced by trigonal deformations (see Fig. 3), but again the trigonal elongation and chelate-ring puckering appear to be counteracting effects which cannot be disparted one from the other.

The splitting of $^2T_1$ is insensitive towards both the changes in chelate-ring conformations and the lowering of the overall symmetry of $[Cr(ox)_3]$. These deformations, however, influence the splitting of $^2T_2$. Hoggard[6] predicted a $^2T_2$ splitting of about 1000 cm^{-1}, as opposed to the value estimated[23] from the analysis of experimental spectra, which is about 120 cm^{-1} for the potassium salt. We were not able to obtain $^2T_2$ splittings greater than 580 cm^{-1} with any sensible set of parameters (see below). Moreover, our lower limit to this value was about 180 cm^{-1} which is comparable to Coleman's findings.[23]

Complete spectrum of $[Cr(ox)_3]^{3-}$

The failure of conventional AOM to account, with a unique set of parameters, both for the doublets and the quartets transitions in the optical spectra of Cr^{III} complexes is well known: a number of suggestions on how to cope with this problem have appeared in the literature.[6,31]

Another problem, which did not receive such attention, stems from the necessity to simultaneously fit data of different experimental accuracies: sharp doublet lines (which are sometimes not unambiguously assigned) and broad quartet bands (which are sometimes insufficiently resolved).

A single modification of AOM that significantly improved the overall fit was the introduction of Trees' correction in the form as described in the preceeding paper.[1(a)] Trees' parameter α causes an

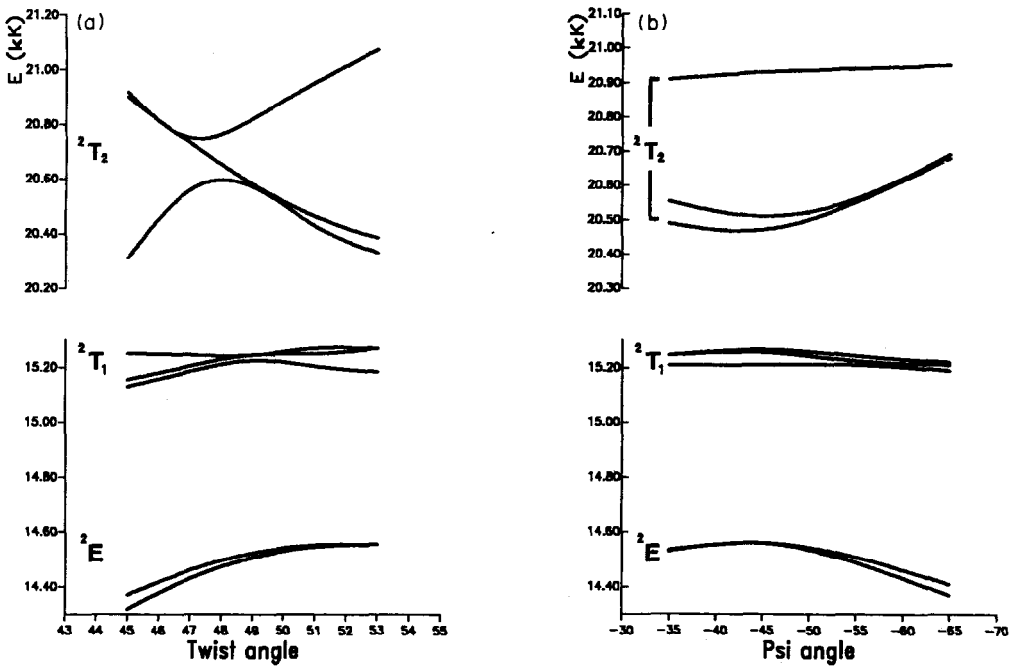

Fig. 3. The influence of trigonal deformations and chelate-ring conformation on the positions and splittings of doublets transitions. Left: Simultaneous change of θ and ω at $\alpha = 82.31°$. Right: The effect of skew-boat puckering of all three chelate rings in $[Cr(ox)_3]^{3-}$ structure. For both diagrams the best-fit parameter set for the whole spectrum was used. $F_2 = 1118.5$ cm^{-1}, $F_4 = 71.7$ cm^{-1}, $\zeta = 115$ cm^{-1}, α(Trees) $= 230$ cm^{-1}, $e(\sigma) = 6540$ cm^{-1}, and $e(\pi c) = 600$ cm^{-1}.

increase in energies of low-lying doublet states, it does not influence the position of the first quartet ($^4T_{2g}$) but it reduces the energy of the second quartet state ($^4T_{1g}$). It also increases slightly the splitting of ^2E and $^2T_{1g}$ and, most importantly, it decreases the difference $\Delta E(^2E - {}^2T_{2g})$. Introduction of parameter α, of course, requires the reoptimization of the other parameters. Thus, it calls for modification of electron repulsion parameters (F_2 and F_4), and a slight decrease in $e(\pi c)$ in order to reproduce ^2E splitting, the change of $e(\sigma)$ in order to reproduce the baricentre of $^4T_{1g}$, and readjustment of other parameters in order to improve the overall fit to the quartet transitions.

The optimized value for α (about 230 cm^{-1}) is larger than the one used[32,33] for the analysis of free Cr^{III} ion spectra. However, similarly large values of Trees' parameter were suggested before[6,31,34] in the case of Cr^{III} complexes.

Table 6. Final results of ligand-field analysis on the complete spectrum of $[Cr(ox)_3]^{3-}$ (in cm^{-1})

Level	Exptl[a]	Calc.[b]		
^2E	14443	14443[c]		14332[d]
	14525	14525		14493
	15187	15192		15117
$^2T_{1g}$	15272	15215		15201
	15305	15235		15227
	20508	20510		20452
$^2T_{2g}$	20596	20700		20754
	20628	20750		20873
$^4T_{2g}$	17630 *A*	17580 *A*[e]	17540 *E*[f]	17077 *A*
	18060 *E*	17870 *E*	17940 *A*	17724 *E*
$^4T_{1g}$	23830 *E*	24030 *E*	23860 *E*	23695 *E*
	25160 *A*	24150 *A*	24230 *A*	24237 *A*

[a] Doublets: 1% $[Cr(ox)_3]^{3-}$ in $K3[Al(ox)_3]\cdot 3H_2O$ at 77 K;[22,23] Quartets: $NaMg[Cr(ox)_3]\cdot 9H_2O$ at 25 K.[21]

[b] Geometry of the CROXKH.[16]

[c] $F_2 = 1118.5\ cm^{-1}$, $F_4 = 72\ cm^{-1}$, $e(\sigma) = 6490\ cm^{-1}$, $e(\pi c) = 600\ cm^{-1}$, $e(\pi s) = 0$, $\zeta = 115\ cm^{-1}$, α(Trees) $= 227\ cm^{-1}$.

[d] $F_2 = 1118.5\ cm^{-1}$, $F_4 = 71.7\ cm^{-1}$, $e(\sigma) = 6540\ cm^{-1}$, $e(\pi c) = 600\ cm^{-1}$, $e(\pi s) = 0$, $\zeta = 115\ cm^{-1}$, α(Trees) $= 230\ cm^{-1}$, together with 17 nearest neighbour atoms (5 potassium and 12 water oxygens) from the crystal lattice.

[e] Quartets were calculated with mean idealized geometry of all crystal structures. Agreement with experimental values is better than with crystal structure CROXKH [cf. note [f] below].

[f] Results obtained on CROXKH with parameter set [c] given in order to enable comparison with the parameter set [d] in which the counterion interactions are included.

The final results are presented in Table 6. A somewhat eclectic nature of the data (Table 6) stemmed from the fact that it was necessary to combine spectral and structural information from various sources in a consistent way. Thus, the calculation with the best-fit parameter set (data column 2 of Table 6) was done on the crystal structure CROXKH for doublets and on the mean idealized geometry for quartets since the exact geometry corresponding to the quartets spectra is not known. Furthermore, the parameter set which included the counterion contributions, was applied onto CROXKH structure both for doublets and for quartets (data column 4 of Table 6). So, for the sake of comparison of the two parameter sets, calculated quartets spectra for CROXKH are also given (data column 3 of Table 6).

An attempt to include contributions to AOM from the outersphere. Following Coleman's[22] suggestion that the second coordination sphere should be considered when analysing the shifts and splittings of sharp doublet lines, we made an attempt to extend the present AOM treatment by including contributions from the counterions and oxygens from water molecules from crystal lattices of $[Cr(ox)_3]^{3-}$ salts.

The smallest interatomic distance between the Cr^{III} centre and a counterion or H_2O in any of known crystal structures is greater than 4 Å. Therefore, interactions were treated as isotropic with $e(\pi c) = e(\pi s) = 0$.

The value of the parameter $e(\sigma)$ for a counterion or water oxygen was taken to be inversely proportional to a power of the interatomic distance. R^{-3} and R^{-5} dependence was proposed by Hoggard,[34] but R^{-7} and R^{-9} were also used.[35,36] Our calculations were performed assuming R^{-5} law. For the nearest water oxygen (approx. 4.2 Å) it gives $e(\sigma)$ of approx. 200 cm^{-1}. For the positive potassium ion, in CROXKH[16] we used $e(\sigma)$ parameters of similar magnitude and opposite sign, in line with general relations between AOM and point charge crystal-field parameters.[37-39]

These corrections increase splittings of all doublet states (^2E, $^2T_{1g}$, and $^2T_{2g}$) as well as the trigonal splitting of $^4T_{2g}$, and lower the energies of all ligand-field states. Unfortunately, for certain combinations of additional parameters, inversions in the order of trigonal components of $^4T_{1g}$ states are observed. By and large, this increase in parameter space demonstrated the necessity for reoptimization of the entire set of parameters, reasserting that for such an endeavour one needs self-consistent sets of accurate structural and spectral data, which are not available at present.

Acknowledgements—This work was supported by the Serbian Research Fund. Computer resources were generously made available by the Serbian State Institute of Statistics (RZS) through the Computer Laboratory of the Univeristy of Belgrade.

REFERENCES

1. (a) S. Zarić and S. R. Niketić, *Polyhedron* 1991, **10**, 2665; (b) S. Zarić and S. R. Niketić, *1st Yugoslav Conf. on Molecular Sciences*, Zagreb, Yugoslavia, May 1986, p. 165; S. Zarić, N. Mitić and S. R. Niketić, *6th Yugoslav-Italian Crystallographic Conf.*, Pula, Yugoslavia, May 1989, Paper O24, p. S88; S. Zarić, M.Sc. Thesis, University of Belgrade (1990).
2. S. S. Eaton, T. D. Yager and G. R. Eaton, *J. Chem. Educ.* 1979, **56**, 635.
3. W. F. Coleman, *J. Chem. Educ.* 1982, **59**, 643.
4. M. A. Atanasov, T. Schonherr and H.-H. Schmidtke, *Theor. Chim. Acta* 1987, **71**, 59.
5. T. Schonherr, J. Spanier and H.-H. Schmidtke, *J. Phys. Chem.* 1989, **93**, 5969.
6. P. E. Hoggard, *Coord. Chem. Rev.* 1986, **70**, 85.
7. C. E. Schaffer and C. K. Jorgensen, *Math. fys. Medd. Dan. Vid. Selsk*, 34, No. 13, (1965).
8. C. E. Schaffer, *Struct. Bond.* 1968, **5**, 68.
9. C. E. Schaffer, *Pure Appl. Chem.* 1970, **24**, 361.
10. C. E. Schaffer, *Struct. Bond.* 1973, **14**, 69.
11. W. Urland, *Chem. Phys. Letts* 1977, **46**, 457.
12. M. L. Ellzey Jr, *Comput. Phys. Commun.* 1975, **10**, 133.
13. S. R. Niketić and W. Urland, *Polyhedron* 1987, **6**, 947.
14. Cambridge Structural Database. For description see, e.g. (a) F. H. Allen, S. Bellard, M. D. Brice, B. A. Cartwright, A. Doubleday, H. Higgs, T. Hummelnik, B. G. Hummelnik-Peters, O. Kennard, W. D. S. Motherwell, J. R. Rogers and D. G. Watson, *Acta Cryst.* 1973, **B35**, 2331; (b) F. H. Allen, O. Kennard and R. Taylor, *Accts Chem. Res.* 1983, **16**, 146.
15. J. N. van Niekerk and F. R. L. Schoening, *Acta Cryst.* 1952, **5**, 499.
16. D. Taylor, *Aust. J. Chem.* 1978, **31**, 1455.
17. N. Bulc, L. Golic and J. Siftar, *Vestn. Slov. Kem. Drus.* 1985, **32**, 221.
18. N. Bulc, L. Golic and J. Siftar, *Vestn. Slov. Kem. Drus.* 1982, **29**, 211.
19. E. H. Merrachi, B. F. Mentzen and F. Chassagneux, *Rev. Chim. Miner.* 1986, **23**, 329.
20. T. S. Piper and R. L. Carlin, *J. Chem. Phys.* 1960, **33**, 608; 1961, **35**, 1809.
21. O. S. Mortensen, *J. Chem. Phys.* 1967, **47**, 4215.
22. W. F. Coleman, *J. Luminesc.* 1975, **10**, 163.
23. W. F. Coleman, *J. Luminesc.* 1980, **22**, 17.
24. R. D. Gillard, D. J. Shepherd and D. A. Tarr, *J. Chem. Soc., Dalton Trans.* 1976, 594.
25. K. R. Butler and M. R. Snow, *J. Chem. Soc., Dalton Trans.* 1976, 251.
26. R. W. Olliff, D. B. Rands and D. Shooter, *Aust. J. Chem.* 1974, **27**, 2057.
27. W. M. Walace and P. E. Hoggard, *Inorg. Chem.* 1983, **22**, 491.
28. C. D. Flint and A. P. Matthews, *J. Chem. Soc., Farad. Trans.* (2) 1973, **69**, 419.
29. H.-H. Schmidtke, H. Adamsky and T. Schonherr, *Bull. Chem. Soc. Japan* 1988, **61**, 59.
30. L. Dubicki and P. Day, *Inorg. Chem.* 1971, **10**, 2043.
31. K.-W. Lee and P. E. Hoggard, *Inorg. Chem.* 1988, **27**, 907.
33. J. Ferguson, *Progr. Inorg. Chem.* 1970, **12**, 159.
34. P. E. Hoggard and K.-W. Lee, *Inorg. Chem.* 1988, **27**, 2335.
36. C. Linares, A. Louat and M. Blanchard, *J. Chem. Phys.* 1982, **68**, 453.
37. M. Kibler, G. Grenet and R. Chatterjee, *J. Luminesc.* 1979, **18/19**, 609.
38. P. J. Steenkamp and J. W. Gonsalves, *Aust. J. Chem.* 1980, **33**, 1705.
39. M. Kibler, *Aust. J. Chem.* 1982, **35**, 231.

Polyhedron Vol. 10, No. 23/24, pp. 2683–2686, 1991
Printed in Great Britain

0277–5387/91 $3.00+.00
© 1991 Pergamon Press plc

THE COORDINATIVE INTERACTION OF A DIORGANOTIN DIHALIDE WITH N-(*META*-SUBSTITUTED PHENYL)-2-HYDROXYNAPHTHALIDENEIMINE

SIANG-GUAN TEOH,* SOON-BENG TEO and GUAN-YEOW YEAP

School of Chemical Sciences, Universiti Sains Malaysia, 11800 Penang, Malaysia

and

JEAN-PAUL DECLERCQ

Laboratoire de Chimie Physique et de Cristallographie, Université Catholique de Louvain, Place L. Pasteur, 1, B-1348, Louvain-la-Neuve, Belgium

(*Received* 8 *May* 1991; *accepted* 1 *August* 1991)

Abstract—The reaction of 1-[3′-methoxyphenylimino)methyl]-2-naphthol with dimethyltin(IV) dichloride yields an addition compound having 2:1 stoichiometry (ligand: organotin). The complex formed has been characterized by elemental analysis, ^{1}H and ^{13}C NMR spectroscopy, IR spectroscopy and X-ray analysis. Coordination of the Schiff base to the metal occurs via the phenolic oxygen atom. This preferred mode of bonding is associated with the shift of the phenolic proton towards the azomethine atom resulting in a zwitterionic configuration for the ligand.

Over the last two decades, studies on the coordination of Schiff bases to inorganic and organometallic tin compounds have received considerable attention.[1–7] Both aliphatic[3,5] and aromatic Schiff bases[4–9] in their neutral and deprotonated forms have been used to react with organotin as well as inorganic tin(II) and tin(IV) halides and pseudohalides. The complexes that are formed exhibit variable stoichiometry in the ligand to metal ratio and different modes of coordination which have been explained on the basis of inductive and steric effects of the substituents on the aromatic ring. However, studies on the structural effects of the *meta*-substituents on the atomatic ring have not been carried out. Structural correlation studies on some of the tin complexes of aldehydes and ketones have contributed to the understanding of the preferred geometry of the tin atom and the conformation of the ligands bonded to the metal.[10] In order to provide more information on the effect of substituents on the nature of the complex formed, we carried out the reaction of the *meta*-substituted 2-hydroxynaphthalideneimine Schiff base 1-[(3′-methoxyphenylimino)-methyl]-2-naphthol with dimethyl tin(IV) dichloride.

* Author to whom correspondence should be addressed.

EXPERIMENTAL

Synthesis of ligand 1-[(3′-*methoxyphenylimino*) *methyl*]-2-*naphthol*

2-Hydroxy-1-naphthaldehyde (50 mmol) was dissolved in a 50 cm^3 mixture (2:1) of CH_2Cl_2 and 95% ethanol. It was then filtered and added to an ethanolic solution of *m*-anisidine (50 mmol). The mixture was stirred for 20 min, whereupon the yellow precipitate which formed was recrystallized from ethanol. M.p. 94–96°C.

Synthesis of the complex $[(CH_3)_2SnCl_2 \cdot 2HOC_{10}H_6CH:NC_6H_4OCH_3]$

A solution of the ligand (6 mmol) dissolved in CH_2Cl_2 (40 cm^3) was added to dimethyltin(IV) dichloride in 10 cm^3 of the same solvent. The mixture was stirred and on standing at room temperature orange crystals were formed. M.p. 146–148°C. Found: C, 59.0; H, 4.7; N, 3.6. Calc. for $C_{38}H_{36}N_2O_4Cl_2Sn$: C, 58.9; H, 4.7; N, 3.6%.

Physical measurements

IR absorption spectra of the compounds were recorded using a Beckman IR 20A IR spectrophotometer in the frequency range 4000–250 cm^{-1}. Samples were prepared as KBr discs. The ^1H and ^{13}C NMR spectra were obtained with a Bruker 300 MHz AC-P NMR spectrometer. Microanalysis was carried out at the School of Chemical Sciences, Universiti Sains Malaysia, Penang, Malaysia.

Crystal structure determination of $[(CH_3)_2SnCl_2 \cdot 2HOC_{10}H_6CH : NC_6H_4OCH_3]$

Intensity data for a crystal with dimensions $0.6 \times 0.4 \times 0.3$ mm were measured at room temperature on a Huber diffractometer fitted with graphite monochromated Mo-K_α radiation, $\lambda = 0.71069$ Å. The θ–2θ scan was employed to measure a total of 4955 reflections such that $\theta_{max} \leqslant 30°$. No significant decomposition occurred during the data collection. Corrections were applied for Lorentz and polarization effects but not for absorption. There were 4955 unique data of which 4778 satisfied the $F \geqslant 2.5\sigma(F)$ criterion of observability and were used in the subsequent analysis. Crystal data are listed in Table 1.

The structure was solved by using SHELXS86[11] and refined by a full-matrix least-squares procedure based on F using SHELX76.[12] The tin atom coincides with a crystallographic centre of symmetry, so that there is only one molecule in the unit cell. All non-hydrogen atoms were refined with anisotropic thermal parameters and hydrogen atoms were included in their idealized positions (C—H = 0.96 Å) and refined isotropically. A weighting scheme of the form $w = k/[\sigma^2(F)+gF^2]$ was used and the refinement continued to final $R = 0.030$, $R_w = 0.033$ for $k = 1.94$ and $g = 0.0008$. The analysis of variance showed no special features and the maximum residual electron density peak in the final difference map was 0.89 e $Å^{-3}$ (near the tin atom). The scattering factors for all the atoms were used as incorporated in SHELX76.

Lists of atomic coordinates, thermal parameters and observed and calculated structure factors have been deposited as supplementary material with the Editor from whom copies are available on request.

Table 1. Crystal data and details of structure refinement for $(CH_3)_2SnCl_2 \cdot 2HOC_{10}H_6CH : NC_6H_4OCH_3$

Formula	$C_{38}H_{36}N_2O_4Cl_2Sn$
Formula weight	774.31
Crystal system	triclinic
Space group	$P\bar{1}$
a (Å)	7.684(1)
b (Å)	9.042(1)
c (Å)	13.502(2)
α (°)	75.80(1)
β (°)	73.35(2)
γ (°)	74.43(1)
V (Å^3)	851.3(2)
Z	1
D_c (g cm^{-3})	1.510
$F(000)$	394
μ (cm^{-1})	9.58
Data collected	4955
Unique data	4955
Data with $F > 2.5\sigma(F)$	4778
R	0.030
R_w	0.033
w	$k/[\sigma^2(F_o)+gF_o^2]$
k	1.94
g	0.0008
$(\Delta\rho)_{max}$	0.89

RESULTS AND DISCUSSION

The ν(C=N) frequency which is found at 1615 cm^{-1} in the IR spectrum of the complex appears at almost the same position in the spectrum of the ligand. This observation indicates that the nitrogen atom is not involved in coordination to the tin atom. The band found at 1270 cm^{-1} in the spectrum of the ligand owing to the phenolic C—O stretching vibration[13,14] is shifted towards a higher frequency (1290 cm^{-1}) upon complex formation, consistent with the coordination of the phenolic oxygen atom to the tin atom. Two additional bands which appear in the spectrum of the complex at 450 and 340 cm^{-1},

Table 2. Selected ^1H and ^{13}C chemical shifts (ppm) of 1-[(3′-methoxyphenylimino)methyl]-2-naphthol and its dimethyltin dichloride complex

	^1H			^{13}C	
	δ(OH)	δ(CH : N)	δ(Sn—CH_3)	δ(C—O)	δ(C=N)
Ligand	13.8	9.2	—	171.4	160.7
Complex	14.0[a]	9.2	1.27	173.2	160.7

[a] Broad.

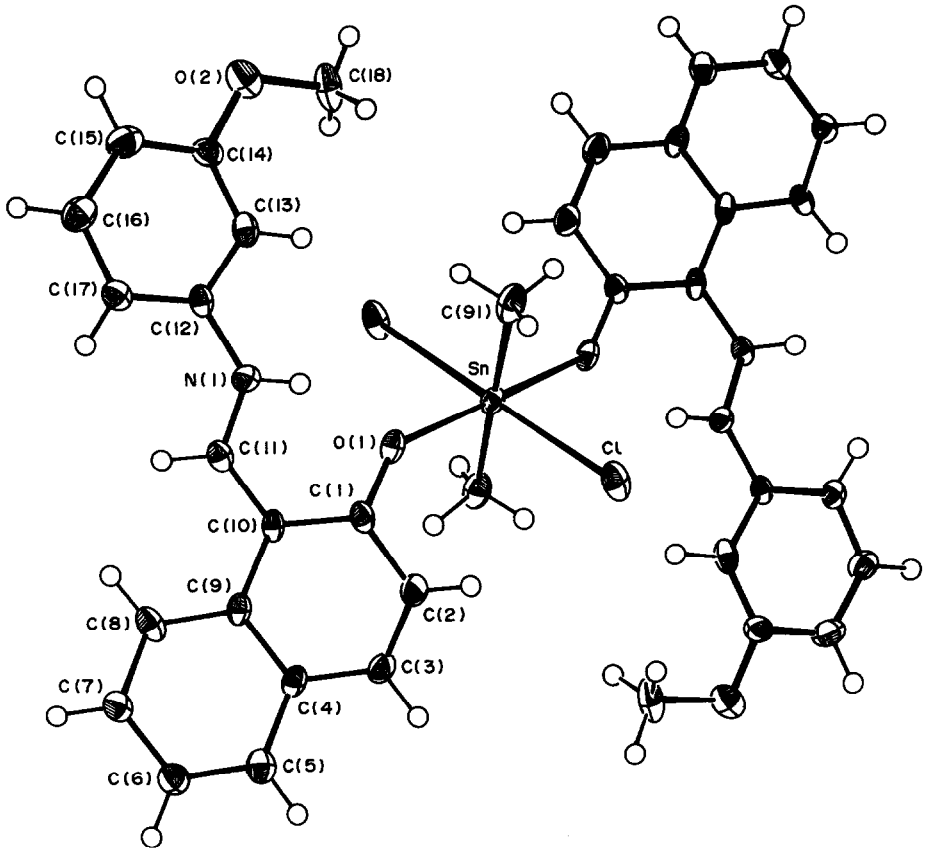

Fig. 1. A perspective view of the molecule.

Table 3. Bond distances (Å) and angles (°) with esds in parentheses

Cl···Sn	2.588(1)	C(9)···C(8)	1.415(2)
C(91)···Sn	2.110(2)	C(10)···C(9)	1.457(2)
O(1)···Sn	2.258(1)	C(11)···C(10)	1.409(2)
C(1)···O(1)	1.299(2)	N(1)···C(11)	1.314(2)
C(2)···C(1)	1.430(2)	C(12)···N(1)	1.417(2)
C(10)···C(1)	1.434(2)	C(13)···C(12)	1.395(2)
C(3)···C(2)	1.361(2)	C(17)···C(12)	1.392(2)
C(4)···C(3)	1.426(2)	C(14)···C(13)	1.390(2)
C(5)···C(4)	1.414(2)	C(15)···C(14)	1.391(3)
C(9)···C(4)	1.416(2)	O(2)···C(14)	1.366(2)
C(6)···C(5)	1.376(3)	C(16)···C(15)	1.384(3)
C(7)···C(6)	1.395(3)	C(17)···C(16)	1.391(2)
C(8)···C(7)	1.385(2)	C(18)···O(2)	1.421(3)

C(91)—Sn—Cl	89.9(1)	C(10)—C(9)—C(8)	123.3(1)
O(1)—Sn—Cl	95.4(1)	C(9)—C(10)—C(1)	119.5(1)
O(1)—Sn—C(91)	86.0(1)	C(11)—C(10)—C(1)	120.3(1)
C(1)—O(1)—Sn	136.8(1)	C(11)—C(10)—C(9)	120.1(1)
C(2)—C(1)—O(1)	120.3(1)	N(1)—C(11)—C(10)	124.2(1)
C(10)—C(1)—O(1)	120.5(1)	C(12)—N(1)—C(11)	128.2(1)
C(10)—C(1)—C(2)	119.1(1)	C(13)—C(12)—N(1)	115.5(1)
C(3)—C(2)—C(1)	120.8(1)	C(17)—C(12)—N(1)	122.9(1)
C(4)—C(3)—C(2)	122.0(1)	C(17)—C(12)—C(13)	121.6(1)
C(5)—C(4)—C(3)	120.3(1)	C(14)—C(13)—C(12)	119.1(1)
C(9)—C(4)—C(3)	119.6(1)	C(15)—C(14)—C(13)	120.1(2)
C(9)—C(4)—C(5)	120.1(1)	O(2)—C(14)—C(13)	123.6(2)
C(6)—C(5)—C(4)	120.8(2)	O(2)—C(14)—C(15)	116.3(2)
C(7)—C(6)—C(5)	119.4(1)	C(16)—C(15)—C(14)	119.8(2)
C(8)—C(7)—C(6)	121.0(2)	C(17)—C(16—C(15)	121.4(2)
C(9)—C(8)—C(7)	120.9(1)	C(16)—C(17)—C(12)	117.9(2)
C(8)—C(9)—C(4)	117.8(1)	C(18)—O(2)—C(14)	117.4(2)
C(10)—C(9)—C(4)	118.9(1)		

respectively, may be attributed to the Sn—O and Sn—Cl vibrations, respectively.

Selected spectral assignments for the ^{1}H and ^{13}C NMR spectra[15] of the ligand and complex are shown in Table 2. The chemical shift corresponding to the carbon from the imine group remains the same for the complex as in the ligand. However, the shifting of the δ(C—O) value of the ligand downfield by 1.8 ppm upon complex formation is again characteristic of the coordination of the phenolic oxygen atom to the tin. A notable feature of the ^{1}H NMR spectrum of the complex is the broadening of the phenolic proton peak due to the weakening of the O—H bond and a strengthening of the C=N—H hydrogen bond.[1]

The structure of the complex and the atom labelling scheme is shown in Fig. 1. The bond lengths and angles are listed in Table 3. The geometry about the tin atom is all *trans*-octahedral with the two methyl groups and the two chlorine atoms occupying the equatorial positions. Coordination of the two ligands to the tin atom occurs via the phenolic oxygen atoms which are located at the axial positions. The bond lengths and angles between the tin and the donor atoms are comparable to those found for similar complexes.[16,17] The phenolic hydrogen of the ligand was found to have shifted to the imine nitrogen atom. This phenomenon of migration of the hydrogen atom has been well substantiated by Bullock *et al.*[18]

REFERENCES

1. K. Kawakami, M. Miya-uchi and T. Tanaka, *J. Inorg. Nucl. Chem.* 1971, **33**, 3733.
2. K. Kawakami and T. Tanaka, *J. Organomet. Chem.* 1973, **49**, 409.
3. J. N. R. Ruddick and J. R. Sams, *J. Organomet. Chem.* 1973, **60**, 233.
4. T. N. Srivastava, G. Srivastava and A. K. S. Chauhan, *J. Inorg. Nucl. Chem.* 1977, **39**, 371.
5. B. S. Saraswat, G. Srivastava and R. C. Mehrotra, *Inorg. Chim. Acta* 1989, **36**, 289.
6. L. E. Khoo, J. P. Charland, E. J. Gabe and F. E. Smith, *Inorg. Chim. Acta* 1987, **128**, 139.
7. L. E. Khoo and F. E. Smith, *Polyhedron* 1982, **1**, 213.
8. B. S. Saraswat, G. Srivastava and R. C. Mehrotra, *J. Organomet. Chem.* 1977, **129**, 155.
9. J. P. Charland, F. L. Lee, E. J. Gabe, L. E. Khoo and F. E. Smith, *Inorg. Chim. Acta* 1987, **130**, 55.
10. S. Shambayati, W. E. Crowe and S. L. Schreiber, *Angew. Chem., Int. Edn Engl.* 1990, **29**, 256.
11. G. M. Sheldrick, SHELXS86. *A Program for Crystal Structure Determination.* University of Gottingen, F.R.G. (1986).
12. G. M. Sheldrick, SHELX76. *A Program for Crystal Structure Determination and Refinement.* Cambridge University, U.K. (1976).
13. C. S. Marvel, S. A. Aspey and A. Dudley, *J. Am. Chem. Soc.* 1956, **78**, 4909.
14. J. E. Kovacic, *Spectrochim. Acta* 1967, **23A**, 183.
15. G. C. Levy, R. L. Lichter and G. L. Nelson, *Carbon-13 Nuclear Magnetic Resonance Spectroscopy*, 2nd edn, p. 163. Wiley Interscience Publication, New York (1980).
16. M. E. Kamwaya and L. E. Khoo, *Acta Cryst.* 1985, **C41**, 1027.
17. H. K. Fun, S. B. Teo, S. G. Teoh and G. Y. Yeap, *Acta Cryst.* 1991, **C47**, 1602.
18. J. I. Bullock, M. F. C. Ladd, D. C. Povey and H. A. Tajmir-Riahi, *Acta Cryst.* 1979, **B35**, 2013.

Polyhedron Vol. 10, No. 23/24, pp. 2687–2691, 1991
Printed in Great Britain

0277–5387/91 $3.00+.00
© 1991 Pergamon Press plc

METAL–BETAINE INTERACTIONS—X. PREPARATION AND CRYSTAL STRUCTURES OF BIS(TRIETHYL BETAINE)BIS(NITRATO)DISILVER(I) AND *CATENA*-BIS(TRIETHYL BETAINE)DISILVER(I) DIPERCHLORATE*

WEI-YUAN HUANG and LONG LÜ

Shanghai Institute of Organic Chemistry, Academia Sinica, 345 Lingling Lu, Shanghai 200032, P.R.C.

and

XIAO-MING CHEN and THOMAS C. W. MAK†

Department of Chemistry, The Chinese University of Hong Kong, Shatin, New Territories, Hong Kong

(*Received* 8 *May* 1991; *accepted* 1 *August* 1991)

Abstract—Two silver(I) complexes of triethyl betaine ($Et_3N^+CH_2COO^-$, Et_3BET) have been prepared and characterized by X-ray crystallography. Both complexes, $[Ag_2(Et_3BET)_2(NO_3)_2]$ (**1**) and $[Ag_2(Et_3BET)_2]_n(ClO_4)_{2n}$ (**2**), contain centrosymmetric bis-carboxylato-bridged Ag_2(carboxylato-O,O′)$_2$ dimers (Ag—O = 2.16–2.23 Å). The dimeric unit in **1** is bound to a chelating nitrato group [Ag—O = 2.524(3), 2.619(3) Å] at each axial site, resulting in a discrete molecule. In **2** the dimers are extended into a stair-like cationic chain via the coordination of each metal centre by a carboxylato oxygen atom [Ag—O = 2.565(5) Å] from an adjacent unit. The intra-dimer Ag···Ag distance is 2.928(1) Å for **1** and 2.856(2) Å for **2**.

The paucity of crystallographic data for silver(I) carboxylates has been ascribed to the poor solubility and light-sensitive nature of such compounds.[2] The known crystal structures have been classified into four types depending on the coordination motif:[3] type A consists of discrete Ag_2(carboxylato-O,O′)$_2$ dimers without any axial ligand; types B and C have similar dimeric structures with the axial site(s) occupied by one and two ligands, respectively, and they are commonly polymeric species; type D comprises dimeric subunits that are extended into a step polymer through the linkage of each metal centre to a carboxylato oxygen of an adjacent dimer, while modified type D has an additional axial ligand attached to each metal atom.[4] Two unusual polymeric structures that are not based on dimeric units have been classified as the fifth type, type E.[5]

As structural analogues of the corresponding carboxylate anions, the zwitterionic betaine ligands can be used to prepare carboxylate-like silver(I) complexes that have very good solubility in water and even in ethanol, and are quite stable under exposure to X-ray radiation. In previous studies we have determined the crystal structures of three silver(I) betaine complexes, namely $[Ag_2(BET)_2(H_2O)_2(NO_3)_2]_n$ (**3**), $[Ag_2(pyBET)_2(ClO_4)_2]_n$ (**4**) and $[Ag(pyBET)(NO_3)]_n$ (**5**) (BET = betaine, $Me_3N^+CH_2COO^-$; pyBET = pyridine betaine, $C_5H_5N^+CH_2COO^-$).[4,5] Both complexes (**3**) and (**4**) adopt modified type D dimeric structures,[4] whereas complex (**5**) has the type E polymeric structure.[5] The study has now been extended to include the preparation and single-crystal X-ray analysis of two silver(I) complexes of a new betaine derivative, triethyl betaine ($Et_3N^+CH_2COO^-$, Et_3BET; IUPAC name: triethylammonioacetate), namely bis(triethyl betaine)bis(nitrato)disilver(I), $[Ag_2(Et_3BET)_2(NO_3)_2]$ (**1**) and *catena*-bis(triethyl betaine)

* For part IX, see ref. 1.

† Author to whom correspondence should be addressed.

disilver(I) diperchlorate, $[Ag_2(Et_3BET)_2]_n(ClO_4)_{2n}$ (**2**).

EXPERIMENTAL

Preparation

Triethyl betaine was synthesized according to a method reported previously.[6] A mixture of 2-bromoacetic acid (13.9 g, 0.10 mol), triethylamine (22.0 g, 0.22 mol) and distilled water (100 cm^3) was stirred at 50–60°C for 4 h. After removal of the excess triethylamine under reduced pressure, the solution was passed through an anion-exchange resin (OH^- form) column (3 × 35 cm) and eluted with distilled water (400 cm^3). The eluate was evaporated to dryness under reduced pressure with a water bath below 80°C to give a pure product (15.6 g, 98% yield) which is very hydroscopic. MS data, m/z: 160 (M + 1), 159 (M); ^1H NMR data (δ, ppm; in D_2O): 1.20 (9H, t, $3CH_3$), 3.47 (6H, q, $3CH_2N$), 3.68 (2H, s, CH_2CO).

Complex **1** was prepared by dissolving $AgNO_3$ (0.170 g, 1.0 mmol) and triethyl betaine (0.159 g, 1.0 mmol) in 90% ethanol solution (4 cm^3) with stirring at 60°C. After cooling to room temperature, colourless prismatic crystals were afforded by slow evaporation in a desiccator charged with silica gel for several days.

Complex **2** was prepared by mixing $AgClO_4$ (0.207 g, 1.0 mmol) and triethyl betaine (0.159 g, 1.5 mmol) in a water–ethanol solution (3 cm^3, v/v 1:1) with stirring at about 60°C to give a clear solution. Evaporation of the solution in air at room temperature for a week yielded colourless grain-like crystals.

Crystallography

Densities of the crystals were measured by flotation in 1,2-dibromoethane/CCl_4. Diffraction intensities for both complexes (**1**) and (**2**) were collected at 21°C on a Nicolet R3m/V diffractometer using the ω-scan (2.9–14.6° min^{-1}) mode.[7] Data processing, absorption corrections, structure solution, and full-matrix least-squares refinement were performed with the SHELXTL-PLUS program package[8,9] (detailed parameters given in Table 1) on a DEC MicroVAX-II computer. The non-hydrogen atoms were refined anisotropically, except the oxygen atoms of the two-fold orientationally disordered perchlorate group in complex (**2**) which were subjected to inter-atomic distance constraints of Cl—O = 1.40 ± 0.01 Å and O···O = 2.26 ± 0.01 Å, assigned site occupancy factors of 0.5, and refined isotropically. All the hydrogen atoms were generated geometrically (C—H = 0.96 Å), assigned isotropic temperature factors and included in the structure-factor calculations. Analytic expressions of neutral-atom scattering factors were employed, and anomalous dispersion corrections were incorporated.[10] The final discrepancy indices and other parameters at the conclusion of refinement are given in Table 1, and selected inter-atomic distances and bond angles in Table 2.

Supplementary materials including non-hydrogen and hydrogen atomic coordinates and thermal parameters have been deposited at the Cambridge Crystallographic Data Centre, and observed and calculated structure factors are available upon request from the corresponding author.

RESULTS AND DISCUSSION

$[Ag_2(Et_3BET)_2(NO_3)_2]$ (**1**)

As illustrated in Fig. 1, the crystal structure of complex (**1**) consists of discrete bis(carboxylato-O,O′)-bridged centrosymmetric $Ag_2(Et_3BET)_2$ dimers, with the carboxylato group acting in the symmetric *syn–syn* bridging mode [C—O = 1.239(5), 1.235(5) Å, O—C—O = 126.2(4)°]. The Ag···Ag separation [2.929(1) Å] in the dimer is significantly larger than that [2.89 Å] in metallic silver, thus indicating a weak or negligible metal–metal interaction. The intra-dimer Ag—O distances and O—Ag—O angle are 2.162(3), 2.207(3) Å and 160.9(1)°, respectively, which are comparable to those found in the dimeric structures of known silver(I) carboxylates. The coordination sphere is completed by an unsymmetrical chelating nitrato group at each axial site of the dimer with Ag—O(nitrato) = 2.524(3) and 2.619(3) Å, which are significantly longer than those [Ag—O(nitrato) = 2.248(2) and 2.41(1) Å] of the

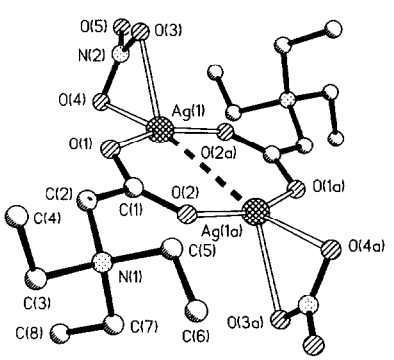

Fig. 1. Perspective view showing the molecular and crystal structure of $[Ag_2(Et_3BET)_2(NO_3)_2]$ (**1**) and the atom numbering scheme. Symmetry code: (a) $1-x, -y, -z$.

Table 1. Data collection and processing parameters

Complex	1	2
Formula	$C_{16}H_{34}N_4Ag_2O_{10}$	$C_{16}H_{34}N_2Ag_2O_{12}Cl_2$
Formula weight	658.21	733.09
a (Å)	8.263(2)	11.469(4)
b (Å)	7.482(2)	14.686(2)
c (Å)	19.400(7)	15.026(4)
β (°)	91.33(2)	
V (Å^3)	1199.1(2)	2530.9(4)
Z	2	4
D_{meas} (Mg m^{-3})	1.812	1.918
D_{calc} (Mg m^{-3})	1.823	1.924
Space group	$P2_1/c$ (No. 14)	$Pcca$ (No. 54)
Radiation	Mo-K_α (λ = 0.71073 Å)	
μ (cm^{-1})	16.7	18.0
Crystal size (mm)	0.18 × 0.22 × 0.32	0.22 × 0.26 × 0.32
Transmission factors	0.521 to 0.595	0.483 to 0.514
Collection range	$h, k, \pm l$; $2\theta_{max} = 55°$	h, k, l; $2\theta_{max} = 50°$
Unique data measured	1808	2232
Observed data with $I \geqslant 3\sigma(I)$ (n)	1483	1507
Number of variables (p)	128	154
$R_F = \Sigma\|\|F_o\|-\|F_c\|\|/\Sigma\|F_o\|$	0.032	0.045
Weighting scheme (w)	$[\sigma^2(F_o)+0.0003\|F_o\|^2]^{-1}$	$[\sigma^2(F_o)+0.0001\|F_o\|^2]^{-1}$
$R_G = [\Sigma w(\|F_o\|-\|F_c\|)^2/\Sigma w\|F_o\|^2]^{1/2}$	0.037	0.047
$S = [\Sigma w(\|F_o\|-\|F_c\|)^2/(n-p)]^{1/2}$	1.512	2.118
Residual extrema in final difference map (e Å^{-3})	+0.31 to −0.34	+0.65 to −0.61

$[Ag(NO_3)_2]^-$ anion found in the double metal salt $[Rh(py)_4Cl_2][Ag(NO_3)_2]$, where the nitrato groups act in the unsymmetrical chelating mode.[11] The longer Ag—O(nitrato) bonds may be attributed to the fact that the axial Ag—O bonds are significantly longer (>2.50 Å in general) than the other Ag—O bonds in the dimeric structure of silver(I) carboxylates. The presence of chelating nitrato ligands in complex (**1**) makes it unique among the $AgNO_3$ complexes containing carboxylate ligands that are presently known, although the directly-bound nitrato ligand is not without precedent in this series. For example, the nitrate groups act as unidentate ligands in complex (**5**) (type E),[5] and as bidentate bridging ligands extending type C dimers into a polymeric structure in alanine silver(I) nitrate.[12] Furthermore, complex (**1**) is the first example of a non-polymeric structure among silver(I) complexes of betaine ligands.

$[Ag_2(Et_3BET)_2]_n(ClO_4)_{2n}$ (2)

Complex (**2**) is a polymer based on bis(carboxylato-O,O′)-bridged centrosymmetric $Ag_2(Et_3BET)_2$ dimers (Fig. 2), with the carboxylato group of Et_3BET serving in the symmetric *syn–syn* bridging mode [C—O = 1.242(8), 1.243(8) Å, O—C—O = 127.5(6)°] as found in complex **1**. The Ag···Ag separation [2.856(2) Å] is smaller than that [2.89 Å] in metallic silver, suggesting a comparable extent of metal–metal interaction. The intra-dimer Ag—O distances and O—Ag—O angle are 2.222(4), 2.232(4) Å and 163.6(1)°, respectively, which are comparable to those found in complex **1** and the other dimeric structures of several known silver(I) carboxylates.[4] The present structure is extended into a stair-like cationic polymer running parallel to the a-axis via metal–carboxylate linkages [Ag(1)—O(2e) = 2.565(5) Å] between adjacent dimers, generating centrosymmetric rhombic Ag_2O_2 units as found in type D and the modified type D structures, e.g. in both complexes **3** and **4**.[4] The perchlorate group has no association shorter

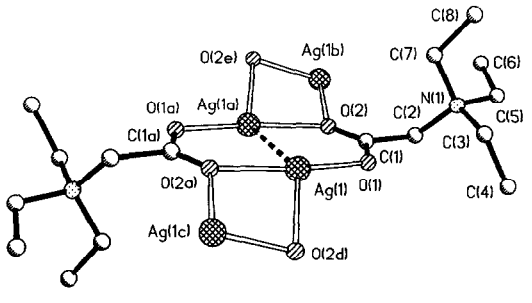

Fig. 2. Perspective view showing the dimeric unit and polymeric structure of the cationic chain in $[Ag_2(Et_3BET)_2]_n(ClO_4)_{2n}$ (**2**) and the atom numbering scheme. Symmetry codes are given in Table 2.

Table 2. Selected inter-atomic distances (Å) and bond angles (°)

Complex **1**			
Ag(1)—O(1)	2.162(3)	Ag(1)—O(3)	2.524(3)
Ag(1)—O(4)	2.619(3)	Ag(1a)—O(2)	2.207(4)
Ag(1)···Ag(1a)	2.929(1)		
O(3)—Ag(1)—O(1)	116.8(1)	O(3)—Ag(1)···Ag(1a)	144.8(1)
O(1)—Ag(1)···Ag(1a)	85.7(1)	O(3)—Ag(1)—O(2a)	80.7(1)
O(1)—Ag(1)—O(2a)	160.9(1)	O(3)—Ag(1)—O(4)	48.8(2)
O(1)—Ag(1)—O(4)	118.8(2)	O(4)—Ag(1)—O(2a)	77.9(2)
Ag(1a)···Ag(1)—O(2a)	75.3(1)	Ag(1a)···Ag(1)—O(4)	144.4(2)
Ag(1)—O(3)—N(2)	96.3(2)	Ag(1)—O(1)—C(1)	120.6(3)
C(1)—O(2)—Ag(1a)	132.1(3)		
O(3)—N(2)	1.243(5)	O(4)—N(2)	1.234(5)
O(5)—N(2)	1.230(5)	O(1)—C(1)	1.239(5)
O(2)—C(1)	1.235(6)	C(1)—C(2)	1.524(6)
C(2)—N(1)	1.517(5)		
O(3)—N(2)—O(4)	118.1(4)	O(3)—N(2)—O(5)	119.3(4)
O(4)—N(2)—O(5)	122.6(4)	O(1)—C(1)—O(2)	126.2(4)
O(1)—C(1)—C(2)	113.2(4)	O(2)—C(1)—C(2)	120.6(4)
C(1)—C(2)—N(1)	116.7(3)		
Complex **2**			
Ag(1)—O(1)	2.222(4)	Ag(1)—O(2a)	2.232(4)
Ag(1)—O(2d)	2.565(5)	Ag(1)···Ag(1a)	2.856(2)
O(1)—Ag(1)···Ag(1a)	81.5(1)	O(1)—Ag(1)—O(2a)	163.6(2)
Ag(1a)···Ag(1)—O(2a)	82.3(1)	O(1)—Ag(1)—O(2d)	118.6(1)
Ag(1a)—Ag(1)—O(2d)	144.9(1)	O(2a)—Ag(1)—O(2d)	74.6(2)
Ag(1)—O(1)—C(1)	124.8(4)	C(1)—O(2)—Ag(1a)	123.4(4)
C(1)—O(2)—Ag(1b)	132.2(4)	Ag(1a)—O(2)—Ag(1b)	103.1(2)
O(1)—C(1)	1.242(8)	O(2)—C(1)	1.243(8)
C(1)—C(2)	1.537(9)	C(2)—N(1)	1.508(8)
O(1)—C(1)—O(2)	127.5(6)	O(1)—C(1)—C(2)	117.8(6)
O(2)—C(1)—C(2)	114.6(5)	C(1)—C(2)—N(1)	114.7(5)

Symmetry codes:
For **1** (a) $1-x, -y, -z$.
For **2** (a) $-x, -y, -z$; (b) $-\frac{1}{2}+x, y, -z$; (c) $\frac{1}{2}-x, -y, z$; (d) $\frac{1}{2}+x, y, -z$; (e) $-\frac{1}{2}-x, -y, z$.

than 2.70 Å with the silver(I) atom, so that complex **2** belongs to the type D dimeric structure. In contrast, perchlorate groups have been found to be unidentate axial ligands in complex **4** (type D),[4] and in di-μ-[(2-chlorophenoxy)ethanoato]disilver(I)-silver(I) perchlorate (type B).[13] This difference may arise from the fact that the greater steric bulk of the triethylamino groups may only allow the axial site to be approached by smaller ligands such as the planar nitrato group in complex (**1**). Another type D dimeric structure has been found in a silver(I) complex of an amino acid, glycine silver(I) nitrate,[14] where the nitrate group is bound to the amino group via hydrogen bonds and has no direct association with the silver(I) atom.

REFERENCES

1. X.-M. Chen and T. C. W. Mak, *Inorg. Chim. Acta* 1991, in press.
2. R. J. Lancashire, in *Comprehensive Coordination Chemistry* (Edited by G. Wilkinson, R. D. Gillard and J. A. McCleverty), Vol. V, p. 808. Pergamon Press, Oxford (1987).
3. T. C. W. Mak, W. H. Yip, C. H. L. Kennard, G. Smith and E. J. O'Reilly, *Aust. J. Chem.* 1986, **39**, 541.
4. X.-M. Chen and T. C. W. Mak, *J. Chem. Soc., Dalton Trans.* 1991, 1219.
5. X.-M. Chen and T. C. W. Mak, *Polyhedron* 1991, **10**, 1723.
6. Y. Utsunomiya, *Yakuguku Zasshi* 1967, **87**, 1442; N. E. Miller, *Inorg. Chem.* 1976, **15**, 1735.

7. R. A. Sparks, in *Crystallographic Computing Techniques* (Edited by F. R. Ahmed), p. 452. Munksgaard, Copenhagen (1976).
8. G. M. Sheldrick, in *Computational Crystallography* (Edited by D. Sayre), p. 506. Oxford University Press, New York (1982).
9. G. M. Sheldrick, in *Crystallographic Computing* 3: *Data Collection, Structure Determination, Proteins, and Databases* (Edited by G. M. Sheldrick, C. Krüger and R. Goddard), p. 175. Oxford University Press, New York (1982).
10. *International Tables for X-ray Crystallography*, Vol. IV, pp. 55, 99, 149. Kynoch Press, Birmingham (1974). (Now distributed by Kluwer Academic Publishers, Dordrecht, The Netherlands.)
11. R. D. Gillard, L. R. Hanton and S. H. Mitchell, *Polyhedron* 1990, **9**, 2127.
12. M. E. Kamwaya, E. Papavinasam, S. G. Teoh and R. K. Rajaram, *Acta Cryst.* 1984, **40C**, 1381.
13. T. C. W. Mak, W. H. Yip, C. H. L. Kennard, G. Smith and E. J. O'Reilly, *J. Chem. Soc., Dalton Trans.* 1988, 2353.
14. J. K. M. Rao and M. A. Viswamitra, *Acta Cryst.* 1972, **28B**, 1484.

Polyhedron Vol. 10, No. 23/24, pp. 2693–2697, 1991
Printed in Great Britain

0277–5387/91 $3.00+.00
© 1991 Pergamon Press plc

PREPARATIVE AND SPECTRAL INVESTIGATIONS ON *ORTHO*-TELLURATED PHENOLS AND THEIR MERCURY(III), PALLADIUM(II) AND PLATINUM(II) PHENOXIDES CHELATED THROUGH TELLURIUM

A. K. SINGH,* S. THOMAS and B. L. KHANDELWAL*

Department of Chemistry, Indian Institute of Technology, New Delhi 110 016, India

(*Received* 27 *March* 1991; *accepted* 1 *August* 1991)

Abstract—Bis(2-hydroxy-5-methylphenyl)telluride (**1**) and (2-hydroxy-5-methylphenyl) aryltelluride (**2**) have been synthesized from *p*-cresol by direct reaction with $TeCl_4$ followed by reduction of the Ar_2TeCl_2 type compound and *ortho*-mercuration followed by *trans*-metallation and reduction, respectively. The ligation behaviour of **1** and **2** has been explored. Compound **1** forms a polymeric mercury(II) complex which on reaction with PPh_3 gives [(PPh_3)HgCl(**1**-H)]. Compound **2** forms with mercury(II), palladium(II) and platinum(II) chelated phenoxides of stoichiometry $[MCl(\mathbf{2}\text{-H})]_2$, which have been found to be dimeric containing chloro bridges. ^1H and ^{13}C NMR and IR spectra of **1** and **2** are characteristic. The electronic spectra support square planar geometry around palladium(II)/platinum(II). IR and ^1H NMR spectra of the metal complexes indicate that **1** acts as a uni-negative bidentate ligand in [(PPh_3)HgCl(**1**-H)] coordinating through oxygen and tellurium. Similar behaviour was found for **2** in all its metal complexes.

Tellurium ligands favour strongly those metals which are designated as Class B in the Arhland, Chatt, Davies classification.[1] The extension of the ligand chemistry of tellurium should be possible if such ligands containing another donor atom, which is hard in the Pearson classification,[2] are synthesized and investigated for their complexation reactions. We have been working on the development of (Te, N)[3,4] and (Te, O)[5] donors for the last 4–5 years. At least five other tellurides[6] are already known which may behave as a (Te, O) donor but only the metal complexes of 2-(4-ethoxyphenyltelluro)benzoate[6] have been isolated and investigated in some detail. As part of our research programme of the development of hybrid organotellurium ligands, we have synthesized the *ortho* tellurated phenols, i.e. (Te, O) ligands **1** and **2** and investigated their ligand chemistry. The synthesis of **1** and **2**, reactions of **1** with $HgCl_2$, and mercury(II), palladium(II) and platinum(II) complexes of **2** are the subject of the present paper.

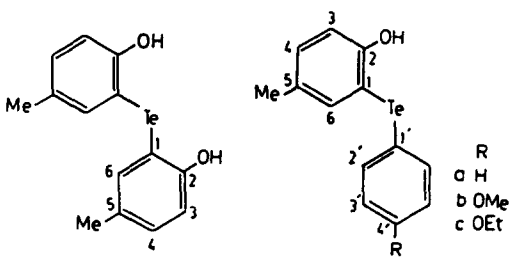

1 2

EXPERIMENTAL

Published methods were used to synthesize bis (2-hydroxy-5-methylphenyl)tellurium(IV) chloride,[7] aryltellurium(IV)chloride[8] (aryl = C_6H_5, 4-$MeOC_6H_4$ or 4-$EtOC_6H_4$) and 1-(chloromercury)-2-hydroxy-5-methylbenzene.[9] The chlorine and tellurium were estimated by standard methods.[10] The carbon, hydrogen and nitrogen analyses were carried out with a Perkin–Elmer 240C elemental analyser. The ^1H and $^{13}C\{^1H\}$ NMR spectra in $CDCl_3$ and DMSO-d_6 were recorded at 25°C on a

* Authors to whom correspondence should be addressed.

JEOL FX-100 FT-NMR spectrometer at 99.55 and 25 MHz, respectively. IR spectra (of Nujol mulls between CsI windows or CsI/KBr discs) in the range 200–4000 cm^{-1} were recorded on a Nicolet 5DX FT-IR spectrometer. Electronic spectra were recorded on a Hitachi UV–vis spectrophotometer model 350. Far IR spectra (up to 50 cm^{-1}) in polyethylene were recorded on a Perkin Elmer far IR spectrometer model 1700X.

Synthesis of bis(2-hydroxy-5-methylphenyl)telluride (**1**)

A suspension of bis(2-hydroxy-5-methylphenyl) tellurium(IV) chloride (4.12 g, 10 mmol), prepared by the published method, in a 50% ethanol–water mixture (25–30 cm^3) was treated with hydrazine hydrate (1.5 g, 3 mmol) dissolved in 10–15 cm^3 ethanol. The resulting mixture was stirred for 10 min and poured into water. The pale yellow telluride was extracted with diethyl ether. The ether extract was washed with water, dried over Na_2SO_4 and concentrated to dryness. Yield, 65%. After recrystallization from methanol the m.p. of the pale yellow telluride was 90°C. Found: C, 47.6; H, 4.1; Te, 38.1. Calc. for $C_{14}H_{14}O_2Te$: C, 47.1; H, 4.1; Te, 37.6%. NMR: ^1H, $CDCl_3$, 25°C: δ, 2.20(s, 6H, CH_3), 6.85(bs, OH), 6.97–7.36(m, 6H, phenyl). $^{13}C\{^1H\}$, $CDCl_3$, 25°C: δ, 20.0(CH_3), 102.1(C_1), 114.0(C_3), 131.3(C_4), 131.8(C_5), 139.9(C_6), 154.0(C_2).

Synthesis of $[HgCl_2 \cdot \mathbf{1}]_n$ *and* $(PPh_3)HgCl_2 \cdot \mathbf{1}$

Mercury(II) chloride (0.27 g, 1 mmol) was refluxed with **1** (0.34 g, 1 mmol) in methanol with stirring for 2–3 h. The yellow precipitate separated out was filtered, washed with methanol and dried *in vacuo*. Yield 80%.

The suspension of $HgCl_2 \cdot \mathbf{1}$ (0.5 mmol) in 10 cm^3 methanol was mixed with triphenylphosphine (1 mmol) dissolved in methanol (10 cm^3). The reaction mixture was refluxed with stirring for 2–3 h. The suspended mercury-complex dissolved. The solution was filtered and the filtrate concentrated to 5–

Table 1. Elemental analysis, m.p. and ^1H NMR data of complexes of **1** and **2**

Complex	m.p. (°C)	Analysis: Found (Calc.)(%) C	H	Te	Cl	Metal	Chemical shift (δ, ppm) at 25°C[a]
$[HgCl_2 \cdot \mathbf{1}]_n$	—	27.8 (27.4)	2.1 (2.3)	21.4 (20.7)	11.4 (11.8)	30.8 (32.6)	Solubility inadquate for NMR
$[(PPh_3)(HgCl_2 \cdot \mathbf{1})]$	110	20.9 (20.0)	1.8 (1.7)	16.0 (15.2)	4.9 (4.2)	24.6 (23.8)	2.14(s, 6H, CH_3), 6.93(bs, OH), 7.01–7.60(m, 21H, ArH)
$[HgCl(\mathbf{2a}\text{-}H)]_2$	154	27.6 (28.5)	2.2 (2.0)	23.4 (23.3)	6.5 (6.5)	37.7 (36.7)	2.2(s, 3H, CH_3), 6.8–7.8(m, 8H, ArH)
$[HgCl(\mathbf{2b}\text{-}H)]_2$	142	27.9 (29.1)	2.3 (2.2)	23.5 (22.1)	7.1 (6.1)	34.8 (34.8)	2.3(s, 3H, CH_3), 3.7(s, 3H, OCH_3), 6.7–6.5(m, 7H, ArH)
$[HgCl(\mathbf{2c}\text{-}H)]_2$	165	30.7 (30.5)	2.4 (2.5)	22.0 (21.6)	6.1 (6.0)	34.6 (34.0)	1.30–1.45(t, 3H, CH_3 of OEt), 2.2(s, 3H, CH_3), 3.8–4.0(q, 2H, OCH_2), 6.6–7.8(m, 7H, ArH)
$[PdCl(\mathbf{2a}\text{-}H)]_2$	151	33.5 (34.5)	2.4 (2.4)	—	—	—	2.2(s, 3H, CH_3), 6.8–8.1(m, 8H, ArH)
$[PdCl(\mathbf{2b}\text{-}H)]_2$	158	33.6 (34.8)	2.4 (2.7)	—	—	—	2.2(s, 3H, CH_3), 3.9(s, 3H, OCH_3), 6.9–7.2, 8.0–8.2(m, 7H, ArH)
$[PdCl(\mathbf{2c}\text{-}H)]_2$	142	36.2 (36.3)	3.0 (3.0)	—	—	—	1.3–1.5(t, 3H, CH_3 of OEt), 2.2(s, 3H, CH_3), 4.0–4.2(q, 2H, OCH_2), 6.9–7.9, 8.1–8.2(m, 7H, ArH)
$[PtCl(\mathbf{2a}\text{-}H)]_2$	178	28.2 (28.8)	2.0 (2.0)	—	—	—	2.3(s, 3H, CH_3), 6.8–8.1(m, 8H, ArH)
$[PtCl(\mathbf{2b}\text{-}H)]_2$	160	28.9 (29.4)	2.1 (2.3)	—	—	—	2.2(s, 3H, CH_3), 3.8(s, 3H, OCH_3), 7.0–8.3(m, 7H, ArH)
$[PtCl(\mathbf{2c}\text{-}H)]_2$	164	29.6 (30.8)	2.5 (2.6)	—	—	—	1.2–1.5(t, 3H, CH_3 of OEt), 2.2(s, 3H, CH_3), 3.9–4.1(q, 2H, OCH_2), 6.8–8.2(m, 7H, ArH)

[a] In $CDCl_3$ for $(Ph_3P)(HgCl_2 \cdot \mathbf{1})$ and DMSO-d_6 for others.

7 cm^3. The solid was separated, washed with hexane and recrystallized from chloroform. Yield, 75%. Elemental analysis and ^1H NMR data are given in Table 1.

Synthesis of (2-hydroxy-5-methylphenyl)(aryl) tellurium(IV) *chlorides*

1-(Chloromercury)-2-hydroxy-5-methylbenzene (10 mmol) and an equimolar amount of aryltellurium(IV) chloride (aryl = C_6H_5, 4-$MeOC_6H_4$ or 4-$EtOC_6H_4$) were refluxed in dry dioxane for 3–4 h under a dinitrogen atmosphere. The solution was filtered hot and the filtrate cooled to 0–5°C for 2–3 h. The $HgCl_2$·dioxane adduct separated out and was filtered off. The filtrate was concentrated to 5 cm^3 and hexane (50 cm^3) was added to the concentrate. The white precipitate resulted, which was filtered, washed with cold ethanol, dried and recrystallized from chloroform. Yield, 75–80%. M.p., elemental analyses, ^1H and $^{13}C\{^1H\}$ NMR (in $CDCl_3$ at 25°C) spectra are given below.

a(Aryl = C_6H_5): m.p. 172°C. Found: C, 41.1; H, 3.1; Te, 33.4; Cl, 18.7. Calc. for $C_{13}H_{12}OCl_2Te$: C, 40.8; H, 3.1; Te, 33.4; Cl, 18.5%. NMR (^1H): δ, 2.2(s, 3H, CH_3), 6.7–7.2, 7.4–7.8(m, 9H, ArH+OH); ($^{13}C\{^1H\}$): δ, 21.3(CH_3), 116.2(C_3), 123.3(C_1'), 128.6(C_3'), 133.1(C_5), 133.8(C_4), 134.5(C_4'), 139.1(C_2'), 141.4(C_6), 155.2(C_2). C_1 merges with the C_2' or C_6 signal.

b(Aryl = 4-$MeOC_6H_4$): m.p. 184°C. Found: C, 40.1; H, 3.4; Te, 31.6; Cl, 17.1. Calc. for $C_{14}H_{14}O_2Cl_2Te$: C, 40.7; H, 3.4; Te, 30.9; Cl, 17.2%. NMR: ^1H: δ, 2.2(s, 3H, CH_3), 3.9(s, 3H, OCH_3), 6.8–7.2, 8.1–8.2(m, 8H, ArH+OH). $^{13}C\{^1H\}$: δ, 21.8(CH_3), 55.7(OCH_3), 115.6(C_3), 124.2(C_1'), 128.2(C_3'), 133.2(C_5), 133.9(C_4), 134.4(C_4'), 139.6(C_2'), 141.5(C_6), 155.0(C_2). C_1 merges with the C_2' or C_6 signal.

c(Aryl = 4-$EtOC_6H_4$): m.p. 167°C. Found: C, 42.8; H, 3.7; Te, 30.0; Cl, 16.6. Calc. for $C_{15}H_{16}O_2Cl_2Te$: C, 42.2; H, 3.7; Te, 29.9; Cl, 16.8%. NMR: ^1H: δ, 1.4–1.5(t, 3H, CH_3 of OEt), 2.2(s, 3H, CH_3), 3.7–4.1(q, 2H, OCH_2), 6.8–7.2, 8.1–8.2(m, 8H, ArH+OH). $^{13}C\{^1H\}$: δ, 14.5(CH_3 of OEt), 21.4(CH_3), 62.1(OCH_2), aryl carbon signals are similar to that of **b**.

Synthesis of (2-hydroxy-5-methylphenyl)(aryl) telluride (**2**)

(2-Hydroxy-5-methylphenyl)tellurium(IV) chloride (**a**, **b** or **c**) (10 mmol) was suspended in water (100 cm^3) and cooled to 0–5°C. Sodium metabisulphite (10 mmol) dissolved in 50 cm^3 water or hydrazine hydrate (10 mmol) in 50 cm^3 ethanol was slowly added to the suspension with stirring. The mixture was further stirred for 2–3 h, keeping the temperature below 5°C. The yellow precipitate of the telluride thus formed was filtered, washed several times with water, dried and recrystallized from chloroform as yellow crystals. Yield, 75–78%. M.p., elemental analyses, ^1H and $^{13}C\{^1H\}$ NMR spectra (in $CDCl_3$ at 25°C) are given below.

2a: m.p. 92°C. Found: C, 50.3; H, 4.0; Te, 40.5. Calc. for $C_{13}H_{12}OTe$: C, 50.1; H, 3.8; Te, 40.9%. NMR: ^1H: δ, 2.2(s, 3H, CH_3), 6.7–7.8(m, 9H, ArH+OH). $^{13}C\{^1H\}$: δ, 20.4(CH_3), 103.1(C_1), 114.2(C_3, C_1'), 128.9(C_4'), 131.2(C_3'), 131.9(C_4), 139.8(C_5), 140.4(C_2'), 141.6(C_6), 154.6(C_2).

2b: m.p. 98°C. Found: C, 49.6; H, 4.1; Te, 38.0. Calc. for $C_{14}H_{14}O_2Te$: C, 49.2; H, 4.1; Te, 37.3%. NMR: ^1H: δ, 2.2(s, 3H, CH_3), 3.8(s, 3H, OCH_3), 6.7–6.9, 7.4–7.5(m, 7H, ArH). $^{13}C\{^1H\}$: δ, 21.0(CH_3), 55.6 (OCH_3), 102.1(C_1), 114.3(C_3, C_1'), 128.4(C_4'), 131.2(C_3'), 131.8(C_4), 139.6(C_5), 140.1(C_2'), 141.4(C_6'), 154.4(C_2).

2c: m.p. 80°C. Found: C, 50.6; H, 4.5; Te, 36.1. Calc. for $C_{16}H_{16}O_2Te$: C, 50.6; H, 4.5; Te, 35.9%. NMR: ^1H: δ, 1.3–1.4(t, 3H, CH_3 of OEt), 2.2(s, 3H, CH_3), 3.9–4.0(q, 2H, OCH_2), 6.6–7.5(m, 7H, ArH). $^{13}C\{^1H\}$: δ, 14.5(CH_3 of OEt), 20.8(CH_3), 61.8(OCH_2), aryl carbons are similar to that of **2b**.

Synthesis of mercury(II), *palladium*(II) *and platinum*(II) *complexes of* **2**

Mercuric chloride (1 mmol) dissolved in 10 cm^3 of acetone was added to a solution of **2** (**a**, **b** or **c**) (1 mmol) in acetone (10 cm^3) and the mixture was stirred at 40°C for 2 h. The resulting precipitate was filtered, washed with acetone thoroughly and dried *in vacuo*. Yield, 75–80%.

Palladium(II) complexes were synthesized by stirring **2** with $(C_6H_5CN)_2PdCl_2$ in chloroform in a manner described above. After stirring 25–30 cm^3 of petroleum ether (40–60°C) was added to this mixture and the resulting red–brown precipitate was filtered. It was washed with petroleum ether thoroughly and dried *in vacuo*. Yield, 83–85%.

To synthesize platinum(II) complexes the stirring of a metal ion–ligand mixture was carried out as described above for the mercury complexes, except **2** which was dissolved in acetone and K_2PtCl_4 in water. Thereafter, the volume of mixture was reduced to 5–7 cm^3 *in vacuo*. The reddish precipitate was filtered, washed with an acetone–water mixture (1 : 1), dried and recrystallized from chloroform. Yield, 85–90%.

Elemental analyses, m.p. and ^1H NMR data of all the complexes of **2** are given in Table 1.

RESULTS AND DISCUSSION

The reaction of 1-hydroxy-4-methylbenzene with tellurium tetrachloride always results in an Ar_2TeCl_2 type of compound[7] which can easily be reduced with hydrazine to **1**. The *ortho*-mercuration of 1-hydroxy-4-methyl benzene followed by *trans*-metallation with $ArTeCl_3$ results in a good yield of the precursor chloride of **2**, which can be reduced to **2** in good yield using $Na_2S_2O_5$. The OH signal in the ^1H NMR spectrum of **1** is shielded with respect to OH of their precursor chlorides by 1.1 ppm. This may be due to a decrease in the Te ← O secondary interaction and change in the inductive effect of tellurium, when the chlorides are reduced to tellurides. The OH signal of **2** and its precursor chloride could not be identified separately in the multiplet of phenyl protons with which it merges. However, its shielding on reduction of the precursor chlorides into **2** seems to be lower than that observed in the case of **1**, as it does not separate out from the multiplet.

Compound **1** reacts with $HgCl_2$ forming a complex of stoichiometry [HgCl(**1**-H)] which has defied all attempts to identify its structure, presumably due to its polymeric nature as it does not dissolve in any organic solvent. However, on refluxing its suspension in methanol with an equimolar amount of PPh_3, a complex [Ph_3PHgCl(**1**-H)] results which is soluble in polar organic solvents. The ^1H NMR spectrum of this complex exhibits an OH signal which is negligibly downfield than that of **1**. The aromatic protons of **1** on complexation with mercury undergo deshielding (0.1–0.2 ppm), indicating the involvement of tellurium in coordination. Thus, **1** behaves as a uni-negative bidentate ligand in this complex (Structure A). Most probably it also does so in the complex [HgCl(**1**-H)] and mercury completes the expected four-coordination number with the chlorine or oxygen of the OH group of the neighbouring molecule, which ultimately results in polymerization. It appears that in the absence of free OH most probably the extended polymerization is not sustained. This has been supported by the absence of a ν(Hg-Cl(terminal)) band[11] around 300 cm^{-1} in the IR spectrum of [HgCl(**1**-H)], whereas this band appears in the IR spectrum of [Ph_3 PHgCl(**1**-H)] at 315 cm^{-1} which supports Structure A for this compound. The occurrence of ν(Te—C)[12] around 250 cm^{-1} in the IR spectrum of this mixed complex further authenticates its formation. The ν(OH) was noticed in the IR spectra of all these complexes around 3300–3400 cm^{-1}, supporting the ligation of **1** in a bidentate mode.

Since of the two OH groups present in **1** only one participates in its ligation with metal ions, it was thought worthwhile to examine the ligation of **2** because the extended polymerization, complicating the structure of [HgCl(**1**-H)], due to the presence of an additional OH group would be avoided. Compound **2** reacts with mercury(II), palladium(II) and platinum(II) forming complexes of stoichiometry [MCl(**2**-H)]. In the ^1H NMR of **2** the OH signal was found merged with phenyl, as indicated by enhanced integration of these protons with respect to that of CH_3. On complexation such an enhancement was absent, indicating the loss of an OH proton on ligation. The aryl protons were deshielded (0.1–0.8 ppm) when **2** ligated with palladium(II) and platinum(II). The deshielding was small in the case of the mercury complex (<0.3 ppm). These observations after taking into account the solvent effect also suggest that in all three complexes **2** coordinates through tellurium; the Hg—Te bond is weaker than the Pd/Pt—Te bond and, therefore, the magnitude of deshielding differs. To complete the coordination number four the species having stoichiometry [MCl(**2**-H)] most probably dimerize, as depicted in Structure B. Most probably the geometry of ligands around mercury(II) is tetrahedral. The coordination number of M as four has been supported in the case of platinum/palladium(II) by the electronic spectra of their complexes in DMSO, which exhibit a band around 27 kK, characteristic of square planar geometry around the metal ion. The dimeric formulation of Struct. B has been supported by the presence of ν(M—Cl(bridging)) bands[11] around 200, 250 and 270 cm^{-1} in the IR spectra of the mercury(II), palladium(II) and platinum(II) complexes, respectively. The ν(Te—C) undergoes a red shift (~10–15 cm^{-1}) on complexation of **2** with palladium/platinum(II). This further supports the involvement of tellurium in chelation. The occurrence of only one ν(M—Cl—M) band in the IR spectra of all three complexes suggests that the

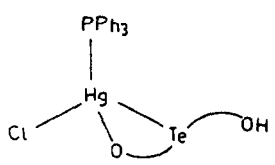

(A)

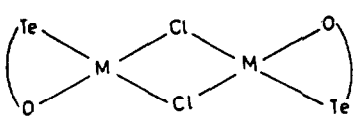

M = Hg, Pd or Pt

(B)

structures of $[Pd/PtCl(2\text{-}H)]_2$ are centrosymmetric (Struct. B).

Acknowledgement—We thank CSIR (India) for the research grant to carry out this work.

REFERENCES

1. S. Ahrland, J. Chatt and N. R. Davies, *Q. Rev. Chem. Soc.* 1958, **12**, 165.
2. R. G. Pearson, *J. Am. Chem. Soc.* 1963, **85**, 3533.
3. A. K. Singh, V. Srivastava and B. L. Khandelwal, *Polyhedron* 1990, **9**, 495 and 851.
4. B. L. Khandelwal, A. K. Singh, V. Srivastava, D. C. Povey and G. W. Smith, *Polyhedron* 1990, **9**, 2041.
5. A. K. Singh, S. Thomas and B. L. Khandelwal, *J. Coord. Chem.* 1990, **21**, 71.
6. N. I. Al-Salim and W. T. McWhinnie, *Inorg. Chim. Acta* 1989, **155**, 2131.
7. B. L. Khandelwal, K. Kumar and K. Raina, *Synth. React. Met.-Org. Chem.* 1981, **11**, 65.
8. K. J. Irgolic and R. A. Zingaro, *Organomet. React.* 1971, **2**, 117.
9. L. G. Makarova and A. N. Nesmeyanov, The organic chemistry of mercury compounds, in *Methods of Elementary Organic Chemistry* (Edited by A. N. Nesmeyanov and K. A. Kocheshkov), Vol. 4, Ch. 5, p. 94. North Holland, Amsterdam (1967).
10. F. H. Kruse, R. E. Sanftner and J. F. Suttle, *Analyt. Chem.* 1953, **25**, 500; A. I. Vogel, *A Text Book of Quantitative Inorganic Analysis*, 3rd edn. Longmans, London (1961).
11. K. Nakamoto, *Infrared and Raman Spectra of Inorganic and Coordination Compounds*, 4th edn, pp. 199–324. John Wiley and Sons, New York (1986).
12. K. J. Irgolic, *The Organic Chemistry of Tellurium*, p. 325. Gordon and Breach, New York (1974).

Polyhedron Vol. 10, No. 23/24, pp. 2699–2709, 1991
Printed in Great Britain

0277–5387/91 $3.00+.00
© 1991 Pergamon Press plc

OLIGOMERIZATION AND STRUCTURAL VARIATION OF ALKALI METAL SILYLOXIDES

MICHAEL J. McGEARY, KIRSTEN FOLTING, WILLIAM E. STREIB, JOHN C. HUFFMAN and KENNETH G. CAULTON*

Department of Chemistry and Molecular Structure Center, Indiana University, Bloomington, IN 47405, U.S.A.

(*Received* 16 *July* 1991; *accepted* 26 *July* 1991)

Abstract—Lithium and potassium silyloxide complexes $[Li(OSiPh_3)]_n$ (**1**), $[K(thf)_{0.2}(OSiPh_3)]_n$ (**3**) and $[K(OSiMe_2{}^tBu)]_n$ (**6**) were prepared by deprotonation of $HOSiPh_3$ or $HOSiMe_2{}^tBu$ with [Li("Bu)] in hexane or KH in THF, respectively. Crystalline DME adducts $[Li(\mu\text{-}OSiPh_3)(\eta^2\text{-}DME)]_2$ (**2**) and $[K_4(\mu_3\text{-}OSiPh_3)_3(\mu_3\text{-}OSiPh_2(\eta^1\text{-}Ph))(\eta^2\text{-}DME)]_2(\mu\text{-}DME)$ (**4**) were prepared by dissolving **1** or **3**, respectively, in dimethoxyethane followed by precipitation with alkane. The potassium-sequestered complexes $[K(18\text{-crown-6})(OSiPh_3)]_2$ (**5**) and $[K(18\text{-crown-6})(OSiMe_2{}^tBu)]_n$ (**7**) were prepared from **3** or **5**, respectively, and one equiv. of 18-crown-6 ether. The complexes were characterized by single-crystal X-ray diffraction: $[Li(\mu\text{-}OSiPh_3)(\eta^2\text{-}DME)]_2$ (**2**): a dimer featuring tetrahedral lithium centres linked by bridging —$OSiPh_3$ ligands. [Crystal data (−156°C): space group $P\bar{1}$, $a = 14.238(6)$, $b = 15.182(7)$, $c = 11.796(5)$ Å, $\alpha = 110.57(2)$, $\beta = 112.02(2)$, $\gamma = 63.02(1)$ Å, $V = 2055.33$ Å^3, $Z = 2$.] $[K_4(\mu_3\text{-}OSiPh_3)_3\{\mu_3\text{-}OSiPh_2(\eta^1\text{-}Ph)\}(\eta^2\text{-}DME)]_2(\mu\text{-}DME)$ (**4**): (1) two cubanes each having every potassium vertex chemically distinct; (2) one chelating DME ligand, one DME ligand bridging between two cubanes; and (3) a K-*ipso*-phenyl carbon contact. [Crystal data (−133°C): $a = 14.246(4)$, $b = 30.939(9)$, $c = 17.981(5)$ Å, $\beta = 112.33(1)°$ with $Z = 2$ in space group $P2_1/c$.] $[K(18\text{-crown-6})OSiPh_3]_2$ (**5**): A dimer with slipped face-to-face stacking of the quasi-planar $K(18\text{-crown-6})^+$ part of the two $Ph_3SiOK(18\text{-crown-6})$ molecules; these are linked by a dative bond from one ether oxygen of a given crown to potassium contained in the other crown. [Crystal data (−155°C): $a = 9.324(2)$, $b = 17.640(5)$, $c = 18.148(15)$ Å, $\beta = 91.60(1)°$ with $Z = 4$ in space group $P2_1/c$.]

Although alkali metal alkoxide chemistry has a long tradition in both organic and inorganic chemistry,[1] alkali metal silyloxide chemistry is comparatively underdeveloped.[2,3,4] We were motivated to explore the synthesis and structural features of lithium and potassium silyloxide complexes for the following reasons:

(1) The reduced basicity of the R_3SiO^- ligand in comparison to the R_3CO^- ligand was expected to diminish the capacity of R_3SiO^- to adopt bridging modes, thereby resulting in new structural types compared to the related alkoxide complexes.

(2) We are evaluating the utility of heterometallic silyloxide complexes as reagents for the preparation of mixed-metal solid-state materials.[5] One aspect of our synthetic strategy for the production of the required heterometallic silyloxide reagents centred on the condensation of a Lewis acidic metal silyloxide complex, $M(OSiR_3)_x$, with a nucleophilic-at-O silyloxide complex, $M'(OSiR_3)_y$ [eq. (1)].

$$M(OSiR_3)_x + M'(OSiR_3)_y \longrightarrow MM'(OSiR_3)_{x+y} \quad (1)$$

Because of the absence of an energetically-accessible vacant d_π manifold, we anticipated that alkali metal silyloxide complexes could serve as efficient $OSiR_3^-$ transfer agents. Indeed this expectation has been fulfilled and we have prepared a series of potassium/tin silyloxide derivatives using $KOSiR_3$ reagents.[6] Furthermore, with the availability of alkali metal/other metal heterometallic silyloxide

* Author to whom correspondence should be addressed.

complexes, synthetic routes to new heterometallic silyloxide complexes not containing the alkali metal can be envisioned based on salt elimination reactions [eq. (2)].

$$MM'(OSiR_3)_{x+y} + M''(X)L_n \longrightarrow MM''(L)_n(OSiR_3)_{x+y} + M'X; \quad (2)$$

where M, M'' = metals, M' = an alkali metal and X = a leaving group (e.g. a halide).

In this paper we report the synthesis and characterization of lithium and potassium silyloxide complexes which we have employed in our work on developing heterometallic silyloxides as molecular precursors to materials: $[Li(OSiPh_3)]_n$ (**1**), $[K(THF)_{0.2}(OSiPh_3)]$ (**3**) and $[K(OSiMe_2{}^tBu)]_n$ (**6**). These compounds were used as reagents to prepare a series of "organic soluble" ether adducts: $[Li(\mu\text{-}OSiPh_3)(\eta^2\text{-}DME)]_2$ (**2**), $[K_4(\mu_3\text{-}OSiPh_3)_3\{\mu_3\text{-}OSiPh_2(\eta^1\text{-}Ph)\}(\eta^2\text{-}DME)]_2(\mu\text{-}DME)$ (**4**), [K(18-crown-6)$(OSiPh_3)]_2$ (**5**) and [K(18-crown-6)$(OSiMe_2{}^tBu)]_n$ (**7**). X-ray structural characterization is presented for $[Li(\mu\text{-}OSiPh_3)(\eta^2\text{-}DME)]_2$, $[K_4(\mu_3\text{-}OSiPh_3)_3\{\mu_3\text{-}OSiPh_2(\eta^1Ph)\}(\eta^2\text{-}DME)]_2(\mu\text{-}DME)$ and [K(18-crown-6)$(OSiPh_3)]_2$.

EXPERIMENTAL

Materials and procedures

All manipulations were performed using standard Schlenk techniques either *in vacuo* or in an atmosphere of nitrogen or using a nitrogen-filled dry-box. Solvents were dried over appropriate desiccants (potassium, benzophenone ketyl for diethyl ether, pentane, hexane, dimethoxyethane, toluene, benzene and tetrahydrofuran; P_2O_5 for dichloromethane and chloroform; KOH for pyridine), distilled under nitrogen or *in vacuo* and subjected to freeze–evacuate–thaw cycles prior to use. The reagents Ph_3SiOH, $Me_2(^tBu)SiOH$, [Li][n-Bu] (1.6 N in hexane), KH and 18-crown-6 ether were obtained commercially (Aldrich). Potassium hydride was purified by washing repeatedly with hexane, followed by drying *in vacuo*; $Me_2(^tBu)SiOH$ was vacuum distilled prior to use; 18-crown-6 ether was sublimed prior to use. Triphenylsilanol and [Li][n-Bu] (1.6 N in hexane) were used as received.

Physical measurements

IR spectra were recorded as Nujol mulls using a Perkin–Elmer 283 spectrophotometer. ^1H and ^{13}C NMR spectra were recorded on a Bruker AM500 (^1H at 500.14 MHz, ^{13}C at 125.76 MHz) instrument and referenced to $SiMe_4$. NMR sample temperatures were monitored using a thermocouple. Elemental analyses were performed by Oneida Research Services, Inc. Combustion aides were used in an effort to discourage carbide formation. The results of carbon, hydrogen, nitrogen combustion analyses were sometimes variable and not always within expectations even for crystalline samples, authenticated by X-ray diffraction.

$[Li(OSiPh_3)]_n$ (1)

A 100 cm^3 Schlenk flask was charged with $HOSiPh_3$ (1.38 g, 5.00 mmol) and toluene (30 cm^3). The solution was chilled to 0°C whereupon [Li(n-Bu)] (4 cm^3, 1.6 N) was added via a pipette. A white solid precipitated immediately. The mixture was stirred for 2 h. The solid was then decanted, washed with pentane and dried *in vacuo*. IR (Nujol): no ν(OH); ν(CH) 3035, 3040; aromatic overtones; 1950, 1880, 1820, 1760; other bands 1110, 975, 705, 695 cm^{-1}. Lack of solubility in solvents with which **1** did not react (e.g. C_6D_6) precluded NMR characterization.

$[Li(\mu\text{-}OSiPh_3)(\eta^2\text{-}DME)]_2$ (2)

A 100 cm^3 Schlenk flask was charged with a small amount of $[Li(OSiPh_3)]_n$. DME (*ca* 30 cm^3) was distilled onto the lithium reagent. The mixture was stirred for 3 h, whereupon the volume of solvent was reduced *in vacuo*. Hexane was added so as to form a layer. Large, colourless crystals suitable for X-ray diffraction precipitated after standing for 24 h. IR (Nujol): no ν(OH); ν(CH) 3040; aromatic overtones: 1950, 1870, 1810; other bands: 1095, 1070, 695 cm^{-1}. ^1H NMR (C_6D_6): δ 7.98 (d, 6.4 Hz, 12H, *ortho*), 7.30–7.25 (structured m, 18H, *meta*, *para*), 3.09 (s, 8H, OCH_2), 3.03 (s, 12H, OCH_3). ^{13}C NMR (C_6D_6): δ 144.6 (*ipso*) 136.0 (*ortho*), 128.6 (*para*), 127.2 (*meta*), 71.6 (OCH_2), 58.7 (OCH_3). Found: C, 71.1; H, 6.7. Calc. for $C_{44}H_{50}Li_2O_6Si_2$: C, 70.9; H, 6.8%.

Structure determination of $[Li(\mu\text{-}OSiPh_3)(\eta^2\text{-}DME)]_2$. A crystal of suitable size was cleaved from a large piece of the sample in a nitrogen atmosphere. The crystal was mounted using silicone grease and was then transferred to a goniostat where it was cooled to −156°C for characterization (Table 1) and data collection.[7] A systematic search of a limited hemisphere of reciprocal space revealed no symmetry or systematic absences. Following intensity data collection ($6° \leqslant 2\theta \leqslant 45°$), data processing gave a residual of 0.034 for 223 unique intensities which has been measured more than once. Four standards measured every 300 data showed no significant trends. No correction was made for absorp-

tion. An initial choice of the centrosymmetric space group $P\bar{1}$ was made based on E-value statistics and was later proven correct by the successful solution of the structure.

Table 1. Crystallographic data for $[Li(DME)OSiPh_3]_2$

Chemical formula	$C_{44}H_{50}Li_2O_6Si_2$
a (Å)	14.238(6)
b (Å)	15.182(7)
c (Å)	11.796(5)
β (°)	112.02(2)
V (Å^3)	2055.33
Z	2
Formula weight	744.93
Space group	$P\bar{1}$
T (°C)	−156
λ (Å)	0.71069
ρ_{calcd} (g cm^{-3})	1.20
μ(Mo-K_α) (cm^{-1})	1.26
R	0.0782
R_w	0.0726

The structure was solved by a combination of direct methods and Fourier techniques. After the non-hydrogen atoms had been located and partially refined, a difference Fourier revealed most of the hydrogen positions. In the final cycles of least-squares refinement, the non-hydrogen atoms were varied with anisotropic thermal parameters and the hydrogen atoms were varied with isotropic thermal parameters. The final difference map was essentially featureless, the largest residual peak being 0.47 e Å^{-3}. The refined C—H distances ranged from 0.89(6) to 1.08(9) Å. Selected bond lengths and bond angles are shown in Table 2 and the structure depicted in Figs 1 and 2. Additional information is available as supplementary material.

$[K(THF)_x(OSiPh_3)]$ (3)

A 200 cm^3 Schlenk flask was charged with KH (0.58 g, 14.46 mmol) and tetrahydrofuran (50 cm^3). Triphenylsilanol (2.78 g, 10.06 mmol) was added in

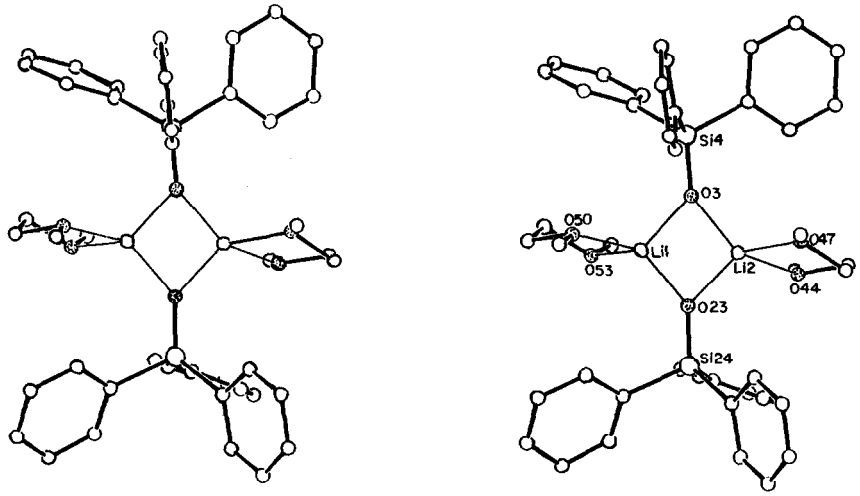

Fig. 1. Stereo ORTEP drawing of the non-hydrogen atoms in $[Li(MeOC_2H_4OMe)OSiPh_3]_2$, showing selective atom labelling. Ether carbons follow the labelling sequence shown. Oxygen atoms are stippled.

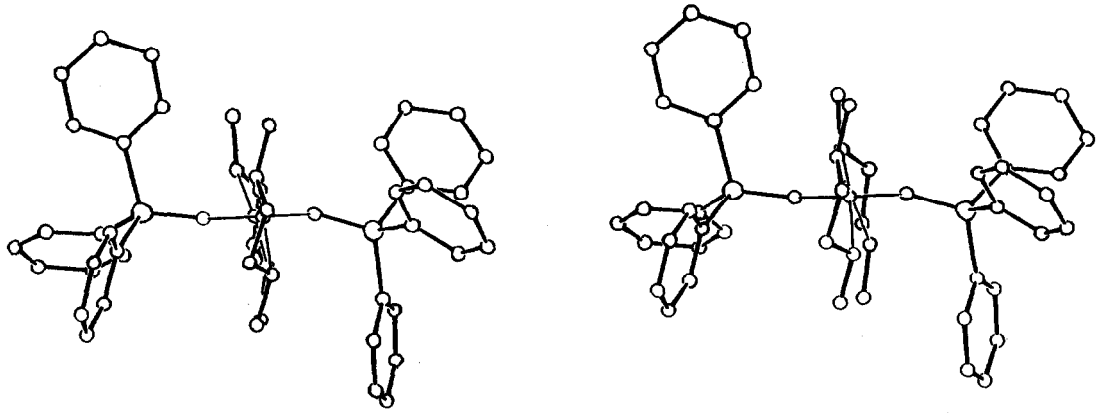

Fig. 2. Stereo ORTEP drawing of the non-hydrogen atoms in $[Li(MeOC_2H_4OMe)OSiPh_3]_2$, viewed down the lithium/lithium direction, showing bending at silyloxide oxygens.

Table 2. Selected bond distances (Å) and angles (°) for $[Li(DME)OSiPh_3]_2$

Si(4)—O(3)	1.587(4)	O(44)—C(45)	1.403(8)
Si(4)—C(5)	1.901(6)	O(44)—Li(2)	2.033(10)
Si(4)—C(11)	1.886(6)	O(47)—C(46)	1.431(7)
Si(4)—C(17)	1.912(5)	O(47)—C(48)	1.421(8)
Si(24)—O(23)	1.580(4)	O(47)—Li(2)	2.056(10)
Si(24)—C(25)	1.888(6)	O(50)—C(49)	1.431(8)
Si(24)—C(31)	1.897(6)	O(50)—C(51)	1.435(8)
Si(24)—C(37)	1.901(6)	O(50)—Li(1)	2.063(10)
O(3)—Li(1)	1.904(9)	O(53)—C(52)	1.411(8)
O(3)—Li(2)	1.881(10)	O(53)—C(54)	1.446(9)
O(23)—Li(1)	1.887(10)	O(53)—Li(1)	1.989(10)
O(23)—Li(2)	1.910(9)	C(45)—C(46)	1.474(9)
O(44)—C(43)	1.436(7)	C(51)—C(52)	1.511(11)
O(3)—Si(4)—C(5)	112.18(23)	C(48)—O(47)—Li(2)	127.3(5)
O(3)—Si(4)—C(11)	114.79(22)	C(49)—O(50)—C(51)	111.3(5)
O(3)—Si(4)—C(17)	110.71(22)	C(49)—O(50)—Li(1)	129.4(5)
C(5)—Si(4)—C(11)	103.26(24)	C(51)—O(50)—Li(1)	110.6(5)
C(5)—Si(4)—C(17)	107.66(23)	C(52)—O(53)—C(54)	112.7(6)
C(11)—Si(4)—C(17)	107.75(25)	C(52)—O(53)—Li(1)	110.8(5)
O(23)—Si(24)—C(25)	112.30(24)	C(54)—O(53)—Li(1)	116.0(5)
O(23)—Si(24)—C(31)	111.00(23)	O(44)—C(45)—C(46)	108.6(5)
O(23)—Si(24)—C(37)	113.81(22)	O(47)—C(46)—C(45)	108.7(5)
C(25)—Si(24)—C(31)	104.40(24)	O(50)—C(51)—C(52)	107.7(5)
C(25)—Si(24)—C(37)	106.63(25)	O(53)—C(52)—C(51)	107.0(6)
C(31)—Si(24)—C(37)	108.15(25)	O(3)—Li(1)—O(23)	97.9(4)
Si(4)—O(3)—Li(1)	133.0(4)	O(3)—Li(1)—O(50)	118.1(5)
Si(4)—O(3)—Li(2)	143.5(4)	O(3)—Li(1)—O(53)	116.4(5)
Li(1)—O(3)—Li(2)	82.2(4)	O(23)—Li(1)—O(50)	130.0(5)
Si(24)—O(23)—Li(1)	137.7(4)	O(23)—Li(1)—O(53)	114.1(5)
Si(24)—O(23)—Li(2)	133.4(4)	O(50)—Li(2)—O(53)	81.0(4)
Li(1)—O(23)—Li(2)	81.9(4)	O(3)—Li(2)—O(23)	97.9(4)
C(43)—O(44)—C(45)	113.8(5)	O(3)—Li(2)—O(44)	129.7(5)
C(43)—O(44)—Li(2)	123.4(5)	O(3)—Li(2)—O(47)	115.0(5)
C(45)—O(44)—Li(2)	114.5(4)	O(23)—Li(2)—O(44)	111.2(5)
C(46)—O(47)—C(48)	113.1(5)	O(23)—Li(2)—O(47)	126.6(5)
C(46)—O(47)—Li(2)	109.9(4)	O(44)—Li(2)—O(47)	79.4(4)

portions via a solids addition tube. Hydrogen gas evolved. The mixture was stirred for 12 h. After filtration through a 2 cm thick plug of Celite to remove unreacted KH, the solvent was evaporated. The oily residue was triturated to a fine powder with pentane. The solvent was decanted away and the powder dried *in vacuo*. IR (Nujol): no ν(OH); ν(CH) 3020; aromatic overtones 1940, 1870, 1810; other bands 1245, 1095, 985, 780, 735, 685 cm^{-1}. ^1H NMR (C_6D_6): δ 7.60 (m, phenyl), 7.19 (m, phenyl), 3.47 (m, α CH_2 of THF), 1.46 (β CH_2 of THF). Integration shows $x = 0.2$.

$[K_4(\mu_3\text{-}OSiPh_3)_3\{\mu_3\text{-}OSiPh_2(\eta^1\text{-}Ph)\}(\eta^2\text{-}DME)]_2(\mu\text{-}DME)$ (**4**)

A 100 cm^3 Schlenk flask was charged with a small amount of $[K(thf)_{0.2}(OSiPh_3)]$. DME (*ca* 30 cm^3) was then distilled onto the potassium reagent. The mixture was stirred for 2 h whereupon the solvent volume was reduced *in vacuo*. Hexane was added so as to form a layer. Large, colourless crystals suitable for X-ray diffraction precipitated upon standing at 0°C. IR (Nujol): no ν(OH); ν(CH) 3020; aromatic overtones: 1940, 1870, 1810, 1750; other bands: 1080, 980, 680 cm^{-1}. ^1H NMR (C_6D_6): δ 7.61 (m, 24H, *ortho*), 7.20 (m, 36H, *meta, para*), 3.20 (s, 6H, OCH_2), 3.02 (s, 9H, OCH_3). ^{13}C NMR (C_6D_6): δ 144.3 (*ipso*), 134.9 (*ortho*), 128.6 (*meta*), 128.2 (*para*), 72.0 (OCH_2), 58.6 (OCH_3). Found: C, 69.7; H, 5.1. Calc. for $C_{78}H_{75}K_4O_7Si_4$: C, 67.2; H, 5.4%. The tendency of this compound to lose DME frustrated accurate analysis.

X-ray diffraction study of $[K_4(\mu_3\text{-}OSiPh_3)_3\{\mu_3\text{-}OSiPh_2(\eta^1\text{-}Ph)\}(\eta^2\text{-}DME)]_2(\mu\text{-}DME)$. A relatively large single crystal was selected from the bulk sample

Table 3. Crystallographic data for $K_8(OSiPh_3)_8(DME)_3$

Chemical formula	$C_{156}H_{150}K_8O_{14}Si_8$
a (Å)	14.246(4)
b (Å)	30.939(9)
c (Å)	17.981(5)
β (°)	112.33(1)
V (Å^3)	7330.73
Z	2
Formula weight	2786.36
Space group	$P2_1/c$
T (°C)	−133
λ (Å)	0.71069
$\rho_{calcd.}$ (g cm^{-3})	1.262
μ(Mo-K_α) (cm^{-1})	3.56
R	0.0479
R_w	0.0490

using inert atmosphere handling techniques. The crystal was transferred to the goniostat where it was cooled to −132°C for characterization (Table 3) and data collection. A systematic search of a limited hemisphere of reciprocal space yielded a set of reflections which exhibited monoclinic ($2/m$) symmetry. The systematic extinction of $0k0$ for $k = 2n+1$ and of $h0l$ for $l = 2n+1$ uniquely identified the space group as $P2_1/c$. A plot of the standards showed no systematic trends. No absorption correction was deemed necessary. The structure was solved by the usual combination of direct methods and Fourier techniques. The four unique potassium atoms were located in the initial E-map and the remaining non-hydrogen atoms were located in successive difference maps phased with the already located atoms. The molecule possesses a crystallographic centre of inversion. Almost all of the hydrogen atoms were evident in a difference map. They were introducted in fixed idealized positions for the final cycles of refinement during which all of the non-hydrogen atoms were refined using anisotropic thermal parameters. An overall isotropic extinction parameter was also refined. The total number of variables was 839.

The final difference map was essentially featureless, the largest peak was 0.58 e Å^{-3}. Selected bond lengths and bond angles are shown in Table 4 and the structure is depicted in Fig. 3.

Further details are available as supplementary material.

Table 4. Selected bond distances (Å) and angles (°) for $K_8(OSiPh_3)_8(MeOC_2H_4OMe)_3$

K(1)—O(5)	2.7271(27)	K(2)—O(92)	2.680(3)
K(1)—O(6)	2.7569(28)	K(3)—O(5)	2.740(3)
K(1)—O(7)	2.6563(27)	K(3)—O(7)	2.6072(26)
K(1)—O(86)	2.884(3)	K(3)—O(8)	2.5920(26)
K(1)—O(89)	2.958(3)	K(4)—O(6)	2.6064(28)
K(2)—O(5)	2.6045(27)	K(4)—O(7)	2.7341(26)
K(2)—O(6)	2.6293(28)	K(4)—O(8)	2.6419(27)
K(2)—O(8)	2.650(3)	K(4)—C(73)	3.078(4)
O(5)—K(1)—O(6)	86.55(8)	O(6)—K(4)—O(7)	87.24(8)
O(5)—K(1)—O(7)	91.48(8)	O(6)—K(4)—O(8)	90.92(8)
O(5)—K(1)—O(86)	109.73(9)	O(6)—K(4)—C(73)	134.47(10)
O(5)—K(1)—O(89)	127.48(9)	O(7)—K(4)—O(8)	83.32(8)
O(6)—K(1)—O(7)	85.79(8)	O(7)—K(4)—C(73)	58.35(9)
O(6)—K(1)—O(86)	163.57(9)	O(8)—K(4)—C(73)	111.32(9)
O(6)—K(1)—O(89)	111.00(8)	O(5)—Si(9)—C(10)	113.87(16)
O(7)—K(1)—O(86)	95.65(8)	O(5)—Si(9)—C(16)	111.28(15)
O(7)—K(1)—O(89)	136.99(8)	O(5)—Si(9)—C(22)	114.13(16)
O(86)—K(1)—O(89)	57.64(8)	O(6)—Si(28)—C(29)	111.64(16)
O(5)—K(2)—O(6)	91.83(8)	O(6)—Si(28)—C(35)	112.21(16)
O(5)—K(2)—O(8)	94.07(8)	O(6)—Si(28)—C(41)	114.69(16)
O(5)—K(2)—O(92)	113.58(10)	O(8)—Si(47)—C(48)	111.46(16)
O(6)—K(2)—O(8)	90.24(8)	O(8)—Si(47)—C(54)	112.83(15)
O(6)—K(2)—O(92)	123.45(10)	O(8)—Si(47)—C(60)	113.61(16)
O(8)—K(2)—O(91)	133.50(10)	O(7)—Si(66)—C(67)	113.63(15)
O(5)—K(3)—O(7)	92.26(8)	O(7)—Si(66)—C(73)	109.51(15)
O(5)—K(3)—O(8)	92.25(8)	O(7)—Si(66)—C(79)	112.74(15)
O(7)—K(3)—O(8)	86.86(8)		

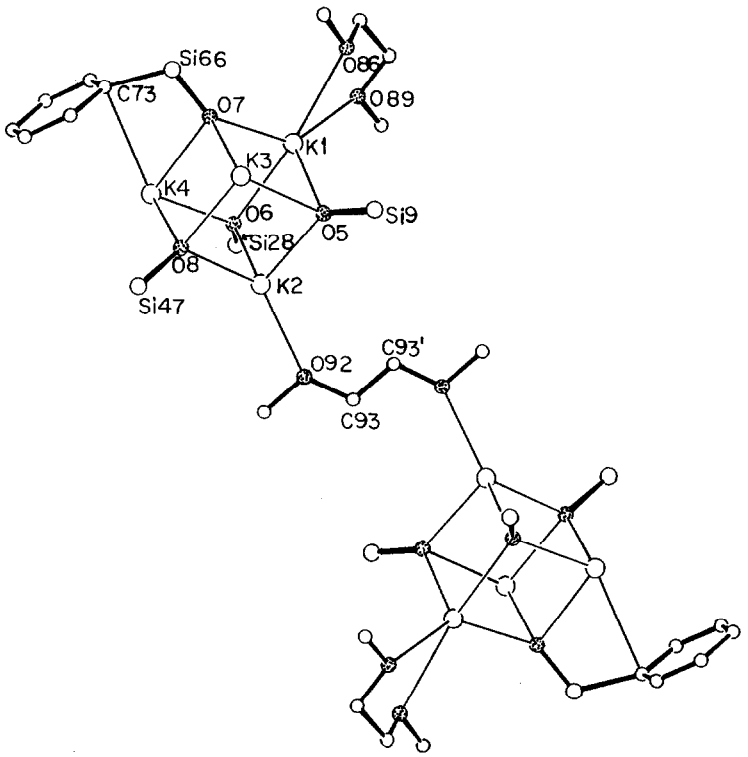

Fig. 3. ORTEP drawing of the non-hydrogen atoms of $K_8(OSiPh_3)_8(MeOC_2H_4OMe)_3$, omitting most phenyl rings for clarity. A crystallographic centre of symmetry lies between C(93) and C(93').

[K(18-crown-6)($OSiPh_3$)] (**5**)

A 100 cm^3 Schlenk flask was charged with $[K(thf)_{0.2}(OSiPh_3)]$ (0.32 g, 1.00 mmol) and 18-crown-6 ether (0.26 g, 1.00 mmol). Toluene (20 cm^3) was then added, resulting in a colourless solution. The mixture was stirred for 3 h, after which time it was concentrated *in vacuo*. Upon standing for 12 h at 0°C, large colourless crystals precipitated. These were isolated by decantation, washed with pentane and dried *in vacuo*. Yield, 90%. IR (Nujol): no ν(OH); ν(CH) 3020; aromatic overtones 1940, 1870, 1810, 1750; other bands 1290, 1270, 1245, 1235, 1100, 1030, 1010, 945, 825, 735, 690 cm^{-1}. ^1H NMR (C_6D_6): δ 8.17 (d, 6.8 Hz, 6H, *ortho*), 7.33 (t, 7.3 Hz, 3H, *para*), 3.16 (s, 24H, OCH_2). ^{13}C NMR (C_6D_6): δ 148.5 (*ipso*), 136.2 (*ortho*), 127.0 (*para*), 126.9 (*meta*), 70.0 (OCH_2). Found: C, 62.5; H, 6.6. Calc. for $C_{30}H_{39}KO_7Si$: C, 62.2; H, 6.8%.

X-ray structure determination of [K(18-crown-6)$OSiPh_3$]$_2$. A suitable crystal was located and transferred to the goniostat using standard inert atmosphere handling techniques and cooled to −155°C for characterization and data collection (Table 5). A systematic search of a limited hemisphere of reciprocal space located a set of diffraction maxima with symmetry and systematic absences corresponding to the unique monoclinic space group $P2_1/c$. Subsequent solution and refinement of the structure confirmed this choice. Data were collected ($6° < 2\theta < 45°$) in the usual manner using a continuous θ–2θ scan with fixed backgrounds.

Table 5. Crystallography data for [K(18-crown-6)$OSiPh_3$]$_2$

Chemical formula	$C_{30}H_{39}KSiO_7$
a (Å)	9.324(2)
b (Å)	17.650(5)
c (Å)	18.147(5)
β (°)	91.60(1)
V (Å^3)	2983.64
Z	4
Formula weight	578.82
Space group	$P2_1/c$
T (°C)	−155
λ (Å)	0.71069
ρ_{calcd} (g cm^{-3})	1.289
μ(Mo-K_α) (cm^{-1})	2.57
R	0.0378
R_w	0.0420

Data were reduced to a unique set of intensities and associated sigmas in the usual manner. The structure was solved by a combination of direct methods (MULTAN78) and Fourier techniques. All hydrogen atoms were clearly visible in a difference Fourier synthesis phased on the non-hydrogen parameters. All hydrogen atoms were refined isotropically and non-hydrogen atoms anisotropically in the final cycles. Final C—H distances ranged from 0.87(3) to 1.01(3) Å. No absorption correction was performed. A final difference Fourier was featureless, with the largest peak being 0.54 e $Å^{-3}$. Selected bond lengths and bond angles are given in Table 6 and the structure is depicted in Figs 4 and 5. Further details are available as supplementary material.

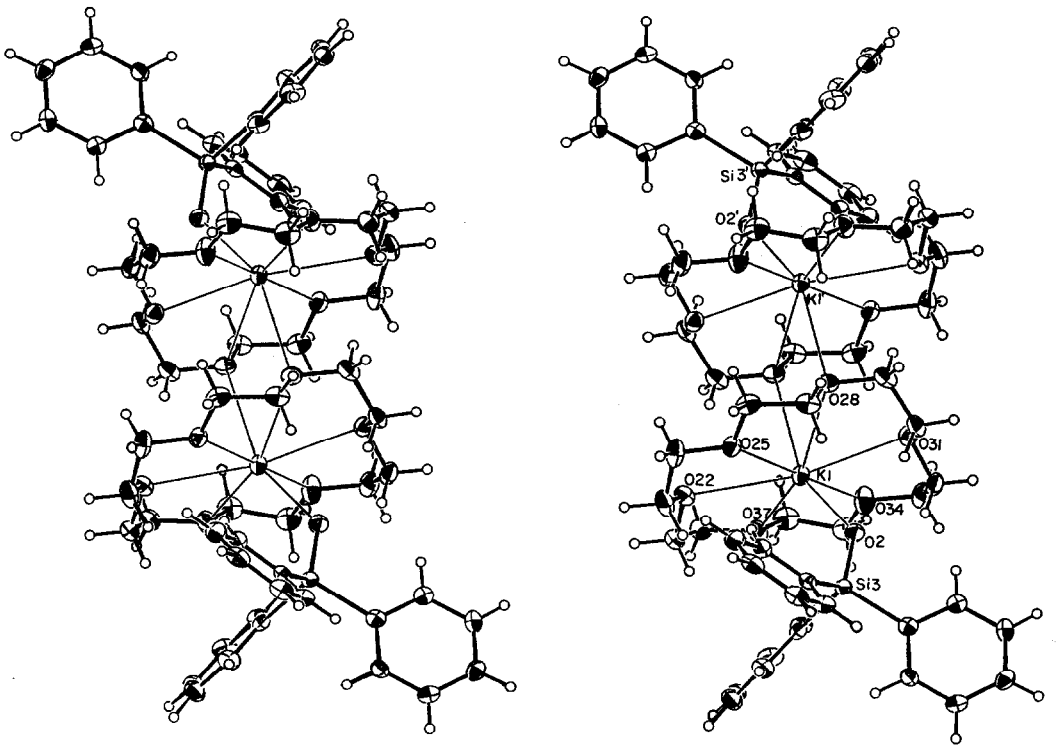

Fig. 4. Stereo ORTEP drawing of $[K(18\text{-crown-6})OSiPh_3]_2$, showing selected atom labelling, bending at silyloxide oxygen, and ether bridging.

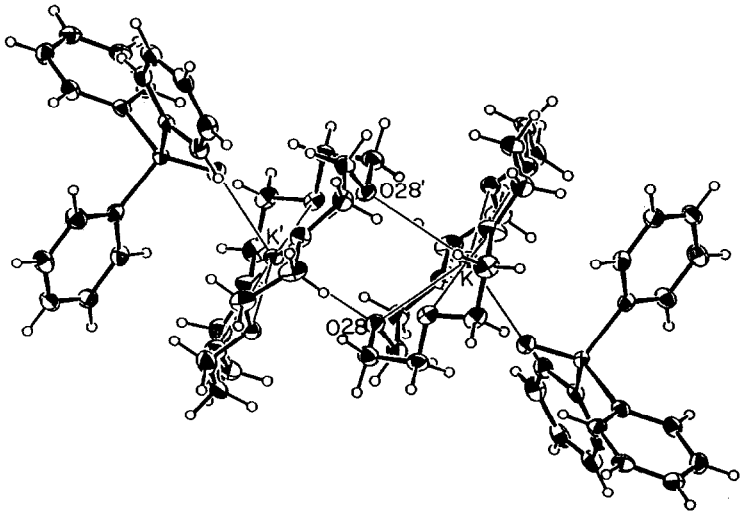

Fig. 5. ORTEP drawing of $[K(18\text{-crown-6})OSiPh_3]_2$ showing face-to-face stacking of crown rings and the "slip" of these rings to allow ether bridging.

Table 6. Selected bond distances (Å) and angles (°) for $[K(18\text{-crown-6})OSiPh_3]_2$

K(1)—O(2)	2.6247(19)	O(22)—C(23)	1.420(4)
K(1)—O(22)	2.9403(20)	O(22)—C(39)	1.436(4)
K(1)—O(25)	2.6981(20)	O(25)—C(24)	1.417(3)
K(1)—O(28)	2.9180(20)	O(25)—C(26)	1.433(3)
K(1)—O(28)′	3.1123(20)	O(28)—C(27)	1.438(3)
K(1)—O(31)	2.8415(20)	O(28)—C(29)	1.427(3)
K(1)—O(34)	2.7013(21)	O(31)—C(30)	1.432(3)
K(1)—O(37)	2.8586(21)	O(31)—C(32)	1.427(3)
Si(3)—O(2)	1.5726(20)	O(34)—C(33)	1.420(4)
Si(3)—C(4)	1.9071(27)	O(34)—C(35)	1.410(4)
Si(3)—C(10)	1.9019(27)	O(37)—C(36)	1.410(4)
Si(3)—C(16)	1.8996(27)	O(37)—C(38)	1.424(4)

O(2)—K(1)—O(22)	116.32(6)	O(25)—K(1)—O(28)	62.35(6)
O(2)—K(1)—O(25)	88.37(6)	O(25)—K(1)—O(31)	123.16(6)
O(2)—K(1)—O(28)′	155.40(6)	O(25)—K(1)—O(34)	175.02(6)
O(2)—K(1)—O(28)	86.91(6)	O(25)—K(1)—O(37)	117.48(6)
O(2)—K(1)—O(31)	76.48(6)	O(28)′—K(1)—O(28)	71.77(6)
O(2)—K(1)—O(34)	96.48(6)	O(28)′—K(1)—O(31)	82.67(6)
O(2)—K(1)—O(37)	116.01(6)	O(28)—K(1)—O(31)	62.39(6)
O(22)—K(1)—O(25)	58.53(5)	O(28)′—K(1)—O(34)	83.78(6)
O(22)—K(1)—O(28)′	84.47(5)	O(28)—K(1)—O(34)	118.89(6)
O(22)—K(1)—O(28)	114.38(6)	O(28)—K(1)—O(37)	156.96(6)
O(22)—K(1)—O(31)	167.08(5)	O(28)′—K(1)—O(37)	85.35(5)
O(22)—K(1)—O(34)	117.86(6)	O(31)—K(1)—O(34)	59.46(6)
O(22)—K(1)—O(37)	59.07(6)	O(31)—K(1)—O(37)	118.41(6)
O(25)—K(1)—O(28)′	92.28(6)		

$[K(OSiMe_2{}^tBu)]_n$ (**6**)

A 100 cm^3 Schlenk flask was charged with KH (0.50 g) and THF (30 cm^3). To the resultant suspension was added $HOSiMe_2{}^tBu$ (1.0 cm^3, 6.4 mmol) via a pipette. Gas evolution occurred immediately. The mixture was stirred for 3 h, whereupon the filtration was performed to remove excess unreacted KH reagent. The solvent was evaporated *in vacuo* from the colourless solution thus obtained, leaving a white solid. The solid was dissolved in pentane. Upon standing at −20°C, colourless crystals precipitated. Yield: 60%. IR (Nujol): no ν(OH); major bands: 1235, 995, 970, 815, 740, 625 cm^{-1}. ^1H NMR (C_6D_6): δ 0.96 (s, 9H, ^{t}Bu), −0.10 (s, 6H, $SiMe_2$). ^{13}C NMR (C_6D_6): δ 27.6 [q, J(CH) 120.9 Hz, —C(CH_3)$_3$], 19.6 (s, —CMe_3), 0.17 [q, J(CH) 114.8 Hz, $SiMe_2$]. Found: C, 42.0; H, 8.9. Calc. for $C_6H_{15}KOSi$: C, 42.3; H, 8.9%.

$[K(18\text{-crown-6})(OSiMe_2{}^tBu)]_n$(**7**)

A 100 cm^3 Schlenk flask was charged with $[K(OSiMe_2{}^tBu)]_n$ (0.85 g, 5.0 mmol), 18-crown-6 ether (1.32 g, 5.00 mmol) and toluene (20 cm^3). A solution was obtained initially. Gradually, the reaction mixture grew turbid and a waxy solid precipitated. The reaction mixture was stirred for 70 h, whereupon the solvent was removed *in vacuo*. The residue was washed with hexane and dried *in vacuo*. Yield: 80%. IR (Nujol): no ν(OH), ν(CH) 2923; other bands: 1287, 1252, 1230, 1220, 1138, 1105, 1024, 962, 839, 819, 800, 770, 738, 634 cm^{-1}. ^1H NMR (C_6D_6): δ 3.26 (s, 24H, crown), 1.47 (s, 9H, ^{t}Bu), 0.49 (s, 6H, $SiMe_2$). ^{13}C NMR (C_6D_6): δ 70.1 (crown), 28.7 [—C(CH_3)$_3$], 20.8 (—CMe_3), 1.31 ($SiMe_2$). Found: C, 48.1; H, 9.1. Calc. for $C_{18}H_{39}KO_7Si$: C, 49.7; H, 9.1%.

RESULTS

Syntheses

Alkali metal silyloxide reagents $[Li(OSiPh_3)]_n$, $[K(thf)_{0.2}(OSiPh_3)]$ and $[K(OSiMe_2{}^tBu)]$ were prepared by deprotonation of Ph_3SiOH or $Me_2{}^t$BuSiOH using Li(^{n}Bu) in hexane and KH in THF, respectively. Crystalline DME adducts $[Li(\mu\text{-}OSiPh_3)(\eta^2\text{-DME})]_2$ and $[K_4(\mu_3\text{-}OSiPh_3)_3\{\mu_3\text{-}OSiPh_2(\eta^1\text{-Ph})\}(\eta^2\text{-DME})]_2(\mu\text{-DME})$ were prepared by dissolving $[Li(OSiPh_3)]_n$ or $[K(thf)_{0.2}$(OSi

Ph_3)], respectively, in dimethoxyethane followed by precipitation with alkane. Toluene-soluble [K(18-crown-6)($OSiPh_3$)]$_2$ and [(18-crown-6)(OSi$Me_2{}^tBu$)]$_n$, respectively, were prepared from [K$(thf)_{0.2}$($OSiPh_3$)] or [K($OSiMe_2{}^tBu$)]$_n$ and equivalent amounts of 18-crown-6 ether in toluene.

Spectroscopic properties

NMR spectroscopy. Both the ^1H and ^{13}C NMR spectra of the dimeric lithium complex [Li(μ-$OSiPh_3$)(η^2-DME)]$_2$ revealed a simple mono-substituted aromatic pattern along with resonances expected for the dimethoxyethane co-ligand. The base-free lithium silyloxide complex [Li($OSiPh_3$)]$_n$ was too insoluble in non-coordinating solvents to permit collection of NMR data.

The NMR spectra for the potassium triphenylsilyloxide complexes were unexpectedly simple given the solid-state structures (see below). The observation of a singlet resonance (by ^1H and ^{13}C NMR) for the 18-crown-6 ether moiety in [K(18-crown-6)($OSiPh_3$)]$_2$, (**5**) indicates that either the ethereal oxygen bridges are not maintained in solution or that a fluxional process equilibrates all 18-crown-6 atoms on the NMR time scale. Similarly, the ^1H and ^{13}C NMR measurements for [K_4(μ_3-$OSiPh_3$)$_3$(μ_3-$OSiPh_2$(η^2-Ph))(η^2-DME)]$_2$(μ-DME) (**4**) showed only one type of —$OSiPh_3$ group and one type of DME co-ligand. The implication here is that ligand reorganization processes are facile on the NMR time scale in solution.

The ^1H and ^{13}C NMR spectra for [K(OSi$Me_2{}^tBu$)]$_n$ (**6**) revealed only the expected —$OSiMe_2{}^tBu$-based signals. The absence of Lewis base co-ligands together with the solid-state characterization of [K($OSiMe_3$)]$_4$ as a cubane[4] implies a similar cubane structural formulation for **6**. The NMR results for [K(18-crown-6)($OSiMe_2{}^tBu$)]$_n$ (**7**) were analogous to those for the triphenylsilyloxide complex **5**: a singlet resonance for the 18-crown-6 ether and a single set of —$OSiMe_2{}^tBu$-based resonances.

IR spectroscopy. All triphenylsilyloxide complexes reported here shared a set of IR active absorptions, namely aromatic ν(CH) modes near 3030 cm^{-1} and mono-substituted aromatic overtone patterns between 1950 and 1780 cm^{-1}. Additionally, intense bands between 1100 and 950 cm^{-1} were detected in each spectrum and were attributed to ν(OSi) modes. Complexes bearing the —$OSiMe_2{}^tBu$ ligand revealed intense absorptions near 1240 cm^{-1}, assigned as δ_s ($SiCH_3$) modes, as well as very intense absorptions between 1050 and 950 cm^{-1}, assigned as ν(SiO) modes. No high energy ν(OH) bands were observed in any of the complexes reported in this study.

Solid-state structure of [Li(μ-$OSiPh_3$)(η^2-DME)]$_2$

The compound adopts a dimeric structure based on a symmetric (Li—O distances are equal to within 3σ) Li_2O_2 rhombus, a structural type reminiscent of lithium alkoxide chemistry.[8] (Fig. 1). This ring is obtuse at lithium [angle 97.9(4)°] and acute at the siloxide oxygen [angles 81.9(4)° and 82.2(4)°]. Bidentate coordination of one DME to each Li^+ gives this element coordination number four. The Si—O vectors do not precisely bisect the Li—O—Li angles, but the deviations are small. The two Si—O distances are equal (mean value 1.584 Å), and are identical to the values of a number of Y^{III}/$OSiPh_3$ compounds.[5] The Li—O(DME) bond distances are equal to within 3σ, and they are over 0.1 Å longer than the Li—O($SiPh_3$) distances. The DME/lithium rings are both puckered, the oxygens in these rings are distinctly pyramidal (angles at oxygen sum to 339.5–351.7°), and the ring conformation puts all terminal methyls in *trans* equatorial positions (Fig. 2). The Li—O(Si) distances (mean value 1.871 Å) are somewhat longer than those to phenoxides in [(Et_2O)Li(O-4-Me, 2,6-$^tBu_2C_6H_2$)]$_2$ [1.828(7) and 1.868(7) Å], where Li^+ is only three-coordinate.[9] Both siloxide oxygens are pyramidal (Fig. 2), but this is less dramatic at O(3) (sum of angles = 358.7°) than at O(23) (353.0°).

Solid-state structure of [K_4(μ_3-$OSiPh_3$)$_3$\{μ_2-$OSiPh_2$(η^1-Ph)\}(η^2-DME)]$_2$(μ-DME)

This molecule exists in the solid state as two K_4($OSiPh_3$)$_4$(η^2-DME) cubane units linked by a bridging DME (Fig. 3). A crystallographic centre of symmetry, located between the two methylene carbons of the bridging DME, relates the two cubane units. All Ph_3SiO^- groups are triply bridging within the cube. As a result, the four K^+ ions in the asymmetric unit have only a total of three terminal ligands: one oxygen of the DME which bridges two cubes and the two oxygens of one DME which is bidentate to a single K^+.

Potassium–oxygen bond lengths expand systematically as metal coordination number increases. This holds for K—OSi and also K—O(ether) distances. The latter are systematically longer than the former. The bridging ether binds to K^+ with a remarkably (0.20–0.27 Å) shorter distance than does the chelating ether. This may be due to a combination of chelate ring strain and the higher K^+ coordination number of the chelate/K^+ site.

There is good evidence that K4 binds to one phenyl *ipso* carbon attached to Si66. The K/C(73) distance of 3.078(4) Å is comparable to that in

potassium-intercalated graphite.[10] Moreover, the smallest of the 12 O—Si—C angles in the structure [109.51(15)°] is to C(73), although the other angles are not much larger [111.28(15)–114.69(16)°]. This K(4)/C(73) distance is only 0.1 Å longer than one of the K(1)—O(ether) distances. Atom K(3) remains only three-coordinate.

Solid state structure of $[K(18\text{-crown-6})OSiPh_3]_2$

The X-ray diffraction study reveals that K(18-crown-6)$OSiPh_3$ is an intimate ion pair in the solid state, and that it forms a dimer by bridging via ether oxygen (Figs 4 and 5). Potassium thereby achieves coordination number eight. The siloxide oxygen and the six oxygens of one crown ether furnish only seven donors. Space-filling drawings show that steric hindrance makes $OSiPh_3$ bridging impossible. Consequently, the eighth coordination site on potassium is occupied by an oxygen on the second crown ether in the dimer. This is accomplished by stacking the crown ether rings face-to-face in the dimeric structure (Fig. 5). This ether oxygen bridging is complementary (because the dimer possesses a crystallographic centre of symmetry), which leads to a "slipped" stacking of the macrocycle ring planes (Fig. 5). The bridging ether oxygen is involved in the longest (3.112 Å) and the third longest (2.918 Å) K—O distances in the structure. The K—OSi distance is the shortest (2.625 Å), and is *trans* to the bridging ether oxygen. The remaining five K—O distances range from 2.698 to 2.940 Å.

The ether oxygens are generally pyramidal, not planar, and they are "ruffled" somewhat out of their mean plane. The K—OSi vector is not perpendicular to this mean plane.

DISCUSSION

This work permits a number of conclusions about solid-state structure:

(1) The comparison of Li^+ and K^+ with $OSiPh_3^-$ and DME as ligands reveals that the larger potassium cation encourages a greater degree of aggregation. Aggregation does not follow uniquely from larger cation size, but is a consequence of ligands recruited into bridging roles, since a formulation like $K(DME)_n^+$ $OSiPh_3^-$ is, in principle, an alternative to aggregation. Indeed, we have reported $[K(\eta^2\text{-DME})_3(\eta^1\text{DME})][Y(OSiPh_3)_4(DME)]$ as an example.[5] Thus, it follows that:

(2) Ph_3SiO^- is abundantly capable of bridging between alkali metals. Not only μ_2- but also μ_3-possibilities are viable. Both bridging modes may be enabled because of minimal $O \rightarrow M^+$ π-donation when M^+ is an alkali metal (i.e. absence of empty *d* orbitals). Such a terminal siloxide remains quite nucleophilic at oxygen.

(3) The larger K^+ ion displays remarkable tolerance towards variable coordination number (and, consequently, geometry). Particularly illustrative of this point is the compound $[K_4(\mu_3\text{-}OSiPh_3)_3\{\mu_3\text{-}OSiPh_2(\eta^1\text{-Ph})\}(\eta^2\text{-DME})]_2(\mu\text{-DME})$, where coordination numbers five, four, "three-plus-one" (three oxygens and one carbon), and three co-exist. The three-coordinate potassium (K3) is also noteworthy because it is pyramidal, not the more stable planar geometry.

(4) The K—O distances show no regular variation with changing coordination number. This contrasts with the situation for transition metal siloxides. This may be a sign of predominately ionic bonding for K^+. Nevertheless, while individual K—O interactions may be largely coulombic in character, such polarity is effectively masked by the hydrocarbon periphery of these molecules and they are therefore hydrocarbon-soluble. Their utility as synthetic reagents in non-coordination solvents is thus established.

(5) The compact ligand 18-crown-6 permits the highest coordination number (eight) for K^+. The ability of an ether oxygen to bridge two metals expands the structural potential of crown ethers.

Supplementary materials available. Full crystallographic details, and atomic coordinates and anisotropic thermal parameters and observed and calculated structure factors for $[LiOSiPh_3(DME)]_2$, $K_8(OSiPh_3)_8(DME)_3$ and K(18-crown-6)$(OSiPh_3)$.

Acknowledgements—This work was supported by DOE grant DE-FGO2-88ER-13906. We thank Scott Horn for skilled technical assistance.

REFERENCES

1. M. H. Chisholm and I. P. Rothwell, in *Comprehensive Coordination Chemistry* (Edited by G. Wilkinson, R. D. Gillard and J. A. McCleverty), Vol. 2, p. 335. Pergamon, Oxford (1987).
2. H. Schmidbaur, *Angew. Chem.* 1965, **77**, 206.
3. D. C. Bradley, *Coord. Chem. Rev.* 1967, **2**, 299.
4. E. Weiss, K. Hoffmann and H.-F. Grutzmacher, *Chem. Ber.* 1970, **103**, 1190.
5. M. J. McGeary, P. S. Coan, K. Folting, W. E. Streib and K. G. Caulton, *Inorg. Chem.* 1991, **30**, 1723.
6. M. J. McGeary, R. H. Cayton, K. Folting, J. C. Huffman and K. G. Caulton, *Polyhedron*, submitted.

7. J. C. Huffman, L. N. Lewis and K. G. Caulton, *Inorg. Chem.* 1980, **19**, 1840.
8. J. C. Huffman, R. L. Geerts and K. G. Caulton, *J. Cryst. Spectrosc. Res.* 1984, **14**, 541.
9. B. Cetinkaya, I. Gumrukcu, M. F. Lappert and J. L. Atwood, *J. Am. Chem. Soc.* 1980, **102**, 2086.
10. S. A. Solin, *Adv. Chem. Phys.* 1982, **49**, 455.

Polyhedron Vol. 10, No. 23/24, pp. 2711–2715, 1991
Printed in Great Britain

0277–5387/91 $3.00+.00
© 1991 Pergamon Press plc

KINETIC AND SPECTROSCOPIC STUDY OF THE FORMATION OF AN INTERMEDIATE RUTHENIUM(III) ASCORBATE COMPLEX IN THE OXIDATION OF L-ASCORBIC ACID

M. M. TAQUI KHAN* and R. S. SHUKLA

Discipline of Coordination Chemistry and Homogeneous Catalysis,
Central Salt and Marine Chemicals Research Institute, Bhavnagar 364 002, India

(*Received* 4 *April* 1991; *accepted* 26 *July* 1991)

Abstract—The formation of an intermediate ruthenium(III) ascorbate complex (**1**) by the interaction of L-ascorbic acid and dichlorotetraaquoruthenium(III) is reported in the temperature range 25–40°C. The kinetics and mechanism of the formation of **1** were studied as a function of $[Ru^{III}Cl_2(H_2O)_4]^+$, [ascorbic acid], pH, ionic strength and temperature. The rate of formation of **1** was found to be first order in $[Ru^{III}Cl_2(H_2O)_4]^+$ and [ascorbic acid]. The rate has an inverse dependence on hydrogen ion concentration. Ionic strength dependence indicated the formation of **1** by monoanionic and cationic species in solution. Decomposition of **1** takes place slowly and gives the products dehydroascorbic acid and $[Ru^{II}Cl_2(H_2O)_4]$. A detailed discussion of the kinetic data and a comparison of rate and equilibrium constants are presented with activation and thermodynamic parameters.

The study of the formation of an intermediate complex during a reaction is of fundamental interest in the understanding of the kinetics and mechanism of the reaction. The chemistry of ascorbic acid complexes took on new importance when a *cis*-diammine platinum ascorbate complex was synthesized[1] and found to be an efficient anti-cancer agent. Evidence of the transient appearance of the metal-ascorbate complexes has been reported in a few cases[2–5] but lacks the detailed study of complex formation. Our recent studies on ruthenium(III) chloride in aqueous solution[6–10] showed that $[Ru^{III}Cl_2(H_2O)_4]^+$ is the most stable chloro species present in solution (pH 1.0–2.5). Stoichiometric[11] and catalytic[12] oxidation of L-ascorbic acid by ruthenium(III) has been studied previously. In this paper we report an investigation of the kinetics of the formation of the ruthenium(III) ascorbate complex using fast kinetic methods and visible spectroscopy.

EXPERIMENTAL

All the solutions were prepared using freshly prepared, doubly distilled water. L-ascorbic acid was an AR grade sample and was used without further purification. A stock solution of ruthenium(III) was prepared[6] by dissolving an appropriate amount of ruthenium trichloride trihydrate $[RuCl_3 \cdot 3H_2O]$ in 1 M hydrochloric acid. AR grade potassium nitrate was used to maintain the ionic strength of the solution at 0.02–0.15 M. The desired pH (0.5–2.75) of the experimental reaction mixture was adjusted by adding either carbonate-free standard NaOH or HCl to the reaction solution. Corrections due to ionic strength were applied in calculating hydrogen ion concentration from the pH data.

pH measurements were performed with a digital pH meter (±0.01 pH) equipped with combined glass and calomel electrodes. The desired temperature (±0.1°C) was maintained in the reaction cell with a circulating water bath. A temperature-controlled Shimadzu 160 UV–vis spectrophotometer was used for all spectrophotometric experiments. Fast kinetic measurements were performed on a thermostated (±0.1°C) stopped-flow spectrophotometer Model S4-51 (HiTech) coupled with an Apple data processor as a function of [ascorbic acid], $[Ru^{III}Cl_2(H_2O)_4]^+$, pH, ionic strength and temperature. An excess of ascorbic acid was used in all cases to ensure pseudo first-order kinetic conditions and the corresponding rate constants

* Author to whom correspondence should be addressed.

were evaluated from the plots of $\log(A_\infty - A_t)$ vs time. All reported rate constants are the mean values of at least four determinations and subjected to an average error limit of $\pm 3\%$.

RESULTS AND DISCUSSION

The oxidation of L-ascorbic acid (H_2A) by $[Ru^{III}Cl_2(H_2O)_4]^+$ leads to the formation of L-dehydroascorbic acid (A) according to the overall reaction in eq. (1).

$$2[Ru^{III}Cl_2(H_2O)_4]^+ + H_2A \longrightarrow 2[Ru^{II}Cl_2(H_2O)_4] + A + 2H^+. \quad (1)$$

The stoichiometry of the reaction is similar to many other ascorbic acid oxidation reactions[13–16] by metal complexes. The reactivity of ascorbic acid depends on the actual species, H_2A, HA^- or A^{2-}, participating in the rate-determining step. In general, the reactivity increases in the order $H_2A < HA^- < A^{2-}$.[17] H_2A and HA^- are the reactive species of ascorbic acid in acidic medium.[18–22] The completely dissociated species exist only above pH 9.00.

Preliminary experiments with ascorbic acid and $[Ru^{III}Cl_2(H_2O)_4]^+$ in the pH range 0.5–2.5 indicated the rapid formation of an intermediate ascorbate complex (Fig. 1), which subsequently decomposed to the products dehydroascorbic acid and $[Ru^{II}Cl_2(H_2O)_4]$. It was possible to record the spectrum of intermediate species (ruthenium(III) ascorbate complex) during the formation and decomposition processes, from which it follows that the complex has a maximum absorption at 510 nm.

Since both the reactants $[Ru^{III}Cl_2(H_2O)_4]^+$ and HA^- in the present study are highly pH sensitive, the molar extinction coefficient of the ruthenium(III) ascorbate complex was determined by measuring the maximum absorbance reached at 510 nm as a function of pH, $[H_2A]$ and $[RuCl_2(H_2O)_4]^+$. The absorption spectrum of the complex formed between ascorbic acid (2×10^{-3} M) and $[RuCl_2(H_2O)_4]^+$ (2×10^{-4} M) in 0.1 M KNO_3 at different pH values (0.5–2.5) (Fig. 1) was obtained by performing spectrophotometric titrations from pH 0.5 to 2.5. The absorbance at 510 nm increases with pH up to 2.0. At pH > 2.0, the pH dependence on absorbance at 510 nm was found to be non-linear. It is clear from Table 1 that after pH 2.5 the absorbance starts decreasing. The dual nature of the pH dependence on complex formation, below and above pH 2.0 may be assigned to the presence of chloro and hydroxo species of ruthenium(III) in aqueous solution, because at higher pH (> 2.0) hydrolysis of the chloro complexes of ruthenium(III) takes place. Hence, at pH 2 the formation of the ruthenium(III) ascorbate complex results from the interaction of $[Ru^{III}Cl_2(H_2O)_4]^+$ and ascorbate monoanion (HA^-). In a 10-fold excess of ascorbic acid, assuming all the $[RuCl_2(H_2O)_4]^+$ in solution is involved in the formation of the ruthenium ascorbate complex, the molar extinction coefficient at 510 nm (ε_{max}^{510}) at pH 2 is 805 M^{-1} cm^{-1}.

In an attempt to measure the stoichiometry of the ruthenium(III) ascorbate complex, we have undertaken experiments in which $[Ru^{III}Cl_2(H_2O)_4]^+$, at constant concentration, was mixed with ascorbate at known but variable concentrations in the stopped-flow apparatus. The total absorbance change due to complex formation was monitored, thus giving a measure of the complex concentration as a function of ascorbate concentration. Under these conditions and at pH 2 and $\mu = 0.1$ M KNO_3, we observed a single kinetic progress curve leading to the formation of a 1 : 1 ruthenium(III) ascorbate complex at 510 nm. The method of cal-

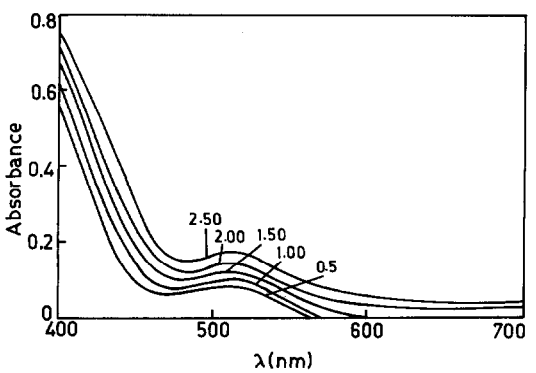

Fig. 1. Absorption spectrum of the intermediate complex formed at 510 nm at different pH values as indicated with $[Ru^{III}Cl_2(H_2O)_4]^+ = 2 \times 10^{-4}$ M, [ascorbic acid] = 2×10^{-3} M and $\mu = 0.1$ M KNO_3 at 30°C.

Table 1. pH dependence for the maximum absorbance of the complex formed at 510 nm, $\mu = 0.1$ M KNO_3, $[RuCl_2(H_2O)_4]^+ = 2 \times 10^{-4}$ M, $[H_2A] = 2 \times 10^{-3}$ M at 30°C

pH	Absorbance	pH	Absorbance
0.5	0.135	2.00	0.165
1.0	0.140	2.25	0.168
1.25	0.145	2.50	0.170
1.50	0.150	2.75	0.165
1.75	0.155	2.80	0.149

Table 2. Rate data as a function of $[RuCl_2(H_2O)_4]^+$, $[H_2A]$ and temperature for complex formation at pH = 2.00 and μ = 0.1 M KNO_3

$[RuCl_2(H_2O)_4]^+$ ($M \times 10^3$)	$[H_2A]$ ($M \times 10^3$)	Temperature (°C)	k_{obs} (s^{-1})	$10^{-3} \times k_1$[a] ($M^{-1} s^{-1}$)
2.00	1.00	35	8.4±0.2	68.3±1.9
2.00	2.00	35	17.0±0.3	69.2±0.9
2.00	4.00	35	32.9±0.4	69.2±1.2
2.00	5.00	35	40.1±0.4	65.4±1.0
2.00	6.00	35	47.48±0.5	64.6±0.9
4.00	2.00	35	16.8±0.2	68.6±0.4
8.00	2.00	35	17.0±0.3	69.4±0.8
2.00	2.00	25	10.9±0.2	55.0±0.8
2.00	2.00	30	14.0±0.2	63.0±0.9
2.00	2.00	40	22.2±0.3	76.3±1.9

[a] Calculated using eq. (4).

culation for the formation constant of the complex is reported in our previous publications.[7-11]

An appropriate quantity of ruthenium(III) chloride from its stock solution (solution A) and solutions containing suitable amounts of 1 M KNO_3, 0.1 M carbonate-free sodium hydroxide and L-ascorbic acid (solution B) were made in separate containers at the required temperatues. On mixing solutions A and B a rapid increase in absorbance in the visible spectrum at 510 nm was observed, indicating rapid formation of the ruthenium(III) ascorbate complex.

The complex formation reaction was carried out by a stopped-flow apparatus as a function of pH, H_2A, μ and temperature and the kinetic data are given in Table 2. Pseudo first-order rate constants k_{obs} are independent of the concentration of $RuCl_2(H_2O)_4^+$ and increased linearly (first order) on increasing ascorbic acid concentration. The pH dependence of the reaction (Table 3) was studied in the pH range 1.50–2.50 and the rate of complex formation was found to increase with pH showing inverse dependence of $[H^+]$. This dependence is explained in terms of eqs (2) and (3).

Table 3. pH dependence for ruthenium(III) ascorbate complex formation at 35°C, μ = 0.1 M KNO_3, $[RuCl_2(H_2O)_4]^+ = 2 \times 10^{-3}$ M and $[H_2A] = 2 \times 10^{-2}$ M

pH	k_{obs} (s^{-1})	k_1 ($10^{-3} \times M^{-1} s^{-1}$)
1.50	5.4±0.1	69.1±1.2
1.75	9.6±0.2	68.9±1.2
2.00	17.0±0.3	69.2±1.5
2.25	28.6±0.5	69.9±1.8
2.50	47.6±0.8	64.0±1.6

$$H_2A \overset{K_a}{\rightleftharpoons} HA^- + H^+ \quad (2)$$

$$[Ru^{III}Cl_2(H_2O)_4]^+ + HA^- \xrightarrow{k_1} \text{complex} \quad (3)$$

The rate expression for the reaction in terms of k_{obs} is written as

$$k_{obs} = k_1 K_a [H_2A]_T (K_a + H^+); \quad (4)$$

where

$$[H_2A]_T = [H_2A] + [HA^-]. \quad (5)$$

Inversing eq. (4) we obtain

$$k_{obs}^{-1} = 1/k_1[H_2A]_T + [H^+]/k_1 K_a [H_2A]_T. \quad (6)$$

The dissociation constants K_a obtained directly by potentiometric titrations at the different temperatures reported[12] at μ = 0.1 M KNO_3 are: $K_a \times 10^5$(°C): 10.05(25), 11.22(30), 12.40(35) and 14.79M(40). Substituting K_a in the slope of the plot of k_{obs}^{-1} vs $[H^+]$ [eq. (6)], the rate constant k_1 calculated at 35°C was $69.6 \pm 0.5 \times 10^3$ $M^{-1} s^{-1}$. The rate constant k_1 computed using the dissociation constant K_a in eq. (4) is fairly constant with regards to the variation of ascorbic acid, $[RuCl_2(H_2O)_4]^+$ and hydrogen ion concentration with an average value of $k_1 = (67.8 \pm 0.2) \times 10^3$ $M^{-1} s^{-1}$, which is in excellent agreement with the rate constant calculated from eq. (6). These results indicate that there is no significant reaction of $[RuCl_2(H_2O)_4]^+$ with undissociated H_2A under the present experimental conditions. The ionic strength (0.02–0.15 M) dependence plot of $\log k_1$ vs $\mu^{1/2}/(1+\mu^{1/2})$ gave

Table 4. Thermodynamic and activation parameters for interaction of $[RuCl_2(H_2O)_4]^+$ and ascorbic acid

Thermodynamic parameters[a]	For equilibrium constants K_a	K
$\Delta H^\ominus$ (kcal mol^{-1})	6.9±0.1	4.0±0.1
$\Delta S^\ominus$ (cal K^{-1} mol^{-1})	6±1	31±3
$\Delta G^\ominus$ (kcal mol^{-1})	5.5±0.1	−5.1±0.1
Activation parameters	For rate constants k_1	k_2[a]
$\Delta H^{\ominus\,b}$ (kcal mol^{-1})	3.3±0.1	6.0±0.1
$\Delta S^{\ominus\,b}$ (cal K^{-1} mol^{-1})	−26±2	−54±3

[a] See ref. 11.
[b] Calculated at 25°C.

a slope of −1, confirming that the complex formation takes place through the interaction of a monocationic and an anionic species [eq. (3)].

Oxidation of ascorbic acid slowly takes place by the decomposition of the complex as given in eqs (7) and (8).

$$\text{Complex} \xrightarrow{k_2} [Ru^{II}Cl_2(H_2O)_4] + HA^{\cdot} \quad (7)$$

$$[Ru^{III}Cl_2(H_2O)_4]^+ + HA^{\cdot} \xrightarrow{\text{fast}} [Ru^{II}Cl_2(H_2O)_4] + H^+ + A; \quad (8)$$

where $HA^{\cdot}$ is the ascorbate radical. The detailed kinetic study of the oxidation of ascorbic acid by the present system has been reported.[11] The formation constant K given by eq. (9) directly calculated by the spectrophotometric method[23] at different temperatures is: $K \times 10^{-3}$(°C): 5.99(25), 6.91(30), 7.81(35) and 8.70 M^{-1}(40).

$$[RuCl_2(H_2O)_4]^+ + HA^- \rightleftharpoons \underset{\text{complex}}{[RuCl_2(H_2O)_2HA]} + 2H_2O \quad (9)$$

The thermodynamic parameters given in Table 4 corresponding to the dissociation constant K_a show that dissociation is highly endothermic with positive values of $\Delta H^\ominus$ and $\Delta G^\ominus$. The formation of the ascorbate complex is highly favourable with a negative value for $\Delta G^\ominus$. The enthalpy of the formation is endothermic and entropy is favourable for its decomposition. A comparison of activation parameters (Table 4) corresponding to the rate constants k_1 and k_2 indicate that the activation process is enthalpy-controlled, since enthalpy is more for slower reactions. The negative values of entropy of activation are in line with an associatively-activated process.

CONCLUSIONS

From the results of the investigation on the ruthenium(III) ascorbate reaction we conclude that intermediate **1** observed in the reaction is a dichloroascorbatodiaquoruthenium(III) complex which maximally forms near pH 2.2. The increase in absorbance at 510 nm observed in the stopped-flow apparatus corresponds to the build up of this complex. Spectrophotometric tirations of the chloro species $[RuCl_2(H_2O)_4]^+$ with ascorbate suggested that the mixed ligand complex formation reaches a maximum at a ruthenium(III) to ascorbate ratio of 1:1 and after that the addition of ascorbic acid does not much affect the complex formation.

REFERENCES

1. L. S. Hollis, A. R. Amundson and E. W. Stern, *J. Am. Chem. Soc.* 1985, **107**, 274.
2. (a) M. M. Taqui Khan and A. E. Martell, *J. Am. Chem. Soc.* 1967, **89**, 4176, 1704; (b) 1968, **90**, 3386, 6011; (c) 1969, **91**, 4668 and refs therein.
3. (a) D. M. Wagnerova, E. Schwertnerava and J. Veprek-Siska, *Collect. Czech. Chem. Commun.* 1976, **41**, 2473; (b) R. J. Jameson and N. J. Blackburn, *J. Inorg. Nucl. Chem.* 1975, **37**, 809.
4. (a) E. F. Kries, *Russ. J. Inorg. Chem.* 1978, **23**, 1004; (b) D. M. Wagnerova, J. Blanck, G. Smetten and J. Veprek-Siska, *Collect. Czech. Chem. Commun.* 1981, **59**, 132; (c) R. N. Gupta and B. K. Sen, *Inorg. Nucl. Chem.* 1975, **37**, 1548.
5. (a) P. Martinez, J. Zuluga, D. Uribe and R. Vaneldik, *Inorg. Chim. Acta* 1987, **136**, 11; (b) H. Keypour, J. Silver, M. T. Wilson and M. Y. Hamed, *Inorg. Chim. Acta* 1986, **125**, 97.
6. M. M. Taqui Khan, G. Ramachandraiah and A. Prakash Rao, *Inorg. Chem.* 1986, **25**, 665.
7. M. M. Taqui Khan and R. S. Shukla, *J. Molec. Catal.* 1986, **34**, 19.
8. M. M. Taqui Khan, G. Ramachandraiah and R. S. Shukla, *Inorg. Chem.* 1988, **27**, 3274.
9. M. M. Taqui Khan, G. Ramachandraiah and R. S. Shukla, *Inorg. Chem.*, submitted.
10. J. A. Rard, *Chem. Rev.* 1985, **85**, 1.
11. M. M. Taqui Khan and R. S. Shukla, *Inorg. Chim. Acta* 1988, **149**, 89.
12. M. M. Taqui Khan and R. S. Shukla, *J. Molec. Catal.* 1986, **37**, 269.
13. U. S. Mehrotra, M. C. Agrawal and S. P. Mushran, *J. Inorg. Nucl. Chem.* 1970, **32**, 2325.

14. S. P. Mushran and R. M. Mehrotra, *J. Chem. Soc., Dalton Trans.* 1974, 1460.
15. R. A. Rickman, R. L. Sorenson, K. O. Watkins and G. Davies, *Inorg. Chem.* 1977, **16**, 1570.
16. A. McAuley, L. Spencer and P. R. West, *Can. J. Chem.* 1985, **63**, 1198.
17. N. H. Williams and J. K. Yandell, *Aust. J. Chem.* 1982, **35**, 1133; 1983, **36**, 2377.
18. E. Pelizzetti and E. Mentasti, *J. Chem. Soc., Dalton Trans.* 1978, 61.
19. M. Kimura, A. Kabayashi and K. Boku, *Bull. Chem. Soc. Japan* 1982, **55**, 2068.
20. R. Sanehi, R. M. Mehrotra and S. P. Mushran, *J. Inorg. Nucl. Chem.* 1975, **37**, 1753.
21. K. Kustin and D. L. Topper, *Inorg. Chem.* 1973, **12**, 1404.
22. E. Pelizzetti, E. Mentasti and E. Praamauro, *Inorg. Chem.* 1978, **17**, 1181.
23. K. L. Brown, *Inorg. Chim. Acta* 1979, **37**, L513.

Polyhedron Vol. 10, No. 23/24, pp. 2717–2724, 1991
Printed in Great Britain

0277–5387/91 $3.00+.00
© 1991 Pergamon Press plc

SYNTHESIS, GEOMETRICAL AND ABSOLUTE CONFIGURATION OF THE TRIS(*S*-ARGININE)COBALT(III) TRINITRATE ISOMERS AND SYNTHESIS AND MOLECULAR STRUCTURE OF $(-)_{589}$-*anti*(N)-Δ-*cis*(N),*cis*(O)-Λ-*cis*(N),*cis*(O)-DI-μ-HYDROXO-TETRAKIS(*S*-ARGININE)DICOBALT(III) TETRANITRATE TETRAHYDRATE

P. N. RADIVOJŠA, N. JURANIĆ* and M. B. ČELAP

Chemical Faculty, University of Belgrade, P.O. Box 550, 11001 Belgrade, Yugoslavia

and

K. TORIUMI

Department of Material Science, Faculty of Science, Himeji Institute of Technology, Harima Science Park City, Kamigori-cho, Hyogo 678-12, Japan

and

K. SAITO

International Christian University, Natural Science Building, 3-10-2 Osawa, Mitaka, Tokyo, Japan

(*Received* 30 *May* 1991; *accepted* 25 *July* 1991)

Abstract—In a direct synthesis reaction of the tris(aminocarboxylato)cobalt(III) complexes with *S*-arginine all four theoretically possible tris(*S*-arginine)cobalt(III) diastereomers were obtained as tripositive complex ions. Besides, one out of 24 theoretically possible isomers of di-μ-hydroxo-tetrakis(*S*-arginine)dicobalt(III) tetrapositive ion was obtained. Geometrical and absolute configurations of the tris(*S*-arginine)cobalt(III) isomers were determined by electronic and CD spectroscopy. The molecular structure of the $(-)_{589}$-*anti*(N)-Δ-*cis*(N),*cis*(O)-Λ-*cis*(N),*cis*(O)-di-μ-hydroxo-tetrakis(*S*-arginine)dicobalt(III) ion was solved by X-ray crystal structure analysis. The complexes obtained represent the first examples of cationic aminocarboxylato complexes of this type. For the first time the formation of the di-μ-hydroxo-tetrakis(aminocarboxylato)dicobalt(III) complex has been observed as a reaction concurrent to the formation of tris(aminocarboxylato)cobalt(III) complexes. Finally, the stereoselectivity of *S*-arginine in the tris(*S*-arginine)cobalt(III) isomers synthesis was discussed.

Arginine has a unique character among α-amino-carboxylates. It exists exclusively as a zwitter ion in the crystalline state,[1] presumably because the guanidino group is much more basic than the α-amino group. The only complex of arginine so far isolated is *cis*(NO_2),*trans*(NH_2)-bis(*S*-arginine) dinitrocobalt(III) nitrate,[2] and the arginine is indeed in the zwitter ion form.[3]

In order to investigate the structure of cobalt(III) complexes of arginine in more detail, we have undertaken the synthesis of such cobalt(III) complexes that have arginine as the exclusive ligand. It is expected that the tris(bidentate) type complex would have a tripositive charge, in contrast to neutral or anionic species formed with other α-amino-

* Author to whom correspondence should be addressed.

carboxylates.[4-6] It is also worthwhile to elucidate the stereoselectivity associated by the complex formation, with special reference to the influence of separated charges brought about by the coordination of this ligand.

EXPERIMENTAL

Synthetic procedure

To a solution of cobalt(II) nitrate (2.91 g, 10 mmol) in water (25 cm^3) a warm solution (50°C) of *S*-arginine (5.22 g, 30 mmol) in water (30 cm^3) was added. A stream of air, previously passed through a 25% solution of potassium hydroxide, was bubbled through the reaction mixture for 4.5 h. Then, 65% nitric acid (0.7 cm^3, $\rho = 1.43$ g cm^{-3}) was added to the reaction mixture, which was heated on a water bath for 2.5 h. After standing at room temperature for about 15 h, about 3 g of crystalline compound was obtained, which was filtered off by suction and washed with ethanol and ether. The crystals were dissolved in 30 cm^3 of water and the solution was poured on the cationic exchange resin "Sephadex" C-25 column (35 cm length and 3.5 cm o.d.) in potassium form. The column was washed with 50 cm^3 of water, and eluted with a 0.2 mol dm^{-3} solution of potassium nitrate. The eluate of the first zone was concentrated in a rotatory vacuum evaporator at 60°C until crystallization began, to give 2.3 g (29%) of violet crystals of meridional Λ-$(+)_{589}$-tris(*S*-arginine)cobalt(III) trinitrate dihydrate (**1**), $[\alpha]_D^{20°} = +490°$ (*ca* 0.1% in water). Found: C, 26.8; H, 5.8; N, 26.2. Calc. for $C_{18}H_{46}N_{15}O_{17}Co$: C, 26.9; H, 5.7; N, 26.1%.

Concentration of the eluate of the second zone in a rotatory vacuum evaporator at 60°C afforded blue crystals of $(-)_{589}$-*anti*(N)-Δ-*cis*(N),*cis*(O)-Λ-*cis*(N),*cis*(O)-di-μ-hydroxo-tetrakis(*S*-arginine) dicobalt(III) tetranitrate tetrahydrate (**2**) in a yield of 2.7 g (24%), $[\alpha]_D^{20°} = -216°$ (*ca* 0.1% in water). The substance for analysis was heated at 105°C for 2 h. Found: C, 26.1; H, 5.5; N, 25.3. Calc. for $C_{24}H_{58}N_{20}O_{26}Co_2$: C, 26.3; H, 5.3; N, 25.5%.

The filtrate of the reacted solution was also poured on a cationic "Sephadex" C-25 column (35 cm length and 4.5 cm o.d.). After washing with 50 cm^3 of water, the elution was carried out with a 0.1 mol dm^{-3} solution of potassium nitrate. Eluates of three small zones, containing unidentified substances, came out of the column. On elution with a 0.2 mol dm^{-3} solution of potassium nitrate three zones formed on the column. On concentrating the eluate of the first zone in a vacuum evaporator at 60°C a violet solid of meridional Δ-$(-)_{589}$-tris(*S*-arginine)cobalt(III) trinitrate trihydrate (**3**) was obtained, in a yield of 0.7 g (2%), $[\alpha]_D^{20°} = -400°$ (*ca* 0.1% in water). Found: C, 26.4; H, 5.9; N, 25.4. Calc. for $C_{18}H_{48}N_{15}O_{18}Co$: C, 26.3; H, 5.8; N, 25.6%.

The concentration of the eluate of the second zone gave a red solid of facial Λ-$(+)_{589}$-tris(*S*-arginine)cobalt(III) trinitrate dihydrate (**4**) in a yield of 0.4 g (5%), $[\alpha]_D^{20°} = +200°$ (*ca* 0.1% in water). Found: C, 26.8; H, 5.8; N, 26.2. Calc. for $C_{18}H_{46}H_{15}O_{17}Co$: C, 26.9; H, 5.7; N, 26.1%.

The third zone contained only a small amount of the product, so that the eluates from three repeated procedures were collected, to give 0.7 g of the red solid of facial Δ-$(-)_{589}$-tris(*S*-arginine)cobalt(III) trinitrate dihydrate (**5**) (the estimated yield is about 3%), $[\alpha]_D^{20°} = -325°$ (*ca* 0.1% in water). Found: C, 26.7; H, 5.6; N, 26.0. Calc. for $C_{18}H_{46}N_{15}O_{17}Co$: C, 26.9; H, 5.7; N, 26.1%.

X-ray crystal structure analysis of complex **2**

A trigonal prismatic crystal of **2** with dimensions of $0.28 \times 0.28 \times 0.18$ mm and recrystallized from water was used for data collection. It was coated with thin layers of paraffin and epoxy resin, since the crystal easily loses water of crystallization. Intensity data were collected on a Rigaku AFC-5 diffractometer at 25°C, by use of the θ–2θ scan technique and graphite monochromated Mo-K_α radiation ($\lambda = 0.71073$ Å). The intensities were corrected for Lorentz-polarization factors and the absorption effect, but not for extinction. The cell dimensions were determined by the least-squares calculation using 50 2θ values ($25° < 2\theta < 30°$), measured on the diffractometer. Crystallographic data, other data collection and refinement informations are summarized in Table 1.

The structure was solved by the conventional heavy-atom method and refined by the full-matrix least-squares program RADIEL.[7] All the non-hydrogen atoms were located from the successive Fourier syntheses and included in the refinement. The structure analysis was first performed for the space group of $P1$ and converged to $R = 0.088$ and $R_w = 0.120$. The ^{13}C NMR spectrum of **2** in dimethylsulphoxide indicated that the complex has no centre of symmetry. This coincides with the use of optically active *S*-arginine ligand. Further analysis was carried out by considering the space group $P\bar{1}$. Since the crystal structure has a pseudo-centre of symmetry, strong correlations were found between parameters of the atoms which were related by the pseudo-symmetry. Hence, the final refinement was performed on the assumption that the thermal parameters of the related atoms were equal. The final refinement with anisotropic thermal par-

Table 1. Crystallographic data for $[Co_2(OH)_2(S\text{-arginine})_4](NO_3)_4 \cdot 4H_2O$

Formula weight	1168.83
$F(000)$	612
Crystal system	Triclinic
a (Å)	11.878(1)
b (Å)	12.310(1)
c (Å)	8.651(1)
α (°)	85.35(1)
β (°)	92.43(1)
γ (°)	100.74(1)
V (Å^3)	1238.3(3)
Space group	$P\bar{1}$
Z	1
D(calcd) (g cm^{-3})	1.567
Temperature (°C)	25
Radiation (Å)	0.71073
μ (cm^{-1})	8.07
Scan type	θ–2θ
Scan range (°)	1.3+0.5 tan
Max 2θ (°)	55
hkl range	$-15 < h < 0$, $-15 < k < 15$, $-12 < l < 11$
Number of reflections measured	6126
Number of reflections observed with $\|F_o\| > 3\sigma(F_o)$	3840
Weighting scheme	$[\sigma_c^2 + (0.020\|F_o\|)^2]^{-1}$
R	0.063
R_w[a]	0.076
GOF[b]	2.04

[a] $R_w = [\Sigma w(|F_o| - |F_c|)^2 / \Sigma w|F_o|^2]^{1/2}$.
[b] GOF $= [\Sigma w(|F_o| - |F_c|)^2/(NO - NV)]^{1/2}$; NO = number of reflections; NV = number of variables.

ameters converged to $R = 0.063$ and $R_w = 0.076$ for 3840 independent reflections. The scattering factors and anomalous scattering corrections were taken from ref. 8. The selected bond distances and angles are shown in Table 2.

All the calculations were carried out on a HITAC M-680 computer at the Computer Centre of Institute for Molecular Science with the Universal Crystallographic Computation Program System UNICS III.[9]

Other physical measurements

^{1}H and ^{13}C NMR spectra (DMSO) were recorded on a JEOL GX-400 spectrometer operating at 400 MHz. Optical rotations, UV, vis and CD spectra were recorded on a Perkin–Elmer MC polarimeter, Varian Super Scan 3 spectrometer and JASCO J-500 A spectropolarimeter, respectively.

RESULTS AND DISCUSSION

Synthesis

As seen from the experiment, we succeeded in obtaining five stereochemically interesting substances in one chemical reaction, namely all four theoretically possible diastereomers of the tris(*S*-arginine)cobalt(III) ion (**1**, **3**–**5**), as well as one of the 24 theoretically possible isomers of the di-μ-hydroxo-tetrakis(*S*-arginine)dicobalt(III) ion, i.e. the $(-)_{589}$-*anti*(N)-Δ-*cis*(N),*cis*(O)-Λ-*cis*(N),*cis*(O)-isomer (**2**). On the basis of the yields obtained, the stoichiometry of the reaction is estimated to be:

$$4Co(NO_3)_2 + 10(S\text{-argH}) + 2HNO_3 + O_2 \longrightarrow [Co_2(OH)_2(S\text{-argH})_4](NO_3)_4 + 2[Co(S\text{-argH})_3](NO_3)_3.$$

The total yield of the reaction is very high (82%), although each isomer is obtained in relatively low yields (see Experimental). Hence, the present reaction is a very simple and efficient synthetic procedure for a simultaneous preparation of the tris(*S*-arginine)cobalt(III) complexes. They are the first examples of cationic tris(aminocarboxylato)cobalt(III) complexes. Their conversion into neutral complexes was not possible at a very high pH, since at these conditions cobalt(III) hydroxide was separated. Although di-μ-hydroxo-tetrakis(aminocarboxylato)dicobalt(III) complexes with glycine, *S*-alanine and *S*-valine have already been synthesized,[10] none of the authors, as far as we know, mentioned the formation of such complexes in a direct synthesis of the tris(aminocarboxylato)cobalt(III) complexes.

Geometrical configuration of the tris(S-arginine)cobalt(III) diastereomers

Two geometrical isomers, meridional and facial ones, are possible for a tris(aminocarboxylato)cobalt(III) complex. Each of them could be resolved into diastereomers for optically active ligands. All the four possible diastereomers of tris(*S*-arginine)cobalt(III) were successfully obtained. Their geometrical configurations were determined from their electronic spectra (Figs 1 and 2). Two red isomers **4** and **5** exhibit relatively narrow and symmetrical bands at 520 nm. On the other hand, the two violet isomers **1** and **3** display relatively wider bands with pronounced inflection in the similar wavelength region. It can be concluded that the red isomers **4** and **5** possess facial, whereas the violet ones **1** and **3** meridional configuration.[11]

Table 2. Selected bond distances (Å) and angles (°), and their mean values calculated for chemically equivalent bond distances or angles

	Moiety A	Moiety B	Mean value
Co(A)···Co(B)	2.852(1)		2.852(1)
Co—N(1)	1.917(15)	1.944(15)	
Co—N(5)	1.953(13)	1.943(13)	1.939(16)
Co—O(2)	1.870(10)	1.914(10)	
Co—O(3)	1.902(12)	1.905(12)	1.898(19)
Co—O(5A)	1.912(10)	1.885(10)	
Co—O(5B)	1.929(10)	1.932(10)	1.915(22)
N(1)—C(2)	1.53(2)	1.46(2)	
N(5)—C(8)	1.55(2)	1.46(2)	1.50(5)
O(2)—C(1)	1.29(2)	1.30(2)	
O(3)—C(7)	1.27(2)	1.33(2)	1.29(3)
O(1)—C(1)	1.24(2)	1.22(2)	
O(4)—C(7)	1.25(2)	1.20(2)	1.23(2)
C(1)—C(2)	1.51(2)	1.50(2)	
C(7)—C(8)	1.54(2)	1.48(2)	1.51(3)
O(5A)—Co—O(5B)	83.4(4)	84.0(4)	83.7(3)
O(5A)—Co—O(2)	91.6(4)	93.0(4)	
O(5A)—Co—O(3)	91.7(5)	90.6(5)	91.7(10)
O(5B)—Co—O(2)	174.8(4)	176.8(4)	175.8(10)
O(5B)—Co—O(3)	91.7(5)	88.6(5)	90.2(15)
O(5A)—Co—N(1)	89.2(5)	88.3(5)	88.8(5)
O(5A)—Co—N(5)	175.7(5)	174.3(5)	175.0(7)
O(5B)—Co—N(1)	91.9(5)	94.8(5)	
O(5B)—Co—N(5)	93.0(5)	92.6(5)	93.1(12)
N(1)—Co—O(2)	86.8(5)	84.0(5)	
N(5)—Co—O(3)	86.0(5)	84.8(5)	85.4(12)
O(2)—Co—N(5)	92.1(5)	90.5(5)	91.3(8)
N(1)—Co—N(5)	93.3(6)	96.5(6)	94.9(16)
O(2)—Co—O(3)	89.6(5)	92.6(5)	91.1(15)
N(1)—Co—O(3)	176.4(6)	176.3(6)	176.4(6)
Co(A)—O(5)—Co(B)	97.4(5)	95.3(4)	96.4(11)
Co—N(1)—C(2)	110.7(9)	107.0(9)	
Co—N(5)—C(8)	106.1(8)	109.7(9)	108.4(21)
Co—O(2)—C(1)	115.7(10)	114.0(10)	
Co—O(3)—C(7)	116.7(9)	114.4(9)	115.2(12)

Absolute configuration of the tris(S-*arginine*)*cobalt* (III) *diastereomers*

CD spectra of the isomers were recorded and shown in Figs 1 and 2. The CD spectra of the corresponding diastereomers of the tris(*S*-alaninato)cobalt(III) complex are also shown, of which the configurations had been determined by the X-ray structure analyses. The crystal structures of $(+)_{589}$-mer-[Co(S-ala)$_3$] and $(-)_{589}$-mer-[Co(S-ala)$_3$] $\cdot 3H_2O$ have been determined by Drew *et al.*[12] and Herak *et al.*,[13] respectively. They confirmed the assignments of Denning and Piper, in which the absolute configurations of these diastereomers were determined on the basis of the CD spectra of these isomers and those of Λ-*mer*-[Co(*S*-proline)$_3$].[14] Denning and Piper (l.c.) also assigned the absolute configuration of the corresponding facial diastereomers.[14] As shown in Fig. 2, the CD spectra of the two meridional isomers of the *S*-arginine complex show similar features to those of the corresponding alanine complexes with the same CoN_3O_3 chromophore. Therefore, it would be reasonable to assign the absolute configuration of the meridional isomers by comparison of their CD spectra, that the $(+)_{589}$-diastereomers possess the Λ configuration and the $(-)_{589}$-diastereomer, the Δ configuration. In an analogous manner, we also assigned the absolute configuration of the facial isomers that the $(+)_{589}$-diastereomer has Λ configuration and the $(-)_{589}$-diastereomer, Δ configuration.

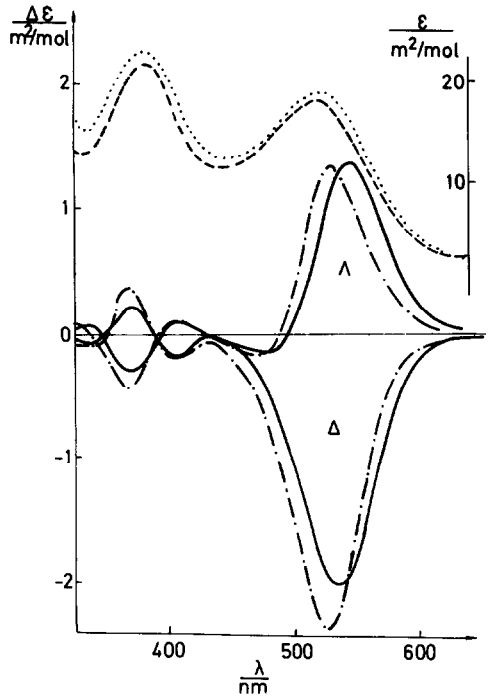

Fig. 1. Electronic absorption spectra of the facial Δ-$(-)_{589}$-(····) (**5**) and Λ-$(+)_{589}$-(————) [Co(S-argH)$_3$]$^{3+}$ (**4**) diastereomers and their CD spectra (————), as well as the CD spectra of the corresponding *S*-alanine complexes (— · — · —).

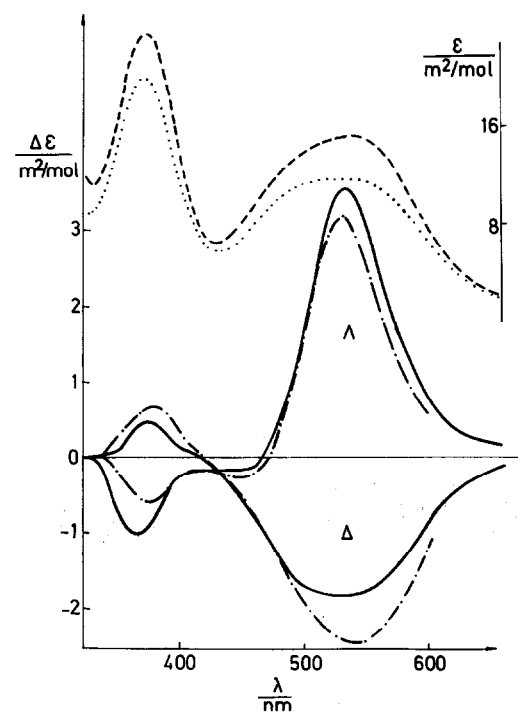

Fig. 2. Electronic absorption spectra of the meridional Δ-$(-)_{589}$-(····) (**3**) and Λ-$(+)_{589}$-(————) [Co(S-argH)$_3$]$^{3+}$ (**1**) diastereomers and their CD spectra (————), as well as the CD spectra of the corresponding *S*-alanine complexes (— · — · —).

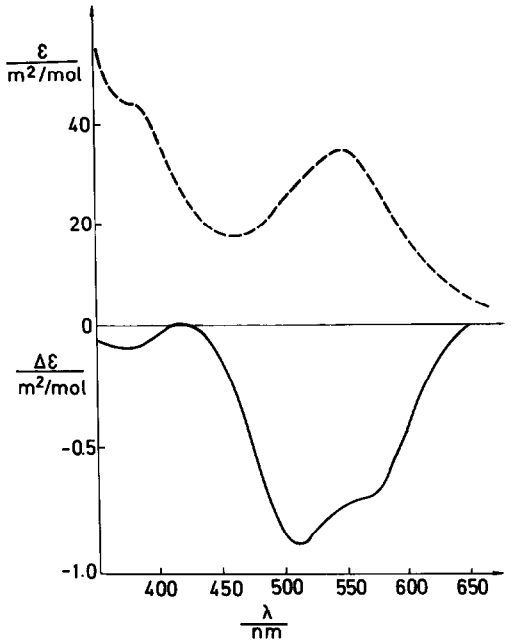

Fig. 3. Electronic absorption (————) and CD spectra (————) of the $(-)_{589}$-*anti*(N),Δ-*cis*(N),*cis*(O),Λ-*cis*(N),*cis*(O)-di-μ-hydroxo-tetrakis(*S*-arginine)dicobalt(III) complex (**2**).

^{13}C *NMR spectra of the dinuclear complex*

Owing to the asymmetric carbon atom of arginine ligand, two halves of the di-μ-hydroxo-tetrakis(*S*-arginine)dicobalt(III) complex are in a diastereomeric relationship. Therefore, a different chemical shift is expected for each carbon atom belonging to the arginine ligands. As shown in Fig. 4, ^{13}C NMR of the dinuclear complex **2** shows more than 12 signals, indicating that the observed molecular structure is essentially retained in solution. The chelate ring carbons which are close to the asymmetric centre exhibit distinctly different chemical shifts. The chemical shifts of the guanidinium moieties are, however, partially degenerate and only two signals are observable. This may be due to the fact that positively-charged moieties of the guanidinium group are separated from each other and are far apart from the asymmetric centres.

Electronic absorption and CD spectra of the dinuclear complex

The *cis*(N),*cis*(O)-configuration around each metal centre produces symmetric *d–d* absorption bands in the energy region characteristic of the CoN_2O_4 chromophore (Fig. 3). The di-μ-hydroxo bridge causes a charge-transfer band, which over-

Table 3. Spectroscopic properties of the tetrakis(aminocarboxylato)dihydroxo-bridged dinuclear complexes of cobalt(III)

	S-ala[a]	*S*-val[a]	*S*-arg[b]
λ_{max} (nm)	526	530	540
ε (m^2 mol^{-1})	22.7	15.0	35.0
λ_{CD} (nm)	495	520	512
$\Delta\varepsilon$ (m^2 mol^{-1})	−0.099	−0.143	−0.088

[a] Values taken from ref. 10.
[b] Our results.

laps partially the second *d–d* transition band (Table 3).

The CD spectra of the di-μ-hydroxo complex indicates a weak optical activity in comparison with that of the tris(*S*-arginine)cobalt(III) complexes. Because of the opposite absolute configuration of the bis(bidentate) pairs around two metal centres, only the vicinal contribution of the ligands is observed.

Structure of the dinuclear complex

No X-ray crystal structure of a dinuclear di-μ-hydroxo-tetrakis(aminocarboxylato)dicobalt(III) complex has been reported. Two crystal structures have been known for the corresponding chromium(III) complexes: *anti*(N)-Δ-*cis*(N),*cis*(O)-Λ-*cis*(N),*cis*(O)-di-μ-hydroxo-tetrakis(glycinato) dichromium(III)[15] and Δ-*trans*(N),Δ-*trans*(O)-di-μ-hydroxo-tetrakis(*S*-prolinato)chromium(III).[16] A special stability of these isomers out of 24 theoretically possible isomers was ascribed to the formation of two intramolecular NH···O hydrogen bonds, which are almost parallel to the chromium/chromium direction. Preferential formation of the geometrical isomers with *cis*(N),*cis*(O) configuration was also pointed out by Oki and Yoneda.[16] The molecular and crystal structure of **2** and its tetranitrate are shown in Figs 5 and 6, respectively.

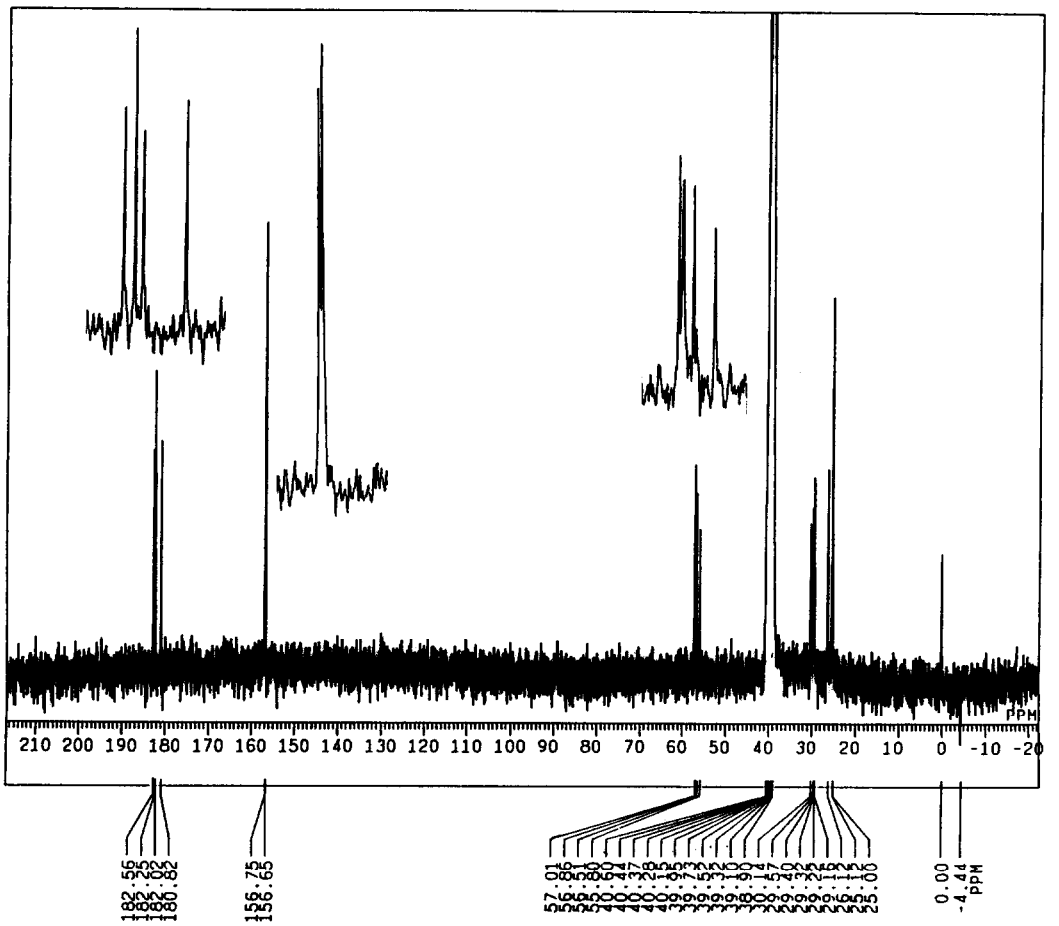

Fig. 4. ^{13}C NMR spectrum of *anti*(N),Δ-*cis*(N),*cis*(O),Λ-*cis*(N),*cis*(O)-di-μ-hydroxo-tetrakis(*S*-arginine)dicobalt(III) tetranitrate tetrahydrate (**2**), expanded in the region of the carboxylic carbon (180–183 ppm), guanidinium group carbon (156–157 ppm) and methyne group carbon (55–57 ppm).

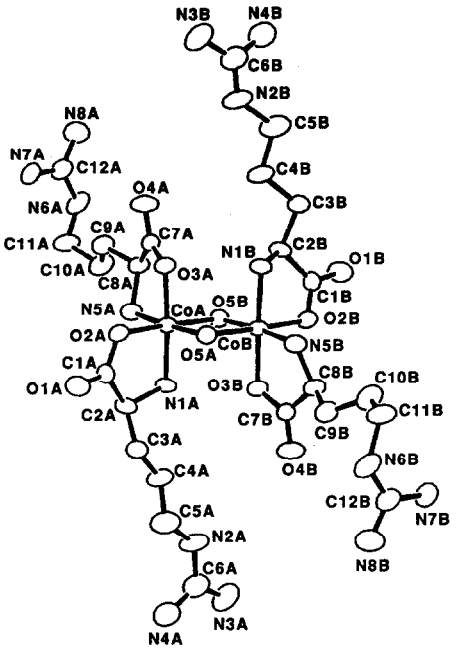

Fig. 5. Molecular structure of $(-)_{589}$-*anti*(N),Δ-*cis*(N), *cis*(O),Λ-*cis*(N),*cis*(O)-di-μ-hydroxo-tetrakis(*S*-arginine) dicobalt(III) (tetrapositive cation of complex **2**).

The present dinuclear complex also has the *cis*(N),*cis*(O)-configuration around each cobalt(III) ion. For bis- or tris-(prolinato) complexes of cobalt (III) and chromium(III), contribution of steric hindrance due to the pyrrolidine ring is very significant.[10,14] In the present complex the C_3 side-chains on the asymmetric carbon atoms extend rather straight, and no apparent steric hindrance coming from the guanidinopropyl group is seen on the chelate structure. The guanidine groups seem to be rather parallel to each other in the crystal. The counter-ions situate in the opening surrounded by the guanidinopropyl chains. It seems as if the electronic charge is compensated separately at the tris(aminocarboxylato)cobalt(III) moiety and the guanidinium nitrate ion pairs. Although the location of protons is not known from the X-ray analysis, it is clear that the arginine ligand is in a zwitter ion form in the coordinated state.

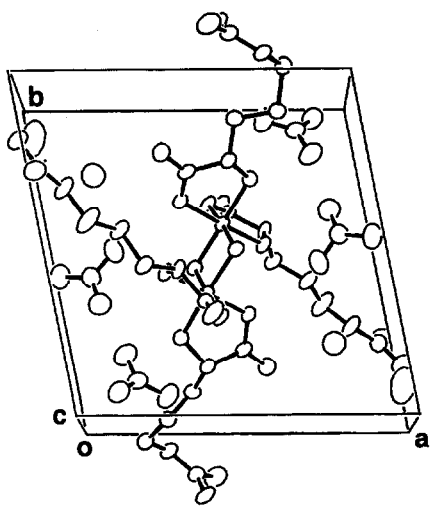

Fig. 6. Crystal structure of $(-)_{589}$-*anti*(N),Δ-*cis*(N),*cis*(O), Λ - *cis*(N),*cis*(O) - di - μ - hydroxo - tetrakis(*S* - arginine) dicobalt(III) tetranitrate tetrahydrate (**2**).

As already mentioned, Gillard[10] reported the synthesis of the di-μ-hydroxo-tetrakis(*S*-aminocarboxylato)dicobalt(III) complexes with *S*-alanine and *S*-valine. From the nature of the Cotton effect at the long wavelength *d–d* band he tentatively concluded that the Δ configuration predominates at both cobalt centres in these dinuclear complexes. We are now able to check this conclusion by comparison of the spectroscopic data of these complexes with the X-ray and spectroscopic data of our dinuclear arginine complex (Table 3). As it is seen, spectroscopic properties of all complexes are similar indicating similar geometries. Therefore, we suggest that Gillard isolated complexes with configurations on two metal centres opposite to each other, as it is in the case of the complex of arginine reported here.

Stereoselectivity

There has been a great deal of discussion about the stereoselective formation of geometrical and optical isomers of tris(aminocarboxylato) cobalt(III) complexes. It is generally understood that aminocarboxylates with short chains exhibit very different geometrical stereoselectivities in the preparation of tris(aminocarboxylato)cobalt(III) complexes. The most pronounced difference is noted when they are prepared by direct synthesis [air oxidation of a mixture of cobalt(II) salt and aminocarboxylato ligand in aqueous solution] and by ligand substitution in hexaamminecobalt(III) complex ion in water at elevated temperature.[4,14,17] On the other hand, Gillard *et al.*[10] reported that tris(*S*-lysinato)cobalt(III) is formed preferentially in the *mer* form when prepared by both methods. It was discussed that the long *S*-lysinato aminobutyl side chain in the α-carbon atom is responsible for the selectivity. Arginine is similar to lysine in the sense that both have rather long carbon chains with terminal basic functional groups. The present tris(arginine) complexes are obtained by direct synthesis more in the *mer* form than in the *fac* and our preliminary results show the same preference of the *mer* form in the reaction between *S*-arginine and

$[Co(NH_3)_6]^{3+}$. Hence, the importance of a long side-chain with a terminal basic group in an aminocarboxylato ligand for the exceptional stereoselectivity in the complex formation seems to be substantiated.

Shibata *et al.*[7] discussed the stereoselectivity involved in the formation of various bis(aminocarboxylato)diamine and tris(aminocarboxylato) cobalt(III) complexes with special reference to the hydrogen-bond formation between a ligated amino group and the free carboxyl group of *S*-aspartate. If the guanidinium moiety in the tris (arginine)cobalt(III) complex has formed hydrogen bonds with the free oxygen atom of coodinated carboxylate, appreciable stereoselectivity might be brought about. The X-ray structure of tris (arginine)cobalt(III) is not known. However, analogy to the structure of the dinuclear species suggests that the guanidinopropyl moieties on the ligands would be present in the extended form. Hence, the guanidinium group will be situated apart from the coordinated carboxylate, and there will be little possibility of forming hydrogen bonds.

We have thus demonstrated that arginine is a unique aminocarboxylato ligand, coodinated to the cobalt(III) ion in the neutral form, as a zwitter ion, to give a tripositive tris(bidentate)-type complex cation. The ligand can be reckoned as if it has the aminocarboxylate and the guanidinium moiety separately. In the crystalline state their electric charges are individually compensated by the central metal ion and the counter-ions, respectively. A similar structure must be maintained in aqueous solutions, because the electronic absorption and circular dichroism spectra are similar to those of other anionic or neutral tris(aminocarboxylato) complexes of cobalt(III).

Supplementary material available: Table of positional parameters and anisotropic thermal parameters for non-hydrogen atoms and a list of structure factors.

REFERENCES

1. J. L. Karle and J. Karle, *Acta Cryst.* 1964, **17**, 835.
2. B. A. Kamberi, M. B. Ćelap and T. J. Janjić, *Glasnik hem. društva Beograd* 1978, **43**, 149 (in English).
3. W. H. Watson, D. R. Johnson, M. B. Ćelap and B. A. Kamberi, *Inorg. Chim. Acta* 1972, **6**, 591.
4. (a) L. D. Gillard and N. C. Payne, *J. Chem. Soc.* (*A*) 1969, 1197; (b) M. Mori, M. Shibata, E. Kyuno and M. Kanaya, *Bul. Chem. Soc. Japan* 1961, **34**, 1837; (c) B. E. Douglas and S. Yamada, *Inorg. Chem.* 1965, **4**, 1561; (d) F. Hursik, F. Petru and B. Hajek, Proc. XIII ICCC, p. 315. Cracow-Zakopane, Poland (1970).
5. M. Shibata, H. Nishikawa and K. Hosaka, *Bull. Chem. Soc. Japan* 1967, **40**, 236.
6. J. Lifshitz, *Proc. Roy. Acad. Sci.* 1936, 1192.
7. P. Coppens, T. N. Guru Row, P. Leung, E. D. Stevens, P. J. Becker and Y. W. Yang, *Acta Cryst.* (*A*) 1979, **35**, 63.
8. *International Tables for X-ray Crystallography*, Vol. IV. Kynoch, Birmingham (1974).
9. T. Sakurai, K. Kabayashi and Rikagaku Kenkyusho Hokoku, *Rep. Inst. Phys. Chem. Res.* 1979, **55**, 69.
10. R. D. Gillard, S. H. Lourie, D. C. Price, D. A. Phipps and C. F. Weick, *J. Chem. Soc., Dalton Trans.* 1974, 1385.
11. F. Basolo, C. J. Ballhausen and J. Bjerum, *Acta Chem. Scand.* 1955, **9**, 810.
12. M. J. B. Drew, J. H. Dunlop, R. D. Gillard and D. J. Rogers, *J. Chem. Soc., Chem. Commun.* 1966, 42.
13. R. Herak, B. Prelesnik, Lj. Manojlović-Muir and K. W. Muir, *Acta Cryst.* (*B*) 1974, **B30**, 229.
14. R. G. Denning and T. S. Piper, *Inorg. Chem.* 1966, **5**, 1056.
15. J. T. Veal, W. E. Matifield, D. Y. Jeter, J. C. Hempel and P. D. Madgson, *Inorg. Chem.* 1973, **12**, 342.
16. H. Oki and H. Yoneda, *Inorg. Chem.* 1981, **20**, 3875.
17. (a) K. Kawasaki, J. Yoshii and M. Shibata, *Bull. Chem. Soc. Japan* 1970, **43**, 3819; (b) T. Matsuda, T. Okumoto and M. Shibata, *Bull. Chem. Soc. Japan* 1972, **45**, 802; (c) K. Kawasaki and M. Shibata, *Bull. Chem. Soc. Japan* 1972, **45**, 3100; (d) T. Matsuda and M. Shibata, *Bull. Chem. Soc. Japan* 1973, **46**, 3104; (e) M. Takeuchi and M. Shibata, *Bull. Chem. Soc. Japan* 1974, **47**, 2797.

Polyhedron Vol. 10, No. 23/24, pp. 2725–2728, 1991
Printed in Great Britain

0277–5387/91 $3.00+.00
© 1991 Pergamon Press plc

FERROMAGNETIC EXCHANGE INTERACTIONS IN TWO NEW BINUCLEAR NICKEL(II) COMPLEXES: $[Ni(pymep)(X)_2]_2 \cdot nH_2O$ {X = N_3, NCS; $n = 2, 0$; pymep = N-(6-METHYL-2-PYRIDYLMETHYLENE)-2-(2-PYRIDYL) ETHYLAMINE}

T. ROJO,* R. CORTES, J. I. R. LARRAMENDI, L. LEZAMA and J. L. MESA

Departamento de Química Inorgánica, Universidad del Pais Vasco, Aptdo. 644, 48080 Bilbao, Spain

(*Received* 6 *June* 1991; *accepted* 24 *July* 1991)

Abstract—The $[Ni(pymep)(N_3)_2]_2 \cdot 2H_2O$ and $[Ni(pymep)(NCS)_2]_2$ compounds [pymep = N-(6-methyl-2-pyridylmethylene)-2-(2-pyridyl) ethylamine] have been synthesized and magnetic susceptibility measurements (3–200 K) show the existence of ferromagnetic exchange interactions in the two complexes, with the following exchange parameters: $J = +21.4$, $D = -7.6$ cm^{-1} (N_3) and $J = +4.8$, $D = -10.4$, $z'J' = 0.3$ cm^{-1} (NCS). Both spectroscopic and magnetic results suggest for the azide complex a dimeric structure with the nickel centres being linked through one-end azide bridges, while for the thiocyanate compound bridging involves an end-to-end thiocyanate mode.

Intramolecular magnetic interactions in transition metal dimers have been extensively studied in the past in order to understand the exchange interaction phenomena.[1] In particular, nickel(II) dimers have been the focal points of several recent magnetic susceptibility studies. Antiferromagnetic exchange interactions as well as ferromagnetic interactions have been found in this kind of complex.[2–4]

N-(6-methyl-2-pyridylmethylene)-2-(2-pyridyl) ethylamine (pymep) is a tridentate ligand which forms mono-complexes with transition metals (metal : ligand ratio 1 : 1) which have been characterized as discrete or polynuclear molecules.[5–7]

The N_3 and NCS pseudohalide groups are known to coordinate metals as terminal or bridging ligands, and inside of this latter category they can act as one-end or end-to-end bridging groups, giving a wide range of magnetic behaviours in the compounds in which they are taking part.

Here we report the synthesis, IR spectroscopy, reflectance spectra, and magnetic properties of the $[Ni(pymep)(X_2)] \cdot nH_2O$ (X = N_3, NCS; $n = 2, 0$) polynuclear compounds.

* Author to whom correspondence should be addressed.

EXPERIMENTAL

Synthesis of the complexes

The compound $[Ni(pymep)(N_3)_2] \cdot H_2O$ was prepared by adding an excess of a saturated NaN_3 aqueous solution to an aqueous solution containing 0.200 g (0.5 mmol) of the $Ni(pymep)Cl_2 \cdot 2H_2O$ complex, previously prepared (by mixing equimolar amounts of $NiCl_2 \cdot nH_2O$ and pymep ligand in a water/acetone solution). Within a few minutes a yellowish-green solid precipitated, which was isolated after filtration, washed with water, and dried *in vacuo* over P_2O_5 for 48 h. A similar procedure was employed to obtain the $[Ni(pymep)(NCS_2)_2]$ compound, by mixing a saturated KNCS aqueous solution with another containing 0.200 g (0.5 mmol) of the complex $Ni(pymep)Cl_2 \cdot 2H_2O$ dissolved in water. The green precipitate immediately obtained was filtered, washed with water, and dried over P_2O_5 during 48 h. Several attempts to obtain X-ray quality crystals of both compounds were unsuccessful. Found: C, 43.9; N, 32.5; H, 4.5; Ni, 15.1. Calc. for $C_{14}H_{15}N_3NiN_6H_2O$: C, 43.5; N, 32.7; H, 4.4; Ni, 15.2%. Found: C, 47.9; N, 16.8; H, 3.7; Ni, 14.6. Calc. for $C_{14}H_{15}N_3NiN_2C_2S_2$: C, 48.1;

N, 17.0; H, 3.7; Ni, 14.7%. Thermogravimetric analysis show that the water molecule in the azide compound is lost over the range 50–80°C.

Physical measurements

Water was determined thermogravimetrically using a Perkin–Elmer system 7 thermobalance. The IR spectra were recorded, with KBr pellets in the 4000–250 cm^{-1} region, using a Perkin–Elmer 1430 spectrophotometer. Reflectance spectra were recorded on a Perkin–Elmer lambda 9 UV-vis/NIR spectrophotometer. Magnetic susceptibility measurements were carried out on powdered samples in the temperature range 4.2–200 K using a DSM8 susceptometer/magnetometer, in a magnetic field of 0.1 T, a value at which the magnetization vs magnetic field curves were still linear at 4.2 K. The susceptibilities were corrected for the diamagnetism of the constituent atoms [-159.7×10^{-6} cm^3 mol^{-1} (N_3) and -215.2×10^{-6} cm^3 mol^{-1} (NCS)] and for the temperature-independent paramagnetism (TIP), estimated to be 100×10^{-6} cm^3 mol^{-1} per nickel(II) ion.

RESULTS AND DISCUSSION

The IR spectra of both compounds have been analysed paying attention to the bands due to the N_3 and NCS pseudohalide groups. The position in the bands corresponding to the $\nu_{as}(N_3)$ and ν(CN) stretching vibrations of these groups can illustrate its coordination to the metal ions, because its energy depends on the degree of symmetry of these groups. The IR spectrum of the $[Ni(pymep)(N_3)_2]\cdot H_2O$ compound exhibits two bands at 2050 and 2020 cm^{-1} due to the $\nu_{as}(N_3)$ stretching vibrations. The frequencies of these bands are similar to that exhibited by the dimeric $[Ni(terpy)(N_3)_2]_2\cdot 2H_2O$ related compound,[8] which contains two terminal azide groups and two one-end azide bridging groups. The azide symmetric stretch, $\nu_s(N_3)$, is observed at about 1300 cm^{-1} and the two signals at 620, 605 cm^{-1} correspond to the azide bending vibrations (δ). In the IR spectrum of the [Ni(pymep)$(NCS)_2$] compound the bands corresponding to the ν(CN) stretching vibrations appear at 2130 and 2100 cm^{-1}, these high frequencies of the stretching vibrations are very similar to those observed in the related [Ni(terpy)$(NCS)_2$] compound[9] which exhibits normal end-to-end NCS bridges, and quite different to those observed in the related [Cu(paphy)(NCS)(SCN)] complex[10] which exhibits unusual one-end two N-thiocyanate bridging groups. The band corresponding to the ν(CS) stretching vibration appears at 785 cm^{-1} and the δ(NCS) bending mode is observed at 465 cm^{-1}.

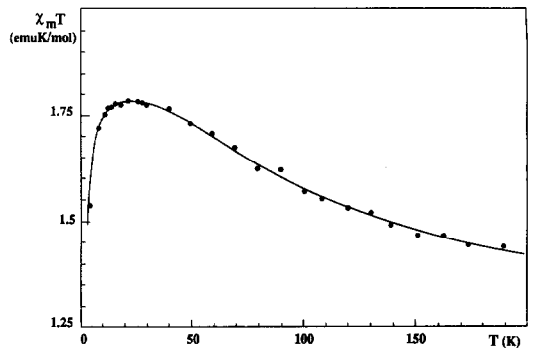

Fig. 1. Thermal evolution of the product $\chi_m T$ for the $[Ni(pymep)(N_3)_2]_2\cdot 2H_2O$ compound.

The reflectance spectra exhibit three bands at 9750, 16,000, 26,000 cm^{-1}, and 10,800, 16,850, 26,000 cm^{-1} for the N_3 and NCS compounds, respectively. These values are in agreement with those given in the literature for octahedral Ni^{II} compounds.[11,12] The bands have been ascribed to $d\rightarrow d$ transitions in a symmetry near to O_h[$^3A_{2g}\rightarrow {}^3T_{2g}$; $^3A_{2g}\rightarrow {}^3T_{1g}$(F); $^3A_{2g}\rightarrow {}^3T_{1g}$(P)]. The calculated[12] nephelauxetic parameters β are 0.81 and 0.85 for the azide and thiocyanate compounds, respectively.

Figures 1 and 2 show the magnetic susceptibility behaviour, represented as the variation of $\chi_m T$ vs T ($\chi_m T = \mu_{eff}^2/8$), for the azide and thiocyanate compounds. The product $\chi_m T$ increases, in both cases, with decreasing temperature reaching a maximum of 1.82 cm^3 K mol^{-1} at 22 K (N_3) and 1.91 cm^3 K mol^{-1} at 5.5 K (NCS), after which it rapidly decreases at lower temperatures. The positive values of the Weiss temperatures ($\theta = +19$ and $+7.7$ K for the azide and thiocyanate complexes, respectively) indicate that the main magnetic interactions are ferromagnetic.

The experimental data were fitted to the analytic

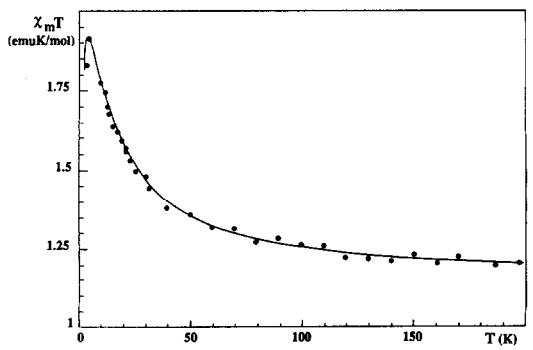

Fig. 2. Thermal evolution of the product $\chi_m T$ for the

The IR spectrum of the clay-bound Rh^{II}-

Table 1. Structural and magnetic parameters of octahedrally coordinated dipseudohalide(NXY)-bridged nickel(II) dimers (NXY = NCO, NCS, NCSe, NNN)

	Compound	Ni—Y—X (°)	X—N—Ni (°)	Ni—Ni (Å)	Ni—N (Å)	Ni—Y (Å)	J (cm^{-1})	D (cm^{-1})	d (Ni-bridge plane) (Å)	Ref.
1	$[Ni(terpy)(NCO)(H_2O)]_2(PF_6)_2$	97.7(3)		3.19(2)	2.04(2)	2.19(3)	+4.6	−12.2	0.01	4
2	$[Ni(terpy)(N_3)_2]_2 \cdot 2H_2O$	101.3(3)		3.268	2.038(6)	2.198(8)	+20.1	−12.5	0.01	8
3	$[Ni(pymep)(N_3)_2]_2 \cdot 2H_2O$						+21.4	−7.6		This work
4	$[Ni(en)_2(NCS)]_2I_2$	100	167	5.78	2.04	2.61	+4.5	−3.3	0.05	14
5	$[Ni(tren)(NCS)]_2(BPh_4)_2$	100	167	5.78	2.04	2.61	+2.4	−0.4	0.05	3
6	$[Ni(tren)(NCSe)]_2(BPh_4)_2$						+1.6	−0.5		3
7	$[Ni(tren)(NCO)]_2(BPh_4)_2$	117.1(5)	155.0(5)	5.385(1)	2.018(7)	2.336(5)	−4.4	−10.1	0.25	[a], 3
8	$[Ni(tren)(N_3)]_2(BPh_4)_2$	135.3(7)	122.3(3)	5.220(2)	2.069(8)	2.195(7)	−35.1	+6.8	0.52	15
9	$[Ni(L)(N_3)_2]_2$	138.4(3)	124.4(2)		2.135(3)	2.167(3)	−90	0[b]	0.02	16
10	$[Ni(terpy)(NCS)_2]_2$	100.0(8)	159(2)	5.633(3)	2.04(2)	2.625(5)	+4.9	−4.3	0.56	9
11	$[Ni(pymep)(NCS)_2]_2$						+4.8	−10.4		This work
12	$[Ni(terpy)(NCSe)_2]_2$						+10.1	−10.0		9

[a] D. M. Duggan and D. N. Hendrickson, *Inorg. Chem.* 1974, **13**, 2056.

Abbreviations: terpy = 2,2′:6′,2″-terpyridine; pymep = N-(6-methyl-2-pyridylmethylene)-2-(2-pyridyl)ethylamine; en = ethylenediamine; tren = 2,2′,2″-triaminoethylamine; L = 1,5,9-triazacyclododecane. The complexes **1–3** exhibit end-on bridging modes. In the dimers **4–12** the bridges are of end-to-end type.

[b] Magnetic susceptibility data have been analysed using the simple isotropic Heisenberg dimer model assuming a zero-field parameter $D = 0$.

expression given by Ginsberg *et al.*[13] for a magnetically isotropic nickel(II) dimer. This fit allowed us to evaluate the intradimer exchange integral J, the nickel(II) single-ion zero-field splitting D, and the interdimer magnetic exchange J' for both compounds. The solid curves in the $\chi_m T$ vs T representations of Figs 1 and 2 show excellent agreement between observed and calculated values of $\chi_m T$ obtained with the following parameters:

$J = +21.4\ cm^{-1}$; $D = -7.6\ cm^{-1}$;

$Z'J' = 0.0\ cm^{-1}$; $g = 2.19$ (N_3)

$J = +4.8\ cm^{-1}$; $D = -10.4\ cm^{-1}$;

$Z'J' = 0.3\ cm^{-1}$; $g = 2.16$ (NCS).

As is usual in this type of fitting the D and $Z'J'$ parameters are approximated, because their effects are most important in the low-temperature region where the experimental uncertainties are greatest, while the calculated J values appear accurately determined. These behaviours indicate the existence of intradimeric ferromagnetic exchange interactions which increase the $\chi_m T$ values, by population of the ground state $S = 2$, with decreasing temperature in both compounds. The single-ion zero-field splittings cause a depopulation to a diamagnetic ground state and consequently the decrease of the $\chi_m T$ values at lower temperatures.

The values of the J and D parameters obtained for the azide and thiocyanate compounds have been compiled in Table 1 with those corresponding to other related complexes, some of them with known crystal structures. The results of the azide compound are in accord with those observed in the azide-terpy related complex, while those observed in the thiocyanate compound show a good accord with those corresponding to the related thiocyanate-terpy complex (see Table 1).

The above spectroscopic and magnetic results allow us to propose ferromagnetically coupled dimeric structures for both compounds; in the case of the azide complex the nickel centres being linked through one-end azide bridges, while in the thiocyanate compound the metallic centres are linked by an end-to-end thiocyanate mode.

Acknowledgements—This work was financially supported in part by a grant of the Universidad del Pais Vasco (UPV/90) which we gratefully acknowledge.

REFERENCES

1. R. D. Willet, D. Gatteschi and O. Kahn (Eds) *Magneto-Structural Correlations in Exchange Coupled Systems*. NATO ASI Series C: Mathematical and Physical Science, Vol. 140, Reidel, Dordrecht (1985).
2. D. M. Duggan and D. N. Hendrickson, *Inorg. Chem.* 1973, **12**, 2422.
3. D. M. Duggan and D. N. Hendrickson, *Inorg. Chem.* 1974, **13**, 2929.
4. M. I. Arriortua, R. Cortés, J. L. Mesa, L. Lezama, T. Rojo and G. Villeneuve, *Trans. Metal Chem.* 1988, **13**, 371.
5. J. I. R. Larramendi, B. Diaz, J. L. Mesa, J. Vía, M. I. Arriortua and T. Rojo, *Acta Cryst. C.* 1991, **47**, 943.
6. T. Rojo, J. I. R. Larramendi, I. Durán, J.L. Mesa, J. Vía and M. I. Arriortua, *Polyhedron* 1990, **9**, 2693.
7. M. I. Arriortua, J. Vía, J. I. R. Larramendi, B. Díaz, L. Lezama and T. Rojo, *Polyhedron* 1991, **10**, 495.
8. M. I. Arriortua, R. Cortés, L. Lezama, T. Rojo, X. Soláns and M. Font-Bardía, *Inorg. Chim. Acta* 1990, **174**, 263.
9. T. Rojo, R. Cortés, L. Lezama, M. I. Arriortua, K. Urtiaga and G. Villeneuve, *J. Chem. Soc., Dalton Trans.* 1991, 1779.
10. J. L. Mesa, T. Rojo, M. I. Arriortua, G. Villeneuve, J. V. Folgado, A. Beltrán and D. Beltrán, *J. Chem. Soc., Dalton Trans.* 1989, 53.
11. W. Henke and D. Reinen, *Z. Anorg. Allg. Chem.* 1977, **436**, 187.
12. A. B. P. Lever, *Inorganic Electronic Spectroscopy*. Elsevier, Amsterdam (1986).
13. A. P. Ginsberg, R. L. Martin, R. W. Brookes and R. C. Sherwood, *Inorg. Chem.* 1972, **11**, 2884.
14. A. E. Shvelashvili, M. A. Porai-Koshits and A. S. Antsyshkina, *J. Struct. Chem.* (Engl. Transl.) 1969, **10**, 552.
15. C. G. Pierpont, D. N. Hendrickson, D. M. Duggan, F. Wagner and E. K. Barefield, *Inorg. Chem.* 1975, **14**, 604.
16. P. Chaudhuri, M. Guttmann, D. Ventur, K. Weighardt, B. Nuber and J. Weiss, *J. Chem. Soc., Chem. Commun.* 1985, 1618.

Polyhedron Vol. 10, No. 23/24, pp. 2729–2736, 1991
Printed in Great Britain

0277-5387/91 $3.00+.00
© 1991 Pergamon Press plc

FORMATION OF A RHODIUM(II) MONOHYDRIDO COMPLEX DERIVED FROM WILKINSON'S COMPLEX $RhCl(PPh_3)_3$ IN THE INTERLAMELLAR SPACES OF MONTMORILLONITE AND CATALYTIC HYDROGENATION OF CYCLOHEXENE

M. M. TAQUI KHAN*, S. A. SAMAD, M. R. H. SIDDIQUI, H. C. BAJAJ and G. RAMACHANDRAIAH

Discipline of Coordination Chemistry and Homogeneous Catalysis,
Central Salt and Marine Chemicals Research Institute, Bhavnagar 364 002, India

(*Received* 25 *June* 1991; *accepted* 22 *July* 1991)

Abstract—The interaction of molecular hydrogen with $[Rh(PPh_3)_3]^+$ (**1a**) "immobilized" in the interlamellar spaces of montmorillonite resulted in the formation of a monohydrido complex, $[Rh^{II}H(PPh_3)_3]$ (**2a**), characterized by electrochemical data of the clay-loaded electrode, IR, EPR and hydrogen absorption studies. Heterogenized homogeneous catalytic hydrogenation of cyclohexene catalysed by **1a** was investigated in the temperature range 283–313 K. The order of reaction with respect to cyclohexene and hydrogen concentration is fractional and first order with respect to catalyst concentration. Thermodynamic parameters ΔH^0 and ΔS^0 corresponding to the formation of the monohydrido species were found to be 18 kcal mol^{-1} and 61 e.u., respectively. The activation enthalpy, $\Delta H^{\ddagger}$, and entropy, $\Delta S^{\ddagger}$, for the hydrogenation of cyclohexene by the Rh^{II}—H complex in clay are more negative by about 2 kcal mol^{-1} and 7 e.u. compared to Wilkinson's catalyst, $RhCl(PPh_3)_3$ (**1**), in homogeneous solution.

Heterogenized homogeneous catalysis by transition metal ions in the intracrystal matrix of naturally occurring swelling layers of lattice silicates has been the subject matter of extensive studies in recent years.[1–6] A variety of metal complex catalysts can be immobilized in smectite clays.[7] The bound or immobilized complex catalyst is often more selective and reactive than the analogous reaction of the complex in homogeneous solution. The steric requirements of the surface transition states[8] or the position of surface equilibria[9] can provide the basis for enhanced catalytic selectivity. Recently, swelling types of layered silicate clays such as montmorillonite and hectorite have been employed as alternative supports for immobilization of cationic transition metal complexes in the interlayers of clay to study solution-like reactions in the solid state.[10] The hydrogenation of olefins by the cationic rhodium complex $[Rh(COD)(PPh_3)_2]^+$ intercalated in synthetic mica[11] was studied and recently, a heterogeneous, anchored $PdCl_2$ in montmorillonite[12,13] was used for the hydrogenation of styrene and of terminal alkenes and alkynes in ambient conditions. In a previous publication we reported the synthesis and characterization of bound $RhCl(PPh_3)_3$ in montmorillonite[14] and its interaction with molecular oxygen to produce a Rh^{II}-μ-peroxo complex. The present paper describes the formation of a rhodium(II) monohydrido complex $RhH(PPh_3)_3^+$ in the interlamellar space of montmorillonite and the kinetics of the heterogenized homogeneous hydrogenation of cyclohexene by $RhCl(PPh_3)_3$ immobilized in montmorillonite. The reaction for the formation of the Rh^{II}—H complex **2a** is compared with those of the corresponding homogeneous system. Unlike the homogeneous hydrogenation reaction with $RhCl(PPh_3)_3$, where the reaction with molecular hydrogen proceeds through the formation of the well-established dihydrido rhodium(III) complex $Rh(H)_2Cl(PPh_3)_3$ (**2b**) by oxidative addition[15] of hydrogen to **1**, the reaction of **1a** with hydrogen

* Author to whom correspondence should be addressed.

results in the formation of Rh^{II}—H, possibly through an intermediate Rh^{I}—μH_2—Rh^{I} species.

EXPERIMENTAL

Rhodium trichloride was purchased from Johnson Matthey, triphenylphosphine and montmorillonite clay were obtained from Fluka AG. The average chemical composition of the acid-washed montmorillonite, converted to the sodium form by treating with NaOH, used in the present investigation is SiO_2, 70%; Al_2O_3, 15%; Fe_2O_3, 1.5%; CaO, 2.5%; MgO, 3.0%; Na_2O, 0.59%; and K_2O, 1.5% (loss of ignition 6%). All organic solvents used were obtained from BDH and were purified by known methods[16] prior to use. Argon was used for the maintenance of an inert atmosphere and was used without purification. The montmorillonite-bound complex mont-$Rh(PPh_3)_3$ was synthesized and characterized by ^{27}Al, ^{29}Si and ^{31}P solid-state NMR according to published procedures.[14]

The IR spectrum of the clay-bound Rh^{II}-hydrido complex was measured in the form of a pellet on a Perkin–Elmer IR spectrometer. Electrochemical studies on the clay-loaded electrode were conducted with an EG&G Princeton Applied Research Model 174A polarographic analyser, a 175 Universal programmer which was employed with a three-electrode cell assembly of Model 303 SMDE/HMDE and a precision *X–Y* recorder of Model RE 0089. A hanging mercury drop (HMDE) to record sampled DC and differential pulse polarograms (DPP) was used as a working electrode. A medium sized drop of effective surface area 0.017 cm^2 was used at a flow rate 2 s per drop. A glass carbon electrode (GCE) of single surfaced area *ca* 0.012 cm^2 was used as a working electrode. A platinum wire of 0.5 mm diameter as the counter electrode and Ag/AgCl in aqueous tetraethyl ammonium chloride 1 M and SCE as the reference electrode were used. The clay-loaded electrode was prepared according to the published procedure.[17] A slurry of pure clay/mont-$Rh(PPh_3)_3$ (5–15 g dm^{-3}) and PVA (5 g dm^{-3}) in a 1 : 1 water–methanol mixture was prepared and a drop (0.01–0.05 cm^3) of the material spread over a glassy carbon electrode and dried overnight at room temperature. The EPR spectra were recorded on an X-band Bruker ESP-300 spectrometer. The magnetic field calibration was checked with TCNE for a *g* value of 2.0028. Cyclohexene was freshly prepared according to a published method.[16] The experimental details of the hydrogenation reactions are similar to those described in an earlier publication.[18] The concentration of catalyst used was in the range 1.15×10^{-5}–5.85×10^{-5} M and the hydrogen partial pressure varied over the range 0.4–1 atmos. The hydrogenation reactions were carried out in a 7 : 3 benzene–ethanol mixture in the temperature range 283–313 K. The solubility of hydrogen in a 7 : 3 benzene–ethanol mixture was calculated[19] and was considered to be constant for every run at a particular temperature. The rate of absorption of hydrogen was obtained from the tangent of the plot of the number of moles of hydrogen absorbed vs time at the desired reaction condition.

RESULTS AND DISCUSSION

The $Rh(PPh_3)_3$-intercalated clay was characterized by ^{27}Al, ^{29}Si and ^{31}P MAS NMR spectroscopy. The ^{27}Al NMR spectrum of clay gave a peak at 7.87 ppm which is shifted downfield by 1.11 ppm and the peak observed at −99.1 ppm in the ^{29}Si NMR spectrum of clay due to the $Si(O\text{-}Si)_3OAl$ site is shifted downfield by 4 ppm on intercalation. The ^{31}P NMR spectrum gave two doublets centred at 50.5 and −28 ppm for the mont-$Rh(PPh_3)_3$ due to PPh_3 *trans* to each other and PPh_3 *trans* to $Si(O\text{-}Si)_3OAl$, respectively. The complex $RhCl(PPh_3)_3$ undergoes dissociation of Cl^- and is absorbed as the cationic species $Rh(PPh_3)^{3+}$ in the intralamellar region of montmorillonite as shown in Structure I.

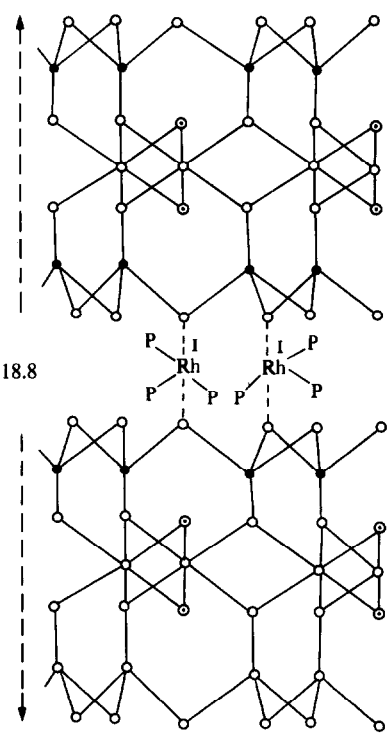

Structure I

The stoichiometry of hydrogen absorption was studied manometrically with a slurry of mont-$Rh(PPh_3)_3$ in benzene–ethanol (7:3) solvent at different temperatures. The absorption of hydrogen is very rapid in the beginning and levels off after 30 min. The total amount of hydrogen absorbed, about 1 mol of hydrogen per 2 mol of catalyst corresponds to the stoichiometry:

$$2[Rh(PPh_3)_3]^+ + H_2 \longrightarrow 2[Rh(PPh_3)_3H].$$
$$\textbf{1a} \qquad\qquad \textbf{2a}$$

The formation of the cationic rhodium(II) hydrido complex $[Rh^{II}(PPh_3)_3H]^+$ (**2a**), which is the actual catalytic species in the hydrogenation, was confirmed by IR and EPR spectra of the hydrido complex $[Rh^{II}(PPh_3)_3H]$ (**2a**). The IR spectrum of complex **2a** shows a single peak at 2028 cm^{-1}, confirming (Fig. 1) the formation of a monohydride. In order to ensure the monohydrido species ^2H labelling experiments were carried out for the hydrogenation of the complex using deuterium obtained by the reaction of zinc with DCl in 99.8% D_2O, supplied by Aldrich Chemicals USA. The liberated deuterium was bubbled through the bonded complex **1a** in a montmorillonite suspension in 7:3 benzene–ethanol for 30 min. The deuterated complex was characterized by IR spectroscopy. The IR spectrum clearly shows a single peak at 1480 cm^{-1} which is assigned to the monodeuterido species $RhD(PPh_3)_3^+$. These labelling results confirm the formation of a rhodium(II) monohydride species.

The formation of the monohydride **2a** by the hydrogenation of **1a** is completely different from the hydrogenation of **1** in CH_2Cl_2 which gives the dihydride $Rh(H)_2Cl(PPh_3)_3$ (**2b**). The IR spectrum of the dihydrido species **2b** gives two IR peaks of the dihydride at 2099 and 2065 cm^{-1}. The ^1H NMR of the dihydride gave peaks[20] at −26.8 and −31.25 ppm. Attempts to take the solid-state deuterium NMR of **2a** by conducting deuteration of **1a** by D_2O failed because of the paramagnetism of rhodium(II).

The bonded $[Rh(PPh_3)_3]^+$ (**1a**) complex in montmorillonite after hydrogenation becomes EPR active. At room temperature a broad signal centred at $g_{iso} = 2.3$ was observed. However, at 77 K, the compound gave a signal resolved into three components: $g_1 = 2.49$, $g_2 = 2.34$ and $g_3 = 2.20$ (Fig. 2). The absence of detectable hyperfine coupling to ^{103}Rh suggests very low values of the Rh—H coupling, *ca* 5–10 G. Recently, some of the mixed valent Rh_2^{3+} complexes such as $[Rh_2(\mu\text{-EE}')_2(^t\text{BuNC})(\mu\text{-Z})(PF_6)_2]$ (where EE′ = dppm, dapm, dpam; Z = P_2, 4mP_2, 3,5-dpp, 4-bromo, 3,5-dmp, 3,4,5-tribromo pyrazole = 3,4,5-tP) were reported.[21] The EPR spectra of these complexes showed three g values around 2.02, 2.19 and 2.22 characteristic of an orthorhombic system with hyperfine coupling of 20 G for ^{103}Rh only in the case of $Rh_2(\mu\text{-dppm})_2(^t\text{BuNC})_2(3,4,5\text{-tP})$ at −196°C. The EPR of rhodium(II) observed[21] for the rhodium(II)-μ-peroxo complex in montmorillonite gave $g_\perp = 2.03$, $g_\parallel = 1.98$ with $g_{av} = 2.01$.

Electrochemistry of the clay electrode of complex **1a**

The cyclic voltammetric responses of the clay electrode with mont-$Rh(PPh_3)_3$(**1a**-PVA) in a deaerated solution of phosphate buffer (pH 7) in the absence and presence of hydrogen were recorded. These results are shown in Fig. 3. The reproduciblity of these results was checked at least three times with freshly prepared electrodes. Figures 3(a) and (b) indicate that the pure clay-coated electrode

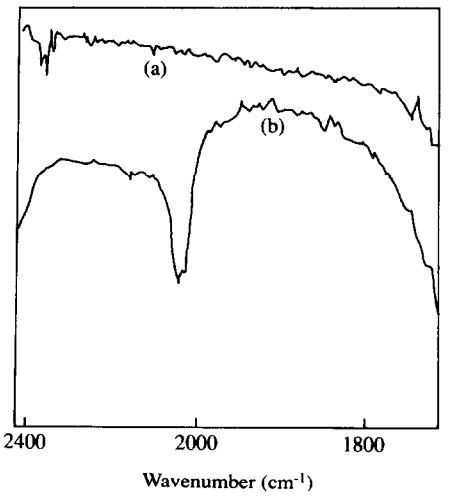

Fig. 1. IR spectrum of mont-$Rh(PPh_3)_3$ (a) before and (b) after hydrogenation.

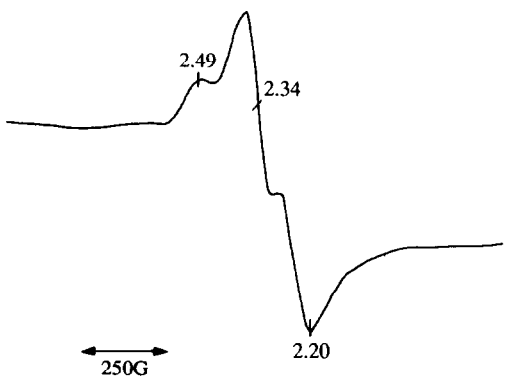

Fig. 2. EPR spectrum of the hydrogenated mont-$[Rh(PPh_3)_3]$ at 77 °K.

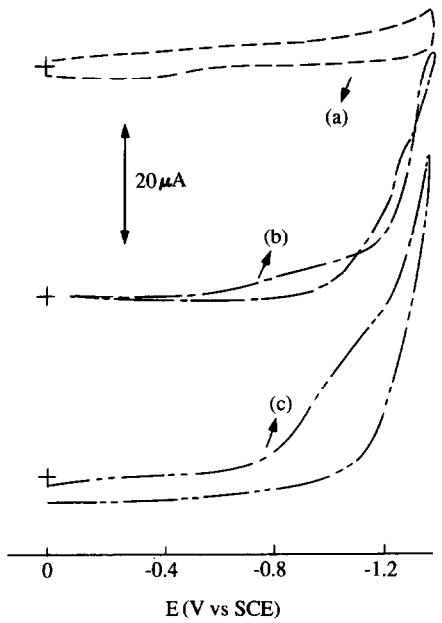

Fig. 3. Cyclic voltammogram of the glassy carbon electrode coated with a thin layer of montmorillonite, (a) and mont-[$Rh(PPh_3)_3$] under nitrogen, (b) and under hydrogen, and (c) in a phosphate buffer of pH 7.

with **1a** under an argon atmosphere did not show any reduction/oxidation step between the potentials 0.0 to −1.2 V. However, the clay-loaded electrode with **1a** under a hydrogen atmosphere showed a single cathodic reduction peak around −1.0 V (Fig. 3c) with no anodic counterpart corresponding to a Rh^{II}/Rh^{I} potential.

In order to bring out the difference in the reaction of hydrogen with **1a** and $RhCl(PPh_3)_3$ (**1**) in homogeneous solution, a solution of Wilkinson's complex (**1**) was prepared in CH_2Cl_2 containing 0.1 M TBAP (tetrabutylammonium perchlorate). The DC and DPP at dme and CV of this solution at HMDE/GCE under an argon atmosphere was recorded. The solution was then purged with hydrogen gas for about 1 h and the electrochemical responses recorded (Fig. 4) again. The solution of complex **1** under an argon atmosphere did not show any electrochemical response at DME or GCE. However, the same solution after hydrogenation showed an anodic wave at −0.1 V (dpp peak potential) and two reduction steps at −0.78 and −1.1 V (Fig. 4a) at the mercury cathode. The cyclic voltammogram (Fig. 4b) at HMDE indicates that the anodic step at −0.1 V was reversible and the reduction steps at −0.78 and −1.1 V were irreversible. This corresponds to the irreversible Rh^{III}/Rh^{II} and Rh^{II}/Rh^{I} couples at 0.78 and −1.1 V, respectively. This confirms the formation of rhodium(II) species in the hydrogenation of **1a**.

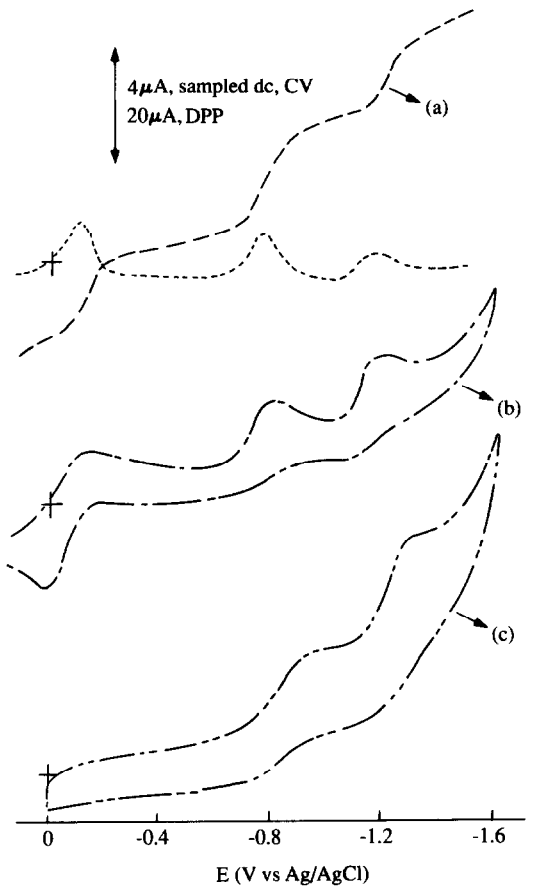

Fig. 4. Electrochemical responses of [$Rh(PPh_3)_3Cl$] (1 mmol) in CH_2Cl_2 under a hydrogen atmosphere. (a) Sampled DC, (b) CV at HMDE, and (c) CV at GCE.

From the above electrochemical, EPR and IR data one can conclude that molecular hydrogen reacts with **1a** in the clay lattice to form the Rh^{II}—H species **2a**. One can speculate on the formation of **2a** from **1a** through the formation of an unstable μ-H_2 complex, [$Rh^{I}(\mu$-$H_2)Rh^{I}$] (Structure II), which then undergoes a cleavage of the H—H bond to give **2a** (Structure III) in a concerted manner. Recently, Collman *et al.*[22] reported this type of (μ-H_2) bonding in cofacial porphyrin ruthenium(II). The ordering of rhodium(I) centres in a clay lattice can easily promote the formation of such an unstable complex which immediately reverts to **2a**. The formation of complex **2a** is reversible. On heating a slurry of complex **2a** at 80°C, the slurry became EPR inactive losing molecular hydrogen and reverting back to the rhodium(I) complex **1a**.

Hydrogenation of cyclohexene catalysed by **1a**

(1) *Dependence of rate of hydrogenation on cyclohexene concentration.* A plot of reciprocal rate

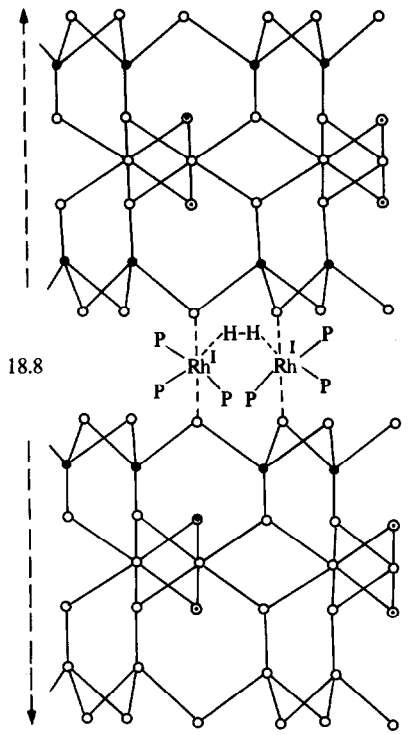

Structure II

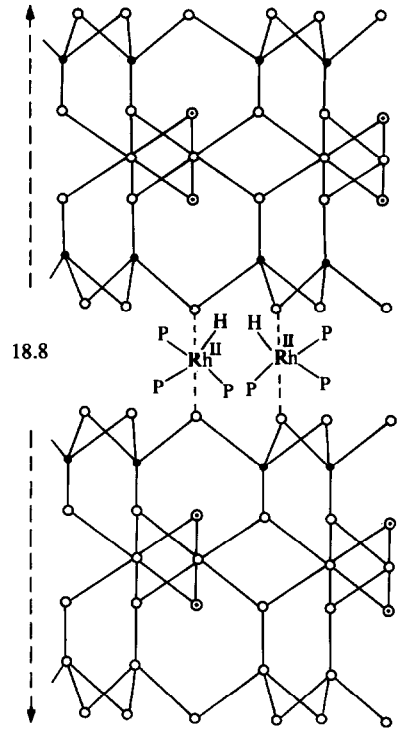

Structure III

vs reciprocal cyclohexene concentration at a particular catalyst concentration, temperature and hydrogen pressure is linear with a positive intercept on the ordinate. Figure 5 shows such a plot of 1/rate

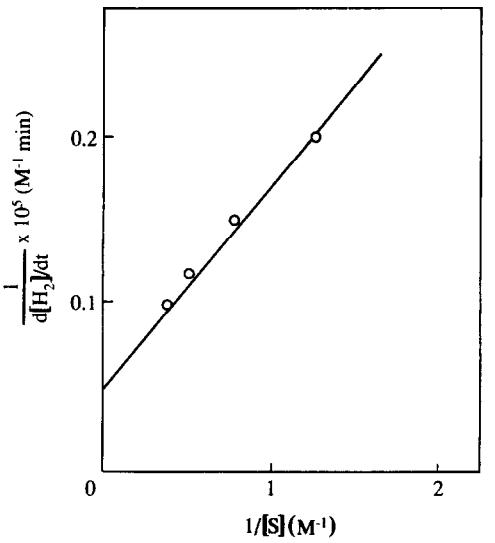

Fig. 5. A plot of $-1/d[H_2]/dt$ vs $1/[S]$.

vs 1/[cyclohexene] at 20°C and 1 atmos. of hydrogen pressure. This plot indicates that the observed rate of hydrogenation is of fractional order with respect to cyclohexane concentration and is related to the same by the following equation:

$$\frac{1}{R} = a\frac{1}{[S]} + b;$$

where R = rate, [S] is the concentration of cyclohexene a and b are the slope and intercept of the plot of 1/R vs 1/[S]. Similar types of plots were obtained at other temperatures studied: 10, 30 and 40°C.

(2) *Dependence of rate on hydrogen concentration.* Figure 6 shows the dependence of the rate of hydrogenation of cyclohexene on the concentration of

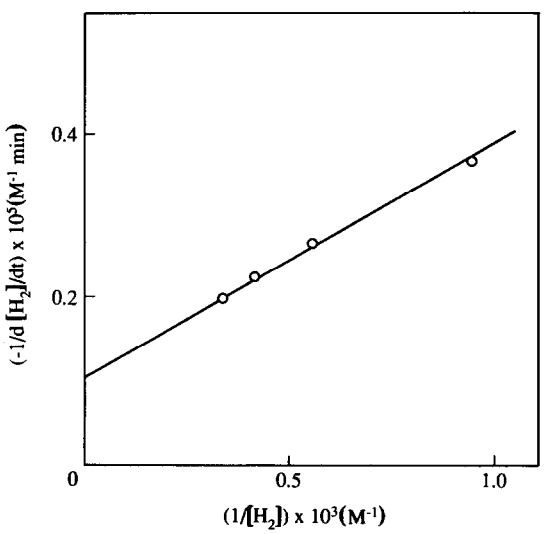

Fig. 6. A plot of $-1/d[H_2]/dt$ vs $1/[H_2]$.

molecular hydrogen in solution at 20°C. The rate was found to be of fractional order. Similar types of plots were obtained at the different temperatures studied.

(3) *Dependence of rate on catalyst concentrations.* The dependence of the rate of hydrogenation of cyclohexene on catalyst concentration was studied by adding a calculated quantity of mont-$Rh(PPh_3)_3$ (**1a**) to the reaction mixture. A first-order dependence on catalyst concentration was observed at 20°C. Similar plots were obtained at the different temperatures studied.

(4) *Dependence of rate on temperature.* The rate of hydrogenation of cyclohexene was measured in the temperature range 10–40°C at 1 atmos. of hydrogen pressure. Linear plots were obtained in all cases, the slope of which is equal to $-(E_a/2.303R)$. Based on the above rate data, stoichiometry of hydrogen absorption and EPR and electrochemical studies, the following mechanism was proposed for the catalytic hydrogenation of olefins:

$$2[Rh(PPh_3)_3]^+ + H_2 \overset{K_1}{\rightleftharpoons} 2[Rh(PPh_3)_3(H)]$$
1a **2a**

K_2 ⇕ S ; k' ↓ [2S]

$$2[Rh(PPh_3)_3(S)]^+ \xrightarrow[H_2]{k''} 2[Rh(PPh_3)_3(H)(S)]$$
4 **3**

↓ fast

$$2[Rh(PPh_3)_3]^+ + \text{Paraffin}$$
5

where S = cyclohexene. In the mechanism proposed, the complex mont-$Rh(PPh_3)_3$ (**1a**) interacts with hydrogen in a pre-equilibrium step K_1 to form the monohydrido rhodium(II) complex **2a**. The EPR and electrochemical studies support the formation of **2a**, Rh^{II}—H. The rhodium(II) hydride **2a** interacts with the substrate cyclohexene in the rate-determining step to form a mixed ligand metal–olefin–hydrido complex (**3**). The formation of **3** is also possible by the interaction of **1a** wth an olefin to form a metal–olefin complex (**4**) in another equilibrium step K_2. Species **4** reacts with molecular hydrogen in another rate-determining step k'' to form the metal–olefin hydrido species **3**. Therefore, the rate-determining step of the reaction involves the formation of the mixed ligand olefin complex **3**, which then transfers a hydrogen atom in a fast step to the coordinated olefin to form the paraffin and catalytically active species **1a**. The metal–olefin complex **4** synthesized separately was found to be inactive in the activation of molecular hydrogen. The alternative pathway k'' is therefore not operative.

From the mechanism proposed for the hydrogenation of cyclohexene a rate law for the reaction can be derived as:

$$-d[H_2]/dt = \frac{k'K_1[H_2][C][S]}{(1+K_1[H_2])(1+K_2[S])}. \quad (1)$$

The above equation can be rearranged in two forms as follows:

$$\frac{1}{-d[H_2]/dt} = \frac{1+K_1[H_2]}{k'K_1[H_2][C][S]} + \frac{1+K_1[H_2]}{k'K_1[H_2][C]} \times K_2 \quad (2)$$

or

$$\frac{1}{-d[H_2]/dt} = \frac{1+K_2[S]}{k'K_2[S][C][H_2]} + \frac{1+K_2[S]}{k'K_2[S][C]} \times K_2. \quad (3)$$

Plots of reciprocal rate vs 1/[S] [eq. (2) Fig. 5] and reciprocal of rate vs $1/[H_2]$ [Fig. 6, eq. (3)] gave straight lines from which the values of K_1 and K_2 were computed, respectively. Substituting the values of K_1 and K_2 in eq. (1), the values of the rate constant k' were calculated at different temperatures. The data are presented in Table 1.

The enthalpy of formation ($\Delta H^{\ominus}$) corresponding to the equilibrium constants K_1 and K_2 were evaluated from the slopes of the plots of $\log K_1$ or K_2 vs $1/T$ and presented in Table 2. Gibb's free energy was calculated from the equation:

$$\Delta G^{\ominus} = -2.303RT \log K. \quad (4)$$

$\Delta S^{\ominus}$ was obtained from the relationship:

$$\Delta S^{\ominus} = \frac{\Delta H^{\ominus} - \Delta G^{\ominus}}{T}. \quad (5)$$

The activation parameter E_a was calculated from the slopes of the plots of $\log k'$ vs $1/T$. The par-

Table 1. Equilibrium and kinetic data for the catalytic hydrogenation of cyclohexene catalysed by mont-$Rh(PPh_3)_3$

Temperature (K)	K_1 (M^{-1})	K_2 (M^{-1})	K' ($M^{-1}\,min^{-1}$)
283	294.5	0.22	1.99
293	408.2	0.33	11.48
303	844.6	0.40	18.19
313	1412.5	0.55	26.91

ameters $\Delta H^{\ddagger}$ and $\Delta S^{\ddagger}$ were obtained from the following equations.

$$\Delta H^{\ddagger} = E_a - RT \quad (6)$$

$$2.303 \log k' = 2.303 \log \frac{RT}{Nh} + \frac{\Delta S^{\ddagger}}{R} - \frac{\Delta H^{\ddagger}}{RT}; \quad (7)$$

where N is Avagadro's number, h is Planck's constant and R is the gas constant.

The thermodynamic parameters corresponding to the formation of the hydrido species are presented in Table 2. The activation parameters corresponding to the rate constant k' are presented in Table 3. The enthalpy ($\Delta H^{\ominus}$) of the formation of the hydrido complex mont-RhH(PPh_3)$_3$ (**2a**) of 18 kcal mol^{-1} is more endothermic than that of the dihydrido[20] complex Rh(H)$_2$Cl(PPh_3)$_3$ (**2b**) (15 kcal mol^{-1}).

The free energy of the hydride complex formation ($\Delta G^{\ominus}$) also shows a decrease for the formation of the dihydrido species **2b** which is much more stable than **2a**. The monohydride is only possible in a clay matrix which is properly oriented to provide formation of a μ-hydrogen complex (Rh^{I}—H_2—Rh^{I}) and its subsequent homolytic cleavage to **2a**. As expected the entropy is highly negative for the formation of **2a** as compared to **2b**. The thermodynamic parameters for the formation of the olefin complex Rh^{I}(olefin) both for **1a** and **1** are about the same indicating no particular preference of the binding of olefins in a clay matrix.

The stable hydrido complex in solution reacts with the olefin to form the mixed ligand–olefin complex. This complex may be considered to be formed either by the reaction of the hydrido complex with the olefin (k') or the interaction of hydrogen with the olefin complex (k''). The latter route had been ruled out on the basis of kinetic evidence of a fractional-order dependence on both substrate and hydrogen concentration. The activation parameters $\Delta H^{\ddagger}$ and $\Delta S^{\ddagger}$ are given in Table 3. The difference in the reactivities of the complexes towards hydrogenation of cyclohexene in homogeneous and heterogenized homogeneous cases may be sought in the ease of formation of the mixed ligand hydrido–olefin complex in clay and subsequent fast insertion of the olefin into the M—H bond. The enthalpy of activation ($\Delta H^{\ddagger}$) is about 2 kcal mol^{-1} more negative than the homogeneous hydrogenation[20] involving **1**, indicating the ease of cleavage of the H—H bond in a 2:1 complex (Rh^{I}—H_2—Rh^{I}) rather than a 1:1 complex η^2-H_2—Rh^{I}.

Table 2. Thermodynamic data for the formation of hydrido and olefin complexes for the catalytic hydrogenation of cyclohexene catalysed by mont-Rh(PPh_3)$_3$

	$\Delta H^{\ominus}$ (kcal mol^{-1})	$\Delta S^{\ominus}$ (e.u.)	$\Delta G^{\ominus}$ (kcal mol^{-1})
K_1	18.11	61.03	−3.95
K_2	6.05	18.16	0.55

Table 3. Activation parameters for the catalytic hydrogenation of cyclohexene by mont-Rh(PPh_3)$_3$

E_a (kcal mol^{-1})	$\Delta H^{\ddagger}$ (kcal mol^{-1})	$\Delta S^{\ddagger}$ (e.u.)
16.8	16.2	−5.72

REFERENCES

1. T. J. Pinnavaia and P. K. Welty, *J. Am. Chem. Soc.* 1975, **97**, 3819.
2. F. Farzaraeh and T. J. Pinnavaia, *Inorg. Chem.* 1983, **22**, 2216.
3. J. A. Ballantine, W. Jones, J. H. Purnell, D. T. B. Tennokoon and J. M. Thomas, *Chem. Lett.* 1985, 963.
4. J. M. Thomas, *Intercalation Chemistry*, pp. 59–99. Academic Press Inc., New York (1982).
5. J. A. Ballantine, M. Navis, J. H. Purnell, M. Rayanakoon, J. M. Thomas and K. J. Williams, *J. Chem. Soc., Chem. Commun.* 1981, 427.
6. E. P. Giannolis, E. G. Lighter and T. J. Pinnavaia, *J. Am. Chem. Soc.* 1988, **110**, 3880.
7. R. Raythatha and T. J. Pinnavaia, *J. Org. Met. Chem.* 1986, **218**, 115.
8. T. J. Pinnavaia, R. Raythatha, J. G. S. Lee, J. L. Halloman and J. F. Hoffman, *J. Am. Chem. Soc.* 1979, **101**, 6891.
9. R. Raythatha and T. J. Pinnavaia, *J. Molec. Catal.* 1983, **80**, 47.
10. T. J. Pinnavaia, *Science* 1983, **220**, 365.
11. T. Miyazaki, A. Truboi, H. Urata, H. Suzuki, V. Moritana, Y. Morooka and I. Ikaiva, *Chem. Lett.* 1985, 793.
12. K. R. Kumar, B. M. Chaudhary, Z. Jamil and G. Thyagarajan, *J. Chem. Soc., Chem. Commun.* 1986, 130.
13. B. M. Chaudhary, K. R. Kumar, Z. Jamil and G. Thyagarajan, *J. Chem. Soc., Chem. Commun.* 1985, 937.
14. M. M. Taqui Khan, M. R. H. Siddiqui and S. A. Samad, *Inorg. Chem.* 1990, **29**, 4427.
15. J. A. Osborn, F. H. Jardine, J. P. Young and G. Wilkinson, *J. Chem. Soc. (A)* 1966, 1711.
16. A. Vogel, *Practical Organic Chemistry*, p. 245. Longman Green, London (1951).
17. (a) D. Ege, P. K. Ghosh, J. R. White, J. F. Equey and A. D. Bard, *J. Am. Chem. Soc.* 1985, **107**, 5644;

(b) P. K. Ghosh and A. J. Bard, *J. Am. Chem. Soc.* 1983, **105**, 5691.
18. M. M. Taqui Khan, S. A. Samad and M. R. H. Siddiqui, *J. Molec. Catal.* 1989, **53**, 23.
19. H. Stephen and T. Stephen, *Solubility of Inorganic and Organic Compounds*, Vol. I, Part I. Pergamon Press, New York (1963).
20. M. M. Taqui Khan, B. Taqui Khan, E. Rama Rao, M. R. H. Siddiqui, S. Begum, S. Mustafa Ali and J. R. Reddy, *J. Molec. Catal.* 1988, **45**, 35.
21. C. Woods, L. J. Tortorelli, D. P. Rillena, J. L. E. Burn and J. C. Depriest, *Inorg. Chem.* 1989, **28**, 1673.
22. J. P. Collman, J. E. Hutchison, P. S. Wagenknechts, N. S. Lewis, M. A. Lopez and R. Guilard, *J. Am. Chem. Soc.* 1990, 8206.

Polyhedron Vol. 10, No. 23/24, pp. 2737–2742, 1991
Printed in Great Britain

0277–5387/91 $3.00+.00
© 1991 Pergamon Press plc

A PHOSPHORUS-CONTAINING SUBSTITUENT GROUP DISPLAYING BOTH DONOR AND ACCEPTOR PROPERTIES. X-RAY CRYSTAL STRUCTURE OF ITS COMPLEX WITH $PtCl_2$*

REINHARD SCHMUTZLER† and LUTZ HEUER

Institut für Anorganische und Analytische Chemie der Technischen Universität, Hagenring 30, 3300 Braunschweig, Germany

and

DIETMAR SCHOMBURG

Gesellschaft für Biotechnologische Forschung, Mascheroder Weg 1, 3300 Braunschweig, Germany

(*Received* 25 *March* 1991; *accepted* 22 *July* 1991)

Abstract—2-Dimethylaminomethyl-6-methoxyphenyldifluorophosphine, **1** was prepared from 2-dimethylaminomethyl-6-methoxyphenyllithium and PF_2Cl. The ^{19}F and ^{31}P NMR parameters of **1** showed significant differences from those of other aryldifluorophosphines, and it is suggested that an intramolecular donor–acceptor interaction exists between the nitrogen atom of the NMe_2 group and the trivalent phosphorus atom. Strong non-bonding P–N-interactions have also been observed for a coordination compound of **1** with platinum(II), $[2\text{-}Me_2NCH_2\text{-}6\text{-}MeOC_6H_3PF_2]_2PtCl_2$, **7**, for which a single crystal X-ray diffraction study is reported.

Difluorophosphines have long been known to function as excellent donors in transition metal complexes.[1] They resemble phosphorus trifluoride and, to some extent, carbon monoxide in their donor properties towards transition metals. By contrast, the acceptor character of phosphorus trifluoride (and, presumably, of difluorophosphines, RPF_2, with R = hydrocarbon group) is much less pronounced. A donor–acceptor complex, $Me_3N \cdot PF_3$ (vapour pressure at −78.5°C, 8.0 mm), has been reported.[2] In the present paper we describe the synthesis and NMR characterization of an aromatic difluorophosphine whose phosphorus atom apparently displays both donor and acceptor properties. Furthermore, the synthesis and single crystal X-ray structure determination of a Pt^{II} complex of this difluorophosphine are reported.

The synthesis of the difluorophosphine **1**

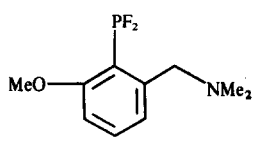

1

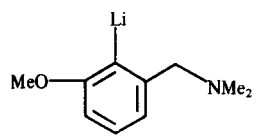

2

followed the previously described route.[3] The preparation of the required 1-lithio precursor compound, **2** was based on the following sequence [eqs (1) and (2)].

* Dedicated to Dr Herbert Naarmann (BASF AG, Ludwigshafen) on the occasion of his 60th birthday.

† Author to whom correspondence should be addressed.

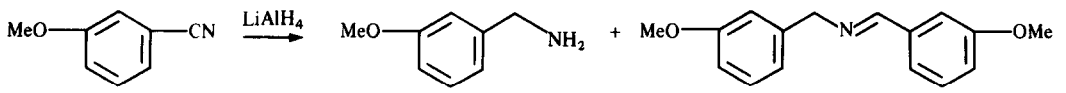

(1)

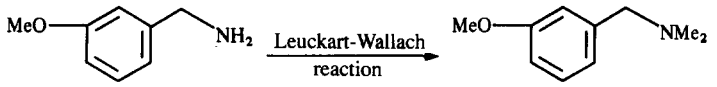

(2)

It should be noted that the $LiAlH_4$ reduction of **3** produced not only the desired amine **4** but also the Schiff base derivative **5**, originating, formally, from the reaction of **4** and 3-methoxybenzaldehyde.

4 was converted to **6** in a Leuckart–Wallach type reaction.[5]

The aromatic difluorophosphine, **1**, was synthesized by lithiation of **6**, followed by reaction of the lithio derivative **2** with PF_2Cl [eq. (3)].

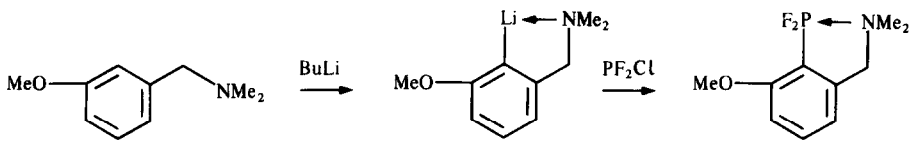

(3)

The difluorophosphine **1** is a thermally unstable oil, which could not be purified by distillation. The compound was not isolated and was characterized as the crude product by ^{19}F and ^{31}P NMR spectroscopy only.

As a result of an apparent interaction between the nitrogen atom in the side chain and phosphorus, the δ_P and $^1J(PF)$ values of **1** deviate significantly [high-field shift of δ_P, decrease in $^1J(PF)$] from the values of other aryldifluorophosphines,[3]

$$\delta_P + 166 \text{ ppm}; \quad {}^1J(PF)\ 1081 \text{ Hz}.$$

These parameters usually fall in the ranges $\delta_P + 190$ to $+220$ ppm and $^1J(PF)$ 1180 ± 30 Hz.[3] The spontaneous redox disproportionation characteristic of many difluorophosphines[4] was not observed for **1**. We believe this to be associated with intramolecular, rather than intermolecular interactions, i.e. N—P instead of P—P.

The reaction of crude **1** with dichloro-(η^4-1,5-cyclooctadiene), $Cl_2Pt(COD)$platinum(II) (COD = cyclooctadiene)furnished the complex, **7** [eq. (4)],

$$Cl_2Pt(COD) + 2\ 2\text{-}Me_2NCH_2\text{-}6\text{-}MeOC_6H_3PF_2 \longrightarrow \underset{\mathbf{1}}{}$$

$$Cl_2Pt(2\text{-}Me_2NCH_2\text{-}6\text{-}MeOC_6H_3PF_2)_2 + COD. \quad (4)$$
$$\mathbf{7}$$

Because of its poor solubility in common organic solvents, the characterization of **7** by NMR spectroscopy was unsatisfactory. A single crystal X-ray structural study of **7** was therefore conducted.

The X-ray crystal structure determination of **7** indicates a strong attractive interaction between phosphorus and nitrogen in the difluorophosphine ligand. The bonding geometry around the central platinum atom is essentially planar (sum of the bond angles around platinum = 360.6°). The bond lengths of platinum to phosphorus and to chlorine are normal. As is observed in other *cis*-dichlorobis(phosphine)platinum(II) complexes, the Cl—Pt—Cl bond angle is smaller than 90° (88.4°) whereas the P—Pt—P bond angle is significantly larger (P—Pt—P 94.0°).

An analysis of the non-bonding distances reveals that there is a non-bonding interaction between phosphorus and nitrogen in the coordinated difluorophosphine (248.7 pm, as against the sum of the van der Waals radii of 335 pm[6]). This donor–acceptor interaction causes a pronounced distortion of the tetrahedral geometry around phos-

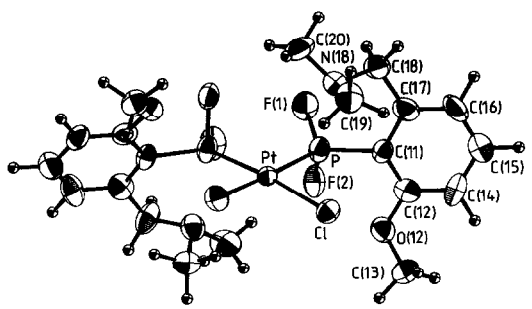

Fig. 1. Structure of **7** in the crystal.

Table 1. Bond lengths and angles in 7

Cl—Pt	233.1(3)	P—Pt	220.3(4)
F(1)—P	158.3(9)	F(2)—P	155.8(9)
C(11)—P	180.2(14)	C(12)—C(11)	134.8(21)
C(17)—C(11)	141.2(18)	O(12)—C(12)	134.9(16)
C(14)—C(12)	136.2(23)	C(13)—O(12)	144.2(19)
C(15)—C(14)	141.6(23)	C(16)—C(15)	137.1(26)
C(17)—C(16)	140.4(26)	C(18)—C(17)	154.3(23)
N(18)—C(18)	144.4(20)	C(19)—N(18)	148.6(21)
C(20)—N(18)	144.7(22)		

P—Pt—Cl	89.1(1)	Cl—Pt—Cl	88.4(2)
F(1)—P—Pt	117.6(4)	F(2)—P—Pt	105.1(4)
F(2)—P—F(1)	90.9(5)	C(11)—P—Pt	128.2(4)
C(11)—P—F(1)	107.9(5)	C(11)—P—F(2)	97.3(6)
P—Pt—P	94.0(2)	C(12)—C(11)—P	121.8(11)
C(17)—C(11)—P	117.2(11)	C(17)—C(11)—C(12)	120.9(14)
O(12)—C(12)—C(11)	118.2(15)	C(14)—C(12)—C(11)	119.9(14)
C(14)—C(12)—O(12)	121.9(16)	C(13)—O(12)—C(12)	118.2(14)
C(15)—C(14)—C(12)	121.5(17)	C(16)—C(15)—C(14)	118.7(17)
C(17)—C(16)—C(15)	120.0(15)	C(16)—C(17)—C(11)	118.9(16)
C(18)—C(17)—C(11)	119.3(15)	C(18)—C(17)—C(16)	121.3(14)
N(18)—C(18)—C(17)	108.1(12)	C(19)—N(18)—C(18)	108.2(14)
C(20)—N(18)—C(18)	111.7(13)	C(20)—N(18)—C(19)	109.6(14)

phorus in the direction of a trigonal bipyramid. This can clearly be seen by comparing bond angles that should be equivalent for tetrahedral geometry (109.5°) but are expected to be different for the trigonal bipyramid (90°, 120°);

F(1)—P—Pt 117.6° F(2)—P—Pt 105.1°

F(1)—P—C(11) 107.9° F(2)—P—C(11) 97.3°.

From these values it can be seen that F(2) is located in a pseudo-axial position whereas F(1) occupies a pseudo-equatorial position at trigonal-bipyramidal phosphorus.

In addition to this attractive interaction between phosphorus and nitrogen, the phosphorus atom is forced into close contact with the two *ortho* substituent atoms (P···O(12) 296.0 ppm; P···C(18) 302.2 ppm). Bond lengths and angles for **7** are listed in Table 1.

The molecule displays crystallographic C_2 symmetry. Because of the observed pseudo-penta-coordination of the phosphorus atom of the coordinated fluorophosphine in the solid state, the resultant

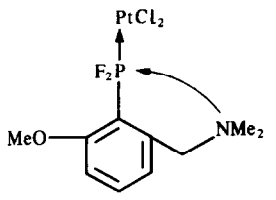

7

λ^5P^{III} moiety represents a chiral unit. The five-membered ring in **7** occupies one axial and one equatorial position at trigonal–bipyramidal phosphorus,[7] and the remaining axial position is occupied by a fluorine atom (see e.g. ref. 8). **7** is found to be present as one of three conceivable stereoisomers (at platinum), as illustrated in Fig. 2.

We believe that for steric reasons (interactions between the bulky NMe_2 groups in **C**) only enantiomers **A** and **B** (and not the diastereomer **C**) form stable crystals.

The N···P interaction in solutions of **7** is weak and it is impossible to establish it unambiguously solely by NMR spectroscopy. It must further be noted that there is a change of symmetry of the chiral compound upon breaking the N···P interaction, giving rise to different diastereomers.

The dynamic stereochemistry of **7** should resemble that, e.g. of

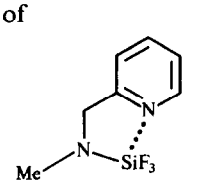

observed by Klebe,[9] and discussed more generally in a review by Corriu and Guerin.[10]

EXPERIMENTAL

The usual precautions required in handling air- and moisture-sensitive substances were observed in

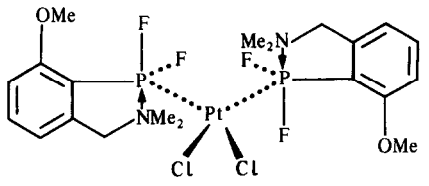

(A)

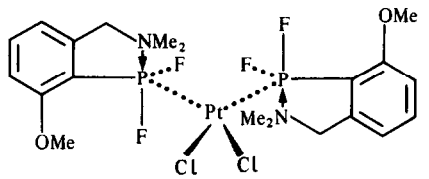

(B)

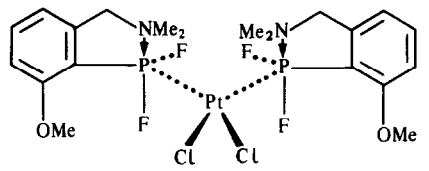

(C)

Fig. 2. Proposed diastereomers of **7**, A–C.

the course of the experimental work. Solvents were purified by standard procedures.[11] Magnetic stirring was employed throughout.

NMR spectra were recorded on the instruments BRUKER AM 200, BRUKER AM 300, and BRUKER AC 400 in $CDCl_3$ as a solvent. Shift values (positive sign for downfield shifts, negative sign for highfield shifts) are given, relative to the following reference compounds: int. TMS (^1H); $CDCl_3$ = 77.05; the multiplicity refers to proton-coupled ^{13}C NMR spectra (^{13}C); ext. CCl_3F (^{19}F); ext. 85% H_3PO_4 (^{31}P).

Starting materials: 3-Methoxybenzonitrile: ALDRICH CHEMICAL Co.; *n*-butyllithium: CHEMETALL GmbH; PF_2Cl;[13] $(COD)PtCl_2$.[14]

Synthesis of 3-*methoxybenzylamine*, **4** (*and of the Schiff base* **5**)

3-Methoxybenzonitrile, **3** (51.0 g; 0.38 mole) was added dropwise with stirring over 1 h to a suspension of 7.6 g (0.20 mole) of lithium aluminium hydride in 200 cm^3 of ether. Stirring was continued at room temperature for 14 h and at reflux for 1 h. About 50 cm^3 of water was cautiously added (0.5 h), followed by aluminium oxide (Woelm Grade A; 15 g). Subsequently, the reaction mixture was filtered through a sintered glass disc. The solid residue was washed with a total of 500 cm^3 of ether (in 100 cm^3 portions). The combined liquid products were concentrated *in vacuo*, and were finally distilled *in vacuo* (Vigreux column). The products, **4** (b.p. 131°C/26 mm; 27.4 g, 52%), and **5** (b.p. 231–232°C/5.5 mm; 10.6 g, 22%) were obtained as colourless liquids.

Compound **4** has previously been reported,[12] and was characterized by ^1H and ^{13}C NMR spectroscopy only:

^1H (300 MHz): δ (aromat.) 7.20 ("t", ^3J(HH) 8 Hz, 1H); δ(H1, 5) 6.86–6.82 (m, 2H); δ(H3) 6.75 ("d", ^3J(HH) 8 and 2.5 Hz, 1H); $\delta(CH_2)$ 3.76 (s, 2H); δ(MeO) 3.75 (s, 3H); $\delta(NH_2)$ 1.46 (exchangeable with D_2O). ^{13}C (75.5 MHz): δ(1) 112.3 (d); δ(2) 159.4 (s); δ(3) 111.8 (d); δ(4) 129.1 (d); δ(5) 118.9 (d); δ(6) 144.8 (s); δ(MeO) 54.7 (q); $\delta(CH_2)$ 46.1.

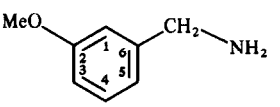

4

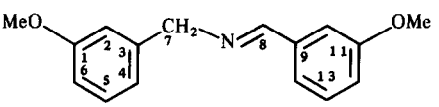

5

Compound **5**: $C_{16}H_{17}NO_2$ (255.3).
Found: C, 75.6; H, 7.3; N, 5.6.
Calc.: C, 75.3; H, 6.7; N, 5.5%.

^1H NMR (400 MHz): δ(H8) 8.27 ("s", 1H); δ(H aromat.) 7.37 ("s", 1H); 7.26 (m, 2H); 7.22 ("t", ^3J(HH) 7.5 Hz, 1H); 6.96–6.87 (m, 3H); 6.76 ("d", ^3J(HH) 7.5 Hz, 1H), $\delta(CH_2)$ 4.73 (s, 2H); δ(MeO) 3.74 (s, 3H); 3.73 (s, 3H).

^{13}C (100 MHz): δ(C1, 11) 159.5, 159.4 (s); δ(C3) 140.6 (s); δ(C5, 13) 129.1, 129.0 (d); δ(C6, 12) 111.5, 111.9 (d); δ(C7) 64.3 (t); δ(C8) 161.3 (d); δ(C9) 137.3 (s); δ(C15.16) 54.6, 54.5 (q); δ(C2, 4, 10, 14) 121.0, 119.8, 116.8, 113.3 (d).

Leuckart–Wallach-reaction of **4**: *preparation of* **6**

A mixture of **4** (27.4 g; 0.2 mole) and formic acid (46.0 g; 1 mole) was prepared with cooling (ice bath) in a r.b. flask, fitted with a reflux condenser and a dropping funnel. Subsequently, 44 cm^3 of a 30% aqueous solution of formaldehyde (0.44 mole)

was added, and the reaction mixture was stirred with gentle heating.

A vigorous reaction ensued, accompanied by evolution of CO_2, and heating was temporarily suspended (*ca* 15 min). After a 7 h reflux period the reaction mixture was left at room temperature for 15 h. Concentrated HCl (40 cm^3) was added to the yellow reaction mixture with ice cooling. Subsequently the mixture was pumped to dryness (20 mm). The residue was dissolved in a solution of 15 g NaOH in 50 cm^3 of water, cooled with ice. This solution was extracted five times with 120 cm^3 portions of ether. The organic layer was dried over K_2CO_3, and was distilled *in vacuo*; b.p. 95–96°C/6.50 mm; yield of **6**, 31.3 g (95%).

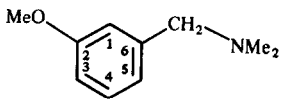

6

$C_{10}H_{15}NO$ (165.23).
Found: C, 72.9; H, 9.1; N, 8.3.
Calc.: C, 72.7; H, 9.1; N, 8.5%.

^{1}H NMR spectrum (400 MHz): δ(4) 7.20 ("t", ^3J(HH) 8.0, 1H); δ(1, 5) 6.89–6.86 (m, 2H); δ(3) 6.78 ("dd", ^3J(HH) 8.0; ^4J(HH) 2.5, 1.0, 1H); δ(OMe) 3.78 (s, 3H); $\delta(CH_2)$ 3.38 (s, 2H); $\delta(NMe_2)$ 2.24 (s, 6H).

Synthesis of 2-dimethylaminomethyl-6-methoxyphenyl-difluorophosphine, **1**

A mixture of 40 cm^3 of ether, 5.0 g (0.03 mole) of 3-methoxy-N,N′-dimethylbenzylamine, **6**, and of 11.5 g (*ca* 0.027 mole) of *n*-butyllithium (15% in hexane) was stirred in a heavy-wall glass tube, fitted with a TEFLON® stopcock, for 20 h at room temperature. Subsequently, PF_2Cl[13] (3.6 g; 0.035 mole) was condensed onto the reaction mixture at −196°C. The reaction tube was sealed, and its contents were stirred for 12 h at room temperature. Products volatile at room temperature *in vacuo* (0.01 mm) were pumped off (0.5 h) and dichloromethane (50 cm^3) was added to the residue. Lithium chloride was removed by centrifugation, and the NMR spectra of the supernatant liquid were recorded. The yield of **1** (estimated from the CH_2 resonance in the ^{1}H NMR spectrum) was *ca* 1 g (14%).

^{19}F NMR data: δ −95.2 ppm; ^1J(PF) 1069 Hz; ^{31}P NMR data: δ +166 ppm; ^1J(PF) 1081 Hz.

Synthesis of the platinum(II) complex, **7**

The difluorophosphine, **1** (0.7 g; 3.1 mole) was added to a solution of 0.5 g (1.34 mmole) of $Cl_2Pt(COD)$[14] in 40 cm^3 of dichloromethane. The crystalline product formed after 2 days was collected by filtration, and was washed with 10 cm^3 of dichloromethane. Yield 0.42 g (42%); m.p. 194–195°C. $C_{20}H_{28}Cl_2F_4O_4P_2Pt$ (732.4). Found: C, 32.9; H, 3.8; P, 8.5. Calc.: C, 32.8; H, 3.8; P, 8.4%.

^{1}H NMR spectrum (400 MHz; CD_2Cl_2 solution): δ(aromat.) 7.45 ("q", J 8 Hz, 2H); 7.11 ("dt", J 6, 8 Hz, 2H); 6.92–6.83 (m, 2H); $\delta(CH_2)$ 4.61–4.41 (m, 4H); δ(MeO) 4.03 and 3.97 (two s, 6H); $\delta(NMe_2)$ 3.0–2.6 (m, 12H; the multiplet comprises three doublets in the ratio 3 : 2 : 1, all J 6 Hz.

X-ray crystal structure analysis of **7**

Crystals of **7**, obtained from dichloromethane, are of tetragonal symmetry; space group $P4_32_12$. The unit cell, with the parameters, a = 825.4 (6); c = 3697.3 (33) pm, contains four molecules, yielding a calculated density of 1.931 g/cm^3. The data were collected at 20°C on a SYNTEX $P2_1$ diffractometer, using graphite-monochromated Mo-K_α radiation (λ = 71.07 pm) in the $\theta-2\theta$ mode, in the range $3° < 2\theta < 50°$, at a scan speed ranging between 2.93 and 29.3°/min, depending on the intensity of the reflection.

The data were corrected for Lorentz, polarization, and absorption effects (μ = 6.337 mm^{-1}). The structure was solved by direct methods and difference Fourier syntheses. Hydrogen atom positions were calculated from those of the directly bound atoms and were refined as "riding atoms". The refinement, using 2183 out of 2765 measured independent reflections [$F > 4.0\ \delta(F)$] converged at R = 0.061 (R_w = 0.058). A final difference map displayed no electron density higher than $0.25 \cdot 10^{-6}$ e/pm^3. The program SHELX-76[15] and our own programs were used. Complex atom scattering factors[16] were employed.

Acknowledgements—We are grateful to BASF AG, BAYER AG, CHEMETALL GmbH, DEGUSSA AG, and HOECHST AG for gifts of chemicals used in this research, and to Fonds der Chemischen Industrie for financial support. Professor L. Ernst is thanked for recording NMR spectra. L.H. acknowledges a maintenance grant awarded by Land Niedersachsen.

REFERENCES

1. J. F. Nixon, *Adv. Inorg. Chem. Radiochem.* 1985, **29**, 41.

2. R. R. Holmes and R. P. Wagner, *Inorg. Chem.* 1963, **2**, 384.
3. L. Heuer and R. Schmutzler, *J. Fluorine Chem.* 1988, **39**, 197.
4. J. F. Liebman, O. Stelzer and R. Schmutzler, *J. Fluorine Chem.* 1984, **25**, 289.
5. (a) M. L. Moore, *Org. Reactions* 1949, **5**, 301. (b) L. F. Tietze and T. Eicher, *Reaktionen und Synthesen im organisch-chemischen Praktikum.* Thieme, Stuttgart (1981).
6. A. Bondi, *J. Phys. Chem.* 1964, **68**, 441.
7. W. Becker, Ph.D. Dissertation, Technische Universität Braunschweig (1989).
8. E. L. Muetterties, W. Mahler and R. Schmutzler, *Inorg. Chem.* 1963, **2**, 613.
9. G. Klebe, M. Nix and K. Hensen, *Chem. Ber.* 1984, **117**, 797.
10. R. J. P. Corriu and G. Guerin, *J. Organomet. Chem.* 1980, **198**, 231.
11. D. D. Perrin, W. L. F. Armarego and D. R. Perrin, *Purification of Laboratory Chemicals.* Pergamon Press, Oxford (1966).
12. G. Grethe, H. L. Lee, M. Uskovic and A. Brossi, *J. Org. Chem.* 1988, **53**, 491.
13. W. Albers, W. Krüger, W. Storzer and R. Schmutzler, *Synth. React. Inorg. Metal-Org. Chem.* 1985, **15**, 187.
14. H. C. Clark and L. E. Manzer, *J. Organomet. Chem.* 1973, **59**, 411.
15. G. M. Sheldrick, private communication to D. S.
16. D. T. Cromer and J. T. Waber, in *International Tables for Crystallography*, Vol. IV, pp. 99 and 149. Kynoch Press, Birmingham (1974).

Polyhedron Vol. 10, No. 23/24, pp. 2743–2755, 1991
Printed in Great Britain

0277–5387/91 $3.00+.00
© 1991 Pergamon Press plc

THE DESIGNED SYNTHESIS AND CHARACTERIZATION OF TWO NOVEL HETEROMETALLIC TRINUCLEAR INCOMPLETE CUBANE-LIKE CLUSTERS $[(CH_3CH_2)_4N]\{M_2CuS_4\}(S_2C_2H_4)_2(PPh_3)$ (M = Mo, W)

NIANYONG ZHU, YIFAN ZHENG and XINTAO WU*

Fuzhou Laboratory of Structural Chemistry, Fujian Institute of Research on Structure of Matter, Chinese Academy of Sciences, Fuzhou, Fujian 350002, P.R.C.

(*Received* 18 *February* 1991; *accepted* 22 *July* 1991)

Abstract—Two novel heterometallic trinuclear incomplete cubane-like clusters $[(CH_3CH_2)_4N][\{M_2CuS_4\}(edt)_2(PPh_3)]$ (M = Mo, W) have been synthesized by reaction of $[(CH_3CH_2)_4N]_2[M_2S_4(edt)_2]$ (M = Mo, W) with $Cu(PPh_3)_2(dtp)$ [where edt is 1,2-ethanedithiolato ligand, dtp is $S_2P(OCH_2CH_3)_2^-$]. The two crystals are isomorphous in space group $P\bar{1}$ (No. 1). The unit cell contains two independent molecules, but the two discrete anions have the same orientation for the PPh_3 ligands along one axis so the space group is undoubtedly non-centrosymmetric. The discrete anion contains two edt ligands and one PPh_3 ligand attached to one incomplete cubane-like cluster core $\{M_2CuS_4\}^{3+}$ (M = Mo, W). The bond lengths of Mo—Mo[W—W] and the two Mo—Cu[W—Cu] are 2.852(2)[2.844(1)], 2.802(2)[2.765(3)], 2.760(2)[2.762(3)] Å, respectively. The $M_2S_4(edt)_2$ (M = Mo, W) moiety remains almost unchanged, except that for the compound **1** the Mo=S double bond length elongates from av. 2.10 to av. 2.165 Å. The title clusters provide a new type of unsymmetric μ_2-bridging sulphido ligand. The incomplete cubane-like cluster core $\{Mo_2CuS_4\}^{3+}$ of compound **1** is distorted because the two Cu—μ_2—S bond lengths are significantly different (2.313 Å and 2.409 Å), but the core $\{W_2CuS_4\}^{3+}$ of compound **2** has approximately C_s symmetry. The IR spectra of the two title clusters and two starting materials are assigned.

In recent years, three aspects of the synthetic and structural chemistry of transition metal clusters containing sulphido ligand(s) have developed rapidly.[1–3] (1) In bioinorganic chemistry, research on the synthetic analogue $[Fe_4S_4(SR)_4]^{2-}$ [4] of the redox sites of iron-sulphido proteins has stimulated research on other analogues of active sites of metal enzymes,[5–7] for example the Mo-containing enzymes, and on the Mo—Cu antagonism;[8] (2) research on the catalysts of hydrodesulphurization (HDS) has also prompted the development of transition metal sulphido clusters;[9–11] (3) study of superconductive materials has also attracted interest in transition metal sulphido clusters.[12]

A large number of heterometallic cubane-like clusters containing sulphido ligand(s) have been synthesized, such as $\{M_3CuS_4\}^{5+}$,[13,14] $\{Mo_3FeS_4\}^{4+}$,[15] $\{M_2Cu_2S_4\}^{4+}$,[16] $\{M_2Co_2S_4\}^{2+}$,[17] $\{MFe_3S_4\}^{n+}$,[18] $\{MCu_3S_3X\}$[19,20] (M = Mo, W; X = Cl, Br; n = 2, 3, 4, 5, 6), etc., by various methods. The research on homometallic trinuclear incomplete cubane-like clusters is extensive,[21,22] but research on heterometallic incomplete cubane-like clusters is only beginning.

We have proposed that the "unit-construction"[23] is a convenient method for the rational synthesis of transition metal clusters by the use of reactive fragments as building blocks. It was shown that the "unit", which contains sulphido ligand(s) with lone-pair electrons and unsaturated coordination, may add to another metal complex which has initial unsaturated coordination positions or easily displaceable ligand(s). To use the cluster containing active sulphido ligands with lone-pair electrons and unsaturated coordination as a starting material is a rational method. Recently, we have succeeded in employing triangular trinuclear incomplete cubane-like core clusters $[M_3S_4][S_2P(OCH_2CH_3)_2]_4 \cdot H_2O$

* Author to whom correspondence should be addressed.

($M = Mo$[21f], W[24]) to obtain a series of cubane-like core $\{M_3CuS_4\}^{5+}$ ($M = Mo$[13], W[14]) clusters.

According to the idea of "unit construction", the title compounds are a successful addition by using $[M_2S_4(edt)_2]^{2-}$[25] (M = Mo, W) and $Cu(PPh_3)^+$ as building blocks. In this paper, we report in detail the synthesis and characterization of the previously communicated $[(CH_3CH_2)_4N]\{M_2CuS_4\}(S_2C_2H_4)_2(PPh_3)$[26] ($M$ = Mo, W). In the communicated paper the crystal structure of the W complex was not reported.

EXPERIMENTAL

Synthesis

The chemicals in this research were used as purchased. The dinuclear complexes $[Et_4N]_2M_2S_4(edt)_2$ (M = Mo, W) were prepared under a dinitrogen atmosphere according to the procedure of Stiefel *et al.*[25] Elemental analysis were carried out by the Elemental Analysis Laboratories of our Institute. Visible and UV electronic spectra were obtained on a Schimadzu UV-3000 spectrophotometer. IR spectra were recorded on Perkin–Elmer 577 spectrometer.

$Cu(PPh_3)_2[S_2P(OCH_2CH_3)_2]$: Triphenylphosphine (94.32 g, 0.323 mol) dissolved in 250 cm^3 CH_2Cl_2 solution was added slowly to a solution of $CuCl_2\cdot 2H_2O$ (20.4 g, 0.120 mol) in 200 cm^3 of EtOH to obtain a solution. Solid P_2S_5 (13.32 g, 0.060 mol) was dissolved in 100 cm^3 of EtOH (warmed up to increase the dissolution of the solid), the resultant solution was then added slowly to the above Cu/PPh_3 solution. The resultant solution was allowed to stand for 4 h, then filtered, and the crystals were washed with EtOH and ether and air-dried. Yield: 84.5 g (92.1%). Found: Cu, 8.7; S, 7.8; P, 12.5; C, 61.8; H, 5.1. Calc. for $CuS_2P_3OC_{40}H_{40}$: Cu, 8.2; S, 8.3; P, 12.0; C, 62.1; H, 5.2%.

$[Et_4N]\{Mo_2CuS_4\}(edt)_2(PPh_3)$ (**1**): $Cu(PPh_3)_2[S_2P(OCH_2CH_3)_2]$ (3.85 g, 5 mmol) dissolved in 50 cm^3 of CH_2Cl_2 was added to a solution of $[Et_4N]_2Mo_2S_4(edt)_2$ (3.80 g, 5 mmol) in 200 cm^3 of CH_3CN, stirred and filtered. The filtrate was allowed to evaporate in air. After standing for 1.5 h, brown–red needle-shaped crystals formed, which were isolated by filtration and washed with isopropanol and ether. Yield 3.27 g (68.9%) analytically pure crystals which were suitable for X-ray measurements. Found: Mo, 19.7; Cu, 6.9; S, 26.3; C, 38.0; N, 2.1; H, 4.8. Calc. for $Mo_2CuS_8PNC_{30}H_{43}$: Mo, 20.0; Cu, 6.6; S, 26.7; C, 37.5; N, 1.5; H, 4.8%.

$[Et_4N]\{W_2CuS_4\}(edt)_2(PPh_3)$ (**2**): $Cu(PPh_3)_2[S_2P(OCH_2CH_3)_2]$ (0.77 g, 1 mmol) dissolved in 30 cm^3 of CH_2Cl_2 was added to a solution of $[Et_4N]_2W_2S_4(edt)_2$ (0.94 g, 1 mmol) in 40 cm^3 CH_3CN. The resulting solution was filtered and the filtrate was allowed to evaporate in the air. After 1 day, some yellow precipitate was filtered off. Subsequent evaporation of the filtrate in the air for 3 days, produced 0.20 g (17.6% yield) of orange–red crystals which were filtered and washed with isopropanol and ether. The crystals were analytically pure and suitable for X-ray measurements. Additional evaporation produced more orange–red crystals. Found: W, 33.1; Cu, 5.5; S, 21.6; C, 31.7; H, 3.8; P, 2.8. Calc. for $W_2CuS_8PNC_{30}H_{43}$: W, 32.4; Cu, 5.6; S, 22.5; C, 31.7; H, 3.8; N, 1.2; P, 2.7%.

X-ray structure determination

(a) $[Et_4N]\{Mo_2CuS_4\}(edt)_2(PPh_3)$ (**1**): A crystal with dimensions $0.33\times0.13\times0.1$ mm was mounted in random orientation on a glass fibre. Some experimental conditions are reported in Table 1. Diffraction data were collected on a CAD-4 K-geometry diffractometer using graphite-monochromated Mo-K_α radiation ($\lambda = 0.71073$ Å). Cell constants were obtained by least-squares fit to 25 diffraction maxima ($24° < 2\theta < 28°$). The intensities were corrected for Lorentz and polarization factors and for absorption by using empirical scan data and DIFABS.[27] A total 7154 reflections were collected, and 6122 reflections with $I > 3\sigma(I)$ were used in the refinement. No extinction correction was applied.

The structure was solved by direct methods using MULTAN 11/82[28] and the positions of six heavy atoms were obtained from the E map. The remaining non-hydrogen atoms were located in the succeeding difference Fourier synthesis, except for some C atoms of one disordered cation which were located geometrically in their calculated positions and allowed to refine. The refinement was based on F. The scattering factors were taken from Cromer and Waber.[29] The structure was refined by full-matrix least-squares technique with anisotropic thermal parameters for the 32 atoms of the cores and isotropic thermal parameters for the remaining non-H atoms (527 variables). $R = \Sigma\|F_o|-|F_c\|/\Sigma|F_o| = 0.056$, $Rw = (\Sigma w(|F_o|-|F_c|)^2/\Sigma wF_o^2)^{1/2} = 0.065$, $S = [\Sigma w(|F_o|-|F_c|)^2/(N_{obs}-N_{var})]^{1/2} = 1.27$, $w = 1/[\sigma(F_o)^2+(PWT\cdot F_o)^2+QWT]-F_o$ (for PWT = 0.020, QWT = 1.0),[30] the function minimized was $\Sigma w(|F_o|-|F_c|)^2$. All calculations were performed on a VAX 785 computer using the SDP program package.[31]

Table 1. Crystallographic data for $[(CH_3CH_2)_4N]\{M_2CuS_4\}(PPh_3)(edt)_2$ (M = Mo, **1**; W, **2**)

Compound	1	2
Chemical formula:	$Mo_2CuS_8PC_{30}NH_{43}$	$W_2CuS_8PC_{30}NH_{43}$
Formula weight	959.4	1135.2
Crystal colour	Dark-red	Orange-red
Crystal system	Triclinic	Triclinic
Space group	$P\bar{1}$ (#1)	$P\bar{1}$ (#1)
Unit cell paramaters		
a =	9.671(3) Å	9.671(2) Å
b =	12.341(2) Å	12.325(7) Å
c =	16.857(3) Å	16.837(3) Å
α =	83.91(1)°	83.97(3)°
β =	86.40(4)°	86.23(2)°
γ =	79.30(3)°	79.02(3)°
V =	1963.8 Å^3	1957(1) Å^3
Z =	2	2
Crystal dimensions	0.33 × 0.13 × 0.1 mm	0.40 × 0.20 × 0.15 mm
μ =	16.2 cm^{-1}	70.05 cm^{-1}
$F(000)$	886	1100
$2\theta_{max}$	50.0°	50.1°
$d_{cald.}$ =	1.55 g cm^{-3}	1.93 g cm^{-3}
Temperature	296 K	296 K
Diffractometer	Enraf–Nonius CAD4	Rigaku AFC5R
Radiation	Mo-K_α (λ = 0.71073 Å)	Mo-K_α (λ = 0.71069 Å)
Collected octants	$-11 \leqslant h \leqslant 11$	$-12 \leqslant h \leqslant 12$
	$-14 \leqslant k \leqslant 14$	$0 \leqslant k \leqslant 15$
	$0 \leqslant l \leqslant 20$	$-20 \leqslant l \leqslant 20$
Max./min. transmission factors	0.893/1.114	0.905/1.232
Solution method	direct methods	direct methods
Correction	Lp, ψ, DIFABS	Lp, ψ, DIFABS
Residuals: R, Rw	0.056, 0.065	0.050, 0.071
Goodness of fit: S	1.27	1.94
No. of unique data	7154	6927
No. of obs. with $I > 3$ [$\sigma(I)$]	6122	6275
Max. shift $(\Delta/\sigma)_{max}$ in final cycle	0.68	0.90
Largest/smallest peaks in final diff. map	1.01/−0.92 e Å^{-3}	1.57/−1.95 e Å^{-3}
Scan type	ω	ω
Max. scan speed	7° min^{-1}	32° min^{-1}
Scan width	0.47° + 0.35° tan cθ	1.575° + 0.30° tan cθ
Extinction coefficient	—	2.103×10^{-7}

(b) $[Et_4N]\{W_2CuS_4\}(edt)_2(PPh_3)$: An orange–red crystal with dimensions 0.40 × 0.20 × 0.15 mm was mounted in random orientation on a glass fibre. Some experimental conditions are reported in Table 1. Data were collected using a RIGAKU AFC5R diffractometer[32] using Mo-K_α radiation at *ca* 296 K. Cell constants were obtained by least-squares analysis on 20 diffraction maxima ($20° < 2\theta < 26°$). Scan speed varied on the basis of SEARCH intensity. A total 7281 (of which 6927 were unique) reflections were collected. Three standard reflections were measured periodically, the absence of random deviations of intensity indicated crystal and electronic stability. A linear decay correction was not applied. The collected intensity was defined as $C\text{-}1/2(t_c/t_b)(b_1+b_2)$, where C = total number of counts, t_c = time spent counting peak intensity, t_b = time spent counting one side of the background, b_1 = high-angle background counts and b_2 = low-angle background counts; the intensity error was defined as $\sigma(F^2) = [C+1/4(t_c/t_b)^2(b_1+b_2)+(pI)^2]^{1/2}$, where I is the intensity and p is the factor that downweighs strong reflections, taken to be 0.05. The data were corrected for Lorentz and polarization factors and for absorption using empirical scan data and DIFABS. 6275 reflections

with $I \geqslant 3\sigma(I)$ were considered observed, and used in the refinement. An extinction correction was applied.

The structure was solved by direct methods using MITHRIL;[33] the W and Cu atoms were located in the E map. Most non-hydrogen atoms were located using the succeeding DIRDIF program;[34] some non-hydrogen atoms were located in the succeeding difference Fourier syntheses, while the positions for some C atoms in the disordered cation were calculated in geometrically reasonable positions and then refined. The structure was refined by full-matrix least-squares techniques with anisotropic thermal parameters for all W, Cu, S, P atoms, and isotropic thermal parameters for all C atoms (487 variables in all). Final $R = \Sigma||F_o|-|F_c||/\Sigma|F_o| = 0.050$, $wR = [\Sigma(|F_o|-|F_c|)^2/\Sigma wF_o^2]^{1/2} = 0.071$ and $S = [\Sigma w(|F_o|-|F_c|)^2/(N_o-N)]^{1/2} = 1.940$, $w = 1/\sigma^2(F_o)$. $(\Delta/\sigma)_{max} = 0.90$ in the final difference electron density synthesis largest and smallest heights were 1.57 and -1.95 e Å^{-3} which were in the vicinity of the W atom. All calculations were performed on a VAX 785 computer using the TEXSAN (1985) program package.[35] Non-hydrogen scattering factors were taken from Cromer and Waber.[30]

RESULTS AND DISCUSSION

Synthesis

For synthesis of the Mo-compound (**1**), we had tried some Cu/PPh_3 complexes, e.g. $Cu(PPh_3)_3Cl$[36] or $CuCl_2 \cdot 2H_2O/PPh_3$ (1:1.5) in CH_3CN/CH_2Cl_2 solution. The reaction was carried out under anaerobic condition and the products were crystallized by gaseous diffusion of ether. The resulting crystals are very stable in air, but obtaining them took much time. If the above reaction solution was under air, the yield is very low and the products are contaminated by a black precipitate. However, when we tried the $Cu(PPh_3)_2[S_2P(OCH_2CH_3)_2]$ in an open container, it was surprising to find that the reaction solution is stable in air. The yield is high in a relatively short time and the products are of analytical purity. This means that, although the ligand $S_2P(OCH_2CH_3)_2^-$ does not exist in the products, it may have some helpful functon in the synthesis in preventing the solution from being oxidized by air. Correspondingly, the halogen ligand does not have this kind of function in the solution.

The synthesis of the W-complex can also be done under air, but it takes a few days and the yield is low.

The reaction is easily followed because the colour of the solution changes quickly from orange–red to brown–red or from orange to orange–red. The reaction procedures can be outlined in Scheme 1.

Scheme 1 implies that this procedure is a convenient one for synthesizing the incomplete cubane-like clusters from other metal complexes. If a new metal complex is used to substitute the Cu/PPh_3 complex, a novel heterometallic incomplete cubane-like clusters could be expected to be obtained.

The trimolybdenum clusters with the incomplete cubane-like cluster core $\{Mo_3S_4\}^{4+}$[21] have attracted much attention, not only because the $\{Mo_3S_4\}^{4+}$ aquo ion is especially stable,[37] but also because it may be employed as a starting material to react with many metals, e.g. Fe,[15] Cu,[13,14] Ni,[38] etc., to form cubane-like clusters, or to dimerize to form an Mo_6S_8 cluster.[12] The cores $\{Mo_2CuS_4\}^{3+}$ and $\{W_2CuS_4\}^{3+}$ of the title compounds are very similar to the cores $\{M_3S_4\}^{4+}$ (M = Mo, W). They are the first two heterometallic incomplete cubane-like cluster cores. The reactivity of the homo- and hetero-clusters of the above compounds are expected to be similar. Recently, the cubane-like core $\{M_2Cu_2S_4\}^{4+}$[16] (M = Mo, W) clusters have been synthesized, this justifies this expectation. Therefore, a procedure to design synthesis of sulphido-bridging cubane-like clusters has been outlined by the experiments, which is $[1+1] = 2$, $[2+1] = 3$, $[3+1] = 4$. Many dinuclear complexes containing the $\{M_2S_4\}^{2+}$ (M = Mo, W) core have been synthesized,[25,39] which are from the step of $[1+1] = 2$. Scheme 1 shows the second step of $[2+1] = 3$ for the incomplete cubane-like clusters. The third step of $[3+1] = 4$ for cubane-like clusters has been verified in many papers.[13–15,38]

IR spectra

The Mo=S and W=S vibration absorptions of dinuclear complexes have been identified.[25] According to the procedures of "unit-construction", the IR spectra comparison of the di-, tri-, tetra-clusters (i.e. M_2S_4, M_2CuS_4, $M_2Cu_2S_4$)[16] help us to assign all the absorptions. The results are shown in Table 2.

For the Mo-compound, the three bands at around 520, 510 and 495 cm^{-1} are obviously

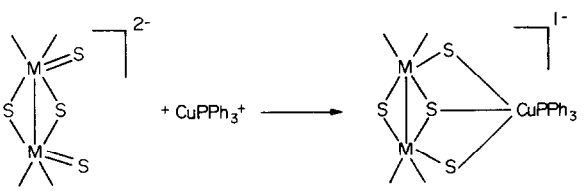

Scheme 1.

Table 2. IR spectra data of four compounds (cm^{-1})

Compound	ν(M—S)	ν(Cu—P)	ν(M—μ_2-S)	ν(M—μ_3-S)	ν(M—SR)$_{edt}$
$\{Mo_2S_4\}^{2+}$	515(s)	—	465(w), 430(w) 325(m)	—	340(w), 295(w)
$\{Mo_2CuS_3\}^{3+}$	495(s)	520(s) 510(s)	465(w), 430(w) 325(w)	465(w), 430(w)	350(w), 310(w)
$\{W_2S_4\}^{2+}$	505(s)	—	465(w), 425(w) 330(s)	—	343(w), 300(w)
$\{W_2CuS_4\}^{3+}$	500(m)	520(s) 508(s)	465(w), 425(w) 330(w)	480(s), 425(w)	350(m), 310(m)

isolated. The first two are assigned to ν(Cu—P) and the other to ν(Mo—S). The first two bands also exist in the compound of $Cu(PPh_3)_2[S_2P(OCH_2CH_3)_2]$. The two bands at 460(w) and 430(w) are due to asymmetric stretching vibrations of a sulphur bridged[40] MoS_2Mo group. The vibration absorptions of Mo—μ_3—S groups are overlapping around 460 and 430 cm^{-1}. From dinuclear complex to trinuclear compound, the band at 325 cm^{-1} becomes weak (in the cubane-like $\{Mo_2Cu_2S_4\}^{4+}$ cluster the band disappeared); this band is assigned to symmetric stretching vibration of a sulphur bridged[40] MoS_2Mo group. The two bands at 340 (350) and 295 (310) cm^{-1} of dimolybdenum complex (trinuclear compound) are attributed[41] to ν(Mo—SR). The vibrational coupling of the two SR groups of the edt ligand at the Mo atom causes the absorption to separate into two bands. The assignment of the IR spectra of the W-compound is similar to that of the Mo-compound, except that the band at 480 cm^{-1} is assigned to ν(W—μ_3—S); this is because the bond length of W—μ_3—S is shorter than that of W—μ_2—S.

Electronic spectra

For comparison, the electronic spectra of the cubane-like core $\{M_2Cu_2S_4\}^{4+}$ [16] (M = Mo, W) clusters were also shown in Table 3. The right peaks

Table 3. Electronic spectra [in CH_2Cl_2 solution, $\lambda(\varepsilon)$ nm ($M^{-1}\cdot cm^{-1}$)]

Compound	Left peak	Centre peak	Right peak
$\{Mo_2S_4\}^{2+}$	228(37,000)	306(26,000)	445(24,000)
$\{Mo_2CuS_4\}^{3+}$	228(49,000)	305(23,000)	482(8600)
$\{Mo_2Cu_2S_4\}^{4+}$	230(60,000)	315(26,000)	510(8900)
$\{W_2S_4\}^{2+}$	235(24,000)	284(20,000)	362(6600)
$\{W_2CuS_4\}^{3+}$	228(44,000)	280(30,700)	405(11,000)
$\{W_2Cu_2S_4\}^{4+}$	230(37,000)	275(37,000)	428(10,600)

of these clusters are broad and rather low. With the increasing of the nuclei, the right peak shifts to a larger wavelength. The longest wavelength peak is attributed to the S_t–M charge transition. The red shift tendency of the S_t–M charge transition with the increasing of the Cu group has also been found elsewhere[42–45] in a series of Mo(W)/Cu/S complexes.

Cyclic voltammetry

The cyclic voltammography[46] has been done in the range 0.0 to −1.75 V. Compound **1** displays a pair of redox waves at −1.28 to −1.07 V while compound **2** displays no electron transfer process in this range. The two starting compounds also show no waves in this range. As reported, the $[Et_4N]_2Mo_2S_4(SCH_2CH_2S)_2$ displays[47] a reversible one-electron transfer at −1.88 V. When the positively $CuPPh_3^+$ group is added, it results in the less negative reduction potentials because of the decreasing of the electron density on the $\{Mo_2S_4\}$ moiety.

Description of the structure

The ORTEP drawings of the two independent anions of $\{Mo_2CuS_4(edt)_2(PPh_3)\}^-$ are shown in Figs 1(a) and (b). Figures 1(c) and (d) show the drawings of the two independent anions of $\{W_2CuS_4\}(edt)_2(PPh_3)^-$. The packing drawing of the unit cell for $[(CH_3CH_2)_4N][Mo_2CuS_4(edt)_2(PPh_3)]$ is shown in Fig. 2. The unit cell contains two discrete anions and two cations. The two discrete anions have the same orientation for the $CuPPh_3$ groups along one axis, so that the space group is undoubtedly noncentrosymmetric. The PPh_3 ligands of the two independent anions have some difference in conformation. One of the two cations $[(CH_3CH_2)_4N]^+$ in the unit cell is disordered. In the unit cell, the dihedral angle of the two triangular Mo_2Cu (or

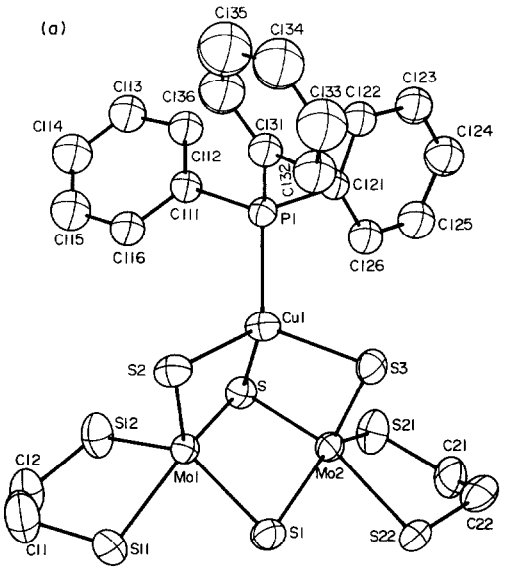

Fig. 1. (a) The ORTEP drawing of the first independent anion of $\{Mo_2CuS_4\}(edt)_2(PPh_3)^-$.

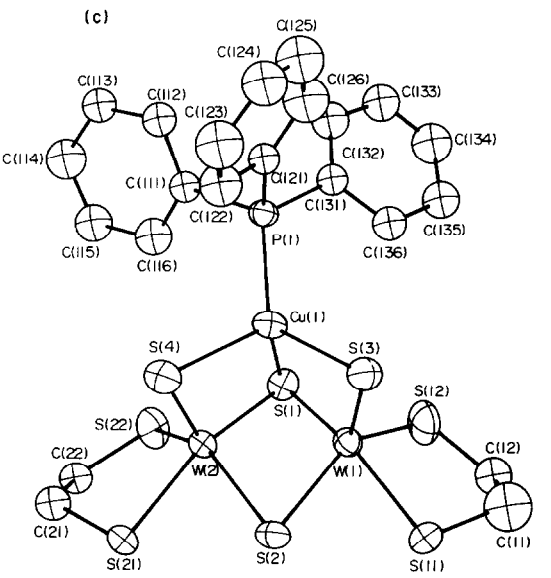

Fig. 1. (c) The ORTEP drawing of the first independent anion of $\{W_2CuS_4\}(edt)_2(PPh_3)^-$.

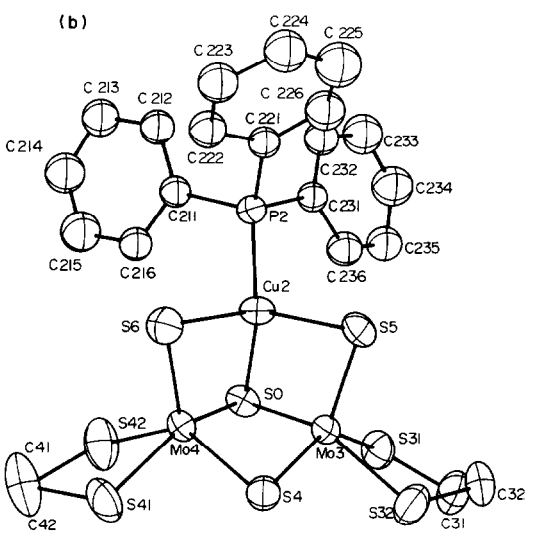

Fig. 1. (b) The ORTEP drawing of the second independent anion of $\{Mo_2CuS_4\}(edt)_2(PPh_3)^-$.

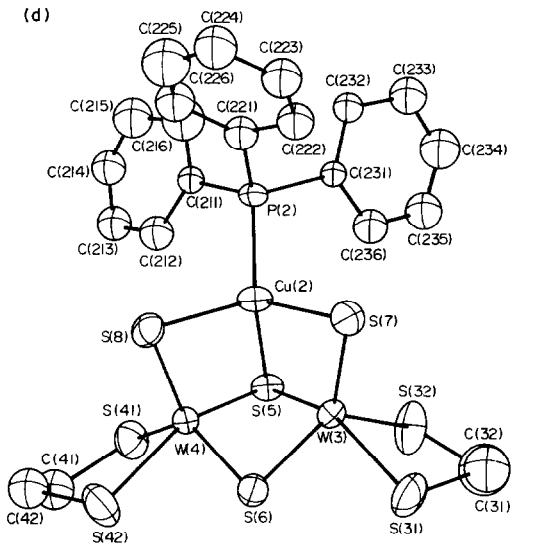

Fig. 1. (d) The ORTEP drawing of the second independent anion of $\{W_2CuS_4\}(edt)_2(PPh_3)^-$.

W_2Cu) metallic planes of the two anions is 173.5° (or 173.9°). If one anion is rotated and overlapped on the other anion, it is found that the two cores of the two anions are extremely similar in structure.

Except for the structural difference of the PPh_3 ligands of the two independent anions, the two cores of the two anions are very similar, so only one core of the anion is discussed below. Selected bond lengths appear in Table 4 and the selected bond angles in Table 5.

The idealized symmetry of the anion is C_s (exclusive of the methylene groups of the edt ligands). Each Mo(W) atom displays tetragonal–pyramidal coordination (TP) by five sulphurs; one μ_3-S atom, two μ_2-S atoms and two terminal sulphurs of the edt ligand, which is the same as in the isolated dinuclear compound.[25,48] The axial position of each TP is occupied by a μ_2-S_t (in the dinuclear complexes the S_t atom is the terminal sulphido atom and the S_b below is the bridging sulphido atom), the equatorial positions are occupied by bridging sulphido ligands (μ_3-S, μ_2-S_b) and the sulphur atoms from the edt ligand. The Mo(W) atom is mean 0.71 Å (0.74 Å) above the basal plane of TP.

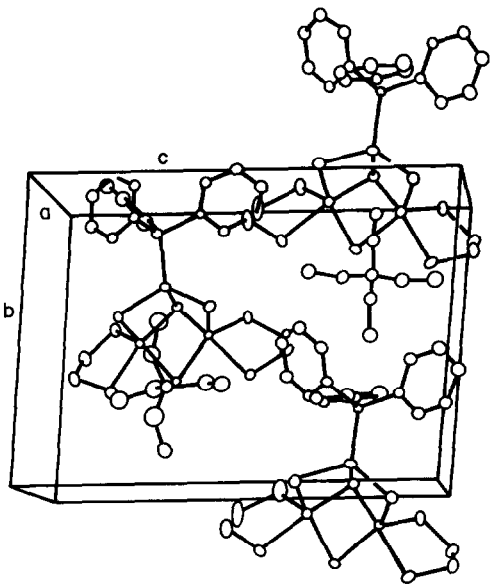

Fig. 2. The packing drawing of the unit cell of compound $[Et_4N]\{W_2CuS_4\}(edt)_2(PPh_3)$ (for clarity only one structure of the disordered cation was drawn).

The deviations from planarity of the four sulphur atoms is shown in Table 6. The large deviations from their least-squares planes show the slight distortion of each TP toward trigonal–bipyramidal coordination. The Cu atom was tetrahedrally coordinated by one μ_3-S atom, two μ_2-S atoms and one PPh_3 ligand.

For the Mo compound (**1**), the dihedral angle of the two Mo/S/S in the Mo_2S_2 ring is almost unchanged (av. 146.8° for compound **1**, 146.9° for the starting dimolybdenum complex). If the Mo_2S_2 ring is used as a frame of reference, the results of the reaction are that the μ_3-bridging sulphido atom side moves toward the two S_t atoms while S(12) and S(21) atoms side rotate away from the two S_t atoms (see Table 5). The resultant S(2)—Mo(1)—S and S(3)—Mo(2)—S angles are less than 5–8° smaller than the corresponding S(2)—Mo(1)—S(1) and S(3)—Mo(2)—S(1) angles, meanwhile the resultant S(2)—Mo(1)—S(12) and S(3)—Mo(2)—S(21) angles are more than 6–7° larger than the corresponding S(2)—Mo(1)—S(11) and S(3)—Mo(2)—S(22). Except for some slight change, the bond lengths and bond angles of the $Mo_2S_4(edt)_2$ moiety in the trinuclear cluster are almost the same as in the isolated dinuclear complex.[48] Only the Mo—S_t double bond lengths elongate from av. 2.10 to av. 2.165 Å, when the terminal S atom becomes μ_2-S atom. This result is con-

Table 4(a). Selected bond lengths (Å) for **1**

Atom	Atom	Distance	Atom	Atom	Distance
Mo(1)	Mo(2)	2.852(2)	Cu(1)	S	2.265(4)
Mo(3)	Mo(4)	2.863(2)	Cu(1)	S(2)	2.409(5)
Mo(1)	Cu(1)	2.802(2)	Cu(1)	S(3)	2.313(5)
Mo(2)	Cu(1)	2.760(2)	Cu(1)	P(1)	2.228(4)
Mo(3)	Cu(2)	2.743(2)	Cu(2)	S(O)	2.267(4)
Mo(4)	Cu(2)	2.779(2)	Cu(2)	S(5)	2.295(4)
Mo(1)	S	2.353(4)	Cu(2)	S(6)	2.385(4)
Mo(1)	S(1)	2.307(4)	Cu(2)	P(2)	2.198(4)
Mo(1)	S(2)	2.169(4)	S(11)	C(11)	1.80(2)
Mo(1)	S(11)	2.387(5)	S(12)	C(12)	1.81(2)
Mo(1)	S(12)	2.382(4)	S(21)	C(21)	1.82(2)
Mo(2)	S	2.358(4)	S(22)	C(22)	1.83(2)
Mo(2)	S(1)	2.316(4)	S(31)	C(31)	1.83(2)
Mo(2)	S(3)	2.161(4)	S(32)	C(32)	1.82(2)
Mo(2)	S(21)	2.360(4)	S(41)	C(41)	1.72(2)
Mo(2)	S(22)	2.389(4)	S(42)	C(42)	1.87(2)
Mo(3)	S(O)	2.375(4)	P(1)	C(111)	1.84(1)
Mo(3)	S(4)	2.319(4)	P(1)	C(121)	1.86(1)
Mo(3)	S(5)	2.156(4)	P(1)	C(131)	1.83(1)
Mo(3)	S(31)	2.361(5)	P(2)	C(211)	1.82(1)
Mo(3)	S(32)	2.368(4)	P(2)	C(221)	1.83(1)
Mo(4)	S(O)	2.363(4)	P(2)	C(231)	1.80(1)
Mo(4)	S(4)	2.312(4)	C(11)	C(12)	1.58(3)
Mo(4)	S(6)	2.169(4)	C(21)	C(22)	1.46(2)
Mo(4)	S(41)	2.376(4)	C(31)	C(32)	1.49(3)
Mo(4)	S(42)	2.366(5)	C(41)	C(42)	1.43(3)

Table 4(b). Selected bond lengths (Å) for **2**

Atom	Atom	Distance	Atom	Atom	Distance
W(1)	W(2)	2.844(1)	Cu(1)	S(1)	2.304(7)
W(3)	W(4)	2.853(1)	Cu(1)	S(3)	2.398(7)
W(1)	Cu(1)	2.765(3)	Cu(1)	S(4)	2.378(7)
W(2)	Cu(1)	2.762(3)	Cu(2)	S(5)	2.315(6)
W(3)	Cu(2)	2.737(3)	Cu(2)	S(7)	2.357(7)
W(4)	Cu(2)	2.730(3)	Cu(2)	S(8)	2.350(7)
W(1)	S(1)	2.311(6)	Cu(1)	P(1)	2.190(7)
W(1)	S(2)	2.356(6)	Cu(2)	P(2)	2.161(6)
W(1)	S(3)	2.139(6)	S(11)	C(11)	1.83(4)
W(1)	S(11)	2.449(7)	S(12)	C(12)	1.81(3)
W(1)	S(12)	2.351(8)	S(21)	C(21)	1.80(3)
W(2)	S(1)	2.320(6)	S(22)	C(22)	1.84(3)
W(2)	S(2)	2.384(6)	S(31)	C(31)	1.73(4)
W(2)	S(4)	2.124(6)	S(32)	C(32)	1.82(5)
W(2)	S(21)	2.431(6)	S(41)	C(41)	1.87(3)
W(2)	S(22)	2.313(7)	S(42)	C(42)	1.83(3)
W(3)	S(5)	2.327(6)	C(11)	C(12)	1.54(5)
W(3)	S(6)	2.381(6)	C(21)	C(22)	1.52(4)
W(3)	S(7)	2.123(6)	C(31)	C(32)	1.53(6)
W(3)	S(31)	2.405(7)	C(41)	C(42)	1.47(5)
W(3)	S(32)	2.343(8)	P(1)	C(111)	1.83(3)
W(4)	S(5)	2.330(6)	P(1)	C(121)	1.83(2)
W(4)	S(6)	2.357(6)	P(1)	C(131)	1.83(2)
W(4)	S(8)	2.107(6)	P(2)	C(211)	1.79(2)
W(4)	S(41)	2.359(7)	P(2)	C(221)	1.83(2)
W(4)	S(42)	2.441(7)	P(2)	C(231)	1.82(3)

Table 5(a). Selected bond angles (°) for **1**

Atom 1	Atom 2	Atom 3	Angle	Atom 1	Atom 2	Atom 3	Angle
Mo(2)	Mo(1)	Cu(1)	58.44(5)	S(5)	Cu(2)	S(6)	107.7(1)
Mo(1)	Mo(2)	Cu(1)	59.88(5)	S(5)	Cu(2)	P(2)	111.5(1)
Mo(1)	Cu(1)	Mo(2)	61.68(5)	S(6)	Cu(2)	P(2)	109.4(1)
Mo(4)	Mo(3)	Cu(2)	59.38(5)	Mo(3)	S(0)	Mo(4)	74.3(2)
Mo(3)	Mo(4)	Cu(2)	58.17(5)	Mo(3)	S(0)	Cu(2)	72.4(1)
Mo(3)	Cu(2)	Mo(4)	62.44(5)	Mo(4)	S(0)	Cu(2)	73.7(1)
S	Mo(1)	S(1)	101.1(1)	Mo(1)	S	Mo(2)	74.6(2)
S	Mo(1)	S(2)	105.0(1)	Mo(1)	S	Cu(1)	74.7(1)
S	Mo(1)	S(11)	148.4(2)	Mo(2)	S	Cu(1)	73.4(1)
S	Mo(1)	S(12)	77.8(1)	Mo(1)	S(1)	Mo(2)	76.2(2)
S(1)	Mo(1)	S(2)	110.5(2)	Mo(1)	S(2)	Cu(1)	75.3(1)
S(1)	Mo(1)	S(11)	78.7(1)	Mo(2)	S(3)	Cu(1)	76.1(1)
S(1)	Mo(1)	S(12)	137.8(2)	Mo(3)	S(4)	Mo(4)	76.4(1)
S(2)	Mo(1)	S(11)	104.6(2)	Mo(3)	S(5)	Cu(2)	76.0(1)
S(2)	Mo(1)	S(12)	110.5(2)	Mo(4)	S(6)	Cu(2)	75.0(1)
S(11)	Mo(1)	S(12)	81.7(2)	Mo(1)	S(11)	C(11)	105.0(7)
S	Mo(2)	S(1)	100.7(1)	Mo(1)	S(12)	C(12)	110.0(7)
S	Mo(2)	S(3)	103.9(1)	Mo(2)	S(21)	C(21)	107.2(6)
S	Mo(2)	S(21)	77.7(1)	Mo(2)	S(22)	C(22)	99.5(5)
S	Mo(2)	S(22)	150.7(1)	Mo(3)	S(31)	C(31)	107.2(6)
S(1)	Mo(2)	S(3)	111.9(2)	Mo(3)	S(32)	C(32)	102.7(6)
S(1)	Mo(2)	S(21)	136.5(2)	Mo(4)	S(41)	C(41)	105.3(9)
S(1)	Mo(2)	S(22)	79.4(1)	Mo(4)	S(42)	C(42)	105.4(9)
S(3)	Mo(2)	S(21)	110.6(2)	Cu(1)	P(1)	C(111)	112.6(5)
S(3)	Mo(2)	S(22)	103.2(1)	Cu(1)	P(1)	C(121)	111.8(4)
S(21)	Mo(2)	S(22)	82.4(1)	Cu(1)	P(1)	C(131)	115.6(5)
S(0)	Mo(3)	S(4)	100.4(1)	C(111)	P(1)	C(121)	104.4(6)
S(0)	Mo(3)	S(5)	103.8(1)	C(111)	P(1)	C(131)	106.3(6)
S(0)	Mo(3)	S(31)	79.2(1)	C(121)	P(1)	C(131)	105.2(6)
S(0)	Mo(3)	S(32)	152.3(2)	Cu(2)	P(2)	C(211)	113.8(5)
S(4)	Mo(3)	S(5)	112.0(2)	Cu(2)	P(2)	C(221)	110.8(4)
S(4)	Mo(3)	S(31)	136.7(2)	Cu(2)	P(2)	C(231)	113.7(5)
S(4)	Mo(3)	S(32)	79.1(2)	C(211)	P(2)	C(221)	106.3(6)
S(5)	Mo(3)	S(31)	110.1(2)	C(211)	P(2)	C(231)	103.5(6)
S(5)	Mo(3)	S(32)	101.9(2)	C(221)	P(2)	C(231)	108.1(6)
S(31)	Mo(3)	S(32)	82.5(2)	S(11)	C(11)	C(12)	109(1)
S(0)	Mo(4)	S(4)	100.9(1)	S(12)	C(12)	C(11)	111(1)
S(0)	Mo(4)	S(6)	104.7(1)	S(21)	C(21)	C(22)	112(1)
S(0)	Mo(4)	S(41)	151.7(2)	S(22)	C(22)	C(21)	111(1)
S(0)	Mo(4)	S(42)	78.6(2)	S(31)	C(31)	C(32)	112(1)
S(4)	Mo(4)	S(6)	111.6(2)	S(32)	C(32)	C(31)	109(1)
S(4)	Mo(4)	S(41)	79.0(2)	S(41)	C(41)	C(42)	112(2)
S(4)	Mo(4)	S(42)	136.5(2)	S(42)	C(42)	C(41)	115(1)
S(6)	Mo(4)	S(41)	101.4(2)	P(1)	C(111)	C(112)	123(1)
S(6)	Mo(4)	S(42)	110.4(2)	P(1)	C(111)	C(116)	116(2)
S(41)	Mo(4)	S(42)	82.3(2)	P(1)	C(121)	C(122)	120(2)
S	Cu(1)	S(2)	100.3(1)	P(1)	C(121)	C(126)	117(2)
S	Cu(1)	S(3)	102.1(1)	P(1)	C(131)	C(132)	114(2)
S	Cu(1)	P(1)	116.5(1)	P(1)	C(131)	C(136)	124(1)
S(2)	Cu(1)	S(3)	106.2(2)	P(2)	C(211)	C(212)	122(2)
S(2)	Cu(1)	P(1)	116.8(1)	P(2)	C(211)	C(216)	117(2)
S(3)	Cu(1)	P(1)	113.2(1)	P(2)	C(221)	C(222)	118(2)
S(0)	Cu(2)	S(5)	103.0(1)	P(2)	C(221)	C(226)	123(1)
S(0)	Cu(2)	S(6)	101.0(1)	P(2)	C(231)	C(232)	124(1)
S(0)	Cu(2)	P(2)	123.1(1)	P(2)	C(231)	C(236)	119(2)

Table 5(b). Selected bond angles (°) for **2**

Atom	Atom	Atom	Angle	Atom	Atom	Atom	Angle
Cu(1)	W(1)	W(2)	58.98(7)	S(5)	W(3)	S(6)	100.2(2)
Cu(1)	W(2)	W(1)	59.09(7)	S(5)	W(3)	S(31)	149.2(3)
W(2)	Cu(1)	W(1)	61.93(7)	S(5)	W(3)	S(32)	79.9(3)
Cu(2)	W(3)	W(4)	58.44(7)	S(6)	W(3)	S(31)	76.1(3)
Cu(2)	W(4)	W(3)	58.65(7)	S(6)	W(3)	S(32)	134.3(3)
W(4)	Cu(2)	W(3)	62.91(7)	S(7)	W(3)	S(5)	107.6(2)
S(1)	W(1)	S(2)	101.5(2)	S(7)	W(3)	S(6)	110.6(3)
S(1)	W(1)	S(11)	147.7(3)	S(7)	W(3)	S(31)	102.1(3)
S(1)	W(1)	S(12)	79.3(3)	S(7)	W(3)	S(32)	112.8(3)
S(2)	W(1)	S(11)	76.2(2)	S(32)	W(3)	S(31)	81.4(3)
S(2)	W(1)	S(12)	135.4(3)	S(5)	W(4)	S(6)	100.9(2)
S(3)	W(1)	S(1)	107.8(2)	S(5)	W(4)	S(41)	79.7(2)
S(3)	W(1)	S(2)	109.8(3)	S(5)	W(4)	S(42)	151.2(3)
S(3)	W(1)	S(11)	103.1(3)	S(6)	W(4)	S(41)	133.9(3)
S(3)	W(1)	S(12)	112.3(3)	S(6)	W(4)	S(42)	76.4(2)
S(11)	W(1)	S(12)	80.5(3)	S(8)	W(4)	S(5)	107.3(2)
S(1)	W(2)	S(2)	100.3(2)	S(8)	W(4)	S(6)	112.2(3)
S(1)	W(2)	S(21)	149.6(2)	S(8)	W(4)	S(41)	111.4(3)
S(1)	W(2)	S(22)	78.5(2)	S(8)	W(4)	S(42)	100.0(3)
S(2)	W(2)	S(21)	77.6(2)	S(41)	W(4)	S(42)	82.0(3)
S(2)	W(2)	S(22)	134.6(3)	S(1)	Cu(1)	S(3)	99.8(2)
S(4)	W(2)	S(1)	107.1(2)	S(1)	Cu(1)	S(4)	99.7(2)
S(4)	W(2)	S(2)	111.3(3)	S(4)	Cu(1)	S(3)	106.0(3)
S(4)	W(2)	S(21)	101.6(3)	P(1)	Cu(1)	S(1)	116.3(2)
S(4)	W(2)	S(22)	112.3(3)	P(1)	Cu(1)	S(3)	119.3(3)
S(22)	W(2)	S(21)	81.9(3)	P(1)	Cu(1)	S(4)	113.2(3)
S(5)	Cu(2)	S(7)	100.5(2)	S(5)	Cu(2)	S(8)	100.1(2)
S(8)	Cu(2)	S(7)	108.5(3)	P(2)	Cu(2)	S(5)	123.2(2)
P(2)	Cu(2)	S(8)	111.3(3)	P(2)	Cu(2)	S(7)	111.8(3)
Cu(1)	S(1)	W(1)	73.6(2)	Cu(1)	S(1)	W(2)	73.4(2)
W(1)	S(1)	W(2)	75.8(2)	W(1)	S(2)	W(2)	73.7(2)
W(1)	S(3)	Cu(1)	74.8(2)	W(2)	S(4)	Cu(1)	75.5(2)
Cu(2)	S(5)	W(3)	72.3(2)	Cu(2)	S(5)	W(4)	72.0(2)
W(3)	S(5)	W(4)	75.6(2)	W(4)	S(6)	W(3)	74.0(2)
W(3)	S(7)	Cu(2)	75.1(2)	W(4)	S(8)	Cu(2)	75.3(2)
C(111)	P(1)	C(121)	104(1)	C(111)	P(1)	C(131)	105(1)
C(121)	P(1)	C(131)	106(1)	C(211)	P(2)	C(231)	108(1)
C(211)	P(2)	C(221)	107(1)	C(231)	P(2)	C(221)	106(1)

sistent with the IR spectra, which show that the vibration of the Mo—S double bond decreases from 515 to 495 cm^{-1}. The Mo—Cu bonds are av. 2.771 Å, which is in the range of effectively bonding. The Cu—μ_3-S bond length is 2.265 Å, but the two Cu—μ_2-S bond lengths are significantly different. One Cu—μ_2-S is 2.313 Å and the other 2.409 Å. This lowers the overall symmetry of the core from C_s to C_1.

Comparing the W-compound (**2**) with the starting ditungsten complex, the dihedral angle in the W_2S_2 ring changes a little from 148.9(1)° to 143.8(3)°. As pointed out for the dinuclear tungsten complex,[25] the two terminal sulphido atoms are in a *cis* position relative to the $S_2WS_2WS_2$ unit. The product atoms are in a *cis* position relative to the $S_2WS_2WS_2$ unit. The product compound also has this *cis* configuration, but the $CuPPh_3^+$ group is only attached to one side (see Table 5). At the μ_3-S side with reference to the W_2S_2 ring, the angles of S(3)—W(1)—S(12) and S(4)—W(2)—S(22) are approximately 10° larger than the corresponding angles S(3)—W(1)—S(11) and S(4)—W(2)—S(21), respectively. Unlike the Mo-compound (**1**), the W—S_t double bond does not elongate, in fact it seems to be somewhat stronger (from av. 2.144 Å to av. 2.123 Å). However, the vibrational frequency of the W—S double bond is slightly reduced from

Table 6. Crystallographic equations[a] for least-squares planes in the Mo- and W-trinuclear clusters

Atom	Distance, Å	Atom	Distance, Å
Mo-compound			
Plane 1: $8.4110x+6.3041y-4.2337z-6.3896=0$			
S	−0.100	S(12)	0.115
S(1)	0.099	Mo(1)	−0.711
S(11)	−0.114		
r.m.s. deviation of the fitted atoms from the plane 1 is 0.113 Å.			
Plane 2: $-8.6393x-7.4346y-2.7905z+11.9430=0$			
S	0.136	S(22)	0.153
S(1)	−0.133	Mo(2)	0.703
S(21)	−0.157		
r.m.s. deviation of the fitted atoms from the plane 2 is 0.145 Å.			
Plane 3: $-8.1747x-7.8550y-5.3258z+4.1212=0$			
S(0)	0.143	S(32)	0.166
S(4)	−0.144	Mo(3)	0.687
S(31)	−0.166		
r.m.s. deviation of the fitted atoms from the plane 3 is 0.155 Å.			
Plane 4: $8.1135x+8.2389y-0.9030z-2.7611=0$			
S(0)	−0.141	S(42)	0.164
S(4)	0.141	Mo(4)	−0.691
S(41)	−0.163		
r.m.s. deviation of the fitted atoms from the plane 4 is 0.152 Å.			
W-compound			
Plane 5: $6.4728x-4.3190y-8.5760z+0.8994=0$			
S(1)	−0.105	S(12)	0.123
S(2)	0.103	W(1)	−0.757
S(11)	−0.122		
r.m.s. deviation of the fitted atoms from the plane 5 is 0.113 Å.			
Plane 6: $7.3754x+2.7118y-8.5920z-1.1864=0$			
S(1)	−0.134	S(22)	0.155
S(2)	0.130	W(2)	−0.730
S(21)	−0.152		
r.m.s. deviation of the fitted atoms from the plane 6 is 0.143 Å.			
Plane 7: $8.2752x-1.1613y-8.2292z-1.8444=0$			
S(5)	−0.130	S(32)	0.152
S(6)	0.129	W(3)	−0.753
S(31)	−0.150		
r.m.s. deviation of the fitted atoms from the plane 7 is 0.140 Å.			
Plane 8: $7.7369x-5.2155y-7.9873z-6.2958=0$			
S(5)	−0.147	S(42)	−0.170
S(6)	0.149	W(4)	−0.712
S(41)	0.167		
r.m.s. deviation of the fitted atoms from the plane 8 is 0.158 Å.			

[a] Equations were fitted to the sulphur atoms only.

504 to 498 cm^{-1}. The Cu—μ_3-S bond length is 2.304(7) Å, and the other two Cu—μ_2-S bond lengths are 2.398(7) and 2.378(7) Å, respectively. The overall symmetry of the core is approximately C_s.

DISCUSSION

The title compounds both have three metal—metal bonds. The short Mo—Mo or W—W bonds are comparable to the dinuclear complexes and can also be interpreted in terms of a metal—metal σ bond. The Mo—Cu or W—Cu bonds are much weaker but the bond lengths are somewhat shorter than Mo—Mo or W—W bonds. The M—μ_2-S_t bonds are very short and can be regarded as double bonds. Meanwhile, the Cu—μ_2-S_t bonds are relatively long, for example they are even approximately 0.1 Å longer than the Cu—μ_3-S bond. Therefore, in the $\{Mo_2CuS_4\}^{3+}$ and $\{W_2CuS_4\}^{3+}$ core there are two unsymmetrical μ_2-bridging sulphido atoms, respectively, in which the two bridging bonds are double bond and single bond. It is noted that the Cu—μ_3-S is shorter than the Cu—μ_2-S_t. This may be because the Cu—μ_3-S bond is approximately parallel to the two M—μ_2-S_t double bonds. Association with the organic olefin chemistry, the reduced short Cu—μ_3-S bond and the two M—μ_2-S_t double bonds may form a large conjugation system due to the approximately space parallel. The conjugation system is stereoscopic because of the participation of the *d* orbitals.

The two title clusters are examples which have new unsymmetrical μ_2-bridging sulphido atoms.[1,23] The M—μ_2-S_t double bonds play an important role in the structure of the $\{M_2CuS_4\}^{3+}$ cores. Very similar to the property of withdrawing electrons through the C—C double bond in organic chemistry, one positively metallic atom (Cu^+ here) may also withdraw electrons through the bridging double bond (Mo—μ_2-S_t or W—μ_2-S_t), which causes the bond of Mo—S_{edt} or W—S_{edt} to become stronger. The result of withdrawing electrons through Mo—μ_2-S_t or W—μ_2-S_t double bonds is consistent with the bond length changes (see Table 4) and the shifts of the IR vibrational bands (see Table 2) of Mo—S_{edt} or W—S_{edt}. Association with the bond lengths and IR spectra of $[M_2Cu_2S_4]^{4+}$, it makes the phenomenon more obvious (for clarity, Table 7 lists the bond changes and the IR shifts). Scheme 2 shows the flow of the electrons when the $CuPPh_3^+$ group withdraws the lone-pair electrons from the sulphido atoms to its 4*s*, 4*p* orbitals through the M—μ_2-S_t double bond to make the M—S_{edt} bond shorter.

Table 7. Bond lengths changing and IR spectra shift of $(M—SR)_{edt}$[a] bonds from dinuclear complexes to cubane-like clusters

Compound	Av. bond length of M—S_{edt}		IR bands of ν(M—SR), cm^{-1}	
$\{Mo_2S_4\}^{2+}$	2.406(3) Å		340(w), 295(w)	
$\{Mo_2CuS_4\}^{3+}$	2.380(4), 2.368(4)[b]	[c]	350(w), 310(w)	[d]
$\{Mo_2Cu_2S_4\}^{4+}$	2.360(2)		360(m), 320(w)	
$\{W_2S_4\}^{2+}$	2.404(2)		343(w), 300(w)	
$\{W_2CuS_4\}^{3+}$	2.386(7), 2.387(7)[b]	[c]	350(m), 310(m)	[d]
$\{W_2Cu_2S_4\}^{4+}$	2.346(4)		365(s), 324(m)	

[a] M = Mo, W.
[b] The two average bond lengths are from two discrete anions, respectively.
[c] The bond lengths become shorter in order.
[d] The corresponding absorption bands shift to higher frequency in order.

Table 8. Comparison of bond lengths and angles of four incomplete cubane-like clusters

	$\{Mo_3S_4\}^{4+}$ [a]	$\{Mo_2CuS_4\}^{3+}$ [b]	$\{W_3S_4\}^{4+}$ [c]	$\{W_2CuS_4\}^{3+}$ [b]
M—M	2.7632(8)	2.858(2)	2.7393(6)	2.849(1)
M—M	2.6817(9)	—	2.6728(6)	—
M—M	2.7452(8)	—	2.7497(6)	—
M—Cu	—	2.752(2)	—	2.751(1)
M—Cu	—	2.791(2)	—	2.746(1)
M—μ_2-S	2.286(3), 2.280(2)	2.169(4), 2.310(4)	2.295(3), 2.301(3)	2.131(6), 2.368(6)
M—μ_2-S	2.286(2), 2.273(2)	2.159(4), 2.318(4)	2.293(3), 2.303(3)	2.116(6), 2.371(6)
M—μ_2-S	2.293(2), 2.285(2)	—	2.290(3), 2.304(4)	—
Cu—μ_2-S	—	2.397(4), 2.304(4)	—	2.378(7), 2.364(7)
M—μ_3-S	2.340(2)	2.358(4)	2.343(2)	2.319(6)
M—μ_3-S	2.336(2)	2.367(4)	2.346(2)	2.325(6)
M—μ_3-S	2.327(2)	—	2.340(2)	—
Cu—μ_3-S	—	2.266	—	2.310(7)
μ_2-S···μ_2-S	3.444	3.779	3.489	3.818
μ_2-S···μ_2-S	3.327	3.710	3.361	3.716
μ_2-S···μ_2-S	3.312	3.693	3.357	3.693
M—M—M	60.47(2)°	58.31(5)	61.06(2)	58.71(7)
M—M—M	58.30(2)	59.63(5)	58.28(8)	58.87(7)
M—M—M	61.24(2)	—	60.66(1)	—
M—Cu—M	—	62.06(5)	—	62.42(7)
M—μ_2-S—M	74.36(6)	76.3(2)	73.21(7)	73.9(2)
M—μ_2-S—M	73.84(6)	—	71.21(8)	—
M—μ_2-S—M	71.96(6)	—	73.29(8)	—
M—μ_2-S—Cu	—	75.2(1)	—	75.0(2)
M—μ_2-S—Cu	—	76.1(1)	—	75.4(2)
M—μ_3-S—M	72.46(5)	74.5(1)	71.48(7)	74.8(2)
M—μ_3-S—M	70.15(5)	—	69.61(7)	—
M—μ_3-S—M	72.05(5)	—	71.86(7)	—
M—μ_3-S—Cu	—	74.2(1)	—	73.0(2)
M—μ_3-S—Cu	—	72.9(1)	—	72.7(2)
μ_2-S—M—μ_2—S	93.55(8)	111.1(2)	94.0(1)	110.2(3)
μ_2-S—M—μ_2—S	98.12(7)	112.0(2)	98.63(9)	111.8(3)
μ_2-S—M—μ_2—S	92.70(7)	—	94.0(1)	—
μ_2-S—Cu—μ_2—S	—	107.0(2)	—	107.3(3)

[a] The data are from ref. 49.
[b] The bond lengths and angles are averaged from those of two independent anions.
[c] The data are from ref. 21(j).

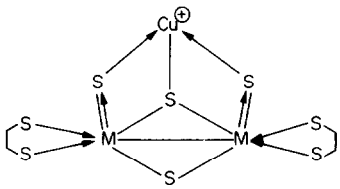

Scheme 2.

Scheme 2 shows that the function of the double bond is very similar to the C=C double bond in transmitting electron density. However, the pattern of the flow of electrons here may also be more three-dimensional because of the participation of *d* orbitals of the Mo atom or W atom.

For comparison, the major average bond distances and bond angles of the four homo- and heterometallic incomplete cubane-like clusters are listed in Table 8. In homometallic clusters with $\{M_3S_4\}^{4+}$, the six M—μ_2-S bonds are approximately identical and they are shorter than the M—μ_3-S bonds. The $M_3S_4{}^{4+}$ cores are about C_{3v} symmetry with the regular six-membered puckered M_3S_3 ring. However, in the two heterometallic clusters with the $\{M_2CuS_4\}^{3+}$ cores, the six bonds of the six-membered M_2CuS_4 puckered ring are quite different. The three separated μ_2-S atoms in the heterometallic cluster cores have distances 0.3–0.5 Å longer than those in the homometallic cluster cores. In the $W_2CuS_4{}^{3+}$ core, the bond length of W—μ_3-S_b is exceptionally shorter than that of W—μ_2-S_b. Additionally, the long bond length of the W—μ_2-S is unusual.

Based on the stability, substitution, addition and oxidation, quantum calculation, etc., the quasi-aromaticity hypothesis in the $Mo_3(\mu_2\text{-}S)_3$ structural unit of the $Mo_3S_4{}^{4+}$ core has been proposed by Huang *et al.*,[50] which has been pictured[51] by the quantum chemistry using the three-centre two-electron *d*(Mo)-*p*(S)-*d*(Mo) π bond. The detailed structure of the $M_2Cu(\mu_2\text{-}S)_3$ unit of the $M_2CuS_4{}^{3+}$ (M = Mo, W) core is different from the Mo_3S_3 unit. The main reason is that the Cu^+ has d^{10} configuration which has no vacant *d* orbital. But other bonds in the core have been strengthened.

Acknowledgements—This research has been supported by grants from the Structural Chemistry Research Laboratory of the Fujian Institute of Research on the Structure of Matter, Chinese Academy of Sciences and the National Science Foundation of China.

REFERENCES

1. H. Vahrenkamp, *Angew. Chem., Int. Edn Engl.* 1975, **14**, 322.
2. A. Müller, E. Diemann, R. Jostes and H. Bögge, *Angew. Chem., Int. Edn Engl.* 1981, **20**, 934.
3. I. G. Dance, *Polyhedron* 1986, **5**, 1037.
4. (a) J. M. Berg, R. H. Holm, in *Iron–Sulfur Proteins* (Edited by T. G. Spiro), Ch. 1. John Wiley, New York (1989). (b) C. D. Stout, *ibid.*, Ch. 3.
5. E. I. Stiefel, *Prog. Inorg. Chem.* 1977, **22**, 1.
6. (a) T. E. Wolff, T. M. Berg, C. Warrick, K. O. Hodgson and R. H. Holm, *J. Am. Chem. Soc.* 1978, **100**, 4630. (b) T. E. Wolff, T. M. Berg, K. O. Hodgson, R. B. Frankel and R. H. Holm, *ibid.*, 1979, **101**, 4140. (c) T. E. Wolff, T. M. Berg, P. P. Power, K. O. Hodgson, R. H. Holm and R. B. Frankel, *ibid.*, 1979, **101**, 5454.
7. (a) D. Coucouvanis, E. D. Simhon, D. Swenson and N. C. Baenziger, *J. Chem. Soc., Chem. Commun.* 1979, 361. (b) D. Coucouvanis, D. Swenson, A. Simopoulos, A. Kostikas, V. Petrouleas and V. Papaefthymiou, *J. Am. Chem. Soc.* 1980, **102**, 1732. (c) D. Coucouvanis, A. Kostikas, A. Simoploulos, V. Petrouleas and V. Papaefthymiou, *ibid.*, 1980, **102**, 1730. (d) C. H. Tieckelmann and B. A. Averill, *Inorg. Chim. Acta* 1980, **46**, 135.
8. S. Sarkar and S. B. S. Mishra, *Coord. Chem. Rev.* 1984, **59**, 239.
9. D. Coucouvanis, A. Hadjikyriacou, M. Draganjac, M. G. Kanatzidis and O. Ileperuma, *Polyhedron* 1986, **5**, 349.
10. M. R. Dubois, *J. Am. Chem. Soc.* 1983, **105**, 3170.
11. M. Draganjac and T. B. Rauchfuss, *Angew. Chem., Int. Edn Engl.* 1985, **24**, 742.
12. T. Saito, N. Yamamoto, T. Yamagata and H. Imoto, *J. Am. Chem. Soc.* 1988, **110**, 1646.
13. (a) X.-T. Wu, S.-F. Lu, N.-Y. Zhu, Q.-J. Wu and J.-X. Lu, *Inorg. Chim. Acta* 1987, **133**, 39. (b) X.-T. Wu, Y.-F. Zheng, N.-Y. Zhu and J.-X. Lu, *JIEGOU HUAXUE* (*J. Struct. Chem.*) 1988, **7**, 137 (English). (c) S.-F. Lu, N.-Y. Zhu, X.-T. Wu, Q.-J. Wu and J.-X. Lu, *J. Molec. Struct.* 1989, **197**, 15. (d) Y.-F. Zheng, N.-Y. Zhu and X.-T. Wu, *Acta Cryst.* 1989, **C45**, 1988.
14. (a) H.-Q. Zhan, Y.-F. Zheng, X.-T. Wu and J.-X. Lu, *Inorg. Chim. Acta* 1989, **156**, 277. (b) Y.-F. Zheng, H.-Q. Zhan, X.-T. Wu and J.-X. Lu, *Trans. Met. Chem.* 1989, **14**, 161. (c) Y.-F. Zheng, H.-Q. Zhan and X.-T. Wu, *Acta Cryst.* 1989, **C45**, 1990. (d) X.-T. Wu, H.-Q. Zhan, Y.-F. Zheng and J.-X. Lu, *J. Molec. Struct.* 1989, **197**, 33.
15. T. Shibahara, H. Akashi and H. Kuroya, *J. Am. Chem. Soc.* 1986, **108**, 1342.
16. (a) N.-Y. Zhu, Y.-F. Zheng and X.-T. Wu, *J. Chem. Soc., Chem. Commun.* 1990, 780. (b) N.-Y. Zhu, R.-C. Wu and X.-T. Wu, *Acta Cryst.* 1991, In press.
17. T. R. Halbert, S. A. Cohen and E. I. Stiefel, *Organometallics* 1985, **4**, 1689.
18. (a) R. E. Palermo, R. Singh, J. K. Bashkin and R. H. Holm, *J. Am. Chem. Soc.* 1984, **106**, 2600 and references therein. (b) Q.-T. Liu, L.-R. Huang, Y. Yang and J.-X. Lu, *Acta Chimica Sinica* (*HUAXUE XUEBAO*) 1988, **46**, 286 (English) and references therein.

19. (a) A. Müller, H. Bögge and U. Schimanski, *Angew. Chem., Int. Edn Engl.* 1980, **19**, 654. (b) A. Müller, H. Bögge and U. Schimanski, *Inorg. Chim. Acta* 1983, **69**, 5.
20. (a) X.-T. Wu, Y.-F. Zheng, S.-W. Du and N.-Y. Zhu, *Trans. Met. Chem.* 1989, **14**, 157. (b) X.-T. Wu, Y.-F. Zheng and S.-W. Du, *Acta Cryst.* 1989, **C45**, 1070. (e) N.-Y. Zhu, J.-H. Wu and X.-T. Wu, *Acta Cryst.* 1991, in press.
21. (a) P. J. Vergamini, H. Vahrenkamp and L. F. Dahl, *J. Am. Chem. Soc.* 1971, **93**, 6327. (b) A. Müller and U. Reinsch, *Angew. Chem., Int. Edn Engl.* 1980, **19**, 72. (c) T. R. Halbert, K. McGauley, W. H. Pan, R. S. Czernuszewicz and E. I. Stiefel, *J. Am. Chem. Soc.* 1984, **106**, 1849. (d) F. A. Cotton, Z. Dori, R. Llusar and W. Schwotzer, *Inorg. Chem.* 1986, **25**, 3654. (e) P. Kathirgamanathan, M. Martinez and M. A. G. Sykes, *J. Chem. Soc., Chem. Commun.* 1985, 1437. (f) X.-T. Lin, Y.-H. Lin, J.-L. Huang and J.-Q. Huang, *KEXUE TONGBAO* 1987, **32**, 810 (English). (g) T. Shibahara and H. Kuroya, *Polyhedron* 1986, **5**, 357. (h) T. Shibahara, K. Kohda, A. Ohtsuji, K. Yasuda and H. Kuroya, *J. Am. Chem. Soc.* 1986, **108**, 2757. (i) T. Shibahara, A. Takeuchi, A. Ohtsuji, K. Kohda and H. Kuroya, *Inorg. Chim. Acta* 1987, **127**, L45. (j) H.-Q. Zhan, Y.-F. Zheng, X.-T. Wu and J.-X. Lu, *J. Molec. Struct.* 1989, **196**, 241. (k) Y.-F. Zheng, H.-Q. Zhan and X.-T. Wu, *Acta Cryst.* 1989, **C45**, 1424.
22. A. Müller, R. Jostes and F. A. Cotton, *Angew. Chem., Int. Edn Engl.* 1980, **19**, 875.
23. X.-T. Wu and J.-X. Lu, *JIEGOU HUAXUE (J. Struct. Chem.)* 1989, **8**, 399 (Chinese).
24. H.-Q. Zhang, Master thesis of Fujian Institute of Research on Structure of Matter, 1989 (Chinese).
25. W. H. Pan, T. Chandler, J. H. Enemark and E. I. Stiefel, *Inorg. Chem.* 1984, **23**, 4265.
26. N.-Y. Zhu, Y.-F. Zheng and X.-T. Wu, *Inorg. Chem.* 1990, **29**, 2750.
27. N. Walker and D. Stuart, *Acta Cryst.* 1983, **A39**, 159.
28. P. Main, S. J. Fiske, S. E. Hull, L. Lessinger, G. Germain, J. P. Declercq and M. M. Woolfson, *MULTAN* 11/82. *A System of Computer Programs for the Automatic Solution of Crystal Structures from X-ray Diffraction Data.* Univ. of York, England, and Univ. of Louvain, Belgium (1982).
29. D. T. Cromer and J. T. Waber, *International Tables for X-ray Crystallography*, Vol. IV, Tables 2.2a, 2.3.1. Kynoch Press, Birmingham (1974).
30. R. C. G. Killean and J. L. Lawrance, *Acta Crystallogr.* 1969, **B25**, 1750.
31. B. A. Frenz, The Enraf–Nonius CAD4 SDP—A real-time system for concurrent X-ray data collect and crystal structure determination, in *Computing in Crystallography* (Edited by H. Schenk, R. Olthof-Hazekamp, H. van Konigsveld and G. C. Bassi), pp. 64–71. Delft University Press, Delft (1978).
32. *CONTROL, An Automation Package for Rigaku AFC Single Crystal Diffractometers.* Molecular Structure Corp., College Station, TX 77840 (1986).
33. C. J. Gilmore, *MITHRIL: A Computer Program for the Automatic Solution of Crystal Structures from X-ray Data.* University of Glasgow, Glasgow (1983).
34. P. T. Beirskens, *DIRDIF: Direct Methods for Difference Structures—An Automatic Procedure for Phase Extension and Refinement of Difference Structure Factors*; Technical Report 1984/1; Crystallography Laboratory, Toernooiveld, The Netherlands (1984).
35. TEXSAN, *TEXRAY Structure Analysis Package.* Molecular Structure Corp., Texas (1985).
36. S. J. Lippard and D. A. Ucko, *Inorg. Chem.* 1968, **7**, 1051.
37. F. A. Cotton, Z. Dori, R. Llusar and W. Schwotzer, *J. Am. Chem. Soc.* 1985, **107**, 6734.
38. T. Shibahara and H. Kuroya, Abstracts of papers, 1987 International Miniconference for Young Chemists in Tokyo Macrocyclic and Coordination Chemistry, Tokyo, July 1987.
39. K. S. Nagaraja and M. R. Udupa, *Polyhedron* 1985, **4**, 649.
40. F. A. Schultz, V. R. Ott, D. S. Rollison, D. C. Bravard, J. W. McDonald and W. E. Newton, *Inorg. Chem.* 1978, **17**, 1758.
41. F. W. Moore and M. L. Larson, *Inorg. Chem.* 1967, **6**, 998.
42. S. F. Gheller, T. W. Hambley, J. R. Rodgers, R. T. C. Brownlee, M. J. O'connor, M. R. Snow and A. G. Wedd, *Inorg. Chem.* 1984, **23**, 2519.
43. F. Secheresse, M. Salis, C. Potvin and J. M. Manoli, *Inorg. Chim. Acta* 1986, **114**, L19.
44. S. R. Acott, C. D. Garner, J. R. Nicholson and W. Clegg, *J. Chem. Soc., Dalton Trans.* 1983, 713.
45. J. M. Manoli, C. Potvin, F. Scheresse and S. Marzak, *Inorg. Chim. Acta* 1988, **150**, 257.
46. 2mM solution in 0.1 M Bu_4NClO_4 vs standard calomel electrode in CH_2Cl_2 solution with a platinum electrode (scan rate 0.1 V/s).
47. K. F. Miller, A. E. Bruce, J. L. Corbin, S. Wherland and E. I. Stiefel, *J. Am. Chem. Soc.* 1980, **102**, 5102.
48. G. Bunzey and J. H. Enemark, *Inorg. Chem.* 1978, **17**, 682.
49. Y.-F. Zheng, N.-Y. Zhu, H.-Q. Zhan and X.-T. Wu, *Acta Cryst.* 1989, **C45**, 1632.
50. J.-Q. Huang, S.-F. Lu, M.-Y. Shang, X.-T. Lin, M.-D. Huang, Y.-H. Lin, D.-M. Wu, H.-H. Zhuang, J.-L. Huang and J.-X. Lu, *JIEGOU HUAXUE (J. Struct. Chem.)* 1987, **6**, 219 (Chinese).
51. J.-X. Lu, *JIEGOU HUAXUE (J. Struct. Chem.)* 1989, **8**, 327 (Chinese).

Polyhedron Vol. 10, No. 23/24, pp. 2757–2769, 1991
Printed in Great Britain

0277–5387/91 $3.00+.00
© 1991 Pergamon Press plc

SYNTHESIS, VIBRATIONAL SPECTROSCOPY AND EXAFS ANALYSIS OF SOME DIVALENT AND TRIVALENT TRIFLUOROMETHANESULPHONATO COMPLEXES

K. BOUMIZANE, M. H. HERZOG-CANCE, D. J. JONES, J. L. PASCAL,* J. POTIER and J. ROZIERE

Laboratoire des Agrégats Moléculaires et Matériaux Inorganiques, URA CNRS 79 CC015, Université Montpellier II, Sciences et Techniques du Languedoc, 34095 Montpellier Cédex 5, France

(*Received* 4 *February* 1991; *accepted* 22 *July* 1991)

Abstract—The syntheses of trifluoromethanesulphonato (OTf) complexes of Co^{II}, Ni^{II}, Cu^{II}, Fe^{III} and Ga^{III} by the reaction of simple metal salts (Cl^-, Br^-, CO_3^{2-}, ClO_4^-) or metallic gallium with trifluoromethanesulphonic acid have been systematically investigated.

Comparison of the vibrational spectra of coordinated OTf in these complexes with that in simple ionic salts indicates the ligand to be bridging bidentate in $M(OTf)_3$, M = Ga, Fe and in $M(OTf)_2$, M = Cu and bridging tridentate in $M'(OTf)_2$, M′ = Co, Ni, Cd. EXAFS spectroscopic data can be interpreted in terms of layered structural arrangements for Co, Ni, Cd and Ga trifluoromethanesulphonato complexes, similar to that of the corresponding anhydrous metal perchlorates studied previously. In $Cu(OTf)_2$, however, the copper atom is in a square planar environment. The short metal–oxygen distances, 1.96–2.09 Å are consistent with strong interactions between the ligand and metallic centre.

Research on the coordinating ability of weakly basic ligands, such as fluorosulphonate FSO_3^-, trifluoromethanesulphonate $CF_3SO_3^-$ and perchlorate ClO_4^- ions, has been considerably developed since the 1970s.[1–6] More recently the use of these weakly coordinated complexes in cationic polymerization,[7,8b] dehydration processes,[9] oxidation,[10] and superacid chemistry[8a] has been reported. Comparison of the Hammett acidities H_0 of their conjugate acids: $FSO_3H \sim CF_3SO_3H \sim -14$[11]; $HClO_4 \sim -17$[12] suggests that development of the chemistry of the $CF_3SO_3^-$ group along lines similar to that of ClO_4^- should be possible, with the clear advantage of avoiding the risks of manipulation associated with the oxidizing and instability properties of the latter.

Many advances have been made in recent years on the synthesis of ClO_4^- complexes and in obtaining structural information on them. For the $CF_3SO_3^-$ ligand only the synthetic aspect has been relatively well developed.[5,13] Complexes $M(OTf)_n$ (OTf = CF_3SO_3) are usually prepared from anhydrous CF_3SO_3H (HOTf) or aqueous HOTf solutions, however no study has yet compared these methods with other possible synthetic routes. Furthermore, structural data on the complexes so isolated is often restricted to that deducible from vibrational and electronic spectroscopies[5] or, more infrequently, from Mössbauer spectroscopy.[14]

The crystal structures of HOTf[15] and its oxonium[16] and alkali metal[17] salts are known, as well as that of $SeO(CF_3SO_3)_2$.[18] Only limited information on coordinated metal–oxygen distances is thus available, growth of single crystals containing coordinated OTf to the exclusion of other ligands being of great difficulty. An analogous situation exists in perchlorate chemistry, where classical methods of recrystallization frequently lead to the introduction of more basic solvent molecules into the coordination sphere.[19]

The contribution of EXAFS spectroscopy, applicable to polycrystalline compounds, in obtaining not only metal–oxygen but also metal to next-nearest-neighbour interatomic distances, has been considerable and has allowed the derivation

* Author to whom correspondence should be addressed.

of three-dimensional structural arrangements in favourable cases. The technique has been applied to perchlorate complexes,[20–22] for example, with success.

In the present paper, various synthetic routes to metal trifluoromethanesulphonate complexes $M(OTf)_n$ ($M = Ni^{II}$, Co^{II}, Cd^{II}, Ga^{III} and Fe^{III}) are discussed, and vibrational and EXAFS spectroscopic results are reported. Here the choice of M was directed such as to enable a comparative study of the perchlorate and trifluoromethanesulphonate ligands.

EXPERIMENTAL

All syntheses were performed in a Pyrex vacuum line analogous to that described for the preparation of anhydrous perchlorate complexes.[3] This set-up allows purification of trifluoromethanesulphonic acid or its anhydride, elimination of gases produced by the reactions and IR analysis by *in situ* deposition in a cell described previously.[23]

Trifluoromethanesulphonic acid and the corresponding anhydride (Merck) were distilled at room temperature under dynamic vacuum (10^{-2} torr). HOTf was mixed with sulphuric acid (36N) prior to distillation, while $(CF_3SO_2)_2O$ was subsequently stored over P_2O_5. The reaction of HOTf on different anhydrous or hydrated salts were conducted as described previously.[3,24]

Synthesis

OTf complexes have often been prepared by replacement of the *m*-bromobenzoate ligand,[25] a reaction which necessitates the prior synthesis of the appropriate benzoate and by which $Co(OTf)_2$ cannot be obtained.[26] In an attempt to avoid this intermediate step, alternative readily available metal salts—such as chlorides or carbonates—were used. Furthermore, the influence of the metal and the ligand to be substituted, and the source of the OTf ligand were examined in order to identify the best synthetic routes. Initial studies have concentrated on the following groups of metals: Ni/Co/Cd; Cu; Fe/Ga and on two distinct types of reaction:

(1) $ML_n + m(HOTf \cdot xH_2O) \longrightarrow nHL + M(OTf)_n \cdot m - n[H(mxH_2O)OTf]$

M = Co, Fe	L = Cl	
M = Ga	L = Br	$x \geqslant 0$
M = Cd	$L = CO_3$	
M = Cd	$L = NO_3$	
M = Cu, Ni	$L = CO_3$, OH	
M = Co	$L = ClO_4$	$(x = 0)$.

(2) $M + m(HOTf \cdot xH_2O) \longrightarrow n/2H_2 + M(OTf)_n \cdot m - n[H(mxH_2O)OTf]$,

n being the oxidation state of the metal.

The second of these general reactions[7] was adapted, in the present study, by using anhydrous HOTf and metallic gallium.

The use of hydrated salts, or of aqueous HOTf solutions, necessitates the subsequent elimination of H_3OOTf by heating, while with nitrates removal of NO_2OTf is required. As far as possible, reactions were performed using anhydrous salts—including $FeCl_3$, $CoCl_2$, $GaBr_3$ and $Co(ClO_4)_2$—to avoid this additional step.

A summary of the experimental conditions, the formation of intermediate complexes, the obtention of trifluoromethanesulphonatometal from them and elemental analyses of the products is given in Table 1.

Chemical analyses

Elemental analyses were carried out according to the method established for perchlorate ions[3] (in order to avoid all losses, dissolutions, in water, of the complexes are performed at low temperature, 90 K). Ni, Co, Cu and Fe were determined by complexation, Ga by atomic absorption spectroscopy, OTf by the acid–base conductimetric method developed by one of us[28] and halide ions by $AgNO_3$ potentiometry.

Vibrational spectroscopy

Vibrational spectroscopic data were recorded at temperatures between 80 and 298 K depending on the $M(OTf)_n$ complex (see below). IR spectra, reproduced in Fig. 1, were recorded on powdered samples between silicon windows on a Perkin–Elmer 180 instrument. Spectral resolution was 1–5 cm^{-1} at 1400 cm^{-1} and 7 cm^{-1} at 300 cm^{-1}. Raman spectra were obtained using a Dilor spectrometer coupled to a Tracor multichannel analyser with an argon laser (5145 Å, 150 mW), (Fig. 2). The powdered compounds were held in 5 mm o.d. Pyrex tubes. Spectral resolution was 0.5–1.0 cm^{-1} over the entire spectral range.

UV–vis spectroscopy

The UV–vis reflectance spectra of Cu, Co and Ni triflato complexes were recorded on a Cary-Varian 2300 spectrophotometer. The finely powdered samples were held in a teflon cell capped with an infrasil window.[24]

Table 1. Synthetic details and analyses of Ni^{II}, Co^{II}, Cu^{II}, Cd^{II}, Fe^{III} and Ga^{III} trifluoromethanesulphonato complexes

Starting reagent	HOTf	T[a]	Final product	Colour	M	Analysis%[b] OTf	X
Ga metal[c]	excess	rt	$Ga(OTf)_3$	white	13.2 (13.5)	86.8 (86.5)	
$GaBr_3$[d]	deficient	rt	$GaBr_2OTf$	white	18.3 (18.4)	39.1 (39.4)	42.7 (42.2)[e]
$GaBr_2OTf$	excess	rt	$Ga(OTf)_3$	white	13.5 (13.5)	86.5 (86.5)	
$FeCl_3$[f]	excess (48 hours)	rt	$Fe(OTf)_3$	yellow	11.2 (11.1)	88.8 (88.9)	
$CdCO_3$[f]	excess	rt	$Cd(OTf)_2$, $nH(H_2O)_nOTf$[g]	white			
$Cd(OTf)_2$, $nH(H_2O)_nOTf$	—	543	$Cd(OTf)_2$	white	27.4 (27.3)	72.6 (72.7)	
$CdCO_3$[f]	aqueous[h] solution	373	$Cd(OTf)_2$, nH_2O[g]				
$Cd(OTf)_2$, nH_2O	—	423	$Cd(OTf)_2$	white	27.4 (27.3)	72.6 (72.7)	
$Cd(NO_3)\cdot 4H_2O$[f]	oleum	rt	$Cd(OTf)_2$, NO_2OTf, H_3OOTf				
$Cd(OTf)_2$, NO_2OTf, H_3OOTf	—	373	$Cd(OTf)_2$	white	27.7 (27.3)	72.3 (72.7)	
$NiCO_3\cdot 2Ni(OH)_2\cdot 4H_2O$[f]	excess	rt	$Ni(OTf)_2$, $3H_3OOTf$	yellow	07.3 (06.9)	86.0 (86.5)	6.5 (6.6)[i]
$Ni(OTf)_2$, $3H_3OOTf$	—	523	$Ni(OTf)_2$	yellow	16.8 (16.4)	83.2 (83.5)	
$CoCl_2\cdot 6H_2O$[f]	aqueous solution	373	$Co(OTf)_2$, xH_3OOTf				
$Co(OTf)_2$, xH_3OOTf	—	523	$Co(OTf)_2$	pink	16.5 (16.5)	83.5 (83.5)	
$CoCl_2\cdot 2H_2O$[f]	excess	rt	$Co(OTf)_2$, $CoCl_2$, $1.28H_3OOTf$	blue	16.8 (16.5)[k]	69.6 (83.5)[k]	10.1[l] 3.7[i]
$CoCl_2\cdot 6H_2O$	excess	rt	$Co(OTf)_2$, $0.46CoCl_2$, $0.5H_3OOTf$	blue	17.2 (16.5)[k]	74.4 (83.5)[k]	6.5[l] 1.9[i]
$Co(ClO_4)_2$[m]	excess	rt	$Co(OTf)_2$	pink	16.6 (16.5)	83.4 (83.5)	
$CuCO_3Cu(OH)_2$[f]	excess	rt	$2Cu(OTf)_2$, $4H_3OOTf$	—			
$2Cu(OTf)_2$, $4H_3OOTf$	—	253	$Cu(OTf)_2$	blue white	17.9 (17.6)	82.1 (82.4)	

[a] Decomposition temperature (K; rt, room temperature; under vacuum 10^{-2} torr).
[b] Calculated values in parentheses.
[c] Rhône Poulenc-Pechiney 99.999% used as received.
[d] Laboratory synthesis.[27]
[e] X = Br.
[f] Merck product for analysis.
[g] As detected gravimetrically and spectroscopically.
[h] The solution was boiled to dryness.
[i] X = H_3OOTf.
[j] $CoCl_2\cdot 6H_2O \xrightarrow[\text{vacuum}]{\Delta = 320} CoCl_2$.
[k] Values in parentheses refer to $Co(OTf)_2$.
[l] X = Cl.
[m] Prepared as in ref. 3(a).

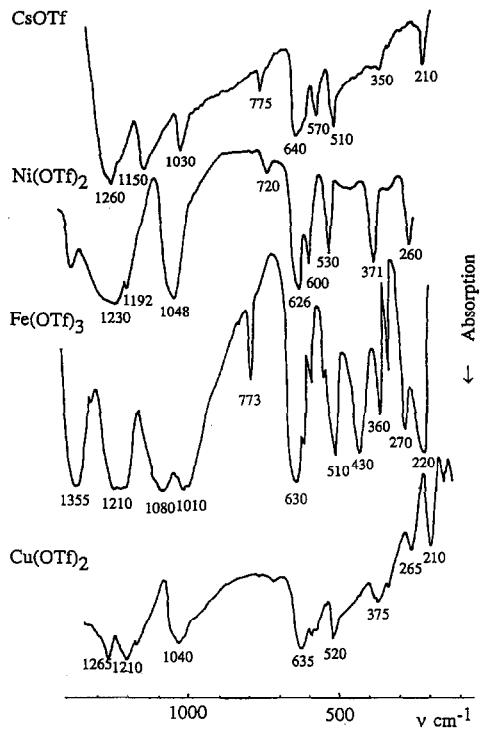

Fig. 1. Typical IR spectra of the bidentate and tridentate OTf complexes. CsOTf (given as reference); $Ni(OTf)_2$—tridentate; $Fe(OTf)_3$—bidentate and $Cu(OTf)_2$—bidentate.

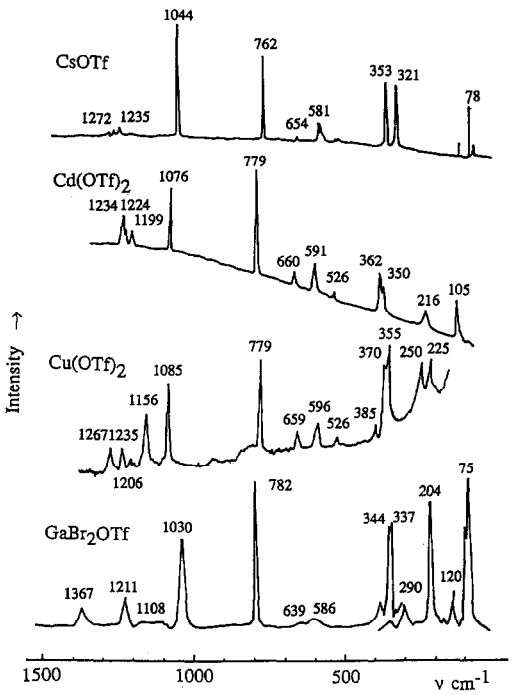

Fig. 2. Typical Raman spectra of the bidentate and tridentate OTf complexes. CsOTf (given as reference); $Cd(OTf)_2$—tridentate; $Cu(OTf)_2$—bidentate and $GaBr_2OTf$—bidentate.

ESR spectrum

The X-band ESR spectrum of $Cu(OTf)_2$ sealed in a 5 mm Pyrex tube was recorded at room temperature and at 77 K.*

EXAFS spectroscopy

X-ray absorption spectra were recorded at the Fe (7112 eV), Co (7709 eV), Ni (8333 eV) and Ga (10367 eV) K edges at 77 K on the EXAFS I spectrometer at the French synchrotron facility, DCI at LURE under typical beam conditions (1.85 GeV, 200 mA). The X-ray beam was monochromatized with a channel-cut Si (331) crystal. No additional measures were taken to eliminate harmonics. After calibration of the spectrometer using appropriate metal foils (Fe, Co, Ni), spectra were recorded in transmission mode in three energy regions: the first from 100 to 20 eV before the edge (stepsize 4 eV), the second from here to 50 eV after the edge (stepsize 1 eV) and thereafter in steps of 2 eV to at least 700 eV above the absorption edge.

Complexes $M(OTf)_n$ were prepared as thick mulls with parafilm oil stored over molecular sieves, and were pressed between the parafilm windows of stainless steel sample cells to form homogeneous thin films. Air-filled ionization chambers were used to measure the incident and transmitted X-ray flux. In each case at least three spectra were recorded to maximize the signal/noise ratio in subsequent data analysis.

All mathematical analysis was performed using the programmes developed by Michalowicz.[30] Normalization was typically performed after background subtraction using a 5th or 6th order polynomial in the $\mu_{1\,exp.} - \mu_{0\,exp.}$ formalism. The resulting spectra $\chi(k)$ vs k are reported in Fig. 3. Fourier transformation (FT) was carried out over a range typically 3–13 $Å^{-1}$ using a Hamming window and k^3 weighting, Fig. 4. Quantitative analysis using curve fitting procedures was performed on Fourier-filtered back-transformed spectra. Phase and amplitude functions were the *ab initio* values of McKale[31] (curved wave–small atom formalism).

Quantitative analysis in each case was approached by Fourier filtration of individual peaks in the FT and backtransformation to k-space. Simulation of the experimental spectra by introduction

* The spectra were recorded on a home built ESR spectrometer.[29]

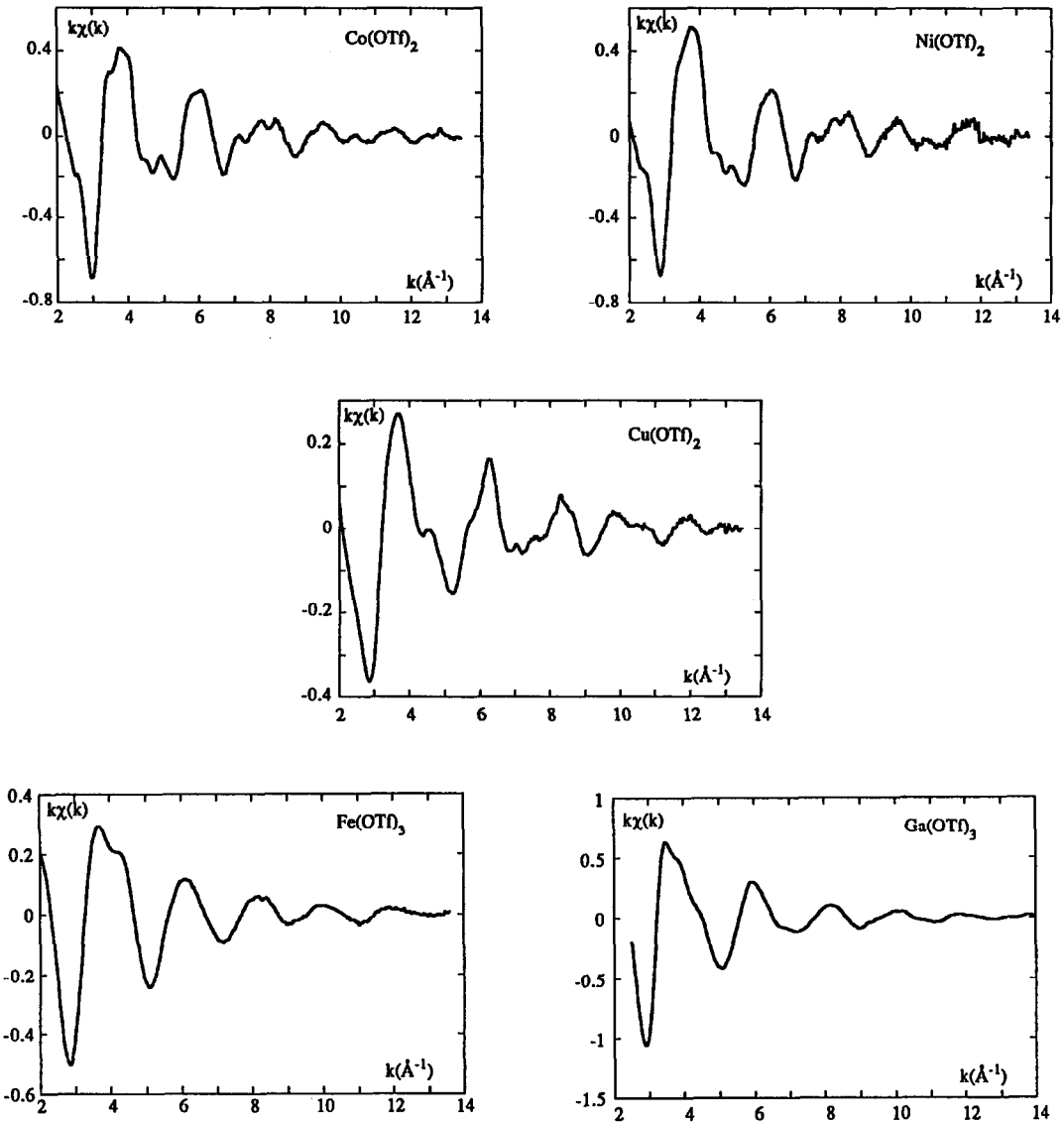

Fig. 3. EXAFS spectra of $Ni(OTf)_2$, $Co(OTf)_2$, $Cu(OTf)_2$, $Fe(OTf)_3$ and $Ga(OTf)_3$ after background substraction and normalization.

of the coordination number, N, absorber–backscatter distance, R (Å), Debye–Waller factor, σ (Å), energy offset, E_0 (eV) and phase and amplitude parameters into the EXAFS equation, was followed by curve-fitting (minimization) routines. After satisfactory convergence had been obtained for individual shells, two shell refinements were performed on the Ni, Co and Cu complexes.

RESULTS AND DISCUSSION

Syntheses

In general the syntheses (Table 1) suffer from the absence of a satisfactorily reactive source of the OTf ligand; only HOTf and the corresponding anhydride are available and neither is particularly efficient: the latter is rather inert[32,37] and HOTf only mildly reactive such that, for example, the synthesis of certain trifluoromethanesulphonato complexes from anhydrous or hydrated chlorides is not achieved. An analogous problem arises in the preparation of perchlorate complexes from chlorides,[3] where an explanation in terms of the compactness of the crystal lattices was suggested.

However the relative electronegativity of the halides must also be considered: the preparation of trifluoromethanesulphonato complexes is easier from bromides than the corresponding chlorides.[8b]

In general, the results obtained using metal chlor-

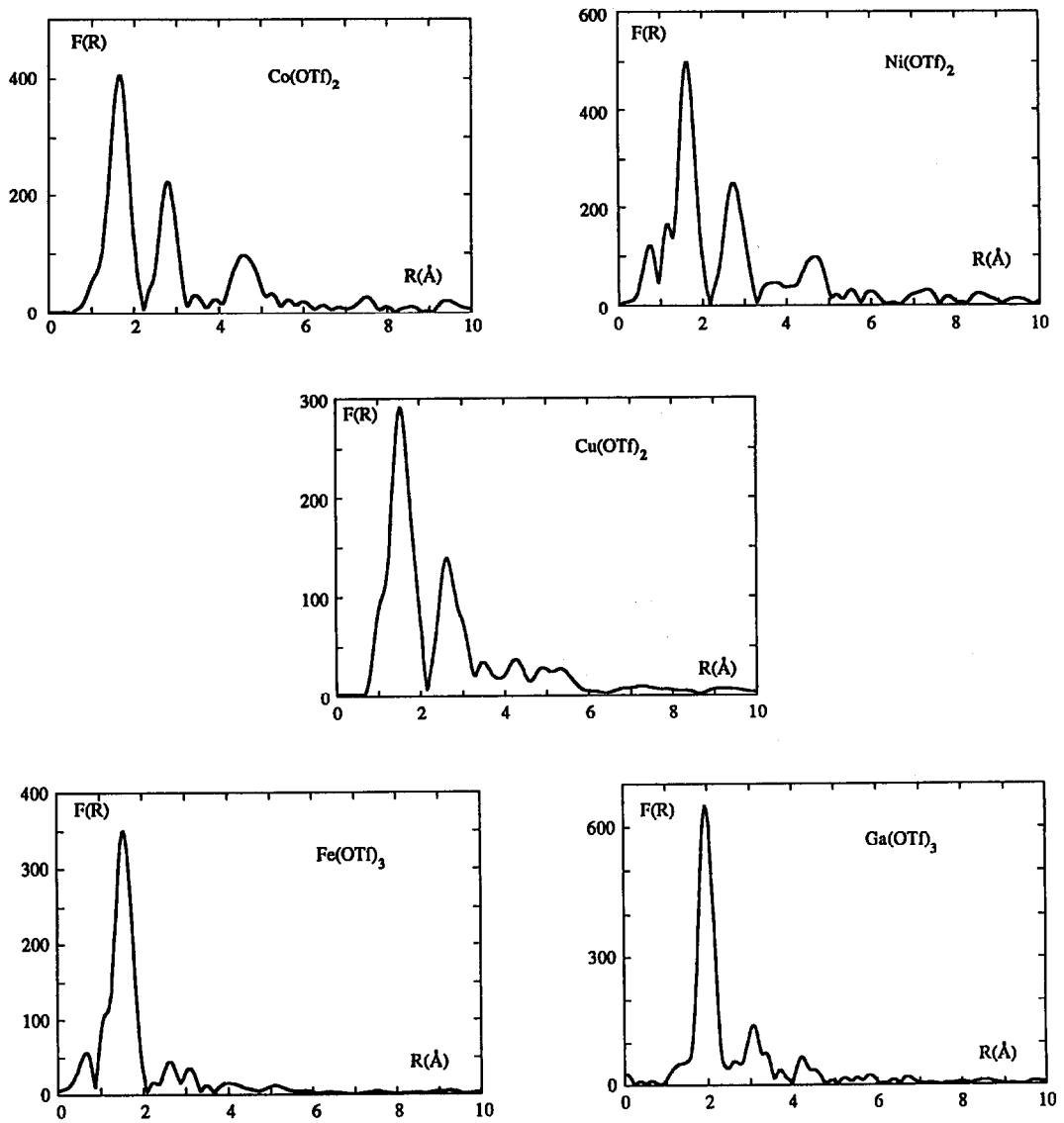

Fig. 4. Fourier transforms of the weighted EXAFS spectra.

ides, bromides and carbonates (basic or neutral) agree with those reported by other workers. The formation of $Ga(OTf)_3$ from $GaBr_3$ occurs via the partially substituted $GaBr_2OTf$. Partial replacement of this type was also observed in the synthesis of boron, gallium and germanium perchlorates from the corresponding chlorides.[4,33,34]

The preparation of OTf complexes from anhydrous perchlorates, although considered inadvisable by certain authors[13] can be succeeded without particular danger if performed in the absence of organic solvents. Progressive formation of $HClO_4$ during the reaction can be detected spectroscopically.[35] The substitution of ClO_4^- by $CF_3SO_3^-$ can be explained by their different basicities (or degrees of hardness according to Pearson).[36] ClO_4 is highly labile and very hard (or weakly basic) and is replaceable by the softer, more basic CF_3SO_3.[37] Although the nitrates are more basic still, they are easily replaced by OTf, as NO_2^+ is formed in strong acid media (see, eg. ref. 38). Thus the reaction of HOTf with $Cd(NO_3)_2 \cdot nH_2O$, $n \leqslant 4$ can lead to the nitryl salt, $(NO_2)_xCd(OTf)_{2+x}$, as demonstrated by vibrational spectroscopy.[28] This reaction is not always reproducible however and frequently leads to a mixture x NO_2OTf,$Cd(OTf)_2$ from which $Cd(OTf)_2$ is obtained by sublimation of NO_2OTf above 360 K, according to methods previously published.[24] As such, nitrates represent an excellent source of the nitrating agent NO_2OTf.

The positive and facile reaction of HOTf with metallic gallium presents the advantage of avoiding the formation of intermediate salts. It is limited, unfortunately, since closely related to the ionization potential of the metal and the redox equilibrium in the metal–acid reaction. For example, whereas HPO_2F_2 reacts with copper metal to give $Cu(PO_2F_2)_2$,[38] HOTf is inactive.[37] Furthermore, passivation phenomena due to the formation of surface oxide can slow down or completely prevent reaction by this route.

Vibrational spectroscopy

The trifluoromethanesulphonate ion has been comprehensively studied by IR and Raman.[5,6,40] Miles[41] and Burger[42] have pointed out the superposition of spectral zones in which internal vibrations of both the pyramidal groups, CF_3 and SO_3, are expected, in particular for the asymmetric CF_3 and SO_3 stretching modes $\nu_{as}CF_3$, $\nu_{as}SO_3$. The latter has been reported to occur at 1150 or at 1270 cm^{-1}, and both positions are consistent with force field calculations.[42] In similar compounds containing the SO_3 group, $\nu_{as}SO_3$ has been identified at 1200, 1254 and 1287 cm^{-1} in CH_3SO_3,[43] CCl_3SO_3[42] and FSO_3,[44] respectively. Consideration of the relative polarizing powers of CH_3, CCl_3, F and CF_3 groups allows the tentative prediction of $\nu_{as}SO_3$ in CF_3SO_3 as ~ 1260 cm^{-1}. Coupling of the A_1 modes is expected, with $\delta_s CF_3$ and νCS being particularly affected. For example potential energy calculations indicate a high contribution of νCS to a band in IR situated at 320 cm^{-1}; that at 770 cm^{-1} is dominated by δCF_3.

Vibrations of the OTf anion are sensitive also to the polarizing power of the countercation.[28] The symmetric stretch ν_sOTf is displaced by ~ 50 cm^{-1} in the series from the lithium to the caesium salts, to a position similar to that observed in the corresponding series of nitrates.[45] Indeed the weak polarizing power of caesium allows the vibrational spectrum of CsOTf to be considered as a "reference".

Coordination of OTf to a metal ion is expected to induce marked spectral changes owing to changes in geometry and symmetry, with vibrations of the SO_3 group being particularly affected.

Finally, in addition to the internal vibrations of OTf, skeletal vibrational modes of the metal—oxygen polyhedron MO_x are expected below 300 cm^{-1}.

Typical IR and Raman spectra of $M(OTf)_2$, and $M(OTf)_3$ complexes, the Raman spectrum of $GaBr_2OTf$ and the vibrational spectra of CsOTf for comparison, are reproduced in Figs 1 (IR) and 2 (Raman). If, as suggested above, CsOTf is regarded as a point of reference, close resemblence is found between its IR spectrum and those of $M(OTf)_2$ M = Ni, Co, Cd. Some significant differences are observed, however, with the spectra of $M'(OTf)_3$, M = Ga, Fe and $Cu(OTf)_2$. Here, for example, four bands occur between 900 and 1400 cm^{-1}, whilst there are only three in the spectrum of CsOTf. This loss of degeneracy strongly suggests that in the presence of Ga, Fe or Cu, OTf is bidentate, whereas retention of degeneracy in the Ni, Co and Cd salts is indicative of tridentate trifluoromethanesulphonate where the SO_3 group has essentially retained its C_{3v} symmetry. Rather similar conclusions reported previously were limited to $M(OTf)_2$ M = Cu, Co[28,46] and $M'(OTf)_3$ M′ = Fe[28,46], Ga.[8]

In the tridentate series of Ni, Co and Cd trifluoromethanesulphonates, two characteristic vibrational bands are displaced: νCS to a higher frequency ($+50$ cm^{-1}), and νSO_b—the average stretching vibration of bridging SO—to a lower frequency (-40 cm^{-1}). These shifts may be interpreted in terms of an elongation of the three SO_b bonds and concomitant shortening of the C—S bond, both modifications induced by coordination.

For the bidentate series, three frequency shifts are observed: νSO_b by -130 cm^{-1}, νSO_t—the stretching vibration of the terminal SO bond—by $+140$ cm^{-1} and νCS by $+15$ cm^{-1} implying that the induced shortening of the C—S bond is less in the bidentate than in the tridentate salts. Indeed, the sensitivity of the position of this band to the nature of metal–oxygen coordination justifies its assignment to νCS. In Fe, Ga and Cu trifluoromethanesulphonato complexes, the bands or lines around 430 cm^{-1} are assigned to the rocking mode of terminal SO_3, only present in the spectrum of bidentate CF_3SO_3, they could be useful in detecting this type of coordination. The M—O stretching vibrations, observed for trifluoromethanesulphonate salts for the first time in this study, are ~ 20 cm^{-1} lower than in the corresponding metal perchlorates.

$GaBr_2OTf$: from the similarity of the vibrational spectra of $GaBr_2OTf$ and $Ga(OTf)_3$ it may be deduced that the OTf ligand in the former compound is bidentate. In addition, vibrations occur at positions characteristic of the $GaBr_2$ group. For example, an intense line in the Raman spectrum at 204 cm^{-1} indicates a GaBrGa bridge while the line at 75 cm^{-1} is a breathing mode of the Ga_2Br_2 ring. No terminal Ga—Br_t bands are present, in accordance with the absence of absorption in UR at 348 cm^{-1}.

Vibrational frequencies for the trifluoromethanesulphonate complexes and their assignments are reported in Tables 2 and 3.

Table 2. IR and Raman spectra of tridentate OTf complexes: assignments

$Ni(OTf)_2$		$Co(OTf)_2$		$Cd(OTf)_2$		
IR	R	IR	R	IR	R	Assignments
1250s,br	1239s	1230sh	1236sh		1234s	$\nu_s CF_3$
1230s,br	1227sh		1226s	1220s,br	1224m	$\nu_{as} SO_3$
1192sh	1203m	1180sh	1202w	1170sh	1199m 1194sh	$\nu_{as} CF_3$
1055s,sh	1094s	1070s	1086s	1060s	1076s	$\nu_s SO_3$
1048s		1040sh		1040sh		
771w	786s		778s		779s	$\delta_s CF_3 + \nu(C—S)$
720w				720w		
	668w		687w			$\delta_{as} SO_3$
626s		650s	657w	640s	660w	
600s	601w	593s	591w	585s	591m	$\delta_s SO_3$
				575sh		+
530s		523s	519?	520s	526w	$\delta_{as} CF_3$
	474s,br[a]		445s,br[a]			
371s	371s	370s	365s	365s	362m	$\nu(C—S) + \delta_s CF_3$
	356sh		358sh			
	335sh			350sh	350m	$\rho_r SO_3$
260s	248w	250s	251s			$\nu MO + \rho_r CF_3$
	233w		225w	235w	216w	
	138m		122s		105m	lattice + δMO_6

[a] Dominating fluorescence.

UV–vis spectra

UV–vis spectra of the Ni, Co and Cu complexes are characterized by broad bands which are located respectively at:

7142–7535, 12,195 and 24,390 cm^{-1} [$Ni(OTf)_2$]; 6945–7690, 13,890 and 18,870 cm^{-1} [$Co(OTf)_2$]; 7935 and 10,525 cm^{-1} [$Cu(OTf)_2$].

The observed frequencies are in agreement with the previous results on the triflato[25,26] and the perchlorato[3] complexes.

The absorptions are consistent with a regular octahedral surrounding of the core atoms for the Ni and Co complexes which is well supported by EXAFS spectroscopic results (see below). Assignments for the absorption bands were given previously.[24,25]

The ligand field parameter Dq (735 cm^{-1}) for $Ni(OTf)_2$ is higher than that observed for the corresponding ClO_4 complex ($\Delta\nu = +45$ cm^{-1}) since the basicity of $CF_3SO_3^-$ is stronger than that of ClO_4^-.

The interpretation of the spectra of $Cu(OTf)_2$ developed by other authors[25] describes a Cu atom closely surrounded by four oxygen atoms, this is entirely consistent with our ESR and EXAFS results.

ESR spectrum

The electron paramagnetic resonance spectrum of $Cu(OTf)_2$[28] gives a two component spectrum with sharp lines and no temperature dependence. The g values, $g_\parallel$: 2.4282, $g_\perp$: 2.0774, are consistent with the presence of copper in a square planar or in a compressed tetrahedral environment, and the value of the gyromagnetic tensor G, 5.53, indicates an axial symmetry with probably a $d_{x^2-y^2}$ ground state, where the principal tetragonal axes are parallel, excluding all possibility of exchange interaction between metal centres, as observed previously for $Cu(ClO_4)_2$.[20]

EXAFS spectroscopy

The EXAFS spectra (Fig. 3) of $Ni(OTf)_2$ and $Co(OTf)_2$ obtained after background subtraction and normalization are almost identical (and different from that of $Cu(OTf)_2$), suggesting the same mode of coordination in the two former complexes. Similarly, the frequency and amplitude of EXAFS oscillations of $M(OTf)_3$, M = Fe, Ga are highly comparable and their relative simplicity (absence of beats characteristic of the superposition of several

Table 3. IR and Raman spectra of bidentate OTf complexes: assignments

$Fe(OTf)_3$		$Ga(OTf)_3$		$GaBr_2OTf$		$Cu(OTf)_2$		Assignments
IR	R	IR	R[a]	IR	R	IR	R	
				1450w[b]				
	1382s		1385w					
1355s		1360s		1345sh	1367m			
1305w		1310w		1320m		1310sh		νSO_t
	1280w					1265s	1267m	
					1211m			
1235w		1230sh				1235sh	1235m	$\nu_s CF_3$
1210s,br		1210s	1209m	1205s		1210s	1206w	$\nu_{as} CF_3$
					1152w[b]			
	1114s	1110s		1090m	1108w	1175s	1156s	
1080s	1071s		1069s					
								$\nu_s + \nu_{as} SO_b$
1010s		1000s,br		1000m	1030s	1040s,br	1085s	
990sh								
				870w[b]				
				810w[b]				
773m	782s	773m	779s		782w		779s	$\delta_s CF_3$
								+
				735m		740w		ν(C—S)
630s	634w	635s			639w	635sh	659m	$\rho_r SO$
	626w	620s			604w	625s	596m	$\rho_w SO$
597s		600s		600s	595w	605s		δSO_{2b}
570m		578m			586w		586sh	
530m		527m			535w	520s	526w,sh	$\delta_{as} CF_3$
510s		500s		515m				
430s		440s		430m		475w	430w,br	$\rho_t SO_3$
360m		360m		375s	363m	390sh	385m	$\rho_w CF_3$
					344s		370sh	
330m		330m				340m	355m	ν(C—S) + δCF_3
					337s			
270s		265m		260m		265s	250m	
	244w				244m			ν(M—O)
220s		200s		210m		210s	225m	$\rho_r(CF_3)$
					290w			ν_{as}GaBrGa
					204s			ν_sGaBrGa
					159w			$\delta GaBr_2$
					120m			
					84s			Lattice
					75s			

[a] The recording of Raman spectra of $Fe(OTf)_3$ and $Ga(OTf)_3$ presents great difficulty due to dominating fluorescence; the main lines of $Ga(OTf)_3$ could however be seen on a complimentary FT Raman spectrum recorded at Nicolet.

[b] h,c harmonic, combination.

EXAFS contributions), compared to the spectra of the M^{II} complexes, is striking.

An alternative representation of the EXAFS data is obtained by Fourier transformation, which allows visualization of the various atom shells and an estimate of their distance from the absorbing atom in direct space. The FT of all five OTf complexes are displayed in Fig. 4, where the similarities observable in the EXAFS spectra are even more apparent. The FT of $Ni(OTf)_2$ and $Co(OTf)_2$ consist of three distinct shells of atoms at 1.58 (1.66, Co), 2.71 (2.75, Co) and 4.42 (4.50, Co) Å before phase correction, corresponding to backscattering from oxygen, sulphur and metal atom shells, respectively. Only two maxima (metal–oxygen, metal–sulphur) are closely observable in the FT of $Cu(OTf)_2$

Table 4. Results of the fitting procedure for Ni^{II}, Co^{II}, Cu^{II}, Fe^{III} and Ga^{III} trifluoromethanesulphonato complexes

	N	σ (Å)	R (Å)	ΔE_0 (eV)	R (Å) $M(ClO_4)_2$[a]
$Ni(OTf)_2$					
Ni—O	6	0.020	2.04	1.5	2.04
Ni—S	5	0.045	3.23	−5.4	3.24 (Cl)
Ni---Ni	—	—	4.88	—	4.80
$Co(OTf)_2$					
Co—O	6	0.045	2.08	3.2	2.09
Co—S	5	0.055	3.26	−4.2	3.26 (Cl)
Co---Co	—	—	4.96	—	4.80
$Cu(OTf)_2$					
Cu—O	4	0.014	1.96	0.0	1.96
Cu—S	4	0.038	3.14	−9.0	2.73 (Cl)
Cu—O	2	0.050	3.35	8.5	2.68
$Fe(OTf)_3$					
Fe—O	5	0.042	1.99	−0.3	—
$Ga(OTf)_3$					
Ga—O	6	0.041	1.96	3.1	1.95

The quality of the fit as estimated from the residual factor R ($R = \Sigma_k(\chi_{exp} - \chi_{calc})/\Sigma_k\chi^2_{exp}$) is 2.2% $Ni(OTf)_2$, 1.2% $Co(OTf)_2$, 2.7% $Cu(OTf)_2$ (1st and 2nd shells), 1.3% $Fe(OTf)_3$, 2.8% $Ga(OTf)_3$ (1st shell). Standard deviations derived from the calculations for the first and second shells of atoms are N±1; $\sigma \pm 0.005$ Å; R±0.02 Å; $E_0 \pm 2$ eV).

[a] Bond lengths obtained previously for the corresponding metal perchlorates are included for comparison (M = Ni^{II},[21] Co^{II},[21] Cu^{II},[20] Ga^{III}[22]).

and structural information in the gallium and iron complexes is essentially limited to the first shell, where the metal–oxygen contribution produces an intense first peak and the metal–sulphur only a broad, relatively very weak second peak in the FT.

The results of curve fitting to the experimental EXAFS of $Ni(OTf)_2$ and $Co(OTf)_2$ containing first and second shell contributions are reported in Table 4. In both compounds the first shell includes six oxygen atoms at a distance of 2.04 Å in the nickel complex and 2.08 Å in the cobalt analogue. The low Debye–Waller factors attest to little distribution about these mean values and regular octahedral environments may be assumed. The second shell is composed of five–six sulphur atoms, situated at 3.23 Å (Ni), 3.26 Å (Co) from the metal absorber. Although curve fitting methods were not attempted on the third shell, metal—metal distances could be obtained directly from the FT after phase correction and adjustment of the energy offset until coincidence of the maxima of the imaginary part and modulus of the FT, and the zero of the real component was obtained,[47] giving intermetallic separations of 4.88 Å (Ni) and 4.96 Å (Co). All of these values are almost identical to those observed previously in $Ni(ClO_4)_2$ and $Co(ClO_4)_2$ by EXAFS measurements (Ni—O 2.04, Ni—Cl 3.24, Ni---Ni 4.80 Å; Co—O 2.08, Co—Cl 3.26, Co---Co 4.80 Å).[21] Bond lengths and coordination numbers are compatible in both the perchlorates and trifluoromethanesulphonates with bridging tridentate ligands in an arrangement in which the ligand lies alternatively above and below a plane defined by the metal atoms.

For $Cu(OTf)_2$, quantitative analysis shows that the first peak in the FT is due to four nearest neighbour oxygen atoms at 1.96 Å with a low Debye–Waller factor, 0.014 Å, (Table 4). This Cu–O distance is identical to that observed in the majority of copper compounds[48] and indicates the presence of strongly coordinated CF_3SO_3. As for the nickel and cobalt complexes above, least squares refinements were satisfactory with the second shell containing sulphur atoms alone (4, at 3.14 Å from Cu),

although a slight improvement in overall agreement between experimental and calculated curves was obtained (Fig. 5) when a second oxygen atom shell was included (Cu—O_{long}) to account for the "4+2" environment frequently observed in oxygen-containing copper salts. Refinement of this model was performed by fixing all structural parameters of the first oxygen shell, and varying only those (S and O_{long}) in the second coordination sphere. The Cu—O distance so obtained, 3.35 Å, is too long for these oxygens to be considered as directly coordinated (compare, for example with the corresponding value of 2.68 Å obtained from EXAFS in $Cu(ClO_4)_2$,[20] or 2.62 Å in $Cu(O_2PF_2)_2$ from X-ray diffraction).[39] It is therefore concluded that in $Cu(OTf)_2$, steric hindrance by the bulky CF_3SO_3 ligand restricts the immediate oxygen environment of copper to square planar, in agreement with the result obtained from ESR measurements. The four oxygen–four sulphur atom surroundings are compatible with the presence of bridging bidentate ligands, and are consistent with conclusions from vibrational spectroscopy.

EXAFS is able to provide first shell information only in the case of $Fe(OTf)_3$ and $Ga(OTf)_3$. Indeed, the first shell filtered and backtransformed EXAFS spectrum is essentially that of the raw (non-filtered, total) EXAFS of these compounds. In both complexes the metal–oxygen distances are short: Fe–O = 1.99; Ga–O = 1.96 Å, and it may be concluded from the coordination numbers, 5–6, that the metal atoms are octahedrally surrounded by oxygen. Furthermore, consideration of the coordination number and the stoichiometry of the metal(III) complexes allows bidentate CF_3SO_3 to be assumed, which may be bridging or chelating.

The absence of longer distance information for these latter complexes may be due to a high static component to the Debye–Waller factor, either through a broad distribution of M^{III}—S distances or through, for example, orientational disorder. Such effects would cause rapid dampening of the EXAFS signal. Alternatively, an explanation in terms of destructive interference of EXAFS signals may be invoked. Calculation of the single scattering EXAFS of oxygen and sulphur at the same distance from iron, for example, clearly shows a phase difference of approximately $\pi(\phi(Fe—S)-\phi(Fe—O) = 3.16$ rad.), which would therefore drastically reduce or even cancel the overall signal. Occurrence of oxygen and sulphur atoms at identical (or almost) distances is possible in the iron or gallium trifluoromethanesulphonate complexes in view of the bidentate coordination of CF_3SO_3 to the metal centre, and consequent freedom of the third —SO_3 oxygen atom. Finally, the possibility of the destruction of the single scattering EXAFS from sulphur through interference with a multiple scattering process involving the Fe—O—S triad cannot be excluded. This has been observed in other metal salts containing tetrahedral oxyanions: $CaHPO_4$,[49] $Ca_5(PO_4)_3OH$,[49] $CaHPO_4 \cdot 2H_2O$[49] and $Zr(HPO_4)_2 \cdot H_2O$.[50]

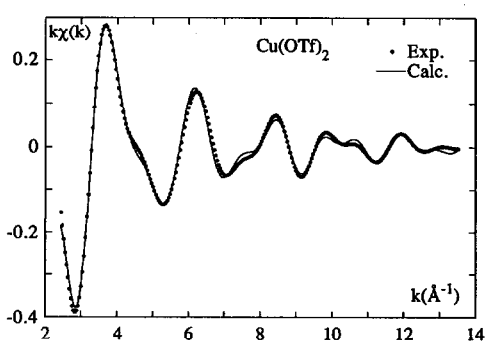

Fig. 5. K space filtered spectrum (dotted line) with the corresponding calculated curve (solid line) for $Cu(OTf)_2$.

CONCLUSION

Systematic investigation of the synthetic routes to known trifluoromethanesulphonato complexes of di- and trivalent metals (Ni^{II}, Co^{II}, Cd^{II}, Cu^{II}, Fe^{III}, Ga^{III}) has led to identification of novel routes using the reaction of trifluoromethanesulphonic acid with metal nitrates, perchlorates and, in one case only, the metal itself (Ga).

The key to the successful preparation of such coordination complexes lies in the availability of an efficient, reactive source of $CF_3SO_3^-$, and research for a reagent more energetic than CF_3SO_3H or its anhydride continues.

The simultaneous availability of spectroscopic data from IR, Raman and EXAFS measurements has facilitated their interpretation. Whilst vibrational spectroscopies have indicated the mode of coordination (bridging bidentate in $Cu(OTf)_2$, $Ga(OTf)_3$, $Fe(OTf)_3$; tridentate in $Ni(OTf)_2$ and $Co(OTf)_2$), EXAFS has provided metal–oxygen and metal–sulphur bond lengths, and corroboration of the ligand arrangement through coordination numbers of the first and second shells of atoms. $Ni(OTf)_2$ and $Co(OTf)_2$ both exhibit the same local structure as observed previously in the corresponding anhydrous perchlorates. Considerable differences however exist between the metal environments in $Cu(OTf)_2$ and $Cu(ClO_4)_2$. In certain cases, structural information is limited to the first shell only for reasons inherent to the geometry of the metal–ligand complex and to the nature of

the EXAFS process; here extension of the structural data available awaits the isolation of single crystalline products.

Acknowledgements—We are grateful to Rhône Poulenc-Péchiney for the gift of metallic gallium. We thank the CEA/CENG/CNRS for access to experimental stations at LURE, and the CNRS for financially supporting this project.

REFERENCES

1. (a) S. P. Mallela, K. Lee, P. F. Gehrs, J. I. Christensen, J. R. Sams and F. Aubke, *Can. J. Chem.* 1986, **65**, 2649 and references therein; (b) D. G. Niyogi, S. Singh and R. D. Verma, *Can. J. Chem.* 1989, **67**, 1895.
2. Z. K. Nikitina, N. V. Krivtsov and V. Ya. Rosolovski, *Russ. J. Inorg. Chem.* (*Engl. Tr.*) 1989, **34**, 686 and references therein.
3. J.-L. Pascal, J. Potier and C. S. Zhang, *J. Chem. Soc., Dalton Trans.* 1985, **2**, 297.
4. M. Fourati, M. Chaabouni, J-L. Pascal and J. Potier, *Can. J. Chem.* 1989, **6**, 1693 and references therein.
5. G. A. Lawrance, *Chem. Rev.* 1986, **86**, 17 and references therein.
6. R. Kapoor, P. Wadkawon, V. Katyal, V. R. Sood and P. Kapoor, *Can. J. Chem.* 1989, **67**, 1760.
7. (a) J. Collomb, A. Gandini and H. Cheradame, *Makromol. Chem. Rapid Commun.* 1980, **1**, 489; (b) J. Collomb, B. Morin, A. Gandini and H. Cheradame, *Europ. Polymer. J.* 1980, **16**, 1135; (c) J. Collomb, P. Arland, A. Gandini and H. Cheradame, *Cationic Polymerisation and Related Processes*, Int. Symp. 6th, p. 49. Academic Press, London (1984).
8. (a) G. A. Olah, K. Laali and O. Farooq, *J. Org. Chem.* 1984, **49**, 4591; (b) G. A. Olah, O. Farooq, S. Moorteza, F. Farnia and J. A. Olah, *J. Am. Chem. Soc.* 1988, **110**, 2560.
9. K. Laali, R. J. Gerzina, C. M. Flajnik, C. M. Geric and A. M. Dombroska, *Helv. Chim. Acta* 1987, **70**, 607.
10. T. Imamoto, Y. Koide and S. Hiyama, *Chem. Lett.* 1990, 1445.
11. R. J. Gillespie and T. E. Peel, *Adv. Org. Chem.* 1971, **9**, 1.
12. A. Potier and J. Potier, unpublished work.
13. N. E. Dixon, G. A. Lawrance, P. A. Lay, A. M. Sargeson and H. Taube, in *Inorganic Syntheses*, Vol. 24, p. 243. John Wiley, New York (1986).
14. R. J. Batchelor, J. N. Ruddick, J. R. Sams and F. Aubke, *Inorg. Chem.* 1977, **16**, 1414.
15. K. Bartmann and D. Mootz, *Acta Cryst.* 1990, **C46**, 319.
16. (a) J. B. Spencer and J. O. Lundgren, *Acta Cryst.* 1973, **B29**, 1923; (b) R. G. Delaplane, J. O. Lundgren and I. Olovsson, *Acta Cryst.* 1975, **B31**, 2202, 2208; (c) J. O. Lundgren, *Acta Cryst.* 1978, **B34**, 2428.
17. (a) F. A. Schröder, B. Gänswein and G. Brauer, *Z. Anorg. Allg. Chem.* 1972, **391**, 295; (b) H. Schumann, J. A. Meese-Marktscheffel and J. Loebel, *Z. Naturforsh.* 1990, **45b**, 1304.
18. R. Kapoor, P. Wadhawan, P. Kapoor and J. F. Sawyer, *Can. J. Chem.* 1988, **66**, 2367.
19. M. Fourati, M. Chaabouni, C. Belin, M. Charbonnel, J.-L. Pascal and J. Potier, *Inorg. Chem.* 1986, **25**, 1386 and references therein.
20. J.-L. Pascal, J. Potier, D. J. Jones, J. Rozière and A. Michalowicz, *Inorg. Chem.* 1984, **23**, 2068.
21. J.-L. Pascal, J. Potier, D. J. Jones, J. Rozière and A. Michalowicz, *Inorg. Chem.* 1985, **24**, 238.
22. J. Potier, A. Seigneurin, J. Rozière, D. J. Jones, J.-L. Pascal and A. Michalowicz, *New J. Chem.* 1987, **11**, 641.
23. J.-L. Pascal, Thesis, University of Montpellier II (1978).
24. C. S. Zhang, Thesis, University of Montpellier II (1984).
25. A. L. Arduini, M. Garnett, R. C. Thompson and T. C. T. Wong, *Can. J. Chem.* 1975, **53**, 3812.
26. M. T. Jansky and J. T. Yoke, *J. Inorg. Nucl. Chem.* 1971, **41**, 1707.
27. E. Chemouni, Thesis, University of Montpellier II (1970).
28. K. Boumizane, Thesis, University of Montpellier II (1989).
29. J. V. Zanchetta, University of Montpellier II, France.
30. A. Michalowicz, Summer School CNRS, *Structures Fines d'Absorption X en Chimie.* Garchy 1988, Vol. 3. *Logiciel d'Analyse de Données d'Absorption X: EXAFS pour le Mac* (Edited by A. Michalowicz, H. Dexpert and M. Verdaguer).
31. A. G. McKale, *J. Am. Chem. Soc.* 1988, **110**, 3763.
32. D. G. Niyogi, S. Singh, S. Gill and R. D. Verma, *J. Fluor. Chem.* 1990, **48**, 421.
33. T. Chausse, J.-L. Pascal, A. Potier and J. Potier, *Nouv. J. Chim.* 1981, **5**, 261.
34. M. Chaabouni, J.-L. Pascal, A. Potier and J. Potier, *J. Chem. Res.* 1977, 80; (b) *J. Chim. Phys.* 1977, **74**, 1083.
35. A. C. Pavia, *Rev. Chim. Min.* 1970, **7**, 471.
36. R. G. Pearson, *Coord. Chem. Rev.* 1990, **100**, 403 and references therein.
37. J.-L. Pascal and M. M. Hamidi, unpublished results.
38. G. Olah, G. K. S. Prakash and J. Sommer, in *Superacids.* John Wiley, New York (1986).
39. M. J. Begley, M. F. A. Dove, R. C. Hibbert, N. Logan, M. Nunn and D. B. Sowerby, *J. Chem. Soc., Dalton Trans.* 1985, 2433.
40. H. Sutcliffe and A. Thornton, *J. Fluor. Chem.* 1985, **28**, 171.
41. M. G. Miles, G. Doyle, R. P. Conney and R. J. Tobias, *Spectrochim. Acta* 1969, **25A**, 1515.
42. H. Bürger, K. Burcyk and A. Blaschette, *Monatsh. für Chem.* 1970, 101.
43. S. M. Chackalckal and F. E. Stafford, *J. Am. Chem. Soc.* 1966, **88**, 4815.
44. H. Siebert, Anwendungen der Schwingungsspektroskopie und Anorganischen Chemie, in *Anorganische*

und Allgemeine Chemie, Vol. VII. Springer, Berlin (1966).
45. D. W. James, in *Molten Salt Chemistry*, p. 507 (Edited by M. Blander). Interscience, New York (1964).
46. J. S. Haynes, J. R. Sams and R. C. Thompson, *Can. J. Chem.* 1981, **59**, 669.
47. P. A. Lee and J. B. Pendry, *Phys. Rev. B* 1975, **11**, 2795.
48. B. J. Hathaway, *Copper(II). From Copper in Comprehensive Coordination Chemistry*, Vol. 5, p. 533. Pergamon Press, Oxford (1987).
49. J. E. Harries, D. W. L. Hukins and S. S. Hasnain, *J. Phys.* 1986, **C8**, 603.
50. D. J. Jones and J. Rozière, *X-ray Absorption Fine Structure* (Edited by S. S. Hasnain), pp. 405–407. Ellis Horwood, New York (1991).

Polyhedron Vol. 10, No. 23/24, pp. 2771–2777, 1991
Printed in Great Britain

0277–5387/91 $3.00+.00
© 1991 Pergamon Press plc

REACTION OF (±)-1,1′-BINAPHTHYL-2,2′-DIYL HYDROGEN PHOSPHATE {(±)-PhosH} WITH COPPER(II), COBALT(II) AND IRON(II) COMPOUNDS; IDENTIFICATION BY X-RAY DIFFRACTION OF $[Co(CH_3OH)_4(H_2O)_2][(+)\text{-Phos}][(-)\text{-Phos}] \cdot 2CH_3OH \cdot H_2O$

MALACHY McCANN* and EAMONN MURPHY

Chemistry Department, St. Patrick's College, Maynooth, Co. Kildare, Ireland

and

CHRISTINE CARDIN* and MAIRE CONVERY

Chemistry Department, Trinity College, Dublin, Ireland

(*Received* 14 *January* 1991; *accepted* 22 *July* 1991)

Abstract—$[Cu_2(\mu\text{-}O_2CCH_3)_4(H_2O)_2]$, $[CuCO_3 \cdot Cu(OH)_2]$, $[CoSO_4 \cdot 7H_2O]$, [Co((+)-tartrate)], and $[FeSO_4 \cdot 7H_2O]$ react with excess racemic (±)-1,1′-binaphthyl-2,2′-diyl hydrogen phosphate {(±)-PhosH} to give mononuclear Cu^{II}, Co^{II} and Fe^{II} products. The cobalt product, $[Co(CH_3OH)_4(H_2O)_2]((+)\text{-Phos})((-)\text{-Phos}) \cdot 2CH_3OH \cdot H_2O$ (**7**), has been identified by X-ray diffraction. The high-spin, octahedral Co^{II} atom is ligated by four equatorial methanol molecules and two axial water molecules. A (+)- and a (−)-$Phos^-$ ion are associated with each molecule of the complex but are not coordinated to the metal centre. For the other Co^{II}, Cu^{II} and Fe^{II} samples of similar formulation to (**7**) it is also thought that the $Phos^-$ ions are not bonded directly to the metal. When some of the Cu^{II} and Co^{II} samples are heated under high vacuum there is evidence that the $Phos^-$ ions are coordinated directly to the metals in the products.

The axially disymmetric binaphthyl skeleton (Fig. 1a) has been shown to have very good chirality recognition properties and has found increasing use in enantiomeric resolution and asymmetric synthesis.[1] Specifically, (+) and (−) enantiomers of 1,1′-binaphthyl-2,2′-diyl hydrogen phosphate (PhosH) (Fig. 1b) are known to be extremely effective for the resolution of racemic organic bases,[2] and they have also been employed as chiral shift reagents for NMR spectroscopy.[3] In addition, Mikeš and Boshart[4] have linked PhosH to silica gel and used it as the chiral stationary phase in HPLC columns for the resolution of helicenes. More recently, (R)-(−)- and (S)-(+)-PhosH have each been used effectively in the asymmetric synthesis of acids via the palladium-catalyzed hydrocarboxylation of olefins.[5] The present paper details our investigations into the potential coordination chemistry of the $Phos^-$ anion towards Cu^{II}, Co^{II} and Fe^{II} centres.

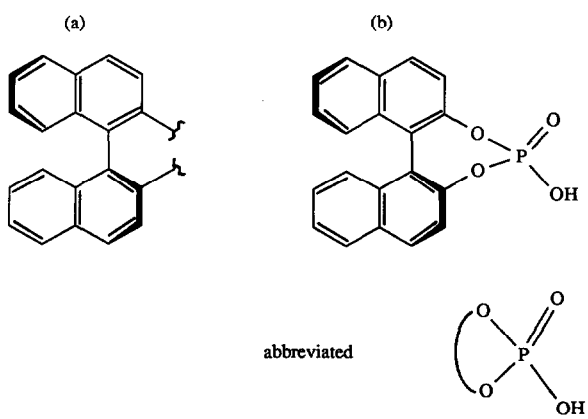

Fig. 1. (a) The binaphthyl skeleton; (b) 1,1′-binaphthyl-2,2′-diyl hydrogen phosphate (PhosH).

* Authors to whom correspondence should be addressed.

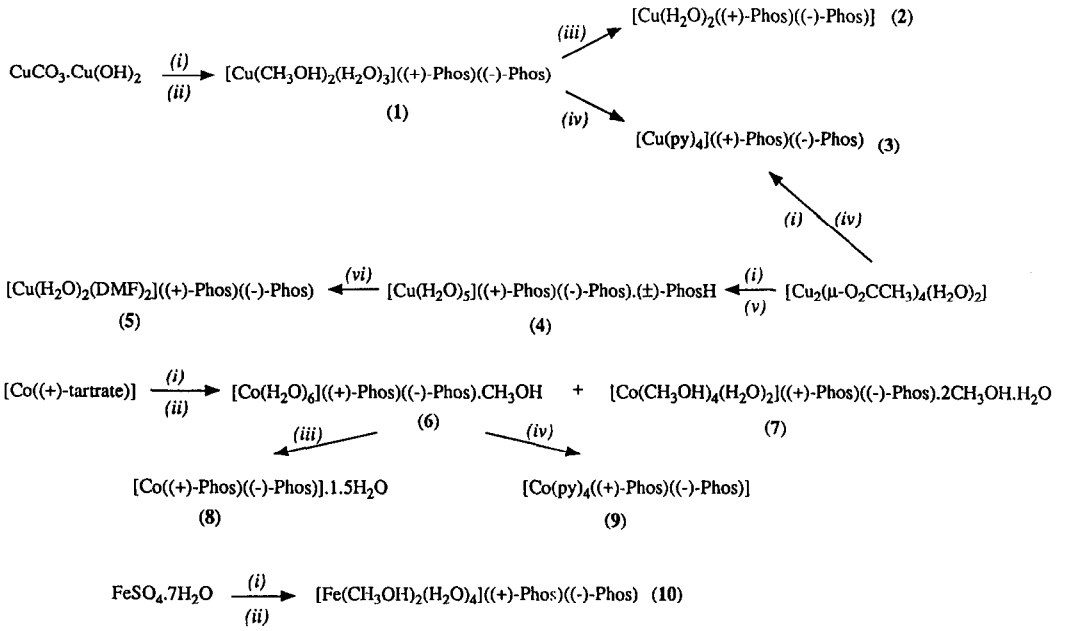

Scheme 1. (i) (±)-PhosH; (ii) methanol; (iii) heat and vacuum; (iv) pyridine; (v) THF; (vi) DMF.

RESULTS AND DISCUSSION

Racemic mixtures of PhosH (i.e. (±)-PhosH) were used throughout this study, and the synthetic routes to the products are summarized in Scheme 1. In general, the complexes were found to be insoluble in water and other common polar solvents, The tetrapyridine complexes **3** and **9** behaved as weak electrolytes in methanol, and in cases where the complexes were soluble in chloroform they were found to be non-electrolytes in that solvent. (±)-PhosH itself was only partially ionized in methanol and remained undissociated in chloroform. Allowing for the spectral differences caused by the presence of either methanol or pyridine all of the complexes were found to have essentially identical IR spectra. As with the sodium salt, Na^+Phos^-, the ν(PO) band for the compounds was present at 1100 cm^{-1} (1110 cm^{-1} for **8** and **10**). The magnetic moments of the complexes were in the ranges expected for normal Cu^{II}, high-spin Co^{II} and high-spin Fe^{II}.[6]

A crystal of the cobalt complex **7** was examined by X-ray diffraction.* The structure is shown in Figs 2(a) and (b). The metal is octahedrally coordinated as $[Co(CH_3OH)_4(H_2O)_2]^{2+}$, and the (+)-$Phos^-$ and (−)-$Phos^-$ ions are not directly bonded to the metal (although there is a network of hydrogen bonds linking the terminal oxygens of the $Phos^-$ ions to the coordinated and uncoordinated methanol and water molecules).

When a sample of the pale-pink solid **6** was placed under high vacuum and heated (120°C) for 12 h, it changed to the dark blue solid **8**. The IR spectrum of **8** did not contain a ν(CO) (methanol) band and there was a significant decrease in the relative intensity of the ν(OH) band when compared to the spectrum of **6**. A small shift in the ν(PO) band was also noted on going from **6** to **8**. The visible spectra of **6** (in wet DMF) and **8** (in dry CH_2Cl_2) were as expected for high-spin octahedral and tetrahedral cobalt(II), respectively (see page 730 in ref. 6). Prolonged exposure of the blue solid to the atmosphere caused it to revert back to the original pink colour. These colour changes suggest that the following equilibrium is operative, and that the $Phos^-$ ions

*X-ray crystallographic data for complex **7**: $C_{46}H_{54}O_{17}CoP_2$, $Mr = 999.77$. Monoclinic, $C2/c$ (no. 15), $a = 41.93(3)$, $b = 8.683(2)$, $c = 13.21(1)$ Å; $\beta = 105.41(4)°$. $V = 4636(5)$ Å. $D_c = 1.426$ g cm $^{-3}$, $z = 4$; $F(000) = 1619.96$, $\lambda = 0.71069$, μ(Mo-K_α) = 4.51 cm^{-1}. The complex crystallized as very thin, fragile, pink plates. Data were collected to 20° on an Enraf–Nonius CAD4 diffractometer on a capillary-mounted sample. All non-hydrogen atoms could be unambiguously identified, but the structure could only be refined to R = 0.13 using 1577 unique data for which $I > \sigma(I)$. The low precision of the data is attributed to the smallness of the largest available crystals and their thinness. The data have therefore not been deposited with the Cambridge Crystallographic Data Centre.

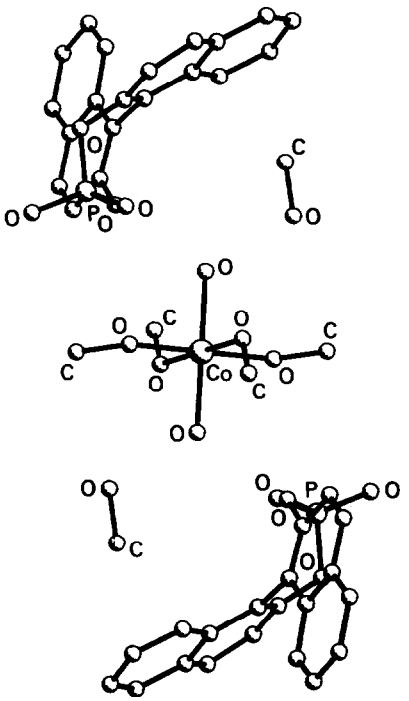

Fig. 2. X-ray structure of $[Co(CH_3OH)_4(H_2O)_2]((+)\text{-Phos})((-)\text{-Phos})\cdot 2CH_3OH\cdot H_2O$ (7) view of one asymmetric unit (excluding water molecule).

are coordinated to the metal in the blue solid **8**:

$$[Co(H_2O)_6]((+)\text{-Phos})((-)\text{-Phos}) \rightleftarrows [Co((+)\text{-Phos})((-)\text{-Phos})] + 6H_2O$$

O_h, pink — T_d, blue

Further evidence for the coordination of $Phos^-$ to the metal comes from the FAB mass spectrum of the Cu^{II} complex **2**, which contained peaks for the following ions: $[Cu(Phos)]^+$ (*m/z* 410); $[Cu_2(Phos)]^+$ (473); $[Cu(Phos)_2]^+$ (757); $[Cu_2(Phos)_2]^+$ (820); $[Cu_3(Phos)_2]^+$ (883).* Some of the possible monomeric and polymeric structures for $[M((\pm)\text{-Phos})_2]$ are illustrated in Fig. 3.

The thermogravimetric (TG) analysis curve for a sample of (±)-PhosH contained a well-defined thermal event between *ca* 200–440°C which correlated with the loss of dinaphtho[2,1-b:1′,2′-d]furan (Fig. 4).† At higher temperatures the remaining residue underwent multistage decomposition in which stable intermediates were not formed.[7] The TG curves for the tetrapyridine complexes **3** and **9** each contained two thermal events, the first of which corresponded to the loss of the four pyridine ligands in a single stage between *ca* 120–280°C. Single stage decomposition of the $Phos^-$ groups (loss of dinaphtho[2,1-b:1′,2′-d]furan) then took place at *ca* 320–480°C for the copper complex **3**, and at *ca* 400–600°C for the cobalt sample **9**.

The cyclic voltammogram of **3** in the potential range +212 to −788 mV [vs the ferrocene/ferrocenium (Fc/Fc^+) couple] showed a reversible, one-electron Cu^{2+}/Cu^+ couple (peaks AB in Fig. 5: $\Delta E = 87$ mV; $E_{1/2} = -407$ mV; $i_{P_c}/i_{P_a} = 1$), and the $E_{1/2}$ value of the couple suggested that the isolation of an air-stable Cu^I Phos compound would be thermodynamically unfavourable. Indeed, the reduction of **3** using the tetraphenylborate ion[8] did appear to give a Cu^I species. Addition of excess $Na[BPh_4]$ to a methanolic solution of **3** (under N_2) produced an immediate pale blue to light yellow colour change, and subsequent concentration of the solution caused the precipitation of a creamy-yellow solid. This solid (presumably a Cu^I species) was found to be extremely air-sensitive and turned green almost immediately on exposure to air. When the scan range of the voltammetry experiment was extended to −1388 mV (Fig. 6) two additional peaks appeared. Peak C was due to the irreversible reduction process, $Cu^+ + e \rightarrow Cu$ ($E_c = -1002$ mV), and the large peak D arose from the anodic stripping reaction, $Cu \rightarrow Cu^+ + e$ ($E_a = -451$ mV).‡

In summary, it appears that in the presence of donor solvents (methanol, water, pyridine) the $Phos^-$ ion does not coordinate directly to Cu^{II}, Co^{II} or Fe^{II} centres. However, in the case of some of the Cu^{II} and Co^{II} compounds there is evidence to suggest that when the compounds are de-solvated (by heating under high vacuum) the $Phos^-$ ions do then coordinate to the metals. Our current efforts are being directed towards the preparation of a sample of a coordinated $Phos^-$ complex for X-ray crystal structure determination in order to establish the coordination mode of the $Phos^-$ ligand.

EXPERIMENTAL

Except where specified all chemicals were reagent grade and were used without further purification. (±)-1,1′-Binaphthyl-2,2′-diyl hydrogen phosphate {(±)-PhosH} was prepared from (±)-1,1′-bi-2-naphthol[9] by using the method outlined by Cramm *et al.*[10] The sodium salt, Na^+Phos^- [ν(PO) = 1100 cm^{-1}], was made by treating a suspension of (±)-PhosH in water with an equimolar amount of NaOH. Most of the $Phos^-$ compounds which were

* The *m/z* values listed are based on the Cu^{63} isotope.

† In the mass spectrum (electron-impact) of (±)-PhosH (probe temperature = 380°C) the base peak was given by the (dinaphtho[2,1-b:1′,2′-d]furan)$^+$ ion (see Fig. 5).

‡ (±)-PhosH was electroinactive in the potential range +212 to −1388 mV (versus Fc/Fc^+).

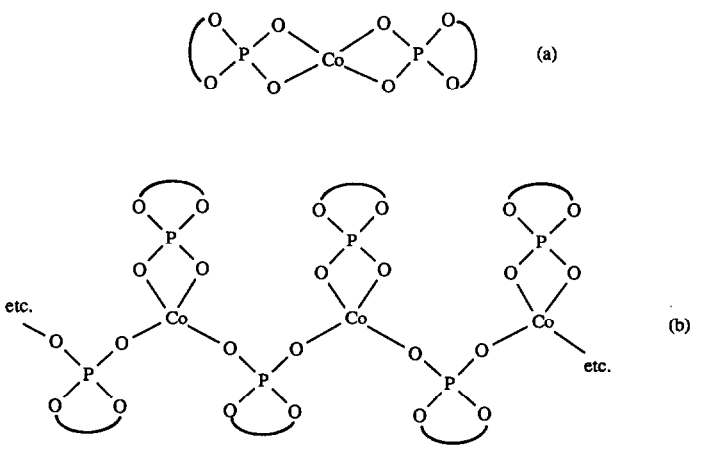

Fig. 3. Some of the possible structures of [Co((+)-Phos)((−)-Phos)] · 1.5H_2O (**8**) (tetrahedral Co^{II}): (a) monomeric, (b) polymeric. (Water molecules not shown.)

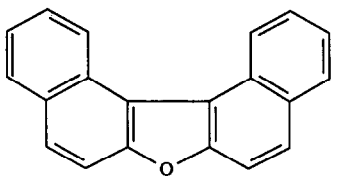

Fig. 4. Dinaphtho[2,1-b : 1′,2′-d]furan.

prepared were found to be hygroscopic. [Co(+)-tartrate] (i.e. [Co((+)-$C_4H_4O_6$)]) was prepared by reacting $CoCO_3$ with a refluxing aqueous solution of [(2*R*,3*R*)-(+)-tartaric acid]. Elemental analyses were performed by the Microanalytical Laboratory, University College Cork, Ireland. FAB mass spectra were run on a Varian MAT711 A spectrometer,

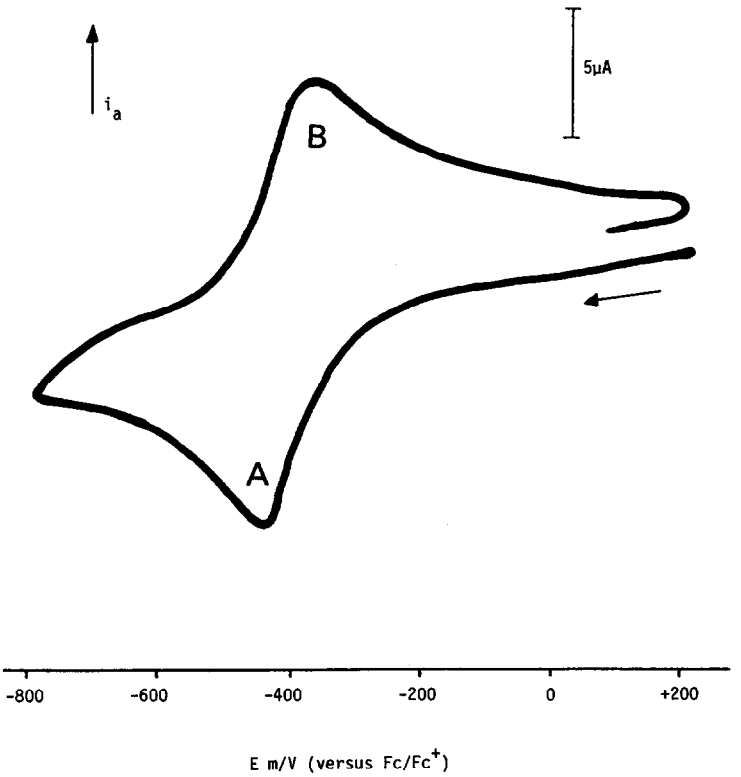

Fig. 5. Cyclic voltammogram of (3) in the potential range +212 to −788 mV (vs Fc/Fc^+). Scan rate = 50 mV s^{-1}.

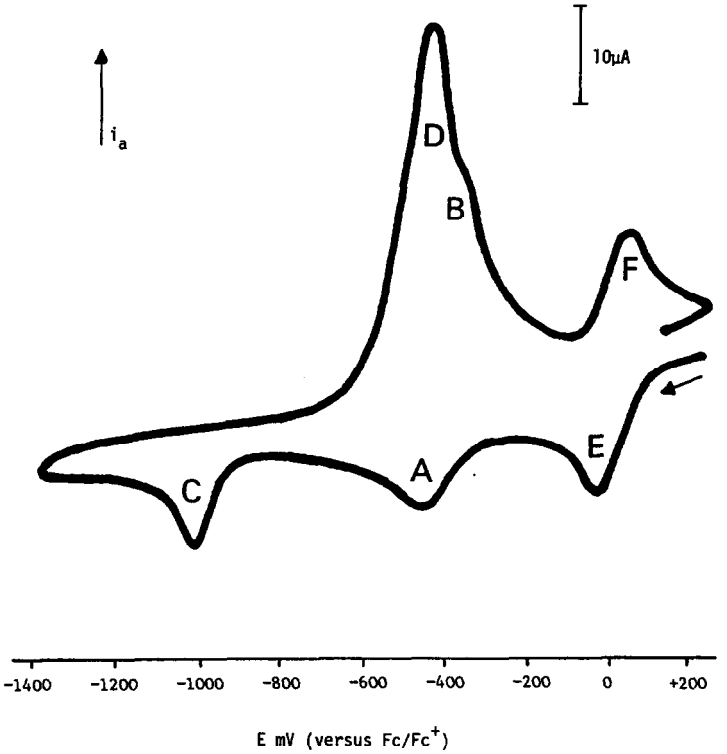

Fig. 6. Cyclic voltammogram of **3** in the potential range +212 to −1388 mV (vs Fc/Fc^+). Scan rate = 50 mV s^{-1}.

and electron-impact mass spectra were obtained using an AEI MS30 instrument equipped with an MSS data system. IR spectra (KBr disc) were recorded in the region 4000–200 cm^{-1} on a Perkin–Elmer 783 grating spectrometer, and solid-state, room-temperature magnetic susceptibility measurements were made using a Johnson Matthey magnetic susceptibility balance. Cyclic voltammograms (*ca* 20°C and under N_2) were recorded using an EG&G model 264A polarographic analyser in combination with an EG&G PARC model 303 electrode assembly. A glassy carbon disc and a platinum wire were used as the working and reference electrodes, respectively. Potentials (mV) were measured with respect to an internal reference standard,[11] the ferrocene/ferrocenium(1+) (Fc/Fc^+) couple. The voltammetry data was analysed with the aid of the EG&G Condecon (TM) 300 system (software iRu compensation was used). Tetraethylammonium perchlorate in dry DMF (1.0×10^{-1} M) was used as the supporting electrolyte/solvent system, and complex **3** and ferrocene were each used at a concentration of 2.0×10^{-3} M. Conductivities (1.0×10^{-3} M in methanol or chloroform) were measured using an AGB Scientific Ltd model 10 conductivity meter. A Milton Roy Spectronic 3000 Array instrument was used for recording UV–vis spectra. Thermogravimetric analyses (under N_2) were done on a Stanton Redcroft TG750/770 instrument which was coupled to a Houston Instrument Omniscribe (series D5000) recorder. The heating rate was 10°C min^{-1}.

$[Cu(CH_3OH)_2(H_2O)_3]((+)$-*Phos*$)((-)$-*Phos*$)$ (**1**)

A mixture of $CuCO_3 \cdot Cu(OH)_2$ (0.16 g, 0.72 mmol), (±)-PhosH (2.02 g, 5.80 mmol) and methanol (40 cm^3) was refluxed for 48 h. The hot suspension was filtered, and the white solid product was then washed with methanol and allowed to air-dry. Yield: 1.11 g (88%). Found: C, 58.9; H, 4.4. Calc: C, 57.6; H, 4.4%. IR: 3600–2600 (OH), 1100 (PO), 1020 cm^{-1} (CO of CH_3OH); $\mu_{eff.}$ = 1.9 BM (17°C); non-electrolyte in $CHCl_3$.

$[Cu(H_2O)_2((+)$-*Phos*$)((-)$-*Phos*$)]$ (**2**)

Complex **1** was heated (*ca* 50°C) under high vacuum for 8 h to give the white solid **2**. Found: C, 60.4; H, 3.5. Calc: C, 60.5; H, 3.5%. IR: 3600–2600 (OH), 1100 cm^{-1} (PO), no methanol (CO) band.

$[Cu(py)_4]((+)$-*Phos*$)((-)$-Phos) (**3**)

Method (*a*). Complex **1** (0.29 g, 0.33 mmol) was refluxed in pyridine (py) (15 cm^3) for 1 h. The resulting suspension was allowed to cool to room temperature and the blue product was then removed by filtration. The solid was washed well with diethyl ether and then air-dried. Yield: 0.27 g (76%).

Method (*b*). $[Cu_2(\mu\text{-}O_2CCH_3)_4(H_2O)_2]$ (0.10 g, 0.25 mmol), (±)-PhosH (0.53 g, 1.52 mmol) and pyridine (40 cm^3) were refluxed together for 2 h. The product was then recovered from the resulting suspension as described in Method (a) above. Yield: 0.49 g (91%). Found: C, 66.1; H, 4.3; N, 4.6. Calc: C, 67.1; H, 4.1; N, 5.2%. IR: 1100 (PO), 1605 cm^{-1} (py); $\mu_{eff.}$ = 1.8 BM (26°C); Λ_M = 56 S cm^2 mol^{-1} (in MeOH): non-electrolyte in $CHCl_3$.

$[Cu(H_2O)_5]((+)$-*Phos*$)((-)$-*Phos*$)\cdot(\pm)$-*Phos*H (**4**)

$[Cu_2(\mu\text{-}O_2CCH_3)_4(H_2O)_2]$ (0.45 g, 1.13 mmol), (±)-PhosH (2.53 g, 7.26 mmol) and THF (30 cm^3) were refluxed together for 3 h. The resulting suspension was allowed to cool to room temperature and the white product was removed by filtration. The solid was washed with THF and then allowed to air-dry. Yield: 1.95 g (72%). Found: C, 60.0; H, 4.1. Calc: C, 60.2; H, 4.0%. IR: 3600–2600 (OH), 1100 cm^{-1} (PO); $\mu_{eff.}$ = 2.0 BM (17°C).

$[Cu(H_2O)_2(DMF)_2]((+)$-*Phos*$)((-)$-*Phos*) (**5**)

Complex **4** (1.52 g, 1.27 mmol) was dissolved in hot dimethylformamide (DMF) (250 cm^3). The resulting brown solution was reduced in volume to *ca* 120 cm^3 by vacuum distillation, and on cooling the white product precipitated. The solid was filtered off, washed with diethyl ether and then allowed to air-dry. Yield: 0.46 g (39%). Found: C, 58.8; H, 4.5; N, 3.2. Calc: C, 58.8; H, 4.5; N, 3.0%. IR: 3600–2600 (OH), 1100 (PO), 1705 cm^{-1} (CO of DMF); $\mu_{eff.}$ = 1.8 BM (17°C).

$[CO(H_2O)_6]((+)$-*Phos*$)((-)$-*Phos*$)\cdot CH_3OH$ (**6**) *and* $[Co(CH_3OH)_4(H_2O)_2]((+)$-*Phos*$)((-)$-*Phos*$)\cdot 2CH_3OH\cdot H_2O$ (**7**)

A mixture comprising [Co(+)-tartrate)] (0.10 g, 0.48 mmol), (±)-PhosH (0.67 g, 1.92 mmol) and methanol (25 cm^3) were refluxed together for 15 min, and the mixture was then allowed to stir overnight at room temperature. The suspension was filtered, and the pale pink product **6** was washed with methanol and then air-dried. Yield: 0.35 g (81%). Found: C, 55.0; H, 4.2. Calc: C, 55.1; H, 4.5%. IR: 3600–2600 (OH), 1100 (PO), 1020 cm^{-1} (CO of CH_3OH); $\mu_{eff.}$ = 4.6 BM (22°C); non-electrolyte in $CHCl_3$. A crystal suitable for X-ray analysis (i.e. **7**) was obtained by allowing the above reaction filtrate to concentrate by slow evaporation in the fume cupboard.

$[Co((+)$-*Phos*$)((-)$-*Phos*$)]\cdot 1.5H_2O$ (**8**)

A sample of the pale pink solid **6** was heated (120°C) under high vacuum for 12 h to give the dark blue solid **8**. Found: C, 61.5; H, 3.3. Calc: C, 61.5; H, 3.5%. IR: 3600–3100 (OH), 1110 cm^{-1} (PO); $\mu_{eff.}$ = 4.8 BM (15°C). Complex **8** slowly turns pink again when it is exposed to the atmosphere. When **8** is reacted with concentrated HCl white, crystalline (±)-PhosH is recovered.

$[Co(py)_4((+)$-*Phos*$)((-)$-*Phos*$)]$ (**9**)

Complex (**6**) (0.60 g, 0.67 mmol) was refluxed in pyridine (15 cm^3) for 1 h and the resulting suspension was then allowed to cool to room temperature. The pink solid was filtered off, washed with diethyl ether and then dried under high vacuum (without heat). Yield: 0.22 g (31%). Found: C, 67.3; H, 3.9; N, 5.2. Calc: C, 67.4; H, 4.1; N, 5.2%. IR: 1100 (PO), 1608 cm^{-1} (py); $\mu_{eff.}$ = 4.7 BM (18°C); Λ_M = 59 S cm^2 mol^{-1} (in MeOH); non-electrolyte in $CHCl_3$.

$[Fe(CH_3OH)_2(H_2O)_4]((+)$-*Phos*$)((-)$-*Phos*) (**10**)

$FeSO_4\cdot 7H_2O$ (0.26 g, 0.94 mmol), (±)-PhosH (1.50 g, 4.31 mmol) and methanol (50 cm^3) were refluxed together for 1.5 h. The resulting suspension was filtered, and the white product was washed with methanol and dried under vacuum (without heating). Yield: 0.76 g (91%). Found: C, 57.9; H, 4.6. Calc: C, 56.9; H. 4.5%. IR: 3500–2600 (OH), 1100 (PO), 1020 cm^{-1} (CO of CH_3OH); $\mu_{eff.}$ = 4.6 BM (16°C); non-electrolyte in $CHCl_3$.

Acknowledgements—M. C. acknowledges financial support from the Krieble Fund, EOLAS and the Federation of Irish Chemical Industries.

REFERENCES

1. For example: (a) D. J. Cramm and J. M. Cramm, *Accts Chem. Res.* 1978, **11**, 8. (b) M. Sépulchre, N. Spassky, C. Mark and V. Schurig, *Makromol. Chem. Rapid Commun.* 1981, **2**, 261. (c) S. Kanoh, Y. Hongoh, M. Motol and H. Suda, *J. Chem. Soc., Chem. Commun.* 1988, 405. (d) R. Noyori, I. Tomino and Y. Tanimoto, *J. Am. Chem. Soc.* 1979, **101**, 3129. (e) S. Tomoda and M. Iwaoka, *J. Chem. Soc.*,

Chem. Commun. 1988, 1283. (f) R. Noyori and H. Takaya, *Accts Chem. Res.* 1990, **23**, 345.
2. For example: (a) E. Mohacsi and J. P. O'Brien, U.S. patent 4808580, 1989. (b) J. Knabe and P. Lampen, *Arch. Pharm. (Weinheim. Ger.)* 1987, **320**, 719. (c) W. Arnold, J. J. Daly, R. Imhof and E. Kyburz, *Tetrahedron Lett.* 1983, **24**, 343. (d) A. Garnier-Suillerot, J.-P. Albertini, A. Collet, L. Faury, J.-M. Pastor and L. Tosi, *J. Chem. Soc., Dalton Trans.* 1981, 2544. (e) J. Jacques, C. Fouquey and R. Viterbo, *Tetrahedron Lett.* 1971, 4617.
3. M. J. Shapiro, A. E. Archinal and M. A. Jarema, *J. Org. Chem.* 1989, **54**, 5826.
4. F. Mikeš and G. Boshart, *J. Chem. Soc., Chem. Commun.* 1978, 173.
5. H. Alper and N. Hamel, *J. Am. Chem. Soc.* 1990, **112**, 2803.
6. F. A. Cotton and G. K. Wilkinson, *Advanced Inorganic Chemistry*, 5th edn. Wiley, New York (1988).
7. M. E. Brown, *Introduction to Thermal Analysis: Techniques and Applications*, p. 17. Chapman & Hall, London (1988).
8. M. G. B. Drew, M. McCann and S. M. Nelson, *J. Chem. Soc., Dalton Trans.* 1981, 1868.
9. (a) A. I. Vogel, *Practical Organic Chemistry*, 3rd edn., p. 668. Longmans, London (1967). (b) R. Pummerer, E. Prell and A. Rieche, *Chem. Ber.* 1926, **59**, 2159.
10. E. P. Kyba, G. W. Gokel, F. de Jong, K. Koga, L. R. Sousa, M. G. Siegel, L. Kaplan, G. D. Y. Sogah and D. J. Cramm, *J. Org. Chem.* 1977, **42**, 4173.
11. R. R. Gagné, C. L. Spiro, T. J. Smith, C. A. Hamann, W. R. Thies and A. K. Shiemke, *J. Am. Chem. Soc.* 1981, **103**, 4073.

Polyhedron Vol. 10, No. 23/24, pp. 2779–2783, 1991
Printed in Great Britain

0277–5387/91 $3.00+.00
© 1991 Pergamon Press plc

BUTYRYLHYDRAZINE CHELATES OF LANTHANIDE DODECAHYDRODODECABORATES

XIN-LAN CHEN and LUN ZHANG*

Department of Chemistry, Wuhan University, Wuhan 430072, China

(*Received* 2 *January* 1991; *accepted* 22 *July* 1991)

Abstract—The butyrylhydrazine[buhy, $CH_3CH_2CH_2C(O)NHNH_2$] chelates of lanthanide dodecahydrododecaborates were synthesized by the reaction of butyrylhydrazine with lanthanide dodecahydrododecaborates. They have the formula $[Ln(buhy)_4]_2(B_{12}H_{12})_3nH_2O$. When Ln = La, Sm, Gd, $n = 5$; and when Ln = Ho, Er, Tm, Yb, $n = 4$. The IR, UV, ^1H NMR spectra and TG-DTA graphs of these chelates were recorded and are discussed.

Recently, we have described the benzoyl- and butyrylhydrazine complexes of first-row transition metal and IIB group metal hydroborates,[1] and the benzoylhydrazine complexes of lanthanide dodecahydrododecaborates.[2] The metal complexes have the formulae $[M(bh)_3]B_nH_n$ and $[M(buhy)_3]B_nH_n$, respectively; where bh is benzoylhydrazine and buhy is butyrylhydrazine; M = Mn, Fe, Co, Ni, Cu, Zn, Cd, and Hg; and $n = 10$ and 12. The formula of the lanthanide complexes is $[Ln(bh)_4]_2B_{12}H_{12}$ and Ln = La, Pr, Nd, Sm, Eu, Gd, Tb, Ho, Er, Tm and Yb. Some of these complexes exhibit biological activity and are able to inhibit the growth of cancer cells.[3]

As a continuation of our previous work, we report here the synthesis of butyrylhydrazine chelates of lanthanide dodecahydrododecaborates, and their spectral and thermal properties.

EXPERIMENTAL

Materials

Synthesis of butyrylhydrazine. An aqueous solution of hydrazine monohydrate (300 mmol, 17 cm^3) was mixed with ethyl butyrate (250 mmol, 34 cm^3) and stirred at room temperature until the reaction mixture became homogeneous. Then the mixture was heated to about 120°C to distill off the by-products and unreacted materials. The residue was cooled to −5°C and crystallized. Recrystallization from ethanol gave needle crystals (yield 80%, 200 mmol). Its m.p. (43–44°C) and IR spectra (see Table 2) are in accordance with the literature data.[4]

Preparation of dodecahydrododecaboric acid. A solution of bis(tetramethylammonium) dodecahydrododecaborate (3.50 mmol) in 50 cm^3 of cold water was passed through a column containing H-form cation exchange resin (100–200 mesh, 50 × 2 cm) and the effused dodecahydrododecaboric acid aqueous solution was collected and used for the preparation of $Ln_2(B_{12}H_{12})_3xH_2O$.

The ethyl butyrate (98%, $d = 0.878$) and hydrazine monohydrate (85%, $d = 1.032$) of reagent grade were used. The lanthanide oxides, all of 99.9% purity, were obtained from Yun Long Chemical Plant (Shanghai). Bis(tetramethylammonium) dodecahydrododecaborate was prepared by a known method.[5]

Physical measurements

IR spectra were obtained on a Shimadzu IR-450 spectrophotometer using KBr discs. UV spectra were recorded in H_2O with a Shimadzu UV-300 spectrophotometer. ^1H NMR spectra were recorded in CD_3CN with a JEOL JNM-90Q spectrometer using tetramethylsilane as internal standard. TG-DTA graphs were recorded on a Beijing LCT-1 TG-DTA instrument at a heating rate of 10°C min^{-1} in dynamic nitrogen of 60 cm^3 min^{-1} over a temperature range from 25°C to about 500°C.

* Author to whom correspondence should be addressed.

Synthesis of the chelates

All the chelates were synthesized using a general procedure that is illustrated below by the synthesis of $[La(buhy)_4]_2(B_{12}H_{12})_3 5H_2O$.

La_2O_3 (0.31 mmol) was dissolved in 16 cm^3 of about 0.07 M dodecahydrododecaboric acid solution. $La_2(B_{12}H_{12})_3 xH_2O$ solid was obtained after concentration of the solution to dryness under reduced pressure at 70°C. The solid $La_2(B_{12}H_{12})_3 xH_2O$ obtained from 0.31 mmol La_2O_3 was dissolved in 10 cm^3 of methanol and to this solution the butyrylhydrazine (7.40 mmol) was added with stirring. After 6 h, the reaction mixture was slowly heated to remove methanol under reduced pressure. The viscose residue was obtained and recrystallized from methanol—ether. The product was filtered, washed twice with small quantities of ether and dried *in vacuo*. A complete list of the chelates, yields and microanalyses are given in Table 1.

$$Ln_2O_3 + 3H_2B_{12}H_{12} \xrightarrow[60^\circ C]{H_2O} Ln_2(B_{12}H_{12})_3 \cdot xH_2O$$

$$[Ln(buhy)_4]_2(B_{12}H_{12})_3 \cdot nH_2O \xleftarrow[\text{Room temperature}]{CH_3OH} \text{buhy}$$

Ln = La, Sm, Gd. $n = 5$; Ln = Ho, Er, Tm, Yb, $n = 4$

Scheme 1.

RESULTS AND DISCUSSION

Syntheses and properties

The synthesis of the butyrylhydrazine chelates of lanthanide dodecahydrododecaborates is outlined in Scheme 1.

Microanalytical data for the chelates (Table 1) show that all the chelates have a 4:1 ratio of buhy to Ln^{3+}, which is independent of the ratio of reactants.

All these chelates are white hygroscopic solids, which are soluble in water, methanol and acetonitrile, and insoluble in ether and acetone.

IR spectra. Since these chelates have similar IR spectra, only the spectral data of buhy, lanthanum dodecahydrododecaborate hydrates, and lanthanum chelate chosen as a representative are listed in Table 2. The detailed vibrational frequencies (4000–400 cm^{-1}) with possible assignments are given.

The important changes observed after chelation are: (1) the splitting and shift of amide I and II frequencies from 1660 to 1610 cm^{-1} in the parent ligand to 1646 cm^{-1} (Amide I) and 1600 cm^{-1} (Amide II); (2) the shifts of the $\nu(N—N)$ vibrations from 995 and 920 cm^{-1} in the ligand to 948 and 905 cm^{-1}, respectively; (3) two bands around 645 and 475 cm^{-1} being found for all chelates, which may be attributed to $\nu(N \rightarrow Ln)$ and $\nu(O \rightarrow Ln)$ vibrations, respectively. These important changes suggest that buhy is coordinated with the lanthanide ions through its carbonyl oxygen and nitrogen atoms, forming five-membered chelate rings.

In comparison with $La_2(B_{12}H_{12})_3 xH_2O$, no change for the characteristic vibration bands of $B_{12}H_{12}^{2-}$ in all chelates were observed. It shows that all *closo*-$B_{12}H_{12}^{2-}$ are outer sphere anions.

UV spectra. The UV spectral data of buhy and its lanthanide chelates are given in Table 3. No absorption was observed in the visible region (900–400 nm) for the ligand and any of its chelates. The spectra of the chelates are similar to the spectrum of the ligand and all of them exhibit only one band due to C=O and $—NH_2$ groups. The absorption maximum (λ_{max}) of the ligand undergoes red shifts of 1–6 nm in the chelates. However, the values of the molar extinction coefficient (ε) of the chelates measured at identical wavelength show significant

Table 1. Yields and microanalyses data for chelates

$[Ln(buhy)_4]_2$ Ln	$(B_{12}H_{12})_3 nH_2O$ n[b]	Yield[a] %	Microanalyses, found (calc.) Ln (%)	B (%)	C (%)	H (%)	N (%)
La	5	47	17.2(17.3)	23.7(24.2)	24.1(23.9)	8.1(7.9)	13.5(13.9)
Sm	5	61	18.6(18.4)	23.5(23.8)	23.9(23.5)	7.6(7.8)	13.4(13.7)
Gd	5	46	18.7(19.1)	23.9(23.6)	24.0(23.3)	7.6(7.7)	13.5(13.6)
Ho	4	78	20.3(20.1)	23.3(23.7)	23.6(23.4)	7.4(7.6)	13.7(13.6)
Er	4	78	20.3(20.3)	23.1(23.6)	23.5(23.3)	7.2(7.6)	13.2(13.6)
Tm	4	69	20.1(20.5)	23.1(23.5)	23.1(23.2)	7.8(7.6)	13.3(13.6)
Yb	4	47	21.0(20.8)	23.6(23.4)	22.5(23.1)	7.2(7.5)	13.6(13.5)

[a] Based on the weight of Ln_2O_3 used.
[b] Determined by TG method (Table 5).

Table 2. IR absorption data (cm^{-1}) of buhy, $La_2(B_{12}H_{12})_3xH_2O$ and $[La(buhy)_4]_2(B_{12}H_{12})_35H_2O$

buhy	$La_2(B_{12}H_{12})_3xH_2O$	La-chelate	Possible assignment
	3360b,vs	3520m	$\nu(H_2O)$
3280s		3300s	ν(NH)
3050sh,w		3050sh,w	ν(NH)
2960m		2960m	ν(CH) saturated
2940m		2940m	ν(CH)
2870m		2870w	ν(CH)
	2470vs	2470vs	ν(BH)
1660–1610b,vs		1646s	ν(C=O) amide **I**
		1600s	δ(NH) + ν(CN) amide **II**
1530m		1530m	δ(—NH—)
1462N		1462m	δ_{as}(CH CH_3)
1380m		1382w	δ_s(CH CH_3)
1332w		1332w	$\delta(NH_2)$
1290w		1290w	$\delta(CH_2)$ wag.
1260w		1260w	$\delta(CH_2)$ wag.
1150w		1153w	$\delta(NH_2)$
1090w		1100m	$\delta(CH_2)$
	1070m	1068m	ν(BB)
1036w		1032w	δ(CH)
995m		948w	ν(NN)
920w		905w	ν(NN)
870w		870w	ν(NN)
806w		810w	
746w		750w	
	720w	720w	δ(BB)
		640w	ν(N → La)
		475w	ν(C → La)

Table 3. UV spectral data of buhy and chelates

Ligand or chelates	λ_{max} (nm)	ε
buhy	206	1919
La	209	14756
Sm	211	14288
Gd	212	12134
Ho	207	18122
Er	207	17777
Tm	211	13250
Yb	209	15127

increments when compared with the value of the ligand. It also suggests that the carbonyl oxygen and amine nitrogen atoms are coordinated to the lanthanide ions.

^1H NMR spectra. The proton signals of ligand (buhy) and lanthanide chelates (Ln = La, Sm, Gd, Ho, Er, Tm and Yb) were recorded (Table 4). Among the lanthanide ions mentioned above, La^{3+} is diamagnetic, while the others containing unpaired $4f$ electrons are all paramagnetic. In the lanthanum ($4f^0$) chelate all the proton signals suffer upfield shifts when compared with that of the free ligand. With the samarium ($4f^5$) chelate the proton signals of the butyryl group suffer downfield shifts. With the gadolinium ($4f^7$) chelate no signal was observed at all, which is similar to that of methylene bis(diphenylphosphine oxide) complex of gadolinium dodecahydrododecaborate.[5] With the holmium ($4f^{10}$) and erbium ($4f^{11}$) chelates all the proton signals suffer downfield shifts and broadening compared with that of the lanthanum chelate. Both the thulium ($4f^{12}$) and ytterbium ($4f^{13}$) chelates display two broad signals, the former centred at 1.50 and 3.92, and the latter at 1.26 and 3.90 ppm, respectively. These spectra with broadened signals may be due to a spin–spin relaxation process arising from the paramagnetic lanthanide ions. Gd^{3+} has the maximum number of unpaired electrons and is strongly paramagnetic, making the signals extremely broad.

Table 4. ^{1}H NMR spectral data of ligand (buhy) and chelates

	Chemical shifts (δ, ppm)[a,b]				
	CH_3—	—CH_2—	—CH_2CO—	—NH—	—NH_2—
buhy[c]	0.96sh,t	1.71m	2.29sh,t	—[d]	9.42br,s
La	0.92sh,t	1.61m	2.23sh,t	9.02br,s	2.58br,s
Sm	1.20sh,t	2.16m	2.74sh,t	8.67br,s	3.90br,s
Ho	1.00br,t	2.18m	3.34br,s	9.96br,s	4.18br,s
Er	1.04br,t	2.12m	3.32br,s	—[d]	4.31br,s

[a] Scanned covering a range of 0–50 ppm at 25°C.
[b] sh, sharp; br, broad; s, singlet; t, triplet; m, multiplet.
[c] Recorded in $CDCl_3$.
[d] Unobserved.

TG-DTA graphs

All the chelates show similar TG-DTA graphs as typically given in Figs 1 and 2 for the Sm- and Yb-chelate respectively.

The TG curve reveals four weight-loss stages. The first two are the dehydration of the chelates, including the loss of crystalline water and coordinated water. The observed weight-loss compares favourably with the calculated values (Table 5). The second two are the decomposition of anhydrous chelates, which are very complex and probably include the partial loss of ligands and the decompo-

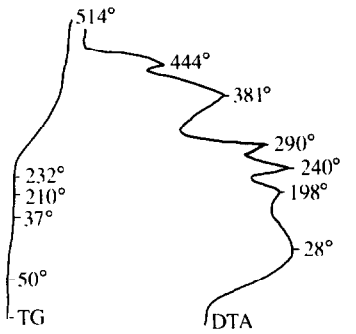

Fig. 1. TG-DTA graph of Sm-chelate.

Table 5. The data for dehydration and decompositon of chelates

	Dehydration					Decomposition		
Chelates	Temperature range (°C)	Weight-Loss (%) Obs.	Calc.	Loss species	DTAPeaks (°C)	Temperature range (°C)	Obs. weight loss (%)	DTA peaks (°C)
La	60–139	4.4	4.5	$4H_2O$	86, 132	237–563	26.5	237, 296
	139–210	1.0	1.1	H_2O				376, 444
Sm	60–137	4.4	4.4	$4H_2O$	88, 198	232–514	26.3	240, 290
	137–210	1.1	1.0	H_2O				381, 444
Gd	60–149	4.3	4.4	$4H_2O$	—, 203	236–519	25.9	—, 288
	149–213	1.1	1.1	H_2O				389, 460
Ho	60–121	3.3	3.3	$3H_2O$	87, 192	231–573	22.3	237, 291
	121–219	0.9	1.1	H_2O				373, 463
Er	60–121	3.0	3.3	$3H_2O$	87, 190	238–543	22.8	237, 293
	121–219	1.1	1.1	H_2O				387, —
Tm	60–133	3.3	3.3	$3H_2O$	85, 204	245–579	22.4	235, 288
	133–213	0.8	1.1	H_2O				382, 473
Yb	60–134	3.2	3.3	$3H_2O$	84, 209	240–579	22.4	242, 296
	134–213	1.0	1.1	H_2O				380, 473

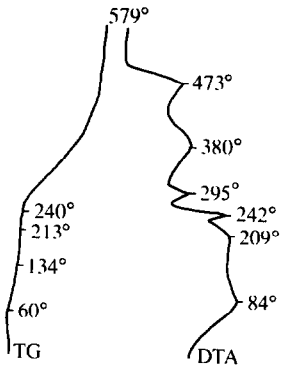

Fig. 2. TGDTA graph of Yb-chelate.

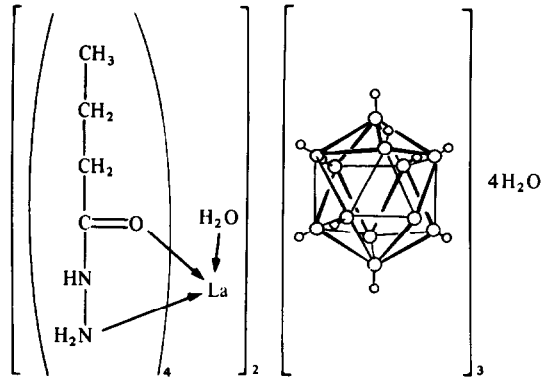

Fig. 3. The proposed structure of La-chelate. ○ = B, ○ = H.

sition of $B_{12}H_{12}^{2-}$ and residual ligands to give an unknown product having an 18:1 ratio of B:Ln. For example, the microanalyses data of the decomposed product of Er-chelate are B(%), 21.8; Er(%), 18.8.

The microanalyses data and all the above results suggest the formulation of these lanthanide chelates as $[Ln(buhy)_4(H_2O)]_2(B_{12}H_{12})_3(n-1)H_2O$. The proposed structure of La-chelate is shown in Fig. 3.

REFERENCES

1. Lun Zhang, Dong-Bao He, Hai-Cheng Zhang and Guo-Min Zhang, *Wuhan Daxue Xuebao, Ziran Kexue Ban* 1984, **3**, 65; *Chem. Abstr.* **103**, 105032h.
2. Lun Zhang, Pei-Zhi Hu, Chun-Hua Qian and Guo-Min Zhang, *Gaodeng xuexiao Huaxue Xuebao* 1984, **5**, 153; *Chem. Abstr.* **100**, 220544d.
3. Guo-Zheng Yuan and Lun Zhang, unpublished results.
4. Sadtler Standard Infrared Grating Spectra, 7684K, Sadtler Research Laboratories Inc. (1969).
5. Xin-Lan Chen, Jia Jiang and Lun Zhang, *Zhongguo Xitu Xuebao* 1988, **6**, 13; *Chem. Abstr.* **110**, 224377f.
6. Lun Zhang, Xin-qin Fang and Guo-Min Zhang, *Synth. React. Inorg. Met.-Org. Chem.* 1988, **18**, 127.

Polyhedron Vol. 10, No. 23/24, pp. 2785–2789, 1991
Printed in Great Britain

0277–5387/91 $3.00+.00
© 1991 Pergamon Press plc

MACROCYCLIC DIVALENT TRANSITION METAL COMPLEXES OF ACETYLACETONE BUCKLED WITH TWO DIFFERENT DIAMINES

K. HUSSAIN REDDY,* G. KRISHNAIAH and Y. SREENIVASULU

Department of Chemistry, Sri Krishnadevaraya University, Anantapur-515 003, India

(*Received* 14 *November* 1990; *accepted* 22 *July* 1991)

Abstract—Metal-mediated condensation of *o*-phenylenediamine with bisacetylacetone-ethylenediimine yields 14-membered tetraaza macrocyclic six-coordinate complexes of the type $[M(mac)Cl_2]$, $[M(mac)SO_4 \cdot H_2O]$ (where M = Fe^{II}, Co^{II} and Cu^{II}; mac = macrocyclic ligand formed in the template reaction). The metal ions are coordinated by four azomethine nitrogen atoms bridged by acetylacetone moieties. The electrical conductance magnetic moments, electronic and IR spectral data of all complexes are discussed.

Several transition-metal macrocyclic complexes either by template or non-template methods have been prepared using different dicarbonyl compounds and diamines. Various synthetic possibilities of the 2,4-pentanedione-1,2-diaminoethane system have been discussed[1] and different macrocyclic ligand complexes have been recently reviewed by Lindoy.[2] Truck and Holm[3] have prepared macrocyclic complexes which are completely conjugated using ethylenediamine and acetylacetone. Similarly, tetraaza macrocyclic transition-metal complexes have been prepared using *o*-phenylenediamine and acetylacetone.[4] Recently,[5] divalent metal complexes with *m*-phenylenediamine and acetylacetone have been prepared and characterized.

However, divalent transition-metal complexes with acetylacetone buckled with both aliphatic and aromatic amines are not reported so far. In continuation[6] of our efforts to derive model compounds using macrocyclic ligands, we report here the synthesis and spectral properties of six-coordinate complexes of tetradentate ligands formed *in situ* in the presence of metal ions with bisacetylacetone-ethylenediimine and *o*-phenylenediamine.

EXPERIMENTAL

All the chemicals and solvents used were of reagent grade.

Ethylenediamine (BDH) was dried over solid potassium hydroxide for 12 h and distilled, the fraction boiling over the range 116–117°C being used in this study. Acetylacetone used in the preparation of complexes was from Germed, Veb Laborchemie and used without further purification. *Ortho* phenylenediamine used in this study was from SD and recrystallized from methanol and used.

The Schiff base bisacetylacetone-ethylenediimine was prepared and purified following the literature procedure[7] (m.p. 111°C; lit. m.p. 111–111.5°C).

Preparation of complexes

To a hot reaction mixture containing *ortho* phenylenediamine (0.002 mol) dissolved in methanol (50 cm^3) and an adequate quantity (0.002 mol) of corresponding metal salt solution, was added bisacetylacetone-ethylenediimine (0.002 mol) dissolved in methanol (25 cm^3). The reaction mixture was then heated under reflux for 2 h in a hot water bath. On cooling the reaction mixture, the product was separated, collected by filtration *in vacuo*, washed with hot water and then with cold methanol and dried. The colour, yield, molar conductance and magnetic moments together with analytical data for all complexes are given in Table 1. Chloro and sulphato complexes were prepared by taking metal chlorides and sulphates, respectively.

The microanalyses of C, H and N were done at the Regional Sophisticated Instrumentation Centre, Central Drug Research Institute, Lucknow, UP, India. The metal contents were estimated using standard EDTA titrations.

* Author to whom correspondence should be addressed.

Table 1. Analytical and magnetic moment data of complexes

Complex	Colour	Yield (%)	Percentage of Carbon Found (Calc.)	Hydrogen Found (Calc.)	Nitrogen Found (Calc.)	Metal Found (Calc.)	μ_{eff} (BM)
$[Fe(C_{18}H_{22}N_4)SO_4H_2O]$	Brown	63	46.1 (46.5)	5.2 (5.2)	12.2 (12.2)	12.5 (12.0)	4.89
$[Fe(C_{18}H_{22}N_4)Cl_2]$	Dark brown	55	49.5 (51.3)	5.2 (5.2)	12.7 (13.3)	13.6 (13.3)	3.61
$[Co(C_{18}H_{22}N_4)SO_4H_2O]$	Black	65	46.4 (46.2)	5.0 (5.1)	12.0 (12.0)	12.7 (12.6)	3.70
$[Co(C_{18}H_{22}N_4)Cl_2]$	Black	57	50.0 (51.0)	5.1 (5.2)	13.6 (13.2)	13.5 (13.9)	3.35
$[Ni(C_{18}H_{22}N_4)]SO_4$	Red	65	46.9 (48.1)	4.8 (4.9)	12.2 (12.5)	13.0 (13.1)	Diamagnetic
$[Ni(C_{18}H_{22}N_4)]Cl_2$	Red	61	50.2 (51.0)	5.5 (5.2)	13.5 (13.2)	13.5 (13.8)	Diamagnetic
$[Cu(C_{18}H_{22}N_4)SO_4]_2$	Black	60	45.1 (45.6)	5.5 (5.5)	12.1 (11.8)	13.8 (13.4)	Diamagnetic
$[Cu(C_{18}H_{22}N_4)Cl_2]$	Black	55	50.2 (50.4)	4.9 (5.1)	13.5 (13.1)	14.5 (14.8)	1.69

Physical measurements

The IR spectra were recorded in the range 4000–180 cm^{-1} using KBr discs. Magnetic susceptibility measurements were made using a vibrating sample magnetometer (VSM) operating at a field strength of 3–8 kg at room temperature. The electronic spectra for all complexes in the UV and visible region were recorded in the range 185–1200 nm on a Carl Zeiss DMR-21 recording spectrophotometer in dimethylformamide (DMF) medium. The electrical conductivity measurements were made in DMF solvent at room temperature (31+2°C) using a Systronic 303 direct-reading conductivity bridge. A suitable quantity of solid complex was weighed and dissolved in DMF to reach a 10^{-3} M concentration. The ^1H NMR spectra were obtained on a Varian XL-300 MHz spectrometer at room temperature.

RESULTS AND DISCUSSION

The colours, analyses, molar conductance and magnetic moment values of the complexes are given in Table 1. Attempts to isolate iron(III) complexes by the procedure described for the preparation of complexes were unsuccessful and resulted in rapid reduction and formation of tetraaza macrocyclic iron(II) complexes.

All the complexes are soluble in hot methanol and DMF. The complexes are stable towards water and unstable either in mineral acids or in alkali.

The analytical data of these complexes show their formulae to be $[M(C_{18}H_{22}N_4)Cl_2]$ and $[M(C_{18}H_{22}N_4)SO_4 \cdot H_2O]$, where M = Fe^{II}, Co^{II} and Cu^{II}. Except [Ni(mac)]Cl_2 (155) and [Ni(mac)]SO_4 (110 Ω^{-1} cm^{-2} mol^{-1}), all the complexes are non-electrolytes in dimethylformamide. Molar conductivity values of nickel complexes are given in parentheses.

Magnetic moments and electronic spectra

Tetraaza macrocyclic iron(II) sulphato and chloro complexes show lower magneton values of 4.89 and 3.61 BM, which may be attributed to the quenching of orbital contribution arising from the lower symmetry.[8] Two bands are observed in the electronic spectrum of iron(II) complexes. Chloro and sulphato macrocyclic iron(II) complexes exhibit bands at 5900, 5200 and 12,800, 12,510 cm^{-1} assigned to $^5A_{1g} \leftarrow {}^5T_{2g}$ and $^5B_{1g} \leftarrow {}^5T_{2g}$ transitions,

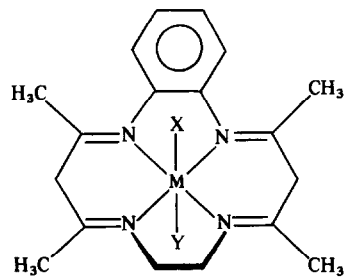

I

where M = Fe^{II}, Co^{II}, Cu^{II}
X = Y = Cl^- or X = H_2O, Y = SO_4^{2-}

Table 2. Electronic spectral data and ligand field parameters of nickel complexes

Complex	Method of evaluation	ν_1	ν_2	ν_3	B_{35}	$\delta\nu^a$	$\beta_{35}{}^b$	10 Dq	$\nu_2-\nu_1$	ν_2/ν_1
[Ni(mac)]SO_4	Observed values	8750	16,540	23,810	—	—	—	8750	7790	1.89
	A	10 Dq	14,231	23,809	786	±2309	0.75	8750	5481	1.67
	B	10 Dq	14,500	25,550	920	±2040	0.88	8750	5750	1.76
[Ni(mac)]Cl_2	Observed values	8820	16,860	24,100	—	—	—	8820	8040	1.91
	A	10 Dq	14,693	24,697	862	±2167	0.83	8820	5873	1.66
	B	10 Dq	14,691	26,259	966	±2169	0.93	8820	5871	1.66

[a] Difference in the observed and calculated value of frequencies.
[b] Ratio of the free ion and of the complex.

respectively, characteristic of six-coordinate iron(II) complexes[9] of the type FeL_4X_2. These complexes exhibit charge-transfer bands at 18,520 (chloro) and 20,830 cm^{-1} (sulphato) with iron(II) t_{2g} electrons being transferred to the empty π-antibonding orbitals of the ligand.

Magnetic moments of [Co(mac)Cl_2] and [Co(mac)$SO_4 \cdot H_2O$] are found to be 3.70 and 3.51 BM, respectively, corresponding to spin-only values for three unpaired electrons of a d^7 system. Most of the octahedral cobalt(II) derivatives are pink or reddish-brown while many of the tetrahedral cobalt (II) complexes are intense blue or green. However, these colours are infallible guides so as to decide the geometry of the complexes. In the electronic spectrum of [Co(mac)Cl_2] and [Co(mac)$SO_4 \cdot H_2O$] three bands are observed at 7300 and 7500, 15,150 and 16,600 and 18,540 and 18,520 cm^{-1}, assigned to $^4T_{2g} \leftarrow {}^4T_{1g}$, $^4A_{2g} \leftarrow {}^4T_{1g}$ and $^4T_{1g}(P) \leftarrow {}^4T_{1g}$ transitions, respectively, in an octahedral geometry.[10] The inter-electronic repulsion (B) and 10 Dq are found to be 786 and 841 and 7850 and 9100 for chloro and sulphato macrocyclic cobalt(II) complexes, respectively. The ratio of observed ν_2 to calculated ν_1 are found to be 2.07 and 2.21 for chloro and sulphato complexes, respectively, as required for an octahedral cobalt(II) complex.[11] The LFSE are calculated and found to be 22.4 and 26.0 kcal mol^{-1} for chloro and sulphato complexes, respectively.

The electronic spectral data for [Ni(mac)]Cl_2 and [Ni(mac)]SO_4 show bands at 8750 and 8820, 16,540 and 16,860 and 23,810 and 24,100 cm^{-1}, attributable to $^3T_{2g}(F) \leftarrow {}^3A_{2g}(F)$, $^3T_{1g}(F) \leftarrow {}^3A_{2g}(F)$ and $^3T_{1g}(F) \leftarrow {}^3A_{2g}(F)$ transitions, respectively. The electronic spectral data suggest an octahedral geometry for these complexes.

The nickel(II) macrocycles are diamagnetic but in DMF the electronic spectral data correspond to octahedral geometry. DMF is known to be a coordinating solvent and presumably coordinates nickel in the axial positions to become six-coordinate. The electronic spectra of the complexes in the solid state correspond to square-planar geometry. The spectral data utilized important ligand field parameters to compute 10 Dq and B_{35}, using the ligand field theory of spin-allowed transitions in a d^8 configuration. The values of B_{35} and 10 Dq were used to calculate ν_2 and ν_3 and the results are given in Table 2.

The diamagnetic nature of the copper(II) sulphato tetraaza macrocyclic complex indicates the possible spin–spin interaction by the overlap of occupied $d_{x^2-y^2}$ orbitals of the two cupric ions to form a δ-type bond similar to that reported in copper(II) acetate monohydrate. The electronic spectrum of this complex shows one broad, strong band at 18,870 cm^{-1} with a more or less pronounced low energy shoulder (17,860 cm^{-1}). Based on the electronic spectrum, this complex seems to be tetragonally distorted.[12] For a copper(II) ion in a tetragonal environment three principal absorption bands are expected, but only in a few complexes[13–15] have these absorption bands been resolved, either by Gaussian analysis or single-crystal polarization studies, and are assigned to the transitions $^2A_{1g} \leftarrow {}^2B_{1g} \cdots (\nu_1)$, $^2B_{2g} \leftarrow {}^2B_{1g} \cdots (\nu_2)$ and $^2E_g \leftarrow {}^2B_{1g} \cdots (\nu_3)$ in order of increasing energy. The low energy shoulder in the present complex can be assigned to[14,15] the splitting of the ^2E_g term. Because of the low intensity of the $^2B_{2g} \leftarrow {}^2B_{2g}$ (which is equal to 10 Dq) band, it is not usually observed as a separate band in tetragonal copper complexes. Another band in the electronic spectrum of this complex is located at 14,600 cm^{-1}, attributable to the $^2E_g \leftarrow {}^2B_{1g}$ transition suggesting octahedral geometry for this complex.[16]

The magnetic moment of the chloro derivative

Table 3. Important IR spectral bands and their assignments

Complex	ν(C=N)+ν(C=C)	ν_{asym}(C—CH_3)	ν_{sym}(C—CH_3)	δ(CH)+ν(C—CH_3)	P_r—CH_3	Anions
[Fe(mac)SO_4H_2O]	1615 1595	1425	1385	1226	1030	1195 1070 1015
[Fe(mac)Cl_2]	1610 1590	1430	1380	1225	1020	290
[Co(mac)SO_4H_2O]	1615 1580	1410	1370	1210	1025	1118 1055 1020
[Co(mac)Cl_2]	1610 1587	1425	1365	1205	1022	300
[Ni(mac)]SO_4	1615 1580	1400	1353	1219	1030	1122 1072 1015
[Ni(mac)]Cl_2	1615 1575	1410	1355	1210	1020	—
[Cu(mac)SO_4]$_2$	1610 1585	1422	1365	1225	1025	1160 1065 1005
[Cu(mac)Cl_2]	1615 1575	1420	1360	1220	1020	283

of the tetraaza macrocyclic copper(II) complex is found to be 1.69 BM, which is very close to the spin-only value for one unpaired electron and is in the range normally observed for copper(II) complexes having an orbitally non-degenerate B_{1g} ground state. This complex shows one band in the visible region with λ_{max} at 15,380 cm^{-1}. This is characteristic of a $^2T_{2g} \leftarrow {}^2E_g$ absorption in octahedral geometry.[17]

IR spectra

The important IR spectral bands of the tetraaza macrocyclic complexes and their assignments are presented in Table 3. In the IR spectra the stretching and deformation vibrations of the NH_2 groups are absent. Strong bands appearing as doublets in the range 1610–1585 cm^{-1} are assigned[18–21] to the coordinated and conjugated $\rangle C{=}N$ group present in all the complexes. The bands characteristic of the acetylacetone moiety (Table 3) are present in all the complexes. The absence of stretching and bending vibrations of the (C—O) group (1525 and 1280 cm^{-1}) indicate the absence of this group in these complexes.[5]

The bands appearing in the spectra of the sulphato complexes, 1120, 1070 and 1020 cm^{-1}, may be assigned to unidentate sulphate groups.[22–24] In the sulphate containing complexes bands in the region 3455–3485 cm^{-1} are assigned to the presence of coordinated water molecules.

Characteristic bands in the far IR spectra of complexes are observed. The chloro complexes exhibit bands at 290, 300 and 283 cm^{-1} and these are assigned to Fe—Cl, Co—Cl and Cu—Cl vibrations, respectively. The appearance of single bands and their regions are consistent with the *trans* octahedral nature of these complexes.[25] In the spectra of all the complexes, bands are observed in the region 440–485 cm^{-1}, assigned to the ν(M—N) vibrations which substantiate the participation of the azomethine nitrogen atom in coordination.[26]

^1H NMR spectra of the nickel complexes: the ^1H NMR spectra of [Ni(mac)]Cl_2 and [Ni(mac)]SO_4 complexes are virtually identical. ^1H NMR ($CDCl_3$): 1.98 (s, 12H, methyl H), 3.23 (s, 4H, methylene H), 3.53 (s, 4H, methylene H), 6.95–7.25 (m, 4H, phenyl H).

Based on the results we have presented so far, structure **I** is assigned for these complexes.

Acknowledgements—The authors thank University Grants Commission, New Delhi for giving financial sup-

port. The authors also thank the authorities of CDRI, Lucknow and RSIC, Madras for providing elemental analyses and spectral data of the complexes.

REFERENCES

1. J. P. Costes, *Polyhedron* 1987, **6**, 2169.
2. L. F. Lindoy, *The Chemistry of Macrocyclic Ligand Complexes*. Cambridge University Press, Cambridge (1989).
3. J. J. Truck and R. H. Holm, *J. Am. Chem. Soc.* 1972, **94**, 4529.
4. V. L. Goedken, J. J. Pluth, S. M. Pang and B. Bursten, *J. Am. Chem. Soc.* 1976, **98**, 8014.
5. V. B. Rana, P. Singh, D. R. Singh and M. P. Teotia, *Polyhedron* 1982, **4**, 177.
6. A. Krishna, K. H. Reddy and D. V. Reddy, *Inorg. Chim. Acta* 1990, **173**, 13.
7. J. McCarthy, R. J. Hovry and A. E. Martell, *J. Am. Chem. Soc.* 1955, **20**, 5821.
8. P. Gutlich, *Struct. Bond. (Berlin)* 1981, **44**, 84.
9. B. N. Figgis, *Introduction to Ligand Fields*, p. 220. Interscience, New York (1966).
10. E. Konig, *Structure and Bonding*, p. 175. Springer, New York (1971).
11. A. B. P. Lever, *Inorganic Electronic Spectroscopy*, pp. 119–332. Elsevier, Amsterdam (1965).
12. M. J. Campbell and R. Grezeskowisk, *J. Chem. Soc.* 1967A, 396.
13. I. M. Procter, B. J. Hathaway and P. Nicholls, *J. Chem. Soc.* 1968A, 1678.
14. A. A. G. Tomlinson, B. J. Hathaway, D. E. Billing and P. Nicholls, *J. Chem. Soc.* 1969A, 65.
15. C. J. Balhausen, *Introduction to Ligand Field Theory*. McGraw-Hill, New York (1962).
16. M. C. Jain, A. K. Srivastava and P. C. Jain, *Inorg. Chim. Acta* 1977, **23**, 199.
17. S. Chandra, B. K. Bharat, K. B. Pandeya and R. P. Singh, *J. Inorg. Nucl. Chem.* 1977, **39**, 2079.
18. D. S. Eggleston and S. C. Jackhls, *Inorg. Chem.* 1980, **19**, 1953.
19. B. K. Coltrain and S. C. Jackhls, *Inorg. Chem.* 1981, **20**, 2032.
20. D. A. Baldwin, R. M. Peiffer, D. W. Richgott and N. J. Rose, *J. Am. Chem. Soc.* 1975, **95**, 515.
21. S. C. Jackhls, K. Farmery, E. K. Barefield, N. J. Rose and D. H. Busch, *Inorg. Chem.* 1972, **11**, 2893.
22. M. Mikami, I. Nagakawa and T. Shimanonchi, *Spectrochim. Acta* 1967, **23A**, 1037.
23. J. E. Finholt, R. W. Anderson, J. A. Fyfe and K. G. Caulton, *Inorg. Chem.* 1965, **4**, 43.
24. K. Nakamoto, *Infrared Spectra of Inorganic and Coordination Compounds*. Wiley, New York (1970).
25. A. M. Tait and D. H. Busch, *Inorg. Chem.* 1976, **15**, 197.
26. J. R. Ferraro, *Low Frequency Vibrations of Inorganic and Coordination Compounds*. Plenum Press, New York (1972).

Polyhedron Vol. 10, No. 23/24, pp. 2791–2798, 1991
Printed in Great Britain

0277-5387/91 $3.00+.00
© 1991 Pergamon Press plc

TITRATION AND SPECTRAL STUDIES OF COMPLEXES BETWEEN FIRST-ROW TRANSITION METALS AND TRIS(2-PYRIDYL)CARBINOL AND BIS(2-PYRIDYL)PHENYLCARBINOL[1]

ROBERT K. BOGGESS,* ANNE H. LAMSON and STEVEN YORK

Department of Chemistry, Radford University, Radford, VA 24142, U.S.A.

(*Received* 1 *March* 1991; *accepted* 16 *July* 1991)

Abstract—Titrations of tris(2-pyridyl)carbinol (py_3COH) and di(2-pyridyl)phenylcarbinol (py_2phCOH) in the presence of first-row transition metals form 2:1 complexes and one —COH group per complex is made acidic. For py_3COH, coordination is via a mixed-mode method, i.e. one ligand is bound in a symmetric N,N′,N″ mode and the second, in which the —COH group is made acidic, in a non-symmetric N,N′,O mode. The cobalt(II) and nickel(II) complexes titrate as a weak acid (pK_a 6.6) and the H^+ is bound to a non-coordinated pyridyl nitrogen. The iron(II) and manganese(II) titrate as strong acids, even through a pyridyl nitrogen is not coordinated. The copper(II) and zinc(II) have both ligands coordinated in a symmetrical fashion and do not consume OH^- until considerably higher pH values. Di(2-pyridyl)phenylcarbinol binds, as it must if it is to be tridentate, exclusively in an N,N′,O fashion and all the complexes titrate as strong acids. The complexes have been characterized by spectroscopic techniques.

Tris(2-pyridyl)carbinol, py_3COH, can coordinate as a tridentate ligand in the N,N′,N″ symmetric mode, **1**, or in an N,N′,O non-symmetric mode, **2**, with first-row transition metals,[2–4] ruthenium,[5]

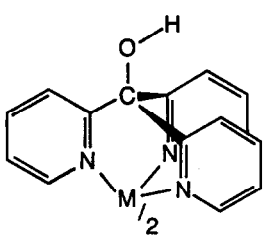

1

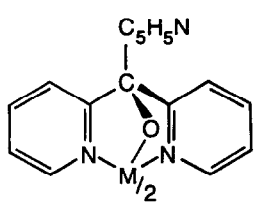

2

methylmercury(II)[6] and monomethylindium.[7] The solution ^1H NMR spectrum in methanol of $(CH_3)_2Au(py_3COH)$ has also suggested bidentate coordination through two pyridyl nitrogens[8] as a mode of coordination for this ligand. Linkage isomers of cobalt(III), with one isomer having both ligands coordinated in the N,N′,N″ symmetric mode[5] while the other has one ligand coordinated in the N,N′,N″ symmetric mode and the second in the N,N′,O non-symmetric mode (the oxygen of the —COH group is deprotonated) to give $[Co(N,N',N''\text{-}py_3COH)(N,N',O\text{-}py_3CO)]^{2+}$ [3] have been reported. The cobalt(II) complex with py_3COH has not been isolated and is unusual in that it is very sensitive to oxygen even though complexes of other py_3X ligands (X is N, P, P=O, or As[9]) are relatively inert toward oxygen and are easily prepared without the necessity of a nitrogen atmosphere and are stable indefinitely in solution. The two ruthenium(II) complexes with py_3COH each have one ligand coordinated in the symmetric mode and the other in the non-symmetric mode, the difference being that the coordinated —COH group is deprotonated in the second complex.

The non-symmetric N,N′,O mode of coor-

* Author to whom correspondence should be addressed.

dination of py_3COH found in many complexes suggested that the carbinol group might be forced upon other transition metals both in the presence and absence of a competing pyridyl group. The latter point was investigated using the ligand bis(2-pyridyl)phenylcarbinol, py_2phCOH, as steric requirements for py_2phCOH and py_3COH should be similar. N,N',O-coordination has been found for py_2phCOH complexes with first-row transition metals[10] and later for monomethylindium[7] complexes. Coordination by both —COH and —CO^- have been reported. A feature of this ligand not found to date for py_3COH is the ability of the oxygen of the —CO^- to bridge two metal ions.[10,7]

Metal-promoted ionizations are important in a number of chemical systems, including many biological ones. An earlier paper attempted to use py_3COH and related ligands as model systems for the active site of carbonic anhydrase.[11] Binding constants for Zn^{2+}, Co^{2+}, Ni^{2+} and Cu^{2+} with several tridentate ligands, including py_3COH, were determined. The authors report that some H^+ were formed as a result of mixing py_3COH with these ions, especially Co^{2+}. However, the acidity was attributed more to M^{2+}-OH_2 than to loss of the proton from the —COH group. Since both py_3COH and py_2phCOH when coordinated can act as a proton donor, we have now investigated the titration curves of these ligands in both the absence and presence of transition metals and report our findings herein.

EXPERIMENTAL

Reagents

All reagents are commercially available and were used as received unless noted below. Bis(2-pyridyl)phenylcarbinol[12] and tris(2-pyridyl)carbinol[13] were prepared as previously reported.

Physical measurements

UV–vis spectra were recorded with a Perkin–Elmer Model 552 or Model 330 spectrophotometer. All titrations were done under nitrogen that had been bubbled through a vanadium(II) solution to remove trace amounts of oxygen and in a mixed ethanol–water (1 : 1 by volume) solution that was also 0.10 M in KCl. A Radiometer titration system (Model 64 pH meter, Model TTT80 automatic titrator, Model 80 autoburet and Model 80 recorder) equipped with a combination electrode was used for all titrations. Electrode calibration was by means of commercially available NBS aqueous buffer solutions (pH 4.00 and pH 7.00). To obtain a measure of the a_{H^+} referred to the standard state in the mixed solvent system, 0.15 log unit was subtracted from each pH meter reading.[14] A typical experiment consisted of adding metal(II) chloride (0.25 mmol) to the ethanol–water mixture (25 cm^3), thoroughly deaerating with nitrogen, adding ligand (0.50 mmol) and titrating with NaOH (1.00 M). Spectra were recorded at specified pH without exposure to the atmosphere. The ^{13}C NMR spectrum was obtained on a Brucker Model WP-200SY instrument at 50.327 MHz. d_3-Acetonitrile was used as the solvent and the spectrum is referenced to TMS at zero ppm.

RESULTS AND DISCUSSION

Titration of a solution containing HCl and py_3COH (3 : 1 molar ratio) or HCl and py_2phCOH (2 : 1 molar ratio) allows the calculation[15] of the pK_a of one pyridyl nitrogen (Table 1) corresponding to the reaction

$$HL^+ \longrightarrow L + H^+ \quad K_a = \frac{[L]a_{H^+}}{[HL]}.$$

The pK_a for py_3COH compares favourably with values reported previously considering that different solvents and different ionic strengths were employed. Titration curves of HCl and HCl-py_3COH (3 : 1 molar ratio) are given in Fig. 1. The complete overlap of the first portion of the titration curves and the near overlap of the middle portion suggests no interaction and only minimal interaction, respectively, of two of the three H^+ with py_3COH, i.e. two of the three pyridyl nitrogens have minimal basic properties. The third pyridyl nitrogen titrates as a typical weak acid. This point is emphasized by the isolation of only the monoprotonated ligand, $py_2(py \cdot H)COH^+$ as the perchlorate salt from a reaction of py_3COH and tetrakis (methylsulphoxide)ruthenium(II) chloride in dilute perchloric acid solution.[16] The crystal structure[17] of this salt has no exceptional features and is similar to that of py_3COH previously reported.[18] The —COH in $[py_2(py \cdot H)COH]ClO_4$ is hydrogen bonded to one pyridine ring with an estimated N—H distance of 1.92(4) Å. In the ruthenium(II) complex with py_3COH[5] (*vide infra*), such hydrogen

Table 1. Acidity constants for py_3COH and py_2phCOH

py_3COH	4.44 ± 0.01	(this work)
	4.7 ± 0.1, 2.1 ± 0.1, 1.5 ± 0.1	($\mu = 0.16$, aqueous solution[11])
	3.98	(50% dioxane–water[6])
py_2phCOH	4.04 ± 0.03	(this work)

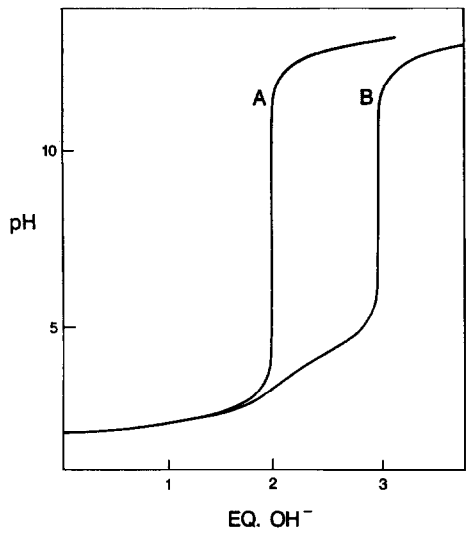

Fig. 1. Titration curves of HCl (A) and HCl:py_3COH (B). Solution A contains 0.500 mmol of HCl, solution B contains 0.750 mmol of HCl and 0.250 mmol of py_3COH.

bonding was used to suggest why the coordinated oxygen rather than an uncoordinated nitrogen of a pyridyl ring is protonated in acid solution.

At high pH values, there is no hint of carbinol ionization in the titration curve of either py_3COH or py_2phCOH nor is any anticipated due to the high pK_a value expected.[19] However, titration curves for solutions containing both py_3COH and metal ion in a 2:1 molar ratio (Fig. 2) do show consumption of one hydroxide per metal ion for manganese(II), iron(II), cobalt(II) and nickel(II) in the pH range 3–8 while for copper(II) and zinc(II), consumption of hydroxide approaches two moles per mole of metal ion at considerably higher pH values. For manganese(II) and iron(II), the titration curves are not those of a typical weak acid and their mathematical analyses[15] confirm this. Cobalt(II) and nickel(II), however, do provide titration curves typical of a weak acid and are clearly distinct from the manganese(II) and iron(II). Except at high pH [> 10 for copper(II) and zinc(II)], no precipitates were observed in any titration. Spectral data for the complexes as a function of pH are given in Table 2.

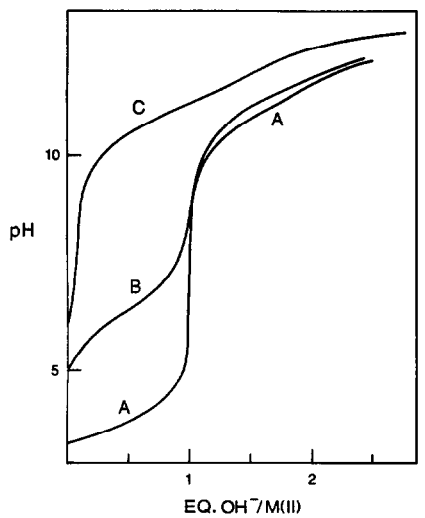

Fig. 2. Titration of py_3COH : metal(II) (2 : 1 molar ratio): Fe(II), A; Ni(II), B; Cu(II), C.

When py_3COH is added to a solution containing iron(II), a complex is formed as indicated by the decrease in pH and the change and increase in the intensity of the colour of the solution. When base is added to this solution, there is considerable darkening of the solution. The intensities of the absorptions for the iron(II) complex indicate that they are change-transfer ones and probably metal-to-ligand.[20] However, neither the band positions nor intensities are those reported previously for $[Fe(N,N',N''\text{-}py_3COH)_2]^{2+}$.[21] Mossbauer data on the solid state of this complex suggested a symmetric arrangement of the ligand and the visible spectrum in acetonitrile was similar to other $[Fe(py_3X)_2]^{2+}$ complexes.[21] The symmetric nature of this isomer in solution has now been confirmed by measuring the ^{13}C NMR spectrum, as only six resonances are observed (Fig. 3) and the bridgehead carbon has a resonance value at 81.3 ppm, almost identical to that in py_3COH and in the symmetric

Table 2. Spectral data as a function of pH. Ligand-to-metal ratio is 2:1

	pH	py_3COH λ (nm) (ε)
Fe^{II}	3.0	441(4500), 385(3550)
	10.2	485(13,400), 425sh(9450)
Co^{II}	5.0	> 800(> 20), 500sh(60), 430sh(180), 378(1300), 350(1180)
	12.5	> 800(> 10), 540sh(30)
Ni^{II}	4.8	890(11), 810sh(9), 570(10), 500(12)
	10.0	860(9), 795(12), 560(12), 495(15)
Cu^{II}	3.0	605(30)
	9.2	620(60)
		py_2phCOH
Fe^{II}	6.4	370(1010)
	11.6	410sh(1040), 335sh(1485)
Co^{II}	3.7	1050(3), 505(20), 490(21), 470(19)
	9.0	1050(7), 620(7), 505(31), 485(35), 470sh(35)
Ni^{II}	4.1	970(7), 600(8), 530sh(5)
	9.8	1020(19), 605(25)

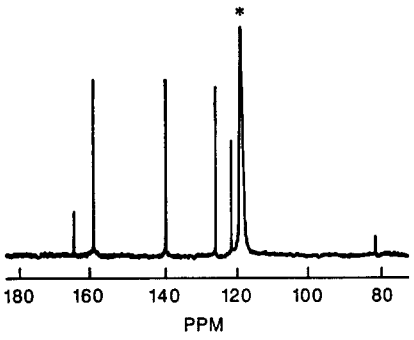

Fig. 3. ^{13}C NMR of $Fe(py_3COH)_2(ClO_4)_2$. The * refers to the carbon of the —CN of the solvent, CD_3CN.

$[Co(N,N',N''\text{-}py_3COH)]^{3+}$ isomer.[4] When the solid is dissolved in the mixed water–ethanol solvent system used in the titration studies, the visible spectrum is unchanged from that of the solid dissolved in acetonitrile, suggesting the symmetric isomer remains intact. However, when the complex is formed by mixing iron(II) chloride and py_3COH in the water–ethanol solvent system, the spectrum is dependent upon the pH of the system (Fig. 4) and is somewhat time-dependent. Since these spectra are different from the symmetric isomer, the species present at pH 3.0 probably has the iron(II) coordinated by two neutral ligands in the mixed-mode fashion while the species present at pH 10.2 is the same mixed-mode coordination with the non-symmetric ligand present as the anion, py_3CO^-. Spectra at intermediate pH are a composite of the pH 3.0 and 10.2 spectra. The spectra at the low and high pH values resemble those for the analogous ruthenium(II) complexes[5] except that for iron(II), the maxima are found at about 35 nm longer wavelengths and the intensity is only about one-fourth at low pH and one-half at high pH. The results indicate a strong tendency for the iron(II) to bind in the mixed-mode fashion and to cause the proton of the —COH group, presumably the one bound to the iron(II), to become a strong acid. A similar result was noted for the analogous ruthenium(II) complex. However, the symmetric isomer, once formed and precipitated as the perchlorate salt, is stable and does not readily change to the mixed-mode isomer even upon redissolving in various solvents. Although spectral data are lacking, the similarity of the titration curves of iron(II) and manganese(II) suggest a similar coordination for the manganese(II).

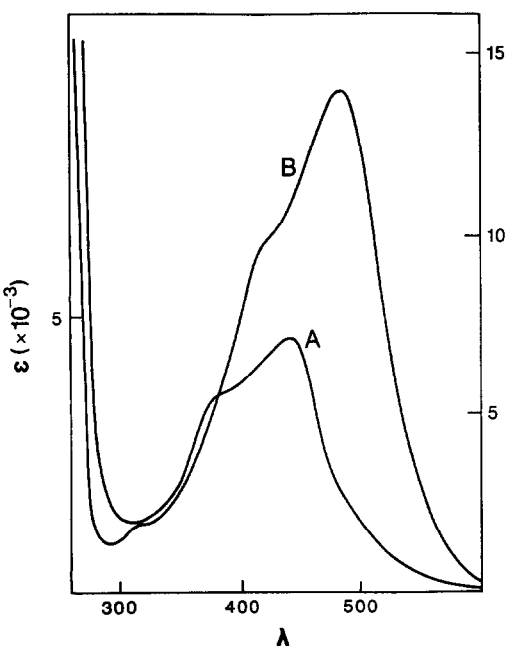

Fig. 4. Visible spectrum of $py_3COH:Fe^{II}$ (2:1 molar ratio). The scale on the left refers to curve A (pH 3.0) and the scale on the right refers to curve B (pH 10.2).

If oxygen is rigorously excluded from the reaction mixture, a cobalt(II) complex with py_3COH is formed and the complex titrates as a weak acid with a pK_a of 6.6(±0.1). The absorption spectrum of this complex does not resemble those of symmetric $[Co(py_3X)_2]^{2+}$ complexes[9] but instead has a maximum absorption at 378 nm (ε 1300) that is part of a more intense band at shorter wavelength. Upon increasing the pH to > 10, the bands between 400 and 300 nm are lost on intense bands below 300 nm. The spectral data strongly suggest that at both the low and high pH, coordination is in the mixed-mode fashion and, unlike the iron(II) and ruthenium(II) complexes, one py_3COH ligand can act as a proton donor but in a weak-acid fashion. What is not clear is whether the proton is being removed directly from a coordinated —COH group, as is claimed in the ruthenium(II) case[5] and above for iron(II), or from the nitrogen of the non-coordinated pyridyl ring. An attempt was made to answer this question by monitoring the ligand absorption bands below 300 nm. For the free ligand, the spectrum between 300 and 225 nm was studied as a function of pH (Fig. 5). At pH 2.9, the spectrum appears as a double-humped band with maximum absorptions at 261 and 267 nm. When the pH is raised, the total intensity of the band decreases with that of the 267 nm band decreasing more rapidly than the 261 nm band and a shoulder at 255 nm becomes more pronounced. A plot of pH vs $\log(\alpha/1-\alpha)$ (α is the fraction of the ligand neutralized) gives a linear plot of slope 0.87, from which a pK_a of 4.5, in reasonable agreement with the titration data of Table 1, is obtained. However, in the same spectral region of the complexes, one

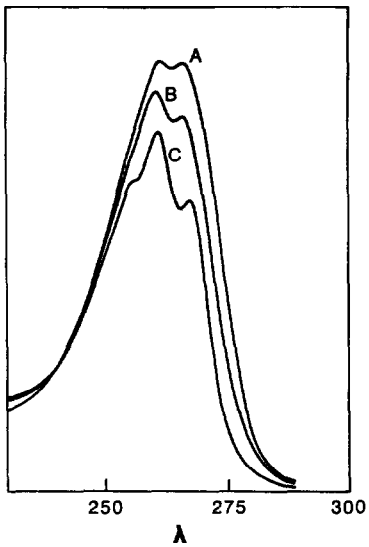

Fig. 5. UV spectra of py_3COH at various pH values: pH 2.9, A; pH 4.4, B; and pH 6.5, C.

cannot distinguish between coordinated pyridyl rings, non-coordinated pyridyl rings, and protonated pyridyl rings due to the broadness and overlap of these bands. Hence, the question of where the proton resides in the cobalt(II) complex is not resolved by these data.

Spectral results from the nickel(II) and py_3COH indicate an octahedral configuration around the metal ion. There are only minor differences in the spectra at low and high pH and the spectra are very similar to that of the symmetric complex previously reported.[2] Much of the discussion of the acid–base characteristics of the cobalt(II) complex above is applicable to the nickel(II) complex as the mixture of nickel(II) and py_3COH also titrates as a weak acid with a pK_a 6.6($\pm$0.1). It is surprising that both cobalt(II) and nickel(II) have the same pK_a and this may be important in determining the site of proton loss. Although not an entirely analogous system, amide deprotonation of a nitrogen coordinated to nickel(II) is approximately 100 times easier when compared to cobalt(II).[22] If this ease of deprotonation was maintained in the py_3COH ligand, the pK_a for nickel(II) should then be significantly lower than for cobalt(II) if the metal ion was competing directly for a basic site. That the pK_as for cobalt(II) and nickel(II) are the same within experimental error would suggest that the removal of the proton is not from a coordinated —COH group. This then leaves the pyridyl nitrogen of the non-coordinated ring as the basic site and suggests that the pK_a of the nitrogen has been increased upon coordination by py_3COH. In fact, metal ion substitution for a proton always increases the pK_a of non-coordinated basic sites elsewhere on the ligand and thus is consistent with these results. Previously mentioned was the result that an analogous situation has been reported for ruthenium(II);[5] based upon bond lengths in the two crystal structures and ^{13}C data on the bridgehead carbon, it was concluded that the basic site was indeed the coordinated —COH group and not a pyridyl nitrogen. However, the pK_a was 3.78, clearly more acidic than either the cobalt(II) or nickel(II) complexes. Thus, based upon titration and spectral evidence, we believe the basic site for the proton in the cobalt(II) and nickel(II) complexes is the pyridyl nitrogen and the coordination is in the mixed-mode fashion. As was the situation for the iron(II) complex, this is in contrast to the structure suggested for the solid state nickel(II) complex. However, a re-examination of these data still suggests the symmetric isomer in the solid state as the stoichiometry of the complex requires a neutral ligand and there is no evidence in the IR spectrum of a protonated pyridyl nitrogen. We have previously reported on complexes with protonated pyridyl nitrogens[23] and there is a very definitive py-H^+ band at 1530 cm^{-1}. No such band appears in the IR spectrum of the solid $[Ni(py_3COH)_2](ClO_4)_2$ complex.

The titration curves for copper(II) and zinc(II) do not show consumption of the hydroxide ion in the acid to neutral pH range but only at pH > 10. The solution spectrum of the copper(II) complex below pH 7 is identical to that of the solid reported earlier.[2] Since no evidence for coordination by the —COH group was observed in the solid and there is no tendency to titrate a proton in the present study, coordination must be by the symmetric mode for the copper(II) and zinc(II) complexes both in the solid and in solution. The ^1H NMR spectrum of $[Zn(py_3COH)_2](ClO_4)_2$ dissolved in d_3-acetonitrile[2] and the complex formed in aqueous solution from Zn^{2+} and py_3COH[11] also suggested a nearly symmetrical mode of coordination. Support for similar coordination here is provided by the titration of solutions containing HCl : py_3COH : copper(II) or zinc(II) in a molar ratio of 6 : 2 : 1. The acid titrates strictly as a strong acid with no evidence for titration of protonated pyridyl rings, whether coordinated or free. With regard to the strong tendency of copper(II) to form complexes with both nitrogen and oxygen ligating atoms,[24] this is especially surprising. Solids isolated at high pH do contain py_3COH but are probably mixed copper(II)—py_3COH—OH^- complexes. No further attempts to characterize these products have been made.

All mixtures of bis(2-pyridyl)phenylcarbinol and metal(II) ions yield an acidic proton (Fig. 6), with most titration curves resembling a strong acid.

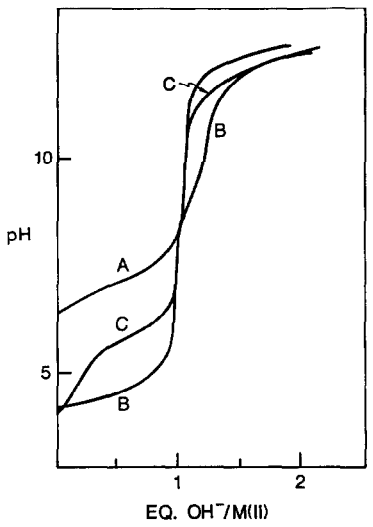

Fig. 6. Titration curves of py_2phCOH : metal(II) (2 : 1 molar ratio): Mn(II), A; Fe(II), B; Ni(II), C.

When n moles of HCl are added to the titration mixture, $n+1$ equivalents of OH^- are consumed in the pH range 3–8; several mixtures consume additional OH^- at higher pH and yield precipitates. Spectral data as a function of pH were recorded (Table 2); generally, the spectra do not show the pH dependence of the py_3COH complexes and most were time-dependent. The results suggest that the —COH of the ligand is coordinated at low pH and that this group titrates in the manner of a strong acid, though not as a completely free proton, as indicated by the different range of pH values for the titration curves.

A 2 : 1 mixture of py_2phCOH : manganese(II) consumed one equivalent of OH^- per manganese(II), beginning about pH 6 and complete by pH 9. Titrations were also carried out using a variety of HCl : py_2phCOH : manganese(II) ratios. For the ratio 4 : 2 : 1, a total of five equivalents of OH^- were consumed, the first two by HCl, the next two by protonated but non-complexed ligand (pK_a 4.0), and the last one by the complex. For the ratio 12 : 4 : 1, a total of 13 equivalents of OH^- were consumed, the first eight by HCl, the next four by protonated but non-complexed ligand (pK_a 4.0), and the last by the complex. The results demonstrate that only one pyridyl nitrogen of non-complexed ligand is protonated and that any interaction between manganese(II) and the ligand is weak although a complex is formed or the $n+1$ OH^- would not be consumed. The solutions are air-sensitive at higher pH and the complex formed is probably a mixture of manganese(II), py_2phCOH, and OH^-. No manganese(II) complex was isolated in the previous study[10] as should be when the weak interaction indicated by the titration data is considered.

The titration curves of py_2phCOH with iron(II), cobalt(II) and zinc(II) in a 2 : 1 molar ratio are nearly identical to each other and are similar to that for manganese(II), the major difference being that the initial pH of the solutions is near 4 and the titrations are complete by pH 6. One equivalent of OH^- is consumed per metal ion.

The py_2phCOH : iron(II) mixture gave spectral results noticeably different than for py_3COH, both in the position and intensity of the bands. Both features are consistent with loss of coordination of a pyridyl nitrogen. For the zinc(II) titrations, the perchlorate salt rather than the chloride was used and upon addition of the ligand, immediate precipitation of $[Zn(py_2phCOH)(py_2phCO)]ClO_4$ occurred. For cobalt(II) chloride, precipitation occurs only at higher pH. There is little difference in the spectrum of the cobalt(II) complex regardless of pH, consistent with the titration data implying that the complex is fully formed at low pH. Spectra at pH 3.7 and 9.0 are typical of octahedral cobalt(II) and closely match that of $[Co(py_2phCOH)(py_2phCO)]ClO_4$[10] and symmetrical octahedral $[Co(py_3X)_2]^{2+}$[9] complexes, the most noticable difference being the partial splitting of the band near 500 nm and the longer wavelength of the absorption bands. These features are consistent with the replacement of two nitrogen atoms of py_3X with two oxygen atoms of py_2phCOH as donor atoms. The cobalt(II) complex with py_2phCOH, unlike that of py_3COH, is relatively inert to oxygen; there is little evidence for oxidation even when a solution at pH 12 is exposed to the atmosphere overnight. The N_5O donor set of the py_3COH complex appears to be the key requirement for oxidation of cobalt(II) as the symmetrical py_3X complexes and the py_2phCOH complex, with N_6 and N_4O_2 donor sets, respectively, are not readily oxidized. Cobalt(II) and zinc(II) complexes previously isolated gave only the stoichiometry $[M(py_2ph(COH)(py_2phCO)]ClO_4$;[10] considering the acidity of the proton, this is reasonable. What is surprising is the inability of zinc(II) to promote ionization in the py_3COH ligand but to promote similar ionization in py_2phCOH to the extent that only the deprotonated complex can be isolated. This in turn argues for the nearly exclusive formation of the symmetrical isomer in $[Zn(py_3COH)_2]^{2+}$.

Titration and spectral results for the py_2phCOH : nickel(II) mixture provide results again consistent with the previous work in which two complexes, $[Ni(py_2phCOH)_2]^{2+}$ and $[Ni(py_2phCOH)(py_2phCO)]^+$, were isolated.[10] The spectra

at pH 4.1 and 9.0 closely match those of the two isolated nickel(II) complexes. The ability of the nickel(II) to promote ionization of the ligand is less than that of either cobalt(II) or zinc(II) and thus both stoichiometries were obtained. In view of this result, the similarity of the cobalt(II) and nickel(II) results with py_3COH (*vide supra*) is even more striking.

Two distinct copper(II) compounds were previously obtained[10] with py_2phCOH, dependent upon the pH and ligand : metal ratio. When mixed in a 1 : 1 molar ratio, a deep blue solution results (λ_{max} 682 nm, ε 67) and one proton is titrated as a strong acid by pH 6.0 to produce a solution of a slightly different blue (λ_{max} 708 nm, ε 130). Some additional consumption of base occurs above pH 9.0 and a light blue precipitate formed about pH 10.0. When acid was added to the final mixture and the pH returned to 3.0, the original spectrum returned. The compound formed by pH 6.0 is probably similar to that isolated,[10] $[Cu(py_2phCO)]ClO_4$, in which bridging oxygen atoms were postulated. If the ligand : metal ratio is 2 : 1 or larger, a purple compound forms after the initial titration of the one proton. This compound is not very soluble in most solvents. Further attempts to ascertain its structure are in progress.

CONCLUSIONS

The ligands py_3COH and py_2phCOH readily coordinate with first-row transition metals. Py_3COH has several possible modes of coordination and the one obtained is dependent upon the method of preparation and/or the pH. In the case of iron(II), three different complexes have been identified. These include one with both ligands coordinated in a symmetric (N,N′,N″) fashion, a second with one ligand bound in a symmetric fashion and the other in a non-symmetric (N,N′,O) protonated fashion, and a third coordinated as the second but with loss of a proton from one ligand. Nickel(II) and cobalt(II) give complexes in which the coordination is by the mixed-mode fashion, i.e. one ligand in the symmetric (N,N′,N″) and the second in the non-symmetric (N,N′,O) mode, with the proton residing on the non-coordinated pyridine and titrating as a weak acid. Copper(II) and zinc(II) form only the symmetric complex with py_3COH and do not promote any ionization of the ligand. Py_2phCOH lacks the third pyridine ring and is forced to coordinate in the N,N′,O mode and complexes with protonated, —COH groups are initially formed. However, the —COH group then titrates as a relatively strong acid, but whose pH range is influenced by the metal of the complex.

Acknowledgements—The authors are grateful to the Jeffress Memorial Trust (J-20) for support of this work, to Mr Gino Iannaccone and Mr Bill Bebout of Virginia Tech for the ^{13}C spectra, to Professor R. Bruce Martin of the University of Virginia for the calculation of the acidity constants, and to Ms Karen Hayes for the spectral determination of the pK_a of py_3COH.

REFERENCES

1. A preliminary report of this work was presented at the 36th Southeastern Regional Meeting of the American Chemical Society, Raleigh, N.C., 1984.
2. R. K. Boggess and S. J. Boberg, *J. Inorg. Nucl. Chem.* 1980, **42**, 21.
3. D. L. White and J. W. Faller, *Inorg. Chem.* 1982, **21**, 3119.
4. D. J. Szalda and F. R. Keene, *Inorg. Chem.* 1986, **25**, 2795.
5. F. R. Keene, D. J. Szalda and T. A. Wilson, *Inorg. Chem.* 1987, **26**, 2211.
6. A. J. Canty, N. Chaichit, B. M. Gatehouse and E. E. George, *Inorg. Chem.* 1981, **20**, 4293.
7. A. J. Canty, L. A. Titcombe, B. W. Skelton and A. H. White, *J. Chem. Soc., Dalton Trans.* 1988, 35.
8. A. J. Canty, N. J. Minchin, P. C. Healy and A. H. White, *J. Chem. Soc., Dalton Trans.* 1982, 1795.
9. R. K. Boggess and D. A. Zatko, *J. Coord. Chem.* 1975, **4**, 217; and refs therein.
10. R. K. Boggess and C. E. Heltzel, *Inorg. Chem.* 1985, **24**, 2947.
11. R. S. Brown and J. Huguet, *Can. J. Chem.* 1980, **58**, 889.
12. A. P. de Jonge, H. J. den Hertog and J. P. Wibaut, *Recl. Trav. Chim. Pays-Bas* 1951, **70**, 989.
13. J. P. Wibaut, A. P. de Jonge, H. G. P. van der Voort and P. Ph. H. L. Otto, *Recl. Trav. Chim. Pays-Bas* 1951, **70**, 1054.
14. R. G. Bates, *Determination of pH*, pp. 222–224. Wiley-Interscience, N.Y. (1964).
15. Calculations performed using a non-linear least-square analysis of the most error prone observable versus an independent variable; carried out by Professor R. Bruce Martin of the University of Virginia.
16. R. K. Boggess, C. E. Heltzel, D. Humphreys, D. Judge, M. McBride, J. Murray and W. Murray, unpublished results.
17. R. K. Boggess, submitted for publication.
18. F. R. Keene, M. R. Snow and E. R. T : Tiekink, *Acta Cryst.* 1988, **44C**, 937.
19. J. P. Wibaut and P. Ph. H. L. Otto, *Recl. Trav. Chim. Pays-Bas* 1958, **77**, 1048. They report a pK_a of 14.77 ± 0.11 for the —COH of py_3COH in aqueous solution.
20. G. M. Bryant, J. E. Fergusson and H. K. J. Powell,

Aust. J. Chem. 1971, **24**, 257; R. A. Palmer and T. S. Piper, *Inorg. Chem.* 1966, **5**, 864.
21. R. K. Boggess, J. W. Hughes, C. W. Chew and J. J. Kemper, *J. Inorg. Nucl. Chem.* 1981, **43**, 939.
22. H. Sigel and R. B. Martin, *Chem. Rev.* 1982, **82**, 385.
23. R. K. Boggess, M. McBride, J. Moulds and D. Judge, 192nd National Meeting of the American Chemical Society, Anaheim, CA, September 1986.
24. R. Griesser and H. Sigel, *Inorg. Chem.* 1971, **10**, 2229.

Polyhedron Vol. 10, No. 23/24, pp. 2799–2807, 1991
Printed in Great Britain

0277–5387/91 $3.00+.00
© 1991 Pergamon Press plc

LOCALIZED MOLECULAR ORBITALS AND THE PROBLEM OF QUASI-AROMATICITY IN TRINUCLEAR MOLYBDENUM CLUSTER COMPOUNDS WITH CORES OF THE TYPE $[Mo_3(\mu_3\text{-}X)(\mu\text{-}Y)_3]^{n+}$ (X, Y = O, S, $n = 4$; X = O, Y = Cl, $n = 5$)

ZHIDA CHEN,* JIAXI LU, CHUNWAN LIU and QIANER ZHANG

Fujian Institute of Research on the Structure of Matter, Fuzhou Research Laboratory of Structural Chemistry, Chinese Academy of Science, Fuzhou, Fujian, China 350002

(*Received* 7 *March* 1991; *accepted* 11 *July* 1991)

Abstract—Calculations of localized molecular orbitals (LMO) and their energy levels for the cluster cores $[Mo_3O_4]^{4+}$, $[Mo_3SO_3]^{4+}$, $[Mo_3OS_3]^{4+}$, $[Mo_3S_4]^{4+}$ and $[Mo_3OCl_3]^{5+}$ have been made by the use of energy-localized CNDO/2-LMO. The results of these LMO calculations show that the six-membered closed and continuous π-conjugated systems around the $[Mo_3Y_3]$ rings, each of which is formed from three synergically connected three-centred two-electron (Mo, Mo, Y) π bonds, is the most significant feature of the electronic structure for the quasi-aromatic clusters $[Mo_3(\mu_3\text{-}Y)(\mu\text{-}X)_3]^{4+}$ (X, Y = O, S), and the size and electronegativity of the bridging Y atoms exhibit significant effects on the degree of quasi-aromaticity of these cluster compounds. For the non-aromatic reference cluster $[Mo_3OCl_3]^{5+}$, the results of our calculations also show a bonding scheme with only one isolated (Mo, Mo, Y) π bond, thus leading to the loss of quasi-aromaticity; and meanwhile, there is a pair of extra electrons localized on the apical molybdenum atom of the Mo_3 triangle, thus with three Mo—Mo single bonds.

During the past decade a number of trinuclear cluster compounds with molybdenum atoms in higher oxidation states with the geometrical configuration of a discrete equilateral triangle have been reported,[1] and a few comprehensive reviews have appeared.[2] Cotton further classified these trinuclear molybdenum cluster compounds into the following two structural types: trigonal pyramidal and trigonal bipyramidal. During the past few years systematic crystal structure analyses and chemical reactivity studies for a series of typical trigonal pyramidal cluster compounds have been carried out in our Institute and Research Laboratory. Thus Huang[3] established on a very sound basis a new concept of quasi-aromaticity, i.e. the puckered six-membered ring $[Mo_3(\mu\text{-}S)_3]^{6+}$ in $[Mo_3(\mu_3\text{-}S)(\mu\text{-}S)_3(\chi\text{-}dtp)_3(\mu\text{-}dtp)(OH_2)]$ (I) [where dtp and χ denote $\{S_2P(OEt)_2\}^{-1}$ and chelating dtp ligands, respectively; cf. Fig. 1] exhibits benzene-like behaviour. Structurally, the six Mo—(μ-S) bonds have an average length of (2.281+0.017) Å, intermediate between the Mo—S single-bond length of 2.44 Å and the Mo=S double-bond 2.08 Å; whereas the six bond angles fall into two sets of (96.6+0.7)° for ∠(μ-S)—Mo—(μ-S) and (74.3+0.8)° for ∠Mo—(μ-S)—Mo. With regard to its chemical reactivity, the reactivity sequence for ligand substitution reactions is H_2O > μ-dtp > χ-dtp ≫ (μ_3-S) ≫ (μ-S), with the $[Mo_3S_3]$ ring kept intact and practically invariant in the course of these reactions. There are two types of addition reactions: simultaneous addition of three sulphur atoms with the formation of three μ-S_2; addition of one metal atom alone to form, for instance, a cubane-like $[(Mo_3S_4)Cu]^{5+}$ or a sandwich-type $[(Mo_3S_4)_2Mo]^{8+}$, with the entire $[Mo_3S_4]^{4+}$ core entering into these reactions as a whole. On the

* Author to whom correspondence should be addressed.

other hand, oxidation of one of the three (μ-S) atoms is at once accompanied by the rupture of two adjoining Mo—(μ-S) bonds and the formation of two new Mo=O bonds. The resemblances to C_6H_6 in all these respects are indeed rather striking. In a series of previous papers[4] we have made comparative studies on the electronic structures of benzene and other aromatic molecules on one hand and the cluster compound **I** on the other hand by the use of the energy-localized CNDO/2 molecular orbital method, it is shown that from a localized bonding point of view, for the well-known aromatic planar six-membered ring C_6H_6, each of the three π-electron pairs is localized on three adjoining carbon atom triads, thus forming three adjoining three-centred two-electron (*p–p–p*) π-bonds. Upon comparing aromatic and quasi-aromatic C_6H_6, $C_3N_3H_3$, $B_3N_3H_6$, and $(B_3O_6)^{3-}$ with the non-aromatic reference molecule $P_3N_3Cl_6$, it is found that a sufficiently large interaction energy between the three (*p–p–p*) or (*d–p–d*) π-bonds is necessary for the formation of a closed continuous π-conjugated system around the ring. Furthermore, it is found that for the $[Mo_3S_3]$ ring in compound **I** there are three three-centred two-electron

π-bonds, with each μ-S atom contributing one pair of electrons from the lone pair occupying the p_z AO perpendicular to the Mo(μ-S)Mo plane and the two adjoining molybdenum atoms contributing one vacant *d* AO each, thus forming a three-centred two-electron (*d–p–d*) π-bond with rather large interaction energy between these π-bonds. This non-planar puckered $[Mo_3S_3]$ ring thus forms a rather interesting three-dimensional closed continuous π-conjugated system. It is obvious that the π-electronic structure of the $[Mo_3S_3]$ ring in compound **I** is quite similar to that of benzene insofar as in either the benzene molecule or the $[Mo_3S_3]$ ring there exists a six-membered closed continuous π-conjugated system formed from three synergically connected three-centred two-electron π bonds around the rings. Huang's[3] further studies have also shown that quasi-aromaticity exists in cluster compounds containing the cores $[Mo_3(\mu_3\text{-}X)(\mu\text{-}Y)_3]^{4+}$ (X, Y = O, S) (cf. Fig. 1). It is interesting to note that Shibahara[5] has recently reported the presence of extra diamagnetic susceptibilities in two molybdenum cluster compounds with the cores $[Mo_3(\mu_3\text{-}S)(\mu\text{-}O)_3]^{4+}$ and $[Mo_3(\mu_3\text{-}S)(\mu\text{-}S)_3]^{4+}$ at very low temperatures.

In the present paper we report the results of our calculations made on $[Mo_3O_4]^{4+}$, $[Mo_3SO_3]^{4+}$, $[Mo_3OS_3]^{4+}$ and $[Mo_3S_4]^{4+}$ by the use of the energy-localized CNDO/2 molecular orbital method. It is interesting to note that replacement of the three bridging oxygen atoms in the $[Mo_3O_4]^{4+}$ cluster by chlorine or bromine atoms to form the $[Mo_3(\mu_3\text{-}O)(\mu\text{-}Y)_3]^{5+}$ (Y = Cl, Br) cluster cores results in loss of such quasi-aromaticity. Thus in the prototype molecule[3,6] $(Me_4N)[Mo_3(\mu_3\text{-}O)(\mu\text{-}Cl)_3(\mu\text{-}O_2CH)_3(Cl_t)_3]$ (t for terminal) the Mo—(μ-Cl)

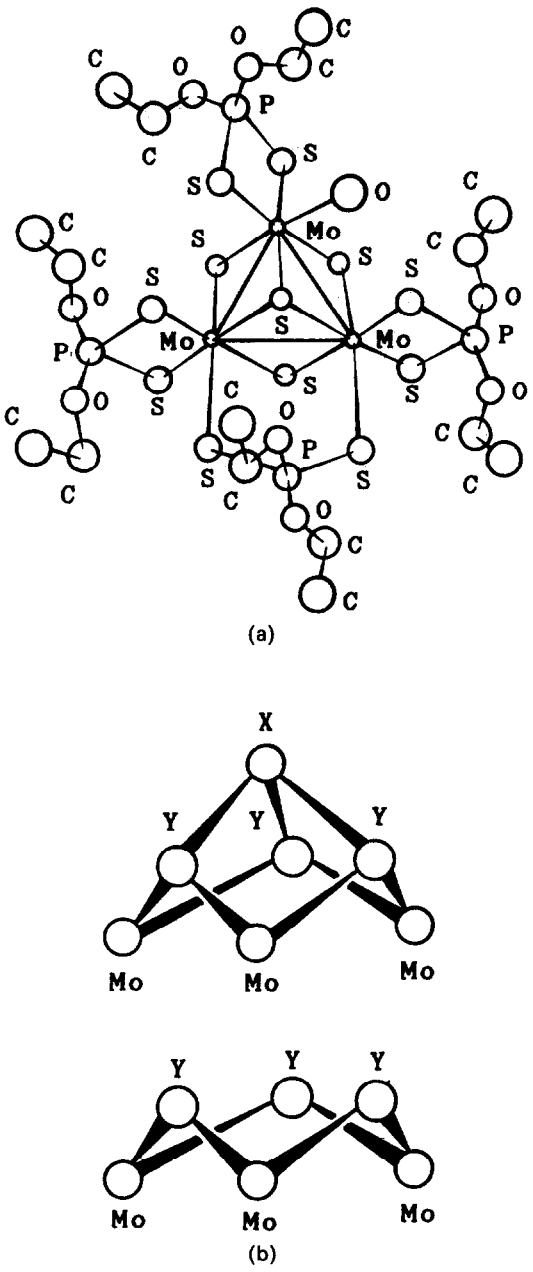

Fig. 1. (a) Configuration of the cluster molecule $[Mo_3(\mu_3\text{-}S)(\mu\text{-}S)_3(\chi\text{-dtp})_3(\mu\text{-dtp})(OH_2)]$; (b) configurations of the cluster cores $[Mo_3(\mu_3\text{-}X)(\mu\text{-}Y)_3]^{n+}$ (X, Y = O, S, $n = 4$; X = O, Y = Cl, $n = 5$) and the six-membered puckered ring $[Mo_3Y_3]$.

2.467 Å) is much longer compared Mo—Cl_t internuclear distance (2.084 Å), longer obeys the rule for the quasi-aromatic $Mo_3(\mu_3\text{-}X)(\mu\text{-}Y)_3]^{4+}$ (X, Y = O, S), in which the Mo—(μ-Y) bond distance lies in between the Mo—Y single and the Mo=Y double bond length. In our calculations this molecule can only be regarded as a non-aromatic reference molecule in order to give a deeper insight into the nature of quasi-aromaticity. In other words, we have attempted to focus our discussion in this paper on the effect of the three bridging Y atoms upon aromaticity, and thus consider only the $[Mo_3(\mu_3\text{-}X)(\mu\text{-}Y)_3]^{n+}$ cores instead of the entire cluster molecules. As discussed in [2] and the previous papers,[4] the core fragment analysis is indeed a good and reasonable approximation in studying the effect of these capping and bridging ligands upon the electronic structures of trinuclear molybdenum cluster compounds.

METHOD OF CALCULATION

The procedure adopted in our calculation is to use the spin unrestricted CNDO/2 method, followed by transformation of the occupied canonical MOs into LMOs by the Edmiston–Ruedenberg energy localized technique, which has been described in [7]. For atoms of non-metal elements n*s* and n*p* AOs are taken as the basis functions; while a complete set of 5*s*, 5*p* and 4*d* valence AOs is taken for each of the molybdenum atoms. The CNDO/2 parameters: orbital exponent ζ, electronegativity χ, bonding parameter β° are listed in Table 1. The geometrical configurations for the cluster cores $[Mo_3O_4]^{4+}$, $[Mo_3SO_3]^{4+}$, $[Mo_3OS_3]^{4+}$, $[Mo_3S_4]^{4+}$ and $[Mo_3OCl_3]^{5+}$ are idealized to C_{3v} symmetry by using bond lengths (cf. Table 3) and angles from the crystal structures of $Cs_2[Mo_3O_4(C_2O_4)_3(H_2O)_3]\cdot 4H_2O\cdot 1/2\,H_2C_2O_4$,[8] $Ba[Mo_3SO_3(Hnta)_3]\cdot 10H_2O$,[9] $[Mo_3OS_3\{S_2P(OEt)_2\}_4]C_3H_3N_2$,[10] $[Mo_3S_4\{\mu\text{—}S_2P(OEt)_2\}\{S_2P(OEt)_2\}_3(H_2O)]$[11] and $(Me_4N)[Mo_3OCl_3(\mu\text{—}O_2CH)_3Cl_3]$,[6] respectively. The atomic contributions for each of the LMOs are obtained by means of Mulliken population analysis, and the non-diagonal elements F_{ij} of the F^{LMO} matrix are regarded as the interaction energies between the *i*th and *j*th LMOs, where

$$F^{LMO} = U^+ F^{CMO} U.$$

F^{CMO} denotes the Fock matrix of the canonical MOs, and U denotes the transformation unitary matrix. All the calculations are carried out on a VAX-11/785 computer.

Table 1. The CNDO/2 calculation parameter[4]

		ζ	χ (eV)	β° (eV)
O	2*s*	2.275	25.390	−31.00
	2*p*	2.275	9.111	−31.00
S	3*s*	1.817	17.650	−18.15
	3*p*	1.817	6.989	−18.15
Cl	3*s*	2.033	21.591	−22.33
	3*p*	2.033	8.708	−22.33
Mo	5*s*	1.710	3.250	−6.00
	5*p*	0.410	0.830	−4.00
	4*d*	2.050	2.580	−6.50

RESULTS AND DISCUSSION

The cluster cores with closed-shell electron configurations have each pair of α- and β-spin occupied LMOs very close to each other. Thus only the α-spin occupied LMOs are listed in Table 2, which gives relative energy levels, main atomic contributions and chemical bond assignments of the LMOs. From our results it is obvious that all the LMOs are localized in two-centred or three-centred σ- and π-bonds or lone electron pairs, thus allowing us to establish one-to-one correspondences between the LMOs and the chemical bonds in the valence bond theory. Figure 2 shows the energy level diagrams of the LMOs for these cluster cores and a diagrammatic representation of the LMOs of the cluster core $[Mo_3S_4]^{4+}$.

$[Mo_3O_4]^{4+}$, $[Mo_3SO_3]^{4+}$, $[Mo_3OS_3]^{4+}$ *and* $[Mo_3S_4]^{4+}$

These four cluster cores have different bridging and capping atoms, although they have quite similar electronic structures in the core frameworks. Of the 19 occupied LMOs, the LMOs for the four lower levels correspond to the four lone pairs of electrons on the bridging and capping atoms. The LMOs of the next nine higher levels correspond obviously to the three σ(Mo—X) and the six σ(Mo—Y), nine polar bonds altogether as viewed from the angle of atomic orbital population. It is important that for all these cores there exist three three-centred two-electron (Mo Mo / Y) π bonds, as described in [4] with each bridging Y atom contributing one pair of electrons from the lone pair occupying the p_z AO perpendicular to the Mo Mo / Y plane and each of the two molyb-

Table 2. α-spin occupied localized molecular orbitals of $[Mo_3O_4]^{4+}$, $[Mo_3SO_3]^{4+}$, $[Mo_3S_4]^{4+}$ and $[Mo_3OCl_3]^{5+}$

Cluster	Mo number	Energy (a.u.)	Per cent atom contribution	Nature of bonding	
$[Mo_3O_4]^{4+}$	1–3	−1.940	O_b(98.99)	$\lambda(O_b)$	(3×)
	4	−1.938	O_c(99.30)	$\lambda(O_c)$	
	5–7	−1.639	Mo(20.95)+O_c(74.41)	σ(Mo—O_c)	(3×)
	8–13	−1.617	Mo(28.24)+O_b(66.64)	σ(Mo—O_b)	(6×)
	14–16	−1.487	Mo(8.35)+O_b(82.85)+Mo′(8.35)	π(Mo, Mo / O_b)	(3×)
	17–19	−1.286	Mo(48.21)+Mo′(48.21)	σ(Mo—Mo)	(3×)
$[Mo_3SO_3]^{4+}$	1–3	−1.927	O_b(98.95)	$\lambda(O_b)$	(3×)
	4	−1.663	S_c(98.98)	$\lambda(S_c)$	
	5–10	−1.596	Mo(28.57)+O_b(66.67)	σ(Mo—O_b)	(6×)
	11–13	−1.473	Mo(26.50)+S_c(69.07)	σ(Mo—S_c)	(3×)
	14–16	−1.464	Mo(8.41)+O_b(82.72)+Mo(8.41)	π(Mo, Mo / O_b)	(3×)
	17–19	−1.266	Mo(48.12)+Mo(48.12)	σ(Mo—Mo)	(3×)
$[Mo_3OS_3]^{4+}$	1	−1.890	O_c(99.00)	$\lambda(O_c)$	
	2–4	−1.609	S_b(98.53)	$\lambda(S_b)$	(3×)
	5–7	−1.557	Mo(22.05)+O_c(72.91)	σ(Mo—O_c)	(3×)
	8–13	−1.415	Mo(34.66)+S_b(61.11)	σ(Mo—S_b)	(6×)
	14–16	−1.299	Mo(10.68)+S_b(77.81)+Mo(10.68)	π(Mo, Mo / S_b)	(3×)
	17–19	−1.222	Mo(47.84)+Mo′(47.84)	σ(Mo—Mo)	(3×)
$[Mo_3S_4]^{4+}$	1	−1.614	S_c(98.50)	λ(Sc)	
	2–4	−1.593	S_b(98.40)	$\lambda(S_b)$	(3×)
	5–7	−1.415	Mo(26.80)+S_c(67.50)	σ(Mo—S_c)	(3×)
	8–13	−1.393	Mo(34.30)+S_b(61.70)	σ(Mo—S_b)	(6×)
	14–16	−1.278	Mo(10.50)+S_b(78.00)+Mo(10.50)	π(Mo, Mo / S_b)	(3×)
	17–19	−1.204	Mo(48.30)+Mo′(48.30)	σ(Mo—Mo)	(3×)
$[Mo_3OCl_3]^{5+}$	1	−2.122	O_c(98.76)	$\lambda(O_c)$	
	2	−1.979	Cl_b(99.10)	$\lambda(Cl_b)$	
	3, 4	−1.974	Cl_b(99.10)	$\lambda(Cl_b)$	(2×)
	5	−1.826	Mo(20.98)+O_c(72.26)	σ(Mo—O_c)	
	6, 7	−1.815	Mo(22.29)+O_c(71.81)	σ(Mo—O_c)	(2×)
	8, 9	−1.675	Mo(24.00)+Cl_b(73.09)	σ(Mo—Cl_b)	(2×)
	10, 11	−1.672	Mo(24.50)+Cl_b(71.79)	σ(Mo—Cl_b	(2×)
	12, 13	−1.663	Mo(25.22)+Cl_b(72.27)	σ(Mo—Cl_b)	(2×)
	14	−1.578	Mo(4.50)+Cl_b(90.83)+Mo′(4.59)	π(Mo, Mo / Cl)	
	15, 16	−1.571	Mo(3.93)+Cl_b(95.50)	$\lambda(Cl_b)$	(2×)
	17	−1.479	Mo(99.15)	λ(Mo)	
	18, 19	−1.453	Mo(42.03)+Mo′(54.59)	σ(Mo—Mo)	(2×)
	20	−1.452	Mo(49.94)+Mo′(49.94)	σ(Mo—Mo)	

λ, σ, π denote lone pair of electrons, σ bond, and π bond, respectively. Subscripts b, c, denote bridging and capping atoms, respectively.

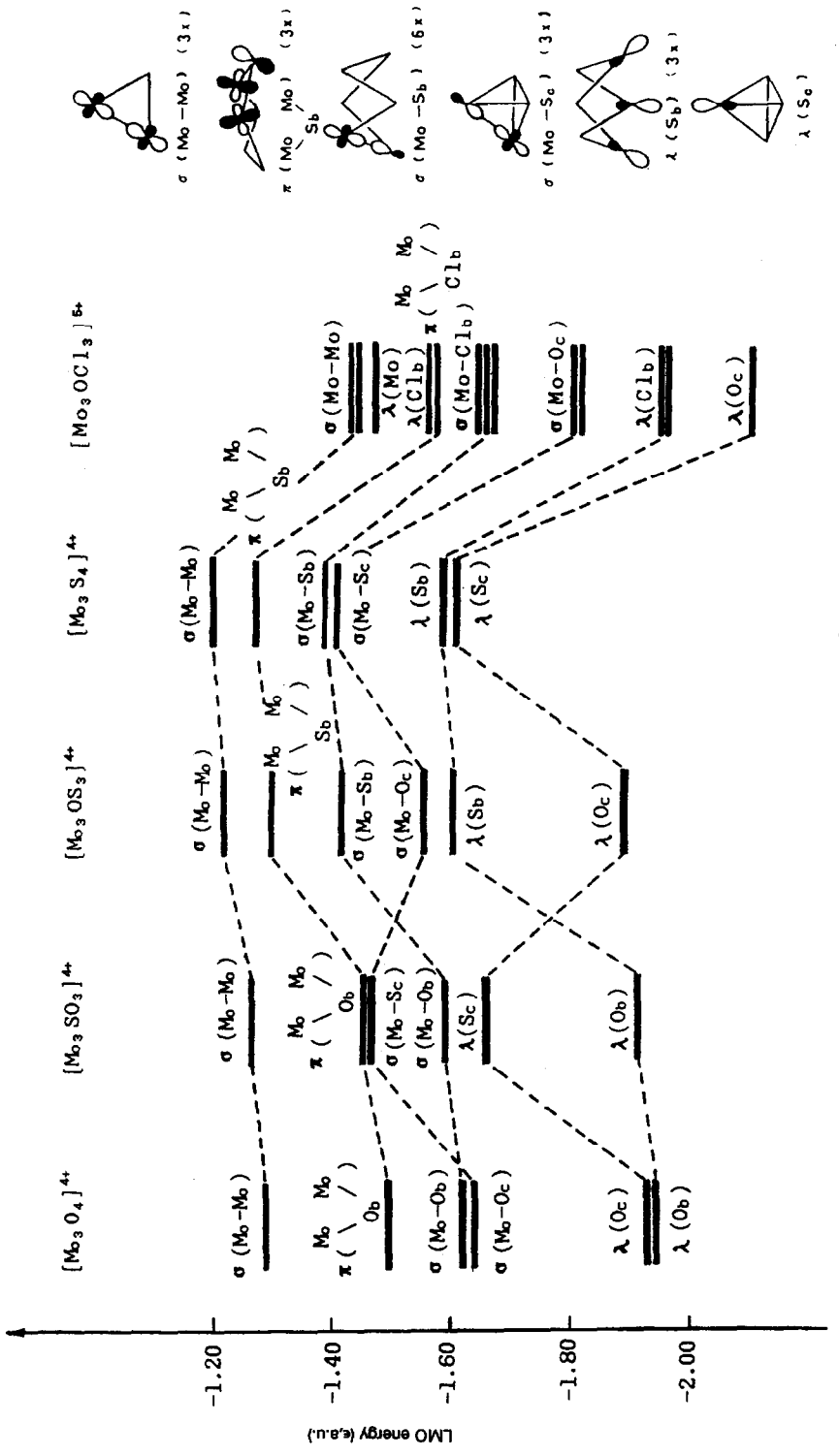

Fig. 2. LMO energy levels of $[Mo_3O_4]^{4+}$, $[Mo_3SO_3]^{4+}$, $[Mo_3OS_3]^{4+}$, $[Mo_3S_4]^{4+}$ and $[Mo_3OCl_3]^{5+}$. Diagrammatic representation of the LMOs of the cluster core $[Mo_3S_4]^{4+}$ (subscripts b, c denote bridging and capping atoms, respectively).

Table 3. Bond lengths in $[Mo_3O_4]^{4+}$, $[Mo_3SO_3]^{4+}$, $[MoOS_3]^{4+}$, $[Mo_3S_4]^{4+}$ and $[Mo_3OCl_3]^{5+}$ (Å)[6,8,9,10,11]

Atom	$[Mo_3O_4]^{4+}$	$[Mo_3SO_3]^{4+}$	$[Mo_3OS_3]^{4+}$	$[Mo_3S_4]^{4+}$	$[Mo_3OCl_3]^{5+}$
Mo—Mo	2.486	2.589	2.638	2.754	2.577
Mo—(μ_3-X)	2.019	2.360	2.027	2.346	1.982
Mo—(μ-Y)	1.921	1.917	2.282	2.283	2.414

denum atoms contributing its unique vacant 4*d* AO, thus forming a (*d*–*p*–*d*) π-bond (cf. Fig. 2). It is seen that the delocalization of the lone pair electrons of the bridging atom onto the two adjoining molybdenum atoms depends mainly on the size and electronegativity of the bridging atom itself. The populations of the bridging atoms in Table 2 show that the degree of delocalization for a bridging sulphur atom is larger than that for a bridging oxygen atom due to the larger atomic volume and smaller electronegativity of the sulphur atom. For the three highest levels, the LMOs correspond obviously to the three two-centred two-electron σ(Mo—Mo) bonds.

Meanwhile, Fig. 2 shows clearly how the energy levels of these cluster cores change with the different bridging and capping atoms. In general, the LMO energy levels for these four cluster cores are raised to some extent as the number of sulphur atoms is increased. In particular, the LMO energy for the σ(Mo—Mo) bonds are only rather inappreciably raised as bridging oxygen atoms are replaced by the sulphur atom. On the other hand, the increasing trends for the LMO energies corresponding to the

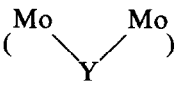

π bonds and the σ(Mo—Y) bonds are much more apparent, arising essentially from the difference in electronegativities between the valence orbitals of the constituent oxygen and sulphur atoms. The Mulliken bond order, in general, decreases as the bond length increases. However, as shown in Tables 3 and 4, for the Mo—Y atom pairs in $[Mo_3O_4]^{4+}$, $[Mo_3SO_3]^{4+}$, $[Mo_3OS_3]^{4+}$ and $[Mo_3S_4]^{4+}$, the Mulliken bond orders are 0.447, 0.449, 0.573 and 0.565 (in unit e), respectively, while their bond lengths are 1.921, 1.917, 2.282 and 2.283 (in unit Å) in the order. It may be seen that though the bond lengths of Mo—(μ-S) in $[Mo_3OS_3]^{4+}$ and $[Mo_3S_4]^{4+}$ are quite larger than of Mo—(μ-O) in $[Mo_3O_4]^{4+}$ and $[Mo_3SO_3]^{4+}$, the Mulliken bond orders of Mo—(μ-S) are unusually large compared to those of Mo—(μ-O). This change of the Mulliken bond orders following the replacement of the bridging oxygen atoms arises indeed from the large delocalization of the lone pair electrons of the bridging sulphur atoms into the vacant 4*d* AO in each of the two adjoining molybdenum atoms, resulting in the stronger bonding in the

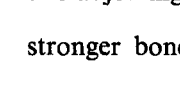

π bonds relative to the

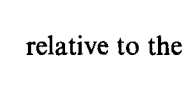

π bonds.

$[Mo_3OCl_3]^{5+}$

In our calculation, the idealized C_{3v} symmetry for the trinuclear molybdenum cluster core is lowered to C_s symmetry with the geometrical configuration of an isosceles triangle for this $[Mo_3OCl_3]^{5+}$ cluster core. From the net charges on the molybdenum atoms (+1.503, +1.503, and +1.542 in unit e) in Table 5, this is not so much a Jahn–Teller distortion with Mulliken bond orders of 0.318 e for the base and 0.370 e for the two other sides. Of the 20 α-spin occupied LMOs, the 13 LMOs of the lower energy levels, similar to the case of the four cluster cores studied above, correspond obviously to the four lone pairs of electrons on the bridging chlorine atoms and capping oxygen atom, the three polar σ(Mo—O) bonds and the six polar σ(Mo—Cl) bonds. It is very interesting to note that the LMOs of the next three energy levels

Table 4. Mulliken bond order in $[Mo_3O_4]^{4+}$, $[Mo_3SO_3]^{4+}$, $[Mo_3OS_3]^{4+}$, $[Mo_3S_4]^{4+}$ and $[Mo_3OCl_3]^{5+}$ (e)

Mo—Mo	0.324	0.321	0.319	0.302	0.318, 0.370(2*x*)
Mo—μ_3X	0.324	0.435	0.322	0.442	0.356, 0.342(2*x*)
Mo—μY	0.447	0.449	0.573	0.565	0.378(2*x*), 0.385(2*x*), 0.395(2*x*)

Table 5. Charges of atoms in $[Mo_3O_4]^{4+}$, $[Mo_3SO_3]^{4+}$, $[MoOS_3]^{4+}$, $[Mo_3S_4]^{4+}$ and $[Mo_3OCl_3]^{5+}$ (e)

	$[Mo_3O_4]^{4+}$	$[Mo_3SO_3]^{4+}$	$[Mo_3OS_3]^{4+}$	$[Mo_3S_4]^{4+}$	$[Mo_3OCl_3]^{5+}$
Mo	1.794	1.674	1.327	1.192	1.542, 1.503(2x)
μ_3-X	−0.473	−0.133	−0.391	−0.020	−0.359
μ-Y	−0.303	−0.297	0.137	0.148	0.300, 0.255(2x)

correspond, respectively, to the (Mo, Mo, Y) (d–p–d) π-bond, and the two lone pairs of π-electrons localized mostly on each of the other two chlorine atoms, with only a little delocalized onto the basal molybdenum atom, instead of the three synergically connected (Mo, Mo, Y) (d–p–d) π-bonds in the cluster cores of the type $[Mo_3(\mu_3\text{-}X)(\mu\text{-}Y)_3]^{4+}$ (X, Y = O, S). The LMOs of the four higher energy levels correspond clearly to the lone pair of electrons localized on the 4d AO of the apical molybdenum atom, and the three σ(Mo—Mo) bonds forming the Mo_3 triangular skeleton. Thus there will be some interaction between this lone pair of the electrons on the apical molybdenum atom and each of the two lone pairs of the π-electron on the adjacent bridging chlorine atoms. This interaction lowers its energy down somewhat below that of the σ(Mo—Mo) bonds. On the other hand, it is seen from Table 2 that the bonding electrons forming the two σ(Mo—Mo) bonds involved in the apical molybdenum atom differ from those of the other σ(Mo—Mo) bonds in the fact that these electrons forming these two polar metal–metal bonds are distinctly inclined to the basal atoms of the Mo_3 triangle. A simple electron-counting scheme gives a total of eight for the valence electrons of the Mo_3 skeleton in the $[Mo_3OCl_3]^{5+}$ cluster core, two more than are found in the core $[Mo_3(\mu_3\text{-}X)(\mu\text{-}Y)_3]^{4+}$ (X, Y = O, S). It is apparent that these two extra electrons must primarily occupy the lone electron pair on the apical molybdenum atom from the LMO point of view, resulting in only single bonds for all the Mo—Mo bonds in the $[Mo_3OCl_3]^{5+}$ cluster core. It is these two extra electrons that lower the idealized C_{3v} symmetry of the $[Mo_3OCl_3]^{5+}$ geometry.

Bridging atom and the degree of quasi-aromaticity

The two types of bonding schemes for the cluster cores $[Mo_3(\mu_3\text{-}X)(\mu\text{-}Y)_3]^{n+}$ (X = O, S; Y = O, S, Cl; n = 4, 5) are represented in Fig. 3, without showing here the lone pair electrons except the lone pair π-electrons.

It has been shown in [4] that for $[Mo_3(\mu_3\text{-}X)(\mu\text{-}Y)_3]^{4+}$ (X, Y = O, S) each of the bridging oxygen and sulphur atoms depopulate the lone pair π-electrons onto each of the two adjacent molybdenum atoms, which contribute their vacant 4d AO to accept electrons from this bridging atom in the mode of bonding [cf. Fig. 3(a)]. However, replace-

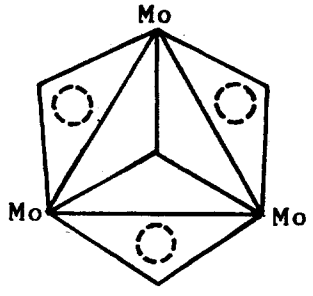

$[Mo_3(\mu_3\text{-}X)(\mu\text{-}Y)_3]^{4+}$ (X, Y = O, S)

(a)

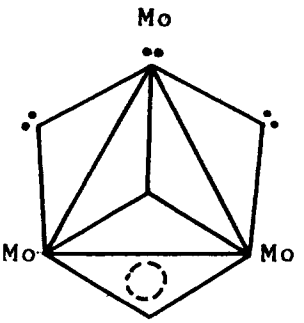

$[Mo_3(\mu_3\text{-}O)(\mu\text{-}Y)_3]^{5+}$ (Y = Cl, Br)

(b)

Fig. 3. Bonding schemes for the cluster cores $[Mo_3(\mu_3\text{-}X)(\mu\text{-}Y)_3]^{n+}$ (n = 4, 5). (a) $[Mo_3(\mu_3\text{-}X)(\mu\text{-}Y)_3]^{4+}$ (X, Y = O, S); (b) $[Mo_3(\mu_3\text{-}O)(\mu\text{-}Y)_3]^{5+}$ (Y = Cl, Br).

Table 6. Inter-(*d–p–d*) π-bond interaction energy and atomic population corresponding to these π bonds in $[Mo_3O_4]^{4+}$, $[Mo_3SO_3]^{4+}$, $[MoOS_3]^{4+}$ and $[M$

Cluster core	$[Mo_3O_4]^{4+}$	$[Mo_3SO_3]^{4+}$	$[Mo_3OS_3]^{4+}$	$[Mo_3S_4]$
Interaction energy (a.u.)	0.045	0.045	0.048	0.050
Mo (%)	8.35	8.41	10.68	10.50
(μ-Y) (%)	82.85	82.72	77.81	78.00

In the previous paper[4] the inter-(*d–p–d*) π-bond interaction energy 0.092 a.u. in $[Mo_3S_4]^{4+}$ is reported for the calculation in which 3*s*, 3*p* and 3*d* AOs are taken as basis functions of the sulphur atom. From the results of *ab initio* calculation followed by Boys localization performed by us, the parameter of the 3*d* AO of the sulphur atom results in an overestimate of the inter-(*d–p–d*) π-bonds interaction energy.

ment of the bridging oxygen and sulphur atoms by the bridging chlorine atom changes the electron count. On the one hand, the six valence electrons for each of the bridging oxygen and sulphur atoms are involved in one lone electron pair, two σ(Mo—O) or σ(Mo—S) bonds, and one three-centred two-electron π-bond; on the other hand, the seven valence electrons for each of the two bridging chlorine between the apical and basal molybdenum atoms are involved in two lone electron pairs and two σ(Mo—Cl) bonds; for the bridging chlorine between the two basal molybdenum atoms one lone electron pair, two σ(Mo—Cl) bonds, and one three-centred two-electron π-bond. Considering the difference of the ionic charges of the cluster cores ($n = 4, 5$), there are still two extra electrons of the Mo_3 skeleton in the $[Mo_3OCl_3]^{5+}$ cluster core, arising from replacement of the chlorine atoms. The two extra electrons enable the $[Mo_3(\mu_3\text{-}O)(\mu\text{-}Cl)_3]^{5+}$ core to adopt another bonding scheme [cf. Fig. 3(b)], in which only one (Mo Cl Mo) π bond is formed between the basal molybdenum atoms of the Mo_3 triangle and the bridging chlorine atom, but the two lone pairs of π-electrons of the two other bridging chlorine atoms remain essentially unchanged in their position without any significant depopulation to the adjacent molybdenum atoms. Thus these two types of bonding schemes would lead the cluster cores in question to exhibit different behaviours. For the case discussed in [4], on one hand, the three three-centred two-electron (Mo Y Mo) π bonds in the $[Mo_3(\mu_3\text{-}X)(\mu\text{-}Y)_3]^{4+}$ (X, Y = O, S) core cooperate actually with each other through each of the common molybdenum atoms, forming a large six-membered closed continuous π-conjugated system around the $[Mo_3Y_3]$ ring. On the other hand, for the other bonding scheme in $[Mo_3(\mu_3\text{-}O)(\mu\text{-}Cl)_3]^{5+}$ only one isolated three-centred two-electron π bond is formed. In the absence of two adjacent (Mo Cl Mo) π bonds, it is impossible to form a large closed continuous π-conjugated system in the $[Mo_3Cl_3]$ ring. Such a cluster core cannot exhibit any quasi-aromaticity at all.

Even though some cluster cores, $[Mo_3O_4]^{4+}$, $[Mo_3SO_3]^{4+}$, $[Mo_3OS_3]^{4+}$ and $[Mo_3S_4]^{4+}$, all have identical bonding schemes, different bridging atoms make these cluster cores exhibit, more or less, different degrees of quasi-aromaticity. The large delocalizability of the lone pair π-electrons in a bridging sulphur atom gives rise to a greater stability of the local delocalized (Mo Y Mo) π bond; but, on the other hand, enhances inter-LMO interaction for the three (Mo Y Mo) π bonds. In Table 6, the inter-bond interaction energy for the (Mo Y Mo) π bonds, and the atomic population for the bridging Y atom and each of the two adjoining molybdenum atoms are also listed. Both the interaction energy and the depopulation of the bridging atom show consistently that the three π bonds with bridging sulphur atoms form a more stabilized π-conjugated system around the $[Mo_3S_3]$ ring than in the case of bridging oxygen atoms. Furthermore, the more labile π-electrons around the $[Mo_3S_3]$ ring give rise to a larger diamagnetic susceptibility than in the $[Mo_3O_3]$ ring. This conclusion is in good agreement with Shibahara's experimental measurements made for $Ba[Mo_3SO_3(Hnta)_3]\cdot 10H_2O$ and $Ca_{1.5}[Mo_3S_4(Hnta)_2(nta)]\cdot 12H_2O$. It is quite apparent that the size and electronegativity of the bridging atoms, which is the decisive factor for the delocalizability of the lone

pair π-electrons in the bridging atom, enable the $[Mo_3Y_3]$ ring (Y = O, S) to exhibit different degrees of quasi-aromaticity in the cluster compounds containing the cores $[Mo_3(\mu_3\text{-}X)(\mu\text{-}Y)_3]^{4+}$ (X, Y = O, S).

Acknowledgement—This research has been supported by a grant from the National Natural Science Foundation of China.

REFERENCES

1. (a) A. Bino, F. A. Cotton and Z. Dori, *J. Am. Chem. Soc.* 1979, **101**, 3842; *Inorg. Chim. Acta* 1979, **33**, L133. (b) F. A. Cotton, T. R. Felthouse and D. G. Lay, *J. Am. Chem. Soc.* 1980, **102**, 1431; (c) X.-T. Lin, Y.-H. Lin, J.-L. Huang and J.-Q. Huang, *Kexue Tongbao* 1987, **32**, 810.
2. B. E. Bursten, F. A. Cotton, M. B. Hall and R. C. Najjar, *Inorg. Chem.* 1982, **21**, 302; R. Jostes, A. Muller and F. A. Cotton, *Angew. Chem., Int. Edn Engl.* 1980, **19**, 875.
3. J.-Q. Huang, J.-L. Huang, M.-Y. Shang, S.-F. Lu, X.-T. Lin, Y.-H. Lin, M.-D. Huang, H.-H. Zhuang and J.-X. Lu, *Pure Appl. Chem.* 1988, **60**, 1185; *Jiegou Huaxue* 1987, **6**, 219 (in Chinese).
4. J.-X. Lu, *Jiegou Huaxue* 1989, **8**, 327 (in Chinese); Z.-D. Chen, J. Li, W.-D. Cheng, J.-Q. Huang, C.-W. Liu, Q.-E. Zhang and J.-X. Lu, *Chin. Sci. Bull.* 1990, **35**, 1698.
5. H. Kobayashi, T. Shibahara and N. Uryu, *Bull. Chem. Soc. Japan* 1990, **63**, 799.
6. X.-T. Lin, J.-L. Huang and J.-Q. Huang, *Acta Chim. Sin.* 1985, **4**, 293.
7. J. Li, J.-Q. Ren, M.-B. Chen and G.-X. Xu, *Acta Sci. Nat. Univ. Pekin.* 1989, **25**, 129.
8. A. Bino, F. A. Cotton and Z. Dori, *J. Am. Chem. Soc.* 1978, **100**, 5252.
9. T. Shibahara, H. Hattori and H. Kuroya, *J. Am. Chem. Soc.* 1984, **106**, 2710.
10. S.-F. Lu, M.-Y. Shang, J.-Q. Huang, J.-L. Huang and J.-X. Lu, *Sci. Sin.* 1988, **31**(B), 147.
11. X.-T. Lin, Y.-H. Lin, J.-L. Huang and J.-Q. Huang, *Kexue Tongbao* 1987, **32**, 810.

Polyhedron Vol. 10, No. 23/24, pp. 2809–2812, 1991
Printed in Great Britain

0277–5387/91 $3.00+.00
© 1991 Pergamon Press plc

SOME COORDINATION POLYMERS OF THORIUM(IV) WITH 4,4′-BIPYRIDYL-*N*,*N*′-DIOXIDE AND 4-ETHOXYCARBONYLAMINOPYRIDINE-*N*-OXIDE*

R. K. AGARWAL† and JAI PRAKASH

Postgraduate Department of Chemistry, Lajpat Rai Postgraduate College, Sahibabad-201 005, Ghaziabad, India

(*Received* 20 *February* 1991; *accepted* 9 *July* 1991)

Abstract—The synthesis and characterization of some coordination polymers of thorium(IV) salts with 4,4′-bipyridyl-*N*,*N*′-dioxide (4,4′-BipyO_2) and 4-ethoxycarbonylaminopyridine *N*-oxide (4-ECAPO) is described. Both ligands form 1:2 (metal:ligand) complexes with thorium(IV) chloride, bromide and thiocyanate but a 1:1 complex with thorium(IV) nitrate. Infrared spectra of these complexes indicate that both ligands are O,O-donors and bridged between two thorium ions to form a polymer chain. The nitrate groups in the nitrato complexes are bidentate chelating. These polymeric chain compounds contain either eight or ten coordinated thorium(IV) depending on the nature of anions.

In recent years a number of coordination polymers have been synthesized from organic ligands and various metal ions.[1] But there is no formal report on thorium(IV) coordination polymers of aromatic amine *N*-oxides.[2,3] In this paper we report our results on some coordination polymers of thorium(IV) with 4,4′-bipyridyl-*N*,*N*′-dioxide (4,4′-BipyO_2) (**I**) and 4-ethoxycarbonylaminopyridine *N*-oxide (4-ECAPO) (**II**).

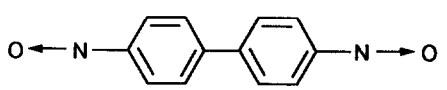

4,4′ – Bipyo$_2$ (I)

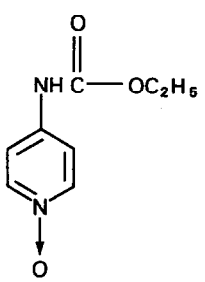

4 – ECAPO (II)

* Presented at National Symposium on Polymer Chemistry, Sardar Patel University, V.V. Nagar, India, 8–10 February 1990.

† Author to whom correspondence should be addressed.

EXPERIMENTAL

$Th(NO_3)_4 \cdot 5H_2O$ (B.D.H., AnalaR) was used as received. Thorium(IV) perchlorate, halo and thiocyanato salts were prepared as reported.[4,5] The ligand 4,4′-bipyridyl-*N*,*N*′-dioxide was prepared by oxidation of 4,4′-bipyridyl (Koch-Light) by the method of Ochiai.[6] The ligand 4-ethoxycarbonylaminopyridine *N*-oxide was prepared from 4-amino pyridine by the method of Katritzky.[7]

Synthesis of coordination polymers

All the complexes were isolated by one of the following methods:

(i) To a solution of the metal salt in ethyl acetate an excess of the ligand in methanol was added and a solid compound was immediately precipitated. It was filtered, washed with ethyl acetate and methanol and finally with solvent ether and dried *in vacuo* over fused $CaCl_2$.

(ii) A solution of Lewis acid in absolute ethanol was treated with an excess of the Lewis base in the same solvent. The mixture was refluxed for *ca* 2 h on the water bath and the excess solvent was removed by distillation. The residual mass on treatment with anhydrous diethyl ether yielded a crystalline solid which was filtered, washed with diethyl ether and dried *in vacuo* over P_4O_{10}.

(iii) A solution of the Lewis acid in ethanol was treated with an excess of the Lewis base on the same solvent. The mixture was refluxed for *ca* 2 h. After cooling the solid mass which settled was filtered, washed with ethanol and solvent ether and dried as above.

All the physicochemical analyses were carried out as reported earlier.[8]

RESULTS AND DISCUSSION

The interaction of 4,4′-$BipyO_2$ and 4-ECAPO with thorium(IV) salts results in the formation of $[ThX_4L_n]$ ($n = 2$; X = Cl, Br or NCS; $n = 1$; X = NO_3 and L = 4,4′-$BipyO_2$ or 4-ECAPO). The analytical data were recorded in Table 1. No absorption bands were observed which could be attributed to water or ethanol thus establishing these complexes to be anhydrous and free from coordinated or lattice water of ethanol. This view was further supported by thermal data. Because of the insolubility of the thorium(IV) complexes studied herein, in suitable organic solvents and in molten camphor, molecular weight determinations could not be carried out.

IR spectra and the nature of coordination

(a) 4,4′-*Bipyridyl* N,N′-*dioxide complexes*. Some IR data for the Th^{IV} complexes of 4,4′-$BipyO_2$ are given in Table 2. IR spectral data indicate that both the donor atoms of 4,4′-$BipyO_2$ are bonded to metal ions and this ligand is bridged between two thorium ions. The steric position of the donor atoms in this ligand precludes chelation but favours coordination to different metal ions thus leading to polymer chain formation. The NO stretching vibration appears as a strong doublet at *ca* 1250 and 1235 cm^{-1} in free 4,4′-$BipyO_2$ shifts to lower frequency region in the complexes indicating a decrease in the π-bond character of the NO bond as a result of oxygen to metal coordination.[1-3] The NO bending vibration appearing as a strong absorption at *ca* 850 and 835 cm^{-1} in the uncoordinated 4,4′-$BipyO_2$ is observed with similar intensity but shifted slightly to the lower frequencies in the IR spectra of the thorium(IV) complexes. Several absorptions associated with C—H out-of-plane deformation modes depending on the number of adjacent hydrogen atoms in the aromatic ring. These absorptions undergo slight positive shifts on complexation due to the decrease of electron density on the aromatic ring. Some new medium or weak bands are also observed in the 410–350 cm^{-1} region due to ν(Th—O).[9,10] These bands further support that oxygens are the only donating centres in 4,4′-$BipyO_2$.

(b) 4-*Ethoxycarbonylaminopyridine* N-*oxide complexes*. This ligand is a potentially multidentate (O, N, O) ligand. Framework molecular models show that it is more likely to bond to different metal ions and thus may act as a bridging rather than a chelating ligand. Some IR data for the 4-ECAPO

Table 1. Analytical data of Th^{IV} complexes of 4,4′-$BipyO_2$ and 4-ECAPO

Complex	M.p. (°C)	Found (Calc.) %				
		Th	C	H	N	Anion
$[ThCl_4(4,4'\text{-}BipyO_2)_2]$	260d	32.0 (30.9)	31.8 (32.0)	2.0 (2.1)	7.3 (7.5)	18.7 (18.9)
$[ThBr_4(4,4'\text{-}BipyO_2)_2]$	240d	25.7 (25.0)	25.4 (25.9)	1.7 (1.7)	5.9 (6.0)	34.0 (34.5)
$[Th(NO_3)_4(4,4'\text{-}BipyO_2)]$	250d	35.3 (34.7)	17.6 (18.0)	1.1 (1.2)	12.5 (12.6)	—
$[Th(NCS)_4(4,4'\text{-}BipyO_2)_2]$	> 260	28.3 (27.6)	34.0 (34.3)	1.8 (1.9)	13.2 (13.3)	27.3 (27.6)
$[ThCl_4(4\text{-}ECAPO)_2]$	> 260	30.8 (31.4)	25.7 (26.0)	2.6 (2.7)	7.1 (7.6)	19.0 (19.2)
$[ThBr_4(4\text{-}ECAPO)_2]$	255d	26.0 (25.3)	20.7 (21.0)	2.1 (2.2)	5.8 (6.1)	34.0 (34.9)
$[Th(NO_3)_4(4\text{-}ECAPO)]$	> 260	35.9 (35.0)	14.3 (14.5)	1.4 (1.5)	12.2 (12.7)	—
$[Th(NCS)_4(4\text{-}ECAPO)_2]$	260d	28.7 (28.0)	28.6 (29.0)	2.3 (2.4)	13.3 (13.5)	27.6 (28.0)

Table 2. Important IR frequencies (cm^{-1}) of thorium(IV) complexes of 4,4′-$BipyO_2$

Assignments	4,4′-$BipyO_2$	[$ThCl_4$(4,4′-$BipyO_2$)$_2$]	[$ThBr_4$(4,4′-$BipyO_2$)$_2$]	[$Th(NO_3)_4$(4,4′-$BipyO_2$)]	[$Th(NCS)_4$(4,4′-$BipyO_2$)$_2$]
(N—O) stretching	1250s 1235s	1220s 1200s	1220s 1205s	1215s 1205s	1222s 1210s
(N—O) bending	850s 835s	840m 825m	845m 827m	840m 820m	835m 815m
C—H out-of-plane deformation	770s 726m	770m 732w	775s 740m	758m	768s 736w 715w
ν(Th—O) (metal–ligand vibration)	—	400m 380m	390m 372w	390m 365m	392m 370m
ν(Th—Cl)	—	255m	—	—	—

complexes of Th^{IV} are given in Table 3. The split bands at 1245 and 1230 cm^{-1} have been assigned to ν(N—O) modes of vibration in free 4-ECAPO which undergo a significant negative shift on complexation. This decrease in frequency is attributed to coordination on the oxygen atom of the base to the metal causing a decrease in π-character of N—O bonding.[9,10] The N—O bending vibration is assigned to *ca* 830 cm^{-1} in free 4-ECAPO.[11,12] The data summarized in Table 3 shows that there is only a slight shift of this vibration in some cases while in others it is unaffected.[13] The absorptions associated with C—H out-of-plane deformation modes depending on the number of adjacent hydrogen atoms in the aromatic ring undergo slight positive shifts on complexation due to decrease of electron density on the aromatic ring. The amide–I band in free 4-ECAPO, appears at 1735 cm^{-1}, which causes a considerable negative shift on complexation suggested coordination through the carbonyl oxygen atom of the free base. The NH stretching absorption in the free ligand occurs at 3200 and 3120 cm^{-1} which remains unaffected after complexation.[14,15] This precludes the possibility of coordination through the imine nitrogen atom.

The steric position of the donor atoms (O, O) in this ligand precludes the possibility of chelation but favours coordination to different metal ions leading

Table 3. Important IR frequencies (cm^{-1}) of thorium(IV) complexes of 4-ECAPO

Assignments	4-ECAPO	[$ThCl_4$ (4-ECAPO)$_2$]	[$ThBr_4$ (4-ECAPO)$_2$]	[$Th(NO_3)_4$ (4-ECAPO)]	[$Th(NCS)_4$ (4-ECAPO)$_2$]
(N—H) stetching	3210m 3160m	3210m 3160m	3205m 3162m	3215m 3155m	3205s 3160m
(C═O) stetching	1740sh 1735s	1650s 1632sh	1650s	1660s 1650sh	1647s 1640m
(N—O) stretching	1248s 1230s	1230m 1210sh	1240m 1190m	1230m 1212sh	1220m 1190m
(N—O) bending	830m	810m	820m	808m	810m
C—H out-of-plane deformation	760m 720m 660w 615	765m 730m 650w 635w	770m 725m 655w 630w	760m 730w 640w	770m 725m 650w 640w
ν(Th—O)	—	420m 395m	410m 387m	405m 380m	420w 392m
ν(Th—Cl)	—	235w	—	—	—

to polymer chain formation. The insolubility and higher decomposition temperature also support this view. The overall IR spectral evidence suggest that 4-ECAPO acts as a bidentate bridging ligand and coordinates through *N*-oxygen and carbonyl oxygen atoms. The bands observed in the 420–380 cm^{-1} region are assigned as ν(Th—O).[9-10]

The spectral bands due to NO_3^- groups in $[Th(NO_3)_4(4,4'\text{-BipyO}_2)]$ and $[Th(NO_3)_4$(4-ECAPO)] complexes which occur at *ca* 1525, 1300, 1040, 820, 750 and 720 cm^{-1} region were compared with the known bands of $Th(NO_3)_4 \cdot 5H_2O$,[16] i.e. 1520 (ν_4), 1290 (ν_1), 1030 (ν_2), 808 (ν_6), 745 (ν_3) and 715 cm^{-1} (ν_5) in which the bidentate character of the nitrato groups has been established by X-ray and neutron diffraction studies.[17] In both the thiocyanato complexes, the three fundamental absorptions C—N stretch (ν_1), C—S stretch (ν_3) and N—C—S bending (ν_2) are identified at *ca* 2050, 830–805 and 460 cm^{-1} respectively. These frequencies are associated with the terminal *N*-bonded isothiocyanate ions.[18]

Thermal studies

The TG and DT curves of these complexes do not show the presence of water molecules. All the complexes decompose endothermically. Thermogravimetric analyses show the following decomposition scheme:

$$[ThX_4L_3] \longrightarrow ThX_4L \longrightarrow ThX_4 \longrightarrow ThOX_2$$

(X = Cl, Br or NCS;
L = 4,4′-$BipyO_2$ or 4-ECAPO)

$$[Th(NO_3)_4L] \longrightarrow [Th(NO_3)_4L_{0.5}] \longrightarrow Th(NO_3)_4 \longrightarrow ThO_2$$

(L = 4,4′-$BipyO_2$ or 4-ECAPO).

On the basis of TG decomposition temperature the order of thermal stability of the complexes is

$$NO_3 > Cl > Br \approx NCS.$$

Structure of the coordination polymers

Thorium(IV) halide (chloride, bromide and thiocyanate) gave 1 : 2 complexes with 4,4′-$BipyO_2$ and 4-ECAPO and the ligands bands indicating the bidentate bridging character of the organic ligands. Thiocyanate (NCS) is *N*-bonded in this complex. On this basis the halide complexes are assigned polymeric chain structures involving eight-coordinated thorium(IV) with eight ligand atoms—four oxygens of the bidentate 4-ECAPO or 4,4′-$BipyO_2$ molecules and 4-chlorine, bromine or nitrogens of the *N*-bonded NCS groups. In nitrato complexes, the bidentate chelating nature of the nitrato ligands and bridging bidentate nature of organic ligands, the 1 : 1 thorium(IV) nitrate complexes are tentatively assigned as polymeric chain structures involving 10-coordinated thorium(IV) with 10 oxygen atoms—two from bidentate bridging 4-ECAPO or 4,4′-$BipyO_2$ molecules and eight from four bidentate chelating nitrate groups.

Acknowledgement—The authors are thankful to the authorities of Lajpat Rai (P.G.) College, Sahibabad, for providing facilities for this work.

REFERENCES

1. I. S. Ahuja, C. L. Yadav and S. Tripathi, *Asian J. Chem.* 1989, **1**, 195.
2. N. M. Karayannis, L. L. Pytlewski and C. M. Mikulski, *Coord. Chem. Rev.* 1973, **11**, 93.
3. N. M. Karayannis, A. N. Speca, D. E. Chasen and L. L. Pytlewski, *Coord. Chem. Rev.* 1976, **20**, 37.
4. P. Ramamurthy and C. C. Patel, *J. Inorg. Nucl. Chem.* 1963, **25**, 310.
5. V. V. Savant and C. C. Patel, *J. Less Common Metals* 1971, **24**, 459.
6. E. Ochiai, *J. Org. Chem.* 1953, **18**, 534.
7. A. R. Katritzky, *J. Chem. Soc.* 1956, 2064.
8. R. K. Agarwal, T. N. Srivastava and A. K. Srivastava, *Trans. Met. Chem.* 1980, **5**, 95.
9. P. A. Vigato, U. Casellato and M. Vidali, *Gazz. Chim.* (Ital.) 1977, **107**, 61.
10. S. K. Madan and A. M. Donohue, *J. Inorg. Nucl. Chem.* 1966, **28**, 1303.
11. A. R. Katritzky and A. R. Handa, *J. Chem. Soc.* 1958, 2195.
12. A. R. Katritzky and R. A. Jones, *J. Chem. Soc.* 1959, 3674.
13. P. Ramamurthy and C. C. Patel, *Can. J. Chem.* 1964, **42**, 856.
14. K. Nakamoto, *Infrared Spectra of Inorganic and Coordination Compounds*. Wiley, New York (1963).
15. L. J. Bellamy, *The Infrared Spectra of Complex Molecules*, 2nd edn. Methuen, London (1958).
16. J. R. Ferraro and A. Walker, *J. Chem. Phys.* 1966, **45**, 550.
17. T. Ueki, A. Zalkin and D. Templeton, *Acta Cryst.* 1966, **20**, 836.
18. J. L. Burmeister, *Coord. Chem. Rev.* 1966, **1**, 205; 1968, **3**, 225.

Polyhedron Vol. 10, No. 23/24, pp. 2813–2820, 1991
Printed in Great Britain

0277–5387/91 $3.00+.00
© 1991 Pergamon Press plc

THE PREPARATION OF DIMOLYBDENUM(V,V) COMPLEXES FROM MOLYBDENUM QUADRUPLY BONDED METAL–METAL DIMERS

JOEL I. DULEBOHN, THEODORE C. STAMATAKOS, DONALD L. WARD, and DANIEL G. NOCERA*

Department of Chemistry, Michigan State University, East Lansing, MI 48824, U.S.A.

(*Received* 24 *June* 1991; *accepted* 5 *July* 1991)

Abstract—Oxidation of quadruply bonded metal–metal dimers in the presence of good π-accepting ligands results in the formation of Mo^{V}—Mo^{V} compounds of the type $[Mo_2(\mu\text{-}X)_2(Y)(Y')]^{2+}$ (X = O or S; Y,Y′ = O,O; S,S; O,S). Reaction of $Mo_2(O_2CCH_3)_4$ with oxygen in the presence of Na_2mnt (mnt = 1,2-dicyanoethylene-2,2-dithiolate) gives $[Mo_2(\mu\text{-}S)_2(O)(S)(mnt)_2]^{2-}$ (**1**). The compound crystallizes in the monoclinic space group $P2_1/c$, with cell dimensions $a = 19.547(4)$, $b = 15.210(4)$, $c = 18.754(6)$ Å, $\beta = 101.69(2)°$, $V = 5460(2)$ Å^3, and $Z = 4$. Similarly, oxidation of *o*-dichlorobenzene solutions of $Mo_2Cl_4(CH_3CN)_4$ and 4,4′-dimethyl-2,2′-dipyridyl (dmpby) or, more directly, the reaction of $Mo_2Cl_4(dmbpy)_2$ with oxygen leads to the formation of a red solid, which was characterized by X-ray crystallography to be $Mo_2(\mu\text{-}O)_2(O)_2(Cl)_2(dmbpy)_2$ (**2**). Red diamond crystals, prepared by slow evaporation of CH_3CN solutions of **2**, are trigonal and in the space group $P3_121$ with cell dimensions $a = 16.135(4)$, $b = 16.135(4)$, $c = 10.709(3)$ Å, $V = 2414.4(13)$ Å^3 and $Z = 3$. In both structures, the geometry about each of the molybdenum atoms is a distorted square pyramid with terminal oxygen or sulphur atoms at the apices and in a *syn* conformation. The molybdenum–molybdenum bond distances of 2.858(1) Å and 2.562(2) Å in structures of **1** and **2**, respectively, are typical of other Mo^{V}—Mo^{V} dimers and indicative of a single Mo—Mo bond.

Quadruply bonded metal–metal complexes are convenient starting materials for binuclear complexes containing oxidized metal cores. A prevalent reaction is the thermal,[1–3] electrochemical[4] or photochemical[5,6] removal of an electron from each metal centre to yield species with a formally reduced bond order. A recurrent theme in M≡M chemistry is that the one-electron oxidation of individual metal atoms is typically accompanied by rearrangement of the ligating sphere to the octahedral coordination geometry[1,2,7] of confacial[8–11] or edge-sharing bioctahedral species.[12–14]

In contrast, multielectron changes in the formal oxidation states of one or both of the metals of M≡M cores is typically accompanied by fragmentation to monomeric species. Nevertheless, the retention of a binuclear core has been observed for some multielectron transformations. For instance Cotton, Walton and co-workers have discovered that quadruply bonded $Re_2^{(III,III)}$ cores disproportionate to yield $Re_2^{(II,IV)}$ mixed-valence species.[15] Four-electron disproportionations of M≡M cores have been observed by Chisholm and co-workers[16] in their pioneering work on $Mo_2^{(II,II)}$ tetraalkoxides to give a $Mo_2^{(0,IV)}$ structure, and most recently by Walton and co-workers who have isolated an $Re_2^{(II,VI)}$ compound from $Re_2^{(III,III)}$ parent complexes.[17]

We now report the conversion of quadruply bonded $Mo_2^{(II,II)}$ complexes to highly oxidized $Mo_2^{(V,V)}$ species of the type $[Mo_2(\mu\text{-}X)_2(Y)(Y')]^{2+}$ (X = O or S; Y,Y′ = O,O; S,S; O,S). This conversion in which the binuclear core is retained may be general when the first coordination sphere of quadruply bonded metal cores are substituted with ligands possessing good π-accepting properties; and indeed this method provides a convenient route to the preparation of this important class[18–20] of binuclear molybdenum compounds.

* Author to whom correspondence should be addressed.

EXPERIMENTAL

Starting materials

The starting compounds $(NH_4)_5Mo_2Cl_9 \cdot H_2O$, disodium 1,2-dicyanoethylene-2,2-dithiolate (Na_2mnt), and $Mo_2(O_2CCH_3)_4$ were prepared by literature methods.[21–23] $(C_4H_9)_4NBr$ and 4,4′-dimethyl-2,2′-dipyridyl (dmpby) were purchased from Aldrich and used as received.

Synthesis of dimolybdenum complexes

$[(C_4H_9)_4(N)]_2[Mo_2(\mu\text{-}S)_2(O)(S)(mnt)_2]$, **1**. A suspension of $Mo_2(O_2CCH_3)_4$ (0.604 g, 1.41 mmol) in 50 cm^3 of dry methanol was charged with 1.06 g of $Na_2[S_2C_2(CN)_2]$ (5.67 mmol) prompting the yellow suspension to turn dark green. After 5 h of stirring, the mixture was filtered and the volume of the filtrate was reduced to 35 cm^3 by rotary evaporation. To this solution, 1.81 g (5.62 mmol) of $(C_4H_9)_4NBr$ was added and the flask was cooled for 12 h in a dry ice–acetone bath. A solid formed, which was collected by filtration in air and washed with methanol. Addition of this solid to refluxing methanol produced a green solution with a red precipitate remaining undissolved. The red precipitate was filtered and recrystallized from hot methanol and acetone. Yield: 0.278 g (0.264 mmol, 19%). X-ray quality crystals of **1** were grown from a solution of CH_2Cl_2 layered with hexane. Crystals grown from the green filtrate were identified by IR and absorption spectra to be the known $[(C_4H_9)_4N]_2Mo(mnt)_3$. Yield: 0.500 g (0.494 mmol, 35%).

$Mo_2(\mu\text{-}O)_2(O)_2(Cl)_2(dmbpy)_2$, **2**. The synthesis of the $Mo_2^{(V,V)}$ compound was achieved from the quadruple bond complex $Mo_2Cl_4(dmbpy)_2$, which was obtained from the modification of the procedure used for the preparation of $Mo_2Cl_4(bpy)_2$.[24] Subsequent addition of 0.500 g of $(NH_4)_5Mo_2Cl_9 \cdot H_2O$ (0.826 mmol) to 2.00 g (10.9 mmol) of dmbpy in 30 cm^3 of methanol with stirring over 90 min yielded a solid. The product was filtered, washed with 10 cm^3 of water, methanol, and three 10 cm^3 portions of ether. The solid was dried *in vacuo*. Yield: 0.406 g (0.578 mmol, 70%).

A suspension of 0.384 g (0.547 mmol) of $Mo_2Cl_4(dmbpy)_2$ in 50 cm^3 of *o*-dichlorobenzene was heated to reflux for 5 h under air. The suspension was cooled to room temperature, and filtered. Hexane was added to the red filtrate and a red precipitate formed, which was filtered, washed with ether, and dried under vacuum. The precipitate was recrystallized from CH_2Cl_2 and hexane. Yield: 0.080 g (0.115 mmol, 21%). X-ray quality crystals of **2** were grown from the slow evaporation of CH_3CN from a solution of the compound.

Instruments

IR spectra were obtained as KBr pellets on a Perkin–Elmer 599 and a Nicolet 740 FT IR spectrophotometer. The diffraction data for the dimolybdenum complexes were collected on a Nicolet P3F diffractometer using graphite-monochromated Mo-K_α ($\lambda = 0.71073$ Å) radiation. All calculations were performed on a VAX 11/750 computer using SDP/VAX.[25]

X-ray crystallographic studies

The intensity data were collected by using θ–2θ scans at a rate of 2° min^{-1} (in 2θ) for **1** and a rate of 4° min^{-1} for **2**. Table 1 lists crystal parameters and details of intensity collection and refinement. Complete tables of positional parameters, bond distances, bond angles, anisotropic thermal parameters, hydrogen atom parameters and structure factors for **1** and **2** are available as Supplementary Material.

A red crystal platelet of **1** (dimensions 0.11 × 0.30 × 0.50 mm) was mounted on a glass fibre in a random orientation. The cell parameters and orientation matrix were obtained from least-square refinement of 21 reflections in the range $15 < 2\theta < 20°$. The space group was determined to be $P2_1/c$. A total of 7767 reflections were collected, of which 7168 were unique and not systematically absent. Three standard reflections were measured every 93 reflections and indicated a decrease of intensity of 0.6%; a linear decay correction was applied. The structure was solved using the direct methods. The two molybdenum atoms were located from an E-map; the remaining atoms were located in succeeding difference Fourier syntheses. The non-hydrogen atoms were refined with anisotropic thermal parameters. The hydrogen atoms were included in the refinement but restrained to ride on the atom to which they are bonded. Anisotropic refinement was used to give $R = 0.044$ and $R_w = 0.046$. The largest shift-to-error was 0.01 σ, and the largest peak in the final difference map was 0.45(7) e Å^{-3}.

A clear red diamond shape crystal of **2** (dimensions 0.10 × 0.15 × 0.20 mm) was mounted on a fibre in a random orientation. The cell constants and orientation matrix were obtained from least-square refinement of 12 reflections in the range $15 < 2\theta < 20°$. From systematic absences and from refinement, the space group was determined to be

Table 1. Data for crystal structure analysis of $[Mo_2(\mu\text{-}S)_2(O)(S)(mnt)_2]^{2-}$ anion and $Mo_2(\mu\text{-}O)_2(O)_2(Cl)_2(dmbpy)_2$

	1	2
Formula	$Mo_2N_6OS_7C_{40}H_{72}$	$Mo_2Cl_2O_4N_4C_{24}H_{24}$
FW	1069.35	695.27
Crystal dimensions (mm)	$0.11 \times 0.30 \times 0.50$	$0.10 \times 0.15 \times 0.20$
Crystal system	monoclinic	trigonal
Space group	$P2_1/c$	$P3_121$
a (Å)	19.547(4)	16.135(4)
b (Å)	15.210(4)	16.135(4)
c (Å)	18.754(6)	10.709(3)
α (°)	90	90
β (°)	101.69(2)	90
γ (°)	90	120
V (Å^3)	5460(2)	2414.4(13)
Z	4	3
ρ_{calc} (g cm^{-3})	1.24	1.43
μ(Mo-K_α) (cm^{-1})	6.3	9.6
λ (Å)	Mo-K_α (0.71073)	Mo-K_α (0.71073)
Temperature (°C)	27(1)	25(1)
Scan method	θ–2θ	θ–2θ
Scan rate (deg min^{-1})	2	4
Number of unique data	7168	2109
Data used [$F_o^2 > 3\sigma(F_o^2)$]	4834	1243
Number of parameters refined	505	167
Min, max transmission factor	0.844, 0.935	0.877, 0.916
R^a	0.044	0.042
$R_w{}^b$	0.046	0.051
GOF^c	2.99	1.68

[a] $R = \Sigma||F_o|-|F_c||/\Sigma|F_o|$.
[b] $R_w = [\Sigma w(|F_o|-|F_c|)^2/\Sigma w|F_o|^2]^{1/2}$; $w = 1/\sigma^2(|F_o|)$.
[c] Goodness of fit $= [\Sigma w(|F_o|-|F_c|)^2/(N_{obsd}-N_{parameters})]^{1/2}$.

$P3_121$. A total of 9353 reflections were collected, of which 2109 were unique and not systematically absent. Three standard reflections were measured every 93 reflections and indicated an increase of intensity of 16.5%; an anisotropic decay correction was applied. The structure was solved by using the Patterson heavy-atom method, which revealed the positions of the molybdenum atoms. The remaining atoms were located in succeeding difference Fourier syntheses. The hydrogen atoms were included in the refinement to ride on the atom to which they are bonded. Complex **2** possesses a crystallographic two-fold axis that passes between the Mo(1), Mo(1)′ atoms; only half of the atoms are crystallographically unique. Anisotropic refinement was used to give $R = 0.042$ and $R_w = 0.051$. The largest shift-to-error was 0.01 σ, and the largest peak in the final difference map was 1.13(12) e Å^{-3}. The refinement performed in the enantiomorphic space group $P3_221$ is slightly inferior with $R = 0.043$, $R_w = 0.052$, and a largest shift-to-error of 0.02 σ. For these reasons we report the results of the refinement for the $P3_121$ enantiomorphic space group.

RESULTS AND DISCUSSION

A common precursor in the preparation of substituted molybdenum quadruple bonded metal–metal dimers is $Mo_2(O_2CCH_3)_4$. Successful synthetic methodologies using this compound have involved the use of Me_3SiCl to remove the acetate ligands.[26–28] However the reaction of Na_2mnt (disodium 1,2-dicyanoethylene-2,2-dithiolate) with $Mo_2(O_2CCH_3)_4$ in the presence of Me_3SiCl yields yet unidentified decomposition products. In the absence of Me_3SiCl, green and orange precipitates form. Elemental analysis and electronic absorption spectra of the green precipitate are identical to that of $[(C_4H_9)_4N]_2Mo(mnt)_3$.[29] The likely alternative product $[(C_4H_9)_4N]_2MoO(mnt)_3$ is not obtained as indicated by the absence of an Mo—O stretch at 930

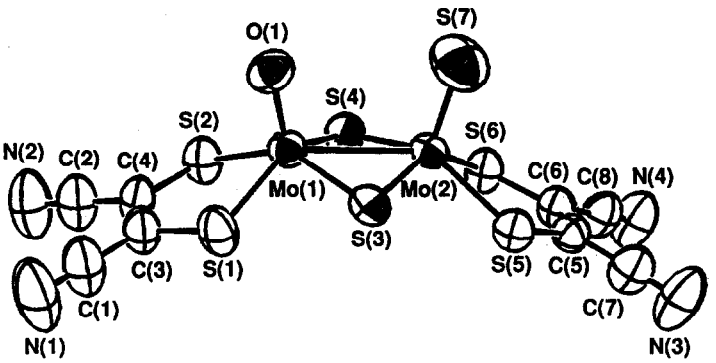

Fig. 1. ORTEP drawing and labelling scheme of $[Mo_2(\mu\text{-}S)_2(O)(S)(mnt)_2]^{2-}$ anion with 50% probability thermal ellipsoids.

cm^{-1}. Spectroscopic analysis of the orange precipitate clearly shows that a binuclear core is retained.

The IR spectrum supports a complex with a $[Mo_2(\mu\text{-}S)_2(O)(S)]^{2+}$ core. Absorptions at 955 and 530 cm^{-1} are characteristic of terminal Mo=O and Mo=S stretching vibrations, respectively.[30-32] A weak band at 340 cm^{-1} and a band at 470 cm^{-1} are assigned to the stretching vibration of di-μ-sulphido bridge, which typically appear with medium intensity in the ~350 and 450 cm^{-1} spectral region.[30] The presence of the mnt^{2-} ligand at the binuclear core is in evidence from the intense C≡N stretch at 2200 cm^{-1}.

The precise nature of the binuclear core ligation sphere was unequivocally determined by solving the X-ray crystal structure. Consistent with spectroscopic data, the molecular structure of **1**, represented by the ORTEP diagram shown in Fig. 1, is determined to be $[(C_4H_9)_4N]_2[Mo_2(\mu\text{-}S)_2(O)(S)(mnt)_2]$. The structure of the dianion displays features that are a composite of those reported by Gelder and Enemark for the symmetric $[Mo_2(\mu\text{-}S)_2(O)_2(i\text{-}mnt)_2]^2$ ion[33] and those observed for the more unusual asymmetric $[Mo_2(\mu\text{-}S)_2(O)(S)]^{2+}$ species.[32,34] The geometry about each of the molybdenum atoms in the $[Mo_2(\mu\text{-}S)_2(O)(S)(mnt)_2]^{2-}$ ion is best described as a distorted square pyramid formed by a terminal oxygen or sulphur atom at the apex and two bridging sulphur atoms and the two sulphur atoms from the mnt^{2-} ligands constituting the basal plane. The bases of the edge-sharing square pyramids are not coplanar but canted towards each other. The axial groups are *cis* to the two bridging ligands and assume a *syn* conformation.

Inspection of selected bond distances and angles listed in Table 2 reveals structural trends that parallel other *syn*-$[Mo_2(\mu\text{-}S)_2(X)(Y)]^{2+}$ (X, Y = O, S) structues. As shown by Tables 3, an $Mo^V\cdots Mo^V$ separation of 2.858(1) Å in **1** is typical of other $Mo^V\cdots Mo^V$ dimers and indicative of a single Mo—Mo bond. The formation of the single Mo—Mo bond in these cores is attributed to the interaction of the single electron occupancy of the d_{xy} orbitals on each molybdenum centre.[20,35] An average Mo—S_b—Mo (S_b = bridging sulphur) bond angle of 76.0°, a Mo—S_b bond distance of 2.321 Å, and a dihedral angle of 148.4° for the Mo_2S_2 unit are characteristic of $[Mo_2(\mu\text{-}S)_2(X)(Y)]^{2+}$ compounds (Table 4), as is the displacement of the Mo atoms 0.706 Å above the basal plane of the square pyramid.[18,32-34,36-39] Despite these similarities, it is noteworthy that the observed apical Mo=O_t = 1.757(5) Å and Mo=S_t = 1.948(3) Å distances are shorter than average Mo—O and Mo—S bond distances but consistent with those cores featuring electron withdrawing ancillary ligands. The good π-accepting properties of the mnt^{2-} ligand will reduce the electron density at the metal thereby enhancing the Mo—O and M—S π-donating interaction. This synergistic effect between the π-accepting and terminal π-donor ligands may well explain the short terminal bond distances.

The origins of the bridging sulphur and terminal sulphur and oxygen atoms have not been resolved. An unidentified intermediate could be oxidized with molecular oxygen to form the terminal oxygen bond. Yet when the reaction was performed under rigorously air-free conditions, $[Mo_2(\mu\text{-}S)_2(O)(S)(mnt)_2]^{2-}$ still formed, albeit in small yield. These results suggest that the oxygen may be delivered from the acetate ligand of the starting complex upon oxidation. Similarly, the bridging and terminal sulphur must come from the oxidation of the Na_2mnt ligand, as this is the only source of sulphur in the reaction. Solutions of $Mo(mnt)_3^{2-}$ and $[Mo_2(\mu\text{-}S)_2(O)(S)(mnt)_2]^{2-}$ do not interconvert under a variety of oxidizing and reducing conditions

Table 2. Selected bond distances (Å) and bond angles (°) for $[Mo_2(\mu\text{-}S)_2(O)(S)(mnt)_2]^{2-}$ anion. Numbers in parentheses are estimated standard deviations in the least significant digits

Distances			
Mo(1)—Mo(2)	2.858(1)	Mo(2)—S(3)	2.325(2)
Mo(1)—S(1)	2.423(2)	Mo(2)—S(4)	2.317(2)
Mo(1)—S(2)	2.430(3)	Mo(2)—S(5)	2.430(2)
Mo(1)—S(3)	2.325(2)	Mo(2)—S(6)	2.429(2)
Mo(1)—S(4)	2.316(2)	Mo(2)—S(7)	1.948(3)
Mo(1)—O(1)	1.757(5)		
Angles			
Mo(1)—Mo(2)—S(3)	52.08(5)	S(1)—Mo(1)—S(4)	142.08(8)
Mo(1)—Mo(2)—S(4)	51.89(5)	S(1)—Mo(1)—O(1)	106.7(2)
Mo(1)—Mo(2)—S(5)	128.46(6)	S(2)—Mo(1)—S(3)	145.56(7)
Mo(1)—Mo(2)—S(6)	127.84(6)	S(2)—Mo(1)—S(4)	78.11(7)
Mo(1)—Mo(2)—S(7)	104.1(1)	S(2)—Mo(1)—O(1)	104.2(2)
Mo(1)—S(1)—C(3)	105.6(3)	S(3)—Mo(1)—S(4)	100.48(7)
Mo(1)—S(2)—C(4)	105.6(3)	S(3)—Mo(1)—O(1)	108.5(2)
Mo(1)—S(3)—Mo(2)	75.83(6)	S(3)—Mo(2)—S(4)	100.42(7)
Mo(1)—S(4)—Mo(2)	76.17(6)	S(3)—Mo(2)—S(5)	78.37(7)
Mo(2)—Mo(1)—S(1)	127.95(6)	S(3)—Mo(2)—S(6)	142.25(7)
Mo(2)—Mo(1)—S(2)	128.14(5)	S(3)—Mo(2)—S(7)	111.7(1)
Mo(2)—Mo(1)—S(3)	52.09(5)	S(4)—Mo(1)—O(1)	109.3(2)
Mo(2)—Mo(1)—S(4)	51.94(6)	S(4)—Mo(2)—S(5)	145.35(7)
Mo(2)—Mo(1)—O(1)	104.6(2)	S(4)—Mo(2)—S(6)	78.83(7)
Mo(2)—S(5)—C(5)	105.7(3)	S(4)—Mo(2)—S(7)	105.5(1)
Mo(2)—S(6)—C(6)	105.6(2)	S(5)—Mo(2)—S(6)	81.68(7)
S(1)—Mo(1)—S(2)	81.90(8)	S(5)—Mo(2)—S(7)	107.0(1)
S(1)—Mo(1)—S(3)	78.81(7)	S(6)—Mo(2)—S(7)	104.7(1)

and, therefore, it is unlikely that they are produced along a concerted reaction pathway.

The susceptibility of the $Mo_2^{(II,II)}$ core towards oxidation when coordinated by good π-accepting cores is further in evidence from the chemistry of $Mo_2Cl_4(dmbpy)_2$, which exhibits greater solubility than its previously prepared bipyridine counterpart. Refluxing *o*-dichlorobenzene solutions of $Mo_2Cl_4(dmbpy)_2$ yields $Mo_2(\mu\text{-}O)_2(O)_2(Cl)_2(dmbpy)_2$, as determined by X-ray crystallography. The ORTEP diagram of **2**, shown in Fig. 2, closely parallels that of $Mo_2(\mu\text{-}O)_2(O)_2(Cl)_2(bpy)_2$,[40] which was prepared from $MoCl_4(bpy)$ monomers. These compounds exhibit

Table 3. Relevant bond distances (Å) for selected complexes with $[Mo_2(\mu\text{-}S)_2(Y)(Y')]^{2+}$ (Y,Y′ = O,O; S,S; O,S) cores. Bridging sulphur is designated by S_b and terminal oxygen and sulphur atoms by O_t and S_t, respectively

$[Mo_2(\mu\text{-}S)_2(Y)(Y')]^{2+}$	Mo—Mo	Mo=O_t	Mo—S_b	Mo=S_t	Mo displacement above basal plane	Ref.
$[Mo_2(\mu\text{-}S)_2(O)(S)(mnt)_2]^{2-}$	2.858(1)	1.757(5)	2.321	1.948(3)	0.706	this work
$[Mo_2(\mu\text{-}S)_2(O)(S)(dtc)_2]^{2-}$	2.826(3)	1.82(2)	2.317	1.98(1)	0.7	32
$[Mo_2(\mu\text{-}S)_2(O)_2(i\text{-}mnt)_2]^{2-}$	2.821(2)	1.664(7)	2.300(4)		0.72	33
$[(\eta^2\text{-}S_2)MoO(\mu\text{-}S)_2MoS(S_4)]^{2-}$	2.850(1)	2.014(5)	2.350	1.862(7)		34
$[Mo_2(\mu\text{-}S)_2(O)_2(SC_2H_4S)]^{2-}$	2.866(3)	1.659(3)	2.341(9)			36
syn-$[Mo_2(\mu\text{-}S)_2(S)_2(SC_2H_4S)_2]^{2-}$	2.855(1)		2.515(2)	2.103(2)		36
$[Mo_2(\mu\text{-}S)_2(O)(S)(S_2)_2]^{2-}$	2.811(1)	1.945(6)	2.314	1.986(6)	0.783	37
$[(\eta^2\text{-}S_2)MoS(\mu\text{-}S)_2MoS(S_4)]^{2-}$	2.3837(1)		2.32(2)	2.110(2)	0.74(2)	38

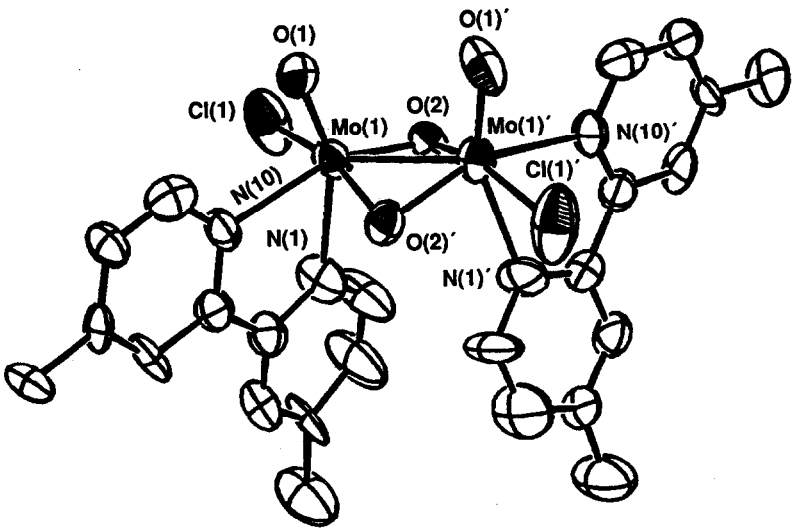

Fig. 2. ORTEP illustration and labelling scheme of the structure of $Mo_2(\mu\text{-}O)_2(O)_2(Cl)_2(dmbpy)_2$ with 50% probability thermal ellipsoids. For clarity hydrogen atoms are not shown.

Table 4. Relevant bond angles (°) for selected complexes with $[Mo_2(\mu\text{-}S)_2(Y)(Y')]^{2+}$ (Y,Y′ = O,O; S,S; O,S) cores. Bridging sulphur is designated by S_b

$[Mo_2(\mu\text{-}S)_2(Y)(Y')]^{2+}$	Mo—S_b—Mo	S_b—Mo—S_b	Dihedral angle of $Mo(S_b)_2$ plane	Ref.
$[Mo_2(\mu\text{-}S)_2(O)(S)(mnt)_2]^{2-}$	76.0	100.45	148.4	this work
$[Mo_2(\mu\text{-}S)_2(O)(S)(dtc)_2]^{2-}$	75.2	101.6	149.4	32
$[Mo_2(\mu\text{-}S)_2(O)_2(i\text{-}mnt)_2]^{2-}$	75.8(1)	101.6(1)	153.1	33
$[(\eta^2\text{-}S_2)MoO(\mu\text{-}S)_2MoS(S_4)]^{2-}$	75.6(1)			34
$[Mo_2(\mu\text{-}S)_2(O)_2(SC_2H_4S)]^{2-}$	75.5(4)	100.5(4)	144.5	36
syn-$[Mo_2(\mu\text{-}S)_2(S)_2(SC_2H_4S)_2]^{2-}$	76.2(1)	100.6(1)	147.2	36
$[Mo_2(\mu\text{-}S)_2(O)(S)(S_2)_2]^{2-}$	74.8(1)	102.45		37
$[(\eta^2\text{-}S_2)MoS(\mu\text{-}S)_2MoS(S_4)]^{2-}$	75.5(1)	102.1(4)	153.2(2)	38

Table 5. Selected bond distances (Å) and bond angles (°) for $Mo_2(\mu\text{-}O)_2(O)_2(Cl)_2(dmbpy)_2$. Atoms designated by the prime (′) symbol are at Y, X, −Z. Numbers in parentheses are estimated standard deviations in the least significant digits

Distances			
Mo(1)—Mo(1)′	2.562(2)	Mo(1)—Cl(1)	2.451(4)
Mo(1)—O(1)	1.682(7)	Mo(1)—N(1)	2.284(8)
Mo(1)—O(2)	1.921(10)	Mo(1)—N(10)	2.253(12)
Mo(1)—O(2)′	1.937(8)		
Angles			
Mo(1)′—Mo(1)—Cl(1)	135.1(1)	Cl(1)—Mo(1)—N(10)	92.7(3)
Mo(1)′—Mo(1)—O(1)	100.5(4)	O(1)—Mo(1)—O(2)	112.9(4)
Mo(1)′—Mo(1)—O(2)	48.7(2)	O(1)—Mo(1)—O(2)′	105.4(4)
Mo(1)′—Mo(1)—O(2)′	48.1(3)	O(1)—Mo(1)—N(1)	155.8(5)
Mo(1)′—Mo(1)—N(1)	102.5(3)	O(1)—Mo(1)—N(10)	89.3(4)
Mo(1)′—Mo(1)—N(10)	130.3(3)	O(2)—Mo(1)—O(2)′	91.7(4)
Mo(1)—O(2)—Mo(1)′	83.2(4)	O(2)—Mo(1)—N(1)	88.1(4)
Cl(1)—Mo(1)—O(1)	90.7(4)	O(2)—Mo(1)—N(10)	157.8(3)
Cl(1)—Mo(1)—O(2)	86.8(3)	O(2)′—Mo(1)—N(1)	84.9(4)
Cl(1)—Mo(1)—O(2)′	163.0(2)	O(2)′—Mo(1)—N(10)	82.2(4)
Cl(1)—Mo(1)—N(1)	78.2(3)	N(1)—Mo(1)—N(10)	70.1(4)

an $[Mo_2(\mu\text{-}O)_2(O)_2(Cl)_2]$ core with a bipyridyl ligand chelating each molybdenum centre. The bond lengths and bond angles for **2** listed in Table 5 compare favourably to those reported for $Mo_2(\mu\text{-}O)_2(O)_2(Cl)_2(bpy)_2$ and the related compound $Mo_2(\mu\text{-}O)_2(O)_2(OPH_2O)_2(bpy)_2$.[41] The strong interaction of the Mo atoms with the terminal oxo ligands is manifested in a pronounced *trans* influence with the Mo—N distances *cis* to the Mo=O_t functionality 0.031 Å shorter than of the *trans* Mo—N distance. The Mo=O_t stretching vibration for **2** appears at 965 cm^{-1} in the IR, and the antisymmetric and symmetric stretching vibrations of the $Mo_2(\mu\text{-}O)_2$ unit are observed at 760 and 440 cm^{-1}, respectively.[42,43] The Mo—Mo bond distances in these compounds are short [d(Mo—Mo) = 2.562(2) Å in **2**, d(Mo—Mo) = 2.565(1) in $Mo_2(\mu\text{-}O)_2(O)_2(Cl)_2(bpy)_2$, and d(Mo—Mo) = 2.554(3) in $Mo_2(\mu\text{-}O)_2(O)_2(OPH_2O)_2(bpy)_2$] and, as is the case for **1**, they are indicative of a Mo—Mo single bond resulting from a d^1—d^1 interaction.[20,35]

There has been significant interest in the role of monomeric and dimeric Mo^V centres coordinated to oxygen and sulphur at the redox-active sites of enzymes.[19,44] The $[Mo_2(\mu\text{-}X)_2(Y)(Y')]^{2+}$ (X = O or S; Y,Y′ = O,O; S,S; O,S) dimeric compounds have frequently been observed as products of reactions directed towards the synthesis of Mo^V model compounds of oxomolybdenum enzymes. Most synthetic strategies involved with the preparation of these compounds have relied on assembling molybdenum monomers in oxidizing environments. Such an approach can be problematic in view of the preponderance of different side reactions competing with dimer formation. In this respect a synthetic design using molybdenum quadruple bond dimers as starting reagents is useful because the bimetallic core acts as a template for the conversion to $[Mo_2(\mu\text{-}X)_2(Y)(Y')]^{2+}$ cores.

Acknowledgements—This work was supported in part by the National Science Foundation (CHE-9100532). D.G.N. is a Presidential Young Investigator Award and Alfred P. Sloan Fellow.

REFERENCES

1. (a) F. A. Cotton, *Polyhedron* 1987, **6**, 667; (b) F. A. Cotton, in *Understanding Molecular Properties* (Edited by J. Avery, J. P. Dahl and A. E. Hansen), p. 17. Reidel, Boston (1987).
2. S. T. Chacon, M. H. Chisholm, W. E. Streib and W. Van Der Sluys, *Inorg. Chem.* 1989, **28**, 5.
3. F. A. Cotton and R. A. Walton, *Multiple Bonds Between Metal Atoms*. Wiley-Interscience, New York (1982).
4. R. A. Walton, *Isr. J. Chem.* 1985, **25**, 196.
5. D. G. Nocera and H. B. Gray, *Inorg. Chem.* 1984, **23**, 3686.
6. (a) C. M. Partigianoni and D. G. Nocera, *Inorg. Chem.* 1990, **29**, 2033; (b) C. M. Partigianoni, I.-J. Chang and D. G. Nocera, *Coord. Chem. Rev.* 1990, **97**, 105.
7. (a) S. Shaik, R. Hoffmann, C. R. Fisel and R. H. Summerville, *J. Am. Chem. Soc.* 1980, **102**, 4555; (b) R. H. Summerville and R. Hoffmann, *J. Am. Chem. Soc.* 1979, **101**, 3821.
8. K. J. Moynihan, X. Gao, P. M. Boorman, J. F. Fait, G. K. W. Freeman, P. Thornton and D. J. Ironmonger, *Inorg. Chem.* 1990, **29**, 1648.
9. S. G. Bott, D. L. Clark, M. L. H. Green and P. Mountford, *J. Chem. Soc., Chem. Commun.* 1989, 418.
10. (a) F. A. Cotton and R. L. Luck, *Inorg. Chem.* 1989, **28**, 182; (b) F. A. Cotton and R. Poli, *Inorg. Chem.* 1987, **26**, 3310.
11. D. J. Bergs, M. H. Chisholm, K. Folting, J. C. Huffman and K. A. Stahl, *Inorg. Chem.* 1988, **27**, 2950.
12. F. A. Cotton, J. L. Eglin, R. L. Luck and K. Son, *Inorg. Chem.* 1990, **29**, 1802.
13. H. D. Mui and R. Poli, *Inorg. Chem.* 1989, **28**, 3609.
14. R. R. Schrock, L. G. Sturgeoff and P. R. Sharp, *Inorg. Chem.* 1983, **22**, 2801.
15. (a) A. R. Chakravarty, F. A. Cotton, A. R. Cutler, S. M. Tetrick and R. A. Walton, *J. Am. Chem. Soc.* 1985, **107**, 4795; (b) A. R. Chakravarty, F. A. Cotton, A. R. Cutler and R. A. Walton, *Inorg. Chem.* 1986, **25**, 3619.
16. M. H. Chisholm, J. C. Huffman and W. G. Van Der Sluys, *J. Am. Chem. Soc.* 1987, **109**, 2514.
17. I. Ara, P. E. Fanwick and R. A. Walton, *J. Am. Chem. Soc.* 1991, **113**, 1429.
18. C. D. Garner and J. M. Charnock, in *Comprehensive Coordination Chemistry* (Edited by G. Wilkinson, R. Gillard and J. A. McCleverty), Vol. 3, Chap. 36.4, p. 1329. Pergamon Press, Oxford (1987).
19. C. D. Garner and S. Bristow, in *Molybdenum Enzymes* (Edited by T. G. Spiro), p. 343. Wiley, New York (1985).
20. E. I. Stiefel, *Prog. Inorg. Chem.* 1977, **22**, 1.
21. J. V. Brencic and F. A. Cotton, *Inorg. Chem.* 1970, **9**, 436.
22. A. Davison and R. H. Holm, *Inorg. Synth.* 1967, **10**, 11.
23. D. Lanton and R. Mason, *J. Am. Chem. Soc.* 1965, **87**, 921.
24. J. San Filippo Jr, H. J. Sniadoch and R. L. Grayson, *Inorg. Chem.* 1974, **13**, 2121.
25. B. A. Frenz, in *Computing in Crystallography* (Edited by H. Schenk, R. Olthof-Hazelkamp, H. Vankonigsveld and G. C. Bassi), p. 64. Delft University Press, Holland (1978).
26. (a) R. E. McCarley, T. R. Ryan, C. C. Torardi, in *Reactivity of Metal–Metal Bonds* (Edited by M. H. Chisholm), ACS Symp. Ser. No. 155, p. 41. American Chemical Society, Washington DC (1981); (b) T. R. Ryan and R. E. McCarley, *Inorg. Chem.* 1982, **21**, 2072.
27. J. D. Arenivar, V. V. Mainz, H. Rubin, R. A. Andersen and A. Zalkin, *Inorg. Chem.* 1982, **21**, 2649.
28. M. L. H. Green, G. Parkin, J. Bashkin, K. Prout, *J. Chem. Soc., Dalton Trans.* 1982, 2519.
29. E. I. Stiefel, L. E. Bennett, Z. Dori, T. H. Crawford, C. Simo and H. B. Gray, *Inorg. Chem.* 1970, **9**, 281.

30. (a) N. Ueyama, N. Nakata, T. Araki, A. Nakamura, S. Yamashita and T. Yamashita, *Chem. Lett.* 1979, 421; (b) N. Ueyama, M. Nakata, T. Araki, A. Nakamura, S. Yamashita and T. Yamashita, *Inorg. Chem.* 1981, **20**, 1934.
31. G. J.-J. Chen, J. W. McDonald, D. C. Bravard and W. E. Newton, *Inorg. Chem.* 1985, **24**, 2327.
32. W. E. Newton, J. W. McDonald, K. Yamanouchi and J. H. Enemark, *Inorg. Chem.* 1979, **18**, 1621.
33. J. I. Gelder and J. H. Enemark, *Inorg. Chem.* 1976, **15**, 1839.
34. X. Xin, N. L. Morris, G. B. Jameson and M. T. Pope, *Inorg. Chem.* 1985, **24**, 3482.
35. K. Wieghardt, M. Hahn, W. Swiridoff and J. Weiss, *Angew. Chem., Int. Edn Engl.* 1983, **22**, 491.
36. T.-C. Hsieh, K. Gebreyes and J. Zubieta, *Trans. Met. Chem.* 1985, **10**, 84.
37. D. Coucouvanis and S.-M. Koo, *Inorg. Chem.* 1989, **28**, 2.
38. W. Clegg, G. Christou, C. D. Garner and G. M. Sheldrick, *Inorg. Chem.* 1981, **20**, 1562.
39. F. A. Cotton, R. L. Luck and C. S. Miertschin, *Inorg. Chem.* 1991, **30**, 1155.
40. J. Beck, W. Hiller, E. Schweda and J. Strahle, *Z. Naturforsch.* 1984, **39b**, 1110.
41. B. M. Gatehouse and E. K. Nunn, *Acta Cryst. B* 1976, **32**, 2627.
42. P. C. H. Mitchell, *J. Inorg. Nucl. Chem.* 1963, **25**, 963.
43. H. K. Saha and M. C. Halder, *J. Inorg. Nucl. Chem.* 1971, **33**, 3719.
44. C. D. Garner, in *Comprehensive Coordination Chemistry* (Edited by G. Wilkinson, R. Gillard and J. A. McCleverty), Vol. 3, Chap. 36.6, p. 1421. Pergamon Press, Oxford (1987).

Polyhedron Vol. 10, No. 23/24, pp. 2821–2825, 1991
Printed in Great Britain

0277–5387/91 $3.00+.00
© 1991 Pergamon Press plc

A NOVEL ROUTE FOR THE SYNTHESIS OF DITHIOCARBAMATE AND XANTHATE NICKEL(II) COMPLEXES STARTING FROM THE DI-μ-HYDROXO-BIS[BIS(PENTAFLUOROPHENYL)NICKELATE(II)] ION

G. LÓPEZ,* G. SÁNCHEZ, G. GARCÍA, J. GARCÍA, A. SANMARTÍN and M. D. SANTANA

Departamento de Química Inorgánica, Universidad de Murcia, 30071 Murcia, Spain

(*Received* 21 *May* 1991; *accepted* 2 *July* 1991)

Abstract—In dichloromethane, $[NBu_4]_2[\{Ni(C_6F_5)_2(\mu\text{-}OH)\}_2]$ reacts with amines [$EtNH_2$, $PrNH_2$, Me_2NH, Et_2NH, pirrolidine (C_4H_8NH), piperidine ($C_5H_{10}NH$) and morpholine (C_4H_8ONH)] or alcohols (MeOH and EtOH) in the presence of carbon disulphide to give the corresponding dithiocarbamate or xanthate complexes $[NBu_4][(C_6F_5)_2Ni(S_2C\text{-}X)]$ [X = NHEt (**1**), NHPr (**2**), NMe_2 (**3**), NEt_2 (**4**), NC_4H_8 (**5**), NC_5H_{10} (**6**), NC_4H_8O (**7**), OMe (**8**) or OEt (**9**)]. In the same solvent, the reaction of the hydroxo-nickel complex with carbon disulphide and $[NBu_4]OH$ leads to the formation of the dithiocarbonate complex $[NBu_4]_2[(C_6F_5)_2Ni(S_2CO)]$ (**10**). The new complexes are air-stable, orange solids which have been studied by conductance measurements and spectroscopic (IR, V–UV, ^1H- and ^{19}F-NMR) methods.

Transition-metal complexes in which a 1,1-dithio ligand forms a four-membered ring with the metal ion have been extensively studied and thoroughly reviewed.[1–4] The general synthetic method for the preparation of these complexes involves the reaction of a transition-metal halocomplex with the alkali metal salt of the corresponding thioacid (eq. 1),

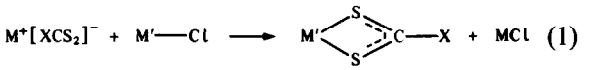

(1)

and the alkali salt is available from the reaction between the amine or alcohol and carbon disulphide in the presence of alkali hydroxide (eq. 2):

$$CS_2 + HX + MOH \longrightarrow M^+[XCS_2]^- + H_2O. \quad (2)$$

On the other hand, the synthesis of the binuclear anionic complexes $[\{M(C_6F_5)_2(\mu\text{-}OH)\}_2]^{2-}$ (M = Ni, Pd or Pt)[5] have been reported recently. These hydroxo complexes react with weak, protic electrophiles H(LL) to give $[\{MR_2(\mu\text{-}LL)\}_2]^{2-}$ or $[MR_2(LL)]^-$ complexes depending on the nature of the $(LL)^-$ ligand (pyrazolate- or beta-diketonate-type ligand respectively).[6] Following our investigations on these hydroxo complexes, we have now found that organometallic dithiocarbamate- and xanthate-nickel(II) complexes can be prepared by reaction of the hydroxo complex $[\{Ni(C_6F_5)_2(\mu\text{-}OH)\}_2]^{2-}$ with amines or alcohols, respectively, in the presence of carbon disulphide.

EXPERIMENTAL

Physical measurements and materials

C, H and N analyses were carried out with a Perkin–Elmer 240 C microanalyser. Melting points were determined on a Reichert microscope. Molar conductivities were measured in acetone solution (conc. $\approx 5 \times 10^{-4}$ M) with a Crison 525 conductimeter. The spectroscopic instruments used were Perkin–Elmer 1430 for IR spectra (Nujol mulls), Hitachi 2000U for UV–vis spectra and Bruker AC 200E (^1H) or Varian FT 80A (^{19}F) for NMR spectra. $SiMe_4$ and $CFCl_3$ were used as internal standards, respectively.

The precursor $[NBu_4]_2[\{Ni(C_6F_5)_2(\mu\text{-}OH)\}_2]$ was prepared as described elsewhere.[5] Solvents were dried by standard methods before use.

* Author to whom correspondence should be addressed.

Synthesis

Dithiocarbamate complexes (**1–7**). In separate experiments, the stoichiometric amount (0.23 mmol) of the corresponding amine was added to a solution of $[NBu_4]_2[\{Ni(C_6F_5)_2(\mu\text{-}OH)\}_2]$ (0.15 g, 0.115 mmol) in dichloromethane (10 cm^3) and carbon disulphide (0.14 cm^3, 0.23 mmol). The solution was stirred at room temperature for 30 min, then concentrated under reduced pressure to half the original volume. Addition of diethyl ether resulted in the precipitation of the expected organo complex as an orange solid which was filtered off, washed with diethyl ether and dried in the air. The compounds were recrystallized from dichloromethane–diethyl ether.

Xanthate complexes (**8**, **9**). Carbon disulphide (1 cm^3) was added to an alcohol (MeOH or EtOH) solution (5 cm^3) containing $[NBu_4]_2[\{Ni(C_6F_5)_2(\mu\text{-}OH)\}_2]$ (0.15 g, 0.115 mmol). The mixture was stirred at room temperature for 1 h, and the solvent was removed *in vacuo*. The residue was extracted with alcohol (MeOH or EtOH) and the addition of water caused the precipitation of an orange–brown solid, which was filtered off, washed with water and dried *in vacuo*.

$[NBu_4]_2[Ni(C_6F_5)_2(S_2CO)]$ (**10**). Carbon disulphide (0.14 cm^3, 0.23 mmol) was added to a mixture of $[NBu_4]_2[\{Ni(C_6F_5)_2(\mu\text{-}OH)\}_2]$ (0.15 g, 0.115 mmol) and $[NBu_4]OH$ (0.30 cm^3 of 20% aqueous solution, 0.23 mmol) in dichloromethane (10 cm^3). The mixture was stirred at room temperature for 1 h, and the solvent was removed *in vacuo*. The resulting solid was treated with 5 cm^3 of dichloromethane and the addition of diethyl ether led to precipitation of an orange solid, which was filtered off, washed with diethyl ether and dried *in vacuo*.

The analytical data and individual yields of the complexes are presented in Table 1.

RESULTS AND DISCUSSION

Previous use[5,7] of the nickel complex $[\{Ni(C_6F_5)_2(\mu\text{-}OH)\}_2]^{2-}$ as a precursor in synthetic work was based on the considerable nucleophilicity of the OH bridges, which is consistent with the high-field proton resonance observed at δ −5.7. In dichloromethane, $[NBu_4]_2[\{Ni(C_6F_5)_2(\mu\text{-}OH)\}_2]$ reacts with amines in the presence of carbon disulphide to give the respective dithiocarbamate complexes **1–7**, according to eq. (3).

$$[NBu_4]_2[\{Ni(C_6F_5)_2(\mu\text{-}OH)\}_2] + 2HX + 2CS_2 \longrightarrow 2[NBu_4]\left[\begin{array}{c} C_6F_5 \\ Ni \\ C_6F_5 \end{array}\right.\!\!\begin{array}{c} S \\ \diagup\!\diagdown \\ S \end{array}\!\!\left.\begin{array}{c} \\ C\!-\!X \\ \end{array}\right] + 2H_2O \quad (3)$$

[X = NHEt (**1**), NHPr (**2**), NMe_2 (**3**), NEt_2 (**4**), NC_4H_8 (**5**), NC_5H_{10} (**6**) or NC_4H_8O (**7**)]

Table 1. Analytical data, yields, decomposition temperatures and molar conductivities for the nickel complexes

Complex	Yield (%)	Analysis [Found (calc.) %] C	H	N	Decomposition temperature (°C)	Λ_M[a]
(**1**) $[NBu_4][Ni(C_6F_5)_2(S_2C\text{-}NHEt)]$	72	49.1 (49.3)	5.7 (5.6)	3.6 (3.7)	147	95
(**2**) $[NBu_4][Ni(C_6F_5)_2(S_2C\text{-}NHPr)]$	77	50.1 (49.9)	5.9 (5.8)	4.0 (3.7)	161	90
(**3**) $[NBu_4][Ni(C_6F_5)_2(S_2C\text{-}NMe_2)]$	71	49.0 (49.3)	5.8 (5.6)	4.0 (3.7)	185	98
(**4**) $[NBu_4][Ni(C_6F_5)_2(S_2C\text{-}NEt_2)]$	75	50.4 (50.6)	6.1 (5.9)	3.6 (3.6)	125	104
(**5**) $[NBu_4][Ni(C_6F_5)_2(S_2C\text{-}NC_4H_8)]$	73	50.3 (50.6)	5.9 (5.6)	4.0 (3.5)	138	94
(**6**) $[NBu_4][Ni(C_6F_5)_2(S_2C\text{-}NC_5H_{10})]$	70	51.1 (51.3)	5.7 (5.8)	3.7 (3.5)	170	99
(**7**) $[NBu_4][Ni(C_6F_5)_2(S_2C\text{-}NC_4H_8O)]$	83	49.8 (49.7)	5.4 (5.6)	3.6 (3.5)	143	94
(**8**) $[NBu_4][Ni(C_6F_5)_2(S_2C\text{-}OMe)]$	86	48.7 (48.5)	5.4 (5.3)	1.9 (1.9)	62	98
(**9**) $[NBu_4][Ni(C_6F_5)_2(S_2C\text{-}OEt)]$	72	49.5 (49.2)	5.6 (5.5)	1.9 (1.9)	87	102
(**10**) $[NBu_4][Ni(C_6F_5)_2(S_2CO)]$	78	55.9 (55.7)	7.5 (7.5)	2.3 (2.9)	121	180

[a] $Ohm^{-1}\,cm^2\,mol^{-1}$ (in acetone solution, conc. $\approx 5\times10^{-4}$ M).

Formally, the hydroxo-nickel complex acts here as the proton acceptor initiating the formation of the dithiocarbamate ion and providing the metal substrate (the $Ni(C_6F_5)_2$ moiety) which is trapped by the 1,1-dithio ligand to form the dithiocarbamate nickel complex.

Similarly, the reaction of the hydroxo-nickel complex with alcohols and carbon disulphide proceeds with the formation of the corresponding xanthate complexes, as represented by eq. (4).

$$[NBu_4]_2[\{Ni(C_6F_5)_2(\mu\text{-}OH)\}_2] + 2ROH + 2CS_2 \longrightarrow$$

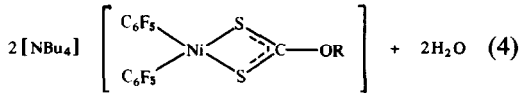

[X = Me (**8**) or Et (**9**)]

However, the reaction of the hydroxo complex with carbon disulphide in the presence of $[NBu_4]OH$ affords a dithiocarbonate complex (eq. 5).

$$[NBu_4]_2[\{Ni(C_6F_5)_2(\mu\text{-}OH)\}_2] + 2CS_2 + 2[NBu_4]OH \longrightarrow$$

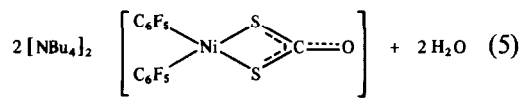

The new pentafluorophenyl–nickel derivatives are air-stable, orange solids and their acetone solutions exhibit conductance values (Table 1) corresponding to 1:1 (dithiocarbamate and xanthate complexes) or 2:1 (dithiocarbonate complex) electrolytes.[8] The IR spectra show the absorptions attributed to the C_6F_5 group[9] at *ca* 1630 m, 1490 vs, 1050 s and 950 vs cm^{-1}, as well as a broad or split band at 780 cm^{-1} for the so-called X-sensitive mode of C_6F_5 which is characteristic of the *cis*-$M(C_6F_5)_2$ fragment.[10]

The most relevant absorption bands in the IR spectra of the dithiocarbamate complexes and their tentative assignments[11–15] are presented in Table 2. The thioureide band near 1500 cm^{-1} indicates considerable double-bond character in the C⋯N bond; this behaviour may be attributed to the electron-releasing ability of the amines, which forces high electron density towards the sulphur atoms, via the π system, thus producing greater double-bond character in the carbon–nitrogen bond, and shifting ν(C⋯N) to higher energy [ν(C=N) = 1690–1640 cm^{-1}; ν(C—N) = 1350–1250 cm^{-1}].[16] This effect should be favoured by the high electronegativity of the C_6F_5 ligands. The band in the 995–970 cm^{-1} region is attributed to the stretching vibration of the C⋯S bonds. The presence of only one band in this region supports the bidentate coordination of the dithio ligand,[17,18] as represented by structure I.

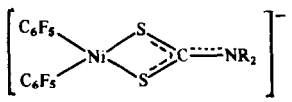

I

Table 2. IR and V–UV data

Complex	IR (cm^{-1})				Electronic spectra (cm^{-1}) (ε_{max})[a]
	ν(N—H)	ν(C⋯N)	ν(C⋯S)	ν(Ni—S)	
(1)	3210m	1520s	970m	340m	21,440 (330)
(2)	3230m	1525s	970m	335m	21,460 (390)
(3)		1545s	980m	360m	21,720 (377)
(4)		1495sh	990m	325m	21,700 (405)
(5)		1500sh	995m	340m	21,480 (399)
(6)		1500sh	995m	340m	21,620 (422)
(7)		1495sh	990m	340m	21,900 (376)
	ν(COC)	ν(CO)	ν(CS)	ν(Ni—S)	
(8)	1235s	1165s	1040s	350	overlapped
(9)	1235s	1125s	1035s	335	overlapped
	$2\nu_{as}$(CS) overtone	ν(CO)	ν_{as}(CS)	ν(Ni—S)	
(10)	1700m	1565vs	850s	380m, 315m	22,800 (448)

[a] Mol^{-1} dm^3 cm^{-1} (in acetone solution).

Table 3. ^1H and ^{19}F NMR data[a]

Complex	^1H, δ (ppm) ($SiMe_4$)[b]	^{19}F (δ/ppm) ($CFCl_3$) F_o	F_p	F_m
(1)	1.16 (t, 3H, CH_3) 3.46 (m, 2H, CH_2)[c] 8.64 (s, 1H, NH)	−112.6	−166.3	−167.2
(2)	0.89 (t, 6H, CH_3) 1.60 (m, 4H, CH_2) 3.34 (m, 4H, NCH_2) 8.68 (s, 1H, NH)	−112.5	−166.2	−167.4
(3)	3.13 (s, 6H, CH_3)	−112.6	−166.3	−167.5
(4)	1.16 (t, 6H, CH_3) 3.63 (q, 4H, CH_2)	−112.5	−166.3	−167.5
(5)	1.97 (m, 4H, CH_2)[c] 3.48 (m, 4H, NCH_2)[c]	−112.5	−166.4	−167.5
(6)	1.57 [m, 6H, $(CH_2)_3$] 3.70 (m, 4H, NCH_2)	−112.5	−166.4	−167.5
(7)	3.62–3.77 (m, 8H)	−112.7	−166.1	−167.4
(8)	4.02 (s, 3H)	−113.3	−165.2	−166.9
(9)	1.36 (t, 3H, CH_3) 4.47 (q, 2H, CH_2)	−113.3	−165.3	−166.9
(10)		−110.5	−168.4	

[a] In $(CD_3)_2CO$.

[b] Additional peaks of $[NBu_4]^+$ are found at δ *ca* 3.7 (t, N—CH_2), 1.8 (m, N—CH_2—CH_2), 1.5 (m, CH_2—CH_3) and 1.0 (t, CH_3), the relative intensities being 8 : 8 : 8 : 12.

[c] Partly overlapped with the peaks of the tetrabutylammonium cation.

The mono-ethyl and -propyl dithiocarbamate derivatives give an additional band in the 3200 cm^{-1} region, due the N—H stretching mode.

The methyl and ethyl xanthate complexes exhibit three IR bands in the 1235–1080 cm^{-1} region (Table 2) which are related to the vibrations of the S_2COR group.[19–22] They are highly coupled and, according to the normal coordinate analysis of $Ni(S_2COEt)_2$,[23] the 1230 cm^{-1} band has a substantial contribution from C—O—C stretching, the band around 1150 cm^{-1} is mainly a contribution of the ν(C—O) mode, and the band around 1050 cm^{-1} is entirely ν(C=S). The ν(Ni—S) mode is assigned to a band located at 350–335 cm^{-1}.

The IR spectrum of the dithiocarbonate complex (Table 2) is consistent with the presence of the bidentate S_2CO group.[19–24] According to Burke and Fackler[24] the band at 1700 cm^{-1} is thought to be due to the first overtone of the carbon–sulphur antisymmetric stretching mode.

The ^1H- and ^{19}F-NMR data for the complexes isolated are listed in Table 3. The ^1H spectra show the expected patterns for the S_2CNHR, S_2CNR_2 or S_2COR ligands. The ^{19}F spectra exhibit the three signals (intensity ratio 4 : 2 : 4) corresponding to the *ortho-*, *para-* and *meta-*F atoms of two equivalent C_6F_5 rings, which supports the assignment of bidentate 1,1-dithio ligand. All the complexes give an absorption band in their electronic spectra (Table 2) which is assigned to the $^1A_{1g} \rightarrow {}^1A_{2g}$ transition in a square-planar ligand field.

Acknowledgements—Financial assistance from the DGICYT (project PB87-0690), Spain, and a grant (to J.G.) from the Dirección Regional de Educación y Universidad, Murcia, are acknowledged.

REFERENCES

1. D. Coucouvanis, *Prog. Inorg. Chem.* 1970, **11**, 233.
2. D. Coucouvanis, *Prog. Inorg. Chem.* 1979, **26**, 301.
3. R. Eisenberg, *Prog. Inorg. Chem.* 1970, **12**, 295.

4. A. M. Bond and R. L. Martin, *Coord. Chem. Rev.* 1984, **54**, 23.
5. G. López, G. García, J. Ruiz, G. Sánchez, J. García and C. Vicente, *J. Chem. Soc., Chem. Commun.* 1989, 1045.
6. G. López, J. Ruiz, G. García, C. Vicente, J. Casabó, E. Molins and C. Miravitlles, *Inorg. Chem.* 1991, **30**, 2605.
7. G. López, G. Sánchez, G. García, J. Ruiz, J. García, M. Martínez-Ripoll, A. Vegas and J. A. Hermoso, *Angew. Chem., Int. Edn Engl.* 1991, **30**, 716.
8. W. J. Geary, *Coord. Chem. Rev.* 1971, **7**, 81.
9. D. A. Long and D. Steele, *Spectrochim. Acta* 1963, 1955.
10. G. López, G. García, C. de Haro, G. Sánchez and M. C. Vallejo, *J. Organomet. Chem.* 1984, **263**, 247.
11. R. Vicente, A. Escuer, J. Ribas, A. Dei, X. Solans and T. Calvet, *Polyhedron* 1990, **9**, 1729.
12. M. B. Hursthouse, M. A. Malik, M. Motevalli and P. O'Brian, *Organometallics* 1991, **10**, 730.
13. C. C. Hadjikostas, G. A. Katsoulos, M. P. Sigalas and C. A. Tsipis, *Inorg. Chim. Acta* 1989, **163**, 173.
14. G. G. Franchini, A. Giusti, C. Preti, L. Tassi and P. Zannini, *Polyhedron* 1985, **4**, 1553.
15. D. Catheline, E. Román and D. Astruc, *Inorg. Chem.* 1984, **23**, 4508.
16. A. C. Fabetti, F. Forghieri, A. Giusti, C. Preti and G. Tosi, *Spectrochim. Acta* 1984, **40A**, 343.
17. F. Bonati and R. Ugo, *J. Organomet. Chem.* 1967, **10**, 257.
18. R. Kellner, G. St. Nikolov and N. Trendafilova, *Inorg. Chim. Acta* 1984, **84**, 233.
19. M. C. Cornock, R. O. Gould, C. L. Jones, J. D. Owen, D. F. Steele and T. A. Stephenson, *J. Chem. Soc., Dalton Trans.* 1977, 497.
20. A. A. M. Aly, M. S. El-Meligy and A. S. A. Zidau, *Trans. Met. Chem.* 1989, **14**, 366.
21. M. Morán, I. Cuadrado, C. Muñoz-Reja, J. R. Masaguer and J. Losada, *J. Chem. Soc., Dalton Trans.* 1988, 149.
22. D. Coucouvanis and J. P. Fackler, *Inorg. Chem.* 1967, **6**, 2047.
23. U. Agarwala and P. B. Rao, *Inorg. Chim. Acta* 1968, **2**, 337.
24. J. M. Burke and J. P. Fackler, *Inorg. Chem.* 1972, **11**, 2744.

Polyhedron Vol. 10, No. 23/24, pp. 2827–2832, 1991
Printed in Great Britain

0277–5387/91 $3.00+.00
© 1991 Pergamon Press plc

THE CYCLIC FIXATION AND REDUCTION OF MOLECULAR NITROGEN WITH $[WH_4(Ph_2PCH_2CH_2PPh_2)_2]$ IN γ-IRRADIATED SOLUTIONS

J. O. DZIĘGIELEWSKI* and J. G. MAŁECKI

Department of Inorganic and Radiation Chemistry, Institute of Chemistry, Silesian University, 40006 Katowice, Szkolna 9, Poland

(*Received* 19 *April* 1991; *accepted* 2 *July* 1991)

Abstract—Yields of NH_3 and N_2H_4 in radiation-catalytic reduction of N_2 by means of a hydride complex of W^{IV} with dppe in thf solution and in mixtures of thf with other solvents have been estimated. A mechanism proposed earlier of reduction of coordinated N_2 has been confirmed and the role of solvent in reduction of N_2 to NH_3 and amines has been explained.

In our recent work it has been shown that the hydride complexes of W^{IV} and Mo^{IV} with $Ph_2PCH_2CH_2PPh_2$(dppe) have higher activity as catalysts in the process of radiation-catalytic reduction of molecular nitrogen when compared with the activity of $[MoOCl(dppe)_2]$ and $[M(dppe)_2]$ (M = Mo, W).[1–4]

Making a comparison between the yields of the redox factors (i.e. H, e_s^-, R) and the yields of H_4N_2 and H_3N it was pointed out that the corresponding complexes formed H^- ions as a result of attachment of H^+ ions to the central ions,[5] and the H^- ions formed could reduce the coordinated N_2.

Using $[WH_4(dppe)_2]$ as a catalyst revealed the formation of $[WH(N_2)_2(dppe)_2]^+$ ions and their reduction to H_4N_2 in a radical process (by means of H atoms from $[WH_5(dppe)_2]^+$ and then to H_3N in an ion involved process (with H^- ions and e^- from the central ion).[2]

In our previous work[2] the remarkable effect of the solvent on the yields of H_3N was shown—the more stable the W—H group the higher the yields of ammonia in the particular solvent.

It is apparent that the role of the solvent cannot be restricted to the thermodynamic aspects of the M—H groups. Especially in the radiation process features such as molecular structure, polarity and polarizability, not to mention the donor–acceptor abilities of the solvent, play a very important role parallel to the stable and unstable radiolysis products.

The influence of the solvent on the yields and the products of the chemical reduction of coordinated N_2 has been reported,[6,7] but not explained so far. Thus, the problem of the solvent choice in the process of nitrogen fixation, especially for a cyclic process in a γ-radiation field is still to be explored. Taking into account the poor solubility of the neutral and ionic complexes of W^{IV} and Mo^{IV} on the one hand and thermodynamic and kinetic properties of the complex solutions including the yields of the stable and unstable radiolysis products on the other, we decided to use tetrahydrofuran (thf) and its mixtures as the most proper solvents. Thf is a medium polarity solvent and the products of its radiolysis are similar to those of the previously applied solvents, i.e. alcohols and cyclohexane.[8] In a mixture of thf with cyclohexane the yields of H_3N are supposed to be higher, while a small addition of water as a polar component can lead to the lower yields of N_2 reduction. The latter suggestion could support the results of our earlier works.

The application of the higher doses is accompanied by a lowering of the yields of ammonia in the solutions of Mo^{IV} and W^{IV} complexes. That fact is to be explained in this paper.

EXPERIMENTAL

Ligand dppe and a complex $[WH_4(dppe)_2]$ were synthesized according to the literature.[9] Thf was

* Author to whom correspondence should be addressed.

purified by refluxing with $LiAlH_4$ and then distilled. Before making solutions, thf and its mixtures with cyclohexane were saturated with N_2+H_2 mixtures or deoxygenated nitrogen.

The complex was dissolved in thf or its mixtures with cyclohexane. The solutions of $[WH_5(dppe)_2]HSO_4$ were obtained by the dissolving of $[WH_4(dppe)_2]$ in 0.1 M or 0.01 M solutions of H_2SO_4 in thf, thf+cyclohexane or thf+H_2O. The solutions of $[WH_5(dppe)_2]HSO_4$ were irradiated in a γ-radiation ^{60}Co source (Issliedowatiel) with simultaneous saturation of the proper solution with deoxygenated nitrogen or a mixture of deoxygenated nitrogen and hydrogen (v/v = 1 : 3). Dose rate was calculated as 7.66×10^{16} eV cm^{-3} min^{-1} in conversion to thf solution on the basis of a Fricke's dosimeter. In order to keep the concentrations of the solutions constant the gases were passed through the scrubbers filled with the proper solvent.

The H_4N_2 and H_3N generated were absorbed in aqueous solutions of H_2SO_4 ($c = 5 \times 10^{-2}$ M). Hydrazine and ammonia were determined by the standard methods, according to the cited papers,[9,10] respectively. For the acidified solutions the products were estimated in the irradiated solutions and in the traps filled with sulphuric acid using the same procedure. The aliphatic amines were detected spectrophotometrically, using salicyl aldehyde.[13] IR spectra were recorded for the irradiated solutions or in KBr pellets (the latter for the substances isolated from the irradiated solutions after evaporation of the solvent). The spectra were made using a Specord 75 IR spectrophotometer. ^1H and ^{31}P NMR spectra were made using a VXR-300 Varian spectrometer. The resonance signals were measured in the irradiated solutions and for the substances isolated from the irradiated solutions. Such substances were dissolved in $CDCl_3$.

RESULTS AND DISCUSSION

The numbers of $(N_2H_6)SO_4$ ions are shown in Fig. 1 and the numbers of $(NH_4)_2SO_4$ molecules in Fig. 2 vs dose and the concentrations of $[WH_5(dppe)_2]^+$ solutions. The radiation yields of ammonia and hydrazine together with the catalytic efficiency of the N_2 reduction are presented in Table 1. The catalytic efficiency of the process equals the number of NH_4^+ ions formed during 1 h irradiation of the $[WH_5(dppe)_2]HSO_4$ solutions. The number of ions is related to 1 mol of $[WH_5(dppe)_2]^+$ ions. Since, according to our earlier work,[2] only 1/3 of the complex is engaged in fixation of N_2, the numbers in column 5 were tripled.

The curves in Fig. 1 are similar to those presented in our earlier papers[1-5] where different complexes

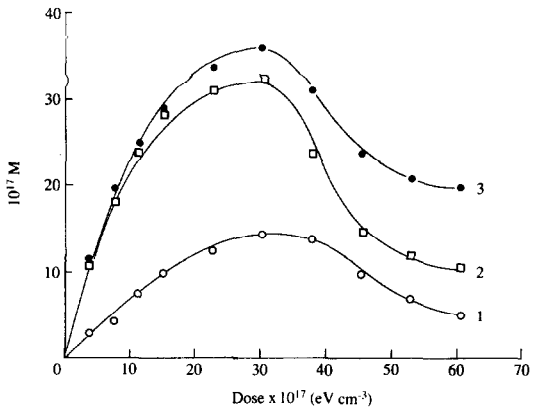

Fig. 1. The numbers of $(N_2H_6)SO_4$ molecules per 1 cm^3 (M) vs dose and concentration of a catalyst in acidified thf solution saturated with N_2+H_2 (1 : 3) mixture. Conc. $[WH_4(dppe)_2]$ = (1, ○) 5×10^{-3} mol dm^{-3}; (2, □) 1×10^{-2} mol dm^{-3}; (3, ●) 5×10^{-2} mol dm^{-3}.

and solvents were applied and the shapes of the curves were explained earlier.[4] The apparent formation of ammonia as a result of reduction of hydrazine was elaborated earlier.[1-5] It is easy to notice from Table 1 and Figs 1 and 2 that the radiation yields of ammonia and hydrazine do not depend directly on the concentrations of the complex. The relative catalytic efficiency (excluding the formation of the W—H groups, H_4N_2 and RNH_2) is increased at the lower concentrations of $[WH_4(dppe)_2]$ and the opposite effect is observed at the higher concentrations. The results presented are likely to be due to the too low dose rate applied. As a consequence, too many molecules of the catalyst

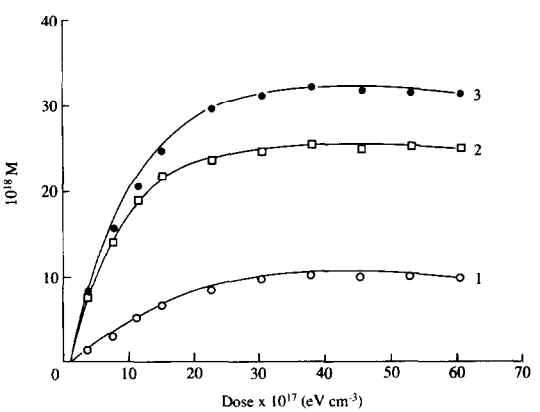

Fig. 2. The numbers of $(NH_4)_2SO_4$ molecules per 1 cm^3 (M) vs dose and concentration of a catalyst in acidified thf solution saturated with N_2+H_2 (1 : 3) mixture. Conc. $[WH_4(dppe)_2]$ = (1, ○) 5×10^{-3} mol dm^{-3}; (2, □) 1×10^{-2} mol dm^{-3}; (3, ●) 5×10^{-2} mol dm^{-3}.

Table 1. The parameters of the catalytic system ([$WH_4(dppe)_2$] dissolved in thf acidified with H_2SO_4 saturated with N_2+H_2)

Concentration of [$WH_4(dppe)_2$] (mol dm^{-3})	Number of $N_2H_6^{2+}$ ions/100 eV	Number of NH_4^+ ions/100 eV	Concentration of NH_4^+ ions after absorption of dose 45.36×10^{17} eV cm^{-3} (mol dm^{-3})	NH_4^+/[$WH_4(dppe)_2$] fixing N_2
5×10^{-3}	77	687	1.67×10^{-2}	10
1×10^{-2}	214	4174	4.24×10^{-2}	13
5×10^{-2}	317	5700	5.29×10^{-2}	3.3

do not take part in the process of fixation and reduction of N_2. The visible induction period (see Figs 2, 4 and 5) was explained earlier.[1-5] The yields of N_2 reduction in the presence of $[WH_5(dppe)_2]^+$ in thf are higher than those in cyclohexane–ethanol and cyclohexane–methanol systems.[2] Our earlier hypothesis that the higher stability of the hydride complex in a low polarity solvent can effect the yields of hydrazine and ammonia seems to be supported by that observation. However, in thf solutions the numbers of NH_4^+ are slightly decreased while increasing the dose as for methanol and methanol–cyclohexane systems.[2,3-5] The observed decrease of the NH_4^+ concentrations was explained earlier[3] as a result of their reactions with the radicals formed in the course of radiolysis of methanol. In the irradiated thf solutions the radicals formed, C_4H_7O,[8,14] can react with NH_4^+ ions and H_3N molecules. It is obvious for the reaction (1) type to go independently of the dose in the γ-radiation field, however in the initial stage of N_2 reduction its rate is much lower than that of the H_3N formation. That is why an increase of the NH_4^+ ions concentration is observed until the plateau starts (see Fig. 2).

$$H_3N+R\longrightarrow RH+NH_2 \quad \text{(ref. 3).} \qquad (1)$$

When the plateau starts, the rate of reaction (1) is greater than the rate of H_3N formation. Thus, the application of greater doses is accompanied by a decrease in the number of NH_4^+ ions. The rate of coordinated nitrogen reduction to ammonia is affected by a concentration of H^- ions.[1,2] The ions can be formed as a result either of the substitution of W—N_2 groups by W—H group or addition of H^+ ions into the central atom.

The equal tangents of the curves from Figs 3 and 4 for the acidified solutions saturated with nitrogen and the non-acidified ones saturated with nitrogen–hydrogen mixture, and, as a consequence, the equal values of $G_{NH_4^+}$ are satisfying supports for the previously proposed two ways of formation of H^- ions and their influence on the reduction of N_2. Regardless of the way H^- ions are formed, they possess the same ability to reduce H_4N_2 to H_3N, i.e. at different oxidation states of the central W ions the $G_{NH_4^+}$ values are equal in the acidified solutions saturated with nitrogen and in the non-acidified ones saturated with nitrogen–hydrogen mixture (see Fig. 4 and Table 2). The association of H^+ ions to W ions is a very rapid process when compared with the process of H^- ion formation to be a result of N_2 elimination using H_2. Therefore, the amount of hydrazine to be reduced to NH_4^+ ions is the lowest in the non-acidified solutions (see Figs 3 and 4). Insufficient concentration of the H^- ions prevents the reduction of all the hydrazine to ammonia (high placed plateau in curve 1 in Fig. 3). Thus, as a consequence, the $G_{NH_4^+}$ in non-acidified solutions is lower than that in the acidified ones and/or solutions saturated with hydrogen (Fig. 4 and Table 2). Hence, the influence of hydrazine amount on the yields of ammonia is supported and the role of H^- and H^+ ions in the process of reduction of molecular nitrogen seems to be explained sat-

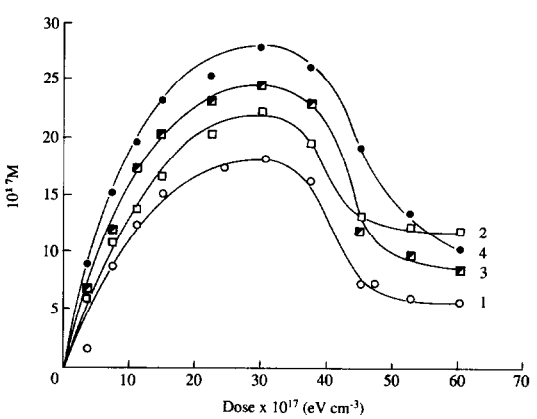

Fig. 3. The numbers of $(N_2H_6)SO_4$ molecules per 1 cm^3 (M) vs dose and concentration of H_2SO_4 (c[$WH_4(dppe)_2$] = 1×10^{-2} mol dm^{-3}) in thf solution. $c_{H_2SO_4}$ = (1) 0 mol dm^{-3} (○)—saturated with N_2+H_2 (1:3); (2) 10^{-2} mol dm^{-3} (□)—saturated with N_2; (3) 10^{-1} mol dm^{-3} (◪)—saturated with N_2; (4) 10^{-2} mol dm^{-3} (●)—saturated with N_2+H_2 (1:3).

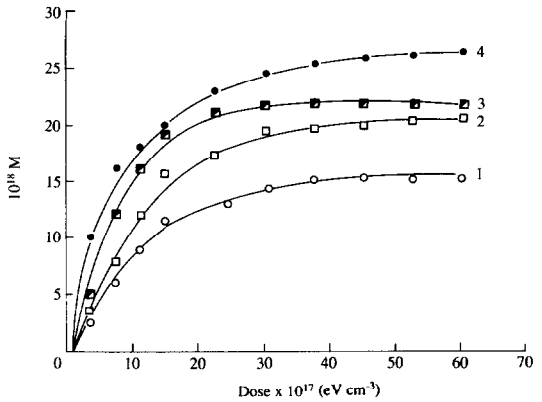

Fig. 4. The numbers of $(NH_4)_2SO_4$ molecules per 1 cm^3 (M) vs dose and concentration of H_2SO_4 ($c[WH_4(dppe)_2] = 1 \times 10^{-2}$ mol dm^{-3}) in thf solution. $c_{H_2SO_4}$ = (1) 0 mol dm^{-3} (○)—saturated with N_2+H_2 (1:3); (2) 10^{-2} mol dm^{-3} (□)—saturated with N_2; (3) 10^{-1} mol dm^{-3} (◪)—saturated with N_2; (4) 10^{-2} mol dm^{-3} (●)—saturated with N_2+H_2 (1:3).

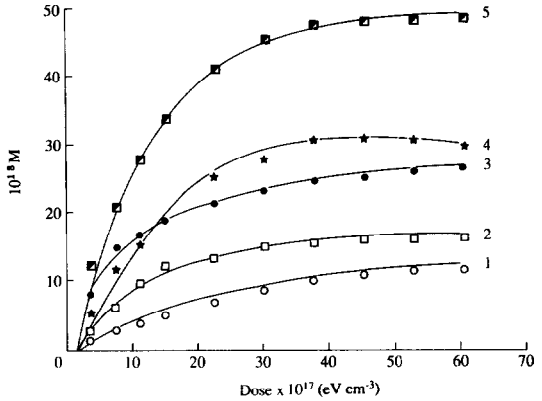

Fig. 5. The numbers of NH_4^+ ions per 1 cm^3 (M) vs dose and concentration of $[WH_4(dppe)_2]$ in different systems. (1,○) $c[WH_4(dppe_2)] = 5 \times 10^{-3}$ mol dm^{-3} in thf+dppe ($c = 5 \times 10^{-3}$ mol dm^{-3}) saturated N_2+H_2 (1:3); (2, □) $c[WH_4(dppe)_2] = 1 \times 10^{-2}$ mol dm^{-3} in thf+dppe ($c = 1 \times 10^{-2}$ mol dm^{-3}) saturated N_2+H_2 (1:3); (3, ●) $c[WH_4(dppe)_2] = 1 \times 10^{-2}$ mol dm^{-3} in thf acidified+dppe ($c = 1 \times 10^{-2}$ mol dm^{-3}) saturated N_2+H_2 (1:3); (4, ★) $c[WH_4(dppe)_2] = 1 \times 10^{-2}$ mol dm^{-3} in thf+C_6H_{12} (1:1) saturated N_2+H_2 (1:3); (5, ◪) $c[WH_4(dppe)_2] = 1 \times 10^{-2}$ mol dm^{-3} in thf acidified+C_6H_{12} (1:1)+dppe ($c = 1 \times 10^{-2}$ mol dm^{-3}) saturated N_2+H_2 (1:3).

isfactorily. Nevertheless, the H^+ ions could protonate the coordinated nitrogen and, indirectly, the other products of reduction. The influence of H^- ions on the mechanism of N_2 reduction (i.e. disproportionation of —NNH_2 group) was observed by the other authors.[15] The influence of the solvent on the coordination sphere of the catalyst is thought to be another reason for the decreasing rate of formation of H_3N when the applied dose is increased.

When free ligand dppe is present in the reaction system it affects the yields of H_4N_2; either in the acidified solutions or in the non-acidified ones the yield of hydrazine is increased about 20% while the yield of NH_4^+ ions is increased about 20% in the acidified solutions only (compare curves 1 and 2 in Fig. 5 with curve 1 in Fig. 4 and the corresponding data from Tables 1–3). The curves in Fig. 5 (excluding curve 4) have permanent tendencies to increase their values, however, at the higher doses the rate of ammonia formation is distinctly lower than at the initial stage of the process. In the non-acidified solutions the presence of dppe does not affect G_{NH_3}, however, due to the relatively high value of $G_{N_2H_4}$ the concentration of NH_3 is increased. These observations suggest that dppe is liberated from the coordination sphere in the two-step competitive pathway (2 and 3) which is as

Table 2. The parameters of the catalytic system ($c[WH_4(dppe)_2] = 10^{-2}$ mol dm^{-3})

Concentration of H_2SO_4 (mol dm^{-3})	Satur. gas	Number of $N_2H_6^{2+}$ ions/100 eV	Number of NH_4^+ ions/100 eV	Concentration of NH_4^+ ions after absorption of dose 45.36×10^{17} eV cm^{-3} (mol dm^{-3})	$NH_4^+/[WH_4(dppe)_2]$ fixation N_2
1×10^{-2}	N_2	141	1218	3.17×10^{-2}	9.6
1×10^{-1}	N_2	176	3130	3.49×10^{-2}	10.6
1×10^{-2}	N_2+H_2 (1:3)	212	3826	3.79×10^{-2}	11.5
0	N_2+H_2 (1:3)	132	1217	2.52×10^{-2}	7.6

Table 3. The parameters of the catalytic system (complex solution ($c = 1 \times 10^{-2}$ or 5×10^{-3} * mol dm^{-3}) saturated with N_2+H_2)

Irradiated system	I	II		III		IV	
Conc.* in thf acidified + dppe ($c = 5 \times 10^{-3}$ mol dm^{-3})	93	800		1.81×10^{-2}		11.3	
Conc. in thf acidified + dppe ($c = 1 \times 10^{-2}$ mol dm^{-3})	282	4400		2.53×10^{-2}		7.7	
Conc. in thf + dppe ($c = 1 \times 10^{-2}$ mol dm^{-3})	159	1217		2.69×10^{-2}		8.1	
Conc. in thf – C_6H_{12} (1:1)	182	2700		5.17×10^{-2}		15.7	
Conc. in thf acidified + C_6H_{12} (1:1) + dppe ($c = 1 \times 10^{-2}$ mol dm^{-3})	388	8380		7.92×10^{-2}		24.0	
Conc. in thf acidified + H_2O (1:1)	11	200		1.04×10^{-2}		3.0	
Conc. in thf + C_6H_{12} (1:1)	78	NH_4^+ 800	RNH_2 116	NH_4^+ 3.53×10^{-2}	RNH_2 10.4×10^{-3}	NH_4^+ 21.2	RNH_2 2.74

I—numbers of $(N_2H_6)SO_4$ molecules per 100 eV.
II—numbers of $(NH_4)_2SO_4$ or RNH_2 molecules per 100 eV.
III—concentrations of NH_4^+ ions or RNH_2 molecules after absorption of 45.36×10^{17} eV cm^{-3} (mol dm^{-3}).
IV—numbers of NH_4^+ ions or RNH_2 molecules per number of $[WH_4(dppe)_2]$ moles fixing N_2.

follows:

$$[WH(N_2)_2(dppe)_2]^+ + [WH_5(dppe)_2]^+ + 2\,HSO_4^- \rightarrow [HWNNH_2(SO_4)(dppe)]^+ + N_2 + [WH_3(dppe)_2]^+ + (dppe\,H_2)SO_4 \quad (2)$$

$$[HWNNH_2(SO_4)(dppe)]^+ \xrightarrow[dppe\,H_2^{2+}]{2thf,\,2H^+} \begin{cases} \xrightarrow{a} [HW(N_2H_4)(thf)_2(dppe)]^+ + SO_4^{-2} \\ \xrightarrow{b} [HW(N_2H_4)(dppe)_2]^+ + H_2SO_4 \end{cases} \quad (3)$$

The products of reaction (2) were not isolated due to their instability and relatively low concentration. The composition of the $[HWNNH_2(SO_4)(dppe)]^+$ product was proposed as the most likely one.

The formation of the hydrazide complexes of type $[WNNH_2(HSO_4)_2L_3]$ was shown by other authors.[16] Since the central ion is protonated the HSO_4^- ion is most likely to act as a bidentate ligand (in a form of SO_4^{2-} ion).[17]

Reactions (2) and (3) are complementary to those presented earlier when $[WH_5(dppe)_2]^+$ was applied as a catalyst.[2] For a process made in thf-cyclohexane system the role of reaction 3a is slightly diminished. The effect is enlarged by the small addition of dppe into the reaction system. The latter is accompanied by the apparent increase of the yields of NH_4^+ ions. On the other hand, the addition of a polar solvent (i.e. H_2O) into thf solution results in a contradictory effect of decreasing yields of hydrazine and ammonia.

The liberation of dppe from the coordination sphere of the complex was monitored by ^{31}P NMR spectroscopy. In a solution of $[WH_4(dppe)_2]$ in thf ($c = 1 \times 10^{-2}$ M) irradiated with a dose 5.4×10^{18} eV cm^{-3} two signals at 33.44 and 27.02 ppm were observed. The former was attributed to $[WH_x(dppe)_2]$ ($x < 4$)[18] complex while the latter was assigned to phosphine oxide[19] which is formed as a result of a liberation of dppe from the coordination sphere of the complex and its oxygenation by oxygen from the air. The chemical shifts of ^{31}P signals of dppe and its oxide were determined for the non-irradiated samples as −12.13 and 27.02 ppm, respectively.[19b] Comparing the integral intensities of the ^{31}P signals one could count the amount of dppe which is effectively exchanged by thf in the coordination sphere to be 10% of the whole amount of the former. Thus, reactions 2 and 3a could not be assumed to have decreased the rate of N_2 reduction to H_3N.

That conclusion seems to be supported by the fact of a relatively high concentration of the bis-dinitrogen complex of W in the irradiated complex solution. In fact, in the IR spectrum of the complex a few characteristic bands appear, e.g. at 1960 cm^{-1} assigned as A_{2u} vibration of a $W(N_2)_2$ group, besides, the lower intensities of the bands at 1830, 1775 and 1730 cm^{-1} attributed to ν(W—H) vibrations are due to the lower concentration of W—H groups in the irradiated solution of $[WH_4(dppe)_2]$. Thus, the other direction of the process of dinitrogen reduction leading neither to hydrazine nor to ammonia could be taken into account. The reduction by the radicals with the simultaneous action of H^+ or H^- ions and H atoms seems to be the alternative explanation of the observed phenomena. As a matter of fact, at the higher doses aliphatic amines are observed (see Table 3). The amines are formed in the acidified solutions, as well. Aromatic amines are not observed. The RNH_2 type amines in the irradiated solution of $[WH_4(dppe)_2]$ saturated with N_2+H_2 were found in the IR spectrum—ν(NH) at 3500 cm^{-1} and δ(NH) at 1640 cm^{-1}.

The other support for the presence of amines is its ^1H NMR spectrum, i.e. the signals at 0.8–1.8 ppm region, in fact, partially overlapped by the signals of dppe. Thus, $[W(N_2)_2(dppe)_2]$ is believed to be reduced by the W—H groups or the radicals R:

$$[W(N_2)_2(dppe)_2] \xrightarrow[R]{H^-} \begin{cases} \xrightarrow{a} H_3N + \\ \xrightarrow{b} [(N_2)W(N_2R)(dppe)_2] \end{cases} \quad (4)$$

More detailed mechanism of the process was presented earlier.[1-5]

The complexes of $[XW(N_2R)(dppe)_2]$ (R = C_6H_{11} or 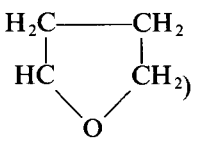) were described in the literature.[20] Our work concerning the formation of diazenide complex and its transformation to amines is in progress. Actually, the probability of reactions 4a and 4b seems to be dependent on the concentration of W—H groups and the lower concentration of the groups the more likely reaction 4b. The yields of the radicals C_6H_{11} and C_4H_7O are lower than 6 ($G_R < 6$) in cyclohexane–thf mixture.[8] If the radicals were formed as a result of the radiation decomposition of the solvents the G_R value should have been higher than 120. Therefore, the radicals are assumed to be formed in the other way without the influence of radiation. This problem will be explained in the next paper. On the other hand, H_3N seems to be the main product of reduction, although the yields of amines are remarkable. Taking into account the entire yields of reduction, i.e. H_3N and RNH_2, the high catalytic ability of the $[WH_4(dppe)_2]$—thf—C_6H_{12}—N_2—H_2 system seems to be obvious.

REFERENCES

1. J. O. Dzięgielewski and R. Grzybek, *Polyhedron* 1990, **9**, 645.
2. J. O. Dzięgielewski, J. Małecki and R. Grzybek, *Polyhedron* 1991, **10**, 1007.
3. J. O. Dzięgielewski and R. Grzybek, *J. Radioanal. Nucl. Chem.* 1989, **132**, 115.
4. J. O. Dzięgielewski, *Polyhedron* 1989, **8**, 1470.
5. J. O. Dzięgielewski, R. Grzybek and R. Gil-Bortnowska, *J. Radioanal. Nucl. Chem.* 1990, **140**, 415.
6. R. J. Burt, D. L. Hughes and G. J. Leigh, *J. Chem. Soc., Dalton Trans.* 1981, 793.
7. S. N. Anderson, J. Chatt, M. E. Fakley and R. L. Richards, *J. Chem. Soc., Dalton Trans.* 1981, 1973.
8. A. K. Pikaev, *Sowremennaa radiaconnaa Khimia*, p. 382. Nauka, Moscow (1986).
9. M. Pares and A. Retit, *Bull. Soc. Chim. France* 1947, 122.
10. G. V. Watt and J. D. Chisp, *Analyt. Chem.* 1952, **24**, 2006.
11. W. T. Bolleter, C. J. Bushmann and P. W. Tidwell, *Analyt. Chem.* 1961, **33**, 592.
12. C. J. Pickett, K. S. Ryder and J. Talarrsnen, *J. Chem. Soc., Dalton Trans.* 1986, 1453.
13. J. M. Korenman, *Fotometricheskij analyz. Methody opredelenia organicheskiyh soedyneney*, p. 149. Khyma, Moscow (1970).
14. J. H. Baxendale, D. Beaumond and M. A. J. Rodgers, *Trans. Faraday Soc.* 1970, 1996.
15. T. A. George and B. B. Kaul, *Inorg. Chem.* 1991, **30**, 882.
16. S. N. Anderson, M. E. Fakley and R. L. Richards, *J. Chem. Soc., Dalton Trans.* 1981, 1973.
17. T. Takahashi, Y. Mizobe, M. Sato, Y. Uchida and M. Hidai, *J. Am. Chem. Soc.* 1980, **102**, 7461.
18. (a) R. Pierantozzi and G. L. Geoffroy, *Inorg. Chem.* 1980, **19**, 1821; (b) L. F. Rhodes, J. D. Zubkowski, K. Folting and J. C. Huffman, *Inorg. Chem.* 1982, **21**, 4185.
19. (a) T. Kupka, A. Wawer, J. O. Dzięgielewski and P. S. Zacharias, *Fresenius. J. Analyt. Chem.* 1991, **339**, 253; (b) J. O. Dzięgielewski, unpublished results.
20. J. Chatt, *New Trends in the Chemistry of Nitrogen Fixation*, pp. 238, 245. Mir, Moscow (1983).

Polyhedron Vol. 10, No. 23/24, pp. 2833–2838, 1991
Printed in Great Britain

0277–5387/91 $3.00+.00
© 1991 Pergamon Press plc

NMR INVESTIGATION OF NICKEL(II) SCHIFF BASE COMPLEXES WITH BENZOYL SUBSTITUENTS

MANABU FUJIWARA,* YOSHIHIDE ICHIKI, SETSUKO KINOSHITA and HISANOBU WAKITA

Department of Chemistry, Faculty of Science, Fukuoka University, Nanakuma, Jonan-ku, Fukuoka 814-01, Japan

(*Received* 5 *February* 1991; *accepted* 21 *June* 1991)

Abstract—The nickel(II) Schiff base complexes with isobutyl chains and benzoyl substituents have been prepared and characterized by ^1H and ^{13}C NMR spectroscopies. In the complex, the donor set of N_2O_2 has a square planar coordination, the benzoyl substituents are perpendicular to the chelate plane and the isobutyl groups move segmentally so that they may approach the benzoyl substituents.

It has been well known that not only the strong interactions such as covalent bonds, coordination bonds or ionic bonds, but also the weak interactions such as hydrogen bonds and hydrophobic interactions play an important role in most biological proceses relating to the regulation of metabolism.[1] In the case of metal complexes, such hydrophobic interactions operating between ligands may provide distinct features in the structure, stability and reactivity of complexes. Fisher and Sigel[2] reported that the interligand interaction operating between aromatic and aliphatic groups increases the stability of the mixed ligand complex with an amino acid having long alkyl chains and bipyridyl or *o*-phenanthroline. Okawa and co-workers[3] reported that the interligand, hydrophobic interactions can be applicable for selective syntheses of geometrical and optical isomers of complexes. In this paper, we report the preparation and characterization of the nickel(II) Schiff base complexes with 2-methylpropyl(isobutyl) chains and benzoyl substituents. Their structures and dynamics in chloroform solution will be discussed from the results of ^1H and ^{13}C NMR spectra, and ^{13}C relaxation-time measurements. It will be made clear that an interaction between isobutyl groups and benzoyl substituents in nickel(II) Schiff base complex is weak but validly affects the characteristic structure and dynamics of isobutyl chains in chloroform solution.

EXPERIMENTAL

Preparation of benzoyl derivatives of nickel(II) Schiff base complexes[4]

To a dry chloroform solution (500 cm^3) of nickel(II) Schiff base complex (0.05 mol) and excess trimethylamine (0.12 mol) was added excess benzoyl chloride (0.12 mol) (benzoyl chloride, *m*-nitrobenzoyl chloride or 3,5-dinitrobenzoyl chloride). The mixture was refluxed for 60 h, and evaporated under reduced pressure. The residue was recrystallized from a mixture of chloroform and methanol (1 : 10) for the derivatives of Ni(Me, Meen), or a mixture of ethanol and diethylether (1 : 1) for the derivatives of Ni(isoBu, Meen). The results of the elemental analyses, IR and electronic spectral data of all complexes indicate that they are quite pure and are consistent with their chemical structures (see Fig. 1).

Measurements

The ^1H NMR, ^{13}C NMR and ^{13}C relaxation-time (T_1) measurements were recorded using a JEOL FX-90 spectrometer at 90 MHz for ^1H and at 22.5 MHz for ^{13}C nuclei. Each sample solution was almost saturated with the respective complexes.

* Author to whom correspondence should be addressed.

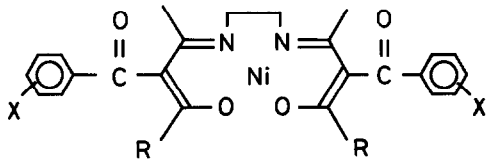

R = Me, X = H : Ni(Me,Meen)-B
X = m-NO_2 : Ni(Me,Meen)-mNO_2B
X = 3,5-$(NO_2)_2$: Ni(Me,Meen)-3,5$(NO_2)_2$B
R = isoBu, X = H : Ni(isoBu,Meen)-B
X = m-NO_2 : Ni(isoBu,Meen)-mNO_2B
X = 3,5-$(NO_2)_2$: Ni(isoBu,Meen)-3,5$(NO_2)_2$B

Fig. 1. Chemical structure of the nickel(II) Schiff base complexes studied.

RESULTS AND DISCUSSION

^{1}H *NMR spectra*

The chemical shift values in the ^{1}H NMR spectra for nickel(II) Schiff base complexes in $CDCl_3$ are summarized in Table 1. For the ^{1}H NMR spectrum of Ni(Me, Meen), three singlet peaks at 1.86, 3.01 and 4.86 ppm were obtained and can be assigned to the overlap of methyl protons attached to azomethine [CH_3(N)] and keto moieties [CH_3(O)], the methylene protons of the ethylenediamine moiety [CH_2(en)], and the methine protons on the γ-positions of the chelate ring, respectively. For the spectra of benzoyl and *m*-nitrobenzoyl derivatives of Ni(Me, Meen), the singlet resonance signals due to CH_3(N) and CH_3(O) are shifted to higher fields, *ca* 0.05 ppm for the benzoyl derivative and 0.02 ppm for the *m*-nitrobenzoyl derivative compared to the parent complex. Other singlet resonance signals due to CH_2(en) are shifted to lower fields, *ca* 0.15, 0.20 and 0.25 ppm, respectively. The shifts were caused by the electron-withdrawing effects of benzoyl substituents which are of the order benzoyl < *m*-nitrobenzoyl < 3,5-dinitrobenzoyl group. However, the shifts to higher field of the signals due to CH_3(N) and CH_3(O) are consequent on the combination of the electron-withdrawing effect and the magnetic anisotropy effect[5] by benzoyl substituents; the latter is associated with higher-field shifts and the former with lower-field shifts. It is evident that the latter effect is stronger than the former in the case of benzoyl and *m*-nitrobenzoyl derivatives, but both are the same in the case of the 3,5-dinitrobenzoyl derivative.

On the other hand, for Ni(isoBu, Meen) the spectrum has a doublet resonance due to the methyl protons of 2-methylpropyl(isobutyl) groups [CH_3(O)] at 0.89 ppm, a singlet due to the methyl protons attached to azomethine moieties [CH_3(N)] at 1.85 ppm, an overlapping multiplet resonance due to the methine and methylene protons of isobutyl groups [CH_2+CH(O)] at 1.95 ppm, a singlet due to CH_2(en) at 3.01 ppm, and a singlet due to the methine protons on the γ-positions of the chelate ring at 4.86 ppm. For the benzoyl, *m*-nitrobenzoyl and 3,5-dinitrobenzoyl derivatives of Ni(isoBu, Meen), similar spectra in the high-field region were obtained (<4.0 ppm), though the signals due to CH_3(N), CH_3(O) and CH_2+CH(O) shifted to higher field and the signals due to CH_2(en) to lower field. These results were caused by exactly the same reasons as in the case for Ni(Me, Meen)s. However, the values of the higher-field shifts on the protons of even methyl and isobutyl groups for Ni(isoBu, Meen)s are larger than those of both methyl groups for Ni(Me, Meen)s, while the values of the lower-field shifts on CH_2(en) are similar for the derivatives of Ni(Me, Meen) and Ni(isoBu, Meen), respectively. This fact is important with respect to the structures of nickel(II) Schiff base complexes in solution. In addition, the ^{1}H NMR chemical shifts and signal features did not depend so much on temperature in the region from −20 to 30°C.

Table 1. ^{1}H NMR spectral data of nickel(II) complexes in $CDCl_3$

Complex	δ (ppm) CH_2(en)	CH_3(N)	CH_3(O)	CH_2+CH(O)
Ni(Me, Meen)	3.01	1.86	1.86	
Ni(Me, Meen)-B	3.16	1.81	1.81	
Ni(Me, Meen)-*m*-NO_2B	3.21	1.83	1.83	
Ni(Me, Meen)-3,5$(NO_2)_2$B	3.26	1.86	1.86	
Ni(isoBu, Meen)	3.01	1.85	0.89	1.95
Ni(isoBu, Meen)-B	3.15	1.76	0.75	1.90
Ni(isoBu, Meen)-*m*-NO_2B	3.21	1.80	0.78	1.91
Ni(isoBu, Meen)-3,5$(NO_2)_2$B	3.25	1.83	0.79	1.91

Table 2. Relaxation times of ^{13}C atoms for nickel(II) complexes at 25°C

^{13}C atom	Ni(Me, Meen) δ (ppm)	Ni(Me, Meen) T_1 (s)	Ni(Me, Meen)-*m*-NO_2B δ (ppm)	Ni(Me, Meen)-*m*-NO_2B T_1 (s)
$CH_3(N)$	21.0	5.3	20.6	1.6
$CH_3(O)$	24.4	5.6	25.6	2.0
$CH_2(en)$	53.1	1.9	53.7	0.4
^{13}C atom	Ni(isoBu, Meen)		Ni(isoBu, Meen)-*m*-NO_2B	
$CH_3(N)$	20.9	2.9	20.5	0.8
$CH_3(O)$	22.7	1.8	22.6	0.9
CH(O)	27.0	2.7	27.0	0.4
$CH_2(O)$	47.3	1.2	46.5	0.6
$CH_2(en)$	53.0	1.1	53.6	0.3

^{13}C *NMR spectra*

The ^{13}C NMR spectrum of Ni(isoBu, Meen) in $CDCl_3$ has eight sharp signals at 21.0, 22.7, 27.0, 47.3, 53.0, 99.8, 164.1 and 179.9 ppm assignable to the methyl carbons attached to azomethine moieties [$CH_3(N)$], methyl carbons of isobutyl groups [$CH_3(O)$], methine carbons of isobutyl groups [CH(O)], methylene carbons of isobutyl groups [$CH_2(O)$], methylene carbons of the ethylenediamine moiety [$CH_2(en)$], methine carbon at γ-positions of the chelate ring, azomethine carbons, and keto carbons, respectively. Similarly, the spectra of its benzoyl, *m*-nitrobenzoyl and 3,5-dinitrobenzoyl derivatives have 13 or 15 sharp signals. The higher-field peaks can be assigned to $CH_3(N)$, $CH_3(O)$, CH(O), $CH_2(O)$, $CH_2(en)$, quarternary carbons at γ-positions of the chelate ring, phenyl carbons of benzoyl substituents (four or six signals), azomethine carbons, keto carbons, and carbonyl carbons of benzoyl substituents, respectively. These results are consistent with the structures of nickel(II) Schiff base complexes shown in Fig. 1.

T_1 *measurements*

The T_1 measurements were obtained using the inversion recovery method[6] for the nickel(II) Schiff base complexes Ni(Me, Meen), Ni(Me, Meen)-*m*-NO_2B, Ni(isoBu, Meen) and Ni(isoBu, Meen)-*m*-NO_2 in $CDCl_3$. The T_1 data for the four nickel(II) complexes are listed in Table 2. It is considered that in large molecules such as the nickel(II) complexes investigated here, the dipole–dipole relaxation is dominant.[7]* It is difficult to extract intramolecular movements such as distortion, the rotation of the benzoyl group or segmental movement of the isobutyl group from the whole movements of the complex molecule. However, the relative difference in intramolecular movements between Ni(Me, Meen) and Ni(isoBu, Meen), or the parent complex and its benzoyl derivative, can be discussed qualitatively based on T_1 data. It can be said that the larger the T_1 value of the ^{13}C atom, the faster its motion. The relaxation times of the methyl, methylene and methine carbons are not the same, even if they have similar mobility. They may be correlated by the following equation:

$$3 \times T_1(\text{methyl}) \fallingdotseq 2 \times T_1(\text{methylene}) = T_1(\text{methine}).$$

All the T_1 values of ^{13}C atoms were reduced greatly owing to the insertion of *m*-nitrobenzoyl groups in the nickel(II) Schiff base complex. This is caused by the reduction of movements such as translation and rotation for the whole complex molecule due to the increase in molecular weight. This effect can be extracted directly from the T_1 value of $CH_2(en)$ because its molecular structure and intramolecular movement may be steady before and after the insertion of benzoyl groups. The T_1 values of $CH_2(en)$ in *m*-nitrobenzoyl derivatives decrease to about a fifth of those in their parent complexes by the insertion of *m*-nitrobenzoyl substituents. However, the magnitude of the decrease in T_1 values for other carbons is not similar to that for $CH_2(en)$.

For Ni(Me, Meen), the T_1 value of $CH_3(N)$ is similar to that of $CH_3(O)$. The T_1 value of $CH_2(en)$ is rather small and it indicates that the chelate plane containing the central nickel(II) ion and chelate rings is rather rigid.

For Ni(Me, Meen)-*m*-NO_2B, the decrease in T_1 values by the insertion of *m*-nitrobenzoyl sub-

* This assumption was confirmed by measuring the NOE factor (η). We have measured this for analogous complexes. The values were found to be within the 2.0 ± 0.1 range for all carbons of the complexes.

stituents is much faster for CH_2(en) than for CH_3(N) and CH_3(O). Therefore, it can be said that the activity of "intramolecular movement", such as the bending and deformation vibrations for both methyl groups, is higher in the *m*-nitrobenzoyl derivative than that in its parent complex. In addition, the T_1 value of CH_3(O) became larger than that of CH_3(N).

On the other hand, for Ni(isoBu, Meen) the T_1 values of both methyl carbons are different even without *m*-nitrobenzoyl substituents, and the T_1 value of CH_3(O) which belongs to the isobutyl chain as its terminal methyl group is much smaller than that of CH_3(N). When *m*-nitrobenzoyl groups are inserted into Ni(isoBu, Meen), the T_1 value of CH_3(N) decreases faster and becomes almost the same as that of CH_3(O). Similarly, the T_1 values for the methylene and methine carbons of the isobutyl group, CH_2(O) and CH(O), decrease by the insertion of *m*-nitrobenzoyl groups, but the degree of the decrease is different. The T_1 value of CH(O) in Ni(isoBu, Meen)-*m*-NO_2B is very small and only *ca* 15% of that in Ni(isoBu, Meen), although values for CH_2(O) and CH_2(en) are *ca* 50 and 27%, respectively. These results indicate that the segmental movement of the isobutyl group, especially the movement at the methine moiety, is restricted by the presence of the *m*-nitrobenzoyl group. Both neighbouring carbons of CH_2(O), the keto carbon in the chelate ring and CH(O) are brought to a standstill, so that like a string the intramolecular movement of CH_2(O) becomes vigorous.

The T_1 values of the phenyl carbons of *m*(3)-nitrobenzoyl substituents at the 2-, 4-, 5- and 6-positions are 0.3, 0.3, 0.2 and 0.2 s, respectively. They are rather small and similar to each other in both the cases of Ni(Me, Meen)-*m*-NO_2B and Ni(isoBu, Meen)-*m*-NO_2B, indicating that *m*-nitrobenzoyl groups are rather rigid.

Temperature dependence of T_1

In order to investigate the temperature dependence of T_1 values, Ni(Me, Meen), Ni(Me, Meen)-*m*-NO_2B, Ni(isoBu, Meen) and Ni(isoBu, Meen)-*m*-NO_2B in $CDCl_3$ solutions were measured at temperatures from −20 to 30°C. For Ni(Me, Meen) and Ni(Me, Meen)-*m*-NO_2B, all T_1 values of CH_3(N), CH_3(O) and CH_2(en) decreased continuously with decreasing temperature (Figs 2 and 3). This is in accordance with the fact that molecular movement such as the internal rotation becomes restricted at lower temperatures.

On the other hand, the result for Ni(isoBu, Meen), which has no benzoyl substituents, is similar to those for Ni(Me, Meen) and Ni(Me, Meen)-*m*-NO_2B as shown in Fig. 4. However, the result for Ni(isoBu, Meen)-*m*-NO_2B (Fig. 5) is different from those for other nickel(II) complexes. All T_1 values of ^{13}C atoms in Ni(isoBu, Meen)-*m*-NO_2B decreased continuously with a decrease in temperature. The magnitude of the decrease in T_1 for CH_3(O) is especially much larger. The T_1 value for CH_3(O) is smaller than for CH_3(N) in the region below 0°C. This result suggests that the intramolecular movement of the isobutyl group in Ni(isoBu, Meen)-*m*-NO_2B in chloroform solution is significantly different from those in the other three complexes. Although the T_1 value of CH(O)

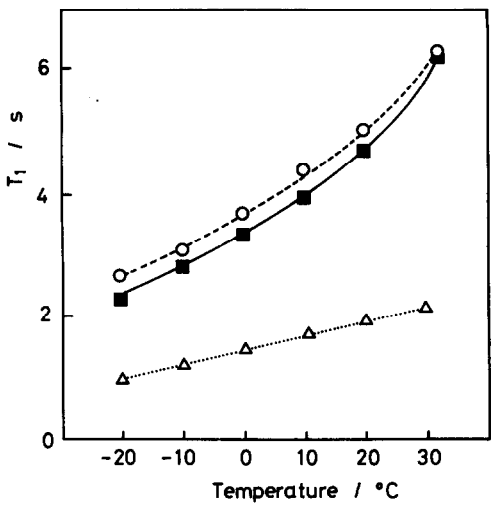

Fig. 2. Temperature dependence of T_1 for Ni(Me, Meen). (---○---): CH_3(O), (——■——): CH_3(N), (···△···): CH_2(en).

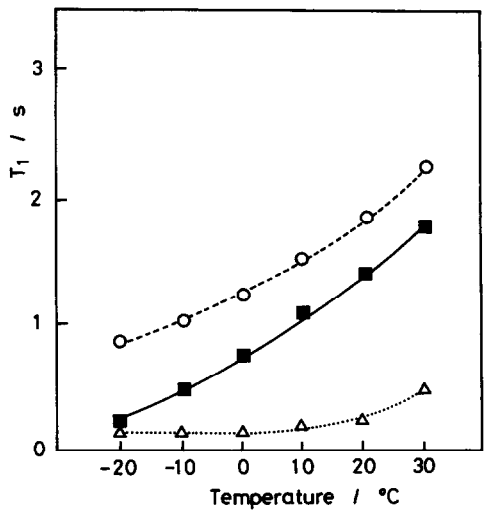

Fig. 3. Temperature dependence of T_1 for Ni(Me, Meen)-*m*-NO_2B. (---○---): CH_3(O), (——■——): CH_3(N), (···△···): CH_2(en).

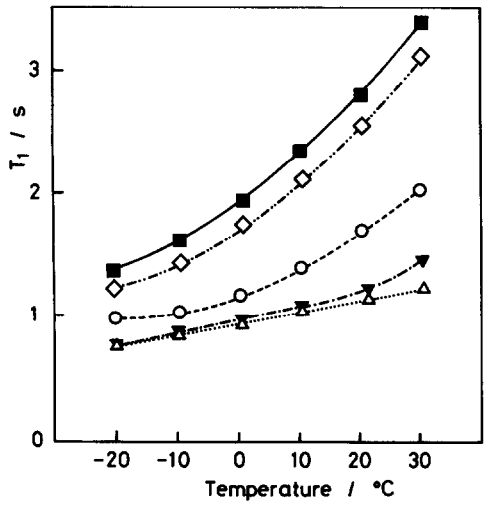

Fig. 4. Temperature dependence of T_1 for Ni(isoBu, Meen). (——■——): CH_3(N), (—··—◇—··—··): CH(O), (---○---): CH_3(O), (—·—▼—·—·—): CH_2(O), (···△···): CH_2(en).

is much larger than that of CH_2(en) in Ni(isoBu, Meen), they are almost the same in Ni(isoBu, Meen)-*m*-NO_2B, indicating that the methine carbon of the isobutyl group is fixed by the inserted *m*-nitrobenzoyl substituent so that the terminal methyl carbons [CH_3(O)] and methylene carbon [CH_2(O)] in the isobutyl group can increase the degree of movement. However, this increase in movement on the methylene and methyl carbons by the insertion of the *m*-nitrobenzoyl substituent diminishes at lower temperature, and the methyl carbons begin to fix in the neighbourhood of the benzoyl group as the methine carbon of the isobutyl group.

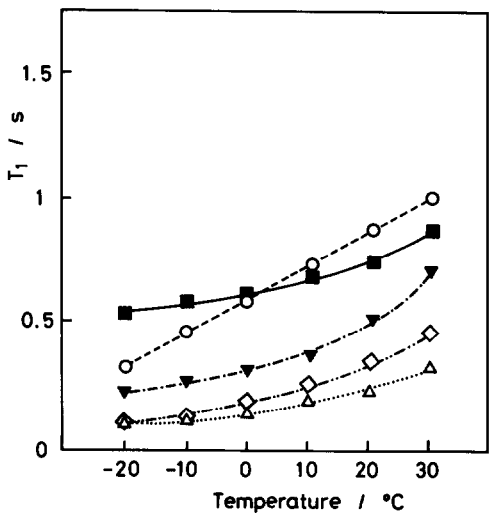

Fig. 5. Temperature dependence of T_1 for Ni(isoBu, Meen)-*m*-NO_2B. (---○---): CH_3(O), (——■——): CH_3(N), (—·—▼—·—·—): CH_2(O), (—··—◇—··—··): CH(O), (···△···): CH_2(en).

Structures and dynamics of nickel(II) complexes in solution

The structures and dynamics of nickel(II) Schiff base complexes in chloroform solution can be proposed from the results of the ^1H and ^{13}C NMR spectra, and ^{13}C relaxation time measurements. In all the nickel(II) complexes studied, the donor sets of N_2O_2 which belong to three chelate rings have a square-planar coordination. Their intramolecular movements are not fast but rather slow. For benzoyl derivatives, the inserted benzoyl groups are perpendicular to the chelate planes containing the nickel(II) ions. There is steric hindrance between benzoyl groups and adjacent isobutyl chains in nickel(II) complexes with both isobutyl and benzoyl groups, and the benzoyl groups are inclined to approach methyl groups attached to azomethine moieties to avoid the isobutyl chains. The isobutyl groups move segmentally so that they may approach the benzoyl groups. The movement of only the methine moiety in the isobutyl group is restricted by the benzoyl substituent but the methylene and terminal methyl moieties move much more actively in benzoyl derivatives than in their parent complexes at room temperature. The movement of the methyl groups became much slower below 0°C. The isobutyl groups may choose some conformations to approach the benzoyl substituents, so that the isobutyl groups can experience the magnetic anisotropy effect of the benzoyl groups for a certain time. The characteristic behaviour of the isobutyl groups may be affected by the so-called CH···π interaction between alkyl and phenyl groups. However, this interaction is so weak in a non-polar organic solvent that the isobutyl groups are not fixed at only one conformation. The isobutyl group is a rather short alkyl chain and its freedom of movement is not naturally high. We are now preparing the nickel(II) Schiff base complexes, with longer alkyl chains such as isopentyl and isohexyl groups, Ni(isoPe, Meen)s and Ni(isoHx, Meen)s and measuring their NMR spectra.

REFERENCES

1. G. Nemethy and H. A. Scheraga, *J. Phys. Chem.* 1962, **66**, 1773; E. Frieden, *J. Chem. Educ.* 1975, **52**, 754.
2. B. E. Fischer and H. Sigel, *J. Am. Chem. Soc.* 1980, **102**, 2998.
3. H. Okawa, K. Ueda and S. Kida, *Inorg. Chem.* 1982, **21**, 1594.

4. J. Eimes, *Polyhedron* 1985, **4**, 943; M. Fujiwara, K. Yokota, H. Wakita, T. Matsushita and T. Shono, *Fukuoka Univ. Sci. Rep.* 1988, **18**, 141.
5. M. Tanaka, R. Ryu, I. Masuda and T. Shono, *Bull. Chem. Soc. Japan* 1977, **50**, 415.
6. K. Mullen and P. S. Pregosin, *Fourier Transform NMR Techniques—A Practical Approach*. Academic Press, London (1976).
7. S. Kinoshita and I. Masuda, *Polyhedron* 1985, **4**, 1245.

Polyhedron Vol. 10, No. 23/24, pp. 2839–2846, 1991
Printed in Great Britain

0277–5387/91 $3.00+.00
© 1991 Pergamon Press plc

THE PREPARATION AND CHARACTERIZATION OF $M_2(OEPh_3)_2(NMe_2)_4$, WHERE M = Mo AND W AND E = C AND Si. THE X-RAY CRYSTAL STRUCTURES OF *GAUCHE*-$W_2(OCPh_3)_2(NMe_2)_4$, *ANTI*-$Mo_2(OCPh_3)_2(NMe_2)_4$ AND *ANTI*-$W_2(OSiPh_3)_2(NMe_2)_4$

M. H. CHISHOLM,† I. P. PARKIN, J. C. HUFFMAN, E. M. LOBKOVSKY and K. FOLTING

Department of Chemistry and Molecular Structure Center, Indiana University, Bloomington, IN 47405, U.S.A.

(*Received* 26 *March* 1991; *accepted* 18 *June* 1991)

Abstract—Reaction of $M_2(NMe_2)_6$ (M = Mo, W) with triphenylmethanol in hexane/ether produces $M_2(OCPh_3)_2(NMe_2)_4$ (**I**) as yellow crystals in high yield (92–97%). $M_2(OCPh_3)_2(NMe_2)_4$ are air-sensitive, soluble in aromatic solvents and decompose around 160°C. The ^1H NMR of **I** is temperature dependent and shows a mixture of *anti* and *gauche* rotamers. The X-ray crystal structures of **I** reveal exclusively the *gauche* isomer for tungsten and the *anti* isomer for molybdenum. The reactions between $M_2(NMe_2)_6$ and triphenylsilanol (2 equiv.) yield $M_2(OSiPh_3)_2(NMe_2)_4$ compounds (M = Mo, W) (**II**) as orange crystals. In the presence of >6 equiv. of Ph_3SiOH the $M_2(NMe_2)_6$ compounds react further to give yellow crystalline compounds, $M_2(OSiPh_3)_4(NMe_2)_2$. In compound **II**, where M = W, the $W_2O_2N_4$ skeleton adopted the *anti* conformation with W—W = 2.2954(6) Å, W—O = 1.925(4) Å, W—N = 1.935(8) Å, W—W—O = 108.1(1)°, W—W—N = 102(1)°. The addition of Ph_3SiOH (>6 equiv.) to $W_2(OBu^t)_6$ yielded the related compound $W_2(OBu^t)_2(OSiPh_3)_4$.

It is well-established that the addition of an alcohol to a metal amide leads to a metal alkoxide and the liberation of an amine and this often provides a synthetic route to metal alkoxides when other routes fail.[1] We have used this reaction extensively in the synthesis of both dinuclear and tetranuclear alkoxides of molybdenum and tungsten starting from the amido compounds $M_2(NMe_2)_6$.[2–5] Though these reactions must surely proceed in a stepwise RO-for-NMe_2 exchange at the M_2 centre with concomitant hydrogen atom transfer no intermediates have been isolated or detected in previous studies. Reasoning that the introduction of a more sterically demanding RO group (relative to NMe_2) might slow the subsequent substitution step we carried out reactions involving Ph_3COH and Ph_3SiOH. These do indeed allow for the isolation of mixed amido-alkoxide M_2-containing compounds as we describe here. These findings complement the recent report by Cotton and co-workers of the synthesis and characterization of the mixed amido perfluoroalkoxide $Mo_2(NMe_2)_2(OC(CF_3)_3)_4$.[6]

RESULTS AND DISCUSSION

Synthesis

Treatment of an ether/hydrocarbon solution of $M_2(NMe_2)_6$ with >six-fold excess of triphenylmethanol produces $M_2(OCPh_3)_2(NMe_2)_4$ (**I**) in high yield [eq. (1)].

$$M_2(NMe_2)_6 + 2HOCPh_3 \xrightarrow[(M = Mo, W)]{RT/hexane/ether} M_2(OCPh_3)_2(NMe_2)_4 + 2HNMe_2 \quad (1)$$

† Author to whom correspondence should be addressed.

When the reaction is followed by ^1H NMR spectroscopy no intermediate is detected. Only $M_2(OCPh_3)_2(NMe_2)_4$, dimethyl-amine and unreacted starting material are observed. The product $M_2(OCPH_3)_2(NMe_2)_4$ (**I**) precipitates from the reaction solution as well-formed yellow crystals. Heating the reaction or using longer reaction times does not enable further substitution and formation of $M_2(OCPh_3)_n(NMe_2)_{6-n}$ ($n \geqslant 3$) species. The reaction shown in eq. (1) is driven by the stronger acidity of triphenylmethanol compared to $HNMe_2$, the entropically-favoured loss of dimethylamine gas and enthalpically by M—O bonds being somewhat stronger than M—N bonds (M = Mo, W).

Compounds **I** are obtained as well-formed yellow crystals which precipitate from the reaction solution on standing. They are air-sensitive, both in the solid state and in solution. However, crystals of **I** are stable for *ca* 2–3 h in air before noticeable decomposition occurs. The decomposition points at 162°C (M = Mo) and 145–7°C (M = W) are comparable with related $M_2(OR)_6$ and $M_2R_2(OR)_4$ compounds.[7]

When $W_2(NMe_2)_6$ is allowed to react with Ph_3SiOH in hydrocarbon/ether solvents the compound $W_2(OSiPh_3)_2(NMe_2)_4$ is formed in a reaction closely related to that of eq. (1). The latter compound is an orange crystalline, hydrocarbon-soluble solid that does react further in the presence of an excess of Ph_3SiOH to yield $W_2(OSiPh_3)_4(NMe_2)_2$. The latter is obtained as a yellow microcrystalline sample only sparingly soluble in hexane.

The addition of $\geqslant 6$ equiv. of Ph_3SiOH to a hydrocarbon solution of $W_2(OBu^t)_6$ gives the mixed siloxide–alkoxide $W_2(OSiPh_3)_4(OBu^t)_2$. Presumably, in this reaction, as in the reaction with $W_2(NMe_2)_6$, the compounds of the formula $W_2(OSiPh_3)_4X_2$, where $X = NMe_2$ or OBu^t, are obtained because further replacement of X by $OSiPh_3$ is prevented by steric hindrance. In reactions with the $W_2(NMe_2)_6$ compound, the replacement of four NMe_2 groups by $OSiPh_3$ relative to two by $OCPh_3$ is also most likely a reflection of the steric effects of the OR ligands. The longer O—Si bonds, relative to O—C, and longer Si—C(phenyl) bonds, relative to C—C(phenyl), make the $OSiPh_3$ less sterically demanding at the metal centre than $OCPh_3$.

Solid-state and molecular structures

Ball-and-stick drawings showing the molecular structures and the atom number scheme for compound **I**, where M = Mo and W, and $W_2(OSiPh_3)_2(NMe_2)_4$ are given in Figs 1, 2 and 3, respectively. Comparisons of the bond distances and bond angles for compounds **I** are given in Table 1, while selected bond distances and angles for $W_2(OSiPh_3)_2(NMe_2)_4$ are given in Table 2. A summary of crystal data for all three compounds is given in Table 3.

The compounds adopt the now familiar staggered ethane-like ground state structures for $M_2X_2Y_4$ (M≡M) compounds.[8] The M—M distances are typical of those found in these types of compounds and most notably the Mo—Mo distance is 0.08 Å shorter than the W—W distance. The M—O and M—N distances are, however, equivalent in all three compounds when the 3σ criteria is applied. This is noteworthy since we see here both *anti* and *gauche* forms of $M_2(OCPh_3)_2(NMe_2)_4$ and the *anti* form of $W_2(OSiPh_3)_2(NMe_2)_4$. Structurally there is very little difference in the bonding in these compounds. The M—O distances are longer than those typically seen in $M_2(OR)_6$ compounds, where R = alkyl, which fall in a very narrow range 1.88(1) Å.[8] Moreover, the M—N distances observed in these compounds are all shorter than those seen in $M_2(NMe_2)_6$ compounds, where M—N = 1.98(1) Å.[9] Thus, the M—O/M—N distances are reflecting the π-bond order of the ligands $Me_2N > OCPh_3$ and $SiPh_3$. Of the M—N distances determined in this study it is also worth noting that those in $W_2(OSiPh_3)_2$

Table 1. Selected bond distances (Å) and angles (°) for the $M_2(OCPh_3)_2(NMe_2)_4$ molecules

	M = Mo	M = W
M(1)—M(1)′	2.2267(16)	2.3072(10)
M(1)—O(2)	1.920(6)	1.963(9)
M(1)—N(22)	1.961(8)	1.937(9)
M(1)—N(25)	1.955(7)	1.954(10)
O(2)—C(3)	1.413(11)	1.436(15)
N(22)—C(23)	1.392(12)	1.471(17)
N(22)—C(24)	1.505(13)	1.469(17)
N(25)—C(26)	1.494(12)	1.466(18)
N(25)—C(27)	1.404(12)	1.468(17)
M(1)—M(1)′—O(2)	112.61(19)	97.99(27)
M(1)—M(1)′—N(22)	101.69(25)	100.98(27)
M(1)—M(1)′—N(25)	102.83(22)	104.7(32)
O(2)—M(1)—N(22)	111.9(3)	118.8(5)
O(2)—M(1)—N(25)	111.3(3)	118.5(4)
N(22)—M(1)—N(25)	115.7(3)	111.8(5)
M(1)—O(2)—C(3)	166.7(6)	140.2(9)
M(1)—N(22)—C(23)	138.6(7)	134.0(8)
M(1)—N(22)—C(24)	112.4(6)	115.8(8)
C(23)—N(22)—C(24)	109.0(8)	109.9(10)
Mo(1)—N(25)—C(26)	130.8(6)	118.8(8)
Mo(1)—N(25)—C(27)	117.5(6)	132.3(9)
C(26)—N(25)—C(27)	111.5(8)	108.7(10)

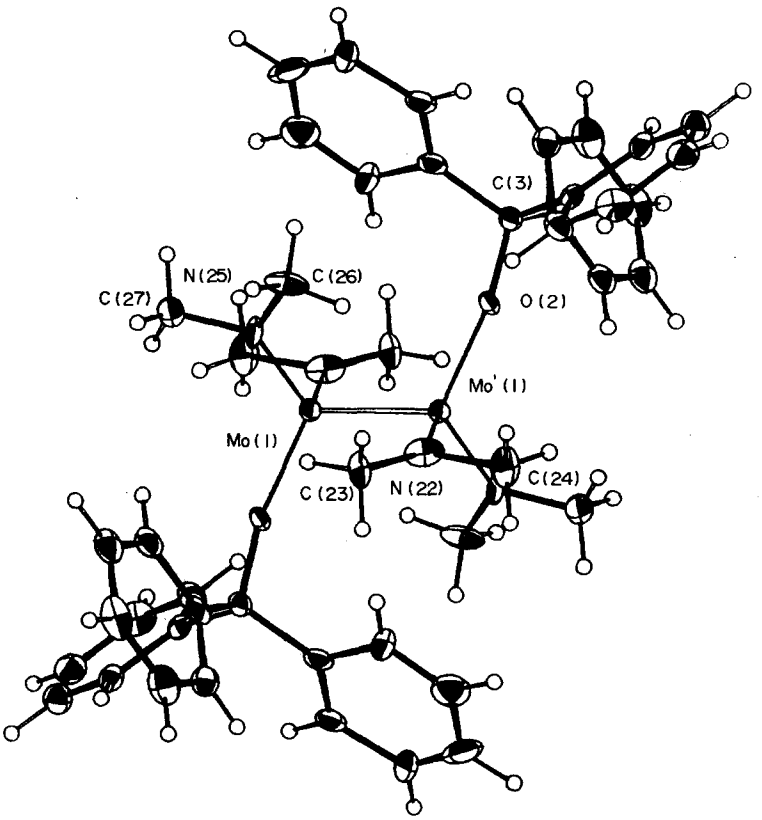

Fig. 1. The molecular structure (ORTEP) of $Mo_2(OCPh_3)_2(NMe_2)_4$ viewed perpendicular to the bond axis.

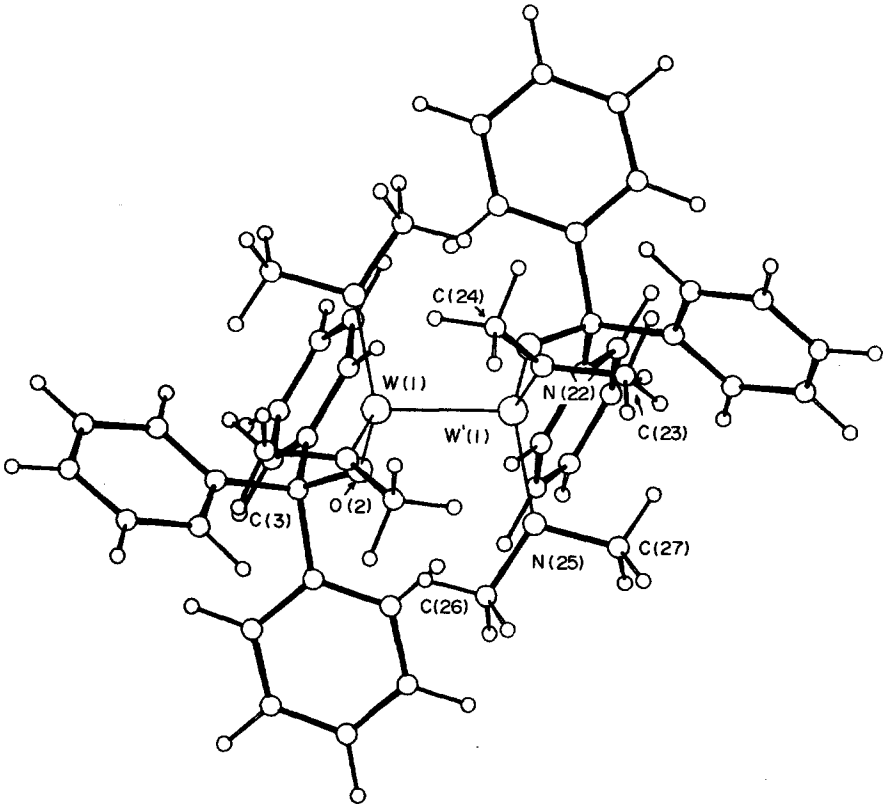

Fig. 2. The molecular structure (ball-and-stick) of $W_2(OCPh_3)_2(NMe_2)_4$ viewed perpendicular to the bond axis.

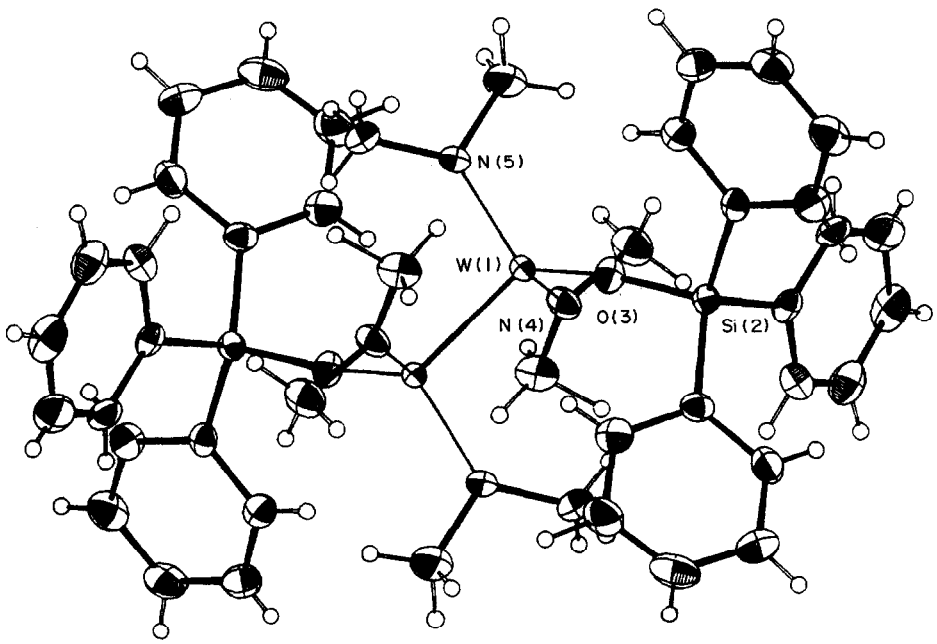

Fig. 3. The molecular structure (ORTEP) of $W_2(OSiPh_3)_2(NMe_2)_4$ viewed perpendicular to the M—M axis.

Table 2. Selected bond distances (Å) and angles (°) for $W_2(OSiPh_3)_2(NMe_2)_4$

Distances (Å)	
W(1)—W(1)′	2.2954(6)
W(1)—O(3)	1.925(4)
W(1)—N(4)	1.932(5)
W(1)—N(5)	1.939(5)
Si(2)—O(3)	1.615(4)
Si—C	1.87(1) (ave)
N—C	1.45(1) (ave)
Angles (°)	
W(1)′—W(1)—O(3)	108.06(13)
W(1)′—W(1)—N(4)	101.47(14)
W(1)′—W(1)—N(5)	102.40(14)
O(3)—W(1)—N(4)	115.51(18)
O(3)—W(1)—N(5)	112.11(18)
N(4)—W(1)—N(5)	115.48(20)
O(3)—Si(2)—C(6)	105.60(23)
O(3)—Si(2)—C(12)	108.76(22)
O(3)—Si(2)—C(18)	108.30(23)
C(6)—Si(2)—C(12)	110.75(25)
C(6)—Si(2)—C(18)	112.55(24)
C(12)—Si(2)—C(18)	110.67(25)
W(1)—O(3)—Si(2)	153.76(24)
W(1)—N(4)—C(24)	132.9(4)
W(1)—N(4)—C(25)	116.4(4)
W(1)—N(5)—C(26)	114.5(4)
W(1)—N(5)—C(27)	134.9(4)

† As with PR_3 ligands this π-bonding can involve Si—C σ^* orbitals.

$(NMe_2)_4$ are the shortest, 1.935(8) Å (ave), which is consistent with the view that the Ph_3SiO ligand is the weakest π-donor as a result of competitive oxygen-to-silicon π-bonding.†

Solution ^{1}H *NMR studies*

As with many other compounds of the general formula 1,2-$X_2M_2(NMe_2)_4$ they exist in equilibria involving *anti* and *gauche* rotamers in solution.[8] Since the M—M π-bonding uses metal d_{xy} and d_{yz} atomic orbitals, the Me_2N ligands are required to π-donate to metal $d_{x^2-y^2}$ and d_{xy} orbitals. This requires that the NC_2 blades of the Me_2N ligands lie along the M—M axis (as found in the X-ray structures). In the low temperature limiting spectrum we observe four N*Me* resonances for the *gauche* rotamer and two for the *anti* as indicated below.

The diamagnetic anisotropy of the M≡≡M bonds[9] leads to a *ca* 2 ppm separation in distal and proximal NMe resonances. On raising the temperature proximal and distal exchange occurs by M—N bond rotation and this leads to coalescence behaviour at higher temperatures. The barriers to M—N bond rotation are influenced by both steric and electronic factors.

Data pertaining to *anti* and *gauche* equilibrium concentrations and M—N rotational barriers are summarized in Table 4. Despite the greater steric pressure at the metal centre that results from $OCPh_3$ relative to $OSiPh_3$ ligands, we see higher barriers to M—N bond rotation for the siloxide. This further

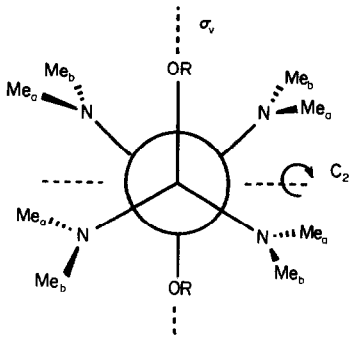

Anti configuration

At low temperature two types of dimethylamide resonances, one at high temperature.

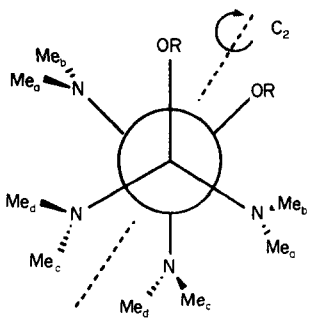

Gauche configuration

At low temperature four resonances, two at high temperature.

Table 3. Summary of crystal data

Empirical formula	$Mo_2C_{46}H_{54}O_2N_4$	$W_2C_{46}H_{54}O_2N_4$	$C_{44}H_{54}N_4O_2Si_2W_2$
Colour of crystal	Pale yellow	brown–yellow	orange
Crystal dimensions (mm)	$0.25 \times 0.30 \times 0.30$	$0.09 \times 0.054 \times 0.09$	$0.16 \times 0.16 \times 0.24$
Space group	$P2_1/n$	*Pbna*	$P2_1/n$
Cell dimensions			
Temperature (°C)	−171	−169	−126
a (Å)	9.528(2)	19.416(5)	9.571(1)
b (Å)	11.133(3)	21.214(5)	15.515(2)
c (Å)	20.602(5)	10.026(3)	15.490(2)
β (deg)	103.24(1)		107.31(2)
Z (molecules/cell)	2	4	2
	2127.17	4129.74	2218.83
Calculated density (g cm^{-3})	1.384	1.700	1.656
Wavelength (Å)	0.71069	0.71069	0.71069
Molecular weight	886.84	1062.66	1094.80
Linear absorption coeff. (cm^{-1})	6.143	57.271	54.387
Detector to sample distance (cm)	22.5	22.5	22.5
Sample to source distance (cm)	23.5	23.5	23.5
Ave Ω scan width at half height	0.25	0.25	0.25
Scan speed (deg/min)	8.0	4.0	8.0
Scan width (deg + dispersion)	2.0	1.8	2.0
Individual background (sec)	4	8	4
Aperture size (mm)	3.0×4.0	3.0×4.0	3.0×4.0
2θ range (deg)	6–45	6–45	6–45
Total number of reflections collected	2994	5196	3272
Number of unique intensities	2785	2686	2892
Number with $F > 0.0$			2791
Number with $F > 3.00\sigma(F)$	2399	1804	
$R(F)$	0.0482	0.0435	0.0253
$R_w(F)$	0.0548	0.0412	0.0275
Goodness of fit for the last cycle	2.105	1.304	1.001
Maximum delta/sigma for last cycle	0.12	0.002	0.19

Table 4. Summary of M—N rotational barriers and equilibrium distribution for *anti-* and *gauche*-$M_2(OCPh_3)_2(NMe_2)_4$ and $W_2(OSiPh_3)_2(NMe_2)_4$ compounds

Compound	[%]	$\Delta G^{\dagger}_{rot}$ kJ mol [T_c][a]
$W_2(OSiPh_3)_2(NMe_2)_4$		
anti	65	63 (60°C)
gauche	35	60 (40°C); 69 (95°C)
$W_2(OCPh_3)_2(NMe_2)_4$		
anti	50	59 (40°C)
gauche	50	50 (0°C); 62 (65°C)
$Mo_2(OCPh_3)_2(NMe_2)_4$		
anti	30	55 (35°C)
gauche	70	58 (25°C); 68 (65°C)

[a] Calculated from

$$K_{ex} = \frac{\pi \Delta v}{2}, \quad \Delta G^{\dagger} = -\ln\left[\frac{K_{ex}h}{KT_c}\right]RT_c.$$

supports the view that Me_2N-to-M π-bonding is stronger in the siloxide derivative than in compounds **I**.

The compounds $M_2(OSiPh_3)_4(NMe_2)_2$ also exist in solution as a mixture of *anti* and *gauche* rotamers, *ca* 60:40, but each has only one NMe_2 ligand. The T_c values fall in the range 30–55°C and 100–115°C. The latter are somewhat higher than the highest value for the $W_2(OSiPh_3)_2(NMe_2)_4$, consistent with the view that replacement of a Me_2N ligand by a $OSiPh_3$ ligand enhances Me_2N-to-M π-bonding in the remaining M-NMe_2 group.

Concluding remarks

The addition of the sterically demanding Ph_3COH and Ph_3SiOH to $M_2(NMe_2)_6$ compounds leads to only partial replacement of the NMe_2 ligands. The compounds $M_2(OEPh_3)_2(NMe_2)_4$, where E = C and Si and M = Mo and W, exist in *anti* and *gauche* rotamers of the now familiar ethane-like 1,2-$M_2X_2Y_4$ compounds (M≡M). The M—N distances are shorter than those in the parent $M_2(NMe_2)_6$ compounds and the M—N rotational barriers are higher supporting the view that the π-bonding order of the ligands is $Me_2N > Ph_3CO > Ph_3SiO$.

EXPERIMENTAL

All reactions were carried out under an inert atmosphere using standard Schlenk techniques. Solvents were distilled under nitrogen prior to use from sodium/benzophenone. Proton NMR spectra were measured on a Varian 300 XL spectrometer operating at 299.66 MHz in d^6-benzene or d^8-toluene and referenced to residual protio impurity at 7.15 and 2.07 ppm, respectively. IR spectra were obtained as pressed KBr pellets on a Perkin–Elmer 283 spectrophotometer. Microanalysis were provided by Oneida Research Services, Whiteboro, New York. $M_2(NMe_2)_6$ compounds were prepared as described previously[9] from WCl_4 or $MoCl_3$ with $LiNMe_2$ and the product was sublimed prior to use. Triphenylmethanol and triphenylsilanol were purchased from Aldrich Chemical Co. and were used as supplied.

The same general procedure and reaction scale was adopted for reactions involving both molybdenum and tungsten as outlined below.

$Mo_2(OCPh_3)_2(NMe_2)_4$

To $Mo_2(NMe_2)_6$ (0.200 g, 0.44 mmol) dissolved in hexane (10 cm^3) at room temperature was added dropwise with stirring over 5 min triphenylcarbinol (0.500 g, 2.0 mmol) in THF/hexane (5/5 cm^3) to generate a green solution. The solution was allowed to stand at room temperature for 2 h then placed in the freezer at −20°C for 3 days. Large yellow crystals of $Mo_2(OCPh_3)_2(NMe_2)_4$ were collected from the solution by removal of solvent via cannula and washing with hexane (5 cm^3) and diethylether (5 cm^3). Obtained $Mo_2(OCPh_3)_2(NMe_2)_4$ (0.380 g, 42.8 mmol, 97%). Found: C, 62.8; H, 6.4; N, 6.1. Calc.: C, 62.3; H, 6.1; N, 6.3%.

IR (cm^{-1}): 3050m, 3020m, 3010m, 2960w, 2940w, 2845s, 2800s, 2760s, 1940w, 1870w, 1790w, 1690w, 1480s, 1440vs, 1420s, 1410s, 1390w, 1310w, 1275w, 1235s, 1195m, 1170m, 1140m, 1100w, 1070m, 1040vs, 1020vs, 950vs, 930vs, 910s, 895s, 840w, 780vs, 760vs, 750vs, 720w, 690vs, 650m, 625s, 550s, 525w, 500w, 480s, 350s. Dec. p. = 162°C.

^{1}H NMR (benzene, 25°C): δ = 7.82 (d, 8H), 7.45 (d, 4H), 7.10 (m, 18H), 4.08 (s, H), 3.6 (br, 8H), 2.4 (br, 8H), 1.82 (4, 4H).

$W_2(OCPh_3)_2(NMe_2)_4$ (0.300 g, 0.283 mmol, 92%). Found: C, 52.9; H, 5.3; N, 4.0. Calc. for residual W_2N: C, 52.8; H, 5.1; N, 4.0%.

^{1}H NMR (benzene, 25°C): δ = 7.85 (d, 8H), 7.56 (d, 8H), 7.10 (m, 14H), 4.15 (s, 3H), 3.65 (s, 9H), 2.5 (s, 9H), 1.84 (s, 3H).

IR (cm^{-1}): 3070m, 3050m, 3020m, 3010m, 2970m, 2950m, 2855vs, 2810vs, 2780vs, 1940w, 1805w, 1795w, 1595m, 1575w, 1492vs, 1440vs, 1420s, 1390m, 1375w, 1310w, 1275w, 1260m, 1243s, 1200m, 1180m, 1160sh, 1155sh, 1150vs, 1110w, 1085s, 1078s, 1045vs, 1025vs, 998s, 955vs, 940vs, 915s, 900s, 865m, 840w, 790vs, 760vs, 750s, 725w,

700vs, 660m, 635s, 630s, 615m, 550m, 530m, 495m, 483s, 345s, 305m, 280w.

$W_2(OSiPh_3)_2(NMe_2)_4$

To $W_2(NMe_2)_6$ (0.500 g, 0.80 mmol) dissolved in hexane (10 cm^3) at 65°C was added $HOSiPh_3$ (0.401 g, 1.45 mmol) in hexane 5 cm^3/ether (5 cm^3)/toluene (1 cm^3). The solution was allowed to cool to room temperature. Five minutes after addition yellow crystals started to form. The solution was left to stand overnight and the filtrate was removed by decanting to leave $W_2(OSiPh_3)_2(NMe_2)_4$ (0.600 g, 0.55 mmol, yield = 68%).

IR (KBr pellet) (cm^{-1}): 3040m, 3020m, 2950m, 2885m, 2840m, 1950w, 1890w, 1810w, 1584s, 1500w, 1470m, 1400m, 1370w, 1340w, 1240s, 1185m, 1140m, 1100s, 910s, 960s, 890m, 800m, 730s, 690s, 540sh, 490vs, 420m, 370w, 350m, 330s, 300m, 286w.

^1H NMR in C_6D_6 at 25°C: δ = 7.8 (m, 12H), 7.1 (m, 12H), 6.8 (m, 6H), 4.1 (s, 3H), 3.9 (s, 6H), 3.15 (s, br, 6H), 2.5 (s, 6H), 2.2 (s, 3H).

V. T. NMR in $C_6D_5CD_3$: T_c-*anti*, 60°C, Δ = 437 Hz, $\Delta G^{\dagger}$ = 62.7 kJ mol^{-1}. T_c-*gauche*, 40°C, Δ = 510 Hz, $\Delta G^{\dagger}$ = 55.5 kJ mol^{-1}. T_c-*gauche*, 95°C, Δ = 325 Hz, $\Delta G^{\dagger}$ = 69.1 kJ mol^{-1}.

$W_2(O^tBu)_2(OSiPh_3)_4$

To $W_2(O^tBu)_6$ (0.250 g, 0.31 mmol) dissolved in hexane (10 cm^3) at room temperature was added triphenylsilanol (0.520 g, 1.88 mmol) in hexane (10 cm^3)/ether (15 cm^3) to generate a dark red–brown solution. The solution was allowed to stand at room temperature for 6 h and then cooled to −20°C for 12 h to produce orange–brown crystals. The filtrate was removed and the solid washed with hexane (10 cm^3) and ether (10 cm^3) to yield $W_2(O^tBu)_2(OSiPh_3)_4$ (0.420 g, 0.269 mmol, yield = 87%). Found: C, 59.4; H, 5.2; N, 0.0. Calc.: C, 59.5; H, 4.8; N, 0.0%. Dec. p. = 132–6°C.

^1H NMR in C_6D_6 at 25°C: δ = 7.63 (d, 24H), 7.13 (t, 12H), 6.97 (t, 24H), 1.40 (s, 18H).

$M_2(OSiPh_3)_4(NMe_2)_2$ (M = Mo, W)

The same general scale and procedure was used for both the molybdenum and tungsten compounds illustrated below for molybdenum.

To $Mo_2(NMe_2)_6$ (0.250 g, 0.55 mmol) dissolved in hexane (15 cm^3) at 65°C was added triphenylsilanol (0.600 g, 2.20 mmol) in diethylether (10 cm^3)/hexane (10 cm^3)/toluene (10 cm^3). This caused an immediate darkening of the solution to a red–brown. The solution was allowed to cool to room temperature overnight, with light orange "rosette" crystals starting to precipitate after 25 min. The filtrate was removed and the crystals washed with hexane (10 cm^3) and diethylether (10 cm^3) and dried briefly *in vacuo* for 10 min. Obtained $Mo_2(OSiPh_3)_4(NMe_2)_2$ (0.724 g, 0.52 mmol, yield = 95%). Found: C, 63.9; H, 5.2; N, 2.0. Calc.: C, 64.3; H, 5.2; N, 2.1%. Dec. p. = 165°C.

IR (cm^{-1}) = 3020s, 2950s, 2900m, 2880s, 2840s, 1940w, 1880w, 1810w, 1580m, 1555w, 1545w, 1470m, 1425vs, 1370m, 1320w, 1295w, 1250s, 1175m, 1145w, 1100vs, 1015, 990s, 920vs, 820sh, 730s, 695vs, 640sh, 505vs, 445m, 410m, 300m.

^1H NMR in C_6D_6 at 25°C: δ = 7.80 (m, 24H), 7.16 (m, 12H), 7.07 (m, 24H), 4.8 (br, 3H), 4.2 (br, 3H), 2.1 (br, 3H), 1.8 (br, 3H).

For $W_2(OSiPh_3)_4(NMe_2)_2$: obtained: 0.575 g, 0.37 mmol, yield = 94% as orange rosettes. Dec. p. = 160°C.

IR (KBr disc) (cm^{-1}) = 3050w, 3020s, 2950s, 2900m, 2880s, 2840s, 1940w, 1880w, 1810w, 1760w, 1580m, 1555w, 1545w, 1476m, 1425vs, 1370m, 1320w, 1295w, 1250s, 1175m, 1145w, 1100vs, 1015s, 990s, 920vs, 820sh, 730s, 695vs, 640sh, 505vs, 435m, 410m, 300m.

^1H NMR in C_6D_6 at 24°C: δ = 7.75 (m, 24H), 6.95 (m, 12H), 6.75 (m, 24H), 3.82 (s, 4H), 2.0 (s, 4H), 1.6 (s, 4H).

Structural determinations

General procedures and a listing of programs used have been reported.[10] Crystal data are summarized in Table 3.

$W_2(OCPh_3)_2(NMe_2)_4$. A suitable small single crystal was selected from the bulk sample using inert-atmosphere handling techniques. The crystal was transferred to the goniostat where it was cooled to −169°C for characterization and data collection. A systematic search of a limited hemisphere of reciprocal space yielded a set of reflections which exhibited orthorhombic symmetry. Unit cell dimensions were determined using 60 unique reflections having two θ values between 12 and 25°. The systematic extinctions of $0kl$ for $k = 2n+l$, of $h0l$ for $h+l = 2n+1$ and of $hk0$ for $h = 2n+1$ identified the space group as *Pbna* [an alternative setting of *Pbcn* (No. 60)]. It should be mentioned that the space group assignment was complicated by the pseudo carbon-centring of the data, all reflections having $h+k = 2n+1$ were quite weak due to the location of the heavy atoms on either side of the two-fold axis. A total of 5196 reflections (including standards and space group extinctions) were col-

lected in the given range. Following the usual data reduction and averaging of equivalent reflections a unique set of 1596 reflections was obtained. 1804 reflections were considered observed by the criterion $F > 3.0\sigma(F)$. A correction for absorption was performed. The R for the averaging was 0.03 for 1586 reflections, measured more than once. A plot of the four standard reflections measured every 400 reflections shows no systematic trends.

The structure was solved after some initial difficulty caused by the pseudo-symmetry. The heavy atom was eventually located by means of a Patterson function as well as by direct methods. The remaining non-hydrogen atoms were located in successive difference maps. Following the initial refinement almost all of the hydrogen atoms were evident in a difference map. The full-matrix least-squares refinement was completed using anisotropic thermal parameters on all non-hydrogen atoms. The hydrogen atoms were introduced in fixed idealized positions using isotropic thermal parameters of 1.0 plus the isotropic equivalent of the parent atom. The final R was 0.044 and $R_w(F)$ was 0.041, using all of the unique data. The total number of variables was 245 giving a ratio of observations to parameters of 10.97.

The final difference map was essentially featureless, the largest peak was about 2 e $Å^{-3}$, in the immediate vicinity of the tungsten atom.

$Mo_2(OCPh_3)_2(NMe_2)_4$. A suitable crystal was located and transferred to the goniostat using standard inert atmosphere handling techniques and cooled to $-171°C$ for characterization and data collection.

A systematic search of a limited hemisphere of reciprocal space located a set of diffraction maxima with symmetry and systematic absences corresponding to the unique monoclinic space group $P2_1/n$. Subsequent solution and refinement of the structure confirmed this choice.

Data were collected using a continuous θ–2θ scan with fixed backgrounds and data were reduced to a unique set of intensities and associated sigmas. The structure was solved by a combination of direct methods (MULTAN78) and Fourier techniques. A difference Fourier synthesis revealed the location of some, but not all, hydrogen atoms. All hydrogen atom positions were therefore calculated using idealized geometries and d(C—H) = 0.95 Å. These calculated positions were fixed for the final cycles of refinement.

A final difference Fourier was featureless, with the largest peak being 0.74 e Å.

$W_2(OSiPh_3)_2(NMe_2)_4$. A crystal of suitable size was mounted using silicon grease and was transferred to a goniostat where it was cooled to $-126°C$ for characterization and data collection. A systematic search of a limited hemisphere of reciprocal space revealed symmetry and systematic absences corresponding to the monoclinic space group $P2_1/n$.

The structure was solved by a usual combination of direct methods (MULTAN78) and Fourier techniques. The tungsten atom position was obtained from an initial E-Map, and the remainder of the non-hydrogen atoms were found in subsequent iterations of least-squares refinement and difference Fourier calculations. After partial refinement of the non-hydrogen atoms, a difference Fourier revealed all hydrogen atoms. Non-hydrogen atoms were refined anisotropically, and hydrogen atoms isotropically to an R-factor equal to 2.5%.

Atomic coordinates have been deposited with the Cambridge Crystallographic Data Centre.

Acknowledgements—We thank the National Science Foundation for support. I.P.P. thanks SERC (U.K.) for support through the form of a NATO fellowship.

REFERENCES

1. M. H. Chisholm and I. P. Rothwell, *Comp. Coord. Chem.* 1987, **2**, 161, 335.
2. M. H. Chisholm, F. A. Cotton, C. A. Murillo and W. W. Reichert, *Inorg. Chem.* 1977, **16**, 1801.
3. M. Akiyama, M. H. Chisholm, F. A. Cotton, M. W. Extine, D. A. Haitko, D. Little and P. E. Fanwick, *Inorg. Chem.* 1979, **18**, 2266.
4. M. H. Chisholm, D. L. Clark, K. Folting, J. C. Huffman and M. J. Hampden-Smith, *J. Am. Chem. Soc.* 1987, **109**, 7750; M. H. Chisholm, D. L. Clark and M. J. Hampden-Smith, *J. Am. Chem. Soc.* 1989, **111**, 574.
5. M. H. Chisholm, K. Folting, C. E. Hammond, M. J. Hampden-Smith and K. G. Moodley, *J. Am. Chem. Soc.* 1989, **111**, 5300.
6. R. G. Abbott, F. A. Cotton and L. R. Favello, *Inorg. Chem.* 1990, **9**, 1829.
7. D. R. Baxter, M. H. Chisholm, J. A. Klang and V. F. DiStasi, *Chem. Materials* 1991, **3**, 221; M. H. Chisholm, V. F. DiStasi and S. Haubrich, unpublished results.
8. M. H. Chisholm, *Angew. Chem., Int. Edn Engl.* 1986, **25**, 21; *Accts. Chem. Res.* 1990, **23**, 419.
9. (a) M = Mo: M. H. Chisholm, F. A. Cotton, B. A. Frenz, W. W. Reichert, L. W. Shive and B. R. Stults, *J. Am. Chem. Soc.* 1976, **98**, 4469; (b) M = W: M. H. Chisholm, F. A. Cotton, M. W. Extine and B. R. Stults, *J. Am. Chem. Soc.* 1976, **98**, 4477.
10. M. H. Chisholm, K. Folting, J. C. Huffman and C. C. Kirkpatrick, *Inorg. Chem.* 1984, **24**, 1021.

Polyhedron Vol. 10, No. 23/24, pp. 2847–2849, 1991
Printed in Great Britain

0277–5387/91 $3.00+.00
Pergamon Press plc

COMMUNICATION

ON THE TRIS((*R*)CYSTEINATE)COBALT(III) AND TRIS((*R*)CYSTEINESULPHINATE)COBALT(III) IONS: A FINALE

A. P. ARNOLD and W. G. JACKSON*

Contribution from the Department of Chemistry, University College (NSW), Australian Defence Force Academy, Northcott Drive, Campbell, ACT 2600, Australia

(*Received* 21 *August* 1991; *accepted* 2 *September* 1991)

Abstract—Responses are offered to a recent critical communication by R. D. Gillard (*Polyhedron* 1991, **10**, 1453) which defend our positions (A. P. Arnold and W. G. Jackson, *Inorg. Chem.* 1990, **29**, 3618) with respect to the stereospecificity in the synthesis of the title complexes.

A paper by Arnold and Jackson published in *Inorganic Chemistry* in 1990,[1] concerning the ions tris(cysteinato)- and tris(cysteinesulphinato) cobalt(III), was the subject of criticism in a communication published very recently in this journal.[2] We prefer not to comment on its tone. Those who have closely read both papers will have assessed the scientific facts for themselves. However, this note serves to clarify some confusion created about our work by Gillard's note, and is directed in particular to those who have read Gillard's communication but not ours.

Our paper[1] addressed the question of specificity in the synthesis of tris(cysteinato)- and tris(cysteinesulphinato)-cobalt(III), while Gillard's note[2] stressed the reliability of the latter complex as a resolving agent when made by a particular method (but asserting that we implied otherwise). He went on to defend earlier claims[3–6] that the tris((*R*)cysteinesulphinate-N,S)cobalt(III) ion could be synthesized by a reliable and stereospecific synthesis.

To summarize the facts: the chiral anion $[Co((R)cysSO_2\text{-}N,S)_3]^{3-}$ can be synthesized in two steps from cobalt(II) or (III) starting materials. The Δ and Λ forms of $[Co((R)cysS\text{-}N,S)_3]^{3-}$ are produced in the first step with a degree of stereoselectivity which depends upon the method of synthesis.[1] Both of these diastereomers are oxidized by H_2O_2 to $[Co((R)cysSO_2\text{-}N,S)_3]^{3-}$, and we demonstrated that this step was stereospecific,[7] as expected.[1]

We consider general points first, and there are two fundamental ones. First, if a substance exists in two isomeric forms and a particular synthesis carried out in solution gives much less than a quantitative yield of a solid complex believed to be a single isomer, it is reasonable to enquire if the other isomer is left in solution. It is not correct to claim that such a synthesis is stereospecific, even if the isolated solid were a single isomer (unless, for all of the material of that particular composition, it was isolated quantitatively). Gillard[2] has defended earlier criticism[1] by stating that he was referring to the isolated solid, but the term to describe such an isolated solid is "pure" or "isomerically pure", not as a solid obtained "stereospecifically". The terms "stereoselective" and "stereospecific", despite differences in inorganic and organic[7] parlance, refer to total product.

The second point is that one cannot know with certainty an isomer distribution, or even establish isomeric purity, if only one of the two isomers has been characterized. For a technique such as NMR spectroscopy, two sets of signals for a product may be diagnostic of composition whereas the observation of one set remains ambiguous. The degree of ambiguity of course depends upon the level of spectroscopic resolution. In summary, where one

* Author to whom correspondence should be addressed.

has characterized just the one isomer, evidence of isomeric composition can only be circumstantial.

Gillard *et al.*,[2-5] and others before them,[8-11] had reported only the one stereoisomer, although there has been recognition that both might have been obtained (by a kinetic route, for example). We, however, have isolated both as pure crystalline solids, for each of the tris(cysteine)- and tris(cysteinesulphinate)-complexes, and despite expressed or implied views to the contrary,[2] this is a significant advance.

Gillard has emphasized the reliability of his synthesis of Schubert's[8] resolving agent. We have never contested this. But there are several synthetic methods,[1,8] not just theirs,[4,5] and we showed that you can and do get isomeric mixtures, depending upon the route you choose.[1] Mindful of this fact, we tested the recrystallization process used by Gillard and others and showed that it does lead to an isomerically pure product. In this regard Gillard takes issue with our use of the word "repeated", in respect of a simple recrystallization. In reference to the $[Co((R)cysSO_2\text{-}N,S)_3]^{3-}$ anion, Gillard stated[2] he always used the Δ form, whereas we[1] used the Δ, the Λ, and a Λ/Δ isomer mixture, and therefore technically we only repeated his work when using the Δ isomer! Actually we may well have repeated his work in the strictest sense since, as already noted, his crude material could have been a mixture; this could never have been known since no one had previously reported that fractionation (or recrystallization) from water/ethanol removes the other isomer.

We feel obliged to respond to his more specific criticisms:[2]

(1) Gillard refers in three places to our "ignorance" of his "extensive reported work". But of course the fact that we did not reference all his work does not mean we were ignorant of it.

(2) In the last paragraph of his communication,[2] he again alludes to our apparent ignorance of the literature, noting our "failure ... to acknowledge relevant, prior work". In particular, he cites a structural paper of a cobalt(III) trinuclear species which contains the tris((*R*)cysteinato)cobalt(III) anion as a ligand,[12] and goes on to say that "... they too" (Okamoto *et al.*) "had gone over the question of the stereoselectivity of the formation of green Δ_{LLL}-*fac*(*S*)-$[Co(L\text{-}cys\text{-}N,S)_3]^{3-}$ but were able to agree in full with our earlier work". We believe that this is misrepresentation of their paper. Okamoto *et al.*[12] discussed the evidence for stereoselectivity of formation for each of two trinuclear species, not that for their precursor. In regard to the latter, Okamoto *et al.*[12] merely noted that the tris(cysteinate)cobalt(III) complex was prepared by the method of Schubert,[8] and stated in two places but without experimental evidence that the Δ_{LLL} isomer was formed selectively (with references to Kita *et al.*[13] and Gillard[3]!).

(3) We suggested[1] that it might be desirable to recrystallize the resolving agent and check its isomeric purity before using it. However, Gillard[2] states that "all that is required is to follow the published directions properly". He fails to accept that there are numerous others routes[1,8] to its synthesis which one might use, and we showed[1] that these can (and often do) give isomeric mixtures. We didn't use his particular method[4,5] (starting from $[Co(NH_3)_6]^{3+}$), and he acknowledged that,[2] and if there were an inference that his method might also give a mixture, it is of no consequence; Gillard *et al.* use recrystallized material,[4,5] and *we showed* (through the characterization of both isomers) that recrystallization as described[4,5] removes any of the other isomeric form.

(4) Gillard[2] singles out a host of remarks from our[1] paper, and deals with these in turn as (i)–(v) on the second page of his communication. With respect to his (i), the "sic" annotation to a quotation from our work is inappropriate. It is true that the ^{13}C NMR spectrum had not been published (prior to our[1] work), although spectral data[5,14] had appeared. Further, Gillard draws attention to a trivial typographical error in our paper, intimating that a temperature difference of 7° as regards chemical shifts might be important; it is our experience that the shift differences between our two isomers were such that temperature could have no possible bearing on the issue; in any event, the spectra of the two isomers were measured at the *same* temperature.

Gillard[2] quotes two sets of chemical shift values he published[5,14] for his complex, stating that they "agree well" with our data. They do not even agree well with each other, let alone our data. Indeed the two sets of values span the shift differences between the authentic two isomers we obtained.[1] From these data, one could even be led to believe that Gillard *et al.* inadvertently obtained the two isomers we described, although we do not think so.

(5) The comments under his (iv)[2] disguise the full truth. We are attributed to having obtained two isomers for the green tris((*R*)cysteinate-N,S) complex *in solution*; the italics are Gillard's.[2] We did,[1] but it is also very clear from our paper that we actually isolated and characterized these as pure solids, and went to some pains to prove this.

(6) Again under (iv), Gillard seems to be equating equilibrium isomer distributions in solution with the isomer or isomers one might crystallize from

solution. They may not be related. We showed[1] one can get a second-order asymmetric transformation in this system, so it is *not* "rather odd[ly]" that we should suggest checking the isolated material for isomeric purity knowing that the equilibrium strongly favours one isomer, but rather for very good reason.

(7) The next paragraph makes a number of statements out of context which convey a very imbalanced account. He suggests[2] there is complete overlap in his and our work, in stating "Jackson and Arnold have confirmed the following facts...". In the light of the present and previous[1] notes, "established" would be a better word than "confirmed". Furthermore, he dismisses the "new facts" about the green compound in a sentence, and totally ignores the new facts about the yellow tris ((*R*)cysteinesulphinate-N,S) compounds, one a new isomer.

Finally, the last paragraph of his note[2] refers to a matter totally unrelated to the cysteine problem, and is clearly directed at discrediting one of us. The readers of the papers[15,16] can make up their own minds, but Gillard's reference to "criticisms and misquotation[7] by Jackson" (ref. 7 is the present ref. 15) again misrepresents a situation. In politest terms, we are unaware of the "misquotation" to which Gillard refers;[2] if there was one,[15,16] it was not by one of us.

REFERENCES

1. A. P. Arnold and W. G. Jackson, *Inorg. Chem.* 1990, **29**, 3618.
2. R. D. Gillard, *Polyhedron* 1991, **10**, 1453.
3. R. D. Gillard and R. Maskill, *J. Chem. Soc., Chem. Commun.* 1968, 160.
4. L. S. Dollimore and R. D. Gillard, *J. Chem. Soc., Dalton Trans.* 1973, 933.
5. P. S. Cartwright, R. D. Gillard and E. R. J. Sillanpaa, *Polyhedron* 1987, **6**, 105.
6. See also other papers cited in ref. 2.
7. E. L. Eliel, *Stereochemistry of Carbon Compounds*, pp. 434–437. McGraw-Hill, New York (1962).
8. M. P. Schubert, *J. Am. Chem. Soc.* 1933, **55**, 3336.
9. R. G. Neville and G. Gorin, *J. Am. Chem. Soc.* 1956, **78**, 4891.
10. R. G. Neville and G. Gorin, *J. Am. Chem. Soc.* 1956, **78**, 4893.
11. G. Gorin, J. E. Spessard and G. A. Wessler, *J. Am. Chem. Soc.* 1959, **81**, 3193.
12. K.-I. Okamoto, S.-I. Aizawa, T. Konno, H. Einaga and J. Hidaka, *Bull. Chem. Soc. Japan* 1986, **59**, 3859.
13. M. Kita, K. Yamanari and Y. Shimura, *Bull. Chem. Soc. Japan* 1982, **55**, 2873.
14. L. S. Dollimore and R. D. Gillard, *J. Chem. Soc., Dalton Trans.* 1975, 369.
15. W. G. Jackson, *Inorg. Chem.* 1987, **26**, 3004.
16. T. L. Brown, *Inorg. Chem.* 1989, **28**, 3229.

Polyhedron Vol. 10, No. 23/24, pp. 2851–2853, 1991
Printed in Great Britain

0277–5387/91 $3.00+.00
Pergamon Press plc

COMMUNICATION

ISOLATION AND CHARACTERIZATION OF A NOVEL MULTIBRIDGED TETRADENTATE DIANIONIC FORM OF PYRIDOXIC ACID. CRYSTAL STRUCTURE OF TETRANUCLEAR $[Cu_4(PAA)_2(Bipyam)_4(H_2O)_2Cl_2](NO_3)_2 \cdot CH_3OH \cdot 10H_2O$*

IRIMPAN I. MATHEWS and HATTIKUDUR MANOHAR†

Department of Inorganic and Physical Chemistry, Indian Institute of Science, Bangalore-560 012, India

(*Received* 19 *July* 1991; *accepted* 27 *August* 1991)

Abstract—The X-ray analysis of the tetranuclear copper(II) complex formed from pyridoxic acid and 2,2′-dipyridylamine reveals a novel metal binding mode of pyridoxic acid as a multibridged tetradentate dianion. Here the pyridoxic acid moiety uses all possible sites except the pyridine nitrogen for metal coordination.

Metal complexes of B_6 vitamins and the Schiff bases derived from them have been an interesting area of study for the bioinorganic chemist.[1] Much research has been concerned with the ligating sites in these compounds. The most common binding sites are phenolic oxygen and the 4-(aminomethyl), 4-(hydroxymethyl) or the 4(-carboxyl) groups of pyridoxamine (PM), pyridoxine (PN) and pyridoxic acid (PA), respectively (Sketch).[2–4] Binding of the metal at other sites like the pyridine nitrogen or the side chain at the 5-position is rare.[3,5] The Vitamin B_6 moiety usually functions as a bidentate and rarely as a tridentate monoanion. The various monoanionic forms, characterized crystallographically, have been discussed in detail recently.[4] Pyridoxic acid is one of the oxidation products of pyridoxal which is an active form of Vitamin B_6. A novel oxidation of pyridoxal to pyridoxic acid was reported earlier from this laboratory during attempts to prepare ternary Schiff base metal complexes with 2,2′-bipyridine as the ternary ligand.[2] The title compound was isolated during studies on the oxidation reaction in metal complexes varying the ternary ligand. The X-ray structure of the complex reveals a novel mode of binding for pyridoxic acid as a multibridged tetradentate dianion where all potential sites except the pyridine nitrogen are used for coordination.

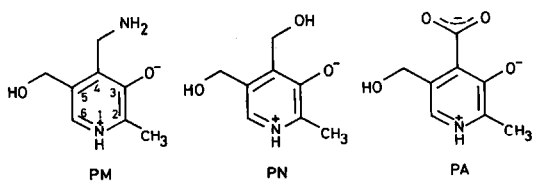

The complex was prepared by treating pyridoxal·HCl with 0.1 N NaOH until the pH reached a value of ~4.1. An aqueous solution of $Cu(NO_3)_2 \cdot 3H_2O$ was then added and the pH raised to ~4.2. This was treated with an aqueous methanolic solution of bipyam and the solution kept aside for slow evaporation. Dark green crystals of the title compound appeared after 4 months.

* PA = pyridoxic acid, PAA = dianionic form of PA, bipyam = 2,2′-dipyridylamine.

† Author to whom correspondence should be addressed.

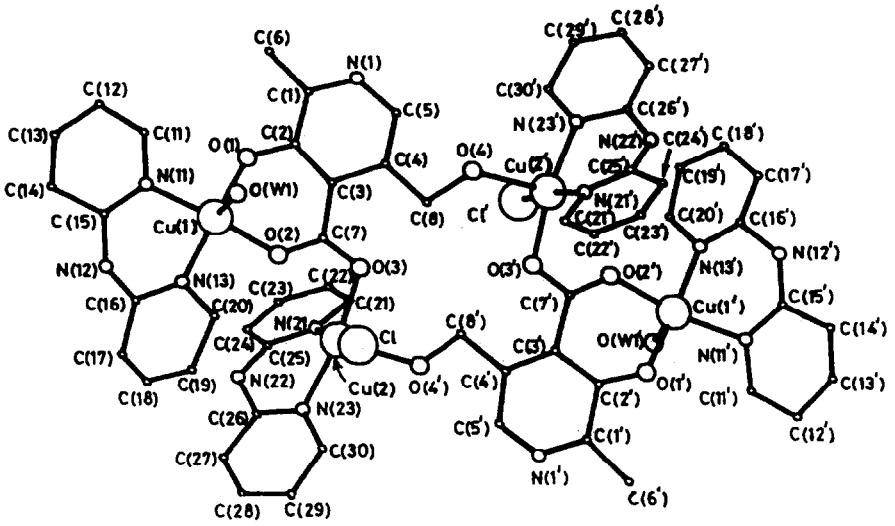

Fig. 1. Molecular structure of $[Cu_4(PAA)_2(Bipyam)_4(H_2O)_2Cl_2]$. Coordinating distances (Å): Cu—N (bipyam) 1.97(2)–2.05(2); Cu—O (carboxylate, phenolic) 1.90(2)–1.99(2); Cu—O(hydroxymethyl) 2.30(2), 2.34(2); Cu—Cl 2.26(1), 2.32(1); Cu—O(water) 2.29(2).

The X-ray structure,* Fig. 1, reveals that the compound is tetranuclear with four square pyramidally coordinated coppers, two PA moieties and four bipyam ligands. The coordinating atoms for Cu(1) and Cu(1′) and Cu(2) and Cu(2′) are similar. The basal sites for the first two are occupied by two bipyam nitrogens, one phenolic oxygen and one carboxylate oxygen. The axial position is filled by a water molecule. On the other hand, for the latter two the phenolic oxygen at the basal site is replaced by a Cl^- ion and a 5-hydroxymethyl oxygen of the pyridoxic acid occupies the axial position. The pyridoxic acid moiety bridges three coppers in both a monodentate and bidentate fashion. The 5-hydroxymethyl oxygen and phenolic oxygen are involved in monodentate coordination, whereas the carboxylate functions as a bridging bidentate. Pyridoxic acid exists as a dianion with carboxylate, phenolate and 5-hydroxymethyl groups deprotonated and the ring nitrogen protonated. The existance of Vitamin B_6 as a dianion and the deprotonation of the 5-hydroxymethyl group are unprecedented. It is interesting to note that the chelation of the metal ions by PAA moieties results in the formation of a 14-membered macrocyclic ring.

To our knowledge this is the first structural study of a tetranuclear complex involving Vitamin B_6 or its derivatives and also of a tetranuclear metal complex involving the chemically important bipyam ligand. Furthermore, this is the first structure of a Vitamin B_6 complex involving bipyam as a ternary ligand.

* *Crystal data*: $C_{57}H_{78}Cl_2N_{16}O_{27}Cu_4$, triclinic, space group $P\bar{1}$, $a = 13.825(6)$, $b = 14.034(6)$, $c = 19.231(5)$ Å, $\alpha = 92.23(3)$, $\beta = 98.89(5)$, $\gamma = 98.47(6)°$; $U = 3639$ Å^3, $Z = 2$, $M = 1743.1$, $D_c = 1.591$ g cm^{-3}, $F(000) = 1797$, μ(Mo-K_α) = 13.64 cm^{-1}, θ range 1.0–20.0° (reflections were very weak at high angles). Final R value 0.098 for 3168 out of 7212 reflections [$I > 2\sigma(I)$], collected on an Enraf–Nonius CAD4 diffractometer. The structure was solved by the heavy-atom method and refined by full-matrix least-squares procedure based on F.[6] Copper, nitrogen and oxygen atoms were refined anisotropically and the carbon atoms isotropically. Hydrogen atoms were located from the electron density maps and used without refinement. One of the nitrate groups showed disorder and was refined with constraints on bond parameters. The molecule shows a pseudo-centre of inversion, but an analysis of the Niggli matrix revealed no higher symmetry. Final atomic coordinates, thermal parameters, bond parameters and structure factor tables have been deposited with the Editor as Supplementary Material. Atomic coordinates have been deposited with the Cambridge Crystallographic Data Centre.

REFERENCES

1. R. H. Holm, *Inorg. Biochem.* 1973, **2**, 1137; A. E. Martell, *Accts Chem. Res.* 1989, **22**, 115.
2. S. P. S. Rao, H. Manohar, K. Aoki, H. Yamazaki and R. Bau, *J. Chem. Soc., Chem. Commun.* 1986, 4; S. P. S. Rao, H. Manohar, K. Aoki and H. Yamazaki, *J. Chem. Soc., Dalton Trans.* 1987, 1009.
3. K. J. Franklin and M. F. Richardson, *Inorg. Chem.* 1980, **19**, 2107.

4. S. P. S. Rao, K. I. Varughese and H. Manohar, *Inorg. Chem.* 1986, **25**, 734 and refs therein.
5. J. F. Cutfield, D. Hall and T. N. Waters, *J. Chem. Soc., Chem. Commun.* 1967, 785; S. P. S. Rao, H. Manohar and R. Bau, *J. Chem. Soc., Dalton Trans.* 1985, 2051; K. Aoki and H. Yamazaki, *J. Chem. Soc., Chem. Commun.* 1987, 1241.
6. G. M. Sheldrick, SHELX-76, Program for Crystal Structure Determination. University of Cambridge, U.K. (1976).

Polyhedron Vol. 10, No. 23/24, p. 2855, 1991
Pergamon Press plc. Printed in Great Britain

BOOK REVIEW

Noble Gas and High Temperature Chemistry (Structure and Bonding 73). Edited by M. J. Clarke, J. D. Dunitz, J. B. Goodenough *et al.* Springer-Verlag, Berlin, 1990, ISBN 3-540-52124-0, 262 pp., DM 148.

The latest volume in this well-established series contains five reviews. Two of these are concerned with Noble Gas (Ng) chemistry, two with stellar elemental synthesis and the remaining one with the chemistry of inorganic vapours. Normally, on realising that the same person was involved in three of the reviews, my reaction would be of scepticism; however, since that author happens to be C. K. Jørgensen, one anticipates a certain panache, and his participation in two pieces on nuclear synthesis in the Big Bang, supernovae, etc. may well be termed a star turn.

A brief first chapter (15 pages) by C. K. Jørgensen and G. Frenking reviewing the history of the discovery of the Noble Gases and their compounds is full of interesting points; with follow-up of initial observations, the Fraunhofer lines might today remember W. H. Wollaston (who discovered palladium and rhodium). Similarly, comments "chemists can never know what may happen tomorrow" and questions—why should an element have only one electronegativity? The review of preparative Ng chemistry beginning with the complicated Xe/PtF_6 reaction "Inorganic chemistry is sometimes too complicated to be easily rationalized by beautiful, but less complicated, ideas" (Reader, what first interested *you* in Inorganic Chemistry?) continues by pointing out that ozone should oxidize xenon at pH 14–15 on thermodynamic grounds, as well as the similarity of isoelectronic Xe^{II} and I^{I}, Xe^{IV} and I^{III}, Xe^{VI} and I^{V} and Xe^{VIII} and I^{VII} couples. Other plausible species include ArO_4 and oxo anions of Kr^{VI} and ^{VIII}, as well as $Xe(CN)_2$.

The second chapter (by G. Frenking and D. Cremer) examines at more length (nearly 80 pages) the chemistry of the more noble Ngs (He, Ne and Ar) of which the authors remark that the common chemical thinking is that they "should be left to physicists and engineers to do work on superconductors and to prepare light bulbs", pointing out that gas-phase species involving these elements have a respectable pedigree (1925 in the case of HeH^+).

The article goes on to look at the role of theoretical predictions in guiding experimentalists, particularly *ab initio* calculations. Species examined include known ones like Ng_2^+ and NgH^+ and polyatomics like $ArCO^+$ (it is pointed out that argon should resemble krypton in its chemistry rather than neon); the scheme used is the donor–acceptor model. A table of predicted stable or metastable species includes neutral NgBeO molecules as well as a range of ions such as $NgCCH^+$ and Ng_2C^{2+}. (Is it not time for a book "Non-existent compounds 30 years on"?)

K. Hilpert's article "Chemistry of inorganic vapours" is a very thorough hundred page survey of the area. It looks mainly at the species present in equilibrium vapours and their dissociation or atomization energies. These results were mainly obtained by Knudsen cells linked to MS, and the methodology is reviewed. Particular developments over the last decade include the identification of complex Zintl compounds, detailed studies of some metal oxides like Li_2O, and various metal halides. It is interesting to note how these gas phase studies can complement solid-state research—i.e. results indicating essentially ionic character in RbAu and CsAu in contrast to LiAu and NaAu; similarly, gas-phase FeI_3 was identified long before the recent successful isolation of the compound in the solid state. Not the least useful feature of the article is the collection of thermodynamic data.

Jørgensen looks at the synthesis of heavy elements in peculiar A-type (A_p) stars. He points out that the vast majority of chemical elements are synthesized in the collapsing core of supernovae; A_p stars have peculiarly high abundances of certain elements, europium for example; others appear to be high in mercury. Various ideas based on neutron irradiation followed by various types of accretion or diffusion have been suggested as explanations. Some A_p stars may have originated in multiple-star systems along with a progenitor that exploded as a supernova.

In the final article, Jørgensen and G. B. Kauffman examine ideas of nuclear synthesis based on high-temperature polymerization of hydrogen (Crookes, 1887) and deviations from mass additivity (Marignac, 1860; Harkins and Wilson, 1915). We are taken through the types of elementary particles, quarks and all, not to mention Dark Matter and WIMPS, together with the possibility of fractionally charged systems. More conventionally, we are given comparative abundances of elements in the solar photosphere and in the earth's crust. We are left to speculate on the intuitive processes of a scientist like Crookes, not to mention universes made up of anti-elements, where presumably antibonding orbitals are desirable.

Thoroughly recommended, but I fear that not enough university libraries in the U.K. are able to afford a standing order to this series, relatively inexpensive though it is.

Felixstowe College **SIMON COTTON**
Felixstowe IP11 7NQ, U.K.

Polyhedron Vol. 10, No. 23/24, p. 2857, 1991
Pergamon Press plc. Printed in Great Britain

ANNOUNCEMENT

MOLECULAR ELECTROCHEMISTRY OF INORGANIC, BIOINORGANIC AND ORGANOMETALLIC COMPOUNDS

Sintra, close to Lisbon, Portugal
25–29 March 1992

Contact: Prof. A. J. L. Pombeiro,
Complexo I, Instituto Superior Técnico,
Av. Rovisco Pais, 1096 Lisbon Codex, Portugal.
Fax: 351-1-3524372. Tel: 351-1-3524303.

Organizing Committee: Profs A. J. L. Pombeiro (Director),
J. McCleverty (Director),
J.-M. Savéant and K. M. Kadish.

General Objective

Assessment of the state-of-the-art in the application of electrochemistry to the investigation of the properties (including synthesis and reactivity) of inorganic, bioinorganic and organometallic complexes, discussion of prospects and formulation of recommendations.

SUBJECT INDEX

(Compiled by Peter Thornton)

A

Ab initio calculations
  S_4N_4, 1935
Acetates and acetato complexes
  cadmium, 1017
  chromium(II), 1237
  copper(II), 805,2035,2613,2867
  europium, 1411
  manganese(III), 2867
  molybdenum(II), 1237
  neodymium, 1411
  nickel(II), 1729
  palladium(II), 2741
  rhenium(II), 743
  rhodium, 1589
  tin(IV), 1331
  tungsten(IV), 11
  uranium(VI), 2987
  yttrium, 1305
Acetone complexes
  cobalt(II), 1375
Acetonitrile complexes
  copper(I), 75,2919
  manganese(II), 1311
  ruthenium(II), 1243
  sodium, 957
  tungsten(0), 2887
  tungsten(VI), 2293
Acetophenone complexes
  aluminium, 233
N-Acetylcysteine, *N*-acetyl-
  penicillamine complexes, Cd, 831
N-Acetylmethionine and -amide
  complexes
  platinum(II), 1975
1-Adamantylamido complex
  aluminium, 257
Alanine complexes
  cadmium, 2437
Alanylalanine, -glycine complexes
  cobalt(II),(III), 2567
Alcohols, oxidation by Ru(VI)
  complexes, 1751
Alcohol complexes
  nickel(II), 535
  osmium(III), 2309
  uranium(IV), 1843
Aldehyde complexes
  aluminium, 233
Alditol complexes
  molybdenum(VI), 1225
Aldol condensations, metal
  enolates in, 223
Alkenes, conversion to alcohols,
  1235
Alkene complexes
  chromium(II), 2193
  tungsten(IV), 23
Alkene dimerisation, 2809
Alkene oligomerization, 2823
Alkenediyl complexes
  Ir(II,III), Rh(II), 2635
Alkenyl complexes
  ruthenium(II), 907
Alkoxides
  aluminium, 227,223,239,253,309,
    371,409
  barium, calcium, 2959
  copper(II), 535,611,2575,2867
  germanium, 2189
  indium(III), 719
  lithium, 227
  manganese(II), 2867
  molybdenum, 619
  molybdenum(III), 1821,2941
  molybdenum(V), 1965
  nickel(II), 2867
  ruthenium(II), 1113
  scandium, 719
  strontium, 2959
  tin(IV), 1331
  tungsten, 2953
  tungsten(III), 1829,2941
  uranium(IV), 1843
  Y, Yb, 719
Alkoxycarbene complexes
  molybdenum, tungsten, 2953
Alkoxycarbonyl complexes
  rhenium(III), 1131
Alkyls
  aluminium, 223,233,239,245,257,
    265,277,289,301,313,371,2205,
    2809
  antimony, arsenic, 921
  boron, 223
  cadmium, 921,1483,2437
  cobalt, 2477
  cobalt(II), 931
  gallium, 223,319,335,343,353,
    2763
  germanium, 227,2263
  hafnium, 301
  indium, 353,361,921
  iridium(III), 1883,2071
  magnesium, 1775
  manganese(I), 921
  mercury, 597,921,2477
  niobium, 1051
  rhenium(V), 957
  rhodium, 2477

rhodium(III), 2047,2071
rhodium(IV), 2071
ruthenium(III), 2071
tantalum, 1051
tellurium(II), 847,921
tin(IV), 2863
titanium(IV), 1423
tungsten(IV), 11,23
tungsten(VI), 1271
zinc, 223,921
zirconium, 301,839,1423
Alkylamides
aluminium, 253,257
chromium(VI), 2625
gallium, 343
mercury, 1765
molybdenum(III), 1821
niobium(V), tantalum(V), 2709
Alkylidene complexes
osmium, tungsten, 1491
Alkylidyne complexes
molybdenum, tungsten, 2953
tungsten(VI), 1271
Alkylimides
chromium(VI), 1009,2625
osmium(VIII), 1009
rhenium(V),(VI),(VII), 2081
tungsten(IV), 603
Alkylsilazalanes, 2205
Alkynes, reactions with trinuclear complexes, 2791
Alkyne complexes
iridium(I), 1867
nickel(I), 581
niobium(I), 1855
Os(0), Ru(0), 1867
tantalum(V), 2709
tungsten(II), 727,2135,2233,2507
tungsten(IV), 603
Allyl complexes
nickel(II), 757
tungsten(IV), 11,23
Aluminium
aldehyde alkyl alkoxide ketone complexes, 233
alkoxide alkylamide amine complexes, 253
alkoxide methyl phenoxide compounds, 239
alkyl chloride, 2809
alkyl enolates, 223
alkyl silyl lithium compounds, 277
alkyl silylamides, 2205
alkylamide arylamide methyl cyclometallated compounds, 257
amine arsine methyl complexes, 289
aniline arylamide chloride methyl cyclometallated complexes, 245
blood plasma speciation, 151,163
butoxides, 227
catechol citrate desferrioxamine hydroxide complexes, 171
chloride ethoxide pyridine complex, 309
chloride tungsten(IV) complex, 11
diketonates, 215
diphosphoglycerate complexes, 189
group 16 complexes, review, 409
hydroxide nitrilotriacetate water complexes, 199
methyl oxo phenoxide compounds, 301
methyl oxo propionate propionic acid propoxide complexes, 371
methyl phosphine-sulphide complexes, 313
methyl pyrazolylborate pyrazolylmethane complexes, 265
niobium(V) oxide, 367
oxo compounds, reviews, 409,429
silicate formation in blood plasma, 193
Aluminohydrides, transition elements, review, 387
"Alumoxanes", review, 429
Americium(III)
crown amine carboxylate ether complexes, 2455
Amide complexes
cobalt(III), 1079
copper(II), 2375
manganese(II), 2699
tin(IV), 125
2-Amidothiophenoxides
rhenium(V), 2211
Amine complexes
aluminium, 253,289
cobalt(II), 2847,2873
cobalt(III), 1079,2803
copper(I), 739,2319
copper(II), 535,611,2375,2463, 2693,2847,2867
gallium, 343
iron(II), 2641
manganese(II), 2873
manganese(III), 2867
mercury, 851,2931
molybdenum(V), 2171
molybdenum(VI), 881
nickel(II), 535,1027,2847,2867, 2873
palladium(II), 495,851
platinum(II), 495,851,2647
rhenium(V), 615
rhodium(III), 2925
ruthenium(II), 1113
tungsten(0), 2887
zinc, 763,2847,2873
Amine synthesis, catalysis by $RuCl_2(PPh_3)_2$, 2517
Aminoacid complexes
cadmium, 665,831
calcium, cobalt(II), 665
cobalt(III), 2149,2245
copper(II) 665,1293,2419
Mg, Ni(II), Pb(II), 665
platinum(II), 1975
vanadium(IV), 81,2101
zinc, 665,1293
Aminoacid ester complexes
mercury, 597
Aminoacid Schiff base complexes
copper(II), zinc, 1293
Aminoalkoxides
aluminium, 409
copper(II), 535,611
Aminoalkyls
gallium, indium, 353
2-Aminobenzenethiol, 2-amino-cyclopentene-1-dithiocarboxylate complexes, Mo(VI), 881

Aminocarbene complexes
chromium(II), 2193
nickel(II), 1447
Aminochlorophosphines, 2619
Aminodiarsines, aminodiphosphines, 2413
2-Aminoethanol complexes
nickel(II), 535
2-Aminoethoxide complexes
copper(II), 535
N-2-Aminoethyl-2-[(2-aminoethyl)thio]acetamide complex, cobalt(III), 1079
2-(2-Aminoethyl)pyridine complexes
copper(II), 1293
Aminophenoltriacetate complexes
Co, Mn, Ni, Zn, 2873
2-Aminophenoxide complexes
lanthanides, 2143
thorium, 1401
zirconium, 1405
Aminopolycarboxylate complexes
aluminium, 199
chromium(III), 137
Ammonia complexes
chromium(III), 119,1175
cobalt(III), 2803
Aniline complexes
aluminium, 245
Anisates
titanium(IV), 783
4-Anisolyl compounds
tellurium(IV), 943
Anthranilate complexes
thorium, 1401
zirconium, 1405,2689
Antiinflammatory drug complexes
copper, zinc, 505
Antimony
alkyls, 921
Arabinitol complexes
molybdenum(VI), 1225
Arene complexes
chromium(0), 1,53,1677
gallium(I), 283
iron(II), 1,2727
ruthenium(II), 1113
Arsenic
alkyls, 921
aryls, 2023
Arsenido complexes
gallium, 319,343
Arsine complexes
aluminium, 289
chromium(0), 1
copper(I), 1609,2919
iron(II), 2433
ruthenium(II), 863,2153
Arsinogallanes, 319
Aryls
arsenic, 2023
cobalt, 2477
gallium, 319
iridium(II,III), 2635
mercury, 2477
palladium(II), 2181
phosphorus, 681
rhenium(V),(VI),(VII), 2081
rhodium, 2477
rhodium(III), 1613
ruthenium(II), 1107,1939
tantalum(V), 963
tellurium(IV), 943
tin(IV), 125,653,2863
Arylamides
aluminium, 245,257
molybdenum, 527,619,687
tugsten, 527
2-Arylazopyridine complexes
silver(I), 2251
Arylimides
technetium(V), 1497
tungsten(IV), 603,669
Ascorbic acid, oxidation by $[Mo(CN)_8]^{3-}$, 113
Aspartate complexes
vanadium(IV), 81
Aspartate peptide complexes
copper(II), nickel(II), 825
Aspirin complexes
copper, zinc, 505
1-Azabicyclo[2.2.2]octane complexes, gallium, 343
Azide complexes
copper(II), 1257,2375,2693
ruthenium(II), 1113
Azole complexes
cadmium, 541,2437
cobalt(II),(III), 2567
copper(I), 1469,2319
copper(II), 713,2035,2981
iron(II), 2971
lanthanides, 751
rhodium(III), 2047
zinc, 1469

B

Barium
alkoxide ether silylamide complexes, 2959
cryptand complexes, 1369
organo compounds, review, 1345
Benzaldehyde complexes
aluminium, 233
Benzene complexes
chromium(0), 1,53
iron(II), 1
ruthenium(II), 1113
Benzoates
rhenium(II), 743
tin(IV), 1331
zirconium(IV), 2689
Benzoins, oxidation by $[Mo(CN)_8]^{3-}$, 2299
Benzoquinone complexes
tellurium(II), 847
Benzotriazolyl(hydro)borates
thallium(I), 63
1-Benzoylacetone complexes
lanthanides, 697
4-Benzoyl-3-methyl-1-phenylpyrazol-5-one complexes
lanthanides, 795
Benzthiazole-2-thiolates
mercury, 2717
Benzyls
tungsten(VI), 1271
zirconium, 839
Benzylidyne complexes
tungsten(VI), 1271
Benzyloxides
aluminium, 233
Bipyrimidine complexes
ruthenium(II), 1243

Bis(acetylacetone)ethylenediamine
complexes
thorium, 1401
zirconium, 1405
Bis(dialkyl)alanylmethane, 277
Bis(dimethylamino)methylarsine
complexes, aluminium, 289
Bis(dimethylphosphino)ethane
complexes
gallium, 343
iron(III), 2139
tungsten(IV), 23
Bis(dimethylphosphino)methane
complexes
osmium(II), 1107
rhenium(III), 1165
ruthenium(II), 1165
Bis(dimethylpyrazolyl)pyridazine
complexes, copper(I), 2603
1,3-Bis(dimethylstibyl)propane
complexes
copper(I), 1609
Bis(diphenylarsino)methane
complexes
rhenium(II), 573,743
rhenium(II,III), 573
Bis(diphenylphosphino)amine
complexes
rhenium(II),(II,III), 573
Bis(diphenylphosphino)cyclopenta-
diene complexes
molybdenum(0), 2469
Bis(diphenylphosphino)ethane
complexes
cadmium selenide, 1913
chromium(VI), 2625
copper(I), 2603
molybdenum(0), 2393
molybdenum(IV), 645
nickel(I), 581
nickel(II), 757
platinum(II), 987
ruthenium(II), 863,2153,2163
technetium(V), 1497
tungsten(II), 2507
1,1-Bis(diphenylphosphino)ethene
complexes, palladium(II), 2741
Bis(diphenylphosphinoethyl)phenyl-
phosphine complexes
molybdenum(IV), 545
Bis(diphenylphosphino)ethyne
complexes, Mo(II), W(II), 801
Bis(diphenylphosphino)ferrocene
complexes,
Cr(0),Mn(0),Mo(0),W(0), 2305
Bis(diphenylphosphino)methane
complexes
cadmium selenide, 1913
copper(I), 2603
iridium(II,III), 2635
nickel, 1487
nickel(0), 2651
nickel(I), 581
nickel(II), 757
palladium, 2767
palladium(II), 2741
platinum, 2767
platinum(II), 2651
rhenium(II), 565,573,743
rhenium(II,III), 573
rhenium(III), 1165
ruthenium(II), 863,2153
tungsten(II), 2135,2233,2507
Bis(diphenylphosphino)propane
complexes
molybdenum(0), 2393
tungsten(II), 2507
Bis(diphenylphosphino)pyridine
reactions and complexes,
Cr(0), Mo(0), W(0), 1757
Bis[(diphenylphosphinyl)methyl]-
phenylphosphine oxide complexes
Mo(II), W(II), 1099
1,3-Bis(diphenylstibyl)propane
complexes
copper(I), 1609
Bis(diphenylthiophosphinoyl)alkane
complexes, aluminium, 313
Bis(di-o-tolylphosphino)ethane
complexes
molybdenum(IV), 645
Bis(4-pyridyl)ethane, -ethene
complexes, iron(II), 1087
Bis(salicylaldehyde)diamine
complexes
thorium(IV), 1401
zirconium(IV), 1405
4,4'-Bis-1,2,4-triazole complex
iron(II), 2971
Bis(trimethylsilyl)amide complexes
titanium, zirconium, 1423
Bis(trimethylsilyl)imide complexes
Ba, Ca, Mg, Mn(II), Sr, 2959
Bis(trimethylsilyl)methyls
aluminium, 277
cobalt(II), 931
Blood plasma speciation modelling
aluminium, 151,163
aluminosilicates in, 193
calcium, copper, 505
gallium, indium, 151,163
zinc, 505
Book reviews
boron compounds, 147
germanium organo compounds, 1779
ligand reactions, 1621
rhenium organo compounds, 899
tin organo compounds, 897,2191
Boranes
molecular orbitals, 1035
Borane complexes
iron, 2359
Boric acid pyrogallol complexes,
789
Boron
in cluster complexes, 1955
compounds, book review, 147
enolate ethyl compound, 223
planar networks, 1901
Bromides and bromo complexes
copper(I), 981,2319
copper(II), 713,1703,2375,2443,
2463,2613,2747
gallium(II), 377
gallium(III), 207
indium(II), 377
lead(II), 2429
magnesium, 1775
mercury, 2041
molybdenum(I), 1187
molybdenum(II), 1099,1209
molybdenum(IV), 545
molybdenum(VI), 881
nickel(II), 2443
palladium(II), 2741
platinum(II), 1683

rhenium(II), 565,573,743
rhenium(II,III), 573
rhenium(III), 1131
rhenium(VI), 2081
ruthenium(VI), 1751
selenium(II), 581,1199
technetium(V), 1497
tellurium(II),(IV), 2879
tin(II), 1187
tin(IV), 1331
tungsten(I), 1187
tungsten(II), 1099
tungsten(IV), 11
uranium(III), 2175
4-Bromobenzenethiolates
chromium(VI), 779
Bromobenzoates
titanium(IV), 783
zirconium(IV), 2689
Butanediolates
molybdenum(V), 1965
Butanethiolates
iron, 1741
Butanoic acid, extraction of metals from clay surface complexes, 2273
Butanol complexes
uranium(IV), 1843
But-3-enyl complexes
tungsten(IV), 23
Butoxides
aluminium, 227,253
lithium, 227
molybdenum, 619
molybdenum(III), 2941
tungsten(III), 2941
uranium(IV), 1843
Butyls
indium, 361
niobium(V), 1051
tin(IV), 361
tungsten(II), 727
tungsten(IV), 23,727
t-Butylamides
chromium(VI), 1009,2625
osmium(VIII), 1009
Butylamine complexes
molybdenum(V), 2171
ruthenium(II), 1113
t-Butylbenzoates
yttrium, 1119
t-Butylhydroperoxide, 487
t-Butylimides
chromium(VI), 1009,2625
osmium(VIII), 1009
rhenium(V),(VI),(VII), 2081
N-Butyliminopropionyl complexes
tungsten(IV), 23
t-Butylisocyanide complexes
chromium(VI), 2625
iridium(II,III), 2635
tungsten(IV), 11
t-Butylphosphine complexes
tungsten(IV), 669
t-Butylphosphinidene complexes
osmium, 1573
3-*t*-Butylpyrazolylborate complexes
magnesium, 1775
4-*t*-Butylpyridine complexes
molybdenum(II), 1209
2-Butyne complexes
iridium(I), 1867
tungsten(II), 2135,2233,2507

C

Cadmium
acetate Schiff base thiolate complexes, 1017
alkyls, 921
alkyl diimine complex, 1483
aminoacid complexes, 665,831
aminoacid imidazole complexes, 2437
dithiolate heterobinuclear complexes, 1441
fluoride complexes, 901
mercaptopyridine mercaptothiazole complexes, 541
mercury telluride precursors, 921
nitrate pyridylpyrazole thiocyanate complexes, 2839
peptide complexes, 831
phenanthroline complexes, 2497
selenide, diphosphine, phosphine complexes, 1913
thiazolylazoresorcinol complexes, 501
thiosemicarbazide complexes, 2029
Caesium
cryptand complexes, 1369
Calcium
alkoxide ether silylamide complexes, 2959
aminoacid complexes, 665
blood serum speciation, effect of polydentate ligands, 505
chloride pyridylketonate copper((II) complexes, 2443
cryptand complexes, 1369
fluoride, hydride, 1919
organo compounds, review, 1345
Carbaboranes, 891,939
Carbaborane complexes
copper(I), gold(I), 2407
molybdenum, tungsten, 2953
1-(2-Carbamylethyl)-2-alkylimidazole complexes, Cu(II), 713,2035
Carbon, in cluster complexes, 1955
Carbonates
nickel(II), 1447
Carbon monoxide, reactions with trinuclear complexes, 2774
Carbonyls
chromium(0), 1,53,703,1479,1677, 1757,2511,2579
chromium(II), 2193
clusters, review, 455
cobalt, 1783,2815
cobalt(-I), 2533
cobalt(I), 1317
copper(I), 2319
iridium(I), 893
iridium(II,III), 2635
iridium(III), 1883,2071
iron, 455,1769,1809,2359,2763,2815
iron(-II), 1127
iron(0), 1045,1337
iron(I), 1187
iron(II), 639,1849
manganese(0), 1479,2305,2579
molecular orbitals, 2001
molybdenum, 619,2763
molybdenum(0),703,1059,1479,1757, 2305,2393,2469,2579,2619,2863, 2901
molybdenum(I), 1187
molybdenum(II), 801,1099,2863,2901

molybdenum(III), 2469
niobium(I), 1855
osmium, 75,455,1491,1573,2385,2759
osmium(0), 1573,1867
rhenium, 623
rhenium(0), 1479
rhenium(II), 565
rhenium(III), 1131
rhodium(I), 969
rhodium(II), 2635
rhodium(III), 1141,2071
ruthenium, 455,623
ruthenium(0), 1867
ruthenium(II), 893,907,2153
semibridging, 1799
substitutions, kinetic studies, review, 1503
tungsten(0), 703,991,1217,1363, 1757,2305,2579,2887
tungsten(I), 1187
tungsten(II), 727,801,1099,2135, 2233,2507,2859
tungsten(IV), 603,727
Carboxylates
aluminium, 371
cadmium, 1017
chromium(II), 1237
cobalt(II), 2873
copper(II), 805,1667,2035,2613,2867
europium, 1411
indium, 361
iron(III), 2675
lanthanides, 1411,2143
manganese(II), 1181,2873
manganese(III), 1181,2867
molybdenum(II), 1237
neodymium, 1411
nickel(II), 1447,1729,2873
palladium(II), 2741
rhenium(II), 743
rhodium, 1589
rhodium(II), 1135
ruthenium(II), 907
ruthenium(II,III), 1723
thorium, 1401
tin(IV), 1331
titanium(IV), 783
tungsten(IV), 11
uranium(VI), 2987
yttrium, 1119,1305
zinc, 2873
zirconium, 1401,2689
Carboxylic acid complexes
aluminium, 371
copper(II), 1667
in extraction of metals from clay surface complexes, 2273
Carrier concentration, indium phosphide, 353
Catecholates
aluminium, 171
rhenium(V),(VII), 1323
silicon, 813
Cation exchange, clays, 517
CD spectra
cobalt peroxidase, 1021
copper(II) peptide complexes, 825
iron(II) carbonyl cyclopentadienyl diphosphine ether complexes, 639
peroxidase, 1021
vanadium(IV) aminoacid oxo complexes, 81,2101
Ceramic glasses, thermolysis, 1709
Cerium(III)
crown ether thiocyanate water complexes, 2371
diketonate pyrazolylborates, 697
phosphotungstates, 1249
Cerium(IV)
oxide, 1919
Chlorides and chloro complexes
aluminium, 245,309,2809
calcium, 2443
chromium(V),(VI), 2625
cobalt(II), 931,2315,2443,2839
cobalt(III), 1379
copper(I), 981,2319
copper(II), 713,1457,1703,2443, 2463,2663,2747
gallium(I), 283
gallium(II), 377
gallium(III), 207,283,353
gold(III), 893,2199
hafnium, 2185
indium, 2533
indium(II), 377
indium(III), 329,353,1297
iridium(I),(III), 893
iron(III), 1065,1695,2139
lanthanides, 479,939,1453
lead(II), 2429
magnesium, 1775,2443
mercury, 851,2041
molybdenum, 527,687,693
molybdenum(II), 1209,1855,2863
molybdenum(IV), 545,2585
molybdenum(V), 2171,2293,2585
molybdenum(VI), 881,2293
nickel(II), 757,1317,2443,2809, 2823,2839
niobium(V), 1051,2709
osmium(II), 1107
osmium(III), 2309
osmium(VIII), 1009
palladium(II), 495,851,1287,1633, 2721,2741
phosphorus(III), 553
platinum(II), 35,495,851,893,1317, 1975,2647,2651,2721
rhenium(II), 565,573,743
rhenium(II,III), 573
rhenium(III), 1131,1165
rhenium(VII), 2081
rhodium, 1589
rhodium(I), 1141
rhodium(II), 2635
rhodium(III), 1141,2127
ruthenium, 2733
ruthenium(II), 893,1107,1113,1243, 2153,2517,2733
ruthenium(II,III), 1723
ruthenium(VI), 1751
selenium(II), 589
tantalum((V), 2709
technetium(III),(V), 1497
thorium, 1645,2987
tin(II), 1187
tin(IV), 125,653,1331,2863
titanium(III), 1617
tungsten(I), 1187
tungsten(III), 669,1829
tungsten(IV), 11,669
tungsten(V), 669
tungsten(VI), 2293
uranium(IV), 69,1645
uranium(VI), 2987

mercury amine thioether macrocyclic complex, 2931
molybdenum arylamide chloride nitrosyl pyrazolylborate complexes, 527
molybdenum arylamide halide nitrosyl phenoxide pyrazolylborate complexes, 687
molybdenum chloride diamide nitrosyl pyrazolylborate complexes, 693
molybdenum(VI) aminothiophenoxide dicarboxylate dithiocarboxylate halide hydroxyquinoline oxo thiocyanate thiosemicarbazide complexes, 881
nickel(II) carboxylate dithiocarbamate macrocyclic tetramine thiocarboxylate xanthate complexes, 1729
osmium(III) chloride diketonate methanol phosphine complexes, 2309
rhenium(II) carbonyl diphosphine halide phosphine complexes, 565
rhenium(II) carboxylate diarsine diphosphine halide complexes, 743
rhenium(II),(II,III) diarsine diphosphine halide complexes, 573
rhenium(VII) catecholate oxo complexes, 1323
rhodium(II),(II,III) carboxylate water complexes, 1135
rhodium(III) amine thioether macrocyclic complex, 2925
rhodium(III) aryl dipyridyl pyridine cyclometallated complex, 1613
ruthenium(II) arsine cyclopentadienyl diphosphine phosphine pyridine pyridine-*N*-oxide complexes, 863
vanadium(IV) diketonate oxo pyrazolylborate complexes, 2483
Cycloarsane, 319
Cyclobutadiene complexes
molybdenum(II), 1855
3-Cyclobutene-1,2-dione-3,4-diolates
copper(II), 2575
Cycloheptatrienyl complexes
molybdenum, 2953
Cyclohexadienyl complexes
rhenium(V), 2081
Cyclohexanone, solvent extraction by, 1717
Cyclohexene
epoxidation by Th(IV) peroxide complexes, 1401
epoxidation by Zr(IV) peroxide complexes, 1405
epoxidation catalysed by CrO_3, 487
Cyclohexenylenolates
Al,B,Ga,Zn, 223
Cyclohexylamine complexes
platinum(II), 2647
Cyclohexylxanthates
nickel(II), 1341
Cyclometallated complexes
aluminium, 245,257
iridium(III), 1883
niobium(V), 1051
palladium(II), 1287,2741
rhenium(VI), 2081
rhodium(III), 1613
tantalum(V), 1051
1,5-Cyclooctadiene complexes
iridium(I), 969
rhodium(I), 1141
Cyclooctatetraene complexes
Ba, Ca, Sr, 1358
Cyclopentadienyls
barium, calcium, 1349
cobalt, 1123,1783,2549
gallium, 2763
hafnium, 301,2185
iridium(III), 1883
iron, 1783,2763
iron(I), 1187
iron(II), 1,639,1091,1849,2727
lanthanides, 479,875,1453,2143
manganese(I),(II), 921
molybdenum, 2763
molybdenum(II), 1855,2901
molybdenum(III), 2469
nickel(I), 581
niobium(I), 1855
rhenium(III), 1131
rhenium(V), 2211
rhodium, 1123
ruthenium, 1783
ruthenium(II), 863,1893,2153,2163
strontium, 1349
titanium(IV), 783,2097
tungsten, 1491
tungsten(II), 2859
tungsten(III),(V), 669
uranium(IV), 69
zirconium, 301,839,2185,2689
Cyclopentadienyldiphenylphosphine complexes, molybdenum(0), 2469
Cyclopolyphosphates
copper(II), 511
Cymene complexes
ruthenium(II), 1113
Cysteine complexes
cadmium, 831
vanadium(IV), 2101
Cysteine ester complexes
cadmium, 831
mercury, 597
Cytochrome *c* complex
platinum(II), 1975

D

DC voltammetry
copper(II) chloride dithiocarbazate ester complexes, 1457
4-Decylanilido complexes
molybdenum, 687
Desferrioxamine complexes
aluminium, 171
Diacetylbenzene complexes
copper(II), zinc, 1293
Diacetylferrocene hydrazones, 2751
Dialkylcarbamoyl complexes
germanium, 227
Dialkylphosphate complexes
cobalt(II), 1147
Diamido complexes
molybdenum, 693
2,2'-Diamidodiethylether complexes
molybdenum, 693

1,3-Diamidopropane complexes
molybdenum, 693
Diamine complexes
cobalt(II), 931
cobalt(III), 1379
copper(I), 2319
copper(II), 611,2937
iridium(III), 2071
lithium, 931
rhodium(III), 2071
Diarsine complexes
rhenium(II), 573,743
rhenium(II,III), 573
1,4-Diazacyclo[2.2.2]octane
complexes, gallium, 343
Diazenide complexes
technetium(III),(V), 1497
Dibenzo-24-crown-8 complexes
lanthanides, 2371
Dibenzotetraazacyclotetradecine
complexes,
ruthenium(0), 1221
tungsten(0), 1217
Dibenzoylmethanide complexes
aluminium, gallium, 215
lanthanides, 697
Dibenzylideneacetone complexes
Pd(0), Pt(0), 1949
Di-*t*-butylaniline complexes
aluminium, 245
Di-*t*-butylcatecholates
rhenium(VII), 1323
Di-*t*-butyldiphosphine, 669
Di-*n*-butyldithiocarbamates
copper(I), 361
Di-*t*-butyl-4-methylphenoxides
aluminium, 233,239,301
Di-*t*-butylphosphido complexes
osmium, 1573
Di-*t*-butylphosphine complexes
osmium, 1573
Di-*t*-butylquinone complexes
ruthenium, 2267
1,2-Dicarba-*closo*-decaborane(12),
nucleoside, 891
7,8-Dicarba-*nido*-nonaborane(11)-
(1-) complexes
copper(I), gold(I), 2407
1,1-Dicarboethoxy-2,2-ethylenedith
iolate complexes
heterobinuclear, 1441
Dicarboxylates
chromium(III), 1175
copper(II), 2035
molybdenum(VI), 881
platinum(II), 1975
Dichlorocatecholate complexes
silicon, 813
Di(*p*-chlorophenyl)triazenides
Ir,Os,Rh,Ru, 1741
1,4-Dicyanobenzene complexes
ruthenium(II), 2153
1,4-Dicyanobutene complexes
ruthenium(II), 2153
Dicyclohexylamine complexes
gallium, 343
Dicyclohexylphosphido complexes
osmium, 1573
Diene complexes
iridium(I), 969
Pd(0), Pt(0), 1949
rhodium(I), 1141
Diethylamido complexes
Nb(V), Ta(V), 2709
Diethylamine complexes
molybdenum(V), 2171
Diethylaminocarbyne, 727
Diethylaminopropyl complexes
gallium, indium, 353
Diethylbenzamide complexes
lithium, 227
N,N-Diethyl-*N'*-*t*-butyldiaminoeth-
yne complexes, W(II), 727
Diethyldithiocarbamates
iron, 1741
nickel(II), 1729
rhodium(II), 2013
Diethylenetriamine complexes
cobalt(III), 2803
Di(2-ethylhexyl)phosphoric acid
complexes, cobalt(II), 1147
Diethyl(phenyl)phosphine complexes
tungsten(II), 2233
Differential pulse polarography
copper(II) dipyridyl hydroxide
pyridine complexes, 629
platinum(II) cytochrome *c*
dipicolinate complex, 1975
ruthenium(II) acetonitrile
chloride diimine nitrite
phosphine complexes, 1243
Difluorobiphenyl complexes
chromium(0), 1
iron(II), 1
Dihydrodiphosphate, rearrangement,
1363
Diimine complexes
cadmium, 1483,2497
chromium(VI), 2625
cobalt(III), 1379
copper(II), 629,2061,2239
lanthanides, 2285
lead, 2497
molybdenum(0), 1059,2863
molybdenum(I), 1187
molybdenum(II), 2863
nickel(I), 581
palladium(II), 1633
rhodium(III), 1613
ruthenium, 2267
ruthenium(II), 893,1243,1939
tin(IV), 125
tungsten(0), 1217
tungsten(I), 1187
Diketonates
aluminium, 215,409
chromium(III), 893
cobalt(II), 2721
copper(II), 2061,2721
Ga, In, 215
lanthanides, 697,751
molybdenum(VI), 1011
nickel(II), 2721,2823
osmium(III), 2309
palladium(II), 1287
scandium, 215
tungsten(IV), 11
vanadium(IV), 1397,1603,2483
yttrium, 1305
Diketone complexes
lanthanides, 795
Dimercaptosuccinic acid ester
complexes, mercury, 597
Dimethoxyphenyls
phosphorus(V), 681
3,3-Dimethylacrylate

ruthenium(II), 907
1,3-Dimethylallyl complexes
tungsten(IV), 23
Dimethylamido complexes
aluminium, 253,257
gallium, 257
molybdenum(III), 1821
tantalum(V), 2709
Dimethylamine complexes
aluminium, 253
Dimethylaminoalkyl complexes
gallium, indium, 353
4-Dimethylaminobenzoates
yttrium, 1119
Dimethylamino(dimethyl)arsine
complexes, aluminium, 289
2-Dimethylaminoethanethiolates
zinc, 763
2-Dimethylaminoethoxide,
i-propoxide, copper(II), 611
N-Dimethylaminoethyl-*N*-methyl-2-
aminoethoxide, copper(II), 611
2,3-Dimethylanthraquinone
complexes, Te(II), 847
Dimethylarsenide complexes
gallium, 343
3,3-Dimethyl-1-butyne complexes
tantalum(V), 2709
5,6-Dimethyl-1,3-dihydro-2-tell-
uraindane, 847
Dimethyldithiocarbamate complexes
iron, 1741
rhodium(II), 2013
Dimethylethylenediamine complexes
copper(II), 2937
Dimethylformamide complexes
tin(IV), 125
Dimethyldithiocarbamate complexes
nickel(II), 1729
Dimethylglyoximates
rhodium(III), 2047
2,6-Dimethylphenoxides
tantalum(V), 963,2709
Dimethyl(phenyl)phosphine
complexes,
chromium(VI), 2625
iridium(I), 1867
iridium(III), 1883
niobium(III), 1689
platinum, 1561
platinum(II), 987,2659
rhenium(III), 1165
tungsten(II), 2233
tungsten(IV), 603
3-(Dimethylphenyl)silyl-2-pyrid-
inethiolate complexes
silver(I), 1429
Dimethylpiperidine complexes
gallium, 343
Dimethylsilylbis(cyclopentadienyl)
complexes, zirconium, 301
Dimethylsulphoxide complexes
tin(IV), 125
vanadium(IV), 1397
N,N-Dimethylthiophenecarbothio-
amide complexes,
palladium(II), 1287
N,N-Dimethylvaline complexes
copper(II), 2419
Dinitrocatecholate complexes
silicon, 813
Dinitrogen, reduction, 645
Dinitrogen complexes
tungsten(IV), 669
Diphenylacetylene complexes
nickel(I), 581
niobium(I), 1855
tantalum(V), 2709
tungsten(IV), 603
Diphenylamido complexes
aluminium, 257
1-Diphenylarsino-2-diphenylphos-
phinoethane complexes,
rhenium(III), 1165
Diphenylketoimine complexes
titanium(IV), 2097
2,6-Diphenylphenol complexes
iridium(I), 969
2,6-Diphenylphenoxides
iridium(I), 969
niobium(V), 1051
rhodium(I), 969
tantalum(V), 1051
titanium(III), 1617
Diphenylphosphido complexes
molybdenum, 2953
molybdenum(II), 2901
molybdenum(III), 2469
tungsten, 2953
Diphenylphosphine complexes
gallium, 335
Diphenylphosphinoferrocene
complexes, tungsten(II), 2233
2-Diphenylphosphinopyridine
complexes,
copper(I), 2603
rhodium(II), 2635
1,3-Diphenyl-1,3-propanedionate
complexes
osmium(III), 2309
vanadium(IV), 2483
Diphenyl(propenyl)phosphine
complexes, tungsten(II), 2233
Diphenyl(tetramethylcyclopentadi-
enyl)phosphine complexes
molybdenum(0), 2901
Diphenyltriazenide complexes
Ir,Os,Rh,Ru, 1737
1,4-Diphosphadiene, formation of
W(0) complex from, 1363
Diphosphines, 669
reactions with trinuclear
complexes, 2780
Diphosphine complexes
cadmium selenide, 1913
chromium(0), 2305
chromium(VI), 2625
copper(I), 2603
gallium, 343
iridium(II,III), 2635
iron(II), 639
manganese(0), 2305
molybdenum(0), 2305,2393,2469
molybdenum(II), 801
molybdenum(IV), 645
nickel, 1487
nickel(0), 2651
nickel(II), 757
osmium(II), 1107
palladium, 2767
palladium(II), 2741
platinum, 2767
platinum(II), 35,987,2651
rhenium(II), 565,573,743
rhenium(II,III), 573
ruthenium(II), 863,1107,2153,
2163
technetium(V), 1497

tungsten(0), 2305
tungsten(II), 801,2135,2233, 2507
tungsten(IV), 11
Diphosphoglycerates
aluminium, zinc, 189
Dipicolinate complexes
platinum(II), 1975
Di-*i*-propylamide complexes
gallium, 343
Di-*i*-propylamine complexes
molybdenum(V), 2171
Dipropyldithiocarbamate complexes
iron, 1741
2,6-Di-*i*-propylphenoxides
tantalum(V), 963,2709
2,2′-Dipyridyl complexes
cadmium, 1483
chromium(VI), 2625
cobalt(III), 1379
copper(II), 629,2061,2239
molybdenum(0), 1059
molybdenum(I), 1187
nickel(I), 581
palladium(II), 1633
rhodium(III), 1613
ruthenium, 2267
ruthenium(II), 893,1939
tin(IV), 125
tungsten(I), 1187
4,4′-Dipyridyl complexes
iron(II), 1087
2,2′-Dipyridylamide complexes
manganese(II), 2699
2,2′-Dipyridylamine complexes
copper(II), 2693
Mo(I), W(I), 1187
Di(2-pyridylethyl)sulphide complexes, Pt(II), 1975
Disulphide complexes
cadmium, 831
molybdenum(IV),(V), 2585
1,4-Dithiins, conversion to dithiolates, 1123
3,3′-Dithiobis(2,4-pentanedionate) complexes
vanadium(IV), 1397
Dithiocarbamates
copper(I), 361
iron, 1741
lanthanides, 859
nickel(II), 1729
rhodium(II), 2013
Dithiocarbazate ester complexes
copper(II), 1457
Dithiocarbazate Schiff base complexes, copper(II), 2981
Dithiocarboxylates
molybdenum(VI), 881
1,3-Dithiolane complexes
Cr(0), Mo(0), W(0), 703
Dithiolates
cobalt, 1123
gold, 1561
heterobinuclear, 1441
molybdenum, 2965
nickel, palladium, 2053
platinum, 1561,2053
rhodium, 1123
Dithionate complexes
nickel(II), 2809,2823
Dithiophosphates
tellurium(IV), 943
Dithiophosphinates
copper(II), nickel(II), 2597
Di(*p*-tolyl)triazenides
Ir,Os,Rh,Ru, 1737
Dodecyl-4-Oxobenzoates
molybdenum, 687
Dysprosium
aminophenoxide carboxylate cyclopentadienyl hydroxyquinolate complexes, 2143
azole diketonate complex, 751
chloride cyclopentadienyl ether complexes, 479
chloride phenoxide water complexes, 939
crown ether thiocyanate water complex, 2371
diketone nitrate complexes, 795
nitrate Schiff base complexes, 2019
phenanthroline polyketonate complexes, 2285
phosphotungstates, 1249

E

Electric conductance
aminophenoltriacetate complexes, 2873
chromium(VI) alkylimide dipyridyl pyridine sulphonate complexes, 2625
cobalt(II) acetone thiocyanate complexes, 1375
cobalt(III) ethylenedibiguanide methionine complexes, 2245
copper(I) diphosphine phosphinopyridine tetraimine binuclear complexes, 2603
copper(II) amine halide tripod Schiff base complexes, 2463
copper(II) aminoacid imidazole pyridine Schiff base complexes, 1293
dithiolate complexes, 1441
iron(III) chloride thiohydrazide thiohydrazone complexes, 1065
lanthanide dithiocarbamate complexes, 859
lanthanide ketoaminophenol complexes, 1639
mercury methyl thioaminoacid ester complexes, 597
molybdenum(VI) diketonate oxime oxo Schiff base complexes, 1011
palladium(II), platinum(II) aminotelluroether chloride complexes, 851
rhenium(II) carbonyl chloride diphosphine phosphine complexes, 565
rhenium(II,III) diarsine diphosphine halide complexes, 573
ruthenium(II) arsine cyclopentadienyl diphosphine phosphine pyridine pyridine-*N*-oxide complexes, 863
ruthenium(II,III) carboxylate chloride ether phosphine oxide pyridine complexes, 1723

thorium chloride Schiff base water complexes, 2987
uranium(VI) acetate chloride hydroxide oxo Schiff base water complexes, 2987
zinc aminoacid Schiff base complex, 1293
Electric conductance (solid state)
molybdenum(VI) oxo thiazolylthiourea complexes, 2449
palladium, platinum dithiolates, 2053
Electrochemistry, carbonyl clusters, review, 455
Electron counting, cluster complexes, 1985
Electron density
arene complexes, 1
Electron diffraction
vanadium(IV) diketonate oxo complex, 1603
Electron mobility, indium phosphide, 353
Electronic spectra
alkali metal germyls, 2263
aminophenoltriacetate complexes, 2873
cadmium acetate Schiff base thiolate complexes, 1017
cadmium thiazolylresorcinol complexes, 501
chromium(III) hydroxide nitrilotriacetate water complexes, 137
chromium(VI) oxo thiolate complex, 779
cobalt(II) acetone thiocyanate complexes, 1375
cobalt(I) azole peptide complexes, 2567
cobalt(II) chloride hydroxide nitrate pyridylpyrazole thiocyanate complexes, 2839
cobalt(II) diethylenetriaminepentaacetate, 99
cobalt(II) diketonate water complexes, 2721
cobalt(II) in lead acetate glasses, 1475
cobalt(II) phthalocyanine, 1021
cobalt(II) salicylaldimine thiocyanate heteropolymetallic complexes, 557
cobalt(III) azole peptide peroxide superoxide complexes, 2567
cobalt(III) complexes on clay surfaces, 2273
cobalt(III) ethylenedibiguanide methionine complexes, 2245
cobalt(III) phthalocyanine, 1021
copper(I) azole Schiff base thioether thiolate complexes, 1469
copper(I) thiolate complexes, 1155,1659
copper(II) acetate azole oxalate sulphate complexes, 2035
copper(II) acetate bromide complexes, 2613
copper(II) amide amine bromide phenoxide pseudohalide thioether water complexes, 2375
copper(II) amine halide tripod Schiff base complexes, 2463
copper(II) aminoethoxide thiocyanate, 535
copper(II) azide dipyridylamine complex, 2693
copper(II) azole halide perchlorate thiocyanate complexes, 713
copper(II) carboxylate phenoxide quinazolone complexes, 805
copper(II) chloride dithiocarbazate ester complexes, 1457
copper(II) chloride oxime complexes, 2663
copper(II) diimine diketonate pyridine complexes, 2061
copper(II) diketonate heterobinuclear complexes, 2721
copper(II) dithiocarbazate imidazole pyridine-*N*-oxide Schiff base complexes, 2981
copper(II) halide triazene oxide binucleating complexes, 1703
copper(II) hydroxycarboxylate water complexes, 1191
copper(II) macrocyclic tetramine complexes, 2221
copper(II) methoxide squarate, 2575
copper(II) peptide complexes, 825
copper(II) polymeric triamine complexes, 2491
copper(II) polyphosphate complexes, 511
copper(II) porphyrin, 2527
copper(II) salicylaldimine thiocyanate heteropolymetallic complexes, 557
copper(II) thioether binuclear macrocyclic complexes, 2911
enzyme inhibition by nitroprusside, 913
group I,II metal crown amine ether complexes, 1747
iron(II) amine thioether macrocyclic complex, 2641
iron(II) phthalocyanine pyridine complexes, 1087
iron(III) chloride phosphine phosphine oxide complexes, 1695
iron(III) chloride thiohydrazide thiohydrazone complexes, 1065
iron(III) phthalocyanine, 1021
lanthanide chloride phenoxide water complexes, 939
lanthanide dithiocarbamate complexes, 859
lanthanide ketoaminophenol complexes, 1639
lanthanide phenanthroline polyketonate complexes, 2285
manganese(II) dipyridylamide complex, 2693
manganese(II),(III) thiosalicylate complexes, 1181
molybdenum dithiolate pyrazolylborate thiocyanate complex, 2965
molybdenum(II) halide pyridine complexes, 1209
molybdenum(VI) aminothiophen-

oxide dicarboxylate dithiocarboxylate halide hydroxyquinoline oxo thiocyanate thiosemicarbazide complexes, 881
molybdenum(VI) oxo thiazolylthiourea complexes, 2449
neodymium hydroxide perchlorate, 659
nickel dithiolates, 2053
nickel(II) aminoethanol thiocyanate complex, 535
nickel(II) carboxylate dithiocarbamate macrocyclic tetramine thiocarboxylate xanthate complexes, 1729
nickel(II) chloride hydroxide nitrate pyridylpyrazole thiocyanate complexes, 2839
nickel(II) complexes on clay surfaces, 2273
nickel(II) diketonate water copper(II) complexes, 2721
nickel(II) peptide complexes, 825
nickel(II) salicylaldimine thiocyanate heteropolymetallic complexes, 557
nickel(II) Schiff base thiolate complexes, 1017
osmium(III) chloride diketonate methanol phosphine complexes, 2309
palladium dithiolates, 2053
palladium(0) dibenzylideneacetone complex, 1949
palladium(II) aminotelluroether chloride complexes, 495,851
peroxidase, 1021
phosphiniminocyclotrithiazenes, 1433
platinum dithiolates, 2053
platinum(0) dibenzylideneacetne complex, 1949
platinum(II) aminoacid chloride cytochrome dipicolinate dipyridyl thioether complexes, 1975
platinum(II) aminotelluroether chloride complexes, 495,851
phenyl-2-picolylketonate polymetallic complexes, 2443
polyphosphate complexes, 2609
rhenium(II),(II,III) diarsine diphosphine halide complexes, 573
rhenium(III) chloride phosphine complexes, 1165
rhodium(II) carboxylate water complexes, 1135
rhodium(II) dithiocarbamate phosphine complexes, 2013
rhodium(II,III) carboxylate water complexes, 1135
rhodium(III) aryl dipyridyl pyridine cyclometallated complex, 1613
rhodium(III) carbonyl chloride telluroether complexes, 1141
ruthenium(II) acetonitrile chloride diimine nitrite phosphine complexes, 1243
ruthenium(II) arsine carbonyl chloride cyclopentadienyl diphosphine hydride nitrile phosphine pyridine complexes, 2153
ruthenium(II) arsine cyclopentadienyl diphosphine phosphine pyridine pyridine-*N*-oxide complexes, 863
ruthenium(III) edta mercaptopyrimidine water complexes, 2681
ruthenium(II) water complex, 1095
ruthenium(II,III) carboxylate chloride ether phosphine oxide pyridine complexes, 1723
saccharinate complexes, 1383
silver(I) pyridine complexes, 2251
tellurium(II) alkyl quinone complexes, 847
thorium chloride Schiff base water complexes, 2987
tin(IV) tetraselenide complex, 1389
tungsten(0) amine carbonyl nitrile phosphine pyridine Schiff base complexes, 2887
tungsten(I) carbonyl diimine halide iron(I) tin(II) complexes, 1187
uranium(IV) alcohol alkoxide oxo complexes, 1843
uranium(VI) acetate chloride hydroxide oxo Schiff base water complexes, 2987
vanadium(IV) aminoacid oxo complexes, 2101
vanadium(IV) aspartate oxo complexes, 81
vanadium(IV) diketonate oxo pyrazolylborate complexes, 2483
vanadium(IV) diketonate oxo pyridine sulphoxide complexes, 1397
yttrium pyridine Schiff base macrocyclic complex, 475
zinc Schiff base thiolate complexes, 1017
Electrophiles, reactions with trinuclear complexes, 2784
Enolates
Al, B, Ga, Zn, 223
Enstatite, 517
Enthalpy of activation
bond rotation, aminophosphines, 2619
fluxionality, dithiolane complexes, 703
fluxionality, spirophosphorane, 1463
methyl exchange, Al - Hf/Zr compounds, 301
pyrolysis, chromium(III) ammonia complex oxalate, 1175
redox, benzoin - $[Mo(CN)_8]^{3-}$, 2299
substitution, chromium(III) ammonia glycine complexes, 119
substitution, ruthenium(III) edta water complex, 2681
Entropy of activation
bond rotation, aminophosphines,

2619
fluxionality, dithiolane complexes, 703
methyl exchange, Al - Hf/Zr compounds, 301
pyrolysis, chromium(III) ammonia complex oxalate, 1175
redox, benzoin - $[Mo(CN)_8]^{3-}$, 2299
substitution, chromium(III) ammonia glycine complexes, 119
substitution, ruthenium(III) edta water complex, 2681
Entropy of formation
monohalide complexes, 2257
Enzyme inhibition by
nitroprusside, 913
Epoxidation, cyclohexene, 1401, 1405
Erbium
chloride cyclopentadienyls, 1453
chloride cyclopentadienyl ether complex, 479
crown ether thiocyanate water complexes, 2371
diketonate pyrazolylborate compounds, 697
nitrate Schiff base complexes, 2019
phenanthroline polyketonate complexes, 2285
phosphotungstates, 1249
Erythritol complexes
molybdenum(VI), 1225
ESR spectra
cobalt(II) alkyl chloride diamine complexes, 931
cobalt(III) imidazole peptide superoxide complexes, 2567
copper(II) acetate azole oxalate sulphate complexes, 2035
copper(II) amide amine bromide phenoxide thioether complexes, 2375
copper(II) amine halide tripod Schiff base complexes, 2463
copper(II) azide dipyridylamine complex, 2693
copper(II) azole halide perchlorate thiocyanate complexes, 713
copper(II) azole Schiff base thioether thiolate complex, 1469
copper(II) carboxylate phenoxide quinazolone complexes, 805
copper(II) chloride oxime complexes, 2663
copper(II) chloride thiouracil complex, 2747
copper(II) in clays, 517
copper(II) diaminodihydroxy tetradentate complexes, 1593
copper(II) dithiophosphinates, 2597
copper(II) halide triazene oxide binucleating complexes, 1703
copper(II) hydroxycarboxylate complexes, 1191
copper(II) peptide complexes, 825
copper(II) saccharinate water complexes, 1383
iron nitrosyl thiolate complexes, 1741
iron(II) azole thiocyanate complex, 2971
iron(III) chloride phosphine phosphine oxide complexes, 1695
iron(III) diaminodihydroxy tetradentate complexes, 1593
lithium diethylbenzamide radical anion, 227
manganese(II) dipyridylamide complex, 2699
nickel(I) alkyne cyclopentadienyl dipyridyl phosphine complexes, 581
osmium(III) chloride diketonate phosphine complexes, 2309
rhenium(II,III) diarsine diphosphine halide complexes, 573
rhenium(VI) bromide oxo cyclometallated complexes, 2081
rhodium(II) dithiocarbamate phosphine complexes, 2013
ruthenium(III) methyl complex, 2071
tellurium(II) quinone complexes, 847
titanium(III) chloride pheoxide complex, 1617
vanadium(IV) aminoacid oxo complexes, 2101
vanadium(IV) aspartate oxo complexes, 81
vanadium(IV) diketonate oxo pyrazolylborate complexes, 2483
vanadium(IV) in glazes, 999
Ester complexes
aluminium, 409
Ethanedithiolates
platinum, 1561
Ethanethiolates
copper(I), 1155
iron, 1741
Ethene complexes
tungsten(IV), 23
Ether complexes
aluminium, 409
barium, calcium, 2959
cobalt(II), copper(II), 2847
gallium, 2763
iron(II), 639
lanthanides, 479
magnesium, manganese(II), 2959
nickel(II), 2847
niobium(V), 2709
ruthenium(II,III), 1723
strontium, 2959
tantalum(V), 2709
zinc, 2847
Ethoxides
aluminium, 309
molybdenum, 619
molybdenum(V), 1965
ruthenium(II), 1113
tungsten, 2953
Ethyls
aluminium, 223,233,2809
boron, 223
gallium, 353
germanium, 227,2263
indium, 353

tungsten(IV), 11,23
zinc, 223
Ethylamine complexes
ruthenium(II), 1113
Ethyldiphenylphosphine complexes
cadmium selenide, 1913
tungsten(II), 2233
Ethylenediamide complexes
molybdenum, 693
Ethylenediamine complexes
cobalt(III), 1379
Ethylenediaminetetraacetates
calcium, copper, 505
hafnium, 2705
ruthenium(III), 2681
zinc, 505
Ethylenedibiguanide complexes
cobalt(III), 2245
Ethylene glycolates
molybdenum(V), 1965
Ethylsulphonate complexes
palladium(II), 1633
Ethyltetramethylcyclopentadienyl
complexes, rhenium(V), 2211
Ethylxanthate complexes
nickel(II), 1729
Ethyne complexes
tungsten(IV), 603
Europium
acetate hexamine macrocyclic
complex, 1411
azole diketonate complex, 751
chloride phenoxide water
complexes, 939
crown amine carboxylate ether
complexes, 2455
crown ether thiocyanate water
complexes, 2371
diketonate nitrate complexes,
795
diketonate pyrazolylborate
compounds, 697
dithiocarbamate complexes, 859
ketoaminophenol complex, 1639
nitrate Schiff base complexes,
2019
phenanthroline polyketonate
complexes, 2285
phosphotungstates, 1249
EXAFS
copper(II) methoxide squarate,
2575
Extended Huckel calculations
boranes, 2359
carbaborane, 2407
iridium(I) alkyne phosphine and
osmium(0), ruthenium(0) alkyne
carbonyl complexes, 1867
metallaboranes, 2359
palladium, platinum trinuclear
complexes, 2767

F

Fenske, R.F., 1781
Fenske - Hall calculations
cyclopentadienyl carbonyl
nitrosyl complexes, 1783
iron carbonyl vinylidene
complexes, 1809
molybdenum(IV),(V) chloride
disulphide thio polynuclear
complexes, 2585
ruthenium(II) dipyridyl
pyridinoaryl complexes, 1939
semibridged complexes, 1799
tungsten(III) alkoxide chloride
oxo complexes, 1829
"two - legged piano stool"
complexes, 2001
Fischer - Tropsch catalysis, 2815
Fluorescence spectra
copper(I) thiolate complexes,
1155
ketoaminophenol, 1639
lanthanide phenanthroline
polyketonate complexes, 2285
neodymium hydroxide perchlorate,
659
palladium(0), platinum(0)
dibenzylideneacetone
complexes, 1949
ruthenium(II) acetonitrile
chloride diimine nitrite
phosphine complexes, 1243
Fluorides and fluoro complexes
cadmium, 901
calcium, 1919
germanium, 1263
lead(II), 2429
magnesium, 1919
tin(IV), 1331
uranium(VI), 47
zinc, 901
zirconium, 1653
Fluorobenzoates
titanium(IV), 783
zirconium(IV), 2689
Fluxionality
aluminium methyl
pyrazolylborate, 265
butyne complexes, 2233
chromium(0) arene carbonyl
complexes, 53
dithiolane complexes, 703
mechanisms, 2221
spirophosphorane, 1463
Force constants
gallium(II), indium(II) halide
complexes, 377
Formates
rhodium(II), 1135
tin(IV), 1331
Formation constants
alkali, alkaline earth cryptand
complexes, 1369
aluminium catechol citrate
desferrioxamine hydroxide
complexes, 171
aluminium diphosphoglycerate
complexes, 189
aluminium hydroxide
nitrilotriacetate water
complexes, 199
americium(III) crown amine
carboxylate ether complexes,
2455
boric acid pyrogallol complexes,
789
cadmium aminoacid azole
complexes, 2437
cadmium aminoacid, peptide
complexes, 825
cadmium fluoride complexes, 901
cadmium phenanthroline
complexes, 2497

cadmium thiazolylazoresorcinol complexes, 501
copper(II) acetate bromide complexes, 2613
copper(II) azide pyridine complexes, 1257
copper(II) diimine macrocyclic complexes, 2239
copper(II) dipyridyl hydroxide pyridine complexes, 629
copper(II) hydroxycarboxylate water complexes, 1191
copper(II) peptide complexes, 831
copper(II) polyphosphate complexes, 511
europium(III) crown amine carboxylate ether complexes, 2455
germanium fluoride hydroxide complexes, 1263
hafnium edta complex, 2705
iron(III) sulphosalicylate complexes, 2675
lanthanide chloride phenoxide water complexes, 939
lead(II) halide complexes, 2429
lead(II) phenanthroline complexes, 2497
leucine, serine complexes, 665
manganese(II),(III) thiosalicylate complexes, 1181
mercury phenoxide complexes, 1537
molybdenum(VI) alditol oxo complexes, 1225
monohalide complexes, 2257
nickel(II) peptide complexes, 825
polyphosphate complexes, 2609
thiosemicarbazide complexes, 2029
tridentate amine ether ligand complexes, 2847
vanadium(IV) aminoacid oxo complexes, 2101
vanadium(IV) aspartate oxo complexes, 81
zinc diphosphoglycerate complexes, 189
zinc fluoride complexes, 901

Free energy of activation
bond rotation, aminophosphines, 2619
fluxionality, butyne complexes, 2233
fluxionality, dithiolane complexes, 703
methyl exchange, Al - Hf/Zr compounds, 301
redox, benzoin - $[Mo(CN)_8]^{3-}$, 2299
substitution, chromium(III) ammonia glycine complexes, 119

Furanaldazine complexes
thorium(IV), uranium(VI), 2987

G

Gadolinium
azole diketonate complex, 751
chloride cyclopentadienyls, 1453
chloride phenoxide water complexes, 939
crown ether thiocyanate water complex, 2371
diketone nitrate complexes, 795
dithiocarbamate complexes, 859
nitrate Schiff base complexes, 2019
phenanthroline polyketonate complex, 2285
phosphotungstates, 1249

Galacticol complexes
molybdenum(VI), 1225

Gallium(I,III)
arene chloride complex, 283

Gallium(II)
halides, review, 377

Gallium(III)
alkyl aminoalkyl chloride complexes, 353
alkyl cyclopentadienyl ether iodide pyridine heterobinuclear complexes, 2763
alkyl diphenylphosphine complexes, 335
alkylamide amine arsenido diphosphine methyl phosphido complexes, 343
arsenido methyl phenyl compounds, 319
in blood plasma, 151,163
citrate halide phosphate sulphate water complexes, 207
diketonates, 215
dimethylamide, 257
enolate methyl compound, 223

Germanium
alkoxide hydrides, 2189
alkyl alkali metal compounds, 2263
alkyl iron(II) complexes, 773
dialkylcarbamoyl ethyl, 227
fluoride hydroxide complexes, 1263
organo compounds, book review, 1779
pyridine iron(-II) complex, 1127

Glasses and glazes, iron(II),(III) and vanadium(IV) in, 999

Glucitol complexes
molybdenum(VI), 1225

Glyceraldehyde-3-phosphate dehydrogenase, 913

Glycine complexes
cadmium, 2437
chromium(III), 119

Glycine glycoside complexes
iron(III), 2895

Glycylalanine, glycylglycine complexes
cobalt(II),(III), 2567

Gold
dithiolate complex, 1561

Gold(I)
carbaborane phosphine complexes, 2407
cyanide complex, 975

Gold(III)
chloride complex, 2199
chloride terpyridine complex, 893

H

Hafnium
chloride cyclopentadienyl pyrazolylborate complex, 2185
cyclopentadienyl methyl compounds, 301
edta hydroxide water complexes, 2705
Hectorite, 517,2273
Heteropolymolybdates, 2023
Heteropolytungstate complexes
lanthanides, 1249
Heteropolyvanadates, 143
Hexafluorobutyne complexes
Os(0), Ru(0), 1867
Hexafluoropentanedionates
aluminium, gallium, 215
osmium(III), 2309
Hexafluoro-i-propoxides
germanium, 2189
1-Hexene
conversion to alcohols, use of rhodium(I) complex, 1235
hydrogenation and isomerization catalysed by aluminohydride complexes, 387
Histamine complexes
copper(II), 1293
Histidine methyl ester complexes
copper(II), 1293
Holmium
aminophenoxide carboxylate cyclopentadienyl hydroxyquinolate complexes, 2143
azole diketonate complex, 751
chloride cyclopentadienyl, 1453
crown ether thiocyanate water complexes, 2371
diketonate pyrazolylborate, 697
nitrate Schiff base complexes, 2019
phenanthroline polyketonate complexes, 2285
phosphotungstates, 1249
Horseradish peroxidase, reactions with phthalocyanines, 1021
Hueckel theory, Kagome nets, 1901
Hydrazide complexes
molybdenum(IV), 545
technetium(V), 1497
Hydride, reaction with trinuclear complexes, 2778
Hydrides and hydro complexes
aluminium, review, 387
calcium, 1919
clusters, 1955
cobalt, 2815
germanium, 2189
iron, 2815
molybdenum(IV), 645
osmium, 1491,1573,2759
rhodium(I), 1235
ruthenium(II), 1107,2153
Hydrotris(pyrazolyl)borates
aluminium, 265
hafnium, 2185
lanthanides, 697
magnesium, 1775,2655
molybdenum, 527,619,687,693,2965
molybdenum(V), 1965
thorium, 1645
tungsten, 527
uranium, 69
uranium(IV), 1645
vanadium(IV), 2483
zirconium(IV), 2185
Hydroxides and hydroxo complexes
aluminium, 171,199
boron, 789
chromium(III), 137
cobalt(II), 2839
cobalt(III), 2803
copper(II), 629
germanium, 1263
hafnium(IV), 2705
iron(III), 2895
neodymium, 659
nickel(II), 2839
rhenium(VII), 2081
tin(IV), 1331
titanium(IV), 2097
uranium(VI), 2987
Hydroxycarboxylates
aluminium, 171
copper(II), 1191
gallium, 207
1-(2-Hydroxyphenyl)propanedionates
Co, Cu, Ni, Pd, Pt, 2721
Hydroxypyridone complexes
aluminium, 409
Hydroxypyrone complexes
copper(II), 2061
Hydroxyquinoline complexes
aluminium, 409
lanthanides, 2143
molybdenum(VI), 881
Hypophosphorous acid, tautomers, 1071

I

Imidazole complexes
cadmium, 2437
cobalt(II),(III), 2567
copper(II), 1293,2981
lanthanides, 751
Imidazolinethione complexes
copper(I), 981
Iminoacyl complexes
chromium(VI), 2625
tungsten(IV), 23
zirconium, 839
Indium(II)
halides, review, 377
Indium(III)
alkoxide oxo compound, 719
alkyls, 921
alkyl aminoalkyl chloride complexes, 353
alkyl carboxylate oxo thiolate copper(I) complexes, 361
blood plasma speciation, 151,163
chloride phosphine cobalt complexes, 2533
chloride phospholyl complex, 329
chloride porphyrin, 1297
diketonates, 215
phosphide, 353
tin oxide [ITO], 361
INDO calculations
iron(II) carbonyl cyanide cyclopentadienyl complexes, 1849
molybdenum(II) chloride cyclobutadiene cyclopentadienyl complex, 1855

niobium(I) alkyne carbonyl cyclopentadienyl complex, 1855
Inelastic neutron scattering
osmium carbonyl hydride, 2759
Iodides and iodo complexes
copper(I), 75,981,2319
gallium(II), 377
gallium(III), 2763
indium(II), 377
lead(II), 2429
molybdenum, 619,687
molybdenum(I), 1187
molybdenum(II), 801,1099
nickel, 1487
platinum(II), 2647
rhenium(III), 1131
tin(II), 1187
tin(IV), 1331
tungsten(I), 1187
tungsten(II), 727,801,1099,2135, 2233,2507
tungsten(IV), 11,727
Iodobenzoates
titanium(IV), 783
zirconium(IV), 2689
IR spectra
alcohol complexes, 1843,2309
alkenyl complexes, 907
alkoxides, 371,2189,2575
alkoxycarbonyl complexes, 1131
alkyls, 301,343,597,2763
alkylamides, 1009
alkylimides, 603
alkyne complexes, 603,727,2135, 2233,2507
amide complexes, 125,2375,2699
amine complexes, 495,851,881, 2171,2641,2931
aminoacid complexes, 119,1293, 1975,2245,2895
aminoacid ester complexes, 597
aminoalcohol complexes, 535
aminophenoxides, 2143
aminothiolate, 763
ammonia complexes, 119,1175
aryls, 2181
arylamides, 245,527,687
arylazopyridine complexes, 2251
arylimides, 603
azide complexes, 1113,2375,2693
azole complexes, 751,2981
bis(diphenylphosphino)pyridine and derivatives, 1757
bromides, 881,1099,1703,1751, 2041,2443,2463,2741
carbonates, 1447
carbonyls, 565,603,727,801,907, 969,1045,1059,1099,1131,1141, 1187,1479,1491,1573,1677,1757, 1883,2135,2153,2193,2233,2305, 2469,2507,2533,2579,2815,2859, 2863,2887,2901
carboxylates, 371,783,907,1017, 1119,1305,1447,1723,2035,2143, 2693,2741,2987
carboxylic acids, 371
carbyne complex, 727
catecholates, 813,1323
chlorides, 495,603,653,851,1065, 1113,1141,1165,1243,1287,1457, 1633,1695,1703,1751,1829,1975, 2081,2163,2171,2309,2443,2463, 2663,2721,2733,2741,2823
crown amine ether, 1747
crown ether complexes, 2371
cyanates, 125,2375,2937
cyclopentadienyls, 479,783,1453, 2143,2689
diamide complexes, 693
diaminodihydroxy tetradentate complexes, 1593
dicarboxylates, 1175,1447
dienen complexes, 1141
diimine complexes, 125,1243,2285
diketonates, 751,795,1011,1305, 1397,2061,2309,2721,2823
dithio- compounds, 1397
dithiocarbamates, 859,881,1729, 2013
dithiocarbazate ester complexes, 1457
dithiolates, 1441,1561,2965
dithionates, 2823
dithiophosphates, 943
ether complexes, 479
ethylenedibiguanide complexes, 2245
fluorides, 1653
hexafluorophosphates, 565,573
hydrates, 475,1633,1639,2463, 2693,2699
hydrides, 2153,2189
hydroxides, 659,2895
hydroxyquinolates, 2143
iminoacyl complexes, 23,2625
isocyanide complexes, 1487,2135, 2663
ketoaminophenol complex, 1639
ketoimine complex, 2097
maltol complexes, 2309
nitrates, 475,795,2019,2443,2839
nitrile complexes, 2153,2887
nitrites, 1243,2375,2591
nitrosyls, 527,687,1741,2081, 2733
oxime complexes, 1011,2663
oxo complexes, 371,779,881,1011, 1323,1397,1541,1653,1751,1829, 2081,2293,2449,2483,2549,2895, 2987
perchlorates, 659,1639,1729, 2251,2981
peroxides, 1653
phenol complexes, 653
phenoxides, 557,687,939,2171, 2375
phosphine complexes, 669,1141, 1243,2823
phosphine oxide complexes, 1099, 1723
phosphiniminato complexes, 2625
phosphiniminocyclotrithiazenes, 1433
phosphinothioformate, 2163
phthalocyanines, 1087
polyketone complexes, 2285
polyphosphines, 35
pyrazolylborates, 63,265,687, 693,1119,2483
pyridine complexes, 475,863, 1087,1723,1975,2251
pyridine-*N*-oxide complexes, 863,2981
pyridylketonate complexes, 2443
quinazolone complexes, 805
quinone complexes, 851

salicylaldimines, 557
Schiff bases, 653
Schiff base complexes, 475,527, 557,1011,1017,1293,2019,2463, 2741,2981,2987
selenium - nitrogen complexes, 1567
silylthiolates, 1659
sulphates, 1633
sulphonates, 1633
sulphoxide complexes, 125,1397
sulphur dioxide complexes, 1633
telluroether complexes, 495,851, 1141,2041
tetramine complexes, 1729
tetrafluoroborates, 1723,2181, 2641
tetraselenide, 1389
thiazolylthiourea complexes, 2449
thio compounds, 2293
thioamide complexes, 1287
thiocyanates, 535,557,713,881, 2371,2375,2839,2965
thioether complexes, 2721
thiohydrazide, thiohydrazone complexes, 1065
thiolates, 597,779,1017,1155, 1659
thiomorpholine complex, 1045
thione complexes, 981,2833
thiosemicarbazide complexes, 2029
thiouracil complexes, 2747
triazenides, 1737
triphosphinomethanides, 2181
tropolonates, 2309
violurates, 2733
water complexes, 2371,2375,2721
xanthate, 1341,1729

Iridium(I)
alkyne phosphine complex, 1867
carbonyl chloride phosphine complex, 893
diene phenol phenoxide complexes, 969

Iridium(II,III)
alkenediyl carbonyl diphosphine isocyanide phenyl complex, 2635

Iridium(III)
alkyl carbonyl cyclpentadienyl phosphine thiolate cyclometallated complexes, 1883
carbonyl diamine methyl complexes, 2071
chloride thioether complexes, 893
triazenides, 1737

Iron
borane carbonyl complexes, 2359
carbide carbonyl nitride phosphine thio cluster complexes, review, 455
carbonyl cluster complexes, 1769
carbonyl cyclopentadienyl gallium complexes, 2763
carbonyl hydride cobalt complexes, 2815
carbonyl vinylidene complexes, 1809
cyanide nitrosyl complex, 913
cyclopentadienyl nitrosyl complexes, 1783
dithiocarbamate nitrosyl thio thiolate thiosulphate complexes, 1741
nitrosyl thio complexes, 2399

Iron(-II)
carbonyl germanium complex, 1127

Iron(0)
carbonyl phosphine silyl complexes, 1337
carbonyl thioether complex, 1045

Iron(I)
carbonyl cyclopentadienyl tin(II) heteropolymetallic complexes, 1187

Iron(II)
amine thioether macrocyclic complex, 2641
arene cyclopentadienyl complexes, 1,2727
arsine cyanide phosphine stibine complexes, 2433
azole thiocyanate complex, 2971
carbonyl cyanide cyclopentadienyl complexes, 1849
carbonyl cyclopentadienyl diphosphine ether complexes, 639
carbonyl cyclopentadienyl germyl complexes, 773
cyclopentadienyls, 1091,2751
cyclopentadienyl heteropolymetallic complexes, 557,2233
in glasses, glazes, 999
phthalocyanine pyridine complexes, 1087
polyphosphate complex, 2609
saccharinate water complexes, 1383

Iron(III)
chloride diphosphine complexes, 2139
chloride phosphine phosphine oxide complexes, 1695
chloride thiohydrazine thiohydrazone complexes, 1065
diaminodihydroxy tetradentate complexes, 1593
in glasses, glazes, 999
glycine glycoside hydroxide oxo complexes, 2895
phthalocyanine, 1021
sulphosalicylate complexes, 2675

Isocyanides, reactions with trinuclear complexes, 2776

Isocyanide complexes
chromium(VI), 2625
iridium(II,III), 2635
nickel, 1487
nickel(0), platinum(II), 2651
tungsten(II), 727,2135
tungsten(IV), 11,727

Isomerism, iron carbonyl cluster complexes, 1769

Isonicotinate complexes
rhenium(II), 743

Isopolymolybdates, 1717

K

Kagome nets, theory and topology, 1901

Ketoaminophenol complexes
europium, terbium, 1639

Ketoimine complexes
titanium(IV), 2097
Ketone complexes
aluminium, 233
cobalt(II), 1375
copper(II), 2747
Kinetic studies
alkene dimerisation catalysis, 2809
enzyme inhibition by nitroprusside, 913
exchange reactions, Rh(III) methyl oxime complexes, 2047
pyrolysis, chromium(III) ammonia complex oxalate salt, 1175
redox, ascorbic acid - $[Mo(CN)_8]^{3-}$, 113
redox, benzoin - $[Mo(CN)_8]^{3-}$, 2299
redox, Co(II) polyaminepolycarboxylate - periodate, 99
solvation, Cr(0) carbonyls, 2511
substitutions, aluminium diketonates, 215
substitutions, carbonyls, review, 1503
substitution, chromium(III) hydroxide nitrilotriacetate water complexes, 137
substitutions, gallium, indium diketonates, 215
substitutions, ruthenium(III) edta water complex, 2681
substitutions, scandium diketonates, 215
tautomerization, hypophosphorous acid, 1021

L

Lanthanides
aminophenoxide carboxylate cyclopentadienyl hydroxyquinolate complexes, 2143
azole diketonate complexes, 751
chloride cyclopentadienyls, 1453
chloride cyclopentadienyl ether complexes, 479
chloride phenoxide complexes, 939
crown ether thiocyanate water complexes, 2371
cyclopentadienyl ylide complexes, 875
diketonate pyrazolylborate compounds, 697
diketone nitrate complexes, 795
dithiocarbamate complexes, 859
nitrate pyridylketonate copper(II) complexes, 2443
nitrate schiff base complexes, 2019
phenanthroline polyketonate complexes, 2285
phosphotungstates, 1249
Lanthanum
chloride cyclopentadienyl, 1453
chloride cyclopentadienyl ether complexes, 479
chloride phenoxide complexes, 939
crown ether thiocyanate water complexes, 2371
diketonate pyrazolylborate compounds, 697
diketone nitrate complexes, 795
dithiocarbamate complexes, 859
nitrate pyridylketonate copper(II) complexes, 2443
phenanthroline polyketonate complexes, 2285
phosphotungstate, 1249
Laponite, 517,1709
Lead(II)
acetate glasses, Co^{2+}, Ni^{2+} in, 1475
aminoacid complexes, 665
dithiolate heterobinuclear complexes, 1441
halide complexes, 2429
phenanthroline complexes, 2497
Leucine complexes
Ca,Cd,Co,Cu,Mg,Ni,Pb,Zn, 665
Ligand reactions
book review, 1621
diketonate, 2061
Ligand synthesis
amino(aminothio)amides, 1079
aminophenoltriacetate, 2873
aminotelluroethers, 495,851
crown amine ether, 1747
cyclopentadienyls, 479,1091
cyclopentadienylphosphines, 2901
diketone - thioether, 2721
diphosphinopyridine, 1757
ketoaminophenol, 1639
macrocyclic tetramine, 2221
oxadiazacycloalkane, 2847
oximes, 2663
polyphosphines, 35
porphyrin, 2527
pyrazolylborates, 63
pyridine schiff base macrocycle, 475
tetradentate Schiff base, 1469
thiadiazolidinethiones, 1017
triamine polymers, 2491
triselenophosphonate, 987
Lithium
butoxides, diethylbenzamide, 227
cryptand complexes, 1369
diamine complex, 931
germyls, 2263
tetrakis(trimethylsilyl)aluminate, 277
Lutetium
crown ether thiocyanate water complexes, 2371
diketonate pyrazolylborate compounds, 697
nitrate Schiff base complexes, 2019
phenanthroline polyketonate complexes, 2285
Lutidine complexes
molybdenum(II), 1209
platinum(II), 2647
Lysidine, interaction with gold(I) complex, 975

M

Macrocyclic complexes
copper(I), 2911
copper(II), 2221,2239,2353,2911, 2919

europium, 1411
iron(II), 2641
mercury, 2931
neodymium, 1411
nickel(II), 1027,1729,2221
rhodium(III), 2925
ruthenium(0), 1221
tetramines, review, 2553
yttrium, 475
Magnesium
aminoacid complexes, 665
chloride nitrate pyridylketonate copper(II) complexes, 2443
crown amine ether complex, 1747
cryptand complexes, 1369
ether silylamide complexes, 2959
fluoride, 1919
halide methyl pyrazolylborate complexes, 1775
polyphosphate complex, 2609
pyrazolylborate siloxide, 2655
reactions with ferrocene derivatives, 1091
Magnetic moments
cobalt(II) amine carboxylate water complexes, 2873
cobalt(II) chloride hydroxide nitrate pyridylpyrazole thiocyanate complexes, 2839
cobalt(II) diketonate water complexes, 2721
cobalt(II) dithiolate hetero-binuclear complexes, 1441
cobalt(II) salicylaldimine thiocyanate heteropolymetallic complexes, 557
cobalt(II) thiosemicarbazide complexes, 2029
copper(II) acetate alkoxide amine pyridine water binucleating complexes, 2867
copper(II) acetate azole oxalate sulphate complexes, 2035
copper(II) amide amin bromide phenoxide pseudohalide thio-ether water complexes, 2375
copper(II) aminoacid imidazole pyridine Schiff base complexes, 1293
copper(II) aminoethoxide thiocyanate, 535
copper(II) azide dipyridylamine complex, 2693
copper(II) azole halide perchlorate thiuocyanate complexes, 713
copper(II) carboxylate phenoxide quinazolinone complexes, 805
copper(II) chloride dithiocarbazate ester complexes, 1457
copper(II) chloride oxime complexes, 2663
copper(II) chloride thiouracil complex, 2747
copper(II) diketonate heterodi-nuclear complexes, 2721
copper(II) dithiolate hetero-binuclear complexes, 1441
copper(II) halide nitrate pyridylketonate heterometallic complexes, 2443
copper(II) halide triazene oxide binucleating complexes, 1703
copper(II) salicylaldimine thiocyanate heteropolymetallic complexes, 557
copper(II) thiosemicarbazide complexes, 2029
iron(II) azole thiocyanate complex, 2971
iron(III) chloride phosphine phosphine oxide complexes, 1695
iron(III) chloride thiohydrazide thiohydrazone complexes, 1065
manganese(II) acetonitrile phenoxide complex, 1311
manganese(II) amine carboxylate water complexes, 2873
manganese(III) acetate alkoxide amine pyridine binucleating complexes, 2867
nickel(II) amine carboxylate water complexes, 2873
nickel(II) aminoethanol thiocyanate complex, 535
nickel(II) chloride hydroxide nitrate pyridylpyrazole thiocyanate complexes, 2839
nickel(II) diketonate water copper(II) complexes, 2721
nickel(II) salicylaldimine thiocyanate heteropolymetallic complexes, 557
nickel(II) Schiff base thiolate complexes, 1017
nickel(II) thiosemicarbazide complexes, 2029
osmium(III) chloride diketonate methanol phosphine complexes, 2309
rhenium(II,III) diarsine diphos-phine halide complexes, 573
rhodium(II) dithiocarbamate phosphine complexes, 2013
ruthenium(II,III) carboxylate chloride ether phosphine oxide pyridine complexes, 1723
saccharinate complexes, 1383
titanium(III) chloride phenoxide complex, 1617
tungsten(IV) chloride phosphine complex, 669
uranium(IV) alkoxide oxo complexes, 1843
vanadium(IV) diketonate oxo pyridine sulphoxide complexes, 1397
Maleonitriledithiolates
cobalt, 1123
gold, 1561
nickel, palladium, 2053
platinum, 1561,2053
rhodium, 1123
Malonates
molybdenum(VI), 881
Maltol complexes
aluminium, 409
osmium(III), 2309
Mandelates
rhodium(II), 1135
Manganese(0)
carbonyl diphosphine complexes, 2305
carbonyl phosphine thioether

complex, 2579
carbonyl phosphinopyridine complex, 1479
Manganese(I)
alkyl carbonyl cyclopentadienyls, 921
Manganese(II)
acetonitrile phenoxide complex, 1311
amine carboxylate water complexes, 2873
cyclopentadienyls, 921
dipyridylamide complex, 2699
ether silylamide complexes, 2959
saccharinate water complexes, 1383
thiosalicylate complexes, 1181
Manganese(III)
acetate alkoxide amine pyridine binucleating complexes, 2867
thiosalicylate complexes, 1181
Mannitol complexes
molybdenum(VI), 1225
Mass spectra
aluminium methyl phenoxide, 239
aminodiarsines, -diphosphines, 2413
cadmium mercaptopyridine mercaptothiazole complexes, 541
chromium(VI) butylimide complex, 1009
cobalt(-I) carbonyl phosphine indium complexes, 2533
copper(I) dithiocarbamate thiolate indium complex, 361
copper(I) thiolate, 1659
copper(II) diimine macrocyclic complexes, 2239
gallium alkylamide arsenido methyl compounds, 343
germanium alkoxide hydrides, 2189
hafnium cyclopentadienyl methyl compounds, 301
indium chloride phosphine cobalt complexes, 2533
indium chloride porphyrin, 1297
iron(0) carbonyl thioether complex, 1045
iron(II) amine thioether macrocyclic complex, 2641
lanthanide aminophenoxide carboxylate cyclopentadienyl hydroxyquinolate complexes, 2143
lanthanide chloride cyclopentadienyl ether complexes, 479
macrocyclic ligand, 475
mercury amine thioether macrocyclic complex, 2931
molybdenum arylamide chloride nitrosyl pyrazolylborate complexes, 527
molybdenum chloride diamide nitrosyl pyrazolylborate complexes, 693
molybdenum dithiolate pyrazolylborate thiocyanate complex, 2965
osmium(VIII) alkylamide alkylimide chloride oxo complexes, 1009
rhenium aryl butylimide nitrosyl complex, 2081
rhodium(III) amine thioether macrocyclic complex, 2925
scandium alkoxide oxo compound, 719
tungsten(II) alkyne carbonyl iodide isocyanide complexes, 727
tungsten(IV) allyl complexes, 11, 23
tungsten(IV) carbonyl carbyne iodide isocyanide complex, 727
vanadium(IV) diketonate oxo pyridine sulphoxide complexes, 1397
ytterbium, yttrium alkoxide oxo compounds, 719
zirconium cyclopentadienyl methyl compounds, 301
Mercaptoacetic acid complexes
mercury, 2717
2-Mercaptobenzoates
manganese(II),(III), 1181
Mercaptobenzothiazole complexes
cadmium, 541
Mercaptoethanol complexes
mercury, 2717
Mercaptopropionic acid complexes
mercury, 2717
Mercaptopropionylglycine complexes
cadmium, 831
Mercaptopyridine complexes
cadmium, 541
Mercaptopyrimidine complexes
ruthenium(III), 2681
Mercury
alkyls, 921
amine thioether macrocyclic complex, 2931
aminotelluroether chloride complexes, 851
cadmium telluride precursors, 921
cyclopentadienyl thiocyanate heteropolymetallic complexes, 557
halide telluroether complexes, 2041
methyl phenyl triphosphorus heterodinuclear complexes, 2477
methyl thioaminoacid - ester complexes, 597
methylhydantoin complex, 1765
phenoxide complexes, 1537
thiolates, thiophenoxide, 2717
Mesityls
rhenium(VII), 2081
Mesitylene selenoxide complexes
Mo(III), W(III), 2941
Methanethiolate complexes
iron, 1741
Methanol complexes
osmium(III), 2309
Methionine complexes
cobalt(III), 2245
platinum(II), 1975
Methionine methyl ester complexes
platinum(II), 1975
Methoxides
copper(II), 2575
molybdenum, 619

molybdenum(V), 1965
rhenium(V), 615
tin(IV), 1331
2-Methoxyethylcyclopentadienyls
lanthanides, 1453
Methyls
aluminium, 223,233,239,245,257, 265,289,301,313,371,2205
cobalt, 2477
exchange reactions, 301
gallium, 223,319,343,353
germanium, 2263
hafnium, 301
indium, 353
iridium(III), 2071
magnesium, 1775
mercury, 597,2477
niobium(V), 1051
rhodium, 2477
rhodium(III), 2047,2071
ruthenium(III), 2071
tantalum(V), 1051
tin(IV), 2863
titanium, 1423
tungsten(IV), 11
zirconium, 301,1423
Methylallyls
nickel(II), 757
tungsten(IV), 23
Methylamine complexes
platinum(II), 2647
4-Methylbenzyls
Nb(V), Ta(V), 1051
Methylcyclopentadienyls
gallium, molybdenum, 2763
ruthenium(II), 2163
titanium(IV), 783
Methyldiphenylphosphine complexes,
iridium(III), 1883
molybdenum(IV), 545
nickel(II), 1341
platinum(II), 987
ruthenium(0), 1221
tungsten(II), 2233
Methylene complexes
molybdenum, tungsten, 2953
Methylenebis(diphenylphosphine oxide) complexes,
Mo(II), W(II), 1099
4-Methylesculetin complexes
lanthanides, 939
1-Methylhydantoin complexes
mercury, 1765
Methylimidazole complexes
rhodium(III), 2047
Methylisocyanide complexes
nickel, 1487,2651
platinum(II), 2651
4-Methoxyphenoxides
zirconium, 2185
4-Methylphenylamides
molybdenum, 619
1-Methylpiperidine-4-thiolates
silver, 769
4-(4'-Methyl-2'-thiazolylazo)-2-methylresorcinol complexes,
cadmium, 501
Methyl thioglycolate complexes
iron, 1741
Microwave dielectric loss heating, synthetic applications, 893
MNDO calculations
polyhedral boranes, metalloboranes, 2359
MOCVD precursors, cadmium mercury telluride, 921
Moessbauer spectra
iron(0) carbonyl thioether complex, 1045
iron(II) arene cyclopentadienyl complexes, 2727
iron(II) cyclopentadienyls, 2751
iron(II),(III) in glasses, glazes, 999
iron(III) chloride thiohydrazide thiohydrazone complexes, 1065
iron(III) diaminodihydroxy tetradentate complexes, 1593
Molecular mechanics
copper(II) aminoacid complexes, 1277,2419
Molecular orbitals
boranes, 1045,2359
carbaborane, 2407
cobalt carbonyl cyclopentadienyl, 1783
iridium(I) alkyne phosphine complex, 1867
iron carbonyl vinylidene complexes, 1809
iron cyclopentadienyl nitrosyl, 1783
iron(II) carbonyl cyanide cyclopentadienyl complexes, 1843
Kagome nets, 1901
metallaboranes, 2359
molybdenum(II) chloride cyclobutadiene cyclopentadienyl complex, 1855
molybdenum(IV),(V) chloride disulphide thio polynuclear complexes, 2585
niobium(I) alkyne carbonyl cyclopentadienyl complex, 1855
osmium(0) alkyne carbonyl complex, 1867
palladium, platinum trinuclear complexes, 2773
ruthenium cyclopentadienyl nitrosyl, 1783
ruthenium(0) alkyne carbonyl complex, 1867
ruthenium(II) dipyridyl pyridinoaryl complexes, 1939
S_4N_4, 1935
semibridged complexes, 1799
sulphur - nitrogen compounds, 107
triatomic molecules, 1919
trinuclear clusters, 1625
tungsten(III) alkoxide chloride oxo complexes, 1829
"two - legged piano stool" complexes, 2001
Molecular rearrangements, 2221
Molybdenum
alkoxide arylamide carbonyl iodide nitrosyl phenoxide pyrazolylborate complexes, 619
alkoxycarbene alkylidyne carbaborane cycloheptatrienyl methylene phosphido tungsten complexes, 2953
arylamide chloride nitrosyl

pyrazolylborate complexes, 527
arylamide halide nitrosyl phenoxide pyrazolylborate complexes, 687
carbonyl cyclopentadienyl gallium complex, 2763
chloride diamide nitrosyl pyrazolylborate complexes, 693
dithiolate pyrazolylborate thiocyanate complex, 2965
Molybdenum(0)
carbonyl diphosphine complexes, 2393,2469
carbonyl diphosphine heterodinuclear complexes, 2305
carbonyl dipyridyl phosphine complexes, 1059
carbonyl dithiolane complexes, 703
carbonyl phosphine complexes, 1479,2619,2901
carbonyl phosphine piperidine complexes, 1757
carbonyl phosphine thioether complex, 2579
Molybdenum(I)
carbonyl diimine halide tin(II) iron(I) complexes, 1187
Molybdenum(II)
acetate chromium(II) compounds, 1237
carbonyl diphosphinoethyne iodide complexes, 801
carbonyl halide phosphine oxide complexes, 1099
carbonyl cyclopentadienyl phosphido complex, 2901
chloride cyclobutadiene cyclopentadienyl complex, 1855
halide pyridine complexes, 1209
Molybdenum(III)
alkoxide selenophenoxides, 2941
carbonyl cyclopentadienyl oxo phosphido complex, 2469
Molybdenum(IV)
chloride disulphide thio complexes, 2585
diphosphine hydride complexes, 645
halide hydrazide phosphine triphosphine complexes, 545
thio water complex, 1671
Molybdenum(V)
alkoxide oxo pyrazolylborate complexes, 1965
amine chloride phenoxide complexes, 2171
chloride disulphide polynuclear complexes, 2585
chloride oxo thio compounds, 2293
cyanide complex, 113,2299
Molybdenum(VI)
alditol oxo complexes, 1225
aminothiophenoxide dicarboxylate dithiocarboxylate halide hydroxyquinoline oxo thiocyanate thiosemicarbazide complexes, 881
dichlorodioxo, 2293
hetropolyanion, 2023
isopolyanions, 1717
nitrilotriacetate oxo polyalkoxide triethanolamine complexes, 1541
oxo thiazolylthiourea complexes, 2449
oxo tripod phosphine oxide cobalt(0) complex, 2549
Monohalide complexes, 2257
Morpholine-4-carbodithioates lanthanides, 859
MOVPE, indium phosphide, 353

N

1,4-Naphthaquinone complexes tellurium(II), 847
Neodymium
acetate hexamine macrocyclic complex, 1411
chloride cyclopentadienyl, 1453
chloride cyclopentadienyl ether complexes, 479
crown ether thiocyanate water complexes, 2371
cyclopentadienyl ylide complexes, 875
diketonate pyrazolylborate, 697
diketone nitrate complexes, 795
dithiocarbamate complexes, 859
hydroxide perchlorate, 659
nitrate pyridylketonate copper(II) complexes, 2443
nitrate Schiff base complexes, 2019
phenanthroline polyketonate complexes, 2285
phosphotungstates, 1249
Neopentyls
rhodium(IV), 2071
Nickel
diphosphine iodide isocyanide complex, 1487
dithiolate complexes, 2053
Nickel(0)
diphosphine isocyanide platinum(II) complex, 2651
Nickel(I)
alkyne cyclopentadienyl dipyridyl phosphine complexes, 581
allyl chloride diphosphine phosphine complexes, 757
Nickel(II)
alkoxide amine pyridine water binucleating complexes, 2867
amine carboxylate water complexes, 2873
amine ether tridentate cyclic complexes, 2847
aminoacid complexes, 665
aminocarbene carbonate carboxylate phosphine complexes, 1447
aminoethanol thiocyanate complex, 535
carboxylate dithiocarbamate macrocyclic tetramine thiocarboxylate xanthate complexes, 1729
chloride dithionate phosphine complexes, 2809,2823
chloride hydroxide nitrate pyridylpyrazole thiocyanate complexes, 2839

chloride polyphosphine Co(I), Pt(II) complexes, 1317
clay surface - adsorbed complexes, 2273
diketonate polymeric complexes, 2823
diketonate water copper(II) complexes, 2721
dithiolate heterobinuclear complexes, 1441
dithiophosphinates, 2597
halide nitrate pyridylketonate copper(II) complexes, 2443
in lead acetate glasses, 1475
macrocyclic tetramine complexes, 2221
peptide complexes, 825
phosphine xanthate complex, 1341
polymeric triamine complexes, 2491
polyphosphate complex, 2609
saccharinate water complexes, 1383
salicylaldimine thiocyanate heteropolymetallic complexes, 557
Schiff base thiolate complexes, 1017
tetramine macrocyclic complex, 1027
thiosemicarbazide complexes, 2029
Niobium(I)
alkyne carbonyl cyclopentadienyl complex, 1855
Niobium(III)
phosphine thio thiolate complexes, 1689
Niobium(V)
alkyl chloride phenoxide cyclometallated complexes, 1051
alkylamide chloride ether complexes, 2709
aluminium oxide, 367
oxide, 367
Nitrates
cadmium, 2839
calcium, 2443
cobalt(II), 2839
cobalt(III), 1079
copper(II), 2443
lanthanides, 795,2019,2443
magnesium, 2443
nickel(II), 2443,2839
platinum(II), 2647
silver(I), 1429,2127
thorium, 491
uranium(VI), 2443
yttrium, 475
zinc, 2839
Nitrile complexes
copper(I), 75
manganese(II), 1311
ruthenium(II), 1243,2153
sodium, 957
tungsten((0), 2887
tungsten(VI), 2293
Nitrilotriacetate complexes
aluminium, 199
chromium(III), 137
molybdenum(VI), 1541
Nitrite complexes
cobalt(III), 1379,2149,2803
copper(II), 2375
palladium(II), 2591
ruthenium(II), 1243
tin(IV), 1331
Nitrobenzoates
titanium(IV), 783
yttrium, 1119
zirconium(IV), 2689
Nitrocatecholates
silicon, 813
Nitrogen - selenium complexes
platinum(II), 1567
Nitrophenoxides
copper(II), 2375
mercury, 1537
zirconium, 2185
Nitrophenyls
arsenic(V), 2023
Nitroprusside, enzyme inhibition, 913
Nitrosyls
iron, 913,1741,1783,2399
molecular orbitals, 2001
molybdenum, 527,619,687,693
rhenium, 2081
rhodium, 1589
ruthenium, 1783,2733
tungsten, 527
NMR (^{1}H) spectra
agostic hydrogens, 23
alkenyl complexes, 907
alkoxides, 233,371,719,1829, 1843,2941,2959
alkoxycarbonyl complexes, 1131
alkyls,11,23,265,277,289,343, 353,371,839,1051,1483,2071, 2263,2477
alkylamides, 1009,2081,2625,2709
alkylidene complexes, 1491
alkylidyne complexes, 1271
alkylimides, 603,1009,2625
alkyne complexes, 603,727,2135, 2233,2597
allyls, 11,23
amide complexes, 125
amidothiophenoxides, 2211
amine complexes, 289,495,739, 2647
aminoacid complexes, 1293,1975
aminoalkyls, 353
aminocarbene complexes, 1447
aminodiarsines, aminodiphosphines, 2413
aminotelluroether complexes, 851
aminothiolate, 763
aniline complex, 245
arene complexes, 1113,1677
arsenido complexes, 343
arsine complexes, 289,1609,2153
arsinogallanes, 319
aryls, 125,943,963,1107,1613, 2081
arylamides, 527,687
arylazopyridine complexes, 2251
arylimides, 603
carbaboranes, 943
carboxylates, 371,743,783,1119, 1331,1411,2741
carboxylic acid complexes, 371
carbyne complexes, 727
catecholates, 813,1323
cyclometallated complexes, 245,

1883
cyclopentadienyls, 479,581,669, 773,783,839,863,875,1131,1883, 1893,2153,2163,2305,2469,2689, 2901
diamide complexes, 693
diarsine complexes, 573,743
diimine complexes, 1483,1613, 2285
diketonates, 697,1011,1305
diphosphadiene, 1363
diphosphine, 669
diphosphine complexes, 565,573, 743,1107,2135,2233,2305,2469, 2507,2603,2741
dipicolinate complexes, 1975
distibine complexes, 1609
dithiocarbamates, 2013
dithiolane complexes, 703,1441, 2965
dithiophosphates, 943
ether complexes, 479,1723
hydrides, 1107,1491,1573
iminoacyls, 839
isocyanide complexes, 2135,2651
ketoaminophenol, 1639
macrocyclic complexes, 1411, 2641,2931
methylene complex, 2953
nitrile complexes, 2153
oxadiazacycloalkane, 2847
oxime complexes, 1011
phenol complexes, 653
phenoxides, 687,839,963,969,1617
phosphido complexes, 343,1573, 2469,2901
phosphiniminocyclotrithiazenes, 1433
phosphine complexes, 11,565,603, 1165,1573,1609,1883,2013,2135, 2153,2469,2579,2901
phosphine oxide complexes, 1099
phosphinidene complexes, 1573
phosphinopyridine complexes, 2603
phosphinothioformate complexes, 2163
phosphite complexes, 1893
phosphonium salts, 129
polyketonates, 2285
polyphosphines, 35
porphyrin complexes, 1297,1331, 2527
pyrazolylborates,63,265,527, 619,687,693,697,1119,2965
pyrazolylmethane complexes, 265
pyridine complexes, 475,863, 1411,1613,1975,2251,2647
pyridine-*N*-oxide complexes, 863
Schiff base, 653
Schiff base complexes, 475,739, 1011,1293,2463,2741,2887,2987
selenophenoxides, 2941
spirophosphorane, 1463
stibine complexes, 1609
sulphonates, 1633
sulphoxide complexes, 125
telluroether complexes, 495,1141 2041
tetraimine complexes, 2603
thioamide complexes, 1287
thiazolylthiourea complexes, 2449
thioether complexes, 1975,2579, 2721
thiolates, 1659
thione complexes, 981
thiourea complexes, 2135
triazenides, 1737
triphosphine complexes, 2477
tripod Schiff base complexes, 2463
ylide complexes, 875
NMR (^{2}H) spectra
pyrazolylborate, 265
NMR (^{11}B) spectra
carbaboranes, 949,2953
NMR (^{13}C) spectra
alditol complexes, 1225
alkoxides, alkoxycarbene complexes, 2953
alkyls, 265,289,353,839,1051, 2263
alkylamides, 1009,2709
alkylidyne complexes, 1271,2953
alkylimides, 603,1009,2625
alkyne complexes, 603,727,2135, 2233
allyls, 757
amine complexes, 289
aminoacid complexes, 1293
aminoalkyls, 353
aminocarbene complexes, 1447, 2193
aminochlorophosphines, 2619
aminotelluroethers, 495
aminotelluroether complexes, 851
aminothiolate, 763
arene complexes, 1677
arsine complexes, 289,2153
aryls, 943,963
bis(diphenylphosphino)pyridine derivatives, 1757
carbaboranes, 943,2953
carbonates, 1447
carbonyls, 727,801,969,1491, 1677,1849,2135,2233,2507
carboxylates, 1411,1447
carbyne complexes, 727
cyanides, 553,913,1849
cyclometallated complex, 245
cyclopentadienyls, 839,863,1849, 2153,2751
dicarboxylates, 1447
diketonates, 1011
diphosphine complexes, 757,801, 2135,2233,2507
dithiocarbamates, 361
dithiolates, 1441
dithiophosphates, 943
hydrazones, 2751
iminoacyls, 23,839
isocyanide complexes, 2135
macrocyclic complexes, 1411, 2221,2641
mercaptothiazole complexes, 541
methylene complexes, 2953
nitrile complexes, 2153
oxime complexes, 1011
phenoxides, 789,839,963
phosphaallyl complex, 2859
phosphine complexes, 603,757, 801,1447,1757,2135,2153,
polyphosphines, 35
pyrazolylborates, 63
pyridine complexes, 863,1411

pyridine-*N*-oxide complexes, 863
Schiff bases, 2751
Schiff base complexes, 1011,1293
telluroether complexes, 2041
thioamide complexes, 1287
thiolates, 1659
thiourea complexes, 2135
tripod Schiff base complexes, 2463
NMR (^{15}N) spectra
cyanides, 1849
NMR (^{17}O) spectra
carbonyls, 1849
heteropolytungstates, 1249
NMR (^{19}F) spectra
aryls, 2181
difluorobiphenyl complexes, 1
NMR (^{23}Na) spectra
clay thermolysis, 517
NMR (^{27}Al) spectra
alumina - laponite reaction, 1709
aluminium methyl oxo propionate propionic acid compounds, 371
aluminium methyl pyrazolylborate pyrazolylmethane complexes, 265
clay thermolysis, 517
NMR (^{29}Si) spectra
ceramic glaze thermolysis, 1709
silicon catecholate complexes, 813
silylthiolate, 1659
NMR (^{31}P) spectra
aminodiphosphines, 2413
bis(diphenylphosphino)pyridine derivatives, 1757
diphosphadiene, 1363
diphosphines, 669
diphosphine complexes, 35,565, 573,639,743,757,801,987,1107, 2305,2469,2603,2651,2741
dithiophosphates, 943
phosphido complexes, 1573,2469, 2901
phosphine complexes, 23,335,565, 603,757,801,863,987,1059,1165, 1287,1447,1561,1573,1609,1757, 2181,2193,2469,2533,2579,2659, 2863,2887,2901
phosphinates, 1555
phosphinidene complexes, 1573
phosphiniminocyclotrithiazenes, 1433
phosphinine complexes, 991
phosphinopyridine complexes, 2603
phosphinothioformate complexes, 2163
phosphonium salts, 129
phosphorus(III) chloride cyanide compounds, 553
phosphorus ylide complexes, 875
phosphotungstates, 1249
polyphosphines, 35
polyphosphine complexes, 1317
triphosphine complexes, 35,2477
triphospinomethanide complexes, 2181
triselenophosphonate complexes, 987
NMR (^{51}V) spectra
vanadium(V) heteropolyanions, 143
NMR (^{59}Co) spectra
cobalt(III) amine ammonia hydroxide nitrite complexes, 2803
cobalt(III) chloride cyanide diamine diimine nitrite sulphite thiourea water complexes, 1379
NMR (^{63}Cu) spectra
copper(I) arsine distibine phosphine stibine complexes, 1609
NMR (^{71}Ga) spectra
gallium citrate halide phosphate sulphate water complexes, 207
NMR (^{77}Se) spectra
selenium(II) halides, 589
selenium sulphides, 1199
tetraselenide, 1389
NMR (^{95}Mo) spectra
molybdenum(0) carbonyl diphosphine complexes, 2393
molybdenum(0) carbonyl dipyridyl phosphine complexes, 1059
molybdenum(VI) alditol oxo complexes, 1225
NMR (^{113}Cd) spectra
cadmium mercaptothiazole complex, 541
NMR (^{125}Te) spectra
tellurium(IV) aryl dialkylene dithiophosphate compounds, 943
NMR (^{183}W) spectra
heteropolytungstates, 1249
tungsten(IV) allyl complexes, 11
NMR (^{195}Pt) spectra
platinum(II) aminoacid dipicolinate complex, 1975
NMR (^{199}Hg) spectra
mercury thiolates, thiophenoxide, 2717
Nucleoside, carbaboranyl, 891

Q

Organobarium compounds, review, 1345
Organocalcium compounds, review, 1345
Organogermanium compounds, book review, 1779
Organorhenium compounds, book review, 897
Organostrontium compounds, review, 1345
Organotin compounds, book reviews, 899,2191
Oscillator strengths
neodymium hydroxide perchlorate, 659
Osmium
alkylidene carbonyl hydride tungsten complex, 1491
carbide carbonyl hydride phosphide phosphine oxo gold complexes, review, 455
carbonyl copper(I) complexes, 75
carbonyl hydride, 2759
carbonyl hydride phosphido phosphine phosphinidene complexes, 1573
carbonyl thio complexes, 2385

Osmium(0)
alkyne carbonyl complex, 1867
carbonyl phosphine complex, 1573
Osmium(II)
chloride diphosphine complex, 1107
Osmium(III)
chloride diketonate methanol phosphine complexes, 2309
triazenides, 1737
Osmium(VIII)
alkylamide alkylimide chloride oxo compounds, 1009
Oxalates
chromium(III), 1175
copper(II), 2035
molybdenum(VI), 881
nickel(II), 1447
Oxaazamacrocyclic complexes
cobalt(II), 2847
copper(II), 2239,2847
nickel(II), zinc, 2847
Oxamine complexes
aluminium, 171
Oxidative additions, trinuclear complexes, 2787
Oxime complexes
copper(II), 2663
molybdenum(VI), 1011
rhodium(III), 2047
Oxo complexes
aluminium, 301,371,409,429
cerium(IV), 1919
chromium(VI), 779
indium, 361,719
iron(III), 2895
molybdenum(III), 2469
molybdenum(V), 1965,2293
molybdenum(VI), 881,1011,1225, 1541,2293,2449,2549
osmium(VIII), 1009
rhenium(V), 615,957,1323,2211
rhenium(VI), 2081
rhenium(VII), 1323,2081,2549
rhodium(IV), 2071
ruthenium(VI), 1751
scandium, 719
sodium, 957
technetium(VII), 2549
tin, 361
tungsten, 1491
tungsten(III), 1829
tungsten(VI), 2293,2549
uranium(IV), 1843
uranium(VI), 2443,2987
vanadium(IV), 81,1397,1603,2101, 2483
ytterbium, yttrium, 719
zirconium, 1653

P

Palladium
diphosphine trinuclear complexes, review, 2767
dithiolate complexes, 2053
Palladium(0)
dibenzylideneacetone complexes, 1949
Palladium(II)
acetate diphosphine halide Schiff base cyclometallated complexes, 2741
aminotelluroether chloride complexes, 495,851
aryl phosphine triphosphinomethanide complexes, 2181
phosphine thioether complex, 2579
chloride diimine sulphate sulphonate sulphur dioxide terpyridyl complexes, 1633
chloride diketonate phosphine pyridine thioamide cyclometallated complexes, 1287
chloride thioether copper(II) complexes, 2721
dithiolate heterobinuclear complexes, 1441
nitrite phosphine complex, 2591
Pamoates
copper(II), 1191
Papain, 913
Parabinate complexes
nickel(II), 1447
PE spectra
cobalt carbonyl cyclopentadienyl complexes, 1783
iron cyclopentadienyl nitrosyl complexes, 1783
molybdenum(V) alkoxide pyrazolylborate complexes, 1965
ruthenium cyclopentadienyl nitrosyl complexes, 1783
Penicillamine complexes
cadmium, 831
copper(II), 505
vanadium(IV), 2101
zinc, 505
Pentafluorophenyls
palladium(II), 2181
Pentamethylcyclopentadienyls
Ba, Ca, 1349
cobalt, 1783
iridium(III), 1883
iron, 1783
lanthanides, 875
rhenium(III), 1135
rhenium(V), 2211
strontium, 1349
titanium(IV), 2097
tungsten(III),(V), 669
zirconium, 301
2,4-Pentanedionates
aluminium, 215
gallium, indium, 215
lanthanides, 697
molybdenum(VI), 1011
osmium(III), 2309
palladium(II), 1287
scandium, 215
tungsten(IV), 11
vanadium(IV), 1603,2483
yttrium, 1305
2,4-Pentanedithionates
nickel(II), 2809,2823
Pentanoic acid, extraction of metals from clay surface complexes, 2273
neo-Pentoxides
Mo(III), W(III), 2941
Pentyls
cadmium, 1483
gallium, 335
rhenium(V), 957

tungsten(IV), 23
tungsten(VI), 1271
Peptide complexes
cadmium, 831
cobalt(III), 2567
copper(II), nickel(II), 825
Perchlorates
copper(II), 713
neodymium, 659
Perfluoro-t-butoxides
molybdenum(III), 1821
Peroxidase, reactions with
phthalocyanines, 1021
Peroxide complexes
cobalt(III), 2567
thorium, 1401
zirconium, 1405,1653
Perturbed angular correlation
hafnium edta complex, 2705
1,10-Phenanthroline complexes
cadmium, 2497
cobalt(III), 1379
copper(II), 2061
lanthanides, 2285
lead, 2497
molybdenum(0), 2863
molybdenum(I), 1187
molybdenum(II), 2863
palladium(II), 1633
tungsten(I), 1187
Phenol complexes
iridium(I), 969
tin(IV), 653
Phenoxides
aluminium, 239,301,409
boron, 789
chromium(II), 1305
copper(II), 805,2375
iridium(I), 969
iron(III), 2675
lanthanides, 939
manganese(II), 1311
mercury, 1537
molybdenum, 619,687
molybdenum(V), 2171
niobium(V), 1051
rhodium(I), 969
tantalum(V), 963,1051,2709
thorium, 1401
tin(IV), 1331
titanium(III), 1617
zirconium, 839,2185
2-Phenoxybenzoate, -benzoic acid
complexes, copper(II), 1667
Phenyls
gallium, 319,353
iridium(II,III), 2635
rhodium(III), 1613
ruthenium(II), 1107
tantalum(V), 963
tellurium(IV), 943
tin(IV), 125,653,2863
Phenylacetylene complexes
nickel(I), 581
tungsten(IV), 603
Phenylalanine complexes
copper(II), 1293
Phenylamido complexes
molybdenum, 619
Phenylbis(tetramethylcyclopentadi-
enyl)phosphine complexes
molybdenum(0), 2901
1-Phenyl-1,3-butanedionates
osmium(III), 2309
vanadium(IV), 2483
Phenylimido complexes
technetium(V), 1497
tungsten(IV), 603,669
2-Phenylphenoxides
zirconium, 2185
Phenyl-2-picolylketonates
heteropolymetallic, 2443
Phenylphosphine complexes
tungsten(V), 669
2-Phenylpyridine complexes
ruthenium(II), 1939
Phenyltriselenophosphonates
platinum(II), 987
Phosphaallyl complexes
tungsten(II), 2859
Phosphametallacycles
chromium(II), 2193
Phosphates
gallium, 207
Phosphido complexes
gallium, 343
molybdenum, 2953
molybdenum(II), 2901
osmium, 1573
tungsten, 2953
Phosphinates
chromium(III), 1555
Phosphines, reactions with
trinuclear complexes, 2775
Phosphine complexes
cadmium selenide, 1913
chromium(0), 1,1479,1757,2579
chromium(II), 2193
chromium(VI), 2625
cobalt, 2549
cobalt(-I), 2533
copper(I), 981,1609,2407,2833,
2919
gallium, 335
gold(I), 2407
indium, 2533
iridium(I), 893,1867
iridium(III), 1883
iron(0), 1337
iron(II), 2433
iron(III), 1695,2139
manganese(0), 1479,2579
molybdenum(0), 1059,1479,1757,
2579,2619,2863,2901
molybdenum(II), 801,2863
molybdenum(IV), 545
nickel(I), 581
nickel(II), 757,1341,1447,2809,
2823
niobium(III), 1689
osmium, 1573
osmium(0), 1573
osmium(III), 2309
palladium(II), 1287,2181,2591
platinum, 1561
platinum(II), 987,1567,1683,2659
rhenium(0), 1479
rhenium(II), 565
rhenium(III), 1165
rhodium, 1589
rhodium(I), 1141,1235
rhodium(II), 2013
rhodium(III), 2047,2071
ruthenium(0), 1221
ruthenium(II), 863,907,1113,
1243,1893,2153,2163,2517

technetium(III),(V), 1497
tungsten(0), 1363,1757,2579, 2887
tungsten(II), 801,2135,2233
tungsten(IV), 11,23,603,669
tungsten(V), 669
Phosphine oxide complexes
aluminium, 409
iron(III), 1695
molybdenum(II), 1099
Mo(VI), Re(VII), 2549
ruthenium(II,III), 1723
ruthenium(VI), 1751
technetium(VII), 2549
tungsten(II), 1099
tungsten(VI), 2549
Phosphine sulphide complexes
aluminium, 313
Phosphinidene complexes
osmium, 1573
Phosphiniminato complexes
chromium(VI), 2625
Phosphiniminocyclotrithiazenes, 1433
Phosphinine complexes
tungsten(0), 991
Phosphinopyridine complexes
copper(I), 2603
manganese(0), 1479
rhodium(II), 2635
Phosphinothioformate complexes
ruthenium(II), 2163
Phospholyls
indium, 329
Phosphonium salts, 129
Phosphorus in cluster complexes, 1955
Phosphorus(III)
chloride cyanide compounds, 553
Phosphorus(V)
aryls, 129
aryl seleno compounds, 681
heteropolytungstate, 1249
Phosphorus trifluoride complexes
tungsten(IV), 11
Phosphorus ylide complexes
lanthanides, 875
Photochemical substitutions
ruthenium(II) diimine complexes, 1243
Phthalocyanines
cobalt(II),(III), 1021
iron(II), 1087
iron(III), 1021
3-Picoline complexes
molybdenum(II), 1209
4-Picoline complexes
copper(II), 1029
molybdenum(II), 1209
platinum(II), 2647
Piperidine complexes
molybdenum(0), 1757
Platinum
diphosphine trinuclear complexes, review, 2767
dithiolate complexes, 2053
dithiolate phosphine complexes, 1561
Platinum(0)
dibenzylideneacetone complexes, 1949
Platinum(II)
amine halide nitrate pyridine complexes, 2647
aminoacid chloride cytochrome dipicolinate dipyridyl - thioether complexes, 1975
aminotelluroether chloride complexes, 495,851
bromide phosphine complex, 1683
chloride diphosphine isocyanide nickel(0) complexes, 2651
chloride diphosphine triphosphine complexes, 35
chloride polyphosphine nickel(II) complexes, 1317
chloride terpyridine complex, 893
chloride thioether complexes, 2721
phosphine selenium - nitrogen complexes, 1567
phosphine tellurium - sulphur - nitrogen complexes, 2659
phosphine triselenophosphonate complexes, 987
Polarography
ruthenium(II) acetonitrile chloride diimine nitrite phosphine complexes, 1243
Polyaminepolycrboxylates
calcium, 505
cobalt(II), 99
Cu(II), Zn, 505
Polyene complexes
molecular orbitals, 2001
Polyhedral boranes, metallaboranes, 2359
Polyketonate complexes
lanthanides, 2285
Polymeric triamine complexes
copper, nickel, zinc, 2491
Polymerization, nickel(II)
macrocyclic tetramine complex, 1027
Polyoxaalkane - enoxide complexes
Ba, Ca, Sr, 2959
Polyphosphates, hydrolysis, 2177
Polyphosphate complexes
copper(II), 511,2609
iron, magnesium, nickel, 2609
Polyphosphine complexes
Co(I), Ni(II), Pt(II), 1317
Polysulphide complexes
ruthenium(II), 1893
Porphyrins
copper(II), 2527
indium, 1297
tin(IV), 1331
Potassium
crown amine ether complex, 1747
cryptand complexes, 1369
germyls, 2263
Potentiometric titrations
boric acid pyrogallol complexes, 789
cadmium, lead phenanthroline complexes, 2497
Praseodymium
azole diketonate complex, 751
chloride cyclopentadienyl ether complexes, 479
crown ether thiocyanate water complexes, 2371
diketonate nitrate complexes, 795
diketonate pyrazolylborate compounds, 697

dithiocarbamate complexes, 859
nitrate Schiff base complexes, 2019
phenanthroline polyketonate complexes, 2285
phosphotungstates, 1249
Prolophos complexes
iron(II), 639
1,3-Propanediolates
molybdenum(V), 1965
Propanethiolates
iron, 1741
Propionates
aluminium, 371
indium, 361
rhenium(II), 743
Propionic acid complexes
aluminium, 371
Propoxides
aluminium, 371
indium(III), 719
molybdenum, 619
molybdenum(V), 1965
scandium, 719
tungsten(III), 1829
Y,Yb, 719
Propyls
gallium, indium, 353
tungsten(IV), 23
Propylamine complexes
molybdenum(V), 2171
Propylene carbonate, solvent extraction by, 1717
i-Propylimido complexes
tungsten(IV), 603
Propylthiolates
copper(I), indium, 361
mercury, 2717
Pseudorotations, 2221
Purinethione complexes
copper(I), 981
Pyrazole complexes
Cd, Co, Ni, Zn, 2839
Pyrazolylborates
aluminium, 265
hafnium, 2185
lanthanides, 697
magnesium, 1775,2655
molybdenum, 527,619,687,693,2965
molybdenum(V), 1965
thallium(I), 63
thorium, 1645
tungsten, 527
uranium(IV), 69,1645
vanadium(IV), 2483
yttrium, 1119
zirconium, 2185
Pyrazolylmethane complexes
aluminium, 265
Pyridinaldazine complexes
thorium, uranium(VI), 2987
Pyridine complexes
aluminium, 309
cadmium, 541,2839
chromium(II), 1311
chromium(VI), 2625
cobalt(II), 2839
copper(I), 2319
copper(II), 629,1029,1257,1293, 2061,2375,2693,2867
europium, 1411
gallium, 2763
germanium, 1127
iron(II), 1087
manganese(II), 2699
manganese(III), 2867
molybdenum(II), 1209
neodymium, 1411
nickel(II), 2839,2867
palladium(II), 1287
platinum(II), 1975,2647
rhodium(III), 1613,2047,2127
ruthenium, 2267
ruthenium(II), 863,1939,2153
ruthenium(II,III), 1723
silver(I), 2251
tungsten(0), 2887
tungsten(IV), 11
tungsten(VI), 1271
vanadium(IV), 1397
yttrium, 475
zinc, 2839
2-Pyridine carboxaldehyde-*N*-oxide Schiff base complexes
copper(II), 2981
Pyridine-*N*-oxide complexes
cobalt(II), 2315
copper(II), 2981
ruthenium(II), 863
Pyridine-2-thionate complexes
copper(I), 2833
rhenium, ruthenium, 623
2-Pyridone complexes
thorium, 491
Pyridoxal, pyridoxamine, pyridoxol complexes, copper(II), 629
2-Pyridyl complexes
ruthenium, 623
4-Pyridylcarbinol complexes
platinum(II), 2647
Pyridylketonate complexes
polymetallic, 2443
2-(2-Pyridyl)phenyl compounds
rhodium(III), 1613
ruthenium(II), 1939
Pyridylphosphine complexes
manganese(0), 1479
Pyridylpyrazole complexes
Cd, Co, Ni, Zn, 2839
10-(4'-*N*-Pyridyl)-5,15,20-triphenylporphinate, indium, 1297
Pyrimidine complexes
copper(II), 2747
ruthenium, 2681,2733
Pyrogallol boric acid complexes, 789
Pyrrolaldazine complexes
thorium, uranium(VI), 2987
Pyrrole, attached to macrocyclic complex, 1027

Q

Quinazolone complexes
copper(II), 805
Quinoline-2-thione complexes
copper(I), 981
Quinone complexes
ruthenium, 2267
tellurium(II), 847
Quinoxalinedithiolates
platinum, 1561

R

Raman spectra
bis(diphenylphosphino)pyridine and derivatives, 1757
bromides, 207,1199
catecholates, 813
chlorides, 207,589,2663
diaminodihydroxy tetradentate complexes, 1593
fluorides, 153
hydroxide, 659
isopolymolybdates, 1717
molybdenum(II) binuclear complexes, 1209
oxime complexes, 2663
oxo complexes, 1653,1751
perchlorate, 659
peroxides, 1653
phosphine complexes, 669
sulphides, 1199
triazenides, 1737
Rhenium
aryl butylimide nitrosyl complex, 2081
carbonyl pyridinethionate thio ruthenium complexes, 623
organo compounds, book review, 899
Rhenium(0)
carbonyl phosphine complex, 1479
Rhenium(II)
carbonyl diphosphine halide phosphine complexes, 565
carboxylate diarsine diphosphine halide complexes, 743
diarsine diphosphine halide complexes, 573
Rhenium(II,III)
diarsine diphosphine halide complexes, 573
Rhenium(III)
alkoxycarbonyl carbonyl cyclopentadienyl halide complexes, 1131
chloride phosphine complexes, 1165
Rhenium(V)
amidothiophenoxide cyclopentadienyl dithiolate thiophenoxide complexes, 2211
aryl butylimide cyclohexadienyl complex, 2081
catecholate oxo complexes, 1323
methoxide oxo tetradentate Schiff base complex, 615
neopentyl oxo sodium complex, 957
Rhenium(VI)
aryl bromide butylimide oxo cyclometallated complexes, 2081
Rhenium(VII)
aryl butylimide chloride hydroxo oxo complexes, 2081
catecholate oxo complexes, 1323
oxo tripod phosphine oxide cobalt(0) complexes, 2549
Rhodium
acetate chloride nitrosyl phosphine complex, 1589
cyclopentadienyl dithiolates, 1123
triphosphine triphosphorus mercury complexes, 2477
Rhodium(I)
carbonyl phenoxide complex, 969
chloride diene phosphine telluroether complexes, 1141
hydride phosphine complex, 1235
Rhodium(II)
alkenediyl carbonyl chloride phosphinopyridine complex, 2635
carboxylate water complexes, 1135
dithiocarbamate phosphine complexes, 2013
Rhodium(II,III)
carboxylate water complexes, 1135
Rhodium(III)
amine thioether macrocyclic complex, 2925
aryl dipyridyl pyridine cyclometallated complex, 1613
azole methyl oxime phosphine pyridine thiourea complexes, 2047
carbonyl chloride telluroether complexes, 1141
carbonyl diamine methyl phosphine thioether complexes, 2071
chloride pyridine complex, 2127
triazenides, 1737
Rhodium(IV)
neopentyl oxo complex, 2071
Ribitol complex
molybdenum(VI), 1225
Rubidium
cryptand complexes, 1369
Ruthenium
carbide carbonyl hydride nitride phosphine cluster complexes, review, 455
carbonyl pyridinethionate pyridyl thio rhenium complexes, 623
cyclopentadienyl nitrosyl, 1783
dipyridyl pyridine quinone complexes, 2267
chloride nitrosyl violurate complexes, 2733
Ruthenium(0)
carbonyl complex, 1867
phosphine tetramine macrocyclic complex, 1221
Ruthenium(II)
acetonitrile chloride diimine nitrite phosphine complexes, 1243
alkenyl carbonyl carboxylate phosphine complexes, 907
amine arene azide chloride ethoxide phosphine complexes, 1113
arsine carbonyl chloride cyclopentadienyl diphosphine hydride nitrile phosphine pyridine complexes, 2153
arsine cyclopentadienyl diphosphine phosphine pyridine pyridine-*N*-oxide complexes, 863
aryl chloride diphosphine hydride complexes, 1107

carbonyl chloride dipyridyl thioether complexes, 893
cyclopentadienyl diphosphine phosphine phosphinothioformate complexes, 2163
cyclopentadienyl phosphite polysulphide complexes, 1893
dipyridyl pyridinoaryl complexes, 1939
violurate water complexes, 2733
water complex, 1095
Ruthenium(II,III)
carboxylate chloride ether phosphine oxide pyridine complexes, 1723
Ruthenium(III)
edta mercaptopyrimidine water complexes, 2681
methyl complex, 2071
triazenides, 1737
Ruthenium(VI)
halide oxide phosphine oxide complexes, 1751

S

Saccharinates
Co,Cu,Fe,Mn,Ni, 1383
Salicylaldimine complexes
lanthanides, 2019
thorium, 1401
zirconium, 1405
Salicylate complexes
copper(II), 1191
iron(III), 2675
nickel(II), 1447
tin(IV), 1331
Salicylideneglycinate ester complexes, tin(IV), 653
Samarium
aminophenoxide carboxylate cyclopentadienyl hydroxyquinolate complexes, 2143
chloride phenoxide water complexes, 939
crown ether thiocyanate water complexes, 2371
cyclopentadienyl ylide complexes, 875
diketonate pyrazolylborate compounds, 697
diketone nitrate complexes, 795
dithiocarbamate complexes, 859
nitrate Schiff base complexes, 2019
phenanthroline polyketonate complexes, 2285
phosphotungstates, 1249
Scandium
alkoxide oxo compound, 719
diketonates, 215
SCF calculations
boranes, 1035
Schiff base complexes
cadmium, 1017
copper(I), 739,1469
copper(II), 1293,2463,2981
europium, 1411
lanthanides, 1411,2019
molybdenum(VI), 1011
neodymium, 1411
nickel(II), 1017
palladium(II), 2741
rhenium(V), 615
thorium, 1401,2987
tungsten(0), 2887
uranium(VI), 2987
yttrium, 475
zinc, 1017,1293,1469
zirconium, 1405
$Se_2N_2^{2-}$ complexes
platinum(II), 1567
Selenide, cadmium, 1913
Selenium - nitrogen complexes
platinum(II), 1567
Selenium sulphides, 1199
Selenium(II)
bromide, 589,1199
halides, 589
Seleno compounds
phosphorus(V), 681
Selenophenoxides
Mo(III), W(III), 2941
Semiquinone complexes
ruthenium, 2267
Serine complexes
Ca,Cd,Co,Cu,Mg,Ni,Pb,Zn, 665
Silicates
aluminium in blood plasma, 193
Silicon
catecholate complexes, 813
Siloxides
aluminium, 409
magnesium, 2655
tungsten(VI), 2293
Silver
dithiolate heterobinuclear complexes, 1441
nitrate complexes, 1429,2127
pyridine complexes, 2251
thiolate complexes, 769,1429
Silyls
aluminium, 277
iron(0), 1337
Silylamides
aluminium 2205
Ba, Ca, Mg, Mn(II), Sr, 2959
titanium, zirconium, 1423
Sodium
acetonitrile oxo rhenium(V) complex, 957
crown amine ether complex, 1747
cryptand complexes, 1369
germyls, 2263
uracil complex, 2199
Solochrome Yellow 2G, reaction with Cr(III) complex, 137
Solvation, $[Cr(CO)_5]$, 2511
Solvent extraction
americium(III), europium(III) crown amine carboxylate ether complexes, 2455
cobalt(II) dialkylphosphate complexes, 1147
isopolymolybdates, 1717
Speciation modelling
Al, Ga, In in blood plasma, 151,163
Spirophosphorane, 1463
Stibine complexes
copper(I), 1609
iron(II), 2433
Strontium
alkoxide ether silylamide complexes, 2959

cryptand complexes, 1369
organo compounds, review, 1345
Sulphates
copper(II), 2035
gallium, 207
palladium(II), 1633
Sulphides
selenium, 1199
Sulphite complexes
cobalt(III), 1379
Sulphonates
chromium(VI), 2625
palladium(II), 1633
tin(IV), 1331
Sulphonated phthalocyanines
Co(II),(III), Fe(III), 1021
5-Sulphosalicylates
iron(III), 2675
Sulphoxide complexes
platinum(II), 2647
tin(IV), 125
vanadium(IV), 1397
Sulphur
nitrogen compounds, 107
Sulphur *compounds, reactions with*
$FeSO_4.7H_2O$ and $NaNO_2$, 2399
Sulphur dioxide complexes
palladium(II), 1633
Superoxide complexes
cobalt(III), 2567

T

Tantalum(V)
alkyl phenoxide cyclometallated complexes, 1051
alkylamide alkyne chloride ether phenoxide complexes, 2709
phenoxide phenyls, 963
$TeSN_2^{2-}$, $TeSN_2H^-$ complexes
platinum(II), 2659
Technetium(III)
chloride diazenide phosphine complex, 1497
Technetium(V)
arylimide diphosphine halide hydrazide phosphine complexes, 1497
Technetium(VII)
oxo tripod phosphine oxide cobalt(0), complexes, 2549
Telluride, cadmium mercury, 921
Tellurium(II)
alkyls, 921
alkyl quinone complexes, 847
bromide thione complex, 2879
Tellurium(IV)
aryl dialkylene dithiophosphate compounds, 943
bromide complex, 2879
Telluroether complexes
mercury, 851,2041
Pd(II), Pt(II), 495,851
rhodium(I),(III), 1141
Terbium
chloride phenoxide water complexes, 939
crown ether thiocyanate water complexes, 2371
diketonate pyrazolylborate compounds, 697
diketone nitrate complexes, 795
ketoaminophenol complex, 1639
nitrate Schiff base complex, 2019
phenanthroline polyketonate complexes, 2285
phosphotungstates, 1249
2,2',2"-Terpyridyl complexes
gold(III), 893
palladium(II), 1633
platinum(II), 893
Tetraazacyclotetradecane complexes
cobalt(III), 2803
Tetracarba-*closo*- [& *nido*-] octaboranes, 949
Tetraethylenepentamine complexes
cobalt(III), 2803
Tetrahydrofuran complexes
group 2 metals, 2959
iron(II), 639
lanthanides, 479
manganese(II), 2959
tantalum(V), 2709
Tetrahydrothiophen complexes
rhodium(III), 2071
Tetraimine complexes
copper(I), 2603
1,2,4,5-Tetramethylbenzene complexes, gallium(I), 283
Tetramethylcyclopentadienyl complexes, molybdenum(II), 2901
Tetramethylethylenediamine complexes,
cobalt(II), 931
iridium(III), 2071
lithium, 931
2,2,6,6-Tetramethyl-3,5-heptanedionates,
chromium(III), 893
lanthanides, 751
Tetramethylthiourea complexes
rhodium(III), 2047
Tetramine complexes
cobalt(III), 2803
copper(II), 2221,2353
nickel(II), 1027,1729,2221
Tetraoxatetraphosphorinane complexes
molybdenum(0), 2619
Tetraphenylporphyrinates
tin(IV), 1331
Tetra(6'-quinolinyl)porphyrins
copper(II), 2527
Tetraselenide, tin(IV), 1389
Tetrasulphide tetranitride, 107, 1935
Thallium(I)
dithiolate heterobinuclear complexes, 1441
pyrazolylborates, 63
Thermal analysis
aluminium niobium(V) oxide, 367
aminophenoltriacetate complexes, 2873
cadmium mercaptopyridine mercaptothiazole complexes, 541
chromium(III) ammonia complex oxalate, 1175
chromium(III) ammonia glycine complexes, 119
copper(I) dithiocarbamate thiolate indium complex, 361
copper(I) thiolate complexes, 1155

iron(III) glycine glycoside hydroxide oxo complexes, 2895
lanthanide chloride phenoxide water complexes, 939
lanthanide crown ether thiocyanate water complexes, 2371
lanthanide dithiocarbamate complexes, 859
lanthanide nitrate Schiff base complexes, 2019
lanthanide phenanthroline polyketonate complexes, 2285
molybdenum arylamide halide nitrosyl phenoxide pyrazolylborate complexes, 687
nickel(II) polymeric complexes, 2823
ruthenium(II) violurate water complexes, 2733
thorium chloride Schiff base water complexes, 2987
tin(IV) tetraselenide complex, 1389
uranium(VI) acetate dioxo chloride hydroxide Schiff base water complexes, 2987
uranium(VI) fluoride complex, 47
Thiazolylazoresorcinol complexes
cadmium, 501
Thiazolylthiourea complexes
molybdenum(VI), 2449
Thio compounds and complexes
iron, 1741,2399
molybdenum(IV), 1671,2585
niobium(III), 1689
osmium, 2385
rhenium, ruthenium, 623
Thioacetate complexes
nickel(II), 1729
Thioamide complexes
cadmium, 831
palladium(II), 1287
Thiobismorpholine complexes
iron(0), 1045
Thiocarbonyl complexes
semibridging, 1799
Thiocarboxylates
nickel(II), 1729
Thiocyanates
cadmium, 2839
cobalt(II), 1375,2839
copper(II), 535,713,1029,2375
iron(II), 2971
lanthanides, 2371
molybdenum, 2965
molybdenum(VI), 881
nickel(II), 535,2839
tin(IV), 1331
zinc, 2839
Thioether complexes
aluminium, 409
chromium(0), 703,2579
cobalt(III), 1079
copper(I), 1469,2911,2919
copper(II), 2375
iridium(III), 893
iron(0), 1045
iron(II), 2641
manganese(0), 2579
mercury, 2931
molybdenum(0), 703,2579
molybdenum(V), 2293
platinum(II), 1975
rhodium(III), 2071,2925
ruthenium(II), 893
tungsten(0), 703,2579
tungsten(VI), 2293
zinc, 1469
Thiohydrazide, thiohydrazone complexes, iron(III), 1065
Thiolates
aluminium, 409
cadmium, 831,1017
chromium(VI), 779
copper(I), 361,1155,1469,1659
indium, 361
iridium(III), 1883
iron, 1741
manganese(II),(III), 1181
mercury, 2717
nickel(II), 1017
niobium(III), 1689
nitroprusside reaction, 913
silver, 769,1429
zinc, 763,1017,1469
Thione complexes
copper(I), 981,2833
tellurium(II), 2879
Thiophenaldazine complexes
Th, U(VI), 2987
Thiophenoxides
aluminium, 409
mercury, 2717
rhenium(V), 2211
Thiosalicylates
manganese(II),(III), 1181
Thiosemicarbazide complexes
Cd, Co, Cu, 2029
molybdenum(VI), 881
Ni, Zn, 2029
Thiosulphate complexes
iron, 1741
Thiouracil complexes
copper(II), 2747
Thiourea complexes
cobalt(III), 1379
molybdenum(VI), 2449
rhodium(III), 2047
tungsten(II), 2135
Thorium
aminophenoxide anthranilate peroxide Schiff base complexes, 1401
chloride pyrazolylborate, 1645
chloride Schiff base water complexes, 2987
nitrate pyridone complex, 491
Threitol complexes
molybdenum(VI), 1225
Thulium
crown ether thiocyanate water complexes, 2371
nitrate Schiff base complexes, 2019
phenanthroline polyketonate complexes, 2285
phosphotungstates, 1249
Tin
organo compounds, book reviews, 897,2191
Tin(II)
halide complexes, reactions with trinuclear complexes, 2777
halide iron(I) molybdenum(I) tungsten(I) complexes, 1187
Tin(IV)

amide aryl chloride cyanate diimine sulphoxide complexes, 125
butyl oxo indium complex, 361
carboxylate halide hydroxide methoxide nitrite phenoxide porphyrin sulphonate thiocyanate complexes, 1331
chloride methyl phenyl molybdenum(II) complexes, 2863
chloride phenol phenyl complexes, 653
tetraselenide complex, 1389
Titanium(III)
chloride phenoxide complex, 1617
Titanium(IV)
carboxylate cyclopentadienyl compounds, 783
cyclopentadienyl hydroxide ketoimine complex, 2097
methyl silylamide complexes, 1423
Toluates
titanium(IV), 783
zirconium(IV), 2689
Toluene complexes
chromium(0), 53
gallium(I), 283
Toluidine complexes
ruthenium(II), 1113
Toluidine Schiff base complexes
lanthanides, 2019
o-Tolyls
rhenium(VII), 2081
p-Tolyls
ruthenium(II), 1107
p-Tolylmethylidene complexes
osmium, tungsten, 1491
Triamine complexes
cobalt(III), 2803
Triatomic molecules, molecular orbitals, 1919
Triazene oxide complexes
copper(II), 1703
Triazenide complexes
Ir(III), Os(III), Rh(III), Ru(III), 1737
Tri(*t*-butoxy)silanethiolates
copper(I), 1659
2,4,6-Tri-*t*-butylbenzoxides
aluminium, 239
2,4,6-Tri-*t*-butylphenoxides
chromium(II), manganese(II), 1311
2,4,6-Tri-*t*-butylphenylamido complexes
aluminium, 245
Tributylphosphate, solvent extraction by, 1717
Tributylphosphine complexes
molybdenum(0), 1059
nickel(I), 581
nickel(II), 2809
palladium(II), 1287
tungsten(II), 2233
Trichlorosilyls
iron(0), 1337
Tricyclohexylphosphine complexes
iron(II), 2433
platinum(II), 1683
Triethanolamine complexes
molybdenum(VI), 1541
Triethylamine complexes
molybdenum(V), 2171
Triethylenetetramine complexes
calcium, 2803
cobalt(II), 2803
copper(II), zinc, 505
Triethylphosphine complexes
platinum, 1561
platinum(II), 987
rhodium(I), 1235
tungsten(II), 2233
Triethylphosphite complexes
nickel(I), 581
rhenium(II), 565
Triethylstibine complexes
copper(I), 1609
Trifluoroacetate complexes
lanthanides, 2143
tin(IV), 1331
tungsten(IV), 11
Trifluoromethanesulphonates
chromium(VI), 2625
tin(IV), 1331
Trifluoropentanedionates
aluminium, gallium, indium, 215
osmium(III), 2309
vanadium(IV), 2483
Trifluoro(thenoyl)butanedionates
vanadium(IV), 2483
Trimethoxyphenyls
phosphorus(V), 681
Trimethylamine complexes
gallium, 343
Trimethylarsine, 289
Trimethylarsine complexes
copper(I), 1609
Trimethylphosphine complexes
chromium(VI), 2625
copper(I), 1609
iridium(III), 1883
molybdenum(0), 1059
nickel(II), 757,1447
niobium(III), 1689
rhenium(II), 565
rhodium(III), 2071
tungsten(II), 2233
tungsten(IV), 11,23,603,669
Trimethylphosphite complexes
nickel(I), 581
rhenium(II), 565
tungsten(IV), 11
Trimethylsiloxy compounds
magnesium, 2655
tungsten(VI), 2293
Trimethylsilyls
aluminium, 277
Trimethylsilylmethoxides
molybdenum, 619
Trimethylsilylmethyls
cobalt(II), 931
gallium, 335
tungsten(VI), 1271
Trimethylsilylmethylarsenido complexes, gallium, 319
Trimethylsilylmethylidyne complexes, W(VI), 1271
Trimethylsilylpropyne complexes
tantalum(V), 2709
Trimethylstibine complexes
copper(I), 1609
Trinuclear cluster complexes, 1625
Triphenylarsine complexes
chromium(0), 1
copper(I), 2919

iron(II), 2433
ruthenium(II), 863 ,2153
Triphenylphosphine complexes
cadmium selenide, 1913
chromium(0), 1
cobalt(-I), 2533
copper(I), 981,2407,2833,2919
gold(I), 2407
indium, 2533
iridium(I), 893
iridium(III), 1883
iron(0), 1337
iron(II), 2433
molybdenum(0), 1059
molybdenum(IV), 545
nickel(I), 581
osmium(III), 2309
platinum, 1561
platinum(II), 1567
rhodium, 1589
rhodium(I), 1141
rhodium(II), 2013
rhodium(III), 2047
ruthenium(II), 863,907,1113, 1243,2153,2163,2517
technetium(III),(V), 1497
tungsten(0), 2887
tungsten(II), 2233
Triphenylphosphine oxide complexes
ruthenium(VI), 1751
Triphenylphosphite complexes
iridium(III), 1883
iron(0), 1337
nickel(I), 581
ruthenium(II), 1893
Triphenylstibine complexes
copper(I), 1609
iron(II), 2433
Triphosphine complexes
cobalt, 2477
molybdenum(IV), 545
platinum(II), 35
rhodium, 2477
Triphosphorus complexes
Co, Hg, Rh, 2477
Tripod phosphine oxide complexes
Mo(VI), Re(VII), Tc(VII), W(VI), 2549
Tripropylphosphine complexes
palladium(II), 2591
tungsten(II), 2233
Tri-*i*-propylphosphite complexes
tungsten(II), 2135
Tris(chlorophenyl)phosphine complexes
iron(II), 2433
molybdenum(0), 1059,2863
molybdenum(II), 2863
Tris(dimethylamino)arsine complexes, aluminium, 289
Tris(dimethylamino)phenylphosphine complexes, Mo(0), 1059
Tris(diphenylphosphino)methane complexes
palladium(II), 2181
Tris(diphenylphosphinomethyl)ethane complexes, Co, Rh, 2477
Triselenophosphonates
platinum(II), 987
Tris(fluorophenyl)phosphine complexes,
iron(II), 2433
molybdenum(0), 1059,2863
molybdenum(II), 2863
nickel(I), 581
Tris(hydroxymethyl)ethane, tris-hydroxymethyl)nitromethane complexes, Mo(VI), 1541
Tris(methoxyphenyl)phosphine complexes,
iron(II), 2433
molybenum(0), 1059,2863
molybdenum(II), 2863
nickel(I), 581
Tris(4-phenyl-3-aza-3-butenyl)-amine complexes, Cu(I), 739
Tris(pyrazolyl)methane complexes
aluminium, 265
Tris(*p*-tolyl)phosphine complexes
iron(II), 2433
molybdenum(0), 1059,2863
molybenum(II), 2863
palladium(II), 1287
Tris(trifluoromethylphenyl)phosphine complexes, iron(II), 2433
Tris(trimethoxyphenyl)phosphine and -phosphine oxide complexes
iron(III), 1695
1,4,7-Trithiacyclononane complexes
Ir(III), Ru(II), 893
Tropolonates
aluminium, 409
osmium(III), 2309
Tungsten
alkoxycarbene alkoxide alkylidyne carbaborane carbonyl methylene phosphido complexes, 2953
alkylidene cyclopentadienyl oxo osmium complex, 1491
arylamide nitrosyl pyrazolylborate complexes, 527
Tungsten(0)
amine carbonyl nitrile phosphine pyridine Schiff base complexes, 2887
carbonyl diimine complex, 1217
carbonyl diphosphine heterobinuclear complexes, 2305
carbonyl dithiolane complexes, 703
carbonyl phosphine complexes, 1363,1757
carbonyl phosphinine complexes, 991
carbonyl phosphine thioether complex, 2579
Tungsten(I)
carbonyl diimine halide tin(II) iron(I) complexes, 1187
Tungsten(II)
alkyne carbonyl diphosphine iodide complex, 2507
alkyne carbonyl diphosphine iodide isocyanide phosphine thiourea complexes, 2135
alkyne carbonyl diphosphine iodide phosphine complexes, 2233
alkyne carbonyl iodide isocyanide complexes, 727
carbonyl cyclopentadienyl phosphaallyl complexes, 2859
carbonyl diphosphinoethyne iodide complexes, 801
carbonyl halide phosphine oxide

complexes, 1099
Tungsten(III)
alkoxide chloride oxo complexes, 1829
alkoxide selenophenoxides, 2941
chloride cyclopentadienyl, 669
Tungsten(IV)
alkene alkyl allyl diphosphine iminoacyl phosphine complexes, 23
alkyl allyl carboxylate diketonate diphosphine halide isocyanide phosphine pyridine aluminium complexes, 11
alkylimide alkyne arylimide carbonyl chloride phosphine complexes, 603
arylimide chloride dinitrogen phosphine complexes, 669
carbonyl carbyne iodide isocyanide complex, 727
Tungsten(V)
chloride cyclopentadienyl phosphine complexes, 669
Tungsten(VI)
alkyl alkylidyne pyridine complexes, 1271
chloride nitrile oxo siloxy thio compounds, 2293
heteropolyanions, 1249
in heteropolyvanadates, 143
oxo tripod phosphine oxide cobalt(0) complexes, 2549
Tyrosine complexes
copper(II), zinc, 1293

U

Uracil complexes
sodium, 2199
Uranium(III)
bromide, 2175
Uranium(IV)
alcohol alkoxide oxo complexes, 1843
chloride cyclopentadienyl pyrazolylborate complexes, 69
chloride pyrazolylborate complexes, 1645
Uranium(VI)
acetate chloride hydroxide oxo Schiff base water complexes, 2987
fluoride complex, 47
nitrate oxo pyridylketonate copper(II) complexes, 2443

V

Valinate complexes
cadmium, 2437
cobalt(III), 2149
Vanadium(IV)
aminoacid oxo complexes, 2101
aspartate oxo complexes, 81
diketonate oxo pyrazolylborate complexes, 2483
diketonate oxo pyridine sulphoxide complexes, 1397
oxo, in glazes, 999
oxo pentanedionate complex, 1603
Vanadium(V)
heteropolyanions, 143
Vanillin Schiff base complexes
lanthanides, 2019
Vapour pressures
alkyls, 921
gallium, indium alkyl aminoalkyl chloride complexes, 353
Vinylidene complexes
iron, 1809
Violurate complexes
ruthenium, 2733

W

Water complexes
aluminium, 199
chromium(III), 137,1555
cobalt(II), 1383,2315,2721,2873
cobalt(III), 1379
copper(II), 1191,1383,2029,2375, 2721,2867
gallium, 207
hafnium, 2705
iron(II), 1383
lanthanides, 2371
manganese(II), 1383,2873
manganese(III), 2867
molybdenum(IV), 1671
nickel(II), 1383,2721,2867,2873
rhodium(II), 1135
ruthenium(II), 1095,2733
thorium, uranium(VI), 2987
yttrium, 1305
zinc, 2873
Water gas shift reaction,
catalysis by trinuclear platinum complex, 2795

X

Xanthate complexes
nickel(II), 1341,1729
XPE spectra
lanthanide aminophenoxide carboxylate cyclopentadienyl hydroxyquinolate complexes, 2143
lanthanide chloride cyclopentadienyls, 1453
lanthanide chloride cyclopentadienyl ether complexes, 479
X - ray crystal structures
aluminium alkoxide alkylamide amine complexes, 253
aluminium alkoxide methyl compound, 239
aluminium alkyl, 277
aluminium alkyl phosphine sulphide complexes, 313
aluminium alkyl silylamides, 2205
aluminium alkylamide arylamide methyl cyclometallated compounds, 257
aluminium arylamide methyl cyclometallated compound, 245
aluminium chloride ethoxide pyridine complex, 309

arsenic(V) aryl heteropolymolybdate, 2023
cadmium mercaptopyridine mercaptothiazole complexes, 541
carbaborane, 2407
chromium(0) arene carbonyl complex, 1677
chromium(0) carbonyl phosphine thioether complex, 2579
chromium(II) alkene aminocarbene carbonyl phosphine complex, 2193
chromium(II) phenoxide pyridine complex, 1311
chromium(VI) alkylimide chloride phosphine pyridine sulphonate complexes, 2625
chromium(VI) oxo thiolate complex, 779
cobalt cyclopentadienyl phosphine rhenium(VII) complex, 2549
cobalt triphosphine triphosphorus mercury complex, 2477
cobalt(-I) carbonyl phosphine indium complex, 2533
cobalt(II) alkyl chloride diamine complexes, 931
cobalt(II) amine carboxylate water complex, 2873
cobalt(II) chloride pyridine-*N*-oxide water complex, 2315
cobalt(III) amide amine nitrite thioether complexes, 1079
cobalt(III) nitrite valinate complex, 2149
copper(I) amine bromide tripod Schiff base complex, 2463
copper(I) amine Schiff base complex, 739
copper(I) arsine nitrile phosphine thioether binuclear macrocyclic complexes, 2919
copper(I) bromide phosphine thione complex, 981
copper(I) diphosphine tetraimine binuclear complex, 2603
copper(I) iodide osmium complexes, 75
copper(I) phosphine thione complex, 2833
copper(I) thioether binuclear macrocyclic complexes, 2911
copper(I) thiolate complexes, 1155,1659
copper(II) acetate alkoxide amine pyridine binucleating complexes, 2867
copper(II) amide amine azide bromide thioether complexes, 2375
copper(II) aminoalkoxides, 611
copper(II) aminoethoxide thiocyanate, 535
copper(II) azide dipyridylamine complex, 2693
copper(II) carboxylate carboxylic acid complex, 1667
copper(II) cyanate diamine complex, 2937
copper(II) diketonate pyridine complex, 2061
copper(II) imidazole Schiff base complex, 2981
copper(II) pyridine thiocyanate complex, 1029
cycloarsane, 319
diacetylferrocene hydrazone, 2751
europium acetate hexamine macrocyclic complex, 1411
europium azole diketonate complex, 751
gallium(I),(III) arene chloride complex, 283
gallium(III) alkyl amine complexes, 343
gallium(III) alkyl cyclopentadienyl ether iodide pyridine heterobinuclear complexes, 2763
gallium(III) alkyl phosphine complexes, 335
gold dithiolate complex, 1561
gold(III) chloride complex, 2199
indium alkoxide oxide, 719
indium chloride phosphine cobalt complex, 2533
indium chloride phospholyl complex, 329
indium(III) chloride porphyrin, 1297
iridium(I) alkyne phosphine complex, 1867
iridium(I) diene phenol phenoxide complex, 969
iridium(II,III) alkenediyl carbonyl diphosphine isocyanide phenyl complex, 2635
iridium((III) alkyl cyclopentadienyl phosphine thiolate cyclometallated complexes, 1883
iron carbonyl cyclopentadienyl gallium complex, 2763
iron carbonyl vinylidene complexes, 1809
iron(-II) carbonyl germanium complex, 1127
iron(0) carbonyl chloride phosphine phosphite silyl complexes, 1337
iron(II) amine thioether macrocyclic complex, 2641
iron(II) azole thiocyanate complex, 2971
iron(II) carbonyl cyclopentadienyl germyl complexes, 773
iron(III) chloride diphosphine complex, 2139
iron(III) chloride phosphine oxide complex, 1695
magnesium chloride pyrazolylborate, 1775
magnesium ether silylamide complex, 2959
magnesium pyrazolylborate siloxide, 2655
manganese(II) acetonitrile phenoxide complex, 1311
manganese(II) dipyridylamide complex, 2699
manganese(II) ether silylamide complex, 2959

mercury amine thioether macrocyclic complex, 2931
mercury bromide telluroether complex, 2041
mercury methylhydantoin complex, 1765
molybdenum alkoxycarbene alkylidyne cycloheptatrienyl methylene tungsten complex, 2953
molybdenum carbonyl cyclopentadienyl gallium compound, 2763
molybdenum dithiolate pyrazolylborate thiocyanate complex, 2965
molybdenum(0) carbonyl diphosphine complexes, 2393
molybdenum(0) carbonyl phosphine complex, 2901
molybdenum(II) bromide pyridine complex, 1209
molybdenum(II) carbonyl cyclopentadienyl phosphido complex, 2901
molybdenum(III) alkoxide alkylamide, 1821
molybdenum(III) alkoxide selenophenoxides, 2941
molybdenum(III) carbonyl cyclopentadienyl oxo phosphido complex, 2469
molybdenum(IV) chloride hydrazide phosphine triphosphine complexes, 545
molybdenum(IV) thio water complex, 1671
molybdenum(VI) nitrilotriacetate oxo polyalkoxide triethanol-amine complexes, 1541
neodymium acetate hexamine macrocyclic complex, 1411
nickel dithiolate complex, 2053
nickel(0) diphosphine isocyanide platinum(II) complex, 2651
nickel(II) aminoethanol thiocyanate complex, 535
nickel(II) diphosphine iodide isocyanide complex, 1487
nickel(II) dithiocarbamate macrocyclic tetramine complex, 1729
nickel(II) dithiophosphinate, 2597
nickel(II) phosphine xanthate complex, 1341
niobium(III) phosphine thio thiolate complexes, 1689
niobium(V) chloride phenoxide cyclometallated complex, 1051
osmium alkylidene carbonyl hydride tungsten complex, 1491
osmium carbonyl copper(I) complexes, 75
osmium carbonyl thio complexes, 2385
osmium(0) alkyne carbonyl complex, 1867
palladium(II) aryl phosphinoe triphosphinomethanide complex, 2181
palladium(II) nitrite phosphine complex, 2591
palladium(II) phosphine thioether complex, 2579
phosphiniminocyclotrithiazenes, 1433
phosphorus(V) aryl seleno compounds, 681
platinum dithiolate phosphine complex, 1561
platinum(II) bromide phosphine complex, 1683
platinum(II) chloride isocyanide nickel(0) complex, 2651
platinum(II) diphosphine triselenophosphonate complex, 987
platinum(II) phosphine selenium - nitrogen complex, 1567
platinum(II) phosphine tellurium - sulphur - nitrogen complex, 2659
rhenium carbonyl pyridinethionate thio ruthenium complexes, 623
rhenium(II) acetate chloride diphosphine complex, 743
rhenium(II) carbonyl chloride diphosphine phosphine complex, 565
rhenium(II) chloride diphosphine complex, 573
rhenium(III) chloride phosphine complexes, 1165
rhenium(V) aryl butylimido cyclohexadienyl complex, 2081
rhenium(V) cyclopentadienyl dithiolate complex, 2211
rhenium(V) methoxide oxo Schiff base complex, 615
rhenium(V) neopentyl oxo sodium complex, 957
rhenium(VI) aryl bromide butylimide oxo cyclometallated complexes, 2081
rhenium(VII) aryl butylimide oxo complex, 2081
rhenium(VII) catecholate oxo complexes, 1323
rhenium(VII) oxo tripod phosphine oxide cobalt(0) complex, 2549
rhodium(I) carbonyl phenoxide complex, 969
rhodium acetate chloride nitrosyl phosphine complex, 1589
rhodium(II) alkenediyl carbonyl chloride phosphinopyridie complex, 2635
rhodium(III) amine thioether macrocyclic complex, 2925
rhodium(III) aryl dipyridyl pyridine cyclometallated complex, 1613
rhodium((III) carbonyl diamine methyl phosphine thioether complexes, 2071
rhodium(III) chloride pyridine complex, 2127
rhodium(IV) neopentyl oxo complex, 2071
ruthenium carbonyl pyridinethionate pyridyl thio rhenium complexes, 623
ruthenium dipyridyl pyridine

quinone complexes, 2267
ruthenium(0) alkyne carbonyl complex, 1867
ruthenum(0) phosphine tetramine macrocyclic complex, 1221
ruthenium(II) alkenyl carbonyl carboxylate phosphine complexes, 907
ruthenium(II) cyclopentadienyl phosphine phosphinothioformate complexes, 2163
ruthenium(II) cyclopentadienyl phosphite polysulphide complexes, 1893
ruthenium(II) violurate complex, 2733
silver nitrate complex, 2127
silver thiolates, 769,1429
sodium acetonitrile oxo rhenium(V) complex, 957
sodium uracil complex, 2199
spirophosphorane, 1463
tantalum(V) alkyl phenoxide cyclometallated complexes, 1051
tantalum(V) phenoxide phenyl, 963
tellurium(II),(IV) romide thione complexes, 2879
thorium chloride pyrazolylborate complex, 1645
thorium nitrate pyridone complex, 491
tin(IV) chloride phenol phenyl complexes, 653
tin(IV) tetraselenide complex, 1389
titanium(III) chloride phenoxide complex, 1617
titanium(IV) carboxylate cyclopentadienyl, 783
titanium(IV) cyclopentadienyl hydroxide ketoimine complex, 2097
titanium(IV) methyl silylamide complexes, 1423
tungsten alkoxycarbene alkylidyne carbaborane methylene molybdenum complex, 2953
tungsten alkylidene cyclopentadienyl oxo osmium complex, 1491
tungsten(0) carbonyl diimine complex, 1217
tungsten(0) carbonyl phosphine complex, 1363
tungsten(0) carbonyl phosphine thioether complex, 2579
tungsten(0) carbonyl phosphinine complex, 991
tungsten(II) carbonyl cyclopentadienyl phosphaallyl complex, 2859
tungsten(III) alkoxide chloride oxo complexes, 1829
tungsten(III) alkoxide selenophenoxides, 2941
tungsten(III) chloride cyclopentadienyl, 669
tungsten(IV) arylimide chloride dinitrogen phosphine complex, 669
tungsten(V) chloride cyclopentadienyl phosphine complex, 669
tungsten(VI) alkyl alkylidyne pyridine complexes, 1271
uranium(IV) chloride cyclopentadienyl pyrazolyl-borate complexes, 69
uranium(IV) chloride pyrazolylborate, 1645
vanadium(IV) diketonate oxo pyrazolylborate complex, 2483
ytterbium alkoxide oxide, 719
yttrium acetate diketonate water complex, 1305
zinc aminothiolate, 763
zirconium benzyl cyclopentadienyl iminoacyl phenoxide compounds, 839
zirconium methyl silylamide complexes, 1423
X - ray diffraction
aluminium niobium(V) oxide, 367
cobalt(III) complexes on clay surfaces, 2273
indium tin oxide, 361
iron(II),(III) in glasses, glazes, 999
nickel(II) complexes on clay surfaces, 2273
uranium(VI) fluoride complex, 47
X - ray fluorescence, clays, 517
Xylitol complexes
molybdenum(VI), 1225
1,1-Xylylenebis(cyclopentadienyl) complexes, lanthanides, 479
Xylyl complexes
rhenium(V),(VI),(VII), 2081

Y

Ylide complexes
lanthanides, 875
Ytterbium(II)
chloride, 1919
Ytterbium(III)
alkoxide oxo compound, 719
aminophenoxide carboxylate cyclopentadienyl hydroxyquin-olate complexes, 2143
azole diketonate compound, 751
chloride cyclopentadienyl, 1453
chloride cyclopentadienyl ether complexes, 479
crown ether thiocyanate water complexes, 2371
diketonate pyrazolylborate compounds, 697
nitrate Schiff base complexes, 2019
phenanthroline polyketonate complex, 2285
phosphotungstates, 1249
Yttrium
acetate diketonate water complex, 1305
alkoxide oxo compound, 719
carboxylate pyrazolylborates, 1119
chloride cyclopentadienyl, 1453
chloride cyclopentadienyl ether complexes, 479

diketonate pyrazolylborate compounds, 697
diketone nitrate complexes, 795
nitrate pyridine Schiff base macrocyclic complex, 475
phenanthroline polyketonate complex, 2285

Z

Zinc
alkyls, 921
amine carboxylate water complexes, 2873
amine ether tridentate cyclic complexes, 2847
aminoacid complexes, 665
aminoacid Schiff base complex, 1293
aminothiolate, 763
azole schiff base thioether thiolate complexes, 1469
in blood serum, effect of polydentate ligands and antiinflammatory drugs, 505
diphosphoglycerate complexes, 189
enolate ethyl compound, 223
fluoride complexes, 901
nitrate pyridylpyrazole thiocyanate complexes, 2839
polymeric triamine complexes, 2491
salicylaldimine thiocyanate heteropolymetallic complexes, 557
Schiff base thiolate complexes, 1017
thiosemicarbazide complexes, 2029
Zirconium
aminophenoxide anthranilate peroxide Schiff base complexes, 1405
benzyl cyclopentadienyl imino-acyl phenoxide compounds, 839
carboxylate chloride cyclopenta-dienyl complexes, 2689
chloride cyclopentadienyl phenoxide pyrazolylborate complexes, 2185
cyclopentadienyl methyl compounds, 301
fluoride oxo peroxide complexes, 1653
methyl silylamide complexes, 1423

AUTHOR INDEX

Abel, E. W. 1603
Adams, R. D. 447
Agarwal, R. K. 2399, 2567, 2809
Ahmed, I. Y. 793
Ahmed, K. J. 1667, 2573
Airoldi, C. 1433
Akasheh, T. S. 1485
Akbar Ali, M. 823, 1327
Akita, M. 1
Al-Dhahir, A. 2051
Al-Dulaymmi, M. F. M. 1549
Al-Juboori, M. A. H. A. 1831
Alarcon, E. 2235
Albach, R. W. 1741
Albada, G. A. van 1091
Alcock, N. W. 1939
Allred, A. L. 1227
Alyea, E. C. 1625
Andersson, C. 2089, 2417
Ando, I. 1139
Andre, J.-J. 687
Andrews, P. C. 1839
Ang, H. G. 881
Ankianiec, B. C. 1411
Annapoorna, K. 2465
Apblett, A. W. 1075
Aragon-Salgado, M. 799
Arancibia, V. 1929
Arbuckle, B. W. 415
Archer, C. M. 1539
Arif, A. M. 543
Arima, K. 2523
Arnold, A. P. 2847
Arnold, D. P. 509
Aronson, R. 1727
Arriortua, M. I. 495, 2451
Arulsamy, N. 731
Asano, T. 2351
Aslanidis, P. 935
Atfah, A. 1485
Attar, S. 1939
Atwood, D. A. 1897
Atwood, J. L. 1897
Aylett, B. J. 1593
Azevedo, M. C. 459

Baird, D. M. 229
Bajaj, H. C. 2729
Baker, D. R. 1839
Baker, P. K. 433, 711, 1663, 2519
Balaji, V. 1265
Ballester-Reventos, L. 1013, 1019
Banbery, H. J. 243
Bandyopadhyay, D. 2605
Barba-Behrens, N. 1333
Barral, M. C. 113
Barron, A. R. 1075
Bartecki, A. 1759, 2179
Bassett, M. 501
Baumeister, U. 2423
Baumgart, F. 1037
Beamish, J. C. 95
Bearden, W. H. 1939
Becalska, A. 877
Beckett, M. A. 1663
Beer, P. D. 1847
Beger, J. 11
Beisheng Kang 2651
Bell, C. F. 613
Bellan, J. 2229
Belsky, K. A. 977
Benetollo, F. 1385, 2171
Benghanem, F. 2529
Bermejo, E. 1579
Bernhardt, P. V. 1373
Berry, D. H. 1189
Bhattacharjee, P. 823
Bhattacharjee, S. S. 779
Björgvinsson, M. 2353
Blake, A. J. 1545
Blaskó, A. 2495
Blau, R. J. 605
Boardman, A. 95
Bodini, M. E. 1929
Boggess, R. K. 2791
Böhland, U. 2423
Bolte, M. 237
Bombieri, G. 1385, 2171
Boncella, J. M. 769
Bontchev, P. R. 763
Bookham, J. L. 2381
Bott, R. C. 1565
Bott, S. G. 1897
Böttcher, H.-C. 2423
Boudjouk, P. 1231
Boumizane, K. 2757
Bradley, D. C. 477, 1049
Brand-Roth, B. 1147
Brničević, N. 2031
Brock, T. H. 459
Bruce, M. I. 277
Bruck, M. 665
Buchholz, E. 1091
Buckner, S. W. 2487

Bukowsky, H. 1591
Bunel, S. 2495
Bunton, C. A. 2495
Burgess, J. 703
Burini, A. 2145
Butou, T. 1449
Buxton, D. P. 747
Byriel, K. A. 873

Cai, Y. M. 881
Calvo, V. 2495
Cammack, J. K. 769
Campbell, J. 2273
Campo, J. A. 133, 2611
Canavan, A. 483
Cano, M. 133, 187, 2611
Capparelli, A. L. 359
Carballo, R. 1579, 1675
Cardin, C. 483, 2771
Carroll, M. T. 1247
Carroll, P. J. 1189
Carrondo, M. A. A. F. de C. T. 73
Cartwright, P. S. 2501
Carvill, A. 2273
Casas, J. M. 1573
Casas, J. S. 1465
Casey, Rev. M. T. 483
Cassoux, P. 687, 2025
Castiñeiras, A. 197, 1579, 1675
Castro, B. de 2541
Castro, R. 197
Caulton, K. G. 1639, 2371, 2699
Celap, M. B. 2717
Cervantes-Lee, F. 1177
Ceulemans, A. 1587
Chagas, A. P. 1433
Chakladar, S. 1513
Chakravarty, A. R. 491, 2483
Chakravorti, M. C. 2605
Chakravortty, V. 33
Chan, H. S. O. 2437
Chaudhry, S. C. 789
Chaudhuri N. R. 2225
Chaudret, B. 2229
Cheatham, L. K. 1075
Chen, J.-T. 629
Chen, X.-M. 273
Chey, J. 1189
Chi, K. M. 2293
Chisholm, M. H. 337, 805, 1215, 1367, 1573, 2309, 2839
Christou, G. 1817, 2255, 2301
Chudzynska, H. 1049
Chunwan Liu 2799
Ciavatta, L. 2587
Cieślak-Golonka, M. 2179
Cifuentes, M. P. 277
Claude-Montigny, B. 1791
Clegg, W. 123, 1839, 1959
Coan, P. S. 2371
Cole-Hamilton, D. J. 993
Compañó, R. 919
Compton, N. A. 123
Connolly, J. W. 841
Constable, E. C. 127, 1395, 1883
Contreras, R. 1333
Convery, M. 2771
Cortes, R. 2725
Coston, C. J. 769
Cotton, F. A. 2145
Cotton, S. 1844, 2083, 2855
Couret, C. 1153
Coutsolelos, A. G. 885
Cowley, A. H. 841, 1897
Cox, P. J. 1085
Craig, D. 41
Crane, J. D. 1809
Crisponi, G. 333
Croux, A. 463
Cruywagen, J. J. 249
Cusick, J. 2629
Cutin, E. H. 653
Czuchajowska, J. 2145

Dai-Zheng Liao 1787
Dali, S. 2529
Dance, I. G. 41, 2629
Danopoulos, A. A. 2241
Daran, J. C. 437, 2045
Das, B. K. 491
Dash, K. C. 33
Davies, D. L. 501
Davies, J. A. 899, 909
Davies, K. M. 1647
Daxu Wu 2651
De Oliveira, D. 1699
Deacon, G. B. 747
Dean, N. S. 1631
Deb, A. K. 1799
Debad, J. D. 1705
Declercq, J.-P. 2683
Deeming, A. J. 837, 1857
Delgado, S. 725
DePriest, J. C. 2153
Derringer, D. R. 79
Dhingra, S. 1069
Di Vaira, M. 2123
Diachenko, O. A. 179
Dias, A. R. 1433
Diaz, B. 495

Díaz, C. 1319
Dickson, R. S. 1995
Dieck, H. tom 255
Dillen, J. L. M. 2535
Dilworth, J. R. 1539
Doherty, S. 1857
Doidge-Harrison, S. M. S. V. 1085
Domingues, D. 2541
Dongmei Wang, 1479
Dorsselaer, A. van 1521
Drake, S. R. 337, 805
Dreisch, K. 2417
Drew, M. G. B. 1883
Dreyer, R. 11
Duan, Z. 2105
Duarte, M. T. L. S. 73
Dubey, R. K. 1733
Duer, M. J. 1749
Duesler, E. N. 645, 2293
Duffield, J. R. 377, 1105, 1113, 1121
Dulebohn, J. I. 2813
Duran, M. L. 197
Dzięgielewski, J. O. 429, 1007, 1459, 2827

Earley, J. E. 829
Edwards, C. F. 61
Efe, G. E. 1611, 1617
Eichhorn, B. W. 2573
Eilmes, J. 1779
Ejfler, J. 2457
El-Erian, M. A. I. 2131
El-Hendawy, A. M. 2137, 2511
El-Hinnawi, M. 2095
El-Khatib, M. 2095
El-Toukhy, A. 535
Elder, S. M. 1395
Ellis, D. 1603
Elsegood, M. R. J. 1727
Enemark, J. H. 665
Errington, R. J. 123, 1959
Escudie, J. 1153
Escuer, A. 2025
Euler, W. B. 859
Evans, D. F. 1131

Fanwick, P. E. 79
Faraglia, G. 351
Faulmann, C. 2025
Fedin, V. P. 997, 1311
Fedorov, V. Ye. 997, 1311
Féliz, M. R. 359
Fendesak, G. 255
Feng, Q. 659
Fenton, D. E. 1809
Ferguson, G. 1625, 1951, 2273
Fernandez, M. J. 1595
Filella, M. 517
Filipek, K. 429, 1459
Finch, A. 1831
Finch, K. P. 963
Fischer, S. 11
Fisher, G. A. 123
Flower, K. R. 711
Folting, K. 1639, 2309, 2699, 2839
Fonda, K. K. 1385
Foulon, J.-D. 1847
Frankel, R. B. 203
Fraústo da Silva, J. J. R. 73
Freire, C. 2541
Fricker, S. P. 1847
Friebel, C. 893
Fuchita, Y. 561, 2037, 2523
Fuentes, G. R. 2371
Fujimoto, H. 1139
Fujiwara, M. 1773, 2833

Gafoor, M. A. 963
Gaj, D. L. 1631
Galema, S. A. 703
Gallagher, B. C. 613
Gallagher, J. 2273
Ganadu, M. L. 333
Gao Yici 1893
García Bugarín, M. 517
Garcia, A. 103
García, G. 2821
García, J. 2821
García-Granda, S. 1717, 2057
García-Tasende, M. S. 517
Garcia-Vazquez, J. A. 197
Gardner, P. J. 1831
Garg, G. 1733
Gaspar, P. P. 1221
Gen-Line Wang 1787
Gencheva, G. 1767
George, T. A. 467
Geraldes, C. F. G. C. 799
Geras'ko, O. A. 997, 1311
Gillard, R. D. 1453, 2051, 2501
Gladysz, J. A. 1903
Gloe, K. 1591
Głowiak, T. 175
Goetz, M. S. 605
Goh, L. Y. 591
Golen, B. S. 789
Golen, J. A. 1343
Gomes, J. 2541
Gomez de Anderez, D. 2225
Goodgame, D. M. L. 1079

Gordon, J. C. 1667
Gordon, M. S. 1247
Goswami, S. 1799
Gou, S. 37, 1363
Graaf, R. A. G. de 1091
Grace, M. R. 2317, 2389
Graham, J. J. 1075
Granados, M. 919
Green, M. L. H. 389
Gregory, N. W. 633
Griffith, W. P. 61
Grillone, M. D. 2171
Grochowski, T. 1473
Groombridge, C. J. 1831
Grumbine, S. D. 1173
Grzybek, R. 1007
Guan-Yeow Yeap 2683
Guinan, P. 483, 2273, 2283
Guo, Z. 351
Gutierrez, A. 1423, 2241
Gutierrez, E. 187
Gutierrez-Alonso, A. 1013, 1019
Gutiérrez-Zorrilla, J. M. 2057

Hader, R. 877
Hadjikakou, S. K. 935
Hage, R. 1091
Hall, I. 1721
Hall, S. W. 261
Hamilton, E. J. M. 471
Hamor, T. A. 243, 1847
Hampden-Smith, M. J. 645, 867, 1145, 2105, 2293
Han Xiaojun, 1491
Handler, A. 2471
Hao, J.-L. 941
Hao, S.-Q. 941
Harada, K. 583
Harman, M. E. 1539
Harrison, A. 1951
Harrod, J. F. 1239
Harston, P. 1085
Hartung, H. 2423
Hasegawa, I. 1097
Hashimoto, M. 649
Hatlee, M. J. 841
Hay-Motherwell, R. S. 1457
Hayashi, H. 2347
He-Fu Guo 2341
Healy, J. 1883
Heaton, D. E. 543
Heinzel, U. 19
Helgesson, G. 1559
Hendrickson, D. N. 2255
Heras, J. V. 187
Herath Banda, R. M. 41
Herdtweck, E. 1741
Herzog-Cance, M. H. 2757
Heuer, L. 1955, 2737
Heyns, J. B. B. 249
Higgins, P. 2273
Hill, R. H. 877, 1705
Hiller, W. 1579
Hinchliffe, J. R. 267
Hiraki, K. 561, 2523
Hitchcock, P. B. 1203, 1549
Hockless, D. C. R. 123, 1959
Hollingshed, G. K. 409
Holm, R. H. 203
Holmes, J. M. 127
Hong, M. 553, 927
Hor, T. S. A. 2437
Houndas, A. 741
Howes, A. J. 477
Howie, R. A. 1085
Hsieh, T.-C. 977
Hsiu-Rong Chang 2255
Huaizhu Ma, 1599
Huang Jian-Quan 2203
Huang Jin-Ling 2203
Huang Zi-Xiang 2203
Huang, J. 403
Huang, L. 553
Huang, Z. 553, 927
Hubbard, C. D. 703
Hubert-Pfalzgraf, L. G. 437, 1559, 1639, 1657, 2045
Huey-Shwu Jang 2069
Huffman, J. C. 1215, 1367, 1817, 2255, 2301, 2573, 2699, 2839
Huggett, P. G. 2131
Humanes, M. 2597
Humphrey, M. G. 277
Hursthouse, M. B. 477, 595, 737, 1049, 1423, 1457, 1539
Husain, M. 779
Huskowska, E. 175
Hussain, W. 243
Hussain-Bates, B. 595, 737, 1423, 1457

Ibarra, C. 2495
Ichida, H. 649
Ichiki, Y. 2833
Igau, A. 1903
Imamura, T. 373
Imura, H. 1405
Insausti, M. 2451
Ioele, M. 2475
Iraqi, A. 993
Ishimori, T. 583

Ismael, M. 1791
Iuliano, M. 2587
Ivanova, I. 1767
Iwamoto, T. 649
Izquierdo, A. 919

Jackson, G. E. 883
Jackson, M. A. 467
Jackson, W. G. 2847
Jacobi, R. 11
Jagner, S. 1559
Jain, A. 1103
Jain, V. K. 851
Jasim, H. A. 1203
Jeffery, J. C. 215
Jelikić-Stankov, M. 455
Jennings, J. R. 2131
Jennings, M. C. 1625
Jensen, C. M. 89, 1343
Jensen, D. 1037
Jesus, F. de 2235
Jeyasubramanian, K. 1687
Jezierska, J. 1653, 2179
Jezierski, A. 2551
Jeżowska-Bojczuk, M. 2331
Jeżowska-Trzebiatowska, B. 429, 1653
Jiang, Z.-H. 101, 941
Jiaxi Lu 2799
Jibril, I. 2095
Jiménez-Aparicio, R. 113
Jobanputra, P. 1539
Johns, J. R. 1121
Johnson, B. F. G. 1955
Jolly, P. W. 459, 1427
Jones, C. J. 243, 1847
Jones, D. J. 2757
Jones, E. L. 1817
Jones, R. A. 543, 1897
Joseph-Nathan, P. 1333
Joslin, F. L. 1713
Juranić, N. 2717
Jyh-Ching Chen 2069
Jyh-Horung Chen 2069

Kabassanov, K. 763
Kaibe Yu 2659
Kaitner, B. 1951
Kaleciński, E. 2551
Kalirai, B. S. 1847
Kamata, Y. 583
Kampf, J. W. 1631
Kanatzidis, M. G. 1069
Kang, B. 553, 927
Kapoor, R. N. 1177
Karagiannidis, P. 935
Karaulov, A. 1539
Karim, M. 837
Kashta, A. 2031
Katsuta, S. 1405
Katz, N. E. 653
Kauffman, G. B. 1843
Kaul, B. B. 467
Kaur, B. 2463
Kawakami, M. 561, 2037
Keder, N. L. 2495
Kehr, G. 1497
Kelly, N. B. 483
Kelly, P. F. 2337
Kendrick, D. ap 433, 2519
Kennard, C. H. L. 509, 873, 1565, 1569
Kenney, C. N. 1955
Kerby, M. C. 2573
Kessler, V. G. 2617
Khaled, A. M. 1079
Khan, A. R. 819, 973
Khan, B. T. 2465
Khan, M. A. 2529
Khan, N. H. 2559
Khan, O. F. Z. 325
Khandelwal, B. L. 2693
Khazaeli, S. 221
Khoo, S. K. 591
Kinoshita, S. 2833
Kirov, R. 393
Kiss, T. 1401
Kitamura, Y. 1449
Klahn, A. H. 1873
Kläui, W. 1091
Koch, K. R. 1721, 2221
Kodas, T. T. 645, 2293
Kolesov, B. A. 997
Kołkowicz, A. 1759
Koner, S. 2225
Konstantinovskii, L. E. 771
Korobov, M. S. 771
Koschmieder, S. U. 135
Kościuszko, B. 945
Kovala-Demertzi, D. 1507
Kozłowski, H. 2331
Krätsmár-Šmogrovič, J. 893
Krishnaiah, G. 2785
Kron, I. 377
Kubica, Z. 2331
Kucheiko, S. I. 2617
Kumar, N. R. S. 365, 579
Kura, G. 697, 1527
Kureshy, R. I. 2559
Kurihara, H. 1139
Kurzak, K. 1759
Kwiatkowski, E. 945

Kwiatkowski, M. 945
Kwik, W. L. 881
Kyrkou, P. 1507

Labarre, M. J. 665
Lachmann, J. 1163
Ladriere, J. 2423
Lai, R. 463
Lal, R. A. 779
Lam, H.-W. 2647
Lamson, A. H. 2791
Lappert, M. F. 1203
Larramendi, J. I. R. 495, 2725
Larson, J. W. 1695
Laschi, F. 2123
Latif Abuhijleh, A. 793
Lawrance, G. A. 409, 1373
Lazraq, M. 1153
Le Bot, S. 463
Legendziewicz, J. 175, 1921
Legros, J. P. 687, 1031
Lei, D. 1221, 2105
Lei, X. 927
Leipoldt, J. G. 1379
Leis, C. 1163
Leiva, A. M. 347
Leiva, C. 1873
Lelj, F. 523, 955, 1911
Leluk, M. 1653
Leong, W. K. 881
Leoni, V. 333
Leung, W.-P. 1203
Lewis, J. 1955
Lezama, L. 495, 2725
Li Jun-Qian 2203
Li, J. 403
Li-Cun Li 1787
Lian-Pin Hwang 2069
Liao, D.-Z. 101, 941
Liebermann Jr, J. 1647
Lin, W. 403
Linder, P. W. 883
Linghong Weng 2651
Lis, T. 2457
Liu, H. 553, 927
Liu, L.-K. 2437
Liu, Q.-Y. 629
Liu, S. 403
Liu, Z.-M. 101
Lobkovsky, E. M. 2839
Lobo, M. A. 187
Loeb, B. 347
Lombao, A. 1579
Long Lü 2687
López, G. 2821
Lott, K. A. K. 613
Lotz, S. 2535
Loubser, C. 2535
Loumrhari, H. 421
Lozano, R. 2235
Lu Can-Zhong 2203
Lu Jia-Xi 2203
Lu Shao-Fang 2203
Ludwig, R. 11
Lun Zhang 2779
Lundeen, M. 2377
Luque, A. 2057
Lynch, D. E. 1569

Ma Yongxiang 2185
Mabille, S. 463
Macazaga, M^{a}J. 725
Macdonald, F. M. 1443
Macías, A. 1465
Maciček, J. 1311
Madelung, S. 2221
Maeder, M. 409
Mague, J. T. 1713
Mahajan, R. K. 789
Mahr, J. A. 1647
Mailhot, G. 237
Mak, T. C. W. 273, 509, 1569, 1723, 2687
Małecki, J. G. 1007, 2827
Malešev, D. 455
Mandair, A.-P. S. 55
Mandal, S. K. 2483
Manohar, H. 2163, 2851
Mapolie, S. F. 717, 963
Marshall, J. E. 1857
Marsicano, F. 1105, 1113, 1121
Martin, R. B. 1401
Martin-Gil, J. 799
Martinez, M. 187
Martinez, M. A. 1031
Martinho Simões, J. A. 1433
Mártire, D. O. 359
Marty, W. 619
Maruyama, H. 561
Masood, Md. A. 811
Massaferro, A. 2075
Massiani, M. C. 437, 1657
Mathews, I. I. 579, 2163, 2851
Mathur, J. N. 47
Matsufuji, S. 107
Matsushita, T. 1773
Matsuzaki, S. 1449
Matt, D. 1521
Mattes, R. 19
Matthews, R. C. 1951

Mazieres, M.-R. 2229
Mazurek, W. 753
McCann, M. 2273, 2283, 2771
McCarley, R. E. 2031
McCleverty, J. A. 243
McFarlane, W. 2381
McGeary, M. J. 2699
McQuillan, G. P. 1085
McWhinnie, W. R. 55
Mechandjiev, D. 763, 1767
Mehrotra, R. C. 949, 1103, 1733, 1967
Mentzafos, D. 935
Mertis, C. 741
Mesa, J. L. 2451, 2725
Meullemeestre, J. 2529
Meyer, G. 1921
Meyer, H. 1379
Michl, J. 1265
Midollini, S. 2123
Mier, G. P. M. van 1963
Miguel, D. 1717
Miki, E. 583
Milosavljevic', E. B. 1939
Minkin, V. I. 179, 771
Mironov, Yu. V. 997
Mitewa, M. 763, 1767
Mizumachi, K. 583
Mochida, K. 2347
Mohanty, R. N. 33
Monfort, M. 103
Monge, A. 113
Monge, M. A. 187
Montauzon, D. de 2025
Morelli, G. 523, 955, 1911
Moreno, C. 725
Moss, J. R. 717, 963
Mossert, K. 1873
Motevalli, M. 1049
Mountford, P. 389
Mtetwa, V. S. B. 389
Mu, Y. 1239
Mühl, P. 1591
Mui, H. D. 1667
Muir, A. S. 2217
Mukherjee, A. K. 2225
Müller, E. P. 2471
Müller, G. 1163
Mullica, D. F. 867
Mulvey, R. E. 1839
Munz, C. 255
Murphy, E. 2771
Musker, W. K. 415
Mutio-Rico, A. M. 1333
Myakishev, K. G. 1311

Nag, K. 1513
Nagai, T. 583
Nagar, M. S. 1683
Nagase, S. 1299
Naiini, A. A. 337, 805
Nakahara, M. 583
Nakamura, A. 1
Nakamura, K. 67
Nakayama, K. 1139
Narula, S. P. 2463
Nazimuddin, M. 823, 1327
Neild, J. 501
Nelson, J. H. 1939
Nethaji, M. 365
Nguyen, K. A. 1247
Nianyong Zhu 2743
Nichols, P. J. 753
Nicholson, J. R. 2255
Nicholson, T. 977
Nieuwenhuyzen, M. 2111
Niketić, S. R. 2665, 2673
Nikolov, G. St. 393
Ning-Hai Hu 2341
Nivorozhkin, A. I. 179
Nivorozhkin, L. E. 179, 771
Nocera, D. G. 2813
Nonoyama, K. 2265
Nonoyama, M. 2265
Norman, N. C. 123
Nurchi, V. 333

O'Brien, P. 325, 567, 575
O'Neil, P. A. 1839
Oczko, G. 1921
Ohta, Y. 2523
Ojo, J. F. 829
Okubo, W. 107
Okuda, J. 1741
Olechnowicz, A. 945
Olekhnovitch, R. Ya. 771
Oliver, J. P. 1631
Olubuyide, O. 829
Orfanopoulos, M. 885
Oro, L. A. 1595
Orpen, A. G. 123
Orrell, K. G. 1603
Ortaggi, G. 2475
Ortiz, J. V. 1285
Ottaviani, M. F. 1911
Oyetunji, A. O. 829

Padilla, E. M. 89, 1343
Palmer, B. J. 877
Pannell, K. H. 1177

Papaefthymiou, G. C. 203
Papiernik, R. 437, 1657
Parker, D. 1951
Parkin, I. P. 1215, 2309, 2839
Pascal, J. L. 2757
Pasteur, E. C. 1545
Patel, R. P. 851
Patil, K. C. 365, 579
Patroniak, V. 683
Paul, P. 1513, 1827
Pedrosa de Jesus, J. 575
Peloso, A. 2191
Pérez-Martínez, J. A. 1717
Peringer, P. 2471
Perlepes, S. P. 2301, 2405
Perpiñan-Vielba, M. F. 1013
Persson, C. 2089
Petit, P. 687
Phang, L.-T. 2437
Pilkington, M. J. 261, 2641
Pillai, M. R. A. 1617
Pinilla, E. 187
Plakatouras, J. C. 2405
Playá, N. 1465
Plesch, G. 893
Plinke, B. 1037
Płuziński, T. 2457
Pohl, S. 1147
Poli, R. 1667
Polo, A. 1385
Pon, G. 1835
Poncelet, O. 1559, 1639, 2045
Porto, R. 2587
Potier, J. 2757
Potts, R. A. 1631
Prakash, J. 2399, 2567, 2809
Prasad, K. M. 323
Pritchard, P. G. 121
Prouse, L. J. S. 501
Pruchnik, F. 2551
Psaroudakis, N. 741
Purcell, W. 1379

Qi Feng, 1527
Qianer Zhang 2799

Radecka-Paryzek, W. 683
Radivojša, P. N. 2717
Radović, Z. 455
Rahman, M. 823
Rai, A. K. 1103, 1203, 1967
Raithby, P. R. 127, 1395
Ramachandraiah, G. 2729
Ramalingam, S. K. 1687
Raman, N. 1687
Raos, N. 2079
Rasmussen, Kj. 2079
Reddy, K. H. 2785
Redshaw, C. 1959
Reedijk, J. 1091
Reid, G. 1545
Reinhold, J. 2423
Reynolds, J. G. 1817
Reynolds, M. S. 203
Ribas, J. 103, 687, 2025
Ricalton, A. 267
Ricciardi, G. 523, 955, 1911
Richards, R. L. 1549
Richmann, P. N. 1343
Riera, V. 1717
Rivera, L. 347
Robinson, W. T. 2111
Rodriguez, M. J. 1595
Roesky, H. W. 2353
Rojo, T. 495, 2451, 2725
Roman, J. 2235
Román, P. 2057
Romanelli, M. 1911
Romero, J. 197
Ros, J. 421
Rosa, A. 523, 955, 1911
Rossignoli, M. 409
Roundhill, D. M. 1713
Royer, E. C. 113
Royle, L. 1951
Roziere, J. 2757
Ru-Ji Wang 2255
Ruan, B. 1025
Rudong Yang, 1479
Rufińska, A. 459
Ruikar, P. B. 1683
Ruiz-Valero, C. 113
Runnacles, J. D. 477
Russanov, V. 763
Russell, D. R. 501
Russo, U. 1353
Rustad, D. S. 633
Ryan, H. 2273
Rzeszotarska, B. 2331

Saak, W. 1147
Sabolović, J. 2079
Saboonchian, V. 595, 737, 1423, 2241
Sachtler, W. M. H. 673
Sadler, P. J. 1443
Sagatys, D. S. 1565
Saito, K. 2717
Sakane, G. 2351
Samad, S. A. 2729
Samath, S. A. 1687

Samochocka, K. 1473
Samuel, E. 1239
Sánchez, A. 1465
Sánchez, G. 2821
Sancho, A. 1031
Sangster, D. F. 1373
Sanmartín, A. 2821
Santana, M. D. 2821
Santos, T. M. dos 575
Sappenfield, E. L. 867
Sasaki, Y. 649
Satge, J. 1153
Saunders, G. C. 1877
Scarsella, M. 2475
Schiebel, H.-M. 2423
Schlemper, E. O. 1611, 1617
Schmutzler, R. 2737
Schneider, W. F. 1631
Schomburg, D. 2737
Schröder, M. 1545
Schroth, G. 459
Schumann, H. 665
Scott, P. 389
Scrimin, P. 1791
Scudder, M. 41
Severs, L. M. 1663
Shankar, R. 2463
Shaohua Gou 2659
Shaowu Wang 1599
Sharma, N. 789
Sharma, S. 1177
Sharp, P. R. 841
Shi Qizhen 1893
Shi-Wei Lu 2341
Shibahara, T. 2351
Shih, K. Y. 229
Shih, K.-Y. 79
Shimoke, K. 2037
Shin, H.-K. 645, 2293
Shinohara, N. 107
Short, E. L. 613
Shterev, I. G. 393
Shukla, R. S. 2711
Siang-Guan Teoh 2683
Sicilia, M. V. 1573
Siddiqui, M. R. H. 2729
Sieler, J. 2423
Sienra, B. 2075
Šik, V. 1603
Sillanpää, E. R. J. 2051, 2501
Silva, J. A. L. 73
Singh, A. 949, 1733
Singh, A. K. 2065, 2693
Singh, K. B. 779
Singh, N. 1803
Singh, N. K. 1803
Sitran, S. 351
Slawin, A. M. Z. 261, 2337, 2641
Sleiter, G. 2475
Smełka, L. 2331
Smith, F. E. 1327
Smith, G. 509, 873, 1565, 1569
Snyder, B. S. 203
Sobota, P. 2457
Sokolov, M. N. 1311
Solujic', L. 1939
Soni, S. 2463
Soon-Beng Teo 2683
Sordo, J. 1465
Soto, L. 1031
Soufiaoui, M. 1153
Sousa, A. 197
Sovago, I. 1401, 2331
Spiccia, L. 619, 1865, 2389
Sreenivasulu, Y. 2785
Srinivas, B. 731
Srinivas, D. 2559
Stålhandske, C. 2417
Stamatakos, T. C. 2813
Staples, R. J. 899, 909
Steed, J. W. 1727
Steudel, R. 1037
Stewart, N. S. 1085
Stone, F. G. A. 215
Stoppioni, P. 2123
Strähle, J. 1579
Streeper, R. T. 221
Streib, W. E. 337, 805, 1573, 1639, 2309, 2371, 2699
Strzelecka, H. 687
Subrahmanyam, G. V. B. 2605
Subramanian, M. S. 1683
Sugaya, H. 373
Suzuki, N. 1405
Švajlenová, O. 893
Svejda, S. A. 1061

Tachibana, J. 373
Takhirov, T. G. 179
Tan, K.-L. 2437
Tanaka, M. 583
Taqui Khan, M. M. 1827, 2559, 2711, 2729
Tarafder, M. T. H. 819, 973
Taylor, R. E. 1203
Tecilla, P. 1791
Teixeira, C. 1433
Terzis, A. 741, 935
Thakur, N. M. 323
Thomas, S. 2065, 2693
Thornton, P. 121

Tilley, T. D. 1173
Tobe, M. L. 2597
Tocher, D. A. 881, 1727, 2597
Tokura, S. 2347
Toma, H. E. 1699
Tondre, C. 1791
Toriumi, K. 2717
Torres, M. R. 421
Toscano, P. J. 977
Toupet, L. 2045
Tregloan, P. A. 2317
Trendafilova, N. 393
Tripathi, U. M. 949
Tripathy, A. N. 323
Troutner, D. E. 1617
Tsay, R.-J. 605
Tuhl, A. H. 1485
Turnbull, M. M. 1835
Turova, N. Ya. 2617

Uhlemann, E. 1591
Ujimoto, K. 1139
Umehara, M. 583
Urbanos, F. A. 113
Urtiaga, M. K. 2451

Valkonen, J. 2501
Vallarino, L. M. 1385
Van Beek, D. A. Jr 1227
VanOrden, S. L. 2487
Varela, J. Ma 1465
Vasca, E. 2587
Vázquez, C. 1675
Venkatasubramanian, K. 851, 1827
Verma, R. 1803
Veselinović, D. 455
Via, J. 495
Vicente, R. 687, 2025
Vidali, M. 1353
Vierling, F. 2529
Voyé, A. 883

Wade, K. 2131
Wagner, F. E. 1741
Wakasa, M. 2347
Waki, H. 659, 1527
Wakita, H. 1773, 2833
Wales, D. J. 1749
Walsh, M. 2273
Walther, B. 2423
Walton, L. 613
Walton, R. A. 79
Wang Genglin 1889
Wang Honggen 1889
Wang Xintang, 1491
Wang Yaoyu 1893
Wang, G.-L. 941
Wang, H.-G. 101
Wang, L. 2477
Wang, Q. 2477
Ward, D. L. 885, 2813
Ward, M. D. 1395
Wardell, J. L. 1085
Watanabe, M. 67
Waters, M. 1113
Wei, G. 553, 927
Wei-Yuan Huang 2687
Weidenbruch, M. 1147
Welch, A. J. 471
Wen, Y.-S. 2437
Wenji Dong, 1479
Wesemann, J. L. 1367
West, B. O. 753
Wexler, P. 665
Whiteley, M. W. 267
Whyte, K. D. 1647
Wilkins, C. J. 2111
Wilkinson, G. 135, 595, 737, 1423, 1457, 2241, 2647
Willett, R. D. 1835
Williams, D. J. 261, 1079, 2241, 2337, 2641, 2647
Williams, D. R. 377, 1105, 1113, 1121
Williams, G. K. 215
Williamson, C. J. 567
Wolfe, T. A. 447
Wong, C. Y. 1131
Woods, C. 2153
Woollins, J. D. 261, 2337, 2641
Worrall, I. J. 95
Wrackmeyer, B. 1497
Wright, M. E. 1061
Wu Ding-Ming 2203
Wu, J. 2477
Wu, W. 447
Wu, Z. 27

Xiao-Ming Chen 1723, 2687
Xiaoheng Zhang 1873
Xiaojing Li, 1479
Xiaozeng You 2659
Xin-Lan Chen 2779
Xintao Wu 2743
Xu, Z. 37, 1363
Xuetai Chen 2651

Yamamoto, H. 1
Yan Shiping 1889
Yan, Y. K. 2437
Yang, H. 1025

Yang, Z. 2477
Yao Xinkan 1889
Yao, X.-K. 101
Yasuda, H. 1
Ye, Z. 27
Yifan Zheng 2743
Yong-Sheng Liu 2341
Yongfei Yu 1599
Yonghan Hu 2651
York, S. 2791
Yoshizawa, C. 2347
You, X. 37, 1363
Young, G. B. 1411
Young-Shen Huang 2229
Yu, K. 37, 1363
Yulang Qi, 1479

Zacharias, P. S. 731, 811
Zafiropoulos, T. F. 2405
Zakharoba, I. 1507
Zakrzewski, U. 1427
Zanello, P. 2123
Zanetti, E. 1085
Zanonato, P. 1353
Zarić, S. 2665, 2673
Zarli, B. 1353
Zhang Yugeng 403
Zhang, C. 1173
Zhang, M. 1025
Zhang, R.-H. 629
Zhang, X. 673, 1025
Zhang, Z.-Y. 941
Zhao Gang 2185
Zhecheva, E. 763, 1767
Zheng Xu 1625, 2659
Zhi-Qiang Wang 2341
Zhida Chen 2799
Zhongwen Ye 1599
Zhongyuan Zhou 2659
Zhou, Z. 37, 1025, 1363
Zhu Ying 1893
Zhu, Y. 2477
Zhuang Hong-Hui 2203
Zipin, H. S. 1189
Zubieta, J. 977
Zybill, C. 1163

Printed in Great Britain at BPCC-AUP Aberdeen Ltd.

VOLUME 10

SUBJECT INDEX

(Compiled by Peter Thornton)

A

Ab initio calculations
  cluster compounds, group 14, 1299
  propellanes, 1247
  silanes, 1265
Acetates and acetato complexes
  cobalt(II), 1333,1395
  copper(II), 793,873,1333,2301
  europium, 1385
  lead(II), 1657
  molybdenum(II), 229,2573
  molybdenum(III,IV), 2203
  palladium(I), 2523
  palladium(II), 2037
  rhenium(II), 79
  rhodium(I,II), 2551
  ruthenium(II), 113
  ruthenium(II,III), 829
  ruthenium(III), 113
  silicon, 1173
  thallium(III), 2069
  uranium(VI), 779,2399,2567
  zinc, 121
Acetohydroxamates
  silicon, 1131
Acetonitrile complexes
  copper(I), 347
  molybdenum(II), 433,1717,2283, 2519
  palladium(II), 1513
  rhenium(I,II),(II), 79
  rhenium(V), 2241
  ruthenium(II),(IV), 1173
  tungsten(II), 433,595
Acetophenone, enantioselective hydrosilation, 1061
Acetyls
  molybdenum(II), 1705
Acetylcyclopentadienyls
  cobalt(III), 725
Acetylferrocene-3-nitrobenzoyl-hydrazone complexes
  lanthanides, 2185
Acetylsalicylates
  tin(IV), 509
Acrylamide polymerization with Cr(VI) and Cu(II), 237
Acrylonitrile complexes
  B, Sb, Sn, Ti, 2131
Acyls
  Co(I),Fe(II),Mn(I), 717
  molybdenum(II), 717,1705
  Re(I),Rh(III), 717
  ruthenium(II), 963
Acylpyrazolonates
  uranium(VI), 1683
Adenosine complexes
  ruthenium(III), 2465
Alanine complexes
  chromium(III), 575
  cobalt(III), 977
Albite, 55
Alcohols, oxidation catalysed by Ru(III) complexes, 2137,2511
Alcohol complexes
  aluminium, 1657
  astatine(I), 11
  bismuth(III), 2617
  cadmium, 2111
  caesium, 337
  lanthanum, 1049
  molybdenum(VI), 2617
  neodymium, 1559
  niobium, 2031
  potassium, 337
  rubidium, 337
  sodium, 2617
  tantalum, 2031
  tungsten(VI), 2617
  yttrium, 1049
Alkanediyl complexes
  iron(II), ruthenium(II), 963
Alkenes
  hydrogenation catalysed by Rh(II) complex, 2729
  polymerisation catalysed by Mo(II) complexes, 2283
Alkene complexes
  iridium(I), 1595
  iron(II), ruthenium(II), 963
  zirconium, 1
Alkenediyl complexes
  palladium(II), 561
Alkenyls
  ruthenium(II), 421
Alkoxides
  aluminium, 1639,1733,1967
  barium, 2045
  bismuth, 437,2617
  caesium, 337
  chromium(III), 2255
  cobalt(II), 1733,2791
  copper(II), 1733,1767,1791,2791
  germanium, 1153
  iron(II), 1163,2791
  lanthanum, 949,1049
  lead(II), 1103,1657
  lithium, 805
  manganese(II), 2791
  mercury, 2065
  molybdenum(III), 2309,2839
  molybdenum(VI), 2617
  neodymium, 1559
  nickel(II), 1733,2791
  Pd(II), Pt(II), 2065
  potassium, rubidium, 337
  silicon, 1097,1173
  sodium, 2617

tungsten(III), 2309,2839
tungsten(VI), 477,2617
yttrium, 1049
zinc, 2791
zirconium, 949
Alkyls
gallium, 1897
germanium, 1153,1221,2347
hafnium, 1177
iron(II), 963,1177
mercury, 1465
molybdenum(II), 1705
phosphorus, 261
platinum(II), 993,1411
ruthenium(II), 963
silicon, 1097,1147,1227,1231
thallium(III), 517,1465
tin(IV), 1085,1497,1717,2683
titanium, 1177
tungsten(II), 1177
zirconium, 1177
Alkylamides
molybdenum(III), 2839
platinum(II), 747
rhenium(VII), 2241
tungsten(III), 1215,2839
tungsten(VI), 477
Alkylidene complexes
tungsten(IV), 215
Alkylidyne complexes
tungsten(IV), 215
Alkylimides
cobalt, 1423
molybdenum(VI), 463
niobium(V), 1959
rhenium, 1423,2241,2647
ruthenium, 291
tungsten(VI), 477
Alkyne complexes
chromium(0), 1427
molybdenum(II), 2519
palladium(I), 2523
platinum(0), 909
rhodium, 1995
tungsten(II), 711
Alkynyl complexes
platinum(II), 2153
Allyls
chromium(I), 1427
molybdenum(II), 605
niobium(III), 1075
tungsten(III),(IV), 459
1-Allylimidazole complexes
molybdenum(VI), 33
Allylphosphido complexes
osmium, 1955
Allyltrimethylsilane, reaction with WCl_6, 2089
Aluminium
alkoxides, aminoalkoxides, carboxylates, diketonates, review, 1967
alkoxide heterometallic complexes, 1733
alkoxide siloxides, 1639
oxide minerals, 55
phosphorus oxyanion water complexes, 659
polyphosphates, 1527
siloxide complexes, 1367
Aluminohydrides
Mo(II), W(II), 595
Amide complexes
cobalt(III), 2075
platinum(II), 1473
sodium, 1877
thorium, 2809
uranium(VI), 1683
Amidopyridine complexes
lanthanides, 2405
Amines, reaction with ruthenium complex, 1799
Amine complexes
astatine(I), 11
cadmium, 409
caesium, 221
cobalt(II), 409
cobalt(III), 977,1449,2075,2597
copper(II), 103,409,495,823,883, 941,1653,1675,1791,1809
europium, 1385
gallium, 1897
iron(II), 409
iron(III), 1809
lead(II), 409
manganese(II), 409
molybdenum(III), 2309
nickel(II), 823,2725
palladium(II), 1521
platinum(II), 799
rhenium(V), 243
rhenium(VII), 2241
rhodium(I), 1061
rhodium(III), 1617
rubidium, 221
ruthenium, 288
sexidentate, 409
silver, 19
tungsten(III), 2309
tungsten(VI), 477
zinc, 409
Aminoacid complexes
chromium(III), 575
cobalt(III), 977,2717,2847
copper(II), 273
palladium(II), 333
Aminoacid Schiff base complexes
copper(II), 2163
Aminoalkoxides
aluminium, review, 1988
barium, 2045
Aminoalkylsalicylaldimine complexes, copper(II), 1653
2-Aminoethylphosphonic acid complexes, lutetium, 175
2-Amino-3-hydroxypyridine complexes
ruthenium(III), 2137
2-Aminoisobutyrates
cobalt(III), 977
Aminophenoxides
ruthenium(III), 2137
titanium(IV), 1847
2-Aminopyrimidine complexes
copper(II), 873
ruthenium(II), 1727
4-Aminopyridine complexes
ruthenium(III), 1139
Aminothiolates
cadmium, 325
Ammonia complexes
cobalt(III), 2075,2317,2495
platinum(II), 799
ruthenium(II), 653,1139,1713
ruthenium(II,III), 653
ruthenium(III), 1139

t-Amyl alcohol, amyloxide
complexes,
lead(II), 1103
yttrium, 1049
t-Amylamine complexes
europium, 1385
Angular overlap calculations
chromium(III) oxalate complexes, 2673
cobalt(III) oxalate complexes, 2665
nickel(II) halide pyridine thiocyanate complexes, 1759
Aniline complexes
europium, 1385
gallium, 1897
Mo(III), W(III), 2309
p-Anisates
ruthenium(II,III), 491
Antimony(V)
chloride nitrile complexes, 2131
Antipyrine Schiff base complexes
thorium(IV), uranium(VI), 2399
Antitumor properties, titanium(IV)
aminophenoxide carboxylate
chloride cyclopentadienyl
thiophenoxide thiosalicylate
complexes, 1847
Arene complexes
potassium, 2353
ruthenium(II), 1091,1727
Arginine complexes
cobalt(III), 2717
Arsenic(V)
chloride phenoxide phenyl complexes, 789
fluoride, in polysilanes, 1227
Arsine complexes
cobalt(I), 2535
iron(II), 2095
molybdenum(II), 665
osmium(III), 2511
ruthenium(III), 2137
Aryls
arsenic(V), 789
germanium, 1153,2347
iridium(IV), 1457
iron(II),717
manganese(I), 717
mercury, 187,1013,1465
molybdenum(VI), 463
nickel(II), 2821
palladium(II), 1513,2037
platinum(II), 909
review, 135
rhenium(I), 717
rhodium(III), 187
silicon, 1173,1231
thallium(III), 1465
tin(IV), 1085
Arylamides
gallium, 1897
molybdenum(III), 2309
platinum(II), 747
potassium, 1839
rhenium(VII), 2241
sodium, 1839
tungsten(III), 2309
Arylimides
rhenium(VI), 1539
ruthenium, 291
Aryliminoisoindoline complexes
molybdenum(II), 229
2-Aryltelluroethoxides,
Hg, Pd(II), Pt(II), 2065
Ascorbate complexes
ruthenium(III), 2711
Ascorbic acid, oxidation catalysed by Cu(II) complexes, 731
ASED - MO calculations
copper dithiolene complexes, 2377
Astatine(I)
halide chelate complexes, 11
Atrolactate complexes
osmium(VI), 61
Azide complexes
chromium(III), 373
cobalt(III), 2597
copper(II), 2451
iron(III), 373
nickel(II), 2659,2725
palladium(II), 1513
Azole complexes
cobalt(II), 1333
copper(II), 893,1333,1767,1809
iron(III), 1809
molybdenum(III), 323
molybdenum(VI), 33
nickel(II), 1031,2659
palladium(II), 1513
platinum(II), 1443
ruthenium(III), 2559
tungsten(II), 711

B

Barium
aminoalkoxide, 2045
diimine pyridine silylamide, 769
oxide in feldspar glass, 55
Benzene complexes
potassium, 2353
ruthenium(II), 1727
Benzene-1,2-dioxydiacetates
calcium, sodium, 1565
Benzenethiolates
palladium(II), 1343
Benzil Schiff base complexes, 973
Benzimidazole complexes
copper(II), 893
molybdenum(III), 323
molybdenum(VI), 33
Benzoates
palladium(I), 2523
samarium, 1599
tin(IV), 509
titanium(IV), 1847
ytterbium, 1599
Benzo-15-crown-5 complexes
potassium, 1025
Benzohydroxamates
silicon, 1131
Benzoic hydrazide complexes
ruthenium(III), 2137
Benzoyldiazenide complexes
rhenium(V), 1539
S-Benzyldithiocarbazate Schiff base complexes, 973
Benzylfluorenyls
germanium, 1153
Betaine complexes
copper(II), 273
silver(I), 1723,2687

Biaryls, formation catalysed by
Pd(II) complex, 2037
Bicyclo[2.2.1]hept-5-ene-2-carboxylate complexes
copper(II), 2273
molybdenum(II), 2273,2283
ruthenium(II,III), 2273
N,N'-Bis(2-aminopropyl)oxamide complexes, Co(II), Cu(II), 1787
N,N'-Bis(3-aminopropyl)oxamide complexes, nickel(II), 103
Bis(arylimino)isoindoline complexes, molybdenum(II), 229
Bis(benzylthio)methane complexes
palladium(I),(II), 561
Bis[bis(2-diphenylphosphinoethyl)-amino]ethane complexes
copper(I), 1827
1,2-Bis[bis(2-methylthiophenyl)-phosphino]ethane complexes
Mo(0),W(0), 1549
1,2-Bis(di-*n*-butylphosphino)ethane complexes, Pt(0),(II), 899
1,4-Bis(dicyclohexylphosphino)butane complexes, Pt(II), 867
1,2-Bis(dicyclohexylphosphino)ethane complexes,
platinum(0),(II), 899,909
Bis(dicyclohexylphosphino)methane complexes, Ru(II),(III), 1713
1,3-Bis(dicyclohexylphosphino)propane complexes, Pt(II), 909
1,2-Bis(dimethylphosphino)ethane complexes
silver(I), 737
tungsten(II),(IV), 595
1,3-Bis(diphenylphosphinoacetyl)-benzene complexes, Pd(II), 1521
1,4-Bis(diphenylphosphino)butane complexes, Pt(II), 1411
1,2-Bis(diphenylphosphino)ethane complexes
cobalt(II), 553
molybdenum(II), 665
molybdenum(V), 1459
niobium(-I), 389
platinum(0), 899,909
platinum(II), 899,909,1411
ruthenium(II), 1019
tungsten(IV), 2827
tungsten(VI), 1311
1,2-Bis(diphenylphosphino)ethene complexes, Pt(II), 993
Bis(2-diphenylphosphinoethyl)ether complexes
molybdenum(IV), 467
Bis(2-diphenylphosphinoethyl)-phenyl)phosphine complexes
platinum(II), 2471
1,1'-Bis(diphenylphosphino)ferrocene complexes
manganese(0), 2437
platinum(II), 1411
rhenium(0), 2437
Bis(diphenylphosphino)methane complexes
cobalt(II), 553
molybdenum(0), 2611
platinum(II), 1411,2153
rhenium(I,II),(II), 79
rhodium(I), 2153
1,3-Bis(diphenylphosphino)-2-methylprop-2-ene complexes
Cr(0), Mo(0), W(0), 2381
1,3-Bis(diphenylphosphino)propane complexes, Pt(II), 1411
1,2-Bis(dipropylphosphino)ethane complexes, Cr(0), 1427
1,2-Bis(di-*o*-tolylphosphino)ethane complexes
tungsten(IV), 1007
Bis(2-hydroxy-5-methylphenyl)telluride complexes, Hg,Pd,Pt, 2693
Bis(2-methylthiophenyl)phenylphosphine complexes, Re(I), 1603
Bismuth
alcohol alkoxide oxo heterometallic complexes, 2617
alkoxide diketonate ether siloxide complexes, 437
chloride heteropolynuclear complexes, 123
Bismuthine complexes
molybdenum(II), 665
1,8-Bis(2-pyridyl)-3,6-dithiaoctane complexes, copper(II), 1647
Bis(pyridyl)triazanonane, -undecane complexes, Co(III), 2597
Bis(trimethylsilyl)amides
barium, 769
germanium, tin(II),(IV), 1203
Bis(trimethylsilyl)cyclopentadienyls, tin(II), 1203
Bis(trimethylsilyl)methyls
germanium, 1153
Bis(trimethylsilyl)phosphides
rhenium(VII), 2241
Bonding and structure, book review, 2083
Boric acid catecholate complexes, 613
Borohydrides
copper(I), 1827
Boron
chloride nitrile complexes, 2131
diimine fluoride complex, 2221
heterocyclic compounds, 1497
Bromides and bromo complexes
astatine(I), 11
cadmium, 2111
copper(II), 823,941,1333,1579, 1675,2301,2529
gallium, 2757
gold(III), 1939
indium, 1069
iron, 203
iron(II), 963
mercury, 351,2611
molybdenum(0), 2611
molybdenum(II), 2283
molybdenum(III), 323,1667
molybdenum(V), 997
nickel(II), 1759
niobium(I), 389
niobium(II,III), 2031
palladium(II), 1507,2265
platinum(II), 909,1443
platinum(IV), 19,2191
rhenium(I), 1603
rhenium(III), 877
rhodium(III), 2265
ruthenium, 583
ruthenium(II), 963
ruthenium(III), 2137

tantalum(II,III), 2031
thorium, 2399,2567,2809
tin(IV), 1497
tungsten(V), 997
tungsten(VI), 1311
uranium(VI), 2399,2567
vanadium(IV), 1817
2-Bromobenzoates
lanthanides, 1599
5-Bromophenanthroline complexes
iron(II), 703
4-Bromothiophenoxides
chromium(VI), 753
Butadiene complexes
chromium(0), 1427
niobium(-I), 389
2-Butanol complexes
Nb(II,III), Ta(II,III), 2031
t-Butanol complexes
caesium, 337
lanthanum, 1049
potassium, rubidium, 337
yttrium, 1049
3-Butenoates
molybdenum(II), 2283
n-Butoxides
lead(II), 1103
t-Butoxides
aluminium, 1733
caesium, 337
cobalt(II), copper((II), 1733
iron(II), 1163
lanthanum, 949,1049
lead(II), 1103,1657
lithium, 805
molybdenum(III), 2309
nickel(II), 1733
potassium, 337
rubidium, 337
tungsten(III), 2309
tungsten(VI), 477
yttrium, 1049
zirconium, 949
n-Butyls
tin(IV), 1717
t-Butyls
gallium, 1897
germanium, 1153
silicon, 1147
t-Butylamides
rhenium(VII), 2241
tungsten(VI), 477
n-,*s*-Butylamine complexes
europium, 1385
t-Butylamine complexes
rhenium(VII), 2241
tungsten(VI), 477
t-Butylcyclopentadienyls
iron(II), 2095
tungsten(III), 459
t-Butyldimethylsiloxides
potassium, 2699
1-Butylimidazole complexes
molybdenum(VI), 33
t-Butylimides
cobalt, 1423
molybdenum(VI), 463
niobium(V), 1959
rhenium, 1423,2241,2647
tungsten(VI), 477
t-Butylisocyanide complexes
molybdenum(0), 267
rhodium(I), 2153
tungsten(0), 267
4-*t*-Butylphenoxides
arsenic(V), 789
4-*t*-Butylpyridine complexes
barium, 769
palladium(II), 2265
n-Butylthiolates
chromium(VI), 753
t-Butylthiolates
chromium(VI), 753
iron(II), 1163
palladium(II), 1343
4-*t*-Butylthiophenoxides
cobalt(II), 553
Butyrylhydrazone complexes
lanthanides, 2779
2-Butyne complexes
chromium(0), 1427
molybdenum(II), 2519
tungsten(II), 711

C

Cadmium
diimine pyridinethionate complexes, 197
dithiocarbamate mercaptoamine thioether complexes, 325
halide methanol pyridine-*N*-oxide complexes, 2111
salicylaldimine thioether sexidentate complexes, 823
Schiff base thiolate complexes, 771
sexidentate amine complex, 409
trifluoromethanesulphonate, 2757
Caesium
alcohol alkoxide complexes, 337
crown ether complexes, 221
hexachlorophosphate, 2217
Calcium
benzenedioxydiacetate sodium complex, 1565
carboxylate crown ether complexes, 1591
dicarboxylate ether water complex, 1569
oxide in feldspar glass, 55
Carbaboranes, 1497
Carbaborane complex
copper(I), 471
Carbene complexes
book review, 1843
cobalt(III), 725
germanium, 1153
2-Carbomethoxyethyls
tin(IV), 1085
Carbon, cluster structures, molecular orbitals, 1299
Carbonates and carbonato complexes
europium, 1385
Carbonyls
chromium, 591
chromium(-I), 2487
chromium(0), 1319,2381
cobalt, 1423
cobalt(I), 717,2535
cobalt(III), 725
iridium(I), 1595
iron(-I), 2487
iron(0), 123,543,2105,2423

iron(I), 2423
iron(II), 841,963,1163,1177,2095
manganese(0), 2437,2487
molybdenum, 1663
molybdenum(0), 123,267,1549,2381, 2611
molybdenum(II), 133,433,665,717, 1549,1705,1717,2519
nickel(0), 2423
niobium(-I), 389
osmium, 881,1955
palladium, 673
rhenium, 1423
rhenium(0), 2437
rhenium(I), 1603,1873
rhenium(I,II), 79
rhenium(II), 79,1873
rhenium(III), 877
rhodium(I), 543,1595,2153
rhodium(III), 187
ruthenium, 277,1013,1955
ruthenium(II), 421,837,963,1019, 1713,2265
ruthenium(III), 2559
tungsten, 1663
tungsten(0), 267,1549,2381
tungsten(II), 433,711,1177,1549, 1717
tungsten(IV), 215
vanadium(-I), 2487
Carboxylates
aluminium, 1985
calcium, 1591
cobalt(II), 1333,1395
copper(II), 793,873,893,1333,1893, 2273,2301
erbium, 1921
europium, 1385
iron(II), 483
lanthanides, 1385,1599,1921
lead(II), 1657
mercury, 133,187
molybdenum(II), 229,2273,2283,2573
molybdenum(III,IV), 2203
neodymium, 1921
palladium(I), 2523
palladium(II), 2037
potassium, 1591
rhenium(II), 79
rhenium(V),(VII), 2241
rhodium(I,II), 2551
rhodium(III), 187
ruthenium(II), 113
ruthenium(II,III), 491,829,2273
ruthenium(III), 113
samarium, 1599
silicon, 1173
silver(I), 1723,2687
sodium, 1591
thallium(III), 2069
tin(IV), 509
titanium(IV), 1847
uranium(VI), 779,2399,2567
ytterbium, 1599
zinc, 121
zirconium, 2341
Catechol, oxidation catalysed by binucleating complexes, 1353
Catecholamine complexes
formation constants, 1401
Catecholates
boron, 613
CD spectra
chromium(III) alanine complex, 575
cobalt(III) arginine hydroxide complexes, 2717
copper(II) aminoacid - pyridoxal phosphate Schiff base complexes, 2163
copper(II) dehydrodipeptide complexes, 2331
Cerium(III)
amidopyridine nitrate perchlorate thiocyanate water complexes, 2405
chloride hydrazone phenanthroline water complexes, 1491
disulphoxide perchlorate complexes, 629
hydrazone complexes, 2185
Chemical speciation modelling, 1105, 1113,1121
Chlorides and chloro complexes
antimony(V), 2131
arsenic(V), 789
astatine(I), 11
bismuth, 123
boron, 2131
cadmium, 2111
chromium(0),(I), 1427
chromium(II), 2541
cobalt(II), 365,811,1333,1733,2785
cobalt(III), 823,977,1449
copper(I), 935
copper(II), 365,495,731,823,1091, 1333,1579,1675,2301,2529,2541, 2785,2851
gold(III), 19,633,1025,1631,1939
hafnium, 1177
iridium(III), 1857
iron, 203
iron(II), 365,2785
lanthanides, 1491,1599
lanthanum, 949,1491
magnesium, 2457
mercury, 351,2065,2611,2693
molybdenum, 429
molybdenum(0), 2611
molybdenum(II), 1717,2519
molybdenum(III), 323,1667
molybdenum(IV), 2799
molybdenum(V), 997,1459,2457,2809
nickel(II), 365,415,1733,1759,2659
niobium(II), 389
niobium(II,III), 2031
niobium(V), 1959
osmium(III), 2511
palladium(I), 561
palladium(II), 89,415,561,579,1343, 1507,1513,1521,2065,2265,2337, 2693
platinum(II), 501,579,747,851,899, 909,1443,1473,1573,2065,2153, 2693,2737
platinum(IV), 1573,2191
rhenium, 1903
rhenium(I), 1603
rhenium(I,II),(II), 79
rhenium(II,III,III), 741
rhenium(V), 243,1539,2241
rhenium(V,VI), 2241
rhodium(I), 1061
rhodium(I,II), 2551
rhodium(III), 717,1611,1617,2229, 2265
ruthenium, 583,1013
ruthenium(II), 837,1019,1091,1699,

1713,1727,2137,2265
ruthenium(II,III), 491,2273
ruthenium(III), 1713,2137,2229, 2511,2559,2711
samarium, 1599
selenium(II), sulphur(II), 1037
tantalum(II,III), 2031
thallium(III), 885
thorium, 2399,2567,2809
tin(II), 1721
tin(IV), 1497,1717,2105,2131,2683
titanium, 1177,1847,2131
tungsten(II), 595,1717
tungsten(V), 595
tungsten(V), 997,2089
tungsten(VI), 477,1311
uranium(VI), 2399,2567
vanadium(IV), 1817
ytterbium, 1599
zirconium, 1177,2341
Chlorodicyclohexylphosphine complexes
nickel(0), 2423
Chlorodiphenylphosphine complexes
nickel(0), 2423
Chlorogenic acid complexes
boron, 613
Chlorophenols, complexes with Co(III)
diketonate, 1405
4-Chlorophenoxides
arsenic(V), 789
Chlorophosphine complexes
nickel(0), 2423
Chromate, in polymerization
photoinitiation, 237
Chromate complexes
copper(II), 2179
Chromium
carbonyl cyclopentadienyl dioxygen seleno complexes, 591
Chromium(-I)
carbonylate anions, 2487
Chromium(0)
alkyne chloride diene diphosphine phosphine complexes, 1427
carbonyl diaminodisulphide complexes, 1319
carbonyl diphosphine complexes, 2381
Chromium(I)
allyl chloride diene phosphine complexes, 1437
Chromium(II)
aryls, 139,150,164
chloride diimine complexes, 2541
Chromium(III)
alanine complex, 575
alkoxythiolate complex, 2255
aryls, 139,150,164
azide porphyrin complex, 373
fluoride complex, 2605
hydroxide water complexes, 619, 1865,2389
oxalate complex, 2673
Chromium(IV)
aryls, 139
Chromium(VI)
chromate, 237
oxo thiolate complexes, 753
Chrysin complexes
silicon, 1131
Ciliatine complex
lutetium, 175
Citrates
osmium(VI), 61
Citrulline complexes
palladium(II), 333
Clays, absorption of methyl salicylate, 567
Cluster complexes
book reviews, 2083,2085
carbon and nitrogen centred, 1749
group 14, molecular orbitals, 1299
ruthenium, review, 277
CNDO calculations
molybdenum(IV) chloride oxo thio trinuclear complexes, 2799
Cobalt
alkylimide carbonyl complex, 1423
phosphine seleno thio complexes, 927
Cobalt(-I)
aryls, 156
Cobalt(0)
aryls, 156
Cobalt(I)
acyl carbonyl phosphine complex, 717
arsine carbonyl phosphine stannyl complexes, 2535
Cobalt(II)
acetate quinquepyridine complex, 1395
alkoxide chloride aluminium complexes, 1733
amine chloride complex, 1449
aryls, 143,156
azole carboxylate chloride complexes, 1333
chloride hydrazinium water complex, 365
chloride phenanthroline entwined complexes, 811
chloride sulphate tetraimine macrocyclic complexes, 2785
cysteinesulphinate complex, 1453
diarylphosphate methanol pyridine water complexes, 2771
diimine oxamide copper(II) complexes, 1787
diphosphine thiolate complexes, 553
fluoride complex, 2605
hydride triphosphine triphosphorus complexes, 2123
hydroxyketone binucleating complexes, 1353
phenanthroline complex, 1803
pyridylcarbinol complexes, 2791
sexidentate amine complex, 409
sulphonates, 2757
tetramine macrocyclic complexes, 1779
Cobalt(III)
amide amine ammonia sulphoxide complexes, 2075
amine aminoacid chloride nitrite pyridine thioether complexes, 977
amine azide pyridine thiocyanate complexes, 2597
ammonia malate complex, 2495
ammonia molybdate complex, 2317
arginine hydroxide complexes, 2717
carbene carbonyl cyclopentadienyl tetracyanoethene complex, 725
chloride salicylaldimine thioether

sexidentate complexes, 823
cysteine sulphinate complexes, 2847
diketonate phenol complexes, 1405
hydroxide peroxide tetramine complexes, 107
ketoimine complexes, 1687
oxalate complex, 829,2665
porphyrin water complex, 1379
pyridine tetramine macrocyclic complex, 1779
pyridine-*N*-oxide thiolate compounds, 2651
Conductimetric titrations
heteropolymetallic alkoxides, 2617
Controlled potential electrolysis
nickel(II) dithiocarbamate triamine complexes, 2025
platinum(II) chloride diphosphine complexes, 899
Copper
diiminate iodide complexes, 955
dithiolene complex, 2377
iodide tetraazaannulene complexes, 1911
Copper(I)
acetonitrile perchlorate phosphine complexes, 347
aryls, 145,159,167
borohydride polyphosphine complex, 1827
carbaborane phosphine complex, 471
chloride phosphine thione complexes, 935
diene diketonate complexes, 2293
diketonate phosphine complexes, 645
phosphine iron(0) complex, 2423
phosphine thio heterometallic complexes, 2743
pyrazine complex, 1835
tetramine macrocyclic binucleating complexes, 1373
Copper(II)
acetate pyridine complexes, 793
acetate pyrimidine complex, 873
alkoxide aluminium complexes, 1733
amine halide salicylaldimine thiocyanate thioether polydentate complexes, 823
amine oxamide nickel(II) complexes, 103
aminoacid complex, 273
aminoacid - pyridoxal phosphate Schiff base complexes, 2163
aminoalkylsalicylaldimine complexes, 1653
amino(hydroxymethyl)pyridine hydroxyquinoline complexes, 1791
azide terpyridyl complex, 2451
azole carboxylate halide hydroxide nitrate complexes, 1333
azole carboxylate salicylaldimine complexes, 893
bromide hexamine water binucleating complex, 941
carboxylates, 2273
carboxylate dipyridyl halide hydroxide complexes, 2301
carboxylate dipyridyl water complex, 1893
chloride diazoleaminophenoxide nitrate perchlorate complexes, 1809
chloride diimine complexes, 2541
chloride dimethylphosphite ruthenium(II) complex, 1091
chloride dipyridylamine pyridoxate water complex, 2851
chloride dipyridylamine water complex, 495
chloride hydrazinium water complex, 365
chloride phenoxide Schiff base complexes, 731
chloride sulphate tetraimine macrocyclic complexes, 2785
chromate diimine complexes, 2179
creatinine methoxide complexes, 1767
dehydropeptide complexes, 2331
diamine diketonate complexes, 1773
diamine nitrate complex, 2225
diaminooxamide cobalt(II) complexes, 1787
diaminopyridine halide nitrate water complexes, 1675
diarylphosphate dimethylformamide methanol pyridine water complexes, 2771
diimine pyridine Schiff base thiolate complexes, 1327
diimine pyridine-*N*-oxide-dithiocarbazate complexes, 1363
dipyridyl complex, 101
dipyridyl saccharinate complex, 403
four coordinate, molecular mechanics, 2079
halide complexes, 2529
halide nitrate quinoline - thioether water complexes, 1579
hydroxyketone binucleating complexes, 1353
ketoimine complexes, 1687
ketoimine pyridine thiolate complexes, 535
ketooxime complexes, 919
nitrate pyridine-*N*-oxide thiosemicarbazone complex, 1625
oxidation of diaminodisulphides, 1319
pyridine thioether complex, 1647
pyridylcarbinol complexes, 2791
salicylaldiminate, 2051
sexidentate amine complex, 409
sulphonates, 2757
tetramine complexes, 523,883,1373
thio water molybdenum(III,IV) complex, 2351
water complex in polymerization termination, 237
Copper(III)
tetramine macrocyclic binucleating complexes, 1373
Creatinine complexes
copper(II), 1767
platinum(II), 799
Crotonitrile complexes
B, Sb, Sn, Ti, 2131
Crown ligand complexes
caesium, 221
calcium, 1591
gadolinium, 1889
iron(II),(III), 763
mercury, 1545
potassium, 1025,1591,2699

rubidium, 221
ruthenium(II),(III), 1139
sodium, 1591,1877
Cubic complexes, 393
Cyanides and cyano complexes
iron(II), 653
mercury, 1013,2611
molybdenum(0), 2611
phosphorus(III), 1831
platinum(II), 909,2153
ruthenium, 1013
zinc, 1105
4-Cyanopyridine complexes
iron(II), 653
ruthenium(II),(II,III), 653
Cyanotrihydroborate complexes
rhenium(II), 79
Cyclam complexes
nickel(II), 103
Cyclic voltammetry
cobalt phosphine seleno thio complexes, 927
cobalt(II) acetate quinquepyridine complex, 1395
cobalt(II) chloride phenanthroline entwined complexes, 811
cobalt(II) hydride triphosphine triphosphorus complexes, 2123
copper diiminate iodide complexes, 955
copper(I) acetonitrile perchlorate phosphine complexes, 347
copper(I) phosphine thio heterometallic complexes, 2743
copper(II) chloride phenoxide Schiff base complexes, 731
copper(II) diarylphosphate dimethylformamide methanol pyridine water complexes, 2771
copper(II) tetramine macrocyclic complexes, 523
ferrocenes, 1741
iridium(IV) mesityl, 1457
iron(II) cyclopentadienyls, 483
manganese(II) quinizarine complexes, 1929
mercury thioether complex, 1545
molybdenum(III,IV) acetate dithiophosphate oxo thio complexes, 2203
molybdenum(V) dithiolate thio copper(I) complex, 2743
molybdenum(VI) azole oxo salicylaldimine complex, 33
nickel(II) dithiocarbamate triamine complexes, 2025
osmium(III) chloride phosphine quinone complex, 2511
platinum(II) chloride diphosphine complexes, 899
pyridine-*N*-oxide-2-thiol complexes, 2651
rhenium(II) carboxylate chloride cyanotrihydroborate diphosphine nitrile complexes, 79
rhenium(VI) arylimide maltol phosphine complex, 1539
rhodium(II) hydride phosphine complex, 2729
ruthenium(II) ammonia crown ether pyridine complexes, 1139
ruthenium(II) arene chloride dimethylphosphite copper(II) complex, 1091
ruthenium(II) chloride hydrazide phosphine complexes, 2137
ruthenium(II) chloride pyrazine sulphoxide complexes, 1699
ruthenium(II) diimine complexes, 1485
ruthenium(III) aminophenoxide arsine halide hydroxyquinoline complexes, 2137
ruthenium(III) ammonia crown ether pyridine complexes, 1139
ruthenium(III) arsine chloride quinone complex, 2511
tungsten(V) dithiolate thio copper(I) complex, 2743
Cycloheptatrienyls
molybdenum(0), 267
niobium(-I),(0),(I),(II), 389
tungsten(0), 267
Cyclohexanethiolates
palladium(II), 89
Cyclohexyl iodide complexes
rhenium, 1903
Cyclometallated compounds
palladium(II), 1513,1521
platinum(II), 255
1,5-Cyclooctadiene complexes
copper(I), 2293
iridium(I), 1595
rhodium(I), 543,1069,1595
Cyclooctene complexes
iridium(I), 1595
Cyclopentadienyls
chromium, 591
cobalt(III), 725
hafnium, 1177
iron(0), 123,2105
iron(II), 483,717,963,1177,1741, 2095,2437
lanthanides, 27,1599
manganese(0), 2487
molybdenum(0), 123
molybdenum(II), 133,665,717,1705
molybdenum(IV), 1189
niobium(0),(I),(II), 389
niobium(III), 1075
rhenium, 1903
rhenium(I),(II), 1873
rhenium(III), 877
rhenium(VII), 2241
ruthenium(II), 963,1173,1713,2483
ruthenium(III), 1713
ruthenium(IV), 1173
samarium, 1599
tin(II), 1203
titanium, 1177,1847
tungsten(II), 1177
tungsten(III), 459
tungsten(IV), 459,1189
ytterbium, 1599
zirconium, 1,1177,2341
Cyclopentanones, template synthesis with Zr compounds, 1
Cyclosilselenanes, 1231
Cysteine complexes
cobalt(III), 2847
Cysteinesulphinates
cobalt(III), 1453,2847
Cytidine complexes
ruthenium(III), 2465

D

Dehydrocoupling for element - element bond formation, review, 1239
Dehydropeptide complexes
copper(II), 2331
Diamine complexes
cobalt(II), 1787
copper(II), 1773,2225
gold(III), 19
molybdenum(II), 2573
molybdenum(VI), 2057
nickel(II), 103,859
platinum(II), 747,2191
platinum(IV), 2191
potassium, 1839
silver, 19
sodium, 1839
1,4-Diaminobutane complexes
copper(II), 1773
Diaminodisulphide complexes
chromium(0), 1319
1,3-Diaminopropane complexes
copper(II), 1773
molybdenum(II), 2573
nickel(II), 103
Diaminopyridine complexes
copper(II), 1675
O,O'-Diarylphosphates
Co(II), Cu(II), Fe(II), 2771
Diazadiene complexes
platinum(II), 255
4,7-Diaza-1-thiacyclononane complexes, Ag,Au(III),Pt(IV), 19
Diazenide complexes
rhenium(V), 1539
1,4-Diboracyclhexa-2,5-diene, 1497
3,5-Di-*t*-butylcatechol, oxidation catalysed by Cu(II) complexes, 731
Di-*t*-butylchlorophosphine complexes, nickel(0), 2423
1,3-Di-*t*-butylcyclopentadienyls
iron(II), 2095
Di-*t*-butylphosphide complexes
iron(0), 543,2423
iron(0,I),(I), 2423
rhodium(I), 543
Di-*t*-butylphosphine complexes
rhodium(I), 543
Di-*i*-butyl sulphide complexes
palladium(II), 2037
1,1-Dicarboethoxy-2,2-ethylenedithiolates, Fe(IV), Mn(IV), 1803
Dicarboxylates
calcium, 1569
chromium(III), 2673
cobalt(III), 829,2665
titanium(III), 829
Dichloromethane complexes
platinum(II), 993
Dichromate, hydrolysis, 753
Dichromate complexes
copper(II), 2179
1,2-Dicyanobenzene complexes
rhenium(II), 79
1,2-Dicyanoethene-1,2-dithiolates
molybdenum(V), 2813
Dicyclohexylphosphido complexes
iron(0),(I), 2423
Diene complexes
chromium(0),(I), 1427
copper(I), 2293
iridium(I), 1595
niobium(-I), 389
rhodium(I), 543,1061,1595
zirconium, 1
Diethyldithiocarbamates
cadmium, 325
molybdenum(VI), 1311
nickel(II), 2025,2821
ruthenium(II), 421,1019
vanadium(IV), 1817
Diethyldithiophosphates
Mo(III,IV), W(III,IV), 2203
Diethyl ether complexes
tungsten(V), 2089
Differential pulse voltammetry
cobalt(II) chloride phenanthroline entwined complexes, 811
Difluoro[dimethylaminomethyl(methoxy)]phenylphosphine complexes
platinum(II), 2737
Digermanoxanes, 2347
Dihydrazone complexes
nickel(II), 859
3,4-Dihydroxybenzoic acid complexes, boron, 613
3,4-Dihydroxycinnamic acid complexes, boron, 613
2,3-Dihydroxypyridine complexes
silicon, 1131
Diimine complexes
barium, 769
boron, 2221
cadmium, 197
chromium(II), 2541
cobalt(II), 1803
copper(II), 101,403,1327,1363, 1893,2179,2301,2541
europium, 1385
iron(II), 703,1803
lanthanides, 1385,1491
molybdenum(0), 2611
molybdenum(II), 2519
molybdenum(V), 2813
nickel(II), 103,859,1327,1803
palladium(II), 1513,2037
platinum(II), 255
rhodium(I,II), 2551
ruthenium, 298,303
ruthenium(II), 653,1485
ruthenium(II,III), 653
vanadium(IV), 73
yttrium, 2171
zinc, 197,1803
Diketonates
aluminium, review, 1980
bismuth, 437
cobalt(III), 1405
copper(I), 645,2293
copper(II), 1773
molybdenum(II), 433,605
palladium(II), 1513
silicon, 1131,2463
tungsten(III), 433
uranium(VI), 1683
zinc, 121
1,2-Dimethoxyethane complexes
lithium, potassium, 2699
tungsten(VI), 2417
Dimethylacetylene dicarboxylate complexes, palladium(I), 2523
Dimethylamides

molybdenum(III), 2839
rhenium(VII), 2241
tungsten(III), 1215,2839
2-Dimethylaminomethylphenyls
palladium(II), 1521
4-Dimethylaminopyridine complexes
barium, 769
ruthenium(III), 1139
2,3-Dimethylbutadiene complexes
chromium(0), 1427
4,4'-Dimethyl-2,2'-dipyridyl
complexes, Mo(V), 2813
Dimethyldithiocarbamates
nickel(II), 2025,2821
nickel(III), 2025
palladium(II), 1513
vanadium(IV), 1817
Dimethylethylenediamine complexes
copper(II), 2225
molybdenum(II), 2573
platinum(II),(IV), 2191
Dimethylformamide complexes
cobalt(III), 2075
N,N-Dimethylfurancarboselenoamide
complexes
Pd(II), Rh(III), Ru(II), 2265
2,9-Dimethylphenanthroline
complexes, molybdenum(0), 2611
4,7-Dimethylphenanthroline
complexes, iron(II), 703
Dimethyl(phenyl)arsine complexes
platinum(II), 851
Dimethyl(phenyl)methoxides
lithium, 805
Dimethyl(phenyl)phosphine
complexes
chromium(0),(I), 1427
iridium(III), 1857
iron(II), 963
molybdenum(II), 665
molybdenum(III), 1667
platinum(II), 1411
rhenium(I), 1873
ruthenium(II), 963
Dimethyl(phenyl)siloxides
potassium, 2353
Dimethyl(phenyl)silylmethyls
platinum(II), 1411
Dimethylphosphido complexes
iron(0),(0,I),(I), 2423
2,6-Dimethyl-4H-pyran-4-one
complexes
mercury, 351
2,6-Dimethyl-4H-pyran-4-thione
complexes
mercury, 351
2,3-Dimethylpyrazine complexes
copper(I), 1835
2,6-Dimethylpyrazine complexes
ruthenium(II), 1699
3,5-Dimethylpyrazolates
Pt(II), Rh(I), 2153
Dimethylsilyls
molybdenum(IV), 1189
Dimethylsulphoxide complexes
cobalt(III), 2075
ruthenium(II), 1699
Dinitrogen, reactions catalysed by
W(IV) complexes, 1007,2827
Dinitrogen complexes
ruthenium, 313
Dioxahexaazacyclotetracosane
complexes. copper(II), 941
1,4-Dioxan complexes
gallium(II), 95
Dioxygen complexes
chromium, 591
Diphenylacetylene complexes
chromium(0), 1427
platinum(0), 909
Diphenylamides
rhenium(VII), 2241
Diphenylarsino(diphenylphosphino)-
methane complexes
Pt(II), Rh(I), 2153
1,5-Diphenyl-1,5-diphosphacyclo-
octane complexes
Ni(II), Pd(II), 415
Diphenyldiselenophosphinates
sodium, 2641
Diphenylethenyl complexes
platinum(0), 909
ruthenium(II), 421
Diphenylphosphido complexes
rhenium(VII), 2241
Diphenylphosphino(phenylmethyl-
thio)methane complexes
palladium(I), 2523
Diphenyl(tolyl)phosphine complexes
platinum(II), 1411
Diphenyl(trifluoromethylphenyl)-
phosphine complexes
platinum(II), 1411
Diphosphazene complexes
osmium, 881
Diphosphine complexes
chromium(0), 1427,2381
cobalt(II), 553
molybdenum(0), 1549,2381,2611
molybdenum(II), 665,1549
molybdenum(V), 1459
nickel(II), 415
niobium(-I), 389
palladium(II), 415
platinum(0), 899,909
platinum(II), 867,899,909,993,
1411,2153
rhenium(I,II),(II), 79
rhodium(I), 2153
ruthenium(II), 1019,1713
ruthenium(III), 1713
silver(I), 737
tungsten(0), 1549,2381
tungsten(II), 595,1549
tungsten(IV), 595,1007,2827
tungsten(V), 595
tungsten(VI), 1311
Diphosphine selenide, sulphide
synthesis, 2381
Diphosphinoether complexes
molybdenum(IV), 467
2,2'-Dipyridyl complexes
barium, 769
boron, 2221
cobalt(II), 1787
copper(II), 101,403,1327,1363,
1893,2179,2301
europium, 1385
iron(II), 703
molybdenum(0), 2611
molybdenum(II), 2519
nickel(II), 103,1327
palladium(II), 1513,2037
rhodium(I,II), 2551
ruthenium(II),(II,III), 653
vanadium(IV), 73

zinc, 197
Dipyridylamine complexes
copper(II), 2851
nickel(II), 2725
4,4'-Dipyridyl-*N,N'*-dioxide complexes, thorium, 2809
Di(2-pyridyl)phenylcarbinol complexes, Co,Cu,Fe,Mn,Ni,Zn, 2791
Dipyridylpyridazine complexes
ruthenium(II), 1485
Disilacyclobutanediimines, 1147
Disulphide complexes
astatine(I), 11
lanthanides, 629
Mo(V), W(V), 997
1,4-Dithiane complexes
gallium(II), 95
Dithiapyranylidene complexes
nickel dithiolate, 687
Dithiocarbamates
cadmium, 325
molybdenum(VI), 1311
nickel(II), 2025,2821
nickel(III), 2025
palladium(II), 1513
ruthenium(II), 421,1019
tungsten(II), 711
vanadium(IV), 1817
Dithiocarbazate complexes
copper(II), 1363
nickel(II), 37
Dithiocarbazate ester Schiff base complexes, Cu,Ni, 1327
Dithiocarbonates
nickel(II), 2821
Dithiolates (dithiolenes)
copper, 2377
Fe(IV), Mn(IV), 1803
molybdenum(V), 2743,2813
nickel, 687
tungsten(V), 2743
Dithiophosphates
Mo(III,IV), W(III,IV), 2203
Dithiouracil complexes
copper(I), 935
Dodecahedral complexes, 393
Dodecahydrododecaborates
lanthanides, 2779
Double helical complex
silver(I), 127
Doxycycline complexes
Mo(VI), W(VI), 455
Dysprosium
amidopyridine nitrate thiocyanate complexes, 2405
chloride hydrazone phenanthroline water complexes, 1491
disulphoxide perchlorate complex, 629
hydrazone complexes, 2185

E

Eight coordination, interligand repulsions, 393
Electric conductance
cobalt(II) diimine oxamide copper(II) complexes, 1787
copper diiminate iodide complexes, 955
copper iodide tetraazaannulenes, 1911
copper(II) diaminooxamide cobalt(II) complexes, 1787
copper(II) diaminopyridine halide nitrate water complexes, 1675
copper(II) nitrate quinoline - thioether water complexes, 1579
iron(IV) dithiolate complexes, 1803
lanthanide chloride hydrazone phenanthroline water complexes, 1491
lanthanide disulphoxide perchlorate complexes, 629
manganese(IV) dithiolate complexes, 1803
molybdenum(0) carbonyl diimine diphosphine halide pseudohalide mercury complexes, 2611
nickel(II) aryl dithiocarbamate dithiocarbonate xanthate complexes, 2821
palladium(II) halide pyrimidinethione complexes, 1507
polysilanes doped with AsF_5, 1227
rhenium(II) chloride diphosphine nitrile complexes, 79
ruthenium(III) chloride pyridylphosphonate zinc complexes, 2229
ruthenium(III) edta nucleoside complexes, 2465
Electrochemical syntheses
fluorides, 2605
Electron, solvated, reaction with Mo(V) complex, 1459
Electronic spectra
boric acid catecholate complexes, 613
chromium(0) carbonyl diaminodisulphide complexes, 1319
chromium(II) chloride diimine complexes, 2541
chromium(III) alkoxythiolate complex, 2255
chromium(III) azide porphyrin complex pyrolysis products, 373
chromium(III) oxalate complex, 2673
chromium(VI) - copper(III) mixture on irradiation, 237
chromium(VI) oxo thiolate complexes, 753
cobalt(II) alkoxide chloride aluminium complexes, 1733
cobalt(II) azole carboxylate chloride complexes, 1333
cobalt(II) chloride phenanthroline entwined complexes, 811
cobalt(II) diarylphosphate methanol pyridine water complexes, 2771
cobalt(II) diimine oxamide copper(II) complexes, 1787
cobalt(III) amide amine ammonia sulphoxide complexes, 2075

cobalt(III) amine aminoacid chloride nitrite pyridine thioether complexes, 977
cobalt(III) arginine hydroxide complexes, 2717
cobalt(III) hydroxide peroxide tetramine complexes, 107
cobalt(III) ketoimine complexes, 1687
cobalt(III) oxalate complex, 2665
copper diiminate iodide complexes, 955
copper(I) chloride phosphine thione complexes, 935
copper(I) phosphine thio heterometallic complexes, 2743
copper(I) tetramine macrocyclic complexes, 1373
copper(II) acetate dipyridyl halide hydroxide complexes, 2301
copper(II) acetate pyridine complexes, 793
copper(II) alkoxide aluminium complexes, 1733
copper(II) azole carboxylate halide hydroxide nitrate complexes, 1333
copper(II) azole carboxylate salicylaldimine complexes, 893
copper(II) chloride diimine complexes, 2541
copper(II) chloride dimethylphosphite ruthenium(II) complex, 1091
copper(II) chloride phenoxide Schiff base complexes, 731
copper(II) chromate diimine complexes, 2179
copper(II) creatinine methoxide complexes, 1767
copper(II) dehydropeptide complexes, 2331
copper(II) diamine diketonate complexes, 1773
copper(II) diaminooxamide cobalt(II) complexes, 1787
copper(II) diaminopyridine halide nitrate water complexes, 1675
copper(II) diimine pyridine Schiff base thiolate complexes, 1327
copper(II) diimine pyridine-*N*-oxide dithiocarbazate complexes, 1363
copper(II) dipyridyl saccharinate complex, 403
copper(II) halide complexes, 2529
copper(II) halide nitrate quinoline - thioether water complexes, 1579
copper(II) ketoimine complexes, 1687
copper(II) ketoimine pyridine thiolate complexes, 535
copper(II) pyridine thioether complex, 1647
copper(II) tetramine complexes, 883
copper(II) tetramine macrocyclic complexes, 523,1373
copper(II) thio water molybdenum complex, 2351
disilacyclobutanediimines, 1147
ferrocenes, 1741
germoxy radicals, 2347
gold(III) chloride, 633
hydrazinium complexes, 365
iron(II) cyanide nitrile ruthenium(II) complex, 653
iron(III) azide porphyrin complex pyrolysis products, 373
iron(III) chloride diazoleaminophenoxide methanol thiocyanate water complexes, 1809
iron(IV) dithiolate complexes, 1803
lanthanide amidopyridine nitrate perchlorate thiocyanate water complexes, 2405
lanthanide carboxylate water complexes, 1921
lanthanide chloride hydrazone phenanthroline water complexes, 1491
lanthanide disulphoxide perchlorate complexes, 629
lanthanide hydrazone complexes, 2185
lanthanide hydrazone water complexes, 2779
lanthanide nitrate sexadentate Schiff base water complexes, 683
macrocyclic tetraimine complexes, 2785
manganese(II) quinizarine complexes, 1929
manganese(IV) dithiolate complexes, 1803
methyl salicylate on clay minerals, 567
molybdenum chloride hydride nitrosyl complex, 429
molybdenum(II) acetate aryliminoisoindoline complexes, 229
molybdenum(II,III,III) hydride iodide phosphine tetrahydrofuran complexes, 2145
molybdenum(III) azole halide thiocyanate complexes, 323
molybdenum(III,IV) acetate dithiophosphate oxo thio complexes, 2203
molybdenum(III,IV) thio water copper(II) complex, 2351
molybdenum(V) chloride diphosphine oxo complex, 1459
molybdenum(V) dithiolate thio copper(I) complex, 2743
nickel(II) alkoxide chloride aluminium complexes, 1733
nickel(II) aryl dithiocarbamate dithiocarbonate xanthate complexes, 2821
nickel(II) azole chloride pseudohalide pyridine pyridine-*N*-oxide-dithiocarbazates, 2659
nickel(II) azole thiocyanate thioether complex, 1031
nickel(II) diamine dihydrazone

diimine complexes, 859
nickel(II) diimine pyridine Schiff base thiolate complexes, 1327
nickel(II) dithiocarbamate triamine complexes, 2025
nickel(II) halide pyridine thiocyanate complexes, 1759
nickel(II) ketoimine complexes, 1687
nickel(II) ketoimine pyridine thiolate complexes, 535
osmium(III) chloride phosphine quinone complex, 2511
palladium(II) chloride hydrazinium complex, 579
palladium(II) chloride phenoxide telluroether complexes, 2693
platinum(II) chloride hydrazinium complex, 579
platinum(II) diamine complexes, 2191
platinum(IV) diamine halide complexes, 2191
potassium crown ether - gold chloride complexes, 1025
pyridylcarbinol complexes, 2809
rhenium(II,III,III) chloride sulphate complex, 741
rhodium(III) hydride tin(II) complex, 1721
ruthenium halide hydroxyquinoline nitrosyl complexes, 583
ruthenium(II) ammonia crown ether pyridine complexes, 1139
ruthenium(II) ammonia cyanopyridine dipyridyl pyridine iron(II) complexes, 653
ruthenium(II) chloride hydrazide phosphine complexes, 2137
ruthenium(II) chloride pyrazine sulphoxide complex, 1699
ruthenium(II) diimine complexes, 1485
ruthenium(II,III) ammonia cyanopyridine dipyridyl pyridine iron(II) complexes, 653
ruthenium(III) aminophenoxide arsine halide hydroxyquinoline complexes, 2137
ruthenium(III) ammonia crown ether pyridine complexes, 1139
ruthenium(III) arsine chloride quinone complex, 2511
ruthenium(III) ascorbate chloride water complex, 2711
ruthenium(III) azole carbonyl chloride phenoxide Schiff base complexes, 2559
ruthenium(III) edta nucleoside complexes, 2465
sexadentate salicylaldimine thioether complexes, 823
terbium(IV) phosphate water complex, 1479
thallium halide porphyrins, 885
trifluoromethanesulphonates, 2757
tungsten(V) dithiolate thio copper(I) complex, 2743
tungsten(V) oxo thio xanthate complexes, 2235
tungsten(VI) bromide diphosphine seleno complexes, 1311
uranium(VI) carboxylate dioxo hydrazone phenoxide pyridine water zinc complexes, 779
vanadate hydrolysis, 249
Endothall complex
calcium, 1569
Enolate complexes
palladium(II), 1521
Enol ether complexes
silicon, 1173
Enthalpy of activation
absorption of methyl salicylate on clay minerals, 567
addition reactions, cobalt(I) carbonyl cyclopentadienyl and carbene precursor,725
alkene hydrogenation catalysed by Ru(II) complex, 2729
chromium(III) hydroxide water complexes interconversion, 619,1865
complexation, copper(II) acetate pyridine complexes, 793
complexation, ruthenium(III) ascorbate chloride water complex, 2711
complex dissociation, iron(II) - diimines, 703
fluxional behaviour, cadmium, zinc Schiff base thiolate complexes, 771
fluxional behaviour, iron(II) carbonyl hydride phosphite silyl complexes, 841
fluxional behaviour, rhenium(I) carbonyl halogen phosphino-thioether complexes, 1603
hydrolysis and ionization, fluorophosphorous acid, 1695
redox, carbonyls - O^-, 2487
redox, platinum(II) - platinum(IV) complexes, 2191
solvent extraction, potassium crown ether - gold chloride complexes ion pair, 1025
substitutions, cobalt(III) porphyrin water ccomplex, 1379
vanadate dimerization, 249
Enthalpy of formation
metal halides, 1433
uranium(VI) oxo phosphate complexes, 47
Enthalpy of vapourization
gold(III) chloride, 633
Entropy of activation
addition reactions, cobalt(I) carbonyl cyclopentadienyls and carbene precursor, 703
alkene hydrogenation catalysed by Ru(II) complex, 2729
chromium(III) hydroxide water complexes interconversion, 619,1865
complexation, copper(II) acetate pyridine complexes, 793
complexation, ruthenium(III) ascorbate chloride water complex, 2711
complex dissociation, iron(II) - diimines, 703
fluxional behaviour, cadmium,

zinc Schiff base thiolate complexes, 771
fluxional behaviour, iron(II) carbonyl hydride phosphite silyl complexes, 841
fluxional behaviour, rhenium(I) carbonyl halogen phosphino-thioether complexes, 1603
hydrolysis and ionization, fluorophosphorous acid, 1695
redox, platinum(II) - platinum(IV) complexes, 2191
substitutions, cobalt(III) porphyrin water complex, 1379
vanadate dimerization, 249
Entropy of formation
uranium(VI) oxo phosphate complexes, 47
Entropy of vapourization
gold(III) chloride, 633
Entwined complexes
cobalt(II) chloride phenanthroline, 811
Erbium
amidopyridine nitrate thiocyanate complexes, 2405
carboxylate water complexes, 1921
chloride hydrazone phenanthroline water complex, 1491
disulphoxide perchlorate complex, 629
hydrazone complexes, 2185
hydrazone water complex, 2779
lactam nitrate mercury complex, 1079
ESR spectra
boric acid catecholate oxidised complexes, 613
chromium carbonyl cyclopentadienyl dioxygen seleno complexes, 591
chromium(VI) - copper(II) irradiated mixture, 237
cobalt(II) acetate quinquepyridine complex, 1395
cobalt(II) diimine oxamide copper(II) complexes, 1787
cobalt(II) phenanthroline complex, 1803
cobalt(II) triphosphine triphosphorus complex, 2123
copper diiminate iodide complexes, 955
copper iodide tetraazaannulene complexes, 1911
copper(II) aminoalkylsalicyl-aldimine complexes, 1653
copper(II) azole carboxylate salicylaldimine complexes, 893
copper(II) bromide hexamine water binucleating complex, 941
copper(II) chloride diimine complexes, 2541
copper(II) chloride dimethyl-phosphite Ru(II) complex, 1091
copper(II) chloride dipyridylamine water complex, 495
copper(II) chloride phenoxide Schiff base complexes, 731
copper(II) chromate diimine complexes, 2179
copper(II) creatinine methoxide complexes, 1767
copper(II) dehydropeptide complexes, 2331
copper(II) diaminooxamide cobalt(II) complexes, 1787
copper(II) diimine pyridine Schiff base thiolate complexes, 1327
copper(II) ketoimine pyridine thiolate complexes, 535
copper(II) ketoxime complexes, 919
copper(II) sulphonates, 2757
copper(II) tetramine macrocyclic complexes, 523
iridium(IV) mesityl, 1457
iron halide phosphine seleno thio thiolate complexes, 203
iron sexadentate amine complex, 763
manganese(IV) dithiolate complex, 1803
molybdenum(III,IV) acetate dithiophosphate oxo thio complexes, 2203
nickel dithiolate - dithiapyr-anylidene complex, 687
nickel(III) dithiocarbamate triamine complexes, 2025
osmium(III) chloride phosphine quinone complex, 2511
polysilanes doped with AsF_5, 1227
rhodium(I,II) carboxylate chloride diimine complexes, 2551
rhodium(II) hydride phosphine complex, 2729
ruthenium(III) aminophenoxide arsine halide hydroxyquinoline complexes, 2137
ruthenium(III) arsine chloride quinone complex, 2511
ruthenium(III) azole carbonyl chloride phenoxide Schiff base complexes, 2559
ruthenium(III) chloride pyridylphosphonate zinc complexes, 2229
tungsten(V) chloride diphosphine complex, 595
Ester complexes
tin(IV), 1085
Ethane-1,2-dithiolates
molybdenum(V), tungsten(V), 2743
Ethanol complexes
bismuth(III), 2617
niobium(II,III), 2031
sodium, 2617
tantalum(II,III), 2031
tungsten(VI), 2617
Ethenyl complexes
ruthenium(II), 421
Ether complexes
astatine(I), 11
bismuth, 437
caesium, 221
calcium, 1565,1569
gadolinium, 1889
gallium(II), 95
lithium, 2699

magnesium, 2457
molybdenum(II,III,III), 2145
molybdenum(V), 2457
potassium, 2699
rhodium(III), 1611
rubidium, 221
sodium, 1877,2641
tungsten(V), 2089
tungsten(VI), 2417
yttrium, 1049
Ethoxides
aluminium, 1733
bismuth(III), 2617
cobalt(II), copper(II), 1733
lead(II), 1657
nickel(II), 1733
silicon, 1097
sodium, tungsten(VI), 2617
4-Ethoxycarbonylaminopyridine-*N*-oxide complexes, thorium, 2809
Ethyls
silicon, 1231
Ethylacetoacetate complexes
palladium(II), 1513
Ethylenediamine complexes
copper(II), 1773
europium, 1385
molybdenum(VI), 2057
nickel(II), 859
platinum(II),(IV), 2191
Ethylenediaminetetraacetates
ruthenium(III), 2465
Ethyldithiocarbamates
nickel(II), 2821
1-Ethylimidazole complexes
molybdenum(VI), 33
2-Ethylimidazole complexes
copper(II), 893
2-Ethyl-4-methylimidazole complexes, Cu(II), 893
Ethyl sulphide complexes
gallium(II), 95
4-Ethyl-2,6,7-trioxa-1-phosphabicyclo[2.2.2.]octane complexes
ruthenium(II), 2265
Ethyl xanthates
nickel(II), 2821
ruthenium(II), 1019
tungsten(V), 2235
Europium
acetate amine carbonate diamine diimine pyridine Schiff base macrocyclic complexes, 1385
amidopyridine nitrate perchlorate thiocyanate water complexes, 2405
chloride hydrazone phenanthroline water complexes, 1491
hydrazone complexes, 2185
EXAFS, sulphonates, 2757
Extended Hueckel calculations
iron carbonyl hydride phosphide heterometallic complexes, 2423
ruthenium(III) azole carbonyl chloride phenoxide Schiff base complexes, 2559

F

Feldspar glass, 55
Ferrocenes
alkyl silyl, 1741
book review, 1844
Ferrocenecarbonylhydrazone complexes, lanthanides, 1491
Fluorenone complexes
tungsten(V), 2089
Fluorenyl complexes
germanium, 1153
tungsten(IV), 459
Fluorenylidene complexes
germanium, 1153
Fluorescence spectra
europium amidopyridine nitrate perchlorate thiocyanate water complexes, 2405
lanthanide carboxylate water complexes, 1921
ruthenium(II) diimine complexes, 1485
Fluorides and fluoro complexes
boron, 2221
electrochemical synthesis, 2605
germanium, 1153
rhenium(V,VI), 2241
thallium(III), 885
2-Fluorobenzoate complexes
samarium, ytterbium, 1599
Fluorophosphorous acid, 1695
Fluxional behaviour
cadmium, zinc Schiff base thiolate complexes, 771
copper(I) diene diketonate complexes, 2293
iridium(III) chloride phosphine complexes, 1857
iron(II) carbonyl hydride phosphite silyl complexes, 841
platinum(IV) metallacyclic compounds, 1587
rhenium(I) carbonyl halogen phosphinothioether complexes, 1603
sodium crown amide ether complex, 1877
thallium(III) acetate porphyrin, 2069
Formate complexes
rhodium(I,II), 2551
Formation constants
aluminium polyphosphates, 1527
astatine(I) halide chelate complexes, 11
caesium crown complexes, 221
calcium carboxylate crown ether complexes, 1591
cobalt(III) ammonia molybdate complex, 2317
cobalt(III) diketonate phenol complexes, 1405
copper(II) dehydropeptide complexes, 2331
copper(II) halide complexes, 2529
copper(II) ketoxime complexes, 919
copper(II) pyridine thioether complexes, 1647
copper(II) tetramine complexes, 883
molybdenum(VI) doxycycline complexes, 455
nickel(II) ketoxime complexes, 919

phosphate anions, 2587
potassium carboxylate crown complexes, 1591
rubidium crown complexes, 221
sexidentate amine complexes, 409
sodium carboxylate crown complexes, 1591
thallium(III) methyl thiobarbiturate complexes, 517
tin(II),(IV) pyrophosphate complexes, 377
tin(IV) alkyl aryl iodide pyridine complex, 1085
tungsten(VI) doxycycline complexes, 455
uranium(VI) oxo phosphate complexes, 47
Free energy of activation
alkene hydrogenation catalysed by Ru(II) complex, 2729
alkylamide M - N bond rotation, 2839
complexation, ruthenium(III) ascorbate chloride water complex, 2711
fluxional behaviour, Cd, Zn Schiff base thiolate complexes, 771
fluxional behaviour, copper(I) diene diketonate complexes, 2293
fluxional behaviour, iridium(III) chloride phosphine complexes, 1857
fluxional behaviour, iron(II) carbonyl hydride phosphite silyl complexes, 841
fluxional behaviour, rhenium(I) carbonyl halogen phosphino-thioether complexes, 1603
fluxional behaviour, thallium(III) acetate porphyrin, 2069
hydrolysis, fluorophosphorous acid, 1695
hydrolysis, polyphosphate, 697
vanadate dimerization, 249
Free energy of formation
uranium(VI) oxo phosphate complexes, 47
Fuller's earth, 567

G

Gadolinium
amidopyridine nitrate perchlorate thiocyanate complexes, 2405
chloride hydrazone phenanthroline water complex, 1491
crown ether thiocyanate water complex, 1889
disulphoxide perchlorate complex, 629
hydrazone complexes, 2185
hydrazone water complexes, 2779
Gallium(II)
ether iodide phosphine thioether complexes, 95
Gallium(III)
alkyl amine arylamide complexes, 1897
bromide sulphonates, 2757
triamine complex, 1951
Gel filtration chromatography, ^{105}Rh complex incorporation into globulin, 1617
Germanium
alkoxide alkyl aryl carbene fluoride complexes, 1153
alkyl aryl oxo compounds and radicals, 2347
chalcogenide silylamide compounds, 1203
cluster structures, molecular orbitals, 1299
hydride propellanes, 1247
methyl metallacyclic compounds, 1221
Germenes, 1153
Germyls
molybdenum(II), 2519
tungsten(III), 1215
Glycine complexes
cobalt(III), 977
Glycine Schiff base complexes
copper(II), 893
Glycolates
osmium(VI), 61
Gold(I)
aryls, 145,160,167
phosphine iron(0) complex, 2423
Gold(III)
aryls, 145,160
bromide chloride phosphine complexes, 1929
chloride, 633
chloride complex, 1025
chloride diamine complexes, 19
chloride iminoether complexes, 1631
Guanosine complex
ruthenium(III), 2465

H

Hafnium
chloride cyclopentadienyl disylylmethyls, 1177
Halides, enthalpies of formation, 1433
Herbicide complexes
calcium, 1569
2,4-Hexadiene complexes
zirconium, 1
Hexafluoropentanedionates
copper(I), 645,2293
molybdenum(II), 605
Hexagonal bipyramidal complexes, interligand repulsions, 393
Hexamethylbenzene complexes
ruthenium(II), 1091
Hexamethylphosphoramide complexes
iron(II), 1163
Hexaphosphates
aluminium, 1527
HFS calculations
copper(II) tetramine macrocyclic complexes, 523

High temperature chemistry, book review, 2851
Holmium
amidopyridine nitrate thiocyanate complexes, 2405
chloride hydrazone phenanthroline water complexes, 1491
disulphoxide perchlorate complex, 629
hydrazone complexes, 2185,2779
HPLC
ruthenium(II) chloride pyrazine sulphoxide complexes, 1699
selenium(II) chloride thiochloride, 1037
Hydrazide complexes
molybdenum(IV), 467
ruthenium(II), 2137
Hydrazine, hydrazinecarboxylate complexes, iron(II), 483
Hydrazinium complexes
Co, Cu, Fe, Ni, 365
Pd(II), Pt(II), 579
Hydrazone complexes
lanthanides, 1491,2185,2779
manganese(II), 2477
silver(I), 127
uranium(VI), 779
Hydride complexes
cobalt(II), 2123
iron(0,I), 2423
iron(II), 841
molybdenum, 429,2145
osmium, 1955
platinum(II), 867,909
rhodium(I), 543
rhodium(II), 2729
rhodium(III), 1721
ruthenium, 1955
ruthenium(II), 1019,1713
silicon, 1173
tungsten(II), 595
tungsten(IV), 595,1007,2827
Hydrosilation, enantioselective of acetophenone, 1061
Hydrotrispyrazolylborates
iridium(I), 1595
tungsten(IV), 215
Hydroxamates
silicon, 1131
Hydroxides and hydroxo complexes
chromium(III), 619,2389
cobalt(III), 107,2717
copper(II), 1333,2301
iron(III), 1121
palladium(II), 1507
platinum(II), 799,1473
tin(IV), 509
yttrium, 2171
Hydroxycarboxylates
cobalt(III), 2495
osmium(VI), 61
2-Hydroxyethanethiol complexes
chromium(III), 2255
N-Hydroxyethylsalicylidene-imine complexes, Mo(VI), 33
Hydroxyketone complexes
silicon, 1131
2-Hydroxynaphthaldehyde Schiff base complexes
Cu, Ni, 1327
Th, U, 2399
2-Hydroxy-1,4-naphthaquinone complexes, Mo,Os,Ru,U, 2511
8-Hydroxyquinoline complexes
copper(II), 1791
ruthenium, 583
ruthenium(III), 2137
8-Hydroxyquinoline-*N*-oxide complexes, silicon, 1131

I

Imidazole complexes
copper(II), 893
molybdenum(III), 323
molybdenum(VI), 33
nickel(II), 1031,2659
palladium(II), 1513
ruthenium(III), 2559
tungsten(II), 711
Iminodiacetate complexes
vanadium(IV), 73
Iminoether complexes
gold(III), 1631
platinum(II),(IV), 1573
Iminyls
silicon, 1147
Indenyl complexes
tungsten(II), 1177
tungsten(IV), 459
Indium
bromide polysulphide complex, 1069
triamine complex, 1951
Inosine complexes
ruthenium(III), 2465
Iodides and iodo complexes
cadmium, 2111
copper, 955,1911
gallium(II), 95
iron, 203
iron(II), 963
mercury, 351,2611
molybdenum(0), 2611
molybdenum(II), 433
molybdenum(II,III,III), 2145
molybdenum(III), 1667
nickel(II), 823,1759
niobium(0), 389
palladium(II), 2265
platinum(II), 747,909,1443
rhenium, 1903
rhenium(I), 1603
rhenium(II), 1873
ruthenium(II), 963
thorium, 2399
tin(IV), 1085
tungsten(II), 433
uranium(VI), 2399
Iodoalkane complexes
rhenium, 1903
2-Iodobenzoates
lanthanides, 1599
Ion cyclotron resonance spectroscopy, carbonylate anions, 2487
Ion mobility
astatine (I) halide chelate complexes, 11
Ion pairs
potassium crown ether - gold chloride complexes, 1025

IR spectra
acyls, 1705
alcohol complexes, 1049,2031, 2065
alcohol solvate, 2045
alkenyl complexes, 421
alkoxides, 949,1733,2065,2309
alkyls, 1411,1465
alkylamides, 477
alkylammonium salt, 2057
alkyne complexes, 711,1427,2519
allyls, 459,605
amide complexes, 403,1683,1877, 2075,2265,2809
amidopyridine complexes, 2405
amine complexes, 243,477,823, 859,1653,1675,1897,2025,2309
aminoacid complexes, 333
aminophenoxides, 2137
ammines, 653,2075,2317
arylamides, 1897,2309
arylimides, 1539
azides, 1513,2659,2725
azole complexes, 323,711,1031, 1333,1767,2559
binuclear complexes, 997
binucleating hydroxyketone complexes, 1353
borohydride, 1827
bromides, 351,1311,1507,1579, 1939,2137,2265,2541
carbonyls, 133,187,215,267,389, 421,543,665,673,711,725,837, 877,963,1013,1019,1163,1177, 1319,1549,1595,1603,1663,1705, 1713,1717,1873,2095,2153,2265, 2423,2559,2611
carboxylates, 121,133,187,779, 1333,1599,1657,1723,1809,2273, 2283,2301,2523,2573
chlorides, 351,561,595,731,789, 949,997,1013,1019,1311,1507, 1573,1579,1631,1675,1699,1939, 2065,2089,2137,2217,2265,2337, 2457,2501,2511,2541,2559,2573, 2659,2683,2693
chromates, 2179
creatinine complexes, 1767
cyanides, 1013,2611
cyanotrihydroborate complexes, 79
cyclopentadienyls, 27,1847
diamine complexes, 1773,2057
diaminodisulphide complexes, 1319
diarylphosphates, 2771
diazenides, 1539
dicarboxylates, 61
diimine complexes, 653,859,1363, 2171,2179,2541
diketonates, 437,605,1683,1773, 2463
diselenide complexes, 1311
disulphide complexes, 997
disulphoxides, 629
dithiocarbamates, 421,1019,1513, 1817,2025,2821
dithiocarbazates, 37,1363,2659
dithiocarbonates, 2821
dithiolates, 1803,2813
dodecahydrododecaborates, 2779
edta complexes, 2465
ester complexes, 1085
ether complexes, 95,1049,2417, 2457
gallium(II) compounds, 95
hexafluorophosphates, 79,495
hydrates, 653,1507,1779,2301, 2779
hydrazide complexes, 467,2137
hydrazinium complexes, 365,579
hydrazone complexes, 127,779, 1491,2185,2477,2779
hydrides, 429,543,595,1019,1713, 2729
hydroxides, 1333,2171,2301
hydroxycarboxylates, 61
hydroxyketone complexes, 1353
imine complex, 2051
iminoether complexes, 1573,1631
iodides, 95,351,2265
isocyanide complexes, 267
ketoimine complexes, 535,1327, 1687
ketone complexes, 1779
maltol complexes, 1539
mercaptothiazolinate, 325
metallaboranes, 1663
methyl salicylate on clay minerals, 567
molybdates, 2317
nitrates, 683,1579,1675,1809, 2399,2405,2567,2809
nitrile complexes, 79,595,653, 1513,1717,2131,2241,2519
nitrogen - sulphur complexes, 2337
nitroimidazole complexes, 1333
nitrophenoxides, 27
nitrosophenoxides, 27
nitrosyls, 429,583,1013
nucleoside complexes, 2465
oxamide complexes, 103,1787
oxo complexes, 33,61,243,477, 753,819,973,997,1353,1683, 2057,2203,2235,2399,2417,2457, 2511,2567,2813
penicillin complexes, 1473
perchlorates, 103,629,1579,1675, 1809,1835,2025,2317,2399,2405, 2659
peroxo complexes, 819,973
phenol complex, 2683
phenoxides, 731,779,789,1653, 1847,2693
phosphine complexes, 543,673, 1411
phosphiniminates, 2241
phosphinoenolates, 1521
phosphinothiolate, 1019
phosphonates, 2229
phosphorus - selenium compound, 261
polyketones, 993
polysulphides, 1069,2501
pyrazine complexes, 1699
pyrimidinethione complexes, 1507
pyridine complexes, 535,653,683, 1579,1675,2089
pyridine-*N*-oxide complexes, 37, 1363,2651,2659,2809
pyridinethionates, 197
quinone complexes, 2511
quinquepyridine complexes, 1395
rhodanine complexes, 1465
saccharin complexes, 403

Schiff base, 2683
Schiff base complexes, 33,37, 683,731,819,823,859,973,1327, 1653,2399,2559,2785
siloxides, 1367,2699
sulphate, 649
sulphonates, 2241,2757
sulphoxide complexes, 1699,2075, 2567
telluroether complexes, 2693
tetraazaannulene complexes, 1911
tetracyanoethene complexes, 725
tetrafluorobrates, 1779
tetramine complexes, 523
tetrafluoroborates, 79
tetraimine complexes, 2785
tetraphenylphosphonium salt, 2501
thio complexes, 997,2203,2235, 2743,2813
thiocarbonyls, 1019
thiocarboxylates, 2095
thiocyanates, 323,1031,1809, 2399,2405,2463,2567,2611,2659, 2725,2809
thioether complexes, 95,823, 1031,1579
thiolates, 535,753,973,1327,2651
thione complexes, 351,935,1507
water complexes, 187,495,683, 1579,1675,1809,2171,2771
xanthates, 421,1019,2235,2821

Iridium(I)
alkene carbonyl diene hydropyrazolylborate tripyrazolylamine complexes, 1595

Iridium(III)
chloride phosphine complexes, 1857

Iridium(IV)
mesityl, 1457

Iron
halide phosphine seleno thio thiolate complexes, 203
organo compounds, book reviews, 1845,2086

Iron(-I)
carbonylate anions, 2487

Iron(0)
aryls, 154
carbonyl cyclopentadienyl bismuth complex, 123
carbonyl cyclopentadienyl tin complexes, 2105
carbonyl phosphide heterometallic complexes, 543,2423
carbonyl phosphide rhodium(I) complexes, 543
tetracarbonyl, fluxionality, 1587

Iron(0,I),(I)
carbonyl hydride phosphide complexes, 2423

Iron(II)
acyl aryl carbonyl cyclopentadienyl phosphine sulphinyl complexes, 717
alkanediyl alkene carbonyl cyclopentadienyl halide phosphine sulphinate complexes, 963
alkoxide carbonyl phosphine oxide silylene thiolate complexes, 1163
alkyl carbonyl cyclopentadienyl silyl complexes, 1177
arsine carbonyl cyclopentadienyl phosphine stibine thiocarboxylate complexes, 2095
aryls, 142,154,166
carbonyl hydride phosphite silyl complexes, 841
carboxylate hydrazine complex, 483
chloride hydrazinium water complex, 365
chloride sulphate tetraimine macrocyclic complexes, 2785
cyanide nitrile ruthenium(II) complex, 653
cyclopentadienyls, 483,1741
diarylphosphate methanol water complexes, 2771
diimine complexes, 703,1803
pyridylcarbinol complexes, 2791
sexidentate amine complexes, 409,763

Iron(II,III)
fluoride water complex, 2605

Iron(III)
aryls, 154
azide porphyrin complex, 373
chloride diazoleaminophenoxide methanol thiocyanate water complexes, 1809
cyclopentadienyls, 1741
fluoride complex, 2605
hydroxide hydroxyketone binucleating complexes, 1353
hydroxide oxide, 1121
pyridine-*N*-oxide thiolate, 2651
sexidentate amine complexes, 763
trifluoromethanesulphonate, 2757

Iron(IV)
dithiolate complexes, 1803

Isocyanide complexes
iron(II), 963
molybdenum(0), 267
rhodium(I), 2153
tungsten(0), 267

Isoleucine complexes
cobalt(III), 977

Isonicotinamide complexes
ruthenium(II), 1139

Isopolytungstate, 649

J

Jahn - Teller effect, permutational isomerism, 1587

K

Ketoimine complexes
cobalt(III), 1687
copper(II), 535,1687
nickel(II), 535,1687,2833

Ketone complexes
mercury, 351
tungsten(V), 2089

Ketoxime complexes
copper(II), nickel(II), 919

Kinetic studies
addition reactions, cobalt(I) carbonyl cyclopentadienyls and carbene precursor, 725
chromium(III) hydroxide water complexes interconversion, 619
complexation, cobalt(III) ammonia molybdate complex, 2317
complexation, copper(II) amino-(hydroxymethyl)pyridine hydroxyquinoline complexes, 1791
complexation, ruthenium(III) ascorbate chloride water complex, 2711
complex dissociation, iron(II) - diimines, 703
fluxional behaviour, cadmium, zinc Schiff base thiolate complexes, 771
fluxional behaviour, iron(II) carbonyl hydride phosphite silyl complexes, 841
fluxional behaviour, rhenium(I) carbonyl halogen phosphino-thioether complexes, 1603
fluxional behaviour, thallium(III) acetate porphyrin, 2069
hydrolysis, chromium(III) hydroxide water complexes, 1865,2389
hydrolysis, diketonates, 753
hydrolysis, polyphosphates, 697
isomerization, platinum(II) azole halide complexes, 1443
photochemistry, cobalt(III) hydroxide peroxide tetramine complexes, 107
photochemistry, germanoxanes, 2347
redox, carbonyls - O^-, 2487
redox, cobalt(III), ruthenium(II,III) - $Ti(C_2O_4)_2^-$, 829
redox, copper(II) pyridine thioether complex - ferrocene, 1647
redox, molybdenum(V) - solvated electron, 1459
redox, molybdenum(V) - vanadium(V) oxo complexes, 359
redox, ozone - terbium(III), 1479
redox, platinum(II) - platinum(IV) complexes, 2191
substitution, cobalt(III) chloride pentamine complex, 1449
substitution, cobalt(III) porphyrin water complex, 1379
substitution, molybdenum thio water heterometallic cubane complexes, 2351

L

Lactam complexes
erbium, mercury, 1079
Lactates
osmium(VI), 61
Lanthanides
amidopyridine nitrate perchlorate thiocyanate water complexes, 2405
aryls, 136,147,162
carboxylate chloride cyclopentadienyls, 1599
carboxylate water complexes, 1921
chloride hydrazone phenanthroline water complexes, 1491
cyclopentadienyl nitrophenoxide nitrosophenoxide complexes, 27
disulphoxide perchlorate complexes, 629
hydrazone complexes, 2185
hydrazone water complexes, 2779
nitrate sexadentate Schiff base water complexes, 683
Lanthanum
alcohol alkoxide complexes, 1049
alkoxide chloride zirconium compounds, 949
amidopyridine nitrate perchlorate thiocyanate water complex, 2405
chloride hydrazone phenanthroline water complex, 1491
disulphoxide perchlorate complex, 629
hydrazone water complex, 2779
nitrate sexadentate Schiff base water complex, 683
Lawsone complexes
Mo(VI), Os(III), Ru(III), U(VI), 2511
Lead
cluster structures, molecular orbitals, 1299
organo compounds, book review, 1963
Lead(II)
alcohol alkoxide carboxylate oxide compounds, 1657
alkoxides, 1103
sexidentate amine complex, 409
Leucine complexes
cobalt(III), 977
Ligand synthesis
aminophosphines, 501,2737
benzil Schiff base, 973
binucleating hydroxyketone, 1353
carboxylates, 2273
diaminopyridine, 1675
diazoleaminophenol, 1809
diphosphines, 1713,2381
N-fluoroarylethanediamines, 747
hydrazone, 2477
iminoether, 1631
ketoimine tetradentates, 2833
macrocyclic tetramines, 523
methoxyiminodiacetate, 73
phenol, 2683
phosphinoamines, 501,2737
phosphinoaminophenoxide, 243
salicylaldimine sexadentates, 823
salicylaldimine tetradentates, 819
tellurophenols, 2693
Lithium
alkoxides, 805
ether siloxide complexes, 2699

oxides in feldspar glass, 55
polyphosphates, 67
Lutetium
chloride hydrazone phenanthroline water complex, 1491
hydrazone complexes, 2185
phosphonate complex, 175

M

Macrocyclic complexes
cobalt(II), 1779,2785
cobalt(III), 1779
copper(II), 523,1373,2785
europium, 1385
iron(II), 2785
nickel(II), 103
Magnesium
chloride ether oxo molybdenum(V) complexes, 2457
terpyridyl complex, 1883
Magnetochemistry
binucleating hydroxyketone complexes, 1353
chromium(II) chloride diimine complexes, 2541
chromium(III) alkoxythiolate complex, 2255
cobalt(II) acetate quinquepyridine complex, 1395
cobalt(II) alkoxide chloride aluminium complexes, 1733
cobalt((II) azole carboxylate chloride complexes, 1333
cobalt(II) chloride phenanthroline entwined complexes, 811
cobalt(II) diimine oxamide copper(II) complexes, 1787
cobalt(II) diphosphine thiolate complexes, 553
cobalt(II) phenanthroline complex, 1803
cobalt(II) tetramine macrocyclic complexes, 1779
cobalt(II) triphosphine triphosphorus complex, 2123
copper diiminate iodide complexes, 955
copper iodide tetraazaannulene complexes, 1911
copper(II) alkoxide aluminium complexes, 1733
copper(II) amine halide salicylaldimine thioether complexes, 823
copper(II) amine oxamide nickel(II) complexes, 103
copper(II) aminoalkylsalicylaldimine complexes, 1653
copper(II) azole carboxylate halide hydroxide nitrate complexes, 1333
copper(II) bromide hexamine water binucleating complex, 941
copper(II) carboxylate dipyridyl halide hydroxide complexes, 2301
copper(II) chloride diimine complexes, 2541
copper(II) chloride phenoxide Schiff base complexes, 731
copper(II) creatinine methoxide complexes, 1767
copper(II) diamine nitrate complex, 2225
copper(II) diaminooxamide cobalt(II) complexs, 1787
copper(II) diaminopyridine halide nitrate water complexes, 1675
copper(II) diazoleaminophenoxide complexes, 1809
copper(II) diimine pyridine Schiff base thiolate complexes, 1327
copper(II) halide nitrate quinoline - thioeher water complexes, 1579
copper(II) ketoimine pyridine thiolate complexes, 535
copper(II) salicylaldiminate, 2051
copper(II) tetramine macrocyclic complexes, 523
hydrazinium complexes, 365
iron halide phosphine seleno thio thiolate complexes, 203
iron(II),(III) sexadentate amine complexes, 763
iron(IV) dithiolate complex, 1803
lanthanide amidopyridine nitrate perchlorate thiocyanate water complexes, 2405
lanthanide disulphoxide perchlorate complexes, 629
macrocyclic tetraimine complexes, 2785
manganese(IV) dithiolate complex, 1803
molybdenum(III) halide phosphine complexes, 1667
molybdenum(V) chloride ether oxo magnesium complexes, 2457
nickel(II) alkoxide chloride aluminium complexes, 1733
nickel(II) amine salicylaldimine thiocyanate thioether complexes, 823
nickel(II) azole thiocyanate thiether complex, 1031
nickel(II) diamine diimide oxamide tetramine copper(II) complexes, 103
nickel(II) dipyridylamine pseudohalide complexes, 2725
nickel(II) phenanthroline complex, 1803
nickel(II) pyridine-*N*-oxide-dithiocarbazates, 2659
ruthenium(III) azole carbonyl chloride phenoxide Schiff base complexes, 2559
ruthenium(III) chloride pyridylphosphonate zinc complexes, 2229
tungsten(II) acetonitrile aluminohydride chloride diphosphine hydride complexes, 595
tungsten(V) chloride diphosphine complex, 595
Malates

cobalt(III), 2495
Maleonitriledithiolates
molybdenum(V), 2813
Maltol complexes
rhenium(V),(VI), 1539
silicon, 1131
Mandelates
rhodium(I),(II), 2551
Manganese
coordination compounds, book review, 2086
Manganese(0)
carbonyl cyclopentadienyl complex, 2487
carbonyl diphosphinoferrocene complexes, 2437
Manganese(I)
acyl aryl carbonyl phosphine sulphinyl complexes, 717
Manganese(II)
aryls, 141,152,166
fluoride complex, 2605
hydrazone water complex, 2477
pyridine-*N*-oxide thiolate compounds, 2651
pyridylcarbinol complexes, 2791
quinazarine complexes, 1929
sexidentate amine complex, 409
Manganese(III)
aryls, 152
fluoride complex, 2605
Manganese(IV)
dithiolate complex, 1803
Mass spectra
aluminium alkoxide siloxides, 1639
binucleating hydroxyketone, 1353
cadmium mercaptothiazolates, 325
carbonylate anions, 2487
chromium(0) carbonyl diaminodisulphide complexes, 1319
cobalt(II) tetramine macrocyclic complexes, 1779
cobalt(III) pyridine tetramine macrocyclic complex, 1779
copper(II) diaminopyridine halide nitrate water complexes, 1675
copper(II) diarylphosphate, 2771
copper(II) diazoleaminophenoxide complexes, 1809
copper(II) salicylaldiminate, 2051
germanium alkoxide alkyl aryl carbene fluoride compounds, 1153
iron(II) aryl carbonyl cyclopentadienyl complexes, 717
iron(III) diazoleaminophenoxide complexes, 1809
lanthanide cyclopentadienyl nitrophenoxide nitrosophenoxide complexes, 27
lanthanum alcohol alkoxide complexes, 1049
lanthanum nitrate sexadentate Schiff base complex, 683
lead(II) alkoxide oxide compounds, 1657
lithium alkoxides, 805
magnesium terpyridyl complex, 1883
manganese(I) aryl carbonyl complexes, 717
mercury methyl phenyl rhodanine complexes, 1465
mercury thioether complex, 1545
molybdenum(0) carbonyl cycloheptatrienyl isocyanide complexes, 267
osmium(VI) hydroxycarboxylate oxalate oxo pyridine complexes, 61
palladium(II) phosphinoenolate, 1521
phosphorus - selenium cyclic compound, 261
rhenium(I) aryl carbonyl complexes, 717
ruthenium halide hydroxyquinoline nitrosyl complexes, 583
ruthenium(II) cyclopentadienyl diphosphine hydride complex, 1713
ruthenium(III) acetate oxo phosphine complex, 113
selenium - phosphorus cyclic compound, 261
selenium(II) chloride thiochloride, 1037
silicon tris-bidentate complexes, 1131
siloxanes, 1097
thallium methyl phenyl rhodanine complexes, 1465
tungsten(0) carbonyl cycloheptatrienyl isocyanide complexes, 267
yttrium alcohol alkoxide ether pyridine complexes, 1049
Mercaptoamine complexes
cadmium, 325
Mercury
alkoxide chloride telluroether complexes, 2065
carboxylate molybdenum(II) complexes, 133
chloride phenoxide phosphine telluroether complexes, 2693
cyanide phenyl thiocyanate ruthenium complexes, 1013
halide ketone thione complexes, 351
halide pseudohalide molybdenum(0) complexes, 2611
lactam erbium complex, 1079
methyl phenyl rhodanine complexes, 1465
phenyl trifluoroacetate rhodium(III) complexes, 187
thio complex, 41
thioether complex, 1539
Mesityls
germanium, 1153
iridium(IV), 1457
molybdenum(VI), 463
palladium(II), 2037
Mesitylphosphido complexes
rhenium(VII), 2241
Metallaboranes
molybdenum, tungsten, 1663
Metallacycles
germanium, 1221
tin(IV), 1203,1497
Methacrylates

copper(II), 1893
Methacrylonitrile complexes
B,Sb,Sn,Ti, 2131
Methanethiolates
palladium(II), 1343
Methanol complexes
cadmium, 2111
Co(II), Cu(II), Fe(II), 2771
Nb, Ta(II,III), 2031
Methoxides
copper(II), 1767
germanium, 1153
silicon, 1097
2-Methoxybenzoates
samarium, ytterbium, 1599
Methoxydimethylsilyls
molybdenum(IV), 1189
2-Methoxyethanol complexes
Bi, Mo(III), Na, W(VI), 2617
2-Methoxyethoxides
bismuth, 437,2617
Mo(VI), Na, W(VI), 2617
N-Methoxyiminodiacetate complexes
vanadium(IV), 73
3-Methoxy-3-methyl-2-butanone
oxime complexes, Rh(III), 1611
4-Methoxyphenoxides
arsenic(V), 789
Methyls
germanium, 1221,2347
mercury, 1465
molybdenum(II), 1705
phosphorus, 261
silicon, 1097,1227,1231
thallium(III), 517,1465
tin(IV), 1497,2683
tungsten(II), 1177
Methylamine complexes
cobalt(III), 2075
2-Methylbenzimidazole complexes
molybdenum(III), 323
Methylcyclopentadienyl complexes
iron(II), 963
manganese(0), 2487
niobium(III), 1075
tungsten(III), 459
zirconium, 2341
2-(3-Methyl-3,6-diazaheptyl)pyridine complexes, copper(II), 1675
Methyldiphenylphosphine complexes
iridium(III), 1857
iron(II), 963
manganese(I), 717
molybdenum(II), 665
molybdenum(IV), 467
platinum(II), 1411
ruthenium(II), 963
Methylethylenediamine complexes
molybdenum(II), 2573
platinum(II),(IV), 2191
Methylfluorenyls
germanium, 1153
1-Methylimidazole complexes
copper(II), 893
2-Methylimidazole complexes
copper(II), 893
molybdenum(III), 323
molybdenum(VI), 33
ruthenium(III), 2559
tungsten(II), 711
4-Methylimidazole complexes
tungsten(II), 711
Methylisocyanide complexes
iron(II), 963
molybdenum(0), 267
tungsten(0), 267
N-Methylmorpholine complexes
gallium(II), 95
2-Methylpent-4-enoates
molybdenum(II), 2283
4-Methylphenanthroline complexes
iron(II), 703
Methylphosphido complexes
osmium, 1955
2-Methylpropenoates
molybdenum(II), 2273,2283
ruthenium(II,III), 2273
1-Methyl-4-*i*-propylbenzene
complexes, ruthenium(II), 1727
6-Methylpyridine-2-thione
complexes, ruthenium(II), 837
N-Methylsalicylaldimine complexes
palladium(II), 1513
Methyl salicylate, absorption by
clays, 567
Methyl sulphide complexes
gallium(II), 95
(2-Methylthiophenyl)diphenylphosphine complexes
rhenium(I), 1603
Methylxanthate complexes
nickel(II), 2821
Metiamide complexes
nickel(II), 1031
Metronidazole complexes
platinum(II), 1443
Moessbauer spectra
ferrocenes, 1741
iron carbonyl hydride phosphide hetyerometallic complexes, 2423
iron halide phosphine seleno thio thiolate complexes, 203
iron(II),(III) sexadentate amine complexes, 763
iron(III) hydroxide hydroxyketone binucleating complexes, 1353
Molecular mechanics
copper dithiolene complex, 2377
copper(II) four coordination, 2079
Molecular orbitals
cluster compounds, group 14, 1299
copper(II) tetramine macrocyclic complexes, 523
iron carbonyl hydride phosphide heterometallic complexes, 2423
molybdenum(IV) chloride oxo thio trinuclear complexes, 2799
nickel(II) halide pyridine thiocyanate complexes, 1759
propellanes, 1247
ruthenium(III) azole carbonyl chloride phenoxide Schiff base complexes, 2559
silanes, 1265,1285
Molybdates
cobalt(III), 2317
Molybdenum
carbonyl phosphine polyhedral borane complex, 1663
chloride hydride nitrosyl complex, 429
Molybdenum(0)
carbonyl cycloheptatrienyl

isocyanide complexes, 267
carbonyl cyclopentadienyl bismuth complex, 123
carbonyl diimine diphosphine halide pseudohalide mercury complexes, 2611
carbonyl diphosphine complexes, 2381
carbonyl diphosphine thioether complexes, 1549
Molybdenum(II)
acetate aryliminoisoindoline complexes, 229
acetate diamine complexes, 2573
acetonitrile carbonyl diketonate iodide phosphine complexes, 433
acetyl carbonyl cyclopentadienyl methyl phosphine complexes, 1705
acyl carbonyl cyclopentadienyl complexes, 717
alkyne carbonyl chloride diimine germyl nitrile phosphine complexes, 2519
allyl diketonates, 605
aluminohydride diphosphine hydride complex, 595
arsine bismuthine carbonyl cyclopentadienyl diphosphine stibine complexes, 665
aryls, 151,165
bromide carboxylate nitrile complexes, 2283
carbonyl chloride nitrile phosphine tin(IV) complexes, 1717
carbonyl cyclopentadienyl mercury complexes, 133
carboxylates, 2273
Molybdenum(II,III,III)
hydride iodide phosphine tetrahydrofuran complexes, 2145
Molybdenum(III)
alkoxide alkylamide siloxide compounds, 2839
alkoxide amine arylamide complexes, 2309
azole halide thiocyanate complexes, 323
halide phosphine complexes, 1667
Molybdenum(III,IV)
acetate dithiophosphate oxo thio complexes, 2203
thio water copper(II) complex, 2351
Molybdenum(IV)
aryls, 139,151
chloride oxo thio trinuclear complexes, 2799
diphosphinoether hydrazide phosphine complexes, 467
Molybdenum(V)
chloride diimine dithiolate oxo thio complexes, 2813
chloride diphosphine oxo complex, 1459
chloride ether oxo magnesium complexes, 2457
cyclopentadienyl hydride silyl compounds, 1189
disulphide halide oxo thio complexes, 997
dithiolate thio copper(I) complex, 2743
oxo complexes, 359
Molybdenum(VI)
alcohol alkoxide oxo complexes, 2617
alkyl chloride mesityl oxo complexes, 463
azole oxo salicylaldimine complex, 33
dithiocarbamate seleno complex, 1311
doxycycline oxo complexes, 455
ethylenediamine oxo complex, 2057
oxo peroxide salicylaldimine complexes, 819
oxo peroxide Schiff base thiolate complexes, 973
oxo quinone complexes, 2511
Montmorillonites, 567,2729
Morpholine complexes
gallium(II), 95
Morpholinedithiocarbamate complexes, nickel(II), 2821

N

Naphthaldehyde Schiff base complexes, ruthenium(III), 2559
α-Naphthoxy compounds
zirconium, 2341
Neodymium
alcohol alkoxide oxo complexes, 1559
amidopyridine nitrate perchlorate thiocyanate water complexes, 2405
carboxylate water complexes, 1921
chloride hydrazone phenanthroline water complexes, 1491
cyclopentadienyl nitrophenoxide nitrosophenoxide complex, 27
disulphoxide perchlorate complex, 629
hydrazone complexes, 2185
sexadentate Schiff base water complex, 683
Nickel
dithiolate - dithiapyranylidene complex, 687
Nickel(0)
carbonyl chlorophosphine complexes, 2423
Nickel(II)
alkoxide chloride aluminium complexes, 1733
amine halide salicylaldimine thiocyanate thioether polydentate complexes, 823
aryls, 144,157
aryl dithiocarbamate dithiocarbonate xanthate complexes, 2821
azole chloride pseudohalide pyridine pyridine-*N*-oxide-dithiocarbazates, 2659
azole thiocyanate thioether complex, 1031

chloride diphosphine complex, 415
chloride hydrazinium water complex, 365
diamine dihydrazone diimine complexes, 859
diamine diimine oxamide tetramine Cu(II) complexes, 103
diimine pyridine Schiff base thiolate complexes, 1327
dipyridylamine pseudohalide complexes, 2725
dithiocarbamate triamine complexes, 2025
fluoride complex, 2605
halide pyridine thiocyanate complexes, 1759
hydroxyketone binucleating complexes, 1353
ketoimine complexes, 1687,2833
ketoimine pyridine thiolate complexes, 535
ketoxime complexes, 919
phenanthroline complex, 1803
pyridine pyridine-*N*-oxide-dithiocarbazate complex, 37
pyridine-*N*-oxide thiolate compound, 2651
pyridylcarbinol complexes, 2791
Schiff base thionate complexes, 179
sulphonates, 2757
Nickel(III)
dithiocarbamate triamine complexes, 2025
Niobium
aryls, 148
Niobium(-I)
carbonyl cycloheptatriene diene diphosphine phosphine complexes, 389
Niobium(0)
cycloheptatriene cyclopentadienyl iodide phosphine complexes, 389
Niobium(I)
bromide cycloheptatriene cyclopentadienyl complex, 389
Niobium(II)
chloride cycloheptatriene phosphine complex, 389
Niobium(II,III)
alcohol halide complexes, 2031
Niobium(III)
allyl cyclopentadienyl complex, 1075
Niobium(V)
alkylimide chloride pyridine complex, 1959
fluoride oxo complexes, 2605
Nitrates and nitrato complexes
copper(II), 1333,1579,1625,1675, 2225
erbium, 1079
lanthanides, 683,2405
silver(I), 1723,2687
thorium, 2399,2567,2809
uranium(VI), 2399,2567
Nitric oxide, oxidation of, 429
Nitride complexes
ruthenium, 311
Nitriles, alcoholysis, 1631
Nitrile complexes
antimony(V), boron, 2131
copper(I), 347
iron(II), 653
molybdenum(II), 433,1717,2283, 2519
palladium(II), 1513
rhenium(I,II),(II), 79
rhenium(V), 2241
ruthenium, 286
ruthenium(II,III), 653
tin(IV), titanium(IV), 2131
tungsten(II), 433,595,1717
Nitrite complexes
cobalt(III), 977
ruthenium, 1799
Nitrogen donor complexes
ruthenium clusters, 277
Nitrogen - selenium compounds, review, 2353
Nitrogen - sulphur ligand complexes, Pd(II), 2337
Nitrogen - tellurium compounds, review, 2353
3-Nitro-2,4-pentanedionates
copper(II), 1773
5-Nitrophenanthroline complexes
cobalt(II), 1787
iron(II), 703
2-Nitrophenoxides
lanthanides, 27
titanium, 1847
3-Nitrophenoxides
titanium, 1847
4-Nitrophenoxides
arsenic(V), 789
titanium, 1847
Nitrosophenoxides
lanthanides, 27
Nitrosyls
molybdenum, 429
rhenium, 1903
ruthenium, 309,583,1013,1799
NMR (^{1}H) spectra
acyls, 717,963
alcohol complexes, 337,1049
alkene complexes, 963
alkenediyl complexes, 561
alkenyl complexes, 421
alkoxides, 337,477,805,949,1049, 1153,1163,1173,1639,2065,2309
alkyls, 1147,1153,1411,1465,1897
alkylamides, 747,1215,2839
alkylidene complexes, 215
alkylidyne complexes, 215
alkylimides, 477,1423,2241
alkyne complexes, 711,2519,2523
allyls, 459,605,1075
aluminohydrides, 595
amide complexes, 1683,2075,2265
amidopyridine complexes, 2405
amine complexes, 859,977,1385, 1617,1897,2309
aminoacid complexes, 333,977
aminopyridine complexes, 1727
ammonia complexes, 2075,2495
arene complexes, 1727
arsine complexes, 2095,2523
aryls, 717,789,1153,1173,1513, 2037
arylamides, 747,1897,2241,2309
azole complexes, 33,711
binucleating hydroxyketone ligand, 1353

borane polyhderal anions, 2779
borohydrides, 1827
carbaboranes, 1497
carbaborane complex, 471
carbene complexes, 1153
carboxylates, 79,113,121,1173, 2069,2203,2283,2523
crown ligand complexes, 1545, 1877
cyanotrihydroborates, 79
cycloheptatrienyl complexes, 267
cyclometallated complexes, 255, 1203,1497,1513
cyclopentadienyls, 459,717,963, 1173,1847,1873,1903,2095,2105, 2483
diamine complexes, 1385
diaminodisulphide complexes, 1319
diboracyclohexadienes, 1497
diene complexes, 1595,2293
diimine complexes, 197,255,769, 859,1385,1491
diketonates, 121,605,1683,2293, 2463
diphosphine complexes,79,737, 867,1411,1549,1713
dithiocarbamates, 711,1311,2821
dithiophosphates, 2203
edta complexes, 2465
enol ether complexes, 1173
ether complexes, 1611,2417,2699
germyls, 1215
hydrazide complexes, 467
hydrazone complexes, 127,779, 1491,2185
hydrides, 543,595,867,1173,1189, 1713,1955,2123,2145,2729
hydroxycarboxylates, 2495
iminoether complexes, 1573,1631
iminyls, 1147
iodoalkane, 1903
isocyanide complexes, 267,963
ketoimine complexes, 535,1687
macrocyclic tetramine complexes, 1779
maltol complexes, 1539
metallaboranes, 1663
nitrile complexes, 347,595,2131, 2283
nucleoside complexes, 2465
oxime complexes, 1611,1617
penicillin complexes, 1473
phenol complexes, 1405,2683
phenoxides, 789,1847,2693
phosphido complexes, 1955,2423
phosphine complexes, 89,113,187, 467,477,543,851,963,1173,1411, 1663,1667,1857,1903,1955,2095, 2423,2483,2523
phosphine oxide complexes, 1163
phosphinoamines, 501
phosphinoenolate, 1521
phosphinothioether complexes, 1603
phosphonates, 2229
polyketones, 993
polyphosphine complexes, 1827
porphyrins, 509,885,2069
pyrazine complexes, 1699
pyrazolylamine complexes, 1595
pyrazolylborates, 215
pyridine complexes, 127,535,683, 747,769,977,1385,1727,1779
pyridine-*N*-oxide complexes, 2651
pyridinethionates, 197,837
pyridylhydrazone complexes, 2483
pyrimidinethione complexes, 1507
quinone complexes, 2511
rhodanine complexes, 1465
salicylaldimine complexes, 33
Schiff base complexes, 33,683, 771,859,1513,2833
siloxides, 1639,2699
silyls, 867,1189
silylamide complexes, 769,1203
silylene complexes, 1163
stannyl complexes, 2535
sulphinates, 963
sulphoxide complexes, 1699,2075
telluroether complexes, 2065, 2693
terpyridine complex, 1883
thiocarboxylates, 2095
thioether complexes, 561,977
thiolates, 89,535,771,851,1163, 2651
thione complexes, 351,935,1507
thiophenoxides, 851
triphosphine complexes, 2123
xanthates, 2821
ylide complexes, 1189
NMR (^{7}Li) spectra
lithium alkoxides, 805
NMR (^{11}B) spectra
boric acid catecholate complexes, 613
boron diimine fluoride complex, 2221
carbaboranes, 1497
carbaborane complex, 471
cyanotrihydroborate, 79
metallaboranes, 1663
NMR (^{13}C) spectra
acyls, 963
alcohol complexes, 337
alkene complexes, 963
alkenediyl complexes, 561
alkoxides, 337,805,949,1049, 1153,2065
alkyls, 1,1147,1153,1411,1465
alkylamides, 477
alkylidene complexes, 215
alkylidyne complexes, 215
alkylimides, 477
alkyne complexes, 711,1427,2519
allyls, 605,1075
amidate complexes, 463
amide complexes, 2265
amine complexes, 477,977
aminoacid complexes, 333,977, 2717
aminophosphine, 2737
arsine complexes, 2539
aryls, 463,717,1013,1153
azole complexes, 711
carbaboranes, 1497
carbene complexes, 1153
carbide carbonyl clusters, 1749
carbonyls, 267,433,665,711,717, 841,963,1749,1873,2105,2265, 2381
carboxylates, 113,2069
crown ligand complexes, 1545, 1877
cyanides, 1013

cycloheptatrienyls, 267
cyclometallated compounds, 255
cyclopentadienyls, 1,963,1075, 1903
diene complexes, 2293
diimine complexes, 197,255
diketonates, 605,2293,2463
diphosphine complexes, 1411, 1713,2381
dithiocarbamates, 711
edta complexes, 2465
ether complexes, 2417,2699
hydroxycarboxylates, 61,2495
hydroxyquinoline complexes, 583
iminyls, 1147
iodoalkane complexes, 1903
isocyanide complexes, 267,963
metallacycles, 1203,1497
methyl salicylate on clay minerals, 567
nucleoside complexes, 2465
penicillin complexes, 1473
phenol complex, 2683
phosphine complexes, 113,963, 1013,1411,1903,2535
phosphinoamines, 501
phosphinoenolate complexes 1521
phosphite complexes, 841
phosphonates, 2229
polyketones, 993
polyphosphine complexes, 1827
porphyrins, 2069
pyrazolylborates, 215
pyridine complexes, 977
pyridinethionate complexes, 197
pyridylcarbinol complexes, 2791
quinone complexes, 2511
rhodanine complexes, 1465
Schiff base, 2683
Schiff base complexes, 771,1327, 2833
siloxides, 2699
silyls, 841
silylamides, 769,1203
stannyl complexes, 2535
sulphinate complexes, 963
telluroether complexes, 2065
thioether complexes, 561,977
thiolates, 771
thione complexes, 351

NMR (^{15}N) spectra
nitride centred clusters, 1749

NMR (^{19}F) spectra
alkylamides, 747
allyls, 605
arylamides, 747
diketonates, 605
fluoroboron complexes, 2221
pentafluorophenyls, 2821

NMR (^{23}Na) spectra
feldspar glasses, 55
sodium crown amide ether complex, 1877

NMR (^{27}Al) spectra
aluminium alkoxide siloxides, 1639
aluminium polyphosphates, 1527
aluminohydrides, 595
feldspar glasses, 55

NMR (^{29}Si) spectra
feldspar glasses, 55
silicon diketonate thiocyanate, 2463
silicon tris- bidentate complexes, 1131
siloxanes, 1097
silyls, silylalkyls, 1177
silylene complexes, 1163

NMR (^{31}P) spectra
arsinophosphine complexes, 2153
diphosphazene complexes, 881
diphosphine complexes, 79,595, 737,899,909,1311,1411,1549, 1713,2153,2381,2611
diphosphinoether complexes, 467
hexachlorophosphate, 2217
phosphates, phosphinates, 659
phosphido complexes, 2241,2423
phosphine complexes, 89,113,187, 347,421,467,477,851,1013,1019, 1173,1411,1539,1663,1717,1857, 1903,1939,2145,2265,2423,2437, 2471,2519,2535,2641
phosphine oxide, 2437
phosphine oxide complexes, 2471
phosphine selenide, - sulphide complexes,2471
phosphinoamines, 501
phosphinoenolate complexes, 1521
phosphinothioether complexes, 1549,1603,2523
phosphinothiolate complexes, 1019
phosphites, 659
phosphite complexes, 1717
phosphonates, 2229
phosphorus methyl selenium cyclic compound, 261
phosphorus tricyanide, 1831
polyphosphates, 1527
polyphosphine complexes, 1827
triphosphine complexes, 2123
triphosphorus complexes, 2123
ylide complexes, 1189

NMR (^{63}Cu) spectra
copper(I) pyrazine complex, 1835

NMR (^{77}Se) spectra
diphosphine selenides, 2381
phosphine selenide complexes, 2471
polyselenides, 2629
selenium(II) chloride thiochloride, 1037

NMR (^{89}Y) spectra
yttrium alkoxides, 1049

NMR (^{93}Nb) spectra
niobium(III) allyl cyclopentadienyl complex, 1075

NMR (^{95}Mo) spectra
molybdenum(0) carbonyl diphosphine complexes, 2381
molybdenum(II) arsine bismuthine carbonyl cyclopentadienyl diphosphine stibine complexes, 665

NMR (^{113}Cd) spectra
cadmium dithiocarbamate mercaptoamine thioether complexes, 325

NMR (^{119}Sn) spectra
stannyl complexes, 2535
tin(II) chloride rhodium(III) complex, 1721
tin(II) cyclopentadienyl silylamides, 1203

tin(IV) chalcogenide silylamide metallacyclic compounds, 1203
tin(IV) chloride iron(0) compounds, 2105
tin(IV) halide methyl metallacyclic compounds, 1497
NMR (^{133}Cs) spectra
caesium crown ether complexes, 221
NMR (^{183}W) spectra
tungsten(0) carbonyl diphosphine complexes, 2381
NMR (^{195}Pt) spectra
platinum(II) ammonia creatinine hydroxide complexes, 799
platinum(II) azole halide complexes, 1443
platinum(II) phosphine phosphine - chalcogenide complexes, 2471
NMR (^{205}Tl) spectra
thallium methyl rhodanine complex, 1465
NMR(^{207}Pb) spectra
lead(II) alcohol alkoxide carboxylate oxide compounds, 1657
Noble gas chemistry, book review, 2851
Nomenclature, book review, 1843
Nucleoside complexes
ruthenium(III), 2465

Q

Octaethylporphyrinates, octamethylporphyrinates, Tl(III), 885
Organoiron compounds, book reviews, 1844,2086
Organolead compounds, book review, 1963
Organometallic compounds in organic synthesis, book review, 2084
Organometallic radicals, book review, 1845
Organosilanes, dehydrocoupling, 1239
Osmium
carbonyl diphosphazene complex, 881
carbonyl hydride phosphide phosphine complexes, 1955
Osmium(III)
chloride phosphine quinone complex, 2511
Osmium(IV)
aryls, 142
Osmium(VI)
hydroxycarboxylate oxalate oxo pyridine complexes, 61
Oxalate complexes
chromium(III), 2673
cobalt(III), 829,2665
osmium(VI), 61
rhodium(I,II), 2551
titanium(III), 829
Oxamide complexes
cobalt(II), 1787
copper(II), 103,1787
nickel(II), 103
Oxides and oxo complexes
chromium(VI), 753
germanium, 2347
iron(III), 1121
lead(II), 1657
magnesium, 2457
molybdenum(III,IV), 2203
molybdenum(IV), 2799
molybdenum(V), 359,997,1459, 2457,2813
molybdenum(VI), 33,455,463,819, 2057,2511,2617
neodymium, 1559
niobium(V), 2605
osmium(VI), 61
rhenium(V), 243
rhenium(VII), 2241,2647
ruthenium(III), 113
tungsten(V), 997,2235
tungsten(VI), 455,477,649,819, 2417,2617
uranium(VI), 47,779,819,1683, 2399,2511,2567
vanadium(IV), 73,2605
vanadium(V), 359
Oxime complexes
rhodium(III), 1611,1617
Oxoisobutyrates
osmium(VI), 61

P

Paeonol complexes
copper(II), 2051
Palladium
carbonyl phosphine complexes in zeolite, 673
Palladium(0)
phosphine complex, 2475
Palladium(I)
alkyne carboxylate phosphinothioether complexes, 2523
chloride thioether complexes, 561
Palladium(II)
alkenediyl chloride thioether complexes, 561
alkoxide chloride telluroether complexes, 2065
amine chloride phosphinoenolate cyclometallated complexes, 1521
aminoacid complex, 333
aryls, 145,157,166
aryl azide azole chloride diimine diketonate dithiocarbamate nitrile perchlorate pyridine salicylaldimine Schiff base cyclometallated complexes, 1513
aryl carboxylate dipyridyl thioether complexes, 2037
chloride diphosphine complex, 415
chloride hydrazinium complex, 579
chloride nitrogen - sulphur complexes, 2337
chloride phenoxide telluroether complexes, 2693

chloride phosphine thiolate complexes, 89,1343
halide hydroxide pyrimidine-thione complexes, 1507
halide phosphine pyridine selenoamide complexes, 2265
Paracyclophane complexes
ruthenium(II), 1727
PE spectra
lanthanide carboxylates, 1599
Penicillin complexes
platinum(II), 1473
Pentafluorophenyls
nickel(II), 2821
Pentaiodides
copper, 1911
Pentamethylcyclopentadienyl complexes
iron(II), 963,1177
rhenium(I),(II), 1873
rhenium(III), 877
ruthenium(II),(IV), 1173
Pentamethyldisilylmethyls
Fe(II),Hf,Ti,W(II),Zr, 1177
Pentamethylene sulphoxide complexes, Th(IV), U(VI), 2567
2,4-Pentanedionates
cobalt(III), 1405
copper(I), 645,2293
molybdenum(II), 433,605
palladium(II), 1513
silicon, 1131,2463
tungsten(II), 433
zinc, 121
2,4-Pentanedionate Schiff base complexes, Cu,Ni, 1687
Pentasulphide complexes
platinum(IV), 2501
Penta(trifluoroacetato)cyclopentadienyls, molybdenum(II), 133
Perchlorate complexes
copper(I), 347
lanthanides, 629,2405
palladium(II), 1513
Permethylpolyazine complexes
nickel(II), 859
Permutational isomerism, Jahn - Teller effect, 1587
Peroxo complexes
cobalt(III), 107
molybdenum(VI), thorium, 819,973
tungsten(VI), 649,819,973
uranium(VI), 819,973
zinc, 819
Phase transfer catalysis, Pd(0), Pt(0) phosphine complex synthesis, 2475
1,10-Phenanthroline complexes
boron, 2221
cadmium, 197
cobalt(II), 811,1787,1803
copper(II), 1327,1363,2179
europium, 1385
iron(II), 703,1803
lanthanides, 1385,1491
molybdenum(0), 2611
nickel(II), 103,1327,1803
rhodium(I,II), 2551
yttrium, 2171
zinc, 197,1803
Phenol complexes
Co(III) diketonate, 1405
tin(IV), 2683
Phenoxides
arsenic(V), 789
copper(II), 731,1653,1809
iron(III), 1809
rhenium(V), 243
ruthenium(III), 2559
titanium(IV), 1847
uranium(VI), 779
Phenyls
arsenic(V), 789
germanium, 2347
mercury, 187,1013,1465
platinum(II), 909
review, 135
rhodium(III), 187
silicon, 1231
thallium(III), 1465
tin(IV), 1085
Phenylalanine Schiff base complexes, copper(II), 2163
Phenylamido complexes
gallium, 1897
Mo(II), W(III), 2309
2-Phenylazopyridine complexes
ruthenium, 1799
1-Phenyl-1,3-butanedionates
molybdenum(II), 433
tungsten(II), 433
1-Phenyl-1,3-butanedione Schiff base complexes
cobalt(III), 1687
Cu(II), Ni(II), 1327,1687
1-Phenyldibenzophosphole complexes
gold(III), 1939
1-Phenyl-3,4-dimethylphosphole complexes, gold(III), 1939
Phenylene complexes
Fe(II), Mn(I), Re(I), 717
o-Phenylenediimine complexes
copper, 955
Phenylethenyl complexes
ruthenium(II), 421
2-Phenylethylamine Schiff base complexes, Co(III), Cu(II), Ni(II), 1687
Phenylethynyl complexes
platinum(II), 2153
2-Phenylimidazole complexes
copper(II), 893
Phenylimido complexes
rhenium(VI), 1539
Phenyl isocyanate, reaction with molybdenum(VI) complexes, 463
1-Phenyl-1,2-propanedione-2-oxime complexes, Cu(II), Ni(II), 919
2-Phenylpropionate complexes
palladium(I), 2523
Phenyl(2-pyridyl)amides
potassium, sodium, 1839
Phosphates and phosphato complexes
aluminium, 659,1527
lithium, 67
sodium, 67,2587
terbium(IV), 1479
uranium(VI), 47
Phosphido complexes
iron, 543,2423
osmium, 1955
rhenium(VII), 2241
rhodium(I), 543
ruthenium, 1955
Phosphinate complexes
aluminium, 659

Phosphine (PH_3) complexes
osmium(0), 1955
Phosphine (PR_3) complexes
chromium(0),(I), 1427
cobalt, 927
cobalt(I), 717,2535
copper(I), 347,471,645,935,2423, 2743
gallium(II), 95
gold(I), 2423
gold(III), 1939
iridium(III), 1857
iron, 203
iron(II), 717,963,2095
manganese(0), 2437
manganese(I), 717
molybdenum, 1663
molybdenum(II), 433,1705,1717, 2519
molybdenum(II,III,III), 2145
molybdenum(III), 1667
molybdenum(IV), 467
niobium(-I),(0),(II), 389
palladium, 673
palladium(0), 2475
palladium(II), 89,1343,2265
platinum(0), 2475
platinum(II), 851,1411,2153, 2471,2737
rhenium, 1903
rhenium(0), 2437
rhenium(I), 1603,1873
rhenium(V), 243,1539
rhenium(VI), 1539
rhodium(I), 543
rhodium(II), 2729
rhodium(III), 187,717,2265
ruthenium, 1013
ruthenium(II), 113,421,963,1019, 1173,2137,2265,2483
ruthenium(III), 113,2511
ruthenium(IV), 1173
silver(I), 2423
tungsten, 1663
tungsten(II), 433,1177,1717
tungsten(VI), 477
Phosphine oxide complexes
copper(II), 1091
iron(II), 1163
platinum(II), 2471
Phosphine selenides, 2641
Phosphine selenide, sulphide complexes, platinum(II), 2471
Phosphiniminates
rhenium(VII), 2241
Phosphinoamine complexes
platinum(II), 501
Phosphinoenolates
palladium(II), 1521
Phosphinothioether complexes
palladium(I), 2523
Phosphinothiolates
ruthenium(II), 1019
Phosphites
aluminium, 659
Phosphite (organo) complexes
iron(II), 841
rhenium(I), 1873
ruthenium(II), 1091
Phosphonates
lutetium, 175
Phosphorus
methyl selenium cyclic compound, 261
Phosphorus(III)
fluoroacid, 1695
tricyano-, 1831
Phosphorus(V)
chloride complex, 2217
Photochemistry
cobalt(III) hydroxide peroxide tetramine complexes, 107
molybdenum(II) carbonyl cyclopentadienyl phosphine complexes, 1705
rhenium(III) bromide carbonyl cyclopentadienyls, 877
Phthaloyl complexes
Co(I), Fe(II), Mn(I), Mo(II), Re(I), Rh(III), 717
Picolinates
rhodium(III), 187
2-Picoline complexes
gallium(II), 95
3-Picoline complexes
copper(II), 793
gallium(II), 95
osmium(VI), 61
4-Picoline complexes
copper(II), 793
gallium(II), 95
palladium(II), 1513
Platinum(0)
alkyne diphosphine complexes, 909
diphosphine complexes, 899
phosphine complex, 2475
Platinum(II)
alkoxide chloride telluroether complexes, 2065
alkyl diphosphine halocarbon complex, 993
alkyl diphosphine phosphine complexes, 1411
alkynyl aryl cyanide diphosphine halide hydride complexes, 909
alkynyl chloride cyanide diphosphine phosphine pyrazolate complexes, 2153
ammonia creatinine hydroxide complexes, 799
arsine chloride phosphine pyridine thiolate thiophenoxide binuclear complexes, 851
aryls, 145,157,166
azole halide complexes, 1443
chloride diphosphine complexes, 899
chloride hydroxide penicillin complexes, 1473
chloride hydrazinium complex, 579
chloride iminoether complexes, 1573
chloride phenoxide telluroether complexes, 2693
chloride phosphine complex, 2737
chloride phosphinoamine complexes, 501
diamine complexes, 2191
diamine halide organoamide pyridine complexes, 747
diimine cyclometallated complexes, 255
diphosphine hydride silyl

complex, 867
phosphine phosphine chalcogenide complexes, 2471
Platinum(III)
aryls, 157
Platinum(IV)
bromide diamine thioether cyclic complex, 19
chloride iminoether complex, 1573
diamine halide complexes, 2191
metallacyclic compounds, fluxionality, 1587
pentasulphide complex, 2501
Polarography
ruthenium(III) azole carbonyl chloride phenoxide Schiff base complexes, 2559
ruthenium(III) edta nucleoside complexes, 2465
Polyamine complexes
cobalt(III), 1449
Polyazine complex
nickel(II), 859
Polybutadiene oxidation, 993
Polycarboxylates
calcium, sodium, 1565
Poly(dimethylsilylenes), 1227
Polyketone synthesis, 993
Polyphosphates
aluminium, 1527
hydrolysis, 697
lithium, sodium, 67
Polyselenides, 2629
Polysulphide complexes
indium, 1069
Porphyrins
chromium(III), 373
cobalt(III), 1379
iron(III), 373
ruthenium, 315
thallium, 885,2069
tin(IV), 509
Potassium
alcohol alkoxide complexes, 337
arene siloxide complex, 2353
arylamide diamine pyridine complexes, 1839
carboxylate crown ether complexes, 1591
crown ether complex, 1025
crown ligand ether siloxide complexes, 2699
Potentiometric titrations
palladium aminoacid complex, 333
pyridylcarbinol complexes, 2791
Praseodymium
amidopyridine nitrate perchlorate thiocyanate water complexes, 2405
chloride hydrazone phenanthroline water complexes, 1491
disulphoxide perchlorate complex, 629
hydrazone complexes, 2185
sexadentate Schiff base water complex, 683
Propanediamine complexes
platinum(II),(IV), 2191
2-Propanol, solvent for copper(II) halide complexes, 2529
2-Propanol complexes
molybdenum(VI), 2617
neodymium, 1559
niobium(II,III), 2031
sodium, 2617
tantalum(II,III), 2031
tungsten(VI), 2617
Propenoates
molybdenum(II), 2273,2283
ruthenium(II,III), 2273
Propionitrile complexes
rhenium(I,II),(II), 79
tungsten(II), 1717
i-Propoxides
aluminium, 1639,1733
cobalt(II), 1733
lanthanum, 949
lead(II), 1103,1657
molybdenum(VI), 2617
neodymium, 1559
nickel(II), 1733
sodium, 2617
tungsten(VI), 477,2617
zirconium, 949
Propyldithiocarbamates
nickel(II), 2821
i-Propylthiolates
platinum(II), 851
i-Propylxanthate complexes
ruthenium(II), 421
Pulse radiolysis
copper(II) tetramine macrocyclic binucleating complex, 1373
Purine-6-thione complexes
copper(I), 935
Pyrazine complexes
copper(I), 1835
ruthenium(II), 1139,1699
Pyrazolates
platinum(II), 2153
rhenium(VII), 2241
rhodium(I), 2153
Pyrazole complexes
palladium(II), 1513
Pyrazole Schiff base thione complexes, nickel(II), 179
Pyrazolyl complexes
ruthenium, 315
Pyrazolylborates
iridium(I), 1595
tungsten(IV), 215
Pyridine complexes
barium, 769
cobalt(II), 2791
cobalt(III), 977,1779,2597
copper(II), 495,535,793,1327, 1579,1647,1675,1791,2791
europium, 1385
iron(II), 2791
lanthanides, 683,1385,2405
nickel(II), 37,535,1327,1759, 2659,2725,2791
niobium(V), 1959
osmium(VI), 61
palladium(II), 1513,2265
platinum(II), 747,851
potassium, 1839
rhodium(I), 1061
rhodium(III), 187
ruthenium, 1799
ruthenium(II), 653,1139,1727
ruthenium(II,III), 653
ruthenium(III), 1139
silver(I), 127

sodium, 1839
tin(IV), 1085
tungsten(V), 2089
uranium(VI), 779
yttrium, 1049
zinc, 2791
4-Pyridinecarboxylic acid hydrazone complexes
manganese(II), 2477
Pyridine-*N*-oxide complexes
cadmium, 2111
copper(II), 1363,1625
nickel(II), 37
thorium, 2809
Pyridine-*N*-oxidedithiocarbazates
nickel(II), 2659
Pyridine-*N*-oxide-2-thiolates
Co(III),Fe(III),Mn(II),Ni(II), 2651
Pyridinethionate complexes
cadmium, 197
ruthenium(II), 837
zinc, 197
Pyridinoacetates
silver(I), 1723
Pyridoxal phosphate Schiff base complexes, copper(II), 2163
Pyridoxates
copper(II), 2851
2-Pyridyl complexes
ruthenium, 302
2,2′-Pyridylbenzimidazole complexes, Cr(II), Cu(II), 2541
Pyridyl-2-diethylphosphonates
Rh(III), Ru(III), Zn, 2229
Pyridylhydrazone complexes
silver(I), 127
2,2′-Pyridylimidazole, -oline complexes, Cr(II), Cu(II), 2541
N-(2-Pyridyl)methyl-2-(2-aminoethyl)thioacetamide complexes, cobalt(III), 977
Pyridyl-2-phenylhydrazone complexes, ruthenium(II), 2483
N-(2-Pyridyl)pyridine-2′-carboxamide complexes
lanthanides, 2405
Pyrimidine complexes
copper(II), 873
Pyrimidinethione complexes
palladium(II), 1507
Pyrophosphates
tin(II),(IV), 377
Pyrrolidinedithiocarbamate complexes
cadmium, 325
nickel(II), 2025,2821
nickel(III), 2025
tungsten(II), 711
vanadium(IV), 1817
Pyruvic acid hydrazone complexes
manganese(II), 2477

Q

Quinaldinates
rhodium(III), 187
Quinates
osmium(VI), 61
Quinizarine complexes
manganese(II), 1929
Quinoline thioether complexes
copper(II), 1579
Quinoline-2-thione complexes
ruthenium(II), 837
Quinone complexes
manganese(II), 1929
Mo(VI), Os(III), Ru(III), U(VI), 2511
Quinquepyridine complexes
cobalt(II), 1395

R

Racemisation, aminoacids, 2163
Radiation - catalytic reduction, dinitrogen, 1007
Raman spectra
ammonia complex, 2317
binuclear complexes, 997
bromides, 997,2757
chlorides, 997,1699,2217
dicarboxylate, 61
disulphide complexes, 997
ether complexes, 95
gallium(II) compounds, 95
hydroxycarboxylates, 61
iodides, 95
molybdate, 2317
oxo complexes, 61,997
perchlorate, 2317
phosphates, phosphinates, phosphites, 659
polyiodides, 1911
pyrazine complexes, 1699
selenium(II) chloride thiochloride, 1037
sulphonates, 2757
sulphoxide complexes, 1699
thio complexes, 997
thioether complexes, 95
Relaxation times
nickel(II) ketoimine tetradentate complexes, 2833
Rhenium
alkylimide carbonyl complex, 1473
cyclopentadienyl halide haloalkane nitrosyl phosphine complexes, 1903
Rhenium(0)
carbonyl diphosphinoferrocene complexes, 2437
Rhenium(I)
carbonyl cyclopentadienyl phosphine complexes, 1873
carbonyl halogen phosphino-thioether complexes, 1603
Rhenium(I,II)
carbonyl chloride diphosphine nitrile complex, 79
Rhenium(II)
acyl aryl carbonyl sulphinyl complexes, 717
aryls, 166
carbonyl carboxylate chloride cyanotrihydroborate diphosphine nitrile complexes, 79
carbonyl cyclopentadienyl iodide phosphine complexes, 1873
Rhenium(II,III,III)
chloride sulphate complex, 741

Rhenium(III)
aryls, 152
bromide carbonyl cyclopentadienyls, 877
Rhenium(IV)
aryls, 141
Rhenium(V)
alkylimide carboxylate chloride nitrile siloxide complexes, 2241
amine chloride oxo phenoxide phosphine Schiff base complexes, 243
chloride diazenide maltol phosphine complex, 1539
Rhenium(V,VI)
alkylimide halide complexes, 2241
Rhenium(VI)
alkylimide, 2241
arylimide maltol phosphine complex, 1539
Rhenium(VII)
alkylamide alkylimide amine arylamide carboxylate cyclopentadienyl oxo phosphide phosphiniminate pyrazolate siloxide complexes, 2241
alkylimide oxo sulphonate complex, 2647
Rhodanine complexes
mercury, thallium(III), 1465
Rhodium
alkyne complexes, review, 1995
Rhodium-105, incorporation into globulin, 1617
Rhodium(I)
amine chloride diene pyridine complexes, 1061
arsine carbonyl diphosphine isocyanide pyrazolate complexes, 2153
carbonyl diene hydride phosphide phosphine iron(0) complexes, 543
carbonyl diene tripyrazolylamine complexes, 1595
Rhodium(I,II)
carboxylate chloride diimine complexes, 2551
Rhodium(II)
hydride phosphine complex, 2729
Rhodium(III)
acyl chloride phosphine complex, 717
aryls, 144,156
aryl carbonyl carboxylate phosphine pyridinecarboxylate water mercury complexes, 187
chloride amine oxime complexes, 1617
chloride ether oxime complexes, 1611
chloride pyridylphosphonate zinc complexes, 2229
halide phosphine selenoamide complexes, 2265
hydride tin(II) complex, 1721
Rubidium
alcohol alkoxide complexes, 337
crown ether complexes, 221
Ruthenium
carbonyl chloride cyanide nitrosyl phosphine thiocyanate mercury complexes, 1013
carbonyl hydride phosphide complex, 1955
carbonyl nitrogen donor cluster complexes, review, 277
carbonyl phosphine thio tungsten complexes, 447
halide hydroxyquinoline nitrosyl complexes, 583
nitrite nitrosyl phenylazopyridine complex, 1799
Ruthenium(II)
acetate phosphine complex, 113
acetonitrile cyclopentadienyl phosphine complex, 1173
acyl alkanediyl alkene carbonyl cyclopentadienyl halide phosphine complexes, 963
alkenyl carbonyl dithiocarbamate phosphine xanthate complexes, 421
aminopyridine arene chloride complexes, 1727
ammonia carbonyl chloride cyclopentadienyl diphosphine hydride complexes, 1713
ammonia crown ether pyridine complexes, 1139
ammonia dipyridyl pyridine iron(II) complexes, 653
arene chloride dimethylphosphite Cu(II) complex, 1091
carbonyl chloride diphosphine dithiocarbamate hydride phosphine phosphinothiolate thiocarbonyl xanthate complexes, 1019
carbonyl chloride phosphine selenoamide complexes, 2265
carbonyl chloride pyridinethione complexes, 837
chloride hydrazide phosphine complexes, 2137
chloride pyrazine sulphoxide complex, 1699
cyclopentadienyl phosphine pyridylhydrazone complexes, 2483
diimine complexes, 1485
Ruthenium(II),(III)
acetate complex, 829
ammonia cyanopyridine dipyridyl pyridine iron(II) complexes, 653
carboxylate chlorides, 491,2273
Ruthenium(III)
acetate oxo phosphine complex, 113
aminophenoxide arsine halide hydroxyquinoline complexes, 2137
ammonia crown ether pyridine complexes, 1139
arsine chloride quinone complex, 2511
ascorbate chloride water complex, 2711
azole carbonyl chloride phenoxide Schiff base complexes, 2559
chloride cyclopentadienyl

diphosphine complex, 1713
chloride pyridylphosphonate zinc complex, 2229
edta nucleoside complexes, 2465
Ruthenium(IV)
acetonitrile cyclopentadienyl phosphine silylene complex, 1173
aryls, 142

S

S_2N_2, $S_3N_2^{2-}$ complexes
palladium(II), 2337
Saccharinates
copper(II), 403
Salicylaldimine complexes
Cd, Co, 823
copper(II), 823,893,1653,2051
molybdenum(VI), 33,819
nickel(II), 823
palladium(II), 1513
rhenium(V), 243
thorium, 819
tungsten(VI), 819
uranium(VI), 771,819
zinc, 819,823
Salicylates
tin(IV), 509
Samarium
amidopyridine nitrate perchlorate thiocyanate water complexes, 2405
carboxylate chloride cyclopentadienyls, 1599
chloride hydrazone phenanthroline water complexes, 1491
disulphoxide perchlorate complex, 629
hydrazone complexes, 2185
hydrazone water complex, 2779
Sarcosine complexes
cobalt(III), 977
SCF - CI calculations, silanes, 1265
Schiff base complexes
cadmium, 771,823
cobalt(II), 823,1779,2785
cobalt(III), 1687,1779
copper(II), 731,823,893,1327, 1653,1687,2051,2163,2785
europium, 1385
iron(II), 2785
lanthanides, 683,1385
molybdenum(VI), 33,819,973
nickel(II), 37,179,823,859,1327, 1687,2833
palladium(II), 1513
rhenium(V), 243
ruthenium, 314
ruthenium(III), 2559
thorium, 819,973,2399
tungsten(VI), 973
uranium(VI), 779,819,973,2399
zinc, 771,823
zirconium, 819,973
Selenium
chloride thiochloride, 1037
nitrogen compounds, review, 2353
phosphorus cyclic compound, 261
polynuclear anions, 2629
sulphides, 1037
Seleno complexes
chromium, 591
cobalt, 927
germanium, 1203
iron, 203
molybdenum(VI), 1311
silicon, 1231
tin(IV), 1203
tungsten(VI), 1311
Selenoamide complexes
Pd(II), Rh(III), Ru(II), 2265
Semibenzoquinonediiminate complexes, copper, 955
Semiquinone complexes
manganese(II), 1929
Sexidentate amine complexes
Cd,Co,Cu, 409,823
iron(II), 409
lanthanides, 683
manganese(II), 409
nickel(II), 823
lead, zinc, 409
Silanes, molecular orbitals, 1265, 1285
Silicon
acetate alkoxide aryl enol-ether hydride compounds, 1173
alkoxide alkyl oxo anions, 1097
alkyls, doped with AsF_5, 1227
alkyl aryl seleno compounds, 1231
alkyl iminyls, 1147
cluster structures, molecular orbitals, 1299
diketonate thiocyanate, 2463
hydride propellanes, 1247
nitrogen compounds, book review, 1593
oxide minerals, 55
tris-bidentate complexes, 1131
Siloxanes, 1097
Siloxides
aluminium, 1367,1639
bismuth, 437
lithium, 2699
molybdenum(III), 2839
potassium, 2353,2699
rhenium(V),(VII), 2241
tungsten(III), 2839
Silver
amine thioether complex, 19
aryls, 145,160
betaine nitrate complexes, 1723, 2687
diphosphine complex, 737
phosphine iron(0) complex, 2423
pyridine pyridylhydrazone double helical complex, 127
Silyls
in dehydrocoupling reactions, 1239
iron(II), 841,1177
molybdenum(IV), 1189
platinum(II), 867
tungsten(II), 1177
tungsten(IV), 1189
Silylamides
barium, 769
Ge, Sn(II),(IV), 1203
Silylene complexes
iron(II) 1163

Sodium
alcohol alkoxide heterometallic complexes, 2617
arylamide diamine pyridine complexes, 1839
benzenedioxyacetate water calcium complex, 1565
carboxylate crown ether complexes, 1591
crown amide ether complex, 1877
diphenyldiselenophosphinate ether water complex, 2641
phosphates, 67,2587
Solid formation and dissolution modelling, 1121
Solubility diagrams
heteropolymetallic alkoxides, 2617
Solubility products
tin pyrophosphate complexes, 377
Solvated electron, reaction with Mo(V) complex, 1459
Solvent extraction
cobalt(III) diketonate phenol complexes, 1405
copper(II), nickel(II) ketoxime complexes, 919
potassium crown ether - gold chloride complex ioron pairs, 1025
rhodium(III) hydride tin(II) complex, 1721
Square antiprismatic complexes, interligand repulsions, 393
Stannyls
cobalt(I), 2535
Stibine complexes
iron(II), 2095
molybdenum(II), 665
Strontium
oxide in feldspar glass, 55
Sulphates
Co(II), Cu(II), Fe(II), 2785
rhenium(II,III,III), 741
tungsten(VI), 649
Sulphinates
cobalt(III), 1453,2847
Sulphinyl complexes
iron(II), 717,963
Mn(I), Re(I), 717
Sulphonates
Cd, Co, Cu, Fe, Ga, Ni, 2757
rhenium(VII), 2647
Sulphoxide complexes
cobalt(III), 2075
ruthenium(II), 1699
thorium(IV), uranium(VI), 2567
Sulphur - nitrogen complexes
palladium(II), 2337
Sulphur(II)
chloride selenochloride, 1037

T

Tantalum(II,III)
alcohol halide complexes, 2031
Tantalum(IV)
aryls, 148
Tantalum(V)
aryls, 138,148
fluoride complex, 2605
Tartrate complexes
osmium(VI), 61
Tellurium - nitrogen compounds, review, 2353
Telluro compounds
germanium, tin(IV), 1203
Telluroether complexes
Hg(II),Pd(II),Pt(II), 2065,2693
Terbium(III)
amidopyridine nitrate thiocyanate complexes, 2405
chloride hydrazone phenanthroline water complexes, 1491
disulphoxide perchlorate complexes, 629
hydrazone complexes, 2185
Terbium(IV)
phosphate water complex, 1479
Terpyridine complexes
copper(II), 2451
magnesium, 1883
Tetraazaannulene complexes
copper, 1911
2,3,4,5-Tetracarbahexaboranes(6), 1497
Tetracyanoethene complexes
cobalt(III), 725
Tetraethylenepentamine complexes
cobalt(III), 1449
Tetrahydrofuran complexes
bismuth, 437
gallium(II), 95
magnesium, 2457
molybdenum(II,III,III), 2145
molybdenum(V), 2457
potassium, 2699
sodium, 2641
tungsten(V), 2089
tungsten(VI), 2417
yttrium, 1049
Tetrahydropyran complexes
gallium(II), 95
Tetrahydrothiophene complexes
gallium(II), 95
Tetrakis(trimethylammoniumphenyl)-porphyrinates, Co(III), 1379
Tetramethyldiphosphine complexes
gallium(II), 95
Tetramethylethylenediamine complexes
platinum(II),(IV), 2191
potassium, sodium, 1839
2,2,6,6-Tetramethyl-3,5-heptane-dionate complexes
bismuth, 437
Tetramethylphenyls
palladium(II), 2037
2,4,4,9-Tetramethyl-1,5,9-triaza-cyclododec-1-ene complexes
nickel(II),(III), 2025
Tetramine complexes
cobalt(II), 1779,2785
cobalt(III), 107,1779
copper(II), 523,883,1373,2785
iron(II), 2785
nickel(II), 103
Tetraphenylporphyrin complexes
chromium(III), 373
iron(III), 373
thallium(III), 885,2069
tin(IV), 509
Tetraphosphates

aluminium, 1527
1,4,8,11-Tetrathiaundecane
complexes, cadmium, 325
Thallium(III)
acetate porphyrin, 2069
halide porphyrins, 885
methyl phenyl rhodanine
complexes, 1465
methyl thiobarbiturate
complexes, 517
Thenoyltrifluoroacetonates
uranium(VI), 1683
Thermal analysis
alkali polyphosphates, 67
chloride hydrazinium water
complexes, 365
chromium(III) azide porphyrin
complexes, 373
cobalt(II) diarylphosphonate
pyridine complex, 2771
copper iodide tetraazaannulene
complexes, 1911
copper(II) creatinine methoxide
complexes, 1767
copper(II) diarylphosphonate
pyridine complex, 2771
indium bromide polysulphide
complex, 1069
iron(III) azide porphyrin
complexes, 373
lanthanide chloride hydrazone
phenanthroline water
complexes, 1491
lanthanide disulphoxide
perchlorate complexes, 629
lanthanide hydrazone complexes,
2185
lanthanide water complexes, 2779
manganese(0) carbonyl diphos-
phinoferrocene complexes, 2437
mercury halide ketone thione
complexes, 351
methyl salicylate on clay
minerals, 567
molybdenum chloride hydride
nitrosyl complex, 429
molybdenum(II) acetate diamine
complexes, 2573
molybdenum(VI) ethylenediamine
oxo complex, 2057
palladium(II) hydroxide pyrim-
idinethione complexes, 1507
platinum(II) azole halide
complexes, 1443
rhenium(0) carbonyl diphosphino-
ferrocene complexes, 2437
thorium amide halide nitrate
pyridine-*N*-oxide thiocyanate
complexes, 2809
thorium halide nitrate
sulphoxide thiocyanate
complexes, 2567
tungsten(V) oxo thio xanthate
complexes, 2235
uranium(VI) acetate halide
nitrate oxo sulphoxide
thiocyanate complexes, 2567
uranium(VI) amide diketonate oxo
complexes, 1683
uranium(VI) carboxylate halide
nitrate oxo Schiff base
thiocyanate complexes,2399
Thermodynamic database
compilation, 1105,1113, 1121
Thiazolidinethione complexes
copper(I), 935
Thio complexes
cobalt, 927
copper(I), 2743
copper(II), 2351
germanium, 1203
iron, 203
mercury, 41
molybdenum(III,IV), 2203,2351
molybdenum(IV), 2799
molybdenum(V), 997,2743
tin(IV), 1203
tungsten(III,IV), 2203
tungsten(V), 997,2235,2743
tungsten(VI), 1311
Thioacetates
iron(II), 2095
Thiobarbiturates
thallium(III), 517
Thiobenzoates
iron(II), 2095
Thiocarbonyls
ruthenium(II), 1019
Thiocarboxylates
iron(II), 2095
Thiocresolates
cobalt(II), 553
Thiocyanates
cobalt(III), 2597
lanthanides, 1889,2405
mercury, 1013,2611
molybdenum(0), 2611
molybdenum(III), 323
nickel(II), 823,1031,1759,2659,
2725
ruthenium, 1013
silicon, 2463
thorium, 2399,2567,2809
uranium(VI), 2399,2567
Thioether complexes
astatine(I), 11
cadmium, 325,823
caesium, 221
cobalt(II), 823
cobalt(III), 977
copper(II), 823,1579,1647
gallium(II), 95
mercury, 1545
molybdenum(0),(II), 1549
nickel(II), 823,1031
palladium(I), 561,2523
palladium(II), 561, 2037
platinum(II), 1473
platinum(IV), 19
rhenium(I), 1603
rubidium, 221
silver, 19
tungsten(0),(II), 1549
zinc, 823
Thiolates
cadmium, 325,771
chromium(III), 2255
chromium(VI), 753
cobalt(II), 553
cobalt(III), 2651
copper(II), 535
iron, 203
iron(II), 1163
iron(III), manganese(II), 2651
molybdenum(VI), 973
nickel(II), 535,2651

palladium(II), 89,1343
platinum(II), 851
Th, W(VI), U(VI), 973
zinc, 771
zirconium, 973
Thionate, thione complexes
astatine(I), 11
cadmium, 197
copper(I), 935
mercury, 351
nickel(II), 179
palladium(II), 1507
zinc, 197
Thiophenoxides
chromium(VI), 753
cobalt(II), 553
iron, 203
platinum(II), 851
titanium(IV), 1847
Thiosalicylates
titanium(IV), 1847
Thiosemicarbazone complexxes
copper(II), 1625
1,4-Thioxan complexes
gallium(II), 95
Thiourea complexes
copper(I), 935
Thorium
amide halide nitrate
pyridine-*N*-oxide thiocyanate complexes, 2809
antipyrine-hydroxynaphthaldehyde Schiff base halide nitrate thiocyanate complexes, 2399
halide nitrate sulphoxide thiocyanate complexes, 2567
peroxide salicylaldimine complexes, 819
peroxide Schiff base thiolate complexes, 973
Thulium
amidopyridine nitrate perchlorate thiocyanate water complexes, 2405
chloride hydrazone phenanthroline water complexes, 1491
hydrazone complexes, 2185
hydrazone water complex, 2779
Tin
cluster structures, molecular orbitals, 1299
Tin(II)
chloride, reaction with Mo(IV) hydrazide complex, 467
chloride rhodium(III) complex, 1721
cyclopentadienyl silylamides, 1203
pyrophosphate complexes, 377
Tin(IV)
alkyl aryl ester iodide pyridine complexes, 1085
butyl chloride molybdenum(II) tungsten(II) complexes, 1717
carboxylate hydroxide porphyrinate water complexes, 509
chalcogenide silylamide metallacyclic compounds, 1203
chloride iron(0) compounds, 2105
chloride methyl phenol complex, 2683
chloride nitrile complexes, 2131
halide methyl metallacyclic compounds, 1497
hydride propellanes, 1247
pyrophosphate complexes, 377
Titanium(III)
aryls, 163
oxalate complexes, 829
Titanium(IV)
aminophenoxide carboxylate chloride cyclopentadienyl phenoxide thiophenoxide thiosalicylate complexes, 1847
aryls, 136,148
chloride cyclopentadienyl disilylmethyls, 1177
chloride nitrile complexes, 2131
cyclopentadienyl silyls, in dehydrocoupling reactions, 1239
fluoride complex, 2605
Tolyls
palladium(II), 2037
Triamine complexes
gallium, indium, 1951
nickel(II),(III), 2025
Triazene complexes
ruthenium, 314
3,4,5-Tribromopyrazolates
platinum(II), rhodium(I), 2153
Tri(*t*-butyl)methanol complexes
lead(II), 1657
Tri(*t*-butyl)methoxides
lead(II), 1657
Tributylphosphine complexes
molybdenum(II), 1705
palladium(II), 2265
platinum(II), 851
Rh(III), Ru(II), 2265
Trichloroacetates
erbium, neodymium, 1921
Trichlorogermyls
molybdenum(II), 2519
Tri(4-chlorophenyl)phosphine complexes
rhodium(III), 187
Trichlorosilyls
iron(II), 841
Triethanolamine complexes
barium, 2045
Triethyl betaine complexes
silver(I), 2687
Triethylenetetramine complexes
cobalt(III), 107
Triethylphosphine complexes
chromium(0), 1427
iron, 203
molybdenum(II), 665
molybdenum(II,III,III), 2145
palladium(II), 1343
platinum(II), 1411
Triethylphosphite complexes
molybdenum(II), 1705,1717
rhenium(I), 1873
tungsten(II), 1717
Trifluoroacetates
mercury, 133,187
rhenium(V),(VII), 2241
rhodium(III), 187
Trifluoromethyls
platinum(II), 993
Trifluoromethylsulphonates
Cd, Co, Cu, Fe, Ga, Ni, 2757

rhenium(VII), 2647
Trifluoropentanedionates
copper(I), 645,2293
molybdenum(II), 605
Tri(4-fluorophenyl)phosphine complexes
rhodium(III), 187
Trigonal bicapped prismatic complexes, interligand repulsions, 393
Triiodide complexes
copper, 1911
Tri(4-methoxyphenyl)phosphine complexes
rhodium(III), 187
2,4,6-Trimethylphenyls
iridium(IV), 1457
Trimethylphosphine complexes
chromium(0),(I), 1427
copper(I), 645
iridium(III), 1857
molybdenum(II), 665
niobium(-I),(0),(II), 389
palladium, 673
palladium(II), 89,1343
platinum(II), 1411
ruthenium(II),(IV), 1173
tungsten(VI), 477
Trimethylphosphite complexes
Mo(II), W(II), 1717
Trimethylsiloxides
aluminium, 1367,1639
rhenium(V),(VII), 2241
Trimethylsilyls
iron(II), 841
silicon, 1231
Trimethylsilylcyclopentadienyls
tin(II), 1203
Trimethylstannyls
cobalt(I), 2535
2,4,4-Trimethyl-1,5,9-triazacyclododec-1-ene complexes
nickel(II),(III), 2025
Triphenylarsine complexes
cobalt(I), 2535
iron(II), 2095
molybdenum(II), 665
osmium(III), 2511
platinum(II), 851
ruthenium(III), 2137
Triphenylbismuthine complexes
molybdenum(II), 665
Triphenylgermyls
tungsten(III), 1215
Triphenylmethoxides
Mo(III), W(III), 2839
tungsten(VI), 477
Triphenylphosphine complexes
cobalt, 927
cobalt(I), 717,2535
copper(I), 347,471,2423,2743
gold(I), 2423
gold(III), 1939
iron(II), 717,2095
manganese(I), 717
molybdenum, 1663
molybdenum(II), 433,665,1705, 2519
molybdenum(II,III,III), 2145
molybdenum(IV), 467
palladium(0), platinum(0), 2475
platinum(II), 851,1411
rhenium, 1903
rhenium(I), 1873
rhenium(V),(VI), 1539
rhodium(II), 2729
rhodium(III), 717
ruthenium, 1013
ruthenium(II), 113,421,963,1019, 2137,2483
ruthenium(III), 113,2511
silver(I), 2423
tungsten, 1663
tungsten(II), 433,1177
Triphenylphosphiniminates
rhenium(VII), 2241
Triphenylphosphite complexes
cobalt(I), 2535
iron(II), 841
molybdenum(II), 665
rhenium(I),(II), 1873
Triphenylsiloxides
bismuth, 437
lithium, potassium, 2699
molybdenum(III), 2839
potassium, 2699
tungsten(III), 2839
Triphenylsilyls
iron(II), 841
platinum(II), 867
Triphenylstibine complexes
iron(II), 2095
molybdenum(II), 665
Triphosphate, aluminium, 1527
Triphosphine complexes
cobalt(I), 2123
Triphosphorus complexes
cobalt(I), 2123
Tris(2-cyanoethyl)phosphine complexes,
ruthenium, 1013
ruthenium(II), 1019
1,1,1-Tris(diphenylphosphinomethyl)ethane complexes, Co(I), 2123
Tris(1-pyrazolylmethyl)amine complexes, Ir(I),Rh(I), 1595
Tris(2-pyridyl)carbinol complexes
Co,Cu,Fe,Mn,Ni,Zn, 2791
Tri-*o*-tolylphosphine complexes
platinum(II), 1411
Tri-*p*-tolylphosphine complexes
copper(I), 935
platinum(II), 851,1411
rhodium(III), 187
Tropolonates
silicon, 1131
Tungsten
book review, 2084
carbonyl phosphine polyhedral borane complex, 1663
carbonyl phosphine thio ruthenium complexes, 447
electrochemistry, book review, 1845
Tungsten(0)
carbonyl cyclopentadienyl isocyanide complexes, 267
carbonyl diphosphine complexes, 2381
carbonyl diphosphine thioether complexes, 1549
Tungsten(II)
acetonitrile aluminohydride chloride diphosphine hydride complexes, 595
acetonitrile carbonyl diketonate

iodide phosphine complexes, 433
alkyl carbonyl cyclopentadienyl silyl compounds, 1177
alkyne azole carbonyl dithiocarbamate complexes, 711
carbonyl chloride nitrile phosphine tin(IV) complexes, 1717
Tungsten(III)
alkoxide alkylamide siloxide compounds, 2839
alkoxide amine arylamide complexes, 2309
alkylamide germyl, 1215
allyl cyclopentadienyl compounds, 459
Tungsten(III,IV)
dithiophosphate thio complexes, 2203
Tungsten(IV)
alkylidene alkylidyne carbonyl pyrazolylborate complexes, 215
allyl cyclopentadienyl compounds, 459
aryls, 139,151
cyclopentadienyl silyl compounds, 1189
diphosphine hydride complexes, 595,1007,2827
Tungsten(V)
aryls, 139
chloride diphosphine complex, 595
chloride ether fluorenone pyridine complexes, 2089
dithiolate thio copper(I) complex, 2743
oxo thio xanthate complexes, 2235
Tungsten(VI)
alcohol alkoxide oxo heterometallic complexes, 2617
alkoxide alkylamide alkylimide amine chloride oxo phosphine complexes, 477
chloride ether oxo complex, 2417
diphosphine halide seleno thio complexes, 1311
disulphide halide oxo thio complexes, 997
doxycycline oxo complexes, 455
oxo peroxo salicylaldimine complexes, 819
oxo peroxo Schiff base thiolate complexes, 973
oxo peroxo sulphate complex, 649
Tyrosine Schiff base complexes
copper(II), 2163

U

Ultraphosphates, Li, Na, 67
Uranium(IV)
aryls, 147
Uranium(VI)
acetate halide nitrate oxo sulphoxide thiocyanate complexes, 2567
amide diketonate oxo complexes, 1683
antipyrine - hydroxynaphthaldehyde Schiff base halide nitrate thiocyanate complexes, 2399
carboxylate hydrazone oxo phenoxide pyridine water zinc complexes, 779
oxo peroxide salicylaldimine complexes, 819
oxo peroxide Schiff base thiolate complexes, 973
oxo phosphate complexes, 47
oxo quinone complexes, 2511
Uridine complexes
ruthenium(III), 2465

V

Vanadates
hydrolysis, 249
Vanadium(-I)
carbonylate anions, 2487
Vanadium(II)
aryls, 148,163
Vanadium(III)
aryls, 148,163
Vanadium(IV)
aryls, 137
dipyridyl iminodiacetate oxo complex, 73
dithiocarbamate halide complexes, 1817
fluoride oxo complex, 2605
hydroxyketone oxo binucleating complexes, 1353
Vanadium(V)
hydroxide hydroxyketone sulphate binucleating complexes, 1353
oxo cations, 359
vanadates, 249
Vapours, inorganic, book review, 2851
Vapour pressure
antimony(V), boron, chloride nitrile complexes, 2131
gold(III) chloride, 633
tin(IV), titanium(IV), chloride nitrile complexes, 2131
Vinyls
ruthenium(II), 421
1-Vinylimidazole complexes
molybdenum(VI), 33
Volume of activation
iron(II) diimine complex dissociation, 703
substitution, cobalt(III) chloride pentamine complex, 1449
substitution, cobalt(III) porphyrin water complex, 1379

W

Water complexes
aluminium, 659
calcium, 1569
chromium(III), 619,2389
cobalt(II), 365,2771
cobalt(III), 1379

copper(II), 365,495,941,1579, 1675,1893,2351,2771,2851
iron(II), 365,2771
iron(II,III), 2605
lanthanides, 683,1479,1491,1889, 1921,2405,2779
manganese(II), 2477
molybdenum(III,IV), 2351
nickel(II), 365
rhodium(III), 187
ruthenium(III), 2711
sodium, 1565,2641
terbium(IV), 1479
tin(IV), 509
uranium(VI), 779
yttrium, 2171
Westonite, 567

X

Xanthates
nickel(II), 2821
ruthenium(II), 421,1019
tungsten(V), 2235
Xanthosine complexes
ruthenium(III), 2465
XPE spectra
molybdenum(III,IV) acetate dithiophosphate oxo thio complexes, 2203
osmium(VI) hydroxycarboxylate oxalate oxo pyridine complexes, 61
rhenium(0) carbonyl diphosphinoferrocene complexes, 2437
X-ray crystal structures
aluminium alkoxide siloxides, 1639
aluminium siloxide, 1367
barium aminoalkoxide, 2045
bismuth alkoxide ether siloxide complexes, 437
bismuth chloride heteropoly-nuclear complexes, 123
cadmium halide pyridine-*N*-oxide complexes, 2111
calcium benzenedioxydiacetate sodium complex, 1565
calcium dicarboxylate ether water complex, 1569
chromium(III) alkoxythiolate complex, 2255
cobalt alkylimide carbonyl complex, 1423
cobalt phosphine seleno thio complexes, 927
cobalt(I) arsine carbonyl phosphine stannyl complexes, 2535
cobalt(II) acetate quinquepyridine complex, 1395
cobalt(II) diarylphosphate methanol water complex, 2771
cobalt(II) diphosphine thiolate complexes, 553
cobalt(II) hydride triphosphine triphosphorus complex, 2123
cobalt(III) amine aminoacid chloride nitrite pyridine thioether complexes, 977
cobalt(III) ammonia malate complex, 2495
cobalt(III) amine azide pyridine thiocyanate complexes, 2597
cobalt(III) arginine hydroxide complex, 2717
copper(I) borohydride polyphosphine complex, 1827
copper(I) carbaborane phosphine complex, 471
copper(I) chloride phosphine thione complex, 935
copper(I) diene diketonate complex, 2293
copper(I) diketonate phosphine complexes, 645
copper(I) phosphine thio heterometallic complexes, 2743
copper(I) pyrazine complex, 1835
copper(II) acetate chloride dipyridyl hydroxide complex, 2301
copper(II) acetate pyrimidine complex, 873
copper(II) aminoacid complex, 273
copper(II) aminoacid - pyridoxal phosphate Schiff base complexes, 2163
copper(II) azide terpyridyl complex, 2451
copper(II) azole chloride complexes, 1333
copper(II) bromide hexamine water binucleating complex, 941
copper(II) carboxylate dipyridyl water complex, 1893
copper(II) chloride diamino-pyridine complex, 1675
copper(II) chloride dimethyl-phosphite ruthenium(II) complex, 1091
copper(II) chloride dipyridylamine pyridoxate water complex, 2851
copper(II) chloride dipyrid-ylamine water complex, 495
copper(II) diamine nitrate complex, 2225
copper(II) dipyridyl complex, 101
copper(II) dipyridyl saccharinate complex, 403
copper(II) nitrate pyridine-*N*-oxide thiosemicarbazone complex, 1625
copper(II) nitrate quinoline-thioether water complex, 1579
copper(II) phenanthroline pyridine-*N*-oxide-dithiocarbazate complex, 1363
copper(II) salicylaldiminate, 2051
erbium lactam nitrate mercury complex, 1079
europium acetate carbonate pyridine Schiff base macrocyclic complex, 1385
gadolinium crown ether thiocyanate water complex, 1889
gallium alkyl amine arylamide complexes, 1897
germanium silylamide telluro

compound, 1203
gold chloride diamine complex, 19
gold(III) bromide chloride phosphine complex, 1939
gold(III) chloride complex, 1631
iminoether salt, 1631
indium bromide polysulphide complex, 1069
indium triamine complex, 1951
iridium(III) chloride phosphine complexes, 1857
iridium(IV) mesityl, 1457
iron(0) carbonyl cyclopentadienyl bismuth complex, 123
iron(0) carbonyl phosphide rhodium(I) complex, 543
iron(0) carbonyl phosphide silver(I) complex, 2423
iron(II) carbonyl hydride phosphite silyl complex, 841
iron(II) carbonyl phosphine oxide silylene thiolate complex, 1163
iron(II) carboxylate cyclopentadienyl hydrazine complexes, 483
iron(II) chloride hydrazinium water complex, 365
iron(III) cyclopentadienyl, 1741
lanthanum alcohol alkoxide complex, 1049
lithium alkoxide, 805
lithium ether siloxide complex, 2699
lutetium phosphonate complex, 175
magnesium chloride ether oxo molybdenum(V) complexes, 2457
magnesium terpyridyl complex, 1883
manganese(0) carbonyl diphosphinoferrocene complex, 2437
manganese(II) hydrazone water complex, 2477
mercury lactam erbium complex, 1079
mercury thio complex, 41
mercury thioether complex, 1545
molybdenum(0) carbonyl cyclopentadienyl bismuth complex, 123
molybdenum(II) acetate diamine complexes, 2573
molybdenum(II) aluminohydride diphosphine hydride complex, 595
molybdenum(II) carbonyl chloride phosphine stannyl complex, 1717
molybdenum(II) carbonyl cyclopentadienyl phosphine complex, 665
molybdenum(II,III,III) hydride iodide phosphine complexes, 2145
molybdenum(III) alkoxide alkylamide compounds, 2833
molybdenum(III) alkoxide amine arylamide complexes, 2309
molybdenum(III) halide phosphine complexes, 1667
molybdenum(III,IV) acetate dithiophosphate oxo thio complexes, 2203
molybdenum(IV) cyclopentadienyl hydride silyl compounds, 1189
molybdenum(V) chloride diimine dithiolate oxo thio complexes, 2813
molybdenum(V) chloride ether oxo magnesium complexes, 2457
molybdenum(V) dithiolate thio copper(I) complex, 2743
molybdenum(VI) alcohol alkoxide oxo heterometallic complex, 2617
molybdenum(VI) ethylenediamine oxo complex, 2057
neodymium alcohol alkoxide oxo complex, 1559
nickel dithiolate dithiapyranylidene complex, 687
nickel(II) azole thiocyanate thioether complex, 1031
nickel(II) chloride diphosphine complex, 415
nickel(II) imidazole pyridine-*N*-oxide - dithiocarbazate complex, 2659
nickel(II) pyridine-*N*-oxide thiolate complex, 2651
nickel(II) pyridine pyridine-*N*-oxide dithiocarbazate complex, 37
nickel(II) Schiff base thionate complexes, 179
niobium(-I) carbonyl cycloheptatrienyl diphosphine complex, 389
niobium(0) cycloheptatrienyl iodide phosphine complex, 389
niobium(III) allyl cyclopentadienyl complex, 1075
niobium(V) alkylimide chloride pyridine complex, 1959
osmium carbonyl diphosphazene complex, 881
palladium(II) chloride diphosphine complex, 415
palladium(II) chloride nitrogen - sulphur complexes, 2337
palladium(II) chloride phosphine thiolate complexes, 89,1343
phosphorus methyl selenium cyclc compound, 261
platinum(II) alkynyl diphosphine pyrazolate rhodium(I) complex, 2153
platinum(II) chloride hydrazinium complex, 579
platinum(II) chloride iminoether complex, 1573
platinum(II) chloride phosphinoamine complex, 501
platinum(II) chloride phosphine complex, 2737
platinum(II) chloride phosphine thiolate complex, 851
platinum(II) diimine cyclometallated compound, 255
platinum(IV) bromide diamine thioether cyclic complex, 19
platinum(IV) pentasulphide complex, 2501
potassium alcohol alkoxide

complex, 337
potassium arene siloxide complex, 2353
potassium arylamide diamine pyridine complexes, 1839
potassium crown ligand ether siloxide complex, 2699
rhenium alkylimide carbonyl complex, 1423
rhenium(0) carbonyl diphosphinoferrocene complex, 2437
rhenium(II) carboxylate chloride cyanotrihydroborate diphosphine nitrile complexes, 79
rhenium(II,III,III) chloride sulphate complex, 741
rhenium(V) amine chloride oxo phenoxide phosphine Schiff base complexes, 243
rhenium(V) chloride diazenide maltol phosphine complex, 1539
rhenium(VI) arylimide maltol phosphine complex, 1539
rhenium(VII) alkylimide amine carboxylate oxo phosphide siloxide complexes, 2241
rhenium(VII) alkylimide oxo sulphonate complex, 2647
rhodium(I) carbonyl diene hydride phosphide phosphine iron(0) complexes, 543
rhodium(I) carbonyl diphosphine pyrazolate platinum(II) complex, 2153
rhodium(III) carboxylate phosphine quinaldate water complex, 187
rhodium(III) chloride amine oxime complex, 1617
rhodium(III) chloride ether oxime complex, 1611
rubidium alcohol alkoxide complex, 337
ruthenium bromide hydroxyquinoline nitrosyl complex, 583
ruthenium carbonyl phosphine thio tungsten complexes, 447
ruthenium(II) aminopyridine arene chloride complexes, 1727
ruthenium(II) arene chloride dimethylphosphite copper(II) complex, 1091
ruthenium(II) cyclopentadienyl phosphine pyridylhydrazone complex, 2483
ruthenium(II,III) carboxylate chlorides, 491,2273
ruthenium(III) acetate oxo phosphine complex, 113
ruthenium(III) chloride cyclopentadienyl diphosphine complex, 1713
silicon alkyl iminyls, 1147
silver amine thioether complex, 19
silver betaine nitrate complexes, 1723,2687
silver diphosphine complex, 737
silver phosphine iron(0) complex, 2423
silver pyridine pyridylhydrazone double helical complex, 127
sodium alcohol alkoxide heterometallic complexes, 2617
sodium arylamide pyridine complexes, 1839
sodium benzenedioxydiacetate water calcium complex, 1565
sodium diphenyldiselenophosphinate ether water complex, 2641
thallium(III) fluoride porphyrin, 885
thallium(III) methyl rhodanine complex, 1465
tin(IV) alkyl aryl ester iodide complex, 1085
tin(IV) alkyl chloride phenol complex, 2683
tin(IV) carboxylate hydroxide porphyrin water complexes, 509
tin(IV) silylamide metallacyclic compound, 1203
titanium(IV) cyclopentadienyl phenoxide, 1847
tungsten carbonyl phosphine thio ruthenium complexes, 447
tungsten(0) carbonyl diphosphine thioether complex, 1549
tungsten(II) carbonyl cyclopentadienyl phosphine silyl silylalkyl complexes, 1177
tungsten(III) alkoxide alkylamide siloxide compounds, 2839
tungsten(III) alkoxide amine arylamide complexes, 2309
tungsten(III) alkylamide germyl, 1215
tungsten(III,IV) dithiophosphate thio complexees, 2203
tungsten(V) chloride diphosphine complex, 595
tungsten(V) dithiolate thio copper(I) complex, 2743
tungsten(VI) alcohol alkoxide oxo sodium complex, 2617
tungsten(VI) alkoxide alkylimide amine chloride complex, 477
tungsten(VI) chloride ether oxo complex, 2417
tungsten(VI) chloride thio complex, 1311
tungsten(VI) oxo peroxo sulphate complex, 649
vanadium(IV) dipyridyl iminodiacetate oxo complex, 73
vanadium(IV) dithiocarbamate halide complexes, 1817
yttrium hydroxide phenanthroline water complex, 2171
zinc phenanthroline pyridinethionate complex, 197
zirconium carboxylate chloride cyclopentadienyl complex, 2341
X-ray diffraction
cadmium(II) halide pyridine-*N*-oxide complexes, 2111
cadmium(II) mercaptothiazolate, 325
niobium, tantalum alcohol halide complexes, 2031
Xylyls
palladium(II), 2037

Y

Ytterbium
amidopyridine nitrate thiocyanate complexes, 2405
chloride hydrazone phenanthroline water complex, 1491
cyclopentadienyl nitrophenoxide nitrosophenoxide complexes, 27
disulphoxide perchlorate complex, 629
hydrazone complex, 2185
hydrazone water complex, 2779
Yttrium
alcohol alkoxide ether pyridine complexes, 1049
carboxylate chloride cyclopentadienyls, 1599
chloride hydrazone phenanthroline water complex, 1491
hydroxide phenanthroline water complexes, 2171

Z

Zeolite Y, formation of palladium carbonyl phosphine complexes in, 673
Zinc
carboxylate diketonate, 121
cyanide solubility product, 1105
diimine pyridinethionate complexes, 197
hydrazone phenoxide uranium(VI) complex, 779
phenanthroline complex, 1803
phosphonate ruthenium(III) complex, 2229
pyridylcarbinol complex, 2791
salicylaldimine thioether sexidentate complexes, 823
Schiff base thiolate complexes, 771
sexidentate amine complex, 409
Zirconium
alkene cyclopentadienyl diene complexes, 1
alkoxide lanthanum compounds, 949
aryls, 137
carboxylate chloride cyclopentadienyl complex, 2341
chloride cyclopentadienyl disilylmethyls, 1177
cyclopentadienyl silyls, in dehydrocoupling reactions, 1239
peroxide salicylaldimine complexes, 819
peroxo Schiff base thiolate complexes, 973